The Grand Unified Theory of Classical Physics

Dr. Randell L. Mills

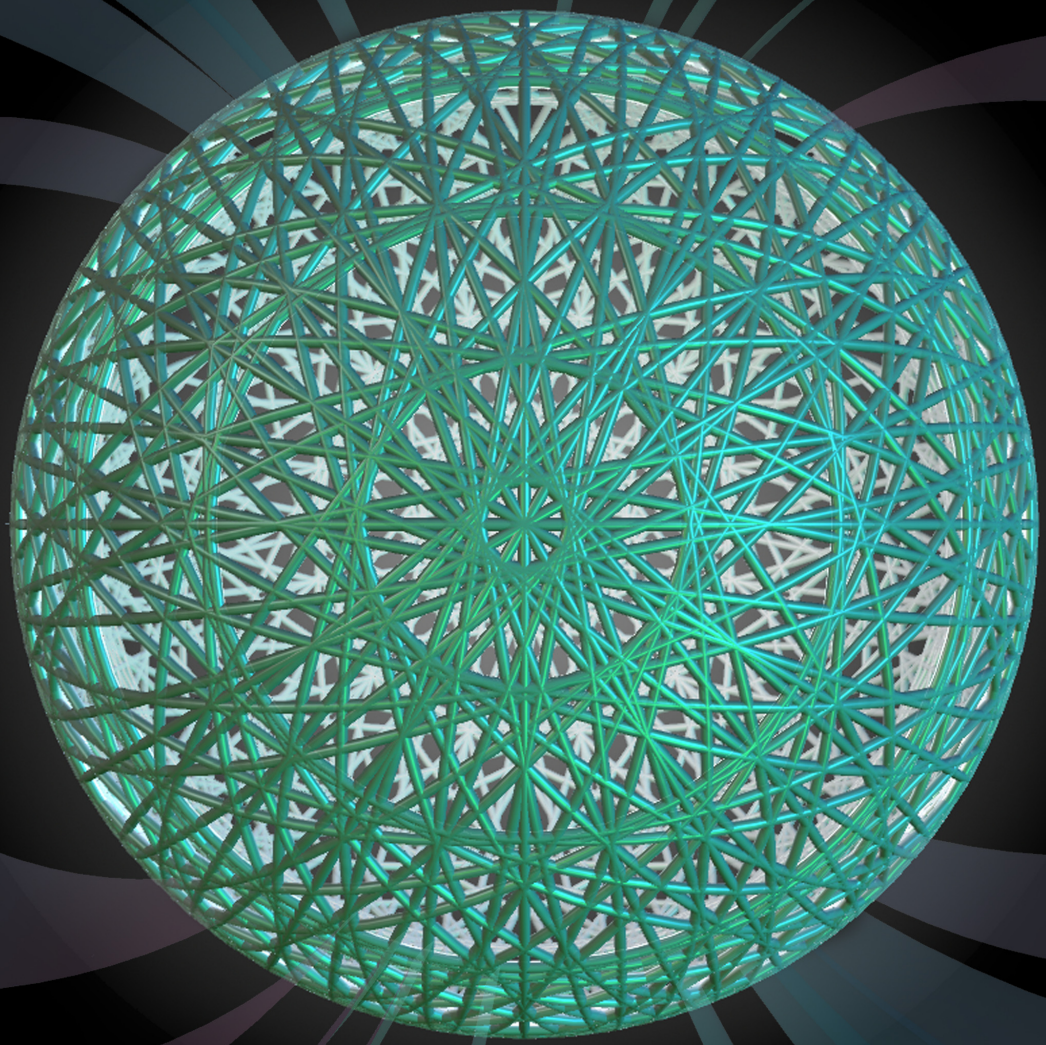

Volume I: Atomic Physics

THE GRAND UNIFIED THEORY OF CLASSICAL PHYSICS

Volume 1 of 3

THE GRAND UNIFIED THEORY OF CLASSICAL PHYSICS

BY

Dr. Randell L. Mills

April 2023 Edition
Volume 1 of 3

ISBN 979-8-218-17988-5
Library of Congress Control Number 2023905641

To Agueda, Aurora, and Randell Jr. Love you now. Will love you again in a trillion years.

TABLE OF CONTENTS

VOLUME 1 ATOMIC PHYSICS

TABLE OF CONTENTS

VOLUME 2 MOLECULAR PHYSICS Part A

TABLE OF CONTENTS

VOLUME 2 MOLECULAR PHYSICS Part B

TABLE OF CONTENTS

VOLUME 3 COLLECTIVE PHENOMENA, HIGH-ENERGY PHYSICS, & COSMOLOGY

APPENDICES

SYMBOLS

μ_0	permeability of free-space
ε_0	permittivity or capacitivity of free-space
$\eta = \sqrt{\frac{\mu_0}{\varepsilon_0}}$	intrinsic impedance of free-space
$c = \sqrt{\frac{1}{\mu_0 \varepsilon_0}}$	speed of light
$\alpha = \frac{\mu_0 e^2 c}{2h}$	fine structure constant
g	electron g factor
h	Planck constant
$\hbar$	Planck constant bar
e	fundamental charge
m_e	mass of the electron
$\mu_e = \frac{m_e m_P}{m_e + m_P}$	reduced mass of the electron
$a_0 = \frac{4\pi\varepsilon_0 \hbar^2}{e^2 m_e} = \frac{\alpha}{4\pi R_\infty}$	Bohr radius
$a_H = \frac{4\pi\varepsilon_0 \hbar^2}{e^2 \mu_e} = \frac{\alpha}{4\pi R}$	radius of the hydrogen atom
R_∞	Rydberg constant with m_e
R	Rydberg constant with μ_e
$\mu_B = \frac{e\hbar}{2m_e}$	Bohr magneton
$\Phi_0 = \frac{h}{2e}$	magnetic flux quantum
$\mu_N = \frac{e\hbar}{2m_P}$	nuclear magneton
$\lambda\!\!\!^{-}_C = \frac{\lambda_C}{2\pi} = \frac{\hbar}{mc}$	Compton wavelength bar
$\lambda\!\!\!^{-}_{Ce} = \frac{\lambda_{Ce}}{2\pi} = \alpha a_0 = \frac{\hbar}{m_e c} = \frac{\alpha^2}{4\pi R_\infty}$	electron Compton wavelength bar
G	Newtonian gravitational constant
m_μ	rest mass of the muon
m_τ	rest mass of the tau
m_N	rest mass of the neutron
m_P	rest mass of the proton

Apparently there is color, apparently sweetness, apparently bitterness; actually there are only atoms and the void.

Democritus 420 BC

And God said, “Let there be light”; and there was light. And God saw that the light was good; and God separated the light from the darkness.

Genesis 1:3

All truth goes through three steps. First, it is ridiculed. Second, it is violently opposed, and finally it is accepted as self-evident.

Arthur Schopenhauer
German philosopher

We must be grateful to God that He created the world in such a way that everything simple is true and everything complicated is untrue.

Gregory Skovoroda
18th-century Ukrainian philosopher

One of the principal objects of theoretical research in any department of knowledge is to find the point of view from which the subject appears in its greatest simplicity.

Josiah Willard Gibbs

PREFACE

Typically freshman students are introduced to classical laws that they apply to physical problems that can be understood intuitively and solved in closed form. As they advance to the second year, they are introduced to a contradictory view—that the atomic-scale world is nonphysical, counterintuitive, and incapable of being understood in physical, intuitive terms. In addition, they are asked to take for granted many fantastical concepts such as electrons being probability waves having an infinite number of energies and positions simultaneously, until measured, spooky actions at a distance, and virtual particles which occupy every point in space but can not be detected. With the introduction of quantum mechanics, which is not a theory of physical reality, students are taught to abandon all that they initially learned for laboratory scale systems and to accept that these laws do not apply to atomic systems; even though, they learned by direct experimental observation that these laws worked perfectly well and that laboratory scale objects are made up of atoms.

This non-physical treatment of atomic electrons is propagated into molecular theory. Repulsion between opposite charges is an undeniable reality; yet quantum theoreticians teach the opposite: chemical bonding is due to negative charges overlapping wherein the more negative charges occupying the same space, the stronger the bond; except that the electrons are also simultaneously repulsive requiring the addition of quantum mechanical wave function electron-electron repulsion terms. Even regions of empty space devoid of nuclei and electrons together with many other ad hoc, inconsistent, often nonphysical, and non-unique terms further comprise the quantum mechanical treatment of the nature of the chemical bond.

Many paradoxes and internal inconsistencies arise in quantum mechanics such as the requirement that two or more contradictory results exist simultaneously, the existence of infinities, non-locality, and violation of causality, to mention a few. Unlike the solutions learned in the freshman year, none of the solutions are unique—algorithms to remove infinities and to add fantastical corrections are totally discretionary [1-17]. One exception is the one-electron atom, but the Schrödinger equation is not a directly experimentally testable relationship. Rather, it is postulated. The solutions make no physical sense. Electron spin is missed completely. And, in many cases, the solutions contradict experimental observations [1-17].

To add to this confusion, Newton's Laws of mechanics are presented as invalid. With the assumption of Galilean transformations, they fail to remain invariant at high speed. Special relativity is introduced as an independent mechanics theory based on the constant maximum of the speed of light, which was demonstrated by the Michelson-Morley experiment. But, this experiment addressed light propagation and not mechanics, except for disproving the ether and a universal reference frame in the sense of the speed of light. Maxwell's equations, which govern light propagation, remain since they are consistent with special relativity and predict c based on universal properties of spacetime. No connection to mass or mechanics is given despite the result of the equivalence of mass and electromagnetic energy from special relativity. There is no connection to particle masses and atomic theory. And, the infinite sea of virtual particles of atomic theory is paradoxically an ether which was abandoned with special relativity.

Furthermore, it is taught that the validity of Maxwell's equations is restricted only to the macro-scale and that they do not apply to the atomic scale. This is inconsistent with the application of special relativity to the mechanics of atomic particles at high speed and the radiation of accelerating atomic particles wherein, paradoxically, Maxwell's equations give the electromagnetic wave equation that governs the emitted radiation. Yet, when the particle motion is thought of as a current, Maxwell's equations predict the radiation of atomic particles as well. Then, contradictory, postulated quantum mechanical rules apply to the radiation or stability of electrons in atoms, which should be treated electrodynamically. Neither a special relativistic or Maxwellian approach to the radiation is deemed to apply even though the Maxwellian Coulomb potential and special relativistic corrections to the electron mass are invoked. Even more disconcerting is that supposedly special relativity is the basis of electron spin in the Dirac equation. But, the solution requires an infinite sea of virtual particles that is equivalent to the ether. This constitutes a glaring internal inconsistency because the absence of both an ether and an absolute frame is the basis of special relativity in the first place. In addition, considering the simplest atom, hydrogen, no physical mechanism for the existence of

discrete radiative energy levels or the stability of the $n = 1$ state exists—only circular reasoning between the empirical data and a postulated wave equation with an infinite number of solutions that was parameterized to match the Rydberg lines [1-17].

Furthermore, the elimination of absolute frame by special relativity results in the elimination of inertial mass and Newton's Second law, foundations of mechanics, and gives rise to the twin paradox and an infinite number of energy inventories of the universe based on the completely arbitrary definition of the observer's frame of reference. Newton's Law of gravitation is also to be unlearned. It is replaced by a postulated tensor relationship that only applies to massive gravitating objects. The replacement theory is explained in terms of warping of spacetime without any connection to the physical laws learned as a freshman or any connection to atoms that make up the massive gravitating bodies. General relativity predicts singularities and a deceleration cosmology—the opposite of that which is observed [18-19]. It is to be accepted with quantum mechanics as the correct atomic theory even though these theories are mutually incompatible. It is further disconcerting that the Uncertainty Principle of quantum mechanics—one of its fundamental tenets—predicts a continuum of particle masses and gives no mechanism for the existence of atomic particles of precise inertial and gravitational mass in the first place. And, the infinite sea of virtual particles and vacuum energy fluctuations throughout the entire universe requires an infinite cosmological constant that is obviously not observed [20].

This confused approach to physics is not due to nature, and it can be avoided. Physics can become transparent and intuitive on all scales and understood conceptually at all levels of specialization. The same is true for chemistry wherein the multitudes of ad hoc, nonphysical, inconsistent, nonunique, adjustable atomic and molecular modeling algorithms of quantum theory are replaced by exact physical solutions comprising fundamental constants only [3-7]. The fundamental laws of physics and chemistry of Maxwell's equations and Newton's Laws of mechanics and gravitation were developed after direct experimental observation of phenomena such as electricity and magnetism, mechanics, and gravity. Electricity and magnetism were unified with the prediction and later confirmation of electromagnetic waves. These laws, developed in the mid 1800's, with the extension to the atomic scale and taking into account the appropriate spacetime metric are sufficient for describing all phenomena in the universe. For objects moving with speeds approaching the speed of light, Newton's Laws must include the limiting maximum speed that is inherent in Maxwell's equations and determined by the permeability and permittivity of spacetime. In mechanics, the metric is Minkowskian wherein the speed relative to light speed must be invoked and Galilean transformations become Lorentzian. Similarly, when a photon transforms to a particle, any signal capable of transporting energy with a limiting velocity must propagate as a light wave front, and the limiting velocity is the speed of light. Thus, for particle production, the electromagnetic front of the photon and the gravitational front due to the particle must have a limiting speed c, the speed of light. As a consequence, the metric is required to be the Schwarzschild metric rather than Minkowskian. Specifically, fundamental particle production occurs when the energy of the particle given by the Planck equation, Maxwell's Equations, and Special Relativity is equal to mc^2, and the proper time is equal to the coordinate time according to Schwarzschild metric. The gravitational equations with the equivalence of the particle production energies permit the equivalence of mass-energy and the absolute spacetime wherein a *"clock" is defined which measures "clicks" on an observable in one aspect, and in another, it is the ruler of spacetime of the universe with the implicit dependence of spacetime on matter-energy conversion*. The masses of the leptons, the bosons, the quarks, and nucleons are derived from this metric of spacetime. Then, the gravitational equations with the equivalence of the particle production energies require the conservation relationship of mass-energy, $E = mc^2$, and spacetime, $\frac{c^3}{4\pi G} = 3.22\ X\ 10^{34}\ \frac{kg}{\sec}$. Spacetime expands as mass is released as energy which provides the basis of absolute space and the atomic, thermodynamic, and cosmological arrows of time. The observations of the acceleration of the cosmic expansion, the absence of time dilation in redshifted quasars, and the absence of a Big Bang origin of the universe confirm the absolute nature of spacetime.

With the conditions of the metric being Minkowskian for Newtonian mechanics and the Schwarzschild metric for Newtonian gravity, all of the fundamental laws of nature are directly derived from experiments. The universe is not mathematical; it is physical. A separate theory for near light speed mechanics, special relativity as it now exists, is unnecessary and incomplete. For example, in addition to the problems raised previously, the famous equation $E = mc^2$ does not predict fundamental particle masses, inertial or gravitational or why they are equivalent. Furthermore, separate theories of atomic physics such as quantum mechanics and quantum electrodynamics, separate nuclear theories such as quantum chromodynamics, a separate theory for particles such as the standard model, a separate theory for gravity, general relativity as it now exists, and separate theories for cosmology such as the Big Bang, inflation, and dark energy are artificial, internally inconsistent, incorrect, incomplete, and not based on physical laws. The correct basis of the spacetime relationships of special relativity and general relativity are inherent in the classical laws that further predict all natural phenomena of physics and chemistry and compositions of matter and energy of any complexity from the scale of quarks to the cosmos in terms of the fundamental constants of nature only.

REFERENCES

1. R. L. Mills, "Classical Quantum Mechanics," Physics Essays, Vol. 16, No. 4, December, (2003), pp. 433-498.
2. R. L. Mills, "Physical Solutions of the Nature of the Atom, Photon, and Their Interactions to Form Excited and Predicted Hydrino States," Phys. Essays, Vol. 20, No. 3, (2007), pp.403-460.

3. R. L. Mills, "Exact Classical Quantum Mechanical Solutions for One- Through Twenty-Electron Atoms," Physics Essays, Vol. 18, (2005), pp. 321-361.
4. R. L. Mills, "The Nature of the Chemical Bond Revisited and an Alternative Maxwellian Approach," Physics Essays, Vol. 17, (2004), pp. 342-389.
5. W. Xie, R. L. Mills, W. Good, A. Makwana, B. Holverstott, N. Hogle, "Millsian 2.0: A Molecular Modeling Software for Structures, Charge Distributions and Energetics of Biomolecules," Physics Essays, Vol. 24, (2011) 200–212.
6. R. L. Mills, B. Holverstott, W. Good, A. Makwana, "Total Bond Energies of Exact Classical Solutions of Molecules Generated by Millsian 1.0 Compared to Those Computed Using Modern 3-21G and 6-31G* Basis Sets," Phys. Essays, Vol. 23, (2010), 153–199; doi: 10.4006/1.3310832.
7. https://millsian.com.
8. R. L. Mills, "Maxwell's Equations and QED: Which is Fact and Which is Fiction," Vol. 19, (2006), pp. 225-262.
9. R. L. Mills, "Exact Classical Quantum Mechanical Solution for Atomic Helium Which Predicts Conjugate Parameters from a Unique Solution for the First Time," Phys. Essays, Vol. 21, No. 2, pp. 103-141.
10. R. L. Mills, "The Fallacy of Feynman's Argument on the Stability of the Hydrogen Atom According to Quantum Mechanics," Annales de la Fondation Louis de Broglie, Vol. 30, No. 2, (2005), pp. 129-151.
11. R. Mills, "The Grand Unified Theory of Classical Quantum Mechanics," Int. J. Hydrogen Energy, Vol. 27, No. 5, (2002), pp. 565-590.
12. R. Mills, "The Nature of Free Electrons in Superfluid Helium—a Test of Quantum Mechanics and a Basis to Review its Foundations and Make a Comparison to Classical Theory," Int. J. Hydrogen Energy, Vol. 26, No. 10, (2001), pp. 1059-1096.
13. R. Mills, "The Hydrogen Atom Revisited," Int. J. of Hydrogen Energy, Vol. 25, Issue 12, December, (2000), pp. 1171-1183.
14. V. F. Weisskopf, Reviews of Modern Physics, Vol. 21, No. 2, (1949), pp. 305-315.
15. P. Pearle, Foundations of Physics, "Absence of radiationless motions of relativistically rigid classical electron," Vol. 7, Nos. 11/12, (1977), pp. 931-945.
16. A. Einstein, B. Podolsky, N. Rosen, Phys. Rev., Vol. 47, (1935), p. 777.
17. F. Laloë, "Do we really understand quantum mechanics? Strange correlations, paradoxes, and theorems," Am. J. Phys. 69 (6), June 2001, 655-701.
18. R. M. Wald, *General Relativity*, University of Chicago Press, Chicago, (1984), pp. 91-101.
19. N. A. Bahcall, J. P. Ostriker, S. Perlmutter, P. J. Steinhardt, Science, May 28, 1999, Vol. 284, pp. 1481-1488.
20. M. M. Waldrop, Science, Vol. 242, December 2, (1988), pp. 1248-1250.

INTRODUCTION

GENERAL CONSIDERATIONS

Toward the end of the 19th century, many physicists believed that all of the principles of physics had been discovered. The accepted principles, now called ***classical physics***, included laws relating to Newton's mechanics, Gibbs' thermodynamics, LaGrange's and Hamilton's elasticity and hydrodynamics, Maxwell-Boltzmann molecular statistics, and Maxwell's equations. However, the discovery that the intensity of blackbody radiation goes to zero, rather than infinity as predicted by the prevailing laws, provided an opportunity for new principles to be discovered. In 1900, Planck made the revolutionary assumption that energy levels were quantized, and that atoms of the blackbody could emit light energy only in amounts given by $h\nu$, where ν is the radiation's frequency and h is a proportionality constant (now called Planck's constant). This assumption also led to our understanding of the photoelectric effect and ultimately to the concept of light as a particle called a photon. A similar course arose in the development of the model of the electron. In 1923, de Broglie suggested that the motion of an electron has a wave aspect where the wavelength, λ, is inversely proportional to the electron's momentum, p, as $\lambda = \frac{h}{p}$. This concept seemed unlikely according to the familiar properties of electrons such as charge, mass and adherence to the laws of particle mechanics. But the wave nature of the electron was confirmed by Davisson and Germer in 1927, by observing diffraction effects when electrons were reflected from metals.

Experiments by the early part of the 20th century had revealed that both light and electrons behave as waves in certain instances and as particles in others. This was unanticipated from preconceptions about the nature of light and the electron. Early 20th century theoreticians proclaimed that light and atomic particles have a "wave-particle duality" that was unlike anything in our common-day experience. The wave-particle duality is the central mystery of the presently accepted atomic model, ***quantum mechanics*** (QM), the one to which all other mysteries could ultimately be reduced. The central equation, the Schrödinger equation, and its associated postulates, are now the basis of quantum mechanics, and it is the basis for the world view that the atomic realm including the electron and photon cannot be described in terms of "pure" wave and "pure" particle but in terms of a wave-particle duality. The wave-particle duality based on the fundamental principle that physics on an atomic scale is very different from physics on a macroscopic scale is central to present day atomic theory [1]. Further founding assumptions maintained from the earlier theories of Bohr and Schrödinger to what is dubbed "modern quantum mechanics" are that phenomena such as stability, quantization, and spin are intrinsic aspects of matter at the atomic scale and the electron is a probability wave requiring that the electron have infinite numbers of positions and energies including negative and infinite energies simultaneously. It is inherent that physical laws such as Maxwell's equations, Newton's laws, conservation of energy and angular momentum are not exactly obeyed. The exactness and determinism of classical physics are replaced by the Heisenberg Uncertainty Principle, an inequality defining the limitations of the existence of physical reality that has recently been tested for the first time and experimentally disproved [2]. Recently a new measuring technique that exploits superposition (i.e. interference) of two short pulses of light with different wavelengths circumvented the limitation formulated by the father of quantum physics, Werner Heisenberg, in 1927. According to Heisenberg's uncertainty principle (HUP), it is not possible to determine the position and the speed of an electron at the same instant. However, Isinger et al. [3] have shown definitively that it can be done and thereby experimentally disproving the HUP. Since the HUP is an inherent consequence of the theory of quantum mechanics (QM), QM is proven wrong as well.

The Schrödinger equation was originally postulated in 1926 as having a solution of the one-electron atom. It gives the principal energy levels of the hydrogen atom as eigenvalues of eigenfunction solutions of the Laguerre differential equation. But, as the principal quantum number n>>1, the eigenfunctions become nonsensical. Despite its wide acceptance, on deeper

inspection, the Schrödinger solution is plagued with many failings as well as difficulties in terms of physical interpretations that have caused it to remain controversial since its inception. Only the one-electron atom may be solved without approximations, but it fails to predict electron spin, leads to models with nonsensical consequences such as negative energy states of the vacuum, infinities, and negative kinetic energy, and it fails to predict the stability of the atomic hydrogen $n=1$ state except for an arbitrary definition[1] [4-15]. In addition to many predictions that simply do not agree with observations even regarding the one-electron atom [4-20], the Schrödinger equation predicts noncausality, nonlocality, spooky actions at a distance or quantum telepathy, perpetual motion, and many internal inconsistencies where contradicting statements have to be taken true simultaneously. The behavior of free electrons in superfluid helium is but one example of a phenomenon that forces the issue of the meaning of the wavefunction. Electrons form bubbles in superfluid helium, which reveal that the electron is real and that a physical interpretation of the wavefunction is necessary. Furthermore, when irradiated with light of energy of about a 0.5 to several eV [21], the electrons carry current at different rates as if they exist with different sizes. It has been proposed that the behavior of free electrons in superfluid helium can be explained in terms of the electron breaking into pieces at superfluid helium temperatures [21]. Yet, the electron has proven to be indivisible even under particle accelerator collisions at 90 GeV (LEPII). The nature of the wavefunction must now be addressed. It is time for the physical rather than the mathematical nature of the wavefunction to be determined.

A new approach has been developed to explain the seemingly mysterious physics of the atomic scale. The theory of ***classical physics*** (CP) now applied correctly to solving the structure of the electron is based on the foundation that laws of physics valid in the macroworld *do hold true* in the microworld of the atom. In the present case, the predictions, which arise from the equations of light and atomic particles are completely consistent with observation, including the wave-particle duality of light and atomic particles. Furthermore, it is shown herein that the quantization of atomic energy levels arises classically without invoking new physics. Continuous motion such as electronic transitions between quantized states and translational motion restores continuity and causality with the continuous nature of spacetime itself restored consistent with first principles and observation. Using Maxwell's equations, *the structure of the electron is derived as a boundary-value problem wherein the electron comprises the source current of time-varying electromagnetic fields during transitions with the constraint that the bound* $n=1$ *state electron cannot radiate energy*. The postulates and mathematical constructs of quantum mechanics are erroneous. Physical laws are shown to apply to the atomic scale in refutation to QM. This issue of treating the wavefunction physically is even more imperative given that classical physics predicts hydrogen atomic transitions below the inalienable quantum "ground state" and these predictions are experimentally confirmed [22-42] with the further result that the corresponding fractional principal quantum states match the observations of free electrons in superfluid helium [14]. (See Free Electrons in Superfluid Helium are Real in the Absence of Measurement Requiring a Connection of ψ to Physical Reality section.)

QM has never dealt with the nature of fundamental particles. Rather, it postulates the impossible situation that they occupy no volume; yet are everywhere at once. In contrast, CP solves the structure of the electron using the constraint of nonradiation based on Maxwell's equations. CP gives closed-form physical solutions for the electron in atoms, the free electron, and excited states that match the observations. With these solutions, conjugate parameters can be solved for the first time, and atomic theory is at last made predictive and intuitive. Application of Maxwell's equations precisely predicts hundreds of fundamental spectral observations and atomic and molecular solutions in exact equations with no adjustable parameters (fundamental constants only). Moreover, unification of atomic and large-scale physics, the ultimate objective of natural theory, is enabled. The result gives a natural relationship between Maxwell's equations, special relativity, and general relativity. CP holds over a scale of spacetime of 85 orders of magnitude—it correctly predicts the nature of the universe from the scale of the quarks to that of the cosmos.

The Maxwellian approach allows the solution of previously intractable problems such as the equations of the masses of fundamental particles. Exemplary relations between fundamental particles are shown in Table I.1.

[1] The Schrödinger equation can only yield integer eigenvalue solutions by selection or definition from an infinite number of possibilities since the solution is over all space with no boundary (i.e. 0 to ∞). In contrast, wave equation solutions with integers are common for boundary-constrained systems such as waveguides and resonators.

Table I.1. The relations between the lepton masses and neutron to electron mass ratio are given in terms of the dimensionless fine structure constant α only.

$$\frac{m_\mu}{m_e}=\left(\frac{\alpha^{-2}}{2\pi}\right)^{\frac{2}{3}}\frac{\left(1+2\pi\frac{\alpha^2}{2}\right)}{\left(1+\frac{\alpha}{2}\right)}=206.76828 \qquad (206.76827)^{a}$$

$$\frac{m_\tau}{m_\mu}=\left(\frac{\alpha^{-1}}{2}\right)^{\frac{2}{3}}\frac{\left(1+\frac{\alpha}{2}\right)}{\left(1-4\pi\alpha^2\right)}=16.817 \qquad (16.817)$$

$$\frac{m_\tau}{m_e}=\left(\frac{\alpha^{-3}}{4\pi}\right)^{\frac{2}{3}}\frac{\left(1+2\pi\frac{\alpha^2}{2}\right)}{\left(1-4\pi\alpha^2\right)}=3477.2 \qquad (3477.3)$$

$$\frac{m_N}{m_e}=\frac{12\pi^2}{1-\alpha}\sqrt{\frac{\sqrt{3}}{\alpha}}\frac{\left(1+2\pi\frac{\alpha^2}{2}\right)}{\left(1-2\pi\frac{\alpha^2}{2}\right)}=1838.67 \qquad (1838.68)$$

[a] Experimental according to the 1998 CODATA and the Particle Data Group [43-44].

CP successfully predicted the mass of the top quark before it was reported and correctly predicted the acceleration of the expansion of the universe before it was observed [45]. It correctly predicts the behavior of free electrons in superfluid helium and further predicts the existence of new states of hydrogen that are lower in energy than the $n=1$ state that represents a new energy source and a new field of chemistry that has far reaching technological implications in power generation, materials, lighting, and lasers. The existence of such states has been confirmed by the data presented in over 100 published journal articles and over 50 independent test reports and articles [22].

CP APPROACH TO THE SOLUTION OF THE BOUND ELECTRON

CP solves the electron by a different approach than that used to solve the Schrödinger wave equation. Rather than using a postulated wave equation with time eliminated in terms of the energy of the electron in a Coulomb field and solving the charge wave (Schrödinger interpretation) or the probability wave (Born interpretation), the solution for the scalar (charge) and vector potential (current) functions of the electron are sought based on first principles. Since the hydrogen atom is stable and nonradiative, the electron has constant energy. Furthermore, it is time dynamic with a corresponding current that serves as a source of electromagnetic radiation during transitions. The wave equation solutions of the radiation fields permit the source currents to be determined as a boundary-value problem. These source currents match the field solutions of the wave equation for two dimensions plus time when the nonradiation condition is applied. Then, the mechanics of the electron can be solved from the two-dimensional wave equation plus time in the form of an energy equation wherein it provides for conservation of energy and angular momentum, as given in the Electron Mechanics and the Corresponding Classical Wave Equation for the Derivation of the Rotational Parameters of the Electron section.

Specifically, CP first assumes that the functions that physically describe the mass and charge of the electron in space and time comprise time-harmonic multipole source currents of time-varying electromagnetic fields between transitions. Rather than use the postulated Schrödinger boundary condition: "$\Psi\to 0$ as $r\to\infty$," which leads to a purely mathematical model of the electron, the constraint is based on the experimental observation that the moving charge must not radiate in the $n=1$ state of hydrogen. The condition for nonradiation based on Maxwell's equations after Haus [46] is that its spacetime Fourier transform does not possess components that are synchronous with waves traveling at the speed of light. Jackson [47] gives a generalized expansion in vector spherical waves that are convenient for electromagnetic boundary-value problems possessing spherical symmetry properties and for analyzing multipole radiation from a localized source distribution. The special case of nonradiation determines that the current functions are confined to two-spatial dimensions plus time and match the electromagnetic wave-equation solutions for these dimensions. The boundary-value solutions for the current-density functions comprise spherical harmonic functions and time harmonic functions confined to two dimensions (θ and ϕ) plus time. In order for the current to be positive definite, a constant function corresponding to the electron spin function is added to each of the spherical harmonic functions corresponding to orbital angular momentum to give the charge (mass)-density functions of the bound electron as a

function of time called an electron atomic orbital. The integral of the constant function over the atomic orbital is the total charge (mass) of the electron. The integral of a spherical harmonic function over the atomic orbital is zero; thus, it modulates the spin function. These functions comprise the well-known s, p, d, f, etc. electrons or orbitals. In the case that such an electron state arises as an excited state by photon absorption, it is radiative due to a radial dipole term in its current-density function since it possesses spacetime Fourier components synchronous with waves traveling at the speed of light, as shown in the Instability of the Excited States section.

The excited states involving the corresponding multipole photon radiation are solved including the radii of the atomic orbitals using Maxwell's equations with the traditional source current boundary constraints at the electron. Quantization arises from the equation of the photon and the electron—not from the solution of the electron alone. After all, each solution models an excited state created by the absorption of a photon. The solutions are analogous to those of excited resonator modes except that the cavity is dynamic. The photon field is described by a Dirac delta function at the radius of the electron, $\delta(r-r_n)$, and due to relativistic effects the field is radially local at the electron. The field lines from the proton superimpose with those of the photon at the electron and end on the current-density function of the electron such that the electric field is zero for $r > r_n$, where r_n is the radius of the electron. The trapped photons are solutions of Maxwell's equations. The electrodynamic field of the photon is a constant function plus a time and spherical harmonic function that is in phase with source currents at the electron, which is given by a constant plus a time and spherical harmonic function. Only particular solutions are possible as resonant photons of the electron, which is a dynamic resonator cavity. The results are in agreement with first principle physics and experimental observations of the hydrogen atom, excited states, free electron, and free space photon including the wave particle duality aspects.

SPIN AND ORBITAL PARAMETERS ARISE FROM FIRST PRINCIPLES ONLY IN THE CASE OF CP

An electron is a two-dimensional spherical surface, called an *electron atomic orbital*, that can exist in a bound state only at specific radii r_n from the nucleus. (See Figures I.1 and I.2 for a pictorial representation of an atomic orbital.) The result for the $n=1$ state of hydrogen is that the charge-density function remains constant with each point on the surface moving at the same angular and linear velocity. The constant function corresponds to the spin function that has a corresponding spin angular momentum that may be calculated from $\mathbf{r}\times\mathbf{p}$ applied directly to the current-density function that describes the electron. The radius of the nonradiative ($n=1$) state is solved using the electromagnetic force equations of Maxwell relating the charge and mass-density functions wherein the angular momentum of the electron is $\hbar$ (Eq. (1.253)). The reduced mass arises naturally from an electrodynamic interaction between the electron and the proton, rather than from a point mass revolving around a point nucleus in the case of Schrödinger wave equation solutions, which presents an internal inconsistency since the wave functions are spherically symmetrical.

CP gives closed form solutions for the resonant photons and excited state electron functions. The free space photon also comprises a radial Dirac delta function, and the angular momentum of the photon given by $\mathbf{m}=\int\frac{1}{8\pi c}\mathrm{Re}\left[\mathbf{r}\times(\mathbf{E}\times\mathbf{B}^*)\right]dx^4=\hbar$ in the Photon section is conserved for the solutions for the resonant photons and excited state electron functions. It can be demonstrated that the resonance condition between these frequencies is to be satisfied in order to have a net change of the energy field [48]. In the present case, the correspondence principle holds. That is the change in angular frequency of the electron is equal to the angular frequency of the resonant photon that excites the resonator cavity mode corresponding to the transition, and the energy is given by Planck's equation. The predicted energies, Lamb shift, fine structure splitting, hyperfine structure, resonant line shape, line width, selection rules, etc., are in agreement with observation.

The radii of excited states are solved using the electromagnetic force equations of Maxwell relating the field from the charge of the proton, the electric field of the photon, and charge and mass-density functions of the electron wherein the angular momentum of the electron is $\hbar$ (Eq. (1.253)).

For excited states of the hydrogen atom, the constant function corresponds to the spin function. Each spherical harmonic function modulates the constant spin function and corresponds to an orbital function of a specific excited state with a corresponding phase-matched trapped photon and orbital angular momentum. Thus, the spherical harmonic function behaves as a charge-density wave, which travels time harmonically on the surface of the atomic orbital about a specific axis. (See Figure 1.2 for a pictorial representation for several ℓ values.) The amplitude of the corresponding orbital energy may be calculated from Maxwell's equations. Since the constant function is modulated harmonically, the time average of the orbital energy is zero except in the presence of a magnetic field. Nondegeneracy of energy levels arises from spin, orbital, and spin-orbit coupling interactions with the applied field. The electrodynamic interaction with the magnetic field gives rise to the observed hyperfine splitting of the hydrogen spectrum.

Many inconsistencies arise in the case of the corresponding solutions of the Schrödinger wave equation. For example, where is the photon in excited states given by the Schrödinger equation? A paradox also arises for the change in angular momentum due to photon absorption. The Schrödinger equation solutions for the kinetic energy of rotation K_{rot} is given by Eq. (10) of Ref. [14] and the value of the electron angular momentum L for the state $Y_{lm}(\theta,\phi)$ is given by Eq. (11) of Ref. [14]. They predict that the excited state rotational energy levels are nondegenerate as a function of the ℓ quantum number even in the

absence of an applied magnetic field, and the predicted energy is over six orders of magnitude of the observed nondegenerate energy in the presence of a magnetic field. In the absence of a magnetic field, no preferred direction exists. In this case, the ℓ quantum number is a function of the orientation of the atom with respect to an arbitrary coordinate system. Therefore, the nondegeneracy is nonsensical and violates conservation of angular momentum of the photon.

In quantum mechanics, the spin angular momentum of the electron is called the "intrinsic angular momentum" since no physical interpretation exists. The Schrödinger equation is not Lorentz invariant in violation of special relativity. It fails to predict the results of the Stern-Gerlach experiment that indicates the need for an additional quantum number. Quantum Electrodynamics (QED) was proposed by Dirac in 1926 to provide a generalization of quantum mechanics for high energies in conformity with the theory of special relativity and to provide a consistent treatment of the interaction of matter with radiation. It is fatally flawed. From Weisskopf [16], "Dirac's quantum electrodynamics gave a more consistent derivation of the results of the correspondence principle, but it also brought about a number of new and serious difficulties." Quantum electrodynamics: (i) *does not explain nonradiation of bound electrons*; (ii) contains an internal inconsistency with special relativity regarding the classical electron radius—the electron mass corresponding to its electric energy is infinite (the Schrödinger equation fails to predict the classical electron radius); (iii) it admits solutions of negative rest mass and negative kinetic energy; (iv) the interaction of the electron with the predicted zero-point field fluctuations leads to infinite kinetic energy and infinite electron mass; (v) Dirac used the unacceptable states of negative mass for the description of the vacuum; yet, infinities still arise. Dirac's equation, which was postulated to explain spin, relies on the unfounded notions of negative energy states of the vacuum, virtual particles, and gamma factors. All of these features are untenable or are inconsistent with observation. These problems regarding spin and orbital angular momentum and energies and the classical electron radius are nonexistent with CP solutions.

From the time of its inception, quantum mechanics (QM) has been controversial because its foundations are in conflict with physical laws and are internally inconsistent. Interpretations of quantum mechanics such as hidden variables, multiple worlds, consistency rules, and spontaneous collapse have been put forward in an attempt to base the theory in reality. Unfortunately, many theoreticians ignore the requirement that the wave function must be real and physical in order for it to be considered a valid description of reality. These issues and other such flawed philosophies and interpretations of experiments that arise from quantum mechanics are discussed in the Retrospect section and Ref. [10, 12, 14]. Reanalysis of old experiments and many new experiments including electrons in superfluid helium and data confirming the existence of hydrinos challenge the Schrödinger equation predictions. Many noted physicists rejected quantum mechanics, even those whose work undermined classical laws. Feynman attempted to use first principles including Maxwell's Equations to discover new physics to replace quantum mechanics [49] and Einstein searched to the end. "Einstein [...] insisted [...] that a more detailed, wholly deterministic theory must underlie the vagaries of quantum mechanics [50]." He believed scientists were misinterpreting the data. Examples of quantum mechanical misinterpretations of experiments are given in Box I.1. (See the following sections: The One-Electron Atom, Electron in Free Space, Classical Photon and Electron Scattering, Three- Through Twenty-Electron Atoms, Superconductivity, Gravity, Wave-Particle Duality, and Refs. [9, 10, 12].)

BOX I.1 MISINTERPRETATIONS OF OBSERVATIONS AS WEIRDNESS OF QUANTUM MECHANICS IS REVEALED TO BE DUE TO ATOMIC-SCALE CLASSICAL PHYSICS

QM: The rise in current of free electrons in superfluid helium when irradiated with low-energy light and the formation of an unexpected plethora of exotic negative charge carriers in superfluid helium with mobilities greater than that of the normal electron are due to the electron breaking into fractional pieces.

CP: Fractional principal quantum energy states of the electron in liquid helium match the photoconductivity and mobility observations without requiring that the electron is divisible.

QM: Virtual particles surround the electron, and as the electron's center is approached, they shield the electron's charge less effectively.

CP: The electron is an extended particle, rather than a point, and the charge density is greatest in the center.

QM: Spooky actions at a distance are predicted.

CP: Photon momentum is conserved on a photon-by-photon basis rather than statistically as predicted by quantum mechanics which predicts photon coincidence counts at separated detectors (Aspect experiment).

QM: The purely postulated Hund's Rule and the Pauli Exclusion Principle of the assignment of unique quantum numbers to all electrons are "weird spooky action" phenomena unique to quantum mechanics that require all electrons in the universe to have instantaneous communication and coordination with no basis in physical laws such as Maxwell's equations.

CP: The observations that all electrons have unique quantum numbers and that the electron configuration of atoms follows a pattern based on solutions of Laplace's equation are phenomenological consequences of physical laws such as Maxwell's equations.

QM: Since fundamental particles are probability waves and their position and energy are uncertain according to the Uncertainty Principle, they can "magically" appear on the other side of a supposedly insurmountable energy barrier based on their energy on the initial side of the barrier; thus, they defy physical laws and tunnel through the barrier.

CP: Fundamental particles such as an electron are real, extended particles each of size equal to its de Broglie wavelength, rather than a point-particle-probability-wave. Potential energy is gained as the particle traverses the barrier that is cleared; even though its initial kinetic energy was less than the barrier height. Energy conservation is obeyed at all times. Tunneling arises from physical laws.

QM: A $^{9}Be^{+}$ ion may be in two separate locations at once.

CP: The fluorescence emission spectrum of a Penning trapped $^{9}Be^{+}$ ion shows interference peaks due to coupling between oscillator modes and a Stern Gerlach transition.

QM: Supercurrent may go in both directions at once.

CP: The energy difference of a superconducting loop observed by Friedman et al. [1] matches the energy corresponding to the flux linkage of the magnetic flux quantum by the ensemble of superconducting electrons in their entirety with a reversal of the corresponding macroscopic current.

QM: O'Connell et al. [2] claimed to have achieved a quantum state of motion for a mechanical object by causing a Josephson junction qbit to be entangled with a macroscopic mechanical resonator and thereby extending, in their opinion, the weird rules of quantum mechanics such as zero-order vibration and entanglement to the macroworld.

CP: In reality, the device that O'Connell's team fabricated and tested is no more than a variant of a SQUID, a known classical (Chp. 42) macrodevice, except that it uniquely exploits piezoelectricity to form the weak link of a superconducting loop to enable the device. It demonstrates quantized excitation independently of the qbit and cannot exhibit zero-order vibration due to the nature of the SQUID; moreover, zero-order vibration is experimentally shown to be nonexistent in measurements with the qbit.

QM: Perpetual motion is predicted.

CP: Perpetual motion is not permitted nor observed.

QM: A weak force is observed between the two precision-machined plates with minuscule separation because the plates serve to limit the number of virtual particle modes between the plates, as opposed to those outside the plates, and the resulting imbalance in pressure between two infinite quantities gives rise to the feeble force known as the Casimir effect.

CP: The Casimir effect is predicted by Maxwell's equations wherein the attractive force is due only to the interactions of the material bodies themselves. Charge and current fluctuations in a material body with a general susceptibility serve as source terms for Maxwell's equations, i.e. classical fields, subject to the boundary conditions presented by the body surfaces. In the limiting case of rarefied media, the van der Waals force of interaction between individual atoms is obtained [3-4].

QM: The *postulated* Quantum Electrodynamics (QED) theory of $\frac{g}{2}$ is based on the determination of the terms of a *postulated* power series in α/π where each *postulated* virtual particle is a source of *postulated* vacuum polarization that gives rise to a *postulated* term. The algorithm involves scores of *postulated* Feynman diagrams corresponding to thousands of matrices with thousands of integrations per matrix requiring decades to reach a consensus on the "appropriate" *postulated* algorithm to remove the intrinsic infinities.

CP: The remarkable agreement between Eqs. (1.236) and (1.237) of the Electron g Factor section demonstrates that $\frac{g}{2}$ may be derived in closed form from Maxwell's equations in a simple straight forward manner that yields a result with eleven-figure agreement with experiments—the limit of the experimental capability is the measurement of the fundamental constants that determine α.

QM: The muon g factor g_{μ} is required to be different from the electron g factor in the standard model due to the mass dependent interaction of each lepton with vacuum polarizations due to virtual particles. The BNL Muon (g-2)

Collaboration used a "magic" $\gamma = 29.3$ which satisfied the BMT equation identically for the theoretical value of $\frac{g_\mu}{2}$ with assumption that $\frac{g_\mu}{2} \neq \frac{g_e}{2}$ and obtained a measured result that was internally consistent.

CP: Rather than indicating an expanded plethora of postulated super-symmetry virtual particles, which make contributions such as smuon-neutralino and sneutrino-chargino loops, the muon, like the electron, is a lepton with $\hbar$ of angular momentum, and the muon and electron g factors are predicted by classical physics to be identical. Using the experimental "magic" $\gamma = 29.3$ and $\frac{g_\mu}{2} = \frac{g_e}{2}$ in the BMT equation, the predicted measurement exactly matched $\frac{g_\mu}{2}$ measured by the BNL Muon (g-2) Collaboration proving that their assumption that the $\gamma = 29.3$ condition eliminated the effect of the electrostatic field on ω_a was flawed and showed the equivalence of the muon and electron g factors.

QM: The expansion of the universe is accelerating due to the presence of "dark energy" throughout all space.

CP: The constant maximum speed c for the propagation of light and gravity results in the conservation relationship of mass-energy, $E = mc^2$ and spacetime, $\frac{c^3}{4\pi G} = 3.22\ X\ 10^{34}\ \frac{kg}{\text{sec}}$. Spacetime expands as mass is converted to energy, and the predictions match the observed Hubble constant and the acceleration of the expansion.

QM: In the double-slit experiment, single electrons break into pieces, go through both slits at once, and interfere with themselves over all space.

CP: Electrons are not divisible and comprise an extended current distribution with $\hbar$ of angular momentum that is conserved with the electrodynamic interaction of the charged propagating electron with the conducting electrons of the material of the slits such that an angular momentum vector change corresponds to a translational displacement. In the far-field, the transverse momentum pattern is given by the Fourier transform of the slit aperture pattern, and the characteristic interference pattern is observed even with single electrons over time.

QM: In photon diffraction through slits, light-wave crests and troughs superimpose to cancel to give dark spots; whereas, superposition of crest with crest and trough with trough reinforces the intensity and gives bright spots.

CP: Photons are not destroyed by other photons. They interact with the electrons of the slit material, and the electrodynamic currents reradiate the light to give the characteristic interference pattern as by the Fourier transform of the slit aperture pattern.

QM: According to Nesvizhevsky et al. [5], a step in the transmission of falling neutrons through a variable-height channel comprising a mirror on the bottom and an absorber at the top occurred at a height of $13\ \mu m$ because neutrons fell in quantized jumps.

CP: The de Broglie wavelength in the vertical direction corresponding to the scattering of a falling neutron from the mirror to the absorber was given by $\lambda = z_1 = \frac{1}{2}\left(\frac{h}{m_n}\right)^{2/3} (g)^{-1/3} = 12.6\ \mu m$ where h is Planck's constant, m_n is the mass of the neutron, and g is the acceleration due to gravity. For absorber heights greater than $13\ \mu m$, the height was greater than the de Broglie wavelength; thus, a step in the transmission of falling neutrons occurred at $13\ \mu m$. The observed transmission matched identically that predicted by Newton's Law of Gravitation; no quantum gravity effect was observed.

QM: The nature of the chemical bond is based on a nonphysical "exchange integral," a "strictly quantum mechanical phenomena," that is a consequence of a postulated linear combination of product wavefunctions wherein it is implicit that each point electron with infinite self-electric-and-magnetic-field energies must exist as a "probability-wave cloud" and be in two places at the same time (i.e. centered on two nuclei simultaneously).

CP: The nature of the chemical bond solved using first principles including stability to radiation requires that the electron charge of the molecular orbital is a prolate spheroid, a solution of the Laplacian as an equipotential minimum energy surface in the natural ellipsoidal coordinates compared to spheroidal in the atomic case, and the current is time harmonic and obeys Newton's laws of mechanics in the central field of the nuclei at the foci of the spheroid.

QM: The electron clouds mutually shield the nuclear charge to provide an adjustable parameter, "effective nuclear charge"; yet, neither has any self-shielding effect; even though the clouds are mutually indistinguishable and must classically result in a self-interaction force equivalent to 1/2 the central attractive force. Furthermore, the electron–electron

repulsion term in the Hamiltonian can be infinite in atoms and molecules; yet, electron overlap is the basis of bonding in molecules.

CP: Electrons are concentric spherical shells in atoms and two-dimensional prolate spheroids in molecules such that there is no electron-electron repulsion, and bonding is due to the attraction between the oppositely charged electrons and nuclei at the origin and foci of the spheroids, respectively.

QM: The lowest energy vibrational state of any molecule is not zero rather, in violation of the second law of thermodynamics and experimental observation such as the formation of a Bose-Einstein condensate of molecules, it is the zero order vibration of $\frac{1}{2}h\nu = \frac{1}{2}\sqrt{\frac{k}{\mu}}$ that is equivalent to zero point energy. Moreover, the basis of zero order vibration, the Heisenberg Uncertainty Principle, has been experimentally disproved [6].

CP: The lowest energy vibrational state of any molecule is zero as its lowest vibrational and rotational energies, and the molecules can be solved using first principles in closed form equations in agreement with experimental observations including the difference in bond energies and vibrational energies with isotope substitution.

QM: Since flux is linked by a superconducting loop with a weak link in quantized units of the magnetic flux quantum, $\Phi_0 = \frac{h}{2e}$, the basis of superconductivity is interpreted as arising from the formation of electron pairs corresponding to the $2e$ term in the denominator; the so-called Cooper pairs form even though electrons repel each other, the electron repulsion should increase the resistance to electron flow, and such pairs cannot form at the critical temperature of high T_c superconductors.

CP: To conserve the electron's invariant angular momentum of $\hbar$, flux is linked by each electron in quantized units of the magnetic flux quantum, $\Phi_0 = \frac{h}{2e}$, and the basis of superconductivity is a correlated flow of an ensemble of individual electrons such that no energy is dissipated (i.e. superconductivity arises when the lattice is a band-pass for the magnetic field of an array of magnetic dipoles; therefore, no energy is dissipated with current flow).

QM: In a realization of Wheeler's delayed-choice gedanken experiment, modulated output is observed at two orthogonal detectors that has a trigonometric dependence on the phase angle with a relative phase angle of π between the outputs when an electro-optical modulator (EOM) is active because the absence of knowledge determines that each single photon must travel back in time, change history, travel along two paths simultaneously, and interfere with itself.

CP: An EOM is not a time machine. The interference results are predicted in terms of the classical nature of each linearly polarized single photon being comprised of two oppositely circular polarized components that conserve angular momentum when each interacts with the EOM at a tilt angle $\frac{\pi}{4}$ relative to the axis of linear polarization. The orthogonal circular polarizations input to the EOM each rotate in opposite directions by $\frac{\pi}{4}$, and the action of the EOM on the opposite circular polarized component vectors is antisymmetrical about the axes with the interchange of initial direction of the linear polarization from E_y to E_x to cause the appearance of interference at the outputs.

REFERENCES

1. J. R. Friedman, V. Patella, W. Hen, S. K. Tolpygo, J. E. Lukens, "Quantum superposition of distinct macroscopic states," Nature, Vol. 406, July, 6, (2000), pp. 43-45.
2. A. D. O'Connell, M. Hofheinz, M. Ansmann, R. C. Bialczak, M. Lenander, E. Lucero, M. Neeley, D. Sank, H. Wang, M. Weides, J. Wenner, J. M. Martinis, A. N. Cleland, "Quantum ground state and single-phonon control of a mechanical resonator," Nature, Vol. 464, (2010), pp. 697-703.
3. A. W. Rodriguez, A. P. McCauley, J. D. Joannopoulos, S. G. Johnson,"Casimir forces in the time domain: Theory," Phys. Rev. A,Vol. 80, (2009), p. 012115.
4. E. M. Lifshitz and L. P. Pitaevskii, Statistical Physics: Part 2 (Pergamon, Oxford, 1980).
5. V. V. Nesvizhevsky, H. G. Borner, A. K. Petukhov, H. Abele, S. Baebler, F. J. Rueb, T. Stoferele, A. Westphal, A. M. Gagarski, G. A. Petrov, A. V. Strelkov, "Quantum states of neutrons in the Earth's gravitational field," Nature, Vol. 415, (2002), pp. 297-299.
6. L. A. Rozema, A. Darabi, D. H. Mahler, A. Hayat, Y. Soudagar, A. M. Steinberg, "Violation of Heisenberg's Measurement-Disturbance Relationship by Weak Measurements," Phys. Rev. Lett., 109 (2012), 100404.

THREE ATOMIC THEORIES

It is possible to arrive at the Rydberg formula using the wrong physics. The statement "the results justify the means" is a fundamental argument for the validity of quantum mechanics no matter how strained the explanations or the consequences. Consider that in fact, the mathematics of the three theories of Bohr, Schrödinger, and presently CP converge to Eq. (I.1) as the principal energy levels of the hydrogen atom.

$$E_n = -\frac{e^2}{n^2 8\pi\varepsilon_0 a_H} = -\frac{13.598\ eV}{n^2} \tag{I.1}$$

$$n = 1, 2, 3, ... \tag{I.2}$$

where a_H is the Bohr radius for the hydrogen atom (52.947 pm), e is the magnitude of the charge of the electron, and ε_o is the vacuum permittivity. The theories of Bohr and Schrödinger depend on specific postulates to yield Eq. (I.1). A mathematical relationship exists between the theories of Bohr and Schrödinger with respect to CP that involves these postulates. CP solves the source currents of spherical multipole radiation fields. The current-density functions are the same as the spherical-harmonic and time-harmonic functions of the spherical electromagnetic waves, but are confined to a two-dimensional sphere of fixed radius except between transitions involving emission or absorption of the corresponding multipole radiation. Then, the currents match the wave equation solutions for two dimensions, the angular and time-dependent solutions of the wave equation. The Fourier transform of the current-density function is a solution of the three-dimensional wave equation in frequency (k,ω) space. Whereas, the Schrödinger-equation solutions are three dimensional in spacetime. The energy is given by:

$$\int_{-\infty}^{\infty} \psi^* H \psi dv = E \int_{-\infty}^{\infty} \psi^2 dv; \tag{I.3}$$

$$\int_{-\infty}^{\infty} \psi^2 dv = 1 \tag{I.4}$$

Thus,

$$\int_{-\infty}^{\infty} \psi^* H \psi dv = E \tag{I.5}$$

In the case that the potential energy of the Hamiltonian, H, is a constant times the wavenumber, the Schrödinger equation becomes the well-known Bessel equation. Then, with one of the solutions for ψ, Eq. (I.5) is equivalent to an inverse Fourier transform. According to the duality and scale change properties of Fourier transforms, the energy equation of CP and that of quantum mechanics are identical, the energy of a radial Dirac delta function of radius equal to an integer multiple of the radius of the hydrogen atom (Eq. (I.1)). Bohr obtained the same energy formula by postulating nonradiative states with angular momentum

$$L_z = m\hbar \tag{I.6}$$

and solving the energy equation classically.

The mathematics of all three theories result in Eq. (I.1). However, the physics is quite different. CP is derived from first principles and holds over a scale of spacetime of 85 orders of magnitude—it correctly predicts the nature of the universe from the scale of quarks to that of the cosmos. The two other theories are more or less mathematical curve fits to the Rydberg formula with inherent physical and mathematical flaws.

Specifically, the Bohr theory has inherent physical shortcomings such as failing to predict the spectrum of hydrogen in a magnetic field and the inability to solve helium and other multi-electron atoms and the nature of the chemical bond as well as the prediction of infinite angular momentum according to Eq. (I.6). Its success can be attributed to the rigging of the angular momentum to give rise to the Rydberg formula with the dismissal of the radiative stability problem.

The electron in the Schrödinger model is a singularity that exists over all space simultaneously at each instantaneous time point that is physically impossible and violates all first principles including stability to radiation. It is not relativistically invariant and fails to predict electron spin, the electron's magnetic moment, the g factor, the Stern-Gerlach experimental results, the Lamb shift, the fine structure, and the hyperfine structure. Furthermore, the Schrödinger equation is mathematically inconsistent in the excited state quantum numbers and does not give the proper quantization of the one-electron atom energy states.

In contrast, the stable electron current at the $n = 1$ state and the quantized excited states and their lifetimes can be solved precisely in closed-form equations containing fundamental constants only using physical laws that do not miss the Lamb shift, fine structure, hyperfine structure, magnetic moment, Stern Gerlach experimental results, g factor, and relativistic invariance as the Schrödinger equation does. Eq. (I.100) is also the de Broglie matter wave condition used heuristically in the Bohr model to give the Rydberg formula, but in this case, the standing wave involves the photon. Furthermore, the quantization involves excitation of discrete resonator modes imposed by the spherical cavity. In quantum mechanics, quantization is purely mathematical, but similarly dependent on the integer spherical periodicity of the spherical harmonics, and the principal quantum is defined in a manner to give integer angular quantum numbers of complete harmonic wavelengths as well as fit the Rydberg formula. However, the result is not even mathematically consistent. The principal quantum number is defined as the integer radial quantum number minus the integer angular quantum number. But, experimentally the angular or orbital quantum number is multi-valued for any principal quantum number causing the internal inconsistency that the radial quantum number must be multi-valued for a given principal quantum number [51]. In contrast, as shown by Eq. (I.103), Eq. (I.100) gives the angular

harmonic solutions and the corresponding integer radial and angular quantum numbers for physical states.

Specifically, there is an inescapable inconsistency in the mathematics of quantum mechanics identified in Section 11.3 of Margenau and Murphy [51] regarding the definition of the quantum numbers in the solutions of the Schrödinger equation. With the mathematical constraints of normalization and power series termination, the hydrogen atomic energy levels given by Margenau and Murphy are:

$$W = \frac{1}{2}\frac{me^4}{\left(n^* - l\right)^2 \hbar^2} \tag{I.7}$$

wherein n^* is the quantum number of the solution of separable radial function and l is the independent quantum number of the solution of the separable angular function. The quantity $\left(n^* - l\right)$ is then denoted by n and called the total quantum number such that the energy states of the hydrogen atom may be written as:

$$W = \frac{1}{2}\frac{me^4}{n^2\hbar^2} \tag{I.8}$$

Now, let's say that the hydrogen atom is in the $n = 5$ state. If the angular quantum number is $l = 0$, then the radial quantum number must be $n^* = 5$, but if the mathematically independent angular quantum number is $l = 1$, then the radial quantum number must be $n^* = 6$. Thus, an internal inconsistency arises due to the mathematics of the separable functions and independent quantum numbers of the corresponding solutions such as the requirement that the radial quantum number be both $n^* = 5$ and $n^* = 6$ for the state $n = 5$. Indeed as $n \to \infty$, each principal quantum state has the possibility of an infinite number of radial functions corresponding to the degenerate energy level of that state which is impossible. Specifically, it is impossible for the different radial wave functions having different expectation values for the radius of a given energy state to be both physical and energy degenerate for an electron in an inverse-squared Coulomb field.

Other problems exist with QM. QM makes inescapable predictions that do not match observations. For example, at page 365, Margenau and Murphy [51] state:

> *but with the term* $\frac{\ell(\ell+1)\hbar^2}{2mr^2}$ *added to the normal potential energy. What is the meaning of that term? In classical mechanics, the energy of a particle moving in three dimensions differs from that of a one-dimensional particle by the kinetic energy of rotation,* $\frac{1}{2}mr^2\omega^2$. *This is precisely the quantity* $\frac{\ell(\ell+1)\hbar^2}{2mr^2}$, *for we have seen that* $\ell(\ell+1)\hbar^2$ *is the certain value of the square of the angular momentum for the state* Y_ℓ, *in classical language* $\left(mr^2\omega\right)^2$ *which is divided by* $2mr^2$, *gives exactly the kinetic energy of rotation.*

From these equations, zero rotational energy and zero angular momentum are predicted for the $n = 1$ state, but these conditions are impossible since the electron is bound in a Coulomb field and must have nonzero instantaneous motion. Thus, the Schrödinger equation solutions further predict that the ionized electron may have infinite angular momentum. The Schrödinger equation solutions also predict that the excited state rotational energy levels are nondegenerate as a function of the ℓ quantum number even in the absence of an applied magnetic field, and the predicted energy is over six orders of magnitude greater than the typically observed nondegenerate energy in the presence of a magnetic field. In the absence of a magnetic field, no preferred direction exists. In this case, the ℓ quantum number is a function of the orientation of the atom with respect to an arbitrary coordinate system. Therefore, the nondegeneracy is nonsensical and violates conservation of angular momentum of the photon. Furthermore, as the principal quantum number and therefore ℓ go to infinity, the rotational energy and angular momentum become infinite while the wavefunction becomes sinusoidal over all space and is not normalizable [51]. In the latter case, a strict mathematical constraint of the founding postulates is violated. Thus, the theory is not mathematically consistent besides being physically impossible. It does not properly give rise to the observed quantized states of the hydrogen atom.

Moreover, only CP predicts reciprocal integers as "allowed" in the Rydberg energy equation. Explicitly, CP gives Eq. (I.1) as the energy-level equation for atomic hydrogen, but the restriction on "n," Eq. (I.2), should be replaced by Eq. (I.9).

$$n = 1, 2, 3, ..., \text{ and, } n = \frac{1}{2}, \frac{1}{3}, \frac{1}{4}, ... \tag{I.9}$$

Experimental observations lead to the conclusion that atomic hydrogen can exist in fractional quantum states that are at lower energies than the traditional "ground" ($n = 1$) state [22-42], and the observation of 54.4 eV and 122.4 eV short-wavelength-cutoff continuum radiation from hydrogen alone [23-29, 31] confirms CP in the prediction of hydrinos and directly disproves atomic theories such as the Bohr theory and the Schrödinger and Dirac equations based on the definition of $n = 1$ as the ground state, the defined state below which it is impossible to go. Thus, postulates were established to give the correct formula for the principal energies of the excited states of atomic hydrogen, but being devoid of the correct physics, the resulting mathematical models failed to predict unanticipated results and are disproved experimentally.

MATHEMATICAL RELATIONSHIP BETWEEN THE THEORIES OF BOHR AND SCHRÖDINGER WITH RESPECT TO CLASSICAL ATOMIC THEORY

The mathematical relationship whereby the Schrödinger equation may be transformed into a form consistent with first principles is shown *infra*. In the case that the potential energy of the Hamiltonian, H, is a constant times the wavenumber, the Schrödinger equation is the well-known Bessel equation. Then, one of the solutions for the wavefunction Ψ (a current-density function rather than a probability wave) is equivalent to an inverse Fourier transform. According to the duality and scale change properties of Fourier transforms, the energy equation of CP and that of quantum mechanics are identical, the energy of a radial Dirac delta function of radius equal to an integer multiple of the radius of the hydrogen atom.

Historically, J. J. Balmer showed, in 1885, that the frequencies for some of the lines observed in the emission spectrum of atomic hydrogen could be expressed with a completely empirical relationship. This approach was later extended by J. R. Rydberg who showed that all of the spectral lines of atomic hydrogen were given by the equation:

$$\bar{\nu} = R\left(\frac{1}{n_f^2} - \frac{1}{n_i^2}\right) \tag{I.10}$$

where $R = 10,967,758\ m^{-1}$, $n_f = 1,2,3,...$, $n_i = 2,3,4,...$, and $n_i > n_f$. In 1911, Rutherford proposed a planetary model for the atom where the electrons revolve about the nucleus (which contained the protons) in various orbits. There was, however, a fundamental conflict with this model and the prevailing classical physics. According to classical electromagnetic theory, an accelerated particle radiates energy as electromagnetic waves. Thus, an electron in a Rutherford orbit, circulating at constant speed but with a continually changing direction of its velocity vector is being accelerated whereby the electron should constantly lose energy by radiating and spiral into the nucleus.

An explanation was provided by Bohr in 1913 when he assumed that the energy levels were quantized and the electron was constrained to move in only one of a number of allowed states. Niels Bohr's theory for atomic hydrogen was based on an unprecedented postulate of stable circular orbits that do not radiate. Although no explanation was offered for the existence of stability for these orbits, the results gave energy levels in agreement with Rydberg's equation. Bohr's theory was a straightforward application of Newton's laws of motion and Coulomb's law of electric force. According to Bohr's model, the point particle electron was held to a circular orbit around the relatively massive point particle nucleus by the balance between the Coulomb force of attraction between the proton and the electron and centrifugal force of the electron.

$$\frac{e^2}{4\pi\varepsilon_0 r^2} = \frac{m_e v^2}{r} \tag{I.11}$$

Bohr postulated the existence of stable orbits in defiance of classical physics (Maxwell's equations), but he applied classical physics according to Eq. (I.11). Bohr then realized that the energy formula Eq. (I.1) was given by postulating nonradiative states with angular momentum

$$L_z = m_e v r = n\hbar \qquad n = 1,2,3... \tag{I.12}$$

and by solving the energy equation classically. The Bohr radius is given by substituting the solution of Eq. (I.12) for v into Eq. (I.11).

$$r = \frac{4\pi\varepsilon_0 \hbar^2 n^2}{m_e e^2} = n^2 a_0 \qquad n = 1,2,3... \tag{I.13}$$

The total energy is the sum of the potential energy and the kinetic energy. In the present case of an inverse squared central field, the total energy (which is the negative of the binding energy) is one half the potential energy [52]. The potential energy, $\phi(\mathbf{r})$, is given by Poisson's equation

$$\phi(\mathbf{r}) = -\int_{V'} \frac{\rho(\mathbf{r}')\,dv'}{4\pi\varepsilon_0 |\mathbf{r} - \mathbf{r}'|} \tag{I.14}$$

For a point charge at a distance r from the nucleus the potential is:

$$\phi(r) = -\frac{e^2}{4\pi\varepsilon_0 r} \tag{I.15}$$

Thus, the total energy is given by:

$$E = -\frac{Z^2 e^2}{8\pi\varepsilon_0 r} \tag{I.16}$$

Substitution of Eq. (I.13) into Eq. (I.16) with the replacement of the electron mass by the reduced electron mass gives Eq. (I.1).

Bohr's model was in agreement with the observed hydrogen spectrum, but it failed with the helium spectrum, and it could not account for chemical bonds in molecules. The prevailing wisdom was that the Bohr model failed because it was based on the application of Newtonian mechanics for discrete particles. Its limited applicability was attributed to the unwarranted assumption that the energy levels are quantized.

In 1923, de Broglie suggested that the motion of an electron has a wave aspect— $\lambda = \frac{h}{p}$. This was confirmed by Davisson and Germer in 1927 by observing diffraction effects when electrons were reflected from metals. Schrödinger reasoned

that if electrons have wave properties, there must be a wave equation that governs their motion. In 1926, he proposed the Schrödinger equation

$$H\Psi = E\Psi \tag{I.17}$$

where Ψ is the wave function, H is the wave operator, and E is the energy of the wave. To give the sought three quantum numbers, the Schrödinger equation solutions are three-dimensional in space and four-dimensional in spacetime.

$$\left[\nabla^2 - \frac{1}{v^2}\frac{\partial^2}{\partial t^2}\right]\Psi(r,\theta,\phi,t) = 0 \tag{I.18}$$

where $\Psi(r,\theta,\phi,t)$ according to quantum theory is the probability-density function of the electron, as described below. When the time harmonic function is eliminated [53-54], the result is

$$-\frac{\hbar^2}{2\mu}\left[\frac{1}{r^2}\frac{\partial}{\partial r}\left(r^2\frac{\partial\Psi}{\partial r}\right) + \frac{1}{r^2\sin\theta}\frac{\partial}{\partial\theta}\left(\sin\theta\frac{\partial\Psi}{\partial\theta}\right)_{r,\phi} + \frac{1}{r^2\sin^2\theta}\left(\frac{\partial^2\Psi}{\partial\phi^2}\right)_{r,\theta}\right] + U(r)\Psi(r,\theta,\phi) = E\Psi(r,\theta,\phi) \tag{I.19}$$

where $U(r)$ is the classical Coulomb potential energy which in MKS units is:

$$U(r) = -\frac{e^2}{4\pi\varepsilon_0 r} \tag{I.20}$$

The Schrödinger equation (Eq. (I.19)) can be transformed into a sum comprising a part that depends only on the radius and a part that is a function of angle only obtained by separation of variables and linear superposition in spherical coordinates. The general form of the solutions for $\psi(r,\theta,\phi)$ is:

$$\psi(r,\theta,\phi) = \sum_{l,m} f_{lm}(r)Y_{lm}(\theta,\phi) \tag{I.21}$$

where l and m are separation constants. The solutions for the full angular part of Eq. (I.19), $Y_{lm}(\theta,\phi)$, are the spherical harmonics.

$$Y_{lm}(\theta,\phi) = \sqrt{\frac{(2l+1)(l-m)!}{4\pi(l+m)!}}P_l^m(\cos\theta)e^{im\phi} \tag{I.22}$$

In general, the Schrödinger equation has an infinite number of solutions. To arrive at the solution, which represents the electron, a suitable boundary condition must be imposed. Schrödinger postulated the boundary condition: "$\Psi \to 0$ as $r \to \infty$," which leads to a purely mathematical model of the electron. In addition, to arrive at the Rydberg series for the principal energy levels, further definitions of constants in the corresponding Laguerre differential equation are required [14-15]. The historical solution [54] may be approached differently to arrive at a solution that is based in physics. The angular part of Eq. (I.19) is the generalized Legendre equation which is derived from the Laplace equation by Jackson ([55] at Eq. (3.9)). For the case that the potential energy is a constant times the wavenumber of the electron, k (a constant times the inverse of the de Broglie wavelength of the electron—$k = \frac{2\pi}{\lambda}$; $\lambda = \frac{h}{p}$), the radial part of Eq. (I.19) is just the Bessel equation, Eq. (3.75) of Jackson [55] with $\upsilon = l + \frac{1}{2}$. (In the present case of an inverse squared central field, the magnitude of each of the binding energy and the kinetic energy is one half the potential energy [52], and the de Broglie wavelength requires that the kinetic energy, $\frac{p^2}{2m_e}$, is a constant times the wavenumber squared.) Thus, the solution for $f_{lm}(r)$ is:

$$f_{lm}(r) = \frac{A_{lm}}{r^{1/2}}J_{l+1/2}(kr) + \frac{B_{lm}}{r^{1/2}}N_{l+1/2}(kr) \tag{I.23}$$

It is customary to define the spherical Bessel, Neumann, and Hankel functions, denoted by $j_l(x)$, $n_l(x)$, $h_l^{(1,2)}(x)$, as follows:

$$\begin{aligned} j_l(x) &= \left(\frac{\pi}{2x}\right)^{1/2}J_{l+1/2}(x) \\ n_l(x) &= \left(\frac{\pi}{2x}\right)^{1/2}N_{l+1/2}(x) \\ h_l^{(1,2)}(x) &= \left(\frac{\pi}{2x}\right)^{1/2}\left[J_{l+1/2}(x) \pm iN_{l+1/2}(x)\right] \end{aligned} \tag{I.24}$$

For $l = 0$ the explicit forms are:

$$j_0(x)=\frac{\sin x}{x}$$
$$n_0(x)=-\frac{\cos x}{x} \tag{I.25}$$
$$h_0^{(1)}(x)=\frac{e^{ix}}{ix}$$

Eq. (I.19) has the general form:

$$H\psi = E\psi \tag{I.26}$$

The energy is given by:

$$\int_{-\infty}^{\infty} \psi H \psi dv = E\int_{-\infty}^{\infty} \psi^2 dv\,; \tag{I.27}$$

Typically, the solutions are normalized.

$$\int_{-\infty}^{\infty} \psi^2 dv = 1 \tag{I.28}$$

thus,

$$\int_{-\infty}^{\infty} \psi H \psi dv = E \tag{I.29}$$

A physical interpretation of Eq. (I.26) is sought. Schrödinger interpreted $e\Psi^*(x)\Psi(x)$ as the charge density or the amount of charge between x and $x+dx$ (Ψ^* is the complex conjugate of Ψ). Presumably, then, he pictured the electron to be spread over large regions of space. Three years after Schrödinger's interpretation, Max Born, who was working with scattering theory, found that this interpretation led to logical difficulties, and he replaced the Schrödinger interpretation with the probability of finding the electron between x and $x+dx$ as:

$$\int \Psi(x)\Psi^*(x)dx \tag{I.30}$$

Born's interpretation is generally accepted. Nonetheless, interpretation of the wave function is a never-ending source of confusion and conflict. Many scientists have solved this problem by conveniently adopting the Schrödinger interpretation for some problems and the Born interpretation for others. This duality allows the electron to be everywhere at one time—yet to have no volume. Alternatively, the electron can be viewed as a discrete particle that moves here and there (from $r=0$ to $r=\infty$), and $\Psi\Psi^*$ gives the time average of this motion. According to the Copenhagen interpretation, every observable exists in a state of superposition of possible states, and observation or the potential for knowledge causes the wavefunction corresponding to the possibilities to collapse into a definite state. The postulate of quantum measurement asserts that the process of measuring an observable forces the state vector of the system into an eigenvector of that observable, and the value measured will be the eigenvalue of that eigenvector. Thus, Eq. (I.26) corresponds to collapsing the wave function, and E is the eigenvalue of the eigenvector.

However, an alternative interpretation of Eq. (I.26) and the corresponding solutions for ψ exists. In this case, ψ is a function given by Eqs. (I.23-I.25), and Eq. (I.19) is equivalent to an inverse Fourier transform. The spacetime inverse Fourier transform in three dimensions in spherical coordinates is given [56-57], as follows:

$$M(s,\Theta,\Phi)=\int_0^{\infty}\int_0^{\pi}\int_0^{2\pi}\rho(r,\theta,\phi)\exp(-i2\pi sr[\cos\Theta\cos\theta+\sin\Theta\sin\theta\cos(\phi-\Phi)])r^2\sin\theta dr d\theta d\phi \tag{I.31}$$

With circular symmetry [56]:

$$M(s,\Theta)=2\pi\int_0^{\infty}\int_0^{\pi}\rho(r,\theta)J_o\left(2\pi sr\sin\Theta\sin\theta\right)\exp\left(-i2\pi sr\cos\Theta\cos\theta\right)r^2\sin\theta dr d\theta \tag{I.32}$$

With spherical symmetry [56],

$$M(s)=4\pi\int_0^{\infty}\rho(r)\mathrm{sinc}\left(2sr\right)r^2dr=4\pi\int_0^{\infty}\rho(r)\frac{\sin 2sr}{2sr}r^2dr \tag{I.33}$$

By substitution of the eigenvalues corresponding to the angular part [54] of Eq. (I.21), the Schrödinger equation becomes the radial equation, $R(r)$, given by:

$$-\frac{\hbar^2}{2\mu r^2}\frac{d}{dr}\left(r^2\frac{dR}{dr}\right)+\left[\frac{\hbar^2 l(l+1)}{2\mu r^2}+U(r)\right]R(r)=ER(r) \tag{I.34}$$

Consider the case that $\ell = 0$, that the potential energy is a constant times the wavenumber, and that the radial function is a spherical Bessel function as given by Eqs. (I.23-I.25). In this case, multiplication of both sides of Eq. (I.34) by $4\pi\left(\frac{\sin 2sr}{2sr}\right)^2$ followed by integration with respect to the radius over its limits (0 to ∞) gives

$$4\pi\int_0^\infty \frac{\sin 2sr}{2sr}\left[-\frac{\hbar^2}{2\mu r^2}\frac{d}{dr}\left(r^2\frac{d}{dr}\right)+U(r)\right]\frac{\sin 2sr}{2sr}r^2dr = E4\pi\int_0^\infty \frac{\sin 2sr}{2sr}\frac{\sin 2sr}{2sr}r^2dr \tag{I.35}$$

Eq. (I.33) is the Fourier transform integral in spherical coordinates with spherical symmetry. The left hand side (LHS) of Eq. (I.35) is equivalent to the LHS of Eq. (I.29) wherein ψ is given by Eq. (I.25). Then the LHS of Eq. (I.35) is the Fourier transform integral of $H\psi$ wherein the kernel is $r^2\frac{\sin 2sr}{2sr}$. The integral of Eq. (I.29) gives E which is a constant. The energy E of Eq. (I.26) is a constant such as b. Thus, $H\psi$ according to Eq. (I.26) is a constant times ψ.

$$H\psi = b\psi \tag{I.36}$$

Since b is an *arbitrary* constant, consider the following case wherein b is the Rydberg quantized energy formula:

$$b = -\frac{Z^2e^2}{8\pi\varepsilon_0 n^2 a_H} \tag{I.37}$$

Then the energy of Eq. (I.29) is that given by Eq. (I.1). However, the Schrödinger equation can be solved to give the energy corresponding to the radial function given by Eq. (I.59) of CP. The radial function used to calculate the energy is a delta function that corresponds to an inverse Fourier transform of the solution for ψ.

$$\Psi(s) = \delta(s - s_n) \tag{I.38}$$

With a change of variable, Eq. (I.38) becomes Eq. (I.59). Eq. (I.35) can be expressed, as follows:

$$4\pi\int_0^\infty \frac{\sin 2sr}{2sr}\left[-\frac{\hbar^2}{2\mu r^2}\frac{d}{dr}\left(r^2\frac{d}{dr}\right)+U(r)\right]\frac{\sin s_n r}{s_n r}r^2dr = E4\pi\int_0^\infty \frac{\sin 2sr}{2sr}\frac{\sin 2s_n r}{2s_n r}r^2dr \tag{I.39}$$

It follows from Eq. (I.33) that the right side integral is the Fourier transform of a radial Dirac delta function:

$$4\pi E\int_0^\infty \frac{\sin 2s_n r}{2s_n r}\frac{\sin 2sr}{2sr}r^2dr = E\frac{\delta(s - s_n)}{4\pi s_n^2} \tag{I.40}$$

Substitution of Eq. (I.36) into Eq. (I.39) gives:

$$4\pi b\int_0^\infty \frac{\sin 2s_n r}{2s_n r}\frac{\sin 2sr}{2sr}r^2dr = b\frac{\delta(s - s_n)}{4\pi s_n^2} \tag{I.41}$$

Substitution of Eq. (I.40) and Eq. (I.41) into Eq. (I.39) gives:

$$b\delta(s - s_n) = E\delta(s - s_n) \tag{I.42}$$

Consider the case where b is given by:

$$b = -\frac{\hbar^2}{2m_e n\frac{a_0}{Z^2}s} = -\frac{\frac{1}{n}Z^2e^2}{8\pi\varepsilon_0 s} \tag{I.43}$$

and s_n is given by:

$$s_n = na_H \tag{I.44}$$

where $r_n = na_H$. According to the duality and change of scale properties of Fourier transforms [58], ***the energy equation of CP and that of QM are identical***, the energy of a radial Dirac delta function of a radius that's equal to an integer multiple of the radius of the hydrogen atom. The total energy of the electron is given by Gauss' law for the potential and the relationship that the total energy is one half the potential energy in the case of an inverse squared central force [52]:

$$E = \int_{-\infty}^{\infty} E\delta(r - r_n)dr = -\int_{-\infty}^{\infty} \delta(r - r_n)\frac{\frac{1}{n}Z^2e^2}{8\pi\varepsilon_0 r}dr = -\frac{\frac{1}{n}Z^2e^2}{8\pi\varepsilon_0 r_n} = -\frac{Z^2e^2}{8\pi\varepsilon_0 n^2 a_H} \tag{I.45}$$

Thus, the mathematical relationship of CP and QM is based on the Fourier transform of the radial function. CP requires that the electron is real and physically confined to a two-dimensional surface comprising source currents that match the wave equation solutions for spherical waves in two dimensions (angular) and time. The corresponding Fourier transform is a wave over all space that is a solution of the three-dimensional wave equation (e.g. the Schrödinger equation). In essence, QM may be considered as a theory dealing with the Fourier transform of an electron, rather than the physical electron. By Parseval's theorem, the energies may be equivalent, but the quantum mechanical case is nonphysical—only mathematical. It may mathematically produce numbers that agree with experimental energies as eigenvalues, but the mechanisms lack internal consistency and conformity with physical laws. If these are the criteria for a valid solution of physical problems, then QM has never successfully solved any problem. The theory of Bohr similarly failed.

SHORTCOMINGS OF QUANTUM THEORY AND REASONS FOR A COMPLETE REVISION OF ATOMIC THEORY

In general, QM has proved to be a deadend towards unification of the fundamental forces including gravity and further failed to give the basis of the inertial and gravitational masses, the equivalence of these masses, predicting the masses of fundamental particles, and the acceleration behavior of the cosmos. Fundamentally, quantum mechanics based on the Schrödinger equation and modifications of the Schrödinger equation has encountered several obstacles that have proved insurmountable even from the beginning with the hydrogen atom, as was the case with the Bohr theory (See the Retrospect section, and Mills' publications [4-15]). The Schrödinger equation mathematically gives the Rydberg equation as a set eigenvalues. On this basis alone, it is justified despite its inconsistency with physical laws and numerous experimental observations such as:

- The appropriate eigenvalue must be postulated and the variables of the Laguerre differential equation must be defined as integers in order to obtain the Rydberg formula.
- The Schrödinger equation is not Lorentz invariant.
- The Schrödinger equation violates first principles, including special relativity and Maxwell's equations [4-20, 59].
- The Schrödinger equation gives no basis why excited states are radiative and the 13.6 eV state is stable. Mathematics does not determine physics; it only models physics.
- The Schrödinger equation solutions, Eq. (36) and Eq. (37) of Ref. [15], predict that the ground state electron has zero angular energy and zero angular momentum, respectively.
- The Schrödinger equation solution, Eq. (37) of Ref. [15], predicts that the ionized electron may have infinite angular momentum.
- The Schrödinger equation solutions, Eq. (36) and Eq. (37) of Ref. [15], predict that the excited state rotational energy levels are nondegenerate as a function of the ℓ quantum number even in the absence of an applied magnetic field, and the predicted energy is over six orders of magnitude of the observed nondegenerate energy in the presence of a magnetic field. In the absence of a magnetic field, no preferred direction exists. In this case, the ℓ quantum number is a function of the orientation of the atom with respect to an arbitrary coordinate system. Therefore, the nondegeneracy is nonsensical and violates conservation of angular momentum of the photon.
- The Schrödinger equation predicts that each of the functions that corresponds to a highly excited state electron is not integrable and cannot be normalized; thus, each is infinite.
- The Schrödinger equation predicts that the ionized electron is sinusoidal over all space and cannot be normalized; thus, it is infinite.
- The Heisenberg Uncertainty Principle arises as the standard deviation in the electron probability wave, but experimentally it is not the basis of wave-particle duality [12, 60].
- The correspondence principle does not hold experimentally.
- The Schrödinger equation does not predict the electron magnetic moment and misses the spin quantum number altogether.
- The Schrödinger equation provides no rational basis for the phenomenon of spin, the Pauli exclusion principle, or Hund's rules. Instantaneous exchange of information between particles is required, which violates special relativity.
- The Schrödinger equation is not a wave equation since it gives the velocity squared proportional to the frequency.
- The Schrödinger equation is not consistent with conservation of energy in an inverse potential field wherein the binding energy is equal to the kinetic energy and the sum of the binding energy and the kinetic energy is equal to the potential energy.
- The Schrödinger equation permits the electron to exist in the nucleus, a state that is physically nonsensical with infinite potential energy and infinite negative kinetic energy.
- The Schrödinger equation interpreted as a probability wave of a point particle cannot explain neutral scattering of electrons from hydrogen.

- The Schrödinger equation interpreted as a probability wave of a point particle gives rise to infinite magnetic and electric energy in the corresponding fields of the electron. For example, the electron must spin in one dimension and give rise to a Bohr magneton; yet, classically the energy of a magnetic moment is $\frac{\mu^2}{r^3}$ which in the present case is infinity (by substitution of $r = 0$ for the model that the electron is a point particle), not the required mc^2. This interpretation is in violation of Special Relativity [61].

- A modification of the Schrödinger equation was developed by Dirac to explain spin.[2] The *postulated* QED theory of $\frac{g}{2}$ is based on the determination of the terms of a *postulated* power series in α/π where each *postulated* virtual particle is a source of *postulated* vacuum polarization that gives rise to a *postulated* term. The algorithm involves scores of *postulated* Feynman diagrams corresponding to thousands of matrices with thousands of integrations per matrix requiring decades to reach a consensus on the "appropriate" *postulated* algorithm to remove the intrinsic infinities.[3]

These failures of QM are attributed to the unwarranted assumption that atomic-size particles obey different physical laws than macroscopic objects. Specifically, QM is incorrect in its basis that first principles such as Maxwell's Equations do not apply to the electron and the notion that the electron is described by a probability distribution function of a point particle. Quantum mechanics is based on engendering the electron with a wave nature, as suggested by the Davisson-Germer experiment and fabricating a set of associated postulates and mathematical rules for wave operators. QM is in violation of Maxwell's equations, as shown through application of the Haus condition to the Schrödinger wave functions (See Schrödinger Wavefunction in Violation of Maxwell's Equation section). Nonradiation based on Maxwell's equations is a necessary boundary constraint, since nonradiation is observed experimentally. The shortcomings of QM regarding violation of Maxwell's equations and other first principles are further discussed in the Retrospect section and Mills' publications [4-15]. These issues indicate that QM atomic theory requires revision.

CLASSICAL ATOMIC THEORY

The physics of numerous phenomena in electricity and magnetism, optics, celestial and orbital mechanics, heat, hydrodynamics, aerodynamics, elasticity, and others obey equations containing the Laplacian:

$$\nabla^2\phi = 0 \qquad \text{is Laplace's equation} \tag{I.46}$$

$$\nabla^2\phi = \frac{1}{a^2}\frac{\partial^2\phi}{\partial t^2} \qquad \text{is the wave equation} \tag{I.47}$$

$$\nabla^2\phi = \frac{1}{a^2}\frac{\partial\phi}{\partial t} \qquad \text{is the diffusion or heat-conduction equation} \tag{I.48}$$

The wave equation is useful to describe electric and magnetic fields and orbiting bodies, as well as in the form of an energy equation wherein it can provide for conservation of energy and angular momentum. Thus, it is the logical choice to solve for the nature of the bound electron as a boundary-value problem. In contrast, the time-dependent Schrödinger equation has the form of Eq. (I.48) and is not a true wave equation. The current QM theory based on the time dependent and time independent Schrödinger equation has many problems, is not based on physical laws, and is not predictive, as discussed previously [4-20]. QM has never dealt with the nature or structure of fundamental particles. They are treated as zero-dimensional points that occupy no volume and are everywhere at once. This view is impossible since occupying no volume would preclude their existence; the inherent infinities are not observed nor are they possible, and the possibility of a particle being everywhere at once violates all physical laws including conservation of energy and causality. Now, a physical approach is followed based on the classical wave equation and the condition for nonradiation from Maxwell's equations.

---

[2] In the old quantum theory the spin angular momentum of the electron is called the "intrinsic angular momentum." This term arises because it is difficult to provide a physical interpretation for the electron's spin angular momentum. Dirac's Quantum Electrodynamics (QED) attempts a physical interpretation by proposing that the "vacuum" contains fluctuating electric and magnetic fields called "zero point energy," negative energy states of the vacuum, virtual particles and their corresponding "polarization" of vacuum space, and arbitrarily disregarding infinities that even Dirac opposed. These aspects render QED fatally flawed in terms of predicting a corresponding inescapable infinite cosmological constant and the unobserved requirement of particle emission by blackholes called Hawking radiation. (See the Wave-Particle Duality section and prior publications [4-15], especially Ref. [10].)

[3] In the Electron g Factor section and Ref. [10], the closed-form Maxwellian result (eleven figure agreement with experiment—the limit of the experimental capability of the measurement of the fundamental constants that determine α) is contrasted with the QED algorithm of invoking virtual particles, zero point fluctuations of the vacuum, and negative energy states of the vacuum.

ONE-ELECTRON ATOMS

NONRADIATION CONDITION

One-electron atoms include the hydrogen atom, He^{+}, Li^{2+}, Be^{3+}, and so on. In each case, the nucleus contains Z protons and the atom has a net positive charge of $(Z-1)e$. To arrive at the solution that represents the electron, a suitable boundary condition must be imposed. It is well known from experiments that the single atomic electron of hydrogen radiates to the same stable state. Thus, CP uses the physical boundary condition of nonradiation of the bound electron to be imposed on the solution for the charge- and current-density functions of the electron. The condition for radiation by a moving point charge given by Haus [46] is that its spacetime Fourier transform possesses components that are synchronous with waves traveling at the speed of light. Conversely, it is proposed that the condition for nonradiation by an ensemble of moving charge that comprises a current-density function is

For non-radiative states, the current-density function must not possess spacetime Fourier components that are synchronous with waves traveling at the speed of light.

The Haus derivation and the condition for nonradiation are given in Appendix I: Nonradiation Condition wherein the nonradiative condition is also derived directly by the determination of the electrodynamic fields with the electron current-density function as the source current. Given the infinite number of possible current-density functions, it is fortuitous that the spherical radiation corresponding to the symmetry and the conditions for emission and absorption of such radiation provide the additional boundary conditions to determine the current-density functions.

ELECTRON SOURCE CURRENT

Since the hydrogen atom is stable and nonradiative, the electron has constant energy. Furthermore, it is time dynamic with a corresponding current that serves as a source of electromagnetic radiation during transitions. The wave equation solutions of the radiation fields permit the source currents to be determined as a boundary-value problem. These source currents match the field solutions of the wave equation for two dimensions plus time and the nonradiative $n = 1$ state when the nonradiation condition is applied. Then, the mechanics of the electron can be solved from the two-dimensional wave equation plus time in the form of an energy equation wherein it provides for conservation of energy and angular momentum, as given in the Electron Mechanics and the Corresponding Classical Wave Equation for the Derivation of the Rotational Parameters of the Electron section. Once the nature of the electron is solved, all problems involving electrons can be solved in principle. Thus, in the case of one-electron atoms, the electron radius, binding energy, and other parameters are solved after solving for the nature of the bound electron.

As shown in Appendix I, for time-varying spherical electromagnetic fields, Jackson [47] gives a generalized expansion in vector spherical waves that are convenient for electromagnetic boundary-value problems possessing spherical symmetry properties and for analyzing multipole radiation from a localized source distribution. The Green function $G(\mathbf{x}',\mathbf{x})$ which is appropriate to the inhomogeneous Helmholtz equation

$$\left(\nabla^2 + k^2\right) G(\mathbf{x}',\mathbf{x}) = -\delta(\mathbf{x}'-\mathbf{x}) \tag{I.49}$$

in the infinite domain with the spherical wave expansion for the outgoing wave Green function is:

$$G(\mathbf{x}',\mathbf{x}) = \frac{e^{-ik|\mathbf{x}-\mathbf{x}'|}}{4\pi|\mathbf{x}-\mathbf{x}'|} = ik\sum_{\ell=0}^{\infty} j_\ell(kr_<)h_\ell^{(1)}(kr_>)\sum_{m=-\ell}^{\ell} Y_{\ell,m}^*(\theta',\phi')Y_{\ell,m}(\theta,\phi) \tag{I.50}$$

Jackson [47] further gives the general multipole field solution to Maxwell's equations in a source-free region of empty space with the assumption of a time dependence $e^{i\omega t}$:

$$\begin{aligned}\mathbf{B} &= \sum_{\ell,m}\left[a_E(\ell,m)\, f_\ell(kr)\mathbf{X}_{\ell,m} - \frac{i}{k}a_M(\ell,m)\nabla\times g_\ell(kr)\mathbf{X}_{\ell,m}\right]\\ \mathbf{E} &= \sum_{\ell,m}\left[\frac{i}{k}a_E(\ell,m)\nabla\times f_\ell(kr)\mathbf{X}_{\ell,m} + a_M(\ell,m)\, g_\ell(kr)\mathbf{X}_{\ell,m}\right]\end{aligned} \tag{I.51}$$

where the cgs units used by Jackson are retained in this section. The radial functions $f_\ell(kr)$ and $g_\ell(kr)$ are of the form:

$$g_\ell(kr) = A_\ell^{(1)}h_\ell^{(1)} + A_\ell^{(2)}h_\ell^{(2)} \tag{I.52}$$

$\mathbf{X}_{\ell,m}$ is the vector spherical harmonic defined by:

$$\mathbf{X}_{\ell,m}(\theta,\phi) = \frac{1}{\sqrt{\ell(\ell+1)}}\mathbf{L}Y_{\ell,m}(\theta,\phi) \tag{I.53}$$

where

$$\mathbf{L} = \frac{1}{i}(\mathbf{r}\times\nabla) \tag{I.54}$$

The coefficients $a_E(\ell,m)$ and $a_M(\ell,m)$ of Eq. (I.51) specify the amounts of electric (ℓ,m) multipole and magnetic (ℓ,m) multipole fields, and are determined by sources and boundary conditions as are the relative proportions in Eq. (I.52). Jackson gives the result of the electric and magnetic coefficients from the sources as

$$a_E(\ell,m)=\frac{4\pi k^2}{i\sqrt{\ell(\ell+1)}}\int Y_\ell^{m*}\left\{\rho\frac{\partial}{\partial r}\left[rj_\ell(kr)\right]+\frac{ik}{c}(\mathbf{r}\cdot\mathbf{J})\,j_\ell(kr)-ik\nabla\cdot(r\times\boldsymbol{M})\,j_\ell(kr)\right\}d^3x \tag{I.55}$$

and

$$a_M(\ell,m)=\frac{-4\pi k^2}{\sqrt{\ell(\ell+1)}}\int j_\ell(kr)Y_\ell^{m*}\mathbf{L}\cdot\left(\frac{\mathbf{J}}{c}+\nabla\times\boldsymbol{M}\right)d^3x \tag{I.56}$$

respectively, where the distribution of charge $\rho(\mathbf{x},t)$, current $\mathbf{J}(\mathbf{x},t)$, and intrinsic magnetization $\boldsymbol{M}(\mathbf{x},t)$ are harmonically varying sources: $\rho(\mathbf{x})e^{-i\omega t}$, $\mathbf{J}(\mathbf{x})e^{-i\omega t}$, and $\boldsymbol{M}(\mathbf{x})e^{-i\omega t}$.

The electron current-density function can be solved as a boundary value problem regarding the time varying corresponding source current $\mathbf{J}(\mathbf{x})e^{-i\omega t}$ that gives rise to the time-varying spherical electromagnetic fields during transitions between states with the further constraint that the electron is nonradiative in a state defined as the $n=1$ state. The potential energy, $V(\mathbf{r})$, is an inverse-radius-squared relationship given by Gauss' law, which for a point charge or a two-dimensional spherical shell at a distance r from the nucleus the potential is:

$$V(r)=-\frac{e^2}{4\pi\varepsilon_0 r} \tag{I.57}$$

Thus, consideration of conservation of energy would require that the electron radius must be fixed. Additional constraints requiring a two-dimensional source current of fixed radius are matching the delta function of Eq. (I.49) with no singularity, no time dependence and consequently no radiation, absence of self-interaction (See Appendix II: Stability and Absence of Self Interaction and Self Energy), and exact electroneutrality of the hydrogen atom wherein the electric field is given by

$$\mathbf{n}\bullet(\mathbf{E}_1-\mathbf{E}_2)=\frac{\sigma_s}{\varepsilon_0} \tag{I.58}$$

where $\mathbf{n}$ is the normal unit vector, $\mathbf{E}_1$ and $\mathbf{E}_2$ are the electric field vectors that are discontinuous at the opposite surfaces, σ_s is the discontinuous two-dimensional surface charge density, and $\mathbf{E}_2=0$. Then, the solution for the radial electron function that satisfies the boundary conditions is a delta function in spherical coordinates—a spherical shell [62]:

$$f(r)=\frac{1}{r^2}\delta(r-r_n) \tag{I.59}$$

where r_n is an allowed radius. This function defines the charge density on a spherical shell of a fixed radius (See Figure I.1), not yet determined, with the charge motion confined to the two-dimensional spherical surface. The integer subscript n here and in Eqs. (I.60-I.62) is *determined during photon absorption* as given in the Excited States of the One-Electron Atom (Quantization) section. It is shown in this section that the force balance between the electric fields of the electron and proton plus any resonantly absorbed photons gives the result that $r_n=nr_1$ wherein n is an integer in an excited state. In general, leptons such as the electron are indivisible, perfectly conducting, and possess an inalienable $\hbar$ of intrinsic angular momentum such that any inelastic perturbation involves the entire particle wherein the intrinsic angular momentum remains unchanged. Bound state transitions are allowed involving the exchange of photons between states, each having $\hbar$ of angular momentum in their fields.

Figure I.1. A bound electron is a constant two-dimensional spherical surface of charge (zero thickness, total charge of $-e$, and total mass of m_e), called *an electron atomic orbital.* The corresponding uniform current-density function having intrinsic angular momentum components of $\mathbf{L}_{xy} = \frac{\hbar}{4}$ and $\mathbf{L}_z = \frac{\hbar}{2}$ following Larmor excitation in a magnetic field give rise to the phenomenon of electron spin.

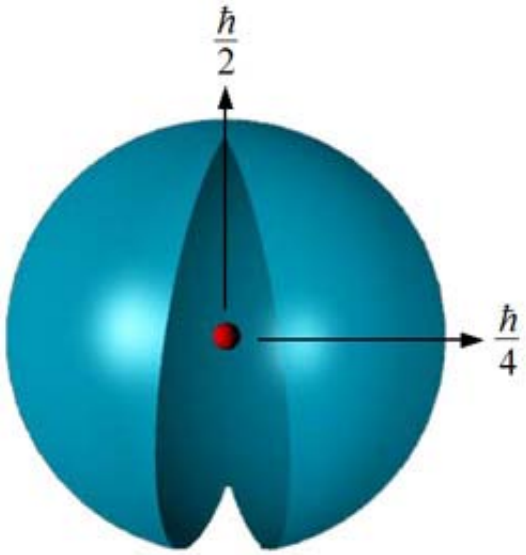

Given time harmonic motion and a radial delta function, the relationship between an allowed radius and the electron wavelength is given by:

$$2\pi r_n = \lambda_n \tag{I.60}$$

Based on conservation of the electron's angular momentum of $\hbar$, the magnitude of the velocity and the angular frequency for *every* point on the surface of the bound electron are:

$$v_n = \frac{h}{m_e \lambda_n} = \frac{h}{m_e 2\pi r_n} = \frac{\hbar}{m_e r_n} \tag{I.61}$$

$$\omega_n = \frac{\hbar}{m_e r_n^2} \tag{I.62}$$

To further match the required multipole electromagnetic fields between transitions of states, the trial nonradiative source current functions are time and spherical harmonics, each having an exact radius and an exact energy. Then, each allowed electron charge-density (mass-density) function is the product of a radial delta function ($f(r) = \frac{1}{r^2}\delta(r - r_n)$), two angular functions (spherical harmonic functions $Y_\ell^m(\theta,\phi) = P_\ell^m(\cos\theta)e^{im\phi}$), and a time-harmonic function $e^{im\omega_n t}$. The spherical harmonic $Y_0^0(\theta,\phi) = 1$ is also an allowed solution that is in fact required in order for the electron charge and mass densities to be positive definite and to give rise to the phenomena of electron spin. The real parts of the spherical harmonics vary between -1 and 1. However, the mass of the electron cannot be negative; and the charge cannot be positive. Thus, to insure that the function is positive definite, the form of the angular solution must be a superposition:

$$Y_0^0(\theta,\phi) + Y_\ell^m(\theta,\phi) \tag{I.63}$$

The current is constant at every point on the surface for the s orbital corresponding to $Y_0^0(\theta,\phi)$. The quantum numbers of the spherical harmonic currents can be related to the observed electron orbital angular momentum states. The currents corresponding to s, p, d, f, etc. orbitals are:

$\ell = 0$

$$\rho(r,\theta,\phi,t) = \frac{e}{8\pi r^2}[\delta(r - r_n)]\left[Y_0^0(\theta,\phi) + Y_\ell^m(\theta,\phi)\right] \tag{I.64}$$

$\ell \neq 0$

$$\rho(r,\theta,\phi,t) = \frac{e}{4\pi r^2}[\delta(r - r_n)]\left[Y_0^0(\theta,\phi) + \mathrm{Re}\left\{Y_\ell^m(\theta,\phi)e^{im\omega_n t}\right\}\right] \tag{I.65}$$

where $Y_\ell^m(\theta,\phi)$ are the spherical harmonic functions that spin about the z-axis with angular frequency ω_n with $Y_0^0(\theta,\phi)$ the

constant function. $\mathrm{Re}\left\{Y_\ell^m(\theta,\phi)e^{i\omega_n t}\right\} = P_\ell^m(\cos\theta)\cos(m\phi + m\omega_n t)$ to keep the form of the spherical harmonic of quantum number m as a traveling wave about the z-axis at angular frequency ω_n.

The Fourier transform of the electron charge-density function is a solution of the four-dimensional wave equation in frequency space (**k**, ω-space). Then, the corresponding Fourier transform of the current-density function $K_\ell^{m_\ell}(s,\Theta,\Phi,\omega)$ is given by multiplying it by the constant angular frequency ω_n given by Eq. (1.36) corresponding to a potentially emitted photon.

$$K_\ell^{m_\ell}(s,\Theta,\Phi,\omega) = 4\pi\omega_n \frac{\sin(2sr_n)}{2sr_n} \otimes G_\ell^{m_\ell}(s,\Theta) \otimes H_\ell^{m_\ell}(s,\Theta,\Phi) \otimes \frac{1}{4\pi}[\delta(\omega-\omega_n)+\delta(\omega+\omega_n)] \tag{I.66}$$

wherein $G_\ell^{m_\ell}(s,\Theta)$ and $H_\ell^{m_\ell}(s,\Theta,\Phi)$ are the spherical-coordinate Fourier transforms of $N_{\ell,m}P_\ell^m(\cos\theta)$ and $e^{im\phi}$, respectively. The motion on the atomic orbital is angular; however, a radial correction exists due to Special Relativistic effects. Consider the wave vector of the sinc function. When the velocity is c corresponding to a potentially emitted photon.

$$\mathbf{s}_n \bullet \mathbf{v}_n = \mathbf{s}_n \bullet \mathbf{c} = \omega_n \tag{I.67}$$

the relativistically corrected wavelength given by Eq. (1.279) is:

$$r_n = \lambda_n \tag{I.68}$$

Substitution of Eq. (I.68) into the sinc function results in the vanishing of the entire Fourier transform of the current-density function. Thus, spacetime harmonics of $\frac{\omega_n}{c} = k$ or $\frac{\omega_n}{c}\sqrt{\frac{\varepsilon}{\varepsilon_0}} = k$, for which the Fourier transform of the current-density function is nonzero, do not exist. Radiation due to charge motion does not occur in any medium when this boundary condition is met. There is acceleration without radiation. (Also see Abbott and Griffiths and Goedecke [63-64]). Nonradiation is also shown directly using Maxwell's equations in Appendix I: Nonradiation Based on the Electromagnetic Fields and the Poynting Power Vector. However, in the case that such a state arises as an excited state by photon absorption, it is radiative due to a radial dipole term in its current-density function since it possesses spacetime Fourier transform components synchronous with waves traveling at the speed of light, as shown in the Instability of Excited States section. The *radiation emitted or absorbed during electron transitions is the multipole radiation given by Eq. (I.50)* as given in the Excited States of the One-Electron Atom (Quantization) section and the Equation of the Photon section wherein Eqs. (4.18-4.23) give a macro-spherical wave in the far-field.

Thus, a bound electron is a constant two-dimensional spherical surface of charge (zero thickness and total charge of $-e$) called an electron atomic orbital that can exist in a bound state at only specified distances from the nucleus determined by an energy minimum for the $n = 1$ state and integer multiples of this radius due to the action of resonant photons as shown in the Determination of Atomic Orbital Radii section and Excited States of the One-Electron Atom (Quantization) section, respectively. The bound electron is not a point, but it is point-like (behaves like a point at the origin). The free electron is continuous with the bound electron as it is ionized and is also point-like, as shown in the Electron in Free Space section. The total function that describes the spinning motion of each electron atomic orbital is composed of two functions. One function, the spin function (see Figure I.1 for the charge function and Figure I.2 for the current function), is spatially uniform over the atomic orbital, where each point moves on the surface with the same quantized angular and linear velocity, and gives rise to spin angular momentum. It corresponds to the nonradiative $n = 1$, $\ell = 0$ state of atomic hydrogen, which is well known as an s state or orbital. The other function, the modulation function, can be spatially uniform—in which case there is no orbital angular momentum and the magnetic moment of the electron atomic orbital is one Bohr magneton—or not spatially uniform—in which case there is orbital angular momentum. The modulation function rotates with a quantized angular velocity about a specific (by convention) z-axis. The constant spin function that is modulated by a time and spherical harmonic function as given by Eq. (I.65) is shown in Figure 1.2 for several ℓ values. The modulation or traveling charge-density wave that corresponds to an orbital angular momentum in addition to a spin angular momentum are typically referred to as p, d, f, etc. orbitals and correspond to an ℓ quantum number not equal to zero.

MOMENT OF INERTIA AND SPIN AND ROTATIONAL ENERGIES

In the derivation of the rotational energy and related parameters, first consider that the electron atomic orbital experiences a constant potential energy because it is fixed at $r = r_n$. The boundary condition is that the modulation of the charge density by a traveling wave is not dissipative corresponding to absence of radiation and further has a time average of zero kinetic energy. The mechanics of motion is such that there is a time and spatially harmonic redistribution of matter and kinetic energy that flows on the surface such that the total of either is unchanged. Wave motion has such behavior and the corresponding equation is a wave equation that is solved with energy degeneracy and a time average of zero for the charge and energy flow as the boundary constraints. In this case, the energy degeneracy is only lifted due to the electrodynamic interaction with an applied field consistent with experimental observations, as given in the Orbital and Spin Splitting section.

The moments of inertia and the rotational energies as a function of the ℓ quantum number for the solutions of the time-dependent electron charge-density functions (Eqs. (I.64-I.65)) are solved using the classical wave equation. With rotation about the designated z-axis, the velocity of the spherical shell depends on the angular position on the surface and consequently is a

function of $Y_0^0(\theta,\phi)$. By expressing the wave equation in the energy form, the angular dependent velocity may be eliminated, and this equation can be solved using the boundary constraints. The corresponding equation is the well known rigid rotor equation [65]:

$$-\frac{\hbar^2}{2I}\left[\frac{1}{\sin\theta}\frac{\partial}{\partial\theta}\left(\sin\theta\frac{\partial}{\partial\theta}\right)_{r,\phi}+\frac{1}{\sin^2\theta}\left(\frac{\partial^2}{\partial\phi^2}\right)_{r,\theta}\right]Y(\theta,\phi)=E_{rot}Y(\theta,\phi) \tag{I.69}$$

The resulting parameters for the spin and orbital angular momentum given in the Rotational Parameters of the Electron (Angular Momentum, Rotational Energy, Moment of Inertia) section are:

$\ell=0$

$$I_z=I_{spin}=\frac{m_e{r_n}^2}{2} \tag{I.70}$$

$$L_z=I\omega\mathbf{i}_z=\pm\frac{\hbar}{2} \tag{I.71}$$

$$E_{rotational}=E_{rotational,\,spin}=\frac{1}{2}\left[I_{spin}\left(\frac{\hbar}{m_e{r_n}^2}\right)^2\right]=\frac{1}{2}\left[\frac{m_e{r_n}^2}{2}\left(\frac{\hbar}{m_e{r_n}^2}\right)^2\right]=\frac{1}{4}\left[\frac{\hbar^2}{2I_{spin}}\right] \tag{I.72}$$

$$T=\frac{\hbar^2}{2m_e r_n^2} \tag{I.73}$$

$\ell\neq 0$

$$I_{orbital}=m_e{r_n}^2\sqrt{\frac{\ell(\ell+1)}{\ell^2+2\ell+1}}=m_e{r_n}^2\sqrt{\frac{\ell}{\ell+1}} \tag{I.74}$$

$$\mathbf{L}_{orbital}=I\omega\mathbf{i}_z=I_{orbital}\omega\mathbf{i}_z=m_e{r_n}^2\sqrt{\frac{\ell(\ell+1)}{\ell^2+2\ell+1}}\omega\mathbf{i}_z=m_e{r_n}^2\frac{\hbar}{m_e{r_n}^2}\sqrt{\frac{\ell}{\ell+1}}\mathbf{i}_z=\hbar\sqrt{\frac{\ell}{\ell+1}}\mathbf{i}_z \tag{I.75}$$

$$E_{rotational\ orbital}=\frac{\hbar^2}{2I}\frac{\ell(\ell+1)}{\ell^2+2\ell+1}=\frac{\hbar^2}{2I}\frac{\ell}{\ell+1}=\frac{\hbar^2}{2m_e{r_n}^2}\frac{\ell}{\ell+1}\qquad \ell=1,2,3,..., \tag{I.76}$$

$$L_{z\ total}=L_{z\ spin}+L_{z\ orbital} \tag{I.77}$$

$$\left\langle L_{z\ orbital}\right\rangle=0 \tag{I.78}$$

$$\left\langle E_{rotational\ orbital}\right\rangle=0 \tag{I.79}$$

The orbital rotational energy arises from a spin function (spin angular momentum) modulated by a spherical harmonic angular function (orbital angular momentum). The time-averaged mechanical angular momentum and rotational energy associated with the wave-equation solution comprising a traveling charge-density wave on the atomic orbital is zero as given in Eqs. (I.78) and (I.79), respectively. Thus, the principal levels are degenerate except when a magnetic field is applied. In the case of an excited state, the angular momentum of $\hbar$ is carried by the fields of the trapped photon. The amplitudes that couple to external magnetic and electromagnetic fields are given by Eq. (I.76) and (I.77), respectively. The rotational energy due to spin is given by Eq. (I.72), and the total kinetic energy is given by Eq. (I.73).

SPIN FUNCTION

It is known from the Stern-Gerlach experiment that a beam of silver atoms is split into two components when passed through an inhomogeneous magnetic field. This implies that the electron is a spin 1/2 particle or fermion with an intrinsic angular momentum of $\pm\frac{\hbar}{2}$ that can only exist parallel or antiparallel to the direction of the applied field (spin axis), and the magnitude of the angular momentum vector, which precesses about the spin axis is $\sqrt{\frac{3}{4}}\hbar$. Furthermore, the magnitude of the splitting implies a magnetic moment of μ_B, a full Bohr magneton, given by Eq. (1.131) corresponding to $\hbar$ of total angular momentum on the axis of the applied field, implying an impossibility of being classically reconciled with the $\pm\frac{\hbar}{2}$ electron angular momentum. Yet, the extraordinary aspects of the magnetic properties and behavior of the electron are the basis to solve its structure that gives rise to these observations. In general, the Maxwell's-equations solution for the source of any magnetic field is unique. Thus, the electron field requires a corresponding unique current according to Maxwell's equations that matches the boundary condition

imposed by the results of the Stern-Gerlach experiment. The solution is given in the Atomic Orbital Equation of Motion For ℓ = 0 Based on the Current Vector Field (CVF) section.

The current density function $Y_0^0(\theta,\phi)$ (Eqs. (I.64-I.65)) that gives rise to the magnetostatic spin of the electron comprises a constant charge (current) density function with moving charge confined to a two-dimensional spherical shell and comprises a uniform complete coverage. It is generated as a continuum of correlated orthogonal great-circle current loops wherein each point charge(current)-density element moves time harmonically with constant angular velocity, ω_n, given by Eq. (I.62) and velocity, v_n, in the direction of the current given by Eq. (I.61). O*rthogonal great-circle current-density elements (one dimensional "current loops")* serve as basis elements to form two distributions of an infinite number of great circles wherein each covers one-half of a two-dimensional spherical shell and is defined as a basis element current vector field ("BECVF") and an atomic orbital current-vector field ("OCVF"). Then, the *continuous* uniform electron current density function $Y_0^0(\theta,\phi)$ (part of Eqs. (I.64-I.65)) that covers the entire spherical surface as a distribution of an infinite number of great circles is generated using the CVFs.

First, the generation of the BECVF is achieved by rotation of two great circle basis elements, one in the x'z'-plane and the other in the y'z'-plane, about the $\left(-\mathbf{i}_x,\mathbf{i}_y,0\mathbf{i}_z\right)$ axis by an infinite set of infinitesimal increments of the rotational angle over a span of π wherein the current direction is such that the resultant angular momentum vector of the basis elements of $\frac{\hbar}{2\sqrt{2}}$ is stationary on this axis.

GENERATION OF THE BECVF

Consider two infinitesimal charge(mass)-density elements at two separate positions or points, one and two, of the first pair of orthogonal great-circle current loops that serve as the basis set for generation of the BECVF as shown in Figure 1.4. The rotating Cartesian coordinates, x',y',z', in which the basis element great circles are fixed is designated the basis-set reference frame. In this frame at time zero, element one is at $x'=0$, $y'=r_n$, and $z'=0$, and element two is at $x'=r_n$, $y'=0$, and $z'=0$. Let element one move on a great circle clockwise toward the -z'-axis, and let element two move counter clockwise on a great circle toward the -z'-axis, as shown in Figure 1.4. . The equations of motion, in the basis-set reference frame with $t=0$ defined at the points (0,1,0) and (1,0,0), respectively, are given by

point one:

$$x_1' = 0 \qquad y_1' = r_n\cos(\omega_n t) \qquad z_1' = -r_n\sin(\omega_n t) \tag{I.80}$$

point two:

$$x_2' = r_n\cos(\omega_n t) \qquad y_2' = 0 \qquad z_2' = -r_n\sin(\omega_n t) \tag{I.81}$$

The great circle basis elements and rotational matrix of the BECVF are given by:

BECVF MATRICES ($R_{\left(-\mathbf{i}_x,\mathbf{i}_y,0\mathbf{i}_z\right)}(\theta)$)

$$\begin{bmatrix} x' \\ y' \\ z' \end{bmatrix} = \begin{bmatrix} \frac{1}{2}+\frac{\cos\theta}{2} & -\frac{1}{2}+\frac{\cos\theta}{2} & -\frac{\sin\theta}{\sqrt{2}} \\ -\frac{1}{2}+\frac{\cos\theta}{2} & \frac{1}{2}+\frac{\cos\theta}{2} & -\frac{\sin\theta}{\sqrt{2}} \\ \frac{\sin\theta}{\sqrt{2}} & \frac{\sin\theta}{\sqrt{2}} & \cos\theta \end{bmatrix} \bullet \left(\begin{bmatrix} 0 \\ r_n\cos\phi \\ -r_n\sin\phi \end{bmatrix} + \begin{bmatrix} r_n\cos\phi \\ 0 \\ -r_n\sin\phi \end{bmatrix} \right) \tag{I.82}$$

GENERATION OF THE OCVF

The generation of the OCVF is achieved by rotation of two great circle basis elements, one in the x'y'-plane and the other in the plane that bisects the x'y'-quadrant and is parallel to the z'-axis, about the $\left(-\frac{1}{\sqrt{2}}\mathbf{i}_x,\frac{1}{\sqrt{2}}\mathbf{i}_y,\mathbf{i}_z\right)$-axis by an infinite set of infinitesimal increments of the rotational angle over a span of π wherein the current direction is such that the resultant angular momentum vector of the basis elements of $\frac{\hbar}{2}$ having components of $\mathbf{L}_{xy}=\frac{\hbar}{2\sqrt{2}}$ and $\mathbf{L}_z=\frac{\hbar}{2\sqrt{2}}$ is stationary on this axis. For the generation of the OCVF, consider two charge(mass)-density elements, point one and two, in the basis-set reference frame at

time zero. Element one is at $x'=\frac{r_n}{\sqrt{2}}$, $y'=\frac{r_n}{\sqrt{2}}$, and $z'=0$, and element two is at $x'=r_n$, $y'=0$, and $z'=0$. Let element one move clockwise on a great circle toward the -z'-axis, and let element two move counter clockwise on a great circle toward the y'-axis as shown in Figure 1.8. The equations of motion, in the basis-set reference frame are given by:

point one:

$$x_1'=r_n\sin\left(\frac{\pi}{4}\right)\cos(\omega_n t)\qquad y_1'=r_n\cos\left(\frac{\pi}{4}\right)\cos(\omega_n t)\qquad z_1'=-r_n\sin(\omega_n t) \tag{I.83}$$

point two:

$$x_2'=r_n\cos(\omega_n t)\qquad y_2'=r_n\sin(\omega_n t)\qquad z_2'=0 \tag{I.84}$$

The great circle basis elements and rotational matrix of the OCVF are given by:

OCVF Matrices ($R_{\left(-\frac{1}{\sqrt{2}}\mathbf{i}_x,\frac{1}{\sqrt{2}}\mathbf{i}_y,\mathbf{i}_z\right)}(\theta)$)

$$\begin{bmatrix}x'\\y'\\z'\end{bmatrix}=\begin{bmatrix}\frac{1}{4}\left(1+3\cos\theta\right) & \frac{1}{4}\left(-1+\cos\theta+2\sqrt{2}\sin\theta\right) & \frac{1}{4}\left(-\sqrt{2}+\sqrt{2}\cos\theta-2\sin\theta\right)\\ \frac{1}{4}\left(-1+\cos\theta-2\sqrt{2}\sin\theta\right) & \frac{1}{4}\left(1+3\cos\theta\right) & \frac{1}{4}\left(\sqrt{2}-\sqrt{2}\cos\theta-2\sin\theta\right)\\ \frac{1}{2}\left(\frac{-1+\cos\theta}{\sqrt{2}}+\sin\theta\right) & \frac{1}{4}\left(\sqrt{2}-\sqrt{2}\cos\theta+2\sin\theta\right) & \cos^2\frac{\theta}{2}\end{bmatrix}\bullet\left(\begin{bmatrix}\frac{r_n\cos\phi}{\sqrt{2}}\\ \frac{r_n\cos\phi}{\sqrt{2}}\\ -r_n\sin\phi\end{bmatrix}+\begin{bmatrix}r_n\cos\phi\\ r_n\sin\phi\\ 0\end{bmatrix}\right) \tag{I.85}$$

GENERATION OF $Y_0^0(\theta,\phi)$

Then, the uniform great-circle distribution $Y_0^0(\theta,\phi)$ is exactly generated from the CVFs. The BECVF is convolved with the OCVF over a 2π span that results in the placement of a BECVF at each great circle of the OCVF. Since the angular momentum vector of the BECVF is matched to twice that of one of the OCVF great circle basis elements and the span is over a 2π, the resultant angular momentum of the distribution is the same as that of the OCVF, except that coverage of the spherical surface is complete. This current vector distribution is normalized by scaling the constant current of each great circle element resulting in the exact uniformity of the distribution independent of time since $\nabla\cdot K=0$ along each great circle. There is no alteration of the angular momentum with normalization since it only affects the density parallel to the angular momentum axis of the distribution, the $\left(-\frac{1}{\sqrt{2}}\mathbf{i}_x,\frac{1}{\sqrt{2}}\mathbf{i}_y,\mathbf{i}_z\right)$-axis. Then, the boundary conditions of $Y_0^0(\theta,\phi)$ having the desired angular momentum components, coverage, element motion, and uniformity are shown to have been achieved by designating the $\left(-\frac{1}{\sqrt{2}}\mathbf{i}_x,\frac{1}{\sqrt{2}}\mathbf{i}_y,\mathbf{i}_z\right)$-axis as the z-axis. Specifically, this uniform spherical shell of current (Figure I.2) meets the boundary conditions of having an angular velocity magnitude at each point on the surface given by Eq. (I.62), and angular momentum projections of $\mathbf{L}_{xy}=+/-\frac{\hbar}{4}$ and $\mathbf{L}_z=\frac{\hbar}{2}$ (Eqs. (1.127-1.128) and Figure 1.23)[4] that give rise to the Stern Gerlach experiment and the phenomenon corresponding to the spin quantum number as shown in the Magnetic Parameters of the Electron (Bohr Magneton) section, and in the Electron g Factor section.

[4] $+/-$ designates both the positive and negative vector directions along an axis in the xy-plane.

Figure I.2. The bound electron exists as a spherical two-dimensional supercurrent (electron *atomic orbital*), an extended distribution of charge and current completely surrounding the nucleus. Unlike a spinning sphere, there is a complex pattern of motion on its surface (indicated by vectors) that generates two orthogonal components of angular momentum (Figure I.1) that give rise to the phenomenon of electron spin. A representation of the $\left(-\frac{1}{\sqrt{2}}\mathbf{i}_x, \frac{1}{\sqrt{2}}\mathbf{i}_y, \mathbf{i}_z\right)$-axis view of the total uniform supercurrent-density pattern of the $Y_0^0(\phi,\theta)$ atomic orbital with 144 vectors overlaid on the continuous bound-electron current density giving the direction of the current of each great circle element (nucleus not to scale) is shown.

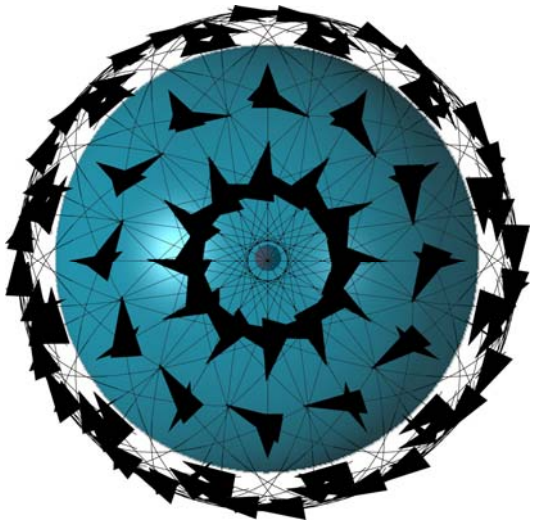

As shown in the Atomic Orbital Equation of Motion for $\ell = 0$ Based on the Current Vector Field (CVF) section, the application of a magnetic field to the atomic orbital gives rise to a precessing angular momentum vector $\mathbf{S}$ directed from the origin of the atomic orbital at an angle of $\theta = \frac{\pi}{3}$ relative to the applied magnetic field. The precession of $\mathbf{S}$ with an angular momentum of $\hbar$ forms a cone in the nonrotating laboratory frame to give a perpendicular projection of $\mathbf{S}_\perp = \pm\sqrt{\frac{3}{4}}\hbar$ (Eq. (1.129)) and a projection onto the axis of the applied magnetic field of $\mathbf{S}_\parallel = \pm\frac{\hbar}{2}$ (Eq. (1.130)). The superposition of the $\frac{\hbar}{2}$ z-axis component of the atomic orbital angular momentum and the $\frac{\hbar}{2}$ z-axis component of $\mathbf{S}$ gives $\hbar$ corresponding to the observed magnetostatic electron magnetic moment of a Bohr magneton. The $\hbar$ of angular momentum along $\mathbf{S}$ has a corresponding precessing magnetic moment of 1 Bohr magneton. The magnetostatic dipole magnetic field corresponding to μ_B is shown in Figure I.3.

Figure I.3. The three-dimensional cut-away representation of the magnetic field of an electron atomic orbital showing the nucleus (not to scale). The field is a dipole outside the atomic orbital.

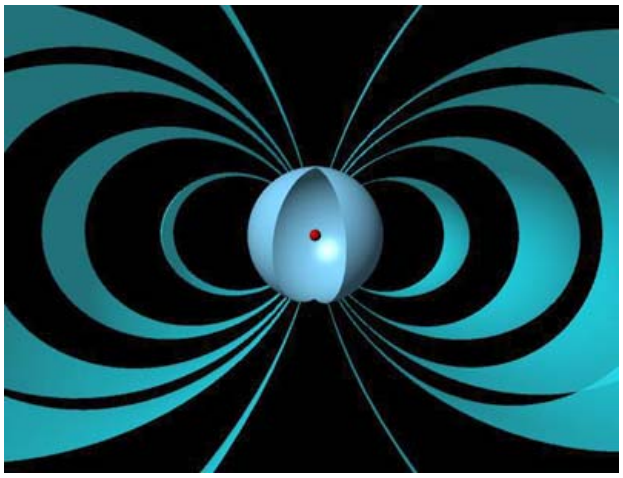

In contrast to the QM and QED cases (See Ref [10]), the fourth quantum number arises naturally in CP as derived in the Electron g Factor section. The Stern-Gerlach experiment implies a magnetic moment of one Bohr magneton and an associated angular momentum quantum number of 1/2. Historically, this quantum number is called the spin quantum number, s ($s=\frac{1}{2};\ m_s=\pm\frac{1}{2}$). Conservation of angular momentum of the atomic orbital permits a discrete change of its "kinetic angular momentum" ($\mathbf{r}\times m\mathbf{v}$) with respect to the field of $\frac{\hbar}{2}$, and concomitantly the "potential angular momentum" ($\mathbf{r}\times e\mathbf{A}$) must change by $-\frac{\hbar}{2}$. The flux change, ϕ, of the atomic orbital for $r<r_n$ is determined as follows:

$$\Delta\mathbf{L}=\frac{\hbar}{2}-\mathbf{r}\times e\mathbf{A} \tag{I.86}$$

$$=\left[\frac{\hbar}{2}-\frac{e2\pi rA}{2\pi}\right]\hat{z} \tag{I.87}$$

$$=\left[\frac{\hbar}{2}-\frac{e\phi}{2\pi}\right]\hat{z} \tag{I.88}$$

In order that the change of angular momentum, $\Delta\mathbf{L}$, equals zero, ϕ must be $\Phi_0=\frac{h}{2e}$, the magnetic flux quantum. Thus, to conserve angular momentum in the presence of an applied magnetic field, the atomic orbital magnetic moment can be parallel or antiparallel to an applied field as observed with the Stern-Gerlach experiment, and the flip between orientations is accompanied by the "capture" of the magnetic flux quantum by the atomic orbital. During the spin-flip transition, power must be conserved. Power flow is governed by the Poynting power theorem,

$$\nabla\bullet(\mathbf{E}\times\mathbf{H})=-\frac{\partial}{\partial t}\left[\frac{1}{2}\mu_0\mathbf{H}\bullet\mathbf{H}\right]-\frac{\partial}{\partial t}\left[\frac{1}{2}\varepsilon_0\mathbf{E}\bullet\mathbf{E}\right]-\mathbf{J}\bullet\mathbf{E} \tag{I.89}$$

Eq. (I.90) derived in the Electron g Factor section gives the total energy of the flip transition, which is the sum of the energy of reorientation of the magnetic moment (1st term), the magnetic energy (2nd term), the electric energy (3rd term), and the dissipated energy of a fluxon treading the atomic orbital (4th term), respectively.

$$\Delta E_{mag}^{spin}=2\left(1+\frac{\alpha}{2\pi}+\frac{2}{3}\alpha^2\left(\frac{\alpha}{2\pi}\right)-\frac{4}{3}\left(\frac{\alpha}{2\pi}\right)^2\right)\mu_B B \tag{I.90}$$

$$\Delta E_{mag}^{spin}=g\mu_B B \tag{I.91}$$

The spin-flip transition can be considered as involving a magnetic moment of g times that of a Bohr magneton. The g factor is now designated the fluxon g factor as opposed to the unwarranted historical anomalous g factor. The calculated value of $\frac{g}{2}$ is $1.001\ 159\ 652\ 137$. The experimental value [66] of $\frac{g}{2}$ is $1.001\ 159\ 652\ 188(4)$.

FORCE BALANCE EQUATION

The radius of the nonradiative ($n=1$) state is solved using the electromagnetic force equations of Maxwell relating the charge and mass density functions wherein the angular momentum of the electron is given by $\hbar$. The reduced mass arises naturally from an electrodynamic interaction between the electron and the proton of mass m_p.

$$\frac{m_e}{4\pi r_1^2}\frac{v_1^2}{r_1} = \frac{e}{4\pi r_1^2}\frac{Ze}{4\pi\varepsilon_0 r_1^2} - \frac{1}{4\pi r_1^2}\frac{\hbar^2}{m_p r_n^3} \tag{I.92}$$

$$r_1 = \frac{a_H}{Z} \tag{I.93}$$

where a_H is the radius of the hydrogen atom and the electron velocity is given by Eq. (I.61).

ENERGY CALCULATIONS

From Maxwell's equations, the potential energy V, kinetic energy T, electric energy or binding energy E_{ele} are:

$$V = \frac{-Ze^2}{4\pi\varepsilon_0 r_1} = \frac{-Z^2e^2}{4\pi\varepsilon_0 a_H} = -Z^2\ X\ 4.3675\ X\ 10^{-18}\ J = -Z^2\ X\ 27.2\ eV \tag{I.94}$$

$$T = \frac{Z^2e^2}{8\pi\varepsilon_0 a_H} = Z^2\ X\ 13.59\ eV \tag{I.95}$$

$$T = E_{ele} = -\frac{1}{2}\varepsilon_0\int_{\infty}^{r_1}\mathbf{E}^2 dv \quad \text{where } \mathbf{E} = -\frac{Ze}{4\pi\varepsilon_0 r^2} \tag{I.96}$$

$$E_{ele} = -\frac{Ze^2}{8\pi\varepsilon_0 r_1} = -\frac{Z^2e^2}{8\pi\varepsilon_0 a_H} = -Z^2\ X\ 2.1786\ X\ 10^{-18}\ J = -Z^2\ X\ 13.598\ eV \tag{I.97}$$

The calculated Rydberg constant is $10{,}967{,}758\ m^{-1}$, and the experimental Rydberg constant is $10{,}967{,}758\ m^{-1}$. For increasing Z, the velocity becomes a significant fraction of the speed of light; thus, special relativistic corrections were included in the calculation of the ionization energies of one-electron atoms that are given by

$$E_B = m_{e0}c^2\left(1-\sqrt{1-(\alpha Z)^2}\right) \tag{I.98}$$

THE NATURE OF THE PHOTON IS THE BASIS OF QUANTIZATION AND EXISTENCE OF EXCITED AND HYDRINO STATES OF ATOMIC HYDROGEN

It is well known that resonator cavities can trap electromagnetic radiation of discrete resonant frequencies. The atomic orbital is a resonator cavity that traps photons of discrete frequencies. The radius of an atomic orbital increases with the absorption of electromagnetic energy. The solutions to Maxwell's equations for modes that can be excited in the atomic orbital resonator cavity give rise to four quantum numbers, and the energies of the modes are the experimentally known hydrogen spectrum including the Lamb shift, fine structure, and hyperfine structure.

The excited states involving the corresponding multipole photon radiation are solved including the radii of the atomic orbitals using Maxwell's equations with the traditional source current boundary constraints at the electron. The "trapped photon" is a "standing electromagnetic wave" which actually is a circulating wave that propagates along the current density of the atomic orbital. The time-function factor, $k(t)$, for the "standing wave" is identical to the time-function factor of the atomic orbital in order to satisfy the boundary (phase) condition at the atomic orbital surface. Thus, the angular frequency of the "trapped photon" has to be identical to the angular frequency of the electron atomic orbital, ω_n. Furthermore, the phase condition requires that the angular functions of the "trapped photon" have to be identical to the spherical harmonic angular functions of the electron atomic orbital. Combining $k(t)$ with the ϕ-function factor of the spherical harmonic gives $e^{i(m\phi - m\omega_n t)}$ for both the electron and the "trapped photon" functions. The photon can be considered a solution of Laplace's equation in spherical coordinates that is "glued" to the inner atomic orbital surface corresponding to a radial Dirac delta function at the electron radius, $\delta(r-r_n)$, and due to relativistic effects the field is radially local at the electron. The field lines from the proton superimpose with those of the photon at the electron and end on the current-density function of the electron such that the electric field is zero for $r > r_n$, where r_n is the radius of the electron. The corresponding photon source current given by Gauss' law in

two dimensions determines the stability condition.

The instability of excited states, as well as the stability of the $n=1$ state arises naturally in CP. The central field of the proton corresponds to an integer charge of one. Excited states comprise an electron with a trapped photon. In all energy states of hydrogen, the photon has an electric field that superposes with the field of the proton. In the $n=1$ state, the sum is one, and the sum is zero in the ionized state. In an excited state, the sum is a fraction of one (i.e. between zero and one), specifically, $\frac{1}{\text{integer}}$. The relationship between the electric field function and the "trapped photon" source charge-density function is given by Gauss' law in two dimensions, Eq. (I.102) where $\mathbf{n}$ is the radial normal unit vector, $\mathbf{E}_1 = 0$ ($\mathbf{E}_1$ is the electric field outside of the atomic orbital), $\mathbf{E}_2$ is given by the total electric field at $r_n = na_H$, and σ_s is the equivalent surface charge density. The electric field of an excited state is fractional; therefore, the source charge function is fractional corresponding to a radiative current-density function. Thus, an excited electron is unstable and decays to the first nonradiative state corresponding to an integer field, $n=1$ (i.e. a field of integer one times the central field of the proton).

Equally valid from first principles are electronic states where the magnitude of the sum of the electric field of the photon and the proton central field are an integer times the central field of the proton. These states are nonradiative. A catalyst can effect a transition between these states via a nonradiative energy transfer to form *hydrinos*, stable hydrogen atoms having energy levels below the ground state and corresponding to principal quantum numbers $n = 1, \frac{1}{2}, \frac{1}{3}, \frac{1}{4}, ..., \frac{1}{p}$; $p \le 137$ replaces the well known parameter $n = \text{integer}$ in the Rydberg equation for hydrogen excited states. *Hydrinos* and the corresponding *hydrino hydride ions* and *molecular hydrinos* have been confirmed experimentally as shown in the Data section. Until now, this predicted discovery was missed entirely due to the erroneous concept of the hydrogen atom "ground state" based on its definition regarding the Schrödinger equation since the Schrödinger equation does not physically explain the observation that spontaneous emission of radiation does not occur for the state having a binding energy of 13.6 eV. Nor, does the Schrödinger equation provide a physical basis for the existence of the $n = \text{integer}$ excited states or absorption or emission of radiation. (See Schrödinger Wavefunction in Violation of Maxwell's Equation section, the Retrospect section, and papers by Mills' [4-15]).

EXCITED STATES

CP gives closed form solutions for the resonant photons and excited state electron functions. The angular momentum of the photon given by

$$\mathbf{m} = \int \frac{1}{8\pi c} \mathrm{Re}\left[\mathbf{r} \times (\mathbf{E} \times \mathbf{B}^*)\right] dx^4 = \hbar \tag{I.99}$$

is conserved [67]. The change in angular velocity of the electron is equal to the angular frequency of the resonant photon. The energy is given by Planck's equation. The predicted energies, Lamb shift, hyperfine structure, resonant line shape, line width, selection rules, etc. are in agreement with observation.

The discretization of the angular momentum of the electron and the photon gives rise to quantized electron radii and energy levels. Transitions occur in integer units of the electron's inalienable intrinsic angular momentum of $\hbar$ (Appendix II) such that the exciting photons carry an integer multiple of $\hbar$. Thus, for $\mathbf{r} \times m_e \mathbf{v}_e = \mathbf{p}$ to be constant, the radius increases by a factor of the integer and the electron velocity decreases by the factor of the integer. This quantization condition is equivalent to that of Bohr except that the electron angular momentum is $\hbar$, the angular momentum of one or more photons that give rise to an excited state is $n\hbar$, and the photon field changes the central force balance. Also, the standing wave regards the photon field and not the electron that comprises an extended current and is not a wave function. Thus, the quantization condition can also be considered as arising from the discretization of the photon standing wave including the integer spherical periodicity of the spherical harmonics of the excited state of the bound electron as a spherical cavity.

The atomic orbital is a dynamic spherical resonator cavity which traps photons of discrete frequencies. The relationship between an allowed radius and the "photon standing wave" wavelength is

$$2\pi r = n\lambda \tag{I.100}$$

where n is an integer. The relationship between an allowed radius and the electron wavelength is:

$$2\pi(nr_1) = 2\pi r_n = n\lambda_1 = \lambda_n \tag{I.101}$$

where $n = 1, 2, 3, 4, \ldots$. The radius of an atomic orbital increases with the absorption of electromagnetic energy due to a corresponding decrease in the central field. *The radii of excited states are solved using the electromagnetic force equations of Maxwell relating the field from the charge of the proton, the electric field of the photon, and charge and mass density functions of the electron wherein the angular momentum of the electron is given by $\hbar$ (Eq. (1.37)).* The solutions to Maxwell's equations for modes that can be excited in the atomic orbital resonator cavity give rise to four quantum numbers, and the energies of the modes are the experimentally known hydrogen spectrum. The relationship between the electric field equation and the "trapped photon" source charge-density function is given by Maxwell's equation in two dimensions.

$$\mathbf{n} \bullet \left(\mathbf{E}_1 - \mathbf{E}_2\right) = \frac{\sigma}{\varepsilon_0} \tag{I.102}$$

The photon standing electromagnetic wave is phase matched with the electron

$$\mathbf{E}_{r\,photon\;\;n,l,m_\ell} = \frac{e\left(na_H\right)^\ell}{4\pi\varepsilon_0}\frac{1}{r^{(\ell+2)}}\left[-Y_0^0\left(\theta,\phi\right)+\frac{1}{n}\left[Y_0^0\left(\theta,\phi\right)+\mathrm{Re}\left\{Y_\ell^m\left(\theta,\phi\right)e^{im\omega_n t}\right\}\right]\right]\delta\left(r-r_n\right)\mathbf{i}_r$$
$$\ell = 0,1,2,...,n-1 \tag{I.103}$$
$$m_\ell = -\ell,-\ell+1,...,0,....+\ell$$

$$\mathbf{E}_{r\,total} = \frac{e}{4\pi\varepsilon_0 r^2}+\frac{e\left(na_H\right)^\ell}{4\pi\varepsilon_0}\frac{1}{r^{(\ell+2)}}\left[-Y_0^0\left(\theta,\phi\right)+\frac{1}{n}\left[Y_0^0\left(\theta,\phi\right)+\mathrm{Re}\left\{Y_\ell^m\left(\theta,\phi\right)e^{im\omega_n t}\right\}\right]\right]\delta\left(r-r_n\right)\mathbf{i}_r \tag{I.104}$$

For $r = na_H$ and $m = 0$, the total radial electric field is:

$$\mathbf{E}_{r\,total} = \frac{1}{n}\frac{e}{4\pi\varepsilon_0\left(na_H\right)^2}\mathbf{i}_r \tag{I.105}$$

When an electron in the $n=1$ state absorbs a photon of energy sufficient to take it to a new resonant state, $n = 2,3,4,...,$ force balance must be maintained with the reduction of the central field caused by the superposition of the electric field of the proton and the photon trapped in the atomic orbital, a spherical resonator cavity. According to Eq. (I.105), the central field is equivalent to that of a central charge of $\frac{e}{n}$, and the excited-state force balance equation is

$$\frac{m_e v_n^2}{r_n} = \frac{\hbar^2}{m_e r_n^3} = \frac{1}{n}\frac{e^2}{4\pi\varepsilon_0 r_n^2} \tag{I.106}$$

where r_1 is the $n=1$ state radius of the electron, r_n is the nth excited state radius of the electron, and the electron velocity is given by Eq. (I.61). The radius of the nth excited state given by Eq. (I.106) is

$$r_n = na_H \tag{I.107}$$

The energy of the photon that excites a mode in the electron spherical resonator cavity from radius a_H to radius na_H is

$$E_{photon} = \frac{e^2}{8\pi\varepsilon_0 a_H}\left[1-\frac{1}{n^2}\right] = h\nu = \hbar\omega \tag{I.108}$$

The change in angular velocity of the atomic orbital for an excitation from $n=1$ to $n=n$ is:

$$\Delta\omega = \frac{\hbar}{m_e\left(a_H\right)^2}-\frac{\hbar}{m_e\left(na_H\right)^2} = \frac{\hbar}{m_e\left(a_H\right)^2}\left[1-\frac{1}{n^2}\right] \tag{I.109}$$

The kinetic energy change of the transition is

$$\frac{1}{2}m_e(\Delta v)^2 = \frac{e^2}{8\pi\varepsilon_0 a_H}\left[1-\frac{1}{n^2}\right] = \hbar\omega \tag{I.110}$$

The change in angular velocity of the electron atomic orbital is identical to the angular velocity of the photon necessary for the excitation, ω_{photon}. The *correspondence principle holds*. It can be demonstrated that the resonance condition between these frequencies is to be satisfied in order to have a net change of the energy field [48].

INSTABILITY OF EXCITED STATES

For the excited energy states of the hydrogen atom, σ_{photon}, the two-dimensional surface charge due to the "trapped photons" at the electron atomic orbital, given by Eq. (I.102) and Eq. (I.103) is:

$$\sigma_{photon} = \frac{e}{4\pi(r_n)^2}\left[Y_0^0\left(\theta,\phi\right)-\frac{1}{n}\left[Y_0^0\left(\theta,\phi\right)+\mathrm{Re}\left\{Y_\ell^m\left(\theta,\phi\right)e^{im\omega_n t}\right\}\right]\right]\delta(r-r_n) \tag{I.111}$$

where $n = 2,3,4,...,$. Whereas, $\sigma_{electron}$, the two dimensional surface charge of the electron atomic orbital given by Eq. (I.65) is

$$\sigma_{electron} = \frac{-e}{4\pi(r_n)^2}\left[Y_0^0\left(\theta,\phi\right)+\mathrm{Re}\left\{Y_\ell^m\left(\theta,\phi\right)e^{im\omega_n t}\right\}\right]\delta(r-r_n) \tag{I.112}$$

The superposition of σ_{photon} (Eq. (I.111)) and $\sigma_{electron}$ (Eq. (I.112)) is equivalent to the sum of a radial electric dipole represented by a doublet function and a radial electric monopole represented by a delta function:

$$\sigma_{photon}+\sigma_{electron} =$$
$$\frac{e}{4\pi(r_n)^2}\left[Y_0^0\left(\theta,\phi\right)\dot{\delta}(r-r_n)-\frac{1}{n}Y_0^0\left(\theta,\phi\right)\delta(r-r_n)-\left(1+\frac{1}{n}\right)\left[\mathrm{Re}\left\{Y_\ell^m\left(\theta,\phi\right)e^{im\omega_n t}\right\}\right]\delta(r-r_n)\right] \tag{I.113}$$

where $n = 2,3,4,...,$. Due to the radial doublet, excited states are radiative since spacetime harmonics of $\frac{\omega_n}{c} = k$ or $\frac{\omega_n}{c}\sqrt{\frac{\varepsilon}{\varepsilon_0}} = k$ do exist for which the spacetime Fourier transform of the current density function is nonzero. An excited state is meta-stable because it is the sum of nonradiative (stable) and radiative (unstable) components and de-excites with a transition probability given by the ratio of the power to the energy of the transition [68]. There is motion in the radial direction only when the energy of the system is changing, and the *radiation emitted or absorbed during electron transitions is the multipole radiation given by Eq. (I.50)* as given in the Excited States of the One-Electron Atom (Quantization) section and the Equation of the Photon section. The discontinuous harmonic radial current in Eq. (I.55) that connects the initial and final states of the transition is:

$$\mathbf{r}\cdot\mathbf{J} = \frac{er}{4\pi r^2}\tau^{-1}\sin\frac{\pi t'}{\tau}\left(u(t') - u(t'-\tau)\right) \tag{I.114}$$

where τ is the lifetime of the transition given by Eq. (2.107) and t' is time during the transition as given in the Excited States of the One-Electron Atom (Quantization) section. The vector potential of the current that connects the initial and final states of a transition, each having currents of the form given by Eq. (1.12), is:

$$\mathbf{A}(r) = \frac{\mu_0}{2\pi}\frac{e\hbar}{m_e}\frac{1}{r_{n_i} - r_{n_f}}\frac{e^{-ik_r r}}{4\pi r}\mathbf{i}_z \tag{I.115}$$

The magnetic and electric fields are derived from the vector potential and are used in the Poynting power vector to give the power. The transition probability or Einstein coefficient A_{ki} for initial state n_i and final state n_f of atomic hydrogen given by the power divided by the energy of the transition is:

$$\frac{1}{\tau} = \frac{1}{m_e c^2}\frac{\eta}{24\pi}\left(\frac{e\hbar}{m_e a_0^2}\right)^2\frac{1}{\left(n_f n_i\right)^2} = 2.678\ X\ 10^9\frac{1}{\left(n_f n_i\right)^2}\ s^{-1} \tag{I.116}$$

which matches the NIST values for all transitions extremely well as shown in Excited States of the One-Electron Atom (Quantization) section.

HYDRINO STATES

EXTENSION OF THE RYDBERG STATES TO LOWER LEVELS

For a spherical resonator cavity, the nonradiative boundary condition and the relationship between the electron and the photon give the hydrogen energy states that are quantized as a function of the parameter n. That is the nonradiative boundary condition and the relationship between an allowed radius and the photon standing wave wavelength (Eq. (I.100)) gives rise to Eq. (I.101), the boundary condition for allowed radii and allowed electron wavelengths as a function of the parameter n. Each value of n corresponds to an allowed transition effected by a resonant photon that excites the transition in the atomic orbital resonator cavity. In addition to the traditional integer values (1, 2, 3,...,) of n, values of $\frac{1}{\text{integer}}$ are allowed by Eq. (I.101) which correspond to transitions with an increase in the central field and decrease in the radius of the atomic orbital. This occurs, for example, when the electron couples to another electronic transition or electron transfer reaction that can absorb energy—an energy sink. This ***transition reaction*** of the electron of hydrogen to a lower energy state occurs by the ***absorption of an energy hole by the hydrogen atom***. The absorption of an energy hole destroys the balance between the centrifugal force and the resulting increased central electric force. Consequently, the electron undergoes a transition to a lower energy nonradiative state.

From energy conservation, the energy hole of a hydrogen atom that excites resonator modes of radial dimensions $\frac{a_H}{m+1}$ is

$$m\cdot 27.2\ eV, \tag{I.117}$$

where m is an integer. After resonant absorption of the energy hole, the radius of the atomic orbital, a_H, shrinks to $\frac{a_H}{m+1}$ and after t cycles of transition, the radius is $\frac{a_H}{mt+1}$. In other words, the radial ground state field can be considered as the superposition of Fourier components. The removal of negative Fourier components of energy $m\cdot 27.2\ eV$, where m is an integer increases the positive electric field inside the spherical shell by m times the charge of a proton. The resultant electric field is a time harmonic solution of Laplace's Equations in spherical coordinates. In this case, the radius at which force balance and nonradiation are achieved is $\frac{a_H}{m+1}$ where m is an integer. In decaying to this radius from the $n=1$ state, a total energy of $[(m+1)^2 - 1^2]\cdot 13.6\ eV$ is released. The process involving the transition reaction is hereafter referred to as the **BlackLight Process**. The source of energy holes may not be consumed in the transition reaction; therefore they serve as a hydrogen catalyst.

The increased-binding-energy hydrogen atom is called a *hydrino atom* having a binding energy of:

$$Binding\ Energy = \frac{13.6\ eV}{n^2} \tag{I.118}$$

where

$$n = \frac{1}{2}, \frac{1}{3}, \frac{1}{4}, ..., \frac{1}{p} \tag{I.119}$$

and p is an integer greater than 1. Hydrino atoms designated as $H(1/p)$ have a radius of a_H / p, the hydrogen atom divided by an integer. The potential energy diagram of the hydrogen atom is extended to lower Rydberg states, as given in Figure I.4.

Figure I.4. Potential energy well of a hydrogen atom.

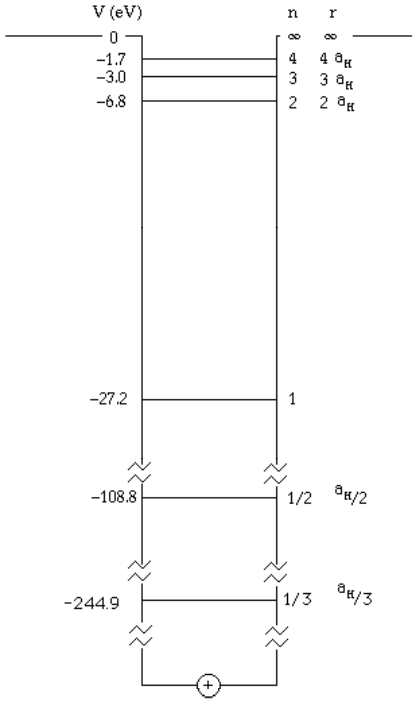

The size of the electron atomic orbital as a function of potential energy is given in Figure I.5.

Figure 1.5. Quantized sizes of hydrogen atoms where n is an integer for excited states and $n = 1/p$ for hydrino states where p is an integer.

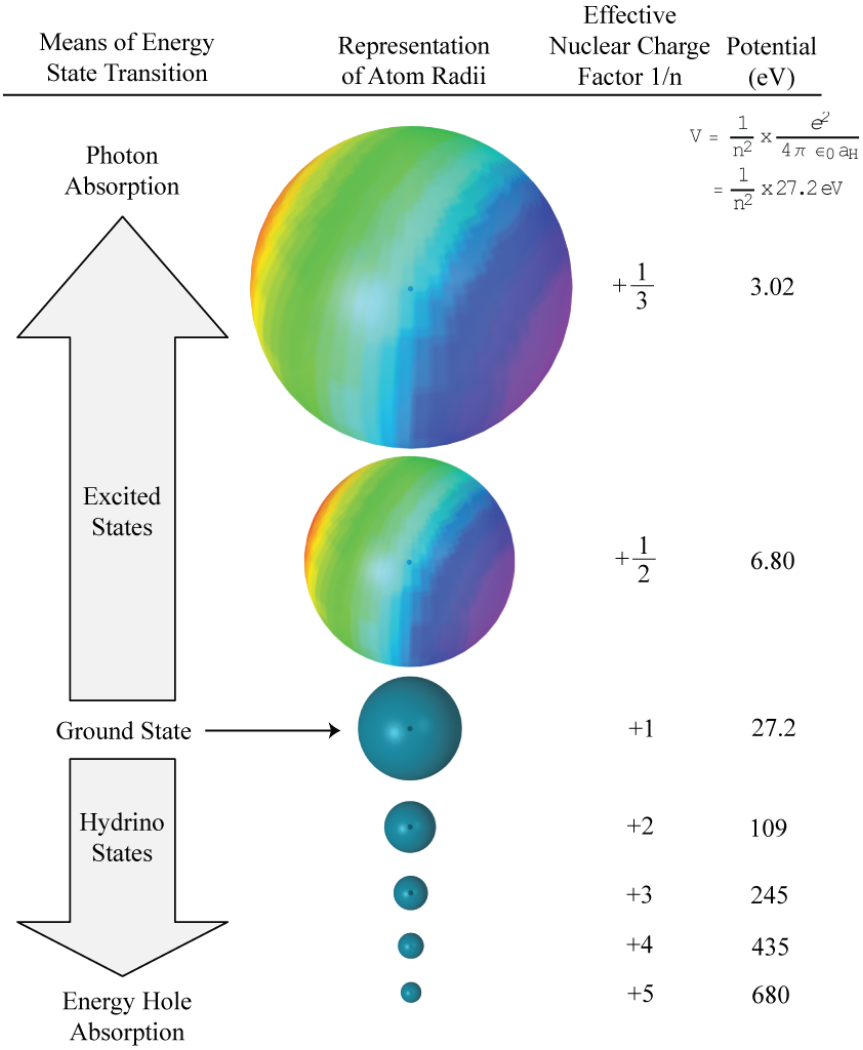

PHOTONIC EQUATION

As shown previously, the hydrino photonic equation must be a solution of Laplace's equation in spherical coordinates. The "trapped photon" field comprises an electric field that provides force balance and a nonradiative state. Following the Maxwellian approach given for excited states in the Excited States section (Eq. (I.103)), the solution to this boundary value problem of the radial photon electric field is:

$$\mathbf{E}_{r\ photon\ n,l,m} = \frac{e\left(na_H\right)^{\ell}}{4\pi\varepsilon_0}\frac{1}{r^{(\ell+2)}}\left[-Y_0^0\left(\theta,\phi\right)+\frac{1}{n}\left[Y_0^0\left(\theta,\phi\right)+\mathrm{Re}\left\{Y_\ell^m\left(\theta,\phi\right)e^{im\omega_n t}\right\}\right]\right]\delta(r-r_n)$$
$$n=\frac{1}{p}$$
$$p=2,3,4,... \qquad (I.120)$$
$$\ell=0,1,2,...,n-1$$
$$m_\ell=-\ell,-\ell+1,...,0,....+\ell$$

The quantum numbers of the electron are p, ℓ, m_ℓ, and m_s as given in the Electron Source Current section and the Excited States section wherein the principal quantum number of excited states is replaced by $n=1/p$. (Also, see Hydrino Theory—BlackLight Process section.)

STABILITY OF THE "GROUND" AND HYDRINO STATES

For the below "ground" (fractional quantum number) energy states of the hydrogen atom, σ_{photon}, the two-dimensional surface charge due to the "trapped photon" at the electron atomic orbital, is given by Eqs. (I.120) and (I.102).

$$\sigma_{photon}=\frac{e}{4\pi(r_n)^2}\left[Y_0^0\left(\theta,\phi\right)-\frac{1}{n}\left[Y_0^0\left(\theta,\phi\right)+\mathrm{Re}\left\{Y_\ell^m\left(\theta,\phi\right)e^{im\omega_n t}\right\}\right]\right]\delta(r-r_n)\quad n=1,\frac{1}{2},\frac{1}{3},\frac{1}{4},..., \qquad (I.121)$$

And, $\sigma_{electron}$, the two-dimensional surface charge of the electron atomic orbital is:

$$\sigma_{electron}=\frac{-e}{4\pi(r_n)^2}\left[Y_0^0\left(\theta,\phi\right)+\mathrm{Re}\left\{Y_\ell^m\left(\theta,\phi\right)e^{im\omega_n t}\right\}\right]\delta(r-r_n) \qquad (I.122)$$

The superposition of σ_{photon} (Eq. (I.121)) and $\sigma_{electron}$, (Eq. (I.122)) where the spherical harmonic functions satisfy the conditions given in the Electron Source Current section is a radial electric monopole represented by a delta function.

$$\sigma_{photon}+\sigma_{electron}=\frac{-e}{4\pi(r_n)^2}\left[\frac{1}{n}Y_0^0\left(\theta,\phi\right)+\left(1+\frac{1}{n}\right)\mathrm{Re}\left\{Y_\ell^m\left(\theta,\phi\right)e^{im\omega_n t}\right\}\right]\delta(r-r_n)\quad n=1,\frac{1}{2},\frac{1}{3},\frac{1}{4},..., \qquad (I.123)$$

As given in the Spacetime Fourier Transform of the Electron Function section, the radial delta function does not possess spacetime Fourier components synchronous with waves traveling at the speed of light (Eqs. (I.66-I.68)). Thus, the below "ground" (fractional quantum) energy states of the hydrogen atom are stable. The "ground" ($n=1$ quantum) energy state is just the first of the nonradiative states of the hydrogen atom; thus, it is the state to which excited states decay.

CATALYTIC LOWER-ENERGY HYDROGEN ELECTRONIC TRANSITIONS

Classical physics gives closed-form solutions of the hydrogen atom, the hydride ion, the hydrogen molecular ion, and the hydrogen molecule and predicts corresponding species having fractional principal quantum numbers. The nonradiative state of atomic hydrogen, which is historically called the "ground state" forms the basis of the boundary condition of CP to solve the bound electron. The solutions for electron states having principal energy levels with quantum numbers that are integers and those where $n=\frac{1}{\text{integer}}$ each reveal the corresponding mechanism of the transitions. In the case of excited states, the superposition given by Eq. (I.113) involves the sum of a delta function with a fractional charge (radial monopole term) and two delta functions of charge plus one and minus one that is a doublet function (radial dipole term). The radial dipole is radiative. Whereas, in the case of lower-energy states, the superposition given by Eq. (I.123) involves integer charge (equivalent) only. As given in Appendix I these states having a radial delta function are nonradiative since spacetime harmonics of $\frac{\omega_n}{c}=k$ or $\frac{\omega_n}{c}\sqrt{\frac{\varepsilon}{\varepsilon_0}}=k$ for which the Fourier transform of the current-density function is nonzero do not exist.

Therefore, for the excited-energy states of atomic hydrogen given by Eq. (I.1) with $n>1$, the $n=1$ state is the "ground" state for spontaneous pure photon transitions, and conversely, the $n=1$ state can absorb a photon and go to an excited electronic state. However, the $n=1$ state cannot directly release a photon and go to a lower-energy electronic state. An electron transition from the $n=1$ state to a lower-energy state is only possible by a nonradiative energy transfer such as multipole coupling or a resonant collision mechanism to form the lower-energy states have fractional quantum numbers, $n=\frac{1}{\text{integer}}$.

Processes such as the transition reaction that occur without photons and that require collisions or nonradiative energy transfer are common. For example, the exothermic chemical reaction of $H+H$ to form H_2 does not occur with the emission of a photon. Rather, the reaction requires a collision with a third body, M, to remove the bond energy- $H+H+M \rightarrow H_2+M^*$ [69]. The third body distributes the energy from the exothermic reaction, and the end result is the H_2 molecule and an increase in the temperature of the system. Some commercial phosphors are based on nonradiative energy transfer involving multipole coupling. For example, the strong absorption strength of Sb^{3+} ions along with the efficient nonradiative transfer of excitation from Sb^{3+} to Mn^{2+}, are responsible for the strong manganese luminescence from phosphors containing these ions [70].

Thus, it is well known that the electric field of an absorbed photon superimposes that of the proton such that the electron of H moves to a higher-energy excited state at a radius that is greater than that of the $n=1$ state. Similarly, in order to conserve energy, a resonant nonradiative energy transfer from H to a catalyst (source of an energy hole) of $m \cdot 27.2\ eV$ results in an increased interaction between the electron and the central field that is equivalent to $m+1$ times that of a proton. The increased interaction then causes the radius to decrease with the further release of energy such that a total energy of $[(m+1)^2-1^2] \cdot 13.6\ eV$ is released.

CATALYST REACTION MECHANISM AND PRODUCTS

Classical physics (CP) gives closed-form solutions of the hydrogen atom, the hydride ion, the hydrogen molecular ion, and the hydrogen molecule and predicts corresponding species having fractional principal quantum numbers. The nonradiative state of atomic hydrogen, which is historically called the "ground state" forms the basis of the boundary condition of CP to solve the bound electron. CP predicts a reaction involving a resonant, nonradiative energy transfer from otherwise stable atomic hydrogen to a catalyst capable of accepting the energy to form hydrogen in lower-energy states than previously thought possible called a ***hydrino atom*** designated as $H\left[\frac{a_H}{p}\right]$ where a_H is the radius of the hydrogen atom. Specifically, CP predicts that atomic hydrogen may undergo a catalytic reaction with certain atoms, excimers, ions, and diatomic hydrides which provide a reaction with a net enthalpy of an integer multiple of the potential energy of atomic hydrogen, $E_h = 27.2\ eV$ where E_h is one Hartree. Specific species (e.g. He^+, Ar^+, Sr^+, K, Li, HCl, NaH, and H_2O) identifiable on the basis of their known electron energy levels are required to be present with atomic hydrogen to catalyze the process. The reaction involves a nonradiative energy transfer of an integer multiple of $27.2\ eV$ from atomic hydrogen to the catalyst followed by $q \cdot 13.6\ eV$ continuum emission or $q \cdot 13.6\ eV$ transfer to another H to form extraordinarily hot, excited-state H and a hydrogen atom that is lower in energy than unreacted atomic hydrogen that corresponds to a fractional principal quantum number. That is, in the formula for the principal energy levels of the hydrogen atom:

$$E_n = -\frac{e^2}{n^2 8\pi\varepsilon_o a_H} = -\frac{13.598\ eV}{n^2} \tag{I.124}$$

$$n = 1, 2, 3, \ldots \tag{I.125}$$

where a_H is the Bohr radius for the hydrogen atom (52.947 pm), e is the magnitude of the charge of the electron, and ε_o is the vacuum permittivity, fractional quantum numbers:

$$n = 1, \frac{1}{2}, \frac{1}{3}, \frac{1}{4}, \ldots, \frac{1}{p}; \quad p \le 137 \text{ is an integer} \tag{I.126}$$

replace the well known parameter $n = \text{integer}$ in the Rydberg equation for hydrogen excited states. Then, similar to an excited state having the analytical solution of Maxwell's equations given by Eq. (2.15), a hydrino atom also comprises an electron, a proton, and a photon as given by Eq. (5.27). However, the electric field of the latter increases the binding corresponding to desorption of energy rather than decreasing the central field with the absorption of energy as in an excited state, and the resultant photon-electron interaction of the hydrino is stable rather than radiative.

The $n=1$ state of hydrogen and the $n = \frac{1}{\text{integer}}$ states of hydrogen are nonradiative, but a transition between two nonradiative states, say $n=1$ to $n=1/2$, is possible via a nonradiative energy transfer. Hydrogen is a special case of the stable states given by Eqs. (I.124) and (I.126) wherein the corresponding radius of the hydrogen or hydrino atom is given by:

$$r = \frac{a_H}{p}, \tag{I.127}$$

where $p = 1, 2, 3, \ldots$. In order to conserve energy, energy must be transferred from the hydrogen atom to the catalyst in units of

$$m \cdot 27.2\ eV,\ m = 1, 2, 3, 4, \ldots. \tag{I.128}$$

and the radius transitions to $\frac{a_H}{m+p}$. The catalyst reactions involve two steps of energy release: a nonradiative energy transfer to the catalyst followed by additional energy release as the radius decreases to the corresponding stable final state. Thus, the general reaction is given by:

$$m \cdot 27.2\ eV + Cat^{q+} + H\left[\frac{a_H}{p}\right] \rightarrow Cat^{(q+r)+} + re^- + H*\left[\frac{a_H}{(m+p)}\right] + m \cdot 27.2\ eV \quad \text{(I.129)}$$

$$H*\left[\frac{a_H}{(m+p)}\right] \rightarrow H\left[\frac{a_H}{(m+p)}\right] + [(p+m)^2 - p^2] \cdot 13.6\ eV - m \cdot 27.2\ eV \quad \text{(I.130)}$$

$$Cat^{(q+r)+} + re^- \rightarrow Cat^{q+} + m \cdot 27.2\ eV \quad \text{(I.131)}$$

And, the overall reaction is:

$$H\left[\frac{a_H}{p}\right] \rightarrow H\left[\frac{a_H}{(m+p)}\right] + [(p+m)^2 - p^2] \cdot 13.6\ eV \quad \text{(I.132)}$$

q, r, m, and p are integers. $H*\left[\frac{a_H}{(m+p)}\right]$ has the radius of the hydrogen atom (corresponding to 1 in the denominator) and a central field equivalent to $(m+p)$ times that of a proton, and $H\left[\frac{a_H}{(m+p)}\right]$ is the corresponding stable state with the radius of $\frac{1}{(m+p)}$ that of H. As the electron undergoes radial acceleration from the radius of the hydrogen atom to a radius of $\frac{1}{(m+p)}$ this distance, energy is released as characteristic light emission or as third-body kinetic energy. The emission may be in the form of an extreme-ultraviolet continuum radiation having an edge at $[(p+m)^2 - p^2 - 2m] \cdot 13.6\ eV$ or $\frac{91.2}{[(p+m)^2 - p^2 - 2m]}\ nm$ and extending to longer wavelengths. In addition to radiation, a resonant kinetic energy transfer to form fast H may occur (See the Dipole-Dipole Coupling section). Subsequent excitation of these fast $H(n=1)$ atoms by collisions with the background H_2 followed by emission of the corresponding $H(n=3)$ fast atoms gives rise to broadened Balmer α emission. Alternatively, fast H is a direct product of H or hydrino serving as the catalyst or source of energy holes as given by Eqs. (5.60), (5.65), (5.70), and (5.83) wherein the acceptance of the resonant energy transfer regards the potential energy rather than the ionization energy. Conservation of energy gives a proton of the kinetic energy corresponding to one half the potential energy in the former case and a catalyst ion at essentially rest in the latter case. The H recombination radiation of the fast protons gives rise to broadened Balmer α emission that is disproportionate to the inventory of hot hydrogen consistent with the excess power balance [22-42].

As given in Disproportionation of Energy States section, hydrogen atoms $H(1/p)$ $p = 1, 2, 3, ...137$ can undergo further transitions to lower-energy states given by Eqs. (I.124) and (I.126) wherein the transition of one atom is catalyzed by a second that resonantly and nonradiatively accepts $m \cdot 27.2\ eV$ with a concomitant opposite change in its potential energy. The overall general equation for the transition of $H(1/p)$ to $H(1/(p+m))$ induced by a resonance transfer of $m \cdot 27.2\ eV$ to $H(1/p')$ given by Eq. (5.87) is represented by:

$$H(1/p') + H(1/p) \rightarrow H + H(1/(p+m)) + \left[2pm + m^2 - p'^2 + 1\right] \cdot 13.6\ eV \quad \text{(I.133)}$$

Hydrogen atoms may serve as a catalyst wherein $m = 1$, $m = 2$, and $m = 3$ for one, two, and three atoms, respectively, acting as a catalyst for another. The rate for the two-atom-catalyst, $2H$, may be high when extraordinarily fast H as reported previously [22-42] collides with a molecule to form the $2H$ wherein two atoms resonantly and nonradiatively accept $54.4\ eV$ from a third hydrogen atom of the collision partners. By the same mechanism, the collision of two hot H_2 provide $3\,H$ to serve as a catalyst of $3 \cdot 27.2\ eV$ for the fourth. The EUV continua at 22.8 nm and 10.1 nm and extraordinary (>100 eV) Balmer α line broadening are observed consistent with predictions [22-42].

The catalyst product, $H(1/p)$, may also react with an electron to form a hydrino hydride ion $H^-(1/p)$, or two $H(1/p)$ may react to form the corresponding molecular hydrino $H_2(1/p)$. Specifically, the catalyst product, $H(1/p)$, may also react with an electron to form a novel hydride ion $H^-(1/p)$ with a binding energy E_B (Eq. (7.74)) derived in the Hydrino Hydride Ion section:

$$E_B = \frac{\hbar^2\sqrt{s(s+1)}}{8\mu_e a_0^2\left[\frac{1+\sqrt{s(s+1)}}{p}\right]^2} - \frac{\pi\mu_0 e^2\hbar^2}{m_e^2}\left(\frac{1}{a_H^3} + \frac{2^2}{a_0^3\left[\frac{1+\sqrt{s(s+1)}}{p}\right]^3}\right) \tag{I.134}$$

where $p = \text{integer} > 1$, $s = 1/2$, $\hbar$ is Planck's constant bar, μ_o is the permeability of vacuum, m_e is the mass of the electron, μ_e is the reduced electron mass given by $\mu_e = \frac{m_e m_p}{\frac{m_e}{\sqrt{\frac{3}{4}}} + m_p}$ where m_p is the mass of the proton, a_o is the Bohr radius, and the ionic radius is $r_1 = \frac{a_0}{p}\left(1+\sqrt{s(s+1)}\right)$ (Eq. (7.73)). From Eq. (I.134), the calculated ionization energy of the hydride ion is $0.75418\ eV$, and the experimental value given by Lykke [71] is $6082.99 \pm 0.15\ cm^{-1}$ (0.75418 eV).

Upfield-shifted NMR peaks are direct evidence of the existence of lower-energy state hydrogen with a reduced radius relative to ordinary hydride ion and having an increase in diamagnetic shielding of the proton. The shift is given by the sum of the contributions of the diamagnetism of the two electrons and the trapped photon field of magnitude p (Eq. (7.87)):

$$\frac{\Delta B_T}{B} = -\mu_0\frac{pe^2}{12m_e a_0\left(1+\sqrt{s(s+1)}\right)}\left(1+p\alpha^2\right) = -\left(p29.9 + p^2 1.59\ X\ 10^{-3}\right)ppm \tag{I.135}$$

where the first term applies to H^- with $p = 1$ and $p = \text{integer} > 1$ for $H^-(1/p)$ and α is the fine structure constant.

$H(1/p)$ may react with a proton and two $H(1/p)$ may react to form $H_2(1/p)^+$ and $H_2(1/p)$, respectively. The hydrogen molecular ion and molecular charge and current density functions, bond distances, and energies were solved in the Nature of the Chemical Bond of Hydrogen-Type Molecules and Molecular Ions section from the Laplacian in ellipsoidal coordinates with the constraint of nonradiation.

$$(\eta-\zeta)R_\xi\frac{\partial}{\partial\xi}(R_\xi\frac{\partial\phi}{\partial\xi}) + (\zeta-\xi)R_\eta\frac{\partial}{\partial\eta}(R_\eta\frac{\partial\phi}{\partial\eta}) + (\xi-\eta)R_\zeta\frac{\partial}{\partial\zeta}(R_\zeta\frac{\partial\phi}{\partial\zeta}) = 0 \tag{I.136}$$

The total energy E_T of the hydrogen molecular ion having a central field of $+pe$ at each focus of the prolate spheroid molecular orbital is (Eqs. (11.192-11.193))

$$E_T = -p^2\left\{\begin{array}{l}\frac{e^2}{8\pi\varepsilon_o a_H}(4\ln 3 - 1 - 2\ln 3)\left[1+\sqrt{\frac{2\hbar\sqrt{\frac{2e^2}{4\pi\varepsilon_o(2a_H)^3}}}{m_e c^2}}\right] \\ -\frac{1}{2}\hbar\sqrt{\frac{\frac{pe^2}{4\pi\varepsilon_o\left(\frac{2a_H}{p}\right)^3} - \frac{pe^2}{8\pi\varepsilon_o\left(\frac{3a_H}{p}\right)^3}}{\mu}}\end{array}\right\} = -p^2 16.2526\ eV \tag{I.137}$$

where p is an integer, c is the speed of light in vacuum, and μ is the reduced nuclear mass. The total energy of the hydrogen molecule having a central field of $+pe$ at each focus of the prolate spheroid molecular orbital is (Eqs. (11.240-11.241)).

$$E_T = -p^2 \left\{ \begin{array}{l} \frac{e^2}{8\pi\varepsilon_o a_0}\left[\left(2\sqrt{2}-\sqrt{2}+\frac{\sqrt{2}}{2}\right)\ln\frac{\sqrt{2}+1}{\sqrt{2}-1}-\sqrt{2}\right]\left[1+\sqrt{\frac{2\hbar\sqrt{\frac{e^2}{4\pi\varepsilon_o a_0^3}m_e}}{m_e c^2}}\right] \\ -\frac{1}{2}\hbar\sqrt{\frac{\frac{pe^2}{8\pi\varepsilon_o\left(\frac{a_0}{p}\right)^3}-\frac{pe^2}{8\pi\varepsilon_o\left(\frac{\left(1+\frac{1}{\sqrt{2}}\right)a_0}{p}\right)^3}}{\mu}} \end{array} \right\} \quad \text{(I.138)}$$

$$= -p^2 31.677\ eV$$

The bond dissociation energy, E_D, of the hydrogen molecule $H_2(1/p)$ is the difference between the total energy of the corresponding hydrogen atoms and E_T

$$E_D = E(2H(1/p)) - E_T \quad \text{(I.139)}$$

where [72]

$$E(2H(1/p)) = -p^2 27.20\ eV \quad \text{(I.140)}$$

E_D is given by Eqs. (I.139-I.140) and (I.138):

$$\begin{aligned} E_D &= -p^2 27.20\ eV - E_T \\ &= -p^2 27.20\ eV - \left(-p^2 31.677\ eV\right) \\ &= p^2 4.478\ eV \end{aligned} \quad \text{(I.141)}$$

The NMR of catalysis-product gas provides a definitive test of the theoretically predicted chemical shift of $H_2(1/p)$. In general, the ^1H NMR resonance of $H_2(1/p)$ is predicted to be upfield from that of H_2 due to the fractional radius in elliptic coordinates wherein the electrons are significantly closer to the nuclei. The predicted shift, $\frac{\Delta B_T}{B}$, for $H_2(1/p)$ is given by the sum of the contributions of the diamagnetism of the two electrons and the trapped photon field of magnitude p (Eqs. (11.415-11.416)).

$$\frac{\Delta B_T}{B} = -\mu_0\left(4-\sqrt{2}\ln\frac{\sqrt{2}+1}{\sqrt{2}-1}\right)\frac{pe^2}{36a_0 m_e}\left(1+p\alpha^2\right) \quad \text{(I.142)}$$

$$\frac{\Delta B_T}{B} = -\left(p28.01 + p^2 1.49\ X\ 10^{-3}\right) ppm \quad \text{(I.143)}$$

where the first term applies to H_2 with $p=1$ and $p=\text{integer}>1$ for $H_2(1/p)$. The experimental absolute H_2 gas-phase resonance shift of -28.0 ppm [73-76] is in excellent agreement with the predicted absolute gas-phase shift of -28.01 ppm (Eq. (I.143)).

The vibrational energies, E_{vib}, for the $\upsilon=0$ to $\upsilon=1$ transition of hydrogen-type molecules $H_2(1/p)$ are (Eq. (11.223))

$$E_{vib} = p^2 0.515902\ eV \quad \text{(I.144)}$$

where p is an integer and the experimental vibrational energy for the $\upsilon=0$ to $\upsilon=1$ transition of H_2, $E_{H_2(\upsilon=0\to\upsilon=1)}$, is given by Beutler [77] and Herzberg [78].

The rotational energies, E_{rot}, for the J to $J+1$ transition of hydrogen-type molecules $H_2(1/p)$ are (Eq. (12.74)).

$$E_{rot} = E_{J+1} - E_J = \frac{\hbar^2}{I}\left[J+1\right] = p^2\left(J+1\right)0.01509\ eV \quad \text{(I.145)}$$

where p is an integer, I is the moment of inertia, and the experimental rotational energy for the $J=0$ to $J=1$ transition of H_2 is given by Atkins [79]. Ro-vibrational emission of $H_2(1/4)$ was observed on e-beam excited molecules in gases and trapped in solid matrix [31, 35] and by Raman spectroscopy [23, 31-35].

The p^2 dependence of the rotational energies results from an inverse p dependence of the internuclear distance and the corresponding impact on the moment of inertia I. The predicted internuclear distance $2c'$ for $H_2(1/p)$ is:

$$2c' = \frac{a_o\sqrt{2}}{p} \tag{I.146}$$

The calculated and experimental parameters of H_2, D_2, H_2^+, and D_2^+ from the Chemical Bond of Hydrogen-Type Molecules section are given in Table I.2.

Table I.2. The Maxwellian closed form calculated and experimental parameters of H_2, D_2, H_2^+ and D_2^+.

Parameter	Calculated	Experimental	Eqs.	Ref. for Exp.
H_2 Bond Energy	4.478 *eV*	4.478 *eV*	11.300	24
D_2 Bond Energy	4.556 *eV*	4.556 *eV*	11.302	24
H_2^+ Bond Energy	2.654 *eV*	2.651 *eV*	11.269	24
D_2^+ Bond Energy	2.696 *eV*	2.691 *eV*	11.271	25
H_2 Total Energy	31.677 *eV*	31.675 *eV*	11.296	24, 30, 19[a]
D_2 Total Energy	31.760 *eV*	31.760 *eV*	11.297	20, 25[b]
H_2 Ionization Energy	15.425 *eV*	15.426 *eV*	11.298	30
D_2 Ionization Energy	15.463 *eV*	15.466 *eV*	11.299	25
H_2^+ Ionization Energy	16.253 *eV*	16.250 *eV*	11.267	24, 19[c]
D_2^+ Ionization Energy	16.299 *eV*	16.294 *eV*	11.268	20, 25[d]
H_2^+ Spin Magnetic Moment	$0.5\mu_B$	$0.5\mu_B$	12.24	31
Absolute H_2 Gas-Phase NMR Shift	-28.0 ppm	-28.0 ppm	11.416	32-33
H_2 Quadrupole Moment	0.4764 X 10^{-16} cm^2	0.38 0.15 X 10^{-16} cm^2	11.430-11.431	46
H_2 Internuclear Distance	0.7411 Å	0.741 Å	12.75	34
D_2 Internuclear Distance	0.7411 Å	0.741 Å	12.75	34
H_2^+ Internuclear Distance	1.0577 Å	1.06 Å	12.81	24
D_2^+ Internuclear Distance	1.0577 Å	1.0559 Å	12.81	25
H_2 Vibrational Energy	0.517 *eV*	0.516 *eV*	11.308	27, 28
D_2 Vibrational Energy	0.371 *eV*	0.371 *eV*	11.313	14, 20
H_2 $\omega_e x_e$	120.4 cm^{-1}	121.33 cm^{-1}	11.310	25
D_2 $\omega_e x_e$	60.93 cm^{-1}	61.82 cm^{-1}	11.314	20
H_2^+ Vibrational Energy	0.270 *eV*	0.271 *eV*	11.277	14, 20
D_2^+ Vibrational Energy	0.193 *eV*	0.196 *eV*	11.281	20
H_2 J=1 to J=0 Rotational Energy	0.01511 *eV*	0.01509 *eV*	12.77	24
D_2 J=1 to J=0 Rotational Energy	0.007557 *eV*	0.00755 *eV*	12.78	24
H_2^+ J=1 to J=0 Rotational Energy	0.00742 *eV*	0.00739 *eV*	12.83	24
D_2^+ J=1 to J=0 Rotational Energy	0.0037095 *eV*	0.003723 *eV*	12.84	25

CATALYSTS

He^+, Ar^+, Sr^+, Li, K, NaH, and H_2O are predicted to serve as catalysts since they meet the catalyst criterion—a chemical or physical process with an enthalpy change equal to an integer multiple of the potential energy of atomic hydrogen, $27.2\ eV$, or have a potential energy of $m \cdot 27.2\ eV$. Specifically, an exemplary catalytic system is provided by the ionization of t electrons from an atom each to a continuum energy level such that the sum of the ionization energies of the t electrons is approximately $m \cdot 27.2\ eV$ where m is an integer. One such catalytic system involves lithium atoms. The first and second ionization energies of lithium are $5.39172\ eV$ and $75.64018\ eV$, respectively [72]. The double ionization ($t = 2$) reaction of Li to Li^{2+} then, has a net enthalpy of reaction of $81.0319\ eV$, which is equivalent to $3 \cdot 27.2\ eV$.

$$81.0319\ eV + Li(m) + H\left[\frac{a_H}{p}\right] \rightarrow Li^{2+} + 2e^- + H\left[\frac{a_H}{(p+3)}\right] + [(p+3)^2 - p^2] \cdot 13.6\ eV \tag{I.147}$$

$$Li^{2+} + 2e^- \rightarrow Li(m) + 81.0319\ eV \tag{I.148}$$

And, the overall reaction is:

$$H\left[\frac{a_H}{p}\right] \rightarrow H\left[\frac{a_H}{(p+3)}\right] + [(p+3)^2 - p^2] \cdot 13.6\ eV \tag{I.149}$$

where $m = 3$ in Eq. (I.128). The energy given off during catalysis is much greater than the energy lost to the catalyst. The energy released is large compared to conventional chemical reactions. For example, when hydrogen and oxygen gases undergo combustion to form water ($H_2\ (g) + \frac{1}{2} O_2\ (g) \rightarrow H_2O\ (l)$) the known enthalpy of formation of water is $\Delta H_f = -286\ kJ / mole$ or 1.48 eV per hydrogen atom. By contrast, each ($n = 1$) ordinary hydrogen atom undergoing a catalysis step to $n = \frac{1}{2}$ releases a net of $40.8\ eV$. Moreover, further catalytic transitions may occur: $n = \frac{1}{2} \rightarrow \frac{1}{3}$, $\frac{1}{3} \rightarrow \frac{1}{4}$, $\frac{1}{4} \rightarrow \frac{1}{5}$, and so on. Once catalysis begins, hydrinos autocatalyze further in a process called disproportionation discussed in the Disproportionation of Energy States section.

Certain molecules may also serve to affect transitions of H to form hydrinos. In general, a compound comprising hydrogen such as MH, where M is an element other than hydrogen, serves as a source of hydrogen and a source of catalyst. A catalytic reaction is provided by the breakage of the $M - H$ bond plus the ionization of t electrons from the atom M each to a continuum energy level such that the sum of the bond energy and ionization energies of the t electrons is approximately $m \cdot 27.2\ eV$, where m is an integer. One such catalytic system involves sodium hydride. The bond energy of NaH is $1.9245\ eV$ [80], and the first and second ionization energies of Na are $5.13908\ eV$ and $47.2864\ eV$, respectively [72]. Based on these energies NaH molecule can serve as a catalyst and H source, since the bond energy of NaH plus the double ionization ($t = 2$) of Na to Na^{2+} is $54.35\ eV$ ($2 \cdot 27.2\ eV$). The concerted catalyst reactions are given by

$$54.35\ eV + NaH \rightarrow Na^{2+} + 2e^- + H\left[\frac{a_H}{3}\right] + [3^2 - 1^2] \cdot 13.6\ eV \tag{I.150}$$

$$Na^{2+} + 2e^- + H \rightarrow NaH + 54.35\ eV \tag{I.151}$$

And, the overall reaction is:

$$H \rightarrow H\left[\frac{a_H}{3}\right] + [3^2 - 1^2] \cdot 13.6\ eV \tag{I.152}$$

With $m = 2$, the product of catalyst NaH is $H(1/3)$ that may further rapidly react to form $H(1/4)$, then molecular hydrino, $H_2(1/4)$. Specifically, in the case of a high hydrogen atom concentration, the further transition given by Eq. (I.133) of $H(1/3)$ ($p = 3$) to $H(1/4)$ ($p + m = 4$) with H as the catalyst ($p' = 1$; $m = 1$) can be fast:

$$H(1/3) \xrightarrow{H} H(1/4) + 95.2\ eV \tag{I.153}$$

A molecule that accepts $m \cdot 27.2\ eV$ from atomic H with a decrease in the magnitude of the potential energy of the molecule by the same energy may serve as a catalyst. For example, the potential energy of H_2O given by Eq. (13.201) is

$$V_e = \left(\frac{3}{2}\right) \frac{-2e^2}{8\pi\varepsilon_0 \sqrt{a^2 - b^2}} \ln \frac{a + \sqrt{a^2 - b^2}}{a - \sqrt{a^2 - b^2}} = -81.8715\ eV \tag{I.154}$$

The catalysis reaction $(m = 3)$ is:

$$81.6\ eV + H_2O + H\left[a_H\right] \rightarrow 2H^+ + O^+ + 3e^- + H*\left[\frac{a_H}{4}\right] + 81.6\ eV \quad \text{(I.155)}$$

$$H*\left[\frac{a_H}{4}\right] \rightarrow H\left[\frac{a_H}{4}\right] + 122.4\ eV \quad \text{(I.156)}$$

$$2H^+ + O^+ + 3e^- \rightarrow H_2O + 81.6\ eV \quad \text{(I.157)}$$

And, the overall reaction is:

$$H\left[a_H\right] \rightarrow H\left[\frac{a_H}{4}\right] + 81.6\ eV + 122.4\ eV \quad \text{(I.158)}$$

wherein $H*\left[\frac{a_H}{4}\right]$ has the radius of the hydrogen atom and a central field equivalent to 4 times that of a proton and $H\left[\frac{a_H}{4}\right]$ is the corresponding stable state with the radius of 1/4 that of H.

Hydrogen and hydrinos may serves as catalysts. As given in the Disproportionation of Energy States section hydrogen atoms $H\left(1/p\right)$ $p = 1,2,3,...137$ can undergo transitions to lower-energy states given by Eqs. (I.124) and (I.126) wherein the transition of one atom is catalyzed by a second that resonantly and nonradiatively accepts $m \cdot 27.2\ eV$ with a concomitant opposite change in its potential energy. The overall general equation for the transition of $H\left(1/p\right)$ to $H\left(1/\left(m+p\right)\right)$ induced by a resonance transfer of $m \cdot 27.2\ eV$ to $H\left(1/p'\right)$ is represented by Eq. (I.133). Thus, hydrogen atoms may serve as a catalyst wherein $m = 1$, $m = 2$, and $m = 3$ for one, two, and three atoms, respectively, acting as a catalyst for another. The rate for the two- or three-atom-catalyst case would be appreciable only when the H density is high. But, high H densities are not uncommon. A high hydrogen atom concentration permissive of 2H or 3H serving as the energy acceptor for a third or fourth may be achieved under several circumstances such as on the surface of the Sun and stars due to the temperature and gravity driven density, on metal surfaces that support multiple monolayers, and in highly dissociated plasmas, especially pinch hydrogen plasmas. Additionally, a three-body H interaction is easily achieved when two H atoms arise with the collision of a hot H with H_2. This event can commonly occur in plasmas having a large population of extraordinarily fast H as reported previously [36-42]. This is evidenced by the unusual intensity of atomic H emission. In such cases, energy transfer can occur from a hydrogen atom to two others within sufficient proximity, being typically a few angstroms as given in the Dipole-Dipole Coupling section. Then, the reaction between three hydrogen atoms whereby two atoms resonantly and nonradiatively accept $54.4\ eV$ from the third hydrogen atom such that $2H$ serves as the catalyst is given by:

$$54.4\ eV + 2H + H \rightarrow 2H^+_{fast} + 2e^- + H*\left[\frac{a_H}{3}\right] + 54.4\ eV \quad \text{(I.159)}$$

$$H*\left[\frac{a_H}{3}\right] \rightarrow H\left[\frac{a_H}{3}\right] + 54.4\ eV \quad \text{(I.160)}$$

$$2H^+_{fast} + 2e^- \rightarrow 2H + 54.4\ eV \quad \text{(I.161)}$$

And, the overall reaction is:

$$H \rightarrow H\left[\frac{a_H}{3}\right] + [3^2 - 1^2] \cdot 13.6\ eV \quad \text{(I.162)}$$

Characteristic continuum emission starting at 22.8 nm ($54.4\ eV$) and continuing to longer wavelengths was observed as predicted for this transition reaction as the energetic hydrino intermediate $H*\left[\frac{a_H}{3}\right]$ decays [23-29, 31]. Alternatively, fast H is producted by the mechanism of Eq. (I.161) or a resonant kinetic energy transfer to form fast H may occur consistent with the observation of extraordinary Balmer α line broadening corresponding to high-kinetic energy H [31, 36-42].

In another H-atom catalyst reaction involving a direct transition to $\left[\frac{a_H}{4}\right]$ state, two hot H_2 molecules collide and dissociate such that three H atoms serve as a catalyst of $3 \cdot 27.2\ eV$ for the fourth. Then, the reaction between four hydrogen atoms whereby three atoms resonantly and nonradiatively accept $81.6\ eV$ from the fourth hydrogen atom such that $3H$ serves as the catalyst is given by:

$$81.6\ eV + 3H + H \rightarrow 3H^+_{fast} + 3e^- + H*\left[\frac{a_H}{4}\right] + 81.6\ eV \quad \text{(I.163)}$$

$$H^{*}\left[\frac{a_H}{4}\right] \rightarrow H\left[\frac{a_H}{4}\right] + 122.4\ eV \tag{I.164}$$

$$3H^{+}_{fast} + 3e^{-} \rightarrow 3H + 81.6\ eV \tag{I.165}$$

And, the overall reaction is:

$$H \rightarrow H\left[\frac{a_H}{4}\right] + [4^2 - 1^2]\cdot 13.6\ eV \tag{I.166}$$

The extreme-ultraviolet continuum radiation band due to the $H^{*}\left[\frac{a_H}{4}\right]$ intermediate of Eq. (I.163) is predicted to have short wavelength cutoff at $122.4\ eV$ (10.1 nm) and extend to longer wavelengths. This continuum band was confirmed experimentally [23-29, 31]. In general, the transition of H to $H\left[\frac{a_H}{p=m+1}\right]$ due by the acceptance of $m\cdot 27.2\ eV$ gives a continuum band with a short wavelength cutoff and energy $E_{\left(H\rightarrow H\left[\frac{a_H}{p=m+1}\right]\right)}$ given by:

$$E_{\left(H\rightarrow H\left[\frac{a_H}{p=m+1}\right]\right)} = m^2\cdot 13.6\ eV \tag{I.167}$$

$$\lambda_{\left(H\rightarrow H\left[\frac{a_H}{p=m+1}\right]\right)} = \frac{91.2}{m^2}\ nm \tag{I.168}$$

and extending to longer wavelengths than the corresponding cutoff. Considering the 91.2 nm continuum shown in Figures 17 and 31 of Ref. [81] and the results shown in Figures 3-8 of Ref. [26], hydrogen may emit the series of 10.1 nm, 22.8 nm, and 91.2 nm continua.

OUTLINE OF THE RESULTS OF THE UNIFIED THEORY DERIVED FROM FIRST PRINCIPLES

To overcome the limitations of quantum mechanics (QM), physical laws that are exact on all scales are sought. Rather than engendering the electron with a wave nature, as suggested by the Davisson-Germer experiment and fabricating a set of associated postulates and mathematical rules for wave operators, a new theory is derived from first principles.

FOUNDATIONS

- Start with first principles
  - Conservation of mass-energy
  - Conservation of linear and angular momentum
  - Maxwell's Equations
  - Newton's Laws
  - Lorentz transforms of Special Relativity

- Highly predictive– application of Maxwell's equations precisely predicts hundreds of fundamental spectral observations in exact equations with no adjustable parameters (fundamental constants only).

- In addition to first principles, the only assumptions needed to predict the Universe over 85 orders of magnitude of scale (Quarks to Cosmos):
  - Four-dimensional spacetime
  - The fundamental constants that comprise the fine structure constant
  - Fundamental particles including the photon have $\hbar$ of angular momentum
  - The Newtonian gravitational constant G
  - The spin of the electron neutrino

Classical Physics (CP) now comprises the unified Maxwell's Equations, Newton's Laws, and General and Special Relativity. The closed form calculations of a broad spectrum of fundamental phenomena containing fundamental constants only are given in subsequent sections. CP gives closed form solutions for the atom that give four quantum numbers, the Rydberg constant, the stability of the $n=1$ state and the instability of the excited states, relativistic invariance of the wave equation, the equations of the photon and electron in excited states, the equations of the free electron, and photon which predict the wave particle duality behavior of particles and light. The current and charge-density functions of the electron may be directly physically interpreted. For example, spin angular momentum results from the motion of negatively charged mass moving systematically, and the equation for angular momentum, $\mathbf{r}\times\mathbf{p}=\hbar$, can be applied directly to the wave function (a current-density

function) that describes the electron. The following observables are derived in closed-form equations based on Maxwell's equations: the magnetic moment of a Bohr magneton, Stern Gerlach experiment, electron and muon g factors, fine structure splitting, Lamb shift, hyperfine structure, muonium hyperfine structure interval, resonant line width and shape, selection rules, correspondence principle, wave particle duality, excited states, reduced mass, rotational energies and momenta, spin-orbit coupling, Knight shift and spin-nuclear coupling, closed form solutions for multielectron atoms, excited states of the helium atom, elastic electron scattering from helium atoms, proton scattering from atomic hydrogen, the nature of the chemical bond, bond energies, vibrational energies, rotational energies, and bond distances of hydrogen-type molecules and molecular ions, the solutions for all major functional groups that give the exact solutions of an infinite number of molecules, solutions to the bonding in the major classes of materials, Davisson Germer experiment, Aspect experiment, Durr experiment on the Heisenberg Uncertainty Principle, Penning trap experiments on single ions, hyperfine structure interval of positronium, magnetic moments of the nucleons, beta decay energy of the neutron, the binding energy of deuterium, and alpha decay. The theory of collective phenomena including statistical mechanics, superconductivity and Josephson junction experiments, integral and fractional quantum Hall effects, and the Aharonov-Bohm effect, is given. The calculations agree with experimental observations.

From the closed form solution of the helium atom, the predicted electron scattering intensity is derived. The closed form scattering equation matches the experimental data; whereas, calculations based on the Born model of the atom utterly fail at small scattering angles. The implications for the invalidity of the Schrödinger and Born models of the atom and the dependent Heisenberg Uncertainty Principle are discussed.

For any kind of wave advancing with limiting velocity and capable of transmitting signals, the equation of front propagation is the same as the equation for the front of a light wave. By applying this condition to electromagnetic and gravitational fields at particle production, the Schwarzschild metric (SM) is derived from the classical wave equation, which modifies general relativity to include conservation of spacetime, in addition to momentum and matter/energy and identifies absolute space. The result gives a natural relationship between Maxwell's equations, special relativity, and general relativity. It gives gravitation from the atom to the cosmos. The gravitational equations with the equivalence of the particle production energies permit the equivalence of mass-energy and the spacetime that determine the nature of absolute space wherein a *"clock" is defined that measures "clicks" on an observable in one aspect, and in another, it is the ruler of spacetime of the universe with the implicit dependence of spacetime on matter-energy conversion*. The masses of the leptons, the quarks, and nucleons are derived from this metric of spacetime that gives the equivalence of the gravitational and inertial masses. The universe is time harmonically oscillatory in matter, energy, and spacetime expansion and contraction with a minimum radius that is the gravitational radius. In closed form equations with fundamental constants only, CP gives the basis of the atomic, thermodynamic, and cosmological arrows of time, the deflection of light by stars, the precession of the perihelion of Mercury, the Hubble constant, the age of the universe, the observed acceleration of the expansion, the power of the universe, the power spectrum of the universe, the microwave background temperature, the primary uniformity of the microwave background radiation, the polarization and microkelvin temperature spatial variation of the microwave background radiation, the observed violation of the GZK cutoff, the mass density of the universe, the large scale structure of the universe, and the identity of dark matter which matches the criteria for the structure of galaxies and emission from interstellar medium and the Sun which have been observed in the laboratory [23-29, 31]. In a special case wherein the gravitational potential energy density of a blackhole equals that of the Planck mass, matter converts to energy and spacetime expands with the release of a gamma ray burst. The singularity in the SM is eliminated. The basis of the antigravitational force is presented with supporting experimental evidence.

In addition to the above known phenomena and characteristics of fundamental particles and forces, the theory predicts the existence of a previously unknown form of matter—hydrogen atoms and molecules having electrons of lower energy than the conventional "ground" state called ***hydrinos*** and ***molecular hydrinos***, respectively, where each energy level corresponds to a fractional quantum number. The existence of hydrinos has been confirmed experimentally proving GUT-CP, and this identity additionally resolves many celestial mysteries [23-29, 31]. It provides resolution to many otherwise inexplicable celestial observations with (a) the identity of dark matter being hydrinos, (b) the hydrino-transition radiation being the radiation source heating the warm-hot interstellar medium (WHIM) and behind the observation that diffuse $H\alpha$ emission is ubiquitous throughout the Galaxy requiring widespread sources of flux shortward of 912 $\AA$, and (c) the energy and radiation from the hydrino transitions being the source of extraordinary temperatures and power regarding the solar corona problem, the cause of sunspots and other solar activity, and why the Sun emits X-rays [23-29, 31].

PHYSICAL CONCEPTS THAT ARISE FROM CP DERIVATIONS ON THE SCALE RANGE OF 85 ORDERS OF MAGNITUDE

Starting from the simple observation that the bound electron of the hydrogen atom is experimentally observed to be stable to radiation, the classical electromagnetic wave equation is used to solve the electron source current by matching it to emitted electromagnetic waves with the constraint that a bound electron in the $n=1$ state cannot radiate energy. The solution is based on Maxwell's equations and other experimentally confirmed physical laws. The resulting CP gives predictions that are unprecedented in success, achieving highly accurate agreement with observations over 85 orders of magnitude from the scale of fundamental particles to that of the cosmos. A summary of some of the salient features of the theory derived in subsequent sections follows:

- Bound electrons are described by a charge-density (mass-density) function which is the product of a radial delta function ($f(r)=\delta(r-r_n)$), angular functions, and a time function. The latter comprise a constant angular function, a time and spherically harmonic function, and linear combinations of these functions. Thus, a bound electron is a constant two-dimensional spherical surface of charge (zero thickness and total charge of $-e$), called an electron atomic orbital that can exist in a bound state at only specified distances from the nucleus determined by the force balance between the electric fields of the electron and proton plus any resonantly absorbed photons.

- The uniform current density function $Y_0^0(\theta,\phi)$ (Eqs. (I.63-I.65)) that gives rise to the spin of the electron is generated from two current-vector fields (CVFs). Each CVF comprises a continuum of correlated *orthogonal great circle current-density elements (one dimensional "current loops")*. The current pattern comprising each CVF is generated over a half-sphere surface by a set of rotations of two orthogonal great circle current loops that serve as basis elements about each of the $\left(-\mathbf{i}_x,\mathbf{i}_y,0\mathbf{i}_z\right)$ and $\left(-\frac{1}{\sqrt{2}}\mathbf{i}_x,\frac{1}{\sqrt{2}}\mathbf{i}_y,\mathbf{i}_z\right)$-axis; the span being π radians. Then, the two CVFs are convoluted, and the result is normalized to exactly generate the *continuous* uniform electron current density function $Y_0^0(\theta,\phi)$ covering a spherical shell and having the three angular momentum components of $\mathbf{L}_{xy}=+/-\frac{\hbar}{4}$ and $\mathbf{L}_z=\frac{\hbar}{2}$.

- Then, the total function that describes the spinning motion of each electron atomic orbital is composed of two functions. One function, the spin function, is spatially uniform over the atomic orbital, where each point moves on the surface with the same quantized angular and linear velocity, and gives rise to spin angular momentum. The other function, the modulation function, can be spatially uniform—in which case there is no orbital angular momentum and the magnetic moment of the electron atomic orbital is one Bohr magneton—or not spatially uniform—in which case there is orbital angular momentum. The modulation function moves harmonically on the surface as a charge-density wave with a quantized angular velocity about a specific (by convention) z-axis. Numerical values for the angular velocity, radii of allowed atomic orbitals, energies, and associated quantities are calculated.

- Atomic orbital radii are calculated by setting the centripetal force equal to the electric and magnetic forces.

- The atomic orbital is a resonator cavity which traps photons of discrete frequencies. The radius of an atomic orbital increases with the absorption of electromagnetic energy. The solutions to Maxwell's equations for modes that can be excited in the atomic orbital resonator cavity give rise to four quantum numbers, and the energies of the modes are the experimentally known hydrogen spectrum. The spectrum of helium is the solution of Maxwell's equations for the energies of modes of this resonator cavity with a contribution from electron-electron spin and orbital interactions.

- Excited states are unstable because the charge-density function of the electron plus photon have a radial doublet function component which corresponds to an electric dipole. The doublet possesses spacetime Fourier components synchronous with waves traveling at the speed of light; thus it is radiative. The charge-density function of the electron plus photon for the $n=1$ principal quantum state of the hydrogen atom as well as for each of the $n=\frac{1}{\text{integer}}$ states mathematically is purely a radial delta function. The delta function does not possess spacetime Fourier components synchronous with waves traveling at the speed of light; thus, each is nonradiative.

- The spectroscopic line-width arises from the classical rise-time band-width relationship, and the Lamb Shift is due to conservation of energy and linear momentum and arises from the radiation reaction force between the electron and the photon.

- The photon is an atomic orbital with electric and magnetic field lines along orthogonal great circles.

- Upon ionization, the atomic orbital radius goes to infinity and the electron becomes a plane wave (consistent with double-slit experiments) with the de Broglie wavelength, $\lambda=h/p$.

- The energy of atoms is stored in their electric and magnetic fields. Chemical bonding occurs when the total energy of

the participant atoms can be lowered with the formation of two-dimensional equipotential energy surfaces (molecular orbitals (MO)) where the current motion in the case of H_2 is along orbits, each comprising an elliptic plane cross section of a spheroidal MO through the foci, and a general form of the nonradiative boundary condition is met.

- Certain atoms and ions serve as catalysts to release energy from hydrogen to produce an increased binding energy hydrogen atom having a binding energy of $\frac{13.6\ eV}{\left(\frac{1}{p}\right)^2}$ where p is an integer greater than 1, designated as $H\left[\frac{a_H}{p}\right]$ where a_H is the radius of the hydrogen atom. Increased binding energy hydrogen atoms called hydrinos are predicted to form by reacting an ordinary hydrogen atom with a catalyst having a net enthalpy of reaction of about the potential energy of hydrogen in its first nonradiative state, $m \cdot 27.2\ eV$, where m is an integer, or have a potential energy of $m \cdot 27.2\ eV$. This catalysis releases energy from the hydrogen atom with a commensurate decrease in size of the hydrogen atom, $r_n = na_H$. For example, the catalysis of $H(n=1)$ to $H(n=1/2)$ releases $40.8\ eV$, and the hydrogen radius decreases from a_H to $\frac{1}{2}a_H$. One such atomic catalytic system involves H itself. The potential energy of H is $27.2\ eV$; thus, one or more (m) H atoms may accept an integer m times $27.2\ eV$ from another that undergoes a transition to a corresponding hydrino state $H\left(1/\left(m+1\right)\right)$. The process is hereafter referred to as the **BlackLight Process**.
- The existence of hydrinos as the product of the BlackLight Process—a new energy source—has been confirmed experimentally.
- For any kind of wave advancing with limiting velocity and capable of transmitting signals, the equation of front propagation is the same as the equation for the front of a light wave. By applying the condition to electromagnetic and gravitational fields at particle production, the Schwarzschild metric (SM) is derived from the classical wave equation, which modifies general relativity to include conservation of spacetime, in addition to momentum and matter/energy. The result gives a natural relationship between Maxwell's equations, special relativity, and general relativity, and defines absolute space that rescues Newton's Second law, resolves the twin paradox, and preserves the energy inventory of the universe. It gives gravitation from the atom to the cosmos.
- The Schwarzschild metric gives the relationship whereby matter causes relativistic corrections to spacetime that determines the curvature of spacetime and is the origin of gravity. The correction is based on the boundary conditions that no signal can travel faster than the speed of light including the gravitational field that propagates following particle production from a photon wherein the particle has a finite gravitational velocity given by Newton's Law of Gravitation.
- The limiting velocity c results in the contraction of spacetime due to particle production. The contraction is given by $2\pi r_g$ where r_g is the gravitational radius of the particle. This has implications for the expansion of spacetime when matter converts to energy.
- The spacetime contraction during particle production is analogous to Lorentz length contraction and time dilation of an object in one inertial frame relative to another moving at constant relative velocity. In the former case, the corresponding correction is a function of the square of the ratio of the gravitational velocity to the speed of light. In the latter case, the corresponding correction is a function of the square of the ratio of the relative velocity of two inertial frames to the speed of light.
- Fundamental particle production occurs when the energy of the particle given by the Planck equation, Maxwell's Equations, and Special Relativity is equal to mc^2, and the proper time is equal to the coordinate time according to the Schwarzschild metric. The gravitational equations with the equivalence of the particle production energies permit the equivalence of mass-energy and the absolute spacetime wherein a *"clock" is defined which measures "clicks" on an observable in one aspect, and in another, it is the ruler of spacetime of the universe with the implicit dependence of spacetime on matter-energy conversion*. The masses of the leptons, the quarks, and nucleons are derived from this metric of spacetime.
- The gravitational equations with the equivalence of the particle production energies require the conservation relationship of mass-energy, $E = mc^2$, and spacetime, $\frac{c^3}{4\pi G} = 3.22\ X\ 10^{34}\ \frac{kg}{\sec}$. Spacetime expands as mass is released as energy which provides the basis of absolute space and the atomic, thermodynamic, and cosmological arrows of time. Entropy and the expansion of the universe are large scale consequences. The universe is closed independently of the total mass of the universe, and different regions of space are isothermal even though they are separated by greater

distances than that over which light could travel during the time of the expansion of the universe. The universe is oscillatory in matter/energy and spacetime with a finite minimum radius, the gravitational radius; thus, the gravitational force causes celestial structures to evolve on a time scale corresponding to the period of oscillation. The equation of the radius of the universe, $\aleph$, is $\aleph = \left(\frac{2Gm_U}{c^2} + \frac{cm_U}{\frac{c^3}{4\pi G}} \right) - \frac{cm_U}{\frac{c^3}{4\pi G}} \cos\left(\frac{2\pi t}{\frac{2\pi G m_U}{c^3}} \right)$ which predicts the observed acceleration of the expansion. The calculated Hubble constant is $H_0 = 78.5 \frac{km}{\sec \cdot Mpc}$. Presently, stars and large-scale structures exist that are older than the elapsed time of the present expansion, as stellar and celestial evolution occurred during the contraction phase. The maximum energy release of the universe that occurs at the beginning of the expansion phase is: $P_U = \frac{c^5}{4\pi G} = 2.88\ X\ 10^{51}\ W$.

- The relationship between inertial and gravitational mass is based on the result that only fundamental particles having an equivalence of the inertial and gravitational masses at particle production are permitted to exist since only in these cases are Maxwell's equations and the conditions inherent in the Schwarzschild metric of spacetime satisfied simultaneously wherein space must be absolute. The equivalence is maintained for any velocity thereafter due to the absolute nature of space and the absolute speed of light. The invariant speed, c, is set by the permittivity and permeability of absolute space, which determines the relativity principle based on propagation of fields and signals as light-wave fronts.
- In addition to the propagation velocity, the intrinsic velocity of the particle and the geometry of this 2-dimensional velocity surface with respect to the limiting speed of light determine that the particle such as an electron may have gravitational mass different from its inertial mass. A constant velocity confined to a spherical surface corresponds to a positive gravitational mass equal to the inertial mass (e.g. particle production or a bound electron). A constant angular velocity function confined to a flat surface corresponds to a gravitational mass less than the inertial mass, which is zero in the limit of an absolutely unbound particle (e.g. absolutely free electron). A hyperbolic velocity function confined to a spherical surface corresponds to a negative gravitational mass (e.g. hyperbolic electron).
- Superconductivity arises when electron plane waves extend throughout the lattice, and the lattice is a band-pass for the magnetic field of an array of magnetic dipoles; so, no energy is dissipated with current flow.
- The Quantum Hall Effect arises when the forces of crossed electric and magnetic fields balance, and the lattice is a band-pass for the magnetic field of an array of magnetic dipoles.
- The vector potential component of the electron's angular momentum gives rise to the Aharonov-Bohm Effect.
- Alpha decay occurs as a transmission of a plane wave through a potential barrier.
- The proton and neutron functions each comprise a linear combination of a constant function and three orthogonal spherical harmonic functions resulting in three quark/gluon functions per nucleon. The nucleons are locally two-dimensional.

SUMMARY OF FOUNDATIONS AND PHYSICAL PHENOMENA SOLVED BY CLASSICAL PHYSICS

The electron current-density functions are solved to match time-harmonic multipole source currents of time-varying electromagnetic fields during transitions with the constraint that a bound electron in the $n = 1$ state cannot radiate energy. The mathematical formulation for zero radiation based on Maxwell's equations follows from a derivation by Haus [46]. The function that describes the motion of the electron corresponding to a potentially emitted photon must not possess spacetime Fourier components that are synchronous with waves traveling at the speed of light. Classical physics gives closed form solutions for the atom including the stability of the $n = 1$ state and the instability of the excited states, relativistic invariance of the wave equation, the equations of the photon and electron in excited states, and the equations of the free electron and photon which also predict the wave-particle duality behavior of particles and light. The current and charge-density functions of the electron may be directly physically interpreted. For example, spin angular momentum results from the motion of negatively charged mass moving systematically, and the equation for angular momentum, $\mathbf{r} \times \mathbf{p} = \hbar$, can be applied directly to the wave function (a current-density function) that describes the electron. A partial listing of well-known and documented phenomena, which are derivable in closed form from classical physics, especially Maxwell's equations are given in Table I.3. The calculations agree with experimental observations.

Table I.3. Partial List of Physical Phenomena Solved by Classical Physics.

- Stability of the atom to radiation
- Magnetic moment of a Bohr magneton and relativistic invariance of each of $\frac{e}{m_e}$ of the electron, the electron angular momentum of $\hbar$, and the electron magnetic moment of μ_B from the spin angular momentum
- De Broglie relationship
- Stern Gerlach experiment
- Electron and muon g factors
- Rotational energies and momenta
- Reduced electron mass
- Ionization energies of multi-electron atoms
- Special relativistic effects
- Excited states
- Resonant line width and shape
- Selection rules
- State Lifetimes and line intensities
- Correspondence principle
- Orbital and spin splitting
- Stark effect
- Lamb Shift
- Knight shift
- Spin-orbit coupling (fine structure)
- Spin-nuclear coupling (hyperfine structure)
- Hyperfine structure interval of muonium
- Nature of the free electron
- Nature of the photon
- Photoelectric effect
- Compton effect
- Wave-particle duality
- Double-slit experiment for photons and electrons
- Davisson Germer experiment
- Elastic electron scattering from helium atoms
- Ionization energies of multielectron atoms
- Hydride ion binding energy and absolute NMR shift
- Hydride lattice parameters and energies
- Excited states of the helium atom with singlet and triplet vector diagrams
- Proton scattering from atomic hydrogen
- Nature of the chemical bond
- Bond energies, vibrational energies, rotational energies, bond distances, magnetic moment and fields of hydrogen-type molecules and molecular ions, absolute NMR shift of H_2
- Molecular Ion and Molecular Excited States
- Parameters of polyatomic molecules
- Superconductivity and Josephson junction experiments
- Integral and fractional quantum Hall effects
- Aharonov-Bohm effect
- Aspect experiment
- Durr experiment on the Heisenberg Uncertainty Principle
- Penning trap experiments on single ions
- Mobility of free electrons in superfluid helium
- Gravitational behavior of neutrons
- Hyperfine structure interval of positronium
- Structure of nucleons
- Magnetic moments of the nucleons
- Beta decay energy of the neutron
- Binding energy of deuterium
- Alpha decay
- Nature of neutrinos
- Proton radius puzzle

For the first time in history, the key building blocks of organic chemistry have been solved from two basic equations. Now, the true physical structure and parameters of an infinite number of organic molecules up to infinite length and complexity can be obtained to permit the engineering of new pharmaceuticals and materials at the molecular level. The solutions of the basic functional groups of organic chemistry were obtained by using generalized forms of a geometrical and an energy equation for the nature of the H-H bond. The geometrical parameters and total bond energies of about 800 exemplary organic molecules were calculated using the functional group composition [4]. The results obtained essentially instantaneously match the experimental values typically to the limit of measurement. The solved functional groups are given in Table I.4.

Table I.4. Partial List of Organic Functional Groups Solved by Classical Physics.

Continuous-Chain Alkanes	N,N-dialkyl Amides	Aniline
Branched Alkanes	Urea	Aryl Nitro Compounds
Alkenes	Carboxylic Acid Halides	Benzoic Acid Compounds
Branched Alkenes	Carboxylic Acid Anhydrides	Anisole
Alkynes	Nitriles	Pyrrole
Alkyl Fluorides	Thiols	Furan
Alkyl Chlorides	Sulfides	Thiophene
Alkyl Bromides	Disulfides	Imidizole
Alkyl Iodides	Sulfoxides	Pyridine
Alkenyl Halides	Sulfones	Pyrimidine
Aryl Halides	Sulfites	Pyrazine
Alcohols	Sulfates	Quinoline
Ethers	Nitroalkanes	Isoquinoline
Primary Amines	Alkyl Nitrates	Indole
Secondary Amines	Alkyl Nitrites	Adenine
Tertiary Amines	Conjugated Alkenes	Fullerene (C_{60})
Aldehydes	Conjugated Polyenes	Graphite
Ketones	Aromatics	Phosphines
Carboxylic Acids	Naphthalene	Phosphine Oxides
Carboxylic Acid Esters	Toluene	Phosphites
Amides	Chlorobenzene	Phosphates
N-alkyl Amides	Phenol	

The two basic equations, one for geometrical parameters and the other for energy parameters that solves organic molecules were applied to bulk forms of matter containing trillions of trillions of electrons. For example, using the same alkane- and alkene-bond solutions as elements in an infinite network, the nature of the solid molecular bond for all known allotropes of carbon (graphite, diamond, C_{60}, and their combinations) were solved. By further extension of this modular approach, the solid molecular bond of silicon and the nature of the semiconductor bond were solved. The nature of other fundamental forms of matter such as the nature of the ionic bond, the metallic bond, and additional major fields of chemistry such as that of silicon, organometallics, and boron were solved exactly such that the position and energy of each and every electron is precisely specified. These results agree with observations to the limit of measurement. The implication of these results is that it is possible using physical laws to solve the structure of all types of matter. Some of the solved forms of matter of infinite extent, as well as additional major fields of chemistry, are given in Table I.5.

Table I.5. Partial List of Additional Molecules and Compositions of Matter Solved by Classical Physics.

- Solid Molecular Bond of the Three Allotropes of Carbon
  - Diamond
  - Graphite
  - Fullerene (C_{60})
- Dipole-Dipole Bonding
  - Hydrogen Bonding
  - Van der Waals Bonding
- Solid Ionic Bond of Alkali-Hydrides
  - Alkali-Hydride Crystal Structures
    - Lithium Hydride
    - Sodium Hydride
    - Potassium Hydride
    - Rubidium & Cesium Hydride
    - Potassium Hydrino Hydride
- Solid Metallic Bond of Alkali Metals
  - Alkali Metal Crystal Structures
    - Lithium Metal
    - Sodium Metal
    - Potassium Metal
    - Rubidium & Cesium Metals
- Alkyl Aluminum Hydrides
- Silicon Groups and Molecules
  - Silanes
  - Alkyl Silanes and Disilanes
- Solid Semiconductor Bond of Silicon
  - Insulator-Type Semiconductor Bond
  - Conductor-Type Semiconductor Bond
- Boron Molecules
  - Boranes
    - Bridging Bonds of Boranes
  - Alkoxy Boranes
- Alkyl Boranes
  - Alkyl Borinic Acids
  - Tertiary Aminoboranes
  - Quaternary Aminoboranes
  - Borane Amines
  - Halido Boranes
- Organometallic Molecular Functional Groups and Molecules
  - Alkyl Aluminum Hydrides
    - Bridging Bonds of Organoaluminum Hydrides
  - Organogermanium and Digermanium
  - Organolead
  - Organoarsenic
  - Organoantimony
  - Organobismuth
- Organic Ions
  - 1° Amino
  - 2° Amino
  - Carboxylate
  - Phosphate
  - Nitrate
  - Sulfate
  - Silicate
- Proteins
  - Amino Acids
  - Peptide Bonds
- DNA
  - Bases
  - 2-deoxyribose
  - Ribose
  - Phosphate Backbone
- Water
- Condensed Noble Gases

For any kind of wave advancing with limiting velocity and capable of transmitting signals, the equation of front propagation is the same as the equation for the front of a light wave. By applying this condition to electromagnetic and gravitational fields at particle production, the Schwarzschild metric (SM) is derived from the classical wave equation, which modifies general relativity to include conservation of spacetime in addition to momentum and mass-energy. The result gives a natural relationship between Maxwell's equations, special relativity, and general relativity and identifies absolute space to give the basis and the equivalence of the inertial and gravitational masses. It gives gravitation from the atom to the cosmos. The universe is time harmonically oscillatory in matter, energy, and spacetime expansion and contraction with a minimum radius that is the gravitational radius. A partial listing of the particle and cosmological phenomena derivable from classical physics in closed form equations with fundamental constants only is given in Table I.6.

Table I.6. Partial List of Particle and Cosmological Phenomena Solved by Classical Physics.

• Equivalence of the inertial and gravitational masses	• Identity of the Diffuse Interstellar Bands (DIBs)
• Newton's second law	• Origin of hot interstellar medium
• Deflection of light by stars	• Solar corona temperature problem
• Precession of the perihelion of Mercury	• Power of the universe
• Lepton masses	• Power spectrum of the universe
• Quark masses	• Microwave background temperature
• Boson masses	• Uniformity of the microwave background radiation
• Hubble constant	• Microkelvin spatial variation of the cosmic microwave background radiation (CMBR)
• Age of the universe	
• Observed acceleration of the expansion	• Polarization of the CMBR data
•Absence of antimatter	• Observed violation of the GZK cutoff
• Absence of a Big Bang origin of the Universe	• Mass density of the universe
• Identity of dark matter	• Web-like, large scale structure of the universe
• Identity of UV crisis/Cosmic EUV continuum emission	

Classical physics further gives the identity of dark matter, which matches the criteria for the structure of galaxies and spectral emission from interstellar medium and the Sun that have been observed in the laboratory [23-29, 31]. In a special case wherein the gravitational potential energy density of a blackhole equals that of the Planck mass, matter converts to energy and spacetime expands with the release of a gamma ray burst. The singularity in the SM is eliminated. The predictions of classical physics are unprecedented in that agreement with observations is achieved over 85 orders of magnitude from the scale of fundamental particles to that of the cosmos.

From the success at predicting the vast scope of known phenomena, it can be appreciated that CP is anticipated to predict new, previously unknown phenomena, as well as now solve previously unsolvable mysteries for which old theories were incapable. In this book, the structure of the bound electron is solved using classical laws and from there a unification theory is developed based on those laws called the Grand Unified Theory of Classical Physics (GUTCP) with results that match observations for the basic phenomena of physics and chemistry from the scale of the quarks to the cosmos. In addition to the observables on the hydrogen atom that are known, it further predicts that atomic hydrogen may undergo a catalytic reaction with certain atomized elements and ions which singly or multiply ionize at integer multiples of the potential energy of atomic hydrogen, $m \cdot 27.2\, eV$ wherein m is an integer or have a potential energy of $m \cdot 27.2\, eV$. Recently, there has been the announcement of some unexpected astrophysical results that support the existence of hydrinos. In the 1995 Edition of the GUTCP, the prediction [45] that the expansion of the universe was accelerating was made from the same equations that correctly predicted the mass of the top quark before it was measured. To the astonishment of cosmologists, this was confirmed by 2000. Another prediction about the nature of dark matter based on GUTCP may be close to being confirmed. Based on recent evidence, Bournaud et al. [82-83] suggest that dark matter is hydrogen in dense molecular form that somehow behaves differently in terms of being unobservable except by its gravitational effects. Theoretical models predict that dwarfs formed from collisional debris of massive galaxies should be free of nonbaryonic dark matter. So, their gravity should tally with the stars and gas within them. By analyzing the observed gas kinematics of such recycled galaxies, Bournaud et al. [82-83] have measured the gravitational masses of a series of dwarf galaxies lying in a ring around a massive galaxy that has recently experienced a collision. Contrary to the predictions of Cold-Dark-Matter (CDM) theories, their results demonstrate that they contain a massive dark component amounting to about twice the visible matter. This baryonic dark matter is argued to be cold molecular hydrogen, but it is distinguished from ordinary molecular hydrogen in that it is not traced at all by traditional methods, such as emission of CO lines. These results match the predictions of the dark matter being molecular hydrino. Additionally, astronomers Jee at al. [84] using data from NASA's Hubble Telescope have mapped the distribution of dark matter, galaxies, and hot gas in the core of the merging galaxy cluster Abell 520 formed from a violent collision of massive galaxy clusters and have determined that the dark matter had collected in a dark core containing far fewer galaxies than would be expected if dark matter was collisionless with dark matter and galaxies anchored together. The collisional debris left behind by the galaxies departing the impact zone behaved as hydrogen did, another indication that the identity of dark matter is molecular hydrino.

The best evidence yet for the existence of dark matter is its direct observation as a source of massive gravitational mass evidenced by gravitational lensing of background galaxies that does not emit or absorb light as shown in Figure I.6 [85]. Hydrogen transitions to hydrinos that comprise the dark matter can be observed celestially and in the laboratory. Characteristic EUV continua of hydrino transitions following radiationless energy transfer with cutoffs at $\lambda_{\left(H\rightarrow H\left[\frac{a_H}{p=m+1}\right]\right)}=\frac{91.2}{m^2}\ nm$ are observed from hydrogen plasmas in the laboratory that match significant celestial observations and further confirm hydrino as the identity of dark matter [23-29, 31]. Hydrinos have been isolated in the laboratory and confirmed by a number of analytical techniques [22-42].

The continua spectra directly and indirectly match significant celestial observations. Hydrogen self-catalysis and disproportionation may be reactions occurring ubiquitously in celestial objects and interstellar medium comprising atomic hydrogen. Stars are sources of atomic hydrogen and hydrinos as stellar wind for interstellar reactions wherein very dense stellar atomic hydrogen and singly ionized helium, He^+, serve as catalysts in stars. Hydrogen continua from transitions to form hydrinos matches the emission from white dwarfs, provides a possible mechanism of linking the temperature and density conditions of the different discrete layers of the coronal/chromospheric sources, and provides a source of the diffuse ubiquitous EUV cosmic background with a 10.1 nm continuum matching the observed intense 11.0-16.0 nm band in addition to resolving the identity of the radiation source behind the observation that diffuse Hα emission is ubiquitous throughout the Galaxy and widespread sources of flux shortward of 912 $\AA$ are required. Moreover, the product hydrinos provides resolution to the identity of dark matter [23-29, 31].

Figure I.6. Dark matter ring in galaxy cluster. This Hubble Space Telescope composite image shows a ghostly "ring" of dark matter in the galaxy cluster Cl 0024+17. The ring is one of the strongest pieces of evidence to date for the existence of dark matter, a prior unknown substance that pervades the universe. Courtesy of NASA/ESA, M.J. Jee and H. Ford (Johns Hopkins University), Nov. 2004.

The recent experimental confirmation of the predictions for transitions of atomic hydrogen to form hydrinos, such as power production and characterization of hydrino reaction products [22-42], as well as pumped catalyst states, fast H, characteristic continuum radiation, and the hydrino product have profound implications theoretically, scientifically, and technologically in that they (1) confirm GUTCP in the prediction of hydrinos, (2) directly disprove atomic theories such as the Schrödinger and Dirac equation theories based on the definition of $n = 1$ as the ground state, the defined state below which it is impossible to go, as expected based on many physical failings and preexisting mathematical inconsistencies [4-20], (3) offer resolution to many otherwise inexplicable celestial observations with (a) the identity of dark matter being hydrinos, (b) the hydrino-transition radiation being the radiation source heating the WHIM and behind the observation that diffuse Hα emission is ubiquitous throughout the Galaxy requiring widespread sources of flux shortward of 912 $\AA$, and (c) the energy and radiation from the hydrino transitions being the source of extraordinary temperatures and power regarding the solar corona problem, the cause of sunspots and other solar activity, and why the Sun emits X-rays [23-29, 31], and (4) directly demonstrate a new field of hydrogen chemistry and a powerful new energy source.

The purpose of a physpcal theory is to not only explain obsservations but predict novel ones such as the acceleration of the expansion of the universe, the absence of a Big Bang origin of the Universe, and the mass of the top quark [45]. Our entire modern technological society was created and depends on engineering using classical physical laws. For example, electromagnetic waves were predicted by Maxwell's equations before they were discovered as a transformational technology. A partial listing of new disruptive technologiues invented using classical physics is given in Table I.7.

Table I.7. Partial List of New Disruptive Technologies Invented Using Classical Physics.

• Hydrino power
• Energetic materials and propellants
• Magnetic materials
• Photonic computer
• Single-molecule super conducting quantum interference devices (SQUIDs)
• Molecular SQUID magnetometer, detectors, switches, gates, logic elements
• Photon torpedoes
• Space drive
• Neutrino communications
• Molecular laser (visible to X-ray wavelength regions)
• Infrared to X-ray light sources
• Hydrino catalyzed fusion tritium production
• Laser wavelength doubler
• High temperature superconductors
• Millsian molecular modeling
• Alternative intelligence

REFERENCES

1. A. Beiser, *Concepts of Modern Physics*, Fourth Edition, McGraw-Hill, New York, (1987), pp. 87-117.
2. L. A. Rozema, A. Darabi, D. H. Mahler, A. Hayat, Y. Soudagar, A. M. Steinberg, "Violation of Heisenberg's Measurement-Disturbance Relationship by Weak Measurements," Phys. Rev. Lett., 109 (2012), 100404.
3. M. Isinger, R. J. Squibb, D. Busto, S. Zhong, A. Harth, D. Kroon, S. Nandi, C. L. Arnold, M. Miranda, J. M. Dahlström, E. Lindroth, R. Feifel, M. Gisselbrecht, A. L'Huillier, "Photoionization in the time and frequency domain," Science, (2017), eaao7043 DOI: 10.1126/science.aao7043MLA.
4. R. L. Mills, B. Holverstott, B. Good, N. Hogle, A. Makwana, J. Paulus, "Total Bond Energies of Exact Classical Solutions of Molecules Generated by Millsian 1.0 Compared to Those Computed Using Modern 3-21G and 6-31G* Basis Sets," Phys. Essays **23**, 153 (2010); doi: 10.4006/1.3310832.
5. W. Xie, R.L. Mills, W. Good, A. Makwana, B. Holverstott, N. Hogle, "Millsian 2.0: A Molecular Modeling Software for Structures, Charge Distributions and Energetics of Biomolecules," Physics Essays, 24 (2011) 200-212.
6. R. L. Mills, "Classical Quantum Mechanics," Physics Essays, Vol. 16, No. 4, December, (2003), pp. 433-498.
7. R. L. Mills, "Physical Solutions of the Nature of the Atom, Photon, and Their Interactions to Form Excited and Predicted Hydrino States," Phys. Essays, Vol. 20, No. 3, (2007), pp. 403-460.
8. R. L. Mills, "Exact Classical Quantum Mechanical Solutions for One- Through Twenty-Electron Atoms," Physics Essays, Vol. 18, (2005), pp. 321-361.
9. R. L. Mills, "The Nature of the Chemical Bond Revisited and an Alternative Maxwellian Approach," Physics Essays, Vol. 17, (2004), pp. 342-389.
10. R. L. Mills, "Maxwell's Equations and QED: Which is Fact and Which is Fiction," Physics Essays, Vol. 19, (2006), pp. 225-262.
11. R. L. Mills, "Exact Classical Quantum Mechanical Solution for Atomic Helium Which Predicts Conjugate Parameters from a Unique Solution for the First Time," Phys. Essays, Vol. 21, No. 2, (2008), pp. 103-141.

12. R. L. Mills, "The Fallacy of Feynman's Argument on the Stability of the Hydrogen Atom According to Quantum Mechanics," Annales de la Fondation Louis de Broglie, Vol. 30, No. 2, (2005), pp. 129-151.
13. R. Mills, "The Grand Unified Theory of Classical Quantum Mechanics," Int. J. Hydrogen Energy, Vol. 27, No. 5, (2002), pp. 565-590.
14. R. Mills, The Nature of Free Electrons in Superfluid Helium—a Test of Quantum Mechanics and a Basis to Review its Foundations and Make a Comparison to Classical Theory, Int. J. Hydrogen Energy, Vol. 26, No. 10, (2001), pp. 1059-1096.
15. R. Mills, "The Hydrogen Atom Revisited," Int. J. of Hydrogen Energy, Vol. 25, Issue 12, December, (2000), pp. 1171-1183.
16. V. F. Weisskopf, Reviews of Modern Physics, Vol. 21, No. 2, (1949), pp. 305-315.
17. P. Pearle, Foundations of Physics, "Absence of radiationless motions of relativistically rigid classical electron," Vol. 7, Nos. 11/12, (1977), pp. 931-945.
18. A. Einstein, B. Podolsky, N. Rosen, Phys. Rev., Vol. 47, (1935), p. 777.
19. F. Laloë, "Do we really understand quantum mechanics? Strange correlations, paradoxes, and theorems," Am. J. Phys. 69 (6), June 2001, pp. 655-701.
20. Z. Merali, "What is really real? A wave of experiments is probing the root of quantum weirdness," Nature, Vol. 521, (2015), pp. 278-280.
21. H. J. Maris, Journal of Low Temperature Physics, Vol. 120, (2000), p. 173.
22. http://www.brilliantlightpower.com/
23. R. Mills, Y. Lu, R. Frazer, "Power Determination and Hydrino Product Characterization of Ultra-low Field Ignition of Hydrated Silver Shots", Chinese Journal of Physics, Vol. 56, (2018), pp. 1667-1717.
24. R. Mills, J. Lotoski, Y. Lu, "Mechanism of soft X-ray continuum radiation from low-energy pinch discharges of hydrogen and ultra-low field ignition of solid fuels", Plasma Science and Technology, Vol. 19, (2017), pp. 1-28.
25. R. L. Mills, R. Booker, Y. Lu, "Soft X-ray Continuum Radiation from Low-Energy Pinch Discharges of Hydrogen," J. Plasma Physics, Vol. 79, (2013), pp 489-507; doi:10.1017/S0022377812001109.
26. R. L. Mills, Y. Lu, "Time-resolved hydrino continuum transitions with cutoffs at 22.8 nm and 10.1 nm," Eur. Phys. J. D, Vol. 64, (2011), pp. 65, DOI: 10.1140/epjd/e2011-20246-5.
27. R. L. Mills, Y. Lu, "Hydrino continuum transitions with cutoffs at 22.8 nm and 10.1 nm," Int. J. Hydrogen Energy, 35 (2010), pp. 8446-8456, doi: 10.1016/j.ijhydene.2010.05.098.
28. R. L. Mills, Y. Lu, K. Akhtar, "Spectroscopic observation of helium-ion- and hydrogen-catalyzed hydrino transitions," Cent. Eur. J. Phys., 8 (2010), pp. 318-339, doi: 10.2478/s11534-009-0106-9.
29. A. Bykanov, "Validation of the observation of soft X-ray continuum radiation from low energy pinch discharges in the presence of molecular hydrogen," http://www.blacklightpower.com/wp-content/uploads/pdf/GEN3_Harvard.pdf.
30. Wilfred R. Hagen, Randell L. Mills, "Electron Paramagnetic Resonance Proof for the Existence of Molecular Hydrino", Vol. 47, No. 56, (2022), pp. 23751-23761; https://www.sciencedirect.com/science/article/pii/S0360319922022406.
31. R. Mills, "Hydrino States of Hydrogen", https://brilliantlightpower.com/pdf/Hydrino_States_of_Hydrogen_Paper.pdf, submitted for publication.
32. R. Mills J. Lotoski, "H_2O-based solid fuel power source based on the catalysis of H by HOH catalyst", Int'l J. Hydrogen Energy, Vol. 40, (2015), 25-37.
33. R. Mills, J. Lotoski, W. Good, J. He, "Solid Fuels that Form HOH Catalyst," Int'l J. Hydrogen Energy, Vol. 39 (2014), pp. 11930–11944 DOI: 10.1016/j.ijhydene.2014.05.170.
34. R. Mills, J. Lotoski, J. Kong, G. Chu, J. He, J. Trevey, "High-Power-Density Catalyst Induced Hydrino Transition (CIHT) Electrochemical Cell." Int. J. Hydrogen Energy, 39 (2014), pp. 14512–14530 DOI: 10.1016/j.ijhydene.2014.06.153.
35. R. Mills, X Yu, Y. Lu, G Chu, J. He, J. Lotoski, "Catalyst induced hydrino transition (CIHT) electrochemical cell," (2012), Int. J. Energy Res., (2013), DOI: 10.1002/er.3142.
36. R. L. Mills, K. Akhtar, "Fast H in Hydrogen Mixed Gas Microwave Plasmas when an Atomic Hydrogen Supporting Surface Was Present," Int. J. Hydrogen Energy, Vol. 35, (2010), pp. 2546–2555, doi: 10.1016/j.ijhydene.2009.12.148.
37. K. Akhtar, J. Scharer, R. L. Mills, "Substantial Doppler Broadening of Atomic Hydrogen Lines in DC and Capactively Coupled RF Plasmas," J. Phys. D: Appl. Phys., Vol. 42, Issue 13 (2009), pp. 135207-135219, doi:10.1088/0022-3727/42/13/135207 42 135207.
38. R. L. Mills, K. Akhtar, "Tests of Features of Field-Acceleration Models for the Extraordinary Selective H Balmer α Broadening in Certain Hydrogen Mixed Plasmas," Int. J. Hydrogen Energy, Vol. 34, (2009), 6465–6477.
39. R. L. Mills, B. Dhandapani, K. Akhtar, "Excessive Balmer α Line Broadening of Water-Vapor Capacitively-Coupled RF Discharge Plasmas," Int. J. Hydrogen Energy, Vol. 33, (2008), 802–815.
40. R. L. Mills, P. Ray, B. Dhandapani, Evidence of an energy transfer reaction between atomic hydrogen and argon II or helium II as the source of excessively hot H atoms in radio-frequency plasmas, J. Plasma Physics, Vol. 72, No. 4, (2006), 469–484.
41. J. Phillips, C. K. Chen, K. Akhtar, B. Dhandapani, R. L. Mills, "Evidence of Catalytic Production of Hot Hydrogen in RF-Generated Hydrogen/Argon Plasmas," Int. J. Hydrogen Energy, Vol. 32(14), (2007), 3010–3025.
42. R. L. Mills, P. C. Ray, R. M. Mayo, M. Nansteel, B. Dhandapani, J. Phillips, "Spectroscopic Study of Unique Line Broadening and Inversion in Low Pressure Microwave Generated Water Plasmas," J. Plasma Physics, Vol. 71, No 6, (2005), 877–888.
43. K. Hagiwara et al., Phys. Rev. D 66, 010001 (2002); http://pdg.lbl.gov/2002/s035.pdf.

44. P. J. Mohr and B. N. Taylor, "CODATA recommended values of the fundamental physical constants: 1998," Reviews of Modern Physics, Vol. 72, No. 2, April, (2000), pp. 351-495.
45. R. L. Mills, *The Grand Unified Theory of Classical Quantum Mechanics*, November 1995 Edition, HydroCatalysis Power Corp., Malvern, PA, Library of Congress Catalog Number 94-077780, ISBN 0-9635171-1-2, Chp. 22.
46. H. A.Haus, "On the radiation from point charges," American Journal of Physics, 54, (1986), pp. 1126-1129.
47. J. D. Jackson, *Classical Electrodynamics*, Second Edition, John Wiley & Sons, New York, (1975), pp. 739-779.
48. M. Mizushima, *Quantum Mechanics of Atomic Spectra and Atomic Structure*, W.A. Benjamin, Inc., New York, (1970), p.17.
49. F. Dyson, "Feynman's proof of Maxwell equations," Am. J. Phys., Vol. 58, (1990), pp. 209-211.
50. J. Horgan, "Quantum Philosophy," Scientific American, July, (1992), p. 96.
51. H. Margenau, G. M. Murphy, *The Mathematics of Chemistry and Physics*, D. Van Nostrand Company, Inc., New York, (1956), Second Edition, pp. 77, 363-367.
52. G. R. Fowles, *Analytical Mechanics*, Third Edition, Holt, Rinehart, and Winston, New York, (1977), pp. 154-156.
53. D. A. McQuarrie, *Quantum Chemistry*, University Science Books, Mill Valley, CA, (1983), pp. 78-79.
54. D. A. McQuarrie, *Quantum Chemistry*, University Science Books, Mill Valley, CA, (1983), pp. 221-225.
55. J. D. Jackson, *Classical Electrodynamics*, Second Edition, John Wiley & Sons, New York, (1975), pp. 84-108.
56. R. N. Bracewell, *The Fourier Transform and Its Applications*, McGraw-Hill Book Company, New York, (1978), pp. 252-253.
57. W. McC. Siebert, *Circuits, Signals, and Systems*, The MIT Press, Cambridge, Massachusetts, (1986), p. 415.
58. W. McC. Siebert, *Circuits, Signals, and Systems*, The MIT Press, Cambridge, Massachusetts, (1986), p. 416.
59. C. A. Fuchs, A. Peres, "Quantum theory needs no 'interpretation,'" Phys. Today, Vol. 53, March, (2000), No. 3, pp. 70-71.
60. S. Durr, T. Nonn, G. Rempe, Nature, September 3, (1998), Vol. 395, pp. 33-37.
61. A. Pais, "George Uhlenbeck and the discovery of electron spin," Physics Today, 42, Dec., (1989), pp. 34-40.
62. J. D. Jackson, *Classical Electrodynamics*, Second Edition, John Wiley & Sons, New York, (1975), p. 111.
63. T. A. Abbott, D. J. Griffiths, Am. J. Phys., Vol. 153, No. 12, (1985), pp. 1203-1211.
64. G. Goedecke, Phys. Rev 135B, (1964), p. 281.
65. D. A. McQuarrie, *Quantum Chemistry*, University Science Books, Mill Valley, CA, (1983), pp. 206-225.
66. R. S. Van Dyck, Jr., P. Schwinberg, H. Dehmelt, "New high precision comparison of electron and positron g factors," Phys. Rev. Lett., Vol. 59, (1987), p. 26-29.
67. J. D. Jackson, *Classical Electrodynamics*, Second Edition, John Wiley & Sons, New York, (1975), pp. 739-779.
68. J. D. Jackson, *Classical Electrodynamics*, Second Edition, John Wiley & Sons, New York, (1975), pp. 758-763.
69. N. V. Sidgwick, *The Chemical Elements and Their Compounds*, Volume I, Oxford, Clarendon Press, (1950), p.17.
70. M. D. Lamb, *Luminescence Spectroscopy*, Academic Press, London, (1978), p. 68.
71. K. R. Lykke, K. K. Murray, W. C. Lineberger, "Threshold photodetachment of H^-," Phys. Rev. A, Vol. 43, No. 11, (1991), pp. 6104-6107.
72. D. R. Lide, *CRC Handbook of Chemistry and Physics*, 86th Edition, CRC Press, Taylor & Francis, Boca Raton, (2005-6), pp. 10-202 to 10-204.
73. K. K. Baldridge, J. S. Siegel, "Correlation of empirical δ(TMS) and absolute NMR chemical shifts predicted by ab initio computations," J. Phys. Chem. A, Vol. 103, (1999), pp. 4038-4042.
74. J. Mason, Editor, *Multinuclear NMR*, Plenum Press, New York, (1987), Chp. 3.
75. C. Suarez, E. J. Nicholas, M. R. Bowman, "Gas-phase dynamic NMR study of the internal rotation in N-trifluoroacetlypyrrolidine," J. Phys. Chem. A, Vol. 107, (2003), pp. 3024-3029.
76. C. Suarez, "Gas-phase NMR spectroscopy," The Chemical Educator, Vol. 3, No. 2, (1998).
77. H. Beutler, Z. Physical Chem., "Die dissoziationswarme des wasserstoffmolekuls H_2, aus einem neuen ultravioletten resonanzbandenzug bestimmt," Vol. 27B, (1934), pp. 287-302.
78. G. Herzberg, L. L. Howe, "The Lyman bands of molecular hydrogen," Can. J. Phys., Vol. 37, (1959), pp. 636-659.
79. P. W. Atkins, *Physical Chemistry*, Second Edition, W. H. Freeman, San Francisco, (1982), p. 589.
80. D. R. Lide, *CRC Handbook of Chemistry and Physics*, 86th Edition, CRC Press, Taylor & Francis, Boca Raton, (2005-6), pp. 9-54 to 9-59.
81. R. Mills, "Spectroscopic Identification of a Novel Catalytic Reaction of Atomic Hydrogen and the Hydride Ion Product," Int. J. Hydrogen Energy, Vol. 26, No. 10, (2001), pp. 1041-1058.
82. F. Bournaud, P. A. Duc, E. Brinks, M. Boquien, P. Amram, U. Lisenfeld, B. Koribalski, F. Walter, V. Charmandaris, "Missing mass in collisional debris from galaxies," Science, Vol. 316, (2007), pp. 1166–1169.
83. B. G. Elmegreen, "Dark matter in galactic collisional debris," Science, Vol. 316, (2007), pp. 32-33.
84. M. J. Jee, A. Mahdavi, H. Hoekstra, A. Babul, J. J. Dalcanton, P. Carroll, P. Capak, "A study of the dark core in A520 with the Hubble Space Telescope: The mystery deepens," Astrophys. J., Vol. 747, No.96, (2012), pp. 96-103.
85. M. J. Jee, et al., "Discovery of a ringlike dark matter structure in the core of the galaxy cluster C1 0024+17," Astrophysical Journal, Vol. 661, (2007), pp. 728-749.

Chapter 1

THE ONE-ELECTRON ATOM

One-electron atoms include the hydrogen atom, He^{+}, Li^{2+}, Be^{3+}, and so on. In each case, the nucleus contains Z protons and the atom has a net positive charge of $(Z-1)e$. The mass-energy and angular momentum of the electron are constant and the flow of current must be conservative and without radiation. A point charge undergoing periodic motion accelerates and as a consequence radiates power according to the Larmor formula. The condition for radiation by a moving point charge derived from Maxwell's equations by Haus [1] is that its spacetime Fourier transform does possess components that are synchronous with waves traveling at the speed of light. The Haus derivation applies to a moving charge-density function as well because charge obeys superposition. Thus, the general condition extended beyond one-dimension is that to radiate, the spacetime Fourier transform of the current-density function must possess components synchronous with waves traveling at the speed of light [1]. Although an accelerated *point* particle radiates, an *extended distribution* modeled as a continuous superposition of accelerating charges does not have to radiate [1-2]. Then, conversely, the nonradiative condition is

For non-radiative states, the current-density function must not possess spacetime Fourier components that are synchronous with waves traveling at the speed of light.

The Haus derivation and the condition for nonradiation are given in Appendix I: Nonradiation Condition wherein the nonradiative condition is also derived directly by the determination of the electrodynamic fields with the electron current-density function as the source current during electron transitions. Given the infinite number of possible current-density functions, it is fortuitous that the spherical radiation corresponding to the symmetry and the conditions for emission and absorption of such radiation provide the additional boundary conditions to determine the current-density functions.

ELECTRON SOURCE CURRENT

Leptons such as the electron (Leptons section) are indivisible, perfectly conducting, and possess an inalienable $\hbar$ of intrinsic angular momentum such that any inelastic perturbation involves the entire particle wherein the intrinsic angular momentum remains unchanged. Bound state transitions are allowed involving the exchange of photons between states, each having $\hbar$ of angular momentum in their fields (Appendix II: Stability and Absence of Self Interaction and Self Energy). A physical approach to solving the structure of the bound electron is followed based on the principles of radiation and the corresponding electron energy state change:

Using Maxwell's equations, the structure of the electron is derived as a boundary-value problem wherein the electron comprises the source current of time-varying electromagnetic fields during transitions with the constraint that the bound $n=1$ state electron cannot radiate energy.

Since the hydrogen atom is stable and nonradiative, the electron has constant energy. Furthermore, it is time dynamic with a corresponding current that serves as a source of electromagnetic radiation during transitions. The wave equation solutions of the radiation fields permit the source currents to be determined as a boundary-value problem. These source currents match the field solutions of the wave equation for two dimensions plus time and the nonradiative $n = 1$ state when the nonradiation condition is applied. Then, the mechanics of the electron can be solved from the two-dimensional wave equation plus time in the form of an energy equation, wherein it provides for conservation of energy and angular momentum as given in the Electron Mechanics and the Corresponding Classical Wave Equation for the Derivation of the Rotational Parameters of the Electron section. Once

the nature of the electron is solved, all problems involving electrons can be solved in principle. Thus, in the case of one-electron atoms, the electron radius, binding energy, and other parameters are solved after solving for the nature of the bound electron.

As shown in Appendix I: Nonradiation Condition, for time-varying spherical electromagnetic fields, Jackson [3] gives a generalized expansion in vector spherical waves that are convenient for electromagnetic boundary-value problems possessing spherical symmetry properties and for analyzing multipole radiation from a localized source distribution. The Green function $G(\mathbf{x}',\mathbf{x})$ that is appropriate to the inhomogenous Helmholtz equation

$$\left(\nabla^2 + k^2\right)G(\mathbf{x}',\mathbf{x}) = -\delta(\mathbf{x}'-\mathbf{x}) \tag{1.1}$$

in the infinite domain with the spherical wave expansion for the outgoing wave Green function is:

$$G(\mathbf{x}',\mathbf{x}) = \frac{e^{-ik|\mathbf{x}-\mathbf{x}'|}}{4\pi|\mathbf{x}-\mathbf{x}'|} = ik\sum_{\ell=0}^{\infty} j_\ell(kr_<)h_\ell^{(1)}(kr_>)\sum_{m=-\ell}^{\ell} Y_{\ell,m}^*(\theta',\phi')Y_{\ell,m}(\theta,\phi) \tag{1.2}$$

Jackson [3] further gives the general multipole field solution to Maxwell's equations in a source-free region of empty space with the assumption of time dependence $e^{i\omega t}$:

$$\begin{aligned}\mathbf{B} &= \sum_{\ell,m}\left[a_E(\ell,m)\,f_\ell(kr)\mathbf{X}_{\ell,m} - \frac{i}{k}a_M(\ell,m)\nabla\times g_\ell(kr)\mathbf{X}_{\ell,m}\right]\\ \mathbf{E} &= \sum_{\ell,m}\left[\frac{i}{k}a_E(\ell,m)\nabla\times f_\ell(kr)\mathbf{X}_{\ell,m} + a_M(\ell,m)\,g_\ell(kr)\mathbf{X}_{\ell,m}\right]\end{aligned} \tag{1.3}$$

where the cgs units used by Jackson are retained in this section. The radial functions $f_\ell(kr)$ and $g_\ell(kr)$ are of the form:

$$g_\ell(kr) = A_\ell^{(1)}h_\ell^{(1)} + A_\ell^{(2)}h_\ell^{(2)} \tag{1.4}$$

$\mathbf{X}_{\ell,m}$ is the vector spherical harmonic defined by:

$$\mathbf{X}_{\ell,m}(\theta,\phi) = \frac{1}{\sqrt{\ell(\ell+1)}}\mathbf{L}Y_{\ell,m}(\theta,\phi) \tag{1.5}$$

where

$$\mathbf{L} = \frac{1}{i}(\mathbf{r}\times\nabla) \tag{1.6}$$

The coefficients $a_E(\ell,m)$ and $a_M(\ell,m)$ of Eq. (1.3) specify the amounts of electric (ℓ,m) multipole and magnetic (ℓ,m) multipole fields, and are determined by sources and boundary conditions as are the relative proportions in Eq. (1.4). Jackson gives the result of the electric and magnetic coefficients from the sources as

$$a_E(\ell,m) = \frac{4\pi k^2}{i\sqrt{\ell(\ell+1)}}\int Y_\ell^{m*}\left\{\rho\frac{\partial}{\partial r}\left[rj_\ell(kr)\right] + \frac{ik}{c}(\mathbf{r}\cdot\mathbf{J})\,j_\ell(kr) - ik\nabla\cdot(r\times\boldsymbol{M})\,j_\ell(kr)\right\}d^3x \tag{1.7}$$

and

$$a_M(\ell,m) = \frac{-4\pi k^2}{\sqrt{\ell(\ell+1)}}\int j_\ell(kr)Y_\ell^{m*}\mathbf{L}\cdot\left(\frac{\mathbf{J}}{c} + \nabla\times\boldsymbol{M}\right)d^3x \tag{1.8}$$

respectively, where the distribution of charge $\rho(\mathbf{x},t)$, current $\mathbf{J}(\mathbf{x},t)$, and intrinsic magnetization $\boldsymbol{M}(\mathbf{x},t)$ are harmonically varying sources: $\rho(\mathbf{x})e^{-i\omega t}$, $\mathbf{J}(\mathbf{x})e^{-i\omega t}$, and $\boldsymbol{M}(\mathbf{x})e^{-i\omega t}$.

The electron current-density function can be solved as a boundary value problem regarding the time varying corresponding source current $\mathbf{J}(\mathbf{x})e^{-i\omega t}$ that gives rise to the time-varying spherical electromagnetic fields during transitions between states with the further constraint that the electron is nonradiative in a state defined as the $n=1$ state. The potential energy, $V(\mathbf{r})$, is an inverse-radius-squared relationship given by Gauss' law, which for a point charge or a two-dimensional spherical shell at a distance r from the nucleus, the potential is:

$$V(r) = -\frac{e^2}{4\pi\varepsilon_0 r} \tag{1.9}$$

Thus, consideration of conservation of energy would require that the electron radius must be fixed. Additional constraints requiring a two-dimensional source current of fixed radius are matching the delta function of Eq. (1.1) with no singularity, no

time dependence and consequently no radiation, absence of self-interaction (See Appendix II: Stability and Absence of Self Interaction and Self Energy), and exact electroneutrality of the hydrogen atom wherein the electric field is given by:

$$\mathbf{n} \bullet \left(\mathbf{E}_1 - \mathbf{E}_2 \right) = \frac{\sigma_s}{\varepsilon_0} \tag{1.10}$$

where $\mathbf{n}$ is the normal unit vector, $\mathbf{E}_1$ and $\mathbf{E}_2$ are the electric field vectors that are discontinuous at the opposite surfaces, σ_s is the discontinuous two-dimensional surface charge density, and $\mathbf{E}_2 = 0$. Then, the solution for the radial electron function, which satisfies the boundary conditions, is a delta function in spherical coordinates—a perfect spherical shell [4]

$$f(r) = \frac{1}{r^2} \delta(r - r_n) \tag{1.11}$$

where r_n is an allowed radius. The perfect spherical nature of a bound electron has been confirmed experimentally by a zero electric dipole moment d_e to an upper limit of $\left| d_e \right| < 10.5 X 10^{-30} e\ m$ [5]. The function of Eq. (1.11) defines the charge density on a spherical shell of a fixed radius, not yet determined where the integer subscript n is *determined during photon absorption,* as given in the Excited States of the One-Electron Atom (Quantization) section. It is shown in this section that the force balance between the electric fields of the electron and proton plus any resonantly absorbed photons gives the result that $r_n = n r_1$ wherein n is an integer in an excited state. To further match the required multipole electromagnetic fields between transitions of states, the trial nonradiative source current functions are time and spherical harmonics, each having an exact radius and an exact energy. Then, each allowed electron charge-density (mass-density) function is the product of a radial delta function ($f(r) = \frac{1}{r^2} \delta(r - r_n)$), two angular functions (spherical harmonic functions), and a time-harmonic function. The corresponding currents $\mathbf{J}$ are

$$\begin{aligned} \mathbf{J} &= \frac{m\omega_n}{2\pi} \frac{e}{4\pi r_n^2} N[\delta(r - r_n)] \mathrm{Re}\left\{ Y_\ell^m(\theta, \phi) \right\} \left[\mathbf{u}(t) \times \mathbf{r} \right] \\ &= \frac{m\omega_n}{2\pi} \frac{e}{4\pi r_n^2} N'[\delta(r - r_n)] \left(P_\ell^m(\cos\theta) \cos\left(m\phi + m\omega_n t \right) \right) \left[\mathbf{u} \times \mathbf{r} \right] \\ &= \frac{m\omega_n}{2\pi} \frac{e}{4\pi r_n^2} N'[\delta(r - r_n)] \left(P_\ell^m(\cos\theta) \cos\left(m\phi + m\omega_n t \right) \right) \sin\theta \hat{\phi} \end{aligned} \tag{1.12}$$

where N and N' are normalization constants. The vectors are defined as:

$$\hat{\phi} = \frac{\hat{u} \times \hat{r}}{\left| \hat{u} \times \hat{r} \right|} = \frac{\hat{u} \times \hat{r}}{\sin\theta}; \qquad \hat{u} = \hat{z} = orbital\ axis \tag{1.13}$$

$$\hat{\theta} = \hat{\phi} \times \hat{r} \tag{1.14}$$

"^" denotes the unit vectors $\hat{u} \equiv \frac{\mathbf{u}}{|\mathbf{u}|}$, non-unit vectors are designated in bold, and the current function is normalized.

The Fourier transform of the radial Dirac delta function is a sinc function as shown in Appendix I. Given time harmonic motion with angular velocity ω_n corresponding to a potentially emitted photon, and a radial delta function, the relationship between an allowed radius and the electron wavelength is given by

$$2\pi r_n = \lambda_n \tag{1.15}$$

Consider the sinc function when the velocity is c corresponding to a potentially emitted photon where Eq. (1.15) applies. In this case, the relativistically corrected wavelength (Eq. (1.279)) is

$$\lambda_n = r_n \tag{1.16}$$

Substitution of Eq. (1.16) into the sinc function results in the vanishing of the entire Fourier transform of the current-density function. Thus, spacetime harmonics of $\frac{\omega_n}{c} = k$ or $\frac{\omega_n}{c} \sqrt{\frac{\varepsilon}{\varepsilon_0}} = k$ do not exist for which the Fourier transform of the current-density function is nonzero. Radiation due to charge motion does not occur in any medium when this boundary condition is met. (Note that in contrast the purely mathematical boundary condition for the solution of the radial function of the hydrogen atom with the Schrödinger equation is $\Psi \to 0$ as $r \to \infty$ wherein the electron exists everywhere at once and has the maximum of the squared wavefunction at the origin inside of the nucleus.)

In addition to satisfaction of the Haus' condition given, the electron currents given by Eq. (1.12) are shown to be nonradiative with the same condition as that of Eq. (1.16) applied to the vector potential based on the electromagnetic fields and the Poynting power vector as shown in Appendix I: Nonradiation Condition. From Eq. (1.12), the charge and intrinsic

magnetization terms are zero. Also, the current $\mathbf{J}(\mathbf{x},t)$ is in the $\hat{\phi}$ direction; thus, the $a_E(\ell,m)$ coefficient given by Eq. (1.7) is zero since $\mathbf{r}\cdot\mathbf{J}=0$. Substitution of Eq. (1.12) into Eq. (1.8) gives the magnetic multipole coefficient $a_M(\ell,m)$:

$$a_M(\ell,m)=\frac{-ek^2}{c\sqrt{\ell(\ell+1)}}\frac{\omega_n}{2\pi}Nj_\ell(kr_n)\Theta\sin(ks) \tag{1.17}$$

For the electron source current given by Eq. (1.12), each comprising a multipole of order (ℓ,m) with a time dependence $e^{i\omega t}$, the far-field solutions to Maxwell's equations given by Eq. (1.3) are:

$$\begin{aligned}\mathbf{B}&=-\frac{i}{k}a_M(\ell,m)\nabla\times g_\ell(kr)\mathbf{X}_{\ell,m}\\ \mathbf{E}&=a_M(\ell,m)g_\ell(kr)\mathbf{X}_{\ell,m}\end{aligned} \tag{1.18}$$

and the time-averaged power radiated per solid angle $\frac{dP(\ell,m)}{d\Omega}$ is:

$$\frac{dP(\ell,m)}{d\Omega}=\frac{c}{8\pi k^2}\left|a_M(\ell,m)\right|^2\left|\mathbf{X}_{\ell,m}\right|^2 \tag{1.19}$$

where $a_M(\ell,m)$ is given by Eq. (1.17). In the case that k is the lightlike k^0, then $k=\omega_n/c$ regarding an emitted photon, in Eq. (1.17), and Eqs. (1.18-1.19) vanishes for:

$$s=vT_n=R=r_n=\lambda_n \tag{1.20}$$

There is no radiation.

There is no radiation due to the azimuthal charge density wave even in an excited state. However, for excited states there exists a radial dipole that is unstable to radiation as shown in the Instability of Excited States section, and this instability gives rise to a radial electric dipole current. In a nonradiative state, there is no emission or absorption of radiation corresponding to the absence of radial motion wherein Eq. (1.7) is zero since $\mathbf{r}\cdot\mathbf{J}=0$. Conversely, there is motion in the radial direction only when the energy of the system is changing, and the *radiation emitted or absorbed during electron transitions is the multipole radiation given by Eq. (1.2)* as given in the Excited States of the One-Electron Atom (Quantization) section and the Equation of the Photon section wherein Eqs. (4.18-4.23) give a macro-spherical wave in the far-field. Thus, radial motion corresponds to the emission or absorption of photons. The form of the radial solution during a transition is then the corresponding electron source current comprising a time-dependent radial Dirac delta function that connects the initial and final states as boundary conditions. The photon carries fields and corresponding angular momentum. The physical characteristics of the photon and the electron are the basis of physically solving for excited states according to Maxwell's equations. The discontinuous harmonic radial current in Eq. (1.7) that connects the initial and final states of the transition is:

$$\mathbf{r}\cdot\mathbf{J}=\frac{er}{4\pi r^2}\tau^{-1}\sin\frac{\pi t'}{\tau}\left(u(t')-u(t'-\tau)\right) \tag{1.21}$$

where τ is the lifetime of the transition given by Eq. (2.107) and t' is time during the transition as given in the Excited States of the One-Electron Atom (Quantization) section. The vector potential of the current that connects the initial and final states of a transition, each having currents of the form given by Eq. (1.12), is:

$$\mathbf{A}(r)=\frac{\mu_0}{2\pi}\frac{e\hbar}{m_e}\frac{1}{r_{n_i}-r_{n_f}}\frac{e^{-ik_r r}}{4\pi r}\mathbf{i}_z \tag{1.22}$$

The magnetic and electric fields are derived from the vector potential and are used in the Poynting power vector to give the power. The transition probability or Einstein coefficient A_{ki} for initial state n_i and final state n_f of atomic hydrogen given by the power divided by the energy of the transition is:

$$\frac{1}{\tau}=\frac{1}{m_e c^2}\frac{\eta}{24\pi}\left(\frac{e\hbar}{m_e a_0^2}\right)^2\frac{1}{\left(n_f n_i\right)^2}=2.678\ X\ 10^9\frac{1}{\left(n_f n_i\right)^2}\ s^{-1} \tag{1.23}$$

which matches the NIST values for all transitions extremely well as shown in Excited States of the One-Electron Atom (Quantization) section.

THE BOUND ELECTRON "ATOMIC ORBITAL"

From Eqs. (1.27-1.29), the electron angular functions are the spherical harmonics, $Y_\ell^m(\theta,\phi)=P_\ell^m(\cos\theta)e^{im\phi}$. The spherical harmonic $Y_0^0(\theta,\phi)=1$ is also an allowed solution that is in fact required in order for the electron charge and mass densities to be

positive definite and to give rise to the phenomena of electron spin. The real parts of the spherical harmonics vary between -1 and 1. But, the mass of the electron cannot be negative, and the charge cannot be positive. Thus, to insure that the function is positive definite, the form of the angular solution must be a superposition:

$$Y_0^0(\theta,\phi)+Y_\ell^m(\theta,\phi) \tag{1.24}$$

(Note that $Y_\ell^m(\theta,\phi)=P_\ell^m(\cos\theta)e^{im\phi}$ are not normalized here as given by Eq. (3.53) of Jackson [6]; however, it is implicit that the magnitude is made to satisfy the boundary condition that the function is positive definite and Eq. (1.26) is satisfied.) $Y_0^0(\theta,\phi)$ is called the angular spin function corresponding to the quantum numbers $s=\frac{1}{2};\ m_s=\pm\frac{1}{2}$ as given in the Atomic Orbital Equation of Motion For $\ell = 0$ Based on the Current Vector Field (CVF) section. Thus, bound electrons are described by a charge-density (mass-density) function that is the product of a radial delta function, Eq. (1.11), two angular functions (spherical harmonic functions), and a time harmonic function. This radial function implies that allowed states are two-dimensional spherical shells (zero thickness [1]) of charge density (and mass density) at specific radii r_n. Thus, a bound electron is a constant two-dimensional spherical surface of charge (zero thickness, total charge of $-e$, and total mass of m_e), called *an electron atomic orbital shown in Figure 1.1, that can exist in a bound state at only specified distances from the nucleus determined by an energy minimum for the n=1 state and integer multiples of this radius due to the action of resonant photons as shown in the Determination of Atomic Orbital Radii section and the Equation of the Electric Field Inside the Atomic Orbital section, respectively.*

Figure 1.1. A bound electron is a constant two-dimensional spherical surface of charge (zero thickness, total charge of $-e$, and total mass of m_e), called *an electron atomic orbital.* For the $n=1$ state of the hydrogen atom, the atomic orbital has the Bohr radius of the hydrogen atom, $r=a_H$. It is a nonradiative, minimum-energy surface, that is absolutely stable except for quantized state changes with the corresponding balanced forces in the $n=1$ state providing a pressure equivalent of twenty million atmospheres.

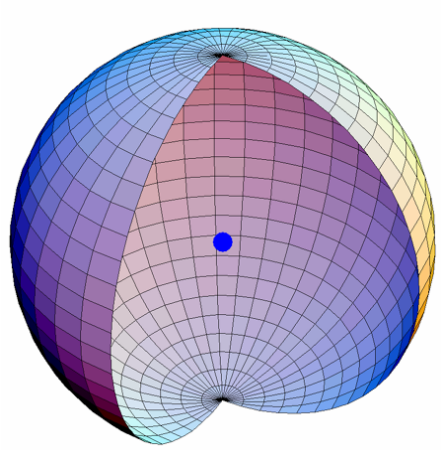

The equipotential, uniform or constant charge-density function (Eq. (1.27)) further comprises a current pattern given in the Atomic Orbital Equation of Motion For $\ell = 0$ Based on the Current Vector Field (CVF) section and corresponds to the spin function of the electron. It also corresponds to the nonradiative $n=1$, $\ell = 0$ state of atomic hydrogen. The uniform current density function $Y_0^0(\theta,\phi)$ (Eqs. (1.27-1.29)) that gives rise to the spin of the electron is generated from two current-vector fields (CVFs). Each CVF comprises a continuum of correlated *orthogonal great circle current-density elements (one dimensional "current loops").* The current pattern comprising each CVF is generated over a half-sphere surface by a set of rotations of two

[1] The atomic orbital has zero thickness, but in order that the speed of light is a constant maximum in any frame including that of the gravitational field that propagates out as a light-wave front at particle production, it gives rise to a spacetime dilation equal to 2π times the Newtonian gravitational or Schwarzschild radius $r_g=\frac{2Gm_e}{c^2}=1.3525\ X\ 10^{-57}\ m$ according to Eqs. (32.36) and (32.140b) and the discussion at the footnote after Eq. (32.40). This corresponds to a spacetime dilation of $8.4980\ X\ 10^{-57}\ m$ or $2.8346\ X\ 10^{-65}\ s$. Although the atomic orbital does not occupy space in the third spatial dimension, its mass discontinuity effectively "displaces" spacetime wherein the spacetime dilation can be considered a "thickness" associated with its gravitational field. The inertial frame of the orbital motion of the bound electron and the atom in motion is with respect to absolute space of the electron and proton as given in the Equivalence of Inertial and Gravitational Masses due Absolute Space and Absolute Light Velocity.

orthogonal great circle current loops that serve as basis elements about each of the $\left(-\mathbf{i}_x, \mathbf{i}_y, 0\mathbf{i}_z\right)$ and $\left(-\frac{1}{\sqrt{2}}\mathbf{i}_x, \frac{1}{\sqrt{2}}\mathbf{i}_y, \mathbf{i}_z\right)$-axis; the span being π radians. Then, the two CVFs are convoluted, and the result is normalized to exactly generate the *continuous* uniform electron current density function $Y_0^0(\theta,\phi)$ covering a spherical shell and having the three angular momentum components of $\mathbf{L}_{xy} = +/-\frac{\hbar}{4}$ and $\mathbf{L}_z = \frac{\hbar}{2}$ (Figure 1.23)[2]. There is acceleration without radiation, in this case, centripetal acceleration. A static charge distribution exists even though there is acceleration along a great circle at each point on the surface. Haus' condition predicts no radiation for the entire ensemble.

In cases of orbitals of heavier elements and excited states of one-electron atoms and atoms or ions of heavier elements which are not constant as given by Eq. (1.29), the constant spin function is modulated by a time and spherical harmonic function. The modulation or traveling charge-density wave corresponds to an orbital angular momentum, in addition to a spin angular momentum. These states are typically referred to as p, d, f, etc. orbitals and correspond to an $\hbar$ quantum number not equal to zero. Haus' condition also predicts nonradiation for a constant spin function modulated by a time and spherically harmonic orbital function. However, in the case that such a state arises as an excited state by photon absorption, it is radiative due to a radial dipole term in its current-density function since it possesses spacetime Fourier transform components synchronous with waves traveling at the speed of light, as given in the Instability of Excited States section.

In the case of an excited state, the charge-density function of the electron atomic orbital can be modulated by the corresponding "trapped" photon to give rise to orbital angular momentum about the z-axis. The "trapped photon" is a "standing electromagnetic wave" which actually is a circulating wave that propagates around the z-axis. Its source current superimposes with the current-density of the atomic orbital at its radius corresponding to a radial Dirac delta function at the electron radius, $\delta(r - r_n)$, and due to relativistic effects the field is radially local at the electron. In order to satisfy the boundary (phase) condition at the atomic orbital surface, the angular and time functions of the photon must match those of its source current which modulates the atomic orbital charge-density function as given in the Equation of the Electric Field Inside the Atomic Orbital section. The time-function factor, *k(t)*, for the photon "standing wave" is identical to the time-function factor of the atomic orbital. Thus, the angular frequency of the "trapped photon" has to be identical to the angular frequency of the electron atomic orbital, ω_n given by Eq. (1.36). However, the linear velocity of the multipole modulation component is not given by Eq. (1.35)—the orbital angular frequency is with respect to the z-axis; thus, the distance from the z-axis, $\rho = r_n \sin\theta$, must be substituted for the atomic orbital radius of Eq. (1.35).

$Y_\ell^m(\theta,\phi)$ is called the angular orbital function corresponding to the quantum numbers $\ell = 0, 1, 2, 3, 4,...;\ m_\ell = -\ell, -\ell + 1, ..., 0, ..., +\ell$. $Y_\ell^m(\theta,\phi)$ can be thought of as a modulation function. The charge density of the entire atomic orbital is the total charge divided by the total area, $\frac{-e}{4\pi r_n^2}$. The fraction of the charge of an electron in any area element is given by:

$$N\left[Y_0^0(\theta,\phi) + Y_\ell^m(\theta,\phi)\right] r_n^2 \sin\theta d\theta d\phi, \tag{1.25}$$

where N is the normalization constant. Therefore, the normalization constant is given by:

$$-e = N r_n^2 \int_0^{\pi}\int_0^{2\pi} \left[Y_0^0(\theta,\phi) + Y_\ell^m(\theta,\phi)\right] \sin\theta d\theta d\phi \tag{1.26}$$

For $\ell = 0$, $N = \frac{-e}{8\pi r_n^2}$. For $\ell \neq 0$, $N = \frac{-e}{4\pi r_n^2}$. The quantum numbers of the spherical harmonic currents can be related to the observed electron orbital angular momentum states. The current is constant at every point on the surface for the s orbital corresponding to $Y_0^0(\theta,\phi)$. The charge-density functions including the time-function factor corresponding to s, p, d, f, etc. orbitals are

$\ell = \mathbf{0}$

$$\rho(r,\theta,\phi,t) = \frac{e}{8\pi r_n^2}[\delta(r - r_n)]\left[Y_0^0(\theta,\phi) + Y_\ell^m(\theta,\phi)\right] \tag{1.27}$$

$\ell \neq \mathbf{0}$

[2] $+/-$ designates both the positive and negative vector directions along an axis in the xy-plane.

$$\rho(r,\theta,\phi,t)=\frac{e}{4\pi r_n^2}[\delta(r-r_n)]\left[Y_0^0(\theta,\phi)+\mathrm{Re}\left\{\pi\left(R_z(\omega_n t)\right)Y_\ell^m(\theta,\phi)\right\}\right] \tag{1.28}$$

$$\rho(r,\theta,\phi,t)=\frac{e}{4\pi r_n^2}[\delta(r-r_n)]\left[Y_0^0(\theta,\phi)+\mathrm{Re}\left\{Y_\ell^m(\theta,\phi)e^{im\omega_n t}\right\}\right] \tag{1.29}$$

where to keep the form of the spherical harmonic as a traveling wave about the z-axis $\pi(R_z)$ is the representation of the rotational matrix about the z-axis R_z (Eq. (1.82)) in the space of functions $\pi\left(R_z(\omega_n t)\right)Y_\ell^m(\theta,\phi)=Y_\ell^m(\theta,\phi+m\omega_n t)$ and $\mathrm{Re}\left\{Y_\ell^m(\theta,\phi)e^{im\omega_n t}\right\}=P_\ell^m(\cos\theta)\cos(m\phi+m\omega_n t)$[3]. Each of the Eqs. (1.28-1.29) represents a traveling charge-density wave that moves on the surface of the atomic orbital about the z-axis with frequency ω_n and modulates the atomic orbital corresponding to $\ell=0$. The latter gives rise to spin angular momentum as given in the Spin Angular Momentum of the Atomic Orbital $Y_0^0(\theta,\phi)$ with $\ell=0$ section. The spin and orbital angular momentum may couple as given in the Orbital and Spin Splitting section. In the cases that $\ell\neq 0$ and $m=0$, the charge is moving or rotating about the z-axis with frequency ω_n, but the charge density is not time dependent. The photon equations that correspond to the atomic orbital states, Eqs. (1.27-1.29), are given in the Excited States of the One-Electron Atom (Quantization) section. It is shown in Appendix I: Nonradiation Condition that in addition to Haus' condition, the atomic orbital states given by Eqs. (1.27-1.29) are nonradiative with the same relationships given by Eqs. (1.15-1.16) applied to the vector potential.

For n = 1, and ℓ = 0, m = 0, and s = 1/2, the charge (and mass) distribution is spherically symmetric and $M_{1,0,0,1/2}=-4.553\ Cm^{-2}$ everywhere on the atomic orbital. Similarly, for $n=2$, ℓ = 0, $m=0$, and $s=1/2$, the charge distribution everywhere on the sphere is $M_{2,0,0,1/2}=-1.138\ Cm^{-2}$. For n = 2, ℓ = 1, m = 0, and s = 1/2, the charge distribution varies with θ. $Y_1^0(\phi,\theta)$ is a maximum at $\theta=0°$ and the charge density is also a maximum at this point, $M_{2,1,0,1/2}(\theta=0°)=-2.276\ Cm^{-2}$. The charge density decreases as θ increases; a minimum in the charge density is reached at $\theta=180°$, $M_{2,1,0,1/2}(\theta=180°)=0\ Cm^{-2}$.

For ℓ = 1 and $m=\pm1$, the spherical harmonics are complex, and the angular functions comprise linear combinations of

$$Y_{1,x}=\sin\theta\cos\phi \tag{1.30}$$

$$Y_{1,y}=\sin\theta\sin\phi \tag{1.31}$$

Each of $Y_{1,x}$ and $Y_{1,y}$ is the component factor part of a phasor. They are not components of a vector; however, the x and y designation corresponds, respectively, to the historical p_x and p_y probability-density functions of quantum mechanics. $Y_{1,x}$ is a maximum at $\theta=90°$ and $\phi=0°$; $M_{2,1,x,1/2}(90°,0°)=-1.138\ Cm^{-2}$. Figure 1.2 gives pictorial representations of how the modulation function changes the electron density on the atomic orbital for several ℓ values[4]. Figure 1.3 gives a pictorial representation of the charge-density wave of a p orbital that modulates the constant spin function and rotates around the z-axis. A single time point is shown for ℓ = 1 and $m=\pm1$ in Eqs. (1.28-1.29).

---

[3] In Eq. (1.28), $Y_0^0(\theta,\phi)$, a constant function, is added to a spherical harmonic function wherein each term $\mathrm{Re}\left\{\pi\left(R_z(\omega_n t)\right)Y_\ell^m(\theta,\phi)\right\}$ and $\mathrm{Re}\left\{Y_\ell^m(\theta,\phi)e^{im\omega_n t}\right\}$ represents a modulation function rotated in time. The latter is defined as a phasor corresponding to the modulation function spinning about the z-axis. This is equivalent to the constant function (first term) modulated by the spherical harmonic function (second term) that spins around the z-axis and comprises a traveling modulation wave. One rotation of the spherical harmonic function occurs in one period.

[4] When the electron charge appears throughout this text in a function involving a linear combination of the spin and orbital functions, it is implicit that the charge is normalized. The integral of the constant mass-density function corresponding to spin over the atomic orbital is the mass of the electron. The integral of any spherical harmonic modulation function corresponding to orbital angular momentum over the atomic orbital is zero. The modulated mass-density function has a lower limit of zero due to the trapped photon that is phase-locked to the modulation function. And, the mass density cannot be negative. Thus, the maximum magnitude of the unnormalized spherical harmonic function over all angles must be one. The summation of the constant function and the orbital function is normalized.

Figure 1.2. The orbital function modulates the constant (spin) function, (shown for t = 0; three-dimensional view).

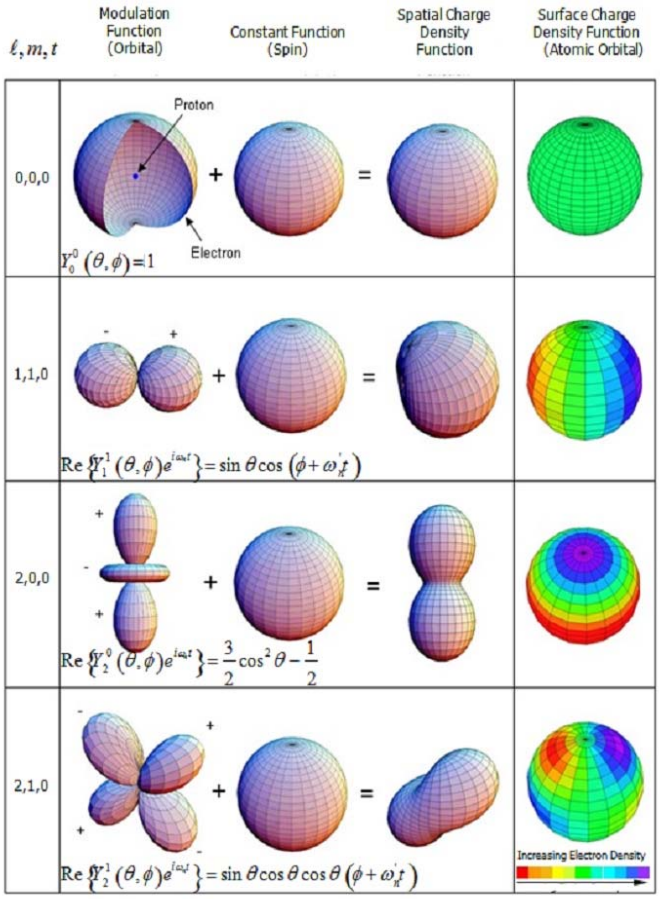

Figure 1.3. A pictorial representation of the charge-density wave of a p orbital that modulates the constant spin function and travels on the surface of the atomic orbital around the z-axis. A single time point is shown for $\ell = 1$ and $m = \pm 1$ in Eq. (1.36). The charge density increases from red to violet. The z-axis is the vertical axis.

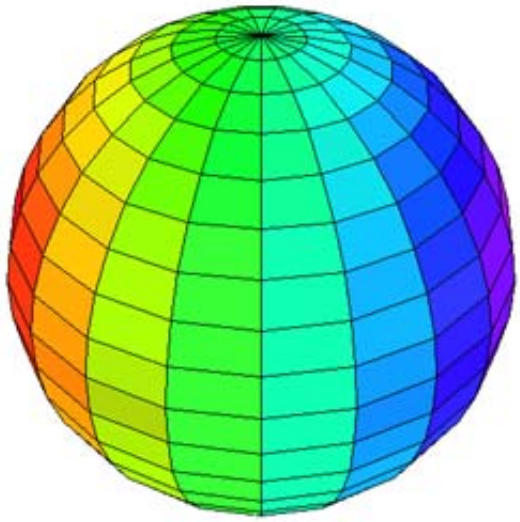

CLASSICAL PHYSICS OF THE DE BROGLIE RELATION

Consider the constant function $Y_0^0(\theta,\phi)$ of Eqs. (1.27-1.29). The angular velocity must be constant (at a given n) because r is constant and the energy and angular momentum are constant. Given time-harmonic motion and a radial delta function, the relationship between an allowed radius and the electron wavelength is given by Eq. (1.15). The allowed angular frequencies are related to the allowed frequencies by:

$$\omega_n = 2\pi\nu_n \tag{1.32}$$

The allowed velocities are related to allowed frequencies and wavelengths by:

$$v_n = \nu_n\lambda_n \tag{1.33}$$

The allowed velocities and angular frequencies are related to r_n by:

$$v_n = 2\pi r_n\nu_n = r_n\omega_n \tag{1.34}$$

such that magnitude of the velocity and the angular frequency for *every* point on the surface of the bound electron and their relationships with the wavelengths and r_n are:

$$v_n = \frac{\hbar}{m_e r_n} = \frac{h}{m_e\lambda_n} = \frac{h}{m_e 2\pi r_n} = \frac{\hbar}{m_e r_n} \tag{1.35}$$

$$\omega_n = \frac{\hbar}{m_e r_n^2} \tag{1.36}$$

where the velocity (Eq. (1.35)) and angular frequency (Eq. (1.36)) are determined by the boundary conditions that the angular momentum density at each point on the surface is constant and the magnitude of the total angular momentum of the atomic orbital $\mathbf{L}$ must also be constant. The constant total is $\hbar$ given by the integral:

$$\begin{aligned}\mathbf{m} &= \int \frac{1}{4\pi r^2}\left|\mathbf{r}\times m_e\mathbf{v}\right|\delta\left(r-r_n\right)dx^3\\ &= m_e r_n\frac{\hbar}{m_e r_n} = \hbar\end{aligned} \tag{1.37}$$

Special relativity requires that the mathematical equations expressing the laws of nature must be covariant, invariant in form, under the transformations of the Lorentz group [7]. The integral of the magnitude of the angular momentum of the electron is always $\hbar$ for any state and is ***relativistically invariant*** since as shown by Eq. (1.37) the angular momentum is invariant of radius or velocity. It is a Lorentz scalar $\mathbf{L} = \hbar$ with respect to the radius of the state. The vector projections of the atomic orbital spin angular momentum relative to the Cartesian coordinates arrived at by summation of the contributions from the electron current elements are given in the Spin Angular Momentum of the Atomic Orbital $Y_0^0(\theta,\phi)$ with $\ell = 0$ section. The same relationship applies to the photon as well as given by Eq. (4.1). Eq. (1.35) also gives the de Broglie relationship:

$$\lambda_n = \frac{h}{p_n} = \frac{h}{m_e v_n} \tag{1.38}$$

The free electron is equivalent to a continuum-excited state with conservation of the parameters of the bound electron. Thus, the de Broglie relationship applied to the free electron is again due to conservation of the electron's angular momentum of $\hbar$. Specifically, it is shown in the Free Electron section that the free electron is a two-dimension lamina of charge with an azimuthal current with a corresponding angular momentum of $\hbar$. The linear velocity of the free electron can be considered to be due to absorption of photons that excite surface currents corresponding to a decreased electron de Broglie wavelength:

$$\lambda_o = \frac{h}{m_e v_z} = 2\pi\rho_0 \tag{1.39}$$

The relationship between the electron wavelength, its radius, ρ_0, and its linear velocity is:

$$\frac{\lambda}{2\pi} = \rho_0 = \frac{\hbar}{m_e v_z} = k^{-1} = \frac{v_z}{\omega_z} \tag{1.40}$$

In this case, the angular frequency ω_z is given by:

$$\omega_z = \frac{\hbar}{m_e\rho_0^2} \tag{1.41}$$

which conserves the photon's angular momentum of $\hbar$ with that of the electron.

It is further shown (Eq. (3.51)) that the total energy E_T, is given by the sum of the change in the free-electron translational kinetic energy, T, the rotational energy of the azimuthal current, E_{rot}, and the corresponding magnetic potential energy, E_{mag}:

$$\begin{aligned} E_T &= T + E_{rot} + E_{mag} \\ &= \frac{1}{2}\frac{\hbar^2}{m_e\rho_0^2} + \frac{5}{4}\frac{\hbar^2}{m_e\rho_0^2} - \frac{5}{4}\frac{\hbar^2}{m_e\rho_0^2} = \frac{1}{2}\frac{\hbar^2}{m_e\rho_0^2} \end{aligned} \tag{1.42}$$

Thus, the total energy, E_T, of the excitation of a free-electron transitional state by a photon having $\hbar$ of angular momentum and an energy given by Planck's equation of $\hbar\omega$ is:

$$E_T = T = \frac{1}{2}m_e v_z^2 = \frac{1}{2}\frac{h^2}{m_e\lambda^2} = \frac{1}{2}\hbar\omega_z \tag{1.43}$$

where λ is the de Broglie wavelength. The angular momentum of the free electron of $\hbar$ is unchanged. The energies in the currents in the plane lamina are balanced so that the total energy is unchanged. The radius ρ_0 decreases to match the de Broglie wavelength and frequency at an increased velocity. At this velocity, the kinetic energy matches the energy provided by the photon wherein the de Broglie frequency matches the photon frequency and both the electron-kinetic energy and the photon energy are given by Planck's equation.

The correspondence principle is the basis of the de Broglie wavelength relationship. The de Broglie relationship is not an independent fundamental property of matter in conflict with physical laws as formalized in the wave-particle-duality-related postulates of quantum mechanics and the corresponding Schrödinger wave equation. The Stern-Gerlach experimental results and the double-slit interference pattern of electrons are also predicted classically as given in the Physics of Classical Electron Diffraction Resolves the Wave-Particle Duality Mystery of Quantum Mechanics section.

ROTATIONAL PARAMETERS OF THE ELECTRON (ANGULAR MOMENTUM, ROTATIONAL ENERGY, AND MOMENT OF INERTIA)

The spin function corresponds to $\ell = 0$. The electron atomic orbital experiences a constant potential energy because it is fixed at $r = r_n$. In general, the kinetic energy for an inverse squared electric force is half the potential energy. It is the rotation of the atomic orbital, projections of the uniform current density, that causes spin angular momentum. The rotational energy of a rotating body, E_{rot}, is

$$E_{rot} = \frac{1}{2}I\omega^2 = \frac{1}{2}I\left(\frac{v}{r}\right)^2 \tag{1.44}$$

where I is the moment of inertia and ω is the angular velocity. The angular momentum is given by:

$$\mathbf{L} = I\omega\mathbf{i}_z \tag{1.45}$$

The angular velocity must be constant (at a given n) because r is constant and the energy and angular momentum are constant. The total kinetic energy, T, of the atomic orbital spin function $Y_0^0(\phi,\theta)$ is:

$$T = \frac{1}{2}m_e v_n^2 \tag{1.46}$$

Substitution of Eq. (1.35) gives:

$$T = \frac{\hbar^2}{2m_e r_n^2} \tag{1.47}$$

One result of the correlated motion along great circles is that some of the kinetic energy is not counted in the rotational energy (i.e. for any spin axis, there will be an infinite number of great circles with planes passing through that axis with θ angles other than $90°$). All points on any one of these great circles will be moving, but not all of that motion will be part of the rotational energy; only that motion perpendicular to the spin axis will be part of the rotational energy. Thus, the rotational kinetic energy will always be less than the total kinetic energy. Furthermore, the following relationships must hold.

$$E_{rotational} = \frac{1}{2}I\omega^2 \le T = \frac{1}{2}m_e v^2 \tag{1.48}$$

$$I\omega \le L = \hbar \tag{1.49}$$

$$I \le m_e r^2 \tag{1.50}$$

Additionally, it is known from the Stern-Gerlach experiment that a beam of silver atoms splits into two components when passed through an inhomogeneous magnetic field. This experiment implies a magnetic moment of one Bohr magneton and an associated angular momentum quantum number of 1/2. Historically, this quantum number is called the spin quantum number, and that designation will be retained. The angular momentum can be thought of as arising from a spin component or equivalently from an orbital component of the spin. The z-axis projection of the spin angular momentum was derived in the Atomic Orbital Equation of Motion For $\ell = 0$ Based on the Current Vector Field (CVF) section and is:

$$\mathbf{L}_z = I\omega\mathbf{i}_z = \pm\frac{\hbar}{2} \tag{1.51}$$

where ω is given by Eq. (1.36); so, for $\ell = 0$

$$\mathbf{L}_z = I\frac{\hbar}{m_e r^2}\mathbf{i}_z = \frac{\hbar}{2}\mathbf{i}_z \tag{1.52}$$

Thus,

$$I_z = I_{spin} = \frac{m_e r_n^{\,2}}{2} \tag{1.53}$$

From Eq. (1.44),

$$E_{rotational\ \ spin} = \frac{1}{2}\left[I_{spin}\omega^2\right] \tag{1.54}$$

From Eqs. (1.36) and (1.53),

$$E_{rotational} = E_{rotational\ \ spin} = \frac{1}{2}\left[I_{spin}\left(\frac{\hbar}{m_e r_n^{\,2}}\right)^2\right] = \frac{1}{2}\left[\frac{m_e r_n^{\,2}}{2}\left(\frac{\hbar}{m_e r_n^{\,2}}\right)^2\right] = \frac{1}{4}\left[\frac{\hbar^2}{2I_{spin}}\right] \tag{1.55}$$

ELECTRON MECHANICS AND THE CORRESPONDING CLASSICAL WAVE EQUATION FOR THE DERIVATION OF THE ROTATIONAL PARAMETERS OF THE ELECTRON

When $\ell \neq 0$, the spherical harmonic is not a constant and the charge-density function is not uniform over the atomic orbital. Thus, the angular momentum can be thought of arising from a spin component and an orbital component. The charge, mass, energy, and angular momentum of the electron are constant, and the flow of current must be conservative and without radiation. The corresponding dynamic charge and mass-density functions are time and spherically harmonic and are interchangeable by the conversion factor of the corresponding ratio m_e / e. In order to match the source current condition of Maxwell's equations, the multipole of the current density must be constant. Then, the spatial and time motion obeys a classical wave equation. The boundary conditions on conservation of kinetic energy and angular momentum, for azimuthal current flow about a defined axis at the angular frequency ω_n given by Eq. (1.36), require classical wave behavior, as well, and the corresponding rotational energy equation is given by the rigid rotor equation [8].

In the derivation of the rotational energy and related parameters, first consider that the electron atomic orbital experiences a constant potential energy because it is fixed at $r = r_n$. The boundary condition is that the modulation of the charge density by a traveling wave is not dissipative corresponding to absence of radiation and further has a time average of zero kinetic energy. The mechanics of motion is such that there is a time and spatially harmonic redistribution of matter and kinetic energy that flows on the surface such that the total of either is unchanged. Wave motion has such behavior and the corresponding equation is a wave equation that is solved with energy degeneracy and a time average of zero for the charge and energy flow as the boundary constraints. In this case, the energy degeneracy is only lifted due to the electrodynamic interaction with an applied field consistent with experiential observations, as given in the Orbital and Spin Splitting section.

The general form of the classical wave equation[5] applies to the mechanics of the bound electron

$$\left[\nabla^2 - \frac{1}{v^2}\frac{\partial^2}{\partial t^2}\right]\rho(r,\theta,\phi,t) = 0 \tag{1.56}$$

where $\rho(r,\theta,\phi,t)$ is the function of the electron in time and space. Here, the current densities of $\rho(r,\theta,\phi,t)$ comprise time

[5] This is not to be confused with the Schrödinger equation that is not a proper wave equation; rather, it is a diffusion equation.

harmonics and the spherical harmonics on a two-dimensional spherical surface (Eqs. (1.28-1.29)) for the temporal and spatial functions. Thus, the mechanics equation is given by

$$\left[\nabla^2_{\theta,\phi}-\frac{1}{v^2}\frac{\partial^2}{\partial t^2}\right]\frac{e}{4\pi r^2}[\delta(r-r_n)]\left[Y_0^0(\theta,\phi)+\mathrm{Re}\left\{Y_\ell^m(\theta,\phi)e^{im\omega_n t}\right\}\right]=0 \tag{1.57}$$

Since the rotation is defined to be about the z-axis, the velocity v in Eq. (1.57) is *not constant*, but has the same angular dependence as the corresponding spherical harmonic $Y_\ell^m(\theta,\phi)$ where the motion is azimuthal to the radius. In general, the spherical harmonic charge density functions satisfy the equation [3]:

$$-\left[\frac{1}{\sin\theta}\frac{\partial}{\partial\theta}\left(\sin\theta\frac{\partial}{\partial\theta}\right)_{r,\phi}+\frac{1}{\sin^2\theta}\left(\frac{\partial^2}{\partial\phi^2}\right)_{r,\theta}\right]Y_{\ell,m_\ell}(\theta,\phi)=\ell(\ell+1)Y_{\ell,m_\ell}(\theta,\phi) \tag{1.58}$$

which may be written in the form:

$$L^2Y_{\ell,m_\ell}(\theta,\phi)=\ell(\ell+1)Y_{\ell,m_\ell}(\theta,\phi) \tag{1.59}$$

The charge/mass flow corresponding to Eq. (1.12) and Eqs. (1.28-1.29) time averages to zero and corresponds to modulation of the constant spin function. Similarly, the current densities are eigenfunctions such that kinetic energy flow time averages to zero and corresponds to the modulation of the constant kinetic energy of the spin function. The amplitude of the orbital rotational energy can be solved from the mechanics equation (Eq. (1.57)) operating on $\mathrm{Re}\left\{Y_\ell^m(\theta,\phi)e^{im\omega_n t}\right\}$. Since the motion of the atomic orbital is transverse to the radius, the motion constitutes an inertial frame that is ***relativistically invariant***, as given in the Special Relativistic Effect on the Electron Radius and the Relativistic Ionization Energies section. The total spin angular momentum of the electron is an invariant Lorentz scalar $\mathbf{L}=\hbar$ [7], as given in the Atomic Orbital Equation of Motion For $\ell=0$ Based on the Current Vector Field (CVF) section, and the time-averaged orbital angular momentum is zero that is also a Lorentz scalar $\mathbf{L}=0$. By expressing the wave equation in the energy form, the angular dependent velocity may be eliminated, and this equation can be solved using the boundary constraints. The time and angular functions are separable.

$$\left[\frac{1}{r_n^2\sin\theta}\frac{\partial}{\partial\theta}\left(\sin\theta\frac{\partial}{\partial\theta}\right)_{r,\phi}+\frac{1}{r_n^2\sin^2\theta}\left(\frac{\partial^2}{\partial\phi^2}\right)_{r,\theta}-\frac{1}{v^2}\frac{\partial^2}{\partial t^2}\right]A(\theta,\phi,t)=0 \tag{1.60}$$

where $\rho(r,\theta,\phi,t)=f(r)A(\theta,\phi,t)=\frac{1}{r^2}\delta(r-r_n)A(\theta,\phi,t)$ *and* $A(\theta,\phi,t)=Y(\theta,\phi)k(t)$. The mass of an electron is superimposable with its charge. That is, the angular mass-density function, $A(\theta,\phi,t)$, is also the angular charge-density function. Elimination of the separable time function of Eq. (1.60) gives:

$$\left[\nabla^2+\frac{\omega^2}{v^2}\right]Y_\ell^m(\theta,\phi)=0 \tag{1.61}$$

Eq. (1.61) can be expressed in terms of the wavenumber and wavelength:

$$\left[\nabla^2+k^2\right]Y_\ell^m(\theta,\phi)=0 \tag{1.62}$$

$$\left[\nabla^2+\left(\frac{2\pi}{\lambda}\right)^2\right]Y_\ell^m(\theta,\phi)=0 \tag{1.63}$$

Using Eq. (1.44) and the de Broglie relationship (Eq. (1.38)) based on conservation of angular momentum gives the relationships:

$$\frac{(2\pi r)^2}{\lambda^2}=\frac{2m_e r_n^2 E_{rot}}{\hbar^2}=\frac{2IE_{rot}}{\hbar^2} \tag{1.64}$$

Substitution of Eq. (1.64) into Eq. (1.63) gives the well-known rigid rotor equation [8]:

$$-\frac{\hbar^2}{2I}\left[\frac{1}{\sin\theta}\frac{\partial}{\partial\theta}\left(\sin\theta\frac{\partial}{\partial\theta}\right)_{r,\phi}+\frac{1}{\sin^2\theta}\left(\frac{\partial^2}{\partial\phi^2}\right)_{r,\theta}\right]Y(\theta,\phi)=E_{rot}Y(\theta,\phi) \tag{1.65}$$

The energies corresponding to Eq. (1.65) are given by [8]:

$$E_{rot}=\frac{\hbar^2\ell(\ell+1)}{2I}=\frac{\hbar^2\ell(\ell+1)}{2m_e r_n^2}\quad \ell=1,2,3,..., \tag{1.66}$$

and the solution of Eq. (1.65) for $\mathbf{L}$, the orbital angular momentum defined to be about the z-axis, is

$$\mathbf{L} = \hbar\sqrt{\ell(\ell+1)}\mathbf{i}_z \tag{1.67}$$

where the moment of inertia, I, assumed by McQuarrie [8] is that of a point particle, mr_n^2. It is demonstrated by Eq. (1.37) that the total integrated magnitude of the angular momentum density over the surface of the electron atomic orbital is $\hbar$; therefore, the magnitude of the angular momentum of an electron atomic orbital about the z-axis must be less than $\hbar$, and the corresponding moment of inertia must be less than that given by $m_e r_n^2$. For example, the moment of inertia of the uniform spherical shell, I_{RS},
is [9]:

$$I_{RS} = \frac{2}{3}mr_n^2 \tag{1.68}$$

The current density of the electron is a two-dimensional shell with a constant or a constant plus a spherical harmonic angular dependence. In this case, the relationships given by Eqs. (1.48-1.50) must hold. Eq. (1.65) can be expressed in terms of the variable x that is substituted for $\cos\theta$. The resulting function $P(x)$ is called Legendre's equation and is a well-known equation in classical physics. It occurs in a variety of problems that are formulated in spherical coordinates. When the power series method of solution is applied to $P(x)$, the series must be truncated in order that the solutions be finite at $x = \pm 1$. The solution to Legendre's equation given by Eq. (1.66) is the maximum term of a series of solutions corresponding to the m_ℓ and ℓ values [8, 10]. The rotational energy must be normalized by the total number of states—each corresponding to a set of quantum numbers of the power series solution. As demonstrated in the Excited States of the One-Electron Atom (Quantization) section, the quantum numbers of the excited states are:

$$\begin{aligned} &n = 2,3,4,... \\ &\ell = 1,2,...,n-1 \\ &m_\ell = -\ell,-\ell+1,...,0,...,+\ell \end{aligned} \tag{1.69}$$

In the case of an atomic orbital excited state, each rotational state solution of Eq. (1.65) (Legendre's equation) corresponds to a multipole moment of the charge-density function (Eqs. (1.28-1.29)). The orbital rotational energy $E_{rotational\ orbital}$ is given by normalizing E_{rot} (Eq. (1.66)) using $N_{\ell,s}$, the total number of multipole moments where each corresponds to an ℓ and m_ℓ quantum number of an energy level corresponding to a principal quantum number of n:

$$N_{\ell,s} = \sum_{\ell=0}^{n-1}\sum_{m_\ell=-\ell}^{+\ell} 1 = \sum_{\ell=0}^{n-1} 2\ell+1 = n^2 = (\ell+1)^2 = \ell^2+2\ell+1 \tag{1.70}$$

Multiplication of Eq. (1.66) by the normalization factor $N_{\ell,s}^{-1}$ given by Eq. (1.70) and substitution of the angular velocity given by Eq. (1.36) results in:

$$E_{rotational\ orbital} = \frac{\hbar^2}{2I}\frac{\ell(\ell+1)}{\ell^2+2\ell+1} = \frac{\hbar^2}{2I}\frac{\ell}{\ell+1} = \frac{\hbar^2}{2m_e r_n^2}\frac{\ell}{\ell+1} \qquad \ell = 1,2,3,..., \tag{1.71}$$

Multiplication of Eq. (1.67) by the normalization factor $N_{\ell,s}^{-1}$ given by Eq. (1.70) and using Eq. (1.36) gives the corresponding orbital angular momentum, $L_{orbital}$, and moment of inertia , $I_{orbital}$, of the atomic orbital where $\ell \neq 0$:

$$\mathbf{L}_{orbital} = I\omega\mathbf{i}_z = I_{orbital}\omega\mathbf{i}_z = m_e {r_n}^2\sqrt{\frac{\ell(\ell+1)}{\ell^2+2\ell+1}}\omega\mathbf{i}_z = m_e {r_n}^2\frac{\hbar}{m_e {r_n}^2}\sqrt{\frac{\ell}{\ell+1}}\mathbf{i}_z = \hbar\sqrt{\frac{\ell}{\ell+1}}\mathbf{i}_z \tag{1.72}$$

$$I_{orbital} = m_e {r_n}^2\sqrt{\frac{\ell(\ell+1)}{\ell^2+2\ell+1}} = m_e {r_n}^2\sqrt{\frac{\ell}{\ell+1}} \tag{1.73}$$

where

$$\sqrt{\frac{\ell}{\ell+1}} < 1 \tag{1.74}$$

consistent with Eq. (1.50).

In the case of the excited states with $\ell \neq 0$, the atomic orbital charge-density functions are given by Eqs. (1.28-1.29), and the total angular momentum is the sum of two functions of equal magnitude. $\mathbf{L}_{ztotal}$ is given by the sum of the spin and orbital angular momentum. The principal energy levels of the excited states are split when a magnetic field is applied. The energy shifts due to spin and orbital angular momentum are given in the Orbital and Spin Splitting section.

$$L_{z\ total} = L_{z\ spin} + L_{z\ orbital} \tag{1.75}$$

Similarly, the orbital rotational energy arises from a spin function (spin angular momentum) modulated by a spherical harmonic angular function (orbital angular momentum). The time-averaged mechanical angular momentum and rotational energy associated with the traveling charge-density wave on the atomic orbital is zero:

$$\langle L_{z\ orbital}\rangle = 0 \tag{1.76}$$

$$\left\langle E_{rotational\ orbital} \right\rangle = 0 \tag{1.77}$$

In the case of an excited state, the angular momentum comprising a Lorentz scalar $\mathbf{L} = \hbar$ is carried by the fields of the trapped photon. The energy and angular momentum amplitudes that couple to external magnetic and electromagnetic fields are given by Eq. (1.71) and (1.72), respectively. The rotational energy due to spin is given by Eq. (1.55), and the total kinetic energy is given by Eq. (1.47).

THE ATOMIC ORBITAL EQUATION OF MOTION FOR ℓ = 0 BASED ON THE CURRENT VECTOR FIELD (CVF)

STERN-GERLACH-EXPERIMENT BOUNDARY CONDITIONS

It is known from the Stern-Gerlach experiment that a beam of silver atoms is split into two components when passed through an inhomogeneous magnetic field. This implies that the electron is a spin 1/2 particle or fermion with an intrinsic angular momentum of $\pm\frac{\hbar}{2}$ that can only exist parallel or antiparallel to the direction of the applied field (spin axis), and the magnitude of the angular momentum vector, which precesses about the spin axis, is $\sqrt{\frac{3}{4}}\hbar$. Furthermore, the magnitude of the splitting implies a magnetic moment of μ_B, a full Bohr magneton, given by Eq. (1.131) corresponding to $\hbar$ of total angular momentum on the axis, implying an impossibility of being classically reconciled with the $\pm\frac{\hbar}{2}$ electron angular momentum. Yet, the extraordinary aspects of the magnetic properties and behavior of the electron are the basis to solve its structure that gives rise to these observations.

Experimentally, the electron has a measured magnetic field and corresponding magnetic moment of a Bohr magneton that can only exist parallel or antiparallel to the direction of the applied magnetic field and behaves as if it possesses only $\frac{\hbar}{2}$ of intrinsic angular momentum. For any magnetic field, the Maxwell's-equations solution for the corresponding source current is unique. Thus, the electron field requires a corresponding unique current according to Maxwell's equations. Several boundary conditions must be satisfied, and the atomic orbital equation of motion for ℓ = 0 is solved as a boundary value problem. The boundary conditions are:

(1) to maintain electroneutrality, force balance, absence of a magnetic or electric multipole, and give the proper Lorentz invariant angular momentum, each point position on the atomic orbital surface designates a charge(mass)-density element, and each point element must have the same magnitude of linear and angular velocity given by Eqs. (1.35) and (1.36), respectively;

(2) according to condition 1, every such infinitesimal point element must move along a great circle and the current-density distribution must be uniform;

(3) the electron magnetic moment must align completely parallel or antiparallel with an applied magnetic field in agreement with the Stern-Gerlach experiment;

(4) it is shown *infra* that according to condition #3, the projection of the intrinsic angular momentum of the atomic orbital onto the z-axis must be $\pm\frac{\hbar}{2}$, and the projection into the transverse plane must be $\pm\frac{\hbar}{4}$ to achieve the spin 1/2 aspect;

(5) it is further shown that the Larmor excitation of the electron in the applied magnetic field must give rise to a component of electron spin angular momentum that precesses about the applied magnetic field such that the contribution along the z-axis is $\pm\frac{\hbar}{2}$ and the projection onto the orthogonal axis which precesses about the z-axis must be $\pm\sqrt{\frac{3}{4}}\hbar$;

(6) due to conditions #4 and #5, the angular momentum components corresponding to the current of the atomic orbital and that due to the Larmor precession give rise to a total angular momentum on the applied-field axis of $\pm\hbar$;

(7) due to condition #6, the precessing electron has a magnetic moment of a Bohr magneton, and

(8) the energy of the transition of the alignment of the magnetic moment with an applied magnetic field must be given by Eqs. (1.226-1.227) wherein the g factor and Bohr magneton factors are due to the extended-nature of the electron such that it links flux in units of the magnetic flux quantum and has a total angular momentum on the applied-field axis of $\pm\hbar$.

The algorithm to generate the spin function designated as $Y_0^0(\theta,\phi)$ (part of Eqs. (1.27-1.29)) and called the electron atomic orbital is developed in this section. It was shown in the Classical Physics of the De Broglie Relationship section that the integral of the magnitude of the angular momentum over the atomic orbital must be constant. The constant is $\hbar$ as given by Eq. (1.37). It is shown in this section that the projection of the intrinsic atomic orbital angular momentum onto the spin axis is $\pm\frac{\hbar}{2}$, and the projection onto **S**, the axis that precesses about the spin axis, is $\hbar$ with a precessing component in the perpendicular plane of $\sqrt{\frac{3}{4}}\hbar$ and a component on the spin axis of $\pm\frac{\hbar}{2}$. Thus, the mystery of an intrinsic angular momentum of $\pm\frac{\hbar}{2}$ and a total angular momentum in a resonant RF experiment of $\mathbf{L}_z = \hbar$ is resolved since the sum of the intrinsic component and the spin-axis projection of the precessing component is $\hbar$. The Stern-Gerlach experiment implies a magnetic moment of one Bohr magneton and an associated angular momentum quantum number of 1/2. Historically, this quantum number is called the spin quantum number, s ($s = \frac{1}{2};\ m_s = \pm\frac{1}{2}$), and that designation is maintained.

Consider the derivation of Eq. (1.65). The moment of inertia of a point particle orbiting an axis is mr^2, and that of a globe spinning about some axis is $I = \frac{2}{3}mr^2$. For $\ell = 0$, the electron mass and charge are uniformly distributed over the atomic orbital, a two-dimensional spherical shell, but the atomic orbital is *not* analogous to a globe. The velocity of a point mass on a spinning globe is a function of θ, but the magnitude of the velocity at each point of the atomic orbital is not a function of θ. To picture the distinction, it is a useful concept to consider that the continuous current density of the atomic orbital is comprised of an infinite number of point elements that move on the spherical surface. Then, each point on the sphere with mass m_i has the same angular velocity, ω_n, the same magnitude of linear velocity, v_n, and the same moment of inertia, $m_i r_n^2$. The motion at each point of the atomic orbital is along a great circle, and the motion along each great circle is correlated with the motion on all other great circles such that the sum of all the contributions of the corresponding angular momentum is different from that of an orbiting point or a globe spinning about an axis. The atomic orbital angular momentum is directed along two orthogonal axes having three angular momentum components of $\mathbf{L}_{xy} = +/-\frac{\hbar}{4}$ and $\mathbf{L}_z = \frac{\hbar}{2}$.

The atomic orbital spin function comprises a constant uniform charge (current) density with moving charge confined to a two-dimensional spherical shell. The current-density is *continuous*, but it may be modeled as a current pattern comprising a superposition of an infinite series of correlated orthogonal great-circle current loops. The equation of motion for each charge-density element (and correspondingly for each mass-density element) corresponds to that of a current on a one-dimensional great circle wherein each point charge(current)-density element moves time harmonically with constant angular velocity, ω_n, given by Eq. (1.36) and has the corresponding velocity, v_n, on the surface in the direction of the current given by Eq. (1.35). The distribution of the great circles is such that all of the boundary conditions are satisfied.

The uniform, equipotential charge-density function of the atomic orbital having only a radial discontinuous field at the surface according to Eq. (1.10) is constant in time due to the motion of the current along great circles. The current flowing into any given point of the atomic orbital equals the current flowing out to satisfy the current continuity condition, $\nabla \cdot J = 0$ as in the case of any macrocurrent carried by an ensemble of electrons. There are many crossings amongst great circle elements at single, zero-dimensional points on the two-dimensional surface of the electron embedded in a three-dimensional space. Thus, the velocity direction is multivalued at each point. But, there is nothing in Maxwell's equations in two dimensions that precludes this result, since these laws only regard fields external to the two-dimensional charge density and current density sources. As in the macro-case, the continuous two-dimensional atomic orbital current density distribution constitutes a uniform, constant two-dimensional *supercurrent* (See Figure 1.22 for the vector supercurrent pattern) wherein the crossings have no effect on the current pattern. Each one-dimensional element is independent of the others, and its contribution to the angular momentum and magnetic field independently superimposes with that of the others.

The aspect of no interaction at local zero-dimensional crossings of a two-dimensional fundamental particle has the same properties as the superposition properties of the electric and magnetic fields of a photon from which the electron forms. Field lines of photons traveling at the speed of light also superimpose with the field- and velocity-direction vectors multivalued at each point that they cross. Indeed, the photon field pattern of a single photon shown in the Equation of the Photon section is very similar to the great-circle pattern of the atomic orbital shown *infra*. As shown in the Excited States of the One-Electron Atom (Quantization), the Creation of Matter from Energy, Pair Production, and the Leptons sections, the angular momentum in the

electric and magnetic fields is conserved in excited states and in the creation of an electron from a photon in agreement with Maxwell's equations. Thus, it is useful to regard an electron as a special-state photon.

Thus, the electron as an indivisible fundamental particle is related to the concepts of current and momentum elements, but the great-circle-current-loop basis elements used to generate and represent the bound electron current corresponding to spin should be considered more fundamentally in terms of sources of electric and magnetic field and sources of momentum that in aggregate gives the corresponding properties of the electron as a whole. In fact, as shown in the Gravity section, all physical observables including the laws of nature and the fundamental constants can ultimately only be related to others and have no independent meaning. Then, the basis elements of an electron are understood in terms of what they do when added in aggregate to constitute an electron. The nomenclature used to describe the elements reflects the analogous macroscopic sources and is adopted for convenience.

GENERATION OF THE ATOMIC ORBITAL CVFS

The atomic orbital spin function comprises a constant charge(current)-density function with moving charge confined to a two-dimensional spherical shell and comprises a uniform complete coverage. The uniform magnetostatic current-density function $Y_0^0(\theta,\phi)$ of the atomic orbital spin function comprises a continuum of correlated orthogonal great-circle current loops wherein each point charge(current)-density element moves time harmonically with constant angular velocity, ω_n, given by Eq. (1.36) and velocity, v_n, in the direction of the current given by Eq. (1.35). The current-density function of the atomic orbital is generated from *orthogonal great-circle current-density elements (one dimensional "current loops")* that serve as basis elements to form two distributions of an infinite number of great circles wherein each covers one-half of a two-dimensional spherical shell and is defined as a basis element current vector field ("BECVF") and an atomic orbital current-vector field ("OCVF"). Then, the *continuous* uniform electron current density function $Y_0^0(\theta,\phi)$ (part of Eqs. (1.27-1.29)) that covers the entire spherical surface as a distribution of an infinite number of great circles is generated using the CVFs.

First, the generation of the BECVF is achieved by rotation of two great circle basis elements, one in the x'z'-plane and the other in the y'z'-plane, about the $\left(-\mathbf{i}_x,\mathbf{i}_y,0\mathbf{i}_z\right)$ axis by an infinite set of infinitesimal increments of the rotational angle wherein the current direction is such that the resultant angular momentum vector of the basis elements of $\frac{\hbar}{2\sqrt{2}}$ is stationary on this axis. The generation of the OCVF is achieved by rotation of two great circle basis elements, one in the x'y'-plane and the other in the plane that bisects the x'y'-quadrant and is parallel to the z'-axis, about the $\left(-\frac{1}{\sqrt{2}}\mathbf{i}_x,\frac{1}{\sqrt{2}}\mathbf{i}_y,\mathbf{i}_z\right)$ axis by an infinite set of infinitesimal increments of the rotational angle wherein the current direction is such that the resultant angular momentum vector of the basis elements of $\frac{\hbar}{2}$ having components of $\mathbf{L}_{xy}=\frac{\hbar}{2\sqrt{2}}$ and $\mathbf{L}_z=\frac{\hbar}{2\sqrt{2}}$ is stationary on this axis. The operator to form each CVF comprises a convolution of the rotational matrix of great circles basis elements with an infinite series of delta functions of argument of the infinitesimal angular increment. Then, the uniform great-circle distribution $Y_0^0(\theta,\phi)$ is exactly generated from the CVFs. The BECVF is convolved with the OCVF over a 2π span that results in the placement of a BECVF at each great circle of the OCVF. Since the angular momentum vector of the BECVF is matched to twice that of one of the OCVF great circle basis elements and the span is over 2π, the resultant angular momentum of the distribution is the same as that of the OCVF, except that coverage of the spherical surface is complete. This current vector distribution is normalized by scaling the constant current of each great circle element resulting in the exact uniformity of the distribution independent of time since $\nabla\cdot K=0$ along each great circle. There is no alteration of the angular momentum by normalization since it only affects the density parallel to the angular momentum axis of the distribution, the $\left(-\frac{1}{\sqrt{2}}\mathbf{i}_x,\frac{1}{\sqrt{2}}\mathbf{i}_y,\mathbf{i}_z\right)$-axis. Then, the boundary conditions of $Y_0^0(\theta,\phi)$ having the desired angular momentum components, coverage, element motion, and uniformity are shown to have been achieved by designating the $\left(-\frac{1}{\sqrt{2}}\mathbf{i}_x,\frac{1}{\sqrt{2}}\mathbf{i}_y,\mathbf{i}_z\right)$-axis as the z-axis. The resulting exact uniform current distribution (Figure 1.22) has the angular momentum components of $\mathbf{L}_{xy}=+/-\frac{\hbar}{4}$ and $\mathbf{L}_z=\frac{\hbar}{2}$ (Eqs. (1.127-1.128) and Figure 1.23).

The z-projection of the angular momentum of a photon given by its orthogonal electric and magnetic fields is $\mathbf{m}=\int\frac{1}{8\pi c}\mathrm{Re}\left[\mathbf{r}\times(\mathbf{E}\times\mathbf{B}^*)\right]dx^4=\hbar$ (Eq. (4.1)). When an electron is formed from a photon as given in the Leptons section, the angular momentum is conserved in the projections of the orthogonal great circle current loops that serve as the basis elements of the atomic orbital. Special relativity requires that the mathematical equations expressing the laws of nature must be covariant, that is, invariant in form, under the transformations of the Lorentz group. As shown by Eq. (1.37) the angular momentum is invariant of radius or velocity. It is a Lorentz scalar $\mathbf{L}=\hbar$ [7] with respect to the radius of the state. The vector projections of

the atomic orbital spin angular momentum relative to the Cartesian coordinates arrived at by summation of the contributions from the electron current elements of the current distribution are given in the Spin Angular Momentum of the Atomic Orbital $Y_0^0(\theta,\phi)$ with $\ell = 0$ section. The *time-independent* current pattern is obtained by defining a basis set for generating the current distribution over the surface of a spherical shell of zero thickness.

As such a basis set, consider that the electron current is distributed within the basis elements and then distributed evenly amongst all great circles such that the final distribution $Y_0^0(\theta,\phi)$ possesses $\hbar$ of angular momentum before and after normalization. First, the basis element BECVF is generated from two orthogonally linked great-circle current loops having $\frac{\hbar}{4}$ apiece and a resultant angular momentum of $\frac{\hbar}{2\sqrt{2}}$. The OCVF is generated from two orthogonally linked great-circle current loops having an angular momentum of $\frac{\hbar}{2\sqrt{2}}$ apiece and a resultant angular momentum of $\frac{\hbar}{2}$. The current pattern of each CVF is generated over the surface by a corresponding infinite set of infinitesimal rotations of the two orthogonal great-circle current loops that serve as basis elements by π radians about the $\left(-\mathbf{i}_x, \mathbf{i}_y, 0\mathbf{i}_z\right)$-axis for the BECVF and $\left(-\frac{1}{\sqrt{2}}\mathbf{i}_x, \frac{1}{\sqrt{2}}\mathbf{i}_y, \mathbf{i}_z\right)$-axis for the OCVF. The BECVF is convolved with the OCVF resulting in the BECVF of matched angular momentum substituting for the great circle basis elements of the OCVF over its great-circle distribution, and the resulting current vector pattern is normalized numerically by individually scaling the current density of each great circle element as given in the Uniformity of $Y_0^0(\theta,\phi)$ section. In the generation of $Y_0^0(\theta,\phi)$, the rotations of the basis elements comprising the convolutions are about the resultant angular momentum axis of the basis elements that leaves the resultant vector unchanged, and the angular momentum is unaffected by normalization. Then, after reorienting the resultant angular momentum vector from along the $\left(-\frac{1}{\sqrt{2}}\mathbf{i}_x, \frac{1}{\sqrt{2}}\mathbf{i}_y, \mathbf{i}_z\right)$-axis to along the z-axis, it is trivial to confirm that the boundary-condition components of having components of $\mathbf{L}_{xy} = +/-\frac{\hbar}{4}$ and $\mathbf{L}_z = \frac{\hbar}{4}$ is met while further achieving the condition that the magnitude of the velocity at any point on the surface is given by Eq. (1.35). Since the final distribution is uniform, the electron charge, current, mass, and angular momentum density can be obtained by equating the surface area integral to $-e$, $-e\omega_n$, m_e, and $\hbar$, respectively. Then, the physical properties are derived in the Spin Angular Momentum of the Atomic Orbital $Y_0^0(\theta,\phi)$ with $\ell = 0$ section and are shown to match the boundary conditions. The derivation of the matrix mechanics to generate the electron spin current distribution called the electron atomic orbital $Y_0^0(\theta,\phi)$ and its uniform charge and current resulting from normalization are considered first and then utilized herein.

GENERATION OF THE BECVF

Next, consider two infinitesimal charge(mass)-density elements at two separate positions or points, one and two, of the first pair of orthogonal great-circle current loops that serve as the basis set for generation of the BECVF as shown in Figure 1.4. The rotating Cartesian coordinates, x',y',z', in which the basis element great circles are fixed is designated the basis-set reference frame. In this frame at time zero, element one is at $x' = 0$, $y' = r_n$, and $z' = 0$, and element two is at $x' = r_n$, $y' = 0$, and $z' = 0$. Let element one move on a great circle clockwise toward the -z'-axis, and let element two move counter clockwise on a great circle toward the -z'-axis, as shown in Figure 1.4. The equations of motion, in the basis-set reference frame with $t = 0$ defined at the points (0,1,0) and (1,0,0), respectively, are given by:

point one:

$$x_1' = 0 \qquad y_1' = r_n \cos(\omega_n t) \qquad z_1' = -r_n \sin(\omega_n t) \tag{1.78}$$

point two:

$$x_2' = r_n \cos(\omega_n t) \qquad y_2' = 0 \qquad z_2' = -r_n \sin(\omega_n t) \tag{1.79}$$

Figure 1.4. The BECVF is generated from two orthogonal great-circle current loops that serve as basis elements. The current on the great circle in the y'z'-plane moves clockwise and the current on the great circle in the x'z'-plane moves counter clockwise as indicated by arrows. Each point or coordinate position on the continuous two-dimensional BECVF defines an infinitesimal charge (mass)-density element, which moves along a geodesic orbit comprising a great circle. Two such infinitesimal charges (masses) are shown at point one, moving clockwise on the great circle in the y'z'-plane, and at point two moving counter clockwise on the great circle in the x'z'-plane. The xyz-system is the laboratory frame, and the orthogonal-current-loop basis set is rigid with respect to the x'y'z'-system that rotates about the $\left(-\mathbf{i}_x, \mathbf{i}_y, 0\mathbf{i}_z\right)$-axis by π radians to generate the elements of the BECVF. The resultant angular momentum vector of the orthogonal great-circle current loops that is stationary in the xy-plane that is evenly distributed over the half-surface is $\frac{\hbar}{2\sqrt{2}}$ in the direction of $\left(-\mathbf{i}_x, \mathbf{i}_y, 0\mathbf{i}_z\right)$.

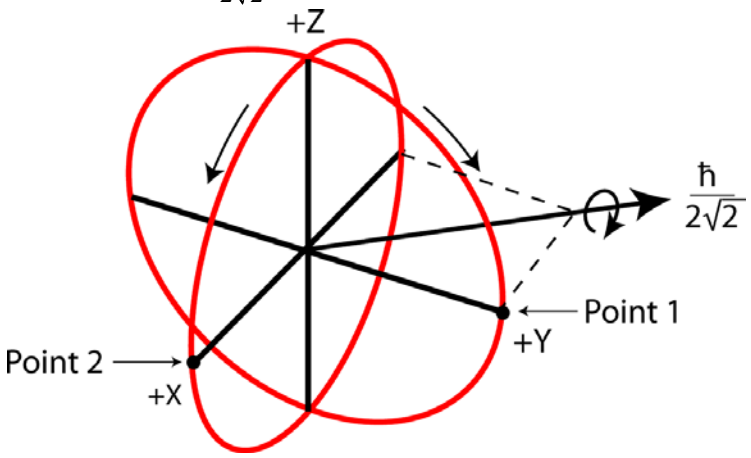

The orthogonal great circle basis set to generate the BECVF is shown in Figure 1.4. It is generated by the rotation of the two orthogonal great circles about the $\left(-\mathbf{i}_x, \mathbf{i}_y, 0\mathbf{i}_z\right)$-axis by an infinite set of infinitesimal increments of the rotational angle totaling a span of π. As shown in Figure 1.4, the current direction is such that the resultant angular momentum vector of the basis elements of magnitude $\frac{\hbar}{2\sqrt{2}}$ is stationary on this axis wherein one basis-element great circle is initially in the yz-plane having angular momentum $\mathbf{L}_x = -\frac{\hbar}{4}$ and the other is initially in the xz-plane having angular momentum $\mathbf{L}_y = \frac{\hbar}{4}$. The operator to form the BECVF comprises a convolution [11] of the rotational matrix of great circles basis elements with an infinite series of delta functions of argument of the infinitesimal angular increment.

The principal rotations in Cartesian coordinates are around each of the orthogonal axes, x, y, and z. Rotations about other axes can be obtained as a noncommutative combination of rotations that rotates one of the principal axes to align on the desired rotational axis relative to the Cartesian coordinates, the principal-axis rotation is applied, and then the matrices to rotate the principal axis to its Cartesian original coordinates are applied. A nonprincipal axis of rotation can be further rotated to a desired position. This can be achieved by rotating the axis about a principal axis relative to the Cartesian coordinates that is unchanged in the process. Principal rotational matrices with a clockwise rotation defined as a positive angle are given in Fowles [12]. The rotational matrix about the x-axis by θ, $R_x(\theta)$, is given by:

$$R_x(\theta) = \begin{bmatrix} 1 & 0 & 0 \\ 0 & \cos(\theta) & \sin(\theta) \\ 0 & -\sin(\theta) & \cos(\theta) \end{bmatrix} \tag{1.80}$$

The rotational matrix about the y-axis by θ, $R_y(\theta)$, is given by:

$$R_y(\theta) = \begin{bmatrix} \cos(\theta) & 0 & -\sin(\theta) \\ 0 & 1 & 0 \\ \sin(\theta) & 0 & \cos(\theta) \end{bmatrix} \tag{1.81}$$

The rotational matrix about the z-axis by θ, $R_z(\theta)$, is given by:

$$R_z(\theta) = \begin{bmatrix} \cos(\theta) & \sin(\theta) & 0 \\ -\sin(\theta) & \cos(\theta) & 0 \\ 0 & 0 & 1 \end{bmatrix} \tag{1.82}$$

The rotational matrix about the $(-\mathbf{i}_x, \mathbf{i}_y, 0\mathbf{i}_z)$-axis by θ, $R_{(-\mathbf{i}_x,\mathbf{i}_y,0\mathbf{i}_z)}(\theta)$, is given by:

$$R_{(-\mathbf{i}_x,\mathbf{i}_y,0\mathbf{i}_z)}(\theta) = R_z\left(\frac{\pi}{4}\right) R_x(-\theta) R_z\left(\frac{-\pi}{4}\right) \tag{1.83}$$

Then, using Eqs. (1.78-1.80, 1.82-1.83), the great circle basis elements and rotational matrix are given by:

BECVF MATRICES ($R_{(-\mathbf{i}_x,\mathbf{i}_y,0\mathbf{i}_z)}(\theta)$)

$$\begin{bmatrix} x' \\ y' \\ z' \end{bmatrix} = \begin{bmatrix} \frac{1}{2}+\frac{\cos\theta}{2} & -\frac{1}{2}+\frac{\cos\theta}{2} & -\frac{\sin\theta}{\sqrt{2}} \\ -\frac{1}{2}+\frac{\cos\theta}{2} & \frac{1}{2}+\frac{\cos\theta}{2} & -\frac{\sin\theta}{\sqrt{2}} \\ \frac{\sin\theta}{\sqrt{2}} & \frac{\sin\theta}{\sqrt{2}} & \cos\theta \end{bmatrix} \bullet \left(\begin{bmatrix} 0 \\ r_n\cos\phi \\ -r_n\sin\phi \end{bmatrix} + \begin{bmatrix} r_n\cos\phi \\ 0 \\ -r_n\sin\phi \end{bmatrix} \right) \tag{1.84}$$

Using Eq. (1.84), the BECVF matrix representation of the convolution is given by:

$$BECVF = \lim_{\Delta\theta\to 0} \sum_{m=1}^{m=\frac{\pi}{|\Delta\theta|}} \left[\left(R_{(-\mathbf{i}_x,\mathbf{i}_y,0\mathbf{i}_z)}(\theta) \bullet \left(GC^{basis}_{(0\mathbf{i}_x,\mathbf{i}_y,\mathbf{i}_z)} + GC^{basis}_{(\mathbf{i}_x,0\mathbf{i}_y,\mathbf{i}_z)} \right) \right) \otimes \delta(\theta - m\Delta\theta_M) \right] \tag{1.85}$$

wherein $R_{(-\mathbf{i}_x,\mathbf{i}_y,0\mathbf{i}_z)}(\theta)$ is the rotational matrix about the $(-\mathbf{i}_x, \mathbf{i}_y, 0\mathbf{i}_z)$-axis, $GC^{basis}_{(0\mathbf{i}_x,\mathbf{i}_y,\mathbf{i}_z)}$ and $GC^{basis}_{(\mathbf{i}_x,0\mathbf{i}_y,\mathbf{i}_z)}$ are the great circle basis elements initially in the yz and xz planes, respectively, and $\otimes$ designates the convolution with the delta function of the infinitesimal incremental angle $m\Delta\theta_M$. The integral form of the convolution is

$$BECVF = \int_0^{\pi} \left(R_{(-\mathbf{i}_x,\mathbf{i}_y,0\mathbf{i}_z)}(\theta) \bullet \left(GC^{basis}_{(0\mathbf{i}_x,\mathbf{i}_y,\mathbf{i}_z)} + GC^{basis}_{(\mathbf{i}_x,0\mathbf{i}_y,\mathbf{i}_z)} \right) \right) \lim_{\Delta\theta\to 0} \sum_{m=1}^{m=\frac{\pi}{|\Delta\theta|}} \delta(\theta - m\Delta\theta_M) d\theta \tag{1.86}$$

The integration gives the infinite sum of great circles that constitute the BECVF:

$$BECVF = \lim_{\Delta\theta\to 0} \sum_{m=1}^{m=\frac{\pi}{|\Delta\theta|}} \left[\left(R_{(-\mathbf{i}_x,\mathbf{i}_y,0\mathbf{i}_z)}(m\Delta\theta_M) \bullet \left(GC^{basis}_{(0\mathbf{i}_x,\mathbf{i}_y,\mathbf{i}_z)} + GC^{basis}_{(\mathbf{i}_x,0\mathbf{i}_y,\mathbf{i}_z)} \right) \right) \right] \tag{1.87}$$

The BECVF given by Eqs. (1.84-1.87) can also be generated by each of rotating a great circle basis element initially in the yz or the xz-planes about the $(-\mathbf{i}_x, \mathbf{i}_y, 0\mathbf{i}_z)$-axis over the range of 0 to 2π as shown in Figures 1.5 and 1.6, respectively. The BECVF of Figure 1.6 with vectors overlaid giving the direction of the current of each great circle element is shown in Figure 1.7. The current pattern of the BECVF generated by the rotations of the orthogonal great-circle current loops is a continuous half coverage of the spherical surface, but it is shown as visual representations using 6 degree increments of θ for Eqs. (1.84) and (1.87) in Figures 1.5-1.7 wherein the incremental angle becomes discrete rather than the actual continuous distribution in the limit that the incremental angle approaches zero. The same applies to the case of the representations of the OCVF and $Y_0^0(\theta,\phi)$ given *infra*.

Figure 1.5. The current pattern of the BECVF given by Eqs. (1.84) and (1.87) shown with 6 degree increments of θ from the perspective of looking along the z-axis. The yz-plane great circle current loop that served as a basis element that was initially in the yz-plane is shown as red.

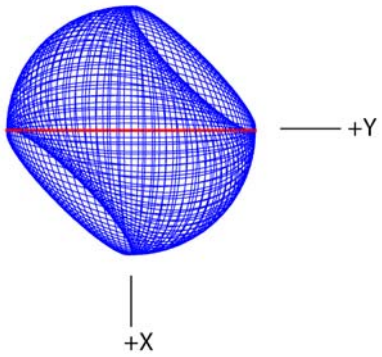

Figure 1.6. The current pattern of the BECVF shown with 6 degree increments of θ from the perspective of looking along the z-axis. The great-circle current loop that served as a basis element that was initially in the xz-plane is shown as red.

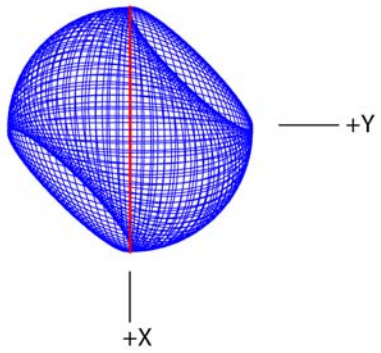

Figure 1.7. A representation of the z-axis perspective view of the BECVF shown in Figure 1.6 with 30 vectors overlaid giving the direction of the current of each great circle element.

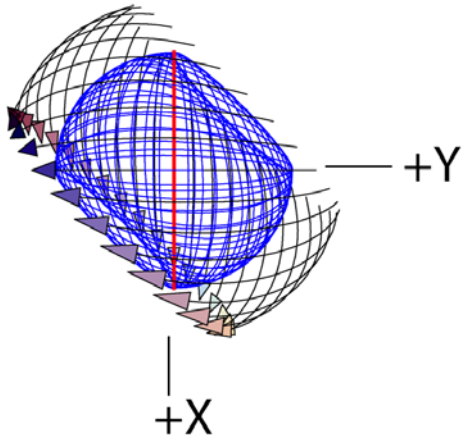

GENERATION OF THE OCVF

For the generation of the OCVF, consider two charge(mass)-density elements, point one and two, in the basis-set reference frame at time zero. Element one is at $x'=\frac{r_n}{\sqrt{2}}$, $y'=\frac{r_n}{\sqrt{2}}$, and $z'=0$, and element two is at $x'=r_n$, $y'=0$, and $z'=0$. Let element one move clockwise on a great circle toward the -z'-axis, and let element two move counter clockwise on a great circle toward the y'-axis as shown in Figure 1.8. The equations of motion, in the basis-set reference frame are given by

point one:

$$x_1'=r_n\sin\left(\frac{\pi}{4}\right)\cos(\omega_n t) \qquad y_1'=r_n\cos\left(\frac{\pi}{4}\right)\cos(\omega_n t) \qquad z_1'=-r_n\sin(\omega_n t) \tag{1.88}$$

point two:

$$x_2'=r_n\cos(\omega_n t) \qquad y_2'=r_n\sin(\omega_n t) \qquad z_2'=0 \tag{1.89}$$

Figure 1.8. In the generation of the OCVF, the current on the great circle in the plane that bisects the x'y'-quadrant and is parallel to the z'-axis moves clockwise, and the current on the great circle in the x'y'-plane moves counter clockwise. Rotation of the great circles about the $\left(-\frac{1}{\sqrt{2}}\mathbf{i}_x,\frac{1}{\sqrt{2}}\mathbf{i}_y,\mathbf{i}_z\right)$-axis by π radians generates the elements of the OCVF. The stationary resultant angular momentum vector of the orthogonal great-circle current loops along the $\left(-\frac{1}{\sqrt{2}}\mathbf{i}_x,\frac{1}{\sqrt{2}}\mathbf{i}_y,\mathbf{i}_z\right)$-axis is $\frac{\hbar}{2}$ corresponding to each of the z and -xy-components of magnitude $\frac{\hbar}{2\sqrt{2}}$.

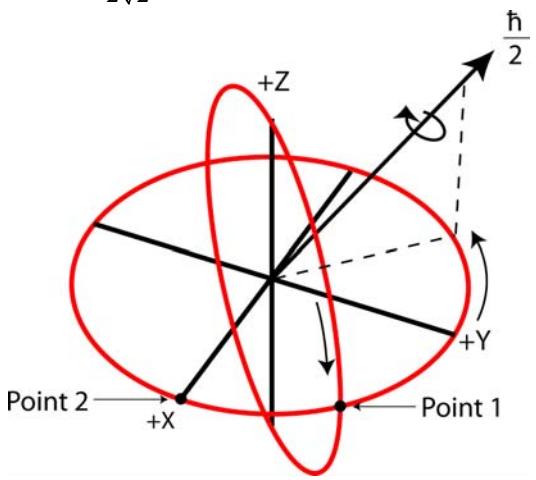

The orthogonal great-circle basis set for the OCVF is shown in Figure 1.8. It is generated by the rotation of the two orthogonal basis-element great circles about the $\left(-\frac{1}{\sqrt{2}}\mathbf{i}_x,\frac{1}{\sqrt{2}}\mathbf{i}_y,\mathbf{i}_z\right)$-axis by an infinite set of infinitesimal increments of the rotational angle totaling a span of π. As shown in Figure 1.8, the current direction is such that the resultant angular momentum vector of the basis elements of magnitude $\frac{\hbar}{2}$ is stationary on this axis wherein one basis-element great circle is initially in the plane that bisects the xy-quadrant and is parallel to the z-axis having angular momentum in the xy plane of $\mathbf{L}_{xy}=\frac{\hbar}{2\sqrt{2}}$ and the other is initially in the xy-plane having angular momentum $\mathbf{L}_z=\frac{\hbar}{2\sqrt{2}}$. The operator to form the OCVF comprises a convolution [11] of the rotational matrix of great circles basis elements with an infinite series of delta functions of argument of the infinitesimal angular increment.

An equivalent distribution to that of the OCVF may be generated by the rotation of a great circle in the yz-plane about the $\left(-\mathbf{i}_x,0\mathbf{i}_y,\mathbf{i}_z\right)$-axis by 2π followed by a rotation about the z-axis by $\frac{\pi}{4}$. The coordinates of the great circle in the yz-plane are given by the matrix:

$$\left[x', y', z'\right]^{\mathrm{T}} = \left[0, r_n \cos\phi, -r_n \sin\phi\right]^{\mathrm{T}} \tag{1.90}$$

The rotational matrix about the $\left(-\mathbf{i}_\mathbf{x}, 0\mathbf{i}_\mathbf{y}, \mathbf{i}_\mathbf{z}\right)$-axis by θ, $R_{\left(-\mathbf{i}_\mathbf{x}, 0\mathbf{i}_\mathbf{y}, \mathbf{i}_\mathbf{z}\right)}(\theta)$, followed by a rotation about the z-axis by $\frac{\pi}{4}$, $R_z(\theta)$, is given by:

$$R_z\left(\frac{\pi}{4}\right) R_{\left(-\mathbf{i}_\mathbf{x}, 0\mathbf{i}_\mathbf{y}, \mathbf{i}_\mathbf{z}\right)}(\theta) = R_z\left(\frac{\pi}{4}\right) R_y\left(\frac{\pi}{4}\right) R_z(\theta) R_y\left(\frac{-\pi}{4}\right) \tag{1.91}$$

In this case, the angular momentum vector of the great circle basis element over a 2π span is not equivalent to a stationary vector on the $\left(-\frac{1}{\sqrt{2}}\mathbf{i}_\mathbf{x}, \frac{1}{\sqrt{2}}\mathbf{i}_\mathbf{y}, \mathbf{i}_\mathbf{z}\right)$-axis. In order to achieve this result, the OCVF is generated by a $R_{\left(-\frac{1}{\sqrt{2}}\mathbf{i}_\mathbf{x}, \frac{1}{\sqrt{2}}\mathbf{i}_\mathbf{y}, \mathbf{i}_\mathbf{z}\right)}(\theta)$ rotation of the great circle basis-element that bisects the xy-quadrant and is parallel to the z-axis over a 2π span. The coordinates of the great circle are given by the matrix that rotates a great circle in the yz-plane about the z-axis by $\frac{\pi}{4}$:

$$\left[x', y', z'\right]^{\mathrm{T}} = \left[\frac{r_n \cos\phi}{\sqrt{2}}, \frac{r_n \cos\phi}{\sqrt{2}}, -r_n \sin\phi\right]^{\mathrm{T}} = R_z\left(\frac{\pi}{4}\right) \bullet \left[0, r_n \cos\phi, -r_n \sin\phi\right]^{\mathrm{T}} \tag{1.92}$$

Since the OCVF is given by the 2π, $R_z\left(\frac{\pi}{4}\right) R_{\left(-\mathbf{i}_\mathbf{x}, 0\mathbf{i}_\mathbf{y}, \mathbf{i}_\mathbf{z}\right)}(\theta)$ rotation of the yz-plane basis-element great circle (Eqs. (1.90-1.91)), the equivalent result may be obtained by first rotating the great circle given by Eq. (1.90) about the z-axis by $-\frac{\pi}{4}$, $R_z\left(-\frac{\pi}{4}\right)$, then applying Eq. (1.91). This combination is equivalent to a rotation about the $\left(-\frac{1}{\sqrt{2}}\mathbf{i}_\mathbf{x}, \frac{1}{\sqrt{2}}\mathbf{i}_\mathbf{y}, \mathbf{i}_\mathbf{z}\right)$-axis by θ, $R_{\left(-\frac{1}{\sqrt{2}}\mathbf{i}_\mathbf{x}, \frac{1}{\sqrt{2}}\mathbf{i}_\mathbf{y}, \mathbf{i}_\mathbf{z}\right)}(\theta)$, and is given by:

$$R_{\left(-\frac{1}{\sqrt{2}}\mathbf{i}_\mathbf{x}, \frac{1}{\sqrt{2}}\mathbf{i}_\mathbf{y}, \mathbf{i}_\mathbf{z}\right)}(\theta) = R_z\left(\frac{\pi}{4}\right) R_y\left(\frac{\pi}{4}\right) R_z(\theta) R_y\left(\frac{-\pi}{4}\right) R_z\left(-\frac{\pi}{4}\right) = R_z\left(\frac{\pi}{4}\right) R_{\left(-\mathbf{i}_\mathbf{x}, 0\mathbf{i}_\mathbf{y}, \mathbf{i}_\mathbf{z}\right)}(\theta) R_z\left(-\frac{\pi}{4}\right) \tag{1.93}$$

Then, the great circle basis-element that bisects the xy-quadrant and is parallel to the z-axis given by Eq. (1.92) is input to the rotational matrix given by Eq. (1.93) to give the desired stationary rotation about the great circle angular momentum axis, the $\left(-\frac{1}{\sqrt{2}}\mathbf{i}_\mathbf{x}, \frac{1}{\sqrt{2}}\mathbf{i}_\mathbf{y}, \mathbf{i}_\mathbf{z}\right)$-axis. The equivalent OCVF is also generated by the rotation of a great circle in the xy-plane about the $\left(-\frac{1}{\sqrt{2}}\mathbf{i}_\mathbf{x}, \frac{1}{\sqrt{2}}\mathbf{i}_\mathbf{y}, \mathbf{i}_\mathbf{z}\right)$-axis by 2π wherein the great circle is given by:

$$\left[x', y', z'\right]^{\mathrm{T}} = \left[r_n \cos\phi, r_n \sin\phi, 0\right]^{\mathrm{T}} \tag{1.94}$$

Then, using Eqs. (1.92-1.94) and Eqs. (1.81-1.82), the great circle basis elements and rotational matrix are given by:

OCVF MATRICES ($R_{\left(-\frac{1}{\sqrt{2}}\mathbf{i}_\mathbf{x}, \frac{1}{\sqrt{2}}\mathbf{i}_\mathbf{y}, \mathbf{i}_\mathbf{z}\right)}(\theta)$)

$$\begin{bmatrix} x' \\ y' \\ z' \end{bmatrix} = \begin{bmatrix} \frac{1}{4}\left(1+3\cos\theta\right) & \frac{1}{4}\left(-1+\cos\theta+2\sqrt{2}\sin\theta\right) & \frac{1}{4}\left(-\sqrt{2}+\sqrt{2}\cos\theta-2\sin\theta\right) \\ \frac{1}{4}\left(-1+\cos\theta-2\sqrt{2}\sin\theta\right) & \frac{1}{4}\left(1+3\cos\theta\right) & \frac{1}{4}\left(\sqrt{2}-\sqrt{2}\cos\theta-2\sin\theta\right) \\ \frac{1}{2}\left(\frac{-1+\cos\theta}{\sqrt{2}}+\sin\theta\right) & \frac{1}{4}\left(\sqrt{2}-\sqrt{2}\cos\theta+2\sin\theta\right) & \cos^2\frac{\theta}{2} \end{bmatrix} \bullet \left(\begin{bmatrix} \frac{r_n\cos\phi}{\sqrt{2}} \\ \frac{r_n\cos\phi}{\sqrt{2}} \\ -r_n\sin\phi \end{bmatrix} + \begin{bmatrix} r_n\cos\phi \\ r_n\sin\phi \\ 0 \end{bmatrix} \right) \tag{1.95}$$

Using Eq. (1.95), the OCVF matrix representation of the convolution is given by:

$$OCVF = \lim_{\Delta\theta\to 0} \sum_{m=1}^{m=\frac{\pi}{|\Delta\theta|}} \left[\left(R_{\left(-\frac{1}{\sqrt{2}}\mathbf{i}_\mathbf{x}, \frac{1}{\sqrt{2}}\mathbf{i}_\mathbf{y}, \mathbf{i}_\mathbf{z}\right)}(\theta) \bullet \left(GC^{basis}_{\left(\frac{1}{\sqrt{2}}\mathbf{i}_\mathbf{x}, \frac{1}{\sqrt{2}}\mathbf{i}_\mathbf{y}, \mathbf{i}_\mathbf{z}\right)} + GC^{basis}_{\left(\mathbf{i}_\mathbf{x}, \mathbf{i}_\mathbf{y}, 0\mathbf{i}_\mathbf{z}\right)} \right) \right) \otimes \delta\left(\theta - m\Delta\theta_M\right) \right] \tag{1.96}$$

wherein $R_{\left(-\frac{1}{\sqrt{2}}\mathbf{i}_\mathbf{x}, \frac{1}{\sqrt{2}}\mathbf{i}_\mathbf{y}, \mathbf{i}_\mathbf{z}\right)}(\theta)$ is the rotational matrix about the $\left(-\frac{1}{\sqrt{2}}\mathbf{i}_\mathbf{x}, \frac{1}{\sqrt{2}}\mathbf{i}_\mathbf{y}, \mathbf{i}_\mathbf{z}\right)$-axis, $GC^{basis}_{\left(\frac{1}{\sqrt{2}}\mathbf{i}_\mathbf{x}, \frac{1}{\sqrt{2}}\mathbf{i}_\mathbf{y}, \mathbf{i}_\mathbf{z}\right)}$ and $GC^{basis}_{\left(\mathbf{i}_\mathbf{x}, \mathbf{i}_\mathbf{y}, 0\mathbf{i}_\mathbf{z}\right)}$ are the great circle basis elements initially in the plane that bisects the xy-quadrant and is parallel to the z-axis and xy-plane, respectively, and $\otimes$ designates the convolution with the delta function of the infinitesimal incremental angle $m\Delta\theta_M$. The integral form of the convolution is:

$$OCVF = \int_0^{\pi}\left(R_{\left(-\frac{1}{\sqrt{2}}\mathbf{i}_x,\frac{1}{\sqrt{2}}\mathbf{i}_y,\mathbf{i}_z\right)}(\theta)\bullet\left(GC^{basis}_{\left(\frac{1}{\sqrt{2}}\mathbf{i}_x,\frac{1}{\sqrt{2}}\mathbf{i}_y,\mathbf{i}_z\right)} + GC^{basis}_{(\mathbf{i}_x,\mathbf{i}_y,0\mathbf{i}_z)}\right)\right)\lim_{\Delta\theta\to 0}\sum_{m=1}^{m=\frac{\pi}{|\Delta\theta|}}\delta(\theta - m\Delta\theta_M)d\theta \tag{1.97}$$

The integration gives the infinite sum of great circles that constitute the OCVF:

$$OCVF = \lim_{\Delta\theta\to 0}\sum_{m=1}^{m=\frac{\pi}{|\Delta\theta|}}\left[\left(R_{\left(-\frac{1}{\sqrt{2}}\mathbf{i}_x,\frac{1}{\sqrt{2}}\mathbf{i}_y,\mathbf{i}_z\right)}(m\Delta\theta_M)\bullet\left(GC^{basis}_{\left(\frac{1}{\sqrt{2}}\mathbf{i}_x,\frac{1}{\sqrt{2}}\mathbf{i}_y,\mathbf{i}_z\right)} + GC^{basis}_{(\mathbf{i}_x,\mathbf{i}_y,0\mathbf{i}_z)}\right)\right)\right] \tag{1.98}$$

The OCVF given by Eq. (1.95) can also be generated by each of rotating a great circle basis element initially in the plane that bisects the xy-quadrant and is parallel to the z-axis or in the xy-plane about the $\left(-\frac{1}{\sqrt{2}}\mathbf{i}_x,\frac{1}{\sqrt{2}}\mathbf{i}_y,\mathbf{i}_z\right)$-axis over the range of 0 to 2π as shown in Figures 1.9 and 1.10, respectively. The OCVF of Figure 1.10 with vectors overlaid giving the direction of the current of each great circle element is shown in Figure 1.11.

Figure 1.9. The current pattern of the OCVF given by Eqs. (1.95) and (1.98) shown with 6 degree increments of θ from the perspective of looking along the z-axis. The great-circle current loop that served as a basis element that was initially in the plane that bisects the xy-quadrant and was parallel to the z-axis is shown as red.

Figure 1.10. The current pattern of the OCVF shown with 6 degree increments of θ from the perspective of looking along the z-axis. The great-circle current loop that served as a basis element that was initially in the xy-plane is shown as red.

Figure 1.11. A representation of the z-axis perspective view of the OCVF shown in Figure 1.10 with 30 vectors overlaid giving the direction of the current of each great circle element.

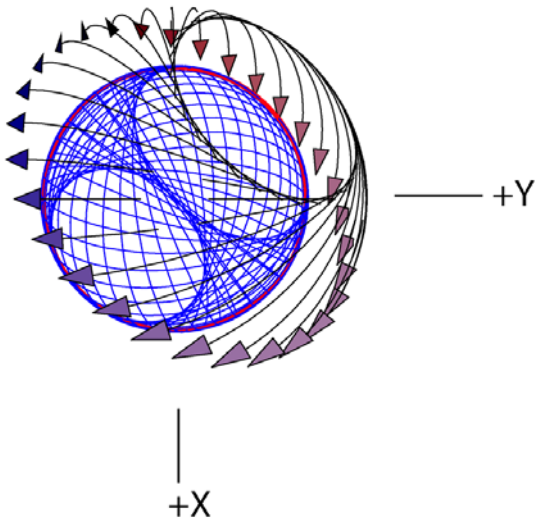

The CVFs, BECVF and OCVF, are used to generate $Y_0^0(\theta,\phi)$. Each CVF involves a unique combination of the initial and final directions of the primed coordinates and orientations of the angular momentum vectors due to the rotation of the basis-element great circles as summarized in Table 1.1. The angular momentum vector of the BECVF is stationary along its rotational

axis, the $\left(-\mathbf{i}_x,\mathbf{i}_y,0\mathbf{i}_z\right)$-axis, and the angular momentum vector of the OCVF is stationary along its rotational axis, the $\left(-\frac{1}{\sqrt{2}}\mathbf{i}_x,\frac{1}{\sqrt{2}}\mathbf{i}_y,\mathbf{i}_z\right)$-axis.

Table 1.1. Summary of the results of the matrix rotations of the two sets of two orthogonal current loops to generate the CVFs.

CVF	Initial Direction of Angular Momentum Components $(\hat{r}\times\hat{K})$[a]	Final Direction of Angular Momentum Components $(\hat{r}\times\hat{K})$[a]	Initial to Final Axis Transformation	$\mathbf{L}_{xy}$	$\mathbf{L}_z$
BECVF	$\left(-\frac{1}{\sqrt{2}}\mathbf{i}_x,\frac{1}{\sqrt{2}}\mathbf{i}_y,0\mathbf{i}_z\right)$	$\left(-\frac{1}{\sqrt{2}}\mathbf{i}_x,\frac{1}{\sqrt{2}}\mathbf{i}_y,0\mathbf{i}_z\right)$	$x'\to -y$ $y'\to -x$ $z'\to -z$	$\frac{\hbar}{2\sqrt{2}}$	0
OCVF	$\left(-\frac{1}{\sqrt{2}}\mathbf{i}_x,\frac{1}{\sqrt{2}}\mathbf{i}_y,\mathbf{i}_z\right)$	$\left(-\frac{1}{\sqrt{2}}\mathbf{i}_x,\frac{1}{\sqrt{2}}\mathbf{i}_y,\mathbf{i}_z\right)$	$x'\to\left(-\frac{1}{2},-\frac{1}{2},-\frac{1}{\sqrt{2}}\right)$ $y'\to\left(-\frac{1}{2},-\frac{1}{2},\frac{1}{\sqrt{2}}\right)$ $z'\to\left(-\frac{1}{\sqrt{2}},\frac{1}{\sqrt{2}},0\right)$	$\frac{\hbar}{2\sqrt{2}}$	$\frac{\hbar}{2\sqrt{2}}$

[a] **K** is the current density, **r** is the polar vector of the great circle, and "^" denotes the unit vectors $\hat{u}\equiv\frac{\mathbf{u}}{|\mathbf{u}|}$.

GENERATION OF $Y_0^{\,0}(\theta,\phi)$

The further constraint that the current density is uniform such that the charge density is uniform, corresponding to an equipotential, minimum energy surface is satisfied by using the CVFs to generate the uniform great-circle distribution $Y_0^{\,0}(\theta,\phi)$ by the convolution of the BECVF with the OCVF followed by normalization. Consider that the BECVF (Eq. (1.84)) for the OCVF convolution can also be generated by rotating a great circle basis element initially in the yz-plane about the $\left(-\mathbf{i}_x,\mathbf{i}_y,0\mathbf{i}_z\right)$-axis by 2π radians as shown in Figure 1.5. Similarly, the OCVF (Eq. (1.95)) can also be generated by rotating a great circle basis element initially in the plane that bisects the xy-quadrant and is parallel to the z-axis about the $\left(-\frac{1}{\sqrt{2}}\mathbf{i}_x,\frac{1}{\sqrt{2}}\mathbf{i}_y,\mathbf{i}_z\right)$-axis over the range of 0 to 2π as shown in Figure 1.9. The convolution operator treats each CVF independently and results in the placement of a BECVF at each great circle of the OCVF such that the resultant angular momentum of the distribution is the same as that of the OCVF. This is achieved by rotating the orientation, phase[6], and vector-matched basis-element, the BECVF, about the same axis as that which generated the OCVF. Thus, the BECVF replaces one great circle basis element, in this case, the one initially in the plane that bisects the xy-quadrant and is parallel to the z-axis. To match to the resultant angular momentum of both great circle basis elements, the angular momentum of the BECVF is $\mathbf{L}_{xy}=\frac{\hbar}{\sqrt{2}}$ (Figure 1.8) along the $\left(-\mathbf{i}_x,\mathbf{i}_y,0\mathbf{i}_z\right)$-axis. Then, $Y_0^{\,0}(\theta,\phi)$ is generated by rotation of the BECVF, about the $\left(-\frac{1}{\sqrt{2}}\mathbf{i}_x,\frac{1}{\sqrt{2}}\mathbf{i}_y,\mathbf{i}_z\right)$-axis by an infinite set of infinitesimal increments of the rotational angle. The current direction is such that the resultant angular momentum vector of the BECVF basis element rotated over the 2π span is equivalent to that of both of the OCVF great circle basis elements, $\frac{\hbar}{2}$ having components of

[6] The resultant angular momentum vector, $\mathbf{L}_\mathbf{R}$, is along $\left(-\mathbf{i}_x,\mathbf{i}_y,0\mathbf{i}_z\right)$; thus, the angular momentum is constant for any rotation about this axis which establishes it as a C_∞-axis relative to the angular momentum. However, rotation about this axis does change the phase (coordinate position relative to the starting position) of the BECVF. For example, a rotation by $|\theta|=\pi$ about the $\left(-\mathbf{i}_x,\mathbf{i}_y,0\mathbf{i}_z\right)$-axis using Eqs. (1.83) and (1.84) causes the BECVF basis-element great circle to rotate by $\frac{\pi}{2}$ about the z-axis such that its position changes between the xz and yz-planes.

$\mathbf{L}_{xy} = \frac{\hbar}{2\sqrt{2}}$ and $\mathbf{L}_z = \frac{\hbar}{2\sqrt{2}}$ that is stationary on the $\left(-\frac{1}{\sqrt{2}}\mathbf{i}_\mathbf{x}, \frac{1}{\sqrt{2}}\mathbf{i}_\mathbf{y}, \mathbf{i}_\mathbf{z}\right)$-axis. Since the resultant angular momentum vector of the BECVF over the 2π span matches that of the replaced great circle basis elements and is stationary on the rotational axis as in the case of the OCVF, the resultant angular momentum of the distribution is the same as that of the OCVF, except that coverage of the spherical surface is complete. The resulting uniformity of the distribution is achieved by normalization as shown in the Uniformity of $Y_0^0(\theta,\phi)$ section.

The operator to form $Y_0^0(\theta,\phi)$ comprises the BECVF convolution [11] of the rotational matrix of great circles basis element about the $\left(-\mathbf{i}_\mathbf{x}, \mathbf{i}_\mathbf{y}, 0\mathbf{i}_\mathbf{z}\right)$-axis with an infinite series of delta functions of argument of the infinitesimal angular increment that is further convolved with the OCVF convolution of the rotational matrix of great circles basis element about the $\left(-\frac{1}{\sqrt{2}}\mathbf{i}_\mathbf{x}, \frac{1}{\sqrt{2}}\mathbf{i}_\mathbf{y}, \mathbf{i}_\mathbf{z}\right)$-axis with an infinite series of delta functions of argument of the infinitesimal angular increment. Using the BECVF matrix representation of its convolution operation (Eq. (1.85)) and the OCVF matrix representation of its convolution operation (Eq. (1.96)), the $Y_0^0(\theta,\phi)$ matrix representation of the convolution is given by:

$$Y_0^0(\theta,\phi) = OCVF \otimes BECVF = \left\{ \begin{array}{l} \left(\lim\limits_{\Delta\theta\to 0} \sum\limits_{m=1}^{m=\frac{2\pi}{|\Delta\theta|}} \left[\left(R_{\left(-\frac{1}{\sqrt{2}}\mathbf{i}_\mathbf{x}, \frac{1}{\sqrt{2}}\mathbf{i}_\mathbf{y}, \mathbf{i}_\mathbf{z}\right)}(\theta) \bullet GC^{basis}_{\left(\frac{1}{\sqrt{2}}\mathbf{i}_\mathbf{x}, \frac{1}{\sqrt{2}}\mathbf{i}_\mathbf{y}, \mathbf{i}_\mathbf{z}\right)} \right) \otimes \delta\left(\theta - m\Delta\theta_M\right) \right] \right) \\ \otimes \left(\lim\limits_{\Delta\theta\to 0} \sum\limits_{n=1}^{n=\frac{2\pi}{|\Delta\theta|}} \left[\left(R_{\left(-\mathbf{i}_\mathbf{x}, \mathbf{i}_\mathbf{y}, 0\mathbf{i}_\mathbf{z}\right)}(\theta) \bullet GC^{basis}_{\left(0\mathbf{i}_\mathbf{x}, \mathbf{i}_\mathbf{y}, \mathbf{i}_\mathbf{z}\right)} \right) \otimes \delta\left(\theta - n\Delta\theta_N\right) \right] \right) \end{array} \right\} \tag{1.99}$$

where the commutative property of convolutions [11] allows for the interchange of the order of CVFs, but the rotational matrices are noncommutative [12]. The integral form of the convolution is

$$Y_0^0(\theta,\phi) = \left\{ \begin{array}{l} \left[\int\limits_0^{2\pi} \left(R_{\left(-\frac{1}{\sqrt{2}}\mathbf{i}_\mathbf{x}, \frac{1}{\sqrt{2}}\mathbf{i}_\mathbf{y}, \mathbf{i}_\mathbf{z}\right)}(\theta) \bullet GC^{basis}_{\left(\frac{1}{\sqrt{2}}\mathbf{i}_\mathbf{x}, \frac{1}{\sqrt{2}}\mathbf{i}_\mathbf{y}, \mathbf{i}_\mathbf{z}\right)} \right) \lim\limits_{\Delta\theta\to 0} \sum\limits_{m=1}^{m=\frac{2\pi}{|\Delta\theta|}} \delta\left(\theta - m\Delta\theta_M^{OCVF}\right) d\theta \right] \\ \otimes \left[\int\limits_0^{2\pi} \left(R_{\left(-\mathbf{i}_\mathbf{x}, \mathbf{i}_\mathbf{y}, 0\mathbf{i}_\mathbf{z}\right)}(\theta) \bullet GC^{basis}_{\left(0\mathbf{i}_\mathbf{x}, \mathbf{i}_\mathbf{y}, \mathbf{i}_\mathbf{z}\right)} \right) \left(\lim\limits_{\Delta\theta\to 0} \sum\limits_{n=1}^{n=\frac{2\pi}{|\Delta\theta|}} \delta\left(\theta - n\Delta\theta_N^{BECVF}\right) \right) d\theta \right] \end{array} \right\} \tag{1.100}$$

$$Y_0^0(\theta,\phi) = \lim_{\Delta\theta\to 0} \sum_{m=1}^{m=\frac{2\pi}{|\Delta\theta|}} \lim_{\Delta\theta\to 0} \sum_{n=1}^{n=\frac{2\pi}{|\Delta\theta|}} \int_0^{2\pi} d\theta_1 \int_0^{2\pi} d\theta_2 R_{\left(-\frac{1}{\sqrt{2}}\mathbf{i}_\mathbf{x}, \frac{1}{\sqrt{2}}\mathbf{i}_\mathbf{y}, \mathbf{i}_\mathbf{z}\right)}(\theta_1) \bullet R_{\left(-\mathbf{i}_\mathbf{x}, \mathbf{i}_\mathbf{y}, 0\mathbf{i}_\mathbf{z}\right)}(\theta_2) \bullet GC^{basis}_{\left(0\mathbf{i}_\mathbf{x}, \mathbf{i}_\mathbf{y}, \mathbf{i}_\mathbf{z}\right)} \delta\left(\theta_1 - m\Delta\theta_M^{OCVF}\right) \delta\left(\theta_2 - n\Delta\theta_N^{BECVF}\right) \tag{1.101}$$

The integration gives the infinite double sum of great circles that constitute $Y_0^0(\theta,\phi)$:

$$Y_0^0(\theta,\phi) = \lim_{\Delta\theta\to 0} \sum_{m=1}^{m=\frac{2\pi}{|\Delta\theta|}} \left[R_{\left(-\frac{1}{\sqrt{2}}\mathbf{i}_\mathbf{x}, \frac{1}{\sqrt{2}}\mathbf{i}_\mathbf{y}, \mathbf{i}_\mathbf{z}\right)}\left(m\Delta\theta_M^{OCVF}\right) \bullet \lim_{\Delta\theta\to 0} \sum_{n=1}^{n=\frac{2\pi}{|\Delta\theta|}} \left[R_{\left(-\mathbf{i}_\mathbf{x}, \mathbf{i}_\mathbf{y}, 0\mathbf{i}_\mathbf{z}\right)}\left(n\Delta\theta_N^{BECVF}\right) \bullet GC^{basis}_{\left(0\mathbf{i}_\mathbf{x}, \mathbf{i}_\mathbf{y}, \mathbf{i}_\mathbf{z}\right)} \right] \right] \tag{1.102}$$

Using Eq. (1.102), a discrete representation of the current distribution $Y_0^0(\theta,\phi)$ that shows a finite number of current elements can be generated by showing the BECVF as a finite sum of the convolved great circle elements using Eqs. (1.84) and (1.87) and by showing the continuous convolution of the BECVF with the OCVF as a superposition of discrete incremental rotations of the position of the BECVF rotated according to Eqs. (1.95) and (1.98) corresponding to the matrix which generated the OCVF. In the case that the discrete representation of the BECVF comprises N great circles and the number of convolved BECVF elements is M, the representation of the current density function showing current loops is given by Eq. (1.103) and shown in Figure 1.12. The $\left(\frac{1}{\sqrt{2}}\mathbf{i}_\mathbf{x}, -\frac{1}{\sqrt{2}}\mathbf{i}_\mathbf{y}, \mathbf{i}_\mathbf{z}\right)$-axis view of this representation with 144 vectors overlaid giving the direction of the current of each great circle element is shown in Figure 1.13. The corresponding mass(momentum) density is also represented by Figures 1.12 and 1.13 wherein the charge and mass are interchangeable by the conversion factor m_e / e.

$$\begin{bmatrix} x' \\ y' \\ z' \end{bmatrix} = \sum_{m=1}^{m=M} \begin{bmatrix} \frac{1}{4}\left(1+3\cos\left(\frac{m2\pi}{M}\right)\right) & \frac{1}{4}\left(-1+\cos\left(\frac{m2\pi}{M}\right)+2\sqrt{2}\sin\left(\frac{m2\pi}{M}\right)\right) & \frac{1}{4}\left(-\sqrt{2}+\sqrt{2}\cos\left(\frac{m2\pi}{M}\right)-2\sin\left(\frac{m2\pi}{M}\right)\right) \\ \frac{1}{4}\left(-1+\cos\left(\frac{m2\pi}{M}\right)-2\sqrt{2}\sin\left(\frac{m2\pi}{M}\right)\right) & \frac{1}{4}\left(1+3\cos\left(\frac{m2\pi}{M}\right)\right) & \frac{1}{4}\left(\sqrt{2}-\sqrt{2}\cos\left(\frac{m2\pi}{M}\right)-2\sin\left(\frac{m2\pi}{M}\right)\right) \\ \frac{1}{2}\left(\frac{-1+\cos\left(\frac{m2\pi}{M}\right)}{\sqrt{2}}+\sin\left(\frac{m2\pi}{M}\right)\right) & \frac{1}{4}\left(\sqrt{2}-\sqrt{2}\cos\left(\frac{m2\pi}{M}\right)+2\sin\left(\frac{m2\pi}{M}\right)\right) & \cos^2\frac{\left(\frac{m2\pi}{M}\right)}{2} \end{bmatrix}$$

$$\bullet \sum_{n=1}^{n=N} \begin{bmatrix} \frac{1}{2}+\frac{\cos\left(\frac{n2\pi}{N}\right)}{2} & -\frac{1}{2}+\frac{\cos\left(\frac{n2\pi}{N}\right)}{2} & -\frac{\sin\left(\frac{n2\pi}{N}\right)}{\sqrt{2}} \\ -\frac{1}{2}+\frac{\cos\left(\frac{n2\pi}{N}\right)}{2} & \frac{1}{2}+\frac{\cos\left(\frac{n2\pi}{N}\right)}{2} & -\frac{\sin\left(\frac{n2\pi}{N}\right)}{\sqrt{2}} \\ \frac{\sin\left(\frac{n2\pi}{N}\right)}{\sqrt{2}} & \frac{\sin\left(\frac{n2\pi}{N}\right)}{\sqrt{2}} & \cos\left(\frac{n2\pi}{N}\right) \end{bmatrix} \begin{bmatrix} 0 \\ r_n\cos\phi \\ -r_n\sin\phi \end{bmatrix} \tag{1.103}$$

Figure 1.12. A representation of the z-axis view of the current pattern of $Y_0^0(\theta,\phi)$ shown with 30 degree increments ($N=M=12$ in Eq. (1.103)) of the angle to generate the BECVF corresponding to Eqs. (1.84) and (1.87) and 30 degree increments of the rotation of this basis element about the $\left(-\frac{1}{\sqrt{2}}\mathbf{i}_x,\frac{1}{\sqrt{2}}\mathbf{i}_y,\mathbf{i}_z\right)$-axis corresponding to Eqs. (1.95) and (1.98).

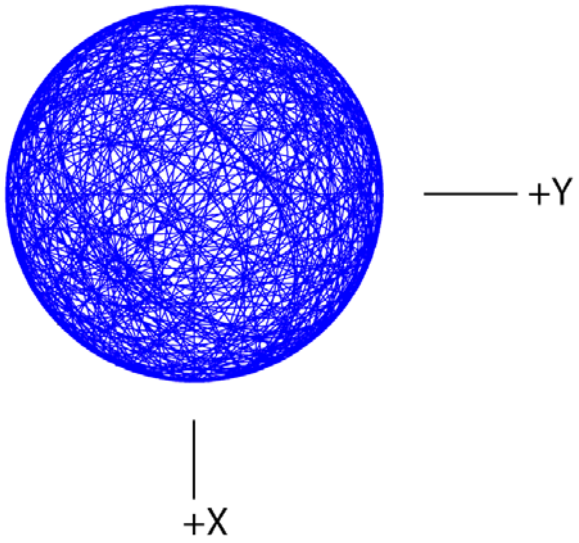

Figure 1.13. A representation of the $\left(\frac{1}{\sqrt{2}}\mathbf{i}_x,-\frac{1}{\sqrt{2}}\mathbf{i}_y,\mathbf{i}_z\right)$-axis view of $Y_0^0(\theta,\phi)$ shown in Figure 1.12 with 144 vectors overlaid giving the direction of the current of each great circle element.

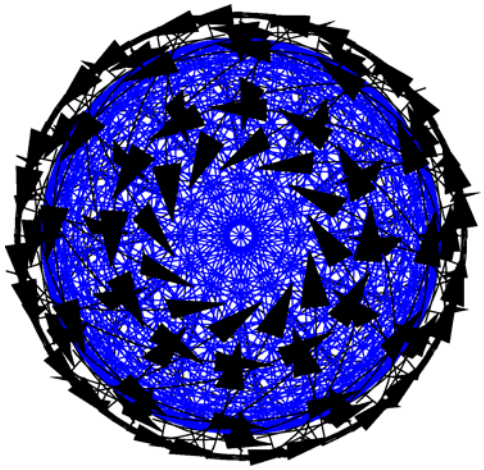

A BECVF can also be generated to replace the great circle basis element of the OCVF that lies in the xy-plane. In the case that the current is counter clockwise with the angular momentum in the direction of the z-axis, the equivalent rotational transformations that maintain the resultant angular momentum stationary on the z-axis over a 2π rotation is the combination of a $-\frac{\pi}{4}$ rotation about the y-axis followed by a 2π rotation of the tilted great circle about the z-axis. The angular-momentum-and-orientation-matched distribution shown in Figure 1.14 is generated by:

$$[x', y', z']^{\mathrm{T}} = R_z(\theta) R_y\left(\frac{-\pi}{4}\right) \bullet [r_n \cos\phi, r_n \sin\phi, 0]^{\mathrm{T}} \tag{1.104}$$

In order to match phase with the OCVF rotational axis, $\left(-\frac{1}{\sqrt{2}}\mathbf{i}_x, \frac{1}{\sqrt{2}}\mathbf{i}_y, \mathbf{i}_z\right)$-axis, Eq. (1.104) must be rotated about the z-axis by $\frac{\pi}{4}$ using $R_z\left(\frac{\pi}{4}\right)$ using Eq. (1.82). In this case, the BECVF is aligned on the xy-plane and the resultant angular momentum vector, $\mathbf{L}_\mathbf{R}$, is also along the z-axis. The final phase-matched distribution shown in Figure 1.15 is given by:

$$[x', y', z']^{\mathrm{T}} = R_z\left(\frac{\pi}{4}\right) R_z(\theta) R_y\left(\frac{-\pi}{4}\right) \bullet [r_n \cos\phi, r_n \sin\phi, 0]^{\mathrm{T}} \tag{1.105}$$

Figure 1.14. The current pattern given by Eq. (1.104) shown with 6 degree increments of θ from the perspective of looking along the z-axis. The great circle current loop that served as a basis element that was initially in the xy-plane is shown as red.

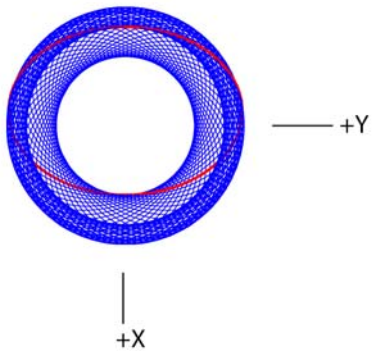

Figure 1.15. The current pattern given by Eq. (1.105) shown with 6 degree increments of θ from the perspective of looking along the z-axis. The great circle current loop that served as a basis element that was initially in the xy-plane is shown as red.

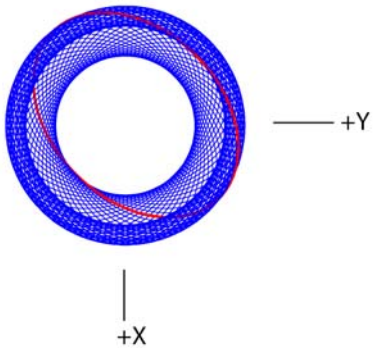

Then, using Eq. (1.105) and Eqs. (1.81-1.82), the great circle basis elements and rotational matrix are given by:

BECVF MATRICES $\left(R_z\left(\frac{\pi}{4}\right) R_z(\theta) R_y\left(\frac{-\pi}{4}\right)\right)$

$$\begin{bmatrix} x' \\ y' \\ z' \end{bmatrix} = \begin{bmatrix} \frac{\cos\theta}{2} - \frac{\sin\theta}{2} & \frac{\sin\theta}{\sqrt{2}} + \frac{\cos\theta}{\sqrt{2}} & \frac{\cos\theta}{2} - \frac{\sin\theta}{2} \\ -\frac{\cos\theta}{2} - \frac{\sin\theta}{2} & -\frac{\sin\theta}{\sqrt{2}} + \frac{\cos\theta}{\sqrt{2}} & -\frac{\cos\theta}{2} - \frac{\sin\theta}{2} \\ -\frac{1}{\sqrt{2}} & 0 & \frac{1}{\sqrt{2}} \end{bmatrix} \begin{bmatrix} r_n \cos\phi \\ r_n \sin\phi \\ 0 \end{bmatrix} \tag{1.106}$$

Using the procedure of Eqs. (1.85-1.87) on Eq. (1.106), the infinite sum of great circles that constitute the BECVF is:

$$BECVF = \lim_{\Delta\theta \to 0} \sum_{m=1}^{m=\frac{2\pi}{|\Delta\theta|}} \left[\left(R_z\left(\frac{\pi}{4}\right) R_z(\theta) R_y\left(\frac{-\pi}{4}\right) (m\Delta\theta_M) \bullet GC^{basis}_{(\mathbf{i}_x, \mathbf{i}_y, 0\mathbf{i}_z)} \right) \right] \tag{1.107}$$

Using Eqs. (1.99-1.102), and (1.107), the corresponding infinite double sum of great circles that constitute $Y_0^0(\theta, \phi)$ is given by:

$$Y_0^{\,0}(\theta,\phi) = \lim_{\Delta\theta\to 0}\sum_{m=1}^{m=\frac{2\pi}{|\Delta\theta|}}\left[R_{\left(-\frac{1}{\sqrt{2}}\mathbf{i}_x,\frac{1}{\sqrt{2}}\mathbf{i}_y,\mathbf{i}_z\right)}\left(m\Delta\theta_M^{OCVF}\right)\bullet\lim_{\Delta\theta\to 0}\sum_{n=1}^{n=\frac{2\pi}{|\Delta\theta|}}\left[R_z\left(\frac{\pi}{4}\right)R_z(\theta)R_y\left(\frac{-\pi}{4}\right)\left(n\Delta\theta_N^{BECVF}\right)\bullet GC^{basis}_{(0\mathbf{i}_x,\mathbf{i}_y,\mathbf{i}_z)}\right]\right] \tag{1.108}$$

Using Eq. (1.108), a discrete representation of the current distribution $Y_0^{\,0}(\theta,\phi)$ that shows a finite number of current elements can be generated by showing the BECVF as a finite sum of the convolved great circle elements using Eqs. (1.106-1.107) and by showing the continuous convolution of the BECVF with the OCVF as a superposition of discrete incremental rotations of the position of the BECVF rotated according to Eqs. (1.95) and (1.98) corresponding to the matrix which generated the OCVF. In the case that the discrete representation of the BECVF comprises N great circles and the number of convolved BECVF elements is M, the representation of the current density function showing current loops is given by Eq. (1.109) and shown in Figure 1.16. The $\left(\frac{1}{\sqrt{2}}\mathbf{i}_x,-\frac{1}{\sqrt{2}}\mathbf{i}_y,\mathbf{i}_z\right)$-axis view of this representation with 144 vectors overlaid giving the direction of the current of each great circle element is shown in Figure 1.17. The corresponding mass(momentum) density is also represented by Figures 1.16 and 1.17 wherein the charge and mass are interchangeable by the conversion factor m_e/e.

$$\begin{bmatrix}x'\\ y'\\ z'\end{bmatrix} = \sum_{m=1}^{m=M}\begin{bmatrix}\frac{1}{4}\left(1+3\cos\left(\frac{m2\pi}{M}\right)\right) & \frac{1}{4}\left(-1+\cos\left(\frac{m2\pi}{M}\right)+2\sqrt{2}\sin\left(\frac{m2\pi}{M}\right)\right) & \frac{1}{4}\left(-\sqrt{2}+\sqrt{2}\cos\left(\frac{m2\pi}{M}\right)-2\sin\left(\frac{m2\pi}{M}\right)\right)\\ \frac{1}{4}\left(-1+\cos\left(\frac{m2\pi}{M}\right)-2\sqrt{2}\sin\left(\frac{m2\pi}{M}\right)\right) & \frac{1}{4}\left(1+3\cos\left(\frac{m2\pi}{M}\right)\right) & \frac{1}{4}\left(\sqrt{2}-\sqrt{2}\cos\left(\frac{m2\pi}{M}\right)-2\sin\left(\frac{m2\pi}{M}\right)\right)\\ \frac{1}{2}\left(\frac{-1+\cos\left(\frac{m2\pi}{M}\right)}{\sqrt{2}}+\sin\left(\frac{m2\pi}{M}\right)\right) & \frac{1}{4}\left(\sqrt{2}-\sqrt{2}\cos\left(\frac{m2\pi}{M}\right)+2\sin\left(\frac{m2\pi}{M}\right)\right) & \cos^2\frac{\left(\frac{m2\pi}{M}\right)}{2}\end{bmatrix}$$

$$\bullet\sum_{n=1}^{n=N}\begin{bmatrix}\frac{\cos\left(\frac{n2\pi}{N}\right)}{2}-\frac{\sin\left(\frac{n2\pi}{N}\right)}{2} & \frac{\sin\left(\frac{n2\pi}{N}\right)}{\sqrt{2}}+\frac{\cos\left(\frac{n2\pi}{N}\right)}{\sqrt{2}} & \frac{\cos\left(\frac{n2\pi}{N}\right)}{2}-\frac{\sin\left(\frac{n2\pi}{N}\right)}{2}\\ -\frac{\cos\left(\frac{n2\pi}{N}\right)}{2}-\frac{\sin\left(\frac{n2\pi}{N}\right)}{2} & -\frac{\sin\left(\frac{n2\pi}{N}\right)}{\sqrt{2}}+\frac{\cos\left(\frac{n2\pi}{N}\right)}{\sqrt{2}} & -\frac{\cos\left(\frac{n2\pi}{N}\right)}{2}-\frac{\sin\left(\frac{n2\pi}{N}\right)}{2}\\ -\frac{1}{\sqrt{2}} & 0 & \frac{1}{\sqrt{2}}\end{bmatrix}\begin{bmatrix}r_n\cos\phi\\ r_n\sin\phi\\ 0\end{bmatrix} \tag{1.109}$$

Figure 1.16. A representation of the z-axis view of the current pattern of the $Y_0^0(\theta,\phi)$ shown with 30 degree increments ($N=M=12$ in Eq. (1.109)) of the angle to generate the BECVF corresponding to Eqs. (1.106) and (1.107) and 30 degree increments of the rotation of this basis element about the $\left(-\frac{1}{\sqrt{2}}\mathbf{i}_x,\frac{1}{\sqrt{2}}\mathbf{i}_y,\mathbf{i}_z\right)$-axis corresponding to Eqs. (1.95) and (1.98). The great circle current loop that served as a basis element of the BECVF is shown as red.

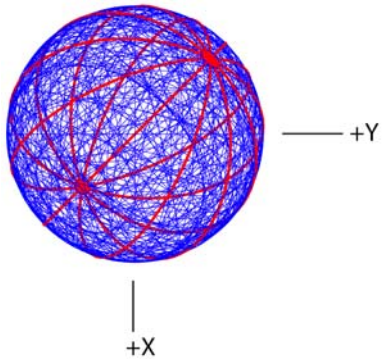

Figure 1.17. A representation of the $\left(\frac{1}{\sqrt{2}}\mathbf{i}_x,-\frac{1}{\sqrt{2}}\mathbf{i}_y,\mathbf{i}_z\right)$-axis view of $Y_0^0(\theta,\phi)$ shown in Figure 1.16 with 144 vectors overlaid giving the direction of the current of each great circle element.

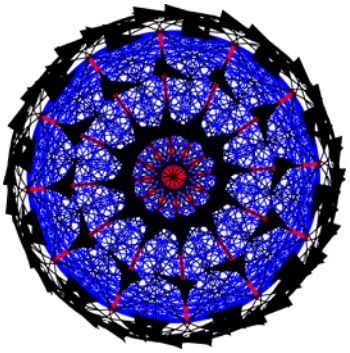

UNIFORMITY OF $Y_0^0(\theta,\phi)$

By using the rotational matrices to generate $Y_0^0(\theta,\phi)$, it is shown to be uniform about the angular momentum axis that is permissive of normalization such that the spherical uniformity and angular momentum boundary conditions are met. Consider the $Y_0^0(\theta,\phi)$ convolution in summation form given by Eqs. (1.99) and (1.102). The BECVF is periodic in θ with a period of π wherein the basis elements interchange. Thus, only one basis need be considered with the range increased to 2π:

$$\begin{bmatrix} x' \\ y' \\ z' \end{bmatrix} = \left(\lim_{\Delta\theta\to 0} \sum_{m=1}^{m=\frac{2\pi}{|\Delta\theta|}} \left[\left(R_{\left(-\frac{1}{\sqrt{2}}\mathbf{i}_x,\frac{1}{\sqrt{2}}\mathbf{i}_y,\mathbf{i}_z\right)}\left(m\Delta\theta_M^{OCVF}\right) \bullet BECVF^{basis}_{\left(\frac{1}{\sqrt{2}}\mathbf{i}_x,\frac{1}{\sqrt{2}}\mathbf{i}_y,\mathbf{i}_z\right)} \right) \right] \right) \tag{1.110}$$

wherein $BECVF^{basis}_{\left(\frac{1}{\sqrt{2}}\mathbf{i}_x,\frac{1}{\sqrt{2}}\mathbf{i}_y,\mathbf{i}_z\right)}$ is the distribution that replaced the great circle basis element of the OCVF distribution in the convolution given by Eqs. (1.87), (1.92), (1.98), and (1.99), respectively. Consider the rotation of both sides of Eq. (1.110) about the $\left(\mathbf{i}_x,\mathbf{i}_y,0\mathbf{i}_z\right)$-axis, the orthogonal axis to that which generated the BECVF, by $\frac{\pi}{4}$:

$$R_{\left(\mathbf{i}_x,\mathbf{i}_y,0\mathbf{i}_z\right)}\left(\frac{\pi}{4}\right)\begin{bmatrix} x' \\ y' \\ z' \end{bmatrix} = \left(R_{\left(\mathbf{i}_x,\mathbf{i}_y,0\mathbf{i}_z\right)}\left(\frac{\pi}{4}\right) \lim_{\Delta\theta\to 0} \sum_{m=1}^{m=\frac{2\pi}{|\Delta\theta|}} \left[\left(R_{\left(-\frac{1}{\sqrt{2}}\mathbf{i}_x,\frac{1}{\sqrt{2}}\mathbf{i}_y,\mathbf{i}_z\right)}\left(m\Delta\theta_M^{OCVF}\right) \bullet BECVF^{basis}_{\left(\frac{1}{\sqrt{2}}\mathbf{i}_x,\frac{1}{\sqrt{2}}\mathbf{i}_y,\mathbf{i}_z\right)} \right) \right] \right) \tag{1.111}$$

The rotation of a sum is the same as the sum of the rotations

$$R_{\left(\mathbf{i}_x,\mathbf{i}_y,0\mathbf{i}_z\right)}\left(\frac{\pi}{4}\right)\begin{bmatrix} x' \\ y' \\ z' \end{bmatrix} = \left(\lim_{\Delta\theta\to 0} \sum_{m=1}^{m=\frac{2\pi}{|\Delta\theta|}} \left[\left(R_{\left(\mathbf{i}_x,\mathbf{i}_y,0\mathbf{i}_z\right)}\left(\frac{\pi}{4}\right) \bullet R_{\left(-\frac{1}{\sqrt{2}}\mathbf{i}_x,\frac{1}{\sqrt{2}}\mathbf{i}_y,\mathbf{i}_z\right)}\left(m\Delta\theta_M^{OCVF}\right) \bullet BECVF^{basis}_{\left(\frac{1}{\sqrt{2}}\mathbf{i}_x,\frac{1}{\sqrt{2}}\mathbf{i}_y,\mathbf{i}_z\right)} \right) \right] \right) \tag{1.112}$$

When the distribution given by Eq. (1.98) having its C_∞-axis along the $\left(-\frac{1}{\sqrt{2}}\mathbf{i}_x,\frac{1}{\sqrt{2}}\mathbf{i}_y,\mathbf{i}_z\right)$-axis is rotated about the $\left(\mathbf{i}_x,\mathbf{i}_y,0\mathbf{i}_z\right)$-axis by $\frac{\pi}{4}$, the resulting distribution having the C_∞-axis along the $\left(-\mathbf{i}_x,\mathbf{i}_y,0\mathbf{i}_z\right)$-axis is equivalent to the distribution given by Eq. (1.87) of matching C_∞-axis. Substitution of Eq. (1.87) into Eq. (1.112) gives:

$$R_{(\mathbf{i}_x,\mathbf{i}_y,0\mathbf{i}_z)}\left(\frac{\pi}{4}\right)\begin{bmatrix}x'\\y'\\z'\end{bmatrix}=\left(\lim_{\Delta\theta\to 0}\sum_{m=1}^{m=\frac{2\pi}{|\Delta\theta|}}\left[\left(R_{(-\mathbf{i}_x,\mathbf{i}_y,0\mathbf{i}_z)}\left(m\Delta\theta_M^{OCVF}\right)\bullet BECVF^{basis}_{\left(\frac{1}{\sqrt{2}}\mathbf{i}_x,\frac{1}{\sqrt{2}}\mathbf{i}_y,\mathbf{i}_z\right)}\right)\right]\right) \tag{1.113}$$

Substitution of Eq. (1.87) for BECVF and using the π periodicity property of the great circle basis elements gives:

$$R_{(\mathbf{i}_x,\mathbf{i}_y,0\mathbf{i}_z)}\left(\frac{\pi}{4}\right)\begin{bmatrix}x'\\y'\\z'\end{bmatrix}=\left(\lim_{\Delta\theta\to 0}\sum_{m=1}^{m=\frac{2\pi}{|\Delta\theta|}}\left[\left(R_{(-\mathbf{i}_x,\mathbf{i}_y,0\mathbf{i}_z)}\left(m\Delta\theta_M\right)\bullet\lim_{\Delta\theta\to 0}\sum_{n=1}^{n=\frac{2\pi}{|\Delta\theta|}}\left[\left(R_{(-\mathbf{i}_x,\mathbf{i}_y,0\mathbf{i}_z)}\left(n\Delta\theta_N\right)\bullet GC^{basis}_{(0\mathbf{i}_x,\mathbf{i}_y,\mathbf{i}_z)}\right)\right]\right)\right]\right) \tag{1.114}$$

Using the distributive property of the double sum gives:

$$R_{(\mathbf{i}_x,\mathbf{i}_y,0\mathbf{i}_z)}\left(\frac{\pi}{4}\right)\begin{bmatrix}x'\\y'\\z'\end{bmatrix}=\lim_{\Delta\theta\to 0}\sum_{m=1}^{m=\frac{2\pi}{|\Delta\theta|}}\lim_{\Delta\theta\to 0}\sum_{n=1}^{n=\frac{2\pi}{|\Delta\theta|}}R_{(-\mathbf{i}_x,\mathbf{i}_y,0\mathbf{i}_z)}\left(m\Delta\theta_M\right)\bullet R_{(-\mathbf{i}_x,\mathbf{i}_y,0\mathbf{i}_z)}\left(n\Delta\theta_N\right)\bullet GC^{basis}_{(0\mathbf{i}_x,\mathbf{i}_y,\mathbf{i}_z)} \tag{1.115}$$

Rotation of the BECVF about its C_∞-axis, the $\left(\mathbf{i}_x,\mathbf{i}_y,0\mathbf{i}_z\right)$-axis, leaves the BECVF distribution unchanged.

$$R_{(\mathbf{i}_x,\mathbf{i}_y,0\mathbf{i}_z)}\left(\frac{\pi}{4}\right)\begin{bmatrix}x'\\y'\\z'\end{bmatrix}=BECVF^{basis}_{\left(\frac{1}{\sqrt{2}}\mathbf{i}_x,\frac{1}{\sqrt{2}}\mathbf{i}_y,\mathbf{i}_z\right)} \tag{1.116}$$

Eq. (1.116) represents the properties of the distribution perpendicular to the $\left(-\frac{1}{\sqrt{2}}\mathbf{i}_x,\frac{1}{\sqrt{2}}\mathbf{i}_y,\mathbf{i}_z\right)$-axis since the distribution was rotated about the $\left(\mathbf{i}_x,\mathbf{i}_y,0\mathbf{i}_z\right)$-axis to align the $\left(-\frac{1}{\sqrt{2}}\mathbf{i}_x,\frac{1}{\sqrt{2}}\mathbf{i}_y,\mathbf{i}_z\right)$-axis with the $\left(-\mathbf{i}_x,\mathbf{i}_y,0\mathbf{i}_z\right)$-axis. This result confirms that the distribution is uniform about the $\left(-\frac{1}{\sqrt{2}}\mathbf{i}_x,\frac{1}{\sqrt{2}}\mathbf{i}_y,\mathbf{i}_z\right)$-axis since the $BECVF^{basis}_{\left(\frac{1}{\sqrt{2}}\mathbf{i}_x,\frac{1}{\sqrt{2}}\mathbf{i}_y,\mathbf{i}_z\right)}$ that served to generate the distribution of $Y_0^0(\theta,\phi)$ is azimuthally uniform. This is an important result since the spherically uniform distribution can be obtained by normalizing the distribution given by Eq. (1.102). Since any density normalization is along the $\left(-\frac{1}{\sqrt{2}}\mathbf{i}_x,\frac{1}{\sqrt{2}}\mathbf{i}_y,\mathbf{i}_z\right)$-axis, there is no change in the angular momentum since the distribution was formed by rotation of the basis elements about the angular momentum axis, the $\left(-\frac{1}{\sqrt{2}}\mathbf{i}_x,\frac{1}{\sqrt{2}}\mathbf{i}_y,\mathbf{i}_z\right)$-axis. Furthermore, the motion on the great circles maintains the uniform distribution since the normalization only scales the constant current on each to achieve uniformity.

Consider the color-scale rendering of the BECVF current density distribution shown in Figure 1.18. It was determined using a computer algorithm [13] that assigns a given number of points to a great circle basis element of Eqs. (1.84) and (1.87), generates the BECVF distribution of points along the great circles using a designated number of rotations about the $\left(-\mathbf{i}_x,\mathbf{i}_y,0\mathbf{i}_z\right)$-axis over a span of 2π radians, and for each point on the half-sphere, it calculates the number of points in a unit circular region in the neighborhood of each point. The radius of each point's neighborhood was taken to be 100 times smaller than the radius of the half-spherical distribution.

Figure 1.18. The numerically determined current density of the BECVF given by Eqs. (1.84) and (1.87) shown with 500 points on the great circle basis element and 0.72 degree increments of θ from the perspective of looking along the z-axis.

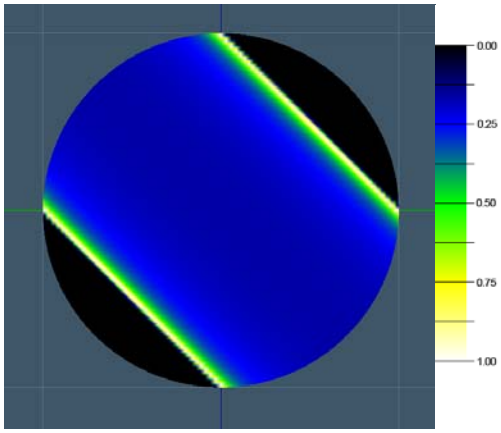

As shown in Figures 1.5 and 1.18 the great circle number of the BECVF is conserved, and the perimeter on the half sphere through which each great circle traverses can be defined by a bisecting plane that is parallel to the σ_v plane and C_2 axis. At the center of the distribution, the circles traverse a perimeter having a circumference of $2\pi r_n$. The corresponding circumference at an angle θ_{sc} from the center of the distribution is $2\pi r_n \cos\theta_{sc}$ wherein θ_{sc} is the spherical coordinate and not the rotational angle θ of the CVFs. This gives rise to a $\cos\theta_{sc}$ dependency of the loop density for $0 \le \theta_{sc} \le \frac{\pi}{4}$. In addition, the great circles converge as the perimeter becomes smaller. Since the distribution of $Y_0^0(\theta,\phi)$ is given by the superposition of the current density of the BECVF as a function of the rotation of the BECVF about the $\left(-\frac{1}{\sqrt{2}}\mathbf{i}_x, \frac{1}{\sqrt{2}}\mathbf{i}_y, \mathbf{i}_z\right)$-axis, the $Y_0^0(\theta,\phi)$ current density is given by the azimuthal integral of the current density of the BECVF. This superposition is difficult to integrate, but a convenient method of determining the density is by numerical integration. The unnormalized $Y_0^0(\theta,\phi)$ current density was determined using the computer algorithm that assigns a given number of points to each great circle basis element, generates the distribution given by Eq. (1.103), and calculates the number of points in a unit circular neighborhood of each point on the surface. The numerically determined density is shown in color scale on the sphere in Figure 1.19. The density distribution is displayed as a distance and a color scale in Figure 1.20.

Figure 1.19. The z-axis view of the numerically determined unnormalized current density of $Y_0^0(\theta,\phi)$ shown with 100 points per great circle basis element, 3.6 degree increments ($N = M = 100$ in Eq. (1.103)) of the angle to generate the BECVF corresponding to Eqs. (1.84) and (1.87), and 3.6 degree increments of the rotation of this basis element about the $\left(-\frac{1}{\sqrt{2}}\mathbf{i}_x, \frac{1}{\sqrt{2}}\mathbf{i}_y, \mathbf{i}_z\right)$-axis corresponding to Eqs. (1.95) and (1.98).

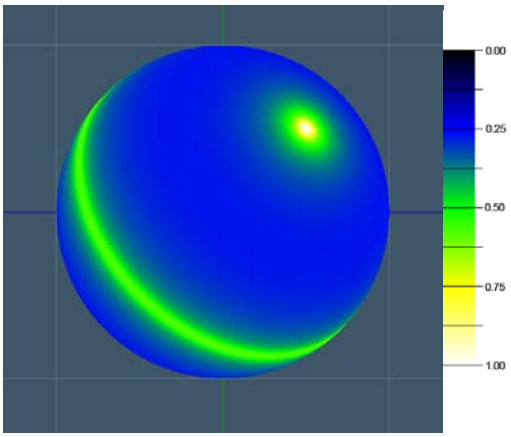

Figure 1.20. The z-axis view of the numerically determined unnormalized current density of $Y_0^0(\theta,\phi)$ wherein the density distribution is displayed as a distance and a color scale, and the view is rotated by 180° relative to Figure 1.19.

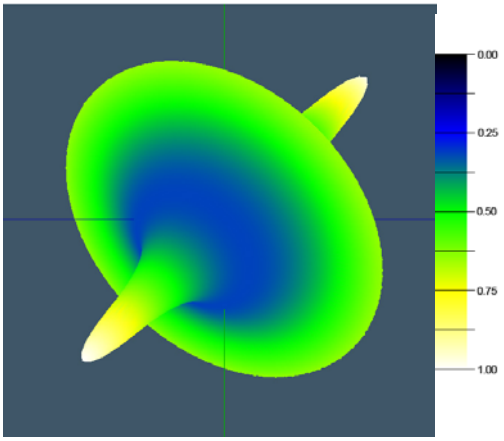

The normalization of the $Y_0^{\,0}(\theta,\phi)$ current pattern given by Eqs. (1.102) and (1.103) was performed using the numerical procedure developed by Bujnak and Hlucha [13]. It is based on forming a uniform great-circle normal-vector distribution. This is equivalent to a uniform great-circle current distribution due to the one-to-one map on the sphere between the former and latter. For a total of N_{GC} great circles distributed over the sphere, the algorithm treats the normal vector of each great circle as coincident with the corresponding angular momentum axis as given by the right hand rule and assigns a dot of integer index i to the intersection of this vector and the spherical shell. For each dot i, the number of other dots D_i within a local neighborhood of dot i are counted, and the corresponding normalization factor N_i^{factor} is given by

$$N_i^{factor} = D_i^{-1} \tag{1.117}$$

Then, the linear current density on the great circle GC_i corresponding to the dot of index i is normalized by N_i^{factor}. The program treats the linear current density as a series of evenly spaced mass(current)-density elements ("points") with the initial condition that the total number of points on each great circle is the constant P_{initial}. Thus, the normalization scales the linear density, and in the discrete case, this is achieved by scaling the mass of each of the points on the great circle by the factor given by Eq. (1.117). This is repeated over all great circles. Since $Y_0^{\,0}(\theta,\phi)$ is given by the superposition of all points, using Eq. (1.117), the final total effective or weighted number of points on the surface $P_{\text{final}}^{Y_0^{\,0}(\theta,\phi)}$ is given by the normalized sum:

$$P_{\text{final}}^{Y_0^{\,0}(\theta,\phi)} = \sum_{i=1}^{N_{GC}} N_i^{factor} P_{\text{initial}} \tag{1.118}$$

Eq. (1.118) is representative of the total mass and current on the surface. The normalization is confirmed by determining the existence of a constant current density at multiple random positions on the sphere. Here, for any point that defines a position on the sphere of integer index k, the factor N_j^{factor} of the other points of integer index j within a local neighborhood of fixed area of position k are counted, and uniformity is confirmed when the following condition is met over many cases:

$$\sum_j N_j^{factor} = \text{constant} \tag{1.119}$$

where j runs through the points in the small circular neighborhood.

The angular momentum components corresponding to the unnormalized and normalized distributions were calculated numerically. According to the numerical algorithm, the total magnitude of the angular momentum over all of the great circles is set equal to $\hbar$ with the initial direction due to the great circle basis element in the y'z'-plane along the $(-1,0,0)$-axis. Then, in the unnormalized case, the magnitude of the contribution from each great circle is given by:

$$\left|L_i\right| = \frac{\hbar}{\sum_{j=1}^{N_{GC}} 1} = \frac{\hbar}{N_{GC}} \tag{1.120}$$

Since the direction of the angular momentum of the other great circles of the distribution are given by $R\left(\theta_i^{BECVF},\theta_i^{OCVF}\right)$, the rotation by the two angles $\theta_i^{BECVF},\theta_i^{OCVF}$ corresponding to the convolution of the respective CVFs, the total angular momentum L_{Total} is given by:

$$L_{Total} = \sum_i^{N_{GC}} L_i = \sum_i^{N_{GC}} \frac{\hbar}{N_{GC}} R\left(\theta_i^{BECVF},\theta_i^{OCVF}\right)\cdot(-1,0,0) \tag{1.121}$$

In the normalized case, the magnitude of the contribution from each great circle is given by:

$$\left|L_i\right| = \frac{N_i^{factor}\hbar}{\sum_{j=1}^{N_{GC}} N_j^{factor}} \tag{1.122}$$

Then, the total angular momentum L_{Total} is given by:

$$L_{Total} = \sum_i^{N_{GC}} L_i = \sum_i^{N_{GC}} \frac{N_i^{factor}\hbar}{\sum_{j=1}^{N_{GC}} N_j^{factor}} R\left(\theta_i^{BECVF},\theta_i^{OCVF}\right)\cdot(-1,0,0) \tag{1.123}$$

In both cases, the calculated results are given as follows:

$$\begin{aligned} L_x^{total} &\sim -0.248\hbar \sim -\frac{\hbar}{4} \\ L_y^{total} &\sim 0.248\hbar \sim \frac{\hbar}{4} \\ L_z^{total} &\sim 0.35\hbar \sim \frac{\hbar}{2\sqrt{2}} \end{aligned} \tag{1.124}$$

$$\left|L_{xyTotal}\right| = \sqrt{\left(L_x^{total}\right)^2 + \left(L_y^{total}\right)^2} \sim 0.35\hbar \sim \frac{\hbar}{2\sqrt{2}} \tag{1.125}$$

$$\left|L_{Total}\right| = \sqrt{\left(L_x^{total}\right)^2 + \left(L_y^{total}\right)^2 + \left(L_z^{total}\right)^2} \sim 0.495\hbar \sim \frac{\hbar}{2} \tag{1.126}$$

These results confirm that the normalization does not affect the angular momentum. The numerically normalized $Y_0^0(\theta,\phi)$ (Figure 1.21) gives the desired spherical uniformity and is permissive of demonstrating the motion of the current in time over the entire surface according to the great circle pattern having constant current per loop each weighted by the normalization algorithm. An ideal representation overlaid with the great-circle pattern showing the vector direction of the current is shown in Figure 1.22.

Figure 1.21. The z-axis view of the numerically normalized current density of $Y_0^0(\theta,\phi)$ shown with 100 points per great circle basis element, 3.6 degree increments ($N = M = 100$ in Eq. (1.103)) of the angle to generate the BECVF corresponding to Eqs. (1.84) and (1.87), and 3.6 degree increments of the rotation of this basis element about the $\left(-\frac{1}{\sqrt{2}}\mathbf{i}_x, \frac{1}{\sqrt{2}}\mathbf{i}_y, \mathbf{i}_z\right)$-axis corresponding to Eqs. (1.95) and (1.98). As the number of points increased and the size of the local neighborhood decreased, the exact uniformity was numerically approached.

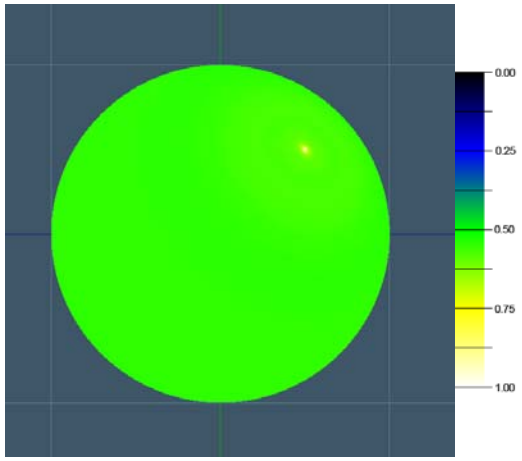

Figure 1.22. An ideal representation of the uniform current pattern of $Y_0^0(\theta,\phi)$ comprising the superposition of an infinite number of great circle elements generated by normalizing the distribution of Eqs. (1.102) and (1.103). The constant uniform current density is overlaid with 144 vectors giving the direction of the current of each great circle element for 30 degree increments ($N = M = 12$ in Eq. (1.103)) of the angle to generate the BECVF corresponding to Eqs. (1.84) and (1.87) and 30 degree increments of the rotation of this basis element about the $\left(-\frac{1}{\sqrt{2}}\mathbf{i}_x, \frac{1}{\sqrt{2}}\mathbf{i}_y, \mathbf{i}_z\right)$-axis corresponding to Eqs. (1.95) and (1.98). The perspective is along the $\left(-\frac{1}{\sqrt{2}}\mathbf{i}_x, \frac{1}{\sqrt{2}}\mathbf{i}_y, \mathbf{i}_z\right)$-axis.

The electron current shown in Figure 1.22 is consistent with Maxwell's equations, other first principles, and the boundary conditions implied by the Stern Gerlach experiment. The crossings reveal an intrinsic property regarding self-interactions of fundamental particles having angular momentum, mass, and an extended nature. Extrinsic fundamental particle scattering interactions depend on the cross section for momentum or energy transfer. These cross sections can vary over an enormous range. Neutrinos and neutrons, for example, have negligible cross sections with condensed matter compared to charged particles. The cross section for interaction amongst photons or field lines within a single photon is zero. The electron is an indivisible special state of a 510 keV photon, and the cross section for momentum transfer amongst current elements of the electron is likewise experimentally zero. This is consistent with the original boundary condition that momentum transfer among fundamental particles having $\hbar$ of angular momentum occurs in quantized units of $\hbar$ requiring that electron momentum transfer must involve its intrinsic angular momentum in its entirety as discussed in Appendix II[7]. Computer modeling of the analytical equations to generate the atomic orbital current vector field and the uniform current (charge) density function $Y_0^0(\theta,\phi)$ is available on the web [13-14]. Also, the precession motion of the free electron over time in the presence of an applied magnetic field generates the equivalent current pattern and the angular momentum of $Y_0^0(\theta,\phi)$ of the bound electron as shown in the Electron in Free Space section and Appendix IV. Given the angular momentum projections of the bound electron shown in Figure 1.23 and that the free electron has $\hbar$ of angular momentum on the z-axis due to in-plane current loops, the free-electron

[7] The angular momentum of neutrinos are $\frac{\hbar}{2}$ which accounts for their negligible interaction cross section as discussed in the Neutrinos section.

angular momentum can be considered to partition into two orthogonal, equal magnitude components of $\frac{\hbar}{2\sqrt{2}}$ and the current, carried on great circle elements, to rescale to form a uniform density due to binding to the central field.

SPIN ANGULAR MOMENTUM OF THE ATOMIC ORBITAL $Y_0^0(\theta,\phi)$ WITH $\ell = 0$

Consider the vector current directions shown in Figure 1.8. The orthogonal great-circle basis set is rotated about the $\left(-\frac{1}{\sqrt{2}}\mathbf{i}_x,\frac{1}{\sqrt{2}}\mathbf{i}_y,\mathbf{i}_z\right)$-axis. The resultant angular momentum vector is along this axis. Thus, the resultant angular momentum vector of magnitude $\frac{\hbar}{2}$ is stationary throughout the rotations that transform the axes as given in Table 1.1. The convolution operation of the BECVF with the OCVF is also about the resultant angular momentum axis, the $\left(-\frac{1}{\sqrt{2}}\mathbf{i}_x,\frac{1}{\sqrt{2}}\mathbf{i}_y,\mathbf{i}_z\right)$-axis. Here, the resultant angular momentum vector of the one BECVF of $\frac{\hbar}{\sqrt{2}}$ in the direction of the $\left(-\mathbf{i}_x,\mathbf{i}_y,0\mathbf{i}_z\right)$-axis over a 2π span is matched to and replaces that of the basis element great circles. Thus, the resultant angular momentum of $\frac{\hbar}{2}$ having components of $\mathbf{L}_{xy}=\frac{\hbar}{2\sqrt{2}}$ and $\mathbf{L}_z=\frac{\hbar}{2\sqrt{2}}$ is stationary on this axis for all rotations. There is no alteration of the angular momentum with normalization since it only affects the density parallel to the angular momentum axis of the distribution, the $\left(-\frac{1}{\sqrt{2}}\mathbf{i}_x,\frac{1}{\sqrt{2}}\mathbf{i}_y,\mathbf{i}_z\right)$-axis. This was proven by numerical integration of the normalized distribution.

Next, it is shown that the properties of $Y_0^0(\theta,\phi)$ match the boundary conditions of having the desired angular momentum components, coverage, element motion, and uniformity by designating the $\left(-\frac{1}{\sqrt{2}}\mathbf{i}_x,\frac{1}{\sqrt{2}}\mathbf{i}_y,\mathbf{i}_z\right)$-axis as the z-axis. The resulting reoriented initial angular momentum component vectors and their new projections relative to the laboratory Cartesian coordinates are shown in Figure 1.23.

Figure 1.23. With the application of a magnetic field the magnetic moment corresponding to the intrinsic angular momentum of the electron of $\frac{\hbar}{2}$ aligns with the applied field direction designated the z-axis. Thus, the resultant angular momentum initially along the $\left(-\frac{1}{\sqrt{2}}\mathbf{i}_x,\frac{1}{\sqrt{2}}\mathbf{i}_y,\mathbf{i}_z\right)$-axis aligns with the z-axis. The new projections relative to the Cartesian coordinates are shown.

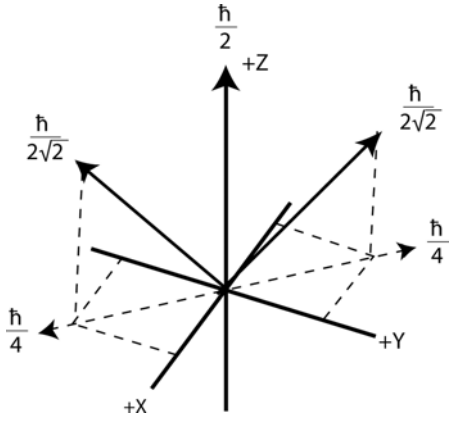

Referring to the new coordinates, the new angular momentum components are $\frac{\hbar}{2}$ along the z-axis, $\frac{\hbar}{2\sqrt{2}}$ along the $\left(\frac{1}{\sqrt{2}}\mathbf{i}_x,-\frac{1}{\sqrt{2}}\mathbf{i}_y,\mathbf{i}_z\right)$ and $\left(-\frac{1}{\sqrt{2}}\mathbf{i}_x,\frac{1}{\sqrt{2}}\mathbf{i}_y,\mathbf{i}_z\right)$-axes, and the xy-plane projections of the latter of $+/-\frac{\hbar}{4}$ along the $\left(\mathbf{i}_x,-\mathbf{i}_y,0\mathbf{i}_z\right)$-axis. (Note that the crossed vectors in Figure 1.22 are the source of the orthogonal components of $\frac{\hbar}{2\sqrt{2}}$.) Then, the Zeeman-splitting-active vector projections of the angular momentum that give rise to the Stern Gerlach phenomenon and other aspects of spin are those components that are onto the xy-plane and the z-axis.

Zeeman L Components

$$\mathbf{L}_{xy}=+/-\frac{\hbar}{4} \tag{1.127}$$

$$\mathbf{L}_{z}=\frac{\hbar}{2} \tag{1.128}$$

where $+/-$ designates both the positive and negative vector directions along an axis in the xy-plane such as the $\left(\mathbf{i}_x,-\mathbf{i}_y,0\mathbf{i}_z\right)$-axis. Consider the behavior of the electron in the presence of an applied magnetic field wherein the Zeeman-active angular momentum of $Y_0^0(\theta,\phi)$ (Figure 1.24) for a right-handed circularly polarized photon is $\mathbf{L}_{xy}=\frac{\hbar}{4}$ and $\mathbf{L}_{z}=\frac{\hbar}{2}$ (Eqs. (1.127-1.128)). As shown in the Resonant Precession of the Spin-1/2-Current-Density Function Gives Rise to the Bohr Magneton section, the electron undergoes resonant Larmor-precession excitation. The angular momentum of the photon of the Larmor excited state electrodynamically interacts with one component of $\mathbf{L}_{xy}$ depending on its handedness to establish a torque balance that results in the orientation of the $\hbar$ of angular momentum of the photon such that its vector projections are $\mathbf{L}_{xy}=\sqrt{\frac{3}{4}}\hbar$ in a Larmor rotating frame and $\mathbf{L}_{z}=\frac{\hbar}{2}$ such that the total angular momentum onto the z-axis, sum of the photon and electron contributions, is $\hbar$. These results meet the boundary condition for the unique current having an angular velocity magnitude at each point on the surface given by Eq. (1.36) and give rise to the result of the Stern Gerlach experiment as shown *infra*, in the Magnetic Parameters of the Electron (Bohr Magneton) section, and in the Electron g Factor section.

Figure 1.24. The atomic orbital is a two dimensional spherical shell of zero thickness with the Bohr radius of the hydrogen atom, $r=a_H$, having intrinsic angular momentum components of $\mathbf{L}_{xy}=\frac{\hbar}{4}$ and $\mathbf{L}_{z}=\frac{\hbar}{2}$ following Larmor excitation in a magnetic field.

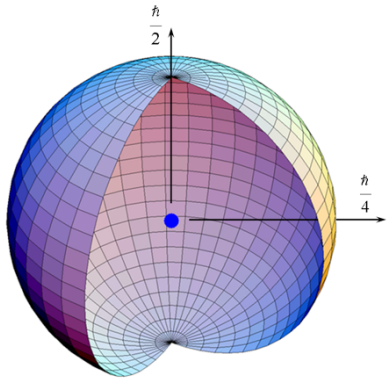

RESONANT PRECESSION OF THE SPIN-1/2-CURRENT-DENSITY FUNCTION GIVES RISE TO THE BOHR MAGNETON

The Stern Gerlach experiment described below demonstrates that the magnetic moment of the electron can only be parallel or antiparallel to an applied magnetic field. In spherical coordinates, this implies a spin quantum number of 1/2 corresponding to an angular momentum on the z-axis of $\frac{\hbar}{2}$. However, the Zeeman splitting energy corresponds to a magnetic moment of μ_B and implies an electron angular momentum on the z-axis of $\hbar$—twice that given by Eq. (1.128). Consider the case of a magnetic field applied to the atomic orbital. As shown in Figure 1.23, the atomic orbital comprises an angular momentum component of $\frac{\hbar}{2}$ along the z-axis and two $\frac{\hbar}{4}$ angular momentum components in opposite directions in the xy-plane. The magnetic moment corresponding to the angular momentum along the z-axis results in the alignment of the z-axis of the atomic orbital with the magnetic field while one of the $\frac{\hbar}{4}$ vectors in the xy-plane causes precession about the applied field. The precession arises from a Larmor excitation by a corresponding resonant photon that couples to one of the $\frac{\hbar}{4}$ angular momentum components to conserve the angular momentum of the photon such that the precession direction matches the handedness of the Larmor photon. An example given in Figure 1.25 regards a right-hand polarized photon that excites the right-handed Larmor precession by coupling to the corresponding $\frac{\hbar}{4}$ angular momentum component as shown. The precession frequency is the Larmor frequency given by the product of the gyromagnetic ratio of the electron, $\frac{e}{2m}$, and the magnetic flux $\mathbf{B}$ [15]. The energy of the precessing electron corresponds to Zeeman splitting—energy levels corresponding to the parallel or antiparallel alignment of the electron magnetic moment with the magnetic field and the excitation of transitions between these states by flipping the orientation along the field by a further resonant photon of the Larmor frequency. Thus, the energy of the transition between these states is that of the resonant photon. The angular momentum of the precessing atomic orbital comprises the initial $\frac{\hbar}{2}$ projection on the z-axis and the initial $\frac{\hbar}{4}$ vector component in the xy-plane that then precesses about the z-axis with the Larmor photon. As shown in the Excited States of the One-Electron Atom (Quantization) section, conservation of the angular momentum of the photon of $\hbar$ gives rise to $\hbar$ of electron angular momentum that gives rise to a $\frac{\hbar}{2}$ contribution to the angular momentum along the magnetic-field or z-axis. The parameters of the photon standing wave for the Zeeman effect are given in the Magnetic Parameters of the Electron (Bohr Magneton) section and Box 1.1.

The angular momentum of the atomic orbital in a magnetic field comprises the static $\frac{\hbar}{2}$ projection on the z-axis (Eq. (1.128)) and the $\frac{\hbar}{4}$ vector component in the xy-plane (Eq. (1.127)) that precesses about the z-axis at the Larmor frequency. The precession at the Larmor frequency as well as the excitation of a spin-flip transition is equivalent to the excitation of an excited state as given in the Excited States of the One-Electron Atom (Quantization) section. Consider the first resonant process. A resonant excitation of the Larmor precession frequency gives rise to a trapped photon with $\hbar$ of angular momentum along a precessing $\mathbf{S}$-axis. In the coordinate system rotating at the Larmor frequency (denoted by the axes labeled X_R, Y_R, and Z_R in Figure 1.25), the X_R-component of magnitude $\frac{\hbar}{4}$ and $\mathbf{S}$ of magnitude $\hbar$ are stationary. The $\frac{\hbar}{4}$ angular momentum along X_R with a corresponding magnetic moment of $\frac{\mu_B}{4}$ (Eq. (28) of Box 1.1) causes $\mathbf{S}$ to rotate in the Y_R Z_R-plane to an angle of $\theta = \frac{\pi}{3}$ such that the torques due to the Z_R-component of $\frac{\hbar}{2}$ and the orthogonal X_R-component of $\frac{\hbar}{4}$ are balanced. Then the Z_R-component due to $\mathbf{S}$ is $\pm\hbar\cos\frac{\pi}{3} = \pm\frac{\hbar}{2}$. The reduction of the magnitude of $\mathbf{S}$ along Z_R from $\hbar$ to $\frac{\hbar}{2}$ corresponds to the ratio of

the X_R-component and the static Z_R-component of $\frac{\frac{\hbar}{4}}{\frac{\hbar}{2}} = \frac{1}{2}$[8]. Since the X_R-component is $\frac{\hbar}{4}$, the Z_R-component of **S** is $\frac{\hbar}{2}$ which adds to the initial $\frac{\hbar}{2}$ component to give a total Z_R-component of $\hbar$.

[8] The torque balance can be appreciated by considering that **S** is aligned with Z_R if the X_R-component is zero, and the three vectors are mutually orthogonal if the X_R-component is $\frac{\hbar}{2}$. The balance can be shown by considering the magnetic energies resulting from the corresponding torques when they are balanced. Using Eqs. (23) and (25) of Box 1.1, the potential energy E_V due to the projection of **S**'s angular momentum of $\hbar$ along Z_R having $\frac{\hbar}{2}$ of angular momentum is

$$E_V = \mu_B B \cos\theta = \mu_B \frac{1}{2} B_{\mu_B} \cos\theta = \frac{1}{2}\hbar\omega_{\mu_B} \cos\theta \tag{1}$$

where B_{μ_B} is the flux due to a magnetic moment of a Bohr magneton and ω_{μ_B} is the corresponding gyromagnetic frequency. The application of a magnetic moment along the X_R-axis causes **S** to precess about the Z_R and X_R-axes. In the $X_R\,Y_R\,Z_R$-frame rotating at ω_{μ_B}, **S** precesses about the X_R-axis. The corresponding precession energy E_{X_R} of **S** about the X_R-component of $\frac{\hbar}{4}$ is the corresponding Larmor energy

$$E_{X_R} = -\frac{1}{4}\hbar\omega_{\mu_B} \tag{2}$$

The energy E_{Z_R} of the magnetic moment corresponding to **S** rotating about Z_R having $\frac{\hbar}{2}$ of angular momentum is the corresponding Larmor energy:

$$E_{Z_R} = \frac{1}{2}\hbar\omega_{\mu_B} \tag{3}$$

At torque balance, the potential energy is equal to the sum of the Larmor energies:

$$E_{Z_R} + E_{X_R} = \hbar\left(\frac{1}{2} - \frac{1}{4}\right)\omega_{\mu_B} = \frac{\hbar}{2}\left(1 - \frac{\frac{1}{4}}{\frac{1}{2}}\right)\omega_{\mu_B} = \frac{1}{2}\hbar\omega_{\mu_B}\cos\theta \tag{4}$$

Balance occurs when $\theta = \frac{\pi}{3}$. Thus, the intrinsic torques are balanced. Furthermore, energy is conserved relative to the external field as well as to the intrinsic, Z_R and X_R-components of the atomic orbital, and the Larmor relationships for both the gyromagnetic ratio and the potential energy of the resultant magnetic moment are satisfied as shown in Box 1.1.

Figure 1.25. The angular momentum components of the atomic orbital and **S** in the rotating coordinate system X_R, Y_R, and Z_R that precesses at the Larmor frequency about Z_R such that the vectors are stationary.

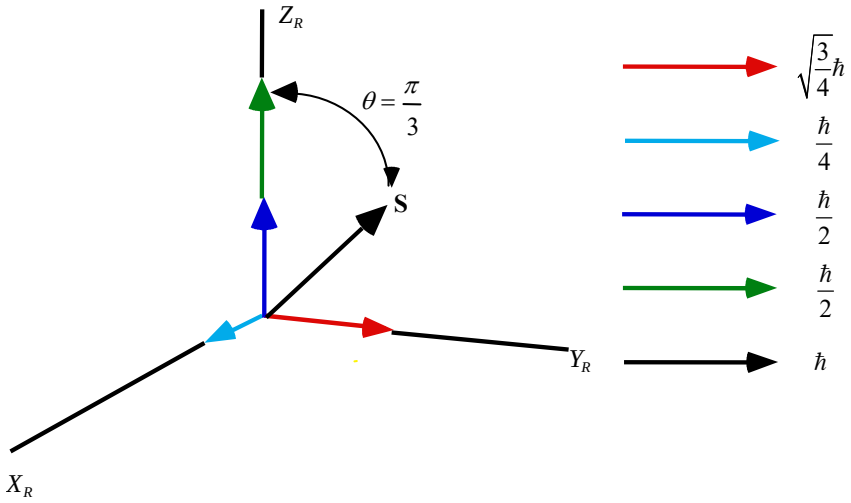

In summary, since the vector **S** that precesses about the z-axis is at an angle of $\theta = \frac{\pi}{3}$ with respect to this axis, has an $X_R\,Y_R$-plane projection at an angle of $\phi = \frac{\pi}{2}$ with respect to $\mathbf{L}_{xy}$ given by Eq. (1.127), and has a magnitude of $\hbar$, the **S** projections in the $X_R\,Y_R$-plane and along the Z_R-axis are:

$$\mathbf{S}_{\perp} = \pm\hbar \sin\frac{\pi}{3} = \pm\sqrt{\frac{3}{4}}\hbar\,\mathbf{i}_{Y_R} \tag{1.129}$$

$$\mathbf{S}_{\parallel} = \pm\hbar \cos\frac{\pi}{3} = \pm\frac{\hbar}{2}\,\mathbf{i}_{Z_R} \tag{1.130}$$

The plus or minus sign of Eqs. (1.129) and (1.130) corresponds to the two possible vector orientations which are observed with the Stern-Gerlach experiment described below. The sum of the torques in the external magnetic field is balanced unless an RF field is applied to cause a Stern-Gerlach transition as discussed in Box 1.1.

Figure 1.26. The angular momentum components of the atomic orbital and **S** in the stationary coordinate system. **S** and the components in the xy-plane precess at the Larmor frequency about the z-axis.

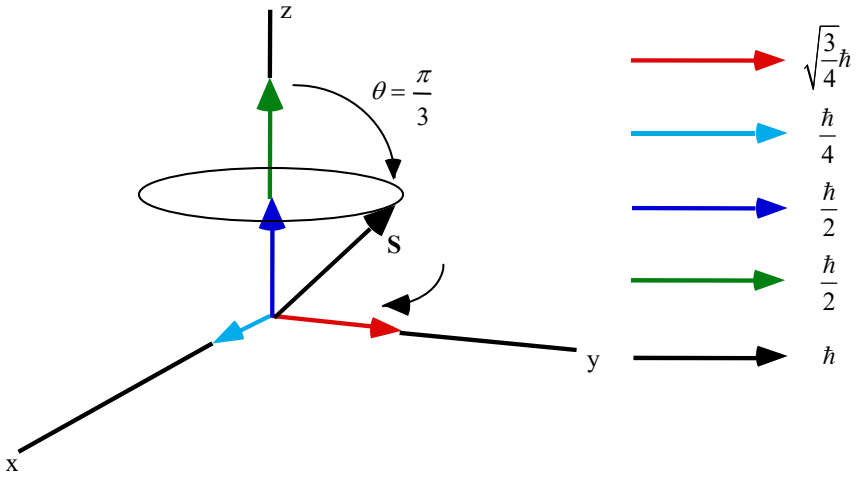

Figure 1.27. The orientation of the atomic orbital and **S** that has the angular momentum components shown in Figure 1.26. The applied magnetic field is in the z-axis direction. The dipole-current spins about the **S**-axis at angular velocity ω_n given by Eq. (1.36) and the atomic orbital and **S** precess at the Larmor frequency about the z-axis.

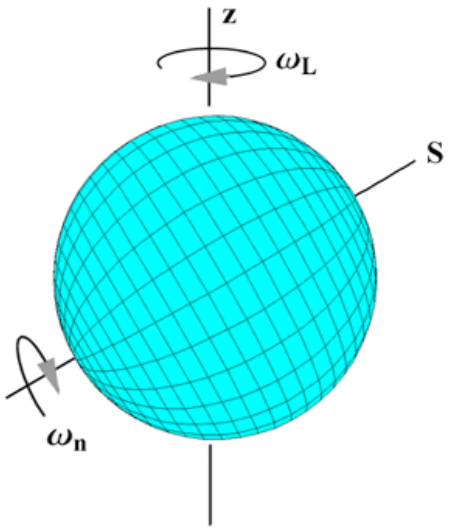

As shown in Figures 1.26 and 1.27, **S** forms a cone in time in the nonrotating laboratory frame with an angular momentum of $\hbar$ that is the source of the known magnetic moment of a Bohr magneton (Eq. (28) of 1.1) as shown in the Magnetic Parameters of the Electron (Bohr Magneton) section. The projection of this angular momentum onto the z-axis of $\frac{\hbar}{2}$ adds to the z-axis component before the magnetic field was applied to give a total of $\hbar$. Thus, in the absence of a resonant precession, the z-component of the angular momentum is $\frac{\hbar}{2}$, but the excitation of the precessing **S** component gives $\hbar$—twice the angular momentum on the z-axis. In addition, rather than a continuum of orientations with corresponding energies, the orientation of the magnetic moment must be only parallel or antiparallel to the magnetic field. This arises from conservation of angular momentum between the "static" and "dynamic" z-axis projections of the angular momentum with the additional constraint that the angular momentum has a "kinetic" as well as a "potential" or vector potential component. To conserve angular momentum, flux linkage by the electron is quantized in units of the magnetic flux quantum, $\Phi_0 = \frac{h}{2e}$, as shown in Box 1.1 and in the Electron g Factor section. Thus, the spin quantum number is $s = \frac{1}{2}$; $m_s = \pm\frac{1}{2}$, but the observed Zeeman splitting corresponds to a full Bohr magneton due to $\hbar$ of angular momentum. This aspect was historically felt to be inexplicable in terms of classical physics and merely postulated in the past.

The demonstration that the boundary conditions of the electron in a magnetic field are met appears in Box 1.1. The observed electron parameters are explained physically. Classical laws give (1) a gyromagnetic ratio of $\frac{e}{2m}$, (2) a Larmor precession frequency of $\frac{e\mathbf{B}}{2m}$, (3) the Stern-Gerlach experimental result of quantization of the angular momentum that implies a spin quantum number of 1/2 corresponding to an angular momentum of $\frac{\hbar}{2}$ on the z-axis, and (4) the observed Zeeman splitting due to a magnetic moment of a Bohr magneton $\mu_B = \frac{e\hbar}{2m_e}$ corresponding to an angular momentum of $\hbar$ on the z-axis. Furthermore, the solution is relativistically invariant as shown in the Special Relativistic Effect on the Electron Radius and the Relativistic Ionization Energies section. Dirac originally attempted to solve the bound electron physically with stability with respect to radiation according to Maxwell's equations with the further constraints that it was relativistically invariant and thus gave rise to electron spin [16]. He was unsuccessful and resorted to the current mathematical probability-wave model that has many problems as discussed in Refs. [17-18].

MAGNETIC PARAMETERS OF THE ELECTRON (BOHR MAGNETON)

THE MAGNETIC FIELD OF AN ATOMIC ORBITAL FROM SPIN

The atomic orbital with $\ell = 0$ is a shell of negative charge current comprising correlated charge motion along great circles. The superposition of the vector projection of the atomic orbital angular momentum on the z-axis is $\frac{\hbar}{2}$ with an orthogonal component of $\frac{\hbar}{4}$. As shown in the Atomic Orbital Equation of Motion For $\ell = 0$ Based on the Current Vector Field (CVF) section, the application of a magnetic field to the atomic orbital gives rise to a precessing angular momentum vector $\mathbf{S}$ directed from the origin of the atomic orbital at an angle of $\theta = \frac{\pi}{3}$ relative to the applied magnetic field. The precession of $\mathbf{S}$ with an angular momentum of $\hbar$ forms a cone in the nonrotating laboratory frame to give a perpendicular projection of $\mathbf{S}_{\perp} = \pm\sqrt{\frac{3}{4}}\hbar$ (Eq. (1.129)) and a projection onto the axis of the applied magnetic field of $\mathbf{S}_{\parallel} = \pm\frac{\hbar}{2}$ (Eq. (1.130)). The superposition of the $\frac{\hbar}{2}$ z-axis component of the atomic orbital angular momentum and the $\frac{\hbar}{2}$ z-axis component of $\mathbf{S}$ gives $\hbar$ corresponding to the observed magnetostatic electron magnetic moment of one Bohr magneton. The $\hbar$ of angular momentum along $\mathbf{S}$ has a corresponding precessing magnetic moment of 1 Bohr magneton [19]:

$$\mu_B = \frac{e\hbar}{2m_e} = 9.274\ X\ 10^{-24}\ JT^{-1} \tag{1.131}$$

The rotating magnetic field of $\mathbf{S}$ is discussed in Box 1.1. The magnetostatic magnetic field corresponding to μ_B derived below is given by

$$\mathbf{H} = \frac{e\hbar}{m_e r_n^3}(\mathbf{i}_r \cos\theta - \mathbf{i}_\theta \sin\theta) \qquad \text{for } r < r_n \tag{1.132}$$

$$\mathbf{H} = \frac{e\hbar}{2m_e r^3}(\mathbf{i}_r 2\cos\theta + \mathbf{i}_\theta \sin\theta) \qquad \text{for } r > r_n \tag{1.133}$$

It follows from Eq. (1.131), the relationship for the Bohr magneton, and relationship between the magnetic dipole field and the magnetic moment $\mathbf{m}$ [20] that Eqs. (1.132) and (1.133) are the equations for the magnetic field due to a magnetic moment of a Bohr magneton, $\mathbf{m} = \mu_B \mathbf{i}_\mathbf{z}$ where $\mathbf{i}_\mathbf{z} = \mathbf{i}_\mathbf{r}\cos\theta - \mathbf{i}_\theta \sin\theta$. Note that the magnetic field is a constant for $r < r_n$. See Figures 1.28 and 1.29. It is shown in the Magnetic Parameters of the Electron (Bohr Magneton) section that the energy stored in the magnetic field of the electron atomic orbital is

$$E_{mag,total} = \frac{\pi\mu_0 e^2\hbar^2}{m_e^2 r_1^3} \tag{1.134}$$

Figure 1.28. The two-dimensional cut-away representation of the magnetic field of an electron atomic orbital. The field is a dipole outside the atomic orbital and uniform inside the atomic orbital.

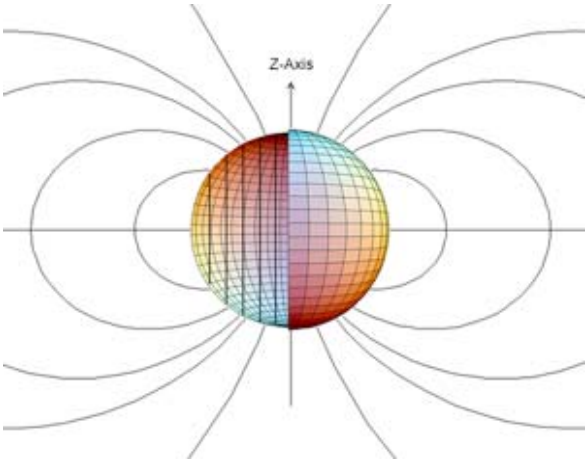

Figure 1.29. The three-dimensional cut-away representation of the magnetic field of an electron atomic orbital. The field is a dipole outside the atomic orbital and uniform inside the atomic orbital.

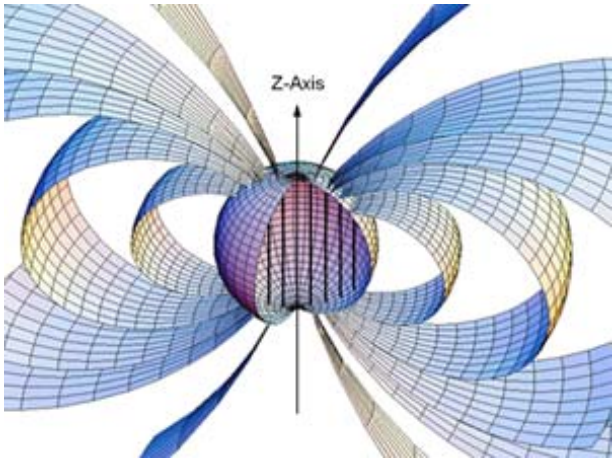

DERIVATION OF THE MAGNETIC FIELD

For convenience the angular momentum vector with a magnitude in the stationary frame of $\hbar$ will be defined as the z-axis as shown in Figures 1.28 and 1.29[9] . The magnetic field must satisfy the following relationships:

$$\nabla \cdot \mathrm{H} = 0 \textit{ in free space} \tag{1.135}$$

$$\mathbf{n}\ X\ (\mathbf{H}_a - \mathbf{H}_b) = \mathbf{K} \tag{1.136}$$

$$\mathbf{n} \cdot (\mathbf{H}_a - \mathbf{H}_b) = 0 \tag{1.137}$$

$$\mathbf{H} = -\nabla \psi \tag{1.138}$$

Since the field is magnetostatic, the current is equivalent to that of current loops extending along the z-axis with the current direction perpendicular to the z-axis. Then, the component of the current about the z-axis, $\mathbf{i}_\phi$, for a current loop of total charge, e, oriented at an angle θ with respect to the z-axis, is given by the product of the charge, the angular velocity given by Eq. (1.36), and $\sin\theta$ since the projection of the current of the atomic orbital perpendicular to the z-axis which carries the incremental current, $\mathbf{i}_\phi$, is a function of $\sin\theta$.

$$\mathbf{i}_\phi = \frac{e\hbar}{m_e {r_n}^2} \sin\theta \hat{i}_\phi \tag{1.139}$$

where $\hat{i}_\phi$ is the unit vector. The angular function of the current density of the atomic orbital is normalized by the geometrical factor N [9] given by:

$$N = \frac{4\pi r_n^3}{2\pi \int_{-r_n}^{r_n} \left(r_n^2 - z^2\right) dz} = \frac{3}{2} \tag{1.140}$$

corresponding to the angular momentum of $\hbar$. (Eq. (1.140) can also be expressed in spherical coordinates for the density of a uniform shell divided by the integral in θ and ϕ of that of a spherical dipole squared [8]. The integration gives $\frac{8\pi}{3}$ which normalized by the uniform mass-density factor of 4π gives the geometrical factor of $\left(\frac{2}{3}\right)^{-1}$.) The current density $\mathbf{K}\hat{i}_\phi$ along the z-axis having a vector orientation perpendicular to the angular momentum vector is given by dividing the magnitude of $\mathbf{i}_\phi$ (Eq. (1.139)) by the length r_n. The current density of the atomic orbital in the incremental length dz is:

$$\mathbf{K}(\rho, \phi, z)\hat{i}_\phi = \hat{i}_\phi N \frac{e\hbar}{m_e {r_n}^3} = \hat{i}_\phi \frac{3}{2} \frac{e\hbar}{m_e {r_n}^3} \tag{1.141}$$

Because

$$z = r\cos\theta \tag{1.142}$$

the differential length is given by:

$$dz = -\sin\theta r_n d\theta \tag{1.143}$$

and so the current density in the differential length $r_n d\theta$ as measured along the periphery of the atomic orbital is a function of $\sin\theta$ as given in Eq. (1.139). From Eq. (1.141), the surface current-density function of the atomic orbital about the z-axis (**S**-axis) is given by:

$$\mathbf{K}(r, \theta, \varphi)\hat{i}_\phi = \hat{i}_\phi \frac{3}{2} \frac{e\hbar}{m_e {r_n}^3} \sin\theta \tag{1.144}$$

Substitution of Eq. (1.144) into Eq. (1.136) gives:

$$H_\theta^a - H_\theta^b = \frac{3}{2} \frac{e\hbar}{m_e {r_n}^3} \sin\theta \tag{1.145}$$

---

[9] As shown in Box 1.1, the angular momentum of $\hbar$ on the **S**-axis is due to a photon standing wave that is phase-matched to a spherical harmonic source current, a spherical harmonic dipole $Y_1^m(\theta, \phi) = \sin\theta$ with respect to the **S**-axis. The dipole spins about the **S**-axis at the angular velocity given by Eq. (1.36). Since the field is magnetostatic in the RF rotating frame, the current is equivalent to current loops along the **S**-axis. Thus, the derivation of the corresponding magnetic field is the same as that of the stationary field given in this section.

To obtain H_θ, the derivative of ψ with respect to θ must be taken, and this suggests that the θ dependence of ψ be taken as $\cos\theta$. The field is finite at the origin and is zero at infinity; so, solutions of Laplace's equation in spherical coordinates are selected because they are consistent with these conditions [21].

$$\Psi = C\left[\frac{r}{r_n}\right]\cos\theta \ ; \qquad r < r_n \tag{1.146}$$

$$\Psi = A\left[\frac{r_n}{r}\right]^2\cos\theta \ ; \qquad r > r_n \tag{1.147}$$

The negative gradients of these potentials are

$$\mathbf{H} = \frac{-C}{r_n}(\mathbf{i}_r\cos\theta - \mathbf{i}_\theta\sin\theta) \quad \text{for } r < r_n \tag{1.148}$$

$$\mathbf{H} = \frac{A}{r_n}\left[\frac{r_n}{r}\right]^3(\mathbf{i}_r 2\cos\theta + \mathbf{i}_\theta\sin\theta) \quad \text{for } r > r_n \tag{1.149}$$

where $\mathbf{i}_r$ and $\mathbf{i}_\theta$ are unit vectors. The continuity conditions of Eqs. (1.136), (1.137), (1.144), and (1.145) are applied to obtain the following relationships among the variables:

$$\frac{-C}{r_n} = \frac{2A}{r_n} \tag{1.150}$$

$$\frac{A}{r_n} - \frac{C}{r_n} = \frac{3}{2}\frac{e\hbar}{m_e r_n^3} \tag{1.151}$$

Solving the variables algebraically gives the magnetic fields of an electron:

$$\mathbf{H} = \frac{e\hbar}{m_e r_n^3}(\mathbf{i}_r\cos\theta - \mathbf{i}_\theta\sin\theta) \qquad \text{for } r < r_n \tag{1.152}$$

$$\mathbf{H} = \frac{e\hbar}{2m_e r^3}(\mathbf{i}_r 2\cos\theta + \mathbf{i}_\theta\sin\theta) \quad \text{for } r > r_n \tag{1.153}$$

The field is that of a Bohr magneton which matches the observed boundary conditions given in the Atomic Orbital Equation of Motion For ℓ = 0 Based on the Current Vector Field (CVF) section including the required spherical symmetry. The demonstration that the boundary conditions of the electron in a magnetic field are met appears in Box 1.1.

DERIVATION OF THE ENERGY

The energy stored in the magnetic field of the electron is:

$$E_{mag} = \frac{1}{2}\mu_0\int_0^{2\pi}\int_0^{\pi}\int_0^{\infty} H^2 r^2\sin\theta dr d\theta d\Phi \tag{1.154}$$

$$E_{mag\ \text{total}} = E_{mag\ \text{external}} + E_{mag\ \text{internal}} \tag{1.155}$$

$$E_{mag\ \text{internal}} = \frac{1}{2}\mu_0\int_0^{2\pi}\int_0^{\pi}\int_0^{r_1}\left[\frac{e\hbar}{m_e r_1^3}\right]^2\left(\cos^2\theta + \sin^2\theta\right)r^2\sin\theta dr d\theta d\Phi \tag{1.156}$$

$$E_{mag\ \text{internal}} = \frac{2\pi\mu_0 e^2\hbar^2}{3m_e^2 r_1^3} \tag{1.157}$$

$$E_{mag\ \text{external}} = \frac{1}{2}\mu_0\int_0^{2\pi}\int_0^{\pi}\int_{r_1}^{\infty}\left[\frac{e\hbar}{2m_e r_1^3}\right]^2\left(4\cos^2\theta + \sin^2\theta\right)r^2\sin\theta dr d\theta d\Phi \tag{1.158}$$

$$E_{mag\ \text{external}} = \frac{\pi\mu_0 e^2\hbar^2}{3m_e^2 r_1^3} \tag{1.159}$$

$$E_{mag\ \text{total}} = \frac{2\pi\mu_0 e^2\hbar^2}{3m_e^2 r_1^3} + \frac{\pi\mu_0 e^2\hbar^2}{3m_e^2 r_1^3} \tag{1.160}$$

$$E_{mag\ \text{total}} = \frac{\pi\mu_0 e^2\hbar^2}{m_e^2 r_1^3} \tag{1.161}$$

$$E_{mag\ \text{total}} = \frac{4\pi\mu_0\mu_B^2}{r_1^3} \tag{1.162}$$

BOX 1.1 BOUNDARY CONDITIONS OF THE ELECTRON IN A MAGNETIC FIELD ARE MET

As shown in the Electron g Factor section, when a magnetic field with flux **B** is applied to an electron in a central field which comprises current loops, the orbital radius of each does not change due to the Lorentz force provided by **B**, but the velocity changes as follows [1]:

$$\Delta v = \frac{erB}{2m_e} \tag{1}$$

corresponding to a precession frequency of

$$\omega = \frac{\Delta v}{r} = \frac{eB}{2m_e} = \gamma_e B \tag{2}$$

where γ_e is the electron gyromagnetic ratio and ω is the Larmor frequency. Eq. (1) applies to the current perpendicular to the magnetic flux. Since the atomic orbital is a uniformly-charged spherical shell, the magnetically induced current according to Lenz' law gives rise to a corresponding moment of inertia I [2], due to circulation about the z-axis of:

$$I = \frac{2}{3} m_e r_1^2 \tag{3}$$

From Eqs. (2) and (3), the corresponding angular momentum L and rotational energy E_{rot} are:

$$L = I\omega = \frac{2}{3} m_e r_1^2 \gamma_e B \tag{4}$$

and

$$E_{rot} = \frac{1}{2} I\omega^2 = \frac{1}{3} m_e r_1^2 \left(\gamma_e B\right)^2 \tag{5}$$

respectively. The change in the magnetic moment corresponding to Eq. (1) is [1]:

$$\Delta\mathbf{m} = -\frac{e^2 r_1^2}{4m_e}\mathbf{B} \tag{6}$$

Using Eqs. (2-6), in the case of a very strong magnetic flux of 10 T applied to atomic hydrogen:

$$\omega = 8.794\ X\ 10^{11}\ rad\cdot\sec^{-1} \tag{7}$$

$$I = 1.701\ X\ 10^{-51}\ kg\cdot m^2 \tag{8}$$

$$L = 1.496\ X\ 10^{-39}\ J\cdot s \tag{9}$$

$$E_{rot} = 6.576\ X\ 10^{-28} J = 4.104\ X\ 10^{-9}\ eV \tag{10}$$

and

$$\Delta m = 1.315\ X\ 10^{-28} J\cdot T^{-1} \tag{11}$$

where the radius is given by Eq. (1.260) and $2/3$, the geometrical factor of a uniformly charged spherical shell [2], was used in the case of Eq. (11). Thus, these effects of the magnetic field are very small when they are compared to the intrinsic angular momentum of the electron of

$$L = \hbar = 1.055\ X\ 10^{-34}\ J\cdot s \tag{12}$$

The electronic angular frequency of hydrogen given by Eqs. (1.36) and (1.260)

$$\omega_1 = \frac{\hbar}{m_e r_1^2} = 4.134\ X\ 10^{16}\ rad\cdot\sec^{-1} \tag{13}$$

the total kinetic energy given by Eq. (1.262)

$$T = 13.606\ eV \tag{14}$$

and the magnetic moment of a Bohr magneton given by Eq. (1.131)

$$\mu_B = \frac{e\hbar}{2m_e} = 9.274\ X\ 10^{-24}\ JT^{-1} \tag{15}$$

E_{rot} is the energy that arises due to the application of the external flux **B**. Thus, the external work required to apply the field is also given by Eq. (10). Since the atomic orbital is uniformly charged and is superconducting, this energy is conserved when the field is removed. It is also independent of the direction of the magnetic moment due to the intrinsic angular momentum of the atomic orbital of $\hbar$. The corresponding magnetic moment given by Eq. (6) does not change when the intrinsic magnetic moment

of the electron changes orientation. Thus, it does not contribute to the energy of a spin-flip transition observed by the Stern Gerlach experiment. It always opposes the applied field and gives rise to the phenomenon of the diamagnetic susceptibility of materials which Eq. (6) predicts with very good agreement with observations [1]. Eq. (6) also predicts the absolute chemical shifts of hydride ions that match experimental observations as shown in the Hydrino Hydride Ion Nuclear Magnetic Resonance Shift section.

As shown in the Spin Angular Momentum of the Atomic Orbital $Y_0^0(\theta,\phi)$ with $\ell = 0$ section, the angular momentum of the atomic orbital in a magnetic field comprises the initial $\frac{\hbar}{2}$ projection on the z-axis and the initial $\frac{\hbar}{4}$ vector component in the xy-plane that precesses about the z-axis. A resonant excitation of the Larmor precession frequency gives rise to an additional component of angular momentum, which is consistent with Maxwell's equations. As shown in the Excited States of the One-Electron Atom (Quantization) section, conservation of the $\hbar$ of angular momentum of a trapped photon can give rise to $\hbar$ of electron angular momentum along the **S**-axis. The photon standing waves of excited states are spherical harmonic functions which satisfy Laplace's equation in spherical coordinates and provide the force balance for the corresponding charge (mass)-density waves. Consider the photon in the case of the precessing electron with a Bohr magneton of magnetic moment along the **S**-axis. The radius of the atomic orbital is unchanged, and the photon gives rise to current on the surface that satisfies the condition

$$\nabla \cdot J = 0 \tag{16}$$

corresponding to a rotating spherical harmonic dipole [3] that phase-matches the current (mass) density of Eq. (1.144). Thus, the electrostatic energy is constant, and only the magnetic energy need be considered as given by Eqs. (23-25). The corresponding central field at the atomic orbital surface given by the superposition of the central field of the proton and that of the photon follows from Eqs. (2.10-2.17):

$$\mathbf{E} = \frac{e}{4\pi\varepsilon_0 r^2}\left[Y_0^0(\theta,\phi)\mathbf{i}_\mathbf{r} + \mathrm{Re}\left\{Y_\ell^m(\theta,\phi)e^{im\omega_n t}\right\}\mathbf{i}_\mathbf{y}\delta(r-r_1)\right] \tag{17}$$

where the spherical harmonic dipole $Y_\ell^m(\theta,\phi) = \sin\theta$ is with respect to the **S**-axis. Force balance according to Eq. (1.253) is maintained by the equivalence of the harmonic modulation of the charge and the mass where e/m_e is invariant as given in the Special Relativistic Effect on the Electron Radius and the Relativistic Ionization Energies section. The dipole spins about the **S**-axis at the angular velocity given by Eq. (1.36). In the frame rotating about the **S**-axis, the electric field of the dipole is

$$\mathbf{E} = \frac{e}{4\pi\varepsilon_0 r^2}\sin\theta\sin\varphi\delta(r-r_1)\mathbf{i}_\mathbf{y} \tag{18}$$

$$\mathbf{E} = \frac{e}{4\pi\varepsilon_0 r^2}\left(\sin\theta\sin\phi\mathbf{i}_\mathbf{r} + \cos\theta\sin\phi\mathbf{i}_\theta + \sin\theta\cos\phi\mathbf{i}_\phi\right)\delta(r-r_1) \tag{19}$$

The resulting current is nonradiative as shown in Appendix I: Nonradiation Condition. Thus, the field in the RF rotating frame is magnetostatic as shown in Figures 1.28 and 1.29 but directed along the **S**-axis. The time-averaged angular momentum and rotational energy due to the charge density wave are zero as given by Eqs. (1.76) and (1.77). However, the corresponding time-dependent surface charge density $\langle\sigma\rangle$ that gives rise to the dipole current of Eq. (1.144) as shown by Haus [4] is equivalent to the current due to a uniformly charged sphere rotating about the **S**-axis at the constant angular velocity given by Eq. (1.36). The charge density is given by Gauss' law at the two-dimensional surface:

$$\sigma = -\varepsilon_0\mathbf{n}\cdot\nabla\Phi|_{r=r_1} = -\varepsilon_0\mathbf{n}\cdot\mathbf{E}|_{r=r_1} \tag{20}$$

From Eq. (19), $\langle\sigma\rangle$ is

$$\langle\sigma\rangle = \frac{e}{4\pi r_1^2}\frac{3}{2}\sin\theta \tag{21}$$

and the current (Eq. (1.144)) is given by the product of Eq. (21) and the constant angular frequency (Eq. (1.36)). The precession of the magnetostatic dipole results in magnetic dipole radiation or absorption during a Stern-Gerlach transition. The application of a magnetic field causes alignment of the intrinsic electron magnetic moment of atoms of a material such that the population of electrons parallel versus antiparallel is a Boltzmann distribution, which depends on the temperature of the material. Following the removal of the field, the original random-orientation distribution is restored as is the original temperature. The distribution may be altered by the application of an RF pulse at the Larmor frequency.

The application of a magnetic field with a resonant Larmor excitation gives rise to a precessing angular momentum vector **S** of magnitude $\hbar$ directed from the origin of the atomic orbital at an angle of $\theta = \frac{\pi}{3}$ relative to the applied magnetic field. **S** rotates about the axis of the applied field at the Larmor frequency. The magnitude of the components of **S** that are parallel and orthogonal to the applied field (Eqs. (1.129-1.130)) are $\frac{\hbar}{2}$ and $\sqrt{\frac{3}{4}}\hbar$, respectively. Since both the RF field and the orthogonal components shown in Figure 1.25 rotate at the Larmor frequency, the RF field that causes a Stern Gerlach transition produces a stationary magnetic field with respect to these components as described by Patz [5].

The component of Eq. (1.130) adds to the initial $\frac{\hbar}{2}$ parallel component to give a total of $\hbar$ in the stationary frame corresponding to a Bohr magneton, μ_B, of magnetic moment. Eqs. (2) and (6) also hold in the case of the Stern Gerlach experiment. Superposition holds for Maxwell's equations, and only the angular momentum given by Eqs. (1.127-1.128) and the source current corresponding to Eq. (17) need be considered. Since it does not change, the diamagnetic component given from Eq. (1) does not contribute to the spin-flip transition as discussed *supra*. The potential energy of a magnetic moment **m** in the presence of flux **B** [6] is:

$$E = \mathbf{m} \cdot \mathbf{B} \tag{22}$$

The angular momentum of the electron gives rise to a magnetic moment of μ_B. Thus, the energy ΔE_{mag}^{spin} to switch from parallel to antiparallel to the field is given by Eq. (1.168)

$$\Delta E_{mag}^{spin} = 2\mu_{\mathbf{B}}\, \mathbf{i}_{\mathbf{z}} \cdot \mathbf{B} = 2\mu_B B \cos\theta = 2\mu_B B \tag{23}$$

In the case of an applied flux of 10 T, Eq. (23) gives:

$$\Delta E_{mag}^{spin} = 1.855\ X\ 10^{-22} J = 1.158 X\ 10^{-3} eV \tag{24}$$

ΔE_{mag}^{spin} is also given by Planck's equation. It can be shown from conservation of angular momentum considerations (Eqs. (26-32)) that the Zeeman splitting is given by Planck's equation and the Larmor frequency based on the gyromagnetic ratio (Eq. (2)). The electron's magnetic moment may only be parallel or antiparallel to the magnetic field rather than at a continuum of angles including perpendicular according to Eq. (22). No continuum of energies predicted by Eq. (22) for a pure magnetic dipole are possible. The energy difference for the magnetic moment to flip from parallel to antiparallel to the applied field is:

$$\Delta E_{mag}^{spin} = 2\hbar\omega = 1.855\ X\ 10^{-22} J = 1.158 X\ 10^{-3} eV \tag{25}$$

corresponding to magnetic dipole radiation.

As demonstrated in the Atomic Orbital Equation of Motion For ℓ = 0 Based on the Current Vector Field (CVF) section, $\frac{\hbar}{2}$ of the atomic orbital angular momentum designated the static component is initially parallel to the field. An additional $\frac{\hbar}{2}$ parallel component designated the dynamic component comes from the $\hbar$ of angular momentum along **S**. The angular momentum in the presence of an applied magnetic field is [7]

$$\mathbf{L} = \mathbf{r} \times (m_e \mathbf{v} + e\mathbf{A}) \tag{26}$$

where **A** is the vector potential evaluated at the location of the atomic orbital. The circular integral of **A** is the flux linked by the electron. During a Stern-Gerlach transition a resonant RF photon is absorbed or emitted, and the $\hbar$ component along **S** reverses direction. It is shown by Eqs. (29-32) that the dynamic parallel component of angular momentum corresponding to the vector potential due to the lightlike transition is equal to the "kinetic angular momentum" $(\mathbf{r} \times m\mathbf{v})$ of $\frac{\hbar}{2}$. Conservation of angular momentum of the atomic orbital requires that the static angular momentum component concomitantly flips. The static component of angular momentum undergoes a spin flip, and concomitantly the "potential angular momentum" $(\mathbf{r} \times e\mathbf{A})$ of the dynamic component must change by $-\frac{\hbar}{2}$ due to the linkage of flux by the electron such that the total angular momentum is conserved.

In spherical coordinates, the relationship between the vector potential **A** and the flux **B** is

$$2\pi r A = \pi r^2 B \tag{27}$$

Eq. (27) can be substituted into Eq. (26) since the magnetic moment m is given [6] as:

$$m = \frac{\text{charge} \cdot \text{angular momentum}}{2 \cdot \text{mass}} \tag{28}$$

and the corresponding energy is consistent with Eqs. (23) and (25) in this case as follows:

$$\Delta \mathbf{m} = -\frac{e(\mathbf{r} \times e\mathbf{A})}{2m_e} = \frac{e\frac{\hbar}{2}}{2m_e} = \frac{\mu_B}{2}\mathbf{i}_z \tag{29}$$

The boundary condition that the angular momentum is conserved is shown by Eqs. (1.165-1.167). It can be shown that Eq. (29) is also consistent with the vector potential along the axis of the applied field [8] given by:

$$\mathbf{A} = \cos\frac{\pi}{3}\mu_0 \frac{e\hbar}{2m_e r^2}\sin\theta \mathbf{i}_\phi = \mu_0 \frac{1}{2}\frac{e\hbar}{2m_e r^2}\sin\theta \mathbf{i}_\phi \tag{30}$$

Substitution of Eq. (30) into Eq. (29) gives:

$$\Delta \mathbf{m} = -\frac{e(\mathbf{r} \times e\mu_0 \frac{1}{2}\frac{e\hbar}{2m_e r^2}\sin\theta \mathbf{i}_\phi)}{2m_e}\mathbf{i}_z = -\frac{1}{2}\left[\frac{\mu_0 e^2}{2m_e r}\right]\frac{e\hbar}{2m_e}\mathbf{i}_z \tag{31}$$

with the geometrical factor of $2/3$ [2] and the current given by Eq. (1.144). Since k is the lightlike k^0, then $k = \omega_n / c$ corresponding to the RF photon field. The relativistic corrections of Eq. (31) are given by Eqs. (1.250) and (1.251) and the relativistic radius $r = \lambda\!\!\!^{-}_c$ given by Eq. (1.249). The relativistically corrected Eq. (31) is:

$$\Delta \mathbf{m} = -\frac{1}{2}(2\pi\alpha)^{-1}\left[\frac{\mu_0 e^2}{2m_e \alpha a_0}\right]\frac{e\hbar}{2m_e} = \frac{\mu_B}{2}\mathbf{i}_z \tag{32}$$

The magnetic flux of the electron is given by:

$$\nabla \times \mathbf{A} = \mathbf{B} \tag{33}$$

Substitution of Eq. (30) into Eq. (33) gives 1/2 the flux of Eq. (1.153).

From Eq. (28), the $\frac{\hbar}{2}$ of angular momentum before and after the field is applied corresponds to an initial magnetic moment on the applied-field-axis of $\frac{\mu_B}{2}$. After the field is applied, the contribution of $\frac{\mu_B}{2}$ from Eq. (29) with Eq. (27) gives a total magnetic moment along the applied-field-axis of μ_B, a Bohr magneton, wherein the additional contribution (Eq. (28)) arises from the angular momentum of $\hbar$ on the $\mathbf{S}$-axis. Thus, even though the magnitude of the vector projection of the angular momentum of the electron in the direction of the magnetic field is $\frac{\hbar}{2}$, the magnetic moment corresponds to $\hbar$ due to the $\frac{\hbar}{2}$ contribution from the dynamic component, and the quantized transition is due to the requirement of angular momentum conservation as given by Eq. (28).

Eq. (22) implies a continuum of energies; whereas, Eq. (29) shows that the static-kinetic and dynamic vector potential components of the angular momentum are quantized at $\frac{\hbar}{2}$. Consequently, as shown in the Electron g Factor section, the flux linked during a spin transition is quantized as the magnetic flux quantum:

$$\Phi_0 = \frac{h}{2e} \tag{34}$$

Only the states corresponding to:

$$m_s = \pm\frac{1}{2} \tag{35}$$

are possible due to conservation of angular momentum. It is further shown using the Poynting power vector with the requirement that flux is linked in units of the magnetic flux quantum, that the factor 2 of Eqs. (23) and (25) is replaced by the electron g factor.

Thus, in terms of flux linkage, the electron behaves as a superconductor with a weak link [9] as described in the Josephson Junction, Weak Link section and the Superconducting Quantum Interference Device (SQUID) section. Consider the case of a current loop with a weak link comprising a large number of superconducting electrons (e.g. 10^{10}). As the applied field increases, the Meissner current increases. In equilibrium, a dissipationless supercurrent can flow around the loop driven by the difference between the flux Φ that threads the loop and the external flux Φ_x applied to the loop. Based on the physics of the electrons carrying the supercurrent, when the current reaches the critical current, the kinetic angular momentum change of $\frac{\hbar}{2}$ equals the magnitude of the potential angular momentum change corresponding to the vector potential according to Eqs. (26) and (31). As a consequence, the flux is linked in units of the magnetic flux quantum as shown in the Electron g Factor section.

REFERENCES

1. E. M. Purcell, *Electricity and Magnetism*, McGraw-Hill, New York, (1965), pp. 370-379.
2. G. R. Fowles, *Analytical Mechanics*, Third Edition, Holt, Rinehart, and Winston, New York, (1977), p. 196.
3. J. D. Jackson, *Classical Electrodynamics*, Second Edition, John Wiley & Sons, New York, (1975), pp. 84-102; 752-763.
4. H. A. Haus, J. R. Melcher, "Electromagnetic Fields and Energy," Department of Electrical Engineering and Computer Science, Massachusetts Institute of Technology, (1985), Sec. 8.6.
5. S. Patz, Cardiovasc. Interven. Radiol., (1986), 8:25, pp. 225-237.
6. D. A. McQuarrie, *Quantum Chemistry*, University Science Books, Mill Valley, CA, (1983), pp. 238-241.
7. E. M. Purcell, *Electricity and Magnetism*, McGraw-Hill, New York, (1965), p. 447.
8. E. M. Purcell, *Electricity and Magnetism*, McGraw-Hill, New York, (1965), pp. 361-367.
9. C. E. Gough, M. S. Colclough, E. M. Forgan, R. G. Jordan, M. Keene, C. M. Muirhead, A. I. M. Rae, N. Thomas, J. S. Abell, S. Sutton, Nature, Vol. 326, (1987), P. 855.

ELECTRON G FACTOR

As demonstrated by Purcell [15], when a magnetic field is applied to an electron in a central field which comprises a current loop, the orbital radius does not change, but the velocity changes as follows:

$$\Delta v = \frac{erB}{2m_e} \tag{1.163}$$

This corresponds to diamagnetism and gives rise to precession with a corresponding resonance as shown in Box 1.1. The angular momentum in the presence of an applied magnetic field is [15]:

$$\mathbf{L} = \mathbf{r} \times (m_e \mathbf{v} + e\mathbf{A}) \tag{1.164}$$

where $\mathbf{A}$ is the vector potential evaluated at the location of the atomic orbital. Conservation of angular momentum of the atomic orbital permits a discrete change of its "kinetic angular momentum" $(\mathbf{r} \times m\mathbf{v})$ with respect to the field of $\frac{\hbar}{2}$, and concomitantly the "potential angular momentum" $(\mathbf{r} \times e\mathbf{A})$ must change by $-\frac{\hbar}{2}$. The flux change, ϕ, of the atomic orbital for $r < r_n$ is determined as follows [15]:

$$\Delta\mathbf{L} = \frac{\hbar}{2} - \mathbf{r} \times e\mathbf{A} \tag{1.165}$$

$$= \left[\frac{\hbar}{2} - \frac{e2\pi rA}{2\pi}\right]\hat{z} \tag{1.166}$$

$$= \left[\frac{\hbar}{2} - \frac{e\phi}{2\pi}\right]\hat{z} \tag{1.167}$$

In order that the change in angular momentum, $\Delta\mathbf{L}$, equals zero, ϕ must be $\Phi_0 = \frac{h}{2e}$, the magnetic flux quantum. Thus, to conserve angular momentum in the presence of an applied magnetic field, the atomic orbital magnetic moment can be parallel or antiparallel to an applied field as observed with the Stern-Gerlach experiment, and the flip between orientations is accompanied by the "capture" of the magnetic flux quantum by the atomic orbital "coils" comprising infinitesimal loops of charge moving along geodesics (great circles). A superconducting loop with a weak link also demonstrates this effect [22].

The energy to flip the orientation of the atomic orbital due to its magnetic moment of a Bohr magneton, μ_B, is:

$$\Delta E_{mag}^{spin\ moment} = 2\mu_B B \tag{1.168}$$

where

$$\mu_B = \frac{e\hbar}{2m_e} \tag{1.169}$$

During the spin-flip transition, power must be conserved. Power flow is governed by the Poynting power theorem,

$$\nabla \bullet (\mathbf{E} \times \mathbf{H}) = -\frac{\partial}{\partial t}\left[\frac{1}{2}\mu_0 \mathbf{H} \bullet \mathbf{H}\right] - \frac{\partial}{\partial t}\left[\frac{1}{2}\varepsilon_0 \mathbf{E} \bullet \mathbf{E}\right] - \mathbf{J} \bullet \mathbf{E} \tag{1.170}$$

STORED MAGNETIC ENERGY

Energy superimposes; thus, the calculation of the spin-flip energy is determined as a sum of contributions. The energy change corresponding to the "capture" of the magnetic flux quantum is derived below. From Eq. (1.161) for one electron,

$$\int_{vol} \frac{1}{2}\mu_0 \mathbf{H} \bullet \mathbf{H} dv = E_{mag}^{fluxon} = \frac{\pi\mu_0 e^2 \hbar^2}{(m_e)^2 r_n^3} \tag{1.171}$$

is the energy stored in the magnetic field of the electron. The atomic orbital is equivalent to a Josephson junction which can trap integer numbers of fluxons where the quantum of magnetic flux is $\Phi_0 = \frac{h}{2e}$. Consider Eq. (1.171). During the flip transition a fluxon treads the atomic orbital at the speed of light; therefore, the radius of the atomic orbital in the lab frame is 2π times the relativistic radius in the fluxon frame as shown in the Special Relativistic Effect on the Electron Radius and the Relativistic Ionization Energies section. Thus, the energy of the transition corresponding to the "capture" of a fluxon by the atomic orbital, E_{mag}^{fluxon}, is:

$$E_{mag}^{fluxon} = \frac{\pi\mu_0 e^2 \hbar^2}{(m_e)^2 (2\pi r_n)^3} \tag{1.172}$$

$$= \frac{\mu_0 e^2}{4\pi^2 m_e r_n}\left(\frac{e\hbar}{2m_e}\right)\left(\frac{h}{2e\pi {r_n}^2}\right) \tag{1.173}$$

$$= \frac{\mu_0 e^2}{4\pi^2 m_e r_n} \mu_B \left(\frac{\Phi_0}{A} \right) \tag{1.174}$$

where A is the area and Φ_0 is the magnetic flux quantum.

$$E_{mag}^{fluxon} = 2\left[\frac{e^2 \mu_0}{2m_e r_n} \right] \frac{1}{4\pi^2} \mu_B B \tag{1.175}$$

where the nth fluxon treading through the area of the atomic orbital is equivalent to the applied magnetic flux. Furthermore, the term in brackets can be expressed in terms of the fine structure constant, α, as follows:

$$\frac{e^2 \mu_0}{2m_e r_n} = \frac{e^2 \mu_0 cv}{2m_e v r_n c} \tag{1.176}$$

Substitution of Eq. (1.35) gives:

$$\frac{e^2 \mu_0}{2m_e r_n} = \frac{e^2 \mu_0 cv}{2\hbar c} \tag{1.177}$$

Substitution of

$$c = \sqrt{\frac{1}{\varepsilon_0 \mu_0}} \tag{1.178}$$

and

$$\alpha = \frac{\mu_0 e^2 c}{2h} \tag{1.179}$$

gives

$$\frac{e^2 \mu_0 cv}{2\hbar c} = 2\pi\alpha \frac{v}{c} \tag{1.180}$$

The fluxon treads the atomic orbital at $v = c$ (k is the lightlike k^0, then $k = \omega_n / c$). Thus,

$$E_{mag}^{fluxon} = 2\frac{\alpha}{2\pi} \mu_B B \tag{1.181}$$

STORED ELECTRIC ENERGY

The superposition of the vector projection of the atomic orbital angular momentum on the z-axis is $\frac{\hbar}{2}$ with an orthogonal component of $\frac{\hbar}{4}$. Excitation of a resonant Larmor precession gives rise to $\hbar$ on an axis **S** that precesses about the spin axis at an angle of $\theta = \frac{\pi}{3}$. **S** rotates about the z-axis at the Larmor frequency. $\mathbf{S}_\perp$, the transverse projection, is $\pm\sqrt{\frac{3}{4}}\hbar$ (Eq. (1.129)), and $\mathbf{S}_\parallel$, the projection onto the axis of the applied magnetic field, is $\pm\frac{\hbar}{2}$ (Eq. (1.130)). As shown in the Spin Angular Momentum of the Atomic Orbital $Y_0^0(\theta,\phi)$ with $\ell = 0$ section, the superposition of the $\frac{\hbar}{2}$ z-axis component of the atomic orbital angular momentum and the $\frac{\hbar}{2}$ z-axis component of **S** gives $\hbar$ corresponding to the observed electron magnetic moment of a Bohr magneton, μ_B. The reorientation of **S** and the atomic orbital angular momentum from parallel to antiparallel due to the magnetic field applied along the z-axis gives rise to a current. The current is acted on by the flux corresponding to Φ_0, the magnetic flux quantum, linked by the electron during the transition which gives rise to a Hall voltage. The electric field corresponding to the Hall voltage corresponds to the electric power term, $\frac{\partial}{\partial t}\left[\frac{1}{2}\varepsilon_0 \mathbf{E} \bullet \mathbf{E}\right]$, of the Poynting power theorem (Eq. (1.170)).

Consider a conductor in a uniform magnetic field and assume that it carries a current driven by an electric field perpendicular to the magnetic field. The current in this case is not parallel to the electric field, but is deflected at an angle to it by the magnetic field. This is the Hall Effect, and it occurs in most conductors. A spin-flip transition is analogous to the Quantum Hall Effect given in the corresponding section wherein the applied magnetic field quantizes the Hall conductance. The current is then precisely perpendicular to the magnetic field, so that no dissipation (that is, no ohmic loss) occurs. This is seen in two-dimensional systems, at cryogenic temperatures, in quite high magnetic fields. Furthermore, the ratio of the total electric potential drop to the total current, the Hall resistance, R_H, is precisely equal to:

$$R_H = \frac{h}{ne^2} \tag{1.182}$$

The factor n is an integer in the case of the Integral Quantum Hall Effect, and n is a small rational fraction in the case of the Fractional Quantum Hall Effect. In an experimental plot [23] as the function of the magnetic field, the Hall resistance exhibits flat steps precisely at these quantized resistance values; whereas, the regular resistance vanishes (or is very small) at these Hall steps. Thus, the quantized Hall resistance steps occur for a transverse superconducting state.

Consider the case that an external magnetic field is applied along the x-axis to a two dimensional superconductor in the yz-plane which exhibits the Integral Quantum Hall Effect. (See Figure 1.30.) Conduction electrons align with the applied field in the x direction as the field permeates the material. The normal current carrying electrons experience a Lorentz force, $\mathbf{F}_L$, due to the magnetic flux. The y-directed Lorentz force on an electron having a velocity $\mathbf{v}$ in the z direction by an x-directed applied flux, **B**, is:

$$\mathbf{F}_L = e\mathbf{v}\times\mathbf{B} \tag{1.183}$$

The electron motion is a cycloid where the center of mass experiences an $\mathbf{E}\times\mathbf{B}$ drift [24]. Consequently, the normal Hall Effect occurs. Conduction electron energy states are altered by the applied field and by the electric field corresponding to the Hall Effect. The electric force, $\mathbf{F}_H$, due to the Hall electric field, $\mathbf{E}_y$, is:

$$\mathbf{F}_H = e\mathbf{E}_y \tag{1.184}$$

When these two forces are equal and opposite, conduction electrons propagate in the z direction alone. For this special case, it is demonstrated in Jackson [24] that the ratio of the corresponding Hall electric field E_H and the applied magnetic flux is:

$$E_H/B = v \tag{1.185}$$

where v is the electron velocity. And, it is demonstrated in the Integral Quantum Hall Effect section that the Hall resistance, R_H, in the superconducting state is given by:

$$R_H = \frac{h}{ne^2} \tag{1.186}$$

where n is an integer.

Figure 1.30. Coordinate system of crossed electric field, $\mathbf{E}_y$, corresponding to the Hall voltage, magnetic flux, $\mathbf{B}_x$, due to applied field, and superconducting current $\mathbf{i}_z$.

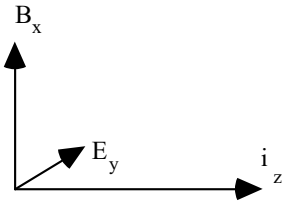

Figure 1.31. Coordinate system of crossed electric field, $\mathbf{E}_r$, corresponding to the Hall voltage, magnetic flux, $\mathbf{B}_\theta$, due to applied field, and superconducting current $\mathbf{i}_\phi$.

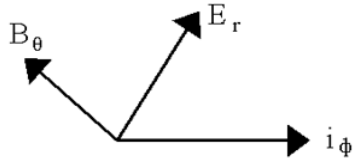

Consider the case of the spin-flip transition of the electron. In the case of an exact balance between the Lorentz force (Eq. (1.183)) and the electric force corresponding to the Hall voltage (Eq. (1.184)), each superconducting point mass-density element of the electron propagates along a great circle where

$$E/B = v \tag{1.187}$$

where v is given by Eq. (1.35). Substitution of Eq. (1.35) into Eq. (1.187) gives:

$$E/B = \frac{\hbar}{m_e r} \tag{1.188}$$

Eq. (1.185) is the condition for superconductivity in the presence of crossed electric and magnetic fields. The electric field corresponding to the Hall voltage corresponds to the electric energy term, E_{ele}, of the Poynting power theorem (Eq. (1.170)).

$$E_{ele} = \frac{1}{2}\int_0^{2\pi}\int_0^{\pi}\int_0^{r_1}\varepsilon_0\mathbf{E}\bullet\mathbf{E}r^2\sin\theta dr d\theta d\phi \tag{1.189}$$

The electric term for this superconducting state is derived as follows using the coordinate system shown in Figure 1.31.

The current is perpendicular to $\mathbf{E}_r$, thus there is no dissipation. This occurs when:

$$e\mathbf{E} = e\mathbf{v}\times\mathbf{B} \tag{1.190}$$

or

$$E/B = v \tag{1.191}$$

The electric field corresponding to the Hall voltage is:

$$\mathbf{E} = \mathbf{v}\times\mathbf{B} \tag{1.192}$$

Substitution of Eq. (1.192) into Eq. (1.189) gives:

$$E_{ele} = \frac{1}{2}\varepsilon_o \int_0^{2\pi}\int_0^{\pi}\int_0^{r_1} (vB)^2 r^2 \sin\theta dr d\theta d\phi \tag{1.193}$$

The spin flip transition may be induced by the absorption of a resonant photon. The velocity is determined from the distance traversed by each point element and the time of the transition due to capture of a photon resonant with the spin-flip transition energy. The current $\mathbf{i}_\phi$ corresponding to the Hall voltage and $\mathbf{E}_r$ is given by the product of the electron charge and the frequency f of the photon where the correspondence principle holds as given in the Photon Absorption section.

$$i = ef \tag{1.194}$$

The resistance of free space for the propagation of a photon is the radiation resistance of free space, η.

$$\eta = \sqrt{\frac{\mu_0}{\varepsilon_0}} \tag{1.195}$$

The power P_r of the electron current induced by the photon as it transitions from free space to being captured by the electron is given by the product of the corresponding current and the resistance R which is given by Eq. (1.195).

$$P_r = i^2 R \tag{1.196}$$

Substitution of Eq. (1.194) and Eq. (1.195) gives

$$P_r = e^2 f^2 \sqrt{\frac{\mu_0}{\varepsilon_0}} \tag{1.197}$$

It follows from the Poynting power theorem (Eq. (1.170)) with spherical radiation that the transition time τ is given by the ratio of the energy and the power of the transition [25].

$$\tau = \frac{energy}{power} \tag{1.198}$$

The energy of the transition, which is equal to the energy of the resonant photon, is given by Planck's equation.

$$E = \hbar\omega = hf \tag{1.199}$$

Substitution of Eq. (1.197) and Eq. (1.199) into Eq. (1.198) gives:

$$\tau = \frac{hf}{e^2 f^2 \sqrt{\frac{\mu_0}{\varepsilon_0}}} \tag{1.200}$$

The distance ℓ traversed by the electron with a kinetic angular momentum change of $\frac{\hbar}{2}$ is:

$$\ell = \frac{2\pi r}{2} = \frac{\lambda}{2} \tag{1.201}$$

where the wavelength is given by Eq. (1.15). The velocity is given by the distance traversed divided by the transition time. Eq. (1.200) and Eq. (1.201) gives:

$$v = \frac{\lambda/2}{\tau} = \frac{\lambda/2}{\dfrac{hf}{e^2 f^2 \sqrt{\frac{\mu_0}{\varepsilon_0}}}} = \frac{\sqrt{\frac{\mu_0}{\varepsilon_0}}e^2}{2h}\lambda f \tag{1.202}$$

The relationship for a photon in free space is:

$$c = \lambda f \tag{1.203}$$

As shown in the Unification of Spacetime, the Forces, Matter, and Energy section, the fine structure constant given by Eq. (1.179) is the dimensionless factor that corresponds to the relativistic invariance of charge.

$$\alpha = \frac{1}{4\pi}\sqrt{\frac{\mu_0}{\varepsilon_0}}\frac{e^2}{\hbar} = \frac{1}{2}\frac{\sqrt{\frac{\mu_0}{\varepsilon_0}}}{\frac{h}{e^2}} = \frac{\mu_0 e^2 c}{2h} \tag{1.204}$$

It is equivalent to one half the ratio of the radiation resistance of free space, $\sqrt{\frac{\mu_0}{\varepsilon_0}}$, and the Hall resistance, $\frac{h}{e^2}$. The radiation resistance of free space is equal to the ratio of the electric field and the magnetic field of the photon (Eq. (4.10)). Substitution of Eq. (1.203) and Eq. (1.204) into Eq. (1.202) gives:

$$v = \alpha c \tag{1.205}$$

Substitution of Eq. (1.205) into Eq. (1.193) gives:

$$E_{ele} = \frac{1}{2}\varepsilon_0 \int_0^{2\pi}\int_0^{\pi}\int_0^{r_1} (\alpha c \mu_0 H)^2 r^2 \sin\theta dr d\theta d\phi \tag{1.206}$$

where

$$B = \mu_0 H \tag{1.207}$$

The relationship between the speed of light, c, and the permittivity of free space, ε_0, and the permeability of free space, μ_0, is

$$c = \frac{1}{\sqrt{\mu_0 \varepsilon_0}} \tag{1.208}$$

Thus, Eq. (1.206) may be written as:

$$E_{ele} = \frac{1}{2}\alpha^2 \int_0^{2\pi}\int_0^{\pi}\int_0^{r_1} \mu_0 H^2 r^2 \sin\theta dr d\theta d\phi \tag{1.209}$$

Substitution of Eq. (1.157) gives

$$E_{ele} = \alpha^2 \frac{2\pi\mu_0 e^2 \hbar^2}{3 m_e^2 r_1^3} \tag{1.210}$$

The magnetic flux, $\mathbf{B}$, is quantized in terms of the Bohr magneton because the electron links flux in units of the magnetic flux quantum,

$$\Phi_0 = \frac{h}{2e} \tag{1.211}$$

Substitution of Eqs. (1.171-1.181) gives:

$$E_{ele} = 2\left(\frac{2}{3}\alpha^2 \frac{\alpha}{2\pi}\mu_B B\right) \tag{1.212}$$

DISSIPATED ENERGY

The $\mathbf{J} \bullet \mathbf{E}$ energy over time is derived from the electron current corresponding to the Larmor excitation and the electric field given by Faraday's law due to the linkage of the magnetic flux of the fluxon during the spin-flip. Consider the electron current due to the external field. The application of a magnetic field with a resonant Larmor excitation gives rise to a precessing angular momentum vector $\mathbf{S}$ of magnitude $\hbar$ directed from the origin of the atomic orbital at an angle of $\theta = \frac{\pi}{3}$ relative to the applied magnetic field. As given in the Spin Angular Momentum of the Atomic Orbital $Y_0^0(\theta,\phi)$ with $\ell = 0$ section, $\mathbf{S}$ rotates about the axis of the applied field at the Larmor frequency. The magnitude of the components of $\mathbf{S}$ that are parallel and orthogonal to the applied field (Eqs (1.129-1.130)) are $\frac{\hbar}{2}$ and $\sqrt{\frac{3}{4}}\hbar$, respectively. Since both the RF field and the orthogonal components shown in Figure 1.25 rotate at the Larmor frequency, the RF field that causes a Stern Gerlach transition produces a stationary magnetic field with respect to these components as described in Box 1.1. The corresponding central field at the atomic orbital surface given by the superposition of the central field of the proton and that of the photon follows from Eqs. (2.10-2.17) and Eq. (17) of Box 1.1:

$$\mathbf{E} = \frac{e}{4\pi\varepsilon_o r^2}\left[Y_0^0(\theta,\phi)\mathbf{i}_\mathbf{r} + \mathrm{Re}\left\{Y_\ell^m(\theta,\phi)e^{im\omega_n t}\right\}\mathbf{i}_\mathbf{y}\delta(r - r_1)\right] \tag{1.213}$$

where the spherical harmonic dipole $Y_\ell^m(\theta,\phi) = \sin\theta$ is with respect to the $\mathbf{S}$-axis. The dipole spins about the $\mathbf{S}$-axis at the angular velocity given by Eq. (1.36). The resulting current is nonradiative as shown in Appendix I: Nonradiation Condition. Thus, the field in the RF rotating frame is magnetostatic as shown in Figures 1.28 and 1.29 but directed along the $\mathbf{S}$-axis. Thus, the corresponding current given by Eq. (1.144) is

$$\mathbf{K}(\rho,\phi,z) = \frac{3}{2}\frac{e\hbar}{m_e r_n^3}\sin\theta \mathbf{i}_\phi \tag{1.214}$$

Next consider Faraday's equation for the electric field

$$\oint_C \mathbf{E} \bullet d\mathbf{s} = -\frac{d}{dt}\int_S \mu_0 \mathbf{H} \bullet d\mathbf{a} \tag{1.215}$$

As demonstrated by Purcell [15], the velocity of the electron changes according to Lenz's law, but the change in centrifugal force is balanced by the change in the central field due to the applied field. The magnetic flux of the electron given by Eq. (1.152) is

$$\mathbf{B} = \mu_0 \mathbf{H} = \frac{\mu_0 e\hbar}{m_e r_1^3}(\mathbf{i}_r \cos\theta - \mathbf{i}_\theta \sin\theta) \qquad \text{for } r < r_n \tag{1.216}$$

From Eq. (1.181), the magnetic flux $B_{\mathbf{J}\bullet\mathbf{E}}$ of the fluxon is:

$$\mathbf{B}_{\mathbf{J}\bullet\mathbf{E}} = \frac{\alpha}{2\pi}\frac{\mu_0 e\hbar}{m_e r_1^3}(\mathbf{i}_r \cos\theta - \mathbf{i}_\theta \sin\theta) = \frac{\alpha}{2\pi}\frac{\mu_0 e\hbar}{m_e r_1^3}\mathbf{i}_z \tag{1.217}$$

The electric field $\mathbf{E}$ is constant about the line integral of the atomic orbital. Using Eq. (1.215) with the change in flux in units of fluxons along the z-axis given by Eq. (1.217) gives:

$$\int_{-r_1}^{+r_1}\oint_C \mathbf{E}\bullet d\mathbf{s}dz = \int_{-r_1}^{+r_1} -\pi r^2 \frac{dB}{dt}dz\mathbf{i}_\phi \tag{1.218}$$

$$2\pi\ \mathbf{E}\int_0^\pi r_1 \sin^2\theta \mathrm{d}\theta\ = -\pi\frac{\Delta B}{\Delta t}r_1^2 \sin^3\theta \mathrm{d}\theta \mathbf{i}_\phi = -\pi r_1^2 \frac{2\Delta B}{3\Delta t}\mathbf{i}_\phi \tag{1.219}$$

Substitution of Eq. (1.217) into Eq. (1.219) gives:

$$\pi r_1\ \mathbf{E} = -\pi r_1^2 \frac{2}{3}\frac{\alpha}{2\pi}\frac{\mu_0 e\hbar}{m_e r_1^3 \Delta t}\mathbf{i}_\phi \tag{1.220}$$

$$\pi r_1\ \mathbf{E} = -\pi \frac{2}{3}\frac{\alpha}{2\pi}\frac{\mu_0 e\hbar}{m_e r_1 \Delta t}\mathbf{i}_\phi \tag{1.221}$$

Thus,

$$\mathbf{E} = -\frac{2}{3}\frac{\alpha}{2\pi}\frac{\mu_0 e\hbar}{m_e r_1^2 \Delta t}\mathbf{i}_\phi \tag{1.222}$$

The dissipative power density $\mathbf{E}\bullet\mathbf{J}$ can be expressed in terms of the surface current density $\mathbf{K}$ as:

$$\int_V (\mathbf{E}\bullet\mathbf{J})\Delta t dv = \int_S (\mathbf{E}\bullet\mathbf{K})\Delta t da \tag{1.223}$$

Using the electric field from Eq. (1.222) and the current density from Eq. (1.214) gives:

$$\int_V (\mathbf{E}\bullet\mathbf{J})\Delta t dv = \int_0^{2\pi}\int_0^{\pi}\left(\frac{2}{3}\frac{\alpha}{2\pi}\frac{\mu_0 e\hbar}{m_e r_1^2 \Delta t}\frac{3}{2}\frac{e\hbar}{m_e r_1^3}\sin^2\theta\right)\Delta t r_1^2 \sin\theta d\theta d\varphi = \frac{4}{3}\frac{\alpha}{2\pi}\frac{\pi\mu_0 e^2\hbar^2}{m_e^2 r_1^3} \tag{1.224}$$

Substitution of Eqs. (1.171-1.181) into Eq. (1.224) gives:

$$\int_V (\mathbf{E}\bullet\mathbf{J})\Delta t dv = 2\left(\frac{4}{3}\right)\left(\frac{\alpha}{2\pi}\right)^2 \mu_B B \tag{1.225}$$

TOTAL ENERGY OF SPIN-FLIP TRANSITION

The principal energy of the transition corresponding to a reorientation of the atomic orbital is given by Eq. (1.168). And, the total energy of the flip transition is the sum of Eq. (1.168), and Eqs. (1.181), (1.212), and (1.225) corresponding to the magnetic energy, the electric energy, and the dissipated energy of a fluxon treading the atomic orbital, respectively.

$$\Delta E_{mag}^{spin} = 2\left(1 + \frac{\alpha}{2\pi} + \frac{2}{3}\alpha^2\left(\frac{\alpha}{2\pi}\right) - \frac{4}{3}\left(\frac{\alpha}{2\pi}\right)^2\right)\mu_B B \tag{1.226}$$

$$\Delta E_{mag}^{spin} = g\mu_B B \tag{1.227}$$

where the stored magnetic energy corresponding to the $\frac{\partial}{\partial t}\left[\frac{1}{2}\mu_0 \mathbf{H}\bullet\mathbf{H}\right]$ term increases, the stored electric energy corresponding to the $\frac{\partial}{\partial t}\left[\frac{1}{2}\varepsilon_0 \mathbf{E}\bullet\mathbf{E}\right]$ term increases, and the $\mathbf{J}\bullet\mathbf{E}$ term is dissipative. The magnetic moment of Eq. (1.168) is twice that from the gyromagnetic ratio as given by Eq. (28) of Box 1.1. The magnetic moment of the electron is the sum of the component

corresponding to the kinetic angular momentum, $\frac{\hbar}{2}$, and the component corresponding to the vector potential angular momentum, $\frac{\hbar}{2}$, (Eq. (1.164)). The spin-flip transition can be considered as involving a magnetic moment of g times that of a Bohr magneton. The g factor is redesignated the fluxon g factor as opposed to the anomalous g factor, and it is given by Eq. (1.226).

$$\frac{g}{2}=1+\frac{\alpha}{2\pi}+\frac{2}{3}\alpha^2\left(\frac{\alpha}{2\pi}\right)-\frac{4}{3}\left(\frac{\alpha}{2\pi}\right)^2 \tag{1.228}$$

For $\alpha^{-1}=137.03604(11)$ [26]

$$\frac{g}{2}=1.001\ 159\ 652\ 120 \tag{1.229}$$

The experimental value [27] is:

$$\frac{g}{2}=1.001\ 159\ 652\ 188(4) \tag{1.230}$$

The calculated and experimental values are within the propagated error of the fine structure constant. Different values of the fine structure constant have been recorded from different experimental techniques, and α^{-1} depends on a circular argument between theory and experiment [28]. One measurement of the fine structure constant based on the electron g factor is $\alpha_{g_e}^{-1}=137.036006(20)$ [29]. This value can be contrasted with equally precise measurements employing solid state techniques such as those based on the Josephson effect [30] ($\alpha_J^{-1}=137.035963(15)$) or the quantized Hall effect [31] ($\alpha_H^{-1}=137.035300(400)$). A method of the determination of α^{-1} that depends on the circular methodology between theory and experiment to a lesser extent is the substitution of the independently measured fundamental constants μ_0, e, c, and h into Eq. (1.204). The following values of the fundamental constants are given by Weast [26]:

$$\mu_0=4\pi\ X\ 10^{-7}\ Hm^{-1} \tag{1.231}$$

$$e=1.6021892(46)\ X\ 10^{-19}C \tag{1.232}$$

$$c=2.99792458(12)\ X\ 10^{8}\ ms^{-1} \tag{1.233}$$

$$h=6.626176(36)\ X\ 10^{-34}\ JHz^{-1} \tag{1.234}$$

For these constants,

$$\alpha^{-1}=137.03603(82) \tag{1.235}$$

Substitution of the α^{-1} from Eq. (1.235) into Eq. (1.228) gives

$$\frac{g}{2}=1.001\ 159\ 652\ 137 \tag{1.236}$$

The experimental value [27] is

$$\frac{g}{2}=1.001\ 159\ 652\ 188(4) \tag{1.237}$$

Conversely, the fine structure calculated for the experimental $\frac{g}{2}$ and Eq. (1.228) is $\alpha^{-1}=137.036\ 032\ 081$.

The *postulated* QED theory of $\frac{g}{2}$ is based on the determination of the terms of a *postulated* power series in α/π where each *postulated* virtual particle is a source of *postulated* vacuum polarization that gives rise to a *postulated* term. The algorithm involves scores of *postulated* Feynman diagrams corresponding to thousands of matrices with thousands of integrations per matrix requiring decades to reach a consensus on the "appropriate" *postulated* algorithm to remove the intrinsic infinities. The solution so obtained using the perturbation series further requires a *postulated* truncation since the series **diverges**. The remarkable agreement between Eqs. (1.236) and (1.237) demonstrates that $\frac{g}{2}$ may be derived in closed form from Maxwell's equations in a simple straightforward manner that yields a result with eleven figure agreement with experiment—the limit of the experimental capability of the measurement of the fundamental constants that determine α. In Ref. [17], the Maxwellian result

is contrasted with the QED algorithm of invoking virtual particles, zero point fluctuations of the vacuum, and negative energy states of the vacuum. Rather than an infinity of radically different QED models, an essential feature is that *Maxwellian solutions are unique*.

The muon, like the electron, is a lepton with $\hbar$ of angular momentum. The magnetic moment of the muon is given by Eq. (1.169) with the electron mass replaced by the muon mass. It is twice that predicted using the gyromagnetic ratio (given in Eq. (2) of Box 1.1) in Eq. (2.65) of the Orbital and Spin Splitting section wherein the intrinsic angular momentum for the spin 1/2 fermion is $\frac{\hbar}{2}$. As is the case with the electron, the magnetic moment of the muon is the sum of the component corresponding to the kinetic angular momentum, $\frac{\hbar}{2}$, and the component corresponding to the vector potential angular momentum, $\frac{\hbar}{2}$, (Eq. (1.164)). The spin-flip transition can be considered as involving a magnetic moment of g times that of a Bohr magneton of the muon. The g factor is equivalent to that of the electron given by Eq. (1.228).

The muon anomalous magnetic moment has been measured in a new experiment at Brookhaven National Laboratory (BNL) [32]. Polarized muons were stored in a superferric ring, and the angular frequency difference ω_a between the spin precession and orbital frequencies was determined by measuring the time distribution of high-energy decay positrons. The dependence of ω_a on the magnetic and electric fields is given by the BMT equation which is the relativistic equation of motion for spin in uniform or slowly varying external fields [33]. The dependence on the electric field is eliminated by storing muons with the "magic" $\gamma = 29.3$, which corresponds to a muon momentum $p = 3.09\ GeV/c$. Hence measurement of ω_a and of B determines the anomalous magnetic moment.

The "magic" γ wherein the contribution to the change of the longitudinal polarization by the electric quadrupole focusing fields are eliminated occurs when

$$\frac{g_\mu \beta}{2} - \frac{1}{\beta} = 0 \tag{1.238}$$

where g_μ is the muon g factor which is required to be different from the electron g factor in the standard model due to the dependence of the mass dependent interaction of each lepton with vacuum polarizations due to virtual particles. For example, the muon is much heavier than the electron, and so high energy (short distance) effects due to strong and weak interactions are more important here [29]. The BNL Muon (g-2) Collaboration [32] used a "magic" $\gamma = 29.3$ which satisfied Eq. (1.238) identically for $\frac{g_\mu}{2}$; however, their assumption that this condition eliminated the effect of the electrostatic field on ω_a is flawed as shown in Appendix III: Muon g Factor. Internal consistency was achieved during the determination of $\frac{g_\mu}{2}$ using the BMT equation with the flawed assumption that $\frac{g_\mu}{2} \neq \frac{g_e}{2}$. The parameter measured by Carey et al. [32] corresponding to $\frac{g_\mu}{2}$ was the sum of a finite electric term as well as a magnetic term. The calculated result based on the equivalence of the muon and electron g factors:

$$\frac{g_\mu}{2} = 1.001\ \ 165\ \ 923 \tag{1.239}$$

is in agreement with the result of Carey et al. [32]:

$$\frac{g_\mu}{2} = 1.001\ \ 165\ \ 925\ \ (15) \tag{1.240}$$

Rather than indicating an expanded plethora of postulated super-symmetry virtual particles which make contributions such as smuon-neutralino and sneutrino-chargino loops as suggested by Brown et al. [34], the deviation of the experimental value of $\frac{g_\mu}{2}$ from that of the standard model prediction simply indicates that the muon g factor is equivalent to the electron g factor.

DETERMINATION OF ATOMIC ORBITAL RADII

The one-electron atomic orbital is a spherical shell of negative charge (total charge = $-e$) of zero thickness at a distance r_n from the nucleus of charge $+Ze$. It is well known that the field of a spherical shell of charge is zero inside the shell and that of a point charge at the origin outside the shell [35]. See Figure 1.32.

Figure 1.32. The point-like electric fields of a proton, a bound electron, and their superposition as the hydrogen atom corresponding to a minimum energy and no electron self interaction. The electron's field is normal and finite only radially distant from its surface, being zero inside of the electron shell according to Gauss' and Faraday's laws which is also consistent with experiments showing zero self field inside of a charged perfect conductor. Thus, only the proton's central field at the electron determines the force balance which causes the flat 2-D geometry of a free electron to transition to the 2-D bubble-like geometry of the atomic orbital.

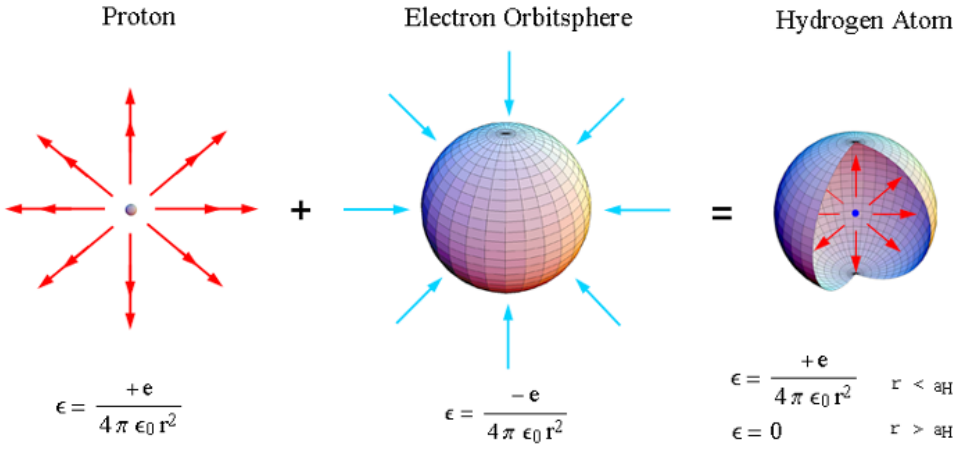

Thus, for a nucleus of charge Z, the force balance equation for the electron atomic orbital is obtained by equating the forces on the mass and charge densities. For the ground state, $n = 1$, the centrifugal force of the electron is given by:

$$\mathbf{F}_{centrifugal} = \frac{m_e}{4\pi r_1^2}\frac{\mathbf{v}_1^2}{r_1} \tag{1.241}$$

where $\frac{m_e}{4\pi r_1^2}$ is the mass density of the atomic orbital. The centripetal force is the electric force, $\mathbf{F}_{ele}$, between the electron and the nucleus.

$$\mathbf{F}_{ele} = \frac{e}{4\pi r_1^2}\frac{Ze}{4\pi\varepsilon_0 r_1^2} \tag{1.242}$$

where ε_0 is the permittivity of free-space.

The second centripetal force is an electrodynamic force or radiation reaction force, a force dependent on the second derivative of charge position, with respect to time, which arises between the electron and the nucleus. This force given in Sections 6.6, 12.10, and 17.3 of Jackson [36] achieves the condition that the sum of the mechanical momentum and electromagnetic momentum is conserved. The motion of each point in the magnetic field of the nucleus will cause a relativistic central force, $\mathbf{F}_{mag}$, which acts on each point mass. The magnetic central force is derived as follows from the Lorentz force, which is relativistically corrected. Each infinitesimal point of the atomic orbital moves on a great circle, and the charge density at each point is $\frac{e}{4\pi r_n^2}$. As given in the Proton and Neutron section, the proton is comprised of a linear combination of three constant functions and three orthogonal spherical harmonic quark/gluon functions. The magnetic field front due to the motion of the electron propagates at the speed of light. From the photon inertial reference frame at the radius of each infinitesimal point of the electron atomic orbital, the proton charge distribution is given as the product of the quark and gluon functions, which gives rise to a uniform distribution. The magnetic flux of the proton in the $v = c$ inertial frame at the electron radius follows from McQuarrie [19]:

$$\mathbf{B} = \frac{\mu_0 e\hbar}{2m_p r_n^3} \tag{1.243}$$

And, the magnetic flux due to a nucleus of charge Z and mass m is:

$$\mathbf{B} = \frac{\mu_0 Ze\hbar}{2mr_n^3} \tag{1.244}$$

The motion of each point will cause a relativistic central force, $\mathbf{F}_{i\,mag}$, which acts on each point mass. The magnetic central force is derived as follows from the Lorentz force which is relativistically corrected. The Lorentz force density on each point moving at velocity $\mathbf{v}$ is:

$$\mathbf{F}_{mag} = \frac{e}{4\pi r_n^2}\mathbf{v}\times\mathbf{B} \tag{1.245}$$

For the hydrogen atom with $Z=1$ and $m=m_p$, substitution of Eq. (1.35) for $\mathbf{v}$ and Eq. (1.244) for $\mathbf{B}$ gives:

$$\mathbf{F}_{mag} = \frac{1}{4\pi r_1^2}\left[\frac{e^2\mu_0}{2m_e r_n}\right]\frac{\hbar^2}{mr_n^3}\hat{r} \tag{1.246}$$

The term in brackets can be expressed in terms the fine structure constant α wherein the radius of the electron relative to the $v=c$ frame (k is the lightlike k^0, then $k=\omega_n/c$ regarding a potentially emitted photon), r_α^*, is the corresponding relativistic radius. From Eq. (1.15), the relationship between the radius and the electron wavelength is:

$$2\pi r = \lambda \tag{1.247}$$

Using the de Broglie Eq. (1.38) with $v=c$

$$\lambda = \frac{h}{mv} = \frac{h}{mc} \tag{1.248}$$

With substitution of Eq. (1.248) into Eq. (1.247)

$$r_\alpha^* = \frac{\hbar}{mc} = \lambda\!\!\!^{-}_c = \alpha a_0 \tag{1.249}$$

The radius of the electron atomic orbital in the $v=c$ frame is $\lambda\!\!\!^{-}_C$, where $v=c$ corresponds to the magnetic field front propagation velocity which is the same in all inertial frames, independent of the electron velocity as shown by the velocity addition formula of special relativity [37]. From Eqs. (1.179) and (1.249),

$$\frac{e^2\mu_0}{2m_e r_n} = 2\pi\alpha \tag{1.250}$$

where $\lambda\!\!\!^{-}_C$ is the Compton wavelength bar substituted for r_n, and a_o is the Bohr radius.

From Lorentz transformations with the electron's invariant angular momentum of $\hbar$ (Eq. (1.37)), it can be shown that the relativistic correction to Eq. (1.246) is the reciprocal of Eq. (1.250). Consider an inertial frame following a great circle of radius r_n with $v=c$ (Here, constant angular velocity as well as constant velocity constitutes an inertial frame for relativistic effects in a general sense, as shown in Chp. 34). The motion is tangential to the radius; thus, r_n is Lorentz invariant. But, as shown in the Special Relativistic Correction to the Ionization Energies section, the tangential distance along a great circle is $2\pi r_n$ in the laboratory frame and r_n in the $v=c$ frame (k is the lightlike k^0, then $k=\omega_n/c$). In addition, the corresponding radius is reduced by α for the light speed radial field. Thus, the term in brackets in Eq. (1.246) is the inverse of the relativistic correction γ' for the electrodynamic central force.

The electron's magnetic moment of a Bohr magneton μ_B given by Eq. (1.131) is also invariant as well as its angular momentum of $\hbar$. The electron is nonradiative due to its angular motion as shown in Appendix I: Nonradiation Condition and the Stability of Atoms and Hydrinos section. Furthermore, the angular momentum of the photon given in the Equation of the Photon section is $\mathbf{m} = \int \frac{1}{8\pi c}\mathrm{Re}\left[\mathbf{r}\times(\mathbf{E}\times\mathbf{B}^*)\right]dx^4 = \hbar$. It is conserved for the solutions for the resonant photons and excited state electron functions given in the Excited States of the One-Electron Atom (Quantization) section and the Equation of the Photon section. Thus, the electrodynamic angular momentum and the inertial angular momentum are matched such that the correspondence principle holds. It follows from the principle of conservation of angular momentum that $\frac{e}{m_e}$ of Eq. (1.131) is invariant. The same applies for the intrinsic magnetic moment μ_B and angular momentum $\hbar$ of the free electron since it is given by the projection of the bound electron into a plane as shown in the Electron in Free Space section. However, special relativity must be applied to physics relative to the electron's center of mass due to the invariance of charge and the invariant

four momentum as given by Purcell [37].

The correction to the term in brackets of Eq. (1.246) also follows from the Lorentz transformation of the electron's invariant magnetic moment as well as its invariant angular momentum of $\hbar$. Consider a great circle of the electron atomic orbital. As shown in the Special Relativistic Effect on the Electron Radius and the Relativistic Ionization Energies section, the tangential distance along a great circle is $2\pi r_n$ in the laboratory frame and r_n in the $v = c$ frame. The corresponding relativistic electron mass density regarding the invariant angular momentum increases by a factor of 2π (Eq. (1.281)). Furthermore, due to invariance of charge under Gauss' Integral Law, with the radius given by (1.209), the charge corresponding to the source current of the magnetic field must be corrected by α^{-1}. Thus, from the perspective of the invariance of μ_B, the term in brackets in Eq. (1.246) is the inverse of the relativistic correction for the electrodynamic central force.

$$\frac{\alpha^{-1}e^2\mu_0}{2(2\pi m_e)r_n} = \frac{\alpha^{-1}e^2\mu_0}{2(2\pi m_e)\lambda\!\!\!^{-}} = \frac{2\pi\alpha^{-1}e^2\mu_0}{2(2\pi m_e)\dfrac{h}{m_e c}} = 1 \tag{1.251}$$

Therefore, the force is given by:

$$\mathbf{F}_{mag} = -\frac{1}{4\pi r_1^2}\frac{\hbar^2}{mr_1^3}\hat{r} \tag{1.252}$$

The force balance equation is given by equating the centrifugal and centripetal force densities:

$$\frac{m_e}{4\pi r_1^2}\frac{v_1^2}{r_1} = \frac{1}{4\pi r_1^2}\frac{\hbar^2}{m_e r_1^3} = \frac{e}{4\pi r_1^2}\frac{Ze}{4\pi\varepsilon_0 r_1^2} - \frac{1}{4\pi r_1^2}\frac{\hbar^2}{mr_1^3} \tag{1.253}$$

where $Z = 1$ and $m = m_p$ for the hydrogen atom and the velocity is given by Eq. (1.35). (Since the surface-area factor cancels in all cases, this factor will be left out in subsequent force calculations throughout this book). From the force balance equation:

$$r_1 = \frac{4\pi\varepsilon_o\hbar^2}{Ze^2\mu_e} \tag{1.254}$$

where the reduced electron mass, μ_e, is:

$$\mu_e = \frac{m_e m}{m_e + m} \tag{1.255}$$

The Bohr radius is:

$$a_0 = \frac{4\pi\varepsilon_0\hbar^2}{e^2 m_e} \tag{1.256}$$

And, the radius given by force balance between the centrifugal force and central electrostatic force alone is:

$$r_1 = \frac{4\pi\varepsilon_o\hbar^2}{Ze^2 m_e} = \frac{a_0}{Z} \tag{1.257}$$

And, for hydrogen, m of Eq. (1.255) is:

$$m = m_p \tag{1.258}$$

Substitution of the reduced electron mass for the electron mass gives, a_H, the Bohr radius of the hydrogen atom.

$$a_H = \frac{4\pi\varepsilon_0\hbar^2}{e^2\mu_e} \tag{1.259}$$

Thus, Eq. (1.254) becomes

$$r_1 = \frac{a_H}{Z} \tag{1.260}$$

where $Z = 1$ for the hydrogen atom. The results can also be arrived at by the familiar minimization of the energy.

ENERGY CALCULATIONS

The potential energy V between the electron and the nucleus separated by the radial distance radius r_1 considering the force balance between the centrifugal force and central electrostatic force alone is

$$V = \frac{-Ze^2}{4\pi\varepsilon_0 r_1} = \frac{-Z^2e^2}{4\pi\varepsilon_0 a_0} = -Z^2 \cdot 4.3598 \; X \; 10^{-18} \; J = -Z^2 \cdot 27.212 \; eV \tag{1.261}$$

Because this is a central force problem, the kinetic energy, T, is $-\frac{1}{2}V$.

$$T = \frac{Z^2e^2}{8\pi\varepsilon_0 a_0} = Z^2 \cdot 13.606 \; eV \tag{1.262}$$

The same result can be obtained from $T = \frac{1}{2} m_e v_1^2$ and Eq. (1.35). Alternatively, the kinetic energy T and the binding energy E_B, which are each equal to the change in stored electric energy, ΔE_{ele}, can be calculated from

$$T = \Delta E_{ele} = -\frac{1}{2}\varepsilon_0 Z \int_{\infty}^{r_1} \mathbf{E}^2 dv \text{ where } \mathbf{E} = -\frac{e}{4\pi\varepsilon_0 r^2}\mathbf{i_r} \tag{1.263}$$

Thus, as the atomic orbital shrinks from ∞ *to* r_1,

$$E_B = -\frac{Ze^2}{8\pi\varepsilon_0 r_1} = -\frac{Z^2e^2}{8\pi\varepsilon_0 a_0} = -Z^2 \cdot 2.1799 \; X \; 10^{-18} \; J = -Z^2 \cdot 13.606 \; eV \tag{1.264}$$

The calculated Rydberg constant R using Eq. (1.259) in Eqs. (1.261-1.264) which includes the relativistic correction corresponding to the magnetic force given by Eq. (1.252) is $10,967,758 \; m^{-1}$. The experimental Rydberg constant is $10,967,758 \; m^{-1}$. Furthermore, a host of parameters can be calculated for the hydrogen atom, as shown in Table 1.2.

Table 1.2. Some calculated parameters for the hydrogen atom ($n = 1$).

radius	$r_1 = a_H$	5.294654 X 10^{-11} m
potential energy	$V = \frac{-e^2}{4\pi\varepsilon_0 a_H}$	–27.196 eV
kinetic energy	$T = \frac{e^2}{8\pi\varepsilon_0 a_H}$	13.598 eV
angular velocity (spin)	$\omega_1 = \frac{\hbar}{m_e r_1^2}$	4.1296 X 10^{16} $rad\ s^{-1}$
linear velocity	$v_1 = r_1\omega_1$	2.1865 X 10^{6} ms^{-1}
wavelength	$\lambda_1 = 2\pi r_1$	3.325 X 10^{-10} m
spin quantum number	$s = \frac{1}{2}$	$\frac{1}{2}$
moment of Inertia	$I = \frac{m_e r_1^2}{2}$	1.277 X 10^{-51} kgm^2
angular kinetic energy	$E_{angular} = \frac{1}{2} I\omega_1^2$	6.795 eV
magnitude of the angular momentum	$\hbar$	1.0545 X 10^{-34} Js
projection of the angular momentum onto the transverse-axis	$\frac{\hbar}{4}$	2.636 X 10^{-35} Js
projection of the angular momentum onto the z-axis	$S_z = \frac{\hbar}{2}$	5.273 X 10^{-35} Js
mass density	$\frac{m_e}{4\pi r_1^2}$	2.589 X 10^{-11} kgm^{-2}
charge density	$\frac{e}{4\pi r_1^2}$	4.553 Cm^{-2}

Table 1.3 gives the radii and energies for some one-electron atoms. In addition to the energies, the wavelength, angular frequency, and the linear velocity can be calculated for any one-electron atom from Eqs. (1.38), (1.36), and (1.35). Values are given in Table 1.4.

Table 1.3. Calculated energies (non-relativistic) and calculated ionization energies for some one-electron atoms.

Atom	Calculated r_1 [a] (a_0)	Calculated Kinetic Energy[b] (eV)	Calculated Potential Energy[c] (eV)	Calculated Ionization Energy[d] (eV)	Experimental Ionization Energy[e] (eV)
H	1.000	13.61	–27.21	13.61	13.59
He^{+}	0.500	54.42	–108.85	54.42	54.42
Li^{2+}	0.333	122.45	–244.90	122.45	122.45
Be^{3+}	0.250	217.69	–435.39	217.69	217.71
B^{4+}	0.200	340.15	–680.29	340.14	340.22
C^{5+}	0.167	489.81	–979.62	489.81	489.98
N^{6+}	0.143	666.68	–1333.37	666.68	667.03
O^{7+}	0.125	870.77	–1741.54	870.77	871.39

[a] from Equation (1.257)
[b] from Equation (1.262)
[c] from Equation (1.261)
[d] from Equation (1.264)
[e] experimental

It is noteworthy that the potential energy is a constant (at a given n) because the electron is at a fixed distance, r_n, from the nucleus. And, the kinetic energy and velocity squared are constant because the atom does not radiate at r_n and the potential energy is constant.

Table 1.4. Calculated radii, angular frequencies, linear velocities, and wavelengths for the n=1 state of some one-electron atoms (non-relativistic).

Atom	r_1 [a] (a_0)	angular[b] velocity ($10^{17}\,rad\,s^{-1}$)	linear[c] velocity ($10^{6}\,ms^{-1}$)	wavelength[d] ($10^{-10}\,m$)
H	1.000	0.413	2.19	3.325
He^{+}	0.500	1.65	4.38	1.663
Li^{2+}	0.333	3.72	6.56	1.108
Be^{3+}	0.250	6.61	8.75	0.831
B^{4+}	0.200	10.3	10.9	0.665
C^{5+}	0.167	14.9	13.1	0.554
N^{6+}	0.143	20.3	15.3	0.475
O^{7+}	0.125	26.5	17.5	0.416

[a] from Equation (1.257)
[b] from Equation (1.36)
[c] from Equation (1.35)
[d] from Equation (1.38)

It should be noted that the linear velocity is an appreciable percentage of the velocity of light for some of the atoms in Table 1.4—5.9% for O^{7+} for example. Relativistic corrections must be applied before a comparison between the total energy and ionization energy (Table 1.3) is made.

SPECIAL RELATIVISTIC EFFECT ON THE ELECTRON RADIUS AND THE RELATIVISTIC IONIZATION ENERGIES

The electron current constitutes an orbit relative to the laboratory frame. Muons and electrons are both leptons. The increase in the lifetime of muonic decay due to relativistic motion in a cyclotron orbit relative to a stationary laboratory frame provides strong confirmation of time dilation and confirms that the electron's frame is an inertial frame [38]. $\frac{eB}{m_e}$ bunching of electrons in a gyrotron [39] occurs because the cyclotron frequency is inversely proportional to the relativistic electron mass. This further demonstrates that the electron frame is an inertial frame and that relativistic electron mass increase and time dilation occur relative to the laboratory frame. The special relativistic relationship in polar coordinates is derived. The result of the treatment of the electron motion relative to the laboratory frame is in excellent agreement with numerous experimental observables such as the electron g factor, the invariance of the electron magnetic moment of μ_B and angular momentum of $\hbar$, the fine structure of the hydrogen atom, and the relativistic ionization energies of one and two electron atoms found *infra* and in the Excited States of the One-Electron Atom (Quantization) and the Two-Electron Atoms sections.

Following the same derivation as given by Beiser [40], it can be shown that the consequences of maintaining a constant maximum speed of light with preservation of physical laws independent of inertial frames of reference for the bound electron requires that the coordinate transformations are Lorentzian. First, the consequences for the electron in its frame are considered. The motion at each infinitesimal point of the atomic orbital is on a great circle as shown in the Atomic Orbital Equation of Motion For $\ell = 0$ Based on the Current Vector Field (CVF) section. The electron motion is tangential to the radius; thus, r_n for the electron-frame is Lorentz invariant. A further consequence of the electron's motion always being perpendicular to its radius is that the electron's angular momentum of $\hbar$ is invariant as shown by Eq. (1.37). The electron's magnetic moment of a Bohr magneton μ_B given by Eq. (1.131) is also invariant as well as its angular momentum of $\hbar$.

Further using the required Lorentz transforms, the special relativistic effects for the laboratory frame are determined on the bound electron by considering lightlike events where there is a decrease in the electron wavelength and period due to relativistic length contraction and time dilation of the electron motion in the laboratory inertial frame relative to the lightlike

frame as shown *infra*[10]. A lightlight event regards the nature of an electron, excited state since only excited states of the bound electron can emit radiation. The nature of excited states depends on the properties of photons as well as the bound electron. The angular momentum of the electric and magnetic fields of the photon given in the Equation of the Photon section is $\hbar$. It is conserved for the solutions for the resonant photons and excited state electron functions given in the Excited States of the One-Electron Atom (Quantization) section and the Equation of the Photon section. The photons emitted during the formation of each one-electron atom are its excited state photons. Thus, the electrodynamic angular momentum and the inertial angular momentum are matched such that the correspondence principle holds. It follows from the principle of conservation of angular momentum of $\hbar$ that $\frac{e}{m_e}$ of Eq. (1.131) is invariant (See the Determination of Atomic Orbital Radii section). Since charge is invariant according to special relativity, the electron mass of the atomic orbital must also be invariant. But, as shown *infra*, the electron radius in the laboratory frame goes to a factor of $\frac{1}{2\pi}$ of that in the lightlike ($v = c$) frame. Thus, the effect of special relativity is to increase the mass and charge densities identically such that $\frac{e}{m_e}$ is a constant invariant. In the present case, the electron mass density increases by factor of 2π relative to that in the lightlike frame. The remarkable agreement between the calculated and observed value of the fine structure of the hydrogen atom which depends on the conditions of the invariance of the electron's charge and charge-to-mass ratio $\frac{e}{m_e}$ as given in the Spin-Orbit Coupling section further confirms the validity of this result. A further consequence of the decrease of the radius of the atomic orbital by a factor of 2π relative to that in the lightlike frame is that the bound electron is nonradiative due to its angular motion even in the case that $\ell \neq 0$. This is shown by using the relativistic wavelength to radius relationship given by Eq. (1.279) in Appendix I: Nonradiation Condition and in the Stability of Atoms and Hydrinos section. The radiative instability of excited states is due to a radial dipole term in the function representative of the excited state due to the interaction of the photon and the excited state electron as shown in the Instability of Excited States section.

Specifically, to derive the relativistic relationships consider that the electron is in constant angular velocity and is an inertial frame of reference relative to absolute space as given in the Equivalence of Inertial and Gravitational Masses Due to Absolute Space and Absolute Light Velocity section. This can be defined as the laboratory frame of the electron's motion upon which the spatial and temporal Lorentzian transforms may be applied. The motion of a possible photon is also relative to absolute space. The nature of an exited state as shown in the Excited States of the One-Electron Atom (Quantization) section is a superposition of an electron and a photon comprising two-dimensional shells of current and field lines, respectively, at the same radius defined by $\delta(r - r_n)$. Due to the further nature of the photon possessing light-speed angular motion, the electron motion and corresponding spatial and temporal parameters may be considered relative to light speed for the laboratory frame of the electron's constant angular velocity. The derivation of Eqs. (1.279) and (1.280) regards the use of Lorentz spatial and temporal transforms for the case of constant angular velocity along a path on a great-circle element. Such transforms are unconventional from the standard transforms on rectilinear motion, but they are perfectly physical as shown in the Newton's Absolute Space Was Abandoned by Special Relativity Because Its Nature Was Unknown section.

The equation of a photon is given in the Equation of the Photon section. An emitted free-space photon comprises a field-line pattern called a photon electric and magnetic vector field (e&mvf) similar to the atomic orbital wherein the former is generated from two orthogonal great circle field lines rather than two great circle current loops as in the case of the electron spin function. The motion along each field line is at light speed. The angular momentum, **m**, of the electric and magnetic fields of the emitted photon given by Eq. (4.1) is $\mathbf{m} = \int \frac{1}{8\pi c} \mathrm{Re}\left[\mathbf{r} \times (\mathbf{E} \times \mathbf{B}^*)\right] dx^4 = \hbar$. The equation of the photon of an exited state is given by Eq. (2.15). The absorption or emission of a photon regards an excited state given in the Excited States of the One-Electron Atom (Quantization) section. The excited state comprises a two-dimension field surface of great-circle field lines at the inner surface of the electron atomic orbital that has a slow component of motion phase-locked with and propagating the electron modulation wave ($\ell \neq 0$) that travels about the z-axis with angular frequency ω_n. The corresponding change in electron angular frequency between states matches the frequency of the photon that excited the transition, and the angular momentum of the fields (Eq. (4.1)) is conserved in the excited state. In addition, the motion along each great-circle field line is at velocity c; so, the

[10] Many problems arise in the case of applying special relativity to standard quantum mechanical solutions for one-electron atoms as discussed in the Quantum Theory Past and Future section, the Shortcomings of Quantum Theory section, and Refs. [16-17]. Spin was missed entirely by the Schrödinger equation, and it was forced by spin matrices in the Dirac equation. It does not arise from first principles, and it results in nonsensical consequences such as infinities and "a sea of virtual particles." These are not consistent with observation and paradoxically the virtual particles constitute an ether, the elimination of which was the basis of special relativity and is the supposed basis of the Dirac equation. In addition, the electron motion in the Schrödinger and Dirac equations is in all directions; consequently, the relativistic increase in electron mass results in an instability since the electron radius is inversely proportional to the electron mass. Since the electron mass in special relativity is not invariant, but the charge is, the electron magnetic moment of a Bohr magneton μ_n as well as its angular momentum of $\hbar$ cannot be invariant in contradiction with experimental observations known to 14-figure accuracy [26].

relative electron to absorbed-photon velocity is c. This is also the velocity that must be considered for the emission of a photon by the bound electron since this state must form in order for emission to occur. The corresponding source current follows from $\mathbf{n} \bullet \left(\mathbf{E}_1 - \mathbf{E}_2\right) = \frac{\sigma}{\varepsilon_0}$ (Eq. (2.11)), and the relativistically corrected wavelength given by Eq. (1.279) is $\lambda_n = r_n$. This is Eq. (41) of the Appendix I that determines the nonradiative property of the atomic orbital and its time and spherically harmonic angular functions as given by Eqs. (38) and (70) and (73) of Appendix I[9]. Emission or absorption corresponds to an energy-state transition. The corresponding change in electron radius with emission or absorption of a photon is the source current for a free-space photon as given in the State Lifetimes and Line Intensities section.

Consider that the motion at each infinitesimal point on the atomic orbital is on a great circle, and that each point-charge element has the charge density $\frac{e}{4\pi r_n^2}$ and mass density $\frac{m_e}{4\pi r_n^2}$ as shown in the Atomic Orbital Equation of Motion For $\ell = 0$ Based on the Current Vector Field (CVF) section. Next, consider a charge-density element (and correspondingly a mass-density element) of a great-circle current loop of the electron atomic orbital in the y'z'-plane as shown in Figure 1.4. The distance on a great circle is given by:

$$\int_0^{2\pi} r_n d\theta = r_n \theta \Big|_0^{2\pi} = 2\pi r_n \tag{1.265}$$

Due to relative motion, the distance along the great circle must contract and the time must dilate due to special relativity. The special relativistic length contraction relationship observed for a laboratory frame relative to an inertial frame moving at constant velocity v is:

$$l = l_o \sqrt{1 - \left(\frac{v}{c}\right)^2} \tag{1.266}$$

Consider a point initially at (0,0,1) moving clockwise on a great circle in the Cartesian y'z'-plane. The relationship between polar and Cartesian coordinates used for special relativity[11] is given by:

$$x_1' = 0 \qquad y_1' = r_n \sin(\omega_n t) \qquad z_1' = r_n \cos(\omega_n t) \tag{1.267}$$

where ω_n is given by Eq. (1.36), r_n is from Eq. (1.257), and

$$\phi = \omega_n t \tag{1.268}$$

Due to relativity, a contracted wavelength arises. The distance on the great circle undergoes length contraction only in the $\hat{\phi}$ direction as $v \to c$. Thus, as $v \to c$ the distance on a great circle approaches its radius which is the relativistically contracted electron wavelength since the relationship between the radius and the wavelength given by Eq. (1.15) is

$$2\pi r_n = \lambda_n \tag{1.269}$$

With $v = c$,

$$r^* = \lambda \tag{1.270}$$

where * indicates the relativistically corrected parameter. Thus,

$$r^* = \frac{r_n}{2\pi} \tag{1.271}$$

The relativistically corrected mass m^* follows from Eq. (1.271) with maintenance of the invariance of the electron angular momentum of $\hbar$ given by Eqs. (1.35) and (1.37).

$$m\mathbf{r} \times \mathbf{v} = m_e r \frac{\hbar}{m_e r} \tag{1.272}$$

[11] The Cartesian coordinate system as compared to general coordinates is special with regard to a fundamental aspect of Lorentz transforms on Cartesian coordinates discussed in the Relativity section.

With Eq. (1.271), the relativistically corrected mass $m*$ corresponding to an increase in its density only is[12]

$$m* = 2\pi m_e \tag{1.273}$$

The effect of the relativistic contraction of the distance along a great circle loop is to change the angle of constant motion in Eq. (1.267) with a corresponding decrease in the electron wavelength. For the point initially at (0,0,1) moving clockwise on a great circle in the Cartesian y'z'-plane as shown in Figure 1.4, the relativistically corrected wavelength that follows from Eqs. (1.265-1.269) is given by the sum of the relativistic electron motion along the great circle (y' direction) and that projected along the radial axis (z' direction):

$$\lambda_n = r^*_{n,y'} \sin\phi^* \int_0^{2\pi} d\phi + \cos\phi^* \int_0^{r^*_{n,z'}} dr \tag{1.274}$$

where the * indices correspond to the relativistically corrected parameters in the y' and z' directions. The length contraction is only in the direction of motion that is orthogonal to the radius and constant as a function of angle. Thus, Eq. (1.268) is given by

$$\lambda_n = 2\pi r'_n \sqrt{1-\left(\frac{v}{c}\right)^2}\sin\phi^* + r'_n \cos\phi^* \tag{1.275}$$

The projection of the angular motion onto the radial axis is determined by determining the relativistic angle ϕ^* corresponding to a decrease in the electron wavelength and period due to relativistic length contraction and time dilation of the electron motion in the laboratory inertial frame. Substitution of Eq. (1.36) into Eq. (1.268) gives:

$$\phi = \omega_n t = \frac{\hbar}{m_e r_n^2} t \tag{1.276}$$

The correction for the time dilation and length contraction due to electron motion gives the relativistic angle ϕ^* as:

$$\phi^* = \omega_n t = \frac{\hbar}{m_e\left(\frac{r_n}{\sqrt{1-\left(\frac{v}{c}\right)^2}}\right)^2} t\sqrt{1-\left(\frac{v}{c}\right)^2} = \frac{\hbar}{m_e r_n^2} t\left(1-\left(\frac{v}{c}\right)^2\right)^{3/2} \tag{1.277}$$

---

[12] The magnitude of the total angular momentum of the atomic orbital $\mathbf{L}$ must be constant. The constant total is $\hbar$ given by the integral

$$\mathbf{m} = \int \frac{1}{4\pi r^2}\left|\mathbf{r}\times m_e\mathbf{v}\right|\delta(r-r_n)\,dx^4 = m_e r_n \frac{\hbar}{m_e r_n} = \hbar \tag{1}$$

where the corresponding velocity is given by Eq. (1.35). The integral of the magnitude of the angular momentum of the electron is $\hbar$ in any inertial frame and is *relativistically invariant*.

According to special relativity, the electron's relative motion with respect to the laboratory frame causes the distance along the great circle to contract and the time to dilate such that a contracted radius arises as given by Eq. (1.280). As $v \to c$ the relativistically corrected radius in the laboratory frame $r*$ is given by

$$r* = \frac{r_n}{2\pi} \tag{2}$$

where r_n is the radius in the electron frame. Eq. (1.271) applies for both the mass and charge densities that are interchangeable by the ratio $\frac{e}{m_e}$. Thus, the ratio is invariant.

However, a relativistically corrected mass $m*$ can be defined from Eq. (1.271) with maintenance of the invariance of the electron angular momentum of $\hbar$ given by Eqs. (1.35) and (1.37). Due to spherical symmetry, the correction is the same along each great circle of the atomic orbital. Thus, the motion of the mass density of the electron along a great circle may be considered. Then,

$$m\mathbf{r}\times\mathbf{v} = m_e r \frac{\hbar}{m_e r} \tag{3}$$

With Eq. (1.271), the relativistically corrected mass $m*$ corresponding to an increase in its density only is

$$m* = 2\pi m_e \tag{4}$$

In other words, the correction of the radius gives an effective relativistic mass as follows:

$$m\mathbf{r}\times\mathbf{v} = m_e \frac{r}{2\pi}\frac{\hbar}{m_e\frac{r}{2\pi}} = 2\pi m_e \frac{r}{2\pi}\frac{\hbar}{m_e r} = m^* \frac{r}{2\pi}\frac{\hbar}{m_e r} = m^* r^* v = \hbar \tag{5}$$

where v is the electron velocity in its frame given by Eq. (1.35).

The period for a wavelength due to electron motion is:

$$T = \frac{2\pi}{\omega} = \frac{\lambda}{v} \tag{1.278}$$

Only the elements of the second y'z'-quadrant need be considered due to symmetry and continuity of the motion. Thus, using Eqs. (1.276-1.277) for a quarter period of time, Eq. (1.275) becomes:

$$\lambda_n = 2\pi r_n' \sqrt{1-\left(\frac{v}{c}\right)^2}\ \sin\left[\frac{\pi}{2}\left(1-\left(\frac{v}{c}\right)^2\right)^{3/2}\right] + r_n' \cos\left[\frac{\pi}{2}\left(1-\left(\frac{v}{c}\right)^2\right)^{3/2}\right] \tag{1.279}$$

Using a phase matching condition, the wavelengths of the electron (Eq. (1.269)) and laboratory (Eq. (1.279)) inertial frames are equated, and the corrected radius is given by:

$$r_n = r_n' \left[\sqrt{1-\left(\frac{v}{c}\right)^2}\ \sin\left[\frac{\pi}{2}\left(1-\left(\frac{v}{c}\right)^2\right)^{3/2}\right] + \frac{1}{2\pi}\cos\left[\frac{\pi}{2}\left(1-\left(\frac{v}{c}\right)^2\right)^{3/2}\right]\right] \tag{1.280}$$

which gives a relativistic factor γ^* of:

$$\gamma^* = \frac{2\pi}{2\pi\sqrt{1-\left(\frac{v}{c}\right)^2}\ \sin\left[\frac{\pi}{2}\left(1-\left(\frac{v}{c}\right)^2\right)^{3/2}\right] + \cos\left[\frac{\pi}{2}\left(1-\left(\frac{v}{c}\right)^2\right)^{3/2}\right]} \tag{1.281}$$

where the velocity is given by Eq. (1.35) with the radius given by Eq. (1.254). Plots of ratio of the radii from Eq. (1.280) and γ^* (Eq. (1.281)) as a function of the electron velocity v relative to the speed of light c are given in Figures 1.33 and 1.34, respectively.

As the electron velocity goes to the speed of light ($v \to c$) corresponding to any real or potentially emitted phase-locked photon, the electron radius in the laboratory frame goes to a factor of $\frac{1}{2\pi}$ of that in the lightlike electron frame ($\frac{r_n}{r_n'} = \frac{1}{2\pi}$). Thus, with $v = c$, due to symmetry the electron motion corresponds to an atomic orbital of radius $\frac{1}{2\pi}$ that of the radius in the lightlike frame. In the case where the velocity is the speed of light, the relativistic behavior predicts that the production masses of leptons are each the rest mass times the speed of light squared calculated from each of the Planck-equation, electric, and magnetic energies in the Leptons section. The radius correction given by Eq. (1.280) and shown in Figure 1.33 also correctly predicts the nonradiation condition, the force corresponding to the reduced electron mass in the radius of the hydrogen atom, spin-orbit coupling, the electron pairing force, and other relativistic observables given in this and subsequent chapters.

Figure 1.33. The normalized radius as a function of v/c due to relativistic contraction.

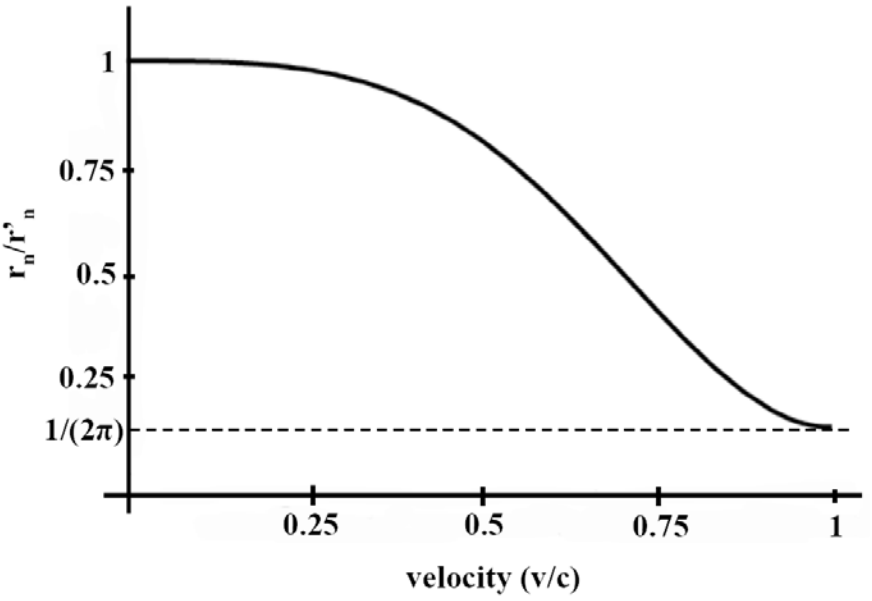

Figure 1.34. The relativistic factor γ^* as a function of v/c.

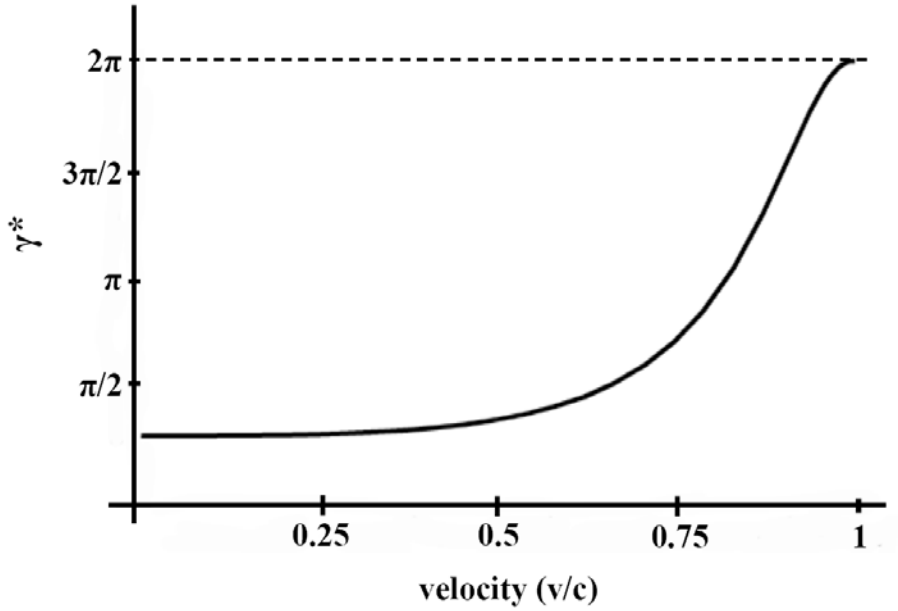

Next, a convenient way to determine the relativistic ionization energies is to use the relativistic total energy equation [41]. Consider the motion of the electron in its frame of reference. Since its motion is perpendicular to the radius, the radius (Eq. (1.260)) is invariant to length contraction, the charge is invariant, and only the dependency of the radius on the relativistic mass needs to be considered. The force balance equation (Eq. (1.253)) given by equating the centrifugal and centripetal force densities applies in the relativistic case as well where $m_e = m_e(v)$ is the relativistic electron mass, Z is the nuclear charge, $m = Am_p$ is the nuclear mass with A being the atomic mass number, and the velocity given by Eq. (1.35) is due to conservation of angular momentum which must be obeyed in the relativistic case as well as the nonrelativistic one. From the force balance equation:

$$r = \frac{4\pi\varepsilon_o\hbar^2}{Ze^2 m_{e0}}\left(\frac{m_{e0}}{m_e} + \frac{m_{e0}}{m_p A}\right) = \frac{a_0}{Z}\frac{m_{e0}}{m_e}\left(1 + \frac{m_e}{m_p A}\right) \tag{1.282}$$

Using the relativistic velocity (Eq. (1.35) with $m_e = m_e(v)$) and the radius from the force balance equation, the relativistic parameter β is:

$$\beta = \frac{v}{c} = \frac{\hbar}{m_e c r} = \frac{\hbar}{m_e c \frac{a_0}{Z}\frac{m_{e0}}{m_e}\left(1+\frac{m_e}{m_p A}\right)} = \frac{\hbar}{m_{e0} c \frac{a_0}{Z}\left(1+\frac{m_e}{m_p A}\right)} \tag{1.283}$$

Eqs. (1.178) and (1.179) give a relationship between the fine structure constant and the constants of Eq. (1.283):

$$\alpha = \frac{\mu_0 e^2 c}{4\pi\hbar} = \frac{e^2}{4\pi\varepsilon_0 \hbar c}\frac{a_0}{a_0} = \frac{e^2}{4\pi\varepsilon_0 \hbar c a_0}\frac{4\pi\varepsilon_0\hbar^2}{e^2 m_{e0}} = \frac{\hbar}{m_{e0} c a_0} \tag{1.284}$$

Then, from Eqs. (1.283) and (1.284), the relativistic parameter β simplifies to:

$$\beta = \frac{v}{c} = \frac{\alpha Z}{\left(1+\frac{m_e}{m_p A}\right)} \tag{1.285}$$

The relativistic mass is given by the Lorentz transformation:

$$m_e(v) = m_e = \frac{m_{e0}}{\sqrt{1-\beta^2}} = \frac{m_{e0}}{\sqrt{1-\frac{v^2}{c^2}}} \tag{1.286}$$

Next, a relationship for the velocity in the relativistic correction for the electron mass is determined from the boundary constraints. In the nonrelativistic limit, Eq. (1.282) reduces to Eq. (1.259) even in the case that Eq. (1.286) is substituted into Eq. (1.285); however, at any finite velocity the spin-nuclear interaction becomes velocity dependent according to Eqs. (1.285-1.286). Since the interaction arises from the invariant magnetic moments corresponding to the invariant angular momentum of the electron and proton, the $m_e = m_e(v)$ parameter in Eq. (1.285) must be the fixed constant of m_{e0}. The corresponding relativistic invariant magnetic moment of the nucleus is the nuclear magneton μ_N given by

$$\mu_N = \frac{e\hbar}{2m_p} \tag{1.287}$$

such that the relativistic mass ratio for the spin-nuclear interaction is $\frac{m_{e0}}{2m_p}$. Thus, Eq. (1.285) is given by:

$$\beta = \frac{v}{c} = \frac{\alpha Z}{\left(1+\frac{m_{e0}}{2m_p A}\right)} \tag{1.288}$$

Thus, from Eqs. (1.282), (1.286), and (1.288), the relativistic radius of the bound electron is given by:

$$r = \frac{a_0}{Z}\left(\sqrt{1-\frac{v^2}{c^2}}+\frac{m_{e0}}{m_p A}\right) = \frac{a_0}{Z}\left(\sqrt{1-\left(\frac{\alpha Z}{\left(1+\frac{m_{e0}}{2m_p A}\right)}\right)^2}+\frac{m_{e0}}{m_p A}\right) \tag{1.289}$$

The ionization energy or ionization potential IP is given by the negative of the sum of the potential V and kinetic energies T:

$$IP = -(V+T) \tag{1.290}$$

The potential energy is given by Eq. (1.261), and the relativistic kinetic energy from Eq. (34.17) is [41]:

$$T = m_{e0}c^2\left(\frac{1}{\sqrt{1-\left(\frac{v}{c}\right)^2}}-1\right) \tag{1.291}$$

Thus, IP is given by:

$$IP = \frac{Ze^2}{4\pi\varepsilon_0 r} - m_{e0}c^2\left(\frac{1}{\sqrt{1-\left(\frac{v}{c}\right)^2}} - 1\right) \tag{1.292}$$

Substitution of Eqs. (1.288-1.289) into Eq. (1.292) gives:

$$\begin{aligned} IP &= \frac{Ze^2}{4\pi\varepsilon_0 \frac{a_0}{Z}\left(\sqrt{1-\left(\frac{\alpha Z}{\left(1+\frac{m_{e0}}{2m_pA}\right)}\right)^2} + \frac{m_{e0}}{m_pA}\right)} - m_{e0}c^2\left(\frac{1}{\sqrt{1-\left(\frac{\alpha Z}{\left(1+\frac{m_{e0}}{2m_pA}\right)}\right)^2}} - 1\right) \\ &= \frac{(\alpha Z)^2 m_{e0}c^2}{\left(\sqrt{1-\left(\frac{\alpha Z}{\left(1+\frac{m_{e0}}{2m_pA}\right)}\right)^2} + \frac{m_{e0}}{m_pA}\right)} - m_{e0}c^2\left(\frac{1}{\sqrt{1-\left(\frac{\alpha Z}{\left(1+\frac{m_{e0}}{2m_pA}\right)}\right)^2}} - 1\right) \end{aligned} \tag{1.293}$$

where Eqs. (28.8-28.9) were used. In the case that the electron spin-nuclear interaction is negligible, Eq. (1.293) reduces to:

$$IP = m_{e0}c^2\left(1-\sqrt{1-(\alpha Z)^2}\right) \tag{1.294}$$

In the special case where the velocity is the speed of light and $Z = \alpha^{-1}$, the relativistic behavior predicts that the production masses of fundamental particles are the same in both the particle and laboratory frames as given in the Leptons and Quarks sections. The energies given by Eq. (1.293) are plotted in Figure 1.35 and are given in Table 1.5. The agreement between the experimental and calculated values is excellent. The small deviation is anticipated to be due to the Lamb shift [42] and experimental error.

Figure 1.35. The relativistic one-electron-atom ionization energies as a function of the nuclear charge Z.

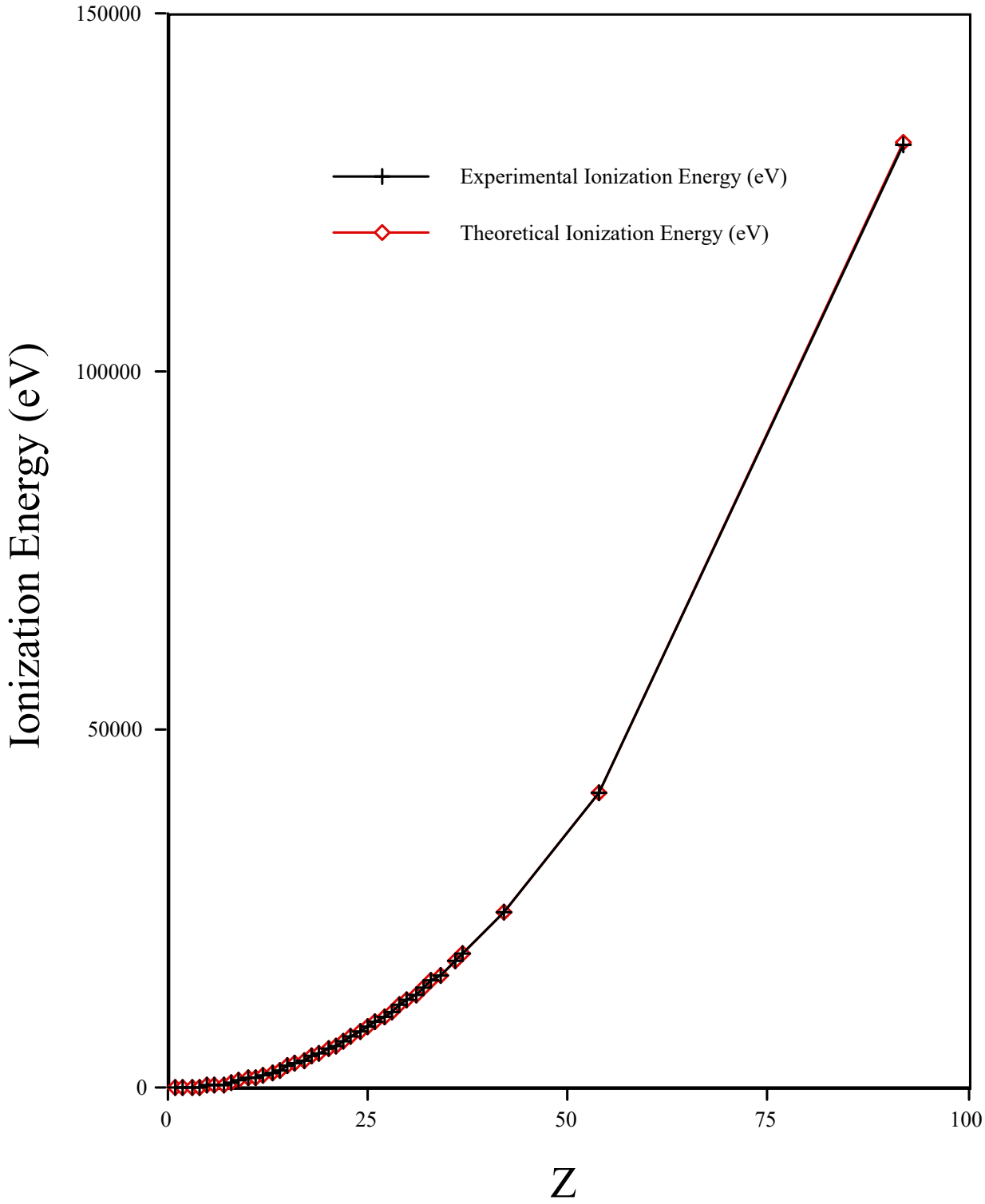

Table 1.5. Relativistic ionization energies for some one-electron atoms.

One e Atom	Z	β (Eq. (1.288))	Theoretical Ionization Energies (eV) (Eq. (1.293))	Experimental Ionization Energies (eV) [a]	Relative Difference between Experimental and Calculated [b]
H	1	0.00730	13.59847	13.59844	-0.000002
He^{+}	2	0.01459	54.41826	54.41778	-0.000009
Li^{2+}	3	0.02189	122.45637	122.45429	-0.000017
Be^{3+}	4	0.02919	217.72427	217.71865	-0.000026
B^{4+}	5	0.03649	340.23871	340.2258	-0.000038
C^{5+}	6	0.04378	490.01759	489.99334	-0.000049
N^{6+}	7	0.05108	667.08834	667.046	-0.000063
O^{7+}	8	0.05838	871.47768	871.4101	-0.000078
F^{8+}	9	0.06568	1103.220	1103.1176	-0.000093
Ne^{9+}	10	0.07297	1362.348	1362.1995	-0.000109
Na^{10+}	11	0.08027	1648.910	1648.702	-0.000126
Mg^{11+}	12	0.08757	1962.945	1962.665	-0.000143
Al^{12+}	13	0.09486	2304.512	2304.141	-0.000161
Si^{13+}	14	0.10216	2673.658	2673.182	-0.000178
P^{14+}	15	0.10946	3070.451	3069.842	-0.000198
S^{15+}	16	0.11676	3494.949	3494.1892	-0.000217
Cl^{16+}	17	0.12405	3947.228	3946.296	-0.000236
Ar^{17+}	18	0.13135	4427.363	4426.2296	-0.000256
K^{18+}	19	0.13865	4935.419	4934.046	-0.000278
Ca^{19+}	20	0.14595	5471.494	5469.864	-0.000298
Sc^{20+}	21	0.15324	6035.681	6033.712	-0.000326
Ti^{21+}	22	0.16054	6628.064	6625.82	-0.000339
V^{22+}	23	0.16784	7248.745	7246.12	-0.000362
Cr^{23+}	24	0.17514	7897.827	7894.81	-0.000382
Mn^{24+}	25	0.18243	8575.426	8571.94	-0.000407
Fe^{25+}	26	0.18973	9281.650	9277.69	-0.000427
Co^{26+}	27	0.19703	10016.63	10012.12	-0.000450
Ni^{27+}	28	0.20432	10780.48	10775.4	-0.000471
Cu^{28+}	29	0.21162	11573.34	11567.617	-0.000495
Zn^{29+}	30	0.21892	12395.35	12388.93	-0.000518
Ga^{30+}	31	0.22622	13246.66	13239.49	-0.000542
Ge^{31+}	32	0.23351	14127.41	14119.43	-0.000565
As^{32+}	33	0.24081	15037.75	15028.62	-0.000608
Se^{33+}	34	0.24811	15977.86	15967.68	-0.000638
Kr^{35+}	36	0.26270	17948.05	17936.21	-0.000660
Rb^{36+}	37	0.27000	18978.49	18964.99	-0.000712
Mo^{41+}	42	0.30649	24592.04	24572.22	-0.000807
Xe^{53+}	54	0.39406	41346.76	41299.7	-0.001140
U^{91+}	92	0.67136	132279.32	131848.5	-0.003268

[a] From theoretical calculations, interpolation of H isoelectronic and Rydberg series, and experimental data [42-45].
[b] (Experimental-theoretical)/experimental.

The electron possesses an invariant angular momentum and magnetic moment of $\hbar$ and a Bohr magneton, respectively. *This invariance feature provides for the stability of multielectron atoms and the existence of excited states wherein electrons magnetically interact* as shown in the Two-Electron Atoms section, the Three- Through Twenty-Electron Atoms section, and the Excited States of Helium section. The electron's motion corresponds to a current which gives rise to a magnetic field with a field strength that is inversely proportional to its radius cubed wherein the magnetic field is a relativistic effect of the electric field as shown by Jackson [46]. As there is *no electrostatic self-energy* as shown in the Determination of Atomic Orbital Radii section and Appendix II, there is also *no magnetic self-energy* for the bound electron since the magnetic moment is invariant for all states and the surface current is the source of the discontinuous field that does not exist inside of the electron as given by Eq. (1.136), $\mathbf{n}\ X\ (\mathbf{H}_a - \mathbf{H}_b) = \mathbf{K}$. No energy term is associated with the magnetic field unless another source of magnetic field is present. In general, the corresponding relativistic correction can be calculated from the effect of the electron's magnetic field on the force balance and energies of other electrons and the nucleus, which also produce magnetic fields. In the case of one-electron atoms, the nuclear-electron magnetic interaction is the only factor. Thus, for example, the effect of the proton was included in the derivation of Eq. (1.260) for the hydrogen atom.

REFERENCES

1. H. A. Haus, "On the radiation from point charges," American Journal of Physics, 54, (1986), pp. 1126-1129.
2. T. A. Abbott, D. J. Griffiths, Am. J. Phys., Vol. 53, No. 12, (1985), pp. 1203-1211.
3. J. D. Jackson, *Classical Electrodynamics*, Second Edition, John Wiley & Sons, New York, (1975), pp. 739-779.
4. J. D. Jackson, *Classical Electrodynamics*, Second Edition, John Wiley & Sons, New York, (1975), p. 111.
5. J. J. Hudson et al., "Improved measurement of the shape of the electron," Nature, Vol. 473, (2011), pp. 493-496.
6. J. D. Jackson, *Classical Electrodynamics*, Second Edition, John Wiley & Sons, New York, (1975), p. 99.
7. J. D. Jackson, *Classical Electrodynamics*, Second Edition, John Wiley & Sons, New York, (1975), p. 532.
8. D. A. McQuarrie, *Quantum Chemistry*, University Science Books, Mill Valley, CA, (1983), pp. 206-225.
9. G. R. Fowles, *Analytical Mechanics*, Third Edition, Holt, Rinehart, and Winston, New York, (1977), p. 196.
10. L. Pauling, E. B. Wilson, *Introduction to Quantum Mechanics with Applications to Chemistry*, McGraw-Hill Book Company, New York, (1935), pp. 118-121.
11. W. McC. Siebert, *Circuits, Signals, and Systems*, The MIT Press, Cambridge, Massachusetts, (1986), pp. 261, 272, 286, 287, 290, 410, 569, 599.
12. G. R. Fowles, *Analytical Mechanics,* Third Edition, Holt, Rinehart, and Winston, New York, (1977), pp. 17-20.
13. T. Bujnak, H. Hlucha personal communication June 2009, http://brilliantlightpower.com/y00-visualization/ density_normalization_angular_momentum_Y00.html.
14. Mathematica modeling of R. Mills' theory by B. Holverstott in "Modeling the Analytical Equations to Generate the Atomic Orbital Current Vector Field and the Uniform Current (Charge) Density Function $Y_0^0(\theta,\phi)$," posted at http://brilliantlightpower.com/atomic-theory/.
15. E. M. Purcell, *Electricity and Magnetism*, McGraw-Hill, New York, (1965), pp. 370-375, 447.
16. P. Pearle, Foundations of Physics, "Absence of radiationless motions of relativistically rigid classical electron," Vol. 7, Nos. 11/12, (1977), pp. 931-945.
17. R. L. Mills, "Maxwell's Equations and QED: Which is Fact and Which is Fiction," Physics Essays, Vol. 19, (2006), pp. 225-262.
18. R. L. Mills, "The Fallacy of Feynman's Argument on the Stability of the Hydrogen Atom According to Quantum Mechanics," Annales de la Fondation Louis de Broglie, Vol. 30, No. 2, (2005), pp. 129-151.
19. D. A. McQuarrie, *Quantum Chemistry*, University Science Books, Mill Valley, CA, (1983), pp. 238-241.
20. J. D. Jackson, *Classical Electrodynamics*, Second Edition, John Wiley & Sons, New York, (1975), p. 178.
21. J. D. Jackson, *Classical Electrodynamics*, Second Edition, John Wiley & Sons, New York, (1975), pp. 194-197.
22. C. E. Gough et al., Nature, Vol. 326, (1987), p. 855.
23. S. Das Sarma, R. E. Prange, Science, Vol. 256, (1992), pp. 1284-1285.
24. J. D. Jackson, *Classical Electrodynamics*, Second Edition, John Wiley & Sons, New York, (1975), pp. 582-584.
25. J. D. Jackson, *Classical Electrodynamics*, Second Edition, John Wiley & Sons, New York, (1975), pp. 758-763.
26. R. C. Weast, *CRC Handbook of Chemistry and Physics*, 68th Edition, CRC Press, Boca Raton, Florida, (1987-88), p. F-186 to p. F-187.
27. R. S. Van Dyck, Jr., P. Schwinberg, H. Dehmelt, "New high precision comparison of electron and positron g factors," Phys. Rev. Lett., Vol. 59, (1987), p. 26-29.
28. P. J. Mohr, B. N. Taylor, "CODATA recommended values of the fundamental physical constants: 1998," Reviews of Modern Physics, Vol. 72, No. 2, April, (2000), pp. 351-495.
29. G. P. Lepage, "Theoretical advances in quantum electrodynamics, International Conference on Atomic Physics, Atomic Physics; Proceedings, Singapore, World Scientific, Vol. 7, (1981), pp. 297-311.
30. E. R. Williams and P. T. Olsen, Phys. Rev. Lett. Vol. 42, (1979), p. 1575.
31. K. V. Klitzing et al., Phys. Rev. Lett. Vol. 45, (1980), p. 494.

32. R. M. Carey et al., Muon (g-2) Collaboration, "New measurement of the anomalous magnetic moment of the positive muon," Phys. Rev. Lett., Vol. 82, (1999), pp. 1632-1635.
33. J. D. Jackson, *Classical Electrodynamics*, Second Edition, John Wiley & Sons, New York, (1975), pp. 556-560.
34. H. N. Brown et al., Muon (g-2) Collaboration, "Precise measurement of the positive muon anomalous magnetic moment," Phys. Rev. D62, 091101 (2000).
35. F. Bueche, *Introduction to Physics for Scientists and Engineers*, McGraw-Hill, (1975), pp. 352-353.
36. J. D. Jackson, *Classical Electrodynamics*, Second Edition, John Wiley & Sons, New York, (1975), pp. 236-240, 601-608, 786-790.
37. E. M. Purcell, *Electricity and Magnetism*, McGraw-Hill, New York, (1985), Second Edition, pp. 451-458.
38. J. Bailey et al., "Final report on the CERN muon storage ring including the anomalous magnetic moment and the electric dipole moment of the muon," and a direct test of relativistic time dilation, Nuclear Physics B150, (1979), pp. 1-75.
39. P. Sprangle, A. T. Drobot, "The linear and self-consistent nonlinear theory of the electron cyclotron maser instability," IEEE Transactions on Microwave Theory and Techniques, Vol. MTT-25, No. 6, June, (1977), pp. 528-544.
40. A. Beiser, *Concepts of Modern Physics*, Fourth Edition, McGraw-Hill, New York, (1987), pp. 1-40.
41. Personal communication, Dr.-Ing. Günther Landvogt, Hamburg, Germany, March, (2004).
42. A. Gemberidze, Th. Stöhlker, D. Banas, K. Beckert, P. Beller, H. F. Beyer, F. Bosch, S. Hafmann, C. Kozhuharov, D. Liesen, F. Nolden, X. Ma, P. H. Mokler, M. Steck, D. Sierpowski, and S. Tashenov, "Quantum electrodynamics in strong electric fields: The ground-state Lamb shift in hydrogenlike uranium," Phys. Rev. Letts., Vol. 94, 223001 (2005).
43. C. E. Moore, "Ionization Potentials and Ionization Limits Derived from the Analyses of Optical Spectra," Nat. Stand. Ref. Data Ser.-Nat. Bur. Stand. (U.S.), No. 34, 1970.
44. D. R. Lide, *CRC Handbook of Chemistry and Physics*, 79th Edition, CRC Press, Boca Raton, Florida, (1998-9), p. 10-175 to p. 10-177.
45. http://physics.nist.gov/PhysRefData/ASD/levels_form.html.
46. J. D. Jackson, *Classical Electrodynamics*, Second Edition, John Wiley & Sons, New York, (1975), pp. 503-561.

Chapter 2

EXCITED STATES OF THE ONE-ELECTRON ATOM (QUANTIZATION)

EQUATION OF THE ELECTRIC FIELD INSIDE THE ATOMIC ORBITAL

It is well known that resonator cavities can trap electromagnetic radiation of discrete resonant frequencies. The atomic orbital is a resonator cavity that traps single photons of discrete frequencies. Thus, photon absorption occurs as an excitation of a resonator mode. The "trapped photon" is a "standing electromagnetic wave" which actually is a circulating wave that propagates around the z-axis, and its source current superimposes with each great circle current loop of the atomic orbital. The time-function factor, $k(t)$, for the "standing wave" is identical to the time-function factor of the atomic orbital in order to satisfy the boundary (phase) condition at the atomic orbital surface. Thus, the angular frequency of the "trapped photon" has to be identical to the angular frequency of the electron atomic orbital, ω_n, given by Eq. (1.36). Furthermore, the phase condition requires that the angular functions of the "trapped photon" have to be identical to the spherical harmonic angular functions of the electron atomic orbital. Combining $k(t)$ with the ϕ-function factor of the spherical harmonic gives $e^{i(m\phi - m\omega_n t)}$ for both the electron and the "trapped photon" function.

Consider the hydrogen atom. The atom and the "trapped photon" caused by a transition to a resonant state other than the $n = 1$ state have neutral charge. As shown *infra*, the photon's electric field superposes that of the proton such that the radial electric field has a magnitude proportional to Z/n at the electron where $n = 1, 2, 3, ...$ for excited states and $n = \frac{1}{2}, \frac{1}{3}, \frac{1}{4}, ..., \frac{1}{137}$ for lower energy states given in the Hydrino Theory—BlackLight Process section. This causes the charge density of the electron to correspondingly decrease and the radius to increase for states higher than 13.6 eV and the charge density of the electron to correspondingly increase and the radius to decrease for states lower than 13.6 eV as shown in Figure 5.2. Thus, the field lines of the proton always end on the electron. A way to conceptualize the effect of the photon "standing wave" in an electronic state other than $n = 1$ is to consider a solution of Laplace's equation in spherical coordinates with source currents "glued" to the electron and to the nucleus and phase-locked to the rotating electron current density with a radial electric field that only exists at the electron. Or, alternatively to a source current at the nucleus, a Poisson equation solution may comprise a delta function inhomogeneity at the origin [1]. Thus, the "trapped photon" is analogous to a gluon described in the Proton and Neutron section and a photon in free space as described in the Equation of the Photon section. However, the true nature of the photon field does not change the nature of the electrostatic field of the nucleus or its energy except at the position of the electron. The photon "standing wave" function further comprises a radial Dirac delta function that "samples" the Laplacian equation solution only at the position infinitesimally inside of the electron current-density function and superimposes with the proton field to give a field of radial magnitude proportional to Z/n, and the Fourier transform of the photon "standing wave" of the electronic states other than the $n = 1$ state is continuous over all frequencies in s_r-space and is given by $\frac{\sin s_r r}{s_r r}$. The free space photon also comprises a radial Dirac delta function, and the angular momentum of the photon given by $\mathbf{m} = \int \frac{1}{8\pi c} \mathrm{Re}\left[\mathbf{r} \times (\mathbf{E} \times \mathbf{B}^*)\right] dx^4 = \hbar$ in the Photon section is conserved [2] for the solutions for the resonant photons and excited state electron functions given *infra*. It can be demonstrated that the resonance condition between these frequencies is to be satisfied in order to have a net change of the electromagnetic energy field [3]. In the present case, the correspondence principle holds. That is the change in angular frequency of the electron is equal to the angular frequency of the resonant photon that excites the resonator cavity mode corresponding to the transition, and the energy is given by Planck's equation. The predicted energies, Lamb shift, fine structure, hyperfine structure, resonant line shape, line width, selection rules, etc. are in agreement with observation as shown *infra*.

The discretization of the angular momentum of the electron and the photon gives rise to quantized electron radii and energy levels. Transitions occur in integer units of the electron's inalienable intrinsic angular momentum of $\hbar$ (Appendix II) wherein the exciting photons carry an integer multiple of $\hbar$. Thus, for $\mathbf{r}\times m_e\mathbf{v}_e=\mathbf{p}$ to be constant, the velocity of the electron source current decreases by a factor of the integer, and the radius increases by the factor of the integer. Concomitantly, the photon field superimposes that of the proton causing a resultant central field of a reciprocal integer that establishes the force balance at the excited state radius. This quantization condition is equivalent to that of Bohr except that the electron angular momentum is $\hbar$, the angular momentum of one or more photons that give to an excited state is $n\hbar$, and the photon field changes the central force balance. Also, the standing wave regards the photon field and not the electron that comprises an extended current and is not a wave function. Thus, the quantization condition can also be considered as arising from the discretization of the photon standing wave including the integer spherical periodicity of the spherical harmonics of the excited state of the bound electron as a spherical cavity.

For a spherical resonator cavity, the relationship between an allowed radius and the "photon standing wave" wavelength is

$$2\pi r_n = n\lambda \tag{2.1}$$

where n is an integer. Now, the question arises: given that this is a resonator cavity, which resonant states are possible where the transition is effected by a "trapped photon?" For the electron atomic orbital, a spherical resonator cavity, the relationship between an allowed radius and the electron wavelength is:

$$2\pi(nr_1) = 2\pi r_n = n\lambda_1 = \lambda_n \tag{2.2}$$

where

$n = 1, 2, 3, 4, \ldots$, and

$$n = \frac{1}{2}, \frac{1}{3}, \frac{1}{4}, \ldots$$

λ_1 is the allowed wavelength for $n=1$

r_1 is the allowed radius for $n=1$

(The mechanism for transitions to the reciprocal integer states involves coupling with another resonator called a catalyst as given in the Hydrino Theory—BlackLight Process section.) An electron in the ground state, $n=1$, is in force balance including the electrodynamic force which is included by using the reduced electron mass as given by Eqs. (1.254), (1.259), and (1.260).

$$\frac{m_e v_1^2}{r_1} = \frac{Ze^2}{4\pi\varepsilon_0 r_1^2} \tag{2.3}$$

When an electron in the ground state absorbs a photon of sufficient energy to take it to a new resonant state, $n = 2, 3, 4, \ldots$, force balance must be maintained. This is possible only if the central field is equivalent to that of a central charge of $\frac{Ze}{n}$, and the excited state force balance equation is:

$$\frac{m_e v_n^2}{r_n} = \frac{1}{n}\frac{Ze^2}{4\pi\varepsilon_0 r_n^2} \tag{2.4}$$

where r_1 is the "ground" state radius of the electron, and r_n is the nth excited state radius of the electron. The radius of the nth excited state follows from Eq. (1.260) and Eq. (2.4).

$$r_n = na_H \tag{2.5}$$

The reduction of the effective charge from Ze to $\frac{Ze}{n}$ is caused by trapping a photon in the atomic orbital, a spherical resonator cavity. (This condition for excited states is also determined by considering the boundary condition for the multipole expansion of the excited states as solutions of Maxwell's equations wherein the angular momentum and energy of each resonant photon are quantized as $\hbar$ and $\hbar\omega$, respectively, as given in the Excited States of Helium section.) The photon's electric field creates a "standing wave" in the cavity with an effective charge of $\left[-1+\frac{1}{n}\right]Ze$ $(at\ r_n)$. The total charge experienced by the electron is the sum of the proton and "trapped photon" charge components. The equation for these "trapped photons" can be solved as a boundary value problem of Laplace's equation. For the hydrogen atom, the boundary conditions are that the electric field is in phase with the atomic orbital and that the radial function for the electric field of the "trapped photon" at r_n is:

$$\mathbf{E}_{r\ photon} = \left[-1+\frac{1}{n}\right]\frac{e}{4\pi\varepsilon_0\left(r_n\right)^2} \qquad n = 2, 3, 4, \ldots, \tag{2.6}$$

The general form of the solution to Laplace's equation in spherical coordinates is:

$$\Phi(r,\theta,\phi)=\sum_{\ell=0}^{\infty}\sum_{m=-\ell}^{\ell}\left[A_{\ell,m}r^{\ell}+B_{\ell,m}r^{-(\ell+1)}\right]\left[Y_0^0(\theta,\phi)+Y_\ell^m(\theta,\phi)\right] \tag{2.7}$$

All $A_{\ell,m}$ are zero because the electric field given by the potential must be inversely proportional to the radius to obtain force balance. The electric field is the gradient of the potential:

$$\mathbf{E}=-\nabla\Phi \tag{2.8}$$

$$\begin{aligned}\mathbf{E}_r&=-\frac{\partial\Phi}{\partial r}\,\hat{i}_r\\ \mathbf{E}_\theta&=-\frac{1}{r}\frac{\partial\Phi}{\partial\theta}\,\hat{i}_\theta\\ \mathbf{E}_\phi&=-\frac{1}{r\sin\theta}\frac{\partial\Phi}{\partial\phi}\,\hat{i}_\phi\end{aligned} \tag{2.9}$$

Thus,

$$\mathbf{E}_r=\sum_{\ell=0}^{\infty}\sum_{m=-\ell}^{\ell}B_{\ell,m}(\ell+1)r^{-(\ell+2)}\left[Y_0^0(\theta,\phi)+Y_\ell^m(\theta,\phi)\right] \tag{2.10}$$

Given that $\mathbf{E}_{proton}=\dfrac{+e}{4\pi\varepsilon_0 r_n^2}$, and that the electric fields of the proton and "trapped photon" must superimpose to yield a field equivalent to a central point charge of $\dfrac{+Ze}{n}$, the "trapped photon" electric field for each mode is determined as follows. The time-function factor and the angular-function factor of the charge-density function of the atomic orbital (Eqs. (1.27) and (1.28-1.29)) at force balance must be in phase with the electric field of the "trapped photon." The relationship between the electric field equation and the "trapped photon" source charge-density function is given by Maxwell's equation in two dimensions.

$$\mathbf{n}\bullet(\mathbf{E}_1-\mathbf{E}_2)=\frac{\sigma}{\varepsilon_0} \tag{2.11}$$

where $\mathbf{n}$ is the radial normal unit vector, $\mathbf{E}_1=0$ ($\mathbf{E}_1$ is the electric field outside of the atomic orbital), $\mathbf{E}_2$ is given by the total electric field at $r_n=na_H$, and σ is the surface charge-density. Thus,

$$\mathbf{E}_{r\ photon\ n,l,m|_{r_n=na_H}}=\frac{e}{4\pi\varepsilon_0(na_H)^2}\left[-1+\frac{1}{n}\left[Y_0^0(\theta,\phi)+\mathrm{Re}\left\{Y_\ell^m(\theta,\phi)e^{im\omega_n t}\right\}\right]\right]\delta(r-r_n) \tag{2.12}$$

$$=\sum_{\ell=0}^{\infty}\sum_{m=-\ell}^{\ell}-B_{\ell,m}(\ell+1)(na_H)^{-(\ell+2)}\left[Y_0^0(\theta,\phi)+\mathrm{Re}\left\{Y_\ell^m(\theta,\phi)e^{im\omega_n t}\right\}\right]\delta(r-r_n) \tag{2.13}$$

Therefore,

$$\sum_{\ell=0}^{\infty}\sum_{m=-\ell}^{\ell}-B_{\ell,m}=\frac{e(na_H)^{\ell}}{4\pi\varepsilon_0(\ell+1)}\left[-1+\frac{1}{n}\right],\ \text{and} \tag{2.14}$$

$$\mathbf{E}_{r\ photon\ n,l,m}=\frac{e(na_H)^{\ell}}{4\pi\varepsilon_0}\frac{1}{r^{(\ell+2)}}\left[-Y_0^0(\theta,\phi)+\frac{1}{n}\left[Y_0^0(\theta,\phi)+\mathrm{Re}\left\{Y_\ell^m(\theta,\phi)e^{im\omega_n t}\right\}\right]\right]\delta(r-r_n) \tag{2.15}$$

$n=1,2,3,4,...$
$\ell=0,1,2,...,n-1$
$m=-\ell,-\ell+1,...,0,...,+\ell$

$\mathbf{E}_{rtotal}$ is the sum of the "trapped photon" and proton electric fields,

$$\mathbf{E}_{rtotal}=\frac{e}{4\pi\varepsilon_0 r^2}+\frac{e(na_H)^{\ell}}{4\pi\varepsilon_0}\frac{1}{r^{(\ell+2)}}\left[-Y_0^0(\theta,\phi)+\frac{1}{n}\left[Y_0^0(\theta,\phi)+\mathrm{Re}\left\{Y_\ell^m(\theta,\phi)e^{im\omega_n t}\right\}\right]\right]\delta(r-r_n) \tag{2.16}$$

For $r=na_H$ and $m=0$, the total radial electric field is:

$$\mathbf{E}_{rtotal}=\frac{1}{n}\frac{e}{4\pi\varepsilon_0(na_H)^2} \tag{2.17}$$

Photons carry electric field, and the direction of field lines change with relative motion as required by special relativity. They increase in the direction perpendicular to the propagation direction. As shown by Eq. (4.9), the linear velocity of each point along a great circle of the photon atomic orbital is c. And, as shown in the Special Relativistic Correction to the Ionization Energies section and by Eq. (1.280), when the velocity along a great circle is light speed, the motion relative to the non-light speed frame is purely radial. In the case of the electric field lines of a trapped resonant photon of an excited state, the relativistic electric field is radial[1]. It is given by Eq. (2.15), and it exists only at $\delta(r-r_n)$. Thus, the photon only changes the radius and energy of the electron directly. Since the electric field of the photon at the electron superimposes that of the nucleus, the excited-state-energy levels are given by Eq. (2.18), and the hydrogen atom, for example, remains neutral.

The spherical harmonic function has a velocity less than light speed given by Eq. (1.35) and is phase-matched with the electron such that angular momentum is conserved during the excited state transition. This radial field can be considered a corresponding surface charge density as given in the Instability of Excited States section and the Stability of Atoms and Hydrinos section. All boundary conditions are met for the electric fields and the wavelengths of the "trapped photon" and the electron. Thus, Eq. (2.16) is the solution for the excited modes of the atomic orbital, a spherical resonator cavity. And, the quantum numbers of the electron are n, ℓ, m_ℓ, and m_s (Described in the Stern-Gerlach Experiment section). A p_x or p_y atomic-hydrogen excited state is shown in Figure 2.1.

Figure 2.1. The electron atomic orbital is a resonator cavity wherein the radii of the excited states are related by integers. The electronic charge-density function of a p_x or p_y atomic-hydrogen excited state is shown with positive and negative charge-density proportional to red intensity and blue intensity, respectively. The function corresponds to a charge density wave on the two-dimensional spherical surface of radius na_0 that travels time harmonically about the z-axis at the angular frequency given by Eq. (1.36). It is comprised of a linear combination of a constant function modulated by time and spherically harmonic functions. The centrifugal force is balanced by the electric field of its photon that is phase-locked to the spinning electron. The brightness corresponds to the intensity of the two-dimensional radial photon field.

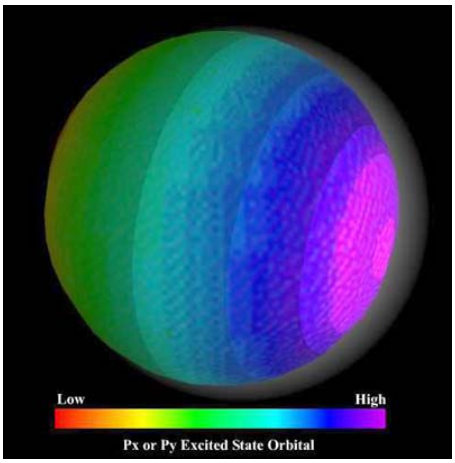

In the limit, the electric field of a photon cancels that of the proton ($n \to \infty$ in Eq. (2.17)), and the electron ionizes. The radius of the spherical shell (electron atomic orbital) goes to infinity as in the case of a spherical wavefront of light emitted from a symmetrical source, but it does not achieve an infinite radius. Rather it becomes ionized as shown in Figure 2.2 with the free electron propagating as a plane wave with linear velocity, v_z, and the size of the electron is the de Broglie wavelength, $\lambda = h/p$, as given in the Electron in Free Space section.

In general, the mechanism of photon absorption to form an excited state is given in the Transitions section wherein ionization is a special case. The extrema excited state photon is annihilated as the electron is ionized. The ionized electron gains kinetic energy with free electron radiation reaction field cancellation of the remnant extrema photon field. Specifically, as the electron radius goes to infinity, the photon field intensity goes to zero, but an infinite radius electron is not physical without interaction. So, the extrema comprising the $n = \infty$ state is a limiting state that cannot be achieved. Instead, the electron is ionized with finite kinetic energy whereby there is a radiation reaction during the corresponding electron acceleration to gain the kinetic energy, and the remnant extrema photon field is annihilated. The field equations follow the superposition of excited states into free states.

---

[1] A positive electric field is given by a trapped photon of an excited state if the velocity of the field lines is in the direction of the field line, and a negative central field is given if they are in opposite directions. The "trapped" photon can be considered the superposition of two free space photons given in the Photon section generated according to Eqs. (4.4-4.7) with the magnetic and electric fields interchanged such that when the two are superposed the great circle electric field lines add and the great circle magnetic field lines cancel.

Photons can transition into particles at rest through a transition state. A transition state atomic orbital of particle production is very similar to a trapped photon of an excited state as given in the Particle Production section, the Lepton section, and the Quarks section.

Figure 2.2. Time-lapsed image of electron ionization. With the absorption of a photon of energy in excess of the binding energy, the bound electron's radius increases and the electron ionizes as a plane-wave with the de Broglie wavelength. Similar to the mechanism of the propagation of a current in a classical conductor, ionization of an inner shell electron proceeds by successive displacement of contiguous outer shell electrons until the most outer shell electron ionizes.

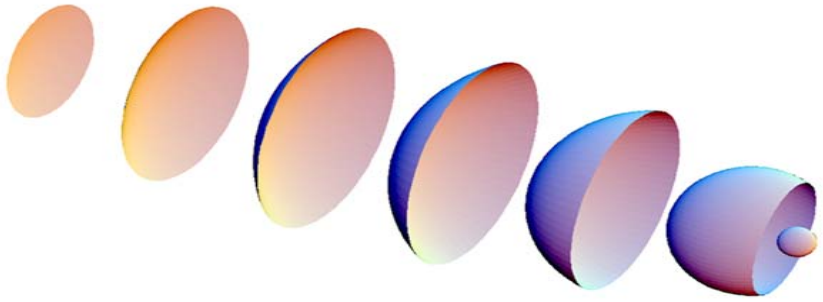

PHOTON ABSORPTION

The energy of the photon, which excites a mode in a stationary spherical resonator cavity from radius a_H to radius na_H is

$$E_{photon} = \frac{e^2}{4\pi\varepsilon_0 a_H}\left[1-\frac{1}{n^2}\right] = h\nu = \hbar\omega \tag{2.18}$$

After multiplying Eq. (2.18) by $\frac{a_H}{a_H} = \frac{4\pi\varepsilon_0\hbar^2}{e^2\mu_e a_H}$, where a_H is given by Eq. (1.259), ω_{photon} is:

$$\omega_{photon} = \frac{\hbar}{m_e a_H^2}\left[1-\frac{1}{n^2}\right] \tag{2.19}$$

In the case of an electron atomic orbital, the resonator possesses kinetic energy before and after the excitation. The kinetic energy is always one-half of the potential energy because the centripetal force is an inverse squared central force. As a result, the energy and angular frequency to excite an electron atomic orbital are only one-half of the values above, Eqs. (2.18) and (2.19). From Eq. (1.36), the angular velocity of an electron atomic orbital of radius na_H is

$$\omega_n = \frac{\hbar}{m_e\left(na_H\right)^2} \tag{2.20}$$

The change in angular velocity of the atomic orbital for an excitation from $n=1$ to $n>1$ is:

$$\Delta\omega = \frac{\hbar}{m_e\left(a_H\right)^2} - \frac{\hbar}{m_e\left(na_H\right)^2} = \frac{\hbar}{m_e\left(a_H\right)^2}\left[1-\frac{1}{n^2}\right] \tag{2.21}$$

The kinetic energy change of the transition is

$$E = \frac{1}{2}m_e(\Delta v)^2 = \frac{1}{2}\frac{e^2}{4\pi\varepsilon_0 a_H}\left[1-\frac{1}{n^2}\right] = \frac{e^2}{8\pi\varepsilon_0 a_H}\left[1-\frac{1}{n^2}\right] = \frac{1}{2}\hbar\omega \tag{2.22}$$

wherein Eq. (2.22) is also the equation for the ionization energy. The change in angular velocity of the electron atomic orbital, Eq. (2.21), is identical to the angular velocity of the photon necessary for the excitation, ω_{photon} (Eq. (2.19)). The energy of the photon necessary to excite the equivalent transition in an electron atomic orbital is one-half of the excitation energy of the stationary cavity because the change in kinetic energy of the electron atomic orbital supplies one-half of the necessary energy. The change in the angular frequency of the atomic orbital during a transition and the angular frequency of the photon corresponding to the superposition of the free space photon and the photon corresponding to the kinetic energy change of the atomic orbital during a transition are equivalent. The correspondence principle holds. It can be demonstrated that the resonance condition between these frequencies is to be satisfied in order to have a net change of the energy field [3]. Similarly photons are emitted when an electron is bound. Relations between the free space photon wavelength, radius, and velocity to the corresponding parameters of a free electron as it is bound are given in the Equation of the Photon section.

The excited states of hydrogen are given in Table 2.1.

Table 2.1. Calculated energies (non-relativistic; no spin-orbit interaction; no electronic spin/nuclear spin interaction) and ionization energies for the hydrogen atom in the ground state and some excited states.

n	Z	Calculated r_n[a] (a_H)	Calculated Kinetic Energy[b] (eV)	Calculated Potential Energy[c] (eV)	Calculated Ionization Energy[d] (eV)	Experimental Ionization Energy[e] (eV)
1	1	1.000	13.598	-27.196	13.598	13.595
2	$\frac{1}{2}$	2.000	3.400	-6.799	3.400	3.393
3	$\frac{1}{3}$	3.000	1.511	-3.022	1.511	1.511
5	$\frac{1}{5}$	5.000	0.544	-1.088	0.544	0.544
10	$\frac{1}{10}$	10.000	0.136	-0.272	0.136	0.136

[a] from Eq. (2.5)

[b] from $T = -\frac{1}{2}V$

[c] from Eq. (1.261)

[d] from Eq. (2.22)

[e] experimental

INSTABILITY OF EXCITED STATES

Satisfaction of the Haus condition [4] of the presence of spacetime Fourier components of the current density synchronous with those traveling at the speed of light, $k = \frac{\omega}{c}$, gives rise to radiation. For the excited (integer quantum number) energy states of the hydrogen atom, σ_{photon}, the two-dimensional surface charge due to the "trapped photons" at the atomic orbital, is given by Eqs. (2.6) and (2.11).

$$\sigma_{photon} = \frac{e}{4\pi(r_n)^2}\left[Y_0^0(\theta,\phi) - \frac{1}{n}\left[Y_0^0(\theta,\phi) + \mathrm{Re}\left\{Y_\ell^m(\theta,\phi)e^{im\omega_n t}\right\}\right]\right]\delta(r-r_n) \quad n = 2,3,4,..., \tag{2.23}$$

Whereas, $\sigma_{electron}$, the two-dimensional surface charge of the electron atomic orbital is

$$\sigma_{electron} = \frac{-e}{4\pi(r_n)^2}\left[Y_0^0(\theta,\phi) + \mathrm{Re}\left\{Y_\ell^m(\theta,\phi)e^{im\omega_n t}\right\}\right]\delta(r-r_n) \tag{2.24}$$

The superposition of σ_{photon} (Eq. (2.23)) and $\sigma_{electron}$ (Eq. (2.24)) where the spherical harmonic functions satisfy the conditions given in the Bound Electron "Atomic Orbital" section is equivalent to the sum of a radial electric dipole represented by a doublet function and an radial electric monopole represented by a delta function.

$$\sigma_{photon} + \sigma_{electron} = \frac{e}{4\pi(r_n)^2}\left[Y_0^0(\theta,\phi)\dot{\delta}(r-r_n) - \frac{1}{n}Y_0^0(\theta,\phi)\delta(r-r_n) - \left(1+\frac{1}{n}\right)\left[\mathrm{Re}\left\{Y_\ell^m(\theta,\phi)e^{im\omega_n t}\right\}\right]\delta(r-r_n)\right] \tag{2.25}$$
$$n = 2,3,4,...,$$

where

$$\left[+\delta(r-r_n) - \delta(r-r_n)\right] = \dot{\delta}(r-r_n) \tag{2.26}$$

is the Dirac doublet function [5] which is defined by the property

$$\begin{aligned} &x(t)\otimes\dot{\delta}(t) = \dot{x}(t) \\ &\int_{-\infty}^{\infty} x(\tau)\dot{\delta}(t-\tau)\,d\tau = \dot{x}(t) \end{aligned} \tag{2.27}$$

or equivalently by the property

$$\int_{-\infty}^{\infty} x(t)\dot{\delta}(t)\,dt = -\dot{x}(0) \tag{2.28}$$

The Dirac doublet is the impulse response of an ideal differentiator and corresponds to the radial electrostatic dipole.

The symbol $\dot{\delta}(t)$ is appropriate since operationally the doublet is the derivative of the impulse.

The doublet does possess spacetime Fourier components synchronous with waves traveling at the speed of light. Whereas, the radial delta function does not. The Spacetime Fourier Transform of the atomic orbital comprising a radial Dirac delta function is given in Appendix I: Nonradiation Condition:

$$M_\ell^{m_\ell}(s,\Theta,\Phi,\omega) = 4\pi \mathrm{sinc}(2sr_n) \otimes G_\ell^{m_\ell}(s,\Theta) \otimes H_\ell^{m_\ell}(s,\Theta,\Phi) \otimes \frac{1}{4\pi}[\delta(\omega-\omega_n)+\delta(\omega+\omega_n)] \tag{2.29}$$

wherein $G_\ell^{m_\ell}(s,\Theta)$ and $H_\ell^{m_\ell}(s,\Theta,\Phi)$ are the spherical-coordinate Fourier transforms of $N_{\ell,m}P_\ell^m(\cos\theta)$ and $e^{im\phi}$, respectively. The radial doublet function is the derivative of the radial Dirac delta function; thus, the Fourier transform of the doublet function can be obtained from the Fourier transform of the Dirac delta function, Eq. (2.29), and the differentiation property of Fourier transforms [6].

$$\begin{array}{lll} x(t) = \int_{-\infty}^{\infty} X(f) e^{j2\pi ft} df & & X(t) = \int_{-\infty}^{\infty} x(t) e^{-j2\pi ft} dt \\ \hline \textit{Differentiation} \quad \dfrac{dx(t)}{dt} & \Leftrightarrow & j2\pi f X(f) \end{array} \tag{2. 30}$$

From Eq. (2.29) and Eq. (2.30), the spacetime Fourier transform of Eq. (2.25), the superposition of σ_{photon} (Eq. (2.23)) and $\sigma_{electron}$ (Eq. (2.24)) is

$$M_\ell^{m_\ell}(s,\Theta,\Phi,\omega) = 4\pi s_n e^{j\frac{\pi}{2}} \frac{\sin(2s_n r_n)}{2s_n r_n} \otimes G_\ell^{m_\ell}(s,\Theta) \otimes H_\ell^{m_\ell}(s,\Theta,\Phi) \otimes \frac{1}{4\pi}[\delta(\omega-\omega_n)+\delta(\omega+\omega_n)] \tag{2.31}$$

$$M_\ell^{m_\ell}(s,\Theta,\Phi,\omega) = 4\pi s_n \frac{\cos(2s_n r_n)}{2s_n r_n} \otimes G_\ell^{m_\ell}(s,\Theta) \otimes H_\ell^{m_\ell}(s,\Theta,\Phi) \otimes \frac{1}{4\pi}[\delta(\omega-\omega_n)+\delta(\omega+\omega_n)] \tag{2.32}$$

In the case of time harmonic motion, the current-density function is given by the time derivative of the charge-density function. Thus, the current-density function is given by the product of the constant angular velocity and the charge-density function. The Fourier transform of the current-density function of the excited-state atomic orbital is given by the product of the constant angular velocity and Eq. (2.32):

$$K_\ell^{m_\ell}(s,\Theta,\Phi,\omega) = 4\pi s_n \omega_n \frac{\cos(2s_n r_n)}{2s_n r_n} \otimes G_\ell^{m_\ell}(s,\Theta) \otimes H_\ell^{m_\ell}(s,\Theta,\Phi) \otimes \frac{1}{4\pi}[\delta(\omega-\omega_n)+\delta(\omega+\omega_n)] \tag{2.33}$$

Consider the wave vector of the cosine function of Eq. (2.33). When the velocity is c corresponding to a potentially emitted photon

$$\mathbf{s}_n \bullet \mathbf{v}_n = \mathbf{s}_n \bullet \mathbf{c} = \omega_n \tag{2.34}$$

the relativistically corrected wavelength (Eq. (1.280)) is:

$$\mathbf{r}_n = \lambda_n \tag{2.35}$$

Substitution of Eq. (2.35) into the cosine function does not result in the vanishing of the Fourier transform of the current-density function. Thus, spacetime harmonics of $\frac{\omega_n}{c} = k$ or $\frac{\omega_n}{c}\sqrt{\frac{\varepsilon}{\varepsilon_0}} = k$ do exist for which the Fourier transform of the current-density function is nonzero. An excited state is metastable because it is the sum of nonradiative (stable) and radiative (unstable) components and de-excites with a transition probability given by the ratio of the power to the energy of the transition [7]. Alternatively, the radiative fields may be considered directly. In the case of the nonradiative currents of nonexcited states, the corresponding far fields have a vanishing Poynting power vector as shown in Appendix I. In contrast, regarding the dipole, the vector -/+ can flip to +/- and radiate the well known current dipole radiation having a finite Poynting power vector in the far field [8].

SOURCE CURRENT OF EXCITED STATES

As shown in Appendix I, for time-varying electromagnetic fields, Jackson [2] gives a generalized expansion in vector spherical waves that are convenient for electromagnetic boundary-value problems possessing spherical symmetry properties and for analyzing multipole radiation from a localized source distribution. The Green function $G(\mathbf{x}',\mathbf{x})$ which is appropriate to the equation:

$$(\nabla^2 + k^2) G(\mathbf{x}',\mathbf{x}) = -\delta(\mathbf{x}'-\mathbf{x}) \tag{2.36}$$

in the infinite domain with the spherical wave expansion for the outgoing wave Green function is:

$$G(\mathbf{x}',\mathbf{x}) = \frac{e^{-ik|\mathbf{x}-\mathbf{x}'|}}{4\pi|\mathbf{x}-\mathbf{x}'|} = ik\sum_{\ell=0}^{\infty} j_\ell(kr_<) h_\ell^{(1)}(kr_>) \sum_{m=-\ell}^{\ell} Y_{\ell,m}^*(\theta',\phi') Y_{\ell,m}(\theta,\phi) \tag{2.37}$$

Jackson [2] further gives the general multipole field solution to Maxwell's equations in a source-free region of empty space with the assumption of a time dependence $e^{i\omega_n t}$:

$$\mathbf{B}=\sum_{\ell,m}\left[a_E(\ell,m)\,f_\ell(kr)\mathbf{X}_{\ell,m}-\frac{i}{k}a_M(\ell,m)\nabla\times g_\ell(kr)\mathbf{X}_{\ell,m}\right]$$
$$\mathbf{E}=\sum_{\ell,m}\left[\frac{i}{k}a_E(\ell,m)\nabla\times f_\ell(kr)\mathbf{X}_{\ell,m}+a_M(\ell,m)g_\ell(kr)\mathbf{X}_{\ell,m}\right] \tag{2.38}$$

where the cgs units used by Jackson are retained in this section. The radial functions $f_\ell(kr)$ and $g_\ell(kr)$ are of the form:

$$g_\ell(kr)=A_\ell^{(1)}h_\ell^{(1)}+A_\ell^{(2)}h_\ell^{(2)} \tag{2.39}$$

$\mathbf{X}_{\ell,m}$ is the vector spherical harmonic defined by:

$$\mathbf{X}_{\ell,m}(\theta,\phi)=\frac{1}{\sqrt{\ell(\ell+1)}}\mathbf{L}Y_{\ell,m}(\theta,\phi) \tag{2.40}$$

where

$$\mathbf{L}=\frac{1}{i}(\mathbf{r}\times\nabla) \tag{2.41}$$

The coefficients $a_E(\ell,m)$ and $a_M(\ell,m)$ of Eq. (2.38) specify the amounts of electric (ℓ,m) multipole and magnetic (ℓ,m) multipole fields, and are determined by sources and boundary conditions as are the relative proportions in Eq. (2.39). Jackson gives the result of the electric and magnetic coefficients from the sources as:

$$a_E(\ell,m)=\frac{4\pi k^2}{i\sqrt{\ell(\ell+1)}}\int Y_\ell^{m*}\left\{\rho\frac{\partial}{\partial r}\left[rj_\ell(kr)\right]+\frac{ik}{c}(\mathbf{r}\cdot\mathbf{J})\,j_\ell(kr)-ik\nabla\cdot(r\times\boldsymbol{M})\,j_\ell(kr)\right\}d^3x \tag{2.42}$$

and

$$a_M(\ell,m)=\frac{-4\pi k^2}{\sqrt{\ell(\ell+1)}}\int j_\ell(kr)Y_\ell^{m*}\mathbf{L}\cdot\left(\frac{\mathbf{J}}{c}+\nabla\times\boldsymbol{M}\right)d^3x \tag{2.43}$$

respectively, where the distribution of charge $\rho(\mathbf{x},t)$, current $\mathbf{J}(\mathbf{x},t)$, and intrinsic magnetization $\boldsymbol{M}(\mathbf{x},t)$ are harmonically varying sources: $\rho(\mathbf{x})e^{-i\omega t}$, $\mathbf{J}(\mathbf{x})e^{-i\omega t}$, and $\boldsymbol{M}(\mathbf{x})e^{-i\omega t}$. The currents corresponding to Eq. (1.27) and the first term of Eqs. (1.28-1.29) are static. Thus, they are trivially nonradiative. The current due to the time dependent term of Eq. (1.29) corresponding to p, d, f, etc. orbitals is:

$$\begin{aligned}\mathbf{J}&=\frac{m\omega_n}{2\pi}\frac{e}{4\pi r_n^2}N[\delta(r-r_n)]\,\mathrm{Re}\left\{Y_\ell^m(\theta,\phi)\right\}\left[\mathbf{u}(t)\times\mathbf{r}\right]\\&=\frac{m\omega_n}{2\pi}\frac{e}{4\pi r_n^2}N'[\delta(r-r_n)]\left(P_\ell^m(\cos\theta)\cos(m\phi+m\omega_n t)\right)\left[\mathbf{u}\times\mathbf{r}\right]\\&=\frac{m\omega_n}{2\pi}\frac{e}{4\pi r_n^2}N'[\delta(r-r_n)]\left(P_\ell^m(\cos\theta)\cos(m\phi+m\omega_n t)\right)\sin\theta\hat{\phi}\end{aligned} \tag{2.44}$$

where N and N' are normalization constants. $\mathbf{J}$ corresponds to a spherical harmonic traveling charge-density wave of quantum number m that moves on the surface of the atomic orbital, spins about the z-axis at angular frequency ω_n, and modulates the constant atomic orbital at frequency $m\omega_n$. The vectors are defined as:

$$\hat{\phi}=\frac{\hat{u}\times\hat{r}}{|\hat{u}\times\hat{r}|}=\frac{\hat{u}\times\hat{r}}{\sin\theta};\qquad \hat{u}=\hat{z}=orbital\ axis \tag{2.45}$$

$$\hat{\theta}=\hat{\phi}\times\hat{r} \tag{2.46}$$

"^" denotes the unit vectors $\hat{u}\equiv\frac{\mathbf{u}}{|\mathbf{u}|}$, non-unit vectors are designed in bold, and the current function is normalized. From Eq. (2.44), the charge and intrinsic magnetization terms are zero. Also, the current $\mathbf{J}(\mathbf{x},t)$ is in the $\hat{\phi}$ direction; thus, the $a_E(\ell,m)$ coefficient given by Eq. (2.42) is zero since $\mathbf{r}\cdot\mathbf{J}=0$. Substitution of Eq. (2.44) into Eq. (2.43) gives the magnetic multipole coefficient $a_M(\ell,m)$:

$$a_M(\ell,m)=\frac{-ek^2}{c\sqrt{\ell(\ell+1)}}\frac{\omega_n}{2\pi}Nj_\ell(kr_n)\Theta\sin(ks) \tag{2.47}$$

For the electron source current given by Eq. (2.44), each comprising a multipole of order (ℓ,m) with a time dependence $e^{i\omega t}$, the far-field solutions to Maxwell's equations given by Eq. (2.38) are:

$$\begin{aligned}\mathbf{B} &= -\frac{i}{k}a_M(\ell,m)\nabla\times g_\ell(kr)\mathbf{X}_{\ell,m}\\ \mathbf{E} &= a_M(\ell,m)\,g_\ell(kr)\mathbf{X}_{\ell,m}\end{aligned} \tag{2.48}$$

and the time-averaged power radiated per solid angle $\frac{dP(\ell,m)}{d\Omega}$ is:

$$\frac{dP(\ell,m)}{d\Omega} = \frac{c}{8\pi k^2}\left|a_M(\ell,m)\right|^2\left|\mathbf{X}_{\ell,m}\right|^2 \tag{2.49}$$

where $a_M(\ell,m)$ is given by Eq. (2.47). In the case that k is the lightlike k^0, then $k=\omega_n/c$ regarding a potentially emitted photon, in Eq. (2.47), and Eqs. (2.48-2.49) vanishes for:

$$s = vT_n = R = r_n = \lambda_n \tag{2.50}$$

There is no radiation. Thus, there is no radiation due to the azimuthal charge density wave even in an excited state. However, for excited states there exists a radial dipole that is unstable to radiation as shown in the Instability of Excited States section. This instability gives rise to a radial electric dipole current considered next.

In a nonradiative state, there is no emission or absorption of radiation corresponding to the absence of radial motion wherein Eq. (2.42) is zero since $\mathbf{r}\cdot\mathbf{J}=0$; conversely, there is motion in the radial direction only when the energy of the system is changing. The same physical consequence can also be easily shown with a matter-wave dispersion relationship. Thus, radial motion corresponds to the emission or absorption of photons. The form of the radial solution during a transition is then the corresponding electron source current comprising a time-dependent radial Dirac delta function that connects the initial and final states as boundary conditions. The photon carries fields and corresponding angular momentum. This aspect is ignored in standard quantum mechanics as shown in the Schrödinger Wavefunction in Violation of Maxwell's Equations section and Refs. [9-17] where the radii of excited states are purely mathematical probability-wave eigenfunctions and are not square integrable, but are infinite in highly-excited states and have many discrepancies with observations as discussed previously [18]. In contrast, the physical characteristics of the photon and the electron are the basis of physically solving for excited states according to Maxwell's equations. The discontinuous harmonic radial current in Eq. (2.42) that connects the initial and final states of the transition is:

$$\mathbf{r}\cdot\mathbf{J} = \frac{er}{4\pi r^2}\tau^{-1}\sin\frac{\pi t'}{\tau}\left(u(t')-u(t'-\tau)\right) \tag{2.51}$$

Where τ is the lifetime of the transition given by Eq. (2.107) and t' is time during the transition.

SELECTION RULES

The multipole fields of a radiating source can be used to calculate the energy and angular momentum carried off by the radiation [19]. For definiteness we consider a linear superposition of electric (ℓ, m) multipoles with different m values, but all having the same ℓ, and following Eq. (16.46) of Jackson [19], write the fields as:

$$\begin{aligned}\mathbf{B}_\ell &= \sum_m a_E(\ell,m)\mathbf{X}_{\ell m}h_\ell^{(1)}(kr)e^{i\omega t}\\ \mathbf{E}_\ell &= \frac{i}{k}\nabla\times\mathbf{B}_\ell\end{aligned} \tag{2.52}$$

For harmonically varying fields, the time-averaged energy density is:

$$u = \frac{1}{16\pi}\left(\mathbf{E}\bullet\mathbf{E}^* + \mathbf{B}\bullet\mathbf{B}^*\right) \tag{2.53}$$

In the radiation zone, the two terms are equal. Consequently, the energy in a spherical shell between r and $(r+dr)$ ($for\ kr>>1$) is:

$$dU = \frac{dr}{8\pi k^2}\sum_{m,m'} a_E^*(\ell,m')\,a_E(\ell,m)\int\mathbf{X}_{\ell m'}^*\bullet\mathbf{X}_{\ell m}d\Omega \tag{2.54}$$

where the asymptotic form (Eq. (16.13) of Jackson [19]) of the spherical Hankel function has been used. With the orthogonality integral (Eq. (16.44) of Jackson [19]) this becomes:

$$\frac{dU}{dr} = \frac{1}{8\pi k^2}\sum_m\left|a_E(\ell,m)\right|^2 \tag{2.55}$$

independent of the radius. For a general superposition of electric and magnetic multipoles, the sum over m becomes a sum over ℓ and m and $|a_E|^2$ becomes $|a_E|^2+|a_M|^2$. The total energy in a spherical shell in the radiation zone is thus an *incoherent sum*

over all multipoles.

The time-averaged angular-momentum density is:

$$m = \frac{1}{8\pi c}\mathrm{Re}\left[\mathbf{r}\times\left(\mathbf{E}\times\mathbf{B}^*\right)\right] \tag{2.56}$$

The triple cross product can be expanded, and the electric field substituted to yield, for a superposition of electric multipoles,

$$m = \frac{1}{8\pi\omega}\mathrm{Re}\left[\mathbf{B}^*\left(\mathbf{L}\bullet\mathbf{B}\right)\right] \tag{2.57}$$

Then the angular momentum in a spherical shell between r and $(r+dr)$ in the radiation zone is:

$$dM = \frac{dr}{8\pi\omega k^2}\mathrm{Re}\sum_{m,m'} a_E^*\left(\ell,m'\right)a_E\left(\ell,m\right)\int\left(\mathbf{L}\bullet\mathbf{X}_{\ell m'}\right)^*\mathbf{X}_{\ell m}d\Omega \tag{2.58}$$

With the explicit form (Eq. (16.43) of Jackson [19]) for X_{lm}, Eq. (2.58) can be written

$$\frac{dM}{dr} = \frac{1}{8\pi\omega k^2}\mathrm{Re}\sum_{m,m'} a_E^*\left(\ell,m'\right)a_E\left(\ell,m\right)\int Y_{\ell m'}^*\mathbf{L}Y_{\ell m}d\Omega \tag{2.59}$$

From the properties of $LY_{\ell m}$ listed in Eq. (16.28) of Jackson [19] and the orthogonality of the spherical harmonics, we obtain the following expressions for the Cartesian components of $\frac{dM}{dr}$

$$\frac{dM_x}{dr} = \frac{1}{16\pi\omega k^2}\mathrm{Re}\left[\sqrt{\left(\ell-m\right)\left(\ell+m+1\right)}a_E^*\left(\ell,m+1\right)+\sqrt{\left(\ell+m\right)\left(\ell-m+1\right)}a_E^*\left(\ell,m-1\right)\right]a_E\left(\ell,m\right) \tag{2.60}$$

$$\frac{dM_y}{dr} = \frac{1}{16\pi\omega k^2}\mathrm{Im}\left[\sqrt{\left(\ell-m\right)\left(\ell+m+1\right)}a_E^*\left(\ell,m+1\right)-\sqrt{\left(\ell+m\right)\left(\ell-m+1\right)}a_E^*\left(\ell,m-1\right)\right]a_E\left(\ell,m\right) \tag{2.61}$$

$$\frac{dM_z}{dr} = \frac{1}{8\pi\omega k^2}\sum_m m\left|a_E\left(\ell,m\right)\right|^2 \tag{2.62}$$

These equations show that for a general ℓ th order electric multipole that consists of a superposition of different m values, only the z component of the angular momentum is relatively simple.

For a multipole with a single m value, M_x and M_y vanish, while a comparison of Eq. (2.62) and Eq. (2.55) shows that

$$\frac{dM_z}{dr} = \frac{m}{\omega}\frac{dU}{dr} \tag{2.63}$$

Independent of r [19]. Experimentally, the photon can carry $\hbar$ units of angular momentum. Thus, during excitation the spin, orbital, or total angular momentum of the atomic orbital can change by zero or $\pm\hbar$. The electron transition rules arise from conservation of angular momentum. The selection rules for multipole transitions between quantum states arise from conservation of total angular momentum and component angular momentum where the photon carries $\hbar$ of angular momentum.

ORBITAL AND SPIN SPLITTING

The ratio of the square of the angular momentum, M^2, to the square of the energy, U^2, for a pure (ℓ,m) multipole follows from Eqs. (2.54-2.55) and Eqs. (2.60-2.62) [19]

$$\frac{M^2}{U^2} = \frac{m^2}{\omega^2} \tag{2.64}$$

The magnetic moment is defined [20] as:

$$\mu = \frac{\text{charge x angular momentum}}{\text{2 x mass}} \tag{2.65}$$

The radiation of a multipole of order (ℓ, m) carries m$\hbar$ units of the z component of angular momentum comprised of $\hbar$ per photon of energy $\hbar\omega$. Thus, the z component of the angular momentum of the corresponding excited state electron atomic orbital is:

$$L_z = m\hbar \tag{2.66}$$

Therefore,

$$\mu_z = \frac{em\hbar}{2m_e} = m\mu_B \tag{2.67}$$

where μ_B is the Bohr magneton. The presence of a magnetic field causes the principal excited state energy levels of the hydrogen atom (Eq. (2.22)) to split by the energy E_{mag}^{orb} corresponding to the interaction of the magnetic flux with the magnetic

moment given by Eq. (2.67). This energy is called orbital splitting.

$$E_{mag}^{orb} = m\mu_B B \tag{2.68}$$

As is the case with spin splitting given by one half the energy of Eq. (1.227) which corresponds to the transition between spin states, the energy of the electron is increased in the case that the magnetic flux is antiparallel to the magnetic moment, or the energy of the electron is decreased in the case that the magnetic flux is parallel to the magnetic moment. The spin and orbital splitting energies superimpose; thus, the principal excited state energy levels of the hydrogen atom (Eq. (2.22)) are split by the energy $E_{mag}^{spin/orb}$

$$E_{mag}^{spin/orb} = m_\ell \frac{e\hbar}{2m_e} B + m_s g \frac{e\hbar}{2m_e} B \tag{2.69}$$

where it follows from Eq. (2.15) that

$$\begin{aligned} &n = 1, 2, 3, 4, ... \\ &\ell = 0, 1, 2, ..., n-1 \\ &m_\ell = -\ell, -\ell+1, ..., 0, ..., +\ell \\ &m_s = \pm 1/2 \end{aligned} \tag{2.70}$$

Based on the vector multipolarity of the corresponding source currents and the quantization of the angular momentum of photons in terms of $\hbar$, the selection rules for the electric dipole transition after Jackson [19] are:

$$\begin{aligned} &\Delta\ell = \pm 1 \\ &\Delta m_\ell = 0, \pm 1 \\ &\Delta m_s = 0 \end{aligned} \tag{2.71}$$

Splitting of the energy levels in addition to that given by Eq. (2.69) occurs due to a relativistic effect described in the Spin-Orbit Coupling (Fine Structure) section. Also, a very small shift that is observable by radio-frequency spectroscopy is due to the radiation reaction force between the electron and the photon and conservation of energy and linear momentum involving recoil during emission. This so-called Lamb shift is described in the Resonant Line Shape, and Hydrogen and Muonic Hydrogen Lamb Shift sections.

Decaying spherical harmonic currents on the surface of the atomic orbital give rise to spherical harmonic radiation fields during emission; conversely, absorbed spherical harmonic radiation fields produce spherical harmonic currents on the surface of the atomic orbital to effect a transition. Excited states are radiative according to Maxwell's equations as given in the Instability of Excited States section, and the transition probabilities or A coefficients are shown to be a function of the initial and final radii in the State Lifetime and Line Intensities section. The distribution of multipole radiation and the multipole moments of the atomic orbital for absorption and emission are derived by Jackson [7]. Some of the simpler angular distributions are listed in Table 2.2.

Table 2.2. Some of the simpler angular distributions of multipole radiation and the multipole moments of the atomic orbital for absorption and emission.

	$\left\|\mathbf{X}_{l,m}(\theta,\phi)\right\|^2$		
ℓ	m		
	0	± 1	± 2
1 Dipole	$\frac{3}{8\pi}\sin^2\theta$	$\frac{3}{16\pi}\left(1+\cos^2\theta\right)$	
2 Quadrupole	$\frac{15}{8\pi}\sin^2\theta\cos^2\theta$	$\frac{5}{16\pi}\left(1-3\cos^2\theta+4\cos^4\theta\right)$	$\frac{5}{16\pi}\left(1-\cos^4\theta\right)$

STARK EFFECT

Similarly to the splitting of the energy levels due to an external applied magnetic field, an applied electric field lifts the degeneracy of the principal energy levels of the one-electron atom to give rise to a splitting called the Stark Effect. Since the magnetic field is a relativistic effect of the electric field as shown by Jackson [21] and the electron's charge, e, charge-to-mass ratio, $\frac{e}{m_e}$, angular momentum of $\hbar$, and the magnetic moment of μ_B are relativistically invariant, it is not surprising as shown in this section that the energy, E_{Stark}, of a one-electron atom in an electric field follows from Eqs. (2.68-2.69) with the magnetic dipole moment replaced by the electric dipole moment and the magnetic flux replaced by the electric field $\mathbf{E}_{applied}$. Considering only an electric dipole $\mathbf{p_z}$ and the direct influence of the external field, the energy is:

$$E_{Stark} = \mathbf{p_z} \cdot \mathbf{E}_{applied} \tag{2.72}$$

The bound electron has a field equivalent to that of a point charge at the origin for a radius greater than that of the atomic orbital as given in the Determination of Atomic Orbital Radii section. The electric field of the nucleus is also equivalent to that of a point particle at the origin. This condition also holds for the spherically and time harmonic excited-state charge-density waves on the surface of the atomic orbital given in the Excited States of the One-Electron Atom (Quantization) section. In these cases, the dipole moment over the angular integrals is zero, but excited-state Stark splittings with the equivalent of the corresponding electric dipole moments given by Eq. (2.72) exist due to the interaction of the applied electric field and the angular momentum of the excited-state photon field.

As further shown in the Excited States of the One-Electron Atom (Quantization) section, quantization is trivial given that the bound electron forms a cavity and the photon has quantized energy and angular momentum corresponding to the multipolarity of the excited-state photon. According to Eq. (2.64), the angular momentum of the excited-state-photon field of energy $\hbar\omega$ carries $m_\ell\hbar$ units of angular momentum to excite the orbital having the quantum number m_ℓ. Then, the transition with $\Delta m_\ell = \pm 1$ of Eq. (2.71) gives the result of Eq. (4.1), and the superposition principle of photons gives the general case corresponding to Eq. (2.64).

The photon-field is phase-locked to the electron charge-density wave of matching multipole moment, and both rotate about the z-axis at the angular velocity given by Eq. (2.20). The rotation is without dissipation; thus, it is a supercurrent. It can be shown that the maintenance of the supercurrent condition and the quantization of the photon-field in terms of $m_\ell\hbar$ quantizes the electric dipole moment of Eq. (2.72) in terms of the quantum number m_ℓ. According to Eq. (2.69), the energy of the excited state due to the orbital angular momentum caused by the excited-state photon in the presence of a magnetic flux B is:

$$E_{mag}^{orb} = m_\ell \frac{e\hbar}{2m_e} B = \frac{m_\ell e}{2}\frac{na_0}{Z}\frac{\hbar}{m_e\frac{na_0}{Z}} B = \frac{3}{2}\frac{m_\ell e}{2}\frac{na_0}{Z} v_n B \sin\theta \tag{2.73}$$

where the velocity, v_n, is given by Eq. (1.35), the geometric factor of $\frac{3}{2}\sin\theta$ is given by Eq. (1.144), and the radii of the excited states are given by Eq. (2.5).

It is shown in the Stored Electric Energy section that during a Stern-Gerlach transition, the applied flux gives rise to a Lorentz force on the atomic orbital current resulting in a crossed electric field corresponding to a Hall voltage. With an exact balance between the Lorentz force (Eq. (1.183)) and the electric force corresponding to the Hall voltage (Eq. (1.184)), each superconducting charge-density element of the electron propagates along a great circle according to Eq. (1.187) which is the condition for superconductivity in the presence of crossed electric and magnetic fields. Consider the case of a Stark-split transition of the electron wherein the applied electric field causes a current that gives rise to a magnetic flux $\mathbf{B}_x$. In this case, the superconductor condition for the vectors shown in Figure 2.3 is

$$E / B = v_n \sin\theta \tag{2.74}$$

Figure 2.3. Coordinate system of crossed electric field, $\mathbf{E}_z$, corresponding to the applied field, magnetic flux, $\mathbf{B}_x$, due to photon field, and superconducting current $\mathbf{i}_y$.

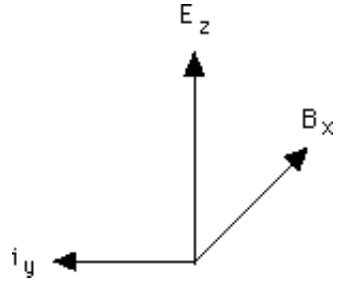

The magnetic field $\mathbf{B}_x$ that is crossed with the applied electric field arises when the electron flips by 180° which doubles the energy of Eq. (2.73). Then, the energies due to an applied electric field are given by the substitution of Eq. (2.74) into Eq. (2.73)

and the multiplication of the result by 2:

$$E_{Stark} = m_\ell \frac{3}{2}\frac{ena_0}{Z} E_{applied} \tag{2.75}$$

From Eqs. (2.72) and (2.75), the eccentric dipole $\mathbf{p}_z$ is:

$$\mathbf{p}_z = m_\ell \frac{3}{2}\frac{ena_0}{Z}\mathbf{i}_z \tag{2.76}$$

wherein m_ℓ is given by Eq. (2.70).

There is no Stark effect unless the charge density is time-dependent modulated by the photon-field. Since the degeneracy is lifted by the external electric field by the induction of an effective electric dipole moment in the atom, transitions between all m_ℓ levels are allowed corresponding to the maximum value of the quantum number ℓ of each level. In this case, the superconductor condition is met since the amplitude of the rotational energy of the charge-density wave given by Eq. (1.71):

$$E_{rotational\ orbital} = \frac{\hbar^2}{2I}\left[\frac{\ell(\ell+1)}{\ell^2+2\ell+1}\right] = \frac{\hbar^2}{2m_e r_n^{\,2}}\left[\frac{\ell}{\ell+1}\right] = \frac{\hbar^2}{2m_e r_n^{\,2}}\left[\frac{n-1}{(n-1)+1}\right] = \frac{\hbar^2}{2m_e r_n^{\,2}}\left[1-\frac{1}{n}\right] = \frac{1}{2}h\nu_n\left[1-\frac{1}{n}\right] \tag{2.77}$$

is that corresponding to the photon as given by Eqs. (2.16) and (2.23), and the corresponding supercurrent component of the photon is given by the frequency (Eqs. (1.32) and (1.36)) times the charge e. Thus, the allowed quantum numbers for the state with principal quantum number n having an effective electric dipole that is a function of principal quantum number n are:

$$\begin{aligned} n &= 1, 2, 3, 4, ... \\ \ell &= n-1 \\ m_\ell &= -\ell, -\ell+1, ..., 0, ..., +\ell \\ m_s &= \pm\frac{1}{2} \end{aligned} \tag{2.78}$$

The splitting of the energy level with principal quantum number n into $(2n-1)$ equidistant sub-levels determined by the quantum number m_ℓ for the $n=1$ to $n=6$ levels is given in Table 2.3. The predictions given by Eq. (2.75) for hydrogen match those given in Ryde [22][2].

---

[2] The theory of the Stark Effect according to quantum mechanics does not arise naturally, rather it must be forced by simultaneously using internally inconsistent spherical and parabolic quantum numbers. The theory also requires the "mutual perturbation" of orbitals involving a single electron in the absence of a transition which is nonphysical [22-23]. Hund's-Rule and Pauli-Exclusion-Principle-type violations are encountered by this "mutual perturbation" as well as by the existence of more than one set of quantum numbers for the same state. Moreover, lines corresponding to the redundant, nonunique quantum numbers are predicted that are not observed.

The agreement between the predictions of Eq. (2.75) and observations also confirms that the radius of the atomic-hydrogen-excited states is given by na_0 rather than $n^2 a_0$ as incorrectly given by the Bohr, Schrödinger, and Dirac equations. These theories are further internally inconsistent because the one-electron-atom wave functions cannot give rise to the electric dipole moments given by Eq. (2.76). In fact, except for the directional orbitals such as np_z, there are no electric dipole moments possible, and the requirement of the localization of the entire charge of the electron along the z-axis violates the Uncertainty Principle as well as all physical laws for a charge bound in a Coulombic central field. Furthermore, mixing of orbitals to give an electric dipole of nea_0 requires the hydrogen atom to have positive and negative poles separated by na_0 in contradiction to the experimental observation that its symmetric neutrality does not change in an electric field.

The argument that such an enormous electric dipole of nea_0 exists only in an excited state does not save the quantum-mechanical basis of the Stark effect. The dielectric susceptibility of any atom is a function of any induced electric dipole moment. Hydrogen has a dielectric constant different from vacuum in the ground state. The physics for the dipole moment of any excited state must also apply to the ground state. Since the experimentally observed susceptibility and thus the induced moment is many orders of magnitude less than that predicted for hydrogen, the quantum mechanical basis for the Stark Effect of electric polarization is disproved. The need to reject the quantum mechanical premise is further easily appreciated by considering the enormous predicted, but unobserved, change in reactivity of hydrogen due to the application of even a very weak electric field.

Table 2.3. The splitting of the energy level with principal quantum number n into $(2n-1)$ equidistant sub-levels determined by the quantum number m_ℓ for the $n=1$ to $n=6$ levels.

n	ℓ	m_ℓ	ΔE [a]
1	0	0	0
2	1	1 0 -1	2a 0 -2a
3	2	2 1 0 -1 -2	6a 3a 0 -3a -6a
4	3	3 2 1 0 -1 -2 -3	12a 8a 4a 0 -4a -8a -12a
5	4	4 3 2 1 0 -1 -2 -3 -4	20a 15a 10a 5a 0 -5a -10a -15a -20a
6	5	5 4 3 2 1 0 -1 -2 -3 -4 -5	30a 24a 18a 12a 6a 0 -6a -12a -18a -24a -30a

[a] Eq. (2.75) with $\frac{3}{2}ea_0E_{applied}$ defined as a.

Here, as shown in the Instability of Excited States section, the excited states are radiative due to a radial electric dipole term. The spectral line emitted as a transition between energy levels n_i and n_f of the hydrogen atom consists of numerous components. The selection rules for electric dipole transitions in the presence of an applied electric field are given by:

$$\begin{aligned}\Delta\ell &= \ell_f - \ell_i = (n_f - 1) - (n_i - 1) = n_f - n_i \\ \Delta m_\ell &= m_{\ell f} - m_{\ell i} = \pm\left(0,1,2....(n_f-1)+(n_i-1)\right) == \pm\left(0,1,2....(n_f+n_i-2)\right)\end{aligned} \tag{2.79}$$

where the subscripts i and f denote the initial and final states, respectively. Due to the vector multipolarity of the corresponding source currents and the quantization of the angular momentum of photons in terms of $\hbar$, these components are either linearly polarized parallel to the vector of the external field, **E**, or circularly polarized in the plane perpendicular to **E**. The polarization is determined by the parity of the sum of the change in the ℓ and m_ℓ quantum numbers after Jackson [19]; so, that

$$\begin{aligned}\Delta\ell + \Delta m_\ell &= \text{even integers} \;\rightarrow\; (\pi\text{-components}) \\ \Delta\ell + \Delta m_\ell &= \text{odd integers} \;\rightarrow\; (\sigma\text{-components})\end{aligned} \tag{2.80}$$

The zero components are forbidden except for the σ-component when $\Delta\ell$ is odd such that the state change conserves the angular momentum of the photon. The intensities of the lines are determined by Eq. (2.107) where the multipolarity of the photon is a z-oriented dipole.

From Table 2.3 and Eq. (2.80), L_α (λ =1215 Å) is split into a triplet comprising a central $\Delta E = 0$, σ-component and

two external $\Delta E = \pm 2a$, π-components. L_β (λ =1025 Å) is split up into two inner $\Delta E = \pm 3a$, σ-components and two $\Delta E = \pm 6a$, π-components having twice the displacement. L_γ (λ =972 Å) comprises 4 π- and three σ-components. The middle undisplaced line being a σ-component and the other alternating π- and σ-components. In general, the number of Lyman lines is equal to the number of sublevels of the initial emitting state $(2n-1)$. The lines comprise n π-components and $n-1$ σ-components except that the zero component is absent when it is a π-component. In this case, $2n-2$ lines are observed comprising each of $n-1$ π- and σ-components. The predicted splitting of the Lyman lines and their corresponding polarizations and energies match those observed experimentally [22].

The three sublevels of L_α form the final states in the emission of Balmer lines. Theoretically, the number of components into which the Balmer lines are split is $3n-1$ π-components and $3n-2$ σ-components except that the zero component is absent when it is a π-component. For H_α (λ =6562 Å), there are eight π-components with $\Delta E = \pm 2a$, $\pm 3a$, $\pm 4a$, and $\pm 8a$, and seven σ-components with $\Delta E = 0$, $\pm 1a$, $\pm 5a$, and $\pm 6a$. Again, the predictions match the experimental data [22].

For H_β (λ =4861Å), ten π-components with $\Delta E = \pm 2a$, $\pm 6a$, $\pm 8a$, $\pm 10a$, and $\pm 14a$, and ten σ-components with $\Delta E = \pm 2a$, $\pm 4a$, $\pm 6a$, $\pm 10a$, and $\pm 12a$ are predicted. All of these lines have been recorded except the faintest ones, the outermost π-components with $\Delta E = \pm 14a$ [22]. For H_γ (λ =4340 Å), the energy shifts of the predicted π- and σ-components are $\Delta E = \pm 2a$, $\pm 5a$, $\pm 8a$, $\pm 12a$, $\pm 15a$, $\pm 18a$, and $\pm 22a$ and $\Delta E = 0$, $\pm 3a$, $\pm 7a$, $\pm 10a$, $\pm 13a$, $\pm 17a$, and $\pm 20a$, respectively. For H_δ (λ =4101 Å), the energy shifts of the predicted π- and σ-components are $\Delta E = \pm 4a$, $\pm 8a$, $\pm 12a$, $\pm 16a$, $\pm 20a$, $\pm 24a$, $\pm 28a$, and $\pm 32a$ and $\Delta E = \pm 2a$, $\pm 6a$, $\pm 10a$, $\pm 14a$, $\pm 18a$, $\pm 22a$, $\pm 26a$, and $\pm 30a$, respectively. All of the theoretically predicted H_γ and H_δ lines have been observed by Stark and others [22-24]. For Balmer lines having odd n, no π- and σ-components coincide, but this does not apply for some components of lines with even n. Such components are consequently partially polarized. Furthermore, zero components only appear in σ-polarization when n is odd (i.e. for H_α, H_γ, H_ε...) corresponding to the case where $\Delta\ell$ is odd. This confirms the basis of the selection and polarization rules as the conservation of angular momentum between the initial and final states and the emitted multipole radiation.

STATE LIFETIMES AND LINE INTENSITIES

The power radiated from an excited state can be calculated from the oscillating current corresponding to the motion of the electron from the initial to the final radius. It is evident from Maxwell's equations that oscillating currents are required in order to generate electromagnetic radiation:

$$\nabla X\mathbf{E} = -i\omega\mu\mathbf{H} \tag{2.81}$$

$$\nabla X\mathbf{H} = \mathbf{J} + i\omega\varepsilon\mathbf{E} \tag{2.82}$$

From the electron-transition current **J**, the electric and magnetic fields can be solved through an auxiliary function to Eqs. (2.81-2.82) called the vector potential **A**:

$$\mathbf{B} = \nabla X\mathbf{A} \tag{2.83}$$

Using Eqs. (2.81-2.83) the inhomogeneous wave equation is derived [25]:

$$\nabla^2\mathbf{A} + \omega^2\mu\varepsilon\mathbf{A} = -\mu\mathbf{J} \tag{2.84}$$

which has the solution

$$\mathbf{A}(r) = \frac{\mu}{4\pi}\iiint_V dV'\frac{\mathbf{J}(r')e^{-ik|\mathbf{r}-\mathbf{r}'|}}{|\mathbf{r}-\mathbf{r}'|} \tag{2.85}$$

where $k = \omega\sqrt{\mu\varepsilon}$, $\mathbf{r}$ is the vector-potential position, **r'** is the position vector of the sources, and $|\mathbf{r}-\mathbf{r}'|$ is the distance between the observation point **r** and the source point **r'**.

The radial current for an electric dipole transition is only finite during the movement of the electron from a state with quantum numbers n_i, ℓ, m_s, m_ℓ and radius r_{n_i} to another state with quantum numbers $n_f, \ell \pm 1, m_s, m_\ell$ and radius r_{n_f}. As shown by Eq. (2.66), the photon carries quantized units of $m\hbar$ of angular momentum along the z-axis. Consequently, for an electric dipole transition, the selection rule on the ℓ quantum number that conserves the angular momentum of the electron and emitted photon given by Eq. (2.71) is

$$\Delta\ell = \pm 1 \tag{2.86}$$

In this case, the multipolarity of the radiation and that of the source current correspond to spherical harmonics that are related by Eq. (2.42). The radial and azimuthal transition currents over the transition lifetime τ are:

$$\mathbf{J}_r = \frac{e}{4\pi r^2}\tau^{-1}\sin\frac{\pi t'}{\tau}\left(u(t') - u(t'-\tau)\right)\mathbf{i}_r \tag{2.87}$$

and

$$\mathbf{J}_\phi = \left(\frac{\omega_n + \Delta\omega_n \sin\frac{\pi t'}{2\tau}}{2\pi}\right)\frac{e}{4\pi r^2}N'\delta\left(r-\left(r_n+\Delta r_n \sin\frac{\pi t'}{2\tau}\right)\right)$$
$$\left(\begin{array}{l}\left(\begin{array}{l}Y_0^0(\theta,\phi)+\\ P_\ell^m(\cos\theta)\cos\left(m\phi+m\omega_n t+\Delta m\omega_n t\sin\frac{\pi t'}{2\tau}\right)\end{array}\right)\cos\frac{\pi t'}{2\tau}\\ +\left(\begin{array}{l}Y_0^0(\theta,\phi)+\\ P_{\ell\pm1}^m(\cos\theta)\cos\left(m\phi+m\omega_n t+\Delta m\omega_n t\sin\frac{\pi t'}{2\tau}\right)\end{array}\right)\sin\frac{\pi t'}{2\tau}\end{array}\right)\left(u(t')-u(t'-\tau)\right)\mathbf{i}_\phi \tag{2.88}$$

respectively, where the lifetime τ of the transition is given by Eq. (2.107), $\Delta\omega = \omega_f - \omega_i$ is the final angular frequency minus the initial, $\Delta r_n = r_f - r_i$ is the final discrete radius minus the initial, t' is time during the transition, and t is the continuous time variable independent of the transition.

As shown in the Photon section, the photon-field equation gives rise to a Green function given by Eqs. (4.18-4.23) with the superposition of many photons. The spherical-wave radiation that propagates in the radial direction has the same form as the source radial current. Due to the spherical symmetry and the time harmonic nature of the electron transition current, the vector potential corresponds to a current dipole at the origin and is a solution of Eq. (2.84). The Green function solution (Eq. (2.85)) matches a spherical radiation wave comprised of photons (Eq. (4.23)) wherein the quantized electron transition current and photon field are basis elements for the macroscopic (continuous) Maxwellian solutions for source current and the corresponding radiation fields.

The vector potential and power can be solved using the constraints of conservation of power and linear and angular momentum between the outgoing discrete (quantized) photon field with the change of the current densities between the initial and final discrete (quantized) states for an electric dipole transition. The electric dipole selection rule is given by Eq. (2.86). In order to conserve the photon's quantized angular momentum along the z-axis, the ℓ quantum number corresponding to the angular momentum of the excited electronic state must change by ±1 corresponding to the transition from initial quantum states n_i, ℓ, m_s, m_ℓ and radius r_{n_i} to the final state with quantum numbers $n_f, \ell\pm1, m_s, m_\ell$ and radius r_{n_f}. The angular dependence of the current which connects the initial and final states is conserved in the photon field. Since there is no special preparation of the states, the radiation pattern is isotropic, and the power and concomitantly, the intensity of each electric dipole transition connecting states with the same initial and final principal quantum numbers are the same. However, the multiplicity of a given ℓ state does change the relative intensities based on statistical population distributions as discussed *infra*.

During an electronic transition, the current-density comprises a radially propagating constant spherical shell of current that is modulated by a traveling charge density wave. The angular integral of the vector potential is given by

$$\begin{aligned}\mathbf{A}(r) &= \frac{\mu_0}{4\pi}\frac{1}{4\pi}\int_0^{2\pi}\int_0^{\pi}\left(Y_0^0(\theta,\phi)+\frac{1}{2}Y_\ell^m(\theta,\phi)+\frac{1}{2}Y_{\ell\pm1}^m(\theta,\phi)\right)\sin\theta\, d\theta\, d\phi\int_{r_n}^{r_{n_f}}\mathbf{J}(r')\frac{e^{-ik_r|\mathbf{r}-\mathbf{r}'|}}{|\mathbf{r}-\mathbf{r}'|}dr'\\ &= \frac{\mu_0}{4\pi}\int_{r_n}^{r_{n_f}}\mathbf{J}(r')\frac{e^{-ik_r|\mathbf{r}-\mathbf{r}'|}}{|\mathbf{r}-\mathbf{r}'|}dr'\end{aligned} \tag{2.89}$$

The radial electric dipole current for the selection-rule condition of Eq. (2.86) is:

$$\frac{\mathbf{r}}{|\mathbf{r}|}\cdot\mathbf{J} = J\mathbf{i}_z \tag{2.90}$$

In order to achieve conservation of energy and power flow as well as angular momentum:

$$J = \frac{e}{4\pi r^2}\frac{\omega}{2\pi} = \frac{e}{4\pi r^2}\frac{\hbar}{2\pi m_e r^2} = \frac{e}{2\pi 4\pi r^2}\frac{v}{r} \tag{2.91}$$

where Eqs. (1.36) and (1.35) were used for the angular and linear velocity, respectively. The current that gives rise to quantized radiation comprises two terms. One corresponds to the quantized angular frequency change that matches the angular frequency of the corresponding emitted photon, and the other corresponds to the quantized wavenumber change with the transition from the initial to final radius. Using Eq. (1.280), the relationship between the electron radius and wavelength in the lightlike frame is given by Eq. (1.16). The radial current from the initial to final radius must be one wavelength in order to be phase-matched with the photon wavelength. Thus, the electron wavenumber corresponding to the propagating photon traveling at $v = c$ is given by the difference in the lightlike electron wavelength in going from the initial to final radius:

$$k_r = k_{r_f} - k_{r_i} = \frac{2\pi}{\lambda_f} - \frac{2\pi}{\lambda_i} = \frac{2\pi}{r_f} - \frac{2\pi}{r_i} \tag{2.92}$$

From Eqs. (2.89-2.92), the quantized current changes in the radial integral of the vector potential are:

$$\mathbf{A}(r) = \frac{\mu_0}{4\pi}\frac{e\hbar}{m_e}\int_{r_{n_i}-r_{n_f}}^{\infty}\frac{1}{2\pi r'^4}\frac{e^{-ik_r|\mathbf{r}-\mathbf{r}'|}}{|\mathbf{r}-\mathbf{r}'|}r'^2\, dr'\mathbf{i}_z \tag{2.93}$$

where the current is a function of $r_{n_i} - r_{n_f}$ in order to conserve the electron and photon angular momentum as in the case of Eq. (1.37). Due to spherical symmetry, the electric dipole current is equivalent to that of a dipole at the origin. With $r' = 0$ in the Green function, $\mathbf{A}(r)$ is:

$$\mathbf{A}(r) = \frac{\mu_0}{2\pi}\frac{e\hbar}{m_e}\int_{r_{n_i}-r_{n_f}}^{\infty}\frac{1}{r'^4}\frac{e^{-ik_r r}}{4\pi r}r'^2\,dr'\mathbf{i}_z = \frac{\mu_0}{2\pi}\frac{e\hbar}{m_e}\frac{1}{r_{n_i}-r_{n_f}}\frac{e^{-ik_r r}}{4\pi r}\mathbf{i}_z \tag{2.94}$$

Applying Eq. (2.83) to $\mathbf{A}(r)$ given by Eq. (2.94) gives the magnetic field **H**:

$$\mathbf{H} = \frac{1}{\mu}\nabla X\mathbf{A} = \frac{e\hbar}{m_e}\frac{1}{r_{n_i}-r_{n_f}}\frac{jk_r}{2\pi}\frac{e^{-ik_r r}}{4\pi r}\left(1+\frac{1}{jk_r r}\right)\sin\theta\mathbf{i}_\phi \tag{2.95}$$

where

$$\mathbf{i}_z = \cos\theta\mathbf{i}_r - \sin\theta\mathbf{i}_\theta \tag{2.96}$$

Outside the dipole source, the corresponding electric field **E** of the radiation with angular frequency ω is given by Ampere's law:

$$\mathbf{E} = \frac{1}{i\omega\varepsilon_0}\nabla X\mathbf{H} = \sqrt{\frac{\mu_0}{\varepsilon_0}}\frac{e\hbar}{m_e}\frac{1}{r_{n_i}-r_{n_f}}\frac{ik_r}{2\pi}\frac{e^{-ik_r r}}{4\pi r}\left\{\begin{array}{l}\left(\frac{1}{ik_r r}+\frac{1}{(ik_r r)^2}\right)2\cos\theta\mathbf{i}_r + \\ \left(1+\frac{1}{ik_r r}+\frac{1}{(ik_r r)^2}\right)\sin\theta\mathbf{i}_\theta\end{array}\right\} \tag{2.97}$$

wherein a further phase match between the electron and photon wavelengths gives the replacement of ω by $k_r c$ corresponding to the Haus condition [4] $k = \frac{\omega}{c}$ given in the Instability of Excited States section. The photon and the electron wave relationships are given in the Equation of the Photon section. For the initial conditions of an unbound electron at rest, the ratio of the linear velocity of the subsequently bound electron to the emitted free-space photon given by (Eq. (4.5)) is:

$$\frac{v_n}{c_{photon}} = \frac{\lambda_n\frac{\omega_n}{2\pi}}{\lambda_{photon}\frac{\omega_{photon}}{2\pi}} = \frac{\lambda_n}{\lambda_{photon}} = \frac{\pi r_n}{r_{photon}} \tag{2.98}$$

where the n subscripts refer to atomic orbital. The relations between the free space photon wavelength, radius, and velocity and the corresponding parameters of a free electron as it is bound are:

(1) $r_{n,photon}$, the radius of the photon electric and magnetic vector field (photon-e&mvf), is equal to $r_n\pi\frac{c}{v_n} = na_H\pi\frac{c}{v_n}$, the electron atomic orbital radius given by Eqs. (2.2) and (2.5) times the product of π and the ratio of the speed of light c and v_n, the velocity of the atomic orbital given by Eq. (1.35):

$$r_{n,photon} = r_n\frac{c}{v_n} = na_H\frac{c}{v_n} \tag{2.99}$$

(2) λ_{photon}, the photon wavelength, is equal to $\lambda_n\frac{c}{v_n}$, where λ_n is the atomic orbital de Broglie wavelength:

$$\lambda_{photon} = \lambda_n\frac{c}{v_n} \tag{2.100}$$

(3) $\omega_{photon} = \frac{2\pi c}{\lambda}$, the photon angular velocity, is equal to ω_n, the atomic orbital angular velocity given by Eq. (1.36):

$$\omega_{photon} = \frac{2\pi c}{\lambda} = \omega_n \tag{2.101}$$

In the far field, the photon radiation is that of a spherical wave as given in the Equation of the Photon section. In this case $k_r r >> 1$, and the terms having powers of $(k_r r)^{-1}$ vanish. The corresponding radiation fields are:

$$\mathbf{H} = \frac{e\hbar}{m_e}\frac{1}{r_{n_i}-r_{n_f}}\frac{ik_r}{2\pi}\frac{e^{-ik_r r}}{4\pi r}\sin\theta\mathbf{i}_\phi \tag{2.102}$$

$$\mathbf{E} = \sqrt{\frac{\mu_0}{\varepsilon_0}}\frac{e\hbar}{m_e}\frac{1}{r_{n_i}-r_{n_f}}\frac{ik_r}{2\pi}\frac{e^{-ik_r r}}{4\pi r}\sin\theta\mathbf{i}_\theta \tag{2.103}$$

The time-averaged power density in the radiation zone is given by

$$\langle \mathbf{S} \rangle = \frac{1}{2}\mathrm{Re}\left[\mathbf{E}\times\mathbf{H}^*\right] = \frac{1}{2}\sqrt{\frac{\mu_0}{\varepsilon_0}}\left|H_\phi\right|^2 = \frac{\eta}{2}\left(\frac{e\hbar}{m_e}\left|\frac{1}{r_{n_i}-r_{n_f}}\right|\frac{k_r}{2\pi}\frac{1}{4\pi r}\right)^2 \sin^2\theta\,\mathbf{i}_r \tag{2.104}$$

The total radiated power P is given by integrating the Poynting power density (Eq. (2.104)) over the surface of a sphere at radius r:

$$P = \int_0^{2\pi}\int_0^{\pi}\langle \mathbf{S} \rangle r^2 \sin\theta d\theta d\phi = \frac{2\pi\eta}{2}\left(\frac{k_r}{2\pi}\frac{e\hbar}{4\pi m_e}\left|\frac{1}{r_{n_i}-r_{n_f}}\right|\right)^2 \int_0^{\pi}\sin^3\theta d\theta = \frac{4\pi}{3}\eta\left|\frac{k_r}{2\pi}\frac{e\hbar}{4\pi m_e}\left(\frac{1}{r_{n_i}-r_{n_f}}\right)\right|^2 \tag{2.105}$$

Eq. (2.105) is the form of the Maxwellian result for continuous fields and the corresponding source current. As shown in the Equation of the Photon section, atomic transitions are quantized and the continuous-field result of Eq. (2.105) is given by the superposition of many photons as the number goes to infinity.

The discrete or quantized power must further include the conservation of linear momentum of the radiating electron with that of the photon. Since power is the energy divided by the lifetime, the correction to the power is the same as that of the energy. The application of the correction for linear momentum conservation given by Eq. (2.153) gives the power of the quantized transition of energy $\hbar\omega$ as:

$$P = \frac{\hbar\omega}{2m_ec^2}\frac{4\pi}{3}\eta\left|\frac{k_r}{2\pi}\frac{e\hbar}{4\pi m_e}\left(\frac{1}{r_{n_i}-r_{n_f}}\right)\right|^2 \tag{2.106}$$

The transition probability $\frac{1}{\tau}$ or A_{ki} coefficient is given by Jackson [7]:

$$\frac{1}{\tau} = A_{ki} = \frac{power}{energy} \tag{2.107}$$

Substitution of Eqs. (2.106) and (2.148) into Eq. (2.107) gives the electric dipole electronic transition probability from initial quantum states n_i, ℓ, m_s, m_ℓ and radius r_{n_i} to the final state with quantum numbers $n_f, \ell\pm1, m_s, m_\ell$ and radius r_{n_f}:

$$\frac{1}{\tau} = \frac{\frac{\hbar\omega}{2m_ec^2}\frac{4\pi}{3}\eta\left|\frac{2\pi\left(\frac{1}{r_{n_f}}-\frac{1}{r_{n_i}}\right)}{2\pi}\frac{e\hbar}{4\pi m_e}\frac{1}{r_{n_i}-r_{n_f}}\right|^2}{\hbar\omega} = \frac{1}{m_ec^2}\frac{\eta}{24\pi}\left(\frac{e\hbar}{m_ea_0^2}\right)^2\left|\frac{1}{n_i-n_f}\left(\frac{1}{n_f}-\frac{1}{n_i}\right)\right|^2 = 2.678\ X\ 10^9\Re\ s^{-1} \tag{2.108}$$

where Eq. (2.5) was used for the radii and $\Re$ is defined as

$$\Re = \left|\frac{1}{n_i-n_f}\left(\frac{1}{n_f}-\frac{1}{n_i}\right)\right|^2 = \left|\frac{1}{n_i-n_f}\left(\frac{n_i-n_f}{n_fn_i}\right)\right|^2 = \frac{1}{\left(n_fn_i\right)^2} \tag{2.109}$$

The reciprocal of Eq. (2.108) gives the mean state lifetime[3]:

$$\tau = 2m_ec^2\frac{3}{4\pi\eta}\left|\frac{2\pi\left(\frac{1}{r_{n_f}}-\frac{1}{r_{n_i}}\right)}{2\pi}\frac{e\hbar}{4\pi m_e}\frac{1}{r_{n_i}-r_{n_f}}\right|^{-2} = m_ec^2\frac{24\pi}{\eta}\left(\frac{e\hbar}{m_ea_0^2}\right)^{-2}\left|\frac{1}{n_i-n_f}\left(\frac{1}{n_f}-\frac{1}{n_i}\right)\right|^{-2} = 3.735\ X\ 10^{-10}\Re^{-1}\ s \tag{2.110}$$

where Eq. (2.5) was used for the radii. Using Eqs. (2.108-2.2110), the parameters of representative hydrogen emission series of lines are given in Tables 2.4-2.16.

Since there is no special preparation of the states, the radiation pattern is isotropic, and the power and concomitantly the intensity of each electric dipole transition connecting states with the same initial and final principal quantum numbers are the same. However, the multiplicity of a given ℓ state does change the relative intensities based on the statistical population of states of the same principal quantum number n, but different ℓ quantum numbers. As given in Jackson, the "sum rule" for the squares of the $Y_{\ell,m}$'s is

$$\sum_{m=-\ell}^{\ell}\left|Y_{\ell,m}(\theta,\phi)\right|^2 = \frac{2\ell+1}{4\pi} \tag{2.111}$$

Furthermore, the total number of states N for a given principal quantum number n is given by (Eq. (1.70)):

$$N = \sum_{\ell=0}^{n-1}\sum_{m_\ell=-\ell}^{+\ell}1 = \sum_{\ell=0}^{n-1}2\ell+1 = n^2 \tag{2.112}$$

[3] A mean lifetime arises due to the superposition of transitions over an ensemble of individual atoms. Each atom has an exact lifetime due to an exact transition involving specific initial, final, and any intermediate ℓ, m states and the corresponding exact photon in space relative to the states. The mean lifetime arises from the mean current given by Eq. (2.87) and the spherical radiation field due to the superposition of emitted photons. Similarly, Maxwell's equations apply to macroscopic fields that are in actuality the superposition of quantized photons. Thus, deterministic physics arises as the aggregate behavior of entities that also in turn obey deterministic physics.

where each state corresponds to an ℓ and m_ℓ quantum number of an energy level corresponding to the principal quantum number n. Consequently, a source comprised of a set of multipoles of order ℓ, independent of m_ℓ gives rise to an isotropic radiation distribution when the multipoles superimpose incoherently. This is the typical case in atomic and nuclear radiative transitions unless the initial state has been prepared in a special way. In the case that the ℓ states can be distinguished, the relative intensities are given statistically by the ratios of the multiplicity of each state divided by the total number of states. Thus, the relative intensity of state ℓ is given by

$$\frac{2\ell+1}{n^2} \tag{2.113}$$

Using Eq. (2.113), the relative line intensities for the transitions ${}^2P^0_{3/2} \to {}^2S_{1/2}$ and ${}^2D_{5/2} \to {}^2P^0_{3/2}$ wherein are $\ell = 1$ and $\ell = 2$ are 3:5 which closely matches the NIST observed relative intensities of 120:180 [26].

Table 2.4. The parameters of the Lyman series of emission lines.

n_i	n_f	$\Re$ [a]	$\Re_{n_i\to 1} / \Re_{2\to 1}$	$1/\tau$ [b]	τ [c]
2	1	2.50E-01	1.00	6.70E+08	1.49E-09
3	1	1.11E-01	0.44	2.98E+08	3.36E-09
4	1	6.25E-02	0.25	1.67E+08	5.97E-09
5	1	4.00E-02	0.16	1.07E+08	9.34E-09
6	1	2.78E-02	0.11	7.44E+07	1.34E-08
7	1	2.04E-02	0.08	5.47E+07	1.83E-08
8	1	1.56E-02	0.06	4.18E+07	2.39E-08
9	1	1.23E-02	0.05	3.31E+07	3.02E-08
10	1	1.00E-02	0.04	2.68E+07	3.73E-08
11	1	8.26E-03	0.03	2.21E+07	4.52E-08
12	1	6.94E-03	0.03	1.86E+07	5.38E-08
13	1	5.92E-03	0.02	1.58E+07	6.31E-08
14	1	5.10E-03	0.02	1.37E+07	7.32E-08
15	1	4.44E-03	0.02	1.19E+07	8.40E-08
16	1	3.91E-03	0.02	1.05E+07	9.56E-08
17	1	3.46E-03	0.01	9.27E+06	1.08E-07
18	1	3.09E-03	0.01	8.27E+06	1.21E-07
19	1	2.77E-03	0.01	7.42E+06	1.35E-07
20	1	2.50E-03	0.01	6.70E+06	1.49E-07

[a] Eq. (2.109).
[b] Eq. (2.108).
[c] Eq. (2.110).

Table 2.5. The parameters of the Balmer series of emission lines.

n_i	n_f	$\Re$ [a]	$\Re_{n_i\to 2}/\Re_{3\to 2}$	$1/\tau$ [b]	τ [c]
3	2	2.78E-02	1.00	7.44E+07	1.34E-08
4	2	1.56E-02	0.56	4.18E+07	2.39E-08
5	2	1.00E-02	0.36	2.68E+07	3.73E-08
6	2	6.94E-03	0.25	1.86E+07	5.38E-08
7	2	5.10E-03	0.18	1.37E+07	7.32E-08
8	2	3.91E-03	0.14	1.05E+07	9.56E-08
9	2	3.09E-03	0.11	8.27E+06	1.21E-07
10	2	2.50E-03	0.09	6.70E+06	1.49E-07
11	2	2.07E-03	0.07	5.53E+06	1.81E-07
12	2	1.74E-03	0.06	4.65E+06	2.15E-07
13	2	1.48E-03	0.05	3.96E+06	2.52E-07
14	2	1.28E-03	0.05	3.42E+06	2.93E-07
15	2	1.11E-03	0.04	2.98E+06	3.36E-07
16	2	9.77E-04	0.04	2.62E+06	3.82E-07
17	2	8.65E-04	0.03	2.32E+06	4.32E-07
18	2	7.72E-04	0.03	2.07E+06	4.84E-07
19	2	6.93E-04	0.02	1.85E+06	5.39E-07
20	2	6.25E-04	0.02	1.67E+06	5.97E-07

[a] Eq. (2.109).
[b] Eq. (2.108).
[c] Eq. (2.110).

Table 2.6. The parameters of the Paschen series of emission lines.

n_i	n_f	$\Re$ [a]	$\Re_{n_i\to 3}/\Re_{4\to 3}$	$1/\tau$ [b]	τ [c]
4	3	6.94E-03	1.00	1.86E+07	5.38E-08
5	3	4.44E-03	0.64	1.19E+07	8.40E-08
6	3	3.09E-03	0.44	8.27E+06	1.21E-07
7	3	2.27E-03	0.33	6.07E+06	1.65E-07
8	3	1.74E-03	0.25	4.65E+06	2.15E-07
9	3	1.37E-03	0.20	3.67E+06	2.72E-07
10	3	1.11E-03	0.16	2.98E+06	3.36E-07
11	3	9.18E-04	0.13	2.46E+06	4.07E-07
12	3	7.72E-04	0.11	2.07E+06	4.84E-07
13	3	6.57E-04	0.09	1.76E+06	5.68E-07
14	3	5.67E-04	0.08	1.52E+06	6.59E-07
15	3	4.94E-04	0.07	1.32E+06	7.56E-07
16	3	4.34E-04	0.06	1.16E+06	8.60E-07
17	3	3.84E-04	0.06	1.03E+06	9.71E-07
18	3	3.43E-04	0.05	9.18E+05	1.09E-06
19	3	3.08E-04	0.04	8.24E+05	1.21E-06
20	3	2.78E-04	0.04	7.44E+05	1.34E-06

[a] Eq. (2.109).
[b] Eq. (2.108).
[c] Eq. (2.110).

Table 2.7. The parameters of the Brackett series of emission lines.

n_i	n_f	$\Re$ [a]	$\Re_{n_i\to 4}/\Re_{5\to 4}$	$1/\tau$ [b]	τ [c]
5	4	2.50E-03	1.00	6.70E+06	1.49E-07
6	4	1.74E-03	0.69	4.65E+06	2.15E-07
7	4	1.28E-03	0.51	3.42E+06	2.93E-07
8	4	9.77E-04	0.39	2.62E+06	3.82E-07
9	4	7.72E-04	0.31	2.07E+06	4.84E-07
10	4	6.25E-04	0.25	1.67E+06	5.97E-07
11	4	5.17E-04	0.21	1.38E+06	7.23E-07
12	4	4.34E-04	0.17	1.16E+06	8.60E-07
13	4	3.70E-04	0.15	9.90E+05	1.01E-06
14	4	3.19E-04	0.13	8.54E+05	1.17E-06
15	4	2.78E-04	0.11	7.44E+05	1.34E-06
16	4	2.44E-04	0.10	6.54E+05	1.53E-06
17	4	2.16E-04	0.09	5.79E+05	1.73E-06
18	4	1.93E-04	0.08	5.17E+05	1.94E-06
19	4	1.73E-04	0.07	4.64E+05	2.16E-06
20	4	1.56E-04	0.06	4.18E+05	2.39E-06

[a] Eq. (2.109).
[b] Eq. (2.108).
[c] Eq. (2.110).

Table 2.8. The parameters of the Pfund series of emission lines.

n_i	n_f	$\Re$ [a]	$\Re_{n_i\to 5}/\Re_{6\to 5}$	$1/\tau$ [b]	τ [c]
6	5	1.11E-03	1.00	2.98E+06	3.36E-07
7	5	8.16E-04	0.73	2.19E+06	4.57E-07
8	5	6.25E-04	0.56	1.67E+06	5.97E-07
9	5	4.94E-04	0.44	1.32E+06	7.56E-07
10	5	4.00E-04	0.36	1.07E+06	9.34E-07
11	5	3.31E-04	0.30	8.85E+05	1.13E-06
12	5	2.78E-04	0.25	7.44E+05	1.34E-06
13	5	2.37E-04	0.21	6.34E+05	1.58E-06
14	5	2.04E-04	0.18	5.47E+05	1.83E-06
15	5	1.78E-04	0.16	4.76E+05	2.10E-06
16	5	1.56E-04	0.14	4.18E+05	2.39E-06
17	5	1.38E-04	0.12	3.71E+05	2.70E-06
18	5	1.23E-04	0.11	3.31E+05	3.02E-06
19	5	1.11E-04	0.10	2.97E+05	3.37E-06
20	5	1.00E-04	0.09	2.68E+05	3.73E-06

[a] Eq. (2.109).
[b] Eq. (2.108).
[c] Eq. (2.110).

Table 2.9. The parameters of the $n_i > 6$ to $n_f = 6$ series of emission lines.

n_i	n_f	$\Re$ [a]	$\Re_{n_i \to 6} / \Re_{7 \to 6}$	$1/\tau$ [b]	τ [c]
7	6	5.67E-04	1.00	1.52E+06	6.59E-07
8	6	4.34E-04	0.77	1.16E+06	8.60E-07
9	6	3.43E-04	0.60	9.18E+05	1.09E-06
10	6	2.78E-04	0.49	7.44E+05	1.34E-06
11	6	2.30E-04	0.40	6.15E+05	1.63E-06
12	6	1.93E-04	0.34	5.17E+05	1.94E-06
13	6	1.64E-04	0.29	4.40E+05	2.27E-06
14	6	1.42E-04	0.25	3.80E+05	2.63E-06
15	6	1.23E-04	0.22	3.31E+05	3.02E-06
16	6	1.09E-04	0.19	2.91E+05	3.44E-06
17	6	9.61E-05	0.17	2.57E+05	3.88E-06
18	6	8.57E-05	0.15	2.30E+05	4.36E-06
19	6	7.69E-05	0.14	2.06E+05	4.85E-06
20	6	6.94E-05	0.12	1.86E+05	5.38E-06

[a] Eq. (2.109).
[b] Eq. (2.108).
[c] Eq. (2.110).

Table 2.10. The parameters of the $n_i > 7$ to $n_f = 7$ series of emission lines.

n_i	n_f	$\Re$ [a]	$\Re_{n_i \to 7} / \Re_{8 \to 7}$	$1/\tau$ [b]	τ [c]
8	7	3.19E-04	1.00	8.54E+05	1.17E-06
9	7	2.52E-04	0.79	6.75E+05	1.48E-06
10	7	2.04E-04	0.64	5.47E+05	1.83E-06
11	7	1.69E-04	0.53	4.52E+05	2.21E-06
12	7	1.42E-04	0.44	3.80E+05	2.63E-06
13	7	1.21E-04	0.38	3.23E+05	3.09E-06
14	7	1.04E-04	0.33	2.79E+05	3.59E-06
15	7	9.07E-05	0.28	2.43E+05	4.12E-06
16	7	7.97E-05	0.25	2.13E+05	4.68E-06
17	7	7.06E-05	0.22	1.89E+05	5.29E-06
18	7	6.30E-05	0.20	1.69E+05	5.93E-06
19	7	5.65E-05	0.18	1.51E+05	6.61E-06
20	7	5.10E-05	0.16	1.37E+05	7.32E-06

[a] Eq. (2.109).
[b] Eq. (2.108).
[c] Eq. (2.110).

Table 2.11. The parameters of the $n_i > 8$ to $n_f = 8$ series of emission lines.

n_i	n_f	$\Re$ [a]	$\Re_{n_i \to 8} / \Re_{9 \to 8}$	$1/\tau$ [b]	τ [c]
9	8	1.93E-04	1.00	5.17E+05	1.94E-06
10	8	1.56E-04	0.81	4.18E+05	2.39E-06
11	8	1.29E-04	0.67	3.46E+05	2.89E-06
12	8	1.09E-04	0.56	2.91E+05	3.44E-06
13	8	9.25E-05	0.48	2.48E+05	4.04E-06
14	8	7.97E-05	0.41	2.13E+05	4.68E-06
15	8	6.94E-05	0.36	1.86E+05	5.38E-06
16	8	6.10E-05	0.32	1.63E+05	6.12E-06
17	8	5.41E-05	0.28	1.45E+05	6.91E-06
18	8	4.82E-05	0.25	1.29E+05	7.74E-06
19	8	4.33E-05	0.22	1.16E+05	8.63E-06
20	8	3.91E-05	0.20	1.05E+05	9.56E-06

[a] Eq. (2.109).
[b] Eq. (2.108).
[c] Eq. (2.110).

Table 2.12. The parameters of the $n_i > 100$ to $n_f = 1$ series of emission lines.

n_i	n_f	$\Re$ [a]	$\Re_{n_i \to 1} / \Re_{101 \to 1}$	$1/\tau$ [b]	τ [c]
101	1	9.80E-05	1.00	2.63E+05	3.81E-06
102	1	9.61E-05	0.98	2.57E+05	3.88E-06
103	1	9.43E-05	0.96	2.52E+05	3.96E-06
104	1	9.25E-05	0.94	2.48E+05	4.04E-06
105	1	9.07E-05	0.93	2.43E+05	4.12E-06
106	1	8.90E-05	0.91	2.38E+05	4.20E-06
107	1	8.73E-05	0.89	2.34E+05	4.28E-06
108	1	8.57E-05	0.87	2.30E+05	4.36E-06
109	1	8.42E-05	0.86	2.25E+05	4.44E-06
110	1	8.26E-05	0.84	2.21E+05	4.52E-06

[a] Eq. (2.109).
[b] Eq. (2.108).
[c] Eq. (2.110).

Table 2.13. The parameters of the $n_i > 100$ to $n_f = 100$ series of emission lines.

n_i	n_f	$\Re$ [a]	$\Re_{n_i \to 100} / \Re_{101 \to 100}$	$1/\tau$ [b]	τ [c]
101	100	9.80E-09	1.00	2.63E+01	3.81E-02
102	100	9.61E-09	0.98	2.57E+01	3.88E-02
103	100	9.43E-09	0.96	2.52E+01	3.96E-02
104	100	9.25E-09	0.94	2.48E+01	4.04E-02
105	100	9.07E-09	0.93	2.43E+01	4.12E-02
106	100	8.90E-09	0.91	2.38E+01	4.20E-02
107	100	8.73E-09	0.89	2.34E+01	4.28E-02
108	100	8.57E-09	0.87	2.30E+01	4.36E-02
109	100	8.42E-09	0.86	2.25E+01	4.44E-02
110	100	8.26E-09	0.84	2.21E+01	4.52E-02

[a] Eq. (2.109).
[b] Eq. (2.108).
[c] Eq. (2.110).

Table 2.14. The parameters of the $n_i > 500$ to $n_f = 1$ series of emission lines.

n_i	n_f	$\Re$ [a]	$\Re_{n_i \to 1} / \Re_{501 \to 1}$	$1/\tau$ [b]	τ [c]
501	1	3.98E-06	1.00	1.07E+04	9.37E-05
502	1	3.97E-06	1.00	1.06E+04	9.41E-05
503	1	3.95E-06	0.99	1.06E+04	9.45E-05
504	1	3.94E-06	0.99	1.05E+04	9.49E-05
505	1	3.92E-06	0.98	1.05E+04	9.52E-05
506	1	3.91E-06	0.98	1.05E+04	9.56E-05
507	1	3.89E-06	0.98	1.04E+04	9.60E-05
508	1	3.88E-06	0.97	1.04E+04	9.64E-05
509	1	3.86E-06	0.97	1.03E+04	9.67E-05
510	1	3.84E-06	0.97	1.03E+04	9.71E-05

[a] Eq. (2.109).
[b] Eq. (2.108).
[c] Eq. (2.110).

Table 2.15. The parameters of the $n_i > 500$ to $n_f = 100$ series of emission lines.

n_i	n_f	$\Re$ [a]	$\Re_{n_i \to 100} / \Re_{501 \to 100}$	$1/\tau$ [b]	τ [c]
501	100	3.98E-10	1.00	1.07E-00	9.37E-01
502	100	3.97E-10	1.00	1.06E-00	9.41E-01
503	100	3.95E-10	0.99	1.06E-00	9.45E-01
504	100	3.94E-10	0.99	1.05E-00	9.49E-01
505	100	3.92E-10	0.98	1.05E-00	9.52E-01
506	100	3.91E-10	0.98	1.05E-00	9.56E-01
507	100	3.89E-10	0.98	1.04E-00	9.60E-01
508	100	3.88E-10	0.97	1.04E-00	9.64E-01
509	100	3.86E-10	0.97	1.03E-00	9.67E-01
510	100	3.84E-10	0.97	1.03E-00	9.71E-01

[a] Eq. (2.109).
[b] Eq. (2.108).
[c] Eq. (2.110).

Table 2.16. The parameters of the $n_i > 500$ to $n_f = 500$ series of emission lines.

n_i	n_f	$\Re$ [a]	$\Re_{n_i \to 500} / \Re_{501 \to 500}$	$1/\tau$ [b]	τ [c]
501	500	1.59E-11	1.00	4.27E-02	2.34E+01
502	500	1.59E-11	1.00	4.25E-02	2.35E+01
503	500	1.58E-11	0.99	4.23E-02	2.36E+01
504	500	1.57E-11	0.99	4.22E-02	2.37E+01
505	500	1.57E-11	0.98	4.20E-02	2.38E+01
506	500	1.56E-11	0.98	4.18E-02	2.39E+01
507	500	1.56E-11	0.98	4.17E-02	2.40E+01
508	500	1.55E-11	0.97	4.15E-02	2.41E+01
509	500	1.54E-11	0.97	4.13E-02	2.42E+01
510	500	1.54E-11	0.97	4.12E-02	2.43E+01

[a] Eq. (2.109).
[b] Eq. (2.108).
[c] Eq. (2.110).

The lifetime of the Balmer α transition of $1.34X\ 10^{-8}\ s$ given in Table 2.5 is in good agreement with the experimental upper limit of $1.5X\ 10^{-8}\ s$ [26-27]. The relative line intensities are dependent on the electron temperature which causes a Boltzmann-distribution skewing [28] of the predominantly lifetime-determined state populations.. However, states that are close in energy are expected to be close to the theoretical limit with greater deviations as the energy differences become larger. The experimental Balmer-series line intensities are given with the calculated intensities in Table 2.17. As expected the predicted and experimental intensities match well for the lowest levels and deviate at the higher levels.

Table 2.17. The parameters of the Balmer series of emission lines.

n_i	n_f	$\Re$ [a]	$\Re_{n_i \to 2} / \Re_{3 \to 2}$	$\Re_{n_i \to 2} / \Re_{3 \to 2}$ X 300	NIST [26] Balmer Line Intensities
3	2	2.78E-02	1.00	300	300
4	2	1.56E-02	0.56	169	160
5	2	1.00E-02	0.36	108	60
6	2	6.94E-03	0.25	75	30
7	2	5.10E-03	0.18	55	8
8	2	3.91E-03	0.14	42	6
9	2	3.09E-03	0.11	33	5

[a] Eq. (2.109).

Ornstein and Burger [29-30] studied the relative emission intensities of Balmer and Paschen lines having the same initial states in order to eliminate the uncertainty of the number of atoms in each initial state. The results of the relative intensities from each state having the same initial number of atoms is given in Table 2.18. The calculated and experimental results agree very well. In contrast, standard quantum mechanics has many shortcomings in this result as well as in general[4].

Table 2.18. The parameter $\Re$ and the calculated and experimental intensity ratios of selected Balmer and Paschen emission lines.

n_i	n_f	$\Re$ [a]	$\Re_{Paschen,n_i} / \Re_{Balmer,n_i}$		Experimental Intensity Ratio [29-30] $\frac{Paschen, n_i}{Balmer, n_i}$
4	2	1.56E-02	$H_\beta / P_\alpha (4 \to 2) : (4 \to 3)$	**2.25**	**2.6**
4	3	6.94E-03			
5	2	1.00E-02	$H_\gamma / P_\beta (5 \to 2) : (5 \to 3)$	**2.25**	**2.5**
5	3	4.44E-03			
6	2	6.94E-03	$H_\delta / P_\gamma (6 \to 2) : (6 \to 3)$	**2.25**	**2**
6	3	3.09E-03			

[a] Eq. (2.109).

The radii of all one-electron atoms are given by Eq. (1.260). For He^+,

[4] The quantum mechanical calculation of the line intensities is also based on classical electrodynamics [32], but there are many internally inconsistent features that arise due to the intrinsic nonphysical aspects peculiar to quantum mechanics. The possibility that $\Delta l = +1$ is not treated. The A coefficients are not symmetrical with respect to excitation and de-excitation as they must be. The $-\sin\theta \mathbf{i}_\theta$ dependence of the current dipole is ignored. The calculation of the current multipole based on integration of the products of wavefunctions over all space is not physical. The electron can not be "everywhere at once," and even the frequency times the average radial displacement during a transition results in an electron velocity that exceeds the speed of light. The calculations are extraordinarily complicated involving hypergeometric series, and the results contain products of terms raised to enormously high and low powers (e.g. power of $\sim \pm 20$ for even the Balmer lines). The results do not match the experimental results by significant factors.

$$r_1 = \frac{a_0}{2} \tag{2.114}$$

Substitution of Eq. (2.114) into Eqs. (2.108) and (2.110) gives the electric dipole electronic transition probability from initial quantum states n_i, ℓ, m_s, m_ℓ and radius r_{n_i} to the final state with quantum numbers $n_f, \ell \pm 1, m_s, m_\ell$ and radius r_{n_f} and the corresponding state lifetime, respectively:

$$\begin{aligned}\frac{1}{\tau} &= \frac{\dfrac{\hbar\omega}{2m_e c^2}\dfrac{4\pi}{3}\eta\left|\dfrac{2\pi\left(\dfrac{1}{r_{n_f}}-\dfrac{1}{r_{n_i}}\right)}{2\pi}\dfrac{e\hbar}{4\pi m_e}\dfrac{1}{r_{n_i}-r_{n_f}}\right|^2}{\hbar\omega} \\ &= \frac{1}{m_e c^2}\frac{\eta}{24\pi}\left(\frac{e\hbar}{m_e\left(\dfrac{a_0}{2}\right)^2}\right)^2\left|\frac{1}{n_i-n_f}\left(\frac{1}{n_f}-\frac{1}{n_i}\right)\right|^2 \\ &= 4.284\ X\ 10^{10}\Re\ s^{-1}\end{aligned} \tag{2.115}$$

$$\begin{aligned}\tau &= 2m_e c^2\frac{3}{4\pi\eta}\left|\frac{2\pi\left(\dfrac{1}{r_{n_f}}-\dfrac{1}{r_{n_i}}\right)}{2\pi}\frac{e\hbar}{4\pi m_e}\frac{1}{r_{n_i}-r_{n_f}}\right|^{-2} \\ &= m_e c^2\frac{24\pi}{\eta}\left(\frac{e\hbar}{m_e\left(\dfrac{a_0}{2}\right)^2}\right)^{-2}\left|\frac{1}{n_i-n_f}\left(\frac{1}{n_f}-\frac{1}{n_i}\right)\right|^{-2} \\ &= 2.334\ X\ 10^{-11}\Re^{-1}\ s\end{aligned} \tag{2.116}$$

where $\Re$ is given by Eq. (2.109). The predicted lifetimes for He^+ are 1/16 those of atomic hydrogen. The equations for the excited-state lifetimes and line intensities can be condensed as given in Box 2.1.

BOX 2.1 CONDENSED FORMULA FOR THE EXCITED-STATE LIFETIMES AND LINE INTENSITIES

Using

$$\alpha = \frac{e^2}{4\pi\varepsilon_0\hbar c} \tag{1}$$

Allows the substitutions

$$a_0 = \frac{4\pi\varepsilon_0\hbar^2}{e^2 m_e} = \frac{\hbar}{\alpha m_e c} \tag{2}$$

and

$$e^2 = 4\pi\varepsilon_0\alpha\hbar c \tag{3}$$

such that the equations for the excited-state lifetimes and line intensities can be condensed [31]. Eq. (2.108) can be written as

$$\frac{1}{\tau} = \frac{1}{2m_e c^2}\cdot\frac{4\pi}{3}\cdot\left(\frac{e\hbar}{4\pi m_e}\right)^2\cdot\frac{1}{\left(r_{nf}r_{ni}\right)^2} \qquad \text{as} \qquad r_{nf} \neq r_{ni} \tag{4}$$

This can be transformed to

$$\begin{aligned}\frac{1}{\tau} &= \frac{1}{6m_e c^2}\sqrt{\frac{\mu_0}{\varepsilon_0}}\frac{e^2\hbar^2}{4\pi m_e^2}\frac{a_0^4}{\left(r_{nf}r_{ni}\right)^2}\left(\frac{e^2 m_e}{4\pi\varepsilon_0\hbar^2}\right)^4 \\ &= \frac{1}{6m_e c^2}\sqrt{\frac{\mu_0}{\varepsilon_0}}\frac{4\pi\varepsilon_0\alpha\hbar c\hbar^2}{4\pi m_e^2}\frac{a_0^4}{\left(r_{nf}r_{ni}\right)^2}\left(\frac{4\pi\varepsilon_0\alpha\hbar c m_e}{4\pi\varepsilon_0\hbar^2}\right)^4 \\ &= \frac{1}{6m_e c^2}\frac{\alpha\hbar^3}{m_e^2}\frac{a_0^4}{\left(r_{nf}r_{ni}\right)^2}\left(\frac{\alpha c m_e}{\hbar}\right)^4 = \frac{1}{6}\alpha^5\frac{m_e c^2}{\hbar}\left(\frac{a_0^2}{r_{nf}r_{ni}}\right)^2\end{aligned} \tag{5}$$

and the corresponding Eq. (2.110) becomes:

$$\tau = 6\alpha^{-5}\frac{\hbar}{m_e c^2}\left(\frac{r_{nf}r_{ni}}{a_0^2}\right)^2 \qquad \text{as} \qquad r_{nf} \neq r_{ni} \tag{6}$$

The result confirms that:

$$\frac{r_{nf}r_{ni}}{a_0^2} = n_f n_i \tag{7}$$

Alternatively, Eq. (2.110) in condensed form is:

$$\tau = 6\alpha^{-5}\cdot\frac{\hbar}{m_e c^2}\cdot\left(n_f n_i\right)^2 = 3.734826\times10^{-10}\,s\cdot\left(n_f n_i\right)^2 \tag{8}$$

And, Eq. (2.116) becomes

$$\tau = \frac{6}{16}\alpha^{-5}\cdot\frac{\hbar}{m_e c^2}\cdot\left(n_f n_i\right)^2 = 2.334266\times10^{-11}\,s\cdot\left(n_f n_i\right)^2 \tag{9}$$

Maxwell made an absolute measurement of the lifetime of excited states of He^+ formed by narrow-beam, electron-impact excitation [30, 33]. The excited He^+ ions were spread by a transverse electric field which did not appreciably affect the ionizing electron beam because a controlling longitudinal magnetic field was applied. The time-of-flight to radiating was recorded as the distance-of-flight and gave the probability distribution of the lifetimes of the excited states. By studying the spatial distribution of the light intensity, Maxwell inferred the mean lifetimes of the excited-state ions. For the $n = 6$ states of He^+, an average lifetime of $\left(1.1 \pm 0.2\right)\ X\ 10^{-8}\ s$ was observed. From Tables 2.4-2.8, the average life time of the $n = 6$ state of H is $1.48\ X\ 10^{-7}\ s$, and from Eq. (2.116), the corresponding average lifetime of He^+ is $9.3X\ 10^{-9}\ s$. The lifetimes of states of He^+ were found to be 1/16 those of H. The agreement between the experimental and calculated results is excellent.

In addition to the electron electric dipole transitions, Eq. (2.107) can be applied to transitions with a multipole distribution in the radial direction such as in the case of nuclear decay given in the Nuclear and X-ray Multipole Radiation section. The transition probability in the case of the electric multipole moment given by Jackson [7] as:

$$Q_{\ell m} = \frac{3}{\ell+3}e\left(na_0\right)^{\ell} \tag{2.117}$$

is [7]:

$$\begin{aligned}
\frac{1}{\tau} &= \frac{power}{energy} \\
\frac{1}{\tau} &= \frac{\left[\dfrac{2\pi c}{\left[\left(2\ell+1\right)!!\right]^2}\left(\dfrac{\ell+1}{\ell}\right)k^{2\ell+1}\left|Q_{\ell m}+Q'_{\ell m}\right|^2\right]}{\left[\hbar\omega\right]} \\
&= 2\pi\left(\frac{e^2}{h}\right)\sqrt{\frac{\mu_0}{\varepsilon_0}}\frac{2\pi}{\left[\left(2\ell+1\right)!!\right]^2}\left(\frac{\ell+1}{\ell}\right)\left(\frac{3}{\ell+3}\right)^2\left(kna_0\right)^{2\ell}\omega
\end{aligned} \tag{2.118}$$

Eq. (2.118) gives very predictive results as shown by Jackson [7].

RESONANT LINE SHAPE

The spectroscopic linewidth arises from the classical rise-time band-width relationship, and the Lamb shift is due to the radiation reaction force between the electron and the photon and conservation of energy and linear momentum involving recoil during emission. It follows from the Poynting Power Theorem (Eq. (7.43)) with spherical radiation that the transition probabilities are given by the ratio of power and the energy of the transition [7]. The lifetime τ for an electric dipole transition is derived in the State Lifetime and Line Intensities section. This rise-time gives rise to Γ, the spectroscopic line-width. The relationship between the rise-time and the band-width is given by Siebert [34].

$$\tau^2 = 4\left[\frac{\int_{-\infty}^{\infty} t^2 h^2(t)dt}{\int_{-\infty}^{\infty} h^2(t)dt} - \left(\frac{\int_{-\infty}^{\infty} t h^2(t)dt}{\int_{-\infty}^{\infty} h^2(t)dt}\right)^2\right] \tag{2.119}$$

$$\Gamma^2 = 4\frac{\int_{-\infty}^{\infty} f^2 \left|H(f)\right|^2 df}{\int_{-\infty}^{\infty} \left|H(f)\right|^2 df} \tag{2.120}$$

By application of the Schwartz inequality, the relationship between the rise-time and the band-width is[5]:

$$\tau\Gamma \geq \frac{1}{\pi} \tag{2.121}$$

From Eq. (2.118), the line-width is proportional to the ratio of the Quantum Hall resistance, $\frac{h}{e^2}$, and, η, the radiation resistance of free space.

$$\eta = \sqrt{\frac{\mu_0}{\varepsilon_0}} \tag{2.122}$$

And, the Quantum Hall resistance given in the Quantum Hall Effect section was derived using the Poynting Power Theorem. Also, from Eq. (2.118), the line-width is proportional to the fine structure constant, α,

$$\alpha = \frac{1}{4\pi}\sqrt{\frac{\mu_0}{\varepsilon_0}}\frac{e^2}{\hbar} \tag{2.123}$$

During a transition, the total energy of the system decays exponentially. Applying Eqs. (2.119) and (2.120) to the case of exponential decay,

$$h(t) = e^{-\alpha t}u(t) = e^{-\frac{2\pi}{T}t}u(t) \tag{2.124}$$

$$\left|H(f)\right| = \frac{1}{\sqrt{\left(\frac{1}{T}\right)^2 + (2\pi f)^2}} \tag{2.125}$$

where the rise-time, τ, is the time required for $h(t)$ of Eq. (2.124) to decay to $1/e$ of its initial value and where the band-width, Γ, is the half-power bandwidth, the distance between points at which:

$$\left|H(f)\right| = \frac{\left|H(0)\right|}{\sqrt{2}} \tag{2.126}$$

From Eq. (2.119) [34],

$$\tau = T \tag{2.127}$$

From Eq. (2.120) [34],

$$\Gamma = \frac{1}{\pi T} \tag{2.128}$$

---

[5] Eq. (2.121) is erroneously interpreted as a physical law of the indeterminate nature of conjugate parameters of atomic particles, such as position and momentum or energy and time. This so called Heisenberg Uncertainty Principle is not a physical law; rather it is a misinterpretation of applying the Schwartz Inequality to a probability-wave model of a particle [35]. The mathematical consequence is that a particle, such as an electron, can have a continuum of momenta and positions with a continuum of energies simultaneously, which cannot be physical. This result is independent of error or limitations introduced by measurement. Jean B. Fourier was the first to discover the relationship between time and frequency compositions of physical measurables. Eq. (2.121) expresses the limitation of measuring these quantities since an impulse contains an infinity of frequencies, and no instrument has such bandwidth. Similarly, an exact frequency requires an infinite measurement time, and all measurements must be finite in length. Thus, Eq. (2.121) is a statement about the limitations of measurement in time and frequency. It is further a conservation statement of energy of a signal in the time and frequency domains. Werner Heisenberg's substitution of momentum and position for a single particle, probability-wave into this relationship says nothing about conjugate parameters of a particle in the absence of their measurement or the validity of the probability-wave model. In fact, this approach was shown to be flawed experimentally (See Wave-Particle Duality section and Refs. [8-11]).

From Eq. (2.127) and Eq. (2.128), the relationship between the rise-time and the band-width for exponential decay is:

$$\tau\Gamma = \frac{1}{\pi} \tag{2.129}$$

Bosons obey Bose-Einstein statistics as given in the Statistical Mechanics section. The emitted radiation, the summation of an ensemble of emitted photons each of an exact frequency and energy given by Eq. (4.8), appears as a wave train with effective length c/Γ. Such a finite pulse of radiation is not exactly monochromatic but has a frequency spectrum covering an interval of the order Γ. The exact shape of the frequency spectrum is given by the square of the Fourier transform of the electric field. Thus, the amplitude spectrum is proportional to

$$\mathbf{E}(\omega) \propto \int_0^\infty e^{-\alpha_t t} e^{-i\omega t} dt = \frac{1}{\alpha_t - i\omega} \tag{2.130}$$

The coefficient α_t corresponds to the spectroscopic linewidth and also to a shift in frequency that arises from the radiation reaction force between the electron and the photon. The energy radiated per unit frequency interval is therefore:

$$\frac{dI(\omega)}{d\omega} = I_0 \frac{\Gamma}{2\pi} \frac{1}{(\omega - \omega_0 - \Delta\omega)^2 + (\Gamma/2)^2} \tag{2.131}$$

where I_0 is the total energy radiated. The spectral distribution is called a resonant line shape. The width of the distribution at half-maximum intensity is called the half-width or line-breadth and is equal to Γ. Shown in Figure 2.4 is such a spectral line. Because of the reactive effects of radiation the line is shifted in frequency. The small radiative shift of the energy levels of atoms was first observed by Lamb in 1947 [36] and is called the Lamb shift in his honor.

Figure 2.4. Broadening of the spectral line due to the rise-time and shifting of the spectral line due to the radiative reaction. The resonant line shape has width Γ. The level shift is $\Delta\omega$.

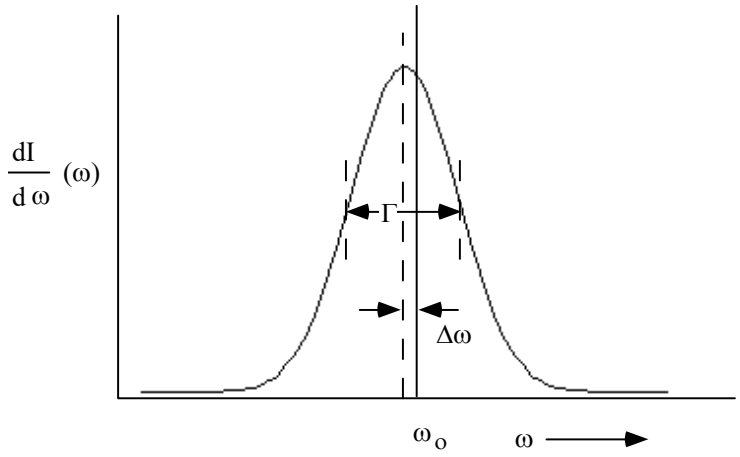

HYDROGEN LAMB SHIFT

The Lamb shift corresponding to the transition energy from the ${}^2P_{1/2}$ state to the ${}^2S_{1/2}$ state of the hydrogen atom having the quantum numbers $n=2,\ \ell=1,\ m_\ell=0$ and $n=2,\ \ell=0,\ m_\ell=0$, respectively, is calculated from the radiation reaction force and the atom recoil energy due to photon emission. For a transition between initial and final states having quantum numbers n_i and n_f, respectively, the time-averaged power density in the radiation zone is given by Eq. (2.104). The total radiated power P given by integrating the Poynting power density (Eq. (2.104)) over the surface of a sphere at radius r is given by Eq. (2.105). The corresponding radiation reaction force is derived from the relativistically corrected fields of the radiated power. Consider that the power is proportional to $\mathbf{E}\times\mathbf{H}$ and then $|H_\phi|^2$ (Eq. (2.104)). A radiation reaction force due to current flow to form the trigonometric current distribution of the $2P_{1/2}$ state from the uniform $2S_{1/2}$ state given in Sections 6.6, 12.10, and 17.3 of Jackson [37] achieves the condition that the sum of the mechanical momentum and electromagnetic momentum is conserved. Since the change in angular momentum between the initial and final atomic states is conserved by the photon's angular momentum, the angular momentum, **m**, of the emitted photon follows from the time-averaged angular-momentum density given by Eq. (24.61) of Jackson [2] in cgs units:

$$\mathbf{m} = \int \frac{1}{8\pi c} \mathrm{Re}\left[\mathbf{r}\times(\mathbf{E}\times\mathbf{B}^*)\right] dx^4 = \hbar \tag{2.132}$$

The corresponding energy, *E*, is given from the Poynting power density [38]:

$$E = \int \frac{c}{4\pi} \mathrm{Re}(\mathbf{E} \times \mathbf{H}^*) dx^4 = \hbar\omega \tag{2.133}$$

As shown by Eqs. (1.280-1.281) and Eq. (29.9), each of the magnetic and electric field is corrected by the product of the factors 2π and α, respectively. Also, the field in excited states scales as $1/n$ due to the corresponding central field from the superposition of the excited-state photon's and proton's fields (Eqs. (2.17)). Thus, using each relativistic and central field correction given by $2\pi\alpha$ and $1/2$, respectively, and using the limit of $r = r_{n_i} - r_{n_f}$ with the radiation reaction perturbation with respect to r, the radiation reaction power P_{RR} given by Eq. (2.105) is

$$P_{RR} = (2\pi\alpha)^2 \left(\frac{1}{2}\right)^2 \frac{\eta}{12\pi} \left(\frac{e\hbar}{m_e r^2}\right)^2 \tag{2.134}$$

The radiation reaction force F_{RR} is given by the power (Eq. (2.108)) divided by the electron velocity v (Eq. (1.35)):

$$\begin{aligned} F_{RR} &= \frac{P_{RR}}{v} \\ &= (2\pi\alpha)^2 \frac{\frac{\eta}{48\pi}\left(\frac{e\hbar}{m_e r^2}\right)^2}{\frac{\hbar}{m_e r}} \\ &= (2\pi\alpha)^2 \frac{\eta}{48\pi} \frac{e^2\hbar}{m_e r^3} \end{aligned} \tag{2.135}$$

The radius of the hydrogen atom given by Eqs. (2.4-2.5) and Eq. (1.253), with $n = 2$, is $r = 2a_H$. The radiation reaction force perturbs the force balance and consequently the radius between the electron and proton relative to the condition in its absence. The outward centrifugal force on the electron is balanced by the electric force and the magnetic force (Eqs. (1.253) and (2.4)), and the radiation reaction force (Eq. (2.135)) corresponding to the current flow to achieve the current distribution of the $2P_{1/2}$ state:

$$\frac{m_e v^2}{r} = \frac{\hbar^2}{m_e r^3} = \frac{0.5e^2}{4\pi\varepsilon_0 r^2} - \frac{\hbar^2}{m_P r^3} + (2\pi\alpha)^2 \frac{\eta}{48\pi} \frac{e^2\hbar}{m_e r^3} \tag{2.136}$$

$$r = 2a_H - (2\pi\alpha)^2 \frac{\hbar}{6m_e c} \tag{2.137}$$

$$r = 1.99999744 a_H \tag{2.138}$$

where Eq. (1.35) was used for the velocity and a_H is the radius of the hydrogen atom given by Eq. (1.259).

ENERGY CALCULATIONS

The change in the electric energy of the electron $\Delta E_{ele}^{H\ Lamb}$ due to the slight shift of the radius of the atom is given by the difference between the electric energies associated with the unperturbed and radiation-reaction-force-perturbed radius. Each electric energy is given by the substitution of the corresponding radius given by Eq. (2.138) into Eqs. (1.264) and (2.4):

$$\Delta E_{ele}^{H\ Lamb} = \frac{-0.5e^2}{8\pi\varepsilon_0}\left[\frac{1}{r_0} - \frac{1}{r_-}\right] = 6.95953\ X\ 10^{-25}\ J \tag{2.139}$$

wherein the unperturbed radius given by Eq. (2.5) is $r_0 = 2a_H$.

In addition, the change in the magnetic energy $\Delta E_{mag}^{H\ Lamb}$ of the electron is given by Eqs. (1.161-1.162) with the substitution of the corresponding radii:

$$\begin{aligned} \Delta E_{mag}^{H\ Lamb} &= \frac{\pi\mu_0 e^2\hbar^2}{m_e^{\ 2}}\left(\frac{1}{r_0^3} - \frac{1}{r_-^3}\right) \\ &= 4\pi\mu_0\mu_B^2\left(\frac{1}{r_0^3} - \frac{1}{r_-^3}\right) \\ &= -4.38449\ X\ 10^{-27}\ J \end{aligned} \tag{2.140}$$

where μ_B is the Bohr magneton.

The $n = 2$ state comprises an electron, a photon, and a proton having the analytical solution of Maxwell's equations given by Eq. (2.15). The recoil energy of this photon gives rise to an energy contribution to the Lamb shift that is calculated by applying conservation of energy and linear momentum to the emitted photon and atom. The photon emitted by an excited state atom carries away energy, linear momentum, and angular momentum. The initial and final values of the energies and

momentum must be conserved between the atom, the electron, and the photon[6]. Consider an isolated atom of mass M having an electron in an excited state level at an energy E. The atom is moving with velocity $\mathbf{V}$ along the direction in which the excited-state photon is to be emitted (the components of motion perpendicular to this direction remain unaffected by the emission and may be ignored). The energy above the "ground" state at rest is

$$\left(E+\frac{1}{2}M\mathbf{V}^2\right) \tag{2.141}$$

When a photon of energy $E_{h\upsilon}$ is emitted, the atom and/or electron recoils and has a new velocity

$$\mathbf{V}+\mathbf{v} \tag{2.142}$$

(which is a vector sum in that $\mathbf{V}$ and $\mathbf{v}$ may be opposed), and a total energy of:

$$\frac{1}{2}M\left(\mathbf{V}+\mathbf{v}\right)^2 \tag{2.143}$$

By conservation of energy,

$$E+\frac{1}{2}M\mathbf{V}^2=E_{h\upsilon}+\frac{1}{2}M\left(\mathbf{V}+\mathbf{v}\right)^2 \tag{2.144}$$

so, that the actual energy of the photon emitted is given by:

$$E_{h\upsilon}=E-\frac{1}{2}M\mathbf{v}^2-M\mathbf{v}\mathbf{V} \tag{2.145}$$

$$E_{h\upsilon}=E-E_R-E_D$$

The photon is thus deficient in energy by a recoil kinetic energy

$$E_R=\frac{1}{2}M\mathbf{v}^2 \tag{2.146}$$

which is independent of the initial velocity $\mathbf{V}$, and by a thermal or Doppler energy

$$E_D=M\mathbf{v}\mathbf{V} \tag{2.147}$$

which depends on $\mathbf{V}$; therefore, it can be positive or negative.

Momentum must also be conserved in the emission process. The energy, E, of the photon is given by Eq. (4.8)

$$E=\hbar\omega=h\frac{\omega}{2\pi}=h\nu=hf=h\frac{c}{\lambda} \tag{2.148}$$

From special relativity,

$$E=\hbar\omega=mc^2 \tag{2.149}$$

Thus, $\mathbf{p}$, the momentum of the photon is:

$$\mathbf{p}=mc=\frac{E_{h\nu}}{c} \tag{2.150}$$

where c is the velocity of light, so that:

$$M\mathbf{V}=M\left(\mathbf{V}+\mathbf{v}\right)+\frac{E_{h\nu}}{c} \tag{2.151}$$

And, the recoil momentum is:

$$M\mathbf{v}=-\frac{E_{h\nu}}{c} \tag{2.152}$$

Thus, the recoil energy is given by:

$$E_R=\frac{E_{h\nu}^2}{2Mc^2} \tag{2.153}$$

and depends on the mass of the atom and the energy of the photon. The Doppler energy, E_D, is dependent on the thermal motion of the atom, and will have a distribution of values which is temperature dependent. A mean value, E_D, can be defined which is related to $\bar{E}_K$, the mean kinetic energy per translational degree of freedom [39-40]:

$$\bar{E}_D\cong\frac{1}{2}kT \tag{2.154}$$

by

$$\bar{E}_D\cong 2\sqrt{E_K E_R}=E_{h\nu}\sqrt{\frac{2\bar{E}_K}{Mc^2}} \tag{2.155}$$

where k is Boltzmann's constant and T is the absolute temperature[7]. As a result, the statistical distribution in energy of the emitted photons is displaced from the true excited-state energy by $-E_R$ and broadened by E_D into a Gaussian distribution of width $2\bar{E}_D$. The distribution for absorption has the same shape but is displaced by $+E_R$.

[6] Conservation of angular momentum is used to derive the photon's equation in the Equation of the Photon section.

[7] This relationship may also apply to an electron undergoing bonding as given in the Doppler Energy Term of Hydrogen-Type Molecular Ions section.

For the photon of the hydrogen atom, the linear momentum of the emitted photon is balanced by the recoil momentum of the entire atom of mass m_H, and the corresponding recoil energy adds to the energy due to the radiation reaction force. The recoil energy $E_{recoil}^{H\ Lamb}$ for the electron in the $n=2$ and the corresponding frequency shift $\Delta f_{recoil}^{H\ Lamb}$ of the hydrogen atom is given by Eq. (2.153):

$$E_{recoil}^{H\ Lamb} = \frac{\left(E_{h\upsilon}\right)^2}{2m_H c^2} = 8.87591\ X\ 10^{-27}\ J \tag{2.156}$$

$$\Delta f_{recoil}^{H\ Lamb} = \frac{\Delta\omega}{2\pi} = \frac{\left(E_{h\upsilon}\right)^2}{2hm_H c^2} = 13.40\ MHz \tag{2.157}$$

where $E_{h\upsilon}$ corresponds to the recoil energy (Eqs. (2.153) and (2.22)) is

$$E_{h\upsilon} = -13.5983\ eV\left(1-\frac{1}{n^2}\right) \tag{2.158}$$

wherein $n=2$ [8].

Then, the total energy of the hydrogen Lamb shift is given by the sum of Eqs. (2.139-2.140) and (2.156):

$$\begin{aligned}\Delta E_{total}^{H\ Lamb} &= \Delta E_{ele}^{H\ Lamb} + \Delta E_{mag}^{H\ Lamb} + E_{recoil}^{H\ Lamb} \\ &= 6.95953\ X\ 10^{-25}\ J - 4.38449\ X\ 10^{-27}\ J + 8.87591\ X\ 10^{-27}\ J \\ &= 7.00445\ X\ 10^{-25}\ J\end{aligned} \tag{2.159}$$

The Planck relationship (Eq. (2.148)) gives $\Delta f_{total}^{H\ Lamb}$, the Lamb shift energy expressed in terms of frequency:

$$\Delta f_{total}^{H\ Lamb} = \frac{\left|\Delta E_{total}^{H\ Lamb}\right|}{h} = 1057.09\ MHz \tag{2.160}$$

The experimental Lamb shift is [42]

$$\Delta f_{total}^{H\ Lamb}\left(\text{experimental}\right) = 1057.845\ MHz \tag{2.161}$$

There is good agreement between the theoretical and experimental values given the 100 MHz natural linewidth of the $2P$ state. The 0.07% relative difference is within the propagated errors in the fundamental constants of the equations. In addition to the Lamb shift, the spectral lines of hydrogen are Zeeman split by spin-orbit coupling and electron-nuclear magnetic interactions given in the Fine Structure and Hyperfine Structure sections, respectively.

MUONIC HYDROGEN LAMB SHIFT

The Lamb shift corresponding to the transition energy from the ${}^2P_{1/2}$ state to the ${}^2S_{1/2}$ state of the muonic hydrogen atom having the quantum numbers $n=2,\ \ell=1,\ m_\ell=0$ and $n=2,\ \ell=0,\ m_\ell=0$, respectively, is also calculated from the radiation reaction force and the atom recoil energy due to photon emission. The radiation reaction force F_{RR} of muonic hydrogen comprises three terms that follow from Eq. (2.135) and arise from lepton-photon-momentum transfer during the ${}^2P_{1/2} \rightarrow {}^2S_{1/2}$ transition wherein the photon couples with the three possible states of the electron mass corresponding to the three possible leptons. The electron, muon, and tau masses are based on the relativistic corrections of the Planck, electric, and magnetic energies, respectively, as given in Eq. (32.48). The masses of the heavier leptons, the muon and tau are dependent on the first lepton's mass, the electron mass, and each can be considered a relativistic effect of the electron mass. Specifically, the muon is a resonant state of an electron given by a relativistic effect of the electron mass as given by Eqs. (36.5-36.6), wherein the muon decays to the electron:

$$2\pi\frac{\hbar}{m_\mu c^2} = 2\pi\sec\sqrt{\frac{2Gm_e\alpha^2 m_\mu}{c\hbar}} \tag{2.162}$$

$$m_\mu = \frac{\hbar}{c}\left(\frac{1}{2Gm_e\left(\alpha\sec\right)^2}\right)^{\frac{1}{3}} = 1.8874\ X\ 10^{-28}\ kg \tag{2.163}$$

Likewise, the tau mass having a dependency on the electron mass is given by Eqs. (36.7-36.8):

$$2\pi\frac{\hbar}{m_\tau c^2} = 2\sec\sqrt{\frac{2Gm_e(2\pi)^2\alpha^4 m_\tau}{c\hbar}} \tag{2.164}$$

$$m_\tau = \frac{\hbar}{c}\left(\frac{1}{2Gm_e}\right)^{\frac{1}{3}}\left(\frac{1}{2\sec\alpha^2}\right)^{\frac{2}{3}} = 3.1604\ X\ 10^{-27}\ kg \tag{2.165}$$

[8] As a further example, conservation of linear momentum of the photon is central to the Mössbauer phenomenon. See Mills patent [41].

Thus, the radiation reaction force of relativistic origin is determined by the action on the electron mass with each mass hierarchy requiring an additional relativistic correction factor of $2\pi\alpha$. Then, using Eqs. (2.135) and (32.48), the first radiation reaction term $(2\pi\alpha)^2$ regards the photon coupling to the electron whose mass is based on the Planck equation. The second term $(2\pi\alpha)^3$ regards the relativistically corrected electric energy whereby the photon couples to the electron via the muon, and the third term $(2\pi\alpha)^4$ regards the magnetic energy which is a relativistic correction to the electric energy whereby the photon couples to the electron via a possible tau state. The first and second radiation reaction terms are negative since the mass-energy of the electron and muon are less than or equal to the mass-energy of the bound particle in muonic H with the lower energy state being relative to the energy of the state involving an electron. The third term is positive since it is a loss term for a possible, but not obtained mass-energy state. The second and third terms involve lepton couplings between two and three leptons, respectively.

Since the magnetic force between the muon and proton magnetic moment given by Eqs. (1.243-1.252) is also a relativistic electrodynamic force involving the lepton mass, it must be corrected by the ratio of the electron to muon mass. The radiation reaction force in the muonic hydrogen atom also perturbs the force balance between the muon and proton relative to the condition in its absence. The outward centrifugal force on the muon is balanced by the electric force and the mass-ratio-corrected magnetic force (Eqs. (1.253) and (2.4)), and the three-term-expanded radiation reaction force (Eq. (2.135)) corresponding to the current flow to achieve the current distribution of the $2S_{1/2}$ from the $2P_{1/2}$ state:

$$\frac{m_\mu v^2}{r} = \frac{\hbar^2}{m_\mu r^3} = \frac{0.5e^2}{4\pi\varepsilon_0 r^2} - \frac{m_e}{m_\mu}\frac{\hbar^2}{m_P r^3} - \left[(2\pi\alpha)^2 + 2(2\pi\alpha)^3 - 3(2\pi\alpha)^4\right]\frac{\eta}{48\pi}\frac{e^2\hbar}{m_e r^3} \tag{2.166}$$

$$r = \frac{4\pi\varepsilon_0}{0.5e^2}\left[\frac{m_e}{m_\mu}\left(\frac{\hbar^2}{m_e} + \frac{\hbar^2}{m_P}\right) + \left[(2\pi\alpha)^2 + 2(2\pi\alpha)^3 - 3(2\pi\alpha)^4\right]\frac{\eta}{48\pi}\frac{e^2\hbar}{m_e}\right] \tag{2.167}$$

$$r = 2a_H\frac{m_e}{m_\mu} + \left[(2\pi\alpha)^2 + 2(2\pi\alpha)^3 - 3(2\pi\alpha)^4\right]\frac{\hbar}{6m_e c} \tag{2.168}$$

$$r = 2.0005735a_{\mu p} = 9.6755983\ X\ 10^{-3}a_H \tag{2.169}$$

where Eq. (1.35) was used for the velocity, a_H is the radius of the hydrogen atom given by Eq. (1.259), and $a_{\mu p}$ is defined as $a_H\frac{m_e}{m_\mu}$. The radius in the absence of the radiation reaction force is $r_0 = 2a_{\mu p} = 9.6728246\ X\ 10^{-3}a_H$.

ENERGY CALCULATIONS

The change in the electric energy of the muon $\Delta E_{ele}^{\mu p\ Lamb}$ due to the slight shift of the radius of the atom is given by the difference between the electric energies associated with the unperturbed and radiation-reaction-force-perturbed radius. Each electric energy is given by the substitution of the corresponding radius given by Eq. (2.167) into Eqs. (1.264) and (2.4):

$$\Delta E_{ele}^{\mu p\ Lamb} = \frac{-0.5e^2}{8\pi\varepsilon_0}\left[\frac{1}{r_0} - \frac{1}{r_+}\right] = -3.22846\ X\ 10^{-20}\ J \tag{2.170}$$

wherein the unperturbed radius given by Eq. (2.5) and Eqs. (1.253-1.259) is $r_0 = 2a_{\mu p}$.

In addition, the change in the magnetic energy $\Delta E_{mag}^{\mu p\ Lamb}$ of the muon is given by Eqs. (1.161-1.162) with the substitution of the corresponding radii

$$\begin{aligned}\Delta E_{mag}^{\mu p\ Lamb} &= \frac{\pi\mu_0 e^2\hbar^2}{m_\mu^{\ 2}}\left(\frac{1}{r_0^3} - \frac{1}{r_+^3}\right)\\ &= 4\pi\mu_0\mu_{B_\mu}^2\left(\frac{1}{r_0^3} - \frac{1}{r_+^3}\right)\\ &= 2.03334\ X\ 10^{-22}\ J\end{aligned} \tag{2.171}$$

where μ_{B_μ} is the muon Bohr magneton.

For the photon of the muonic hydrogen atom, the linear momentum of the emitted photon is balanced by the recoil momentum of the entire atom of mass $m_{\mu p}$, and the corresponding recoil energy adds to the energy due to the radiation reaction force. The recoil energy $E_{recoil}^{\mu p\ Lamb}$ for the muon in the $n = 2$ state and the corresponding frequency shift $\Delta f_{recoil}^{\mu p\ Lamb}$ of the muonic hydrogen atom is given by Eqs. (2.153):

$$E_{recoil}^{\mu p\ Lamb} = -\frac{(E_{h\upsilon})^2}{2m_{\mu p}c^2} = -3.41241\ X\ 10^{-22}\ J \tag{2.172}$$

$$\Delta f_{recoil}^{\mu p\ Lamb} = \frac{\Delta\omega}{2\pi} = \frac{\left(E_{h\upsilon}\right)^2}{\left|2hm_{\mu p}c^2\right|} = 514.99\ GHz \tag{2.173}$$

where $E_{h\upsilon}$ corresponds to the recoil energy (Eqs. (2.153) and (2.22)) for muonic H is:

$$E_{h\upsilon} = -13.5983\frac{m_\mu}{m_e}\ eV\left(1-\frac{1}{n^2}\right) = -2811.67\ eV\left(1-\frac{1}{n^2}\right) \tag{2.174}$$

wherein $n = 2$.

Then, the total energy of the muonic hydrogen Lamb shift corresponding to the transition ${}^2P_{1/2} \rightarrow {}^2S_{1/2}$ is given by the sum of Eqs. (2.170-2.172):

$$\begin{aligned}\Delta E_{total}^{\mu p\ Lamb} &= \Delta E_{ele}^{\mu p\ Lamb} + \Delta E_{mag}^{\mu p\ Lamb} + E_{recoil}^{\mu p\ Lamb} \\ &= -3.22846\ X\ 10^{-20}\ J + 2.03334\ X\ 10^{-22}\ J - 3.41241\ X\ 10^{-22}\ J \\ &= -3.24225\ X\ 10^{-20}\ J\end{aligned} \tag{2.175}$$

The Planck relationship (Eq. (2.148)) gives $\Delta f_{total}^{\mu p\ Lamb}$, the magnitude of the muonic hydrogen Lamb shift energy corresponding to the transition ${}^2P_{1/2} \rightarrow {}^2S_{1/2}$ expressed in terms of frequency:

$$\Delta f_{total}^{\mu p\ Lamb} = \frac{\left|\Delta E_{total}^{\mu p\ Lamb}\right|}{h} = 48{,}931.0\ GHz \tag{2.176}$$

The literature energies for $E_{2P_{3/2}^{F=2}\rightarrow 2P_{1/2}}$, the ${}^2P_{3/2}^{F=2}$ level shift with respect to the unperturbed ${}^2P_{1/2}$ level, and, $E_{2S_{1/2}^{F=1}}$, the ${}^2S_{1/2}^{F=1}$ level shift with respect to the unperturbed ${}^2S_{1/2}$ level, are [43]:

$$E_{2P_{3/2}^{F=2}\rightarrow 2P_{1/2}} = 9.6243\ meV = 1.54199\ X\ 10^{-21}\ J \tag{2.177}$$

$$E_{2S_{1/2}^{F=1}} = 5.7037\ meV = 9.13841\ X\ 10^{-22}\ J \tag{2.178}$$

Then, using Eqs. (2.175) and (2.177-2.178), the total energy of the muonic hydrogen Lamb shift corresponding to the transition ${}^2P_{3/2}\ F=2 \rightarrow {}^2S_{1/2}\ F=1$ is:

$$\begin{aligned}\Delta E_{total}^{\mu p\ Lamb\ {}^2P_{3/2}\ F=2\rightarrow {}^2S_{1/2}\ F=1} &= \Delta E_{total}^{\mu p\ Lamb} - E_{2P_{3/2}^{F=2}\rightarrow 2P_{1/2}} + E_{2S_{1/2}^{F=1}} \\ &= -3.24225\ X\ 10^{-20}\ J - 1.54199\ X\ 10^{-21}\ J + 9.13841\ X\ 10^{-22}\ J \\ &= -3.30507\ X\ 10^{-20}\ J\end{aligned} \tag{2.179}$$

The Planck relationship (Eq. (2.148)) gives $\Delta f_{total}^{\mu p\ Lamb\ {}^2P_{3/2}\ F=2\rightarrow {}^2S_{1/2}\ F=1}$, the magnitude of the muonic hydrogen Lamb shift energy expressed in terms of frequency:

$$\Delta f_{total}^{\mu p\ Lamb\ {}^2P_{3/2}\ F=2\rightarrow {}^2S_{1/2}\ F=1} = \frac{\left|\Delta E_{total}^{\mu p\ Lamb\ {}^2P_{3/2}\ F=2\rightarrow {}^2S_{1/2}\ F=1}\right|}{h} = 49{,}879.0\ GHz \tag{2.180}$$

The magnitude of the experimental muonic hydrogen Lamb shift matching the ${}^2S_{1/2}$ state lower than the ${}^2P_{1/2}$ and states ${}^2P_{3/2}$ is [43]:

$$\Delta f_{total}^{\mu p\ Lamb\ {}^2P_{3/2}\ F=2\rightarrow {}^2S_{1/2}\ F=1}\left(\text{experimental}\right) = 49{,}881.88\ GHz \tag{2.181}$$

There is good agreement between the theoretical and experimental values given the 18.6 GHz natural linewidth of the $2P$ state. The 0.0058% relative difference is within the measurement error and propagated errors in the fundamental constants of the equations. For example, the relative difference is 0.0025% using the 2002 CODATA constants [44]. These results solve the proton radius puzzle wherein QED erroneously invokes the proton radius in computation of the muonic hydrogen Lamb shift.

HYDROGEN SPIN-ORBIT COUPLING (FINE STRUCTURE)

For the $2P$ level, the possible quantum numbers are $n=2,\ \ell=1,\ m_\ell=0$ and $n=2,\ \ell=1,\ m_\ell=\pm 1$ corresponding to the states ${}^2P_{1/2}$ and ${}^2P_{3/2}$, respectively. Thus, for $\ell=1$, the electron may or may not possess orbital angular momentum in addition to spin angular momentum corresponding to $m_\ell=\pm 1$ and $m_\ell=0$, respectively. As a consequence, the energy of the $2P$ level is split by a relativistic interaction between the spin and orbital angular momentum as well as the corresponding radiation reaction force. The corresponding energy for the transition ${}^2P_{1/2} \rightarrow {}^2P_{3/2}$ is known as the hydrogen fine structure.

The electron's motion in the hydrogen atom is always perpendicular to its radius; consequently, as shown by Eq. (1.37), the electron's angular momentum of $\hbar$ is invariant. Furthermore, the electron is nonradiative due to its angular motion as shown in Appendix I and the Stability of Atoms and Hydrinos section. The radiative instability of excited states is due to a radial dipole term in the function representative of the excited state due to the interaction of the photon and the excited-state electron as shown in the Instability of Excited States section. The angular momentum of the photon given in the Equation of the Photon section is given by Eqs. (2.132) and (4.1). It is conserved for the solutions for the resonant photons and excited-state electron functions

given in the Excited States of the One-Electron Atom (Quantization) section and the Equation of the Photon section. Thus, the electrodynamic angular momentum and the inertial angular momentum are matched such that the correspondence principle holds. It follows from the principle of conservation of angular momentum that $\frac{e}{m_e}$ of Eq. (1.131) is invariant (See the Determination of Atomic Orbital Radii section).

A magnetic field is a relativistic effect of the electrical field as shown by Jackson [21]. No energy term is associated with the magnetic field of the electron of the hydrogen atom unless another source of magnetic field is present. In the case of spin-orbit coupling, the invariant $\hbar$ of spin angular momentum and orbital angular momentum each give rise to a corresponding invariant magnetic moment of a Bohr magneton, and their corresponding energies superimpose as given in the Orbital and Spin Splitting section. The interaction of the two magnetic moments gives rise to a relativistic spin-orbit coupling energy. The vector orientations of the momentum must be considered as well as the condition that flux must be linked by the electron in units of the magnetic flux quantum in order to conserve the invariant electron angular momentum of $\hbar$. The energy may be calculated with the additional conditions of the invariance of the electron's charge and charge-to-mass ratio $\frac{e}{m_e}$.

As shown in the Electron g Factor section (Eq. (1.181)), flux must be linked by the electron atomic orbital in units of the magnetic flux quantum that treads the atomic orbital at $v = c$ with a corresponding energy of:

$$E_{mag}^{fluxon} = 2\frac{\alpha}{2\pi}\mu_B B \tag{2.182}$$

As shown in the Atomic Orbital Equation of Motion for $\ell = 0$ Based on the Current Vector Field (CVF) section, the Two-Electron Atoms section, and Appendix VI, the maximum projection of the rotating spin angular momentum of the electron onto an axis is $\sqrt{\frac{3}{4}}\hbar$. From Eq. (2.65), the magnetic flux due to the spin angular momentum of the electron is [20]:

$$\mathbf{B} = \frac{\mu_0 \mu}{r^3} = \frac{\mu_0 e\hbar}{2m_e r_2^3}\sqrt{\frac{3}{4}} \tag{2.183}$$

where μ is the magnetic moment. The maximum projection of the orbital angular momentum onto an axis is $\hbar$ as shown in the Orbital and Spin Splitting section with a corresponding magnetic moment of a Bohr magneton μ_B. Substitution of the magnetic moment of μ_B corresponding to the orbital angular momentum and Eq. (2.183) for the magnetic flux corresponding to the spin angular momentum into Eq. (2.182) gives the spin-orbit coupling energy $E_{s/o}$.

$$E_{s/o} = 2\frac{\alpha}{2\pi}\mu_B B = 2\frac{\alpha}{2\pi}\left(\frac{e\hbar}{2m_e}\right)\frac{\mu_0 e\hbar}{2m_e r^3}\sqrt{\frac{3}{4}} \tag{2.184}$$

The Bohr magneton corresponding to the orbital angular momentum is invariant and the corresponding invariant electron charge e is common with that which gives rise to the magnetic field due to the spin angular momentum. The condition that the magnetic flux quantum treads the atomic orbital at $v = c$ with the maintenance of the invariance of the electron's charge-to-mass ratio $\frac{e}{m_e}$ and electron angular momentum of $\hbar$ requires that the radius and the electron mass of the magnetic field term of Eq. (2.184) be relativistically corrected. As shown by Eq. (1.280) and in Appendix I and the Determination of Atomic Orbital Radii sections, the relativistically corrected radius r^* follows from the relationship between the electron wavelength and the radius.

$$2\pi r = \lambda \tag{2.185}$$

The phase matching condition requires that the electron wavelength be the same for orbital and spin angular momentum. Using Eq. (1.280) with $v = c$:

$$r^* = \lambda \tag{2.186}$$

Thus,

$$r^* = \frac{r}{2\pi} \tag{2.187}$$

The relativistically corrected mass m^* follows from Eq. (2.187) with maintenance of the invariance of the electron angular momentum of $\hbar$ given by Eqs. (1.35) and (1.37).

$$m\mathbf{r} \times \mathbf{v} = m_e r \frac{\hbar}{m_e r} \tag{2.188}$$

With Eq. (2.187), the relativistically corrected mass m^* is:

$$m^* = 2\pi m_e \tag{2.189}$$

With the substitution of Eq. (2.187) and Eq. (2.189) into Eq. (2.184), the spin-orbit coupling energy $E_{s/o}$ is given by

$$E_{s/o} = 2\frac{\alpha}{2\pi}\left(\frac{e\hbar}{2m_e}\right)\frac{\mu_0 e\hbar}{2\left(2\pi m_e\right)\left(\frac{r}{2\pi}\right)^3}\sqrt{\frac{3}{4}} = \frac{\alpha\pi\mu_0 e^2\hbar^2}{m_e^2 r^3}\sqrt{\frac{3}{4}} \tag{2.190}$$

(The magnetic field in this case is equivalent to that of a point electron at the origin with $\sqrt{\frac{3}{4}}\hbar$ of angular momentum.)

In the case that $n=2$, the radius given by Eq. (2.5) is $r=2a_0$. The predicted energy difference between the $^2P_{1/2}$ and $^2P_{3/2}$ levels of the hydrogen atom, $E_{s/o}$, given by Eq. (2.190) is:

$$E_{s/o}=\frac{\alpha\pi\mu_0 e^2\hbar^2}{8m_e^2 a_0^{\,3}}\sqrt{\frac{3}{4}} \tag{2.191}$$

wherein $\ell=1$ and both levels are equivalently Lamb shifted.

$E_{s/o}$ may be expressed in terms of the mass energy of the electron. The energy stored in the magnetic field of the electron atomic orbital (Eq. (1.183)) is:

$$E_{mag}=\frac{\pi\mu_0 e^2\hbar^2}{(m_e)^2 r_n^3} \tag{2.192}$$

As shown in the Pair Production section with the $v=c$ condition, the result of the substitution of $\alpha a_o=\lambda\!\!\!^{-}_C$ for r_n, the relativistic mass, $2\pi m_e$, for m_e, and multiplication by the relativistic correction, α^{-1}, which arises from Gauss' law surface integral and the relativistic invariance of charge is:

$$E_{mag}=m_e c^2 \tag{2.193}$$

Thus, Eq. (2.191) can be expressed as:

$$E_{s/o}=\frac{\alpha^5(2\pi)^2}{8}m_e c^2\sqrt{\frac{3}{4}}=7.24043\ X\ 10^{-24}\ J \tag{2.194}$$

Using the Planck equation, the corresponding frequency, $\Delta f_{s/o}$, is:

$$\Delta f_{s/o}=10{,}927.02\ MHz \tag{2.195}$$

As in the case of the $^2P_{1/2}\rightarrow{}^2S_{1/2}$ transition, an additional term arises in the fine structure interval from the radiation reaction force involving electron-photon-momentum transfer during the $^2P_{1/2}\rightarrow{}^2P_{3/2}$ transition corresponding to the rotating orbital dipole that couples with the spin angular momentum. The radiation reaction force F_{RR} is given by Eq. (2.135) having the additional relativistic correction factor of $2\pi\alpha$ with an additional geometrical correction factor of $\sqrt{\frac{3}{4}}$ matching the rotating projection of the spin angular momentum:

$$F_{RR}=(2\pi\alpha)^3\frac{\eta}{48\pi}\frac{e^2\hbar}{m_e r^3}\sqrt{\frac{3}{4}} \tag{2.196}$$

The outward centrifugal force on the electron is balanced by the electric force and the magnetic force (Eqs. (1.253) and (2.4)), and the radiation reaction force (Eq. (2.196)):

$$\frac{m_e v^2}{r}=\frac{\hbar^2}{m_e r^3}=\frac{0.5e^2}{4\pi\varepsilon_0 r^2}-\frac{\hbar^2}{m_P r^3}+(2\pi\alpha)^3\frac{\eta}{48\pi}\frac{e^2\hbar}{m_e r^3}\sqrt{\frac{3}{4}} \tag{2.197}$$

$$r=2a_H-(2\pi\alpha)^3\frac{\hbar}{6m_e c}\sqrt{\frac{3}{4}} \tag{2.198}$$

$$r=1.99999990a_H \tag{2.199}$$

where Eq. (1.35) was used for the velocity and a_H is the radius of the hydrogen atom given by Eq. (1.259).

ENERGY CALCULATIONS

The change in the electric energy of the electron $\Delta E_{ele}^{H\ FS}$ due to the slight shift of the radius of the atom is given by the difference between the electric energies associated with the unperturbed and radiation-reaction-force-perturbed radius. Each electric energy is given by the substitution of the corresponding radius given by Eq. (2.199) into Eqs. (1.264) and (2.4):

$$\Delta E_{ele}^{H\ FS}=\frac{-0.5e^2}{8\pi\varepsilon_0}\left[\frac{1}{r_0}-\frac{1}{r_-}\right]=2.76347\ X\ 10^{-26}\ J \tag{2.200}$$

wherein the unperturbed radius given by Eq. (2.5) is $r_0=2a_H$.

In addition, the change in the magnetic energy $\Delta E_{mag}^{H\ FS}$ of the electron is given by Eqs. (1.161-1.162) with the substitution of the corresponding radii:

$$\Delta E_{mag}^{H\ FS} = \frac{\pi\mu_0 e^2\hbar^2}{m_e^{\ 2}}\left(\frac{1}{r_0^3}-\frac{1}{r_-^3}\right)$$
$$= 4\pi\mu_0\mu_B^2\left(\frac{1}{r_0^3}-\frac{1}{r_-^3}\right) \tag{2.201}$$
$$= -1.74098\ X\ 10^{-28}\ J$$

where μ_B is the Bohr magneton.

Then, the total radiation reaction energy of the hydrogen fine structure $\Delta E_{RRtotal}^{H\ FS}$ is given by the sum of Eqs. (2.200-2.201):

$$\Delta E_{RRtotal}^{H\ FS} = \Delta E_{ele}^{H\ FS} + \Delta E_{mag}^{H\ FS}$$
$$= 2.76347\ X\ 10^{-26}\ J - 1.74098\ X\ 10^{-28}\ J \tag{2.202}$$
$$= 2.74606\ X\ 10^{-26}\ J$$

The Planck relationship (Eq. (2.148)) gives $\Delta f_{RRtotal}^{H\ FS}$, the radiation reaction energy contribution expressed in terms of frequency:

$$\Delta f_{RRtotal}^{H\ FS} = \frac{\left|\Delta E_{RRtotal}^{H\ FS}\right|}{h} = 41.44\ MHz \tag{2.203}$$

Then, the total energy of the hydrogen fine structure $\Delta E_{total}^{H\ FS}$ is given by the sum of Eqs. (2.194) and (2.202):

$$\Delta E_{total}^{H\ FS} = E_{s/o} + \Delta E_{RRtotal}^{H\ FS}$$
$$= 7.24043\ X\ 10^{-24}\ J + 2.74606\ X\ 10^{-26}\ J \tag{2.204}$$
$$= 7.26789\ X\ 10^{-24}\ J$$

The Planck relationship (Eq. (2.148)) gives $\Delta f_{total}^{H\ FS}$, the fine structure energy expressed in terms of frequency:

$$\Delta f_{total}^{H\ FS} = \frac{\left|\Delta E_{total}^{H\ FS}\right|}{h} = 10,968.46\ MHz \tag{2.205}$$

The experimental hydrogen fine structure is [42]

$$\Delta f_{total}^{H\ FS}\left(\text{experimental}\right) = 10,969.05\ MHz \tag{2.206}$$

The large natural widths of the hydrogen $2P$ levels limits the experimental accuracy [45]; yet, given this limitation, the agreement between the theoretical and experimental fine structure (0.005% relative difference) is excellent and within the cited and propagated errors.

HYDROGEN KNIGHT SHIFT

In an external magnetic field, the unpaired electron of the hydrogen atom gives rise to a uniform magnetic field contribution at the nucleus which is given by Eq. (1.152).

$$\mathbf{H} = \frac{e\hbar}{m_e r_n^3}(\mathbf{i}_r\cos\theta - \mathbf{i}_\theta\sin\theta) \qquad r < r_n \tag{2.207}$$

Multiplication of Eq. (2.207) by the permeability of free space, μ_0, and substitution of the Bohr radius of the hydrogen atom, a_H, given by Eq. (1.259) for r_n of Eq. (2.207) gives the magnetic flux, $\mathbf{B_s}$, at the nucleus due to electron spin.

$$\mathbf{B_s} = \frac{\mu_0 e\hbar}{m_e a_H^3}\mathbf{i}_z = 157.29\ T \tag{2.208}$$

The shift of the NMR frequency of a nucleus by an unpaired electron is called the Knight Shift. The Knight Shift of the hydrogen atom is given by the magnetic flux (Eq. (2.208)) times the proton gyromagnetic ratio of $42.5775\ MHzT^{-1}$. The experimental value is unknown; however, magnetic hyperfine structure shifts of Mössbauer spectra corresponding to magnetic fluxes of 100 T or more due to unpaired electrons are common.

SPIN - NUCLEAR COUPLING (HYPERFINE STRUCTURE)

The radius of the hydrogen atom is increased or decreased very slightly due to the Lorentz force on the electron due to the magnetic field of the proton and its orientation relative to the electron's angular momentum vector. The additional small centripetal magnetic force is the relativistic corrected Lorentz force, $\mathbf{F}_{mag}$, as also given in the Two-Electron Atoms section and the Three- Through Twenty-Electron Atoms section.

The atomic orbital with $\ell = 0$ is a shell of negative charge current comprising correlated charge motion along great circles. The superposition of the vector projection of the atomic orbital angular momentum on the z-axis is $\mathbf{L}_z = \frac{\hbar}{2}$ (Eq. (1.128))

with an orthogonal component of $\mathbf{L}_{xy} = \frac{\hbar}{4}$ (Eq. (1.127)). The magnetic field of the electron at the nucleus due to $\mathbf{L}_z$ after McQuarrie [20] is

$$\mathbf{B} = \frac{\mu_0 e\hbar}{2m_e r^3} \tag{2.209}$$

where μ_0 is the permeability of free-space ($4\pi\ X\ 10^{-7}\ N/A^2$). An electrodynamic force or radiation reaction force, a force dependent on the second derivative of the charge's position with respect to time, arises between the electron and the proton. This force given in Sections 6.6, 12.10, and 17.3 of Jackson [37] achieves the condition that the sum of the mechanical momentum and electromagnetic momentum is conserved.

The magnetic moment of the proton, μ_P, aligns in the direction of $\mathbf{L}_z$, but experiences a torque due to the orthogonal component $\mathbf{L}_{xy}$. As shown in the Atomic Orbital Equation of Motion for $\ell = 0$ Based on the Current Vector Field (CVF) section, the magnetic field of the atomic orbital gives rise to the precession of the magnetic moment vector of the proton directed from the origin of the atomic orbital at an angle of $\theta = \frac{\pi}{3}$ relative to the z-axis. The precession of μ_P forms a cone in the nonrotating laboratory frame to give a perpendicular projection of:

$$\mu_{P\perp} = \pm\sqrt{\frac{3}{4}}\mu_P \tag{2.210}$$

after Eq. (1.129) and a projection onto the z-axis of:

$$\mu_{P\parallel} = \pm\frac{\mu_P}{2} \tag{2.211}$$

after Eq. (1.130). At torque balance, $\mathbf{L}_{xy}$ also precesses about the z-axis at 90° with respect to $\mu_{P\parallel}$. Using Eq. (2.209), the magnitude of the force F_{mag} between the antiparallel field of the electron and μ_P is:

$$F_{mag} = \left|\frac{\mu_P \times \mathbf{B}}{r}\right| = \mu_P \frac{\mu_0 e\hbar}{2m_e r^4} \tag{2.212}$$

The radiation reaction force corresponding to photon emission or absorption is radial as given in the Equation of the Electric Field inside the Atomic Orbital section. The reaction force on the electron due to the force of the electron's field on the magnetic moment of the proton is the corresponding relativistic central force, $\mathbf{F}_{mag}$, which acts uniformly on each charge (mass)-density element of the electron. The magnetic central force is derived as follows from the Lorentz force which is relativistically corrected. The Lorentz force at each point of the electron moving at velocity $\mathbf{v}$ due to a magnetic flux $\mathbf{B}$ is:

$$\mathbf{F}_{mag} = e\mathbf{v} \times \mathbf{B} \tag{2.213}$$

Eqs. (2.212) and (2.213) may be expressed in terms of the electron velocity given by Eq. (1.35):

$$F_{mag} = \frac{\hbar}{m_e r}\frac{e\mu_0\mu_P}{2r^3} = \frac{e}{2}|\mathbf{v} \times \mathbf{B}| \tag{2.214}$$

where $\mathbf{B}$ is the magnetic flux of the proton at the electron. (The magnetic moment $\mathbf{m}$ of the proton is given by Eq. (37.29), and the magnetic field of the proton follows from the relationship between the magnetic dipole field and the magnetic moment $\mathbf{m}$ as given by Jackson [46] where $\mathbf{m} = \mu_P \mathbf{i}_z$.) In the lightlike frame, the velocity $\mathbf{v}$ is the speed of light, and $\mathbf{B}$ corresponds to the time-dependent component of the proton magnetic moment given by Eq. (2.210). Thus, the central force is:

$$\mathbf{F}_{mag} = \pm\frac{e\alpha c}{2}\frac{\mu_0}{r^3}\ \mu_P\sqrt{\frac{3}{4}} \tag{2.215}$$

where the relativistic factor from Eq. (1.249) is α (Eq. (1.205) also gives the velocity as αc), the plus sign corresponds to antiparallel alignment of the magnetic moments of the electron and proton, and the minus sign corresponds to parallel alignment. The outward centrifugal force (Eq. (1.241)) on the electron is balanced by the electric force (Eq. (1.242)) and the magnetic forces given by Eqs. (1.252) and (2.215):

$$\frac{m_e v^2}{r} = \frac{e^2}{4\pi\varepsilon_0 r^2} - \frac{\hbar^2}{mr^3} \pm \frac{e\alpha c}{2}\frac{\mu_0}{r^3}\ \mu_P\sqrt{\frac{3}{4}} \tag{2.216}$$

Using Eq. (1.35),

$$\frac{\hbar^2}{m_e r^3} = \frac{e^2}{4\pi\varepsilon_0 r^2} - \frac{\hbar^2}{mr^3} \pm \frac{e\alpha c}{2}\frac{\mu_0}{r^3}\ \mu_P\sqrt{\frac{3}{4}} \tag{2.217}$$

$$\frac{\hbar^2}{m_e r^3} + \frac{\hbar^2}{mr^3} = \frac{e^2}{4\pi\varepsilon_0 r^2} \pm \frac{e\alpha c}{2}\frac{\mu_0}{r^3}\ \mu_P\sqrt{\frac{3}{4}} \tag{2.218}$$

$$\frac{\hbar^2}{\mu_e} \pm \frac{e\alpha c\mu_0}{2}\ \mu_P\sqrt{\frac{3}{4}} = \frac{e^2}{4\pi\varepsilon_0} r \tag{2.219}$$

$$r = a_H \pm \frac{4\pi\varepsilon_0}{2e^2} e\alpha c\mu_0 \ \mu_P \sqrt{\frac{3}{4}} \tag{2.220}$$

$$r = a_H \pm \frac{2\pi\alpha \ \mu_P}{ec} \sqrt{\frac{3}{4}} \tag{2.221}$$

where μ_e is the reduced electron mass given by Eq. (1.255), a_H is the Bohr radius of the hydrogen atom given by Eq. (1.259), the plus sign corresponds to parallel alignment of the magnetic moments of the electron and proton, and the minus sign corresponds to antiparallel alignment.

ENERGY CALCULATIONS

The magnetic energy to flip the orientation of the proton's magnetic moment, μ_P, from antiparallel to parallel to the direction of the magnetic flux $\mathbf{B}_s$ of the electron (180° rotation of the magnetic moment vector) given by Eqs. (1.168), (2.209), and (2.210) is:

$$\Delta E_{mag}^{\text{proton spin}} = -\frac{\mu_0 e\hbar}{2m_e} \mu_P \sqrt{\frac{3}{4}} \left(\frac{1}{r_+^3} + \frac{1}{r_-^3} \right) = -\mu_0 \mu_B \mu_P \sqrt{\frac{3}{4}} \left(\frac{1}{r_+^3} + \frac{1}{r_-^3} \right) = -1.918365 \ X \ 10^{-24} \ J \tag{2.222}$$

where the Bohr magneton, μ_B, is given by Eq. (1.131).

The change in the electric energy of the electron due to the slight shift of the radius of the electron is given by the difference between the electric energies associated with the two possible orientations of the magnetic moment of the electron with respect to the magnetic moment of the proton, parallel versus antiparallel. Each electric energy is given by the substitution of the corresponding radius given by Eq. (2.221) into Eq. (1.264). The change in electric energy for the flip from antiparallel to parallel alignment, $\Delta E_{ele}^{S/N}$, is:

$$\Delta E_{ele}^{S/N} = \frac{-e^2}{8\pi\varepsilon_0} \left[\frac{1}{r_+} - \frac{1}{r_-} \right] = 9.597048 \ X \ 10^{-25} \ J \tag{2.223}$$

In addition, the interaction of the magnetic moments of the electron and proton increases the magnetic energy, E_{mag}, of the electron given by Eqs. (1.161-1.162). The term of E_{mag} for the hyperfine structure of the hydrogen atom is similar to that of muonium given by Eq. (2.244) in the Muonium Hyperfine Structure Interval section:

$$\begin{aligned} E_{mag} &= -\left(1 + \left(\frac{2}{3} \right)^2 + \alpha \left(\cos\frac{\pi}{3} \right)^2 \right) \frac{\pi\mu_0 e^2\hbar^2}{m_e^2} \left(\frac{1}{r_+^3} - \frac{1}{r_-^3} \right) \\ &= -\left(1 + \left(\frac{2}{3} \right)^2 + \frac{\alpha}{4} \right) 4\pi\mu_0 \mu_B^2 \left(\frac{1}{r_+^3} - \frac{1}{r_-^3} \right) \\ &= 1.748861 \ X \ 10^{-26} \ J \end{aligned} \tag{2.224}$$

where the contribution corresponding to electron spin gives the first term, 1, and the second term, $\left(\frac{2}{3} \right)^2$, corresponds to the rotation of the electron about the z-axis corresponding to the precession of $\mathbf{L}_{xy}$. The geometrical factor of $\frac{2}{3}$ for the rotation is given in the Derivation of the Magnetic Field section in Chapter One (Eq. (1.140)) and by Eq. (11.391), and the energy is proportional to the magnetic field strength squared according to Eq. (1.154). The relativistic factor from Eq. (1.249) and Eqs. (1.161) and (2.190) is α times $\left(\cos\frac{\pi}{3} \right)^2$ where the latter term is due to the nuclear magnetic moment oriented $\theta = \frac{\pi}{3}$ relative to the z-axis. The energy is proportional to the magnetic field strength squared according to Eq. (1.154).

The total energy of the transition from antiparallel to parallel alignment, $\Delta E_{total}^{S/N}$, is given as the sum of Eqs. (2.222-2.224):

$$\begin{aligned} \Delta E_{total}^{S/N} &= \Delta E_{mag}^{\text{proton spin}} + \Delta E_{ele}^{S/N} + E_{mag} \\ &= -1.918365 \ X \ 10^{-24} \ J + 9.597048 \ X \ 10^{-25} \ J + 1.748861 \ X \ 10^{-26} \ J \\ &= -9.411714 \ X \ 10^{-25} \ J \end{aligned} \tag{2.225}$$

The energy is expressed in terms of wavelength using the Planck relationship, Eq. (2.148):

$$\lambda_{total}^{S/N} = \frac{hc}{\Delta E_{total}^{S/N}} = 21.10610\ cm \tag{2.226}$$

The experimental value from the hydrogen maser is [47]:

$$\lambda_{total}^{S/N} = 21.10611\ cm \tag{2.227}$$

The 21 cm line is important in astronomy for the determination of the presence of hydrogen. There is remarkable agreement between the calculated and experimental values of the hyperfine structure that is only limited by the accuracy of the fundamental constants in Eqs. (2.221-2.224).

MUONIUM HYPERFINE STRUCTURE INTERVAL

Muonium (μ^+e^-, M) is the hydrogenlike bound state of a positive muon and an electron. The solution of the ground state ($1^2S_{1/2}$) hyperfine structure interval of muonium, $\Delta\nu_{Mu}$, is similar to that of the hydrogen atom. The electron binds to the muon as both form concentric atomic orbitals with a minimization of energy. The outward centrifugal force (Eq. (1.241)) on the outer electron is balanced by the electric force (Eq. (1.242)) and the magnetic forces due to the inner positive muon given by Eqs. (1.252) and (2.215). The resulting force balance equation is the same as that for the hydrogen atom given by Eq. (2.216) with the muon mass, m_μ, replacing the proton mass, m, and the muon magnetic moment, μ_μ, replacing the proton magnetic moment, μ_P. The radius of the electron, r_2, is given by:

$$\frac{m_e v^2}{r_2} = \frac{e^2}{4\pi\varepsilon_0 r_2^2} - \frac{\hbar^2}{m_\mu r_2^3} \pm \frac{e\alpha c}{2}\frac{\mu_0}{r_2^3}\ \mu_\mu\sqrt{\frac{3}{4}} \tag{2.228}$$

Using Eq. (1.35),

$$\frac{\hbar^2}{m_e r_2^3} = \frac{e^2}{4\pi\varepsilon_0 r_2^2} - \frac{\hbar^2}{m_\mu r_2^3} \pm \frac{e\alpha c}{2}\frac{\mu_0}{r_2^3}\ \mu_\mu\sqrt{\frac{3}{4}} \tag{2.229}$$

$$\frac{\hbar^2}{\mu_{e,\mu}} \pm \frac{e\alpha c\mu_0\ \mu_\mu}{2}\sqrt{\frac{3}{4}} = \frac{e^2}{4\pi\varepsilon_0} r_2 \tag{2.230}$$

$$r_2 = a_\mu \pm \frac{2\pi\alpha\ \mu_\mu}{ec}\sqrt{\frac{3}{4}} \tag{2.231}$$

$$r_{2+} = a_\mu + \frac{2\pi\alpha\ \mu_\mu}{ec}\sqrt{\frac{3}{4}} = 5.31736859\ X\ 10^{-11}\ m \tag{2.232}$$

$$r_{2-} = a_\mu - \frac{2\pi\alpha\ \mu_\mu}{ec}\sqrt{\frac{3}{4}} = 5.31736116\ X\ 10^{-11}\ m \tag{2.233}$$

where $\mu_{e,\mu}$ is the reduced muonium-electron mass given by Eq. (1.255) with the mass of the proton replaced by the mass of the muon, a_μ is the Bohr radius of the muonium atom given by Eq. (1.259) with the reduced electron mass, μ_e (Eq. (1.255)), replaced by $\mu_{e,\mu}$. The plus sign corresponds to parallel alignment of the magnetic moments of the electron and muon, and the minus sign corresponds to antiparallel alignment.

The radii of the muon, r_1, in different spin states can be determined from r_2, the radii of the electron (Eqs. (2.232-2.233)), and the opposing forces on the muon due to the bound electron. The outward centrifugal force (Eq. (1.241)) on the muon is balanced by the reaction forces given by Eq. (2.228):

$$\frac{m_\mu v^2}{r_1} = \frac{\hbar^2}{m_e r_2^3} \pm \frac{e\alpha c}{2}\frac{\mu_0}{r_2^3}\ \mu_\mu\sqrt{\frac{3}{4}} \tag{2.234}$$

Using Eq. (1.35),

$$\frac{\hbar^2}{m_\mu r_1^3} = \frac{\hbar^2}{m_e r_2^3} \pm \frac{e\alpha c}{2}\frac{\mu_0}{r_2^3}\ \mu_\mu\sqrt{\frac{3}{4}} \tag{2.235}$$

$$r_2^3 = \left(\frac{m_\mu}{m_e} \pm \frac{m_\mu e\alpha c}{2\hbar^2}\mu_0\ \mu_\mu\sqrt{\frac{3}{4}}\right) r_1^3 \tag{2.236}$$

$$r_1 = \frac{r_2}{\left(\frac{m_\mu}{m_e} \pm \frac{m_\mu e\alpha c}{2\hbar^2}\mu_0\ \mu_\mu\sqrt{\frac{3}{4}}\right)^{1/3}} \tag{2.237}$$

Using Eqs. (2.232-2.233) for r_2,

$$r_1 = \frac{a_\mu \pm \frac{2\pi\alpha\ \mu_\mu}{ec}\sqrt{\frac{3}{4}}}{\left(\frac{m_\mu}{m_e} \pm \frac{m_\mu e\alpha c}{2\hbar^2}\mu_0\ \mu_\mu\sqrt{\frac{3}{4}}\right)^{1/3}} \tag{2.238}$$

$$r_{1+} = \frac{a_\mu + \frac{2\pi\alpha\ \mu_\mu}{ec}\sqrt{\frac{3}{4}}}{\left(\frac{m_\mu}{m_e} + \frac{m_\mu e\alpha c}{2\hbar^2}\mu_0\ \mu_\mu\sqrt{\frac{3}{4}}\right)^{1/3}} = 8.9922565\ X\ 10^{-12}\ m \tag{2.239}$$

$$r_{1-} = \frac{a_\mu - \frac{2\pi\alpha\ \mu_\mu}{ec}\sqrt{\frac{3}{4}}}{\left(\frac{m_\mu}{m_e} - \frac{m_\mu e\alpha c}{2\hbar^2}\mu_0\ \mu_\mu\sqrt{\frac{3}{4}}\right)^{1/3}} = 8.99224822\ X\ 10^{-12}\ m \tag{2.240}$$

where the plus sign corresponds to parallel alignment of the magnetic moments of the electron and muon and the minus sign corresponds to antiparallel alignment.

ENERGY CALCULATIONS

The magnetic energy, $\Delta E_{mag}^{spin}\left(\Delta\nu_{Mu}\right)$, to flip the orientation of the muon's magnetic moment, μ_μ, from antiparallel to parallel to the direction of the magnetic flux $\mathbf{B}_s$ of the electron (180° rotation of the magnetic moment vector) given by Eq. (2.222) is:

$$\Delta E_{mag}^{spin}\left(\Delta\nu_{Mu}\right) = -\frac{\mu_0 e\hbar}{2m_e}\mu_\mu\sqrt{\frac{3}{4}}\left(\frac{1}{r_{2+}^3} + \frac{1}{r_{2-}^3}\right) = -\mu_0\mu_B\mu_\mu\sqrt{\frac{3}{4}}\left(\frac{1}{r_{2+}^3} + \frac{1}{r_{2-}^3}\right) = -6.02890320\ X\ 10^{-24}\ J \tag{2.241}$$

wherein the muon magnetic moment replaces the proton magnetic moment and the electron Bohr magneton, μ_B, is given by Eq. (1.131).

An electric field equivalent to that of a point charge of magnitude $+e$ at the origin only exists for $r_1 < r \le r_2$. Thus, the change in the electric energy of the electron due to the slight shift of the radius of the electron is given by the difference between the electric energies associated with the two possible orientations of the magnetic moment of the electron with respect to the magnetic moment of the muon, parallel versus antiparallel. Each electric energy is given by the substitution of the corresponding radius given by Eq. (2.231) into Eq. (1.264) or Eq. (2.223). The change in electric energy for the flip from antiparallel to parallel alignment, $\Delta E_{ele}\left(\Delta\nu_{Mu}\right)$, is:

$$\Delta E_{ele}\left(\Delta\nu_{Mu}\right) = \frac{-e^2}{8\pi\varepsilon_0}\left[\frac{1}{r_{2+}} - \frac{1}{r_{2-}}\right] = 3.02903048\ X\ 10^{-24}\ J \tag{2.242}$$

For each lepton, the application of a magnetic field with a resonant Larmor excitation gives rise to a precessing angular momentum vector **S** of magnitude $\hbar$ directed from the origin of the atomic orbital at an angle of $\theta = \frac{\pi}{3}$ relative to the applied magnetic field. As given in the Spin Angular Momentum of the Atomic Orbital $Y_0^0(\theta,\phi)$ with $\ell = 0$ section, **S** rotates about the axis of the applied field at the Larmor frequency. The magnitude of the components of **S** that are parallel and orthogonal to the applied field (Eqs. (1.129-1.130)) are $\frac{\hbar}{2}$ and $\sqrt{\frac{3}{4}}\hbar$, respectively. Since both the RF field and the orthogonal components shown in Figure 1.25 rotate at the Larmor frequency, the RF field that causes a Stern Gerlach transition produces a stationary magnetic field with respect to these components as described by Patz [48]. The corresponding central field at the atomic orbital surface given by the superposition of the central field of the lepton and that of the photon follows from Eqs. (2.10-2.17) and Eq. (17) of Box 1.1:

$$\mathbf{E} = \frac{e}{4\pi\varepsilon_0 r^2}\left[Y_0^0(\theta,\phi)\mathbf{i}_\mathbf{r} + \mathrm{Re}\left\{Y_\ell^m(\theta,\phi)e^{im\omega_n t}\right\}\mathbf{i}_\mathbf{y}\delta(r - r_1)\right] \tag{2.243}$$

where the spherical harmonic dipole $Y_\ell^m(\theta,\phi)=\sin\theta$ is with respect to the **S**-axis. The dipole spins about the **S**-axis at the angular velocity given by Eq. (1.36). The resulting current is nonradiative as shown in Appendix I: Nonradiation Condition. Thus, the field in the RF rotating frame is magnetostatic as shown in Figures 1.28 and 1.29 but directed along the **S**-axis.

The interaction of the magnetic moments of the leptons increases their magnetic energies given by Eqs. (1.161-1.162) with the mass of the corresponding lepton:

$$\begin{aligned} E_{mag,e}^{stored}(\Delta\nu_{Mu}) &= -\left(1+\left(\frac{2}{3}\cos\frac{\pi}{3}\right)^2+\alpha\right)\frac{\pi\mu_0 e^2\hbar^2}{m_e{}^2}\left(\frac{1}{r_{2+}^3}-\frac{1}{r_{2-}^3}\right) \\ &= -\left(1+\left(\frac{2}{3}\cos\frac{\pi}{3}\right)^2+\alpha\right)4\pi\mu_0\mu_B^2\left(\frac{1}{r_{2+}^3}-\frac{1}{r_{2-}^3}\right) \\ &= 4.23209178\ X\ 10^{-26}\ J \end{aligned} \tag{2.244}$$

$$\begin{aligned} E_{mag,\mu}^{stored}(\Delta\nu_{Mu}) &= -\left(1+\left(\frac{2}{3}\cos\frac{\pi}{3}\right)^2+\alpha\right)\frac{\pi\mu_0 e^2\hbar^2}{m_\mu{}^2}\left(\frac{1}{r_{1+}^3}-\frac{1}{r_{1-}^3}\right) \\ &= -\left(1+\left(\frac{2}{3}\cos\frac{\pi}{3}\right)^2+\alpha\right)4\pi\mu_0\mu_{B,\mu}^2\left(\frac{1}{r_{1+}^3}-\frac{1}{r_{1-}^3}\right) \\ &= 1.36122030\ X\ 10^{-28}\ J \end{aligned} \tag{2.245}$$

where (1) the radii of the electron and muon are given by Eq. (2.232-2.233) and Eqs. (2.239-2.240)), respectively, (2) $\mu_{B,\mu}$ is the muon Bohr magneton given by Eq. (1.131) with the electron mass replaced by the muon mass, (3) the first term is due to lepton spin, (4) the second term, $\left(\frac{2}{3}\cos\frac{\pi}{3}\right)^2$ is due to **S**, oriented $\theta=\frac{\pi}{3}$ relative to the z-axis, wherein the geometrical factor of $\frac{2}{3}$ corresponds to the source current of the dipole field (Eq. (2.243)) given in the Derivation of the Magnetic Field section (Eq. (1.140)) and by Eq. (11.391), and the energy is proportional to the magnetic field strength squared according to Eq. (1.154), and (5) the relativistic factor from Eq. (1.249) and Eqs. (1.161) and (2.190) is α.

The energy of the ground state ($1^2S_{1/2}$) hyperfine structure interval of muonium, $\Delta E(\Delta\nu_{Mu})$, is given by the sum of Eqs. (2.241-2.242) and (2.244-2.245):

$$\begin{aligned} \Delta E(\Delta\nu_{Mu}) &= \Delta E_{mag}^{spin}(\Delta\nu_{Mu})+\Delta E_{ele}(\Delta\nu_{Mu})+E_{mag,e}^{stored}(\Delta\nu_{Mu})+E_{mag,\mu}^{stored}(\Delta\nu_{Mu}) \\ &= -6.02890320\ X\ 10^{-24}\ J+3.02903048\ X\ 10^{-24}\ J+4.23209178\ X\ 10^{-26}\ J+1.36122030\ X\ 10^{-28}\ J \\ &= -2.95741568\ X\ 10^{-24}\ J \end{aligned} \tag{2.246}$$

Using Planck's equation (Eq. (2.148)), the interval frequency, $\Delta\nu_{Mu}$, and wavelength, $\Delta\lambda_{Mu}$, are:

$$\Delta\nu_{Mu} = 4.46330328\ GHz \tag{2.247}$$

$$\Delta\lambda_{Mu} = 6.71682919\ \text{cm} \tag{2.248}$$

The experimental hyperfine structure interval of muonium [49] is:

$$\begin{aligned} &\Delta E(\Delta\nu_{Mu}) = -2.957415336\ X\ 10^{-24}\ J \\ &\Delta\nu_{Mu} = 4.463302765(53)\ GHz\ \ (12\,ppm) \\ &\Delta\lambda_{Mu} = 6.71682998\ \text{cm} \end{aligned} \tag{2.249}$$

There is remarkable (7 to 8 significant figure-) agreement between the calculated and experimental values of $\Delta\nu_{Mu}$ that is only limited by the accuracy of the fundamental constants in Eqs. (2.239-2.240), (2.241-2.242), and (2.244-2.245) as shown by using different CODATA values [50-51].

REFERENCES

1. J. D. Jackson, *Classical Electrodynamics*, Second Edition, John Wiley & Sons, New York, (1975), pp. 110-113.
2. J. D. Jackson, *Classical Electrodynamics*, Second Edition, John Wiley & Sons, New York, (1975), pp. 739-779.
3. M. Mizushima, *Quantum Mechanics of Atomic Spectra and Atomic Structure*, W.A. Benjamin, Inc., New York, (1970), p.17.
4. H. A. Haus, "On the radiation from point charges," American Journal of Physics, 54, (1986), pp. 1126-1129.
5. W. McC. Siebert, *Circuits, Signals, and Systems*, The MIT Press, Cambridge, Massachusetts, (1986), pp. 338-339.
6. W. McC. Siebert, *Circuits, Signals, and Systems*, The MIT Press, Cambridge, Massachusetts, (1986), p. 416.
7. J. D. Jackson, *Classical Electrodynamics*, Second Edition, John Wiley & Sons, New York, (1975), pp. 758-763.
8. J. D. Jackson, *Classical Electrodynamics*, Second Edition, John Wiley & Sons, New York, (1975), pp. 394-397.
9. R. L. Mills, "Maxwell's Equations and QED: Which is Fact and Which is Fiction," *Physics Essays*, Vol. 19, No. 2, (2006), 225-262. Posted with spreadsheets at http://www.blacklightpower.com/techpapers.shtml.
10. R. L. Mills, "The Fallacy of Feynman's Argument on the Stability of the Hydrogen Atom According to Quantum Mechanics," Annales de la Fondation Louis de Broglie, Vol. 30, No. 2, (2005), pp.129-151; posted at www.blacklightpower.com/theory/theory.shtml.
11. R. Mills, "The Nature of Free Electrons in Superfluid Helium—a Test of Quantum Mechanics and a Basis to Review its Foundations and Make a Comparison to Classical Theory," Int. J. Hydrogen Energy, Vol. 26, No. 10, (2001), pp. 1059-1096.
12. R. Mills, "The Hydrogen Atom Revisited," Int. J. of Hydrogen Energy, Vol. 25, Issue 12, December, (2000), pp. 1171-1183.
13. J. Daboul and J. H. D. Jensen, Z. Physik, Vol. 265, (1973), pp. 455-478.
14. T. A. Abbott and D. J. Griffiths, Am. J. Phys., Vol. 53, No. 12, (1985), pp. 1203-1211.
15. G. Goedecke, Phys. Rev 135B, (1964), p. 281.
16. P. Pearle, Foundations of Physics, "Absence of radiationless motions of relativistically rigid classical electron," Vol. 7, Nos. 11/12, (1977), pp. 931-945.
17. V. F. Weisskopf, Reviews of Modern Physics, Vol. 21, No. 2, (1949), pp. 305-315.
18. H. Margenau, G. M. Murphy, *The Mathematics of Chemistry and Physics*, D. Van Nostrand Company, Inc., New York, (1956), Second Edition, pp. 363-367.
19. J. D. Jackson, *Classical Electrodynamics*, Second Edition, John Wiley & Sons, New York, (1975), pp. 739-752.
20. D. A. McQuarrie, *Quantum Chemistry*, University Science Books, Mill Valley, CA, (1983), pp. 238-241.
21. J. D. Jackson, *Classical Electrodynamics*, Second Edition, John Wiley & Sons, New York, (1975), pp. 503-561.
22. N. Ryde, *Atoms and Molecules in Electric Fields*, Almqvist & Wiksell International, Stockholm, Sweden, (1976), pp. 168-177.
23. N. Ryde, *Atoms and Molecules in Electric Fields*, Almqvist & Wiksell International, Stockholm, Sweden, (1976), pp. 44-74.
24. J. Stark, do. V. Feinzerlegung der Wasserstoffserie, Ann. d. Phys., Vol. 48, (1915), p. 193.
25. L. C. Shi, J. A. Kong, *Applied Electromagnetism*, Brooks/Cole Engineering Division, Monterey, CA, (1983), pp. 170-209.
26. NIST Atomic Spectra Database, http://physics.nist.gov/PhysRefData/ASD/index.html.
27. S. Djurovic, J. R. Roberts, "Hydrogen Balmer alpha line shapes for hydrogen-argon mixtures in a low-pressure rf discharge," J. Appl. Phys., Vol. 74, No. 11, (1993), pp. 6558-6565.
28. G. Sultan, G. Baravian, M. Gantois, G. Henrion, H. Michel, A. Ricard, "Doppler-broadened H_α line shapes in a dc low-pressure discharge for TiN deposition," Chemical Physics, Vol. 123, (1988), pp. 423-429.
29. L. S. Ornstein, H. C. Burger, Zeits. für Phys., Intensitätsverhältnis von Balmer- und Paschenlinien," Vol. 62, (1930), pp. 636-639.
30. E. U. Condon, G. H. Shortley, *The Theory of Atomic Spectra*, Cambridge University Press, (1967), p. 141.
31. Personal communication, Dr.-Ing. Günther Landvogt, Hamburg, Germany, November, (2005).
32. E. U. Condon, G. H. Shortley, *The Theory of Atomic Spectra*, Cambridge University Press, (1967), Chp. 4 and Chp 5, sections 6 and 7.
33. L. R. Maxwell, "The average life of the ionized helium atom," Phys. Rev., Vol. 38, (1931), pp. 1664-1686.
34. W. McC. Siebert, *Circuits, Signals, and Systems*, The MIT Press, Cambridge, Massachusetts, (1986), pp. 488-502.
35. D. A. McQuarrie, *Quantum Chemistry*, University Science Books, Mill Valley, CA, (1983), pp. 135-140.
36. W. E. Lamb, R. C. Retherford, "Fine Structure of the Hydrogen Atom by a Microwave Method," R. C., Phys. Rev., Vol. 72, No. 3, August 1, (1947), pp. 241-243.
37. D. Jackson, *Classical Electrodynamics*, Second Edition, John Wiley & Sons, New York, (1975), pp. 236-240, 601-608, 786-790.
38. J. D. Jackson, *Classical Electrodynamics*, Second Edition, John Wiley & Sons, New York, (1975), pp. 236-240.
39. T. C. Gibb, *Principles of Mössbauer Spectroscopy*, Chapman and Hall: London (1977), Chp. 1.
40. U. Gonser, From a Strange Effect to Mössbauer Spectroscopy in *Mössbauer Spectroscopy*, U. Gonser, Ed. Springer-Verlag: New York (1975), pp. 1-51.
41. R. L. Mills, EPO Patent Number 86103694.5/0 198 257, Method and Apparatus for Selective Irradiation of Biological Materials, (1986).
42. P. J. Mohr, B. N. Taylor, D. B. Newell, "CODATA recommended values of the fundamental physical constants: 2006," Reviews of Modern Physics, Vol. 80, (2008), pp. 633-730.
43. R. Pohl, A. Antognini, F. N., F. D. Amaro, F. Biraben, J. M. R. Cardoso, D. S. Covita, A. Dax, S. Dhawan, L. M. P. Fernandes, A. Giesen, T. Graf, T. W. Hansch, P. Indelicato, L. Julien, C-Y. Kao, P. Knowles, E-O. Le Bigot, Y-W. Liu, J. A. M. Lopes, L. Ludhova, C. M. B. Monteiro, F. Mulhauser, T. Nebel, P. Rabinowitz, J. M. F. dos Santos, L. A. Schaller, K.

Schuhmann, C. Schwob, D. Taqqu, J. F. C. A. Veloso, F. Kottmann, "The size of the proton," Nature, Vol. 466, (2010), pp. 213-216, doi:10.1038/nature09250.

44. P. J. Mohr, B. N. Taylor, "CODATA recommended values of the fundamental physical constants: 2002," Rev. Mod. Phys. 77, (2005), pp. 1–107, http://dx.doi.org/10.1103/RevModPhys.77.1.
45. P. J. Mohr, B. N. Taylor, "CODATA recommended values of the fundamental physical constants: 1998," Reviews of Modern Physics, Vol. 72, No. 2, April, (2000), p. 418.
46. J. D. Jackson, *Classical Electrodynamics*, Second Edition, John Wiley & Sons, New York, (1975), p. 178.
47. P. J. Mohr, B. N. Taylor, "CODATA recommended values of the fundamental physical constants: 1998," Reviews of Modern Physics, Vol. 72, No. 2, April, (2000), pp. 418-419.
48. S. Patz, Cardiovasc Interven Radiol, (1986), 8:25, pp. 225-237.
49. W. Liu, M. G. Boshier, S. Dhawan, O. van Dyck, P. Egan, X. Fei, M. Grosse Perdekamp, V. W. Hughes, M. Janousch, K. Jungmann, D. Kawall, F. G. Mariam, C. Pillai, R. Prigl, G. zu Putlitz, I. Reinhard, W. Schwarz, P. A. Thompson, K. A. Woodle, "High Precision measurements of the ground state hyperfine structure interval of muonium and the muon magnetic moment," Phys. Rev. Letts., Vol. 82, No. 4, (1999), pp. 711-714.
50. P. J. Mohr, B. N. Taylor, "CODATA recommended values of the fundamental physical constants: 1998," Reviews of Modern Physics, Vol. 72, No. 2, April, (2000), pp. 448-453.
51. P. J. Mohr, B. N. Taylor, "CODATA recommended values of the fundamental physical constants: 2002," Reviews of Modern Physics, Vol. 77, No. 1, (2005), pp. 1-107.

Chapter 3

ELECTRON IN FREE SPACE

CHARGE-DENSITY FUNCTION

The radius of a spherical wavefront of light goes to infinity as it propagates from a spherically-symmetrical source such that its propagation in the far-field is given by the plane-wave equation:

$$\mathbf{E} = E_0 e^{-ik_z z} \tag{3.1}$$

Light and electrons display identical propagation and diffraction behavior. (This is expected because an electron is created from a photon as derived in the Pair Production section). Electrons behave as two-dimensional wavefronts with the de Broglie wavelength, $\lambda = h/p$, in double-slit experiments (Davisson-Germer experiment) [1]. The plane wave nature of free electrons is demonstrated in the Electron Scattering by Helium section[1]. The results of the double-slit experiment are derived classically in the Two-Slit Interference (Wave-Particle Duality) section. Analogous to the behavior of light, the radius of the spherically-symmetrical electron atomic orbital increases with the absorption of electromagnetic energy [2].

Consider an idealized hypothetical state. With the absorption of exactly the ionization energy, the atomic radius *r* goes to infinity, the electron momentum goes to zero, and the de Broglie relationship given by Eq. (1.15) predicts that the electron wavelength concomitantly goes to infinity corresponding to an infinitely large electron. The interaction radius of an infinitely large atom goes to infinity also. Such a state is not physical; so, let's consider the case observed. In order for the atom to become ionized to form a free electron, the atom must absorb energy greater than its ionization energy. The radius of the spherical shell (electron atomic orbital) goes to infinity as in the case of a spherical wavefront of light emitted from a symmetrical source, but it does not achieve an infinite radius. Rather it becomes ionized with the free electron propagating with linear velocity, v_z, and the de Broglie wavelength is finite as shown in Figure 3.1. The ionized electron is a plane wave that propagates as a wavefront with the de Broglie wavelength where the size of the electron is the de Broglie wavelength, $\lambda = h/p$, as shown below.

Figure 3.1. Time-lapsed image of spherical to plane-wave front continuity that determines the boundary conditions for atomic electron ionization. With the absorption of a photon of energy in excess of the binding energy, the bound electron's radius increases, and the electron ionizes as a plane-wave.

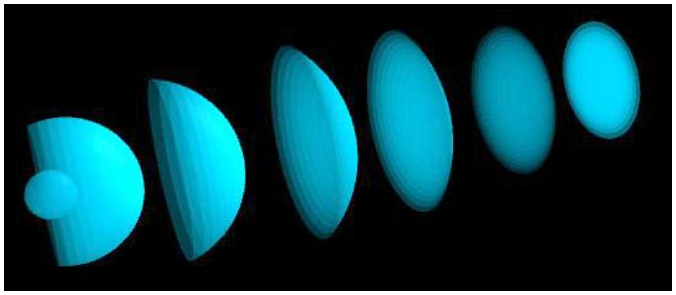

[1] Particles such as the proton and neutron also demonstrate interference patterns during diffraction. The observed far-field position distribution is a picture of the particles' transverse momentum distribution after the interaction. The momentum transfer is given by $\hbar k$ where $k = \frac{2\pi}{\lambda}$ is the wave number. The wavelength λ is the de Broglie wavelength associated with the momentum of the particles which is transferred through interactions. An example is the interference pattern for rubidium atoms given in the Wave-Particle Duality is Not Due to the Uncertainty Principle Section.

The ionized electron traveling at constant velocity, v_z, is nonradiative and is a two-dimensional surface having a total charge of e and a total mass of m_e. The spacetime charge-density function of the ionized electron is solved as a boundary value problem as described previously for the bound electron in the One Electron-Atom section. The de Broglie wavelength relationship given by Eq. (1.38) must hold independent of the radius of the electron. The relationship between the electron atomic orbital radius and its wavelength, is given by Eq. (1.15). The integral of the magnitude of the angular momentum density is $\hbar$ (Eq. (1.37)) independent of the electron radius; thus, for both the bound electron and the free electron, the total magnitude of the angular momentum is $\hbar$. The spacetime plane-wave charge-density function of the free electron is a solution of the classical wave equation (Eq. (1.56)). The current-density function possesses no spacetime Fourier components synchronous with waves traveling at the speed of light; thus it is nonradiative. As shown below, the solution of the boundary value problem of the free electron is given by the projection of the atomic orbital into a plane that linearly propagates along an axis perpendicular to the plane. The velocity of the plane and the atomic orbital is given by Eq. (1.35) where the radius of the atomic orbital in spherical coordinates is equal to the radius of the free electron in cylindrical coordinates.

Consider an electron atomic orbital of radius r_0. The boundary condition that the de Broglie wavelength holds and the angular momentum is conserved as shown *infra* for any electron radius requires that the ionized electron is the projection of the atomic orbital into $\pi(z)$, the Cartesian xy-plane that propagates linearly along the z-axis with the same linear velocity as the electron atomic orbital. The mass-density function, $\sigma_m(\rho,\phi,z)$, of the electron with linear velocity along the z-axis of v_z ***in the inertial frame of the proton***[2] given by Eq. (1.35):

$$\mathbf{v}_z = \frac{\hbar}{m_e r_n} = \frac{\hbar}{m_e r_0} = \frac{\hbar}{m_e \rho_0} \tag{3.2}$$

is given by the projection into the xy-plane of the convolution, $\otimes$, of the xy-plane, $\pi(z)$, with an atomic orbital of radius r_0. The convolution is

$$\pi(z) \otimes \delta(r - r_0) = \sqrt{r_0^2 - z^2}\,\delta(r - \sqrt{r_0^2 - z^2}) \tag{3.3}$$

where the atomic orbital function is given in spherical coordinates. The equation of the free electron is given as the projection of Eq. (3.3) into the xy-plane which in cylindrical coordinates is:

$$\begin{aligned} &\sigma_m(\rho,\phi,z) = N\sqrt{\rho_0^2 - \rho^2}\,\delta(z) \quad for\ 0 \le \rho \le \rho_0 \\ &\sigma_m(\rho,\phi,z) = 0 \qquad\qquad\qquad for\ \rho_0 < \rho \end{aligned} \tag{3.4}$$

where N is the normalization factor for the charge and mass plane-wave defined by $\pi\left(\frac{\rho}{2\rho_0}\right)$ which represents a two-dimensional disc or plane-lamina disc of radius ρ_0. In spherical coordinates, Eq. (3.4) is given by $\sin\theta$, the projection of the charge density of a spherical shell into a plane. The total mass is m_e. Thus, the normalization factor N in Eq. (3.4) is given by:

$$m_e = N\int_0^{2\pi}\int_0^{\rho_0}\sqrt{\rho_0^2 - \rho^2}\,\rho\, d\rho\, d\phi \tag{3.5}$$

$$N = \frac{m_e}{\frac{2}{3}\pi\rho_0^3} \tag{3.6}$$

The mass-density function of a free electron is a two-dimensional disc (essentially zero thickness equal to its Schwarzschild radius $r_g = \frac{2Gm_e}{c^2} = 1.3525\ X\ 10^{-57}\ m$ according to Eqs. (32.36) and (32.140b)). The mass-density distribution, $\sigma_m(\rho,\phi,z)$, and charge-density distribution, $\sigma_e(\rho,\phi,z)$, in the xy-plane at $\delta(z)$ are:

---

[2] The universe is electrically neutral and contains no antimatter according to the particle production equation (Eq. (32.172)) of the contracting phase of the oscillatory universe. Particle production proceeds through a neutron pathway that gives the number of electrons of the universe equal to the number of protons. The wavelength and the radius of the electron must depend on the velocity relative to the proton's inertial frame in order that relativistic invariance of charge holds and the universe is electrically neutral. In the case of an observer in an inertial frame with constant relative motion with respect to the direction perpendicular to the two-dimensional plane containing the free-electron, the de Broglie wavelength of the electron in both the proton frame (the special frame of origin of the free electron) and the second inertial frame are the same. The radius of the electron is also the same in both frames and is given by

$$\rho_0 = \frac{\hbar}{\mathbf{p}_z} \tag{1}$$

where $\mathbf{p}_z$ is the electron momentum in the z-direction relative to the proton. There is no Lorentz contraction in the second frame since the electron is oriented perpendicular to the direction of relative motion. Eq. (1) further satisfies the conditions that the moving electron acquires velocity by acceleration with concomitant photon emission in quantized units of $\hbar$ and that the electric field of the moving electron is no longer that of the electron at rest. Conservation of angular momentum and energy gives rise to the de Broglie relationship as given in the Classical Physics of the de Broglie Relationship section.

$$\sigma_m(\rho,\phi,z) = \frac{m_e}{\frac{2}{3}\pi\rho_0^3}\sqrt{\rho_0^2-\rho^2} = \frac{3}{2}\frac{m_e}{\pi\rho_0^2}\sqrt{1-\left(\frac{\rho}{\rho_0}\right)^2}\,\delta(z) \quad \text{for } 0 \le \rho \le \rho_0$$
$$\sigma_m(\rho,\phi,z) = 0 \quad \text{for } \rho_0 < \rho \tag{3.7}$$

and

$$\sigma_e(\rho,\phi,z) = \frac{e}{\frac{2}{3}\pi\rho_0^3}\sqrt{\rho_0^2-\rho^2} = \frac{3}{2}\frac{e}{\pi\rho_0^2}\sqrt{1-\left(\frac{\rho}{\rho_0}\right)^2}\,\delta(z) \quad \text{for } 0 \le \rho \le \rho_0$$
$$\sigma_e(\rho,\phi,z) = 0 \quad \text{for } \rho_0 < \rho \tag{3.8}$$

respectively, where $\frac{m_e}{\pi\rho_0^2}$ is the average mass density and $\frac{e}{\pi\rho_0^2}$ is the average charge density of the free electron. The magnitude of each distribution is shown in Figure 3.2. ***The charge-density distribution of the free electron given by Eq. (3.8) and shown in Figure 3.2 has recently been confirmed experimentally*** [3,4]. Researchers working at the Japanese National Laboratory for High Energy Physics (KEK) demonstrated that the charge of the free electron increases toward the particle's core and is symmetrical as a function of ϕ.

Figure 3.2A. The angular-momentum-axis view of the magnitude of the continuous mass(charge)-density function in the xy-plane of a polarized free electron propagating along the z-axis and the side view of this electron. For the polarized electron, the angular momentum axis is aligned along the direction of propagation, the z-axis.

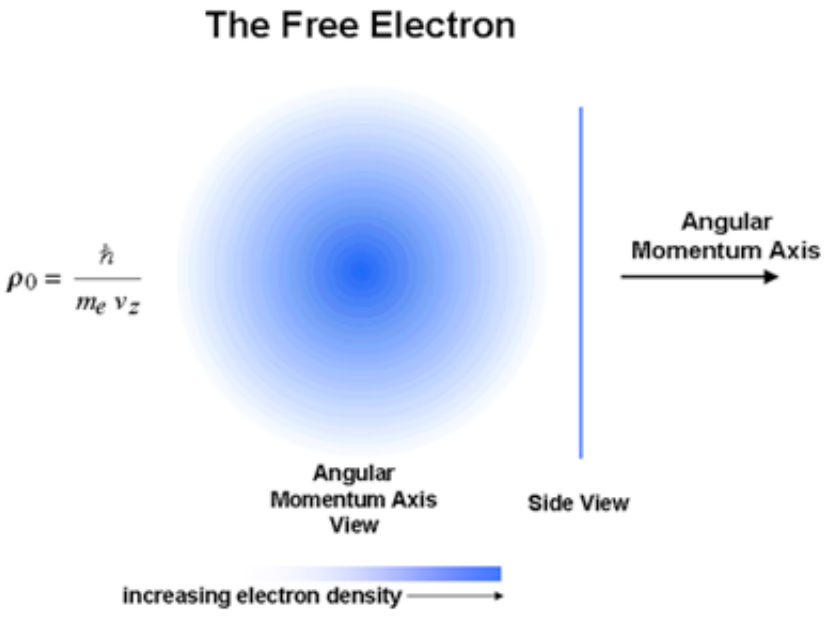

Figure 3.2B. The magnitude plotted along the z-axis of the mass(charge)-density function of the free electron traveling at $10^5\ m/s$ relative to the observer. From Eq. (3.29), the radius of the xy-plane-lamina disc is $1.16\ X\ 10^{-9}\ m$, and from Eqs. (3.7) and (3.8), the maximum mass density and charge density at $\rho = 0$ are $3.25\ X\ 10^{-13}\ kg/m^2$ and $0.0571\ \mathrm{C}/m^2$, respectively.

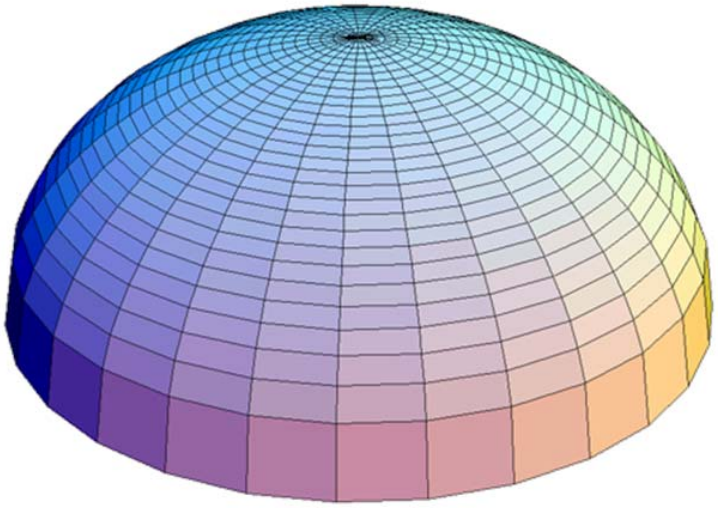

This surface has an electric field equivalent to a point charge at the origin along the z-axis as shown in the Electric Field of a Free Electron section.

ELECTRIC FIELD OF A FREE ELECTRON

The electrical neutrality of the universe must be maintained. A free electron is a continuum excited state of a state bound in an inverse r-squared positive electric field as given in the Excited States of the One-Electron Atom (Quantization). A free electron is tethered to photon electromagnetic field that created the free electron state away from the proton field and changed its radius ρ and velocity v_z according to Eq. (3.45). Specifically, the photon that excites the state is glued to the linearly traveling electron and maintains its radius ρ, charge density function, angular momentum, and velocity as shown in the Force Balance Based on the Radiation-Reaction Force section and the Classical Physics of the de Broglie Relation section. (The only exception to this configuration is when all fields have been cancelled to form a free electron with no gravitational mass as given in the Positive, Zero, and Negative Gravitational Mass section.) As given in the Force Balance Based on the Radiation-Reaction Force section, the current density of the free electron can be modeled as a continuum of circular current elements having the same rotational frequency. The photon field lines propagate along these current elements. The photon field lines and the free electron charge density only exist at the position of the two-dimensional plane of the free electron and superimpose only at that plane. Considering electrodynamic interactions (Eqs. (3.30-3.52)), the charge and current densities are determined to be absent any in-plane forces; thus, the charge density comprises an equipotential such that the electric field lines at the surface of the free electron are normal to the surface. The relationship between the electric field and the source charge density is given by Gauss' law and Faraday's law equation in two dimensions [5-7]:

$$\mathbf{n} \bullet \left(\mathbf{E}_1 - \mathbf{E}_2 \right) = \frac{\sigma}{\varepsilon_0} \tag{3.9}$$

where $\mathbf{n}$ is the radial normal unit vector, $\mathbf{E}_1$ is the electric field on one side of the free electron, $\mathbf{E}_2$ is the electric field on the other side of the free electron, and σ is the surface charge density distribution of the free electron given by Eq. (3.8). Based on symmetry, the condition that the free electron comprises an equipotential surface requiring the absence of an in-plane electric field component at $\delta(z)$, and by using the substitution of $\rho = \rho_0 \sin\theta$ in Eqs. (3.8) and (3.9), the electric field at each surface is given by:

$$\begin{aligned} \mathbf{E}_{\pm z=0} &= \pm \frac{3e}{4\pi\varepsilon_0 \rho_0^2} \cos\theta \delta(z) \mathbf{i}_z \quad \textit{for } 0 \le \rho \le \rho_0 \\ \mathbf{E}_{\pm z=0} &= 0 \qquad\qquad\qquad\qquad\quad \textit{for } \rho_0 < \rho \end{aligned} \tag{3.10}$$

The charge distribution and z-axis field is the spherical harmonic $Y_0^1(\theta,\phi)$, an allowed spherical harmonic solution of an excited state, which is required for the selection rules based on conservation of electron and photon angular momentum and continuity of excited states though the continuum series.

Since the photon field only exists in the two-dimensional plane, the electric potential of a free electron for $z \neq 0$ is given

by Poisson's Equation for a charge-density function, $\rho(x',y',z')$ given by Eq. (3.8):

$$\begin{aligned}\Phi(x,y,z) &= \iiint \frac{\rho(x',y',z')dv'}{4\pi\varepsilon_0\sqrt{(x-x')^2+(y-y')^2+(z-z')^2}} \\ &= -\frac{e}{\frac{2}{3}\pi\rho_0^3}\frac{1}{4\pi\varepsilon_0}\int_{-\infty}^{\infty}\int_{-\rho_0}^{\rho_0}\int_{-\sqrt{\rho_0^2-y'^2}}^{+\sqrt{\rho_0^2-y'^2}}\frac{\sqrt{\rho_0^2-x'^2-y'^2}\,\delta(z')dx'dy'dz'}{\sqrt{(x-x')^2+(y-y')^2+z^2}}\end{aligned} \tag{3.11}$$

For $r=\sqrt{x^2+y^2+z^2} >> \rho_0$, the magnitude of the integral over the charge density is e, and

$$\Phi(r) = -\frac{e}{4\pi\varepsilon_0 r} \tag{3.12}$$

Eq. (3.12) is equivalent to the potential of a point charge at the origin. The electric field, $\mathbf{E}$, is the gradient of the electric potential given by Eqs. (3.11-3.12):

$$\mathbf{E} = -\nabla\Phi \tag{3.13}$$

A numerical plot of the electric field out of plane is shown in Figure 3.3 wherein the plot is discontinuous at the plane wherein the normal direct field at $\delta(z)$ is given by Eq. (3.10) corresponding to an equipotential membrane due to the superposition of the photon field with the electron charge only at the plane of the free electron.

Figures 3.3A-B. The electric potential and electric field of the free electron. A. Three-dimensional cutaway view of the electric potential of a free electron that approaches that of a point charge at the center-of-mass in the far field. B. The two-dimensional cross section of the electric field lines of a free electron. The electric field is symmetrical about the z-axis and approaches that of a point charge at the center-of-mass in the far-field.

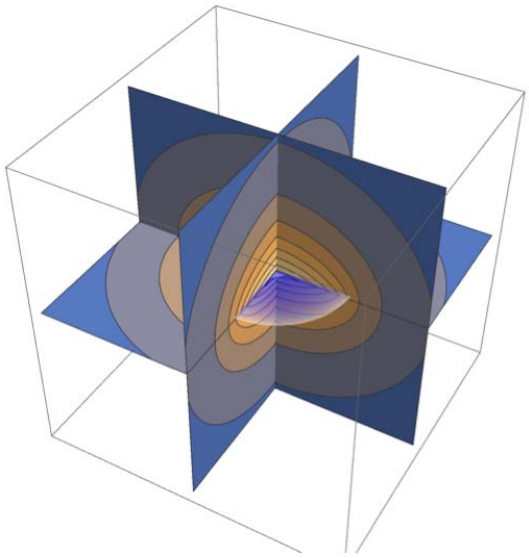

(A)

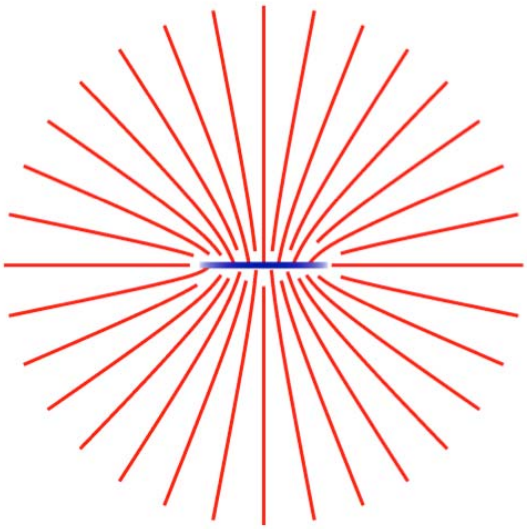

(B)

CURRENT-DENSITY FUNCTION

In general, the current-density function is the product of the charge-density function times the angular velocity function. If the intrinsic electron current was variable over time, then radiation would result, and the electron would be unstable. A current that changes over time is also inconsistent with the Lorentz invariant electron magnetic moment of one Bohr magneton. Thus, in order for the current to be stable over time, the current must be constant as a function of the radial distance and given by the product of ρ, the free-electron charge density (Eq. (3.8)) and a constant angular velocity. The magnitude of the angular velocity of the atomic orbital is given by Eq. (1.36):

$$\omega = \frac{\hbar}{m_e r^2} \tag{3.14}$$

Rather than being confined to a spherical shell, the free electron possesses time harmonic charge motion in the xy-plane at a constant angular frequency. That is, at each point on the free electron, the current moves along a flat current loop time harmonically. This holds for all points such that the current confined to a plane is constant. Since the charge density is determined, the boundary condition on the angular velocity is applied next to solve the current density function of the free electron. Consider the boundary condition that arises during the ionization of a bound electron to form a free electron. During ionization of the electron, the scalar sum of the magnitude of the angular momentum, $\hbar$, must be conserved. The current-density function of a free electron propagating with ***velocity*** v_z ***along the z-axis in the inertial frame of the proton*** is given by the product of the charge density and the constant angular velocity. Since the mass to charge ratio of the electron is invariant, the corresponding boundary condition is that the angular momentum of $\hbar$ is conserved. The projection of the constant angular velocity of the atomic orbital into the plane of the free electron gives the angular velocity of the form

$$\omega = N_\omega \frac{\hbar}{m_e \rho_0^2} \tag{3.15}$$

where N_ω is the normalization constant that gives $\hbar$ of angular momentum. The angular momentum, $\mathbf{L}$, is given by:

$$\mathbf{Li}_z = m_e \rho^2 \omega \tag{3.16}$$

Consider the case that $N_\omega = \frac{5}{2}$ such that:

$$\omega = \frac{5}{2} \frac{\hbar}{m_e \rho_0^2} \tag{3.17}$$

Substitution of the mass density, σ_m, given by Eq. (3.7) and the angular frequency, ω, given by Eq. (3.17) into Eq. (3.16) gives the angular momentum-density function $\mathbf{L}$ which is shown in Figures 3.4A and 3.4B.

$$\mathbf{Li}_z = \frac{m_e}{\frac{2}{3}\pi\rho_0^3} \sqrt{\rho_0^2 - \rho^2}\, \frac{5}{2} \frac{\hbar}{m_e \rho_0^2} \rho^2 \tag{3.18}$$

Figure 3.4A. The plot as a function of ρ of the angular momentum density in the plane of a free electron having $\mathbf{v}_z == 100\ m/s$.

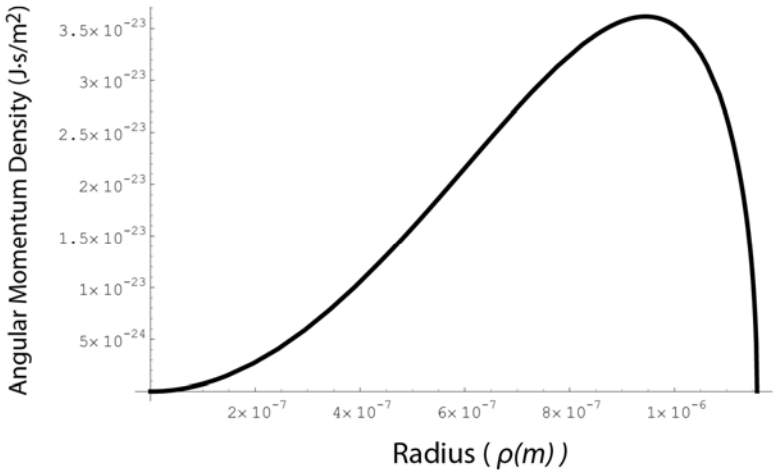

Figure 3.4B. The cut-away, relief view of the angular momentum density in the plane of a free electron having $\mathbf{v}_z == 100\ m/s$.

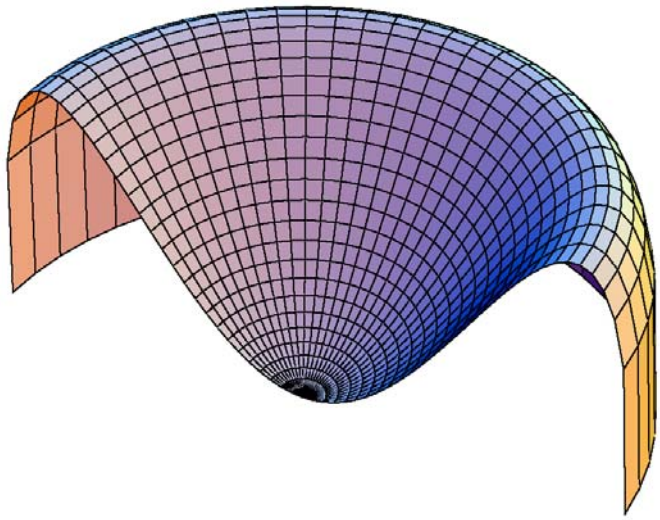

The total angular momentum of the free electron is given by integration over the two-dimensional disc having the angular-momentum density given by Eq. (3.18). Using integral #211 of Lide [8] gives:

$$\mathbf{Li}_z = \int_0^{2\pi}\int_0^{\rho_0} \frac{m_e}{\frac{2}{3}\pi\rho_0^3}\sqrt{\rho_0^2-\rho^2}\,\frac{5}{2}\frac{\hbar}{m_e\rho_0^2}\rho^2\rho d\rho d\phi$$

$$= 2\pi\frac{\hbar}{\frac{2}{3}\pi\rho_0^5}\frac{5}{2}\left(\left(-\frac{1}{5}\rho^2-\frac{2}{15}\rho_0^2\right)\left(\rho_0^2-\rho^2\right)^{3/2}\right)_0^{\rho_0} \tag{3.19}$$

$$= 2\pi\frac{\hbar}{\frac{2}{3}\pi\rho_0^5}\frac{5}{2}\frac{2}{15}\rho_0^5$$

$$\mathbf{Li}_z = \hbar \tag{3.20}$$

Thus, the constant angular velocity at each point on the two-dimensional lamina is given by Eq. (3.17).

The intrinsic current-density function of the free electron is given by the product of the angular velocity ω and the charge-density function given by Eqs. (3.17) and (3.8), respectively. The total current density $\mathbf{J}(\rho,\phi,z,t)$ additionally comprises the component due to translational motion. The total current-density function is given by:

$$\mathbf{J}(\rho,\phi,z,t)=\rho\left[\frac{e}{\frac{2}{3}\pi\rho_0^3}\sqrt{\rho_0^2-\rho^2}\,\frac{5}{2}\frac{\hbar}{m_e\rho_0^2}\,\mathbf{i}_\phi\right]\delta(z)+\frac{e\hbar}{m_e\rho_0}\delta(z-\frac{\hbar}{m_e\rho_0}t)\mathbf{i}_z \tag{3.21}$$

The intrinsic current is shown in Figure 3.5.

Figure 3.5. The magnitude plotted along the z-axis of the current-density function, J, of the free electron traveling at $10^5\ ms^{-1}$ relative to the observer. From Eq. (3.29), the radius of the xy-plane-lamina disc is $1.16X10^{-9}\ m$, and from Eq. (3.21), the maximum current density at $\rho=0$ is $1.23\ X\ 10^{13}\ Am^{-2}$.

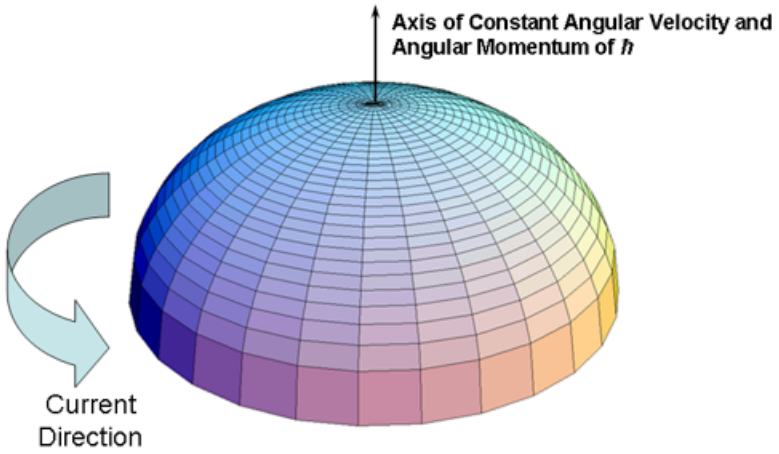

The spacetime Fourier transform of Eq. (3.21) is [9,10]:

$$\frac{e}{\frac{4}{3}\pi\rho_0^3}\frac{\hbar}{m_e}\mathrm{sinc}(s\rho_0)+2\pi e\frac{\hbar}{m_e\rho_0}\delta(\omega-\mathbf{k}_z\bullet\mathbf{v}_z) \tag{3.22}$$

where s is the wavenumber $\frac{2\pi}{\rho_0}$. The condition for nonradiation of a moving charge-density function is that the spacetime Fourier transform of the current-density function must not possess components synchronous with waves traveling at the speed of light, that is synchronous with $\frac{\omega}{c}$ or synchronous with $\frac{\omega}{c}\sqrt{\frac{\varepsilon}{\varepsilon_0}}$ where ε is the dielectric constant of the medium. The Fourier transform of the current-density function of the free electron is given by Eq. (3.22). Consider the radial part of, $J_\perp$, the Fourier transform of the current-density function where the z spatial dimensional transform is not zero:

$$J_\perp\propto\mathrm{sinc}(s\rho_0)=\frac{\sin s\rho_0}{s\rho_0} \tag{3.23}$$

For time harmonic motion corresponding to the electron parameters ω_0 and s_0, Eq. (1.15),

$$2\pi\rho_0=\lambda_0 \tag{3.24}$$

The charge motion of the free electron is angular, and consequently the radius undergoes Lorentz contraction as shown in the Special Relativistic Correction to the Ionization Energies section. Consider the wave vector of the sinc function. When the velocity is c corresponding to a potentially emitted photon, $\mathbf{s}$ is the lightlike $\mathbf{s}^0$ wherein

$$\mathbf{s}\bullet\mathbf{v}=\mathbf{s}\bullet\mathbf{c}=\omega_0 \tag{3.25}$$

The relativistically corrected wavelength given by Eq. (1.280) is:

$$\rho_0=\lambda_0 \tag{3.26}$$

as also shown in Appendix I: Nonradiation Based on the Electromagnetic Fields and the Poynting Power Vector. Substitution of Eq. (3.26) into the sinc function results in the vanishing of the entire Fourier transform of the current-density function. Thus, spacetime harmonics of $\frac{\omega}{c}=k$ *or* $\frac{\omega}{c}\sqrt{\frac{\varepsilon}{\varepsilon_0}}=k$ do not exist. Radiation due to charge motion does not occur in any medium when

this boundary condition is met. Furthermore, consider the z spatial dimensional transform of, $J_\perp$, the Fourier transform of the current-density function:

$$J_\perp \propto 2\pi e \frac{\hbar}{m_e \rho_0} \delta(\omega - \mathbf{k}_z \bullet \mathbf{v}_z) \tag{3.27}$$

The only nonzero Fourier components are for:

$$k_z = \frac{\omega}{v_z \cos\theta} > \frac{\omega}{c} \tag{3.28}$$

where θ is the angle between $\mathbf{k}_z$ and $\mathbf{v}_z$. Thus, no Fourier components that are synchronous with light velocity with the propagation constant $|\mathbf{k}_z| = \frac{\omega}{c}$ exist. Radiation due to charge motion does not occur when this boundary condition is met. It follows from Eq. (3.2) and Eq. (3.24) that the wavelength of the free electron is:

$$\lambda_0 = \frac{h}{m_e v_z} = 2\pi\rho_0 \tag{3.29}$$

which is the de Broglie wavelength.

FORCE BALANCE BASED ON THE RADIATION-REACTION FORCE

Consideration must be made of the free electron as a continuum excited electronic state caused by absorption of a photon. The physics of excited states is continuous with the free electron or continuum excited states. For excited states given in the Equation of the Electric Field inside the Atomic Orbital section, the vector direction of the photon electric field was determined directly by considering the relativistic effect of its motion relative to the electron. In the case of the free electron, the electrodynamic field may be treated as a magnetic field since a magnetic field is a relativistic effect of the corresponding electric field. The free electron is a two-dimensional disc with a charge distribution given by Eq. (3.8) having a radius ρ_0 given by Eq. (3.29) and an in-plane electric field given by Eqs. (3.8 and (3.9). This distribution is a minimum energy, two-dimensional surface[3]. An attractive magnetic force exists between current circles in the xy-plane, and the force balance equation is given by equating the centrifugal and the centripetal forces.

The centripetal force, $\mathbf{F}_{mag}$, between the current loops is the electrodynamic or radiation-reaction magnetic force as given in the One Electron Atom—Determination of Atomic Orbital Radii section and the Two-Electron Atoms section. Here, each infinitesimal point (mass or charge-density element) of the free electron moves azimuthally about the angular-momentum axis on a circle at the same angular velocity given by Eq. (3.17) at a radius $0 \le \rho \le \rho_0$, and each point has the mass density and charge density given by Eqs. (3.7) and (3.8), respectively. Due to the relative motion of the charge-density elements of each electron current loop, a radiation reaction force arises between each loop. This force given in Sections 6.6, 12.10, and 17.3 of Jackson [11] achieves the condition that the sum of the mechanical momentum and electromagnetic momentum is conserved. The magnetic central force is derived from the Lorentz force, which is relativistically corrected. The magnetic field at the

---

[3] This relation shows that only a 2-D geometry meets the criterion for a fundamental particle. This is the nonsingularity geometry that is no longer divisible. It is the dimension from which it is not possible to lower dimensionality. In this case, there is no electrostatic self-interaction since the corresponding potential is continuous across the surface according to Faraday's law in the electrostatic limit, and the field is discontinuous and normal to the charge according to Gauss' law [8-10]. Thus, only the continuous current density function need be considered.

It was shown in the Electron g Factor section that as a requirement of the conservation of angular momentum, the magnetic moment of the electron can only be parallel or antiparallel to an applied magnetic field. Similarly, in order to conserve angular momentum, any internal change in the bound-electron current distribution and its corresponding angular momentum requires emission of a photon that carries angular momentum in its electric and magnetic fields only in discrete units of $\hbar$ as given in the Equation of the Photon section. Conservation of angular momentum also requires that this condition be met for the free electron. Self interaction of the current of the free electron having the angular momentum distribution given in the Current-Density Function section and the Stern-Gerlach Experiment section requires the emission of a photon having an angular momentum that is a fraction of $\hbar$ which is not possible according to Maxwell's equations as given in the Excited States of the One-Electron Atom (Quantization) section. Thus, any self interaction is a radiation-reaction type wherein k is also the lightlike k^0 such that $k = \omega_n / c$. Any such light-like interaction can only be central. Since the velocity of each point of the electron for a given ρ is the same, the current of the atomic orbital is confined to a circle in the $v = c$ frame as well as the lab frame as given by Eq. (1.280). Since the current is orthogonal to the central vector at the same ρ for each circular current-density element, there is no self interaction, but there is an interaction between circular current-density elements for different values of ρ that balances the centrifugal force as given by Eq. (3.30) and Eqs. (3.37-3.38) to maintain the free electron as an equipotential 2-D surface..

As given by Eq. (3.15), the total angular momentum confined to the plane of the free electron is $\hbar$. The radiation reaction force requires conservation of the reaction photon's angular momentum of $\hbar$. Thus, this force is only present for the free electron as opposed to the bound electron since the radial direction in the bound case is perpendicular to the surface and a photon of $\hbar$ of angular momentum may only be emitted through a release of energy due to the central field.

Furthermore, since fundamental particles such as the electron are superconducting, nonresonant collisions cannot change the intrinsic angular momentum. Such collisions involve the entire particle. And, the intrinsic angular momentum remains unchanged, except when a resonant photon is emitted or absorbed according to the Maxwellian-based conservation rules given in the Excited States section and the Equation of the Photon section.

Similar to the case of the electric field, a discontinuity in surface mass density gives rise to a discontinuity in the curvature of spacetime originating at the two-dimensional surface. Thus, in addition to the absence of electric self-interaction (Appendix II), the Virial theorem does not apply regarding gravitational self-interaction. The derivation of the gravitational field is given in the Gravity section.

electron current loop at position $\rho < \rho_0$ due to the electron current loop at position ρ_0 follows from Eq. (1.130) after McQuarrie [12]:

$$\mathbf{B} = \frac{\mu_o e\hbar}{2m_e\rho_0^3} \tag{3.30}$$

wherein the intrinsic angular momentum during photon interaction is the same as that of a bound electron as shown in the Stern-Gerlach Experiment section and μ_0 is the permeability of free-space ($4\pi\ X\ 10^{-7}\ N/A^2$). The motion at each position of the electron loop at radius $\rho < \rho_0$ in the presence of the magnetic field of the current loop at position ρ_0 gives rise to a central force which acts at each charge density element of the former. The Lorentz force at each element moving at velocity $\mathbf{v}$ is

$$\mathbf{F}_{mag} = e\mathbf{v}\times\mathbf{B} = e\rho\omega\times\mathbf{B} \tag{3.31}$$

Substitution of Eq. (3.17) for ω and Eq. (3.30) for $\mathbf{B}$ based on the angular momentum of the free electron of $\hbar$ gives:

$$\mathbf{F}_{mag} = \frac{5}{2}\left(\rho\frac{e\hbar}{m_e\rho_0^2}\right)\frac{\mu_0 e\hbar}{2m_e\rho_0^3} = \frac{5}{2}\left[\frac{e^2\mu_o}{2m_e\rho_0}\right]\frac{\hbar^2\rho}{m_e\rho_0^4} \tag{3.32}$$

Furthermore, the term in brackets can be expressed in terms of the fine structure constant α. The radius of the electron loop in the light-like frame is $\lambda\!\!\!^{-}_C$. From Eq. (1.250)

$$\frac{e^2\mu_o}{2m_e\rho_0} = 2\pi\alpha \tag{3.33}$$

Based on the relativistic invariance of $\frac{e}{m_e}$ corresponding to the invariance of μ_B given by Eq. (1.131) as well as its invariant angular momentum of $\hbar$, it can be shown that the relativistic correction to Eq. (3.32) is the reciprocal of Eq. (3.33). Specifically, as shown previously in the One Electron Atom—Determination of Atomic Orbital Radii section and the Two-Electron Atoms section, the relativistic correction γ' due to the light speed electrodynamic central force is:

$$\gamma' = (2\pi\alpha)^{-1} \tag{3.34}$$

Thus, Eq. (3.32) becomes:

$$\mathbf{F}_{mag} = \frac{5}{2}\frac{\hbar^2\rho}{m_e\rho_0^4} \tag{3.35}$$

Eq. (3.35) gives the force as a function of the radius ρ.

The centrifugal force due to each charge density element on each current loop about the angular-momentum axis is balanced by the centripetal force $\mathbf{F}_{mag}$. During the radiation reaction event, the centrifugal force, $\mathbf{F}_{i\ centrifugal}$, at each point of the free electron of mass m_i is given by:

$$\mathbf{F}_{i\ centrifugal} = m_i\rho\omega^2\mathbf{i}_\rho = m_i\frac{v^2}{\rho}\mathbf{i}_\rho \tag{3.36}$$

(An equation for $\mathbf{F}_{mag}$ that is also proportional to the angular frequency squared that parallels that of Eq. (3.41) is given by expressing the magnetic flux in terms of the current given by the charge times the angular frequency [13].) The velocity $\mathbf{v}$ at each point follows from the angular velocity (Eq. (3.17)) and is given by:

$$\mathbf{v} = \rho\frac{5}{2}\frac{\hbar}{m_e\rho_0^2}\mathbf{i}_\phi \tag{3.37}$$

where ρ is the radius of the point. Substitution of Eq. (3.37) into Eq. (3.36) gives:

$$\mathbf{F}_{i\ centrifugal} = -\frac{m_i}{\rho}\left(\rho\frac{5}{2}\frac{\hbar}{m_e\rho_0^2}\right)^2\mathbf{i}_\rho \tag{3.38}$$

The integral over the density gives the total force $\mathbf{F}_{centrifugal}$. As in the case of $\mathbf{F}_{mag}$, $\mathbf{F}_{centrifugal}$ for the radiation reaction event is linear in ρ such that the force per unit area is equal over the two-dimensional lamina to maintain the constraints that the electron is an equipotential, minimum-energy surface and the corresponding energy is proportional to $\hbar\omega$ of a photon. Thus, $F_{centrifugal}$, the linear factor for $\mathbf{F}_{centrifugal}$ is given by multiplication of Eq. (3.38) by $\frac{\rho}{\rho_0}$, substitution of the mass density (Eq. (3.7)) for m_i, and integration over the plane lamina:

$$F_{centrifugal} = \frac{1}{\rho_0}\left(\frac{5}{2}\frac{\hbar}{m_e\rho_0^2}\right)^2 \int_0^{2\pi}\int_0^{\rho_0} \frac{m_e}{\frac{2}{3}\pi\rho_0^3}\sqrt{\rho_0^2-\rho^2}\,\rho^2\rho d\rho d\phi$$

$$= 2\pi\frac{m_e}{\frac{2}{3}\pi\rho_0^4}\frac{1}{\rho_0}\left(\frac{5}{2}\frac{\hbar}{m_e\rho_0^2}\right)^2\left(\left(-\frac{1}{5}\rho^2-\frac{2}{15}\rho_0^2\right)\left(\rho_0^2-\rho^2\right)^{3/2}\right)_0^{\rho_0} \tag{3.39}$$

$$= \frac{5}{2}2\pi\frac{\hbar^2}{\frac{2}{3}\pi m_e\rho_0^8}\frac{5}{2}\frac{2}{15}\rho_0^5 = \frac{5}{2}\frac{\hbar^2}{m_e\rho_0^3}$$

$F_{centrifugal}$ is also the magnitude of the total centrifugal force of the ensemble of current loops that is equally distributed throughout the plane lamina. It is also given by using Eq. (3.36) in another form:

$$\mathbf{F}_{i\ centrifugal} = m_i\rho^2\omega\frac{\omega}{\rho}\mathbf{i}_\rho \tag{3.40}$$

Substitution of the total angular momentum given by Eqs. (3.18-3.20), the angular velocity given by Eq. (3.17), and the total radius ρ_0 into Eq. (3.40) gives $F_{centrifugal}$:

$$F_{centrifugal} = \hbar\frac{\frac{5}{2}\frac{\hbar}{m_e\rho_0^2}}{\rho_0} = \frac{5}{2}\frac{\hbar^2}{m_e\rho_0^3} \tag{3.41}$$

Using Eq. (3.39) or Eq. (3.41), $\mathbf{F}_{centrifugal}$ is given by:

$$\mathbf{F}_{centrifugal} = \frac{\rho}{\rho_0}\frac{5}{2}\frac{\hbar^2}{m_e\rho_0^3}\mathbf{i}_\rho = \frac{5}{2}\frac{\hbar^2\rho}{m_e\rho_0^4}\mathbf{i}_\rho \tag{3.42}$$

$\mathbf{F}_{centrifugal}$ is further given by the derivative of E_{rot}:

$$F_{centrifugal} = -\frac{\rho}{\rho_0}\frac{\delta E_{rot}}{\delta\rho_0}\mathbf{i}_\rho = -\frac{\rho}{\rho_0}\frac{\delta}{\delta\rho_0}\left(\frac{5}{4}\frac{\hbar^2}{m_e\rho_0^2}\right)\mathbf{i}_\rho = \frac{5}{2}\frac{\hbar^2\rho}{m_e\rho_0^4}\mathbf{i}_\rho \tag{3.43}$$

where E_{rot} is given by Eq. (3.50). From Eqs. (3.42-3.43) and (3.35), the outward centrifugal force, $\mathbf{F}_{centrifugal}$, due to each element on each current loop about the angular-momentum axis is balanced by the centripetal force $\mathbf{F}_{mag}$ due to the magnetic interactions between the current loops.

Furthermore, the free electron possesses a total charge e, a total mass m_e, and an angular momentum of $\hbar$. The magnetic moment is given by Eq. (2.65); thus,

$$\mu_B = \frac{e\hbar}{2m_e} = 9.274\ X\ 10^{-24}\ JT^{-1} \tag{3.44}$$

which is the Bohr magneton. Conservation of angular momentum with the linking of flux in discrete increments of the magnetic flux quantum gives rise to the spin quantum number, m_s, and the g factor which is the same as given previously in the Electron g Factor section. The behavior of the free electron in a magnetic field is given in the Stern-Gerlach Experiment section. It is shown next that the intrinsic angular momentum of $\hbar$ is unchanged as the electron acquires linear velocity with a concomitant change in its de Broglie wavelength.

CLASSICAL PHYSICS OF THE DE BROGLIE RELATIONSHIP

As shown in Appendix IV, the plane-lamina of the free electron generates a spherical current-density pattern over time during the interaction with photons designated $Y_0^0(\theta,\phi)$. The angular momentum of the photon given by $\mathbf{m} = \int\frac{1}{8\pi c}\mathrm{Re}\left[\mathbf{r}\times(\mathbf{E}\times\mathbf{B}^*)\right]dx^4 = \hbar$ in the Photon section is conserved [14] for the solutions for the resonant photons and excited state electron functions given in the Excited States of the One-Electron Atom (Quantization) section. It can be demonstrated that the resonance condition between these frequencies is to be satisfied in order to have a net change of the energy field [15]. In this case, the correspondence principle holds. That is the change in angular frequency of the electron is equal to the angular frequency of the resonant photon that excites the resonator cavity mode corresponding to the transition, and the energy is given by Planck's equation. The same conditions apply to the free electron, and the correspondence between the principles of the bound and free electrons further hold in the case of the Stern-Gerlach experiment as given in the Stern-Gerlach Experiment section.

The linear velocity of the free electron can be considered to be due to absorption of photons that excite surface currents corresponding to a decreased de Broglie wavelength where the free electron is equivalent to a continuum excited state with

conservation of the parameters of the bound electron discussed *supra*. The relationship between the electron wavelength and the linear velocity is

$$\frac{\lambda}{2\pi} = \rho_0 = \frac{\hbar}{m_e v_z} = k^{-1} = \frac{v_z}{\omega_z} \tag{3.45}$$

In this case, the angular frequency ω_z is given by:

$$\omega_z = \frac{\hbar}{m_e \rho^2{}_0} \tag{3.46}$$

which conserves the photon's angular momentum of $\hbar$ with that of the electron relative to its center of mass. The angular momentum conservation relationship of $\hbar$ is the same as that of the bound electron given by Eq. (1.37) where the velocity is v_z given by Eq. (3.2) and the radius is ρ_0 given by Eq. (3.29). In addition, the electron kinetic energy T is given by

$$T = \frac{1}{2} m_e v_z^2 = \frac{1}{2} \frac{\hbar^2}{m_e \rho_0^2} = \frac{1}{2} \hbar \omega_z \tag{3.47}$$

The potential energy, E_{mag}, corresponding to $\mathbf{F}_{mag}$ is given by the integral over the radius:

$$E_{mag} = \int_{\rho_0}^{0} \frac{5}{2} \frac{\hbar^2}{m_e \rho_0^4} \rho d\rho = \frac{5}{2} \frac{\hbar^2}{m_e \rho_0^4} \left(\frac{\rho^2}{2} \right)_{\rho_0}^{0} = -\frac{5}{4} \frac{\hbar^2}{m_e \rho_0^2} \tag{3.48}$$

The rotational kinetic energy, E_{rot}, of the free electron corresponding to the angular momentum given by Eqs. (3.18-3.20) is:

$$E_{rot} = \frac{1}{2} L\omega = \frac{1}{2} I \omega^2 = \frac{1}{2} m_e v^2 \tag{3.49}$$

Using Eqs. (3.17), (3.20), and (3.49) gives:

$$E_{rot} = \frac{1}{2} L\omega = \frac{1}{2} \hbar \frac{5}{2} \frac{\hbar}{m_e \rho_0^2} = \frac{5}{4} \frac{\hbar^2}{m_e \rho_0^2} \tag{3.50}$$

Similarly to Eq. (3.48), E_{rot} is also given by the integral of the corresponding force, $\mathbf{F}_{centrifugal}$, given by Eq. (3.43).

The total energy, E_T, is given by the sum of the change in the free-electron translational kinetic energy, T, the rotational energy, E_{rot}, corresponding to the current of the loops, and the potential energy, E_{mag}, due to the radiation reaction force $\mathbf{F}_{mag}$, the magnetic attractive force between the current loops due to the relative rotational or current motion:

$$E_T = T + E_{rot} + E_{mag} = \frac{1}{2} \frac{\hbar^2}{m_e \rho_0^2} + \frac{5}{4} \frac{\hbar^2}{m_e \rho_0^2} - \frac{5}{4} \frac{\hbar^2}{m_e \rho_0^2} = \frac{1}{2} \frac{\hbar^2}{m_e \rho_0^2} \tag{3.51}$$

Thus, the total energy, E_T, of the excitation of a free-electron transitional state by a photon having $\hbar$ of angular momentum and an energy given by Planck's equation of $\hbar\omega$ is:

$$E_T = T = \frac{1}{2} m_e v_z^2 = \frac{1}{2} \frac{h^2}{m_e \lambda^2} = \frac{1}{2} \hbar \omega_z \tag{3.52}$$

where λ is de Broglie wavelength. The angular momentum of the free electron of $\hbar$ is unchanged, the energies in the currents in the plane lamina are balanced so that the total energy is unchanged, and the radius ρ_0 changes to match the de Broglie wavelength and frequency at an increased velocity. At this velocity, the kinetic energy matches the energy provided by the photon wherein the de Broglie frequency matches the photon frequency and both the electron-kinetic energy and the photon energy are given by Planck's equation.

Eq. (3.52) is identical to Eq. (2.22) that gives the relationship between the energy and frequency of a photon that causes a bound excited state and the corresponding change in the electron's kinetic energy. A photon of the same energy as Eq. (3.52) is emitted due to acceleration of the free electron by an applied electric field to acquire the velocity v_z in agreement with the Abraham-Lorentz equation of motion [16]. This relationship is identical to that of the binding energy and kinetic energy of the bound electron in the central field of the proton given in the Photon Absorption section. The exception is that the photon-bound-electron interaction results in a trapped photon with the electron in a different orbit with a maintained eccentricity of zero and a decreased angular and linear velocity; whereas, the eccentricity of the orbit for the photon-free-electron interaction goes to infinity corresponding to a hyperbolic orbit that approaches rectilinear motion with an increased linear velocity. The angular distribution of radiation emitted by an accelerated charge and the distribution in frequency and angle of energy radiated by accelerated charges is also given classically in Sections 14.3 and 14.5 of Jackson [17,18].

The correspondence principle is the basis of the de Broglie wavelength relationship. Stated in other words, the de Broglie relationship is not an independent fundamental property of matter in conflict with physical laws as formalized in the wave-particle-duality-related postulates of quantum mechanics and the corresponding Schrödinger wave equation. Nothing is waving including probability. The relationship arises from the correspondence principle that is based on Maxwell's equations and conservation of angular momentum and energy. The other fundamental misconceptions of quantum mechanics that serve as its foundations are the impossibility of explaining the Stern-Gerlach experimental results and the double-slit interference pattern

of electrons classically. In contradiction to widely accepted beliefs, these phenomena are also shown to be exactly predicted from first principles (Stern-Gerlach Experiment section and in the Two-Slit Interference (Wave-Particle Duality) section).

STERN-GERLACH EXPERIMENT

The Stern Gerlach experiment demonstrates that the magnetic moment of the electron can only be parallel or antiparallel to an applied magnetic field. This implies a spin quantum number of 1/2 corresponding to an angular momentum on the z-axis of $\frac{\hbar}{2}$. However, the Zeeman splitting energy corresponds to a magnetic moment of a Bohr magneton μ_B and implies an electron angular momentum on the z-axis of $\hbar$—twice that expected. This in turn implies that the gyromagnetic ratio is twice that expected for a classical magnetic moment generated by a current loop. Historically, this dilemma was felt to be inexplicable and could only be resolved by purely mathematical approaches rather than physics. It is shown *infra* that this is not the case. The Stern-Gerlach results are completely predictable from first principles, and the results are intuitive.

The free electron arises during pair production and ionization. In both cases, the production photon or the ionizing photon carries $\hbar$ of angular momentum. The derivations of the parameters of the free electron given *supra* were made with the conservation of the photon angular momentum implicit. The vector and scalar parameters of the bound electron in a magnetic field given in the Atomic Orbital Equation of Motion for $\ell = 0$ Based on the Current Vector Field (CVF) section and the Magnetic Parameters of the Electron (Bohr Magneton) Stern-Gerlach Experiment section are also conserved in the case of a free electron in a magnetic field.

Consider the case of a magnetic field applied to the free electron. The direction of the electron's intrinsic angular momentum of $\hbar$ and the corresponding magnetic moment of μ_B can change orientation with the application of a magnetic field or an electric field. It is also reoriented by interaction with photons. Randomly-directed fields and random photon interactions give rise to random orientations. Thus, in the absence of an applied orienting field or a specific procedure to produce a polarized state, the free electron is unpolarized. The Bohr magneton of magnetic moment of the free electron corresponding to its $\hbar$ of angular momentum is initially in a random direction relative to the z-axis, the axis of an applied magnetic field. The center of mass of the electron propagates at the original constant velocity v_z in Eq. (3.2).

Then, a small diamagnetic azimuthal current in the plane of the lamina opposes an applied field according to Lenz's law as given for the bound electron in Box 1.1. Furthermore, the application of the magnetic field causes a resonant excitation of the Larmor precession as in the case of the bound electron wherein the energy arises from that stored in the applied magnetic field. The excitation can be described in terms of photons in the same manner as in the case of photon emission or absorption due to an applied electric field that causes the free electron to accelerate. The Larmor precession frequency is given by the product of the gyromagnetic ratio of the electron, $\frac{e}{2m}$, and the magnetic flux **B** [19]. As in the case of the bound electron, the precessing free electron is a spin-1/2 particle ($L_z = \frac{\hbar}{2}$), but the stationary resultant angular momentum projection that is either parallel or antiparallel to the applied-field axis is $\hbar$ corresponding to a full Bohr magneton of magnetic moment. Here, each of the resonant photons which excites the Larmor precession and the intrinsic angular momentum of the free electron (Eq. (3.20)) contribute equally to the resultant z-axis projection. As shown in the Excited States of the One-Electron Atom (Quantization) section, conservation of the angular momentum of the photon of $\hbar$ gives rise to $\hbar$ of electron angular momentum in the excited state. The photon having the Larmor frequency corresponding to the energy given by Eq. (1.227) and $\hbar$ of angular momentum initially along an axis in the transverse (xy)-plane causes the electron and the photon to precess about both the z-axis and the transverse-axis. Then, as a time average the angular momentum of the precessing electron contributes one-half of its intrinsic angular momentum of $\hbar$ to the projection on the z-axis, and the photon angular momentum also contributes $\frac{\hbar}{2}$ to the z-projection.

As shown in Appendix IV, with the electron current in the counter clockwise direction, the Larmor precession of the angular momentum vector of the free electron is about two axes simultaneously, the $\left(\mathbf{i}_x, 0\mathbf{i}_y, \mathbf{i}_z\right)$-axis and the laboratory-frame z-axis defined by the direction of the applied magnetic field. The precessions are about the opposite axes with the current in the opposite direction. The motion generates CVFs equivalent to those of the bound electron given in the Atomic Orbital Equation of Motion for $\ell = 0$ Based on the Current Vector Field (CVF) section. Over one time period, the first motion sweeps out the equivalent of a BECVF, and the rotation about the z-axis sweeps out the equivalent of an OCVF. The combined motions sweep out the equivalent of the convolution of the BECVF with the OCVF, an angular-momentum distribution equivalent to $Y_0^0(\theta,\phi)$ of the bound electron. The Larmor excited precessing electron can further interact with another resonant photon that gives rise to Zeeman splitting—energy levels corresponding to flipping of the parallel or antiparallel alignment of the electron magnetic moment of a Bohr magneton with the magnetic field.

The parameters of the photon standing wave for the Larmor precession and the Zeeman effect of the free electron follow from those of the bound electron given in the Magnetic Parameters of the Electron (Bohr Magneton) section and Box 1.1. To cause the Larmor excitation and the spin-flip transition, the corresponding photon gives rise to surface currents in the plane of the free electron that are equivalent to the projection of the time- and spherically-harmonic dipole Larmor currents of the bound

electron into the free-electron plane. The currents cause a precession of the disc to form a time-averaged bi-conical cavity that is azimuthally symmetrical about the $(\mathbf{i}_x, 0\mathbf{i}_y, \mathbf{i}_z)$-axis (Figure 3.8). The time-averaged angular momentum and rotational energy of the currents that are phase-locked to the photon field is zero as given by Eqs. (1.76-1.77), but the photon's angular momentum is $\hbar$ corresponding to a magnetic moment of one Bohr magneton μ_B as shown for the case of the Larmor resonant excitation of a bound electron in Box 1.1.

The $\hbar$ of angular momentum of the photon that excites the Larmor precession is initially along an axis in the transverse (xy)-plane. This causes a torque on the z-axis-directed $\hbar$ of angular momentum of the electron and causes it to rotate into the xy-plane. This in turn causes a torque on the angular momentum of the photon. As a result the electron and the photon undergo mutual precession about both the $(\mathbf{i}_x, 0\mathbf{i}_y, \mathbf{i}_z)$-axis and the z-axis. The motion is more easily analyzed by first considering a coordinate system that rotates about the z-axis. In the coordinate system rotating at the Larmor frequency (denoted by the axes labeled X_R, Y_R, and Z_R in Figure 3.6), the positive X_R-component of magnitude $\hbar$ corresponding to the photon and a negative X_R-component of magnitude $\frac{\hbar}{2}$ (Eq. (3.65)), corresponding to the current generated by the rotation of the free electron about the X_R-axis, are stationary. The angular momentum vector of the free electron of magnitude $\hbar$ corresponding to a magnetic moment of one Bohr magneton μ_B is designated by $\mathbf{S}_z$. The photon's positive $\hbar$ of angular momentum along X_R with a corresponding magnetic moment of μ_B (Eq. (28) of Box 1.1) causes the $\mathbf{S}_z$ to rotate about X_R. As the Z_R-axis precesses about the X_R-axis, it causes a reactive torque such that the X_R-axis also rotates about the Z_R-axis. Consequently, the two vectors shown in Figure 3.6 precess about both the $(\mathbf{i}_x, 0\mathbf{i}_y, \mathbf{i}_z)$-axis and the z-axis.

Figure 3.6. The initial angular momentum components of the free electron and positive and negative X_R components in the rotating coordinate system (X_R, Y_R, Z_R) that precesses at the Larmor frequency about Z_R such that the vectors are stationary. The electron is initially in the $X_R\,Y_R$-plane.

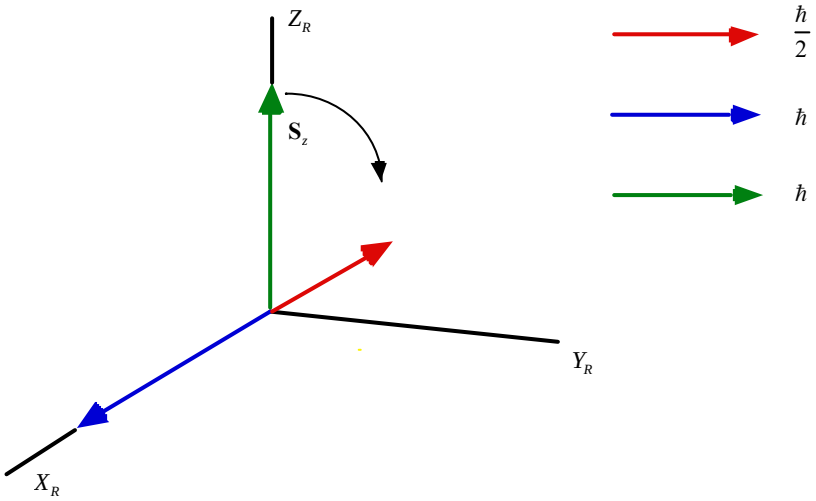

For further convenience, a second primed Cartesian coordinate system refers to the axes that rotate with the $(\mathbf{i}_x, 0\mathbf{i}_y, \mathbf{i}_z)$-axis about the z-axis at the Larmor frequency wherein the x'y'-plane of the plane-lamina disc of the free electron aligns with the xy-plane time harmonically at this frequency. Then, each of the X_R-, Y_R, and Z_R-axis is designated the x'-, y', and z'-axis, respectively. The initial corresponding precession of the plane lamina in the x'y'-plane about each of the z- and x-axes results in a precession about the $(\mathbf{i}_x, 0\mathbf{i}_y, \mathbf{i}_z)$-axis as shown in Figure 3.7. The electron precession motion about the $(\mathbf{i}_x, 0\mathbf{i}_y, \mathbf{i}_z)$-axis which is stationary in the rotating frame generates a BECVF as given in Appendix IV which is a solid version of the BECVF for the case of the bound electron. The rotation of the BECVF in the laboratory frame generates the $Y_0^0(\theta,\phi)$ distribution.

Figure 3.7. In the Larmor-frequency rotating (X_R, Y_R, Z_R) frame, the plane-lamina disc of the free electron rotates about the $\left(\mathbf{i}_x, 0\mathbf{i}_y, \mathbf{i}_z\right)$-axis. The resultant angular momentum vector of $\sqrt{2}\hbar$ (red vector) having projections onto each of the Z_R-axis (green vector) and the X_R-axis (blue vector) of $\hbar$ is stationary on the rotating $\left(\mathbf{i}_x, 0\mathbf{i}_y, \mathbf{i}_z\right)$-axis. The electron precession motion about the $\left(\mathbf{i}_x, 0\mathbf{i}_y, \mathbf{i}_z\right)$-axis generates the free electron BECVF. The green and blue vectors can be assigned to the intrinsic electron and photon angular momentum at $t = 0$, respectively. These components rotate about the $\left(\mathbf{i}_x, 0\mathbf{i}_y, \mathbf{i}_z\right)$-axis and harmonically interchange at each one-half period of rotation. Thus, z-axis component of $\hbar$ comprises a time-averaged contribution of $\frac{\hbar}{2}$ from each of the electron and the photon.

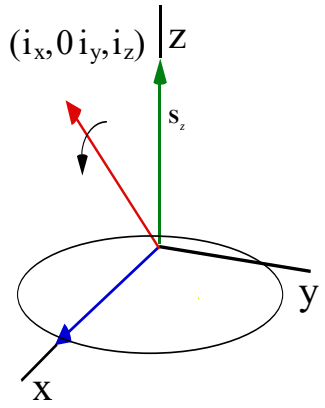

The Larmor excitation comprises a double precession. The z-axis angular momentum projection before and after the excitation of the Larmor precession is $\hbar$, and the energy of the photon to cause the precession of the $\left(\mathbf{i}_x, 0\mathbf{i}_y, \mathbf{i}_z\right)$-axis about the z-axis at the Larmor frequency is given by Eq. (25) of Box 1.1. Therefore, only the torque balance of the precession of the electron about the $\left(\mathbf{i}_x, 0\mathbf{i}_y, \mathbf{i}_z\right)$-axis in the Larmor-frequency rotating (X_R, Y_R, Z_R) frame (Figure 3.7) needs to be considered. The derivation of the corresponding current density about the x'-axis follows that for the bound electron given in the Magnetic Parameters of the Electron (Bohr Magneton) section. The magnetic moment (angular momentum) can be determined from the current (mass)-density function. The magnetic moment of a current loop of area $\pi y'^2$ due to a point charge element of charge e_i that has an angular velocity of $\omega_{x'}\ \mathbf{i}_{x'}$ is given by

$$\mathbf{m}_{x'} = e_i y'^2 \frac{\omega_{x'}}{2}\ \mathbf{i}_{x'} \tag{3.53}$$

The angular momentum of a point mass element of mass m_i at a distance y' from the rotation axis with an angular velocity of $\omega_{x'}\ \mathbf{i}_{x'}$ is given by

$$\mathbf{L}_{x'} = m_i y'^2\ \omega_{x'}\ \mathbf{i}_{x'} = I_x \omega_{x'}\ \mathbf{i}_{x'} \tag{3.54}$$

where I_x is the moment of inertia. If the free electron simply rotated as a rigid plane-lamina disc with the mass density maintained in the plane as given by Eq. (3.7) and as shown in Figure 3.2, then the moment of inertia I_x corresponding to a rotation of the disc about the x'-axis would be given by

$$\begin{aligned} I_{x'} &= 2\frac{m_e}{\frac{2}{3}\pi\rho_0^3}\int_{-\rho_0}^{\rho_0}\int_{0}^{\sqrt{\rho_0^2 - x'^2}} \sqrt{\rho_0^2 - \left(x'^2 + y'^2\right)}\, y'^2\, dy'dx'\ \mathbf{i}_{x'} \\ &= \frac{3}{\pi}\frac{m_e}{\rho_0^3}\int_{-\rho_0}^{\rho_0}\int_{0}^{\sqrt{\rho_0^2 - x'^2}} y'^2 \sqrt{\left(\rho_0^2 - x'^2\right) - y'^2}\, dy'dx'\ \mathbf{i}_{x'} \end{aligned} \tag{3.55}$$

Using the integral with respect to y' given by #210 of Lide [20], Eq. (3.55) becomes

$$I_{x'}=\frac{3}{\pi}\frac{m_e}{\rho_0^3}\int_{-\rho_0}^{\rho_0}\left(\begin{array}{l}-\dfrac{y'}{4}\sqrt{\left(\left(\rho_0^2-x'^2\right)-y'^2\right)^3}+\\ \dfrac{\rho_0^2-x'^2}{8}\left(y'\sqrt{\left(\rho_0^2-x'^2\right)-y'^2}+\left(\rho_0^2-x'^2\right)\arcsin\dfrac{y'}{\left|\sqrt{\rho_0^2-x'^2}\right|}\right)\end{array}\right|_0^{\sqrt{\rho_0^2-x'^2}}dx'\ \mathbf{i}_{x'} \tag{3.56}$$

Evaluation at the integration limits gives

$$I_{x'}=\frac{3}{16}\frac{m_e}{\rho_0^3}\int_{-\rho_0}^{\rho_0}\left(\rho_0^2-x'^2\right)^2dx'\ \mathbf{i}_{x'} \tag{3.57}$$

The multiplication and integration of each term followed by evaluation at the limits gives

$$\begin{aligned}I_{x'}&=\frac{3}{16}\frac{m_e}{\rho_0^3}\left(\rho_0^4x'-\frac{2\rho_0^2x'^3}{3}+\frac{x'^5}{5}\right)_{-\rho_0}^{\rho_0}\ \mathbf{i}_{x'}\\&=\frac{3}{16}\frac{m_e}{\rho_0^3}\left(2\rho_0^5-\frac{4\rho_0^5}{3}+\frac{2\rho_0^5}{5}\right)\ \mathbf{i}_{x'}=\frac{1}{5}m_e\rho_0^2\ \mathbf{i}_{x'}\end{aligned} \tag{3.58}$$

which is 1/2 the moment of inertia of a uniform disc as shown by Fowles [21].

The angular momentum $\mathbf{L}_{x'}$ follows from Eq. (3.54) as Eq. (3.58) times the constant angular velocity $\omega_{x'}\ \mathbf{i}_{x'}$. It is shown *infra* that the torque due to the photon's angular momentum of $\hbar$ initially along the x'-axis does cause $\mathbf{S}_z$ to rotate such that the mass-density function and the magnitude of the angular momentum-density function about the x'-axis are the same as those about the z-axis given by Eqs. (3.7) and (3.17), respectively.

By the perpendicular-axis theorem [21], the corresponding angular momentum about the x'-axis is 1/2 that about the z-axis. This is easily shown since Eq. (3.19) can be expanded as

$$\mathbf{L}\mathbf{i}_z=\int_0^{2\pi}\int_0^{\rho_0}\frac{m_e}{\frac{2}{3}\pi\rho_0^{\,3}}\sqrt{\rho_0^{\,2}-\rho^2}\,\frac{5}{2}\frac{\hbar}{m_e\rho_0^2}\left(x^2+y^2\right)\rho d\rho d\phi\ \mathbf{i}_z \tag{3.59}$$

Then the angular momentum about the x'-axis is

$$\mathbf{L}\mathbf{i}_{x'}=-\int_0^{2\pi}\int_0^{\rho_0}\frac{m_e}{\frac{2}{3}\pi\rho_0^{\,3}}\sqrt{\rho_0^{\,2}-\rho^2}\,\frac{5}{2}\frac{\hbar}{m_e\rho_0^2}\left(y'^2\right)\rho d\rho d\phi\ \mathbf{i}_z \tag{3.60}$$

which is 1/2 that of Eq. (3.59) since the number of symmetrical axes of integration was reduced to 1/2. This result can also be shown directly. Then, the angular momentum along the x'-axis corresponding to a rotation of the mass of the electron about this axis during a Larmor excitation is given by

$$\begin{aligned}\mathbf{L}\mathbf{i}_{x'}&=-\frac{m_e}{\frac{2}{3}\pi\rho_0^{\,3}}\frac{5}{2}\int_{-\rho_0}^{\rho_0}\int_{-\sqrt{\rho_0^2-x'^2}}^{\sqrt{\rho_0^2-x'^2}}\sqrt{\rho_0^2-\left(x'^2+y'^2\right)}\,\frac{\hbar}{m_e\rho_0^2}\,y'^2\,dy'dx'\,\mathbf{i}_{x'}\\&=-\frac{15\hbar}{4\pi\rho_0^{\,5}}\int_{-\rho_0}^{\rho_0}\int_{-\sqrt{\rho_0^2-x'^2}}^{\sqrt{\rho_0^2-x'^2}}\sqrt{\left(\rho_0^2-x'^2\right)-y'^2}\,y'^2\,dy'dx'\,\mathbf{i}_{x'}\end{aligned} \tag{3.61}$$

with the mass density and $\omega_{x'}$ equivalent to that of Eq. (3.19) but directed around the x'-axis and $\rho d\rho d\phi$ was replaced by $dy'dx'$. Using the integral with respect to y' given by # 210 of Lide [20], Eq. (3.61) becomes

$$\mathbf{L}\mathbf{i}_{x'}=-\frac{15\hbar}{4\pi\rho_0^{\,5}}\int_{-\rho_0}^{\rho_0}\left(\begin{array}{l}-\dfrac{y'}{4}\sqrt{\left(\rho_0^2-x'^2-y'^2\right)^3}\\ +\dfrac{\rho_0^2-x'^2}{8}\left(y'\sqrt{\rho_0^2-x'^2-y'^2}+\left(\rho_0^2-x'^2\right)\sin^{-1}\dfrac{y'}{\left|\sqrt{\rho_0^2-x'^2}\right|}\right)\end{array}\right|_{-\sqrt{\rho_0^2-x'^2}}^{\sqrt{\rho_0^2-x'^2}}dx'\mathbf{i}_{x'} \tag{3.62}$$

$$\begin{aligned}\mathbf{L}\mathbf{i}_{x'}&=-\frac{15\hbar}{4\pi\rho_0^{\,5}}\frac{\pi}{8}\int_{-\rho_0}^{\rho_0}\left(\rho_0^2-x'^2\right)^2dx'\ \mathbf{i}_{x'}\\&=-\frac{15\hbar}{32\rho_0^{\,5}}\int_{-\rho_0}^{\rho_0}\left(\rho_0^4-2\rho_0^2x'^2+x'^4\right)dx'\ \mathbf{i}_{x'}\end{aligned} \tag{3.63}$$

The integration of each term with respect to x' followed by evaluation at the limits gives:

$$\mathbf{L}\mathbf{i}_{x'} = -\frac{15\hbar}{32\rho_0^{\,5}}\left(\rho_0^4 x' - 2\frac{\rho_0^2 x'^3}{3} + \frac{x'^5}{5}\right)_{-\rho_0}^{\rho_0} \mathbf{i}_{x'} = -\frac{\hbar}{2}\,\mathbf{i}_{x'} \tag{3.64}$$

which is 1/2 the angular momentum of the free electron given by Eqs. (3.19-3.20).

The torque **N** in rotating coordinates is given by [22]

$$\mathbf{N} = \dot{\mathbf{L}} + \omega\mathbf{i}_{x'} \times \mathbf{L} \tag{3.65}$$

The electron's angular momentum of $\hbar$ is conserved. Thus, the torque $\mathbf{N}_\mathbf{p}$ on the electron's angular momentum of $\hbar$ due to the photon's angular momentum of $\hbar$ and corresponding magnetic moment of μ_B is

$$\mathbf{N}_\mathbf{p} = \omega\hbar\mathbf{i}_{x'} \tag{3.66}$$

The torque $\mathbf{N}_c$ corresponding to the centrifugal force $\mathbf{F}_\mathbf{c}$ for a rotating system is given by:

$$\mathbf{N}_\mathbf{c} = r \times \mathbf{F}_\mathbf{c} = -mr^2\omega^2\mathbf{i}_{x'} = -I_{x'}\omega^2\mathbf{i}_{x'} = -\mathbf{L}_{x'}\omega\mathbf{i}_{x'} \tag{3.67}$$

Substitution of Eq. (3.64) into Eq. (3.67) gives

$$\mathbf{N}_\mathbf{c} = -\frac{\hbar}{2}\omega\mathbf{i}_{x'} \tag{3.68}$$

The rotating mass/charge density gives rise to an angular momentum of $\frac{\hbar}{2}$ (Eq. (3.64)) and a corresponding magnetic moment of $\frac{\mu_B}{2}$ (Eq. (28) of Box 1.1) that opposes the magnetic moment of the photon. The corresponding torque is:

$$\mathbf{N}_{x'} = -\mathbf{L}_{x'}\omega\mathbf{i}_{x'} = -\frac{\hbar}{2}\omega\mathbf{i}_{x'} \tag{3.69}$$

The required torque balance is:

$$\mathbf{N}_\mathbf{p} + \mathbf{N}_c + \mathbf{N}_{x'} = \omega\mathbf{i}_{x'}\left(\hbar - \frac{\hbar}{2} - \frac{\hbar}{2}\right) = 0 \tag{3.70}$$

The result of Eq. (3.70) confirms the match of the mass-density function and magnitude of the angular frequency function of Eqs. (3.59-3.64) with those of Eq. (3.19).

Thus, the application of a magnetic field causes a resonant excitation of the Larmor precession. The $\hbar$ of angular momentum on the z'-axis and the $\hbar$ of angular momentum on the x'-axis gives a resultant stationary projection of $\sqrt{2}\hbar$ onto the $\left(\mathbf{i}_\mathbf{x}, 0\mathbf{i}_\mathbf{y}, \mathbf{i}_\mathbf{z}\right)$-axis. The static projection of the resultant onto the z-axis is $\hbar$. The precessing electron can further interact with a resonant photon directed along the x-axis that rotates the z-axis-directed static projection of the resultant of $\hbar$ such that it flips it to the opposite direction. Thus, absorption of an RF photon gives rise to a Zeeman transition corresponding to flipping of the parallel or antiparallel alignment of the electron magnetic moment of a Bohr magneton with respect to the magnetic field wherein the energy of the transition between Zeeman states is that of the resonant photon given by Eq. (1.227).

The parameters of the photon standing wave for the Zeeman effect of the free electron follow from those of the bound electron given in the Magnetic Parameters of the Electron (Bohr Magneton) section and Box 1.1. The charge density of the free electron is given by the projection of the atomic orbital into a plane as given in the Charge-Density Function section. To cause the Larmor excitation and the spin-flip transition, the corresponding photon gives rise to surface currents in the plane of the free electron that are also equivalent to the projection of the time- and spherically-harmonic dipole Larmor currents of the bound electron into the free-electron plane. Specifically, the photon gives rise to a current on the surface of the disc that corresponds to a rotating time- and polar-harmonic dipole that phase-matches the mass (charge) density of Eqs. (3.7-3.8).

The current of the free electron is initially azimuthally symmetrical about the z-axis. The resonant Larmor photon induces transient currents in the xy-plane to give rise to $\hbar$ of angular momentum initially along the x-axis. The corresponding torque causes the electron to precess about the x- and z-axes giving rise to Larmor precession about the $\left(\mathbf{i}_\mathbf{x}, 0\mathbf{i}_\mathbf{y}, \mathbf{i}_\mathbf{z}\right)$-axis and the z-axis at steady state depending on the initial direction of the free-electron magnetic moment relative to the applied magnetic-field direction. Thus, the currents cause a precession of the disc to form a time-averaged bi-conical cavity shown in Figure 3.8 that is azimuthally symmetrical about the $\left(\mathbf{i}_\mathbf{x}, 0\mathbf{i}_\mathbf{y}, \mathbf{i}_\mathbf{z}\right)$-axis, and this distribution further precesses about the z-axis to generate the $Y_0^{\,0}(\theta,\phi)$ distribution.

The photon-induced surface current satisfies the condition

$$\nabla \cdot J = 0 \tag{3.71}$$

And, the radius, ρ_0, of the free electron is unchanged. The time-averaged angular momentum and rotational energy of the currents that are phase-locked to the photon field are zero as given by Eqs. (1.76-1.77), but the photon's angular momentum is $\hbar$ corresponding to a magnetic moment of one Bohr magneton μ_B as shown for the case of the Larmor resonant excitation of a bound electron in Box 1.1. Thus, the electrostatic energy is constant, and only the magnetic energy need be considered as given by Eqs. (23-25) of Box 1.1.

The photon-field is central according to special relativity as given in the Equation of the Electric Field inside the Atomic Orbital section. The corresponding central field at the free-electron surface follows from Eq. (17) of Box 1.1 and the force balance condition between the centrifugal force and the electric-field force:

$$\mathbf{E} = \frac{3}{\varepsilon_0 2}\frac{e}{\pi\rho_0^3}\sqrt{\rho_0^2-\rho_n^2}\,\mathrm{Re}\left\{Y_\ell^m(\theta,\phi)e^{i\omega t}\right\}\mathbf{i}_\rho\delta(\rho-\rho_n)\delta(z') \tag{3.72}$$

where the spherical harmonic dipole $Y_\ell^m(\theta,\phi)=\sin\theta$ is with respect to the xy-plane of the free electron and gives the magnitude at position ρ_n in the plane, the centrifugal force is given by Eq. (3.67), and ω is given by Eq. (3.17). The mass density given by Eq. (3.7) may be given in terms of spherical coordinates as follows:

Let

$$\rho = \rho_0\cos\theta \tag{3.73}$$

Then

$$\sigma_m(\rho,\phi,z) = \frac{3}{2}\frac{m_e}{\pi\rho_0^2}\sqrt{1-\left(\frac{\rho_0\cos\theta}{\rho_0}\right)^2} = \frac{3}{2}\frac{m_e}{\pi\rho_0^2}\sin\theta \tag{3.74}$$

Force balance is maintained by the equivalence of the harmonic modulation of the charge and the mass where e/m_e is invariant.

The in-plane time- and polar-harmonic dipole further spins about the z-axis at the Larmor frequency, ω_L. By considering the Larmor frequency component and the motion at the frequency given by Eq. (3.17), the free-electron motion in a magnetic field parallels that of the bound electron that also has two components of motion. The angular frequency about the rotation axis of the bound electron is given by Eq. (1.36), and the resulting dipole current rotates about the z-axis at the Larmor frequency. The parallels continue. In the free-electron frame rotating about the z-axis, the electric field of the dipole is

$$\mathbf{E} = \frac{3}{\varepsilon_0 2}\frac{e}{\pi\rho_0^3}\sqrt{\rho_0^2-\rho_n^2}\sin\theta\sin(\varphi-\omega t)\delta(\rho-\rho_n)\delta(z')\mathbf{i}_\rho \tag{3.75}$$

corresponding to Eq. (18) of Box 1.1. From Eqs. (20) and (21), the corresponding photon surface current is equivalent to the projection of the charge of a uniformly-charged spherical shell rotating at constant angular velocity of ω about the z-axis into the free-electron plane. Given that the charge moving azimuthally and time-harmonically at the constant frequency is equivalent to the planar projection of a spherical dipole, the resulting current is nonradiative as shown for this condition in Appendix I. The z-axis directed field in the laboratory frame and the field in frames rotating about the $(\mathbf{i}_x, 0\mathbf{i}_y, \mathbf{i}_z)$-axis are magnetostatic as shown in Figures 1.32 and 1.33 but directed along the respective axis. The precession of the magnetostatic dipole results in magnetic dipole radiation or absorption during a Stern-Gerlach transition.

Consider next the physics of the free-electron Zeeman splitting based on the electron structure and corresponding behavior in magnetic and photon fields based on Maxwell's equations. The free electron is a two-dimensional plane lamina comprised of a series of concentric circular current loops in the xy-plane (ρ-plane) that circulate about the z-axis as given in the Current-Density Function section. Each current loop can be considered a great-circle basis element analogous to those given in the Atomic Orbital Equation of Motion for ℓ = 0 Based on the Current Vector Field (CVF) section. The rotation of each such great circle about the $(\mathbf{i}_x, 0\mathbf{i}_y, \mathbf{i}_z)$- axis by 2π during a period generates the equivalent of the current pattern of a BECVF. Furthermore, the rotation of the free-electron disc having a continuous progression of larger current loops along ρ forms two conical surfaces over a period that join at the origin and face in the opposite directions along the $(\mathbf{i}_x, 0\mathbf{i}_y, \mathbf{i}_z)$-axis, the axis of rotation, as shown in Figure 3.8. At each position of $0<\rho$, there exists a BECVF of that radius that is concentric to the one of infinitesimally larger radius to the limit at $\rho=\rho_0$. The BECVFs at each position ρ generated over a period by the precession about the $(\mathbf{i}_x, 0\mathbf{i}_y, \mathbf{i}_z)$-axis by 2π is given in Appendix IV.

Over one time period, the first motion about the $(\mathbf{i}_x, 0\mathbf{i}_y, \mathbf{i}_z)$-axis by 2π sweeps out the equivalent of a BECVF, and the rotation about the z-axis sweeps out the equivalent of an OCVF. The combined motions sweep out the equivalent of the convolution of the BECVF with the OCVF, an angular-momentum distribution equivalent to $Y_0^0(\theta,\phi)$ of the bound electron. A discrete representation from Appendix IV as a series of great circle current loops is shown in Figure 3.9

Figure 3.8. A view of one of the two conical surfaces formed by rotation of the plane-lamina disc comprised of concentric great circles about the $\left(\mathbf{i}_x, 0\mathbf{i}_y, \mathbf{i}_z\right)$-axis that join at the origin and face in the opposite directions along the axis of rotation, the $\left(\mathbf{i}_x, 0\mathbf{i}_y, \mathbf{i}_z\right)$-axis.

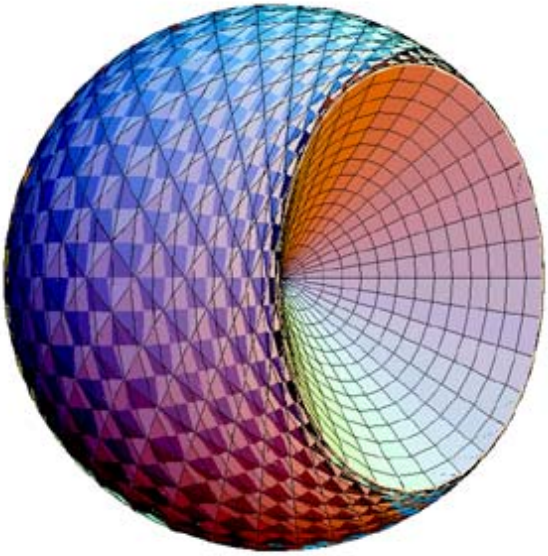

Figure 3.9. A representation of the uniform current pattern of the $Y_0^0(\theta,\phi)$ free electron motion over a period of both precessional motions shown with 30 degree increments of the angle to generate the free electron BECVF and 30 degree increments of the rotation of this basis element about the z-axis. The perspective is along the x-axis. The great circle current loop that served as a basis element that was initially in the xy-plane of each free electron BECVF is shown as red.

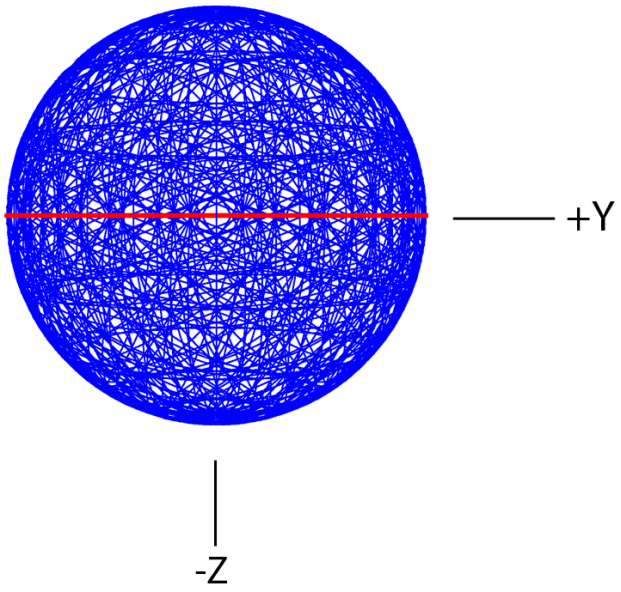

Now, consider the dynamics when the precessing electron further interacts with a resonant photon that gives rise to Zeeman splitting. As shown in Appendix IV, the combined rotations about the $\left(\mathbf{i}_x, 0\mathbf{i}_y, \mathbf{i}_z\right)$-axis and the z-axis generates a distribution over a period of motion that is equivalent to the current pattern and angular momentum of $Y_0^0(\theta,\phi)$ of the bound electron. The absorbed Larmor-frequency-resonant photon provides $\hbar$ of angular momentum along the x-axis that causes the $Y_0^0(\theta,\phi)$ distribution to rotate about the x-axis by π to flip the magnetic moment in the opposite direction while maintaining the distribution with the currents reversed.

Since the Larmor precession sweeps out the form of the $Y_0^0(\theta,\phi)$ distribution for each position of ρ and the current of each concentric shell along ρ obeys superposition, the free electron in aggregate behaves as a shell of charge, current, and angular-momentum density of the free-electron radius ρ_0 having a total magnitude of angular momentum of $\hbar$ and the projection $\mathbf{L}_z = \frac{\hbar}{2}$. Then, the resulting time-averaged azimuthally uniform spherical momentum density interacts with the external applied magnetic field in a manner that is equivalent to that of the atomic orbital equation of motion, $Y_0^0(\theta,\phi)$, of the bound electron of radius $r_n = \rho_0$. Note the parallels between the bound and free electrons wherein the free electron angular momentum was considered as the plane projection of the constant angular momentum density of a bound electron confined to a spherical shell of radius ρ_0 having a total magnitude of angular momentum of $\hbar$ and the projection $\mathbf{L}_z = \frac{\hbar}{2}$ (Eqs. (3.2-3.4) and (3.19-3.20)).

FREE-ELECTRON g FACTOR

Since the projection of the time-averaged intrinsic free electron angular momentum and that of the resonant photon that excites the Larmor precession onto the z-axis are both $\frac{\hbar}{2}$, and the angular motion distribution of the free electron is spherically symmetric, the Larmor-excited free electron behaves equivalently to the bound electron in a magnetic field during a spin flip transition. Flux must be linked in the same manner in units of the magnetic flux quantum, $\Phi_0 = \frac{h}{2e}$. Consequently, the g factor for the free electron is the same as that of the bound electron, and the energy of the transition between these states is that of the resonant photon given by Eq. (1.227).

Consider the bound electron. As demonstrated in the Atomic Orbital Equation of Motion for $\ell = 0$ Based on the Current Vector Field (CVF) section, $\frac{\hbar}{2}$ of the atomic orbital angular momentum designated the static component is initially parallel to the field. An additional $\frac{\hbar}{2}$ parallel component designated the dynamic component comes from the $\hbar$ of angular momentum along $\mathbf{S}$. The angular momentum in the presence of an applied magnetic field is [23]:

$$\mathbf{L} = \mathbf{r} \times (m_e \mathbf{v} + e\mathbf{A}) \tag{3.76}$$

where $\mathbf{A}$ is the vector potential evaluated at the location of the atomic orbital. The circular integral of $\mathbf{A}$ is the flux linked by the atomic orbital. During a Stern-Gerlach transition a resonant RF photon is absorbed or emitted, and the $\hbar$ component along $\mathbf{S}$ reverses direction. Referring to Box 1.1, it is shown by Eqs. (29-32) that the dynamic parallel component of angular momentum corresponding to the vector potential due to the lightlike transition is equal to the "kinetic angular momentum" $(\mathbf{r} \times m\mathbf{v})$ of $\frac{\hbar}{2}$. Conservation of angular momentum of the electron requires that the static angular momentum component concomitantly flips. The static component of angular momentum undergoes a spin flip, and concomitantly the "potential angular momentum" $(\mathbf{r} \times e\mathbf{A})$ of the dynamic component must change by $-\frac{\hbar}{2}$ due to the linkage of flux by the electron such that the total angular momentum is conserved.

In the case of the free electron, the application of a further $\hbar$ component along the x'-axis with the absorption of a resonant photon causes the $Y_0^0(\theta, \phi)$ distribution to flip about the x-axis to reverse the magnetic moment with respect to the applied magnetic field. The photon having $\hbar$ of angular momentum along the positive x'-axis of the free electron has an energy that is equivalent to that of the spin-flip transition given by Eq. (1.227). Here also, the dynamic parallel component of angular momentum corresponding to the vector potential due to the lightlike transition is equal to the "kinetic angular momentum" $(\mathbf{r} \times m\mathbf{v})$ of $\frac{\hbar}{2}$. Conservation of angular momentum of the $Y_0^0(\theta, \phi)$ distribution requires that the static angular momentum component concomitantly flips. The static component of angular momentum undergoes a spin flip, and concomitantly the "potential angular momentum" $(\mathbf{r} \times e\mathbf{A})$ of the dynamic component must change by $-\frac{\hbar}{2}$ due to the linkage of flux by the electron such that the total angular momentum is conserved.

From Eq. (28) of Box 1.1, the $\frac{\hbar}{2}$ of intrinsic angular momentum after the field is applied corresponds to a magnetic moment on the applied-field-axis of $\frac{\mu_B}{2}$ in the case of the free electron as well as the atomic orbital. The resonant Larmor-precession-angular-momentum contribution of $\frac{\hbar}{2}$ corresponds to another $\frac{\mu_B}{2}$ of magnetic moment that gives a total magnetic moment along the applied-field-axis of μ_B, a Bohr magneton. The additional contribution (Eq. (28)) arises from the angular momentum of $\hbar$ on the $\mathbf{S}$-axis and the x'-axis for the atomic orbital and free electron, respectively. Thus, even though the magnitude of the vector projection of the angular momentum of the electron in the direction of the magnetic field is $\frac{\hbar}{2}$, the magnetic moment corresponds to $\hbar$ due to the $\frac{\hbar}{2}$ contribution from the dynamic component, and the quantized transition is due to the requirement of angular momentum conservation as given by Eq. (28) of Box 1.1.

Eq. (22) of Box 1.1 implies a continuum of energies; whereas, Eq. (29) of Box 1.1 shows that the static-kinetic and dynamic vector potential components of the angular momentum are quantized at $\frac{\hbar}{2}$. Consequently, as shown in the Electron g Factor section, the flux linked during a spin transition is quantized as the magnetic flux quantum:

$$\Phi_0 = \frac{h}{2e} \tag{3.77}$$

Only the states corresponding to:

$$m_s = \pm\frac{1}{2} \tag{3.78}$$

are possible due to conservation of angular momentum. It is further shown using the Poynting power vector with the requirement that flux is linked in units of the magnetic flux quantum, that the factor 2 of Eqs. (23) and (25) of Box 1.1 is replaced by the electron g factor.

In summary, since the corresponding properties of the free electron are equivalent to those of the bound electron, conservation of angular momentum of the electron permits a discrete change of its "kinetic angular momentum" $(\mathbf{r}\times m\mathbf{v})$ with respect to the field of $\frac{\hbar}{2}$, and concomitantly the "potential angular momentum" $(\mathbf{r}\times e\mathbf{A})$ must change by $-\frac{\hbar}{2}$ (Eqs. (1.171-1.174)). Consequently, flux linkage by the electron is quantized in units of the magnetic flux quantum, $\Phi_0 = \frac{h}{2e}$, and the electron magnetic moment can be parallel or antiparallel to an applied field as observed with the Stern-Gerlach experiment (See Box 1.1 and in the Electron g Factor section). Rather than a continuum of orientations with corresponding energies, the energy, ΔE_{mag}^{spin}, of the spin flip transition corresponding to the $m_s = \pm\frac{1}{2}$ quantum number is given by Eq. (1.227):

$$\Delta E_{mag}^{spin} = g\mu_B B \tag{3.79}$$

The Stern-Gerlach experiment implies a magnetic moment of one Bohr magneton and an associated angular momentum quantum number of 1/2. Historically, this quantum number is called the spin quantum number, m_s, and that designation is maintained.

The Stern Gerlach experiment was historically felt to be inexplicable in terms of classical physics. Past explanations based on associated postulates were purely mathematical. However, the observed electron parameters are explained physically. Classical laws give (1) a gyromagnetic ratio of $\frac{e}{2m}$, (2) a Larmor precession frequency of $\frac{e\mathbf{B}}{2m}$, (3) the Stern-Gerlach experimental result of quantization of the angular momentum that implies a spin quantum number of 1/2 corresponding to an angular momentum of $\frac{\hbar}{2}$ on the z-axis, and (4) the observed Zeeman splitting due to a magnetic moment of a Bohr magneton $\mu_B = \frac{e\hbar}{2m_e}$ corresponding to an angular momentum of $\hbar$ on the z-axis. Furthermore, the solution is relativistically invariant as shown in the Special Relativistic Correction to the Ionization Energies section. Dirac originally attempted to solve the bound electron physically with stability with respect to radiation according to Maxwell's equations with the further constraints that it was relativistically invariant and gave rise to electron spin [24]. He was unsuccessful and resorted to the current mathematical-probability-wave model that has many problems as discussed in Refs. [25-26].

FREE-ELECTRON BINDING

The free electron comprises a planar disc wherein the azimuthal charge density increases towards the origin of the disc according to Eq. (3.8). When an electron undergoes binding by a nucleus, the opposite of the reversible and time-symmetrical process of electron ionization, any linear kinetic energy is lost as radiation such that the initial de Broglie wavelength and radius ρ_0 are large according to Eq. (3.2). During binding in the nuclear central field, the electron current pattern over time is equivalent to the pattern traced out over time by the planar great circle of radius ρ_0 of a free electron undergoing a precession in a magnetic field during a spin flip transition. In the binding case, as the free electron undergoes a wobble rotational motion, the concentric planar great circles of current shown in Figure 3.2A flow from the disc origin to the perimeter edge at ρ_0 and successively spread the electron charge density over a BECVF such as that shown in Figures 1.5-1.7. Next, a wobble rotational motion of the BECVF spreads the charge over a spherical shell as a uniform density to comprise the bound electron atomic orbital $Y_0^0(\theta,\phi)$ of spherical radius R as shown in Figures 1.12, 1.13, 1.16, 1.17, and 1.22.

Specifically, consider the rotation of the angular momentum vector of the free electron current about two axes, the $\left(\mathbf{i}_x, 0\mathbf{i}_y, \mathbf{i}_z\right)$-axis in a first step and the laboratory-frame z-axis in a second step as shown in Appendix IV. The corresponding motion of the perimeter great circle current loop at ρ_0 in the plane perpendicular to the angular momentum vector generates CVFs equivalent to those of the bound electron given in the Atomic Orbital Equation of Motion for $\ell = 0$ Based on the Current Vector Field (CVF) section. Specifically, the first rotation sweeps out the equivalent of a BECVF (Figure IV.1), wherein the concentric planar great circle current loops shown in Figure 3.2A flow from the disc origin to the perimeter edge at ρ_0 during the rotation to successively spread the charge density over the BECVF. The second rotation of the BECVF sweeps out the equivalent of the convolution of the BECVF with the OCVF given in Figure IV.5. The result is a charge and current density

distribution equivalent to $Y_0^0(\theta,\phi)$ of the bound electron wherein charge density of the bound electron has the same angular frequency and linear velocity everywhere on the surface. During binding, the radii of the great circles of the BECVF and $Y_0^0(\theta,\phi)$ may change with the emssion of the equivalent of at least one excited state photon. However, due to the indivisiblity of the electron and conservation of energy in an inverse squared Coulomb nuclear field, the time average radius of the BECVF or $Y_0^0(\theta,\phi)$ must change as an ensemble wherein the time average of the kinetic energy, $<T>$, for any circular or elliptical motion in an inverse-squared field is $1/2$ that of the time average of the magnitude of the potential energy, $|<V>|$. $<T>=1/2|<V>|$ [27]. The common radial current of a bound electon during an excited state transition and the corresponding lifetime is given in the State Lifetimes and Line Intensities section. The reversible and time-symetric mechanism of the emission or absorption of photons by the bound electron is given in the Transitions section. The uninform charge density is proportional to the spherical coordinate term $\rho_0 \sin\theta$ relative to the z-axis which follows from Eq. (3.8) with the substitution of $\rho = \rho_0 \cos\theta$ as given by Eq. (3.74). Additionally, the bound electron may comprise time and spherical harmonic modulation functions given by Eq. (1.28) depending on the electron configuration. The opposite process to binding described herein occurs during electron ionization.

Specifically, consider the free electron traveling along the z-axis with plane of the electron disc in the xz-plane as it approaches the proton at the origin. The bonding proceeds by the rotation of the angular momentum vector of the free electron current about two axes, the $(\mathbf{i}_x, 0\mathbf{i}_y, \mathbf{i}_z)$-axis in a first step and the laboratory-frame z-axis in a second step as shown in Appendix IV. The corresponding motion of the perimeter great circle current loop at ρ_0 in the plane perpendicular to the angular momentum vector generates CVFs equivalent to those of the bound electron given in the Atomic Orbital Equation of Motion for $\ell = 0$ Based on the Current Vector Field (CVF) section. Specifically, the first rotation sweeps out the equivalent of a BECVF (Figure IV.1), wherein the concentric planar great circle current loops shown in Figure 3.2A flow from the disc origin to the perimeter edge at ρ_0 during the rotation to successively spread the charge density over the BECVF as the disc converters into an annulus with the inner radius increasing to ρ_0 at the step completing the BECVF. The second rotation of the BECVF sweeps out the equivalent of the convolution of the BECVF with the OCVF given in Figure IV.5 to form the uniform charge, mass, current density, and momentum-density function $Y_0^0(\theta,\phi)$.

Electron binding is a continuous process with continuous current flow. An equation providing visualization in discrete steps that generates the angular momentum vectors of the bound electron follows from Eq. (18) of Appendix IV.

$$\begin{bmatrix} x' \\ y' \\ z' \end{bmatrix} = \sum_{m=1}^{m=M} \begin{bmatrix} \cos\left(\frac{m2\pi}{M}\right) & \sin\left(\frac{m2\pi}{M}\right) & 0 \\ -\sin\left(\frac{m2\pi}{M}\right) & \cos\left(\frac{m2\pi}{M}\right) & 0 \\ 0 & 0 & 1 \end{bmatrix} \bullet \delta\left(z-\rho_0\left(1-\frac{n}{N}\right)\right) \sum_{n=1}^{n=N} \begin{bmatrix} \frac{1}{2}+\frac{\cos\left(\frac{n2\pi}{N}\right)}{2} & \frac{\sin\left(\frac{n2\pi}{N}\right)}{\sqrt{2}} & \frac{1}{2}-\frac{\cos\left(\frac{n2\pi}{N}\right)}{2} \\ -\frac{\sin\left(\frac{n2\pi}{N}\right)}{\sqrt{2}} & \cos\left(\frac{n2\pi}{N}\right) & \frac{\sin\left(\frac{n2\pi}{N}\right)}{\sqrt{2}} \\ \frac{1}{2}-\frac{\cos\left(\frac{n2\pi}{N}\right)}{2} & -\frac{\sin\left(\frac{n2\pi}{N}\right)}{\sqrt{2}} & \frac{1}{2}+\frac{\cos\left(\frac{n2\pi}{N}\right)}{2} \end{bmatrix} \begin{bmatrix} \rho\cos\phi \\ \rho\sin\phi \\ 0 \end{bmatrix}_{\substack{\phi=0 \text{ to } 2\pi \\ \rho=\frac{n}{N}\rho_0 \text{ to } \rho_0}} \tag{3.80}$$

Consider that the free electron translates along the z-axis towards the proton at the origin. To maintain an equipotential, the N rotations of the free electron disc (Eq. (3.80)) commences at a distance from the proton equal to the outer radius of the disc ρ_0. The current within the disc flows towards the outer radius ρ_0 to form a set of time-delayed concentric great circles. At each step of the rotation to transfer a great circle current element from the free electron current density to that of the forming BECVF

according to Eq. (Eq. (3.80)), as a great circle of radius ρ_0 is transferred to the forming BECVF a next great circle replaces it such that the remaining electron disc current density forms an annulus with a constant outer radius $\rho = \rho_0$ and an increasing inner radius $\rho = \frac{n}{N}\rho_0$. The center of mass of the forming BECVF/annulus translates a distance of $\frac{\rho_0}{N}$ along the z-axis towards the proton for each n rotation step such that the proton is in the coordinate origin of the BECVF at the end of the N rotations. Next, the M rotations of the BECVF form the spherical shell with the proton at the center. During the formation of the BECVF, each point of the forming BECVF surface and the disc are equipotential relative to the Coulomb field between the proton and electron. Computer modeling of the analytical equations to generate the free electron current vector field, the current vector fields during electron binding, and the azimuthally uniform momentum-density function $Y_0^0(\theta,\phi)$ is available on the web [28]. Excerpts of the animation of the continuous electron binding process are shown in Figure 3.10. The discrete representation of the current distribution $Y_0^0(\theta,\phi)$ that shows a finite number of current elements wherein the BECVF comprises N great circles and the number of convolved BECVF elements is M is shown in Figures 3.11 and 3.12.

Figure 3.10. Representations of stages of the bound electron current pattern of the $Y_0^0(\theta,\phi)$ formed by free electron binding to a proton (Eq. (3.80)) wherein the current density of the free electron disc is converted into great circles covering a two-dimensional spherical shell.

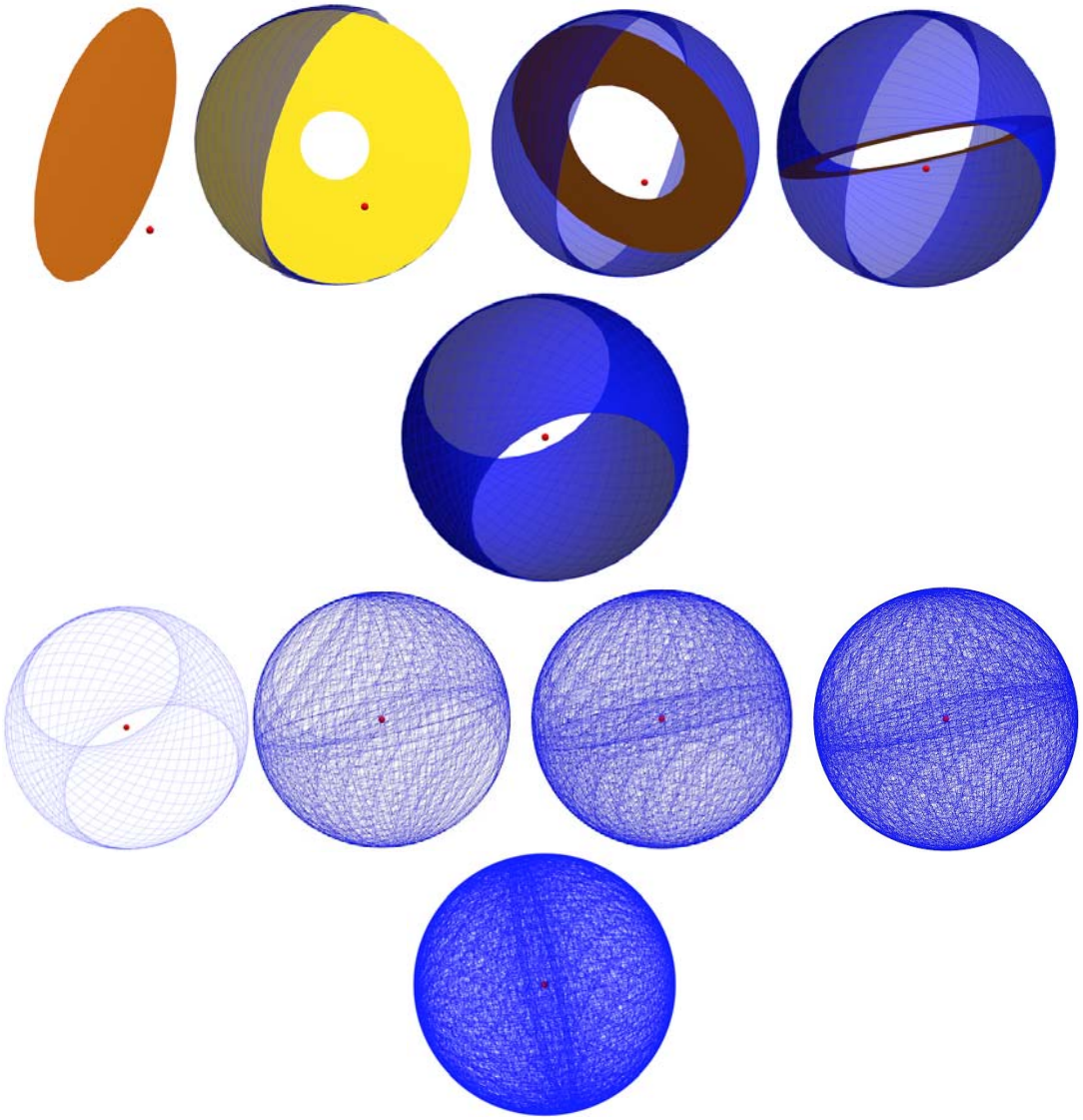

Figures 3.11 and 3.12. Representations of the current pattern of the $Y_0^0(\theta,\phi)$ formed by electron binding with 30 degree increments ($N = M = 12$ in Eq. (3.80)) of the angle to generate the free electron binding BECVF and 30 degree increments of the rotation of this BECVF about the z-axis to form the bound electron current vector field. The free electron disc that served as the source of great circle basis element current loops that was initially in the xy-plane is shown as red

Figure 3.11. The perspective is along the z-axis.

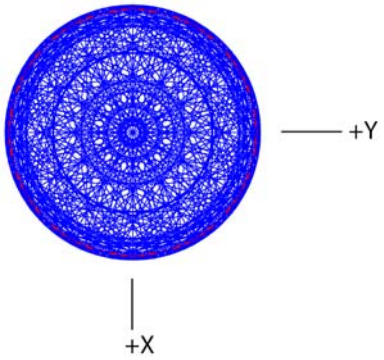

Figure 3.12. The perspective is along the x-axis.

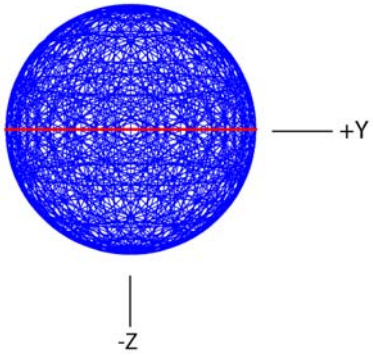

The z-axis view of this representation with 144 vectors overlaid giving the direction of the current of each great circle element is shown in Figure 3.13. The corresponding mass (momentum) density is also represented by Figures 3.11 and 3.12 wherein the charge and mass are interchangeable by the conversion factor m_e / e.

Figure 3.13. An ideal representation of the uniform current pattern of $Y_0^0(\theta,\phi)$ comprising the superposition of an infinite number of great circle elements generated by normalizing the distribution of Eq. (3.80). The constant uniform current density is overlaid with 144 vectors giving the direction of the current of each great circle element for 30 degree increments ($N = M = 12$ in Eq. (3.80)) of the angle to generate the BECVF and 30 degree increments of the rotation of this basis element about the z-axis. The perspective is along the z-axis. The corresponding uniform current-density function having intrinsic angular momentum components of $\mathbf{L}_{xy} = \frac{\hbar}{4}$ and $\mathbf{L}_z = \frac{\hbar}{2}$ following Larmor excitation in a magnetic field give rise to the phenomenon of electron spin.

The result is a charge and current density distribution equivalent to $Y_0^0(\theta,\phi)$ of the bound electron wherein charge density of the bound electron has the same angular frequency and linear velocity everywhere on the surface. During binding, the radii of the great circles of the BECVF and $Y_0^0(\theta,\phi)$ may change with the emssion of the equivalent of at least one excited state photon. However, due to the indivisiblity of the electron and conservation of energy in an inverse squared Coulomb nuclear field, the time average radius of the BECVF or $Y_0^0(\theta,\phi)$ must change as an ensemble wherein the time average of the kinetic energy, $< T >$, for any circular or elliptical motion in an inverse-squared field is $1/2$ that of the time average of the magnitude of the potential energy, $|< V >|$. $< T >= 1/2 |< V >|$ [27]. The common radial current of a bound electon during an excited state

transition and the corresponding lifetime is given in the State Lifetimes and Line Intensities section. The reversible and time-symetric mechanism of the emission or absorption of photons by the bound electron is given in the Transitions section. The uninform charge density is proportional to the spherical coordinate term $\rho_0 \sin\theta$ relative to the z-axis which follows from Eq. (3.8) with the substitution of $\rho = \rho_0 \cos\theta$ as given by Eq. (3.74). Additionally, the bound electron may comprise time and spherical harmonic modulation functions given by Eq. (1.28) depending on the electron configuration. The opposite process to binding described herein occurs during electron ionization.

REFERENCES

1. G. Matteucci, "Electron wavelike behavior: a historical and experimental introduction," Am. J. Phys., 58, No. 12, (1990), pp. 1143-1147.
2. D. Clark, "Very large hydrogen atoms in interstellar space," Journal of Chemical Education, 68, No. 6, (1991), pp. 454-455.
3. J. Gribbin, New Scientist, January, 25, (1997), p. 15.
4. I. Levine, et al., Physical Review Letters, Vol. 78, No. 3, (1997), pp. 424-427.
5. J. A. Stratton, *Electromagnetic Theory*, McGraw-Hill Book Company, (1941), p. 195.
6. J. D. Jackson, Classical Electrodynamics, Second Edition, John Wiley & Sons, New York, (1975), pp. 17-22
7. H. A. Haus, J. R. Melcher, "Electromagnetic Fields and Energy," Department of Electrical Engineering and Computer Science, Massachusetts Institute of Technology, (1985), Sec. 5.3.
8. D. R. Lide, *CRC Handbook of Chemistry and Physics*, 79th Edition, CRC Press, Boca Raton, Florida, (1998-9), pp. A-32 to A-33.
9. R. N. Bracewell, *The Fourier Transform and Its Applications*, McGraw-Hill Book Company, New York, (1978), pp. 248-249.
10. H. A. Haus, "On the radiation from point charges," American Journal of Physics, 54, (1986), pp. 1126-1129.
11. J. D. Jackson, *Classical Electrodynamics*, Second Edition, John Wiley & Sons, New York, (1975), pp. 236-240, 601-608, 786-790.
12. D. A. McQuarrie, *Quantum Chemistry*, University Science Books, Mill Valley, CA, (1983), pp. 238-241.
13. J. D. Jackson, *Classical Electrodynamics*, Second Edition, John Wiley & Sons, New York, (1975), pp. 168-173.
14. J. D. Jackson, *Classical Electrodynamics*, Second Edition, John Wiley & Sons, New York, (1975), pp. 739-779.
15. M. Mizushima, *Quantum Mechanics of Atomic Spectra and Atomic Structure*, W.A. Benjamin, Inc., New York, (1970), p.17.
16. J. D. Jackson, *Classical Electrodynamics*, Second Edition, John Wiley & Sons, New York, (1975), pp. 780-791.
17. J. D. Jackson, *Classical Electrodynamics*, Second Edition, John Wiley & Sons, New York, (1975), pp. 662-665.
18. J. D. Jackson, *Classical Electrodynamics*, Second Edition, John Wiley & Sons, New York, (1975), pp. 668-672.
19. E. M. Purcell, *Electricity and Magnetism*, McGraw-Hill, New York, (1965), pp. 370-375, 447.
20. D. R. Lide, *CRC Handbook of Chemistry and Physics*, 79th Edition, CRC Press, Boca Raton, Florida, (1998-9), p. A-33.
21. G. R. Fowles, *Analytical Mechanics*, Third Edition, Holt, Rinehart, and Winston, New York, (1977), pp. 193-199.
22. G. R. Fowles, *Analytical Mechanics*, Third Edition, Holt, Rinehart, and Winston, New York, (1977), pp. 243-247.
23. E. M. Purcell, *Electricity and Magnetism*, McGraw-Hill, New York, (1965), p. 447.
24. P. Pearle, "Absence of radiationless motions of relativistically rigid classical electron," Foundations of Physics, Vol. 7, Nos. 11/12, (1977), pp. 931-945.
25. R. L. Mills, "Maxwell's Equations and QED: Which is Fact and Which is Fiction," Physics Essays, Vol. 19, (2006), pp. 225-262.
26. R. L. Mills, "The Fallacy of Feynman's Argument on the Stability of the Hydrogen Atom According to Quantum Mechanics," Annales de la Fondation Louis de Broglie, Vol. 30, No. 2, (2005), pp. 129-151.
27. G. R. Fowles, *Analytical Mechanics*, Third Edition, Holt, Rinehart, and Winston, New York, (1977), pp. 145-158.
28. "Modeling of the Analytical Equations of the Binding of a Free Electron to form the Bound Electron Current Vector Field $Y_0^0(\theta,\phi)$ and Corresponding Ionization by Time Reversal" posted at www.brilliantlightpower.com.

Chapter 4

EQUATION OF THE PHOTON

RIGHT AND LEFT HAND CIRCULAR AND ELLIPTICALLY POLARIZED PHOTONS

The equation of the photon in free space is derived as a boundary value problem involving the transition from the ground state to an excited state of the hydrogen atom. The "ground" state function of the hydrogen atom is an atomic orbital given in the Atomic Orbital Equation of Motion $\ell = 0$ Based on the Current Vector Field (CVF) section, and the excited-state function comprising the atomic orbital and a resonant trapped photon is given in the Excited States of the One-Electron Atom (Quantization) section. The atomic orbital CVF equations are given by Eqs. (1.78-1.98), and the CVFs are shown in Figures 1.4-1.11. The "trapped photon" of an excited state is given by Eq. (2.15). The latter gives rise to a corresponding phase-matched source current given by Eq. (2.11). During the transition from the excited state to the ground state, the excited-atomic-state angular momentum given by Eq. (2.66) and the emitted-photon angular momentum are quantized in unit of $\hbar$ such that Eq. (9.2) is obeyed. Since the change in angular momentum between the initial and final atomic states is conserved by the photon's angular momentum, the angular momentum, **m**, of the emitted photon follows from the time-averaged angular-momentum density given by Eq. (16.61) of Jackson [1]:

$$\mathbf{m} = \int \frac{1}{8\pi c} \mathrm{Re}\left[\mathbf{r} \times (\mathbf{E} \times \mathbf{B}^*)\right] dx^4 = \hbar \tag{4.1}$$

Thus, the photon equation is given by the superposition of two atomic orbital-type current-vector fields at the same radius—one with electric field lines, which follow great circles and one with magnetic field lines, which follow great circles. The magnetic current-vector field is rotated $\frac{\pi}{2}$ relative to the electric current-vector field; thus, the magnetic field lines are orthogonal to the electric field lines

$$\nabla X \mathbf{E} = -\frac{\partial \mu_0 \mathbf{H}}{\partial t} \tag{4.2}$$

$$\nabla X \mathbf{H} = \frac{\partial \varepsilon_0 \mathbf{E}}{\partial t} \tag{4.3}$$

where the magnitude of the electric and magnetic fields are give by Eq. (4.1) with the boundary condition that photon angular momentum is $\hbar$.

A photon comprising a field-line pattern called a photon electric and magnetic vector field (e&mvf) similar to the atomic orbital is generated from two orthogonal great circle field lines shown in Figure 4.1 rather than two great circle current loops as in the case of the electron spin function. Consider the fields of the photon to be generated from two orthogonal great circles field lines, one for E and one for B. The Cartesian coordinate system wherein a first great circle magnetic field line lies in the x'z'-plane, and a second great circle electric field line lies in the y'z'-plane is designated the basis-set reference frame, and the xyz Cartesian-coordinate frame is the laboratory frame as given in the Atomic Orbital Equation of Motion $\ell = 0$ Based on the Current Vector Field (CVF) section.

Figure 4.1. The stationary Cartesian coordinate system xyz wherein the first great circle magnetic field line lies initially in the xz-plane, and the second great circle electric field line lies initially in the yz-plane. The rotated coordinates are primed.

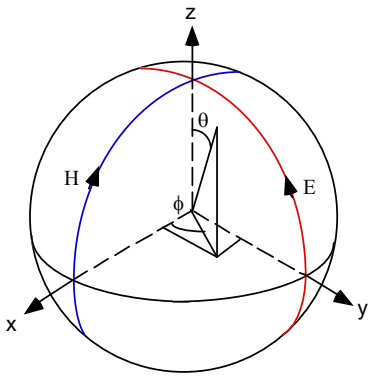

Consider a point on each of the two orthogonal great-circle field lines, one and two, in the basis-set reference frame at time zero wherein initially the first loop lies in the xz-plane, and the second loop lies in the yz-plane. Point one is at $x'=r_n$, $y'=0$, and $z'=0$ and point two is at $x'=0$, $y'=0$, and $z'=r_n$. Let point one move clockwise on the great circle in the x'z'-plane toward the positive z'-axis, and let point two move counterclockwise on the great circle in the y'z'-plane toward the negative y'-axis, as shown in Figure 4.1. The equations of motion, in the sub-basis-set reference frame are given by:

point one (H FIELD):

$$x_2'=r_n\cos(\omega_n t) \qquad y_2'=0 \qquad z_2'=r_n\sin(\omega_n t) \tag{4.4}$$

point two (E FIELD):

$$x_1'=0 \qquad y_1'=-r_n\sin(\omega_n t) \qquad z_1'=r_n\cos(\omega_n t) \tag{4.5}$$

The right-handed-circularly-polarized photon electric and magnetic vector field (RHCP photon-e&mvf) and the left-handed-circularly-polarized photon electric and magnetic vector field (LHCP photon-e&mvf) are generated by rotating the great circles about the $(\mathbf{i}_x,\mathbf{i}_y,0\mathbf{i}_z)$-axis or the $(\mathbf{i}_x,-\mathbf{i}_y,0\mathbf{i}_z)$-axis by $\frac{\pi}{2}$, respectively. The corresponding primed Cartesian coordinate system refers to the axes that rotate with the great circles relative to the xyz-system and determines the basis-element reference frame. The fields are continuous on the spherical surface, but they can be visualized by a discrete-element representation wherein each element of the field-line density function is obtained with each incremental rotation of a series over the span of $\frac{\pi}{2}$. Thus, the two points, one and two, are on the first member pair of the orthogonal great circles of an infinite series that comprises a representation of a photon.

The right-handed-circularly-polarized photon electric and magnetic vector field (RHCP photon-e&mvf) shown in Figure 4.2 is generated by the rotation of the basis elements comprising the great circle magnetic field line in the xz-plane and the great circle electric field line in the yz-plane about the $(\mathbf{i}_x,\mathbf{i}_y,0\mathbf{i}_z)$-axis by $\frac{\pi}{2}$ corresponding to the output of the matrix given by Eq. (4.6).

RHCP PHOTON E FIELD and H FIELD:

$$\begin{bmatrix}x'\\y'\\z'\end{bmatrix}=\begin{bmatrix}\frac{1}{2}+\frac{\cos\theta}{2} & \frac{1}{2}-\frac{\cos\theta}{2} & -\frac{\sin\theta}{\sqrt{2}}\\ \frac{1}{2}-\frac{\cos\theta}{2} & \frac{1}{2}+\frac{\cos\theta}{2} & \frac{\sin\theta}{\sqrt{2}}\\ \frac{\sin\theta}{\sqrt{2}} & -\frac{\sin\theta}{\sqrt{2}} & \cos\theta\end{bmatrix}\bullet\left(\begin{bmatrix}0\\ r_n\cos\phi\\ r_n\sin\phi\end{bmatrix}_{\text{Red}}+\begin{bmatrix}r_n\cos\phi\\ 0\\ r_n\sin\phi\end{bmatrix}_{\text{Blue}}\right) \tag{4.6}$$

The left-handed-circularly-polarized photon electric and magnetic vector field (LHCP photon-e&mvf) is generated by the rotation of the basis elements comprising the great circle magnetic field line in the xz-plane and the great circle electric field line in the yz-plane about the $(\mathbf{i}_x,-\mathbf{i}_y,0\mathbf{i}_z)$-axis by $\frac{\pi}{2}$ corresponding to the output of the matrix given by Eq. (4.7). The mirror image of the RHCP photon-e&mvf, the left-handed circularly polarized photon-e&mvf, is shown with three orthogonal views in Figure 4.3.

LHCP PHOTON E FIELD and H FIELD:

$$\begin{bmatrix} x' \\ y' \\ z' \end{bmatrix} = \begin{bmatrix} \frac{1}{2}+\frac{\cos\theta}{2} & -\frac{1}{2}+\frac{\cos\theta}{2} & \frac{\sin\theta}{\sqrt{2}} \\ -\frac{1}{2}+\frac{\cos\theta}{2} & \frac{1}{2}+\frac{\cos\theta}{2} & \frac{\sin\theta}{\sqrt{2}} \\ -\frac{\sin\theta}{\sqrt{2}} & -\frac{\sin\theta}{\sqrt{2}} & \cos\theta \end{bmatrix} \bullet \left(\begin{bmatrix} 0 \\ r_n\cos\phi \\ r_n\sin\phi \end{bmatrix}_{\text{Red}} + \begin{bmatrix} r_n\cos\phi \\ 0 \\ r_n\sin\phi \end{bmatrix}_{\text{Blue}} \right) \tag{4.7}$$

Figure 4.2. The field-line pattern given by Eq. (4.6) from three orthogonal perspectives of a RHCP photon-e&mvf corresponding to the first great circle magnetic field line and the second great circle electric field line shown with 6 degree increments of the angle θ. (Electric field lines red; Magnetic field lines blue).

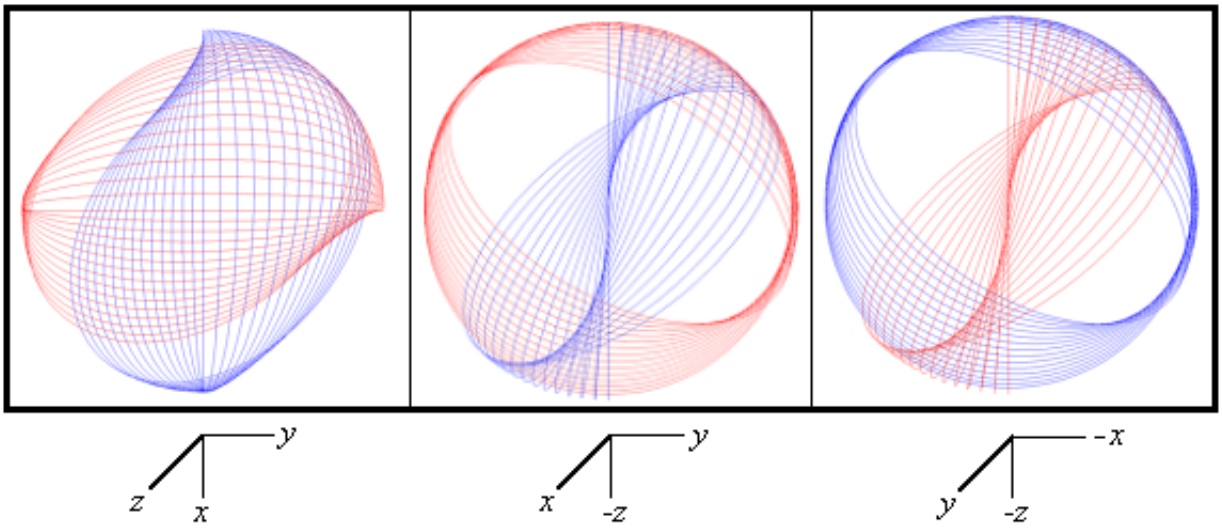

Figure 4.3. The field-line pattern given by Eq. (4.7) from three orthogonal perspectives of a left-handed circularly polarized photon-e&mvf corresponding to the first great circle magnetic field line, and the second great circle electric field line shown with 6 degree increments of the angle θ. (Electric field lines red; Magnetic field lines blue).

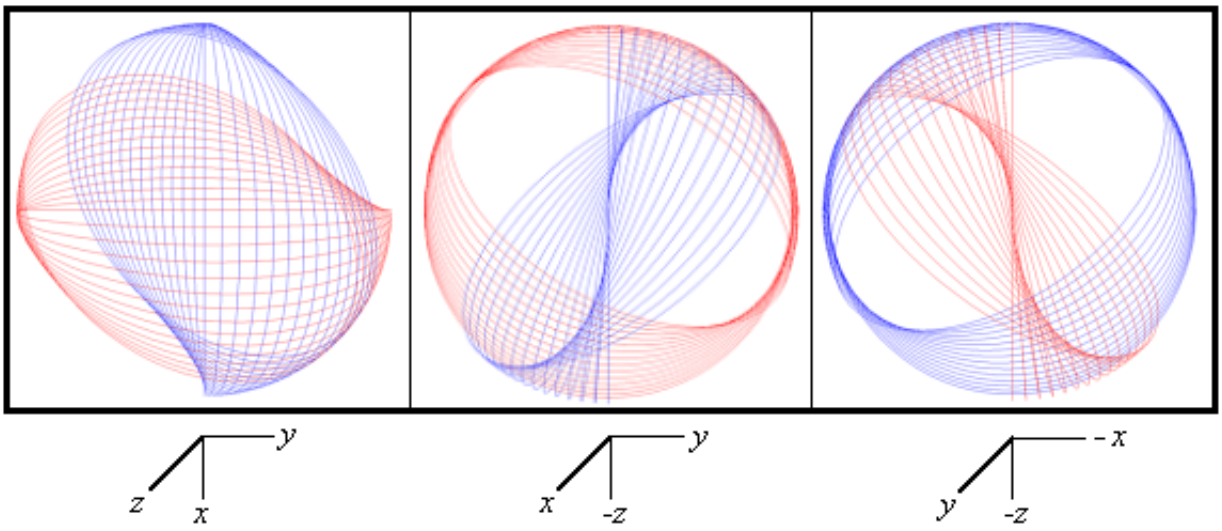

FIELDS BASED ON INVARIANCE UNDER GAUSS' INTEGRAL LAW

The angular velocity of the photon-e&mvf is equal to the change in angular velocity of the electron atomic orbital for a de-excitation from the energy level with principal quantum number $n = n_i$ to $n = n_f$, where $n_i > n_f$, given by Eq. (2.21) for $n_f = 1$. From Eq. (2.22), the photon is an electromagnetic wave that carries energy, E, given by:

$$E = \hbar\omega \tag{4.8}$$

Given the relationships, Eqs. (4.2) and (4.3) for the electric and magnetic fields, the solution of the classical wave equation Eq. (I.45) requires that the linear velocity at each point along a great circle of the photon-e&mvf is c,

$$c = \sqrt{\frac{1}{\varepsilon_0 \mu_0}} \tag{4.9}$$

and, that the velocity of the photon in the lab frame is c. Therefore, with the velocity addition property of special relativity, the velocity in all frames of reference is c including the rest frame. Thus, the zero rest mass concept of the photon can be discarded. The "mass" of the photon in any frame is actually momentum contained in its electric and magnetic fields as given by Eqs. (2.150) and (4.1). An additional consequence of the light speed in all frames is that the radius of the photon is invariant. The field lines in the lab frame follow from the relativistic invariance of charge as given by Purcell [2]. The relationship between the relativistic velocity and the electric field of a moving charge is shown schematically in Figure 4.4A and 4.4B.

Figure 4.4A. The electric field of a moving point charge ($v = \frac{1}{3}c$).

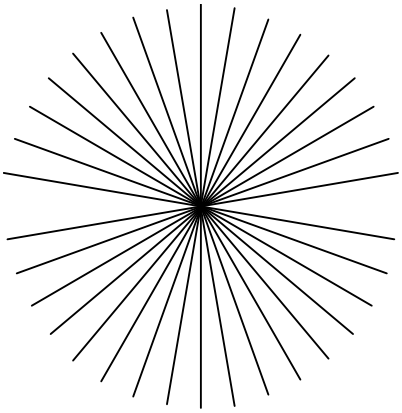

Figure 4.4B. The electric field of a moving point charge ($v = \frac{4}{5}c$).

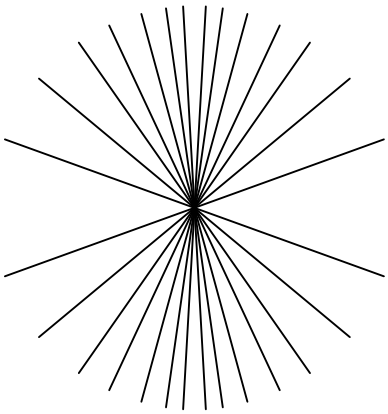

The field invariance under Gauss' Integral Law also applies to the fields of the photon-e&mvf. From Eqs. (4.4-4.7) and as shown in Appendix V, the electric and magnetic fields are harmonic in space and time wherein $c = \lambda \frac{\omega}{2\pi}$ is satisfied which is a solution of the wave equation for an electromagnetic wave, and the fields are orthogonal such that Faraday's and Ampere's Laws are satisfied. The photon equation in the lab frame (shown in Figures 4.5 and 4.6) of a right-handed circularly polarized photon-e&mvf is:

$$\mathbf{E} = \mathbf{E}_0 \left[\mathbf{x} + i\mathbf{y}\right] e^{-jk_z z} e^{-j\omega t}$$
$$\mathbf{H} = \left(\frac{\mathbf{E}_0}{\eta}\right)\left[\mathbf{y} - i\mathbf{x}\right] e^{-jk_z z} e^{-j\omega t} = \mathbf{E}_0 \sqrt{\frac{\varepsilon}{\mu}}\left[\mathbf{y} - i\mathbf{x}\right] e^{-jk_z z} e^{-j\omega t} \tag{4.10}$$

with a wavelength of:

$$\lambda = 2\pi \frac{c}{\omega} \tag{4.11}$$

The relationship between the photon-e&mvf radius and wavelength is:

$$2r_{photon} = \lambda \tag{4.12}$$

The wavelength (radius) changes for moving observers according to the Doppler formula of Lorentz transforms. In terms of Eqs. (4.4-4.7), E_0 of the photon is given by the boundary condition that the angular momentum given by Eq. (4.1) is $\hbar$; thus, the energy is given by Planck's equation (Eq. (2.18)) as shown by Eqs. (2.56-2.64). The relationship between Planck's equation and Maxwell's equations is also consistent with regard to the energies of excited states as given by Eqs. (2.18-2.22).

Figure 4.5. The direction of rotation of the electric field lines of a right-handed circularly polarized photon-e&mvf as seen along the axis of propagation in the lab inertial reference frame as it passes a fixed point.

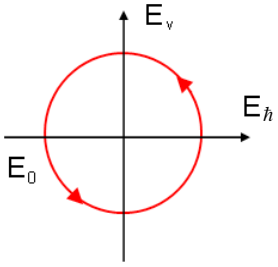

Figure 4.6. The electric field rotation as a function of z of a right-handed circularly polarized photon-e&mvf as seen transverse to the z-axis, axis of propagation, in the lab inertial reference frame at a fixed time wherein $2r_{photon} = \lambda$

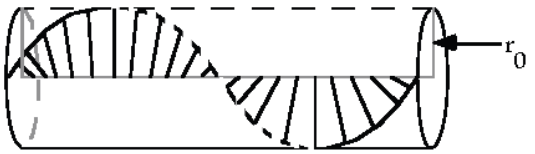

The cross-sectional area, σ, transverse to the propagation direction of the photon is

$$\sigma = \pi\left[\frac{\lambda}{2}\right]^2 \tag{4.13}$$

The geometric cross section (Eq. (4.13)) is consistent with the Rayleigh scattering formula, which is derived from Maxwell's equations [3].

The photon-e&mvf may comprise basis element magnetic and electric field lines that are constant in magnitude as a function of angle over the surface, or the magnitude of the fields of the basis elements may vary as a function of angular position (θ,ϕ) on the photon-e&mvf. The general photon equation for the electric field in its frame is:

$$\mathbf{E}_{\theta,\phi} = \frac{e}{4\pi\varepsilon_0 r_{photon}^2}\left(-1+\frac{1}{n}\left[Y_0^0(\theta,\phi)+\mathrm{Re}\left\{Y_\ell^m(\theta,\phi)e^{im\omega_n t}\right\}\right]\right)\delta\left(r-\frac{\lambda}{2\pi}\right) \tag{4.14}$$

where r_{photon} is the radius of the photon-e&mvf and $\omega_n = \frac{2\pi c}{\lambda}$ is the photon angular velocity which is equal to $\Delta\omega$, the change in atomic orbital angular velocity given by Eq. (2.21) and the light speed changes the direction of the field lines to the transverse direction.

Similarly photons are emitted when an electron is bound. Using Eq. (1.34) for the photon and the electron wave relationships for the initial conditions of an unbound electron at rest, the ratio of the linear velocity of the subsequently bound electron to the emitted free-space photon is given by:

$$\frac{v_n}{c_{photon}} = \frac{\lambda_n\frac{\omega_n}{2\pi}}{\lambda_{photon}\frac{\omega_{photon}}{2\pi}} = \frac{\lambda_n}{\lambda_{photon}} = \frac{\pi r_n}{r_{photon}} \tag{4.15}$$

where the n subscripts refer to atomic orbital quantities and the far-right-hand-side relationship follows from Eq. (2.2) and Eq. (4.12). From Eq. (4.15), the relations between the free space photon wavelength, radius, and velocity and the corresponding parameters of a free electron as it is bound are:

(1) r_{photon}, the radius of the photon-e&mvf, is equal to $r_n\pi\frac{c}{v_n} = na_H\pi\frac{c}{v_n}$, the electron atomic orbital radius given by Eqs. (2.2) and (2.5) times the product of π and the ratio of the speed of light c and v_n, the velocity of the atomic orbital given by Eq. (1.35),

(2) λ_{photon}, the photon wavelength, is equal to $\lambda_n\frac{c}{v_n}$, where λ_n is the atomic orbital de Broglie wavelength, and

(3) $\omega_{photon} = \frac{2\pi c}{\lambda}$, the photon angular velocity, is equal to ω_n, the atomic orbital angular velocity given by Eq. (1.36).

The magnetic field photon-e&mvf is given by Eqs. (4.14) and (4.2). In the case of $Y_\ell^m(\theta,\phi) = 0$ in Eq. (4.14), a right-handed and a left-handed circularly polarized photon-e&mvf are superimposed to comprise a linearly polarized photon-e&mvf. A right-handed or left-handed circularly polarized photon is obtained by attenuating the oppositely polarized component. For Eq. (4.14), the power density per unit area, **S**, is:

$$\mathbf{S} = \mathbf{E}\times\mathbf{B}^* \tag{4.16}$$

LINEAR POLARIZED PHOTONS

The linearly polarized photon is given by the superposition of the right-handed circularly polarized photon-e&mvf shown in Figure 4.2 and its mirror image, the left-handed circularly polarized photon-e&mvf, shown in Figure 4.3. The field-line pattern of a linearly polarized (LP) photon-e&mvf shown from the perspective of looking along the z-axis is shown in Figure 4.7. Thus, the LP photon-e&mvf is obtained by rotation of the basis-element-great-circle electric and magnetic fields lines about each of the $(\mathbf{i}_x, \mathbf{i}_y, 0\mathbf{i}_z)$- and $(\mathbf{i}_x, -\mathbf{i}_y, 0\mathbf{i}_z)$-axes by $\frac{\pi}{2}$. The analytical functions and matrices to generate the RHCP, LHCP, and LP photon-e&mvfs are given in Appendix V, and the RHCP, LHCP, and LP photon-e&mvfs are visually demonstrated by computer simulations [4]. The conditions whereby a photon becomes an electron and a positron are given in the Pair Production and the Leptons sections.

Figure 4.7. The field-line pattern of a linearly polarized photon-e&mvf shown with 6 degree increments of the angle θ from the perspective of looking along the z-axis. (Electric field lines red; Magnetic field lines blue).

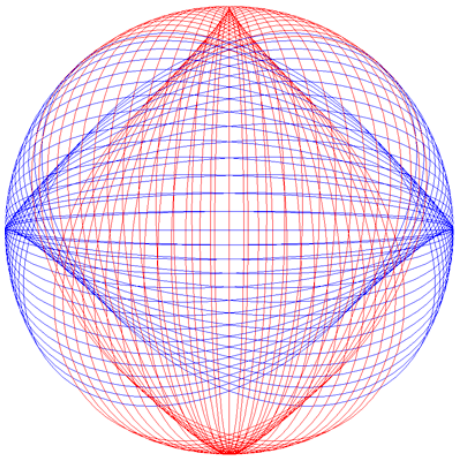

The linearly polarized photon-e&mvf equation in the lab frame is

$$\mathbf{E} = E_0 e^{-jk_z z} e^{-j\omega t} \tag{4.17}$$

In the case of $Y_\ell^m(\theta,\phi) \neq 0$ in Eq. (4.14), a right-handed and a left-handed elliptically polarized photon-e&mvf are superimposed to comprise a linearly polarized photon-e&mvf with the plane of polarization rotated relative to the case of $Y_\ell^m(\theta,\phi) = 0$. A right-handed or left-handed elliptically polarized photon is obtained by attenuating the oppositely polarized component.

SPHERICAL WAVE

Photons superimpose and the amplitude due to N photons is:

$$\mathbf{E}_{total} = \sum_{n=1}^{N} \frac{e^{-ik_r|\mathbf{r}-\mathbf{r}'|}}{4\pi|\mathbf{r}-\mathbf{r}'|} f(\theta,\phi) \tag{4.18}$$

When the observation point is very far from the source as shown in Figure 4.8, the distance in Eq. (4.18) becomes:

$$|\mathbf{r}-\mathbf{r}'| \approx r - \hat{\mathbf{r}} \bullet \mathbf{r}' \tag{4.19}$$

where $\hat{\mathbf{r}}$ is the radial unit vector. Substitution of Eq. (4.19) into Eq. (4.18) gives:

$$\mathbf{E}_{total} = \frac{e^{-ikr}}{r} \sum_{n=1}^{N} e^{-i\mathbf{k}\cdot\mathbf{r}'} f(\theta,\phi) \tag{4.20}$$

where we neglect $\hat{\mathbf{r}} \bullet \mathbf{r}'$ in the denominator, and

$$\mathbf{k} = \hat{\mathbf{r}} k \tag{4.21}$$

For an assembly of incoherent emitters

$$\sum_{n=1}^{N} e^{i\mathbf{k}\cdot\mathbf{r}'} f(\theta,\phi) = 1 \tag{4.22}$$

Thus, in the far field, the emitted wave is a spherical wave

$$\mathbf{E}_{total} = E_0 \frac{e^{-ikr}}{r} \tag{4.23}$$

which is shown by Bonham to be required in order to insure continuity of power flow for wavelets from a single source [5]. Also, as a conservation law at the photon level, the density of photons decreases as the number of photons divided by the area of the outgoing spherical wave front. The Green Function, (Eq. (6.62) of Jackson [1]) is given as the solution of the wave equation

(Eq. (6.58) of Jackson [1]). Thus, the superposition of photons gives the classical result. As r goes to infinity, the spherical wave given by Eq. (4.23) becomes a plane wave. The double slit interference pattern is derived in Eqs. (8.15-8.23). From the equation of a photon (Eqs. (4.4-4.7), the wave-particle duality arises naturally. The energy is always given by Planck's equation; yet, an interference pattern is observed when photons add over time or space.

Figure 4.8. Far field approximation.

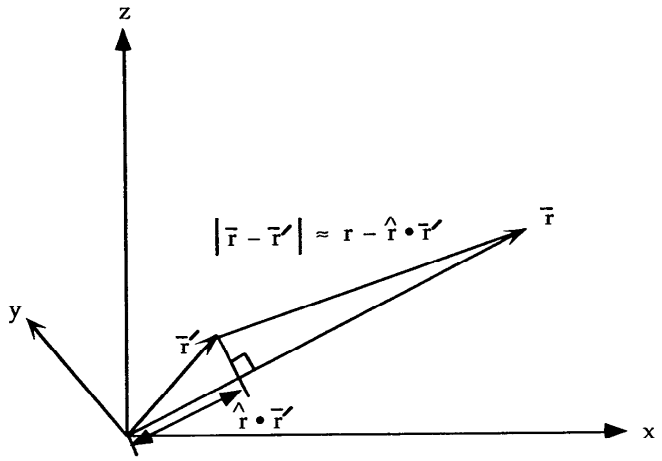

The photon spin angular momentum corresponding to the first term of Eq. (4.14) and the orbital angular momentum corresponding to the second term of Eq. (4.14) are conserved during electronic excitation as described in the Excited States of the One-Electron Atom (Quantization) section. And, the spin and orbital angular momentum of photons superimpose to give the classical result. For example, second harmonic generation has been obtained by Dholakia et al. [6] by use of Laguerre-Gaussian beams in a variety of mode orders. Each mode becomes doubled in frequency and transformed to a higher order, which is shown to be a consequence of the phase-matching conditions. The experiment is consistent with the interpretation that the orbital angular momentum of the Laguerre-Gaussian mode is directly proportional to the azimuthal mode index ℓ where each photon possesses orbital angular momentum of $\ell\hbar$ in addition to any spin angular momentum due to its state of polarization.

The macroscopic Maxwell's equations for reflection and refraction arise from the superposition of individual photon behavior at a bulk material surface. A totally internally reflected photon incident at an angle greater than the critical angle giving rise to a surface wave and an evanescent field arises from charge separation in the reflecting matter. Free or polarization current and charge produce the corresponding purely decaying electric and magnetic fields.

PHOTON TORPEDOES

Recent evidence suggests that energy packets like photon torpedoes are creeping toward reality [7]. The possibility of solutions of the scalar wave equation and Maxwell's equations that describe localized, slowly decaying transmission of energy in spacetime has been suggested by several groups in recent years. These include exact pulse solutions such as focus wave modes [8-9], electromagnetic directed energy pulse trains [10], splash modes [11], transient beams [12], continuous-wave modes (Bessel beams) [13], and asymptotic fields (electromagnetic missiles [14], electromagnetic bullets [15], Gaussian wave packets [16]).

A macroscopic surface current having a distribution given as an atomic orbital transition comprises a means to emit electromagnetic energy having electric and magnetic field lines which comprise a photon-e&mvf. In this case, energy is not diminished in intensity as the electromagnetic wave propagates through space. Thus, "photon torpedoes" can be realized. High power densities can be achieved by increasing the magnitude of the electric and magnetic fields of the photon where the energy is given by Eq. (1.263) and Eq. (1.154). Also, neutrino-type photons described in the Weak Nuclear Force: Beta Decay of the Neutron section represent a means to transfer energy without scattering or attenuation between matched emitters and receivers. Applications in both cases include power transfer, communications, and weapons. An example of a device that produces photon torpedoes is a mode-locked femtosecond laser.

PHOTOELECTRIC EFFECT

Electrons are ejected, and a photocurrent is observed when a clean surface of a metal such as sodium is irradiated with ultraviolet light in the wavelength range 2000–400 Å in an evacuated vessel. The photoelectric current, which is the amount of charge arriving at a collection plate per unit time, is proportional to the rate of liberation of electrons from the metal surface; that is, if Δn_e is the number of free electrons produced in the time interval Δt and i is the current,

$$\frac{\Delta n_e}{\Delta t} = \frac{i}{e} \tag{4.24}$$

To determine the velocity with which the photoelectrons travel, a potential is applied to a grid mounted between the metal surface and the collection plate. The potential creates an electric field, which decelerates the photoelectrons. As the potential difference between the grid and the emitting metal is increased, a *stopping voltage* V_s is observed, the value above which the electrons are stopped before they reach the plate and the current ceases to flow. At the stopping voltage, the initial kinetic energy of the photoelectrons liberated from the metal by the light has all been converted to potential energy; thus

$$\frac{1}{2}mv^2 = eV_s \tag{4.25}$$

The number of electrons produced per second and their maximum kinetic energy as functions of the intensity I and frequency ν of the incident light is determined by measuring i and V_s.

Physicists of the early 20th century had a misconception regarding classical wave theory and the photoelectric effect that has been promulgated to the present. They erroneously predicted that the energy of the radiation should be continuously absorbed by the electrons in the metal. After an electron has absorbed an amount of energy in excess of its binding energy eV_0, it may be ejected from the surface. The adjustable potential V_s is used to stop electrons whose energy exceeds eV_0 by eV_s or less. Since the intensity I of the light is the rate at which energy is propagated by the radiation waves, an increase in intensity should increase the average kinetic energy of ejected electrons which implies that the stopping voltage V_s is proportional to I.

It is experimentally observed that V_s is proportional to the *frequency* of the light and *independent of the intensity*. As shown in Figure 4.9, if the frequency ν is below a certain threshold value ν_0, no photoelectric current is produced. At frequencies greater than ν_0, the empirical equation for the stopping voltage is:

$$V_s = k(\nu - \nu_0) \tag{4.26}$$

where k is a constant independent of the metal used, but ν_0 varies from one metal to another. Although there is no relation between V_s and the light intensity, it is found that the photoelectric current, and therefore the number of electrons liberated per second, is proportional to I.

Figure 4.9. The stopping voltage V_s of photoelectrons as a function of the frequency ν of the incident light.

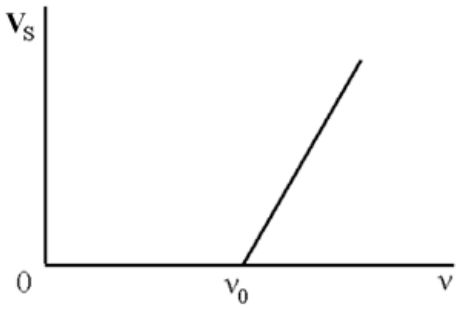

These results are *not* in disagreement with expectations from the classical wave theory based on the equations of a photon (Eqs. (4.4-4.7)). The electric and magnetic fields of a photon carry $\hbar$ of angular momentum as given by Eq. (4.1), and the corresponding energy is given by Planck's equation (Eq. (4.8)). As shown in the Excited States of the One-Electron Atom (Quantization) section, the angular momentum of the photon is conserved [1] for the solutions for the resonant photons and excited state electron functions. It can be demonstrated that the resonance condition between these corresponding frequencies is to be satisfied in order to have a net change of the energy field [17]. Thus, the correspondence principle holds. That is the change in angular frequency of the electron is equal to the angular frequency of the resonant photon that excites the resonator cavity mode corresponding to the transition, and the energy is given by Planck's equation. In the case of photoelectrons, the resonant transition is from a bound state in the metal to a continuum level. Thus, a photon of energy $h\nu$ strikes a bound electron, which may absorb the photon energy. If $h\nu$ is greater than the binding energy (or *work function*) eV_0, the electron is liberated. Thus, the threshold frequency ν_0 is given by:

$$\nu_0 = \frac{eV_0}{h} \tag{4.27}$$

Since V_0 is a characteristic of the particular metal, which is used in the experiment, ν_0 depends upon the metal, in accordance with the experimentally observed result.

For a photon of energy $h\nu$, the total energy of the excited electron is $h\nu$, with the excess over the potential energy eV_0 required to escape from the metal appearing as kinetic energy. Conservation of energy requires that the kinetic energy is the difference between the energy of the absorbed photon and the work function of the metal, which is the binding energy. The relationship is:

$$\frac{1}{2}mv^2 = h\nu - eV_0 = eV_s \tag{4.28}$$

which is identical to Eq. (4.26), with $k = h/e$. The photoelectric effect provides another means to determine Planck's constant h originally used by Planck for blackbody radiation and by Bohr for the hydrogen spectrum.

Furthermore, since the energy of each photon is $h\nu$, the intensity of the radiation is not related to the energy of each photon, but instead determines the number of photons striking the metal surface per second. The rate of electron ejection is expected to be proportional to the rate at which the photons impinge upon the metal surface; thus, an increase in light intensity is predicted to increase the photoelectric current, as observed. Because the amount of energy absorbed by an electron is $h\nu$ regardless of the rate at which photons impinge on the surface, the kinetic energy of the ejected electrons should be independent of the intensity of the light. Thus, all of the predictions of the photon mechanism for the photoelectric effect are in agreement with the experimental results.

COMPTON EFFECT

An experiment that is related to the photoelectric effect is the Compton effect. This experiment, which provides more detailed information about the interaction of radiation and matter was performed in the early 1920's and analyzed by Compton in 1923. The experiment comprises the irradiation of a sample of material such as a paraffin hydrocarbon with X-rays or γ-rays, high-frequency radiation. The photons are scattered from bound electrons, which are ionized. The wavelength of the scattered radiation and the energy of the emitted electron are determined as a function of angle, relative to the incident beam. It is found that the radiation scattered from the material contains not only wavelengths equal to that of the incident radiation λ, but also wavelengths of the order of a few hundredths of an Angstrom longer than λ. The dependence of the scattered wavelength λ' upon the angle θ between the primary and scattered beams is found to be:

$$\lambda' = \lambda + k \sin^2\left(\frac{\theta}{2}\right) \tag{4.29}$$

where k is a constant.

Physicists of the early 20th century had a misconception regarding classical wave theory and the Compton effect that has been promulgated to the present. They erroneously predicted that the wavelength of the radiation would increase based on the Doppler effect since an electron in the sample would be accelerated by the impinging radiation and would therefore emit waves with longer wavelengths. The Doppler effect does not correctly explain the observations, however, since (a) the Doppler shift is proportional to the wavelength of the primary radiation and (b) the Doppler shift increases with the electron velocity and therefore should increase with time, since the electrons are accelerated continuously while they absorb energy during the irradiation. Neither of these predictions is corroborated by the experimental results, not as a consequence of the failure of classical theory, but because of an erroneous misconception about the nature of the photon and its interaction with matter. As was the case for the photoelectric effect, the observations can be explained quantitatively by the photon theory of radiation given *supra* and the laws of conservation of energy and momentum for particles including photons and electrons.

According to Eqs. (2.148-2.150), the incident photon with wavelength λ and frequency $\nu = c/\lambda$ has a momentum $h\nu/c$. Correspondingly, the scattered photon, which has a longer wavelength λ', and therefore a lower frequency $\nu' = c'/\lambda'$, has a lower momentum $h\nu'/c$. Since ν is in the X-ray region $(\lambda \sim 1\text{–}10\ \text{Å})$, the energy $(h\nu \sim 1000\ \text{eV})$ is so much greater than the binding energy of the electrons $(\approx 10\ \text{eV})$ that to a first approximation the latter be neglected. Thus, the electron is ejected in the direction ϕ with a momentum mv, which is calculable from an energy and momentum balance for the process as shown in Figure 4.10. The classical equations of conservation of energy and of the two components of the linear momentum are:

$$h\nu = h\nu' + \frac{1}{2}m_e v^2 \qquad \text{(energy)} \tag{4.30}$$

$$\frac{h\nu}{c} = \frac{h\nu'}{c}\cos\theta + m_e v \cos\phi \qquad (x \text{ component of momentum}) \tag{4.31}$$

$$0 = \frac{h\nu'}{c}\sin\theta - m_e v \sin\phi \qquad (y \text{ component of momentum}) \tag{4.32}$$

Figure 4.10. The Compton effect based on conservation of energy and momentum of a scattered photon and an electron.

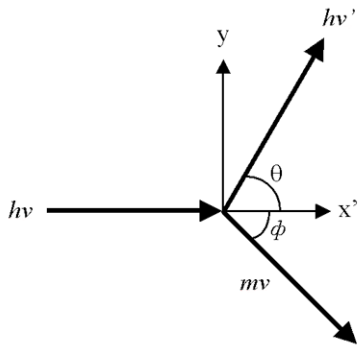

Eliminating ν and ϕ from these equations, introducing λ by the definition $\lambda = c/\nu$, and making the approximation that $\lambda\lambda' \approx \lambda^2$, gives:

$$\Delta\lambda = \lambda' - \lambda = 2\frac{h}{m_e c}\sin^2\left(\frac{\theta}{2}\right) \tag{4.33}$$

in agreement with Eq. (4.29). For λ in Angstroms, Eq. (4.33) gives:

$$\Delta\lambda = 0.0485\ \sin^2\left(\frac{\theta}{2}\right) \tag{4.34}$$

If the ejected electron is treated relativistically with its total energy given by Eq. (34.17):

$$E = \left(m_e^2c^4 + p_e^2c^2\right)^{1/2} = m_e c^2\sqrt{1+\left(\frac{v_e}{c}\right)^2} \tag{4.35}$$

and the kinetic energy is obtained by subtracting the rest energy $m_e c^2$, Eq. (4.33) can be derived without using the approximation that $\lambda' \approx \lambda$. The maximum shift is seen to occur for $\theta = \pi$, where $\Delta\lambda = 0.0485$ Å.

The photon mechanism was tested by using γ-rays of energy $\approx 10^6$ eV, and the scattered photon and the Compton electron were recorded by means of scintillation counters. Cross and Ramsey [18] found that the angles ϕ and θ for an electron and a photon which were simultaneously detected were within $\pm 1^\circ$ of those required by the conservation laws (Eqs. 4.30-4.32)).

The analysis of the photoelectric and Compton effects shows that the particle viewpoint and Newtonian mechanics lead to a simple and quantitatively correct interpretation of these experiments, and that predictions based upon the classical wave theory are *not* wrong, but must be understood from the nature of the photon given by Eqs. (4.4-4.7). Individual photons behave as particles with energy given by Planck's equation (Eq. (4.8)). As shown by Eqs. (4.18-4.23), photons superimpose to give a spherical wave which gives rise to certain other phenomena such as diffraction and interference which are typically ascribed to wave theory with waves as an independent aspect of photons. The character exhibited by radiation, whether wave-like or particle-like, depends upon the type of experiment that is done. If the interaction of radiation with matter produces a measurable change in the matter, such as the ejection of an electron, the phenomenon appears to require the photon theory for its interpretation. If the interaction produces a measurable change in the spatial distribution of the radiation, such as diffraction at a slit, but produces no measurable change in the matter, invoking the wave theory seems appropriate as shown in the Classical Scattering of Electromagnetic Radiation section. Superficially, these results suggest that a synthesis of the two points of view is required which takes into account the nature of the experiment being analyzed; that is, the measuring process itself must be included in the theory. In actuality, both particle and wave aspects arise naturally from the particle-like photons which superimpose in time or space to form a wave which accounts precisely for the wave-particle duality of light.

TRANSITIONS

Other interactions involving electromagnetic radiation and matter are given classically wherein the photon carries $\hbar$ of angular momentum in its electric and magnetic fields as given by Eq. (4.1) with a corresponding energy given by Planck's equation (Eq. (4.8)). Bremsstrahlung radiation is given classically as radiation due to acceleration of charged particles by Jackson [19]. *Cherenkov radiation* occurs when charges moving at constant velocity in a medium different from vacuum possess spacetime Fourier components of the current that are synchronous with a wave traveling at the speed of light as given by a radiative condition derived from Maxwell's equations by Haus [20]. That is spacetime harmonics of $\frac{\omega_n}{c}\sqrt{\frac{\varepsilon}{\varepsilon_0}} = k$ do exist for which the Fourier transform of the current-density function is nonzero [20].

Although Einstein did not anticipate the physics of the lifetimes of excited states as given in the State Lifetimes and Line Intensities section, lasing, or laser devices, the concept of stimulated emission originated in 1917, ten years before the Schrödinger equation was postulated, when Einstein proposed that Planck's formula for blackbody radiation could better curve fit the data if an ensemble of atoms with quantized energy levels underwent stimulated as well as spontaneous emission [21]. Stimulated emission can occur for an inverted population in a suitable resonator cavity to such an extent that amplification or lasing occurs. The *maser* and its extension to shorter wavelengths, the *laser*, are predicted by Maxwell's equations[1] as shown by Lamb [23] and Townes [24], respectively. From this approach, Townes invented first the maser, and he latter extended his work to optical wavelengths with the invention of the laser. The B_{ki} coefficient for lasing can be calculated from the A_{ki} coefficient using Eq. (6) of Carmichael [25]. The A_{ki} coefficient given by Eq. (2.108) is calculated from the excited-state electron source current in the State Lifetimes and Line Intensities section.

Photons possess both wave and particle characteristics. The physical basis of the wave behavior is given in the Spherical Wave section, and particle behavior is observed during the photoelectron and Compton effects given in the corresponding sections. Another manifestation of particle behavior is the absorption and emission of indivisible photons each having an irreducible quantized angular momentum of $\hbar$ (Eq. (4.1)). Electrons and photons both have conserved angular momentum of $\hbar$ such that the inalienability of the quantization is intrinsic to the transition partners and the conservative physical laws. Except for the case of particle production, the radius of two-dimensional sphere of the photon comprising the photon-e&mvf and being proportional to the photon wavelength is typically orders of magnitude larger than the dimensions of the photon-absorbing electron (Eqs. (2.98-2.101)). The photon travels at light speed and a collision with an electron can only initially involve a small fraction of the photon-e&mvf; yet, the entire photon is either elastically scattered or entirely absorbed. Consider the relationship between the radius and wavelength of an electron and a photon of the resonant frequency that excites an electronic transition of the electron to form an electronic excited state given by Eq. (4.15) wherein the photon angular frequency and energy match the change in energy and angular frequency of the electron that is excited by the photon (Eqs. (2.18-2.22)). When the photon collides with the electron, the photon excites a resonator mode of the spherical superconducting electron resonator cavity such that the photon wavelength decreases to match the dimensions of the electron absorbing the photon akin to the process of total internal reflection wherein the two-dimensional ensemble of field lines propagates along the inner surface of the electron membrane. In the case of a macrocavity excitation, the field comprises the superposition of many photons with fields ending on time-dependent surface source charges and currents. In contrast, each electric field line of the quantum excitation by a single photon is closed onto itself. Moreover, uniquely the energy in the electric and magnetic fields of a free-space photon are equal, and the magnetic field is dependent on the electric field with both propagating at light speed. Consequently, as the photon initially traveling in free space at the speed of light is trapped by the atomic, ionic, or molecular electron undergoing excitation, the photon magnetic field lines transition to electric field lines. The result is a corresponding transition-state-evf (TS-evf) comprising only the electric field lines of the free space photon with the intensity increased by a factor or $\sqrt{2}$ corresponding an increase in the electric energy by a factor of 2 according to Eq. (1.189). For example, consider the left-handed-circularly-polarized photon electric and magnetic vector field (LHCP photon-e&mvf) given by the output of the matrix of Eq. (4.7) and shown in Figure 4.3. With the transition of the magnetic field to electric field according to Faraday's law (Eq. (4.2)), the corresponding left-handed-transition-state electric vector field (LHTS-evf) is generated by the rotation of a basis element comprising a great circle electric field line in the yz-plane about the $\left(\mathbf{i}_x,-\mathbf{i}_y,0\mathbf{i}_z\right)$-axis by $\frac{\pi}{2}$ wherein the radius r_n is equal to the spherical radius of the excited state atomic or ionic electron or the ellipsoidal radius ξ_n of the excited state molecular orbital, respectively.

[1] The development of the laser was impeded by quantum mechanics since its existence disproves the Heisenberg Uncertainty Principle as discussed by Carver Meade [22]:

> As late as 1956, Bohr and Von Neumann, the paragons of quantum theory, arrived at the Columbia laboratories of Charles Townes, who was in the process of describing his invention. With the transistor, the laser is one of the most important inventions of the twentieth century. Designed into every CD player and long-distance telephone connection, lasers today are manufactured by the billions. At the heart of laser action is perfect alignment of the crests and troughs of myriad waves of light. Their location and momentum must be theoretically knowable. But this violates the holiest canon of Copenhagen theory: Heisenberg Uncertainty. Bohr and Von Neumann proved to be true believers in Heisenberg's rule. Both denied that the laser was possible. When Townes showed them one in operation, they retreated artfully.

LH TRANSITION STATE E FIELD:

$$\begin{bmatrix} x' \\ y' \\ z' \end{bmatrix} = \sqrt{2}\begin{bmatrix} \frac{1}{2}+\frac{\cos\theta}{2} & -\frac{1}{2}+\frac{\cos\theta}{2} & \frac{\sin\theta}{\sqrt{2}} \\ -\frac{1}{2}+\frac{\cos\theta}{2} & \frac{1}{2}+\frac{\cos\theta}{2} & \frac{\sin\theta}{\sqrt{2}} \\ -\frac{\sin\theta}{\sqrt{2}} & -\frac{\sin\theta}{\sqrt{2}} & \cos\theta \end{bmatrix} \bullet \begin{bmatrix} 0 \\ r_n\cos\phi \\ r_n\sin\phi \end{bmatrix}_{\text{Red}} ;\ \theta \text{ to } \frac{\pi}{2} \tag{4.36}$$

Free space photons, transition states, and excited state photons carry electric field as given by Eqs. (4.6), (4.7), (4.36), and (2.15). The directions of field lines change with relative motion as required by special relativity. They increase in the direction perpendicular to the propagation direction. As shown by Eq. (4.9), the linear velocity of each point along a great circle of the photon atomic orbital is c. The same applies to the transition state. And, as shown in the Special Relativistic Correction to the Ionization Energies section and by Eq. (1.280), when the velocity along a great circle is light speed, the motion relative to the non-light speed frame is purely radial. In the case of the electric field lines of a trapped resonant photon of an excited state, the relativistic electric field is radial. It is given by Eq. (2.15), and it exists only at $\delta(r-r_n)$ wherein r_n is the radius of the excited electron.

The bound electron is an equipotential, equi-energy surface comprising the uniform current density function $Y_0^0(\theta,\phi)$. The radial field of the TS-evf only covers 1/4th of the inner surface of the electron membrane. Thus, the imbalance in central force on the spherical surface gives rise to a rotation over the range of $\frac{\pi}{2}$ to 2π about the axis that forms the TS-evf. In the case of excitation by a RHCP photon, the rotation is about the $(\mathbf{i}_x,\mathbf{i}_y,0\mathbf{i}_z)$-axis to form the corresponding right-handed transition state basis element electric vector field (RHTSBE-evf). In turn, the RHTSBE-evf undergoes a transition that distributes the field lines uniformly over the surface of a spherical electric field vector membrane corresponding to a convolution operator acting on the RHTSBE-evf about the $\left(\frac{1}{\sqrt{2}}\mathbf{i}_x,\frac{1}{\sqrt{2}}\mathbf{i}_y,\mathbf{i}_z\right)$ -axis. In the case of excitation by a LHCP photon the rotation is about the $(\mathbf{i}_x,-\mathbf{i}_y,0\mathbf{i}_z)$-axis to form the corresponding left-handed transition state basis element electric vector field (LHTSBE-evf). Likewise, the LHTSBE-evf is transitioned to the uniform field distribution by the convolution operator acting on the LHTSBE-evf about the $\left(\frac{1}{\sqrt{2}}\mathbf{i}_x,-\frac{1}{\sqrt{2}}\mathbf{i}_y,\mathbf{i}_z\right)$-axis. Both are convolved over the range 0 to 2π to form the uniform excited state electric vector field (ES-evf) that matches the uniform current density distribution of the electron wherein each convolution is normalized to produce a central field given by Eq. (2.15).

The uniform distribution current density function $Y_0^0(\theta,\phi)$ corresponds to electron's spin that is matched by the ES-evf corresponds to electron spin (Eq. (1.27-1.28)). Consider the exemplary case to generate the ES-evf using the same the matrices as those used to generate the electron spin current density function given in the Generation of the Atomic Orbital CVFS section. Two current loops, one in the yz-plane and one in the xz-plane, serve as great circle basis elements for the electron current density pattern called the basis element current vector field (BECVF) that is formed by the rotation of the basis elements about the $(-\mathbf{i}_x,\mathbf{i}_y,0\mathbf{i}_z)$-axis as given by Eqs. (1.84) and (1.87). The LHCP photon and corresponding LHTS-evf and LHTSBE-evf may also be generated by rotation of the electric and magnetic field basis elements and the electric field basis element, respectively, about the $(-\mathbf{i}_x,\mathbf{i}_y,0\mathbf{i}_z)$-axis wherein the current loop in the yz-plane is replaced with an electric field great circle, the current loop in the xz-plane is replaced with a magnetic field great circle, and θ of the $(\mathbf{i}_x,-\mathbf{i}_y,0\mathbf{i}_z)$-axis rotation (Eqs. (1.84) and (1.87)) is replaced by $-\theta$. With E_0 given by Eq. (29) of Appendix V and $H_0=\frac{E_0}{\eta}$ according to Eq. (19) of Appendix V, the LHCP photon-e&mvf is given by Eq. (4.37) for $a_1=1;\ a_2=1,\ \theta=0$ to $\theta=-\frac{\pi}{2}$; the LHTS-evf given by Eq. (4.37) for $a_1=\sqrt{2};\ a_2=0$, $\theta=0$ to $\theta=-\frac{\pi}{2}$, and the LHTSBE-evf is given by Eq. (4.37) for $a_1=\sqrt{2};\ a_2=0,\ \theta=0$ to $\theta=-2\pi$. The LHTSBE-evf is shown in Figure 4.11.

$$\begin{bmatrix} x' \\ y' \\ z' \end{bmatrix} = a_1 E_0 \begin{bmatrix} \frac{1}{2}+\frac{\cos\theta}{2} & -\frac{1}{2}+\frac{\cos\theta}{2} & -\frac{\sin\theta}{\sqrt{2}} \\ -\frac{1}{2}+\frac{\cos\theta}{2} & \frac{1}{2}+\frac{\cos\theta}{2} & -\frac{\sin\theta}{\sqrt{2}} \\ \frac{\sin\theta}{\sqrt{2}} & \frac{\sin\theta}{\sqrt{2}} & \cos\theta \end{bmatrix} \bullet \begin{bmatrix} 0 \\ r_n\cos\phi \\ r_n\sin\phi \end{bmatrix}_{\text{Red}} + a_2 H_0 \begin{bmatrix} \frac{1}{2}+\frac{\cos\theta}{2} & -\frac{1}{2}+\frac{\cos\theta}{2} & -\frac{\sin\theta}{\sqrt{2}} \\ -\frac{1}{2}+\frac{\cos\theta}{2} & \frac{1}{2}+\frac{\cos\theta}{2} & -\frac{\sin\theta}{\sqrt{2}} \\ \frac{\sin\theta}{\sqrt{2}} & \frac{\sin\theta}{\sqrt{2}} & \cos\theta \end{bmatrix} \bullet \begin{bmatrix} r_n\cos\phi \\ 0 \\ r_n\sin\phi \end{bmatrix}_{\text{Blue}} \tag{4.37}$$

Figure 4.11. The photon electric field pattern of the LHTSBE-evf corresponding to the electron BECVF shown with 6-degree increments of θ from the perspective of looking along the z-axis. The yz-plane great circle electric field loop that served as a basis element that was initially in the yz-plane is shown as red.

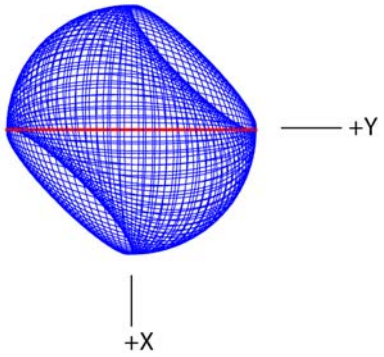

The exemplary transition of the LHTSBE-evf to the uniform distribution that matches the equipotential, equi-energy condition of the atomic orbital is given by the convolution of the output of Eq. (4.37) with the matrix given by Eq. (1.95) corresponding to a convolution about the $\left(-\frac{1}{\sqrt{2}}\mathbf{i}_x, \frac{1}{\sqrt{2}}\mathbf{i}_y, \mathbf{i}_z\right)$-axis wherein the output of the matrix of Eq. (1.95) called the orbital current vector field (OCVF) used to generate the uniform electron current distribution corresponding to electron spin. Due to symmetry over a range of 2π, the LHTSBE-evf is also given for θ positive in Eq. (4.37). Using (1.103), a discrete representation of the electric field distribution $Y_0^0(\theta,\phi)$ is generated. The continuous convolution of the LHTSBE-evf about the $\left(-\frac{1}{\sqrt{2}}\mathbf{i}_x, \frac{1}{\sqrt{2}}\mathbf{i}_y, \mathbf{i}_z\right)$-axis to form the ES-evf is shown as a superposition of discrete incremental rotations of the position of the LHTSBE-evf rotated according to Eqs. (1.95) and (1.98) corresponding to the matrix which generated the OCVF of the electron spin current function. In the case that the discrete representation of the LHTSBE-evf comprises N great circle electric field element and the number of convolved RHTSBE-evf elements is M, the representation of the ES-evf function showing electric field loops is given by Eq. (4.38) with E_0 given by Eq. (2.15), and the $\left(\frac{1}{\sqrt{2}}\mathbf{i}_x, -\frac{1}{\sqrt{2}}\mathbf{i}_y, \mathbf{i}_z\right)$-axis view with 144 vectors overlaid giving the initial free-photon-frame direction of each great circle electric field element is shown in Figure 4.12.

$$\begin{bmatrix} x' \\ y' \\ z' \end{bmatrix} = E_0 \sum_{m=1}^{m=M} \begin{bmatrix} \frac{1}{4}\left(1+3\cos\left(\frac{m2\pi}{M}\right)\right) & \frac{1}{4}\left(-1+\cos\left(\frac{m2\pi}{M}\right)+2\sqrt{2}\sin\left(\frac{m2\pi}{M}\right)\right) & \frac{1}{4}\left(-\sqrt{2}+\sqrt{2}\cos\left(\frac{m2\pi}{M}\right)-2\sin\left(\frac{m2\pi}{M}\right)\right) \\ \frac{1}{4}\left(-1+\cos\left(\frac{m2\pi}{M}\right)-2\sqrt{2}\sin\left(\frac{m2\pi}{M}\right)\right) & \frac{1}{4}\left(1+3\cos\left(\frac{m2\pi}{M}\right)\right) & \frac{1}{4}\left(\sqrt{2}-\sqrt{2}\cos\left(\frac{m2\pi}{M}\right)-2\sin\left(\frac{m2\pi}{M}\right)\right) \\ \frac{1}{2}\left(\frac{-1+\cos\left(\frac{m2\pi}{M}\right)}{\sqrt{2}}+\sin\left(\frac{m2\pi}{M}\right)\right) & \frac{1}{4}\left(\sqrt{2}-\sqrt{2}\cos\left(\frac{m2\pi}{M}\right)+2\sin\left(\frac{m2\pi}{M}\right)\right) & \cos^2\frac{\left(\frac{m2\pi}{M}\right)}{2} \end{bmatrix}$$

$$\bullet \sum_{n=1}^{n=N} \begin{bmatrix} \frac{1}{2}+\frac{\cos\left(\frac{n2\pi}{N}\right)}{2} & -\frac{1}{2}+\frac{\cos\left(\frac{n2\pi}{N}\right)}{2} & -\frac{\sin\left(\frac{n2\pi}{N}\right)}{\sqrt{2}} \\ -\frac{1}{2}+\frac{\cos\left(\frac{n2\pi}{N}\right)}{2} & \frac{1}{2}+\frac{\cos\left(\frac{n2\pi}{N}\right)}{2} & -\frac{\sin\left(\frac{n2\pi}{N}\right)}{\sqrt{2}} \\ \frac{\sin\left(\frac{n2\pi}{N}\right)}{\sqrt{2}} & \frac{\sin\left(\frac{n2\pi}{N}\right)}{\sqrt{2}} & \cos\left(\frac{n2\pi}{N}\right) \end{bmatrix} \begin{bmatrix} 0 \\ r_n \cos\phi \\ r_n \sin\phi \end{bmatrix} \tag{4.38}$$

Figure 4.12. A representation of the $\left(\frac{1}{\sqrt{2}}\mathbf{i}_x, -\frac{1}{\sqrt{2}}\mathbf{i}_y, \mathbf{i}_z\right)$-axis view of ES-evf comprising the $Y_0^0(\theta,\phi)$ distribution matching the electron spin function shown with 144 vectors overlaid giving the initial free-photon-frame direction of the electric field of each great circle basis element.

As shown by Eq. (2.11) and (2.15) the ES-evf obeys some of the properties of electrostatic charge. In addition to matching the spin function of the excited electron, the $\hbar$ angular momentum in the electric and magnetic fields of the excitation photon given by Eq. (4.1) must be conserved as electron angular momentum. Thus, the ES-evf must possess a spherical harmonic modulation component that matches an allowed spherical harmonic electron current distribution given by Eqs. (1.27-1.29) wherein the ES-evf obeys the corresponding properties of rotating electrostatic charge. The spherical harmonic function has a velocity less than light speed given by Eq. (1.35) and is phase-matched with the electron such that angular momentum is conserved during the excited state transition. The multipole of the photon is conserved in the spherical harmonic of the excited state having the corresponding orbital angular momentum given by Eq. (1.72). Moreover, the radial field can be considered a corresponding surface charge density according to Eq. (2.11)). The effect of the nature of this photon charge-equivalent on the stability and lifetime of excited states is given in the Instability of Excited States section, the State Lifetimes and Line Intensities section, and the Stability of Atoms and Hydrinos section. All boundary conditions are met for the electric fields and the wavelengths of the "trapped photon" and the electron. Eq. (2.16) is the solution for the excited modes of the atomic orbital, a spherical resonator cavity. And, the quantum numbers of the electron are n, ℓ, m_ℓ, and m_s (Described in the Stern-Gerlach

Experiment section). A p_x or p_y atomic-hydrogen excited state is shown in Figure 4.13.

Figure 4.13. The electron atomic orbital is a resonator cavity wherein the radii of the excited states are related by integers. The electronic charge-density function of a p_x or p_y atomic-hydrogen excited state is shown with positive and negative charge-density proportional to red intensity and blue intensity, respectively. The function corresponds to a charge density wave on the two-dimensional spherical surface of radius na_0 that travels time harmonically about the z-axis at the angular frequency given by Eq. (1.36). It is comprised of a linear combination of a constant function modulated by time and spherically harmonic functions. The centrifugal force is balanced by the electric field of its photon that is phase-locked to the rotating electron. The brightness corresponds to the intensity of the two-dimensional radial photon field.

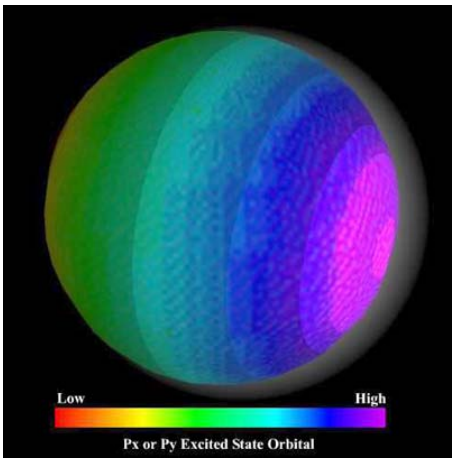

Regarding the energy balance of the transition to an excited state, the effect of the deceleration of the electron during the transition and the consequence for the ES-evf must be considered. Upon collision of a photon with an electron, the photon electric fields induce a decelerating current component along impacted great circle basis elements of the current vector field (CVF) of the electron given in the Generation of $Y_0^0(\theta,\phi)$ section. Decelerating current results in radiation. Given the indivisibility of the electron, the deceleration current produces a field along every great circle current element of the electron. The photon scatters elastically except in the case that the correspondence principle holds whereby the frequency of the photon matches the allowed frequency change of the electron as given in the Photon Absorption section. In the latter resonance case, the photon e&mvfs transition to the ES-evf, and the superposition of the field energy of the photon and the equivalent radiation field energy from the decrease in kinetic energy due to resonant electron current deceleration gives rise to the central photonic field along every great circle. The lifetime τ of this process is very small based on the time for a resonant photon to transverse the dimensions of a bound electron at lightspeed (e.g. $3\,X\,10^{-19}\,s$ for a 1 Å diameter electron). In superposition, the photon field reduces central nuclear field at the position of the electron only. In case of the hydrogen atom, the excitation photon decreases the central spherical field to that of a reciprocal integer of the fundamental charge at the central nucleus, wherein ½ of the excitation energy is contributed by the resonant photon and ½ of the energy is contributed by the decrease in kinetic energy due to electron deceleration during the transition as shown by Eqs. (2.18-2.22). Consequently, the radius of the electron increases to give rise to a radial current. The energy and angular momentum of the photon given by Eqs. (4.1) and (4.8), respectively, are conserved in the corresponding excited electronic state. The multipole of the photon is conserved in the spherical harmonic of the excited state having the corresponding orbital angular momentum given by Eq. (1.72). The transition probability and state lifetime are given by the ratio of the power and energy of the transition determined by the radial and angular source currents of photon absorption and emission events as given in the State Lifetimes and Line Intensities section. Absorption and emission of a photon are reversible, time-symmetrical processes wherein the opposite process to a that described herein occurs during photon emission. Computer modeling of the analytical equations of the mechanism of photon absorption and corresponding emission by time reversal is available on the web [26].

FREE ELECTRON PHOTON ABSORPTION

Consider next the physics of the free-electron photon absorption based on the free electron structure and corresponding behavior in the electric and magnetic photon fields based on Maxwell's equations. The free electron is a two-dimensional plane lamina comprised of a series of concentric circular current loops in the xy-plane (ρ-plane) that circulate about the z-axis as given in the Current-Density Function section. The circulation corresponds to rotational kinetic energy, and additionally the free electron center of mass may undergo linear translation corresponding to linear kinetic energy wherein the sum of these two components comprises the total energy of the free electron. With conservation of photon energy, the rotational and linear kinetic energies of a free electron can be arbitrarily large starting from a bound electron by absorption of a single high energy photon or starting from a bound electron that is ionized to form a low-energy free electron that then absorbs a series of photons. In either

case, the ionization of a bound electron to produce a free electron of any final total energy may proceed through a series of excited state levels each having a principal, orbital, and spin quantum number wherein the orbital quantum number ℓ may comprise a superposition of ℓ quantum numbers. The superposition may comprise a Fourier series of corresponding spherical harmonics wherein the orbital quantum number ℓ may approach infinity as the principal quantum number approaches infinity. In general, the physics of photon emission and absorption obeys time-reversal symmetry and superposition of states akin to Hess's law on a macroscopic scale. Consider the physics of the bound-electron absorption of a photon having energy excess of the ionization energy to form a free electron. The energy excess of the ionization energy is conserved in the free electron rotational energy, corresponding to the plane-lamina circular current with $\hbar$ of angular momentum, and the linear kinetic energy, corresponding to a linear velocity that derive from Eqs. (3.29) and (3.52). From a bound electronic state, free electron total energies each comprising a given set of rotational and linear kinetic energy states of arbitrary high energies can be achieved by absorption of a photon equal to the sum of the bound electron ionization energy and the total energy of the free electron. Alternatively, a free electron may absorb a plurality of photons with a concomitant increase in its rotational and linear kinetic energies to any final total energy that may be achieved starting from a bound state wherein the summation of the photon energies is conserved.

As shown by Eqs. (3.29) and (3.52), the radius ρ_0 decreases and the linear velocity increases to match the conservation condition that the change in the disc radius $\Delta\rho_0$ is given by Eq. (3.29), and the velocity increase corresponds to a kinetic energy increase that is exactly ½ the energy of the photon (Eq. (3.52)). The resulting energy balance is given by Eqs. (3.51) and (3.52). Specifically, using Eqs. (3.29) and (3.52), the absorption of a photon of frequency ω_{photon} by a free electron with an initial velocity along the z-axis of v_z gives rise to the radius decrease $\Delta\rho_0$ and the linear velocity increase Δv_z of

$$\Delta\rho_0 = \frac{\hbar}{m_e}\left(\frac{1}{v_z + \Delta v_z} - \frac{1}{v_z}\right) \tag{4.39}$$

wherein based on the kinetic energy increase (Eq. 3.52)) for velocities $v_z << c$:

$$\Delta v_z = \sqrt{\frac{\hbar\omega_{photon}}{m_e}} \tag{4.40}$$

Substitution of Eq. (4.40) into Eq. (4.39) gives

$$\Delta\rho_0 = \frac{\hbar}{m_e}\left(\frac{1}{v_z + \sqrt{\frac{\hbar\omega_{photon}}{m_e}}} - \frac{1}{v_z}\right) \tag{4.41}$$

To obey time time-reversal symmetry and superposition of states, the mechanism of absorption or emission of a photon by a free electron with a change in the free electron rotational and linear kinetic energies involves the formation of a transient, free-electron excited state. The spherically symmetric electronic state comprises a photon that provides the binding radial electric field force; whereafter the state decays as the photon applies equal average magnitude radial and linear forces on the excited state electron. The electric field of an exited state photon given in the Equation of the Electric Field inside the Atomic Orbital section comprises electric field great circles that are matched to each great circle of the bound electron and further circulate at light speed along each electron great circle wherein additionally the photon field intensity is modulated by time and spherical harmonics that are phase matched to any modulation of the electron current. Consequentially, the relativistic direction of the photon electric field lines is radial. To match the boundary conditions on nature of electron excited states and the required direction of the photon-electric-field-sourced radial and linear electronic forces, the excited electronic state electron comprises a charge and current density distribution equivalent to $Y_0^0(\theta,\phi)$ of the bound electron that is modulated by a Fourier series of time and spherically harmonic functions. The $Y_0^0(\theta,\phi)$ current density of the bound electron has the same angular frequency and linear velocity everywhere on the surface corresponding to electron spin, and the time and spherically harmonic modulation current densities correspond to orbital angular momentum. The photon modulated current density function that provides the required forces can be determined by considering the corresponding modulation of each great circle current of the free electron excited state. The modulated current density that matches the boundary conditions of the resultant photon force fields can be generated from an initial free electron great circle basis element with cylindrical radius $\rho = \rho_0$ comprising a constant function modulated by a time-constant trigonometric function that undergoes the series of BECVF and OCVF rotations to generate the free electron excited state. With the conversion of energy of the photon field to angular and linear kinetic energies as the electron ionizes to a new free state, each electron great circle transitions to a smaller radius, and the free electron is linearly accelerated in the direction perpendicular to the plane of the initial free electron basis element reference frame.

Specifically, consider the incidence of a linearly polarized photon having $\hbar$ of angular momentum aligned on the x-axis and propagating along the x-axis with a free electron in the xy-plane having $\hbar$ of angular momentum aligned on the z-axis and propagating along the z-axis. The photon angular momentum of the free electron creates a torque to cause the rotation of the angular momentum vector of the free electron current about two axes, the $\left(\mathbf{i}_x, 0\mathbf{i}_y, \mathbf{i}_z\right)$-axis in a first step and the laboratory-frame z-axis in a second step. The corresponding motion of the perimeter great circle current loop at ρ_0 in the plane perpendicular to

the angular momentum vector generates CVFs equivalent to those of the bound electron given in the Atomic Orbital Equation of Motion for $\ell = 0$ Based on the Current Vector Field (CVF) section. Specifically, as given by Eq. (3.80) and shown in Figure 3.10 the first rotation sweeps out the equivalent of a BECVF, wherein the concentric planar great circle current loops shown in Figure 3.2A flow from the disc origin to the perimeter edge at ρ_0. The remaining electron disc current density at each rotational angle forms an annulus with a constant outer radius $\rho = \rho_0$ and an increasing inner radius during the rotation to successively spread the charge density over the BECVF. The second rotation of the BECVF sweeps out the equivalent of the convolution of the BECVF with the OCVF. The result is a charge and current density distribution equivalent to $Y_0^{\,0}(\theta,\phi)$ of the bound electron wherein charge density of the bound electron has the same angular frequency and linear velocity everywhere on the surface.

The field of a bound photon replaces the proton as the source of central field to create equivalent event as the binding of the electron to a proton as given Eq. (3.80) and shown in Figure 3.10 wherein the equations of a free linearly polarized and bound photon are given by Eqs. (4.6-4.7) and (4.38), and Figures 4.7 and 4.12, respectively. In the absence of the central field of a nucleus, the trapped photon field from Eq. (2.16) has the form:

$$\mathbf{E}_r = \mathrm{Re}\left\{Y_0^0(\theta,\phi) + Y_\ell^m(\theta,\phi)e^{im\omega_n t}\right\}\delta(r - r_n) \tag{4.42}$$

except that the trapped photon of a free electron comprises a Fourier series of spherical harmonics that result in a central force and a linear force along the z-axis wherein the orthogonal components are equal on average. The photon field of the free electron excited state comprises a Fourier series of time harmonic and spherically harmonic functions that can be constructed from a great circle electric field basis element having a time-constant trigonometrically modulated photon intensity along the great circle current basis element. The corresponding time-constant, relativistic radial electrical field of the photon field basis element that is phase matched to the great circle current basis element is given by:

$$\mathbf{E}_\rho = (1 - \cos\theta)\delta(\rho - \rho_0) \tag{4.43}$$

wherein for when $\theta = \pi$, the vector $\mathbf{i}_\rho$ is in the direction of the positive x-axis of the original free electron reference frame before excitation by the incident photon. The electron great circle current density is spatially modulated in phase with the electric field modulation wherein the spatial modulation is constant in time. Electron ionization of the free electron excited state is a continuous process with continuous current flow. An equation providing visualization in discrete steps that generates the angular momentum vectors of the bound electron is given by Eq. (3.80), but time reversed with the spherical and cylindrical radii scaled sequentially according to the average of the forces acting of the electron current during each step of the event. The visualization of the ionization event is given by the reverse sequence shown in Figure 3.10 with the excited state photon substituting for the proton and with a scaling factor applied. The scaling factor S of the spatial dimensions that multiples the output of the reverse sequence of Eq. (3.80) corresponding the indices in the direction m = M to m = 1 and n= N to n = 1 is given by

$$S = \left(1 - \left(1 - \frac{n-1}{N}\right)\frac{\Delta\rho_0}{\rho_0}\right) \tag{4.44}$$

Considering the translational acceleration over the ionization event, the linear velocity concomitantly incrementally increases by the factor S':

$$S' = \left(1 + \frac{n-1}{N}\frac{\Delta v_z}{v_z}\right) \tag{4.45}$$

The absorbed photon must form a spherical bound state in the moving reference frame of the free electron to result in an inelastic event. Time reversal symmetry resulting in ionization favors the photon kinetic energy contribution to add positively to the initial velocity of the free electron. Additionally, conservation of energy for a single absorption event favors the absorbed photon contributing the positive addition to the initial velocity. Consider the magnitude of the increase in electron linear momentum due to photon absorption compared to the linear momentum of the absorbed photon of angular frequency ω given by

$$p = \frac{\hbar\omega}{c} \tag{4.46}$$

The relativistic three vector momentum for rectilinear motion along the z-axis (Eq. (34.12)) is

$$p = \frac{m_{e0}}{\sqrt{1 - \left(\frac{v}{c}\right)^2}}v \tag{4.47}$$

wherein v is the three velocities. Considering that ½ of the energy of an absorbed photon is converted to electron linear kinetic energy, the increase in electron linear kinetic energy T corresponding to an increase in linear velocity v from rest in the electron's absolute frame given by Eqs. (1.291) and (3.52) is

$$T = \frac{\hbar\omega}{2} = m_{e0}c^2\left(\frac{1}{\sqrt{1-\left(\frac{v}{c}\right)^2}}-1\right) \tag{4.48}$$

Using Eq. (4.48), the increase in linear velocity is given by

$$v = c\sqrt{1-\left(\frac{m_{e0}}{\left(\frac{\hbar\omega}{2c^2}+m_{e0}\right)}\right)^2} \tag{4.49}$$

Using Eq. (4.47), the relativistic three vector momentum for rectilinear motion along the z-axis is

$$p = \left(\frac{\hbar\omega}{2c^2}+m_{e0}\right)c\sqrt{1-\left(\frac{m_{e0}}{\left(\frac{\hbar\omega}{2c^2}+m_{e0}\right)}\right)^2} \tag{4.50}$$

Consider the case of a microwave photon of frequency f of 5 GHz ($3.3\,X\,10^{-24}\,J$). The corresponding photon linear momentum (Eq. (4.50)) is $1.1\,X\,10^{-32}\,kgms^{-1}$ and the corresponding increase in electron linear momentum is $1.73\,X\,10^{-27}\,kgms^{-1}$ which is five orders of magnitude greater.

A free space photon having $\hbar$ in its electric and magnetic fields is not divisible, and the electric field of a photon cannot be translated by an external action due to the properties of spacetime. Photon propagation in free space at an exact velocity of $c = \frac{1}{\sqrt{\mu_0\varepsilon_0}}$ is based on the permittivity ε_0 and permeability μ_0 of free space. The relationship between the energies of a photon as it converts to mass due to angular frequency, electric field, magnetic field, gravitational energy, and space time contraction are given by Eqs. (32.48a-32.48b) wherein the relationship between spacetime contraction and expansion due to energy to matter conversion and vice versa is given by Eqs. (32.140a-32.140b). Kinetic energy contributes to the inertial mass of an electron according to Eq. (1.291). Photons and free electrons each have zero gravitational mass; consequently, there is no violation of particle production laws by the absorption of a photon by an electron to increase its kinetic mass/energy.

In effect spacetime of the photon field-free electron interaction serves as the body that conserves momentum from the free-electron photon absorption event wherein the photon angular momentum is partially converted to linear momentum. This phenomenon is enabling of a novel propulsion device that drives against spacetime called space drive.

The mechanisms of technologies almost without exception are also observed in Nature. This is also the case with space-drive phenomenon as the mechanism of the formation of ***sprites*** formed during lightning storms. Specifically, electrons are accelerated to relativistic energies in the direction away from the Earth during atmospheric discharges called red sprites and blue jets (Figure 4.14). These comprise large-scale vertically ascending pillars of emission from electrons accelerated from the tops of thunderclouds out into space that are associated with gamma ray bursts during lightning events. The Italian Space Agency's AGILE observatory found that the energy spectrum of terrestrial gamma-ray flashes extends up to 100 MeV. These otherwise inexplicable observations can be resolved as being due to the space drive mechanism. The high voltage within clouds or between clouds and Earth directionally accelerates electrons during a lightening discharge. The high current of lightning causes a strong vector magnetic field. The directional relativistic electron flow directly and the flow in the presence of the directional magnetic field results in the emission of microwaves that are absorbed by an upward (downward) flow of plasma causing the electrons to accelerate selectively in the upward (downward) direction by the space-drive effect. Ions such as H_3^+ are dragged by the directionally accelerated electrons. Predominantly collisional air molecular excitation as well as recombination of upward ion and electron flow in the high-altitude atmosphere emit the high-altitude light emission of a sprite. In addition to the traditional colliding counter flowing ice particles mechanism, the upward space drive current may serve to further positively charge clouds to achieve run-away relativistic electron energies of greater than 100 MeV to give rise to the extraordinarily 100 MeV gamma ray flashes.

Figure 4.14. Upward jet of electrons accelerated away from the Earth at near light speed associated with gamma ray bursts during lightning events.

The same mechanism may be the source of the gamma rays of extraordinary energies of over 1 TeV emitted by the Sun [27], beyond those anticipated from magnetic field acceleration of electrons [28].

REFERENCES

1. J. D. Jackson, *Classical Electrodynamics*, Second Edition, John Wiley & Sons, New York, (1975), pp. 739-779.
2. E. Purcell, *Electricity and Magnetism*, McGraw-Hill, New York, (1965), pp. 156-167.
3. L. C. Shi, J. A. Kong, *Applied Electromagnetism*, Brooks/Cole Engineering Division, Monterey, CA, (1983), pp. 210-215.
4. Mathematica modeling of R. Mills' theory by B. Holverstott in "Analytical-Equation Derivation of the Photon Electric and Magnetic Fields," posted at http://www.blacklightpower.com.
5. R. A. Bonham, M. Fink, *High Energy Electron Scattering*, ACS Monograph, Van Nostrand Reinhold Company, New York, (1974), pp. 1-3.
6. K. Dholakia, N. B. Simpson, M. J. Padgett, L. Allen, Physical Review A, Volume 54, Number 5, (1996), pp. R3742-R3745.
7. R. W. Ziolkowski, K. D. Lewis, Phys. Rev. Letts., Vol. 62, No. 2, (1989), pp. 147-150.
8. J. B. Brittingham, J. Appl. Phys., Vol. 54, (1983), p. 1179.
9. R. W. Ziolkowski, J. Math. Phys., Vol. 26, (1985), p. 861.
10. R. W. Ziolkowski, *Microwave and Particle Beam Sources and Propagation*, edited by N. Rostoker, SPIE Conference Proceedings, No. 873, (SPIE, Bellingham, WA, 1988).
11. P. Hillion, J. Appl. Phys., Vol. 60, (1986), p. 2981; P. Hillion, J. Math. Phys., Vol. 28, (1987), p. 1743.
12. E. Heyman, L. B. Felsen, IEEE Trans. Antennas Propag., Vol. 34, (1986), p. 1062; E. Heyman, B. Z. Steinberg, J. Opt. Soc. Am. A, Vol. 4, (1987), p. 473; E. Heyman, B. Z. Steinberg, L. P. Felsen, J. Opt. Soc. Am. A, Vol. 4, (1987), p. 2081.
13. J. Durnin, Opt. Soc. Am. A, Vol. 4, (1987), p. 651; J. Durnin, J. Miceli, J. H. Eberly, Phys. Rev. Lett., Vol. 58, (1987), p. 1499.
14. T. T. Wu, J. Appl. Phys., Vol. 57, (1985), p. 2370; T. T. Wu, R. W. P. King, H. Shen, J. Appl. Phys., Vol. 62, (1987), p. 4036; H. Shen, *Microwave and Particle Beam Sources and Propagation*, edited by N. Rostoker, SPIE Conference Proceedings, No. 873, (SPIE, Bellingham, WA, 1988).
15. H. E. Moses, J. Math. Phys., Vol. 25, (1984), p. 1905; H. E. Moses, R. T. Prosser, IEEE Trans. Antennas Propag., Vol. 34, (1986), p. 188.
16. A. N. Norris, B. White, S. Schrieffer, Proc. Roy. Soc. London A, Vol. 412, (1987), p. 93.
17. M. Mizushima, *Quantum Mechanics of Atomic Spectra and Atomic Structure*, W.A. Benjamin, Inc., New York, (1970), p.17.
18. W. G. Cross, N. F. Ramsey, Phys. Rev., Vol. 80, (1950), p. 929.
19. J. D. Jackson, *Classical Electrodynamics*, Second Edition, John Wiley & Sons, New York, (1975), Chp. 15.
20. H. A. Haus, "On the radiation from point charges," Am. J. Phys., 54, (1986), pp. 1126-1129.
21. A. Einstein, Phys. Z, Vol. 18, (1917), 121.
22. "The Interview Carver Meade," The American Spectator, September/October, (2001).
23. W. E. Lamb, "Theory of an optical maser," Phys. Rev., Vol. 134, No. 6A, (1964), pp. A1429-1450.
24. A. L. Schawlow, C. H. Townes, "Infrared and optical masers," Phys. Rev., Vol. 112, (1958), pp. 1940-1949.
25. H. J. Carmichael, "Quantum theory of the laser," Proc. of the International School on Lasers and Quantum Optics, Laser and Quantum Optics, L. M. Narducci, E. J. Quell, J. R. Tredicce, Editors, CIF Series Vol. 13, Mar del Plata, Argentina, 22-31 Aug., (1988), pp. 52-85.
26. "Modeling of the Analytical Equations of the Mechanism of Photon Absorption and Corresponding Emission by Time Reversal" posted at www.brilliantlightpower.com.
27. Ravisetti, "Sun blasts out highest-energy radiation ever recorded, raising questions for solar physics"SPACE.com, August 6, 2023, https://www.space.com/sun-blasts-highest-energy-radiation-ever-recorded-raising-questions-solar-physics.
28. J. A. Miller, R. Reuven, "Relativistic Electron Transport and Bremsstrahlung Production in Solar Flares", Astrophysical Journal, Vol. 344, (1989), p. 973.

Chapter 5

HYDRINO THEORY – BLACKLIGHT PROCESS

BLACKLIGHT PROCESS

Classical physics (CP) gives closed-form solutions of the hydrogen atom, the hydride ion, the hydrogen molecular ion, and the hydrogen molecule and predicts corresponding species having fractional principal quantum numbers. The nonradiative state of atomic hydrogen, which is historically called the "ground state" forms the basis of the boundary condition of CP to solve the bound electron. CP predicts a reaction involving a resonant, nonradiative energy transfer from otherwise stable atomic hydrogen to a catalyst capable of accepting the energy to form hydrogen in lower-energy states than previously thought possible called a ***hydrino atom*** designated as $H\left[\frac{a_H}{p}\right]$ where a_H is the radius of the hydrogen atom. Specifically, CP predicts that atomic hydrogen may undergo a catalytic reaction with certain atoms, excimers, ions, and diatomic hydrides which provide a reaction with a net enthalpy of an integer multiple of the potential energy of atomic hydrogen, $E_h = 27.2\ eV$ where E_h is one Hartree. Specific species (e.g. He^+, Ar^+, Sr^+, K, Li, HCl, NaH, and H_2O) identifiable on the basis of their known electron energy levels are required to be present with atomic hydrogen to catalyze the process. The reaction involves a nonradiative energy transfer of an integer multiple of $27.2\ eV$ from atomic hydrogen to the catalyst followed by $q \cdot 13.6\ eV$ continuum emission or $q \cdot 13.6\ eV$ transfer to another H to form extraordinarily hot, excited-state H and a hydrogen atom that is lower in energy than unreacted atomic hydrogen that corresponds to a fractional principal quantum number. That is, in the formula for the principal energy levels of the hydrogen atom:

$$E_n = -\frac{e^2}{n^2 8\pi\varepsilon_o a_H} = -\frac{13.598\ eV}{n^2} \tag{5.1}$$

$$n = 1, 2, 3, \ldots \tag{5.2}$$

where a_H is the Bohr radius for the hydrogen atom (52.947 pm), e is the magnitude of the charge of the electron, and ε_o is the vacuum permittivity, fractional quantum numbers:

$$n = 1, \frac{1}{2}, \frac{1}{3}, \frac{1}{4}, \ldots, \frac{1}{p};\quad p \le 137 \text{ is an integer} \tag{5.3}$$

replace the well known parameter $n = \text{integer}$ in the Rydberg equation for hydrogen excited states. Then, similar to an excited state having the analytical solution of Maxwell's equations given by Eq. (2.15), a hydrino atom also comprises an electron, a proton, and a photon as given by Eq. (5.27). However, the electric field of the latter increases the binding corresponding to desorption of energy rather than decreasing the central field with the absorption of energy as in an excited state, and the resultant photon-electron interaction of the hydrino is stable rather than radiative.

The $n = 1$ state of hydrogen and the $n = \frac{1}{\text{integer}}$ states of hydrogen are nonradiative, but a transition between two nonradiative states, say $n = 1$ to $n = 1/2$, is possible via a nonradiative energy transfer. Hydrogen is a special case of the stable states given by Eqs. (5.1) and (5.3) wherein the corresponding radius of the hydrogen or hydrino atom is given by:

$$r = \frac{a_H}{p}, \tag{5.4}$$

where $p = 1, 2, 3, \ldots$. In order to conserve energy, energy must be transferred from the hydrogen atom to the catalyst in units of

$$m \cdot 27.2\ eV,\ m = 1, 2, 3, 4, \ldots. \tag{5.5}$$

and the radius transitions to $\frac{a_H}{m+p}$. The catalyst reactions involve two steps of energy release: a nonradiative energy transfer to the catalyst followed by additional energy release as the radius decreases to the corresponding stable final state. Thus, the general reaction is given by:

$$m \cdot 27.2\ eV + Cat^{q+} + H\left[\frac{a_H}{p}\right] \rightarrow Cat_{fast}^{(q+r)+} + re^- + H*\left[\frac{a_H}{(m+p)}\right] + m \cdot 27.2\ eV \tag{5.6}$$

$$H*\left[\frac{a_H}{(m+p)}\right] \rightarrow H\left[\frac{a_H}{(m+p)}\right] + [(p+m)^2 - p^2] \cdot 13.6\ eV - m \cdot 27.2\ eV \tag{5.7}$$

$$Cat_{fast}^{(q+r)+} + re^- \rightarrow Cat^{q+} + m \cdot 27.2\ eV \tag{5.8}$$

And, the overall reaction is:

$$H\left[\frac{a_H}{p}\right] \rightarrow H\left[\frac{a_H}{(m+p)}\right] + [(p+m)^2 - p^2] \cdot 13.6\ eV \tag{5.9}$$

q, r, m, and p are integers. $H*\left[\frac{a_H}{(m+p)}\right]$ has the radius of the hydrogen atom (corresponding to $p = 1$) and a central field equivalent to $(m+p)$ times that of a proton, and $H\left[\frac{a_H}{(m+p)}\right]$ is the corresponding stable state with the radius of $\frac{1}{(m+p)}$ that of H. As the electron undergoes radial acceleration from the radius of the hydrogen atom to a radius of $\frac{1}{(m+p)}$ this distance, energy is released as characteristic light emission or as third-body kinetic energy. The emission may be in the form of an extreme-ultraviolet continuum radiation having an edge at $[(p+m)^2 - p^2 - 2m] \cdot 13.6\ eV$ or $\frac{91.2}{[(p+m)^2 - p^2 - 2m]}\ nm$ and extending to longer wavelengths. In addition to radiation, a resonant kinetic energy transfer to form fast H may occur. Subsequent excitation of these fast $H(n=1)$ atoms by collisions with the background H_2 followed by emission of the corresponding $H(n=3)$ fast atoms gives rise to broadened Balmer α emission.

As given in Disproportionation of Energy States section, hydrogen atoms $H(1/p)$ $p = 1, 2, 3, \ldots 137$ can undergo further transitions to lower-energy states given by Eqs. (5.1) and (5.3) wherein the transition of one atom is catalyzed by a second that resonantly and nonradiatively accepts $m \cdot 27.2\ eV$ with a concomitant opposite change in its potential energy. The overall general equation for the transition of $H(1/p)$ to $H(1/(p+m))$ induced by a resonance transfer of $m \cdot 27.2\ eV$ to $H(1/p')$ given by Eq. (5.75) is represented by:

$$H(1/p') + H(1/p) \rightarrow H + H(1/(p+m)) + \left[2pm + m^2 - p'^2 + 1\right] \cdot 13.6\ eV \tag{5.10}$$

Hydrogen atoms may serve as a catalyst wherein $m = 1$, $m = 2$, and $m = 3$ for one, two, and three atoms, respectively, acting as a catalyst for another. The rate for the two-atom-catalyst, $2H$, may be high when extraordinarily fast H as reported previously [1-7] collides with a molecule to form the $2H$ wherein two atoms resonantly and nonradiatively accept $54.4\ eV$ from a third hydrogen atom of the collision partners. By the same mechanism, the collision of two hot H_2 provide $3\,H$ to serve as a catalyst of $3 \cdot 27.2\ eV$ for the fourth. The EUV continua at 22.8 nm and 10.1 nm and extraordinary (>100 eV) Balmer α line broadening are observed consistent with predictions [1-9].

The catalyst product, $H(1/p)$, may also react with an electron to form a hydrino hydride ion $H^-(1/p)$, or two $H(1/p)$ may react to form the corresponding molecular hydrino $H_2(1/p)$. Specifically, the catalyst product, $H(1/p)$, may also react with an electron to form a novel hydride ion $H^-(1/p)$ with a binding energy E_B (Eq. (7.74)) derived in the Hydrino Hydride Ion section:

$$E_B = \frac{\hbar^2\sqrt{s(s+1)}}{8\mu_e a_0^2\left[\frac{1+\sqrt{s(s+1)}}{p}\right]^2} - \frac{\pi\mu_0 e^2\hbar^2}{m_e^2}\left(\frac{1}{a_H^3} + \frac{2^2}{a_0^3\left[\frac{1+\sqrt{s(s+1)}}{p}\right]^3}\right) \tag{5.11}$$

where $p = \text{integer} > 1$, $s = 1/2$, $\hbar$ is Planck's constant bar, μ_o is the permeability of vacuum, m_e is the mass of the electron, μ_e is the reduced electron mass given by $\mu_e = \frac{m_e m_p}{\frac{m_e}{\sqrt{\frac{3}{4}}} + m_p}$ where m_p is the mass of the proton, a_o is the Bohr radius, and the ionic radius is $r_1 = \frac{a_0}{p}\left(1+\sqrt{s\left(s+1\right)}\right)$ (Eq. (7.73)). From Eq. (5.11), the calculated ionization energy of the hydride ion is $0.75418\ eV$, and the experimental value given by Lykke [10] is $6082.99 \pm 0.15\ cm^{-1}$ (0.75418 eV).

Upfield-shifted NMR peaks are direct evidence of the existence of lower-energy state hydrogen with a reduced radius relative to ordinary hydride ion and having an increase in diamagnetic shielding of the proton. The shift is given by the sum of the contributions of the diamagnetism of the two electrons and the trapped photon field of magnitude p (Eq. (7.87)):

$$\frac{\Delta B_T}{B} = -\mu_0\frac{pe^2}{12m_e a_0\left(1+\sqrt{s\left(s+1\right)}\right)}\left(1+p\alpha^2\right) = -\left(p29.9 + p^2 1.59\ X\ 10^{-3}\right)\ ppm \tag{5.12}$$

where the first term applies to H^- with $p = 1$ and $p = \text{integer} > 1$ for $H^-\left(1/p\right)$ and α is the fine structure constant.

$H\left(1/p\right)$ may react with a proton and two $H\left(1/p\right)$ may react to form $H_2\left(1/p\right)^+$ and $H_2\left(1/p\right)$, respectively. The hydrogen molecular ion and molecular charge and current density functions, bond distances, and energies were solved in the Nature of the Chemical Bond of Hydrogen-Type Molecules and Molecular Ions section from the Laplacian in ellipsoidal coordinates with the constraint of nonradiation.

$$(\eta-\zeta)R_\xi\frac{\partial}{\partial\xi}(R_\xi\frac{\partial\phi}{\partial\xi}) + (\zeta-\xi)R_\eta\frac{\partial}{\partial\eta}(R_\eta\frac{\partial\phi}{\partial\eta}) + (\xi-\eta)R_\zeta\frac{\partial}{\partial\zeta}(R_\zeta\frac{\partial\phi}{\partial\zeta}) = 0 \tag{5.13}$$

The total energy E_T of the hydrogen molecular ion having a central field of $+pe$ at each focus of the prolate spheroid molecular orbital is (Eqs. (11.192-11.193))

$$\begin{aligned} E_T &= -p^2\left\{\begin{array}{l} \frac{e^2}{8\pi\varepsilon_o a_H}(4\ln 3 - 1 - 2\ln 3)\left[1+\sqrt{\frac{2\hbar\sqrt{\frac{2e^2}{4\pi\varepsilon_o\left(2a_H\right)^3}}}{m_e c^2}}\right] \\ -\frac{1}{2}\hbar\sqrt{\frac{\frac{pe^2}{4\pi\varepsilon_o\left(\frac{2a_H}{p}\right)^3} - \frac{pe^2}{8\pi\varepsilon_o\left(\frac{3a_H}{p}\right)^3}}{\mu}} \end{array}\right\} \\ &= -p^2 16.2526\ eV \end{aligned} \tag{5.14}$$

where p is an integer, c is the speed of light in vacuum, and μ is the reduced nuclear mass. The total energy of the hydrogen molecule having a central field of $+pe$ at each focus of the prolate spheroid molecular orbital is (Eqs. (11.240-11.241))

$$E_T = -p^2\left\{\begin{array}{l}\dfrac{e^2}{8\pi\varepsilon_o a_0}\left[\left(2\sqrt{2}-\sqrt{2}+\dfrac{\sqrt{2}}{2}\right)\ln\dfrac{\sqrt{2}+1}{\sqrt{2}-1}-\sqrt{2}\right]\left[1+\sqrt{\dfrac{2\hbar\sqrt{\dfrac{e^2}{4\pi\varepsilon_o a_0^3}}}{m_e c^2}}\right] \\ -\dfrac{1}{2}\hbar\sqrt{\dfrac{\dfrac{pe^2}{8\pi\varepsilon_o\left(\dfrac{a_0}{p}\right)^3}-\dfrac{pe^2}{8\pi\varepsilon_o\left(\dfrac{\left(1+\dfrac{1}{\sqrt{2}}\right)a_0}{p}\right)^3}}{\mu}}\end{array}\right\} \quad (5.15)$$

$$= -p^2 31.677\ eV$$

The bond dissociation energy, E_D, of the hydrogen molecule $H_2(1/p)$ is the difference between the total energy of the corresponding hydrogen atoms and E_T

$$E_D = E(2H(1/p)) - E_T \quad (5.16)$$

where [11]

$$E(2H(1/p)) = -p^2 27.20\ eV \quad (5.17)$$

E_D is given by Eqs. (5.16-5.17) and (5.15):

$$\begin{aligned} E_D &= -p^2 27.20\ eV - E_T \\ &= -p^2 27.20\ eV - \left(-p^2 31.677\ eV\right) \\ &= p^2 4.478\ eV \end{aligned} \quad (5.18)$$

The calculated and experimental parameters of H_2, D_2, H_2^+, and D_2^+ are given in Table 11.1.

The NMR of catalysis-product gas provides a definitive test of the theoretically predicted chemical shift of $H_2(1/p)$. In general, the ^1H NMR resonance of $H_2(1/p)$ is predicted to be upfield from that of H_2 due to the fractional radius in elliptic coordinates wherein the electrons are significantly closer to the nuclei. The predicted shift, $\frac{\Delta B_T}{B}$, for $H_2(1/p)$ is given by the sum of the contributions of the diamagnetism of the two electrons and the trapped photon field of magnitude p (Eqs. (11.415-11.416)):

$$\frac{\Delta B_T}{B} = -\mu_0\left(4-\sqrt{2}\ln\frac{\sqrt{2}+1}{\sqrt{2}-1}\right)\frac{pe^2}{36a_0 m_e}\left(1+p\alpha^2\right) \quad (5.19)$$

$$\frac{\Delta B_T}{B} = -\left(p28.01 + p^2 1.49\ X\ 10^{-3}\right) ppm \quad (5.20)$$

where the first term applies to H_2 with $p=1$ and $p=\text{integer}>1$ for $H_2(1/p)$. The experimental absolute H_2 gas-phase resonance shift of -28.0 ppm [12-15] is in excellent agreement with the predicted absolute gas-phase shift of -28.01 ppm (Eq. (5.20)).

The vibrational energies, E_{vib}, for the $\upsilon=0$ to $\upsilon=1$ transition of hydrogen-type molecules $H_2(1/p)$ are (Eq. (11.223))

$$E_{vib} = p^2 0.515902\ eV \quad (5.21)$$

where p is an integer and the experimental vibrational energy for the $\upsilon=0$ to $\upsilon=1$ transition of H_2, $E_{H_2(\upsilon=0\rightarrow\upsilon=1)}$, is given by Beutler [16] and Herzberg [17].

The rotational energies, E_{rot}, for the J to $J+1$ transition of hydrogen-type molecules $H_2(1/p)$ are (Eq. (12.74))

$$E_{rot} = E_{J+1} - E_J = \frac{\hbar^2}{I}\left[J+1\right] = p^2\left(J+1\right)0.01509\ eV \quad (5.22)$$

where p is an integer, I is the moment of inertia, and the experimental rotational energy for the $J=0$ to $J=1$ transition of H_2 is given by Atkins [18].

The p^2 dependence of the rotational energies results from an inverse p dependence of the internuclear distance and the corresponding impact on the moment of inertia I. The predicted internuclear distance $2c'$ for $H_2(1/p)$ is:

$$2c' = \frac{a_o\sqrt{2}}{p} \tag{5.23}$$

The data from a broad spectrum of investigational techniques strongly and consistently indicates that hydrogen can exist in lower-energy states than previously thought possible and support the existence of these states called hydrino, for "small hydrogen", and the corresponding hydride ions and molecular hydrino. Some of these prior related studies supporting the possibility of a novel reaction of atomic hydrogen, which produces hydrogen in fractional quantum states that are at lower energies than the traditional "ground" ($n=1$) state, include extreme ultraviolet (EUV) spectroscopy, characteristic emission from catalysts and the hydride ion products, lower-energy hydrogen emission, chemically-formed plasmas, Balmer α line broadening, population inversion of H lines, elevated electron temperature, anomalous plasma afterglow duration, power generation, and analysis of novel chemical compounds.

ENERGY TRANSFER MECHANISM

Consider the excited energy states of ***atomic*** hydrogen given by Eq. (5.1) with $n=2,3,4,...$ (Eq. (5.2)). The $n=1$ state is the "ground" state for "pure" photon transitions (the $n=1$ state can absorb a photon and go to an excited electronic state, but it cannot release a photon and go to a lower-energy electronic state). However, an electron transition from the $n=1$ state to a lower-energy state hydrino state is possible by a nonradiative energy transfer such as multipole coupling or a resonant collision mechanism. Processes that occur without photons and that require collisions are common. For example, the exothermic chemical reaction of $H+H$ to form H_2 does not occur with the emission of a photon. Rather, the reaction requires a collision with a third body, M, to remove the bond energy: $H+H+M \rightarrow H_2+M^*$ [19]. The third body distributes the energy from the exothermic reaction, and the end result is the H_2 molecule and an increase in the temperature of the system. Further exemplary of an inelastic collision with resonant energy transfer is the Franck-Hertz experiment wherein an excited state atom [20] is formed. Additionally, some commercial phosphors are based on nonradiative energy transfer involving multipole coupling. For example, the strong absorption strength of Sb^{3+} ions along with the efficient nonradiative transfer of excitation from Sb^{3+} to Mn^{2+} are responsible for the strong manganese luminescence from phosphors containing these ions [21][1]. Another example of resonant, nonradiative energy transfer involves atomic hydrogen wherein resonant energy transfer from excited Ne_2^* excimer formed in high pressure microhollow cathode discharges to hydrogen atoms in the ground state occurs with high efficiency to give predominantly Lyman α and Lyman β emission [22-24] in the absence of excimer emission observed with pure neon plasmas. Thus, the normal emission is consequently quenched as H emits.

Similarly, the $n=1$ state of hydrogen and the $n=\frac{1}{\text{integer}}$ states of hydrogen are nonradiative, but a transition between two nonradiative states is possible via a nonradiative energy transfer, say $n=1$ to $n=1/4$. In these cases, during the transition the H electron couples to another electron transition, electron transfer reaction, or inelastic scattering reaction that can absorb the

---

[1] An example of *nonradiative energy transfer* is the basis of commercial fluorescent lamps. Consider Mn^{2+} which when excited sometimes emits yellow luminescence. The absorption transitions of Mn^{2+} are spin-forbidden. Thus, the absorption bands are weak, and the Mn^{2+} ions cannot be efficiently raised to excited states by direct optical pumping. Nevertheless, Mn^{2+} is one of the most important luminescence centers in commercial phosphors. For example, the double-doped phosphor $Ca_5(PO_4)_3F:Sb^{3+},Mn^{2+}$ is used in commercial fluorescent lamps where it converts mainly ultraviolet light from a mercury discharge into visible radiation. When 2536 Å mercury radiation falls on this material, the radiation is absorbed by the Sb^{3+} ions rather than the Mn^{2+} ions. Some excited Sb^{3+} ions emit their characteristic blue luminescence, while other excited Sb^{3+} ions transfer their energy to Mn^{2+} ions. These excited Mn^{2+} ions emit their characteristic yellow luminescence. The efficiency of transfer of ultraviolet photons through the Sb^{3+} ions to the Mn^{2+} ions can be as high as 80%. The strong absorption strength of Sb^{3+} ions along with the efficient transfer of excitation from Sb^{3+} to Mn^{2+} are responsible for the strong manganese luminescence from this material.

This type of *nonradiative energy transfer* is common. The ion which emits the light and which is the active element in the material is called the *activator*; and the ion that helps to excite the activator and makes the material more sensitive to pumping light is called the *sensitizer*. Thus, the sensitizer ion absorbs the radiation and becomes excited. Because of a coupling between sensitizer and activator ions, the sensitizer transmits its excitation to the activator, which becomes excited, and the activator may release the energy as its own characteristic radiation. The sensitizer to activator transfer is *not* a radiative emission and absorption process, rather a *nonradiative transfer*. The nonradiative transfer may be by electric or magnetic multipole interactions. In the transfer of energy between dissimilar ions, the levels will, in general, not be in resonance, and some of the energy is released as a phonon or phonons. In the case of similar ions the levels should be in resonance, and phonons are not needed to conserve energy.

Sometimes the host material itself may absorb (usually in the ultraviolet) and the energy can be transferred nonradiatively to dopant ions. For example, in $YVO_4:Eu^{3+}$, the vanadate group of the host material absorbs ultraviolet light, then transfers its energy to the Eu^{3+} ions which emit characteristic Eu^{3+} luminescence.

exact amount of energy that must be removed from the hydrogen atom to initiate the transition. These reactions comprise a resonant energy sink generally referred to as an ***energy hole***. Thus, a ***catalyst*** is a source of an energy hole because it provides a net positive enthalpy of reaction of $m \cdot 27.2\ eV$ (i.e. it absorbs or provides an energy sink of $m \cdot 27.2\ eV$). The reaction of hydrogen-type atoms to lower-energy states may also be referred to as a ***transition reaction***. The certain atoms or ions that serve as transition reaction catalysts resonantly accept energy from hydrogen atoms and release the energy to the surroundings to effect electronic transitions to hydrino states comprising energy levels corresponding to fractional quantum numbers in the Rydberg formula. The catalysis of hydrogen involves the nonradiative transfer of energy from atomic hydrogen to a catalyst to form an intermediate (Eq. (5.7)) that may then release the additional energy by radiative and nonradiative mechanisms. Thus, as a consequence of the nonradiative energy transfer, the hydrogen atom becomes unstable and emits further energy until it achieves a lower-energy nonradiative state having a principal energy level given by Eqs. (5.1) and (5.3). Characteristic continuum radiation and extraordinary (>100 eV) Balmer α line broadening corresponding to fast H observed from mixed hydrogen plasmas containing a hydrino catalyst [1-9] are signatures of the reaction to form hydrinos. The latter release may occur via a collisional or nonradiative energy transfer from the corresponding formed metastable intermediate to yield the fast $H\left(n=1\right)$. The mechanism of energy release may be akin to a quenching reaction [25-26] that is selection rule dependent.

ENERGY HOLE CONCEPT

For a spherical resonator cavity, the nonradiative boundary condition and the relationship between the electron and the photon give the "allowed" hydrogen energy states that are quantized as a function of the parameter n. That is, the nonradiative boundary condition and the relationship between an allowed radius and the photon standing wave wavelength (Eq. (2.1)) give rise to Eq. (2.2), the boundary condition for allowed radii and allowed electron wavelengths as a function of the parameter n. Each value of n corresponds to an allowed transition caused by a resonant photon, which excites the transition in the atomic orbital resonator cavity from the initial to the final state. In addition to the traditional integer values (1, 2, 3,...) of n, fractional values are allowed by Eq. (2.2) which correspond to transitions between energy states with an increase in the central field (effective charge) and decrease in the radius of the atomic orbital. This occurs, for example, when the atomic orbital couples to another resonator cavity, which can absorb energy. This is the ***absorption of an energy hole by the hydrogen-type atom***. The absorption of an energy hole destroys the balance between the centrifugal force and the increased central electric force. Consequently, the electron undergoes a transition to a stable lower energy state. Thus, the corresponding reaction from an initial energy state to a lower energy state requiring an energy hole is called a ***transition reaction*** and the resonant energy acceptor including a catalyst that is unchanged in the over all reaction to form hydrinos can generally be considered a ***source of energy holes***.

From energy conservation, the energy hole of a hydrogen atom, which excites resonator modes of radial dimensions $\frac{a_H}{m+1}$ is:

$$m \cdot 27.2\ eV, \quad \text{where } m = 1, 2, 3, 4, ... \tag{5.24}$$

After resonant absorption of the energy hole, the radius of the atomic orbital, a_H, shrinks to $\frac{a_H}{m+1}$ and after t cycles of transition, the radius is $\frac{a_H}{mt+1}$. In other words, the radial ground state field can be considered as the superposition of Fourier components. The removal of negative Fourier components of energy $m \cdot 27.2\ eV$, where m is an integer, increases the positive electric field inside the spherical shell by m times that of a proton charge. The resultant electric field is a time harmonic solution of Laplace's Equations in spherical coordinates. In this case, the radius at which force balance and nonradiation are achieved is $\frac{a_H}{m+1}$ where m is an integer. In decaying to this radius from the "ground" state, a total energy of $[(m+1)^2 - 1^2] \cdot 13.6\ eV$ is released. The process is called the **Atomic BlackLight Process.**

For the hydrogen atom, the radius of the ground state atomic orbital is a_H. This atomic orbital contains no photonic waves and the centrifugal force and the electric force balance including the electrodynamic force, which is included by using the reduced electron mass as given by Eqs. (1.254), (1.259), and (1.260) is:

$$\frac{m_e v_1^2}{a_H} = \frac{e^2}{4\pi\varepsilon_0 a_H^2} \tag{5.25}$$

where v_1 is the velocity in the "ground" state. It was shown in the Excited States of the One-Electron Atom (Quantization) section that the electron atomic orbital is a resonator cavity, which can trap electromagnetic radiation of discrete frequencies. The photon electric field functions are solutions of Laplace's equation. The "trapped photons" decrease the effective nuclear charge or nuclear charge factor Z_{eff} to $1/n$ and increase the radius of the atomic orbital to na_H. The new configuration is also in force balance.

$$\frac{\hbar^2}{m_e r_n^3} = \frac{Z_{eff} e^2}{4\pi\varepsilon_0 r_n^2} \tag{5.26}$$

Similarly a transition to a hydrino state occurs because the effective nuclear charge increases by an integer, m, when Eqs. (5.26-5.28) are satisfied by the introduction of an energy hole. The source of energy holes may not be consumed in the transition reaction; therefore it serves as a catalyst. The catalyst provides energy holes and causes the transition from the initial radius $\frac{a_H}{p}$ and an effective nuclear charge of p to the second radius $\frac{a_H}{p+m}$ and an effective nuclear charge of $p+m$. Energy conservation and the boundary condition that "trapped photons" must be a solution to Laplace's equation determine that the energy hole to cause a transition is given by Eq. (5.24). As a result of coupling, the hydrogen atom nonradiatively transfers $m \cdot 27.2\ eV$ to the catalyst.

Stated another way, the hydrogen atom absorbs an energy hole of $m \cdot 27.2\ eV$. The energy hole absorption causes a standing electromagnetic wave ("photon") to be trapped in the hydrogen atom electron atomic orbital having the same form of Maxwellian solution of electromagnetic radiation of discrete energy trapped in a resonator cavity as for excited states given in the Excited States of the One-Electron Atom (Quantization) section. As shown previously, the photonic equation must be a solution of Laplace's equation in spherical coordinates. The "trapped photon" field comprises an electric field, which provides force balance and a nonradiative electron current. Following that given for excited states (Eq. (2.15)), the solution to this boundary value problem of the radial photon electric field is given by:

$$\mathbf{E}_{r\ photon\ n,l,m} = \frac{e(na_H)^{\ell}}{4\pi\varepsilon_0} \frac{1}{r^{(\ell+2)}} \left[-Y_0^0(\theta,\phi) + \frac{1}{n}\left[Y_0^0(\theta,\phi) + \mathrm{Re}\left\{ Y_\ell^m(\theta,\phi) e^{im\omega_n t} \right\} \right] \right] \delta(r - r_n) \tag{5.27}$$

$$n = \frac{1}{p}$$

$$2 \le p \le 137$$

$$\ell = 0, 1, 2, ..., p-1$$

$$m_\ell = -\ell, -\ell + 1, ..., 0, ..., +\ell$$

$$m_s = \pm\frac{1}{2}$$

The quantum numbers of the electron are p, ℓ, m_ℓ, and m_s as described in the Excited States of the One-Electron Atom (Quantization) section wherein the principal quantum number of excited states is replaced by $n = \frac{1}{p}$. It is apparent from this equation that given an initial radius of $\frac{a_H}{p}$ and a final radius of $\frac{a_H}{p+m}$, the central field is increased by m with the absorption of an energy hole of $m \cdot 27.2\ eV$. The potential energy decreases by this energy; thus, energy is conserved. However, the force balance equation is not initially satisfied as the effective nuclear charge increases by m. Further energy is emitted as force balance is achieved at the final radius. By replacing the initial radius with the final radius, and by increasing the charge by m in Eq. (5.26).

$$[p+m]^3 \frac{\hbar^2}{m_e a_H^3} = [p+m]^2 \frac{((p+m)e)e}{4\pi\varepsilon_0 a_H^2} \tag{5.28}$$

Force balance is achieved and the electron is non-radiative. The energy balance for $m = 1$ is as follows. An initial energy of $27.2\ eV$ is transferred as the energy hole absorption event. This increases the nuclear charge (effective nuclear charge factor) by one elementary charge unit and decreases the potential by $27.2\ eV$. More energy is emitted until the total energy released is $[(p+1)^2 - p^2] \cdot 13.6\ eV$. The potential energy diagram of the electron is given in Figure 5.1.

Figure 5.1. Potential Energy well of a Hydrogen Atom.

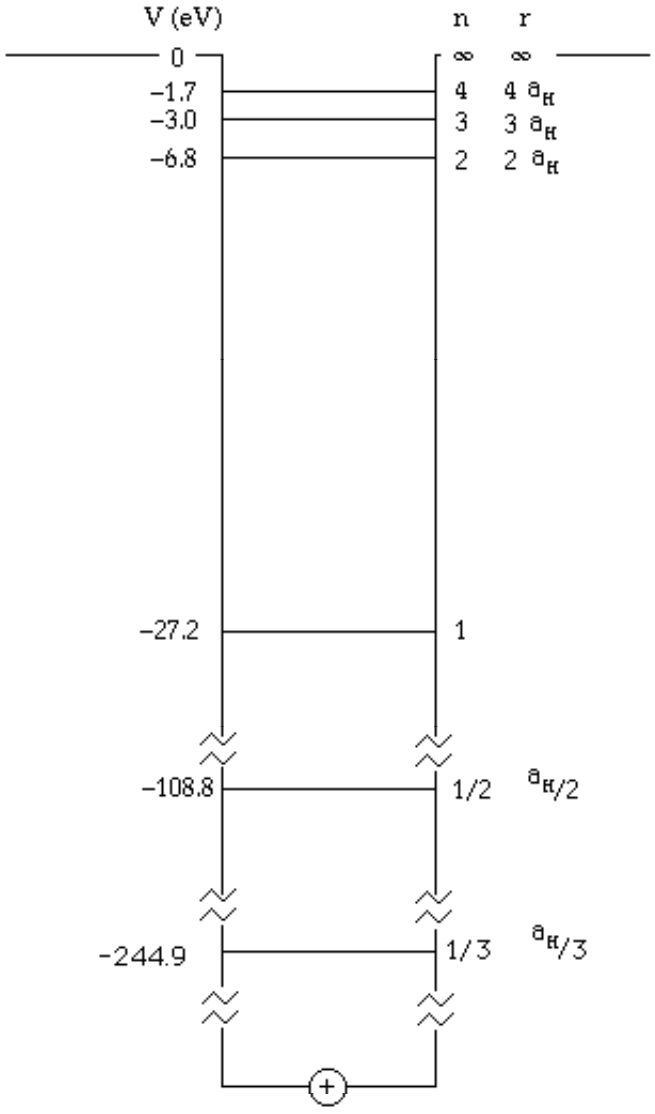

The energy hole ($m \cdot 27.2\ eV$) required to cause a hydrogen atom to undergo a transition reaction to form a given hydrino atom ($H\left(\frac{a_H}{m+1}\right)$) as well as the corresponding radius ($\frac{a_H}{(m+1)}$), effective nuclear charge factor ($Z_{eff} = m+1$) and energy parameters of several states of atomic hydrogen are given in Table 5.1.

Table 5.1. Principal quantum number, radius, potential energy, kinetic energy, effective nuclear charge factor, energy hole required to form the hydrino from atomic hydrogen (n=1), and hydrino binding energy, respectively, for several states of hydrogen.

$H(n)$	R	V (eV)	T (eV)	Z_{eff}	Energy Hole (eV)	Binding Energy (eV)
1	a_H	-27.2	13.6	1	0	13.6
$\frac{1}{2}$	$\frac{a_H}{2}$	-108.8	54.4	2	27.2	54.4
$\frac{1}{3}$	$\frac{a_H}{3}$	-244.9	122.4	3	54.4	122.4
$\frac{1}{4}$	$\frac{a_H}{4}$	-435.4	217.7	4	81.6	217.7
$\frac{1}{5}$	$\frac{a_H}{5}$	-680.2	340.1	5	108.8	340.1
$\frac{1}{6}$	$\frac{a_H}{6}$	-979.6	489.6	6	136.1	489.6
$\frac{1}{7}$	$\frac{a_H}{7}$	-1333.3	666.4	7	163.3	666.4
$\frac{1}{8}$	$\frac{a_H}{8}$	-1741.4	870.4	8	190.5	870.4
$\frac{1}{9}$	$\frac{a_H}{9}$	-2204.0	1101.6	9	217.7	1101.6
$\frac{1}{10}$	$\frac{a_H}{10}$	-2721.0	1360.5	10	244.9	1360.5

The size of the electron atomic orbital as a function of potential energy is given in Figure 5.2.

Figure 5.2. Quantized sizes of hydrogen atoms where n is an integer for excited states and $n = 1/p$. for hydrino states where p is an integer.

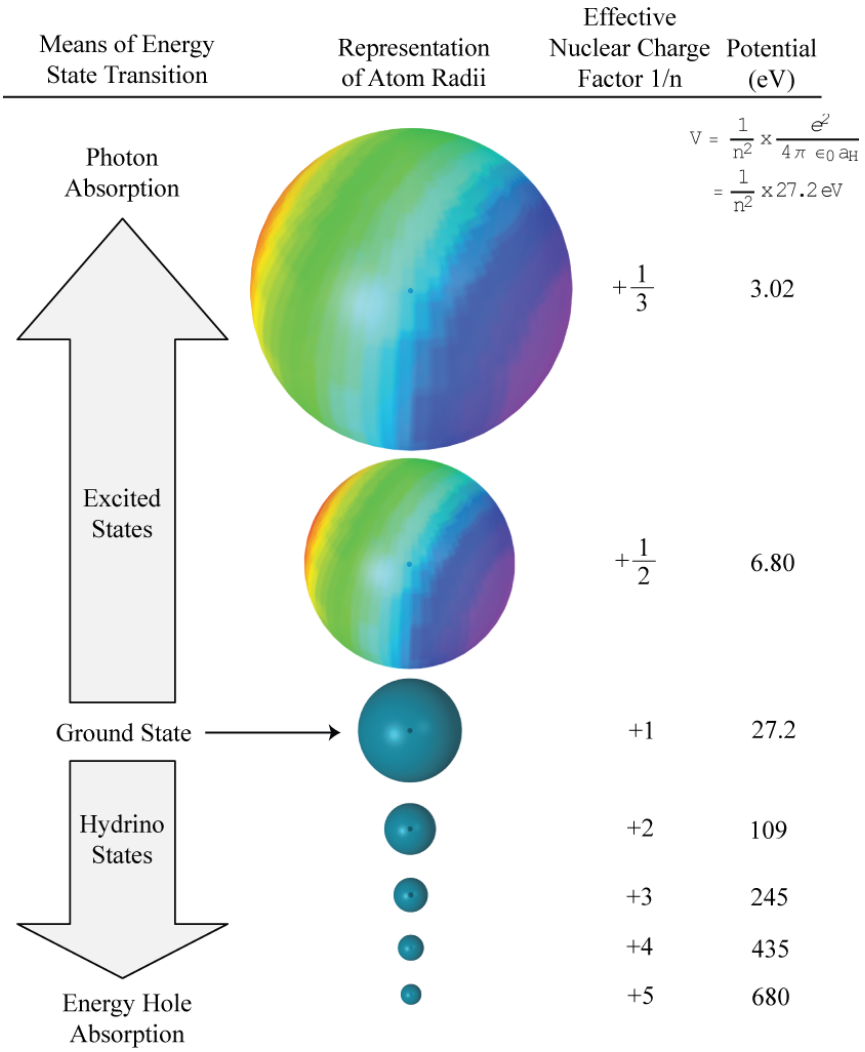

CATALYSTS

A source of energy holes that is not consumed in the reaction serves as a catalyst that provides a net positive enthalpy of reaction of $m \cdot 27.2\ eV$ (i.e. it resonantly accepts the nonradiative energy transfer from hydrogen atoms and releases the energy to the surroundings to affect electronic transitions to fractional quantum energy levels). K, He^+, Ar^+, Sr^+, Li, K, NaH, and H_2O, for example, are predicted to serve as catalysts since they meet the catalyst criterion—a chemical or physical process with an enthalpy change equal to an integer multiple of the potential energy of atomic hydrogen, $27.2\ eV$, or have a potential energy of $m \cdot 27.2\ eV$. Specifically, an exemplary catalytic system is provided by the ionization of t electrons from an atom each to a continuum energy level such that the sum of the ionization energies of the t electrons is approximately $m \cdot 27.2\ eV$ where m is an integer. One such catalytic system involves potassium atoms. K can serve as a catalyst since the ionization of K to K^{3+} is about $81.6\ eV$ ($3 \cdot 27.2\ eV$). As a consequence of the nonradiative energy transfer, the hydrogen atom becomes unstable and emits further energy until it achieves a lower-energy nonradiative state having a principal energy level given by Eqs. (5.1) and (5.3). Thus, the catalysis releases energy from the hydrogen atom with a commensurate decrease in size of the hydrogen atom, $r_n = na_H$ where n is given by Eq. (5.3). For example, the catalysis of $H(n=1)$ to $H(n=1/4)$ releases $204\ eV$, and the hydrogen radius decreases from a_H to $\frac{1}{4}a_H$. Specifically, the first, second, and third ionization energies of potassium are $4.34066\ eV$, $31.63\ eV$, $45.806\ eV$, respectively [11]. The triple ionization ($t=3$) reaction of K to K^{3+}, then, has a net enthalpy of reaction of $81.7767\ eV$, which is equivalent to $m=3$ in Eq. (5.24).

$$81.7767\ eV + K(m) + H\left[\frac{a_H}{p}\right] \rightarrow K^{3+} + 3e^- + H\left[\frac{a_H}{(p+3)}\right] + [(p+3)^2 - p^2] \cdot 13.6\ eV \tag{5.29}$$

$$K^{3+} + 3e^- \rightarrow K(m) + 81.7767\ eV \tag{5.30}$$

And, the overall reaction is

$$H\left[\frac{a_H}{p}\right] \rightarrow H\left[\frac{a_H}{(p+3)}\right] + [(p+3)^2 - p^2] \cdot 13.6\ eV \tag{5.31}$$

The potassium-atom catalyst (K) and the $3+$ ion (K^{3+}) that arises from the resonant energy transfer are solved in the Three-Through Twenty-Electron Atoms section and are shown in Figure 5.3.

Figure 5.3. Cross Section of Charge-Density Functions of K and K^{3+} Shown in Color Scale. The electrons of multielectron atoms exist as concentric atomic orbitals ("bubble-like" charge-density functions) of discrete radii, which are given by r_n of the radial Dirac delta function, $\delta(r-r_n)$ and serve as resonator cavities during the resonant nonradiative energy transfer that gives rise to ionization. Each s orbital is a constant current-density function which gives rise to spin, and the charge-density of each p orbital is a superposition of a constant and a spherical and time harmonic function. The corresponding charge-density wave on the surface gives rise to electron orbital angular momentum that superimposes the spin angular momentum. The insert on the right shows the atom and ions at a lower magnification to view the outer 4s electron of K.

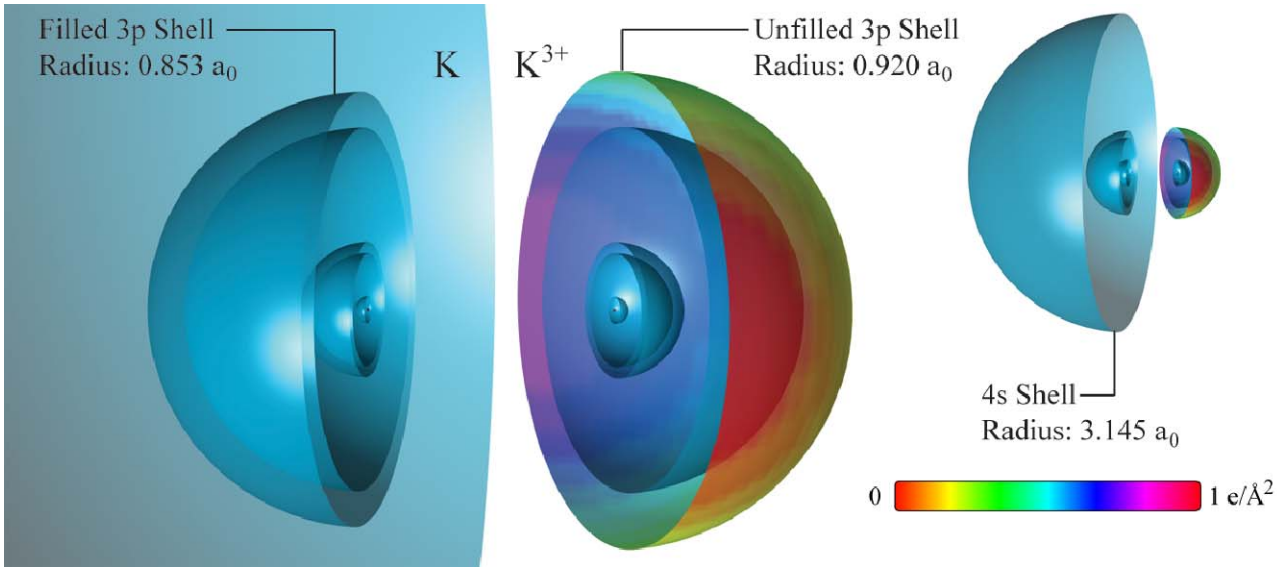

The energy given off during catalysis is much greater than the energy lost to the catalyst. The energy released is large as compared to conventional chemical reactions. For example, when hydrogen and oxygen gases undergo combustion to form water ($H_2(g)+\frac{1}{2}O_2(g)\rightarrow H_2O(l)$) the known enthalpy of formation of water is $\Delta H_f=-286\ kJ/mole$ or 1.48 eV per hydrogen atom. By contrast, each ($n=1$) ordinary hydrogen atom undergoing a catalysis step to $n=\frac{1}{2}$ releases a net of $40.8\ eV$. Moreover, further catalytic transitions may occur: $n=\frac{1}{2}\rightarrow\frac{1}{3}$, $\frac{1}{3}\rightarrow\frac{1}{4}$, $\frac{1}{4}\rightarrow\frac{1}{5}$, and so on. Once catalysis begins, hydrinos autocatalyze further in a process called disproportionation discussed in the Disproportionation of Energy States section.

Helium ions can serve as a catalyst because the second ionization energy of helium is $54.417\ eV$, which is equivalent to $2\cdot 27.2\ eV$. In this case, $54.417\ eV$ is transferred nonradiatively from atomic hydrogen to He^+ which is resonantly ionized. The electron decays to the $n=1/3$ state with the further release of $54.417\ eV$ as given in Eq. (5.7). The full catalysis reaction invoving an energetic intermediate formed by the energy transfer to the catalyst is:

$$54.417\ eV+He^++H\left[a_H\right]\rightarrow He^{2+}+e^-+H^*\left[\frac{a_H}{3}\right]+54.4\ eV \tag{5.32}$$

$$H^*\left[\frac{a_H}{3}\right]\rightarrow H\left[\frac{a_H}{3}\right]+54.4\ eV \tag{5.33}$$

$$He^{2+}+e^-\rightarrow He^++54.417\ eV \tag{5.34}$$

And, the overall reaction is:

$$H\left[a_H\right]\rightarrow H\left[\frac{a_H}{3}\right]+54.4\ eV+54.4\ eV \tag{5.35}$$

wherein $H^*\left[\frac{a_H}{3}\right]$ has the radius of the hydrogen atom and a central field equivalent to 3 times that of a proton and $H\left[\frac{a_H}{3}\right]$ is the corresponding stable state with the radius of 1/3 that of H. As the electron undergoes radial acceleration from the radius of the hydrogen atom to a radius of 1/3 this distance, energy is released as characteristic light emission or as third-body kinetic energy.

Hydrogen catalysts capable of providing a net enthalpy of reaction of approximately $m\cdot 27.2\ eV$ where m is an integer to produce a hydrino (whereby t electrons are ionized from an atom or ion) are given in Table 5.2. The atoms or ions given in

the first column are ionized to provide the net enthalpy of reaction of $m \cdot 27.2\ eV$ given in the tenth column where m is given in the eleventh column. The electrons that participate in ionization are given with the ionization potential (also called ionization energy or binding energy). The ionization potential of the nth electron of the atom or ion is designated by IP_n and is given by the CRC [11]. That is for example, $Li + 5.39172\ eV \rightarrow Li^+ + e^-$ and $Li^+ + 75.6402\ eV \rightarrow Li^{2+} + e^-$. The first ionization potential, $IP_1 = 5.39172\ eV$, and the second ionization potential, $IP_2 = 75.6402\ eV$, are given in the second and third columns, respectively. The net enthalpy of reaction for the double ionization of Li is $81.0319\ eV$ as given in the tenth column, and $m = 3$ in Eq. (5.24) as given in the eleventh column.

Table 5.2. Hydrogen Catalysts.

Catalyst	IP1	IP2	IP3	IP4	IP5	IP6	IP7	IP8	Enthalpy	m
Li	5.39172	75.6402							81.032	3
Be	9.32263	18.2112							27.534	1
K	4.34066	31.63	45.806						81.777	3
Ca	6.11316	11.8717	50.9131	67.27					136.17	5
Ti	6.8282	13.5755	27.4917	43.267	99.3				190.46	7
V	6.7463	14.66	29.311	46.709	65.2817				162.71	6
Cr	6.76664	16.4857	30.96						54.212	2
Mn	7.43402	15.64	33.668	51.2					107.94	4
Fe	7.9024	16.1878	30.652						54.742	2
Fe	7.9024	16.1878	30.652	54.8					109.54	4
Co	7.881	17.083	33.5	51.3					109.76	4
Co	7.881	17.083	33.5	51.3	79.5				189.26	7
Ni	7.6398	18.1688	35.19	54.9	76.06				191.96	7
Ni	7.6398	18.1688	35.19	54.9	76.06	108			299.96	11
Cu	7.72638	20.2924							28.019	1
Zn	9.39405	17.9644							27.358	1
Zn	9.39405	17.9644	39.723	59.4	82.6	108	134	174	625.08	23
As	9.8152	18.633	28.351	50.13	62.63	127.6			297.16	11
Se	9.75238	21.19	30.8204	42.945	68.3	81.7	155.4		410.11	15
Kr	13.9996	24.3599	36.95	52.5	64.7	78.5			271.01	10
Kr	13.9996	24.3599	36.95	52.5	64.7	78.5	111		382.01	14
Rb	4.17713	27.285	40	52.6	71	84.4	99.2		378.66	14
Rb	4.17713	27.285	40	52.6	71	84.4	99.2	136	514.66	19
Sr	5.69484	11.0301	42.89	57	71.6				188.21	7
Nb	6.75885	14.32	25.04	38.3	50.55				134.97	5
Mo	7.09243	16.16	27.13	46.4	54.49	68.8276			220.10	8
Mo	7.09243	16.16	27.13	46.4	54.49	68.8276	125.664	143.6	489.36	18
Pd	8.3369	19.43							27.767	1
Sn	7.34381	14.6323	30.5026	40.735	72.28				165.49	6
Te	9.0096	18.6							27.61	1
Te	9.0096	18.6	27.96						55.57	2
Cs	3.8939	23.1575							27.051	1
Ce	5.5387	10.85	20.198	36.758	65.55				138.89	5
Ce	5.5387	10.85	20.198	36.758	65.55	77.6			216.49	8
Pr	5.464	10.55	21.624	38.98	57.53				134.15	5
Sm	5.6437	11.07	23.4	41.4					81.514	3
Gd	6.15	12.09	20.63	44					82.87	3
Dy	5.9389	11.67	22.8	41.47					81.879	3
Pb	7.41666	15.0322	31.9373						54.386	2
Pt	8.9587	18.563							27.522	1
He^+		54.4178							54.418	2
Na^+		47.2864	71.6200	98.91					217.816	8
Rb^+		27.285							27.285	1
Fe^{3+}				54.8					54.8	2
Mo^{2+}			27.13						27.13	1
Mo^{4+}					54.49				54.49	2
In^{3+}				54					54	2
Ar^+		27.62							27.62	1
Sr^+		11.03	42.89						53.92	2
$2K^+$ to K and K^{2+}	4.34	31.63							27.28	1
$2Ba^{2+}$ to Ba^+ and Ba^{3+}	5.21	10	37.3						27.3	1

Certain molecules may also serve to affect transitions of H to form hydrinos. In general, a compound comprising hydrogen such as MH, where M is an element other than hydrogen, serves as a source of hydrogen and a source of catalyst. A catalytic reaction is provided by the breakage of the $M-H$ bond plus the ionization of t electrons from the atom M each to a continuum energy level such that the sum of the bond energy and ionization energies of the t electrons is approximately

$m \cdot 27.2\ eV$, where m is an integer. One such catalytic system involves sodium hydride. The bond energy of NaH is $1.9245\ eV$ [27], and the first and second ionization energies of Na are $5.13908\ eV$ and $47.2864\ eV$, respectively [11]. Based on these energies NaH molecule can serve as a catalyst and H source, since the bond energy of NaH plus the double ionization ($t = 2$) of Na to Na^{2+} is $54.35\ eV$ ($2 \cdot 27.2\ eV$). The concerted catalyst reactions are given by:

$$54.35\ eV + NaH \rightarrow Na^{2+} + 2e^- + H\left[\frac{a_H}{3}\right] + [3^2 - 1^2] \cdot 13.6\ eV \tag{5.36}$$

$$Na^{2+} + 2e^- + H \rightarrow NaH + 54.35\ eV \tag{5.37}$$

And, the overall reaction is:

$$H \rightarrow H\left[\frac{a_H}{3}\right] + [3^2 - 1^2] \cdot 13.6\ eV \tag{5.38}$$

A molecule that accepts $m \cdot 27.2\ eV$ from atomic H with a decrease in the magnitude of the potential energy of the molecule by the same energy may serve as a catalyst. For example, the potential energy of H_2O given by Eq. (13.201) is:

$$V_e = \left(\frac{3}{2}\right)\frac{-2e^2}{8\pi\varepsilon_0\sqrt{a^2 - b^2}} \ln\frac{a + \sqrt{a^2 - b^2}}{a - \sqrt{a^2 - b^2}} = -81.8715\ eV \tag{5.39}$$

The full catalysis reaction $(m = 3)$ is:

$$81.6\ eV + H_2O + H\left[a_H\right] \rightarrow 2H^+_{fast} + O^+ + 3e^- + H*\left[\frac{a_H}{4}\right] + 81.6\ eV \tag{5.40}$$

$$H*\left[\frac{a_H}{4}\right] \rightarrow H\left[\frac{a_H}{4}\right] + 122.4\ eV \tag{5.41}$$

$$2H^+_{fast} + O^+ + 3e^- \rightarrow H_2O + 81.6\ eV \tag{5.42}$$

And, the overall reaction is:

$$H\left[a_H\right] \rightarrow H\left[\frac{a_H}{4}\right] + 81.6\ eV + 122.4\ eV \tag{5.43}$$

wherein $H*\left[\frac{a_H}{4}\right]$ has the radius of the hydrogen atom and a central field equivalent to 4 times that of a proton and $H\left[\frac{a_H}{4}\right]$ is the corresponding stable state with the radius of 1/4 that of H.

ENERGY HOLE AS A MULTIPOLE EXPANSION

The potential energy (Eq. (1.261)) of the hydrino states of radius $\frac{a_H}{p}$ having a central field of magnitude p is:

$$-p^2 \cdot 27.2\ eV \tag{5.44}$$

where p is an integer. The potential energy is given as the superposition of ℓ energy-degenerate quantum states corresponding to a multipole expansion of the central electromagnetic field. Based on the selection rules given in the Excited States of the One-Electron Atom (Quantization) section that are enabled by multipole coupling, one multipole moment of all those possible, need be excited to stimulate the below "ground" state transition. The total number, N, of multipole moments where each corresponds to an ℓ and m_ℓ quantum number of an energy level corresponding to a principal quantum number of p is:

$$N = \sum_{\ell=0}^{p-1} \sum_{m_\ell=-\ell}^{+\ell} 1 = \sum_{\ell=0}^{n-1} 2\ell + 1 = p^2 \tag{5.45}$$

Thus, the energy hole to stimulate a transition of a hydrogen atom from radius $\frac{a_H}{p}$ to radius $\frac{a_H}{p+1}$ with an increase in the central field from p to $p+1$ where p is an integer is:

$$(p+1)^2 \cdot 27.2 \cdot \frac{1}{(p+1)^2} = 27.2\ eV \tag{5.46}$$

Eq. (5.46) obeys superposition such that the energy hole for the excitation of m multipoles is $m \cdot 27.2\ eV$. Energy conservation occurs during the absorption of an energy hole. For a hydrogen atom with a principal quantum number of p having a radius of $\frac{a_H}{p}$, the absorption of an energy hole of $m \cdot 27.2\ eV$ instantaneously decreases the potential energy by $m \cdot 27.2\ eV$. The calculation of the instantaneous electric field of the photon standing wave corresponding to the absorbed energy hole is determined by the conservation of the potential energy change due to the absorption of the energy hole of equal but opposite

energy. It is given by the summation over all possible multipoles of the integral of the product of the electric field of the photon standing wave and the multipoles of the electron charge-density function. The multipole of the photon standing wave and each multipole of the electron charge-density function correspond to an ℓ and m_ℓ quantum number.

DISPROPORTIONATION OF ENERGY STATES

Hydrogen and hydrinos may serves as catalysts. As given *infra* hydrogen atoms $H\left(1/p\right)$ $p=1,2,3,...137$ can undergo transitions to lower-energy states given by Eqs. (5.1) and (5.3) wherein the transition of one atom is catalyzed by a second that resonantly and nonradiatively accepts $m\cdot 27.2\ eV$ with a concomitant opposite change in its potential energy. The overall general equation for the transition of $H\left(1/p\right)$ to $H\left(1/\left(m+p\right)\right)$ induced by a resonance transfer of $m\cdot 27.2\ eV$ to $H\left(1/p'\right)$ is represented by (Eq. (5.75))

$$H\left(1/p'\right)+H\left(1/p\right)\rightarrow H+H\left(1/(m+p)\right)+\left[2pm+m^2-p'^2+1\right]\cdot 13.6\ eV \tag{5.47}$$

Thus, hydrogen atoms may serve as a catalyst wherein $m=1$, $m=2$, and $m=3$ for one, two, and three atoms, respectively, acting as a catalyst for another. The rate for the two- or three-atom-catalyst case would be appreciable only when the H density is high. But, high H densities are not uncommon. A high hydrogen atom concentration permissive of 2H or 3H serving as the energy acceptor for a third may be achieved under several circumstances such as on the surface of the Sun and stars due to the temperature and gravity driven density, on metal surfaces that support multiple monolayers, and in highly dissociated plasmas, especially pinched hydrogen plasmas. Additionally, a three-body H interaction is easily achieved when two H atoms arise with the collision of a hot H with H_2. This event can commonly occur in plasmas having a large population of extraordinarily fast H as reported previously [1-7]. This is evidenced by the unusual intensity of atomic H emission. In such cases, energy transfer can occur from a hydrogen atom to two others within sufficient proximity, being typically a few angstroms as given in the Dipole-Dipole Coupling section. Then, the reaction between three hydrogen atoms whereby two atoms resonantly and nonradiatively accept $54.4\ eV$ from the third hydrogen atom such that $2H$ serves as the catalyst is given by:

$$54.4\ eV+2H+H\rightarrow 2H^+_{fast}+2e^-+H*\left[\frac{a_H}{3}\right]+54.4\ eV \tag{5.48}$$

$$H*\left[\frac{a_H}{3}\right]\rightarrow H\left[\frac{a_H}{3}\right]+54.4\ eV \tag{5.49}$$

$$2H^+_{fast}+2e^-\rightarrow 2H+54.4\ eV \tag{5.50}$$

And, the overall reaction is:

$$H\rightarrow H\left[\frac{a_H}{3}\right]+[3^2-1^2]\cdot 13.6\ eV \tag{5.51}$$

$H*\left[\frac{a_H}{2+1}\right]$ has the radius of the hydrogen atom (corresponding to the 1 in the denominator) and a central field equivalent to 3 times that of a proton, and $H\left[\frac{a_H}{3}\right]$ is the corresponding stable state with the radius of 1/3 that of H. As the electron undergoes radial acceleration from the radius of the hydrogen atom to a radius of 1/3 this distance, energy is released as characteristic light emission or as third-body kinetic energy. The emission may be in the form of an extreme-ultraviolet continuum radiation having an edge at $54.4\ eV$ (22.8 nm) and extending to longer wavelengths. Alternatively, H is the lightest atom; thus, it is the most probable fast species in collisional energy exchange from the H intermediate (e.g. $H*\left[\frac{a_H}{2+1}\right]$). Additionally, H is unique with regard to the energetic transition state intermediate (generally represented by $H*\left[\frac{a_H}{m+p}\right]$) in that all these species are energy states of hydrogen with corresponding harmonic frequencies. Thus, the cross section for H excitation by a nonradiative energy transfer to form fast H is predicted to be large since it is a resonant process. Efficient energy transfer can occur by common through-space mechanisms such as dipole-dipole interactions as described by Förster's theory *infra*. Consequently, in addition to radiation, a resonant kinetic energy transfer to form fast H may occur. Alternatively, fast H is a direct product of H or hydrino serving as the catalyst or source of energy holes as given by Eqs. (5.48), (5.53), (5.58), and (5.71) wherein the acceptance of the resonant energy transfer regards the potential energy rather than the ionization energy. Conservation of energy gives a proton of

the kinetic energy corresponding to one half the potential energy in the former case and a catalyst ion at essentially rest in the latter case. The H recombination radiation of the fast protons gives rise to broadened Balmer α emission that is disproportionate to the inventory of hot hydrogen consistent with the excess power balance. Conservation of momentum in the formation of fast protons also gives rise to hot hydrinos that heat H. Subsequent excitation of these fast $H(n=1)$ atoms by collisions with the background H_2 followed by emission of the corresponding $H(n=3)$ fast atoms gives rise to broadened Balmer α emission but of less intensity than directly formed hot protons that emit by recombination. With increasingly lower-energy states formed over time as the reaction progresses, very large kinetic energies are predicted throughout the cell. Only isotropic non-directional broadening of hydrogen atomic lines is predicted with an increase in fast H with time. These features have been confirmed experimentally [1-7], especially regarding closed hydrogen plasmas or water vapor plasmas that become predominantly H plasmas in time [1-3]. Overall, the EUV continuum radiation and fast H were observed with hydrogen plasmas wherein 2H served as the catalyst [8-9]. Astrophysical soft X-ray continuum radiation bands are observed at 10.1 nm, 22.8 nm, and 91.2 nm as predicted for mH catalyst, $m=1$, $m=2$, and $m=3$, respectively [8]. Soft X-ray continuum radiation having a 10.1 nm cutoff was also observed in the laboratory as predicted for H_2O catalyst [8]. Thus, the predictions corresponding to transitions of atomic hydrogen to form hydrinos were experimentally confirmed.

The predicted product of 2H (Eqs. (5.48-5.51)) catalyst reaction is $H(1/3)$. In the case of a high hydrogen atom concentration, the further transition given by Eq. (5.47) of $H(1/3)$ ($p=3$) to $H(1/4)$ ($m+p=4$) with H as the catalyst ($p'=1$; $m=1$) can be fast:

$$H(1/3) \xrightarrow{H} H(1/4) + 95.2\ eV \tag{5.52}$$

In another H-atom catalyst reaction involving a direct transition to $\left[\frac{a_H}{4}\right]$ state, two hot H_2 molecules collide and dissociate such that three H atoms serve as a catalyst of $3 \cdot 27.2\ eV$ for the fourth. Then, the reaction between four hydrogen atoms whereby three atoms resonantly and nonradiatively accept $81.6\ eV$ from the fourth hydrogen atom such that $3H$ serves as the catalyst is given by:

$$81.6\ eV + 3H + H \rightarrow 3H^+_{fast} + 3e^- + H*\left[\frac{a_H}{4}\right] + 81.6\ eV \tag{5.53}$$

$$H*\left[\frac{a_H}{4}\right] \rightarrow H\left[\frac{a_H}{4}\right] + 122.4\ eV \tag{5.54}$$

$$3H^+_{fast} + 3e^- \rightarrow 3H + 81.6\ eV \tag{5.55}$$

And, the overall reaction is

$$H \rightarrow H\left[\frac{a_H}{4}\right] + [4^2 - 1^2] \cdot 13.6\ eV \tag{5.56}$$

The extreme-ultraviolet continuum radiation band due to the $H*\left[\frac{a_H}{3+1}\right]$ intermediate of Eq. (5.53) is predicted to have short wavelength cutoff at $122.4\ eV$ (10.1 nm) and extend to longer wavelengths. This continuum band also formed by H_2O catalyst was confirmed experimentally [8]. In general, the transition of H to $H\left[\frac{a_H}{p=m+1}\right]$ due by the acceptance of $m \cdot 27.2\ eV$ gives a continuum band with a short wavelength cutoff and energy $E_{\left(H \rightarrow H\left[\frac{a_H}{p=m+1}\right]\right)}$ given by:

$$\begin{aligned} E_{\left(H \rightarrow H\left[\frac{a_H}{p=m+1}\right]\right)} &= m^2 \cdot 13.6\ eV \\ \lambda_{\left(H \rightarrow H\left[\frac{a_H}{p=m+1}\right]\right)} &= \frac{91.2}{m^2}\ nm \end{aligned} \tag{5.57}$$

and extending to longer wavelengths than the corresponding cutoff. The radiation band is in the region from zero to the cutoff wavelength with a Bremsstrahlung profile that is predominantly in the high-energy region.

Consistent with Eq. (5.57) with $m=1$, a 91.2 nm continuum in argon plasma with trace hydrogen was observed where the catalyst reaction Ar^+ to Ar^{2+} has a net enthalpy of reaction of $27.63\ eV$ [28]. Two hydrogen atoms may react to give the

same continuum band by a reaction similar to those given by Eqs. (5.48-5.51). The reaction whereby one H resonantly and nonradiatively accepts $27.2\ eV$ from the other hydrogen atom such that it serves as the catalyst is given by:

$$27.2\ eV + H + H \rightarrow H^{+}_{fast} + e^{-} + H*\left[\frac{a_H}{2}\right] + 27.2\ eV \tag{5.58}$$

$$H*\left[\frac{a_H}{2}\right] \rightarrow H\left[\frac{a_H}{2}\right] + 13.6\ eV \tag{5.59}$$

$$H^{+}_{fast} + e^{-} \rightarrow H + 27.2\ eV \tag{5.60}$$

And, the overall reaction is:

$$H \rightarrow H\left[\frac{a_H}{2}\right] + [2^2 - 1^2]\cdot 13.6\ eV \tag{5.61}$$

The emission from Eq. (5.59) may be in the form of an extreme-ultraviolet continuum radiation having an edge at $13.6\ eV$ (91.2 nm) and extending to longer wavelengths. This band was also observed in pulsed pure hydrogen plasmas using the normal incidence spectrometer, but temporal studies are required in order to eliminate the background hydrogen molecular band. These bands were eliminated previously in the argon plasma with trace hydrogen [28] wherein H is highly dissociated. Hydrogen may emit the series of 10.1 nm, 22.8 nm, and 91.2 nm continua as shown in Ref. [8].

Since the products of the catalysis reactions (e.g. Eqs. (5.48-5.51)) have binding energies of $m\cdot 27.2\ eV$, they may further serve as catalysts. Thus, further catalytic transitions may occur: $n=\frac{1}{3}\rightarrow\frac{1}{4}$, $\frac{1}{4}\rightarrow\frac{1}{5}$, and so on. Thus, lower-energy hydrogen atoms, *hydrinos*, can act as catalysts by resonantly and nonradiatively accepting energy of $m\cdot 27.2\ eV$ from another H or hydrino atom (Eq. (5.24)). The process can occur by several mechanisms: metastable excitation, resonance excitation, and ionization energy of a hydrino atom is $m\cdot 27.2\ eV$ (Eq. (5.24)). The transition reaction mechanism of a first hydrino atom affected by a second hydrino atom involves the resonant coupling between the atoms of m degenerate multipoles each having $27.2\ eV$ of potential energy. (See the Energy Hole as a Multipole Expansion section).

The energy transfer of $m\cdot 27.2\ eV$ from the first hydrino atom to the second hydrino atom causes the central field of the first to increase by m and the electron of the first to drop m levels lower from a radius of $\frac{a_H}{p}$ to a radius of $\frac{a_H}{p+m}$. The second lower-energy hydrogen is excited to a metastable state, excited to a resonance state, or ionized by the resonant energy transfer. The resonant transfer may occur in multiple stages. For example, a nonradiative transfer by multipole coupling may occur wherein the central field of the first increases by m, then the electron of the first drops m levels lower from a radius of $\frac{a_H}{p}$ to a radius of $\frac{a_H}{p+m}$ with further resonant energy transfer. The energy transferred by multipole coupling may occur by a mechanism that is analogous to photon absorption involving an excitation to a virtual level. Or, the energy transferred by multipole coupling during the electron transition of the first hydrino atom may occur by a mechanism that is analogous to two-photon absorption involving a first excitation to a virtual level and a second excitation to a resonant or continuum level [29-31]. Similarly to the case with H as the catalyst, the transition energy greater than the energy transferred to the second hydrino atom may appear as a characteristic light emission in a vacuum medium or extraordinary fast H.

The transition of the hydrino intermediate from its radius to the corresponding hydrino radius gives rise to continuum radiation. By time reversal symmetry, the hydrino can serve as a catalyst to accept the energy difference between its state and a corresponding intermediate state at the radius of the intermediate wherein the decay to the hydrino radius releases the transferred energy. The release may be as continuum radiation or fast H.

For example, $H\left[\frac{a_H}{p'}\right]$ may serve as a source of energy holes for $H\left[\frac{a_H}{p}\right]$. In general, the transition of $H\left[\frac{a_H}{p}\right]$ to $H\left[\frac{a_H}{p+m}\right]$ induced by a resonance transfer of $m\cdot 27.2\ eV$ (Eq. (5.24)) with a metastable state excited in $H\left[\frac{a_H}{p'}\right]$ is represented by:

$$m\cdot 27.2\ eV + H\left[\frac{a_H}{p'}\right] + H\left[\frac{a_H}{p}\right] \rightarrow H*\left[\frac{a_H}{p'}\right] + H*\left[\frac{a_H}{p+m}\right] + m\cdot 27.2\ eV \tag{5.62}$$

$$H*\left[\frac{a_H}{p'}\right] \rightarrow H\left[\frac{a_H}{p'}\right] + m\cdot 27.2\ eV \tag{5.63}$$

$$H*\left[\frac{a_H}{p+m}\right] \rightarrow H\left[\frac{a_H}{p+m}\right] + \left[(p+m)^2 - p^2\right]\cdot 13.6\ eV - m\cdot 27.2\ eV \tag{5.64}$$

where p, p', and m are integers and the asterisk represents an excited metastable state. And, the overall reaction is:

$$H\left[\frac{a_H}{p}\right] \rightarrow H\left[\frac{a_H}{p+m}\right] + [(p+m)^2 - p^2] \cdot 13.6\ eV \tag{5.65}$$

The short-wavelength cutoff energy of the continuum radiation given by Eq. (5.57) is the maximum energy release of the hydrino intermediate as it decays. For example, both the reaction of H with $H\left[\frac{a_H}{p'}\right]$ as the source of an energy hole of $3 \cdot 27.2\ eV$ to form $H\left[\frac{a_H}{4}\right]$ and the reaction of $H\left[\frac{a_H}{5}\right]$ with $H\left[\frac{a_H}{p'}\right]$ as the source of an energy hole of $27.2\ eV$ to form $H\left[\frac{a_H}{6}\right]$ gives rise to a cutoff of 10.1 nm (122.4 eV) wherein the magnitude of the potential energy of $H\left[\frac{a_H}{p'}\right]$ is greater than $m \cdot 27.2\ eV$ for each case.

In another mechanism, the transition of $H\left[\frac{a_H}{p}\right]$ to $H\left[\frac{a_H}{p+m}\right]$ induced by a multipole resonance transfer of $m \cdot 27.2\ eV$ (Eq. (5.24)) and a transfer of $[(p')^2 - (p'-m')^2] \cdot 13.6\ eV - m \cdot 27.2\ eV$ with a resonance state of $H\left[\frac{a_H}{p'-m'}\right]$ excited in $H\left[\frac{a_H}{p'}\right]$ is represented by:

$$H\left[\frac{a_H}{p'}\right] + H\left[\frac{a_H}{p}\right] \rightarrow H\left[\frac{a_H}{p'-m'}\right] + H\left[\frac{a_H}{p+m}\right] + [\left((p+m)^2 - p^2\right) - \left(p'^2 - (p'-m')^2\right)] \cdot 13.6\ eV \tag{5.66}$$

where p, p', m, and m' are integers.

In two other mechanisms, the hydrino atom that serves as the source of the energy hole may be ionized by the resonant energy transfer. Consider the transition cascade for the pth cycle of the hydrogen-type atom, $H\left[\frac{a_H}{p}\right]$, with the hydrogen-type atom, $H\left[\frac{a_H}{p'}\right]$, that is ionized as the source of energy holes that causes the transition. The equation for the absorption of an energy hole of $m \cdot 27.2\ eV$ (Eq. (5.24)) equivalent to the binding energy of $H\left[\frac{a_H}{p'}\right]$, is represented by:

$$m \cdot 27.2\ eV + H\left[\frac{a_H}{p'}\right] + H\left[\frac{a_H}{p}\right] \rightarrow H^+ + e^- + H^*\left[\frac{a_H}{p+m}\right] + m \cdot 27.2\ eV \tag{5.67}$$

$$H^*\left[\frac{a_H}{p+m}\right] \rightarrow H\left[\frac{a_H}{p+m}\right] + \left[(p+m)^2 - p^2\right] \cdot 13.6\ eV - m \cdot 27.2\ eV \tag{5.68}$$

$$H^+ + e^- \rightarrow + H\left[\frac{a_H}{1}\right] + 13.6\ eV \tag{5.69}$$

And, the overall reaction is:

$$H\left[\frac{a_H}{p'}\right] + H\left[\frac{a_H}{p}\right] \rightarrow H\left[\frac{a_H}{1}\right] + H\left[\frac{a_H}{(p+m)}\right] + \left[2pm + m^2 - p'^2 + 1\right] \cdot 13.6\ eV \tag{5.70}$$

wherein $m \cdot 27.2\ eV = p'^2 \cdot 13.6\ eV$.

Alternatively, the energy transfer may affect the potential energy of the acceptor rather than the total energy. The energy transfer from a first hydrogen-type atom $H\left[\frac{a_H}{p}\right]$ to a second acceptor hydrogen-type atom $H\left[\frac{a_H}{p'}\right]$ serving as a catalyst causes the electric potential energy of the acceptor hydrogen-type atom to become zero, and the energy conservation gives rise to a hot proton with the ionization of the energy acceptor hydrogen-type atom. The transition reaction equation for the pth cycle transition cascade of the hydrogen-type atom, $H\left[\frac{a_H}{p}\right]$, with the hydrogen-type atom, $H\left[\frac{a_H}{p'}\right]$, that is ionized with the absorption of an energy hole of $m \cdot 27.2\ eV$ (Eq. (5.24)) equivalent to its potential energy, is represented by:

$$m\cdot 27.2\ eV + H\left[\frac{a_H}{p'}\right] + H\left[\frac{a_H}{p}\right] \rightarrow H^+_{fast} + e^- + H*\left[\frac{a_H}{p+m}\right] + m\cdot 27.2\ eV \tag{5.71}$$

$$H*\left[\frac{a_H}{p+m}\right] \rightarrow H\left[\frac{a_H}{p+m}\right] + \left[(p+m)^2 - p^2\right]\cdot 13.6\ eV - m\cdot 27.2\ eV \tag{5.72}$$

$$H^+_{fast} + e^- \rightarrow H\left[\frac{a_H}{1}\right] + (m+1)\cdot 13.6\ eV \tag{5.73}$$

And, the overall reaction is:

$$H\left[\frac{a_H}{p'}\right] + H\left[\frac{a_H}{p}\right] \rightarrow H\left[\frac{a_H}{1}\right] + H\left[\frac{a_H}{(p+m)}\right] + \left[2pm + m^2 - m + 1\right]\cdot 13.6\ eV \tag{5.74}$$

wherein $m\cdot 27.2\ eV = p'^2\cdot 27.2\ eV$. Consider all stable states of hydrogen and their ability to serve as a source of energy holes regarding a general reaction involving a transition of hydrogen to a lower-energy state caused by another hydrogen or hydrino. In the case that H is the source of energy hole involving either mechanism (Eq (5.70) or Eq. (5.74)), the reaction is given by

$$H(1/p') + H(1/p) \rightarrow H + H(1/(m+p)) + \left[2pm + m^2 - p'^2 + 1\right]\cdot 13.6\ eV \tag{5.75}$$

where p, p', and m are integers with $m = p' = 1$.

The laboratory results of the formation of hydrinos with emission of continuum radiation has celestial implications. Hydrogen self-catalysis and disproportionation may be reactions occurring ubiquitously in celestial objects and interstellar medium comprising atomic hydrogen. Stars are sources of atomic hydrogen and hydrinos as stellar wind for interstellar reactions wherein very dense stellar atomic hydrogen and singly ionized helium, He^+, serve as catalysts in stars. H_2O catalyst may also be active in interstellar medium. Hydrogen continua from transitions to form hydrinos matches the emission from white dwarfs, provides a possible mechanism of linking the temperature and density conditions of the different discrete layers of the coronal/chromospheric sources, and provides a source of the diffuse ubiquitous EUV cosmic background with a 10.1 nm continuum matching the observed intense 11.0-16.0 nm band in addition to resolving the identity of the radiation source behind the observation that diffuse H_α emission is ubiquitous throughout the Galaxy and widespread sources of flux shortward of 912Å are required. Moreover, the product hydrinos provides resolution to the identity of dark matter [8-9].

Disproportionation reactions of hydrinos are predicted to given rise to features in the X-ray region. As shown by Eqs. (5.40-5.43) the reaction product of HOH catalyst is $H\left[\frac{a_H}{4}\right]$. Consider a likely transition reaction in hydrogen clouds containing H_2O gas wherein the first hydrogen-type atom $H\left[\frac{a_H}{p}\right]$ is an H atom and the second acceptor hydrogen-type atom $H\left[\frac{a_H}{p'}\right]$ serving as a catalyst is $H\left[\frac{a_H}{4}\right]$. Since the potential energy of $H\left[\frac{a_H}{4}\right]$ is $4^2\cdot 27.2\ eV = 16\cdot 27.2\ eV = 435.2\ eV$, the transition reaction is represented by:

$$16\cdot 27.2\ eV + H\left[\frac{a_H}{4}\right] + H\left[\frac{a_H}{1}\right] \rightarrow H^+_{fast} + e^- + H*\left[\frac{a_H}{17}\right] + 16\cdot 27.2\ eV \tag{5.76}$$

$$H*\left[\frac{a_H}{17}\right] \rightarrow H\left[\frac{a_H}{17}\right] + 3481.6\ eV \tag{5.77}$$

$$H^+_{fast} + e^- \rightarrow H\left[\frac{a_H}{1}\right] + 231.2\ eV \tag{5.78}$$

And, the overall reaction is:

$$H\left[\frac{a_H}{4}\right] + H\left[\frac{a_H}{1}\right] \rightarrow H\left[\frac{a_H}{1}\right] + H\left[\frac{a_H}{17}\right] + 3712.8\ eV \tag{5.79}$$

The extreme-ultraviolet continuum radiation band due to the $H*\left[\frac{a_H}{p+m}\right]$ intermediate (e.g. Eq. (5.72) and Eq. (5.7) is predicted to have a short wavelength cutoff and energy $E_{\left(H\rightarrow H\left[\frac{a_H}{p+m}\right]\right)}$ given by:

$$E_{\left(H\rightarrow H\left[\frac{a_H}{p+m}\right]\right)} = \left[\left(p+m\right)^2 - p^2\right]\cdot 13.6\ eV - m\cdot 27.2\ eV$$
$$\lambda_{\left(H\rightarrow H\left[\frac{a_H}{p+m}\right]\right)} = \frac{91.2}{\left[\left(p+m\right)^2 - p^2\right] - 2m}\ nm \tag{5.80}$$

and extending to longer wavelengths than the corresponding cutoff. Here the extreme-ultraviolet continuum radiation band due to the decay of the $H*\left[\frac{a_H}{17}\right]$ intermediate is predicted to have a short wavelength cutoff at $E = 3481.6\ eV;\ 0.35625\ nm$ and extending to longer wavelengths. A broad X-ray peak with a 3.48 keV cutoff was recently observed in the Perseus Cluster by NASA's Chandra X-ray Observatory and by the XMM-Newton [32-34] that has no match to any known atomic transition. The 3.48 keV feature assigned to dark matter of unknown identity by BulBul et al. [32, 34] matches the $H\left[\frac{a_H}{4}\right] + H\left[\frac{a_H}{1}\right] \rightarrow H\left[\frac{a_H}{17}\right]$ transition and further confirms hydrinos as the identity of dark matter.

DIPOLE-DIPOLE COUPLING

The process referred to as the Atomic BlackLight Process described in the Hydrino Theory—BlackLight Process section comprises the transition of ordinarily stable hydrogen atoms with $n = 1$ in Eq. (5.1) to lower-energy stable states via an initial resonant nonradiative energy transfer to an acceptor comprising a source of an energy hole. Comparing the implications of the source-current-to-stability relationship (Eqs. (2.23-2.25) and (6.7-6.9)) of Rydberg transitions to excited $n = 1, 2, 3, ...$ states as opposed to the transitions to hydrino states having $n = 1, \frac{1}{2}, \frac{1}{3}, \frac{1}{4}, ..., \frac{1}{p}$, it can be appreciated that the former transitions directly involve photons; whereas, the latter do not. Transitions are symmetric with respect to time. Current-density functions, which give rise to photons are created by photons by the reverse process. Excited energy states correspond to this case. And, current-density functions, which do not directly give rise to photons are not created by photons by the reverse process. Hydrino energy states correspond to this case. But, radiationless processes generally classified as atomic collisions involving an energy hole can cause a stable H state to undergo a transition to a lower-energy stable state. Examples of radiationless energy transfer mechanisms are given in the Energy Transfer Mechanism section.

Since the initial state in each case is not a radiative multipole as described in the Excited States of the One-Electron Atom (Quantization) section, the transitions to lower energy states of hydrogen are forbidden. However, forbidden transitions can become allowed by coupling. For example, forbidden electronic transitions in transition metal complexes couple to vibrational transitions with a dramatic increase in the absorption cross section that results in absorption. This is well known as vibronic coupling [35]. In addition to direct physical collision, several interactions can be generally classified as "collisions" that perturb the current density function of a hydrogen atom. Catalyst ions can electrostatically polarize the current density of the hydrogen atom. Similarly induced polarization may occur by the same mechanism that gives rise to van der Waals forces. In addition, all hydrogen atoms and hydrinos have a single unpaired electron that can interact through a magnetic dipole interaction. Once the current density function is altered energy transfer may occur between the hydrogen atom or hydrino and the catalyst.

In an otherwise radiative system containing two fluorescent species such that the emission spectrum of one (the "donor") overlaps the absorption spectrum of the other (the "acceptor"), the excitation energy of the donor atoms may be transferred by a resonance Coulombic electromagnetic interaction mechanism over relatively large distances to the acceptor species (energy hole) rather than the donors radiating into free space. The total Coulombic interaction may be taken as the sum of terms including dipole-dipole, dipole-quadrupole, and terms involving higher order multipoles. Multipole-multipole resonance such as dipole-dipole resonance initially occurs in the electro and magnetostatic limit rather than involving transverse fields as in the case of pure radiation coupling. The Förster theory [36-40] is general to dipole-dipole energy transfer, which is often predominant. A modification of Förster theory applies to the case of transitions to or between hydrino states. The mechanism for the coupling between the $n = 1/p$ ($p = 1, 2, 3, ...$)-state electron of the hydrogen atom and the catalyst may involve direct coupling between existing multipoles, or the catalyst may induce a multipole in the reactant H or hydrino atom. Mechanisms for the catalyst to induce a multipole in the electron current include collisional perturbations and polarizations by electric or magnetic field interactions.

The hydrogen-type electron atomic orbital is a spherical shell of negative charge (total charge = $-e$) of zero thickness at a distance r_n from the nucleus (charge = $+Ze$). It is well known that the field of a spherical shell of charge is zero inside the shell and that of a point charge at the origin outside the shell [41]. The electric field of the proton is that of a point charge at the origin. And, the superposition, $\mathbf{E}$, of the electric fields of the electron and the proton is that of a point charge inside the shell and zero outside.

$$\mathbf{E} = \frac{e}{4\pi\varepsilon_0 r^2} \qquad \text{for } r < r_n \tag{5.81}$$

$$\mathbf{E} = 0 \qquad \text{for } r > r_n \tag{5.82}$$

The magnetic field of the electron, $\mathbf{H}$, is derived in the Derivation of the Magnetic Field section:

$$\mathbf{H} = \frac{e\hbar}{m_e r_n^3}(\mathbf{i}_r \cos\theta - \mathbf{i}_\theta \sin\theta) \qquad \text{for } r < r_n \tag{5.83}$$

$$\mathbf{H} = \frac{e\hbar}{2m_e r^3}(\mathbf{i}_r 2\cos\theta - \mathbf{i}_\theta \sin\theta) \qquad \text{for } r > r_n \tag{5.84}$$

Power flow is governed by the Poynting power theorem,

$$\nabla \bullet (\mathbf{E} \times \mathbf{H}) = -\frac{\partial}{\partial t}\left[\frac{1}{2}\mu_0 \mathbf{H} \bullet \mathbf{H}\right] - \frac{\partial}{\partial t}\left[\frac{1}{2}\varepsilon_0 \mathbf{E} \bullet \mathbf{E}\right] - \mathbf{J} \bullet \mathbf{E} \tag{5.85}$$

It follows from Eqs. (5.81-5.85) that $\nabla \bullet (\mathbf{E} \times \mathbf{H})$ is zero until an interaction occurs between a hydrogen-type atom and a catalyst. Here, a nonradiative transition can couple to one that is radiative. As given in Jackson [42], each current distribution can be written as a multipole expansion. A catalytic interaction or collision gives rise to radiative terms including a dipole term. (There is at least current in the radial direction until force balance is achieved again at the next nonradiative level). Förster's theory [36] gives the following equation for $n(R)$, the nonradiative transfer rate constant:

$$n(R) = \frac{9000(\ln 10)\kappa^2 \Phi_D}{128\pi^5 n^4 N_A \tau_D R^6} \int_0^\infty f_D(\bar{\nu}) \varepsilon_A(\bar{\nu}) \frac{d\bar{\nu}}{\bar{\nu}^4} \tag{5.86}$$

where $\varepsilon_A(\bar{\nu})$ is the molar decadic extinction coefficient of the acceptor (at wave-number $\bar{\nu}$), $f_D(\bar{\nu})$ is the spectral distribution of the fluorescence of the donor (measured in quanta and normalized to unity on a wave-number scale), N_A is Avogadro's number, τ_D is the mean lifetime of the excited state, Φ_D is the quantum yield of the fluorescence of the donor, n is the refractive index , R is the distance between the donor and acceptor, and κ is an orientation factor which for a random distribution equals $\left(\frac{2}{3}\right)^{\frac{1}{2}}$.

Adaptation of Förster's theory gives the transfer rate constant. In this case, the form of the equation is the same except that $\varepsilon_A(\bar{\nu})$ is the molar decadic energy acceptor cross section (at wave-number $\bar{\nu}$), $f_D(\bar{\nu})$ is the spectral distribution of the transferred energy of the donor (measured in quanta and normalized to unity on a wave-number scale), τ_D is the mean lifetime of the transition, and κ is a factor dependent on the mutual orientation of the donor and acceptor transition moments which for a random distribution equals $\left(\frac{2}{3}\right)^{\frac{1}{2}}$. Φ_D is the transition probability of the donor that is dependent on establishing a radiative state in both the acceptor and donor via the nonradiative resonant energy transfer. Φ_D is analogous to the excitation probability to a doubly excited state.

The collision of two hydrino atoms will result in an elastic collision, an inelastic collision with a hydrogen-type molecular reaction, or an inelastic collision with a disproportionation reaction as described in the Disproportionation of Energy States section**.** An estimate of the transition probability for electric multipoles is given by Eq. (16.104) of Jackson [43]. For an electric dipole $\ell = 1$, and Eq. (16.104) of Jackson is:

$$\frac{1}{\tau_E} \cong \left(\frac{e^2}{\hbar c}\right)\frac{\pi}{16}(ka)^2 \omega \tag{5.87}$$

where a is the radius of the hydrogen-type atom, and k is the wave-number of the transition. Substitution of:

$$k = \frac{\omega}{c} \tag{5.88}$$

into Eq. (5.87) gives:

$$\frac{1}{\tau_E} \cong \left(\frac{e^2}{\hbar c}\right)\frac{\pi}{16}\left(\frac{a}{c}\right)^2 \omega^3 \tag{5.89}$$

From Eq. (5.89), the transition probability is proportional to the frequency cubed. Thus, the disproportionation reaction of hydrinos is favored over molecular bond formation because it is the most energetic transition for the donor hydrino atom, and bond formation further requires a third body to remove the bond energy.

In one example wherein nonradiative energy transfer occurs between two hydrino atoms, the mean lifetime of the transition of Eq. (5.86), τ_D, is taken as the vibrational period of the corresponding dihydrino molecule that serves as a model of the transition state. The lifetime follows from Eq. (11.223) and Planck's Equation (Eq. (2.148)). The distance between the donor and acceptor, R, is given by the internuclear distance which is twice c' of Eq. (11.203), and the orientation factor, κ,

equals one because of the spherical symmetry of the hydrino atoms. Electronic transitions of hydrino atoms occur only by an initial nonradiative energy transfer, and the transition probability based on a physical collision approaches one in the limit. Thus, Φ_D, is set equal to one. Ideally, in free space, the overlap integral between the frequency-dependent energy acceptor cross-section and the transferred energy of the donor (energy of $m \cdot 27.2\ eV$ given by Eq. (5.24)) is also one.

Consider the following disproportionate reaction where the additional energy release for the transition given by $m = 1$, $m' = 2$ and $p = 2$ in Eqs. (5.67-5.70) involving the absorption of an energy hole of $27.21\ eV$, $m = 1$ in Eq. (5.24), is $13.6\ eV$.

$$H\left[\frac{a_H}{2}\right] \xrightarrow{H\left[\frac{a_H}{2}\right]} H\left[\frac{a_H}{3}\right] \tag{5.90}$$

The transfer rate constant, $n(R)$, for Eq. (5.90) using Eq. (5.86) is:

$$n(R) = \frac{9000(\ln 10)(1)^2 1}{128\pi^5 (1)^4 \left(6.02\ X\ 10^{23}\right)\left(1.77\ X\ 10^{-15}\right)\left(3.73\ X\ 10^{-11}\right)^6 \left(6.91\ X\ 10^{7}\right)^4} = 8\ X\ 10^{21}\ \text{sec}^{-1} \tag{5.91}$$

According to the adaptation of Förster's theory [40], the efficiency E of such nonradiative energy transfer given by the product of the transfer rate constant and the mean lifetime of the transition may be expressed by:

$$E = \frac{1}{1 + \left[\frac{r}{R_0}\right]^6} \tag{5.92}$$

$$R_0^6 = \left(8.8\ X\ 10^{-25}\right) J \eta^{-4} \phi_D \kappa^2$$

where r is the distance between the donor and the acceptor, J is the overlap integral between the frequency-dependent energy acceptor cross section and the transferred energy of the donor, and η is the dielectric constant. In the case that the radius of Eq. (5.91) is a fraction of the Bohr radius, the efficiency of energy transfer may be high and approaches one in the limit.

The reaction rate of oxygen with carbon and hydrocarbons is very low at room temperature; however, once the material is ignited, the oxidation reaction can be very fast. This is due to the formation of free radicals that cause a chain reaction known as pyrolysis, which dominates the reaction rate. The formation of hydrinos by a first catalyst such as He^+, Li, K, nH, or H_2O gives rise to subsequent disproportionation reactions to additional lower energy states. Analogously, the latter reactions may dominate the power released if a substantial concentration of hydrinos may be maintained as shown in the Power Density of Gaseous Reactions section.

INTERSTELLAR DISPROPORTIONATION RATE

Disproportionation may be the predominant mechanism of hydrogen electronic transitions to lower energy levels of interstellar hydrogen and hydrinos. The reaction rate is dependent on the collision rate between the reactants and the coupling factor for resonant energy transfer. The collision rate can be calculated by determining the collision frequency. The collision frequency, f, and the mean free path, ℓ, for a gas containing n_u spherical particles per unit volume, each with radius r and velocity v is given by Bueche [44].

$$f = 4\pi\sqrt{2} n_u r^2 v \tag{5.93}$$

$$\ell = \frac{1}{4\pi\sqrt{2} n_u r^2} \tag{5.94}$$

The average velocity, v_{avg}, can be calculated from the temperature, T, [44].

$$\frac{1}{2} m_H v_{avg}^2 = \frac{3}{2} kT \tag{5.95}$$

where k is Boltzmann's constant. Substitution of Eq. (5.95) into Eq. (5.93) gives the collision rate, $f_{H\left[\frac{a_H}{p}\right]}$, in terms of the temperature, T, the number of hydrogen or hydrino atoms per unit volume, n_H, and the radius of each hydrogen atom or hydrino, $\frac{a_H}{p}$.

$$f_{H\left[\frac{a_H}{p}\right]} = 4\pi\sqrt{2} n_H \left(\frac{a_H}{p}\right)^2 \sqrt{\frac{3kT}{m_H}} \tag{5.96}$$

The rate constant of the disproportionation reaction, $k_{m,m',p}$, to the transition reaction, Eqs. (5.67-5.70), is given by the product of the collision rate per atom, Eq. (5.96), and the coupling factor for resonant energy transfer, $g_{m,m',p}$.

$$k_{m,m',p} = g_{m,p} 4\pi\sqrt{2} n_H \left(\frac{a_H}{p}\right)^2 \sqrt{\frac{3kT}{m_H}} \tag{5.97}$$

Using an upper limit of the coupling factor $g_{m,m',p}$ for resonant energy transfer consistent with the efficiencies of dipole-dipole resonant energy transfers [36-40], an estimate of the rate constant of the disproportionation reaction, $k_{m,m',p}$, to cause the transition reaction, Eqs. (5.67-5.70), is given by substitution of $g_{m,m',p} = 1$ into Eq. (5.97).

$$k_{m,m',p} = 4\pi\sqrt{2} n_H \left(\frac{a_H}{p}\right)^2 \sqrt{\frac{3kT}{m_H}} \ \text{sec}^{-1} \tag{5.98}$$

The rate of the disproportionation reaction, $r_{m,m',p}$, to cause the transition reaction, Eqs. (5.67-5.70), is given by the product of the rate constant, $k_{m,m',p}$ given by Eq. (5.98), and the total number of hydrogen or hydrino atoms, N_H.

$$r_{m,m',p} = N_H 4\pi \frac{1}{2}\sqrt{2} n_H \left(\frac{a_H}{p}\right)^2 \sqrt{\frac{3kT}{m_H}} \ \frac{transitions}{\text{sec}} \tag{5.99}$$

The factor of one half in Eq. (5.99) corrects for double counting of collisions [45]. The power, $P_{m,m',p}$, is given by the product of the rate of the transition, Eq. (5.99), and the energy of the transition, Eq. (5.70).

$$P_{m,m',p} = \frac{N_H^2}{V} \frac{4\pi}{\sqrt{2}} \left(\frac{a_H}{p}\right)^2 \sqrt{\frac{3kT}{m_H}} \left[2mp + m^2 - p'^2 + 1\right] X\, 2.2X10^{-18} \ W \tag{5.100}$$

where V is the volume.

POWER DENSITY OF GASEOUS REACTIONS

The reaction of atomic hydrogen or hydrinos to lower-energy states releases energy intermediate that of typical chemical reactions and nuclear reactions. However, in order to be consequential as a power source celestially in processes such as heating the corona of the Sun [9] or terrestrially as an alternative to conventional sources such as combustion or nuclear power, the rate of the reaction must be nontrivial. A hydrino is formed by reaction of atomic hydrogen with a source of energy holes, and hydrinos may subsequently undergo transitions to successively lower states in reactions involving the initial source of energy holes or by disproportionation. Once it starts, the latter process has the potential to be a predominant source of power depending on the maintenance of a substantial concentration of hydrinos in steady state. The power contribution can be conservatively calculated considering only a single relative low-energy transition.

The disproportionation reaction rate, $r_{m,m',p}$, Eqs. (5.67-5.70), is dependent on the collision rate between the reactants and the efficiency of resonant energy transfer. It is given by the product of the rate constant, $k_{m,m',p}$,(Eq. (5.98)), the total number of hydrogen or hydrino atoms, N_H, and the efficiency, E, of the transfer of the energy from the donor hydrino atom to the energy hole provided by the acceptor hydrino atom given by Eq. (5.93). Thus, the rate of the disproportionation reaction, $r_{m,m',p}$, to cause a transition reaction is

$$r_{m,m',p} = E\ N_H 4\pi \frac{1}{2}\sqrt{2} n_H \left(\frac{a_H}{p}\right)^2 \sqrt{\frac{3kT}{m_H}} \tag{5.101}$$

The factor of one half in Eq. (5.101) corrects for double counting of collisions [45]. The power, $P_{m,m',p}$, is given by the product of the rate of the transition, Eq. (5.101), and the energy of the disproportionation reaction (Eq. (5.70)).

$$P_{m,m',p} = E\ \frac{N_H^2}{V} 4\pi \frac{1}{\sqrt{2}} \left(\frac{a_H}{p}\right)^2 \sqrt{\frac{3kT}{m_H}} \left[2pm + m^2 - p'^2 + 1\right] \cdot 2.2X10^{-18} \ W \tag{5.102}$$

where V is the volume. For a disproportionation reaction in the gas phase with Φ_D and the overlap integral both equal to one, the energy transfer efficiency is one as given by Eq. (5.92). The power given by substitution of

$$E = 1,\ p = 2,\ m = 1,\ p' = 2,\ V = 1\ m^3,\ N = 3\ X\ 10^{19},\ T = 675\ K \tag{5.103}$$

into Eq. (5.102) is:

$$P_{m,m',p} = 100\ kW \tag{5.104}$$

corresponding to $100\ mW / cm^3$.

Next, the power due to a reaction involving a catalyst such as an atom to form hydrinos is considered. In the case that the reaction of hydrogen to lower-energy states occurs by the reaction of a catalytic source of energy holes with hydrogen or hydrino atoms, the reaction rate is dependent on the collision rate between the reactants and the efficiency of resonant energy transfer.

The hydrogen-or-hydrino-atom/catalyst-atom collision rate per unit volume, $Z_{H\left[\frac{a_H}{p}\right]\text{ Catalyst}}$, for a gas containing n_H hydrogen or hydrino atoms per unit volume, each with radius $\frac{a_H}{p}$ and velocity v_H and n_C catalyst atoms per unit volume, each with radius r_{Catalyst} and velocity v_C is given by the general equation of Levine [45] for the collision rate per unit volume between atoms of two dissimilar gases.

$$Z_{H\left[\frac{a_H}{p}\right]\text{ Catalyst}} = \pi\left(\frac{a_H}{p} + r_{\text{Catalyst}}\right)^2 \left[\left\langle v_H \right\rangle^2 + \left\langle v_C \right\rangle^2\right]^{1/2} n_H n_C \tag{5.105}$$

The average velocity, v_{avg}, can be calculated from the temperature, T, [46].

$$\frac{1}{2} m_H v_{avg}^2 = \frac{3}{2} kT \tag{5.106}$$

where k is Boltzmann's constant. Substitution of Eq. (5.106) into Eq. (5.105) gives the collision rate per unit volume, $Z_{H\left[\frac{a_H}{p}\right]\text{ Catalyst}}$, in terms of the temperature, T.

$$Z_{H\left[\frac{a_H}{p}\right]\text{ Catalyst}} = \pi\left(\frac{a_H}{p} + r_{\text{Catalyst}}\right)^2 \left[3kT\left(\frac{1}{m_H} + \frac{1}{m_C}\right)\right]^{1/2} n_H n_C \tag{5.107}$$

The rate of the catalytic reaction, $r_{m,p}$, to cause a transition reaction is given by the product of the collision rate per unit volume, $Z_{H\left[\frac{a_H}{p}\right]\text{ Catalyst}}$, the volume, V, and the efficiency, E, of resonant energy transfer given by Eq. (5.92).

$$r_{m,p} = E\ \ \pi\left(\frac{a_H}{p} + r_{\text{Catalyst}}\right)^2 \left[3kT\left(\frac{1}{m_H} + \frac{1}{m_C}\right)\right]^{1/2} \frac{N_H N_C}{V} \tag{5.108}$$

The power, $P_{m,p}$, is given by the product of the rate of the transition, Eq. (5.108), and the energy of the transition, Eq. (5.9).

$$P_{m,p} = E\pi\left(\frac{a_H}{p} + r_{\text{Catalyst}}\right)^2 \left[3kT\left(\frac{1}{m_H} + \frac{1}{m_C}\right)\right]^{1/2} \frac{N_H N_C}{V}\left[2mp + m^2\right] \cdot 2.2X10^{-18}\ W \tag{5.109}$$

In the exemplary case that the efficiency is $E = 10^{-4}$, the power for the Li catalyst reaction given by Eqs. (5.32-5.34) with the substitution of

$$\begin{aligned} &E = 10^{-4},\ p = 1,\ m = 3,\ V = 1\ m^3,\ N_H = 3\ X\ 10^{21},\ N_C = 3\ X\ 10^{19}, \\ &m_C = 1.15\ X\ 10^{-26}\ \text{kg},\ r_C = 1.35\ X\ 10^{-10}\ \text{m},\ T = 675\ K \end{aligned} \tag{5.110}$$

into Eq. (5.109) is:

$$P_{m,p} = 144\ kW \tag{5.111}$$

corresponding to $144\ mW / cm^3$.

HYDRINO CATALYZED FUSION (HCF)

Fusion reaction rates are extraordinarily small [47]. In fact, fusion is virtually impossible in the laboratory. A high relative kinetic energy corresponding to extraordinary temperatures of the participating nuclei must be sufficient to overcome their repulsive potential energy. The recent NIF experimental results confirm that so called "ignition" requires 250,000,000°C and a deuterium-tritium density of ten times that of lead to achieve about 0.2% fusion power over that input to the NIF lasers. In this case, the lasers consumed 500 trillion watts of power, 33 times the peak power of the entire world![1]

Cold fusion regarding hydrogen loading, excess hydrogen absorbed in a metal lattice, to force nuclei together is not possible since the Coulombic energy barrier is 0.1 MeV [47]. Whereas the vibrational energies within crystals are much less, about 0.01 eV. Coulombic screening is also not plausible based on the known crystalline structure of metal hydrides. Given the relationship between temperature and energy, 11,600 K/eV, the disparity in temperature in both cases is 1.16 X 10^7 versus 116 K, a factor of one hundred thousand.

Albeit, it is still high-energy physics involving colliders, muonic catalyzed fusion may propagate at a high rate at more conventional plasma temperatures. Rather than directly using high temperature and density conditions, fusion occurs by a muonic catalyzed mechanism involving forming muons in a high-energy accelerator that transiently replace electrons in atoms and molecules (time scale of the muon half-life of 2.2 μs). In muon catalyzed fusion [48-49], the internuclear separation of muonic H_2 is reduced by a factor of 207 that of electron H_2 (the muon to electron mass ratio), and the fusion rate increases by about 80 orders of magnitude. A few hundred fusion events can occur per muon (vanishingly small compared to Avogadro's number of $6.022\,X10^{23}$). To be permissive of even this miniscule rate of fusion, the muonic molecules provide the same conditions as those at high energies. Correspondingly, the vibrational energies regarding the movement of the nuclei towards each other in an oscillating linear manner can be very large in the muonic hydrogen case, $E_{vib} \approx v207X\ 0.517\ eV = v107\ eV$ wherein v is the vibrational quantum number. During the close approach of the vibrational compression phase, the nuclei can assume an orientation that allows the mutual electric fields to induce multipoles in the quarks and gluons to trigger a transition to a fusion product. The highest vibrational energy states such as the state $v = 9$ with $E_{vib} \approx v107\ eV = 9X107\ eV = 963\ eV$ are at the bond dissociation limit. Given the extraordinary confinement time in a bound state, these muonic molecules have sufficiently large kinetic energy to overcome the Coulombic barrier for fusion of the heavy hydrogen isotopes of tritium with deuterium at just detectable rates.

Fusion in the Sun occurs due to extreme gravitational compression and thermal temperatures that provide sufficient confinement time, enormous reactant densities, and incredible energies. But even here, the Sun considered as a fusion machine of $1.412\,X10^{30}$ *liter* outputting $3.846\,X10^{26}$ *W* corresponds to a feeble $272\ \mu W/liter$. Fusion bombs (e.g. Tsar Bomba) require ignition by a fission bomb that produces power density on the order of $\frac{240X10^{15}\ J}{\left(10^{-3}\ s\right)\left(2.7X10^{7}\ liters\right)} = 8.8X10^{12}\ W/liter$, $3.2X10^{16}$ times the average power density of the Sun.[2]

Next, consider the feasibility of hydrino catalyzed fusion (HCF) based on a similar mechanism to that of muonic catalyzed fusion. Once a deuterium or tritium hydrino atom is formed by a catalyst, further catalytic transitions $n = \frac{1}{2} \to \frac{1}{3},\ \frac{1}{3} \to \frac{1}{4},\ \frac{1}{4} \to \frac{1}{5},$ and so on may occur to a limited extent in competition with molecular hydrino formation that terminates this cascade. The hydrino atom radius can be reduced to $1/p$ that of the $n = 1$ state atom. Analogous to muonic catalyzed fusion, the internuclear separation in the corresponding hydrino molecules is $1/p$ that of ordinary molecular hydrogen as given in the Nature of the Chemical Bond of Hydrogen-Type Molecules and Molecular Ions section (Eq. (11.204)). As the internuclear separation decreases due to high p states, fusion is more probable. As p becomes large, relativistic effects become appreciable for the energy transferred from a hydrino atom and accepted by the catalyst that provides the corresponding energy hole. As in the nonrelativistic case, the energy transferred is the potential energy of the hydrogen-type atom $H(1/p)$ that transitions to a lower energy state, divided by p^2, the total number of multipole modes of the state according to Eq. (5.45). Due to similar relativistic effects in hydrino atoms of similar p states, hydrino atoms may serve as the catalyst by disproportionation reactions such as ones given by Eqs. (5.62-5.80). Disproportionation reactions may propagate or cascade to very low hydrino energy states of corresponding very high p values. The corresponding hydrino molecules have vastly shorter

[1] It is also remarkable that the NIF device cost $3.5B, and the fusion pellet cost $1M for a single shot that requires months to repeat. The product was less than one cents worth of radioactive thermal as an explosive shock wave.

[2] Arc current detonation of hydrated silver shots and other conductive solid fuels comprising a source of hydrogen and a source of HOH catalyst yielded power densities comparable to those of nuclear weapons [50-54].

internuclear distances (Eq. (11.204)) such that finite rates of nuclear reactions may occur in the case of heavy hydrogen isotopes, deuterium and tritium.

In the case that the electron spin-nuclear interaction is negligible, using Eq. (1.292), the relativistic potential energy of a hydrino atom $H\left(1/p\right)$ of a given state p is

$$V=\frac{Ze^2}{4\pi\varepsilon_0 r}=\frac{Z^2e^2}{4\pi\varepsilon_0 a_0\sqrt{1-(\alpha Z)^2}}=\frac{(\alpha p)^2 m_{e0}c^2}{\sqrt{1-(\alpha p)^2}} \tag{5.112}$$

wherein the radius given by Eq. (1.289) is

$$r=\frac{a_0}{p}\sqrt{1-(\alpha p)^2} \tag{5.113}$$

and Eqs. (28.8-28.9) were used. Thus, the energy hole according to Eqs. (5.112), (5.5), and (5.45) is

$$m\frac{\alpha^2 m_{e0}c^2}{\sqrt{1-(\alpha p)^2}} \tag{5.114}$$

which in the low-speed limit is $m\cdot 27.2\ eV$ given by Eq. (5.5). Using Eq. (1.294) and Eqs. (5.6-5.9), the energy released from a hydrino state p during the transition involving an energy hole of quanta m is given by the difference in ionization energies between the initial and final energy states wherein the final p_f state is $p_f = p+m$:

$$\Delta E = m_{e0}c^2\left(\sqrt{1-(\alpha p)^2}-\sqrt{1-\left(\alpha\left(p+m\right)\right)^2}\right) \tag{5.115}$$

In the low-speed-limit the energy released is given by Eq. (5.9). Note as given previously, $p=137$ is the highest value of p physically possible corresponding to a minimum radius of $0.022926\alpha a_0 = 8.853X10^{-15}m = 8.853\,fm$, 8.9 times times the radius of a proton of 1 fm, and one thirtieth the radius of the muonic atom.

The non-relativistic vibrational energies are given by Eq. (11.223) as $E_{vib} = p^2 0.517\ eV$, and the relativistic atomic radii are given by Eq. (5.113). A sufficiently high p can provide vibrational energies and close approach of nuclei of corresponding molecules sufficient for fusion to ensue. Considering the p^2 dependency of the vibrational energies of $H_2\left(1/p\right)$, and excitation of highest vibrational energy state at the bond dissociation limit (e.g. $v=9$), the state $p=15$ can achieve comparable vibrational energies as muonic molecules; yet, the $p=15$ hydrino atomic radius (Eq. (5.113) and corresponding molecular hydrino internuclear distance are about 14 times greater than those of the muonic species. The p state that achieves comparable dimensions to those of muonic atoms and molecules is $p=115$ (Eq. (5.113)) which has a corresponding nonrelativistic vibrational energy of 6840 eV. Only the lowest energy vibrational state would likely be populated with the energy from bond formation $p^2 4.478eV$ (Eq. 11.252)) since the temperature required to excite 7 keV vibrational modes is on the order of 10^8 K, compared to an ordinary plasma temperature of about 1000 K. Considering that each muon catalyzes hundreds of fusion events, the cross section to populate the molecule hydrino vibration state is essential to match fusion rates comparable to muonic catalyzed fusion of tritium with deuterium since hydrino catalyzed fusion occurs as single events.

Consider the limit of the highest p value for a hydrino state $H\left(1/p\right)$. Using Eq. (5.115), the energy for the cascade of two hydrogen atoms, each to the final state of $H\left(1/137\right)$ results in an energy release of $1X10^6\ eV$. In comparison, the fusion equation for deuterium and tritium is

$$^2H + {}^3H \rightarrow n\left(14.1MeV\right) + {}^4He\left(3.5MeV\right) \tag{5.116}$$

Nuclear fusion (i) requires accelerator-produced, radioactive tritium, (ii) it is a highly radioactive dangerous process, and (iii) it requires a steam cycle involving massive scale and a water-body coolant source such as a river as well as an electrical distribution grid. Production of chemical power as light and supersonic plasma flow enabling compact photovoltaic and magnetohydrodynamic conversion, respectively, that is devoid of any fuels or distribution infrastructure is much more practical and economically competitive as a commercial power technology.

Fusion has other utility such as production of (i) neutrons (D + T and D + D fusion), and (ii) ^3He, tritium, and high energy protons (D + D fusion) which have industrial applications. In the case of extraordinarily high p states approaching p = 137, bonding with inner shell electrons may result in fusion of heavier elements than hydrogen isotopes. Energetic fusion products may also initiate subsequent nuclear reactions. Using heavy hydrogen, trace production of tritium by HCF may be competitive with atomic accelerators and hot fusion reactors. According to a study by Kovari [55], D-D tritium breeding might cost $2 billion per kilogram produced. Tritium stockpiles are projected to be depleted near term wherein Savannah River's tritium facilities are the United States' only source of tritium, an essential component in nuclear weapons.

Fusion requires a hydrino transition reaction cascade such as one propagated by disproportionation reactions to hydrino states of high p. The cascade is favored by (i) massive kinetics, (ii) hydrino and plasma confinement, and (iii) increasing duration of the hydrino reaction. One exemplary system to cause massive kinetics and hydrino and plasma confinement is detonation of hydrino reactant solid fuels under arc current conditions [50-54]. Hydrino confinement is achieved by using as a component of the hydrino reactant mixture at least one of (i) a solid material to absorb hydrino atoms such as a metal surface or bulk such as one that also absorbs H atoms (e.g. Ni, Ti, Pd, Pt, Nb, or Ta) [54], (ii) a magnetic material such as FeOOH or Fe_2O_3, that favors magnetic bonding of hydrinos [54], and (iii) an oxide such as a metal oxide such as GaOOH or Ga_2O_3 that binds hydrinos [56].

MOLECULAR BLACKLIGHT PROCESS

BELOW "GROUND" STATE TRANSITIONS OF HYDROGEN-TYPE MOLECULES AND MOLECULAR IONS

As is the case with the hydrogen atom, higher and lower molecular energy states are equally valid wherein the central field of molecular hydrogen ions and molecules can also be a reciprocal integer or an integer value of that of the ordinary states corresponding to molecular excited states and molecular hydrino states as given in the Diatomic Molecular Energy States section and the Nature of the Chemical Bond of Hydrogen-Type Molecules and Molecular Ions section, respectively. The photon changes the effective charge at the MO surface where the central field is ellipsoidal and arises from the protons at the foci and the "trapped photon" as effectively at the foci of the MO. Force balance is achieved at a series of two-dimensional ellipsoidal equipotential surfaces. The "trapped photons" are solutions of the Laplacian in ellipsoidal coordinates, Eq. (11.27). Thus, each molecular state comprises two electrons, two protons, and a photon, but the excited states are radiative; whereas, the hydrino states are stable. Excited and hydrino electronic states are created when photons of discrete frequencies are trapped in the ellipsoidal resonator cavity of the MO by resonant photon absorption and resonant nonradiative energy transfer, respectively.

ENERGY HOLES

From Eqs. (11.207) and (11.208), the magnitude of the elliptic field corresponding to a below "ground state" transition of the hydrogen molecule is an integer. The potential energy equations of hydrogen-type molecules are:

$$V_e = \frac{-p2e^2}{8\pi\varepsilon_0\sqrt{a^2-b^2}}\ln\frac{a+\sqrt{a^2-b^2}}{a-\sqrt{a^2-b^2}} \tag{5.117}$$

$$V_p = \frac{pe^2}{8\pi\varepsilon_0\sqrt{a^2-b^2}} \tag{5.118}$$

where

$$a = \frac{a_0}{p} \tag{5.119}$$

$$b = \frac{1}{p\sqrt{2}}a_0 \tag{5.120}$$

$$c' = \sqrt{a^2-b^2} = \frac{\sqrt{2}a_0}{2p} \tag{5.121}$$

and where p is an integer. The quantum number p is a scaling parameter of the molecular dimensions and energies. In the latter case it corresponds to the effective nuclear charge factor. Using the convention defined in the Energy Hole Concept section, this factor $Z_{effective}$ is given by $Z_{effective} = 1/\mathrm{n} = p$ where the principal quantum number $n = 1/p$. From energy conservation, the resonance energy hole of a hydrogen-type molecule which causes the transition

$$H_2\left[2c' = \frac{\sqrt{2}a_0}{p}\right] \rightarrow H_2\left[2c' = \frac{\sqrt{2}a_0}{p+m}\right] \tag{5.122}$$

is

$$mp^2\ X\ 48.6\ eV \tag{5.123}$$

where m and p are integers. During the transition, the elliptic field is increased from magnitude p to magnitude $p+m$. The corresponding potential energy change equals the energy absorbed by the energy hole.

$$Energy\ hole = -V_e - V_p = mp^2\ X\ 48.6\ eV \tag{5.124}$$

Further energy is released by the hydrogen-type molecule as the internuclear distance "shrinks." The total energy, E_T, released during the transition is:

$$E_T = -13.6\ eV\left[\left(2(m+p)^2\sqrt{2} - (m+p)^2\sqrt{2} + \frac{(m+p)^2\sqrt{2}}{2}\right)\ln\frac{\sqrt{2}+1}{\sqrt{2}-1} - (m+p)^2\sqrt{2}\right] \quad (5.125)$$

$$+13.6\ eV\left[\left(2p^2\sqrt{2} - p^2\sqrt{2} + \frac{p^2\sqrt{2}}{2}\right)\ln\frac{\sqrt{2}+1}{\sqrt{2}-1} - p^2\sqrt{2}\right]$$

A schematic drawing of the total energy well of hydrogen-type molecules and molecular ions is given in Figure 5.4. The exothermic reaction involving transitions from one potential energy level to a lower level is also hereafter referred to as the Molecular BlackLight Process.

Figure 5.4. The total energy well of hydrogen-type molecules and molecular ions.

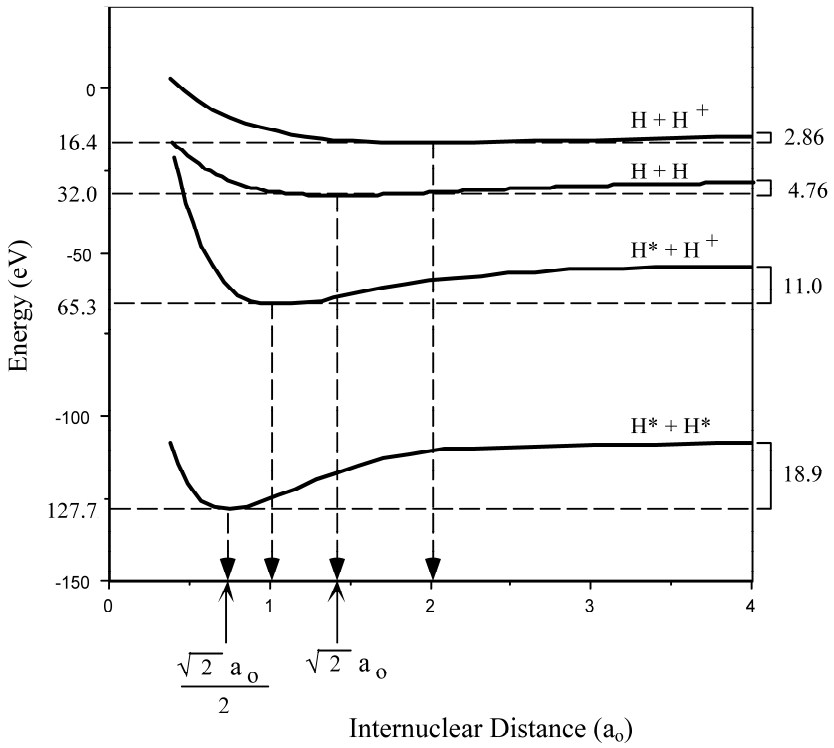

A hydrogen-type molecule with its electrons in a lower than "ground state" energy level corresponding to a fractional quantum number is hereafter referred to as a dihydrino molecule. The designation for a dihydrino molecule of internuclear distance, $2c' = \frac{\sqrt{2}a_0}{p}$, where p is an integer, is $H_2\left[2c' = \frac{\sqrt{2}a_0}{p}\right]$. A schematic drawing of the size of hydrogen-type molecules as a function of total energy is given in Figure 5.5.

Figure 5.5. The size of hydrogen-type molecules as a function of total energy where $n = 1/p$ for dihydrino states, p is an integer, and 2c' is the internuclear distance.

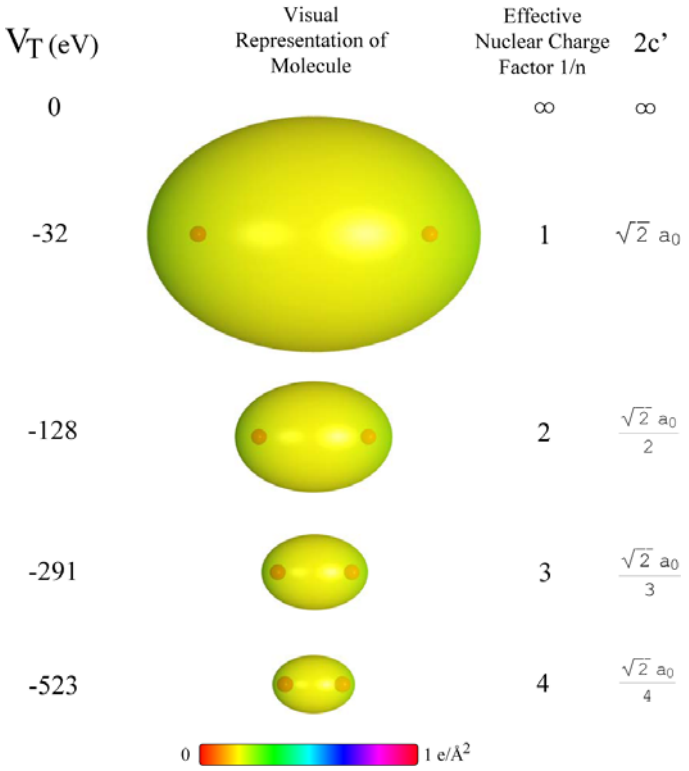

The magnitude of the elliptic field corresponding to the first below "ground state" transition of the hydrogen molecule is 2 times the magnitude of a reference field defined by two elementary charges e at a distance of $2c'$ from each other. From energy conservation, the resonance energy hole of a hydrogen molecule, which excites the transition of the hydrogen molecule with internuclear distance $2c' = \sqrt{2}a_o$ to the first below "ground state" with internuclear distance $2c' = \frac{1}{\sqrt{2}}a_0$ is given by Eqs. (5.112-5.116) where the elliptic field is increased from magnitude one to magnitude two:

$$V_e = \frac{-2e^2}{8\pi\varepsilon_0\sqrt{a^2-b^2}}\ln\frac{a+\sqrt{a^2-b^2}}{a-\sqrt{a^2-b^2}} = -67.836\ eV \tag{5.126}$$

$$V_p = \frac{e^2}{8\pi\varepsilon_0\sqrt{a^2-b^2}} = 19.24\ eV \tag{5.127}$$

$$Energy\ hole = -V_e - V_p = 48.6\ eV \tag{5.128}$$

In other words, the elliptic "ground state" field of the hydrogen molecule can be considered as the superposition of Fourier components. The removal of negative Fourier components of energy

$$m\ X\ \ 48.6\ eV \tag{5.129}$$

where m is an integer, increases the positive electric field inside the ellipsoidal shell by m times the charge of a proton at each focus. The resultant electric field is a time harmonic solution of the Laplacian in ellipsoidal coordinates. The corresponding potential energy change equals the energy absorbed by the energy hole.

$$Energy\ hole = -V_e - V_p = m\ X\ \ 48.6\ eV \tag{5.130}$$

Further energy is released by the hydrogen molecule as the internuclear distance "shrinks." The hydrogen molecule with internuclear distance $2c' = \sqrt{2}a_o$ is caused to undergo a transition to the below "ground state" level, and the internuclear distance for which force balance and nonradiation are achieved is $2c' = \frac{\sqrt{2}a_0}{1+m}$. In decaying to this internuclear distance from the "ground state," a total energy of:

$$-13.6\ eV\left[\left(2(1+m)^2\sqrt{2}-(1+m)^2\sqrt{2}+\frac{(1+m)^2\sqrt{2}}{2}\right)\ln\frac{\sqrt{2}+1}{\sqrt{2}-1}-(1+m)^2\sqrt{2}\right]$$
$$+13.6\ eV\left[\left(2\sqrt{2}-\sqrt{2}+\frac{\sqrt{2}}{2}\right)\ln\frac{\sqrt{2}+1}{\sqrt{2}-1}-\sqrt{2}\right] \quad (5.131)$$

is released.

CATALYTIC ENERGY HOLES FOR HYDROGEN-TYPE MOLECULES

An efficient catalytic system that hinges on the coupling of three resonator cavities involves iron and lithium. For example, the fourth ionization energy of iron is $54.8\ eV$. This energy hole is obviously too high for resonant absorption. However, Li^+ releases $5.392\ eV$ when it is reduced to Li. The combination of Fe^{3+} to Fe^{4+} and Li^+ to Li, then, has a net energy change of $49.4\ eV$.

$$49.4\ eV + Fe^{3+} + Li^+ + H_2\left[2c' = \sqrt{2}a_0\right] \rightarrow Fe^{4+} + Li + H_2\left[2c' = \frac{\sqrt{2}a_0}{2}\right] + 94.9\ eV \quad (5.132)$$

$$Li + Fe^{4+} \rightarrow Li^+ + Fe^{3+} + 49.4\ eV \quad (5.133)$$

And, the overall reaction is:

$$H_2\left[2c' = \sqrt{2}a_0\right] \rightarrow H_2\left[2c' = \frac{\sqrt{2}a_0}{2}\right] + 94.9\ eV \quad (5.134)$$

Note that the energy given off as the molecule shrinks is much greater than the energy lost to the energy hole. And, the energy released is large compared to conventional chemical reactions.

An efficient catalytic system that hinges on the coupling of three resonator cavities involves scandium. For example, the fourth ionization energy of scandium is $73.47\ eV$. This energy hole is obviously too high for resonant absorption. However, Sc^{3+} releases $24.76\ eV$ when it is reduced to Sc^{2+}. The combination of Sc^{3+} to Sc^{4+} and Sc^{3+} to Sc^{2+}, then, has a net energy change of $48.7\ eV$.

$$48.7\ eV + Sc^{3+} + Sc^{3+} + H_2\left[2c' = \sqrt{2}a_0\right] \rightarrow Sc^{4+} + Sc^{2+} + H_2\left[2c' = \frac{\sqrt{2}a_0}{2}\right] + 94.9\ eV \quad (5.135)$$

$$Sc^{2+} + Sc^{4+} \rightarrow Sc^{3+} + Sc^{3+} + 48.7\ eV \quad (5.136)$$

And, the overall reaction is:

$$H_2\left[2c' = \sqrt{2}a_0\right] \rightarrow H_2\left[2c' = \frac{\sqrt{2}a_0}{2}\right] + 94.9\ eV \quad (5.137)$$

An efficient catalytic system that hinges on the coupling of three resonator cavities involves gallium and lead. For example, the fourth ionization energy of gallium is $64.00\ eV$. This energy hole is obviously too high for resonant absorption. However, Pb^{2+} releases $15.03\ eV$ when it is reduced to Pb^+. The combination of Ga^{3+} to Ga^{4+} and Pb^{2+} to Pb^+, then, has a net energy change of $48.97\ eV$.

$$48.97\ eV + Ga^{3+} + Pb^{2+} + H_2\left[2c' = \sqrt{2}a_0\right] \rightarrow Ga^{4+} + Pb^+ + H_2\left[2c' = \frac{\sqrt{2}a_0}{2}\right] + 94.9\ eV \quad (5.138)$$

$$Ga^{4+} + Pb^+ \rightarrow Ga^{3+} + Pb^{2+} + 48.97\ eV \quad (5.139)$$

And, the overall reaction is:

$$H_2\left[2c' = \sqrt{2}a_0\right] \rightarrow H_2\left[2c' = \frac{\sqrt{2}a_0}{2}\right] + 94.9\ eV \quad (5.140)$$

The rate of an electronic transition of a molecule is a function of the change in internuclear distance during the transition. Transitions between electronic states that have equivalent internuclear distances at some point during their vibrational cycles have much greater rates than transitions that require the energy level of the electrons to change as well as the internuclear distance to change simultaneously. As shown in Figure 5.4, the transition from the $n = 1$ state to the $n = 1/2$ state of molecular hydrogen is not favored for this reason. A more likely transition pathway is a vibrational excitation of molecular hydrogen ($n = 1$) that breaks the bond, followed by a transition reaction of each of the hydrogen atoms via a $27.2\ eV$ energy hole catalyst as given in the Hydrino Theory—BlackLight Process section, followed by reaction of the two hydrino atoms ($n = 1/2$) to form a dihydrino molecule ($n = 1/2$).

REFERENCES

1. K. Akhtar, J. Scharer, R. L. Mills, Substantial Doppler broadening of atomic-hydrogen lines in DC and capacitively coupled RF plasmas**,** J. Phys. D, Applied Physics, Vol. 42, (2009), 42 135207 (2009) doi:10.1088/0022-3727/42/13/135207.
2. R. Mills, K. Akhtar, "Tests of Features of Field-Acceleration Models for the Extraordinary Selective H Balmer α Broadening in Certain Hydrogen Mixed Plasmas," Int. J. Hydrogen Energy, Vol. 34, (2009), pp. 6465-6477.
3. R. L. Mills, B. Dhandapani, K. Akhtar, "Excessive Balmer α Line Broadening of Water-Vapor Capacitively-Coupled RF Discharge Plasmas," Int. J. Hydrogen Energy, Vol. 33, (2008), pp. 802-815.
4. R. Mills, P. Ray, B. Dhandapani, "Evidence of an Energy Transfer Reaction Between Atomic Hydrogen and Argon II or Helium II as the Source of Excessively Hot H Atoms in RF Plasmas," Journal of Plasma Physics, (2006), Vol. 72, Issue 4, pp. 469-484.
5. J. Phillips, C-K Chen, K. Akhtar, B. Dhandapani, R. Mills, "Evidence of Catalytic Production of Hot Hydrogen in RF Generated Hydrogen/Argon Plasmas," International Journal of Hydrogen Energy, Vol. 32(14), (2007), 3010-3025.
6. R. L. Mills, P. C. Ray, R. M. Mayo, M. Nansteel, B. Dhandapani, J. Phillips, "Spectroscopic Study of Unique Line Broadening and Inversion in Low Pressure Microwave Generated Water Plasmas," J. Plasma Physics, Vol. 71, Part 6, (2005), pp. 877-888.
7. R. L. Mills, K. Akhtar, "Fast H in Hydrogen Mixed Gas Microwave Plasmas when an Atomic Hydrogen Supporting Surface Was Present," Int. J. Hydrogen Energy, 35 (2010), pp. 2546-2555, doi:10.1016/j.ijhydene.2009.12.148.
8. R. Mills, Y. Lu, "Mechanism of soft X-ray continuum radiation from low-energy pinch discharges of hydrogen and ultra-low field ignition of solid fuels," submitted.
9. R. L. Mills, R. Booker, Y. Lu, "Soft X-ray Continuum Radiation from Low-Energy Pinch Discharges of Hydrogen," J. Plasma Physics, Vol. 79, (2013), pp 489-507; doi:10.1017/S0022377812001109.
10. K. R. Lykke, K. K. Murray, W. C. Lineberger, "Threshold photodetachment of H^-," Phys. Rev. A, Vol. 43, No. 11, (1991), pp. 6104-6107.
11. D. R. Lide, *CRC Handbook of Chemistry and Physics*, 86th Edition, CRC Press, Taylor & Francis, Boca Raton, (2005-6), pp. 10-202 to 10-204.
12. K. K. Baldridge, J. S. Siegel, "Correlation of empirical δ(TMS) and absolute NMR chemical shifts predicted by ab initio computations," J. Phys. Chem. A, Vol. 103, (1999), pp. 4038-4042.
13. J. Mason, Editor, *Multinuclear NMR*, Plenum Press, New York, (1987), Chp. 3.
14. C. Suarez, E. J. Nicholas, M. R. Bowman, "Gas-phase dynamic NMR study of the internal rotation in N-trifluoroacetlypyrrolidine," J. Phys. Chem. A, Vol. 107, (2003), pp. 3024-3029.
15. C. Suarez, "Gas-phase NMR spectroscopy," The Chemical Educator, Vol. 3, No. 2, (1998).
16. H. Beutler, Z. Physical Chem., "Die dissoziationswarme des wasserstoffmolekuls H_2, aus einem neuen ultravioletten resonanzbandenzug bestimmt," Vol. 27B, (1934), pp. 287-302.
17. G. Herzberg, L. L. Howe, "The Lyman bands of molecular hydrogen," Can. J. Phys., Vol. 37, (1959), pp. 636-659.
18. P. W. Atkins, *Physical Chemistry*, Second Edition, W. H. Freeman, San Francisco, (1982), p. 589.
19. N. V. Sidgwick, *The Chemical Elements and Their Compounds*, Volume I, Oxford, Clarendon Press, (1950), p.1
20. A. Beiser, *Concepts of Modern Physics*, Fourth Edition, McGraw-Hill Book Company, New York, (1978), pp. 153-155.
21. M. D. Lamb, *Luminescence Spectroscopy*, Academic Press, London, (1978), p. 68.
22. P. Kurunczi, H. Shah, and K. Becker, "Excimer formation in high-pressure microhollow cathode discharge plasmas in helium initiated by low-energy electron collisions," Int. J. Mass Spectrosc., Vol. 205, (2001), pp. 277-283.
23. P. F. Kurunczi, K. H. Becker, "Microhollow Cathode Discharge Plasma: Novel Source of Monochromatic Vacuum Ultraviolet Radiation," Proc. Hakone VII, Int. Symp. High Pressure, Low Temperature Plasma Chemistry, Greifswald, Germany, Sept. 10 - 13, (2000), Vol. 2, p. 491.
24. P. Kurunczi, H. Shah, and K. Becker, "Hydrogen Lyman-α and Lyman-β emissions from high-pressure microhollow cathode discharges in $Ne-H_2$ mixtures," J. Phys. B: At. Mol. Opt. Phys., Vol. 32, (1999), L651-L658.
25. J. Wieser, D. E. Murnick, A. Ulrich, H. A Higgins, A. Liddle, W. L. Brown, "Vacuum ultraviolet rare gas excimer light source," Rev. Sci. Instrum., Vol. 68, No. 3, (1997), pp. 1360-1364.
26. A. Ulrich, J. Wieser, D. E. Murnick, "Excimer Formation Using Low Energy Electron Beam Excitation," Second International Conference on Atomic and Molecular Pulsed Lasers, Proceedings of SPIE, Vol. 3403, (1998), pp. 300-307.

27. D. R. Lide, *CRC Handbook of Chemistry and Physics*, 86th Edition, CRC Press, Taylor & Francis, Boca Raton, (2005-6), pp. 9-54 to 9-59.
28. R. Mills, "Spectroscopic Identification of a Novel Catalytic Reaction of Atomic Hydrogen and the Hydride Ion Product," Int. J. Hydrogen Energy, Vol. 26, No. 10, (2001), pp. 1041-1058.
29. B. J. Thompson, *Handbook of Nonlinear Optics*, Marcel Dekker, Inc., New York, (1996), pp. 497-548.
30. Y. R Shen, *The Principles of Nonlinear Optics*, John Wiley & Sons, New York, (1984), pp. 203-210.
31. B. de Beauvoir, F. Nez, L. Julien, B. Cagnac, F. Biraben, D. Touahri, L. Hilico, O. Acef, A. Clairon, and J. J. Zondy, Physical Review Letters, Vol. 78, No. 3, (1997), pp. 440-443.
32. E. Bulbul, M. Markevitch, A. Foster, R. K. Smith, M. Loewenstein, S. W. Randall, "Detection of an unidentified emission line in the stacked X-Ray spectrum of galaxy clusters," The Astrophysical Journal, Volume 789, Number 1, (2014).
33. A. Boyarsky, O. Ruchayskiy, D. Iakubovskyi, J. Franse, "An unidentified line in X-ray spectra of the Andromeda galaxy and Perseus galaxy cluster," (2014),arXiv:1402.4119 [astro-ph.CO].
34. Nico Cappelluti, Esra Bulbul, Adam Foster, Priyamvada Natarajan, Megan C. Urry, Mark W. Bautz, Francesca Civano, Eric Miller, Randall K. Smith, "Searching for the 3.5 keV Line in the Deep Fields with Chandra: The 10 ms Observations," The Astrophysical Journal, Vol. 854 (2), (2018), p. 179 DOI: 10.3847/1538-4357/aaaa68.
35. F. A. Cotton, "Chemical applications of Group Theory," 2nd Edition, Wiley Interscience, (1963), pp. 280-283.
36. F. Wilkinson, "Intramolecular Electronic Energy Transfer Between Organic Molecules," *Luminescence in Chemistry*, Edited by E. J. Bowen, D. Van Nostrand Co. Ltd., London, (1968), Chapter 8, pp. 154-182.
37. H. Morawetz, Science, 240, (1988), pp. 172-176.
38. O. Schnepp, Levy, M., J. Am. Chem. Soc., 84, (1962), pp. 172-177.
39. F. Wilkinson, *Luminescence in Chemistry*, Edited by E. J. Bowen, D. Van Nostrand Co. Ltd., London, (1968), pp. 155-182.
40. Th. Förster, *Comparative Effects of Radiation*, Report of a Conference held at the University of Puerto Rico, San Juan, February 15-19, (1960), sponsored by the National Academy of Sciences; National Research Council, Edited by Milton Burton, J. S. Kirby-Smith, and John L. Magee, John Wiley & Sons, Inc., New York pp. 300-325.
41. F. Bueche, *Introduction to Physics for Scientists and Engineers*, McGraw-Hill, (1975), pp. 352-353.
42. J. D. Jackson, *Classical Electrodynamics*, Second Edition, John Wiley & Sons, New York, (1975), pp. 739-747.
43. J. D. Jackson, *Classical Electrodynamics*, Second Edition, John Wiley & Sons, New York, (1975), pp. 758-760.
44. F. J. Bueche, *Introduction to Physics for Scientists and Engineers*, McGraw-Hill Book Company, New York, (1986), pp. 261-265.
45. I. Levine, *Physical Chemistry*, McGraw-Hill Book Company, New York, (1978), pp. 420-421.
46. F. J. Bueche, *Introduction to Physics for Scientists and Engineers*, McGraw-Hill Book Company, New York, (1986), pp. 261-265.
47. http://en.wikipedia.org/wiki/Nuclear_fusion.
48. L. I. Ponomarev, "Muon catalyzed fusion," Contemporary Physics, Vol. 31, No. 4, (1990), pp. 219-245.
49. J. Zmeskal, P. Kammel, A. Scrinzi, W. H. Breunlich, M. Cargnelli, J. Marton, N. Nagele, J. Werner, W. Bertl, and C. Petitjean, "Muon-catalyzed dd fusion between 25 and 150 K: experiment," Phys. Rev. A, Vol. 42, (1990), pp. 1165-1177.
50. R. Mills, Y. Lu, R. Frazer, "Power Determination and Hydrino Product Characterization of Ultra-low Field Ignition of Hydrated Silver Shots", Chinese Journal of Physics, Vol. 56, (2018), pp. 1667-1717.
51. R. Mills J. Lotoski, "H_2O-based solid fuel power source based on the catalysis of H by HOH catalyst", Int'l J. Hydrogen Energy, Vol. 40, (2015), 25-37.
52. https://brilliantlightpower.com/pdf/Spectroscopy_Nansteel_Report_040219.pdf.
53. https://www.brilliantlightpower.com/wp-content/uploads/pdf/Free-Air-TNT-Analysis.pdf.
54. R. Mills, "Hydrino States of Hydrogen", https://brilliantlightpower.com/pdf/Hydrino_States_of_Hydrogen.pdf, submitted for publication.
55. https://www.science.org/content/article/fusion-power-may-run-fuel-even-gets-started#:~:text=According%20to%20Kovari's%20study%2C%20D%2DD,%242%20billion%20per%20kilogram%20produced.
56. Wilfred R. Hagen, Randell L. Mills, "Electron Paramagnetic Resonance Proof for the Existence of Molecular Hydrino", Vol. 47, No. 56, (2022), pp. 23751-23761; https://www.sciencedirect.com/science/article/pii/S0360319922022406.

Chapter 6

STABILITY OF ATOMS AND HYDRINOS

The central field of the proton corresponds to integer one charge. Excited states comprise an electron with a trapped photon. In all energy states of hydrogen, the photon has an electric field that superposes with the field of the proton. In the $n=1$ state, the sum is one, and the sum is zero in the ionized state. In an excited state, the sum is a fraction of one (i.e. between zero and one). Derivations from first principles given in the Excited States of the One-Electron Atom section demonstrate that each "allowed" fraction corresponding to an excited state is $\frac{1}{\text{integer}}$. Following the derivation given in the Excited States of the One-Electron Atom (Quantization) section, the relationship between the electric field equation and the "trapped photon" source charge-density function is given by Maxwell's equation in two-dimensions.

$$\mathbf{n} \bullet \left(\mathbf{E}_1 - \mathbf{E}_2 \right) = \frac{\sigma}{\varepsilon_0} \tag{6.1}$$

where $\mathbf{n}$ is the radial normal unit vector, $\mathbf{E}_1 = 0$ ($\mathbf{E}_1$ is the electric field outside of the atomic orbital), $\mathbf{E}_2$ is given by the total electric field at $r_n = na_H$, and σ is the surface charge-density. The electric field of an excited state is fractional; therefore, the source charge function is fractional. It is well known that fractional charge is not "allowed." The reason given in the Instability of Excited States section is that fractional charge typically corresponds to a radiative current-density function. The excited states of the hydrogen atom are examples. They are radiative; consequently, they are not stable. Thus, an excited electron decays to the first nonradiative state corresponding to an integer field, $n=1$ (i.e. a field of integer one times the central field of the proton). Specifically, the superposition of σ_{photon} (Eq. (2.23)) and $\sigma_{electron}$ (Eq. (2.24)) is equivalent to the sum of a radial electric dipole represented by a doublet function and a radial electric monopole represented by a delta function given in Eq. (2.25). Due to the radial doublet, excited states are radiative since spacetime harmonics of $\frac{\omega_n}{c} = k$ or $\frac{\omega_n}{c}\sqrt{\frac{\varepsilon}{\varepsilon_0}} = k$ do exist for which the spacetime Fourier transform of the current density function is nonzero.

Equally valid from first principles are electronic states where the magnitude of the sum of the electric field of the photon and the proton central field are an integer greater than one times the central field of the proton. These states are nonradiative. A catalyst can effect a transition between these states as described in the Hydrino Theory—BlackLight Process section.

The condition for radiation by a moving charge is derived from Maxwell's equations. To radiate, the spacetime Fourier transform of the current-density function must possess components synchronous with waves traveling at the speed of light [1]. Alternatively,

> *For non-radiative states, the current-density function must not possess spacetime Fourier components that are synchronous with waves traveling at the speed of light.*

As given in the One-Electron Atom section, the relationship between the radius and the wavelength of the electron is:

$$v_n = \lambda_n f_n \tag{6.2}$$

$$v_n = 2\pi r_n f_n = \lambda_n f_n \tag{6.3}$$

$$2\pi r_n = \lambda_n \tag{6.4}$$

Consider the wave vector of the sinc function of Eq. (38) of Appendix I, the Spacetime Fourier Transform of the Electron Function. When the velocity is c corresponding to a potentially emitted photon

$$\mathbf{s}_n \bullet \mathbf{v}_n = \mathbf{s}_n \bullet \mathbf{c} = \omega_n \tag{6.5}$$

the relativistically corrected wavelength (Eq. (1.280)) is given by:

$$\mathbf{r}_n = \lambda_n \tag{6.6}$$

Substitution of Eq. (6.6) into the sinc function results in the vanishing of the entire Fourier transform of the current-density function. Thus, spacetime harmonics of $\frac{\omega_n}{c} = k$ or $\frac{\omega_n}{c}\sqrt{\frac{\varepsilon}{\varepsilon_0}} = k$ do not exist for which the Fourier transform of the current-density function is nonzero.

In the case of below "ground" (fractional quantum number) energy states, the sum of the source current corresponding to the photon and the electron current results in a radial Dirac delta function as shown in the Stability of Atoms and Hydrinos section. Whereas, in the case of above "ground" or excited (integer quantum number) energy states, the sum of the source current corresponding to the photon and the electron current results in a radial doublet function which has Fourier components of $\frac{\omega_n}{c} = k$. Thus, excited states are radiative as shown in the Instability of Excited States section.

STABILITY OF "GROUND" AND HYDRINO STATES

For the below "ground" (fractional quantum number) energy states of the hydrogen atom, σ_{photon}, the two-dimensional surface charge due to the "trapped photon" at the electron atomic orbital, is given by Eqs. (5.27) and (2.11).

$$\sigma_{photon} = \frac{e}{4\pi(r_n)^2}\left[Y_0^0(\theta,\phi) - \frac{1}{n}\left[Y_0^0(\theta,\phi) + \mathrm{Re}\left\{Y_\ell^m(\theta,\phi)e^{im\omega_n t}\right\}\right]\right]\delta(r-r_n) \quad n = 1, \frac{1}{2}, \frac{1}{3}, \frac{1}{4}, \ldots \tag{6.7}$$

And, $\sigma_{electron}$, the two-dimensional surface charge of the electron atomic orbital is:

$$\sigma_{electron} = \frac{-e}{4\pi(r_n)^2}\left[Y_0^0(\theta,\phi) + \mathrm{Re}\left\{Y_\ell^m(\theta,\phi)e^{im\omega_n t}\right\}\right]\delta(r-r_n) \tag{6.8}$$

The superposition of σ_{photon} (Eq. (6.7)) and $\sigma_{electron}$, (Eq. (6.8)) where the spherical harmonic functions satisfy the conditions given in the Bound Electron "Atomic Orbital"section is a radial electric monopole represented by a delta function.

$$\sigma_{photon} + \sigma_{electron} = \frac{-e}{4\pi(r_n)^2}\left[\frac{1}{n}Y_0^0(\theta,\phi) + \left(1+\frac{1}{n}\right)\mathrm{Re}\left\{Y_\ell^m(\theta,\phi)e^{im\omega_n t}\right\}\right]\delta(r-r_n) \quad n = 1, \frac{1}{2}, \frac{1}{3}, \frac{1}{4}, \ldots \tag{6.9}$$

In the case of lower-energy states or hydrino states, the superposition given by Eq. (6.9) involves integer charge only. Whereas, in the case of excited states, the superposition given by Eq. (2.25) involves the sum of a delta function with a fractional charge (radial monopole term) and two delta functions of charge plus one and minus one which is a doublet function (radial dipole term). As given in the Spacetime Fourier Transform of the Electron Function section, the radial delta function does not possess spacetime Fourier components synchronous with waves traveling at the speed of light. Thus, the below "ground" (fractional quantum number) energy states of the hydrogen atom are stable. The "ground" ($n = 1$ quantum number) energy state is just the first of the nonradiative states of the hydrogen atom; thus, it is the state to which excited states decay based on the nature of photon and corresponding electron source current of excited as opposed to the hydrino states as given in the Excited States of the One-Electron Atom (Quantization) section and Hydrino Theory—BlackLight Process section, respectively. The stability is also shown using the Poynting power theorem applied to the electric and magnetic fields from the electron source current as shown in Appendix I.

NEW "GROUND" STATE

Hydrogen atoms can undergo transitions to energy states below the $n = 1$ state until the potential energy of the proton is converted to kinetic energy and total energy (the negative of the binding energy), and a state is formed, which is stable to both radiation and nonradiative energy transfer. The potential energy V of the electron and the proton separated by the radial distance radius r_1 is:

$$V = \frac{-e^2}{4\pi\varepsilon_0 r_1} \tag{6.10}$$

where the radius r_1 is the proton radius given by Eq. (29.1)

$$r_p = 1.3\ X\ 10^{-15}\ m \tag{6.11}$$

Substitution of Eq. (6.11) into Eq. (6.10) gives the total potential energy V of the electron and the proton

$$V = \frac{-e^2}{4\pi\varepsilon_0 r_p} = 1.1\ \mathrm{X}\ 10^6\ \mathrm{eV} \tag{6.12}$$

In the present case of an inverse squared central field, the binding energy and the kinetic energy are each equal to one half the potential energy [2] in the electron frame, and the lab-frame relativistic correction is given by correcting the radius as given in the Special Relativistic Correction to the Ionization Energies section. The relativistic invariance of the magnetic moment μ_B and angular momentum $\hbar$ of the electron may be used to characterize the limiting $v = c$ case as shown in the One-Electron Atom—Determination of Atomic Orbital Radii section. Considering the consequences of special relativity, the size of a

hydrogen atom in the true ground state is limited not to be less than $\lambda\!\!\!^{-}$, the electron Compton wavelength bar,

$$\lambda\!\!\!^{-}' = r' = \frac{\hbar}{m_e c} = \alpha a_0 \tag{6.13}$$

$$\lambda\!\!\!^{-} = r = \frac{\hbar}{\gamma^* m_e c} = \frac{\alpha a_0}{2\pi} = 6.14\ X\ 10^{-14} m \tag{6.14}$$

since the tangential electron velocity (Eq. (1.35)) is the speed of light at this radius. Eq. (1.35) and Eq. (1.254) gives the relationship between the electron speed and the speed of light, which gives the limit on the quantum state p as:

$$\frac{v}{c} = \alpha pZ \qquad p = 1, 2, 3... \tag{6.15}$$

With $Z = 1$, $p \le 137$ due to the limiting speed of light. In Eq. (6.13) $\lambda\!\!\!^{-}'$ is the radius in the electron frame, and $\lambda\!\!\!^{-}$ in Eq. (6.14) is the radius in the laboratory frame according to Eq. (1.280). From Eq. (6.14), the proton radius given by Eq. (6.11) cannot be reached. As given previously in the Hydrino Catalyzed Fusion (HCF) section, $p = 137$ is the highest value of p physically possible corresponding to a minimum radius of $0.022926\alpha a_0 = 8.853X10^{-15} m = 8.853\, fm$, 8.9 times the radius of a proton of 1 fm, and one thirtieth the radius of the muonic atom.

As shown in the Spacetime Fourier Transform of the Electron Function section and the Special Relativistic Correction to the Ionization Energies section, there can be no radiation from the electron at light speed in the laboratory inertial frame. Nonradiative energy transfer is also forbidden since this requires the impossible formation of a photon standing wave at light speed relative to the electron at light speed. Electronic transitions below the $H\left[\frac{a_H}{\alpha^{-1}}\right]$ state are not possible since no energy transfer mechanism is possible.

However, for this electronic state, it may be possible for the proton to decay to gamma rays with the capture of the electron. With electron capture, the electron atomic orbital superimposes that of the proton, and a neutral particle is formed that is energy deficient with respect to the neutron. To conserve spin, electron capture requires the concurrent capture of an electron antineutrino with decay to a photon and an electron neutrino as given in the Gravity section. Disproportionation reactions to the lowest-energy states of hydrogen followed by electron capture with gamma ray emission may be a source of nonthermal γ-ray bursts from interstellar regions [3]. A branch of the decay path may also be similar to that of the π^0 meson. Gamma and pair production decay would result in characteristic 511 keV annihilation energy emission. This emission has been recently been identified with dark matter [4-5]. Alternatively, the diffuse 511 keV radiation by interstellar medium is consistent with the role of hydrino as dark matter in pair production from incident cosmic radiation [6-8].

Hydrinos present in neutron stars may facilitate HCF. This may be the mechanism of gamma emission by neutron stars. With sufficient energy/mass release, a chain reaction of neutron decay to release electron antineutrinos, which react with hydrinos according to Eq. (24.173) may be the cause of γ-ray bursts. Another more likely mechanism based on a particle of the Planck Mass is given in the Gravity section.

SPIN-NUCLEAR AND ORBITAL-NUCLEAR COUPLING OF HYDRINOS

The "trapped photon" given by Eq. (5.27) is a "standing electromagnetic wave" which actually is a circulating wave that propagates along each great circle current loop of the atomic orbital. The time-function factor, $k(t)$, for the "standing wave" is identical to the time-function factor of the atomic orbital in order to satisfy the boundary (phase) condition at the atomic orbital surface. Thus, the angular frequency of the "trapped photon" has to be identical to the angular frequency of the electron atomic orbital, ω_n. Furthermore, the phase condition requires that the angular functions of the "trapped photon" have to be identical to the spherical harmonic angular functions of the electron atomic orbital.

Photons obey Maxwell's equations. At the two-dimensional surface of the atomic orbital containing a "trapped photon," the relationship between the photon's electric field and its two-dimensional charge density at the atomic orbital is:

$$\mathbf{n} \bullet \left(\mathbf{E}_1 - \mathbf{E}_2\right) = \frac{\sigma}{\varepsilon_0} \tag{6.16}$$

Thus, the photon's electric field acts as surface charge. According to Eq. (6.16), the "photon standing wave" in the electron atomic orbital resonator cavity gives rise to a two-dimensional surface charge at the atomic orbital two dimensional surface. The surface charge is given by Eq. (6.16) for a central field strength equal in magnitude to that of a central charge pe. This surface charge possesses the same angular velocity as the atomic orbital; thus, it is a current with a corresponding magnetic field. The rotational parameters of the surface current of the "photon standing wave" are given in the Rotational Parameters of the Electron (Angular Momentum, Rotational Energy, Moment of Inertia) section. The solution to Legendre's equation given by Eq. (1.66) is the maximum term of a series of solutions corresponding to the m and ℓ values [9-10]. From Eq. (1.72), $\mathbf{L}$, the amplitude of the orbital angular momentum along the z-axis is

$$\mathbf{L} = \pm\hbar\sqrt{\frac{\ell}{\ell+1}}\mathbf{i}_z \tag{6.17}$$

Therefore, from Eq. (2.65), the corresponding magnetic moment is:

$$\mu = \pm\frac{e\hbar}{2m_e}\sqrt{\frac{\ell}{\ell+1}}\mathbf{i}_z = \pm\mu_B\sqrt{\frac{\ell}{\ell+1}}\mathbf{i}_z \tag{6.18}$$

where μ_B is the Bohr magneton. The magnetic moment gives rise to a magnetic field at the nucleus, which superimposes that due to spin. Thus, from Eqs. (2.215) and (6.18), the central force after the derivations in the Spin-Nuclear Coupling (Hyperfine Structure) section is:

$$\mathbf{F}_{mag} = \pm e\alpha c\frac{\mu_0}{r^3}\ \mu_P\sqrt{\frac{3}{4}}\left(\frac{1}{2}+\sqrt{\frac{\ell}{\ell+1}}\right) \tag{6.19}$$

where the plus corresponds to antiparallel alignment of the magnetic moments of the electron and proton, and the minus corresponds to parallel alignment. The outward centrifugal force (Eq. (1.241)) on the electron is balanced by the electric force (Eq. (1.242)) and the magnetic force given by Eq. (6.19)

$$\frac{m_e v^2}{r} = \frac{pe^2}{4\pi\varepsilon_0 r^2} - \frac{\hbar^2}{m_P r^3} \pm pe\alpha c\frac{\mu_0}{r^3}\ \mu_P\sqrt{\frac{3}{4}}\left(\frac{1}{2}+\sqrt{\frac{\ell}{\ell+1}}\right) \tag{6.20}$$

where the central field of the hydrino atom has a magnitude that is equivalent to p times that of the "ground" state ($n = p = 1$) hydrogen atom and m_P is the mass of the proton. Using Eq. (1.35),

$$\frac{\hbar^2}{m_e r^3} = \frac{pe^2}{4\pi\varepsilon_0 r^2} - \frac{\hbar^2}{m_P r^3} \pm pe\alpha c\frac{\mu_0}{r^3}\ \mu_P\sqrt{\frac{3}{4}}\left(\frac{1}{2}+\sqrt{\frac{\ell}{\ell+1}}\right) \tag{6.21}$$

$$r = \frac{a_H}{p} \pm \frac{4\pi\alpha\ \mu_P}{ec}\sqrt{\frac{3}{4}}\left(\frac{1}{2}+\sqrt{\frac{\ell}{\ell+1}}\right) \tag{6.22}$$

where a_H is the radius of the hydrogen atom and the plus corresponds to parallel alignment of the magnetic moments of the electron and proton, and the minus corresponds to antiparallel alignment.

ENERGY CALCULATIONS

The magnetic energy $\Delta E_{magdipole}$ to flip the orientation of the proton's magnetic moment, μ_P, from parallel to antiparallel to the direction of the magnetic flux $\mathbf{B}_s$ due to electron spin and the magnetic flux $\mathbf{B}_o$ due to the orbital angular momentum of the electron (180° rotation of the magnet moment vector) given by Eqs. (1.168), (2.222), (2.210), and (6.18) is:

$$\Delta E_{magdipole} = -\frac{p\mu_0 e\hbar}{m_e}\mu_P\sqrt{\frac{3}{4}}\left(\frac{1}{2}+\sqrt{\frac{\ell}{\ell+1}}\right)\left(\frac{1}{r_+^3}+\frac{1}{r_-^3}\right) = -2p\mu_0\mu_B\mu_P\sqrt{\frac{3}{4}}\left(\frac{1}{2}+\sqrt{\frac{\ell}{\ell+1}}\right)\left(\frac{1}{r_+^3}+\frac{1}{r_-^3}\right) \tag{6.23}$$

where the Bohr magneton, μ_B, is given by Eq. (1.131), the radius of the hydrino atom is $\frac{a_H}{p}$, and the central field of the hydrino atom has a magnitude that is equivalent to p times that of the "ground" state ($n = p = 1$) hydrogen atom.

The change in the electric energy of the electron due to the slight shift of the radius of the electron due to spin-nuclear and orbital-nuclear interactions is given by the difference between the electric energies associated with the two possible orientations of the magnetic moment of the electron with respect to the magnetic moment of the proton, parallel versus antiparallel. The electric energy is given by the substitution of the corresponding radius given by Eq. (6.22) into Eq. (1.264) where $Z = p$. The change in electric energy for the flip from antiparallel to parallel alignment, $\Delta E_{ele}^{S/N\ O/N}$, is:

$$\Delta E_{ele}^{S/N\ O/N} = \frac{-pe^2}{8\pi\varepsilon_0}\left[\frac{1}{r_+}-\frac{1}{r_-}\right] \tag{6.24}$$

In addition, the interaction of the magnetic moments of the electron and proton increases the magnetic energy of the electron given by Eq. (2.224). The change in the magnetic energy of the electron $\Delta E_{mag}^{S/N\ O/N}$ due to the slight shift of the radius of the electron due to spin-nuclear and orbital-nuclear interactions is:

$$\begin{aligned}\Delta E_{mag}^{S/N\ O/N} &= -\left(1+\left(\frac{2}{3}\right)^2+\alpha\left(\cos\frac{\pi}{3}\right)^2\right)\frac{\pi\mu_0 e^2\hbar^2}{m_e^2}\left(\frac{1}{r_+^3}-\frac{1}{r_-^3}\right)\\ &= -\left(1+\left(\frac{2}{3}\right)^2+\frac{\alpha}{4}\right)4\pi\mu_0\mu_B^2\left(\frac{1}{r_+^3}-\frac{1}{r_-^3}\right)\end{aligned} \tag{6.25}$$

The orbital rotational energy arises from a spin function (spin angular momentum) modulated by a spherical harmonic angular function (orbital angular momentum). The amplitude of the orbital rotational energy $E_{rotational\ orbital}$ is:

$$E_{rotational\ \ orbital} = \frac{\hbar^2}{2m_e r_n^{\ 2}}\left[\frac{\ell}{\ell+1}\right] \tag{6.26}$$

However, the time-averaged mechanical angular momentum and rotational energy associated with the traveling charge-density wave on the atomic orbital is zero:

$$\left\langle L_{z\ orbital}\right\rangle = 0 \tag{6.27}$$

$$\left\langle E_{rotational\ \ orbital}\ \right\rangle = 0 \tag{6.28}$$

Thus, a term corresponding to Eq. (6.26) was not added to Eq. (6.25). Only the coupling of the dynamic angular momentum to the radiative reaction need be considered as given in Eqs. (6.19) and (6.23).

The total energy of the transition from antiparallel to parallel alignment due to spin-nuclear and orbital-nuclear interactions, $\Delta E_{total}^{S/N\ O/N}$, is given as the sum of Eqs. (6.23-6.25):

$$\Delta E_{total}^{S/N\ O/N} = \Delta E_{magdipole} + \Delta E_{ele}^{S/N\ O/N} + \Delta E_{mag}^{S/N\ O/N} \tag{6.29}$$

$$\begin{aligned}\Delta E_{total}^{S/N\ O/N} &= -2p\mu_0\mu_B\mu_P\sqrt{\frac{3}{4}}\left(\frac{1}{2}+\sqrt{\frac{\ell}{\ell+1}}\right)\left(\frac{1}{r_+^3}+\frac{1}{r_-^3}\right)\\ &-\frac{pe^2}{8\pi\varepsilon_0}\left[\frac{1}{r_+}-\frac{1}{r_-}\right]-\left(1+\left(\frac{2}{3}\right)^2+\frac{\alpha}{4}\right)4\pi\mu_0\mu_B^2\left(\frac{1}{r_+^3}-\frac{1}{r_-^3}\right)\end{aligned} \tag{6.30}$$

For the case that $\ell = 0$, the hydrino hyperfine structure radius and energy $\Delta E_{total}^{S/N}$ given by Eqs. (2.221) and (2.225) respectively, are the same as those of ordinary hydrogen with $p = 1$ in Eqs. (6.22) and (6.31):

$$\Delta E_{total}^{S/N} = -p\mu_0\mu_B\mu_P\sqrt{\frac{3}{4}}\left(\frac{1}{r_+^3}+\frac{1}{r_-^3}\right)-\frac{pe^2}{8\pi\varepsilon_0}\left[\frac{1}{r_+}-\frac{1}{r_-}\right]-\left(1+\left(\frac{2}{3}\right)^2+\frac{\alpha}{4}\right)4\pi\mu_0\mu_B^2\left(\frac{1}{r_+^3}-\frac{1}{r_-^3}\right) \tag{6.31}$$

The frequency, f, can be determined from the energy using the Planck relationship, Eq. (2.148).

$$f = \frac{-\Delta E_{total}^{S/N\ O/N}}{h} \tag{6.32}$$

From Eqs. (6.22), (6.30), (6.31), and the Planck relationship, Eq. (2.148), the energy, the wavelength, and the frequency corresponding to the spin-nuclear and orbital-nuclear coupling energy of the hydrino atom with the lower energy state quantum numbers p and ℓ and with the radius $\frac{a_H}{p}$ are given in Table 6.1.

Table 6.1. The spin-nuclear and orbital-nuclear coupling energies of the hydrino atom with the lower energy state quantum numbers p and ℓ and with the radius $\frac{a_H}{p}$.

p	ℓ	Energy ($J\ X\ 10^{-23}$)	Wavelength (cm)	Wave Number (cm^{-1})	Frequency (GHz)
1	0	0.094117	21.106	0.047380	1.4204
2	0	2.2736	0.87369	1.1446	34.314
2	1	5.4890	0.36189	2.7633	82.840
3	0	12.806	0.15512	6.4466	193.27
3	1	30.916	0.064253	15.564	466.58
3	2	33.718	0.058914	16.974	508.87
4	0	42.520	0.046718	21.405	641.71
4	1	102.65	0.019351	51.677	1549.2
4	2	111.96	0.017743	56.360	1689.6
4	3	116.17	0.017100	58.480	1753.2
5	0	106.81	0.018598	53.769	1611.9
5	1	257.86	0.0077036	129.81	3891.6
5	2	281.23	0.0070635	141.57	4244.2
5	3	291.81	0.0068074	146.90	4403.9
5	4	297.87	0.0066688	149.95	4495.5

A COEFFICIENT

An estimate of the transition probability for magnetic multipoles is given by Eq. (16.105) of Jackson [11]. For a magnetic dipole $\ell = 1$, and Eq. (16.105) of Jackson is:

$$\frac{1}{\tau_M} \cong \left(\frac{g}{mc}\right)^2 \left(\frac{\hbar e^2}{c}\right) \frac{\pi}{4} k^2 \omega \tag{6.33}$$

where τ_M is the mean life of the magnetic multipole. Substitution of:

$$k = \frac{\omega}{c} \tag{6.34}$$

into Eq. (6.33) gives

$$\frac{1}{\tau_M} \cong \left(\frac{g}{mc}\right)^2 \left(\frac{\hbar e^2}{c}\right) \frac{\pi}{4} \frac{\omega^3}{c^2} \tag{6.35}$$

From Eq. (6.35), the transition probability is proportional to the frequency cubed. The experimental A coefficient for hydrogen $H\left(n=1\right)$ [12] is

$$A = 2.87\ X\ 10^{-15}\ \text{sec}^{-1} \tag{6.36}$$

The frequencies for the spin/nuclear hyperfine transition of hydrogen $H\left(n=1\right)$ and hydrino $H\left(n=1/2\right)$ are given in Table 6.1. The A coefficient for hydrino $H\left(n=1/2\right)$ is given by Eq. (6.35) and Eq. (6.36) and the frequencies of Table 6.1.

$$A_{H(n=1/2)} = A_{H(n=1)} \left(\frac{\omega_{H(n=1/2)}}{\omega_{H(n=1)}}\right)^3 = 2.87\ X\ 10^{-15} \left(\frac{34.31}{1.420}\right)^3 \text{sec}^{-1} = 4.05\ X\ 10^{-11}\ \text{sec}^{-1} \tag{6.37}$$

INTENSITY OF SPIN-NUCLEAR AND ORBITAL-NUCLEAR COUPLING TRANSITIONS OF HYDRINOS

The intensity, I, of spin-nuclear and orbital-nuclear coupling transitions of hydrinos can be calculated from the column density of hydrino atoms, $N(H)$, and the A coefficient, A_{ul}. The column density is given by the product of the number of hydrino atoms per unit volume, n_H, and the path length, ℓ, which is calculated in steradians from its integral.

$$I = \frac{1}{4\pi} A_{ul} N(H) = \frac{1}{4\pi} A_{ul} n_H \ell \tag{6.38}$$

wherein A_{ul} is given by Eq. (6.37). The number of hydrino atoms per unit volume, n_H, can be estimated from the experimental results of the integrated continuum emission for a selected transition from a celestial source. The number of electronic transitions per atom per second, k_1 (Eq. (5.105)), estimated to be equivalent to the number of photons per atom per second (A_{ul} (Eq. (6.38)) for the hydrino transition). Equating intensities of integrated photon flux (Eq. (6.38)) and the rate of the disproportionation reaction, $r_{m,m',p}$ Eq. (5.106), gives:

$$I = \frac{1}{4\pi} A_{ul} N(H) = \frac{1}{\sqrt{2}} n_H \left(\frac{a_H}{p}\right)^2 \sqrt{\frac{3kT}{m_H}} N(H) \tag{6.39}$$

where $N(H) = n_H \ell$ is the column density and $g_{m,p} = 1$ (the result is equivalent to Förster's theory for the efficiencies of dipole-dipole resonant energy transfers). $N(H)$, the column density of hydrino atoms, $H\left(\frac{a_H}{p}\right)$, can be calculated along the selected sight-line and substituted into Eq. (6.38) to give the intensity of the spin-nuclear and orbital-nuclear coupling transitions of hydrinos as a function of the path length, ℓ, which is calculated in steradians from its integral.

REFERENCES

1. H. A. Haus, "On the radiation from point charges," Am. J. Phys., 54, (1986), pp. 1126-1129.
2. G. R. Fowles, *Analytical Mechanics*, Third Edition, Holt, Rinehart, and Winston, New York, (1977), pp. 154-156.
3. K. Hurley, et. al., Nature, 372, (1994), pp. 652-654.
4. M. Chown, "Astronomers claim dark matter breakthrough," NewScientist.com, Oct. 3, (2003).
5. C. Boehm, D. Hooper, J. Silk, M. Casse, J. Paul, "MeV dark matter: Has it been detected," Phys. Rev. Lett., Vol. 92, (2004), p. 101301.
6. G. H. Share, "Recent results on celestial gamma radiation from SMM", Advances in Space Research, Vol.11, Issue 8, (1991), pp. 85-94.
7. G. H. Share, R. L. Kinzer, D. C. Messina, W. R. Purcell, E. L. Chupp, D. J. Forrest, E. Rieger, "Observations of galactic gamma-radiation with the SMM spectrometer", Advances in Space Research, Vol. 6, Issue 4, (1986), pp. 145-148.
8. B. Kozlovsky, R. E. Lingenfelter, R. Ramaty, "Positrons from accelerated particle interactions," The Astrophysical Journal, Vol. 316, (1987), pp. 801-818.
9. D. A. McQuarrie, *Quantum Chemistry*, University Science Books, Mill Valley, CA, (1983), pp. 206-221.
10. L. Pauling, E. Wilson, *Introduction to Quantum Mechanics with Applications to Chemistry*, McGraw-Hill Book Company, New York, (1935), pp. 118-121.
11. J. D. Jackson, *Classical Electrodynamics*, Second Edition, John Wiley & Sons, New York, (1975), pp. 758-760.
12. C. W. Allen, *Astrophysical Quantities*, 3rd Edition, (1973), University of London, The Athlone Press, p. 79.

Chapter 7

TWO-ELECTRON ATOMS

As is the case for one-electron atoms shown in the corresponding section, two-electron atoms can also be solved exactly. Two-electron atoms comprise two indistinguishable electrons bound to a nucleus of $+Z$. Each electron experiences a centrifugal force, and the balancing centripetal force (on each electron) is produced by the electric force between the electron and the nucleus and the magnetic force between the two electrons causing the electrons to pair.

DETERMINATION OF ATOMIC ORBITAL RADII

As shown in the One-Electron Atom section, bound electrons are described by a charge-density (mass-density) function, which is the product of a radial delta function ($f(r)=\delta(r-r_n)$), two angular functions (spherical harmonic functions), and a time harmonic function. Thus, an electron is a two-dimensional spherical current-density surface that can exist in a bound state at only specified distances from the nucleus. More explicitly, the uniform current-density function $Y_0^0(\theta,\phi)$ (Eqs. (1.27-1.29)) called the electron atomic orbital (shown in Figure 1.22) that gives rise to the spin of the electron is generated from two current-vector fields (CVFs). Each CVF comprises a continuum of correlated *orthogonal great circle current-density elements (one dimensional "current loops")*. The current pattern comprising each CVF is generated over a half-sphere surface by a set of rotations of two orthogonal great circle current loops that serve as basis elements about each of the $\left(-\mathbf{i}_x,\mathbf{i}_y,0\mathbf{i}_z\right)$ and $\left(-\frac{1}{\sqrt{2}}\mathbf{i}_x,\frac{1}{\sqrt{2}}\mathbf{i}_y,\mathbf{i}_z\right)$-axis; the span being π radians. Then, the two CVFs are convoluted, and the result is normalized to exactly generate the *continuous* uniform electron current density function $Y_0^0(\theta,\phi)$ covering a spherical shell and having the three angular momentum components of $\mathbf{L}_{xy}=+/-\frac{\hbar}{4}$ and $\mathbf{L}_z=\frac{\hbar}{2}$ (Figure 1.23)[1].

Each one-electron atomic orbital is a static two-dimensional spherical shell of moving negative charge (total charge $=-e$) of zero thickness at a distance r_n from the nucleus (charge $=+Ze$). It is well known that the field of a spherical shell of charge is zero inside the shell and that of a point charge at the origin outside the shell [1] (See Figure 1.32). Thus, for a nucleus of charge Z, the force balance equation for the electron atomic orbital is obtained by equating the forces on the mass and charge densities. The centrifugal force of each electron is given by[2]

$$\mathbf{F}_{centrifugal}=\frac{m_e}{4\pi r_n^{\,2}}\frac{\mathbf{v}_n^{\,2}}{r_n} \tag{7.1}$$

where r_n is the radius of electron n which has velocity $\mathbf{v}_n$. In order to be nonradiative, the velocity for every point on the atomic orbital is given by Eq. (1.35).

$$\mathbf{v}_n=\frac{\hbar}{m_e r_n} \tag{7.2}$$

Helium can be formed by the binding of two electrons simultaneously to He^{2+}. It can also be formed by the binding of an electron to He^{+}. The same boundary condition, that helium has no spin, applies in both cases. The forces must be consistent with the binding of both electrons at the same radius such that their currents corresponding to spin are identical mirror images

[1] $+/-$ designates both the positive and negative vector directions along an axis in the xy-plane.

[2] In this section, $n=1$ *or* 2 for electron one and electron two, respectively, not to be confused with the previous use of n as the principal quantum number.

and consequently identically cancel. This implies that the forces at balance are equivalent for the two electrons. As an approach to the helium solution using these constraints, now consider electron 1 initially at $r = r_1 = \frac{a_0}{Z}$ (the radius of the one-electron atom of charge Z given in the One-Electron Atom section where $a_0 = \frac{4\pi\varepsilon_0\hbar^2}{e^2 m_e}$ and the spin-nuclear interaction corresponding to the electron reduced mass (Eq. (1.255)) is not used here since the electrons have no field at the nucleus upon pairing) and electron 2 initially at $r_n = \infty$. Each electron can be treated as $-e$ charge at the nucleus with $\mathbf{E} = \frac{-e}{4\pi\varepsilon_0 r^2}$ for $r > r_n$ and $\mathbf{E} = 0$ for $r < r_n$ where r_n is the radius of the electron atomic orbital. The centripetal force is the electric force, $\mathbf{F}_{ele}$, between the electron and the nucleus. Thus, the electric force between electron 2 and the nucleus is:

$$\mathbf{F}_{ele(electron\ 2)} = \frac{(Z-1)e^2}{4\pi\varepsilon_0 r_2^2} \tag{7.3}$$

where ε_0 is the permittivity of free-space. The second centripetal force, $\mathbf{F}_{mag}$, on the electron 2 (initially at infinity) from electron 1 (at r_1) is the magnetic force. Each infinitesimal point (mass or charge-density element) of each atomic orbital moves on a great circle, and each point has the charge density $\frac{e}{4\pi r_n^2}$. Due to the relative motion of the charge-density elements of each electron, a radiation reaction force arises between the two electrons. This force given in Sections 6.6, 12.10, and 17.3 of Jackson [2] achieves the condition that the sum of the mechanical momentum and electromagnetic momentum is conserved[3]. The magnetic central force is derived from the Lorentz force that is relativistically corrected.

The magnetic force is derived by first determining the interaction of the two electrons due to the field of the outer electron 2 acting on the magnetic moments of electron 1 and vice versa. Insight to the behavior is given by considering the physics of a single bound electron in an externally applied uniform magnetic field. As shown in the Resonant Precession of the Spin-1/2-Current-Density Function Gives Rise to the Bohr Magneton section, the angular momentum of the atomic orbital in the magnetic field of an external applied field $B\mathbf{i}_z$ comprises the static $\frac{\hbar}{2}$ projection on the z-axis (Eq. (1.128)) and the $\frac{\hbar}{4}$ vector component in the xy-plane (Eq. (1.127)) that precesses about the z-axis at the Larmor frequency, ω_L. A resonant excitation of the Larmor precession frequency gives rise to a trapped photon with $\hbar$ of angular momentum along the precessing $\mathbf{S}$-axis. As shown in Box 1.1, the photon standing wave is phase-matched to a spherical harmonic source current, a spherical harmonic dipole $Y_\ell^m(\theta,\phi) = \sin\theta$ with respect to the $\mathbf{S}$-axis. The dipole spins about the $\mathbf{S}$-axis at the angular velocity given by Eq. (1.36).

In the coordinate system rotating at the Larmor frequency (denoted by the axes labeled X_R, Y_R, and Z_R in Figure 7.1), the X_R-component of magnitude $\frac{\hbar}{4}$ and $\mathbf{S}$ of magnitude $\hbar$ are stationary. The $\frac{\hbar}{4}$ angular momentum along X_R with a corresponding magnetic moment of $\frac{\mu_B}{4}$ (Eq. (28) of Box 1.1) causes $\mathbf{S}$ to rotate in the Y_R Z_R-plane to an angle of $\theta = \frac{\pi}{3}$ such that the torques due to the Z_R-component of $\frac{\hbar}{2}$ and the orthogonal X_R-component of $\frac{\hbar}{4}$ are balanced. Then the Z_R-component due to $\mathbf{S}$ is $\pm\hbar\cos\frac{\pi}{3} = \pm\frac{\hbar}{2}$, and the Y_R-component of $\mathbf{S}$ is $\pm\hbar\sin\frac{\pi}{3} = \pm\sqrt{\frac{3}{4}}\hbar$.

[3] The angular momentum of the two electrons cancels with pairing, and the conserved angular momentum is carried with the $\hbar$ of angular momentum of the photon corresponding to the radiation reaction force and energy. The energy of the Coulombic field is also conserved with the emission of photons of quantized energy wherein the radial acceleration during binding gives rise to the radiation as given in the Excited States of the One-Electron Atom (Quantization) section.

Figure 7.1. The angular momentum components of the atomic orbital and $\mathbf{S}$ in the rotating coordinate system X_R, Y_R, and Z_R that precesses at the Larmor frequency about Z_R such that the vectors are stationary.

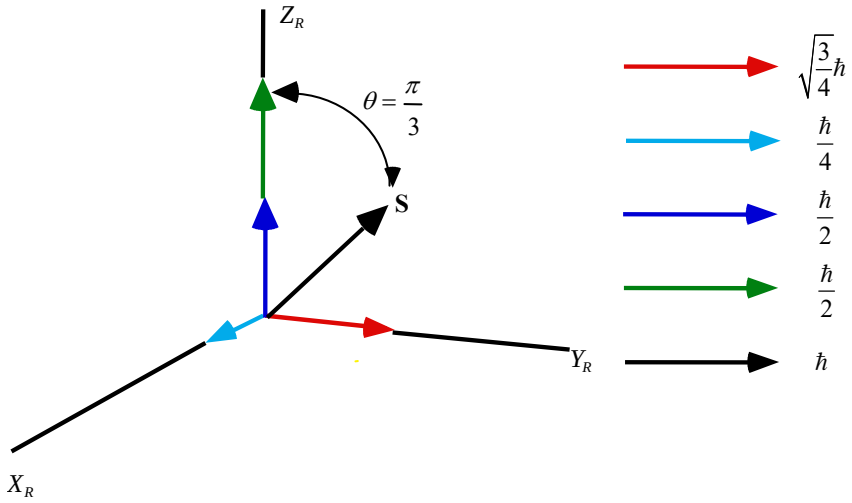

As shown in Figure 7.2, $\mathbf{S}$ forms a cone in time in the nonrotating laboratory frame with an angular momentum of $\hbar$ that is the source of the known magnetic moment of a Bohr magneton (Eq. (2.65)) as shown in the Magnetic Parameters of the Electron (Bohr Magneton) section. The projection of this angular momentum onto the z-axis of $\frac{\hbar}{2}$ adds to the z-axis component before the magnetic field was applied to give a total of $\hbar$. Thus, in the absence of a resonant precession, the z-component of the angular momentum is $\frac{\hbar}{2}$, but the excitation of the precessing $\mathbf{S}$ component gives $\hbar$—twice the angular momentum on the z-axis.

Figure 7.2. The angular momentum components of the atomic orbital and $\mathbf{S}$ in the stationary coordinate system. $\mathbf{S}$ and the components in the xy-plane precess at the Larmor frequency about the z-axis.

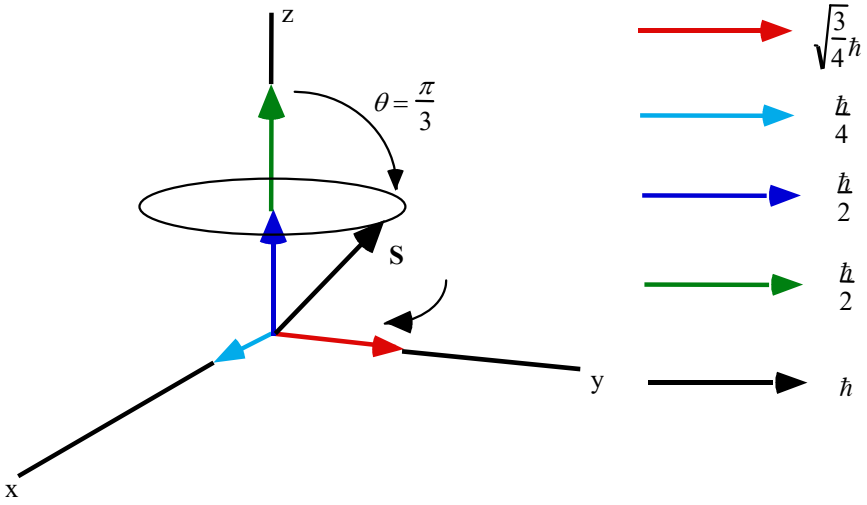

In summary, since the vector $\mathbf{S}$ that precesses about the z-axis at an angle of $\theta = \frac{\pi}{3}$ and an angle of $\phi = \frac{\pi}{2}$ with respect to $\mathbf{L}_{xy}$ given by Eq. (1.127) and has a magnitude of $\hbar$, the $\mathbf{S}$ projections in the $X_R\,Y_R$-plane and along the Z_R-axis (Eqs. (1.129-1.130)) are

$$\mathbf{S}_{\perp} = \hbar \sin\frac{\pi}{3} = \pm\sqrt{\frac{3}{4}}\hbar\ \mathbf{i}_{Y_R} \tag{7.4}$$

$$\mathbf{S}_{\parallel} = \pm\hbar\cos\frac{\pi}{3} = \pm\frac{\hbar}{2}\ \mathbf{i}_{Z_R} \tag{7.5}$$

The plus or minus sign of Eqs. (7.4) and (7.5) corresponds to the two possible vector orientations.

Consider the case that the external field is due to electron 2 on the moments of electron 1 and vice versa. In the limit, the magnetic moments of electrons 1 and 2 will cancel as they spin pair to form an energy minimum. In this case, the radii will be equal (i.e. $r_1 = r_2$). Cases other than the bound case correspond to excited states, which are solved for helium in the Excited States of Helium section. These states correspond to the atom having trapped photons. The central magnetic force to determine the bound state with $r_1 = r_2$ is derived by first determining the magnetic moments and fields of the interacting electrons from the corresponding angular momenta due to the trapped photons.

Unlike the external-applied-field case, each of the two interacting electrons have two orthogonal components of angular momentum. Each has $\frac{\hbar}{2}$ along the principal-axis (Eq. (1.128)) and $\frac{\hbar}{4}$ along an axis in the transverse-plane (Eq. (1.127)). For each electron, torque balance is also achieved when a photon standing wave is phase-matched to a spherical harmonic source current, a spherical harmonic dipole $Y_\ell^m(\theta,\phi) = \sin\theta$ with respect to the $\mathbf{S}$-axis. The dipole spins about the $\mathbf{S}$-axis at the angular velocity given by Eq. (1.36) as in the external-applied-field case, but the orientations are as shown in Figures 7.3A and 7.3B rather than that shown in Figures 7.1 and 7.2.

In the stationary coordinate system of electron 2 (denoted by the axes labeled X, Y, and Z in Figure 7.3A), the $\frac{\hbar}{4}$ of intrinsic angular momentum is along X, the $\frac{\hbar}{2}$ of intrinsic angular momentum is along Y, and the photon angular momentum vector $\mathbf{S}_2$ of magnitude $\hbar$ is in the XZ-plane at an angle of $\theta = \frac{\pi}{6}$ relative to the Z-axis. The Z-axis projection of $\mathbf{S}_2$ is $\sqrt{\frac{3}{4}}\hbar$, and the X-axis projection of $\mathbf{S}_2$ is $-\frac{\hbar}{2}$.

In the stationary coordinate system of electron 1 (denoted by the axes labeled X', Y', and Z' in Figure 7.3B), the $\frac{\hbar}{4}$ of intrinsic angular momentum is along X', the $\frac{\hbar}{2}$ of intrinsic angular momentum is along Y', and the photon angular momentum vector $\mathbf{S}_1$ of magnitude $\hbar$ is in the $Y'Z'$-plane at an angle of $\theta = \frac{\pi}{3}$ relative to the Y'-axis. The Z'-axis projection of $\mathbf{S}_1$ is $\sqrt{\frac{3}{4}}\hbar$, and the Y'-axis projection of $\mathbf{S}_1$ is $\frac{\hbar}{2}$.

The torques from the corresponding magnetic moments given by Eq. (2.65) are balanced in the absence of Larmor precession for the angular momentum projections of electron 2 shown in Figure 7.3A relative to those of electron 1 shown in Figure 7.3B. The photonic $-\frac{\hbar}{2}$ X-axis projection of $\mathbf{S}_2$ with a corresponding magnetic moment of $-\frac{\mu_B}{2}$ cancels the superposition of the $\frac{\hbar}{4}$ of intrinsic angular momentum of electrons 1 and 2 along X' and X, respectively, each with a corresponding magnetic moment of $\frac{\mu_B}{4}$ (Eq. (2.65)). The $\frac{\hbar}{2}$ of intrinsic angular momentum of electron 2 along Y gives rise to a magnetic field corresponding to $\frac{\mu_B}{2}$ in the direction of the $\sqrt{\frac{3}{4}}\hbar$ Z'-axis projection of $\mathbf{S}_1$ of electron 1. The $\frac{\hbar}{2}$ of intrinsic angular momentum of electron 1 along Y' and the Y'-axis projection of $\mathbf{S}_1$ of $\frac{\hbar}{2}$ gives rise to a magnetic field corresponding to μ_B in the direction of the $\sqrt{\frac{3}{4}}\hbar$ Z-axis projection of $\mathbf{S}_2$ of electron 2.

Figure 7.3. The relative angular momentum components of electron 1 and electron 2 to determine the magnetic interactions and the central magnetic force. (A) The atomic orbital and $\mathbf{s}_2$ of electron 2 in the stationary coordinate system *X*,*Y*,*Z* that is designated the unprimed spherical coordinate system relative to the *Z*-axis as shown. The photon angular momentum vector $\mathbf{s}_2$ of magnitude $\hbar$ is in the *XZ*-plane at an angle of $\theta = \frac{\pi}{6}$ relative to the *Z*-axis. (B) The angular momentum components of the atomic orbital and $\mathbf{s}_1$ of electron 1 in the stationary coordinate system *X*′,*Y*′,*Z*′ that is designated the primed spherical coordinate system relative to the *Z*′-axis as shown. The photon angular momentum vector $\mathbf{s}_1$ of magnitude $\hbar$ is in the *Y*′*Z*′-plane at an angle of $\theta = \frac{\pi}{3}$ relative to the *Y*′-axis.

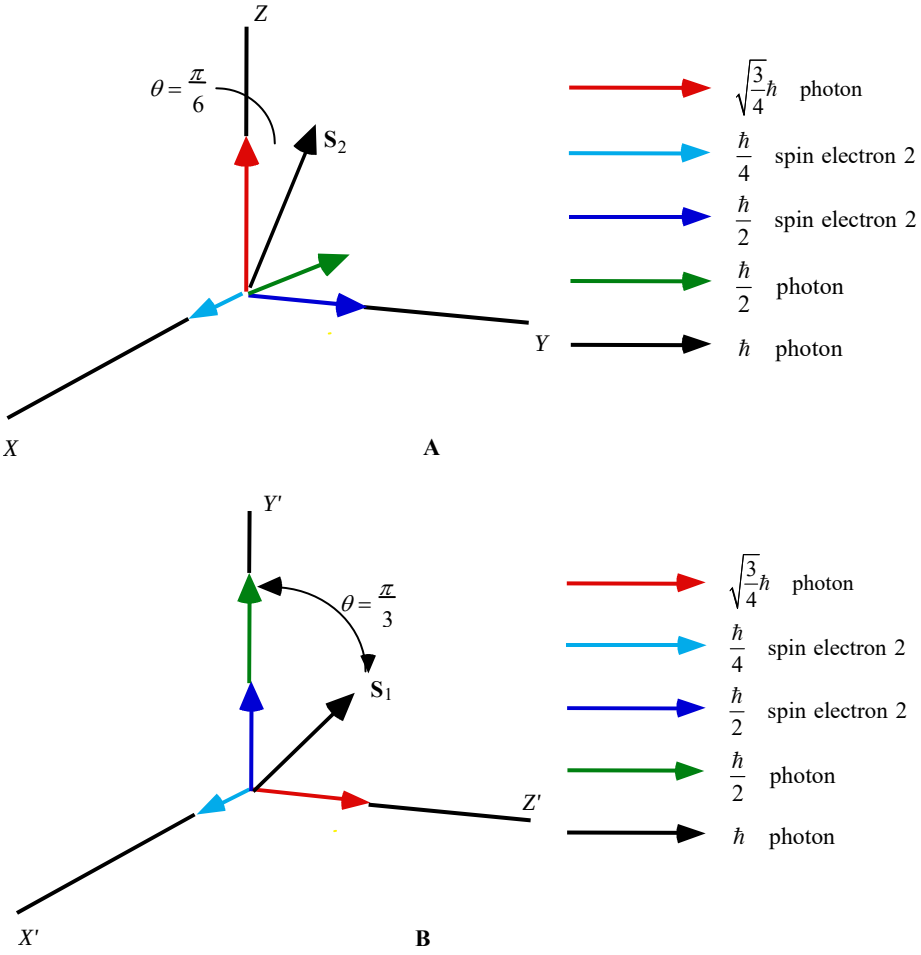

When the electrons pair, the photon is emitted as the corresponding excited state decays and the orientation of the magnetic moments of electron 1 relative to those of electron 2 rotate as shown in Figure 7.4 compared to Figures 7.3A and 7.3B. In the paired orientation, the angular momenta and the corresponding magnetic fields identically cancel.

Figure 7.4. The angular momentum components of the superimposed atomic orbitals of electron 1 and 2 in the stationary coordinate system *X,Y,Z* when binding occurs and the magnetic moments cancel.

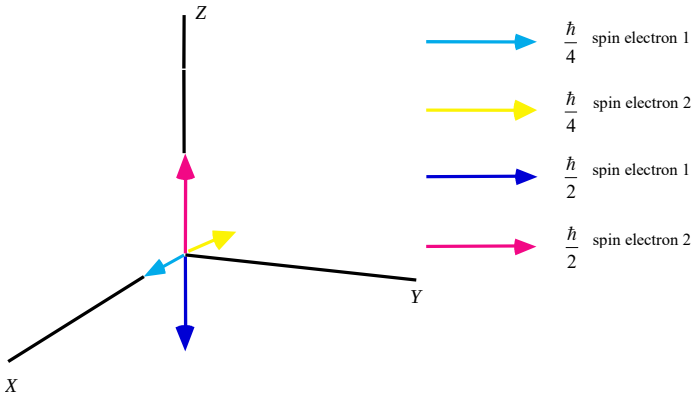

The magnetic central force is due to the interaction of the magnetic field of the electron 2 and the current dipole of the photon at the radius of electron 1 and vice versa. Considering the angular momentum vectors given in Figures 7.3A and 7.3B, the magnetostatic magnetic flux of electron 2 and electron 1 corresponding to $\frac{\mu_B}{2}$ and μ_B, respectively, follow from Eqs. (1.132) and (1.133) and after McQuarrie [3]:

$$\mathbf{B} = \frac{\mu_0 e\hbar}{2m_e r_2^3}(\mathbf{i}_{r'}\cos\theta - \mathbf{i}_{\theta'}\sin\theta) \tag{7.6}$$

$$\mathbf{B} = \frac{\mu_0 e\hbar}{2m_e r^3}(\mathbf{i}_r 2\cos\theta + \mathbf{i}_\theta \sin\theta) \tag{7.7}$$

where μ_0 is the permeability of free-space ($4\pi\ X\ 10^{-7}\ N/A^2$) and the coordinates of the magnetic field due to electron 2 acting on the magnetic moments of electron 1 is designated as the primed system and the magnetic field of electron 1 acting on the magnetic moments of electron 2 is designated as the unprimed system. It follows from Eq. (1.131), the relationship for the Bohr magneton, and relationship between the magnetic dipole field and the magnetic moment $\mathbf{m}$ [4] that Eqs. (1.132) and (1.137) are the equations for the magnetic field due to a magnetic moment of one half a Bohr magneton, $\mathbf{m} = \frac{\mu_B}{2}\mathbf{i}_\mathbf{z}$ and one Bohr magneton, $\mathbf{m} = \mu_B \mathbf{i}_\mathbf{z}$, respectively, where $\mathbf{i}_\mathbf{z} = \mathbf{i}_\mathbf{r}\cos\theta - \mathbf{i}_\theta \sin\theta$. In each case, the spherical harmonic dipole $Y_\ell^m(\theta,\phi) = \sin\theta$ spins about the **S**-axis at the angular velocity given by Eq. (1.36). Thus, angular velocity $\hat{\omega}$ and linear velocity $\mathbf{v}$ projections onto each $Z(Z')$-axis are:

$$\hat{\omega} = \frac{\hbar}{m_e r_1^2}\sqrt{\frac{3}{4}}\mathbf{i}_{Z,Z'} \tag{7.8}$$

$$\mathbf{v} = \frac{\hbar}{m_e r_1}\sqrt{\frac{3}{4}}\sin\theta\mathbf{i}_{\phi,\phi'} \tag{7.9}$$

The Lorentz force density at each point moving at velocity $\mathbf{v}$ given by Eq. (7.9) is

$$\mathbf{F}_{mag} = \frac{e}{4\pi r_2^2}\mathbf{v}\times\mathbf{B} \tag{7.10}$$

Substitution of Eq. (7.9) and Eqs. (7.6-7.7) into Eq. (7.10) while maintaining the designation of the coordinates of the magnetic field of electron 2 acting on the magnetic moments of electron 1 as the primed system and the coordinates of the magnetic field of electron 1 acting on the magnetic moments of electron 2 as the unprimed system gives:

$$\mathbf{F}_{mag} = -\frac{e}{4\pi r_2^2}\left(\begin{array}{l}\frac{\hbar}{m_e r_1}\sqrt{\frac{3}{4}}\sin\theta\mathbf{i}_{\phi'}\times\frac{\mu_0 e\hbar}{2m_e r_2^3}(\mathbf{i}_{r'}\cos\theta - \mathbf{i}_{\theta'}\sin\theta) \\ +\frac{\hbar}{m_e r_2}\sqrt{\frac{3}{4}}\sin\theta\mathbf{i}_\phi\times\frac{\mu_0 e\hbar}{2m_e r_2^3}(\mathbf{i}_r 2\cos\theta + \mathbf{i}_\theta\sin\theta)\end{array}\right) \tag{7.11}$$

As shown in Eqs. (7.16-7.24), the relativistic form of Eq. (7.11) results in the equivalence of the velocity at the two radii; thus, r_1 may be substituted for r_2 in the velocity factor of the second term to give:

$$\begin{aligned}\mathbf{F}_{mag} &= -\frac{1}{4\pi r_2^{\,2}}\frac{\mu_0 e^2\hbar^2}{2r_1 m_e^2 r_2^3}\sqrt{\frac{3}{4}}\begin{pmatrix}\sin\theta\mathbf{i}_{\phi'}\times\left(\mathbf{i}_{r'}\cos\theta-\mathbf{i}_{\theta'}\sin\theta\right)\\+\sin\theta\mathbf{i}_{\phi}\times\left(\mathbf{i}_{r}2\cos\theta+\mathbf{i}_{\theta}\sin\theta\right)\end{pmatrix}\\ &= -\frac{1}{4\pi r_2^{\,2}}\frac{\mu_0 e^2\hbar^2}{2r_1 m_e^2 r_2^3}\sqrt{\frac{3}{4}}\begin{pmatrix}-\sin\theta\cos\theta\mathbf{i}_{\theta'}+\sin^2\theta\mathbf{i}_{r'}\\+2\sin\theta\cos\theta\mathbf{i}_{\theta}+\sin^2\theta\mathbf{i}_{r}\end{pmatrix}\end{aligned} \tag{7.12}$$

The $\mathbf{i}_{r'}$ unit vector is transformed to $\mathbf{i}_r$ by substituting θ with $\theta+\frac{\pi}{2}$ in the second term of Eq. (7.12):

$$\begin{aligned}\mathbf{F}_{mag} &= -\frac{1}{4\pi r_2^{\,2}}\frac{\mu_0 e^2\hbar^2}{2r_1 m_e^2 r_2^3}\sqrt{\frac{3}{4}}\begin{pmatrix}-\sin\theta\cos\theta\mathbf{i}_{\theta'}+\sin^2\left(\theta+\frac{\pi}{2}\right)\mathbf{i}_{r'}\\+2\sin\theta\cos\theta\mathbf{i}_{\theta}+\sin^2\theta\mathbf{i}_{r}\end{pmatrix}\\ &= -\frac{1}{4\pi r_2^{\,2}}\frac{\mu_0 e^2\hbar^2}{2r_1 m_e^2 r_2^3}\sqrt{\frac{3}{4}}\begin{pmatrix}-\sin\theta\cos\theta\mathbf{i}_{\theta'}+\left(\sin^2\theta+\cos^2\theta\right)\mathbf{i}_{r}\\+2\sin\theta\cos\theta\mathbf{i}_{\theta}\end{pmatrix}\\ &= -\frac{1}{4\pi r_2^{\,2}}\frac{\mu_0 e^2\hbar^2}{2r_1 m_e^2 r_2^3}\sqrt{\frac{3}{4}}\left(-\sin\theta\cos\theta\mathbf{i}_{\theta'}+2\sin\theta\cos\theta\mathbf{i}_{\theta}+\mathbf{i}_{r}\right)\\ &= -\frac{1}{4\pi r_2^{\,2}}\frac{\mu_0 e^2\hbar^2}{2r_1 m_e^2 r_2^3}\sqrt{\frac{3}{4}}\left(-\frac{1}{2}\sin 2\theta\mathbf{i}_{\theta'}+\sin 2\theta\mathbf{i}_{\theta}+\mathbf{i}_{r}\right)\end{aligned} \tag{7.13}$$

The $F_{mag}\mathbf{i}_{\theta}$ and $F_{mag}\mathbf{i}_{\theta'}$ average to zero over the surface for $0\le\theta\le\pi$. The relativistic correction given *infra.* is based on quantized-angular-momentum conservation with the emission of a photon. The relativistic correction for the lightlike frame causes the circumferential distances on the surface to dilate to the radial dimension alone as given *infra.* and in the Special Relativistic Correction to the Ionization Energies section. This causes the angular force to vanish since it averages to zero such that only the radial force remains. Since there is no net angular force on the electron, only the resultant radial force need be considered:

$$\mathbf{F}_{mag} = -\frac{1}{4\pi r_2^{\,2}}\frac{\mu_0 e^2\hbar^2}{2r_1 m_e^2 r_2^3}\sqrt{\frac{3}{4}}\mathbf{i}_r \tag{7.14}$$

Eq. (7.14) may be written in the form

$$\mathbf{F}_{mag} = -\frac{1}{4\pi r_2^{\,2}}\left[\frac{e^2\mu_0}{2m_e r_1}\right]\frac{\hbar^2}{m_e r_2^{\,3}}\sqrt{s(s+1)}\mathbf{i}_r \tag{7.15}$$

where $s=1/2$ and $\sqrt{s(s+1)}=\sqrt{\frac{3}{4}}$ is the historical designation of the spin-angular momentum magnitude factor.

Furthermore, the term in brackets can be expressed in terms of the fine structure constant α. The radius of the electron atomic orbital in the $v=c$ frame[4] is $\lambda\!\!\!^{-}_C$, where $v=c$ corresponds to the magnetic field front propagation velocity which is the same in all inertial frames, independent of the electron velocity as shown by the velocity addition formula of special relativity [5]. From Eq. (1.35) and Eqs. (1.179-1.180)

$$\frac{e^2\mu_0}{2m_e r_1} = 2\pi\alpha\frac{v}{c} \tag{7.16}$$

where $v=c$. Based on the relativistic invariance of the electron's magnetic moment of a Bohr magneton μ_B given by Eq. (1.131) as well as its invariant angular momentum of $\hbar$, it can be shown that the relativistic correction to Eq. (7.15) is $\frac{1}{Z}$ times the reciprocal of Eq. (7.16). As shown previously in the One-Electron Atom—Determination of Atomic Orbital Radii section, the radius term in the brackets of Eq. (7.15) is relativistically corrected due to invariance of charge under Gauss' Integral Law [6]. The radius of the electron relative to the $v=c$ frame, r_α^*, is relativistically corrected as follows. The wave equation relationship is:

$$v = \lambda\frac{\omega}{2\pi} \tag{7.17}$$

[4] For the radiation-reaction force, v in Eq. (7.10) is not the electron velocity relative to the laboratory frame.

It can be demonstrated that the velocity of the electron atomic orbital satisfies the relationship for the velocity of a wave by substitution of Eqs. (1.15) and (1.36) into Eq. (7.17), which gives Eq. (1.35). The result of the substitution into Eq. (7.17) of c for v_n, λ_n given by Eq. (2.2):

$$2\pi(nr_1) = 2\pi r_n = n\lambda_1 = \lambda_n \tag{7.18}$$

with r_1 given by Eq. (1.260):

$$r_1 = \frac{a_0}{Z} \tag{7.19}$$

for λ, and of ω_n given by Eq. (1.36)

$$\omega_n = \frac{\hbar}{m_e r_n^2} \tag{7.20}$$

for ω is

$$c = 2\pi \frac{\gamma^* a_0}{Z} \frac{\hbar}{m_e \left[\frac{\gamma^* a_0}{Z}\right]^2 2\pi} \tag{7.21}$$

$$\gamma^* = \frac{Z\hbar}{m_e c a_0} = \frac{Z\sqrt{\varepsilon_0\mu_0}\hbar}{m_e} \frac{e^2 m_e}{4\pi\varepsilon_0\hbar^2} = Z\frac{1}{4\pi}\sqrt{\frac{\mu_0}{\varepsilon_0}}\frac{e^2}{\hbar} = \alpha Z \tag{7.22}$$

where γ^* is the relativistic factor corresponding to the radius, c is given by Eq. (1.178), and α is given by Eq. (2.123). It follows from Eq. (7.22) that the radius r_1 of Eq. (7.15) must be corrected by the factor $(\alpha Z)^{-1}$.

Due to relativistic invariance of $\frac{e}{m_e}$ corresponding to the invariance of μ_B, the correction of the electron mass of the bracketed term of Eq. (7.15) is 2π as given in the One-Electron Atom—Determination of Atomic Orbital Radii section (Eq. (1.273)). By correcting the radius and the mass, the relativistic correction γ' due to the light speed electrodynamic central force is

$$\gamma' = \left(2\pi\alpha Z\frac{v}{c}\right)^{-1} \tag{7.23}$$

where $v = c$ [5]. Thus, $\frac{1}{Z}$ is substituted for the term in brackets in Eq. (7.15). Thus, Eq. (7.15) becomes:

$$\mathbf{F}_{mag} = -\frac{1}{4\pi r_2^2}\frac{1}{Z}\frac{\hbar^2}{m_e r_2^3}\sqrt{s(s+1)}\mathbf{i}_r \tag{7.24}$$

The radiation-reaction force between the two electrons that achieves the condition that the sum of the mechanical momentum and electromagnetic momentum is conserved can also be derived from the relativistically invariant relationship between momentum and energy. As shown in the Excited States of the One-Electron Atom (Quantization) section and the Excited States of Helium section, in general, for a macroscopic multipole with a single m value, a comparison of Eq. (2.62) and Eq. (2.55) shows that the relationship between the angular momentum M_z, energy U, and angular frequency ω is given by Eq. (2.63):

$$\frac{dM_z}{dr} = \frac{m}{\omega}\frac{dU}{dr} \tag{7.25}$$

independent of r where m is an integer. Furthermore, the ratio of the square of the angular momentum, M^2, to the square of the energy, U^2, for a pure (ℓ, m) multipole follows from Eq. (2.55) and Eqs. (2.60-2.62) as given by Eq. (2.64):

$$\frac{M^2}{U^2} = \frac{m^2}{\omega^2} \tag{7.26}$$

From Jackson [7], the quantum mechanical interpretation is that the radiation from such a multipole of order (ℓ, m) carries off $m\hbar$ units of the z component of angular momentum per photon of energy $\hbar\omega$. However, the photon and the electron can each possess only $\hbar$ of angular momentum which requires that Eqs. (7.25-7.26) correspond to a state of the radiation field containing m photons. Then, the magnetic energy due to the interaction of the magnetic moment of each electron and the magnetic field of the opposite member of the pair is quantized in terms of the magnetic field as well as the magnetic moment as opposed to being a continuous function of magnetic flux B in the case of the energy due to an applied field. In the applied-field case, the energy ΔE_{mag} of interaction of a magnetic moment **m** and flux **B** is given by Eq. (1.168)

[5] The same relativistic correction is obtained by consideration of the kinetic and vector potential components of the angular momentum in the light-like frame as shown in Box 1.1.

$$\Delta E_{mag} = \mathbf{m} \cdot \mathbf{B} = mB\cos\theta \tag{7.27}$$

In the case of the interaction of the magnetic moments of two electrons of two-electron atoms, Eq. (7.27) does not apply due to the result of Eq. (7.26).

The quantized energy for an electron ΔE_{mag}^{spin} to switch from parallel to antiparallel to an applied field $\mathbf{B}$ is given by Eq. (1.168)

$$\Delta E_{mag}^{spin} = 2\mu_{\mathbf{B}}\, \mathbf{i_z} \cdot \mathbf{B} = 2\mu_B B\cos\theta = 2\mu_B B = 2\hbar\omega_L \tag{7.28}$$

where ω_L is the Larmor frequency given by Eq. (2) of Box 1.1. In the case of the interaction between the two electrons, the frequency must satisfy Eq. (7.26). From Eq. (7.8), the angular velocity $\hat{\omega}_L$ is:

$$\hat{\omega}_L = \frac{\hbar}{m_e r_2^2}\sqrt{\frac{3}{4}}\mathbf{i}_Z \tag{7.29}$$

Energy is conserved between the electric and magnetic energies of the helium atom as shown by Eq. (7.42). Since charge is relativistically invariant under Gauss' Integral Law, the relationships between the parameters of Eqs. (7.25) and (7.26) due to quantization of angular momentum $\hbar$ and energy $\hbar\omega$ requires the normalization of the energy U by the central field Z such that the magnetic-force dependence on the nuclear charge is the reciprocal of that of the electric force. Then, the radial electric field has a magnitude proportional to Z and the magnetic interaction has a magnitude of $\frac{1}{Z}$ such that the corresponding magnetic energy U is decreased by the factor of $\frac{1}{Z^2}$ corresponding to the electric energy given by Eqs. (1.263-1.264). Using Eqs. (7.26) and (7.29) with $m = 2$ for the magnetic dipole interaction and the invariance of charge gives

$$\Delta E_{mag}^{spin} = \frac{\hbar\omega_L}{2Z} = \frac{\hbar^2}{2Zm_e r_2^2}\sqrt{\frac{3}{4}} \tag{7.30}$$

The corresponding magnetic force is given as the gradient of the energy:

$$\mathbf{F}_{mag} = \frac{1}{4\pi r_2^{\,2}}\nabla\left(\Delta E_{mag}^{spin}\right) = \frac{1}{4\pi r_2^{\,2}}\frac{\delta\Delta E_{mag}^{spin}}{\delta r_2}\mathbf{i}_r = -\frac{1}{4\pi r_2^{\,2}}\frac{\hbar^2}{Zm_e r_2^3}\sqrt{\frac{3}{4}}\mathbf{i}_r \tag{7.31}$$

The outward centrifugal force on electron 2 (Eqs. (7.1-7.2)) is balanced by the electric force (Eq. (7.3)) and the magnetic force (on electron 2) (Eqs. (7.24) and (7.31)):

$$\frac{m_e}{4\pi r_2^2}\frac{v_2^2}{r_2} = \frac{e}{4\pi r_2^2}\frac{(Z-1)e}{4\pi\varepsilon_0 r_2^2} + \frac{1}{4\pi r_2^2}\frac{\hbar^2}{Zm_e r_2^3}\sqrt{s(s+1)} \tag{7.32}$$

From Eq. (1.35) and Eq. (7.2)

$$v_2^2 = \frac{\hbar^2}{m_e^2 r_2^2} \tag{7.33}$$

Then,

$$\frac{m_e v_2^2}{r_2} = \frac{\hbar^2}{m_e r_2^3} = \frac{(Z-1)e^2}{4\pi\varepsilon_0 r_2^2} + \frac{1}{Z}\frac{\hbar^2}{m_e r_2^3}\sqrt{s(s+1)} \tag{7.34}$$

Solving for r_2,

$$r_2 = r_1 = a_0\left(\frac{1}{Z-1} - \frac{\sqrt{s(s+1)}}{Z(Z-1)}\right);\ s = \frac{1}{2} \tag{7.35}$$

That is, the final radius of electron 2, r_2, is given by Eq. (7.35); this is also the final radius of electron 1. The energies and radii of several two-electron atoms are given in Table 7.1.

(Since the density factor always cancels, it will not be used in subsequent force balance equations).

ENERGY CALCULATIONS

The electric work to bring electron 2 to $r_2 = r_1$ is given by the integral of the electric force from infinity to r_1,

$$work(electric, electron2) = \frac{(Z-1)e^2}{8\pi\varepsilon_0 r_1} \tag{7.36}$$

And, the electric energy is the negative of the electric work,

$$E(electric) = \frac{-(Z-1)e^2}{8\pi\varepsilon_0 r_1} \tag{7.37}$$

The potential energy of each electron at $r = r_1$, is given as:

$$V = \frac{-(Z-1)e^2}{4\pi\varepsilon_0 r_1} \tag{7.38}$$

The kinetic energy is $\frac{1}{2}m_e v^2$, where v is given by Eq. (1.35).

$$T = \frac{1}{2}\frac{\hbar^2}{m_e r_1^2} \tag{7.39}$$

The magnetic work is the integral of the magnetic force from infinity to r_1,

$$work(magnetic, electron2) = -\frac{1}{2}\frac{1}{Z}\frac{\hbar^2}{m_e r_1^2}\sqrt{s(s+1)} \tag{7.40}$$

CONSERVATION OF ENERGY

Energy is conserved. Thus, the potential energy (electron 2 at r_1) with the nucleus plus the magnetic work (electron 2 going from infinity to r_1) must equal the sum of the negative of the electric work (electron 2 going from infinity to r_1) and the kinetic energy (electron 2 at r_1). This is shown below with Eq. (7.41) and Eq. (7.42).

$$V(electron\ 2\ at\ r_1) = \frac{-(Z-1)e^2}{8\pi\varepsilon_0 r_1} + \frac{1}{2}\frac{1}{Z}\frac{\hbar^2}{m_e r_1^2}\sqrt{s(s+1)} - \frac{1}{2}\frac{\hbar^2}{m_e r_1^2} \tag{7.41}$$

and using r_1 from Eq. (7.35),

$$V(electron\ 2\ at\ r_1) = -\frac{(Z-1)e^2}{4\pi\varepsilon_0 r_1} \tag{7.42}$$

This is also the potential energy of electron 1 where their potential energies are indistinguishable when $r_1 = r_2$, but once one is excited they are distinguishable [6].

---

[6] The decrease in the central force of electron 1 from that corresponding to Z to that corresponding to $Z-1$ as given by Eq. (7.42) allows the potential energies of the two electrons to match upon pairing. This is possible according to Maxwell's equations by the relationship between the two-dimensional surface charge density of each binding electron and the field:

$$\mathbf{n} \bullet \left(\mathbf{E}_1 - \mathbf{E}_2 \right) = \frac{\sigma}{\varepsilon_0} \tag{1}$$

Whenever there is a potential energy difference in any perfect conductor, current will flow to redistribute the charge and, thus, the field lines, until an equipotential is achieved. This is true even in the case of the two-dimensional layer of charge of paired electrons. However, in this case, the orientation of the field lines changes since current flow in the radial direction is not possible. Reverse-directed field lines partially cancel the central field of the nucleus at the shell such that the equipotential condition is met for the shell.

In the case of helium for example, the two spin-paired electrons comprise a single two-dimensional shell (zero thickness) at radius $0.566987a_0$. They satisfy Maxwell's source charge equation (Eq. (1)) and Gauss' law (Eq. (33.6)) while achieving a minimum energy, equipotential surface with one half of the combined field lines directed radial inward and one half directed radial outward from the surface of the shell. The inward-directed lines are cancelled by those of the $+2e$ charged nucleus. The result is that each electron of the superposition of the two comprising the shell of $-2e$ total charge experiences a central field of $+e$. The minimum energy is achieved by spin pairing with a significant reduction in the radius of the initial electron 2 due to the spin pairing force (Eq. (7.24)) in Eq. (7.34) relative to the pure Lorentz force (Eq. (7.15)). Using $r_1 = 0.5a_0$ from Eq. (1.260) as a first-order approximation of the multibody unpaired-electron problem, the corresponding radius without spin pairing is $0.999a_0$. Using Eq. (7.37), the corresponding binding energy of electron 2 is $13.61\ eV$ compared to the case with spin pairing of $24.58750\ eV$. Thus, spin pairing lowers the total energy of the system of interacting electrons by $10.98\ eV$ even though the electrons become indistinguishable upon pairing.

As a consequence of the spin-pairing interaction and associated stabilization, it is not possible to assign an independent energy to any single electron of He. Rather, the total system must be considered. Only for a one-electron atom is the electron's energy equal to the total energy. Specifically, the electrons of He in the ground state are paired in the same shell and are indistinguishable. That does not mean that the ionization of He to He^{2+} is twice $24.58750\ eV$. Both electrons cannot be ionized from the position $r_1 = r_2 = 0.566987a_0$ to a continuum level without becoming unpaired since paired free electrons at the same position is energetically unobtainable. In excited states, the electrons are distinguishable; yet, dependent in terms of their positions and energies. With photon absorption, one electron moves to a greater radius and the other moves closer to the nucleus. It is a sequential quantized process as shown in the Excited States of Helium section. In the limit, the total energy of the photon required for one of the initially indistinguishable electrons to be ionized with the other moving to the radius of $0.5a_0$ is $24.58750\ eV$ (Eqs. (7.44-7.46)). The corresponding He^+ ion has an ionization energy of $54.423\ eV$ (Eqs. (1.260) and (1.264))). Thus, the total binding energy of He in the ground state is $24.58750\ eV + 54.423\ eV$.

An energy balance can be assigned to the two electrons. From Eq. (1.264), the binding energy of He^+ is

$$E_B\left(He^+\right) = 54.423\ eV \tag{2}$$

The spin pairing of the two electrons with the binding of an electron 2 to He^+ with an electron 1 causes an energy change corresponding to the central field at electron 1 to decrease by an integer such that both electrons are bound with the same force and are equivalent. The binding or ionization energy change given by Eq. (1.264) is

$$\Delta E_B = -\Delta \frac{Ze^2}{8\pi\varepsilon_0 r_1} = -\frac{e^2}{8\pi\varepsilon_0 a_0}\left(\frac{2}{0.5} - \frac{1}{0.566987}\right) = -30.42654\ eV \tag{3}$$

where the radius of He^+ (Eq. (1.260)) is $0.5a_0$ and the radius of He is $0.566987a_0$ (Eq. (7.35)). From Eq. (7.45), the electric energy of either of the equivalent electrons at $r_1 = r_2 = 0.566987a_0$ is

$$E(electric) = -\frac{e^2}{8\pi\varepsilon_0 0.566987a_0} = -23.996467\ eV \tag{4}$$

With the contribution of the magnetic energy (Eqs. (7.44) and (7.46))), the binding energy of **either** of the equivalent electrons of helium (Eqs. (7.44-7.46)) is

$$E_B\left(He\right) = 24.58741\ eV \tag{5}$$

With the ionization of either electron 1 or electron 2, the central field of the unionized electron, say electron 1, increases by one. The electric and magnetic fields are conservative, and the energy $E_B\left(e_1\right)$ of the unionized electron is given by the negative of the sum of Eqs. (3) and (4):

$$E_B\left(e_1\right) = -\left(\Delta E_B + E(electric)\right) = -\left(-30.42654\ eV - 23.996467\ eV\right) = 54.423\ eV \tag{6}$$

which matches Eq. (2). Thus, the total ionization energy of helium $E_{BT}\left(He\right)$ given by the sum of the first and second ionization energies is

$$E_{BT}\left(He\right) = IP_1 + IP_2 = 54.423\ eV + 24.58741\ eV = 79.011\ eV \tag{7}$$

where IP is the ionization potential.

The central field lines of the nucleus of two-electron atoms end equally on each electron. Thus, the difference in energy of electron 1 before and after pairing given by Eq. (3) can be considered the energy of pairing that is conserved upon unpairing of the electrons such that the binding energy is increased by the negative of Eq. (3). In general, the matched potential of the binding electrons is that which achieves a minimum energy of the atom, ion, molecular ion, or molecule and obeys Maxwell's source charge equation (Eq. (1)) and Gauss' law (Eq. (33.6)) for the total charge and total fields across the shell comprised of two or more electrons bound by at least one of spin- and orbital- interactions. Further examples of the application of the equal potential condition for the binding of multi-electrons per shell are the cases of the hydride ion, three- through twenty-electron atoms, and molecules given in the corresponding sections.

IONIZATION ENERGIES

During ionization, power must be conserved. Power flow is governed by the Poynting power theorem,

$$\nabla \bullet (\mathbf{E} \times \mathbf{H}) = -\frac{\partial}{\partial t}\left[\frac{1}{2}\mu_0 \mathbf{H} \bullet \mathbf{H}\right] - \frac{\partial}{\partial t}\left[\frac{1}{2}\varepsilon_0 \mathbf{E} \bullet \mathbf{E}\right] - \mathbf{J} \bullet \mathbf{E} \tag{7.43}$$

Energy is superposable; thus, the calculation of the ionization energy is determined as a sum of the electric and magnetic contributions. Energy must be supplied to overcome the electric force of the nucleus, and this energy contribution is the negative of the electric work given by Eq. (7.37). Additionally, the electrons are initially spin-paired at $r_1 = r_2 = 0.566987a_0$ producing no magnetic fields; whereas, following ionization, the electrons possess magnetic fields and corresponding energies. For helium, the contribution to the ionization energy is given as the energy stored in the magnetic fields of the two electrons at the initial radius where they become spin-unpaired. Part of this energy and the corresponding relativistic term corresponds to the precession of the outer electron about the z-axis due to the spin angular momentum of the inner electron. These terms are the same as those of the corresponding terms of the hyperfine structure interval of muonium as given in the Muonium Hyperfine Structure Interval section. Thus, for helium, which has no electric field beyond r_1 the ionization energy is given by the general formula:

$$Ionization\ Energy(He) = -E(electric) + E(magnetic)\left(1 - \frac{1}{2}\left(\left(\frac{2}{3}\cos\frac{\pi}{3}\right)^2 + \alpha\right)\right) \tag{7.44}$$

where,

$$E(electric) = -\frac{(Z-1)e^2}{8\pi\varepsilon_0 r_1} \tag{7.45}$$

$$E(magnetic) = \frac{2\pi\mu_0 e^2\hbar^2}{m_e^2 r_1^3} = \frac{8\pi\mu_0\mu_B^2}{r_1^3} \tag{7.46}$$

Eq. (7.46) is derived for each of the two electrons as Eq. (1.161) of the Magnetic Parameters of the Electron (Bohr Magneton) section with the radius given by Eq. (7.35). By substituting the radius given by Eq. (7.35) into Eq. (1.35), the velocity v is given by:

$$v = \frac{\hbar}{\frac{4\pi\varepsilon_0\hbar^2}{e^2}\left(\frac{1}{Z-1} - \frac{\sqrt{\frac{3}{4}}}{Z(Z-1)}\right)} = \frac{\alpha c(Z-1)}{\left(1 - \frac{\sqrt{\frac{3}{4}}}{Z}\right)} \tag{7.47}$$

with $Z > 1$ where Eqs. (1.204) and (1.208) were used. For increasing Z, the velocity becomes a significant fraction of the speed of light; thus, special relativistic corrections were included in the calculation of the ionization energies of two-electron atoms given in Table 7.1. The relativistic corrections follow from those given in the Special Relativistic Correction to the Ionization Energies section wherein the nuclear-electron magnetic interactions as well as the electron-electron interactions of two-electron atoms must be included to be precise.

For a nuclear charge Z greater than two, a central electric field equal to that of an elementary charge quanta of $Z-2$ exists outside of the atomic orbital of the unionized atom. During ionization, the energy contribution of the expansion of the atomic orbital of the ionized electron (electron 2) from r_1 to infinity in the presence of the electric fields present inside and outside of the atomic orbital is calculated as the $\mathbf{J} \bullet \mathbf{E}$ term of the Poynting theorem. This energy contribution can be determined by designing an energy cycle and considering the individual contributions of each electron (electron 1 and electron 2) in going from the initial unionized to the final ionized state. Consider two paired atomic orbitals. Expansion of an atomic orbital in the presence of an electric field which is positive in the outward radial direction requires energy, and contraction of an atomic orbital in this field releases energy. Thus, the contribution of the $\mathbf{J} \bullet \mathbf{E}$ term to ionization is the difference in the energy required to expand one atomic orbital (electron 2) from r_1 to infinity and to contract one atomic orbital (electron 1) from infinity to r_1. The energy contribution for the expanding atomic orbital follows the derivation of Eq. (1.225) of the Electron g Factor section as follows (the vector direction is taken to give a positive dissipated energy).

DISSIPATED ENERGY

The $\mathbf{J} \bullet \mathbf{E}$ energy over time is derived from the central electric field from the nucleus against which electron 2 expands and the current of the expanding electron 2 wherein the latter is dependent on the magnetic field of the inner electron 1. The magnetic field of electron 1 gives rise to a Lorentz force on electron 2, and the dissipative current density of electron 2 depends on this force wherein the superconducting condition given by Eq. (1.187) is maintained with the electric field of electron 1. The magnitude of the magnetic flux at electron 2 due to electron 1 is given by that of the Bohr magneton at the origin that follows from McQuarrie [3]:

$$B = \frac{\mu_0 e\hbar}{2m_e r_2^3} \tag{7.48}$$

The magnetic force on electron 2 due to the magnetic field of electron 1 is the Lorentz force given by Eq. (1.183). Substitution of Eq. (1.35) for $\mathbf{v}$ and Eq. (7.48) for the magnetic flux into Eq. (1.183) gives

$$\mathbf{F}_{mag} = \frac{\mu_0 e^2\hbar^2}{2m_e^2 r_2^4}\mathbf{i}_r \tag{7.49}$$

Furthermore, the velocity of electron 1 is proportional to the nuclear charge as given by Eqs. (1.35) and (1.257). Thus, in order to maintain the superconducting condition given by Eq. (1.187), the magnetic force corresponding to B must be given by

$$\mathbf{F}_{mag} = \frac{1}{Z}\frac{\mu_0 e^2\hbar^2}{2m_e^2 r_2^4}\mathbf{i}_r \tag{7.50}$$

The expansion of the atomic orbital of electron 2 produces a current. The current over time $\Delta t\mathbf{J}$ is:

$$\Delta t\mathbf{J} = \Delta t\sigma\ \mathbf{E}_f \tag{7.51}$$

where $\mathbf{J}$ is the current density, Δt is the time interval, σ is the conductivity, and $\mathbf{E}_f$ is the effective electric field defined as follows:

$$\mathbf{F} = q(\theta,\phi)\mathbf{E}_f \tag{7.52}$$

where $\mathbf{F}$ is the magnetic force given by Eq. (7.50), and $q(\theta,\phi)$ is the angular charge density given as follows:

$$q(\theta,\phi) = \frac{e}{4\pi} \tag{7.53}$$

The orbit expands in free space; thus, the relation for the conductivity is:

$$\Delta t\sigma = \varepsilon_0 \tag{7.54}$$

The electric field provided by the nucleus for the expanding atomic orbital is:

$$\mathbf{E} = \frac{(Z-2)e}{4\pi\varepsilon_0 r_2^2}\mathbf{i}_r \tag{7.55}$$

where ε_0 is the permittivity of free space ($8.854\ X\ 10^{-12}\ C^2 / N \cdot m^2$). Using Eqs. (7.50-7.55), the $\mathbf{J} \bullet \mathbf{E}$ energy density over time for the expansion of electron 2 with the contraction of electron 1 is:

$$\Delta t(\mathbf{J} \bullet \mathbf{E}) = \frac{(Z-2)}{Z}\frac{\mu_0 e^2\hbar^2}{2m_e^2 r_2^6} \tag{7.56}$$

The $\mathbf{J} \bullet \mathbf{E}$ energy over time is the volume integral of the energy density over time

$$[\Delta t(\mathbf{J} \bullet \mathbf{E})]_{energy\ external} = \int_0^{2\pi}\int_0^{\pi}\int_{\infty}^{r_1}\frac{(Z-2)}{Z}\frac{\mu_0 e^2\hbar^2}{2m_e^2 r_2^6} r^2 \sin\theta dr d\theta d\Phi \tag{7.57}$$

$$[\Delta t(\mathbf{J} \bullet \mathbf{E})]_{energy\ external} = \frac{(Z-2)}{Z}\frac{2\pi\mu_0 e^2\hbar^2}{3m_e^2 r_1^3} \tag{7.58}$$

The $\mathbf{J} \bullet \mathbf{E}$ energy over time involving the electric field external to the atomic orbital of electron 2 is $\frac{(Z-2)}{Z}$ times the magnetic energy stored in the space external to the atomic orbital as given by Eq. (1.170). The left and right sides of the Poynting theorem must balance. Given the form of the $\mathbf{J} \bullet \mathbf{E}$ energy over time involving the electric field external to the atomic orbital of electron 2 and given that the electric field inside of the atomic orbital is $Z-1$ times the electric field of a point charge, the $\mathbf{J} \bullet \mathbf{E}$ energy over time involving the electric field internal to the atomic orbital of electron 2 is $\frac{(Z-1)}{Z}$ times the magnetic energy stored inside of the atomic orbital as given by Eq. (1.159). This energy is

$$[\Delta t(\mathbf{J} \bullet \mathbf{E})]_{energy\ internal} = \frac{(Z-1)}{Z}\frac{4\pi\mu_0 e^2\hbar^2}{3m_e^2 r_1^3} \tag{7.59}$$

Thus, the total $\mathbf{J} \bullet \mathbf{E}$ energy over time of electron 2 is the sum of Eqs. (7.58) and (7.59).

The $\mathbf{J} \bullet \mathbf{E}$ energy over time of electron 1 during contraction from infinity to r_1 is negative, and the equations for the external and internal contributions are of the same form as Eqs. (7.58) and (7.59) where the appropriate effective charge is

substituted. The $\mathbf{J} \bullet \mathbf{E}$ energy over time involving the electric field external to the atomic orbital of electron 1 is

$$[\Delta t(\mathbf{J} \bullet \mathbf{E})]_{energy\ external} = \frac{(Z-1)}{Z} \frac{2\pi\mu_0 e^2 \hbar^2}{3m_e^2 r_1^3} \tag{7.60}$$

And, the $\mathbf{J} \bullet \mathbf{E}$ energy over time involving the electric field internal to the atomic orbital of electron 1 is:

$$[\Delta t(\mathbf{J} \bullet \mathbf{E})]_{\text{energy } internal} = \frac{Z}{Z} \frac{4\pi\mu_0 e^2 \hbar^2}{3m_e^3 r_1^3} \tag{7.61}$$

The difference, Δ, between the $\mathbf{J} \bullet \mathbf{E}$ energy over time for expanding electron 2 from r_1 to infinity and contracting electron 1 from infinity to r_1 is $-\frac{1}{Z}$ times the stored magnetic energy given by Eq. (7.46).

$$\Delta = -\frac{1}{Z} \frac{2\pi\mu_0 e^2 \hbar^2}{m_e^2 r_1^3} \tag{7.62}$$

Thus, the ionization energies are given by

$$Ionization\ Energy = -Electric\ Energy - \frac{1}{Z} Magnetic\ Energy \tag{7.63}$$

The energies of several two-electron atoms are given in Table 7.1. The relativistic factor γ^* involving the spin pairing between the two electrons is derived in the Special Relativistic Effect on the Electron Radius and the Relativistic Ionization Energies section.

Table 7.1. Relativistically corrected ionization energies for some two-electron atoms.

2 e Atom	Z	r_1 (a_o) [a]	Electric Energy [b] (eV)	Magnetic Energy [c] (eV)	Velocity (m/s) [d]	γ^* [e]	Theoretical Ionization Energies [f] (eV)	Experimental Ionization Energies [g] (eV)	Relative Error [h]
He	2	0.566987	23.996467	0.590536	3.85845E+06	1.000021	24.58750	24.58741	-0.000004
Li^{+}	3	0.35566	76.509	2.543	6.15103E+06	1.00005	75.665	75.64018	-0.0003
Be^{2+}	4	0.26116	156.289	6.423	8.37668E+06	1.00010	154.699	153.89661	-0.0052
B^{3+}	5	0.20670	263.295	12.956	1.05840E+07	1.00016	260.746	259.37521	-0.0053
C^{4+}	6	0.17113	397.519	22.828	1.27836E+07	1.00024	393.809	392.087	-0.0044
N^{5+}	7	0.14605	558.958	36.728	1.49794E+07	1.00033	553.896	552.0718	-0.0033
O^{6+}	8	0.12739	747.610	55.340	1.71729E+07	1.00044	741.023	739.29	-0.0023
F^{7+}	9	0.11297	963.475	79.352	1.93649E+07	1.00057	955.211	953.9112	-0.0014
Ne^{8+}	10	0.10149	1206.551	109.451	2.15560E+07	1.00073	1196.483	1195.8286	-0.0005
Na^{9+}	11	0.09213	1476.840	146.322	2.37465E+07	1.00090	1464.871	1465.121	0.0002
Mg^{10+}	12	0.08435	1774.341	190.652	2.59364E+07	1.00110	1760.411	1761.805	0.0008
Al^{11+}	13	0.07778	2099.05	243.13	2.81260E+07	1.00133	2083.15	2085.98	0.0014
Si^{12+}	14	0.07216	2450.98	304.44	3.03153E+07	1.00159	2433.13	2437.63	0.0018
P^{13+}	15	0.06730	2830.11	375.26	3.25043E+07	1.00188	2810.42	2816.91	0.0023
S^{14+}	16	0.06306	3236.46	456.30	3.46932E+07	1.00221	3215.09	3223.78	0.0027
Cl^{15+}	17	0.05932	3670.02	548.22	3.68819E+07	1.00258	3647.22	3658.521	0.0031
Ar^{16+}	18	0.05599	4130.79	651.72	3.90705E+07	1.00298	4106.91	4120.8857	0.0034
K^{17+}	19	0.05302	4618.77	767.49	4.12590E+07	1.00344	4594.25	4610.8	0.0036
Ca^{18+}	20	0.05035	5133.96	896.20	4.34475E+07	1.00394	5109.38	5128.8	0.0038
Sc^{19+}	21	0.04794	5676.37	1038.56	4.56358E+07	1.00450	5652.43	5674.8	0.0039
Ti^{20+}	22	0.04574	6245.98	1195.24	4.78241E+07	1.00511	6223.55	6249	0.0041
V^{21+}	23	0.04374	6842.81	1366.92	5.00123E+07	1.00578	6822.93	6851.3	0.0041
Cr^{22+}	24	0.04191	7466.85	1554.31	5.22005E+07	1.00652	7450.76	7481.7	0.0041
Mn^{23+}	25	0.04022	8118.10	1758.08	5.43887E+07	1.00733	8107.25	8140.6	0.0041
Fe^{24+}	26	0.03867	8796.56	1978.92	5.65768E+07	1.00821	8792.66	8828	0.0040
Co^{25+}	27	0.03723	9502.23	2217.51	5.87649E+07	1.00917	9507.25	9544.1	0.0039
Ni^{26+}	28	0.03589	10235.12	2474.55	6.09529E+07	1.01022	10251.33	10288.8	0.0036
Cu^{27+}	29	0.03465	10995.21	2750.72	6.31409E+07	1.01136	11025.21	11062.38	0.0034

[a] From Eq. (7.35).

[b] From Eq. (7.45).

[c] From Eq. (7.46), except Eq. (7.44) for neutral He.

[d] From Eq. (7.47).

[e] From Eq. (1.281) with the velocity given by Eq. (7.47).

[f] From Eq. (7.44) for neutral atom helium, and ions from Eq. (7.63) with $E(electric)$ of Eq. (7.45) relativistically corrected by γ^* according to Eq. (1.281).

[g] From theoretical calculations for ions Ne^{8+} to Cu^{27+} [8-9].

[h] (Experimental-theoretical)/experimental.

The agreement between the experimental and calculated values of Table 7.1 is within the experimental capability of the spectroscopic determinations at large Z, which relies on X-ray spectroscopy. In this case, the experimental capability is three to four significant figures, which is consistent with the last column. The helium atom isoelectronic series is given in Table 7.1 [8-9] to much higher precision than the capability of X-ray spectroscopy, but these values are based on theoretical and interpolation techniques rather than data alone. Ionization energies are difficult to determine since the cut-off of the Rydberg series of lines at the ionization energy is often not observed, and the ionization energy must be determined from theoretical calculations, interpolation of He isoelectronic and Rydberg series, as well as direct experimental data.

The theoretical values for low Z can be improved by calculating the spin-nuclear relativistic factor, which corresponds to the reduced mass for one-electron atoms given in the Determination of Atomic Orbital Radii section.

HYDRIDE ION

The hydride ion comprises two indistinguishable electrons bound to a proton of $Z = +1$. Each electron experiences a centrifugal force, and the balancing centripetal force (on each electron) is produced by the electric force between the electron and the nucleus. In addition, a magnetic force exists between the two electrons causing the electrons to pair.

DETERMINATION OF THE ATOMIC ORBITAL RADIUS, R_N

Consider the binding of a second electron to a hydrogen atom to form a hydride ion. The second electron experiences no central electric force because the electric field is zero outside of the radius of the first electron. However, the second electron experiences a magnetic force due to electron 1 causing it to pair with electron 1. Thus, electron 1 experiences the reaction force of electron 2 which acts as a centrifugal force. The force balance equation can be determined by equating the total forces acting on the two bound electrons taken together. The force balance equation for the paired electron atomic orbital is obtained by equating the forces on the mass and charge densities. The centrifugal force of both electrons is given by Eq. (7.1) and Eq. (7.2) where the mass is $2m_e$. Electric field lines end on charge. Since both electrons are paired at the same radius, the number of field lines ending on the charge density of electron 1 equals the number that end on the charge density of electron 2. The electric force is proportional to the number of field lines; thus, the centripetal electric force, $\mathbf{F}_{ele}$, between the electrons and the nucleus is

$$\mathbf{F}_{ele(electron\ 1,2)} = \frac{\frac{1}{2}e^2}{4\pi\varepsilon_0 r_n^2} \tag{7.64}$$

where ε_0 is the permittivity of free space. The outward magnetic force on the two paired electrons is given by the negative of Eq. (7.24) where the mass is $2m_e$. The outward centrifugal force and magnetic forces on electrons 1 and 2 are balanced by the electric force

$$\frac{\hbar^2}{2m_e r_2^3} = \frac{\frac{1}{2}e^2}{4\pi\varepsilon_0 r_2^2} - \frac{1}{Z}\frac{\hbar^2}{2m_e r_2^3}\sqrt{s(s+1)} \tag{7.65}$$

where $Z = 1$. Solving for r_2,

$$r_2 = r_1 = a_0\left(1+\sqrt{s\left(s+1\right)}\right);\ s = \frac{1}{2} \tag{7.66}$$

where a_0 is given by Eq. (1.256). That is, the final radius of electron 2, r_2, is given by Eq. (7.66); this is also the final radius of electron 1.

IONIZATION ENERGY

Since the hydrogen atom is neutral, the ionization energy of the hydride ion is determined from the magnetic energy balance. During ionization, electron 2 is moved to infinity. By the selection rules for absorption of electromagnetic radiation dictated by conservation of angular momentum, absorption of a photon causes the spin axes of the antiparallel spin-paired electrons to become parallel. The unpairing energy, $E_{unpairing}(magnetic)$, is given by Eq. (7.46) and Eq. (7.66) multiplied by two because the magnetic energy is proportional to the square of the magnetic field as derived in Eqs. (1.154-1.161). The magnetic energy of electron 1 following ionization of the hydride ion, $E_{electron\ 1\ final}(magnetic)$, is given by Eq. (1.161) and Eq. (1.260).

In addition, a third ionization energy term arises from the interaction of the two electrons during ionization. A magnetic force exists on the electron to be ionized due to the spin-spin interaction. The energy to move electron 2 to a radius which is infinitesimally greater than that of electron 1 is zero. In this case, the only force acting on electron 2 is the magnetic force. Due to conservation of energy, the potential energy change to move electron 2 to infinity to ionize the hydride ion can be calculated from the magnetic force of Eq. (7.65). The magnetic work, $E_{magwork}$, is the negative integral of the magnetic force (the second term on the right side of Eq. (7.65)) from r_2 to infinity,

$$E_{magwork} = \int_{r_2}^{\infty} \frac{\hbar^2}{2m_e r^3}\sqrt{s(s+1)}dr \tag{7.67}$$

where r_2 is given by Eq. (7.66). The result of the integration is:

$$E_{magwork} = \frac{\hbar^2\sqrt{s(s+1)}}{4m_e a_0^2\left[1+\sqrt{s(s+1)}\right]^2} \tag{7.68}$$

where $s = \frac{1}{2}$. By moving electron 2 to infinity, electron 1 moves to the radius $r_1 = a_H$, and the corresponding magnetic energy, $E_{electron\ 1\ final}(magnetic)$, is given by Eq. (7.46). In the present case of an inverse squared central field corresponding to the reaction force on electron 1, the magnitude of the binding energy is one half the magnitude of the potential energy [10], which is equivalent to that of Eq. (7.68). Thus, the ionization energy is given by subtracting the two magnetic energy terms from one half the magnetic work (Eq. (7.68)) wherein m_e is the electron reduced mass $\mu_e = \frac{m_e m_p}{\frac{m_e}{\sqrt{\frac{3}{4}}} + m_p}$ due to the electrodynamic magnetic

energy that arises from the force between the unpaired electrons and the nucleus which follows from Eqs. (1.253-1.255) and Eq. (7.67)[7]. The electrodynamic force goes to zero as the two electrons pair due to the cancellation of the electron currents and magnetic fields. Thus, the corresponding reduced mass only appears in the $E_{magwork}$ term and in the magnetic energy of the free hydrogen atom term, $E_{electron\ 1\ final}(magnetic)$. Thus, the ionization energy of the hydride ion is given by:

$$Ionization\ Energy = \frac{1}{2}E_{magwork} - E_{electron\ 1\ final}(magnetic) - E_{unpairing}(magnetic)$$

$$= \frac{\hbar^2\sqrt{s(s+1)}}{8\mu_e a_0^2\left[1+\sqrt{s(s+1)}\right]^2} - \frac{\pi\mu_0 e^2\hbar^2}{m_e^2}\left(\frac{1}{a_H^3} + \frac{2^2}{a_0^3\left[1+\sqrt{s(s+1)}\right]^3}\right) \tag{7.69}$$

From Eq. (7.69), the calculated ionization energy of the hydride ion is 0.75418 eV.

The experimental value given by Lykke [11] is $6082.99 \pm 0.15\ cm^{-1}$ **(0.75418 eV).**

Without deriving the details of the nuclear structure of the deuterium nucleus and its magnetic moment, the electrodynamic magnetic energy term of the deuterium hydride ion due to the corresponding force between the interacting electrons and the nucleus with two nucleons may be taken as twice that of hydrogen, which has only one nucleon. From Eqs. (1.253-1.255) and Eq. (7.68), the corresponding reduced electron mass in Eq. (7.69) is $\mu_e = \frac{m_e m_p}{\frac{2m_e}{\sqrt{\frac{3}{4}}} + m_p}$.

From Eq. (7.69), the calculated ionization energy of the deuterium hydride ion is 0.75471 eV.

The experimental value given by Lykke [11] is $6086.2 \pm 0.6\ cm^{-1}$ **(0.75457 eV).**

---

[7]The electrodynamic force between the unpaired electrons and the nucleus which follows from Eqs. (1.253-1.255) goes to zero as the two electrons pair due to the cancellation of the electron currents and magnetic fields. During ionization, the corresponding energy due to the unpaired electrons is given by

$$E_{electrodynamic\ magwork} = \frac{\hbar^2}{2m_p r_1^2}\sqrt{s(s+1)} - \int_{r_2}^{\infty}\frac{\hbar^2}{2m_p r^3}\sqrt{s(s+1)}dr \tag{1}$$

where the mass in Eq. (1.246) is $2m_e$. Eq. (7.67) with the inclusion of the electrodynamic energy given by Eq. (1) is

$$E_{magwork} = \int_{r_2}^{\infty}\frac{\hbar^2}{2r^3}\sqrt{s(s+1)}\left(\frac{1}{m_e} + \frac{1}{m_p\sqrt{s(s+1)}}\right)dr \tag{2}$$

Thus, Eq. (7.68) with the electrodynamic energy is given by

$$E_{magwork} = \frac{\hbar^2\sqrt{s(s+1)}}{4\mu_e a_0^2\left[1+\sqrt{s(s+1)}\right]^2} \tag{3}$$

where the reduced electron mass is

$$\mu_e = \frac{m_e m_p}{\frac{m_e}{\sqrt{\frac{3}{4}}} + m_p} \tag{4}$$

HYDRINO HYDRIDE ION

The hydrino atom $H\left(1/2\right)$ can form a stable hydride ion. The central field is twice that of the hydrogen atom, and it follows from Eq. (7.65) that the radius of the hydrino hydride ion $H^-\left(n=1/2\right)$ is one half that of atomic hydrogen hydride, $H^-\left(n=1\right)$, given by Eq. (7.66).

$$r_2 = r_1 = \frac{a_0}{2}\left(1+\sqrt{s\left(s+1\right)}\right);\ s=\frac{1}{2} \tag{7.70}$$

The energy follows from Eq. (7.69) and Eq. (7.70) where due to the invariance of e/m and $\hbar$ for lower-energy states as well as excited states as shown in the Spin-Orbit Coupling section, the relativistic correction to the binding of the electron to a hydrogen atom or hydrino atom is the energy stored in the magnetic field of the hydrogen atom.

$$\begin{aligned} Ionization\ Energy &= \frac{1}{2}E_{magwork} - E_{electron\ 1\ final}(magnetic) - E_{unpairing}(magnetic) \\ &= \frac{\hbar^2\sqrt{s(s+1)}}{8\mu_e a_0^2\left[\frac{1+\sqrt{s(s+1)}}{2}\right]^2} - \frac{\pi\mu_0 e^2\hbar^2}{m_e^2}\left(\frac{1}{a_H^3}+\frac{2^2}{a_0^3\left[\frac{1+\sqrt{s(s+1)}}{2}\right]^3}\right) \end{aligned} \tag{7.71}$$

From Eq. (7.71), the calculated ionization energy of the hydrino hydride ion $H^-\left(n=1/2\right)$ is $3.047\ eV$ which corresponds to a wavelength of $\lambda = 407\ nm$.

In general, the central field of hydrino atom $H\left(n=1/p\right);\ p=\text{integer}$ is p times that of the hydrogen atom. Thus, the force balance equation is:

$$\frac{\hbar^2}{2m_e r_2^3} = \frac{\frac{p}{2}e^2}{4\pi\varepsilon_0 r_2^2} - \frac{1}{Z}\frac{\hbar^2}{2m_e r_2^3}\sqrt{s(s+1)} \tag{7.72}$$

where $Z=1$ because the field is zero for $r > r_1$. Solving for r_2,

$$r_2 = r_1 = \frac{a_0}{p}\left(1+\sqrt{s\left(s+1\right)}\right);\ s=\frac{1}{2} \tag{7.73}$$

From Eq. (7.73), the radius of the hydrino hydride ion $H^-\left(n=1/p\right);\ p=\text{integer}$ is $\frac{1}{p}$ that of atomic hydrogen hydride, $H^-\left(n=1\right)$, given by Eq. (7.66). The energy follows from Eq. (7.69) and Eq. (7.73).

$$\begin{aligned} Ionization\ Energy &= \frac{1}{2}E_{magwork} - E_{electron\ 1\ final}(magnetic) - E_{unpairing}(magnetic) \\ &= \frac{\hbar^2\sqrt{s(s+1)}}{8\mu_e a_0^2\left[\frac{1+\sqrt{s(s+1)}}{p}\right]^2} - \frac{\pi\mu_0 e^2\hbar^2}{m_e^2}\left(\frac{1}{a_H^3}+\frac{2^2}{a_0^3\left[\frac{1+\sqrt{s(s+1)}}{p}\right]^3}\right) \end{aligned} \tag{7.74}$$

From Eq. (7.74), the calculated ionization energy of the hydrino hydride ion $H^-\left(n=1/p\right)$ as a function of p is given in Table 7.2.

Table 7.2. The ionization energy of the hydrino hydride ion $H^-\left(n=1/p\right)$ as a function of *p*.

Hydride Ion	r_1 (a_o)[a]	Cal. Ionization Energy (eV)[b]	Cal. Wavelength (nm)
$H^-\left(n=1\right)$	1.8660	0.7542	1644
$H^-\left(n=1/2\right)$	0.9330	3.047	406.9
$H^-\left(n=1/3\right)$	0.6220	6.610	187.6
$H^-\left(n=1/4\right)$	0.4665	11.23	110.4
$H^-\left(n=1/5\right)$	0.3732	16.70	74.23
$H^-\left(n=1/6\right)$	0.3110	22.81	54.35
$H^-\left(n=1/7\right)$	0.2666	29.34	42.25
$H^-\left(n=1/8\right)$	0.2333	36.09	34.46
$H^-\left(n=1/9\right)$	0.2073	42.84	28.94
$H^-\left(n=1/10\right)$	0.1866	49.38	25.11
$H^-\left(n=1/11\right)$	0.1696	55.50	22.34
$H^-\left(n=1/12\right)$	0.1555	60.98	20.33
$H^-\left(n=1/13\right)$	0.1435	65.63	18.89
$H^-\left(n=1/14\right)$	0.1333	69.22	17.91
$H^-\left(n=1/15\right)$	0.1244	71.55	17.33
$H^-\left(n=1/16\right)$	0.1166	72.40	17.12
$H^-\left(n=1/17\right)$	0.1098	71.56	17.33
$H^-\left(n=1/18\right)$	0.1037	68.83	18.01
$H^-\left(n=1/19\right)$	0.0982	63.98	19.38
$H^-\left(n=1/20\right)$	0.0933	56.81	21.82
$H^-\left(n=1/21\right)$	0.0889	47.11	26.32
$H^-\left(n=1/22\right)$	0.0848	34.66	35.76
$H^-\left(n=1/23\right)$	0.0811	19.26	64.36
$H^-\left(n=1/24\right)$	0.0778	0.6945	1785
$H^-\left(n=1/25\right)$		not stable[c]	

[a] from Eq. (7.73).
[b, c] from Eq. (7.74).

HYDRINO HYDRIDE ION NUCLEAR MAGNETIC RESONANCE SHIFT

The proton gyromagnetic ratio, $\gamma_p/2\pi$, is

$$\gamma_P/2\pi = 42.57602\ MHz\ T^{-1} \tag{7.75}$$

The NMR frequency, f, is the product of the proton gyromagnetic ratio given by Eq. (7.75) and the magnetic flux, $\mathbf{B}$.

$$f = \gamma_P/2\pi\mathbf{B} = 42.57602\ MHz\ T^{-1}\mathbf{B} \tag{7.76}$$

A typical radio frequency (RF) is $400\ MHz$. According to Eq. (7.76) this corresponds to a flux of $9.39496\ T$ provided by a superconducting NMR magnet. With a constant magnetic field, the frequency is scanned to yield the spectrum where the frequency scan is typically achieved using a Fourier transform on the free induction decay signal following a radio frequency pulse. Historically, the radiofrequency was held constant, the applied magnetic field, H_0 ($H_0 = \frac{B}{\mu_0}$), was varied over a small range, and the frequency of energy absorption was recorded at the various values for H_0. By convention based on this historic mode of operation, the radiofrequency spectrum is converted into the corresponding applied magnetic field, H_0 ($H_0 = \frac{B}{\mu_0}$), of energy absorption and displayed as a function of increasing H_0. The protons that would absorb energy at a lower H_0 give rise

to a downfield absorption peak; whereas, the protons that would absorb energy at a higher H_0 give rise to an upfield absorption peak. The electrons of the compound of a sample influence the field at the nucleus such that it deviates slightly from the applied value. For the case that the chemical environment has no NMR effect, the value of H_0 at resonance with the radiofrequency held constant at $400\ MHz$ is

$$\frac{2\pi f}{\mu_0\gamma_P} = \frac{(2\pi)(400\ MHz)}{\mu_0 42.57602\ MHz\ T^{-1}} = H_0 \tag{7.77}$$

In the case that the chemical environment has a NMR effect, a different value of H_0 is required for resonance. This chemical shift is proportional to the electronic magnetic flux change at the nucleus due to the applied field that in the case of each hydrino hydride ion is a function of its radius.

The change in the magnetic moment, $\Delta\mathbf{m}$, of each electron of the hydride ion due to an applied magnetic flux $\mathbf{B}$ is [12]

$$\Delta\mathbf{m} = -\frac{e^2 r^2 \mathbf{B}}{4m_e} \tag{7.78}$$

The two electrons are spin-paired and the velocities are mirror opposites. Thus, the change in velocity of each electron treated individually (Eq. (10.3)) due to the applied field would be equal and opposite. However, as shown in the Three Electron Atom section, the two paired electrons may be treated as one with twice the mass where m_e is replaced by $2m_e$ in Eq. (7.78). In this case, the paired electrons spin together about the applied field axis, the z-axis, to cause a reduction in the applied field according to Lenz's law. Then, the radius in Eq. (7.78) corresponds to the coordinate ρ in cylindrical coordinates since it is perpendicular to the direction of the applied field along the z-axis. The integral over the entire flux linked by the hydride ion atomic orbital is given by

$$\Delta\mathbf{m} = -\frac{e^2\mathbf{B}}{8m_e}\frac{\int_{-r_1}^{r_1}\left(r_1^2 - z^2\right)dz}{2r_1} = -\frac{2}{3}\frac{e^2 r_1^2\mathbf{B}}{8m_e} \tag{7.79}$$

where r_1 is the radius of the hydride ion [13]. The change in magnetic flux $\Delta\mathbf{B}$ at the nucleus due to the change in magnetic moment, $\Delta\mathbf{m}$, given by Eq. (7.79) follows from Eq. (1.132).

$$\Delta\mathbf{B} = \mu_0\frac{\Delta m}{r_1^3}(\mathbf{i}_r\cos\theta - \mathbf{i}_\theta\sin\theta) \qquad \text{for } r < r_n \tag{7.80}$$

where μ_0 is the permeability of vacuum. Substitution of Eq. (7.79) into Eq. (7.80) gives the absolute upfield chemical shift $\frac{\Delta B}{B}$ of $H^-(1/p)$ relative to a bare proton:

$$\frac{\Delta B_T}{B} = -\mu_0\frac{pe^2}{12m_e a_0\left(1+\sqrt{s(s+1)}\right)} = -p29.9\ ppm \tag{7.81}$$

where p is an integer.

It follows from Eqs. (7.73) and (7.81) that the diamagnetic flux (flux opposite to the applied field) at the nucleus is inversely proportional to the radius, $r_1 = \frac{a_0}{p}\left(1+\sqrt{s(s+1)}\right)$. For resonance to occur, ΔH_0, the change in applied field from that given by Eq. (7.77), must compensate by an equal and opposite amount as the field due to the electrons of the hydrino hydride ion. According to Eq. (7.73), the ratio of the radius of the hydrino hydride ion $H^-(1/p)$ to that of the ordinary hydride ion H^- is the reciprocal of an integer p. It follows from Eqs. (7.75-7.81) that compared to a proton with no chemical shift, the ratio of ΔH_0 for resonance of the proton of the hydrino hydride ion $H^-(1/p)$ to that of the ordinary hydride ion H^- is a positive integer. That is, if only the size is considered, the absolute absorption peak of the hydrino hydride ion (i.e. relative to a proton with no shift) occurs at a value of ΔH_0 that is a multiple of p times the value that is resonant for H^-. However, the source current of the state must be considered in addition to the reduced radius.

As shown in the Stability of "Ground" and Hydrino States section, for the below "ground" (fractional quantum number) energy states of the hydrogen atom, σ_{photon}, the two-dimensional surface charge due to the "trapped photon" at the electron atomic orbital and phase-locked with the electron atomic orbital current, is given by Eqs. (6.7) and (6.8) wherein the principal quantum number of excited states is replaced by $n = \frac{1}{p}$.

$$\sigma_{photon} = \frac{e}{4\pi(r_n)^2}\left[Y_0^0(\theta,\phi) - \frac{1}{n}\left[Y_0^0(\theta,\phi) + \mathrm{Re}\left\{Y_\ell^m(\theta,\phi)e^{im\omega_n t}\right\}\right]\right]\delta(r-r_n)$$
$$n = \frac{1}{p};\ \ell = 0,1,2,...,p-1;\ m_\ell = -\ell,-\ell+1,...,0,...+\ell;\ m_s = \pm\frac{1}{2} \tag{7.82}$$

And, $\sigma_{electron}$, the two-dimensional surface charge of the electron atomic orbital is

$$\sigma_{electron} = \frac{-e}{4\pi(r_n)^2}\left[Y_0^0(\theta,\phi) + \mathrm{Re}\left\{Y_\ell^m(\theta,\phi)e^{im\omega_n t}\right\}\right]\delta(r-r_n) \tag{7.83}$$

The superposition of σ_{photon} (Eq. (7.82)) and $\sigma_{electron}$, (Eq. (7.83)) where the spherical harmonic functions satisfy the conditions given in the Bound Electron "Atomic Orbital" section is:

$$\sigma_{photon} + \sigma_{electron} = \frac{-e}{4\pi(r_n)^2}\left[\frac{1}{n}Y_0^0(\theta,\phi) + \left(1+\frac{1}{n}\right)\mathrm{Re}\left\{Y_\ell^m(\theta,\phi)e^{im\omega_n t}\right\}\right]\delta(r-r_n) \tag{7.84}$$

The ratio of the total charge distributed over the surface at the radius of the hydride ion of the hydrino hydride ion $H^-(1/p)$ to that of the ordinary hydride ion H^- is an integer p , and the corresponding total source current of the hydrino hydride ion is equivalent to an integer p times that of an electron. The "trapped photon" obeys the phase-matching condition given in Excited States of the One-Electron Atom (Quantization) section, and the source current of the state must be considered in addition to the reduced radius.

In the case that the photons and corresponding source current spin in opposite directions for the two electrons, the orbital magnetic moments cancel. However, as given in the Pair Production section, a photon having an energy equivalent to that of the mass energy of the electron may undergo particle production to form an electron. To maintain continuity, the photon surface current of a hydrino hydride state must behave as the charge equivalent to its energy during the interaction of the electrons and the phased locked photon-field surface current with the external magnetic field such that the photon component gives rise to a proportional diamagnetic effect as well. The photon diamagnetic component is given by Eqs. (29.10-29.11) as the charge equivalent to its energy that superimposes with the diamagnetism of the two electrons. The relativistic term after Eq. (29.10) and the central field magnitude term for the hydrino hydride state having principle quantum number p are α^2 and p , respectively. The photon contribution to the change in flux $\Delta\mathbf{B}_{SR}$ for hydrino hydride $H^-(1/p)$ given by applying the corresponding relativistic factor of $\gamma_{SR} = \alpha^2$ to Eq. (7.80) is

$$\Delta\mathbf{B}_{SR} = -p\alpha^2\mu_0\frac{\Delta m}{r_n^3}(\mathbf{i}_r\cos\theta - \mathbf{i}_\theta\sin\theta) \qquad \text{for } r < r_n \tag{7.85}$$

Thus, using Eqs. (7.81) and (7.86), the upfield chemical shift $\frac{\Delta B_{SR}}{B}$ due to the photon contribution of the ion $H^-(1/p)$ corresponding to the lower-energy state with principal quantum energy state p is given by:

$$\frac{\Delta B_{SR}}{B} = -p\alpha^2\mu_0\frac{pe^2}{12m_e a_0\left(1+\sqrt{s(s+1)}\right)} \tag{7.86}$$

The total shift $\frac{\Delta B_T}{B}$ for $H^-(1/p)$ is given by the sum of that of the two electrons given by Eq. (7.81) and that of the photon given by Eq. (7.86):

$$\frac{\Delta B_T}{B} = -\mu_0\frac{pe^2}{12m_e a_0\left(1+\sqrt{s(s+1)}\right)}\left(1+p\alpha^2\right) = -\left(p29.9 + p^2 1.59\ X\ 10^{-3}\right)ppm \tag{7.87}$$

where the first term applies to H^- with $p=1$ and $p=\text{integer}>1$ for $H^-(1/p)$. The experimental absolute resonance shift of TMS is -31.5 ppm relative to the proton's gyromagnetic frequency [14-15]. Thus, the theoretical shift of $H^-(1/p)$ relative to TMS standard is given by the difference of Eq. (7.87) and -31.5 ppm.

Hydrino Hydride Ion Hyperfine Lines

For the ordinary hydride ion H^-, a continuum is observed at shorter wavelengths of the ionization or binding energy referred to as the bound-free continuum. For typical conditions in the photosphere, Figure 4.5 of Stix [16] shows the continuous absorption coefficient $\kappa_C(\lambda)$ of the Sun. In the visible and infrared spectrum, the hydride ion H^- is the dominant absorber. Its free-free continuum starts at $\lambda = 1.645\ \mu m$, corresponding to the ionization energy of $0.745\ eV$ for H^- with strongly increasing absorption towards the far infrared. The ordinary hydride spectrum recorded on the Sun is representative of the hydride spectrum in a very hot plasma.

The reaction of a hydrogen atom with a second electron to form ordinary hydride ion comprising two paired electrons in a single shell releases continuum radiation to longer wavelengths with a cutoff of the binding energy of the second electron of the hydride ion as shown by Stix [16]. However, hydrino hydride ion and the corresponding emission of a hydrino atom binding a second electron are unique. Hydrino hydride ion comprises an unpaired electron which results the emission of the binding energy of the second electron being released with additional quantized units of energy based on linkage of flux increments of the fluxon or magnet flux quantum $\frac{h}{2e}$. Specifically, hydrino $H^-(1/p)$comprises (i) two electrons bound in a minimum energy, equipotential, spherical, two-dimensional current membrane wherein the electrons of $H^-(1/p)$ are unpaired in the same shell at the same position r and (ii) a photon that increases the central field by an integer of the fundamental charge at the nucleus centered on the origin of the sphere. The interaction of the hydrino state photon electric field with each electron gives rise to a nonradiative radial monopole such that the state is stable. The combination of two electrons into a single atomic orbital (AO) while maintaining the radiationless integer photonic central field gives rise to the special case of a doublet AO state in hydrino hydride ion rather than a singlet state as in the case of ordinary hydride ion. The singlet state is nonmagnetic; whereas, the doublet state has a net magnetic moment of a Bohr magneton μ_B.

Specifically, the basis element of the current of the atomic orbital is a great circle as shown in the Generation of the Atomic Orbital-CVFS section. As shown in the Equation of the Electric Field inside the Atomic Orbital section, (i) photons carry electric field and comprise closed field line loops, (ii) a hydrino atom comprises a trapped photon wherein the photon field-line loops each travel along a mated great circle current loop basis element in the same vector direction, (iii) the direction of each field line increases in the direction perpendicular to the propagation direction with relative motion as required by special relativity, and (iv) since the linear velocity of each point along a field line loop of a trapped photon is light speed c, the electric field direction relative to the laboratory frame is purely perpendicular to its mated current loop and it exists only at $\delta(r - r_n)$. The paired electrons of the H^- atomic orbital comprise a singlet state having no net magnetic moment. However, the photon field lines of a hydrino hydride ion can only propagate in one direction to avoid cancellation and give rise to a central field to provide force balance between the centrifugal and central forces (Eq. (7.72)). This special case gives rise to a doublet state in hydrino hydride ion.

The hydrino hydride AO may be treated as a linear combination of the great circles that comprise the current density function of each electron as given in the Generation of the Orbitsphere-CVFS section. To meet the boundary conditions that the photon is matched in direction with the electron current and that the electron angular momentum is $\hbar$ are satisfied, one half of electron 1 and one half of electron 2 may be spin up and matched with the photon, and the other half of electron 1 may be spin up and the other half of electron 2 may be spin down such that one half of the currents are paired and one half of the currents are unpaired. Given the indivisibility of each electron and the condition that the AO comprises two identical electrons, the force of the photon is transferred to the totality of the electron AO comprising a linear combination of the two identical electrons to satisfy Eq. (7.72). The resulting angular momentum and magnetic moment of the unpaired current density are $\hbar$ and a Bohr magneton μ_B, respectively. As given in the Electron g Factor section, flux is linked by an unpaired electron in quantized units of the fluxon or magnetic flux quantum $\frac{h}{2e}$.

Hydride ions formed by the reaction of hydrogen or hydrino atoms with free electrons with a kinetic energy distribution give rise to the bound-free emission band to shorter wavelengths than the ionization or binding energy due to the release of the electron kinetic energy and the hydride ion binding energy. As shown by Eq. (7.74) compared to Eq. (7.71), the energies for the formation of hydrino hydride ions are much greater, and with sufficient spectroscopic resolution, it may be possible to resolve the unique hyperfine structure in the corresponding bound-free band due to interactions of the free and bound electrons during the formation of hydrino hydride ion. The derivation of the hyperfine lines of the unique doublet state follows.

Consider a free electron binding to a hydrino atom to form a hydrino hydride ion. The total angular momentum of an electron is $\hbar$. During binding of the free electron, the bound electron produces a magnetic field at the free electron given by Eq. (1.133). Thus, for radial distances greater than the radius of the hydride ion, the magnetic field is equivalent to that of a magnetic dipole of a Bohr magneton at the origin. The energy of interaction of a magnetic dipole with the magnetic field of the bound electron E_{ss}, the spin-spin energy, is given by Eq. (1.227)—the product of the electron g factor given by Eq. (1.226), the magnetic moment of the free electron, a Bohr magneton given by Eq. (1.131), and the magnetic flux which follows from Eq. (1.133).

$$E_{ss} = g\mu_B\mu_0 H = g\mu_B B = g\frac{\mu_0}{r^3}\left(\frac{e\hbar}{2m_e}\right)^2 \tag{7.88}$$

where μ_0 is the permeability of free space, r is the radius of the hydride ion $H^-(1/p)$ given by Eq. (7.73), and p is an integer. E_{ss} for $H^-(1/2)$ is given by

$$E_{ss} = 0.011223\ eV \tag{7.89}$$

where the radius given by Eq. (7.73) for $p = 2$ is:

$$r_1 = 0.93301 a_0 \tag{7.90}$$

From Eqs. (7.74) and (7.73), the binding energy E_B of $H^-(1/2)$ is:

$$E_B = 3.0471\ eV\ \ (4069.0\ \text{Å}) \tag{7. 91}$$

When a free electron binds to the hydrino atom $H(1/2)$ to form a hydride ion $H^-(1/2)$, a photon is emitted with a minimum energy equal to the binding energy ($E_B = 3.0471\ eV$). Any kinetic energy that the free electron possesses must increase the energy of the emitted photon. The interaction of the two electrons quantizes this emission by the same mechanism as that observed in the Stern Gerlach experiment—quantization of flux linkage. Superconducting Quantum Interference Devices (SQUIDs) or wire loops linked to SQUIDs also show quantization of flux and the corresponding energies as shown in the Schrödinger Fat Cats—Another Flawed Interpretation section.

In the Stern-Gerlach experiment, a magnetic field is applied along the z-axis called the spin axis. The superposition of the vector projection of the atomic orbital angular momentum on the z-axis is $\frac{\hbar}{2}$ with an orthogonal component of $\frac{\hbar}{4}$. Excitation of a resonant Larmor precession gives rise to $\hbar$ on an axis $\mathbf{S}$ that precesses about the spin axis at an angle of $\theta = \frac{\pi}{3}$. $\mathbf{S}$ rotates about the z-axis at the Larmor frequency. $\mathbf{S}_\perp$, the transverse projection (Y_R-axis of Figure 1.25), is $\pm\sqrt{\frac{3}{4}}\hbar$, and $\mathbf{S}_\parallel$, the projection onto the axis of the applied magnetic field (z-axis), is $\pm\frac{\hbar}{2}$. As shown in the Spin Angular Momentum of the Atomic Orbital $Y_0^0(\theta,\phi)$ section, the superposition of the $\frac{\hbar}{2}$ z-axis component of the atomic orbital angular momentum and the $\frac{\hbar}{2}$ z-axis component of $\mathbf{S}$ gives $\hbar$ corresponding to the observed electron magnetic moment of a Bohr magneton, μ_B. As given in the Electron g Factor section, the electron links flux in units of the magnetic flux quantum $\Phi_0 = \frac{h}{2e}$ during a Stern-Gerlach transition, which conserves the angular momentum of the electron of $\hbar$. Due to the field of the bound electron, the free electron possessing kinetic energy will precess about the z-axis as it orbits the bound electron giving an additional component of angular momentum. A resonance exists when the transverse precessional angular momentum along the Y_R-axis of Figure 1.25 is an integer number of $\frac{\hbar}{\sqrt{s(s+1)}}$ such that its projection onto the $\mathbf{S}$-axis is $\hbar$. In order to conserve angular momentum of both electrons as the bound electron links an integer number of fluxons due to the free electron, the corresponding fluxon energy E_Φ due the free electron's Y_R-axis component of $j\frac{\hbar}{\sqrt{s(s+1)}}$ follows from Eq. (1.226) wherein the angular momentum corresponding to the Bohr magneton, $\hbar$, is replaced by $j\frac{\hbar}{\sqrt{s(s+1)}}$, and the magnetic flux density B is given by the ratio of the flux to the area.

$$\begin{aligned} E_\Phi &= j(g-2)\frac{\mu_B}{\sqrt{s(s+1)}}B = j(g-2)\frac{\mu_B}{\sqrt{s(s+1)}}\left(\frac{j\Phi_0}{A}\right) = j^2(g-2)\frac{\mu_B}{\sqrt{s(s+1)}}B \\ &= j^2(g-2)\frac{\mu_B}{\sqrt{s(s+1)}}\frac{\mu_0}{r^3}\left(\frac{e\hbar}{2m_e}\right) \end{aligned} \tag{7.92}$$

where j is an integer, $s = 1/2$, and A is the area linked by the integer number of fluxons as given in the Electron g Factor section. The additional angular momentum due to the kinetic energy of the binding free electron is conserved in rotational energy of the resulting hydride ion. The flux linkage energy applies to each of the two electrons; thus, a factor of two in Eq. (7.92) is required. This is analogous to mutual induction. The electrons flip in opposite directions and conserve angular momentum by linking flux in integer units of the magnetic flux quantum, which corresponds to the term $(g-2)$. With the

radius given by Eq. (7.73), the fluxon energy E_Φ of $H^-(1/2)$ for both electrons is given by

$$E_\Phi = j^2 2(g-2)\frac{\mu_B}{\sqrt{s(s+1)}}\frac{\mu_0}{r^3}\left(\frac{e\hbar}{2m_e}\right) = j^2 3.00213\ X\ 10^{-5}\ eV \tag{7.93}$$

The energies of the hyperfine lines E_{HF}, are given by the sum of the binding energy (Eqs. (7.74) and (7.91)), the spin-spin energy (Eqs. (7.88) and (7.89)), and the fluxon energy (Eqs. (7.92) and (7.93)).

$$\begin{aligned} E_{HF} &= E_\Phi + E_{ss} + E_B = \left(j^2 3.00213\ X\ 10^{-5} + 0.011223 + 3.0471\right)\ eV \\ &= \left(j^2 3.00213\ X\ 10^{-5} + 3.0583\right)\ eV \end{aligned} \qquad (j \text{ is an integer}) \tag{7.94}$$

The observation of bound-free hyperfine peaks requires an electron-binding threshold with a large cross section. Ordinary hydride ion does not have a fine structure transition; thus, it shows only a hydride binding energy continuum [17]. The existence of fine structure transitions in $H(1/2)$ provides a mechanism to observe a peak corresponding to the formation of a free hydride ion by the binding of an electron. The predicted energy difference between the $1/2P_{1/2}$, $1/2S_{1/2}$ and $1/2P_{3/2}$ levels of the hydrogen atom, the fine structure splitting given by Eq. (2.194), is:

$$E_{s/o} = 8\alpha^5(2\pi)^2 m_e c^2\sqrt{\frac{3}{4}} = 2.8922\ X\ 10^{-3}\ eV \tag{7.95}$$

From Eq. (2.69) and the Spin-Nuclear Coupling section, the spin-orbit coupling is proportional to the applied flux due to spin and orbital angular momentum. With the requirement of the quantization of flux in integer units of the magnetic flux quantum during binding as shown in the Electron g Factor section, the corresponding emission is at a longer wavelength having an energy of the binding energy minus an integer times the fine structure energy. The peak due to the binding energy (Eqs. (7.91)) with excitation of the fine structure splitting (Eq. (7.95)) is given by:

$$E_{Bs/o} = E_B - E_{s/o} = 3.0471\ eV - 2.8922\ X\ 10^{-3}\ eV = 3.0442\ eV\ \ (\lambda_{air} = 4071.7\ \text{Å}) \tag{7.96}$$

The $1/2P_{3/2}$, $1/2P_{1/2}$, and $1/2S_{1/2}$ levels are also split by spin-nuclear and orbital-nuclear coupling. $1/2S_{1/2}$—$1/2P_{3/2}$ and $1/2P_{1/2}$—$1/2P_{3/2}$ transitions occur between hyperfine levels; thus, the transition energy is the sum of the fine structure and the corresponding hyperfine energy. The hyperfine splitting of $H(1/2)$ given in the Spin-Nuclear Coupling section are $1.4191\ X\ 10^{-4}\ eV$ and $3.426\ X\ 10^{-4}\ eV$ for $\ell = 0$ and $\ell = 1$, respectively. In addition to a continuum, the binding of an electron to $H(1/2)$ has a resonance emission with excitation of transitions between hyperfine levels of the fine structure levels.

The ionization of Rb^+ and an electron transfer between two K^+ ions (Eqs. (5.6-5.9)) provide a reaction with a net enthalpy of an integer multiple of the potential energy of atomic hydrogen, $27.2\ eV$. The corresponding Group I nitrates provide these reactants as volatilized ions directly or as atoms by undergoing decomposition or reduction to the corresponding metals that are ionized in a plasma. The presence of each of the reactants identified as providing an enthalpy of $27.2\ eV$ formed a low-applied temperature, extremely-low-voltage plasma in atomic hydrogen called a resonant transfer or rt-plasma having strong vacuum ultraviolet (VUV) emission [18-20]. The catalyst product of Rb^+ and two K^+, $H(1/2)$, was predicted to be a highly reactive intermediate which further reacts to form a hydrino hydride ion $H^-(1/2)$.

$H^-(1/2)$ ions form by the reaction of $H(1/2)$ atoms with free electrons that have a kinetic energy distribution. The release of the electron kinetic energies and the hydrino hydride ion binding energy gives rise to the bound-free emission band to shorter wavelengths than the ionization or binding energy of the corresponding hydride ion. Due to the requirement that flux is linked by $H(1/2)$ in integer units of the magnetic flux quantum, the energy is quantized, and the emission due to $H^-(1/2)$ formation comprises a series of hyperfine lines in the corresponding bound-free band. From the electron g factor and using the observed binding energy peak E_B^*, the bound-free hyperfine structure lines due to interactions of the free and bound electrons have predicted energies E_{HF} given by the sum of the fluxon energy E_Φ, the spin-spin energy E_{ss}, and the observed binding energy peak E_B^*:

$$\begin{aligned} E_{HF} &= E_\Phi + E_{ss} + E_B^* \\ &= j^2 2(g-2)\frac{\mu_B}{\sqrt{s(s+1)}}\frac{\mu_0}{r^3}\left(\frac{e\hbar}{2m_e}\right) + g\frac{\mu_0}{r^3}\left(\frac{e\hbar}{2m_e}\right)^2 + E_B^* \\ &= \left(j^2 3.00213\ X\ 10^{-5} + 0.011223 + 3.0451\right)\ eV \\ &= \left(j^2 3.00213\ X\ 10^{-5} + 3.0563\right)\ eV \end{aligned} \tag{7.97}$$

where j = integer. This is compared to $E_{HF} = \left(j^2 3.00213\ X\ 10^{-5} + 3.0583 \right) eV$ with the unperturbed E_B given by Eqs. (7.73) and (7.74). The predicted spectrum is an inverse Rydberg-type series that converges at increasing wavelengths and terminates at 3.0563 eV, the hydride binding energy with the fine structure plus the spin-pairing energies. The high-resolution visible plasma emission spectra in the region of 4000 Å to 4060 Å shown in FIGURE 62 matched the predicted emission lines to 1 part in 10^5.

Specifically, the predicted $3.0471\ eV$ binding energy of $H^- \left(1/2 \right)$ was observed as a continuum threshold at 3.047 eV ($\lambda_{air} = 4068$ Å). The experimental $H^- \left(1/2 \right)$ peak E_B^* at 4070.6 Å (air wavelength) was used to calculate the peak positions of the bound-free hyperfine lines by substitution of the corresponding energy of 3.0451 eV into Eq. (7.97) for E_B to give the bound-free hyperfine structure lines of $H^- \left(1/2 \right)$. The high resolution visible plasma emission lines in the region of 3995 Å to 4060 Å, comprising an inverse Rydberg-type series from 3.0563 eV to 3.1012 eV matched the predicted hyperfine splitting emission energies E_{HF} given by Eq. (7.97) for $j = 1$ to $j = 39$ with the series edge at 3996.3 Å up to 1 part in 10^5 [18-20]. The flat intensity profile matches that of Josephson junctions such as ones of superconducting quantum interference devices (SQUIDs) that also link magnetic flux in quantized units of the magnetic flux quantum $\frac{h}{2e}$.

REFERENCES

1. F. Bueche, *Introduction to Physics for Scientists and Engineers*, McGraw-Hill, (1975), pp. 352-353.
2. J. D. Jackson, *Classical Electrodynamics*, Second Edition, John Wiley & Sons, New York, (1975), pp. 236-240, 601-608, 786-790.
3. D. A. McQuarrie, *Quantum Chemistry*, University Science Books, Mill Valley, CA, (1983), pp. 238-241.
4. J. D. Jackson, *Classical Electrodynamics*, Second Edition, John Wiley & Sons, New York, (1975), p. 178.
5. E. M. Purcell, *Electricity and Magnetism*, McGraw-Hill, New York, (1985), Second Edition, pp. 451-458.
6. E. M. Purcell, *Electricity and Magnetism*, McGraw-Hill, New York, (1985), Second Edition, pp. 176-178.
7. J. D. Jackson, *Classical Electrodynamics*, Second Edition, John Wiley & Sons, New York, (1975), pp. 747-752.
8. C. E. Moore, "Ionization Potentials and Ionization Limits Derived from the Analyses of Optical Spectra," Nat. Stand. Ref. Data Ser.-Nat. Bur. Stand. (U.S.), No. 34, 1970.
9. R. C. Weast, CRC Handbook of Chemistry and Physics, 58 Edition, CRC Press, West Palm Beach, Florida, (1977), p. E-68.
10. G. R. Fowles, *Analytical Mechanics*, Third Edition, Holt, Rinehart, and Winston, New York, (1977), pp. 154-156.
11. K. R. Lykke, K. K. Murray, W. C. Lineberger, "Threshold photodetachment of H^-," Phys. Rev. A, Vol. 43, No. 11, (1991), pp. 6104-6107.
12. E. Purcell, *Electricity and Magnetism*, McGraw-Hill, New York, (1985), pp. 413-418.
13. G. R. Fowles, *Analytical Mechanics*, Third Edition, Holt, Rinehart, and Winston, New York, (1977), p. 195-196.
14. K. K. Baldridge, J. S. Siegel, "Correlation of empirical δ(TMS) and absolute NMR chemical shifts predicted by ab initio computations," J. Phys. Chem. A, Vol. 103, (1999), pp. 4038-4042.
15. J. Mason, Editor, *Multinuclear NMR*, Plenum Press, New York, (1987), Chp. 3.
16. M. Stix, *The Sun*, Springer-Verlag, Berlin, (1991), p. 136
17. K. R. Lykke, K. K. Murray, W. C. Lineberger, "Threshold photodetachment of H^-," Phys. Rev. A, Vol. 43, No. 11, (1991), pp. 6104-6107.
18. R. L. Mills, P. Ray, "A Comprehensive Study of Spectra of the Bound-Free Hyperfine Levels of Novel Hydride Ion $H^-\left(1/2\right)$, Hydrogen, Nitrogen, and Air", Int. J. Hydrogen Energy, Vol. 28, No. 8, (2003), pp. 825-871.
19. R. Mills, W. Good, P. Jansson, J. He, "Stationary Inverted Lyman Populations and Free-Free and Bound-Free Emission of Lower-Energy State Hydride Ion formed by and Exothermic Catalytic Reaction of Atomic Hydrogen and Certain Group I Catalysts," Cent. Eur. J. Phys., Vol. 8, (2010), 7–16, doi: 10.2478/s11534-009-0052-6.
20. R. L. Mills, P. Ray, "Stationary Inverted Lyman Population and a Very Stable Novel Hydride Formed by a Catalytic Reaction of Atomic Hydrogen and Certain Catalysts," J. Opt. Mat., 27, (2004), 181–186.
21. R. L. Mills, P. C. Ray, R. M. Mayo, M. Nansteel, W. Good, P. Jansson, B. Dhandapani, J. He, "Hydrogen Plasmas Generated Using Certain Group I Catalysts Show Stationary Inverted Lyman Populations and Free-Free and Bound-Free Emission of Lower-Energy State Hydride," Res. J. Chem Env., Vol. 12(2), (2008), 42–72.

Chapter 8

CLASSICAL PHOTON AND ELECTRON SCATTERING

CLASSICAL SCATTERING OF ELECTROMAGNETIC RADIATION

Light is an electromagnetic disturbance that is propagated by vector wave equations that are readily derived from Maxwell's equations. The Helmholtz wave equation results from Maxwell's equations. The Helmholtz equation is linear; thus, superposition of solutions is allowed. Huygens' principle is that a point source of light will give rise to a spherical wave emanating equally in all directions. Superposition of this particular solution of the Helmholtz equation permits the construction of a general solution. An arbitrary wave shape may be considered as a collection of point sources whose strength is given by the amplitude of the wave at that point. The field, at any point in space, is simply a sum of spherical waves. Applying Huygens' principle to a disturbance across a plane aperture gives the amplitude of the far field as the Fourier transform of the aperture distribution, i.e., apart from constant factors,

$$\psi(x,y) = \int\int A(\xi,\eta)\exp\left[\frac{-ik}{f}(\xi \mathrm{x} + \eta \mathrm{y})\right] d\xi d\eta \tag{8.1}$$

Here $A(\xi,\eta)$ describes the amplitude and phase distribution across the aperture and $\psi(x,y)$ describes the far field [1] where f is the focal length.

DELTA FUNCTION

In many diffraction and interference problems, it proves convenient to make use of the Dirac delta function. This function is defined by the following property: let $f(\xi)$ be any function (satisfying some very weak convergence conditions which need not concern us here) and let $\delta(\xi - \xi')$ be a delta function centered at the point ξ'; then:

$$\int_a^b f(\xi)\delta(\xi - \xi')d\xi = f(\xi') \qquad (a < \xi' < b);\ 0\ \textit{otherwise} \tag{8.2}$$

We note, therefore, that:

$$\int_{-\infty}^{\infty} \delta(\xi - \xi')d\xi = 1 \tag{8.3}$$

the Fourier transform of the delta function is given by:

$$\psi(x) = \int \delta(\xi - \xi')\exp\left[\frac{-ik\mathrm{x}\xi}{f}\right] d\xi \tag{8.4}$$

which by definition of the delta function becomes:

$$\psi(x) = \exp\left[\frac{-ik\mathrm{x}\xi'}{f}\right] \tag{8.5}$$

The amplitude is constant and the phase function $\left(\frac{-ik\mathrm{x}\xi'}{f}\right)$ depends on the origin.

THE ARRAY THEOREM

A large number of interference problems involve the mixing of similar diffraction patterns. That is, they arise in the study of the combined diffraction patterns of an array of similar diffracting apertures. This entire class of interference effects can be described by a single equation, the array theorem. This unifying theorem is easily developed as follows: Let $\psi(\xi)$ represent the amplitude and phase distribution across one aperture centered in the diffraction plane, and let the total diffracting aperture consist of a collection of these elemental apertures at different locations ξ_n. We require first a method of representing such an array. The appropriate representation is obtained readily by means of the delta function. Thus, if an elemental aperture is positioned such that its center is at the point ξ_n, the appropriate distribution function is $\psi(\xi-\xi_n)$. The combining property of the delta function allows us to represent this distribution as follows:

$$\psi(\xi-\xi_n)=\int\psi(\xi-\alpha)\delta(\alpha-\xi_n)d\alpha \tag{8.6}$$

The integral in Eq. (8.6) is termed a "convolution" integral and plays an important role in Fourier analysis. Thus, if we wish to represent a large number N of such apertures with different locations, we could write the total aperture distribution $\Psi(\xi)$ as a sum, i.e.,

$$\Psi(\xi)=\sum_{n=1}^{N}\psi(\xi-\xi_n) \tag{8.7}$$

Or in terms of the delta function we could write, combining the features of Eqs. (8.6) and (8.7),

$$\Psi(\xi)=\sum_{n=1}^{N}\int\psi(\xi-\alpha)\delta(\alpha-\xi_n)d\alpha \tag{8.8}$$

Eq. (8.8) may be put in a more compact form by introducing the notation

$$A(\alpha)=\sum_{n=1}^{N}\delta(\alpha-\xi_n) \tag{8.9}$$

thus, Eq. (8.8) becomes:

$$\Psi(\xi)=\int\psi(\xi-\alpha)A(\alpha)d\alpha \tag{8.10}$$

which is physically pleasing in the sense that $A(\alpha)$ characterizes the array itself. That is, $A(\alpha)$ describes the location of the apertures and $\psi(\xi)$ describes the distribution across a single aperture. We are in a position to calculate the far field or Fraunhofer diffraction pattern associated with the array. We have the theorem that the Fraunhofer pattern is the Fourier transform of the aperture distribution. Thus, the Fraunhofer pattern $\tilde{\Psi}(\mathrm{x})$ of the distribution $\Psi(\xi)$ is given by

$$\tilde{\Psi}(\mathrm{x})=\int\Psi(\xi)\exp\left(\frac{-2\pi i\xi\cdot\mathbf{x}}{\lambda \mathrm{f}}\right)d\xi \tag{8.11}$$

substituting from Eq. (8.10) gives:

$$\tilde{\Psi}(\mathrm{x})=\left[\iint\psi(\xi-\alpha)A(\alpha)d\alpha\right]\exp\left(\frac{-2\pi i\xi\cdot\mathbf{x}}{\lambda \mathrm{f}}\right)d\xi \tag{8.12}$$

A very important theorem of Fourier analysis states that the Fourier transform of a convolution is the product of the individual Fourier transforms [1]. Thus, Eq. (8.12) may be written as:

$$\tilde{\Psi}(\mathrm{x})=\tilde{\psi}(\mathrm{x})\tilde{A}(\mathrm{x}) \tag{8.13}$$

where $\tilde{\psi}(\mathrm{x})$ and $\tilde{A}(\mathrm{x})$ are the Fourier transforms of $\psi(\xi)$ and $A(\alpha)$. Eq. (8.13) is the array theorem and states that the diffraction pattern of an array of similar apertures is given by the product of the elemental pattern $\tilde{\psi}(\mathrm{x})$ and the pattern that would be obtained by a similar array of point sources, $\tilde{A}(\mathrm{x})$. Thus, the separation that first arose in Eq. (8.10) is retained. To analyze the complicated patterns that arise in interference problems of this sort, one may analyze separately the effects of the array and the effects of the individual apertures.

APPLICATIONS OF THE ARRAY THEOREM

TWO-SLIT INTERFERENCE (WAVE-PARTICLE DUALITY)

Photons superimpose such that in the far field, the emitted wave is a spherical wave where the total electric field is given by Eq. (4.23):

$$\mathbf{E}_{total}=E_0\frac{e^{-ikr}}{r} \tag{8.14}$$

which is shown by Bonham to be required in order to insure continuity of power flow for wavelets from a single source [2]. The Green Function, (Eq. (6.62) of Jackson [3]) is given as the solution of the wave equation (Eq. (6.58) of Jackson [3]). Thus, the superposition of photons gives the classical result. As r goes to infinity, the spherical wave given by Eq. (8.14) or Eq. (4.23) becomes a plane wave. The double slit interference pattern is derived in Eqs. (8.15-8.23). From the equations of a photon given in the Equation of the Photon section, the wave-particle duality arises naturally. The energy is always given by Planck's equation as also shown in the Equation of the Photon section; yet, an interference pattern is observed when photons add over time or space.

Similarly, rather than a point, the electron is an extended particle which may impinge on a double slit one electron at a

time. As shown in the Electron in Free Space section, the ionized electron is a plane-lamina disc of charge (mass)-density given by Eqs. (3.7-3.8) and current (momentum)-density given by Eqs. (3.19) and (3.20) with a radius ρ_0 such that $2\pi\rho_0 = \lambda_0$ wherein λ_0 is the de Broglie wavelength. In the case that the electron de Broglie wavelength (Eq. (3.24)) and therefore the size of the electron is comparable to the slit size and/or separation, the resulting intensity pattern of electrons striking a detector beyond the slits is equivalent to a wave interference pattern. This result arises even though the electrons are not physically interacting with each other. Nothing is actually interfering. As in the case of the photon, the wave-particle duality nature of the electron arises classically.

The electron-slit interaction is mediated by photons, each of which have quantized angular momentum in units of $\hbar$. This angular momentum and the $\hbar$ of angular momentum of the electron is conserved during the interaction such that the de Broglie relationship holds as given in the Classical Physics of the de Broglie Relationship section. For photon diffraction, the $\hbar$ of angular momentum of the photon is conserved during an interaction directly. In each case, the pattern in the far-field is a map of the conserved momentum density of the particles incident on the slit or slits.

We use Eq. (8.13) to describe the simplest of interference experiments, Young's double-slit experiment in one dimension. The individual aperture will be described by

$$\Psi(\xi) = (C \quad |\xi| < a; \qquad 0 \quad |\xi| > a) = rec(\xi \,|\, a) \tag{8.15}$$

Here C is a constant representing the amplitude transmission of the apertures. This is essentially a one-dimensional problem and the diffraction integral may be written as

$$\tilde{\Psi}(\mathrm{x}) = \int \Psi(\xi) \exp\left(\frac{-ik\xi\cdot\mathbf{x}}{\mathrm{f}}\right) d\xi = C\int_{-a}^{a} \exp\left(\frac{-ik\xi\cdot\mathbf{x}}{\mathrm{f}}\right) d\xi \tag{8.16}$$

The integral in Eq. (8.16) is readily evaluated to give:

$$\tilde{\Psi}(\mathrm{x}) = \frac{-Cf}{ik\mathrm{x}}\left[\exp\left(\frac{-ika\mathrm{x}}{\mathrm{f}}\right) - \exp\left(\frac{+ika\mathrm{x}}{\mathrm{f}}\right)\right] = 2aC\,\frac{\sin\left(\frac{ka\mathrm{x}}{\mathrm{f}}\right)}{\left(\frac{ka\mathrm{x}}{\mathrm{f}}\right)} \tag{8.17}$$

The notation $\mathrm{sinc}\,\theta = \dfrac{\sin\theta}{\theta}$ is frequently used and in terms of this function $\tilde{\Psi}(\mathrm{x})$ may be written as:

$$\tilde{\Psi}(\mathrm{x}) = 2aC\ \mathrm{sinc}\left(\frac{ka\mathrm{x}}{\mathrm{f}}\right) \tag{8.18}$$

Thus, the result is that the elemental distribution in the Fraunhofer plane is Eq. (8.18). The array in this case is simply two delta functions; thus,

$$A(\xi) = \delta(\xi - b) + \delta(\xi + b) \tag{8.19}$$

The array pattern is, therefore,

$$\tilde{A}(\mathrm{x}) = \int\left[\delta(\xi - b) + \delta(\xi + b)\right]\exp\left(\frac{-2\pi i\xi\cdot\mathbf{x}}{\lambda\mathrm{f}}\right) d\xi \tag{8.20}$$

Eq. (8.20) is readily evaluated by using the combining property of the delta function, thus,

$$\tilde{A}(\mathrm{x}) = \exp\left(\frac{2\pi ib\mathrm{x}}{\lambda\mathrm{f}}\right) + \exp\left(\frac{-2\pi ib\mathrm{x}}{\lambda\mathrm{f}}\right) = 2\cos\left(\frac{2\pi b\mathrm{x}}{\lambda\mathrm{f}}\right) \tag{8.21}$$

Finally, the diffraction pattern of the array of two slits is:

$$\tilde{\Psi}(\mathrm{x}) = 4aC\ \mathrm{sinc}\left(\frac{2\pi a\mathrm{x}}{\lambda\mathrm{f}}\right)\cos\left(\frac{2\pi b\mathrm{x}}{\lambda\mathrm{f}}\right) \tag{8.22}$$

The intensity is

$$I(\mathrm{x}) = 16a^2C^2\mathrm{sinc}^2\left(\frac{2\pi a\mathrm{x}}{\lambda f}\right)\cos^2\left(\frac{2\pi b\mathrm{x}}{\lambda f}\right) \tag{8.23}$$

From Eq. (8.23), it is clear that the resulting pattern has the appearance of cosine-squared fringes of period $\lambda f / b$ with an envelope $\mathrm{sinc}^2\left(2\pi a\mathrm{x} / \lambda f\right)$.

In the case of photon diffraction, the far field interference pattern given by Eqs. (8.22-8.23) is due to conservation of angular momentum of the photon interaction with the slits. The pattern is not due to constructive and destructive interference of photon electric fields. Photons cannot be created or destroyed by superimposing. If this were true, it would be possible to cool a room or to cloak an object by illumination. Constructive and destructive interference violates the first and second laws of thermodynamics[1]. The correct physics is based on conservation of the $\hbar$ of photon angular momentum and $\hbar\omega$ of photon energy.

The incident photons have a size comparable to their wavelength as given in the Equation of the Photon section. A

[1] Similarly, the constructive and destructive interference of probability waves makes no sense. Nor does negative probability or probability that is based on noncausality. The interference pattern is a map of the momentum density. This physical basis applies to photon and particle diffraction as given *infra.* wherein the particle, photon, and consequently the slit interaction is quantized in units of $\hbar$. The double-slit experiment is predicted by classical laws that dispel the belief that quantum weirdness must be invoked to explain the double-slit experiment.

diffraction pattern is observed when the slit dimensions are comparable to the photon wavelength. The physical basis of the mechanism is that each photon interacts with the slit apparatus to give rise to an electron or polarization current. Each photon is reemitted, and the regions of high and low intensity due to more or less photons impinging at locations of the detector are generated, as the number of photons diffracted grows large. The pattern is based on conservation of the momentum of the slit-source currents and re-emitted photon distribution. Here, in the case of each incident and diffracted photon, the transverse displacement is related to the change in the transverse component of the angular momentum of the photon. The corresponding pattern is representative of the aggregate momentum distribution of slit-apparatus current induced by many photon interactions. The same physics of momentum conservation in the electric and magnetic radiation fields determines the radiation pattern of a multipole source as given in the Excited States of the One-Electron Atom (Quantization) section. Photon diffraction is shown schematically in Figure 8.1.

Figure 8.1. (A) The incident photon is emitted from a source and travels to the slit apparatus in the distance. The photon's electric and magnetic fields are confined on its two-dimensional surface. (B) The photon contacts the double slit apparatus. (C) The photon's electric and magnetic fields give rise to electron or polarization currents at both slits (blue). As in the case with the application of a voltage to an object, there is an effect at a distance. The transition of the photon's fields from incident to transmitted is shown translucently. (D) The slit's currents cause reemission of a photon in the direction of the detector in the far field. (E) The transverse displacement of the reemitted photon conserves the angular momentum of the source current. The superposition of reemitted photons from the interaction of many incident photons over time forms a photon field characteristic of the slits as their source. The source is equivalent to a uniform-electric-field silhouette of the slits given by Eqs. (8.15) and (8.19). (F) In the far field, the distribution of photons corresponding to the intensity pattern is the Fourier transform of the slit pattern.

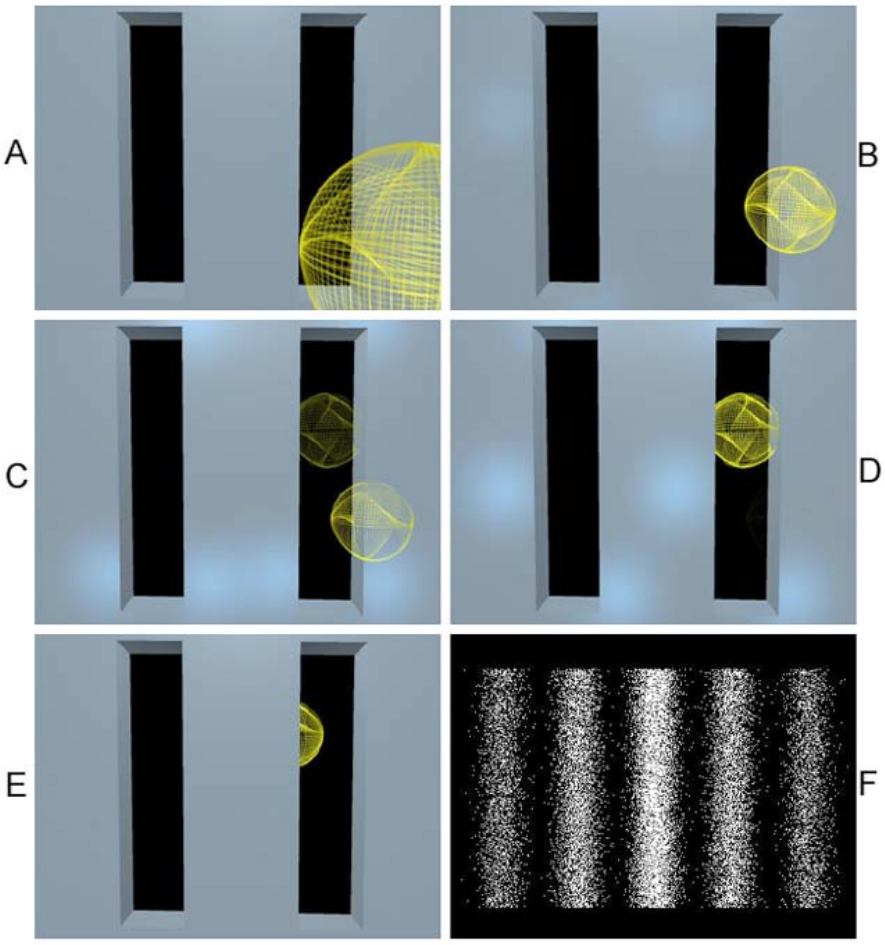

Eq. (8.22) also applies to two-slit diffraction of other particles as well as photons wherein the amplitude reflects the transverse momentum density of the particles. The proton and neutron as well as photons and electrons demonstrate interference patterns during diffraction. An example is the interference pattern for rubidium atoms given in the Wave-Particle Duality is Not Due to the Uncertainty Principle Section. Particle-particle interactions may be involved, and in other cases the interference pattern arises without fundamental-particle-particle interaction. In these cases, the pattern-generating interaction can be attributed to that between the particle and the diffraction apparatus with conservation of the angular momentum of the particle and any photons involved in mediating the interaction wherein even neutral particles such as neutrons comprise charged sub-

particles such as quarks and also possess magnetic moments that can give rise to induced electrodynamic currents and fields of a scatterer during interaction.

Conservation of the photon's angular momentum of $\hbar$ gives rise to the de Broglie relationship of the electron as given in the Classical Physics of the de Broglie Relationship section. This result also applies to other fundamental particles. Since all particle-slit interactions are mediated by photons, and the angular momentum change must be conserved in the far-field, the corresponding amplitude function that arises from the electron-aperture function is equivalent to that of a corresponding photon-front aperture function. Both amplitude functions are given by Eq. (8.22).

In Michelson interferometry, photons interact with the optical elements wherein the velocity is slower than free space. There is dispersion in velocity based on phase such that photons speed up and slow down relative to each other and are bunched to create a pattern of concentration or compression and rarefaction of photon spatial density over each period of the incident electromagnetic wave. The redistribution is observed as dark and light bands that repeat every photon wavelength based on the periodicity of the light wave comprising an ensemble of photons. The distribution pattern observed with diffracting electrons is equivalent to that for diffracting light. Note that Eq. (8.16) represents a plane wave. In the case of the Davison-Germer experiment, the intensity is given by Eq. (8.13) as the product of the Fourier transforms of the elemental pattern corresponding to a plane wave of wavelength $\lambda = h/p$ and the array pattern of the nickel crystal.

In general, the observed far-field position distribution is a picture of the particle transverse momentum distribution after the interaction. As shown in the Classical Wave Theory of Electron Scattering section, the phase of the amplitude of the angular-momentum-distribution function contains the term $(\mathbf{k}_i - \mathbf{k}_s)\cdot\mathbf{r}_l$, where $\mathbf{k}_i - \mathbf{k}_s$ is proportional to the momentum change of the incident particle upon scattering, since $\hbar\mathbf{k}_i$ is the initial momentum and $\hbar\mathbf{k}_s$ is the final momentum of the scattered particle such as an electron. The wavelength, λ, is the de Broglie wavelength associated with the momentum of the particle which is transferred through interactions corresponding to the wavenumber $k = \frac{2\pi}{\lambda}$. Since the two-slit aperture pattern is the convolution of the single-slit pattern with two delta functions, the intensity of the two-slit experiment is given as cosine squared fringes of the single-slit pattern as given by Eq. (8.23) wherein the extended particle interacts with both slits with conservation of momentum to give the modulation of the single-slit momentum pattern.

The energy is proportional to the square of the momentum. The conservation of power flow requires that the intensity distribution representing the number of particles incident on the detector at a given position is given by the amplitude of the momentum-distribution function squared.

During electron diffraction, the initially unpolarized electron becomes polarized to minimize the energy of interaction with the slit such that the angular momentum of the polarized free electron is parallel or antiparallel to the direction of propagation. If the forward momentum is unchanged, then the electron is detected at $\mathrm{x} = 0$ in the far field. However, the interaction with the slit can cause momentum transfer to the transverse direction that can be mediated by photons having $\hbar$ of angular momentum. Each photon provides a torque to change the direction of the angular momentum vector; concomitantly, the linear momentum is redirected to have a transverse component. The momentum transfer from the z-axis to the transverse or x-axis in the far field depends on the strength and the time duration of a photon-generated torque as given in the Stern-Gerlach Experiment subsection of the Free Electron section. The spatial distribution of the electron positions is determined by the conservation of momentum. With sufficient application of torque the angular momentum vector is reversed. The interaction of the free electron with the slit to reverse the angular momentum corresponds to a sign change of the amplitude, and periodic reversals of the angular momentum gives rise to maximum and minima of the amplitude. Since the magnitude of the angular momentum change depends on the strength and duration of the torque, which has a finite half-life, the amplitude decreases steeply as a function of transverse momentum.

CLASSICAL WAVE THEORY OF ELECTRON SCATTERING

The following mathematical development of scattering is adapted from Bonham [4] with the exception that the CP model is a Fourier optics derivation for an exact elemental pattern, a plane wave, and an exact array pattern, an atomic orbital. In contrast, Bonham derives similar scattering equations for an incident plane wave via an averaged probability density function description of the electron, the Born model.

In scattering experiments in which Fraunhofer diffraction is the most important mode for scattering, measurements are made in momentum or reciprocal space. The data is then transformed in terms of real space, where the structure of the scatterer is expressed in terms of distances from its center of mass. There are, fortunately, well known mathematical techniques for making this transformation. If we are given a model of the scattering system, we can, in general, uniquely calculate the results to be expected in reciprocal space for scattering from the model. Unfortunately, the converse—deducing the nature of the scatterer uniquely by transforming the experimental results obtained in reciprocal space—is not always possible. But, as we will see, certain possibilities can be eliminated because they violate fundamental physical laws such as Special Relativity.

In classical optics, a diffraction pattern results whenever light is scattered by a slit system whose dimensions are small compared to the wavelength of light. In order to develop a mathematical model for diffraction scattering, let us represent the amplitude of an incident plane wave traveling from left to right as $e^{i(\mathbf{k}\cdot\mathbf{r}-\omega t)}$, where the absolute magnitude of the wave vector $\mathbf{k}$ is $|\mathbf{k}| = \frac{2\pi}{\lambda}$. The quantity λ is the wavelength of the incident radiation and $\hbar\mathbf{k}$ is the momentum $\mathbf{p}$. The vector $\mathbf{r}$ represents the position in real space at which the amplitude is evaluated, and ω and t are the angular frequency and time, respectively. A

plane wave traveling in the opposite direction is $e^{-i(\mathbf{k}\cdot\mathbf{r}+\omega t)}$ where the sign of $\mathbf{k}\cdot\mathbf{r}$ changes, but not the sign of t. That is, we may reflect a wave from a mirror and reverse its direction, but we cannot change the sign of the time since that would indicate a return to the past. The intensity of a classical wave is the square magnitude of the amplitude, and thus the intensity of a plane wave is constant in space and time. If a plane wave is reflected back on itself by a perfectly reflecting mirror, then the resultant amplitude is $e^{i(\mathbf{k}\cdot\mathbf{r}-\omega t)}+e^{-i(\mathbf{k}\cdot\mathbf{r}+\omega t)}=e^{-i\omega t}2\cos\mathbf{k}\cdot\mathbf{r}$, and the intensity is $I=4\cos^2\mathbf{k}\cdot\mathbf{r}e^{i\omega t}e^{-i\omega t}$ which is independent of time and given as $4\cos^2\mathbf{k}\cdot\mathbf{r}$ which clearly exhibits maxima and minima dictated by the wavelength of the radiation and the position in space at which intensity is measured.

In an experiment, we measure the intensity of scattered particles, which is related to plane waves in a simple fashion. To see this, consider a collimated plane-wave source, whose width is small compared to the scattering angle region where the scattering is to be investigated, incident upon a diffraction grating. If we integrate the incident intensity over a time interval Δt, we obtain a number proportional to the energy content of the incident wave. We may safely assume in most cases that the scattering power of the diffraction image does not change with time, so that a constant fraction of the incident radiation and hence constant energy will be transferred into the scattered wave. We further assume that the effect of the diffraction grating on the incident radiation occurs only in a region very close to the grating in comparison to its distance from the detection point. For elastic scattering (no energy transfer to the grating), once the scattered portion of the wave has left the field of influence of the scatterer, all parts of the scattered amplitude at the same radial distance from the scatterer must travel at the velocity of the incident wave. For simplicity, we neglect resonance effects, which can introduce significant time delays in the scattering process even if the waves are scattered elastically. The effects of resonance states on the scattering at high energies, is usually negligible and hence will not be discussed here. In the case of inelastic scattering, in which waves are scattered with various velocities, we can focus our attention successively on parts of the outgoing scattered radiation that have velocities falling within a certain narrow band, and the following argument will hold for each such velocity segment. The result of the integration of a constant-velocity segment of the scattered intensity over the volume element,

$$\int_R^{R+\Delta R} r^2 dr \int_0^{\pi} \sin\theta d\theta \int_0^{2\pi} d\Phi \tag{8.24}$$

is proportional to the energy content in that portion of the scattered wave, and the result must be independent of R. This restriction, which is a direct consequence of conservation of energy, then demands that the outgoing scattered waves have in polar coordinates the form:

$$\Psi_{sc}(R,\theta,\phi)=\frac{e^{ikR}}{R}f(\theta,\phi) \tag{8.25}$$

where the term $1/R$ is a dilution effect to guarantee energy on an ever-spreading wave.

Ψ_{sc} only describes the scattered amplitude after the scattered wave has left the field of influence of the scatterer and is thus an asymptotic form. The function $f(\theta,\varphi)$ is called the scattered amplitude and depends on the nature of the scatterer. The classical theory tells us that the scattered intensity is proportional to the square magnitude of the scattered amplitude; so, the intensity will be directly proportional to $\frac{|f(\theta,\varphi)|^2}{R^2}$.

Let us next consider the expression for the scattering of a plane wave by a number of disturbances in some fixed arrangement in space. Consider the scatterers comprising a nucleus and electrons; this would correspond to a plane wave scattered by an atom.

We shall choose the center of mass of the scatterer as our origin and shall for the most part consider dilute-gas electron scattering in the keV energy range, where the electron wavelength λ lies in the range $0.03\ \text{Å}<\lambda<0.1\ \text{Å}$. The scattering experimental conditions are such that to a high degree of approximation, at least within 0.1% or better, we can consider the scattering as a single electron scattered by a single atom. Note also that no laboratory to center-of-mass coordinate system transformation is required because the ratio of the electron mass to the mass of the target will be on the order of 10^{-3} or smaller.

Let us consider an ensemble of scattering centers as shown in Figure 8.2.

Figure 8.2. An ensemble of scattering centers.

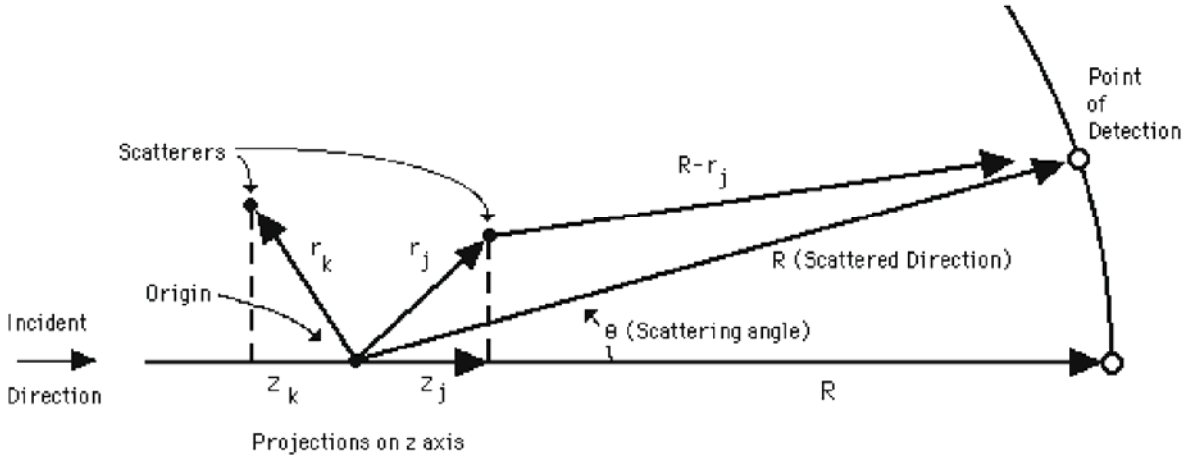

We may write the total scattered amplitude in the first approximation as a sum of amplitudes, each of which is produced by scattering from one of the single scattering centers. In this view, we generally neglect multiple scattering, the re-scattering of portions of the primary scattered amplitudes whenever they come in contact with other centers, except in the case of elastic scattering in the heavier atoms. Clearly a whole hierarchy of multiple-scattering processes may result. The incident wave may experience a primary scattering from one center, a portion of the scattered amplitude may re-scatter from a second center, and part of this amplitude may in turn be scattered by a third center (which can even be the first center), and so on.

An incident plane wave will obviously travel a distance along the incident direction before scattering from a particular center, depending on the instantaneous location of that center. To keep proper account of the exact amplitude and phase of the incident wave at the instant it scatters from a particular center, we select our origin, as mentioned previously, to lie at the center of mass. The phase of the scattered wave depends on the total distance traveled from the center of mass to the detector. We can now write the scattered amplitude as:

$$\Psi_{total} = \sum_{l=1}^{N} \left(\frac{\exp\left[ik\left(z_l + \left|\mathbf{R} - \mathbf{r}_l\right| \right) \right]}{\left|\mathbf{R} - \mathbf{r}_l\right|} \right) f_l\left(\theta, \phi\right) \tag{8.26}$$

where $z_l + \left|\mathbf{R} - \mathbf{r}_l\right|$ is the distance traveled from a plane perpendicular to the incident direction and passing through the center of mass and $f_l\left(\theta, \phi\right)$ is the scattered amplitude characteristic of the $l-th$ scattering center. It should be clear at this point that the term $\left(\frac{\exp\left[ik\left|\mathbf{R} - \mathbf{r}_l\right| \right]}{\left|\mathbf{R} - \mathbf{r}_l\right|} \right) f_l\left(\theta, \phi\right)$ is made up of a plane wave in the scattered direction with the dilution factor $\frac{1}{\left|\mathbf{R} - \mathbf{r}_l\right|}$ to account for energy conservation and with allowances made through $f_l\left(\theta, \phi\right)$ for any special influence that the scatterer may have on the scattering because of the detailed structure of the scatterer. The additional term e^{ikz_l} enters whenever two or more scattering centers are encountered and accounts for the fact that the instantaneous location of our scattering centers may not coincide with planes of equal amplitude of the incident plane wave. That is, in a two-center case, the first particle may scatter a plane wave of amplitude +1 while at the same time a second scatterer may encounter an amplitude of -1. The amplitudes of the incident plane wave which the various particles encounter depend on their separation from each other along the z-axis and on the wavelength of the incident radiation. By adding to the phase, the projections of the various $\mathbf{r}_l$ vectors onto the incident direction, referenced to the same origin, this problem is automatically corrected. As long as our composite scatterer is on the order of atomic dimensions, the magnitude of R will be enormously larger than either $\mathbf{z}_l$ or $\mathbf{r}_l$. This allows us to expand $\left|\mathbf{R} - \mathbf{r}_l\right|$ in a binomial expansion through first-order terms as $R - \left(\frac{\mathbf{R}}{\left|\mathbf{R}\right|} \cdot \mathbf{r}_l \right)$. In the denominator, the first-order correction term R can be neglected but not in the phase.

To see this, suppose that R is π X 10^6 and $\frac{\mathbf{R}}{\left|\mathbf{R}\right|} \cdot \mathbf{r}_l$ is $\pi/2$. Clearly $\pi/2$ would seem negligible compared to π X 10^6, but look what a difference the value of a sine or cosine function has if $\pi/2$ is retained or omitted from the sum of the two terms. The product kz_l may be rewritten as $\mathbf{k_i} \cdot \mathbf{r}_l$, where the subscript i on $\mathbf{k}$ denotes the fact that $\mathbf{k}_i$ is a vector parallel to the incident

direction magnitude $k = \frac{2\pi}{\lambda}$. Similarly, since $\frac{\mathbf{R}}{|\mathbf{R}|}$ is a unit vector whose sense is essentially in the direction of the scattered electron, we may write $k\frac{\mathbf{R}}{|\mathbf{R}|}\cdot\mathbf{r}_l$ as $\mathbf{k}_s\cdot\mathbf{r}_l$ where $\mathbf{k}_s$ is a wave vector in the scattering direction. The phase of Eq. (8.26) now contains the term $(\mathbf{k}_i - \mathbf{k}_s)\cdot\mathbf{r}_l$, where $\mathbf{k}_i - \mathbf{k}_s$ must be proportional to the momentum change of the incident particle on scattering, since $\hbar\mathbf{k}_i$ is the initial momentum and $\hbar\mathbf{k}_s$ is the final momentum of the scattered electron. This vector difference is labeled by the symbol $\mathbf{s}$. The asymptotic total amplitude is now expressible as:

$$\Psi_{total} = \frac{e^{ikR}}{R}\sum_{l=1}^{N} e^{i\mathbf{s}\cdot\mathbf{r}_l} f_l(\theta,\phi) \tag{8.27}$$

CLASSICAL WAVE THEORY APPLIED TO SCATTERING FROM ATOMS AND MOLECULES

Let us first apply Eq. (8.27) to scattering from atoms. We will consider the theoretical side of high-energy electron scattering and X-ray scattering from gaseous targets as well. In the X-ray case, the intensity for an X-ray scattered by an electron is found experimentally to be a constant, usually denoted by I_{cl}, which varies inversely as the square of the mass of the scatterer where I_{cl} is the Thompson X-ray scattering constant. This means that X-rays are virtually un-scattered by the nucleus, since the ratio of electron to nuclear scattering will be greater than $\left[\frac{m_p}{m_e}\right]^2 \cong \left[\frac{1X\ 10^{-24}}{9X10^{-28}}\right]^2 \sim 10^6$, where m_p is the proton rest mass and m_e is the electron rest mass. The total amplitude for X-ray scattering by an atom can then be written as:

$$\Psi_{total}^{\text{xr}} = \sqrt{I_{cl}}\ e^{i\eta_{cl}} e^{ikR}\sum_{l=1}^{N} e^{i\mathbf{s}\cdot\mathbf{r}_l} \tag{8.28}$$

where η_{cl} is a phase factor introduced because of a possibility that the X-ray scattered amplitude may be complex. The intensity can be written as:

$$I_{total}^{xr} = I_{cl}(N + \sum_{l\neq k}^{N}\sum_{l\neq k}^{N} e^{i\mathbf{s}\cdot\mathbf{r}_{l\,k}}) \tag{8.29}$$

where $\mathbf{r}_{lk} = \mathbf{r}_l - \mathbf{r}_k$ is an inter-electron distance. Both expressions, Eqs. (8.28) and (8.29), correspond to a fixed arrangement of electrons in space. For electrons, the intensity of scattering by another charged particle proceeds according to the Rutherford experimental law $I = \frac{I_e Z^2}{s^4}$, where Z is the charge of the scatterer and I_e is a characteristic constant. Note that both I_{cl} and I_e include the $\frac{1}{R^2}$ dilution factor and depend on the incident X-ray or electron beam flux I_0 and on the number N_0 of target particles per cubic centimeter in the path of the incident beam as the product $I_0 N_0$. We may take $f_l(\theta,\phi) = \sqrt{I_e}\left(\frac{Z}{s^2}\right)\exp\left[i\eta(Z)\right]$,where $\eta(Z)$ is again an unknown phase shift introduced because of the possibility that the amplitude may be complex. In the X-ray case for scattering by an atom, the intensity is independent of the phase η_{cl}, and we need not investigate it further. In electron scattering, this term is different for electrons and nuclei since they contain charges of opposite sign and usually different magnitude. The amplitude for this case is:

$$\Psi_{total}^{ed} = \sqrt{I_e}\left(\frac{e^{ikR}}{s^2}\right)\left[Ze^{(i\eta(Z)+i\mathbf{s}\cdot\mathbf{r}_n)} + \sum_{i=1}^{N} e^{(i\eta(-1)+i\mathbf{s}\cdot\mathbf{r}_i)}\right] \tag{8.30}$$

which for an atom simplifies further, since the nuclear position vector $\mathbf{r}_n$ is zero because the nucleus lies at the center of mass. The term $\eta(Z)$ is the nuclear phase and $\eta(-1)$ is the phase for scattering by an individual electron. The notation -1 signifies a unit negative charge on each electron as opposed to $+Z$ on the nucleus, where Z is the atomic number. The intensity with $\mathbf{r}_n = 0$ becomes:

$$I_{total}^{ed} = \left(\frac{I_e}{s^4}\right)\{Z^2 + 2Z\sum_{i=1}^{N}\cos[\eta(Z) - \eta(-1) - \mathbf{s}\cdot\mathbf{r}_i] + N + \sum_{i\neq j}^{N}\sum_{i\neq j}^{N} e^{i\mathbf{s}\cdot\mathbf{r}_{i\,j}}\} \tag{8.31}$$

Note that the last two terms on the right in Eq. (8.31) are identical to those in Eq. (8.29).

According to Huygens' principle, the function $\sum_{i=1}^{N} e^{i\mathbf{s}\cdot\mathbf{r}_i}$ of Eq. (8.30) represents the sum over each spherical wave source arising from the scattering of an incident plane wave from each point of the electron function where the wavelength of the incident plane wave is given by the de Broglie equation $\lambda = h/p$. The sum is replaced by the integral over ρ and ϕ of the single point element aperture distribution function. The single point element aperture distribution function, $a(\rho,\phi,z)$, for the

scattering of an incident plane wave by an atom is given by the convolution of a plane wave function with the electron atomic orbital function. The convolution is $a(\rho,\phi,z)=\pi(z)\otimes[\delta(r-r_0)]Y_\ell^m(\theta,\phi)$ where $a(\rho,\phi,z)$ is given in cylindrical coordinates, $\pi(z)$, the xy-plane wave is given in Cartesian coordinates with the propagation direction along the z-axis, and the atomic orbital function, $[\delta(r-r_0)]Y_\ell^m(\theta,\phi)$, is given in spherical coordinates. Using cylindrical coordinates,

$$\sum_{i=1}^{N} e^{i\mathbf{s}\cdot\mathbf{r}_i}=\int_0^\infty\int_0^{2\pi}\int_{-\infty}^{\infty} a(\rho,\phi,z)e^{-i[s\rho\cos(\phi-\Phi)+wz]}\rho^2\rho d\rho d\phi dz \tag{8.32}$$

The general Fourier transform integral is given in reference [5].

For an aperture distribution with circular symmetry, $F(s)$, the Fourier transform of the aperture array distribution function, $A(z)$, is [5]:

$$\sum_{i=1}^{N} e^{i\mathbf{s}\cdot\mathbf{r}_i}=2\pi\int_0^\infty\int_{-\infty}^{\infty} a(\rho,z)J_0(s\rho)e^{-iwz}\rho d\rho dz \tag{8.33}$$

$$=\int_0^\infty A(z)e^{-iwz}dz \tag{8.34}$$

$$=F(s) \tag{8.35}$$

The same derivation applies for the two-point term $\sum_{i\neq j}^{N}\sum_{i\neq j}^{N} e^{i\mathbf{s}\cdot\mathbf{r}_{ij}}$ of Eq. (8.31). The sum is replaced by the integral over ρ and ϕ of the single point element autocorrelation function, $\mathsf{r}(\rho,\phi,z)$, of the single point element aperture distribution function. For circular symmetry [5] :

$$\mathsf{r}(\rho,\phi,z)=a(\rho,\phi,z)\otimes a(\rho,\phi,z) \tag{8.36}$$

and

$$\sum_{i\neq j}^{N}\sum_{i\neq j}^{N} e^{i\mathbf{s}\cdot\mathbf{r}_{ij}}=2\pi\int_0^\infty\int_{-\infty}^{\infty}\mathsf{r}(\rho,z)J_0(s\rho)e^{-iwz}\rho d\rho dz \tag{8.37}$$

$$=\int_0^\infty R(z)e^{-iwz}dz \tag{8.38}$$

and

$$R(z)=A(z)A(z) \tag{8.39}$$

For closed shell atoms in single states such as rare gases, $Y(\theta,\phi)$, the spherical harmonic angular function of the electron function is a constant, and only two expressions are possible from all orders of averaging over all possible orientations in space. For the X-ray case the scattered intensities are:

$$I_1^{xr}=I_{cl}[\int_0^\infty A(z)e^{-iwz}dz]^2=I_{cl}F(s)^2 \tag{8.40}$$

and

$$I_2^{xr}=I_{cl}[N+\int_0^\infty R(z)e^{-iwz}dz] \tag{8.41}$$

while for electrons, the scattered intensities are:

$$I_1^{ed}=\left[\frac{I_e}{s^4}\right]\{Z^{2+}2Z\cos[\eta(Z)-\eta(-1)]F(s)+F(s)^2\} \tag{8.42}$$

and

$$I_2^{ed}=\left[\frac{I_e}{s^4}\right]\{Z^2+2Z\cos[\eta(Z)-\eta(-1)]F(s)+N+\int_0^\infty R(z)e^{-iwz}dz\} \tag{8.43}$$

where the subscript 1 denotes an amplitude derivation and 2 an intensity derivation. The aperture function of the nucleus is a delta function of magnitude Z, the nuclear charge. The Fourier transform is a constant of magnitude Z as appears in Eqs. (8.42) and (8.43). Note that the Fourier convolution theorem proves the equivalence of Eq. (8.40) and Eq. (8.41) and the equivalence of Eq. (8.42) and Eq. (8.43).

The aperture array distribution function, $A(z)$, Eq. (8.34), corresponds to the electron radial distribution function of Bonham, and the aperture array autocorrelation function $R(z)$, Eq. (8.38), corresponds to the electron pair correlation function of Bonham [4].

ELECTRON SCATTERING EQUATION FOR THE HELIUM ATOM BASED ON THE ATOMIC ORBITAL MODEL

The closed form solution of all two electron atoms is given in the Two Electron Atom section. In the helium ground state, both electrons atomic orbitals are at a radius where:

$$r_1 = 0.567a_0 \tag{8.44}$$

The helium atom comprises a central nucleus of charge $+2e$ which is at the center of an infinitely thin spherical shell comprising two bound electrons of $-2e$. Thus, the helium atom is neutrally charged, and the electric field of the atom is zero for $r > 0.567a_0$. The Rutherford scattering equation for isolated charged particles does *not* apply. The appropriate scattering equation for helium in the ground state can be derived as a Fourier optics problem as given in the Classical Scattering of Electromagnetic Radiation section. The incident plane-wave free electron given in the Electron in Free Space section scatters from the helium atom by time-symmetrically deforming onto and from the surface of the helium atom as shown in Figure 8.3 such that the far field intensity pattern of many electrons is modeled by Huygens's Principle.

Figure 8.3. The time-symmetrical elastic scattering behavior of a free electron from a helium atom.

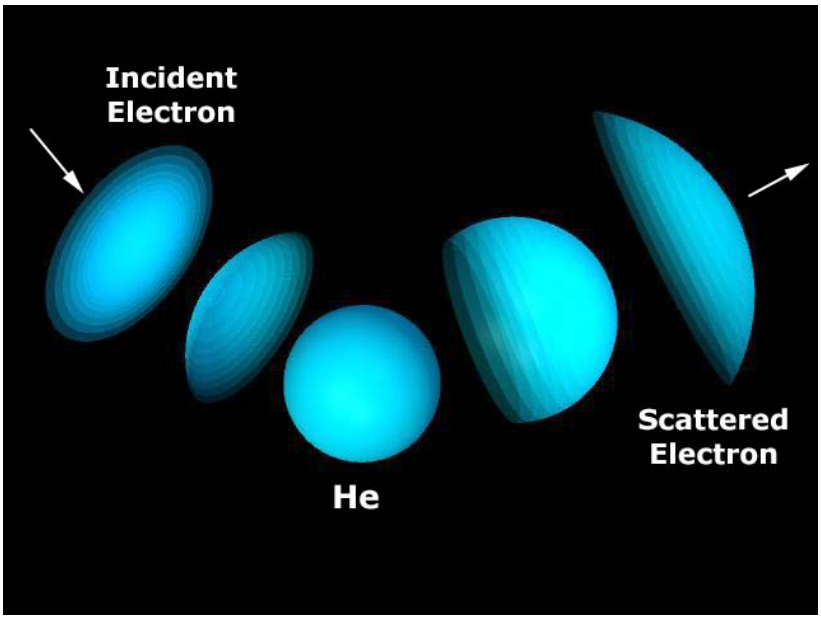

The aperture distribution function, $a(\rho,\phi,z)$, for the scattering of an incident plane wave by the He atom is given by the convolution of the plane wave function with the two electron atomic orbital Dirac delta function of $radius = 0.567a_0$ and charge/mass density of $\frac{2}{4\pi(0.567a_0)^2}$. For radial units in terms of a_0

$$a(\rho,\phi,z) = \pi(z) \otimes \frac{2}{4\pi(0.567a_0)^2}[\delta(r - 0.567a_0)] \tag{8.45}$$

where $a(\rho,\phi,z)$ is given in cylindrical coordinates, $\pi(z)$, the xy-plane wave is given in Cartesian coordinates with the propagation direction along the z-axis, and the He atom atomic orbital function, $\frac{2}{4\pi(0.567a_0)^2}[\delta(r - 0.567a_0)]$, is given in spherical coordinates.

$$a(\rho,\phi,z) = \frac{2}{4\pi(0.567a_0)^2}\sqrt{(0.567a_0)^2 - z^2}\,\delta(r - \sqrt{(0.567a_0)^2 - z^2}) \tag{8.46}$$

For circular symmetry [5],

$$F(s) = \frac{2}{4\pi(0.567a_0)^2} 2\pi \int_0^{\infty}\int_{-\infty}^{\infty} \sqrt{(0.567a_0)^2 - z^2}\,\delta(\rho - \sqrt{(0.567a_0)^2 - z^2})J_0(s\rho)e^{-iwz}\rho d\rho dz \tag{8.47}$$

Eq. (8.47) may be expressed as:

$$F(s) = \frac{4\pi}{4\pi(0.567a_0)^2}\int_{-z_0}^{z_0}(z_0^2 - z^2)J_0(s\sqrt{z_0^2 - z^2}))e^{-iwz}dz \;\; ; \;\; z_0 = 0.567a_0 \tag{8.48}$$

Substitute $\frac{z}{z_0} = -\cos\theta$

$$F(s) = \frac{4\pi z_0^2}{4\pi z_0^2}\int_0^{\pi} \sin^3\theta J_0(sz_0\sin\theta)e^{iz_0 w\cos\theta}d\theta \tag{8.49}$$

Substitution of the recurrence relationship,

$$J_0(\mathrm{x}) = \frac{2J_1(\mathrm{x})}{\mathrm{x}} - J_2(\mathrm{x}) \;\; ; \;\; \mathrm{x} = sz_0\sin\theta \tag{8.50}$$

into Eq. (8.49), and, using the general integral of Apelblat [6] :

$$\int_0^{\pi} (\sin\theta)^{\upsilon+1} J_{\upsilon}(b\sin\theta)e^{ia\cos\theta}d\theta = \left[\frac{2\pi}{a^2+b^2}\right]^{\frac{1}{2}}\left[\frac{b}{a^2+b^2}\right]^{\upsilon} J_{\upsilon+1/2}\left[(a^2+b^2)^{\frac{1}{2}}\right] \tag{8.51}$$

with $a = z_0 w$ and $b = z_0 s$ gives:

$$F(s) = \left[\frac{2\pi}{(z_0 w)^2 + (z_0 s)^2}\right]^{\frac{1}{2}}$$

$$\left\{2\left[\frac{z_0 s}{(z_0 w)^2 + (z_0 s)^2}\right] J_{3/2}\left[((z_0 w)^2 + (z_0 s)^2)^{1/2}\right] - \left[\frac{z_0 s}{(z_0 w)^2 + (z_0 s)^2}\right]^2 J_{5/2}\left[((z_0 w)^2 + (z_0 s)^2)^{1/2}\right]\right\} \tag{8.52}$$

The magnitude of the single point element autocorrelation function, $|\mathrm{r}(\rho,\phi,z)|$, is given by the convolution of the magnitude of the single point element aperture distribution function, $a(\rho,\phi,z)$, with itself.

$$|\mathrm{r}(\rho,\phi,z)| = |a(\rho,\phi,z)| \otimes |a(\rho,\phi,z)| \tag{8.53}$$

The Fourier convolution theorem permits Eq. (8.53) to be determined by Fourier transformation.

$$|\mathrm{r}(\rho,\phi,z)| = \int_0^{\infty} e^{i\mathbf{w}\bullet\mathbf{z}}\left[\int_0^{\infty}\sqrt{\left(0.567a_0\right)^2 - z^2}\,e^{-i\mathbf{w}\bullet\mathbf{z}}dz\right]^2 dw \tag{8.54}$$

$$|\mathrm{r}(\rho,\phi,z)| = -e^{i\pi}\left\{\int_0^{\infty}\sin\left(\mathbf{w}\bullet\mathbf{z}\right)\left[\frac{J_1\left(0.567a_0 w\right)}{w}\right]^2 dw\right\} + C \tag{8.55}$$

where C is an integration constant for which $R(\rho)$ equals zero at $r = 1.134a_o$

$$\left|\mathrm{r}(\rho,\phi,z)\right| = \left[\frac{1}{2} - \left(\frac{4z_0}{3\pi}\right)\left[\left(1+\frac{z^2}{4z_0^2}\right)E\left(\frac{z}{2z_0}\right) + \left(1-\frac{z^2}{4z_0^2}\right)K\left(\frac{z}{2z_0}\right)\right]\right] + C \tag{8.56}$$

$$0 < z \le 2z_0;\; z_0 = 0.567a_0$$

Eq. (8.56) was derived from a similar transform by Bateman [7]. The electron elastic scattering intensity is given by a constant times the square of the amplitude given by Eq. (8.52).

$$I_1^{ed} = I_e\left\{\begin{array}{l}\left[\dfrac{2\pi}{(z_0 w)^2 + (z_0 s)^2}\right]^{\frac{1}{2}} \\ \left\{2\left[\dfrac{z_0 s}{(z_0 w)^2 + (z_0 s)^2}\right] J_{3/2}\left[((z_0 w)^2 + (z_0 s)^2)^{1/2}\right] - \left[\dfrac{z_o s}{(z_0 w)^2 + (z_0 s)^2}\right]^2 J_{5/2}\left[((z_0 w)^2 + (z_0 s)^2)^{1/2}\right]\right\}\end{array}\right\}^2 \tag{8.57}$$

$$s = \frac{4\pi}{\lambda}\sin\frac{\theta}{2};\; w = 0 \;(\textit{units of } \mathring{A}^{-1}) \tag{8.58}$$

RESULTS

The magnitude of the single point element aperture distribution function, $a(\rho,\phi,z)$, convolved with the function $\delta(z-0.567a_0)$ is shown graphically in Figure 8.4 in units of a_0. The function was normalized to 2.

The magnitude of the single point element autocorrelation function, $\mathsf{r}(\rho,\phi,z)$, convolved with the function $\delta(z-1.134a_0)$ is shown graphically in Figure 8.5 in units of a_0. The function was normalized to 2 and the constant of 0.352183 was added to meet the boundary condition for the convolution integral.

The experimental setup for the measuring the intensity of elastically scattered 500 eV electrons from an atomic beam of helium is shown in Figure 8.6.

The experimental results of Bromberg [8], the extrapolated experimental data of Hughes [8], the small angle data of Geiger [9], and the semi-experimental results of Lassettre [8] for the elastic differential cross section for the elastic scattering of electrons by helium atoms are shown graphically in Figure 8.7. The elastic differential cross section as a function of angle numerically calculated by Khare [8] using the first Born approximation and first-order exchange approximation also appear in Figure 8.7.

Figure 8.4. The magnitude of the single point element aperture distribution function, $a(\rho,\phi,z)$, convolved with the function $\delta(z-0.567a_0)$ in units of a_0.

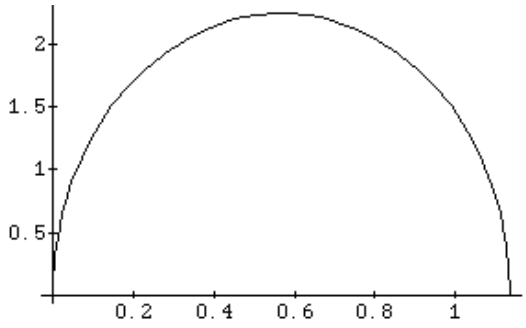

Figure 8.5. The magnitude of the single point element autocorrelation function, $\mathsf{r}(\rho,\phi,z)$, convolved with the function $\delta(z-1.134a_0)$ is shown graphically in units of a_0.

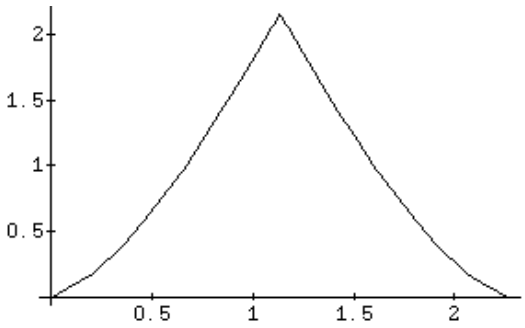

Figure 8.6. The incident electron and electron beams intersect and the scattered free electrons are detected in the far field.

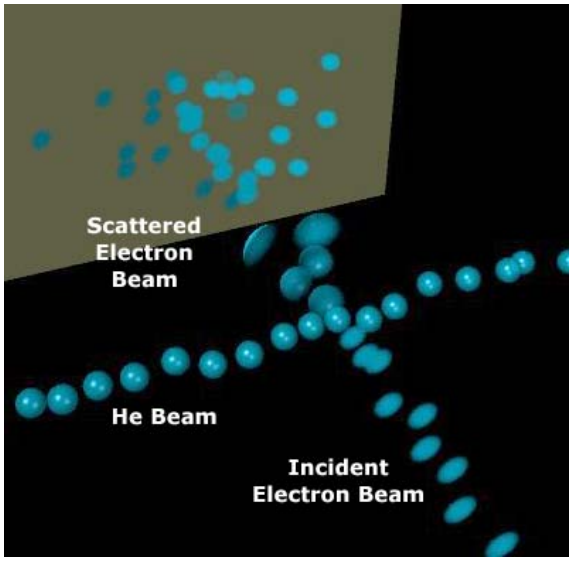

Figure 8.7. The experimental results of Bromberg [8], the extrapolated experimental data of Hughes [8], the small angle data of Geiger [9], and the semi-experimental results of Lassettre [8] for the elastic differential cross section for the elastic scattering of electrons by helium atoms and the elastic differential cross section as a function of angle numerically calculated by Khare [8] using the first Born approximation and first-order exchange approximation.

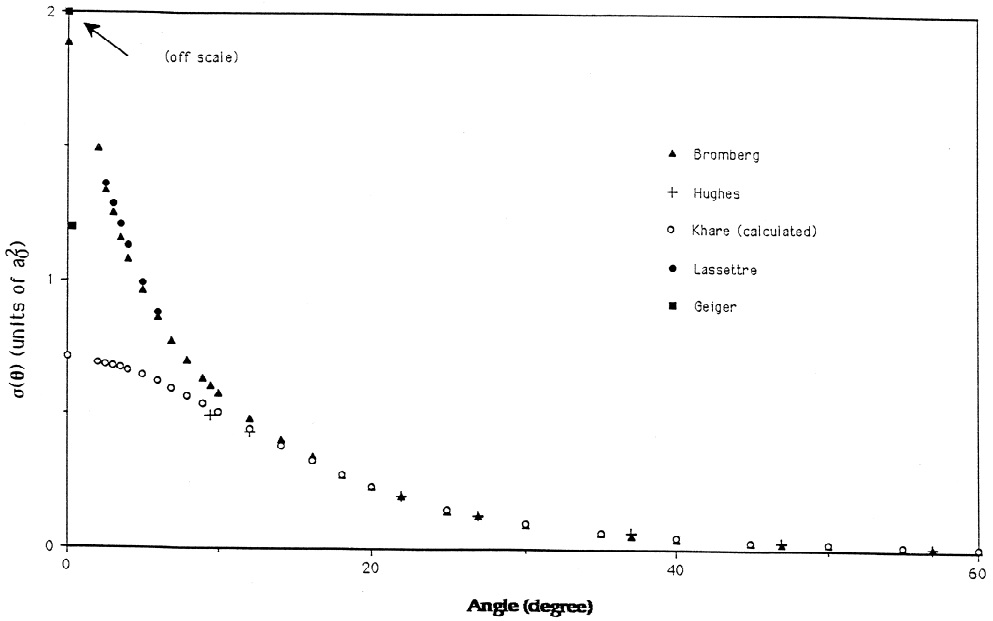

These results, which are based on a quantum mechanical model, are compared with experimentation [8, 9]. The closed-form function (Eqs. (8.57) and (8.58)) for the elastic differential cross section for the elastic scattering of electrons by helium atoms is shown graphically in Figure 8.8. The scattering amplitude function, $F(s)$ (Eq. (8.52)), is shown as an insert.

Figure 8.8. The closed form function (Eqs. (8.57) and (8.58)) for the elastic differential cross section for the elastic scattering of electrons by helium atoms. The scattering amplitude function, $F(s)$ (Eq. (8.52)), is shown as an insert.

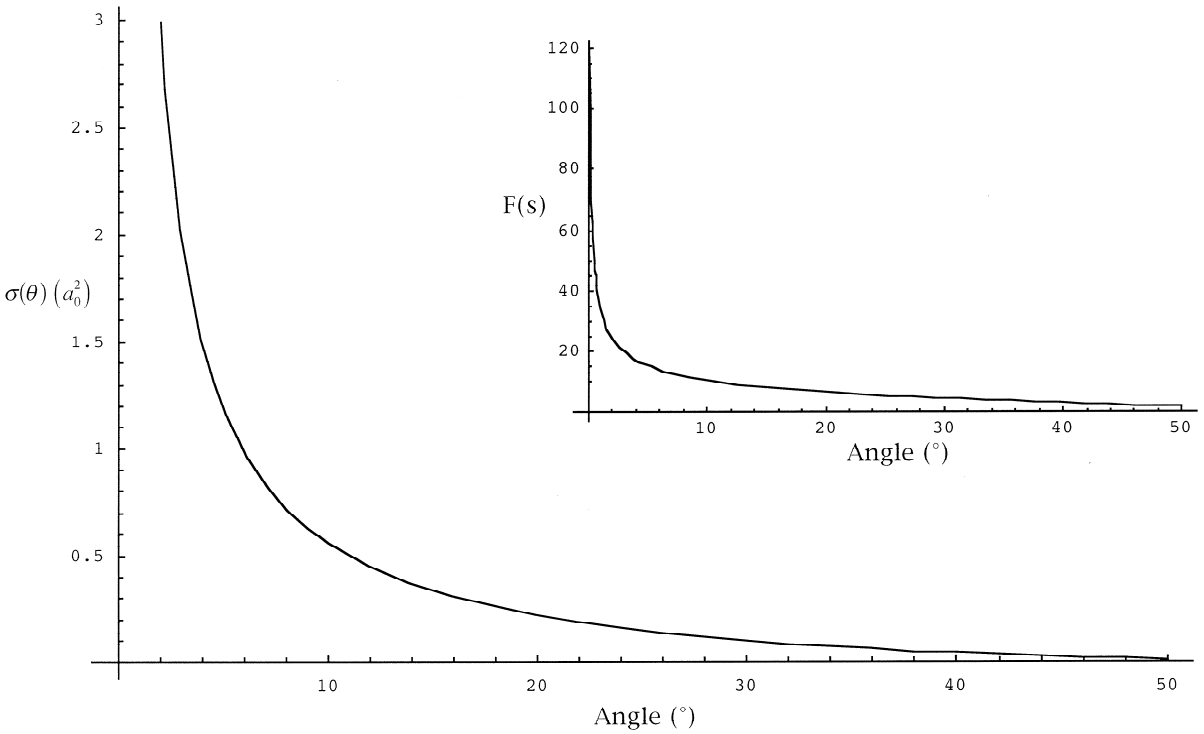

DISCUSSION

The magnitude of the single point element autocorrelation function, $\mathsf{r}(\rho,\phi,z)$, convolved with the function $\delta(z-1.134a_0)$ (Figure 8.5) and the electron pair correlation function, $P(r)$, of Bonham [10] are similar. According to Bonham [10], the electron radial distribution function, $D(r)$, calculated from properly correlated CI wave functions for He is similar in shape to the $P(r)$ function but its maximum occurs at a value of r almost exactly half of that for $P(r)$. Thus, the function $D(r)$ is similar to the magnitude of the single point element aperture distribution function, $a(r,\theta,z)$, (Figure 8.4). $D(r)$ and $P(r)$ lead to a most probable structure for the He atom in which the electrons and the nucleus are collinear with the nucleus lying between the two electrons [4]. This is an average picture that is an ad hoc modification of the true model involving a three-point-body atom and a point-particle incident electron for which it is impossible to get neutral scattering, let alone the observed pattern shown in Figure 8.7. Furthermore, even with this unjustified modification, it is apparent from Figure 8.7 that the modified quantum mechanical calculations fail completely at predicting the experimental results at small scattering angles; whereas, Eq. (8.57) predicts the correct scattering intensity as a function of angle. Another problem for the quantum mechanical model is that the helium wave equation used to calculate the scattering is not the solution of the Schrödinger equation for the helium atom that gives the correct ionization energy. Since it involves three bodies, the exact solution is impossible to be obtained. Many solutions have been obtained with great effort using various perturbation and adjustable-parameter methods as given by McQuarrie [11]. Such solutions are very dubious in that they are non-unique, not based on physical laws, and are better classified as curve fitting techniques in that they use up to 1000 adjustable parameters to obtain the ionization energy [11].

In the far field, the solution of the Schrödinger equation for the amplitude of the scattered plane wave incident on a three dimensional static potential field $U(r)$ is identical to Eq. (8.26) only if one assumes a continuous distribution of individual scattering points and replaces the sum over ℓ in Eq. (8.26) with an integral over the scattering power f_l of point ℓ replaced by the instantaneous value of the potential at the same point. This result is the basis of the failures of Schrödinger's interpretation that $\Psi(x)$ is the amplitude of the electron over three-dimensional space in some sense since the entire electron must correspond to each point ℓ and the superseding interpretation of Born that $\Psi(x)$ represents a probability function of a point electron. The Born interpretation can only be valid if the speed of the electron is equal to infinity. (The electron must be in all positions weighted by the probability density function during the time of the scattering event). The correct aperture function for the Born interpretation is a Dirac delta function, $\delta(r)$, having a Fourier transform of a constant divided by $\mathbf{s}^2$ which is equivalent to the case of the point nucleus (Rutherford Equation). The Born interpretation must be rejected because the electron velocity cannot exceed c without violating special relativity.

Solutions to the Schrödinger equation involve the set of Laguerre functions, spherical Bessel functions, and Newmann functions. From the infinite set of solutions to real problems, a linear combination of functions and the amplitude and phases of these functions are sought which gives results that are consistent with scattering experiments. The Schrödinger equation is a statistical model representing an approximation to the actual nature of the bound electron. Statistical models are good at predicting averages as exemplified by the reasonable agreement between the calculated and experimental scattering results at large angles. However, in the limit of zero scattering angle, the results calculated via the Schrödinger equation are not in agreement with experimentation. In the limit, the "blurred" representation cannot be averaged, and only the exact description of the electron will yield scattering predictions which are consistent with the experimental results.

Also, a contradiction arises in the quantum mechanical scattering calculation. For hydrogen electron orbitals, the $n=\infty$ orbital is equivalent to an ionized electron. According to the quantum mechanical scattering model, the incident ionized electron is a plane wave. However, substitution of $n=\infty$ into the solution of the Schrödinger equation yields a radial function that has an infinite number of nodes and exists over all space. The hydrogen-like radial functions have $n-\ell-1$ nodes between $r=0$ and $r=\infty$. In fact, as $n\to\infty$ the Schrödinger equation becomes the equation of a linear harmonic oscillator [12]. The wavefunction shows sinusoidal behavior; thus, the wavefunction for the free electron can not be normalized and is infinite. In addition, the angular momentum of the free electron is infinite since it is given by $\ell(\ell+1)\hbar^2$ where $\ell\to\infty$. The results of the Davison-Germer experiment confirm that the ionized electron is a plane wave. In contrast, for the present atomic orbital model, as n goes to infinity the electron is a plane wave with wavelength $\lambda=h/p$ as shown in the Electron in Free Space section.

Although there are parallels in the mathematical derivations wherein the Schwartz inequality is invoked, the physics of the Heisenberg Uncertainty Principle is quite distinct from the physics of the rise-time/band-width relationship of classical mechanics [13] as given in the Resonant Line Shape and Lamb Shift section. The Heisenberg Uncertainty Principle is derived from the probability model of the electron by applying the Schwartz inequality [14] to obtain the "indefiniteness" in the conjugate electron position and momentum in the absence of measurement; whereas, the physical rise-time/band-width relationship of classical mechanics is an energy conservation statement according to Parseval's Theorem. The Born model of the electron violates Special Relativity. The failure of the Born and Schrödinger model of the electron to provide a consistent representation of the states of the electron from a bound state to an ionized state to a scattered state also represents a failure of the dependent Heisenberg Uncertainty Principle.

In contrast, the Maxwellian, exact atomic orbital model provides a continuous representation of all states of the electron including the ionized state as a plane wave having the de Broglie wavelength as given in the Electron in Free Space section. Using the exact, unique solution of the helium atom given in the Two-Electron Atom section, in a closed-form solution, the Maxwellian model predicts the experimental results of the electron scattering from helium for all angles. The solution of the helium atom is further proven to be correct since it is used to solve up through twenty-electron atoms in the Three- Through

Twenty-Electron Atoms section and 100 excited-state energy levels in the Excited States of Helium section. In the former case, the physical approach was applied to multielectron atoms that were solved exactly disproving the deep-seated view that such exact solutions cannot exist according to quantum mechanics. The predictions from general solutions for one through twenty-electron atoms are in remarkable agreement with the experimental values known for 400 atoms and ions. In the latter case, the results given for any given n and ℓ quantum number in the equations agree remarkably well—up to 6 significant figures where the data is obtainable to that accuracy. These consistent results and the failure of the true quantum mechanical model as well as the unphysical Born approximation disprove the nature of the electron as a point particle which further disproves the primary assumption of quantum mechanics. The results directly prove that the electron is an extended particle and specifically show, in the case of the helium atom, that the electron function comprises two paired, electron atomic orbitals at a radius given by Eq. (8.44) as derived in the Two-Electron Atom section. Furthermore, the deep-seated notion that probability waves are required to explain the nature of the double-slit experiment is dispelled by classical predictions using the correct nature of the electron considered next.

PHYSICS OF CLASSICAL ELECTRON DIFFRACTION RESOLVES THE WAVE-PARTICLE DUALITY MYSTERY OF QUANTUM MECHANICS

The beginning of the Wave-Particle Duality section describes how early 20th century theoreticians proclaimed that light and atomic particles have a wave-particle duality that was unlike anything in our common everyday experience. The wave-particle duality is the central mystery of quantum mechanics—the one to which all others could ultimately be reduced. The current mental picture of the two-slit experiment is shown in Figures 42.1-42.4. The classical depiction of the two-slit-experiment shown in Figures 8.9-8.11 is very similar to the depiction of the quantum notion of the wave-particle duality shown in Figure 42.4. In fact, the mathematics of the quantum mechanical and classical pictures is essentially identical including the relationship between the transverse momentum and position given by Eqs. (8.60) and (8.61). However, what is very different is the physics. Consider the quantum conundrum due to the nature of the photon and electron being point particles. If each electron passes individually through one slit, with what does it "interfere?" Although each electron arrives at the target at a single place and a single time, it seems that each has passed through—or somehow felt the presence of both slits at once. Thus, the electron is understood in terms of a wave-particle duality as represented in Figure 42.4.

Here, the point electron or photon is everywhere at once—rather than being local to the slits of nanometer dimensions it exits as a probability wave of equal amplitude from positive to negative infinity, simultaneously! It is incident to and transmitted through both slits simultaneously, "guided" by the probability wave over all space with a phase that depends on the Heisenberg Uncertainty Principle:

$$\Delta x \Delta \mathbf{p} \geq \frac{\hbar}{2} \tag{8.59}$$

The phase contains the term $(\mathbf{k}_i - \mathbf{k}_s)\cdot\mathbf{r}_l$, where $\Delta p = \mathbf{k}_i - \mathbf{k}_s$ is interpreted as the contribution to the *uncertainty in the momentum of the incident particle on scattering*, since $\hbar\mathbf{k}_i$ is the initial momentum and $\hbar\mathbf{k}_s$ is the final momentum of the scattered particle such as an electron. In the classical picture, the phase also contains the term $(\mathbf{k}_i - \mathbf{k}_s)\cdot\mathbf{r}_l$, where $\mathbf{k}_i - \mathbf{k}_s$ is the *physical momentum change of the incident particle on scattering*, since $\hbar\mathbf{k}_i$ is the initial momentum and $\hbar\mathbf{k}_s$ is the final momentum of the scattered particle. In both cases, Δx corresponds to the transverse displacement of the particle due to diffraction.

Furthermore, each electron only goes through one slit classically, but it is imprinted with the wave character of the photon that it creates across both slits due to its interaction with the slit. An electromagnetic wave exits. Quantum mechanics reproduces the mathematics that corresponds to this physical electromagnetic wave by invoking a nonsensical waving probability. Thus, it is stuck with the unfortunate result that the "wave-particle duality is unlike anything in our common everyday experience." Physics can now be reinstated over mysticism for this simple experiment based on an understanding of the physical nature of fundamental particles. An outline of the classical explanation of the observations made on the double-slit experiment is shown in Figures 8.9A-F, 8.10, and 8.11.

Figure 8.9. The electron-slit interaction is mediated by electron-induced radiation of photons from the split aperture that causes transverse electron displacements with the photon-momentum distribution imprinted onto that of the diffracting electrons such that the transverse momentum distribution in the far-field is a result of this interaction and is characteristic of the slit pattern. (A) The approaching charged electron interacts with both slits by inducing slit mirror currents (blue). (B) The slit's electron mirror currents that mediate its interaction with the approaching charged electron cause emission of photons. (C) The superposition of the photons forms a photon field characteristic of the slits as its source. (D) The electron angular momentum vector precesses about that of an absorbed photon from the slit photon field. (E) The photon is readmitted and the electron gained transverse momentum depending on the strength and duration of the electron's interaction with the photon field wherein the photon's angular momentum is conserved according to the change in the electron's de Broglie wavelength. (F) Rather than uncertainty in position and momentum according to the Uncertainty Principle: $\Delta x \Delta \mathbf{p} \geq \frac{\hbar}{2}$, Δp is the physical momentum change of the incident electron and Δx is the physical distance change from the incident direction such that the electron distribution in the far field is the Fourier transform of the slit pattern.

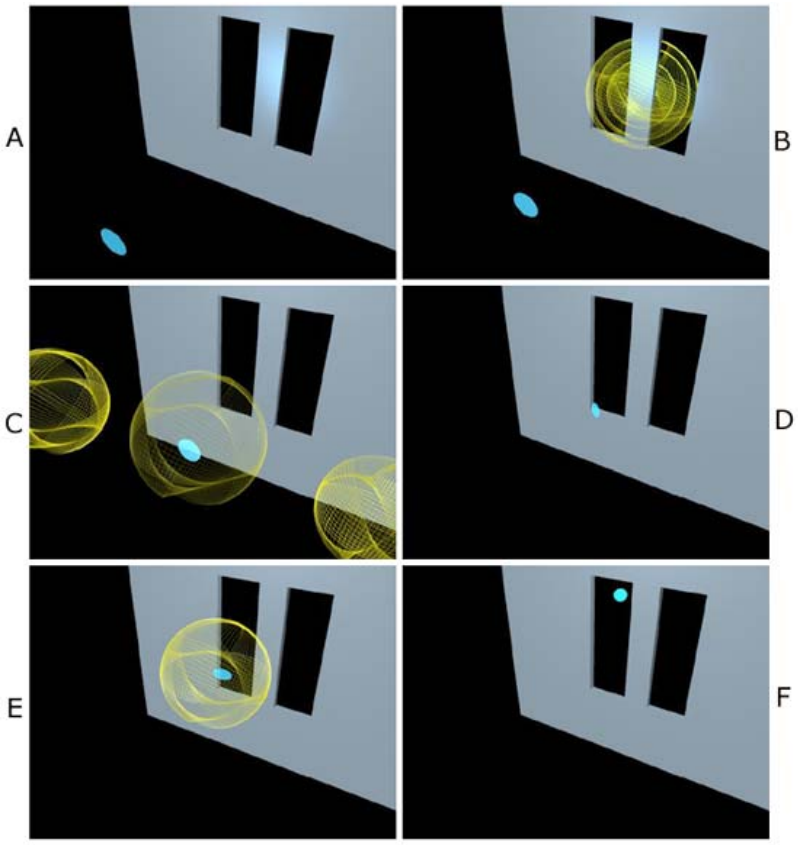

Consider a beam of electrons propagating in the z-axis direction. The electron is a plane-wave with momentum $k_z\hbar$ initially along the z-axis only. The $\hbar$ of angular momentum of the free electron is perpendicular to the plane lamina and is initially in a random orientation relative to the z-axis. To minimize the energy of interaction, the slit polarizes the electron such that its angular momentum becomes aligned parallel or antiparallel to the z-axis (Figure 8.9A). The slit is comprised of matter having electrons that can provide image charges due to the electric field of the incident electron (Figure 8.9A). The slit's electron-mirror currents that mediate its interaction with the approaching charged electron cause emission of photons (Figure 8.9B). When one interacts with the electron (Figure 8.9C), the electron angular-frequency change corresponding to the elctron-de-Broglie-wavelength change matches the frequency of the photon as given in the Classical Physics of the de Broglie Relationship section. The result of this interaction over time is the reorientation and transverse displacement of the electron's angular elastic diffraction, the energies are low, and the photons are large, encompassing and emanating from both slits. Each photon has a quantized angular momentum of $\hbar$. The $\hbar$ of angular momentum of the electron precesses about the $\hbar$ of angular momentum vector of the absorbed photon to cause a momentum transfer from the z-axis to the transverse axis. The photon is reemitted (Figure 8.9E), and the electron gained transverse momentum depending on the strength and duration of the electron's interaction with the photon field wherein the photon's angular momentum is conserved according to the change in the electron's de Broglie wavelength.

Over time, the electron beam statistically produces a uniform distribution across the slits. (Here, the statistics are deterministic and local/causal unlike the quantum mechanical case.) The photon pattern is also uniform across the slit. Since the electron and each photon that mediates the slit-electron interaction have quantized angular momentum in units of $\hbar$, the photon far-field pattern is imprinted on the electron beam pattern over time. The resulting transverse-momentum map is given by the Fourier transform of the two-slit aperture which arises classically from a consideration of conservation of power flow. The amplitude is periodically positive and negative corresponding to the cyclical reversal of the electron angular momentum as shown in Figure 8.10. The amplitude decreases from the center line due to the requirement of an increasing momentum transfer along the transverse axis from the center line with a decreasing probability for a long-duration photon-electron interaction or coupling with multiple photons to achieve increasing transverse momentum transfer.

Figure 8.10. The amplitude of the transverse electron momentum is a sinc function due to the decreasing probability of photon interactions causing a periodic reversal of the electron's angular momentum vector with an increasing transverse momentum transfer.

Since the number of electrons hitting a given position over time goes as the electron kinetic energy, the intensity pattern is given by the square of the amplitude. The predicted result shown in Figure 8.11 is the observed classical double slit interference pattern.

Figure 8.11. The classically predicted far-field electron distribution of the two-slit experiment matches that observed.

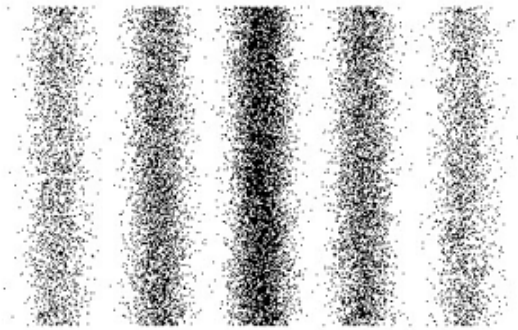

EQUATIONS OF CLASSICAL DIFFRACTION

Consider the double-slit electron diffraction experiment shown in Figure 8.9. The interaction with the slit can cause momentum transfer to the transverse direction that can be mediated by photons having $\hbar$ of angular momentum. If the forward momentum is unchanged, then the electron is detected at $\mathrm{x} = 0$ in the far field. However, momentum transfer from the z-axis to along the x-axis in the far field may occur depending on the strength and the time duration of a photon-generated torque as given in the Stern-Gerlach Experiment subsection of the Free Electron section. Also see Patz [15] and Slichter [16]. The spatial distribution of the electron position is determined by the conservation of momentum. Thus, the electron source at the aperture is analogous to an antenna, and the spatial electron-density pattern has as a parallel to the radiation pattern of the antenna as given by Kong [17]. If each point on the electron across a diffraction slit can act as a point source of a spherical wave according to Huygens' Principle, then the momentum pattern in the far field is given as the Fourier transform of the momentum-aperture function, and the electron density is given as the square of the amplitude of the Fourier transform.

Thus, the result of the double-slit experiment given by Eq. (8.23) can be interpreted as the positions of the electrons due to conservation of momentum following a semi-elastic interaction with the slit apparatus. The interaction is a time-dynamic equipotential and the forces statistically[2] cause the electrons over time to propagate as spherical waves from each point of a Laplacian surface according to Huygens' Principle. The incident pattern over time is determined by the superposition of the position and momenta of the incident individual electrons. The Fourier transform result given by Eq. (8.23) can be shown to arise by considering the diffraction of each electron individually.

The free electron is unpolarized, but the minimum energy constraint with slit-interrelations causes the polarization of the incident electrons. The angular momentum of the polarized electron may be parallel or antiparallel (negative direction) with respect to the z-axis. As shown in the Electron in Free Space section, there is a correspondence between the properties of the states of the free electron based on interactions with photons and those of bound-excited-state electrons. The time- and spherical harmonic current-density functions of bound and free-electron states comprise source currents for electromagnetic fields that are solutions of the wave equation as given in the Electron Source Current section. As shown in the Selection Rules section, multipole fields of an electron follow the same Maxwellian physics as that of a macroscopic radiating source. The radiation of a multipole of order $(\ell,\ m_\ell)$ carries $m\hbar$ units of the z component of angular momentum comprised of $\hbar$ per photon of energy $\hbar\omega$.

The distribution as a function of the position of the detector must conserve the angular momentum of the electron having an intrinsic angular momentum of $\hbar$ and an induced multipole of order $(\ell,\ m_\ell)$. The asymptotic electron-momentum total amplitude in the far field due to the scattering interactions of N electrons with the slit mediated by photons with $\hbar$ of angular momentum follows from Eq. (8.27) given in the Classical Wave Theory of Electron Scattering section and Eq. (8.32) in the Classical Wave Theory Applied to Scattering from Atoms and Molecules section. Consider the assembly of N coherently scattered electrons. The slit-electron interaction is an energy minimum or equipotential. The angular terms of Eq. (8.27) sum to unity. According to Huygens' principle, the function $\sum_{\mathrm{i}=1}^{N} e^{i\mathbf{s}\cdot\mathbf{r}_i}$ of Eq. (8.32) represents the sum over each spherical wave source arising from the scattering of an incident plane wave from each point of the slit where the wavelength of the incident plane wave is given by the de Broglie equation $\lambda = h/p$. (The Green Function of Eqs. (8.25-8.27), is also given by Eq. (6.62) of Jackson [3] as the solution of the wave equation (Eq. (6.58) of Jackson [3]) as given in the Spherical Wave subsection of the Equation of the Photon section.) The sum is replaced by the integral over ξ of the single point element aperture distribution function. For the case of a single slit, the aperture function is given by Eq. (8.15). Then, the amplitude of the scattering in the far field given by Eqs. (8.16) and (8.32) is:

$$\tilde{\Psi}(\mathrm{x}) = \sum_{i=1}^{N} e^{i\mathbf{s}\cdot\mathbf{r}_i} = \int \Psi(\xi) \exp\left(\frac{-ik\xi\cdot\mathbf{x}}{\mathrm{f}}\right) d\xi = C\int_{-a}^{a} \exp\left(\frac{-ik\xi\cdot\mathbf{x}}{\mathrm{f}}\right) d\xi \tag{8.60}$$

wherein the phase contains the term $(\mathbf{k}_i - \mathbf{k}_s)\cdot\mathbf{r}_l$, where $\mathbf{k}_i - \mathbf{k}_s$ is proportional to the momentum change of the incident particle on scattering, since $\hbar\mathbf{k}_i$ is the initial momentum and $\hbar\mathbf{k}_s$ is the final momentum of the scattered electron. This vector difference labeled by the symbol $\mathbf{s}$ is given by:

$$-i\mathbf{s}\cdot\mathbf{r}_i = \left(\frac{-ik\xi\cdot\mathbf{x}}{\mathrm{f}}\right) \tag{8.61}$$

The single-slit-momentum-amplitude pattern is then given by Eq. (8.22). The intensity of electrons is proportional to their kinetic energy which carry the electrons to the analyzer where it was shown by Bonham to be required in order to insure continuity of power flow for wavelets from a single source [4] and was used as the basis of Eqs. (8.27) and (8.32). The intensity pattern of electrons is then given as the square of the amplitude and, thus, the square of the momentum which is proportional to the electron energy. It follows that the single-slit pattern is given as the square of Eq. (8.18) and the double-slit pattern is given

[2] Here, the underlying physics is deterministic. Quantum mechanics postulates that the electron is a point-particle-probability wave wherein its sampling or measurement creates the statistics corresponding to a stochastic reality. In general, the theory of statistics is based on deterministic but unknown information. The concepts of quantum mechanics of an underlying distribution in a state of indeterminism as well as negative probability are nonsensical and are not a part of this classical result.

by Eq. (8.23).

The double-slit experiment may be modeled physically, and a computer simulation outlined in the Computer Simulation of Classical Electron Diffraction section is posted on the web [18]. The interaction of each incoming electron with the slit or slits causes a redistribution of the incident momentum that is shown visually as a corresponding trajectory from the aperture to the detector. The algorithm uses N electrons that statistically form a uniform distribution at the aperture. To get the points of impact, the momentum-distribution pattern is calculated using Eq. (8.22) that arise from classical statistics. For diffraction at a single slit, the transverse-momentum-density map is given by:

$$2aC\sin\left(\mathbf{k}\cdot\mathbf{x}\right) \tag{8.62}$$

which is spatially diluted according to $\mathbf{k}\cdot\mathbf{x}$ and scaled according to the far field factor of $\frac{a}{f}$. The sine dependence of Eq. (8.62) is equivalent to that of the dot product of the plane lamina of the free electron with the z-axis. Each incident electron that is initially polarized by the slit interaction precesses due to the photon mediated, interaction-generated torque to reorient the plane lamina wherein the cross section of the interaction is proportional to this dot product. The sine dependence can easily be appreciated by considering that the interaction is concentrated at one end of the plane-lamina free electron when it is oriented perpendicularly to the slit; whereas, it is evenly distributed throughout the plane lamina when it is parallel to the slit.

The intensity of the one-slit pattern is then given as the square of the amplitude. Since the two-slit aperture pattern is the convolution of the single-slit pattern with two delta functions, the intensity of the two-slit experiment is given as cosine squared fringes of the single-slit pattern as given by Eq. (8.23) wherein the extended electron interacts with both slits with conservation of momentum to give the modulation of the single-slit momentum pattern. Thus, the superposition of electrons gives the classical result. The double-slit interference pattern associated with the wave-particle duality arises naturally whether electrons add over time or space.

CP predicts that the angular momentum of electrons or photons periodically reverses direction as a function of the transverse distance in the far field of the one-, two- or n-slit diffraction experiment. The pattern is not due to constructive interference of electron- or photon-probability waves; rather it is a map of the transverse momentum. The intensity is given by the amplitude squared, since energy and, thus, the number of electrons or photons is proportional to the amplitude of the momentum squared. The amplitude varies from a maximum to a minimum at which point the angular momentum of the photon or electron reverses direction, then it goes to a maximum again over a periodic cycle. The amplitude decreases away from the longitudinal axis of the slit in the transverse direction since the probability of multiple reversals is low. The amplitude also decreases when there is a large change in the angular momentum that is redirected to a transverse momentum component corresponding to a large torque or a long interaction time.

This can be tested with electrons by polarizing a beam using a Stern-Gerlach analyzer before the slit to select only electrons polarized parallel or antiparallel to the z-axis (the propagation direction of the beam). These electrons are then analyzed in the far field with a second Stern-Gerlach-type analyzer, which determines the polarization as a function of position in the transverse plane or along a transverse axis. Alternate polarization as a function of transverse distance confirms this mechanism of the n-slit pattern.

Recently, it was shown that the induction of surface currents on a metal sheet parallel to the propagation direction of the electron beam of a double-slit experiment interfered with the pattern as expected [19-20]. Furthermore, the double slit experiment has been demonstrated on a macroscopic scale using droplets bouncing on a vertically vibrated bath [21]. Here the localized droplets are coupled to surface waves generated in the bath and random transverse deviations imposed by restrictions of two slits results in a double slit pattern over many flights of droplets to a detector analogous to the transverse deviations of localized electrons or photons during flight due to interactions with the slits and corresponding currents and electromagnetic waves described here. In other recent experiments, the classical mechanism of the double slit experiment has been directly confirmed for photons. The results of Kocsis et al. [22] are consistent with the interpretation that photons have a determined position and momentum, and with an appropriately sensitive measurement apparatus, the causal transverse momentum and position change imparted by close double slits over an ensemble of photons that individually travel through a slit of the pair can be determined wherein the far-field pattern of the superposition of the transverse displacements imparted by the slit interaction over the ensemble is an interference pattern. The old view of constructive and destructive interference of waves is disproved. Photons cannot be created or destroyed by constructive or destructive interference, respectively. The pattern is merely due to photon trajectories corresponding to conservation of momentum altered by photons propagating through close slits. The uncertainty principle as the mechanism of the double-slit interference pattern is similarly disproved by the experiments of Durr et al. [23] as shown in the Wave-Particle Duality is Not Due to the Uncertainty Principle section. Again, the appearance and cancellation of the interference pattern, which in this case involves ^{85}Rb atoms diffracted from standing light waves as the atomic states are manipulated, is predicted classically as a transverse position density pattern corresponding to the transverse momentum distribution caused by the interaction of the manipulated states in the atoms with the standing light waves.

REFERENCES

1. G. O. Reynolds, J. B. DeVelis, G. B. Parrent, B. J. Thompson, *The New Physical Optics Notebook*, SPIE Optical Engineering Press, (1990).
2. R. A. Bonham, M. Fink, *High Energy Electron Scattering*, ACS Monograph, Van Nostrand Reinhold Company, New York, (1974), pp. 1-3.
3. J. D. Jackson, *Classical Electrodynamics,* Second Edition, John Wiley & Sons, New York, (1975), pp. 739-779.
4. R. A. Bonham, M. Fink, *High Energy Electron Scattering*, ACS Monograph, Van Nostrand Reinhold Company, New York, (1974).
5. R. N. Bracewell, *The Fourier Transform and Its Applications*, McGraw-Hill Book Company, New York, (1978), pp. 252-253.
6. A. Apelblat, *Table of Definite and Infinite Integrals*, Elsevier Scientific Publishing Company, Amsterdam, (1983).
7. H. Bateman, *Tables of Integral Transforms*, Vol. I, McGraw-Hill Book Company, New York, (1954).
8. P. J. Bromberg, "Absolute differential cross sections of elastically scattered electrons. I. He, N_2, and CO at 500 eV," The Journal of Chemical Physics, Vol. 50, No. 9, (1969), pp. 3906-3921.
9. J. Geiger, "Elastische und unelastische streuung von elektronen an gasen," Zeitschrift fur Physik, Vol. 175, (1963), pp. 530-542.
10. E. M. Peixoto, C. F. Bunge, R. A. Bonham, "Elastic and inelastic scattering by He and Ne atoms in their ground states," Physical Review, Vol. 181, (1969), pp. 322-328.
11. D. A. McQuarrie, *Quantum Chemistry*, University Science Books, Mill Valley, CA, (1983), p. 291.
12. H. Margenau, G. M. Murphy, *The Mathematics of Chemistry and Physics*, D. Van Nostrand Company, Inc., New York, (1943), pp. 363-367.
13. W. McC. Siebert, *Circuits, Signals, and Systems*, The MIT Press, Cambridge, Massachusetts, (1986), pp. 488-502.
14. D. A. McQuarrie, *Quantum Chemistry*, University Science Books, Mill Valley, CA, (1983), p. 139.
15. S. Patz, Cardiovasc Interven Radiol, (1986), 8:25, pp. 225-237.
16. C. P. Slichter, *Principles of Magnetic Resonance*, Harper & Row, New York, (1963), pp. 1-44.
17. L. C. Shi, J. A. Kong, *Applied Electromagnetism*, Brooks/Cole Engineering Division, Monterey, CA, (1983), pp. 170-209.
18. Mathematica modeling of R. Mills' theory by B. Holverstott in "Computer Simulation of Classical Electron Diffraction," posted at www.blacklightpower.com.
19. D. Castelvecchi, Science News, Vol. 171, (2007), p. 292.
20. P. Sonnentag, F. Hasselbach, "Measurement of decoherence of electron waves and visualization of the quantum-classical transition," Phys. Rev. Letts., Vol. 98, May 18, (2007), 200402-1-200402-4.
21. Y. Couder and E. Fort, "Single-particle diffraction and interference at a macroscopic scale," Phys. Rev. Letts., Vol. 97, (2006), pp. 154101-1-154101-4.
22. S. Kocsis, B. Braverman, S. Ravets, M. J. Stevens, R. P. Mirin, L. K. Shalm, A. M. Steinberg, "Observing the average trajectories of single photons in a two-slit interferometer," Science 332, (2011), 1170.
23. S. Durr, T. Nonn, G. Rempe, "Origin of quantum-mechanical complementarity probed by a 'which-way' experiment in an atom interferometer," Nature, September 3, (1998), Vol. 395, pp. 33-37.

Chapter 9

EXCITED STATES OF HELIUM

Bound electrons are described by a charge-density (mass-density) function that is the product of a radial delta function ($f(r)=\delta(r-r_n)$), two angular functions (spherical harmonic functions), and a time harmonic function. Thus, a bound electron is a dynamic "bubble-like" charge and current-density function. The two-dimensional spherical surface can exist in a bound state at only specified distances from the nucleus. More explicitly, the uniform current-density function $Y_0^0(\theta,\phi)$ (Eqs. (1.27-1.29)) called the electron atomic orbital that gives rise to the spin of the electron is generated from two current-vector fields (CVFs). Each CVF comprises a continuum of correlated *orthogonal great circle current-density elements (one dimensional "current loops")*. The current pattern comprising each CVF is generated over a half-sphere surface by a set of rotations of two orthogonal great circle current loops that serve as basis elements about each of the $\left(-\mathbf{i}_x,\mathbf{i}_y,0\mathbf{i}_z\right)$ and $\left(-\frac{1}{\sqrt{2}}\mathbf{i}_x,\frac{1}{\sqrt{2}}\mathbf{i}_y,\mathbf{i}_z\right)$-axis; the span being π radians. Then, the two CVFs are convoluted, and the result is normalized to exactly generate the *continuous* uniform electron current density function $Y_0^0(\theta,\phi)$ covering a spherical shell and having the three angular momentum components of $\mathbf{L}_{xy}=+/-\frac{\hbar}{4}$ and $\mathbf{L}_z=\frac{\hbar}{2}$ (Figure 1.23)[1].

The spin function of the electron corresponds to the nonradiative $n=1$, $\ell=0$ state which is well known as an s state or orbital. (See Figure 1.1 for the charge function and Figure 1.22 for the current function.) In cases of orbitals of excited states with the ℓ quantum number not equal to zero and which are not constant as given by Eq. (1.27), the constant spin function is modulated by a time and spherical harmonic function as given by Eq. (1.29) and shown in Figure 1.2. The modulation or traveling charge-density wave corresponds to an orbital angular momentum in addition to a spin angular momentum. These states are typically referred to as p, d, f, etc. orbitals.

Each atomic orbital is a spherical shell of negative charge (total charge $=-e$) of zero thickness at a distance r_n from the nucleus (charge $=+Ze$). It is well known that the field of a spherical shell of charge is zero inside the shell and that of a point charge at the origin outside the shell [1] (See Figure 1.32). The field of each electron can be treated as that corresponding to a $-e$ charge at the origin with $\mathbf{E}=\frac{-e}{4\pi\varepsilon_0 r^2}$ for $r>r_n$ and $\mathbf{E}=0$ for $r<r_n$ where r_n is the radius of the electron atomic orbital. Thus, as shown in the Two-Electron Atoms section, the central electric fields due to the helium nucleus are $\mathbf{E}=\frac{2e}{4\pi\varepsilon_0 r^2}$ and $\mathbf{E}=\frac{e}{4\pi\varepsilon_0 r^2}$ for $r<r_1$ and $r_1<r<r_2$, respectively. In the ground state of the helium atom, both electrons are at $r_1=r_2=0.567a_0$. When a photon is absorbed, one of the initially indistinguishable electrons called electron 1 moves to a smaller radius, and the other called electron 2 moves to a greater radius. In the limiting case of the absorption of an ionizing photon, electron 1 moves to the radius of the helium ion, $r_1=0.5a_0$, and electron 2 moves to a continuum radius, $r_2=\infty$. When a photon is absorbed by the ground state helium atom it generates an effective charge, Z_{P-eff}, within the second atomic orbital such that the electrons move in opposite radial directions while conserving energy and angular momentum. We can determine Z_{P-eff} of the "trapped photon" electric field by requiring that the resonance condition is met for photons of discrete energy, frequency, and wavelength for electron excitation in an electromagnetic potential energy well.

[1] $+/-$ designates both the positive and negative vector directions along an axis in the xy-plane.

It is well known that resonator cavities can trap electromagnetic radiation of discrete resonant frequencies. The atomic orbital is a resonator cavity that traps single photons of discrete frequencies. Thus, photon absorption occurs as an excitation of a resonator mode. The free space photon also comprises a radial Dirac delta function, and the angular momentum of the photon given by $\mathbf{m} = \int \frac{1}{8\pi c} \mathrm{Re}\left[\mathbf{r} \times (\mathbf{E} \times \mathbf{B}^*)\right] dx^4 = \hbar$ in the Photon section is conserved [2] for the solutions for the resonant photons and excited state electron functions as shown for one-electron atoms in the Excited States of the One-Electron Atom (Quantization) section. The correspondence principle holds. That is the change in angular frequency of the electron is equal to the angular frequency of the resonant photon that excites the resonator cavity mode corresponding to the transition, and the energy is given by Planck's equation. It can be demonstrated that the resonance condition between these frequencies is to be satisfied in order to have a net change of the energy field [3].

In general, for a macroscopic multipole with a single m value, a comparison of Eq. (2.62) and Eq. (2.55) shows that the relationship between the angular momentum M_z, energy U, and angular frequency ω is given by Eq. (2.63):

$$\frac{dM_z}{dr} = \frac{m}{\omega}\frac{dU}{dr} \tag{9.1}$$

independent of r where m is an integer. Furthermore, the ratio of the square of the angular momentum, M^2, to the square of the energy, U^2, for a pure (ℓ, m) multipole follows from Eq. (2.55) and Eqs. (2.60-2.62) as given by Eq. (2.64):

$$\frac{M^2}{U^2} = \frac{m^2}{\omega^2} \tag{9.2}$$

From Jackson [4], the quantum mechanical interpretation is that the radiation from such a multipole of order (ℓ, m) carries off $m\hbar$ units of the z component of angular momentum per photon of energy $\hbar\omega$. However, the photon and the electron can each possess only $\hbar$ of angular momentum which requires that Eqs. (9.1-9.2) correspond to a state of the radiation field containing m photons.

As shown in the Excited States of the One-Electron Atom (Quantization) section during excitation the spin, orbital, or total angular momentum of the atomic orbital can change by zero or $\pm\ \hbar$. The selection rules for multipole transitions between quantum states arise from conservation of the photon's multipole moment and angular momentum of $\hbar$. In an excited state, the time-averaged mechanical angular momentum and rotational energy associated with the traveling charge-density wave on the atomic orbital is zero (Eqs. (1.76-1.77)), and the angular momentum of $\hbar$ of the photon that excites the electronic state is carried by the fields of the trapped photon. The amplitudes of the rotational energy, angular momentum, and moment of inertia that couple to external magnetic and electromagnetic fields are given by Eqs. (1.71), (1.72), and (1.73), respectively. Furthermore, the electron charge-density waves are nonradiative due to the angular motion as shown in the Appendix I: Nonradiation Condition. But, excited states are radiative due to a radial dipole that arises from the presence of the trapped photon as shown in the Instability of Excited States section corresponding to $m = 1$ in Eqs. (9.1-9.2).

Then, as shown in the Excited States of the One-Electron Atom (Quantization) section and the Electron Mechanics and the Corresponding Classical Wave Equation for the Derivation of the Rotational Parameters of the Electron section, the total number of multipoles, $N_{\ell,s}$, of an energy level corresponding to a principal quantum number n where each multipole corresponds to an ℓ and m_ℓ quantum number is:

$$N_{\ell,s} = \sum_{\ell=0}^{n-1} \sum_{m_\ell=-\ell}^{+\ell} 1 = \sum_{\ell=0}^{n-1} 2\ell + 1 = \left(\ell + 1\right)^2 = \ell^2 + 2\ell + 1 = n^2 \tag{9.3}$$

Any given state may be due to a direct transition or due to the sum of transitions between all intermediate states wherein the multiplicity of possible multipoles increases with higher states. Then, the relationships between the parameters of Eqs. (9.1) and (9.2) due to transitions of quantized angular momentum $\hbar$, energy $\hbar\omega$, and radiative via a radial dipole are given by substitution of $m = 1$ and normalization of the energy U by the total number of degenerate multipoles, n^2. This requires that the photon's electric field superposes that of the nucleus for $r_1 < r < r_2$ such that the radial electric field has a magnitude proportional to e/n at the electron 2 where $n = 2, 3, 4, \ldots$ for excited states such that U is decreased by the factor of $1/n^2$.

Energy is conserved between the electric and magnetic energies of the helium atom as shown by Eq. (7.42). The helium atom and the "trapped photon" corresponding to a transition to a resonant excited state have neutral charge and obey Maxwell's equations. Since charge is relativistically invariant, the energies in the electric and magnetic fields of the electrons of the helium atom must be conserved as photons are emitted or absorbed. The corresponding forces are determined from the requirement that the radial excited-state electric field has a magnitude proportional to e/n at electron 2.

The "trapped photon" is a "standing electromagnetic wave" which actually is a traveling wave that propagates on the surface around the z-axis, and its source current is only at the atomic orbital. The time-function factor, $k(t)$, for the "standing wave" is identical to the time-function factor of the atomic orbital in order to satisfy the boundary (phase) condition at the atomic orbital surface. Thus, the angular frequency of the "trapped photon" has to be identical to the angular frequency of the electron atomic orbital, ω_n, given by Eq. (1.36). Furthermore, the phase condition requires that the angular functions of the "trapped photon" have to be identical to the spherical harmonic angular functions of the electron atomic orbital. Combining $k(t)$ with the ϕ-function factor of the spherical harmonic gives $e^{i(m\phi - \omega_n t)}$ for both the electron and the "trapped photon" function.

The photon "standing wave" in an excited electronic state is a solution of Laplace's equation in spherical coordinates

with source currents given by Eq. (2.11) "glued" to the electron and phase-locked to the electron current density wave that travel on the surface with a radial electric field. As given in the Excited States of the One-Electron Atom (Quantization) section, the photon field is purely radial since the field is traveling azimuthally at the speed of light even though the spherical harmonic function has a velocity less than light speed given by Eq. (1.35). The photon field does not change the nature of the electrostatic field of the nucleus or its energy except at the position of the electron. The photon "standing wave" function comprises a radial Dirac delta function that "samples" the Laplace equation solution only at the position infinitesimally inside of the electron current-density function and superimposes with the proton field to give a field of radial magnitude corresponding to a charge of e/n where $n = 2,3,4,\ldots$.

The electric field of the nucleus for $r_1 < r < r_2$ is:

$$\mathbf{E}_{nucleus} = \frac{e}{4\pi\varepsilon_0 r^2} \tag{9.4}$$

From Eq. (2.15), the equation of the electric field of the "trapped photon" for $r = r_2$ where r_2 is the radius of electron 2, is:

$$\mathbf{E}_{r\ photon\ \ n,l,m|_{r=r_2}} = \frac{e}{4\pi\varepsilon_0 r_2^2}\left[-1+\frac{1}{n}\left[Y_0^0(\theta,\phi)+\mathrm{Re}\left\{Y_\ell^m(\theta,\phi)e^{im\omega_n t}\right\}\right]\right]\delta(r-r_n) \tag{9.5}$$

The total central field for $r = r_2$ is given by the sum of the electric field of the nucleus and the electric field of the "trapped photon."

$$\mathbf{E}_{total} = \mathbf{E}_{nucleus} + \mathbf{E}_{photon} \tag{9.6}$$

Substitution of Eqs. (9.4) and (9.5) into Eq. (9.6) gives for $r = r_2$,

$$\begin{aligned}\mathbf{E}_{r\,total} &= \frac{e}{4\pi\varepsilon_0 r^2} + \frac{e}{4\pi\varepsilon_0 r_2^2}\left[-1+\frac{1}{n}\left[Y_0^0(\theta,\phi)+\mathrm{Re}\left\{Y_\ell^m(\theta,\phi)e^{im\omega_n t}\right\}\right]\right]\delta(r-r_n)\\ &= \frac{1}{n}\frac{e}{4\pi\varepsilon_0 r_2^2}\left[Y_0^0(\theta,\phi)+\mathrm{Re}\left\{Y_\ell^m(\theta,\phi)e^{im\omega_n t}\right\}\right]\delta(r-r_n)\end{aligned} \tag{9.7}$$

For $r = r_2$ and $m = 0$, the total radial electric field is:

$$\mathbf{E}_{r\,total} = \frac{1}{n}\frac{e}{4\pi\varepsilon_0 r^2} \tag{9.8}$$

The result is equivalent to Eq. (2.17) of the Excited States of the One-Electron Atom (Quantization) section.

In contrast to shortcomings of quantum-mechanical equations, with classical physics (CP), all excited states of the helium atom can be exactly solved in closed form. The radii of electron 2 are determined from the force balance of the electric, magnetic, and centrifugal forces that corresponds to the minimum of energy of the system. The excited-state energies are then given by the electric energies at these radii. All singlet and triplet states with $\ell = 0$ or $\ell \neq 0$ are solved exactly except for small terms corresponding to the magnetostatic energies in the magnetic fields of excited-state electrons, spin-nuclear interactions, and the very small term due to spin-orbit coupling. Spin-nuclear interactions resulted in the use of a_{He} calculated from Eq. (1.259) using the reduced electron mass (Eqs. (1.252-1.255)) rather than a_0 given by Eq. (1.255). Furthermore, a table of the spin-orbit energies was calculated for $\ell = 1$ to compare to the effect of different ℓ quantum numbers. For over 100 states, the agreement between the predicted and experimental results is remarkable.

SINGLET EXCITED STATES WITH $\ell = 0$ $(1s^2 \rightarrow 1s^1(ns)^1)$

With $\ell = 0$, the electron source current in the excited state is a constant function given by Eq. (1.27) that spins as a globe about the z-axis:

$$\rho(r,\theta,\phi,t) = \frac{e}{8\pi r^2}[\delta(r-r_n)]\left[Y_0^0(\theta,\phi)+Y_\ell^m(\theta,\phi)\right] \tag{9.9}$$

As given in the Derivation of the Magnetic Field section in Chapter One and by Eq. (11.391), the current is a function of $\sin\theta$ which gives rise to a correction of 2/3 to the field given by Eq. (7.6) and, correspondingly, the magnetic force of two-electron atoms given by Eq. (7.24). The vector orientations of the electrons and the derivation of the magnetic force is given in Appendix VI. The balance between the centrifugal and electric and magnetic forces follows from Eq. (7.32):

$$\frac{m_e v^2}{r_2} = \frac{\hbar^2}{m_e r_2^3} = \frac{1}{n}\frac{e^2}{4\pi\varepsilon_0 r_2^2} + \frac{2}{3}\frac{1}{n}\frac{\hbar^2}{2m_e r_2^3}\sqrt{s(s+1)} \tag{9.10}$$

with the exceptions that the electric and magnetic forces are reduced by a factor of $\frac{1}{n}$ since the corresponding charge from Eq. (9.8) is $\frac{e}{n}$ and the magnetic force is further corrected by the factor of 2/3. With $s = \frac{1}{2}$,

$$r_2 = \left[n - \frac{\sqrt{\frac{3}{4}}}{3}\right]a_{He} \qquad n = 2,3,4,\ldots \tag{9.11}$$

The excited-state energy is the energy stored in the electric field, E_{ele}, given by Eqs. (1.263), (1.264), and (10.102) which is the energy of electron 2 relative to the ionized electron at rest having zero energy:

$$E_{ele} = -\frac{1}{n}\frac{e^2}{8\pi\varepsilon_0 r_2} \tag{9.12}$$

where r_2 is given by Eq. (9.11) and from Eq. (9.8), $Z = 1/n$ in Eq. (1.264). The energies of the various singlet excited states of helium with $\ell = 0$ appear in Table 9.1.

As shown in the Special Relativistic Correction to the Ionization Energies section the electron possesses an invariant charge-to-mass ratio ($\frac{e}{m_e}$) angular momentum of $\hbar$, and magnetic moment of a Bohr magneton (μ_B). *This invariance feature provides for the stability of multielectron atoms* as shown in the Two-Electron Atoms section and the Three- Through Twenty-Electron Atoms section. This feature also permits *the existence of excited states wherein electrons magnetically interact*. The electron's motion corresponds to a current which gives rise to a magnetic field with a field strength that is inversely proportional to its radius cubed as given in Eq. (9.10) wherein the magnetic field is a relativistic effect of the electric field as shown by Jackson [5]. Since the forces on electron 2 due to the nucleus and electron 1 (Eq. (9.10)) are radial/central, invariant of r_1, and independent of r_1 with the condition that $r_1 < r_2$, r_2 can be determined without knowledge of r_1. But, once r_2 is determined, r_1 can be solved using the equal and opposite magnetic force of electron 2 on electron 1 and the central Coulombic force corresponding to the nuclear charge of $2e$. Using Eq. (9.10), the force balance between the centrifugal and electric and magnetic forces is

$$\frac{m_e v^2}{r_1} = \frac{\hbar^2}{m_e r_1^3} = \frac{2e^2}{4\pi\varepsilon_0 r_1^2} - \frac{1}{3n}\frac{\hbar^2}{m_e r_2^3}\sqrt{s(s+1)} \tag{9.13}$$

With $s = \frac{1}{2}$,

$$r_1^3 - \left(\frac{12n}{\sqrt{3}}r_2^3\right)r_1 + \frac{6n}{\sqrt{3}}r_2^3 = 0 \qquad n = 2,3,4,... \tag{9.14}$$

where r_2 is given by Eq. (9.11) and r_1 and r_2 are in units of a_{He}. To obtain the solution of cubic Eq. (9.14) [6], let

$$g = \frac{6n}{\sqrt{3}}r_2^3 \qquad n = 2,3,4,... \tag{9.15}$$

Then, Eq. (9.14) becomes:

$$r_1^3 - 2gr_1 + g = 0 \tag{9.16}$$

and the roots are:

$$r_{11} = A + B \tag{9.17}$$

$$r_{12} = -\frac{A+B}{2} + \frac{A-B}{2}i\sqrt{3} \tag{9.18}$$

$$r_{13} = -\frac{A+B}{2} - \frac{A-B}{2}i\sqrt{3} \tag{9.19}$$

where

$$A = \sqrt[3]{-\frac{g}{2} + \sqrt{\frac{g^2}{4} - \frac{8g^3}{27}}} = \sqrt[3]{\frac{g}{2}}\sqrt[3]{z} \tag{9.20}$$

and

$$B = \sqrt[3]{-\frac{g}{2} - \sqrt{\frac{g^2}{4} - \frac{8g^3}{27}}} = \sqrt[3]{\frac{g}{2}}\sqrt[3]{\bar{z}} \tag{9.21}$$

The complex number z is defined by

$$z = -1 + i\sqrt{\frac{32}{27}g - 1} = re^{i\theta} = r\left(\cos\theta + i\sin\theta\right) \tag{9.22}$$

where the modulus, r, and argument, θ, are

$$r = \sqrt{\frac{32}{27}g} \tag{9.23}$$

and

$$\theta = \frac{\pi}{2} + \sin^{-1}(1/r) \tag{9.24}$$

respectively. The cube roots are:

$$\sqrt[3]{z} = \sqrt[3]{r}e^{i\theta/3} = \sqrt[3]{r}\left(\cos\frac{\theta}{3} + i\sin\frac{\theta}{3}\right) \tag{9.25}$$

$$\sqrt[3]{\bar{z}} = \sqrt[3]{r}e^{-i\theta/3} = \sqrt[3]{r}\left(\cos\frac{\theta}{3} - i\sin\frac{\theta}{3}\right) \tag{9.26}$$

so,

$$A = \sqrt[3]{\frac{g}{2}r}\left(\cos\frac{\theta}{3} + i\sin\frac{\theta}{3}\right) \tag{9.27}$$

and

$$B = \sqrt[3]{\frac{g}{2}r}\left(\cos\frac{\theta}{3} - i\sin\frac{\theta}{3}\right) \tag{9.28}$$

The physical root r_1 is from the roots that are real and distinct:

$$r_{11} = 2\left(\frac{8}{27}\right)^{1/6}\sqrt{g}\cos\frac{\theta}{3}; r_{12} = -\left(\frac{8}{27}\right)^{1/6}\sqrt{g}\left(\cos\frac{\theta}{3} + \sqrt{3}\sin\frac{\theta}{3}\right); r_{13} = -\left(\frac{8}{27}\right)^{1/6}\sqrt{g}\left(\cos\frac{\theta}{3} - \sqrt{3}\sin\frac{\theta}{3}\right) \tag{9.29}$$

Table 9.1. Calculated and experimental energies of He I singlet excited states with $\ell = 0$ $(1s^2 \rightarrow 1s^1(ns)^1)$.

n	r_1 (a_{He}) [a]	r_2 (a_{He}) [b]	**Term Symbol**	E_{ele} CP He I Energy Levels [c] (eV)	NIST He I Energy Levels [d] (eV)	Difference CP-NIST (eV)	Relative Difference [e] (CP-NIST)
2	0.501820	1.71132	1s2s ^{1}S	-3.97465	-3.97161	-0.00304	0.00077
3	0.500302	2.71132	1s3s ^{1}S	-1.67247	-1.66707	-0.00540	0.00324
4	0.500088	3.71132	1s4s ^{1}S	-0.91637	-0.91381	-0.00256	0.00281
5	0.500035	4.71132	1s5s ^{1}S	-0.57750	-0.57617	-0.00133	0.00230
6	0.500016	5.71132	1s6s ^{1}S	-0.39698	-0.39622	-0.00076	0.00193
7	0.500009	6.71132	1s7s ^{1}S	-0.28957	-0.2891	-0.00047	0.00163
8	0.500005	7.71132	1s8s ^{1}S	-0.22052	-0.2202	-0.00032	0.00144
9	0.500003	8.71132	1s9s ^{1}S	-0.17351	-0.1733	-0.00021	0.00124
10	0.500002	9.71132	1s10s ^{1}S	-0.14008	-0.13992	-0.00016	0.00116
11	0.500001	10.71132	1s11s ^{1}S	-0.11546	-0.11534	-0.00012	0.00103
					Avg.	**-0.00144**	**0.00175**

[a] Radius of the inner electron 1 from Eq. (9.29).
[b] Radius of the outer electron 2 from Eq. (9.11).
[c] Classical physics (CP) calculated energy levels given by the electric energy (Eq. (9.12)).
[d] Experimental NIST levels [7] with the ionization potential defined as zero.
[e] (Theoretical-Experimental)/Experimental.

TRIPLET EXCITED STATES WITH $\ell = 0$ $(1s^2 \rightarrow 1s^1(ns)^1)$

For the $\ell = 0$ singlet state, the time-averaged spin angular momentum of electron 2 is zero as given in Appendix VI. A triplet state requires the further excitation to unpair the spin states of the two electrons. The angular momentum corresponding to the excited state is $\hbar$ and the angular momentum change corresponding to the spin-flip is also $\hbar$ as given in the Magnetic Parameters of the Electron (Bohr Magneton) section. Then, the triplet state comprises spin interaction terms between the two electrons plus a contribution from the unpairing photon. As shown in the Resonant Precession of the Spin-1/2-Current-Density Function Gives Rise to the Bohr Magneton section, the electron spin angular momentum gives rise to a trapped photon with $\hbar$ of angular momentum along an $\mathbf{S}$-axis. Then, the spin state of each of electron 1 and 2 comprises a photon standing wave that is phase-matched to a spherical harmonic source current, a spherical harmonic dipole $Y_\ell^m(\theta,\phi) = \sin\theta$ with respect to the $\mathbf{S}$-axis. The dipole spins about the $\mathbf{S}$-axis at the angular velocity given by Eq. (1.36) with $\hbar$ of angular momentum. To conserve angular momentum, electron 2 rotates in the opposite direction about $\mathbf{S}$, the axis of the photon angular momentum due to the spin, and this rotation corresponds to $-\frac{2}{3}\hbar$ of angular momentum relative to $\mathbf{S}$. The corresponding angular momentum components of electron 2 due to spin, unpairing, and rotation are:

$$\mathbf{S}_Z = \left(\sqrt{\frac{3}{4}}\hbar + \sqrt{\frac{3}{4}}\hbar - \frac{2}{3}\sqrt{\frac{3}{4}}\hbar\right)\mathbf{i}_Z = \frac{4}{3}\sqrt{\frac{3}{4}}\hbar\mathbf{i}_Z \tag{9.30a}$$

$$\mathbf{S}_Y = \left(\frac{\hbar}{2} + \frac{\hbar}{2} - \frac{2}{3}\frac{\hbar}{2}\right)\mathbf{i}_Y = \frac{4}{3}\frac{\hbar}{2}\mathbf{i}_Y \tag{9.30b}$$

The corresponding angular momentum components of electron 1 are $\hbar$ and $\sqrt{\frac{3}{4}}\hbar$, respectively. The magnetic interaction of each electron is equivalent to the magnetic field corresponding to a magnetic moment of μ_B interacting with an aligned magnetic momentum of $\frac{4}{3}\sqrt{\frac{3}{4}}\mu_B$. Since the triplet electron-electron interactions are twice those of the singlet case, the triplet magnetic force for electron 2 is twice that of the singlet states as shown in Appendix VI:

$$\frac{m_e v^2}{r_2} = \frac{\hbar^2}{m_e r_2^3} = \frac{1}{n}\frac{e^2}{4\pi\varepsilon_0 r_2^2} + 2\frac{2}{3}\frac{1}{n}\frac{\hbar^2}{2m_e r_2^3}\sqrt{s(s+1)} \tag{9.31}$$

With $s = \frac{1}{2}$,

$$r_2 = \left[n - \frac{2\sqrt{\frac{3}{4}}}{3}\right]a_{He} \qquad n = 2,3,4,... \tag{9.32}$$

The excited-state energy is the energy stored in the electric field, E_{ele}, given by Eq. (9.12) where r_2 is given by Eq. (9.32). The energies of the various triplet excited states of helium with $\ell = 0$ appear in Table 9.2.

Using r_2 (Eq. (9.32)), r_1 can be solved using the equal and opposite magnetic force of electron 2 on electron 1 and the central Coulombic force corresponding to the nuclear charge of $2e$. Using Eq. (9.31), the force balance between the centrifugal and electric and magnetic forces is:

$$\frac{m_e v^2}{r_1} = \frac{\hbar^2}{m_e r_1^3} = \frac{2e^2}{4\pi\varepsilon_0 r_1^2} - \frac{2}{3n}\frac{\hbar^2}{m_e r_2^3}\sqrt{s(s+1)} \tag{9.33}$$

With $s = \frac{1}{2}$,

$$r_1^3 - \left(\frac{6n}{\sqrt{3}}r_2^3\right)r_1 + \frac{3n}{\sqrt{3}}r_2^3 = 0 \qquad n = 2,3,4,... \tag{9.34}$$

where r_2 is given by Eq. (9.32) and r_1 and r_2 are in units of a_{He}. To obtain the solution of cubic Eq. (9.34), let

$$g = \frac{3n}{\sqrt{3}}r_2^3 \qquad n = 2,3,4,... \tag{9.35}$$

Then, Eq. (9.34) becomes:

$$r_1^3 - 2gr_1 + g = 0 \tag{9.36}$$

Using Eqs. (9.16-9.29), the physical root r_1 is from the roots that are real and distinct:

$$r_{11} = 2\left(\frac{8}{27}\right)^{1/6}\sqrt{g}\cos\frac{\theta}{3}; r_{12} = -\left(\frac{8}{27}\right)^{1/6}\sqrt{g}\left(\cos\frac{\theta}{3} + \sqrt{3}\sin\frac{\theta}{3}\right); r_{13} = -\left(\frac{8}{27}\right)^{1/6}\sqrt{g}\left(\cos\frac{\theta}{3} - \sqrt{3}\sin\frac{\theta}{3}\right) \tag{9.37}$$

Table 9.2. Calculated and experimental energies of He I triplet excited states with $\ell = 0$ $(1s^2 \rightarrow 1s^1(ns)^1)$.

n	r_1 (a_{He}) [a]	r_2 (a_{He}) [b]	**Term Symbol**	E_{ele} CP He I Energy Levels [c] (eV)	NIST He I Energy Levels [d] (eV)	Difference CP-NIST (eV)	Relative Difference [e] (CP-NIST)
2	0.506514	1.42265	1s2s ^{3}S	-4.78116	-4.76777	-0.01339	0.00281
3	0.500850	2.42265	1s3s ^{3}S	-1.87176	-1.86892	-0.00284	0.00152
4	0.500225	3.42265	1s4s ^{3}S	-0.99366	-0.99342	-0.00024	0.00024
5	0.500083	4.42265	1s5s ^{3}S	-0.61519	-0.61541	0.00022	-0.00036
6	0.500038	5.42265	1s6s ^{3}S	-0.41812	-0.41838	0.00026	-0.00063
7	0.500019	6.42265	1s7s ^{3}S	-0.30259	-0.30282	0.00023	-0.00077
8	0.500011	7.42265	1s8s ^{3}S	-0.22909	-0.22928	0.00019	-0.00081
9	0.500007	8.42265	1s9s ^{3}S	-0.17946	-0.17961	0.00015	-0.00083
10	0.500004	9.42265	1s10s ^{3}S	-0.14437	-0.1445	0.00013	-0.00087
11	0.500003	10.42265	1s11s ^{3}S	-0.11866	-0.11876	0.00010	-0.00087
					Avg.	**-0.00152**	**-0.00006**

[a] Radius of the inner electron 1 from Eq. (9.37).
[b] Radius of the outer electron 2 from Eq. (9.32).
[c] Classical physics (CP) calculated energy levels given by the electric energy (Eq. (9.12)).
[d] Experimental NIST levels [7] with the ionization potential defined as zero.
[e] (Theoretical-Experimental)/Experimental.

SINGLET EXCITED STATES WITH $\ell \neq 0$

With $\ell \neq 0$, the electron source current in the excited state is the sum of constant and time-dependent functions where the latter, given by Eq. (1.29), travels about the z-axis. The current due to the time dependent term of Eq. (1.29) corresponding to p, d, f, etc. orbitals is:

$$\begin{aligned}\mathbf{J} &= \frac{m\omega_n}{2\pi}\frac{e}{4\pi r_n^2}N[\delta(r-r_n)]\mathrm{Re}\left\{Y_\ell^m(\theta,\phi)\right\}\left[\mathbf{u}(t)\times\mathbf{r}\right] = \frac{m\omega_n}{2\pi}\frac{e}{4\pi r_n^2}N'[\delta(r-r_n)]\left(P_\ell^m(\cos\theta)\cos\left(m\phi+m\omega_n t\right)\right)\left[\mathbf{u}\times\mathbf{r}\right] \\ &= \frac{m\omega_n}{2\pi}\frac{e}{4\pi r_n^2}N'[\delta(r-r_n)]\left(P_\ell^m(\cos\theta)\cos\left(m\phi+m\omega_n t\right)\right)\sin\theta\hat{\phi}\end{aligned} \tag{9.38}$$

where to keep the form of the spherical harmonic as a traveling wave about the z-axis, $\omega_n' = m\omega_n$ and N and N' are normalization constants. The vectors are defined as:

$$\hat{\phi} = \frac{\hat{u}\times\hat{r}}{\left|\hat{u}\times\hat{r}\right|} = \frac{\hat{u}\times\hat{r}}{\sin\theta}; \qquad \hat{u} = \hat{z} = orbital\ axis \tag{9.39}$$

$$\hat{\theta} = \hat{\phi}\times\hat{r} \tag{9.40}$$

"^" denotes the unit vectors $\hat{u} \equiv \dfrac{\mathbf{u}}{|\mathbf{u}|}$, non-unit vectors are designated in bold, and the current function is normalized.

Jackson [8] gives the general multipole field solution to Maxwell's equations in a source-free region of empty space with the assumption of a time dependence $e^{i\omega_n t}$:

$$\begin{aligned}\mathbf{B} &= \sum_{\ell,m}\left[a_E(\ell,m)\,f_\ell(kr)\mathbf{X}_{\ell,m} - \frac{i}{k}a_M(\ell,m)\nabla\times g_\ell(kr)\mathbf{X}_{\ell,m}\right] \\ \mathbf{E} &= \sum_{\ell,m}\left[\frac{i}{k}a_E(\ell,m)\nabla\times f_\ell(kr)\mathbf{X}_{\ell,m} + a_M(\ell,m)\,g_\ell(kr)\mathbf{X}_{\ell,m}\right]\end{aligned} \tag{9.41}$$

where the cgs units used by Jackson are retained in this section. The radial functions $f_\ell(kr)$ and $g_\ell(kr)$ are of the form:

$$g_\ell(kr) = A_\ell^{(1)}h_\ell^{(1)} + A_\ell^{(2)}h_\ell^{(2)} \tag{9.42}$$

$\mathbf{X}_{\ell,m}$ is the vector spherical harmonic defined by:

$$\mathbf{X}_{\ell,m}(\theta,\phi) = \frac{1}{\sqrt{\ell(\ell+1)}}\mathbf{L}Y_{\ell,m}(\theta,\phi) \tag{9.43}$$

where

$$\mathbf{L}=\frac{1}{i}(\mathbf{r}\times\nabla) \tag{9.44}$$

The coefficients $a_E(\ell,m)$ and $a_M(\ell,m)$ of Eq. (9.41) specify the amounts of electric (ℓ,m) multipole and magnetic (ℓ,m) multipole fields, and are determined by sources and boundary conditions as are the relative proportions in Eq. (9.42). Jackson gives the result of the electric and magnetic coefficients from the sources as

$$a_E(\ell,m)=\frac{4\pi k^2}{i\sqrt{\ell(\ell+1)}}\int Y_\ell^{m*}\left\{\rho\frac{\delta}{\delta r}\left[rj_\ell(kr)\right]+\frac{ik}{c}(\mathbf{r}\cdot\mathbf{J})\,j_\ell(kr)-ik\nabla\cdot(r\times\boldsymbol{M})\,j_\ell(kr)\right\}d^3x \tag{9.45}$$

and

$$a_M(\ell,m)=\frac{-4\pi k^2}{\sqrt{\ell(\ell+1)}}\int j_\ell(kr)Y_\ell^{m*}\mathbf{L}\cdot\left(\frac{\mathbf{J}}{c}+\nabla\times\boldsymbol{M}\right)d^3x \tag{9.46}$$

respectively, where the distribution of charge $\rho(\mathbf{x},t)$, current $\mathbf{J}(\mathbf{x},t)$, and intrinsic magnetization $\boldsymbol{M}(\mathbf{x},t)$ are harmonically varying sources: $\rho(\mathbf{x})e^{-\omega_n t}$, $\mathbf{J}(\mathbf{x})e^{-\omega_n t}$, and $\boldsymbol{M}(\mathbf{x})e^{-\omega_n t}$. From Eq. (9.38), the charge and intrinsic magnetization terms are zero. Since the source dimensions are very small compared to a wavelength ($kr_{\max}<<1$), the small argument limit can be used to give the magnetic multipole coefficient $a_M(\ell,m)$ as:

$$a_M(\ell,m)=\frac{-4\pi k^{\ell+2}}{(2\ell+1)!!}\left(\frac{\ell+1}{\ell}\right)^{1/2}\left(M_{\ell,m}+M'_{\ell,m}\right)=\frac{-4\pi k^{\ell+2}}{\frac{(2\ell+1)!}{2^\ell\ell!}}\left(\frac{\ell+1}{\ell}\right)^{1/2}\left(M_{\ell,m}+M'_{\ell,m}\right) \tag{9.47}$$

where $(2\ell+1)!!=(2\ell+1)(2\ell-1)(2\ell-3)\cdots(5)\cdot(3)\cdot(1)=\frac{(2\ell+1)!}{2^\ell\ell!}$ and the magnetic multipole moments are:

$$M_{\ell,m}=-\frac{1}{\ell+1}\int r^\ell Y^*_{\ell,m}\nabla\cdot\left(\frac{\mathbf{r}\times\mathbf{J}}{c}\right)d^3x$$

$$M'_{\ell,m}=-\int r^\ell Y^*_{\ell,m}\nabla\cdot\boldsymbol{M}d^3x \tag{9.48}$$

From Eq. (1.140), the geometrical factor of the surface current-density function of the atomic orbital about the z-axis is $\left(\frac{2}{3}\right)^{-1}$. Using the geometrical factor, Eqs. (9.47-9.48), and Eqs. (24.101) and (24.102) of Jackson [9], the multipole coefficient $a_{Mag}(\ell,m)$ of the magnetic force of Eq. (7.24) is:

$$a_{Mag}(\ell,m)=\frac{\frac{3}{2}}{(2\ell+1)!!}\frac{1}{\ell+2}\left(\frac{\ell+1}{\ell}\right)^{1/2} \tag{9.49}$$

For singlet states with $\ell\neq0$, a minimum energy is achieved with conservation of the photon's angular momentum of $\hbar$ when the magnetic moments of the corresponding angular momenta relative to the electron velocity (and corresponding Lorentz forces given by Eq. (7.10)) superimpose negatively such that the spin component is radial ($\mathbf{i}_r$-direction) and the orbital component is central ($-\mathbf{i}_r$-direction). The amplitude of the orbital angular momentum $\mathbf{L}_{rotational\ orbital}$, given by Eq. (1.76) is:

$$\mathbf{L}=I\omega\mathbf{i}_z=\hbar\left[\frac{\ell(\ell+1)}{\ell^2+2\ell+1}\right]^{\frac{1}{2}}=\hbar\sqrt{\frac{\ell}{\ell+1}} \tag{9.50}$$

Thus, using Eqs. (7.24), (9.8), (9.49-9.50), and Eq. (36) of Appendix VI, the magnetic force between the two electrons is:

$$\mathbf{F}_{mag}=\frac{1}{n}\frac{\frac{3}{2}}{(2\ell+1)!!}\frac{1}{\ell+2}\left(\frac{\ell+1}{\ell}\right)^{1/2}\frac{1}{2}\frac{\hbar^2}{m_e r^3}\left(\sqrt{s(s+1)}-\sqrt{\frac{\ell}{\ell+1}}\right)\mathbf{i}_r \tag{9.51}$$

and the force balance equation from Eq. (7.32) which achieves the condition that the sum of the mechanical momentum and electromagnetic momentum is conserved as given in Sections 6.6, 12.10, and 17.3 of Jackson [10] is:

$$\frac{m_e v^2}{r_2}=\frac{\hbar^2}{m_e r_2^3}=\frac{1}{n}\frac{e^2}{4\pi\varepsilon_0 r_2^2}-\frac{1}{n}\frac{\frac{3}{2}}{(2\ell+1)!!}\left(\frac{\ell+1}{\ell}\right)^{1/2}\frac{1}{\ell+2}\frac{1}{2}\frac{\hbar^2}{m_e r^3}\left(\sqrt{s(s+1)}-\sqrt{\frac{\ell}{\ell+1}}\right) \tag{9.52}$$

with $s=\frac{1}{2}$,

$$r_2 = \left[n + \frac{\frac{3}{4}}{(2\ell+1)!!}\frac{1}{\ell+2}\left(\frac{\ell+1}{\ell}\right)^{1/2}\left(\sqrt{\frac{3}{4}} - \sqrt{\frac{\ell}{\ell+1}}\right)\right] a_{He} \qquad n = 2,3,4,... \tag{9.53}$$

The excited-state energy is the energy stored in the electric field, E_{ele}, given by Eq. (9.12) where r_2 is given by Eq. (9.53). The energies of the various singlet excited states of helium with $\ell \neq 0$ appear in Table 9.3.

Using r_2 (Eq. (9.53)), r_1 can be solved using the equal and opposite magnetic force of electron 2 on electron 1 and the central Coulombic force corresponding to the nuclear charge of $2e$. Using Eq. (9.52), the force balance between the centrifugal and electric and magnetic forces is:

$$\frac{m_e v^2}{r_1} = \frac{\hbar^2}{m_e r_1^3} = \frac{2e^2}{4\pi\varepsilon_0 r_1^2} + \frac{1}{n}\frac{\frac{3}{2}}{(2\ell+1)!!}\left(\frac{\ell+1}{\ell}\right)^{1/2}\frac{1}{\ell+2}\frac{1}{2}\frac{\hbar^2}{m_e r_2^3}\left(\sqrt{s(s+1)} - \sqrt{\frac{\ell}{\ell+1}}\right) \tag{9.54}$$

with $s = \frac{1}{2}$,

$$\begin{aligned} &r_1^3 + \frac{n8r_1r_2^3}{3\left(\sqrt{\frac{3}{4}} - \sqrt{\frac{\ell}{\ell+1}}\right)}(2\ell+1)!!\left(\frac{\ell}{\ell+1}\right)^{1/2}(\ell+2) \\ &\quad - \frac{n4r_2^3}{3\left(\sqrt{\frac{3}{4}} - \sqrt{\frac{\ell}{\ell+1}}\right)}(2\ell+1)!!\left(\frac{\ell}{\ell+1}\right)^{1/2}(\ell+2) = 0 \\ &\quad n = 2,3,4,... \end{aligned} \tag{9.55}$$

where r_2 is given by Eq. (9.53) and r_1 and r_2 are in units of a_{He}. To obtain the solution of cubic Eq. (9.55), let

$$g = -\frac{n4r_2^3}{3\left(\sqrt{\frac{3}{4}} - \sqrt{\frac{\ell}{\ell+1}}\right)}(2\ell+1)!!\left(\frac{\ell}{\ell+1}\right)^{1/2}(\ell+2) \qquad n = 2,3,4,... \tag{9.56}$$

Then, Eq. (9.55) becomes:

$$r_1^3 - 2gr_1 + g = 0 \tag{9.57}$$

Three distinct cases arise depending on the value of ℓ. For $\ell = 1$ or $\ell = 2$, g of Eq. (9.56) is negative and A and B of Eqs. (9.20) and (9.21), respectively, are real:

$$A = \sqrt[3]{-\frac{g}{2}}\sqrt[3]{1 + \sqrt{1 - \frac{32}{27}g}} \tag{9.58}$$

and

$$B = -\sqrt[3]{-\frac{g}{2}}\sqrt[3]{\sqrt{1 - \frac{32}{27}g} - 1} \tag{9.59}$$

The only real root is:

$$r_1 = r_{11} = \sqrt[3]{-\frac{g}{2}}\left\{\sqrt[3]{1 + \sqrt{1 - \frac{32}{27}g}} - \sqrt[3]{\sqrt{1 - \frac{32}{27}g} - 1}\right\} \tag{9.60}$$

while r_{12} and r_{13} are complex conjugates. When $\ell = 3$ the magnetic force term (2nd term on RHS) of Eq. (9.52) is zero, and the force balance trivially gives:

$$r_1 = 0.5a_{He} \tag{9.61}$$

When $\ell = 4,5,6...$, g (Eq. (9.56)) is positive; so, all three roots are real, but, the physical root is r_{13}. In this case, note that $n \geq 5$, $\ell \geq 4$; so, the factor g of Eq. (9.56) is large ($> 10^8$). Expanding r_{13} (Eq. (9.29)) for large values of g gives:

$$r_1 = r_{13} = -\left(\frac{8}{27}\right)^{1/6}\sqrt{g}\left(\cos\frac{\theta}{3} - \sqrt{3}\sin\frac{\theta}{3}\right) = \frac{1}{2} + \frac{1}{16g} + O\left(g^{-3/2}\right) \approx \frac{1}{2} \tag{9.62}$$

Table 9.3. Calculated and experimental energies of He I singlet excited states with $\ell \neq 0$.

n	ℓ	r_1 (a_{He}) [a]	r_2 (a_{He}) [b]	**Term Symbol**	E_{ele} CP He I Energy Levels [c] (eV)	NIST He I Energy Levels [d] (eV)	Difference CP-NIST (eV)	Relative Difference [e] (CP-NIST)
2	1	0.499929	2.01873	1s2p $^1P^0$	-3.36941	-3.36936	-0.0000477	0.0000141
3	2	0.499999	3.00076	1s3d ^1D	-1.51116	-1.51331	0.0021542	-0.0014235
3	1	0.499986	3.01873	1s3p $^1P^0$	-1.50216	-1.50036	-0.0017999	0.0011997
4	2	0.500000	4.00076	1s4d ^1D	-0.85008	-0.85105	0.0009711	-0.0011411
4	3	0.500000	4.00000	1s4f $^1F^0$	-0.85024	-0.85037	0.0001300	-0.0001529
4	1	0.499995	4.01873	1s4p $^1P^0$	-0.84628	-0.84531	-0.0009676	0.0011446
5	2	0.500000	5.00076	1s5d ^1D	-0.54407	-0.54458	0.0005089	-0.0009345
5	3	0.500000	5.00000	1s5f $^1F^0$	-0.54415	-0.54423	0.0000764	-0.0001404
5	4	0.500000	5.00000	1s5g ^1G	-0.54415	-0.54417	0.0000159	-0.0000293
5	1	0.499998	5.01873	1s5p $^1P^0$	-0.54212	-0.54158	-0.0005429	0.0010025
6	2	0.500000	6.00076	1s6d ^1D	-0.37784	-0.37813	0.0002933	-0.0007757
6	3	0.500000	6.00000	1s6f $^1F^0$	-0.37788	-0.37793	0.0000456	-0.0001205
6	4	0.500000	6.00000	1s6g ^1G	-0.37788	-0.37789	0.0000053	-0.0000140
6	5	0.500000	6.00000	1s6h $^1H^0$	-0.37788	-0.37788	-0.0000045	0.0000119
6	1	0.499999	6.01873	1s6p $^1P^0$	-0.37671	-0.37638	-0.0003286	0.0008730
7	2	0.500000	7.00076	1s7d ^1D	-0.27760	-0.27779	0.0001907	-0.0006864
7	3	0.500000	7.00000	1s7f $^1F^0$	-0.27763	-0.27766	0.0000306	-0.0001102
7	4	0.500000	7.00000	1s7g ^1G	-0.27763	-0.27763	0.0000004	-0.0000016
7	5	0.500000	7.00000	1s7h $^1H^0$	-0.27763	-0.27763	0.0000006	-0.0000021
7	6	0.500000	7.00000	1s7i ^1I	-0.27763	-0.27762	-0.0000094	0.0000338
7	1	0.500000	7.01873	1s7p $^1P^0$	-0.27689	-0.27667	-0.0002186	0.0007900
						Avg.	**0.0000240**	**-0.0000220**

[a] Radius of the inner electron 1 from Eq. (9.60) for $\ell = 1$ or $\ell = 2$, Eq. (9.61) for $\ell = 3$, and Eq. (9.62) for $\ell = 4, 5, 6...$.

[b] Radius of the outer electron 2 from Eq. (9.53).

[c] Classical physics (CP) calculated energy levels given by the electric energy (Eq. (9.12)).

[d] Experimental NIST levels [7] with the ionization potential defined as zero.

[e] (Theoretical-Experimental)/Experimental.

TRIPLET EXCITED STATES WITH $\ell \neq 0$

For triplet states with $\ell \neq 0$, a minimum energy is achieved with conservation of the photon's angular momentum of $\hbar$ when the magnetic moments of the corresponding angular momenta superimpose negatively such that the spin component is central and the orbital component is radial. Furthermore, as given for the triplet states with $\ell = 0$, the spin component in Eqs. (9.51) and (9.52) is doubled. Thus, the force balance equation derived in Appendix VI is given by:

$$\frac{m_e v^2}{r_2} = \frac{\hbar^2}{m_e r_2^3} = \frac{1}{n}\frac{e^2}{4\pi\varepsilon_0 r_2^2} + \frac{1}{n}\frac{\frac{3}{2}}{(2\ell+1)!!}\left(\frac{\ell+1}{\ell}\right)^{1/2}\frac{1}{\ell+2}\frac{1}{2}\frac{\hbar^2}{m_e r^3}\left(2\sqrt{s(s+1)} - \sqrt{\frac{\ell}{\ell+1}}\right) \tag{9.63}$$

With $s = \frac{1}{2}$,

$$r_2 = \left[n - \frac{\frac{3}{4}}{(2\ell+1)!!}\frac{1}{\ell+2}\left(\frac{\ell+1}{\ell}\right)^{1/2}\left(2\sqrt{\frac{3}{4}} - \sqrt{\frac{\ell}{\ell+1}}\right)\right]a_{He} \tag{9.64}$$

$$n = 2, 3, 4, ...$$

The excited-state energy is the energy stored in the electric field, E_{ele}, given by Eq. (9.12) where r_2 is given by Eq. (9.64). The energies of the various triplet excited states of helium with $\ell \neq 0$ appear in Table 9.4.

Using r_2 (Eq. (9.64)), r_1 can be solved using the equal and opposite magnetic force of electron 2 on electron 1 and the central Coulombic force corresponding to the nuclear charge of $2e$. Using Eq. (9.63), the force balance between the centrifugal and electric and magnetic forces is:

$$\frac{m_e v^2}{r_1} = \frac{\hbar^2}{m_e r_1^3} = \frac{2e^2}{4\pi\varepsilon_0 r_1^2} - \frac{1}{n}\frac{\frac{3}{2}}{(2\ell+1)!!}\left(\frac{\ell+1}{\ell}\right)^{1/2}\frac{1}{\ell+2}\frac{1}{2}\frac{\hbar^2}{m_e r_2^3}\left(2\sqrt{s(s+1)} - \sqrt{\frac{\ell}{\ell+1}}\right) \tag{9.65}$$

with $s = \frac{1}{2}$,

$$r_1^3 - \frac{n8r_1r_2^3}{3\left(\sqrt{\frac{3}{4}} - \sqrt{\frac{\ell}{\ell+1}}\right)}(2\ell+1)!!\left(\frac{\ell}{\ell+1}\right)^{1/2}(\ell+2) + \frac{n4r_2^3}{3\left(\sqrt{\frac{3}{4}} - \sqrt{\frac{\ell}{\ell+1}}\right)}(2\ell+1)!!\left(\frac{\ell}{\ell+1}\right)^{1/2}(\ell+2) = 0 \tag{9.66}$$

$$n = 2,3,4,...$$

where r_2 is given by Eq. (9.64) and r_1 and r_2 are in units of a_{He}. To obtain the solution of cubic Eq. (9.66), let:

$$g = \frac{n4r_2^3}{3\left(\sqrt{3} - \sqrt{\frac{\ell}{\ell+1}}\right)}(2\ell+1)!!\left(\frac{\ell}{\ell+1}\right)^{1/2}(\ell+2) \qquad n = 2,3,4,... \tag{9.67}$$

Then, Eq. (9.66) becomes:

$$r_1^3 - 2gr_1 + g = 0 \tag{9.68}$$

Using Eqs. (9.16-9.29), g (Eq. (9.67)) is positive, and the physical root r_1 is from the roots that are real and distinct:

$$r_{11} = 2\left(\frac{8}{27}\right)^{1/6}\sqrt{g}\cos\frac{\theta}{3}; r_{12} = -\left(\frac{8}{27}\right)^{1/6}\sqrt{g}\left(\cos\frac{\theta}{3} + \sqrt{3}\sin\frac{\theta}{3}\right); r_{13} = -\left(\frac{8}{27}\right)^{1/6}\sqrt{g}\left(\cos\frac{\theta}{3} - \sqrt{3}\sin\frac{\theta}{3}\right) \tag{9.69}$$

Table 9.4. Calculated and experimental energies of He I triplet excited states with $\ell \neq 0$.

n	ℓ	r_1 (a_{He}) [a]	r_2 (a_{He}) [b]	**Term Symbol**	E_{ele} CP He I Energy Levels [c] (eV)	NIST He I Energy Levels [d] (eV)	Difference CP-NIST (eV)	Relative Difference [e] (CP-NIST)
2	1	0.500571	1.87921	1s2p $^3P^0_2$	-3.61957	-3.6233	0.0037349	-0.0010308
2	1	0.500571	1.87921	1s2p $^3P^0_1$	-3.61957	-3.62329	0.0037249	-0.0010280
2	1	0.500571	1.87921	1s2p $^3P^0_0$	-3.61957	-3.62317	0.0036049	-0.0009949
3	1	0.500105	2.87921	1s3p $^3P^0_2$	-1.57495	-1.58031	0.0053590	-0.0033911
3	1	0.500105	2.87921	1s3p $^3P^0_1$	-1.57495	-1.58031	0.0053590	-0.0033911
3	1	0.500105	2.87921	1s3p $^3P^0_0$	-1.57495	-1.58027	0.0053190	-0.0033659
3	2	0.500011	2.98598	1s3d $^3D_3$	-1.51863	-1.51373	-0.0049031	0.0032391
3	2	0.500011	2.98598	1s3d $^3D_2$	-1.51863	-1.51373	-0.0049031	0.0032391
3	2	0.500011	2.98598	1s3d $^3D_1$	-1.51863	-1.51373	-0.0049031	0.0032391
4	1	0.500032	3.87921	1s4p $^3P^0_2$	-0.87671	-0.87949	0.0027752	-0.0031555
4	1	0.500032	3.87921	1s4p $^3P^0_1$	-0.87671	-0.87949	0.0027752	-0.0031555
4	1	0.500032	3.87921	1s4p $^3P^0_0$	-0.87671	-0.87948	0.0027652	-0.0031442
4	2	0.500003	3.98598	1s4d $^3D_3$	-0.85323	-0.85129	-0.0019398	0.0022787
4	2	0.500003	3.98598	1s4d $^3D_2$	-0.85323	-0.85129	-0.0019398	0.0022787

n	ℓ	r_1 (a_{He}) [a]	r_2 (a_{He}) [b]	**Term Symbol**	E_{ele} CP He I Energy Levels [c] (eV)	NIST He I Energy Levels [d] (eV)	Difference CP-NIST (eV)	Relative Difference [e] (CP-NIST)
4	2	0.500003	3.98598	$1s4d\ ^3D_1$	-0.85323	-0.85129	-0.0019398	0.0022787
4	3	0.500000	3.99857	$1s4f\ ^3F^0_3$	-0.85054	-0.85038	-0.0001638	0.0001926
4	3	0.500000	3.99857	$1s4f\ ^3F^0_4$	-0.85054	-0.85038	-0.0001638	0.0001926
4	3	0.500000	3.99857	$1s4f\ ^3F^0_2$	-0.85054	-0.85038	-0.0001638	0.0001926
5	1	0.500013	4.87921	$1s5p\ ^3P^0_2$	-0.55762	-0.55916	0.0015352	-0.0027456
5	1	0.500013	4.87921	$1s5p\ ^3P^0_1$	-0.55762	-0.55916	0.0015352	-0.0027456
5	1	0.500013	4.87921	$1s5p\ ^3P^0_0$	-0.55762	-0.55915	0.0015252	-0.0027277
5	2	0.500001	4.98598	$1s5d\ ^3D_3$	-0.54568	-0.54472	-0.0009633	0.0017685
5	2	0.500001	4.98598	$1s5d\ ^3D_2$	-0.54568	-0.54472	-0.0009633	0.0017685
5	2	0.500001	4.98598	$1s5d\ ^3D_1$	-0.54568	-0.54472	-0.0009633	0.0017685
5	3	0.500000	4.99857	$1s5f\ ^3F^0_3$	-0.54431	-0.54423	-0.0000791	0.0001454
5	3	0.500000	4.99857	$1s5f\ ^3F^0_4$	-0.54431	-0.54423	-0.0000791	0.0001454
5	3	0.500000	4.99857	$1s5f\ ^3F^0_2$	-0.54431	-0.54423	-0.0000791	0.0001454
5	4	0.500000	4.99988	$1s5g\ ^3G_4$	-0.54417	-0.54417	0.0000029	-0.0000054
5	4	0.500000	4.99988	$1s5g\ ^3G_5$	-0.54417	-0.54417	0.0000029	-0.0000054
5	4	0.500000	4.99988	$1s5g\ ^3G_3$	-0.54417	-0.54417	0.0000029	-0.0000054
6	1	0.500006	5.87921	$1s6p\ ^3P^0_2$	-0.38565	-0.38657	0.0009218	-0.0023845
6	1	0.500006	5.87921	$1s6p\ ^3P^0_1$	-0.38565	-0.38657	0.0009218	-0.0023845
6	1	0.500006	5.87921	$1s6p\ ^3P^0_0$	-0.38565	-0.38657	0.0009218	-0.0023845
6	2	0.500001	5.98598	$1s6d\ ^3D_3$	-0.37877	-0.37822	-0.0005493	0.0014523
6	2	0.500001	5.98598	$1s6d\ ^3D_2$	-0.37877	-0.37822	-0.0005493	0.0014523
6	2	0.500001	5.98598	$1s6d\ ^3D_1$	-0.37877	-0.37822	-0.0005493	0.0014523
6	3	0.500000	5.99857	$1s6f\ ^3F^0_3$	-0.37797	-0.37793	-0.0000444	0.0001176
6	3	0.500000	5.99857	$1s6f\ ^3F^0_4$	-0.37797	-0.37793	-0.0000444	0.0001176
6	3	0.500000	5.99857	$1s6f\ ^3F^0_2$	-0.37797	-0.37793	-0.0000444	0.0001176
6	4	0.500000	5.99988	$1s6g\ ^3G_4$	-0.37789	-0.37789	-0.0000023	0.0000060
6	4	0.500000	5.99988	$1s6g\ ^3G_5$	-0.37789	-0.37789	-0.0000023	0.0000060
6	4	0.500000	5.99988	$1s6g\ ^3G_3$	-0.37789	-0.37789	-0.0000023	0.0000060
6	5	0.500000	5.99999	$1s6h\ ^3H^0_4$	-0.37789	-0.37788	-0.0000050	0.0000133
6	5	0.500000	5.99999	$1s6h\ ^3H^0_5$	-0.37789	-0.37788	-0.0000050	0.0000133
6	5	0.500000	5.99999	$1s6h\ ^3H^0_6$	-0.37789	-0.37788	-0.0000050	0.0000133
7	1	0.500003	6.87921	$1s7p\ ^3P^0_2$	-0.28250	-0.28309	0.0005858	-0.0020692
7	1	0.500003	6.87921	$1s7p\ ^3P^0_1$	-0.28250	-0.28309	0.0005858	-0.0020692
7	1	0.500003	6.87921	$1s7p\ ^3P^0_0$	-0.28250	-0.28309	0.0005858	-0.0020692
7	2	0.500000	6.98598	$1s7d\ ^3D_3$	-0.27819	-0.27784	-0.0003464	0.0012468
7	2	0.500000	6.98598	$1s7d\ ^3D_2$	-0.27819	-0.27784	-0.0003464	0.0012468
7	2	0.500000	6.98598	$1s7d\ ^3D_1$	-0.27819	-0.27784	-0.0003464	0.0012468
7	3	0.500000	6.99857	$1s7f\ ^3F^0_3$	-0.27769	-0.27766	-0.0000261	0.0000939
7	3	0.500000	6.99857	$1s7f\ ^3F^0_4$	-0.27769	-0.27766	-0.0000261	0.0000939
7	3	0.500000	6.99857	$1s7f\ ^3F^0_2$	-0.27769	-0.27766	-0.0000261	0.0000939

n	ℓ	r_1 (a_{He}) [a]	r_2 (a_{He}) [b]	**Term Symbol**	E_{ele} CP He I Energy Levels [c] (eV)	NIST He I Energy Levels [d] (eV)	Difference CP-NIST (eV)	Relative Difference [e] (CP-NIST)
7	4	0.500000	6.99988	$1s7g\ ^3G_4$	-0.27763	-0.27763	-0.0000043	0.0000155
7	4	0.500000	6.99988	$1s7g\ ^3G_5$	-0.27763	-0.27763	-0.0000043	0.0000155
7	4	0.500000	6.99988	$1s7g\ ^3G_3$	-0.27763	-0.27763	-0.0000043	0.0000155
7	5	0.500000	6.99999	$1s7h\ ^3H^0_5$	-0.27763	-0.27763	0.0000002	-0.0000009
7	5	0.500000	6.99999	$1s7h\ ^3H^0_6$	-0.27763	-0.27763	0.0000002	-0.0000009
7	5	0.500000	6.99999	$1s7h\ ^3H^0_4$	-0.27763	-0.27763	0.0000002	-0.0000009
7	6	0.500000	7.00000	$1s7\ i^3I_5$	-0.27763	-0.27762	-0.0000094	0.0000339
7	6	0.500000	7.00000	$1s7i\ ^3I6$	-0.27763	-0.27762	-0.0000094	0.0000339
7	6	0.500000	7.00000	$1s7i\ ^3I_7$	-0.27763	-0.27762	-0.0000094	0.0000339
						Avg.	**0.0002768**	**-0.0001975**

[a] Radius of the inner electron 1 from Eq. (9.69).
[b] Radius of the outer electron 2 from Eq. (9.64).
[c] Classical physics (CP) calculated energy levels given by the electric energy (Eq. (9.12)).
[d] Experimental NIST levels [7] with the ionization potential defined as zero.
[e] (Theoretical-Experimental)/Experimental.

ALL EXCITED HE I STATES

The combined energies of the various states of helium appear in Table 9.5. A plot of the predicted and experimental energies of levels assigned by NIST [7] appears in Figure 9.1.

Figure 9.1. A plot of the predicted and experimental energies of levels assigned by NIST [7].

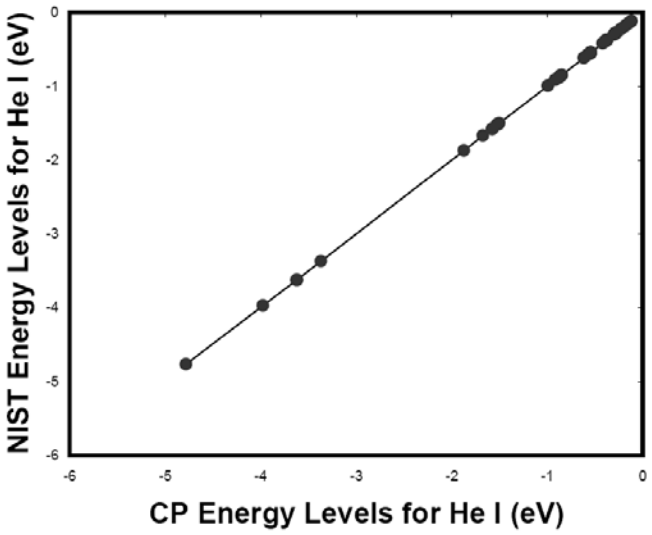

For over 100 states, the r-squared value is 0.999994, and the typical average relative difference is about 5 significant figures, which is within the error of the experimental data. The agreement is remarkable. The color scale, translucent views of the charge densities of exemplary spherical harmonics that modulate the time-independent spin function are shown in Figure 9.2. For $\ell \neq 0$, the modulation functions propagate about the z-axis as spatially and temporally harmonic charge-density waves.

Figure 9.2. Exemplary color scale, translucent views of the charge-densities of the inner and outer electrons of helium excited states. The outer-electron orbital function modulates the time-constant (spin) function, (shown for t = 0; three-dimensional view). The inner electron is essentially that of He^+ (nuclei red, not to scale).

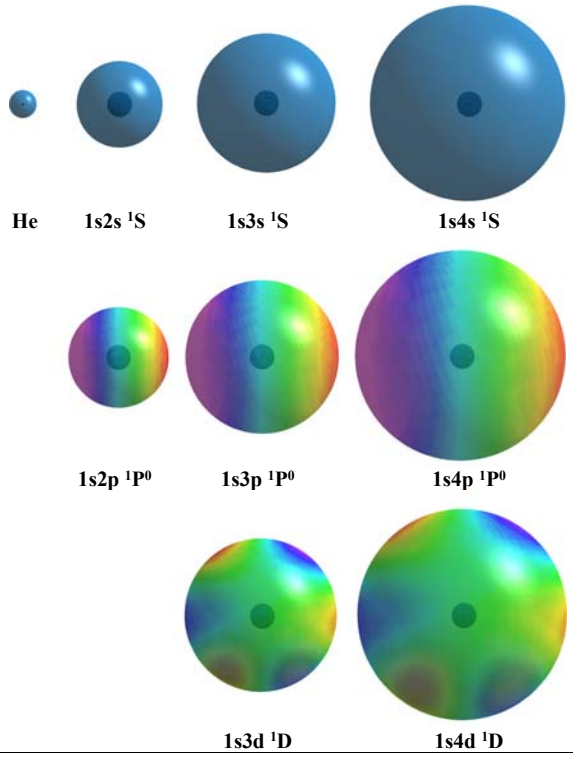

The hydrino states given in the Hydrino Theory—BlackLight Process section are strongly supported by the calculation of the helium excited states as well as the hydrogen excited states given in the Electron Atom (Quantization) Excited States of the One-model is the same in both the section since the electron-photon energy states of hydrogen except excited states and in the lower-central field of magnitude n in that the photon provides a excited-state case. the hydrino case and $1/n$ in the

Table 9.5. Calculated and experimental energies of states of helium.

n	ℓ	r_1 (a_{He}) [a]	r_2 (a_{He}) [b]	**Term Symbol**	E_{ele} CP He I EnergyLevels [c] (eV)	NIST He I Energy Levels [d] (eV)	Difference CP-NIST (eV)	Relative Difference [e] (CP-NIST)
1	0	0.56699	0.566987	$1s^2\ ^1S$	-24.58750	-24.58741	-0.000092	0.0000038
2	0	0.506514	1.42265	$1s2s\ ^3S$	-4.78116	-4.76777	-0.0133929	0.0028090
2	0	0.501820	1.71132	$1s2s\ ^1S$	-3.97465	-3.97161	-0.0030416	0.0007658
2	1	0.500571	1.87921	$1s2p\ ^3P^0_2$	-3.61957	-3.6233	0.0037349	-0.0010308
2	1	0.500571	1.87921	$1s2p\ ^3P^0_1$	-3.61957	-3.62329	0.0037249	-0.0010280
2	1	0.500571	1.87921	$1s2p\ ^3P^0_0$	-3.61957	-3.62317	0.0036049	-0.0009949
2	1	0.499929	2.01873	$1s2p\ ^1P^0$	-3.36941	-3.36936	-0.0000477	0.0000141
3	0	0.500850	2.42265	$1s3s\ ^3S$	-1.87176	-1.86892	-0.0028377	0.0015184
3	0	0.500302	2.71132	$1s3s\ ^1S$	-1.67247	-1.66707	-0.0054014	0.0032401
3	1	0.500105	2.87921	$1s3p\ ^3P^0_2$	-1.57495	-1.58031	0.0053590	-0.0033911
3	1	0.500105	2.87921	$1s3p\ ^3P^0_1$	-1.57495	-1.58031	0.0053590	-0.0033911
3	1	0.500105	2.87921	$1s3p\ ^3P^0_0$	-1.57495	-1.58027	0.0053190	-0.0033659
3	2	0.500011	2.98598	$1s3d\ ^3D_3$	-1.51863	-1.51373	-0.0049031	0.0032391
3	2	0.500011	2.98598	$1s3d\ ^3D_2$	-1.51863	-1.51373	-0.0049031	0.0032391
3	2	0.500011	2.98598	$1s3d\ ^3D_1$	-1.51863	-1.51373	-0.0049031	0.0032391
3	2	0.499999	3.00076	$1s3d\ ^1D$	-1.51116	-1.51331	0.0021542	-0.0014235
3	1	0.499986	3.01873	$1s3p\ ^1P^0$	-1.50216	-1.50036	-0.0017999	0.0011997
4	0	0.500225	3.42265	$1s4s\ ^3S$	-0.99366	-0.99342	-0.0002429	0.0002445
4	0	0.500088	3.71132	$1s4s\ ^1S$	-0.91637	-0.91381	-0.0025636	0.0028054

n	ℓ	r_1 (a_{He}) [a]	r_2 (a_{He}) [b]	**Term Symbol**	E_{ele} CP He I EnergyLevels [c] (eV)	NIST He I Energy Levels [d] (eV)	Difference CP-NIST (eV)	Relative Difference [e] (CP-NIST)
4	1	0.500032	3.87921	$1s4p\ ^3P^0_2$	-0.87671	-0.87949	0.0027752	-0.0031555
4	1	0.500032	3.87921	$1s4p\ ^3P^0_1$	-0.87671	-0.87949	0.0027752	-0.0031555
4	1	0.500032	3.87921	$1s4p\ ^3P^0_0$	-0.87671	-0.87948	0.0027652	-0.0031442
4	2	0.500003	3.98598	$1s4d\ ^3D_3$	-0.85323	-0.85129	-0.0019398	0.0022787
4	2	0.500003	3.98598	$1s4d\ ^3D_2$	-0.85323	-0.85129	-0.0019398	0.0022787
4	2	0.500003	3.98598	$1s4d\ ^3D_1$	-0.85323	-0.85129	-0.0019398	0.0022787
4	2	0.500000	4.00076	$1s4d\ ^1D$	-0.85008	-0.85105	0.0009711	-0.0011411
4	3	0.500000	3.99857	$1s4f\ ^3F^0_3$	-0.85054	-0.85038	-0.0001638	0.0001926
4	3	0.500000	3.99857	$1s4f\ ^3F^0_4$	-0.85054	-0.85038	-0.0001638	0.0001926
4	3	0.500000	3.99857	$1s4f\ ^3F^0_2$	-0.85054	-0.85038	-0.0001638	0.0001926
4	3	0.500000	4.00000	$1s4f\ ^1F^0$	-0.85024	-0.85037	0.0001300	-0.0001529
4	1	0.499995	4.01873	$1s4p\ ^1P^0$	-0.84628	-0.84531	-0.0009676	0.0011446
5	0	0.500083	4.42265	$1s5s\ ^3S$	-0.61519	-0.61541	0.0002204	-0.0003582
5	0	0.500035	4.71132	$1s5s\ ^1S$	-0.57750	-0.57617	-0.0013253	0.0023002
5	1	0.500013	4.87921	$1s5p\ ^3P^0_2$	-0.55762	-0.55916	0.0015352	-0.0027456
5	1	0.500013	4.87921	$1s5p\ ^3P^0_1$	-0.55762	-0.55916	0.0015352	-0.0027456
5	1	0.500013	4.87921	$1s5p\ ^3P^0_0$	-0.55762	-0.55915	0.0015252	-0.0027277
5	2	0.500001	4.98598	$1s5d\ ^3D_3$	-0.54568	-0.54472	-0.0009633	0.0017685
5	2	0.500001	4.98598	$1s5d\ ^3D_2$	-0.54568	-0.54472	-0.0009633	0.0017685
5	2	0.500001	4.98598	$1s5d\ ^3D_1$	-0.54568	-0.54472	-0.0009633	0.0017685
5	2	0.500000	5.00076	$1s5d\ ^1D$	-0.54407	-0.54458	0.0005089	-0.0009345
5	3	0.500000	4.99857	$1s5f\ ^3F^0_3$	-0.54431	-0.54423	-0.0000791	0.0001454
5	3	0.500000	4.99857	$1s5f\ ^3F^0_4$	-0.54431	-0.54423	-0.0000791	0.0001454
5	3	0.500000	4.99857	$1s5f\ ^3F^0_2$	-0.54431	-0.54423	-0.0000791	0.0001454
5	3	0.500000	5.00000	$1s5f\ ^1F^0$	-0.54415	-0.54423	0.0000764	-0.0001404
5	4	0.500000	4.99988	$1s5g\ ^3G_4$	-0.54417	-0.54417	0.0000029	-0.0000054
5	4	0.500000	4.99988	$1s5g\ ^3G_5$	-0.54417	-0.54417	0.0000029	-0.0000054
5	4	0.500000	4.99988	$1s5g\ ^3G_3$	-0.54417	-0.54417	0.0000029	-0.0000054
5	4	0.500000	5.00000	$1s5g\ ^1G$	-0.54415	-0.54417	0.0000159	-0.0000293
5	1	0.499998	5.01873	$1s5p\ ^1P^0$	-0.54212	-0.54158	-0.0005429	0.0010025
6	0	0.500038	5.42265	$1s6s\ ^3S$	-0.41812	-0.41838	0.0002621	-0.0006266
6	0	0.500016	5.71132	$1s6s\ ^1S$	-0.39698	-0.39622	-0.0007644	0.0019291
6	1	0.500006	5.87921	$1s6p\ ^3P^0_2$	-0.38565	-0.38657	0.0009218	-0.0023845
6	1	0.500006	5.87921	$1s6p\ ^3P^0_1$	-0.38565	-0.38657	0.0009218	-0.0023845
6	1	0.500006	5.87921	$1s6p\ ^3P^0_0$	-0.38565	-0.38657	0.0009218	-0.0023845
6	2	0.500001	5.98598	$1s6d\ ^3D_3$	-0.37877	-0.37822	-0.0005493	0.0014523
6	2	0.500001	5.98598	$1s6d\ ^3D_2$	-0.37877	-0.37822	-0.0005493	0.0014523
6	2	0.500001	5.98598	$1s6d\ ^3D_1$	-0.37877	-0.37822	-0.0005493	0.0014523
6	2	0.500000	6.00076	$1s6d\ ^1D$	-0.37784	-0.37813	0.0002933	-0.0007757
6	3	0.500000	5.99857	$1s6f\ ^3F^0_3$	-0.37797	-0.37793	-0.0000444	0.0001176
6	3	0.500000	5.99857	$1s6f\ ^3F^0_4$	-0.37797	-0.37793	-0.0000444	0.0001176

n	ℓ	r_1 (a_{He}) [a]	r_2 (a_{He}) [b]	**Term Symbol**	E_{ele} CP He I EnergyLevels [c] (eV)	NIST He I Energy Levels [d] (eV)	Difference CP-NIST (eV)	Relative Difference [e] (CP-NIST)
6	3	0.500000	5.99857	$1s6f\ ^3F^0_2$	-0.37797	-0.37793	-0.0000444	0.0001176
6	3	0.500000	6.00000	$1s6f\ ^1F^0$	-0.37788	-0.37793	0.0000456	-0.0001205
6	4	0.500000	5.99988	$1s6g\ ^3G_4$	-0.37789	-0.37789	-0.0000023	0.0000060
6	4	0.500000	5.99988	$1s6g\ ^3G_5$	-0.37789	-0.37789	-0.0000023	0.0000060
6	4	0.500000	5.99988	$1s6g\ ^3G_3$	-0.37789	-0.37789	-0.0000023	0.0000060
6	4	0.500000	6.00000	$1s6g\ ^1G$	-0.37788	-0.37789	0.0000053	-0.0000140
6	5	0.500000	5.99999	$1s6h\ ^3H^0_4$	-0.37789	-0.37788	-0.0000050	0.0000133
6	5	0.500000	5.99999	$1s6h\ ^3H^0_5$	-0.37789	-0.37788	-0.0000050	0.0000133
6	5	0.500000	5.99999	$1s6h\ ^3H^0_6$	-0.37789	-0.37788	-0.0000050	0.0000133
6	5	0.500000	6.00000	$1s6h\ ^1H^0$	-0.37788	-0.37788	-0.0000045	0.0000119
6	1	0.499999	6.01873	$1s6p\ ^1P^0$	-0.37671	-0.37638	-0.0003286	0.0008730
7	0	0.500019	6.42265	$1s7s\ ^3S$	-0.30259	-0.30282	0.0002337	-0.0007718
7	0	0.500009	6.71132	$1s7s\ ^1S$	-0.28957	-0.2891	-0.0004711	0.0016295
7	1	0.500003	6.87921	$1s7p\ ^3P^0_2$	-0.28250	-0.28309	0.0005858	-0.0020692
7	1	0.500003	6.87921	$1s7p\ ^3P^0_1$	-0.28250	-0.28309	0.0005858	-0.0020692
7	1	0.500003	6.87921	$1s7p\ ^3P^0_0$	-0.28250	-0.28309	0.0005858	-0.0020692
7	2	0.500000	6.98598	$1s7d\ ^3D_3$	-0.27819	-0.27784	-0.0003464	0.0012468
7	2	0.500000	6.98598	$1s7d\ ^3D_2$	-0.27819	-0.27784	-0.0003464	0.0012468
7	2	0.500000	6.98598	$1s7d\ ^3D_1$	-0.27819	-0.27784	-0.0003464	0.0012468
7	2	0.500000	7.00076	$1s7d\ ^1D$	-0.27760	-0.27779	0.0001907	-0.0006864
7	3	0.500000	6.99857	$1s7f\ ^3F^0_3$	-0.27769	-0.27766	-0.0000261	0.0000939
7	3	0.500000	6.99857	$1s7f\ ^3F^0_4$	-0.27769	-0.27766	-0.0000261	0.0000939
7	3	0.500000	6.99857	$1s7f\ ^3F^0_2$	-0.27769	-0.27766	-0.0000261	0.0000939
7	3	0.500000	7.00000	$1s7f\ ^1F^0$	-0.27763	-0.27766	0.0000306	-0.0001102
7	4	0.500000	6.99988	$1s7g\ ^3G_4$	-0.27763	-0.27763	-0.0000043	0.0000155
7	4	0.500000	6.99988	$1s7g\ ^3G_5$	-0.27763	-0.27763	-0.0000043	0.0000155
7	4	0.500000	6.99988	$1s7g\ ^3G_3$	-0.27763	-0.27763	-0.0000043	0.0000155
7	4	0.500000	7.00000	$1s7g\ ^1G$	-0.27763	-0.27763	0.0000004	-0.0000016
7	5	0.500000	6.99999	$1s7h\ ^3H^0_5$	-0.27763	-0.27763	0.0000002	-0.0000009
7	5	0.500000	6.99999	$1s7h\ ^3H^0_6$	-0.27763	-0.27763	0.0000002	-0.0000009
7	5	0.500000	6.99999	$1s7h\ ^3H^0_4$	-0.27763	-0.27763	0.0000002	-0.0000009
7	5	0.500000	7.00000	$1s7h\ ^1H^0$	-0.27763	-0.27763	0.0000006	-0.0000021
7	6	0.500000	7.00000	$1s7\ i^3I_5$	-0.27763	-0.27762	-0.0000094	0.0000339
7	6	0.500000	7.00000	$1s7i\ ^3I_6$	-0.27763	-0.27762	-0.0000094	0.0000339
7	6	0.500000	7.00000	$1s7i\ ^3I_7$	-0.27763	-0.27762	-0.0000094	0.0000339
7	6	0.500000	7.00000	$1s7i\ ^1I$	-0.27763	-0.27762	-0.0000094	0.0000338
7	1	0.500000	7.01873	$1s7p\ ^1P^0$	-0.27689	-0.27667	-0.0002186	0.0007900
8	0	0.500011	7.42265	$1s8s\ ^3S$	-0.22909	-0.22928	0.0001866	-0.0008139
8	0	0.500005	7.71132	$1s8s\ ^1S$	-0.22052	-0.2202	-0.0003172	0.0014407
9	0	0.500007	8.42265	$1s9s\ ^3S$	-0.17946	-0.17961	0.0001489	-0.0008291
9	0	0.500003	8.71132	$1s9s\ ^1S$	-0.17351	-0.1733	-0.0002141	0.0012355

n	ℓ	r_1 (a_{He}) [a]	r_2 (a_{He}) [b]	**Term Symbol**	E_{ele} CP He I EnergyLevels [c] (eV)	NIST He I Energy Levels [d] (eV)	Difference CP-NIST (eV)	Relative Difference [e] (CP-NIST)
10	0	0.500004	9.42265	1s10s ^{3}S	-0.14437	-0.1445	0.0001262	-0.0008732
10	0	0.500002	9.71132	1s10s ^{1}S	-0.14008	-0.13992	-0.0001622	0.0011594
11	0	0.500003	10.42265	1s11s ^{3}S	-0.11866	-0.11876	0.0001037	-0.0008734
11	0	0.500001	10.71132	1s11s ^{1}S	-0.11546	-0.11534	-0.0001184	0.0010268
						Avg.	**-0.000112**	**0.0000386**

[a] Radius of the inner electron 1 of singlet excited states with $\ell = 0$ from Eq. (9.29); triplet excited states with $\ell = 0$ from Eq. (9.37); singlet excited states with $\ell \neq 0$ from Eq. (9.60) for $\ell = 1$ or $\ell = 2$ and Eq. (9.61) for $\ell = 3$, and Eq. (9.62) for $\ell = 4, 5, 6...$; triplet excited states with $\ell \neq 0$ from Eq. (9.69), and $1s^2\ ^1S$ from Eq. (7.35).

[b] Radius of the outer electron 2 of singlet excited states with $\ell = 0$ from Eq. (9.11); triplet excited states with $\ell = 0$ from Eq. (9.32); singlet excited states with $\ell \neq 0$ from Eq. (9.53); triplet excited states with $\ell \neq 0$ from Eq. (9.64), and $1s^2\ ^1S$ from Eq. (7.35).

[c] Classical physics (CP) calculated excited-state energy levels given by the electric energy (Eq. (9.12)) and the energy level of $1s^2\ ^1S$ is given by Eqs. (7.44-7.46).

[d] Experimental NIST levels [7] with the ionization potential defined as zero.

[e] (Theoretical-Experimental)/Experimental.

SPIN-ORBIT COUPLING OF EXCITED STATES WITH $\ell \neq 0$

The energy of the $2P$ level is split by a relativistic interaction between the spin and orbital angular momentum as well as the corresponding radiation reaction force. The corresponding energy $\Delta E_{total}^{H\ FS}$ and frequency $\Delta f_{total}^{H\ FS}$ for the transition $^2P_{1/2} \rightarrow {}^2P_{3/2}$ is known as the hydrogen fine structure and is given by the sum of the spin-orbital coupling energy (Eq. (2.194)):

$$E_{s/o} = \frac{\alpha^5 (2\pi)^2}{8} m_e c^2 \sqrt{\frac{3}{4}} = 7.24043\ X\ 10^{-24}\ J \tag{9.70}$$

and the radiation reaction force that shifts the H radius from $r_0 = 2a_H$ to:

$$r = 2a_H - (2\pi\alpha)^3 \frac{\hbar}{6m_e c} \sqrt{\frac{3}{4}} = 1.99999990 a_H \tag{9.71}$$

given by Eqs. (2.198-2.199). The radiation reaction energy of the hydrogen fine structure $\Delta E_{RRtotal}^{H\ FS}$ is given as the sum of the electric and magnetic energy changes (Eqs. (2.200-2.202)):

$$\begin{aligned} \Delta E_{RRtotal}^{H\ FS} &= \frac{-0.5e^2}{8\pi\varepsilon_0}\left[\frac{1}{r_0} - \frac{1}{r_-}\right] + 4\pi\mu_0\mu_B^2\left(\frac{1}{r_0^3} - \frac{1}{r_-^3}\right) = 2.76347\ X\ 10^{-26}\ J - 1.74098\ X\ 10^{-28}\ J \\ &= 2.74606\ X\ 10^{-26}\ J \end{aligned} \tag{9.72}$$

Then, the total energy of the hydrogen fine structure $\Delta E_{total}^{H\ FS}$ is given by the sum (Eq. (2.204)):

$$\Delta E_{total}^{H\ FS} = E_{s/o} + \Delta E_{RRtotal}^{H\ FS} = 7.24043\ X\ 10^{-24}\ J + 2.74606\ X\ 10^{-26}\ J = 7.26789\ X\ 10^{-24}\ J \tag{9.73}$$

The fine structure energy expressed in terms of frequency (Eq. (2.205)) is

$$\Delta f_{total}^{H\ FS} = 10{,}968.46\ MHz \tag{9.74}$$

The experimental hydrogen fine structure (Eq. (2.206)) is:

$$\Delta f_{total}^{H\ FS}(\text{experimental}) = 10{,}969.05\ MHz \tag{9.75}$$

Given the large natural linewidth of the $2P$ state, the 0.005% relative difference is within the measurement error and propagated errors in the fundamental constants of the equations. Using r_2 given by Eq. (9.53), the spin-orbital energies were calculated for $\ell = 1$ using Eq. (9.70) to compare to the effect of different ℓ quantum numbers. There is agreement between the magnitude of the predicted results given in Table 9.6 and the experimental dependence on the ℓ quantum number as given in Table 9.5.

Table 9.6. Calculated spin-orbital energies of He I singlet excited states with $\ell = 1$ as a function of the radius of the outer electron.

n	r_2 (a_{He}) [a]	Term Symbol	$E_{s/o}$ spin-orbit coupling [b] (eV)
2	2.01873	$1s2p\ ^1P^0$	0.0000439
3	3.01873	$1s3p\ ^1P^0$	0.0000131
4	4.01873	$1s4p\ ^1P^0$	0.0000056
5	5.01873	$1s5p\ ^1P^0$	0.0000029
6	6.01873	$1s6p\ ^1P^0$	0.0000017
7	7.01873	$1s7p\ ^1P^0$	0.0000010

[a] Radius of the outer electron 2 from Eq. (9.53).

[b] The spin-orbit coupling energy of electron 2 from Eq. (9.70) using r_2 from Eq. (9.53).

REFERENCES

1. F. Bueche, *Introduction to Physics for Scientists and Engineers*, McGraw-Hill, (1975), pp. 352-353.
2. J. D. Jackson, *Classical Electrodynamics*, Second Edition, John Wiley & Sons, New York, (1975), pp. 739-779.
3. M. Mizushima, *Quantum Mechanics of Atomic Spectra and Atomic Structure*, W.A. Benjamin, Inc., New York, (1970), p.17.
4. J. D. Jackson, *Classical Electrodynamics*, Second Edition, John Wiley & Sons, New York, (1975), pp. 747-752.
5. J. D. Jackson, *Classical Electrodynamics*, Second Edition, John Wiley & Sons, New York, (1975), pp. 503-561.
6. M. W. Nansteel, personal communication, cube root formulas using the method given in CRC Standard Mathematical Tables, 15th Ed., (1967), p.85, and also Abramowitz and Stegun, Handbook of Mathematical Functions, 9th printing, (1972), p.17, November, (2018).
7. NIST Atomic Spectra Database, www.physics.nist.gov/cgi-bin/AtData/display.ksh.
8. J. D. Jackson, *Classical Electrodynamics*, Second Edition, John Wiley & Sons, New York, (1975), pp. 739-779.
9. J. D. Jackson, *Classical Electrodynamics*, Second Edition, John Wiley & Sons, New York, (1975), p. 759.
10. J. D. Jackson, *Classical Electrodynamics*, Second Edition, John Wiley & Sons, New York, (1975), pp. 236-240, 601-608, 786-790.

Chapter 10

THREE- THROUGH TWENTY-ELECTRON ATOMS

Three- through twenty-electron atoms are solved in this section with supporting material on the magnetic forces given in the Two-Electron Atoms section and Appendix VI. The charge-density functions of one- through twenty-electron atoms and their corresponding positive ions are shown in Figures 10.1 and 10.2, respectively. The electrons of multielectron atoms and ions exist as concentric atomic orbitals ("bubble-like" charge-density functions) of discrete radii that are given by r_n of the radial Dirac delta function, $\delta(r-r_n)$ as shown by the exemplary sectional view of the potassium atom in Figure 10.3.

THREE-ELECTRON ATOMS

As is the case for one and two-electron atoms shown in the corresponding sections, three through ten-electron atoms can also be solved exactly using the results of the solutions of the preceding atoms. For example, three-electron atoms can be solved exactly using the results of the solutions of the one and two-electron atoms.

THE LITHIUM ATOM

For Li^+, there are two spin-paired electrons in an atomic orbital with:

$$r_1 = r_2 = a_0\left[\frac{1}{2}-\frac{\sqrt{\frac{3}{4}}}{6}\right] \tag{10.1}$$

as given by Eq. (7.35) where r_n is the radius of electron n which has velocity v_n. The next electron is added to a new atomic orbital because of the repulsive diamagnetic force between the two spin-paired electrons and the spin-unpaired electron. This repulsive diamagnetic force is due to the interaction of the magnetic field of the outer spin-unpaired electron on the electron current of the two spin-paired electrons of the inner shell. The diamagnetic force on the outer electron is determined by first considering the central force on each electron of the inner shell due to the magnetic flux B of the outer electron that follows from Purcell [1]:

$$\mathbf{F} = \frac{2m_e v_n \Delta v}{r}\mathbf{i}_\mathbf{r} \tag{10.2}$$

where $\mathbf{i}_\mathbf{r}$ is defined as the radial vector in the direction of the central electric field of the nucleus and

$$\frac{\Delta v}{r} = \frac{eB}{2m_e} \tag{10.3}$$

Figure 10.1. Charge-Density Functions Shown in Color Scale of One- Through Twenty-Electron Atoms. The electrons of multielectron atoms exist as concentric atomic orbitals (“ bubble-like” charge-density functions) of discrete radii, which are given by r_n of the radial Dirac delta function, $\delta(r - r_n)$. The electron configuration for one through twenty-electron atoms that achieves an energy minimum is: $1s < 2s < 2p < 3s < 3p < 4s$ wherein each s orbital is a constant current-density function which gives rise to spin, and the charge-density of each p orbital is a superposition of a constant and a spherical and time harmonic function. The corresponding charge-density wave on the surface gives rise to electron orbital angular momentum that superimposes the spin angular momentum. To achieve an energy minimum, electrons of an atom with the same principal and ℓ quantum numbers align parallel until each of the m_ℓ levels are occupied, and then pairing occurs until each of the m_ℓ levels contain paired electrons.

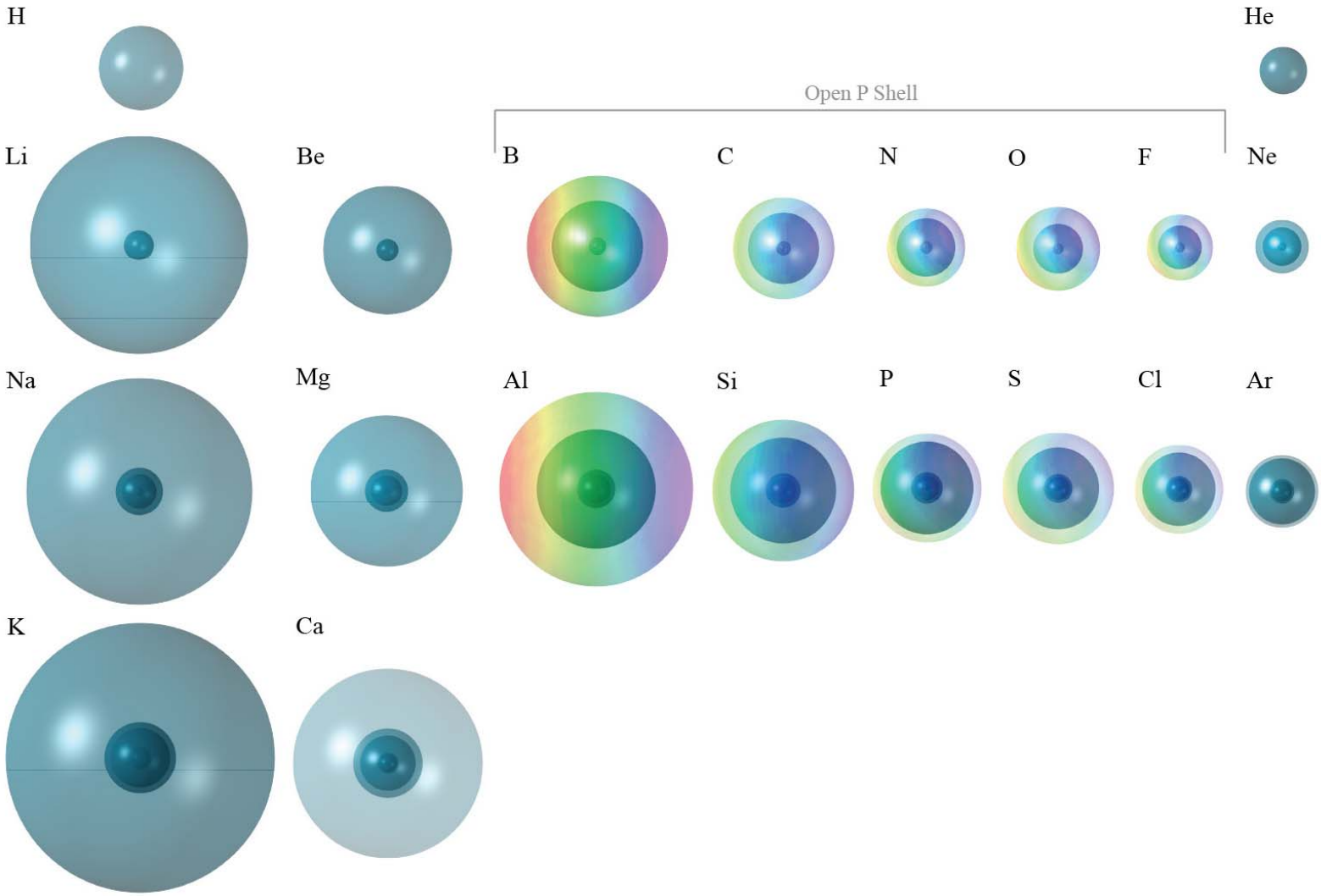

Figure 10.2. Charge-Density Functions Shown in Color Scale of One- Through Twenty-Electron-Plus-One Ions. The electrons of multielectron ions also exist as concentric atomic orbitals (" bubble-like" charge-density functions) of discrete radii which are given by r_n of the radial Dirac delta function, $\delta(r - r_n)$, and the electron configuration follows the same principles as that for one through twenty-electron atoms: 1s < 2s < 2p < 3s < 3p < 4s wherein electrons of an ion with the same principal and ℓ quantum numbers align parallel until each of the m_ℓ levels are occupied, and then pairing occurs until each of the m_ℓ levels contain paired electrons.

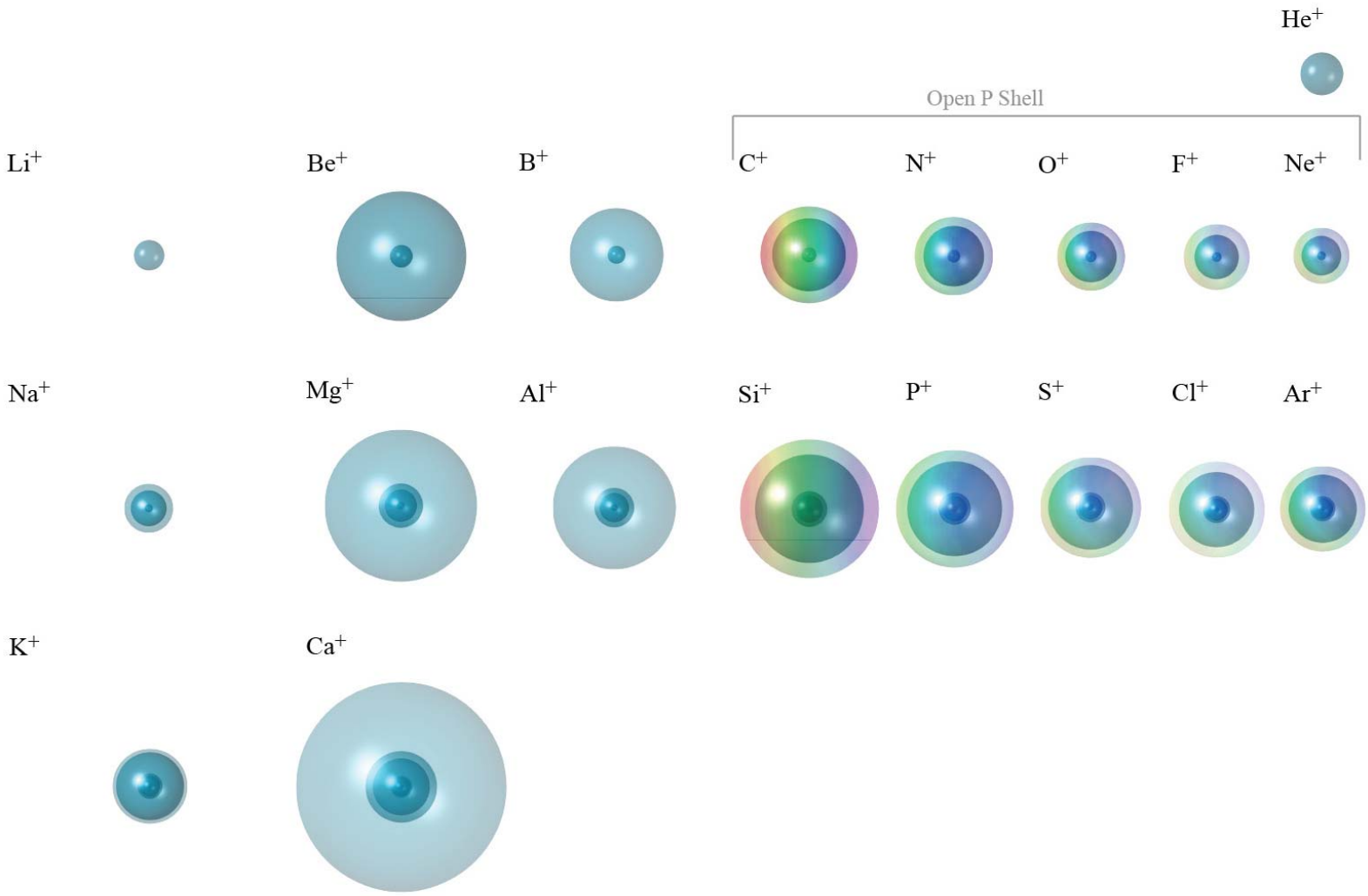

Figure 10.3. A sectional view of the potassium atom showing the radii of the paired 1s, paired 2s, three sets of paired 2p, paired 3s, and three sets of paired 3p inner electrons and the unpaired 4s outer electron.

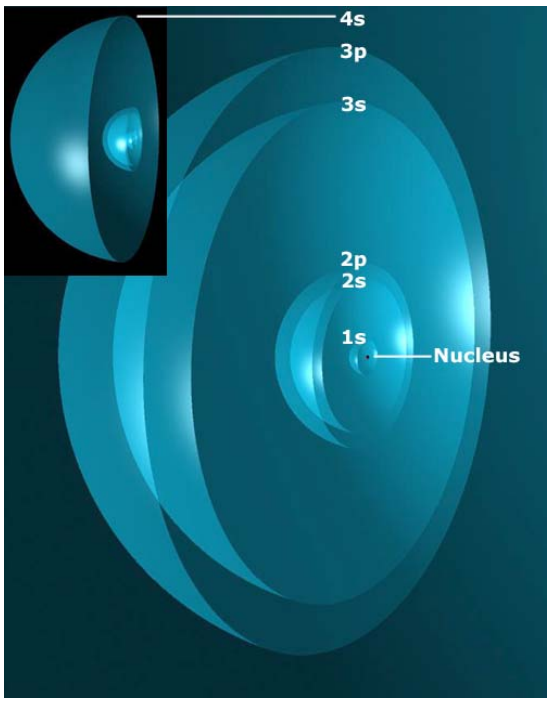

The velocity v_n is given by the boundary condition for no radiation as follows:

$$v_1 = \frac{\hbar}{m_e r_1} \tag{10.4}$$

where r_1 is the radius of the first atomic orbital; therefore, the force on each of the inner electrons is given as follows:

$$\mathbf{F} = \frac{\hbar e B}{m_e r_1}\mathbf{i}_\mathbf{r} \tag{10.5}$$

The change in magnetic moment, Δm, of each electron of the inner shell due to the magnetic flux B of the outer electron is [1]:

$$\Delta m = -\frac{e^2 r_1^2 B}{4m_e} \tag{10.6}$$

The diamagnetic force on the outer electron due to the two inner shell electrons is in the opposite direction of the force given by Eq. (10.5), and this diamagnetic force on the outer electron is proportional to the sum of the changes in magnetic moments of the two inner electrons due to the magnetic flux B of the outer electron. The two electrons are spin-paired and the velocities are mirror opposites. Thus, the change in velocity of each electron treated individually (Eq. (10.3)) due to the magnetic flux B would be equal and opposite. However, the two paired electrons may be treated as one with twice the mass where m_e is replaced by $2m_e$ in Eq. (10.6). In this case, the paired electrons spin together about the field axis to cause a reduction in the flux according to Lenz's law. It is then apparent that the force given by Eq. (10.5) is proportional to the flux B of the outer electron; whereas, the total of the change in magnetic moments of the inner shell electrons given by Eq. (10.6) applied to the combination of the inner electrons is proportional to one eighth of the flux, B. Thus, the force on the outer electron due to the reaction of the inner shell to the flux of the outer electron is given as follows:

$$\mathbf{F}_{diamagnetic} = -\frac{\hbar}{8r_1}\frac{eB}{m_e}\mathbf{i}_\mathbf{r} \tag{10.7}$$

where r_1 is the radial distance of the first atomic orbital from the nucleus. The magnetic flux, B, is supplied by the constant field inside the atomic orbital of the outer electron at radius r_3 and is given by the product of μ_0 times Eq. (1.152).

$$B = \frac{\mu_0 e\hbar}{m_e r_3^3} \tag{10.8}$$

The result of substitution of Eq. (10.8) into Eq. (10.7) is:

$$\mathbf{F}_{diamagnetic} = -\left[\frac{e^2\mu_0}{2m_e r_3}\right]\frac{\hbar^2}{4m_e r_1 r_3^2}\mathbf{i}_\mathbf{r} \tag{10.9}$$

The term in brackets can be expressed in terms of the fine structure constant, α. From Eqs. (1.176-1.180)

$$\frac{e^2\mu_0}{2m_e r_3} = 2\pi\alpha\frac{v}{c} \tag{10.10}$$

It is demonstrated in the Two-Electron Atoms section that the relativistic correction to Eq. (10.9) is $\frac{1}{Z}$ times the reciprocal of Eq. (10.10). Z for electron three is one; thus, one is substituted for the term in brackets in Eq. (10.9).

The force must be corrected for the $\sqrt{s(s+1)} = \sqrt{\frac{3}{4}}$ vector projection of the velocity onto the z-axis as given in the Two-Electron Atoms section and Appendix VI. Thus, Eq. (10.9) becomes:

$$\mathbf{F}_{diamagnetic} = -\frac{\hbar^2}{4m_e r_3^2 r_1}\sqrt{s(s+1)}\mathbf{i}_\mathbf{r} \tag{10.11}$$

THE RADIUS OF THE OUTER ELECTRON OF THE LITHIUM ATOM

The radius for the outer electron is calculated by equating the outward centrifugal force to the sum of the electric and diamagnetic forces as follows:

$$\frac{m_e v_3^2}{r_3} = \frac{e^2}{4\pi\varepsilon_0 r_3^2} - \frac{\hbar^2}{4m_e r_3^2 r_1}\sqrt{s(s+1)} \tag{10.12}$$

With $v_3 = \frac{\hbar}{m_e r_3}$ (Eq. (1.35)), $r_1 = a_0\left[\frac{1}{2} - \frac{\sqrt{\frac{3}{4}}}{6}\right]$ (Eq. (7.35)), and $s = \frac{1}{2}$, we solve for r_3.

$$r_3 = \frac{a_0}{\left[1 - \frac{\sqrt{3/4}}{4\left(\frac{1}{2} - \frac{\sqrt{3/4}}{6}\right)}\right]} \tag{10.13}$$

$$r_3 = 2.5559\ a_0$$

THE IONIZATION ENERGY OF LITHIUM

From Eq. (1.264), the magnitude of the energy stored in the electric field is:

$$\frac{e^2}{8\pi\varepsilon_0 r_3} = 5.318\ eV \tag{10.14}$$

The magnetic field of the outer electron changes the angular velocities of the inner electrons. However, the magnetic field of the outer electron provides a central Lorentz force that exactly balances the change in centrifugal force because of the change in angular velocity [1]. Thus, the electric energy of the inner atomic orbital is unchanged upon ionization. The magnetic field of the outer electron, however, also changes the magnetic moment, m, of each of the inner atomic orbital electrons. From Eq. (10.6), the change in magnetic moment, Δm, (per electron) is:

$$\Delta m = -\frac{e^2 r_1^2}{4m_e} B \tag{10.15}$$

where B is the magnetic flux of the outer electron given by the product of μ_o times Eq. (1.152).

$$B = \frac{\mu_0 e\hbar}{m_e r_3^3} \tag{10.16}$$

Substitution of Eq. (10.16) and $2m_e$ for m_e (because there are two electrons) into Eq. (10.15) gives:

$$\Delta m = -\left[\frac{e^2\mu_0}{2m_e r_3}\right]\frac{e\hbar r_1^2}{4m_e r_3^2} \tag{10.17}$$

Furthermore, we know from Eqs. (10.9) and (10.11) that the term in brackets is replaced by $\sqrt{s(s+1)}$.

$$\Delta m = -\frac{e\hbar r_1^2}{4m_e r_3^2}\sqrt{s(s+1)} \tag{10.18}$$

Substitution of Eq. (10.1) for r_1, Eq. (10.13) for r_3, and given that the magnetic moment of an electron is one Bohr magneton according to Eq. (1.131),

$$\mu_B = \frac{e\hbar}{2m_e} \tag{10.19}$$

the fractional change in magnetic moment of an inner shell electron, Δm_f, is given as follows:

$$\Delta m_f = \frac{\dfrac{e\hbar r_1^2\sqrt{s(s+1)}}{4m_e r_3^2}}{\dfrac{e\hbar}{2m_e}} \tag{10.20}$$

$$= \frac{1}{2}\frac{r_1^2}{r_3^2}\sqrt{s(s+1)} \tag{10.21}$$

With r_1 given by Eq. (10.1), r_3 given by Eq. (10.13), and $s = \frac{1}{2}$, the fractional change in magnetic moment of the two inner shell electrons is:

$$\Delta m_f = \frac{\left(a_0\left[\frac{1}{2} - \frac{\sqrt{\frac{3}{4}}}{6}\right]\right)^2\sqrt{\frac{3}{4}}}{\left(\frac{a_0}{1 - \frac{\sqrt{\frac{3}{4}}}{4\left(\frac{1}{2} - \frac{\sqrt{\frac{3}{4}}}{6}\right)}}\right)^2} \tag{10.22}$$

$$\Delta m_f = 0.016767$$

We add one (corresponding to m_f) to Δm_f which is the fractional change in the magnetic moment. The energy stored in the magnetic field is proportional to the magnetic field strength squared as given by Eq. (1.144); thus, the sum is squared

$$(1.016767)^2 = 1.033815 \tag{10.23}$$

Thus, the change in magnetic energy of the inner atomic orbital is $3.382\ \%$, so that the corresponding energy ΔE_{mag} is

$$\Delta E_{mag} = (0.033815)(2.543\ eV) = 0.08599\ eV \tag{10.24}$$

where the magnetic energy of the inner electrons given in Table 7.1 is $2.543\ eV$. Then the ionization energy of the lithium atom is given by Eqs. (10.13-10.14) and (10.24):

$$E(ionization;\ Li) = \frac{(Z-2)e^2}{8\pi\varepsilon_0 r_3} + \Delta E_{mag} \tag{10.25}$$

$$= 5.3230\ eV + 0.08599\ eV = 5.4090\ eV$$

The experimental ionization energy of lithium is $5.392\ eV$ [2-3].

THREE ELECTRON ATOMS WITH A NUCLEAR CHARGE Z>3

Three-electron atoms having $Z > 3$ possess an electric field of:

$$\mathbf{E} = \frac{(Z-3)e}{4\pi\varepsilon_0 r^2}\mathbf{i}_r \tag{10.26}$$

for $r > r_3$. For three-electron atoms having $Z > 3$, the diamagnetic force given by Eq. (10.11) is unchanged. However, for three-electron atoms having $Z > 3$, an electric field exists for $r > r_3$. This electric field gives rise to an additional diamagnetic force term which adds to Eq. (10.11). The additional diamagnetic force is derived as follows. The diamagnetic force repels the third (outer) electron, and the electric force attracts the third electron. Consider the reverse of ionization where the third electron is at infinity and the two spin-paired electrons are at $r_1 = r_2$ given by Eq. (7.35).

Power must be conserved as the net force of the diamagnetic and electric forces cause the third electron to move from infinity to its final radius. Power flow is given by the Poynting Power Theorem:

$$\nabla \bullet (\mathbf{E}\times\mathbf{H}) = -\frac{\partial}{\partial t}\left[\frac{1}{2}\mu_0\mathbf{H}\bullet\mathbf{H}\right] - \frac{\partial}{\partial t}\left[\frac{1}{2}\varepsilon_0\mathbf{E}\bullet\mathbf{E}\right] - \mathbf{J}\bullet\mathbf{E} \tag{10.27}$$

During binding, the radius of electron three decreases. The electric force where:

$$\mathbf{F}_{ele} = \frac{(Z-2)e^2}{4\pi\varepsilon_0 r_3^2}\mathbf{i}_r \tag{10.28}$$

increases the stored electric energy which corresponds to the power term, $-\frac{\partial}{\partial t}\left[\frac{1}{2}\varepsilon_0\mathbf{E}\bullet\mathbf{E}\right]$, of Eq. (10.27). The diamagnetic

force given by Eq. (10.7) changes the stored magnetic energy which corresponds to the power term, $-\frac{\partial}{\partial t}\left[\frac{1}{2}\mu_0 \mathbf{H} \bullet \mathbf{H}\right]$, of Eq. (10.27). An additional diamagnetic force arises when $Z-3>0$. This diamagnetic force corresponds to that given by Purcell [1] for a charge moving in a central field having an imposed magnetic field perpendicular to the plane of motion. The second diamagnetic force $\mathbf{F}_{diamagnetic\ 2}$ is given by

$$\mathbf{F}_{diamagnetic\ 2} = -2\frac{m_e \Delta v^2}{r_1}\mathbf{i}_\mathbf{r} \tag{10.29}$$

where Δv is derived from Eq. (10.3). The result of substitution of Δv into Eq. (10.29) is:

$$\mathbf{F}_{diamagnetic\ 2} = -\frac{2m_e}{r_1}\left[\frac{er_1 B}{2m_e}\right]^2 \mathbf{i}_\mathbf{r} \tag{10.30}$$

The magnetic flux, B, at electron three for $r < r_3$ is given by the product of μ_o times Eq. (1.152). The result of the substitution of the flux into Eq. (10.30) is:

$$\mathbf{F}_{diamagnetic\ 2} = -2\left[\frac{e^2\mu_0}{2m_e r_3}\right]^2 \frac{r_1\hbar^2}{m_e r_3^4}\mathbf{i}_\mathbf{r} \tag{10.31}$$

The term in brackets can be expressed in terms of the fine structure constant, α. From Eqs. (1.176-1.181)

$$\frac{Z_1 e^2\mu_0}{2m_e r_3} = 2\pi\alpha Z_1 \frac{v}{c} \tag{10.32}$$

It is demonstrated in the Two-Electron Atoms section that the relativistic correction to Eq. (10.31) is $\frac{1}{Z}$ times the reciprocal of Eq. (10.32). Consider the case wherein Z_1 of Eq. (10.32) is different from $Z = Z_2$ of Eq. (7.22) in order to maintain relativistic invariance of the electron angular momentum and magnetic moment. The relativistic correction to Eq. (10.31) can be considered the product of two corrections—a correction of electron three relative to electron one and two, and electron one and two relative to electron three. In the former case, Z_1 and $Z_2 = 1$ which corresponds to electron three. In the latter case, $Z_1 = Z-3$, and $Z_2 = Z-2$ which corresponds to r_3^+, infinitesimally greater than the radius of the outer atomic orbital and r_3^-, infinitesimally less than the radius of the outer atomic orbital, respectively, where Z is the nuclear charge. Thus, $\frac{Z-3}{Z-2}$ is substituted for the term in brackets in Eq. (10.31). The force must be corrected for the $\sqrt{s(s+1)} = \sqrt{\frac{3}{4}}$ vector projection of the velocity onto the z-axis as given in the Two-Electron Atoms section and Appendix VI. Thus, Eq. (10.31) becomes:

$$\mathbf{F}_{diamagnetic\ 2} = -2\frac{(Z-3)r_1\hbar^2}{(Z-2)m_e r_3^4}\sqrt{s(s+1)}\mathbf{i}_\mathbf{r} \tag{10.33}$$

As given previously in the Two Electron section, this force corresponds to the dissipation term of Eq. (10.27), $\mathbf{J} \bullet \mathbf{E}$. The current $\mathbf{J}$ is proportional to the sum of one for the outer electron and two times two—the number of spin-paired electrons. For the inner electrons, the factor of two arises because they possess mutual inductance which doubles their contribution to $\mathbf{J}$. (Recall the general relationship that the current is equal to the flux divided by the inductance.) Thus, the second diamagnetic force is:

$$\mathbf{F}_{diamagnetic\ 2} = -2\left[\frac{Z-3}{Z-2}\right]\frac{(1+4)r_1\hbar^2}{m_e r_3^4}\sqrt{s(s+1)}\mathbf{i}_\mathbf{r};\quad s=\frac{1}{2} \tag{10.34}$$

$$\mathbf{F}_{diamagnetic\ 2} = -\left[\frac{Z-3}{Z-2}\right]\frac{r_1\hbar^2}{m_e r_3^4}10\sqrt{3/4}\mathbf{i}_\mathbf{r} \tag{10.35}$$

THE RADIUS OF THE OUTER ELECTRON OF THREE-ELECTRON ATOMS WITH A NUCLEAR CHARGE Z>3

The radius of the outer electron is calculated by equating the outward centrifugal force to the sum of the electric and diamagnetic forces as follows:

$$\frac{m_e v_3^2}{r_3} = \frac{(Z-2)e^2}{4\pi\varepsilon_0 r_3^2} - \frac{\hbar^2}{4m_e r_3^2 r_1}\sqrt{s(s+1)} - \left[\frac{Z-3}{Z-2}\right]\frac{r_1\hbar^2}{r_3^4 m_e}10\sqrt{s(s+1)} \tag{10.36}$$

With $v_3 = \frac{\hbar}{m_e r_3}$ (Eq. (1.35)), $r_1 = a_0\left(\frac{1}{Z-1} - \frac{\sqrt{s(s+1)}}{Z(Z-1)}\right)$ (Eq. (7.35), and $s = \frac{1}{2}$, we solve for r_3 using the quadratic formula or reiteratively.

$$r_3 = \frac{\left[1+\left[\frac{Z-3}{Z-2}\right]\frac{r_1}{r_3}10\sqrt{\frac{3}{4}}\right]}{\left[\frac{(Z-2)}{a_0} - \frac{\sqrt{\frac{3}{4}}}{4r_1}\right]} \tag{10.37}$$

The quadratic equation corresponding to Eq. (10.37) is:

$$r_3^2 - \frac{r_3}{\left[\frac{(Z-2)}{a_0} - \frac{\sqrt{\frac{3}{4}}}{4r_1}\right]} - \frac{\left[\frac{Z-3}{Z-2}\right]r_1 10\sqrt{\frac{3}{4}}}{\left[\frac{(Z-2)}{a_0} - \frac{\sqrt{\frac{3}{4}}}{4r_1}\right]} = 0 \tag{10.38}$$

The solution of Eq. (10.38) using the quadratic formula is:

$$r_3 = \frac{\frac{a_0}{\left[(Z-2) - \frac{\sqrt{\frac{3}{4}}}{4r_1}\right]} \pm a_0\sqrt{\frac{1}{\left[(Z-2) - \frac{\sqrt{\frac{3}{4}}}{4r_1}\right]^2} + 4\frac{\left[\frac{Z-3}{Z-2}\right]r_1 10\sqrt{\frac{3}{4}}}{\left[(Z-2) - \frac{\sqrt{\frac{3}{4}}}{4r_1}\right]}}}{2}, \quad r_1 \text{ in units of } a_0 \tag{10.39}$$

$$r_3 = \frac{\frac{a_0}{\left[(Z-2) - \frac{\sqrt{3/4}}{4r_1}\right]}\left[1 \pm \sqrt{1+4\left[\frac{Z-3}{Z-2}\right]r_1 10\sqrt{\frac{3}{4}}\left[(Z-2) - \frac{\sqrt{\frac{3}{4}}}{4r_1}\right]}\right]}{2}, \quad r_1 \text{ in units of } a_0 \tag{10.40}$$

$$r_3 = \frac{\frac{a_o}{\left[(Z-2) - \frac{\sqrt{3/4}}{4r_1}\right]}\left[1 \pm \sqrt{1+4(Z-3)r_1 10\sqrt{\frac{3}{4}} - \left[\frac{Z-3}{Z-2}\right]\frac{30}{4}}\right]}{2}, \quad r_1 \text{ in units of } a_0 \tag{10.41}$$

$$r_3 = \frac{\frac{a_0}{\left[(Z-2) - \frac{\sqrt{3/4}}{4\left(\frac{1}{Z-1} - \frac{\sqrt{3/4}}{Z(Z-1)}\right)}\right]}\left[1 \pm \sqrt{1+4(Z-3)\left(\frac{1}{Z-1} - \frac{\sqrt{3/4}}{Z(Z-1)}\right)10\sqrt{\frac{3}{4}} - \left[\frac{Z-3}{Z-2}\right]\frac{30}{4}}\right]}{2} \tag{10.42}$$

The positive root of Eq. (10.42) must be taken in order that $r_3 > 0$.

THE IONIZATION ENERGIES OF THREE-ELECTRON ATOMS WITH A NUCLEAR CHARGE Z>3

The energy stored in the electric field, $E(electric)$, is:

$$E(electric) = -\frac{(Z-2)e^2}{8\pi\varepsilon_0 r_3} \tag{10.43}$$

where r_3 is given by Eq. (10.42). The magnetic field of the outer electron changes the velocities of the inner electrons. However, the magnetic field of the outer electron provides a central Lorentz field which balances the change in centrifugal force because of the change in velocity. Thus, the electric energy of the inner atomic orbital is unchanged upon ionization. The change in the velocities of the inner electrons upon ionization gives rise to a change in kinetic energies of the inner electrons. The change in velocity, Δv, is given by Eq. (10.3)

$$\Delta v = \frac{er_1 B}{2m_e} \tag{10.44}$$

Substitution of the flux, B, given by the product of μ_0 and Eq. (1.152), into Eq. (10.44) is:

$$\Delta v = \left[\frac{e^2\mu_0}{2m_e r_1}\right]\frac{r_1^2\hbar}{m_e r_3^3} \tag{10.45}$$

It is demonstrated in the One-Electron Atom section and the Two-Electrons Atom section (at Eq. (7.23)) that the relativistic correction to Eq. (10.45) is $\frac{1}{Z}$ times the reciprocal of the term in brackets. In this case, Z corresponding to electron three is one; thus, one is substituted for the term in brackets in Eq. (10.45). Thus, Eq. (10.45) becomes,

$$\Delta v = \frac{r_1^2\hbar}{r_3^3 m_e} \tag{10.46}$$

wherein r_1 given by Eq. (7.35), and r_3 is given by Eq. (10.42). The change in kinetic energy, ΔE_T, of the two inner shell electrons is given by:

$$\Delta E_T = 2\frac{1}{2}m_e\Delta v^2 \tag{10.47}$$

The ionization energy is the sum of the electric energy, Eq. (10.43), and the change in the kinetic energy, Eq. (10.47), of the inner electrons.

$$E(Ionization) = E(Electric) + E_T \tag{10.48}$$

The relativistic correction to Eq. (10.48) is given by (1) relativistically correcting the radius of the inner paired electrons r_1, (2) using the relativistically corrected r_1 to determine r_3 which is then relativistically corrected. The relativistically corrected r_1 is given by dividing the radius given Eq. (7.35) by γ^* of Eq. (1.281)

$$r_2 = r_1 = \frac{r_1'}{\gamma^*} = \frac{a_0\left(\frac{1}{Z-1} - \frac{\sqrt{s(s+1)}}{Z(Z-1)}\right)}{2\pi}\Bigg/\frac{2\pi\sqrt{1-\left(\frac{v}{c}\right)^2}\sin\left[\frac{\pi}{2}\left(1-\left(\frac{v}{c}\right)^2\right)^{3/2}\right]+\cos\left[\frac{\pi}{2}\left(1-\left(\frac{v}{c}\right)^2\right)^{3/2}\right]}{2\pi}, \; s=\frac{1}{2} \tag{10.49}$$

where the velocity is given by Eq. (1.35) with the radius given by Eq. (7.35). Similarly, the relativistically corrected r_3 is given by dividing the radius given Eq. (10.41) by γ^* of Eq. (1.281)

$$r_3 = \frac{r_3'}{\gamma^*} = \frac{\frac{a_0}{\left[(Z-2)-\frac{\sqrt{3/4}}{4r_1}\right]}\left[1+\sqrt{1+4(Z-3)r_1 10\sqrt{\frac{3}{4}}-\left[\frac{Z-3}{Z-2}\right]\frac{30}{4}}\right]}{\frac{2}{2\pi}}\Bigg/\frac{2\pi\sqrt{1-\left(\frac{v}{c}\right)^2}\sin\left[\frac{\pi}{2}\left(1-\left(\frac{v}{c}\right)^2\right)^{3/2}\right]+\cos\left[\frac{\pi}{2}\left(1-\left(\frac{v}{c}\right)^2\right)^{3/2}\right]}{2\pi}, \; r_1 \text{ in units of } a_0 \tag{10.50}$$

where r_1 is given by Eq. (10.49) and the velocity is given by Eq. (1.35) with the radius given by Eq. (10.42). The ionization energies are given by Eq. (10.48) wherein the relativistically corrected radii given by Eqs. (10.49-10.50) are used in the sum of the electric energy, Eq. (10.43), and the change in the kinetic energy, Eq. (10.47), of the inner electrons. The ionization energies for several three-electron atoms are given in Table 10.1.

Table 10.1. Ionization energies for some three-electron atoms.

3 e Atom	Z	r_1 (a_0) [a]	r_3 (a_0) [b]	Electric Energy [c] (eV)	Δv [d] (m/s)	ΔE_T [e] (eV)	Theoretical Ionization Energies [f] (eV)	Experimental Ionization Energies [g] (eV)	Relative Error [h]
Li	3	0.35566	2.55606	5.3230	1.6571E+04	1.5613E-03	5.40390	5.39172	-0.00226
Be^{+}	4	0.26116	1.49849	18.1594	4.4346E+04	1.1181E-02	18.1706	18.21116	0.00223
B^{2+}	5	0.20670	1.07873	37.8383	7.4460E+04	3.1523E-02	37.8701	37.93064	0.00160
C^{3+}	6	0.17113	0.84603	64.3278	1.0580E+05	6.3646E-02	64.3921	64.4939	0.00158
N^{4+}	7	0.14605	0.69697	97.6067	1.3782E+05	1.0800E-01	97.7160	97.8902	0.00178
O^{5+}	8	0.12739	0.59299	137.6655	1.7026E+05	1.6483E-01	137.8330	138.1197	0.00208
F^{6+}	9	0.11297	0.51621	184.5001	2.0298E+05	2.3425E-01	184.7390	185.186	0.00241
Ne^{7+}	10	0.10149	0.45713	238.1085	2.3589E+05	3.1636E-01	238.4325	239.0989	0.00279
Na^{8+}	11	0.09213	0.41024	298.4906	2.6894E+05	4.1123E-01	298.9137	299.864	0.00317
Mg^{9+}	12	0.08435	0.37210	365.6469	3.0210E+05	5.1890E-01	366.1836	367.5	0.00358
Al^{10+}	13	0.07778	0.34047	439.5790	3.3535E+05	6.3942E-01	440.2439	442	0.00397
Si^{11+}	14	0.07216	0.31381	520.2888	3.6868E+05	7.7284E-01	521.0973	523.42	0.00444
P^{12+}	15	0.06730	0.29102	607.7792	4.0208E+05	9.1919E-01	608.7469	611.74	0.00489
S^{13+}	16	0.06306	0.27132	702.0535	4.3554E+05	1.0785E+00	703.1966	707.01	0.00539
Cl^{14+}	17	0.05932	0.25412	803.1158	4.6905E+05	1.2509E+00	804.4511	809.4	0.00611
Ar^{15+}	18	0.05599	0.23897	910.9708	5.0262E+05	1.4364E+00	912.5157	918.03	0.00601
K^{16+}	19	0.05302	0.22552	1025.6241	5.3625E+05	1.6350E+00	1027.3967	1033.4	0.00581
Ca^{17+}	20	0.05035	0.21350	1147.0819	5.6993E+05	1.8468E+00	1149.1010	1157.8	0.00751
Sc^{18+}	21	0.04794	0.20270	1275.3516	6.0367E+05	2.0720E+00	1277.6367	1287.97	0.00802
Ti^{19+}	22	0.04574	0.19293	1410.4414	6.3748E+05	2.3106E+00	1413.0129	1425.4	0.00869
V^{20+}	23	0.04374	0.18406	1552.3606	6.7135E+05	2.5626E+00	1555.2398	1569.6	0.00915
Cr^{21+}	24	0.04191	0.17596	1701.1197	7.0530E+05	2.8283E+00	1704.3288	1721.4	0.00992
Mn^{22+}	25	0.04022	0.16854	1856.7301	7.3932E+05	3.1077E+00	1860.2926	1879.9	0.01043
Fe^{23+}	26	0.03867	0.16172	2019.2050	7.7342E+05	3.4011E+00	2023.1451	2023	-0.00007
Co^{24+}	27	0.03723	0.15542	2188.5585	8.0762E+05	3.7084E+00	2192.9020	2219	0.01176
Ni^{25+}	28	0.03589	0.14959	2364.8065	8.4191E+05	4.0300E+00	2369.5803	2399.2	0.01235
Cu^{26+}	29	0.03465	0.14418	2547.9664	8.7630E+05	4.3661E+00	2553.1987	2587.5	0.01326

[a] Radius of the paired inner electrons of three-electron atoms from Eq. (10.49).

[b] Radius of the unpaired outer electron of three-electron atoms from Eq. (10.50).

[c] Electric energy of the outer electron of three-electron atoms from Eq. (10.43).

[d] Change in the velocity of the paired inner electrons due to the unpaired outer electron of three-electron atoms from Eq. (10.46).

[e] Change in the kinetic energy of the paired inner electrons due to the unpaired outer electron of three-electron atoms from Eq. (10.47).

[f] Calculated ionization energies of three-electron atoms from Eq. (10.48) for $Z > 3$ and Eq. (10.25) for *Li*.

[g] From theoretical calculations, interpolation of isoelectronic and spectral series, and experimental data [2-3].

[h] (Experimental-theoretical)/experimental.

The agreement between the experimental and calculated values of Table 10.1 is well within the experimental capability of the spectroscopic determinations including the values at large Z which relies on X-ray spectroscopy. In this case, the experimental capability is three to four significant figures, which is consistent with the last column. The lithium atom isoelectronic series is given in Table 10.1 [2-3] to much higher precision than the capability of X-ray spectroscopy, but these values are based on theoretical and interpolation techniques rather than data alone. Ionization energies are difficult to determine since the cut-off of the Rydberg series of lines at the ionization energy is often not observed, and the ionization energy must be determined from theoretical calculations, interpolation of Li isoelectronic and Rydberg series, as well as direct experimental data.

The ionization energies of four- through twenty-electron atoms are calculated next using the electric energy at the radius of the force balance between the outward centrifugal force and the sum of the Coulombic force and any magnetic forces to the order r^{-3}. The agreement between the experimental and calculated values is excellent, but could even be improved, especially for lower Z ions, by considering higher order magnetic terms involving the interaction between the outer electron and any lower-lying inner shell electrons.

FOUR-ELECTRON ATOMS

Four-electron atoms can be solved exactly using the results of the solutions of one, two, and three-electron atoms.

RADII OF THE OUTER ELECTRONS OF FOUR-ELECTRON ATOMS

For each three-electron atom having a central charge of Z times that of the proton, there are two indistinguishable spin-paired electrons in an atomic orbital with radii r_1 and r_2 both given by Eq. (7.35):

$$r_1 = r_2 = a_0\left[\frac{1}{Z-1} - \frac{\sqrt{\frac{3}{4}}}{Z(Z-1)}\right] \tag{10.51}$$

and an unpaired electron with a radius r_3 given by Eq. (10.42). For $Z \geq 4$, the next electron which binds to form the corresponding four-electron atom becomes spin-paired with the outer electron such that they become indistinguishable with the same radius $r_3 = r_4$. The corresponding spin-pairing force $\mathbf{F}_{mag}$ is given by Eq. (7.24):

$$\mathbf{F}_{mag} = \frac{1}{Z}\frac{\hbar^2}{m_e r_4^3}\sqrt{s(s+1)}\mathbf{i}_\mathbf{r} \tag{10.52}$$

The central forces given by Eq. (10.36) and Eq. (10.52) act on the outer electron to cause it to bind wherein the electric force on the outer-most electron due to the nucleus and the inner three electrons is given by Eq. (10.28) with the appropriate charge and radius:

$$\mathbf{F}_{ele} = \frac{(Z-3)e^2}{4\pi\varepsilon_0 r_4^2}\mathbf{i}_\mathbf{r} \tag{10.53}$$

for $r > r_3$.

In addition to the paramagnetic spin-pairing force between the third electron initially at radius r_3, the pairing causes the diamagnetic interaction between the outer electrons and the inner electrons given by Eq. (10.11) to vanish, except for an electrodynamic effect for $Z > 4$ described in the Two-Electron Atoms section, since upon pairing the magnetic field of the outer electrons becomes zero. Therefore, the corresponding force $\mathbf{F}_{mag\ 2}$ is in the same direction as the spin-pairing force and is given by substitution of Eq. (7.6) with the radius r_4 into Eq. (10.5):

$$\mathbf{F}_{mag\ 2} = \frac{\hbar eB}{2m_e r_1} = \frac{\mu_0 e^2 \hbar^2}{2m_e^2 r_1 r_4^3}\mathbf{i}_\mathbf{r} \tag{10.54}$$

Then, from Eqs. (10.54) and (7.6-7.24), the paramagnetic force is given by:

$$\mathbf{F}_{mag\ 2} = \frac{1}{Z}\frac{\hbar^2}{m_e r_1 r_4^2}\sqrt{s(s+1)}\mathbf{i}_\mathbf{r} \tag{10.55}$$

The outward centrifugal force on electron 4 is balanced by the electric force and the magnetic forces (on electron 4). The radius of the outer electron is calculated by equating the outward centrifugal force to the sum of the electric (Eq. (10.53)), diamagnetic (Eqs. (10.11) and (10.35) for r_4), and paramagnetic (Eqs. (10.52) and (10.55)) forces as follows:

$$\frac{m_e v_4^2}{r_4} = \frac{(Z-3)e^2}{4\pi\varepsilon_0 r_4^2} - \frac{\hbar^2}{4m_e r_4^2 r_1}\sqrt{s(s+1)} + \frac{\hbar^2}{Zm_e r_4^2 r_1}\sqrt{s(s+1)} - \left[\frac{Z-3}{Z-2}\right]\frac{r_1\hbar^2}{r_4^4 m_e}10\sqrt{s(s+1)} + \frac{\hbar^2}{Zm_e r_4^3}\sqrt{s(s+1)} \tag{10.56}$$

Substitution of $v_4 = \dfrac{\hbar}{m_e r_4}$ (Eq. (1.35)) and $s = \dfrac{1}{2}$ into Eq. (10.56) gives:

$$\frac{\hbar^2}{m_e r_4^3} = \frac{(Z-3)e^2}{4\pi\varepsilon_0 r_4^2} - \frac{\hbar^2}{4m_e r_4^2 r_1}\sqrt{\frac{3}{4}} + \frac{\hbar^2}{Zm_e r_4^2 r_1}\sqrt{\frac{3}{4}} - \left[\frac{Z-3}{Z-2}\right]\frac{r_1\hbar^2}{r_4^4 m_e}10\sqrt{\frac{3}{4}} + \frac{\hbar^2}{Zm_e r_4^3}\sqrt{\frac{3}{4}} \tag{10.57}$$

$$\left(\frac{(Z-3)e^2}{4\pi\varepsilon_0} - \left(\frac{1}{4}-\frac{1}{Z}\right)\frac{\hbar^2}{m_e r_1}\sqrt{\frac{3}{4}}\right)\frac{1}{r_4^2} - \left[\frac{Z-3}{Z-2}\right]\frac{r_1\hbar^2}{r_4^4 m_e}10\sqrt{\frac{3}{4}} - \frac{\hbar^2}{m_e r_4^3}\left(1 - \frac{\sqrt{\frac{3}{4}}}{Z}\right) = 0 \tag{10.58}$$

The quadratic equation corresponding to Eq. (10.58) is

$$\left(\frac{(Z-3)e^2}{4\pi\varepsilon_0} - \left(\frac{1}{4}-\frac{1}{Z}\right)\frac{\hbar^2}{m_e r_1}\sqrt{\frac{3}{4}}\right)r_4^2 - \frac{\hbar^2}{m_e}\left(1 - \frac{\sqrt{\frac{3}{4}}}{Z}\right)r_4 - \left[\frac{Z-3}{Z-2}\right]\frac{r_1\hbar^2}{m_e}10\sqrt{\frac{3}{4}} = 0 \tag{10.59}$$

$$r_4^2-\frac{\dfrac{\hbar^2}{m_e}\left(1-\dfrac{\sqrt{\dfrac{3}{4}}}{Z}\right)}{\left(\dfrac{(Z-3)e^2}{4\pi\varepsilon_0}-\left(\dfrac{1}{4}-\dfrac{1}{Z}\right)\dfrac{\hbar^2}{m_e r_1}\sqrt{\dfrac{3}{4}}\right)}r_4-\frac{\left[\dfrac{Z-3}{Z-2}\right]\dfrac{r_1\hbar^2}{m_e}10\sqrt{\dfrac{3}{4}}}{\left(\dfrac{(Z-3)e^2}{4\pi\varepsilon_0}-\left(\dfrac{1}{4}-\dfrac{1}{Z}\right)\dfrac{\hbar^2}{m_e r_1}\sqrt{\dfrac{3}{4}}\right)}=0 \tag{10.60}$$

$$r_4^2-\frac{\left(1-\dfrac{\sqrt{\dfrac{3}{4}}}{Z}\right)}{\left(\dfrac{(Z-3)}{a_0}-\left(\dfrac{1}{4}-\dfrac{1}{Z}\right)\dfrac{\sqrt{\dfrac{3}{4}}}{r_1}\right)}r_4-\frac{\left[\dfrac{Z-3}{Z-2}\right]r_1 10\sqrt{\dfrac{3}{4}}}{\left(\dfrac{(Z-3)}{a_0}-\left(\dfrac{1}{4}-\dfrac{1}{Z}\right)\dfrac{\sqrt{\dfrac{3}{4}}}{r_1}\right)}=0 \tag{10.61}$$

The solution of Eq. (10.61) using the quadratic formula is:

$$r_4=r_3=\frac{\dfrac{a_0\left(1-\dfrac{\sqrt{\dfrac{3}{4}}}{Z}\right)}{\left((Z-3)-\left(\dfrac{1}{4}-\dfrac{1}{Z}\right)\dfrac{\sqrt{\dfrac{3}{4}}}{r_1}\right)}\pm a_0\sqrt{\dfrac{\left(1-\dfrac{\sqrt{\dfrac{3}{4}}}{Z}\right)^2}{\left((Z-3)-\left(\dfrac{1}{4}-\dfrac{1}{Z}\right)\dfrac{\sqrt{\dfrac{3}{4}}}{r_1}\right)^2}+4\dfrac{\left[\dfrac{Z-3}{Z-2}\right]r_1 10\sqrt{\dfrac{3}{4}}}{\left((Z-3)-\left(\dfrac{1}{4}-\dfrac{1}{Z}\right)\dfrac{\sqrt{\dfrac{3}{4}}}{r_1}\right)}}}{2},\ r_1\ in\ units\ of\ a_0 \tag{10.62}$$

where r_1 is given by Eq. (10.51) and also Eq. (7.35). The positive root of Eq. (10.62) must be taken in order that $r_4>0$. The final radius of electron 4, r_4, is given by Eq. (10.62); this is also the final radius of electron 3. The radii of several four-electron atoms are given in Table 10.2.

ENERGIES OF THE BERYLLIUM ATOM

The energy stored in the electric field, $E(electric)$, is given by Eq. (10.43) with the appropriate charge and radius:

$$E(electric)=-\frac{(Z-3)e^2}{8\pi\varepsilon_0 r_4} \tag{10.63}$$

The ionization energy is given by the sum of the electric energy and the diamagnetic and paramagnetic energy terms. The magnetic energy, $E(magnetic)$, for an electron corresponding to a radius r_n given by Eq. (7.46) is:

$$E(magnetic)=\frac{2\pi\mu_0 e^2\hbar^2}{m_e^2 r_n^3} \tag{10.64}$$

Since there is no source of dissipative power, $\mathbf{J}\bullet\mathbf{E}$ of Eq. (10.27), to compensate for any potential change in the magnetic moments, Δm, of the inner electrons due to the ionization of an outer electron of the beryllium atom, there is a diamagnetic energy term in the ionization energy for this atom that follows from the corresponding term for the lithium atom. This term is given by Eqs. (10.15-10.24) wherein r_1 is given by Eq. (10.51) with $Z=4$ and $r_3=r_4$ is given by Eq. (10.62). Thus, the change in magnetic energy of the inner atomic orbital is $5.144\ \%$, so that the corresponding energy ΔE_{mag} is:

$$\Delta E_{mag}=0.05144\ X\ 6.42291\ eV=0.33040\ eV \tag{10.65}$$

where the magnetic energy of the inner electrons is $6.42291\ eV$. In addition, there is a paramagnetic energy term $E(magnetic)$ corresponding to the ionization of a spin-paired electron from a neutral atom with a closed s-shell. The energy follows from that given for helium by Eqs. (7.44) and (7.46) wherein the electron radius for helium is replaced by the radius r_4 of Eq. (10.62). Then, the ionization energy of the beryllium atom is given by Eqs. (7.44), (7.46), (10.25), and (10.62-10.65):

$$E(ionization;\ Be)=\frac{(Z-3)e^2}{8\pi\varepsilon_0 r_4}+\frac{2\pi\mu_0 e^2\hbar^2}{m_e^2 r_4^3}+\Delta E_{mag}=8.9216\ eV+0.03226\ eV+0.33040\ eV=9.28430\ eV \tag{10.66}$$

The experimental ionization energy of beryllium is $9.32263\ eV$ [3].

THE IONIZATION ENERGIES OF FOUR-ELECTRON ATOMS WITH A NUCLEAR CHARGE Z>4

The ionization energies for the four-electron atoms with $Z > 4$ are given by the sum of the electric energy, $E(electric)$, given by Eq. (10.63) and the magnetic energies. The paramagnetic energy term corresponding to the ionization of a spin-paired electron from an atom with an external electric field is given by Eqs. (7.46) and (7.63) wherein the electron radius for helium is replaced by the radius r_4 of Eq. (10.62):

$$Ionization\ Energy = -Electric\ Energy - \frac{1}{Z} Magnetic\ Energy \tag{10.67}$$

Once the outer electrons of four-electron atoms with $Z > 4$ become spin unpaired during ionization, the corresponding magnetic field changes the velocities of the inner electrons in the same manner as shown for the case of the outer electron of three-electron atoms with $Z > 3$. The magnetic effect is calculated for the remaining electron 3 at the radius r_4 corresponding to condition of the derivation of Eq. (10.67) that follows from Eqs. (7.46) and (7.63). Thus, change in velocity, Δv, in the four-electron-atom case is that of three-electron atoms given by Eq. (10.46) wherein the electron radius r_3 is replaced by the radius r_4 of Eq. (10.62).

Since the velocities of electrons one and two decrease during ionization in the case of four-electron atoms rather than increase as in the case of three-electron atoms, the corresponding kinetic energy decreases and the kinetic energy term given by Eq. (10.47) is the opposite sign in Eq. (10.48). Thus, the ionization energies of four-electron atoms with $Z > 4$ given by Eqs. (10.48) and (10.67) with the electric energy (Eq. (10.63)), the magnetic energy (Eq. (10.64)), and the change in the kinetic energy of the inner electrons (Eq. (10.47)) are

$$E(Ionization) = -Electric\ Energy - \frac{1}{Z} Magnetic\ Energy - E_T \tag{10.68}$$

The ionization energies for several four-electron atoms are given in Table 10.2. Since the radii, r_4, are greater than 10% of a_0 corresponding to a velocity of less than $1.5 \times 10^7\ m/s$, the relativistic corrections are negligible and are not included in Table 10.2.

Table 10.2. Ionization energies for some four-electron atoms.

4 e Atom	Z	r_1 (a_0) [a]	r_3 (a_0) [b]	Electric Energy [c] (eV)	Magnetic Energy [d] (eV)	Δv [e] (m/s X 10^{-5})	ΔE_T [f] (eV)	Theoretical Ionization Energies [g] (eV)	Experimental Ionization Energies [h] (eV)	Relative Error [i]
Be	4	0.26116	1.52503	8.9178	0.03226	0.4207	0.0101	9.28430	9.32263	0.0041
B^{+}	5	0.20670	1.07930	25.2016	0.0910	0.7434	0.0314	25.1627	25.15484	-0.0003
C^{2+}	6	0.17113	0.84317	48.3886	0.1909	1.0688	0.0650	48.3125	47.8878	-0.0089
N^{3+}	7	0.14605	0.69385	78.4029	0.3425	1.3969	0.1109	78.2765	77.4735	-0.0104
O^{4+}	8	0.12739	0.59020	115.2148	0.5565	1.7269	0.1696	115.0249	113.899	-0.0099
F^{5+}	9	0.11297	0.51382	158.8102	0.8434	2.0582	0.2409	158.5434	157.1651	-0.0088
Ne^{6+}	10	0.10149	0.45511	209.1813	1.2138	2.3904	0.3249	208.8243	207.2759	-0.0075
Na^{7+}	11	0.09213	0.40853	266.3233	1.6781	2.7233	0.4217	265.8628	264.25	-0.0061
Mg^{8+}	12	0.08435	0.37065	330.2335	2.2469	3.0567	0.5312	329.6559	328.06	-0.0049
Al^{9+}	13	0.07778	0.33923	400.9097	2.9309	3.3905	0.6536	400.2017	398.75	-0.0036
Si^{10+}	14	0.07216	0.31274	478.3507	3.7404	3.7246	0.7888	477.4989	476.36	-0.0024
P^{11+}	15	0.06730	0.29010	562.5555	4.6861	4.0589	0.9367	561.5464	560.8	-0.0013
S^{12+}	16	0.06306	0.27053	653.5233	5.7784	4.3935	1.0975	652.3436	652.2	-0.0002
Cl^{13+}	17	0.05932	0.25344	751.2537	7.0280	4.7281	1.2710	749.8899	749.76	-0.0002
Ar^{14+}	18	0.05599	0.23839	855.7463	8.4454	5.0630	1.4574	854.1849	854.77	0.0007
K^{15+}	19	0.05302	0.22503	967.0007	10.0410	5.3979	1.6566	965.2283	968	0.0029
Ca^{16+}	20	0.05035	0.21308	1085.0167	11.8255	5.7329	1.8687	1083.0198	1087	0.0037
Sc^{17+}	21	0.04794	0.20235	1209.7940	13.8094	6.0680	2.0935	1207.5592	1213	0.0045
Ti^{18+}	22	0.04574	0.19264	1341.3326	16.0032	6.4032	2.3312	1338.8465	1346	0.0053
V^{19+}	23	0.04374	0.18383	1479.6323	18.4174	6.7384	2.5817	1476.8813	1486	0.0061
Cr^{20+}	24	0.04191	0.17579	1624.6929	21.0627	7.0737	2.8450	1621.6637	1634	0.0075
Mn^{21+}	25	0.04022	0.16842	1776.5144	23.9495	7.4091	3.1211	1773.1935	1788	0.0083
Fe^{22+}	26	0.03867	0.16165	1935.0968	27.0883	7.7444	3.4101	1931.4707	1950	0.0095
Co^{23+}	27	0.03723	0.15540	2100.4398	30.4898	8.0798	3.7118	2096.4952	2119	0.0106
Ni^{24+}	28	0.03589	0.14961	2272.5436	34.1644	8.4153	4.0264	2268.2669	2295	0.0116
Cu^{25+}	29	0.03465	0.14424	2451.4080	38.1228	8.7508	4.3539	2446.7858	2478	0.0126

[a] Radius of the paired inner electrons of four-electron atoms from Eq. (10.51).

[b] Radius of the paired outer electrons of four-electron atoms from Eq. (10.62).

[c] Electric energy of the outer electrons of four-electron atoms from Eq. (10.63).

[d] Magnetic energy of the outer electrons of four-electron atoms upon unpairing from Eq. (7.46) and Eq. (10.64).

[e] Change in the velocity of the paired inner electrons due to the unpaired outer electron of four-electron atoms during ionization from Eq. (10.46).

[f] Change in the kinetic energy of the paired inner electrons due to the unpaired outer electron of four-electron atoms during ionization from Eq. (10.47).

[g] Calculated ionization energies of four-electron atoms from Eq. (10.68) for $Z > 4$ and Eq. (10.66) for *Be*.

[h] From theoretical calculations, interpolation of isoelectronic and spectral series, and experimental data [2-3].

[i] (Experimental-theoretical)/experimental.

The agreement between the experimental and calculated values of Table 10.2 is well within the experimental capability of the spectroscopic determinations including the values at large Z which relies on X-ray spectroscopy. In this case, the experimental capability is three to four significant figures which is consistent with the last column. The beryllium atom isoelectronic series is given in Table 10.2 [2-3] to much higher precision than the capability of X-ray spectroscopy, but these values are based on theoretical and interpolation techniques rather than data alone. Ionization energies are difficult to determine since the cut-off of the Rydberg series of lines at the ionization energy is often not observed, and the ionization energy must be determined from theoretical calculations, interpolation of Be isoelectronic and Rydberg series, as well as direct experimental data.

2P-ORBITAL ELECTRONS BASED ON AN ENERGY MINIMUM

For each four-electron atom having a central charge of Z times that of the proton, there are two indistinguishable spin-paired electrons in an atomic orbital with radii r_1 and r_2 both given by Eq. (7.35) (Eq. (10.51)) and two indistinguishable spin-paired electrons in an atomic orbital with radii r_3 and r_4 both given by Eq. (10.62). For $Z \geq 5$, the next electron which binds to form the corresponding five-electron atom is attracted by the central Coulomb field and is repelled by diamagnetic force due to the spin-paired inner electrons such that it forms an unpaired atomic orbital at radius r_5.

The central Coulomb force, $\mathbf{F}_{ele}$, acts on the outer electron to cause it to bind wherein this electric force on the outer-most electron due to the nucleus and the inner four electrons is given by Eq. (10.28) with the appropriate charge and radius:

$$\mathbf{F}_{ele} = \frac{(Z-4)e^2}{4\pi\varepsilon_0 r_5^2}\mathbf{i}_\mathbf{r} \tag{10.69}$$

for $r > r_4$. The same form of force equation also applies to six through ten-electron atoms as well as five-electron atoms:

$$\mathbf{F}_{ele} = \frac{(Z-n)e^2}{4\pi\varepsilon_0 r_n^2}\mathbf{i}_\mathbf{r} \tag{10.70}$$

for $r > r_{n-1}$ where n corresponds to the number of electrons of the atom and Z is its atomic number. In each case, the magnetic field of the binding outer electron changes the angular velocities of the inner electrons. However, in each case, the magnetic field of the outer electron provides a central Lorentz force which exactly balances the change in centrifugal force because of the change in angular velocity [1]. The inner electrons remain at their initial radii, but cause a diamagnetic force according to Lenz's law.

The diamagnetic force, $\mathbf{F}_{diamagnetic}$, for the formation of an s orbital given by Eq. (10.11) with the appropriate radii is:

$$\mathbf{F}_{diamagnetic} = -\frac{\hbar^2}{4m_e r_n^2 r_3}\sqrt{s(s+1)}\mathbf{i}_\mathbf{r} \tag{10.71}$$

However, with the formation of a third shell, a nonuniform distribution of charge is possible that achieves an energy minimum. Minimum energy configurations are given by solutions to Laplace's Equation. The general form of the solution (Eq. (10.449)) is:

$$\Phi(r,\theta,\phi) = \sum_{\ell=0}^{\infty}\sum_{m=-\ell}^{\ell} B_{\ell,m} r^{-(\ell+1)} Y_\ell^m(\theta,\phi) \tag{10.72}$$

As shown in the Excited States of the One-Electron Atom (Quantization) section, this general solution in the form of a source matching the wave-equation gives the functions of the resonant photons of excited states. From Eqs. (2.15-2.16):

$$\mathbf{E}_{r\,photon\;\,n,l,m} = \frac{e(na_H)^\ell}{4\pi\varepsilon_0}\frac{1}{r^{(\ell+2)}}\left[-Y_0^0(\theta,\phi) + \frac{1}{n}\left[Y_0^0(\theta,\phi) + \mathrm{Re}\left\{Y_\ell^m(\theta,\phi)e^{im\omega_n t}\right\}\right]\right]\delta(r-r_n) \tag{10.73}$$

$n = 1,2,3,4,\ldots$

$\ell = 1,2,\ldots,n-1$

$m = -\ell, -\ell+1,\ldots,0,\ldots,+\ell$

$\mathbf{E}_{rtotal}$ is the sum of the "trapped photon" and proton electric fields,

$$\mathbf{E}_{rtotal} = \frac{e}{4\pi\varepsilon_0 r^2} + \frac{e(na_H)^\ell}{4\pi\varepsilon_0}\frac{1}{r^{(\ell+2)}}\left[-Y_0^0(\theta,\phi) + \frac{1}{n}\left[Y_0^0(\theta,\phi) + \mathrm{Re}\left\{Y_\ell^m(\theta,\phi)e^{im\omega_n t}\right\}\right]\right]\delta(r-r_n) \tag{10.74}$$

As shown in the Bound Electron "Atomic Orbital" section and the Instability of Excited States section, the angular part of the charge-density functions are eigenfunctions of Eq. (1.59), match the angular functions of the inhomogeneous Helmholtz equation, and include the time-harmonic function factor (Eqs. (1.27-1.29)) that comprises the electron source current of the corresponding electromagnetic waves. The latter are solutions of the wave-equation (Eqs. (1.1)) and arise with a change in electron radius:

$\ell = \mathbf{0}$

$$\rho(r,\theta,\phi,t) = \frac{e}{8\pi r^2}[\delta(r-r_n)]\left[Y_0^0(\theta,\phi) + Y_\ell^m(\theta,\phi)\right] \tag{10.75}$$

$\ell \neq \mathbf{0}$

$$\rho(r,\theta,\phi,t) = \frac{e}{4\pi r^2}[\delta(r-r_n)]\left[Y_0^0(\theta,\phi) + \mathrm{Re}\left\{\pi\left(R_z(\omega_n t)\right)Y_\ell^m(\theta,\phi)\right\}\right] \tag{10.76}$$

$$\rho(r,\theta,\phi,t) = \frac{e}{4\pi r^2}[\delta(r-r_n)]\left[Y_0^0(\theta,\phi) + \mathrm{Re}\left\{Y_\ell^m(\theta,\phi)e^{im\omega_n t}\right\}\right] \tag{10.77}$$

where to keep the form of the spherical harmonic as a traveling wave about the z-axis $\pi(R_z)$ is the representation of the rotational matrix about the z-axis R_z (Eq. (1.82)) in the space of functions $\pi\left(R_z(\omega_n t)\right)Y_\ell^m(\theta,\phi) = Y_\ell^m(\theta,\phi + m\omega_n t)$ and

$\mathrm{Re}\left\{Y_\ell^m(\theta,\phi)e^{im\omega_n t}\right\} = P_\ell^m(\cos\theta)\cos(m\phi + m\omega_n t)$. In the cases that $m \neq 0$, Eq. (10.77) is a traveling charge-density wave that moves on the surface of the atomic orbital about the z-axis with frequency ω_n and modulates the atomic orbital corresponding to $\ell = 0$ at $m\omega_n$. These functions comprise the well known s, p, d, f, etc. orbitals wherein the constant function $Y_0^0(\theta,\phi)$ corresponds to the spin function having spin angular momentum and the modulation function $\mathrm{Re}\left\{Y_\ell^m(\theta,\phi)e^{im\omega_n t}\right\}$ corresponds to the orbital function having orbital angular momentum as given in the Bound Electron "Atomic Orbital" section and the Rotational Parameters of the Electron (Angular Momentum, Rotational Energy, Moment of Inertia) section.

Similar to the phenomenon observed for spherical conductors [4-5], spherical harmonic charge-density waves may be induced in the inner electron atomic orbitals with the addition of one or more outer electrons, each having an orbital quantum number $\ell \neq 0$ as given by Eq. (10.77). With $Z > 5$, an energy minimum is achieved when the fifth through tenth electrons of each five through ten-electron atom fills a p orbital with the formation of orthogonal complementary charge-density waves in the inner shell electrons. To maintain the symmetry of the central charge and the energy minimum condition given by solutions to Laplace's equation (Eq. (10.72)), the charge-density waves on electron atomic orbitals at r_1 and r_3 complement those of the outer orbitals when the outer p orbitals are not all occupied by at least one electron, and the complementary charge-density waves are provided by electrons at r_3 when this condition is met. Since the angular harmonic charge-density waves are nonradiative as shown in Appendix I: Nonradiation Condition, the time-averaged central field is inverse r-squared even though the central field is modulated by the concentric charge-density waves. The modulated central field maintains the spherical harmonic orbitals that maintain the spherical-harmonic phase according to Eq. (10.72). For $\ell = 1$ and $m = \pm 1$, the spherical harmonics $Y_\ell^m(\theta,\phi)$ given by Eqs. (1.30-1.31) are:

$$Y_{1,x} = \sin\theta\cos\phi \tag{10.78}$$

$$Y_{1,y} = \sin\theta\sin\phi \tag{10.79}$$

wherein the x and y designation corresponds, respectively, to the historical p_x and p_y probability-density functions of quantum mechanics. The p_x and p_y charge-density waves rotate in the same direction such that their individual contributions to the diamagnetic force add, or they rotate in opposite directions such that their contributions cancel. In addition, for $\ell = 1$ and $m = 0$, the spherical harmonic $Y_\ell^m(\theta,\phi)$ is:

$$Y_{1,z} = \cos\theta \tag{10.80}$$

wherein the z designation corresponds to the historical p_z probability-density function of quantum mechanics.

As shown by Eq. (10.9), the diamagnetic force is dependent on the integral of the charge-density squared over the surface of the atomic orbital with the further constant of the invariance of charge under Gauss's integral law. The correction to the force due to a time and spatially-dependent spherical harmonic current-density wave is given by the normalization term for spherical harmonics given by Eq. (3.53) of Jackson [6] and Eq. (6-76) of McQuarrie [7]:

$$\frac{(\ell+|m|)!}{(2\ell+1)(\ell-|m|)!} \tag{10.81}$$

Since the spin function is constant and the orbital function is a traveling wave, only the latter contributes to the diamagnetic and paramagnetic-force contributions of an unpaired electron. Substitution of Eq. (10.81) into Eq. (10.11) gives the contribution of each orbital to the diamagnetic force, $\mathbf{F}_{diamagnetic}$, which is summed over the orbitals:

$$\mathbf{F}_{diamagnetic} = -\sum_m \frac{(\ell+|m|)!}{(2\ell+1)(\ell-|m|)!}\frac{\hbar^2}{4m_e r_n^2 r_3}\sqrt{s(s+1)}\mathbf{i}_\mathbf{r} \tag{10.82}$$

where the contributions from orbitals having $|m| = 1$ add positively or negatively.

For each five-electron atom having a central charge of Z times that of the proton, there are two indistinguishable spin-paired electrons in an atomic orbital with radii r_1 and r_2 both given by Eq. (7.35) (Eq. (10.51)), two indistinguishable spin-paired electrons in an atomic orbital with radii r_3 and r_4 both given by Eq. (10.62), and an unpaired electron in an atomic orbital at r_5 given by Eq. (10.113). For $Z \geq 6$, the next electron which binds to form the corresponding six-electron atom is attracted by the central Coulomb field and is repelled by diamagnetic force due to the spin-paired inner electrons. A paramagnetic spin-pairing force to form a filled s orbital is also possible, but the force due to the spin-pairing of the electrons (Eq. (7.24) with the radius r_6) reduces the energy of the atom less than that due to the alternative forces on two unpaired p electrons in an atomic orbital at the same radius r_6.

In general, a nonuniform distribution of charge achieves an energy minimum with the formation of a third shell due to the dependence of the magnetic forces on the nuclear charge and orbital energy (Eqs. (10.52), (10.55), and (10.93)). The outer electrons of atoms and ions that are isoelectronic with the series boron through neon half-fill a 2p level with unpaired electrons at nitrogen, then fill the level with paired electrons at neon. *Thus, it is found that the purely postulated Hund's Rule and the Pauli Exclusion Principle of the assignment of unique quantum numbers to all electrons are not "weird spooky action" phenomena unique to quantum mechanics that require all electrons in the universe to have instantaneous communication and coordination*

with no basis in physical laws such as Maxwell's equations. Rather they are phenomenological consequences of those laws.

Each outer 2p electron contributes spin as well as orbital angular momentum. The former gives rise to spin pairing to another 2p electron when an energy minimum is achieved. The corresponding force, $\mathbf{F}_{mag\ 2}$, given by Eq. (10.52) is:

$$\mathbf{F}_{mag\ 2} = \frac{1}{Z}\frac{\hbar^2}{m_e r_n^2 r_3}\sqrt{s(s+1)}\mathbf{i}_\mathbf{r} \tag{10.83}$$

The orbital angular momenta of spin-paired electrons may add to double the spin-pairing force of each individual p electron such that the resultant force is four times that of Eq. (10.83) in agreement with the energy (and force) relationship of magnetic fields (Eq. (1.154)):

$$\mathbf{F}_{mag\ 2} = \frac{1}{Z}\frac{4\hbar^2}{m_e r_n^2 r_3}\sqrt{s(s+1)}\mathbf{i}_\mathbf{r} \tag{10.84}$$

Or, the orbital angular momenta of spin-paired electrons may add negatively to cancel such that $\mathbf{F}_{mag\ 2}$ due to the contribution from spin-pairing alone is equivalent to that given by Eq. (10.83).

The electron velocity given by Eq. (1.35) is:

$$v_n = \frac{\hbar}{m_e r_n} \tag{10.85}$$

The velocity (Eq. (1.35)) and angular frequency (Eq. (1.36)) are determined by the boundary conditions that the angular momentum density at each point on the surface is constant and the magnitude of the total angular momentum of the atomic orbital $\mathbf{L}$ must also be constant. The constant total is $\hbar$ given by the integral:

$$\mathbf{m} = \int \frac{1}{4\pi r^2}\left|\mathbf{r} \times m_e \mathbf{v}\right|\delta\left(r - r_n\right)dx^4 = m_e r_n \frac{\hbar}{m_e r_n} = \hbar \tag{10.86}$$

The integral of the magnitude of the angular momentum of the electron is $\hbar$ in any inertial frame and is ***relativistically invariant*** as a Lorentz scalar $\mathbf{L} = \hbar$. The vector projections of the atomic orbital spin angular momentum relative to the Cartesian coordinates are given in the Spin Angular Momentum of the Atomic Orbital $Y_0^0(\theta,\phi)$ with $\ell = 0$ section. The orbital and spin angular momentum of excited states is also quantized in units of $\hbar$ as shown in the Orbital and Spin Splitting section. The orbital moment of inertia, $I_{orbital}$, corresponding to orbital quantum number ℓ (Eq. (1.147)) is:

$$I_{orbital} = m_e {r_n}^2\left[\frac{\ell(\ell+1)}{\ell^2+2\ell+1}\right]^{\frac{1}{2}} = m_e {r_n}^2\sqrt{\frac{\ell}{\ell+1}} \tag{10.87}$$

The spin and orbital angular momentum can superimpose positively or negatively:

$$L_{z\ total} = L_{z\ spin} + L_{z\ orbital} \tag{10.88}$$

Thus, the contribution of the orbital angular momentum to the paramagnetic force is also that given by Eq. (10.83).

$$\mathbf{F}_{mag\ 2} = \frac{1}{Z}\frac{\hbar^2}{m_e r_n^2 r_3}\sqrt{s(s+1)}\mathbf{i}_\mathbf{r} \tag{10.89}$$

And, the total force is given as the sum over the orbital and spin angular momenta that may add positively or negatively to achieve an energy minimum while maintaining the conservation of angular momentum.

The amplitude of the corresponding rotational energy, $E_{rotational\ \text{orbital}}$, given by Eq. (1.71) is:

$$E_{rotational\ \text{orbital}} = \frac{\hbar^2}{2m_e {r_n}^2}\left[\frac{\ell(\ell+1)}{\ell^2+2\ell+1}\right]^{\frac{1}{2}} = \frac{\hbar^2}{2m_e {r_n}^2}\sqrt{\frac{\ell}{\ell+1}} \tag{10.90}$$

Since the orbital rotational energy arises from a spin function (spin angular momentum) modulated by a spherical harmonic angular function (orbital angular momentum), the time-averaged orbital rotational energy having an amplitude given by Eq. (1.71) (Eq. (10.90)) is zero:

$$\left\langle E_{rotational\ \text{orbital}} \right\rangle = 0 \tag{10.91}$$

However, the orbital energy is nonzero in the presence of a magnetic field.

N-electron atoms having $Z > n$ possess an electric field of:

$$\mathbf{E} = \frac{(Z-n)e}{4\pi\varepsilon_0 r^2}\mathbf{i}_\mathbf{r} \tag{10.92}$$

for $r > r_n$. Since there is a source of dissipative power, $\mathbf{J} \bullet \mathbf{E}$ of Eq. (10.27), the magnetic moments of the inner electrons may change due to the outer electron such that the energy of the n-electron atom is lowered. The diamagnetic force, $\mathbf{F}_{diamagnetic\ 2}$, due to a relativistic effect with an electric field for $r > r_n$ (Eq. (10.35)) is dependent on the amplitude of the orbital energy. Using the orbital energy with $\ell = 1$ (Eq. (10.90)), the energy $m_e \Delta v^2$ of Eq. (10.29) is reduced by the factor of $\left(1 - \frac{\sqrt{2}}{2}\right)$ due to the contribution of the charge-density wave of the inner electrons at r_3. Thus, $\mathbf{F}_{diamagnetic\ 2}$ is given by:

$$\mathbf{F}_{diamagnetic\ 2} = -\left[\frac{Z-n}{Z-(n-1)}\right]\left(1-\frac{\sqrt{2}}{2}\right)\frac{r_3\hbar^2}{m_e r_n^4}10\sqrt{s(s+1)}\mathbf{i}_{\mathbf{r}} \tag{10.93}$$

Using the forces given by Eqs. (10.70), (10.82-10.84), (10.89), (10.93), and the radii r_3 given by Eq. (10.62), the radii of the 2p electrons of all five through ten-electron atoms may be solved exactly. The electric energy given by Eq. (10.102) gives the corresponding exact ionization energies. $\mathbf{F}_{ele}$ and $\mathbf{F}_{diamagnetic\ 2}$ given by Eqs. (10.70) and (10.93), respectively, are of the same form for all atoms with the appropriate nuclear charges and atomic radii. $\mathbf{F}_{diamagnetic}$ given by Eq. (10.82) and $\mathbf{F}_{mag\ 2}$ given by Eqs. (10.83-10.84) and (10.89) are of the same form with the appropriate factors that depend on the minimum-energy electron configuration. The general equation and the summary of the parameters that determine the exact radii and ionization energies of all five through ten-electron atoms are given the General Equation For The Ionization Energies of Five Through Ten-Electron Atoms section and in Table 10.9.

FIVE-ELECTRON ATOMS

Five-electron atoms can be solved exactly using the results of the solutions of one, two, three, and four-electron atoms.

RADIUS AND IONIZATION ENERGY OF THE OUTER ELECTRON OF THE BORON ATOM

For each four-electron atom having a central charge of Z times that of the proton, there are two indistinguishable spin-paired electrons in an atomic orbital with radii r_1 and r_2 both given by Eq. (7.35) (Eq. (10.51)) and two indistinguishable spin-paired electrons in an atomic orbital with radii r_3 and r_4 both given by Eq. (10.62). For $Z \geq 5$, the next electron which binds to form the corresponding five-electron atom is attracted by the central Coulomb field and is repelled by diamagnetic force due to the spin-paired inner electrons such that it forms an unpaired atomic orbital at radius r_5. The resulting electron configuration is $1s^2 2s^2 2p^1$, and the orbital arrangement is:

2p state

$$\begin{array}{ccc} \uparrow & & \\ \hline 1 & 0 & -1 \end{array} \tag{10.94}$$

corresponding to the ground state ${}^2P^0_{1/2}$.

The central Coulomb force acts on the outer electron to cause it to bind wherein this electric force on the outer-most electron due to the nucleus and the inner four electrons is given by Eq. (10.70) with the appropriate charge and radius:

$$\mathbf{F}_{ele} = \frac{(Z-4)e^2}{4\pi\varepsilon_0 r_5^2}\mathbf{i}_{\mathbf{r}} \tag{10.95}$$

for $r > r_4$.

The single p orbital of the boron atom produces a diamagnetic force equivalent to that of the formation of an s orbital due to the induction of complementary and spherically symmetrical charge-density waves on electron atomic orbitals at r_1 and r_3 in order to achieve a solution of Laplace's equation (Eq. (10.72)). The inner electrons remain at their initial radii, but cause a diamagnetic force according to Lenz's law that is two times that of Eqs. (10.11) and (10.71) since the two electrons at $r_1 = r_2$ act on the two electrons at $r_3 = r_4$ which in turn act of the outer electron. $\mathbf{F}_{diamagnetic}$ is also given by Eq. (10.82) with $\ell = 0$ and the appropriate radii when the contributions from the three orthogonal spherical harmonics are summed over including those induced:

$$\mathbf{F}_{diamagnetic} = -\frac{2\hbar^2}{4m_e r_5^2 r_3}\sqrt{s(s+1)}\mathbf{i}_{\mathbf{r}} \tag{10.96}$$

The charge induction forms complementary mirror charge-density waves which must have opposing angular momenta such that momentum is conserved. In this case, $\mathbf{F}_{mag\ 2}$ given by Eq. (10.89) is zero:

$$\mathbf{F}_{mag\ 2} = 0 \tag{10.97}$$

The outward centrifugal force on electron 5 is balanced by the electric force and the magnetic force (on electron 5). The radius of the outer electron is calculated by equating the outward centrifugal force to the sum of the electric (Eq. (10.95)) and diamagnetic (Eq. (10.96)) forces as follows:

$$\frac{m_e v_5^2}{r_5} = \frac{(Z-4)e^2}{4\pi\varepsilon_0 r_5^2} - \frac{2\hbar^2}{4m_e r_5^2 r_3}\sqrt{s(s+1)} \tag{10.98}$$

Substitution of $v_5 = \frac{\hbar}{m_e r_5}$ (Eq. (1.35)) and $s = \frac{1}{2}$ into Eq. (10.98) gives:

$$\frac{\hbar^2}{m_e r_5^3} = \frac{(Z-4)e^2}{4\pi\varepsilon_0 r_5^2} - \frac{\hbar^2}{2m_e r_5^2 r_3}\sqrt{\frac{3}{4}} \tag{10.99}$$

$$r_5 = \frac{a_0}{\left((Z-4)-\frac{\sqrt{\frac{3}{4}}}{2r_3}\right)},\ r_3 \textit{ in units of } a_0 \tag{10.100}$$

Substitution of $\frac{r_3}{a_0} = 1.07930$ (Eq. (10.62) with $Z = 5$) into Eq. (10.100) gives:

$$r_5 = 1.67000351 a_0 \tag{10.101}$$

In general, the energy stored in the electric field, $E(electric)$, is given by Eq. (10.43) with the appropriate charge and radius:

$$E(electric) = -\frac{(Z-(n-1))e^2}{8\pi\varepsilon_0 r_n} \tag{10.102}$$

where n corresponds to the number of electrons of the atom and Z is its atomic number. The ionization energy is given by the sum of the electric energy and the energy corresponding to the change in magnetic-moments of the inner shell electrons. Since there is no source of dissipative power, $\mathbf{J} \bullet \mathbf{E}$ of Eq. (10.27), to compensate for any potential change in the magnetic moments, Δm, of the inner electrons due to the ionization of the outer electron of the boron atom, there is a diamagnetic energy term in the ionization energy for this atom that follows from the corresponding term for the lithium atom. Since the diamagnetic force for the boron atom (Eq. (10.96)) is twice that of the corresponding force (Eq. (10.11)) of the lithium atom, this term is given by twice that of Eqs. (10.15-10.24), with $Z = 5$, r_3 given by Eq. (10.62), and r_5 given by Eq. (10.101). Thus, the change in magnetic energy of the inner atomic orbital at r_3 is 85.429321 %, so that the corresponding energy ΔE_{mag} is:

$$\Delta E_{mag} = 2\left(0.85429321\ X\ 0.09100214\ eV\right) = 0.15548501\ eV \tag{10.103}$$

where the magnetic energy of the inner electrons is $0.09100214\ eV$ (Eqs. (10.64) and (10.101)). Then, the ionization energy of the boron atom is given by Eqs. (10.101-10.102) and (10.103):

$$\begin{aligned} E(ionization;\ B) &= \frac{(Z-4)e^2}{8\pi\varepsilon_0 r_5} + \Delta E_{mag} \\ &= 8.147170901\ eV + 0.15548501\ eV = 8.30265592\ eV \end{aligned} \tag{10.104}$$

The experimental ionization energy of the boron atom is $8.29803\ eV$ [3].

THE IONIZATION ENERGIES OF FIVE-ELECTRON ATOMS WITH A NUCLEAR CHARGE Z>5

Five-electron atoms having $Z > 5$ possess an external electric field given by Eq. (10.92). In this case, an energy minimum is achieved with conservation of momentum when the orbital angular momentum is such that $\mathbf{F}_{diamagnetic}$ is minimized while $\mathbf{F}_{mag\ 2}$ is maximized. From Eq. (10.82), the diamagnetic force, $\mathbf{F}_{diamagnetic}$, is given by the sum of the contributions from the p_x, p_y, and p_z orbitals corresponding to m = 1, -1, and 0, respectively:

$$\mathbf{F}_{diamagnetic} = -\left(\frac{2}{3}+\frac{2}{3}+\frac{1}{3}\right)\frac{\hbar^2}{4m_e r_5^2 r_3}\sqrt{s(s+1)}\mathbf{i}_\mathbf{r} = -\left(\frac{5}{3}\right)\frac{\hbar^2}{4m_e r_5^2 r_3}\sqrt{s(s+1)}\mathbf{i}_\mathbf{r} \tag{10.105}$$

With $Z > 5$, the charge induction forms complementary mirror charge-density waves such that the angular momenta do not cancel. From Eq. (10.89), $\mathbf{F}_{mag\ 2}$ corresponding to the orbital angular momentum of the single p_x electron is

$$\mathbf{F}_{mag\ 2} = \frac{1}{Z}\frac{\hbar^2}{m_e r_5^2 r_3}\sqrt{s(s+1)}\mathbf{i}_\mathbf{r} \tag{10.106}$$

The second diamagnetic force, $\mathbf{F}_{diamagnetic\ 2}$, due to the binding of the p-orbital electron having an electric field outside of its radius is given by Eq. (10.93):

$$\mathbf{F}_{diamagnetic\ 2} = -\left[\frac{Z-5}{Z-4}\right]\left(1-\frac{\sqrt{2}}{2}\right)\frac{r_3\hbar^2}{m_e r_5^4}10\sqrt{s(s+1)}\mathbf{i}_\mathbf{r} \tag{10.107}$$

In the case that $Z > 5$, the radius of the outer electron is calculated by equating the outward centrifugal force to the sum of the electric (Eq. (10.95)) and diamagnetic (Eqs. (10.105) and (10.107)), and paramagnetic (Eq. (10.106)) forces as follows:

$$\frac{m_e v_5^2}{r_5} = \frac{(Z-4)e^2}{4\pi\varepsilon_0 r_5^2} - \frac{5\hbar^2}{12m_e r_5^2 r_3}\sqrt{s(s+1)} + \frac{\hbar^2}{Zm_e r_5^2 r_3}\sqrt{s(s+1)} - \left[\frac{Z-5}{Z-4}\right]\left(1-\frac{\sqrt{2}}{2}\right)\frac{r_3\hbar^2}{r_5^4 m_e}10\sqrt{s(s+1)} \tag{10.108}$$

Substitution of $v_5 = \frac{\hbar}{m_e r_5}$ (Eq. (1.35)) and $s = \frac{1}{2}$ into Eq. (10.108) gives:

$$\frac{\hbar^2}{m_e r_5^3}=\frac{(Z-4)e^2}{4\pi\varepsilon_0 r_5^2}-\frac{5\hbar^2}{12m_e r_5^2 r_3}\sqrt{\frac{3}{4}}+\frac{\hbar^2}{Zm_e r_5^2 r_3}\sqrt{\frac{3}{4}}-\left[\frac{Z-5}{Z-4}\right]\left(1-\frac{\sqrt{2}}{2}\right)\frac{r_3\hbar^2}{r_5^4 m_e}10\sqrt{\frac{3}{4}} \tag{10.109}$$

The quadratic equation corresponding to Eq. (10.109) is:

$$\left(\frac{(Z-4)e^2}{4\pi\varepsilon_0}-\left(\frac{5}{12}-\frac{1}{Z}\right)\frac{\hbar^2}{m_e r_3}\sqrt{\frac{3}{4}}\right)r_5^2-\frac{\hbar^2}{m_e}r_5-\left[\frac{Z-5}{Z-4}\right]\left(1-\frac{\sqrt{2}}{2}\right)\frac{r_3\hbar^2}{m_e}10\sqrt{\frac{3}{4}}=0 \tag{10.110}$$

$$r_5^2-\frac{\dfrac{\hbar^2}{m_e}}{\left(\dfrac{(Z-4)e^2}{4\pi\varepsilon_0}-\left(\dfrac{5}{12}-\dfrac{1}{Z}\right)\dfrac{\hbar^2}{m_e r_3}\sqrt{\dfrac{3}{4}}\right)}r_5-\frac{\dfrac{\hbar^2}{m_e}\left[\dfrac{Z-5}{Z-4}\right]\left(1-\dfrac{\sqrt{2}}{2}\right)r_3 10\sqrt{\dfrac{3}{4}}}{\left(\dfrac{(Z-4)e^2}{4\pi\varepsilon_0}-\left(\dfrac{5}{12}-\dfrac{1}{Z}\right)\dfrac{\hbar^2}{m_e r_3}\sqrt{\dfrac{3}{4}}\right)}=0 \tag{10.111}$$

The solution of Eq. (10.111) using the quadratic formula is:

$$r_5=\frac{\dfrac{\dfrac{\hbar^2}{m_e}}{\left(\dfrac{(Z-4)e^2}{4\pi\varepsilon_0}-\left(\dfrac{5}{12}-\dfrac{1}{Z}\right)\dfrac{\hbar^2}{m_e r_3}\sqrt{\dfrac{3}{4}}\right)}\pm\sqrt{\left(\dfrac{\dfrac{\hbar^2}{m_e}}{\left(\dfrac{(Z-4)e^2}{4\pi\varepsilon_0}-\left(\dfrac{5}{12}-\dfrac{1}{Z}\right)\dfrac{\hbar^2}{m_e r_3}\sqrt{\dfrac{3}{4}}\right)}\right)^2+4\dfrac{\dfrac{\hbar^2}{m_e}\left[\dfrac{Z-5}{Z-4}\right]\left(1-\dfrac{\sqrt{2}}{2}\right)r_3 10\sqrt{\dfrac{3}{4}}}{\left(\dfrac{(Z-4)e^2}{4\pi\varepsilon_0}-\left(\dfrac{5}{12}-\dfrac{1}{Z}\right)\dfrac{\hbar^2}{m_e r_3}\sqrt{\dfrac{3}{4}}\right)}}}{2} \tag{10.112}$$

$$r_5=\frac{\dfrac{a_0}{\left((Z-4)-\left(\dfrac{5}{24}-\dfrac{1}{2Z}\right)\dfrac{\sqrt{3}}{r_3}\right)}\pm a_0\sqrt{\left(\dfrac{1}{\left((Z-4)-\left(\dfrac{5}{24}-\dfrac{1}{2Z}\right)\dfrac{\sqrt{3}}{r_3}\right)}\right)^2+\dfrac{20\sqrt{3}\left(\left[\dfrac{Z-5}{Z-4}\right]\left(1-\dfrac{\sqrt{2}}{2}\right)r_3\right)}{\left((Z-4)-\left(\dfrac{5}{24}-\dfrac{1}{2Z}\right)\dfrac{\sqrt{3}}{r_3}\right)}}}{2},\ r_3\ \textit{in units of}\ a_0 \tag{10.113}$$

where r_3 is given by Eq. (10.62). The positive root of Eq. (10.113) must be taken in order that $r_5>0$. The radii of several five-electron atoms are given in Table 10.3.

The ionization energies for the five-electron atoms with $Z>5$ are given by the electric energy, $E(electric)$, (Eq. (10.102) with the radii, r_5, given by Eq. (10.113)):

$$E(Ionization)=-Electric\ Energy=\frac{(Z-4)e^2}{8\pi\varepsilon_0 r_5} \tag{10.114}$$

Since the relativistic corrections were small, the nonrelativistic ionization energies for experimentally measured five-electron atoms are given in Table 10.3.

Table 10.3. Ionization energies for some five-electron atoms.

5 e Atom	Z	r_1 (a_o) [a]	r_3 (a_o) [b]	r_5 (a_o) [c]	Theoretical Ionization Energies [d] (eV)	Experimental Ionization Energies [e] (eV)	Relative Error [f]
B	5	0.20670	1.07930	1.67000	8.30266	8.29803	-0.00056
C^{+}	6	0.17113	0.84317	1.12092	24.2762	24.38332	0.0044
N^{2+}	7	0.14605	0.69385	0.87858	46.4585	47.44924	0.0209
O^{3+}	8	0.12739	0.59020	0.71784	75.8154	77.41353	0.0206
F^{4+}	9	0.11297	0.51382	0.60636	112.1922	114.2428	0.0179
Ne^{5+}	10	0.10149	0.45511	0.52486	155.5373	157.93	0.0152
Na^{6+}	11	0.09213	0.40853	0.46272	205.8266	208.5	0.0128
Mg^{7+}	12	0.08435	0.37065	0.41379	263.0469	265.96	0.0110
Al^{8+}	13	0.07778	0.33923	0.37425	327.1901	330.13	0.0089
Si^{9+}	14	0.07216	0.31274	0.34164	398.2509	401.37	0.0078
P^{10+}	15	0.06730	0.29010	0.31427	476.2258	479.46	0.0067
S^{11+}	16	0.06306	0.27053	0.29097	561.1123	564.44	0.0059
Cl^{12+}	17	0.05932	0.25344	0.27090	652.9086	656.71	0.0058
Ar^{13+}	18	0.05599	0.23839	0.25343	751.6132	755.74	0.0055
K^{14+}	19	0.05302	0.22503	0.23808	857.2251	861.1	0.0045
Ca^{15+}	20	0.05035	0.21308	0.22448	969.7435	974	0.0044
Sc^{16+}	21	0.04794	0.20235	0.21236	1089.1678	1094	0.0044
Ti^{17+}	22	0.04574	0.19264	0.20148	1215.4975	1221	0.0045
V^{18+}	23	0.04374	0.18383	0.19167	1348.7321	1355	0.0046
Cr^{19+}	24	0.04191	0.17579	0.18277	1488.8713	1496	0.0048
Mn^{20+}	25	0.04022	0.16842	0.17466	1635.9148	1644	0.0049
Fe^{21+}	26	0.03867	0.16165	0.16724	1789.8624	1799	0.0051
Co^{22+}	27	0.03723	0.15540	0.16042	1950.7139	1962	0.0058
Ni^{23+}	28	0.03589	0.14961	0.15414	2118.4690	2131	0.0059
Cu^{24+}	29	0.03465	0.14424	0.14833	2293.1278	2308	0.0064

[a] Radius of the first set of paired inner electrons of five-electron atoms from Eq. (10.51).

[b] Radius of the second set of paired inner electrons of five-electron atoms from Eq. (10.62).

[c] Radius of the outer electron of five-electron atoms from Eq. (10.113) for $Z > 5$ and Eq. (10.101) for B.

[d] Calculated ionization energies of five-electron atoms given by the electric energy (Eq. (10.114)) for $Z > 5$ and Eq. (10.104) for B.

[e] From theoretical calculations, interpolation of isoelectronic and spectral series, and experimental data [2-3].

[f] (Experimental-theoretical)/experimental.

The agreement between the experimental and calculated values of Table 10.3 is well within the experimental capability of the spectroscopic determinations including the values at large Z which relies on X-ray spectroscopy. In this case, the experimental capability is three to four significant figures which is consistent with the last column. The boron atom isoelectronic series is given in Table 10.3 [2-3] to much higher precision than the capability of X-ray spectroscopy, but these values are based on theoretical and interpolation techniques rather than data alone. Ionization energies are difficult to determine since the cut-off of the Rydberg series of lines at the ionization energy is often not observed, and the ionization energy must be determined from theoretical calculations, interpolation of B isoelectronic and Rydberg series, as well as direct experimental data.

SIX-ELECTRON ATOMS

Six-electron atoms can be solved exactly using the results of the solutions of one, two, three, four, and five-electron atoms.

RADIUS AND IONIZATION ENERGY OF THE OUTER ELECTRON OF THE CARBON ATOM

For each five-electron atom having a central charge of Z times that of the proton, there are two indistinguishable spin-paired electrons in an atomic orbital with radii r_1 and r_2 both given by Eq. (7.35) (Eq. (10.51)), two indistinguishable spin-paired electrons in an atomic orbital with radii r_3 and r_4 both given by Eq. (10.62), and an unpaired electron in an atomic orbital at r_5 given by Eq. (10.113). For $Z \geq 6$, the next electron which binds to form the corresponding six-electron atom is attracted by the central Coulomb field and is repelled by diamagnetic force due to the spin-paired inner electrons. A paramagnetic spin-pairing force to form a filled s orbital is also possible, but the force due to the spin-pairing of the electrons (Eq. (7.24) with the radius r_6) reduces the energy of the atom less than that due to the alternative forces on two unpaired p electrons in an atomic orbital at the same radius r_6. The resulting electron configuration is $1s^2 2s^2 2p^2$, and the orbital arrangement is:

2p state

$$\underset{1}{\uparrow} \quad \underset{0}{\uparrow} \quad \underset{-1}{\_\_} \tag{10.115}$$

corresponding to the ground state ${}^3P_0$.

The central Coulomb force acts on the outer electron to cause it to bind wherein this electric force on the outer-most electron due to the nucleus and the inner five electrons is given by Eq. (10.70) with the appropriate charge and radius:

$$\mathbf{F}_{ele} = \frac{(Z-5)e^2}{4\pi\varepsilon_0 r_6^2}\mathbf{i}_\mathbf{r} \tag{10.116}$$

for $r > r_5$.

The two orthogonal electrons form charge-density waves such that the total angular momentum of the two outer electrons is conserved which determines the diamagnetic force according to Eq. (10.82). $\mathbf{F}_{diamagnetic}$ is:

$$\mathbf{F}_{diamagnetic} = -\left(\frac{2}{3}\right)\frac{\hbar^2}{4m_e r_6^2 r_3}\sqrt{s(s+1)}\mathbf{i}_\mathbf{r} \tag{10.117}$$

corresponding to $m = 1$.

The charge induction forms complementary mirror charge-density waves which must have opposing angular momenta such that momentum is conserved. In this case, $\mathbf{F}_{mag\ 2}$ given by Eq. (10.89) is zero:

$$\mathbf{F}_{mag\ 2} = 0 \tag{10.118}$$

The outward centrifugal force on electron 6 is balanced by the electric force and the magnetic forces (on electron 6). The radius of the outer electron is calculated by equating the outward centrifugal force to the sum of the electric (Eq. (10.116)) and diamagnetic (Eq. (10.117)) forces as follows:

$$\frac{m_e v_6^2}{r_6} = \frac{(Z-5)e^2}{4\pi\varepsilon_0 r_6^2} - \frac{\hbar^2}{6m_e r_6^2 r_3}\sqrt{s(s+1)} \tag{10.119}$$

Substitution of $v_6 = \frac{\hbar}{m_e r_6}$ (Eq. (1.35)) and $s = \frac{1}{2}$ into Eq. (10.119) gives:

$$\frac{\hbar^2}{m_e r_6^3} = \frac{(Z-5)e^2}{4\pi\varepsilon_0 r_6^2} - \frac{\hbar^2}{6m_e r_6^2 r_3}\sqrt{\frac{3}{4}} \tag{10.120}$$

$$r_6 = \frac{a_0}{\left((Z-5) - \frac{\sqrt{\frac{3}{4}}}{6r_3}\right)},\ r_3 \textit{ in units of } a_0 \tag{10.121}$$

Substitution of $\frac{r_3}{a_0} = 0.84317$ (Eq. (10.62) with $Z = 6$) into Eq. (10.121) gives:

$$r_6 = 1.20654 a_0 \tag{10.122}$$

The ionization energy of the carbon atom is given by the electric energy, $E(electric)$, (Eq. (10.102) with the radius, r_6, given by Eq. (10.122)):

$$E(ionization;\ C) = -Electric\ Energy = \frac{(Z-5)e^2}{8\pi\varepsilon_0 r_6} = 11.27671\ eV \tag{10.123}$$

where $r_6 = 1.20654 a_0$ (Eq. (10.122)) and $Z = 6$. The experimental ionization energy of the carbon atom is 11.2603 eV [3].

THE IONIZATION ENERGIES OF SIX-ELECTRON ATOMS WITH A NUCLEAR CHARGE Z>6

Six-electron atoms having $Z > 6$ possess an external electric field given by Eq. (10.92). In this case, an energy minimum is achieved with conservation of momentum when the orbital angular momentum is such that $\mathbf{F}_{diamagnetic}$ is minimized while $\mathbf{F}_{mag\ 2}$ is maximized. From Eq. (10.82), the diamagnetic force, $\mathbf{F}_{diamagnetic}$, is given by the sum of the contributions from the p_x, p_y, and p_z orbitals corresponding to $m = 1,\ -1,$ and $0,$ respectively:

$$\mathbf{F}_{diamagnetic} = -\left(\frac{2}{3}+\frac{2}{3}+\frac{1}{3}\right)\frac{\hbar^2}{4m_e r_6^2 r_3}\sqrt{s(s+1)}\mathbf{i}_{\mathbf{r}} = -\left(\frac{5}{3}\right)\frac{\hbar^2}{4m_e r_6^2 r_3}\sqrt{s(s+1)}\mathbf{i}_{\mathbf{r}} \tag{10.124}$$

With $Z > 6$, the charge induction forms complementary mirror charge-density waves such that the angular momenta do not cancel. From Eq. (10.89), $\mathbf{F}_{mag\ 2}$ corresponding to the orbital angular momentum of the two p electrons in addition to complementary charge-density waves is:

$$\mathbf{F}_{mag\ 2} = 2\frac{1}{Z}\frac{2\hbar^2}{m_e r_6^2 r_3}\sqrt{s(s+1)}\mathbf{i}_{\mathbf{r}} = \frac{1}{Z}\frac{4\hbar^2}{m_e r_6^2 r_3}\sqrt{s(s+1)}\mathbf{i}_{\mathbf{r}} \tag{10.125}$$

The second diamagnetic force, $\mathbf{F}_{diamagnetic\ 2}$, due to the binding of the p-orbital electron having an electric field outside of its radius, is given by Eq. (10.93):

$$\mathbf{F}_{diamagnetic\ 2} = -\left[\frac{Z-6}{Z-5}\right]\left(1-\frac{\sqrt{2}}{2}\right)\frac{r_3\hbar^2}{m_e r_6^4}10\sqrt{s(s+1)}\mathbf{i}_{\mathbf{r}} \tag{10.126}$$

In the case that $Z > 6$, the radius of the outer electron is calculated by equating the outward centrifugal force to the sum of the electric (Eq. (10.116)), diamagnetic (Eqs. (10.124) and (10.126)), and paramagnetic (Eq. (10.125)) forces as follows:

$$\frac{m_e v_6^2}{r_6} = \frac{(Z-5)e^2}{4\pi\varepsilon_0 r_6^2} - \frac{5\hbar^2}{12m_e r_6^2 r_3}\sqrt{s(s+1)} + \frac{4\hbar^2}{Zm_e r_6^2 r_3}\sqrt{s(s+1)} - \left[\frac{Z-6}{Z-5}\right]\left(1-\frac{\sqrt{2}}{2}\right)\frac{r_3\hbar^2}{m_e r_6^4}10\sqrt{s(s+1)} \tag{10.127}$$

Substitution of $v_6 = \dfrac{\hbar}{m_e r_6}$ (Eq. (1.35)) and $s = \dfrac{1}{2}$ into Eq. (10.127) gives:

$$\frac{\hbar^2}{m_e r_6^3} = \frac{(Z-5)e^2}{4\pi\varepsilon_0 r_6^2} - \frac{5\hbar^2}{12m_e r_6^2 r_3}\sqrt{\frac{3}{4}} + \frac{4\hbar^2}{Zm_e r_6^2 r_3}\sqrt{\frac{3}{4}} - \left[\frac{Z-6}{Z-5}\right]\left(1-\frac{\sqrt{2}}{2}\right)\frac{r_3\hbar^2}{r_6^4 m_e}10\sqrt{\frac{3}{4}} \tag{10.128}$$

The quadratic equation corresponding to Eq. (10.128) is:

$$\left(\frac{(Z-5)e^2}{4\pi\varepsilon_0} - \left(\frac{5}{12}-\frac{4}{Z}\right)\frac{\hbar^2}{m_e r_3}\sqrt{\frac{3}{4}}\right)r_6^2 - \frac{\hbar^2}{m_e}r_6 - \left[\frac{Z-6}{Z-5}\right]\left(1-\frac{\sqrt{2}}{2}\right)\frac{r_3\hbar^2}{m_e}10\sqrt{\frac{3}{4}} = 0 \tag{10.129}$$

$$r_6^2 - \frac{\dfrac{\hbar^2}{m_e}}{\left(\dfrac{(Z-5)e^2}{4\pi\varepsilon_0} - \left(\dfrac{5}{12}-\dfrac{4}{Z}\right)\dfrac{\hbar^2}{m_e r_3}\sqrt{\dfrac{3}{4}}\right)}r_6 - \frac{\dfrac{\hbar^2}{m_e}\left[\dfrac{Z-6}{Z-5}\right]\left(1-\dfrac{\sqrt{2}}{2}\right)r_3 10\sqrt{\dfrac{3}{4}}}{\left(\dfrac{(Z-5)e^2}{4\pi\varepsilon_0} - \left(\dfrac{5}{12}-\dfrac{4}{Z}\right)\dfrac{\hbar^2}{m_e r_3}\sqrt{\dfrac{3}{4}}\right)} = 0 \tag{10.130}$$

The solution of Eq. (10.130) using the quadratic formula is:

$$r_6 = \frac{\dfrac{\dfrac{\hbar^2}{m_e}}{\left(\dfrac{(Z-5)e^2}{4\pi\varepsilon_0} - \left(\dfrac{5}{12}-\dfrac{4}{Z}\right)\dfrac{\hbar^2}{m_e r_3}\sqrt{\dfrac{3}{4}}\right)} \pm \sqrt{\left(\dfrac{\dfrac{\hbar^2}{m_e}}{\left(\dfrac{(Z-5)e^2}{4\pi\varepsilon_0} - \left(\dfrac{5}{12}-\dfrac{4}{Z}\right)\dfrac{\hbar^2}{m_e r_3}\sqrt{\dfrac{3}{4}}\right)}\right)^2 + 4\dfrac{\dfrac{\hbar^2}{m_e}\left[\dfrac{Z-6}{Z-5}\right]\left(1-\dfrac{\sqrt{2}}{2}\right)r_3 10\sqrt{\dfrac{3}{4}}}{\left(\dfrac{(Z-5)e^2}{4\pi\varepsilon_0} - \left(\dfrac{5}{12}-\dfrac{4}{Z}\right)\dfrac{\hbar^2}{m_e r_3}\sqrt{\dfrac{3}{4}}\right)}}}{2} \tag{10.131}$$

$$r_6 = \frac{\dfrac{a_0}{\left((Z-5)-\left(\dfrac{5}{24}-\dfrac{2}{Z}\right)\dfrac{\sqrt{3}}{r_3}\right)} \pm a_0 \sqrt{\left(\dfrac{1}{\left((Z-5)-\left(\dfrac{5}{24}-\dfrac{2}{Z}\right)\dfrac{\sqrt{3}}{r_3}\right)}\right)^2 + \dfrac{20\sqrt{3}\left(\left[\dfrac{Z-6}{Z-5}\right]\left(1-\dfrac{\sqrt{2}}{2}\right)r_3\right)}{\left((Z-5)-\left(\dfrac{5}{24}-\dfrac{2}{Z}\right)\dfrac{\sqrt{3}}{r_3}\right)}}}{2}, r_3 \text{ in units of } a_0 \tag{10.132}$$

where r_3 is given by Eq. (10.62). The positive root of Eq. (10.132) must be taken in order that $r_6 > 0$. The final radius of electron 6, r_6, is given by Eq. (10.132); this is also the final radius of electron 5. The radii of several six-electron atoms are given in Table 10.4.

The ionization energies for the six-electron atoms with $Z > 6$ are given by the electric energy, $E(electric)$, (Eq. (10.102) with the radii r_6, given by Eq. (10.132)):

$$E(Ionization) = -Electric\ Energy = \frac{(Z-5)e^2}{8\pi\varepsilon_0 r_6} \tag{10.133}$$

Since the relativistic corrections were small, the nonrelativistic ionization energies for experimentally measured six-electron atoms are given in Table 10.4.

Table 10.4. Ionization energies for some six-electron atoms.

6 e Atom	Z	r_1 (a_0) [a]	r_3 (a_0) [b]	r_6 (a_0) [c]	Theoretical Ionization Energies [d] (eV)	Experimental Ionization Energies [e] (eV)	Relative Error [f]
C	6	0.17113	0.84317	1.20654	11.27671	11.2603	-0.0015
N^{+}	7	0.14605	0.69385	0.90119	30.1950	29.6013	-0.0201
O^{2+}	8	0.12739	0.59020	0.74776	54.5863	54.9355	0.0064
F^{3+}	9	0.11297	0.51382	0.63032	86.3423	87.1398	0.0092
Ne^{4+}	10	0.10149	0.45511	0.54337	125.1986	126.21	0.0080
Na^{5+}	11	0.09213	0.40853	0.47720	171.0695	172.18	0.0064
Mg^{6+}	12	0.08435	0.37065	0.42534	223.9147	225.02	0.0049
Al^{7+}	13	0.07778	0.33923	0.38365	283.7121	284.66	0.0033
Si^{8+}	14	0.07216	0.31274	0.34942	350.4480	351.12	0.0019
P^{9+}	15	0.06730	0.29010	0.32081	424.1135	424.4	0.0007
S^{10+}	16	0.06306	0.27053	0.29654	504.7024	504.8	0.0002
Cl^{11+}	17	0.05932	0.25344	0.27570	592.2103	591.99	-0.0004
Ar^{12+}	18	0.05599	0.23839	0.25760	686.6340	686.1	-0.0008
K^{13+}	19	0.05302	0.22503	0.24174	787.9710	786.6	-0.0017
Ca^{14+}	20	0.05035	0.21308	0.22772	896.2196	894.5	-0.0019
Sc^{15+}	21	0.04794	0.20235	0.21524	1011.3782	1009	-0.0024
Ti^{16+}	22	0.04574	0.19264	0.20407	1133.4456	1131	-0.0022
V^{17+}	23	0.04374	0.18383	0.19400	1262.4210	1260	-0.0019
Cr^{18+}	24	0.04191	0.17579	0.18487	1398.3036	1396	-0.0017
Mn^{19+}	25	0.04022	0.16842	0.17657	1541.0927	1539	-0.0014
Fe^{20+}	26	0.03867	0.16165	0.16899	1690.7878	1689	-0.0011
Co^{21+}	27	0.03723	0.15540	0.16203	1847.3885	1846	-0.0008
Ni^{22+}	28	0.03589	0.14961	0.15562	2010.8944	2011	0.0001
Cu^{23+}	29	0.03465	0.14424	0.14970	2181.3053	2182	0.0003

[a] Radius of the first set of paired inner electrons of six-electron atoms from Eq. (10.51).

[b] Radius of the second set of paired inner electrons of six-electron atoms from Eq. (10.62).

[c] Radius of the two unpaired outer electrons of six-electron atoms from Eq. (10.132) for $Z > 6$ and Eq. (10.122) for C.

[d] Calculated ionization energies of six-electron atoms given by the electric energy (Eq. (10.133)).
[e] From theoretical calculations, interpolation of isoelectronic and spectral series, and experimental data [2-3].
[f] (Experimental-theoretical)/experimental.

The agreement between the experimental and calculated values of Table 10.4 is well within the experimental capability of the spectroscopic determinations including the values at large Z which relies on X-ray spectroscopy. In this case, the experimental capability is three to four significant figures which is consistent with the last column. The carbon atom isoelectronic series is given in Table 10.4 [2-3] to much higher precision than the capability of X-ray spectroscopy, but these values are based on theoretical and interpolation techniques rather than data alone. Ionization energies are difficult to determine since the cut-off of the Rydberg series of lines at the ionization energy is often not observed, and the ionization energy must be determined from theoretical calculations, interpolation of C isoelectronic and Rydberg series, as well as direct experimental data.

SEVEN-ELECTRON ATOMS

Seven-electron atoms can be solved exactly using the results of the solutions of one, two, three, four, five, and six-electron atoms.

RADIUS AND IONIZATION ENERGY OF THE OUTER ELECTRON OF THE NITROGEN ATOM

For each six-electron atom having a central charge of Z times that of the proton, there are two indistinguishable spin-paired electrons in an atomic orbital with radii r_1 and r_2 both given by Eq. (7.35) (Eq. (10.51)), two indistinguishable spin-paired electrons in an atomic orbital with radii r_3 and r_4 both given by Eq. (10.62), and two unpaired electrons in an atomic orbital at r_6 given by Eq. (10.132). For $Z \geq 7$, the next electron which binds to form the corresponding seven-electron atom is attracted by the central Coulomb field and is repelled by diamagnetic force due to the spin-paired inner electrons. A paramagnetic spin-pairing force is also possible, but the force due to the spin-pairing of the electrons (Eq. (7.24) with the radius r_7) reduces the energy of the atom less than that due to the alternative forces on three unpaired p electrons in an atomic orbital at the same radius r_7. The resulting electron configuration is $1s^2 2s^2 2p^3$, and the orbital arrangement is:

2p state		
$\uparrow$	$\uparrow$	$\uparrow$
1	0	-1

(10.134)

corresponding to the ground state ${}^4S^0_{3/2}$.

The central Coulomb force acts on the outer electron to cause it to bind wherein this electric force on the outer-most electron due to the nucleus and the inner six electrons is given by Eq. (10.70) with the appropriate charge and radius:

$$\mathbf{F}_{ele} = \frac{(Z-6)e^2}{4\pi\varepsilon_0 r_7^2}\mathbf{i}_\mathbf{r} \tag{10.135}$$

for $r > r_6$.

The energy is minimized with conservation of angular momentum when the angular momenta of the two orthogonal p_x and p_y electrons cancel such that the diamagnetic force (Eq. (10.82)), $\mathbf{F}_{diamagnetic}$, is:

$$\mathbf{F}_{diamagnetic} = -\left(\frac{1}{3}\right)\frac{\hbar^2}{4m_e r_7^2 r_3}\sqrt{s(s+1)}\mathbf{i}_\mathbf{r} \tag{10.136}$$

corresponding to $m = 0$.

From Eq. (10.89), $\mathbf{F}_{mag\ 2}$ corresponding to the orbital angular momentum of the p_z electron is:

$$\mathbf{F}_{mag\ 2} = \frac{1}{Z}\frac{\hbar^2}{m_e r_7^2 r_3}\sqrt{s(s+1)}\mathbf{i}_\mathbf{r} \tag{10.137}$$

The outward centrifugal force on electron 7 is balanced by the electric force and the magnetic forces (on electron 7). The radius of the outer electron is calculated by equating the outward centrifugal force to the sum of the electric (Eq. (10.135)), diamagnetic (Eq. (10.136)), and paramagnetic (Eq. (10.137)) forces as follows:

$$\frac{m_e v_7^2}{r_7} = \frac{(Z-6)e^2}{4\pi\varepsilon_0 r_7^2} - \frac{\hbar^2}{12m_e r_7^2 r_3}\sqrt{s(s+1)} + \frac{\hbar^2}{Zm_e r_7^2 r_3}\sqrt{s(s+1)} \tag{10.138}$$

Substitution of $v_7 = \frac{\hbar}{m_e r_7}$ (Eq. (1.35)) and $s = \frac{1}{2}$ into Eq. (10.138) gives:

$$\frac{\hbar^2}{m_e r_7^3} = \frac{(Z-6)e^2}{4\pi\varepsilon_0 r_7^2} - \frac{\hbar^2}{12m_e r_7^2 r_3}\sqrt{\frac{3}{4}} + \frac{\hbar^2}{Zm_e r_7^2 r_3}\sqrt{\frac{3}{4}} \tag{10.139}$$

$$r_7 = \frac{\frac{\hbar^2}{m_e}}{\frac{(Z-6)e^2}{4\pi\varepsilon_0} - \frac{\hbar^2}{12m_e r_3}\sqrt{\frac{3}{4}} + \frac{\hbar^2}{Zm_e r_3}\sqrt{\frac{3}{4}}} \tag{10.140}$$

$$r_7 = \frac{a_0}{(Z-6) - \left(\frac{1}{12} - \frac{1}{Z}\right)\frac{\sqrt{\frac{3}{4}}}{r_3}},\ r_3 \text{ in units of } a_0 \tag{10.141}$$

Substitution of $\frac{r_3}{a_0} = 0.69385$ (Eq. (10.62) with $Z = 7$) into Eq. (10.141) gives:

$$r_7 = 0.93084 a_0 \tag{10.142}$$

The ionization energy of the nitrogen atom is given by the electric energy, $E(electric)$, (Eq. (10.102) with the radius, r_7, given by Eq. (10.142)):

$$E(ionization;\ N) = -Electric\ Energy = \frac{(Z-6)e^2}{8\pi\varepsilon_0 r_7} = 14.61664\ eV \tag{10.143}$$

where $r_7 = 0.93084 a_0$ (Eq. (10.142)) and $Z = 7$. The experimental ionization energy of the nitrogen atom is 14.53414 eV [3].

THE IONIZATION ENERGIES OF SEVEN-ELECTRON ATOMS WITH A NUCLEAR CHARGE Z>7

Seven-electron atoms having $Z > 7$ possess an external electric field given by Eq. (10.92). In this case, an energy minimum is achieved with conservation of momentum when the orbital angular momentum is such that $\mathbf{F}_{diamagnetic}$ is minimized while $\mathbf{F}_{mag\ 2}$ is maximized. From Eq. (10.82), the diamagnetic force, $\mathbf{F}_{diamagnetic}$, is given by the sum of the contributions from the p_x, p_y, and p_z orbitals corresponding to m = 1, -1, and 0, respectively:

$$\mathbf{F}_{diamagnetic} = -\left(\frac{2}{3} + \frac{2}{3} + \frac{1}{3}\right)\frac{\hbar^2}{4m_e r_7^2 r_3}\sqrt{s(s+1)}\mathbf{i}_\mathbf{r} = -\left(\frac{5}{3}\right)\frac{\hbar^2}{4m_e r_7^2 r_3}\sqrt{s(s+1)}\mathbf{i}_\mathbf{r} \tag{10.144}$$

With $Z > 6$, the charge induction forms complementary mirror charge-density waves such that the angular momenta do not cancel. From Eq. (10.89), $\mathbf{F}_{mag\ 2}$ corresponding to the orbital angular momentum of the three p electrons in addition complementary charge-density waves is

$$\mathbf{F}_{mag\ 2} = 2\frac{1}{Z}\frac{3\hbar^2}{m_e r_7^2 r_3}\sqrt{s(s+1)}\mathbf{i}_\mathbf{r} \tag{10.145}$$

The second diamagnetic force, $\mathbf{F}_{diamagnetic\ 2}$, due to the binding of the p-orbital electron having an electric field outside of its radius is given by Eq. (10.93):

$$\mathbf{F}_{diamagnetic\ 2} = -\left[\frac{Z-7}{Z-6}\right]\left(1 - \frac{\sqrt{2}}{2}\right)\frac{r_3\hbar^2}{m_e r_7^4}10\sqrt{s(s+1)}\mathbf{i}_\mathbf{r} \tag{10.146}$$

In the case that $Z > 7$, the radius of the outer electron is calculated by equating the outward centrifugal force to the sum of the electric (Eq. (10.135)), diamagnetic (Eqs. (10.10.144) and (10.146)), and paramagnetic (Eq. (10.145)) forces as follows:

$$\frac{m_e v_7^2}{r_7} = \frac{(Z-6)e^2}{4\pi\varepsilon_0 r_7^2} - \frac{5\hbar^2}{12m_e r_7^2 r_3}\sqrt{s(s+1)} + \frac{6\hbar^2}{Zm_e r_7^2 r_3}\sqrt{s(s+1)} - \left[\frac{Z-7}{Z-6}\right]\left(1 - \frac{\sqrt{2}}{2}\right)\frac{r_3\hbar^2}{m_e r_7^4}10\sqrt{s(s+1)} \tag{10.147}$$

Substitution of $v_7 = \frac{\hbar}{m_e r_7}$ (Eq. (1.35)) and $s = \frac{1}{2}$ into Eq. (10.147) gives:

$$\frac{\hbar^2}{m_e r_7^3} = \frac{(Z-6)e^2}{4\pi\varepsilon_0 r_7^2} - \frac{5\hbar^2}{12m_e r_7^2 r_3}\sqrt{\frac{3}{4}} + \frac{6\hbar^2}{Zm_e r_7^2 r_3}\sqrt{\frac{3}{4}} - \left[\frac{Z-7}{Z-6}\right]\left(1 - \frac{\sqrt{2}}{2}\right)\frac{r_3\hbar^2}{r_7^4 m_e}10\sqrt{\frac{3}{4}} \tag{10.148}$$

The quadratic equation corresponding to Eq. (10.148) is

$$\left(\frac{(Z-6)e^2}{4\pi\varepsilon_0} - \left(\frac{5}{12} - \frac{6}{Z}\right)\frac{\hbar^2}{m_e r_3}\sqrt{\frac{3}{4}}\right)r_7^2 - \frac{\hbar^2}{m_e}r_7 - \left[\frac{Z-7}{Z-6}\right]\left(1 - \frac{\sqrt{2}}{2}\right)\frac{r_3\hbar^2}{m_e}10\sqrt{\frac{3}{4}} = 0 \tag{10.149}$$

$$r_7^2 - \frac{\frac{\hbar^2}{m_e}}{\left(\frac{(Z-6)e^2}{4\pi\varepsilon_0} - \left(\frac{5}{12} - \frac{6}{Z}\right)\frac{\hbar^2}{m_e r_3}\sqrt{\frac{3}{4}}\right)}r_7 - \frac{\frac{\hbar^2}{m_e}\left[\frac{Z-7}{Z-6}\right]\left(1 - \frac{\sqrt{2}}{2}\right)r_3 10\sqrt{\frac{3}{4}}}{\left(\frac{(Z-6)e^2}{4\pi\varepsilon_0} - \left(\frac{5}{12} - \frac{6}{Z}\right)\frac{\hbar^2}{m_e r_3}\sqrt{\frac{3}{4}}\right)} = 0 \tag{10.150}$$

The solution of Eq. (10.150) using the quadratic formula is:

$$r_7 = \frac{\dfrac{\dfrac{\hbar^2}{m_e}}{\left(\dfrac{(Z-6)e^2}{4\pi\varepsilon_0} - \left(\dfrac{5}{12} - \dfrac{6}{Z}\right)\dfrac{\hbar^2}{m_e r_3}\sqrt{\dfrac{3}{4}}\right)} \pm \sqrt{\left(\dfrac{\dfrac{\hbar^2}{m_e}}{\left(\dfrac{(Z-6)e^2}{4\pi\varepsilon_0} - \left(\dfrac{5}{12} - \dfrac{6}{Z}\right)\dfrac{\hbar^2}{m_e r_3}\sqrt{\dfrac{3}{4}}\right)}\right)^2 + 4\dfrac{\dfrac{\hbar^2}{m_e}\left[\dfrac{Z-7}{Z-6}\right]\left(1-\dfrac{\sqrt{2}}{2}\right)r_3 10\sqrt{\dfrac{3}{4}}}{\left(\dfrac{(Z-6)e^2}{4\pi\varepsilon_0} - \left(\dfrac{5}{12} - \dfrac{6}{Z}\right)\dfrac{\hbar^2}{m_e r_3}\sqrt{\dfrac{3}{4}}\right)}}}{2} \tag{10.151}$$

$$r_7 = \frac{\dfrac{a_0}{\left((Z-6) - \left(\dfrac{5}{24} - \dfrac{3}{Z}\right)\dfrac{\sqrt{3}}{r_3}\right)} \pm a_0\sqrt{\left(\dfrac{1}{\left((Z-6) - \left(\dfrac{5}{24} - \dfrac{3}{Z}\right)\dfrac{\sqrt{3}}{r_3}\right)}\right)^2 + \dfrac{20\sqrt{3}\left(\left[\dfrac{Z-7}{Z-6}\right]\left(1-\dfrac{\sqrt{2}}{2}\right)r_3\right)}{\left((Z-6) - \left(\dfrac{5}{24} - \dfrac{3}{Z}\right)\dfrac{\sqrt{3}}{r_3}\right)}}}{2}, \; r_3 \text{ in units of } a_0 \tag{10.152}$$

where r_3 is given by Eq. (10.62). The positive root of Eq. (10.152) must be taken in order that $r_7 > 0$. The final radius of electron 7, r_7, is given by Eq. (10.152); this is also the final radius of electrons 5 and 6. The radii of several seven-electron atoms are given in Table 10.5.

The ionization energies for the seven-electron atoms with $Z > 7$ are given by the electric energy, $E(electric)$, (Eq. (10.102) with the radii, r_7, given by Eq. (10.152)):

$$E(Ionization) = -Electric\ Energy = \frac{(Z-6)e^2}{8\pi\varepsilon_0 r_7} \tag{10.153}$$

Since the relativistic corrections were small, the nonrelativistic ionization energies for experimentally measured seven-electron atoms are given in Table 10.5.

Table 10.5. Ionization energies for some seven-electron atoms.

7 e Atom	Z	r_1 (a_0) [a]	r_3 (a_0) [b]	r_7 (a_0) [c]	Theoretical Ionization Energies [d] (eV)	Experimental Ionization Energies [e] (eV)	Relative Error [f]
N	7	0.14605	0.69385	0.93084	14.61664	14.53414	-0.0057
O^{+}	8	0.12739	0.59020	0.78489	34.6694	35.1173	0.0128
F^{2+}	9	0.11297	0.51382	0.67084	60.8448	62.7084	0.0297
Ne^{3+}	10	0.10149	0.45511	0.57574	94.5279	97.12	0.0267
Na^{4+}	11	0.09213	0.40853	0.50250	135.3798	138.4	0.0218
Mg^{5+}	12	0.08435	0.37065	0.44539	183.2888	186.76	0.0186
Al^{6+}	13	0.07778	0.33923	0.39983	238.2017	241.76	0.0147
Si^{7+}	14	0.07216	0.31274	0.36271	300.0883	303.54	0.0114
P^{8+}	15	0.06730	0.29010	0.33191	368.9298	372.13	0.0086
S^{9+}	16	0.06306	0.27053	0.30595	444.7137	447.5	0.0062
Cl^{10+}	17	0.05932	0.25344	0.28376	527.4312	529.28	0.0035
Ar^{11+}	18	0.05599	0.23839	0.26459	617.0761	618.26	0.0019
K^{12+}	19	0.05302	0.22503	0.24785	713.6436	714.6	0.0013
Ca^{13+}	20	0.05035	0.21308	0.23311	817.1303	817.6	0.0006
Sc^{14+}	21	0.04794	0.20235	0.22003	927.5333	927.5	0.0000
Ti^{15+}	22	0.04574	0.19264	0.20835	1044.8504	1044	-0.0008
V^{16+}	23	0.04374	0.18383	0.19785	1169.0800	1168	-0.0009
Cr^{17+}	24	0.04191	0.17579	0.18836	1300.2206	1299	-0.0009
Mn^{18+}	25	0.04022	0.16842	0.17974	1438.2710	1437	-0.0009
Fe^{19+}	26	0.03867	0.16165	0.17187	1583.2303	1582	-0.0008
Co^{20+}	27	0.03723	0.15540	0.16467	1735.0978	1735	-0.0001
Ni^{21+}	28	0.03589	0.14961	0.15805	1893.8726	1894	0.0001
Cu^{22+}	29	0.03465	0.14424	0.15194	2059.5543	2060	0.0002

[a] Radius of the first set of paired inner electrons of seven-electron atoms from Eq. (10.51).

[b] Radius of the second set of paired inner electrons of seven-electron atoms from Eq. (10.62).

[c] Radius of the three unpaired paired outer electrons of seven-electron atoms from Eq. (10.152) for $Z > 7$ and Eq. (10.142) for N.

[d] Calculated ionization energies of seven-electron atoms given by the electric energy (Eq. (10.153)).

[e] From theoretical calculations, interpolation of isoelectronic and spectral series, and experimental data [2-3].

[f] (Experimental-theoretical)/experimental.

The agreement between the experimental and calculated values of Table 10.5 is well within the experimental capability of the spectroscopic determinations including the values at large Z which relies on X-ray spectroscopy. In this case, the experimental capability is three to four significant figures which is consistent with the last column. The nitrogen atom isoelectronic series is given in Table 10.5 [2-3] to much higher precision than the capability of X-ray spectroscopy, but these values are based on theoretical and interpolation techniques rather than data alone. Ionization energies are difficult to determine since the cut-off of the Rydberg series of lines at the ionization energy is often not observed, and the ionization energy must be determined from theoretical calculations, interpolation of N isoelectronic and Rydberg series, as well as direct experimental data.

EIGHT-ELECTRON ATOMS

Eight-electron atoms can be solved exactly using the results of the solutions of one, two, three, four, five, six, and seven-electron atoms.

RADIUS AND IONIZATION ENERGY OF THE OUTER ELECTRON OF THE OXYGEN ATOM

For each seven-electron atom having a central charge of Z times that of the proton, there are two indistinguishable spin-paired electrons in an atomic orbital with radii r_1 and r_2 both given by Eq. (7.35) (Eq. (10.51)), two indistinguishable spin-paired electrons in an atomic orbital with radii r_3 and r_4 both given by Eq. (10.62), and three unpaired electrons in an atomic orbital at r_7 given by Eq. (10.152). For $Z \geq 8$, the next electron which binds to form the corresponding eight-electron atom is attracted by the central Coulomb field and is repelled by diamagnetic force due to the spin-paired inner electrons. A paramagnetic spin-pairing force that results in the formation of a filled s orbital is also possible, but the force due to the spin-pairing of the electrons (Eq. (7.24) with the radius r_8) reduces the energy of the atom less than that due to the alternative forces on two paired electrons in a p_x orbital and two unpaired electrons in p_y and p_z orbitals of an atomic orbital at the same radius r_8. The resulting electron configuration is $1s^2 2s^2 2p^4$, and the orbital arrangement is:

2p state		
$\uparrow\downarrow$	$\uparrow$	$\uparrow$
1	0	-1

(10.154)

corresponding to the ground state ${}^3P_2$.

The central Coulomb force acts on the outer electron to cause it to bind wherein this electric force on the outer-most electron due to the nucleus and the inner seven electrons is given by Eq. (10.70) with the appropriate charge and radius:

$$\mathbf{F}_{ele} = \frac{(Z-7)e^2}{4\pi\varepsilon_0 r_8^2}\mathbf{i}_\mathbf{r} \tag{10.155}$$

for $r > r_7$.

The energy is minimized with conservation of angular momentum by the cancellation of the orbital angular momentum of a p_x electron by that of the p_y electron with the pairing of electron eight to fill the p_x orbital. Then, the diamagnetic force is that of N given by Eq. (10.136) corresponding to the p_z-orbital electron (Eq. (10.82) with $m = 0$) as the source of diamagnetism with an additional contribution from the uncanceled p_x electron (Eq. (10.82) with $m = 1$). $\mathbf{F}_{diamagnetic}$ for the oxygen atom is:

$$\mathbf{F}_{diamagnetic} = -\left(\frac{1}{3}+\frac{2}{3}\right)\frac{\hbar^2}{4m_e r_8^2 r_3}\sqrt{s(s+1)}\mathbf{i}_\mathbf{r} = -\frac{\hbar^2}{4m_e r_8^2 r_3}\sqrt{s(s+1)}\mathbf{i}_\mathbf{r} \tag{10.156}$$

From Eqs. (10.83) and (10.89), $\mathbf{F}_{mag\ 2}$ is

$$\mathbf{F}_{mag\ 2} = (1+1)\frac{1}{Z}\frac{\hbar^2}{m_e r_8^2 r_3}\sqrt{s(s+1)}\mathbf{i}_\mathbf{r} = \frac{1}{Z}\frac{2\hbar^2}{m_e r_8^2 r_3}\sqrt{s(s+1)}\mathbf{i}_\mathbf{r} \tag{10.157}$$

corresponding to the spin-angular-momentum contribution alone of the p_x electron and the orbital angular momentum of the p_z electron, respectively.

The outward centrifugal force on electron 8 is balanced by the electric force and the magnetic forces (on electron 8). The radius of the outer electron is calculated by equating the outward centrifugal force to the sum of the electric (Eq. (10.155)), diamagnetic (Eq. (10.156)), and paramagnetic (Eq. (10.157)) forces as follows:

$$\frac{m_e v_8^2}{r_8} = \frac{(Z-7)e^2}{4\pi\varepsilon_0 r_8^2} - \frac{\hbar^2}{4m_e r_8^2 r_3}\sqrt{s(s+1)} + \frac{2\hbar^2}{Zm_e r_8^2 r_3}\sqrt{s(s+1)} \tag{10.158}$$

Substitution of $v_8 = \frac{\hbar}{m_e r_8}$ (Eq. (1.35)) and $s = \frac{1}{2}$ into Eq. (10.158) gives:

$$\frac{\hbar^2}{m_e r_8^3} = \frac{(Z-7)e^2}{4\pi\varepsilon_0 r_8^2} - \frac{\hbar^2}{4m_e r_8^2 r_3}\sqrt{\frac{3}{4}} + \frac{2\hbar^2}{Zm_e r_8^2 r_3}\sqrt{\frac{3}{4}} \tag{10.159}$$

$$r_8 = \frac{\frac{\hbar^2}{m_e}}{\frac{(Z-7)e^2}{4\pi\varepsilon_0} - \frac{\hbar^2}{4m_e r_3}\sqrt{\frac{3}{4}} + \frac{2\hbar^2}{Zm_e r_3}\sqrt{\frac{3}{4}}} \tag{10.160}$$

$$r_8 = \frac{a_0}{(Z-7)-\left(\frac{1}{4}-\frac{2}{Z}\right)\frac{\sqrt{\frac{3}{4}}}{r_3}},\ r_3 \text{ in units of } a_0 \tag{10.161}$$

Substitution of $\frac{r_3}{a_0} = 0.59020$ (Eq. (10.62) with $Z = 8$) into Eq. (10.161) gives:

$$r_8 = a_0 \tag{10.162}$$

The ionization energy of the oxygen atom is given by the negative of $E(electric)$ given by Eq. (10.102) with the appropriate charge and radius:

$$E(ionization;\ O) = -Electric\ Energy = \frac{(Z-7)e^2}{8\pi\varepsilon_0 r_8} = 13.60580\ eV \tag{10.163}$$

where $r_8 = a_0$ (Eq. (10.162)) and $Z = 8$. The experimental ionization energy of the oxygen atom is $13.6181\ eV$ [3].

THE IONIZATION ENERGIES OF EIGHT-ELECTRON ATOMS WITH A NUCLEAR CHARGE Z>8

Eight-electron atoms having $Z > 8$ possess an external electric field given by Eq. (10.92). In this case, an energy minimum is achieved with conservation of momentum when the orbital angular momentum is such that $\mathbf{F}_{diamagnetic}$ is minimized while $\mathbf{F}_{mag\ 2}$ is maximized. From Eq. (10.82), the diamagnetic force, $\mathbf{F}_{diamagnetic}$, is given by the sum of the contributions from the p_x, p_y, and p_z orbitals corresponding to m = 1, -1, and 0, respectively:

$$\mathbf{F}_{diamagnetic} = -\left(\frac{2}{3}+\frac{2}{3}+\frac{1}{3}\right)\frac{\hbar^2}{4m_e r_8^2 r_3}\sqrt{s(s+1)}\mathbf{i}_\mathbf{r} = -\left(\frac{5}{3}\right)\frac{\hbar^2}{4m_e r_8^2 r_3}\sqrt{s(s+1)}\mathbf{i}_\mathbf{r} \tag{10.164}$$

The filled p orbitals with the maintenance of symmetry according to Eq. (10.72) requires that the diamagnetic force is only due to the electrons at r_3. From Eqs. (10.84) and (10.89), $\mathbf{F}_{mag\ 2}$ is:

$$\mathbf{F}_{mag\ 2} = (4+1+1)\frac{1}{Z}\frac{\hbar^2}{m_e r_8^2 r_3}\sqrt{s(s+1)}\mathbf{i}_\mathbf{r} = \frac{1}{Z}\frac{6\hbar^2}{m_e r_8^2 r_3}\sqrt{s(s+1)}\mathbf{i}_\mathbf{r} \tag{10.165}$$

corresponding to the spin and orbital angular momenta of the paired p_x electrons and the orbital angular momentum of each of the p_y and p_z electrons, respectively.

The second diamagnetic force, $\mathbf{F}_{diamagnetic\ 2}$, due to the binding of the p-orbital electron having an electric field outside of its radius is given by Eq. (10.93).

$$\mathbf{F}_{diamagnetic\ 2} = -\left[\frac{Z-8}{Z-7}\right]\left(1-\frac{\sqrt{2}}{2}\right)\frac{r_3\hbar^2}{m_e r_8^4}10\sqrt{s(s+1)}\mathbf{i}_\mathbf{r} \tag{10.166}$$

In the case that $Z > 8$, the radius of the outer electron is calculated by equating the outward centrifugal force to the sum of the electric (Eq. (10.155)), diamagnetic (Eqs. (10.164) and (10.166)), and paramagnetic (Eq. (10.165)) forces as follows:

$$\frac{m_e v_8^2}{r_8} = \frac{(Z-7)e^2}{4\pi\varepsilon_0 r_8^2} - \frac{5\hbar^2}{12m_e r_8^2 r_3}\sqrt{s(s+1)} + \frac{6\hbar^2}{Zm_e r_8^2 r_3}\sqrt{s(s+1)} - \left[\frac{Z-8}{Z-7}\right]\left(1-\frac{\sqrt{2}}{2}\right)\frac{r_3\hbar^2}{m_e r_8^4}10\sqrt{s(s+1)} \tag{10.167}$$

Substitution of $v_8 = \frac{\hbar}{m_e r_8}$ (Eq. (1.35)) and $s = \frac{1}{2}$ into Eq. (10.167) gives:

$$\frac{\hbar^2}{m_e r_8^3} = \frac{(Z-7)e^2}{4\pi\varepsilon_0 r_8^2} - \frac{5\hbar^2}{12m_e r_8^2 r_3}\sqrt{\frac{3}{4}} + \frac{6\hbar^2}{Zm_e r_8^2 r_3}\sqrt{\frac{3}{4}} - \left[\frac{Z-8}{Z-7}\right]\left(1-\frac{\sqrt{2}}{2}\right)\frac{r_3\hbar^2}{r_8^4 m_e}10\sqrt{\frac{3}{4}} \tag{10.168}$$

The quadratic equation corresponding to Eq. (10.168) is

$$\left(\frac{(Z-7)e^2}{4\pi\varepsilon_0} - \left(\frac{5}{12}-\frac{6}{Z}\right)\frac{\hbar^2}{m_e r_3}\sqrt{\frac{3}{4}}\right)r_8^2 - \frac{\hbar^2}{m_e}r_8 - \left[\frac{Z-8}{Z-7}\right]\left(1-\frac{\sqrt{2}}{2}\right)\frac{r_3\hbar^2}{m_e}10\sqrt{\frac{3}{4}} = 0 \tag{10.169}$$

$$r_8^2 - \frac{\frac{\hbar^2}{m_e}}{\left(\frac{(Z-7)e^2}{4\pi\varepsilon_0} - \left(\frac{5}{12}-\frac{6}{Z}\right)\frac{\hbar^2}{m_e r_3}\sqrt{\frac{3}{4}}\right)}r_8 - \frac{\frac{\hbar^2}{m_e}\left[\frac{Z-8}{Z-7}\right]\left(1-\frac{\sqrt{2}}{2}\right)r_3 10\sqrt{\frac{3}{4}}}{\left(\frac{(Z-7)e^2}{4\pi\varepsilon_0} - \left(\frac{5}{12}-\frac{6}{Z}\right)\frac{\hbar^2}{m_e r_3}\sqrt{\frac{3}{4}}\right)} = 0 \tag{10.170}$$

The solution of Eq. (10.170) using the quadratic formula is:

$$r_8 = \frac{\dfrac{\dfrac{\hbar^2}{m_e}}{\left(\dfrac{(Z-7)e^2}{4\pi\varepsilon_0} - \left(\dfrac{5}{12} - \dfrac{6}{Z}\right)\dfrac{\hbar^2}{m_e r_3}\sqrt{\dfrac{3}{4}}\right)} \pm \sqrt{\left(\dfrac{\dfrac{\hbar^2}{m_e}}{\left(\dfrac{(Z-7)e^2}{4\pi\varepsilon_0} - \left(\dfrac{5}{12} - \dfrac{6}{Z}\right)\dfrac{\hbar^2}{m_e r_3}\sqrt{\dfrac{3}{4}}\right)}\right)^2 + 4\dfrac{\dfrac{\hbar^2}{m_e}\left[\dfrac{Z-8}{Z-7}\right]\left(1-\dfrac{\sqrt{2}}{2}\right)r_3 10\sqrt{\dfrac{3}{4}}}{\left(\dfrac{(Z-7)e^2}{4\pi\varepsilon_0} - \left(\dfrac{5}{12} - \dfrac{6}{Z}\right)\dfrac{\hbar^2}{m_e r_3}\sqrt{\dfrac{3}{4}}\right)}}}{2} \tag{10.171}$$

$$r_8 = \frac{\dfrac{a_0}{\left((Z-7) - \left(\dfrac{5}{24} - \dfrac{3}{Z}\right)\dfrac{\sqrt{3}}{r_3}\right)} \pm a_0\sqrt{\left(\dfrac{1}{\left((Z-7) - \left(\dfrac{5}{24} - \dfrac{3}{Z}\right)\dfrac{\sqrt{3}}{r_3}\right)}\right)^2 + \dfrac{20\sqrt{3}\left(\left[\dfrac{Z-8}{Z-7}\right]\left(1-\dfrac{\sqrt{2}}{2}\right)r_3\right)}{\left((Z-7) - \left(\dfrac{5}{24} - \dfrac{3}{Z}\right)\dfrac{\sqrt{3}}{r_3}\right)}}}{2}, \; r_3 \text{ in units of } a_0 \tag{10.172}$$

where r_3 is given by Eq. (10.62). The positive root of Eq. (10.172) must be taken in order that $r_8 > 0$. The final radius of electron 8, r_8, is given by Eq. (10.172); this is also the final radius of electrons 5, 6, and 7. The radii of several eight-electron atoms are given in Table 10.6.

The ionization energies for the eight-electron atoms with $Z > 8$ are given by the electric energy, $E(electric)$, (Eq. (10.102) with the radii, r_8, given by Eq. (10.172)):

$$E(Ionization) = -Electric\ Energy = \frac{(Z-7)e^2}{8\pi\varepsilon_0 r_8} \tag{10.173}$$

Since the relativistic corrections were small, the nonrelativistic ionization energies for experimentally measured eight-electron atoms are given in Table 10.6.

Table 10.6. Ionization energies for some eight-electron atoms.

8 e Atom	Z	r_1 (a_0) [a]	r_3 (a_0) [b]	r_8 (a_0) [c]	Theoretical Ionization Energies [d] (eV)	Experimental Ionization Energies [e] (eV)	Relative Error [f]
O	8	0.12739	0.59020	1.00000	13.60580	13.6181	0.0009
F^+	9	0.11297	0.51382	0.7649	35.5773	34.9708	-0.0173
Ne^{2+}	10	0.10149	0.45511	0.6514	62.6611	63.45	0.0124
Na^{3+}	11	0.09213	0.40853	0.5592	97.3147	98.91	0.0161
Mg^{4+}	12	0.08435	0.37065	0.4887	139.1911	141.27	0.0147
Al^{5+}	13	0.07778	0.33923	0.4338	188.1652	190.49	0.0122
Si^{6+}	14	0.07216	0.31274	0.3901	244.1735	246.5	0.0094
P^{7+}	15	0.06730	0.29010	0.3543	307.1791	309.6	0.0078
S^{8+}	16	0.06306	0.27053	0.3247	377.1579	379.55	0.0063
Cl^{9+}	17	0.05932	0.25344	0.2996	454.0940	455.63	0.0034
Ar^{10+}	18	0.05599	0.23839	0.2782	537.9756	538.96	0.0018
K^{11+}	19	0.05302	0.22503	0.2597	628.7944	629.4	0.0010
Ca^{12+}	20	0.05035	0.21308	0.2434	726.5442	726.6	0.0001
Sc^{13+}	21	0.04794	0.20235	0.2292	831.2199	830.8	-0.0005
Ti^{14+}	22	0.04574	0.19264	0.2165	942.8179	941.9	-0.0010
V^{15+}	23	0.04374	0.18383	0.2051	1061.3351	1060	-0.0013
Cr^{16+}	24	0.04191	0.17579	0.1949	1186.7691	1185	-0.0015
Mn^{17+}	25	0.04022	0.16842	0.1857	1319.1179	1317	-0.0016
Fe^{18+}	26	0.03867	0.16165	0.1773	1458.3799	1456	-0.0016
Co^{19+}	27	0.03723	0.15540	0.1696	1604.5538	1603	-0.0010
Ni^{20+}	28	0.03589	0.14961	0.1626	1757.6383	1756	-0.0009
Cu^{21+}	29	0.03465	0.14424	0.1561	1917.6326	1916	-0.0009

[a] Radius of the first set of paired inner electrons of eight-electron atoms from Eq. (10.51).

[b] Radius of the second set of paired inner electrons of eight-electron atoms from Eq. (10.62).

[c] Radius of the two paired and two unpaired outer electrons of eight-electron atoms from Eq. (10.172) for $Z > 8$ and Eq. (10.162) for O.

[d] Calculated ionization energies of eight-electron atoms given by the electric energy (Eq. (10.173)).

[e] From theoretical calculations, interpolation of isoelectronic and spectral series, and experimental data [2-3].

[f] (Experimental-theoretical)/experimental.

The agreement between the experimental and calculated values of Table 10.6 is well within the experimental capability of the spectroscopic determinations including the values at large Z that relies on X-ray spectroscopy. In this case, the experimental capability is three to four significant figures which is consistent with the last column. The oxygen atom isoelectronic series is given in Table 10.6 [2-3] to much higher precision than the capability of X-ray spectroscopy, but these values are based on theoretical and interpolation techniques rather than data alone. Ionization energies are difficult to determine since the cut-off of the Rydberg series of lines at the ionization energy is often not observed, and the ionization energy must be determined from theoretical calculations, interpolation of O isoelectronic and Rydberg series, as well as direct experimental data.

NINE-ELECTRON ATOMS

Nine-electron atoms can be solved exactly using the results of the solutions of one, two, three, four, five, six, seven, and eight-electron atoms.

RADIUS AND IONIZATION ENERGY OF THE OUTER ELECTRON OF THE FLUORINE ATOM

For each eight-electron atom having a central charge of Z times that of the proton, there are two indistinguishable spin-paired electrons in an atomic orbital with radii r_1 and r_2 both given by Eq. (7.35) (Eq. (10.51)), two indistinguishable spin-paired electrons in an atomic orbital with radii r_3 and r_4 both given by Eq. (10.62), and two paired and unpaired electrons in an atomic orbital at r_8 given by Eq. (10.172). For $Z \geq 9$, the next electron which binds to form the corresponding nine-electron atom is attracted by the central Coulomb field and is repelled by diamagnetic force due to the spin-paired inner electrons. A paramagnetic spin-pairing force that results in the formation of a filled s orbital is also possible, but the force due to the spin-pairing of the electrons (Eq. (7.24) with the radius r_9) reduces the energy of the atom less than that due to the alternative forces on an unpaired electron in a p_y orbital and two pairs of electrons of opposite spin in p_x and p_z orbitals of an atomic orbital at the same radius r_9. The resulting electron configuration is $1s^2 2s^2 2p^5$, and the orbital arrangement is:

2p state

$$\underset{1}{\underline{\uparrow\downarrow}} \quad \underset{0}{\underline{\uparrow\downarrow}} \quad \underset{-1}{\underline{\uparrow}} \tag{10.174}$$

corresponding to the ground state ${}^2P^0_{3/2}$.

The central Coulomb force acts on the outer electron to cause it to bind wherein this electric force on the outer-most electron due to the nucleus and the inner eight electrons is given by Eq. (10.70) with the appropriate charge and radius:

$$\mathbf{F}_{ele} = \frac{(Z-8)e^2}{4\pi\varepsilon_0 r_9^2}\mathbf{i}_\mathbf{r} \tag{10.175}$$

for $r > r_8$.

The energy is minimized and the angular momentum is conserved with the pairing of electron nine to fill the p_z orbital when the orbital angular momenta of each set of p_x and p_z spin-paired electrons adds negatively to cancel. Then, the diamagnetic force (Eq. (10.82)), $\mathbf{F}_{diamagnetic}$, is:

$$\mathbf{F}_{diamagnetic} = -\left(\frac{2}{3}\right)\frac{\hbar^2}{4m_e r_9^2 r_3}\sqrt{s(s+1)}\mathbf{i}_\mathbf{r} \tag{10.176}$$

corresponding to $m = -1$ for the unpaired p_y electron.

From Eqs. (10.83) and (10.89), $\mathbf{F}_{mag\ 2}$ is:

$$\mathbf{F}_{mag\ 2} = (1+1+1)\frac{1}{Z}\frac{\hbar^2}{m_e r_9^2 r_3}\sqrt{s(s+1)}\mathbf{i}_\mathbf{r} = \frac{1}{Z}\frac{3\hbar^2}{m_e r_9^2 r_3}\sqrt{s(s+1)}\mathbf{i}_\mathbf{r} \tag{10.177}$$

corresponding to the spin-angular-momentum contribution alone from each of the p_x and p_z orbitals and the orbital-angular-momentum contribution of the p_y electron, respectively.

The outward centrifugal force on electron 9 is balanced by the electric force and the magnetic forces (on electron 9). The radius of the outer electron is calculated by equating the outward centrifugal force to the sum of the electric (Eq. (10.175)), diamagnetic (Eq. (10.176)), and paramagnetic (Eq. (10.177)) forces as follows:

$$\frac{m_e v_9^2}{r_9} = \frac{(Z-8)e^2}{4\pi\varepsilon_0 r_9^2} - \frac{\hbar^2}{6m_e r_9^2 r_3}\sqrt{s(s+1)} + \frac{3\hbar^2}{Zm_e r_9^2 r_3}\sqrt{s(s+1)} \tag{10.178}$$

Substitution of $v_9 = \frac{\hbar}{m_e r_9}$ (Eq. (1.35)) and $s = \frac{1}{2}$ into Eq. (10.178) gives:

$$\frac{\hbar^2}{m_e r_9^3} = \frac{(Z-8)e^2}{4\pi\varepsilon_0 r_9^2} - \frac{\hbar^2}{6m_e r_9^2 r_3}\sqrt{\frac{3}{4}} + \frac{3\hbar^2}{Zm_e r_9^2 r_3}\sqrt{\frac{3}{4}} \tag{10.179}$$

$$r_9 = \frac{\frac{\hbar^2}{m_e}}{\frac{(Z-8)e^2}{4\pi\varepsilon_0} - \frac{\hbar^2}{6m_e r_3}\sqrt{\frac{3}{4}} + \frac{3\hbar^2}{Zm_e r_3}\sqrt{\frac{3}{4}}} \tag{10.180}$$

$$r_9 = \frac{a_0}{(Z-8)-\left(\frac{1}{6}-\frac{3}{Z}\right)\frac{\sqrt{\frac{3}{4}}}{r_3}},\ r_3 \text{ in units of } a_0 \tag{10.181}$$

Substitution of $\frac{r_3}{a_0} = 0.51382$ (Eq. (10.62) with $Z = 9$) into Eq. (10.181) gives:

$$r_9 = 0.78069 a_0 \tag{10.182}$$

The ionization energy of the fluorine atom is given by the negative of $E(electric)$ given by Eq. (10.102) with the appropriate charge and radius:

$$E(ionization;\ F) = -Electric\ Energy = \frac{(Z-8)e^2}{8\pi\varepsilon_0 r_9} = 17.42782\ eV \tag{10.183}$$

where $r_9 = 0.78069 a_0$ (Eq. (10.183)) and $Z = 9$. The experimental ionization energy of the fluorine atom is 17.42282 eV [3].

THE IONIZATION ENERGIES OF NINE-ELECTRON ATOMS WITH A NUCLEAR CHARGE Z>9

Nine-electron atoms having $Z > 9$ possess an external electric field given by Eq. (10.92). In this case, an energy minimum is achieved with conservation of momentum when the orbital angular momentum is such that $\mathbf{F}_{diamagnetic}$ is minimized while $\mathbf{F}_{mag\ 2}$ is maximized. From Eq. (10.82), the diamagnetic force, $\mathbf{F}_{diamagnetic}$, is given by the sum of the contributions from the p_x, p_y, and p_z orbitals corresponding to $m = 1,\ -1$, and 0, respectively:

$$\mathbf{F}_{diamagnetic} = -\left(\frac{2}{3}+\frac{2}{3}+\frac{1}{3}\right)\frac{\hbar^2}{4m_e r_9^2 r_3}\sqrt{s(s+1)}\mathbf{i}_\mathbf{r} = -\left(\frac{5}{3}\right)\frac{\hbar^2}{4m_e r_9^2 r_3}\sqrt{s(s+1)}\mathbf{i}_\mathbf{r} \tag{10.184}$$

The filled p orbitals with the maintenance of symmetry according to Eq. (10.72) requires that the diamagnetic force is only due to the electrons at r_3. From Eqs. (10.84) and (10.89), $\mathbf{F}_{mag\ 2}$ is:

$$\mathbf{F}_{mag\ 2} = (4+4+1)\frac{1}{Z}\frac{\hbar^2}{m_e r_9^2 r_3}\sqrt{s(s+1)}\mathbf{i}_\mathbf{r} = \frac{1}{Z}\frac{9\hbar^2}{m_e r_9^2 r_3}\sqrt{s(s+1)}\mathbf{i}_\mathbf{r} \tag{10.185}$$

corresponding to the spin and orbital angular momenta of the paired p_x and p_z electrons and the orbital angular momentum of the unpaired p_y electron, respectively.

The second diamagnetic force, $\mathbf{F}_{diamagnetic\ 2}$, due to the binding of the p-orbital electron having an electric field outside of its radius is given by Eq. (10.93):

$$\mathbf{F}_{diamagnetic\ 2} = -\left[\frac{Z-9}{Z-8}\right]\left(1-\frac{\sqrt{2}}{2}\right)\frac{r_3\hbar^2}{m_e r_9^4}10\sqrt{s(s+1)}\mathbf{i}_\mathbf{r} \tag{10.186}$$

In the case that $Z > 9$, the radius of the outer electron is calculated by equating the outward centrifugal force to the sum of the electric (Eq. (10.175)), diamagnetic (Eqs. (10.184) and (10.186)), and paramagnetic (Eq. (10.185)) forces as follows:

$$\frac{m_e v_9^2}{r_9} = \frac{(Z-8)e^2}{4\pi\varepsilon_0 r_9^2} - \frac{5\hbar^2}{12 m_e r_9^2 r_3}\sqrt{s(s+1)} + \frac{9\hbar^2}{Z m_e r_9^2 r_3}\sqrt{s(s+1)} - \left[\frac{Z-9}{Z-8}\right]\left(1-\frac{\sqrt{2}}{2}\right)\frac{r_3\hbar^2}{m_e r_9^4}10\sqrt{s(s+1)} \tag{10.187}$$

Substitution of $v_9 = \frac{\hbar}{m_e r_9}$ (Eq. (1.35)) and $s = \frac{1}{2}$ into Eq. (10.187) gives:

$$\frac{\hbar^2}{m_e r_9^3} = \frac{(Z-8)e^2}{4\pi\varepsilon_0 r_9^2} - \frac{5\hbar^2}{12 m_e r_9^2 r_3}\sqrt{\frac{3}{4}} + \frac{9\hbar^2}{Z m_e r_9^2 r_3}\sqrt{\frac{3}{4}} - \left[\frac{Z-9}{Z-8}\right]\left(1-\frac{\sqrt{2}}{2}\right)\frac{r_3\hbar^2}{r_9^4 m_e}10\sqrt{\frac{3}{4}} \tag{10.188}$$

The quadratic equation corresponding to Eq. (10.188) is

$$\left(\frac{(Z-8)e^2}{4\pi\varepsilon_0} - \left(\frac{5}{12}-\frac{9}{Z}\right)\frac{\hbar^2}{m_e r_3}\sqrt{\frac{3}{4}}\right)r_9^2 - \frac{\hbar^2}{m_e}r_9 - \left[\frac{Z-9}{Z-8}\right]\left(1-\frac{\sqrt{2}}{2}\right)\frac{r_3\hbar^2}{m_e}10\sqrt{\frac{3}{4}} = 0 \tag{10.189}$$

$$r_9^2 - \frac{\frac{\hbar^2}{m_e}}{\left(\frac{(Z-8)e^2}{4\pi\varepsilon_0} - \left(\frac{5}{12}-\frac{9}{Z}\right)\frac{\hbar^2}{m_e r_3}\sqrt{\frac{3}{4}}\right)}r_9 - \frac{\frac{\hbar^2}{m_e}\left[\frac{Z-9}{Z-8}\right]\left(1-\frac{\sqrt{2}}{2}\right)r_3 10\sqrt{\frac{3}{4}}}{\left(\frac{(Z-8)e^2}{4\pi\varepsilon_0} - \left(\frac{5}{12}-\frac{9}{Z}\right)\frac{\hbar^2}{m_e r_3}\sqrt{\frac{3}{4}}\right)} = 0 \tag{10.190}$$

The solution of Eq. (10.190) using the quadratic formula is:

$$r_9 = \frac{\dfrac{\dfrac{\hbar^2}{m_e}}{\left(\dfrac{(Z-8)e^2}{4\pi\varepsilon_0} - \left(\dfrac{5}{12} - \dfrac{9}{Z}\right)\dfrac{\hbar^2}{m_e r_3}\sqrt{\dfrac{3}{4}}\right)} \pm \sqrt{\left(\dfrac{\dfrac{\hbar^2}{m_e}}{\left(\dfrac{(Z-8)e^2}{4\pi\varepsilon_0} - \left(\dfrac{5}{12} - \dfrac{9}{Z}\right)\dfrac{\hbar^2}{m_e r_3}\sqrt{\dfrac{3}{4}}\right)}\right)^2 + 4\dfrac{\dfrac{\hbar^2}{m_e}\left[\dfrac{Z-9}{Z-8}\right]\left(1-\dfrac{\sqrt{2}}{2}\right)r_3 10\sqrt{\dfrac{3}{4}}}{\left(\dfrac{(Z-8)e^2}{4\pi\varepsilon_0} - \left(\dfrac{5}{12} - \dfrac{9}{Z}\right)\dfrac{\hbar^2}{m_e r_3}\sqrt{\dfrac{3}{4}}\right)}}}{2} \tag{10.191}$$

$$r_9 = \frac{\dfrac{a_0}{\left((Z-8) - \left(\dfrac{5}{24} - \dfrac{9}{2Z}\right)\dfrac{\sqrt{3}}{r_3}\right)} \pm a_0\sqrt{\left(\dfrac{1}{\left((Z-8) - \left(\dfrac{5}{24} - \dfrac{9}{2Z}\right)\dfrac{\sqrt{3}}{r_3}\right)}\right)^2 + \dfrac{20\sqrt{3}\left(\left[\dfrac{Z-9}{Z-8}\right]\left(1-\dfrac{\sqrt{2}}{2}\right)r_3\right)}{\left((Z-8) - \left(\dfrac{5}{24} - \dfrac{9}{2Z}\right)\dfrac{\sqrt{3}}{r_3}\right)}}}{2}, \; r_3 \text{ in units of } a_0 \tag{10.192}$$

where r_3 is given by Eq. (10.62). The positive root of Eq. (10.192) must be taken in order that $r_9 > 0$. The final radius of electron 9, r_9, is given by Eq. (10.192); this is also the final radius of electrons 5, 6,7, and 8. The radii of several nine-electron atoms are given in Table 10.7.

The ionization energies for the nine-electron atoms with $Z > 9$ are given by the electric energy, $E(electric)$, (Eq. (10.102) with the radii, r_9, given by Eq. (10.192)):

$$E(Ionization) = -Electric\ Energy = \frac{(Z-8)e^2}{8\pi\varepsilon_0 r_9} \tag{10.193}$$

Since the relativistic corrections were small, the nonrelativistic ionization energies for experimentally measured nine-electron atoms are given in Table 10.7.

Table 10.7. Ionization energies for some nine-electron atoms.

9 e Atom	Z	r_1 (a_0) [a]	r_3 (a_0) [b]	r_9 (a_0) [c]	Theoretical Ionization Energies [d] (eV)	Experimental Ionization Energies [e] (eV)	Relative Error [f]
F	9	0.11297	0.51382	0.78069	17.42782	17.42282	-0.0003
Ne^{+}	10	0.10149	0.45511	0.64771	42.0121	40.96328	-0.0256
Na^{2+}	11	0.09213	0.40853	0.57282	71.2573	71.62	0.0051
Mg^{3+}	12	0.08435	0.37065	0.50274	108.2522	109.2655	0.0093
Al^{4+}	13	0.07778	0.33923	0.44595	152.5469	153.825	0.0083
Si^{5+}	14	0.07216	0.31274	0.40020	203.9865	205.27	0.0063
P^{6+}	15	0.06730	0.29010	0.36283	262.4940	263.57	0.0041
S^{7+}	16	0.06306	0.27053	0.33182	328.0238	328.75	0.0022
Cl^{8+}	17	0.05932	0.25344	0.30571	400.5466	400.06	-0.0012
Ar^{9+}	18	0.05599	0.23839	0.28343	480.0424	478.69	-0.0028
K^{10+}	19	0.05302	0.22503	0.26419	566.4968	564.7	-0.0032
Ca^{11+}	20	0.05035	0.21308	0.24742	659.8992	657.2	-0.0041
Sc^{12+}	21	0.04794	0.20235	0.23266	760.2415	756.7	-0.0047
Ti^{13+}	22	0.04574	0.19264	0.21957	867.5176	863.1	-0.0051
V^{14+}	23	0.04374	0.18383	0.20789	981.7224	976	-0.0059
Cr^{15+}	24	0.04191	0.17579	0.19739	1102.8523	1097	-0.0053
Mn^{16+}	25	0.04022	0.16842	0.18791	1230.9038	1224	-0.0056
Fe^{17+}	26	0.03867	0.16165	0.17930	1365.8746	1358	-0.0058
Co^{18+}	27	0.03723	0.15540	0.17145	1507.7624	1504.6	-0.0021
Ni^{19+}	28	0.03589	0.14961	0.16427	1656.5654	1648	-0.0052
Cu^{20+}	29	0.03465	0.14424	0.15766	1812.2821	1804	-0.0046

[a] Radius of the first set of paired inner electrons of nine-electron atoms from Equation (10.51).

[b] Radius of the second set of paired inner electrons of nine-electron atoms from Equation (10.62).

[c] Radius of the one unpaired and two sets of paired outer electrons of nine-electron atoms from Eq. (10.192) for $Z > 9$ and Eq. (10.182) for F.

[d] Calculated ionization energies of nine-electron atoms given by the electric energy (Eq. (10.193)).

[e] From theoretical calculations, interpolation of isoelectronic and spectral series, and experimental data [2-3].

[f] (Experimental-theoretical)/experimental.

The agreement between the experimental and calculated values of Table 10.7 is well within the experimental capability of the spectroscopic determinations including the values at large Z which relies on X-ray spectroscopy. In this case, the experimental capability is three to four significant figures which is consistent with the last column. The fluorine atom isoelectronic series is given in Table 10.7 [2-3] to much higher precision than the capability of X-ray spectroscopy, but these values are based on theoretical and interpolation techniques rather than data alone. Ionization energies are difficult to determine since the cut-off of the Rydberg series of lines at the ionization energy is often not observed, and the ionization energy must be determined from theoretical calculations, interpolation of F isoelectronic and Rydberg series, as well as direct experimental data.

TEN-ELECTRON ATOMS

Ten-electron atoms can be solved exactly using the results of the solutions of one, two, three, four, five, six, seven, eight, and nine-electron atoms.

RADIUS AND IONIZATION ENERGY OF THE OUTER ELECTRON OF THE NEON ATOM

For each nine-electron atom having a central charge of Z times that of the proton, there are two indistinguishable spin-paired electrons in an atomic orbital with radii r_1 and r_2 both given by Eq. (7.35) (Eq. (10.51)), two indistinguishable spin-paired electrons in an atomic orbital with radii r_3 and r_4 both given by Eq. (10.62), and two sets of paired and an unpaired electron in an atomic orbital at r_9 given by Eq. (10.192). For $Z \geq 10$, the next electron which binds to form the corresponding ten-electron atom is attracted by the central Coulomb field and is repelled by diamagnetic force due to the spin-paired inner electrons. A paramagnetic spin-pairing force that results in the formation of a filled s orbital is also possible, but the force due to the spin-pairing of the electrons (Eq. (7.24) with the radius r_{10}) reduces the energy of the atom less than that due to the alternative forces on three pairs of electrons of opposite spin in p_x, p_y, and p_z orbitals of an atomic orbital at the same radius r_{10}. The resulting electron configuration is $1s^2 2s^2 2p^6$, and the orbital arrangement is:

$$\begin{array}{ccc} & \text{2p state} & \\ \underline{\uparrow\ \downarrow} & \underline{\uparrow\ \downarrow} & \underline{\uparrow\ \downarrow} \\ 1 & 0 & -1 \end{array} \tag{10.194}$$

corresponding to the ground state ${}^1S_0$.

The central Coulomb force acts on the outer electron to cause it to bind wherein this electric force on the outer-most electron due to the nucleus and the inner nine electrons is given by Eq. (10.70) with the appropriate charge and radius:

$$\mathbf{F}_{ele} = \frac{(Z-9)e^2}{4\pi\varepsilon_0 r_{10}^2}\mathbf{i}_\mathbf{r} \tag{10.195}$$

for $r > r_9$.

The energy is minimized and the angular momentum is conserved with the pairing of electron ten to fill the p_y orbital when the orbital angular momenta of each set of the p_x, p_y, and p_z spin-paired electrons add negatively to cancel. Then, the diamagnetic force (Eq. (10.82)), $\mathbf{F}_{diamagnetic}$, is zero:

$$\mathbf{F}_{diamagnetic} = 0 \tag{10.196}$$

From Eq. (10.83), $\mathbf{F}_{mag\ 2}$ is

$$\mathbf{F}_{mag\ 2} = (1+1+1)\frac{1}{Z}\frac{\hbar^2}{m_e r_{10}^2 r_3}\sqrt{s(s+1)}\mathbf{i}_\mathbf{r} = \frac{1}{Z}\frac{3\hbar^2}{m_e r_{10}^2 r_3}\sqrt{s(s+1)}\mathbf{i}_\mathbf{r} \tag{10.197}$$

corresponding to the spin-angular-momentum contribution alone from each of the p_x, p_y, and p_z orbitals.

The outward centrifugal force on electron 10 is balanced by the electric force and the magnetic forces (on electron 10). The radius of the outer electron is calculated by equating the outward centrifugal force to the sum of the electric (Eq. (10.195)), diamagnetic (Eq. (10.196)), and paramagnetic (Eq. (10.197)) forces as follows:

$$\frac{m_e v_{10}^2}{r_{10}} = \frac{(Z-9)e^2}{4\pi\varepsilon_0 r_{10}^2} + \frac{3\hbar^2}{Z m_e r_{10}^2 r_3}\sqrt{s(s+1)} \tag{10.198}$$

Substitution of $v_{10} = \dfrac{\hbar}{m_e r_{10}}$ (Eq. (1.35)) and $s = \dfrac{1}{2}$ into Eq. (10.198) gives:

$$\frac{\hbar^2}{m_e r_{10}^3} = \frac{(Z-9)e^2}{4\pi\varepsilon_0 r_{10}^2} + \frac{3\hbar^2}{Z m_e r_{10}^2 r_3}\sqrt{\frac{3}{4}} \tag{10.199}$$

$$r_{10} = \frac{\dfrac{\hbar^2}{m_e}}{\dfrac{(Z-9)e^2}{4\pi\varepsilon_0} + \dfrac{3\hbar^2}{Z m_e r_3}\sqrt{\dfrac{3}{4}}} \tag{10.200}$$

$$r_{10} = \frac{a_0}{(Z-9) + \dfrac{3}{Z}\dfrac{\sqrt{\dfrac{3}{4}}}{r_3}},\ r_3 \textit{ in units of } a_0 \tag{10.201}$$

Substitution of $\frac{r_3}{a_0} = 0.45511$ (Eq. (10.62) with $Z = 10$) into Eq. (10.201) gives:

$$r_{10} = 0.63659 a_0 \tag{10.202}$$

The ionization energy of the neon atom is given by the negative of $E(electric)$ given by Eq. (10.102) with the appropriate charge and radius:

$$E(ionization;\ Ne) = -Electric\ Energy = \frac{(Z-9)e^2}{8\pi\varepsilon_0 r_{10}} = 21.37296\ eV \tag{10.203}$$

where $r_{10} = 0.63659 a_0$ (Eq. (10.202)) and $Z = 10$. The experimental ionization energy of the neon atom is $21.56454\ eV$ [3].

THE IONIZATION ENERGIES OF TEN-ELECTRON ATOMS WITH A NUCLEAR CHARGE Z>10

Ten-electron atoms having $Z > 10$ possess an external electric field given by Eq. (10.92). In this case, an energy minimum is achieved with conservation of momentum when the orbital angular momentum is such that $\mathbf{F}_{diamagnetic}$ is minimized while $\mathbf{F}_{mag\ 2}$ is maximized. From Eq. (10.82), the diamagnetic force, $\mathbf{F}_{diamagnetic}$, is given by the sum of the contributions from the p_x, p_y, and p_z orbitals corresponding to m = 1, -1, and 0, respectively:

$$\mathbf{F}_{diamagnetic} = -\left(\frac{2}{3}+\frac{2}{3}+\frac{1}{3}\right)\frac{\hbar^2}{4m_e r_{10}^2 r_3}\sqrt{s(s+1)}\mathbf{i}_\mathbf{r} = -\left(\frac{5}{3}\right)\frac{\hbar^2}{4m_e r_{10}^2 r_3}\sqrt{s(s+1)}\mathbf{i}_\mathbf{r} \tag{10.204}$$

The filled p orbitals with the maintenance of symmetry according to Eq. (10.72) requires that the diamagnetic force is only due to the electrons at r_3. From Eq. (10.84), $\mathbf{F}_{mag\ 2}$ is

$$\mathbf{F}_{mag\ 2} = \left(4+4+4\right)\frac{1}{Z}\frac{\hbar^2}{m_e r_{10}^2 r_3}\sqrt{s(s+1)}\mathbf{i}_\mathbf{r} = \frac{1}{Z}\frac{12\hbar^2}{m_e r_{10}^2 r_3}\sqrt{s(s+1)}\mathbf{i}_\mathbf{r} \tag{10.205}$$

corresponding to the spin and orbital angular momenta of the paired p_x, p_y, and p_z electrons.

The second diamagnetic force, $\mathbf{F}_{diamagnetic\ 2}$, due to the binding of the p-orbital electron having an electric field outside of its radius is given by Eq. (10.93):

$$\mathbf{F}_{diamagnetic\ 2} = -\left[\frac{Z-10}{Z-9}\right]\left(1-\frac{\sqrt{2}}{2}\right)\frac{r_3\hbar^2}{m_e r_{10}^4}10\sqrt{s(s+1)}\mathbf{i}_\mathbf{r} \tag{10.206}$$

In the case that $Z > 10$, the radius of the outer electron is calculated by equating the outward centrifugal force to the sum of the electric (Eq. (10.195)), diamagnetic (Eqs. (10.204) and (10.206)), and paramagnetic (Eq. (10.205)) forces as follows:

$$\frac{m_e v_{10}^2}{r_{10}} = \frac{(Z-9)e^2}{4\pi\varepsilon_0 r_{10}^2} - \frac{5\hbar^2}{12m_e r_{10}^2 r_3}\sqrt{s(s+1)} + \frac{12\hbar^2}{Zm_e r_{10}^2 r_3}\sqrt{s(s+1)} - \left[\frac{Z-10}{Z-9}\right]\left(1-\frac{\sqrt{2}}{2}\right)\frac{r_3\hbar^2}{m_e r_{10}^4}10\sqrt{s(s+1)} \tag{10.207}$$

Substitution of $v_{10} = \frac{\hbar}{m_e r_{10}}$ (Eq. (1.35)) and $s = \frac{1}{2}$ into Eq. (10.207) gives:

$$\frac{\hbar^2}{m_e r_{10}^3} = \frac{(Z-9)e^2}{4\pi\varepsilon_0 r_{10}^2} - \frac{5\hbar^2}{12m_e r_{10}^2 r_3}\sqrt{\frac{3}{4}} + \frac{12\hbar^2}{Zm_e r_{10}^2 r_3}\sqrt{\frac{3}{4}} - \left[\frac{Z-10}{Z-9}\right]\left(1-\frac{\sqrt{2}}{2}\right)\frac{r_3\hbar^2}{r_{10}^4 m_e}10\sqrt{\frac{3}{4}} \tag{10.208}$$

The quadratic equation corresponding to Eq. (10.208) is

$$\left(\frac{(Z-9)e^2}{4\pi\varepsilon_0} - \left(\frac{5}{12}-\frac{12}{Z}\right)\frac{\hbar^2}{m_e r_3}\sqrt{\frac{3}{4}}\right)r_{10}^2 - \frac{\hbar^2}{m_e}r_{10} - \left[\frac{Z-10}{Z-9}\right]\left(1-\frac{\sqrt{2}}{2}\right)\frac{r_3\hbar^2}{m_e}10\sqrt{\frac{3}{4}} = 0 \tag{10.209}$$

$$r_{10}^2 - \frac{\frac{\hbar^2}{m_e}}{\left(\frac{(Z-9)e^2}{4\pi\varepsilon_0} - \left(\frac{5}{12}-\frac{12}{Z}\right)\frac{\hbar^2}{m_e r_3}\sqrt{\frac{3}{4}}\right)}r_{10} - \frac{\frac{\hbar^2}{m_e}\left[\frac{Z-10}{Z-9}\right]\left(1-\frac{\sqrt{2}}{2}\right)r_3 10\sqrt{\frac{3}{4}}}{\left(\frac{(Z-9)e^2}{4\pi\varepsilon_0} - \left(\frac{5}{12}-\frac{12}{Z}\right)\frac{\hbar^2}{m_e r_3}\sqrt{\frac{3}{4}}\right)} = 0 \tag{10.210}$$

The solution of Eq. (10.210) using the quadratic formula is:

$$r_{10} = \frac{\dfrac{\dfrac{\hbar^2}{m_e}}{\left(\dfrac{(Z-9)e^2}{4\pi\varepsilon_0} - \left(\dfrac{5}{12} - \dfrac{12}{Z}\right)\dfrac{\hbar^2}{m_e r_3}\sqrt{\dfrac{3}{4}}\right)} \pm \sqrt{\left(\dfrac{\dfrac{\hbar^2}{m_e}}{\left(\dfrac{(Z-9)e^2}{4\pi\varepsilon_0} - \left(\dfrac{5}{12} - \dfrac{12}{Z}\right)\dfrac{\hbar^2}{m_e r_3}\sqrt{\dfrac{3}{4}}\right)}\right)^2 + 4\dfrac{\dfrac{\hbar^2}{m_e}\left[\dfrac{Z-10}{Z-9}\right]\left(1-\dfrac{\sqrt{2}}{2}\right)r_3 10\sqrt{\dfrac{3}{4}}}{\left(\dfrac{(Z-9)e^2}{4\pi\varepsilon_0} - \left(\dfrac{5}{12} - \dfrac{12}{Z}\right)\dfrac{\hbar^2}{m_e r_3}\sqrt{\dfrac{3}{4}}\right)}}}{2} \tag{10.211}$$

$$r_{10} = \frac{\dfrac{a_0}{\left((Z-9) - \left(\dfrac{5}{24} - \dfrac{6}{Z}\right)\dfrac{\sqrt{3}}{r_3}\right)} \pm a_0\sqrt{\left(\dfrac{1}{\left((Z-9) - \left(\dfrac{5}{24} - \dfrac{6}{Z}\right)\dfrac{\sqrt{3}}{r_3}\right)}\right)^2 + \dfrac{20\sqrt{3}\left(\left[\dfrac{Z-10}{Z-9}\right]\left(1-\dfrac{\sqrt{2}}{2}\right)r_3\right)}{\left((Z-9) - \left(\dfrac{5}{24} - \dfrac{6}{Z}\right)\dfrac{\sqrt{3}}{r_3}\right)}}}{2}, \; r_3 \text{ in units of } a_0 \tag{10.212}$$

where r_3 is given by Eq. (10.62). The positive root of Eq. (10.212) must be taken in order that $r_{10} > 0$. The final radius of electron 10, r_{10}, is given by Eq. (10.62); this is also the final radius of electrons 5, 6, 7, 8, and 9. The radii of several ten-electron atoms are given in Table 10.8.

The ionization energies for the ten-electron atoms with $Z > 10$ are given by the electric energy, $E(electric)$, (Eq. (10.102) with the radii, r_{10}, given by Eq. (10.212)):

$$E(Ionization) = -Electric\ Energy = \frac{(Z-9)e^2}{8\pi\varepsilon_0 r_{10}} \tag{10.213}$$

Since the relativistic corrections were small, the nonrelativistic ionization energies for experimentally measured ten-electron atoms are given in Table 10.8.

Table 10.8. Ionization energies for some ten-electron atoms.

10 e Atom	Z	r_1 (a_0) [a]	r_3 (a_0) [b]	r_{10} (a_0) [c]	Theoretical Ionization Energies [d] (eV)	Experimental Ionization Energies [e] (eV)	Relative Error [f]
Ne	10	0.10149	0.45511	0.63659	21.37296	21.56454	0.00888
Na^{+}	11	0.09213	0.40853	0.560945	48.5103	47.2864	-0.0259
Mg^{2+}	12	0.08435	0.37065	0.510568	79.9451	80.1437	0.0025
Al^{3+}	13	0.07778	0.33923	0.456203	119.2960	119.992	0.0058
Si^{4+}	14	0.07216	0.31274	0.409776	166.0150	166.767	0.0045
P^{5+}	15	0.06730	0.29010	0.371201	219.9211	220.421	0.0023
S^{6+}	16	0.06306	0.27053	0.339025	280.9252	280.948	0.0001
Cl^{7+}	17	0.05932	0.25344	0.311903	348.9750	348.28	-0.0020
Ar^{8+}	18	0.05599	0.23839	0.288778	424.0365	422.45	-0.0038
K^{9+}	19	0.05302	0.22503	0.268844	506.0861	503.8	-0.0045
Ca^{10+}	20	0.05035	0.21308	0.251491	595.1070	591.9	-0.0054
Sc^{11+}	21	0.04794	0.20235	0.236251	691.0866	687.36	-0.0054
Ti^{12+}	22	0.04574	0.19264	0.222761	794.0151	787.84	-0.0078
V^{13+}	23	0.04374	0.18383	0.210736	903.8853	896	-0.0088
Cr^{14+}	24	0.04191	0.17579	0.19995	1020.6910	1010.6	-0.0100
Mn^{15+}	25	0.04022	0.16842	0.19022	1144.4276	1134.7	-0.0086
Fe^{16+}	26	0.03867	0.16165	0.181398	1275.0911	1266	-0.0072
Co^{17+}	27	0.03723	0.15540	0.173362	1412.6783	1397.2	-0.0111
Ni^{18+}	28	0.03589	0.14961	0.166011	1557.1867	1541	-0.0105
Cu^{19+}	29	0.03465	0.14424	0.159261	1708.6139	1697	-0.0068
Zn^{20+}	30	0.03349	0.13925	0.153041	1866.9581	1856	-0.0059

[a] Radius of the first set of paired inner electrons of ten-electron atoms from Equation (10.51).
[b] Radius of the second set of paired inner electrons of ten-electron atoms from Equation (10.62).
[c] Radius of three sets of paired outer electrons of ten-electron atoms from Eq. (10.212) for $Z > 10$ and Eq. (10.202) for *Ne*.
[d] Calculated ionization energies of ten-electron atoms given by the electric energy (Eq. (10.213)).
[e] From theoretical calculations, interpolation of isoelectronic and spectral series, and experimental data [2-3].
[f] (Experimental-theoretical)/experimental.

The agreement between the experimental and calculated values of Table 10.8 is well within the experimental capability of the spectroscopic determinations, including the values at large Z, which rely on X-ray spectroscopy. In this case, the experimental capability is three to four significant figures, which is consistent with the last column. The neon atom isoelectronic series is given in Table 10.8 [2-3] to much higher precision than the capability of X-ray spectroscopy, but these values are based on theoretical and interpolation techniques rather than data alone. Ionization energies are difficult to determine since the cut-off of the Rydberg series of lines at the ionization energy is often not observed, and the ionization energy must be determined from theoretical calculations, interpolation of Ne isoelectronic and Rydberg series, as well as direct experimental data.

GENERAL EQUATION FOR THE IONIZATION ENERGIES OF FIVE THROUGH TEN-ELECTRON ATOMS

Using the forces given by Eqs. (10.70), (10.82-10.84), (10.89), (10.93), and the radii r_3 given by Eq. (10.62), the radii of the 2p electrons of all five through ten-electron atoms may be solved exactly. The electric energy given by Eq. (10.102) gives the corresponding exact ionization energies. A summary of the parameters of the equations that determine the exact radii and ionization energies of all five through ten-electron atoms is given in Table 10.9.

$\mathbf{F}_{ele}$ and $\mathbf{F}_{diamagnetic\ 2}$ given by Eqs. (10.70) and (10.93), respectively, are of the same form for all atoms with the appropriate nuclear charges and atomic radii. $\mathbf{F}_{diamagnetic}$ given by Eq. (10.82) and $\mathbf{F}_{mag\ 2}$ given by Eqs. (10.83-10.84) and (10.89) are of the same form with the appropriate factors that depend on the electron configuration wherein the electron configuration must be a minimum of energy.

For each n-electron atom having a central charge of Z times that of the proton and an electron configuration $1s^2 2s^2 2p^{n-4}$, there are two indistinguishable spin-paired electrons in an atomic orbital with radii r_1 and r_2 both given by Eqs. (7.35) and (10.51):

$$r_1 = r_2 = a_0\left[\frac{1}{Z-1} - \frac{\sqrt{\frac{3}{4}}}{Z(Z-1)}\right] \tag{10.214}$$

two indistinguishable spin-paired electrons in an atomic orbital with radii r_3 and r_4 both given by Eq. (10.62):

$$r_4 = r_3 = \frac{\dfrac{a_0\left(1-\dfrac{\sqrt{\frac{3}{4}}}{Z}\right)}{\left((Z-3)-\left(\frac{1}{4}-\frac{1}{Z}\right)\frac{\sqrt{\frac{3}{4}}}{r_1}\right)} \pm a_o\sqrt{\dfrac{\left(1-\dfrac{\sqrt{\frac{3}{4}}}{Z}\right)^2}{\left((Z-3)-\left(\frac{1}{4}-\frac{1}{Z}\right)\frac{\sqrt{\frac{3}{4}}}{r_1}\right)^2} + 4\dfrac{\left[\frac{Z-3}{Z-2}\right]r_1 10\sqrt{\frac{3}{4}}}{\left((Z-3)-\left(\frac{1}{4}-\frac{1}{Z}\right)\frac{\sqrt{\frac{3}{4}}}{r_1}\right)}}}{2}, \quad r_1 \text{ in units of } a_o \tag{10.215}$$

where r_1 is given by Eq. (10.214), and $n-4$ electrons in an atomic orbital with radius r_n given by:

$$r_n = \frac{\dfrac{a_0}{\left((Z-(n-1))-\left(\frac{A}{8}-\frac{B}{2Z}\right)\frac{\sqrt{3}}{r_3}\right)} \pm a_0\sqrt{\dfrac{1}{\left((Z-(n-1))-\left(\frac{A}{8}-\frac{B}{2Z}\right)\frac{\sqrt{3}}{r_3}\right)^2} + \dfrac{20\sqrt{3}\left(\left[\frac{Z-n}{Z-(n-1)}\right]\left(1-\frac{\sqrt{2}}{2}\right)r_3\right)}{\left((Z-(n-1))-\left(\frac{A}{8}-\frac{B}{2Z}\right)\frac{\sqrt{3}}{r_3}\right)}}}{2}, \quad r_3 \text{ in units of } a_0 \tag{10.216}$$

where r_3 is given by Eq. (10.215), the parameter A given in Table 10.9 corresponds to the diamagnetic force, $\mathbf{F}_{diamagnetic}$, (Eq. (10.82)), and the parameter B given in Table 10.9 corresponds to the paramagnetic force, $\mathbf{F}_{mag\ 2}$ (Eqs. (10.83-10.84) and (10.89)). The positive root of Eq. (10.216) must be taken in order that $r_n > 0$. The radii of several n-electron atoms are given in Tables 10.3-10.8.

The ionization energy for the boron atom is given by Eq. (10.104). The ionization energies for the n-electron atoms are given by the negative of the electric energy, $E(electric)$, (Eq. (10.102) with the radii, r_n, given by Eq. (10.216)).

$$E(Ionization) = -Electric\ Energy = \frac{(Z-(n-1))e^2}{8\pi\varepsilon_0 r_n} \tag{10.217}$$

Since the relativistic corrections were small, the nonrelativistic ionization energies for experimentally measured n-electron atoms are given by Eqs. (10.217) and (10.216) in Tables 10.3-10.8.

Table 10.9. Summary of the parameters of five through ten-electron atoms.

Atom Type	Electron Configuration	Ground State Term [a]	Orbital Arrangement of 2p Electrons (2p state)	Diamagnetic Force Factor A [b]	Paramagnetic Force Factor B [c]
Neutral 5 e Atom B	$1s^2 2s^2 2p^1$	$^2P^0_{1/2}$	$\underline{\uparrow}\ \underline{\ }\ \underline{\ }$ 1 0 -1	2	0
Neutral 6 e Atom C	$1s^2 2s^2 2p^2$	$^3P_0$	$\underline{\uparrow}\ \underline{\uparrow}\ \underline{\ }$ 1 0 -1	$\frac{2}{3}$	0
Neutral 7 e Atom N	$1s^2 2s^2 2p^3$	$^4S^0_{3/2}$	$\underline{\uparrow}\ \underline{\uparrow}\ \underline{\uparrow}$ 1 0 -1	$\frac{1}{3}$	1
Neutral 8 e Atom O	$1s^2 2s^2 2p^4$	$^3P_2$	$\underline{\uparrow\downarrow}\ \underline{\uparrow}\ \underline{\uparrow}$ 1 0 -1	1	2
Neutral 9 e Atom F	$1s^2 2s^2 2p^5$	$^2P^0_{3/2}$	$\underline{\uparrow\downarrow}\ \underline{\uparrow\downarrow}\ \underline{\uparrow}$ 1 0 -1	$\frac{2}{3}$	3
Neutral 10 e Atom Ne	$1s^2 2s^2 2p^6$	$^1S_0$	$\underline{\uparrow\downarrow}\ \underline{\uparrow\downarrow}\ \underline{\uparrow\downarrow}$ 1 0 -1	0	3
5 e Ion	$1s^2 2s^2 2p^1$	$^2P^0_{1/2}$	$\underline{\uparrow}\ \underline{\ }\ \underline{\ }$ 1 0 -1	$\frac{5}{3}$	1
6 e Ion	$1s^2 2s^2 2p^2$	$^3P_0$	$\underline{\uparrow}\ \underline{\uparrow}\ \underline{\ }$ 1 0 -1	$\frac{5}{3}$	4
7 e Ion	$1s^2 2s^2 2p^3$	$^4S^0_{3/2}$	$\underline{\uparrow}\ \underline{\uparrow}\ \underline{\uparrow}$ 1 0 -1	$\frac{5}{3}$	6
8 e Ion	$1s^2 2s^2 2p^4$	$^3P_2$	$\underline{\uparrow\downarrow}\ \underline{\uparrow}\ \underline{\uparrow}$ 1 0 -1	$\frac{5}{3}$	6
9 e Ion	$1s^2 2s^2 2p^5$	$^2P^0_{3/2}$	$\underline{\uparrow\downarrow}\ \underline{\uparrow\downarrow}\ \underline{\uparrow}$ 1 0 -1	$\frac{5}{3}$	9
10 e Ion	$1s^2 2s^2 2p^6$	$^1S_0$	$\underline{\uparrow\downarrow}\ \underline{\uparrow\downarrow}\ \underline{\uparrow\downarrow}$ 1 0 -1	$\frac{5}{3}$	12

[a] The theoretical ground state terms match those given by NIST [8].

[b] Eq. (10.82).

[c] Eqs. (10.83-10.84) and (10.89).

ELEVEN-ELECTRON ATOMS

Eleven-electron atoms can be solved exactly using the results of the solutions of one, two, three, four, five, six, seven, eight, nine, and ten-electron atoms.

RADIUS AND IONIZATION ENERGY OF THE OUTER ELECTRON OF THE SODIUM ATOM

For each ten-electron atom having a central charge of Z times that of the proton, there are two indistinguishable spin-paired electrons in an atomic orbital with radii r_1 and r_2 both given by Eq. (7.35) (Eq. (10.51)), two indistinguishable spin-paired electrons in an atomic orbital with radii r_3 and r_4 both given by Eq. (10.62), and three sets of paired electrons in an atomic orbital at r_{10} given by Eq. (10.212). For $Z \geq 11$, the next electron which binds to form the corresponding eleven-electron atom is attracted by the central Coulomb field and is repelled by diamagnetic forces due to the 3 sets of spin-paired inner electrons such that it forms an unpaired atomic orbital at radius r_{11}.

The central Coulomb force acts on the outer electron to cause it to bind wherein this electric force on the outer-most electron due to the nucleus and the inner ten electrons is given by Eq. (10.70) with the appropriate charge and radius:

$$\mathbf{F}_{ele} = \frac{(Z-10)e^2}{4\pi\varepsilon_0 r_{11}^2}\mathbf{i}_r \tag{10.218}$$

for $r > r_{10}$.

The spherically symmetrical closed 2p shell of eleven-electron atoms produces a diamagnetic force, $\mathbf{F}_{diamagnetic}$, that is equivalent to that of a closed s shell given by Eq. (10.11) with the appropriate radii. The inner electrons remain at their initial radii, but cause a diamagnetic force according to Lenz's law that is

$$\mathbf{F}_{diamagnetic} = -\frac{\hbar^2}{4m_e r_{11}^2 r_{10}}\sqrt{s(s+1)}\mathbf{i}_\mathbf{r} \tag{10.219}$$

In addition to the spin-spin interaction between electron pairs, the three sets of 2p electrons are orbitally paired. The single s orbital of the sodium atom produces a magnetic field at the position of the three sets of spin-paired 2p electrons. In order for the electrons to remain spin and orbitally paired, a corresponding diamagnetic force, $\mathbf{F}_{diamagnetic\ 3}$, on electron eleven from the three sets of spin-paired electrons is given by:

$$\mathbf{F}_{diamagnetic\ 3} = -8\left[\frac{e^2\mu_0}{2m_e r_{10}}\right]\frac{\hbar^2}{m_e r_{11}^{\ 3}}\mathbf{i}_\mathbf{r} \tag{10.220}$$

corresponding to the p_x and p_y electrons with no interaction from the orthogonal p_z electrons (Eq. (10.84)). As demonstrated by Eqs. (7.15-7.23), the maintenance of the invariance of the electron's angular momentum of $\hbar$, mass to charge ratio, $\frac{e}{m_e}$, and corresponding magnetic moment of a Bohr magneton, μ_B, requires that the term in brackets is be replaced by $\frac{1}{Z}$ corresponding to the relativistic correction given by Eq. (7.23). Thus, $\mathbf{F}_{diamagnetic\ 3}$ is given by:

$$\mathbf{F}_{diamagnetic\ 3} = -\frac{1}{Z}\frac{8\hbar^2}{m_e r_{11}^{\ 3}}\sqrt{s(s+1)}\mathbf{i}_\mathbf{r} \tag{10.221}$$

where the vector projection of the spin interaction of $\sqrt{s(s+1)} = \sqrt{\frac{3}{4}}$ is given in the Two-Electron Atoms section and Appendix VI.

The outward centrifugal force on electron 11 is balanced by the electric force and the magnetic forces (on electron 11). The radius of the outer electron is calculated by equating the outward centrifugal force to the sum of the electric (Eq. (10.218)) and diamagnetic (Eqs. (10.219) and (10.221)) forces as follows:

$$\frac{m_e v_{11}^2}{r_{11}} = \frac{(Z-10)e^2}{4\pi\varepsilon_0 r_{11}^2} - \frac{\hbar^2}{4m_e r_{11}^2 r_{10}}\sqrt{s(s+1)} - \frac{8\hbar^2}{Zm_e r_{11}^3}\sqrt{s(s+1)} \tag{10.222}$$

Substitution of $v_{11} = \frac{\hbar}{m_e r_{11}}$ (Eq. (1.35)) and $s = \frac{1}{2}$ into Eq. (10.222) gives:

$$\frac{\hbar^2}{m_e r_{11}^3} = \frac{(Z-10)e^2}{4\pi\varepsilon_0 r_{11}^2} - \frac{\hbar^2}{4m_e r_{11}^2 r_{10}}\sqrt{\frac{3}{4}} - \frac{8\hbar^2}{Zm_e r_{11}^3}\sqrt{\frac{3}{4}} \tag{10.223}$$

$$r_{11} = \frac{\frac{\hbar^2}{m_e}\left(1+\frac{8}{Z}\sqrt{\frac{3}{4}}\right)}{\frac{(Z-10)e^2}{4\pi\varepsilon_0} - \frac{\hbar^2}{4m_e r_{10}}\sqrt{\frac{3}{4}}} \tag{10.224}$$

$$r_{11} = \frac{a_0\left(1+\frac{8}{Z}\sqrt{\frac{3}{4}}\right)}{(Z-10) - \frac{\sqrt{\frac{3}{4}}}{4r_{10}}},\ r_{10}\ \textit{in units of}\ a_0 \tag{10.225}$$

Substitution of $\frac{r_{10}}{a_0} = 0.56094$ (Eq. (10.212) with $Z = 11$) into Eq. (10.225) gives:

$$r_{11} = 2.65432a_0 \tag{10.226}$$

The ionization energy of the sodium atom is given by the negative of $E(electric)$ given by Eq. (10.102) with the appropriate charge and radius:

$$E(ionization;\ Na) = -Electric\ Energy = \frac{(Z-10)e^2}{8\pi\varepsilon_0 r_{11}} = 5.12592\ eV \tag{10.227}$$

where $r_{11} = 2.65432a_0$ (Eq. (10.226)) and $Z = 11$. The experimental ionization energy of the sodium atom is $5.13908\ eV$ [3].

THE IONIZATION ENERGIES OF ELEVEN-ELECTRON ATOMS WITH A NUCLEAR CHARGE Z>11

Eleven-electron atoms having $Z>11$ possess an external electric field given by Eq. (10.92). Since there is a source of dissipative power, $\mathbf{J}\bullet\mathbf{E}$ of Eq. (10.27), the magnetic moments of the inner electrons may change due to the outer electron such that the energy of the eleven-electron atom is lowered. The orbital angular momenta of the paired p_x and p_y electrons give rise to the paramagnetic force given by Eq. (10.89), which is also equivalent to that given by Eq. (10.55):

$$\mathbf{F}_{mag\ 2}=\frac{1}{Z}\frac{4\hbar^2}{m_e r_{11}^2 r_{10}}\sqrt{s(s+1)}\mathbf{i}_{\mathbf{r}} \tag{10.228}$$

The diamagnetic force, $\mathbf{F}_{diamagnetic\ 2}$, due to a relativistic effect with an electric field for $r>r_n$ (Eq. (10.35)) may be determined by considering the corresponding force due to the binding of a 2p electron. It was shown in the Five-Electron Atom section, that $\mathbf{F}_{diamagnetic\ 2}$ for five through ten-electron atoms, is dependent on the amplitude of the orbital energy. Using the orbital energy with $\ell=1$ (Eq. (10.90)), the energy $m_e\Delta v^2$ of Eq. (10.29) is reduced by the factor of $\left(1-\frac{\sqrt{2}}{2}\right)$ due to the contribution of the charge-density wave of the inner electrons at r_3. Thus, $\mathbf{F}_{diamagnetic\ 2}$ is given by Eq. (10.93). Conversely, the binding of a 3s electron increases the energy $m_e\Delta v^2$ of Eq. (10.29) by the factor of $\left(1+\frac{\sqrt{2}}{2}\right)$ such that $\mathbf{F}_{diamagnetic\ 2}$ becomes

$$\mathbf{F}_{diamagnetic\ 2}=-\left[\frac{Z-11}{Z-10}\right]\left(1+\frac{\sqrt{2}}{2}\right)\frac{r_{10}\hbar^2}{m_e r_{11}^4}10\sqrt{s(s+1)}\mathbf{i}_{\mathbf{r}} \tag{10.229}$$

In the case that $Z>11$, the radius of the outer electron is calculated by equating the outward centrifugal force to the sum of the electric (Eq. (10.218)), diamagnetic (Eq. (10.229)), and paramagnetic (Eq. (10.228)) forces as follows:

$$\begin{aligned}\frac{m_e v_{11}^2}{r_{11}}=&\frac{(Z-10)e^2}{4\pi\varepsilon_0 r_{11}^2}-\frac{\hbar^2}{4m_e r_{11}^2 r_{10}}\sqrt{s(s+1)}+\frac{4\hbar^2}{Zm_e r_{11}^2 r_{10}}\sqrt{s(s+1)}\\&-\frac{8\hbar^2}{Zm_e r_{11}^3}\sqrt{s(s+1)}-\left[\frac{Z-11}{Z-10}\right]\left(1+\frac{\sqrt{2}}{2}\right)\frac{r_{10}\hbar^2}{m_e r_{11}^4}10\sqrt{s(s+1)}\end{aligned} \tag{10.230}$$

Substitution of $v_{11}=\frac{\hbar}{m_e r_{11}}$ (Eq. (1.35)) and $s=\frac{1}{2}$ into Eq. (10.230) gives:

$$\frac{\hbar^2}{m_e r_{11}^3}=\frac{(Z-10)e^2}{4\pi\varepsilon_0 r_{11}^2}-\frac{\hbar^2}{4m_e r_{11}^2 r_{10}}\sqrt{\frac{3}{4}}+\frac{4\hbar^2}{Zm_e r_{11}^2 r_{10}}\sqrt{\frac{3}{4}}-\frac{8\hbar^2}{Zm_e r_{11}^3}\sqrt{\frac{3}{4}}-\left[\frac{Z-11}{Z-10}\right]\left(1+\frac{\sqrt{2}}{2}\right)\frac{r_{10}\hbar^2}{m_e r_{11}^4}10\sqrt{\frac{3}{4}} \tag{10.231}$$

The quadratic equation corresponding to Eq. (10.231) is

$$\left(\frac{(Z-10)e^2}{4\pi\varepsilon_0}-\left(\frac{1}{4}-\frac{4}{Z}\right)\frac{\hbar^2}{m_e r_{10}}\sqrt{\frac{3}{4}}\right)r_{11}^2-\frac{\hbar^2}{m_e}\left(1+\frac{8\sqrt{\frac{3}{4}}}{Z}\right)r_{11}-\left[\frac{Z-11}{Z-10}\right]\left(1+\frac{\sqrt{2}}{2}\right)\frac{r_{10}\hbar^2}{m_e}10\sqrt{\frac{3}{4}}=0 \tag{10.232}$$

$$r_{11}^2-\frac{\frac{\hbar^2}{m_e}\left(1+\frac{8\sqrt{\frac{3}{4}}}{Z}\right)}{\left(\frac{(Z-10)e^2}{4\pi\varepsilon_0}-\left(\frac{1}{4}-\frac{4}{Z}\right)\frac{\hbar^2}{m_e r_{10}}\sqrt{\frac{3}{4}}\right)}r_{11}-\frac{\left[\frac{Z-11}{Z-10}\right]\left(1+\frac{\sqrt{2}}{2}\right)\frac{r_{10}\hbar^2}{m_e}10\sqrt{\frac{3}{4}}}{\left(\frac{(Z-10)e^2}{4\pi\varepsilon_0}-\left(\frac{1}{4}-\frac{4}{Z}\right)\frac{\hbar^2}{m_e r_{10}}\sqrt{\frac{3}{4}}\right)}=0 \tag{10.233}$$

The solution of Eq. (10.233) using the quadratic formula is:

$$r_{11}=\frac{\dfrac{\dfrac{\hbar^2}{m_e}\left(1+\dfrac{8\sqrt{\dfrac{3}{4}}}{Z}\right)}{\left(\dfrac{(Z-10)e^2}{4\pi\varepsilon_0}-\left(\dfrac{1}{4}-\dfrac{4}{Z}\right)\dfrac{\hbar^2}{m_e r_{10}}\sqrt{\dfrac{3}{4}}\right)}\pm\sqrt{\left(\dfrac{\dfrac{\hbar^2}{m_e}\left(1+\dfrac{8\sqrt{\dfrac{3}{4}}}{Z}\right)}{\left(\dfrac{(Z-10)e^2}{4\pi\varepsilon_0}-\left(\dfrac{1}{4}-\dfrac{4}{Z}\right)\dfrac{\hbar^2}{m_e r_{10}}\sqrt{\dfrac{3}{4}}\right)}\right)^2+4\dfrac{\left[\dfrac{Z-11}{Z-10}\right]\left(1+\dfrac{\sqrt{2}}{2}\right)\dfrac{r_{10}\hbar^2}{m_e}10\sqrt{\dfrac{3}{4}}}{\left(\dfrac{(Z-10)e^2}{4\pi\varepsilon_0}-\left(\dfrac{1}{4}-\dfrac{4}{Z}\right)\dfrac{\hbar^2}{m_e r_{10}}\sqrt{\dfrac{3}{4}}\right)}}}{2} \tag{10.234}$$

$$r_{11}=\frac{\dfrac{a_0\left(1+\dfrac{4\sqrt{3}}{Z}\right)}{\left((Z-10)-\left(\dfrac{1}{8}-\dfrac{2}{Z}\right)\dfrac{\sqrt{3}}{r_{10}}\right)}\pm a_0\sqrt{\left(\dfrac{1+\dfrac{4\sqrt{3}}{Z}}{\left((Z-10)-\left(\dfrac{1}{8}-\dfrac{2}{Z}\right)\dfrac{\sqrt{3}}{r_{10}}\right)}\right)^2+\dfrac{20\sqrt{3}\left(\left[\dfrac{Z-11}{Z-10}\right]\left(1+\dfrac{\sqrt{2}}{2}\right)r_{10}\right)}{\left((Z-10)-\left(\dfrac{1}{8}-\dfrac{2}{Z}\right)\dfrac{\sqrt{3}}{r_{10}}\right)}}}{2},\ r_{10}\ \textit{in units of}\ a_0 \tag{10.235}$$

where r_{10} is given by Eq. (10.212). The positive root of Eq. (10.235) must be taken in order that $r_{11}>0$. The radii of several eleven-electron atoms are given in Table 10.10.

The ionization energies for the eleven-electron atoms with $Z>11$ are given by the electric energy, $E(electric)$, (Eq. (10.102) with the radii, r_{11}, given by Eq. (10.235)):

$$E(Ionization)=-Electric\ Energy=\frac{(Z-10)e^2}{8\pi\varepsilon_0 r_{11}} \tag{10.236}$$

Since the relativistic corrections were small, the nonrelativistic ionization energies for experimentally measured eleven-electron atoms are given in Table 10.10.

Table 10.10. Ionization energies for some eleven-electron atoms.

11 e Atom	Z	r_1 (a_o) [a]	r_3 (a_o) [b]	r_{10} (a_o) [c]	r_{11} (a_o) [d]	Theoretical Ionization Energies [e] (eV)	Experimental Ionization Energies [f] (eV)	Relative Error [g]
Na	11	0.09213	0.40853	0.560945	2.65432	5.12592	5.13908	0.0026
Mg^{+}	12	0.08435	0.37065	0.510568	1.74604	15.5848	15.03528	-0.0365
Al^{2+}	13	0.07778	0.33923	0.456203	1.47399	27.6918	28.44765	0.0266
Si^{3+}	14	0.07216	0.31274	0.409776	1.25508	43.3624	45.14181	0.0394
P^{4+}	15	0.06730	0.29010	0.371201	1.08969	62.4299	65.0251	0.0399
S^{5+}	16	0.06306	0.27053	0.339025	0.96226	84.8362	88.0530	0.0365
Cl^{6+}	17	0.05932	0.25344	0.311903	0.86151	110.5514	114.1958	0.0319
Ar^{7+}	18	0.05599	0.23839	0.288778	0.77994	139.5577	143.460	0.0272
K^{8+}	19	0.05302	0.22503	0.268844	0.71258	171.8433	175.8174	0.0226
Ca^{9+}	20	0.05035	0.21308	0.251491	0.65602	207.3998	211.275	0.0183
Sc^{10+}	21	0.04794	0.20235	0.236251	0.60784	246.2213	249.798	0.0143
Ti^{11+}	22	0.04574	0.19264	0.222761	0.56631	288.3032	291.500	0.0110
V^{12+}	23	0.04374	0.18383	0.210736	0.53014	333.6420	336.277	0.0078
Cr^{13+}	24	0.04191	0.17579	0.19995	0.49834	382.2350	384.168	0.0050
Mn^{14+}	25	0.04022	0.16842	0.19022	0.47016	434.0801	435.163	0.0025
Fe^{15+}	26	0.03867	0.16165	0.181398	0.44502	489.1753	489.256	0.0002
Co^{16+}	27	0.03723	0.15540	0.173362	0.42245	547.5194	546.58	-0.0017
Ni^{17+}	28	0.03589	0.14961	0.166011	0.40207	609.1111	607.06	-0.0034
Cu^{18+}	29	0.03465	0.14424	0.159261	0.38358	673.9495	670.588	-0.0050
Zn^{19+}	30	0.03349	0.13925	0.153041	0.36672	742.0336	738	-0.0055

[a] Radius of the first set of paired inner electrons of eleven-electron atoms from Eq. (10.51).
[b] Radius of the second set of paired inner electrons of eleven-electron atoms from Eq. (10.62).
[c] Radius of three sets of paired inner electrons of eleven-electron atoms from Eq. (10.212).
[d] Radius of unpaired outer electron of eleven-electron atoms from Eq. (10.235) for $Z > 11$ and Eq. (10.226) for *Na*.
[e] Calculated ionization energies of eleven-electron atoms given by the electric energy (Eq. (10.236)).
[f] From theoretical calculations, interpolation of isoelectronic and spectral series, and experimental data [2-3].
[g] (Experimental-theoretical)/experimental.

The agreement between the experimental and calculated values of Table 10.10 is well within the experimental capability of the spectroscopic determinations including the values at large Z, which relies on X-ray spectroscopy. In this case, the experimental capability is three to four significant figures, which is consistent with the last column. The sodium atom isoelectronic series is given in Table 10.10 [2-3] to much higher precision than the capability of X-ray spectroscopy, but these values are based on theoretical and interpolation techniques rather than data alone. Ionization energies are difficult to determine since the cut-off of the Rydberg series of lines at the ionization energy is often not observed, and the ionization energy must be determined from theoretical calculations, interpolation of Na isoelectronic and Rydberg series, as well as direct experimental data.

TWELVE-ELECTRON ATOMS

Twelve-electron atoms can be solved exactly using the results of the solutions of one, two, three, four, five, six, seven, eight, nine, ten, and eleven-electron atoms.

RADIUS AND IONIZATION ENERGY OF THE OUTER ELECTRON OF THE MAGNESIUM ATOM

For each eleven-electron atom having a central charge of Z times that of the proton, there are two indistinguishable spin-paired electrons in an atomic orbital with radii r_1 and r_2 both given by Eq. (7.35) (Eq. (10.51)), two indistinguishable spin-paired electrons in an atomic orbital with radii r_3 and r_4 both given by Eq. (10.62), three sets of paired electrons in an atomic orbital at r_{10} given by Eq. (10.212), and an unpaired electron in an atomic orbital at r_{11}. For $Z \geq 12$, the next electron which binds to form the corresponding twelve-electron atom is attracted by the central Coulomb field and the spin-pairing force with the unpaired 3s inner electron and is repelled by diamagnetic forces due to the 3 sets of spin-paired inner electrons such that it forms an unpaired atomic orbital at radius r_{12}.

The central Coulomb force acts on the outer electron to cause it to bind wherein this electric force on the outer-most electron due to the nucleus and the inner eleven electrons is given by Eq. (10.70) with the appropriate charge and radius:

$$\mathbf{F}_{ele} = \frac{(Z-11)e^2}{4\pi\varepsilon_0 r_{12}^2}\mathbf{i}_\mathbf{r} \tag{10.237}$$

for $r > r_{11}$.

The outer electron which binds to form the corresponding twelve-electron atom becomes spin-paired with the unpaired inner electron such that they become indistinguishable with the same radius $r_{11} = r_{12}$ corresponding to a filled 3s shell. The corresponding spin-pairing force $\mathbf{F}_{mag}$ is given by Eq. (7.24).

$$\mathbf{F}_{mag} = \frac{1}{Z}\frac{\hbar^2}{m_e r_{12}^3}\sqrt{s(s+1)}\mathbf{i}_\mathbf{r} \tag{10.238}$$

The spherically symmetrical closed 2p shell of twelve-electron atoms produces a diamagnetic force, $\mathbf{F}_{diamagnetic}$, that is equivalent to that of a closed s shell given by Eq. (10.11) with the appropriate radii. The inner electrons remain at their initial radii, but cause a diamagnetic force according to Lenz's law that is:

$$\mathbf{F}_{diamagnetic} = -\frac{\hbar^2}{4m_e r_{12}^2 r_{10}}\sqrt{s(s+1)}\mathbf{i}_\mathbf{r} \tag{10.239}$$

In addition to the paramagnetic spin-pairing force between the eleventh electron initially at radius r_{11}, the pairing causes the diamagnetic interaction between the outer electrons and the inner electrons given by Eq. (10.11) to vanish, except for an electrodynamic effect for $Z > 12$ described in the Two-Electron Atoms section, since upon pairing the magnetic field of the outer electrons becomes zero. Using Eq. (10.55), $\mathbf{F}_{mag\ 2}$ due to the three 2p orbitals is given by:

$$\mathbf{F}_{mag\ 2} = \frac{3}{Z}\frac{\hbar^2}{m_e r_{10} r_{12}^2}\sqrt{s(s+1)}\mathbf{i}_\mathbf{r} \tag{10.240}$$

In addition to the spin-spin interactions between electron pairs, the three sets of 2p electrons are orbitally paired. The s electrons of the magnesium atom produce a magnetic field at the position of the three sets of spin-paired 2p electrons. In order for the electrons to remain spin and orbitally paired, the corresponding diamagnetic force, $\mathbf{F}_{diamagnetic\ 3}$ (Eq. (10.221)), on electron twelve from the three sets of spin-paired electrons is given by:

$$\mathbf{F}_{diamagnetic\ 3} = -\frac{1}{Z}\frac{12\hbar^2}{m_e r_{12}^3}\sqrt{s(s+1)}\mathbf{i}_\mathbf{r} \tag{10.241}$$

corresponding to the p_x, p_y, and p_z electrons.

The outward centrifugal force on electron 12 is balanced by the electric force and the magnetic forces (on electron 12). The radius of the outer electron is calculated by equating the outward centrifugal force to the sum of the electric (Eq. (10.237)), diamagnetic (Eqs. (10.239) and (10.241)) and paramagnetic (Eqs. (10.238) and (10.240)) forces as follows:

$$\frac{m_e v_{12}^2}{r_{12}} = \frac{(Z-11)e^2}{4\pi\varepsilon_0 r_{12}^2} - \frac{\hbar^2}{4m_e r_{12}^2 r_{10}}\sqrt{s(s+1)} + \frac{3\hbar^2}{Zm_e r_{12}^2 r_{10}}\sqrt{s(s+1)} \tag{10.242}$$

$$-\frac{12\hbar^2}{Zm_e r_{12}^3}\sqrt{s(s+1)} + \frac{\hbar^2}{Zm_e r_{12}^3}\sqrt{s(s+1)}$$

Substitution of $v_{12} = \frac{\hbar}{m_e r_{12}}$ (Eq. (1.35)) and $s = \frac{1}{2}$ into Eq. (10.242) gives:

$$\frac{\hbar^2}{m_e r_{12}^3} = \frac{(Z-11)e^2}{4\pi\varepsilon_0 r_{12}^2} - \frac{\hbar^2}{4m_e r_{12}^2 r_{10}}\sqrt{\frac{3}{4}} + \frac{3\hbar^2}{Zm_e r_{12}^2 r_{10}}\sqrt{\frac{3}{4}} - \frac{12\hbar^2}{Zm_e r_{12}^3}\sqrt{\frac{3}{4}} + \frac{\hbar^2}{Zm_e r_{12}^3}\sqrt{\frac{3}{4}} \tag{10.243}$$

$$r_{12} = \frac{\frac{\hbar^2}{m_e}\left(1 + \frac{11\sqrt{\frac{3}{4}}}{Z}\right)}{\frac{(Z-11)e^2}{4\pi\varepsilon_0} - \left(\frac{1}{4} - \frac{3}{Z}\right)\frac{\hbar^2}{m_e r_{10}}\sqrt{\frac{3}{4}}} \tag{10.244}$$

$$r_{12} = \frac{a_0\left(1 + \frac{11\sqrt{\frac{3}{4}}}{Z}\right)}{(Z-11) - \left(\frac{1}{4} - \frac{3}{Z}\right)\frac{\sqrt{\frac{3}{4}}}{r_{10}}},\ r_{10}\ \textit{in units of}\ a_0 \tag{10.245}$$

Substitution of $\frac{r_{10}}{a_0} = 0.51057$ (Eq. (10.212) with $Z = 12$) into Eq. (10.245) gives:

$$r_{12} = 1.79386 a_0 \tag{10.246}$$

The ionization energy of the magnesium atom is given by the electric energy, $E(electric)$, (Eq. (10.102) with the radius, r_{12}, given by Eq. (10.246)).

$$E(ionization;\ Mg) = -Electric\ Energy = \frac{(Z-11)e^2}{8\pi\varepsilon_0 r_{12}} = 7.58467\ eV \tag{10.247}$$

where $r_{12} = 1.79386 a_0$ (Eq. (10.246)) and $Z = 12$. The experimental ionization energy of the magnesium atom is $7.64624\ eV$ [3].

THE IONIZATION ENERGIES OF TWELVE-ELECTRON ATOMS WITH A NUCLEAR CHARGE Z>12

Twelve-electron atoms having $Z > 12$ possess an external electric field given by Eq. (10.92). Since there is a source of dissipative power, $\mathbf{J} \bullet \mathbf{E}$ of Eq. (10.27), the magnetic moments of the inner electrons may change due to the outer electron such that the energy of the twelve-electron atom is lowered with conservation of angular momentum. Of the possible forces based on Maxwell's equations, those that give rise to an energy minimum are used to calculate the atomic radii and energies. With this constraint, the only paramagnetic force is that given by Eq. (10.89) due to the spin angular momenta of the paired 2 p_x, p_y, and p_z electrons interacting equivalently with each of the 3s electrons. This force, which is also equivalent to that given by Eq. (10.145), is:

$$\mathbf{F}_{mag\ 2} = 2\frac{1}{Z}\frac{3\hbar^2}{m_e r_{12}^2 r_{10}}\sqrt{s(s+1)}\mathbf{i}_{\mathbf{r}} \tag{10.248}$$

From Eq. (10.229), the diamagnetic force, $\mathbf{F}_{diamagnetic\ 2}$, due to a relativistic effect with an electric field for $r > r_{12}$ (Eq. (10.35)) is:

$$\mathbf{F}_{diamagnetic\ 2} = -\left[\frac{Z-12}{Z-11}\right]\left(1+\frac{\sqrt{2}}{2}\right)\frac{r_{10}\hbar^2}{m_e r_{12}^4}10\sqrt{s(s+1)}\mathbf{i}_{\mathbf{r}} \tag{10.249}$$

In the case that $Z > 12$, the radius of the outer electron is calculated by equating the outward centrifugal force to the sum of the electric (Eq. (10.237)), diamagnetic (Eq. (10.249)), and paramagnetic (Eq. (10.248)) forces as follows:

$$\frac{m_e v_{12}^2}{r_{12}} = \frac{(Z-11)e^2}{4\pi\varepsilon_0 r_{12}^2} - \frac{\hbar^2}{4m_e r_{12}^2 r_{10}}\sqrt{s(s+1)} + \frac{6\hbar^2}{Z m_e r_{12}^2 r_{10}}\sqrt{s(s+1)} - \left[\frac{Z-12}{Z-11}\right]\left(1+\frac{\sqrt{2}}{2}\right)\frac{r_{10}\hbar^2}{m_e r_{12}^4}10\sqrt{s(s+1)} \tag{10.250}$$

Substitution of $v_{12} = \frac{\hbar}{m_e r_{12}}$ (Eq. (1.35)) and $s = \frac{1}{2}$ into Eq. (10.250) gives:

$$\frac{\hbar^2}{m_e r_{12}^3} = \frac{(Z-11)e^2}{4\pi\varepsilon_0 r_{12}^2} - \frac{\hbar^2}{4m_e r_{12}^2 r_{10}}\sqrt{\frac{3}{4}} + \frac{6\hbar^2}{Z m_e r_{12}^2 r_{10}}\sqrt{\frac{3}{4}} - \left[\frac{Z-12}{Z-11}\right]\left(1+\frac{\sqrt{2}}{2}\right)\frac{r_{10}\hbar^2}{m_e r_{12}^4}10\sqrt{\frac{3}{4}} \tag{10.251}$$

The quadratic equation corresponding to Eq. (10.251) is

$$\left(\frac{(Z-11)e^2}{4\pi\varepsilon_0} - \left(\frac{1}{4}-\frac{6}{Z}\right)\frac{\hbar^2}{m_e r_{10}}\sqrt{\frac{3}{4}}\right)r_{12}^2 - \frac{\hbar^2}{m_e}r_{12} - \left[\frac{Z-12}{Z-11}\right]\left(1+\frac{\sqrt{2}}{2}\right)\frac{r_{10}\hbar^2}{m_e}10\sqrt{\frac{3}{4}} = 0 \tag{10.252}$$

$$r_{12}^2 - \frac{\frac{\hbar^2}{m_e}}{\left(\frac{(Z-11)e^2}{4\pi\varepsilon_0} - \left(\frac{1}{4}-\frac{6}{Z}\right)\frac{\hbar^2}{m_e r_{10}}\sqrt{\frac{3}{4}}\right)}r_{12} - \frac{\left[\frac{Z-12}{Z-11}\right]\left(1+\frac{\sqrt{2}}{2}\right)\frac{r_{10}\hbar^2}{m_e}10\sqrt{\frac{3}{4}}}{\left(\frac{(Z-11)e^2}{4\pi\varepsilon_0} - \left(\frac{1}{4}-\frac{6}{Z}\right)\frac{\hbar^2}{m_e r_{10}}\sqrt{\frac{3}{4}}\right)} = 0 \tag{10.253}$$

The solution of Eq. (10.253) using the quadratic formula is:

$$r_{12} = \frac{\dfrac{\dfrac{\hbar^2}{m_e}}{\left(\dfrac{(Z-11)e^2}{4\pi\varepsilon_0} - \left(\dfrac{1}{4} - \dfrac{6}{Z}\right)\dfrac{\hbar^2}{m_e r_{10}}\sqrt{\dfrac{3}{4}}\right)} \pm \sqrt{\left(\dfrac{\dfrac{\hbar^2}{m_e}}{\left(\dfrac{(Z-11)e^2}{4\pi\varepsilon_0} - \left(\dfrac{1}{4} - \dfrac{6}{Z}\right)\dfrac{\hbar^2}{m_e r_{10}}\sqrt{\dfrac{3}{4}}\right)}\right)^2 + 4\dfrac{\left[\dfrac{Z-12}{Z-11}\right]\left(1+\dfrac{\sqrt{2}}{2}\right)\dfrac{r_{10}\hbar^2}{m_e}10\sqrt{\dfrac{3}{4}}}{\left(\dfrac{(Z-11)e^2}{4\pi\varepsilon_0} - \left(\dfrac{1}{4} - \dfrac{6}{Z}\right)\dfrac{\hbar^2}{m_e r_{10}}\sqrt{\dfrac{3}{4}}\right)}}}{2} \tag{10.254}$$

$$r_{12} = \frac{\dfrac{a_0}{\left((Z-11) - \left(\dfrac{1}{8} - \dfrac{3}{Z}\right)\dfrac{\sqrt{3}}{r_{10}}\right)} \pm a_0 \sqrt{\left(\dfrac{1}{\left((Z-11) - \left(\dfrac{1}{8} - \dfrac{3}{Z}\right)\dfrac{\sqrt{3}}{r_{10}}\right)}\right)^2 + \dfrac{20\sqrt{3}\left(\left[\dfrac{Z-12}{Z-11}\right]\left(1+\dfrac{\sqrt{2}}{2}\right)r_{10}\right)}{\left((Z-11) - \left(\dfrac{1}{8} - \dfrac{3}{Z}\right)\dfrac{\sqrt{3}}{r_{10}}\right)}}}{2}, \; r_{10} \textit{ in units of } a_0 \tag{10.255}$$

where r_{10} is given by Eq. (10.212). The positive root of Eq. (10.255) must be taken in order that $r_{12} > 0$. The radii of several twelve-electron atoms are given in Table 10.11.

The ionization energies for the twelve-electron atoms with $Z > 12$ are given by the electric energy, $E(electric)$, (Eq. (10.102) with the radii, r_{12}, given by Eq. (10.255)).

$$E(Ionization) = -Electric\ Energy = \frac{(Z-11)e^2}{8\pi\varepsilon_0 r_{12}} \tag{10.256}$$

Since the relativistic corrections were small, the nonrelativistic ionization energies for experimentally measured twelve-electron atoms are given in Table 10.11.

Table 10.11. Ionization energies for some twelve-electron atoms.

12 e Atom	Z	r_1 (a_o) [a]	r_3 (a_o) [b]	r_{10} (a_o) [c]	r_{12} (a_o) [d]	Theoretical Ionization Energies [e] (eV)	Experimental Ionization Energies [f] (eV)	Relative Error [g]
Mg	12	0.08435	0.37065	0.51057	1.79386	7.58467	7.64624	0.0081
Al^{+}	13	0.07778	0.33923	0.45620	1.41133	19.2808	18.82856	-0.0240
Si^{2+}	14	0.07216	0.31274	0.40978	1.25155	32.6134	33.49302	0.0263
P^{3+}	15	0.06730	0.29010	0.37120	1.09443	49.7274	51.4439	0.0334
S^{4+}	16	0.06306	0.27053	0.33902	0.96729	70.3296	72.5945	0.0312
Cl^{5+}	17	0.05932	0.25344	0.31190	0.86545	94.3266	97.03	0.0279
Ar^{6+}	18	0.05599	0.23839	0.28878	0.78276	121.6724	124.323	0.0213
K^{7+}	19	0.05302	0.22503	0.26884	0.71450	152.3396	154.88	0.0164
Ca^{8+}	20	0.05035	0.21308	0.25149	0.65725	186.3102	188.54	0.0118
Sc^{9+}	21	0.04794	0.20235	0.23625	0.60857	223.5713	225.18	0.0071
Ti^{10+}	22	0.04574	0.19264	0.22276	0.56666	264.1138	265.07	0.0036
V^{11+}	23	0.04374	0.18383	0.21074	0.53022	307.9304	308.1	0.0006
Cr^{12+}	24	0.04191	0.17579	0.19995	0.49822	355.0157	354.8	-0.0006
Mn^{13+}	25	0.04022	0.16842	0.19022	0.46990	405.3653	403.0	-0.0059
Fe^{14+}	26	0.03867	0.16165	0.18140	0.44466	458.9758	457	-0.0043
Co^{15+}	27	0.03723	0.15540	0.17336	0.42201	515.8442	511.96	-0.0076
Ni^{16+}	28	0.03589	0.14961	0.16601	0.40158	575.9683	571.08	-0.0086
Cu^{17+}	29	0.03465	0.14424	0.15926	0.38305	639.3460	633	-0.0100
Zn^{18+}	30	0.03349	0.13925	0.15304	0.36617	705.9758	698	-0.0114

[a] Radius of the first set of paired inner electrons of twelve-electron atoms from Eq. (10.51).

[b] Radius of the second set of paired inner electrons of twelve-electron atoms from Eq. (10.62).

[c] Radius of three sets of paired inner electrons of twelve-electron atoms from Eq. (10.212).

[d] Radius of paired outer electrons of twelve-electron atoms from Eq. (10.255) for $Z > 12$ and Eq. (10.246) for *Mg*.

[e] Calculated ionization energies of twelve-electron atoms given by the electric energy (Eq. (10.256)).

[f] From theoretical calculations, interpolation of isoelectronic and spectral series, and experimental data [2-3].

[g] (Experimental-theoretical)/experimental.

The agreement between the experimental and calculated values of Table 10.11 is well within the experimental capability of the spectroscopic determinations including the values at large Z which relies on X-ray spectroscopy. In this case, the experimental capability is three to four significant figures, which is consistent with the last column. The magnesium atom isoelectronic series is given in Table 10.11 [2-3] to much higher precision than the capability of X-ray spectroscopy, but these values are based on theoretical and interpolation techniques rather than data alone. Ionization energies are difficult to determine since the cut-off of the Rydberg series of lines at the ionization energy is often not observed, and the ionization energy must be determined from theoretical calculations, interpolation of Mg isoelectronic and Rydberg series, as well as direct experimental data.

3P-ORBITAL ELECTRONS BASED ON AN ENERGY MINIMUM

For each thirteen through eighteen-electron atom having a central charge of Z times that of the proton, there are two indistinguishable spin-paired electrons in an atomic orbital with radii r_1 and r_2 both given by Eq. (7.35) (Eq. (10.51)), two indistinguishable spin-paired electrons in an atomic orbital with radii r_3 and r_4 both given by Eq. (10.62), three sets of paired electrons in an atomic orbital at r_{10} given by Eq. (10.212), and two indistinguishable spin-paired electrons in an atomic orbital with radii r_{11} and r_{12} both given by Eq. (10.255). For $Z \geq 12$, the next electron which binds to form the corresponding n-electron atom $(13 \leq n \leq 18)$ is attracted by the central Coulomb field and is repelled by diamagnetic forces and attracted by paramagnetic forces due to the 3 sets of spin-paired inner 2p electrons and two spin-paired inner 3s electrons such that it forms an atomic orbital comprising all of the 3p electrons at radius r_n. The resulting electron configuration is $1s^2 2s^2 2p^6 3s^2 3p^{n-12}$.

The central Coulomb force, $\mathbf{F}_{ele}$, acts on the outer electron to cause it to bind wherein this electric force on the outer-most electron due to the nucleus and the inner $n-1$ electrons is given by Eq. (10.70).

$$\mathbf{F}_{ele} = \frac{(Z-(n-1))e^2}{4\pi\varepsilon_0 r_n^2}\mathbf{i}_r \tag{10.257}$$

for $r > r_{n-1}$ where n corresponds to the number of electrons of the atom and Z is its atomic number. In each case, the magnetic field of the binding outer electron changes the angular velocities of the inner electrons. However, in each case, the magnetic field of the outer electron provides a central Lorentz force which exactly balances the change in centrifugal force because of the change in angular velocity [1]. The inner electrons remain at their initial radii, but cause a diamagnetic force according to Lenz's law.

As shown in the 2P-Orbital Electrons Based on an Energy Minimum section the quantum numbers $\ell = 1 \quad m = \pm 1$ and $\ell = 1 \quad m = 0$ correspond to spherical harmonics solutions, $Y_\ell^m(\theta,\phi)$, of Laplace's equation designated the $2\,p_x$, $2\,p_y$, and $2\,p_z$ orbitals, respectively. Similarly, for $13 \le n \le 18$, the energy may be lowered by filling 3p orbitals in the same manner to achieve an energy minimum relative to other configurations and arrangements. In general, a nonuniform distribution of charge achieves an energy minimum with the formation of a fifth shell due to the dependence of the magnetic forces on the nuclear charge and orbital energy (Eqs. (10.70), (10.258-10.264), and (10.268)). The outer electrons of atoms and ions that are isoelectronic with the series aluminum through argon half-fill a 3p level with unpaired electrons at phosphorous, then fill the level with paired electrons at argon.

Similarly to the case of the 2p orbitals, spherical harmonic charge-density waves may be induced in the inner electron atomic orbitals with the addition of one or more outer electrons to the 3p orbitals. An energy minimum is achieved when the thirteenth through eighteenth electrons of each thirteen through eighteen-electron atom fills a 3p orbital with the formation of orthogonal complementary charge-density waves in the inner shell 2p and 3s electrons. To maintain the symmetry of the central charge and the energy minimum condition given by solutions to Laplace's equation (Eq. (10.72)), the charge-density waves on electron atomic orbitals at r_{10} and r_{12} complement those of the outer orbitals when the outer 3p orbitals are not all occupied by at least one electron, and the complementary charge-density waves are provided by electrons at r_{12} when this condition is met. In the case of the 3p electrons, an exception to the trends in 2p orbital forces arises due to the interaction between the 2p, 3s, and 3p electrons due to magnetic fields independent of induced complementary charge-density waves. The spin and angular momenta of the 2p electrons give rise to corresponding magnetic fields that interact with the two 3s electrons. The filled 2p orbitals with the maintenance of symmetry according to Laplace's equation (Eq. (10.72)) requires that the 2p as well as the 3s electrons contribute forces to the 3p electrons due to the electrons at r_{10} acting on the electrons at r_{12} which complies with the reactive force, $\mathbf{F}_{diamagnetic\ 2}$, having the factor $\left(1+\frac{\sqrt{2}}{2}\right)$ and given by Eq. (10.229).

The total orbital contribution to the diamagnetic force, $\mathbf{F}_{diamagnetic}$, given by Eq. (10.82) is:

$$\mathbf{F}_{diamagnetic} = -\sum_m \frac{(\ell+|m|)!}{(2\ell+1)(\ell-|m|)!}\frac{\hbar^2}{4m_e r_n^2 r_{12}}\sqrt{s(s+1)}\mathbf{i}_\mathbf{r} \tag{10.258}$$

where the contributions from orbitals having $|m| = 1$ add positively or negatively. From Eq. (10.204), the diamagnetic force, $\mathbf{F}_{diamagnetic}$, contribution from the 2p electrons is given by the sum of the contributions from the p_x, p_y, and p_z orbitals corresponding to m = 1, -1, and 0, respectively:

$$\mathbf{F}_{diamagnetic} = -\left(\frac{2}{3}+\frac{2}{3}+\frac{1}{3}\right)\frac{\hbar^2}{4m_e r_n^2 r_{12}}\sqrt{s(s+1)}\mathbf{i}_\mathbf{r} = -\left(\frac{5}{3}\right)\frac{\hbar^2}{4m_e r_n^2 r_{12}}\sqrt{s(s+1)}\mathbf{i}_\mathbf{r} \tag{10.259}$$

where r_{12} is given by Eq. (10.255). Due to the 2p-3s-3p interaction, the 3s electrons provide spin or orbital angular momentum in order conserve angular momentum of the interacting orbitals. In the case that an energy minimum is achieved with 3s orbital angular momentum, the diamagnetic force, $\mathbf{F}_{diamagnetic}$, contribution is given by Eqs. (10.82) and (10.258) where m = 1, -1, or 0 corresponding to induced charge-density waves. The contribution from the 3s orbital is added to the contributions from the 3p and the 2p orbitals until the 3p orbitals are at least half filled. Then the diamagnetic force is only due to 3p and 3s electrons since the induced charge-density waves only involve the inner-most shell, the 3s orbital.

As given by Eq. (10.89), the contribution of the orbital angular momentum of an unpaired 3p electron to the paramagnetic force, $\mathbf{F}_{mag\ 2}$, is:

$$\mathbf{F}_{mag\ 2} = \frac{1}{Z}\frac{\hbar^2}{m_e r_n^2 r_{12}}\sqrt{s(s+1)}\mathbf{i}_\mathbf{r} \tag{10.260}$$

Each outer 3p electron contributes spin as well as orbital angular momentum. The former gives rise to spin pairing to another 3p electron when an energy minimum is achieved. In the case that the orbital angular momenta of paired 3p electrons cancel, the contribution to $\mathbf{F}_{mag\ 2}$ due to spin alone given by Eq. (10.83) is equivalent to that due to orbital angular momentum alone (Eq. (10.260)). Due to the 2p-3s-3p interaction, the 3s electrons can also provide a paramagnetic force, $\mathbf{F}_{mag\ 2}$, contribution given by Eqs. (10.82) and (10.260) due to spin angular momentum corresponding to induced charge-density waves.

N-electron atoms having $Z > n$ possess an electric field given by Eq. (10.92) for $r > r_n$. Since there is a source of dissipative power, $\mathbf{J} \bullet \mathbf{E}$ of Eq. (10.27), the magnetic moments of the inner electrons may change due to the outer electron such that the energy of the n-electron atom is lowered. $\mathbf{F}_{diamagnetic}$, is given by Eqs. (10.82) and (10.258). Due to the 2p-3s-3p interaction, the 2p level contributes to the forces even when the filling of the 3p level is half or greater, and the 3s electrons may

provide orbital angular momentum in order conserve angular momentum of the interacting orbitals. In the case that an energy minimum is achieved with 3s orbital angular momentum, the diamagnetic force, $\mathbf{F}_{diamagnetic}$, contribution is given by Eqs. (10.82) and (10.258) where m = 1, -1, or 0 corresponding to induced charge-density waves. The contribution from the 3s orbital is added to the contributions from the 3p and the 2p orbitals.

Due to the 2p-3s-3p interaction with $Z > n$, $\mathbf{F}_{mag\ 2}$ has a contribution from the 2p, 3s, and 3p orbitals. The filled 2p orbitals with the maintenance of symmetry according to Eq. (10.72) requires that the diamagnetic force, $\mathbf{F}_{mag\ 2}$, contribution is:

$$\mathbf{F}_{mag\ 2} = \left(4+4+4\right)\frac{1}{Z}\frac{\hbar^2}{m_e r_n^2 r_{12}}\sqrt{s(s+1)}\mathbf{i}_{\mathbf{r}} = \frac{1}{Z}\frac{12\hbar^2}{m_e r_n^2 r_{12}}\sqrt{s(s+1)}\mathbf{i}_{\mathbf{r}} \tag{10.261}$$

corresponding to the spin and orbital angular momenta of the paired 2 p_x, p_y, and p_z electrons (Eq. (10.205)). The 3s electrons can provide a $\mathbf{F}_{mag\ 2}$ contribution of:

$$\mathbf{F}_{mag\ 2} = \frac{1}{Z}\frac{4\hbar^2}{m_e r_n^2 r_{12}}\sqrt{s(s+1)}\mathbf{i}_{\mathbf{r}} \tag{10.262}$$

corresponding to coupling to the spin and induced orbital angular momentum wherein the orbitals interact such that this contribution superimposes negatively or positively to the contributions from the 2p and 3p orbitals. Each outer 3p electron contributes spin as well as orbital angular momentum. Each unpaired 3p electron can spin and orbitally pair with a 2p orbital. The corresponding force, $\mathbf{F}_{mag\ 2}$, contribution given by Eq. (10.84) is:

$$\mathbf{F}_{mag\ 2} = \frac{1}{Z}\frac{4\hbar^2}{m_e r_n^2 r_{12}}\sqrt{s(s+1)}\mathbf{i}_{\mathbf{r}} \tag{10.263}$$

The 3p electrons spin-pair upon further filling of the 3p orbital. Two spin-paired 3p electrons interacting with two spin-paired 2p orbital electrons double the corresponding force, $\mathbf{F}_{mag\ 2}$, contribution:

$$\mathbf{F}_{mag\ 2} = \frac{1}{Z}\frac{8\hbar^2}{m_e r_n^2 r_{12}}\sqrt{s(s+1)}\mathbf{i}_{\mathbf{r}} \tag{10.264}$$

The sum of the magnitude of the angular momentum of the electron is $\hbar$ in any inertial frame and is relativistically invariant. The vector projections of the atomic orbital spin angular momentum relative to the Cartesian coordinates are given in the Spin Angular Momentum of the Atomic Orbital $Y_0^0(\theta,\phi)$ with ℓ = 0 section. The magnitude of the z-axis projection of the spin angular momentum, $\left|L_z\right|$, the moment of inertia about the z-axis, I_z, and the rotational energy about the z-axis, $E_{rotational\ \ spin}$, given by Eqs. (1.51-1.55) are:

$$\left|L_z\right| = I\frac{\hbar}{m_e r^2} = \frac{\hbar}{2} \tag{10.265}$$

$$I_z = I_{spin} = \frac{m_e r_n^{\ 2}}{2} \tag{10.266}$$

$$E_{rotational} = E_{rotational\ \ spin} = \frac{1}{4}\left[\frac{\hbar^2}{2I_{spin}}\right] = \frac{1}{4}\left[\frac{\hbar^2}{m_e r_n^{\ 2}}\right] \tag{10.267}$$

N-electron atoms having $Z > n$ possess an electric field given by Eq. (10.92) for $r > r_n$. Since there is a source of dissipative power, $\mathbf{J} \bullet \mathbf{E}$ of Eq. (10.27), the magnetic moments of the inner electrons may change due to the outer electron such that the energy of the n-electron atom is lowered. As shown in the P-Orbital Electrons Based on an Energy Minimum section for $\mathbf{F}_{diamagnetic\ 2}$ given by Eq. (10.93), the corresponding diamagnetic force for 2p electrons, $\mathbf{F}_{diamagnetic\ 2}$, due to a relativistic effect with an electric field for $r > r_n$ (Eq. (10.35)) is dependent on the amplitude of the orbital energy. Using the orbital energy with $\ell = 1$ (Eq. (10.90)), the energy $m_e \Delta v^2$ of Eq. (10.29) is reduced by the factor of $\left(1-\frac{\sqrt{2}}{2}\right)$ due to the contribution of the charge-density wave of the inner electrons at r_{12}. In addition, the two 3s electrons contribute an energy factor based on Eq. (1.55) since the filled 2p orbitals with the maintenance of symmetry according to Eq. (10.72) requires that the diamagnetic force is due to the electrons at r_{10} acting on the electrons at r_{12} which complies with the reactive force, $\mathbf{F}_{diamagnetic\ 2}$, given by Eq. (10.229). Thus, $\mathbf{F}_{diamagnetic\ 2}$ for 3p electrons with $Z > n$ is given by:

$$\mathbf{F}_{diamagnetic\ 2} = -\left[\frac{Z-n}{Z-\left(n-1\right)}\right]\left(1-\frac{\sqrt{2}}{2}+\frac{1}{2}\right)\frac{r_{12}\hbar^2}{m_e r_n^4}10\sqrt{s(s+1)}\mathbf{i}_{\mathbf{r}} \tag{10.268}$$

The total diamagnetic and paramagnetic forces are given as the sum over the orbital and spin angular momenta that may add positively or negatively while maintaining the conservation of angular momentum. Of the possible forces based on Maxwell's equations, those which give rise to an energy minimum are used to calculated the atomic radii and energies. In general, an energy minimum is achieved by minimizing $\mathbf{F}_{diamagnetic}$ while maximizing $\mathbf{F}_{mag\ 2}$ with conservation of angular

momentum.

Using the forces given by Eqs. (10.257-10.264), (10.268), and the radii r_{12} given by Eq. (10.255), the radii of the 3p electrons of all thirteen through eighteen-electron atoms may be solved exactly. The electric energy given by Eq. (10.102) gives the corresponding exact ionization energies. $\mathbf{F}_{ele}$ and $\mathbf{F}_{diamagnetic\ 2}$ given by Eqs. (10.257) and (10.268), respectively, are of the same form for all atoms with the appropriate nuclear charges and atomic radii. $\mathbf{F}_{diamagnetic}$ given by Eq. (10.258) and $\mathbf{F}_{mag\ 2}$ given by Eqs. (10.260-10.264) are of the same form with the appropriate factors that depend on the minimum-energy electron configuration. The general equation and the summary of the parameters that determine the exact radii and ionization energies of all thirteen through eighteen-electron atoms are given the General Equation For The Ionization Energies of Thirteen Through Eighteen-Electron Atoms section and in Table 10.18.

THIRTEEN-ELECTRON ATOMS

Thirteen-electron atoms can be solved exactly using the results of the solutions of one, two, three, four, five, six, seven, eight, nine, ten, eleven, and twelve-electron atoms.

RADIUS AND IONIZATION ENERGY OF THE OUTER ELECTRON OF THE ALUMINUM ATOM

For each twelve-electron atom having a central charge of Z times that of the proton, there are two indistinguishable spin-paired electrons in an atomic orbital with radii r_1 and r_2 both given by Eq. (7.35) (Eq. (10.51)), two indistinguishable spin-paired electrons in an atomic orbital with radii r_3 and r_4 both given by Eq. (10.62), three sets of paired electrons in an atomic orbital at r_{10} given by Eq. (10.212), and two indistinguishable spin-paired electrons in an atomic orbital with radii r_{11} and r_{12} both given by Eq. (10.255). For $Z \geq 13$, the next electron which binds to form the corresponding thirteen-electron atom is attracted by the central Coulomb field and is repelled by diamagnetic forces due to the 3 sets of spin-paired inner 2p electrons and two spin-paired inner 3s electrons such that it forms an unpaired atomic orbital at radius r_{13}. The resulting electron configuration is $1s^2 2s^2 2p^6 3s^2 3p^1$, and the orbital arrangement is:

3p state

$$\begin{array}{ccc} \uparrow & & \\ \hline 1 & 0 & -1 \end{array} \tag{10.269}$$

corresponding to the ground state ${}^2P^0_{1/2}$.

The central Coulomb force acts on the outer electron to cause it to bind wherein this electric force on the outer-most electron due to the nucleus and the inner twelve electrons is given by Eq. (10.70) with the appropriate charge and radius:

$$\mathbf{F}_{ele} = \frac{(Z-12)e^2}{4\pi\varepsilon_0 r_{13}^2}\mathbf{i}_{\mathbf{r}} \tag{10.270}$$

for $r > r_{12}$.

As in the case of the boron atom given in the Five-Electron Atom section, the single p orbital of the aluminum atom produces a diamagnetic force equivalent to that of the formation of an s orbital due to the induction of complementary and spherically symmetrical charge-density waves on electron atomic orbitals at r_{10} and r_{12} in order to achieve a solution of Laplace's equation (Eq. (10.72)). The inner electrons remain at their initial radii, but cause a diamagnetic force according to Lenz's law that is given by Eq. (10.96) with the appropriate radii. In addition, the contribution of the diamagnetic force, $\mathbf{F}_{diamagnetic}$, due to the 2p electrons is given by Eqs. (10.105) and (10.259) as the sum of the contributions from the p_x, p_y, and p_z orbitals corresponding to m = 1, -1, and 0, respectively. Thus, $\mathbf{F}_{diamagnetic}$ is given by:

$$\mathbf{F}_{diamagnetic} = -\left(2+\frac{2}{3}+\frac{2}{3}+\frac{1}{3}\right)\frac{\hbar^2}{4m_e r_{13}^2 r_{12}}\sqrt{s(s+1)}\mathbf{i}_{\mathbf{r}} = -\left(\frac{11}{3}\right)\frac{\hbar^2}{4m_e r_{13}^2 r_{12}}\sqrt{s(s+1)}\mathbf{i}_{\mathbf{r}} \tag{10.271}$$

The charge induction forms complementary mirror charge-density waves which must have opposing angular momenta such that momentum is conserved. In this case, $\mathbf{F}_{mag\ 2}$ given by Eq. (10.260) is zero:

$$\mathbf{F}_{mag\ 2} = 0 \tag{10.272}$$

The outward centrifugal force on electron 13 is balanced by the electric force and the magnetic force (on electron 13). The radius of the outer electron is calculated by equating the outward centrifugal force to the sum of the electric (Eq. (10.270)) and diamagnetic (Eq. (10.271)) forces as follows:

$$\frac{m_e v_{13}^2}{r_{13}} = \frac{(Z-12)e^2}{4\pi\varepsilon_o r_{13}^2} - \frac{\frac{11}{3}\hbar^2}{4m_e r_{13}^2 r_{12}}\sqrt{s(s+1)} \tag{10.273}$$

Substitution of $v_{13} = \frac{\hbar}{m_e r_{13}}$ (Eq. (1.35)) and $s = \frac{1}{2}$ into Eq. (10.273) gives:

$$\frac{\hbar^2}{m_e r_{13}^3} = \frac{(Z-12)e^2}{4\pi\varepsilon_0 r_{13}^2} - \frac{11\hbar^2}{12 m_e r_{13}^2 r_{12}}\sqrt{\frac{3}{4}} \tag{10.274}$$

$$r_{13} = \frac{a_0}{\left((Z-12) - \dfrac{11\sqrt{\dfrac{3}{4}}}{12 r_{12}}\right)},\ r_{12}\ in\ units\ of\ a_0 \tag{10.275}$$

Substitution of $\frac{r_{12}}{a_0} = 1.41133$ (Eq. (10.255) with $Z = 13$) into Eq. (10.275) gives:

$$r_{13} = 2.28565 a_0 \tag{10.276}$$

The energy stored in the electric field of the aluminum atom, $E(electric)$, is given by Eq. (10.102) with the appropriate with the radius, r_{13}, given by Eq. (10.276)):

$$E(electric;\ Al) = -\frac{(Z-12)e^2}{8\pi\varepsilon_0 r_{13}} = 5.95270\ eV \tag{10.277}$$

where $r_{13} = 2.28565 a_0$ (Eq. (10.276)) and $Z = 13$. The ionization energy is given by the sum of the electric energy and the energy corresponding to the change in magnetic-moments of the inner shell electrons. Since there is no source of dissipative power, $\mathbf{J} \bullet \mathbf{E}$ of Eq. (10.27), to compensate for any potential change in the magnetic moments, Δm, of the inner electrons due to the ionization of the outer electron of the aluminum atom, there is a diamagnetic energy term in the ionization energy for this atom that follows from the corresponding term for the lithium atom given by Eqs. (10.15-10.24), with $Z = 13$, r_{12} given by Eq. (10.255), and r_{13} given by Eq. (10.276). Thus, the change in magnetic energy of the inner atomic orbital at r_{12} is 76.94147 %, so that the corresponding energy ΔE_{mag} is

$$\Delta E_{mag} = 0.7694147\ X\ 0.04069938\ eV = 0.0313147\ eV \tag{10.278}$$

where the magnetic energy of the inner electrons is $0.04069938\ eV$ (Eqs. (10.64) and (10.276)). Then, the ionization energy of the aluminum atom is given by Eqs. (10.276-10.278):

$$E(ionization;\ Al) = \frac{(Z-12)e^2}{8\pi\varepsilon_0 r_{13}} + \Delta E_{mag} = 5.95270\ eV + 0.031315\ eV = 5.98402\ eV \tag{10.279}$$

The experimental ionization energy of the boron atom is $5.98577\ eV$ [3].

THE IONIZATION ENERGIES OF THIRTEEN-ELECTRON ATOMS WITH A NUCLEAR CHARGE Z>13

Thirteen-electron atoms having $Z > 13$ possess an external electric field given by Eq. (10.92). In this case, an energy minimum is achieved with conservation of momentum when the orbital angular momentum is such that $\mathbf{F}_{diamagnetic}$ is minimized while $\mathbf{F}_{mag\ 2}$ is maximized. From Eq. (10.258), the diamagnetic force, $\mathbf{F}_{diamagnetic}$, is given by the sum of the contributions from the 2 p_x, p_y, and p_z orbitals corresponding to m = 1, -1, and 0, respectively:

$$\mathbf{F}_{diamagnetic} = -\left(\frac{2}{3} + \frac{2}{3} + \frac{1}{3}\right)\frac{\hbar^2}{4 m_e r_{13}^2 r_{12}}\sqrt{s(s+1)}\mathbf{i}_{\mathbf{r}} = -\left(\frac{5}{3}\right)\frac{\hbar^2}{4 m_e r_{13}^2 r_{12}}\sqrt{s(s+1)}\mathbf{i}_{\mathbf{r}} \tag{10.280}$$

wherein the contribution due to the 3 p_x (m = 1) is canceled by the mirror charge-density wave with m = -1 induced in the 3s orbital according to Eq. (10.258).

With $Z > 13$, the charge induction forms complementary mirror charge-density waves such that the angular momenta do not cancel. The filled 2p orbitals with the maintenance of symmetry according to Eq. (10.72) requires that the diamagnetic force is due to the electrons at r_{10} acting on the electrons at r_{12} which complies with the reactive force, $\mathbf{F}_{diamagnetic\ 2}$, given by Eq. (10.249). From Eq. (10.261), $\mathbf{F}_{mag\ 2}$ is:

$$\mathbf{F}_{mag\ 2} = (4+4+4)\frac{1}{Z}\frac{\hbar^2}{m_e r_{13}^2 r_{12}}\sqrt{s(s+1)}\mathbf{i}_{\mathbf{r}} = \frac{1}{Z}\frac{12\hbar^2}{m_e r_{13}^2 r_{12}}\sqrt{s(s+1)}\mathbf{i}_{\mathbf{r}} \tag{10.281}$$

corresponding to the spin and orbital angular momenta of the paired 2 p_x, p_y, and p_z electrons wherein the contribution due to the 3 p_x (m = 1) is canceled by the mirror charge-density wave with $m = -1$ induced in the 3s orbital according to Eq. (10.262).

The diamagnetic force, $\mathbf{F}_{diamagnetic\ 2}$, due to the binding of the 3p-orbital electron having an electric field outside of its radius is given by Eq. (10.268):

$$\mathbf{F}_{diamagnetic\ 2} = -\left[\frac{Z-13}{Z-12}\right]\left(1 - \frac{\sqrt{2}}{2} + \frac{1}{2}\right)\frac{r_{12}\hbar^2}{m_e r_{13}^4}10\sqrt{s(s+1)}\mathbf{i}_{\mathbf{r}} \tag{10.282}$$

In the case that $Z > 13$, the radius of the outer electron is calculated by equating the outward centrifugal force to the sum

of the electric (Eq. (10.270)) and diamagnetic (Eqs. (10.280) and (10.282)), and paramagnetic (Eq. (10.281)) forces as follows:

$$\frac{m_e v_{13}^2}{r_{13}} = \frac{(Z-12)e^2}{4\pi\varepsilon_0 r_{13}^2} - \frac{5\hbar^2}{12 m_e r_{13}^2 r_{12}}\sqrt{s(s+1)} + \frac{12\hbar^2}{Z m_e r_{13}^2 r_{12}}\sqrt{s(s+1)}$$
$$-\left[\frac{Z-13}{Z-12}\right]\left(1-\frac{\sqrt{2}}{2}+\frac{1}{2}\right)\frac{r_{12}\hbar^2}{r_{13}^4 m_e}10\sqrt{s(s+1)} \tag{10.283}$$

Substitution of $v_{13} = \dfrac{\hbar}{m_e r_{13}}$ (Eq. (1.35)) and $s = \dfrac{1}{2}$ into Eq. (10.283) gives:

$$\frac{\hbar^2}{m_e r_{13}^3} = \frac{(Z-12)e^2}{4\pi\varepsilon_0 r_{13}^2} - \frac{5\hbar^2}{12 m_e r_{13}^2 r_{12}}\sqrt{\frac{3}{4}} + \frac{12\hbar^2}{Z m_e r_{13}^2 r_{12}}\sqrt{\frac{3}{4}} - \left[\frac{Z-13}{Z-12}\right]\left(1-\frac{\sqrt{2}}{2}+\frac{1}{2}\right)\frac{r_{12}\hbar^2}{r_{13}^4 m_e}10\sqrt{\frac{3}{4}} \tag{10.284}$$

The quadratic equation corresponding to Eq. (10.284) is:

$$\left(\frac{(Z-12)e^2}{4\pi\varepsilon_0} - \left(\frac{5}{12}-\frac{12}{Z}\right)\frac{\hbar^2}{m_e r_{12}}\sqrt{\frac{3}{4}}\right)r_{13}^2 - \frac{\hbar^2}{m_e}r_{13} - \left[\frac{Z-13}{Z-12}\right]\left(1-\frac{\sqrt{2}}{2}+\frac{1}{2}\right)\frac{r_{12}\hbar^2}{m_e}10\sqrt{\frac{3}{4}} = 0 \tag{10.285}$$

$$r_{13}^2 - \frac{\dfrac{\hbar^2}{m_e}}{\left(\dfrac{(Z-12)e^2}{4\pi\varepsilon_0} - \left(\dfrac{5}{12}-\dfrac{12}{Z}\right)\dfrac{\hbar^2}{m_e r_{12}}\sqrt{\dfrac{3}{4}}\right)}r_{13} - \frac{\left[\dfrac{Z-13}{Z-12}\right]\left(1-\dfrac{\sqrt{2}}{2}+\dfrac{1}{2}\right)\dfrac{r_{12}\hbar^2}{m_e}10\sqrt{\dfrac{3}{4}}}{\left(\dfrac{(Z-12)e^2}{4\pi\varepsilon_o} - \left(\dfrac{5}{12}-\dfrac{12}{Z}\right)\dfrac{\hbar^2}{m_e r_{12}}\sqrt{\dfrac{3}{4}}\right)} = 0 \tag{10.286}$$

The solution of Eq. (10.286) using the quadratic formula is:

$$r_{13} = \frac{\dfrac{\dfrac{\hbar^2}{m_e}}{\left(\dfrac{(Z-12)e^2}{4\pi\varepsilon_0} - \left(\dfrac{5}{12}-\dfrac{12}{Z}\right)\dfrac{\hbar^2}{m_e r_{12}}\sqrt{\dfrac{3}{4}}\right)} \pm \sqrt{\left(\dfrac{\dfrac{\hbar^2}{m_e}}{\left(\dfrac{(Z-12)e^2}{4\pi\varepsilon_0} - \left(\dfrac{5}{12}-\dfrac{12}{Z}\right)\dfrac{\hbar^2}{m_e r_{12}}\sqrt{\dfrac{3}{4}}\right)}\right)^2 + 4\dfrac{\dfrac{\hbar^2}{m_e}\left[\dfrac{Z-13}{Z-12}\right]\left(1-\dfrac{\sqrt{2}}{2}+\dfrac{1}{2}\right)r_{12}10\sqrt{\dfrac{3}{4}}}{\left(\dfrac{(Z-12)e^2}{4\pi\varepsilon_0} - \left(\dfrac{5}{12}-\dfrac{12}{Z}\right)\dfrac{\hbar^2}{m_e r_{12}}\sqrt{\dfrac{3}{4}}\right)}}}{2} \tag{10.287}$$

$$r_{13} = \frac{\dfrac{a_0}{\left((Z-12) - \left(\dfrac{5}{24}-\dfrac{6}{Z}\right)\dfrac{\sqrt{3}}{r_{12}}\right)} \pm a_0\sqrt{\left(\dfrac{1}{\left((Z-12) - \left(\dfrac{5}{24}-\dfrac{6}{Z}\right)\dfrac{\sqrt{3}}{r_{12}}\right)}\right)^2 + \dfrac{20\sqrt{3}\left(\left[\dfrac{Z-13}{Z-12}\right]\left(1-\dfrac{\sqrt{2}}{2}+\dfrac{1}{2}\right)r_{12}\right)}{\left((Z-12) - \left(\dfrac{5}{24}-\dfrac{6}{Z}\right)\dfrac{\sqrt{3}}{r_{12}}\right)}}}{2}, \; r_{12} \text{ in units of } a_0 \tag{10.288}$$

where r_{12} is given by Eq. (10.255). The positive root of Eq. (10.288) must be taken in order that $r_{13} > 0$. The radii of several thirteen-electron atoms are given in Table 10.12.

The ionization energies for the thirteen-electron atoms with $Z > 13$ are given by the electric energy, $E(electric)$, (Eq. (10.102) with the radii, r_{13}, given by Eq. (10.288)).

$$E(Ionization) = -Electric\ Energy = \frac{(Z-12)e^2}{8\pi\varepsilon_0 r_{13}} \tag{10.289}$$

Since the relativistic corrections were small, the nonrelativistic ionization energies for experimentally measured thirteen-electron

atoms are given in Table 10.12.

Table 10.12. Ionization energies for some thirteen-electron atoms.

13 e Atom	Z	r_1 (a_o) [a]	r_3 (a_o) [b]	r_{10} (a_o) [c]	r_{12} (a_o) [d]	r_{13} (a_o) [e]	Theoretical Ionization Energies [f] (eV)	Experimental Ionization Energies [g] (eV)	Relative Error [h]
Al	13	0.07778	0.33923	0.45620	1.41133	2.28565	5.98402	5.98577	0.0003
Si^{+}	14	0.07216	0.31274	0.40978	1.25155	1.5995	17.0127	16.34585	-0.0408
P^{2+}	15	0.06730	0.29010	0.37120	1.09443	1.3922	29.3195	30.2027	0.0292
S^{3+}	16	0.06306	0.27053	0.33902	0.96729	1.1991	45.3861	47.222	0.0389
Cl^{4+}	17	0.05932	0.25344	0.31190	0.86545	1.0473	64.9574	67.8	0.0419
Ar^{5+}	18	0.05599	0.23839	0.28878	0.78276	0.9282	87.9522	91.009	0.0336
K^{6+}	19	0.05302	0.22503	0.26884	0.71450	0.8330	114.3301	117.56	0.0275
Ca^{7+}	20	0.05035	0.21308	0.25149	0.65725	0.7555	144.0664	147.24	0.0216
Sc^{8+}	21	0.04794	0.20235	0.23625	0.60857	0.6913	177.1443	180.03	0.0160
Ti^{9+}	22	0.04574	0.19264	0.22276	0.56666	0.6371	213.5521	215.92	0.0110
V^{10+}	23	0.04374	0.18383	0.21074	0.53022	0.5909	253.2806	255.7	0.0095
Cr^{11+}	24	0.04191	0.17579	0.19995	0.49822	0.5510	296.3231	298.0	0.0056
Mn^{12+}	25	0.04022	0.16842	0.19022	0.46990	0.5162	342.6741	343.6	0.0027
Fe^{13+}	26	0.03867	0.16165	0.18140	0.44466	0.4855	392.3293	392.2	-0.0003
Co^{14+}	27	0.03723	0.15540	0.17336	0.42201	0.4583	445.2849	444	-0.0029
Ni^{15+}	28	0.03589	0.14961	0.16601	0.40158	0.4341	501.5382	499	-0.0051
Cu^{16+}	29	0.03465	0.14424	0.15926	0.38305	0.4122	561.0867	557	-0.0073
Zn^{17+}	30	0.03349	0.13925	0.15304	0.36617	0.3925	623.9282	619	-0.0080

[a] Radius of the paired 1s inner electrons of thirteen-electron atoms from Eq. (10.51).

[b] Radius of the paired 2s inner electrons of thirteen-electron atoms from Eq. (10.62).

[c] Radius of the three sets of paired 2p inner electrons of thirteen-electron atoms from Eq. (10.212).

[d] Radius of the paired 3s inner electrons of thirteen-electron atoms from Eq. (10.255).

[e] Radius of the unpaired 3p outer electron of thirteen-electron atoms from Eq. (10.288) for $Z > 13$ and Eq. (10.276) for *Al*.

[f] Calculated ionization energies of thirteen-electron atoms given by the electric energy (Eq. (10.289)) for $Z > 13$ and Eq. (10.279) for *Al*.

[g] From theoretical calculations, interpolation of isoelectronic and spectral series, and experimental data [2-3].

[h] (Experimental-theoretical)/experimental.

The agreement between the experimental and calculated values of Table 10.12 is well within the experimental capability of the spectroscopic determinations including the values at large Z, which relies on X-ray spectroscopy. In this case, the experimental capability is three to four significant figures, which is consistent with the last column. The aluminum atom isoelectronic series is given in Table 10.12 [2-3] to much higher precision than the capability of X-ray spectroscopy, but these values are based on theoretical and interpolation techniques rather than data alone. Ionization energies are difficult to determine since the cut-off of the Rydberg series of lines at the ionization energy is often not observed, and the ionization energy must be determined from theoretical calculations, interpolation of Al isoelectronic and Rydberg series, as well as direct experimental data.

FOURTEEN-ELECTRON ATOMS

Fourteen-electron atoms can be solved exactly using the results of the solutions of one, two, three, four, five, six, seven, eight, nine, ten, eleven, twelve, and thirteen-electron atoms.

RADIUS AND IONIZATION ENERGY OF THE OUTER ELECTRON OF THE SILICON ATOM

For each thirteen-electron atom having a central charge of Z times that of the proton, there are two indistinguishable spin-paired electrons in an atomic orbital with radii r_1 and r_2 both given by Eq. (7.35) (Eq. (10.51)), two indistinguishable spin-paired electrons in an atomic orbital with radii r_3 and r_4 both given by Eq. (10.62), three sets of paired electrons in an atomic orbital at r_{10} given by Eq. (10.212), two indistinguishable spin-paired electrons in an atomic orbital with radii r_{11} and r_{12} both given by Eq. (10.255), and an unpaired electron in an atomic orbital with radius r_{13} given by Eq. (10.288). For $Z \geq 14$, the next electron which binds to form the corresponding fourteen-electron atom is attracted by the central Coulomb field and is repelled by diamagnetic forces due to the 3 sets of spin-paired inner 2p electrons and two spin-paired inner 3s electrons. A paramagnetic spin-pairing force to form a filled s orbital is also possible, but the force due to the spin-pairing of the electrons (Eq. (7.24) with the radius r_{14}) reduces the energy of the atom less than that due to the alternative forces on two unpaired 3p electrons in an atomic orbital at the same radius r_{14}. The resulting electron configuration is $1s^2 2s^2 2p^6 3s^2 3p^2$, and the orbital arrangement is:

3p state

↑	↑	
1	0	-1

(10.290)

corresponding to the ground state ${}^3P_0$.

The central Coulomb force acts on the outer electron to cause it to bind wherein this electric force on the outer-most electron due to the nucleus and the inner thirteen electrons is given by Eq. (10.70) with the appropriate charge and radius:

$$\mathbf{F}_{ele} = \frac{(Z-13)e^2}{4\pi\varepsilon_0 r_{14}^2}\mathbf{i}_\mathbf{r} \tag{10.291}$$

for $r > r_{13}$.

As in the case of the carbon atom given in the Six-Electron Atom section, the two orthogonal 3p electrons form charge-density waves such that the total angular momentum of the two outer electrons is conserved which determines the diamagnetic force according to Eq. (10.82) (Eq. (10.258)). The contribution is given by Eq. (10.117) corresponding to $m = 1$. In addition, the contribution of the diamagnetic force, $\mathbf{F}_{diamagnetic}$, due to the 2p electrons is given by Eq. (10.105) (Eq. (10.259)) as the sum of the contributions from the 2 p_x, p_y, and p_z orbitals corresponding to m = 1, -1, and 0, respectively. Thus, $\mathbf{F}_{diamagnetic}$ is given by:

$$\mathbf{F}_{diamagnetic} = -\left(\frac{2}{3}+\frac{2}{3}+\frac{2}{3}+\frac{1}{3}\right)\frac{\hbar^2}{4m_e r_{14}^2 r_{12}}\sqrt{s(s+1)}\mathbf{i}_\mathbf{r} = -\left(\frac{7}{3}\right)\frac{\hbar^2}{4m_e r_{14}^2 r_{12}}\sqrt{s(s+1)}\mathbf{i}_\mathbf{r} \tag{10.292}$$

The charge induction forms complementary mirror charge-density waves which must have opposing angular momenta such that momentum is conserved. In this case, $\mathbf{F}_{mag\ 2}$ given by Eq. (10.89) (Eq. (10.260)) is zero:

$$\mathbf{F}_{mag\ 2} = 0 \tag{10.293}$$

The outward centrifugal force on electron 14 is balanced by the electric force and the magnetic forces (on electron 14). The radius of the outer electron is calculated by equating the outward centrifugal force to the sum of the electric (Eq. (10.291)) and diamagnetic (Eq. (10.292)) forces as follows:

$$\frac{m_e v_{14}^2}{r_{14}} = \frac{(Z-13)e^2}{4\pi\varepsilon_0 r_{14}^2} - \frac{7\hbar^2}{12m_e r_{14}^2 r_{12}}\sqrt{s(s+1)} \tag{10.294}$$

Substitution of $v_{14} = \frac{\hbar}{m_e r_{14}}$ (Eq. (1.35)) and $s = \frac{1}{2}$ into Eq. (10.294) gives:

$$\frac{\hbar^2}{m_e r_{14}^3} = \frac{(Z-13)e^2}{4\pi\varepsilon_0 r_{14}^2} - \frac{7\hbar^2}{12m_e r_{14}^2 r_{12}}\sqrt{s(s+1)} \tag{10.295}$$

$$r_{14} = \frac{a_0}{\left((Z-13) - \frac{7\sqrt{\frac{3}{4}}}{12r_{12}}\right)},\ r_{12}\ \textit{in units of}\ a_0 \tag{10.296}$$

Substitution of $\frac{r_{12}}{a_0} = 1.25155$ (Eq. (10.255) with $Z = 14$) into Eq. (10.296) gives:

$$r_{14} = 1.67685 a_0 \tag{10.297}$$

The ionization energy of the silicon atom is given by the electric energy, $E(electric)$, (Eq. (10.102) with the radius, r_{14}, given by Eq. (10.297)):

$$E(ionization;\ Si) = -Electric\ Energy = \frac{(Z-13)e^2}{8\pi\varepsilon_0 r_{14}} = 8.11391\ eV \tag{10.298}$$

where $r_{14} = 1.67685a_0$ (Eq. (10.297)) and $Z = 14$. The experimental ionization energy of the silicon atom is $8.15169\ eV$ [3].

THE IONIZATION ENERGIES OF FOURTEEN-ELECTRON ATOMS WITH A NUCLEAR CHARGE Z>14

Fourteen-electron atoms having $Z > 14$ possess an external electric field given by Eq. (10.92). In this case, an energy minimum is achieved with conservation of momentum when the orbital angular momentum is such that $\mathbf{F}_{diamagnetic}$ is minimized while $\mathbf{F}_{mag\ 2}$ is maximized. With a half-filled 3p shell, the diamagnetic force due to the orbital angular momenta of the 3p electrons cancels that of the 2p electrons. Thus, $\mathbf{F}_{diamagnetic}$ is minimized by the formation of a charge-density wave in the 3s orbital corresponding to $m = -1$ in Eq. (10.258) to form the equivalent of a half-filled 3p shell such that the contribution due to the 2p shell is canceled. From Eq. (10.258), the diamagnetic force, $\mathbf{F}_{diamagnetic}$, is given by the sum of the contributions from the 3 p_x and p_z orbitals corresponding to m = 1 and 0, respectively, and the negative contribution due to the charge-density wave with m = -1 induced in the 3s orbital according to Eq. (10.258):

$$\mathbf{F}_{diamagnetic} = -\left(\frac{2}{3}+\frac{1}{3}-\frac{2}{3}\right)\frac{\hbar^2}{4m_e r_{14}^2 r_{12}}\sqrt{s(s+1)}\mathbf{i}_{\mathbf{r}} = -\left(\frac{1}{3}\right)\frac{\hbar^2}{4m_e r_{14}^2 r_{12}}\sqrt{s(s+1)}\mathbf{i}_{\mathbf{r}} \tag{10.299}$$

From Eq. (10.261), $\mathbf{F}_{mag\ 2}$ corresponding to the spin and orbital angular momenta of the paired 2 p_x, p_y, and p_z electrons is:

$$\mathbf{F}_{mag\ 2} = \left(4+4+4\right)\frac{1}{Z}\frac{\hbar^2}{m_e r_{14}^2 r_{12}}\sqrt{s(s+1)}\mathbf{i}_{\mathbf{r}} = \frac{1}{Z}\frac{12\hbar^2}{m_e r_{14}^2 r_{12}}\sqrt{s(s+1)}\mathbf{i}_{\mathbf{r}} \tag{10.300}$$

and the contribution from the 3p shell is

$$\mathbf{F}_{mag\ 2} = \left(4+4-4\right)\frac{1}{Z}\frac{\hbar^2}{m_e r_{14}^2 r_{12}}\sqrt{s(s+1)}\mathbf{i}_{\mathbf{r}} = \frac{1}{Z}\frac{4\hbar^2}{m_e r_{14}^2 r_{12}}\sqrt{s(s+1)}\mathbf{i}_{\mathbf{r}} \tag{10.301}$$

corresponding to the 3 p_x and p_z electrons wherein the contribution due to the 3 p_x (m = 1) electron is canceled by the mirror charge-density wave with $m = -1$ induced in the 3s orbital (Eq. (10.262)). Thus, the total of $\mathbf{F}_{mag\ 2}$ is

$$\mathbf{F}_{mag\ 2} = \frac{1}{Z}\frac{16\hbar^2}{m_e r_{14}^2 r_{12}}\sqrt{s(s+1)}\mathbf{i}_{\mathbf{r}} \tag{10.302}$$

The diamagnetic force, $\mathbf{F}_{diamagnetic\ 2}$, due to the binding of the 3p-orbital electron having an electric field outside of its radius is given by Eq. (10.268):

$$\mathbf{F}_{diamagnetic\ 2} = -\left[\frac{Z-14}{Z-13}\right]\left(1-\frac{\sqrt{2}}{2}+\frac{1}{2}\right)\frac{r_{12}\hbar^2}{m_e r_{14}^4}10\sqrt{s(s+1)}\mathbf{i}_{\mathbf{r}} \tag{10.303}$$

In the case that $Z > 14$, the radius of the outer electron is calculated by equating the outward centrifugal force to the sum of the electric (Eq. (10.291)), diamagnetic (Eqs. (10.299) and (10.303)), and paramagnetic (Eq. (10.302)) forces as follows:

$$\frac{m_e v_{14}^2}{r_{14}} = \frac{(Z-13)e^2}{4\pi\varepsilon_0 r_{14}^2} - \frac{\hbar^2}{12m_e r_{14}^2 r_{12}}\sqrt{s(s+1)} + \frac{16\hbar^2}{Zm_e r_{14}^2 r_{12}}\sqrt{s(s+1)} - \left[\frac{Z-14}{Z-13}\right]\left(1-\frac{\sqrt{2}}{2}+\frac{1}{2}\right)\frac{r_{12}\hbar^2}{m_e r_{14}^4}10\sqrt{s(s+1)} \tag{10.304}$$

Substitution of $v_{14} = \dfrac{\hbar}{m_e r_{14}}$ (Eq. (1.35)) and $s = \dfrac{1}{2}$ into Eq. (10.304) gives:

$$\frac{\hbar^2}{m_e r_{14}^3} = \frac{(Z-13)e^2}{4\pi\varepsilon_0 r_{14}^2} - \frac{\hbar^2}{12m_e r_{14}^2 r_{12}}\sqrt{\frac{3}{4}} + \frac{16\hbar^2}{Zm_e r_{14}^2 r_{12}}\sqrt{\frac{3}{4}} - \left[\frac{Z-14}{Z-13}\right]\left(1-\frac{\sqrt{2}}{2}+\frac{1}{2}\right)\frac{r_{12}\hbar^2}{m_e r_{14}^4}10\sqrt{\frac{3}{4}} \tag{10.305}$$

The quadratic equation corresponding to Eq. (10.305) is

$$\left(\frac{(Z-13)e^2}{4\pi\varepsilon_0} - \left(\frac{1}{12}-\frac{16}{Z}\right)\frac{\hbar^2}{m_e r_{12}}\sqrt{\frac{3}{4}}\right)r_{14}^2 - \frac{\hbar^2}{m_e}r_{14} - \left[\frac{Z-14}{Z-13}\right]\left(1-\frac{\sqrt{2}}{2}+\frac{1}{2}\right)\frac{r_{12}\hbar^2}{m_e}10\sqrt{\frac{3}{4}} = 0 \tag{10.306}$$

$$r_{14}^2 - \frac{\dfrac{\hbar^2}{m_e}}{\left(\dfrac{(Z-13)e^2}{4\pi\varepsilon_0} - \left(\dfrac{1}{12}-\dfrac{16}{Z}\right)\dfrac{\hbar^2}{m_e r_{12}}\sqrt{\dfrac{3}{4}}\right)} r_{14} - \frac{\dfrac{\hbar^2}{m_e}\left[\dfrac{Z-14}{Z-13}\right]\left(1-\dfrac{\sqrt{2}}{2}+\dfrac{1}{2}\right)r_{12}10\sqrt{\dfrac{3}{4}}}{\left(\dfrac{(Z-13)e^2}{4\pi\varepsilon_0} - \left(\dfrac{1}{12}-\dfrac{16}{Z}\right)\dfrac{\hbar^2}{m_e r_{12}}\sqrt{\dfrac{3}{4}}\right)} = 0 \tag{10.307}$$

The solution of Eq. (10.307) using the quadratic formula is:

$$r_{14} = \frac{\dfrac{\dfrac{\hbar^2}{m_e}}{\left(\dfrac{(Z-13)e^2}{4\pi\varepsilon_0} - \left(\dfrac{1}{12}-\dfrac{16}{Z}\right)\dfrac{\hbar^2}{m_e r_{12}}\sqrt{\dfrac{3}{4}}\right)} \pm \sqrt{\left(\dfrac{\dfrac{\hbar^2}{m_e}}{\left(\dfrac{(Z-13)e^2}{4\pi\varepsilon_0} - \left(\dfrac{1}{12}-\dfrac{16}{Z}\right)\dfrac{\hbar^2}{m_e r_{12}}\sqrt{\dfrac{3}{4}}\right)}\right)^2 + 4\dfrac{\dfrac{\hbar^2}{m_e}\left[\dfrac{Z-14}{Z-13}\right]\left(1-\dfrac{\sqrt{2}}{2}+\dfrac{1}{2}\right)r_{12}10\sqrt{\dfrac{3}{4}}}{\left(\dfrac{(Z-13)e^2}{4\pi\varepsilon_0} - \left(\dfrac{1}{12}-\dfrac{16}{Z}\right)\dfrac{\hbar^2}{m_e r_{12}}\sqrt{\dfrac{3}{4}}\right)}}}{2} \tag{10.308}$$

$$r_{14} = \frac{\dfrac{a_0}{\left((Z-13) - \left(\dfrac{1}{24}-\dfrac{8}{Z}\right)\dfrac{\sqrt{3}}{r_{12}}\right)} \pm a_0\sqrt{\left(\dfrac{1}{\left((Z-13) - \left(\dfrac{1}{24}-\dfrac{8}{Z}\right)\dfrac{\sqrt{3}}{r_{12}}\right)}\right)^2 + \dfrac{20\sqrt{3}\left(\left[\dfrac{Z-14}{Z-13}\right]\left(1-\dfrac{\sqrt{2}}{2}+\dfrac{1}{2}\right)r_{12}\right)}{\left((Z-13) - \left(\dfrac{1}{24}-\dfrac{8}{Z}\right)\dfrac{\sqrt{3}}{r_{12}}\right)}}}{2}, \; r_{12} \text{ in units of } a_0 \tag{10.309}$$

where r_{12} is given by Eq. (10.255). The positive root of Eq. (10.309) must be taken in order that $r_{14} > 0$. The final radius of electron 14, r_{14}, is given by Eq. (10.309); this is also the final radius of electron 13. The radii of several fourteen-electron atoms are given in Table 10.13.

The ionization energies for the fourteen-electron atoms with $Z > 14$ are given by the electric energy, $E(electric)$, (Eq. (10.102) with the radii r_{14}, given by Eq. (10.309)).

$$E(Ionization) = -Electric\ Energy = \frac{(Z-13)e^2}{8\pi\varepsilon_0 r_{14}} \tag{10.310}$$

Since the relativistic corrections were small, the nonrelativistic ionization energies for experimentally measured fourteen-electron atoms are given in Table 10.13.

Table 10.13. Ionization energies for some fourteen-electron atoms.

14 e Atom	Z	r_1 (a_o) [a]	r_3 (a_o) [b]	r_{10} (a_o) [c]	r_{12} (a_o) [d]	r_{14} (a_o) [e]	Theoretical Ionization Energies [f] (eV)	Experimental Ionization Energies [g] (eV)	Relative Error [h]
Si	14	0.07216	0.31274	0.40978	1.25155	1.67685	8.11391	8.15169	0.0046
P^{+}	15	0.06730	0.29010	0.37120	1.09443	1.35682	20.0555	19.7694	-0.0145
S^{2+}	16	0.06306	0.27053	0.33902	0.96729	1.21534	33.5852	34.790	0.0346
Cl^{3+}	17	0.05932	0.25344	0.31190	0.86545	1.06623	51.0426	53.4652	0.0453
Ar^{4+}	18	0.05599	0.23839	0.28878	0.78276	0.94341	72.1094	75.020	0.0388
K^{5+}	19	0.05302	0.22503	0.26884	0.71450	0.84432	96.6876	99.4	0.0273
Ca^{6+}	20	0.05035	0.21308	0.25149	0.65725	0.76358	124.7293	127.2	0.0194
Sc^{7+}	21	0.04794	0.20235	0.23625	0.60857	0.69682	156.2056	158.1	0.0120
Ti^{8+}	22	0.04574	0.19264	0.22276	0.56666	0.64078	191.0973	192.10	0.0052
V^{9+}	23	0.04374	0.18383	0.21074	0.53022	0.59313	229.3905	230.5	0.0048
Cr^{10+}	24	0.04191	0.17579	0.19995	0.49822	0.55211	271.0748	270.8	-0.0010
Mn^{11+}	25	0.04022	0.16842	0.19022	0.46990	0.51644	316.1422	314.4	-0.0055
Fe^{12+}	26	0.03867	0.16165	0.18140	0.44466	0.48514	364.5863	361	-0.0099
Co^{13+}	27	0.03723	0.15540	0.17336	0.42201	0.45745	416.4021	411	-0.0131
Ni^{14+}	28	0.03589	0.14961	0.16601	0.40158	0.43277	471.5854	464	-0.0163
Cu^{15+}	29	0.03465	0.14424	0.15926	0.38305	0.41064	530.1326	520	-0.0195
Zn^{16+}	30	0.03349	0.13925	0.15304	0.36617	0.39068	592.0410	579	-0.0225

[a] Radius of the paired 1s inner electrons of fourteen-electron atoms from Eq. (10.51).

[b] Radius of the paired 2s inner electrons of fourteen-electron atoms from Eq. (10.62).

[c] Radius of the three sets of paired 2p inner electrons of fourteen-electron atoms from Eq. (10.212).

[d] Radius of the paired 3s inner electrons of fourteen-electron atoms from Eq. (10.255).

[e] Radius of the two unpaired 3p outer electrons of fourteen-electron atoms from Eq. (10.309) for $Z > 14$ and Eq. (10.297) for *Si*.

[f] Calculated ionization energies of fourteen-electron atoms given by the electric energy (Eq. (10.310)).

[g] From theoretical calculations, interpolation of isoelectronic and spectral series, and experimental data [2-3].

[h] (Experimental-theoretical)/experimental.

The agreement between the experimental and calculated values of Table 10.13 is well within the experimental capability of the spectroscopic determinations including the values at large Z which relies on X-ray spectroscopy. In this case, the experimental capability is three to four significant figures which is consistent with the last column. The silicon atom isoelectronic series is given in Table 10.13 [2-3] to much higher precision than the capability of X-ray spectroscopy, but these values are based on theoretical and interpolation techniques rather than data alone. Ionization energies are difficult to determine since the cut-off of the Rydberg series of lines at the ionization energy is often not observed, and the ionization energy must be determined from theoretical calculations, interpolation of Si isoelectronic and Rydberg series, as well as direct experimental data.

FIFTEEN-ELECTRON ATOMS

Fifteen-electron atoms can be solved exactly using the results of the solutions of one, two, three, four, five, six, seven, eight, nine, ten, eleven, twelve, thirteen and fourteen-electron atoms.

RADIUS AND IONIZATION ENERGY OF THE OUTER ELECTRON OF THE PHOSPHOROUS ATOM

For each fourteen-electron atom having a central charge of Z times that of the proton, there are two indistinguishable spin-paired electrons in an atomic orbital with radii r_1 and r_2 both given by Eq. (7.35) (Eq. (10.51)), two indistinguishable spin-paired electrons in an atomic orbital with radii r_3 and r_4 both given by Eq. (10.62), three sets of paired electrons in an atomic orbital at r_{10} given by Eq. (10.212), two indistinguishable spin-paired electrons in an atomic orbital with radii r_{11} and r_{12} both given by Eq. (10.255), and two unpaired electrons in an atomic orbital with radius r_{14} given by Eq. (10.288). For $Z \geq 15$, the next electron which binds to form the corresponding fifteen-electron atom is attracted by the central Coulomb field and is repelled by diamagnetic forces due to the 3 sets of spin-paired inner 2p electrons and two spin-paired inner 3s electrons. A paramagnetic spin-pairing force to form a filled s orbital is also possible, but the force due to the spin-pairing of the electrons (Eq. (7.24) with the radius r_{15}) reduces the energy of the atom less than that due to the alternative forces on three unpaired 3p electrons in an atomic orbital at the same radius r_{15}. The resulting electron configuration is $1s^2 2s^2 2p^6 3s^2 3p^3$, and the orbital arrangement is

3p state

$$\underset{1}{\uparrow} \quad \underset{0}{\uparrow} \quad \underset{-1}{\uparrow} \tag{10.311}$$

corresponding to the ground state ${}^4S^0_{3/2}$.

The central Coulomb force acts on the outer electron to cause it to bind wherein this electric force on the outer-most electron due to the nucleus and the inner fourteen electrons is given by Eq. (10.70) with the appropriate charge and radius:

$$\mathbf{F}_{ele} = \frac{(Z-14)e^2}{4\pi\varepsilon_0 r_{15}^2}\mathbf{i}_\mathbf{r} \tag{10.312}$$

for $r > r_{14}$.

The diamagnetic force, $\mathbf{F}_{diamagnetic}$, is only due to 3p and 3s electrons when the 3p shell is at least half filled since the induced charge-density waves only involve the inner-most shell, the 3s orbital. Thus, $\mathbf{F}_{diamagnetic}$, is given by Eq. (10.259) as the sum of the contributions from the 3 p_x, p_y, and p_z orbitals corresponding to m = 1, -1, and 0, respectively:

$$\mathbf{F}_{diamagnetic} = -\left(\frac{2}{3}+\frac{2}{3}+\frac{1}{3}\right)\frac{\hbar^2}{4m_e r_{15}^2 r_{12}}\sqrt{s(s+1)}\mathbf{i}_\mathbf{r} = -\left(\frac{5}{3}\right)\frac{\hbar^2}{4m_e r_{15}^2 r_{12}}\sqrt{s(s+1)}\mathbf{i}_\mathbf{r} \tag{10.313}$$

The energy is minimized with conservation of angular momentum when the spin angular momentum of the 3s orbital superimposes negatively with the orbital angular momentum of the 3p orbitals. From Eq. (10.260), $\mathbf{F}_{mag\ 2}$ corresponding to the orbital angular momentum of the 3 p_x, p_y, and p_z orbitals minus the contribution from the 3s orbital is

$$\mathbf{F}_{mag\ 2} = (1+1+1-1)\frac{1}{Z}\frac{\hbar^2}{m_e r_{15}^2 r_{12}}\sqrt{s(s+1)}\mathbf{i}_\mathbf{r} = \frac{1}{Z}\frac{2\hbar^2}{m_e r_{15}^2 r_{12}}\sqrt{s(s+1)}\mathbf{i}_\mathbf{r} \tag{10.314}$$

The outward centrifugal force on electron 15 is balanced by the electric force and the magnetic forces (on electron 15). The radius of the outer electron is calculated by equating the outward centrifugal force to the sum of the electric (Eq. (10.312)), diamagnetic (Eq. (10.313)), and paramagnetic (Eq. (10.314)) forces as follows:

$$\frac{m_e v_{15}^2}{r_{15}} = \frac{(Z-14)e^2}{4\pi\varepsilon_0 r_{15}^2} - \frac{5\hbar^2}{12m_e r_{15}^2 r_{12}}\sqrt{s(s+1)} + \frac{2\hbar^2}{Zm_e r_{15}^2 r_{12}}\sqrt{s(s+1)} \tag{10.315}$$

Substitution of $v_{15} = \dfrac{\hbar}{m_e r_{15}}$ (Eq. (1.35)) and $s = \dfrac{1}{2}$ into Eq. (10.315) gives:

$$\frac{\hbar^2}{m_e r_{15}^3} = \frac{(Z-14)e^2}{4\pi\varepsilon_0 r_{15}^2} - \frac{5\hbar^2}{12m_e r_{15}^2 r_{12}}\sqrt{\frac{3}{4}} + \frac{2\hbar^2}{Zm_e r_{15}^2 r_{12}}\sqrt{\frac{3}{4}} \tag{10.316}$$

$$r_{15} = \frac{\dfrac{\hbar^2}{m_e}}{\dfrac{(Z-14)e^2}{4\pi\varepsilon_0} - \dfrac{5\hbar^2}{12m_e r_{12}}\sqrt{\dfrac{3}{4}} + \dfrac{2\hbar^2}{Zm_e r_{12}}\sqrt{\dfrac{3}{4}}} \tag{10.317}$$

$$r_{15} = \frac{a_0}{(Z-14) - \left(\dfrac{5}{12}-\dfrac{2}{Z}\right)\dfrac{\sqrt{\dfrac{3}{4}}}{r_{12}}},\ r_{12}\ in\ units\ of\ a_0 \tag{10.318}$$

Substitution of $\dfrac{r_{12}}{a_0} = 1.09443$ (Eq. (10.255) with $Z = 15$) into Eq. (10.318) gives:

$$r_{15} = 1.28900 a_0 \tag{10.319}$$

The ionization energy of the phosphorous atom is given by the electric energy, $E(electric)$, (Eq. (10.102) with the radius, r_{15}, given by Eq. (10.319)):

$$E(ionization;\ P) = -Electric\ Energy = \frac{(Z-14)e^2}{8\pi\varepsilon_0 r_{15}} = 10.5554\ eV \tag{10.320}$$

where $r_{15} = 1.28900 a_0$ (Eq. (10.319)) and $Z = 15$. The experimental ionization energy of the phosphorous atom is 10.48669 eV [3].

THE IONIZATION ENERGIES OF FIFTEEN-ELECTRON ATOMS WITH A NUCLEAR CHARGE Z>15

Fifteen-electron atoms having $Z>15$ possess an external electric field given by Eq. (10.92). In this case, an energy minimum is achieved with conservation of momentum when the orbital angular momentum is such that $\mathbf{F}_{diamagnetic}$ is minimized while $\mathbf{F}_{mag\ 2}$ is maximized. With a half-filled 3p shell, the diamagnetic force due to the orbital angular momenta of the 3p electrons cancels that of the 2p electrons. Thus, the diamagnetic force (Eq. (10.258)), $\mathbf{F}_{diamagnetic}$, is zero:

$$\mathbf{F}_{diamagnetic}=0 \tag{10.321}$$

From Eqs. (10.205) and (10.261), $\mathbf{F}_{mag\ 2}$ corresponding to the spin and orbital angular momenta of the paired 2 p_x, p_y, and p_z electrons is:

$$\mathbf{F}_{mag\ 2}=\left(4+4+4\right)\frac{1}{Z}\frac{\hbar^2}{m_e r_{15}^2 r_{12}}\sqrt{s(s+1)}\mathbf{i}_{\mathbf{r}}=\frac{1}{Z}\frac{12\hbar^2}{m_e r_{15}^2 r_{12}}\sqrt{s(s+1)}\mathbf{i}_{\mathbf{r}} \tag{10.322}$$

and the contribution from the 3p level is:

$$\mathbf{F}_{mag\ 2}=\left(4+4+4\right)\frac{1}{Z}\frac{\hbar^2}{m_e r_{15}^2 r_{12}}\sqrt{s(s+1)}\mathbf{i}_{\mathbf{r}}=\frac{1}{Z}\frac{12\hbar^2}{m_e r_{15}^2 r_{12}}\sqrt{s(s+1)}\mathbf{i}_{\mathbf{r}} \tag{10.323}$$

corresponding to the 3 p_x, p_y, and p_z electrons. Thus, the total of $\mathbf{F}_{mag\ 2}$ is:

$$\mathbf{F}_{mag\ 2}=\frac{1}{Z}\frac{24\hbar^2}{m_e r_{15}^2 r_{12}}\sqrt{s(s+1)}\mathbf{i}_{\mathbf{r}} \tag{10.324}$$

The diamagnetic force, $\mathbf{F}_{diamagnetic\ 2}$, due to the binding of the 3p-orbital electron having an electric field outside of its radius is given by Eq. (10.268):

$$\mathbf{F}_{diamagnetic\ 2}=-\left[\frac{Z-15}{Z-14}\right]\left(1-\frac{\sqrt{2}}{2}+\frac{1}{2}\right)\frac{r_{12}\hbar^2}{m_e r_{15}^4}10\sqrt{s(s+1)}\mathbf{i}_{\mathbf{r}} \tag{10.325}$$

In the case that $Z>15$, the radius of the outer electron is calculated by equating the outward centrifugal force to the sum of the electric (Eq. (10.312)), diamagnetic (Eqs. (10.321) and (10.325)), and paramagnetic (Eq. (10.324)) forces as follows:

$$\frac{m_e v_{15}^2}{r_{15}}=\frac{(Z-14)e^2}{4\pi\varepsilon_0 r_{15}^2}+\frac{24\hbar^2}{Zm_e r_{15}^2 r_{12}}\sqrt{s(s+1)}-\left[\frac{Z-15}{Z-14}\right]\left(1-\frac{\sqrt{2}}{2}+\frac{1}{2}\right)\frac{r_{12}\hbar^2}{m_e r_{15}^4}10\sqrt{s(s+1)} \tag{10.326}$$

Substitution of $v_{15}=\dfrac{\hbar}{m_e r_{15}}$ (Eq. (1.35)) and $s=\dfrac{1}{2}$ into Eq. (10.326) gives:

$$\frac{\hbar^2}{m_e r_{15}^3}=\frac{(Z-14)e^2}{4\pi\varepsilon_0 r_{15}^2}+\frac{24\hbar^2}{Zm_e r_{15}^2 r_{12}}\sqrt{\frac{3}{4}}-\left[\frac{Z-15}{Z-14}\right]\left(1-\frac{\sqrt{2}}{2}+\frac{1}{2}\right)\frac{r_{12}\hbar^2}{m_e r_{15}^4}10\sqrt{\frac{3}{4}} \tag{10.327}$$

The quadratic equation corresponding to Eq. (10.327) is:

$$\left(\frac{(Z-14)e^2}{4\pi\varepsilon_0}+\frac{24\hbar^2}{Zm_e r_{12}}\sqrt{\frac{3}{4}}\right)r_{15}^2-\frac{\hbar^2}{m_e}r_{15}-\left[\frac{Z-15}{Z-14}\right]\left(1-\frac{\sqrt{2}}{2}+\frac{1}{2}\right)\frac{r_{12}\hbar^2}{m_e}10\sqrt{\frac{3}{4}}=0 \tag{10.328}$$

$$r_{15}^2-\frac{\dfrac{\hbar^2}{m_e}}{\left(\dfrac{(Z-14)e^2}{4\pi\varepsilon_0}+\dfrac{24\hbar^2}{Zm_e r_{12}}\sqrt{\dfrac{3}{4}}\right)}r_{15}-\frac{\dfrac{\hbar^2}{m_e}\left[\dfrac{Z-15}{Z-14}\right]\left(1-\dfrac{\sqrt{2}}{2}+\dfrac{1}{2}\right)r_{12}10\sqrt{\dfrac{3}{4}}}{\left(\dfrac{(Z-14)e^2}{4\pi\varepsilon_0}-\dfrac{24\hbar^2}{Zm_e r_{12}}\sqrt{\dfrac{3}{4}}\right)}=0 \tag{10.329}$$

The solution of Eq. (10.329) using the quadratic formula is:

$$r_{15}=\frac{\dfrac{\dfrac{\hbar^2}{m_e}}{\left(\dfrac{(Z-14)e^2}{4\pi\varepsilon_0}+\dfrac{24\hbar^2}{Zm_e r_{12}}\sqrt{\dfrac{3}{4}}\right)}\pm\sqrt{\left(\dfrac{\dfrac{\hbar^2}{m_e}}{\left(\dfrac{(Z-14)e^2}{4\pi\varepsilon_0}+\dfrac{24\hbar^2}{Zm_e r_{12}}\sqrt{\dfrac{3}{4}}\right)}\right)^2+4\dfrac{\dfrac{\hbar^2}{m_e}\left[\dfrac{Z-15}{Z-14}\right]\left(1-\dfrac{\sqrt{2}}{2}+\dfrac{1}{2}\right)r_{12}10\sqrt{\dfrac{3}{4}}}{\left(\dfrac{(Z-14)e^2}{4\pi\varepsilon_0}+\dfrac{24\hbar^2}{Zm_e r_{12}}\sqrt{\dfrac{3}{4}}\right)}}}{2} \tag{10.330}$$

$$r_{15}=\frac{\dfrac{a_0}{\left((Z-14)+\dfrac{12\sqrt{3}}{Zr_{12}}\right)}\pm a_0\sqrt{\left(\dfrac{1}{\left((Z-14)+\dfrac{12\sqrt{3}}{Zr_{12}}\right)}\right)^2+\dfrac{20\sqrt{3}\left(\left[\dfrac{Z-15}{Z-14}\right]\left(1-\dfrac{\sqrt{2}}{2}+\dfrac{1}{2}\right)r_{12}\right)}{\left((Z-14)+\dfrac{12\sqrt{3}}{Zr_{12}}\right)}}}{2},\ r_{12}\ in\ units\ of\ a_0 \tag{10.331}$$

where r_{12} is given by Eq. (10.255). The positive root of Eq. (10.331) must be taken in order that $r_{15}>0$. The final radius of electron 15, r_{15}, is given by Eq. (10.331); this is also the final radius of electrons 13 and 14. The radii of several fifteen-electron atoms are given in Table 10.14.

The ionization energies for the fifteen-electron atoms with $Z>15$ are given by the electric energy, $E(electric)$, (Eq. (10.102) with the radii r_{15}, given by Eq. (10.331)):

$$E(Ionization)=-Electric\ Energy=\frac{(Z-14)e^2}{8\pi\varepsilon_0 r_{15}} \tag{10.332}$$

Since the relativistic corrections were small, the nonrelativistic ionization energies for experimentally measured fifteen-electron atoms are given in Table 10.14.

Table 10.14. Ionization energies for some fifteen-electron atoms.

15 e Atom	Z	r_1 (a_o) [a]	r_3 (a_o) [b]	r_{10} (a_o) [c]	r_{12} (a_o) [d]	r_{15} (a_o) [e]	Theoretical Ionization Energies [f] (eV)	Experimental Ionization Energies [g] (eV)	Relative Error [h]
P	15	0.06730	0.29010	0.37120	1.09443	1.28900	10.55536	10.48669	-0.0065
S^+	16	0.06306	0.27053	0.33902	0.96729	1.15744	23.5102	23.3379	-0.0074
Cl^{2+}	17	0.05932	0.25344	0.31190	0.86545	1.06759	38.2331	39.61	0.0348
Ar^{3+}	18	0.05599	0.23839	0.28878	0.78276	0.95423	57.0335	59.81	0.0464
K^{4+}	19	0.05302	0.22503	0.26884	0.71450	0.85555	79.5147	82.66	0.0381
Ca^{5+}	20	0.05035	0.21308	0.25149	0.65725	0.77337	105.5576	108.78	0.0296
Sc^{6+}	21	0.04794	0.20235	0.23625	0.60857	0.70494	135.1046	138.0	0.0210
Ti^{7+}	22	0.04574	0.19264	0.22276	0.56666	0.64743	168.1215	170.4	0.0134
V^{8+}	23	0.04374	0.18383	0.21074	0.53022	0.59854	204.5855	205.8	0.0059
Cr^{9+}	24	0.04191	0.17579	0.19995	0.49822	0.55652	244.4799	244.4	-0.0003
Mn^{10+}	25	0.04022	0.16842	0.19022	0.46990	0.52004	287.7926	286.0	-0.0063
Fe^{11+}	26	0.03867	0.16165	0.18140	0.44466	0.48808	334.5138	330.8	-0.0112
Co^{12+}	27	0.03723	0.15540	0.17336	0.42201	0.45985	384.6359	379	-0.0149
Ni^{13+}	28	0.03589	0.14961	0.16601	0.40158	0.43474	438.1529	430	-0.0190
Cu^{14+}	29	0.03465	0.14424	0.15926	0.38305	0.41225	495.0596	484	-0.0229
Zn^{15+}	30	0.03349	0.13925	0.15304	0.36617	0.39199	555.3519	542	-0.0246

[a] Radius of the paired 1s inner electrons of fifteen-electron atoms from Eq. (10.51).

[b] Radius of the paired 2s inner electrons of fifteen-electron atoms from Eq. (10.62).

[c] Radius of the three sets of paired 2p inner electrons of fifteen-electron atoms from Eq. (10.212).

[d] Radius of the paired 3s inner electrons of fifteen-electron atoms from Eq. (10.255).

[e] Radius of the three unpaired 3p outer electrons of fifteen-electron atoms from Eq. (10.331) for $Z>15$ and Eq. (10.319) for P.

[f] Calculated ionization energies of fifteen-electron atoms given by the electric energy (Eq. (10.332)).

[g] From theoretical calculations, interpolation of isoelectronic and spectral series, and experimental data [2-3].

[h] (Experimental-theoretical)/experimental.

The agreement between the experimental and calculated values of Table 10.14 is well within the experimental capability of the spectroscopic determinations including the values at large Z which relies on X-ray spectroscopy. In this case, the experimental capability is three to four significant figures which is consistent with the last column. The phosphorous atom isoelectronic series is given in Table 10.14 [2-3] to much higher precision than the capability of X-ray spectroscopy, but these values are based on theoretical and interpolation techniques rather than data alone. Ionization energies are difficult to determine since the cut-off of the Rydberg series of lines at the ionization energy is often not observed, and the ionization energy must be determined from theoretical calculations, interpolation of P isoelectronic and Rydberg series, as well as direct experimental data.

SIXTEEN-ELECTRON ATOMS

Sixteen-electron atoms can be solved exactly using the results of the solutions of one, two, three, four, five, six, seven, eight, nine, ten, eleven, twelve, thirteen, fourteen, and fifteen-electron atoms.

RADIUS AND IONIZATION ENERGY OF THE OUTER ELECTRON OF THE SULFUR ATOM

For each fifteen-electron atom having a central charge of Z times that of the proton, there are two indistinguishable spin-paired electrons in an atomic orbital with radii r_1 and r_2 both given by Eq. (7.35) (Eq. (10.51)), two indistinguishable spin-paired electrons in an atomic orbital with radii r_3 and r_4 both given by Eq. (10.62), three sets of paired electrons in an atomic orbital at r_{10} given by Eq. (10.212), two indistinguishable spin-paired electrons in an atomic orbital with radii r_{11} and r_{12} both given by Eq. (10.255), and three unpaired electrons in an atomic orbital with radius r_{15} given by Eq. (10.331). For $Z \geq 16$, the next electron which binds to form the corresponding sixteen-electron atom is attracted by the central Coulomb field and is repelled by diamagnetic forces due to the 3 sets of spin-paired inner 2p electrons and two spin-paired inner 3s electrons. A paramagnetic spin-pairing force to form a filled s orbital is also possible, but the force due to the spin-pairing of the electrons (Eq. (7.24) with the radius r_{16}) reduces the energy of the atom less than that due to the alternative forces on a set of paired and two unpaired 3p electrons in an atomic orbital at the same radius r_{16}. The resulting electron configuration is $1s^2 2s^2 2p^6 3s^2 3p^4$, and the orbital arrangement is:

3p state

$$\begin{array}{cccc} \uparrow\downarrow & \uparrow & \uparrow & \\ \underline{\quad\quad} & \underline{\quad\quad} & \underline{\quad\quad} & \\ 1 & 0 & -1 & \end{array} \tag{10.333}$$

corresponding to the ground state ${}^3P_2$.

The central Coulomb force acts on the outer electron to cause it to bind wherein this electric force on the outer-most electron due to the nucleus and the inner fifteen electrons is given by Eq. (10.70) with the appropriate charge and radius:

$$\mathbf{F}_{ele} = \frac{(Z-15)e^2}{4\pi\varepsilon_0 r_{16}^2}\mathbf{i}_\mathbf{r} \tag{10.334}$$

for $r > r_{15}$.

The diamagnetic force, $\mathbf{F}_{diamagnetic}$, is only due to 3p and 3s electrons when the 3p shell is at least half filled since the induced charge-density waves only involve the inner-most shell, the 3s orbital. The energy is minimized with conservation of angular momentum when the induced orbital angular momentum of the 3s orbital superimposes positively with the orbital angular momenta of the other 3 p_x and the 3 p_z-orbital electrons and the orbital angular momentum of one of the spin-paired 3 p_x electrons is canceled by the 3 p_y electron. Thus, $\mathbf{F}_{diamagnetic}$, is given by Eq. (10.258) as the sum of the contributions from the 3 p_x and p_z orbitals corresponding to m = 1 and 0, respectively, and the induced contribution from the 3s orbital corresponding to m = 0:

$$\mathbf{F}_{diamagnetic} = -\left(\frac{2}{3}+\frac{1}{3}+\frac{1}{3}\right)\frac{\hbar^2}{4m_e r_{16}^2 r_{12}}\sqrt{s(s+1)}\mathbf{i}_\mathbf{r} = -\left(\frac{4}{3}\right)\frac{\hbar^2}{4m_e r_{16}^2 r_{12}}\sqrt{s(s+1)}\mathbf{i}_\mathbf{r} \tag{10.335}$$

The energy is minimized with conservation of angular momentum when the spin angular momentum the 3s orbital superimposes negatively with the spin angular momentum of the 3 p_x orbital-electron and the orbital angular momentum of the 3 p_z-orbital electron. From Eq. (10.260), $\mathbf{F}_{mag\ 2}$ corresponding to the orbital angular momentum of the 3 p_x, p_y, and p_z orbitals minus the contribution from the 3s orbital is:

$$\mathbf{F}_{mag\ 2} = (1+1-1)\frac{1}{Z}\frac{\hbar^2}{m_e r_{16}^2 r_3}\sqrt{s(s+1)}\mathbf{i}_\mathbf{r} = \frac{1}{Z}\frac{\hbar^2}{m_e r_{16}^2 r_{12}}\sqrt{s(s+1)}\mathbf{i}_\mathbf{r} \tag{10.336}$$

The outward centrifugal force on electron 16 is balanced by the electric force and the magnetic forces (on electron 16). The radius of the outer electron is calculated by equating the outward centrifugal force to the sum of the electric (Eq. (10.334)), diamagnetic (Eq. (10.335)), and paramagnetic (Eq. (10.336)) forces as follows:

$$\frac{m_e v_{16}^2}{r_{16}} = \frac{(Z-15)e^2}{4\pi\varepsilon_0 r_{16}^2} - \frac{4\hbar^2}{12 m_e r_{16}^2 r_{12}}\sqrt{s(s+1)} + \frac{\hbar^2}{Z m_e r_{16}^2 r_{12}}\sqrt{s(s+1)} \tag{10.337}$$

Substitution of $v_{16} = \frac{\hbar}{m_e r_{16}}$ (Eq. (1.35)) and $s = \frac{1}{2}$ into Eq. (10.337) gives:

$$\frac{\hbar^2}{m_e r_{16}^3} = \frac{(Z-15)e^2}{4\pi\varepsilon_0 r_{16}^2} - \frac{4\hbar^2}{12 m_e r_{16}^2 r_{12}}\sqrt{\frac{3}{4}} + \frac{\hbar^2}{Z m_e r_{16}^2 r_{12}}\sqrt{\frac{3}{4}} \tag{10.338}$$

$$r_{16} = \frac{\frac{\hbar^2}{m_e}}{\frac{(Z-15)e^2}{4\pi\varepsilon_0} - \frac{4\hbar^2}{12 m_e r_{12}}\sqrt{\frac{3}{4}} + \frac{\hbar^2}{Z m_e r_{12}}\sqrt{\frac{3}{4}}} \tag{10.339}$$

$$r_{16} = \frac{a_0}{(Z-15) - \left(\frac{4}{12} - \frac{1}{Z}\right)\frac{\sqrt{\frac{3}{4}}}{r_{12}}},\ r_{12}\ in\ units\ of\ a_0 \tag{10.340}$$

Substitution of $\frac{r_{12}}{a_0} = 0.96729$ (Eq. (10.255) with $Z = 16$) into Eq. (10.340) gives:

$$r_{16} = 1.32010 a_0 \tag{10.341}$$

The ionization energy of the sulfur atom is given by the electric energy, $E(electric)$, (Eq. (10.102) with the radius, r_{16}, given by Eq. (10.341)).

$$E(ionization;\ S) = -Electric\ Energy = \frac{(Z-15)e^2}{8\pi\varepsilon_0 r_{16}} = 10.30666\ eV \tag{10.342}$$

where $r_{16} = 1.32010 a_0$ (Eq. (10.341)) and $Z = 16$. The experimental ionization energy of the sulfur atom is $10.36001\ eV$ [3].

THE IONIZATION ENERGIES OF SIXTEEN-ELECTRON ATOMS WITH A NUCLEAR CHARGE Z>16

Sixteen-electron atoms having $Z > 16$ possess an external electric field given by Eq. (10.92). In this case, an energy minimum is achieved with conservation of momentum when the orbital angular momentum is such that $\mathbf{F}_{diamagnetic}$ is minimized while $\mathbf{F}_{mag\ 2}$ is maximized. With a half-filled 3p shell, the diamagnetic force due to the orbital angular momenta of the 3p electrons cancels that of the 2p electrons. Thus, $\mathbf{F}_{diamagnetic}$ is minimized by the formation of a charge-density wave in the 3s orbital corresponding to $m = 1$ in Eq. (10.258) that cancels the orbital angular momentum of one of the $3\,p_x$ electrons to form the equivalent of a half-filled 3p shell. Then, the contribution due to the 2p level is canceled. From Eq. (10.82), the diamagnetic force, $\mathbf{F}_{diamagnetic}$, is given by the sum of the contributions from the $3\,p_y$ and p_z orbitals corresponding to $m = -1,$ and $0,$ respectively, and the negative contribution due to the charge-density wave with $m = 1$ induced in the 3s orbital (Eq. (10.258)).

$$\mathbf{F}_{diamagnetic} = -\left(\frac{2}{3} + \frac{1}{3} - \frac{2}{3}\right)\frac{\hbar^2}{4 m_e r_{16}^2 r_{12}}\sqrt{s(s+1)}\mathbf{i}_{\mathbf{r}} = -\left(\frac{1}{3}\right)\frac{\hbar^2}{4 m_e r_{16}^2 r_{12}}\sqrt{s(s+1)}\mathbf{i}_{\mathbf{r}} \tag{10.343}$$

From Eq. (10.261), $\mathbf{F}_{mag\ 2}$ corresponding to the spin and orbital angular momenta of the paired $2\,p_x$, p_y, and p_z electrons is

$$\mathbf{F}_{mag\ 2} = (4+4+4)\frac{1}{Z}\frac{\hbar^2}{m_e r_{16}^2 r_{12}}\sqrt{s(s+1)}\mathbf{i}_{\mathbf{r}} = \frac{1}{Z}\frac{12\hbar^2}{m_e r_{16}^2 r_{12}}\sqrt{s(s+1)}\mathbf{i}_{\mathbf{r}} \tag{10.344}$$

and the contribution from the 3p level is:

$$\mathbf{F}_{mag\ 2} = (8+4+4-4)\frac{1}{Z}\frac{\hbar^2}{m_e r_{16}^2 r_{12}}\sqrt{s(s+1)}\mathbf{i}_{\mathbf{r}} = \frac{1}{Z}\frac{12\hbar^2}{m_e r_{16}^2 r_{12}}\sqrt{s(s+1)}\mathbf{i}_{\mathbf{r}} \tag{10.345}$$

corresponding to the $3\,p_x$ (Eq. (10.264)) and p_z (Eq. (10.263)) electrons wherein the contribution due to the $3\,p_x$ ($m = 1$) electron is canceled by the mirror charge-density wave with $m = 1$ induced in the 3s orbital (Eq. (10.262)). Thus, the total of $\mathbf{F}_{mag\ 2}$ is

$$\mathbf{F}_{mag\ 2} = \frac{1}{Z}\frac{24\hbar^2}{m_e r_{16}^2 r_{12}}\sqrt{s(s+1)}\mathbf{i}_{\mathbf{r}} \tag{10.346}$$

The diamagnetic force, $\mathbf{F}_{diamagnetic\ 2}$, due to the binding of the 3p-orbital electron having an electric field outside of its radius is given by Eq. (10.268):

$$\mathbf{F}_{diamagnetic\ 2} = -\left[\frac{Z-16}{Z-15}\right]\left(1-\frac{\sqrt{2}}{2}+\frac{1}{2}\right)\frac{r_{12}\hbar^2}{m_e r_{16}^4}10\sqrt{s(s+1)}\mathbf{i}_{\mathbf{r}} \tag{10.347}$$

In the case that $Z>16$, the radius of the outer electron is calculated by equating the outward centrifugal force to the sum of the electric (Eq. (10.334)), diamagnetic (Eqs. (10.343) and (10.347)), and paramagnetic (Eq. (10.346)) forces as follows:

$$\frac{m_e v_{16}^2}{r_{16}} = \frac{(Z-15)e^2}{4\pi\varepsilon_0 r_{16}^2} - \frac{\hbar^2}{12 m_e r_{16}^2 r_{12}}\sqrt{s(s+1)} + \frac{24\hbar^2}{Z m_e r_{16}^2 r_{12}}\sqrt{s(s+1)} - \left[\frac{Z-16}{Z-15}\right]\left(1-\frac{\sqrt{2}}{2}+\frac{1}{2}\right)\frac{r_{12}\hbar^2}{m_e r_{16}^4}10\sqrt{s(s+1)} \tag{10.348}$$

Substitution of $v_{16} = \dfrac{\hbar}{m_e r_{16}}$ (Eq. (1.35)) and $s=\dfrac{1}{2}$ into Eq. (10.348) gives:

$$\frac{\hbar^2}{m_e r_{16}^3} = \frac{(Z-15)e^2}{4\pi\varepsilon_0 r_{16}^2} - \frac{\hbar^2}{12 m_e r_{16}^2 r_{12}}\sqrt{\frac{3}{4}} + \frac{24\hbar^2}{Z m_e r_{16}^2 r_{12}}\sqrt{\frac{3}{4}} - \left[\frac{Z-16}{Z-15}\right]\left(1-\frac{\sqrt{2}}{2}+\frac{1}{2}\right)\frac{r_{12}\hbar^2}{m_e r_{16}^4}10\sqrt{\frac{3}{4}} \tag{10.349}$$

The quadratic equation corresponding to Eq. (10.349) is

$$\left(\frac{(Z-15)e^2}{4\pi\varepsilon_0} - \left(\frac{1}{12}-\frac{24}{Z}\right)\frac{\hbar^2}{m_e r_{12}}\sqrt{\frac{3}{4}}\right)r_{16}^2 - \frac{\hbar^2}{m_e}r_{16} - \left[\frac{Z-16}{Z-15}\right]\left(1-\frac{\sqrt{2}}{2}+\frac{1}{2}\right)\frac{r_{12}\hbar^2}{m_e}10\sqrt{\frac{3}{4}} = 0 \tag{10.350}$$

$$r_{16}^2 - \frac{\dfrac{\hbar^2}{m_e}}{\left(\dfrac{(Z-15)e^2}{4\pi\varepsilon_0} - \left(\dfrac{1}{12}-\dfrac{24}{Z}\right)\dfrac{\hbar^2}{m_e r_{12}}\sqrt{\dfrac{3}{4}}\right)}r_{16} - \frac{\dfrac{\hbar^2}{m_e}\left[\dfrac{Z-16}{Z-15}\right]\left(1-\dfrac{\sqrt{2}}{2}+\dfrac{1}{2}\right)r_{12}10\sqrt{\dfrac{3}{4}}}{\left(\dfrac{(Z-15)e^2}{4\pi\varepsilon_0} - \left(\dfrac{1}{12}-\dfrac{24}{Z}\right)\dfrac{\hbar^2}{m_e r_{12}}\sqrt{\dfrac{3}{4}}\right)} = 0 \tag{10.351}$$

The solution of Eq. (10.351) using the quadratic formula is:

$$r_{16} = \frac{\dfrac{\dfrac{\hbar^2}{m_e}}{\left(\dfrac{(Z-15)e^2}{4\pi\varepsilon_0} - \left(\dfrac{1}{12}-\dfrac{24}{Z}\right)\dfrac{\hbar^2}{m_e r_{12}}\sqrt{\dfrac{3}{4}}\right)} \pm \sqrt{\left(\dfrac{\dfrac{\hbar^2}{m_e}}{\left(\dfrac{(Z-15)e^2}{4\pi\varepsilon_0} - \left(\dfrac{1}{12}-\dfrac{24}{Z}\right)\dfrac{\hbar^2}{m_e r_{12}}\sqrt{\dfrac{3}{4}}\right)}\right)^2 + 4\dfrac{\dfrac{\hbar^2}{m_e}\left[\dfrac{Z-16}{Z-15}\right]\left(1-\dfrac{\sqrt{2}}{2}+\dfrac{1}{2}\right)r_{12}10\sqrt{\dfrac{3}{4}}}{\left(\dfrac{(Z-15)e^2}{4\pi\varepsilon_0} - \left(\dfrac{1}{12}-\dfrac{24}{Z}\right)\dfrac{\hbar^2}{m_e r_{12}}\sqrt{\dfrac{3}{4}}\right)}}}{2} \tag{10.352}$$

$$r_{16} = \frac{\dfrac{a_0}{\left((Z-15) - \left(\dfrac{1}{24}-\dfrac{12}{Z}\right)\dfrac{\sqrt{3}}{r_{12}}\right)} \pm a_0\sqrt{\left(\dfrac{1}{\left((Z-15) - \left(\dfrac{1}{24}-\dfrac{12}{Z}\right)\dfrac{\sqrt{3}}{r_{12}}\right)}\right)^2 + \dfrac{20\sqrt{3}\left(\left[\dfrac{Z-16}{Z-15}\right]\left(1-\dfrac{\sqrt{2}}{2}+\dfrac{1}{2}\right)r_{12}\right)}{\left((Z-15) - \left(\dfrac{1}{24}-\dfrac{12}{Z}\right)\dfrac{\sqrt{3}}{r_{12}}\right)}}}{2}, \quad r_{12}\ \textit{in units of}\ a_0 \tag{10.353}$$

where r_{12} is given by Eq. (10.255). The positive root of Eq. (10.353) must be taken in order that $r_{16}>0$. The final radius of electron 16, r_{16}, is given by Eq. (10.353); this is also the final radius of electrons 13, 14, and 15. The radii of several sixteen-electron atoms are given in Table 10.15.

The ionization energies for the sixteen-electron atoms with $Z>16$ are given by the electric energy, $E(electric)$, (Eq. (10.102) with the radii r_{16}, given by Eq. (10.353)).

$$E(Ionization) = -Electric\ Energy = \frac{(Z-15)e^2}{8\pi\varepsilon_0 r_{16}} \tag{10.354}$$

Since the relativistic corrections were small, the nonrelativistic ionization energies for experimentally measured sixteen-electron atoms are given in Table 10.15.

Table 10.15. Ionization energies for some sixteen-electron atoms.

16 e Atom	Z	r_1 (a_o) [a]	r_3 (a_o) [b]	r_{10} (a_o) [c]	r_{12} (a_o) [d]	r_{16} (a_o) [e]	Theoretical Ionization Energies [f] (eV)	Experimental Ionization Energies [g] (eV)	Relative Error [h]
S	16	0.06306	0.27053	0.33902	0.96729	1.32010	10.30666	10.36001	0.0051
Cl^+	17	0.05932	0.25344	0.31190	0.86545	1.10676	24.5868	23.814	-0.0324
Ar^{2+}	18	0.05599	0.23839	0.28878	0.78276	1.02543	39.8051	40.74	0.0229
K^{3+}	19	0.05302	0.22503	0.26884	0.71450	0.92041	59.1294	60.91	0.0292
Ca^{4+}	20	0.05035	0.21308	0.25149	0.65725	0.82819	82.1422	84.50	0.0279
Sc^{5+}	21	0.04794	0.20235	0.23625	0.60857	0.75090	108.7161	110.68	0.0177
Ti^{6+}	22	0.04574	0.19264	0.22276	0.56666	0.68622	138.7896	140.8	0.0143
V^{7+}	23	0.04374	0.18383	0.21074	0.53022	0.63163	172.3256	173.4	0.0062
Cr^{8+}	24	0.04191	0.17579	0.19995	0.49822	0.58506	209.2996	209.3	0.0000
Mn^{9+}	25	0.04022	0.16842	0.19022	0.46990	0.54490	249.6938	248.3	-0.0056
Fe^{10+}	26	0.03867	0.16165	0.18140	0.44466	0.50994	293.4952	290.2	-0.0114
Co^{11+}	27	0.03723	0.15540	0.17336	0.42201	0.47923	340.6933	336	-0.0140
Ni^{12+}	28	0.03589	0.14961	0.16601	0.40158	0.45204	391.2802	384	-0.0190
Cu^{13+}	29	0.03465	0.14424	0.15926	0.38305	0.42781	445.2492	435	-0.0236
Zn^{14+}	30	0.03349	0.13925	0.15304	0.36617	0.40607	502.5950	490	-0.0257

[a] Radius of the paired 1s inner electrons of sixteen-electron atoms from Eq. (10.51).

[b] Radius of the paired 2s inner electrons of sixteen-electron atoms from Eq. (10.62).

[c] Radius of the three sets of paired 2p inner electrons of sixteen-electron atoms from Eq. (10.212).

[d] Radius of the paired 3s inner electrons of sixteen-electron atoms from Eq. (10.255).

[e] Radius of the two paired and two unpaired 3p outer electrons of sixteen-electron atoms from Eq. (10.353) for $Z > 16$ and Eq. (10.341) for *S*.

[f] Calculated ionization energies of sixteen-electron atoms given by the electric energy (Eq. (10.354)).

[g] From theoretical calculations, interpolation of isoelectronic and spectral series, and experimental data [2-3].

[h] (Experimental-theoretical)/experimental.

The agreement between the experimental and calculated values of Table 10.15 is well within the experimental capability of the spectroscopic determinations including the values at large Z which relies on X-ray spectroscopy. In this case, the experimental capability is three to four significant figures which is consistent with the last column. The sulfur atom isoelectronic series is given in Table 10.15 [2-3] to much higher precision than the capability of X-ray spectroscopy, but these values are based on theoretical and interpolation techniques rather than data alone. Ionization energies are difficult to determine since the cut-off of the Rydberg series of lines at the ionization energy is often not observed, and the ionization energy must be determined from theoretical calculations, interpolation of S isoelectronic and Rydberg series, as well as direct experimental data.

SEVENTEEN-ELECTRON ATOMS

Seventeen-electron atoms can be solved exactly using the results of the solutions of one, two, three, four, five, six, seven, eight, nine, ten, eleven, twelve, thirteen, fourteen, fifteen, and sixteen-electron atoms.

RADIUS AND IONIZATION ENERGY OF THE OUTER ELECTRON OF THE CHLORINE ATOM

For each sixteen-electron atom having a central charge of Z times that of the proton, there are two indistinguishable spin-paired electrons in an atomic orbital with radii r_1 and r_2 both given by Eq. (7.35) (Eq. (10.51)), two indistinguishable spin-paired electrons in an atomic orbital with radii r_3 and r_4 both given by Eq. (10.62), three sets of paired electrons in an atomic orbital at r_{10} given by Eq. (10.212), two indistinguishable spin-paired electrons in an atomic orbital with radii r_{11} and r_{12} both given by Eq. (10.255), and two paired and two unpaired electrons in an atomic orbital with radius r_{16} given by Eq. (10.353). For $Z \geq 17$, the next electron which binds to form the corresponding seventeen-electron atom is attracted by the central Coulomb field and is repelled by diamagnetic forces due to the 3 sets of spin-paired inner 2p electrons and two spin-paired inner 3s electrons. A paramagnetic spin-pairing force to form a filled s orbital is also possible, but the force due to the spin-pairing of the electrons

(Eq. (7.24) with the radius r_{17}) reduces the energy of the atom less than that due to the alternative forces on two sets of paired electrons and an unpaired 3p electron in an atomic orbital at the same radius r_{17}. The resulting electron configuration is $1s^2 2s^2 2p^6 3s^2 3p^5$, and the orbital arrangement is:

3p state

$$\underset{1}{\uparrow\downarrow}\quad \underset{0}{\uparrow\downarrow}\quad \underset{-1}{\uparrow} \tag{10.355}$$

corresponding to the ground state ${}^2P^0_{3/2}$.

The central Coulomb force acts on the outer electron to cause it to bind wherein this electric force on the outer-most electron due to the nucleus and the inner sixteen electrons is given by Eq. (10.70) with the appropriate charge and radius:

$$\mathbf{F}_{ele} = \frac{(Z-16)e^2}{4\pi\varepsilon_0 r_{17}^2}\mathbf{i}_\mathbf{r} \tag{10.356}$$

for $r > r_{16}$.

The diamagnetic force, $\mathbf{F}_{diamagnetic}$, is only due to 3p and 3s electrons when the 3p shell is at least half filled since the induced charge-density waves only involve the inner-most shell, the 3s orbital. Thus, $\mathbf{F}_{diamagnetic}$, is given by Eq. (10.258) as the contribution from the 3 p_y orbital corresponding to $m = -1$ with the cancellation of the orbital angular momenta of the spin-paired 3 p_x and p_z electrons:

$$\mathbf{F}_{diamagnetic} = -\left(\frac{2}{3}\right)\frac{\hbar^2}{4m_e r_{17}^2 r_{12}}\sqrt{s(s+1)}\mathbf{i}_\mathbf{r} \tag{10.357}$$

The energy is minimized with conservation of angular momentum when the spin angular momentum of the 3s orbital superimposes negatively with the angular momenta of the 3p orbitals. From Eq. (10.260), $\mathbf{F}_{mag\ 2}$ corresponding to the sum of the spin angular momenta of the 3 p_x and 3 p_z orbitals and the orbital angular momentum of the 3 p_y orbital, minus the contribution from the 3s orbital is:

$$\mathbf{F}_{mag\ 2} = (1+1+1-1)\frac{1}{Z}\frac{\hbar^2}{m_e r_{17}^2 r_{12}}\sqrt{s(s+1)}\mathbf{i}_\mathbf{r} = \frac{1}{Z}\frac{2\hbar^2}{m_e r_{17}^2 r_{12}}\sqrt{s(s+1)}\mathbf{i}_\mathbf{r} \tag{10.358}$$

The outward centrifugal force on electron 17 is balanced by the electric force and the magnetic forces (on electron 17). The radius of the outer electron is calculated by equating the outward centrifugal force to the sum of the electric (Eq. (10.356)), diamagnetic (Eq. (10.357)), and paramagnetic (Eq. (10.358)) forces as follows:

$$\frac{m_e v_{17}^2}{r_{17}} = \frac{(Z-16)e^2}{4\pi\varepsilon_0 r_{17}^2} - \frac{2\hbar^2}{12m_e r_{17}^2 r_{12}}\sqrt{s(s+1)} + \frac{2\hbar^2}{Zm_e r_{17}^2 r_{12}}\sqrt{s(s+1)} \tag{10.359}$$

Substitution of $v_{17} = \dfrac{\hbar}{m_e r_{17}}$ (Eq. (1.35)) and $s = \dfrac{1}{2}$ into Eq. (10.359) gives:

$$\frac{\hbar^2}{m_e r_{17}^3} = \frac{(Z-16)e^2}{4\pi\varepsilon_0 r_{17}^2} - \frac{2\hbar^2}{12m_e r_{17}^2 r_{12}}\sqrt{\frac{3}{4}} + \frac{2\hbar^2}{Zm_e r_{17}^2 r_{12}}\sqrt{\frac{3}{4}} \tag{10.360}$$

$$r_{17} = \frac{\dfrac{\hbar^2}{m_e}}{\dfrac{(Z-16)e^2}{4\pi\varepsilon_0} - \dfrac{2\hbar^2}{12m_e r_{12}}\sqrt{\dfrac{3}{4}} + \dfrac{2\hbar^2}{Zm_e r_{12}}\sqrt{\dfrac{3}{4}}} \tag{10.361}$$

$$r_{17} = \frac{a_0}{(Z-16) - \left(\dfrac{2}{12} - \dfrac{2}{Z}\right)\dfrac{\sqrt{\frac{3}{4}}}{r_{12}}},\ r_{12}\ in\ units\ of\ a_0 \tag{10.362}$$

Substitution of $\dfrac{r_{12}}{a_0} = 0.86545$ (Eq. (10.255) with $Z = 17$) into Eq. (10.362) gives:

$$r_{17} = 1.05158 a_0 \tag{10.363}$$

The ionization energy of the chlorine atom is given by the electric energy, $E(electric)$, (Eq. (10.102) with the radius, r_{17}, given by Eq. (10.363)):

$$E(ionization;\ Cl) = -Electric\ Energy = \frac{(Z-16)e^2}{8\pi\varepsilon_0 r_{17}} = 12.93841\ eV \tag{10.364}$$

where $r_{17} = 1.05158 a_0$ (Eq. (10.363)) and $Z = 17$. The experimental ionization energy of the chlorine atom is 12.96764 eV [3].

THE IONIZATION ENERGIES OF SEVENTEEN-ELECTRON ATOMS WITH A NUCLEAR CHARGE Z>17

Seventeen-electron atoms having $Z>17$ possess an external electric field given by Eq. (10.92). In this case, an energy minimum is achieved with conservation of momentum when the orbital angular momentum is such that $\mathbf{F}_{diamagnetic}$ is minimized while $\mathbf{F}_{mag\ 2}$ is maximized. With a filled 3p shell, the diamagnetic force due to the orbital angular momenta of the 3p electrons cancels that of the 2p electrons. Thus, $\mathbf{F}_{diamagnetic}$ is minimized by the formation of a charge-density wave in the 3s orbital corresponding to two electrons with m = -1 in Eq. (10.258) to form the equivalent of a filled 3p level such that the contribution due to the 2p level is canceled. From Eq. (10.82), the diamagnetic force, $\mathbf{F}_{diamagnetic}$, is given by the contribution due to the charge-density wave with m = -1 induced in the 3s orbital according to Eq. (10.258).

$$\mathbf{F}_{diamagnetic} = -\left(\frac{2}{3}\right)\frac{\hbar^2}{4m_e r_{17}^2 r_{12}}\sqrt{s(s+1)}\mathbf{i}_{\mathbf{r}} \tag{10.365}$$

From Eqs. (10.205) and (10.261), $\mathbf{F}_{mag\ 2}$ corresponding to the spin and orbital angular momenta of the paired 2 p_x, p_y, and p_z electrons is

$$\mathbf{F}_{mag\ 2} = (4+4+4)\frac{1}{Z}\frac{\hbar^2}{m_e r_{17}^2 r_{12}}\sqrt{s(s+1)}\mathbf{i}_{\mathbf{r}} = \frac{1}{Z}\frac{12\hbar^2}{m_e r_{17}^2 r_{12}}\sqrt{s(s+1)}\mathbf{i}_{\mathbf{r}} \tag{10.366}$$

and the contribution from the paired 3 p_x, p_y, and p_z electrons given by Eq. (10.264) is

$$\mathbf{F}_{mag\ 2} = (8+8+8)\frac{1}{Z}\frac{\hbar^2}{m_e r_{17}^2 r_{12}}\sqrt{s(s+1)}\mathbf{i}_{\mathbf{r}} = \frac{1}{Z}\frac{24\hbar^2}{m_e r_{17}^2 r_{12}}\sqrt{s(s+1)}\mathbf{i}_{\mathbf{r}} \tag{10.367}$$

wherein the contribution due to the charge-density wave with m = -1 induced in the 3s orbital (Eq. (10.262)) provides the equivalent of a filled 3 p_y orbital and adds a negative contribution of:

$$\mathbf{F}_{mag\ 2} = -\frac{1}{Z}\frac{4\hbar^2}{m_e r_{17}^2 r_{12}}\sqrt{s(s+1)}\mathbf{i}_{\mathbf{r}} \tag{10.368}$$

Thus, the total of $\mathbf{F}_{mag\ 2}$ is:

$$\mathbf{F}_{mag\ 2} = \frac{1}{Z}\frac{32\hbar^2}{m_e r_{17}^2 r_{12}}\sqrt{s(s+1)}\mathbf{i}_{\mathbf{r}} \tag{10.369}$$

The diamagnetic force, $\mathbf{F}_{diamagnetic\ 2}$, due to the binding of the 3p-orbital electron having an electric field outside of its radius is given by Eq. (10.268):

$$\mathbf{F}_{diamagnetic\ 2} = -\left[\frac{Z-17}{Z-16}\right]\left(1-\frac{\sqrt{2}}{2}+\frac{1}{2}\right)\frac{r_{12}\hbar^2}{m_e r_{17}^4}10\sqrt{s(s+1)}\mathbf{i}_{\mathbf{r}} \tag{10.370}$$

In the case that $Z>17$, the radius of the outer electron is calculated by equating the outward centrifugal force to the sum of the electric (Eq. (10.356)), diamagnetic (Eqs. (10.365) and (10.370)), and paramagnetic (Eq. (10.369)) forces as follows:

$$\frac{m_e v_{17}^2}{r_{17}} = \frac{(Z-16)e^2}{4\pi\varepsilon_0 r_{17}^2} - \frac{2\hbar^2}{12m_e r_{17}^2 r_{12}}\sqrt{s(s+1)} + \frac{32\hbar^2}{Zm_e r_{17}^2 r_{12}}\sqrt{s(s+1)} - \left[\frac{Z-17}{Z-16}\right]\left(1-\frac{\sqrt{2}}{2}+\frac{1}{2}\right)\frac{r_{12}\hbar^2}{m_e r_{17}^4}10\sqrt{s(s+1)} \tag{10.371}$$

Substitution of $v_{17} = \dfrac{\hbar}{m_e r_{17}}$ (Eq. (1.35)) and $s = \dfrac{1}{2}$ into Eq. (10.371) gives:

$$\frac{\hbar^2}{m_e r_{17}^3} = \frac{(Z-16)e^2}{4\pi\varepsilon_0 r_{17}^2} - \frac{2\hbar^2}{12m_e r_{17}^2 r_{12}}\sqrt{\frac{3}{4}} + \frac{32\hbar^2}{Zm_e r_{17}^2 r_{12}}\sqrt{\frac{3}{4}} - \left[\frac{Z-17}{Z-16}\right]\left(1-\frac{\sqrt{2}}{2}+\frac{1}{2}\right)\frac{r_{12}\hbar^2}{m_e r_{17}^4}10\sqrt{\frac{3}{4}} \tag{10.372}$$

The quadratic equation corresponding to Eq. (10.372) is

$$\left(\frac{(Z-16)e^2}{4\pi\varepsilon_0} - \left(\frac{2}{12}-\frac{32}{Z}\right)\frac{\hbar^2}{m_e r_{12}}\sqrt{\frac{3}{4}}\right)r_{17}^2 - \frac{\hbar^2}{m_e}r_{17} - \left[\frac{Z-17}{Z-16}\right]\left(1-\frac{\sqrt{2}}{2}+\frac{1}{2}\right)\frac{r_{12}\hbar^2}{m_e}10\sqrt{\frac{3}{4}} = 0 \tag{10.373}$$

$$r_{17}^2 - \frac{\dfrac{\hbar^2}{m_e}}{\left(\dfrac{(Z-16)e^2}{4\pi\varepsilon_0} - \left(\dfrac{2}{12}-\dfrac{32}{Z}\right)\dfrac{\hbar^2}{m_e r_{12}}\sqrt{\dfrac{3}{4}}\right)}r_{17} - \frac{\dfrac{\hbar^2}{m_e}\left[\dfrac{Z-17}{Z-16}\right]\left(1-\dfrac{\sqrt{2}}{2}+\dfrac{1}{2}\right)r_{12}10\sqrt{\dfrac{3}{4}}}{\left(\dfrac{(Z-16)e^2}{4\pi\varepsilon_0} - \left(\dfrac{2}{12}-\dfrac{32}{Z}\right)\dfrac{\hbar^2}{m_e r_{12}}\sqrt{\dfrac{3}{4}}\right)} = 0 \tag{10.374}$$

The solution of Eq. (10.374) using the quadratic formula is:

$$r_{17}=\frac{\dfrac{\dfrac{\hbar^2}{m_e}}{\left(\dfrac{(Z-16)e^2}{4\pi\varepsilon_0}-\left(\dfrac{2}{12}-\dfrac{32}{Z}\right)\dfrac{\hbar^2}{m_e r_{12}}\sqrt{\dfrac{3}{4}}\right)}\pm\sqrt{\left(\dfrac{\dfrac{\hbar^2}{m_e}}{\left(\dfrac{(Z-16)e^2}{4\pi\varepsilon_0}-\left(\dfrac{2}{12}-\dfrac{32}{Z}\right)\dfrac{\hbar^2}{m_e r_{12}}\sqrt{\dfrac{3}{4}}\right)}\right)^2+4\dfrac{\dfrac{\hbar^2}{m_e}\left\lfloor\dfrac{Z-17}{Z-16}\right\rfloor\left(1-\dfrac{\sqrt{2}}{2}+\dfrac{1}{2}\right)r_{12}10\sqrt{\dfrac{3}{4}}}{\left(\dfrac{(Z-16)e^2}{4\pi\varepsilon_0}-\left(\dfrac{2}{12}-\dfrac{32}{Z}\right)\dfrac{\hbar^2}{m_e r_{12}}\sqrt{\dfrac{3}{4}}\right)}}}{2} \tag{10.375}$$

$$r_{17}=\frac{\dfrac{a_0}{\left((Z-16)-\left(\dfrac{1}{12}-\dfrac{16}{Z}\right)\dfrac{\sqrt{3}}{r_{12}}\right)}\pm a_0\sqrt{\left(\dfrac{1}{\left((Z-16)-\left(\dfrac{1}{12}-\dfrac{16}{Z}\right)\dfrac{\sqrt{3}}{r_{12}}\right)}\right)^2+\dfrac{20\sqrt{3}\left(\left\lfloor\dfrac{Z-17}{Z-16}\right\rfloor\left(1-\dfrac{\sqrt{2}}{2}+\dfrac{1}{2}\right)r_{12}\right)}{\left((Z-16)-\left(\dfrac{1}{12}-\dfrac{16}{Z}\right)\dfrac{\sqrt{3}}{r_{12}}\right)}}}{2},\ r_{12}\ in\ units\ of\ a_0 \tag{10.376}$$

where r_{12} is given by Eq. (10.255). The positive root of Eq. (10.376) must be taken in order that $r_{17}>0$. The final radius of electron 17, r_{17}, is given by Eq. (10.376); this is also the final radius of electrons 13, 14, 15, and 16. The radii of several seventeen-electron atoms are given in Table 10.16.

The ionization energies for the seventeen-electron atoms with $Z>17$ are given by the electric energy, $E(electric)$, (Eq. (10.102) with the radii r_{17}, given by Eq. (10.376)).

$$E(Ionization)=-Electric\ Energy=\frac{(Z-16)e^2}{8\pi\varepsilon_0 r_{17}} \tag{10.377}$$

Since the relativistic corrections were small, the nonrelativistic ionization energies for experimentally measured seventeen-electron atoms are given in Table 10.16.

Table 10.16. Ionization energies for some seventeen-electron atoms.

17 e Atom	Z	r_1 (a_o) [a]	r_3 (a_o) [b]	r_{10} (a_o) [c]	r_{12} (a_o) [d]	r_{17} (a_o) [e]	Theoretical Ionization Energies [f] (eV)	Experimental Ionization Energies [g] (eV)	Relative Error [h]
Cl	17	0.05932	0.25344	0.31190	0.86545	1.05158	12.93841	12.96764	0.0023
Ar^+	18	0.05599	0.23839	0.28878	0.78276	0.98541	27.6146	27.62967	0.0005
K^{2+}	19	0.05302	0.22503	0.26884	0.71450	0.93190	43.8001	45.806	0.0438
Ca^{3+}	20	0.05035	0.21308	0.25149	0.65725	0.84781	64.1927	67.27	0.0457
Sc^{4+}	21	0.04794	0.20235	0.23625	0.60857	0.77036	88.3080	91.65	0.0365
Ti^{5+}	22	0.04574	0.19264	0.22276	0.56666	0.70374	116.0008	119.53	0.0295
V^{6+}	23	0.04374	0.18383	0.21074	0.53022	0.64701	147.2011	150.6	0.0226
Cr^{7+}	24	0.04191	0.17579	0.19995	0.49822	0.59849	181.8674	184.7	0.0153
Mn^{8+}	25	0.04022	0.16842	0.19022	0.46990	0.55667	219.9718	221.8	0.0082
Fe^{9+}	26	0.03867	0.16165	0.18140	0.44466	0.52031	261.4942	262.1	0.0023
Co^{10+}	27	0.03723	0.15540	0.17336	0.42201	0.48843	306.4195	305	-0.0047
Ni^{11+}	28	0.03589	0.14961	0.16601	0.40158	0.46026	354.7360	352	-0.0078
Cu^{12+}	29	0.03465	0.14424	0.15926	0.38305	0.43519	406.4345	401	-0.0136
Zn^{13+}	30	0.03349	0.13925	0.15304	0.36617	0.41274	461.5074	454	-0.0165

[a] Radius of the paired 1s inner electrons of seventeen-electron atoms from Eq. (10.51).

[b] Radius of the paired 2s inner electrons of seventeen-electron atoms from Eq. (10.62).

[c] Radius of the three sets of paired 2p inner electrons of seventeen-electron atoms from Eq. (10.212).

[d] Radius of the paired 3s inner electrons of seventeen-electron atoms from Eq. (10.255).

[e] Radius of the two sets of paired and an unpaired 3p outer electron of seventeen-electron atoms from Eq. (10.376) for $Z > 17$ and Eq. (10.363) for *Cl*.

[f] Calculated ionization energies of seventeen-electron atoms given by the electric energy (Eq. (10.377)).

[g] From theoretical calculations, interpolation of isoelectronic and spectral series, and experimental data [2-3].

[h] (Experimental-theoretical)/experimental.

The agreement between the experimental and calculated values of Table 10.16 is well within the experimental capability of the spectroscopic determinations including the values at large Z which relies on X-ray spectroscopy. In this case, the experimental capability is about two to four significant figures which is consistent with the last column. Ionization energies are difficult to determine since the cut-off of the Rydberg series of lines at the ionization energy is often not observed. Thus, the chlorine atom isoelectronic series given in Table 10.16 [2-3] relies on theoretical calculations and interpolation of the Cl isoelectronic and Rydberg series as well as direct experimental data to extend the precision beyond the capability of X-ray spectroscopy. But, no assurances can be given that these techniques are correct, and they may not improve the results. The error given in the last column is very reasonable given the quality of the data.

EIGHTEEN-ELECTRON ATOMS

Eighteen-electron atoms can be solved exactly using the results of the solutions of one, two, three, four, five, six, seven, eight, nine, ten, eleven, twelve, thirteen, fourteen, fifteen, sixteen, and seventeen-electron atoms.

RADIUS AND IONIZATION ENERGY OF THE OUTER ELECTRON OF THE ARGON ATOM

For each seventeen-electron atom having a central charge of Z times that of the proton, there are two indistinguishable spin-paired electrons in an atomic orbital with radii r_1 and r_2 both given by Eq. (7.35) (Eq. (10.51)), two indistinguishable spin-paired electrons in an atomic orbital with radii r_3 and r_4 both given by Eq. (10.62), three sets of paired electrons in an atomic orbital at r_{10} given by Eq. (10.212), two indistinguishable spin-paired electrons in an atomic orbital with radii r_{11} and r_{12} both given by Eq. (10.255), and two sets of paired and an unpaired electron in an atomic orbital with radius r_{17} given by Eq. (10.376). For $Z \geq 18$, the next electron which binds to form the corresponding eighteen-electron atom is attracted by the central Coulomb field and is repelled by diamagnetic forces due to the 3 sets of spin-paired inner 2p electrons and two spin-paired inner 3s electrons. A paramagnetic spin-pairing force to form a filled s orbital is also possible, but the force due to the spin-pairing of the electrons (Eq. (7.24) with the radius r_{18}) reduces the energy of the atom less than that due to the alternative forces on three sets of paired 3p electrons in an atomic orbital at the same radius r_{18}. The resulting electron configuration is $1s^2 2s^2 2p^6 3s^2 3p^6$, and the orbital arrangement is:

3p state

$$\underline{\uparrow\ \downarrow}\quad \underline{\uparrow\ \downarrow}\quad \underline{\uparrow\ \downarrow} \tag{10.378}$$

1 0 -1

corresponding to the ground state $^1S_0$.

The central Coulomb force acts on the outer electron to cause it to bind wherein this electric force on the outer-most electron due to the nucleus and the inner seventeen electrons is given by Eq. (10.70) with the appropriate charge and radius:

$$\mathbf{F}_{ele} = \frac{(Z-17)e^2}{4\pi\varepsilon_0 r_{18}^2}\mathbf{i}_\mathbf{r} \tag{10.379}$$

for $r > r_{17}$.

As in the case on the neon atom, the energy of the argon atom is minimized and the angular momentum is conserved with the pairing of electron eighteen to fill the 3 p_y orbital when the orbital angular momenta of each set of the 3 p_x, p_y, and p_z spin-paired electrons adds negatively to cancel. Then, the diamagnetic force (Eq. (10.258)), $\mathbf{F}_{diamagnetic}$, is given by the induced orbital angular momentum of the 3s orbital alone which conserves angular momentum.

$$\mathbf{F}_{diamagnetic} = -\left(\frac{1}{3}\right)\frac{\hbar^2}{4m_e r_{18}^2 r_{12}}\sqrt{s(s+1)}\mathbf{i}_\mathbf{r} \tag{10.380}$$

From Eq. (10.260), $\mathbf{F}_{mag\ 2}$ is:

$$\mathbf{F}_{mag\ 2} = (1+1+1+1)\frac{1}{Z}\frac{\hbar^2}{m_e r_{18}^2 r_{12}}\sqrt{s(s+1)}\mathbf{i}_\mathbf{r} = \frac{1}{Z}\frac{4\hbar^2}{m_e r_{18}^2 r_{12}}\sqrt{s(s+1)}\mathbf{i}_\mathbf{r} \tag{10.381}$$

corresponding to the spin-angular-momentum contribution alone from each of the 3 p_x, p_y, and p_z orbitals and the spin angular momentum of the 3s orbital.

The outward centrifugal force on electron 18 is balanced by the electric force and the magnetic forces (on electron 18). The radius of the outer electron is calculated by equating the outward centrifugal force to the sum of the electric (Eq. (10.379)), diamagnetic (Eq. (10.380)), and paramagnetic (Eq. (10.381)) forces as follows:

$$\frac{m_e v_{18}^2}{r_{18}} = \frac{(Z-17)e^2}{4\pi\varepsilon_0 r_{18}^2} - \frac{\hbar^2}{12m_e r_{18}^2 r_{12}}\sqrt{s(s+1)} + \frac{4\hbar^2}{Zm_e r_{18}^2 r_{12}}\sqrt{s(s+1)} \tag{10.382}$$

Substitution of $v_{18} = \dfrac{\hbar}{m_e r_{18}}$ (Eq. (1.35)) and $s = \dfrac{1}{2}$ into Eq. (10.382) gives:

$$\frac{\hbar^2}{m_e r_{18}^3} = \frac{(Z-17)e^2}{4\pi\varepsilon_0 r_{18}^2} - \frac{\hbar^2}{12m_e r_{18}^2 r_{12}}\sqrt{\frac{3}{4}} + \frac{4\hbar^2}{Zm_e r_{18}^2 r_{12}}\sqrt{\frac{3}{4}} \tag{10.383}$$

$$r_{18} = \frac{\dfrac{\hbar^2}{m_e}}{\dfrac{(Z-17)e^2}{4\pi\varepsilon_0} - \dfrac{\hbar^2}{12m_e r_{12}}\sqrt{\dfrac{3}{4}} + \dfrac{4\hbar^2}{Zm_e r_{12}}\sqrt{\dfrac{3}{4}}} \tag{10.384}$$

$$r_{18} = \frac{a_0}{(Z-17) - \left(\dfrac{1}{12} - \dfrac{4}{Z}\right)\dfrac{\sqrt{\frac{3}{4}}}{r_{12}}},\ r_{12}\ in\ units\ of\ a_0 \tag{10.385}$$

Substitution of $\dfrac{r_{12}}{a_0} = 0.78276$ (Eq. (10.255) with $Z = 18$) into Eq. (10.385) gives:

$$r_{18} = 0.86680 a_0 \tag{10.386}$$

The ionization energy of the argon atom is given by the electric energy, $E(electric)$, (Eq. (10.102) with the radius, r_{18}, given by Eq. (10.386)).

$$E(ionization;\ Ar) = -Electric\ Energy = \frac{(Z-17)e^2}{8\pi\varepsilon_0 r_{18}} = 15.69651\ eV \tag{10.387}$$

where $r_{18} = 0.86680 a_0$ (Eq. (10.386)) and $Z = 18$. The experimental ionization energy of the argon atom is 15.75962 eV [3].

THE IONIZATION ENERGIES OF EIGHTEEN-ELECTRON ATOMS WITH A NUCLEAR CHARGE Z>18

Eighteen-electron atoms having $Z>18$ possess an external electric field given by Eq. (10.92). In this case, an energy minimum is achieved with conservation of momentum when the orbital angular momentum is such that $\mathbf{F}_{diamagnetic}$ is minimized while $\mathbf{F}_{mag\ 2}$ is maximized. With a filled 3p shell, the diamagnetic force due to the orbital angular momenta of the 3p electrons cancels that of the 2p electrons. Thus, the diamagnetic force (Eq. (10.258)), $\mathbf{F}_{diamagnetic}$, is zero:

$$\mathbf{F}_{diamagnetic}=0 \tag{10.388}$$

From Eqs. (10.205) and (10.261), $\mathbf{F}_{mag\ 2}$ corresponding to the spin and orbital angular momenta of the paired 2 p_x, p_y, and p_z electrons is:

$$\mathbf{F}_{mag\ 2}=\left(4+4+4\right)\frac{1}{Z}\frac{\hbar^2}{m_e r_{18}^2 r_{12}}\sqrt{s(s+1)}\mathbf{i}_{\mathbf{r}}=\frac{1}{Z}\frac{12\hbar^2}{m_e r_{18}^2 r_{12}}\sqrt{s(s+1)}\mathbf{i}_{\mathbf{r}} \tag{10.389}$$

the contribution from the 3p level (Eq. (10.264)) is:

$$\mathbf{F}_{mag\ 2}=\left(8+8+8\right)\frac{1}{Z}\frac{\hbar^2}{m_e r_{18}^2 r_{12}}\sqrt{s(s+1)}\mathbf{i}_{\mathbf{r}}=\frac{1}{Z}\frac{24\hbar^2}{m_e r_{18}^2 r_{12}}\sqrt{s(s+1)}\mathbf{i}_{\mathbf{r}} \tag{10.390}$$

and the contribution due to the spin and induced orbital angular momentum of the 3s orbital that achieves conservation of angular momentum given by Eq. (10.262) is:

$$\mathbf{F}_{mag\ 2}=\frac{1}{Z}\frac{4\hbar^2}{m_e r_{18}^2 r_{12}}\sqrt{s(s+1)}\mathbf{i}_{\mathbf{r}} \tag{10.391}$$

Thus, the total of $\mathbf{F}_{mag\ 2}$ is

$$\mathbf{F}_{mag\ 2}=\frac{1}{Z}\frac{40\hbar^2}{m_e r_{18}^2 r_{12}}\sqrt{s(s+1)}\mathbf{i}_{\mathbf{r}} \tag{10.392}$$

The diamagnetic force, $\mathbf{F}_{diamagnetic\ 2}$, due to the binding of the 3p-orbital electron having an electric field outside of its radius is given by Eq. (10.268).

$$\mathbf{F}_{diamagnetic\ 2}=-\left[\frac{Z-18}{Z-17}\right]\left(1-\frac{\sqrt{2}}{2}+\frac{1}{2}\right)\frac{r_{12}\hbar^2}{m_e r_{18}^4}10\sqrt{s(s+1)}\mathbf{i}_{\mathbf{r}} \tag{10.393}$$

In the case that $Z>18$, the radius of the outer electron is calculated by equating the outward centrifugal force to the sum of the electric (Eq. (10.379)), diamagnetic (Eqs. (10.388) and (10.393)), and paramagnetic (Eq. (10.392)) forces as follows:

$$\frac{m_e v_{18}^2}{r_{18}}=\frac{(Z-17)e^2}{4\pi\varepsilon_0 r_{18}^2}+\frac{40\hbar^2}{Zm_e r_{18}^2 r_{12}}\sqrt{s(s+1)}-\left[\frac{Z-18}{Z-17}\right]\left(1-\frac{\sqrt{2}}{2}+\frac{1}{2}\right)\frac{r_{12}\hbar^2}{m_e r_{18}^4}10\sqrt{s(s+1)} \tag{10.394}$$

Substitution of $v_{18}=\dfrac{\hbar}{m_e r_{18}}$ (Eq. (1.35)) and $s=\dfrac{1}{2}$ into Eq. (10.394) gives:

$$\frac{\hbar^2}{m_e r_{18}^3}=\frac{(Z-17)e^2}{4\pi\varepsilon_0 r_{18}^2}+\frac{40\hbar^2}{Zm_e r_{18}^2 r_{12}}\sqrt{\frac{3}{4}}-\left[\frac{Z-18}{Z-17}\right]\left(1-\frac{\sqrt{2}}{2}+\frac{1}{2}\right)\frac{r_{12}\hbar^2}{m_e r_{18}^4}10\sqrt{\frac{3}{4}} \tag{10.395}$$

The quadratic equation corresponding to Eq. (10.395) is:

$$\left(\frac{(Z-17)e^2}{4\pi\varepsilon_0}+\frac{40\hbar^2}{Zm_e r_{12}}\sqrt{\frac{3}{4}}\right)r_{18}^2-\frac{\hbar^2}{m_e}r_{18}-\left[\frac{Z-18}{Z-17}\right]\left(1-\frac{\sqrt{2}}{2}+\frac{1}{2}\right)\frac{r_{12}\hbar^2}{m_e}10\sqrt{\frac{3}{4}}=0 \tag{10.396}$$

$$r_{18}^2-\frac{\dfrac{\hbar^2}{m_e}}{\left(\dfrac{(Z-17)e^2}{4\pi\varepsilon_0}+\dfrac{40\hbar^2}{Zm_e r_{12}}\sqrt{\dfrac{3}{4}}\right)}r_{18}-\frac{\dfrac{\hbar^2}{m_e}\left[\dfrac{Z-18}{Z-17}\right]\left(1-\dfrac{\sqrt{2}}{2}+\dfrac{1}{2}\right)r_{12}10\sqrt{\dfrac{3}{4}}}{\left(\dfrac{(Z-17)e^2}{4\pi\varepsilon_0}+\dfrac{40\hbar^2}{Zm_e r_{12}}\sqrt{\dfrac{3}{4}}\right)}=0 \tag{10.397}$$

The solution of Eq. (10.397) using the quadratic formula is:

$$r_{18}=\frac{\dfrac{\dfrac{\hbar^2}{m_e}}{\left(\dfrac{(Z-17)e^2}{4\pi\varepsilon_0}+\dfrac{40\hbar^2}{Zm_e r_{12}}\sqrt{\dfrac{3}{4}}\right)}\pm\sqrt{\left(\dfrac{\dfrac{\hbar^2}{m_e}}{\left(\dfrac{(Z-17)e^2}{4\pi\varepsilon_0}+\dfrac{40\hbar^2}{Zm_e r_{12}}\sqrt{\dfrac{3}{4}}\right)}\right)^2+4\dfrac{\dfrac{\hbar^2}{m_e}\left[\dfrac{Z-18}{Z-17}\right]\left(1-\dfrac{\sqrt{2}}{2}+\dfrac{1}{2}\right)r_{12}10\sqrt{\dfrac{3}{4}}}{\left(\dfrac{(Z-17)e^2}{4\pi\varepsilon_0}+\dfrac{40\hbar^2}{Zm_e r_{12}}\sqrt{\dfrac{3}{4}}\right)}}}{2} \tag{10.398}$$

$$r_{18}=\frac{\dfrac{a_0}{\left((Z-17)+\dfrac{20\sqrt{3}}{Zr_{12}}\right)}\pm a_0\sqrt{\left(\dfrac{1}{\left((Z-17)+\dfrac{20\sqrt{3}}{Zr_{12}}\right)}\right)^2+\dfrac{20\sqrt{3}\left(\left[\dfrac{Z-18}{Z-17}\right]\left(1-\dfrac{\sqrt{2}}{2}+\dfrac{1}{2}\right)r_{12}\right)}{\left((Z-17)+\dfrac{20\sqrt{3}}{Zr_{12}}\right)}}}{2},\ r_{12}\ \textit{in units of}\ a_0 \tag{10.399}$$

where r_{12} is given by Eq. (10.255). The positive root of Eq. (10.399) must be taken in order that $r_{18}>0$. The final radius of electron 18, r_{18}, is given by Eq. (10.399); this is also the final radius of electrons 13, 14, 15, 16, and 17. The radii of several eighteen-electron atoms are given in Table 10.17.

The ionization energies for the eighteen-electron atoms with $Z>18$ are given by the electric energy, $E(electric)$, (Eq. (10.102) with the radii r_{18}, given by Eq. (10.399)).

$$E(Ionization)=-Electric\ Energy=\frac{(Z-17)e^2}{8\pi\varepsilon_0 r_{18}} \tag{10.400}$$

Since the relativistic corrections were small, the nonrelativistic ionization energies for experimentally measured eighteen-electron atoms are given in Table 10.17.

Table 10.17. Ionization energies for some eighteen-electron atoms.

18 e Atom	Z	r_1 (a_o) [a]	r_3 (a_o) [b]	r_{10} (a_o) [c]	r_{12} (a_o) [d]	r_{18} (a_o) [e]	Theoretical Ionization Energies [f] (eV)	Experimental Ionization Energies [g] (eV)	Relative Error [h]
Ar	18	0.05599	0.23839	0.28878	0.78276	0.86680	15.69651	15.75962	0.0040
K^+	19	0.05302	0.22503	0.26884	0.71450	0.85215	31.9330	31.63	-0.0096
Ca^{2+}	20	0.05035	0.21308	0.25149	0.65725	0.82478	49.4886	50.9131	0.0280
Sc^{3+}	21	0.04794	0.20235	0.23625	0.60857	0.76196	71.4251	73.4894	0.0281
Ti^{4+}	22	0.04574	0.19264	0.22276	0.56666	0.70013	97.1660	99.30	0.0215
V^{5+}	23	0.04374	0.18383	0.21074	0.53022	0.64511	126.5449	128.13	0.0124
Cr^{6+}	24	0.04191	0.17579	0.19995	0.49822	0.59718	159.4836	160.18	0.0043
Mn^{7+}	25	0.04022	0.16842	0.19022	0.46990	0.55552	195.9359	194.5	-0.0074
Fe^{8+}	26	0.03867	0.16165	0.18140	0.44466	0.51915	235.8711	233.6	-0.0097
Co^{9+}	27	0.03723	0.15540	0.17336	0.42201	0.48720	279.2670	275.4	-0.0140
Ni^{10+}	28	0.03589	0.14961	0.16601	0.40158	0.45894	326.1070	321.0	-0.0159
Cu^{11+}	29	0.03465	0.14424	0.15926	0.38305	0.43379	376.3783	369	-0.0200
Zn^{12+}	30	0.03349	0.13925	0.15304	0.36617	0.41127	430.0704	419.7	-0.0247

[a] Radius of the paired 1s inner electrons of eighteen-electron atoms from Eq. (10.51).

[b] Radius of the paired 2s inner electrons of eighteen-electron atoms from Eq. (10.62).

[c] Radius of the three sets of paired 2p inner electrons of eighteen-electron atoms from Eq. (10.212).

[d] Radius of the paired 3s inner electrons of eighteen-electron atoms from Eq. (10.255).

[e] Radius of the three sets of paired 3p outer electrons of eighteen-electron atoms from Eq. (10.399) for $Z > 18$ and Eq. (10.386) for Ar.

[f] Calculated ionization energies of eighteen-electron atoms given by the electric energy (Eq. (10.400)).

[g] From theoretical calculations, interpolation of isoelectronic and spectral series, and experimental data [2-3].

[h] (Experimental-theoretical)/experimental.

The agreement between the experimental and calculated values of Table 10.17 is well within the experimental capability of the spectroscopic determinations including the values at large Z which relies on X-ray spectroscopy. In this case, the experimental capability is about two to four significant figures which is consistent with the last column. Ionization energies are difficult to determine since the cut-off of the Rydberg series of lines at the ionization energy is often not observed. Thus, the argon atom isoelectronic series given in Table 10.17 [2-3] relies on theoretical calculations and interpolation of the Ar isoelectronic and Rydberg series as well as direct experimental data to extend the precision beyond the capability of X-ray spectroscopy. But, no assurances can be given that these techniques are correct, and they may not improve the results. The error given in the last column is very reasonable given the quality of the data.

GENERAL EQUATION FOR THE IONIZATION ENERGIES OF THIRTEEN THROUGH EIGHTEEN-ELECTRON ATOMS

Using the forces given by Eqs. (10.257-10.264), (10.268), and the radii r_{12} given by Eq. (10.255), the radii of the 3p electrons of all thirteen through eighteen-electron atoms may be solved exactly. The electric energy given by Eq. (10.102) gives the corresponding exact ionization energies. A summary of the parameters of the equations that determine the exact radii and ionization energies of all thirteen through eighteen-electron atoms is given in Table 10.18.

$\mathbf{F}_{ele}$ and $\mathbf{F}_{diamagnetic\ 2}$ given by Eqs. (10.257) and (10.268), respectively, are of the same form for all atoms with the appropriate nuclear charges and atomic radii. $\mathbf{F}_{diamagnetic}$ given by Eq. (10.258) and $\mathbf{F}_{mag\ 2}$ given by Eqs. (10.259-10.264) are of the same form with the appropriate factors that depend on the electron configuration wherein the electron configuration must be a minimum of energy.

For each n-electron atom having a central charge of Z times that of the proton and an electron configuration $1s^2 2s^2 2p^6 3s^2 3p^{n-12}$, there are two indistinguishable spin-paired electrons in an atomic orbital with radii r_1 and r_2 both given by Eq. (7.35) and (10.51).

$$r_1 = r_2 = a_0 \left[\frac{1}{Z-1} - \frac{\sqrt{\frac{3}{4}}}{Z(Z-1)} \right] \tag{10.401}$$

two indistinguishable spin-paired electrons in an atomic orbital with radii r_3 and r_4 both given by Eq. (10.62):

$$r_4 = r_3 = \frac{\dfrac{a_0\left(1-\dfrac{\sqrt{\frac{3}{4}}}{Z}\right)}{\left((Z-3)-\left(\frac{1}{4}-\frac{1}{Z}\right)\frac{\sqrt{\frac{3}{4}}}{r_1}\right)} \pm a_0\sqrt{\dfrac{\left(1-\dfrac{\sqrt{\frac{3}{4}}}{Z}\right)^2}{\left((Z-3)-\left(\frac{1}{4}-\frac{1}{Z}\right)\frac{\sqrt{\frac{3}{4}}}{r_1}\right)^2}+4\dfrac{\left[\frac{Z-3}{Z-2}\right]r_1 10\sqrt{\frac{3}{4}}}{\left((Z-3)-\left(\frac{1}{4}-\frac{1}{Z}\right)\frac{\sqrt{\frac{3}{4}}}{r_1}\right)}}}{2} \qquad (10.402)$$

r_1 *in units of* a_0

where r_1 is given by Eqs. (10.51) and (10.401), three sets of paired indistinguishable electrons in an atomic orbital with radius r_{10} given by Eq. (10.212).

$$r_{10} = \frac{\dfrac{a_0}{\left((Z-9)-\left(\frac{5}{24}-\frac{6}{Z}\right)\frac{\sqrt{3}}{r_3}\right)} \pm a_0\sqrt{\dfrac{\left(\frac{1}{\left((Z-9)-\left(\frac{5}{24}-\frac{6}{Z}\right)\frac{\sqrt{3}}{r_3}\right)}\right)^2}{+\dfrac{20\sqrt{3}\left(\left[\frac{Z-10}{Z-9}\right]\left(1-\frac{\sqrt{2}}{2}\right)r_3\right)}{\left((Z-9)-\left(\frac{5}{24}-\frac{6}{Z}\right)\frac{\sqrt{3}}{r_3}\right)}}}}{2}, \; r_3 \text{ in units of } a_0 \qquad (10.403)$$

where r_3 is given by Eqs. (10.62) and (10.402), two indistinguishable spin-paired electrons in an atomic orbital with radius r_{12} given by Eq. (10.255).

$$r_{12} = \frac{\dfrac{a_0}{\left((Z-11)-\left(\frac{1}{8}-\frac{3}{Z}\right)\frac{\sqrt{3}}{r_{10}}\right)} \pm a_0\sqrt{\dfrac{\left(\frac{1}{\left((Z-11)-\left(\frac{1}{8}-\frac{3}{Z}\right)\frac{\sqrt{3}}{r_{10}}\right)}\right)^2}{+\dfrac{20\sqrt{3}\left(\left[\frac{Z-12}{Z-11}\right]\left(1+\frac{\sqrt{2}}{2}\right)r_{10}\right)}{\left((Z-11)-\left(\frac{1}{8}-\frac{3}{Z}\right)\frac{\sqrt{3}}{r_{10}}\right)}}}}{2}, \; r_{10} \text{ in units of } a_0 \qquad (10.404)$$

where r_{10} is given by Eq. (10.212), and $n-12$ electrons in a 3p atomic orbital with radius r_n given by:

$$r_n = \frac{\dfrac{a_0}{\left((Z-(n-1))-\left(\frac{A}{8}-\frac{B}{2Z}\right)\frac{\sqrt{3}}{r_{12}}\right)} \pm a_0\sqrt{\dfrac{\left(\frac{1}{\left((Z-(n-1))-\left(\frac{A}{8}-\frac{B}{2Z}\right)\frac{\sqrt{3}}{r_{12}}\right)}\right)^2}{+\dfrac{20\sqrt{3}\left(\left[\frac{Z-n}{Z-(n-1)}\right]\left(1-\frac{\sqrt{2}}{2}+\frac{1}{2}\right)r_{12}\right)}{\left((Z-(n-1))-\left(\frac{A}{8}-\frac{B}{2Z}\right)\frac{\sqrt{3}}{r_{12}}\right)}}}}{2}, \; r_{12} \text{ in units of } a_0 \qquad (10.405)$$

where r_{12} is given by Eqs. (10.255) and (10.404), the parameter A given in Table 10.18 corresponds to the diamagnetic force, $\mathbf{F}_{diamagnetic}$, (Eq. (10.258)), and the parameter B given in Table 10.18 corresponds to the paramagnetic force, $\mathbf{F}_{mag\,2}$ (Eqs. (10.260-10.264)). The positive root of Eq. (10.405) must be taken in order that $r_n > 0$. The radii of several n-electron 3p atoms are given in Tables 10.10-10.17.

The ionization energy for the aluminum atom is given by Eq. (10.227). The ionization energies for the n-electron 3p atoms are given by the negative of the electric energy, $E(electric)$, (Eq. (10.102) with the radii, r_n, given by Eq. (10.405)):

$$E(Ionization) = -Electric\ Energy = \frac{(Z-(n-1))e^2}{8\pi\varepsilon_0 r_n} \tag{10.406}$$

Since the relativistic corrections were small, the nonrelativistic ionization energies for experimentally measured n-electron 3p atoms are given by Eqs. (10.405) and (10.406) in Tables 10.10-10.17.

Table 10.18. Summary of the parameters of thirteen through eighteen-electron atoms.

Atom Type	Electron Configuration	Ground State Term [a]	Orbital Arrangement of 3p Electrons (3p state)	Diamagnetic Force Factor A [b]	Paramagnetic Force Factor B [c]
Neutral 13 e Atom *Al*	$1s^2 2s^2 2p^6 3s^2 3p^1$	$^2P^0_{1/2}$	$\underline{\uparrow}\ \ \underline{\ \ }\ \ \underline{\ \ }$ 1 0 -1	$\frac{11}{3}$	0
Neutral 14 e Atom *Si*	$1s^2 2s^2 2p^6 3s^2 3p^2$	$^3P_0$	$\underline{\uparrow}\ \ \underline{\uparrow}\ \ \underline{\ \ }$ 1 0 -1	$\frac{7}{3}$	0
Neutral 15 e Atom *P*	$1s^2 2s^2 2p^6 3s^2 3p^3$	$^4S^0_{3/2}$	$\underline{\uparrow}\ \ \underline{\uparrow}\ \ \underline{\uparrow}$ 1 0 -1	$\frac{5}{3}$	2
Neutral 16 e Atom *S*	$1s^2 2s^2 2p^6 3s^2 3p^4$	$^3P_2$	$\underline{\uparrow\downarrow}\ \ \underline{\uparrow}\ \ \underline{\uparrow}$ 1 0 -1	$\frac{4}{3}$	1
Neutral 17 e Atom *Cl*	$1s^2 2s^2 2p^6 3s^2 3p^5$	$^2P^0_{3/2}$	$\underline{\uparrow\downarrow}\ \ \underline{\uparrow\downarrow}\ \ \underline{\uparrow}$ 1 0 -1	$\frac{2}{3}$	2
Neutral 18 e Atom *Ar*	$1s^2 2s^2 2p^6 3s^2 3p^6$	$^1S_0$	$\underline{\uparrow\downarrow}\ \ \underline{\uparrow\downarrow}\ \ \underline{\uparrow\downarrow}$ 1 0 -1	$\frac{1}{3}$	4
13 e Ion	$1s^2 2s^2 2p^6 3s^2 3p^1$	$^2P^0_{1/2}$	$\underline{\uparrow}\ \ \underline{\ \ }\ \ \underline{\ \ }$ 1 0 -1	$\frac{5}{3}$	12
14 e Ion	$1s^2 2s^2 2p^6 3s^2 3p^2$	$^3P_0$	$\underline{\uparrow}\ \ \underline{\uparrow}\ \ \underline{\ \ }$ 1 0 -1	$\frac{1}{3}$	16
15 e Ion	$1s^2 2s^2 2p^6 3s^2 3p^3$	$^4S^0_{3/2}$	$\underline{\uparrow}\ \ \underline{\uparrow}\ \ \underline{\uparrow}$ 1 0 -1	0	24
16 e Ion	$1s^2 2s^2 2p^6 3s^2 3p^4$	$^3P_2$	$\underline{\uparrow\downarrow}\ \ \underline{\uparrow}\ \ \underline{\uparrow}$ 1 0 -1	$\frac{1}{3}$	24
17 e Ion	$1s^2 2s^2 2p^6 3s^2 3p^5$	$^2P^0_{3/2}$	$\underline{\uparrow\downarrow}\ \ \underline{\uparrow\downarrow}\ \ \underline{\uparrow}$ 1 0 -1	$\frac{2}{3}$	32
18 e Ion	$1s^2 2s^2 2p^6 3s^2 3p^6$	$^1S_0$	$\underline{\uparrow\downarrow}\ \ \underline{\uparrow\downarrow}\ \ \underline{\uparrow\downarrow}$ 1 0 -1	0	40

[a] The theoretical ground state terms match those given by NIST [8].
[b] Eq. (10.258).
[c] Eqs. (10.260-10.264).

NINETEEN-ELECTRON ATOMS

Nineteen-electron atoms can be solved exactly using the results of the solutions of one, two, three, four, five, six, seven, eight, nine, ten, eleven, twelve, thirteen, fourteen, fifteen, sixteen, seventeen, and eighteen-electron atoms.

RADIUS AND IONIZATION ENERGY OF THE OUTER ELECTRON OF THE POTASSIUM ATOM

For each eighteen-electron atom having a central charge of Z times that of the proton, there are two indistinguishable spin-paired electrons in an atomic orbital with radii r_1 and r_2 both given by Eq. (7.35) (Eq. (10.51)), two indistinguishable spin-paired electrons in an atomic orbital with radii r_3 and r_4 both given by Eq. (10.62), three sets of paired electrons in an atomic orbital at r_{10} given by Eq. (10.212), two indistinguishable spin-paired electrons in an atomic orbital with radii r_{11} and r_{12} both given by Eq. (10.255), and three sets of paired electrons in an atomic orbital with radius r_{18} given by Eq. (10.399). For $Z \geq 19$, the next electron which binds to form the corresponding nineteen-electron atom is attracted by the central Coulomb field and is repelled by diamagnetic forces due to the 3 sets of spin-paired inner 3p electrons such that it forms an unpaired atomic orbital at radius r_{19}.

The central Coulomb force acts on the outer electron to cause it to bind wherein this electric force on the outer-most electron due to the nucleus and the inner eighteen electrons is given by Eq. (10.70) with the appropriate charge and radius:

$$\mathbf{F}_{ele} = \frac{(Z-18)e^2}{4\pi\varepsilon_0 r_{19}^2}\mathbf{i}_\mathbf{r} \tag{10.407}$$

for $r > r_{18}$.

The spherically symmetrical closed 3p shell of nineteen-electron atoms produces a diamagnetic force, $\mathbf{F}_{diamagnetic}$, that is equivalent to that of a closed s shell given by Eq. (10.11) with the appropriate radii except that the force is doubled due to the interaction of the 4s and 3p electrons as given by Eq. (10.96). The inner electrons remain at their initial radii, but cause a diamagnetic force according to Lenz's law that is:

$$\mathbf{F}_{diamagnetic} = -\frac{2\hbar^2}{4m_e r_{19}^2 r_{18}}\sqrt{s(s+1)}\mathbf{i}_\mathbf{r} \tag{10.408}$$

In addition to the spin-spin interaction between electron pairs, the three sets of 3p electrons are orbitally paired. As in the case of the sodium atom with the corresponding radii, the single 4s orbital of the potassium atom produces a magnetic field at the position of the three sets of spin-paired 3p electrons. In order for the electrons to remain spin and orbitally paired, a corresponding diamagnetic force, $\mathbf{F}_{diamagnetic\ 3}$, on electron nineteen from the three sets of spin-paired electrons that follows from the deviation given in the Eleven-Electron Atom section (Eq. (10.221)) is:

$$\mathbf{F}_{diamagnetic\ 3} = -\frac{1}{Z}\frac{12\hbar^2}{m_e r_{19}^3}\sqrt{s(s+1)}\mathbf{i}_\mathbf{r} \tag{10.409}$$

corresponding to the 3 p_x, p_y, and p_z electrons.

The outward centrifugal force on electron 19 is balanced by the electric force and the magnetic forces (on electron 19). The radius of the outer electron is calculated by equating the outward centrifugal force to the sum of the electric (Eq. (10.407)) and diamagnetic (Eqs. (10.408) and (10.409)) forces as follows:

$$\frac{m_e v_{19}^2}{r_{19}} = \frac{(Z-18)e^2}{4\pi\varepsilon_0 r_{19}^2} - \frac{2\hbar^2}{4m_e r_{19}^2 r_{18}}\sqrt{s(s+1)} - \frac{12\hbar^2}{Zm_e r_{19}^3}\sqrt{s(s+1)} \tag{10.410}$$

Substitution of $v_{19} = \frac{\hbar}{m_e r_{19}}$ (Eq. (1.35)) and $s = \frac{1}{2}$ into Eq. (10.410) gives:

$$\frac{\hbar^2}{m_e r_{19}^3} = \frac{(Z-18)e^2}{4\pi\varepsilon_0 r_{19}^2} - \frac{2\hbar^2}{4m_e r_{19}^2 r_{18}}\sqrt{\frac{3}{4}} - \frac{12\hbar^2}{Zm_e r_{19}^3}\sqrt{\frac{3}{4}} \tag{10.411}$$

$$r_{19} = \frac{\frac{\hbar^2}{m_e}\left(1+\frac{12}{Z}\sqrt{\frac{3}{4}}\right)}{\frac{(Z-18)e^2}{4\pi\varepsilon_0} - \frac{\hbar^2}{2m_e r_{18}}\sqrt{\frac{3}{4}}} \tag{10.412}$$

$$r_{19} = \frac{a_0\left(1+\frac{12}{Z}\sqrt{\frac{3}{4}}\right)}{(Z-18) - \frac{\sqrt{\frac{3}{4}}}{2r_{18}}},\ r_{18}\ \textit{in units of}\ a_0 \tag{10.413}$$

Substitution of $\frac{r_{18}}{a_0} = 0.85215$ (Eq. (10.399) with $Z = 19$) into Eq. (10.413) gives:

$$r_{19} = 3.14515 a_0 \tag{10.414}$$

The ionization energy of the potassium atom is given by the electric energy, $E(electric)$, (Eq. (10.102) with the radius, r_{19}, given by Eq. (10.414)).

$$E(ionization;\ K) = -Electric\ Energy = \frac{(Z-18)e^2}{8\pi\varepsilon_0 r_{19}} = 4.32596\ eV \tag{10.415}$$

where $r_{19} = 3.14515 a_0$ (Eq. (10.414)) and $Z = 19$. The experimental ionization energy of the potassium atom is $4.34066\ eV$ [3].

THE IONIZATION ENERGIES OF NINETEEN-ELECTRON ATOMS WITH A NUCLEAR CHARGE Z>19

Nineteen-electron atoms having $Z > 19$ possess an external electric field given by Eq. (10.92). Since there is a source of dissipative power, $\mathbf{J} \bullet \mathbf{E}$ of Eq. (10.27), the magnetic moments of the inner electrons may change due to the outer electron such that the energy of the nineteen-electron atom is lowered. The spherically symmetrical closed 3p shell of nineteen-electron atoms produces a diamagnetic force, $\mathbf{F}_{diamagnetic}$, that is equivalent to that of a closed s shell given by Eq. (10.11) with the appropriate radii except that the force is tripled due to the interaction of the 2p, 3s, and 3p electrons as discussed in the 3P-Orbital Electrons Based on an Energy Minimum section. The inner electrons remain at their initial radii, but cause a diamagnetic force according to Lenz's law that is:

$$\mathbf{F}_{diamagnetic} = -\frac{3\hbar^2}{4 m_e r_{19}^2 r_{18}} \sqrt{s(s+1)}\,\mathbf{i}_{\mathbf{r}} \tag{10.416}$$

In addition to the spin-spin interaction between electron pairs, the six sets of 2p and 3p electrons are orbitally paired. As in given in the Eleven-Electron Atom section, the single 4s orbital of each nineteen-electron atoms having $Z > 19$ produces a magnetic field at the position of the six sets of spin-paired 2p and 3p electrons. In order for the electrons to remain spin and orbitally paired, a corresponding diamagnetic force, $\mathbf{F}_{diamagnetic\ 3}$, on electron nineteen from the six sets of spin-paired electrons that follows from the deviation given in the Eleven-Electron Atom section (Eq. (10.221)) is:

$$\mathbf{F}_{diamagnetic\ 3} = -\frac{1}{Z}\frac{24\hbar^2}{m_e r_{19}^{\ 3}} \sqrt{s(s+1)}\,\mathbf{i}_{\mathbf{r}} \tag{10.417}$$

corresponding to the 2 and 3 p_x, p_y, and p_z electrons.

As shown in the P-Orbital Electrons Based on an Energy Minimum section for $\mathbf{F}_{diamagnetic\ 2}$ given by Eq. (10.93), the corresponding diamagnetic force for 2p electrons due to a relativistic effect with an electric field for $r > r_n$ (Eq. (10.35)) is dependent on the amplitude of the orbital energy. Using the orbital energy with $\ell = 1$ (Eq. (10.90)), the energy $m_e \Delta v^2$ of Eq. (10.29) is reduced by the factor of $\left(1 - \frac{\sqrt{2}}{2}\right)$ due to the contribution of the charge-density wave of the inner electrons at r_3. In addition, it was shown in the 3P-Orbital Electrons Based on an Energy Minimum section that the two 3s electrons contribute an energy factor based on Eq. (1.55) since the filled 2p orbitals with the maintenance of symmetry according to Eq. (10.72) requires that the diamagnetic force is due to the electrons at r_{10} acting on the electrons at r_{12} which complies with the reactive force, $\mathbf{F}_{diamagnetic\ 2}$, given by Eq. (10.229). Thus, $\mathbf{F}_{diamagnetic\ 2}$ for the factor from 3p electrons with $Z > n$ is reduced by the factor of $\left(1 - \frac{\sqrt{2}}{2} + \frac{1}{2}\right)$. Similarly, the factor for 4s electrons due to the inner 2p, 3s, and 3p electrons is cumulative. Thus, $\mathbf{F}_{diamagnetic\ 2}$ for 4s electrons with $Z > n$ is:

$$\mathbf{F}_{diamagnetic\ 2} = -\left[\frac{Z-n}{Z-(n-1)}\right]\left(1 - \frac{\sqrt{2}}{2} + \frac{1}{2} - \frac{\sqrt{2}}{2} + \frac{1}{2}\right)\frac{r_{18}\hbar^2}{m_e r_n^4} 10\sqrt{s(s+1)}\,\mathbf{i}_{\mathbf{r}} \tag{10.418}$$

For $n = 19$, $\mathbf{F}_{diamagnetic\ 2}$ is

$$\mathbf{F}_{diamagnetic\ 2} = -\left[\frac{Z-19}{Z-18}\right]\left(1 - \frac{\sqrt{2}}{2} + \frac{1}{2} - \frac{\sqrt{2}}{2} + \frac{1}{2}\right)\frac{r_{18}\hbar^2}{m_e r_{19}^4} 10\sqrt{s(s+1)}\,\mathbf{i}_{\mathbf{r}} \tag{10.419}$$

In the case that $Z > 19$, the radius of the outer electron is calculated by equating the outward centrifugal force to the sum of the electric (Eq. (10.407)) and diamagnetic (Eqs. (10.416), (10.417), and (10.419)) forces as follows:

$$\frac{m_e v_{19}^2}{r_{19}} = \frac{(Z-18)e^2}{4\pi\varepsilon_0 r_{19}^2} - \frac{3\hbar^2}{4m_e r_{19}^2 r_{18}}\sqrt{s(s+1)} - \frac{24\hbar^2}{Zm_e r_{19}^3}\sqrt{s(s+1)}$$

$$-\left[\frac{Z-19}{Z-18}\right]\left(1-\frac{\sqrt{2}}{2}+\frac{1}{2}-\frac{\sqrt{2}}{2}+\frac{1}{2}\right)\frac{r_{18}\hbar^2}{m_e r_{19}^4}10\sqrt{s(s+1)} \tag{10.420}$$

Substitution of $v_{19} = \dfrac{\hbar}{m_e r_{19}}$ (Eq. (1.35)) and $s = \dfrac{1}{2}$ into Eq. (10.420) gives:

$$\frac{\hbar^2}{m_e r_{19}^3} = \frac{(Z-18)e^2}{4\pi\varepsilon_0 r_{19}^2} - \frac{3\hbar^2}{4m_e r_{19}^2 r_{18}}\sqrt{\frac{3}{4}} - \frac{24\hbar^2}{Zm_e r_{19}^3}\sqrt{\frac{3}{4}} - \left[\frac{Z-19}{Z-18}\right]\left(1-\frac{\sqrt{2}}{2}+\frac{1}{2}-\frac{\sqrt{2}}{2}+\frac{1}{2}\right)\frac{r_{18}\hbar^2}{m_e r_{19}^4}10\sqrt{\frac{3}{4}} \tag{10.421}$$

The quadratic equation corresponding to Eq. (10.421) is

$$\left(\frac{(Z-18)e^2}{4\pi\varepsilon_0} - \frac{3\hbar^2}{4m_e r_{18}}\sqrt{\frac{3}{4}}\right)r_{19}^2 - \frac{\hbar^2}{m_e}\left(1+\frac{24\sqrt{\frac{3}{4}}}{Z}\right)r_{19} - \left[\frac{Z-19}{Z-18}\right]\left(1-\frac{\sqrt{2}}{2}+\frac{1}{2}-\frac{\sqrt{2}}{2}+\frac{1}{2}\right)\frac{r_{18}\hbar^2}{m_e}10\sqrt{\frac{3}{4}} = 0 \tag{10.422}$$

$$r_{19}^2 - \frac{\dfrac{\hbar^2}{m_e}\left(1+\dfrac{24\sqrt{\frac{3}{4}}}{Z}\right)}{\left(\dfrac{(Z-18)e^2}{4\pi\varepsilon_0} - \dfrac{3\hbar^2}{4m_e r_{18}}\sqrt{\frac{3}{4}}\right)}r_{19} - \frac{\left[\dfrac{Z-19}{Z-18}\right]\left(1-\dfrac{\sqrt{2}}{2}+\dfrac{1}{2}-\dfrac{\sqrt{2}}{2}+\dfrac{1}{2}\right)\dfrac{r_{18}\hbar^2}{m_e}10\sqrt{\frac{3}{4}}}{\left(\dfrac{(Z-18)e^2}{4\pi\varepsilon_0} - \dfrac{3\hbar^2}{4m_e r_{18}}\sqrt{\frac{3}{4}}\right)} = 0 \tag{10.423}$$

The solution of Eq. (10.423) using the quadratic formula is:

$$r_{19} = \frac{\dfrac{\dfrac{\hbar^2}{m_e}\left(1+\dfrac{24\sqrt{\frac{3}{4}}}{Z}\right)}{\left(\dfrac{(Z-18)e^2}{4\pi\varepsilon_0} - \dfrac{3\hbar^2}{4m_e r_{18}}\sqrt{\frac{3}{4}}\right)} \pm \sqrt{\left(\dfrac{\dfrac{\hbar^2}{m_e}\left(1+\dfrac{24\sqrt{\frac{3}{4}}}{Z}\right)}{\left(\dfrac{(Z-18)e^2}{4\pi\varepsilon_0} - \dfrac{3\hbar^2}{4m_e r_{18}}\sqrt{\frac{3}{4}}\right)}\right)^2 + 4\dfrac{\left[\dfrac{Z-19}{Z-18}\right]\left(1-\dfrac{\sqrt{2}}{2}+\dfrac{1}{2}-\dfrac{\sqrt{2}}{2}+\dfrac{1}{2}\right)\dfrac{r_{18}\hbar^2}{m_e}10\sqrt{\frac{3}{4}}}{\left(\dfrac{(Z-18)e^2}{4\pi\varepsilon_0} - \dfrac{3\hbar^2}{4m_e r_{18}}\sqrt{\frac{3}{4}}\right)}}}{2} \tag{10.424}$$

$$r_{19} = \frac{\dfrac{a_0\left(1+\dfrac{12\sqrt{3}}{Z}\right)}{\left((Z-18)-\dfrac{3\sqrt{3}}{8r_{18}}\right)} \pm a_0\sqrt{\left(\dfrac{1+\dfrac{12\sqrt{3}}{Z}}{\left((Z-18)-\dfrac{3\sqrt{3}}{8r_{18}}\right)}\right)^2 + \dfrac{20\sqrt{3}\left(\left[\dfrac{Z-19}{Z-18}\right]\left(1-\dfrac{\sqrt{2}}{2}+\dfrac{1}{2}-\dfrac{\sqrt{2}}{2}+\dfrac{1}{2}\right)r_{18}\right)}{\left((Z-18)-\dfrac{3\sqrt{3}}{8r_{18}}\right)}}}{2}, \; r_{18} \text{ in units of } a_0 \tag{10.425}$$

where r_{18} is given by Eq. (10.399). The positive root of Eq. (10.425) must be taken in order that $r_{19} > 0$. The radii of several nineteen-electron atoms are given in Table 10.19.

The ionization energies for the nineteen-electron atoms with $Z > 19$ are given by the electric energy, $E(electric)$, (Eq. (10.102) with the radii r_{19}, given by Eq. (10.425)):

$$E(Ionization) = -Electric\ Energy = \frac{(Z-18)e^2}{8\pi\varepsilon_0 r_{19}} \tag{10.426}$$

Since the relativistic corrections were small, the nonrelativistic ionization energies for experimentally measured nineteen-electron atoms are given in Table 10.19.

Table 10.19. Ionization energies for some nineteen-electron atoms.

19 e Atom	Z	r_1 (a_o) [a]	r_3 (a_o) [b]	r_{10} (a_o) [c]	r_{12} (a_o) [d]	r_{18} (a_o) [e]	r_{19} (a_o) [f]	Theoretical Ionization Energies [g] (eV)	Experimental Ionization Energies [h] (eV)	Relative Error [i]
K	19	0.05302	0.22503	0.26884	0.71450	0.85215	3.14515	4.32596	4.34066	0.0034
Ca^{+}	20	0.05035	0.21308	0.25149	0.65725	0.82478	2.40060	11.3354	11.87172	0.0452
Sc^{2+}	21	0.04794	0.20235	0.23625	0.60857	0.76196	1.65261	24.6988	24.75666	0.0023
Ti^{3+}	22	0.04574	0.19264	0.22276	0.56666	0.70013	1.29998	41.8647	43.2672	0.0324
V^{4+}	23	0.04374	0.18383	0.21074	0.53022	0.64511	1.08245	62.8474	65.2817	0.0373
Cr^{5+}	24	0.04191	0.17579	0.19995	0.49822	0.59718	0.93156	87.6329	90.6349	0.0331
Mn^{6+}	25	0.04022	0.16842	0.19022	0.46990	0.55552	0.81957	116.2076	119.203	0.0251
Fe^{7+}	26	0.03867	0.16165	0.18140	0.44466	0.51915	0.73267	148.5612	151.06	0.0165
Co^{8+}	27	0.03723	0.15540	0.17336	0.42201	0.48720	0.66303	184.6863	186.13	0.0078
Ni^{9+}	28	0.03589	0.14961	0.16601	0.40158	0.45894	0.60584	224.5772	224.6	0.0001
Cu^{10+}	29	0.03465	0.14424	0.15926	0.38305	0.43379	0.55797	268.2300	265.3	-0.0110
Zn^{11+}	30	0.03349	0.13925	0.15304	0.36617	0.41127	0.51726	315.6418	310.8	-0.0156

[a] Radius of the paired 1s inner electrons of nineteen-electron atoms from Eq. (10.51).

[b] Radius of the paired 2s inner electrons of nineteen-electron atoms from Eq. (10.62).

[c] Radius of the three sets of paired 2p inner electrons of nineteen-electron atoms from Eq. (10.212).

[d] Radius of the paired 3s inner electrons of nineteen-electron atoms from Eq. (10.255).

[e] Radius of the three sets of paired 3p inner electrons of nineteen-electron atoms from Eq. (10.399).

[f] Radius of the unpaired 4s outer electron of nineteen-electron atoms from Eq. (10.425) for $Z > 19$ and Eq. (10.414) for K.

[g] Calculated ionization energies of nineteen-electron atoms given by the electric energy (Eq. (10.426)).

[h] From theoretical calculations, interpolation of isoelectronic and spectral series, and experimental data [2-3].

[i] (Experimental-theoretical)/experimental.

The agreement between the experimental and calculated values of Table 10.19 is well within the experimental capability of the spectroscopic determinations including the values at large Z which relies on X-ray spectroscopy. In this case, the experimental capability is about three to four significant figures which is consistent with the last column. Ionization energies are difficult to determine since the cut-off of the Rydberg series of lines at the ionization energy is often not observed. Thus, the potassium atom isoelectronic series given in Table 10.19 [2-3] relies on theoretical calculations and interpolation of the K isoelectronic and Rydberg series as well as direct experimental data to extend the precision beyond the capability of X-ray spectroscopy. But, no assurances can be given that these techniques are correct, and they may not improve the results. The error given in the last column is very reasonable given the quality of the data.

TWENTY-ELECTRON ATOMS

Twenty-electron atoms can be solved exactly using the results of the solutions of one, two, three, four, five, six, seven, eight, nine, ten, eleven, twelve, thirteen, fourteen, fifteen, sixteen, seventeen, eighteen, and nineteen-electron atoms.

RADIUS AND IONIZATION ENERGY OF THE OUTER ELECTRON OF THE CALCIUM ATOM

For each nineteen-electron atom having a central charge of Z times that of the proton, there are two indistinguishable spin-paired electrons in an atomic orbital with radii r_1 and r_2 both given by Eq. (7.35) (Eq. (10.51)), two indistinguishable spin-paired electrons in an atomic orbital with radii r_3 and r_4 both given by Eq. (10.62), three sets of paired electrons in an atomic orbital at r_{10} given by Eq. (10.212), two indistinguishable spin-paired electrons in an atomic orbital with radii r_{11} and r_{12} both given by Eq. (10.255), three sets of paired electrons in an atomic orbital with radius r_{18} given by Eq. (10.399), and an unpaired electron in an atomic orbital with radius r_{19} given by Eq. (10.425). For $Z \geq 20$, the next electron which binds to form the corresponding twenty-electron atom is attracted by the central Coulomb field and the spin-pairing force with the unpaired 4s inner electron and is repelled by diamagnetic forces due to the 3 sets of spin-paired inner 3p electrons such that it forms an unpaired atomic orbital at radius r_{20}.

The central Coulomb force acts on the outer electron to cause it to bind wherein this electric force on the outer-most electron due to the nucleus and the inner nineteen electrons is given by Eq. (10.70) with the appropriate charge and radius:

$$\mathbf{F}_{ele} = \frac{(Z-19)e^2}{4\pi\varepsilon_0 r_{20}^2}\mathbf{i}_\mathbf{r} \tag{10.427}$$

for $r > r_{19}$.

The forces for the calcium atom follow from those of the magnesium atom given in the Twelve-Electron Atom section. The outer electron which binds to form the corresponding twenty-electron atom becomes spin-paired with the unpaired inner electron such that they become indistinguishable with the same radius $r_{19} = r_{20}$ corresponding to a filled 4s shell. The corresponding spin-pairing force $\mathbf{F}_{mag}$ is given by Eqs. (7.24) and (10.239).

$$\mathbf{F}_{mag} = \frac{1}{Z}\frac{\hbar^2}{m_e r_{20}^3}\sqrt{s(s+1)}\mathbf{i}_\mathbf{r} \tag{10.428}$$

The spherically symmetrical closed 3p shell of twenty-electron atoms produces a diamagnetic force, $\mathbf{F}_{diamagnetic}$, that is equivalent to that of a closed s shell given by Eq. (10.11) with the appropriate radii. The inner electrons remain at their initial radii, but cause a diamagnetic force according to Lenz's law that is

$$\mathbf{F}_{diamagnetic} = -\frac{\hbar^2}{4m_e r_{20}^2 r_{18}}\sqrt{s(s+1)}\mathbf{i}_\mathbf{r} \tag{10.429}$$

In addition to the paramagnetic spin-pairing force between the nineteenth electron initially at radius r_{19}, the pairing causes the diamagnetic interaction between the outer electrons and the inner electrons given by Eq. (10.11) to vanish, except for an electrodynamic effect for $Z > 20$ described in the Two-Electron Atoms section, since upon pairing the magnetic field of the outer electrons becomes zero. Using Eqs. (10.55) and (10.240), $\mathbf{F}_{mag\ 2}$ due to the three 3p orbitals is given by:

$$\mathbf{F}_{mag\ 2} = \frac{3}{Z}\frac{\hbar^2}{m_e r_{20} r_{18}^2}\sqrt{s(s+1)}\mathbf{i}_\mathbf{r} \tag{10.430}$$

In addition to the spin-spin interactions between electron pairs, the three sets of 2p and 3p electrons are orbitally paired. The 4s electrons of the calcium atom produce a magnetic field at the position of the six sets of spin-paired 2p and 3p electrons which interact as described in the P-Orbital Electrons Based on an Energy Minimum section. In order for the electrons to remain spin and orbitally paired, the corresponding diamagnetic force, $\mathbf{F}_{diamagnetic\ 3}$, on electron twenty from the six sets of spin-paired electrons that follows from the deviation given in the Eleven-Electron Atom section (Eq. (10.221)) is:

$$\mathbf{F}_{diamagnetic\ 3} = -\frac{1}{Z}\frac{24\hbar^2}{m_e r_{20}^{\ 3}}\sqrt{s(s+1)}\mathbf{i}_\mathbf{r} \tag{10.431}$$

corresponding to the 2 and 3 p_x, p_y, and p_z electrons.

The outward centrifugal force on electron 20 is balanced by the electric force and the magnetic forces (on electron 20). The radius of the outer electron is calculated by equating the outward centrifugal force to the sum of the electric (Eq. (10.427)), diamagnetic (Eq. (10.428-10.429) and (10.431)), and paramagnetic (Eq. (10.430)) forces as follows:

$$\frac{m_e v_{20}^2}{r_{20}} = \frac{(Z-19)e^2}{4\pi\varepsilon_0 r_{20}^2} - \frac{\hbar^2}{4m_e r_{20}^2 r_{18}}\sqrt{s(s+1)} + \frac{3\hbar^2}{Zm_e r_{20}^2 r_{18}}\sqrt{s(s+1)} - \frac{24\hbar^2}{Zm_e r_{20}^3}\sqrt{s(s+1)} + \frac{\hbar^2}{Zm_e r_{20}^3}\sqrt{s(s+1)} \tag{10.432}$$

Substitution of $v_{20} = \frac{\hbar}{m_e r_{20}}$ (Eq. (1.35)) and $s = \frac{1}{2}$ into Eq. (10.432) gives:

$$\frac{\hbar^2}{m_e r_{20}^3} = \frac{(Z-19)e^2}{4\pi\varepsilon_0 r_{20}^2} - \frac{\hbar^2}{4m_e r_{20}^2 r_{18}}\sqrt{\frac{3}{4}} + \frac{3\hbar^2}{Zm_e r_{20}^2 r_{18}}\sqrt{\frac{3}{4}} - \frac{24\hbar^2}{Zm_e r_{20}^3}\sqrt{\frac{3}{4}} + \frac{\hbar^2}{Zm_e r_{20}^3}\sqrt{\frac{3}{4}} \tag{10.433}$$

$$r_{20} = \frac{\frac{\hbar^2}{m_e}\left(1 + \frac{23\sqrt{\frac{3}{4}}}{Z}\right)}{\frac{(Z-19)e^2}{4\pi\varepsilon_0} - \left(\frac{1}{4} - \frac{3}{Z}\right)\frac{\hbar^2}{m_e r_{18}}\sqrt{\frac{3}{4}}} \tag{10.434}$$

$$r_{20} = \frac{a_0\left(1+\frac{23\sqrt{\frac{3}{4}}}{Z}\right)}{(Z-19)-\left(\frac{1}{4}-\frac{3}{Z}\right)\frac{\sqrt{\frac{3}{4}}}{r_{18}}},\ r_{18}\ in\ units\ of\ a_0 \tag{10.435}$$

Substitution of $\frac{r_{18}}{a_0} = 0.82478$ (Eq. (10.399) with $Z = 20$) into Eq. (10.435) gives:

$$r_{20} = 2.23009 a_0 \tag{10.436}$$

The ionization energy of the calcium atom is given by the electric energy, $E(electric)$, (Eq. (10.102) with the radius, r_{20}, given by Eq. (10.435)).

$$E(ionization;\ Ca) = -Electric\ Energy = \frac{(Z-19)e^2}{8\pi\varepsilon_0 r_{20}} = 6.10101\ eV \tag{10.437}$$

where $r_{20} = 2.23009 a_0$ (Eq. (10.435)) and $Z = 20$. The experimental ionization energy of the calcium atom is $6.11316\ eV$ [3].

THE IONIZATION ENERGIES OF TWENTY-ELECTRON ATOMS WITH A NUCLEAR CHARGE Z>20

Nineteen-electron atoms having $Z > 20$ possess an external electric field given by Eq. (10.92). Since there is a source of dissipative power, $\mathbf{J} \bullet \mathbf{E}$ of Eq. (10.27), the magnetic moments of the inner electrons may change due to the outer electron such that the energy of the nineteen-electron atom is lowered. The spherically symmetrical closed 3p shell of twenty-electron atoms produces a diamagnetic force, $\mathbf{F}_{diamagnetic}$, that is equivalent to that of a closed s shell given by Eq. (10.11) with the appropriate radii except that the force is doubled (Eq. (10.96)) due to the interaction of the 2p, 3s, and 3p electrons as discussed in the 3P-Orbital Electrons Based on an Energy Minimum section with the cancellation of the contribution of the 3s orbital by the 4s orbital. The inner electrons remain at their initial radii, but cause a diamagnetic force according to Lenz's law that is:

$$\mathbf{F}_{diamagnetic} = -\frac{2\hbar^2}{4m_e r_{20}^2 r_{18}}\sqrt{s(s+1)}\mathbf{i}_\mathbf{r} \tag{10.438}$$

In addition to the spin-spin interaction between electron pairs, the six sets of 2p and 3p electrons are orbitally paired. As in given in the Eleven-Electron Atom section, the single 4s orbital of each twenty-electron atoms having $Z > 20$ produces a magnetic field at the position of the six sets of spin-paired 2p and 3p electrons. In order for the electrons to remain spin and orbitally paired, the corresponding diamagnetic force, $\mathbf{F}_{diamagnetic\ 3}$, on electron twenty from the six sets of spin-paired electrons given by Eq. (10.221) is:

$$\mathbf{F}_{diamagnetic\ 3} = -\frac{1}{Z}\frac{24\hbar^2}{m_e r_{20}^{\ 3}}\sqrt{s(s+1)}\mathbf{i}_\mathbf{r} \tag{10.439}$$

corresponding to the 2 and 3 p_x, p_y, and p_z electrons.

From Eq. (10.418), the diamagnetic force, $\mathbf{F}_{diamagnetic\ 2}$, due to a relativistic effect with an electric field for $r > r_{20}$ (Eq. (10.35)) is:

$$\mathbf{F}_{diamagnetic\ 2} = -\left[\frac{Z-20}{Z-19}\right]\left(1-\frac{\sqrt{2}}{2}+\frac{1}{2}-\frac{\sqrt{2}}{2}+\frac{1}{2}\right)\frac{r_{18}\hbar^2}{m_e r_{20}^4}10\sqrt{s(s+1)}\mathbf{i}_\mathbf{r} \tag{10.440}$$

In the case that $Z > 20$, the radius of the outer electron is calculated by equating the outward centrifugal force to the sum of the electric (Eq. (10.427)) and diamagnetic (Eqs. (10.438-10.440)) forces as follows:

$$\frac{m_e v_{20}^2}{r_{20}} = \frac{(Z-19)e^2}{4\pi\varepsilon_0 r_{20}^2} - \frac{2\hbar^2}{4m_e r_{20}^2 r_{18}}\sqrt{s(s+1)} - \frac{24\hbar^2}{Z m_e r_{20}^3}\sqrt{s(s+1)}$$
$$-\left[\frac{Z-20}{Z-19}\right]\left(1-\frac{\sqrt{2}}{2}+\frac{1}{2}-\frac{\sqrt{2}}{2}+\frac{1}{2}\right)\frac{r_{18}\hbar^2}{m_e r_{20}^4}10\sqrt{s(s+1)} \tag{10.441}$$

Substitution of $v_{20} = \frac{\hbar}{m_e r_{20}}$ (Eq. (1.35)) and $s = \frac{1}{2}$ into Eq. (10.441) gives:

$$\frac{\hbar^2}{m_e r_{20}^3}=\frac{(Z-19)e^2}{4\pi\varepsilon_0 r_{20}^2}-\frac{2\hbar^2}{4m_e r_{20}^2 r_{18}}\sqrt{\frac{3}{4}}-\frac{24\hbar^2}{Zm_e r_{20}^3}\sqrt{\frac{3}{4}}$$
$$-\left[\frac{Z-20}{Z-19}\right]\left(1-\frac{\sqrt{2}}{2}+\frac{1}{2}-\frac{\sqrt{2}}{2}+\frac{1}{2}\right)\frac{r_{18}\hbar^2}{m_e r_{20}^4}10\sqrt{\frac{3}{4}} \tag{10.442}$$

The quadratic equation corresponding to Eq. (10.442) is:

$$r_{20}^2-\frac{\dfrac{\hbar^2}{m_e}\left(1+\dfrac{24\sqrt{\frac{3}{4}}}{Z}\right)}{\left(\dfrac{(Z-19)e^2}{4\pi\varepsilon_0}-\dfrac{2\hbar^2}{4m_e r_{18}}\sqrt{\frac{3}{4}}\right)}r_{20}-\frac{\left[\dfrac{Z-20}{Z-19}\right]\left(1-\dfrac{\sqrt{2}}{2}+\dfrac{1}{2}-\dfrac{\sqrt{2}}{2}+\dfrac{1}{2}\right)\dfrac{r_{18}\hbar^2}{m_e}10\sqrt{\frac{3}{4}}}{\left(\dfrac{(Z-19)e^2}{4\pi\varepsilon_0}-\dfrac{2\hbar^2}{4m_e r_{18}}\sqrt{\frac{3}{4}}\right)}=0 \tag{10.443}$$

The solution of Eq. (10.443) using the quadratic formula is:

$$r_{20}=\frac{\dfrac{\dfrac{\hbar^2}{m_e}\left(1+\dfrac{24\sqrt{\frac{3}{4}}}{Z}\right)}{\left(\dfrac{(Z-19)e^2}{4\pi\varepsilon_0}-\dfrac{2\hbar^2}{4m_e r_{18}}\sqrt{\frac{3}{4}}\right)}\pm\sqrt{\left(\dfrac{\dfrac{\hbar^2}{m_e}\left(1+\dfrac{24\sqrt{\frac{3}{4}}}{Z}\right)}{\left(\dfrac{(Z-19)e^2}{4\pi\varepsilon_0}-\dfrac{2\hbar^2}{4m_e r_{18}}\sqrt{\frac{3}{4}}\right)}\right)^2+4\dfrac{\left[\dfrac{Z-20}{Z-19}\right]\left(1-\dfrac{\sqrt{2}}{2}+\dfrac{1}{2}-\dfrac{\sqrt{2}}{2}+\dfrac{1}{2}\right)\dfrac{r_{18}\hbar^2}{m_e}10\sqrt{\frac{3}{4}}}{\left(\dfrac{(Z-19)e^2}{4\pi\varepsilon_0}-\dfrac{2\hbar^2}{4m_e r_{18}}\sqrt{\frac{3}{4}}\right)}}}{2} \tag{10.444}$$

$$r_{20}=\frac{\dfrac{a_0\left(1+\dfrac{12\sqrt{3}}{Z}\right)}{\left((Z-19)-\dfrac{\sqrt{3}}{4r_{18}}\right)}\pm a_0\sqrt{\left(\dfrac{1+\dfrac{12\sqrt{3}}{Z}}{\left((Z-19)-\dfrac{\sqrt{3}}{4r_{18}}\right)}\right)^2+\dfrac{20\sqrt{3}\left(\left[\dfrac{Z-20}{Z-19}\right]\left(1-\dfrac{\sqrt{2}}{2}+\dfrac{1}{2}-\dfrac{\sqrt{2}}{2}+\dfrac{1}{2}\right)r_{18}\right)}{\left((Z-19)-\dfrac{\sqrt{3}}{4r_{18}}\right)}}}{2},\ r_{18}\ \textit{in units of}\ a_0 \tag{10.445}$$

where r_{18} is given by Eq. (10.399). The positive root of Eq. (10.445) must be taken in order that $r_{20}>0$. The final radius of electron 20, r_{20}, is given by Eq. (10.445); this is also the final radius of electron 19. The radii of several twenty-electron atoms are given in Table 10.20. The general equation for the ionization energies of atoms having an outer s-shell is given in the General Equation for the Ionization Energies of Atoms Having an Outer S-Shell section.

The ionization energies for the twenty-electron atoms with $Z>20$ are given by the electric energy, $E(electric)$, (Eq. (10.102) with the radii r_{20}, given by Eq. (10.445)).

$$E(Ionization)=-Electric\ Energy=\frac{(Z-19)e^2}{8\pi\varepsilon_0 r_{20}} \tag{10.446}$$

Since the relativistic corrections were small, the nonrelativistic ionization energies for experimentally measured twenty-electron atoms are given in Table 10.20.

Table 10.20. Ionization energies for some twenty-electron atoms.

20 e Atom	Z	r_1 (a_o) [a]	r_3 (a_o) [b]	r_{10} (a_o) [c]	r_{12} (a_o) [d]	r_{18} (a_o) [e]	r_{20} (a_o) [f]	Theoretical Ionization Energies [g] (eV)	Experimental Ionization Energies [h] (eV)	Relative Error [i]
Ca	20	0.05035	0.21308	0.25149	0.65725	0.82478	2.23009	6.10101	6.11316	0.0020
Sc^{+}	21	0.04794	0.20235	0.23625	0.60857	0.76196	2.04869	13.2824	12.79967	-0.0377
Ti^{2+}	22	0.04574	0.19264	0.22276	0.56666	0.70013	1.48579	27.4719	27.4917	0.0007
V^{3+}	23	0.04374	0.18383	0.21074	0.53022	0.64511	1.19100	45.6956	46.709	0.0217
Cr^{4+}	24	0.04191	0.17579	0.19995	0.49822	0.59718	1.00220	67.8794	69.46	0.0228
Mn^{5+}	25	0.04022	0.16842	0.19022	0.46990	0.55552	0.86867	93.9766	95.6	0.0170
Fe^{6+}	26	0.03867	0.16165	0.18140	0.44466	0.51915	0.76834	123.9571	124.98	0.0082
Co^{7+}	27	0.03723	0.15540	0.17336	0.42201	0.48720	0.68977	157.8012	157.8	0.0000
Ni^{8+}	28	0.03589	0.14961	0.16601	0.40158	0.45894	0.62637	195.4954	193	-0.0129
Cu^{9+}	29	0.03465	0.14424	0.15926	0.38305	0.43379	0.57401	237.0301	232	-0.0217
Zn^{10+}	30	0.03349	0.13925	0.15304	0.36617	0.41127	0.52997	282.3982	274	-0.0307

[a] Radius of the paired 1s inner electrons of twenty-electron atoms from Eq. (10.51).

[b] Radius of the paired 2s inner electrons of twenty-electron atoms from Eq. (10.62).

[c] Radius of the three sets of paired 2p inner electrons of twenty-electron atoms from Eq. (10.212)).

[d] Radius of the paired 3s inner electrons of twenty-electron atoms from Eq. (10.255)).

[e] Radius of the three sets of paired 3p inner electrons of twenty-electron atoms from Eq. (10.399).

[f] Radius of the paired 4s outer electrons of twenty-electron atoms from Eq. (10.445) for $Z > 20$ and Eq. (10.436) for *Ca*.

[g] Calculated ionization energies of twenty-electron atoms given by the electric energy (Eq. (10.446)).

[h] From theoretical calculations, interpolation of isoelectronic and spectral series, and experimental data [2-3].

[i] (Experimental-theoretical)/experimental.

The agreement between the experimental and calculated values of Table 10.20 is well within the experimental capability of the spectroscopic determinations including the values at large Z which relies on X-ray spectroscopy. In this case, the experimental capability is about three to four significant figures which are consistent with the last column. Ionization energies are difficult to determine since the cut-off of the Rydberg series of lines at the ionization energy is often not observed. Thus, the calcium atom isoelectronic series given in Table 10.20 [2-3] relies on theoretical calculations and interpolation of the Ca isoelectronic and Rydberg series as well as direct experimental data to extend the precision beyond the capability of X-ray spectroscopy. But, no assurances can be given that these techniques are correct, and they may not improve the results. The error given in the last column is very reasonable given the quality of the data.

GENERAL EQUATION FOR THE IONIZATION ENERGIES OF ATOMS HAVING AN OUTER S-SHELL

The derivation of the radii and energies of the 1s, 2s, 3s, and 4s electrons is given in the One-Electron Atoms, the Two-Electron Atoms, the Three-Electron Atoms, the Four-Electron Atoms, the Eleven-Electron Atoms, the Twelve-Electron Atoms, the Nineteen-Electron Atoms, and the Twenty-Electron Atoms sections. Similarly, to Eqs. (10.216) and (10.405), the general equation for the radii of s electrons is given by

$$r_n = \frac{\dfrac{a_0\left(1+(C-D)\dfrac{\sqrt{3}}{2Z}\right)}{\left((Z-(n-1))-\left(\dfrac{A}{8}-\dfrac{B}{2Z}\right)\dfrac{\sqrt{3}}{r_m}\right)} \pm a_0\sqrt{\left(\dfrac{\left(1+(C-D)\dfrac{\sqrt{3}}{2Z}\right)}{\left((Z-(n-1))-\left(\dfrac{A}{8}-\dfrac{B}{2Z}\right)\dfrac{\sqrt{3}}{r_m}\right)}\right)^2 + \dfrac{20\sqrt{3}\left(\left[\dfrac{Z-n}{Z-(n-1)}\right]Er_m\right)}{\left((Z-(n-1))-\left(\dfrac{A}{8}-\dfrac{B}{2Z}\right)\dfrac{\sqrt{3}}{r_m}\right)}}}{2} \qquad (10.447)$$

r_m *in units of* a_0

where Z is the nuclear charge, n is the number of electrons, r_m is the radius of the preceding filled shell, the parameter A given

in Table 10.21 corresponds to the diamagnetic force, $\mathbf{F}_{diamagnetic}$, (Eq. (10.11)), the parameter B given in Table 10.21 corresponds to the paramagnetic force, $\mathbf{F}_{mag\ 2}$ (Eq. (10.55)), the parameter C given in Table 10.21 corresponds to the diamagnetic force, $\mathbf{F}_{diamagnetic\ 3}$, (Eq. (10.221)), the parameter D given in Table 10.21 corresponds to the paramagnetic force, $\mathbf{F}_{mag}$, (Eq. (7.24)), and the parameter E given in Table 10.21 corresponds to the diamagnetic force, $\mathbf{F}_{diamagnetic\ 2}$, (Eqs. (10.35), (10.229), and (10.418)). The positive root of Eq. (10.447) must be taken in order that $r_n > 0$. The radii of several n-electron atoms having an outer s shell are given in Tables 1.3, 1.5, 7.1, 10.1, 10.2, 10.10, 10.11, 10.19, and 10.20.

The ionization energy for atoms having an outer s-shell are given by the negative of the electric energy, $E(electric)$, (Eq. (10.102) with the radii, r_n, given by Eq. (10.447)).

$$E(Ionization) = -Electric\ Energy = \frac{(Z-(n-1))e^2}{8\pi\varepsilon_0 r_n} \tag{10.448}$$

except that minor corrections due to the magnetic energy must be included in cases wherein the s electron does not couple to p electrons as given in Eqs. (7.44), (7.63), (10.25), (10.48), (10.66), and (10.68). Since the relativistic corrections were small except for one, two, and three-electron atoms, the nonrelativistic ionization energies for experimentally measured n-electron, s-filling atoms are given in most cases by Eqs. (10.447) and (10.448). The ionization energies of several n-electron atoms having an outer s shell are given in Tables 1.3, 1.5, 7.1, 10.1, 10.2, 10.10, 10.11, 10.19, and 10.20.

Table 10.21. Summary of the parameters of atoms filling the 1s, 2s, 3s, and 4s orbitals.

Atom Type	Electron Configuration	Ground State Term [a]	Orbital Arrangement of s Electrons (s state)	Diamag. Force Factor A [b]	Paramag. Force Factor B [c]	Diamag. Force Factor C [d]	Paramag. Force Factor D [e]	Diamag. Force Factor E [f]
Neutral 1 e Atom *H*	$1s^1$	$^2S_{1/2}$	$\underline{\uparrow}$ 1s	0	0	0	0	0
Neutral 2 e Atom *He*	$1s^2$	$^1S_0$	$\underline{\uparrow\ \downarrow}$ 1s	0	0	0	1	0
Neutral 3 e Atom *Li*	$2s^1$	$^2S_{1/2}$	$\underline{\uparrow}$ 2s	1	0	0	0	0
Neutral 11 e Atom *Na*	$1s^2 2s^2 2p^6 3s^1$	$^2S_{1/2}$	$\underline{\uparrow}$ 3s	1	0	8	0	0
Neutral 12 e Atom *Mg*	$1s^2 2s^2 2p^6 3s^2$	$^1S_0$	$\underline{\uparrow\ \downarrow}$ 3s	1	3	12	1	0
Neutral 19 e Atom *K*	$1s^2 2s^2 2p^6 3s^2 3p^6 4s^1$	$^2S_{1/2}$	$\underline{\uparrow}$ 4s	2	0	12	0	0
Neutral 20 e Atom *Ca*	$1s^2 2s^2 2p^6 3s^2 3p^6 4s^2$	$^1S_0$	$\underline{\uparrow\ \downarrow}$ 4s	1	3	24	1	0
1 e Ion	$1s^1$	$^2S_{1/2}$	$\underline{\uparrow}$ 1s	0	0	0	0	0
2 e Ion	$1s^2$	$^1S_0$	$\underline{\uparrow\ \downarrow}$ 1s	0	0	0	1	0

Atom Type	Electron Configuration	Ground State Term [a]	Orbital Arrangement of s Electrons (s state)	Diamag. Force Factor A [b]	Paramag. Force Factor B [c]	Diamag. Force Factor C [d]	Paramag. Force Factor D [e]	Diamag. Force Factor E [f]
3 e Ion	$2s^1$	${}^2S_{1/2}$	$\underline{\uparrow}$ 2s	1	0	0	0	1
4 e Ion	$2s^2$	${}^1S_0$	$\underline{\uparrow\downarrow}$ 2s	1	0	0	1	1
11 e Ion	$1s^2 2s^2 2p^6 3s^1$	${}^2S_{1/2}$	$\underline{\uparrow}$ 3s	1	4	8	0	$1+\frac{\sqrt{2}}{2}$
12 e Ion	$1s^2 2s^2 2p^6 3s^2$	${}^1S_0$	$\underline{\uparrow\downarrow}$ 3s	1	6	0	0	$1+\frac{\sqrt{2}}{2}$
19 e Ion	$1s^2 2s^2 2p^6 3s^2 3p^6 4s^1$	${}^2S_{1/2}$	$\underline{\uparrow}$ 4s	3	0	24	0	$2-\sqrt{2}$
20 e Ion	$1s^2 2s^2 2p^6 3s^2 3p^6 4s^2$	${}^1S_0$	$\underline{\uparrow\downarrow}$ 4s	2	0	24	0	$2-\sqrt{2}$

[a] The theoretical ground state terms match those given by NIST [8].
[b] Eq. (10.11).
[c] Eq. (10.55).
[d] Eq. (10.221).
[e] Eq. (7.24).
[f] Eqs. (10.35), (10.229), and (10.418).

The physical approach was applied to multielectron atoms that were solved exactly disproving the deep-seated view that such exact solutions cannot exist according to quantum mechanics. The predictions of the ionization energies for one through twenty-electron atoms are in remarkable agreement with the experimental values known for 400 atoms and ions. The trends of the radii also generally agree with those published [9], but the radii cannot be taken as the contact radii based on nuclear separation in molecules and solids. If the outer most electron of the negative ion was at the location of that of the positive ion, then the potential energies would be the same. Since the ionization energies of positive ions are much greater than the electron affinities of negative ions, the positive ions must have smaller radii. Furthermore the size taken as the contact distance can not be correct since the electron-electron repulsion energies would be dominant.

THE ELECTRON CONFIGURATION OF ATOMS

The electrons of multielectron atoms all exist as atomic orbitals of discrete radii which are given by r_n of the radial Dirac delta function, $\delta(r-r_n)$. These electron atomic orbitals may be paired or unpaired depending on the force balance that applies to each electron. Ultimately, the electron configuration must be a minimum of energy. Minimum energy configurations are given by solutions to Laplace's Equation. The general form of the solution is:

$$\Phi(r,\theta,\phi)=\sum_{\ell=0}^{\infty}\sum_{m=-\ell}^{\ell}B_{\ell,m}r^{-(\ell+1)}Y_{\ell}^{m}(\theta,\phi) \tag{10.449}$$

As demonstrated previously, this general solution gives the functions of the resonant photons. As shown in the One-Electron Atom section, the Two-Electron Atom section, and the Three- Through Twenty-Electron Atoms section, the electron configuration of an atom essentially parallels that of the excited modes of the helium atom: $1s<2s<2p<3s<3p<4s<3d<4p<5s<4d$. (See Excited States of Helium section.)

In general, electrons of an atom with the same principal and ℓ quantum numbers align parallel until each of the m_ℓ levels are occupied, and then pairing occurs until each of the m_ℓ levels contain paired electrons. Exceptions occur due to the relative importance of spin and orbital interactions and paramagnetic, diamagnetic, and electric forces for a given atom or ion.

The predictions of the ionization energies of one through twenty-electron atoms using Maxwell's equations are given in the One-Electron Atom section, the Two-Electron Atom section, and the Three- Through Twenty-Electron Atoms section. The agreement between the experimental ionization energies and the classical predictions based on concentric dynamical atomic orbitals ("bubble-like" charge-density functions) wherein the charge-density waves on the surface are time and spherically harmonic is remarkable. The classical shell model of atomic electrons is also being confirmed by studying electron dynamics using coherent short-pulse laser excitation [10-12].

REFERENCES

1. E. Purcell, *Electricity and Magnetism*, McGraw-Hill, New York, (1965), pp. 370-389.
2. C. E. Moore, "Ionization Potentials and Ionization Limits Derived from the Analyses of Optical Spectra," Nat. Stand. Ref. Data Ser.-Nat. Bur. Stand. (U.S.), No. 34, 1970.
3. R. C. Weast, CRC Handbook of Chemistry and Physics, 58th Edition, CRC Press, West Palm Beach, Florida, (1977), p. E-68.
4. A. O. Wistrom, A. V. M. Khachatourian, "Coulomb motor by rotation of spherical conductors via the electrostatic force," Applied Physics Letters, Volume 80, No. 15, (2002), pp. 2800-2802.
5. A. V. M. Khachatourian, A. O. Wistrom, "A sum rule for associated Legendre polynomials with spherical triangles," Journal of Mathematical Physics, Vol. 44(2), (2003), pp. 849-852.
6. J. D. Jackson, *Classical Electrodynamics*, Second Edition, John Wiley & Sons, New York, (1975), p. 99.
7. D. A. McQuarrie, *Quantum Chemistry*, University Science Books, Mill Valley, CA, (1983), p. 215.
8. NIST Atomic Spectra Database, www.physics.nist.gov/cgi-bin/AtData/display.ksh.
9. M. Karplus, R. N. Porter, *Atoms and Molecules an Introduction for Students of Physical Chemistry*, The Benjamin/Cummings Publishing Company, Menlo Park, California, (1970), pp. 202-207.
10. S. N. Pisharody, R. R. Jones, "Probing two electron dynamics of an atom," Science, Vol. 303, (2004), pp. 813-815.
11. C. R. Stroud, "Pas de deux for atomic electrons," Science, Vol. 303, (2004), pp. 778-779.
12. H. Maeda, D. V. L. Norum, T. F. Gallagher, "Microwave manipulation of an atomic electron in a classical orbit," Science, Vol. 307, (2005), pp. 1757-1760.

The Grand Unified Theory of Classical Physics

Dr. Randell L. Mills

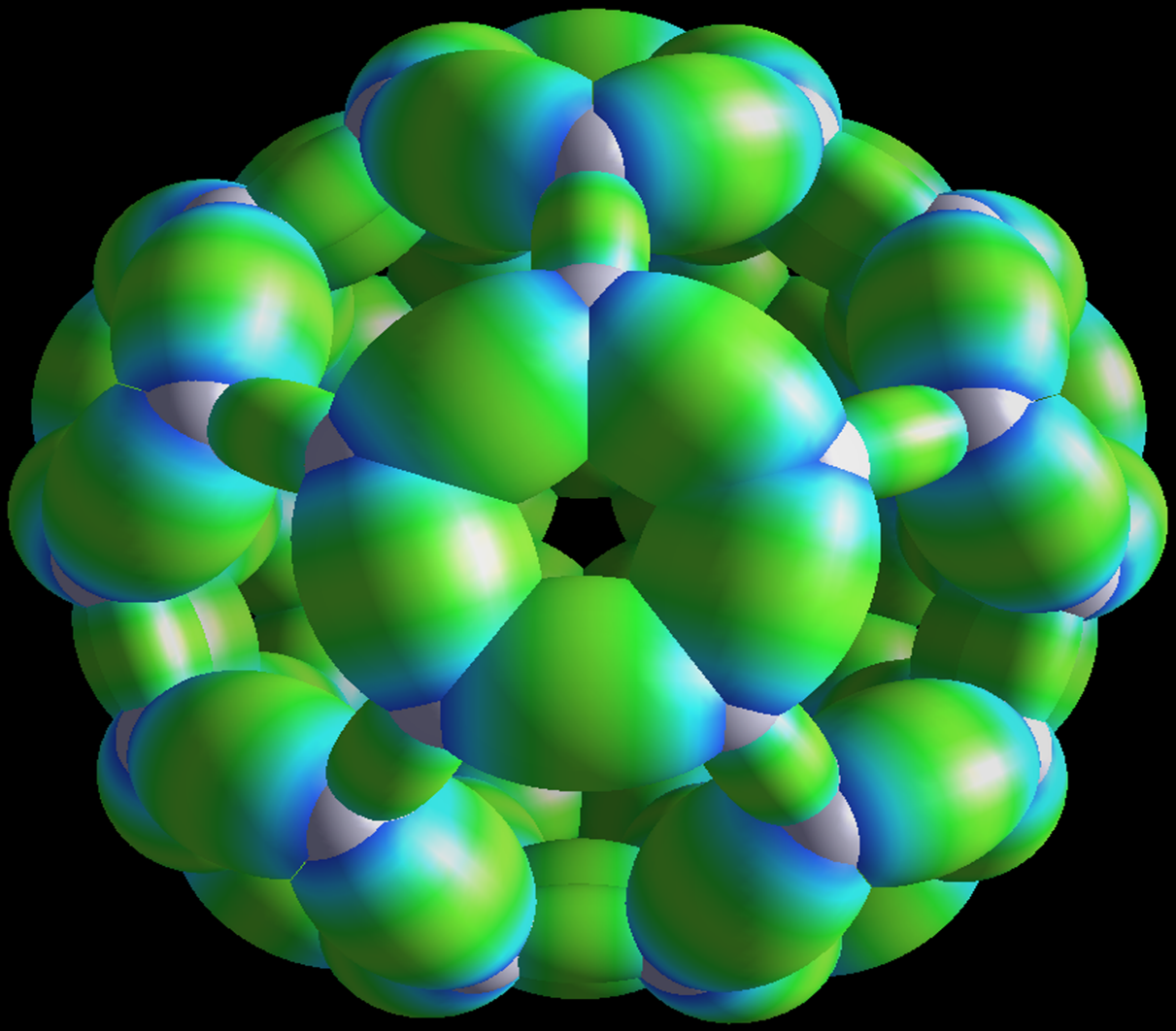

Volume II:
Part A
Molecular Physics

THE GRAND UNIFIED THEORY OF CLASSICAL PHYSICS

Volume 2A of 3

THE GRAND UNIFIED THEORY OF CLASSICAL PHYSICS

BY

Dr. Randell L. Mills

April 2023 Edition
Volume 2A of 3

ISBN 979-8-218-17988-5
Library of Congress Control Number 2023905641

TABLE OF CONTENTS

VOLUME 2 MOLECULAR PHYSICS Part A

Chapter 11

THE NATURE OF THE CHEMICAL BOND OF HYDROGEN-TYPE MOLECULES AND MOLECULAR IONS

With regard to the Hydrino Theory—BlackLight Process section, the possibility of states with $n=1/p$ is also predicted in the case of hydrogen molecular species wherein $H(1/p)$ reacts with a proton or two $H(1/p)$ atoms react to form $H_2^+(1/p)$ and $H_2(1/p)$, respectively. The natural molecular-hydrogen coordinate system based on symmetry is ellipsoidal coordinates. The magnitude of the central field in the derivations of molecular hydrogen species is taken as the general parameter p wherein p may be an integer which may be predictive of new possibilities. Thus, p replaces the effective nuclear charge of quantum mechanics and corresponds to the physical field of a resonant photon superimposed with the field of the proton. The case with $p=1$ is evaluated and compared with the experimental results for hydrogen species in Table 11.1, and the consequences that $p=$ integer are considered in the Nuclear Magnetic Resonance Shift section.

Two hydrogen atoms react to form a diatomic molecule, the hydrogen molecule.

$$2H\left[a_H\right]\rightarrow H_2\left[2c'=\sqrt{2}a_0\right] \tag{11.1}$$

where $2c'$ is the internuclear distance. Also, two hydrino atoms react to form a diatomic molecule, a dihydrino molecule.

$$2H\left[\frac{a_H}{p}\right]\rightarrow H_2\left[2c'=\frac{\sqrt{2}a_0}{p}\right] \tag{11.2}$$

where p is an integer.

Hydrogen molecules form hydrogen molecular ions when they are singly ionized.

$$H_2\left[2c'=\sqrt{2}a_0\right]\rightarrow H_2\left[2c'=2a_0\right]^+ + e- \tag{11.3}$$

Also, dihydrino molecules form dihydrino molecular ions when they are singly ionized.

$$H_2\left[2c'=\frac{\sqrt{2}a_0}{p}\right]\rightarrow H_2\left[2c'=\frac{2a_0}{p}\right]^+ + e- \tag{11.4}$$

HYDROGEN-TYPE MOLECULAR IONS

Each hydrogen-type molecular ion comprises two protons and an electron where the equation of motion of the electron is determined by the central field that is p times that of a proton at each focus (p is one for the hydrogen molecular ion, and p is an integer greater than one for each $H_2^+(1/p)$, called a dihydrino molecular ion). The differential equations of motion in the case of a central field are [1]

$$m(\ddot{r}-r\dot{\theta}^2)=f(r) \tag{11.5}$$

$$m(2\dot{r}\dot{\theta}+r\ddot{\theta})=0 \tag{11.6}$$

The second or transverse equation, Eq. (11.6), gives the result that the angular momentum is constant.

$$r^2\dot{\theta}=\text{constant}=L/m \tag{11.7}$$

where L is the angular momentum ($\hbar$ in the case of the electron). The central force equations can be transformed into an orbital equation by the substitution, $u=\frac{1}{r}$. The differential equation of the orbit of a particle moving under a central force is

$$\frac{\partial^2 u}{\partial\theta^2}+u=\frac{-1}{\frac{mL^2u^2}{m^2}}f(u^{-1}) \tag{11.8}$$

Because the angular momentum is constant, motion in only one plane need be considered; thus, the orbital equation is given in polar coordinates. The solution of Eq. (11.8) for an inverse-squared force

$$f(r)=-\frac{k}{r^2} \tag{11.9}$$

is

$$r=r_0\frac{1+e}{1+e\cos\theta} \tag{11.10}$$

$$e=A\frac{m\frac{L^2}{m^2}}{k} \tag{11.11}$$

$$r_0=\frac{m\frac{L^2}{m^2}}{k(1+e)} \tag{11.12}$$

where e is the eccentricity of the ellipse and A is a constant. The equation of motion due to a central force can also be expressed in terms of the energies of the orbit. The square of the speed in polar coordinates is

$$v^2=(\dot{r}^2+r^2\dot{\theta}^2) \tag{11.13}$$

Since a central force is conservative, the total energy, E, is equal to the sum of the kinetic, T, and the potential, V, and is constant. The total energy is:

$$\frac{1}{2}m(\dot{r}^2+r^2\dot{\theta}^2)+V(r)=E=\text{ constant} \tag{11.14}$$

Substitution of the variable $u=\frac{1}{r}$ and Eq. (11.7) into Eq. (11.14) gives the orbital energy equation.

$$\frac{1}{2}m\frac{L^2}{m^2}\left(\left(\frac{\partial u}{\partial\theta}\right)^2+u^2\right)+V(u^{-1})=E \tag{11.15}$$

Because the potential energy function $V(r)$ for an inverse-squared force field is:

$$V(r)=-\frac{k}{r}=-ku \tag{11.16}$$

the energy equation of the orbit, Eq. (11.15),

$$\frac{1}{2}m\frac{L^2}{m^2}\left(\left(\frac{\partial u}{\partial\theta}\right)^2+u^2\right)-ku=E \tag{11.17}$$

which has the solution

$$r=\frac{m\frac{L^2}{m^2}k^{-1}}{1+\left(1+2Em\frac{L^2}{m^2}k^{-2}\right)^{1/2}\cos\theta} \tag{11.18}$$

where the eccentricity, e, is:

$$e=\left(1+2Em\frac{L^2}{m^2}k^{-2}\right)^{1/2} \tag{11.19}$$

Eq. (11.19) permits the classification of the orbits according to the total energy, E, as follows:

$E<0,$	$e<1$	closed orbits (ellipse or circle)
$E=0,$	$e=1$	parabolic orbit
$E>0,$	$e>1$	hyperbolic orbit

Since $E=T+V$ and is constant, the closed orbits are those for which $T<|V|$, and the open orbits are those for which $T\geq|V|$. It can be shown that the time average of the kinetic energy, $<T>$, for elliptical motion in an inverse-squared field is $1/2$ that of the time average of the magnitude of the potential energy, $|<V>|$. $<T>=1/2|<V>|$ [1].

As demonstrated in the One-Electron Atom section, the electric inverse-squared force is conservative; thus, the angular momentum of the electron, $\hbar$, and the energy of atomic atomic orbitals are constant. In addition, the atomic orbitals are nonradiative when the boundary condition is met.

The central force equation, Eq. (11.14), has orbital solutions, which are circular, elliptical, parabolic, or hyperbolic. The former two types of solutions are associated with atomic and molecular orbitals. These solutions are nonradiative. The

boundary condition for nonradiation given in the One-Electron Atom section, is the absence of components of the spacetime Fourier transform of the current-density function synchronous with waves traveling at the speed of light. The boundary condition is met when the velocity for the charge density at every coordinate position on the atomic orbital is:

$$v_n = \frac{\hbar}{m_e r_n} \tag{11.20}$$

The allowed velocities and angular frequencies are related to r_n by:

$$v_n = r_n \omega_n \tag{11.21}$$

$$\omega_n = \frac{\hbar}{m_e r_n^2} \tag{11.22}$$

As demonstrated in the One-Electron Atom section and by Eq. (11.22), this condition is met for the product function of a radial Dirac delta function and a time harmonic function where the angular frequency, ω, is constant and given by Eq. (11.22).

$$\omega_n = \frac{\hbar}{m_e r_n^2} = \frac{\frac{\pi L}{m_e}}{A} \tag{11.23}$$

where L is the angular momentum and A is the area of the closed orbit. Consider the solution of the central force equation comprising the product of a two-dimensional ellipsoid and a time harmonic function. The spatial part of the product function is the convolution of a radial Dirac delta function with the equation of an ellipsoid. The Fourier transform of the convolution of two functions is the product of the individual Fourier transforms of the functions; thus, the boundary condition is met for an ellipsoidal-time harmonic function when,

$$\omega_n = \frac{\pi\hbar}{m_e A} = \frac{\hbar}{m_e ab} \tag{11.24}$$

where the area of an ellipse is

$$A = \pi ab \tag{11.25}$$

where b and $2b$ are the lengths of the semiminor and minor axes, respectively, and a and $2a$ are the lengths of the semimajor and major axes, respectively. The geometry of molecular hydrogen is ellipsoidal with the internuclear axis as the principal axis; thus, the electron orbital is a two-dimensional ellipsoidal-time harmonic function. The mass follows an elliptical path, time harmonically as determined by the central field of the protons at the foci. Rotational symmetry about the internuclear axis further determines that the orbital is a prolate spheroid. In general, ellipsoidal orbits of molecular bonding, hereafter referred to as ellipsoidal molecular orbitals (MOs), have the general equation:

$$\frac{x^2}{a^2} + \frac{y^2}{b^2} + \frac{z^2}{c^2} = 1 \tag{11.26}$$

The semiprincipal axes of the ellipsoid are a, b, c.

In ellipsoidal coordinates the Laplacian is:

$$(\eta - \zeta) R_\xi \frac{\partial}{\partial \xi}\left(R_\xi \frac{\partial \phi}{\partial \xi}\right) + (\zeta - \xi) R_\eta \frac{\partial}{\partial \eta}\left(R_\eta \frac{\partial \phi}{\partial \eta}\right) + (\xi - \eta) R_\zeta \frac{\partial}{\partial \zeta}\left(R_\zeta \frac{\partial \phi}{\partial \zeta}\right) = 0 \tag{11.27}$$

An ellipsoidal MO is equivalent to a charged perfect conductor (i.e. no dissipation to current flow) whose surface is given by Eq. (11.26). It is a two-dimensional equipotential membrane where each MO is supported by the outward centrifugal force due to the corresponding angular velocity, which conserves its angular momentum of $\hbar$. It satisfies the boundary conditions for a discontinuity of charge in Maxwell's equations, Eq. (11.48). It carries a total charge $q = -e$, and it's potential is a solution of the Laplacian in ellipsoidal coordinates, Eq. (11.27).

Excited states of atomic orbitals are discussed in the Excited States of the One-Electron Atom (Quantization) section. In the case of ellipsoidal MOs, excited electronic states are created when photons of discrete frequencies are trapped in the ellipsoidal resonator cavity of the MO. The photon changes the effective charge at the MO surface where the central field is ellipsoidal and arises from the protons and the effective charge of the "trapped photon" at the foci of the MO. Force balance is achieved at a series of ellipsoidal equipotential two-dimensional surfaces confocal with the ground state ellipsoid. The "trapped photons" are solutions of the Laplacian in ellipsoidal coordinates, Eq. (11.27).

As is the case with the atomic orbital, higher and lower energy states are equally valid. The photon standing wave in both cases is a solution of the Laplacian in ellipsoidal coordinates. For an ellipsoidal resonator cavity, the relationship between an allowed circumference, $4aE$, and the photon standing wavelength, λ, is:

$$4aE = n\lambda \tag{11.28}$$

where n is an integer and where the elliptic integral E of Eq. (11.28) is given by:

$$E(k) = \int_0^{\frac{\pi}{2}} \sqrt{1 - k^2 \sin^2\phi}\, d\phi \tag{11.29}$$

$$k = e = \frac{\sqrt{a^2 - b^2}}{a} \tag{11.30}$$

Applying Eqs. (11.28) and (11.29-11.30), the relationship between an allowed angular frequency given by Eq. (11.24) and the

photon standing wave angular frequency, ω, is:

$$\frac{\pi\hbar}{m_e A} = \frac{\hbar}{m_e n a_1 n b_1} = \frac{\hbar}{m_e a_n b_n} = \frac{1}{n^2}\omega_1 = \omega_n \tag{11.31}$$

where $n = 1, 2, 3, 4, ...$ ($n = \frac{1}{2}, \frac{1}{3}, \frac{1}{4}, ...$ for molecular hydrino states); ω_1 is the allowed angular frequency for $n = 1$

a_1 and b_1 are the allowed semimajor and semiminor axes for $n = 1$. Using the boundary conditions, the excited states are solved in the Excited States of the Hydrogen Molecular Ion and Excited States of the Hydrogen Molecule sections.

The potential, ϕ, and distribution of charge, σ, over the conducting surface of an ellipsoidal MO are sought given the conditions: 1.) the potential is equivalent to that of a charged ellipsoidal conductor whose surface is given by Eq. (11.26), 2.) it carries a total charge $q = -e$, and 3.) initially there is no external applied field. To solve this problem, a potential function must be found which satisfies Eq. (11.27), which is regular at infinity, and which is constant over the given ellipsoid. The solution is well known and is given after Stratton [2]. Consider that the Laplacian is solved in ellipsoidal coordinates wherein ξ is the parameter of a family of ellipsoids all confocal with the standard surface $\xi = 0$ whose axes have the specified values a, b, c. The variables ζ and η are the parameters of confocal hyperboloids and as such serve to measure position on any ellipsoid $\xi = \text{constant}$. On the surface $\xi = 0$; therefore, ϕ must be independent of ζ and η. Due to the uniqueness property of solutions of the Laplacian, a function which satisfies Eq. (11.27), behaves properly at infinity, and depends only on ξ, can be adjusted to represent the potential correctly at any point outside the ellipsoid $\xi = 0$.

Thus, it is assumed that $\phi = \phi(\xi)$. Then, the Laplacian reduces to:

$$\frac{\partial}{\partial\xi}(R_\xi \frac{\partial\phi}{\partial\xi}) = 0 \qquad R_\xi = \sqrt{(\xi + a^2)(\xi + b^2)(\xi + c^2)} \tag{11.32}$$

which on integration leads to:

$$\phi(\xi) = C_1 \int_\xi^\infty \frac{\partial\xi}{R_\xi} \tag{11.33}$$

where C_1 is an arbitrary constant. The upper limit is selected to ensure the proper behavior at infinity. When ξ becomes very large, R_ξ approaches $\xi^{3/2}$ and,

$$\phi \sim \frac{2C_1}{\sqrt{\xi}} \qquad (\xi \to \infty) \tag{11.34}$$

Furthermore, the equation of an ellipsoid can be written in the form:

$$\frac{x^2}{1 + \frac{a^2}{\xi}} + \frac{y^2}{1 + \frac{b^2}{\xi}} + \frac{z^2}{1 + \frac{c^2}{\xi}} = \xi \tag{11.35}$$

If $r^2 = x^2 + y^2 + z^2$ is the distance from the origin to any point on the ellipsoid ξ, it is apparent that as ξ becomes very large $\xi \to r^2$. Thus, at great distances from the origin, the potential becomes that of a point charge at the origin:

$$\phi \sim \frac{2C_1}{r} \tag{11.36}$$

The solution Eq. (11.33) is, therefore, regular at infinity, and the constant C_1 is then determined. It has been shown by Stratton [2] that whatever the distribution, the dominant term of the expansion at remote points is the potential of a point charge at the origin equal to the total charge of the distribution—in this case q. Hence $C_1 = \frac{q}{8\pi\varepsilon_o}$, and the potential at any point is:

$$\phi(\xi) = \frac{q}{8\pi\varepsilon_0} \int_\xi^\infty \frac{\partial\xi}{R_\xi} \tag{11.37}$$

The equipotential surfaces are the ellipsoids $\xi = \text{constant}$. Eq. (11.37) is an elliptic integral and its values have been tabulated [3].

Since the distance along a curvilinear coordinate u^1 is measured not by du^1 but by $h_1 du^1$, the normal derivative in ellipsoidal coordinates is given by:

$$\frac{\partial\phi}{\partial n} = \frac{1}{h_1}\frac{\partial\phi}{\partial\xi} = \frac{-q}{4\pi\varepsilon_0} \frac{1}{\sqrt{(\xi - \eta)(\xi - \zeta)}} \tag{11.38}$$

where

$$h_1 = \frac{1}{2}\frac{\sqrt{(\xi - \eta)(\xi - \zeta)}}{R_\xi} \tag{11.39}$$

The density of charge, σ, over the surface $\xi = 0$ is:

$$\sigma = \varepsilon_0 \left(\frac{\partial \phi}{\partial n} \right)_{\xi=0} = \frac{q}{4\pi\sqrt{\eta\zeta}} \tag{11.40}$$

Defining x, y, z in terms of ξ, η, ζ we put $\xi = 0$, it may be easily verified that,

$$\frac{x^2}{a^4} + \frac{y^2}{b^4} + \frac{z^2}{c^4} = \frac{\zeta\eta}{a^2b^2c^2} \qquad (\xi = 0) \tag{11.41}$$

Consequently, the charge density in rectangular coordinates is:

$$\sigma = \frac{q}{4\pi abc} \frac{1}{\sqrt{\frac{x^2}{a^4} + \frac{y^2}{b^4} + \frac{z^2}{c^4}}} \tag{11.42}$$

(The mass-density function of an MO is equivalent to its charge-density function where m replaces q of Eq. (11.42)). The equation of the plane tangent to the ellipsoid at the point x_0, y_0, z_0 is:

$$X\frac{x_0}{a^2} + Y\frac{y_0}{b^2} + Z\frac{z_0}{c^2} = 1 \tag{11.43}$$

where X, Y, Z are running coordinates in the plane. After dividing through by the square root of the sum of the squares of the coefficients of X, Y, and Z, the right member is the distance D from the origin to the tangent plane. That is,

$$D = \frac{1}{\sqrt{\frac{x^2}{a^4} + \frac{y^2}{b^4} + \frac{z^2}{c^4}}} \tag{11.44}$$

so that for an electron MO:

$$\sigma = \frac{-e}{4\pi abc} D \tag{11.45}$$

In other words, the surface density at any point on a charged ellipsoidal conductor is proportional to the perpendicular distance from the center of the ellipsoid to the plane tangent to the ellipsoid at the point. The charge is thus greater on the more sharply rounded ends farther away from the origin.

In the case of hydrogen-type molecules and molecular ions, rotational symmetry about the internuclear axis requires that two of the axes be equal. Thus, the MO is a spheroid, and Eq. (11.37) can be integrated in terms of elementary functions. If $a > b = c$, the spheroid is prolate, and the potential is given by:

$$\phi = \frac{1}{8\pi\varepsilon_0} \frac{-e}{\sqrt{a^2 - b^2}} \ln \frac{\sqrt{\xi + a^2} + \sqrt{a^2 - b^2}}{\sqrt{\xi + a^2} - \sqrt{a^2 - b^2}} \tag{11.46}$$

SPHEROIDAL FORCE EQUATIONS

ELECTRIC FORCE

The spheroidal MO is a two-dimensional surface of constant potential given by Eq. (11.46) for $\xi = 0$. For an isolated electron MO the electric field inside is zero as given by Gauss' Law:

$$\int_S \mathbf{E} dA = \int_V \frac{\rho}{\varepsilon_0} dV \tag{11.47}$$

where the charge density, ρ, inside the MO is zero. Gauss' Law at a two-dimensional surface with continuity of the potential across the surface according to Faraday's law in the electrostatic limit [4-6] is:

$$\mathbf{n} \bullet \left(\mathbf{E}_1 - \mathbf{E}_2 \right) = \frac{\sigma}{\varepsilon_0} \tag{11.48}$$

$\mathbf{E}_2$ is the electric field inside which is zero. The electric field of an ellipsoidal MO with semimajor and semiminor axes a and $b = c$, respectively, is given by substituting σ given by Eq. (11.38-11.42) into Eq. (11.48).

$$\mathbf{E} = \frac{\sigma}{\varepsilon_0}\mathbf{i}_\xi = \frac{-e}{4\pi\varepsilon_0} \frac{1}{\sqrt{(\xi - \eta)(\xi - \zeta)}} \mathbf{i}_\xi = \frac{-e}{4\pi\varepsilon_0 abc} D\mathbf{i}_\xi = \frac{-e}{4\pi\varepsilon_o abc} \frac{1}{\sqrt{\frac{x^2}{a^4} + \frac{y^2}{b^4} + \frac{z^2}{c^4}}} \mathbf{i}_\xi \tag{11.49}$$

wherein the ellipsoidal-coordinate parameter $\xi = 0$ at the surface of the MO and D is the distance from the origin to the tangent plane given by Eq. (11.44). The electric field and thus the force and potential energy between the protons and the electron MO can be solved based on three principles: (1) Maxwell's equations require that the electron MO is an equipotential energy surface that is a function of ξ alone; thus, it is a prolate spheroid, (2) stability to radiation, and conservation first principles require that the angular velocity is constant and given in polar coordinates with respect to the origin by Eq. (11.24), and (3) the equations of motion due to the central force of each proton (Eqs. (11.5-11.19) and Eqs. (11.68-11.70)) also determine that the current is ellipsoidal, and based on symmetry, the current is a prolate spheroid. Thus, based on Maxwell's equations, conservation principles, and Newton's Laws for the equations of motion, the electron MO constraints and the motion under the force of the

protons both give rise to a prolate spheroid. Since the energy of motion is determined from the Coulombic central field (Eqs. (11.5-11.19), the protons give rise to a prolate spheroidal energy surface (a surface of constant energy) that is matched to the equipotential, prolate spheroidal electron MO.

The electron cannot emit radiation; thus, it maintains the prolate spheroidal shape based on the overall conservation of angular momentum and energy (Appendix II: Stability and Absence of Self Interaction and Self Energy). Chapter 36 (Leptons) provides the conditions for the creation of an electron from a photon that forbid the electron from being severable. These properties that maintain the stability of an electron molecular orbital are invoked and provide that the integral of the physical properties such as the angular momentum of $\hbar$ (Eq. (11.101)) and energies in the inverse r-squared electric field originating at each focus over the entire electron match the boundary conditions. Consequently, the electron MO behaves as if it has rigidity based on the integrated conserved angular momentum of $\hbar$ (Eq. (11.101) as well as kinetic energy T (Eq. (11.119)) wherein T is one-half the magnitude of V_e (Eq. (11.117)) as required for an inverse-squared force [1] wherein V_e is the source of T. As in the case of an atomic orbital, a MO comprises a current density surface with flow along paths. An algorithm given in the Force Balance of Hydrogen-Type Molecules section solves the distribution wherein the velocity distribution on each path of the current distribution is variable to match the boundary conditions.

The force balance equation between the average ellipsoidal central field of the protons at the foci and the ellipsoidal electron MO is solved to give the position of the foci. Then, the total energy is determined including the repulsive energy between the two protons at the foci to determine whether the original assumption of an elliptic orbit was valid. If the condition $E<0$ is met, then the problem of the stable elliptic orbit is solved. In any case that this condition is not found to be met, then a stable orbit cannot be formed. The force and energy equations of a point charge (mass) (Eqs. (11.5-11.24)) are reformulated in term of densities for charge, current, mass, momentum, and potential, kinetic, and total energies. Consider an elliptical orbit shown in Figure 11.1 that applies to a point charge (mass) as well as a point on a continuous elliptical current loop that comprises a basis element of the continuous current density of the ellipsoidal MO. The tangent plane at any point on the ellipsoid makes equal angles with the foci radii at that point and the sum of the distance to the foci is a constant, $2a$. Thus, the normal is the bisector of the angle between the foci radii at that point as shown in Figure 11.1.

Figure 11.1. An elliptical current element of the prolate spheroidal MO showing the semimajor axis a, the semiminor axis b, the foci F_1 and F_2, and the vector $r(t)$ from the origin to a point (x,y,z). The radial vectors from the foci to a point on the ellipse have a total length of $2a$ and make equal angles α with the tangent such that the normal vector is the bisector of the interior angle 2β.

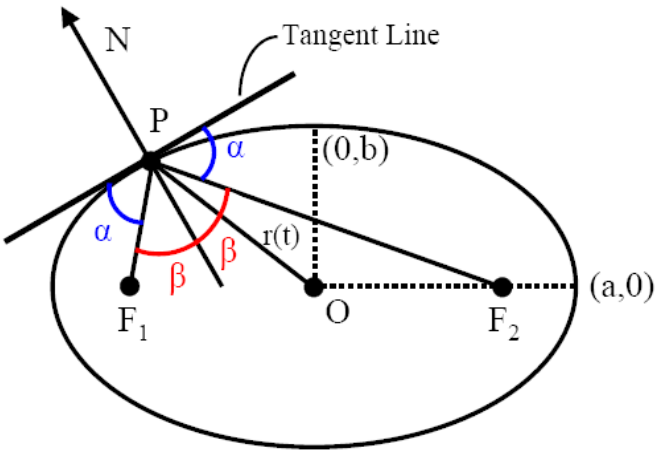

The unit vector normal to the ellipsoidal MO at a point (x,y,z) is:

$$\hat{\mathbf{d}}=\frac{\left(\frac{x}{a^2},\frac{y}{b^2},\frac{z}{b^2}\right)}{\sqrt{\frac{x^2}{a^4}+\frac{y^2}{b^4}+\frac{z^2}{c^4}}} \tag{11.50}$$

$F_1(r(t))$ and $F_2(r(t))$ are defined as the components of the central forces centered on F_1 and F_2. The components of the central forces that are normal to the ellipsoidal MO in the direction of $\hat{\mathbf{d}}$, the unit vector in the $\mathbf{i}_\xi$-direction are defined as

$F_{1\perp}\left(r\left(t\right)\right)$ and $F_{2\perp}\left(r\left(t\right)\right)$. The normalized projections or projection factor of the sum of these central forces in the $\hat{\mathbf{d}}$-direction at the point $\left(x,y,z\right)$ is:

$$\begin{aligned}\frac{F_{1\perp}\left(r\left(t\right)\right)+F_{2\perp}\left(r\left(t\right)\right)}{\left|F_1\left(r\left(t\right)\right)+F_2\left(r\left(t\right)\right)\right|}&=\frac{\left(\mathbf{r}_1+\mathbf{r}_2\right)\cdot\hat{\mathbf{d}}}{2a}\\&=\frac{\left(\left(x-c,y,z\right)+\left(x+c,y,z\right)\right)\cdot\left(\frac{x}{a^2},\frac{y}{b^2},\frac{z}{b^2}\right)}{2a\sqrt{\frac{x^2}{a^4}+\frac{y^2}{b^4}+\frac{z^2}{c^4}}}\\&=\frac{\left(\frac{x^2-cx}{a^2}+\frac{y^2}{b^2}+\frac{z^2}{b^2}\right)+\left(\frac{x^2+cx}{a^2}+\frac{y^2}{b^2}+\frac{z^2}{b^2}\right)}{2a\sqrt{\frac{x^2}{a^4}+\frac{y^2}{b^4}+\frac{z^2}{c^4}}}\\&=\frac{1}{a\sqrt{\frac{x^2}{a^4}+\frac{y^2}{b^4}+\frac{z^2}{c^4}}}\end{aligned}\tag{11.51}$$

where $\mathbf{r}_1$ and $\mathbf{r}_2$ are the radial vectors of the central forces from the corresponding focus to the point $\left(x,y,z\right)$ on the ellipsoidal MO.

The polar-coordinate elliptical orbit of a point charge due to its motion in a central inverse-squared-radius field is given by Eqs. (11.10-11.12) as the solution of the polar-coordinate-force equations, Eqs. (11.5-11.19) and (11.68-11.70). The orbit is also completely specified in Cartesian coordinates by the solution of Eqs. (11.5-11.19) and (11.68-11.70) for the semimajor and semiminor axes. Then, the corresponding polar-coordinate elliptical orbit is given as a plane cross section through the foci of the Cartesian-coordinate-system ellipsoid having the same axes given by Eq. (11.26) where $c=b$. Thus, the Coulumbic central force can be determined in terms of the general Cartesian coordinates from the polar-coordinate central force equations (Eqs. (11.5-11.19)). Consider separately the elliptical solution at each focus given in polar coordinates by Eq. (11.10).

$$r_1=a\left(1-e\right)\frac{1+e}{1+e\cos\theta}=\frac{a\left(1-e^2\right)}{1+e\cos\theta}\tag{11.52}$$

$$r_2=\frac{a\left(1-e^2\right)}{1+e\cos\left(\theta+\pi\right)}=\frac{a\left(1-e^2\right)}{1-e\cos\theta}\tag{11.53}$$

where

$$r_0=a-c'=a\left(1-\frac{c'}{a}\right)=a\left(1-e\right)\tag{11.54}$$

The magnitude of the sum of the central forces centered on F_1 and F_2 that are normal to the ellipsoidal MO are:

$$\begin{aligned}\left|F_1\left(r_1\right)\right|+\left|F_2\left(r_2\right)\right|&=\frac{k}{r_1^2}+\frac{k}{r_2^2}\\&=k\frac{\left(1+e\cos\theta\right)^2+\left(1-e\cos\theta\right)^2}{a^2\left(1-e^2\right)^2}\\&=k\frac{1+2e\cos\theta+e^2\cos^2\theta+1-2e\cos\theta+e^2\cos^2\theta}{a^2\left(1-e^2\right)^2}\\&=k\frac{1+e^2\cos^2\theta+1+e^2\cos^2\theta}{a^2\left(1-e^2\right)^2}\\&=k\frac{2+2e^2\cos^2\theta}{a^2\left(1-e^2\right)^2}\end{aligned}\tag{11.55}$$

The vector central forces centered on F_1 and F_2 that are normal to the ellipsoidal MO are then given by the product of the corresponding magnitude and vector projection given by Eqs. (11.55) and (11.51), respectively,

$$\mathbf{F}_{1\perp}\left(r_1\right)+\mathbf{F}_{2\perp}\left(r_2\right)=k\frac{2+2e^2\cos^2\theta}{a^2\left(1-e^2\right)^2}\frac{1}{a\sqrt{\frac{x^2}{a^4}+\frac{y^2}{b^4}+\frac{z^2}{c^4}}}\mathbf{i}_\xi\tag{11.56}$$

Eq. (11.56) is based on a single point charge e. For a charge-density distribution that is given as an ellipsoidal equipotential, the θ-dependence must vanish. In addition to the elliptical orbit being completely specified in Cartesian coordinates by the solution of Eqs. (11.5-11.19) and Eqs. (11.68-11.70) for the semimajor and semiminor axes in Eq. (11.26), the polar-coordinate elliptical orbit is also completely specified by the total constant total energy E and the angular momentum which for the electron is the constant $\hbar$. Considering Eq. (11.56), the corresponding total energy of the electron is conserved and is determined by the integration over the MO to give the average:

$$\mathbf{F}_{1\perp}(r_1)+\mathbf{F}_{2\perp}(r_2)=k\frac{2+e^2}{a^2\left(1-e^2\right)^2}\frac{1}{a\sqrt{\frac{x^2}{a^4}+\frac{y^2}{b^4}+\frac{z^2}{c^4}}}\mathbf{i}_\xi \tag{11.57}$$

Eq. (11.57) is transformed from a two-centered-central force to a one-centered-central force to match the form of the potential of the ellipsoidal MO. In this case,

$$\mathbf{r}_1,\mathbf{r}_2\to r(t)\mathbf{i}_\xi \tag{11.58}$$

In the case that

$$r_1=r_2=a \tag{11.59}$$

then,

$$r(t)=b \tag{11.60}$$

and the one-centered-central force is in the $\mathbf{i}_\xi$-direction. Consider the current motion on the great circle in the yz-plane containing the semiminor axes, each of length b, as shown in Figure 11.2. In order to match the average elliptic force for the condition of Eq. (11.60), Eq. (11.57) transforms as

$$\begin{aligned}\mathbf{F}_{1\perp}(r(t))+\mathbf{F}_{2\perp}(r(t)) &= k\frac{\left(2+e^2\right)}{b^2\left(1-e^2\right)^2}\frac{1}{a\sqrt{\frac{x^2}{a^4}+\frac{y^2}{b^4}+\frac{z^2}{c^4}}}\\ &=\frac{2+e^2}{\left(1-e^2\right)^2}k\frac{1}{ab^2\sqrt{\frac{x^2}{a^4}+\frac{y^2}{b^4}+\frac{z^2}{c^4}}}\mathbf{i}_\xi\end{aligned} \tag{11.61}$$

Eq. (11.61) has the same form as that of the electric field of the ellipsoidal MO given by Eq. (11.49), except for the scaling factor of two-centered coordinates h_{2cc}:

$$h_{2cc}=\frac{2+e^2}{\left(1-e^2\right)^2} \tag{11.62}$$

As shown in the case of the derivation of the Laplacian charge-density and electric field, if $r^2=x^2+y^2+z^2$ is the distance from the origin to any point on the ellipsoid ξ, it is apparent that as ξ becomes very large $\xi\to r^2$. Thus, at great distances from the origin, the potential becomes that of a point charge at the origin as given by Eq. (11.36). The same boundary condition applies to the potential and field of the protons. The limiting case is also given as $e\to 0$. Then, to transform the scale factor to that of one-centered coordinates for an ellipsoidal MO, the reciprocal of the scaling factor multiplies the Laplacian-MO-electric-field term. The reciprocal of Eq. (11.62) is:

$$h_{2cc}^{-1}=\frac{\left(1-e^2\right)^2}{2+e^2} \tag{11.63}$$

such that as $e\to 0$, $h_{2cc}^{-1}\to\frac{1}{2}$. This transform scale factor corresponds to the interchange of the points of highest and lowest velocity on the surface and the distribution of the charge-density in the opposite manner as shown *infra*. The charge-density distribution corrects the angular variation in central force over the surface such that a solution of the central force equation of motion and the Laplacian MO are solved simultaneously. It can also be considered as a multipole normalization factor such as those of the spherical harmonics and the spherical geometric factor of atomic electrons that gives the central force as a function of ξ only.

The reciprocal of the h_{2cc} form-factor with the dependence of the charge density on the distance parameter $r(t)$ gives:

$$\mathbf{F}_{1\perp}(r(t))+\mathbf{F}_{2\perp}(r(t))=k\frac{\left(1-e^2\right)^2}{b^2\left(2+e^2\right)}\frac{1}{a\sqrt{\frac{x^2}{a^4}+\frac{y^2}{b^4}+\frac{z^2}{c^4}}}\mathbf{i}_\xi \tag{11.64}$$

From Eq. (11.31), the magnitude of the ellipsoidal field corresponding to a below "ground state" hydrogen-type molecular ion is an integer p. The integer is one in the case of the hydrogen molecular ion and an integer greater than one in the case of each dihydrino molecular ion. The central-electric-force constant, k, from the two protons that includes the central-field contribution due to photons of lower-energy states is:

$$k = \frac{Ze^2}{4\pi\varepsilon_0} = \frac{p2e^2}{4\pi\varepsilon_0} \tag{11.65}$$

Substitution of Eq. (11.65) for k in Eq. (11.64) gives the one-center-coordinate electric force $\mathbf{F}_{ele}$ between the protons and the ellipsoidal MO:

$$\mathbf{F}_{ele} = \mathbf{F}_{1\perp}\left(r(t)\right) + \mathbf{F}_{2\perp}\left(r(t)\right) = \frac{2pe^2}{4\pi\varepsilon_0} \frac{\left(1-\left(\frac{c'}{a}\right)^2\right)^2}{ab^2\left(2+\left(\frac{c'}{a}\right)^2\right)} \frac{1}{\sqrt{\frac{x^2}{a^4}+\frac{y^2}{b^4}+\frac{z^2}{c^4}}} \mathbf{i}_\xi \tag{11.66}$$

where e is the charge and with the distance from the origin to a nucleus at a focus defined as c', the eccentricity, e, is:

$$e = \frac{c'}{a} \tag{11.67}$$

From the orbital equations in polar coordinates, Eqs. (11.10-11.12), the following relationship can be derived [1]:

$$a = \frac{m\frac{L^2}{m^2}}{k(1-e^2)} \tag{11.68}$$

For any ellipse,

$$b = a\sqrt{1-e^2} \tag{11.69}$$

thus,

$$b = a\sqrt{\frac{\frac{L^2}{m^2}m}{ka}} \text{ (point charge (mass) in polar coordinates)} \tag{11.70}$$

From, the equal energy condition, it can be shown that b for the motion of a point charge (mass) in polar coordinates due to a proton at one focus corresponds to:

$$c' = \sqrt{a^2 - b^2} \tag{11.71}$$

of the MO in ellipsoidal coordinates, and k_1 of one attracting focus is replaced by $k = 2k_1$ of ellipsoidal coordinates with two attracting foci. In ellipsoidal coordinates, k is given by Eq. (11.65) and L for the electron equals $\hbar$.

Consider the force balance equation for the point on the ellipse at the intersection of the semiminor axis b with the ellipse. At this point called $(0,b)$, the distances from each focus, r_1 and r_2, to the ellipse are equal. The relationship for the sum of the distances from the foci to any point on the ellipse is:

$$r_1 + r_2 = 2a \tag{11.72}$$

Thus, at point $(0,b)$,

$$r_1 = r_2 = a \tag{11.73}$$

Using Eq. (11.5), the magnitude of the force balance in the radial ($r(t)$) direction, from the origin, is given by:

$$mr\dot{\theta}^2 = \frac{2pe^2}{4\pi\varepsilon_0 a^2}\sin\theta = \frac{2pe^2}{4\pi\varepsilon_0 a^2}\frac{b}{a} \tag{11.74}$$

wherein the $m\ddot{r}$ term of Eq. (11.5) is zero and θ is the angle from the focus to point $(0,b)$. Using Eqs. (11.24), (11.94), and (11.95), Eq. (11.74) becomes:

$$mr\omega^2 = mb\frac{\hbar^2}{m^2a^2b^2} = \frac{2pe^2}{4\pi\varepsilon_0 a^2}\frac{b}{a} \tag{11.75}$$

In order for the prolate spheroidal MO to be an equipotential surface, the mass and charge density must be according to Eq. (11.45). In this case, the mass and charge density along the ellipse is such that the magnitudes of the radial and transverse forces components at point $(0,b)$ are equivalent. Furthermore, according to Eq. (11.5), the central force of each proton at a focus is separable and symmetrical to that at the other focus. Based on symmetry, the transverse forces of the two protons are in opposite directions and the radial components are in the same direction. But, the relationship between the magnitudes must still hold wherein at point $(0,b)$ the transverse force is equivalent to that due to the sum of the charges at one focus. The sum of the magnitudes of the transverse forces which is equivalent to a force of $2e$ at each focus in turn is:

$$\left|f(r)e_\theta\right| = \frac{2pe^2}{4\pi\varepsilon_0 a^2}\cos\theta = \frac{2pe^2}{4\pi\varepsilon_0 a^2}\frac{c'}{a} \tag{11.76}$$

Thus, using the mass and charge-density scaling factor, $\frac{\frac{c'}{a}}{\frac{b}{a}}=\frac{c'}{b}$, to match the equipotential condition in Eq. (11.75) gives:

$$b\frac{\hbar^2}{m_e\frac{c'}{b}a^2b^2}=\frac{2\frac{c'}{b}pe^2}{4\pi\varepsilon_0 a^2}\frac{b}{a} \tag{11.77}$$

$$c'^2=\frac{\hbar^2 4\pi\varepsilon_0 a}{m_e 2pe^2} \tag{11.78}$$

Using Eq. (1.256)

$$c'=a\sqrt{\frac{\hbar^2 4\pi\varepsilon_0}{me^2 2pa}}=\sqrt{\frac{aa_0}{2p}} \tag{11.79}$$

Then, the length of the semiminor axis of the prolate spheroidal MO, $b=c$, is:

$$b=\sqrt{a^2-c'^2} \tag{11.80}$$

Correspondingly, c' is given by Eq. (11.71).

Substitution of Eq. (11.79) into Eq. (11.66) gives the electric force:

$$\begin{aligned}\mathbf{F}_{ele}&=\frac{2pe^2}{4\pi\varepsilon_0}\frac{\left(1-\left(\frac{\sqrt{\frac{aa_0}{2p}}}{a}\right)^2\right)^2}{ab^2\left(2+\left(\frac{\sqrt{\frac{aa_0}{2p}}}{a}\right)^2\right)}\frac{1}{\sqrt{\frac{x^2}{a^4}+\frac{y^2}{b^4}+\frac{z^2}{c^4}}}\mathbf{i}_\xi\\&=\frac{2pe^2}{4\pi\varepsilon_0}\frac{\left(1-\frac{a_0}{2ap}\right)^2}{ab^2\left(2+\frac{a_0}{2ap}\right)}\frac{1}{\sqrt{\frac{x^2}{a^4}+\frac{y^2}{b^4}+\frac{z^2}{c^4}}}\mathbf{i}_\xi\\&=\frac{2pe^2}{4\pi\varepsilon_0}\frac{\left(1-\frac{a_0}{2ap}\right)^2}{ab^2\left(2+\frac{a_0}{2ap}\right)}D\mathbf{i}_\xi\end{aligned} \tag{11.81}$$

CENTRIFUGAL FORCE

The centrifugal force along the radial vector from each proton at each focus of the ellipsoid is given by the $mr\dot{\theta}^2$ term of Eq. (11.5). The tangent plane at any point on the ellipsoid makes equal angles with the foci radii at that point and the sum of the distance to the foci is a constant, $2a$. Thus, the normal is the bisector of the angle between the foci radii at that point as shown in Figure 11.1. In order to satisfy the equation of motion for an equal energy surface for both foci, the transverse component of the central force of one foci at any point on the elliptic orbit due to the central force of the other (Eq. (11.5)) must cancel on average and vice versa. Thus, the centrifugal force due to the superposition of the central forces in the direction of each foci must be normal to an ellipsoidal surface in the direction perpendicular to the direction of motion. Thus, it is in the ξ-direction. This can only be achieved by a time rate of change of the momentum density that compensates for the variation of the distances from each focus to each point on an elliptical cross section. Since the angular momentum must be conserved, there can be no net force in the direction transverse to the elliptical path over each orbital path. The total energy must also be conserved; thus, as shown *infra.* the distribution of the mass must also be a solution of Laplace's equation in the parameter ξ only. Thus, the mass-density constraint is the same as the charge-density constraint. As further shown *infra.*, the distribution and concomitantly the centrifugal force is a function of D, the time-dependent distance from the center of the ellipsoid to a tangent plane given by Eq. (11.44) where D and the Cartesian coordinates are the time-dependent parameters.

Each point or coordinate position on the continuous two-dimensional electron MO defines an infinitesimal mass-density element which moves along an orbit comprising an elliptical plane cross section of the spheroidal MO through the foci. The kinetic energy of the electron is conserved. Then, the corresponding radial conservative force balance equation is

$$m(\ddot{r}+C_1 r)=0 \tag{11.82}$$

The motion is such that the eccentric angle, θ, changes at a constant rate at each point. That is $\theta=\omega t$ at time t where the angular velocity ω is a constant. The solution of the homogeneous equation with $C_1=\omega^2$ is:

$$r(t) = \mathbf{i}a\cos\omega t + \mathbf{j}b\sin\omega t \tag{11.83}$$

where a is the semimajor axis, b is semiminor axis, and the boundary conditions of $r(t) = a$ for $\omega t = 0$ and $r(t) = b$ for $\omega t = \frac{\pi}{2}$ were applied. Eq. (11.83) is the parametric equation of the ellipse of the orbit. The velocity is given by the time derivative of the parametric position vector:

$$v(t) = \dot{r}(t) = -\mathbf{i}a\omega\sin\omega t + \mathbf{j}b\omega\cos\omega t \tag{11.84}$$

The velocity is $\frac{\pi}{2}$ out of phase with the charge density at $r(t) = a$ ($\omega t = 0$) and $r(t) = b$ ($\omega t = \frac{\pi}{2}$) such that the lowest charge density has the highest velocity and the highest charge density has the lowest velocity. In this case, it can be shown that the current is constant along each elliptical path of the MO. Recall that nonradiation results when $\omega = \text{constant}$ given by Eq. (11.24) that corresponds to a constant current, which further maintains the current continuity condition.

Consider Eq. (11.32) for the prolate spheroidal MO. From this equation, the mass and current-densities, the angular momentum, and the potential and kinetic energies are a function of ξ alone, and any dependence on the orthogonal coordinate parameters averages to unity. From Eq. (11.32).

$$R_\xi \frac{\partial\phi}{\partial\xi} = C_1 \tag{11.85}$$

Substitution of Eq. (11.40) into Eq. (11.85) gives:

$$\int_\xi^\infty R_\xi h_1 \frac{e}{4\pi\sqrt{\eta\zeta}}\delta(\xi)\,d\xi = \varepsilon_0 C_1 = \frac{e}{8\pi} \tag{11.86}$$

where C_1 is from Eq. (11.36). Substitution of Eq. (11.39) into Eq. (11.86) gives:

$$\int_\xi^\infty R_\xi \frac{e}{4\pi\sqrt{\eta\zeta}}\frac{1}{2}\frac{\sqrt{(\xi-\eta)(\xi-\zeta)}}{R_\xi}\delta(\xi)\,d\xi = \frac{e}{8\pi} \tag{11.87}$$

Comparison of Eq. (11.86) with Eq. (11.87) demonstrates that:

$$8\pi\int_\xi^\infty R_\xi \frac{e}{4\pi\sqrt{\eta\zeta}}\frac{1}{2}\frac{\sqrt{(\xi-\eta)(\xi-\zeta)}}{R_\xi}\delta(\xi)\,d\xi = e \tag{11.88}$$

The current density J is given by the product of the constant frequency (Eq. (11.24)) and the charge density (Eq. (11.40)).

$$J = \frac{\hbar}{2\pi m_e ab}\frac{e}{4\pi\sqrt{\eta\zeta}} \tag{11.89}$$

The total constant current is dependent on ξ alone according to Eq. (11.32). Then, applying the result of Eq. (11.88) to Eq. (11.89) gives:

$$\mathbf{i} = 8\pi\int_\xi^\infty R_\xi \frac{\hbar}{2\pi m_e ab}\frac{e}{4\pi\sqrt{\eta\zeta}}\frac{1}{2}\frac{\sqrt{(\xi-\eta)(\xi-\zeta)}}{R_\xi}\delta(\xi)\,d\xi\ \mathbf{e}_\zeta\times\mathbf{e}_\xi = \frac{e\hbar}{2\pi m_e ab}\ \mathbf{e}_\eta \tag{11.90}$$

the constant current that is nonradiative.

If $\mathbf{a}(t)$ denotes the acceleration vector, then

$$\mathbf{a}(t) = -\omega^2 r(t)\mathbf{i}_r \tag{11.91}$$

In other words, the acceleration is centrifugal as in the case of circular motion with constant angular speed ω. The dot product of $\mathbf{r}(t)$ with $\hat{\mathbf{d}}$, the unit vector normal to the ellipsoidal MO at a point (x,y,z) given by Eq. (11.50), is:

$$\mathbf{r}(t)\cdot\hat{\mathbf{d}} = \frac{(x,y,z)\cdot\left(\frac{x}{a^2},\frac{y}{b^2},\frac{z}{b^2}\right)}{\sqrt{\frac{x^2}{a^4}+\frac{y^2}{b^4}+\frac{z^2}{c^4}}} = \frac{\left(\frac{x^2}{a^2}+\frac{y^2}{b^2}+\frac{z^2}{b^2}\right)}{\sqrt{\frac{x^2}{a^4}+\frac{y^2}{b^4}+\frac{z^2}{c^4}}} \tag{11.92}$$

Using Eq. (11.26), the normal component projection is:

$$\mathbf{r}(t)\cdot\hat{\mathbf{d}} = \frac{1}{\sqrt{\frac{x^2}{a^4}+\frac{y^2}{b^4}+\frac{z^2}{c^4}}} = D \tag{11.93}$$

where D, the distance from the origin to the tangent plane, is given by Eq. (11.44).

The centrifugal force, $\mathbf{F}_{ci}$, on mass element m_i [7] given by the second term of Eq. (11.82) is:

$$\mathbf{F}_{ci} = m_i a = -m_i\omega^2 r(t) \tag{11.94}$$

Substitution of the angular velocity given by Eq. (11.24) and m_e for m into Eq. (11.94) gives the centrifugal force $\mathbf{F}_c$ on the electron that is normal to the MO surface according to Eq. (11.93).

$$\mathbf{F}_c = \frac{-\hbar^2}{m_e a^2 b^2}\mathbf{r}(t)\cdot\hat{\mathbf{d}}\mathbf{i}_\xi = \frac{-\hbar^2}{m_e a^2 b^2} D\mathbf{i}_\xi \tag{11.95}$$

$\mathbf{F}_c$ has an equivalent dependence on D as the electric force based on the charge distribution (Eq. (11.45)). This is expected based on the invariance of $\frac{e}{m_e}$ which results in the same distribution of the mass and charge.

The equipotential charge-density distribution gives rise to the constant current condition. It also gives rise to a constant total kinetic energy condition wherein the angular velocity given by Eq. (11.24) is a constant. Recall from Eq. (11.32), that on the surface $\xi = 0$; ϕ must be independent of ζ and η and depend only on ξ at any point outside the ellipsoid $\xi = 0$. Since the current and total kinetic energy are also constant on the surface $\xi = 0$, the total kinetic energy depends only on ξ. Thus, the centrifugal force on the mass of the electron, m_e, must be in the same direction as the electric field corresponding to ϕ, normal to the electron surface wherein any tangential component in Eq. (11.94) averages to zero over the electron MO by the mass distribution given by Eqs. (11.40) and (11.45) with m_e replacing e.

The cancellation of tangential acceleration over each elliptical path maintains the charge density distribution given by Eq. (11.40) with constant current at each point on each elliptical path of the MO. Since the centrifugal force is given by Eq. (11.94), the multiplication of the mass density by the scaling factor h_1 and integration with respect to ξ gives a constant net centrifugal force. Thus, the result matches those of the determination of the constant current (Eq. (11.90)) and angular momentum shown *infra.* (Eq. (11.101)) wherein the charge and mass densities given in Eqs. (11.90-11.91) and (11.100), respectively, were integrated over.

Specifically, consider the normal-directed centrifugal force, $\mathbf{F}_{ci}$, on mass element m_i:

$$\mathbf{F}_{ci} = -m_i\omega^2 D\mathbf{i}_\xi \tag{11.96}$$

The mass density is given by Eq. (11.40) with m_e replacing e. Then, the substitution of the mass density for m_i in Eq. (11.96) and using Eq. (11.24) for ω gives the centrifugal force density $\mathbf{F}_{ca}$:

$$\mathbf{F}_{ca} = \frac{m_e}{4\pi\sqrt{\eta\zeta}}\frac{\hbar^2}{m_e^2 a^2 b^2} D\mathbf{i}_\xi \tag{11.97}$$

Eq. (11.32) determines that the centrifugal force is a function of ξ alone, and any dependence on the transverse coordinate parameters averages to zero. Using the result of Eq. (11.88) gives the net centrifugal force $\mathbf{F}_c$:

$$\mathbf{F}_c = 8\pi\int_\xi^\infty \frac{1}{4\pi\sqrt{\eta\zeta}}\frac{\hbar^2}{m_e a^2 b^2} R_\xi \frac{1}{2}\frac{\sqrt{(\xi-\eta)(\xi-\zeta)}}{R_\xi} D\delta(\xi)\,d\xi\mathbf{i}_\xi = \frac{\hbar^2}{m_e a^2 b^2} D\mathbf{i}_\xi \tag{11.98}$$

In the limit as the ellipsoidal coordinates go over into spherical coordinates, Eq. (11.95) reduces to the centrifugal force of the spherical atomic orbital given by Eq. (1.253) with Eq. (1.35). This condition must be and is met as a further boundary condition that parallels that of Eqs. (11.32-11.37). Using the same dependence of the total mass (charge) on the scale factor h_1 according to Eqs. (11.32-11.40), the further boundary conditions on the angular momentum and kinetic energy are met.

Specifically, the constant potential and current conditions and the use of Eq. (11.32) in the derivation of Eq. (11.95) also satisfy another condition, the conservation of $\hbar$ of angular momentum of the electron. The angular momentum $\mathbf{p}_i$ at each point i of mass m_i is

$$\begin{aligned}\mathbf{p}_i(t) &= m_i\mathbf{r}(t)\times\mathbf{v}(t)\\ &= m_i\left(\mathbf{i}a\cos\omega t + \mathbf{j}b\sin\omega t\right)\times\left(-\mathbf{i}a\omega\sin\omega t + \mathbf{j}b\omega\cos\omega t\right)\\ &= m_i ab\omega\left(\cos^2\omega t + \sin^2\omega t\right)\mathbf{i}\times\mathbf{j}\\ &= m_i ab\omega\mathbf{k}\end{aligned} \tag{11.99}$$

The mass density is given by Eq. (11.40) with m_e replacing e. Then, substitution of m_i in Eq. (11.99) by the mass density and using Eq. (11.24) for ω gives the angular momentum density $\mathbf{p}(t)$:

$$\mathbf{p}(t) = ab\omega\frac{m_e}{4\pi\sqrt{\eta\zeta}}\mathbf{k} = ab\frac{\hbar}{m_e ab}\frac{m_e}{4\pi\sqrt{\eta\zeta}}\mathbf{k} \tag{11.100}$$

Using the result of Eq. (11.88) gives the total constant angular momentum $\mathbf{L}$:

$$\mathbf{L} = 8\pi\int_\xi^\infty \hbar\frac{1}{4\pi\sqrt{\eta\zeta}} R_\xi \frac{1}{2}\frac{\sqrt{(\xi-\eta)(\xi-\zeta)}}{R_\xi}\delta(\xi)\,d\xi\mathbf{k} = \hbar\mathbf{k} \tag{11.101}$$

Eq. (11.101) demonstrates conservation of angular momentum that is a function of ξ alone that parallels the case of atomic electrons where $\mathbf{L}$ conservation is a function of the radius r alone as given by Eq. (1.37).

Similarly, the kinetic energy $T(t)$ at each point i of mass m_i is:

$$\begin{aligned} T(t) &= \frac{1}{2} m_i v(t)^2 \\ &= \frac{1}{2} m_i \left(-\mathbf{i} a\omega \sin\omega t + \mathbf{j} b\omega \cos\omega t\right)^2 \\ &= \frac{1}{2} m_i \omega^2 \left(a^2 \sin^2 \omega t + b^2 \cos^2 \omega t\right) \end{aligned} \tag{11.102}$$

In Eqs. (11.96-11.98), m_i was replaced by the mass density and the ξ integral was determined to give the centrifugal force in terms of the mass of the electron. The kinetic energy can also be determined from the ξ integral of the centrifugal force:

$$T = h_{2cc} F_c \frac{ab^2}{2D} \int_{\xi}^{\infty} \frac{d\xi}{R_\xi} \tag{11.103}$$

The result is given in Eq. (11.119). From Eq. (11.102), the kinetic energy is time (position) dependent, but the total kinetic energy corresponding to the centrifugal force given by Eq. (11.95) satisfies the condition that the time-averaged kinetic energy is 1/2 the time-averaged potential energy for elliptic motion in an inverse-squared central force [1]. (Here, the potential and total kinetic energies are constant and correspond to the time-averaged energies of the general case.) Thus, as shown by Eqs. (11.122) (11.124), (11.262), and (11.264) energy is conserved.

FORCE BALANCE OF HYDROGEN-TYPE MOLECULAR IONS

Consider the case of spheroidal coordinates based on the rotational symmetry about the semimajor axis [2]. In the limit, as the focal distance $2c$ and the eccentricity of the series of confocal ellipses approaches zero, spheroidal coordinates go over into spherical coordinates with $\xi \to r$ and $\eta \to \cos\theta$. The field of an equipotential two-dimensional charge surface of constant radius $r = R$ is equivalent to that of a point charge of the total charge of the spherical shell at the origin. The force balance between the centrifugal force and the central Coulomb force for spherical symmetry is given by Eq. (1.253).

Similarly, the centrifugal force is in the direction of ξ and balances the central Coulombic force between the protons at the foci and the electron MO. In the case of the prolate spheroidal MO, the inhomogeneous equation given by Eq. (11.5) must hold for each fixed position of $r(t)$ since the MO is static in time due to the constant current condition. With $r(t)$ fixed, the $m\ddot{r}$ term of Eq. (11.5) is zero, and the force balanced equation is the balance between the centrifugal force and the Coulombic force which are both normal to the surface of the elliptic orbit:

$$mr\dot{\theta}^2 = f(r) \tag{11.104}$$

Substitution of Eq. (11.81) and Eq. (11.95) into Eq. (11.104) gives the force balance between the centrifugal and electric central forces:

$$\frac{\hbar^2}{m_e a^2 b^2} D = \frac{2pe^2}{4\pi\varepsilon_0} \frac{\left(1 - \frac{a_0}{2ap}\right)^2}{ab^2\left(2 + \frac{a_0}{2ap}\right)} D \tag{11.105}$$

$$\frac{\hbar^2 4\pi\varepsilon_0}{m_e e^2 2ap}\left(2 + \frac{a_0}{2ap}\right) = \left(1 - \frac{a_0}{2ap}\right)^2 \tag{11.106}$$

$$\frac{a_0}{ap} + \left(\frac{a_0}{2ap}\right)^2 = \left(1 - \frac{a_0}{2ap}\right)^2 \tag{11.107}$$

$$\frac{a_0}{ap} + \left(\frac{a_0}{2ap}\right)^2 = 1 - \frac{a_0}{ap} + \left(\frac{a_0}{2ap}\right)^2 \tag{11.108}$$

$$a = 2\frac{a_0}{p} \tag{11.109}$$

Substitution of a given by Eq. (11.109) into Eq. (11.79) gives:

$$c' = \frac{a_0}{p} \tag{11.110}$$

The internuclear distance from Eq. (11.110) is:

$$2c' = \frac{2a_0}{p} \tag{11.111}$$

Substitution of $a = \frac{2a_0}{p}$ and $c' = \frac{a_0}{p}$ into Eq. (11.80) gives the length of the semiminor axis of the prolate spheroidal MO, $b = c$:

$$b = \frac{\sqrt{3}}{p} a_0 \tag{11.112}$$

Substitution of $a = \frac{2a_0}{p}$ and $c' = \frac{a_0}{p}$ into Eq. (11.67) gives the eccentricity, e:

$$e = \frac{1}{2} \tag{11.113}$$

From Eqs. (11.63-11.65), the result of Eq. (11.113) can be used to the obtain the electric force $\mathbf{F}_{ele}$ between the protons and the ellipsoidal MO as:

$$\mathbf{F}_{ele} = Ze\mathbf{E}\mathbf{i}_\xi = h_{2cc}^{-1} \frac{p2e^2}{4\pi\varepsilon_0 ab^2} D\mathbf{i}_\xi = \frac{pe^2}{8\pi\varepsilon_0 ab^2} D\mathbf{i}_\xi \tag{11.114}$$

where the electric field $\mathbf{E}$ of the MO is given by Eq. (11.49). Then, the force balance of the hydrogen-type molecular ion is given by:

$$\frac{\hbar^2}{m_e a^2 b^2} D = \frac{pe^2}{8\pi\varepsilon_0 ab^2} D \tag{11.115}$$

which has the parametric solution given by Eq. (11.83) when:

$$a = \frac{2a_0}{p} \tag{11.116}$$

The solutions for the prolate spheroidal axes and eccentricity are given by Eqs. (11.109-11.113).

ENERGIES OF HYDROGEN-TYPE MOLECULAR IONS

From Eq. (11.31), the magnitude of the ellipsoidal field corresponding to a below "ground state" hydrogen-type molecule is an integer, p. The force balance equation (Eq. (11.115)) applies for each point of the electron MO having non-constant charge (mass)-density and velocity over the equipotential and equal energy surface. The electron potential and kinetic energies are thus determined from an ellipsoidal integral.

The potential energy is doubled due to the transverse electric force. The force normal to the MO is given by the dot product of the sum of the force vectors from each focus with $\hat{\mathbf{d}}$ where the angle β is $\beta = \frac{\pi}{2} - \alpha$, and the transverse forces are given by the cross product with $\hat{\mathbf{d}}$. As shown in Figure 11.1, equivalently, the transverse projection is given with the angle α replacing β where the range of α is the same as β. The two contributions to the potential energy doubles it. The potential energy, V_e, of the electron MO in the field of magnitude p times that of the two protons at the foci is:

$$\begin{aligned} V_e &= 2\frac{-2pe^2}{4\pi\varepsilon_0} D \frac{ab^2}{2D} \int_\xi^\infty \frac{d\xi}{R_\xi} \\ &= \frac{-4pe^2}{8\pi\varepsilon_0} \int_\xi^\infty \frac{d\xi}{(\xi + b)\sqrt{\xi + a}} \\ &= \frac{-4pe^2}{8\pi\varepsilon_0 \sqrt{a^2 - b^2}} \ln \frac{a + \sqrt{a^2 - b^2}}{a - \sqrt{a^2 - b^2}} \\ &= \frac{-4pe^2}{8\pi\varepsilon_0 c'} \ln \frac{a + c'}{a - c'} \end{aligned} \tag{11.117}$$

where

$$\sqrt{a^2 - b^2} = c' \tag{11.118}$$

$2c'$ is the distance between the foci which is the internuclear distance. The kinetic energy, T, of the electron MO follows from the same type of integral as V_e using Eqs. (7-14) of Stratton [8], Eqs. (11.37-11.46), and integral #147 of Lide [9]. T is given by the corresponding integral of the centrifugal force (LHS of Eq. (11.115)) with the constraint that the current motion allows the equipotential and equal energy condition with a central field due to the protons; thus, it is corrected by the scale factor h_{2cc} given by Eq. (11.62). The h_{2cc} correction can be considered the scaling factor of the moment of inertia such that the kinetic energy is equivalent to the rotational energy for constant angular frequency ω. The kinetic energy, T, of the electron MO is given by

$$T = h_{2cc} \frac{-\hbar^2}{m_e a^2 b^2} D \frac{ab^2}{2D} \int_\xi^\infty \frac{d\xi}{R_\xi} = \frac{-4\hbar^2}{2m_e a} \int_\xi^\infty \frac{d\xi}{(\xi + b)\sqrt{\xi + a}} = \frac{2\hbar^2}{m_e a\sqrt{a^2 - b^2}} \ln \frac{a + \sqrt{a^2 - b^2}}{a - \sqrt{a^2 - b^2}} \tag{11.119}$$

The potential energy, V_p, due to proton-proton repulsion in the field of magnitude p times that of the protons at the foci ($\xi = 0$) is:

$$V_p = \frac{pe^2}{8\pi\varepsilon_0\sqrt{a^2 - b^2}} \tag{11.120}$$

The total energy, E_T, is given by the sum of the energy terms

$$E_T = V_e + V_p + T \tag{11.121}$$

Substitution of a and b given by Eqs. (11.109) and (11.112), respectively, into Eqs. (11.117), (11.119), (11.120), and (11.121) gives:

$$V_e = \frac{-4p^2e^2}{8\pi\varepsilon_0 a_0}\ln 3 \tag{11.122}$$

$$V_p = \frac{p^2e^2}{8\pi\varepsilon_0 a_0} \tag{11.123}$$

$$T = \frac{2p^2e^2}{8\pi\varepsilon_0 a_0}\ln 3 \tag{11.124}$$

$$E_T = -13.6\ eV(4p^2\ln 3 - p^2 - 2p^2\ln 3) = -p^2 16.28\ eV \tag{11.125}$$

The total energy, which includes the proton-proton-repulsion term is negative which justifies the original treatment of the force balance using the analytical-mechanics equations of an ellipse that considered only the binding force between the protons and the electron and the electron centrifugal force. T is one-half the magnitude of V_e as required for an inverse-squared force [1] wherein V_e is the source of T.

VIBRATION OF HYDROGEN-TYPE MOLECULAR IONS

A charge, q, oscillating according to $\mathbf{r}_0(t) = \mathbf{d}\sin\omega_0 t$ has a Fourier spectrum

$$\mathbf{J}(\mathbf{k},\omega) = \frac{q\omega_0 d}{2} J_m(k\cos\theta d)\{\delta[\omega - (m+1)\omega_0] + \delta[\omega - (m-1)\omega_0]\} \tag{11.126}$$

where J_m's are Bessel functions of order m. These Fourier components can, and do, acquire phase velocities that are equal to the velocity of light [10]. The protons of hydrogen-type molecular ions and molecules oscillate as simple harmonic oscillators; thus, vibrating protons will radiate. Moreover, non-oscillating protons may be excited by one or more photons that are resonant with the oscillatory resonance frequency of the molecule or molecular ion, and oscillating protons may be further excited to higher energy vibrational states by resonant photons. The energy of a photon is quantized according to Planck's equation

$$E = \hbar\omega \tag{11.127}$$

The energy of a vibrational transition corresponds to the energy difference between the initial and final vibrational states. Each state has an electromechanical resonance frequency, and the emitted or absorbed photon is resonant with the difference in frequencies. Thus, as a general principle, quantization of the vibrational spectrum is due to the quantized energies of photons and the electromechanical resonance of the vibrationally excited ion or molecule.

It is shown by Fowles [11] that a perturbation of the orbit determined by an inverse-squared force results in simple harmonic oscillatory motion of the orbit. In a circular orbit in spherical coordinates, the transverse equation of motion gives

$$\dot{\theta} = \frac{L/m}{r^2} \tag{11.128}$$

where L is the angular momentum. The radial equation of motion is:

$$m\left(\ddot{r} - r\dot{\theta}^2\right) = f(r) \tag{11.129}$$

Substitution of Eq. (11.128) into Eq. (11.129) gives:

$$m\ddot{r} - \frac{m(L/m)^2}{r^3} = f(r) \tag{11.130}$$

For a circular orbit, r is a constant and $\ddot{r} = 0$. Thus, the radial equation of motion is given by:

$$-\frac{m(L/m)^2}{a^3} = f(a) \tag{11.131}$$

where a is the radius of the circular orbit for central force $f(a)$ at $r = a$. A perturbation of the radial motion may be expressed in terms of a variable x defined by:

$$x = r - a \tag{11.132}$$

The differential equation can then be written as

$$m\ddot{x} - m(L/m)^2(x+a)^{-3} = f(x+a) \tag{11.133}$$

Expanding the two terms involving $x + a$ as a power series in x, gives:

$$m\ddot{x} - m(L/m)^2 a^{-3}\left(1 - 3\frac{x}{a} + \ldots\right) = f(a) + f'(a)x + \ldots \tag{11.134}$$

Substitution of Eq. (11.131) into Eq. (11.134) and neglecting terms involving x^2 and higher powers of x gives:

$$m\ddot{x}+\left[\frac{-3}{a}f(a)-f'(a)\right]x=0 \tag{11.135}$$

For an inverse-squared central field, the coefficient of x in Eq. (11.135) is positive, and the equation is the same as that of the simple harmonic oscillator. In this case, the particle, if perturbed, oscillates harmonically about the circle $r=a$, and an approximation of the angular frequency of this oscillation is:

$$\omega=\sqrt{\frac{\left[\frac{-3}{a}f(a)-f'(a)\right]}{m}}=\sqrt{\frac{k}{m}} \tag{11.136}$$

An apsis is a point in an orbit at which the radius vector assumes an extreme value (maximum or minimum). The angle swept out by the radius vector between two consecutive apsides is called the apsidal angle. Thus, the apsidal angle is π for elliptical orbits under the inverse-squared law of force. In the case of a nearly circular orbit, Eq. (11.135) shows that r oscillates about the circle $r=a$, and the period of oscillation is given by:

$$\tau_r=2\pi\sqrt{\frac{m}{-\left[\frac{3}{a}f(a)+f'(a)\right]}} \tag{11.137}$$

The apsidal angle in this case is just the amount by which the polar angle θ increases during the time that r oscillates from a minimum value to the succeeding maximum value which is τ_r. From Eq. (11.128), $\dot{\theta}=\frac{L/m}{r^2}$; therefore, θ remains constant, and Eq. (11.131) gives:

$$\dot{\theta}\approx\frac{L/m}{a^2}=\left[-\frac{f(a)}{ma}\right]^{1/2} \tag{11.138}$$

Thus, the apsidal angle is given by

$$\psi=\frac{1}{2}\tau_r\dot{\theta}=\pi\left[3+a\frac{f'(a)}{f(a)}\right]^{-1/2} \tag{11.139}$$

Thus, the power force of $f(r)=-cr^n$ gives:

$$\psi=\pi(3+n)^{-1/2} \tag{11.140}$$

The apsidal angle is independent of the size of the orbit in this case. The orbit is re-entrant, or repetitive, in the case of the inverse-squared law ($n=-2$) for which $\psi=\pi$.

A prolate spheroid MO and the definition of axes are shown in Figures 11.5A and 11.5B, respectively. Consider the two nuclei A and B, each at a focus of the prolate spheroid MO. From Eqs. (11.115), (11.117), and (11.119), the attractive force between the electron and each nucleus at a focus is:

$$f(a)=-\frac{pe^2}{4\pi\varepsilon_0 a^2} \tag{11.141}$$

and

$$f'(a)=\frac{2pe^2}{4\pi\varepsilon_0 a^3} \tag{11.142}$$

In addition to the attractive force between the electron and the nuclei, there is a repulsive force between the two nuclei that is the source of a corresponding reactive force on the reentrant electron orbit. Consider an elliptical orbital plane cross section of the MO in the xy-plane with a nucleus A at (-c', 0) and a nucleus B at (c', 0). For B acting as the attractive focus, the reactive repulsive force at the point (a, 0), the positive semimajor axis, depends on the distance from (a, 0) to nucleus A at (-c', 0) (i.e. the distance from the position of the electron MO at the semimajor axis to the opposite nuclear repelling center at the opposite focus). The distance is given by the sum of the semimajor axis, a, and c', 1/2 the internuclear distance. The contribution from the repulsive force between the two protons is:

$$f(a+c')=\frac{pe^2}{8\pi\varepsilon_0(a+c')^2} \tag{11.143}$$

and

$$f'(a+c')=-\frac{pe^2}{4\pi\varepsilon_0(a+c')^3} \tag{11.144}$$

Thus, from Eqs. (11.136) and (11.141-11.144), the angular frequency of this oscillation is:

$$\omega = \sqrt{\frac{\frac{pe^2}{4\pi\varepsilon_0 a^3} - \frac{pe^2}{8\pi\varepsilon_0 (a+c')^3}}{\mu}}$$

$$= \sqrt{\frac{\frac{pe^2}{4\pi\varepsilon_0 \left(\frac{2a_H}{p}\right)^3} - \frac{pe^2}{8\pi\varepsilon_0 \left(\frac{3a_H}{p}\right)^3}}{\mu}} \tag{11.145}$$

$$= p^2 4.44865\ X\ 10^{14}\ rad/s$$

where the semimajor axis, a, is $a = \frac{2a_H}{p}$ according to Eq. (11.116) and c' is $c' = \frac{a_H}{p}$ according to Eq. (11.110).

In the case of a hydrogen molecule or molecular ion, the electrons which have a mass of 1/1836 that of the protons move essentially instantaneously, and the charge density is that of a continuous membrane. Thus, a stable electron orbit is maintained with oscillatory motion of the protons. Hydrogen molecules and molecular ions are symmetrical along the semimajor axis; thus, the oscillatory motion of protons is along this axis. Let x be the increase in the semimajor axis due to the reentrant orbit with a corresponding displacement of the protons along the semimajor axis from the position of the initial foci of the stationary state. The equation of proton motion due to the perturbation of an orbit having a central inverse-squared central force [1] and neglecting terms involving x^2 and higher is given by

$$\mu\ddot{x} + kx = 0 \tag{11.146}$$

which has the solution in terms of the maximum amplitude of oscillation, A, the reduced nuclear mass, μ, the restoring constant or spring constant, k, the resonance angular frequency, ω_0, and the vibrational energy, E_{vib}, [12]

$$A\cos\omega_0 t \tag{11.147}$$

where

$$\omega_0 = \sqrt{\frac{k}{\mu}} \tag{11.148}$$

For a symmetrical displacement x, the potential energy corresponding to the oscillation E_{Pvib} is given by:

$$E_{Pvib} = 2\left(\frac{1}{2}kx^2\right) = kx^2 \tag{11.149}$$

The total energy of the oscillating molecular ion, $E_{Totalvib}$, is given as the sum of the kinetic and potential energies

$$E_{Totalvib} = \frac{1}{2}\mu\dot{x}^2 + kx^2 \tag{11.150}$$

The velocity is zero when x is the maximum amplitude, A. The total energy of the oscillating molecular ion, $E_{Totalvib}$, is then given as the potential energy with $x = A$

$$E_{Totalvib} = kA^2 \tag{11.151}$$

thus,

$$A = \sqrt{\frac{E_{Totalvib}}{k}} \tag{11.152}$$

It is shown in the Excited States of the One-Electron Atom (Quantization) section that the change in angular frequency of the electron atomic orbital (Eq. (2.21)) is identical to the angular frequency of the photon necessary for the excitation, ω_{photon} (Eq. (2.19)). The energy of the photon necessary to excite the equivalent transition in an electron atomic orbital is one-half of the excitation energy of the stationary cavity because the change in kinetic energy of the electron atomic orbital supplies one-half of the necessary energy. The change in the angular frequency of the atomic orbital during a transition and the angular frequency of the photon corresponding to the superposition of the free space photon and the photon corresponding to the kinetic energy change of the atomic orbital during a transition are equivalent. The correspondence principle holds. It can be demonstrated that the resonance condition between these frequencies is to be satisfied in order to have a net change of the energy field [13]. The bound electrons are excited with the oscillating protons. Thus, the mechanical resonance frequency, ω_0, is only one-half that of the electromechanical frequency which is equal to the frequency of the free space photon, ω, which excites the vibrational mode of the hydrogen molecule or hydrogen molecular ion. The vibrational energy, E_{vib}, corresponding to the photon is given by:

$$E_{vib} = \hbar\omega = \hbar\omega_0 = \hbar\sqrt{\frac{k}{\mu}} = 2kA^2 \tag{11.153}$$

where Planck's equation (Eq. (11.127)) was used. The reduced mass is given by:

$$\mu = \frac{m_1 m_2}{m_1 + m_2} \tag{11.154}$$

Thus,

$$A = \sqrt{\frac{\hbar\omega_0}{2k}} \tag{11.155}$$

Since the protons and electron are not fixed, but vibrate about the center of mass, the maximum amplitude is given by the reduced amplitude, $A_{reduced}$, given by

$$A_{reduced} = \frac{A_1 A_2}{A_1 + A_2} \tag{11.156}$$

where A_n is the amplitude n if the origin is fixed. Thus, Eq. (11.155) becomes:

$$A_{reduced} = \frac{1}{2}\sqrt{\frac{\hbar\omega_0}{2k}} \tag{11.157}$$

and from Eq. (11.148), $A_{reduced}$ is:

$$A_{reduced} = \frac{1}{2}\sqrt{\frac{\hbar\omega_0}{2k}} = \frac{1}{2}\sqrt{\frac{\hbar}{2k}}\left(\frac{k}{\mu}\right)^{1/4} = \frac{\sqrt{\hbar}}{2^{3/2}(k\mu)^{1/4}} \tag{11.158}$$

Then, from Eq. (11.67), $A_{c'}$, the displacement of c' is the eccentricity e given by Eq. (11.113) times $A_{reduced}$ (Eq. (11.158)):

$$A_{c'} = eA_{reduced} = \frac{A_{reduced}}{2} = \frac{\sqrt{\hbar}}{2^{5/2}(k\mu)^{1/4}} \tag{11.159}$$

Thus, during bond formation, the perturbation of the orbit determined by an inverse-squared force results in simple harmonic oscillatory motion of the orbit, and the corresponding frequency, $\omega(0)$, for a hydrogen-type molecular ion $H_2^+(1/p)$ given by Eqs. (11.136) and (11.145) is

$$\omega(0) = p^2\sqrt{\frac{k(0)}{\mu}} = p^2\sqrt{\frac{165.51\ Nm^{-1}}{\mu}} = p^2 4.449\ X\ 10^{14}\ radians/s \tag{11.160}$$

where the reduced nuclear mass of hydrogen given by Eq. (11.154) is:

$$\mu = 0.5 m_p \tag{11.161}$$

and the spring constant, $k(0)$, given by Eqs. (11.136) and (11.145) is:

$$k(0) = p^4 165.51\ Nm^{-1} \tag{11.162}$$

The transition-state vibrational energy, $E_{vib}(0)$, is given by Planck's equation (Eq. (11.127)):

$$E_{vib}(0) = \hbar\omega = \hbar p^2 4.44865\ X\ 10^{14}\ rad/s = p^2 0.2928\ eV \tag{11.163}$$

The amplitude of the oscillation, $A_{reduced}(0)$, given by Eq. (11.158) and Eqs. (11.161-11.162) is:

$$A_{reduced}(0) = \frac{\sqrt{\hbar}}{2^{3/2}\left(p^4 165.51\ Nm^{-1}\mu\right)^{1/4}} = \frac{5.952\ X\ 10^{-12}\ m}{p} = 0.1125\frac{a_0}{p} \tag{11.164}$$

Then, from Eq. (11.67), $A_{c'}(0)$, the displacement of c' is the eccentricity e given by Eq. (11.113) times $A_{reduced}(0)$ (Eq. (11.164)).

$$A_{c'}(0) = eA_{reduced}(0) = \frac{A_{reduced}(0)}{2} = \frac{\sqrt{\hbar}}{2^{5/2}(k\mu)^{1/4}} = \frac{0.05624 a_0}{p} \tag{11.165}$$

The spring constant and vibrational frequency for the formed molecular ion are then obtained from Eqs. (11.136) and (11.141-11.145) using the increases in the semimajor axis and internuclear distances due to vibration in the transition state. The vibrational energy, $E_{vib}(1)$, for the $H_2^+(1/p)$ $\upsilon = 1 \rightarrow \upsilon = 0$ transition given by adding $A_{c'}(0)$ (Eq. (11.159)) to the distances a and $a + c'$ in Eqs. (11.145) and (11.163) is:

$$E_{vib}(1) = p^2 0.270\ eV \tag{11.166}$$

where υ is the vibrational quantum number.

A harmonic oscillator is a linear system as given by Eq. (11.146). In this case, the predicted resonant vibrational frequencies and energies, spring constants, and amplitudes for $H_2^+(1/p)$ for vibrational transitions to higher energy $\upsilon_i \rightarrow \upsilon_f$ are given by $(\upsilon_f - \upsilon_i)$ times the corresponding parameters given by Eq. (11.160) and Eqs. (11.162-11.164). However, excitation of vibration of the molecular ion by external radiation causes the semimajor axis and, consequently, the internuclear distance to increase as a function of the vibrational quantum number υ. Consequently, the vibrational energies of hydrogen-type molecular ions are nonlinear as a function of the vibrational quantum number υ. The lines become more closely spaced and the change in

amplitude, $\Delta A_{reduced}$, between successive states becomes larger as higher states are excited due to the distortion of the molecular ion in these states. The energy difference of each successive transition of the vibrational spectrum can be obtained by considering nonlinear terms corresponding to anharmonicity.

The harmonic oscillator potential energy function can be expanded about the internuclear distance and expressed as a Maclaurin series corresponding to a Morse potential after Karplus and Porter (K&P) [14] and after Eq. (11.134). Treating the Maclaurin series terms as anharmonic perturbation terms of the harmonic states, the energy corrections can be found by perturbation methods. The energy $\tilde{\nu}_\upsilon$ of state υ is:

$$\tilde{\nu}_\upsilon = \upsilon\omega_0 - \upsilon(\upsilon-1)\omega_0 x_0, \quad \upsilon = 0,1,2,3... \tag{11.167}$$

where

$$\omega_0 x_0 = \frac{hc\omega_0^2}{4D_0} \tag{11.168}$$

ω_0 is the frequency of the $\upsilon = 1 \to \upsilon = 0$ transition corresponding to Eq. (11.166), and D_0 is the bond dissociation energy given by Eq. (11.198). From Eqs. (11.166), (11.168), and (11.198),

$$\omega_0 x_0 = \frac{100hc\left(8.06573X10^3 \ \frac{cm^{-1}}{eV} p^2 0.270 \ eV\right)^2}{4e\left(p^2 2.535 \ eV + p^3 0.118755 \ eV\right)} cm^{-1} \tag{11.169}$$

The vibrational energies of successive states are given by Eqs. (11.166-11.167) and (11.169).

Using Eqs. (11.145), (11.158-11.160), (11.162-11.169), and (11.199) the corresponding parameters for deuterium-type molecular ions with:

$$\mu = m_p \tag{11.170}$$

are

$$\omega(0) = p^2\sqrt{\frac{k(0)}{\mu}} = p^2\sqrt{\frac{165.65 \ Nm^{-1}}{\mu}} = p^2 3.147 \ X \ 10^{14} \ radians/s \tag{11.171}$$

$$k(0) = p^4 165.65 \ Nm^{-1} \tag{11.172}$$

$$E_{vib}(0) = p^2 0.20714 \ eV \tag{11.173}$$

$$A_{reduced}(0) = \frac{\sqrt{\hbar}}{2^{3/2}\left(p^4 165.65 \ Nm^{-1}\mu\right)^{1/4}} = \frac{5.004 \ X \ 10^{-12} \ m}{p} = 0.09457\frac{a_0}{p} \tag{11.174}$$

$$E_{vib}(1) = p^2 0.193 \ eV \tag{11.175}$$

$$\omega_0 x_0 = \frac{100hc\left(8.06573X10^3 \ \frac{cm^{-1}}{eV} p^2 0.193 \ eV\right)^2}{4e\left(p^2 2.5770 \ eV + p^3 0.118811 \ eV\right)} cm^{-1} \tag{11.176}$$

The vibrational energies of successive states are given by Eqs. (11.167) and (11.175-11.176).

THE DOPPLER ENERGY TERM OF HYDROGEN-TYPE MOLECULAR IONS

As shown in the Vibration of Hydrogen-type Molecular Ions section, the electron orbiting the nuclei at the foci of an ellipse may be perturbed such that a stable reentrant orbit is established that gives rise to a vibrational state corresponding to time harmonic oscillation of the nuclei and electron. The perturbation is caused by a photon that is resonant with the frequency of oscillation of the nuclei wherein the radiation is electric dipole with the corresponding selection rules.

Oscillation may also occur in the transition state. The perturbation arises from the decrease in internuclear distance as the molecular bond forms. Relative to the unperturbed case given in the Force Balance of Hydrogen-type Molecular Ions section, the reentrant orbit may give rise to a decrease in the total energy while providing a transient kinetic energy to the vibrating nuclei. However, as an additional condition for stability, radiation must be considered. Regarding the potential for radiation, the nuclei may be considered point charges. A point charge undergoing periodic motion accelerates and as a consequence radiates according to the Larmor formula (cgs units) [15]:

$$P = \frac{2e^2}{3c^3}\left|\dot{\mathbf{v}}\right|^2 \tag{11.177}$$

where e is the charge, $\dot{\mathbf{v}}$ is its acceleration, and c is the speed of light. The radiation has a corresponding force that can be determined based on conservation of energy with radiation. The radiation reaction force, $\mathbf{F}_{\mathbf{rad}}$, given by Jackson [16] is:

$$\mathbf{F}_{\mathbf{rad}} = \frac{2}{3}\frac{e^2}{c^3}\ddot{\mathbf{v}} \tag{11.178}$$

Then, the Abraham-Lorentz equation of motion is given by [16]:

$$m\left(\dot{\mathbf{v}}-\frac{2}{3}\frac{e^2}{mc^3}\ddot{\mathbf{v}}\right)=\mathbf{F}_{\mathbf{ext}} \tag{11.179}$$

where $\mathbf{F}_{\mathbf{ext}}$ is the external force and m is the mass. The external force for the vibrating system is given by Eq. (11.146).

$$\mathbf{F}_{\mathbf{ext}}=kx \tag{11.180}$$

where x is the displacement of the protons along the semimajor axis from the position of the initial foci of the stationary state in the absence of vibration with a reentrant orbit of the electron. A nonradiative state must be achieved after the emission due to transient vibration wherein the nonradiative condition given by Eq. (11.24) must be satisfied.

As shown in the Resonant Line Shape and Lamb Shift section, the spectroscopic linewidth arises from the classical rise-time band-width relationship, and the Lamb Shift is due to conservation of energy and linear momentum and arises from the radiation reaction force between the electron and the photon. The radiation reaction force in the case of the vibration of the molecular ion in the transition state corresponds to a Doppler energy, E_D, that is dependent on the motion of the electron and the nuclei. The Doppler energy of the electron is given by Eq. (2.155) after Gibb [17]:

$$\bar{E}_D \cong 2\sqrt{E_K E_R}=E_{h\nu}\sqrt{\frac{2\bar{E}_K}{Mc^2}} \tag{11.181}$$

where E_R is the recoil energy which arises from the photon's linear momentum given by Eq. (2.153), E_K is the vibrational kinetic energy of the reentrant orbit in the transition state, and M is the mass of the electron m_e.

As given in the Vibration of Hydrogen-Type Molecular Ions section, for an inverse-squared central field, the coefficient of x in Eq. (11.135) is positive, and the equation is the same as that of the simple harmonic oscillator. Since the electron of the hydrogen molecular ion is perturbed as the internuclear separation decreases with bond formation, it oscillates harmonically about the semimajor axis given by Eq. (11.116), and an approximation of the angular frequency of this oscillation is

$$\omega=\sqrt{\frac{\left[\frac{-3}{a}f(a)-f'(a)\right]}{m_e}}=\sqrt{\frac{k}{m_e}} \tag{11.182}$$

From Eqs. (11.115), (11.117), and (11.119), the central force terms between the electron MO and the two protons are:

$$f(a)=-\frac{2pe^2}{4\pi\varepsilon_0 a^2} \tag{11.183}$$

and

$$f'(a)=\frac{4pe^2}{4\pi\varepsilon_0 a^3} \tag{11.184}$$

Thus, the angular frequency of this oscillation is:

$$\omega=\sqrt{\frac{\frac{2pe^2}{4\pi\varepsilon_0\left(\frac{2a_H}{p}\right)^3}}{m_e}}=p^2\,2.06538\;X\;10^{16}\;rad/s \tag{11.185}$$

where the semimajor axis, a, is $a=\frac{2a_H}{p}$ according to Eq. (11.116) including the reduced electron mass. The kinetic energy, E_K, is given by Planck's equation (Eq. (11.127)).

$$\bar{E}_K=\hbar\omega=\hbar p^2\,2.06538\;X\;10^{16}\;rad/s=p^2 13.594697\;eV \tag{11.186}$$

In Eq. (11.181), substitution of the total energy of the hydrogen molecular ion, E_T, (Eq. (11.125)) for $E_{h\nu}$, the mass of the electron, m_e, for M, and the kinetic energy given by Eq. (11.186) for $\bar{E}_K$ divided by p^2, the number of multipoles of a molecular hydrino state p (Eq. (5.45)) gives the Doppler energy of the electron for the reentrant orbit.

$$\bar{E}_D \cong E_{h\nu}\sqrt{\frac{2\bar{E}_K}{Mc^2}}=-p^2 16.28034\;eV\sqrt{\frac{2e\left(p^2 13.594697\;eV\right)}{p^2 m_e c^2}}=-p^2 0.118755\;eV \tag{11.187}$$

The total energy of the molecular ion is decreased by $\bar{E}_D$.

In addition to the electron, the nuclei also undergo simple harmonic oscillation in the transition state at their corresponding frequency given in the Vibration of Hydrogen-Type Molecular Ions section. On average, the total energy of vibration is equally distributed between kinetic energy and potential energy [18]. Thus, the average kinetic energy of vibration corresponding to the Doppler energy of the electrons, $\bar{E}_{Kvib}$, is 1/2 of the vibrational energy of the molecular ion given by Eq. (11.166). The decrease in the energy of the hydrogen molecular ion due to the reentrant orbit in the transition state

corresponding to simple harmonic oscillation of the electron and nuclei, $\bar{E}_{osc}$, is given by the sum of the corresponding energies, $\bar{E}_D$ and $\bar{E}_{Kvib}$. Using Eq. (11.187) and E_{vib} from Eq. (11.163) gives:

$$\bar{E}_{osc} = \bar{E}_D + \bar{E}_{Kvib} = \bar{E}_D + \frac{1}{2}\hbar p^2\sqrt{\frac{k}{\mu}} \tag{11.188}$$

$$\bar{E}_{osc} = -p^2 0.118755\ eV + \frac{1}{2}p^2\left(0.29282\ eV\right) \tag{11.189}$$

To the extent that the MO dimensions are the same, the electron reentrant orbital energies $\bar{E}_K$ are the same independent of the isotope of hydrogen, but the vibrational energies are related by Eq. (11.148). Thus, the differences in bond energies are essentially given by 1/2 the differences in vibrational energies. Using Eq. (11.187) with the deuterium reduced electron mass for E_T and $\bar{E}_D$, and E_{vib} for $D_2^+(1/p)$ given by Eq. (11.173), that corresponds to the deuterium reduced nuclear mass (Eq. (11.170)), the corresponding $\bar{E}_{osc}$ is:

$$\bar{E}_{osc} = -p^2 0.118811\ eV + \frac{1}{2}p^2\left(0.20714\ eV\right) \tag{11.190}$$

TOTAL, IONIZATION, AND BOND ENERGIES OF HYDROGEN AND DEUTERIUM MOLECULAR IONS

The total energy of the hydrogen molecular ion which is equivalent to the negative of the ionization energy is given by the sum of E_T (Eqs. (11.121) and (11.125)) and $\bar{E}_{osc}$ given by Eqs. (11.185-11.188). Thus, the total energy of the hydrogen molecular ion having a central field of $+pe$ at each focus of the prolate spheroid molecular orbital including the Doppler term is:

$$E_T = V_e + V_p + T + \bar{E}_{osc} \tag{11.191}$$

$$\begin{aligned} E_T &= -p^2\left\{\frac{e^2}{8\pi\varepsilon_0 a_H}(4\ln 3 - 1 - 2\ln 3)\left[1+\sqrt{\frac{2\hbar\sqrt{\frac{2e^2}{4\pi\varepsilon_0\left(2a_H\right)^3}}{m_e}}{m_e c^2}}\right] - \frac{1}{2}\hbar\sqrt{\frac{k}{\mu}}\right\} \\ &= -p^2 16.2803\ eV - p^2 0.118755\ eV + \frac{1}{2}p^2\hbar\sqrt{\frac{k}{\mu}} \end{aligned} \tag{11.192}$$

From Eqs. (11.189) and (11.191-11.192), the total energy for hydrogen-type molecular ions is:

$$\begin{aligned} E_T &= -p^2 16.28033\ eV + \bar{E}_{osc} \\ &= -p^2 16.28033\ eV - p^2 0.118755\ eV + \frac{1}{2}p^2\left(0.29282\ eV\right) \\ &= -p^2 16.252675\ eV \end{aligned} \tag{11.193}$$

The total energy of the deuterium molecular ion is given by the sum of E_T (Eq. (11.125)) corrected for the reduced electron mass of D and $\bar{E}_{osc}$ given by Eq. (11.190).

$$\begin{aligned} E_T &= -p^2 16.284\ eV + \bar{E}_{osc} \\ &= -p^2 16.284\ eV - p^2 0.118811\ eV + \frac{1}{2}p^2\left(0.20714\ eV\right) \\ &= -p^2 16.2988\ eV \end{aligned} \tag{11.194}$$

The bond dissociation energy, E_D, is the difference between the total energy of the corresponding hydrogen atom or $H(1/p)$ atom [19-20], called hydrino atom having a principal quantum number $1/p$ where p is an integer, and E_T.

$$E_D = E(H(1/p)) - E_T \tag{11.195}$$

where [19]

$$E(H(1/p)) = -p^2 13.59844\ eV \tag{11.196}$$

and [20]

$$E(D(1/p)) = -p^2 13.603\ eV \tag{11.197}$$

The hydrogen molecular ion bond energy, E_D, is given by Eq. (11.193) with the reduced electron mass and Eqs. (11.195-11.196):

$$\begin{aligned} E_D &= -p^2 13.59844 - E_T \\ &= -p^2 13.59844 - \left(-p^2 16.252675\ eV\right) \\ &= p^2 2.65424\ eV \end{aligned} \tag{11.198}$$

The deuterium molecular ion bond energy, E_D, is given by Eq. (11.194) with the reduced electron mass of D and Eqs. (11.195) and (11.197).

$$\begin{aligned} E_D &= -p^2 13.603 - E_T \\ &= -p^2 13.603 - \left(-p^2 16.2988\ eV\right) \\ &= p^2 2.6958\ eV \end{aligned} \tag{11.199}$$

HYDROGEN-TYPE MOLECULES

FORCE BALANCE OF HYDROGEN-TYPE MOLECULES

Hydrogen-type molecules comprise two indistinguishable electrons bound by an elliptic field. Each electron experiences a centrifugal force. The balancing centripetal force (on each electron) is produced by the electric force between the electron and the elliptic electric field and the magnetic force between the two electrons causing the electrons to pair wherein the interaction between the pairing electrons involves a magnetic moment of a Bohr magneton, μ_B, as given in the Magnetic Moment of an Ellipsoidal MO section. The internal field is uniform along the major axis, and the far field is that of a dipole as shown in the Magnetic Field of an Ellipsoidal MO section. The magnetic force is derived by first determining the interaction of the two electrons due to the field of the outer electron 2 acting on the magnetic moments of electron 1 and vice versa. Insight into the behavior is given by considering the physics of a single bound electron in an externally applied uniform magnetic field as discussed in the Two-Electron Atoms section. The uniform current- (charge-) density function $Y_0^0(\theta,\phi)$ was given in the Atomic Orbital Equation of Motion for $\ell = 0$ Based on the Current Vector Field (CVF) section. The resultant angular momentum projections of the spherically-symmetric atomic orbital current density, $Y_0^0(\theta,\phi)$, corresponding to the interaction are $\mathbf{L}_{xy} = \frac{\hbar}{4}$ and $\mathbf{L}_z = \frac{\hbar}{2}$. As shown in the Resonant Precession of the Spin-1/2-Current-Density Function Gives Rise to the Bohr Magneton section, the electron spin angular momentum gives rise to a trapped photon with $\hbar$ of angular momentum along an $\mathbf{S}$-axis. Then, the spin state of an atomic orbital comprises a photon standing wave that is phase-matched to a spherical harmonic source current, a spherical harmonic dipole $Y_\ell^m(\theta,\phi) = \sin\theta$ with respect to the $\mathbf{S}$-axis. The dipole spins about the $\mathbf{S}$-axis at the angular velocity given by Eq. (1.36) with $\hbar$ of angular momentum. $\mathbf{S}$ rotates about the z-axis at the Larmor frequency at $\theta = \frac{\pi}{3}$ such that it has a static projection of the angular momentum of $\mathbf{S}_{\|} = \pm\hbar\cos\frac{\pi}{3} = \pm\frac{\hbar}{2}\,\mathbf{i}_{Z_R}$ as given by Eq. (1.97), and from Eq. (1.96), the projection of $\mathbf{S}$ onto the transverse plane (xy-plane) is $\mathbf{S}_{\perp} = \hbar\sin\frac{\pi}{3} = \pm\sqrt{\frac{3}{4}}\hbar\,\mathbf{i}_{Y_R}$. Then, the vector projection of the radiation-reaction-type magnetic force of the Two Electron Atom section given by Eqs. (7.24) and (7.31) contain the factor $\sqrt{\frac{3}{4}}\hbar$. This represents the maximum projection of the time-dependent magnetic moment onto an axis of the spherical-central-force system.

The atomic orbital can serve as a basis element to form a molecular orbital (MO). The total magnitude of the angular momentum of $\hbar$ is conserved for each member of the linear combinations of $Y_0^0(\theta,\phi)$'s in the transition from the $Y_0^0(\theta,\phi)$'s to the MO. Since the charge and current densities have the same distribution, the equipotential energy surface solution of Laplace's equation for the charge distribution also determines the current distribution. Newton's laws determine the angular frequency and the velocity of the charge motion corresponding to the current. Specifically, the further constraint from Newton's laws that the orbital surface is a constant total energy surface and the condition of nonradiation provide that the motion is periodic with a constant period and that the current is continuous and constant over a period. These boundary conditions determine the corresponding velocity function. In non-spherical coordinates, the nonuniform charge distribution given by Laplace's equation is compensated by a nonuniform velocity distribution such that the constant current condition is met. Then, the conservation of the angular momentum is provided when symmetrically stretching the current density of an atomic $Y_0^0(\theta,\phi)$ current density along the semimajor axis of the MO so formed.

The angular momentum projection may be determined by first considering the case of the hydrogen molecular ion. Specifically, the angular momentum must give the results of the Stern-Gerlach experiment as shown for atomic electrons and free electrons in the Resonant Precession of the Spin-1/2-Current-Density Function Gives Rise to the Bohr Magneton section and Stern-Gerlach Experiment section, respectively. The hydrogen-molecular-ion MO, and all MOs in general, have cylindrical symmetry along the bond axis. Then, in general, $Y_0^0(\theta,\phi)$ can serve as a basis element for an MO having cylindrical symmetry along the semimajor axis. This defines the axis for stretching the $Y_0^0(\theta,\phi)$ basis element to form the MO (Figure 11.2) while conserving the angular momentum. The charge and current distribution is normalized by applying the method given in the

Uniformity of $Y_0^0(\theta,\phi)$ section according to the distribution given by Eq. (11.42). This gives rise to an ellipsoidal surface comprised of the equivalent of elliptical-orbit, plane cross sections in the direction parallel to the semimajor axis with the conserved angular momentum projections along the orthogonal semiminor axes.

Figure 11.2. The bound electron MO, a prolate spheroidal two-dimensional supercurrent comprising an extended continuous distribution of charge and current completely surrounding the nuclei at the foci, obtained by stretching $Y_0^0(\theta,\phi)$ along the semimajor axis. Unlike a spinning top, there is a complex pattern of motion on its surface that generates two orthogonal components of angular momentum (Figure 11.4) that give rise to the phenomenon of electron spin. A. The z-axis view of the MO current paths having $\mathbf{L}_z = \frac{\hbar}{2}$ matching the angular momentum projection on the $\left(-\frac{1}{\sqrt{2}}\mathbf{i}_x, \frac{1}{\sqrt{2}}\mathbf{i}_y, \mathbf{i}_z\right)$-axis of the basis element $Y_0^0(\theta,\phi)$. B. A representation of the z-axis view of the continuous charge-density and supercurrent-density distributions of the MO with 144 vectors overlaid giving the direction of the currents (nuclei not to scale).

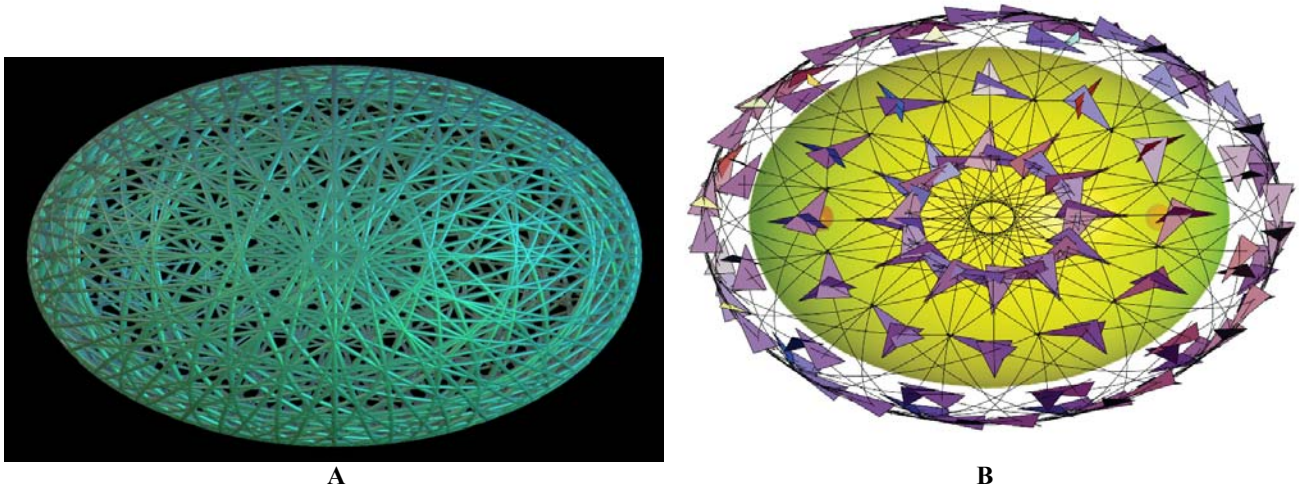

A **B**

As shown in the Atomic Orbital Equation of Motion for $\ell = 0$ Based on the Current Vector Field (CVF) section, the atomic orbital is comprised of the uniform function $Y_0^0(\theta,\phi)$ with the intrinsic angular momentum directed along two orthogonal axes having three angular momentum components of $\mathbf{L}_{xy} = +/-\frac{\hbar}{4}$ and $\mathbf{L}_z = \frac{\hbar}{2}$. Then, $Y_0^0(\theta,\phi)$ serves as the basis element for the formation of a MO with conservation of the total magnitude of the angular momentum of $\hbar$ (Eq. (1.37)) and the orthogonal projections $\mathbf{L}_{xy}$ and $\mathbf{L}_z$ of $Y_0^0(\theta,\phi)$ directed along the semiminor axes of the MO. Since the direction of the stretching of the great-circle elements of $Y_0^0(\theta,\phi)$ having a radius of the semiminor axes is perpendicular to the angular momentum axes, the conserved angular momentum projections of the MO are $\mathbf{L}_y = +/-\frac{\hbar}{4}$ and $\mathbf{L}_z = \frac{\hbar}{2}$ as shown in Figure 11.4. The transform is that of a minimum energy, equipotential spherical to prolate spheroidal surface. A convenient method to perform the stretching is numerically using a computer instead of using basis elements, convolutions, and rotational matrices in ellipsoidal coordinates following the method for construction of $Y_0^0(\theta,\phi)$ given in the Generation of the Atomic Orbital CVFs section. As shown for the $Y_0^0(\theta,\phi)$ normalization algorithm in the Uniformity of $Y_0^0(\theta,\phi)$ section, the equipotential charge density of the MO can be obtained by stretching and weighting the total constant current on each current loop without changing the angular momentum distribution since the changes are orthogonal to the angular momentum axes. In addition, the current distribution along each loop is adjusted to achieve the equipotential charge density (Eq. (11.42)) wherein the current is constant due to a corresponding variable velocity with position on the loop (Eqs. (11.84) and (11.23-11.24) using the area A of the elliptic plane section of the prolate spheroid).

The algorithm for generating the charge and current density numerically may be an adaptation of computed tomography algorithms such as the original: Apply an Affine transform to the atomic electron current pattern to form an initial current distribution. Calculate the density at each point area from the initial distribution, substrate it from the prolate spheroid distribution, add the normalized error to the current of each contributing loop, distribute the current correction along each loop in a manner to match Eq. (11.45), and repeat over all point areas repetitively until the error goes to zero. Alternatively, a numerical spheroid to ellipsoidal transform may be applied to the numerically normalized atomic current motion wherein the angular momentum of each current loop is conserved and the constant current is based on the corresponding velocity variation on the ellipsoidal surface. Specifically, normalization was achieved using a transformation that transforms an ellipsoidal MO into the

AO atomic orbital $Y_0^0(\theta,\phi)$. Then, sample points of the normalized sphere were used to numerically perform the transform in reverse using the inverse of the ellipsoidal MO to $Y_0^0(\theta,\phi)$ transformation to give the current densities shown in Figure 11.3 [21]. The change in velocity is inherently compensated by the mass/charge density such that the overall flow of increments of mass/charge on each ellipse is constant, and the transform of each ellipse to a circle is such that the angular momentum remains the same. The radius of the sphere is the same as the semiminor axis, but could be arbitrary in the normalization algorithm since densities are computed (corresponding to the number of samples in a certain solid angle).

Figure 11.3. The y-axis view of the numerically normalized current density of the ellipsoidal MO using the inverse of the ellipsoidal MO to $Y_0^0(\theta,\phi)$ transformation.

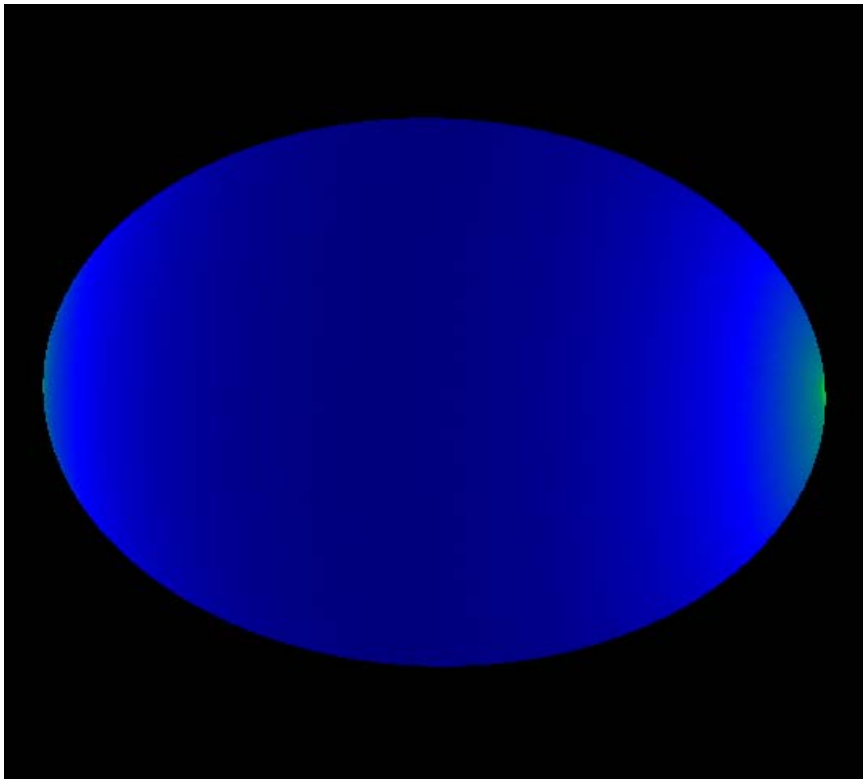

Now consider the behavior of the hydrogen molecular ion in a magnetic field. As shown in the Resonant Precession of the Spin-1/2-Current-Density Function Gives Rise to the Bohr Magneton section, in general, the photon angular momentum corresponding to the resonant excitation of the Larmor excited state is $\hbar$, and the angular momentum change corresponding to the spin-flip transition is also $\hbar$. In the case of the hydrogen molecular ion, the Larmor-excitation photon carries $\hbar$ of angular momentum that gives rise to a prolate spheroidal dipole current about an $\mathbf{S}$-axis in the same manner as in the case of the spherical dipole of the Larmor excited atomic orbital shown in Figures 1.15 and 1.16. The former are given by the prolate angular function, which comprises an associated Legendre function $P_\ell^m(\eta)$ [22], and the latter comprises the spherical harmonic dipole $Y_\ell^m(\theta,\phi)=\sin\theta$. Both are with respect to the $\mathbf{S}$-axis. For hydrogen molecular ion, $\mathbf{L}_y=+/-\frac{\hbar}{4}$ and $\mathbf{L}_z=\frac{\hbar}{2}$ of intrinsic spin are along the semiminor axes of the prolate spheroidal MO and $\mathbf{S}$ is along the semimajor axis as shown in Figure 11.4. Thus, the Larmor excitation is constrained by Maxwell's equations to be along the semimajor axis. In general, all bonds are cylindrically symmetrical about the internuclear or semimajor axis; thus, the Larmor precession occurs about the bond axis of an MO wherein the intrinsic angular momentum components rotate about $\mathbf{S}$ at the Larmor frequency and are not stationary relative to the magnetic field. In the coordinate system rotating at the Larmor frequency (denoted by the axes labeled X_R, Y_R, and Z_R in Figure 11.2), the angular momentum of $\mathbf{S}$ of magnitude $\hbar$ is stationary. The Y_R-components of magnitude $+/-\frac{\hbar}{4}$ and the Z_R-component of magnitude $\frac{\hbar}{2}$ rotate about $\mathbf{S}$ at the Larmor frequency. The opposing intrinsic magnetic moments of $\pm\frac{\mu_B}{4}$ along the Y_R-axis corresponding to the angular momentum of $\mathbf{L}_y=+/-\frac{\hbar}{4}$ (Eq. (28) of Box 1.1 and Eq. (2.65)) balances the torque on the $\frac{\hbar}{2}$ angular momentum component along the Z_R-axis, and all of the components have the necessary orthogonality.

Then, the **S**-axis is the direction of the magnetic moment of each unpaired electron of a molecule or molecular ion. The magnetic moment of **S** of μ_B corresponding to its $\hbar$ of angular momentum is consistent with the Stern-Gerlach experiment. The Larmor excitation can only be parallel or antiparallel to the magnetic field in order to conserve the angular momentum of the electron as well as the $\hbar$ of angular momentum of each of the photon corresponding to the Larmor excitation and the photon that causes a 180° flip of the direction of **S**. The result is the same as that for the atomic electron and the free electron given in the Resonant Precession of the Spin-1/2-Current-Density Function Gives Rise to the Bohr Magneton section and Stern-Gerlach Experiment section, respectively. The magnetic field is given in the Magnetic Field of an Ellipsoidal Molecular Orbital section.

Figure 11.4. The angular momentum components of the MO and **S** in the rotating coordinate system X_R, Y_R, and Z_R that precesses at the Larmor frequency about **S** such that the **S** vector is stationary.

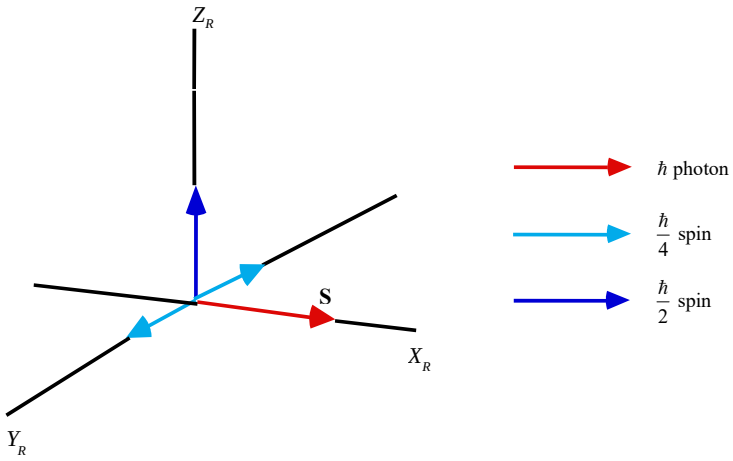

Next, consider the magnetic-pairing force of the hydrogen molecule due to the spin-angular-momentum components. The magnetic moments of electrons 1 and 2 of the hydrogen molecule cancel, as they are spin paired to form an energy minimum at the distance ξ (i.e. $\xi_1 = \xi_2$). The molecular magnetic force follows from the derivation for that between the electrons of two-electron atoms as given in the Two-Electron Atoms section. The latter force was derived by first determining the interaction of the two electrons due to the field of the outer electron 2 acting on the magnetic moment of electron 1 and vice versa. It was also given by the relationship between the angular momentum, energy, and frequency for the transition of electron 2 from the continuum to the ground state of the two-electron atom. The molecular magnetic force follows from Eqs. (7.25-7.31) with the conversion to ellipsoidal coordinates. The conversion is apparent from comparing the centrifugal forces for each coordinate system given by Eq. (11.98) and Eqs. (7.1-7.2). In the present case of hydrogen-type molecules, the radiation-reaction-type magnetic force arises between the electrons, each having the components shown in Figure 11.4. With the photon angular momentum projection of $\hbar$ and the total nuclear charge (non-photon-field) of 2, the magnitude of the magnetic force between the two electrons is 1/2 that of the centrifugal force given by Eq. (11.95). This force is a term in the overall force balance.

In addition to the spin pairing force between the two electrons, the electric and centrifugal forces must be considered in the force balance. In the hydrogen-type molecule, the two electrons are bound by the central electric field as in the case of the molecular ion. The hydrogen-type molecule is formed by the binding of an electron 2 to the hydrogen-type molecular ion comprising two protons at the foci of the prolate spheroidal MO of electron 1. The ellipsoids of electron 1 and electron 2 are confocal; thus, the electric fields and the corresponding forces are normal to each MO of electron 1 and electron 2. The field of the protons is ellipsoidal on average, and the binding of electron 2 requires a quantized energy release in units of $\hbar$. The magnetic force is also quantized in terms of $\hbar$. The final bound electrons must have the same angular momentum and be paired in the same orbit; thus, they must have the same eccentricity. This is only possible according to Eq. (11.11) if they have the same central force. Consequently, to conserve angular momentum, the electric force on electron 2 must be the same as that as on electron 1. Due to the magnetic pairing force between electron 2 and electron 1 as well as the central electric force, the balance between the centrifugal force and the central field of electron 2 of the hydrogen-type molecule formed by electron 2 binding to a hydrogen-type molecular ion is the same as that given by Eq. (11.115). Then, the force balance between the centrifugal force and the sum of the Coulombic and additionally the magnetic spin-pairing forces to solve for the semimajor axis is:

$$\frac{\hbar^2}{m_e a^2 b^2} D = \frac{pe^2}{8\pi\varepsilon_0 ab^2} D + \frac{\hbar^2}{2m_e a^2 b^2} D \tag{11.200}$$

$$\frac{2a_0}{pa} - \frac{a_0}{pa} = 1 \tag{11.201}$$

$$a = \frac{a_0}{p} \tag{11.202}$$

Substitution of Eq. (11.202) into Eq. (11.79) is:

$$c' = \frac{1}{p\sqrt{2}} a_0 \tag{11.203}$$

The internuclear distance given by multiplying Eq. (11.203) by two is:

$$2c' = \frac{a_0\sqrt{2}}{p} \tag{11.204}$$

Substitution of Eqs. (11.202-11.203) into Eq. (11.80) is:

$$b = c = \frac{1}{p\sqrt{2}} a_0 \tag{11.205}$$

Substitution of Eqs. (11.202-11.203) into Eq. (11.67) is:

$$e = \frac{1}{\sqrt{2}} \tag{11.206}$$

For hydrogen, $r(t) = D$ for $\theta = n\frac{\pi}{2}$, $n = 0,1,2,3,4$. Thus, there is no dipole moment, and the molecule is not predicted to be infrared active. However, it is predicted to be Raman active due to the quadrupole moment. The liquefaction temperature of H_2 is also predicted to be significantly higher than isoelectronic helium.

ENERGIES OF HYDROGEN-TYPE MOLECULES

The energy components defined previously for the molecular ion, Eqs. (11.117), (11.119), (11.120), and (11.121), apply in the case of the corresponding molecule except that all of the field lines of the protons must end on the MO comprising two-paired electrons. With spin pairing of the mirror-image-current electrons, the scaling factors due to the non-ellipsoidal variation of the electric field of the protons is unity as in the case of the sum of squares of spherical harmonics. Thus, the hydrogen-type molecular energies are given by the integral of the forces without correction. Then, each molecular-energy component is given by the integral of corresponding force in Eq. (11.200) where each energy component is the total for the two equivalent electrons with the central-force action at the position of the electron MO where the parameters a and b are given by Eqs. (11.202) and (11.205), respectively.

The potential energy, V_e, of the two-electron MO comprising equivalent electrons in the field of magnitude p times that of the two protons at the foci is:

$$\begin{aligned} V_e &= 2\frac{-pe^2}{4\pi\varepsilon_0} D\frac{ab^2}{2D}\int_{\xi}^{\infty}\frac{d\xi}{R_\xi} \\ &= \frac{-2pe^2}{8\pi\varepsilon_0}\int_{\xi}^{\infty}\frac{d\xi}{(\xi+b)\sqrt{\xi+a}} \\ &= \frac{-2pe^2}{8\pi\varepsilon_0\sqrt{a^2-b^2}}\ln\frac{a+\sqrt{a^2-b^2}}{a-\sqrt{a^2-b^2}} \end{aligned} \tag{11.207}$$

which is equivalent to $Ze = 2pe$ times the potential of the MO given by Eq. (11.46) after Eq. (11.114). The potential energy, V_p, due to proton-proton repulsion in the field of magnitude p times that of the protons at the foci ($\xi = 0$) is

$$V_p = \frac{p}{8\pi\varepsilon_0}\frac{e^2}{\sqrt{a^2-b^2}} \tag{11.208}$$

The kinetic energy, T, of the two-electron MO of total mass $2m_e$ is:

$$\begin{aligned} T &= 2\frac{-\hbar^2}{2m_e a^2 b^2} D\frac{ab^2}{2D}\int_{\xi}^{\infty}\frac{d\xi}{R_\xi} \\ &= \frac{-\hbar^2}{2m_e a}\int_{\xi}^{\infty}\frac{d\xi}{(\xi+b)\sqrt{\xi+a}} \\ &= \frac{\hbar^2}{2m_e a\sqrt{a^2-b^2}}\ln\frac{a+\sqrt{a^2-b^2}}{a-\sqrt{a^2-b^2}} \end{aligned} \tag{11.209}$$

The magnetic energy, V_m, of the two-electron MO of total mass $2m_e$ corresponding to the magnetic force of Eq. (11.200) is:

$$\begin{aligned} V_m &= 2\frac{-\hbar^2}{2(2m_e)a^2b^2}D\frac{ab^2}{2D}\int_{\xi}^{\infty}\frac{d\xi}{R_\xi} \\ &= \frac{-\hbar^2}{4m_e a}\int_{\xi}^{\infty}\frac{d\xi}{(\xi+b)\sqrt{\xi+a}} \\ &= \frac{-\hbar^2}{4m_e a\sqrt{a^2-b^2}}\ln\frac{a+\sqrt{a^2-b^2}}{a-\sqrt{a^2-b^2}} \end{aligned} \tag{11.210}$$

The total energy, E_T, is given by the sum of the energy terms (Eqs. (11.207-11.210)).

$$E_T = V_e + T + V_m + V_p \tag{11.211}$$

$$E_T = -13.60\ eV\left[\left(2p^2\sqrt{2} - p^2\sqrt{2} + \frac{p^2\sqrt{2}}{2}\right)\ln\frac{\sqrt{2}+1}{\sqrt{2}-1} - p^2\sqrt{2}\right] = -p^2 31.63 \tag{11.212}$$

where a and b are given by Eqs. (11.202) and (11.205), respectively. The total energy, which includes the proton-proton-repulsion term is negative which justifies the original treatment of the force balance using the analytical mechanics equation of an ellipse that considered only the binding force between the protons and the electrons and the electron centrifugal force. As shown by Eqs. (11.290) and (11.292), T is one-half the magnitude of V_e as required for an inverse-squared force [1] wherein V_e is the source of T.

VIBRATION OF HYDROGEN-TYPE MOLECULES

The vibrational energy levels of hydrogen-type molecules may be solved in the same manner as hydrogen-type molecular ions given in the Vibration of Hydrogen-type Molecular Ions section. The corresponding central force terms of Eq. (11.136) are:

$$f(a) = -\frac{pe^2}{8\pi\varepsilon_0 a^2} \tag{11.213}$$

and

$$f'(a) = \frac{pe^2}{4\pi\varepsilon_0 a^3} \tag{11.214}$$

The distance for the reactive nuclear-repulsive terms is given by the sum of the semimajor axis, a, and c', 1/2 the internuclear distance. The contribution from the repulsive force between the two protons is:

$$f(a+c') = \frac{pe^2}{8\pi\varepsilon_0 (a+c')^2} \tag{11.215}$$

and

$$f'(a+c') = -\frac{pe^2}{4\pi\varepsilon_0 (a+c')^3} \tag{11.216}$$

Thus, from Eqs. (11.136) and (11.213-11.216), the angular frequency of the oscillation is:

$$\omega = \sqrt{\frac{\frac{pe^2}{8\pi\varepsilon_0 a^3} - \frac{pe^2}{8\pi\varepsilon_0 (a+c')^3}}{\mu}} = \sqrt{\frac{\frac{pe^2}{8\pi\varepsilon_0\left(\frac{a_0}{p}\right)^3} - \frac{pe^2}{8\pi\varepsilon_0\left(\frac{\left(1+\frac{1}{\sqrt{2}}\right)a_0}{p}\right)^3}}{\mu}} = p^2 8.62385\ X\ 10^{14}\ rad/s \tag{11.217}$$

where the semimajor axis, a, is $a = \frac{a_0}{p}$ according to Eq. (11.202) and c' is $c' = \frac{a_0}{p\sqrt{2}}$ according to Eq. (11.203). Thus, during bond formation, the perturbation of the orbit determined by an inverse-squared force results in simple harmonic oscillatory motion of the orbit, and the corresponding frequency, $\omega(0)$, for a hydrogen-type molecule $H_2(1/p)$ given by Eqs. (11.136) and (11.145) is:

$$\omega(0) = p^2\sqrt{\frac{k(0)}{\mu}} = p^2\sqrt{\frac{621.98\ Nm^{-1}}{\mu}} = p^2 8.62385\ X\ 10^{14}\ radians/s \tag{11.218}$$

where the reduced nuclear mass of hydrogen is given by Eq. (11.161) and the spring constant, $k(0)$, given by Eqs. (11.136) and (11.217) is:

$$k(0) = p^4 621.98\ Nm^{-1} \tag{11.219}$$

The transition-state vibrational energy, $E_{vib}(0)$, is given by Planck's equation (Eq. (11.127)):

$$E_{vib}(0) = \hbar\omega = \hbar p^2 8.62385\ X\ 10^{14}\ rad/s = p^2 0.56764\ eV \tag{11.220}$$

The amplitude of oscillation, $A_{reduced}(0)$, given by Eqs. (11.158), (11.161), and (11.219) is:

$$A_{reduced}(0) = \frac{\sqrt{\hbar}}{2^{3/2}\left(p^4 621.98\ Nm^{-1}\mu\right)^{1/4}} = \frac{4.275\ X\ 10^{-12}\ m}{p} = 0.08079\frac{a_0}{p} \tag{11.221}$$

Then, from Eq. (11.67), $A_{c'}(0)$, the displacement of c' is the eccentricity e given by Eq. (11.206) times $A_{reduced}(0)$ (Eq. (11.221)):

$$A_{c'}(0) = eA_{reduced}(0) = \frac{A_{reduced}(0)}{\sqrt{2}} = \frac{\sqrt{\hbar}}{4(k\mu)^{1/4}} = \frac{0.05713a_0}{p} \tag{11.222}$$

The spring constant and vibrational frequency for the formed molecule are then obtained from Eqs. (11.136) and (11.213-11.222) using the increases in the semimajor axis and internuclear distances due to vibration in the transition state. The vibrational energy, $E_{vib}(1)$, for the $H_2(1/p)$ $\upsilon = 1 \to \upsilon = 0$ transition given by adding $A_{c'}(0)$ (Eq. (11.222)) to the distances a and $a + c'$ in Eqs. (11.213-11.220) is:

$$E_{vib}(1) = p^2 0.517\ eV \tag{11.223}$$

where υ is the vibrational quantum number. Using Eq. (11.176) with Eqs. (11.223) and (11.252), the anharmonic perturbation term, $\omega_0 x_0$, of $H_2(1/p)$ is

$$\omega_0 x_0 = \frac{100hc\left(8.06573X10^3\ \frac{cm^{-1}}{eV}\ p^2 0.517\ eV\right)^2}{4e\left(p^2 4.151\ eV + p^3 0.326469\ eV\right)} cm^{-1} \tag{11.224}$$

where ω_0 is the frequency of the $\upsilon = 1 \to \upsilon = 0$ transition corresponding to Eq. (11.223) and D_0 is the bond dissociation energy given by Eq. (11.252). The vibrational energies of successive states are given by Eqs. (11.167) and (11.223-11.224).

Using the reduced nuclear mass given by Eq. (11.170), the corresponding parameters for deuterium-type molecules $D_2(1/p)$ (Eqs. (11.213-11.224) and (11.253)) are:

$$\omega(0) = p^2\sqrt{\frac{k(0)}{\mu}} = p^2\sqrt{\frac{621.98\ Nm^{-1}}{\mu}} = p^2 6.09798\ X\ 10^{14}\ radians/s \tag{11.225}$$

$$k(0) = p^4 621.98\ Nm^{-1} \tag{11.226}$$

$$E_{vib}(0) = p^2 0.4014\ eV \tag{11.227}$$

$$A_{reduced}(0) = \frac{\sqrt{\hbar}}{2^{3/2}\left(p^4 621.98\ Nm^{-1}\mu\right)^{1/4}} = \frac{3.595\ X\ 10^{-12}\ m}{p} = 0.06794\frac{a_0}{p} \tag{11.228}$$

$$E_{vib}(1) = p^2 0.371\ eV \tag{11.229}$$

$$\omega_0 x_0 = \frac{100hc\left(8.06573X10^3\ \frac{cm^{-1}}{eV}\ p^2 0.371\ eV\right)^2}{4e\left(p^2 4.229\ eV + p^3 0.326469\ eV\right)} cm^{-1} \tag{11.230}$$

The vibrational energies of successive states are given by Eqs. (11.167) and (11.229-11.230).

THE DOPPLER ENERGY TERM OF HYDROGEN-TYPE MOLECULES

The radiation reaction force in the case of the vibration of the molecule in the transition state also corresponds to the Doppler energy, E_D, given by Eq. (11.181) that is dependent on the motion of the electrons and the nuclei. Here, a nonradiative state must also be achieved after the emission due to transient vibration wherein the nonradiative condition given by Eq. (11.24) must be satisfied. Typically, a third body is required to form hydrogen-type molecules. For example, the exothermic chemical reaction of $H+H$ to form H_2 does not occur with the emission of a photon. Rather, the reaction requires a collision with a third body, M, to remove the bond energy—$H+H+M \rightarrow H_2+M^*$ [23]. The third body distributes the energy from the exothermic reaction, and the end result is the H_2 molecule and an increase in the temperature of the system. Thus, a third body removes the energy corresponding to the additional force term given by Eq. (11.180). From Eqs. (11.200), (11.207) and (11.209), the central force terms between the electron MO and the two protons are:

$$f(a) = -\frac{pe^2}{4\pi\varepsilon_0 a^2} \tag{11.231}$$

and

$$f'(a) = \frac{2pe^2}{4\pi\varepsilon_0 a^3} \tag{11.232}$$

Thus, the angular frequency of this oscillation is:

$$\omega = \sqrt{\frac{\frac{pe^2}{4\pi\varepsilon_0\left(\frac{a_0}{p}\right)^3}}{m_e}} = p^2 4.13414\ X\ 10^{16}\ rad/s \tag{11.233}$$

where the semimajor axis, a, is $a = \frac{a_0}{p}$ according to Eq. (11.202). The kinetic energy, E_K, is given by Planck's equation (Eq. (11.127)):

$$\overline{E}_K = \hbar\omega = \hbar p^2 4.13414\ X\ 10^{16}\ rad/s = p^2 27.2116\ eV \tag{11.234}$$

In Eq. (11.181), substitution of the total energy of the hydrogen molecule, E_T, (Eq. (11.212)) for E_{hv}, the mass of the electron, m_e, for M, and the kinetic energy given by Eq. (11.234) for $\overline{E}_K$ divided by p^2, the number of multipoles of a molecular hydrino state p (Eq. (5.45)), gives the Doppler energy of the electrons for the reentrant orbit.

$$\overline{E}_D \cong E_{hv}\sqrt{\frac{2\overline{E}_K}{Mc^2}} = -31.635p^2\ eV\sqrt{\frac{2e\left(p^2 27.2116\ eV\right)}{p^2 m_e c^2}} = -p^2 0.326469\ eV \tag{11.235}$$

The total energy of the molecule is decreased by $\overline{E}_D$.

In addition to the electrons, the nuclei also undergo simple harmonic oscillation in the transition state at their corresponding frequency given in the Vibration of Hydrogen-Type Molecules section. On average, the total energy of vibration is equally distributed between kinetic energy and potential energy [18]. Thus, the average kinetic energy of vibration corresponding to the Doppler energy of the electrons, $\overline{E}_{Kvib}$, is 1/2 of the vibrational energy of the molecule given by Eq. (11.148). The decrease in the energy of the hydrogen molecule due to the reentrant orbit in the transition state corresponding to simple harmonic oscillation of the electrons and nuclei, $\overline{E}_{osc}$, is given by the sum of the corresponding energies, $\overline{E}_D$ and $\overline{E}_{Kvib}$. Using Eq. (11.235) and E_{vib} from Eq. (11.220) gives:

$$\overline{E}_{osc} = \overline{E}_D + \overline{E}_{Kvib} = \overline{E}_D + \frac{1}{2}\hbar p^2\sqrt{\frac{k}{\mu}} \tag{11.236}$$

$$\overline{E}_{osc} = -p^2 0.326469\ eV + \frac{1}{2}p^2\left(0.56764\ eV\right) \tag{11.237}$$

To the extent that the MO dimensions are the same, the electron reentrant orbital energies, $\overline{E}_K$, are the same independent of the isotope of hydrogen, but the vibrational energies are related by Eq. (11.148). Thus, the differences in bond energies are essentially given by 1/2 the differences in vibrational energies. Using Eq. (11.235) and E_{vib} for $D_2\left(1/p\right)$ given by Eq. (11.227), that corresponds to the deuterium reduced nuclear mass (Eq. (11.170)), the corresponding $\overline{E}_{osc}$ is:

$$\overline{E}_{osc} = -p^2 0.326469\ eV + \frac{1}{2}p^2\left(0.401380\ eV\right) \tag{11.238}$$

TOTAL, IONIZATION, AND BOND ENERGIES OF HYDROGEN AND DEUTERIUM MOLECULES

The total energy of the hydrogen molecule is given by the sum of E_T (Eqs. (11.211-11.212)) and $\bar{E}_{osc}$ given in Eqs. (11.233-11.236). Thus, the total energy of the hydrogen molecule having a central field of $+pe$ at each focus of the prolate spheroid molecular orbital including the Doppler term is:

$$E_T = V_e + T + V_m + V_p + \bar{E}_{osc} \tag{11.239}$$

$$\begin{aligned} E_T &= -p^2 \left\{ \frac{e^2}{8\pi\varepsilon_0 a_0} \left[\left(2\sqrt{2} - \sqrt{2} + \frac{\sqrt{2}}{2} \right) \ln \frac{\sqrt{2}+1}{\sqrt{2}-1} - \sqrt{2} \right] \left[1 + \sqrt{\frac{2\hbar \sqrt{\frac{e^2}{4\pi\varepsilon_0 a_0^3}}}{m_e c^2}} \right] - \frac{1}{2}\hbar\sqrt{\frac{k}{\mu}} \right\} \\ &= -p^2 31.635\ eV - p^2 0.326469\ eV + \frac{1}{2}\hbar\sqrt{\frac{k}{\mu}} \end{aligned} \tag{11.240}$$

From Eqs. (11.237) and (11.239-11.240), the total energy for hydrogen-type molecules is:

$$\begin{aligned} E_T &= -p^2 31.635\ eV + \bar{E}_{osc} \\ &= -p^2 31.635\ eV - p^2 0.326469\ eV + \frac{1}{2} p^2 \left(0.56764\ eV \right) \\ &= -p^2 31.6775\ eV \end{aligned} \tag{11.241}$$

The total energy of the deuterium molecule is given by the sum of E_T (Eq. (11.212)) and $\bar{E}_{osc}$ given by Eq. (11.238).

$$\begin{aligned} E_T &= -p^2 31.6354\ eV + \bar{E}_{osc} \\ &= -p^2 31.6354\ eV - p^2 0.326469\ eV + \frac{1}{2} p^2 \left(0.401380\ eV \right) \\ &= -p^2 31.760\ eV \end{aligned} \tag{11.242}$$

The total energy, which includes the proton-proton-repulsion term is negative which justifies the original treatment of the force balance using the analytical mechanics equation of an ellipse that considered only the binding force between the protons and the electrons, the spin-pairing force, and the electron centrifugal force.

The first ionization energy of the hydrogen molecule, IP_1,

$$H_2(1/p) \rightarrow H_2^+(1/p) + e^- \tag{11.243}$$

is given by the difference of Eqs. (11.193) and (11.241).

$$\begin{aligned} IP_1 &= E_T\left(H_2^+(1/p)\right) - E_T\left(H_2(1/p)\right) \\ &= -p^2 16.2527\ eV - \left(-p^2 31.6775\ eV\right) \\ &= p^2 15.4248\ eV \end{aligned} \tag{11.244}$$

The second ionization energy, IP_2, is given by the negative of Eq. (11.193).

$$IP_2 = p^2 16.2527\ eV \tag{11.245}$$

The first ionization energy of the deuterium molecule, IP_1,

$$D_2(1/p) \rightarrow D_2^+(1/p) + e^- \tag{11.246}$$

is given by the difference of Eqs. (11.194) and (11.242).

$$\begin{aligned} IP_1 &= E_T\left(D_2^+(1/p)\right) - E_T\left(D_2(1/p)\right) \\ &= -p^2 16.2988\ eV - \left(-p^2 31.761\ eV\right) \\ &= p^2 15.4627\ eV \end{aligned} \tag{11.247}$$

The second ionization energy, IP_2, is given by the negative of Eq. (11.194).

$$IP_2 = p^2 16.2988\ eV \tag{11.248}$$

The bond dissociation energy, E_D, is the difference between the total energy of the corresponding hydrogen atoms and E_T

$$E_D = E(2H(1/p)) - E_T \tag{11.249}$$

where [19]:

$$E(2H(1/p)) = -p^2 27.20\ eV \tag{11.250}$$

and [20]:

$$E(2D(1/p)) = -p^2 27.206\ eV \tag{11.251}$$

The hydrogen bond energy, E_D, is given by Eqs. (11.249-11.250) and (11.241):

$$\begin{aligned} E_D &= -p^2 27.20\ eV - E_T \\ &= -p^2 27.20\ eV - \left(-p^2 31.677\ eV\right) \\ &= p^2 4.478\ eV \end{aligned} \tag{11.252}$$

The deuterium bond energy, E_D, is given by Eqs. (11.249), (11.251), and (11.242):

$$\begin{aligned} E_D &= -p^2 27.206\ eV - E_T \\ &= -p^2 27.206\ eV - \left(-p^2 31.760\ eV\right) \\ &= p^2 4.556\ eV \end{aligned} \tag{11.253}$$

THE HYDROGEN MOLECULAR ION $\mathbf{H_2}\left[\mathbf{2c' = 2a_0}\right]^+$

FORCE BALANCE OF HYDROGEN MOLECULAR ION

Force balance between the electric and centrifugal forces is given by Eq. (11.115) where $p = 1$

$$\frac{\hbar^2}{m_e a^2 b^2} D = \frac{e^2}{8\pi\varepsilon_0 a b^2} D \tag{11.254}$$

which has the parametric solution given by Eq. (11.83) when:

$$a = 2a_0 \tag{11.255}$$

The semimajor axis, a, is also given by Eq. (11.116) where $p = 1$. The internuclear distance, $2c'$, which is the distance between the foci is given by Eq. (11.111) where $p = 1$.

$$2c' = 2a_0 \tag{11.256}$$

The experimental internuclear distance is $2a_o$. The semiminor axis is given by Eq. (11.112) where $p = 1$.

$$b = \sqrt{3} a_0 \tag{11.257}$$

The eccentricity, e, is given by Eq. (11.113).

$$e = \frac{1}{2} \tag{11.258}$$

ENERGIES OF THE HYDROGEN MOLECULAR ION

The potential energy, V_e, of the electron MO in the field of the protons at the foci ($\xi = 0$) is given by Eq. (11.117) where $p = 1$

$$V_e = \frac{-4e^2}{8\pi\varepsilon_0\sqrt{a^2 - b^2}} \ln\frac{a + \sqrt{a^2 - b^2}}{a - \sqrt{a^2 - b^2}} \tag{11.259}$$

The potential energy, V_p, due to proton-proton repulsion is given by Eq. (11.120) where $p = 1$

$$V_p = \frac{e^2}{8\pi\varepsilon_0\sqrt{a^2 - b^2}} \tag{11.260}$$

The kinetic energy, T, of the electron MO is given by Eq. (11.119) where $p = 1$

$$T = \frac{2\hbar^2}{m_e a\sqrt{a^2 - b^2}} \ln\frac{a + \sqrt{a^2 - b^2}}{a - \sqrt{a^2 - b^2}} \tag{11.261}$$

Substitution of a and b given by Eqs. (11.255) and (11.257), respectively, into Eqs. (11.259-11.261) is:

$$V_e = \frac{-4e^2}{8\pi\varepsilon_0 a_H} \ln 3 = -59.7575\ eV \tag{11.262}$$

$$V_p = \frac{e^2}{8\pi\varepsilon_0 a_H} = 13.5984\ eV \tag{11.263}$$

$$T = \frac{2e^2}{8\pi\varepsilon_0 a_H} \ln 3 = 29.8787\ eV \tag{11.264}$$

The Doppler term, $\bar{E}_{osc}$, for hydrogen and deuterium are given by Eqs. (11.189) and (11.190), respectively, where $p = 1$

$$\bar{E}_{osc}\left(H_2^+\right) = \bar{E}_D + \bar{E}_{Kvib} = -0.118755\ eV + \frac{1}{2}\left(0.29282\ eV\right) = 0.027655\ eV \tag{11.265}$$

$$\bar{E}_{osc}\left(D_2^+\right) = -0.118811\ eV + \frac{1}{2}\left(0.20714\ eV\right) = -0.01524\ eV \tag{11.266}$$

The total energy, E_T, for the hydrogen molecular ion given by Eqs. (11.191-11.193) is:

$$E_T = -\left\{\frac{e^2}{8\pi e_0 a_H}(4\ln 3 - 1 - 2\ln 3)\left[1 + \sqrt{\frac{2\hbar\sqrt{\frac{2e^2}{4\pi\varepsilon_0\left(2a_H\right)^3}}{m_e}}{m_e c^2}}\right] - \frac{1}{2}\hbar\sqrt{\frac{k}{m}}\right\}$$

$$= -16.2803\ eV - 0.118755\ eV + \frac{1}{2}\left(0.29282\ eV\right) \tag{11.267}$$

$$= -16.2527\ eV$$

where in Eqs. (11.262-11.267), the radius of the hydrogen atom a_H (Eq. (1.259)) was used in place of a_0 to account for the corresponding electrodynamic force between the electron and the nuclei as given in the case of the hydrogen atom by Eq. (1.252). The negative of Eq. (11.267) is the ionization energy of H_2^+ and the second ionization energy, IP_2, of H_2. From Eqs. (11.191-11.192) and (11.194), the total energy, E_T, for the deuterium molecular ion (the ionization energy of D_2^+ and the second ionization energy, IP_2, of D_2) is:

$$E_T = -16.284\ eV - 0.118811\ eV + \frac{1}{2}\left(0.20714\ eV\right) = -16.299\ eV \tag{11.268}$$

The bond dissociation energy, E_D, is the difference between the total energy of the corresponding hydrogen atom and E_T. The hydrogen molecular ion bond energy, E_D, including the reduced electron mass given by Eq. (11.198) where $p = 1$ is

$$E_D = 2.535\ eV + 0.118755\ eV = 2.654\ eV \tag{11.269}$$

The experimental bond energy of the hydrogen molecular ion [24] is:

$$E_D = 2.651\ eV \tag{11.270}$$

From Eq. (11.199) where $p = 1$, the deuterium molecular ion bond energy, E_D, including the reduced electron mass of D is

$$E_D = 2.5770\ eV + 0.118811\ eV = 2.6958\ eV \tag{11.271}$$

The experimental bond energy of the deuterium molecular ion [25] is:

$$E_D = 2.691\ eV \tag{11.272}$$

VIBRATION OF THE HYDROGEN MOLECULAR ION

It can be shown that a perturbation of the orbit determined by an inverse-squared force results in simple harmonic oscillatory motion of the orbit [11]. The resonant vibrational frequency for H_2^+ given by Eq. (11.160) is:

$$\omega(0) = \sqrt{\frac{k(0)}{\mu}} = \sqrt{\frac{165.51\ Nm^{-1}}{\mu}} = 4.449\ X\ 10^{14}\ radians/s \tag{11.273}$$

wherein $p = 1$. The spring constant, $k(0)$, for H_2^+ given by Eq. (11.162) is:

$$k(0) = 165.51\ Nm^{-1} \tag{11.274}$$

The vibrational energy, $E_{vib}(0)$, of H_2^+ during bond formation given by Eq. (11.163) is:

$$E_{vib}(0) = 0.29282\ eV \tag{11.275}$$

The amplitude of oscillation given by Eq. (11.164) is:

$$A(0) = \frac{\sqrt{\hbar}}{2^{3/2}\left(165.51\ Nm^{-1}\mu\right)^{1/4}} = 5.952\ X\ 10^{-12}\ m = 0.1125 a_o \tag{11.276}$$

The vibrational energy for the H_2^+ $\upsilon = 1 \rightarrow \upsilon = 0$ transition given by Eq. (11.166) is:

$$E_{vib}(1) = 0.270\ eV \tag{11.277}$$

The experimental vibrational energy of H_2^+ [14, 20] is:

$$E_{vib} = 0.271\ eV \tag{11.278}$$

The anharmonicity term of H_2^+ given by Eq. (11.169) is:

$$\omega_0 x_0 = 55.39\ cm^{-1} \tag{11.279}$$

The experimental anharmonicity term of H_2^+ from NIST [20] is:

$$\omega_e x_e = 66.2\ cm^{-1} \tag{11.280}$$

The vibrational energy for the D_2^+ $\upsilon = 1 \to \upsilon = 0$ transition given by Eq. (11.175) is:

$$E_{vib} = 0.193\ eV \tag{11.281}$$

The vibrational energy of the D_2^+ [20] based on calculations from experimental data is:

$$E_{vib} = 0.196\ eV \tag{11.282}$$

The anharmonicity term of D_2^+ given by Eq. (11.176) is:

$$\omega_0 x_0 = 27.86\ cm^{-1} \tag{11.283}$$

The experimental anharmonicity term of D_2^+ for the state $X\ {}^2\sum_g{}^{+1}s\sigma$ is not given, but the term for state $B\ {}^2\sum_g{}^{+3}d\sigma$ from NIST [20] is:

$$\omega_e x_e = 2.62\ cm^{-1} \tag{11.284}$$

THE HYDROGEN MOLECULE $\mathbf{H_2}\left[\mathbf{2c' = \sqrt{2}a_0}\right]$

FORCE BALANCE OF THE HYDROGEN MOLECULE

The force balance equation for the hydrogen molecule is given by Eq. (11.200) where $p = 1$

$$\frac{\hbar^2}{m_e a^2 b^2} D = \frac{e^2}{8\pi\varepsilon_0 a b^2} D + \frac{\hbar^2}{2 m_e a^2 b^2} D \tag{11.285}$$

which has the parametric solution given by Eq. (11.83) when,

$$a = a_0 \tag{11.286}$$

The semimajor axis, a, is also given by Eq. (11.202) where $p = 1$. The internuclear distance, $2c'$, which is the distance between the foci is given by Eq. (11.204) where $p = 1$.

$$2c' = \sqrt{2} a_0 \tag{11.287}$$

The experimental internuclear distance is $\sqrt{2}a_0$. The semiminor axis is given by Eq. (11.205) where $p = 1$.

$$b = \frac{1}{\sqrt{2}} a_0 \tag{11.288}$$

The eccentricity, e, is given by Eq. (11.206).

$$e = \frac{1}{\sqrt{2}} \tag{11.289}$$

The finite dimensions of the hydrogen molecule are evident in the plateau of the resistivity versus pressure curve of metallic hydrogen [26].

ENERGIES OF THE HYDROGEN MOLECULE

The energies of the hydrogen molecule are given by Eqs. (11.207-11.210) where $p = 1$

$$V_e = \frac{-2e^2}{8\pi\varepsilon_0 \sqrt{a^2 - b^2}} \ln \frac{a + \sqrt{a^2 - b^2}}{a - \sqrt{a^2 - b^2}} = -67.8358\ eV \tag{11.290}$$

$$V_p = \frac{e^2}{8\pi\varepsilon_0 \sqrt{a^2 - b^2}} = 19.2415\ eV \tag{11.291}$$

$$T = \frac{\hbar^2}{2 m_e a \sqrt{a^2 - b^2}} \ln \frac{a + \sqrt{a^2 - b^2}}{a - \sqrt{a^2 - b^2}} = 33.9179\ eV \tag{11.292}$$

The energy, V_m, of the magnetic force is

$$V_m = \frac{-\hbar^2}{4 m_e a \sqrt{a^2 - b^2}} \ln \frac{a + \sqrt{a^2 - b^2}}{a - \sqrt{a^2 - b^2}} = -16.9589\ eV \tag{11.293}$$

The Doppler terms, $\bar{E}_{osc}$, for hydrogen and deuterium molecules are given by Eqs. (11.237) and (11.238), respectively, where $p = 1$

$$\bar{E}_{osc}\left(H_2\right) = \bar{E}_D + \bar{E}_{Kvib} = -0.326469\ eV + \frac{1}{2}\left(0.56764\ eV\right) = -0.042649\ eV \tag{11.294}$$

$$\bar{E}_{osc}\left(D_2\right) = -0.326469\ eV + \frac{1}{2}\left(0.401380\ eV\right) = -0.125779\ eV \tag{11.295}$$

The total energy, E_T, for the hydrogen molecule given by Eqs. (11.239-11.241) is

$$\begin{aligned} E_T &= -\left\{ \frac{e^2}{8\pi\varepsilon_0 a_0}\left[\left(2\sqrt{2}-\sqrt{2}+\frac{\sqrt{2}}{2}\right)\ln\frac{\sqrt{2}+1}{\sqrt{2}-1}-\sqrt{2}\right]\left[1+\sqrt{\frac{2\hbar\sqrt{\frac{e^2}{4\pi\varepsilon_0 a_0^3}}}{m_e c^2}}\right]-\frac{1}{2}\hbar\sqrt{\frac{k}{\mu}}\right\} \\ &= -31.635\ eV - 0.326469\ eV + \frac{1}{2}\left(0.56764\ eV\right) \\ &= -31.6776\ eV \end{aligned} \tag{11.296}$$

From Eqs. (11.239-11.240) and (11.242), the total energy, E_T, for the deuterium molecule is:

$$E_T = -31.635\ eV - 0.326469\ eV + \frac{1}{2}\left(0.401380\ eV\right) = -31.7608\ eV \tag{11.297}$$

The first ionization energies of the hydrogen and deuterium molecules, IP_1, (Eqs. (11.243) and (11.246)) are given by the differences in the total energy of corresponding molecular ions and molecules which are given by Eqs. (11.244) and (11.247), respectively, where $p = 1$:

$$IP_1\left(H_2\right) = 15.4248\ eV \tag{11.298}$$

$$IP_1\left(D_2\right) = 15.4627\ eV \tag{11.299}$$

The bond dissociation energy, E_D, is the difference between the total energy of two of the corresponding hydrogen atoms and E_T. The hydrogen molecular bond energy, E_D, given by Eq. (11.252) where $p = 1$ is:

$$E_D = 4.478\ eV \tag{11.300}$$

The experimental bond energy of the hydrogen molecule [23] is:

$$E_D = 4.478\ eV \tag{11.301}$$

The deuterium molecular bond energy, E_D, given by Eq. (11.253) where $p = 1$ is:

$$E_D = 4.556\ eV \tag{11.302}$$

The experimental bond energy of the deuterium molecule [23] is:

$$E_D = 4.556\ eV \tag{11.303}$$

VIBRATION OF THE HYDROGEN MOLECULE

It can be shown that a perturbation of the orbit determined by an inverse-squared force results in simple harmonic oscillatory motion of the orbit [11]. The resonant vibrational frequency for H_2 given by Eq. (11.218) is:

$$\omega(0) = \sqrt{\frac{k(0)}{\mu}} = \sqrt{\frac{621.98\ Nm^{-1}}{\mu}} = 8.62385\ X\ 10^{14}\ radians/s \tag{11.304}$$

The spring constant, $k(0)$, for H_2 given by Eq. (11.219) is:

$$k(0) = 621.98\ Nm^{-1} \tag{11.305}$$

wherein $p = 1$. The vibrational energy, $E_{vib}(0)$, of H_2 during bond formation given by Eq. (11.220) is:

$$E_{vib}(0) = 0.56764\ eV \tag{11.306}$$

The amplitude of oscillation given by Eq. (11.221) is:

$$A(0) = \frac{\sqrt{\hbar}}{2^{3/2}\left(621.98\ Nm^{-1}\mu\right)^{1/4}} = 4.275\ X\ 10^{-12}\ m = 0.08079 a_o \tag{11.307}$$

The vibrational energy for the H_2 $\upsilon = 1 \rightarrow \upsilon = 0$ transition given by Eq. (11.223) is:

$$E_{vib}(1) = 0.517\ eV \tag{11.308}$$

The experimental vibrational energy of H_2 [27-28] is:

$$E_{vib}(1) = 0.5159\ eV \tag{11.309}$$

The anharmonicity term of H_2 given by Eq. (11.224) is:

$$\omega_0 x_0 = 120.4\ cm^{-1} \tag{11.310}$$

The experimental anharmonicity term of H_2 from Huber and Herzberg [25] is:

$$\omega_e x_e = 121.33\ cm^{-1} \tag{11.311}$$

The vibrational energy for the D_2 $\upsilon = 1 \to \upsilon = 0$ transition given by Eq. (11.229) is:

$$E_{vib} = 0.371\ eV \tag{11.312}$$

The experimental vibrational energy of D_2 [14, 20] is:

$$E_{vib} = 0.371\ eV \tag{11.313}$$

The anharmonicity term of D_2 given by Eq. (11.230) is:

$$\omega_0 x_0 = 60.93\ cm^{-1} \tag{11.314}$$

The experimental anharmonicity term of D_2 from NIST [20] is:

$$\omega_e x_e = 61.82\ cm^{-1} \tag{11.315}$$

The results of the determination of the bond, vibrational, total, and ionization energies, and internuclear distances for hydrogen and deuterium molecules and molecular ions are given in Table 11.1. The calculated results are based on first principles and given in closed form equations containing fundamental constants only. The agreement between the experimental and calculated results is excellent.

Despite the predictions of standard quantum mechanics that preclude the imaging of a molecule orbital, the full three-dimensional structure of the outer molecular orbital of N_2 has been recently tomographically reconstructed [29]. The charge-density surface observed is similar to that shown in Figure 11.6 for H_2 which is direct evidence that electrons are not point-particle probability waves that have no form until they are "collapsed to a point" by measurement. Rather they are physical, two-dimensional equipotential charge density surfaces.

Table 11.1. The calculated and experimental parameters of H_2, D_2, H_2^+ and D_2^+.

Parameter	Calculated	Experimental	Eqs.	Ref. for Exp.
H_2 Bond Energy	4.478 *eV*	4.478 *eV*	11.300	24
D_2 Bond Energy	4.556 *eV*	4.556 *eV*	11.302	24
H_2^+ Bond Energy	2.654 *eV*	2.651 *eV*	11.269	24
D_2^+ Bond Energy	2.696 *eV*	2.691 *eV*	11.271	25
H_2 Total Energy	31.677 *eV*	31.675 *eV*	11.296	24, 30, 19[a]
D_2 Total Energy	31.760 *eV*	31.760 *eV*	11.297	20, 25[b]
H_2 Ionization Energy	15.425 *eV*	15.426 *eV*	11.298	30
D_2 Ionization Energy	15.463 *eV*	15.466 *eV*	11.299	25
H_2^+ Ionization Energy	16.253 *eV*	16.250 *eV*	11.267	24, 19[c]
D_2^+ Ionization Energy	16.299 *eV*	16.294 *eV*	11.268	20, 25[d]
H_2^+ Spin Magnetic Moment	$0.5\mu_B$	$0.5\mu_B$	12.24	31
Absolute H_2 Gas-Phase NMR Shift	-28.0 ppm	-28.0 ppm	11.416	32-33
H_2 Quadrupole Moment	0.4764 X 10^{-16} cm^2	0.38 0.15 X 10^{-16} cm^2	11.430-11.431	46
H_2 Internuclear Distance	0.7411 Å	0.741 Å	12.75	34
D_2 Internuclear Distance	0.7411 Å	0.741 Å	12.75	34
H_2^+ Internuclear Distance	1.0577 Å	1.06 Å	12.81	24
D_2^+ Internuclear Distance	1.0577 Å	1.0559 Å	12.81	25
H_2 Vibrational Energy	0.517 *eV*	0.516 *eV*	11.308	27, 28
D_2 Vibrational Energy	0.371 *eV*	0.371 *eV*	11.313	14, 20
H_2 $\omega_e x_e$	120.4 cm^{-1}	121.33 cm^{-1}	11.310	25
D_2 $\omega_e x_e$	60.93 cm^{-1}	61.82 cm^{-1}	11.314	20
H_2^+ Vibrational Energy	0.270 *eV*	0.271 *eV*	11.277	14, 20
D_2^+ Vibrational Energy	0.193 *eV*	0.196 *eV*	11.281	20
H_2 J=1 to J=0 Rotational Energy	0.01511 *eV*	0.01509 *eV*	12.77	24
D_2 J=1 to J=0 Rotational Energy	0.007557 *eV*	0.00755 *eV*	12.78	24
H_2^+ J=1 to J=0 Rotational Energy	0.00742 *eV*	0.00739 *eV*	12.83	24
D_2^+ J=1 to J=0 Rotational Energy	0.0037095 *eV*	0.003723 *eV*	12.84	25

[a] The experimental total energy of the hydrogen molecule is given by adding the first (15.42593 *eV*) [30] and second (16.2494 *eV*) ionization energies where the second ionization energy is given by the addition of the ionization energy of the hydrogen atom (13.59844 *eV*) [19] and the bond energy of H_2^+ (2.651 *eV*) [24].

[b] The experimental total energy of the deuterium molecule is given by adding the first (15.466 *eV*) [25] and second (16.294 *eV*) ionization energies where the second ionization energy is given by the addition of the ionization energy of the deuterium atom (13.603 *eV*) [20] and the bond energy of D_2^+ (2.692 *eV*) [25].

[c] The experimental second ionization energy of the hydrogen molecule, IP_2, is given by the sum of the ionization energy of the hydrogen atom (13.59844 *eV*) [19] and the bond energy of H_2^+ (2.651 *eV*) [24].

[d] The experimental second ionization energy of the deuterium molecule, IP_2, is given by the sum of the ionization energy of the deuterium atom (13.603 *eV*) [20] and the bond energy of D_2^+ (2.692 *eV*) [25].

THE DIHYDRINO MOLECULAR ION $\mathbf{H_2}\left[\mathbf{2c'=a_0}\right]^+$

FORCE BALANCE OF THE DIHYDRINO MOLECULAR ION

Force balance between the electric and centrifugal forces of $H_2^+(1/2)$ is given by Eq. (11.115) where $p=2$

$$\frac{\hbar^2}{m_e a^2 b^2} D = \frac{2e^2}{8\pi\varepsilon_0 a b^2} D \tag{11.316}$$

which has the parametric solution given by Eq. (11.83) when:

$$a = a_0 \tag{11.317}$$

The semimajor axis, a, is also given by Eq. (11.116) where $p=2$. The internuclear distance, $2c'$, which is the distance between the foci is given by Eq. (11.111) where $p=2$.

$$2c' = a_0 \tag{11.318}$$

The semiminor axis is given by Eq. (11.112) where $p=2$.

$$b = \frac{\sqrt{3}}{2} a_0 \tag{11.319}$$

The eccentricity, e, is given by Eq. (11.113).

$$e = \frac{1}{2} \tag{11.320}$$

ENERGIES OF THE DIHYDRINO MOLECULAR ION

The potential energy, V_e, of the electron MO in the field of magnitude twice that of the protons at the foci ($\xi = 0$) is given by Eq. (11.117) where $p=2$

$$V_e = \frac{-8e^2}{8\pi\varepsilon_0\sqrt{a^2-b^2}} \ln\frac{a+\sqrt{a^2-b^2}}{a-\sqrt{a^2-b^2}} \tag{11.321}$$

The potential energy, V_p, due to proton-proton repulsion in the field of magnitude twice that of the protons at the foci ($\xi = 0$) is given by Eq. (11.120) where $p=2$

$$V_p = \frac{2e^2}{8\pi\varepsilon_0\sqrt{a^2-b^2}} \tag{11.322}$$

The kinetic energy, T, of the electron MO is given by Eq. (11.119) where $p=2$

$$T = \frac{2\hbar^2}{m_e a\sqrt{a^2-b^2}} \ln\frac{a+\sqrt{a^2-b^2}}{a-\sqrt{a^2-b^2}} \tag{11.323}$$

Substitution of a and b given by Eqs. (11.317) and (11.319), respectively, into Eqs. (11.321-11.323) and using Eqs. (11.191-11.193) with $p=2$ gives:

$$V_e = \frac{-16e^2}{8\pi\varepsilon_0 a_0} \ln 3 = -239.16\ eV \tag{11.324}$$

$$V_p = \frac{4e^2}{8\pi\varepsilon_0 a_0} = 54.42\ eV \tag{11.325}$$

$$T = \frac{8e^2}{8\pi\varepsilon_0 a_0} \ln 3 = 119.58\ eV \tag{11.326}$$

$$E_T = V_e + V_p + T + \overline{E}_{osc} \tag{11.327}$$

$$E_T = -2^2\left\{\frac{e^2}{8\pi\varepsilon_0 a_H}(4\ln 3 - 1 - 2\ln 3)\left[1+\sqrt{\frac{2\hbar\sqrt{\dfrac{2e^2}{4\pi\varepsilon_0(2a_H)^3}}}{p^2 m_e c^2}}\right] - \frac{1}{2}\hbar\sqrt{\frac{k}{\mu}}\right\} \tag{11.328}$$

$$= -2^2(16.2527\ eV) = -65.01\ eV$$

where Eqs. (11.324-11.326) are equivalent to Eqs. (11.122-11.124) with $p=2$. The bond dissociation energy, E_D, given by Eq. (11.198) with $p=2$ is the difference between the total energy of the corresponding hydrino atom and E_T given by Eq. (11.328):

$$E_D = E_T(H(1/p)) - E_T(H_2^+(1/p)) = 2^2(2.654\ eV) = 10.62\ eV \tag{11.329}$$

VIBRATION OF THE DIHYDRINO MOLECULAR ION

It can be shown that a perturbation of the orbit determined by an inverse-squared force results in simple harmonic oscillatory motion of the orbit [11]. The resonant vibrational frequency for $H_2^+(1/2)$ from Eq. (11.160) is:

$$\omega(0) = 2^2\sqrt{\frac{165.51\ Nm^{-1}}{\mu}} = 1.78\ X\ 10^{15}\ radians/s \tag{11.330}$$

wherein $p = 2$. The spring constant, $k(0)$, for $H_2^+(1/2)$ from Eq. (11.162) is:

$$k(0) = 2^4 165.51\ Nm^{-1} = 2648\ Nm^{-1} \tag{11.331}$$

The amplitude of oscillation from Eq. (11.164) is:

$$A(0) = \frac{\sqrt{\hbar}}{2^{3/2}\left(2^4(165.51)\ Nm^{-1}\mu\right)^{1/4}} = \frac{5.952\ X\ 10^{-12}\ m}{2} = \frac{0.1125a_o}{2} \tag{11.332}$$

The vibrational energy, $E_{vib}(1)$, for the $\upsilon = 1 \rightarrow \upsilon = 0$ transition given by Eq. (11.166) is:

$$E_{vib}(1) = 2^2(0.270\ eV) = 1.08\ eV \tag{11.333}$$

THE DIHYDRINO MOLECULE $\mathbf{H_2}\left[\mathbf{2c' = \frac{a_0}{\sqrt{2}}}\right]$

FORCE BALANCE OF THE DIHYDRINO MOLECULE

The force balance equation for the dihydrino molecule $H_2(1/2)$ is given by Eq. (11.200) where $p = 2$

$$\frac{\hbar^2}{m_e a^2 b^2} D = \frac{2e^2}{8\pi\varepsilon_0 a b^2} D + \frac{\hbar^2}{2m_e a^2 b^2} D \tag{11.334}$$

which has the parametric solution given by Eq. (11.83) when

$$a = \frac{a_0}{2} \tag{11.335}$$

The semimajor axis, a, is also given by Eq. (11.202) where $p = 2$. The internuclear distance, $2c'$, which is the distance between the foci is given by Eq. (11.204) where $p = 2$.

$$2c' = \frac{1}{\sqrt{2}} a_0 \tag{11.336}$$

The semiminor axis is given by Eq. (11.205) where $p = 2$.

$$b = c = \frac{1}{2\sqrt{2}} a_0 \tag{11.337}$$

The eccentricity, e, is given by Eq. (11.206).

$$e = \frac{1}{\sqrt{2}} \tag{11.338}$$

ENERGIES OF THE DIHYDRINO MOLECULE

The energies of the dihydrino molecule $H_2(1/2)$ are given by Eqs. (11.207-11.210) and Eqs. (11.239-11.241) with $p = 2$

$$V_e = \frac{-4e^2}{8\pi\varepsilon_0\sqrt{a^2 - b^2}} \ln\frac{a + \sqrt{a^2 - b^2}}{a - \sqrt{a^2 - b^2}} = -271.34\ eV \tag{11.339}$$

$$V_p = \frac{2}{8\pi\varepsilon_0}\frac{e^2}{\sqrt{a^2 - b^2}} = 76.97\ eV \tag{11.340}$$

$$T = \frac{\hbar^2}{2m_e a\sqrt{a^2 - b^2}} \ln\frac{a + \sqrt{a^2 - b^2}}{a - \sqrt{a^2 - b^2}} = 135.67\ eV \tag{11.341}$$

The energy, V_m, of the magnetic force is

$$V_m = \frac{-\hbar^2}{4m_e a\sqrt{a^2 - b^2}} \ln\frac{a + \sqrt{a^2 - b^2}}{a - \sqrt{a^2 - b^2}} = -67.84\ eV \tag{11.342}$$

$$E_T = V_e + T + V_m + V_p + \bar{E}_{osc} \tag{11.343}$$

$$E_T = -2^2\left\{\frac{e^2}{8\pi\varepsilon_0 a_0}\left[\left(2\sqrt{2}-\sqrt{2}+\frac{\sqrt{2}}{2}\right)\ln\frac{\sqrt{2}+1}{\sqrt{2}-1}-\sqrt{2}\right]\left[1+\sqrt{\frac{2\hbar\sqrt{\frac{e^2}{4\pi\varepsilon_0 a_0^3}}}{p^2 m_e c^2}}\right]-\frac{1}{2}\hbar\sqrt{\frac{k}{\mu}}\right\}$$
$$= -2^2\left(31.677\ eV\right) \tag{11.344}$$
$$= -126.71\ eV$$

where Eqs. (11.339-11.342) are equivalent to Eqs. (11.207-11.210) with $p=2$. The bond dissociation energy, E_D, given by Eq. (11.252) with $p=2$ is the difference between the total energy of the corresponding hydrino atoms and E_T given by Eq. (11.344).

$$E_D = E_T(2H(1/p)) - E_T(H_2(1/p)) = 2^2\left(4.478\ eV\right) = 17.91\ eV \tag{11.345}$$

VIBRATION OF THE DIHYDRINO MOLECULE

It can be shown that a perturbation of the orbit determined by an inverse-squared force results in simple harmonic oscillatory motion of the orbit [11]. The resonant vibrational frequency for the $H_2(1/2)$ from Eq. (11.218) is

$$\omega(0) = 2^2\sqrt{\frac{k}{\mu}} = 2^2\sqrt{\frac{621.98\ Nm^{-1}}{\mu}} = 3.45\ X\ 10^{15}\ radians/s \tag{11.346}$$

wherein $p=2$. The spring constant, $k(0)$, for $H_2(1/2)$ from Eq. (11.219) is:

$$k(0) = 2^4 621.98\ Nm^{-1} = 9952\ Nm^{-1} \tag{11.347}$$

The amplitude of oscillation from Eq. (11.221) is:

$$A(0) = \frac{\sqrt{\hbar}}{2^{3/2}\left(2^4\left(621.98\right)\ Nm^{-1}\mu\right)^{1/4}} = \frac{4.275\ X\ 10^{-12}\ m}{2} = \frac{0.08079 a_o}{2} \tag{11.348}$$

The vibrational energy, $E_{vib}(1)$, of $H_2(1/2)$ from Eq. (11.223) is:

$$E_{vib}(1) = 2^2\left(0.517\right)\ eV = 2.07\ eV \tag{11.349}$$

GEOMETRY

The internuclear distance can also be determined geometrically. The spheroidal MO of the hydrogen molecule is an equipotential energy surface, which is an energy minimum surface. For the hydrogen molecule, the electric field is zero for $\xi > 0$. Consider two hydrogen atoms A and B approaching each other. Consider that the two electrons form a spheroidal MO as the two atoms overlap, and the charge is distributed such that an equipotential two-dimensional surface is formed. The electric fields of atoms A and B add vectorially as the atoms overlap. The energy at the point of intersection of the overlapping atomic orbitals decreases to a minimum as they superimpose and then rises with further overlap. When this energy is a minimum the internuclear distance is determined. It can be demonstrated [35] that when two hydrogen atomic orbitals superimpose such that the radial electric field vector from nucleus A and B makes a $45°$ angle with the point of intersection of the two original atomic orbitals, the electric energy of interaction between atomic orbitals given by

$$E_{\text{interaction}} = 2\ X\ \frac{1}{2}\varepsilon_0\int \Delta\mathbf{E}^2 dv \tag{11.350}$$

is a minimum (Figure 7.1 of [35]). The MO is a minimum potential energy surface; therefore, a minimum of energy of one point on the surface is a minimum for the entire surface of the MO. Thus,

$$R_{H_2} = \sqrt{2}a_0 = 0.748\text{Å} \tag{11.351}$$

The experimental internuclear bond distance is $0.746\ \text{Å}$.

DIHYDRINO IONIZATION ENERGIES

The first ionization energy, IP_1, of the dihydrino molecule

$$H_2(1/p) \rightarrow H_2^+(1/p) + e^- \tag{11.352}$$

is given by Eq. (11.244) with $p = 2$.

$$IP_1 = E_T\left(H_2^+(1/p)\right) - E_T\left(H_2(1/p)\right) \tag{11.353}$$

$$IP_1 = 2^2(15.4248\ eV) = 61.70\ eV \tag{11.354}$$

The second ionization energy, IP_2, is given by Eq. (11.245) with $p = 2$.

$$IP_2 = 2^2(16.2527\ eV) = 65.01\ eV \tag{11.355}$$

A hydrino atom can react with a hydrogen, deuterium, or tritium nucleus to form a dihydrino molecular ion that further reacts with an electron to form a dihydrino molecule.

$$H(1/p) + H^+ + e- \rightarrow H_2(1/p) \tag{11.356}$$

The energy released is

$$E = E(H(1/p)) - E_T \tag{11.357}$$

where E_T is given by Eq. (11.241).

A hydrino atom can react with a hydrogen, deuterium, or tritium atom to form a dihydrino molecule.

$$H(1/p) + H \rightarrow H_2(1/p) \tag{11.358}$$

The energy released is

$$E = E\left(H(1/p)\right) + E(H) - E_T \tag{11.359}$$

where E_T is given by Eq. (11.241).

SIZES OF REPRESENTATIVE ATOMS AND MOLECULES

ATOMS

Figure 11.5. Cross-section of an atomic orbital.

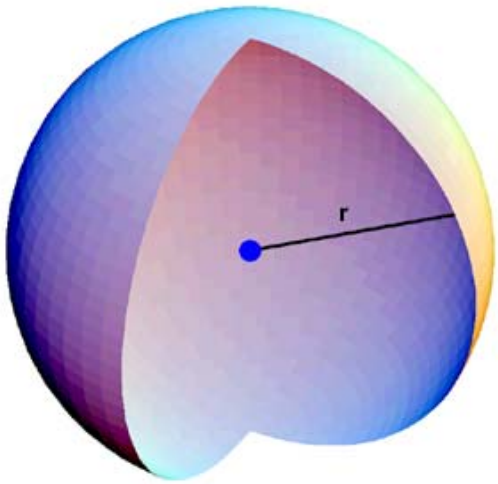

Helium Atom (He)

Helium comprises the nucleus at the origin and two electrons as a spherical shell at $r = 0.567a_0$.

Hydrogen Atom ($\mathbf{H}[\mathbf{a_H}]$)

Hydrogen comprises the nucleus at the origin and the electron as a spherical shell at $r = a_H$.

Hydrino Atom ($\mathbf{H}\left[\frac{\mathbf{a_H}}{\mathbf{2}}\right]$)

Hydrino atom (1/2) comprises the nucleus at the origin and the electron as a spherical shell at $r = \frac{a_H}{2}$.

MOLECULES

Figure 11.6. **A**. Prolate spheroid MO. **B**. Prolate spheroid parameters of molecules and molecular ions where a is the semimajor axis, $2a$ is the total length of the molecule or molecular ion along the principal axis, $b = c$ is the semiminor axis, $2b = 2c$ is the total width of the molecule or molecular ion along the minor axis, c' is the distance from the origin to a focus (nucleus), $2c'$ is the internuclear distance, and the protons are at the foci.

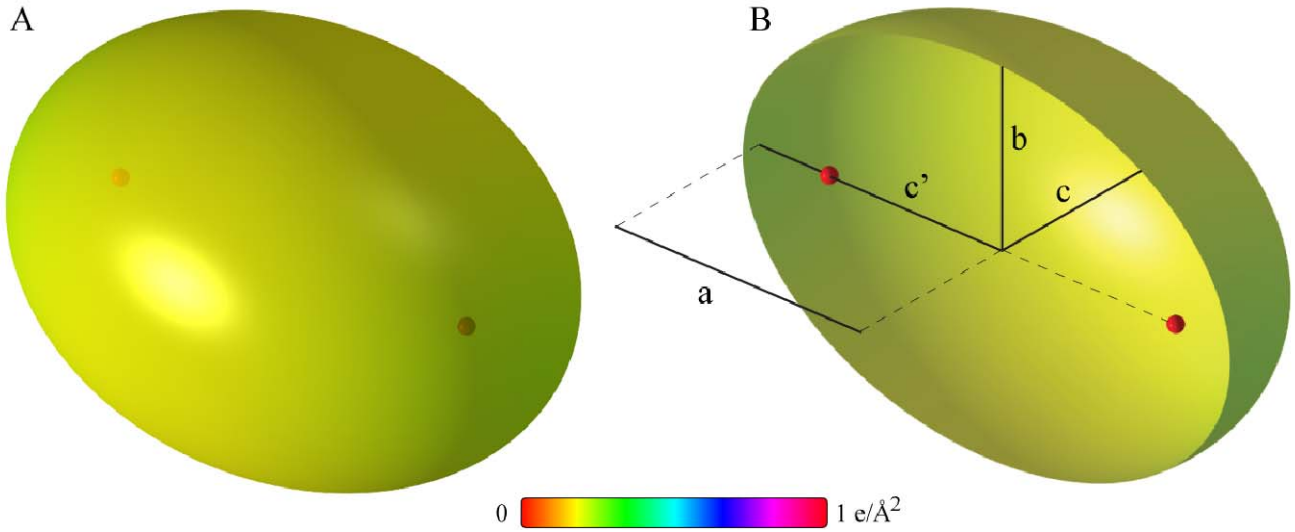

Hydrogen Molecular Ion ($\mathbf{H_2}\left[\mathbf{2c' = 2a_0}\right]^+$)

$$a = 2a_0$$

$$b = c = \sqrt{3}a_0$$

$$c' = a_0$$

$$2c' = 2a_0$$

Dihydrino Molecular Ion ($\mathbf{H_2}\left[\mathbf{2c' = a_0}\right]^+$)

$$a = a_0$$

$$b = c = \frac{\sqrt{3}}{2}a_0$$

$$c' = \frac{1}{2}a_0$$

$$2c' = a_0$$

Hydrogen Molecule ($\mathbf{H_2}\left[\mathbf{2c' = \sqrt{2}a_0}\right]$)

$$a = a_0$$

$$b = c = \frac{1}{\sqrt{2}}a_0$$

$$c' = \frac{1}{\sqrt{2}}a_0$$

$$2c' = \sqrt{2}a_0$$

Dihydrino Molecule ($\mathbf{H_2}\left[\mathbf{2c' = \frac{1}{\sqrt{2}}a_0}\right]$)

$$a = \frac{1}{2}a_0$$

$$b = c = \frac{1}{2\sqrt{2}}a_0$$

$$c' = \frac{1}{2\sqrt{2}}a_0$$

$$2c' = \frac{1}{\sqrt{2}}a_0$$

NUCLEAR SPIN-SPIN TRANSITION OF HYDROGEN-TYPE MOLECULES

Each proton of hydrogen-type molecules possesses a magnetic moment, which is derived in the Proton and Neutron section and is given by

$$\mu_P = \frac{\left(\frac{2}{3}\right)^2 e\hbar}{2\frac{m_p}{2\pi}} \tag{11.360}$$

The magnetic moment, $\mathbf{m}$, of the proton is given by Eq. (11.360), and the magnetic field of the proton follows from the relationship between the magnetic dipole field and the magnetic moment, $\mathbf{m}$, as given by Jackson [36] where $\mathbf{m} = \mu_P \mathbf{i}_z$.

$$\mathbf{H} = \frac{\mu_P}{r^3}(\mathbf{i}_r 2\cos\theta - \mathbf{i}_\theta \sin\theta) \tag{11.361}$$

Multiplication of Eq. (11.361) by the permeability of free space, μ_0, gives the magnetic flux, $\mathbf{B}$, due to proton one at proton two.

$$\mathbf{B} = \frac{\mu_0\mu_P}{r^3}(\mathbf{i}_r 2\cos\theta - \mathbf{i}_\theta \sin\theta) \tag{11.362}$$

$\Delta E_{mag}^{\text{ortho/para}}$, the magnetic energy to flip the orientation of proton two's magnetic moments, μ_P, from parallel magnetic moments to antiparallel magnetic moments with respect to the direction of the magnetic moment of proton one with corresponding magnetic flux $\mathbf{B}$ is:

$$\Delta E_{mag}^{\text{ortho/para}} = -2\mu_P \mathbf{B} = \frac{-2\mu_0{\mu_P}^2}{r^3} \tag{11.363}$$

where r is the internuclear distance 2c' where c' is given by Eq. (11.204). Substitution of the internuclear distance into Eq. (11.363) for r gives:

$$\Delta E_{mag}^{\text{ortho/para}} = -2\mu_P \mathbf{B} = \frac{-2\mu_0{\mu_P}^2 p^3}{\left(\sqrt{2}a_0\right)^3} \tag{11.364}$$

$\Delta E_{mag}^{\text{ortho/para}}$ corresponds to a force that causes the internuclear distance and concomitantly the other dimensions of the H_2 MO to change thereby having a relatively substantial effect on the energy difference of the ortho and para states. A useful parameter, the ro-vibrational ortho-para splitting, can easily be calculated from the result of Lavrov and Weber [37] for $H_2(1/4)$ using the Morse-potential expansion with an inter nuclear distance of 1/4 that of H_2 for $H_2(1/4)$:

$$\frac{\Delta_{H_2(1/4)}}{\Delta_{H_2}} = \frac{\frac{12(256)B_e^2}{\hbar 16\omega_e}\left(\frac{4a\hbar}{\mu 256\omega_e^2}\sqrt{\frac{2}{\mu 16 B_e}} - 1\right)}{\frac{12B_e^2}{\hbar\omega_e}\left(\frac{a\hbar}{\mu\omega_e^2}\sqrt{\frac{2}{\mu B_e}} - 1\right)} \tag{11.365}$$

In the case that $1 << \frac{a\hbar}{\mu\omega_e^2}\sqrt{\frac{2}{\mu B_e}}$, $\Delta_{H_2(1/4)} = 16\Delta_{H_2} = 4^2\Delta_{H_2} = 1418\ cm^{-1}$ where the calculated H_2 result of 88.61 cm^{-1} (Ref. [38]) allowed for the cancellation of the curve-fit parameter a and where ω_e and B_e are the vibartional and rotational parameters given by Eqs. (11.217) and (12.89), respectively.

NUCLEAR MAGNETIC RESONANCE SHIFT

The proton gyromagnetic ratio, $\gamma_p / 2\pi$, is

$$\gamma_P / 2\pi = 42.57602\ MHz\ T^{-1} \tag{11.366}$$

The NMR frequency, f, is the product of the proton gyromagnetic ratio given by Eq. (11.366) and the magnetic flux, $\mathbf{B}$.

$$f = \gamma_P / 2\pi \mathbf{B} = 42.57602\ MHz\ T^{-1}\mathbf{B} \tag{11.367}$$

A typical radio frequency (RF) is 400 MHz. According to Eq. (11.367) this corresponds to a flux of 9.39496 T provided by a superconducting NMR magnet. With a constant magnetic field, the frequency is scanned to yield the spectrum where the frequency scan is typically achieved using a Fourier transform on the free induction decay signal following a radio frequency pulse. Historically, the radiofrequency was held constant, the applied magnetic field, H_0 ($H_0 = \frac{B}{\mu_0}$), was varied over a small range, and the frequency of energy absorption was recorded at the various values for H_0. By convention based on this historic

mode of operation, the radiofrequency spectrum is converted into the corresponding applied magnetic field, H_0 ($H_0 = \frac{B}{\mu_0}$), of energy absorption and displayed as a function of increasing H_0. The protons that would absorb energy at a lower H_0 give rise to a downfield absorption peak; whereas, the protons that would absorb energy at a higher H_0 give rise to an upfield absorption peak. The electrons of the compound of a sample influence the field at the nucleus such that it deviates slightly from the applied value. For the case that the chemical environment has no NMR effect, the value of H_0 at resonance with the radiofrequency held constant at $400\ MHz$ is:

$$\frac{2\pi f}{\mu_0 \gamma_P} = \frac{(2\pi)(400\ MHz)}{\mu_0 42.57602\ MHz\ T^{-1}} = H_0 \tag{11.368}$$

In the case that the chemical environment has a NMR effect, a different value of H_0 is required for resonance. This chemical shift is proportional to the electronic magnetic flux charge at the nucleus due to the applied field, which in the case of each dihydrino molecule is a function of its semimajor and semiminor axes as shown *infra*.

Consider the application of a z-axis-directed uniform external magnetic flux, $\mathbf{B}_z$, to a dihydrino molecule comprising prolate spheroidal electron MOs with two spin-paired electrons. The diamagnetic reaction current increases or decreases the MO current to counteract any applied flux according to Lenz's law as shown in the Hydrino Hydride Ion Nuclear Magnetic Resonance Shift section. The current of hydrogen-type molecules is along elliptical orbits parallel to the semimajor axis. Thus, each nuclear magnetic moment must be in the direction of the semiminor axis for the electronic interaction with the nuclei. Thus, the nuclei are NMR active towards $\mathbf{B}_z$ when the orientation of the semimajor axis, a, is along the x-axis, and the semiminor axes, $b = c$, are along the y-axis and z-axis, respectively. The flux is applied over the time interval $\Delta t = t_i - t_f$ such that the field increases at a rate dB/dt. The electric field, $\mathbf{E}$, along a perpendicular elliptic path of the dihydrino MO at the plane $z = 0$ is given by

$$\oint E \cdot ds = \int \frac{dB}{dt} \cdot dA \tag{11.369}$$

The induced electric field must be constant along the path; otherwise, compensating currents would flow until the electric field is constant. Thus, Eq. (11.369) becomes

$$E = \frac{\int \frac{dB}{dt} \cdot dA}{\oint ds} = \frac{\int \frac{dB}{dt} \cdot dA}{4aE(k)} = \frac{\pi ab \frac{dB}{dt}}{4aE(k)} \tag{11.370}$$

where $E(k)$ is the elliptic integral given by:

$$E(k) = \int_0^{\frac{\pi}{2}} \sqrt{1 - k \sin^2 \phi}\, d\phi = 1.2375 \tag{11.371}$$

$$k = e = \frac{\sqrt{a^2 - b^2}}{a} = \frac{\sqrt{2}}{2} \tag{11.372}$$

the area of an ellipse, A, is

$$A = \pi ab \tag{11.373}$$

the perimeter of an ellipse, s, is:

$$s = 4aE(k) \tag{11.374}$$

a is the semimajor axis given by Eq. (11.202), b is the semiminor axis given by Eq. (11.205), and e is the eccentricity given by Eq. (11.206). The acceleration along the path, dv/dt, during the application of the flux is determined by the electric force on the charge density of the electrons:

$$m_e \frac{dv}{dt} = eE = \frac{e\pi ab}{4aE(k)} \frac{dB}{dt} \tag{11.375}$$

Thus, the relationship between the change in velocity, v, and the change in B is:

$$dv = \frac{e\pi ab}{4aE(k) m_e} dB \tag{11.376}$$

Let Δv represent the net change in v over the time interval $\Delta t = t_i - t_f$ of the application of the flux. Then,

$$\Delta v = \int_{v_0}^{v_0 + \Delta v} dv = \frac{e\pi ab}{4aE(k) m_e} \int_0^B dB = \frac{e\pi abB}{4aE(k) m_e} \tag{11.377}$$

The average current, I, of a charge moving in time harmonically along an ellipse is:

$$I = ef = \frac{ev}{4aE(k)} \tag{11.378}$$

where f is the frequency. The corresponding magnetic moment is given by:

$$m = AI = \pi abI = \frac{\pi abev}{4aE(k)} \tag{11.379}$$

Thus, from Eqs. (11.377) and (11.379), the change in the magnetic moment, $\Delta\mathbf{m}$, due to an applied magnetic flux, $\mathbf{B}$, is [39]

$$\Delta\mathbf{m} = -\frac{(e\pi ab)^2\,\mathbf{B}}{(4aE(k))^2\,m_e} \tag{11.380}$$

Next, the contribution from all plane cross-sections of the prolate spheroid MO must be integrated along the z-axis. The spheroidal surface is given by

$$\frac{x^2}{a^2}+\frac{y^2}{b^2}+\frac{z^2}{b^2}=1 \tag{11.381}$$

The intersection of the plane $z = z'$ $(-b \le z' \le b)$ with the spheroid determines the curve

$$\frac{x^2}{a^2}+\frac{y^2}{b^2}=1-\frac{z'^2}{b^2} \tag{11.382}$$

or

$$\frac{x^2}{a^2\left(1-\frac{z'^2}{b^2}\right)}+\frac{y^2}{b^2\left(1-\frac{z'^2}{b^2}\right)}=1 \tag{11.383}$$

Eq. (11.383) is an ellipse with semimajor axis, a', and semiminor axis, b', given by:

$$a' = a\sqrt{1-\frac{z'^2}{b^2}} \tag{11.384}$$

$$b' = b\sqrt{1-\frac{z'^2}{b^2}} \tag{11.385}$$

The eccentricity, e', is given by

$$e' = \frac{\sqrt{a^2\left(1-\frac{z'^2}{b^2}\right)-b^2\left(1-\frac{z'^2}{b^2}\right)}}{a\sqrt{1-\frac{z'^2}{b^2}}} = \frac{\sqrt{a^2-b^2}}{a} = e \tag{11.386}$$

where e is given by Eq. (11.372). The area, A', is given by:

$$A' = \pi a'b' \tag{11.387}$$

and the perimeter, s', is given by

$$s' = 4a'E(k) = 4aE(k)\sqrt{1-\frac{z'^2}{b^2}} = s\sqrt{1-\frac{z'^2}{b^2}} \tag{11.388}$$

where s is given by Eq. (11.374). The differential magnetic moment change along the z-axis is:

$$d\Delta\mathbf{m} = -\frac{1}{2b}\frac{(e\pi a'b')^2\,\mathbf{B}}{(4a'E(k))^2\,m_e}dz' \tag{11.389}$$

Using Eq. (11.385) for the parameter b', the change in magnetic moment for the dihydrino molecule is given by the integral over $-b \le b' \le b$:

$$\Delta\mathbf{m} = -\frac{1}{2b}\int_{-b}^{b}\frac{\left(e\pi a'b\sqrt{1-\frac{z'^2}{b^2}}\right)^2\mathbf{B}}{(4a'E(k))^2\,m_e}dz' = -C_1\frac{1}{m_e}\left(\frac{\pi e}{4E(k)}\right)^2\mathbf{B} \tag{11.390}$$

Then, the integral to correct for the z-dependence of b' is:

$$C_1 = \frac{\int_{-b}^{b}\left(b^2-z^2\right)dz}{2b} = \frac{2}{3}b^2 = \frac{a_0^2}{3p^2} \tag{11.391}$$

where the semiminor axis, $b = \frac{a_0}{p\sqrt{2}}$, given by Eq. (11.205) was used.

The change in magnetic moment would be given by the substitution of Eq. (11.391) into Eq. (11.390), if the charge density were constant along the path of Eqs. (11.370) and (11.378), but it is not. The charge density of the MO in rectangular coordinates (Eq. (11.42)) is

$$\sigma = \frac{e}{4\pi abc}\frac{1}{\sqrt{\frac{x^2}{a^4}+\frac{y^2}{b^4}+\frac{z^2}{c^4}}} \tag{11.392}$$

(The mass-density function of an MO is equivalent to its charge-density function where m replaces q of Eq. (11.42)). The equation of the plane tangent to the ellipsoid at the point $x_0,\ y_0,\ z_0$ is:

$$X\frac{x_0}{a^2}+Y\frac{y_0}{b^2}+Z\frac{z_0}{c^2} = 1 \tag{11.393}$$

where $X,\ Y,\ Z$ are running coordinates in the plane. After dividing through by the square root of the sum of the squares of the coefficients of $X,\ Y,$ and Z, the right member is the distance D from the origin to the tangent plane. That is,

$$D = \frac{1}{\sqrt{\frac{x^2}{a^4}+\frac{y^2}{b^4}+\frac{z^2}{c^4}}} \tag{11.394}$$

so that

$$\sigma = \frac{e}{4\pi abc}D \tag{11.395}$$

In other words, the surface density at any point on the ellipsoidal MO is proportional to the perpendicular distance from the center of the ellipsoid to the plane tangent to the ellipsoid at the point. The charge is thus greater on the more sharply rounded ends farther away from the origin. In order to maintain current continuity, the diamagnetic velocity of Eq. (11.377) must be a constant along any given path integral corresponding to a constant electric field. Consequently, the charge density must be the minimum value of that given by Eq. (11.392). The minimum corresponds to $y = b$ and $x = z = 0$ such that the charge density is:

$$\sigma = \frac{e}{4\pi ab^2}\frac{1}{\sqrt{\frac{0^2}{a^4}+\frac{b^2}{b^4}+\frac{0^2}{b^4}}} = \frac{e}{4\pi ab} \tag{11.396}$$

The MO is an equipotential surface, and the current must be continuous over the two-dimensional surface. Continuity of the surface current density, K, due to the diamagnetic effect of the applied magnetic field on the MO and the equipotential boundary condition require that the current of each elliptical curve determined by the intersection of the plane $z = z'$ ($-b \le z' \le b$) with the spheroid be the same. The charge density is spheroidally symmetrical about the semimajor axis. Thus, λ, the charge density per unit length along each elliptical path cross section of Eq. (11.383) is given by distributing the surface charge density of Eq. (11.396) uniformly along the z-axis for $-b \le z' \le b$. So, $\lambda(z'=0)$, the linear charge density λ in the plane $z' = 0$, is:

$$\lambda(z'=0) = \frac{\sigma}{\frac{1}{2b}} = \frac{e}{4\pi ab}2b = \frac{e}{2\pi a} \tag{11.397}$$

And, the linear charge density must be equally distributed over each elliptical path cross-section corresponding to each plane $z = z'$. The current is independent of z' when the linear charge density, $\lambda(z')$, is normalized for the path length:

$$\lambda(z') = \frac{e}{2\pi a}\frac{4aE(k)}{4a'E(k')} = \frac{e}{2\pi a'} \tag{11.398}$$

where the equality of the eccentricities of each elliptical plane cross section given by Eq. (11.386) was used. Substitution of Eq. (11.398) for the corresponding charge density, $\frac{e}{4a'E(k)}$, of Eq. (11.390) and using Eq. (11.391) gives:

$$\Delta\mathbf{m} = \frac{2}{3}\frac{e^2b^2\mathbf{B}}{4m_e} = \frac{e^2a_0^2\mathbf{B}}{12p^2m_e} \tag{11.399}$$

The two electrons are spin-paired and the velocities are mirror opposites. Thus, the change in velocity of each electron treated individually (Eq. (10.3)) due to the applied field would be equal and opposite. However, as shown in the Three Electron Atom section, the two paired electrons may be treated as one with twice the mass where m_e is replaced by $2m_e$ in Eq. (11.399). In this case, the paired electrons spin together about the applied field axis, the z-axis, to cause a reduction in the applied field according to Lenz's law. Thus, from Eq. (11.399), the change in magnetic moment is given by:

$$\Delta\mathbf{m} = \frac{e^2a_0^2\mathbf{B}}{24p^2m_e} \tag{11.400}$$

The opposing diamagnetic flux is uniform, parallel, and opposite the applied field as given by Stratton [40]. Specifically, the change in magnetic flux, $\Delta\mathbf{B}$, at the nucleus due to the change in magnetic moment, $\Delta\mathbf{m}$, is:

$$\Delta\mathbf{B} = \mu_0 A_2 \Delta\mathbf{m} \tag{11.401}$$

where μ_0 is the permeability of vacuum,

$$A_2 = \int_0^\infty \frac{ds}{\left(s+b^2\right)R_s} \tag{11.402}$$

is an elliptic integral of the second kind given by Whittaker and Watson [41], and

$$R_s = (s+b^2)\sqrt{(s+a^2)} \tag{11.403}$$

Substitution of Eq. (11.403) into Eq. (11.402) gives:

$$A_2 = \int_0^\infty \frac{ds}{\left(s+b^2\right)^2\left(s+a^2\right)^{1/2}} \tag{11.404}$$

From integral 154 of Lide [42]:

$$A_2 = -\left\{\frac{1}{a^2-b^2}\frac{\sqrt{s+a^2}}{s+b^2}\right\}_0^\infty - \frac{1}{2}\frac{1}{a^2-b^2}\int_0^\infty \frac{ds}{\left(s+b^2\right)\sqrt{s+a^2}} \tag{11.405}$$

The evaluation at the limits of the first integral is

$$-\left\{\frac{1}{a^2-b^2}\frac{\sqrt{s+a^2}}{s+b^2}\right\}_0^\infty = \frac{a}{b^2\left(a^2-b^2\right)} \tag{11.406}$$

From integral #147 of Lide [9], the second integral is:

$$-\frac{1}{2}\frac{1}{a^2-b^2}\int_0^\infty \frac{ds}{\left(s+b^2\right)\sqrt{s+a^2}} = \left\{\frac{1}{2}\frac{1}{\left(a^2-b^2\right)^{3/2}}\ln\frac{\sqrt{s+a^2}+\sqrt{a^2-b^2}}{\sqrt{s+a^2}-\sqrt{a^2-b^2}}\right\}_0^\infty \tag{11.407}$$

Evaluation at the limits of the second integral gives:

$$-\frac{1}{2}\frac{1}{\left(a^2-b^2\right)^{3/2}}\ln\frac{a+\sqrt{a^2-b^2}}{a-\sqrt{a^2-b^2}} \tag{11.408}$$

Combining Eq. (11.406) and Eq. (11.408) gives:

$$A_2 = \frac{a}{b^2\left(a^2-b^2\right)} - \frac{1}{2}\frac{1}{\left(a^2-b^2\right)^{3/2}}\ln\frac{a+\sqrt{a^2-b^2}}{a-\sqrt{a^2-b^2}} = \frac{p^3 4}{a_0^3} - \frac{p^3\sqrt{2}}{a_0^3}\ln\frac{\sqrt{2}+1}{\sqrt{2}-1} \tag{11.409}$$

where the semimajor axis, $a = \frac{a_0}{p}$, given by Eq. (11.202) and the semiminor axis, $b = \frac{a_0}{p\sqrt{2}}$, given by Eq. (11.205) were used.

Substitution of Eq. (11.400) and Eq. (11.409) into Eq. (11.401) gives:

$$\Delta\mathbf{B} = -\mu_0\left(\frac{p^3 4}{a_0^3} - \frac{p^3\sqrt{2}}{a_0^3}\ln\frac{\sqrt{2}+1}{\sqrt{2}-1}\right)\frac{a_0^2 e^2\mathbf{B}}{24p^2 m_e} \tag{11.410}$$

Additionally, it is found both theoretically and experimentally that the dimensions, r^2, of the molecule corresponding to the area in Eqs. (11.369) and (11.379) used to derive Eq. (11.410) must be replaced by an average, $\left\langle r^2\right\rangle$, that takes into account averaging over the orbits isotropically oriented. The correction of 2/3 is given by Purcell [39] (also Eq (11.391)). In the case of hydrogen-type molecules, the electronic interaction with the nuclei require that each nuclear magnetic moment is in the direction of the semiminor axis. But free rotation about each of three axes results in an isotropic averaging of 2/3 where the rotational frequencies of hydrogen-type molecules are much greater than the corresponding NMR frequency (e.g. 10^{12} *Hz* versus 10^8 *Hz*). Thus, Eq. (11.410) gives the absolute upfield chemical shift, $\frac{\Delta B}{B}$, of $H_2(1/p)$ relative to a bare proton:

$$\begin{aligned}\frac{\Delta\mathbf{B}}{\mathbf{B}} = \frac{\Delta B}{B} &= -\mu_0\left(\frac{p^3 4}{a_0^3} - \frac{p^3\sqrt{2}}{a_0^3}\ln\frac{\sqrt{2}+1}{\sqrt{2}-1}\right)\frac{a_0^2 e^2}{36p^2 m_e} \\ &= -\mu_0\left(4-\sqrt{2}\ln\frac{\sqrt{2}+1}{\sqrt{2}-1}\right)\frac{pe^2}{36a_0 m_e} \\ &= -p28.01\ ppm\end{aligned} \tag{11.411}$$

where p is an integer.

For resonance to occur, ΔH_0, the change in applied field from that given by Eq. (11.368), must compensate by an equal and opposite amount as the field due to the electrons of molecular hydrino. Compared to protons with no chemical shift, the ratio of ΔH_0 for resonance of the protons of the dihydrino molecule $H_2(1/p)$ to that of H_2 is a positive integer. According to Eq. (11.202), the ratio of the semimajor axis of the dihydrino molecule $H_2(1/p)$ to that of the hydrogen molecule H_2 is the reciprocal of an integer p. It follows from Eqs. (11.202) and (11.411) that the diamagnetic flux (flux opposite to the applied

field) at each nucleus is inversely proportional to the semimajor radius, $a = \frac{a_0}{p}$. That is, if only the size is considered, the absolute absorption peak of the dihydrino molecule (i.e. relative to a proton with no shift) occurs at a value of ΔH_0 that is a multiple of p times the value that is resonant for H_2. However, the source current of the state must be considered in addition to the reduced geometrical dimensions.

As shown in the Stability of "Ground" and Hydrino States section, for the below "ground" (fractional quantum number) energy states of the hydrogen atom, σ_{photon}, the two-dimensional surface charge due to the "trapped photon" at the electron atomic orbital and phase-locked with the electron atomic orbital current, is given by Eqs. (5.27) and (2.11). The excited states of the hydrogen molecule are solved using the same approach as those of the excited states of atoms wherein the corresponding geometry is prolate spheroid rather than spherical and the photon fields are modeled by associated Legendre functions or ellipsoidal spherical harmonics with regard to the semimajor axis as given in the Excited States of the Hydrogen Molecule section. The total central ellipsoidal field of the molecule at the position of the molecular orbital (MO) due to the superposition of the field of the nuclei and the photon field is equivalent to an integer p times that of the nuclei at the foci of the prolate spheroidal MO. The photon source current gives rise to an additional contribution to the diamagnetism of the two electrons that is a function of p.

As given in the Excited States of the Hydrogen Molecule section, the current of the paired electrons of the MO are phase locked to the photon field of magnitude p of the dihydrino state. For the spherical harmonics, the quantum number of the electron are p, ℓ, m_ℓ, and m_s as described in the Excited States of the One-Electron Atom (Quantization) section wherein the principal quantum number of excited states is replaced by $n = \frac{1}{p}$. From Eq. (5.27),

$$n = \frac{1}{p};\ \ell = 0,1,2,...,p-1;\ m_\ell = -\ell,-\ell+1,...,0,...+\ell;\ m_s = \pm\frac{1}{2} \tag{11.412}$$

In the case that the photons and corresponding source current spin in opposite directions for the two electrons, the orbital magnetic moments cancel. However, as given in the Pair Production section, a photon having an energy equivalent to that of the mass energy of the electron may undergo particle production to form an electron. To maintain continuity, the photon surface current of a dihydrino state must behave as the charge equivalent to its energy during the interaction of the electrons and the phased locked photon-field surface current with the external magnetic field such that the photon component gives rise to a proportional diamagnetic effect as well. The photon diamagnetic component is given by Eqs. (29.10-29.11) as the charge equivalent to its energy that superimposes with the diamagnetism of the two electrons. The relativistic term after Eq. (29.10) and the central field magnitude term for the dihydrino state having principle quantum number p are α^2 and p, respectively. The photon contribution to the change in flux $\Delta\mathbf{B}_{SR}$ for molecular hydrino $H_2(1/p)$ given by applying the corresponding relativistic factor of $\gamma_{SR} = \alpha^2$ to Eq. (11.401) is

$$\Delta\mathbf{B}_{SR} = -p\alpha^2\mu_0 A_2 \Delta\mathbf{m} \tag{11.413}$$

Thus, using Eq. (11.411) and Eq. (11.413), the upfield chemical shift, $\frac{\Delta B_{SR}}{B}$, due to the photon contribution of the molecule $H_2(1/p)$ corresponding to the lower-energy state with principal quantum energy state p is given by:

$$\frac{\Delta B_{SR}}{B} = -p\alpha^2\mu_0\left(4-\sqrt{2}\ln\frac{\sqrt{2}+1}{\sqrt{2}-1}\right)\frac{pe^2}{36a_0m_e} \tag{11.414}$$

The total shift, $\frac{\Delta B_T}{B}$, for $H_2(1/p)$ is given by the sum of that of the electrons given by Eq. (11.411) and that of the photon given by Eq. (11.414):

$$\frac{\Delta B_T}{B} = -\mu_0\left(4-\sqrt{2}\ln\frac{\sqrt{2}+1}{\sqrt{2}-1}\right)\frac{pe^2}{36a_0m_e}\left(1+p\alpha^2\right) \tag{11.415}$$

$$\frac{\Delta B_T}{B} = -\left(p28.01 + p^2 1.49\ X\ 10^{-3}\right)ppm \tag{11.416}$$

where the first term applies to H_2 with $p=1$ and $p=\text{integer}>1$ for $H_2(1/p)$.

H_2 has been characterized by gas phase ^1H NMR. The experimental absolute resonance shift of gas-phase TMS relative to the proton's gyromagnetic frequency is -28.5 ppm [32]. The experimental absolute resonance shift of TMS is -31.5 ppm relative to the proton's gyromagnetic frequency [43-44]. H_2 was observed at 0.48 ppm compared to gas phase TMS set at 0.00 ppm [33]. Thus, the corresponding absolute H_2 gas-phase resonance shift of -28.0 ppm (-28.5 + 0.48) ppm was in excellent agreement with the predicted absolute gas-phase shift of -28.01 ppm given by Eq. (11.411). The solution NMR of H_2 has a

chemical shift of about +4.65 ppm relative to TMS in many solvents [45] corresponding to a solvent or matrix shift of about +1 ppm. The chemical shift of $H_2(1/p)$ is given by the difference of Eq. (11.416) and -31.5 ppm plus any solvent shift.

As given in the Parameters and Magnetic Energies Due to the Spin Magnetic Moment of $H_2(1/4)$ section $H_2(1/p)$ has an unpaired electron such that it is paramagnetic. The paramagnetism contributes to the difficulty of observing molecular hydrino NMR peaks directly. However molecular hydrino states can give rise to a matrix shift in the MAS NMR spectrum when the matrix comprises NMR active H species such as a matrix having waters of hydration or an alkaline hydroxide solid matrix wherein a local interaction with $H_2(1/p)$ causes an upfield matrix shift. This effect may be enhanced for H species capable of rapid H exchange wherein the local $H_2(1/p)$ interaction influences a larger population due to the rapid H exchange.

QUADRUPOLE MOMENT

The quadrupole moment Q_{33} of a charge distribution $\rho(\vec{r})$ along the z-axis is given by

$$Q_{zz} = \iiint d\vec{r}\,\rho(\vec{r})\left[3z^2 - r^2\right] \tag{11.417}$$

In cylindrical coordinates, the quadrupole moment is given by

$$Q_{zz} = \int dz \int d\phi \int dr r\left[2z^2 - r^2\right]\sigma \tag{11.418}$$

wherein from Eqs. (11.26), (11.45), and (11.46) the electron charge distribution σ is

$$\sigma = \frac{-2e}{4\pi abc}\frac{1}{\sqrt{\frac{x^2}{a^4}+\frac{y^2}{b^4}+\frac{z^2}{b^4}}}; \qquad \frac{x^2}{a^2}+\frac{y^2}{b^2}+\frac{z^2}{b^2} = 1 \tag{11.419}$$

Consider that the prolate spheroid is aligned with the major axis along the z-axis such that the magnitude of the charge density of the hydrogen-type molecular orbital is

$$\sigma = \frac{-2e}{4\pi ab^2}\frac{1}{\sqrt{\frac{r^2}{b^4}+\frac{z^2}{a^4}}}; \qquad \frac{r^2}{b^2}+\frac{z^2}{a^2} = 1 \tag{11.420}$$

Substitution of Eq. (11.419) into Eq. (11.418) gives the electron contribution to the quadrupole moment Q_{zze}:

$$Q_{zze} = \frac{-2e}{4\pi ab^2}\int_{-a}^{a}\int_{0}^{2\pi}\frac{\int_0^\infty r\left(2z^2 - r^2\right)}{\sqrt{\frac{z^2}{a^4}+\frac{r^2}{b^4}}}\delta\left(r - b\sqrt{1-\frac{z^2}{a^2}}\right)drd\phi dz \tag{11.421}$$

Integration with respect to r and ϕ gives

$$Q_{zze} = \frac{-e}{ab^2}\int_{-a}^{a}\frac{2z^2 b\sqrt{1-\frac{z^2}{a^2}} - b^3\left(1-\frac{z^2}{a^2}\right)^{3/2}}{\sqrt{\frac{z^2}{a^4}+\frac{\left(1-\frac{z^2}{a^2}\right)}{b^2}}}dz \tag{11.422}$$

With the substitution of the semimajor axis (Eq. (11.202)), semiminor axis (Eq. (11.205)), and $z' = z/a$ into Eq. (11.422), Q_{zze} becomes

$$Q_{zze} = -e\frac{a_0^2}{p^2}\int_{-1}^{1}\frac{2^{3/2}z'^2\sqrt{1-z'^2} - \frac{1}{\sqrt{2}}\left(1-z'^2\right)^{3/2}}{\sqrt{2-z'^2}}dz' \tag{11.423}$$

Integral (11.423) given by Mathematica is

$$\frac{Q_{zze}}{e} = -0.298728\frac{a_0^2}{p^2} = \frac{-8.36523X10^{-22}m^2}{p^2} = \frac{-8.36523X10^{-18}cm^2}{p^2} \tag{11.424}$$

Next, consider the quadrupole moment contribution of the two protons of hydrogen-type molecules wherein the protons are aligned along the z-axis with a separation of the internuclear distance $2c'$ given by Eq. (11.204). The quadrupole moment tensor is given by [46]:

$$Q_{ij} = \int d^3x\,\rho(\mathbf{x})\left(3x_i x_j - r^2\delta_{ij}\right) \tag{11.425}$$

The charge densities of the protons are given by

$$\rho(\mathbf{x}) = e\left(\delta^3\left(\mathbf{x} - c'\mathbf{k}\right) + \delta^3\left(\mathbf{x} + c'\mathbf{k}\right)\right) \tag{11.426}$$

The quadrupole moment may be easily evaluated in Cartesian coordinates wherein the Dirac delta functions become

$$\delta^3\left(\mathbf{x}-c'\mathbf{k}\right)+\delta^3\left(\mathbf{x}+c'\mathbf{k}\right)=\delta\left(z-c'\right)\delta\left(x\right)\delta\left(y\right)+\delta\left(z+c'\right)\delta\left(x\right)\delta\left(y\right) \tag{11.427}$$

Substitution of Eqs. (11.426-11.427) into Eq. (11.425) gives the proton quadrupole contribution Q_{zzp}:

$$\begin{aligned} Q_{zzp} &= \int_{-\infty}^{\infty} dx \int_{-\infty}^{\infty} dy \int_{-\infty}^{\infty} dz \rho(\mathbf{x})\left(3z^2-\left(x^2+y^2+z^2\right)\right) \\ &= e\int_{-\infty}^{\infty} dx \int_{-\infty}^{\infty} dy \int_{-\infty}^{\infty} dz \left(\delta\left(z-c'\right)\delta\left(x\right)\delta\left(y\right)+\delta\left(z+c'\right)\delta\left(x\right)\delta\left(y\right)\right)\left(2z^2-x^2-y^2\right) \\ &= 4ec'^2 \end{aligned} \tag{11.428}$$

The charge-normalized quadrupole moment of hydrogen-type molecule $\frac{Q_{zzH_2(1/p)}}{e}$ is given by the sum of the charge-normalized quadrupole moment contributions of the protons, $\frac{Q_{zzp}}{e}$ given by Eq. (11.428), and the electrons, $\frac{Q_{zze}}{e}$ given by Eq. (11.424):

$$\frac{Q_{zzH_2(1/p)}}{e}=\frac{Q_{zzp}}{e}+\frac{Q_{zze}}{e}=4c'^2-0.29873\frac{a_0^2}{p^2}=\left(2-0.29873\right)\frac{a_0^2}{p^2}=1.70127\frac{a_0^2}{p^2} \tag{11.429}$$

wherein the distance of each proton from the origin c' is given by Eq. (11.203). In the case of H_2 wherein $p=1$, the charge-normalized quadrupole moment given by Eq. (11.429) is

$$\frac{Q_{zzH_2}}{e}=1.70127a_0^2=0.476404X10^{-16}cm^2 \tag{11.430}$$

which agrees with the experimental results of Ramsey [47]:

$$\frac{Q_{zzH_2}}{e}=0.38\pm0.15X10^{-16}cm^2 \tag{11.431}$$

In the case of $H_2\left(1/4\right)$ wherein $p=4$, the charge-normalized quadrupole moment given by Eq. (11.429) is

$$\frac{Q_{zzH_2(1/4)}}{e}=1.70127\frac{a_0^2}{4^2}=2.97752X10^{-18}cm^2 \tag{11.432}$$

REFERENCES

1. G. R. Fowles, *Analytical Mechanics*, Third Edition, Holt, Rinehart, and Winston, New York, (1977), pp. 145-158.
2. J. A. Stratton, *Electromagnetic Theory*, McGraw-Hill Book Company, (1941), pp. 38-59; 195-267.
3. Jahnke-Emde, *Tables of Functions*, 2nd ed., Teubner, (1933).
4. J. D. Jackson, Classical Electrodynamics, Second Edition, John Wiley & Sons, New York, (1975), pp. 17-22.
5. H. A. Haus, J. R. Melcher, "Electromagnetic Fields and Energy," Department of Electrical Engineering and Computer Science, Massachusetts Institute of Technology, (1985), Sec. 5.3.
6. J. A. Stratton, *Electromagnetic Theory*, McGraw-Hill Book Company, (1941), p. 195.
7. G. R. Fowles, *Analytical Mechanics*, Third Edition, Holt, Rinehart, and Winston, New York, (1977), pp. 119-124.
8. J. A. Stratton, *Electromagnetic Theory*, McGraw-Hill Book Company, (1941), pp. 38-54; 207-209.
9. D. R. Lide, *CRC Handbook of Chemistry and Physics*, 79th Edition, CRC Press, Boca Raton, Florida, (1998-9), p. A-29.
10. H. A. Haus, "On the radiation from point charges," American Journal of Physics, 54, (1986), pp. 1126-1129.
11. G. R. Fowles, *Analytical Mechanics*, Third Edition, Holt, Rinehart, and Winston, New York, (1977), pp. 161-164.
12. G. R. Fowles, *Analytical Mechanics*, Third Edition, Holt, Rinehart, and Winston, New York, (1977), pp. 57-66.
13. M. Mizushima, *Quantum Mechanics of Atomic Spectra and Atomic Structure*, W.A. Benjamin, Inc., New York, (1970), p.17.
14. M. Karplus, R. N. Porter, *Atoms and Molecules an Introduction for Students of Physical Chemistry*, The Benjamin/Cummings Publishing Company, Menlo Park, California, (1970), pp. 447-484.
15. J. D. Jackson, *Classical Electrodynamics*, Second Edition, John Wiley & Sons, New York, (1975), p. 659.
16. J. D. Jackson, *Classical Electrodynamics*, Second Edition, John Wiley & Sons, New York, (1975), pp. 780-786.
17. T. C. Gibb, *Principles of Mössbauer Spectroscopy,* Wiley, (1976), pp. 1-5.
18. D. A. McQuarrie, *Quantum Chemistry*, University Science Books, Mill Valley, CA, (1983), p. 172.
19. D. R. Lide, *CRC Handbook of Chemistry and Physics*, 79th Edition, CRC Press, Boca Raton, Florida, (1998-9), p. 10-175.
20. NIST Atomic Spectra Database, www.physics.nist.gov/cgi-bin/AtData/display.ksh.
21. T. Bujnak, personal communication July 2010.
22. M. Abramowitz, I. A. Stegun (Editors), *Handbook of Mathematical Functions with Formulas, Graphs, and Mathematical Tables*, Dover Publications, Inc, New York, (1970), pp. 753-759
23. N. V. Sidgwick, *The Chemical Elements and Their Compounds*, Volume I, Oxford, Clarendon Press, (1950), p.17.
24. P. W. Atkins, *Physical Chemistry*, Second Edition, W. H. Freeman, San Francisco, (1982), p. 589.
25. K. P. Huber, G. Herzberg, *Molecular Spectra and Molecular Structure, IV. Constants of Diatomic Molecules*, Van Nostrand Reinhold Company, New York, (1979).
26. W. J. Nellis, "Making Metallic Hydrogen," Scientific American, May, (2000), pp. 84-90.

27. H. Beutler, Z. Physical Chem., "Die dissoziationswarme des wasserstoffmolekuls H_2, aus einem neuen ultravioletten resonanzbandenzug bestimmt," Vol. 27B, (1934), pp. 287-302.
28. G. Herzberg, L. L. Howe, "The Lyman bands of molecular hydrogen," Can. J. Phys., Vol. 37, (1959), pp. 636-659.
29. J. Itatani, J. Levesque, D. Zeidler, H. Niikura, H. Pepin, J. C. Kieffer, P. B. Corkum, D. M. Villeneuve, "Tomographic imaging of molecular orbitals," Nature, Vol. 432, (2004), pp. 867-871.
30. D. R. Lide, *CRC Handbook of Chemistry and Physics*, 79th Edition, CRC Press, Boca Raton, Florida, (1998-9), p. 10-181.
31. R. Loch, R. Stengler, G. Werth, "Measurement of the electronic g factor of H_2^+," Phys. Rev. A, Vol. 38, No. 11, (1988), pp. 5484-5488.
32. C. Suarez, E. J. Nicholas, M. R. Bowman, "Gas-phase dynamic NMR study of the internal rotation in N-trifluoroacetlypyrrolidine," J. Phys. Chem. A, Vol. 107, (2003), pp. 3024-3029.
33. C. Suarez, "Gas-phase NMR spectroscopy," The Chemical Educator, Vol. 3, No. 2, (1998).
34. D. R. Lide, *CRC Handbook of Chemistry and Physics*, 79th Edition, CRC Press, Boca Raton, Florida, (1998-9), p. 9-82.
35. R. L. Mills, J. J. Farrell, *The Grand Unified Theory*, Science Press, (1989), pp. 46-47; 117-119.
36. J. D. Jackson, *Classical Electrodynamics*, Second Edition, John Wiley & Sons, New York, (1975), p. 178.
37. E. V. Lavrov, J. Weber, "Ortho and Para Interstitial H_2 in Silicon," Phys. Rev. Letts., 89(21), (2002), pp. 215501 to 1–215501-4.
38. Liquefaction of "Permanent" Gases" (PDF of lecture notes). 2011. Retrieved 2017-10-16 (Reference 5 of "Spin isomers of hydrogen", Wikipedia, https://en.wikipedia.org/wiki/Spin_isomers_of_hydrogen, Retrieved 2018-11-28.
39. E. Purcell, *Electricity and Magnetism*, McGraw-Hill, New York, (1965), pp. 370-389.
40. J. A. Stratton, *Electromagnetic Theory*, McGraw-Hill Book Company, (1941), pp. 211-215, 257-258.
41. Whittaker and Watson, *Modern Analysis*, 4th Edition, Cambridge University Press, (1927), pp. 512ff.
42. D. R. Lide, *CRC Handbook of Chemistry and Physics*, 79th Edition, CRC Press, Boca Raton, Florida, (1998-9), p. A-30.
43. K. K. Baldridge, J. S. Siegel, "Correlation of empirical δ(TMS) and absolute NMR chemical shifts predicted by ab initio computations," J. Phys. Chem. A, Vol. 103, (1999), pp. 4038-4042.
44. J. Mason, Editor, *Multinuclear NMR*, Plenum Press, New York, (1987), Chp. 3.
45. G. R. Fulmer, A. J. M. Miller, N. H. Sherden, H. E. Gottlieb, A. Nudelman, B. M. Stoltz, J. E. Bercaw, K. I. Goldberg, "NMR chemical shifts of trace impurities: common laboratory solvents, organics, and gases in deuterated solvents relevant to the organometallic chemist," Organometallics, Vol. 29 (9), (2010), pp. 2176-2179, DOI: 10.1021/om100106e.
46. "Multipole moments," November 9, 2015, http://www.physics.usu.edu/Wheeler/EM3600/Notes12MultipoleMoments.pdf.
47. N. F. Ramsey, "Quadrupole moment of the electron distribution in hydrogen molecules", Physical Review, Vol. 78, No. 3, (1950), pp. 221-222.

Chapter 12

DIATOMIC MOLECULAR ENERGY STATES

EXCITED ELECTRONIC STATES OF ELLIPSOIDAL MOLECULAR ORBITALS

Excited states of atomic orbitals are discussed in the Excited States of the One-Electron Atom (Quantization) section and the Excited States of Helium section. In the case of ellipsoidal MOs, excited electronic states are created when photons of discrete frequencies are trapped in the ellipsoidal resonator cavity of the MO of the outer excited-state electron. The photon changes the effective charge at the MO surface where the central field is ellipsoidal and arises from both the net field of the nuclei at the foci of the inner MO and the trapped photon of the outer. The "trapped photons" are solutions of the two-dimensional Laplacian in ellipsoidal coordinates given by Eq. (11.27). The excited-state photon's electric field at the outer electron (Eq. (2.15) except ellipsoidal coordinates) superimposes that of the net field of the nuclei at the foci of the inner MO and inner MO charge such that the net electric field has a magnitude proportional to Z/n in the direction of $\mathbf{i}_\xi$ at the outer electron where $n = 2,3,4,...$ for excited states. Force balance is achieved at a series of ellipsoidal equipotential two-dimensional surfaces with an increased distance ξ. The state geometrical parameters are solved from the force balance equation and the relationships among the ellipsoidal parameters given in the Derivation of the General Geometrical and Energy Equations of Organic Chemistry section. The force balance of the outer excited-state electron is given by balance between the centrifugal force, the central Coulombic force corresponding to the effective central field due to the superposition of photon field at the outer electron and the net field of the nuclei at the foci of the inner MO, and the magnetic forces in the case of paired electrons in the unexcited state. The energies corresponding to the excited electron are given by the prolate spheroidal energy equations given in the Derivation of the General Geometrical and Energy Equations of Organic Chemistry section except for a correction corresponding to a single electron, and the electric terms are scaled according to the effective central field.

EXCITED STATES OF THE HYDROGEN MOLECULAR ION

FORCE BALANCE OF THE EXCITED STATES OF THE HYDROGEN MOLECULAR ION

The excited states of the hydrogen molecular ion are determined by the same physics as those of one and two electron atoms. The excited-state photon's electric field superposes that of the protons at the foci of the MO such that the excited-state electric field has a magnitude proportional to e/n in the direction of $\mathbf{i}_\xi$ at the electron MO where $n = 2,3,4,...$ for excited states. Balance between the centrifugal and the Coulomb forces is achieved at a series of MOs, ellipsoidal equipotential two-dimensional surfaces, confocal with the $n = 1$-state ellipsoid MO wherein the corresponding Coulombic force that balances the centrifugal force meets the requirement that the excited-state electric field has a magnitude proportional to e/n at the electron. Thus, force balance between the electric and centrifugal forces given by Eq. (11.115) where $p = 1/n$ is

$$\frac{\hbar^2}{m_e a^2 b^2} D = \frac{1}{n} \frac{e^2}{8\pi\varepsilon_0 a b^2} D \tag{12.1}$$

which has the parametric solution given by Eq. (11.83) when semimajor axis, a, is:

$$a = 2na_0 \tag{12.2}$$

The internuclear distance, $2c'$, which is the distance between the foci is given by Eq. (11.111) where $p = 1/n$.

$$2c' = 2na_0 \tag{12.3}$$

The semiminor axis is given by Eq. (11.112) where $p = 1/n$.

$$b = \sqrt{3}na_0 \tag{12.4}$$

The eccentricity, e, is given by Eq. (11.113).

$$e = \frac{1}{2} \tag{12.5}$$

ENERGIES OF THE EXCITED STATES OF THE HYDROGEN MOLECULAR ION

The potential energy, V_e, of the electron MO in the field of the protons at the foci ($\xi = 0$) is given by Eq. (11.117) where $p = 1/n$

$$V_e = \frac{-\left(\frac{1}{n}\right)4e^2}{8\pi\varepsilon_0\sqrt{a^2-b^2}} \ln\frac{a+\sqrt{a^2-b^2}}{a-\sqrt{a^2-b^2}} \tag{12.6}$$

To match the condition that electric field has a magnitude proportional to Z/n in the direction of $\mathbf{i}_\xi$ at the electrons, the corresponding potential energy, V_p, due to proton-proton repulsion is given by Eq. (11.120) where $p = 1/n$

$$V_p = \frac{\frac{1}{n}e^2}{8\pi\varepsilon_0\sqrt{a^2-b^2}} \tag{12.7}$$

The kinetic energy, T, of the electron MO is given by Eq. (11.119)

$$T = \frac{2\hbar^2}{m_e a\sqrt{a^2-b^2}} \ln\frac{a+\sqrt{a^2-b^2}}{a-\sqrt{a^2-b^2}} \tag{12.8}$$

Substitution of a and b given by Eqs. (12.2) and (12.4), respectively, into Eqs. (12.6-12.8) is:

$$V_e = \frac{-4e^2}{n^2 8\pi\varepsilon_0 a_H} \ln 3 = \frac{-59.7575\ eV}{n^2} \tag{12.9}$$

$$V_p = \frac{e^2}{n^2 8\pi\varepsilon_0 a_H} = \frac{13.5984\ eV}{n^2} \tag{12.10}$$

$$T = \frac{2e^2}{n^2 8\pi\varepsilon_0 a_H} \ln 3 = \frac{29.8787\ eV}{n^2} \tag{12.11}$$

The Doppler term, $\bar{E}_{osc}$, for hydrogen is given by Eq. (11.189) where $p = 1/n$

$$\bar{E}_{osc}\left(H_2^+\right) = \bar{E}_D + \bar{E}_{Kvib} = -\left(\frac{1}{n}\right)^3 0.118755\ eV + \frac{1}{2}\left(\frac{1}{n}\right)^2 \left(0.29282\ eV\right) \tag{12.12}$$

The total energy, E_T, for the hydrogen molecular ion given by Eqs. (11.191-11.193) is:

$$\begin{aligned} E_T &= -\left(\frac{1}{n}\right)^2 \left\{ \frac{e^2}{8\pi\varepsilon_0 a_H}(4\ln 3 - 1 - 2\ln 3)\left[1 + \left(\frac{1}{n}\right)\sqrt{\frac{2\hbar\sqrt{\frac{2e^2}{4\pi\varepsilon_0(2a_H)^3}}}{m_e c^2}}\right] - \frac{1}{2}\hbar\sqrt{\frac{k}{\mu}} \right\} \\ &= -\left(\frac{1}{n}\right)^2 16.2803\ eV - \left(\frac{1}{n}\right)^3 0.118755\ eV + \frac{1}{2}\left(\frac{1}{n}\right)^2 \hbar\sqrt{\frac{k}{\mu}} \\ &= -\left(\frac{1}{n}\right)^2 16.13392\ eV - \left(\frac{1}{n}\right)^3 0.118755\ eV \end{aligned} \tag{12.13}$$

The negative of Eq. (12.13) is the ionization energy of the excited state of H_2^+. The energy T_e from the $n = 1$ state (also referred to as the state X) to the energy of the n^{th} excited state is given by the difference of E_T given by Eq. (12.13) and the energy of unexcited H_2^+ given by Eq. (12.13) with $n = 1$:

$$T_e = -16.13392\ eV\left(\frac{1}{n^2} - 1\right) - 0.118755\ eV\left(\frac{1}{n^3} - 1\right) \tag{12.14}$$

These states are much higher in energy than the bond dissociation energy and cannot be observed. This result is consistent with observations wherein the excited state spectrum of H_2^+ comprises only excited vibrational levels and levels within a van der Waals state [1–3].

VIBRATION OF THE EXCITED STATES OF THE HYDROGEN MOLECULAR ION

It can be shown that a perturbation of the orbit determined by an inverse-squared force results in simple harmonic oscillatory motion of the orbit [4]. The resonant vibrational frequency for H_2^+ given by Eq. (11.160) is

$$\omega(0)=\left(\frac{1}{n}\right)^2\sqrt{\frac{k(0)}{\mu}}=\left(\frac{1}{n}\right)^2\sqrt{\frac{165.51\ Nm^{-1}}{\mu}}=\left(\frac{1}{n}\right)^2 4.449\ \times\ 10^{14}\ radians/s \tag{12.15}$$

wherein $p=1/n$. The spring constant, $k(0)$, for H_2^+ excited states given by Eq. (11.162) is:

$$k(0)=\left(\frac{1}{n}\right)^4 165.51\ Nm^{-1} \tag{12.16}$$

The vibrational energy, $E_{vib}(0)$, of the H_2^+ excited state for the determination of $\bar{E}_{osc}$ given by Eq. (11.163) is:

$$E_{vib}(0)=\left(\frac{1}{n}\right)^2 0.2928\ eV \tag{12.17}$$

The amplitude of oscillation given by Eq. (11.164) is:

$$A_{reduced}(0)=n0.1125a_0 \tag{12.18}$$

The vibrational energy for the H_2^+ excited-state $\upsilon=1\rightarrow\upsilon=0$ transition given by Eq. (11.166) is:

$$E_{vib}(1)=\left(\frac{1}{n}\right)^2 0.270\ eV \tag{12.19}$$

The anharmonicity term of the H_2^+ excited state given by Eq. (11.169) is:

$$\omega_0 x_0=\frac{100hc\left(8.06573\times10^3\ \frac{cm^{-1}}{eV}\left(\frac{1}{n}\right)^2 0.270\ eV\right)^2}{4e\left(\left(\frac{1}{n}\right)^2 2.535\ eV+\left(\frac{1}{n}\right)^3 0.118755\ eV\right)}cm^{-1} \tag{12.20}$$

MAGNETIC MOMENT OF AN ELLIPSOIDAL MOLECULAR ORBITAL

The magnetic dipole moment, μ, of a current loop is:

$$\mu=iA \tag{12.21}$$

where i is the current and A is the area of the loop. For any elliptic orbital due to a central field, the frequency, f, is:

$$f=\frac{\frac{L}{m}}{2A}=\frac{\frac{L}{m}}{2\pi ab} \tag{12.22}$$

where L is the angular momentum, m is the mass, and the area A of an ellipse is given by Eq. (11.25). The current, i, is:

$$i=ef=\frac{\frac{eL}{m_e}}{2\pi ab} \tag{12.23}$$

where e is the charge. The magnetic moment is given by substitution of Eqs. (12.23) and (11.25) into Eq. (12.21) where $L=\frac{\hbar}{2}$ is the intrinsic electron angular momentum of the ellipsoidal MO given in the Force Balance of Hydrogen-type Molecules section:

$$\mu=\frac{1}{2}\frac{e\hbar}{2m_e}=\frac{\mu_B}{2} \tag{12.24}$$

where μ_B is the Bohr magneton. In a Larmor excited state, the electron gains $L=\hbar$ along the semimajor axis as the intrinsic angular momentum precesses about this axis at the Larmor frequency. The magnetic moment of the Larmor excited state of cylindrical symmetry is given by Eq. (2.65):

$$\mu=\frac{e\hbar}{2m_e}=\mu_B \tag{12.25}$$

which is the Bohr magneton.

MAGNETIC FIELD OF AN ELLIPSOIDAL MOLECULAR ORBITAL

The magnetic field can be solved as a magnetostatic boundary value problem, which is equivalent to that of a uniformly magnetized ellipsoid. The magnetic scalar potential inside the ellipsoidal MO, ϕ^-, [5] and outside of the MO, ϕ^+, [6] are

$$\phi^- = \frac{e\hbar}{2m_e}\int_0^\infty \frac{ds}{(s+a^2)R_\xi} \tag{12.26}$$

and

$$\phi^+ = \frac{3e\hbar}{8\pi m_e}\frac{\xi}{a^2-b^2}\left(\frac{\eta}{2}\ln\frac{\eta+1}{\eta-1}-1\right) \tag{12.27}$$

respectively, where R_ξ for a prolate spheroid given by Stratton [7] (Eq. (11.32)) is:

$$R_\xi = \left(\xi+b^2\right)\sqrt{\left(\xi+a^2\right)} \tag{12.28}$$

and the spheroidal [7] parameters for Eq. (12.27) after Chang [6] are:

$$\eta = \sqrt{\frac{1}{2}\left[\left(1+x^2+y^2+z^2\right)+\sqrt{\left(1+x^2+y^2+z^2\right)^2-4x^2}\right]} \tag{12.29}$$

$$\xi = \frac{x}{\eta} \tag{12.30}$$

The magnetic field inside the ellipsoidal MO, $\mathbf{H}_x^-$, is [5]:

$$\begin{aligned}\mathbf{H}_x^- &= -\frac{\delta\phi^-}{\delta x}\\ &= \frac{-e\hbar}{2m_e}\int_0^\infty \frac{ds}{(s+a^2)R_\xi}\\ &= \frac{-e\hbar}{2m_e}\int_0^\infty \frac{ds}{(s+b^2)(s+a^2)^{3/2}}\\ &= \frac{e\hbar}{2m_e}\frac{1}{a^3\left(1-\frac{b^2}{a^2}\right)^{3/2}}\left(2\sqrt{1-\frac{b^2}{a^2}}+\ln\frac{1+\sqrt{1-\frac{b^2}{a^2}}}{1-\sqrt{1-\frac{b^2}{a^2}}}\right)\end{aligned} \tag{12.31}$$

The magnetic field inside the ellipsoidal MO is uniform and parallel to the semimajor axis. The Cartesian-coordinate magnetic field components outside the ellipsoidal MO, $\mathbf{H}_{x,y,z}^+$, are obtained by taking the gradient of ϕ^+ given by Eq. (12.27):

$$\mathbf{H}_{x,y,z}^+ = -\nabla\phi^+ = -\sum_{j=1}^{3}\frac{\delta\phi^+}{\delta u^j}\mathbf{i}_j \tag{12.32}$$

where

$$u^1 = x \qquad u^2 = y \qquad u^3 = z \tag{12.33}$$

Substitution of Eq. (12.27) into Eq. (12.32) gives [6]

$$\mathbf{H}_x^+ = -\frac{3e\hbar}{8\pi m_e\left(a^2-b^2\right)^{3/2}}\left(\frac{1}{2}\ln\frac{\eta+1}{\eta-1}-\frac{\eta}{\eta^2-\xi^2}\right) \tag{12.34}$$

$$\mathbf{H}_y^+ = \frac{3e\hbar}{8\pi m_e\left(a^2-b^2\right)^{3/2}}\frac{\xi\sqrt{1-\xi^2}}{\sqrt{\eta^2-1}\left(\eta^2-\xi^2\right)}\cos\theta \tag{12.35}$$

$$\mathbf{H}_z^+ = \frac{3e\hbar}{8\pi m_e\left(a^2-b^2\right)^{3/2}}\frac{\xi\sqrt{1-\xi^2}}{\sqrt{\eta^2-1}\left(\eta^2-\xi^2\right)}\sin\theta \tag{12.36}$$

where

$$\theta = \arctan\frac{z}{y} \tag{12.37}$$

A plot of the field lines of the magnetic dipole due to a resonant Larmor excitation of the prolate-spheroidal H_2^+ MO is shown in Figures 12.1A-C.

Figure 12.1A. The two-dimensional cross-section of the field lines of the magnetic dipole due to a resonant Larmor excitation of the prolate-spheroidal H_2^+ MO. The internal field is uniform, and the field external to the prolate spheroidal MO is a dipole field.

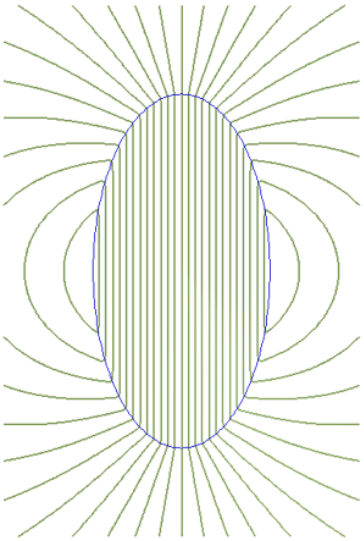

Figure 12.1B. The field lines of the magnetic dipole due to a resonant Larmor excitation of the prolate-spheroidal H_2^+ MO. The field external to the prolate spheroidal MO is a dipole field.

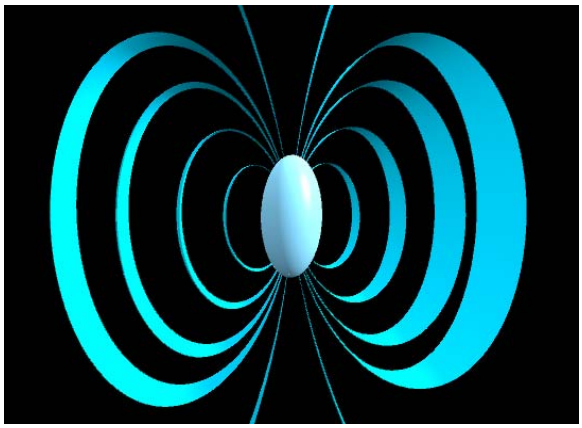

Figure 12.1C. The field lines of the magnetic dipole due to a resonant Larmor excitation of the prolate-spheroidal H_2^+ MO with the MO partially cut-away to show the uniform internal field lines.

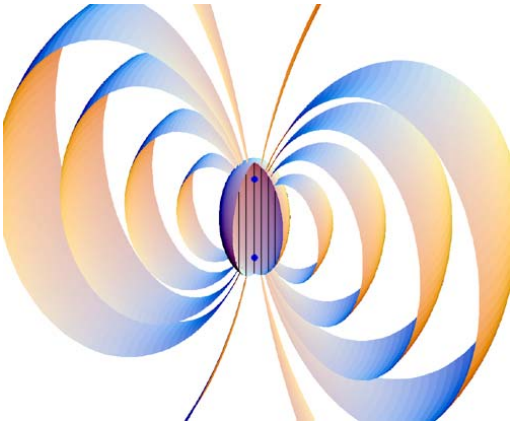

Chapter 12

EXCITED STATES OF THE HYDROGEN MOLECULE

FORCE BALANCE OF THE EXCITED STATES OF THE HYDROGEN MOLECULE

In the mathematical limit, as the eccentricity goes to zero the hydrogen molecule becomes the helium atom. The excited states of the hydrogen molecule are determined by the same physics as those of the helium atom. It was shown in the Excited States of Helium section that the inner atomic orbital is essentially that of He^+ for all excited states with the exact result upon ionization. The infinite H_2 excited state corresponds to a free electron with the inner MO and protons comprising H_2^+. Implicit in the calculation of the energy of the outer electron of each H_2 excited state is that the inner electron has the geometrical parameters, component energies, and the total energy of H_2^+ as shown to very good approximation for the inner atomic electron of helium excited states. For H_2, the excited-state photon's two-dimensional ellipsoidal electric field at the outer electron superimposes that of the field of the nuclei at the foci of the inner MO and inner MO charge such that the resultant electric field has a magnitude e/n in the direction of $\mathbf{i}_\xi$ at the outer electron where $n = 2,3,4,...$ for excited states. Then, the force balance of the outer excited-state electron is given by the balance between the centrifugal force, the central Coulombic force corresponding to the effective central field due to the superposition of the photon field at the outer electron and the net field of the protons at the foci of the inner MO, and the magnetic forces for the particular spin and orbital state. The geometrical parameters for H_2 are determined from the semimajor axis given by the force balance and the relationships among the ellipsoidal parameters. The energies corresponding to the excited electron are given by the prolate spheroidal energy equations given in the Derivation of the General Geometrical and Energy Equations of Organic Chemistry section except for a 1/2 correction corresponding to a single electron, and the electric terms are scaled according to the effective central field of $1/n$.

SINGLET EXCITED STATES

$\ell = 0$

The force balance between the electric, magnetic, and centrifugal forces of the outer electron given by Eqs. (9.10) and (11.285) is:

$$\frac{\hbar^2}{m_e a^2 b^2} D = \frac{1}{n} \frac{e^2}{8\pi\varepsilon_0 a b^2} D + \frac{1}{n} \frac{2m}{3} \frac{1}{2} \frac{\hbar^2}{2 m_e a^2 b^2} D \tag{12.38}$$

where the geometrical factor due to the electron rotation about the semimajor axis is given by Eq. (11.391) and m is a positive or negative integer wherein the inner and outer electron may rotate relative to each other to quantized the magnetic force such that net relative motion obeys the condition $\ell = 0$. The parametric solution given by Eq. (11.83) occurs when semimajor axis, a, is:

$$a = a_0 \left(2n - \frac{m}{3} \right) \tag{12.39}$$

The internuclear distance, $2c'$, which is the distance between the foci is given by Eq. (11.79) where $p = 1/n$.

$$2c' = 2\sqrt{\frac{a a_0}{2p}} = 2a_0 \sqrt{\frac{n\left(2n - \frac{m}{3} \right)}{2}} \tag{12.40}$$

The semiminor axis is given by Eq. (11.80).

$$b = \sqrt{a^2 - c'^2} = a_0 \left(2n - \frac{m}{3} \right) \sqrt{1 - \frac{n}{2\left(2n - \frac{m}{3} \right)}} \tag{12.41}$$

The eccentricity, e, is given by Eq. (11.67).

$$e = \frac{c'}{a} = \sqrt{\frac{n}{2\left(2n - \frac{m}{3} \right)}} \tag{12.42}$$

$\ell \neq 0$

The excited singlet states of the hydrogen molecule for $\ell \neq 0$ are solved using the same approach as those of the excited states of the helium atom given in the corresponding section, wherein the force balance due to the $a_{Mag}(\ell, m)$ terms corresponding to prolate spheroid geometry rather than spherical are also associated Legendre functions or spherical harmonics with regard to the semimajor axis as given by Li, Kang, and Leong [8].

The magnetic forces comprise the component of Eq. (12.38) corresponding to the nondynamic current and the $a_{Mag}(\ell, m)$ component due to the time dynamic modulation current and its interaction with electron spin. The force balance between the electric, magnetic, and centrifugal forces of the outer electron given by Eqs. (12.38) and (9.52) is

$$\frac{\hbar^2}{m_e a^2 b^2} D = \frac{1}{n}\frac{e^2}{8\pi\varepsilon_0 a b^2} D + \frac{1}{n}\frac{m}{3}\frac{\hbar^2}{2m_e a^2 b^2} D - \frac{1}{n}\frac{\frac{3}{2}}{(2\ell+1)!!}\left(\frac{\ell+1}{\ell}\right)^{1/2}\frac{1}{\ell+2}\frac{1}{2}\frac{\hbar^2}{m_e a^2 b^2}\left(1-\sqrt{\frac{\ell}{\ell+1}}\right) D \tag{12.43}$$

where the $\sqrt{3/4}$ and r^{-3} terms are replaced by one and $Da^{-2}b^{-2}$ as given in the Force Balance of Hydrogen-Types Molecules section. The parametric solution given by Eq. (11.83) occurs when semimajor axis, a, is:

$$a = a_0\left(2n - \frac{m}{3} + \frac{\frac{3}{2}}{(2\ell+1)!!}\left(\frac{\ell+1}{\ell}\right)^{1/2}\frac{1}{\ell+2}\left(1-\sqrt{\frac{\ell}{\ell+1}}\right)\right) \tag{12.44}$$

The internuclear distance, $2c'$, which is the distance between the foci is given by Eq. (11.79) where $p = 1/n$.

$$2c' = 2\sqrt{\frac{aa_0}{2p}} = 2a_0\sqrt{\frac{n\left(2n - \frac{m}{3} + \frac{\frac{3}{2}}{(2\ell+1)!!}\left(\frac{\ell+1}{\ell}\right)^{1/2}\frac{1}{\ell+2}\left(1-\sqrt{\frac{\ell}{\ell+1}}\right)\right)}{2}} \tag{12.45}$$

The semiminor axis is given by Eq. (11.80).

$$b = \sqrt{a^2 - c'^2} = a_0\left(\left(2n - \frac{m}{3} + \frac{\frac{3}{2}}{(2\ell+1)!!}\left(\frac{\ell+1}{\ell}\right)^{1/2}\frac{1}{\ell+2}\left(1-\sqrt{\frac{\ell}{\ell+1}}\right)\right)\sqrt{1-\frac{n}{2\left(2n - \frac{m}{3} + \frac{\frac{3}{2}}{(2\ell+1)!!}\left(\frac{\ell+1}{\ell}\right)^{1/2}\frac{1}{\ell+2}\left(1-\sqrt{\frac{\ell}{\ell+1}}\right)\right)}}\right) \tag{12.46}$$

The eccentricity, e, is given by Eq. (11.67).

$$e = \frac{c'}{a} = \sqrt{\frac{n}{2\left(2n - \frac{m}{3} + \frac{\frac{3}{2}}{(2\ell+1)!!}\left(\frac{\ell+1}{\ell}\right)^{1/2}\frac{1}{\ell+2}\left(1-\sqrt{\frac{\ell}{\ell+1}}\right)\right)}} \tag{12.47}$$

TRIPLET EXCITED STATES

$\ell = 0$

The force-balance equation and semimajor-axis solution of triplet excited states for $\ell = 0$ are equivalent to those of the corresponding singlet excited states given by Eqs. (12.38-12.39). However, due to the triplet spin state, the magnetic force in Eq. (12.38) is increased by a factor of two as in the case of the corresponding helium excited states given in Eq. (9.31). Thus, m is replaced by $2m$. Then, the force balance between the electric, magnetic, and centrifugal forces of the outer electron is

$$\frac{\hbar^2}{m_e a^2 b^2} D = \frac{1}{n}\frac{e^2}{8\pi\varepsilon_0 a b^2} D + \frac{1}{n}\frac{4m}{3}\frac{1}{2}\frac{\hbar^2}{2m_e a^2 b^2} D \tag{12.48}$$

The parametric solution given by Eq. (11.83) occurs when semimajor axis, a, is:

$$a = a_0\left(2n - \frac{2m}{3}\right) \tag{12.49}$$

The internuclear distance, $2c'$, which is the distance between the foci is given by Eq. (11.79) where $p = 1/n$.

$$2c' = 2\sqrt{\frac{aa_0}{2p}} = 2a_0\sqrt{\frac{n\left(2n - \frac{2m}{3}\right)}{2}} \tag{12.50}$$

The semiminor axis is given by Eq. (11.80).

$$b = \sqrt{a^2 - c'^2} = a_0\left(2n - \frac{2m}{3}\right)\sqrt{1-\frac{n}{2\left(2n - \frac{2m}{3}\right)}} \tag{12.51}$$

The eccentricity, e, is given by Eq. (11.67).

$$e = \frac{c'}{a} = \sqrt{\frac{n}{2\left(2n - \frac{2m}{3}\right)}} \tag{12.52}$$

$\ell \neq 0$

The magnetic forces of triplet excited molecular states having $\ell \neq 0$ comprise the nondynamic-current component of Eq. (12.43) with the parameter m of the magnetic force of Eq. (12.38) increased by a factor of two and the $a_{Mag}\left(\ell,m\right)$ component due to the time dynamic modulation current and its interaction with electron spin. The latter is solved using the same approach as that of the triplet excited states of the helium atom given in the corresponding section. The force balance between the electric, magnetic, and centrifugal forces of the outer electron given by Eqs. (12.48) and (9.63) is

$$\frac{\hbar^2}{m_e a^2 b^2} D = \frac{1}{n}\frac{e^2}{8\pi\varepsilon_0 a b^2} D + \frac{1}{n}\frac{2m}{3}\frac{\hbar^2}{2m_e a^2 b^2} D + \frac{1}{n}\frac{\frac{3}{2}}{(2\ell+1)!!}\left(\frac{\ell+1}{\ell}\right)^{1/2}\frac{1}{\ell+2}\frac{1}{2}\frac{\hbar^2}{m_e a^2 b^2}\left(2-\sqrt{\frac{\ell}{\ell+1}}\right) D \tag{12.53}$$

where the $\sqrt{3/4}$ and r^{-3} terms are replaced by one and $Da^{-2}b^{-2}$ as given in the Force Balance of Hydrogen-Types Molecules section. The parametric solution given by Eq. (11.83) occurs when semimajor axis, a, is:

$$a = a_0\left(2n - \frac{2m}{3} - \frac{\frac{3}{2}}{(2\ell+1)!!}\left(\frac{\ell+1}{\ell}\right)^{1/2}\frac{1}{\ell+2}\left(2-\sqrt{\frac{\ell}{\ell+1}}\right)\right) \tag{12.54}$$

The internuclear distance, $2c'$, which is the distance between the foci is given by Eq. (11.79) with the 2 factor and $p = 1/n$.

$$2c' = 2\sqrt{\frac{aa_0}{2p}} = 2a_0\sqrt{\frac{n\left(2n - \frac{2m}{3} - \frac{\frac{3}{2}}{(2\ell+1)!!}\left(\frac{\ell+1}{\ell}\right)^{1/2}\frac{1}{\ell+2}\left(2-\sqrt{\frac{\ell}{\ell+1}}\right)\right)}{2}} \tag{12.55}$$

The semiminor axis is given by Eq. (11.80).

$$b = \sqrt{a^2 - c'^2} = a_0\left(\left(2n - \frac{2m}{3} - \frac{\frac{3}{2}}{(2\ell+1)!!}\left(\frac{\ell+1}{\ell}\right)^{1/2}\frac{1}{\ell+2}\left(2-\sqrt{\frac{\ell}{\ell+1}}\right)\right)\sqrt{1 - \frac{n}{2\left(2n - \frac{2m}{3} - \frac{\frac{3}{2}}{(2\ell+1)!!}\left(\frac{\ell+1}{\ell}\right)^{1/2}\frac{1}{\ell+2}\left(2-\sqrt{\frac{\ell}{\ell+1}}\right)\right)}}\right) \tag{12.56}$$

The eccentricity, e, is given by Eq. (11.67).

$$e = \frac{c'}{a} = \sqrt{\frac{n}{2\left(2n - \frac{2m}{3} - \frac{\frac{3}{2}}{(2\ell+1)!!}\left(\frac{\ell+1}{\ell}\right)^{1/2}\frac{1}{\ell+2}\left(2-\sqrt{\frac{\ell}{\ell+1}}\right)\right)}} \tag{12.57}$$

ENERGIES OF THE EXCITED STATES OF THE HYDROGEN MOLECULE

The component energies of the outer electron of the hydrogen molecule of the excited state corresponding to quantum number n are given by Eqs. (11.290-11.293) and (11.233-11.236) where the energies are each multiplied by a factor of 1/2 since the outer MO comprises only one electron, and those corresponding to charge are multiplied by effective-charge factor of $1/n$:

$$V_e = \frac{1}{n}\frac{1}{2}\frac{-2e^2}{8\pi\varepsilon_0\sqrt{a^2-b^2}}\ln\frac{a+\sqrt{a^2-b^2}}{a-\sqrt{a^2-b^2}} \tag{12.58}$$

$$V_p = 0 \tag{12.59}$$

$$T = \frac{1}{2}\frac{\hbar^2}{2m_e a\sqrt{a^2-b^2}}\ln\frac{a+\sqrt{a^2-b^2}}{a-\sqrt{a^2-b^2}} \tag{12.60}$$

$$V_m = \frac{1}{n}\frac{1}{2}\frac{-\hbar^2}{4m_e a\sqrt{a^2-b^2}}\ln\frac{a+\sqrt{a^2-b^2}}{a-\sqrt{a^2-b^2}} \tag{12.61}$$

$$\bar{E}_{osc}\left(H_2\right) = \bar{E}_D + \bar{E}_{Kvib} = -\left(V_e + T + V_m + V\right)\sqrt{\frac{2\hbar\sqrt{\frac{1}{n^4}\frac{1}{2}\frac{e^2}{4\pi\varepsilon_0 a_0^3}}}{m_e}}\frac{}{m_e c^2} + \bar{E}_{Kvib} \tag{12.62}$$

where with regard to Eq. (12.62), the angular frequency of reentrant oscillation ω and corresponding energies E_K, $\bar{E}_D$, and $\bar{E}_{osc}$ are given by Eqs. (11.233-11.236) with $p = 1/n$ and the factor of 1/2 was applied since the outer MO comprises only one electron. The potential energy, V_p, due to proton-proton repulsion (Eq. 12.59)) is zero. The repulsive term applies only to the total energy of H_2^+ which is implicit in the calculation of the energy of the outer electron of the H_2 excited state as in the case with the energy of the helium excited states given in the Excited States of Helium section. The total energy, E_T, for the hydrogen molecular excited state given by Eqs. (11.239-11.240) is:

$$E_T = V_e + T + V_m + V_p + \bar{E}_{osc} \tag{12.63}$$

$$E_T = -\left\{\left(\frac{-e^2}{8\pi\varepsilon_0} - \frac{n\hbar^2}{4m_e a} + \frac{\hbar^2}{8m_e a}\right)\frac{1}{n\sqrt{a^2-b^2}}\ln\frac{a+\sqrt{a^2-b^2}}{a-\sqrt{a^2-b^2}}\left[1+\sqrt{\frac{2\hbar\sqrt{\frac{e^2}{n^4 8\pi\varepsilon_0 a_0^3}}}{m_e c^2}}\right] - \bar{E}_{Kvib}\right\} \tag{12.64}$$

The negative of Eq. (12.64) is the ionization energy of the excited state of H_2. The energy T_e from the $n=1$ state (also referred to as the state X) to the energy of the n^{th} excited state is given by the sum of E_T given by Eq. (12.64) and IP_1 of H_2 given by Eq. (11.298):

$$T_e(H_2) = E_T + 15.4248\ eV \tag{12.65}$$

The geometrical (Eqs. (12.38-12.55) and energy (Eqs. (12.56-12.62)) parameters of singlet and triplet excited states of molecular hydrogen are given in Tables 12.1 and 12.2, respectively, where $\bar{E}_{Kvib}$ was given to very good approximation by ω_e of H_2^+ (the $n=\infty$ state) since there is a close match with ω_e of each excited state [9]. The color scale, translucent views of the charge densities of exemplary ellipsoidal spherical harmonics that modulate the time independent spin function are shown in Figure 12.2. The modulation functions propagate about the major axis as spatially and temporally harmonic charge-density waves.

Figure 12.2. Overhead-view of exemplary color scale, translucent views of the charge-densities of the inner and outer electrons of molecular-hydrogen excited states. The outer-electron orbital function modulates the time-constant (spin) function, (shown for t = 0; three-dimensional view). The inner electron is essentially that of H_2^+ (nuclei red, not to scale).

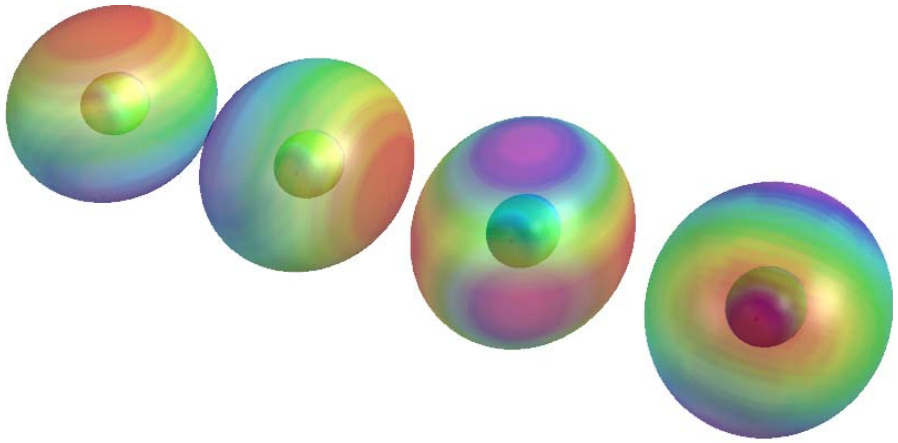

Table 12.1. The geometrical and energy parameters of the singlet excited states of molecular hydrogen compared to the experimental energies [9].

n	m	l	$a\,(a_0)$	$a\,(m)$	$b,c\,(m)$	$c'\,(m)$	$2c'\,(m)$	e	$V_e\,(eV)$	$V_p\,(eV)$	$T\,(eV)$	$V_m\,(eV)$	$E_T(H_2MO)\,(eV)$	$\bar{E}_{Kvib}\,(eV)$	$\omega\,(10^{15}\,rad/s)$	$E_K\,(eV)$	$\bar{E}_D\,(eV)$	$\bar{E}_{osc}\,(eV)$	$IP_1(H_2)\,(eV)$	$Cal.\,T_e\,(eV)$	$Exp.\,T_e\,(eV)$	State	$Exp.\,T_e\,(cm^{-1})$	Relative Error
2	4	1	2.73570	1.44767E-10	1.15312E-10	8.75257E-11	1.75051E-10	0.60460	-5.76118	0	2.10592	-0.52648	-4.18174	0.28479	7.30819	4.81038	-1.81447E-02	0.12425	15.424814	11.3673	11.36819	B	91689.9	0.00008
2	1	1	3.73570	1.97685E-10	1.69169E-10	1.02279E-10	2.04558E-10	0.51739	-4.03193	0	1.07930	-0.26982	-3.22245	0.28479	7.30819	4.81038	-1.39823E-02	0.12841	15.424814	12.3308	12.40385	C	100043.0	0.00589
2	0	0	4.00000	2.11671E-10	1.83312E-10	1.05835E-10	2.11671E-10	0.50000	-3.73688	0	0.93422	-0.23355	-3.03621	0.28479	7.30819	4.81038	-1.31742E-02	0.12922	15.424814	12.5178	12.40631	E	100062.8	-0.00899
2	-2	0	4.66667	2.46949E-10	2.18897E-10	1.14315E-10	2.28631E-10	0.46291	-3.15548	0	0.67618	-0.16904	-2.64835	0.28479	7.30819	4.81038	-1.14913E-02	0.13091	15.424814	12.9074	12.82999	F	103480	-0.00603
3	4	0	4.66667	2.46949E-10	2.03426E-10	1.40007E-10	2.80014E-10	0.56695	-2.20446	0	0.70858	-0.11810	-1.61398	0.28479	3.24809	2.13795	-4.66874E-03	0.13773	15.424814	13.9486	13.96780	K	112657	0.00138
3	4	1	4.73570	2.50603E-10	2.07146E-10	1.41039E-10	2.82078E-10	0.56280	-2.16761	0	0.68657	-0.11443	-1.59546	0.28479	3.24809	2.13795	-4.61517E-03	0.13778	15.424814	13.9671	13.98466	G	112793	0.00125
3	3	0	5.00000	2.64589E-10	2.21371E-10	1.44921E-10	2.89842E-10	0.54772	-2.03734	0	0.61120	-0.10187	-1.52801	0.28479	3.24809	2.13795	-4.42004E-03	0.13798	15.424814	14.0348	14.01839	I	113065	-0.00117
3	3	2	5.00562	2.64886E-10	2.21673E-10	1.45003E-10	2.90005E-10	0.54742	-2.03474	0	0.60974	-0.10162	-1.52663	0.28479	3.24809	2.13795	-4.41606E-03	0.13798	15.424814	14.0362	14.02818	Q	113144	-0.00057
3	3	1	5.06904	2.68242E-10	2.25081E-10	1.45918E-10	2.91836E-10	0.54398	-2.00588	0	0.59357	-0.09893	-1.51124	0.28479	3.24809	2.13795	-4.37155E-03	0.13803	15.424814	14.0516	14.06042	J	113404	0.00063
3	2	0	5.33333	2.82228E-10	2.39270E-10	1.49674E-10	2.99348E-10	0.53033	-1.89402	0	0.53269	-0.08878	-1.45011	0.28479	3.24809	2.13795	-4.19471E-03	0.13820	15.424814	14.1129	14.12043	D	113888	0.00053
3	2	1	5.40237	2.85881E-10	2.42973E-10	1.50639E-10	3.01279E-10	0.52693	-1.86685	0	0.51834	-0.08639	-1.43490	0.28479	3.24809	2.13795	-4.15070E-03	0.13825	15.424814	14.1282	14.12055	H	113889	-0.00054
3	1	0	5.66667	2.99867E-10	2.57134E-10	1.54280E-10	3.08561E-10	0.51450	-1.76971	0	0.46845	-0.07808	-1.37933	0.28479	3.24809	2.13795	-3.98998E-03	0.13841	15.424814	14.1839	14.19631	L	114500	0.00087
3	1	1	5.73570	3.03520E-10	2.60830E-10	1.55217E-10	3.10434E-10	0.51139	-1.74599	0	0.45661	-0.07610	-1.36548	0.28479	3.24809	2.13795	-3.94992E-03	0.13845	15.424814	14.1978	14.21540	M	114654	0.00124
3	-3	1	7.06904	3.74077E-10	3.32025E-10	1.72316E-10	3.44633E-10	0.46064	-1.38755	0	0.29443	-0.04907	-1.14219	0.28479	3.24809	2.13795	-3.30401E-03	0.13909	15.424814	14.4217	14.41551	N	116268	-0.00043
4	4	1	6.73570	3.56438E-10	2.98872E-10	1.94226E-10	3.88452E-10	0.54491	-1.13268	0	0.33632	-0.04204	-0.83840	0.28479	1.82705	1.20259	-1.81892E-03	0.14058	15.424814	14.7270	14.71581	R	118690	-0.00076
4	1	2	7.67229	4.06000E-10	3.49094E-10	2.07290E-10	4.14580E-10	0.51057	-0.97861	0	0.25510	-0.03189	-0.75539	0.28479	1.82705	1.20259	-1.63883E-03	0.14076	15.424814	14.8102	14.81549	T	119494	0.00036
4	1	1	7.73570	4.09356E-10	3.52488E-10	2.08145E-10	4.16290E-10	0.50847	-0.96969	0	0.25070	-0.03134	-0.75032	0.28479	1.82705	1.20259	-1.62783E-03	0.14077	15.424814	14.8153	14.81772	P	119512	0.00017
4	-1	0	8.33333	4.40981E-10	3.84438E-10	2.16036E-10	4.32071E-10	0.48990	-0.89305	0	0.21433	-0.02679	-0.70551	0.28479	1.82705	1.20259	-1.53061E-03	0.14087	15.424814	14.8602	14.85591	S	119820	-0.00029
4	-1	1	8.40237	4.44634E-10	3.88126E-10	2.16929E-10	4.33857E-10	0.48788	-0.88497	0	0.21065	-0.02633	-0.70066	0.28479	1.82705	1.20259	-1.52008E-03	0.14088	15.424814	14.8650	14.85975	O	119851	-0.00036
																						Avg. Rel. Error		-0.00035

Table 12.2. The geometrical and energy parameters of the triplet excited states of molecular hydrogen compared to the experimental energies [9].

n	m	l	$a\,(a_0)$	$a\,(m)$	$b,c\,(m)$	$c'\,(m)$	$2c'\,(m)$	e	$V_e\,(eV)$	$V_p\,(eV)$	$T\,(eV)$	$V_m\,(eV)$	$E_T(H_2MO)\,(eV)$	$\bar{E}_{Kvib}\,(eV)$	$\omega\,(10^{15}\,rad/s)$	$E_K\,(eV)$	$\bar{E}_D\,(eV)$	$\bar{E}_{osc}\,(eV)$	$IP_1(H_2)\,(eV)$	$Cal.\,T_e\,(eV)$	$Exp.\,T_e\,(eV)$	State	$Exp.\,T_e\,(cm^{-1})$	Relative Error
2	1	1	3.02860	1.60266E-10	1.31165E-10	9.20919E-11	1.84184E-10	0.57462	-5.11612	0	1.68927	-0.42232	-3.84916	0.28479	7.30819	4.81038	-1.67016E-02	0.12570	15.424814	11.7013	11.87084	c	95744	0.01428
2	1	0	3.33333	1.76392E-10	1.47580E-10	9.66141E-11	1.93228E-10	0.54772	-4.58402	0	1.37520	-0.34380	-3.55261	0.28479	7.30819	4.81038	-1.54149E-02	0.12698	15.424814	11.9992	11.89489	a	95938	-0.00877
3	4	1	3.02860	1.60266E-10	1.13859E-10	1.12789E-10	2.25578E-10	0.70376	-3.72248	0	1.84367	-0.30728	-2.18609	0.28479	3.24809	2.13795	-6.32367E-03	0.13607	15.424814	13.3748	13.36275	e	107777	-0.00090
3	2	2	4.63043	2.45032E-10	2.01471E-10	1.39462E-10	2.78925E-10	0.56916	-2.22432	0	0.72056	-0.12009	-1.62386	0.28479	3.24809	2.13795	-4.69732E-03	0.13770	15.424814	13.9387	13.97338	d	112702	0.00249
3	2	0	4.56667	2.46949E-10	2.03426E-10	1.40007E-10	2.80014E-10	0.56695	-2.20446	0	0.70858	-0.11810	-1.61398	0.28479	3.24809	2.13795	-4.66874E-03	0.13773	15.424814	13.9486	13.98181	h	112770	0.00238
3	1	1	5.02860	2.66102E-10	2.22908E-10	1.45335E-10	2.90670E-10	0.54616	-2.02419	0	0.60380	-0.10063	-1.52102	0.28479	3.24809	2.13795	-4.39984E-03	0.13800	15.424814	14.0418	13.98268	g	112777	-0.00423
3	1	2	5.29710	2.80310E-10	2.37326E-10	1.49165E-10	2.98329E-10	0.53214	-1.90861	0	0.54047	-0.09008	-1.45822	0.28479	3.24809	2.13795	-4.21816E-03	0.13818	15.424814	14.1048	14.01132	i	113008	-0.00667
3	1	0	5.33333	2.82228E-10	2.39270E-10	1.49674E-10	2.99348E-10	0.53033	-1.89402	0	0.53269	-0.08878	-1.45011	0.28479	3.24809	2.13795	-4.19471E-03	0.13820	15.424814	14.1129	14.03488	j	113198	-0.00556
4	4	1	5.02860	2.66102E-10	2.06512E-10	1.67818E-10	3.35637E-10	0.63065	-1.59277	0	0.63349	-0.07919	-1.03847	0.28479	1.82705	1.20259	-2.25298E-03	0.14014	15.424814	14.5265	14.47007	f	116708	-0.00390
4	3	1	5.59526	3.01380E-10	2.42762E-10	1.78596E-10	3.57193E-10	0.59260	-1.37400	0	0.48251	-0.06031	-0.95181	0.28479	1.82705	1.20259	-2.06497E-03	0.14033	15.424814	14.6133	14.66658	v	118293	0.00363
4	3	2	5.96376	3.15589E-10	2.57285E-10	1.82758E-10	3.65516E-10	0.57910	-1.30225	0	0.43672	-0.05459	-0.92012	0.28479	1.82705	1.20259	-1.99621E-03	0.14040	15.424814	14.6451	14.67625	k	118371	0.00212
4	2	1	6.36193	3.36659E-10	2.78763E-10	1.88760E-10	3.77520E-10	0.56069	-1.20882	0	0.38002	-0.04750	-0.87630	0.28479	1.82705	1.20259	-1.90115E-03	0.14050	15.424814	14.6890	14.68915	p	118475	0.00001
4	2	0	6.56667	3.52785E-10	2.95161E-10	1.93228E-10	3.86456E-10	0.54772	-1.14600	0	0.34380	-0.04298	-0.84518	0.28479	1.82705	1.20259	-1.83363E-03	0.14056	15.424814	14.7202	14.69250	s	118502	-0.00189
4	1	1	7.02860	3.71937E-10	3.14600E-10	1.98404E-10	3.96808E-10	0.53343	-1.07948	0	0.30717	-0.03840	-0.81070	0.28479	1.82705	1.20259	-1.75884E-03	0.14064	15.424814	14.7547	14.70155	r	118575	-0.00362
4	1	0	7.33333	3.88063E-10	3.30941E-10	2.02659E-10	4.05319E-10	0.52223	-1.02923	0	0.28070	-0.03509	-0.78362	0.28479	1.82705	1.20259	-1.70007E-03	0.14070	15.424814	14.7819	14.79379	m	119319	0.00080
5	3	1	7.59526	4.07216E-10	3.34593E-10	2.32104E-10	4.64208E-10	0.56998	-0.80341	0	0.26101	-0.02610	-0.56850	0.28479	1.16931	0.76966	-9.86698E-04	0.14141	15.424814	14.9977	14.99651	n	120954	-0.00008
5	3	2	7.96376	4.21424E-10	3.49065E-10	2.36119E-10	4.72237E-10	0.56029	-0.77238	0	0.24247	-0.02425	-0.55416	0.28479	1.16931	0.76966	-9.61808E-04	0.14143	15.424814	15.0121	15.01449	q	121099	0.00016
5	2	1	8.36193	4.42494E-10	3.70488E-10	2.41949E-10	4.83898E-10	0.54679	-0.73059	0	0.21843	-0.02184	-0.53401	0.28479	1.16931	0.76966	-9.26832E-04	0.14147	15.424814	15.0323	15.03879	t	121295	0.00043
6	-4	0	14.66667	7.76126E-10	6.92214E-10	3.51016E-10	7.02033E-10	0.45227	-0.33334	0	0.06818	-0.00568	-0.27084	0.28479	0.812021	0.53449	-3.91731E-04	0.14201	15.424814	15.2960	15.31031	u	123485	0.00094
																						Avg. Rel. Error		-0.00044

DIATOMIC MOLECULAR ROTATION

A molecule with a permanent dipole moment can resonantly absorb a photon, which excites a rotational mode about the center of mass of the molecule. Momentum must be conserved with excitation of a rotational mode. The photon carries $\hbar$ of angular momentum; thus, the rotational angular momentum of the molecule changes by $\hbar$. And, the rotational charge-density function is equivalent to the rigid rotor problem considered in the Rotational Parameters of the Electron (Angular Momentum, Rotational Energy, Moment of Inertia) section with the exception that for a diatomic molecule having atoms of masses m_1 and m_2, the moment of inertia is:

$$I = \mu r^2 \tag{12.66}$$

where μ is the reduced mass

$$\mu = \frac{m_1 m_2}{m_1 + m_2} \tag{12.67}$$

and where r is the distance between the centers of the atoms, the internuclear distance. The rotational energy levels follow from Eq. (1.71)

$$E_{rotational\ orbital} = \frac{\hbar^2}{2I} J(J+1) \tag{12.68}$$

where J is an integer. For Eq. (12.68), $J = 0$ corresponds to rotation about the z-axis where the internuclear axis is along the x-axis, and $J \neq 0$ corresponds to a linear combination of rotations about the z and y-axis (Figure 11.4).

As given in the Selection Rules section, the radiation of a multipole of order (ℓ, m_ℓ) carries $m\hbar$ units of the z component of angular momentum per photon of energy $\hbar\omega$. Thus, the z component of the angular momentum of the corresponding excited rotational state is

$$L_z = m\hbar \tag{12.69}$$

Thus, the selection rule for rotational transitions is:

$$\Delta J = \pm 1 \tag{12.70}$$

In addition, the molecule must possess a permanent dipole moment. In the case of absorption of electromagnetic radiation, the molecule goes from a state with a quantum number J to one with a quantum number of $J+1$. Using Eq. (12.68), the energy difference is:

$$\Delta E = E_{J+1} - E_J = \frac{\hbar^2}{I}\left[J+1\right] \tag{12.71}$$

DIATOMIC MOLECULAR ROTATION OF HYDROGEN-TYPE MOLECULES

The reduced mass of hydrogen-type molecular ions and molecules, μ_{H_2}, having two protons is given by Eq. (12.67) where $m_1 = m_2 = m_p$, and m_p is the mass of the proton.

$$\mu_{H_2} = \frac{m_p m_p}{m_p + m_p} = \frac{1}{2} m_p \tag{12.72}$$

The moment of inertia of hydrogen-type molecules is given by substitution of the reduced mass (Eq. (12.72)) for μ of Eq. (12.66) and substitution of the internuclear distance (Eq. (11.204)) for r of Eq. (12.66).

$$I = m_p \frac{a_0^2}{p^2} \tag{12.73}$$

where p is an integer which corresponds to $H_2(1/p)$. The Doppler energy term, $\bar{E}_D$, of the bond energy (Eqs. (11.235), and (11.240-11.241)) decreases the internuclear distance, r, of Eq. (12.66), which increases the rotational energy. To determine the internuclear distance considering the correction for $\bar{E}_D$, consider that the contribution of $\bar{E}_D$ to the binding energy is one-half the magnitude of the potential energy contribution as required for an inverse-squared force [10] wherein $\bar{E}_D$ is the source of the additional binding energy term. Then, the sum of ½ $\bar{E}_D$ and the unperturbed total energy comprising the sum of the inverse-squared field terms given by Eqs. (11.207-11.211) is subtracted from the total energy given by Eqs. (11.207-11.211) with the semimajor axis a comprising a variable. The difference is equated to zero, and the resulting Eq. (12.74) is solved reiteratively for the semimajor axis a with the prolate other spheroidal dimensions dependent on the semimajor axis given by Eqs. (11.79-11.80) and (11.67).

$$\left\{\begin{aligned}&\left[\left(\frac{-2pe^2}{8\pi\varepsilon_0\sqrt{a^2-b^2}} + \frac{\hbar^2}{2m_e a\sqrt{a^2-b^2}}\frac{-\hbar^2}{4m_e a\sqrt{a^2-b^2}}\right)\ln\frac{a+\sqrt{a^2-b^2}}{a-\sqrt{a^2-b^2}} + \frac{p}{8\pi\varepsilon_0}\frac{e^2}{\sqrt{a^2-b^2}}\right]\\ &+ep^2\left(31.63536831+\left(0.5\right)p0.326469\right)\end{aligned}\right\} = 0 \tag{12.74}$$

internuclear distance for $p = 1$ is

$$2c' = 0.7411\ \text{Å} \tag{12.75}$$

Eq. (12.75) is also the internuclear distance for molecular hydrogen isotopes such as D_2. To a high degree of accuracy, the general result for hydrogen-type molecules is

$$2c' = \frac{0.7411}{p}\ \text{Å} \tag{12.76}$$

Using Eqs. (12.66), (12.71-12.72), and (12.76), the rotational energy absorbed by a hydrogen-type molecule with the transition from the state with the rotational quantum number J to one with the rotational quantum number $J+1$ is:

$$\Delta E_{J\to J+1} = E_{J+1} - E_J = \frac{p^2\hbar^2}{0.5m_p\left(7.411X10^{-11}m\right)^2}\left[J+1\right] = p^2\left[J+1\right]0.01511\ eV\ = \left[J+1\right]p^2 121.89\ cm^{-1} \tag{12.77}$$

The result of Eq. (12.77) without the correction for centrifugal distortion compares well to the experimental value of $\Delta E = 0.01509\ eV\left(121.7\ cm^{-1}\right)$ for $p=1$ [11].

Using the reduced mass for molecular deuterium which to a high level of accuracy is twice that of molecular hydrogen given by Eq. (12.72) and the internuclear distance given by Eq. (12.76) in Eq. (12.71) gives the rotational energy of deuterium-type molecules as:

$$\Delta E_{J\to J+1} = E_{J+1} - E_J = \frac{p^2\hbar^2}{m_p\left(7.411X10^{-11}m\right)^2}\left[J+1\right] = p^2\left[J+1\right]0.007557\ eV\ = \left[J+1\right]p^2 60.95\ cm^{-1} \tag{12.78}$$

The result of Eq. (12.78) without the correction for centrifugal distortion compares well to the experimental value of $\Delta E = 0.00755\ eV\left(60.90\ cm^{-1}\right)$ for $p=1$ [11].

DIATOMIC MOLECULAR ROTATION OF HYDROGEN-TYPE MOLECULAR IONS

The moment of inertia of hydrogen-type molecular ions is given by substitution of the reduced mass (Eq. (12.72)) for μ of Eq. (12.66) and substitution of the internuclear distance (Eq. (11.111)) for r of Eq. (12.66).

$$I = m_p\frac{2a_0^2}{p^2} \tag{12.79}$$

where p is an integer which corresponds to $H_2^+\left(1/p\right)$. The Doppler energy term, $\bar{E}_D$, of the bond energy (Eqs. (11.187), and (11.192-11.193)) decreases the internuclear distance, r, of Eq. (12.66), which increases the rotational energy. To determine the internuclear distance considering the correction for $\bar{E}_D$, consider that the contribution of $\bar{E}_D$ to the binding energy is one-half the magnitude of the potential energy contribution as required for an inverse-squared force [10] wherein $\bar{E}_D$ is the source of the additional binding energy term. Then, the sum of ½ $\bar{E}_D$ and the unperturbed total energy comprising the sum of the inverse-squared field terms given by Eqs. (11.117-11.121) with the semimajor axis given by Eq. (11.116) is subtracted from the total energy given by Eqs. (11.117-11.121) with the semimajor axis a comprising a variable. The difference is equated to zero, and the resulting Eq. (12.80) is solved reiteratively for the semimajor axis a with the prolate other spheroidal dimensions dependent on the semimajor axis given by Eqs. (11.79-11.80) and (11.67).

$$\left\{\begin{aligned}&\frac{-4pe^2}{8\pi\varepsilon_0\sqrt{a^2-b^2}}\ln\frac{a+\sqrt{a^2-b^2}}{a-\sqrt{a^2-b^2}} + \frac{pe^2}{8\pi\varepsilon_0\sqrt{a^2-b^2}}\\ &+\frac{2\hbar^2}{m_e a\sqrt{a^2-b^2}}\ln\frac{a+\sqrt{a^2-b^2}}{a-\sqrt{a^2-b^2}} + ep^2\left[16.28\ eV + e\left(0.5\right)p0.11875\right]\end{aligned}\right\} = 0 \tag{12.80}$$

internuclear distance for $p=1$ is

$$2c' = 1.0577\ \text{Å} \tag{12.81}$$

Eq. (12.81) is also the internuclear distance for molecular hydrogen isotopes such as D_2^+. To a high degree of accuracy, the general result for hydrogen-type molecular ions is

$$2c' = \frac{1.0577}{p}\ \text{Å} \tag{12.82}$$

Using Eqs. (12.66), (12.71-12.72), and (12.82), the rotational energy absorbed by a hydrogen-type molecular ion with the transition from the state with the rotational quantum number J to one with the rotational quantum number $J+1$ is:

$$\begin{aligned}\Delta E_{J\to J+1} = E_{J+1} - E_J &= \frac{p^2\hbar^2}{0.5m_p\left(1.0577X10^{-10}m\right)^2}\left[J+1\right]\\ &= p^2\left[J+1\right]0.00742\ eV\ = \left[J+1\right]p^2 59.84\ cm^{-1} = \left[J+1\right]p^2 167.12\ \mu m\end{aligned} \tag{12.83}$$

The result of Eq. (12.83) without the correction for centrifugal distortion is a good match to the experimentally observed wavelength of 169 μm [11]. The rotational wavelength for $p = 6$ is 4.7 μm. A broad 4.7 μm solar chromospheric absorption line is observed which was previously assigned to cool carbon monoxide clouds; however, the temperature of the chromosphere, $> 6000\ K$, is higher than that at which carbon monoxide completely decomposes into carbon and oxygen, $< 4000\ K$ [12]. The assignment of the 4.7 μm absorption line to the Doppler-broadened $J = 0$ to $J = 1$ rotational transition of $H_2^+\left[2c' = \frac{a_0}{3}\right]$ provides a resolution of the problem of cool carbon monoxide clouds.

Using the reduced mass for molecular deuterium which to a high level of accuracy is twice that of molecular hydrogen given by Eq. (12.72) and the internuclear distance given by Eq. (12.82) in Eq. (12.71) gives the rotational energy of deuterium-type molecular ions as:

$$\Delta E_{J\to J+1} = E_{J+1} - E_J = \frac{p^2\hbar^2}{m_p\left(1.0577X10^{-10}m\right)^2}\left[J+1\right] = p^2\left[J+1\right]0.0037095\ eV\ = \left[J+1\right]p^2 29.92\ cm^{-1} \tag{12.84}$$

The result of Eq. (12.84) without the correction for centrifugal distortion compares well to the experimental value of $\Delta E = 0.003723\ eV\left(30.03\ cm^{-1}\right)$ for $p = 1$ [13].

CENTRIFUGAL DISTORTION

The equilibrium internuclear distance of the hydrogen molecular ion and hydrogen molecule can increase as a result of a centrifugal force due to rotation. Since the centrifugal distortion increases as a function of J, the rotational term given by Eq. (12.68) can be added as a centrifugal potential to the harmonic oscillator potential energy relationship (Eq. (11.146)) to give $E_J(r)$, a combined potential dependent on the internuclear separation [14]. From Eq. (11.146) and Eq. (12.68),

$$E_J(r) = \frac{1}{2}k_0\left(r - r_e\right)^2 + \frac{\hbar^2}{2I}J(J+1) \tag{12.85}$$

where r_e is the equilibrium internuclear distance with $J = 0$ and k_0 is the spring constant with $\upsilon = 0$. Let r_e' be the equilibrium internuclear distance for which $E_J(r)$ is a minimum. A relationship between the distorted equilibrium internuclear distance r_e' and J is derived from $E_J(r)$ by taking the derivative with respect to r, setting the derivative equal to zero corresponding to the minimum, and evaluating the equation at r_e'. The result using Eq. (12.66) is:

$$\left.\frac{dE_J(r)}{dr}\right|_{r=r_e'} = k_0\left(r_e' - r_e\right) - \frac{\hbar^2}{\mu\left(r_e'\right)^3}J(J+1) = 0 \tag{12.86}$$

Since the deviation due to centrifugal distortion is small such that $\frac{r_e' - r_e}{r_e} << 1$, r_e' may be determined as a function of J, and r_e' may be solved from Eq. (12.86) by successive approximation. Little accuracy is lost by the first-order correction resulting from the substitution of $r_e' = r_e$ in the rotational term of Eq. (12.86) to give:

$$r_e' = r_e + \frac{hB_e}{2\pi^2\nu_0^2\mu r_e}J(J+1) \tag{12.87}$$

where

$$B_e = \frac{\hbar^2}{2I_e h} \tag{12.88}$$

and

$$\nu_0 = \frac{1}{2\pi}\left(\frac{k_0}{\mu}\right)^{1/2} \tag{12.89}$$

Then, r_e can be replaced by r_e' in the relationship for $E_J(r)$ (Eq. (12.85)) to determine the correction to the rotational energy due to centrifugal distortion.

$$E_J(r) = \frac{\hbar^2}{2\mu\left(r_e'\right)^2}J(J+1) + \frac{1}{2}k_0\left(r_e' - r_e\right)^2 \tag{12.90}$$

By substitution of r_e' given by Eq. (12.87) into Eq. (12.90), expanding the result in powers of $J(J+1)$, and retaining only the first two terms which are predominant, $E_J(r)$ is given by:

$$E_J = J(J+1)hc\tilde{B}_e - \left[J(J+1)\right]^2 hc\tilde{D}_e \tag{12.91}$$

where the centrifugal distortion term $\tilde{D}_e$ is given by:

$$\tilde{D}_e = \frac{4\tilde{B}_e^3}{\omega_0^2} \tag{12.92}$$

and

$$\tilde{B}_e = \frac{B_e}{c} = \frac{\hbar^2}{2I_e hc} \tag{12.93}$$

For most molecules, the corrections due to centrifugal distortion represented by $\tilde{D}_e$ are relatively small except for high J values. From Eqs. (11.223), (12.72),(12.75), and (12.92-12.93), $\tilde{D}_e$ for H_2 is:

$$\tilde{D}_e = \frac{4\tilde{B}_e^3}{\omega_0^2} = \frac{4\left(\frac{\hbar^2}{2I_e hc}\right)^3}{\omega_0^2} = \frac{\hbar^3}{10^6\,(2)\left(\pi\mu r_e^2 c\right)^3 \omega_0^2}$$

$$= \frac{\hbar^3}{10^6\,(2)\left(\pi m_p\left(\sqrt{2}a_0\right)^2 c\right)^3 \left(8.06573\times10^3\ \frac{cm^{-1}}{eV}0.517\ eV\right)^2} = 0.0491\ cm^{-1} \tag{12.94}$$

The experimental $\tilde{D}_e$ of H_2 [15,16] is:

$$\tilde{D}_e = 0.0465\ cm^{-1} \tag{12.95}$$

From Eq. (11.170), (11.287), (11.312), (12.66), and (12.92-12.93), $\tilde{D}_e$ for D_2 is:

$$\tilde{D}_e = \frac{4\tilde{B}_e^3}{\omega_0^2} = \frac{4\left(\frac{\hbar^2}{2I_e hc}\right)^3}{\omega_0^2} = \frac{\hbar^3}{10^6\,(2)\left(2\pi\mu r_e^2 c\right)^3 \omega_0^2}$$

$$= \frac{\hbar^3}{10^6\,(2)\left(2\pi m_p\left(\sqrt{2}a_0\right)^2 c\right)^3 \left(8.06573\times10^3\ \frac{cm^{-1}}{eV}0.371\ eV\right)^2} = 0.0119\ cm^{-1} \tag{12.96}$$

The experimental $\tilde{D}_e$ of D_2 [15,16] is:

$$\tilde{D}_e = 0.01159\ cm^{-1} \tag{12.97}$$

There is good agreement between the calculated and experimental values of $\tilde{D}_e$.

REFERENCES

1. A. Carrington, I. R. McNab, C. A. Montgomerie, Spectroscopy of the hydrogen molecular ion, J. Phys. B, 22, (1989), 3551–3586.
2. A. Carrington, I. R. McNab, C. A. Montgomerie, R. Kennedy, Electronic spectrum ($2p\sigma_u$–$1s\sigma_g$) of the D_2^+ ion, Mol. Phys., 67, (1989), 711–738.
3. C. A. Leach, R. E. Moss, Spectroscopy and quantum mechanics of the hydrogen molecular cation: A test of molecular quantum mechanics, Annu. Rev. Phys. Chem., 46, (1995), 55–82.
4. G. R. Fowles, *Analytical Mechanics*, Third Edition, Holt, Rinehart, and Winston, New York, (1977), pp. 161-164.
5. J. A. Stratton, *Electromagnetic Theory*, McGraw-Hill Book Company, (1941), pp. 211-215; 257-258.
6. H. Chang, "Fields external to open-structure magnetic devices represented by ellipsoid or spheroid," British Journal of Applied Physics, Vol. 12, (1961). pp. 160-163.
7. J. A. Stratton, *Electromagnetic Theory*, McGraw-Hill Book Company, (1941), pp. 56-59.
8. L-W. Li, X-K. Kang, M-S Leong, *Spheroidal Wave Functions in Electromagnetic Theory*, Wiley Series in Microwave and Optical Engineering, K. Chang, Editor, John Wiley & Sons, Inc., New York, (2002).
9. G. Herzberg, *Molecular Spectra and Molecular Structure I. Spectra of Diatomic Molecules*, Krieger Publishing Company, Malabar, FL, 2nd Ed., (1989), pp. 530-534.
10. G. R. Fowles, *Analytical Mechanics*, Third Edition, Holt, Rinehart, and Winston, New York, (1977), pp. 145-158.
11. P. W. Atkins, *Physical Chemistry*, 2nd Ed., W. H. Freeman, San Francisco, (1982), p. 589.
12. J. H. Phillips, *Guide to the Sun*, Cambridge University Press, Cambridge (1992), pp. 126-127; 360.
13. K. P. Huber, G. Herzberg, *Molecular Spectra and Molecular Structure, IV. Constants of Diatomic Molecules*, Van Nostrand Reinhold Company, New York, (1979).
14. M. Karplus, R. N. Porter, *Atoms and Molecules. An Introduction for Students of Physical Chemistry*, The Benjamin/Cummings Publishing Company, Menlo Park, California, (1970), pp. 480-481.
15. M. Karplus, R. N. Porter, *Atoms and Molecules. An Introduction for Students of Physical Chemistry*, The Benjamin/Cummings Publishing Company, Menlo Park, California, (1970), pp. 469.
16. G. Herzberg, *Spectra of Diatomic Molecules*, Van Nostrand, Princeton, NJ, (1950).

Chapter 13

GENERAL DIATOMIC AND POLYATOMIC MOLECULAR IONS AND MOLECULES

Non-hydrogen diatomic and polyatomic molecular ions and molecules can be solved using the similar principles as those used to solve hydrogen molecular ions and molecules wherein the hydrogen molecular orbitals (MOs) and hydrogen atomic orbitals serve as basis functions for the MOs of the general diatomic and polyatomic molecular ions or molecules. The MO must (1) be a solution of Laplace's equation to give a equipotential energy surface, (2) correspond to an orbital solution of the Newtonian equation of motion in an inverse-radius-squared central field having a constant total energy, (3) be stable to radiation, and (4) conserve the electron angular momentum of $\hbar$. Energy of the MO must be matched to that of the outermost atomic orbital of a bonding heteroatom in the case where a minimum energy is achieved with a direct bond to the atomic orbital (AO). In the case that an independent MO is formed, the AO force balance causes the remaining electrons to be at lower energy and a smaller radius. The atomic orbital may hybridize in order to achieve a bond at an energy minimum. At least one molecule or molecular ion representative of each of these cases was solved. Specifically, the results of the determination of bond parameters of H_3^+, D_3^+, OH, OD, H_2O, D_2O, NH, ND, NH_2, ND_2, NH_3, ND_3, CH, CD, CH_2, CH_3, CH_4, N_2, O_2, F_2, Cl_2, CN, CO, and NO are given in Table 13.1. The calculated results for homo- and hetero-diatomic radicals and molecules, and polyatomic molecular ions and molecules are based on first principles and given in closed-form, exact equations containing fundamental constants only. The agreement between the experimental and calculated results is excellent.

TRIATOMIC MOLECULAR HYDROGEN-TYPE ION (H_3^+)

The polyatomic molecular ion $H_3^+(1/p)$ is formed by the reaction of a proton with a hydrogen-type molecule

$$H_2(1/p)+H^+ \rightarrow H_3^+(1/p) \tag{13.1}$$

and by the exothermic reaction

$$H_2^+(1/p)+H_2(1/p) \rightarrow H_3^+(1/p)+H(1/p) \tag{13.2}$$

FORCE BALANCE OF H_3^+-TYPE MOLECULAR IONS

$H_3^+(1/p)$-type molecular ions comprise two indistinguishable spin-paired electrons bound by three protons. The ellipsoidal molecular orbital (MO) satisfies the boundary constraints as shown in the Nature of the Chemical Bond of Hydrogen-Type Molecules section. Since the protons are indistinguishable, ellipsoidal MOs about each pair of protons taken one at a time are indistinguishable. $H_3^+(1/p)$ is then given by a superposition or linear combinations of three equivalent ellipsoidal MOs that form a equilateral triangle where the points of contact between the prolate spheroids are equivalent in energy and charge density. The outer perimeter of the superposition of three prolate spheroids is the $H_3^+(1/p)$ MO with the protons at the foci that bind and maintain the electron MO.

As in the case for $H_2^+(1/p)$ and $H_2(1/p)$ shown in the Nature of the Chemical Bond of Hydrogen-Type Molecules section, the stability of $H_3^+(1/p)$ is due to the dependence of the charge density of the distance D from the origin to the tangent plane. That is,

$$D = \frac{1}{\sqrt{\frac{x^2}{a^4} + \frac{y^2}{b^4} + \frac{z^2}{c^4}}} \tag{13.3}$$

so that

$$\sigma = \frac{e}{4\pi ab^2} D \tag{13.4}$$

In other words, the surface density at any point on a charged ellipsoidal conductor is proportional to the perpendicular distance from the center of the ellipsoid to the plane tangent to the ellipsoid at the point. The charge is thus greater on the more sharply rounded ends farther away from the origin. This distribution places the charge closest to the protons to give a minimum energy.

The balanced forces also depend on D as shown in the Nature of the Chemical Bond of Hydrogen-Type Molecules section. The D-dependence of the charge density as well as the centrifugal and Coulombic central field of two nuclei at the foci of the ellipsoid applies to each ellipsoid which is given from any other by a rotation of $|\phi| = \frac{\pi}{3}$ about an axis at a focus that is perpendicular to the plane of the equilateral triangle defined by the three foci. Since the centrifugal, Coulombic, and magnetic forces relate mass and charge densities which are interchangeable by the ratio e/m_e, the conditions at any point on any given ellipsoid is applicable to any other point on the ellipsoid. Furthermore, this condition can be generalized to any point of the other members of the set of three ellipsoids due to equivalence. As a further constraint to maintain the force balance between the three protons and the $H_3^+(1/p)$ MO comprising the superposition of the three $H_2(1/p)$-type ellipsoidal MOs, the total charge of the two electrons must be normalized over the three basis set $H_2(1/p)$-type ellipsoidal MOs. In this case, the parameters of each basis element $H_2(1/p)$-type ellipsoidal MO is solved, and the energies are given by the electron charge where it appears multiplied by a factor of $3/2$ (three MOs normalized by the total charge of two electrons).

Consider each $H_2(1/p)$-type ellipsoidal MO. At each point on the $H_3^+(1/p)$ MO, the electron experiences a centrifugal force, and the balancing centripetal force (on each electron) is produced by the electric force between the electron and the ellipsoidal electric field and the radiation-reaction-type magnetic force between the two electrons causing the electrons to pair. The force balance equation derived in Force Balance of Hydrogen-Type Molecules section is given by Eq. (11.200):

$$\frac{\hbar^2}{m_e a^2 b^2} D = \frac{pe^2}{8\pi\varepsilon_0 ab^2} D + \frac{\hbar^2}{2m_e a^2 b^2} D \tag{13.5}$$

$$\frac{2a_0}{pa} - \frac{a_0}{pa} = 1 \tag{13.6}$$

$$a = \frac{a_0}{p} \tag{13.7}$$

Substitution of Eq. (13.7) into Eq. (11.79) is:

$$c' = \frac{1}{p\sqrt{2}} a_0 \tag{13.8}$$

The internuclear distance given by multiplying Eq. (13.8) by two is:

$$2c' = \frac{a_0\sqrt{2}}{p} \tag{13.9}$$

Substitution of Eqs. (13.7-13.8) into Eq. (11.80) is:

$$b = c = \frac{1}{p\sqrt{2}} a_0 \tag{13.10}$$

Substitution of Eqs. (13.7-13.8) into Eq. (11.67) is:

$$e = \frac{1}{\sqrt{2}} \tag{13.11}$$

Using the parameters given by Eqs. (13.7-13.11), the resulting $H_3^+(1/p)$ MO comprising the superposition of three $H_2(1/p)$-type ellipsoidal MOs is shown in Figure 13.1. The outer surface of the superposition comprises charge density of the MO. The equilateral triangular structure was confirmed experimentally [1]. The $H_3^+(1/p)$ MO having no distinguishable electrons is consistent with the absence of strong excited states observed for H_3^+ [1]. It is also consistent with the absence of a permanent dipole moment [1].

Figure 13.1. The equilateral triangular $H_3^+(1/p)$ MO formed by the superposition of three $H_2(1/p)$-type ellipsoidal MOs with the protons at the foci. (A)-(B) Oblique and top views of the charge-density shown in color scale showing the ellipsoid surfaces and the nuclei (red, not to scale). (C) Cross sectional view with one proton cut away.

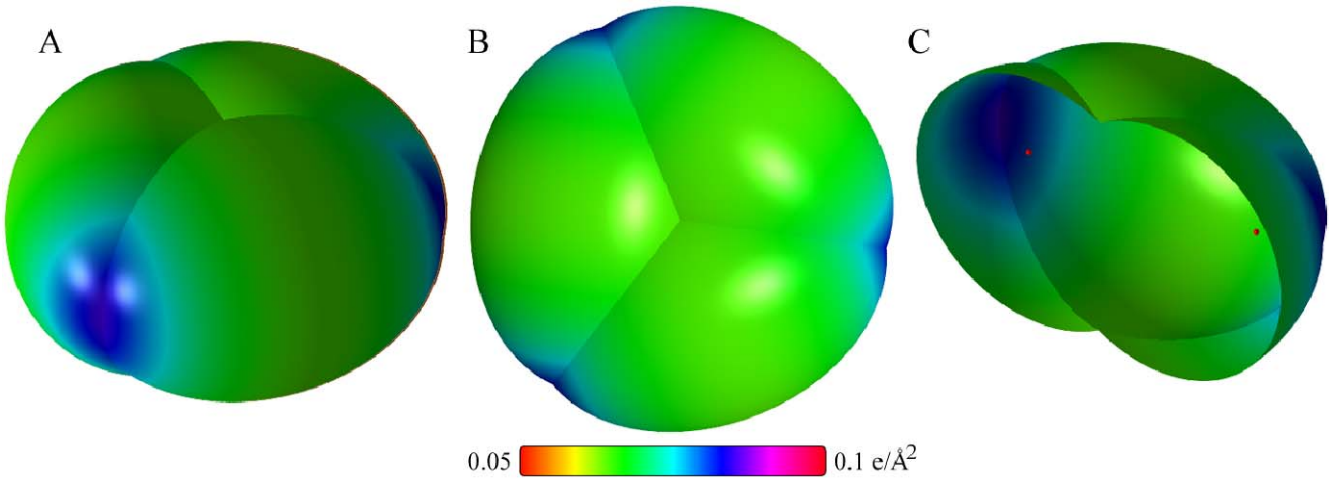

ENERGIES OF H_3^+-TYPE MOLECULAR IONS

Due to the equivalence of the $H_2(1/p)$-type ellipsoidal MOs and the linear superposition of their energies, the energy components defined previously for the molecule, Eqs. (11.207-11.212) apply in the case of the corresponding $H_3^+(1/p)$ molecular ion. And, each molecular energy component is given by the integral of corresponding force in Eq. (13.5). Each energy component is the total for the two equivalent electrons with the exception that the total charge of the two electrons is normalized over the three basis set $H_2(1/p)$-type ellipsoidal MOs. Thus, the energies are those given for $H_2(1/p)$ in the Energies of Hydrogen-Type Molecules section with the electron charge, where it appears, multiplied by a factor of $3/2$. In addition, the three sets of equivalent proton-proton pairs give rise to a factor of three times the proton-proton repulsion energy given by Eq. (11.208). The parameters a and b are given by Eqs. (13.7) and (13.10), respectively.

$$V_e = \frac{3}{2}\frac{-2pe^2}{8\pi\varepsilon_0\sqrt{a^2-b^2}}\ln\frac{a+\sqrt{a^2-b^2}}{a-\sqrt{a^2-b^2}} \tag{13.12}$$

$$V_p = 3\frac{p}{8\pi\varepsilon_0}\frac{e^2}{\sqrt{a^2-b^2}} \tag{13.13}$$

$$T = \frac{\hbar^2}{2m_e a\sqrt{a^2-b^2}}\ln\frac{a+\sqrt{a^2-b^2}}{a-\sqrt{a^2-b^2}} \tag{13.14}$$

The energy, V_m, corresponding to the magnetic force of Eq. (13.5) is:

$$V_m = \frac{3}{2}\frac{-\hbar^2}{4m_e a\sqrt{a^2-b^2}}\ln\frac{a+\sqrt{a^2-b^2}}{a-\sqrt{a^2-b^2}} \tag{13.15}$$

$$E_T = V_e + T + V_m + V_p \tag{13.16}$$

$$E_T = -\frac{e^2}{8\pi\varepsilon_0 a_0}\left[\left(3p^2\sqrt{2}-p^2\sqrt{2}+3\frac{p^2\sqrt{2}}{4}\right)\ln\frac{\sqrt{2}+1}{\sqrt{2}-1}-3p^2\sqrt{2}\right] = -p^2 35.54975\ eV \tag{13.17}$$

where the charge e appears in the magnetic energy V_m according to Eqs. (7.14-7.24) as discussed in the Force Balance of Hydrogen-Type Molecules section.

VIBRATION OF H_3^+-TYPE MOLECULAR IONS

The vibrational energy levels of H_3^+-type molecular ions may be solved as three equivalent coupled harmonic oscillators by developing the Lagrangian, the differential equation of motion, and the eigenvalue solutions [2] wherein the spring constants are derived from the central forces as given in the Vibration of Hydrogen-Type Molecular Ions section and the Vibration of Hydrogen-Type Molecules section.

THE DOPPLER ENERGY TERM OF H_3^+-TYPE MOLECULAR IONS

As shown in the Vibration of Hydrogen-type Molecular Ions section, the electron orbiting the nuclei at the foci of an ellipse may be perturbed such that a stable reentrant orbit is established that gives rise to a vibrational state corresponding to time harmonic oscillation of the nuclei and electron. The perturbation is caused by a photon that is resonant with the frequency of oscillation of the nuclei wherein the radiation is electric dipole with the corresponding selection rules.

Oscillation may also occur in the transition state. The perturbation arises from the decrease in internuclear distance as the molecular bond forms. Relative to the unperturbed case given in the Force Balance of Hydrogen-type Molecular Ions section, the reentrant orbit may give rise to a decrease in the total energy while providing a transient kinetic energy to the vibrating nuclei. However, as an additional condition for stability, radiation must be considered. A nonradiative state must be achieved after the emission due to transient vibration wherein the nonradiative condition given by Eq. (11.24) must be satisfied. The radiation reaction force due to the vibration of $H_2^+(1/p)$ and $H_2(1/p)$ in the transition state was derived in the Doppler Energy Term of Hydrogen-type Molecular Ions section and the Doppler Energy Term of Hydrogen-type Molecules section, respectively, and corresponds to a Doppler energy, E_D, that is dependent on the motion of the electron and the nuclei. The radiation reaction force in the case of the vibration of $H_3^+(1/p)$ in the transition state also corresponds to the Doppler energy, E_D, given by Eq. (11.181) that is dependent on the motion of the electrons and the nuclei. Here, a nonradiative state must also be achieved after the emission due to transient vibration wherein the nonradiative condition given by Eq. (11.24) must be satisfied. Typically, a third body is required to form H_3^+-type molecular ions. For example, the exothermic chemical reaction of $H+H$ to form H_2 does not occur with the emission of a photon. Rather, the reaction requires a collision with a third body, M, to remove the bond energy- $H+H+M \rightarrow H_2+M^*$ [3]. The third body distributes the energy from the exothermic reaction, and the end result is the H_2 molecule and an increase in the temperature of the system. Thus, a third body removes the energy corresponding to the additional force term given by Eq. (11.180).

The kinetic energy of the transient vibration is derived from the corresponding central forces. From Eqs. (13.5) and (13.12), the central force terms between the electron MO and the protons of each of the three $H_2(1/p)$-type ellipsoidal MOs are

$$f(a) = -\frac{3}{2}\frac{pe^2}{4\pi\varepsilon_0 a^2} \tag{13.18}$$

and

$$f'(a) = \frac{3}{2}\frac{2pe^2}{4\pi\varepsilon_0 a^3} \tag{13.19}$$

Thus, using Eqs. (11.136) and (13.18-13.19), the angular frequency of this oscillation is:

$$\omega = \sqrt{\frac{\frac{3}{2}\frac{pe^2}{4\pi\varepsilon_0\left(\frac{a_0}{p}\right)^3}}{m_e}} = p^2\, 5.06326\ X\ 10^{16}\ rad/s \tag{13.20}$$

where the semimajor axis, a, is $a = \frac{a_0}{p}$ according to Eq. (13.7). The kinetic energy, E_K, is given by Planck's equation (Eq. (11.127)):

$$\overline{E}_K = \hbar\omega = \hbar p^2\, 5.06326\ X\ 10^{16}\ rad/s = p^2\, 33.3273\ eV \tag{13.21}$$

In Eq. (11.181), substitution of the total energy of the H_3^+-type molecular ion, E_T, (Eq. (13.17)) for $E_{h\nu}$, the mass of the electron, m_e, for M, and the kinetic energy given by Eq. (13.21) for $\overline{E}_K$ gives the Doppler energy of the electrons for the reentrant orbit.

$$\overline{E}_D \cong E_{h\nu}\sqrt{\frac{2\overline{E}_K}{Mc^2}} = -35.54975\, p^2\ eV\sqrt{\frac{2e\left(p^2\, 33.3273\ eV\right)}{m_e c^2}} = -p^3\, 0.406013\ eV \tag{13.22}$$

The total energy of the H_3^+-type molecular ion is decreased by $\overline{E}_D$.

In addition to the electrons, the nuclei also undergo simple harmonic oscillation in the transition state at their corresponding frequency. On average, the total energy of vibration is equally distributed between kinetic energy and potential energy [4]. Thus, the average kinetic energy of vibration corresponding to the Doppler energy of the electrons, $\overline{E}_{Kvib}$, is 1/2 of the vibrational energy of the H_3^+-type molecular ion given by Eq. (11.148). The decrease in the energy of the molecular ion due to the reentrant orbit in the transition state corresponding to simple harmonic oscillation of the electrons and nuclei, $\overline{E}_{osc}$, is given by the sum of the corresponding energies, $\overline{E}_D$ and $\overline{E}_{Kvib}$. Using Eq. (13.22) and the experimental vibrational energy H_3^+ of $E_{vib} = 2521.31\ cm^{-1} = 0.312605\ eV$ [1] gives:

$$\bar{E}_{osc} = \bar{E}_D + \bar{E}_{Kvib} = \bar{E}_D + \frac{1}{2}\hbar p^2\sqrt{\frac{k}{\mu}} \tag{13.23}$$

$$\bar{E}_{osc} = -p^3 0.406013\ eV + \frac{1}{2}p^2\left(0.312605\ eV\right) \tag{13.24}$$

The reentrant orbit for the binding of a proton to $H_2(1/p)$ causes two bonds to oscillate by increasing and decreasing in length along opposite sides of the equilateral triangle at a relative phase angle of 180°. Since the vibration and reentrant oscillation is along two lengths of the equilateral triangular MO with E symmetry, $\bar{E}_{osc}$ for $H_3^+(1/p)$, $\bar{E}_{osc}\left(H_3^+(1/p)\right)$, is:

$$\bar{E}_{osc}\left(H_3^+(1/p)\right) = 2\left(\bar{E}_D + \frac{1}{2}\hbar p^2\sqrt{\frac{k}{\mu}}\right) = 2\left(-p^3 0.406013\ eV + \frac{1}{2}p^2\left(0.312605\ eV\right)\right) \tag{13.25}$$

To the extent that the MO dimensions are the same, the electron reentrant orbital energies, $\bar{E}_K$, are the same independent of the isotope of hydrogen, but the vibrational energies are related by Eq. (11.148). Thus, the differences in bond energies are essentially given by 1/2 the differences in vibrational energies per bond. Using Eq. (13.22), Eq. (13.25), and the experimental vibrational energy D_3^+ of $E_{vib} = 1834.67\ cm^{-1} = 0.227472\ eV$ [1], the corresponding $\bar{E}_{osc}\left(D_3^+(1/p)\right)$ is:

$$\bar{E}_{osc}\left(D_3^+(1/p)\right) = 2\left(-p^3 0.406013\ eV + \frac{1}{2}p^2\left(0.227472\ eV\right)\right) \tag{13.26}$$

TOTAL AND BOND ENERGIES OF $H_3^+(1/p)$- AND $D_3^+(1/p)$-TYPE MOLECULAR IONS

The total energy of the $H_3^+(1/p)$-type molecular ion is given by the sum of E_T (Eqs. (13.16-13.17)) and $\bar{E}_{osc}\left(H_3^+(1/p)\right)$ given Eqs. (13.20-13.25). Thus, the total energy of $H_3^+(1/p)$ having a central field of $+pe$ at each focus of the prolate spheroid molecular orbital including the Doppler term is

$$E_T = V_e + T + V_m + V_p + \bar{E}_{osc}\left(H_3^+(1/p)\right) \tag{13.27}$$

$$\begin{aligned} E_T &= -p^2\left\{\frac{e^2}{8\pi\varepsilon_0 a_0}\left[\left(3\sqrt{2}-\sqrt{2}+\frac{3\sqrt{2}}{4}\right)\ln\frac{\sqrt{2}+1}{\sqrt{2}-1}-3\sqrt{2}\right]\left[1+2p\sqrt{\frac{2\hbar\sqrt{\frac{3}{2}\frac{e^2}{4\pi\varepsilon_0 a_0^3}}}{m_e c^2}}\right]-2\left(\frac{1}{2}\hbar\sqrt{\frac{k}{\mu}}\right)\right\} \\ &= -p^2 35.54975 - 2p^3 0.406013\ eV + 2p^2\left(\frac{1}{2}\hbar\sqrt{\frac{k}{\mu}}\right) \end{aligned} \tag{13.28}$$

From Eqs. (13.24-13.25) and (13.27-13.28), the total energy of the H_3^+-type molecular ion is:

$$\begin{aligned} E_T &= -p^2 35.54975\ eV + \bar{E}_{osc}\left(H_3^+(1/p)\right) \\ &= -p^2 35.54975 - 2p^3 0.406013\ eV + 2\left(\frac{1}{2}p^2\left(0.312605\ eV\right)\right) \\ &= -p^2 35.23714\ eV - p^3 0.812025\ eV \end{aligned} \tag{13.29}$$

The total energy of the D_3^+-type molecular ion is given by the sum of E_T (Eq. (13.17)) and $\bar{E}_{osc}\left(D_3^+(1/p)\right)$ given by Eq. (13.26).

$$\begin{aligned} E_T &= -p^2 35.54975\ eV + \bar{E}_{osc}\left(D_3^+(1/p)\right) \\ &= -p^2 35.54975 - 2p^3 0.406013\ eV + 2\left(\frac{1}{2}p^2\left(0.227472\ eV\right)\right) \\ &= -p^2 35.32227\ eV - p^3 0.812025\ eV \end{aligned} \tag{13.30}$$

The bond dissociation energy, E_D, is the difference between the total energy of the corresponding hydrogen molecule and E_T

$$E_D = E(H_2(1/p)) - E_T \tag{13.31}$$

where $E\left(H_2(1/p)\right)$ is given by Eq. (11.241):

$$E\left(H_2(1/p)\right) = -p^2 31.351\ eV - p^3 0.326469\ eV \tag{13.32}$$

and $E\left(D_2(1/p)\right)$ is given by Eq. (11.242):

$$E\left(D_2(1/p)\right) = -p^2 31.4345\ eV - p^3 0.326469\ eV \tag{13.33}$$

The H_3^+ bond dissociation energy, E_D, is given by Eqs. (13.31-13.32) and (13.29):

$$\begin{aligned} E_D &= -p^2 31.351\ eV - p^3 0.326469\ eV - E_T \\ &= -p^2 31.351\ eV - p^3 0.326469\ eV - \left(-p^2 35.23714\ eV - p^3 0.812025\ eV\right) \\ &= p^2 3.88614\ eV + p^3 0.485556\ eV \end{aligned} \tag{13.34}$$

The D_3^+ bond dissociation energy, E_D, is given by Eqs. (13.31), (13.33), and (13.30):

$$\begin{aligned} E_D &= -p^2 31.4345\ eV - p^3 0.326469\ eV - E_T \\ &= -p^2 31.4345\ eV - p^3 0.326469\ eV - \left(-p^2 35.32227\ eV - p^3 0.812025\ eV\right) \\ &= p^2 3.88777\ eV + p^3 0.485556\ eV \end{aligned} \tag{13.35}$$

THE H_3^+ MOLECULAR ION

FORCE BALANCE OF THE H_3^+ MOLECULAR ION

The force balance equation for H_3^+ is given by Eq. (13.5) where $p=1$

$$\frac{\hbar^2}{m_e a^2 b^2} D = \frac{e^2}{8\pi\varepsilon_0 a b^2} D + \frac{\hbar^2}{2 m_e a^2 b^2} D \tag{13.36}$$

which has the parametric solution given by Eq. (11.83) when:

$$a = a_0 \tag{13.37}$$

The semimajor axis, a, is also given by Eq. (13.7) where $p=1$. The internuclear distance, $2c'$, which is the distance between the foci is given by Eq. (13.9) where $p=1$.

$$2c' = \sqrt{2} a_0 \tag{13.38}$$

The semiminor axis is given by Eq. (13.10) where $p=1$.

$$b = \frac{1}{\sqrt{2}} a_0 \tag{13.39}$$

The eccentricity, e, is given by Eq. (13.11).

$$e = \frac{1}{\sqrt{2}} \tag{13.40}$$

ENERGIES OF THE H_3^+ MOLECULAR ION

The energies of H_3^+ are given by Eqs. (13.12-13.15) where $p=1$

$$V_e = \frac{3}{2} \frac{-2e^2}{8\pi\varepsilon_0 \sqrt{a^2 - b^2}} \ln \frac{a + \sqrt{a^2 - b^2}}{a - \sqrt{a^2 - b^2}} = -101.7538\ eV \tag{13.41}$$

$$V_p = 3 \frac{e^2}{8\pi\varepsilon_0 \sqrt{a^2 - b^2}} = 57.7245\ eV \tag{13.42}$$

$$T = \frac{\hbar^2}{2 m_e a \sqrt{a^2 - b^2}} \ln \frac{a + \sqrt{a^2 - b^2}}{a - \sqrt{a^2 - b^2}} = 33.9179\ eV \tag{13.43}$$

The energy, V_m, of the magnetic force is

$$V_m = \frac{3}{2} \frac{-\hbar^2}{4 m_e a \sqrt{a^2 - b^2}} \ln \frac{a + \sqrt{a^2 - b^2}}{a - \sqrt{a^2 - b^2}} = -25.4384\ eV \tag{13.44}$$

The Doppler terms, $\bar{E}_{osc}\left(H_3^+(1/p)\right)$ and $\bar{E}_{osc}\left(D_3^+(1/p)\right)$ are given by Eqs. (13.25) and (13.26), respectively, where $p=1$

$$\bar{E}_{osc}\left(H_2^+\right) = 2\left(\bar{E}_D + \bar{E}_{Kvib}\right) = 2\left(-0.406013\ eV + \frac{1}{2}\left(0.312605\ eV\right)\right) = -0.499420\ eV \tag{13.45}$$

$$\bar{E}_{osc}\left(D_2\right) = 2\left(-0.406013\ eV + \frac{1}{2}\left(0.227472\ eV\right)\right) = -0.584553\ eV \tag{13.46}$$

The total energy, E_T, for H_3^+ given by Eqs. (13.27-13.29) is:

$$E_T = -\left\{ \frac{e^2}{8\pi\varepsilon_0 a_0} \left[\left(3\sqrt{2} - \sqrt{2} + \frac{3\sqrt{2}}{4} \right) \ln \frac{\sqrt{2}+1}{\sqrt{2}-1} - 3\sqrt{2} \right] \left[1 + 2\sqrt{\frac{2\hbar\sqrt{\frac{3}{2}\frac{e^2}{4\pi\varepsilon_0 a_0^3}}}{m_e c^2}} \right] - 2\left(\frac{1}{2}\hbar\sqrt{\frac{k}{\mu}} \right) \right\}$$

$$= -35.54975 - 2(0.406013\ eV) + 2\left(\frac{1}{2}(0.31260516\ eV) \right) \tag{13.47}$$

$$= -36.049167\ eV$$

From Eqs. (13.27-13.28) and (13.30), the total energy, E_T, for D_3^+ is:

$$E_T = -35.54975 - 2(0.406013\ eV) + 2\left(\frac{1}{2}(0.227472\ eV) \right) = -36.134300\ eV \tag{13.48}$$

The bond dissociation energy, E_D, is the difference between the total energy of H_2 or D_2 and E_T. The H_3^+ molecular bond dissociation energy, E_D, given by the difference between the experimental total energy of H_2 [5-7] [1] and the total energy of H_3^+ (Eqs. (13.29) where $p = 1$ and (13.47)) is

$$E_D = -31.675\ eV\ -(-36.049167\ eV) = 4.374167\ eV \tag{13.49}$$

The H_3^+ bond dissociation energy, E_D, given by Eq. (13.34) where $p = 1$ is:

$$E_D = 3.88614\ eV + 0.485556\ eV = 4.37170\ eV \tag{13.50}$$

The experimental bond dissociation energy of H_3^+ [8] is:

$$E_D = 4.373\ eV \tag{13.51}$$

The difference between the results of Eqs. (13.49) and (13.50) is within the experimental and propagated errors in the different calculations. The calculated results are based on first principles and given in closed-form equations containing fundamental constants only. The agreement between the experimental and calculated results for the H_3^+ bond dissociation energy is excellent.

The predicted D_3^+ molecular bond dissociation energy, E_D, given by the difference between the total energy of D_3^+ (Eqs. (13.30) where $p = 1$ and (13.48)) and the experimental total energy of D_2 [9-10][2] is:

$$E_D = -31.76\ eV - (-36.134300\ eV) = 4.374300\ eV \tag{13.52}$$

The D_3^+ bond dissociation energy, E_D, given by Eq. (13.35) where $p = 1$ is:

$$E_D = 3.88777\ eV + 0.485556\ eV = 4.373331\ eV \tag{13.53}$$

The results of the determination of bond parameters of H_3^+ are given in Table 13.1. The calculated results are based on first principles and given in closed-form, exact equations containing fundamental constants only. The agreement between the experimental and calculated results is excellent.

HYDROXYL RADICAL (OH)

The water molecule can be solved by first considering the solution of the hydroxyl radical which is formed by the reaction of a hydrogen atom and an oxygen atom:

$$H + O \rightarrow OH \tag{13.54}$$

The hydroxyl radical OH can be solved using the same principles as those used to solve the hydrogen molecule wherein the diatomic molecular orbital (MO) developed in the Nature of the Chemical Bond of Hydrogen-Type Molecules and Molecular Ions section serves as basis function in linear combination with an oxygen atomic orbital (AO) to form the MO of OH. The MO must (1) be a solution of Laplace's equation to give a equipotential energy surface, (2) correspond to an orbital solution of the Newtonian equation of motion in an inverse-radius-squared central field having a constant total energy, (3) be stable to radiation, and (4) conserve the electron angular momentum of $\hbar$. A further constraint with the substitution of a heteroatom (O) for one of the hydrogen atoms is that the constant energy of the MO must match the energy of the heteroatom.

---

[1] The experimental total energy of the hydrogen molecule is given by adding the first (15.42593 eV) [5] and second (16.2494 eV) ionization energies where the second ionization energy is given by the addition of the ionization energy of the hydrogen atom (13.59844 eV) [6] and the bond energy of H_2^+ (2.651 eV) [7].

[2] The experimental total energy of the deuterium molecule is given by adding the first (15.466 eV) [9] and second (16.294 eV) ionization energies where the second ionization energy is given by the addition of the ionization energy of the deuterium atom (13.603 eV) [10] and the bond energy of D_2^+ (2.692 eV) [9].

FORCE BALANCE OF *OH*

OH comprises two spin-paired electrons in a chemical bond between the oxygen atom and the hydrogen atom such that one electron on O remains unpaired. The OH radical MO is determined by considering properties of the binding atoms and the boundary constraints. The prolate spheroidal H_2 MO developed in the Nature of the Chemical Bond of Hydrogen-Type Molecules section satisfies the boundary constraints; thus, the H-atom electron forms a H_2-type ellipsoidal MO with one of the O-atom electrons. The O electron configuration given in the Eight-Electron Atoms section is $1s^2 2s^2 2p^4$, and the orbital arrangement is:

2p state

$$\underline{\uparrow\downarrow}\quad\underline{\uparrow}\quad\underline{\uparrow} \qquad (13.55)$$

1 0 -1

corresponding to the ground state ${}^3P_2$.

In determining the central forces for O in the Radius and Ionization Energy of the Outer Electron of the Oxygen Atom section, it was shown that the energy is minimized with conservation of angular momentum by the cancellation of the orbital angular momentum of a p_x electron by that of the p_y electron with the pairing of electron eight to fill the p_x orbital. Then, the diamagnetic force is given by Eq. (10.156) is that of atomic nitrogen (Eq. (10.136) corresponding to the p_z-orbital electron (Eq. (10.82) with $m = 0$) as the source of diamagnetism with an additional contribution from the uncanceled p_x electron (Eq. (10.82) with $m = 1$). From Eqs. (10.83) and (10.89), the paramagnetic force, $\mathbf{F}_{mag\ 2}$, is given by Eq. (10.157) corresponding to the spin-angular-momentum contribution alone of the p_x electron and the orbital angular momentum of the p_z electron, respectively. The diamagnetic and paramagnetic forces cancel such that the central force is purely the Coulombic force. This central force is maintained with bond formation such that the energy of the $O2p$ shell is unchanged. Thus, the angular momentum of each electron of the $O2p$ shell is conserved with bond formation. The central paramagnetic force due to spin is provided by the spin-pairing force of the OH MO that has the symmetry of an s orbital that superimposes with the $2p$ orbitals such that the corresponding angular momenta of the $O2p$ orbitals are unchanged.

The $O2p_y$ electron combines with the $H1s$ electron to form a molecular orbital. The proton of the H atom is along the internuclear axis. Due to symmetry, the other O electrons are equivalent to point charges at the origin. (See Eqs. (19-38) of Appendix II.) Thus, the energies in the OH MO involve only the $O2p_y$ and $H1s$ electrons and the change in the magnetic energy of the $O2p_y$ electron with the other O electrons (Eq. (13.152)) with the formation of the OH MO. The forces are determined by these energies.

As in the case of H_2, the MO is a prolate spheroid with the exception that the ellipsoidal MO surface cannot extend into O atom for distances shorter than the radius of the $2p$ shell. Otherwise, the electric field of the other $O2p$ electrons would be perturbed, and the $2p$ shell would not be stable. The corresponding increase in energy of O would not be offset by any energy decrease in the OH MO based on the distance from the O nucleus to the $H1s$ electron compared to those of the $O2p$ electrons. Thus, the MO surface comprises a prolate spheroid at the H proton that is continuous with the $2p$ shell at the O atom. The energy of the prolate spheroid is matched to that of the $O2p$ shell.

The orbital energy E for each elliptical cross section of the prolate spheroidal MO is given by the sum of the kinetic T and potential V energies. $E = T + V$ is constant, and the closed orbits are those for which $T < |V|$, and the open orbits are those for which $T \geq |V|$. It can be shown that the time average of the kinetic energy, $< T >$, for elliptic motion in an inverse-squared field is $1/2$ that of the time average of the magnitude of the potential energy, $|< V >|$. $< T >= 1/2 |< V >|$ [11]. In the case of an atomic orbital (AO), $E = T + V$, and for all points on the AO, $|E| = T = 1/2 |V|$. As shown in the Hydrogen-type Molecular Ions section, each point or coordinate position on the continuous two-dimensional electron MO defines an infinitesimal mass-density element which moves along an orbit comprising an elliptic plane cross section of the spheroidal MO through the foci. The motion is such that eccentric angle, θ, changes at a constant rate at each point. That is $\theta = \omega t$ at time t where ω is a constant, and

$$r(t) = \mathbf{i}a\cos\omega t + \mathbf{j}b\sin\omega t \qquad (13.56)$$

Consider the boundary condition that the MO of OH comprises a linear combination of an oxygen AO and a H_2-type ellipsoidal MO. The charge density of an H_2-type ellipsoidal MO given by Eq. (13.4) maintains that the surface is an equipotential; however, the potential and kinetic energy of a point on the surface changes as it orbits the central field. The potential energy is a maximum and the kinetic energy is a minimum at the semimajor axis, and the reverse occurs at the semiminor axis. Since the time average of the kinetic energy, $< T >$, for elliptic motion in an inverse-squared field is $1/2$ that of the time average of the magnitude of the potential energy, by symmetry, the $< T >= 1/2 < |V| >$ condition holds for 1/2 of the

H_2-type ellipsoidal MO having the H focus and ending at the plane defined by the semiminor axes. The O nucleus comprises the other focus of the OH MO. The $O2p$ AO obeys the energy relationship for all points. Since the H atomic orbital is at the Coulombic energy between the electron and proton given by Eq. (1.264), the energy matching condition is achieved while maintaining an energy match to the $O2p$ AO orbital with the charge density of 1/2e on the $O2p$ AO, corresponding to a donation of 0.25e from each MO electron. Then, the charge in the MO force balance corresponds to that of $-2\left(0.75\right)e=-1.5e$. Thus, the linear combination of the H_2-type ellipsoidal MO with the $O2p$ AO must involve a 25% contribution from the H_2-type ellipsoidal MO to the $O2p$ AO in order to match the energy relationships. Thus, the OH MO must comprise 75% of a H_2-type ellipsoidal MO (1/2 +25%) and an oxygen AO:

$$1\,O2p_y\ AO+0.75\,H_2\ MO\rightarrow OH\ MO \tag{13.57}$$

The force balance of the OH MO is determined by the boundary conditions that arise from the linear combination of orbitals according to Eq. (13.57). The force constant k of a H_2-type ellipsoidal MO due to the equivalent of two point charges of at the foci is given by Eq. (11.65).

$$k=\frac{2e^2}{4\pi\varepsilon_0} \tag{13.58}$$

Since the H_2-type ellipsoidal MO comprises 75% of the OH MO, the electron charge density in Eq. (13.58) is given by $-0.75e$. Thus, k' of the H_2-type-ellipsoidal-MO component of the OH MO is

$$k'=\frac{\left(0.75\right)2e^2}{4\pi\varepsilon_0} \tag{13.59}$$

L for the electron equals $\hbar$; thus, the distance from the origin of the OH MO to each focus c' is given by Eqs. (11.79) and (13.59):

$$c'=a\sqrt{\frac{\hbar^2 4\pi\varepsilon_0}{m_e e^2 1.5a}}=\sqrt{\frac{2aa_0}{3}} \tag{13.60}$$

The internuclear distance from Eq. (13.60) is:

$$2c'=2\sqrt{\frac{2aa_0}{3}} \tag{13.61}$$

The length of the semiminor axis of the prolate spheroidal OH MO $b=c$ given by Eq. (11.80) is:

$$b=\sqrt{a^2-c'^2} \tag{13.62}$$

The eccentricity, e, is:

$$e=\frac{c'}{a} \tag{13.63}$$

Then, the solution of the semimajor axis a allows for the solution of the other axes of the prolate spheroidal and eccentricity of the OH MO.

The general equation of the ellipsoidal MO having semiprincipal axes a, b, c given by:

$$\frac{x^2}{a^2}+\frac{y^2}{b^2}+\frac{z^2}{c^2}=1 \tag{13.64}$$

is also completely determined by the total energy E given by Eq. (11.18):

$$r=\frac{m\frac{L^2}{m^2}k^{-1}}{1+\left(1+2Em\frac{L^2}{m^2}k^{-2}\right)^{1/2}\cos\theta} \tag{13.65}$$

The energy of the oxygen $2p$ shell is the negative of the ionization energy of the oxygen atom given by Eq. (10.163). Experimentally, the energy is [12]:

$$E\left(2p\ shell\right)=-E(ionization;\ O)=-13.6181\ eV \tag{13.66}$$

Since the prolate spheroidal MO transitions to the O AO, the energy E in Eq. (13.66) adds to that of the H_2-type ellipsoidal MO to give the total energy of the OH MO. From the energy equation and the relationship between the axes given by Eqs. (13.60-13.63), the dimensions of the OH MO are solved.

The energy components derived previously for the hydrogen molecule, Eqs. (11.207-11.212), apply in the case of the H_2-type ellipsoidal MO. As in the case of the energies of $H_3^+\left(1/\ p\right)$ given by Eqs. (13.12-13.16), each energy component of the H_2-type ellipsoidal MO is the total for the two equivalent electrons with the exception that the total charge and energies of the two electrons is normalized by the percentage composition given by Eq. (13.57):

$$V_e = \left(\frac{3}{4}\right)\frac{-2e^2}{8\pi\varepsilon_0\sqrt{a^2-b^2}}\ln\frac{a+\sqrt{a^2-b^2}}{a-\sqrt{a^2-b^2}} \tag{13.67}$$

$$V_p = \frac{e^2}{8\pi\varepsilon_0\sqrt{a^2-b^2}} \tag{13.68}$$

$$T = \left(\frac{3}{4}\right)\frac{\hbar^2}{2m_e a\sqrt{a^2-b^2}}\ln\frac{a+\sqrt{a^2-b^2}}{a-\sqrt{a^2-b^2}} \tag{13.69}$$

$$V_m = \left(\frac{3}{4}\right)\frac{-\hbar^2}{4m_e a\sqrt{a^2-b^2}}\ln\frac{a+\sqrt{a^2-b^2}}{a-\sqrt{a^2-b^2}} \tag{13.70}$$

$$E_T = V_e + T + V_m + V_p \tag{13.71}$$

$$E_T = -\frac{e^2}{8\pi\varepsilon_0\sqrt{a^2-b^2}}\left[\left(\frac{3}{2}-\frac{3}{4}\frac{a_0}{a}+\frac{3}{8}\frac{a_0}{a}\right)\ln\frac{a+\sqrt{a^2-b^2}}{a-\sqrt{a^2-b^2}}-1\right] \tag{13.72}$$

$$E_T = -\frac{e^2}{8\pi\varepsilon_0 c'}\left[\left(\frac{3}{2}-\frac{3}{8}\frac{a_0}{a}\right)\ln\frac{a+c'}{a-c'}-1\right] \tag{13.73}$$

Since the prolate spheroidal MO transitions to the O AO and the energy of the $O2p$ shell must remain constant and equal to the negative of the ionization energy given by Eq. (13.66), the total energy $E_T(OH)$ of the OH MO is given by the sum of the energies of the orbitals corresponding to the composition of the linear combination of the O AO and the H_2-type ellipsoidal MO that forms the OH MO as given by Eq. (13.57):

$$E_T(OH) = E_T + E(2p\ shell) = E_T - E(ionization;\ O) = -\frac{e^2}{8\pi\varepsilon_0 c'}\left[\left(\frac{3}{2}-\frac{3}{8}\frac{a_0}{a}\right)\ln\frac{a+c'}{a-c'}-1\right]-13.6181\ eV \tag{13.74}$$

To match the boundary condition that the total energy of the entire H_2-type ellipsoidal MO is given by Eq. (11.212):

$$E_T(H_2) = -\frac{e^2}{8\pi\varepsilon_0 a_0}\left[\left(2\sqrt{2}-\sqrt{2}+\frac{\sqrt{2}}{2}\right)\ln\frac{\sqrt{2}+1}{\sqrt{2}-1}-\sqrt{2}\right] = -31.63536831\ eV \tag{13.75}$$

$E_T(OH)$ given by Eq. (13.74) is set equal to Eq. (13.75):

$$E_T(OH) = -\frac{e^2}{8\pi\varepsilon_0 c'}\left[\left(\frac{3}{2}-\frac{3}{8}\frac{a_0}{a}\right)\ln\frac{a+c'}{a-c'}-1\right]-13.6181\ eV = -31.63536831\ eV \tag{13.76}$$

From the energy relationship given by Eq. (13.76) and the relationship between the axes given by Eqs. (13.60-13.63), the dimensions of the OH MO can be solved.

Substitution of Eq. (13.60) into Eq. (13.76) gives:

$$\frac{e^2}{8\pi\varepsilon_0\sqrt{\frac{2aa_0}{3}}}\left[\left(\frac{3}{2}-\frac{3}{8}\frac{a_0}{a}\right)\ln\frac{a+\sqrt{\frac{2aa_0}{3}}}{a-\sqrt{\frac{2aa_0}{3}}}-1\right] = e18.01726831 \tag{13.77}$$

The most convenient way to solve Eq. (13.77) is by the reiterative technique using a computer. The result to within the round-off error with five-significant figures is:

$$a = 1.26430a_0 = 6.69039\ X\ 10^{-11}\ m \tag{13.78}$$

Substitution of Eq. (13.78) into Eq. (13.60) gives:

$$c' = 0.91808a_0 = 4.85826\ X\ 10^{-11}\ m \tag{13.79}$$

The internuclear distance given by multiplying Eq. (13.79) by two is:

$$2c' = 1.83616a_0 = 9.71651\ X\ 10^{-11}\ m \tag{13.80}$$

The experimental bond distance is [13]:

$$2c' = 9.71\ X\ 10^{-11}\ m \tag{13.81}$$

Substitution of Eqs. (13.78-13.79) into Eq. (13.62) gives:

$$b = c = 0.86925a_0 = 4.59985\ X\ 10^{-11}\ m \tag{13.82}$$

Substitution of Eqs. (13.78-13.79) into Eq. (13.63) gives:

$$e = 0.72615 \tag{13.83}$$

The nucleus of the H atom and the nucleus of the O atom comprise the foci of the H_2-type ellipsoidal MO. The parameters of the point of intersection of the H_2-type ellipsoidal MO and the $O2p_y$ AO can be determined from the polar equation of the ellipse (Eq. (11.10)).

$$r = r_0 \frac{1+e}{1+e\cos\theta'} \tag{13.84}$$

The radius of the $O2p_y$ AO given by Eq. (10.162) is $r_8 = a_0$, and the polar radial coordinate of the ellipse and the radius of the $O2p_y$ AO are equal at the point of intersection. Thus, Eq. (13.84) becomes:

$$r = (a-c')\frac{1+\frac{c'}{a}}{1+\frac{c'}{a}\cos\theta'} \tag{13.85}$$

where $r = a_0$ for O such that the polar angle θ' is given by:

$$\theta' = \cos^{-1}\left(\frac{a}{c'}\left((a-c')\frac{1+\frac{c'}{a}}{a_0}-1\right)\right) \tag{13.86}$$

Substitution of Eqs. (13.78-13.79) into Eq. (13.86) gives:

$$\theta' = 123.65° \tag{13.87}$$

Then, the angle θ_{O2p_yAO} the radial vector of the $O2p_y$ AO makes with the internuclear axis is

$$\theta_{O2p_yAO} = 180° - 123.65° = 56.35° \tag{13.88}$$

as shown in Figure 13.2.

Figure 13.2. The cross section of the OH MO showing the axes, angles, and point of intersection of the H_2-type ellipsoidal MO with the $O2p_y$ AO. The continuation of the H_2-type-ellipsoidal-MO basis element beyond the intersection point with the $O2p$ shell is shown as dashed since it only serves to solve the energy match with the $O2p$ shell and does not represent charge density. Similarly, the vertical dashed line only designates the parameters of the intersection point. The actual charge density is shown by the solid lines. Legend: a: semimajor axis, b: semiminor axis, c': internuclear distance, $d_1 : d_{H_2MO}$, $\theta_1 : \theta_{O2p_yAO}$, and $d_2 : d_{O2pAO}$.

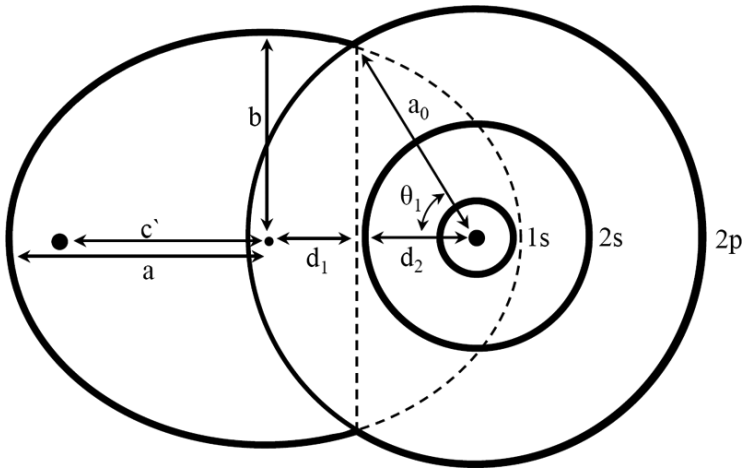

The Cartesian **i**-coordinate of the interception point of the MO and the AO can be calculated using the MO ellipsoidal parameters by first calculating the parametric angle in Eq. (11.83) that matches Cartesian **j**-coordinate components at the point of intersection. Thus, the matching elliptic parametric angle $\omega t = \theta_{H_2MO}$ satisfies the following relationship:

$$a_0 \sin\theta_{O2p_yAO} = b\sin\theta_{H_2MO} \tag{13.89}$$

such that

$$\theta_{H_2MO} = \sin^{-1}\frac{a_0 \sin 56.35°}{b} \tag{13.90}$$

with the use of Eq. (13.88). Substitution of Eq. (13.82) into Eq. (13.90) gives:

$$\theta_{H_2MO} = 73.27° \tag{13.91}$$

Then, the distance d_{H_2MO} along the internuclear axis from the origin of H_2-type ellipsoidal MO to the point of intersection of the orbitals is given by:

$$d_{H_2MO} = a\cos\theta_{H_2MO} \tag{13.92}$$

Substitution of Eqs. (13.78) and (13.91) into Eq. (13.92) gives:

$$d_{H_2MO} = 0.36397a_0 = 1.92606\ X\ 10^{-11}\ m \tag{13.93}$$

The distance d_{O2pAO} along the internuclear axis from the origin of the O atom to the point of intersection of the orbitals is given by

$$d_{O2pAO} = c' - d_{H_2MO} \tag{13.94}$$

Substitution of Eqs. (13.79) and (13.93) into Eq. (13.94) gives:

$$d_{O2pAO} = 0.55411a_0 = 2.93220\ X\ 10^{-11}\ m \tag{13.95}$$

As shown in Eq. (13.57), in addition to the p-orbital charge-density modulation, the uniform charge-density in the p_y orbital is increased by a factor of 0.25 and the H-atom density is decreased by a factor of 0.25. The internuclear axis of the $O-H$ bond is perpendicular to the bonding p_y orbital. Using the orbital composition of OH (Eq. (13.57)), the radii of $O1s = 0.12739a_0$ (Eq. (10.51)), $O2s = 0.59020a_0$ (Eq. (10.62)), and $O2p = a_0$ (Eq. (10.162)) shells, and the parameters of the OH MO given by Eqs. (13.3-13.4), (13.78-13.80), (13.82-13.83), and (13.87-13.95), the dimensional diagram and charge-density of the OH MO comprising the linear combination of the H_2-type ellipsoidal MO and the O AO according to Eq. (13.57) are shown in Figures 13.2 and 13.3, respectively.

In this case as well as in general, the current of the ellipsoidal MO and spherical AOs maintain spin pairing and current continuity. The current may comprise a linear combination of the MO current onto the AO and the AO currents that may comprise standing-wave components with current reflection at the interceptions of the surfaces. Thus, the current may flow equally in opposite directions between interception lines comprising mirror currents such that there is no net spin current. The linear combination gives a minimum equipotential energy surface of spin-paired electrons. Any asymmetrical charge distribution in the molecule corresponding to energy matching of the orbitals gives rise to a bond moment that is calculated in the Bond and Dipole Moment section.

Figure 13.3. OH MO comprising the superposition of the H_2-type ellipsoidal MO and the $O2p_y$ AO with a relative charge-density of 0.75 to 1.25; otherwise, the $O2p_y$ is the same as that of the oxygen atom. (A) Side-on, color scale, translucent view of the charge-density of the OH MO and the nuclei (shown red, not to scale). The ellipsoidal surface of the H_2-type ellipsoidal MO that transitions to the $O2p_y$ AO, the $O2p$ shell, the $O2s$ shell, the $O1s$ shell, and the nuclei are shown. (B) Cut-away view showing the inner most $O1s$ shell, and moving radially, the $O2s$ shell, the $O2p$ shell, and the H_2-type ellipsoidal MO that transitions to the $O2p_y$ AO.

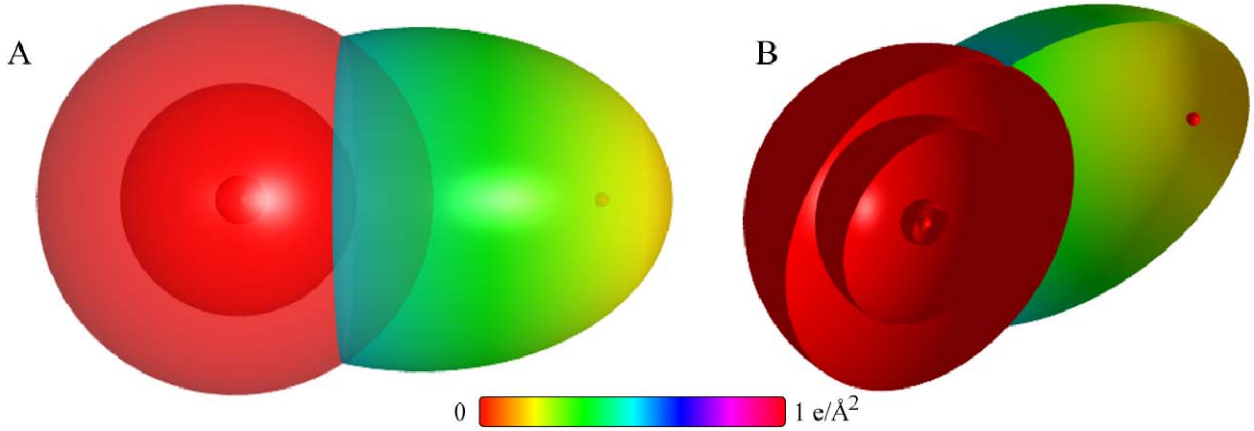

ENERGIES OF *OH*

The energies of OH given by the substitution of the semiprincipal axes (Eqs. (13.78-13.80) and (13.82)) into the energy equations (Eqs. (13.67-13.73)) are:

$$V_e = \left(\frac{3}{4}\right)\frac{-2e^2}{8\pi\varepsilon_0\sqrt{a^2-b^2}}\ln\frac{a+\sqrt{a^2-b^2}}{a-\sqrt{a^2-b^2}} = -40.92709\ eV \tag{13.96}$$

$$V_p = \frac{e^2}{8\pi\varepsilon_0\sqrt{a^2-b^2}} = 14.81988\ eV \tag{13.97}$$

$$T = \left(\frac{3}{4}\right)\frac{\hbar^2}{2m_e a\sqrt{a^2-b^2}}\ln\frac{a+\sqrt{a^2-b^2}}{a-\sqrt{a^2-b^2}} = 16.18567\ eV \tag{13.98}$$

$$V_m = \left(\frac{3}{4}\right)\frac{-\hbar^2}{4m_e a\sqrt{a^2-b^2}}\ln\frac{a+\sqrt{a^2-b^2}}{a-\sqrt{a^2-b^2}} = -8.09284\ eV \tag{13.99}$$

$$E_T(OH) = -\frac{e^2}{8\pi\varepsilon_0 c'}\left[\left(\frac{3}{2}-\frac{3}{8}\frac{a_0}{a}\right)\ln\frac{a+c'}{a-c'}-1\right] - 13.6181\ eV = -31.63247\ eV \tag{13.100}$$

where $E_T(OH)$ is given by Eq. (13.74) which is reiteratively matched to Eq. (13.75) within five-significant-figure round-off error.

VIBRATION AND ROTATION OF *OH*

The vibrational energy of OH may be solved in the same manner as that of hydrogen-type molecular ions and hydrogen molecules given in the Vibration of Hydrogen-type Molecular Ions section, and the Vibration of Hydrogen-type Molecules section, respectively, except that the orbital composition and the requirement that the *O*2*p* shell remain at the same energy and radius in the OH MO as it is in the *O* atom must be considered. Each *p*-orbital comprises the sum of a constant function and a spherical harmonic function as given by Eq. (1.29). In addition to the *p*-orbital charge-density modulation, the uniform charge-density in p_y orbital is increased by a factor of 0.25, and the *H*-atom electron density is decreased by a factor of 0.25. The force between the electron density of the H_2-type ellipsoidal MO and the nuclei determines the vibrational energy. With the radius of the orbit at the oxygen atom fixed at

$$r_8 = a_0 \tag{13.101}$$

according to Eq. (10.162), the central-force terms for the reentrant orbit between the electron density and the nuclei of the H_2-type ellipsoidal MO are given by Eqs. (11.213-11.214), except that the corresponding charge of –0.75*e* replaces the charge of –*e* of Eqs. (11.213-11.214). Furthermore, due to condition that the *O*2*p* shell remain at the same energy and radius in the OH MO as it is in the *O* atom, the oscillation of H_2-type ellipsoidal is along the semiminor axis with the apsidal angle of Eq. (11.140) given by $\psi = \pi$. Thus, the semimajor axis *a* of Eqs. (11.213-11.214) is replaced by the semiminor axis b:

$$f(b) = -\frac{0.75e^2}{8\pi\varepsilon_0 b^2} \tag{13.102}$$

and

$$f'(b) = \frac{0.75e^2}{4\pi\varepsilon_0 b^3} \tag{13.103}$$

Here, the force factor of 0.75 is equal to the equivalent term of Eq. (13.59). As the H_2-type ellipsoidal oscillates along b, the internuclear distance changes 180° out of phase. Thus, the distance for the reactive nuclear-repulsive terms is given by internuclear distance $2c'$ (Eq. (13.80)). Similar to that of Eqs. (11.215-11.216), the contribution from the repulsive force between the two nuclei is

$$f(2c') = \frac{e^2}{8\pi\varepsilon_0(2c')^2} \tag{13.104}$$

and

$$f'(2c') = -\frac{e^2}{4\pi\varepsilon_0(2c')^3} \tag{13.105}$$

Thus, from Eqs. (11.136), (11.213-11.217), and (13.102-13.105), the angular frequency of the oscillation is

$$\omega = \sqrt{\frac{\frac{0.75e^2}{8\pi\varepsilon_0 b^3} - \frac{e^2}{8\pi\varepsilon_0 (2c')^3}}{\mu}} = \sqrt{\frac{\frac{0.75e^2}{8\pi\varepsilon_0 (0.86925a_0)^3} - \frac{e^2}{8\pi\varepsilon_0 (1.83616a_0)^3}}{\frac{16}{17}m_p}} = 6.96269\ X\ 10^{14}\ rad/s \tag{13.106}$$

where b is given by Eq. (13.82), $2c'$ is given by Eq. (13.80), and the reduced mass of ^{16}OH is given by:

$$\mu_{^{16}OH} = \frac{m_1 m_2}{m_1 + m_2} = \frac{(1)(16)}{1+16} m_p \tag{13.107}$$

where m_p is the proton mass. Thus, during bond formation, the perturbation of the orbit determined by an inverse-squared force results in simple harmonic oscillatory motion of the orbit, and the corresponding frequency, $\omega(0)$, for ^{16}OH given by Eqs. (11.136), (11.148), and (13.106) is:

$$\omega(0) = \sqrt{\frac{k(0)}{\mu}} = \sqrt{\frac{763.18\ Nm^{-1}}{\mu}} = 6.96269\ X\ 10^{14}\ radians/s \tag{13.108}$$

where the reduced nuclear mass of ^{16}OH is given by Eq. (13.107) and the spring constant, $k(0)$, given by Eqs. (11.136) and (13.106) is:

$$k(0) = 763.18\ Nm^{-1} \tag{13.109}$$

The ^{16}OH transition-state vibrational energy, $E_{vib}(0)$, given by Planck's equation (Eq. (11.127)) is:

$$E_{vib}(0) = \hbar\omega = \hbar 6.96269\ X\ 10^{14}\ rad/s = 0.4583\ eV = 3696.38\ cm^{-1} \tag{13.110}$$

Zero-order or zero-point vibration is not physical and is not observed experimentally as discussed in the Diatomic Molecular Vibration section; yet, there is a term ω_e of the old point-particle-probability-wave-mechanics that can be compared to $E_{vib}(0)$. From Herzberg [14], ω_e, from the experimental curve fit of the vibrational energies of ^{16}OH is:

$$\omega_e = 3735.21\ cm^{-1} \tag{13.111}$$

As shown in the Vibration of Hydrogen-type Molecular Ions section, the harmonic oscillator potential energy function can be expanded about the internuclear distance and expressed as a Maclaurin series corresponding to a Morse potential after Karplus and Porter (K&P) [15] and after Eq. (11.134). Treating the Maclaurin series terms as anharmonic perturbation terms of the harmonic states, the energy corrections can be found by perturbation methods. The energy $\tilde{\nu}_\upsilon$ of state υ is:

$$\tilde{\nu}_\upsilon = \upsilon\omega_0 - \upsilon(\upsilon - 1)\omega_0 x_0, \quad \upsilon = 0,1,2,3... \tag{13.112}$$

where

$$\omega_0 x_0 = \frac{hc\omega_0^2}{4D_0} \tag{13.113}$$

ω_0 is the frequency of the $\upsilon = 1 \to \upsilon = 0$ transition, and D_0 is the bond dissociation energy given by Eq. (13.162). From Eq. (13.112), ω_0 is given by:

$$\omega_0 = E_{vib}(0) - 2\omega_0 x_0 \tag{13.114}$$

Substitution of Eq. (13.113) into Eq. (13.114) gives:

$$\omega_0 = E_{vib}(0) - 2\frac{hc\omega_0^2}{4D_0} \tag{13.115}$$

Eq. (13.115) can be expressed as:

$$\omega_0^2 + \frac{2D_0}{hc}\omega_0 - \frac{2D_0}{hc}E_{vib}(0) = 0 \tag{13.116}$$

which can be solved by the quadratic formula:

$$\omega_0 = \frac{-\frac{2D_0}{hc} \pm \sqrt{\left(\frac{2D_0}{hc}\right)^2 + 4\frac{2D_0}{hc}E_{vib}(0)}}{2} \tag{13.117}$$

Only the positive root is real, physical; thus,

$$\omega_0\left(cm^{-1}\right)=\frac{-\frac{2D_0}{100hc}+\sqrt{\left(\frac{2D_0}{100hc}\right)^2+4\frac{2D_0}{100hc}E_{vib}(0)}}{2}$$
$$=\frac{-\frac{2e(4.4104\ eV)}{100hc}+\sqrt{\left(\frac{2e(4.4104\ eV)}{100hc}\right)^2+4\frac{2e(4.4104\ eV)}{100hc}\left(3696.37\ cm^{-1}\right)}}{2} \tag{13.118}$$
$$=3522.02\ cm^{-1}$$

where $E_{vib}(0)$ is given by Eq. (13.110) and D_0 is given by Eq. (13.156). The corresponding ^{16}OH $\upsilon=1\rightarrow\upsilon=0$ vibrational energy, $E_{vib}(1)$, in electron volts is:

$$E_{vib}(1)=0.43666\ eV \tag{13.119}$$

The experimental vibrational energy of ^{16}OH is [16-17]:

$$E_{vib}(1)=0.4424\ eV \qquad \left(3568\ cm^{-1}\right) \tag{13.120}$$

Using Eqs. (13.118-13.119) with Eq. (13.113), the anharmonic perturbation term, ω_0x_0, of ^{16}OH is:

$$\omega_0x_0=\frac{100hc\left(8.06573X10^3\ \frac{cm^{-1}}{eV}0.43666\ eV\right)^2}{4e(4.4104\ eV)}cm^{-1}=87.18\ cm^{-1} \tag{13.121}$$

The experimental anharmonic perturbation term, ω_0x_0, of ^{16}OH [14] is:

$$\omega_0x_0=82.81\ cm^{-1} \tag{13.122}$$

The vibrational energies of successive states are given by Eqs. (13.110), (13.112), and (13.121).
Using the reduced nuclear mass of ^{16}OD given by

$$\mu_{^{16}OD}=\frac{m_1m_2}{m_1+m_2}=\frac{(2)(16)}{2+16}m_p \tag{13.123}$$

where m_p is the proton mass, the corresponding parameters for deuterated hydroxyl radical ^{16}OD (Eqs. (13.102-13.121) and (13.162)) are:

$$\omega(0)=\sqrt{\frac{k(0)}{\mu}}=\sqrt{\frac{763.18\ Nm^{-1}}{\mu}}=5.06610\ X\ 10^{14}\ radians/s \tag{13.124}$$

$$k(0)=763.18\ Nm^{-1} \tag{13.125}$$

$$E_{vib}(0)=\hbar\omega=\hbar5.06610\ X\ 10^{14}\ rad/s=0.33346\ eV=2689.51\ cm^{-1} \tag{13.126}$$

$$\omega_0\left(cm^{-1}\right)=\frac{-\frac{2D_0}{100hc}+\sqrt{\left(\frac{2D_0}{100hc}\right)^2+4\frac{2D_0}{100hc}E_{vib}(0)}}{2}$$
$$=\frac{-\frac{2e(4.4687\ eV)}{100hc}+\sqrt{\left(\frac{2e(4.4687\ eV)}{100hc}\right)^2+4\frac{2e(4.4687\ eV)}{100hc}\left(2689.51\ cm^{-1}\right)}}{2} \tag{13.127}$$
$$=2596.02\ cm^{-1}$$

$$E_{vib}(1)=0.3219\ eV \tag{13.128}$$

$$\omega_0x_0=\frac{100hc\left(8.06573X10^3\ \frac{cm^{-1}}{eV}0.3219\ eV\right)^2}{4e(4.4687\ eV)}cm^{-1}=46.75\ cm^{-1} \tag{13.129}$$

From Herzberg [14], ω_e, from the experimental curve fit of the vibrational energies of ^{16}OD is:

$$\omega_e=2720.9\ cm^{-1} \tag{13.130}$$

The experimental vibrational energy of ^{16}OD is [16-17]:

$$E_{vib}(1)=0.3263\ eV \qquad \left(2632.1\ cm^{-1}\right) \tag{13.131}$$

and the experimental anharmonic perturbation term, ω_0x_0, of ^{16}OD [14] is:

$$\omega_0x_0=44.2\ cm^{-1} \tag{13.132}$$

which match the predictions given by Eqs. (13.126), (13.127-13.128), and (13.129), respectively.

The B_e rotational parameters for ^{16}OH and ^{16}OD are given by:

$$B_e = \frac{\hbar^2}{2I_e hc} \tag{13.133}$$

where

$$I = \mu r^2 \tag{13.134}$$

and B_e is $\tilde{B}_e$ (Eq. (12.89) rather than Eq. (12.84)) to give units of cm^{-1}.

Using the internuclear distance, $r = 2c'$, and reduced mass of ^{16}OH given by Eqs. (13.80) and (13.107), respectively, the corresponding B_e is:

$$B_e = 18.835\ cm^{-1} \tag{13.135}$$

The experimental B_e rotational parameter of ^{16}OH is [14]:

$$B_e = 18.871\ cm^{-1} \tag{13.136}$$

Using the internuclear distance, $r = 2c'$, and reduced mass of ^{16}OD given by Eqs. (13.80) and (13.123), respectively, the corresponding B_e is

$$B_e = 9.971\ cm^{-1} \tag{13.137}$$

The experimental B_e rotational parameter of ^{16}OD is [14]:

$$B_e = 10.01\ cm^{-1} \tag{13.138}$$

THE DOPPLER ENERGY TERMS OF ^{16}OH AND ^{16}OD

The radiation reaction force in the case of the vibration of ^{16}OH in the transition state corresponds to the Doppler energy, E_D, given by Eq. (11.181) and Eq. (13.22) that is dependent on the motion of the electrons and the nuclei. The kinetic energy of the transient vibration is derived from the corresponding central forces. Following the same consideration as those used to derive Eqs. (13.102-13.103) and Eqs. (11.231-11.232), the central force terms between the electron density and the nuclei of ^{16}OH MO with the radius of the orbit at the oxygen atom fixed at:

$$r_8 = a_0 \tag{13.139}$$

according to Eq. (10.162) are:

$$f(b) = -\frac{0.75e^2}{4\pi\varepsilon_0 b^2} \tag{13.140}$$

and

$$f'(b) = \frac{(0.75)2e^2}{4\pi\varepsilon_0 b^3} \tag{13.141}$$

wherein the oscillation of H_2-type ellipsoidal MO is along the semiminor axis b with the apsidal angle of Eq. (11.140) given by $\psi = \pi$ due to condition that the $O2p$ shell remain at the same energy and radius in the OH MO as it is in the O atom. Thus, using Eqs. (11.136) and (13.140-13.141), the angular frequency of this oscillation is:

$$\omega = \sqrt{\frac{\frac{0.75e^2}{4\pi\varepsilon_0 b^3}}{m_e}} = 4.41776\ X\ 10^{16}\ rad/s \tag{13.142}$$

The kinetic energy, E_K, is given by Planck's equation (Eq. (11.127)):

$$\bar{E}_K = \hbar\omega = \hbar 4.41776\ X\ 10^{16}\ rad/s = 29.07844\ eV \tag{13.143}$$

In Eq. (11.181), substitution of the total energy of OH, $E_T(OH)$, (Eq. (13.76)) for $E_{h\nu}$, the mass of the electron, m_e, for M, and the kinetic energy given by Eq. (13.143) for $\bar{E}_K$ gives the Doppler energy of the electrons for the reentrant orbit.

$$\bar{E}_D \cong E_{h\nu}\sqrt{\frac{2\bar{E}_K}{Mc^2}} = -31.63537\ eV\sqrt{\frac{2e(29.07844\ eV)}{m_e c^2}} = -0.33749\ eV \tag{13.144}$$

The total energy of OH is decreased by $\bar{E}_D$.

In addition to the electrons, the nuclei also undergo simple harmonic oscillation in the transition state at their corresponding frequency. On average, the total energy of vibration is equally distributed between kinetic energy and potential energy [4]. Thus, the average kinetic energy of vibration corresponding to the Doppler energy of the electrons, $\bar{E}_{Kvib}$, is 1/2 of the vibrational energy of OH given by Eq. (13.120). The decrease in the energy of the OH due to the reentrant orbit in the transition state corresponding to simple harmonic oscillation of the electrons and nuclei, $\bar{E}_{osc}$, is given by the sum of the

corresponding energies, $\bar{E}_D$ and $\bar{E}_{Kvib}$. Using Eq. (13.144) and the experimental ^{16}OH ω_e of 3735.21 cm^{-1} $\left(0.463111\ eV\right)$ [16-17] gives:

$$\bar{E}_{osc}\left(^{16}OH\right)=\bar{E}_D+\bar{E}_{Kvib}=\bar{E}_D+\frac{1}{2}\hbar\sqrt{\frac{k}{\mu}} \tag{13.145}$$

$$\bar{E}_{osc}\left(^{16}OH\right)=-0.33749\ eV+\frac{1}{2}\left(0.463111\ eV\right)=-0.10594\ eV \tag{13.146}$$

To the extent that the MO dimensions are the same, the electron reentrant orbital energies, $\bar{E}_K$, are the same independent of the isotope of hydrogen, but the vibrational energies are related by Eq. (11.148). Thus, the differences in bond energies are essentially given by 1/2 the differences in vibrational energies per bond. Using Eq. (13.144), Eqs. (13.145-13.146), and the experimental ^{16}OD ω_e of 2720.9 cm^{-1} $\left(0.33735\ eV\right)$ [16-17], the corresponding $\bar{E}_{osc}\left(^{16}OD\right)$ is:

$$\bar{E}_{osc}\left(^{16}OD\right)=-0.33749\ eV+\frac{1}{2}\left(0.33735\ eV\right)=-0.16881\ eV \tag{13.147}$$

TOTAL AND BOND ENERGIES OF ^{16}OH AND ^{16}OD RADICALS

$E_{T+osc}\left(^{16}OH\right)$, the total energy of the ^{16}OH radical including the Doppler term, is given by the sum of $E_T\left(OH\right)$ (Eq. (13.76)) and $\bar{E}_{osc}\left(^{16}OH\right)$ given by Eqs. (13.142-13.146):

$$E_{T+osc}\left(^{16}OH\right)=V_e+T+V_m+V_p+E\left(2p\ shell\right)+\bar{E}_{osc}\left(^{16}OH\right)=E_T\left(OH\right)+\bar{E}_{osc}\left(^{16}OH\right) \tag{13.148}$$

$$\begin{aligned}E_{T+osc}\left(^{16}OH\right)&=\left\{\frac{-e^2}{8\pi\varepsilon_0 c'}\left[\left(\frac{3}{2}-\frac{3}{8}\frac{a_0}{a}\right)\ln\frac{a+c'}{a-c'}-1\right]-13.6181\ eV\right\}\left[1+\sqrt{\frac{2\hbar\sqrt{\frac{3}{4}\frac{e^2}{4\pi\varepsilon_0 b^3}}}{m_e}}{m_e c^2}\right]+\frac{1}{2}\hbar\sqrt{\frac{k}{\mu}}\\&=-31.63537\ eV-0.33749\ eV+\frac{1}{2}\hbar\sqrt{\frac{k}{\mu}}\end{aligned} \tag{13.149}$$

From Eqs. (13.145-13.146) and (13.148-13.149), the total energy of ^{16}OH is:

$$\begin{aligned}E_{T+osc}\left(^{16}OH\right)&=-31.63537\ eV+\bar{E}_{osc}\left(^{16}OH\right)\\&=-31.63537\ eV-0.33749\ eV+\frac{1}{2}\left(0.463111\ eV\right)\\&=-31.74130\ eV\end{aligned} \tag{13.150}$$

where the experimental ω_e was used for the $\hbar\sqrt{\frac{k}{\mu}}$ term. $E_{T+osc}\left(^{16}OD\right)$, the total energy of ^{16}OD including the Doppler term, isgiven by the sum of $E_T\left(OD\right)=E_T\left(OH\right)$ (Eq. (13.76)) and $\bar{E}_{osc}\left(^{16}OD\right)$ given by Eq. (13.147):

$$\begin{aligned}E_{T+osc}\left(^{16}OD\right)&=-31.63537\ eV+\bar{E}_{osc}\left(^{16}OD\right)\\&=-31.63537\ eV-0.33749\ eV+\frac{1}{2}\left(0.33735\ eV\right)\\&=-31.80418\ eV\end{aligned} \tag{13.151}$$

where the experimental ω_e was used for the $\hbar\sqrt{\frac{k}{\mu}}$ term. The dissociation of the bond of the hydroxyl radical forms a free hydrogen atom with one unpaired electron and an oxygen atom with two unpaired electrons as shown in Eq. (13.55) which interact to stabilize the atom as shown by Eq. (10.161-10.162). The lowering of the energy of the reactants decreases the bond energy. Thus, the total energy of oxygen is reduced by the energy in the field of the two magnetic dipoles given by Eq. (7.46) and Eq. (13.101):

$$E(magnetic)=\frac{2\pi\mu_0 e^2\hbar^2}{m_e^2 a_0^3}=\frac{8\pi\mu_0\mu_B^2}{a_0^3}=0.114411\ eV \tag{13.152}$$

The corresponding bond dissociation energy, E_D, is given by the sum of the total energies of the oxygen atom and the corresponding hydrogen atom minus the sum of $E_{T+osc}\left(^{16}OH\right)$ and $E(magnetic)$:

$$E_D=E(^{16}O)+E(H)-E_{T+osc}\left(^{16}OH\right)-E\left(magnetic\right) \tag{13.153}$$

$E(^{16}O)$ is given by Eq. (13.66), $E_D\left(H\right)$ [18]is:

$$E(H) = -13.59844\ eV \tag{13.154}$$

and $E_D(D)$ [19] is:

$$E(D) = -13.603\ eV \tag{13.155}$$

The ^{16}OH bond dissociation energy, $E_D\left(^{16}OH\right)$, is given by Eqs. (13.150) and (13.152-13.155):

$$\begin{aligned} E_D\left(^{16}OH\right) &= -\left(13.6181\ eV + 13.59844\ eV\right) - \left(E\left(magnetic\right) + E_{T+osc}\left(^{16}OH\right)\right) \\ &= -27.21654\ eV - \left(0.114411\ eV - 31.74130\ eV\right) \\ &= 4.4104\ eV \end{aligned} \tag{13.156}$$

The experimental ^{16}OH bond dissociation energy is [20]:

$$E_D\left(^{16}OH\right) = 4.41174\ eV \tag{13.157}$$

The ^{16}OD bond dissociation energy, $E_D\left(^{16}OD\right)$, is given by Eqs. (13.151-13.153):

$$\begin{aligned} E_D\left(^{16}OD\right) &= -\left(13.6181\ eV + 13.603\ eV\right) - \left(E\left(magnetic\right) + E_{T+osc}\left(^{16}OD\right)\right) \\ &= -27.2211\ eV - \left(0.114411\ eV - 31.804183\ eV\right) \\ &= 4.4687\ eV \end{aligned} \tag{13.158}$$

The experimental ^{16}OD bond dissociation energy is [21-22]:

$$E_D\left(^{16}OD\right) = 4.454\ eV \tag{13.159}$$

The results of the determination of bond parameters of OH and OD are given in Table 13.1. The calculated results are based on first principles and given in closed-form, exact equations containing fundamental constants only. The agreement between the experimental and calculated results is excellent.

WATER MOLECULE (H_2O)

The water molecule H_2O is formed by the reaction of a hydrogen atom with a hydroxyl radical:

$$OH + H \rightarrow H_2O \tag{13.160}$$

The water molecule can be solved using the same principles as those used to solve the hydrogen molecule, H_3^+, and OH wherein the diatomic molecular orbital (MO) developed in the Nature of the Chemical Bond of Hydrogen-Type Molecules and Molecular Ions section serves as basis function in a linear combination with an oxygen atomic orbital (AO) to form the MO of H_2O. The solution is very similar to that of OH except that there are two OH bonds in water.

FORCE BALANCE OF H_2O

H_2O comprises two chemical bonds between oxygen and hydrogen. Each $O-H$ bond comprises two spin-paired electrons with one from an initially unpaired electron of the oxygen atom and the other from the hydrogen atom. The H_2O MO is determined by considering properties of the binding atoms and the boundary constraints. The H_2 prolate spheroidal MO satisfies the boundary constraints as shown in the Nature of the Chemical Bond of Hydrogen-Type Molecules section; thus, each H-atom electron forms a H_2-type ellipsoidal MO with one of the initially unpaired O-atom electrons. The initial O electron configuration given in the Eight-Electron Atoms section is $1s^2 2s^2 2p^4$, and the orbital arrangement is given by Eqs. (10.154) and Eq. (13.55).

As shown in the case of OH in the Force Balance of OH section, the forces that determine the radius and the energy of the $O2p$ shell are unchanged with bond formation. Thus, the angular momentum of each electron of the $O2p$ is conserved with bond formation. The central paramagnetic force due to spin of each $O-H$ bond is provided by the spin-pairing force of the H_2O MO that has the symmetry of an s orbital that superimposes with the $O2p$ orbitals such that the corresponding angular momenta are unchanged.

Each of the $O2p_z$ and $O2p_x$ electron combines with a $H1s$ electron to form a molecular orbital. The proton of the H atom is along the internuclear axis. Due to symmetry, the other O electrons are equivalent to point charges at the origin. (See Eqs. (19-38) of Appendix II.) Thus, the energies in the H_2O MO involve only each $O2p$ and each $H1s$ electron with the formation of each $O-H$ bond. The forces are determined by these energies.

As in the case of H_2, each of two $O-H$-bond MOs is a prolate spheroid with the exception that the ellipsoidal MO surface cannot extend into the O atom for distances shorter than the radius of the $2p$ shell. Otherwise, the electric field of the other $O2p$ electrons would be perturbed, and the $2p$ shell would not be stable. The corresponding increase in energy of O would not be offset by any energy decrease in the $O-H$-bond MO based on the distance from the O nucleus to the $H1s$

electron compared to those of the $O2p$ electrons. Thus, the MO surface comprises a prolate spheroid at each H proton that is continuous with the $2p$ shell at the O atom. The sum of the energies of the prolate spheroids is matched to that of the $2p$ shell.

The orbital energy E for each elliptical cross section of the prolate spheroidal MO is given by the sum of the kinetic T and potential V energies. $E = T + V$ is constant, and the closed orbits are those for which $T < |V|$, and the open orbits are those for which $T \geq |V|$. It can be shown that the time average of the kinetic energy, $< T >$, for elliptic motion in an inverse-squared field is $1/2$ that of the time average of the magnitude of the potential energy, $|< V >|$. $< T >= 1/2 |< V >|$ [11]. In the case of an atomic orbital (AO), $E = T + V$, and for all points on the AO, $|E| = T = 1/2|V|$. As shown in the Hydrogen-type Molecular Ions section, each point or coordinate position on the continuous two-dimensional electron MO defines an infinitesimal mass-density element which moves along an orbit comprising an elliptic plane cross section of the spheroidal MO through the foci. The motion is such that the eccentric angle, θ, changes at a constant rate at each point. That is $\theta = \omega t$ at time t where ω is a constant, and

$$r(t) = \mathbf{i}a\cos\omega t + \mathbf{j}b\sin\omega t \tag{13.161}$$

Consider the boundary condition that the MO of H_2O comprises a linear combination of an oxygen AO and two H_2-type ellipsoidal MOs, one for each $O-H$ -bond. The charge density of each H_2-type ellipsoidal MO given by Eqs. (11.44-11.45) and (13.3-13.4) maintains that the surface is an equipotential; however, the potential and kinetic energy of a point on the surface changes as it orbits the central field. The potential energy is a maximum and the kinetic energy is a minimum at the semimajor axis, and the reverse occurs at the semiminor axis. Since the time average of the kinetic energy, $< T >$, for elliptic motion in an inverse-squared field is $1/2$ that of the time average of the magnitude of the potential energy, by symmetry, the $< T >= 1/2 < |V| >$ condition holds for 1/2 of each H_2-type ellipsoidal MO having the H focus and ending at the plane defined by the semiminor axes. The O nucleus comprises the other focus of each OH -MO component of the H_2O MO. The $O2p$ AO obeys the energy relationship for all points. Thus, the linear combination of the H_2-type ellipsoidal MO with the $O2p$ AO must involve a 25% contribution from the H_2-type ellipsoidal MO to the $O2p$ AO in order to match the energy relationships. Thus, the H_2O MO must comprise two $O-H$ -bonds with each comprising 75% of a H_2-type ellipsoidal MO (1/2 +25%) and an oxygen AO:

$$\left[1\ O2p_z\ AO + 0.75\ H_2\ MO\right] + \left[1\ O2p_y\ AO + 0.75\ H_2\ MO\right] \rightarrow H_2O\ MO \tag{13.162}$$

The force balance of the H_2O MO is determined by the boundary conditions that arise from the linear combination of orbitals according to Eq. (13.162). The force constant k of a H_2-type ellipsoidal MO due to the equivalent of two point charges at the foci is given by Eq. (11.65).

$$k = \frac{2e^2}{4\pi\varepsilon_0} \tag{13.163}$$

Since each H_2-type ellipsoidal MO comprises 75% of the $O-H$ -bond MO, the electron charge density in Eq. (13.163) is given by $-0.75e$. Thus, k' of each H_2-type-ellipsoidal-MO component of the H_2O MO is:

$$k' = \frac{(0.75)2e^2}{4\pi\varepsilon_0} \tag{13.164}$$

L for the electron equals $\hbar$; thus, the distance from the origin of each $O-H$ -bond MO to each focus c' is given by Eqs. (11.79) and (13.164):

$$c' = a\sqrt{\frac{\hbar^2 4\pi\varepsilon_0}{m_e e^2 1.5a}} = \sqrt{\frac{2aa_0}{3}} \tag{13.165}$$

The internuclear distance from Eq. (13.165) is:

$$2c' = 2\sqrt{\frac{2aa_0}{3}} \tag{13.166}$$

The length of the semiminor axis of the prolate spheroidal $O-H$ -bond MO $b = c$ given by Eq. (11.80) is:

$$b = \sqrt{a^2 - c'^2} \tag{13.167}$$

The eccentricity, e, is:

$$e = \frac{c'}{a} \tag{13.168}$$

The solution of the semimajor axis a then allows for the solution of the other axes of the prolate spheroid and eccentricity of the $O-H$ -bond MO.

The general equation of the ellipsoidal MO having semiprincipal axes a, b, c given by:

$$\frac{x^2}{a^2} + \frac{y^2}{b^2} + \frac{z^2}{c^2} = 1 \tag{13.169}$$

is also completely determined by the total energy E given by Eq. (11.18).

$$r = \frac{m\frac{L^2}{m^2}k^{-1}}{1+\left(1+2Em\frac{L^2}{m^2}k^{-2}\right)^{1/2}\cos\theta} \tag{13.170}$$

The energy of the oxygen $2p$ shell is the negative of the ionization energy of the oxygen atom given by Eqs. (10.163) and (13.66). Experimentally, the energy is [12]

$$E\left(2p\ shell\right) = -E(ionization;\ O) = -13.6181\ eV \tag{13.171}$$

Since each of the two prolate spheroidal $O-H$ -bond MOs comprises a H_2-type-ellipsoidal MO that transitions to the O AO, the energy E in Eq. (13.171) adds to that of the two corresponding H_2-type ellipsoidal MOs to give the total energy of the H_2O MO. From the energy equation and the relationship between the axes given by Eqs. (13.165-13.168), the dimensions of the H_2O MO are solved.

The energy components defined previously for Hydrogen-Type Molecules, Eqs. (11.207-11.212), apply in the case of H_2O. Since the H_2O MO comprises two equivalent $O-H$ -bond MOs, each a linear combination of a H_2-type-ellipsoidal MO and an $O2p$ AO, the corresponding energy component of the H_2O MO is given by the linear superposition of the component energies. Thus, the energy scale factor is given as two times the force factor, the term in parentheses in Eq. (13.164). In addition to the equivalence and linearity principles, this factor also arises from the consideration of the nature of each bond and the linear combination that forms the H_2O MO. Each $O-H$ -bond-energy component is the total for the two equivalent electrons with the exception that the total charge of the two electrons is normalized over the three basis set functions, two $O-H$ -bond MOs (OH -type ellipsoidal MOs given in the Energies of OH section) and one $O2p$ AO. Thus, the contribution of the $O-H$ -bond MOs to the H_2O MO energies are those given for $H_2\left(1/p\right)$ in the Energies of Hydrogen-Type Molecules multiplied by a factor of $3/2$ as in the case with H_3^+ (Eqs. (13.12), (13.15), (13.18-13.20)). In addition, the two sets of equivalent nuclear-point-charge pairs give rise to a factor of two times the proton-proton repulsion energy given by Eq. (11.208). Thus, the component energies of the H_2O MO are twice the corresponding energies of the OH MO given by Eqs. (13.67-13.73). The parameters a, b, and c' are given by Eqs. (13.165-13.167), respectively.

$$V_e = 2\left(\frac{3}{4}\right)\frac{-2e^2}{8\pi\varepsilon_0\sqrt{a^2-b^2}}\ln\frac{a+\sqrt{a^2-b^2}}{a-\sqrt{a^2-b^2}} = \left(\frac{3}{2}\right)\frac{-2e^2}{8\pi\varepsilon_0\sqrt{a^2-b^2}}\ln\frac{a+\sqrt{a^2-b^2}}{a-\sqrt{a^2-b^2}} \tag{13.172}$$

$$V_p = 2\frac{e^2}{8\pi\varepsilon_0\sqrt{a^2-b^2}} \tag{13.173}$$

$$T = 2\left(\frac{3}{4}\right)\frac{\hbar^2}{2m_e a\sqrt{a^2-b^2}}\ln\frac{a+\sqrt{a^2-b^2}}{a-\sqrt{a^2-b^2}} = \left(\frac{3}{2}\right)\frac{\hbar^2}{2m_e a\sqrt{a^2-b^2}}\ln\frac{a+\sqrt{a^2-b^2}}{a-\sqrt{a^2-b^2}} \tag{13.174}$$

$$V_m = 2\left(\frac{3}{4}\right)\frac{-\hbar^2}{4m_e a\sqrt{a^2-b^2}}\ln\frac{a+\sqrt{a^2-b^2}}{a-\sqrt{a^2-b^2}} = \left(\frac{3}{2}\right)\frac{-\hbar^2}{4m_e a\sqrt{a^2-b^2}}\ln\frac{a+\sqrt{a^2-b^2}}{a-\sqrt{a^2-b^2}} \tag{13.175}$$

$$E_T = V_e + T + V_m + V_p \tag{13.176}$$

$$E_T = -\frac{e^2}{4\pi\varepsilon_0\sqrt{a^2-b^2}}\left[\left(\frac{3}{2}-\frac{3}{4}\frac{a_0}{a}+\frac{3}{8}\frac{a_0}{a}\right)\ln\frac{a+\sqrt{a^2-b^2}}{a-\sqrt{a^2-b^2}}-1\right] \tag{13.177}$$

$$E_T = -\frac{e^2}{4\pi\varepsilon_0 c'}\left[\left(\frac{3}{2}-\frac{3}{8}\frac{a_0}{a}\right)\ln\frac{a+c'}{a-c'}-1\right] \tag{13.178}$$

Since the prolate spheroidal H_2-type MO transitions to the O AO and the energy of the $O2p$ shell must remain constant and equal to the negative of the ionization energy given by Eq. (13.171), the total energy $E_T\left(H_2O\right)$ of the H_2O MO is given by the sum of the energies of the orbitals corresponding to the composition of the linear combination of the O AO and the two H_2-type ellipsoidal MOs that forms the H_2O MO as given by Eq. (13.162):

$$E_T\left(H_2O\right) = E_T + E\left(2p\ shell\right) = E_T - E(ionization;\ O) = -\frac{e^2}{4\pi\varepsilon_0 c'}\left[\left(\frac{3}{2}-\frac{3}{8}\frac{a_0}{a}\right)\ln\frac{a+c'}{a-c'}-1\right]-13.6181\ eV \tag{13.179}$$

The two hydrogen atoms and the oxygen atom can achieve an energy minimum as a linear combination of two H_2-type ellipsoidal MOs each having the proton and the oxygen nucleus as the foci. Each $O-H$ -bond MO comprises the same $O2p$ shell of constant energy given by Eq. (13.171). Thus, the energy of the H_2O MO is also given by the sum of that of the two

H_2-type ellipsoidal MOs given by Eq. (11.212) minus the energy of the redundant oxygen atom of the linear combination given by Eq. (13.171):

$$\begin{aligned} E_T\left(2H_2-O\right) &= -2\frac{e^2}{8\pi\varepsilon_0 a_0}\left[\left(2\sqrt{2}-\sqrt{2}+\frac{\sqrt{2}}{2}\right)\ln\frac{\sqrt{2}+1}{\sqrt{2}-1}-\sqrt{2}\right]-E\left(2p\ shell\right) \\ &= 2\left(-31.63536831\ eV\right)-\left(-13.6181\ eV\right) \\ &= -49.652637\ eV \end{aligned} \tag{13.180}$$

$E_T\left(H_2O\right)$ given by Eq. (13.179) is set equal to two times the energy of the H_2-type ellipsoidal MO minus the energy of the $O2p$ shell given by Eq. (13.180):

$$E_T\left(H_2O\right) = -\frac{e^2}{4\pi\varepsilon_0 c'}\left[\left(\frac{3}{2}-\frac{3}{8}\frac{a_0}{a}\right)\ln\frac{a+c'}{a-c'}-1\right]-13.6181\ eV = -49.652637\ eV \tag{13.181}$$

From the energy relationship given by Eq. (13.181) and the relationship between the axes given by Eqs. (13.165-13.167), the dimensions of the H_2O MO can be solved.

Substitution of Eq. (13.165) into Eq. (13.181) gives:

$$\frac{e^2}{4\pi\varepsilon_0\sqrt{\frac{2aa_0}{3}}}\left[\left(\frac{3}{2}-\frac{3}{8}\frac{a_0}{a}\right)\ln\frac{a+\sqrt{\frac{2aa_0}{3}}}{a-\sqrt{\frac{2aa_0}{3}}}-1\right] = e36.034537 \tag{13.182}$$

The most convenient way to solve Eq. (13.182) is by the reiterative technique using a computer. The result to within the round-off error with five-significant figures is:

$$a = 1.2641a_0 = 6.68933\ X\ 10^{-11}\ m \tag{13.183}$$

Substitution of Eq. (13.183) into Eq. (13.165) gives:

$$c' = 0.918005a_0 = 4.85787\ X\ 10^{-11}\ m \tag{13.184}$$

The internuclear distance given by multiplying Eq. (13.184) by two is:

$$2c' = 1.83601a_0 = 9.71574\ X\ 10^{-11}\ m \tag{13.185}$$

The experimental bond distance is [23]:

$$2c' = 9.70 \pm .005\ X\ 10^{-11}\ m \tag{13.186}$$

Substitution of Eqs. (13.183-13.184) into Eq. (13.167) gives:

$$b = c = 0.869031a_0 = 4.59871\ X\ 10^{-11}\ m \tag{13.187}$$

Substitution of Eqs. (13.183-13.184) into Eq. (13.168) gives:

$$e = 0.726212 \tag{13.188}$$

The nucleus of the H atom and the nucleus of the O atom comprise the foci of each H_2-type ellipsoidal MO. The parameters of the point of intersection of each H_2-type ellipsoidal MO and the $O2p_y$ AO or $O2p_z$ AO can be determined from the polar equation of the ellipse (Eq. (11.10)):

$$r = r_0\frac{1+e}{1+e\cos\theta'} \tag{13.189}$$

The radius of the $O2p$ shell given by Eq. (10.162) is $r_8 = a_0$, and the polar radial coordinate of the ellipse and the radius of the $O2p$ shell are equal at the point of intersection. Thus, Eq. (13.189) becomes:

$$a_0 = \left(a-c'\right)\frac{1+\frac{c'}{a}}{1+\frac{c'}{a}\cos\theta'} \tag{13.190}$$

such that the polar angle θ' is given by

$$\theta' = \cos^{-1}\left(\frac{a}{c'}\left(\left(a-c'\right)\frac{1+\frac{c'}{a}}{a_0}-1\right)\right) \tag{13.191}$$

Substitution of Eqs. (13.183-13.184) into Eq. (13.191) gives:

$$\theta' = 123.66° \tag{13.192}$$

Then, the angle θ_{O2pAO} the radial vector of the $O2p$ AO makes with the internuclear axis is:

$$\theta_{O2pAO} = 180° - 123.66° = 56.33° \tag{13.193}$$

as shown in Figure 13.2. The Cartesian $\mathbf{i}$-coordinate of the interception point of the MO and the AO can be calculated using the MO ellipsoidal parameters by first calculating the parametric angle in Eq. (11.83) that matches Cartesian $\mathbf{j}$-coordinate

components at the point of intersection. Thus, the matching elliptic parametric angle $\omega t = \theta_{H_2MO}$ satisfies the following relationship:

$$a_0 \sin\theta_{O2pAO} = b \sin\theta_{H_2MO} \tag{13.194}$$

such that

$$\theta_{H_2MO} = \sin^{-1}\frac{a_0 \sin\theta_{O2pAO}}{b} = \sin^{-1}\frac{a_0 \sin 56.33°}{b} \tag{13.195}$$

with the use of Eq. (13.193). Substitution of Eq. (13.187) into Eq. (13.195) gives:

$$\theta_{H_2MO} = 73.28° \tag{13.196}$$

Then, the distance d_{H_2MO} along the internuclear axis from the origin of the H_2-type ellipsoidal MO to the point of intersection of the orbitals is given by

$$d_{H_2MO} = a\cos\theta_{H_2MO} \tag{13.197}$$

Substitution of Eqs. (13.183) and (13.196) into Eq. (13.197) gives:

$$d_{H_2MO} = 0.3637a_0 = 1.9244\ X\ 10^{-11}\ m \tag{13.198}$$

The distance d_{O2pAO} along the internuclear axis from the origin of the O atom to the point of intersection of the orbitals is given by

$$d_{O2pAO} = c' - d_{H_2MO} \tag{13.199}$$

Substitution of Eqs. (13.184) and (13.198) into Eq. (13.199) gives:

$$d_{O2pAO} = 0.5543a_0 = 2.93343\ X\ 10^{-11}\ m \tag{13.200}$$

In addition to the intersection of the H_2-type MO with the $O2p$ shell, two adjoining ellipsoidal H_2-type MOs intersect at points of equipotential. The angle and distance parameters are given by Eqs. (13.595-13.600) for the limiting methane case wherein four adjoining intersecting H_2-type MOs have the possibility of forming a self-contained two-dimensional equipotential surface of charge and current. Charge continuity can be obeyed for the H_2O MO if the current is continuous between the adjoining H_2-type MOs. However, in the limiting case of methane, the existence of a separate linear combination of the H_2-type MOs comprising four spin-paired electrons, not connected to the bonding carbon heteroatom requires that the electron be divisible. It is possible for an electron to form time-dependent singular points or nodes having no charge as shown by Eqs. (1.28-1.29), and two-dimensional charge distributions having Laplacian potentials and one-dimensional regions of zero charge are possible for macroscopic charge densities and currents as given in Haus and Melcher [24]. However, it is not possible for single electrons to have two-dimensional discontinuities in charge based on internal forces and first principles discussed in Appendix II. Thus, at the points of intersection of the H_2-type MOs of methane, symmetry, electron indivisibility, current continuity, and conservation of energy and angular momentum require that the current between the points of mutual contact and the carbon atom be projected onto and flow along the radial vector to the surface of the $C2sp^3$ shell. This current designated the bisector current (BC) meets the $C2sp^3$ surface and does not travel to distances shorter than its radius. The methane result must also apply in the case of other bonds including that of the water molecule. Here, the H_2-type MOs intersect and the ellipsoidal current is projected onto the radial vector to the $O2p$ shell and does not travel to distances shorter than its radius as in the case of a single $O-H$ bond.

As shown in Eq. (13.162), in addition to the p-orbital charge-density modulation, the uniform charge-density in the p_z and p_y orbitals is increased by a factor of 0.25 and the H atoms are each decreased by a factor of 0.25. Using the orbital composition of H_2O (Eq. (13.162)), the radii of $O1s = 0.12739a_0$ (Eq. (10.51)), $O2s = 0.59020a_0$ (Eq. (10.62)), and $O2p = a_0$ (Eq. (10.162)) shells, and the parameters of the H_2O MO given by Eqs. (13.3-13.4), (13.183-13.185), (13.187-13.188), and (13.192-13.200), the charge-density of the H_2O MO comprising the linear combination of two $O-H$-bond MOs (OH-type ellipsoidal MOs given in the Energies of OH section) according to Eq. (13.162) is shown in Figure 13.4. Each $O-H$-bond MO comprises a H_2-type ellipsoidal MO and an $O2p$ AO having the dimensional diagram shown in Figure 13.4.

Figure 13.4. H_2O MO comprising the linear combination of two $O-H$ -bond MOs. Each $O-H$ -bond MO comprises the superposition of a H_2-type ellipsoidal MO and the $O2p_z$ AO or the $O2p_y$ AO with a relative charge-density of 0.75 to 1.25; otherwise, the $O2p$ orbitals are the same as those of the oxygen atom. The internuclear axis of one $O-H$ bond is perpendicular to the bonding p_y orbital, and the internuclear axis of the other $O-H$ bond is perpendicular to the bonding p_z orbital. (A) Color scale, translucent view of the charge-density of the H_2O MO from the top. For each $O-H$ bond, the ellipsoidal surface of each H_2-type ellipsoidal MO transitions to the $O2p$ AO. The $O2p$ shell, the $O2s$ shell, the $O1s$ shell, and the nuclei (red, not to scale) are shown. (B) Cut-away view showing the innermost $O1s$ shell, and moving radially, the $O2s$ shell, the $O2p$ shell, and the H_2-type ellipsoidal MO that transitions to the $O2p$ AO for each $O-H$ bond. Bisector current not shown.

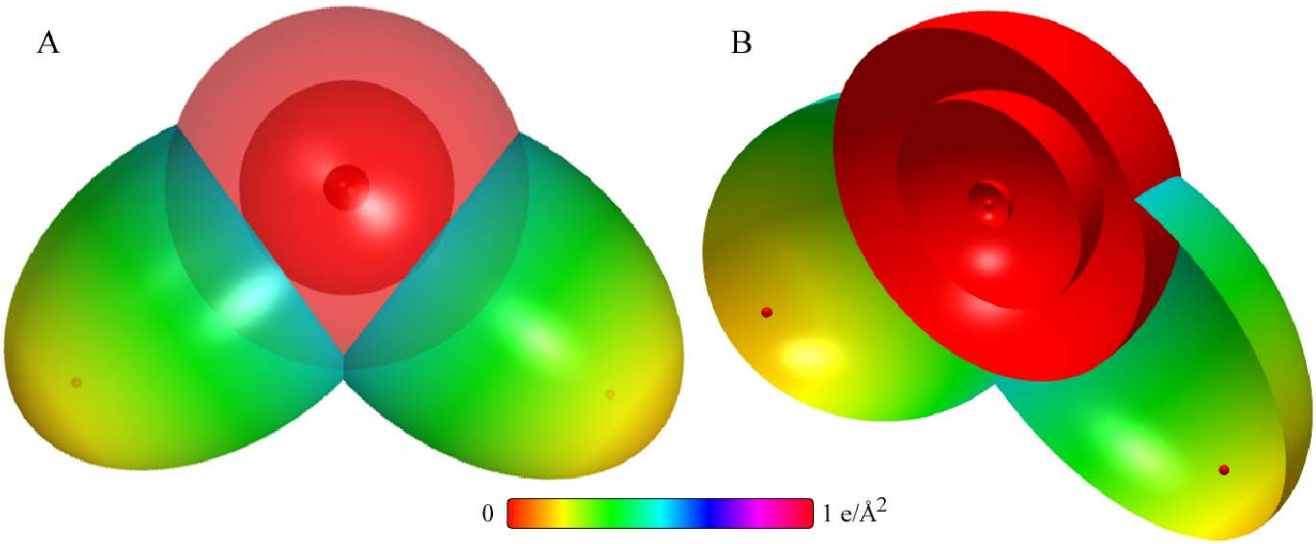

ENERGIES OF H_2O

The energies of H_2O given by the substitution of the semiprincipal axes (Eqs. (13.183-13.185) and (13.187)) into the energy equations (Eqs. (13.172-13.180)) are:

$$V_e = \left(\frac{3}{2}\right)\frac{-2e^2}{8\pi\varepsilon_0\sqrt{a^2-b^2}}\ln\frac{a+\sqrt{a^2-b^2}}{a-\sqrt{a^2-b^2}} = -81.8715\ eV \tag{13.201}$$

$$V_p = 2\frac{e^2}{8\pi\varepsilon_0\sqrt{a^2-b^2}} = 29.6421\ eV \tag{13.202}$$

$$T = \left(\frac{3}{2}\right)\frac{\hbar^2}{2m_e a\sqrt{a^2-b^2}}\ln\frac{a+\sqrt{a^2-b^2}}{a-\sqrt{a^2-b^2}} = 32.3833\ eV \tag{13.203}$$

$$V_m = \left(\frac{3}{2}\right)\frac{-\hbar^2}{4m_e a\sqrt{a^2-b^2}}\ln\frac{a+\sqrt{a^2-b^2}}{a-\sqrt{a^2-b^2}} = -16.1917\ eV \tag{13.204}$$

$$E_T\left(H_2O\right) = -\frac{e^2}{4\pi\varepsilon_0 c'}\left[\left(\frac{3}{2}-\frac{3}{8}\frac{a_0}{a}\right)\ln\frac{a+c'}{a-c'}-1\right]-13.6181\ eV = -49.6558\ eV \tag{13.205}$$

where $E_T\left(H_2O\right)$ is given by Eq. (13.179) which is reiteratively matched to Eq. (13.180) within five-significant-figure round-off error.

VIBRATION OF H_2O

The vibrational energy levels of H_2O may be solved as two equivalent coupled harmonic oscillators by developing the Lagrangian, the differential equation of motion, and the eigenvalue solutions [2] wherein the spring constants are derived from the central forces as given in the Vibration of Hydrogen-Type Molecular Ions section and the Vibration of Hydrogen-Type Molecules section.

THE DOPPLER ENERGY TERM OF H_2O

The radiation reaction force in the case of the vibration of H_2O in the transition state corresponds to the Doppler energy, E_D, given by Eq. (11.181) and Eqs. (13.22) and (13.144) that is dependent on the motion of the electrons and the nuclei. The kinetic energy of the transient vibration is derived from the corresponding central forces. As in the case of H_3^+, the water molecule is a linear combination of three orbitals. The water MO comprises two H_2-type ellipsoidal MOs and the O AO. Thus, the force factor of water in the determination of the Doppler frequency is equivalent to that of the H_3^+ ion given in Eqs. (13.18-13.20) and given by Eq. (13.164). From Eqs. (11.231-11.232) and (13.18-13.20), the central force terms between the electron density and the nuclei of each $O-H$ -bond MO with the radius of the orbit at the oxygen atom fixed at

$$r_8 = a_0 \tag{13.206}$$

according to Eq. (10.162) with the oscillation along the semiminor axis are:

$$f(b) = -\left(\frac{3}{2}\right)\frac{e^2}{4\pi\varepsilon_0 b^2} \tag{13.207}$$

and

$$f'(b) = \left(\frac{3}{2}\right)\frac{2e^2}{4\pi\varepsilon_0 b^3} \tag{13.208}$$

Thus, using Eqs. (11.136) and (13.207-13.208), the angular frequency of this oscillation is:

$$\omega = \sqrt{\frac{\left(\frac{3}{2}\right)\frac{e^2}{4\pi\varepsilon_0 b^3}}{m_e}} = 6.24996\ X\ 10^{16}\ rad/s \tag{13.209}$$

The kinetic energy, E_K, is given by Planck's equation (Eq. (11.127)):

$$\bar{E}_K = \hbar\omega = \hbar 6.24996\ X\ 10^{16}\ rad/s = 41.138334\ eV \tag{13.210}$$

The three basis elements of water, H, H, and O, all have the same Coulombic energy as given by Eqs. (1.264) and (10.163), respectively, such that the Doppler energy involves the total energy of the H_2O MO. Thus, in Eq. (11.181), substitution of the total energy of H_2O, $E_T(H_2O)$, (Eqs. (13.179-13.180) and Eq. (13.181)) for $E_{h\nu}$, the mass of the electron, m_e, for M, and the kinetic energy given by Eq. (13.210) for $\bar{E}_K$ gives the Doppler energy of the electrons for the reentrant orbit:

$$\bar{E}_D \cong E_{h\nu}\sqrt{\frac{2\bar{E}_K}{Mc^2}} = -49.652637\ eV\sqrt{\frac{2e(41.138334\ eV)}{m_e c^2}} = -0.630041\ eV \tag{13.211}$$

The total energy of H_2O is decreased by $\bar{E}_D$.

In addition to the electrons, the nuclei also undergo simple harmonic oscillation in the transition state at their corresponding frequency. On average, the total energy of vibration is equally distributed between kinetic energy and potential energy [4]. Thus, the average kinetic energy of vibration corresponding to the Doppler energy of the electrons, $\bar{E}_{Kvib}$, is 1/2 of the vibrational energy of H_2O. The decrease in the energy of H_2O due to the reentrant orbit in the transition state corresponding to simple harmonic oscillation of the electrons and nuclei, $\bar{E}_{osc}$, is given by the sum of the corresponding energies, $\bar{E}_D$ and $\bar{E}_{Kvib}$. Using Eq. (13.211) and the experimental $H^{16}OH$ vibrational energy of $E_{vib} = 3755.93\ cm^{-1} = 0.465680\ eV$ [25] gives:

$$\bar{E}'_{osc} = \bar{E}_D + \bar{E}_{Kvib} = \bar{E}_D + \frac{1}{2}\hbar\sqrt{\frac{k}{\mu}} \tag{13.212}$$

$$\bar{E}'_{osc} = -0.630041\ eV + \frac{1}{2}(0.465680\ eV) = -0.397201\ eV \tag{13.213}$$

per bond. As in the case for $H_3^+(1/p)$ shown in the Doppler Energy Term of H_3^+-type Molecular Ions section, the reentrant orbit for the binding of a hydrogen atom to a hydroxyl radical causes the bonds to oscillate by increasing and decreasing in length along the two $O-H$ bonds at a relative phase angle of 180°. Since the vibration and reentrant oscillation is along two bonds for the asymmetrical stretch (ν_3), $\bar{E}_{osc}$ for $H^{16}OH$, $\bar{E}_{osc}(H^{16}OH)$, is:

$$\bar{E}_{osc}(H^{16}OH) = 2\left(\bar{E}_D + \frac{1}{2}\hbar\sqrt{\frac{k}{\mu}}\right) = 2\left(-0.630041\ eV + \frac{1}{2}(0.465680\ eV)\right) = -0.794402\ eV \tag{13.214}$$

To the extent that the MO dimensions are the same, the electron reentrant orbital energies, $\bar{E}_K$, are the same independent of the isotope of hydrogen, but the vibrational energies are related by Eq. (11.148). Thus, the differences in bond energies are

essentially given by 1/2 the differences in vibrational energies per bond. Using Eq. (13.211), Eqs. (13.212-13.214), and the experimental $D^{16}OD$ vibrational energy of $E_{vib} = 2787.92\ cm^{-1} = 0.345661\ eV$ [25], the corresponding $\bar{E}_{osc}\left(D^{16}OD\right)$ is:

$$\bar{E}_{osc}\left(D^{16}OD\right) = 2\left(-0.630041\ eV + \frac{1}{2}\left(0.345661\ eV\right)\right) = -0.914421\ eV \tag{13.215}$$

TOTAL AND BOND ENERGIES OF $H^{16}OH$ AND $D^{16}OD$

$E_{T+osc}\left(H_2{}^{16}O\right)$, the total energy of the $H^{16}OH$ including the Doppler term, is given by the sum of $E_T\left(H_2O\right)$ (Eq. (13.181)) and $\bar{E}_{osc}\left(H^{16}OH\right)$ given Eqs. (13.207-13.214).

$$E_{T+osc}\left(H_2{}^{16}O\right) = V_e + T + V_m + V_p + E\left(O2p\right) + \bar{E}_{osc}\left(H^{16}OH\right) = E_T\left(H_2O\right) + \bar{E}_{osc}\left(H^{16}OH\right) \tag{13.216}$$

$$\begin{aligned} E_{T+osc}\left(H_2{}^{16}O\right) &= \left\{\begin{array}{l}\left(\frac{-e^2}{4\pi\varepsilon_0 c'}\left(\left(\frac{3}{2}-\frac{3}{8}\frac{a_0}{a}\right)\ln\frac{a+c'}{a-c'}-1\right)-13.6181\ eV\right)\left(1+2\sqrt{\frac{2\hbar\sqrt{\frac{3}{2}\frac{e^2}{4\pi\varepsilon_0 b^3}}}{m_e c^2}}\right)\\ +2\left(\frac{1}{2}\hbar\sqrt{\frac{k}{\mu}}\right)\end{array}\right\} \\ &= -49.652637\ eV - 2\left(0.630041\ eV - \frac{1}{2}\hbar\sqrt{\frac{k}{\mu}}\right)\end{aligned} \tag{13.217}$$

From Eqs. (13.214) and (13.216-13.217), the total energy of $H^{16}OH$ is:

$$\begin{aligned} E_{T+osc}\left(H_2{}^{16}O\right) &= -49.652637\ eV + \bar{E}_{osc}\left(H^{16}OH\right) \\ &= -49.652637\ eV - 2\left(0.630041\ eV - \frac{1}{2}\left(0.465680\ eV\right)\right) = -50.447039\ eV\end{aligned} \tag{13.218}$$

where the experimental vibrational energy was used for the $\hbar\sqrt{\frac{k}{\mu}}$ term. $E_{T+osc}\left(D_2{}^{16}O\right)$, the total energy of $D^{16}OD$ including the Doppler term is given by the sum of $E_T\left(D_2O\right) = E_T\left(H_2O\right)$ (Eq. (13.181)) and $\bar{E}_{osc}\left(D^{16}OD\right)$ given by Eq. (13.215):

$$\begin{aligned} E_{T+osc}\left(D_2{}^{16}O\right) &= -49.652637\ eV + \bar{E}_{osc}\left(D^{16}OD\right) \\ &= -49.652637\ eV - 2\left(0.630041\ eV - \frac{1}{2}\left(0.345661\ eV\right)\right) = -50.567058\ eV\end{aligned} \tag{13.219}$$

where the experimental vibrational energy was used for the $\hbar\sqrt{\frac{k}{\mu}}$ term. As in the case of the hydroxyl radical, the dissociation of the bond of the water molecule forms a free hydrogen atom and a hydroxyl radical, with one unpaired electron each. The lowering of the energy of the reactants due to the magnetic dipoles decreases the bond energy. Thus, the total energy of oxygen is reduced by the energy in the field of the two magnetic dipoles given by Eq. (13.152). The corresponding bond dissociation energy, E_D, is given by the sum of the total energies of the corresponding hydroxyl radical and hydrogen atom minus the total energy of water, $E_{T+osc}\left(H^{16}OH\right)$, and $E(magnetic)$.

Thus, E_D of $H^{16}OH$ is given by:

$$E_D\left(H^{16}OH\right) = E(H) + E(^{16}OH) - E_{T+osc}\left(H^{16}OH\right) - E(magnetic) \tag{13.220}$$

where $E_T(^{16}OH)$ is given by the sum of the experimental energies of ^{16}O (Eq. (13.171)), H (Eq. (13.154)), and the negative of the bond energy of ^{16}OH (Eq. (13.157)):

$$E(^{16}OH) = -13.59844\ eV - 13.6181\ eV - 4.41174\ eV = -31.62828\ eV \tag{13.221}$$

From Eqs. (13.154), (13.218), and (13.220-13.221), $E_D\left(H^{16}OH\right)$ is

$$\begin{aligned} E_D(H^{16}OH) &= E(H) + E(^{16}OH) - \left(E(magnetic) + E_{T+osc}\left(H^{16}OH\right)\right) \\ &= -13.59844\ eV - 31.62828\ eV - \left(0.114411\ eV - 50.447039\ eV\right) = 5.1059\ eV\end{aligned} \tag{13.222}$$

The experimental $H^{16}OH$ bond dissociation energy is [26]:

$$E_D(H^{16}OH) = 5.0991\ eV \tag{13.223}$$

Similarly, E_D of $D^{16}OD$ is given by:

$$E_D\left(D^{16}OH\right) = E(D) + E(^{16}OD) - \left(E(magnetic) + E_{T+osc}\left(D^{16}OD\right)\right) \tag{13.224}$$

where $E_T(^{16}OD)$ is given by the sum of the experimental energies of ^{16}O (Eq. (13.171)), D (Eq. (13.155)), and the negative of the bond energy of ^{16}OD (Eq. (13.159)):

$$E(^{16}OD) = -13.603\ eV - 13.6181\ eV - 4.454\ eV = -31.6751\ eV \tag{13.225}$$

From Eqs. (13.155), (13.220), and (13.224-13.225), $E_D\left(D^{16}OD\right)$ is

$$E_D(D^{16}OD) = -13.603\ eV - 31.6751\ eV - \left(0.114411\ eV - 50.567058\ eV\right) = 5.178\ eV \tag{13.226}$$

The experimental $D^{16}OD$ bond dissociation energy is [27]:

$$E_D(D^{16}OD) = 5.191\ eV \tag{13.227}$$

BOND ANGLE OF H_2O

The H_2O MO comprises a linear combination of two $O-H$ -bond MOs. Each $O-H$ -bond MO comprises the superposition of a H_2-type ellipsoidal MO and the $O2p_z$ AO or the $O2p_y$ AO with a relative charge-density of 0.75 to 1.25; otherwise, the $O2p$ orbitals are the same as those of the oxygen atom. A bond is also possible between the two H atoms of the $O-H$ bonds. Such $H-H$ bonding would decrease the $O-H$ -bond strength since electron density would be shifted from the $O-H$ bonds to the $H-H$ bond. Thus, the bond angle between the two $O-H$ bonds is determined by the condition that the total energy of the H_2-type ellipsoidal MO between the terminal H atoms of the $O-H$ bonds is zero. Since the two H_2-type ellipsoidal MOs comprise 75% of the H electron density of H_2, the energies and the total energy E_T of the $H-H$ bond is given by Eqs. (13.67-13.73). From Eq. (11.79), the distance from the origin to each focus of the $H-H$ ellipsoidal MO is

$$c' = a\sqrt{\frac{\hbar^2 4\pi\varepsilon_0}{m_e e^2 2a}} = \sqrt{\frac{aa_0}{2}} \tag{13.228}$$

The internuclear distance from Eq. (13.228) is:

$$2c' = 2\sqrt{\frac{aa_0}{2}} \tag{13.229}$$

The length of the semiminor axis of the prolate spheroidal $H-H$ MO $b=c$ is given by Eq. (13.167). Substitution of Eq. (13.228) into Eq. (13.73) gives:

$$E_T = -\frac{e^2}{8\pi\varepsilon_0\sqrt{\frac{aa_0}{2}}}\left[\left(\frac{3}{2} - \frac{3}{8}\frac{a_0}{a}\right)\ln\frac{a+\sqrt{\frac{aa_0}{2}}}{a-\sqrt{\frac{aa_0}{2}}} - 1\right] \tag{13.230}$$

The radiation reaction force in the case of the vibration of $H-H$ in the transition state corresponds to the Doppler energy, E_D, given by Eq. (11.181) that is dependent on the motion of the electrons and the nuclei. The total energy E_T that includes the radiation reaction of the $H-H$ MO is given by the sum of E_T (Eq. (13.73)) and $\bar{E}_{osc}\left(H_2\right)$ given by Eqs. (11.213-11.220), (11.231-11.236), and (11.239-11.240). Thus, the total energy $E_T\left(H-H\right)$ of the $H-H$ MO including the Doppler term is

$$E_T = V_e + T + V_m + V_p + \bar{E}_{osc}\left(H-H\right) \tag{13.231}$$

$$\begin{aligned} E_T &= \frac{-e^2}{8\pi\varepsilon_0\sqrt{\frac{aa_0}{2}}}\left[\left(\frac{3}{2} - \frac{3}{8}\frac{a_0}{a}\right)\ln\frac{a+\sqrt{\frac{aa_0}{2}}}{a-\sqrt{\frac{aa_0}{2}}} - 1\right]\left[1+\sqrt{\frac{2\hbar\sqrt{\frac{0.75e^2}{4\pi\varepsilon_0 a^3}}}{m_e c^2}}\right] + \frac{1}{2}\hbar\sqrt{\frac{k}{\mu}} \\ &= \frac{-e^2}{8\pi\varepsilon_0\sqrt{\frac{aa_0}{2}}}\left[\left(\frac{3}{2} - \frac{3}{8}\frac{a_0}{a}\right)\ln\frac{a+\sqrt{\frac{aa_0}{2}}}{a-\sqrt{\frac{aa_0}{2}}} - 1\right]\left[1+\sqrt{\frac{2\hbar\sqrt{\frac{0.75e^2}{4\pi\varepsilon_0 a^3}}}{m_e c^2}}\right] + \frac{1}{2}\hbar\sqrt{\frac{\frac{0.75e^2}{8\pi\varepsilon_0 a^3} - \frac{e^2}{8\pi\varepsilon_0\left(a+c'\right)^3}}{0.5m_p}} \end{aligned} \tag{13.232}$$

To match the boundary condition that the total energy of the $H-H$ ellipsoidal MO is zero, $E_T\left(H-H\right)$ given by Eq. (13.232) is set equal to zero:

$$0=\left[\frac{-e^2}{8\pi\varepsilon_0\sqrt{\frac{aa_0}{2}}}\left[\left(\frac{3}{2}-\frac{3}{8}\frac{a_0}{a}\right)\ln\frac{a+\sqrt{\frac{aa_0}{2}}}{a-\sqrt{\frac{aa_0}{2}}}-1\right]\left[1+\sqrt{\frac{2\hbar\sqrt{\frac{0.75e^2}{4\pi\varepsilon_0 a^3}}\,m_e}{m_e c^2}}\right]\right.$$
$$\left.+\frac{1}{2}\hbar\sqrt{\frac{\frac{0.75e^2}{8\pi\varepsilon_0 a^3}-\frac{e^2}{8\pi\varepsilon_0\left(a+c'\right)^3}}{0.5m_p}}\right] \tag{13.233}$$

From the energy relationship given by Eq. (13.233) and the relationship between the axes given by Eqs. (13.165-13.167), the dimensions of the $H-H$ MO can be solved.

The most convenient way to solve Eq. (13.233) is by the reiterative technique using a computer. The result to within the round-off error with five-significant figures is

$$a=4.300a_0=2.275\ X\ 10^{-10}\ m \tag{13.234}$$

Substitution of Eq. (13.234) into Eq. (13.228) gives:

$$c'=1.466a_0=7.759\ X\ 10^{-11}\ m \tag{13.235}$$

The internuclear distance given by multiplying Eq. (13.235) by two is:

$$2c'=2.933a_0=1.552\ X\ 10^{-10}\ m \tag{13.236}$$

Substitution of Eqs. (13.234-13.235) into Eq. (13.167) gives:

$$b=c=4.042a_0=2.139\ X\ 10^{-10}\ m \tag{13.237}$$

Substitution of Eqs. (13.234-13.235) into Eq. (13.168) gives:

$$e=0.341 \tag{13.238}$$

Using the distance between the two H atoms when the total energy of the corresponding MO is zero, the corresponding bond angle can be determined from the law of cosines:

$$A^2+B^2-2AB\text{cosine}\,\theta=C^2 \tag{13.239}$$

With $A=B=2c'_{O-H}$, the internuclear distance of each $O-H$ bond given by Eq. (13.185), and $C=2c'_{H-H}$, the internuclear distance of the two H atoms, the bond angle between the $O-H$ bonds is given by

$$\left(2c'_{O-H}\right)^2+\left(2c'_{O-H}\right)^2-2\left(2c'_{O-H}\right)^2\text{cosine}\,\theta=\left(2c'_{H-H}\right)^2 \tag{13.240}$$

$$\theta=\cos^{-1}\left(\frac{2\left(2c'_{O-H}\right)^2-\left(2c'_{H-H}\right)^2}{2\left(2c'_{O-H}\right)^2}\right) \tag{13.241}$$

Substitution of Eqs. (13.185) and (13.236) into Eq. (13.241) gives:

$$\theta=\cos^{-1}\left(\frac{2\left(1.836\right)^2-\left(2.933\right)^2}{2\left(1.836\right)^2}\right) \tag{13.242}$$
$$=\cos^{-1}\left(-0.2756\right)=105.998°$$

The experimental internuclear distance of the two H atoms, $2c'_{H-H}$, is [23]:

$$2c'_{H-H}=1.55\pm0.01\ X\ 10^{-10}\ m \tag{13.243}$$

which matches Eq. (13.236) very well. The experimental angle between the $O-H$ bonds is [23]:

$$\theta=106° \tag{13.244}$$

which matches the predicted angle given by Eq. (13.242).

The results of the determination of bond parameters of H_2O and D_2O are given in Table 13.1. The calculated results are based on first principles and given in closed-form, exact equations containing fundamental constants only. The agreement between the experimental and calculated results is excellent.

HYDROGEN NITRIDE (NH)

The ammonia molecule can be solved by first considering the solution of the hydrogen and dihydrogen nitride radicals. The former is formed by the reaction of a hydrogen atom and a nitrogen atom:

$$H+N\rightarrow NH \tag{13.245}$$

The hydrogen nitride radicals, NH and NH_2, and ammonia, NH_3, can be solved using the same principles as those used to solve OH and H_2O.

FORCE BALANCE OF *NH*

NH comprises two spin-paired electrons in a chemical bond between the nitrogen atom and the hydrogen atom such that two electrons on N remain unpaired. The NH radical molecular orbital (MO) is determined by considering properties of the binding atoms and the boundary constraints. The prolate spheroidal H_2 MO developed in the Nature of the Chemical Bond of Hydrogen-Type Molecules section satisfies the boundary constraints; thus, the H-atom electron forms a H_2-type ellipsoidal MO with one of the N-atom electrons. The N electron configuration given in the Seven-Electron Atoms section is $1s^2 2s^2 2p^3$, and the orbital arrangement is

2p state

$$\underset{1}{\uparrow} \quad \underset{0}{\uparrow} \quad \underset{-1}{\uparrow} \tag{13.246}$$

corresponding to the ground state ${}^4S^0_{3/2}$. The $N2p_x$ electron combines with the $H1s$ electron to form a molecular orbital. The proton of the H atom is along the internuclear axis. Due to symmetry, the other N electrons are equivalent to point charges at the origin. (See Eqs. (19-38) of Appendix II.) Thus, the energies in the NH MO involve only the $N2p_x$ and $H1s$ electrons and the change in the magnetic energy of the $N2p_x$ electron with the other N electrons (Eq. (13.305)) with the formation of the NH MO. The forces are determined by these energies.

As in the case of H_2, the MO is a prolate spheroid with the exception that the ellipsoidal MO surface cannot extend into N atom for distances shorter than the radius of the $2p$ shell. Thus, the MO surface comprises a prolate spheroid at the H proton that is continuous with the $2p$ shell at the N atom whose nucleus serves as the other focus. The energy of the prolate spheroid is matched to that of the $N2p$ shell. As in the case with OH, the linear combination of the H_2-type ellipsoidal MO with the $N2p$ AO must involve a 25% contribution from the H_2-type ellipsoidal MO to the $N2p$ atomic orbital (AO) in order to match potential, kinetic, and orbital energy relationships. Thus, the NH MO must comprise 75% of a H_2-type ellipsoidal MO and a nitrogen AO:

$$1\, N2p_x\ AO + 0.75\, H_2\ MO \rightarrow NH\ MO \tag{13.247}$$

The force balance of the NH MO is determined by the boundary conditions that arise from the linear combination of orbitals according to Eq. (13.247) and the energy matching condition between the hydrogen and nitrogen components of the MO.

Similar to the OH case given by Eq. (13.59), the H_2-type ellipsoidal MO comprises 75% of the NH MO; so, the electron charge density in Eq. (11.65) is given by $-0.75e$. Based on the condition that the electron MO is an equipotential energy surface, Eq. (11.79) gives the ellipsoidal parameter c' in terms of the central force of the foci, the electron angular momentum, and the ellipsoidal parameter a. To meet the equipotential condition of the union of the H_2-type-ellipsoidal-MO and the N AO, the force constant used to determine the ellipsoidal parameter c' is normalized by the ratio of the ionization energy of N $14.53414\ eV$ [6] and $13.605804\ eV$, the magnitude of the Coulombic energy between the electron and proton of H given by Eq. (1.264). This normalizes the force to match that of the Coulombic force alone to meet the force matching condition of the NH MO under the influence of the proton and the N nucleus. Thus, k' of Eq. (11.79) to determine c' is

$$k' = \frac{(0.75)2e^2}{4\pi\varepsilon_0 \frac{14.53414}{13.605804}} = (0.936127)\frac{(0.75)2e^2}{4\pi\varepsilon_0} \tag{13.248}$$

L for the electron equals $\hbar$; thus, the distance from the origin of the NH MO to each focus c' is given by Eqs. (11.79) and (13.248):

$$c' = a\sqrt{\frac{\hbar^2 4\pi\varepsilon_0}{m_e e^2 1.5a(0.936127)}} = \sqrt{\frac{2aa_0}{3(0.936127)}} = \sqrt{0.712154aa_0} \tag{13.249}$$

The internuclear distance from Eq. (13.249) is

$$2c' = 2\sqrt{0.712154aa_0} \tag{13.250}$$

The length of the semiminor axis of the prolate spheroidal NH MO $b = c$ is given by Eqs. (11.80) and (13.62). The eccentricity, e, is given by Eq. (13.63). Then, the solution of the semimajor axis a allows for the solution of the other axes of the prolate spheroidal and eccentricity of the NH MO.

The energy of the nitrogen $2p$ shell is the negative of the ionization energy of the nitrogen atom given by Eq. (10.143). Experimentally, the energy is [6]:

$$E(2p\ shell) = -E(ionization;\ N) = -14.53414\ eV \tag{13.251}$$

Since the prolate spheroidal MO transitions to the N AO, the energy E in Eq. (13.251) adds to that of the H_2-type ellipsoidal MO to give the total energy of the NH MO. From the energy equation and the relationship between the axes given by Eqs. (13.249-13.250) and (13.62-13.63), the dimensions of the NH MO are solved.

The energy components of V_e, V_p, T, V_m, and E_T are the same as those of OH given by Eqs. (13.67-13.73). Similarly to OH, the total energy $E_T(NH)$ of the NH MO is given by the sum of the energies of the orbitals corresponding to the composition of the linear combination of the N AO and the H_2-type ellipsoidal MO that forms the NH MO as given by Eq. (13.247):

$$E_T(NH) = E_T + E(2p\ shell) = E_T - E(ionization;\ N) = -\frac{e^2}{8\pi\varepsilon_0 c'}\left[\left(\frac{3}{2}-\frac{3}{8}\frac{a_0}{a}\right)\ln\frac{a+c'}{a-c'}-1\right]-14.53414\ eV \tag{13.252}$$

To match the boundary condition that the total energy of the entire H_2-type ellipsoidal MO is given by Eqs. (11.212) and (13.75), $E_T(NH)$ given by Eq. (13.252) is set equal to Eq. (13.75):

$$E_T(NH) = -\frac{e^2}{8\pi\varepsilon_0 c'}\left[\left(\frac{3}{2}-\frac{3}{8}\frac{a_0}{a}\right)\ln\frac{a+c'}{a-c'}-1\right]-14.53414\ eV = -31.63536831\ eV \tag{13.253}$$

From the energy relationship given by Eq. (13.252) and the relationship between the axes given by Eqs. (13.249-13.250) and (13.62-13.63), the dimensions of the NH MO can be solved.

Substitution of Eq. (13.249) into Eq. (13.253) gives:

$$\frac{e^2}{8\pi\varepsilon_0\sqrt{0.712154aa_0}}\left[\left(\frac{3}{2}-\frac{3}{8}\frac{a_0}{a}\right)\ln\frac{a+\sqrt{0.712154aa_0}}{a-\sqrt{0.712154aa_0}}-1\right] = e17.10123 \tag{13.254}$$

The most convenient way to solve Eq. (13.254) is by the reiterative technique using a computer. The result to within the round-off error with five-significant figures is

$$a = 1.36275a_0 = 7.21136\ X\ 10^{-11}\ m \tag{13.255}$$

Substitution of Eq. (13.255) into Eq. (13.249) gives:

$$c' = 0.98513a_0 = 5.21310\ X\ 10^{-11}\ m \tag{13.256}$$

The internuclear distance given by multiplying Eq. (13.256) by two is:

$$2c' = 1.97027a_0 = 1.04262\ X\ 10^{-10}\ m \tag{13.257}$$

The experimental bond distance is [28]:

$$2c' = 1.0362\ X\ 10^{-10}\ m \tag{13.258}$$

Substitution of Eqs. (13.255-13.256) into Eq. (13.62) gives:

$$b = c = 0.94159a_0 = 4.98270\ X\ 10^{-11}\ m \tag{13.259}$$

Substitution of Eqs. (13.255-13.256) into Eq. (13.63) gives:

$$e = 0.72290 \tag{13.260}$$

The nucleus of the H atom and the nucleus of the N atom comprise the foci of the H_2-type ellipsoidal MO. The parameters of the point of intersection of the H_2-type ellipsoidal MO and the $N2p_x$ AO are given by Eqs. (13.84-13.95). The polar intersection angle θ' is given by:

$$\theta' = \cos^{-1}\left(\frac{a}{c'}\left(\left(a-c'\right)\frac{1+\frac{c'}{a}}{r_n}-1\right)\right) \tag{13.261}$$

where $r_n = r_7 = 0.93084a_0$ is the radius of the N atom. Substitution of Eqs. (13.255-13.256) into Eq. (13.86) gives:

$$\theta' = 114.61° \tag{13.262}$$

Then, the angle θ_{N2p_xAO} the radial vector of the $N2p_x$ AO makes with the internuclear axis is:

$$\theta_{N2p_xAO} = 180° - 114.61° = 65.39° \tag{13.263}$$

as shown in Figure 13.5.

Figure 13.5. The cross section of the NH MO showing the axes, angles, and point of intersection of the H_2-type ellipsoidal MO with the $N2p_x$ AO. The continuation of the H_2-type-ellipsoidal-MO basis element beyond the intersection point with the $N2p$ shell is shown as dashed since it only serves to solve the energy match with the $N2p$ shell and does not represent charge density. Similarly, the vertical dashed line only designates the parameters of the intersection point. The actual charge density is shown by the solid lines. Legend: a: semimajor axis, b: semiminor axis, c': internuclear distance, $d_1 : d_{H_2MO}$, $\theta_1 : \theta_{N2p_xAO}$, $d_2 : d_{N2pAO}$, and $R : r_7$.

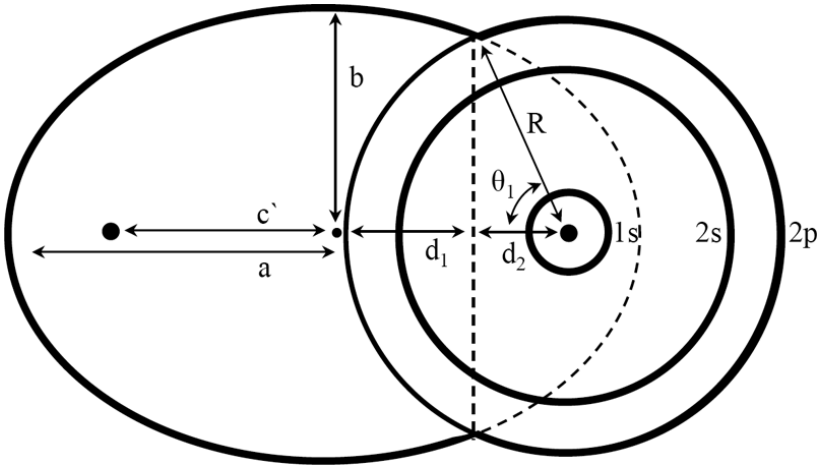

The Cartesian **i**-coordinate of the interception point of the MO and the AO can be calculated using the MO ellipsoidal parameters by first calculating the parametric angle in Eq. (11.83) that matches Cartesian **j**-coordinate components at the point of intersection. Thus, the matching elliptic parametric angle $\omega t = \theta_{H_2MO}$ satisfies the following relationship:

$$r_7 \sin\theta_{N2p_xAO} = 0.93084a_0 \sin\theta_{N2p_xAO} = b\sin\theta_{H_2MO} \tag{13.264}$$

such that

$$\theta_{H_2MO} = \sin^{-1}\frac{0.93084a_0 \sin\theta_{N2p_xAO}}{b} = \sin^{-1}\frac{0.93084a_0 \sin 65.39°}{b} \tag{13.265}$$

with the use of Eq. (13.263). Substitution of Eq. (13.259) into Eq. (13.265) gives:

$$\theta_{H_2MO} = 64.00° \tag{13.266}$$

Then, the distance d_{H_2MO} along the internuclear axis from the origin of H_2-type ellipsoidal MO to the point of intersection of the orbitals is given by:

$$d_{H_2MO} = a\cos\theta_{H_2MO} \tag{13.267}$$

Substitution of Eqs. (13.255) and (13.266) into Eq. (13.267) gives:

$$d_{H_2MO} = 0.59747a_0 = 3.16166\ X\ 10^{-11}\ m \tag{13.268}$$

The distance d_{N2pAO} along the internuclear axis from the origin of the N atom to the point of intersection of the orbitals is given by:

$$d_{N2pAO} = c' - d_{H_2MO} \tag{13.269}$$

Substitution of Eqs. (13.79) and (13.93) into Eq. (13.94) gives:

$$d_{N2pAO} = 0.38767a_0 = 2.05144\ X\ 10^{-11}\ m \tag{13.270}$$

As shown in Eq. (13.247), in addition to the p-orbital charge-density modulation, the uniform charge-density in the p_x orbital is increased by a factor of 0.25 and the H-atom density is decreased by a factor of 0.25. The internuclear axis of the $N-H$ bond is perpendicular to the bonding p_x orbital. Using the orbital composition of NH (Eq. (13.27)), the radii of $N1s = 0.14605a_0$ (Eq. (10.51)), $N2s = 0.69385a_0$ (Eq. (10.62)), and $N2p = 0.93084a_0$ (Eq. (10.142)) shells, and the parameters of the NH MO given by Eqs. (13.3-13.4) and (13.255-13.270), the dimensional diagram and charge-density of the NH MO comprising the linear combination of the H_2-type ellipsoidal MO and the N AO according to Eq. (13.247) are shown in Figures 13.5 and 13.6, respectively.

Figure 13.6. NH MO comprising the superposition of the H_2-type ellipsoidal MO and the $N2p_x$ AO with a relative charge-density of 0.75 to 1.25; otherwise, the $N2p_x$ is the same as that of the nitrogen atom. (A) Side-on, color scale, translucent view of the charge-density of the NH MO. The ellipsoidal surface of the H_2-type ellipsoidal MO that transitions to the $N2p_x$ AO, the $N2p$ shell, the $N2s$ shell, the $N1s$ shell, and the nuclei (red not to scale) are shown. (B) Cut-away view showing the inner most $N1s$ shell, and moving radially, the $N2s$ shell, the $N2p$ shell, and the H_2-type ellipsoidal MO that transitions to the $N2p_x$ AO.

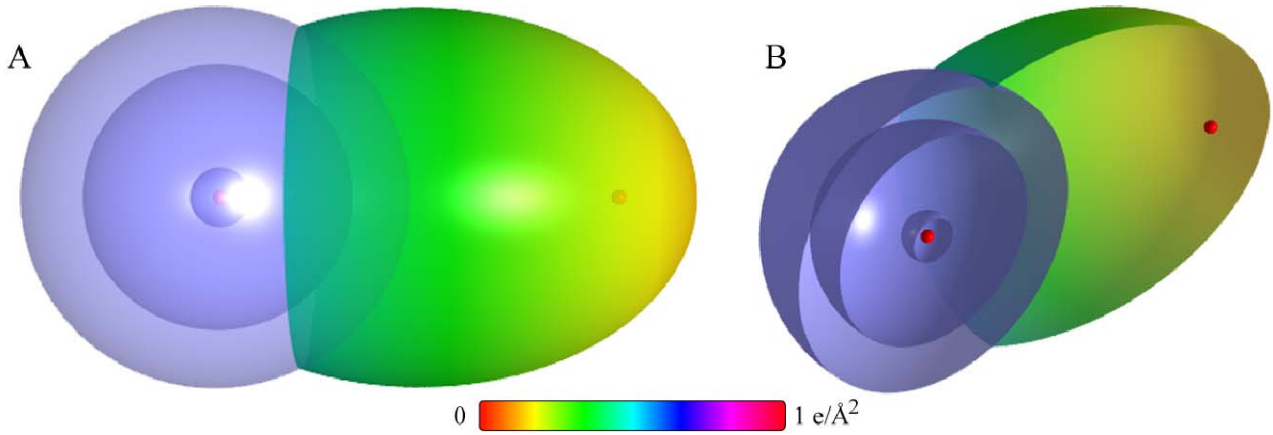

ENERGIES OF NH

The energies of NH given by the substitution of the semiprincipal axes (Eqs. (13.255-13.256) and (13.259)) into the energy equations (Eqs. (13.67-13.73)) are:

$$V_e = \left(\frac{3}{4}\right)\frac{-2e^2}{8\pi\varepsilon_0\sqrt{a^2-b^2}}\ln\frac{a+\sqrt{a^2-b^2}}{a-\sqrt{a^2-b^2}} = -37.85748\ eV \tag{13.271}$$

$$V_p = \frac{e^2}{8\pi\varepsilon_0\sqrt{a^2-b^2}} = 13.81113\ eV \tag{13.272}$$

$$T = \left(\frac{3}{4}\right)\frac{\hbar^2}{2m_e a\sqrt{a^2-b^2}}\ln\frac{a+\sqrt{a^2-b^2}}{a-\sqrt{a^2-b^2}} = 13.89011\ eV \tag{13.273}$$

$$V_m = \left(\frac{3}{4}\right)\frac{-\hbar^2}{4m_e a\sqrt{a^2-b^2}}\ln\frac{a+\sqrt{a^2-b^2}}{a-\sqrt{a^2-b^2}} = -6.94505\ eV \tag{13.274}$$

$$E_T(NH) = -\frac{e^2}{8\pi\varepsilon_0 c'}\left[\left(\frac{3}{2}-\frac{3}{8}\frac{a_0}{a}\right)\ln\frac{a+c'}{a-c'}-1\right] - 14.53414\ eV = -31.63544\ eV \tag{13.275}$$

where $E_T(NH)$ is given by Eq. (13.253) which is reiteratively matched to Eq. (13.75) within five-significant-figure round-off error.

VIBRATION AND ROTATION OF NH

The vibrational energy of NH may be solved in the same manner as that of OH. From Eqs. (13.102-13.106) with the substitution of the NH parameters, the angular frequency of the oscillation is:

$$\omega = \sqrt{\frac{\frac{0.75e^2}{8\pi\varepsilon_0 b^3} - \frac{e^2}{8\pi\varepsilon_0(2c')^3}}{\mu}} = \sqrt{\frac{\frac{0.75e^2}{8\pi\varepsilon_0(0.94159a_0)^3} - \frac{e^2}{8\pi\varepsilon_0(1.97027a_0)^3}}{\frac{14}{15}m_p}} = 6.18700\ X\ 10^{14}\ rad/s \tag{13.276}$$

where b is given by Eq. (13.259), $2c'$ is given by Eq. (13.257), and the reduced mass of ^{14}NH is given by:

$$\mu_{^{14}NH} = \frac{m_1 m_2}{m_1+m_2} = \frac{(1)(14)}{1+14}m_p \tag{13.277}$$

where m_p is the proton mass. Thus, during bond formation, the perturbation of the orbit determined by an inverse-squared force results in simple harmonic oscillatory motion of the orbit, and the corresponding frequency, $\omega(0)$, for ^{14}NH given by Eqs. (11.136), (11.148), and (13.276) is

$$\omega(0)=\sqrt{\frac{k(0)}{\mu}}=\sqrt{\frac{597.59\ Nm^{-1}}{\mu}}=6.18700\ X\ 10^{14}\ radians/s \tag{13.278}$$

where the reduced nuclear mass of ^{14}NH is given by Eq. (13.277) and the spring constant, $k(0)$, given by Eqs. (11.136) and (13.276) is:

$$k(0)=597.59\ Nm^{-1} \tag{13.279}$$

The ^{14}NH transition-state vibrational energy, $E_{vib}(0)$, given by Planck's equation (Eq. (11.127)) is:

$$E_{vib}(0)=\hbar\omega=\hbar 6.18700\ X\ 10^{14}\ rad/s=0.407239\ eV=3284.58\ cm^{-1} \tag{13.280}$$

ω_e, from the experimental curve fit of the vibrational energies of ^{14}NH is [28]:

$$\omega_e=3282.3\ cm^{-1} \tag{13.281}$$

Using Eqs. (13.112-13.118) with $E_{vib}(0)$ given by Eq. (13.280) and D_0 given by Eq. (13.311), the ^{14}NH $\upsilon=1\rightarrow\upsilon=0$ vibrational energy, $E_{vib}(1)$ is:

$$E_{vib}(1)=0.38581\ eV \qquad \left(3111.84\ cm^{-1}\right) \tag{13.282}$$

The experimental vibrational energy of ^{14}NH using ω_e and $\omega_e x_e$ [28] according to K&P [15] is:

$$E_{vib}(1)=0.38752\ eV \qquad \left(3125.5\ cm^{-1}\right) \tag{13.283}$$

Using Eq. (13.113) with $E_{vib}(1)$ given by Eq. (13.282) and D_0 given by Eq. (13.311), the anharmonic perturbation term, $\omega_0 x_0$, of ^{14}NH is:

$$\omega_0 x_0=86.37\ cm^{-1} \tag{13.284}$$

The experimental anharmonic perturbation term, $\omega_0 x_0$, of ^{14}NH [28] is:

$$\omega_0 x_0=78.4\ cm^{-1} \tag{13.285}$$

The vibrational energies of successive states are given by Eqs. (13.280), (13.112), and (13.284).

Using b given by Eq. (13.259), $2c'$ given by Eq. (13.257), D_0 given by Eq. (13.314), and the reduced nuclear mass of ^{14}ND given by

$$\mu_{^{14}ND}=\frac{m_1 m_2}{m_1+m_2}=\frac{(2)(14)}{2+14}m_p \tag{13.286}$$

where m_p is the proton mass, the corresponding parameters for deuterium nitride ^{14}ND (Eqs. (13.102-13.121)) are:

$$\omega(0)=\sqrt{\frac{k(0)}{\mu}}=\sqrt{\frac{597.59\ Nm^{-1}}{\mu}}=4.51835\ X\ 10^{14}\ radians/s \tag{13.287}$$

$$k(0)=579.59\ Nm^{-1} \tag{13.288}$$

$$E_{vib}(0)=\hbar\omega=\hbar 4.51835\ X\ 10^{14}\ rad/s=0.29741\ eV=2398.72\ cm^{-1} \tag{13.289}$$

$$E_{vib}(1)=0.28710\ eV \qquad \left(2305.35\ cm^{-1}\right) \tag{13.290}$$

$$\omega_0 x_0=47.40\ cm^{-1} \tag{13.291}$$

ω_e, from the experimental curve fit of the vibrational energies of ^{14}ND is [28]:

$$\omega_e=2398\ cm^{-1} \tag{13.292}$$

The experimental vibrational energy of ^{14}ND using ω_e and $\omega_e x_e$ [28] according to K&P [15] is:

$$E_{vib}(1)=0.2869\ eV \qquad \left(2314\ cm^{-1}\right) \tag{13.293}$$

and the experimental anharmonic perturbation term, $\omega_0 x_0$, of ^{14}ND [28] is:

$$\omega_0 x_0=42\ cm^{-1} \tag{13.294}$$

which match the predictions given by Eqs. (13.289), (13.290) and (13.291), respectively.

Using Eqs. (13.133-13.134) and the internuclear distance, $r=2c'$, and reduced mass of ^{14}NH given by Eqs. (13.257) and (13.277), respectively, the corresponding B_e is:

$$B_e=16.495\ cm^{-1} \tag{13.295}$$

The experimental B_e rotational parameter of ^{14}NH is [28]:

$$B_e=16.6993\ cm^{-1} \tag{13.296}$$

Using the internuclear distance, $r = 2c'$, and reduced mass of ^{14}ND given by Eqs. (13.257) and (13.286), respectively, the corresponding B_e is:

$$B_e = 8.797\ cm^{-1} \tag{13.297}$$

The experimental B_e rotational parameter of ^{14}ND is [28]:

$$B_e = 8.7913\ cm^{-1} \tag{13.298}$$

THE DOPPLER ENERGY TERMS OF ^{14}NH AND ^{14}ND

The equations of the radiation reaction force of hydrogen and deuterium nitride are the same as those of the corresponding hydroxyl radicals with the substitution of the hydrogen and deuterium nitride parameters. Using Eqs. (11.136) and (13.140-13.141), the angular frequency of the reentrant oscillation in the transition state is

$$\omega = \sqrt{\frac{\frac{0.75e^2}{4\pi\varepsilon_0 b^3}}{m_e}} = 3.91850\ X\ 10^{16}\ rad/s \tag{13.299}$$

where b is given by Eq. (13.259). The kinetic energy, E_K, is given by Planck's equation (Eq. (11.127)):

$$\bar{E}_K = \hbar\omega = \hbar 3.91850\ X\ 10^{16}\ rad/s = 25.79224\ eV \tag{13.300}$$

In Eq. (11.181), substitution of the total energy of NH, $E_T(NH)$, (Eq. (13.253)) for $E_{h\nu}$, the mass of the electron, m_e, for M, and the kinetic energy given by Eq. (13.300) for $\bar{E}_K$ gives the Doppler energy of the electrons for the reentrant orbit:

$$\bar{E}_D \cong E_{h\nu}\sqrt{\frac{2\bar{E}_K}{Mc^2}} = -31.63537\ eV\sqrt{\frac{2e(25.79224\ eV)}{m_e c^2}} = -0.31785\ eV \tag{13.301}$$

In addition to the electrons, the nuclei also undergo simple harmonic oscillation in the transition state at their corresponding frequency. The decrease in the energy of NH due to the reentrant orbit in the transition state corresponding to simple harmonic oscillation of the electrons and nuclei, $\bar{E}_{osc}$, is given by the sum of the corresponding energies, $\bar{E}_D$ given by Eq. (13.301) and $\bar{E}_{Kvib}$, the average kinetic energy of vibration which is 1/2 of the vibrational energy of NH. Using the experimental ^{14}NH ω_e of 3282.3 cm^{-1} $(0.40696\ eV)$ [28] $\bar{E}_{osc}(^{14}NH)$ is:

$$\bar{E}_{osc}(^{14}NH) = \bar{E}_D + \bar{E}_{Kvib} = \bar{E}_D + \frac{1}{2}\hbar\sqrt{\frac{k}{\mu}} \tag{13.302}$$

$$\bar{E}_{osc}(^{14}NH) = -0.31785\ eV + \frac{1}{2}(0.40696\ eV) = -0.11437\ eV \tag{13.303}$$

Using Eqs. (13.301) and the experimental ^{14}ND ω_e of 2398 cm^{-1} $(0.29732\ eV)$ [28] $\bar{E}_{osc}(^{14}ND)$ is:

$$\bar{E}_{osc}(^{14}ND) = -0.31785\ eV + \frac{1}{2}(0.29732\ eV) = -0.16919\ eV \tag{13.304}$$

TOTAL AND BOND ENERGIES OF ^{14}NH AND ^{14}ND

$E_{T+osc}(NH)$, the total energy of the ^{14}NH radical including the Doppler term, is given by the sum of $E_T(NH)$ (Eq. (13.253)) and $\bar{E}_{osc}(^{14}NH)$ given by Eq. (13.303):

$$\begin{aligned} E_{T+osc}(NH) &= V_e + T + V_m + V_p + E(2p\ shell) + \bar{E}_{osc}(^{14}NH) \\ &= E_T(NH) + \bar{E}_{osc}(^{14}NH) \end{aligned} \tag{13.305}$$

$$\begin{aligned} E_{T+osc}(NH) &= \left\{\frac{-e^2}{8\pi\varepsilon_0 c'}\left[\left(\frac{3}{2} - \frac{3}{8}\frac{a_0}{a}\right)\ln\frac{a+c'}{a-c'} - 1\right] - 14.53414\ eV\right\}\left[1 + \sqrt{\frac{2\hbar\sqrt{\frac{3}{4}\frac{e^2}{4\pi\varepsilon_0 b^3}}{m_e}}{m_e c^2}}\right] + \frac{1}{2}\hbar\sqrt{\frac{k}{\mu}} \\ &= -31.63537\ eV - 0.31785\ eV + \frac{1}{2}\hbar\sqrt{\frac{k}{\mu}} \end{aligned} \tag{13.306}$$

From Eqs. (13.302-13.303) and (13.305-13.306), the total energy of ^{14}NH is:

$$\begin{aligned} E_{T+osc}\left(NH\right) &= -31.63537\ eV + \bar{E}_{osc}\left(^{14}NH\right) \\ &= -31.63537\ eV - 0.31785\ eV + \frac{1}{2}\left(0.40696\ eV\right) \\ &= -31.74974\ eV \end{aligned} \tag{13.307}$$

where the experimental ω_e was used for the $\hbar\sqrt{\frac{k}{\mu}}$ term. $E_{T+osc}\left(ND\right)$, the total energy of ^{14}ND including the Doppler term, is given by the sum of $E_T\left(ND\right) = E_T\left(NH\right)$ (Eq. (13.253)) and $\bar{E}_{osc}\left(^{14}ND\right)$ given by Eq. (13.304):

$$\begin{aligned} E_{T+osc}\left(ND\right) &= -31.63537\ eV + \bar{E}_{osc}\left(^{14}ND\right) \\ &= -31.63537\ eV - 0.31785\ eV + \frac{1}{2}\left(0.29732\ eV\right) \\ &= -31.80456\ eV \end{aligned} \tag{13.308}$$

where the experimental ω_e was used for the $\hbar\sqrt{\frac{k}{\mu}}$ term. The dissociation of the bond of the hydrogen nitride forms a free hydrogen atom with one unpaired electron and a nitrogen atom with three unpaired electrons as shown in Eq. (13.246). The p_x and p_y fields cancel and the magnetic energy (Eq. (7.46)) with $r_7 = 0.93084a_0$ is subtracted due to the one component of E_{mag} given by Eq. (10.137):

$$E(magnetic) = \frac{2\pi\mu_0 e^2\hbar^2}{m_e^2\left(0.93084a_0\right)^3} = \frac{8\pi\mu_0\mu_B^2}{\left(0.93084a_0\right)^3} = 0.14185\ eV \tag{13.309}$$

The corresponding bond dissociation energy, E_D, is given by the sum of the total energies of the nitrogen atom and the corresponding hydrogen atom minus the sum of $E_{T+osc}\left(NH\right)$ and $E(magnetic)$:

$$E_D = E(^{14}N) + E(H) - E_{T+osc}\left(NH\right) - E\left(magnetic\right) \tag{13.310}$$

$E(^{14}N)$ is given by Eq. (13.251), $E_D\left(H\right)$ is given by Eq. (13.154), and $E_D\left(D\right)$ is given by Eq. (13.155). The ^{14}NH bond dissociation energy, $E_D\left(^{14}NH\right)$, is given by Eqs. (13.154), (13.251), (13.307), and (13.309-13.310):

$$\begin{aligned} E_D\left(^{14}NH\right) &= -\left(14.53414\ eV + 13.59844\ eV\right) - \left(E\left(magnetic\right) + E_{T+osc}\left(NH\right)\right) \\ &= -28.13258\ eV - \left(0.14185 - 31.74974\ eV\right) \\ &= 3.47530\ eV \end{aligned} \tag{13.311}$$

The experimental ^{14}NH bond dissociation energy from Ref. [29] and Ref. [30] is:

$$E_D\left(^{14}NH\right) = 3.42\ eV \tag{13.312}$$

$$E_D\left(^{14}NH\right) \le 3.47\ eV \tag{13.313}$$

The ^{14}ND bond dissociation energy, $E_D\left(^{14}ND\right)$, is given by Eqs. (13.155), (13.251), (13.308), and (13.309-13.310):

$$\begin{aligned} E_D\left(^{14}ND\right) &= -\left(14.53414\ eV + 13.603\ eV\right) - \left(E\left(magnetic\right) + E_{T+osc}\left(ND\right)\right) \\ &= -28.13714\ eV - \left(0.14185 - 31.80456\ eV\right) \\ &= 3.5256\ eV \end{aligned} \tag{13.314}$$

The experimental ^{14}ND bond dissociation energy from Ref. [31] and Ref. [30] is:

$$E_{D_{298}}\left(^{14}ND\right) \le 339\ kJ/mol = 3.513\ eV \tag{13.315}$$

$$E_D\left(^{14}ND\right) \le 3.54\ eV \tag{13.316}$$

The results of the determination of bond parameters of NH and ND are given in Table 13.1. The calculated results are based on first principles and given in closed-form, exact equations containing fundamental constants only. The agreement between the experimental and calculated results is excellent.

DIHYDROGEN NITRIDE (NH_2)

The dihydrogen nitride radical NH_2 is formed by the reaction of a hydrogen atom with a hydrogen nitride radical:

$$NH + H \rightarrow NH_2 \tag{13.317}$$

NH_2 can be solved using the same principles as those used to solve H_2O. Two diatomic molecular orbitals (MOs) developed in the Nature of the Chemical Bond of Hydrogen-Type Molecules and Molecular Ions section serve as basis functions in a linear combination with two nitrogen atomic orbitals (AOs) to form the MO of NH_2. The solution is very similar to that of NH except that there are two NH bonds in NH_2.

FORCE BALANCE OF NH_2

NH_2 comprises two chemical bonds between nitrogen and hydrogen. Each $N-H$ bond comprises two spin-paired electrons with one from an initially unpaired electron of the nitrogen atom and the other from the hydrogen atom. Each H-atom electron forms a H_2-type ellipsoidal MO with one of the initially unpaired N-atom electrons, $2p_x$ or $2p_y$, such that the proton and the N nucleus serve as the foci. The initial N electron configuration given in the Seven-Electron Atoms section is $1s^2 2s^2 2p^3$, and the orbital arrangement is given by Eqs. (10.134) and (13.246). The radius and the energy of the $N2p$ shell are unchanged with bond formation. The central paramagnetic force due to spin of each $N-H$ bond is provided by the spin-pairing force of the NH_2 MO that has the symmetry of an s orbital that superimposes with the $N2p$ orbitals such that the corresponding angular momenta are unchanged.

As in the case of H_2, each of two $N-H$-bond MOs is a prolate spheroid with the exception that the ellipsoidal MO surface cannot extend into N atom for distances shorter than the radius of the $2p$ shell since it is energetically unfavorable. Thus, the MO surface comprises a prolate spheroid at each H proton that is continuous with the $2p$ shell at the N atom. The energies in the NH_2 MO involve only each $N2p$ and each $H1s$ electron with the formation of each $N-H$ bond. The sum of the energies of the prolate spheroids is matched to that of the $2p$ shell. The forces are determined by these energies. As in the case of NH, the linear combination of each H_2-type ellipsoidal MO with each $N2p$ AO must involve a 25% contribution from the H_2-type ellipsoidal MO to the $N2p$ AO in order to match potential, kinetic, and orbital energy relationships. Thus, the NH_2 MO must comprise two $N-H$ bonds with each comprising 75% of a H_2-type ellipsoidal MO (1/2 +25%) and a nitrogen AO:

$$\left[1\, N2p_x\, AO + 0.75\, H_2\, MO\right] + \left[1\, N2p_y\, AO + 0.75\, H_2\, MO\right] \rightarrow NH_2\, MO \tag{13.318}$$

The force constant k' of each H_2-type-ellipsoidal-MO component of the NH_2 MO is given by Eq. (13.248). The distance from the origin of each $N-H$-bond MO to each focus c' is given by Eq. (13.249). The internuclear distance is given by Eq. (13.250). The length of the semiminor axis of the prolate spheroidal $N-H$-bond MO $b=c$ is given by Eq. (13.62). The eccentricity, e, is given by Eq. (13.63). The solution of the semimajor axis a then allows for the solution of the other axes of each prolate spheroid and eccentricity of each $N-H$-bond MO. Since each of the two prolate spheroidal $N-H$-bond MOs comprises a H_2-type-ellipsoidal MO that transitions to the N AO, the energy E in Eq. (13.251) adds to that of the two corresponding H_2-type ellipsoidal MOs to give the total energy of the NH_2 MO. From the energy equation and the relationship between the axes, the dimensions of the NH_2 MO are solved.

The energy components of V_e, V_p, T, V_m, and E_T are twice those of OH and NH given by Eqs. (13.67-13.73) and equal to those of H_2O given by Eqs. (13.172-13.178). Similarly to H_2O, since each prolate spheroidal H_2-type MO transitions to the N AO and the energy of the $N2p$ shell must remain constant and equal to the negative of the ionization energy given by Eq. (13.251), the total energy $E_T\left(NH_2\right)$ of the NH_2 MO is given by the sum of the energies of the orbitals corresponding to the composition of the linear combination of the N AO and the two H_2-type ellipsoidal MOs that forms the NH_2 MO as given by Eq. (13.318):

$$\begin{aligned} E_T\left(NH_2\right) &= E_T + E\left(2p\ shell\right) = E_T - E(ionization;\ N) \\ &= -\frac{e^2}{4\pi\varepsilon_0 c'}\left[\left(\frac{3}{2}-\frac{3}{8}\frac{a_0}{a}\right)\ln\frac{a+c'}{a-c'}-1\right]-14.53414\ eV \end{aligned} \tag{13.319}$$

The two hydrogen atoms and the nitrogen atom can achieve an energy minimum as a linear combination of two H_2-type ellipsoidal MOs each having the proton and the nitrogen nucleus as the foci. Each $N-H$-bond MO comprises the same $N2p$ shell of constant energy given by Eq. (13.251). Thus, the energy of the NH_2 MO is also given by the sum of that of the two H_2-type ellipsoidal MOs given by Eq. (11.212) minus the energy of the redundant nitrogen atom of the linear combination given by Eq. (13.251):

$$E_T\left(2H_2-N\right)=-2\frac{e^2}{8\pi\varepsilon_0 a_0}\left[\left(2\sqrt{2}-\sqrt{2}+\frac{\sqrt{2}}{2}\right)\ln\frac{\sqrt{2}+1}{\sqrt{2}-1}-\sqrt{2}\right]-E\left(2p\ shell\right)$$
$$=2\left(-31.63536831\ eV\right)-\left(-14.53414\ eV\right)=-48.73660\ eV \tag{13.320}$$

$E_T\left(NH_2\right)$ given by Eq. (13.319) is set equal to two times the energy of the H_2-type ellipsoidal MO minus the energy of the $N2p$ shell given by Eq. (13.320):

$$E_T\left(NH_2\right)=-\frac{e^2}{4\pi\varepsilon_0 c'}\left[\left(\frac{3}{2}-\frac{3}{8}\frac{a_0}{a}\right)\ln\frac{a+c'}{a-c'}-1\right]-14.53414\ eV=-48.73660\ eV \tag{13.321}$$

From the energy relationship given by Eq. (13.321) and the relationship between the axes given by Eqs. (13.248-13.250) and (13.62-13.63), the dimensions of the NH_2 MO can be solved.

Substitution of Eq. (13.249) into Eq. (13.321) gives:

$$\frac{e^2}{4\pi\varepsilon_0\sqrt{0.712154aa_0}}\left[\left(\frac{3}{2}-\frac{3}{8}\frac{a_0}{a}\right)\ln\frac{a+\sqrt{0.712154aa_0}}{a-\sqrt{0.712154aa_0}}-1\right]=e34.20246 \tag{13.322}$$

The most convenient way to solve Eq. (13.322) is by the reiterative technique using a computer. The result to within the round-off error with five-significant figures is

$$a=1.36276a_0=7.21141\ X\ 10^{-11}\ m \tag{13.323}$$

Substitution of Eq. (13.323) into Eq. (13.249) gives:

$$c'=0.98514a_0=5.21312\ X\ 10^{-11}\ m \tag{13.324}$$

The internuclear distance given by multiplying Eq. (13.324) by two is:

$$2c'=1.97027a_0=1.04262\ X\ 10^{-10}\ m \tag{13.325}$$

The experimental bond distance is [32]:

$$2c'=1.024\ X\ 10^{-10}\ m \tag{13.326}$$

Substitution of Eqs. (13.323-13.324) into Eq. (13.62) gives:

$$b=c=0.94160a_0=4.98276\ X\ 10^{-11}\ m \tag{13.327}$$

Substitution of Eqs. (13.323-13.324) into Eq. (13.63) gives:

$$e=0.72290 \tag{13.328}$$

The nucleus of the H atom and the nucleus of the N atom comprise the foci of the H_2-type ellipsoidal MO. The parameters of the point of intersection of each H_2-type ellipsoidal MO and the $N2p_x$ AO or $N2p_y$ AO are given by Eqs. (13.84-13.95) and (13.261-13.270). Using Eqs. (13.323-13.325) and (13.327-13.328), the polar intersection angle θ' given by Eq. (13.261) with $r_n=r_7=0.93084a_0$ is

$$\theta'=114.61° \tag{13.329}$$

Then, the angle θ_{N2pAO} the radial vector of the $N2p_x$ AO or $N2p_y$ AO makes with the internuclear axis is

$$\theta_{N2pAO}=180°-114.61°=65.39° \tag{13.330}$$

as shown in Figure 13.5. The parametric angle θ_{H_2MO} given by Eqs. (13.264-13.265), (13.327), and (13.330) is:

$$\theta_{H_2MO}=64.00° \tag{13.331}$$

Then, the distance d_{H_2MO} along the internuclear axis from the origin of H_2-type ellipsoidal MO to the point of intersection of the orbitals given by Eqs. (13.267), (13.323), and (13.331) is:

$$d_{H_2MO}=0.59748a_0=3.16175\ X\ 10^{-11}\ m \tag{13.332}$$

The distance d_{N2pAO} along the internuclear axis from the origin of the N atom to the point of intersection of the orbitals given by Eqs. (13.269), (13.324), and (13.332) is:

$$d_{N2pAO}=0.38765a_0=2.05137\ X\ 10^{-11}\ m \tag{13.333}$$

As shown in Eq. (13.318), in addition to the p-orbital charge-density modulation, the uniform charge-density in the p_x and p_y orbitals is increased by a factor of 0.25 and the H atoms are each decreased by a factor of 0.25. Using the orbital composition of NH_2 (Eq. (13.318)), the radii of $N1s=0.14605a_0$ (Eq. (10.51)), $N2s=0.69385a_0$ (Eq. (10.62)), and $N2p=0.93084a_0$ (Eq. (10.142)) shells, and the parameters of the NH_2 MO given by Eqs. (13.3-13.4) and (13.323-13.333), the charge-density of the NH_2 MO comprising the linear combination of two $N-H$-bond MOs (NH-type ellipsoidal MOs given in the Energies of NH section) according to Eq. (13.318) is shown in Figure 13.7. Each $N-H$-bond MO comprises a H_2-type ellipsoidal MO and an $N2p$ AO having the dimensional diagram shown in Figure 13.5.

Figure 13.7. NH_2 MO comprising the linear combination of two $N-H$ -bond MOs. Each $N-H$ -bond MO comprises the superposition of a H_2-type ellipsoidal MO and the $N2p_x$ AO or the $N2p_y$ AO with a relative charge-density of 0.75 to 1.25; otherwise, the $N2p$ orbitals are the same as those of the nitrogen atom. The internuclear axis of one $N-H$ bond is perpendicular to the bonding p_x orbital, and the internuclear axis of the other $N-H$ bond is perpendicular to the bonding p_y orbital. (A) Color scale, translucent view of the charge-density of the NH_2 MO from the top. For each $N-H$ bond, the ellipsoidal surface of each H_2-type ellipsoidal MO transitions to a $N2p$ AO. The $N2p$ shell, the $N2s$ shell, the $N1s$ shell, and the nuclei (red, not to scale) are shown. (B) Cut-away view showing the inner most $N1s$ shell, and moving radially, the $N2s$ shell, the $N2p$ shell, and the H_2-type ellipsoidal MO that transitions to a $N2p$ AO for each $N-H$ bond. Bisector current not shown.

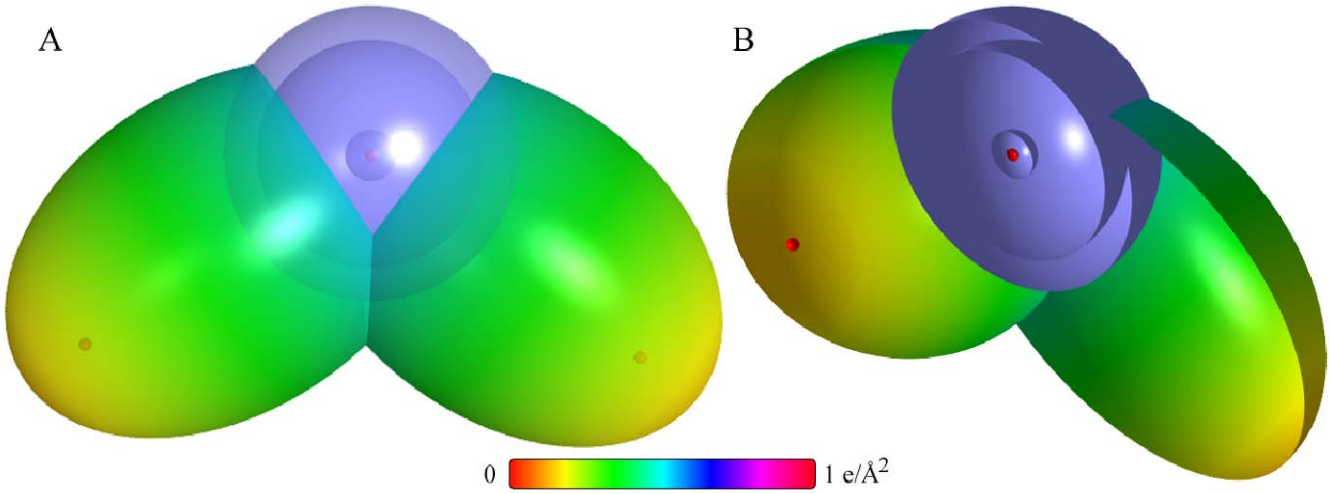

ENERGIES OF NH_2

The energies of NH_2 given by the substitution of the semiprincipal axes ((Eqs. (13.323-13.325) and (13.327)) into the energy equations (Eqs. (13.172-13.176)) are:

$$V_e = \left(\frac{3}{2}\right)\frac{-2e^2}{8\pi\varepsilon_0\sqrt{a^2-b^2}}\ln\frac{a+\sqrt{a^2-b^2}}{a-\sqrt{a^2-b^2}} = -75.71422\ eV \tag{13.334}$$

$$V_p = 2\frac{e^2}{8\pi\varepsilon_0\sqrt{a^2-b^2}} = 27.62216\ eV \tag{13.335}$$

$$T = \left(\frac{3}{2}\right)\frac{\hbar^2}{2m_e a\sqrt{a^2-b^2}}\ln\frac{a+\sqrt{a^2-b^2}}{a-\sqrt{a^2-b^2}} = 27.77974\ eV \tag{13.336}$$

$$V_m = \left(\frac{3}{2}\right)\frac{-\hbar^2}{4m_e a\sqrt{a^2-b^2}}\ln\frac{a+\sqrt{a^2-b^2}}{a-\sqrt{a^2-b^2}} = -13.88987\ eV \tag{13.337}$$

$$E_T\left(NH_2\right) = -\frac{e^2}{4\pi\varepsilon_0 c'}\left[\left(\frac{3}{2}-\frac{3}{8}\frac{a_0}{a}\right)\ln\frac{a+c'}{a-c'}-1\right] - 14.53414\ eV = -48.73633\ eV \tag{13.338}$$

where $E_T\left(NH_2\right)$ is given by Eq. (13.319) which is reiteratively matched to Eq. (13.320) within five-significant-figure round-off error.

VIBRATION OF NH_2

The vibrational energy levels of NH_2 may be solved as two equivalent coupled harmonic oscillators by developing the Lagrangian, the differential equation of motion, and the eigenvalue solutions [2] wherein the spring constants are derived from the central forces as given in the Vibration of Hydrogen-Type Molecular Ions section and the Vibration of Hydrogen-Type Molecules section.

THE DOPPLER ENERGY TERM OF NH_2

The radiation reaction force in the case of the vibration of NH_2 in the transition state corresponds to the Doppler energy, E_D, given by Eq. (11.181) and Eqs. (13.22) and (13.144) that is dependent on the motion of the electrons and the nuclei. The kinetic energy of the transient vibration is derived from the corresponding central forces. The equations of the radiation reaction force of dihydrogen and dideuterium nitride are the same as those of the corresponding water molecules with the substitution of the dihydrogen and dideuterium nitride parameters. Using Eqs. (11.136) and (13.207-13.209), the angular frequency of the reentrant oscillation in the transition state is

$$\omega = \sqrt{\frac{\left(\frac{3}{2}\right)\frac{e^2}{4\pi\varepsilon_0 b^3}}{m_e}} = 5.54150\ X\ 10^{16}\ rad/s \tag{13.339}$$

where b is given by Eq. (13.327). The kinetic energy, E_K, is given by Planck's equation (Eq. (11.127)):

$$\overline{E}_K = \hbar\omega = \hbar 5.54150\ X\ 10^{16}\ rad/s = 36.47512\ eV \tag{13.340}$$

In Eq. (11.181), substitution of $E_T\left(H_2\right)$ (Eqs. (11.212) and (13.75)), the maximum total energy of each H_2-type MO, for $E_{h\nu}$, the mass of the electron, m_e, for M, and the kinetic energy given by Eq. (13.340) for $\overline{E}_K$ gives the Doppler energy of the electrons for the reentrant orbit:

$$\begin{aligned}\overline{E}_D &\cong E_{h\nu}\sqrt{\frac{2\overline{E}_K}{Mc^2}}\\ &= -31.63537\ eV\sqrt{\frac{2e\left(36.47512\ eV\right)}{m_e c^2}}\\ &= -0.37798\ eV\end{aligned} \tag{13.341}$$

In addition to the electrons, the nuclei also undergo simple harmonic oscillation in the transition state at their corresponding frequency. The decrease in the energy of NH_2 due to the reentrant orbit in the transition state corresponding to simple harmonic oscillation of the electrons and nuclei, $\overline{E}_{osc}$, is given by the sum of the corresponding energies, $\overline{E}_D$ given by Eq. (13.341) and $\overline{E}_{Kvib}$, the average kinetic energy of vibration which is 1/2 of the vibrational energy of NH_2. Using the experimental $^{14}NH_2$ vibrational energy of $E_{vib} = 3301.110\ cm^{-1} = 0.40929\ eV$ [33] gives:

$$\overline{E}'_{osc} = \overline{E}_D + \overline{E}_{Kvib} = \overline{E}_D + \frac{1}{2}\hbar\sqrt{\frac{k}{\mu}} \tag{13.342}$$

$$\begin{aligned}\overline{E}'_{osc} &= -0.37798\ eV + \frac{1}{2}\left(0.40929\ eV\right)\\ &= -0.17334\ eV\end{aligned} \tag{13.343}$$

per bond. As in the case for H_2O, the reentrant orbit for the binding of a hydrogen atom to a NH radical causes the bonds to oscillate by increasing and decreasing in length along the two $N-H$ bonds at a relative phase angle of 180°. Since the vibration and reentrant oscillation is along two bonds for the asymmetrical stretch (ν_3), $\overline{E}_{osc}$ for $^{14}NH_2$, $\overline{E}_{osc}\left(^{14}NH_2\right)$, is:

$$\begin{aligned}\overline{E}_{osc}\left(^{14}NH_2\right) &= 2\left(\overline{E}_D + \frac{1}{2}\hbar\sqrt{\frac{k}{\mu}}\right)\\ &= 2\left(-0.37798\ eV + \frac{1}{2}\left(0.40929\ eV\right)\right)\\ &= -0.34668\ eV\end{aligned} \tag{13.344}$$

Using Eq. (13.341), Eqs. (13.342-13.344), and the $^{14}ND_2$ vibrational energy of $E_{vib} = 2410.79\ cm^{-1} = 0.29890\ eV$, calculated from the experimental $^{14}NH_2$ vibrational energy using Eq. (11.148), the corresponding $\overline{E}_{osc}\left(^{14}ND_2\right)$ is:

$$\begin{aligned}\overline{E}_{osc}\left(^{14}ND_2\right) &= 2\left(-0.37798\ eV + \frac{1}{2}\left(0.29890\ eV\right)\right)\\ &= -0.45707\ eV\end{aligned} \tag{13.345}$$

TOTAL AND BOND ENERGIES OF $^{14}NH_2$ AND $^{14}ND_2$

$E_{T+osc}\left(^{14}NH_2\right)$, the total energy of the $^{14}NH_2$ including the Doppler term, is given by the sum of $E_T\left(NH_2\right)$ (Eq. (13.321)) and $\bar{E}_{osc}\left(^{14}NH_2\right)$ given Eqs. (13.339-13.344):

$$E_{T+osc}\left(^{14}NH_2\right) = V_e + T + V_m + V_p + E\left(N2p\right) + \bar{E}_{osc}\left(^{14}NH_2\right) = E_T\left(NH_2\right) + \bar{E}_{osc}\left(^{14}NH_2\right) \tag{13.346}$$

$$E_{T+osc}\left(^{14}NH_2\right) = \left\{\begin{array}{l}\left(\dfrac{-e^2}{4\pi\varepsilon_0 c'}\left[\left(\dfrac{3}{2}-\dfrac{3}{8}\dfrac{a_0}{a}\right)\ln\dfrac{a+c'}{a-c'}-1\right]-14.53414\ eV\right) \\ -2\left(\left(31.63536831\ eV\right)\sqrt{\dfrac{2\hbar\sqrt{\dfrac{\dfrac{3}{2}\dfrac{e^2}{4\pi\varepsilon_0 b^3}}{m_e}}}{m_e c^2}}-\dfrac{1}{2}\hbar\sqrt{\dfrac{k}{\mu}}\right)\end{array}\right\} \tag{13.347}$$

$$= -48.73660\ eV - 2\left(0.37798\ eV - \frac{1}{2}\hbar\sqrt{\frac{k}{\mu}}\right)$$

From Eqs. (13.344) and (13.346-13.347), the total energy of $^{14}NH_2$ is:

$$\begin{aligned} E_{T+osc}\left(^{14}NH_2\right) &= -48.73660\ eV + \bar{E}_{osc}\left(^{14}NH_2\right) \\ &= -48.73660\ eV - 2\left(0.37798\ eV - \frac{1}{2}\left(0.40929\ eV\right)\right) \\ &= -49.08328\ eV \end{aligned} \tag{13.348}$$

where the experimental $^{14}NH_2$ vibrational energy was used for the $\hbar\sqrt{\dfrac{k}{\mu}}$ term. $E_{T+osc}\left(^{14}ND_2\right)$, the total energy of $^{14}ND_2$ including the Doppler term is given by the sum of $E_T\left(ND_2\right) = E_T\left(NH_2\right)$ (Eq. (13.321)) and $\bar{E}_{osc}\left(^{14}ND_2\right)$ given by Eq. (13.345).

$$\begin{aligned} E_{T+osc}\left(^{14}ND_2\right) &= -48.73660\ eV + \bar{E}_{osc}\left(^{14}ND_2\right) \\ &= -48.73660\ eV - 2\left(0.37798\ eV - \frac{1}{2}\left(0.29890\ eV\right)\right) \\ &= -49.19366\ eV \end{aligned} \tag{13.349}$$

where the experimental $^{14}NH_2$ vibrational energy corrected for the reduced mass difference of hydrogen and deuterium was used for the $\hbar\sqrt{\dfrac{k}{\mu}}$ term. The corresponding bond dissociation energy, E_D, is given by the sum of the total energies of the corresponding hydrogen nitride radical and hydrogen atom minus the total energy of dihydrogen nitride, $E_{T+osc}\left(^{14}NH_2\right)$.

Thus, E_D of $^{14}NH_2$ is given by:

$$E_D\left(^{14}NH_2\right) = E(H) + E(^{14}NH) - E_{T+osc}\left(^{14}NH_2\right) \tag{13.350}$$

where $E_T(^{14}NH)$ is given by the of the sum of the experimental energies of ^{14}N (Eq. (13.251)), H (Eq. (13.154)), and the negative of the bond energy of ^{14}NH (Eq. (13.312)):

$$E(^{14}NH) = -13.59844\ eV - 14.53414\ eV - 3.42\ eV = -31.55258\ eV \tag{13.351}$$

From Eqs. (13.154), (13.348), and (13.350-13.351), $E_D\left(^{14}NH_2\right)$ is:

$$\begin{aligned} E_D\left(^{14}NH_2\right) &= E(H) + E(^{14}NH) - E_{T+osc}\left(^{14}NH_2\right) \\ &= -13.59844\ eV - 31.55258\ eV - \left(-49.08328\ eV\right) \\ &= 3.9323\ eV \end{aligned} \tag{13.352}$$

The experimental $^{14}NH_2$ bond dissociation energy from Ref. [34] and Ref. [35] is:

$$E_D(^{14}NH_2) = 88 \pm 4\ kcal/mole = 3.8160\ eV \tag{13.353}$$

$$E_D(^{14}NH_2) = 91.0 \pm 0.5\ kcal/mole = 3.9461\ eV \tag{13.354}$$

Similarly, E_D of $^{14}ND_2$ is given by:

$$E_D\left(^{14}ND_2\right) = E(D) + E(^{14}ND) - \left(E_{T+osc}\left(^{14}ND_2\right)\right) \tag{13.355}$$

where $E_T(^{14}ND)$ is given by the of the sum of the experimental energies of ^{14}N (Eq. (13.251)), D (Eq. (13.155)), and the negative of the bond energy of ^{14}ND (Eq. (13.315)):

$$E(^{14}ND) = -13.603\ eV - 14.53414\ eV - 3.513\ eV = -31.6506\ eV \tag{13.356}$$

From Eqs. (13.155), (13.349), and (13.355-13.356), $E_D\left(^{14}ND_2\right)$ is

$$E_D(^{14}ND_2) = -13.603\ eV - 31.6506\ eV - \left(-49.19366\ eV\right) = 3.9401\ eV \tag{13.357}$$

The $^{14}ND_2$ bond dissociation energy calculated from the average of the experimental bond energies [34-35] and vibrational energy of $^{14}NH_2$ [33] is:

$$\begin{aligned} E_D(^{14}ND_2) &= E_D(^{14}NH_2) + \frac{1}{2}\left(E_{vib}\left(^{14}NH_2\right) - E_{vib}\left(^{14}ND_2\right)\right) \\ &= \frac{1}{2}\left(3.8160\ eV + 3.9461\ eV\right) + \frac{1}{2}\left(0.40929\ eV - 0.29890\ eV\right) = 3.9362\ eV \end{aligned} \tag{13.358}$$

BOND ANGLE OF NH_2

The NH_2 MO comprises a linear combination of two $N-H$ -bond MOs. Each $N-H$ -bond MO comprises the superposition of a H_2-type ellipsoidal MO and the $N2p_x$ AO or the $N2p_y$ AO with a relative charge density of 0.75 to 1.25; otherwise, the $N2p$ AOs are the same as those of the nitrogen atom. A bond is also possible between the two H atoms of the $N-H$ bonds. Such $H-H$ bonding would decrease the $N-H$ bond strength since electron density would be shifted from the $N-H$ bonds to the $H-H$ bond. Thus, the bond angle between the two $N-H$ bonds is determined by the condition that the total energy of the H_2-type ellipsoidal MO between the terminal H atoms of the $N-H$ bonds is zero. From Eqs. (11.79) and (13.228), the distance from the origin to each focus of the $H-H$ ellipsoidal MO is

$$c' = a\sqrt{\frac{\hbar^2 4\pi\varepsilon_0}{m_e e^2 2a}} = \sqrt{\frac{aa_0}{2}} \tag{13.359}$$

The internuclear distance from Eq. (13.229) is:

$$2c' = 2\sqrt{\frac{aa_0}{2}} \tag{13.360}$$

The length of the semiminor axis of the prolate spheroidal $H-H$ MO $b=c$ is given by Eq. (13.167).

Since the two H_2-type ellipsoidal MOs comprise 75% of the H electron density of H_2 and the energy of each H_2-type ellipsoidal MO is matched to that of the $N2p$ AO; the component energies and the total energy E_T of the $H-H$ bond are given by Eqs. (13.67-13.73) except that V_e, T, and V_m are corrected for the energy matching factor of 0.93613 given in Eq. (13.248). Substitution of Eq. (13.359) into Eq. (13.233) with the energy-matching factor gives:

$$0 = \left[\begin{array}{l} \dfrac{-e^2}{8\pi\varepsilon_0\sqrt{\dfrac{aa_0}{2}}}\left[\left(0.93613\right)^{-1}\left(\frac{3}{2} - \frac{3}{8}\frac{a_0}{a}\right)\ln\dfrac{a+\sqrt{\dfrac{aa_0}{2}}}{a-\sqrt{\dfrac{aa_0}{2}}} - 1\right]\left[1+\sqrt{\dfrac{2\hbar\sqrt{\dfrac{0.75e^2}{4\pi\varepsilon_0 a^3}m_e}}{m_e c^2}}\right] \\ + \dfrac{1}{2}\hbar\sqrt{\dfrac{\dfrac{0.75e^2}{8\pi\varepsilon_0 a^3} - \dfrac{e^2}{8\pi\varepsilon_0\left(a+c'\right)^3}}{0.5m_p}} \end{array}\right] \tag{13.361}$$

From the energy relationship given by Eq. (13.361) and the relationship between the axes given by Eqs. (13.359-13.360) and (13.167-13.168), the dimensions of the $H-H$ MO can be solved.

The most convenient way to solve Eq. (13.361) is by the reiterative technique using a computer. The result to within the round-off error with five-significant figures is:

$$a = 4.9500a_0 = 2.6194\ X\ 10^{-10}\ m \tag{13.362}$$

Substitution of Eq. (13.362) into Eq. (13.359) gives:

$$c' = 1.5732a_0 = 8.3251\ X\ 10^{-11}\ m \tag{13.363}$$

The internuclear distance given by multiplying Eq. (13.363) by two is:

$$2c' = 3.1464a_0 = 1.6650\ X\ 10^{-10}\ m \tag{13.364}$$

Substitution of Eqs. (13.362-13.363) into Eq. (13.167) gives:

$$b = c = 4.6933a_0 = 2.4836\ X\ 10^{-10}\ m \tag{13.365}$$

Substitution of Eqs. (13.362-13.363) into Eq. (13.168) gives:

$$e = 0.3178 \tag{13.366}$$

Using, $2c'_{H-H}$ (Eq. (13.364)), the distance between the two H atoms when the total energy of the corresponding MO is zero (Eq. (13.361)), and $2c'_{N-H}$ (Eq. (13.325)), the internuclear distance of each $N-H$ bond, the corresponding bond angle can be determined from the law of cosines. Using, Eq. (13.242), the bond angle θ between the $N-H$ bonds is:

$$\theta = \cos^{-1}\left(\frac{2(1.9703)^2 - (3.1464)^2}{2(1.9703)^2}\right) = \cos^{-1}(-0.2751) = 105.969^\circ \tag{13.367}$$

The experimental angle between the $N-H$ bonds is [32]:

$$\theta = 103.3^\circ \tag{13.368}$$

The results of the determination of bond parameters of NH_2 and ND_2 are given in Table 13.1. The calculated results are based on first principles and given in closed-form, exact equations containing fundamental constants only. The agreement between the experimental and calculated results is excellent.

AMMONIA (NH_3)

Ammonia (NH_3) is formed by the reaction of a hydrogen atom with a dihydrogen nitride radical:

$$NH_2 + H \rightarrow NH_3 \tag{13.369}$$

NH_3 can be solved using the same principles as those used to solve NH_2 except that three rather than two H_2-type prolate spheroidal molecular orbitals (MOs) serve as basis functions in a linear combination with nitrogen atomic orbitals (AOs) to form the MO of NH_3.

FORCE BALANCE OF NH_3

NH_3 comprises three chemical bonds between nitrogen and hydrogen. Each $N-H$ bond comprises two spin-paired electrons with one from an initially unpaired electron of the nitrogen atom and the other from the hydrogen atom. Each H-atom electron forms a H_2-type ellipsoidal MO with one of the initially unpaired N-atom electrons, $2p_x$, $2p_y$, or $2p_z$, such that the proton and the N nucleus serve as the foci. The initial N electron configuration given in the Seven-Electron Atoms section is $1s^2 2s^2 2p^3$, and the orbital arrangement is given by Eqs. (10.134) and (13.246). The radius and the energy of the $N2p$ shell are unchanged with bond formation. The central paramagnetic force due to spin of each $N-H$ bond is provided by the spin-paring force of the NH_3 MO that has the symmetry of an s orbital that superimposes with the $N2p$ orbitals such that the corresponding angular momenta are unchanged.

As in the case of H_2, each of three $N-H$-bond MOs is a prolate spheroid with the exception that the ellipsoidal MO surface cannot extend into the N atom for distances shorter than the radius of the $2p$ shell since it is energetically unfavorable. Thus, the MO surface comprises a prolate spheroid at each H proton that is continuous with the $2p$ shell at the N atom. The energies in the NH_3 MO involve only each $N2p$ and each $H1s$ electron with the formation of each $N-H$ bond. The sum of the energies of the prolate spheroids is matched to that of the $2p$ shell. The forces are determined by these energies. As in the cases of NH and NH_2, the linear combination of each H_2-type ellipsoidal MO with each $N2p$ AO must involve a 25% contribution from the H_2-type ellipsoidal MO to the $N2p$ AO in order to match potential, kinetic, and orbital energy relationships. Thus, the NH_3 MO must comprise three $N-H$ bonds with each comprising 75% of a H_2-type ellipsoidal MO (1/2 +25%) and a nitrogen AO:

$$\left[1\,N2p_x\,AO + 0.75\,H_2\,MO\right] + \left[1\,N2p_y\,AO + 0.75\,H_2\,MO\right] + \left[1\,N2p_z\,AO + 0.75\,H_2\,MO\right] \rightarrow NH_3\,MO \tag{13.370}$$

The force constant k' of each H_2-type-ellipsoidal-MO component of the NH_3 MO is given by Eq. (13.248). The distance from the origin of each $N-H$-bond MO to each focus c' is given by Eq. (13.249). The internuclear distance is given by Eq. (13.250). The length of the semiminor axis of the prolate spheroidal $N-H$-bond MO $b = c$ is given by Eq. (13.62). The eccentricity, e, is given by Eq. (13.63). The solution of the semimajor axis a then allows for the solution of the other axes of each prolate spheroid and eccentricity of each $N-H$-bond MO. Since each of the three prolate spheroidal $N-H$-bond MOs comprises a H_2-type-ellipsoidal MO that transitions to the N AO, the energy E in Eq. (13.251) adds to that of the three corresponding H_2-type ellipsoidal MOs to give the total energy of the NH_3 MO. From the energy equation and the relationship between the axes, the dimensions of the NH_3 MO are solved.

The energy components of V_e, V_p, T, V_m, and E_T are three times those of OH and NH given by Eqs. (13.67-13.73) and 1.5 times those of H_2O given by Eqs. (13.172-13.178). Similarly to H_2O, since each prolate spheroidal H_2-type MO transitions to the N AO and the energy of the $N2p$ shell must remain constant and equal to the negative of the ionization energy given by Eq. (13.251), the total energy $E_T(NH_3)$ of the NH_3 MO is given by the sum of the energies of the orbitals

corresponding to the composition of the linear combination of the N AO and the three H_2-type ellipsoidal MOs that forms the NH_3 MO as given by Eq. (13.370):

$$\begin{aligned} E_T\left(NH_3\right) &= E_T + E\left(2p\ shell\right) \\ &= E_T - E(ionization;\ N) \\ &= -3\frac{e^2}{8\pi\varepsilon_0 c'}\left[\left(\frac{3}{2}-\frac{3}{8}\frac{a_0}{a}\right)\ln\frac{a+c'}{a-c'}-1\right]-14.53414\ eV \end{aligned} \tag{13.371}$$

The three hydrogen atoms and the nitrogen atom can achieve an energy minimum as a linear combination of three H_2-type ellipsoidal MOs each having the proton and the nitrogen nucleus as the foci. Each $N-H$-bond MO comprises the same $N2p$ shell of constant energy given by Eq. (13.251). Thus, an energy term of the NH_3 MO is given by the sum of the three H_2-type ellipsoidal MOs given by Eq. (11.212) minus the energy of the redundant nitrogen atom of the linear combination given by Eq. (13.251). The total sum is determined by the energy matching condition of the binding atoms.

In Eq. (13.248), the equipotential condition of the union of each H_2-type-ellipsoidal-MO and the N AO was met when the force constant used to determine the ellipsoidal parameter c' was normalized by the ratio of the ionization energy of N $14.53414\ eV$ [6] and $13.605804\ eV$, the magnitude of the Coulombic energy between the electron and proton of H given by Eq. (1.264). This normalized the force to match that of the Coulombic force alone to meet the force matching condition of the NH MO under the influence of the proton and the N nucleus. The minimum total energy of the NH_3 MO from the sum of energies of a linear combination from four atoms is determined using the energy matching condition of Eq. (13.248). Since each of the three prolate spheroidal $N-H$-bond MOs of NH_3 comprises a H_2-type-ellipsoidal MO that transitions to the N AO and the energy matching condition is met, the nitrogen energy E (Eq. (13.251)) and the energy (Eq. (1.264)) of a hydrogen atomic orbital (H AO), $E_{Coulomb}\left(H\right)$, corresponding to the Coulombic force of $+e$ from the nitrogen nucleus is subtracted from the sum of the energies of the three corresponding H_2-type ellipsoidal MOs to given an energy minimum. From another perspective, the electron configuration of NH_2 is equivalent to that of OH and is given by Eq. (10.174). NH_2 serves as a one-electron atom that is energy matched by the H AO as a basis element to minimize the energy of NH_3 in the formation of the third $N-H$-bond.

$$\begin{aligned} E_T\left(3H_2-N-H\right) &= \left\{\begin{matrix} -3\frac{e^2}{8\pi\varepsilon_0 a_0}\left[\left(2\sqrt{2}-\sqrt{2}+\frac{\sqrt{2}}{2}\right)\ln\frac{\sqrt{2}+1}{\sqrt{2}-1}-\sqrt{2}\right] \\ -E\left(N2p\ shell\right)-E_{Coulomb}\left(H\right) \end{matrix}\right\} \\ &= 3\left(-31.63536831\ eV\right)-\left(-14.53414\ eV-13.605804eV\right)=-66.76616\ eV \end{aligned} \tag{13.372}$$

$E_T\left(NH_3\right)$ given by Eq. (13.371) is set equal to Eq. (13.372), three times the energy of the H_2-type ellipsoidal MO minus the energy of the $N2p$ shell and the H AO:

$$E_T\left(NH_3\right) = -3\frac{e^2}{8\pi\varepsilon_0 c'}\left[\left(\frac{3}{2}-\frac{3}{8}\frac{a_0}{a}\right)\ln\frac{a+c'}{a-c'}-1\right]-14.53414\ eV = -66.76616\ eV \tag{13.373}$$

From the energy relationship given by Eq. (13.373) and the relationship between the axes given by Eqs. (13.248-13.250) and (13.62-13.63), the dimensions of the NH_3 MO can be solved.

Substitution of Eq. (13.249) into Eq. (13.373) gives:

$$\frac{3e^2}{8\pi\varepsilon_0\sqrt{0.712154aa_0}}\left[\left(\frac{3}{2}-\frac{3}{8}\frac{a_0}{a}\right)\ln\frac{a+\sqrt{0.712154aa_0}}{a-\sqrt{0.712154aa_0}}-1\right]=e52.23202 \tag{13.374}$$

The most convenient way to solve Eq. (13.374) is by the reiterative technique using a computer. The result to within the round-off error with five-significant figures is:

$$a = 1.34750a_0 = 7.13066\ X\ 10^{-11}\ m \tag{13.375}$$

Substitution of Eq. (13.375) into Eq. (13.249) gives:

$$c' = 0.97961a_0 = 5.18385\ X\ 10^{-11}\ m \tag{13.376}$$

The internuclear distance given by multiplying Eq. (13.376) by two is:

$$2c' = 1.95921a_0 = 1.03677\ X\ 10^{-10}\ m \tag{13.377}$$

The experimental bond distance is [32]:

$$2c' = 1.012\ X\ 10^{-10}\ m \tag{13.378}$$

Substitution of Eqs. (13.375-13.376) into Eq. (13.62) gives:

$$b = c = 0.92527a_0 = 4.89633\ X\ 10^{-11}\ m \tag{13.379}$$

Substitution of Eqs. (13.375-13.376) into Eq. (13.63) gives:

$$e = 0.72698 \tag{13.380}$$

The nucleus of the H atom and the nucleus of the N atom comprise the foci of the H_2-type ellipsoidal MO. The parameters of the point of intersection of each H_2-type ellipsoidal MO and the $N2p_x$, $N2p_y$, or $N2p_z$ AO are given by Eqs. (13.84-13.95), (13.261-13.270), and (13.261-13.270). Using Eqs. (13.375-13.377) and (13.379-13.380), the polar intersection angle θ' given by Eq. (13.261) with $r_n = r_7 = 0.93084a_0$ is:

$$\theta' = 115.89° \tag{13.381}$$

Then, the angle θ_{N2pAO} the radial vector of the $N2p_x$, $N2p_y$, or $N2p_z$ AO makes with the internuclear axis is

$$\theta_{N2pAO} = 180° - 115.89° = 64.11° \tag{13.382}$$

as shown in Figure 13.5. The parametric angle θ_{H_2MO} given by Eqs. (13.264-13.265), (13.379), and (13.382) is:

$$\theta_{H_2MO} = 64.83° \tag{13.383}$$

Then, the distance d_{H_2MO} along the internuclear axis from the origin of H_2-type ellipsoidal MO to the point of intersection of the orbitals given by Eqs. (13.267), (13.375), and (13.383) is:

$$d_{H_2MO} = 0.57314a_0 = 3.03292\ X\ 10^{-11}\ m \tag{13.384}$$

The distance d_{N2pAO} along the internuclear axis from the origin of the N atom to the point of intersection of the orbitals given by Eqs. (13.269), (13.376), and (13.384) is:

$$d_{N2pAO} = 0.40647a_0 = 2.15093\ X\ 10^{-11}\ m \tag{13.385}$$

As shown in Eq. (13.370), in addition to the p-orbital charge-density modulation, the uniform charge-density in the p_x, p_y, and p_z orbitals is increased by a factor of 0.25 and the H atoms are each decreased by a factor of 0.25. Using the orbital composition of NH_3 (Eq. (13.370)), the radii of $N1s = 0.14605a_0$ (Eq. (10.51)), $N2s = 0.69385a_0$ (Eq. (10.62)), and $N2p = 0.93084a_0$ (Eq. (10.142)) shells, and the parameters of the NH_3 MO given by Eqs. (13.3-13.4) and (13.375-13.385), the charge-density of the NH_3 MO comprising the linear combination of three $N-H$-bond MOs (NH-type ellipsoidal MOs given in the Energies of NH section) according to Eq. (13.370) is shown in Figure 13.8. Each $N-H$-bond MO comprises a H_2-type ellipsoidal MO and an $N2p$ AO having the dimensional diagram shown in Figure 13.5.

Figure 13.8. NH_3 MO comprising the linear combination of three $N-H$-bonds. Each $N-H$-bond MO comprises the superposition of a H_2-type ellipsoidal MO and the $N2p_x$, $N2p_y$, or $N2p_z$ AO with a relative charge-density of 0.75 to 1.25; otherwise, the $N2p$ orbitals are the same as those of the nitrogen atom. The each internuclear axis of one $N-H$ bond is perpendicular to the bonding p orbital. (A) Color scale, translucent view of the charge-density of the NH_3 MO shown obliquely from the top. For each $N-H$ bond, the ellipsoidal surface of each H_2-type ellipsoidal MO transitions to a $N2p$ AO. The $N2p$ shell, the $N2s$ shell, the $N1s$ shell, and the nuclei (red, not to scale) are shown. (B) Off-center cut-away view showing the complete inner most $N1s$ shell, and moving radially, the cross section of the $N2s$ shell, the $N2p$ shell, and the H_2-type ellipsoidal MO that transitions to a $N2p$ AO for each $N-H$ bond. Bisector current not shown. (C)-(E) Color scale, side-on, top, and bottom translucent views of the charge-density of the NH_3 MO, respectively.

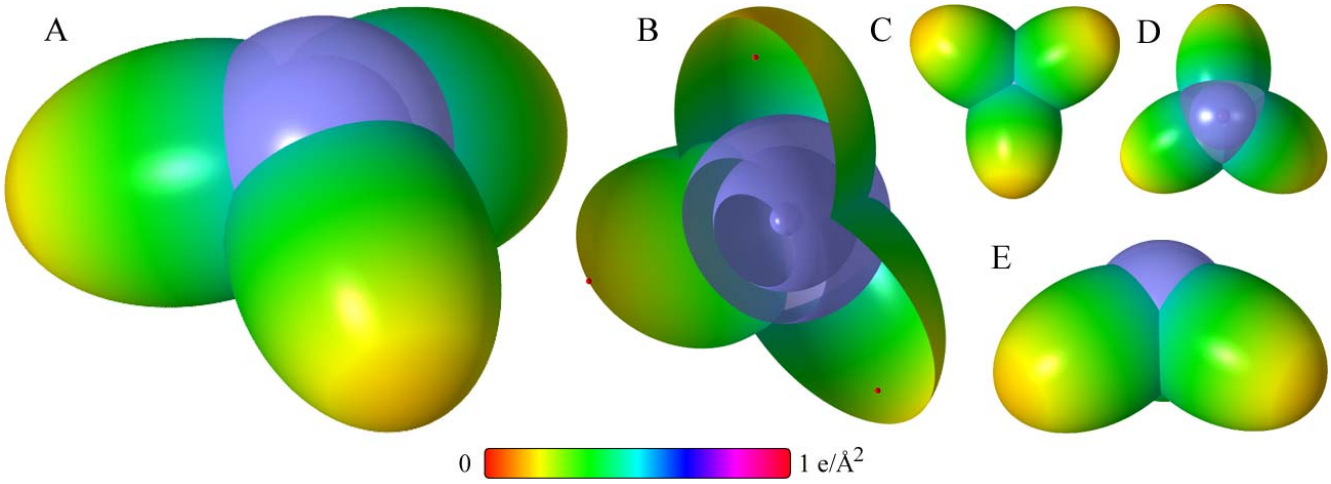

ENERGIES OF NH_3

The energies of NH_3 given by the substitution of the semiprincipal axes ((Eqs. (13.375-13.377) and (13.379)) into the energy equations (Eqs. (13.67-13.73)) multiplied by three are:

$$V_e = 3\left(\frac{3}{4}\right)\frac{-2e^2}{8\pi\varepsilon_0\sqrt{a^2-b^2}}\ln\frac{a+\sqrt{a^2-b^2}}{a-\sqrt{a^2-b^2}} = -115.28799\ eV \tag{13.386}$$

$$V_p = 3\frac{e^2}{8\pi\varepsilon_0\sqrt{a^2-b^2}} = 41.66718\ eV \tag{13.387}$$

$$T = 3\left(\frac{3}{4}\right)\frac{\hbar^2}{2m_e a\sqrt{a^2-b^2}}\ln\frac{a+\sqrt{a^2-b^2}}{a-\sqrt{a^2-b^2}} = 42.77848\ eV \tag{13.388}$$

$$V_m = 3\left(\frac{3}{4}\right)\frac{-\hbar^2}{4m_e a\sqrt{a^2-b^2}}\ln\frac{a+\sqrt{a^2-b^2}}{a-\sqrt{a^2-b^2}} = -21.38924\ eV \tag{13.389}$$

$$E_T\left(NH_3\right) = -3\frac{e^2}{8\pi\varepsilon_0 c'}\left[\left(\frac{3}{2}-\frac{3}{8}\frac{a_0}{a}\right)\ln\frac{a+c'}{a-c'}-1\right] - 14.53414\ eV = -66.76571\ eV \tag{13.390}$$

where $E_T\left(NH_3\right)$ is given by Eq. (13.371) which is reiteratively matched to Eq. (13.372) within five-significant-figure round-off error.

VIBRATION OF NH_3

The vibrational energy levels of NH_3 may be solved as three equivalent coupled harmonic oscillators by developing the Lagrangian, the differential equation of motion, and the eigenvalue solutions [2] wherein the spring constants are derived from the central forces as given in the Vibration of Hydrogen-Type Molecular Ions section and the Vibration of Hydrogen-Type Molecules section.

THE DOPPLER ENERGY TERM OF NH_3

The radiation reaction force in the case of the vibration of NH_3 in the transition state corresponds to the Doppler energy, E_D, given by Eq. (11.181) and Eqs. (13.22) and (13.144) that is dependent on the motion of the electrons and the nuclei. The kinetic energy of the transient vibration is derived from the corresponding central forces. The equations of the radiation reaction force of ammonia are the same as those of the corresponding water and dihydrogen and dideuterium nitride radicals with the substitution of the ammonia parameters. Using Eqs. (11.136) and (13.207-13.209), the angular frequency of the reentrant oscillation in the transition state is

$$\omega = \sqrt{\frac{\left(\frac{3}{2}\right)\frac{e^2}{4\pi\varepsilon_0 b^3}}{m_e}} = 5.68887\ X\ 10^{16}\ rad/s \tag{13.391}$$

where b is given by Eq. (13.379). The kinetic energy, E_K, is given by Planck's equation (Eq. (11.127)):

$$\bar{E}_K = \hbar\omega = \hbar 5.68887\ X\ 10^{16}\ rad/s = 37.44514\ eV \tag{13.392}$$

In Eq. (11.181), substitution of $E_T\left(H_2\right)$ (Eqs. (11.212) and (13.75)), the maximum total energy of each H_2-type MO acting independently due to the D_{3h} symmetry point group, for $E_{h\nu}$, the mass of the electron, m_e, for M, and the kinetic energy given by Eq. (13.392) for $\bar{E}_K$ gives the Doppler energy of the electrons of each of the three bonds for the reentrant orbit:

$$\bar{E}_D \cong E_{h\nu}\sqrt{\frac{2\bar{E}_K}{Mc^2}} = -31.6353683\ eV\sqrt{\frac{2e\left(37.44514\ eV\right)}{m_e c^2}} = -0.38298\ eV \tag{13.393}$$

In addition to the electrons, the nuclei also undergo simple harmonic oscillation in the transition state at their corresponding frequency. The decrease in the energy of NH_3 due to the reentrant orbit in the transition state corresponding to simple harmonic oscillation of the electrons and nuclei, $\bar{E}_{osc}$, is given by the sum of the corresponding energies, $\bar{E}_D$ given by Eq. (13.393) and $\bar{E}_{Kvib}$, the average kinetic energy of vibration which is 1/2 of the vibrational energy of NH_3. Using the experimental $^{14}NH_3$ vibrational energy of $E_{vib} = 3443.59\ cm^{-1} = 0.426954\ eV$ [36] gives:

$$\bar{E}'_{osc} = \bar{E}_D + \bar{E}_{Kvib} = \bar{E}_D + \frac{1}{2}\hbar\sqrt{\frac{k}{\mu}} \tag{13.394}$$

$$\bar{E}'_{osc} = -0.38298\ eV + \frac{1}{2}\left(0.426954\ eV\right) = -0.16950\ eV \tag{13.395}$$

per bond. The reentrant orbit for the binding of a hydrogen atom to a NH_2 radical involves three $N-H$ bonds. Since the vibration and reentrant oscillation is along three bonds, $\bar{E}_{osc}$ for $^{14}NH_3$, $\bar{E}_{osc}\left(^{14}NH_3\right)$, is:

$$\bar{E}_{osc}\left(^{14}NH_3\right) = 3\left(\bar{E}_D + \frac{1}{2}\hbar\sqrt{\frac{k}{\mu}}\right) = 3\left(-0.38298\ eV + \frac{1}{2}\left(0.426954\ eV\right)\right) = -0.50850\ eV \tag{13.396}$$

Using Eq. (13.393), Eqs. (13.394-13.396), and the $^{14}ND_3$ experimental vibrational energy of $E_{vib} = 2563.96\ cm^{-1} = 0.317893\ eV$ [36], the corresponding $\bar{E}_{osc}\left(^{14}ND_2\right)$ is:

$$\bar{E}_{osc}\left(^{14}ND_3\right) = 3\left(-0.38298\ eV + \frac{1}{2}\left(0.317893\ eV\right)\right) = -0.67209\ eV \tag{13.397}$$

TOTAL AND BOND ENERGIES OF $^{14}NH_3$ AND $^{14}ND_3$

$E_{T+osc}\left(^{14}NH_3\right)$, the total energy of the $^{14}NH_3$ including the Doppler term, is given by the sum of $E_T\left(NH_3\right)$ (Eq. (13.373)) and $\bar{E}_{osc}\left(^{14}NH_3\right)$ given Eqs. (13.391-13.396):

$$E_{T+osc}\left(^{14}NH_3\right) = V_e + T + V_m + V_p + E\left(N2p\right) + \bar{E}_{osc}\left(^{14}NH_3\right) = E_T\left(NH_3\right) + \bar{E}_{osc}\left(^{14}NH_3\right) \tag{13.398}$$

$$E_{T+osc}\left(^{14}NH_3\right) = \left\{\begin{array}{l}\left(3\dfrac{-e^2}{8\pi\varepsilon_0 c'}\left[\left(\dfrac{3}{2}-\dfrac{3}{8}\dfrac{a_0}{a}\right)\ln\dfrac{a+c'}{a-c'}-1\right]-14.53414\ eV\right) \\ -3\left(\left(31.63536831\ eV\right)\sqrt{\dfrac{2\hbar\sqrt{\dfrac{\frac{3}{2}\dfrac{e^2}{4\pi\varepsilon_0 b^3}}{m_e}}}{m_e c^2}}-\dfrac{1}{2}\hbar\sqrt{\dfrac{k}{\mu}}\right)\end{array}\right\} \tag{13.399}$$

$$= -66.76616\ eV - 3\left(0.38298\ eV - \frac{1}{2}\hbar\sqrt{\frac{k}{\mu}}\right)$$

From Eqs. (13.396) and (13.398-13.399), the total energy of $^{14}NH_2$ is:

$$\begin{aligned} E_{T+osc}\left(^{14}NH_3\right) &= -66.76616\ eV + \bar{E}_{osc}\left(^{14}NH_3\right) \\ &= -66.76616\ eV - 3\left(0.38298\ eV - \frac{1}{2}\left(0.426954\ eV\right)\right) \\ &= -67.27466\ eV \end{aligned} \tag{13.400}$$

where the experimental $^{14}NH_3$ vibrational energy was used for the $\hbar\sqrt{\frac{k}{\mu}}$ term. $E_{T+osc}\left(^{14}ND_3\right)$, the total energy of $^{14}ND_3$ including the Doppler term is given by the sum of $E_T\left(ND_3\right) = E_T\left(NH_3\right)$ (Eq. (13.373)) and $\bar{E}_{osc}\left(^{14}ND_3\right)$ given by Eq. (13.397):

$$\begin{aligned} E_{T+osc}\left(^{14}ND_3\right) &= -66.76616\ eV + \bar{E}_{osc}\left(^{14}ND_3\right) \\ &= -66.76616\ eV - 3\left(0.38298\ eV - \frac{1}{2}\left(0.317893\ eV\right)\right) \\ &= -67.43780\ eV \end{aligned} \tag{13.401}$$

where the experimental $^{14}ND_3$ vibrational energy was used for the $\hbar\sqrt{\frac{k}{\mu}}$ term. The corresponding bond dissociation energy, E_D, is given by the sum of the total energies of the corresponding dihydrogen nitride radical and hydrogen atom minus the total energy of ammonia, $E_{T+osc}\left(^{14}NH_3\right)$.

Thus, E_D of $^{14}NH_3$ is given by:

$$E_D\left(^{14}NH_3\right) = E(H) + E(^{14}NH_2) - E_{T+osc}\left(^{14}NH_3\right) \tag{13.402}$$

where $E_T(^{14}NH_2)$ is given by the of the sum of the experimental energies of ^{14}N (Eq. (13.251)), two H (Eq. (13.154)), and the negative of the bond energies of ^{14}NH (Eq. (13.312)) and $^{14}NH_2$ (Eq. (13.354)):

$$E(^{14}NH_2) = 2\left(-13.59844\ eV\right) - 14.53414\ eV - 3.42\ eV - 3.946\ eV = -49.09709\ eV \tag{13.403}$$

From Eqs. (13.154), (13.400), and (13.402-13.403), $E_D\left({}^{14}NH_2\right)$ is:

$$\begin{aligned} E_D\left({}^{14}NH_3\right) &= E(H) + E({}^{14}NH_2) - E_{T+osc}\left({}^{14}NH_3\right) \\ &= -13.59844\ eV - 49.09709\ eV - \left(-67.27466\ eV\right) = 4.57913\ eV \end{aligned} \tag{13.404}$$

The experimental ${}^{14}NH_3$ bond dissociation energy [37] is:

$$E_D({}^{14}NH_3) = 4.60155\ eV \tag{13.405}$$

Similarly, E_D of ${}^{14}ND_3$ is given by:

$$E_D\left({}^{14}ND_3\right) = E(D) + E({}^{14}ND_2) - \left(E_{T+osc}\left({}^{14}ND_3\right)\right) \tag{13.406}$$

where $E_T({}^{14}ND_2)$ is given by the of the sum of the experimental energies of ${}^{14}N$ (Eq. (13.251)), two times the energy of D (Eq. (13.155)), and the negative of the bond energies of ${}^{14}ND$ (Eq. (13.315)) and ${}^{14}ND_2$ (Eq. (13.358)):

$$E({}^{14}ND_2) = 2\left(-13.603\ eV\right) - 14.53414\ eV - 3.5134\ eV - 3.9362\ eV = -49.18981\ eV \tag{13.407}$$

From Eqs. (13.155), (13.401), and (13.406-13.407), $E_D\left({}^{14}ND_3\right)$ is:

$$E_D({}^{14}ND_3) = -13.603\ eV - 49.18981\ eV - \left(-67.43780\ eV\right) = 4.64499\ eV \tag{13.408}$$

The experimental ${}^{14}ND_3$ bond dissociation energy [37] is:

$$E_D({}^{14}ND_3) = 4.71252\ eV \tag{13.409}$$

BOND ANGLE OF NH_3

Using, $2c'_{H-H}$ (Eq. (13.364)), the distance between the two H atoms when the total energy of the corresponding MO is zero (Eq. (13.361)), and $2c'_{N-H}$, the internuclear distance of each $N-H$ bond (Eq. (13.377)), the corresponding bond angle can be determined from the law of cosines. Using Eq. (13.367), the bond angle θ between the $N-H$ bonds is:

$$\theta = \cos^{-1}\left(\frac{2\left(1.95921\right)^2 - \left(3.14643\right)^2}{2\left(1.95921\right)^2}\right) = \cos^{-1}\left(-0.28956\right) = 106.67° \tag{13.410}$$

The experimental angle between the $N-H$ bonds is [36]:

$$\theta = 106.67° \tag{13.411}$$

The NH_3 molecule has a pyramidal structure with the nitrogen atom along the z-axis at the apex and the hydrogen atoms at the base in the xy-plane. Since any two $N-H$ bonds form an isosceles triangle, the distance $d_{origin-H}$ from the origin to the nucleus of a hydrogen atom is given by:

$$d_{origin-H} = \frac{2c'_{H-H}}{2\sin 60°} \tag{13.412}$$

Substitution of Eq. (13.364) into Eq. (13.412) gives:

$$d_{origin-H} = 1.81659a_0 \tag{13.413}$$

The height along the z-axis of the pyramid from the origin to N nucleus d_{height} is given by:

$$d_{height} = \sqrt{\left(2c'_{N-H}\right)^2 - \left(d_{origin-H}\right)^2} \tag{13.414}$$

Substitution of Eqs. (13.377) and (13.413) into Eq. (13.414) gives:

$$d_{height} = 0.73383a_0 \tag{13.415}$$

The angle θ_v of each $N-H$ bond from the z-axis is given by:

$$\theta_v = \tan^{-1}\left(\frac{d_{origin-H}}{d_{height}}\right) \tag{13.416}$$

Substitution of Eqs. (13.413) and (13.415) into Eq. (13.416) gives:

$$\theta_v = 68.00° \tag{13.417}$$

The NH_3 MO shown in Figure 13.8 was rendered using these parameters.

The results of the determination of bond parameters of NH_3 and ND_3 are given in Table 13.1. The calculated results are based on first principles and given in closed-form, exact equations containing fundamental constants only. The agreement between the experimental and calculated results is excellent.

HYDROGEN CARBIDE (CH)

The methane molecule can be solved by first considering the solution of the hydrogen carbide, dihydrogen carbide, and methyl radicals. The former is formed by the reaction of a hydrogen atom and a carbon atom:

$$H + C \rightarrow CH \tag{13.418}$$

The hydrogen carbide radicals, CH and CH_2, methyl radical, CH_3, and methane, CH_4, can be solved using the same principles as those used to solve OH, H_2O, NH, NH_2, and NH_3 with the exception that the carbon $2s$ and $2p$ shells hybridize to form a single $2sp^3$ shell as an energy minimum.

FORCE BALANCE OF CH

CH comprises two spin-paired electrons in a chemical bond between the carbon atom and the hydrogen atom. The CH radical molecular orbital (MO) is determined by considering properties of the binding atoms and the boundary constraints. The prolate spheroidal H_2 MO developed in the Nature of the Chemical Bond of Hydrogen-Type Molecules section satisfies the boundary constraints; thus, the H-atom electron forms a H_2-type ellipsoidal MO with one of the C-atom electrons. However, such a bond is not possible with the outer C electrons in their ground state since the resulting H_2-type ellipsoidal MO would have a shorter internuclear distance than the radius of the carbon $2p$ shell, which is not energetically stable. Thus, when bonding the carbon $2s$ and $2p$ shells hybridize to form a single $2sp^3$ shell as an energy minimum.

The C electron configuration given in the Six-Electron Atoms section is $1s^2 2s^2 2p^2$, and the orbital arrangement is:

$$\begin{array}{ccc} & \text{2p state} & \\ \underline{\uparrow} & \underline{\uparrow} & \underline{\quad} \\ 1 & 0 & -1 \end{array} \tag{13.419}$$

corresponding to the ground state ${}^3P_0$. The radius r_6 of the $2p$ shell given by Eq. (10.122) is:

$$r_6 = 1.20654 a_0 \tag{13.420}$$

The energy of the carbon $2p$ shell is the negative of the ionization energy of the carbon atom given by Eq. (10.123). Experimentally, the energy is [12]

$$E\left(C, 2p\ shell\right) = -E(ionization;\ C) = -11.2603\ eV \tag{13.421}$$

The $C2s$ atomic orbital (AO) combines with the $C2p$ AOs to form a single $2sp^3$ hybridized orbital (HO) with the orbital arrangement:

$$\begin{array}{cccc} & & \text{2sp}^3\text{ state} & \\ \underline{\uparrow} & \underline{\uparrow} & \underline{\uparrow} & \underline{\uparrow} \\ 0,0 & 1,-1 & 1,0 & 1,1 \end{array} \tag{13.422}$$

where the quantum numbers (ℓ, m_ℓ) are below each electron. The total energy of the state is given by the sum over the four electrons. The sum $E_T\left(C, 2sp^3\right)$ of calculated energies of C, C^+, C^{2+}, and C^{3+} from Eqs. (10.123), (10.113-10.114), (10.68), and (10.48), respectively, is:

$$E_T\left(C, 2sp^3\right) = 64.3921\ eV + 48.3125\ eV + 24.2762\ eV + 11.27671\ eV = 148.25751\ eV \tag{13.423}$$

which agrees well with the sum of 148.02532 eV from the experimental [6] values. The orbital-angular-momentum interactions cancel such that the energy of the $E_T\left(C, 2sp^3\right)$ is purely Coulombic. By considering that the central field decreases by an integer for each successive electron of the shell, the radius r_{2sp^3} of the $C2sp^3$ shell may be calculated from the Coulombic energy using Eq. (10.102).

$$\begin{aligned} r_{2sp^3} &= \sum_{n=2}^{5} \frac{(Z-n)e^2}{8\pi\varepsilon_0\left(e148.25751\ eV\right)} \\ &= \frac{10e^2}{8\pi\varepsilon_0\left(e148.25751\ eV\right)} \\ &= 0.91771 a_0 \end{aligned} \tag{13.424}$$

Using Eqs. (10.102) and (13.424), the Coulombic energy $E_{Coulomb}\left(C,2sp^3\right)$ of the outer electron of the $C2sp^3$ shell is:

$$E_{Coulomb}\left(C,2sp^3\right)=\frac{-e^2}{8\pi\varepsilon_0 r_{2sp^3}}$$
$$=\frac{-e^2}{8\pi\varepsilon_0 0.91771a_0}=-14.82575\ eV \tag{13.425}$$

During hybridization, the spin-paired $2s$ electrons are promoted to the $C2sp^3$ shell as unpaired electrons. The energy for the promotion is the magnetic energy given by Eq. (13.152) at the initial radius of the $2s$ electrons. From Eq. (10.62) with $Z=6$, the radius r_3 of the $C2s$ shell is

$$r_3=0.84317a_0 \tag{13.426}$$

Using Eqs. (13.152) and (13.426), the unpairing energy is:

$$E(magnetic)=\frac{2\pi\mu_0 e^2\hbar^2}{m_e^2\left(r_3\right)^3}=\frac{8\pi\mu_0\mu_B^2}{\left(0.84317a_0\right)^3}=0.19086\ eV \tag{13.427}$$

Using Eqs. (13.425) and (13.427), the energy $E\left(C,2sp^3\right)$ of the outer electron of the $C2sp^3$ shell is:

$$E\left(C,2sp^3\right)=\frac{-e^2}{8\pi\varepsilon_0 r_{2sp^3}}+\frac{2\pi\mu_0 e^2\hbar^2}{m_e^2\left(r_3\right)^3}$$
$$=-14.82575\ eV+0.19086\ eV=-14.63489\ eV \tag{13.428}$$

The nitrogen atom's $2p$-shell electron configuration given by Eq. (10.134) is the same as that of the $C2sp^3$ shell, and nitrogen's calculated energy of $14.61664\ eV$ given by Eq. (10.143) is a close match with $E\left(C,2sp^3\right)$. Thus, the binding should be very similar except that four bonds to hydrogen can occur with carbon.

The carbon $C2sp^3$ electron combines with the $H1s$ electron to form a molecular orbital. The proton of the H atom and the nucleus of the C atom are along the internuclear axis and serve as the foci. Due to symmetry, the other C electrons are equivalent to point charges at the origin. (See Eqs. (19-38) of Appendix II.) Thus, the energies in the CH MO involve only the $C2sp^3$ and $H1s$ electrons. The forces are determined by these energies.

As in the case of H_2, the MO is a prolate spheroid with the exception that the ellipsoidal MO surface cannot extend into the $C2sp^3$ HO for distances shorter than the radius of the $C2sp^3$ shell. Thus, the MO surface comprises a prolate spheroid at the H proton that is continuous with the $C2sp^3$ shell at the C atom whose nucleus serves as the other focus. The energy of the H_2-type ellipsoidal MO is matched to that of the $C2sp^3$ shell. As in the case with OH and NH, the linear combination of the H_2-type ellipsoidal MO with the $C2sp^3$ HO must involve a 25% contribution from the H_2-type ellipsoidal MO to the $C2sp^3$ HO in order to match potential, kinetic, and orbital energy relationships. Thus, the CH MO must comprise 75% of a H_2-type ellipsoidal MO and a $C2sp^3$ HO:

$$1\ C2sp^3+0.75\ H_2\ MO\rightarrow CH\ MO \tag{13.429}$$

The force balance of the CH MO is determined by the boundary conditions that arise from the linear combination of orbitals according to Eq. (13.429) and the energy matching condition between the hydrogen and $C2sp^3$ HO components of the MO.

As in the case with OH (Eq. (13.57)), the H_2-type ellipsoidal MO comprises 75% of the CH MO; so, the electron charge density in Eq. (11.65) is given by $-0.75e$. The force constant k' to determine the ellipsoidal parameter c' in terms of the central force of the foci is given by Eq. (13.59). The distance from the origin to each focus c' is given by Eq. (13.60). The internuclear distance is given by Eq. (13.61). The length of the semiminor axis of the prolate spheroidal $C-H$-bond MO $b=c$ is given by Eq. (13.62). The eccentricity, e, is given by Eq. (13.63). The solution of the semimajor axis a then allows for the solution of the other axes of each prolate spheroid and eccentricity of the CH MO. Since the CH MO comprises a H_2-type-ellipsoidal MO that transitions to the $C2sp^3$ HO, the energy $E\left(C,2sp^3\right)$ in Eq. (13.428) adds to that of the H_2-type ellipsoidal MO to give the total energy of the CH MO. From the energy equation and the relationship between the axes, the dimensions of the CH MO are solved.

The energy components of V_e, V_p, T, and V_m are those of H_2 (Eqs. (11.207-11.212)) except that they are corrected for electron hybridization. Hybridization gives rise to the $C2sp^3$ HO-shell Coulombic energy $E_{Coulomb}\left(C,2sp^3\right)$ given by Eq. (13.425). To meet the equipotential condition of the union of the H_2-type-ellipsoidal-MO and the $C2sp^3$ HO, the electron energies are normalized by the ratio of $14.82575\ eV$, the magnitude of $E_{Coulomb}\left(C,2sp^3\right)$ given by Eq. (13.425), and $13.605804\ eV$, the magnitude of the Coulombic energy between the electron and proton of H given by Eq. (1.264). This

normalizes the energies to match that of the Coulombic energy alone to meet the energy matching condition of the CH MO under the influence of the proton and the C nucleus. The hybridization energy factor C_{C2sp^3HO} is

$$C_{C2sp^3HO} = \frac{\frac{e^2}{8\pi\varepsilon_0 a_0}}{\frac{e^2}{8\pi\varepsilon_0 r_{2sp^3}}} = \frac{\frac{e^2}{8\pi\varepsilon_0 a_0}}{\frac{e^2}{8\pi\varepsilon_0 0.91771 a_0}} = \frac{13.605804\ eV}{14.82575\ eV} = 0.91771 \tag{13.430}$$

The total energy $E_T(CH)$ of the CH MO is given by the sum of the energies of the orbitals, the H_2-type ellipsoidal MO and the $C2sp^3$ HO, that form the hybridized CH MO. $E_T(CH)$ follows from Eq. (13.74) for OH, but the energy of the $C2sp^3$ HO given by Eq. (13.428) is substituted for the energy of O and the H_2-type-ellipsoidal-MO energies are those of H_2 (Eqs. (11.207-11.212)) multiplied by the electron hybridization factor rather than by the factor of 0.75:

$$\begin{aligned} E_T(CH) &= E_T + E(C, 2sp^3) \\ &= -\frac{e^2}{8\pi\varepsilon_0 c'}\left[(0.91771)\left(2 - \frac{1}{2}\frac{a_0}{a}\right)\ln\frac{a+c'}{a-c'} - 1\right] - 14.63489\ eV \end{aligned} \tag{13.431}$$

To match the boundary condition that the total energy of the entire the H_2-type ellipsoidal MO is given by Eqs. (11.212) and (13.75), $E_T(CH)$ given by Eq. (13.431) is set equal to Eq. (13.75).

$$E_T(CH) = -\frac{e^2}{8\pi\varepsilon_0 c'}\left[(0.91771)\left(2 - \frac{1}{2}\frac{a_0}{a}\right)\ln\frac{a+c'}{a-c'} - 1\right] - 14.63489\ eV = -31.63536831\ eV \tag{13.432}$$

From the energy relationship given by Eq. (13.432) and the relationship between the axes given by Eqs. (13.60-13.63), the dimensions of the CH MO can be solved.

Substitution of Eq. (13.60) into Eq. (13.432) gives:

$$\frac{e^2}{8\pi\varepsilon_0\sqrt{\frac{2aa_0}{3}}}\left[(0.91771)\left(2 - \frac{1}{2}\frac{a_0}{a}\right)\ln\frac{a+\sqrt{\frac{2aa_0}{3}}}{a-\sqrt{\frac{2aa_0}{3}}} - 1\right] = e17.00048 \tag{13.433}$$

The most convenient way to solve Eq. (13.433) is by the reiterative technique using a computer. The result to within the round-off error with five-significant figures is:

$$a = 1.67465a_0 = 8.86186\ X\ 10^{-11}\ m \tag{13.434}$$

Substitution of Eq. (13.434) into Eq. (13.60) gives:

$$c' = 1.05661a_0 = 5.59136\ X\ 10^{-11}\ m \tag{13.435}$$

The internuclear distance given by multiplying Eq. (13.435) by two is:

$$2c' = 2.11323a_0 = 1.11827\ X\ 10^{-10}\ m \tag{13.436}$$

The experimental bond distance is [14]:

$$2c' = 1.1198\ X\ 10^{-10}\ m \tag{13.437}$$

Substitution of Eqs. (13.434-13.435) into Eq. (13.62) gives:

$$b = c = 1.29924a_0 = 6.87527\ X\ 10^{-11}\ m \tag{13.438}$$

Substitution of Eqs. (13.434-13.435) into Eq. (13.63) gives:

$$e = 0.63095 \tag{13.439}$$

The nucleus of the H atom and the nucleus of the C atom comprise the foci of the H_2-type ellipsoidal MO. The parameters of the point of intersection of the H_2-type ellipsoidal MO and the $C2sp^3$ HO are given by Eqs. (13.84-13.95) and (13.261-13.270). The polar intersection angle θ' is given by Eq. (13.261) where $r_n = r_{2sp^3} = 0.91771a_0$ is the radius of the $C2sp^3$ shell. Substitution of Eqs. (13.434-13.435) into Eq. (13.261) gives:

$$\theta' = 81.03° \tag{13.440}$$

Then, the angle θ_{C2sp^3HO} the radial vector of the $C2sp^3$ HO makes with the internuclear axis is:

$$\theta_{C2sp^3HO} = 180° - 81.03° = 98.97° \tag{13.441}$$

as shown in Figure 13.9.

Figure 13.9. The cross section of the CH MO showing the axes, angles, and point of intersection of the H_2-type ellipsoidal MO with the $C2sp^3$ HO. The continuation of the H_2-type-ellipsoidal-MO basis element beyond the intersection point with the $C2sp^3$ shell is shown as dashed since it only serves to solve the energy match with the $C2sp^3$ shell and does not represent charge density. Similarly, the vertical dashed line only designates the parameters of the intersection point. The actual charge density is shown by the solid lines. Legend: a: semimajor axis, b: semiminor axis, c': internuclear distance, $d_1 : d_{H_2MO}$, $\theta_1 : \theta_{C2sp^3HO}$, $d_2 : d_{C2sp^3HO}$, and $R : r_{2sp^3}$.

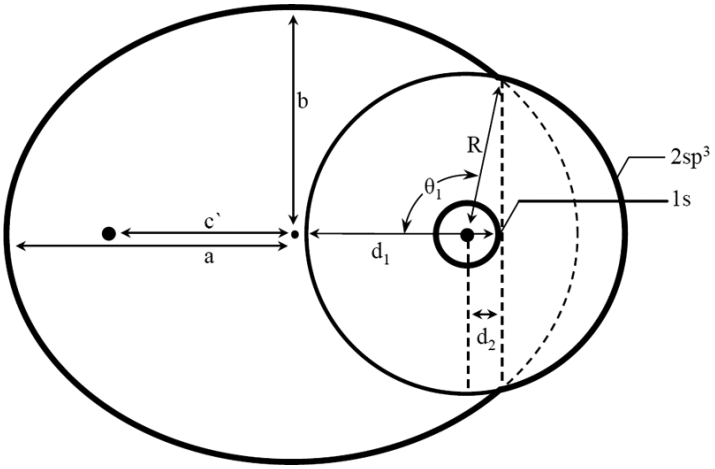

The Cartesian $\mathbf{i}$-coordinate of the interception point of the MO and the AO can be calculated using the MO ellipsoidal parameters by first calculating the parametric angle in Eq. (11.83) that matches Cartesian $\mathbf{j}$-coordinate components at the point of intersection. Thus, the matching elliptic parametric angle $\omega t = \theta_{H_2MO}$ satisfies the following relationship:

$$r_{2sp^3} \sin\theta_{C2sp^3HO} = 0.91771 a_0 \sin\theta_{C2sp^3HO} = b \sin\theta_{H_2MO} \tag{13.442}$$

such that

$$\begin{aligned} \theta_{H_2MO} &= \sin^{-1} \frac{0.91771 a_0 \sin\theta_{C2sp^3HO}}{b} \\ &= \sin^{-1} \frac{0.91771 a_0 \sin 98.97°}{b} \end{aligned} \tag{13.443}$$

with the use of Eq. (13.441). Substitution of Eq. (13.438) into Eq. (13.443) gives:

$$\theta_{H_2MO} = 44.24° \tag{13.444}$$

Then, the distance d_{H_2MO} along the internuclear axis from the origin of H_2-type ellipsoidal MO to the point of intersection of the orbitals is given by

$$d_{H_2MO} = a \cos\theta_{H_2MO} \tag{13.445}$$

Substitution of Eqs. (13.434) and (13.444) into Eq. (13.445) gives:

$$d_{H_2MO} = 1.19968 a_0 = 6.34845\ X\ 10^{-11}\ m \tag{13.446}$$

The distance d_{C2sp^3HO} along the internuclear axis from the origin of the C atom to the point of intersection of the orbitals is given by:

$$d_{C2sp^3HO} = d_{H_2MO} - c' \tag{13.447}$$

Substitution of Eqs. (13.435) and (13.446) into Eq. (13.447) gives:

$$d_{C2sp^3HO} = 0.14307 a_0 = 7.57090\ X\ 10^{-12}\ m \tag{13.448}$$

As shown in Eq. (13.429), the uniform charge-density in the $C2sp^3$ HO is increased by a factor of 0.25 and the H-atom density is decreased by a factor of 0.25. Using the orbital composition of CH (Eq. (13.429)), the radii of $C1s = 0.17113 a_0$ (Eq. (10.51)) and $C2sp^3 = 0.91771 a_0$ (Eq. (13.424)) shells, and the parameters of the CH MO given by Eqs. (13.3-13.4), (13.434-13.436), and (13.438-13.448), the dimensional diagram and charge-density of the CH MO comprising the linear combination of the H_2-type ellipsoidal MO and the $C2sp^3$ HO according to Eq. (13.429) are shown in Figures 13.9 and 13.10, respectively.

Figure 13.10. CH MO comprising the superposition of the H_2-type ellipsoidal MO and the $C2sp^3$ HO with a relative charge-density of 0.75 to 1.25; otherwise, the $C2sp^3$ HO is unchanged. (A) Side-on, color scale, translucent view of the charge-density of the CH MO. The ellipsoidal surface of the H_2-type ellipsoidal MO that transitions to the $C2sp^3$ HO, the $C2sp^3$ HO shell, $C1s$ shell, and the nuclei (red, not to scale) are shown. (B) Cut-away view showing the inner most $C1s$ shell, and moving radially, the $C2sp^3$ shell, and the H_2-type ellipsoidal MO that transitions to the $C2sp^3$ HO.

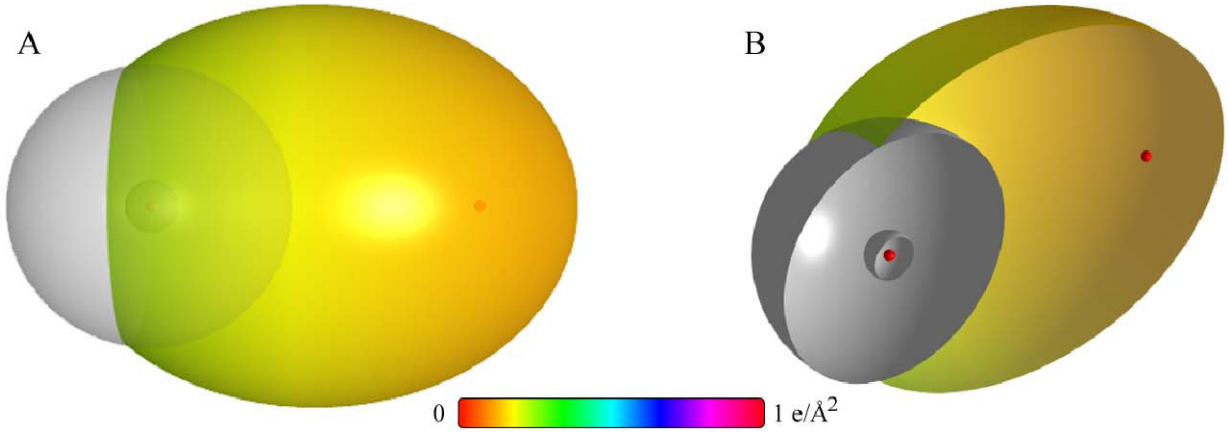

ENERGIES OF *CH*

The energies of CH are given by the substitution of the semiprincipal axes (Eqs. (13.434-13.435) and (13.438)) into the energy equations (Eq. (13.431) and Eqs. (11.207-11.211)) that are corrected for electron hybridization using Eq. (13.430).

$$V_e = (0.91771)\frac{-2e^2}{8\pi\varepsilon_0\sqrt{a^2-b^2}}\ln\frac{a+\sqrt{a^2-b^2}}{a-\sqrt{a^2-b^2}} = -35.12015\ eV \tag{13.449}$$

$$V_p = \frac{e^2}{8\pi\varepsilon_0\sqrt{a^2-b^2}} = 12.87680\ eV \tag{13.450}$$

$$T = (0.91771)\frac{\hbar^2}{2m_e a\sqrt{a^2-b^2}}\ln\frac{a+\sqrt{a^2-b^2}}{a-\sqrt{a^2-b^2}} = 10.48582\ eV \tag{13.451}$$

$$V_m = (0.91771)\frac{-\hbar^2}{4m_e a\sqrt{a^2-b^2}}\ln\frac{a+\sqrt{a^2-b^2}}{a-\sqrt{a^2-b^2}} = -5.24291\ eV \tag{13.452}$$

$$E_T(CH) = -\frac{e^2}{8\pi\varepsilon_0 c'}\left[(0.91771)\left(2-\frac{1}{2}\frac{a_0}{a}\right)\ln\frac{a+c'}{a-c'}-1\right]-14.63489\ eV = -31.63533\ eV \tag{13.453}$$

where $E_T(CH)$ is given by Eq. (13.431) which is reiteratively matched to Eq. (13.75) within five-significant-figure round-off error.

VIBRATION AND ROTATION OF *CH*

The vibrational energy of CH may be solved in the same manner as that of OH and NH except that the force between the electrons and the foci given by Eq. (13.102) is doubled due to electron hybridization of the two shells of carbon after Eq. (11.141). From Eqs. (13.102-13.106) with the substitution of the CH parameters, the angular frequency of the oscillation is

$$\omega = \sqrt{\frac{\frac{0.75e^2}{4\pi\varepsilon_0 b^3}-\frac{e^2}{8\pi\varepsilon_0(2c')^3}}{\mu}} = \sqrt{\frac{\frac{0.75e^2}{4\pi\varepsilon_0(1.29924a_0)^3}-\frac{e^2}{8\pi\varepsilon_0(2.11323a_0)^3}}{\frac{12}{13}m_p}} = 5.39828\ X\ 10^{14}\ rad/s \tag{13.454}$$

where b is given by Eq. (13.438), $2c'$ is given by Eq. (13.436), and the reduced mass of ^{12}CH is given by:

$$\mu_{^{12}CH} = \frac{m_1 m_2}{m_1+m_2} = \frac{(1)(12)}{1+12}m_p \tag{13.455}$$

where m_p is the proton mass. Thus, during bond formation, the perturbation of the orbit determined by an inverse-squared force results in simple harmonic oscillatory motion of the orbit, and the corresponding frequency, $\omega(0)$, for ^{12}CH given by Eqs. (11.136), (11.148), and (13.454) is:

$$\omega(0)=\sqrt{\frac{k(0)}{\mu}}=\sqrt{\frac{449.94\ Nm^{-1}}{\mu}}=5.39828\ X\ 10^{14}\ radians/s \tag{13.456}$$

where the reduced nuclear mass of ^{12}CH is given by Eq. (13.455) and the spring constant, $k(0)$, given by Eqs. (11.136) and (13.454) is:

$$k(0)=449.94\ Nm^{-1} \tag{13.457}$$

The ^{12}CH transition-state vibrational energy, $E_{vib}(0)$, given by Planck's equation (Eq. (11.127)) is:

$$E_{vib}(0)=\hbar\omega=\hbar 5.39828\ X\ 10^{14}\ rad/s=0.35532\ eV=2865.86\ cm^{-1} \tag{13.458}$$

ω_e, from the experimental curve fit of the vibrational energies of ^{12}CH is [14] :

$$\omega_e=2861.6\ cm^{-1} \tag{13.459}$$

Using Eqs. (13.112-13.118) with $E_{vib}(0)$ given by Eq. (13.458) and D_0 given by Eq. (13.488), the ^{12}CH $\upsilon=1\rightarrow\upsilon=0$ vibrational energy, $E_{vib}(1)$ is:

$$E_{vib}(1)=0.33879\ eV \qquad \left(2732.61\ cm^{-1}\right) \tag{13.460}$$

The experimental vibrational energy of ^{12}CH using ω_e and $\omega_e x_e$ [14] according to K&P [15] is:

$$E_{vib}(1)=0.33885\ eV \qquad \left(2733\ cm^{-1}\right) \tag{13.461}$$

Using Eq. (13.113) with $E_{vib}(1)$ given by Eq. (13.460) and D_0 given by Eq. (13.488), the anharmonic perturbation term, $\omega_0 x_0$, of ^{12}CH is:

$$\omega_0 x_0=66.624\ cm^{-1} \tag{13.462}$$

The experimental anharmonic perturbation term, $\omega_0 x_0$, of ^{12}CH [14] is:

$$\omega_0 x_0=64.3\ cm^{-1} \tag{13.463}$$

The vibrational energies of successive states are given by Eqs. (13.458), (13.112), and (13.462).

Using b given by Eq. (13.438), $2c'$ given by Eq. (13.436), D_0 given by Eq. (13.490), and the reduced nuclear mass of ^{12}CD given by:

$$\mu_{^{12}CD}=\frac{m_1 m_2}{m_1+m_2}=\frac{(2)(12)}{2+12}m_p \tag{13.464}$$

where m_p is the proton mass, the corresponding parameters for deuterium carbide ^{12}CD (Eqs. (13.102-13.121)) are:

$$\omega(0)=\sqrt{\frac{k(0)}{\mu}}=\sqrt{\frac{449.94\ Nm^{-1}}{\mu}}=3.96126\ X\ 10^{14}\ radians/s \tag{13.465}$$

$$k(0)=449.94\ Nm^{-1} \tag{13.466}$$

$$E_{vib}(0)=\hbar\omega=\hbar 3.96126\ X\ 10^{14}\ rad/s=0.26074\ eV=2102.97\ cm^{-1} \tag{13.467}$$

$$E_{vib}(1)=0.25173\ eV \qquad \left(2030.30\ cm^{-1}\right) \tag{13.468}$$

$$\omega_0 x_0=36.335\ cm^{-1} \tag{13.469}$$

ω_e, from the experimental curve fit of the vibrational energies of ^{12}CD is [14] :

$$\omega_e=2101.0\ cm^{-1} \tag{13.470}$$

The experimental vibrational energy of ^{12}CD using ω_e and $\omega_e x_e$ [14] according to K&P [15] is:

$$E_{vib}(1)=0.25189\ eV \qquad \left(2031.6\ cm^{-1}\right) \tag{13.471}$$

and the experimental anharmonic perturbation term, $\omega_0 x_0$, of ^{12}CD is [14] :

$$\omega_0 x_0=34.7\ cm^{-1} \tag{13.472}$$

which match the predictions given by Eqs. (13.467), (13.468) and (13.469), respectively.

Using Eqs. (13.133-13.134) and the internuclear distance, $r=2c'$, and reduced mass of ^{12}CH given by Eqs. (13.436) and (13.455), respectively, the corresponding B_e is:

$$B_e=14.498\ cm^{-1} \tag{13.473}$$

The experimental B_e rotational parameter of ^{12}CH is [14]:

$$B_e=14.457\ cm^{-1} \tag{13.474}$$

Using the internuclear distance, $r = 2c'$, and reduced mass of ^{12}CD given by Eqs. (13.436) and (13.464), respectively, the corresponding B_e is:

$$B_e = 7.807\ cm^{-1} \tag{13.475}$$

The experimental B_e rotational parameter of ^{12}CD is [14]:

$$B_e = 7.808\ cm^{-1} \tag{13.476}$$

THE DOPPLER ENERGY TERMS OF ^{12}CH AND ^{12}CD

The equations of the radiation reaction force of hydrogen and deuterium carbide are the same as those of the corresponding hydroxyl and hydrogen nitride radicals with the substitution of the hydrogen and deuterium carbide parameters. Using Eqs. (11.136) and (13.140-13.142), the angular frequency of the reentrant oscillation in the transition state is

$$\omega = \sqrt{\frac{\frac{0.75e^2}{4\pi\varepsilon_0 b^3}}{m_e}} = 2.41759\ X\ 10^{16}\ rad/s \tag{13.477}$$

where b is given by Eq. (13.438). The kinetic energy, E_K, is given by Planck's equation (Eq. (11.127)):

$$\overline{E}_K = \hbar\omega = \hbar 2.41759\ X\ 10^{16}\ rad/s = 15.91299\ eV \tag{13.478}$$

In Eq. (11.181), substitution of the total energy of CH, $E_T(CH)$, (Eq. (13.432)) for E_{hv}, the mass of the electron, m_e, for M, and the kinetic energy given by Eq. (13.478) for $\overline{E}_K$ gives the Doppler energy of the electrons for the reentrant orbit:

$$\overline{E}_D \cong E_{hv}\sqrt{\frac{2\overline{E}_K}{Mc^2}} = -31.63537\ eV\sqrt{\frac{2e(15.91299\ eV)}{m_e c^2}} = -0.24966\ eV \tag{13.479}$$

In addition to the electrons, the nuclei also undergo simple harmonic oscillation in the transition state at their corresponding frequency. The decrease in the energy of CH due to the reentrant orbit in the transition state corresponding to simple harmonic oscillation of the electrons and nuclei, $\overline{E}_{osc}$, is given by the sum of the corresponding energies, $\overline{E}_D$ given by Eq. (13.479) and $\overline{E}_{Kvib}$, the average kinetic energy of vibration which is 1/2 of the vibrational energy of CH. The experimental ^{12}CH ω_e is $2861.6\ cm^{-1}$ $(0.35480\ eV)$ [14] which matches the predicted ω_e of $2865.86\ cm^{-1}$ $(0.35532\ eV)$ given by Eq. (13.458). Using the predicted ω_e for $\overline{E}_{Kvib}$ of the transition state, $\overline{E}_{osc}(^{12}CH)$ is:

$$\overline{E}_{osc}(^{12}CH) = \overline{E}_D + \overline{E}_{Kvib} = \overline{E}_D + \frac{1}{2}\hbar\sqrt{\frac{k}{\mu}} \tag{13.480}$$

$$\overline{E}_{osc}(^{12}CH) = -0.24966\ eV + \frac{1}{2}(0.35532\ eV) = -0.07200\ eV \tag{13.481}$$

The experimental ^{12}CD ω_e is $2101.0\ cm^{-1}$ $(0.26049\ eV)$ [14] which matches the predicted ω_e of $2102.97\ cm^{-1}$ $(0.26074\ eV)$ given by Eq. (13.467). Using Eq. (13.479) and the predicted ω_e for $\overline{E}_{Kvib}$ of the transition state, $\overline{E}_{osc}(^{12}CD)$ is:

$$\overline{E}_{osc}(^{12}CD) = -0.24966\ eV + \frac{1}{2}(0.26074\ eV) = -0.11929\ eV \tag{13.482}$$

TOTAL AND BOND ENERGIES OF ^{12}CH AND ^{12}CD

$E_{T+osc}(^{12}CH)$, the total energy of the ^{12}CH radical including the Doppler term, is given by the sum of $E_T(CH)$ (Eq. (13.432)) and $\overline{E}_{osc}(^{12}CH)$ given by Eq. (13.481):

$$E_{T+osc}(^{12}CH) = V_e + T + V_m + V_p + E(C, 2sp^3) + \overline{E}_{osc}(^{12}CH) = E_T(CH) + \overline{E}_{osc}(^{12}CH) \tag{13.483}$$

$$E_{T+osc}(^{12}CH) = \left\{\left(\frac{-e^2}{8\pi\varepsilon_0 c'}\left[(0.91771)\left(2 - \frac{1}{2}\frac{a_0}{a}\right)\ln\frac{a+c'}{a-c'} - 1\right] - 14.63489\ eV\right)\right\}$$
$$\left\{\left(1 + \sqrt{\frac{2\hbar\sqrt{\frac{3}{4}\frac{e^2}{4\pi\varepsilon_0 b^3}}{m_e}}{m_e c^2}}\right) + \frac{1}{2}\hbar\sqrt{\frac{k}{\mu}}\right\} \tag{13.484}$$

$$= -31.63537\ eV - 0.24966\ eV + \frac{1}{2}\hbar\sqrt{\frac{k}{\mu}}$$

From Eqs. (13.480-13.481) and (13.483-13.484), the total energy of ^{12}CH is:

$$\begin{aligned} E_{T+osc}\left(^{12}CH\right) &= -31.63537\ eV + \bar{E}_{osc}\left(^{12}CH\right) \\ &= -31.63537\ eV - 0.24966\ eV + \frac{1}{2}\left(0.35532\ eV\right) \\ &= -31.70737\ eV \end{aligned} \tag{13.485}$$

where the predicted ω_e (Eq. (13.458)) was used for the $\hbar\sqrt{\frac{k}{\mu}}$ term. $E_{T+osc}\left(^{12}CD\right)$, the total energy of ^{12}CD including the Doppler term, is given by the sum of $E_T\left(CD\right) = E_T\left(CH\right)$ (Eq. (13.432)) and $\bar{E}_{osc}\left(^{12}CD\right)$ given by Eq. (13.482).

$$\begin{aligned} E_{T+osc}\left(^{12}CD\right) &= -31.63537\ eV + \bar{E}_{osc}\left(^{12}CD\right) \\ &= -31.63537\ eV - 0.24966\ eV + \frac{1}{2}\left(0.26074\ eV\right) \\ &= -31.75462\ eV \end{aligned} \tag{13.486}$$

where the predicted ω_e (Eq. (13.467)) was used for the $\hbar\sqrt{\frac{k}{\mu}}$ term.

The CH bond dissociation energy, $E_D\left(^{12}CH\right)$, is given by the sum of the total energies of the $C2sp^3$ HO and the hydrogen atom minus $E_{T+osc}\left(^{12}CH\right)$[3]:

$$E_D\left(^{12}CH\right) = E\left(C,2sp^3\right) + E(H) - E_{T+osc}\left(^{12}CH\right) \tag{13.487}$$

$E\left(C,2sp^3\right)$ is given by Eq. (13.428), and $E_D(H)$ is given by Eq. (13.154). Thus, the ^{12}CH bond dissociation energy, $E_D\left(^{12}CH\right)$, given by Eqs. (13.154), (13.428), (13.485), and (13.487) is:

$$\begin{aligned} E_D\left(^{12}CH\right) &= -\left(14.63489\ eV + 13.59844\ eV\right) - E_{T+osc}\left(CH\right) \\ &= -28.23333\ eV - \left(-31.70737\ eV\right) \\ &= 3.47404\ eV \end{aligned} \tag{13.488}$$

The experimental ^{12}CH bond dissociation energy is [14]:

$$E_D\left(^{12}CH\right) = 3.47\ eV \tag{13.489}$$

which is a close match to that of NH as predicted based on the match between the N and $C2sp^3$ HO energies and electron configurations.

The ^{12}CD bond dissociation energy, $E_D\left(^{12}CD\right)$, is given by the sum of the total energies of the $C2sp^3$ HO and the deuterium atom minus $E_{T+osc}\left(CD\right)$:

$$E_D\left(^{12}CD\right) = E\left(C,2sp^3\right) + E(D) - E_{T+osc}\left(^{12}CD\right) \tag{13.490}$$

$E\left(C,2sp^3\right)$ is given by Eq. (13.428), and $E_D(D)$ is given by Eq. (13.155). Thus, the ^{12}CD bond dissociation energy, $E_D\left(^{12}CD\right)$, given by Eqs. (13.155), (13.428), (13.486), and (13.490) is:

$$\begin{aligned} E_D\left(^{12}CD\right) &= -\left(14.63489\ eV + 13.603\ eV\right) - E_{T+osc}\left(^{12}CD\right) \\ &= -28.23789\ eV - \left(-31.75462\ eV\right) \\ &= 3.51673\ eV \end{aligned} \tag{13.491}$$

The experimental ^{12}CD bond dissociation energy is [14]:

$$E_D\left(^{12}CD\right) = 3.52\ eV \tag{13.492}$$

The results of the determination of bond parameters of CH and CD are given in Table 13.1. The calculated results are based on first principles and given in closed-form, exact equations containing fundamental constants only. The agreement between the experimental and calculated results is excellent.

---

[3] The hybridization energy is the difference between $E\left(C,2p\ shell\right)$ given by Eq. (13.421) and $E\left(C,2sp^3\right)$ given by Eq. (13.428). Since this term adds to $E\left(C,2p\ shell\right)$ to give the total energy from which $E_{T+osc}\left(^{12}CH\right)$ is subtracted to give $E_D\left(^{12}CH\right)$, it is more convenient to simply use $E\left(C,2sp^3\right)$ directly in Eq. (13.487).

DIHYDROGEN CARBIDE (CH_2)

The dihydrogen carbide radical CH_2 is formed by the reaction of a hydrogen atom with a hydrogen carbide radical:

$$CH + H \rightarrow CH_2 \tag{13.493}$$

CH_2 can be solved using the same principles as those used to solve H_2O and NH_2 with the exception that the carbon $2s$ and $2p$ shells hybridize to form a single $2sp^3$ shell as an energy minimum. Two diatomic molecular orbitals (MOs) developed in the Nature of the Chemical Bond of Hydrogen-Type Molecules and Molecular Ions section serve as basis functions in a linear combination with two carbon $2sp^3$ hybridized orbitals (HOs) to form the MO of CH_2. The solution is very similar to that of CH except that there are two CH bonds in CH_2.

FORCE BALANCE OF CH_2

CH_2 comprises two chemical bonds between carbon and hydrogen atoms. Each $C-H$ bond comprises two spin-paired electrons with one from an initially unpaired electron of the carbon atom and the other from the hydrogen atom. Each H-atom electron forms a H_2-type ellipsoidal MO with an unpaired C-atom electrons. However, such a bond is not possible with the outer two C electrons in their ground state since the resulting H_2-type ellipsoidal MO would have a shorter internuclear distance than the radius of the carbon $2p$ shell, which is not energetically stable. Thus, when bonding the carbon $2s$ and $2p$ shells hybridize to form a single $2sp^3$ shell as an energy minimum. The electron configuration and the energy, $E\left(C,2sp^3\right)$, of the $C2sp^3$ shell is given by Eqs. (13.422), and (13.428), respectively.

For each $C-H$ bond, a $C2sp^3$ electron combines with the $H1s$ electron to form a molecular orbital. The proton of the H atom and the nucleus of the C atom are along each internuclear axis and serve as the foci. As in the case of H_2, each of the two $C-H$-bond MOs is a prolate spheroid with the exception that the ellipsoidal MO surface cannot extend into the $C2sp^3$ HO for distances shorter than the radius of the $C2sp^3$ shell since it is energetically unfavorable. Thus, each MO surface comprises a prolate spheroid at the H proton that is continuous with the $C2sp^3$ shell at the C atom whose nucleus serves as the other focus. The radius and the energy of the $C2sp^3$ shell are unchanged with bond formation. The central paramagnetic force due to spin of each $C-H$ bond is provided by the spin-pairing force of the CH_2 MO that has the symmetry of an s orbital that superimposes with the $C2sp^3$ orbitals such that the corresponding angular momenta are unchanged.

The energies in the CH_2 MO involve only each $C2sp^3$ and each $H1s$ electron with the formation of each $C-H$ bond. The sum of the energies of the H_2-type ellipsoidal MOs is matched to that of the $C2sp^3$ shell. As in the cases of OH, H_2O, NH, NH_2, NH_3, and CH the linear combination of each H_2-type ellipsoidal MO with the $C2sp^3$ HO must involve a 25% contribution from the H_2-type ellipsoidal MO to the $C2sp^3$ HO in order to match potential, kinetic, and orbital energy relationships. Thus, the CH_2 MO must comprise two $C-H$ bonds with each comprising 75% of a H_2-type ellipsoidal MO and a $C2sp^3$ HO:

$$\left[1\, C2sp^3 + 0.75\, H_2\ MO\right] + \left[1\, C2sp^3 + 0.75\, H_2\ MO\right] \rightarrow CH_2\ MO \tag{13.494}$$

The force balance of the CH_2 MO is determined by the boundary conditions that arise from the linear combination of orbitals according to Eq. (13.494) and the energy matching condition between the hydrogen and $C2sp^3$ HO components of the MO.

The force constant k' to determine the ellipsoidal parameter c' of the each H_2-type-ellipsoidal-MO component of the CH_2 MO in terms of the central force of the foci is given by Eq. (13.59). The distance from the origin of each $C-H$-bond MO to each focus c' is given by Eq. (13.60). The internuclear distance is given by Eq. (13.61). The length of the semiminor axis of the prolate spheroidal $C-H$-bond MO $b=c$ is given by Eq. (13.62). The eccentricity, e, is given by Eq. (13.63). The solution of the semimajor axis a then allows for the solution of the other axes of each prolate spheroid and eccentricity of each $C-H$-bond MO. Since each of the two prolate spheroidal $C-H$-bond MOs comprises a H_2-type-ellipsoidal MO that transitions to the $C2sp^3$ HO, the energy $E\left(C,2sp^3\right)$ in Eq. (13.428) adds to that of the two corresponding H_2-type ellipsoidal MOs to give the total energy of the CH_2 MO. From the energy equation and the relationship between the axes, the dimensions of the CH_2 MO are solved.

The energy components of V_e, V_p, T, and V_m are twice those of CH corresponding to the two $C-H$ bonds. Since each prolate spheroidal H_2-type MO transitions to the $C2sp^3$ HO and the energy of the $C2sp^3$ shell must remain constant and equal to the $E\left(C,2sp^3\right)$ given by Eq. (13.428), the total energy $E_T\left(CH_2\right)$ of the CH_2 MO is given by the sum of the energies

of the orbitals corresponding to the composition of the linear combination of the $C2sp^3$ HO and the two H_2-type ellipsoidal MOs that forms the CH_2 MO as given by Eq. (13.494). Using Eq. (13.431), $E_T\left(CH_2\right)$ is given by:

$$E_T\left(CH_2\right)=E_T+E\left(C,2sp^3\right)=-\frac{e^2}{4\pi\varepsilon_0 c'}\left[\left(0.91771\right)\left(2-\frac{1}{2}\frac{a_0}{a}\right)\ln\frac{a+c'}{a-c'}-1\right]-14.63489\ eV \tag{13.495}$$

The two hydrogen atoms and the hybridized carbon atom can achieve an energy minimum as a linear combination of two H_2-type ellipsoidal MOs each having the proton and the carbon nucleus as the foci. Hybridization gives rise to the $C2sp^3$ HO-shell Coulombic energy $E_{Coulomb}\left(C,2sp^3\right)$ given by Eq. (13.425). To meet the equipotential condition of the union of the H_2-type-ellipsoidal-MO and the $C2sp^3$ HO, the electron energies in Eq. (13.495) were normalized by the ratio of $14.82575\ eV$, the magnitude of $E_{Coulomb}\left(C,2sp^3\right)$ given by Eq. (13.425), and $13.605804\ eV$, the magnitude of the Coulombic energy between the electron and proton of H given by Eq. (1.264). The factor given by Eq. (13.430) normalized the energies to match that of the Coulombic energy alone to meet the energy matching condition of each $C-H$-bond MO under the influence of the proton and the C nucleus. Each $C-H$-bond MO comprises the same $C2sp^3$ shell having its energy normalized to that of the Coulombic energy between the electron and a charge of $+e$ at the carbon focus of the CH_2 MO. Thus, the energy of the CH_2 MO is also given by the sum of that of the two H_2-type ellipsoidal MOs given by Eq. (11.212) minus the Coulombic energy, $E_{Coulomb}\left(H\right)=-13.605804\ eV$, of the redundant $+e$ of the linear combination:

$$\begin{aligned}E_T\left(2H_2-H\right)&=-\frac{e^2}{4\pi\varepsilon_0 a_0}\left[\left(2\sqrt{2}-\sqrt{2}+\frac{\sqrt{2}}{2}\right)\ln\frac{\sqrt{2}+1}{\sqrt{2}-1}-\sqrt{2}\right]-E_{Coulomb}\left(H\right)\\&=2\left(-31.63536831\ eV\right)-\left(-13.605804\ eV\right)\\&=-49.66493\ eV\end{aligned} \tag{13.496}$$

$E_T\left(CH_2\right)$ given by Eq. (13.495) is set equal to two times the energy of the H_2-type ellipsoidal MO minus the Coulombic energy of H given by Eq. (13.496):

$$\begin{aligned}E_T\left(CH_2\right)&=-\frac{e^2}{4\pi\varepsilon_0 c'}\left[\left(0.91771\right)\left(2-\frac{1}{2}\frac{a_0}{a}\right)\ln\frac{a+c'}{a-c'}-1\right]-14.63489\ eV\\&=-49.66493\ eV\end{aligned} \tag{13.497}$$

From the energy relationship given by Eq. (13.497) and the relationship between the axes given by Eqs. (13.60-13.63), the dimensions of the CH_2 MO can be solved.

Substitution of Eq. (13.60) into Eq. (13.497) gives:

$$\frac{e^2}{4\pi\varepsilon_0\sqrt{\frac{2aa_0}{3}}}\left[\left(0.91771\right)\left(2-\frac{1}{2}\frac{a_0}{a}\right)\ln\frac{a+\sqrt{\frac{2aa_0}{3}}}{a-\sqrt{\frac{2aa_0}{3}}}-1\right]=e35.03004 \tag{13.498}$$

The most convenient way to solve Eq. (13.498) is by the reiterative technique using a computer. The result to within the round-off error with five-significant figures is

$$a=1.64010a_0=8.67903\ X\ 10^{-11}\ m \tag{13.499}$$

Substitution of Eq. (13.499) into Eq. (13.60) gives:

$$c'=1.04566a_0=5.53338\ X\ 10^{-11}\ m \tag{13.500}$$

The internuclear distance given by multiplying Eq. (13.500) by two is:

$$2c'=2.09132a_0=1.10668\ X\ 10^{-10}\ m \tag{13.501}$$

The experimental bond distance is [38]:

$$2c'=1.111\ X\ 10^{-10}\ m \tag{13.502}$$

Substitution of Eqs. (13.499-13.500) into Eq. (13.62) gives:

$$b=c=1.26354a_0=6.68635\ X\ 10^{-11}\ m \tag{13.503}$$

Substitution of Eqs. (13.499-13.500) into Eq. (13.63) gives:

$$e=0.63756 \tag{13.504}$$

The nucleus of the H atom and the nucleus of the C atom comprise the foci of each H_2-type ellipsoidal MO. The parameters of the point of intersection of each H_2-type ellipsoidal MO and the $C2sp^3$ HO are given by Eqs. (13.84-13.95), (13.261-

13.270), and (13.440-13.448). The polar intersection angle θ' is given by Eq. (13.261) where $r_n = r_{2sp^3} = 0.91771a_0$ is the radius of the $C2sp^3$ shell. Substitution of Eqs. (13.499-13.500) into Eq. (13.261) gives:

$$\theta' = 84.54° \tag{13.505}$$

Then, the angle θ_{C2sp^3HO} the radial vector of the $C2sp^3$ HO makes with the internuclear axis is:

$$\theta_{C2sp^3HO} = 180° - 84.54° = 95.46° \tag{13.506}$$

as shown in Figure 13.9. The parametric angle θ_{H_2MO} given by Eqs. (13.442-13.443), (13.503), and (13.506) is:

$$\theta_{H_2MO} = 46.30° \tag{13.507}$$

Then, the distance d_{H_2MO} along the internuclear axis from the origin of H_2-type ellipsoidal MO to the point of intersection of the orbitals given by Eqs. (13.445), (13.499), and (13.507) is:

$$\begin{aligned} d_{H_2MO} &= 1.13305a_0 \\ &= 5.99585\ X\ 10^{-11}\ m \end{aligned} \tag{13.508}$$

The distance d_{C2sp^3HO} along the internuclear axis from the origin of the C atom to the point of intersection of the orbitals given by Eqs. (13.447), (13.500), and (13.508) is:

$$\begin{aligned} d_{C2sp^3HO} &= 0.08739a_0 \\ &= 4.62472\ X\ 10^{-12}\ m \end{aligned} \tag{13.509}$$

As shown in Eq. (13.494), the uniform charge-density in the $C2sp^3$ HO is increased by a factor of 0.25 and the H-atom density is decreased by a factor of 0.25 for by each $C-H$ bond. Using the orbital composition of CH_2 (Eq. (13.494)), the radii of $C1s = 0.17113a_0$ (Eq. (10.51)) and $C2sp^3 = 0.91771a_0$ (Eq. (13.424)) shells, and the parameters of the CH_2 MO given by Eqs. (13.3-13.4), (13.499-13.501), and (13.503-13.509), the charge-density of the CH_2 MO comprising the linear combination of two $C-H$-bond MOs is shown in Figure 13.11. Each $C-H$-bond MO comprises a H_2-type ellipsoidal MO and a $C2sp^3$ HO having the dimensional diagram shown in Figure 13.9.

Figure 13.11. CH_2 MO comprising the linear combination of two $C-H$-bond MOs. Each $C-H$-bond MO comprises the superposition of a H_2-type ellipsoidal MO and a $C2sp^3$ HO with a relative charge-density of 0.75 to 1.25; otherwise, the $C2sp^3$ HO shell is unchanged. (A) Color scale, translucent view of the charge-density of the CH_2 MO from the top. For each $C-H$ bond, the ellipsoidal surface of the H_2-type ellipsoidal MO that transitions to the $C2sp^3$ HO, the $C2sp^3$ HO shell, $C1s$ shell, and the nuclei (red, not to scale) are shown. (B) Cut-away view showing the inner most $C1s$ shell, and moving radially, the $C2sp^3$ shell, and the H_2-type ellipsoidal MO that transitions to the $C2sp^3$ HO for each $C-H$ bond. Bisector current not shown.

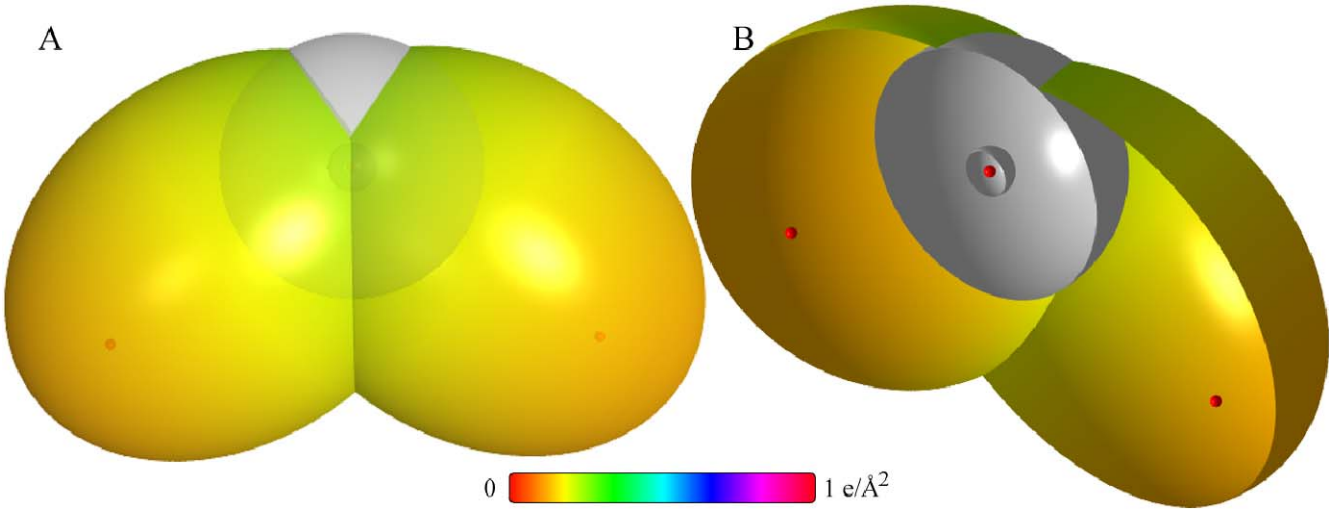

ENERGIES OF CH_2

The energies of CH_2 are two times those of CH and are given by the substitution of the semiprincipal axes (Eqs. (13.499-13.500) and (13.503)) into the energy equations Eq. (13.495) and (Eqs. (13.449-13.452)) that are multiplied by two:

$$V_e = (0.91771)\frac{-2e^2}{4\pi\varepsilon_0\sqrt{a^2-b^2}}\ln\frac{a+\sqrt{a^2-b^2}}{a-\sqrt{a^2-b^2}} = -72.03287\ eV \tag{13.510}$$

$$V_p = \frac{e^2}{4\pi\varepsilon_0\sqrt{a^2-b^2}} = 26.02344\ eV \tag{13.511}$$

$$T = (0.91771)\frac{\hbar^2}{m_e a\sqrt{a^2-b^2}}\ln\frac{a+\sqrt{a^2-b^2}}{a-\sqrt{a^2-b^2}} = 21.95990\ eV \tag{13.512}$$

$$V_m = (0.91771)\frac{-\hbar^2}{2m_e a\sqrt{a^2-b^2}}\ln\frac{a+\sqrt{a^2-b^2}}{a-\sqrt{a^2-b^2}} = -10.97995\ eV \tag{13.513}$$

$$E_T(CH_2) = -\frac{e^2}{4\pi\varepsilon_0 c'}\left[(0.91771)\left(2-\frac{1}{2}\frac{a_0}{a}\right)\ln\frac{a+c'}{a-c'}-1\right]-14.63489\ eV = -49.66437\ eV \tag{13.514}$$

where $E_T(CH_2)$ is given by Eq. (13.495) which is reiteratively matched to Eq. (13.496) within five-significant-figure round-off error.

VIBRATION OF CH_2

The vibrational energy levels of CH_2 may be solved as two equivalent coupled harmonic oscillators by developing the Lagrangian, the differential equation of motion, and the eigenvalue solutions [2] wherein the spring constants are derived from the central forces as given in the Vibration of Hydrogen-Type Molecular Ions section and the Vibration of Hydrogen-Type Molecules section.

THE DOPPLER ENERGY TERMS OF $^{12}CH_2$

The reentrant oscillation of hybridized orbitals in the transition state is not coupled. Therefore, the equations of the radiation reaction force of dihydrogen and dideuterium carbide are the same as those of the corresponding hydrogen carbide radicals with the substitution of the dihydrogen and dideuterium carbide parameters. Using Eqs. (11.136) and (13.140-13.142), the angular frequency of the reentrant oscillation in the transition state is

$$\omega = \sqrt{\frac{\frac{0.75e^2}{4\pi\varepsilon_0 b^3}}{m_e}} = 2.52077\ X\ 10^{16}\ rad/s \tag{13.515}$$

where b is given by Eq. (13.503). The kinetic energy, E_K, is given by Planck's equation (Eq. (11.127)):

$$\bar{E}_K = \hbar\omega = \hbar 2.52077\ X\ 10^{16}\ rad/s = 16.59214\ eV \tag{13.516}$$

In Eq. (11.181), substitution of $E_T(H_2)$ (Eqs. (11.212) and (13.75)), the maximum total energy of each H_2-type MO, for E_{hv}, the mass of the electron, m_e, for M, and the kinetic energy given by Eq. (13.516) for $\bar{E}_K$ gives the Doppler energy of the electrons of each of the two bonds for the reentrant orbit:

$$\bar{E}_D \cong E_{hv}\sqrt{\frac{2\bar{E}_K}{Mc^2}} = -31.63537\ eV\sqrt{\frac{2e(16.59214\ eV)}{m_e c^2}} = -0.25493\ eV \tag{13.517}$$

In addition to the electrons, the nuclei also undergo simple harmonic oscillation in the transition state at their corresponding frequency. The decrease in the energy of CH_2 due to the reentrant orbit of each bond in the transition state corresponding to simple harmonic oscillation of the electrons and nuclei, $\bar{E}_{osc}$, is given by the sum of the corresponding energies, $\bar{E}_D$ given by Eq. (13.517) and $\bar{E}_{Kvib}$, the average kinetic energy of vibration which is 1/2 of the vibrational energy of each $C-H$ bond. Using ω_e given by Eq. (13.458) for $\bar{E}_{Kvib}$ of the transition state having two independent bonds, $\bar{E}'_{osc}(^{12}CH_2)$ per bond is:

$$\bar{E}'_{osc}(^{12}CH_2) = \bar{E}_D + \bar{E}_{Kvib} = \bar{E}_D + \frac{1}{2}\hbar\sqrt{\frac{k}{\mu}} \tag{13.518}$$

$$\bar{E}'_{osc}(^{12}CH_2) = -0.25493\ eV + \frac{1}{2}(0.35532\ eV) = -0.07727\ eV \tag{13.519}$$

Given that the vibration and reentrant oscillation is for two $C-H$ bonds, $\bar{E}_{osc}(^{12}CH_2)$, is:

$$\begin{aligned}\bar{E}_{osc}\left({}^{12}CH_2\right) &= 2\left(\bar{E}_D + \frac{1}{2}\hbar\sqrt{\frac{k}{\mu}}\right) \\ &= 2\left(-0.25493\ eV + \frac{1}{2}\left(0.35532\ eV\right)\right) = -0.15454\ eV\end{aligned} \tag{13.520}$$

TOTAL AND BOND ENERGIES OF ${}^{12}CH_2$

$E_{T+osc}\left({}^{12}CH_2\right)$, the total energy of the ${}^{12}CH_2$ radical including the Doppler term, is given by the sum of $E_T\left(CH_2\right)$ (Eq. (13.497)) and $\bar{E}_{osc}\left({}^{12}CH_2\right)$ given by Eq. (13.520).

$$\begin{aligned}E_{T+osc}\left(CH_2\right) &= V_e + T + V_m + V_p + E\left(C, 2sp^3\right) + \bar{E}_{osc}\left({}^{12}CH_2\right) \\ &= E_T\left(CH_2\right) + \bar{E}_{osc}\left({}^{12}CH_2\right)\end{aligned} \tag{13.521}$$

$$\begin{aligned}E_{T+osc}\left({}^{12}CH_2\right) &= \left\{\begin{array}{l}\left(\frac{-e^2}{4\pi\varepsilon_0 c'}\left[\left(0.91771\right)\left(2-\frac{1}{2}\frac{a_0}{a}\right)\ln\frac{a+c'}{a-c'}-1\right]-14.63489\ eV\right) \\ -2\left(\left(31.63536831\ eV\right)\sqrt{\frac{2\hbar\sqrt{\frac{3}{4}\frac{e^2}{4\pi\varepsilon_0 b^3}}}{m_e c^2}}-\frac{1}{2}\hbar\sqrt{\frac{k}{\mu}}\right)\end{array}\right\} \\ &= -49.66493\ eV - 2\left(0.25493\ eV - \frac{1}{2}\hbar\sqrt{\frac{k}{\mu}}\right)\end{aligned} \tag{13.522}$$

From Eqs. (13.518-13.522), the total energy of ${}^{12}CH_2$ is:

$$\begin{aligned}E_{T+osc}\left({}^{12}CH_2\right) &= -49.66493\ eV + \bar{E}_{osc}\left({}^{12}CH_2\right) \\ &= -49.66493\ eV - 2\left(0.25493\ eV - \frac{1}{2}\left(0.35532\ eV\right)\right) = -49.81948\ eV\end{aligned} \tag{13.523}$$

where ω_e given by Eq. (13.458) was used for the $\hbar\sqrt{\frac{k}{\mu}}$ term.

${}^{12}CH_2$ has the same electronic configuration as ${}^{14}NH$. The dissociation of the bond of the dihydrogen carbide radical forms a free hydrogen atom with one unpaired electron and a $C2sp^3$ HO with three unpaired electrons as shown in Eq. (13.422) wherein the magnetic moments cannot all cancel. Thus, the bond dissociation of ${}^{12}CH_2$ gives rise to ${}^{12}CH$ with the same electronic configuration as N as given by Eq. (10.134). The N configuration is more stable than H as shown in Eqs. (10.141-10.143). The lowering of the energy of the reactants decreases the bond energy. The total energy of carbon is reduced by the energy in the field of the two magnetic dipoles given by Eq. (7.46) and Eq. (13.424).

$$E(magnetic) = \frac{2\pi\mu_0 e^2\hbar^2}{m_e^2\left(r_{2sp^3}\right)^3} = \frac{8\pi\mu_0\mu_B^2}{\left(0.91771a_0\right)^3} = 0.14803\ eV \tag{13.524}$$

The CH_2 bond dissociation energy, $E_D\left({}^{12}CH_2\right)$, is given by the sum of the total energies of the CH radical and the hydrogen atom minus the sum of $E_{T+osc}\left({}^{12}CH_2\right)$ and $E(magnetic)$:

$$E_D\left({}^{12}CH_2\right) = E\left({}^{12}CH\right) + E(H) - E_{T+osc}\left({}^{12}CH_2\right) - E\left(magnetic\right) \tag{13.525}$$

where $E_T({}^{12}CH)$ is given by the sum of the energies of the $C2sp^3$ HO, $E\left(C, 2sp^3\right)$ given by Eq. (13.428), $E_D(H)$ given by Eq. (13.154), and the negative of the bond energy of ${}^{12}CH$ given by Eq. (13.489):

$$E({}^{12}CH) = -13.59844\ eV - 14.63489\ eV - 3.47\ eV = -31.70333\ eV \tag{13.526}$$

Thus, the ${}^{12}CH_2$ bond dissociation energy, $E_D\left({}^{12}CH_2\right)$, given by Eqs. (13.154), and (13.523-13.526) is:

$$\begin{aligned}E_D\left({}^{12}CH_2\right) &= -\left(31.70333\ eV + 13.59844\ eV\right) - \left(E_{T+osc}\left({}^{12}CH_2\right) + E\left(magnetic\right)\right) \\ &= -45.30177\ eV - \left(-49.81948\ eV + 0.14803\ eV\right) = 4.36968\ eV\end{aligned} \tag{13.527}$$

The experimental ${}^{12}CH_2$ bond dissociation energy is [39]:

$$E_D\left({}^{12}CH_2\right) = 4.33064\ eV \tag{13.528}$$

BOND ANGLE OF $^{12}CH_2$

The CH_2 MO comprises a linear combination of two $C-H$ -bond MOs. Each $C-H$ -bond MO comprises the superposition of a H_2 -type ellipsoidal MO and the $C2sp^3$ HO with a relative charge density of 0.75 to 1.25; otherwise, the $C2sp^3$ shell is unchanged. A bond is also possible between the two H atoms of the $C-H$ bonds. Such $H-H$ bonding would decrease the $C-H$ bond strength since electron density would be shifted from the $C-H$ bonds to the $H-H$ bond. Thus, the bond angle between the two $C-H$ bonds is determined by the condition that the total energy of the H_2 -type ellipsoidal MO between the terminal H atoms of the $C-H$ bonds is zero. From Eqs. (11.79) and (13.228), the distance from the origin to each focus of the $H-H$ ellipsoidal MO is

$$c' = a\sqrt{\frac{\hbar^2 4\pi\varepsilon_0}{m_e e^2 2a}} = \sqrt{\frac{aa_0}{2}} \tag{13.529}$$

The internuclear distance from Eq. (13.229) is:

$$2c' = 2\sqrt{\frac{aa_0}{2}} \tag{13.530}$$

The length of the semiminor axis of the prolate spheroidal $H-H$ MO $b=c$ is given by Eq. (13.62).

The bond angle of CH_2 is derived by using the orbital composition and an energy matching factor as in the case with NH_2 and NH_3. Since the two H_2 -type ellipsoidal MOs comprise 75% of the H electron density of H_2 and the energy of each H_2 -type ellipsoidal MO is matched to that of the $C2sp^3$ HO; the component energies and the total energy E_T of the $H-H$ bond are given by Eqs. (13.67-13.73) except that V_e, T, and V_m are corrected for the hybridization-energy-matching factor of 0.91771 given by Eq. (13.430). Substitution of Eq. (13.529) into Eq. (13.233) with the hybridization factor gives:

$$0 = \left[\begin{array}{l} \dfrac{-e^2}{8\pi\varepsilon_0\sqrt{\dfrac{aa_0}{2}}}\left[(0.91771)^{-1}\left(\frac{3}{2}-\frac{3}{8}\frac{a_0}{a}\right)\ln\dfrac{a+\sqrt{\dfrac{aa_0}{2}}}{a-\sqrt{\dfrac{aa_0}{2}}}-1\right]\left[1+\sqrt{\dfrac{2\hbar\sqrt{\dfrac{0.75e^2}{4\pi\varepsilon_0 a^3}}}{m_e c^2}}\right] \\ +\dfrac{1}{2}\hbar\sqrt{\dfrac{\dfrac{0.75e^2}{8\pi\varepsilon_0 a^3}-\dfrac{e^2}{8\pi\varepsilon_0\left(a+c'\right)^3}}{0.5m_p}} \end{array}\right] \tag{13.531}$$

From the energy relationship given by Eq. (13.531) and the relationship between the axes given by Eqs. (13.529-13.530) and (13.62-13.63), the dimensions of the $H-H$ MO can be solved.

The most convenient way to solve Eq. (13.531) is by the reiterative technique using a computer. The result to within the round-off error with five-significant figures is:

$$a = 5.1500a_0 = 2.7253\ X\ 10^{-10}\ m \tag{13.532}$$

Substitution of Eq. (13.532) into Eq. (13.529) gives:

$$c' = 1.6047a_0 = 8.4916\ X\ 10^{-11}\ m \tag{13.533}$$

The internuclear distance given by multiplying Eq. (13.533) by two is:

$$2c' = 3.2094a_0 = 1.6983\ X\ 10^{-10}\ m \tag{13.534}$$

Substitution of Eqs. (13.532-13.533) into Eq. (13.62) gives:

$$b = c = 4.8936a_0 = 2.5896\ X\ 10^{-10}\ m \tag{13.535}$$

Substitution of Eqs. (13.532-13.533) into Eq. (13.63) gives:

$$e = 0.3116 \tag{13.536}$$

Using, $2c'_{H-H}$ (Eq. (13.534)), the distance between the two H atoms when the total energy of the corresponding MO is zero (Eq. (13.531)), and $2c'_{C-H}$ (Eq. (13.501)), the internuclear distance of each $C-H$ bond, the corresponding bond angle can be determined from the law of cosines. Using, Eq. (13.242), the bond angle θ between the $C-H$ bonds is:

$$\theta = \cos^{-1}\left(\frac{2\left(2.09132\right)^2-\left(3.2094\right)^2}{2\left(2.09132\right)^2}\right) = \cos^{-1}\left(-0.1775\right) = 100.22° \tag{13.537}$$

The experimental angle between the $C-H$ bonds is [38]:

$$\theta = 102.4° \tag{13.538}$$

The results of the determination of bond parameters of CH_2 are given in Table 13.1. The calculated results are based on first principles and given in closed-form, exact equations containing fundamental constants only. The agreement between the experimental and calculated results is excellent.

METHYL RADICAL (CH_3)

The methyl radical CH_3 is formed by the reaction of a hydrogen atom with a dihydrogen carbide radical:

$$CH_2 + H \rightarrow CH_3 \tag{13.539}$$

CH_3 can be solved using the same principles as those used to solve NH_3 with the exception that the carbon $2s$ and $2p$ shells hybridize to form a single $2sp^3$ shell as an energy minimum. Three diatomic molecular orbitals (MOs) developed in the Nature of the Chemical Bond of Hydrogen-Type Molecules and Molecular Ions section serve as basis functions in a linear combination with three carbon $2sp^3$ hybridized orbitals (HOs) to form the MO of CH_3. The solution is very similar to that of CH_2 except that there are three CH bonds in CH_3.

FORCE BALANCE OF CH_3

CH_3 comprises three chemical bonds between carbon and hydrogen atoms. Each $C-H$ bond comprises two spin-paired electrons with one from an initially unpaired electron of the carbon atom and the other from the hydrogen atom. Each H-atom electron forms an H_2-type ellipsoidal MO with an unpaired C-atom electron. However, such a bond is not possible with the outer two C electrons in their ground state since the resulting H_2-type ellipsoidal MO would have a shorter internuclear distance than the radius of the carbon $2p$ shell which is not energetically stable, and only two electrons are unpaired. Thus, when bonding the carbon $2s$ and $2p$ shells hybridize to form a single $2sp^3$ shell as an energy minimum. The electron configuration and the energy, $E\left(C,2sp^3\right)$, of the $C2sp^3$ shell is given by Eqs. (13.422), and (13.428), respectively.

For each $C-H$ bond, a $C2sp^3$ electron combines with the $H1s$ electron to form a molecular orbital. The proton of the H atom and the nucleus of the C atom are along each internuclear axis and serve as the foci. As in the case of H_2, each of the three $C-H$-bond MOs is a prolate spheroid with the exception that the ellipsoidal MO surface cannot extend into $C2sp^3$ HO for distances shorter than the radius of the $C2sp^3$ shell since it is energetically unfavorable. Thus, each MO surface comprises a prolate spheroid at the H proton that is continuous with the $C2sp^3$ shell at the C atom whose nucleus serves as the other focus. The radius and the energy of the $C2sp^3$ shell are unchanged with bond formation. The central paramagnetic force due to spin of each $C-H$ bond is provided by the spin-pairing force of the CH_3 MO that has the symmetry of an s orbital that superimposes with the $C2sp^3$ orbitals such that the corresponding angular momenta are unchanged.

The energies in the CH_3 MO involve only each $C2sp^3$ and each $H1s$ electron with the formation of each $C-H$ bond. The sum of the energies of the H_2-type ellipsoidal MOs is matched to that of the $C2sp^3$ shell. As in the cases of OH, H_2O, NH, NH_2, NH_3, CH, and CH_2 the linear combination of each H_2-type ellipsoidal MO with the $C2sp^3$ HO must involve a 25% contribution from the H_2-type ellipsoidal MO to the $C2sp^3$ HO in order to match potential, kinetic, and orbital energy relationships. Thus, the CH_3 MO must comprise three $C-H$ bonds with each comprising 75% of a H_2-type ellipsoidal MO and a $C2sp^3$ HO:

$$3\left[1\ C2sp^3 + 0.75\ H_2\ MO\right] \rightarrow CH_3\ MO \tag{13.540}$$

The force balance of the CH_3 MO is determined by the boundary conditions that arise from the linear combination of orbitals according to Eq. (13.540) and the energy matching condition between the hydrogen and $C2sp^3$ HO components of the MO.

The force constant k' to determine the ellipsoidal parameter c' of each H_2-type-ellipsoidal-MO component of the CH_3 MO in terms of the central force of the foci is given by Eq. (13.59). The distance from the origin of each $C-H$-bond MO to each focus c' is given by Eq. (13.60). The internuclear distance is given by Eq. (13.61). The length of the semiminor axis of the prolate spheroidal $C-H$-bond MO $b=c$ is given by Eq. (13.62). The eccentricity, e, is given by Eq. (13.63). The solution of the semimajor axis a then allows for the solution of the other axes of each prolate spheroid and eccentricity of each $C-H$-bond MO. Since each of the three prolate spheroidal $C-H$-bond MOs comprises a H_2-type-ellipsoidal MO that transitions to the $C2sp^3$ HO, the energy $E\left(C,2sp^3\right)$ in Eq. (13.428) adds to that of the three corresponding H_2-type ellipsoidal MOs to give the total energy of the CH_3 MO. From the energy equation and the relationship between the axes, the dimensions of the CH_3 MO are solved.

The energy components of V_e, V_p, T, and V_m are three times those of CH corresponding to the three $C-H$ bonds. Since each prolate spheroidal H_2-type MO transitions to the $C2sp^3$ HO and the energy of the $C2sp^3$ shell must remain constant and equal to the $E\left(C,2sp^3\right)$ given by Eq. (13.428), the total energy $E_T\left(CH_3\right)$ of the CH_3 MO is given by the sum of the

energies of the orbitals corresponding to the composition of the linear combination of the $C2sp^3$ HO and the three H_2-type ellipsoidal MOs that forms the CH_3 MO as given by Eq. (13.540). Using Eq. (13.431), $E_T\left(CH_3\right)$ is given by:

$$\begin{aligned} E_T\left(CH_3\right) &= E_T + E\left(C,2sp^3\right) \\ &= -\frac{3e^2}{8\pi\varepsilon_0 c'}\left[\left(0.91771\right)\left(2-\frac{1}{2}\frac{a_0}{a}\right)\ln\frac{a+c'}{a-c'}-1\right]-14.63489\ eV \end{aligned} \tag{13.541}$$

The three hydrogen atoms and the hybridized carbon atom can achieve an energy minimum as a linear combination of three H_2-type ellipsoidal MOs each having the proton and the carbon nucleus as the foci. Hybridization gives rise to the $C2sp^3$ HO-shell Coulombic energy $E_{Coulomb}\left(C,2sp^3\right)$ given by Eq. (13.425). To meet the equipotential condition of the union of the H_2-type-ellipsoidal-MO and the $C2sp^3$ HO, the electron energies in Eqs. (13.431), (13.495), and (13.541) were normalized by the ratio of 14.82575 eV, the magnitude of $E_{Coulomb}\left(C,2sp^3\right)$ given by Eq. (13.425), and 13.605804 eV, the magnitude of the Coulombic energy between the electron and proton of H given by Eq. (1.224). The factor given by Eq. (13.430) normalized the energies to match that of the Coulombic energy alone to meet the energy matching condition of each $C-H$-bond MO under the influence of the proton and the C nucleus. Each $C-H$-bond MO comprises the same $C2sp^3$ shell having its energy normalized to that of the Coulombic energy between the electron and a charge of $+e$ at the carbon focus of the CH_3 MO. Thus, the energy of the CH_3 MO is also given by the sum of that of the three H_2-type ellipsoidal MOs given by Eq. (11.212) minus two times the Coulombic energy, $E_{Coulomb}\left(H\right)=-13.605804\ eV$, of the two redundant $+e$'s of the linear combination:

$$\begin{aligned} E_T\left(3H_2-2H\right) &= -\frac{3e^2}{8\pi\varepsilon_0 a_0}\left[\left(2\sqrt{2}-\sqrt{2}+\frac{\sqrt{2}}{2}\right)\ln\frac{\sqrt{2}+1}{\sqrt{2}-1}-\sqrt{2}\right]-2E_{Coulomb}\left(H\right) \\ &= 3\left(-31.63536831\ eV\right)-2\left(-13.605804\ eV\right)=-67.69450\ eV \end{aligned} \tag{13.542}$$

$E_T\left(CH_3\right)$ given by Eq. (13.541) is set equal to three times the energy of the H_2-type ellipsoidal MO minus two times the Coulombic energy of H given by Eq. (13.542).

$$\begin{aligned} E_T\left(CH_3\right) &= -\frac{3e^2}{8\pi\varepsilon_0 c'}\left[\left(0.91771\right)\left(2-\frac{1}{2}\frac{a_0}{a}\right)\ln\frac{a+c'}{a-c'}-1\right]-14.63489\ eV \\ &= -67.69450\ eV \end{aligned} \tag{13.543}$$

From the energy relationship given by Eq. (13.543) and the relationship between the axes given by Eqs. (13.60-13.63), the dimensions of the CH_3 MO can be solved.

Substitution of Eq. (13.60) into Eq. (13.543) gives:

$$\frac{3e^2}{8\pi\varepsilon_0\sqrt{\frac{2aa_0}{3}}}\left[\left(0.91771\right)\left(2-\frac{1}{2}\frac{a_0}{a}\right)\ln\frac{a+\sqrt{\frac{2aa_0}{3}}}{a-\sqrt{\frac{2aa_0}{3}}}-1\right]=e53.05961 \tag{13.544}$$

The most convenient way to solve Eq. (13.544) is by the reiterative technique using a computer. The result to within the round-off error with five-significant figures is

$$a=1.62893a_0=8.61990\ X\ 10^{-11}\ m \tag{13.545}$$

Substitution of Eq. (13.545) into Eq. (13.60) gives:

$$c'=1.04209a_0=5.51450\ X\ 10^{-11}\ m \tag{13.546}$$

The internuclear distance given by multiplying Eq. (13.546) by two is:

$$2c'=2.08418a_0=1.10290\ X\ 10^{-10}\ m \tag{13.547}$$

The experimental bond distance is [38]:

$$2c'=1.079\ X\ 10^{-10}\ m \tag{13.548}$$

Substitution of Eqs. (13.545-13.546) into Eq. (13.62) gives:

$$b=c=1.25198a_0=6.62518\ X\ 10^{-11}\ m \tag{13.549}$$

Substitution of Eqs. (13.545-13.546) into Eq. (13.63) gives:

$$e=0.63974 \tag{13.550}$$

The nucleus of the H atom and the nucleus of the C atom comprise the foci of each H_2-type ellipsoidal MO. The parameters of the point of intersection of each H_2-type ellipsoidal MO and the $C2sp^3$ HO are given by Eqs. (13.84-13.95), (13.261-13.270), and (13.434-13.442). The polar intersection angle θ' is given by Eq. (13.261) where $r_n = r_{2sp^3} = 0.91771a_0$ is the radius of the $C2sp^3$ shell. Substitution of Eqs. (13.545-13.546) into Eq. (13.261) gives:

$$\theta' = 85.65° \tag{13.551}$$

Then, the angle θ_{C2sp^3HO} the radial vector of the $C2sp^3$ HO makes with the internuclear axis is:

$$\theta_{C2sp^3HO} = 180° - 85.65° = 94.35° \tag{13.552}$$

as shown in Figure 13.9. The parametric angle θ_{H_2MO} given by Eqs. (13.442-13.443), (13.549), and (13.552) is:

$$\theta_{H_2MO} = 46.96° \tag{13.553}$$

Then, the distance d_{H_2MO} along the internuclear axis from the origin of H_2-type ellipsoidal MO to the point of intersection of the orbitals given by Eqs. (13.445), (13.545), and (13.553) is:

$$\begin{aligned} d_{H_2MO} &= 1.11172a_0 \\ &= 5.88295\ X\ 10^{-11}\ m \end{aligned} \tag{13.554}$$

The distance d_{C2sp^3HO} along the internuclear axis from the origin of the C atom to the point of intersection of the orbitals given by Eqs. (13.447), (13.546), and (13.554) is:

$$d_{C2sp^3HO} = 0.06963a_0 = 3.68457\ X\ 10^{-12}\ m \tag{13.555}$$

As shown in Eq. (13.540), the uniform charge-density in the $C2sp^3$ HO is increased by a factor of 0.25 and the H-atom density is decreased by a factor of 0.25 for each $C-H$ bond. Using the orbital composition of CH_3 (Eq. (13.540)), the radii of $C1s = 0.17113a_0$ (Eq. (10.51)) and $C2sp^3 = 0.91771a_0$ (Eq. (13.424)) shells, and the parameters of the CH_3 MO given by Eqs. (13.3-13.4), (13.545-13.547), and (13.549-13.555), the charge-density of the CH_3 MO comprising the linear combination of three $C-H$-bond MOs is shown in Figure 13.12. Each $C-H$-bond MO comprises a H_2-type ellipsoidal MO and a $C2sp^3$ HO having the dimensional diagram shown in Figure 13.9.

Figure 13.12. CH_3 MO comprising the linear combination of three $C-H$-bond MOs. Each $C-H$-bond MO comprises the superposition of a H_2-type ellipsoidal MO and a $C2sp^3$ HO with a relative charge-density of 0.75 to 1.25; otherwise, the $C2sp^3$ HO shell is unchanged. (A) Color scale, translucent view of the charge-density of the CH_3 MO from the top. For each $C-H$ bond, the ellipsoidal surface of the H_2-type ellipsoidal MO that transitions to the $C2sp^3$ HO, the $C2sp^3$ HO shell, $C1s$ shell, and the nuclei (red, not to scale) are shown. (B) Cut-away view showing the inner most $C1s$ shell, and moving radially, the $C2sp^3$ shell, and the H_2-type ellipsoidal MO that transitions to the $C2sp^3$ HO for each $C-H$ bond. Bisector current not shown. (C)-(D) Color scale, bottom, top, and side-on translucent views of the charge-density of the CH_3 MO, respectively.

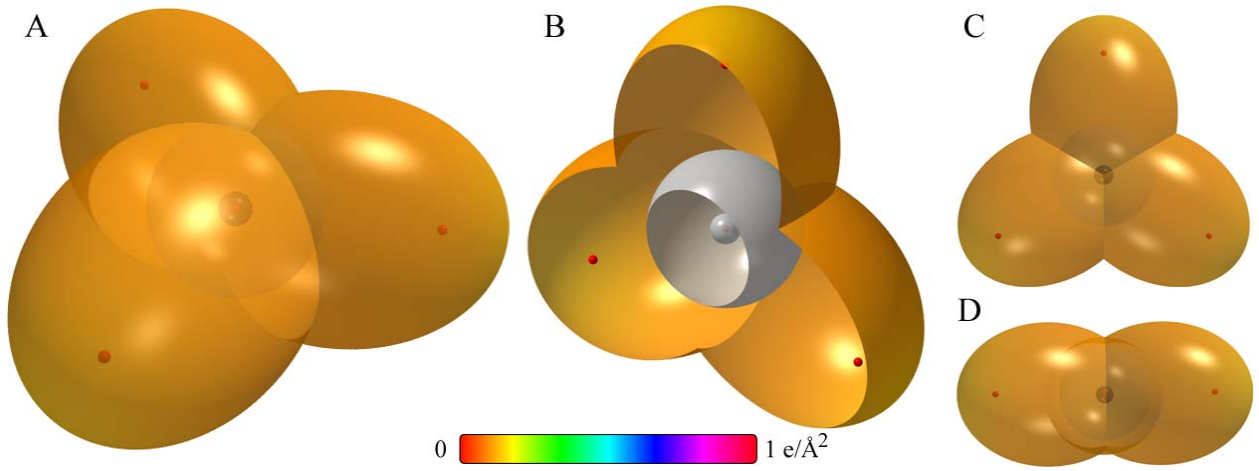

ENERGIES OF CH_3

The energies of CH_3 are three times those of CH and are given by the substitution of the semiprincipal axes (Eqs. (13.545-13.546) and (13.549)) into the energy equations Eq. (13.541) and (Eqs. (13.449-13.452)) that are multiplied by three:

$$V_e = 3(0.91771)\frac{-2e^2}{8\pi\varepsilon_0\sqrt{a^2-b^2}}\ln\frac{a+\sqrt{a^2-b^2}}{a-\sqrt{a^2-b^2}} = -108.94944\ eV \tag{13.556}$$

$$V_p = \frac{3e^2}{8\pi\varepsilon_0\sqrt{a^2-b^2}} = 39.16883\ eV \tag{13.557}$$

$$T = 3(0.91771)\frac{\hbar^2}{2m_e a\sqrt{a^2-b^2}}\ln\frac{a+\sqrt{a^2-b^2}}{a-\sqrt{a^2-b^2}} = 33.44213\ eV \tag{13.558}$$

$$V_m = 3(0.91771)\frac{-\hbar^2}{4m_e a\sqrt{a^2-b^2}}\ln\frac{a+\sqrt{a^2-b^2}}{a-\sqrt{a^2-b^2}} = -16.72107\ eV \tag{13.559}$$

$$E_T(CH_3) = -\frac{3e^2}{8\pi\varepsilon_0 c'}\left[(0.91771)\left(2-\frac{1}{2}\frac{a_0}{a}\right)\ln\frac{a+c'}{a-c'}-1\right]-14.63489\ eV = -67.69444\ eV \tag{13.560}$$

where $E_T(CH_3)$ is given by Eq. (13.541) which is reiteratively matched to Eq. (13.542) within five-significant-figure-round-off-error.

VIBRATION OF CH_3

The vibrational energy levels of CH_3 may be solved as three equivalent coupled harmonic oscillators by developing the Lagrangian, the differential equation of motion, and the eigenvalue solutions [2] wherein the spring constants are derived from the central forces as given in the Vibration of Hydrogen-Type Molecular Ions section and the Vibration of Hydrogen-Type Molecules section.

THE DOPPLER ENERGY TERMS OF $^{12}CH_3$

The reentrant oscillation of hybridized orbitals in the transition state is not coupled. Therefore, the equations of the radiation reaction force of methyl radical are the same as those of the corresponding hydrogen carbide radicals with the substitution of the methyl radical parameters. Using Eqs. (11.136) and (13.140-13.142), the angular frequency of the reentrant oscillation in the transition state is:

$$\omega = \sqrt{\frac{\frac{0.75e^2}{4\pi\varepsilon_0 b^3}}{m_e}} = 2.55577\ X\ 10^{16}\ rad/s \tag{13.561}$$

where b is given by Eq. (13.549). The kinetic energy, E_K, is given by Planck's equation (Eq. (11.127)):

$$\overline{E}_K = \hbar\omega = \hbar 2.55577\ X\ 10^{16}\ rad/s = 16.82249\ eV \tag{13.562}$$

In Eq. (11.181), substitution of $E_T(H_2)$ (Eqs. (11.212) and (13.75)), the maximum total energy of each H_2-type MO, for $E_{h\nu}$, the mass of the electron, m_e, for M, and the kinetic energy given by Eq. (13.562) for $\overline{E}_K$ gives the Doppler energy of the electrons of each of the three bonds for the reentrant orbit:

$$\begin{aligned}\overline{E}_D &\cong E_{h\nu}\sqrt{\frac{2\overline{E}_K}{Mc^2}} \\ &= -31.63537\ eV\sqrt{\frac{2e(16.82249\ eV)}{m_e c^2}} = -0.25670\ eV\end{aligned} \tag{13.563}$$

In addition to the electrons, the nuclei also undergo simple harmonic oscillation in the transition state at their corresponding frequency. The decrease in the energy of CH_3 due to the reentrant orbit of each bond in the transition state corresponding to simple harmonic oscillation of the electrons and nuclei, $\overline{E}_{osc}$, is given by the sum of the corresponding energies, $\overline{E}_D$ given by Eq. (13.563) and $\overline{E}_{Kvib}$, the average kinetic energy of vibration which is 1/2 of the vibrational energy of each $C-H$ bond. Using ω_e given by Eq. (13.458) for $\overline{E}_{Kvib}$ of the transition state having three independent bonds, $\overline{E}'_{osc}(^{12}CH_3)$ per bond is

$$\overline{E}'_{osc}(^{12}CH_3) = \overline{E}_D + \overline{E}_{Kvib} = \overline{E}_D + \frac{1}{2}\hbar\sqrt{\frac{k}{\mu}} \tag{13.564}$$

$$\bar{E}'_{osc}\left({}^{12}CH_3\right) = -0.25670\ eV + \frac{1}{2}\left(0.35532\ eV\right) = -0.07904\ eV \tag{13.565}$$

Given that the vibration and reentrant oscillation is for three $C-H$ bonds, $\bar{E}_{osc}\left({}^{12}CH_3\right)$, is:

$$\begin{aligned}\bar{E}_{osc}\left({}^{12}CH_3\right) &= 3\left(\bar{E}_D + \frac{1}{2}\hbar\sqrt{\frac{k}{\mu}}\right)\\ &= 3\left(-0.25670\ eV + \frac{1}{2}\left(0.35532\ eV\right)\right) = -0.23711\ eV\end{aligned} \tag{13.566}$$

TOTAL AND BOND ENERGIES OF ${}^{12}CH_3$

$E_{T+osc}\left({}^{12}CH_3\right)$, the total energy of the ${}^{12}CH_3$ radical including the Doppler term, is given by the sum of $E_T\left(CH_3\right)$ (Eq. (13.543)) and $\bar{E}_{osc}\left({}^{12}CH_3\right)$ given by Eq. (13.566).

$$E_{T+osc}\left(CH_3\right) = V_e + T + V_m + V_p + E\left(C,2sp^3\right) + \bar{E}_{osc}\left({}^{12}CH_3\right) = E_T\left(CH_3\right) + \bar{E}_{osc}\left({}^{12}CH_3\right) \tag{13.567}$$

$$\begin{aligned}E_{T+osc}\left({}^{12}CH_3\right) &= \left\{\begin{array}{l}\left(\frac{-3e^2}{8\pi\varepsilon_0 c'}\left[\left(0.91771\right)\left(2-\frac{1}{2}\frac{a_0}{a}\right)\ln\frac{a+c'}{a-c'}-1\right]-14.63489\ eV\right)\\ -3\left(\left(31.63536831\ eV\right)\sqrt{\frac{2\hbar\sqrt{\frac{3}{4}\frac{e^2}{4\pi\varepsilon_0 b^3}}}{m_e c^2}}-\frac{1}{2}\hbar\sqrt{\frac{k}{\mu}}\right)\end{array}\right\}\\ &= -67.69450\ eV - 3\left(0.25670\ eV - \frac{1}{2}\hbar\sqrt{\frac{k}{\mu}}\right)\end{aligned} \tag{13.568}$$

From Eqs. (13.564-13.568), the total energy of ${}^{12}CH_3$ is:

$$\begin{aligned}E_{T+osc}\left({}^{12}CH_3\right) &= -67.69450\ eV + \bar{E}_{osc}\left({}^{12}CH_3\right)\\ &= -67.69450\ eV - 3\left(0.25670\ eV - \frac{1}{2}\left(0.35532\ eV\right)\right)\\ &= -67.93160\ eV\end{aligned} \tag{13.569}$$

where ω_e given by Eq. (13.458) was used for the $\hbar\sqrt{\frac{k}{\mu}}$ term.

The CH_3 bond dissociation energy, $E_D\left({}^{12}CH_3\right)$, is given by the sum of the total energies of the CH_2 radical and the hydrogen atom minus $E_{T+osc}\left({}^{12}CH_3\right)$:

$$E_D\left({}^{12}CH_3\right) = E\left({}^{12}CH_2\right) + E(H) - E_{T+osc}\left({}^{12}CH_3\right) \tag{13.570}$$

where $E_T({}^{12}CH_2)$ is given by the sum of the energies of the $C2sp^3$ HO, $E\left(C,2sp^3\right)$ given by Eq. (13.428), $2E_D(H)$ given by Eq. (13.154), and the negative of the bond energies of ${}^{12}CH$ given by Eq. (13.489) and ${}^{12}CH_2$ given by Eq. (13.528):

$$\begin{aligned}E({}^{12}CH_2) &= 2\left(-13.59844\ eV\right) - 14.63489\ eV - 3.47\ eV - 4.33064\ eV\\ &= -49.63241\ eV\end{aligned} \tag{13.571}$$

Thus, the ${}^{12}CH_3$ bond dissociation energy, $E_D\left({}^{12}CH_3\right)$, given by Eqs. (13.154), and (13.569-13.571) is:

$$\begin{aligned}E_D\left({}^{12}CH_3\right) &= +\left(-49.63241\ \ eV - 13.59844\ eV\right) - E_{T+osc}\left({}^{12}CH_3\right)\\ &= -63.23085eV - \left(-67.93160\ eV\right)\\ &= 4.70075\ eV\end{aligned} \tag{13.572}$$

The experimental ${}^{12}CH_3$ bond dissociation energy is [40]

$$E_D\left({}^{12}CH_3\right) = 4.72444\ eV \tag{13.573}$$

BOND ANGLE OF $^{12}CH_3$

Consider the case that all of the MOs can participate in a superposition involving bonding of the terminal atoms. Then, solving for $2c'_{H-H} = 3.61109a_0$, the distance between any adjacent two H atoms when the total energy of the corresponding MO is zero given by Eq. (13.531) with the replacement of the hybridization factor and energy terms with $(0.91771)\left(2-\frac{1}{2}\frac{a_0}{a}\right)$ of Eq. (13.568), and $2c'_{C-H}$, the internuclear distance of each $C-H$ bond (Eq. (13.547)), the corresponding bond angle can be determined from the law of cosines. Using Eq. (13.537), the bond angle θ between the $C-H$ bonds is:

$$\theta = \cos^{-1}\left(\frac{2(2.08418)^2-(3.61109)^2}{2(2.08418)^2}\right) = \cos^{-1}(-0.50099) = 120° \tag{13.574}$$

which is in agreement with D_{3h} symmetry [38].

The CH_3 radical has a pyramidal structure with the carbon atom along the z-axis at the apex and the hydrogen atoms at the base in the xy-plane. The distance $d_{origin-H}$ from the origin to the nucleus of a hydrogen atom given by Eqs. (13.534) and (13.412) is:

$$d_{origin-H} = 2.0848a_0 \tag{13.575}$$

The height along the z-axis of the pyramid from the origin to the C nucleus is d_{height} given by Eqs. (13.414), (13.547), and (13.575) is:

$$d_{height} = 0a_0 \tag{13.576}$$

The angle θ_v of each $C-H$ bond from the z-axis given by Eqs. (13.416), (13.575), and (13.576) is:

$$\theta_v = 90° \tag{13.577}$$

The CH_3 MO shown in Figure 13.12 was rendered using these parameters.

The results of the determination of bond parameters of CH_3 are given in Table 13.1. The calculated results are based on first principles and given in closed-form, exact equations containing fundamental constants only. The agreement between the experimental and calculated results is excellent.

METHANE MOLECULE (CH_4)

The methane molecule CH_4 is formed by the reaction of a hydrogen atom with a methyl radical:

$$CH_3 + H \rightarrow CH_4 \tag{13.578}$$

CH_4 can be solved using the same principles as those used to solve and CH_3 wherein the carbon $2s$ and $2p$ shells hybridize to form a single $2sp^3$ shell as an energy minimum. Four diatomic molecular orbitals (MOs) developed in the Nature of the Chemical Bond of Hydrogen-Type Molecules and Molecular Ions section serve as basis functions in a linear combination with four carbon $2sp^3$ hybridized orbitals (HOs) to form the MO of CH_4. The solution is very similar to that of CH_3 except that there are four CH bonds in CH_4. Methane is the simplest hydrocarbon that can be solved using the results for CH_3. From the solution of CH_2 as well as CH_3, more complex hydrocarbons can be solved using these radicals as basis elements with bonding between the $C2sp^3$ hybridized carbons.

FORCE BALANCE OF CH_4

CH_4 comprises four chemical bonds between carbon and hydrogen atoms. Each $C-H$ bond comprises two spin-paired electrons with one from an initially unpaired electron of the carbon atom and the other from the hydrogen atom. Each H-atom electron forms a H_2-type ellipsoidal MO with an unpaired C-atom electrons. However, such a bond is not possible with the outer two C electrons in their ground state since the resulting H_2-type ellipsoidal MO would have a shorter internuclear distance than the radius of the carbon $2p$ shell which is not energetically stable, and only two electrons are unpaired. Thus, when bonding the carbon $2s$ and $2p$ shells hybridize to form a single $2sp^3$ shell as an energy minimum. The electron configuration and the energy, $E\left(C,2sp^3\right)$, of the $C2sp^3$ shell is given by Eqs. (13.422), and (13.428), respectively.

For each $C-H$ bond, a $C2sp^3$ electron combines with the $H1s$ electron to form a molecular orbital. The proton of the H atom and the nucleus of the C atom are along each internuclear axis and serve as the foci. As in the case of H_2, each of the four $C-H$-bond MOs is a prolate spheroid with the exception that the ellipsoidal MO surface cannot extend into the $C2sp^3$ HO for distances shorter than the radius of the $C2sp^3$ shell since it is energetically unfavorable. Thus, each MO surface comprises a prolate spheroid at the H proton that can be solved as being continuous with the $C2sp^3$ shell at the C atom whose nucleus

serves as the other focus. The radius and the energy of the $C2sp^3$ shell are unchanged with bond formation. The central paramagnetic force due to spin of each $C-H$ bond is provided by the spin-pairing force of the CH_4 MO that has the symmetry of an s orbital that superimposes with the $C2sp^3$ orbitals such that the corresponding angular momenta are unchanged.

The energies in the CH_4 MO involve only each $C2sp^3$ and each $H1s$ electron with the formation of each $C-H$ bond. The sum of the energies of the H_2-type ellipsoidal MOs is matched to that of the $C2sp^3$ shell. As in the cases of OH, H_2O, NH, NH_2, NH_3, CH, CH_2, and CH_3 the CH_4 MO must comprise four $C-H$ bonds with each having 75% of a H_2-type ellipsoidal MO and a $C2sp^3$ HO in a linear combination in order to match potential, kinetic, and orbital energy relationships:

$$4\left[1\,C2sp^3+0.75\,H_2\;MO\right]\rightarrow CH_4\;MO \tag{13.579}$$

The force balance of the CH_4 MO is determined by the boundary conditions that arise from the linear combination of orbitals according to Eq. (13.579) and the energy matching condition between the hydrogen and $C2sp^3$ HO components of the MO.

The force constant k' to determine the ellipsoidal parameter c' of the each H_2-type-ellipsoidal-MO component of the CH_4 MO in terms of the central force of the foci is given by Eq. (13.59). The distance from the origin of each $C-H$-bond MO to each focus c' is given by Eq. (13.60). The internuclear distance is given by Eq. (13.61). The length of the semiminor axis of the prolate spheroidal $C-H$-bond MO $b=c$ is given by Eq. (13.62). The eccentricity, e, is given by Eq. (13.63). The solution of the semimajor axis a then allows for the solution of the other axes of each prolate spheroid and eccentricity of each $C-H$-bond MO. Since each of the four prolate spheroidal $C-H$-bond MOs comprises a H_2-type-ellipsoidal MO that transitions to the $C2sp^3$ HO, the energy $E\left(C,2sp^3\right)$ in Eq. (13.428) adds to that of the four corresponding H_2-type ellipsoidal MOs to give the total energy of the CH_4 MO. From the energy equation and the relationship between the axes, the dimensions of the CH_4 MO are solved.

The energy components of V_e, V_p, T, and V_m are four times those of CH corresponding to the four $C-H$ bonds. Since each prolate spheroidal H_2-type MO transitions to the $C2sp^3$ HO and the energy of the $C2sp^3$ shell must remain constant and equal to the $E\left(C,2sp^3\right)$ given by Eq. (13.428), the total energy $E_T\left(CH_4\right)$ of the CH_4 MO is given by the sum of the energies of the orbitals corresponding to the composition of the linear combination of the $C2sp^3$ HO and the four H_2-type ellipsoidal MOs that forms the CH_4 MO as given by Eq. (13.579). Using Eq. (13.431), $E_T\left(CH_4\right)$ is given by:

$$E_T\left(CH_4\right)=E_T+E\left(C,2sp^3\right)=-\frac{4e^2}{8\pi\varepsilon_0 c'}\left[(0.91771)\left(2-\frac{1}{2}\frac{a_0}{a}\right)\ln\frac{a+c'}{a-c'}-1\right]-14.63489\;eV \tag{13.580}$$

The four hydrogen atoms and the hybridized carbon atom can achieve an energy minimum as a linear combination of four H_2-type ellipsoidal MOs each having the proton and the carbon nucleus as the foci. Hybridization gives rise to the $C2sp^3$ HO-shell Coulombic energy $E_{Coulomb}\left(C,2sp^3\right)$ given by Eq. (13.435). To meet the equipotential condition of the union of the H_2-type-ellipsoidal-MO and the $C2sp^3$ HO, the electron energies in Eqs. (13.431), (13.495), (13.541), and (13.580) were normalized by the ratio of $14.82575\;eV$, the magnitude of $E_{Coulomb}\left(C,2sp^3\right)$ given by Eq. (13.425), and $13.605804\;eV$, the magnitude of the Coulombic energy between the electron and proton of H given by Eq. (1.264). The factor given by Eq. (13.430) normalized the energies to match that of the Coulombic energy alone to meet the energy matching condition of each $C-H$-bond MO under the influence of the proton and the C nucleus. Each $C-H$-bond MO comprises the same $C2sp^3$ shell having its energy normalized to that of the Coulombic energy between the electron and a charge of $+e$ at the carbon focus of the CH_4 MO. Thus, the energy of the CH_4 MO is also given by the sum of that of the four H_2-type ellipsoidal MOs given by Eq. (11.212) minus three times the Coulombic energy, $E_{Coulomb}\left(H\right)=-13.605804\;eV$, of the three redundant $+e$'s of the linear combination:

$$\begin{aligned}E_T\left(4H_2-3H\right)&=-\frac{4e^2}{8\pi\varepsilon_0 a_0}\left[\left(2\sqrt{2}-\sqrt{2}+\frac{\sqrt{2}}{2}\right)\ln\frac{\sqrt{2}+1}{\sqrt{2}-1}-\sqrt{2}\right]-3E_{Coulomb}\left(H\right)\\&=4\left(-31.63536831\;eV\right)-3\left(-13.605804\;eV\right)\\&=-85.72406\;eV\end{aligned} \tag{13.581}$$

$E_T\left(CH_4\right)$ given by Eq. (13.580) is set equal to four times the energy of the H_2-type ellipsoidal MO minus three times the Coulombic energy of H given by Eq. (13.581):

$$E_T\left(CH_4\right)=-\frac{4e^2}{8\pi\varepsilon_0 c'}\left[(0.91771)\left(2-\frac{1}{2}\frac{a_0}{a}\right)\ln\frac{a+c'}{a-c'}-1\right]-14.63489\;eV=-85.72406\;eV \tag{13.582}$$

From the energy relationship given by Eq. (13.582) and the relationship between the axes given by Eqs. (13.60-13.63), the dimensions of the CH_4 MO can be solved.

Substitution of Eq. (13.60) into Eq. (13.543) gives:

$$\frac{4e^2}{8\pi\varepsilon_0\sqrt{\frac{2aa_0}{3}}}\left[(0.91771)\left(2-\frac{1}{2}\frac{a_0}{a}\right)\ln\frac{a+\sqrt{\frac{2aa_0}{3}}}{a-\sqrt{\frac{2aa_0}{3}}}-1\right]=e71.08917 \tag{13.583}$$

The most convenient way to solve Eq. (13.583) is by the reiterative technique using a computer. The result to within the round-off error with five-significant figures is

$$a=1.62340a_0=8.59066\ X\ 10^{-11}\ m \tag{13.584}$$

Substitution of Eq. (13.584) into Eq. (13.60) gives:

$$c'=1.04032a_0=5.50514\ X\ 10^{-11}\ m \tag{13.585}$$

The internuclear distance given by multiplying Eq. (13.585) by two is:

$$2c'=2.08064a_0=1.10103\ X\ 10^{-10}\ m \tag{13.586}$$

The experimental bond distance is [41] :

$$2c'=1.087\ X\ 10^{-10}\ m \tag{13.587}$$

Substitution of Eqs. (13.584-13.585) into Eq. (13.62) gives:

$$b=c=1.24626a_0=6.59492\ X\ 10^{-11}\ m \tag{13.588}$$

Substitution of Eqs. (13.584-13.585) into Eq. (13.63) gives:

$$e=0.64083 \tag{13.589}$$

The nucleus of the H atom and the nucleus of the C atom comprise the foci of each H_2-type ellipsoidal MO. The parameters of the point of intersection of each H_2-type ellipsoidal MO and the $C2sp^3$ HO in the absence of the other three are given by Eqs. (13.84-13.95), (13.261-13.270), (13.434-13.442), and (13.551-13.555). The polar intersection angle θ' is given by Eq. (13.261) where $r_n=r_{2sp^3}=0.91771a_0$ is the radius of the $C2sp^3$ shell. Substitution of Eqs. (13.584-13.585) into Eq. (13.261) gives:

$$\theta'=86.20° \tag{13.590}$$

Then, the angle θ_{C2sp^3HO} the radial vector of the $C2sp^3$ HO makes with the internuclear axis is:

$$\theta_{C2sp^3HO}=180°-86.20°=93.80° \tag{13.591}$$

as shown in Figure 13.9. The parametric angle θ_{H_2MO} given by Eqs. (13.442-13.443), (13.588), and (13.591) is:

$$\theta_{H_2MO}=47.29° \tag{13.592}$$

Then, the distance d_{H_2MO} along the internuclear axis from the origin of H_2-type ellipsoidal MO to the point of intersection of the orbitals given by Eqs. (13.445), (13.584), and (13.592) is:

$$d_{H_2MO}=1.10121a_0=5.82734\ X\ 10^{-11}\ m \tag{13.593}$$

The distance d_{C2sp^3HO} along the internuclear axis from the origin of the C atom to the point of intersection of the orbitals given by Eqs. (13.447), (13.585), and (13.593) is:

$$d_{C2sp^3HO}=0.06089a_0=3.22208\ X\ 10^{-12}\ m \tag{13.594}$$

The H_2-type ellipsoidal MOs do not actually directly contact the $C2sp^3$ HO. As discussed in the Force Balance of H_2O section, with the addition of the fourth $C-H$ bond, the H_2-type ellipsoidal MOs may linearly combine to form a continuous two-dimensional surface of equipotential equivalent to that of the MOs if they did contact the $C2sp^3$ HO. However, Eqs. (13.579-13.580) must hold based on conservation of momentum and the potential, kinetic, and total energy relationships. In order that there is current continuity given the constraints of Eqs. (13.579-13.580), the existence of a self-contained, continuous-current, linear-combination of the H_2-type ellipsoidal MOs requires that electrons are divisible between the combination H_2-type MO and the $C2sp^3$ HO. This is not possible.

Thus, at the points of intersection of the H_2-type MOs of methane symmetry, and in similar geometries such as that of CH_3, representative of the general case, electron indivisibility, current continuity, and conservation of energy and angular momentum require that the current between the $C2sp^3$ shell and points of mutual contact is projected onto and flows along the radial vector to the surface of $C2sp^3$ shell. This current designated the bisector current (BC) meets the $C2sp^3$ surface and does not travel to distances shorter than its radius.

Moreover, an energy minimum is obtained when the H-atom charge-density of each $C-H$-bond MO is decreased by a factor of 0.25 with a corresponding 0.25 increase in that of the three other $C-H$-bond MOs. In this case, the angular momentum components of the transferred current mutually cancel. The geometry of the equivalent bonds is tetrahedral. The symmetry point group is T_d. This geometry is equivalent to the indistinguishable bonds positioned uniformly on a spherical surface or also at the apexes of a cube. The predicted angle θ between the $C-H$ bonds is:

$$\theta = 109.5° \tag{13.595}$$

The experimental bond angle is [41]:

$$\theta = 109.5° \tag{13.596}$$

The polar angle ϕ at which the H_2-type ellipsoidal MOs intersect is given by the bisector of the angle θ between the $C-H$ bonds:

$$\phi = \frac{109.5}{2} = 54.75° \tag{13.597}$$

With the carbon nucleus defined as the origin and one of the $C-H$ bonds defined as the positive x-axis, the polar-coordinate angle of the intersection occurs at:

$$\phi' = 54.75° + 180° = 234.75° \tag{13.598}$$

The polar radius r_i at this angle is given by Eqs. (13.84-13.85):

$$r_i = (a - c')\frac{1 + \frac{c'}{a}}{1 + \frac{c'}{a}\cos\phi'} \tag{13.599}$$

Substitution of Eqs. (13.584-13.585) and (13.589) into Eq. (13.599) gives:

$$r_i = 1.52223a_0 = 8.05530\ X\ 10^{-11}\ m \tag{13.600}$$

Using the orbital composition of CH_4 (Eq. (13.579)), the radii of $C1s = 0.17113a_0$ (Eq. (10.51)) and $C2sp^3 = 0.91771a_0$ (Eq. (13.424)) shells, and the parameters of the CH_4 MO given by Eqs. (13.3-13.4), (13.584-13.586), and (13.588-13.600), the charge-density of the CH_4 MO comprising the linear combination of four $C-H$-bond MOs is shown in Figure 13.13. Each $C-H$-bond MO having the dimensional diagram shown in Figure 13.9 comprises a H_2-type ellipsoidal MO and a $C2sp^3$ HO according to Eq. (13.579). But, based on the T_d symmetry of the H_2-type MOs, the charge is distributed 1:1 between the H_2-type MOs and the $C2sp^3$ shell.

Figure 13.13. CH_4 MO comprising the linear combination of four $C-H$ -bond MOs formed by the superposition of a H_2-type ellipsoidal MO and a $C2sp^3$ HO. (A) Color scale, translucent view of the charge-density of the CH_4 MO. The combined surface of the four H_2-type ellipsoidal MOs from each $C-H$ bond that surrounds the $C2sp^3$ HO, the $C2sp^3$ HO shell, $C1s$ shell, and the nuclei (red, not to scale) are shown. (B) Off-center cut-away view showing the complete inner most $C1s$ shell, and moving radially, the $C2sp^3$ shell, and the H_2-type ellipsoidal MOs that surround the $C2sp^3$ HO. Bisector current not shown. (C) Opaque view. (D)-(E) Additional translucent views.

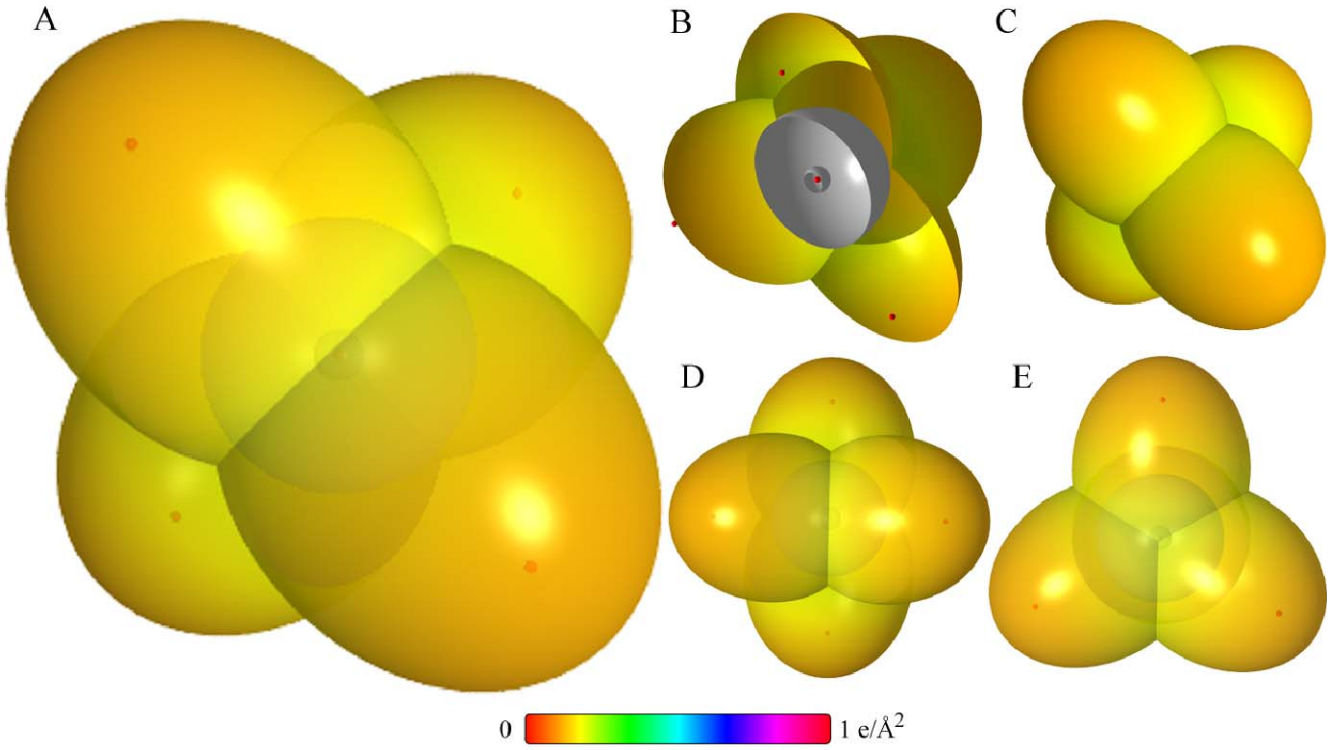

ENERGIES OF CH_4

The energies of CH_4 are four times those of CH and are given by the substitution of the semiprincipal axes (Eqs. (13.584-13.585) and (13.588)) into the energy equations Eq. (13.580) and (Eqs. (13.449-13.452)) that are multiplied by four:

$$V_e = 4(0.91771)\frac{-2e^2}{8\pi\varepsilon_0\sqrt{a^2-b^2}}\ln\frac{a+\sqrt{a^2-b^2}}{a-\sqrt{a^2-b^2}} = -145.86691\ eV \tag{13.601}$$

$$V_p = \frac{4e^2}{8\pi\varepsilon_0\sqrt{a^2-b^2}} = 52.31390\ eV \tag{13.602}$$

$$T = 4(0.91771)\frac{\hbar^2}{2m_e a\sqrt{a^2-b^2}}\ln\frac{a+\sqrt{a^2-b^2}}{a-\sqrt{a^2-b^2}} = 44.92637\ eV \tag{13.603}$$

$$V_m = 4(0.91771)\frac{-\hbar^2}{4m_e a\sqrt{a^2-b^2}}\ln\frac{a+\sqrt{a^2-b^2}}{a-\sqrt{a^2-b^2}} = -22.46318\ eV \tag{13.604}$$

$$\begin{aligned} E_T(CH_4) &= -\frac{4e^2}{8\pi\varepsilon_0 c'}\left[(0.91771)\left(2-\frac{1}{2}\frac{a_0}{a}\right)\ln\frac{a+c'}{a-c'}-1\right]-14.63489\ eV \\ &= -85.72472\ eV \end{aligned} \tag{13.605}$$

where $E_T(CH_4)$ is given by Eq. (13.580) which is reiteratively matched to Eq. (13.581) within five-significant-figure round-off error.

VIBRATION OF CH_4

The vibrational energy levels of CH_4 may be solved as four equivalent coupled harmonic oscillators by developing the Lagrangian, the differential equation of motion, and the eigenvalue solutions [2] wherein the spring constants are derived from the central forces as given in the Vibration of Hydrogen-Type Molecular Ions section and the Vibration of Hydrogen-Type Molecules section.

THE DOPPLER ENERGY TERMS OF $^{12}CH_4$

The reentrant oscillation of hybridized orbitals in the transition state is not coupled. Therefore, the equations of the radiation reaction force of methane are the same as those of OH, CH, CH_2, and CH_3 with the substitution of the methane parameters. Using Eqs. (11.136) and (13.140-13.142), the angular frequency of the reentrant oscillation in the transition state is:

$$\omega = \sqrt{\frac{0.75e^2}{4\pi\varepsilon_0 b^3}} = 2.57338\ X\ 10^{16}\ rad/s \tag{13.606}$$

where b is given by Eq. (13.588). The kinetic energy, E_K, is given by Planck's equation (Eq. (11.127)).

$$\bar{E}_K = \hbar\omega = \hbar 2.57338\ X\ 10^{16}\ rad/s = 16.93841\ eV \tag{13.607}$$

In Eq. (11.181), substitution of $E_T\left(H_2\right)$ (Eqs. (11.212) and (13.75)), the maximum total energy of each H_2-type MO, for $E_{h\nu}$, the mass of the electron, m_e, for M, and the kinetic energy given by Eq. (13.607) for $\bar{E}_K$ gives the Doppler energy of the electrons of each of the four bonds for the reentrant orbit:

$$\begin{aligned}\bar{E}_D &\cong E_{h\nu}\sqrt{\frac{2\bar{E}_K}{Mc^2}} \\ &= -31.63537\ eV\sqrt{\frac{2e(16.93841\ eV)}{m_e c^2}} = -0.25758\ eV\end{aligned} \tag{13.608}$$

In addition to the electrons, the nuclei also undergo simple harmonic oscillation in the transition state at their corresponding frequency. The decrease in the energy of CH_4 due to the reentrant orbit of each bond in the transition state corresponding to simple harmonic oscillation of the electrons and nuclei, $\bar{E}_{osc}$, is given by the sum of the corresponding energies, $\bar{E}_D$ given by Eq. (13.608) and $\bar{E}_{Kvib}$, the average kinetic energy of vibration which is 1/2 of the vibrational energy of each $C-H$ bond. Using ω_e given by Eq. (13.458) for $\bar{E}_{Kvib}$ of the transition state having four independent bonds, $\bar{E}'_{osc}\left(^{12}CH_4\right)$ per bond is:

$$\bar{E}'_{osc}\left(^{12}CH_4\right) = \bar{E}_D + \bar{E}_{Kvib} = \bar{E}_D + \frac{1}{2}\hbar\sqrt{\frac{k}{\mu}} \tag{13.609}$$

$$\bar{E}'_{osc}\left(^{12}CH_4\right) = -0.25758\ eV + \frac{1}{2}(0.35532\ eV) = -0.07992\ eV \tag{13.610}$$

The reentrant orbit for the binding of a hydrogen atom to a CH_3 radical involves four $C-H$ bonds. Since the vibration and reentrant oscillation is along four bonds, $\bar{E}_{osc}$ for $^{12}CH_4$, $\bar{E}_{osc}\left(^{12}CH_4\right)$, is:

$$\begin{aligned}\bar{E}_{osc}\left(^{12}CH_4\right) &= 4\left(\bar{E}_D + \frac{1}{2}\hbar\sqrt{\frac{k}{\mu}}\right) \\ &= 4\left(-0.25758\ eV + \frac{1}{2}(0.35532\ eV)\right) = -0.31967\ eV\end{aligned} \tag{13.611}$$

TOTAL AND BOND ENERGIES OF $^{12}CH_4$

$E_{T+osc}\left(^{12}CH_4\right)$, the total energy of the $^{12}CH_4$ radical including the Doppler term, is given by the sum of $E_T\left(CH_4\right)$ (Eq. (13.582)) and $\bar{E}_{osc}\left(^{12}CH_4\right)$ given by Eq. (13.611).

$$E_{T+osc}\left(CH_4\right)=V_e+T+V_m+V_p+E\left(C,2sp^3\right)+\bar{E}_{osc}\left(^{12}CH_4\right)=E_T\left(CH_4\right)+\bar{E}_{osc}\left(^{12}CH_4\right) \tag{13.612}$$

$$\begin{aligned}E_{T+osc}\left(^{12}CH_4\right)&=\left\{\begin{array}{l}\left(\dfrac{-4e^2}{8\pi\varepsilon_0 c'}\left[\left(0.91771\right)\left(2-\dfrac{1}{2}\dfrac{a_0}{a}\right)\ln\dfrac{a+c'}{a-c'}-1\right]-14.63489\ eV\right)\\ -4\left(\left(31.63536831\ eV\right)\sqrt{\dfrac{2\hbar\sqrt{\dfrac{\frac{3}{4}\dfrac{e^2}{4\pi\varepsilon_0 b^3}}{m_e}}}{m_e c^2}}-\dfrac{1}{2}\hbar\sqrt{\dfrac{k}{\mu}}\right)\end{array}\right\}\\ &=-85.72406\ eV-4\left(0.25758\ eV-\frac{1}{2}\hbar\sqrt{\frac{k}{\mu}}\right)\end{aligned} \tag{13.613}$$

From Eqs. (13.609-13.613), the total energy of $^{12}CH_4$ is:

$$\begin{aligned}E_{T+osc}\left(^{12}CH_4\right)&=-85.72406\ eV+\bar{E}_{osc}\left(^{12}CH_4\right)\\ &=-85.72406\ eV-4\left(0.25758\ eV-\frac{1}{2}\left(0.35532\ eV\right)\right)=-86.04373\ eV\end{aligned} \tag{13.614}$$

where ω_e given by Eq. (13.458) was used for the $\hbar\sqrt{\dfrac{k}{\mu}}$ term.

The CH_4 bond dissociation energy, $E_D\left(^{12}CH_4\right)$, is given by the sum of the total energies of the CH_3 radical and the hydrogen atom minus $E_{T+osc}\left(^{12}CH_4\right)$:

$$E_D\left(^{12}CH_4\right)=E\left(^{12}CH_3\right)+E(H)-E_{T+osc}\left(^{12}CH_4\right) \tag{13.615}$$

where $E_T(^{12}CH_3)$ is given by the sum of the energies of the $C2sp^3$ HO, $E\left(C,2sp^3\right)$ given by Eq. (13.428), $3E_D\left(H\right)$ given by Eq. (13.154), and the negative of the bond energies of ^{12}CH given by Eq. (13.489), $^{12}CH_2$ given by Eq. (13.528), and $^{12}CH_3$ given by Eq. (13.573):

$$E(^{12}CH_3)=\begin{pmatrix}3\left(-13.59844\ eV\right)-14.63489\ eV\\ -3.47\ eV-4.33064\ eV-4.72444\ eV\end{pmatrix}=-67.95529\ eV \tag{13.616}$$

Thus, the $^{12}CH_4$ bond dissociation energy, $E_D\left(^{12}CH_4\right)$, given by Eqs. (13.154), and (13.614-13.616) is:

$$\begin{aligned}E_D\left(^{12}CH_4\right)&=-\left(67.95529\ \ eV+13.59844\ eV\right)-E_{T+osc}\left(^{12}CH_4\right)\\ &=-81.55373\ eV-\left(-86.04373\ eV\right)=4.4900\ eV\end{aligned} \tag{13.617}$$

The experimental $^{12}CH_4$ bond dissociation energy is [40] :

$$E_D\left(^{12}CH_4\right)=4.48464\ eV \tag{13.618}$$

The results of the determination of bond parameters of CH_4 are given in Table 13.1. The calculated results are based on first principles and given in closed-form, exact equations containing fundamental constants only. The agreement between the experimental and calculated results is excellent.

NITROGEN MOLECULE

The nitrogen molecule can be formed by the reaction of two nitrogen atoms:

$$N + N \rightarrow N_2 \tag{13.619}$$

The bond in the nitrogen molecule comprises a H_2-type molecular orbital (MO) with two paired electrons. The force balance equation and radius r_7 of the $2p$ shell of N is derived in the Seven-Electron Atoms section. With the formation of the H_2-type MO by the contribution of a $2p$ electron from each N atom, a diamagnetic force arises between the remaining $2p$ electrons and the H_2-type MO. This force from each N causes the H_2-type MO to move to greater principal axes than would result with the Coulombic force alone. But, the integer increase of the central field and the resulting increased Coulombic as well as magnetic central forces on the remaining $2p$ electrons of each N decrease the radius of the corresponding shell such that the energy minimum is achieved that is lower than that of the reactant atoms. The resulting electron configuration of N_2 is $1s_1^2 1s_2^2 2s_1^2 2s_2^2 2p_1^2 2p_2^2 \sigma_{1,2}^2$ where the subscript designates the N atom, 1 or 2, σ designates the H_2-type MO, and the orbital arrangement is:

σ state

$\uparrow\downarrow$

2p state

$\uparrow\downarrow$	$\uparrow\downarrow$
0	0

2s state

$\uparrow\downarrow$	$\uparrow\downarrow$

1s state

$\uparrow\downarrow$	$\uparrow\downarrow$
$N1$	$N2$

(13.620)

Nitrogen is predicted to be diamagnetic in agreement with observations.

FORCE BALANCE OF THE $2p$ SHELL OF THE NITROGEN ATOMS OF THE NITROGEN MOLECULE

For each N atom, force balance for the outermost $2p$ electron of N_2 (electron 6) is achieved between the centrifugal force and the Coulombic and magnetic forces that arise due to interactions between electron 6 and the other $2p$-shell as well as the $2s$-shell electrons due to spin and orbital angular momentum. The forces used are derived in the Seven-Electron Atoms section. The central Coulomb force on the outer-most $2p$ shell electron of N_2 (electron 6) due to the nucleus and the inner five electrons is given by Eq. (10.70) with the appropriate charge and radius:

$$\mathbf{F}_{ele} = \frac{(Z-5)e^2}{4\pi\varepsilon_0 r_6^2}\mathbf{i}_\mathbf{r} \tag{13.621}$$

for $r > r_5$. The $2p$ shell possess an external electric field given by Eq. (10.92) for $r > r_6$. The energy is minimized with conservation of angular momentum. This condition is met when the diamagnetic force, $\mathbf{F}_{diamagnetic}$, of Eq. (10.82) due to the p-orbital contribution is the same as that of the reactant nitrogen atoms given by Eq. (10.136) with r_6 replacing r_7:

$$\begin{aligned}\mathbf{F}_{diamagnetic} &= -\left(\frac{1}{3}\right)\frac{\hbar^2}{4m_e r_6^2 r_3}\sqrt{s(s+1)}\mathbf{i}_\mathbf{r} \\ &= -\frac{\hbar^2}{12m_e r_6^2 r_3}\sqrt{\frac{3}{4}}\mathbf{i}_\mathbf{r}\end{aligned} \tag{13.622}$$

And, $\mathbf{F}_{mag\ 2}$ corresponding to the conserved orbital angular momentum of the three orbitals is given by Eq. (10.89).

$$\mathbf{F}_{mag\ 2} = \frac{1}{Z}\frac{3\hbar^2}{m_e r_6^2 r_3}\sqrt{s(s+1)}\mathbf{i}_\mathbf{r} \tag{13.623}$$

The electric field external to the $2p$ shell given by Eq. (10.92) for $r > r_6$ gives rise to a second diamagnetic force,

$\mathbf{F}_{diamagnetic\ 2}$, given by Eq. (10.93). $\mathbf{F}_{diamagnetic\ 2}$ due to the binding of the p-orbital electron having an electric field of +1 outside of its radius is:

$$\mathbf{F}_{diamagnetic\ 2} = -\left[\frac{Z-6}{Z-5}\right]\left(1-\frac{\sqrt{2}}{2}\right)\frac{r_3\hbar^2}{m_e r_6^4}10\sqrt{s(s+1)}\mathbf{i}_\mathbf{r} \tag{13.624}$$

In addition, the contribution of a $2p$ electron from each N atom in the formation of the σ MO gives rise to a paramagnetic force on the remaining two $2p$ electrons that pair. The force, $\mathbf{F}_{mag\ 3}$, follows from Eq. (10.11) wherein the two radii are equal to r_6 and the direction is positive, central:

$$\mathbf{F}_{mag\ 3} = \frac{\hbar^2}{4m_e r_6^3}\sqrt{s(s+1)}\mathbf{i}_\mathbf{r} \tag{13.625}$$

$\mathbf{F}_{mag\ 3}$ is present in additional diatomic molecules where its contribution minimizes the energy. This AO spin-pairing force reduces the radius directly to reduce the energy, and it can also cancel the contribution of the corresponding electron to $\mathbf{F}_{diamagnetic}$ to further reduce the energy.

The radius of the $2p$ shell is calculated by equating the outward centrifugal force to the sum of the electric (Eq. (13.621)) and diamagnetic (Eqs. (13.622) and (13.624)), and paramagnetic (Eqs. (13.623) and (13.625)) forces as follows:

$$\frac{m_e v_6^2}{r_6} = \left(\begin{array}{l}\dfrac{(Z-5)e^2}{4\pi\varepsilon_0 r_6^2} - \dfrac{\hbar^2}{12m_e r_6^2 r_3}\sqrt{s(s+1)} + \dfrac{3\hbar^2}{Zm_e r_6^2 r_3}\sqrt{s(s+1)} \\ -\left[\dfrac{Z-6}{Z-5}\right]\left(1-\dfrac{\sqrt{2}}{2}\right)\dfrac{r_3\hbar^2}{r_6^4 m_e}10\sqrt{s(s+1)} + \dfrac{\hbar^2}{4m_e r_6^3}\sqrt{s(s+1)}\end{array}\right) \tag{13.626}$$

Substitution of $v_6 = \dfrac{\hbar}{m_e r_6}$ (Eq. (1.35)) and $s = \dfrac{1}{2}$ into Eq. (13.626) gives:

$$\frac{\hbar^2}{m_e r_6^3} - \frac{\hbar^2}{4m_e r_6^3}\sqrt{\frac{3}{4}} = \frac{(Z-5)e^2}{4\pi\varepsilon_0 r_6^2} - \frac{\hbar^2}{12m_e r_6^2 r_3}\sqrt{\frac{3}{4}} + \frac{3\hbar^2}{Zm_e r_6^2 r_3}\sqrt{\frac{3}{4}} - \left[\frac{Z-6}{Z-5}\right]\left(1-\frac{\sqrt{2}}{2}\right)\frac{r_3\hbar^2}{r_6^4 m_e}10\sqrt{\frac{3}{4}} \tag{13.627}$$

The quadratic equation corresponding to Eq. (13.627) is:

$$r_6^2 - \frac{\dfrac{\hbar^2}{m_e}\left(1-\dfrac{\sqrt{3}}{8}\right)}{\left(\dfrac{(Z-5)e^2}{4\pi\varepsilon_0} - \left(\dfrac{1}{12}-\dfrac{3}{Z}\right)\dfrac{\hbar^2}{m_e r_3}\sqrt{\dfrac{3}{4}}\right)}r_6 - \frac{\dfrac{\hbar^2}{m_e}\left[\dfrac{Z-6}{Z-5}\right]\left(1-\dfrac{\sqrt{2}}{2}\right)r_3 10\sqrt{\dfrac{3}{4}}}{\left(\dfrac{(Z-5)e^2}{4\pi\varepsilon_0} - \left(\dfrac{1}{12}-\dfrac{3}{Z}\right)\dfrac{\hbar^2}{m_e r_3}\sqrt{\dfrac{3}{4}}\right)} = 0 \tag{13.628}$$

The solution of Eq. (13.628) using the quadratic formula is:

$$r_6 = \frac{\dfrac{a_0\left(1-\dfrac{\sqrt{3}}{8}\right)}{\left(\dfrac{(Z-5)-\left(\dfrac{1}{12}-\dfrac{3}{Z}\right)\dfrac{\sqrt{3}}{2r_3}}\right)} \pm a_0\sqrt{\left(\dfrac{\dfrac{1-\dfrac{\sqrt{3}}{8}}{\left(\dfrac{(Z-5)-\left(\dfrac{1}{12}-\dfrac{3}{Z}\right)\dfrac{\sqrt{3}}{2r_3}}\right)}\right)^2 + \dfrac{20\sqrt{3}\left(\left[\dfrac{Z-6}{Z-5}\right]\left(1-\dfrac{\sqrt{2}}{2}\right)r_3\right)}{\left(\dfrac{(Z-5)-\left(\dfrac{1}{12}-\dfrac{3}{Z}\right)\dfrac{\sqrt{3}}{2r_3}}\right)}}}{2}, \; r_3 \text{ in units of } a_0 \tag{13.629}$$

The positive root of Eq. (13.629) must be taken in order that $r_6 > 0$. Substitution of $\dfrac{r_3}{a_0} = 0.69385$ (Eq. (10.62) with $Z = 7$) into Eq. (13.629) gives:

$$r_6 = 0.78402a_0 \tag{13.630}$$

ENERGIES OF THE $2p$ SHELL OF THE NITROGEN ATOMS OF THE NITROGEN MOLECULE

The central forces on the $2p$ shell of each N are increased with the formation of the σ MO, which reduces the shell's radius and increases its total energy. The Coulombic energy terms of the total energy of the two N atoms at the new radius are calculated and added to the energy of the σ MO to give the total energy of N_2. Then, the bond energy is determined from the total N_2 energy.

The radius r_7 of each nitrogen atom before bonding is given by Eq. (10.142).

$$r_7 = 0.93084a_0 \tag{13.631}$$

Using the initial radius r_7 of each N atom and the final radius r_6 of the $N2p$ shell of N_2 (Eq. (13.630)) and by considering that the central Coulombic field decreases by an integer for each successive electron of the shell, the sum $E_T\left(N_2,2p\right)$ of the Coulombic energy change of the $N2p$ electrons of both atoms is determined using Eq. (10.102).

$$E_T\left(N_2,2p\right) = -2\sum_{n=4}^{5}\frac{(Z-n)e^2}{8\pi\varepsilon_0}\left(\frac{1}{r_6}-\frac{1}{r_7}\right) = -2\left(13.60580\ eV\right)\left(0.20118\right)\left(2+3\right) = -27.37174\ eV \tag{13.632}$$

FORCE BALANCE OF THE σ MO OF THE NITROGEN MOLECULE

The $2p$ shell gives rise to two diamagnetic forces on the σ MO. As given for the hydrogen molecule in the Hydrogen-Type Molecules section, the σ MO comprises two electrons, σ electron 1 and σ electron 2, that are bound at $\xi = 0$ as a equipotential prolate spheroidal MO by the central Coulombic field due to the nitrogen atoms at the foci and the spin pairing force on σ electron 2 due to σ electron 1 that initially has smaller semiprincipal axes. The spin-pairing force given in Eq. (11.200) is equal to one half the centrifugal force of the two electrons. The spin-pairing electron of the σ MO is also repelled by the remaining $2p$ electrons of each N according to Lenz law, and the force is based on the total number of these electrons n_e that interact with the binding σ-MO electron. This diamagnetic force $\mathbf{F}_{diamagneticMO1}$ is of the same form as the molecular spin-pairing force but in the opposite direction. The force follows from the derivations of Eqs. (10.219) and (11.200) which gives:

$$\mathbf{F}_{diamagneticMO1} = \frac{n_e\hbar^2}{4m_e a^2b^2}D\mathbf{i}_\xi \tag{13.633}$$

In addition, there is a relativistically corrected Lorentz force $\mathbf{F}_{diamagneticMO2}$ on the pairing electron of the σ MO that follows from Eqs. (7.15) and (11.200):

$$\mathbf{F}_{diamagneticMO2} = \frac{1}{Z}\frac{|L|\hbar}{2m_e a^2b^2}D\mathbf{i}_\xi \tag{13.634}$$

where $|L|$ is the magnitude of the angular momentum of each N atom at a focus that is the source of the diamagnetism at the σ-MO.

The force balance equation for the σ-MO of the nitrogen molecule given by Eq. (11.200) and Eqs. (13.633-13.634) with $n_e = 2$ and $|L| = \hbar$ is:

$$\frac{\hbar^2}{m_e a^2b^2}D = \frac{e^2}{8\pi\varepsilon_0 ab^2}D + \frac{\hbar^2}{2m_e a^2b^2}D - \left(1+\frac{1}{Z}\right)\frac{\hbar^2}{2m_e a^2b^2}D \tag{13.635}$$

$$\frac{\hbar^2}{m_e a^2b^2}D = \frac{e^2}{8\pi\varepsilon_0 ab^2}D - \frac{1}{Z}\frac{\hbar^2}{2m_e a^2b^2}D \tag{13.636}$$

$$\left(2+\frac{1}{Z}\right)\frac{\hbar^2}{2m_e a^2b^2}D = \frac{e^2}{8\pi\varepsilon_0 ab^2}D \tag{13.637}$$

$$a = \left(2+\frac{1}{Z}\right)a_0 \tag{13.638}$$

Substitution of $Z = 7$ into Eq. (13.638) gives:

$$a = 2.14286a_0 = 1.13395\ X\ 10^{-10}\ m \tag{13.639}$$

Substitution of Eq. (13.639) into Eq. (11.79) is:

$$c' = 1.03510a_0 = 5.47750\ X\ 10^{-11}\ m \tag{13.640}$$

The internuclear distance given by multiplying Eq. (13.640) by two is:

$$2c' = 2.07020a_0 = 1.09550\ X\ 10^{-10}\ m \tag{13.641}$$

The experimental bond distance from Ref. [28] and Ref. [43] is:

$$2c' = 1.09769\ X\ 10^{-10}\ m \tag{13.642}$$

$$2c' = 1.094\ X\ 10^{-10}\ m \tag{13.643}$$

Substitution of Eqs. (13.639-13.640) into Eq. (11.80) is:

$$b = c = 1.87628a_0 = 9.92882\ X\ 10^{-11}\ m \tag{13.644}$$

Substitution of Eqs. (13.639-13.640) into Eq. (11.67) is:

$$e = 0.48305 \tag{13.645}$$

Using the electron configuration of N_2 (Eq. (13.620)), the radii of the $N1s = 0.14605a_0$ (Eq. (10.51)), $N2s = 0.69385a_0$ (Eq. (10.62)), and $N2p = 0.78402a_0$ (Eq. (13.630)) shells and the parameters of the σ MO of N_2 given by Eqs. (13.3-13.4), (13.639-13.641), and (13.644-13.645), the dimensional diagram and charge-density of the N_2 MO are shown in Figures 13.14 and 13.15, respectively.

Despite the predictions of standard quantum mechanics that preclude the imaging of a molecular orbital, the full three-dimensional structure of the outer molecular orbital of N_2 has been recently tomographically reconstructed [44]. The charge-density surface observed is consistent with that shown in Figure 13.15. This result constitutes direct evidence that electrons are not point-particle probability waves that have no form until they are "collapsed to a point" by measurement. Rather they are physical, two-dimensional equipotential charge density surfaces.

Figure 13.14. The cross section of the N_2 MO showing the axes, σ MO (H_2-type ellipsoidal MO), with the N $1s$, $2s$, and $2p$ atomic orbitals (AOs). Legend: a: semimajor axis, b: semiminor axis, c': internuclear distance, r_6: radius of the $N2p$ shell having two paired electrons.

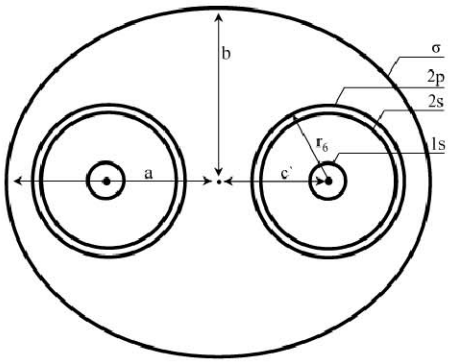

Figure 13.15. N_2 MO comprising the σ MO (H_2-type MO) with N atoms at the foci that have each donated an electron to the σ MO and have smaller radii and higher binding energies as a consequence. (A) Color scale, translucent view of the charge-density of the N_2 MO. (B) Off-center cut-away view showing the complete inner most $N1s$ shell, and moving radially, the $N2s$ shell, the $N2p$ shell, and the σ prolate spheroidal MO that have the N atoms as the foci.

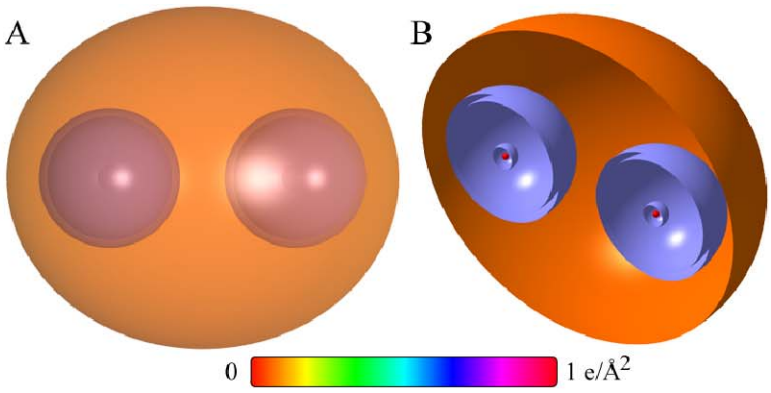

Sum of the Energies of the σ MO and the AOS of the Nitrogen Molecule

The energies of the N_2 σ MO are given by the substitution of the semiprincipal axes (Eqs. (13.639-13.640) and (13.644)) into the energy equations (Eqs. (11.207-11.212)) of H_2:

$$V_e = \frac{-2e^2}{8\pi\varepsilon_0\sqrt{a^2-b^2}}\ln\frac{a+\sqrt{a^2-b^2}}{a-\sqrt{a^2-b^2}} = -27.70586\ eV \tag{13.646}$$

$$V_p = \frac{e^2}{8\pi\varepsilon_0\sqrt{a^2-b^2}} = 13.14446\ eV \tag{13.647}$$

$$T = \frac{\hbar^2}{2m_e a\sqrt{a^2-b^2}}\ln\frac{a+\sqrt{a^2-b^2}}{a-\sqrt{a^2-b^2}} = 6.46470\ eV \tag{13.648}$$

$$V_m = \frac{-\hbar^2}{4m_e a\sqrt{a^2-b^2}}\ln\frac{a+\sqrt{a^2-b^2}}{a-\sqrt{a^2-b^2}} = -3.23235\ eV \tag{13.649}$$

$$E_T = V_e + T + V_m + V_p \tag{13.650}$$

Substitution of Eqs. (11.79) and (13.646-13.649) into Eq. (13.650) gives:

$$E_T\left(N_2,\sigma\right)=\frac{-e^2}{8\pi\varepsilon_0\sqrt{\frac{aa_0}{2}}}\left(\left(2-\frac{1}{2}\frac{a_0}{a}\right)\ln\frac{a+\sqrt{\frac{aa_0}{2}}}{a-\sqrt{\frac{aa_0}{2}}}-1\right) \tag{13.651}$$
$$=-11.32906\ eV$$

where $E_T\left(N_2,\sigma\right)$ is the total energy of the σ MO of N_2. The sum, $E_T\left(N_2\right)$, of $E_T\left(N_2,2p\right)$, the $2p$ (AO) contribution given by Eq. (13.632), and $E_T\left(N_2,\sigma\right)$, the σ MO contribution given by Eq. (13.651) is:

$$E_T\left(N_2\right)=E_T\left(N_2,2p\right)+E_T\left(N_2,\sigma\right) \tag{13.652}$$
$$=-27.37174\ eV-11.32906\ eV=-38.70080\ eV$$

VIBRATION OF N_2

The vibrational energy levels of N_2 may be solved by determining the Morse potential curve from the energy relationships for the transition from two N atoms whose parameters are given by Eqs. (10.134-10.143) to the two N atoms whose parameter r_6 is given by Eq. (13.630) and the σ MO whose parameters are given by Eqs. (13.639-13.641) and (13.644-13.645). As shown in the Vibration of Hydrogen-type Molecular Ions section, the harmonic oscillator potential energy function can be expanded about the internuclear distance and expressed as a Maclaurin series corresponding to a Morse potential after Karplus and Porter (K&P) [15] and after Eq. (11.134). Treating the Maclaurin series terms as anharmonic perturbation terms of the harmonic states, the energy corrections can be found by perturbation methods.

THE DOPPLER ENERGY TERMS OF THE NITROGEN MOLECULE

The equations of the radiation reaction force of nitrogen are the same as those of H_2 with the substitution of the nitrogen parameters. Using Eqs. (11.231-11.233), the angular frequency of the reentrant oscillation in the transition state is:

$$\omega=\sqrt{\frac{e^2}{4\pi\varepsilon_0 a^3 m_e}} \tag{13.653}$$
$$=1.31794\ X\ 10^{16}\ rad/s$$

where a is given by Eq. (13.639). The kinetic energy, E_K, is given by Planck's equation (Eq. (11.127)):

$$\overline{E}_K=\hbar\omega \tag{13.654}$$
$$=\hbar 1.31794\ X\ 10^{16}\ rad/s=8.67490\ eV$$

In Eq. (11.181), substitution of $E_T\left(N_2\right)$ for $E_{h\nu}$, the mass of the electron, m_e, for M, and the kinetic energy given by Eq. (13.654) for $\overline{E}_K$ gives the Doppler energy of the electrons of the reentrant orbit:

$$\overline{E}_D\cong E_{h\nu}\sqrt{\frac{2\overline{E}_K}{Mc^2}} \tag{13.655}$$
$$=-38.70080\ eV\sqrt{\frac{2e\left(8.67490\ eV\right)}{m_e c^2}}=-0.22550\ eV$$

In addition to the electrons, the nuclei also undergo simple harmonic oscillation in the transition state at their corresponding frequency. The decrease in the energy of the N_2 MO due to the reentrant orbit in the transition state corresponding to simple harmonic oscillation of the electrons and nuclei, $\overline{E}_{osc}$, is given by the sum of the corresponding energies, $\overline{E}_D$ given by Eq. (13.655) and $\overline{E}_{Kvib}$, the average kinetic energy of vibration which is 1/2 of the vibrational energy. Using the experimental N_2 ω_e of 2358.57 cm^{-1} $\left(0.29243\ eV\right)$ [28] for $\overline{E}_{Kvib}$ of the transition state, $\overline{E}_{osc}\left(N_2\right)$ is:

$$\overline{E}_{osc}\left(N_2\right)=\overline{E}_D+\overline{E}_{Kvib}=\overline{E}_D+\frac{1}{2}\hbar\sqrt{\frac{k}{\mu}} \tag{13.656}$$

$$\overline{E}_{osc}\left(N_2\right)=-0.22550\ eV+\frac{1}{2}\left(0.29243\ eV\right) \tag{13.657}$$
$$=-0.07929\ eV$$

TOTAL AND BOND ENERGIES OF THE NITROGEN MOLECULE

$E_{T+osc}(N_2)$, the total energy of N_2 including the Doppler term, is given by the sum of $E_T(N_2)$ (Eq. (13.652)) and $\bar{E}_{osc}(N_2)$ given by Eq. (13.657):

$$\begin{aligned} E_{T+osc}(N_2) &= V_e + T + V_m + V_p + E_T(N_2, 2p) + \bar{E}_{osc}(N_2) \\ &= E_T(N_2, \sigma) + E_T(N_2, 2p) + \bar{E}_{osc}(N_2) = E_T(N_2) + \bar{E}_{osc}(N_2) \end{aligned} \tag{13.658}$$

$$E_{T+osc}(N_2) = \left\{ \begin{array}{l} \left(\dfrac{-e^2}{8\pi\varepsilon_0 \sqrt{\dfrac{aa_0}{2}}} \left(\left(2 - \dfrac{1}{2}\dfrac{a_0}{a}\right) \ln \dfrac{a + \sqrt{\dfrac{aa_0}{2}}}{a - \sqrt{\dfrac{aa_0}{2}}} - 1 \right) - 2\sum_{n=4}^{5} \dfrac{(Z-n)e^2}{8\pi\varepsilon_0} \left(\dfrac{1}{r_6} - \dfrac{1}{r_7} \right) \right) \\ \left(1 + \sqrt{\dfrac{2\hbar \sqrt{\dfrac{e^2}{4\pi\varepsilon_0 a^3}}}{m_e c^2}} \right) + \dfrac{1}{2}\hbar\sqrt{\dfrac{k}{\mu}} \end{array} \right\} \tag{13.659}$$

$$= -38.70080\ eV - 0.22550\ eV + \frac{1}{2}\hbar\sqrt{\frac{k}{\mu}}$$

From Eqs. (13.656-13.659), the total energy of the N_2 MO is:

$$\begin{aligned} E_{T+osc}(N_2) &= -38.70080\ eV + \bar{E}_{osc}(N_2) \\ &= -38.70080\ eV - 0.22550\ eV + \frac{1}{2}(0.29243\ eV) = -38.78009\ eV \end{aligned} \tag{13.660}$$

where the experimental ω_e was used for the $\hbar\sqrt{\dfrac{k}{\mu}}$ term.

The N_2 bond dissociation energy, $E_D(N_2)$, is given by the difference in the total energies of the two N atoms and $E_{T+osc}(N_2)$:

$$E_D(N_2) = 2E(N) - E_{T+osc}(N_2) \tag{13.661}$$

where the energy of a nitrogen atom is [6] :

$$E(N) = -14.53414\ eV \tag{13.662}$$

Thus, the N_2 bond dissociation energy, $E_D(N_2)$, given by Eqs. (13.660-13.662) is:

$$E_D(N_2) = -2(14.53414\ eV) - E_{T+osc}(N_2) = -29.06828\ eV - (-38.78009\ eV) = 9.71181\ eV \tag{13.663}$$

The experimental N_2 bond dissociation energy from Ref. [43] and Ref. [45] is:

$$E_D(N_2) = 9.756\ eV \tag{13.664}$$

$$E_D(N_2) = 9.764\ eV \tag{13.665}$$

The results of the determination of bond parameters of N_2 are given in Table 13.1. The calculated results are based on first principles and given in closed-form, exact equations containing fundamental constants only. The agreement between the experimental and calculated results is excellent.

OXYGEN MOLECULE

The oxygen molecule can be formed by the reaction of two oxygen atoms:

$$O + O \rightarrow O_2 \tag{13.666}$$

The bond in the oxygen molecule comprises a H_2-type molecular orbital (MO) with two paired electrons. The force balance equation and radius r_8 of the $2p$ shell of O is derived in the Eight-Electron Atoms section. With the formation of the H_2-type MO by the contribution of a $2p$ electron from each O atom, a diamagnetic force arises between the remaining $2p$ electrons and the H_2-type MO. This force from each O causes the H_2-type MO to move to greater principal axes than would result with the Coulombic force alone. But, the integer increase of the central field and the resulting increased Coulombic as well as magnetic central forces on the remaining $2p$ electrons of each O decrease the radius of the corresponding shell such that the energy minimum is achieved that is lower than that of the reactant atoms. The resulting electron configuration of O_2 is $1s_1^2 1s_2^2 2s_1^2 2s_2^2 2p_1^3 2p_2^3 \sigma_{1,2}^2$ where the subscript designates the O atom, 1 or 2, σ designates the H_2-type MO, and the orbital arrangement is:

σ state

$\uparrow\downarrow$

2p state

$\underset{0}{\uparrow\downarrow}$ $\underset{1}{\uparrow}$ $\underset{0}{\uparrow\downarrow}$ $\underset{1}{\uparrow}$

(13.667)

2s state

$\uparrow\downarrow$ $\uparrow\downarrow$

1s state

$\underset{O1}{\uparrow\downarrow}$ $\underset{O2}{\uparrow\downarrow}$

Oxygen is predicted to be paramagnetic in agreement with observations [42].

FORCE BALANCE OF THE $2p$ SHELL OF THE OXYGEN ATOMS OF THE OXYGEN MOLECULE

For each O atom, force balance for the outermost $2p$ electron of O_2 (electron 7) is achieved between the centrifugal force and the Coulombic and magnetic forces that arise due to interactions between electron 7 and the other $2p$-shell as well as the $2s$-shell electrons due to spin and orbital angular momentum. The forces used are derived in the Eight-Electron Atoms section. The central Coulomb force on the outer-most $2p$ shell electron of O_2 (electron 7) due to the nucleus and the inner six electrons is given by Eq. (10.70) with the appropriate charge and radius:

$$\mathbf{F}_{ele} = \frac{(Z-6)e^2}{4\pi\varepsilon_0 r_7^2}\mathbf{i}_\mathbf{r} \tag{13.668}$$

for $r > r_6$. The $2p$ shell possess an external electric field given by Eq. (10.92) for $r > r_7$. The energy is minimized with conservation of angular momentum. This condition is met when the magnetic forces are the same as those of the reactant oxygen atoms with r_7 replacing r_8. The diamagnetic force, $\mathbf{F}_{diamagnetic}$, of Eq. (10.82) due to the p-orbital contributions is given by Eq. (10.156):

$$\mathbf{F}_{diamagnetic} = -\left(\frac{1}{3}+\frac{2}{3}\right)\frac{\hbar^2}{4m_e r_7^2 r_3}\sqrt{s(s+1)}\mathbf{i}_\mathbf{r} = -\frac{3\hbar^2}{12m_e r_7^2 r_3}\sqrt{\frac{3}{4}}\mathbf{i}_\mathbf{r} \tag{13.669}$$

And, $\mathbf{F}_{mag\ 2}$ corresponding to the conserved spin and orbital angular momentum given by Eq. (10.157) is:

$$\mathbf{F}_{mag\ 2} = \frac{1}{Z}\frac{2\hbar^2}{m_e r_7^2 r_3}\sqrt{s(s+1)}\mathbf{i}_\mathbf{r} \tag{13.670}$$

The electric field external to the $2p$ shell given by Eq. (10.92) for $r > r_7$ gives rise to a second diamagnetic force, $\mathbf{F}_{diamagnetic\ 2}$, given by Eq. (10.93). $\mathbf{F}_{diamagnetic\ 2}$ due to the binding of the p-orbital electron having an electric field of +1 outside of its radius is :

$$\mathbf{F}_{diamagnetic\ 2} = -\left[\frac{Z-7}{Z-6}\right]\left(1-\frac{\sqrt{2}}{2}\right)\frac{r_3\hbar^2}{m_e r_7^4}10\sqrt{s(s+1)}\mathbf{i}_\mathbf{r} \tag{13.671}$$

The radius of the $2p$ shell is calculated by equating the outward centrifugal force to the sum of the electric (Eq. (13.688)) and diamagnetic (Eqs. (13.669) and (13.671)), and paramagnetic (Eq. (13.670)) forces as follows:

$$\frac{m_e v_7^2}{r_7} = \left(\begin{array}{l}\frac{(Z-6)e^2}{4\pi\varepsilon_0 r_7^2} - \frac{3\hbar^2}{12m_e r_7^2 r_3}\sqrt{s(s+1)} + \frac{2\hbar^2}{Zm_e r_7^2 r_3}\sqrt{s(s+1)} \\ -\left[\frac{Z-7}{Z-6}\right]\left(1-\frac{\sqrt{2}}{2}\right)\frac{r_3\hbar^2}{r_7^4 m_e}10\sqrt{s(s+1)}\end{array}\right) \tag{13.672}$$

Substitution of $v_7 = \frac{\hbar}{m_e r_7}$ (Eq. (1.35)) and $s = \frac{1}{2}$ into Eq. (13.672) gives:

$$\frac{\hbar^2}{m_e r_7^3} = \frac{(Z-6)e^2}{4\pi\varepsilon_0 r_7^2} - \frac{3\hbar^2}{12m_e r_7^2 r_3}\sqrt{\frac{3}{4}} + \frac{2\hbar^2}{Zm_e r_7^2 r_3}\sqrt{\frac{3}{4}} - \left[\frac{Z-7}{Z-6}\right]\left(1-\frac{\sqrt{2}}{2}\right)\frac{r_3\hbar^2}{r_7^4 m_e}10\sqrt{\frac{3}{4}} \tag{13.673}$$

The quadratic equation corresponding to Eq. (13.673) is:

$$r_7^2-\frac{\frac{\hbar^2}{m_e}}{\left(\frac{(Z-6)e^2}{4\pi\varepsilon_0}-\left(\frac{3}{12}-\frac{2}{Z}\right)\frac{\hbar^2}{m_e r_3}\sqrt{\frac{3}{4}}\right)}r_7-\frac{\frac{\hbar^2}{m_e}\left[\frac{Z-7}{Z-6}\right]\left(1-\frac{\sqrt{2}}{2}\right)r_3 10\sqrt{\frac{3}{4}}}{\left(\frac{(Z-6)e^2}{4\pi\varepsilon_0}-\left(\frac{3}{12}-\frac{2}{Z}\right)\frac{\hbar^2}{m_e r_3}\sqrt{\frac{3}{4}}\right)}=0 \quad (13.674)$$

The solution of Eq. (13.674) using the quadratic formula is:

$$r_7=\frac{\frac{a_0}{\left((Z-6)-\left(\frac{3}{12}-\frac{2}{Z}\right)\frac{\sqrt{3}}{2r_3}\right)}\pm a_0\sqrt{\left(\frac{1}{\left((Z-6)-\left(\frac{3}{12}-\frac{2}{Z}\right)\frac{\sqrt{3}}{2r_3}\right)}\right)^2+\frac{20\sqrt{3}\left(\left[\frac{Z-7}{Z-6}\right]\left(1-\frac{\sqrt{2}}{2}\right)r_3\right)}{\left((Z-6)-\left(\frac{3}{12}-\frac{2}{Z}\right)\frac{\sqrt{3}}{2r_3}\right)}}}{2},\ r_3 \text{ in units of } a_0 \quad (13.675)$$

The positive root of Eq. (13.675) must be taken in order that $r_7>0$. Substitution of $\frac{r_3}{a_0}=0.59020$ (Eq. (10.62) with $Z=8$) into Eq. (13.675) gives:

$$r_7=0.91088a_0 \quad (13.676)$$

ENERGIES OF THE $2p$ SHELL OF THE OXYGEN ATOMS OF THE OXYGEN MOLECULE

The central forces on the $2p$ shell of each O are increased with the formation of the σ MO, which reduces the shell's radius and increases its total energy. The Coulombic energy terms of the total energy of the two O atoms at the new radius are calculated and added to the energy of the σ MO to give the total energy of O_2. Then, the bond energy is determined from the total O_2 energy.

The radius r_8 of each oxygen atom before bonding is given by Eq. (10.162).

$$r_8=a_0 \quad (13.677)$$

Using the initial radius r_8 of each O atom and the final radius r_7 of the $O2p$ shell of O_2 (Eq. (13.676)) and by considering that the central Coulombic field decreases by an integer for each successive electron of the shell, the sum $E_T(O_2,2p)$ of the Coulombic energy change of the $O2p$ electrons of both atoms is determined using Eq. (10.102):

$$\begin{aligned}E_T(O_2,2p)&=-2\sum_{n=4}^{6}\frac{(Z-n)e^2}{8\pi\varepsilon_0}\left(\frac{1}{r_7}-\frac{1}{r_8}\right) \quad (13.678)\\&=-2(13.60580\ eV)(0.09784)(2+3+4)=-23.96074\ eV\end{aligned}$$

FORCE BALANCE OF THE σ MO OF THE OXYGEN MOLECULE

The force balance equation for the σ-MO of the oxygen molecule given by Eq. (11.200) and Eqs. (13.633-13.634) with $n_e=3$ and $|L|=\sqrt{\frac{3}{4}}\hbar$ is:

$$\frac{\hbar^2}{m_e a^2 b^2}D=\frac{e^2}{8\pi\varepsilon_0 ab^2}D+\frac{\hbar^2}{2m_e a^2 b^2}D-\left(\frac{3}{2}+\frac{\sqrt{\frac{3}{4}}}{Z}\right)\frac{\hbar^2}{2m_e a^2 b^2}D \quad (13.679)$$

$$\frac{\hbar^2}{m_e a^2 b^2}D=\frac{e^2}{8\pi\varepsilon_0 ab^2}D-\left(\frac{1}{2}+\frac{\sqrt{\frac{3}{4}}}{Z}\right)\frac{\hbar^2}{2m_e a^2 b^2}D \quad (13.680)$$

$$\left(\frac{5}{2}+\frac{\sqrt{\frac{3}{4}}}{Z}\right)\frac{\hbar^2}{2m_e a^2 b^2}D=\frac{e^2}{8\pi\varepsilon_0 ab^2}D \tag{13.681}$$

$$a=\left(\frac{5}{2}+\frac{\sqrt{\frac{3}{4}}}{Z}\right)a_0 \tag{13.682}$$

Substitution of $Z=8$ into Eq. (13.682) gives:

$$a=2.60825a_0=1.38023\ X\ 10^{-10}\ m \tag{13.683}$$

Substitution of Eq. (13.683) into Eq. (11.79) is:

$$c'=1.14198a_0=6.04312\ X\ 10^{-11}\ m \tag{13.684}$$

The internuclear distance given by multiplying Eq. (13.684) by two is:

$$2c'=2.28397a_0=1.20862\ X\ 10^{-10}\ m \tag{13.685}$$

The experimental bond distance is [28] :

$$2c'=1.20752\ X\ 10^{-10}\ m \tag{13.686}$$

Substitution of Eqs. (13.683-13.684) into Eq. (11.80) is:

$$\begin{aligned} b=c&=2.34496a_0\\ &=1.24090\ X\ 10^{-10}\ m\end{aligned} \tag{13.687}$$

Substitution of Eqs. (13.683-13.684) into Eq. (11.67) is:

$$e=0.43783 \tag{13.688}$$

Using the electron configuration of O_2 (Eq. (13.667)), the radii of the $O1s=0.12739a_0$ (Eq. (10.51)), $O2s=0.59020a_0$ (Eq. (10.62)), and $O2p=0.91088a_0$ (Eq. (13.676)) shells and the parameters of the σ MO of O_2 given by Eqs. (13.3-13.4), (13.683-13.685), and (13.687-13.688), the dimensional diagram and charge-density of the O_2 MO are shown in Figures 13.16 and 13.17, respectively.

Figure 13.16. The cross section of the O_2 MO showing the axes, σ MO (H_2-type ellipsoidal MO), with the O $1s$, $2s$, and $2p$ atomic orbitals (AOs). Legend: a: semimajor axis, b: semiminor axis, c': internuclear distance, r_7: radius of the $O2p$ shell having two paired electrons.

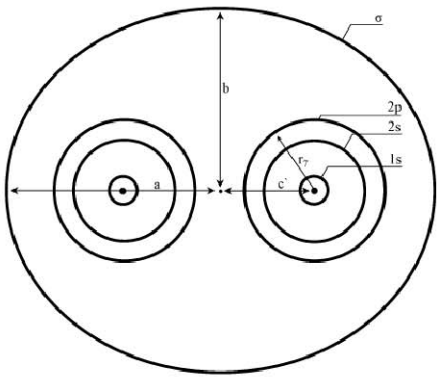

Figure 13.17. O_2 MO comprising the σ MO (H_2-type MO) with O atoms at the foci that have each donated an electron to the σ MO and have smaller radii and higher binding energies as a consequence. (A) Color scale, translucent view of the charge-density of the O_2 MO. (B) Off-center cut-away view showing the complete inner most $O1s$ shell, and moving radially, the $O2s$ shell, the $O2p$ shell, and the σ prolate spheroidal MO that have the O atoms as the foci.

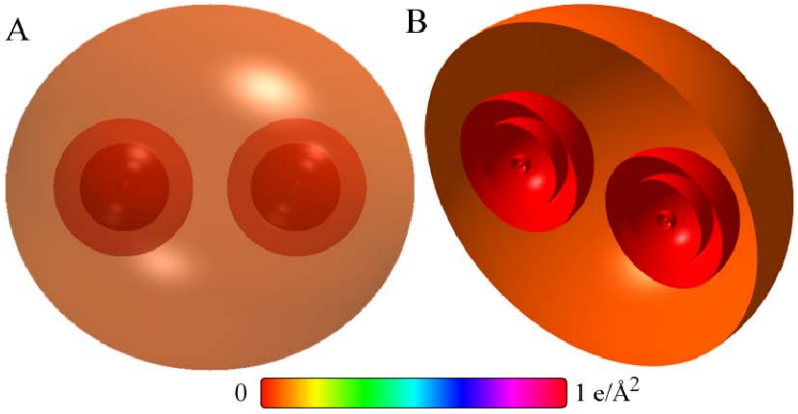

SUM OF THE ENERGIES OF THE σ MO AND THE AOs OF THE OXYGEN MOLECULE

The energies of the O_2 σ MO are given by the substitution of the semiprincipal axes (Eqs. (13.683-13.684) and (13.687)) into the energy equations (Eqs. (11.207-11.212)) of H_2:

$$V_e = \frac{-2e^2}{8\pi\varepsilon_0\sqrt{a^2-b^2}}\ln\frac{a+\sqrt{a^2-b^2}}{a-\sqrt{a^2-b^2}} = -22.37716\ eV \tag{13.689}$$

$$V_p = \frac{e^2}{8\pi\varepsilon_0\sqrt{a^2-b^2}} = 11.91418\ eV \tag{13.690}$$

$$T = \frac{\hbar^2}{2m_e a\sqrt{a^2-b^2}}\ln\frac{a+\sqrt{a^2-b^2}}{a-\sqrt{a^2-b^2}} = 4.28968\ eV \tag{13.691}$$

$$V_m = \frac{-\hbar^2}{4m_e a\sqrt{a^2-b^2}}\ln\frac{a+\sqrt{a^2-b^2}}{a-\sqrt{a^2-b^2}} = -2.14484\ eV \tag{13.692}$$

$$E_T = V_e + T + V_m + V_p \tag{13.693}$$

Substitution of Eqs. (11.79) and (13.689-13.692) into Eq. (13.693) gives:

$$E_T(O_2,\sigma) = \frac{-e^2}{8\pi\varepsilon_0\sqrt{\frac{aa_0}{2}}}\left(\left(2-\frac{1}{2}\frac{a_0}{a}\right)\ln\frac{a+\sqrt{\frac{aa_0}{2}}}{a-\sqrt{\frac{aa_0}{2}}}-1\right) = -8.31814\ eV \tag{13.694}$$

where $E_T(O_2,\sigma)$ is the total energy of the σ MO of O_2. The sum, $E_T(O_2)$, of $E_T(O_2,2p)$, the $2p$ AO contribution given by: Eq. (13.678), and $E_T(O_2,\sigma)$, the σ MO contribution given by Eq. (13.694) is:

$$E_T(O_2) = E_T(O_2,2p) + E_T(O_2,\sigma) = -23.96074\ eV - 8.31814\ eV = -32.27888\ eV \tag{13.695}$$

VIBRATION OF O_2

The vibrational energy levels of O_2 may be solved by determining the Morse potential curve from the energy relationships for the transition from two O atoms whose parameters are given by Eqs. (10.154-10.163) to the two O atoms whose parameter r_7 is given by Eq. (13.676) and the σ MO whose parameters are given by Eqs. (13.683-13.685) and (13.687-13.688). As shown in the Vibration of Hydrogen-type Molecular Ions section, the harmonic oscillator potential energy function can be expanded about the internuclear distance and expressed as a Maclaurin series corresponding to a Morse potential after Karplus and Porter (K&P) [15] and after Eq. (11.134). Treating the Maclaurin series terms as anharmonic perturbation terms of the harmonic states, the energy corrections can be found by perturbation methods.

THE DOPPLER ENERGY TERMS OF THE OXYGEN MOLECULE

The equations of the radiation reaction force of oxygen are the same as those of H_2 with the substitution of the oxygen parameters. Using Eqs. (11.231-11.233), the angular frequency of the reentrant oscillation in the transition state is:

$$\omega = \sqrt{\frac{e^2}{4\pi\varepsilon_0 a^3}} = 9.81432\ X\ 10^{16}\ rad/s \tag{13.696}$$

where a is given by Eq. (13.683). The kinetic energy, E_K, is given by Planck's equation (Eq. (11.127)).

$$\bar{E}_K = \hbar\omega = \hbar 9.81432\ X\ 10^{16}\ rad/s = 6.45996\ eV \tag{13.697}$$

In Eq. (11.181), substitution of $E_T(O_2)$ for $E_{h\nu}$, the mass of the electron, m_e, for M, and the kinetic energy given by Eq. (13.697) for $\bar{E}_K$ gives the Doppler energy of the electrons of the reentrant orbit:

$$\bar{E}_D \cong E_{h\nu}\sqrt{\frac{2\bar{E}_K}{Mc^2}} = -32.27888\ eV\sqrt{\frac{2e(6.45996\ eV)}{m_e c^2}} = -0.16231\ eV \tag{13.698}$$

In addition to the electrons, the nuclei also undergo simple harmonic oscillation in the transition state at their corresponding frequency. The decrease in the energy of the O_2 MO due to the reentrant orbit in the transition state corresponding to simple

harmonic oscillation of the electrons and nuclei, $\bar{E}_{osc}$, is given by the sum of the corresponding energies, $\bar{E}_D$ given by Eq. (13.698) and $\bar{E}_{Kvib}$, the average kinetic energy of vibration which is 1/2 of the vibrational energy. Using the experimental O_2 ω_e of 1580.19 cm^{-1} $(0.19592\ eV)$ [28] for $\bar{E}_{Kvib}$ of the transition state, $\bar{E}_{osc}(O_2)$ is:

$$\bar{E}_{osc}(O_2) = \bar{E}_D + \bar{E}_{Kvib} = \bar{E}_D + \frac{1}{2}\hbar\sqrt{\frac{k}{\mu}} \tag{13.699}$$

$$\bar{E}_{osc}(O_2) = -0.16231\ eV + \frac{1}{2}(0.19592\ eV) = -0.06435\ eV \tag{13.700}$$

TOTAL AND BOND ENERGIES OF THE OXYGEN MOLECULE

$E_{T+osc}(O_2)$, the total energy of O_2 including the Doppler term, is given by the sum of $E_T(O_2)$ (Eq. (13.695)) and $\bar{E}_{osc}(O_2)$ given by Eq. (13.700):

$$\begin{aligned} E_{T+osc}(O_2) &= V_e + T + V_m + V_p + E_T(O_2, 2p) + \bar{E}_{osc}(O_2) \\ &= E_T(O_2, \sigma) + E_T(O_2, 2p) + \bar{E}_{osc}(O_2) \\ &= E_T(O_2) + \bar{E}_{osc}(O_2) \end{aligned} \tag{13.701}$$

$$\begin{aligned} E_{T+osc}(O_2) = &\left\{ \left(\frac{-e^2}{8\pi\varepsilon_0\sqrt{\frac{aa_0}{2}}} \left(\left(2 - \frac{1}{2}\frac{a_0}{a}\right) \ln \frac{a + \sqrt{\frac{aa_0}{2}}}{a - \sqrt{\frac{aa_0}{2}}} - 1 \right) - 2\sum_{n=4}^{6} \frac{(Z-n)e^2}{8\pi\varepsilon_0} \left(\frac{1}{r_7} - \frac{1}{r_8} \right) \right) \right. \\ &\left. \left(1 + \sqrt{\frac{2\hbar\sqrt{\frac{e^2}{4\pi\varepsilon_0 a^3}}}{m_e c^2}} \right) + \frac{1}{2}\hbar\sqrt{\frac{k}{\mu}} \right\} \\ = &-32.27888\ eV - 0.16231\ eV + \frac{1}{2}\hbar\sqrt{\frac{k}{\mu}} \end{aligned} \tag{13.702}$$

From Eqs. (13.699-13.702), the total energy of the O_2 MO is:

$$\begin{aligned} E_{T+osc}(O_2) &= -32.27888\ eV + \bar{E}_{osc}(O_2) \\ &= -32.27888\ eV - 0.16231\ eV + \frac{1}{2}(0.19592\ eV) \\ &= -32.34323\ eV \end{aligned} \tag{13.703}$$

where the experimental ω_e was used for the $\hbar\sqrt{\frac{k}{\mu}}$ term.

The O_2 bond dissociation energy, $E_D(O_2)$, is given by the difference in the total energies of the two O atoms and $E_{T+osc}(O_2)$:

$$E_D(O_2) = 2E(O) - E_{T+osc}(O_2) \tag{13.704}$$

where the energy of an oxygen atom is [6]:

$$E(O) = -13.61806\ eV \tag{13.705}$$

Thus, the O_2 bond dissociation energy, $E_D(O_2)$, given by Eqs. (13.703-13.705) is:

$$E_D(O_2) = -2(13.61806\ eV) - E_{T+osc}(O_2) = -27.23612\ eV - (-32.34323\ eV) = 5.10711\ eV \tag{13.706}$$

The experimental O_2 bond dissociation energy from Ref. [46] and Ref. [47] is:

$$E_D(O_2) = 5.11665\ eV \tag{13.707}$$

$$E_D(O_2) = 5.116696\ eV \tag{13.708}$$

The results of the determination of bond parameters of O_2 are given in Table 13.1. The calculated results are based on first principles and given in closed-form, exact equations containing fundamental constants only. The agreement between the experimental and calculated results is excellent.

FLUORINE MOLECULE

The fluorine molecule can be formed by the reaction of two fluorine atoms:

$$F + F \rightarrow F_2 \tag{13.709}$$

The bond in the fluorine molecule comprises a H_2-type molecular orbital (MO) with two paired electrons. The force balance equation and radius r_9 of the $2p$ shell of F is derived in the Nine-Electron Atoms section. With the formation of the H_2-type MO by the contribution of a $2p$ electron from each F atom, a diamagnetic force arises between the remaining $2p$ electrons and the H_2-type MO. This force from each F causes the H_2-type MO to move to greater principal axes than would result with the Coulombic force alone. But, the integer increase of the central field and the resulting increased Coulombic as well as magnetic central forces on the remaining $2p$ electrons of each F decrease the radius of the corresponding shell such that the energy minimum is achieved that is lower than that of the reactant atoms. The resulting electron configuration of F_2 is $1s_1^2 1s_2^2 2s_1^2 2s_2^2 2p_1^4 2p_2^4 \sigma_{1,2}^2$ where the subscript designates the F atom, 1 or 2, σ designates the H_2-type MO, and the orbital arrangement is:

σ state

$\uparrow\downarrow$

2p state

$\uparrow\downarrow$ $\uparrow\downarrow$ $\uparrow\downarrow$ $\uparrow\downarrow$

0 1 0 1

2s state

$\uparrow\downarrow$ $\uparrow\downarrow$

1s state

$\uparrow\downarrow$ $\uparrow\downarrow$

$F1$ $F2$

(13.710)

Fluorine is predicted to be diamagnetic in agreement with observations [42].

FORCE BALANCE OF THE $2p$ SHELL OF THE FLUORINE ATOMS OF THE FLUORINE MOLECULE

For each F atom, force balance for the outermost $2p$ electron of F_2 (electron 8) is achieved between the centrifugal force and the Coulombic and magnetic forces that arise due to interactions between electron 8 and the other $2p$-shell as well as the $2s$-shell electrons due to spin and orbital angular momentum. The forces used are derived in the Nine-Electron Atoms section. The central Coulomb force on the outer-most $2p$ shell electron of F_2 (electron 8) due to the nucleus and the inner seven electrons is given by Eq. (10.70) with the appropriate charge and radius:

$$\mathbf{F}_{ele} = \frac{(Z-7)e^2}{4\pi\varepsilon_0 r_8^2}\mathbf{i}_\mathbf{r} \tag{13.711}$$

for $r > r_7$. The $2p$ shell possess an external electric field given by Eq. (10.92) for $r > r_8$. The energy is minimized with conservation of angular momentum. This condition is met when the diamagnetic force, $\mathbf{F}_{diamagnetic}$, of Eq. (10.82) due to the p-orbital contributions is the same as that of the reactant fluorine atoms given by Eq. (10.176) with r_8 replacing r_9:

$$\begin{aligned}\mathbf{F}_{diamagnetic} &= -\left(\frac{2}{3}\right)\frac{\hbar^2}{4m_e r_8^2 r_3}\sqrt{s(s+1)}\mathbf{i}_\mathbf{r} \\ &= -\frac{2\hbar^2}{12m_e r_8^2 r_3}\sqrt{\frac{3}{4}}\mathbf{i}_\mathbf{r}\end{aligned} \tag{13.712}$$

Thus, $\mathbf{F}_{diamagnetic}$ due to the two filled $2p$ orbitals per F atom is twice that of N_2 given by Eq. (13.622) having one filled $2p$ orbital per N atom. $\mathbf{F}_{mag\ 2}$ corresponding to the conserved spin and orbital angular momentum is also the same as that of the reactant fluorine atoms given by Eq. (10.177) and that of N_2 given by Eq. (13.623) where the outer radius of the $2p$ shell of the

F atoms of F_2 is r_8.

$$\mathbf{F}_{mag\ 2} = \frac{1}{Z}\frac{3\hbar^2}{m_e r_8^2 r_3}\sqrt{s(s+1)}\mathbf{i}_\mathbf{r} \tag{13.713}$$

The electric field external to the $2p$ shell given by Eq. (10.92) for $r > r_8$ gives rise to a second diamagnetic force, $\mathbf{F}_{diamagnetic\ 2}$, given by Eq. (10.93). $\mathbf{F}_{diamagnetic\ 2}$ due to the binding of the p-orbital electron having an electric field of +1 outside of its radius is :

$$\mathbf{F}_{diamagnetic\ 2} = -\left[\frac{Z-8}{Z-7}\right]\left(1-\frac{\sqrt{2}}{2}\right)\frac{r_3\hbar^2}{m_e r_8^4}10\sqrt{s(s+1)}\mathbf{i}_\mathbf{r} \tag{13.714}$$

In addition, the contribution of a $2p$ electron from each F atom in the formation of the σ MO gives rise to a paramagnetic force on the remaining paired $2p$ electrons. The force $\mathbf{F}_{mag\ 3}$ is given by Eq. (13.625) wherein the radius is r_8:

$$\mathbf{F}_{mag\ 3} = \frac{\hbar^2}{4m_e r_8^3}\sqrt{s(s+1)}\mathbf{i}_\mathbf{r} \tag{13.715}$$

The radius of the $2p$ shell is calculated by equating the outward centrifugal force to the sum of the electric (Eq. (13.711)) and diamagnetic (Eqs. (13.712) and (13.714)), and paramagnetic (Eqs. (13.713) and (13.715)) forces as follows:

$$\frac{m_e v_8^2}{r_8} = \begin{pmatrix} \frac{(Z-7)e^2}{4\pi\varepsilon_0 r_8^2} - \frac{2\hbar^2}{12 m_e r_8^2 r_3}\sqrt{s(s+1)} + \frac{3\hbar^2}{Z m_e r_8^2 r_3}\sqrt{s(s+1)} \\ -\left[\frac{Z-8}{Z-7}\right]\left(1-\frac{\sqrt{2}}{2}\right)\frac{r_3\hbar^2}{r_8^4 m_e}10\sqrt{s(s+1)} + \frac{\hbar^2}{4m_e r_8^3}\sqrt{s(s+1)} \end{pmatrix} \tag{13.716}$$

Substitution of $v_8 = \frac{\hbar}{m_e r_8}$ (Eq. (1.35)) and $s = \frac{1}{2}$ into Eq. (13.716) gives:

$$\frac{\hbar^2}{m_e r_8^3} - \frac{\hbar^2}{4m_e r_8^3}\sqrt{\frac{3}{4}} = \frac{(Z-7)e^2}{4\pi\varepsilon_0 r_8^2} - \frac{2\hbar^2}{12 m_e r_8^2 r_3}\sqrt{\frac{3}{4}} + \frac{3\hbar^2}{Z m_e r_8^2 r_3}\sqrt{\frac{3}{4}} - \left[\frac{Z-8}{Z-7}\right]\left(1-\frac{\sqrt{2}}{2}\right)\frac{r_3\hbar^2}{r_8^4 m_e}10\sqrt{\frac{3}{4}} \tag{13.717}$$

The quadratic equation corresponding to Eq. (13.717) is:

$$r_8^2 - \frac{\frac{\hbar^2}{m_e}\left(1-\frac{\sqrt{3}}{8}\right)}{\left(\frac{(Z-7)e^2}{4\pi\varepsilon_0} - \left(\frac{2}{12}-\frac{3}{Z}\right)\frac{\hbar^2}{m_e r_3}\sqrt{\frac{3}{4}}\right)}r_8 - \frac{\frac{\hbar^2}{m_e}\left[\frac{Z-8}{Z-7}\right]\left(1-\frac{\sqrt{2}}{2}\right)r_3 10\sqrt{\frac{3}{4}}}{\left(\frac{(Z-7)e^2}{4\pi\varepsilon_0} - \left(\frac{2}{12}-\frac{3}{Z}\right)\frac{\hbar^2}{m_e r_3}\sqrt{\frac{3}{4}}\right)} = 0 \tag{13.718}$$

The solution of Eq. (13.718) using the quadratic formula is:

$$r_8 = \frac{\frac{a_0\left(1-\frac{\sqrt{3}}{8}\right)}{\left((Z-7)-\left(\frac{2}{12}-\frac{3}{Z}\right)\frac{\sqrt{3}}{2r_3}\right)} \pm a_0\sqrt{\left(\frac{1-\frac{\sqrt{3}}{8}}{\left((Z-7)-\left(\frac{2}{12}-\frac{3}{Z}\right)\frac{\sqrt{3}}{2r_3}\right)}\right)^2 + \frac{20\sqrt{3}\left(\left[\frac{Z-8}{Z-7}\right]\left(1-\frac{\sqrt{2}}{2}\right)r_3\right)}{\left((Z-7)-\left(\frac{2}{12}-\frac{3}{Z}\right)\frac{\sqrt{3}}{2r_3}\right)}}}{2}, \; r_3 \text{ in units of } a_0 \tag{13.719}$$

The positive root of Eq. (13.719) must be taken in order that $r_8 > 0$. Substitution of $\frac{r_3}{a_0} = 0.51382$ (Eq. (10.62) with $Z = 9$) into Eq. (13.719) gives:

$$r_8 = 0.73318 a_0 \tag{13.720}$$

ENERGIES OF THE $2p$ SHELL OF THE FLUORINE ATOMS OF THE FLUORINE MOLECULE

The central forces on the $2p$ shell of each F are increased with the formation of the σ MO, which reduces the shell's radius and increases its total energy. The Coulombic energy terms of the total energy of the two F atoms at the new radius are calculated and added to the energy of the σ MO to give the total energy of F_2. Then, the bond energy is determined from the total F_2 energy.

The radius r_9 of each fluorine atom before bonding is given by Eq. (10.182):

$$r_9 = 0.78069a_0 \tag{13.721}$$

Using the initial radius r_9 of each F atom and the final radius r_8 of the $F2p$ shell of F_2 (Eq. (13.720)) and by considering that the central Coulombic field decreases by an integer for each successive electron of the shell, the sum $E_T\left(F_2,2p\right)$ of the Coulombic energy change of the $F2p$ electrons of both atoms is determined using Eq. (10.102).

$$\begin{aligned} E_T\left(F_2,2p\right) &= -2\sum_{n=4}^{7}\frac{(Z-n)e^2}{8\pi\varepsilon_0}\left(\frac{1}{r_8}-\frac{1}{r_9}\right) \\ &= -2\left(13.60580\ eV\right)\left(0.08301\right)\left(2+3+4+5\right) = -31.62353\ eV \end{aligned} \tag{13.722}$$

FORCE BALANCE OF THE σ MO OF THE FLUORINE MOLECULE

The relativistic diamagnetic force $\mathbf{F}_{diamagneticMO2}$ of F_2 is one half that of N_2 due to the two versus one filled $2p$ orbitals per atom at the focus. The force balance equation for the σ-MO of the fluorine molecule is given by Eq. (11.200) and Eqs. (13.633-13.634) with the correction of 1/2 due the two $2p$ orbitals per F after Eqs. (10.2-10.11), $n_e = 5$, and $\left|L\right| = \hbar$:

$$\frac{\hbar^2}{m_e a^2 b^2}D = \frac{e^2}{8\pi\varepsilon_0 ab^2}D + \frac{\hbar^2}{2m_e a^2 b^2}D - \left(\frac{5}{2}+\frac{1}{2Z}\right)\frac{\hbar^2}{2m_e a^2 b^2}D \tag{13.723}$$

$$\frac{\hbar^2}{m_e a^2 b^2}D = \frac{e^2}{8\pi\varepsilon_0 ab^2}D - \left(\frac{3}{2}+\frac{1}{2Z}\right)\frac{\hbar^2}{2m_e a^2 b^2}D \tag{13.724}$$

$$\left(\frac{7}{2}+\frac{1}{2Z}\right)\frac{\hbar^2}{2m_e a^2 b^2}D = \frac{e^2}{8\pi\varepsilon_0 ab^2}D \tag{13.725}$$

$$a = \left(\frac{7}{2}+\frac{1}{2Z}\right)a_0 \tag{13.726}$$

Substitution of $Z = 9$ into Eq. (13.726) gives:

$$a = 3.55556a_0 = 1.88152\ X\ 10^{-10}\ m \tag{13.727}$$

Substitution of Eq. (13.727) into Eq. (11.79) is:

$$c' = 1.33333a_0 = 7.05569\ X\ 10^{-11}\ m \tag{13.728}$$

The internuclear distance given by multiplying Eq. (13.728) by two is:

$$2c' = 2.66667a_0 = 1.41114\ X\ 10^{-10}\ m \tag{13.729}$$

The experimental bond distance is [28] :

$$2c' = 1.41193\ X\ 10^{-10}\ m \tag{13.730}$$

Substitution of Eqs. (13.727-13.728) into Eq. (11.80) is:

$$b = c = 3.29609a_0 = 1.74421\ X\ 10^{-10}\ m \tag{13.731}$$

Substitution of Eqs. (13.727-13.728) into Eq. (11.67) is:

$$e = 0.37500 \tag{13.732}$$

Using the electron configuration of F_2 (Eq. (13.710)), the radii of the $F1s = 0.11297a_0$ (Eq. (10.51)), $F2s = 0.51382a_0$ (Eq. (10.62)), and $F2p = 0.73318a_0$ (Eq. (13.720)) shells and the parameters of the σ MO of F_2 given by Eqs. (13.3-13.4), (13.727-13.728), and (13.731-13.732), the dimensional diagram and charge-density of the F_2 MO are shown in Figures 13.18 and 13.19, respectively.

Figure 13.18. The cross section of the F_2 MO showing the axes, σ MO (H_2-type ellipsoidal MO), with the F $1s$, $2s$, and $2p$ atomic orbitals (AOs). Legend: a: semimajor axis, b: semiminor axis, c': internuclear distance, r_8: radius of the $F2p$ shell having two paired electrons.

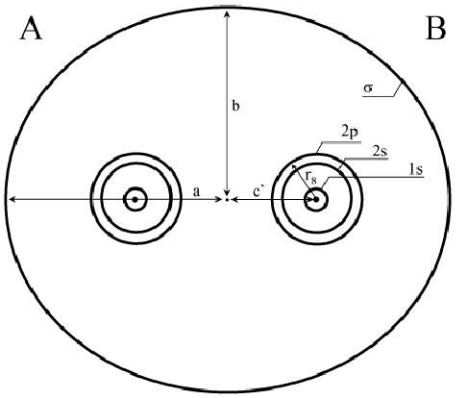

Figure 13.19. F_2 MO comprising the σ MO (H_2-type MO) with F atoms at the foci that have each donated an electron to the σ MO and have smaller radii and higher binding energies as a consequence. (A) Color scale, translucent view of the charge-density of the F_2 MO. (B) Off-center cut-away view showing the complete inner most $F1s$ shell, and moving radially, the $F2s$ shell, the $F2p$ shell, and the σ prolate spheroidal MO that have the F atoms as the foci.

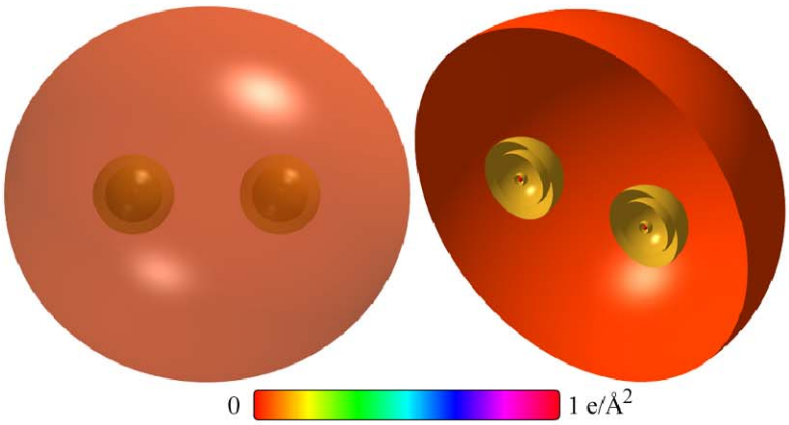

SUM OF THE ENERGIES OF THE σ MO AND THE AOs OF THE FLUORINE MOLECULE

The energies of the F_2 σ MO are given by the substitution of the semiprincipal axes (Eqs. (13.683-13.684) and (13.687)) into the energy equations (Eqs. (11.207-11.212)) of H_2:

$$V_e = \frac{-2e^2}{8\pi\varepsilon_0\sqrt{a^2-b^2}}\ln\frac{a+\sqrt{a^2-b^2}}{a-\sqrt{a^2-b^2}} = -16.09139\ eV \tag{13.733}$$

$$V_p = \frac{e^2}{8\pi\varepsilon_0\sqrt{a^2-b^2}} = 10.20435\ eV \tag{13.734}$$

$$T = \frac{\hbar^2}{2m_e a\sqrt{a^2-b^2}}\ln\frac{a+\sqrt{a^2-b^2}}{a-\sqrt{a^2-b^2}} = 2.26285\ eV \tag{13.735}$$

$$V_m = \frac{-\hbar^2}{4m_e a\sqrt{a^2-b^2}}\ln\frac{a+\sqrt{a^2-b^2}}{a-\sqrt{a^2-b^2}} = -1.13143\ eV \tag{13.736}$$

$$E_T = V_e + T + V_m + V_p \tag{13.737}$$

Substitution of Eqs. (11.79) and (13.733-13.736) into Eq. (13.737) gives:

$$\begin{aligned} E_T(F_2,\sigma) &= \frac{-e^2}{8\pi\varepsilon_0\sqrt{\frac{aa_0}{2}}}\left(\left(2-\frac{1}{2}\frac{a_0}{a}\right)\ln\frac{a+\sqrt{\frac{aa_0}{2}}}{a-\sqrt{\frac{aa_0}{2}}}-1\right) \\ &= -4.75562\ eV \end{aligned} \tag{13.738}$$

where $E_T(F_2,\sigma)$ is the total energy of the σ MO of F_2. The sum, $E_T(F_2)$, of $E_T(F_2,2p)$, the $2p$ AO contribution given by Eq. (13.722), and $E_T(F_2,\sigma)$, the σ MO contribution given by Eq. (13.738) is:

$$\begin{aligned} E_T(F_2) &= E_T(F_2,2p) + E_T(F_2,\sigma) \\ &= -31.62353\ eV - 4.75562\ eV = -36.37915\ eV \end{aligned} \tag{13.739}$$

VIBRATION OF F_2

The vibrational energy levels of F_2 may be solved by determining the Morse potential curve from the energy relationships for the transition from two F atoms whose parameters are given by Eqs. (10.174-10.183) to the two F atoms whose parameter r_8 is given by Eq. (13.720) and the σ MO whose parameters are given by Eqs. (13.727-13.729) and (13.731-13.732). As shown in the Vibration of Hydrogen-type Molecular Ions section, the harmonic oscillator potential energy function can be expanded about the internuclear distance and expressed as a Maclaurin series corresponding to a Morse potential after Karplus and Porter (K&P) [15] and after Eq. (11.134). Treating the Maclaurin series terms as anharmonic perturbation terms of the harmonic states, the energy corrections can be found by perturbation methods.

THE DOPPLER ENERGY TERMS OF THE FLUORINE MOLECULE

The equations of the radiation reaction force of fluorine are the same as those of H_2 with the substitution of the fluorine parameters. Using Eqs. (11.231-11.233), the angular frequency of the reentrant oscillation in the transition state is:

$$\omega = \sqrt{\frac{e^2}{4\pi\varepsilon_0 a^3 m_e}} = 6.16629\ X\ 10^{15}\ rad/s \tag{13.740}$$

where a is given by Eq. (13.727). The kinetic energy, E_K, is given by Planck's equation (Eq. (11.127)):

$$\bar{E}_K = \hbar\omega = \hbar 6.16629\ X\ 10^{15}\ rad/s = 4.05876\ eV \tag{13.741}$$

In Eq. (11.181), substitution of $E_T(F_2)$ for $E_{h\nu}$, the mass of the electron, m_e, for M, and the kinetic energy given by Eq. (13.741) for $\bar{E}_K$ gives the Doppler energy of the electrons of the reentrant orbit:

$$\bar{E}_D \cong E_{h\nu}\sqrt{\frac{2\bar{E}_K}{Mc^2}} = -36.37915\ eV\sqrt{\frac{2e(4.05876\ eV)}{m_e c^2}} = -0.14499\ eV \tag{13.742}$$

In addition to the electrons, the nuclei also undergo simple harmonic oscillation in the transition state at their corresponding frequency. The decrease in the energy of the F_2 MO due to the reentrant orbit in the transition state corresponding to simple harmonic oscillation of the electrons and nuclei, $\bar{E}_{osc}$, is given by the sum of the corresponding energies, $\bar{E}_D$ given by Eq. (13.742) and $\bar{E}_{Kvib}$, the average kinetic energy of vibration which is 1/2 of the vibrational energy. Using the experimental F_2 ω_e of 916.64 cm^{-1} $(0.11365\ eV)$ [28] for $\bar{E}_{Kvib}$ of the transition state, $\bar{E}_{osc}(F_2)$ is:

$$\bar{E}_{osc}(F_2) = \bar{E}_D + \bar{E}_{Kvib} = \bar{E}_D + \frac{1}{2}\hbar\sqrt{\frac{k}{\mu}} \tag{13.743}$$

$$\bar{E}_{osc}(F_2) = -0.14499\ eV + \frac{1}{2}(0.11365\ eV) = -0.08817\ eV \tag{13.744}$$

TOTAL AND BOND ENERGIES OF THE FLUORINE MOLECULE

$E_{T+osc}(F_2)$, the total energy of F_2 including the Doppler term, is given by the sum of $E_T(F_2)$ (Eq. (13.739)) and $\bar{E}_{osc}(F_2)$ given by Eq. (13.744):

$$\begin{aligned} E_{T+osc}(F_2) &= V_e + T + V_m + V_p + E_T(F_2, 2p) + \bar{E}_{osc}(F_2) \\ &= E_T(F_2, \sigma) + E_T(F_2, 2p) + \bar{E}_{osc}(F_2) \\ &= E_T(F_2) + \bar{E}_{osc}(F_2) \end{aligned} \tag{13.745}$$

$$E_{T+osc}(F_2) = \left\{ \begin{array}{l} \left(\dfrac{-e^2}{8\pi\varepsilon_0\sqrt{\dfrac{aa_0}{2}}} \left(\left(2 - \dfrac{1}{2}\dfrac{a_0}{a}\right) \ln \dfrac{a + \sqrt{\dfrac{aa_0}{2}}}{a - \sqrt{\dfrac{aa_0}{2}}} - 1 \right) - 2\sum_{n=4}^{7} \dfrac{(Z-n)e^2}{8\pi\varepsilon_0} \left(\dfrac{1}{r_8} - \dfrac{1}{r_9} \right) \right) \\ \left(1 + \sqrt{\dfrac{2\hbar\sqrt{\dfrac{e^2}{4\pi\varepsilon_0 a^3 m_e}}}{m_e c^2}} \right) + \dfrac{1}{2}\hbar\sqrt{\dfrac{k}{\mu}} \end{array} \right\} \tag{13.746}$$

$$= -36.37915\ eV - 0.14499\ eV + \frac{1}{2}\hbar\sqrt{\frac{k}{\mu}}$$

From Eqs. (13.743-13.746), the total energy of the F_2 MO is:

$$E_{T+osc}(F_2) = -36.37915\ eV + \bar{E}_{osc}(F_2) = -36.37915\ eV - 0.14499\ eV + \frac{1}{2}(0.11365\ eV) = -36.46732\ eV \tag{13.747}$$

where the experimental ω_e was used for the $\hbar\sqrt{\frac{k}{\mu}}$ term.

The F_2 bond dissociation energy, $E_D(F_2)$, is given by the difference in the total energies of the two F atoms and $E_{T+osc}(F_2)$:

$$E_D(F_2) = 2E(F) - E_{T+osc}(F_2) \tag{13.748}$$

where the energy of a fluorine atom is [6]:

$$E(F) = -17.42282\ eV \tag{13.749}$$

Thus, the F_2 bond dissociation energy, $E_D(F_2)$, given by Eqs. (13.747-13.749) is:

$$E_D(F_2) = -2(17.42282\ eV) - E_{T+osc}(F_2) = -34.84564\ eV - (-36.46732\ eV) = 1.62168\ eV \tag{13.750}$$

The experimental F_2 bond dissociation energy is [48]:

$$E_D(F_2) = 1.606\ eV \tag{13.751}$$

The results of the determination of bond parameters of F_2 are given in Table 13.1. The calculated results are based on first principles and given in closed-form, exact equations containing fundamental constants only. The agreement between the experimental and calculated results is excellent.

CHLORINE MOLECULE

The chlorine molecule can be formed by the reaction of two chlorine atoms:

$$Cl + Cl \rightarrow Cl_2 \tag{13.752}$$

The chlorine molecule can be solved by using the hybridization approach used to solve the methane series $CH_{n=1,2,3,4}$. In the methane series, the $2s$ and $2p$ shells of carbon hybridize to form a single $2sp^3$ shell to achieve an energy minimum, and in a likewise manner, the $3s$ and $3p$ shells of chlorine hybridize to form a single $3sp^3$ shell which forms the bonding orbital of Cl_2.

FORCE BALANCE OF Cl_2

Cl_2 has two spin-paired electrons in a chemical bond between the chlorine atoms. The Cl_2 molecular orbital (MO) is determined by considering properties of the binding atoms and the boundary constraints. The prolate spheroidal H_2 MO developed in the Nature of the Chemical Bond of Hydrogen-Type Molecules section satisfies the boundary constraints; thus, each Cl atom could contribute a $3p$ electron to form a σ MO (H_2-type ellipsoidal MO) as in the case of N_2, O_2, and F_2. However, such a bond is not possible with the outer Cl electrons in their ground state since the resulting $3p$ shells of chlorine atoms would overlap which is not energetically stable. Thus, when bonding, the chlorine $3s$ and $3p$ shells hybridize to form a single $3sp^3$ shell to achieve an energy minimum.

The Cl electron configuration given in the Seventeen-Electron Atoms section is $1s^2 2s^2 2p^6 3s^2 3p^5$, and the orbital arrangement is:

3p state

$$\underset{1}{\underline{\uparrow\downarrow}}\quad \underset{0}{\underline{\uparrow\downarrow}}\quad \underset{-1}{\underline{\uparrow}} \tag{13.753}$$

corresponding to the ground state $^2P^0_{3/2}$. The radius r_{17} of the $3p$ shell given by Eq. (10.363) is:

$$r_{17} = 1.05158a_0 \tag{13.754}$$

The energy of the chlorine $3p$ shell is the negative of the ionization energy of the chlorine atom given by Eq. (10.364). Experimentally, the energy is [6]:

$$E(3p\ shell) = -E(ionization;\ Cl) = -12.96764\ eV \tag{13.755}$$

The $Cl3s$ atomic orbital (AO) combines with the $Cl3p$ AOs to form a single $3sp^3$ hybridized orbital (HO) with the orbital arrangement.

$3sp^3$ state

$$\underset{0,0}{\underline{\uparrow\downarrow}}\quad \underset{1,-1}{\underline{\uparrow\downarrow}}\quad \underset{1,0}{\underline{\uparrow\downarrow}}\quad \underset{1,1}{\underline{\uparrow}} \tag{13.756}$$

where the quantum numbers (ℓ, m_ℓ) are below each electron. The total energy of the state is given by the sum over the seven electrons. Using only the largest-force terms of the outer most and next inner shell, the calculated energies for the chlorine atom and the ions: Cl, Cl^+, Cl^{2+}, Cl^{3+}, Cl^{4+}, Cl^{5+} and Cl^{6+} are given in Eqs. (10.363-10.364), (10.353-10.354), (10.331-10.332), (10.309-10.310), (10.288-10.289), (10.255-10.256), and (10.235-10.236), respectively. The sum $E_T\left(Cl,3sp^3\right)$ of the experimental energies of Cl and these ions is [6]:

$$E_T\left(Cl,3sp^3\right)=\begin{pmatrix}12.96764\ eV+23.814\ eV+39.61\ eV+53.4652\ eV\\ +67.8\ eV+97.03\ eV+114.1958\ eV\end{pmatrix}=408.88264\ eV \tag{13.757}$$

The spin and orbital-angular-momentum interactions cancel such that the energy of the $E_T\left(Cl,3sp^3\right)$ is purely Coulombic. By considering that the central field decreases by an integer for each successive electron of the shell, the radius r_{3sp^3} of the $Cl3sp^3$ shell may be calculated from the Coulombic energy using Eq. (10.102):

$$r_{3sp^3}=\sum_{n=10}^{16}\frac{(Z-n)e^2}{8\pi\varepsilon_0\left(e408.8826\ eV\right)}=\frac{28e^2}{8\pi\varepsilon_0\left(e408.8826\ eV\right)}=0.93172a_0 \tag{13.758}$$

where $Z=17$. Using Eqs. (10.102) and (13.758), the Coulombic energy $E_{Coulomb}\left(Cl,3sp^3\right)$ of the outer electron of the $Cl3sp^3$ shell is:

$$E_{Coulomb}\left(Cl,3sp^3\right)=\frac{-e^2}{8\pi\varepsilon_0 r_{3sp^3}}=\frac{-e^2}{8\pi\varepsilon_0 0.93172a_0}=-14.60295\ eV \tag{13.759}$$

The calculated energy of the $C2sp^3$ shell of $14.63489\ eV$ given by Eq. (13.428), and nitrogen's calculated energy of $14.61664\ eV$ given by Eq. (10.143) is a close match with $E_{Coulomb}\left(Cl,3sp^3\right)$.

The unpaired $Cl3sp^3$ electrons from each of two chlorine atoms combine to form a molecular orbital. The nuclei of the Cl atoms are along the internuclear axis and serve as the foci. Due to symmetry, the other Cl electrons are equivalent to point charges at the origin. (See Eqs. (19-38) of Appendix II.) Thus, the energies in the Cl MO involve only the two $Cl3sp^3$ electrons. The forces are determined by these energies.

As in the case of H_2, the MO is a prolate spheroid with the exception that the ellipsoidal MO surface cannot extend into $Cl3sp^3$ HO for distances shorter than the radius of the $Cl3sp^3$ shell of each atom. Thus, the MO surface comprises a partial prolate spheroid in between the nuclei and is continuous with the $Cl3sp^3$ shell at each Cl atom. The energy of the H_2-type ellipsoidal MO is matched to that of the $Cl3sp^3$ shell. As in the case with OH, NH, and CH (where the latter also demonstrates sp^3 hybridization) the linear combination of the H_2-type ellipsoidal MO with each $Cl3sp^3$ HO must involve a 25% contribution from the H_2-type ellipsoidal MO to the $Cl3sp^3$ HO in order to match potential, kinetic, and orbital energy relationships. Thus, the Cl_2 MO must comprise two $Cl3sp^3$ HOs and 75% of a H_2-type ellipsoidal MO divided between the two $Cl3sp^3$ HOs:

$$2\ Cl3sp^3+0.75\ H_2\ MO\rightarrow Cl_2\ MO \tag{13.760}$$

The force balance of the Cl_2 MO is determined by the boundary conditions that arise from the linear combination of orbitals according to Eq. (13.760) and the energy matching condition between the H_2-type-ellipsoidal-MO and $Cl3sp^3$-HO components of the MO.

As in the case with OH (Eq. (13.57)), NH (Eq. (13.247)), and CH (Eq. (13.429)), the H_2-type ellipsoidal MO comprises 75% of the Cl_2 MO; so, the electron charge density in Eq. (11.65) is given by $-0.75e$. Since the chlorine atoms of Cl_2 are hybridized and the k parameter is different from unity in order to meet the boundary constraints, both k and k' must comprise the corresponding hybridization factors. (In contrast, the chlorine atom of a $C-Cl$ bond of an alkyl chloride is not hybridized, and only k' must comprise the corresponding hybridization factor.) The force constant k' to determine the ellipsoidal parameter c' in terms of the central force of the foci is given by Eq. (13.59), except that k' is divided by two since the H_2-type-ellipsoidal-MO is physically divided between two $Cl3sp^3$ HOs. In addition, the energy matching at both $Cl3sp^3$ HOs further requires that k' be corrected with the hybridization factor given by Eq. (13.762). Thus, k' of the H_2-type-ellipsoidal-MO component of the Cl_2 MO is:

$$k'=C_{Cl3sp^3HO}\frac{(0.75)}{2}\frac{2e^2}{4\pi\varepsilon_0}=0.93172\frac{(0.75)}{2}\frac{2e^2}{4\pi\varepsilon_0} \tag{13.761}$$

The distance from the origin to each focus c' is given by Eq. (13.60). The internuclear distance is given by Eq. (13.61). The length of the semiminor axis of the prolate spheroidal $Cl-Cl$-bond $b=c$ is given by Eq. (13.62). The eccentricity, e, is given by Eq. (13.63). The solution of the semimajor axis a then allows for the solution of the other axes of each prolate spheroid and eccentricity of the Cl_2 MO. Since the Cl_2 MO comprises a H_2-type-ellipsoidal MO that transitions to the $Cl3sp^3$ HOs at each end of the molecule, the energy $E\left(Cl,3sp^3\right)$ in Eq. (13.759) adds to that of the H_2-type ellipsoidal MO to give the total energy of the Cl_2 MO. From the energy equation and the relationship between the axes, the dimensions of the Cl_2 MO are solved.

The energy components of V_e, V_p, T, and V_m are those of H_2 (Eqs. (11.207-11.211)) except that they are corrected for electron hybridization. Hybridization gives rise to the $Cl3sp^3$ HO-shell Coulombic energy $E_{Coulomb}\left(Cl,3sp^3\right)$ given by Eq. (13.759). To meet the equipotential condition of the union of the H_2-type-ellipsoidal-MO with each $Cl3sp^3$ HO, the electron energies are normalized by the ratio of $14.60295\,eV$, the magnitude of $E_{Coulomb}\left(Cl,3sp^3\right)$ given by Eq. (13.759), and $13.605804\,eV$, the magnitude of the Coulombic energy between the electron and proton of H given by Eq. (1.264). This normalizes the energies to match that of the Coulombic energy alone to meet the energy matching condition of the Cl_2 MO under the influence of the two $Cl3sp^3$ HOs bridged by the H_2-type-ellipsoidal MO. The hybridization energy factor C_{Cl3sp^3HO} is:

$$C_{Cl3sp^3HO}=\frac{\frac{e^2}{8\pi\varepsilon_0 a_0}}{\frac{e^2}{8\pi\varepsilon_0 r_{3sp^3}}}=\frac{\frac{e^2}{8\pi\varepsilon_0 a_0}}{\frac{e^2}{8\pi\varepsilon_0 0.93172a_0}}$$
$$=\frac{13.605804\ eV}{14.60295\ eV}=0.93172 \tag{13.762}$$

The total energy $E_T\left(Cl_2\right)$ of the Cl_2 MO is given by the sum of the energies of the orbitals, the H_2-type ellipsoidal MO and the two $Cl3sp^3$ HOs, that form the hybridized Cl_2 MO. $E_T\left(Cl_2\right)$ follows from Eq. (13.74) for OH, but the energy of the $Cl3sp^3$ HO given by Eq. (13.759) is substituted for the energy of O and the H_2-type-ellipsoidal-MO energies are those of H_2 (Eqs. (11.207-11.212)) multiplied by the electron hybridization factor rather than by the factor of 0.75:

$$E_T\left(Cl_2\right)=E_T+E_{Coulomb}\left(Cl,3sp^3\right)$$
$$=-\frac{e^2}{8\pi\varepsilon_0 c'}\left[(0.93172)\left(2-\frac{1}{2}\frac{a_0}{a}\right)\ln\frac{a+c'}{a-c'}-1\right]-14.60295\ eV \tag{13.763}$$

To match the boundary condition that the total energy of the entire the H_2-type ellipsoidal MO is given by Eqs. (11.212) and (13.75), $E_T\left(Cl_2\right)$ given by Eq. (13.763) is set equal to Eq. (13.75):

$$E_T\left(Cl_2\right)=-\frac{e^2}{8\pi\varepsilon_0 c'}\left[(0.93172)\left(2-\frac{1}{2}\frac{a_0}{a}\right)\ln\frac{a+c'}{a-c'}-1\right]-14.60295\ eV$$
$$=-31.63537\ eV \tag{13.764}$$

From the energy relationship given by Eq. (13.764) and the relationship between the axes given by Eqs. (13.60-13.63), the dimensions of the Cl_2 MO can be solved.

Substitution of Eqs. (13.60) and (13.761) into Eq. (13.764) gives:

$$\frac{e^2}{8\pi\varepsilon_0\sqrt{\frac{4aa_0}{3(0.93172)}}}\left[(0.93172)\left(2-\frac{1}{2}\frac{a_0}{a}\right)\ln\frac{a+\sqrt{\frac{4aa_0}{3(0.93172)}}}{a-\sqrt{\frac{4aa_0}{3(0.93172)}}}-1\right]=e17.03242 \tag{13.765}$$

The most convenient way to solve Eq. (13.765) is by the reiterative technique using a computer. The result to within the round-off error with five-significant figures is:

$$a=2.46500a_0=1.30442\ X\ 10^{-10}\ m \tag{13.766}$$

Substitution of Eq. (13.766) into Eq. (13.60) gives:

$$c'=1.87817a_0=9.93887\ X\ 10^{-11}\ m \tag{13.767}$$

The internuclear distance given by multiplying Eq. (13.767) by two is:

$$2c' = 3.75635a_0 = 1.98777\ X\ 10^{-10}\ m \tag{13.768}$$

The experimental bond distance is [28] :

$$2c' = 1.988\ X\ 10^{-10}\ m \tag{13.769}$$

Substitution of Eqs. (13.766-13.767) into Eq. (13.62) gives:

$$b = c = 1.59646a_0 = 8.44810\ X\ 10^{-11}\ m \tag{13.770}$$

Substitution of Eqs. (13.766-13.767) into Eq. (13.63) gives:

$$e = 0.76194 \tag{13.771}$$

The Cl nuclei comprise the foci of the H_2-type ellipsoidal MO. The parameters of the point of intersection of the H_2-type ellipsoidal MO and the $Cl3sp^3$ HO are given by Eqs. (13.84-13.95) and (13.261-13.270). The polar intersection angle θ' is given by Eq. (13.261) where $r_n = r_{3sp^3} = 0.93172a_0$ is the radius of the $Cl3sp^3$ shell. Substitution of Eqs. (13.766-13.767) into Eq. (13.261) gives

$$\theta' = 81.72° \tag{13.772}$$

Then, the angle θ_{Cl3sp^3HO} the radial vector of the $Cl3sp^3$ HO makes with the internuclear axis is:

$$\theta_{Cl3sp^3HO} = 180° - 81.72° = 98.28° \tag{13.773}$$

as shown in Figure 13.20. The Cartesian $\mathbf{i}$-coordinate of the interception point of the MO and the AO can be calculated using the MO ellipsoidal parameters by first calculating the parametric angle in Eq. (11.83) that matches Cartesian $\mathbf{j}$-coordinate components at the point of intersection. Thus, the matching elliptic parametric angle $\omega t = \theta_{H_2MO}$ satisfies the following relationship:

$$r_{3sp^3} \sin\theta_{Cl3sp^3HO} = 0.93172a_0 \sin\theta_{Cl3sp^3HO} = b \sin\theta_{H_2MO} \tag{13.774}$$

such that

$$\theta_{H_2MO} = \sin^{-1}\frac{0.93172a_0 \sin\theta_{Cl3sp^3HO}}{b} = \sin^{-1}\frac{0.93172a_0 \sin 98.28°}{b} \tag{13.775}$$

with the use of Eq. (13.773). Substitution of Eq. (13.770) into Eq. (13.775) gives:

$$\theta_{H_2MO} = 35.28° \tag{13.776}$$

Then, the distance d_{H_2MO} along the internuclear axis from the origin of H_2-type ellipsoidal MO to the point of intersection of the orbitals is given by:

$$d_{H_2MO} = a\cos\theta_{H_2MO} \tag{13.777}$$

Substitution of Eqs. (13.766) and (13.776) into Eq. (13.777) gives:

$$d_{H_2MO} = 2.01235a_0 = 1.06489\ X\ 10^{-10}\ m \tag{13.778}$$

The distance d_{Cl3sp^3HO} along the internuclear axis from the origin of each Cl atom to the point of intersection of the orbitals is given by:

$$d_{Cl3sp^3HO} = d_{H_2MO} - c' \tag{13.779}$$

Substitution of Eqs. (13.768) and (13.778) into Eq. (13.779) gives:

$$d_{Cl3sp^3HO} = 0.13417a_0 = 7.10022\ X\ 10^{-12}\ m \tag{13.780}$$

As shown in Eq. (13.760), a factor of 0.25 of the charge-density of the H_2-type ellipsoidal MO is distributed on each $Cl3sp^3$ HO. Using the orbital composition of Cl_2 (Eq. (13.760)), the radii of the $Cl1s = 0.05932a_0$ (Eq. (10.51)), $Cl2s = 0.25344a_0$ (Eq. (10.62)), $Cl2p = 0.31190a_0$ (Eq. (10.212)), and $Cl3sp^3 = 0.93172a_0$ (Eq. (13.758)) shells, and the parameters of the Cl_2 MO given by Eqs. (13.3-13.4), (13.766-13.768), and (13.770-13.771), the dimensional diagram and charge-density of the Cl_2 MO comprising the linear combination of the H_2-type ellipsoidal MO and two $Cl3sp^3$ HOs according to Eq. (13.760) are shown in Figures 13.20 and 13.21, respectively.

Figure 13.20. The cross section of the Cl_2 MO showing the axes, angles, and point of intersection of the H_2-type ellipsoidal MO with the two $Cl3sp^3$ HOs. The continuation of the H_2-type-ellipsoidal-MO basis element beyond the intersection point with each $Cl3sp^3$ shell is shown as dashed since it only serves to solve the energy match with each $Cl3sp^3$ shell and does not represent charge density. Similarly, the vertical dashed line only designates the parameters of the intersection points. The actual charge density is shown by the solid lines. Legend: a: semimajor axis, b: semiminor axis, c': internuclear distance, $d_1 : d_{H_2MO}$, $\theta_1 : \theta_{Cl3sp^3HO}$, $d_2 : d_{Cl3sp^3HO}$, and $R : r_{3sp^3}$.

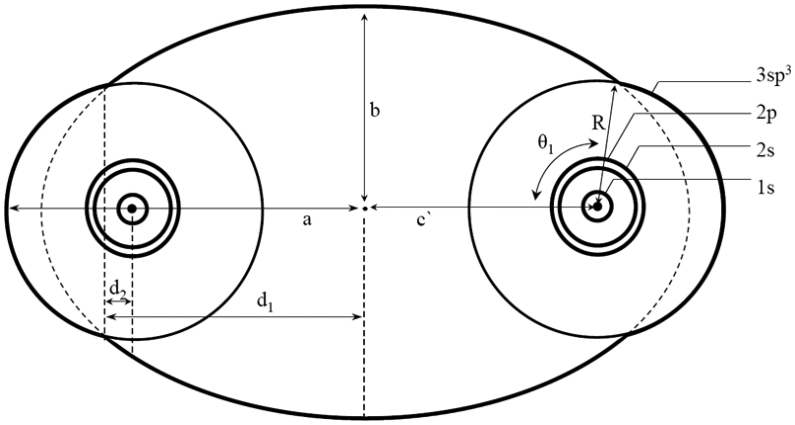

Figure 13.21. Cl_2 MO comprising the superposition of the H_2-type ellipsoidal MO and the two $Cl3sp^3$ HOs, each with a relative charge-density of 0.75 to 1.25 divided between the former and the latter; otherwise, the $Cl3sp^3$ HO is unchanged. (A) Side-on, color scale, translucent view of the charge-density of the Cl_2 MO. The ellipsoidal surface of the H_2-type ellipsoidal MO that transitions to the $Cl3sp^3$ HO, the $Cl3sp^3$ HO, and the $Cl1s$, $Cl2s$, and $Cl2p$ shells of each Cl atom are shown. (B) Cut-away view showing the inner most $Cl1s$ shell, and moving radially, the $Cl2s$, $Cl2p$, and $Cl3sp^3$ shells, and the H_2-type ellipsoidal MO that transitions to the $Cl3sp^3$ HOs.

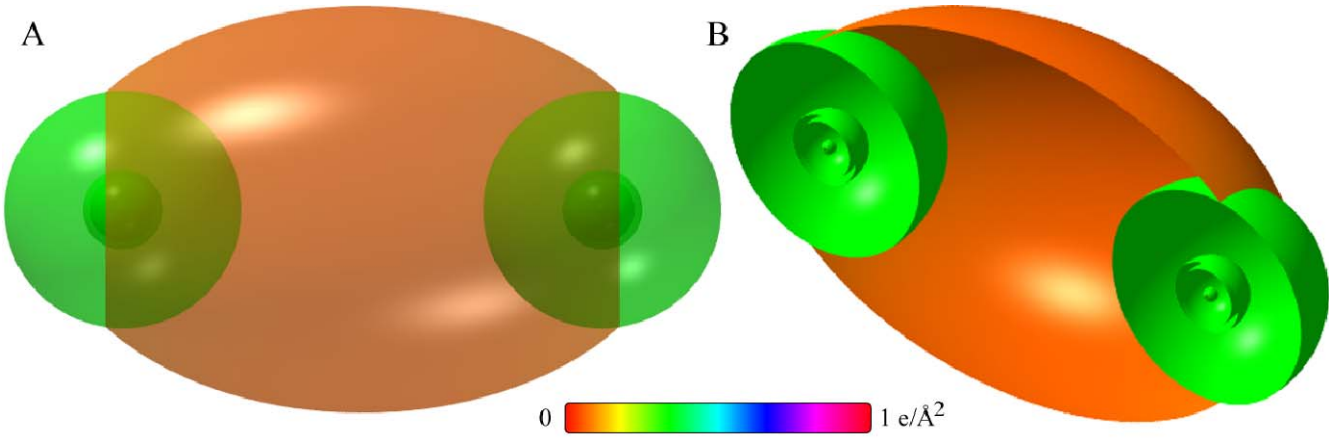

ENERGIES OF Cl_2

The energies of Cl_2 are given by the substitution of the semiprincipal axes (Eqs. (13.766-13.767) and (13.770)) into the energy equations, (Eq. (13.763) and Eqs. (11.207-11.211) of H_2) that are corrected for electron hybridization using Eq. (13.762).

$$V_e = (0.93172)\frac{-2e^2}{8\pi\varepsilon_0\sqrt{a^2-b^2}}\ln\frac{a+\sqrt{a^2-b^2}}{a-\sqrt{a^2-b^2}} = -27.02007\ eV \tag{13.781}$$

$$V_p = \frac{e^2}{8\pi\varepsilon_0\sqrt{a^2-b^2}} = 7.24416\ eV \tag{13.782}$$

$$T = (0.93172)\frac{\hbar^2}{2m_e a\sqrt{a^2-b^2}}\ln\frac{a+\sqrt{a^2-b^2}}{a-\sqrt{a^2-b^2}} = 5.48074\ eV \tag{13.783}$$

$$V_m = (0.93172)\frac{-\hbar^2}{4m_e a\sqrt{a^2-b^2}}\ln\frac{a+\sqrt{a^2-b^2}}{a-\sqrt{a^2-b^2}} = -2.74037\ eV \tag{13.784}$$

$$E_T\left({}^{35}Cl_2\right) = -\frac{e^2}{8\pi\varepsilon_0 c'}\left[(0.93172)\left(2-\frac{1}{2}\frac{a_0}{a}\right)\ln\frac{a+c'}{a-c'}-1\right] - 14.60295\ eV = -31.63537\ eV \tag{13.785}$$

where $E_T(Cl_2)$ is given by Eq. (13.763) which is reiteratively matched to Eq. (13.75) within five-significant-figure round-off error.

VIBRATION AND ROTATION OF Cl_2

In Cl_2, the division of the H_2-type ellipsoidal MO between the two $Cl3sp^3$ HOs and the hybridization must be considered in determining the vibrational parameters. One approach is to use Eq. (13.761) for the force constant and r_{3sp^3} given by Eq. (13.758) for the distance parameter of the central force in Eq. (11.213) since the H_2-type ellipsoidal MO is energy matched to the $Cl3sp^3$ HOs. With the substitution of the Cl_2 parameters in Eqs. (11.213-11.217), the angular frequency of the oscillation is:

$$\begin{aligned}\omega &= \sqrt{\frac{0.93172\frac{(0.75)}{2}\frac{e^2}{8\pi\varepsilon_0\left(r_{3sp^3}\right)^3}-\frac{e^2}{8\pi\varepsilon_0\left(r_{3sp^3}+c'\right)^3}}{\mu}} \\ &= \sqrt{\frac{0.93172\frac{(0.75)}{2}\frac{e^2}{8\pi\varepsilon_0(0.93172)^3}-\frac{e^2}{8\pi\varepsilon_0(0.93172a_0+1.87817a_0)^3}}{\frac{35}{2}m_p}} = 1.01438\ X\ 10^{14}\ rad/s\end{aligned} \tag{13.786}$$

where c' is given by Eq. (13.767), and the reduced mass of ${}^{35}Cl_2$ is given by:

$$\mu_{{}^{35}Cl_2} = \frac{m_1 m_2}{m_1+m_2} = \frac{(35)(35)}{35+35}m_p \tag{13.787}$$

where m_p is the proton mass. Thus, during bond formation, the perturbation of the orbit determined by an inverse-squared force results in simple harmonic oscillatory motion of the orbit, and the corresponding frequency, $\omega(0)$, for ${}^{35}Cl_2$ given by Eqs. (11.136), (11.148), and (13.786) is:

$$\omega(0) = \sqrt{\frac{k(0)}{\mu}} = \sqrt{\frac{301.19\ Nm^{-1}}{\mu}} = 1.01438\ X\ 10^{14}\ radians/s \tag{13.788}$$

where the reduced nuclear mass of ${}^{35}Cl_2$ is given by Eq. (13.787) and the spring constant, $k(0)$, given by Eqs. (11.136) and (13.786) is:

$$k(0) = 301.19\ Nm^{-1} \tag{13.789}$$

The ${}^{35}Cl_2$ transition-state vibrational energy, $E_{vib}(0)$ or ω_e, given by Planck's equation (Eq. (11.127)) is:

$$E_{vib}(0) = \omega_e = \hbar\omega = \hbar 1.01438\ X\ 10^{14}\ rad/s = 0.06677\ eV = 538.52\ cm^{-1} \tag{13.790}$$

ω_e, from the experimental curve fit of the vibrational energies of $^{35}Cl_2$ is [28] :

$$\omega_e = 559.7\ cm^{-1} \tag{13.791}$$

Using Eqs. (13.112-13.118) with $E_{vib}(0)$ given by Eq. (13.790) and D_0 given by Eq. (13.807), the $^{35}Cl_2$ $\upsilon = 1 \rightarrow \upsilon = 0$ vibrational energy, $E_{vib}(1)$ is:

$$E_{vib}(1) = 0.0659\ eV \qquad (531.70\ cm^{-1}) \tag{13.792}$$

The experimental vibrational energy of $^{35}Cl_2$ using ω_e and $\omega_e x_e$ [28] according to K&P [15] is:

$$E_{vib}(1) = 0.0664\ eV \qquad (535.55\ cm^{-1}) \tag{13.793}$$

Using Eq. (13.113) with $E_{vib}(1)$ given by Eq. (13.792) and D_0 given by Eq. (13.807), the anharmonic perturbation term, $\omega_0 x_0$, of $^{35}Cl_2$ is:

$$\omega_0 x_0 = 3.41\ cm^{-1} \tag{13.794}$$

The experimental anharmonic perturbation term, $\omega_0 x_0$, of $^{35}Cl_2$ [28] is:

$$\omega_0 x_0 = 2.68\ cm^{-1} \tag{13.795}$$

The vibrational energies of successive states are given by Eqs. (13.790), (13.112), and (13.794).

Using Eqs. (13.133-13.134) and the internuclear distance, $r = 2c'$, and reduced mass of $^{35}Cl_2$ given by Eqs. (13.768) and (13.787), respectively, the corresponding B_e is:

$$B_e = 0.2420\ cm^{-1} \tag{13.796}$$

The experimental B_e rotational parameter of $^{35}Cl_2$ is [28]:

$$B_e = 0.2440\ cm^{-1} \tag{13.797}$$

THE DOPPLER ENERGY TERMS OF Cl_2

The equations of the radiation reaction force of the symmetrical Cl_2 MO are the given by Eqs. (11.231-11.233) with the substitution of the Cl_2 parameters and the substitution of the force factor of Eq. (13.761). The angular frequency of the reentrant oscillation in the transition state is:

$$\omega = \sqrt{\frac{0.93172\frac{(0.75)}{2}\frac{e^2}{4\pi\varepsilon_0 a^3}}{m_e}} = 6.31418\ X\ 10^{15}\ rad/s \tag{13.798}$$

where a is given by Eq. (13.766). The kinetic energy, E_K, is given by Planck's equation (Eq. (11.127)).

$$\bar{E}_K = \hbar\omega = \hbar 1.6.31418\ X\ 10^{15}\ rad/s = 4.15610\ eV \tag{13.799}$$

In Eq. (11.181), substitution of the total energy of Cl_2, $E_T(Cl_2)$, (Eq. (13.764)) for $E_{h\nu}$, the mass of the electron, m_e, for M, and the kinetic energy given by Eq. (13.799) for $\bar{E}_K$ gives the Doppler energy of the electrons for the reentrant orbit:

$$\bar{E}_D \cong E_{h\nu}\sqrt{\frac{2\bar{E}_K}{Mc^2}} = -31.63537\ eV\sqrt{\frac{2e(4.15610\ eV)}{m_e c^2}} = -0.12759\ eV \tag{13.800}$$

In addition to the electrons, the nuclei also undergo simple harmonic oscillation in the transition state at their corresponding frequency. The decrease in the energy of Cl_2 due to the reentrant orbit in the transition state corresponding to simple harmonic oscillation of the electrons and nuclei, $\bar{E}_{osc}$, is given by the sum of the corresponding energies, $\bar{E}_D$ given by Eq. (13.800) and $\bar{E}_{Kvib}$, the average kinetic energy of vibration which is 1/2 of the vibrational energy of Cl_2. Using the experimental $^{35}Cl_2$ ω_e of 559.7 cm^{-1} $(0.06939\ eV)$ [28] for $\bar{E}_{Kvib}$ of the transition state, $\bar{E}_{osc}(^{35}Cl_2)$ is:

$$\bar{E}_{osc}(^{35}Cl_2) = \bar{E}_D + \bar{E}_{Kvib} = \bar{E}_D + \frac{1}{2}\hbar\sqrt{\frac{k}{\mu}} \tag{13.801}$$

$$\bar{E}_{osc}(^{35}Cl_2) = -0.12759\ eV + \frac{1}{2}(0.06939\ eV) = -0.09289\ eV \tag{13.802}$$

TOTAL AND BOND ENERGIES OF Cl_2

$E_{T+osc}\left({}^{35}Cl_2\right)$, the total energy of the ${}^{35}Cl_2$ radical including the Doppler term, is given by the sum of $E_T\left(Cl_2\right)$ (Eq. (13.764)) and $\overline{E}_{osc}\left({}^{35}Cl_2\right)$ given by Eq. (13.802).

$$E_{T+osc}\left({}^{35}Cl_2\right)=V_e+T+V_m+V_p+E_{Coulomb}\left(Cl,3sp^3\right)+\overline{E}_{osc}\left({}^{35}Cl_2\right)=E_T\left(Cl_2\right)+\overline{E}_{osc}\left({}^{35}Cl_2\right) \tag{13.803}$$

$$\begin{aligned}E_{T+osc}\left({}^{35}Cl_2\right)&=\left\{\left(\frac{-e^2}{8\pi\varepsilon_0 c'}\left[\left(0.93172\right)\left(2-\frac{1}{2}\frac{a_0}{a}\right)\ln\frac{a+c'}{a-c'}-1\right]-14.60295\ eV\right)\right\}\\&\quad+\left\{\left(\sqrt{1+\sqrt{\frac{2\hbar\sqrt{\frac{0.93172\frac{\left(0.75\right)}{2}\frac{e^2}{4\pi\varepsilon_0 a^3}}{m_e}}}{m_e c^2}}}\right)+\frac{1}{2}\hbar\sqrt{\frac{k}{\mu}}\right\}\\&=-31.63537\ eV-0.12759\ eV+\frac{1}{2}\hbar\sqrt{\frac{k}{\mu}}\end{aligned} \tag{13.804}$$

From Eqs. (13.801-13.804), the total energy of ${}^{35}Cl_2$ is:

$$\begin{aligned}E_{T+osc}\left({}^{35}Cl_2\right)&=-31.63537\ eV+\overline{E}_{osc}\left({}^{35}Cl_2\right)\\&=-31.63537\ eV-0.12759\ eV+\frac{1}{2}\left(0.06939\ eV\right)=-31.72826\ eV\end{aligned} \tag{13.805}$$

where the experimental ω_e (Eq. (13.791)) was used for the $\hbar\sqrt{\frac{k}{\mu}}$ term.

The Cl_2 bond dissociation energy, $E_D\left({}^{35}Cl_2\right)$, is given by the difference between the total energies of the two $Cl3sp^3$ HOs and $E_{T+osc}\left({}^{35}Cl_2\right)$:

$$E_D\left({}^{35}Cl_2\right)=2E_{Coulomb}\left(Cl,3sp^3\right)-E_{T+osc}\left({}^{35}Cl_2\right) \tag{13.806}$$

$E_{Coulomb}\left(Cl,3sp^3\right)$ is given by Eq. (13.759); thus, the ${}^{35}Cl_2$ bond dissociation energy, $E_D\left({}^{35}Cl_2\right)$, given by Eqs. (13.759) and (13.805-13.806) is

$$E_D\left({}^{35}Cl_2\right)=-2\left(14.60295\ eV\right)-E_{T+osc}\left({}^{35}Cl_2\right)=-29.20590\ eV-\left(-31.72826\ eV\right)=2.52236\ eV \tag{13.807}$$

The experimental ${}^{35}Cl_2$ bond dissociation energy is [49]:

$$E_D\left({}^{35}Cl_2\right)=2.51412\ eV \tag{13.808}$$

The results of the determination of bond parameters of Cl_2 are given in Table 13.1. The calculated results are based on first principles and given in closed-form, exact equations containing fundamental constants only. The agreement between the experimental and calculated results is excellent.

CARBON NITRIDE RADICAL

The carbon nitride radical can be formed by the reaction of carbon and nitrogen atoms:

$$C+N\rightarrow CN \tag{13.809}$$

The bond in carbon nitride radical comprises a H_2-type molecular orbital (MO) with two paired electrons. The force balance equations and radii, r_6 and r_7, of the $2p$ shell of C and N are derived in the Six-Electron Atoms section and Seven-Electron Atoms section, respectively. With the formation of the H_2-type MO by the contribution of a $2p$ electron from each of the C and N atoms, a diamagnetic force arises between the remaining $2p$ electrons of each atom and the H_2-type MO. This force from each atom causes the H_2-type MO to move to greater principal axes than would result with the Coulombic force alone. But, the integer increase of the central field and the resulting increased Coulombic as well as magnetic central forces on the remaining $2p$ electrons of each atom decrease the radii of the corresponding shells such that the energy minimum is achieved that is lower than that of the reactant atoms. The resulting electron configuration of CN is $C1s^2N1s^2C2s^2N2s^2C2p^1N2p^2\sigma_{C,N}^2$ where σ designates the H_2-type MO, and the orbital arrangement is:

σ state

$\underline{\uparrow\downarrow}$

2p state

$\underline{\uparrow}$ $\underline{\uparrow\downarrow}$

0 0

2s state

$\underline{\uparrow\downarrow}$ $\underline{\uparrow\downarrow}$

1s state

$\underline{\uparrow\downarrow}$ $\underline{\uparrow\downarrow}$

C N (13.810)

The carbon nitride radical is predicted to be weakly paramagnetic.

FORCE BALANCE OF THE $2p$ SHELL OF THE CARBON ATOM OF THE CARBON NITRIDE RADICAL

For the C atom, force balance for the outermost $2p$ electron of CN (electron 5) is achieved between the centrifugal force and the Coulombic and magnetic forces that arise due to interactions between electron 5 and the $2s$-shell electrons due to spin and orbital angular momentum. The forces used are derived in the Six-Electron Atoms section. The central Coulomb force on the outer-most $2p$ shell electron of CN (electron 5) due to the nucleus and the inner four electrons is given by Eq. (10.70) with the appropriate charge and radius:

$$\mathbf{F}_{ele} = \frac{(Z-4)e^2}{4\pi\varepsilon_0 r_5^2}\mathbf{i}_{\mathbf{r}} \tag{13.811}$$

for $r > r_4$. The $2p$ shell possess an external electric field given by Eq. (10.92) for $r > r_5$.

The single unpaired carbon $2p$ electron gives rise to a diamagnetic force on the σ-MO as given by Eqs. (13.835-13.839). The corresponding Newtonian reaction force cancels $\mathbf{F}_{diamagnetic}$, of Eq. (10.82). The energy is minimized with conservation of angular momentum. This condition is met when:

$$\mathbf{F}_{diamagnetic} = 0 \tag{13.812}$$

And, $\mathbf{F}_{mag\ 2}$ corresponding to the maximum orbital angular momentum of the three $2p$ orbitals given by Eq. (10.89) is:

$$\mathbf{F}_{mag\ 2} = \frac{1}{Z}\frac{3\hbar^2}{m_e r_5^2 r_3}\sqrt{s(s+1)}\mathbf{i}_{\mathbf{r}} \tag{13.813}$$

The electric field external to the $2p$ shell given by Eq. (10.92) for $r > r_5$ gives rise to a second diamagnetic force, $\mathbf{F}_{diamagnetic\ 2}$, given by Eq. (10.93). $\mathbf{F}_{diamagnetic\ 2}$ due to the binding of the p-orbital electron having an electric field of +1 outside of its radius is:

$$\mathbf{F}_{diamagnetic\ 2} = -\left[\frac{Z-5}{Z-4}\right]\left(1-\frac{\sqrt{2}}{2}\right)\frac{r_3\hbar^2}{m_e r_5^4}10\sqrt{s(s+1)}\mathbf{i}_{\mathbf{r}} \tag{13.814}$$

The radius of the $2p$ shell is calculated by equating the outward centrifugal force to the sum of the electric (Eq. (13.811)) and diamagnetic (Eqs. (13.812) and (13.814)), and paramagnetic (Eq. (13.813)) forces as follows:

$$\frac{m_e v_5^2}{r_5} = \left(\begin{array}{l}\dfrac{(Z-4)e^2}{4\pi\varepsilon_0 r_5^2} + \dfrac{3\hbar^2}{Z m_e r_5^2 r_3}\sqrt{s(s+1)} \\ -\left[\dfrac{Z-5}{Z-4}\right]\left(1-\dfrac{\sqrt{2}}{2}\right)\dfrac{r_3\hbar^2}{r_5^4 m_e}10\sqrt{s(s+1)}\end{array}\right) \tag{13.815}$$

Substitution of $v_5 = \dfrac{\hbar}{m_e r_5}$ (Eq. (1.35)) and $s = \dfrac{1}{2}$ into Eq. (13.815) gives:

$$\frac{\hbar^2}{m_e r_5^3} = \frac{(Z-4)e^2}{4\pi\varepsilon_0 r_5^2} + \frac{3\hbar^2}{Z m_e r_5^2 r_3}\sqrt{\frac{3}{4}} - \left[\frac{Z-5}{Z-4}\right]\left(1-\frac{\sqrt{2}}{2}\right)\frac{r_3\hbar^2}{r_5^4 m_e}10\sqrt{\frac{3}{4}} \tag{13.816}$$

The quadratic equation corresponding to Eq. (13.816) is:

$$r_5^2-\frac{\frac{\hbar^2}{m_e}}{\left(\frac{(Z-4)e^2}{4\pi\varepsilon_0}+\frac{3\hbar^2}{Zm_e r_3}\sqrt{\frac{3}{4}}\right)}r_5-\frac{\frac{\hbar^2}{m_e}\left[\frac{Z-5}{Z-4}\right]\left(1-\frac{\sqrt{2}}{2}\right)r_3 10\sqrt{\frac{3}{4}}}{\left(\frac{(Z-4)e^2}{4\pi\varepsilon_0}+\frac{3\hbar^2}{Zm_e r_3}\sqrt{\frac{3}{4}}\right)}=0 \tag{13.817}$$

The solution of Eq. (13.817) using the quadratic formula is:

$$r_5=\frac{\frac{a_0}{\left((Z-4)+\frac{3\sqrt{3}}{Z2r_3}\right)}\pm a_0\sqrt{\left(\frac{1}{\left((Z-4)+\frac{3\sqrt{3}}{Z2r_3}\right)}\right)^2+\frac{20\sqrt{3}\left(\left[\frac{Z-5}{Z-4}\right]\left(1-\frac{\sqrt{2}}{2}\right)r_3\right)}{\left((Z-4)+\frac{3\sqrt{3}}{Z2r_3}\right)}}}{2},\ r_3\ \textit{in units of}\ a_0 \tag{13.818}$$

The positive root of Eq. (13.818) must be taken in order that $r_5>0$. Substitution of $\frac{r_3}{a_0}=0.84317$ (Eq. (10.62) with $Z=6$) into Eq. (13.818) gives:

$$r_5=0.88084a_0 \tag{13.819}$$

FORCE BALANCE OF THE $2p$ SHELL OF THE NITROGEN ATOM OF THE CARBON NITRIDE RADICAL

For the N atom, force balance for the outermost $2p$ electron of CN (electron 6) is achieved between the centrifugal force and the Coulombic and magnetic forces that arise due to interactions between electron 6 and the other $2p$-shell as well as the $2s$-shell electrons due to spin and orbital angular momentum. The forces used are derived in the Seven-Electron Atoms section. The central Coulomb force on the outer-most $2p$ shell electron of CN (electron 6) due to the nucleus and the inner five electrons is given by Eq. (10.70) with the appropriate charge and radius:

$$\mathbf{F}_{ele}=\frac{(Z-5)e^2}{4\pi\varepsilon_0 r_6^2}\mathbf{i}_{\mathbf{r}} \tag{13.820}$$

for $r>r_5$. The $2p$ shell possess an external electric field given by Eq. (10.92) for $r>r_6$.

The forces to determine the radius of the $N2p$ shell of N in CN are the same as those of N in N_2 except that in CN there is a contribution from the Newtonian reaction force that arises from the single unpaired carbon $2p$ electron. The energy is minimized with conservation of angular momentum. This condition is met when $\mathbf{F}_{diamagnetic}$ of N in CN is canceled by the σ-MO -reaction force. Eq. (13.622) becomes:

$$\mathbf{F}_{diamagnetic}=0 \tag{13.821}$$

And, $\mathbf{F}_{mag\ 2}$ corresponding to the conserved orbital angular momentum of the three orbitals given by Eq. (10.89) is:

$$\mathbf{F}_{mag\ 2}=\frac{1}{Z}\frac{3\hbar^2}{m_e r_6^2 r_3}\sqrt{s(s+1)}\mathbf{i}_{\mathbf{r}} \tag{13.822}$$

The electric field external to the $2p$ shell given by Eq. (10.92) for $r>r_6$ gives rise to a second diamagnetic force, $\mathbf{F}_{diamagnetic\ 2}$, given by Eq. (10.93). $\mathbf{F}_{diamagnetic\ 2}$ due to the binding of the p-orbital electron having an electric field of +1 outside of its radius is:

$$\mathbf{F}_{diamagnetic\ 2}=-\left[\frac{Z-6}{Z-5}\right]\left(1-\frac{\sqrt{2}}{2}\right)\frac{r_3\hbar^2}{m_e r_6^4}10\sqrt{s(s+1)}\mathbf{i}_{\mathbf{r}} \tag{13.823}$$

The N forces $\mathbf{F}_{ele}$, $\mathbf{F}_{mag\ 2}$, $\mathbf{F}_{diamagnetic\ 2}$, and $\mathbf{F}_{mag\ 3}$ of CN are the same as those of N_2 given by Eqs. (13.621) and (13.623-13.624), respectively. In both cases, the contribution of a $2p$ electron from the N atom in the formation of the σ MO gives rise to a paramagnetic force on the remaining two $2p$ electrons that pair. Thus, the force, $\mathbf{F}_{mag\ 3}$ of CN, given by Eq. (13.625) is:

$$\mathbf{F}_{mag\ 3} = \frac{\hbar^2}{4m_e r_6^3}\sqrt{s(s+1)}\mathbf{i}_\mathbf{r} \tag{13.824}$$

The radius of the $2p$ shell is calculated by equating the outward centrifugal force to the sum of the electric (Eq. (13.820)) and diamagnetic (Eqs. (13.821) and (13.823)), and paramagnetic (Eqs. (13.822) and (13.824)) forces as follows:

$$\frac{m_e v_6^2}{r_6} = \begin{pmatrix} \frac{(Z-5)e^2}{4\pi\varepsilon_0 r_6^2} + \frac{3\hbar^2}{Zm_e r_6^2 r_3}\sqrt{s(s+1)} \\ -\left[\frac{Z-6}{Z-5}\right]\left(1-\frac{\sqrt{2}}{2}\right)\frac{r_3\hbar^2}{r_6^4 m_e}10\sqrt{s(s+1)} + \frac{\hbar^2}{4m_e r_6^3}\sqrt{s(s+1)} \end{pmatrix} \tag{13.825}$$

Substitution of $v_6 = \frac{\hbar}{m_e r_6}$ (Eq. (1.35)) and $s = \frac{1}{2}$ into Eq. (13.626) gives:

$$\frac{\hbar^2}{m_e r_6^3} - \frac{\hbar^2}{4m_e r_6^3}\sqrt{\frac{3}{4}} = \frac{(Z-5)e^2}{4\pi\varepsilon_0 r_6^2} + \frac{3\hbar^2}{Zm_e r_6^2 r_3}\sqrt{\frac{3}{4}} - \left[\frac{Z-6}{Z-5}\right]\left(1-\frac{\sqrt{2}}{2}\right)\frac{r_3\hbar^2}{r_6^4 m_e}10\sqrt{\frac{3}{4}} \tag{13.826}$$

The quadratic equation corresponding to Eq. (13.826) is

$$r_6^2 - \frac{\frac{\hbar^2}{m_e}\left(1-\frac{\sqrt{3}}{8}\right)}{\left(\frac{(Z-5)e^2}{4\pi\varepsilon_0} + \frac{3\hbar^2}{Zm_e r_3}\sqrt{\frac{3}{4}}\right)} r_6 - \frac{\frac{\hbar^2}{m_e}\left[\frac{Z-6}{Z-5}\right]\left(1-\frac{\sqrt{2}}{2}\right)r_3 10\sqrt{\frac{3}{4}}}{\left(\frac{(Z-5)e^2}{4\pi\varepsilon_0} + \frac{3\hbar^2}{Zm_e r_3}\sqrt{\frac{3}{4}}\right)} = 0 \tag{13.827}$$

The solution of Eq. (13.827) using the quadratic formula is:

$$r_6 = \frac{\frac{a_0\left(1-\frac{\sqrt{3}}{8}\right)}{\left((Z-5)+\frac{3\sqrt{3}}{Z2r_3}\right)} \pm a_0\sqrt{\left(\frac{1-\frac{\sqrt{3}}{8}}{\left((Z-5)+\frac{3\sqrt{3}}{Z2r_3}\right)}\right)^2 + \frac{20\sqrt{3}\left(\left[\frac{Z-6}{Z-5}\right]\left(1-\frac{\sqrt{2}}{2}\right)r_3\right)}{\left((Z-5)+\frac{3\sqrt{3}}{Z2r_3}\right)}}}{2},\ r_3 \textit{ in units of } a_0 \tag{13.828}$$

The positive root of Eq. (13.828) must be taken in order that $r_6 > 0$. Substitution of $\frac{r_3}{a_0} = 0.69385$ (Eq. (10.62) with $Z = 7$) into Eq. (13.828) gives:

$$r_6 = 0.76366a_0 \tag{13.829}$$

ENERGIES OF THE $2p$ SHELLS OF THE CARBON AND NITROGEN ATOMS OF THE CARBON NITRIDE RADICAL

The central forces on the $2p$ shell of the C and N atoms are increased with the formation of the σ MO which reduces each shell's radius and increases its total energy. The Coulombic energy terms of the total energy of the C and N atoms at the new radii are calculated and added to the energy of the σ MO to give the total energy of CN. Then, the bond energy is determined from the total CN energy.

The radius r_6 of the carbon atom before bonding is given by Eq. (10.122):

$$r_6 = 1.20654a_0 \tag{13.830}$$

Using the initial radius r_6 of the C atom and the final radius r_5 of the $C2p$ shell of CN (Eq. (13.819)) and by considering that the central Coulombic field decreases by an integer for each successive electron of the shell, the sum $E_T(CN, C2p)$ of the Coulombic energy change of the $C2p$ electron is determined using Eq. (10.102):

$$E_T\left(CN,C2p\right)=-\sum_{n=4}^{4}\frac{(Z-n)e^2}{8\pi\varepsilon_0}\left(\frac{1}{r_5}-\frac{1}{r_6}\right)=-\left(13.60580\ eV\right)\left(0.30647\right)\left(2\right)=-8.33948\ eV \tag{13.831}$$

The radius r_7 of the nitrogen atom before bonding is given by Eq. (10.142).

$$r_7=0.93084a_0 \tag{13.832}$$

Using the initial radius r_7 of the N atom and the final radius r_6 of the $N2p$ shell of CN (Eq. (13.829)) and by considering that the central Coulombic field decreases by an integer for each successive electron of the shell, the sum $E_T\left(CN,N2p\right)$ of the Coulombic energy change of the $N2p$ electron is determined using Eq. (10.102):

$$E_T\left(CN,N2p\right)=-\sum_{n=4}^{5}\frac{(Z-n)e^2}{8\pi\varepsilon_0}\left(\frac{1}{r_6}-\frac{1}{r_7}\right)=-\left(13.60580\ eV\right)\left(0.23518\right)\left(2+3\right)=-15.99929\ eV \tag{13.833}$$

FORCE BALANCE OF THE σ MO OF THE CARBON NITRIDE RADICAL

The diamagnetic force $\mathbf{F}_{diamagneticMO1}$ for the σ-MO of the CN molecule due to the two paired electrons in the $N2p$ shell given by Eq. (13.633) with $n_e=2$ is:

$$\mathbf{F}_{diamagneticMO1}=\frac{\hbar^2}{2m_ea^2b^2}D\mathbf{i}_\xi \tag{13.834}$$

The force $\mathbf{F}_{diamagneticMO2}$ is given by Eq. (13.634) except that the force is summed over the individual diamagnetic-force terms due to each component of angular momentum $\left|L_i\right|$ acting on the electrons of the σ-MO from each atom having a nucleus of charge Z_j at one of the foci of the σ-MO:

$$\mathbf{F}_{diamagneticMO2}=\sum_{i,j}\frac{\left|L_i\right|\hbar}{Z_j2m_ea^2b^2}D\mathbf{i}_\xi \tag{13.835}$$

Using Eqs. (11.200), (13.633-13.634), and (13.834-13.835), the force balance for the σ-MO of the carbon nitride radical comprising carbon with charge $Z_1=6$ and $\left|L_1\right|=\hbar$ and $\left|L_2\right|=\sqrt{\frac{3}{4}}\hbar$ and nitrogen with $Z_2=7$ and $\left|L_3\right|=\hbar$ is:

$$\frac{\hbar^2}{m_ea^2b^2}D=\frac{e^2}{8\pi\varepsilon_0ab^2}D+\frac{\hbar^2}{2m_ea^2b^2}D-\left(1+\frac{1}{Z_1}+\frac{\sqrt{\frac{3}{4}}}{Z_1}+\frac{1}{Z_2}\right)\frac{\hbar^2}{2m_ea^2b^2}D \tag{13.836}$$

$$\frac{\hbar^2}{m_ea^2b^2}D=\frac{e^2}{8\pi\varepsilon_0ab^2}D-\left(\frac{1}{Z_1}+\frac{\sqrt{\frac{3}{4}}}{Z_1}+\frac{1}{Z_2}\right)\frac{\hbar^2}{2m_ea^2b^2}D \tag{13.837}$$

$$\left(2+\frac{1}{Z_1}+\frac{\sqrt{\frac{3}{4}}}{Z_1}+\frac{1}{Z_2}\right)\frac{\hbar^2}{2m_ea^2b^2}D=\frac{e^2}{8\pi\varepsilon_0ab^2}D \tag{13.838}$$

$$a=\left(2+\frac{1}{Z_1}+\frac{\sqrt{\frac{3}{4}}}{Z_1}+\frac{1}{Z_2}\right)a_0 \tag{13.839}$$

Substitution of $Z_1=6$ and $Z_2=7$ into Eq. (13.839) gives:

$$a=2.45386a_0=1.29853\ X\ 10^{-10}\ m \tag{13.840}$$

Substitution of Eq. (13.840) into Eq. (11.79) is:

$$c'=1.10767a_0=5.86153\ X\ 10^{-11}\ m \tag{13.841}$$

The internuclear distance given by multiplying Eq. (13.841) by two is:

$$2c'=2.21534a_0=1.17231\ X\ 10^{-10}\ m \tag{13.842}$$

The experimental bond distance from Ref. [28] is:

$$2c'=1.17181\ X\ 10^{-10}\ m \tag{13.843}$$

Substitution of Eqs. (13.840-13.841) into Eq. (11.80) is:

$$b = c = 2.18964a_0 = 1.15871\ X\ 10^{-10}\ m \tag{13.844}$$

Substitution of Eqs. (13.840-13.841) into Eq. (11.67) is:

$$e = 0.45140 \tag{13.845}$$

Using the electron configuration of CN (Eq. (13.810)), the radii of the $C1s = 0.17113a_0$ (Eq. (10.51)), $C2s = 0.84317a_0$ (Eq. (10.62)), $C2p = 0.88084a_0$ (Eq. (13.819)), $N1s = 0.14605a_0$ (Eq. (10.51)), $N2s = 0.69385a_0$ (Eq. (10.62)), and $N2p = 0.76366a_0$ (Eq. (13.829)) shells and the parameters of the σ MO of CN given by Eqs. (13.3-13.4), (13.840-13.842), and (13.844-13.845), the dimensional diagram and charge-density of the CN MO are shown in Figures 13.22 and 13.23, respectively.

Figure 13.22. The cross section of the CN MO showing the axes, σ MO (H_2-type ellipsoidal MO), with the C $1s$, $2s$, and $2p$ atomic orbitals (AOs) and the N $1s$, $2s$, and $2p$ AOs. Legend: a: semimajor axis, b: semiminor axis, c': internuclear distance, r_5: radius of the $C2p$ shell having one unpaired electron, r_6: radius of the $N2p$ shell having two paired electrons.

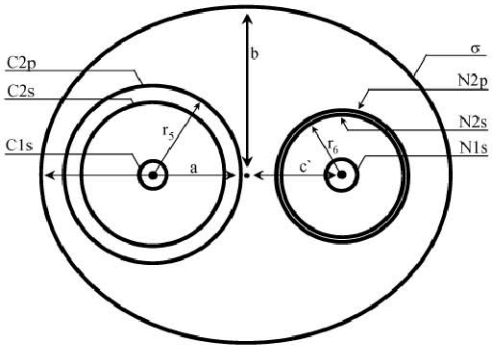

Figure 13.23. CN MO comprising the σ MO (H_2-type MO) with C and N atoms at the foci that have each donated an electron to the σ MO and have smaller radii and higher binding energies as a consequence. (A) Color scale, translucent view of the charge-density of the CN MO. (B) Off-center cut-away view showing the complete inner most $C1s$ shell, and moving radially, the $C2s$ shell, the $C2p$ shell, and the σ prolate spheroidal MO that has the C atom as a focus. Moving radially from the nitrogen-atom focus, the complete inner most $N1s$ shell, the $N2s$ shell, the $N2p$ shell, and the σ prolate spheroidal MO are shown.

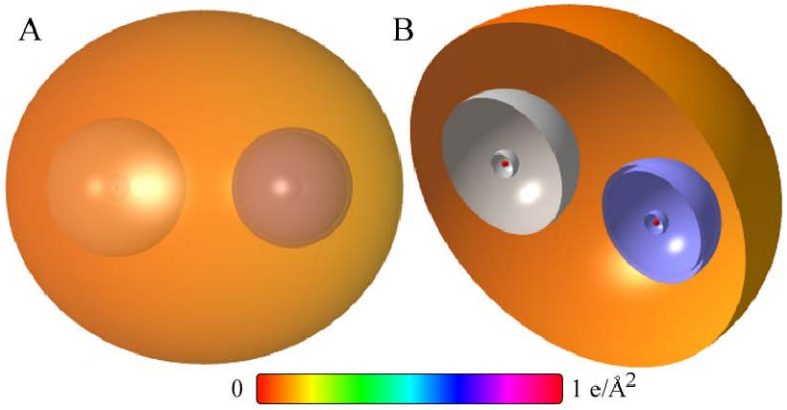

SUM OF THE ENERGIES OF THE σ MO AND THE AOs OF THE CARBON NITRIDE RADICAL

The energies of the CN σ MO are given by the substitution of the semiprincipal axes (Eqs. (13.840-13.841) and (13.844)) into the energy equations (Eqs. (11.207-11.212)) of H_2:

$$V_e = \frac{-2e^2}{8\pi\varepsilon_0\sqrt{a^2-b^2}}\ln\frac{a+\sqrt{a^2-b^2}}{a-\sqrt{a^2-b^2}} = -23.90105\ eV \tag{13.846}$$

$$V_p = \frac{e^2}{8\pi\varepsilon_0\sqrt{a^2-b^2}} = 12.28328\ eV \tag{13.847}$$

$$T = \frac{\hbar^2}{2m_e a\sqrt{a^2-b^2}}\ln\frac{a+\sqrt{a^2-b^2}}{a-\sqrt{a^2-b^2}} = 4.87009\ eV \tag{13.848}$$

$$V_m = \frac{-\hbar^2}{4m_e a\sqrt{a^2-b^2}}\ln\frac{a+\sqrt{a^2-b^2}}{a-\sqrt{a^2-b^2}} = -2.43504\ eV \tag{13.849}$$

$$E_T = V_e + T + V_m + V_p \tag{13.850}$$

Substitution of Eqs. (11.79) and (13.846-13.849) into Eq. (13.850) gives:

$$E_T(CN,\sigma)=\frac{-e^2}{8\pi\varepsilon_0\sqrt{\frac{aa_0}{2}}}\left(\left(2-\frac{1}{2}\frac{a_0}{a}\right)\ln\frac{a+\sqrt{\frac{aa_0}{2}}}{a-\sqrt{\frac{aa_0}{2}}}-1\right)=-9.18273\ eV \tag{13.851}$$

where $E_T(CN,\sigma)$ is the total energy of the σ MO of CN. The sum, $E_T(CN)$, of $E_T(CN,C2p)$, the $C2p$ AO contribution given by Eq. (13.831), $E_T(CN,N2p)$, the $N2p$ AO contribution given by Eq. (13.833), and $E_T(CN,\sigma)$, the σ MO contribution given by Eq. (13.851) is:

$$\begin{aligned}E_T(CN)&=E_T(CN,C2p)+E_T(CN,N2p)+E_T(N_2,\sigma)\\&=-8.33948\ eV-15.99929\ eV-9.18273\ eV\\&=-33.52149\ eV\end{aligned} \tag{13.852}$$

VIBRATION OF *CN*

The vibrational energy levels of CN may be solved by determining the Morse potential curve from the energy relationships for the transition from a C atom and N atom whose parameters are given by Eqs. (10.115-10.123) and (10.134-10.143), respectively, to a C atom whose parameter r_5 is given by Eq. (10.819), a N atom whose parameter r_6 is given by Eq. (13.829), and the σ MO whose parameters are given by Eqs. (13.840-13.842) and (13.844-13.845). As shown in the Vibration of Hydrogen-type Molecular Ions section, the harmonic oscillator potential energy function can be expanded about the internuclear distance and expressed as a Maclaurin series corresponding to a Morse potential after Karplus and Porter (K&P) [15] and after Eq. (11.134). Treating the Maclaurin series terms as anharmonic perturbation terms of the harmonic states, the energy corrections can be found by perturbation methods.

THE DOPPLER ENERGY TERMS OF THE CARBON NITRIDE RADICAL

The equations of the radiation reaction force of CN are the same as those of H_2 with the substitution of the CN parameters. Using Eqs. (11.231-11.233), the angular frequency of the reentrant oscillation in the transition state is:

$$\omega=\sqrt{\frac{\frac{e^2}{4\pi\varepsilon_0 a^3}}{m_e}}=1.07550\ X\ 10^{16}\ rad/s \tag{13.853}$$

where a is given by Eq. (13.840). The kinetic energy, E_K, is given by Planck's equation (Eq. (11.127)).

$$\bar{E}_K=\hbar\omega=\hbar 1.07550\ X\ 10^{16}\ rad/s=7.07912\ eV \tag{13.854}$$

In Eq. (11.181), substitution of $E_T(CN)$ for $E_{h\nu}$, the mass of the electron, m_e, for M, and the kinetic energy given by Eq. (13.854) for $\bar{E}_K$ gives the Doppler energy of the electrons of the reentrant orbit:

$$\begin{aligned}\bar{E}_D&\cong E_{h\nu}\sqrt{\frac{2\bar{E}_K}{Mc^2}}=-33.59603\ eV\sqrt{\frac{2e(7.07912\ eV)}{m_e c^2}}\\&=-0.17684\ eV\end{aligned} \tag{13.855}$$

In addition to the electrons, the nuclei also undergo simple harmonic oscillation in the transition state at their corresponding frequency. The decrease in the energy of the CN MO due to the reentrant orbit in the transition state corresponding to simple harmonic oscillation of the electrons and nuclei, $\bar{E}_{osc}$, is given by the sum of the corresponding energies, $\bar{E}_D$ given by Eq. (13.855) and $\bar{E}_{Kvib}$, the average kinetic energy of vibration which is 1/2 of the vibrational energy. Using the experimental CN ω_e of 2068.59 cm^{-1} $(0.25647\ eV)$ [28] for $\bar{E}_{Kvib}$ of the transition state, $\bar{E}_{osc}(CN)$ is:

$$\begin{aligned}\bar{E}_{osc}(CN)&=\bar{E}_D+\bar{E}_{Kvib}\\&=\bar{E}_D+\frac{1}{2}\hbar\sqrt{\frac{k}{\mu}}\end{aligned} \tag{13.856}$$

$$\begin{aligned}\bar{E}_{osc}(CN)&=-0.17684\ eV+\frac{1}{2}(0.25647\ eV)\\&=-0.04860\ eV\end{aligned} \tag{13.857}$$

TOTAL AND BOND ENERGIES OF THE CARBON NITRIDE RADICAL

$E_{T+osc}(CN)$, the total energy of CN including the Doppler term, is given by the sum of $E_T(CN)$ (Eq. (13.852)) and $\bar{E}_{osc}(CN)$ given by Eq. (13.857):

$$\begin{aligned} E_{T+osc}(CN) &= V_e + T + V_m + V_p + E_T(CN, C2p) + E_T(CN, N2p) + \bar{E}_{osc}(CN) \\ &= E_T(CN, \sigma) + E_T(CN, C2p) + E_T(CN, N2p) + \bar{E}_{osc}(CN) \\ &= E_T(CN) + \bar{E}_{osc}(CN) \end{aligned} \tag{13.858}$$

$$\begin{aligned} E_{T+osc}(CN) = &\left\{ \begin{array}{l} \left(\dfrac{-e^2}{8\pi\varepsilon_0 \sqrt{\dfrac{aa_0}{2}}} \left(\left(2 - \dfrac{1}{2}\dfrac{a_0}{a}\right) \ln \dfrac{a + \sqrt{\dfrac{aa_0}{2}}}{a - \sqrt{\dfrac{aa_0}{2}}} - 1 \right) \right. \\ \left. - \sum_{C,n=4}^{4} \dfrac{(Z-n)e^2}{8\pi\varepsilon_0} \left(\dfrac{1}{r_5} - \dfrac{1}{r_6} \right) - \sum_{N,n=4}^{5} \dfrac{(Z-n)e^2}{8\pi\varepsilon_0} \left(\dfrac{1}{r_6} - \dfrac{1}{r_7} \right) \right) \\ \left(1 + \sqrt{\dfrac{2\hbar \sqrt{\dfrac{e^2}{4\pi\varepsilon_o a^3}}}{m_e c^2}} \right) + \dfrac{1}{2}\hbar\sqrt{\dfrac{k}{\mu}} \end{array} \right\} \\ &= -33.52149\ eV - 0.17684\ eV + \frac{1}{2}\hbar\sqrt{\frac{k}{\mu}} \end{aligned} \tag{13.859}$$

From Eqs. (13.856-13.859), the total energy of the CN MO is:

$$\begin{aligned} E_{T+osc}(CN) &= -33.52149\ eV + \bar{E}_{osc}(CN) \\ &= -33.52149\ eV - 0.17684\ eV + \frac{1}{2}(0.25647\ eV) \\ &= -33.56970\ eV \end{aligned} \tag{13.860}$$

where the experimental ω_e was used for the $\hbar\sqrt{\dfrac{k}{\mu}}$ term.

The CN bond dissociation energy, $E_D(CN)$, is given by the difference between the sum of the energies of the C and N atoms and $E_{T+osc}(CN)$:

$$E_D(CN) = E(C) + E(N) - E_{T+osc}(CN) \tag{13.861}$$

where the energy of a carbon atom is [6]:

$$E(C) = -11.26030\ eV \tag{13.862}$$

and the energy of a nitrogen atom is [6]:

$$E(N) = -14.53414\ eV \tag{13.863}$$

Thus, the CN bond dissociation energy, $E_D(CN)$, given by Eqs. (13.860-13.863) is:

$$\begin{aligned} E_D(CN) &= -(11.26030\ eV + 14.53414\ eV) - E_{T+osc}(CN) \\ &= -25.79444\ eV - (-33.56970\ eV) \\ &= 7.77526\ eV \end{aligned} \tag{13.864}$$

The experimental CN bond dissociation energy is [50]:

$$E_{D298}(CN) = 7.7731\ eV \tag{13.865}$$

The results of the determination of bond parameters of CN are given in Table 13.1. The calculated results are based on first principles and given in closed-form, exact equations containing fundamental constants only. The agreement between the experimental and calculated results is excellent.

CARBON MONOXIDE MOLECULE

The carbon monoxide molecule can be formed by the reaction of carbon and oxygen atoms:

$$C + O \rightarrow CO \tag{13.866}$$

The bond in the carbon monoxide molecule comprises a double bond, a H_2-type molecular orbital (MO) with four paired electrons. The force balance equation and radius r_6 of the $2p$ shell of C is derived in the Six-Electron Atoms section. The force balance equation and radius r_8 of the $2p$ shell of O is derived in the Eight-Electron Atoms section. With the formation of the H_2-type MO by the contribution of two $2p$ electrons from each of the C and O atoms, a diamagnetic force arises between the remaining outer shell atomic electrons, the $2s$ electrons of C and the $2p$ electrons of O, and the H_2-type MO. This force from C and O causes the H_2-type MO to move to greater principal axes than would result with the Coulombic force alone. But, the factor of two increase of the central field and the resulting increased Coulombic as well as magnetic central forces on the remaining $O2p$ electrons decrease the radius of the corresponding shell such that the energy minimum is achieved that is lower than that of the reactant atoms. The resulting electron configuration of CO is $C1s^2O1s^2C2s^2O2s^2O2p^2\sigma_{C,O}^4$ where σ designates the H_2-type MO, and the orbital arrangement is:

σ state

$\underline{\uparrow\downarrow}\ \underline{\uparrow\downarrow}$

2p state

$\underline{\uparrow\downarrow}$

0

2s state

$\underline{\uparrow\downarrow}\qquad\underline{\uparrow\downarrow}$ (13.867)

1s state

$\underline{\uparrow\downarrow}\qquad\underline{\uparrow\downarrow}$

$C\qquad O$

Carbon monoxide is predicted to be diamagnetic in agreement with observations [42].

FORCE BALANCE OF THE $2p$ SHELL OF THE OXYGEN ATOM OF THE CARBON MONOXIDE MOLECULE

For the O atom, force balance for the outermost $2p$ electron of CO (electron 6) is achieved between the centrifugal force and the Coulombic and magnetic forces that arise due to interactions between electron 6 and the other $2p$ electron as well as the $2s$-shell electrons due to spin and orbital angular momentum. The forces used are derived in the Eight-Electron Atoms section. The central Coulomb force on the outer-most $2p$ shell electron of CO (electron 6) due to the nucleus and the inner five electrons is given by Eq. (10.70) with the appropriate charge and radius:

$$\mathbf{F}_{ele} = \frac{(Z-5)e^2}{4\pi\varepsilon_0 r_6^2}\mathbf{i}_r \tag{13.868}$$

for $r > r_5$. The $2p$ shell possesses a +2 external electric field given by Eq. (10.92) for $r > r_6$. The energy is minimized with conservation of angular momentum. This condition is met when the diamagnetic force, $\mathbf{F}_{diamagnetic}$, of Eq. (10.82) due to the p-orbital contribution is given by:

$$\begin{aligned}\mathbf{F}_{diamagnetic} &= -\left(\frac{1}{3}\right)\frac{\hbar^2}{4m_e r_6^2 r_3}\sqrt{s(s+1)}\mathbf{i}_r \\ &= -\frac{\hbar^2}{12m_e r_6^2 r_3}\sqrt{\frac{3}{4}}\mathbf{i}_r\end{aligned} \tag{13.869}$$

And, $\mathbf{F}_{mag\ 2}$ corresponding to the conserved spin and orbital angular momentum given by Eq. (10.157) is:

$$\mathbf{F}_{mag\ 2} = \frac{1}{Z}\frac{2\hbar^2}{m_e r_6^2 r_3}\sqrt{s(s+1)}\mathbf{i}_r \tag{13.870}$$

The electric field external to the $2p$ shell given by Eq. (10.92) for $r > r_6$ gives rise to a second diamagnetic force, $\mathbf{F}_{diamagnetic\ 2}$, given by Eq. (10.93). $\mathbf{F}_{diamagnetic\ 2}$ due to the binding of the p-orbital electron having an electric field of +2 outside of its radius is:

$$\mathbf{F}_{diamagnetic\ 2} = -\left[\frac{Z-6}{Z-5}\right]\left(1-\frac{\sqrt{2}}{2}\right)\frac{r_3\hbar^2}{m_e r_6^4}10\sqrt{s(s+1)}\mathbf{i}_\mathbf{r} \tag{13.871}$$

In addition, the contribution of two $2p$ electrons in the formation of the σ molecular orbital (MO) gives rise to a paramagnetic force on the remaining paired $2p$ electrons. The force $\mathbf{F}_{mag\ 3}$ is given by Eq. (13.625) wherein the radius is r_6:

$$\mathbf{F}_{mag\ 3} = \frac{\hbar^2}{4m_e r_6^3}\sqrt{s(s+1)}\mathbf{i}_\mathbf{r} \tag{13.872}$$

The radius of the $2p$ shell is calculated by equating the outward centrifugal force to the sum of the electric (Eq. (13.868)) and diamagnetic (Eqs. (13.869) and (13.871)), and paramagnetic (Eqs. (13.870) and (13.872)) forces as follows:

$$\frac{m_e v_6^2}{r_6} = \left(\begin{array}{l}\dfrac{(Z-5)e^2}{4\pi\varepsilon_0 r_6^2} - \dfrac{\hbar^2}{12m_e r_6^2 r_3}\sqrt{s(s+1)} + \dfrac{2\hbar^2}{Zm_e r_6^2 r_3}\sqrt{s(s+1)} \\ -\left[\dfrac{Z-6}{Z-5}\right]\left(1-\dfrac{\sqrt{2}}{2}\right)\dfrac{r_3\hbar^2}{r_6^4 m_e}10\sqrt{s(s+1)} + \dfrac{\hbar^2}{4m_e r_6^3}\sqrt{s(s+1)}\end{array}\right) \tag{13.873}$$

Substitution of $v_6 = \dfrac{\hbar}{m_e r_6}$ (Eq. (1.35)) and $s = \dfrac{1}{2}$ into Eq. (13.873) gives:

$$\frac{\hbar^2}{m_e r_6^3} - \frac{\hbar^2}{4m_e r_6^3}\sqrt{\frac{3}{4}} = \frac{(Z-5)e^2}{4\pi\varepsilon_0 r_6^2} - \frac{\hbar^2}{12m_e r_6^2 r_3}\sqrt{\frac{3}{4}} + \frac{2\hbar^2}{Zm_e r_6^2 r_3}\sqrt{\frac{3}{4}} - \left[\frac{Z-6}{Z-5}\right]\left(1-\frac{\sqrt{2}}{2}\right)\frac{r_3\hbar^2}{r_6^4 m_e}10\sqrt{\frac{3}{4}} \tag{13.874}$$

The quadratic equation corresponding to Eq. (13.874) is

$$r_6^2 - \frac{\dfrac{\hbar^2}{m_e}\left(1-\dfrac{\sqrt{3}}{8}\right)}{\left(\dfrac{(Z-5)e^2}{4\pi\varepsilon_0} - \left(\dfrac{1}{12}-\dfrac{2}{Z}\right)\dfrac{\hbar^2}{m_e r_3}\sqrt{\dfrac{3}{4}}\right)}r_6 - \frac{\dfrac{\hbar^2}{m_e}\left[\dfrac{Z-6}{Z-5}\right]\left(1-\dfrac{\sqrt{2}}{2}\right)r_3 10\sqrt{\dfrac{3}{4}}}{\left(\dfrac{(Z-5)e^2}{4\pi\varepsilon_0} - \left(\dfrac{1}{12}-\dfrac{2}{Z}\right)\dfrac{\hbar^2}{m_e r_3}\sqrt{\dfrac{3}{4}}\right)} = 0 \tag{13.875}$$

The solution of Eq. (13.875) using the quadratic formula is:

$$r_6 = \frac{\dfrac{a_0\left(1-\dfrac{\sqrt{3}}{8}\right)}{\left((Z-5) - \left(\dfrac{1}{12}-\dfrac{2}{Z}\right)\dfrac{\sqrt{3}}{2r_3}\right)} \pm a_0\sqrt{\left(\dfrac{1-\dfrac{\sqrt{3}}{8}}{\left((Z-5) - \left(\dfrac{1}{12}-\dfrac{2}{Z}\right)\dfrac{\sqrt{3}}{2r_3}\right)}\right)^2 + \dfrac{20\sqrt{3}\left(\left[\dfrac{Z-6}{Z-5}\right]\left(1-\dfrac{\sqrt{2}}{2}\right)r_3\right)}{\left((Z-5) - \left(\dfrac{1}{12}-\dfrac{2}{Z}\right)\dfrac{\sqrt{3}}{2r_3}\right)}}}{2}, \; r_3 \text{ in units of } a_0 \tag{13.876}$$

The positive root of Eq. (13.876) must be taken in order that $r_6 > 0$. Substitution of $\dfrac{r_3}{a_0} = 0.59020$ (Eq. (10.62) with $Z = 8$) into Eq. (13.876) gives:

$$r_6 = 0.68835a_0 \tag{13.877}$$

ENERGIES OF THE $2s$ AND $2p$ SHELLS OF THE CARBON ATOM AND THE $2p$ SHELL OF THE OXYGEN ATOM OF THE CARBON MONOXIDE MOLECULE

With the formation of the H_2-type MO by the contribution of two $2p$ electrons from the C atom, the remaining outer-shell atomic electrons comprise the $2s$ electrons, which are unchanged by bonding with oxygen. However, the total energy of the CO molecule, which is subtracted from the sum of the energies of the carbon and oxygen atoms to determine the bond energy, is increased by the ionization energies of C^+ and O^+ given by Eqs. (10.113-10.114) and (10.152-10.153), respectively. Experimentally, the energies are [6] :

$$E(ionization;\ C^+) = 24.38332\ eV \tag{13.878}$$

$$E(ionization;\ O^+) = 35.11730\ eV \tag{13.879}$$

In addition, the central forces on the $2p$ shell of the O atom are increased with the formation of the σ MO, which reduces the shell's radius and increases its total energy. The Coulombic energy terms of the total energy of the O atom at the new radius are calculated and added to the ionization energies of C^+ and O^+, and the energy of the σ MO to give the total energy of CO. Then, the bond energy is determined from the total CO energy.

The radius r_8 of the oxygen atom before bonding is given by Eq. (10.162):

$$r_8 = a_0 \tag{13.880}$$

Using the initial radius r_8 of the O atom and the final radius r_6 of the $O2p$ shell (Eq. (13.877)) and by considering that the central Coulombic field decreases by an integer for each successive electron of the shell, the sum $E_T(O,2p)$ of the Coulombic energy change of the $O2p$ electrons of the O atom is determined using Eq. (10.102):

$$E_T(O,2p) = -\sum_{n=4}^{5} \frac{(Z-n)e^2}{8\pi\varepsilon_0}\left(\frac{1}{r_6}-\frac{1}{r_8}\right) = -(13.60580\ eV)(0.45275)(3+4) = -43.11996\ eV \tag{13.881}$$

FORCE BALANCE OF THE σ MO OF THE CARBON MONOXIDE MOLECULE

The force balance can be considered due to a second pair of two electrons binding to a molecular ion having $+2e$ at each focus and a first bound pair. Then, the forces are the same as those of a molecule ion having $+e$ at each focus. The diamagnetic force $\mathbf{F}_{diamagneticMO1}$ for the σ-MO of the CO molecule due to the two paired electrons in each of the $C2s$ and $O2p$ shells is given by Eq. (13.633) with $n_e = 2$:

$$\mathbf{F}_{diamagneticMO1} = \frac{\hbar^2}{2m_e a^2 b^2} D\mathbf{i}_\xi \tag{13.882}$$

The force $\mathbf{F}_{diamagneticMO2}$ is given by Eqs. (13.634) and (13.835) as the sum of the contributions due to carbon with $Z = Z_1$ and oxygen with $Z = Z_2$. $\mathbf{F}_{diamagneticMO1}$ for CO with $|L_i| = \hbar$ is:

$$\mathbf{F}_{diamagneticMO2} = \left(\frac{1}{Z_1}+\frac{1}{Z_2}\right)\frac{\hbar^2}{2m_e a^2 b^2} D\mathbf{i}_\xi \tag{13.883}$$

The force balance equation for the σ-MO of the carbon monoxide molecule given by Eqs. (11.200), (13.633-13.634), and (13.882-13.883) is:

$$\frac{\hbar^2}{m_e a^2 b^2} D = \frac{e^2}{8\pi\varepsilon_0 ab^2} D + \frac{\hbar^2}{2m_e a^2 b^2} D - \left(1+\left(\frac{1}{Z_1}+\frac{1}{Z_2}\right)\right)\frac{\hbar^2}{2m_e a^2 b^2} D \tag{13.884}$$

$$\frac{\hbar^2}{m_e a^2 b^2} D = \frac{e^2}{8\pi\varepsilon_0 ab^2} D - \left(\frac{1}{Z_1}+\frac{1}{Z_2}\right)\frac{\hbar^2}{2m_e a^2 b^2} D \tag{13.885}$$

$$\left(2+\frac{1}{Z_1}+\frac{1}{Z_2}\right)\frac{\hbar^2}{2m_e a^2 b^2} D = \frac{e^2}{8\pi\varepsilon_0 ab^2} D \tag{13.886}$$

$$a = \left(2+\frac{1}{Z_1}+\frac{1}{Z_2}\right)a_0 \tag{13.887}$$

Substitution of $Z_1 = 6$ and $Z_2 = 8$ into Eq. (13.887) gives:

$$a = 2.29167 a_0 = 1.21270\ X\ 10^{-10}\ m \tag{13.888}$$

Substitution of Eq. (13.888) into Eq. (11.79) is:

$$c' = 1.07044a_0 = 5.66450\ X\ 10^{-11}\ m \tag{13.889}$$

The internuclear distance given by multiplying Eq. (13.889) by two is:

$$2c' = 2.14087a_0 = 1.13290\ X\ 10^{-10}\ m \tag{13.890}$$

The experimental bond distance is [28]:

$$2c' = 1.12823\ X\ 10^{-10}\ m \tag{13.891}$$

Substitution of Eqs. (13.888-13.889) into Eq. (11.80) is:

$$b = c = 2.02630a_0 = 1.07227\ X\ 10^{-10}\ m \tag{13.892}$$

Substitution of Eqs. (13.888-13.889) into Eq. (11.67) is:

$$e = 0.46710 \tag{13.893}$$

Using the electron configuration of CO (Eq. (13.867)), the radii of the $C1s = 0.17113a_0$ (Eq. (10.51)), $C2s = 0.84317a_0$ (Eq. (10.62)), $O1s = 0.12739a_0$ (Eq. (10.51)), $O2s = 0.59020a_0$ (Eq. (10.62)), and $O2p = 0.68835a_0$ (Eq. (13.877)) shells and the parameters of the σ MO of CO given by Eqs. (13.3-13.4), (13.888-13.890), and (13.892-13.893), the dimensional diagram and charge-density of the CO MO are shown in Figures 13.24 and 13.25, respectively.

Figure 13.24. The cross section of the CO MO showing the axes, σ MO (H_2-type ellipsoidal MO) with four paired electrons, with the C $1s$ and $2s$ atomic orbitals (AOs) and the O $1s$, $2s$, and $2p$ AOs. Legend: a: semimajor axis, b: semiminor axis, c': internuclear distance, r_4: radius of the $C2s$ shell having two paired electrons, r_6: radius of the $O2p$ shell having two paired electrons.

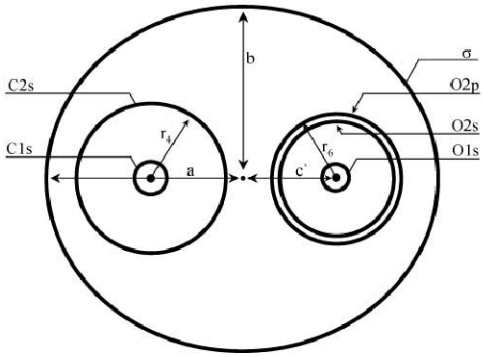

Figure 13.25. CO MO comprising the σ MO (H_2-type MO) with C and O atoms at the foci that have each donated two electrons to the σ MO. Consequently, the outer electrons of the carbon atom comprise the $C2s$ shell, and the $O2p$ shell has a smaller radius and a higher binding energy. (A) Color scale, translucent view of the charge-density of the CO MO. (B) Off-center cut-away view showing the complete inner most $O1s$ shell, and moving radially, the $O2s$ shell, the $O2p$ shell, and the σ prolate spheroidal MO that has the O atom as a focus. Moving radially from the carbon-atom focus, the complete inner most $C1s$ shell, the $C2s$ shell, and the σ prolate spheroidal MO are shown.

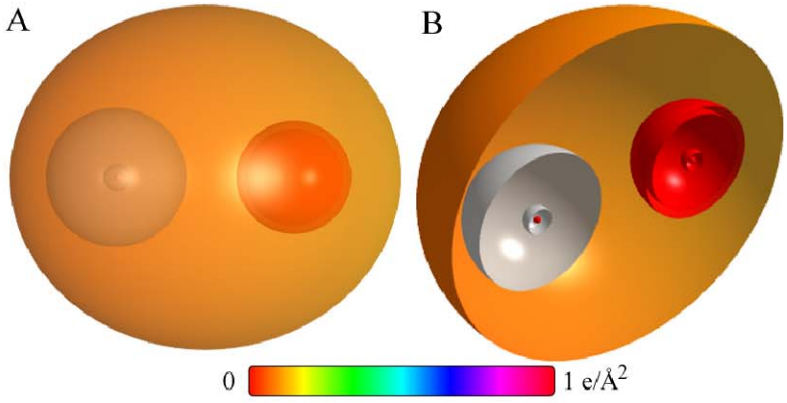

SUM OF THE ENERGIES OF THE σ MO AND THE AOs OF THE CARBON MONOXIDE MOLECULE

The energies of the CO σ MO are given by the substitution of the semiprincipal axes (Eqs. (13.888-13.889) and (13.892)) into the energy equations (Eqs. (11.207-11.212)) of H_2 except that the terms based on charge are multiplied by four and the kinetic energy term is multiplied by two due to the σ-MO double bond with two pairs of paired electrons:

$$V_e = 2^2 \frac{-2e^2}{8\pi\varepsilon_0\sqrt{a^2-b^2}} \ln\frac{a+\sqrt{a^2-b^2}}{a-\sqrt{a^2-b^2}} = -102.97635\ eV \tag{13.894}$$

$$V_p = 2^2 \frac{e^2}{8\pi\varepsilon_0\sqrt{a^2-b^2}} = 50.84210\ eV \tag{13.895}$$

$$T = 2\frac{\hbar^2}{2m_e a\sqrt{a^2-b^2}} \ln\frac{a+\sqrt{a^2-b^2}}{a-\sqrt{a^2-b^2}} = 11.23379\ eV \tag{13.896}$$

$$V_m = 2^2 \frac{-\hbar^2}{4m_e a\sqrt{a^2-b^2}} \ln \frac{a+\sqrt{a^2-b^2}}{a-\sqrt{a^2-b^2}} = -11.23379\ eV \tag{13.897}$$

$$E_T = V_e + T + V_m + V_p \tag{13.898}$$

Substitution of Eqs. (11.79) and (13.894-13.897) into Eq. (13.898) gives:

$$E_T(CO,\sigma) = \frac{-e^2}{8\pi\varepsilon_0\sqrt{\frac{aa_0}{2}}} \left(8\ln \frac{a+\sqrt{\frac{aa_0}{2}}}{a-\sqrt{\frac{aa_0}{2}}} - 4 \right) = -52.13425\ eV \tag{13.899}$$

where $E_T(CO,\sigma)$ is the total energy of the σ MO of CO. The total energy of CO, $E_T(CO)$, is given by the sum of $E(ionization;\ C^+)$, the energy of the second electron of carbon (Eq. (13.878)) donated to the double bond, $E(ionization;\ O^+)$, the energy of the second electron of oxygen (Eq. (13.879)) donated to the double bond, $E_T(O,2p)$, the $O2p$ AO contribution due to the decrease in radius with bond formation (Eq. (13.881)), and $E_T(CO,\sigma)$, the σ MO contribution given by Eq. (13.899):

$$\begin{aligned} E_T(CO) &= E(ionization;\ C^+) + E(ionization;\ O^+) + E_T(O,2p) + E_T(CO,\sigma) \\ &= 24.38332\ eV + 35.11730\ eV - 43.11996\ eV - 52.13425\ eV \\ &= -35.75359\ eV \end{aligned} \tag{13.900}$$

VIBRATION OF *CO*

The vibrational energy levels of CO may be solved by determining the Morse potential curve from the energy relationships for the transition from a C atom and O atom whose parameters are given by Eqs. (10.115-10.123) and (10.154-10.163), respectively, to a C atom whose parameter r_4 is given by Eq. (10.61), an O atom whose parameter r_6 is given by Eq. (13.877), and the σ MO whose parameters are given by Eqs. (13.888-13.890) and (13.892-13.893). As shown in the Vibration of Hydrogen-type Molecular Ions section, the harmonic oscillator potential energy function can be expanded about the internuclear distance and expressed as a Maclaurin series corresponding to a Morse potential after Karplus and Porter (K&P) [15] and after Eq. (11.134). Treating the Maclaurin series terms as anharmonic perturbation terms of the harmonic states, the energy corrections can be found by perturbation methods.

THE DOPPLER ENERGY TERMS OF THE CARBON MONOXIDE MOLECULE

The equations of the radiation reaction force of carbon monoxide are the same as those of H_2 with the substitution of the CO parameters except that there is a factor of four increase in the central force in Eq. (11.231) due to the double bond. Using Eqs. (11.231-11.233), the angular frequency of the reentrant oscillation in the transition state is

$$\omega = \sqrt{\frac{\frac{4e^2}{4\pi\varepsilon_0 a^3}}{m_e}} = 2.38335\ X\ 10^{16}\ rad/s \tag{13.901}$$

where a is given by Eq. (13.888). The kinetic energy, E_K, is given by Planck's equation (Eq. (11.127)).

$$\begin{aligned} \bar{E}_K &= \hbar\omega = \hbar 2.38335\ X\ 10^{16}\ rad/s \\ &= 15.68762\ eV \end{aligned} \tag{13.902}$$

In Eq. (11.181), substitution of $E_T(CO)$ for $E_{h\nu}$, the mass of the electron, m_e, for M, and the kinetic energy given by Eq. (13.902) for $\bar{E}_K$ gives the Doppler energy of the electrons of the reentrant orbit:

$$\begin{aligned} \bar{E}_D &\cong E_{h\nu}\sqrt{\frac{2\bar{E}_K}{Mc^2}} \\ &= -35.75359\ eV\sqrt{\frac{2e(15.68762\ eV)}{m_e c^2}} = -0.28016\ eV \end{aligned} \tag{13.903}$$

In addition to the electrons, the nuclei also undergo simple harmonic oscillation in the transition state at their corresponding frequency. The decrease in the energy of the CO MO due to the reentrant orbit in the transition state corresponding to simple harmonic oscillation of the electrons and nuclei, $\bar{E}_{osc}$, is given by the sum of the corresponding energies, $\bar{E}_D$ given by Eq. (13.903) and $\bar{E}_{Kvib}$, the average kinetic energy of vibration which is 1/2 of the vibrational energy. Using the experimental CO ω_e of 2169.81 cm^{-1} $(0.26902\ eV)$ [28] for $\bar{E}_{Kvib}$ of the transition state, $\bar{E}'_{osc}(CO)$ per bond is:

$$\bar{E}'_{osc}(CO) = \bar{E}_D + \bar{E}_{Kvib} = \bar{E}_D + \frac{1}{2}\hbar\sqrt{\frac{k}{\mu}} \tag{13.904}$$

$$\bar{E}'_{osc}(CO) = -0.28016\ eV + \frac{1}{2}(0.26902\ eV) = -0.14564\ eV \tag{13.905}$$

Since the σ MO bond is a double bond with twice a many electrons as a single bond, $\bar{E}'_{osc}(CO)$ is multiplied by two to give:

$$\bar{E}_{osc}(CO) = -0.29129\ eV \tag{13.906}$$

TOTAL AND BOND ENERGIES OF THE CARBON MONOXIDE MOLECULE

$E_{T+osc}(CO)$, the total energy of CO including the Doppler term, is given by the sum of $E_T(CO)$ (Eq. (13.900)) and $\bar{E}_{osc}(CO)$ given by Eq. (13.906):

$$\begin{aligned} E_{T+osc}(CO) &= \begin{pmatrix} V_e + T + V_m + V_p + E(ionization;\ C^+) \\ +E(ionization;\ O^+) + E_T(O,2p) + \bar{E}_{osc}(CO) \end{pmatrix} \\ &= \begin{pmatrix} E_T(CO,\sigma) + E(ionization;\ C^+) + E(ionization;\ O^+) \\ +E_T(O,2p) + \bar{E}_{osc}(CO) \end{pmatrix} \\ &= E_T(CO) + \bar{E}_{osc}(CO) \end{aligned} \tag{13.907}$$

$$\begin{aligned} E_{T+osc}(CO) = \Bigg\{ & \begin{pmatrix} \dfrac{-e^2}{8\pi\varepsilon_0\sqrt{\dfrac{aa_0}{2}}}\left(8\ln\dfrac{a+\sqrt{\dfrac{aa_0}{2}}}{a-\sqrt{\dfrac{aa_0}{2}}} - 4\right) + E\left(ionization;\ C^+\right) \\ +E\left(ionization;\ O^+\right) - \displaystyle\sum_{O,n=4}^{5} \dfrac{(Z-n)e^2}{8\pi\varepsilon_0}\left(\dfrac{1}{r_6} - \dfrac{1}{r_8}\right) \end{pmatrix} \Bigg\} \\ & \begin{pmatrix} 1 + 2\sqrt{\dfrac{2\hbar\sqrt{\dfrac{4e^2}{4\pi\varepsilon_0 a^3}}}{m_e c^2}} \end{pmatrix} + 2\left(\frac{1}{2}\hbar\sqrt{\frac{k}{\mu}}\right) \\ = & -35.75359\ eV - 2(0.28016\ eV) + 2\left(\frac{1}{2}\hbar\sqrt{\frac{k}{\mu}}\right) \end{aligned} \tag{13.908}$$

From Eqs. (13.906-13.908), the total energy of the CO MO is:

$$\begin{aligned} E_{T+osc}(CO) &= -35.75359\ eV + \bar{E}_{osc}(CO) \\ &= -35.75359\ eV + (-0.29129\ eV) = -36.04488\ eV \end{aligned} \tag{13.909}$$

where the experimental ω_e was used for the $\hbar\sqrt{\frac{k}{\mu}}$ term.

The CO bond dissociation energy, $E_D(CO)$, is given by the difference between the sum of the energies of the C and O atoms and $E_{T+osc}(CO)$:

$$E_D(CO) = E(C) + E(O) - E_{T+osc}(CO) \tag{13.910}$$

where the energy of a carbon atom is [6]:

$$E(C) = -11.26030\ eV \tag{13.911}$$

and the energy of an oxygen atom is [6]:

$$E(O) = -13.61806\ eV \tag{13.912}$$

Thus, the CO bond dissociation energy, $E_D(CO)$, given by Eqs. (13.909-13.912) is:

$$\begin{aligned} E_D(CO) &= -(11.26030\ eV + 13.61806\ eV) - E_{T+osc}(CO) \\ &= -24.87836\ eV - (-36.04488\ eV) = 11.16652\ eV \end{aligned} \tag{13.913}$$

The experimental CO bond dissociation energy is [49]:

$$E_{D298}(CO) = 11.15696\ eV \tag{13.914}$$

The results of the determination of bond parameters of CO are given in Table 13.1. The calculated results are based on first principles and given in closed-form, exact equations containing fundamental constants only. The agreement between the experimental and calculated results is excellent.

NITRIC OXIDE RADICAL

The nitric oxide radical can be formed by the reaction of nitrogen and oxygen atoms:

$$N + O \rightarrow NO \tag{13.915}$$

The bond in the nitric oxide radical comprises a double bond, a H_2-type molecular orbital (MO) with four paired electrons. The force balance equation and radius r_7 of the $2p$ shell of N is derived in the Seven-Electron Atoms section. The force balance equation and radius r_8 of the $2p$ shell of O is derived in the Eight-Electron Atoms section. With the formation of the H_2-type MO by the contribution of two $2p$ electrons from each of the N and O atoms, a diamagnetic force arises between the remaining outer shell atomic electrons, the $2s$ and $2p$ electrons of N and O, and the H_2-type MO. This force from N and O causes the H_2-type MO to move to greater principal axes than would result with the Coulombic force alone. But, the factor of two increase of the central field and the resulting increased Coulombic as well as magnetic central forces on the remaining N and O electrons decrease the radii of the corresponding shells such that the energy minimum is achieved that is lower than that of the reactant atoms. The resulting electron configuration of NO is $N1s^2O1s^2N2s^2O2s^2N2p^1O2p^2\sigma_{N,O}^4$ where σ designates the H_2-type MO, and the orbital arrangement is:

σ state

$\underline{\uparrow\downarrow}\ \underline{\uparrow\downarrow}$

2p state

$\underline{\uparrow}\quad\quad\underline{\uparrow\downarrow}$

0 0

2s state

$\underline{\uparrow\downarrow}\quad\quad\underline{\uparrow\downarrow}$ (13.916)

1s state

$\underline{\uparrow\downarrow}\quad\quad\underline{\uparrow\downarrow}$

$N\quad\quad O$

Nitric oxide is predicted to be weakly paramagnetic in agreement with observations [42].

FORCE BALANCE OF THE $2p$ SHELL OF THE NITROGEN ATOM OF THE NITRIC OXIDE RADICAL

For the N atom, force balance for the outermost $2p$ electron of NO (electron 5) is achieved between the centrifugal force and the Coulombic and magnetic forces that arise due to interactions between electron 5 and the $2s$-shell electrons due to spin and orbital angular momentum. The forces used are derived in the Seven-Electron Atoms section. The central Coulomb force on the outer-most $2p$ shell electron of NO (electron 5) due to the nucleus and the inner four electrons is given by Eq. (10.70) with the appropriate charge and radius:

$$\mathbf{F}_{ele} = \frac{(Z-4)e^2}{4\pi\varepsilon_0 r_5^2}\mathbf{i}_\mathbf{r} \tag{13.917}$$

for $r > r_4$. The $2p$ shell possess a +2 external electric field given by Eq. (10.92) for $r > r_5$. The energy is minimized with conservation of angular momentum. This condition is met when the magnetic forces of N in NO are the same as those of N in the nitrogen molecule with r_5 replacing r_6 and with an increase of the central field by an integer. The diamagnetic force, $\mathbf{F}_{diamagnetic}$, of Eq. (10.82) due to the p-orbital contribution is given by Eq. (13.622) with r_5 replacing r_6:

$$\mathbf{F}_{diamagnetic} = -\left(\frac{1}{3}\right)\frac{\hbar^2}{4m_e r_5^2 r_3}\sqrt{s(s+1)}\mathbf{i}_\mathbf{r} = -\frac{\hbar^2}{12m_e r_5^2 r_3}\sqrt{\frac{3}{4}}\mathbf{i}_\mathbf{r} \tag{13.918}$$

And, $\mathbf{F}_{mag\ 2}$ corresponding to the conserved orbital angular momentum of the three orbitals is also the same as that of N_2 given by Eq. (13.623) with r_5 replacing r_6:

$$\mathbf{F}_{mag\ 2} = \frac{1}{Z}\frac{3\hbar^2}{m_e r_5^2 r_3}\sqrt{s(s+1)}\mathbf{i}_\mathbf{r} \tag{13.919}$$

The electric field external to the $2p$ shell given by Eq. (10.92) for $r > r_5$ gives rise to a second diamagnetic force, $\mathbf{F}_{diamagnetic\ 2}$, given by Eq. (10.93). $\mathbf{F}_{diamagnetic\ 2}$ due to the binding of the p-orbital electron having an electric field of +2 outside of its radius follows from Eq. (13.624).

$$\mathbf{F}_{diamagnetic\ 2} = -\left[\frac{Z-5}{Z-4}\right]\left(1-\frac{\sqrt{2}}{2}\right)\frac{r_3\hbar^2}{m_e r_5^4}10\sqrt{s(s+1)}\mathbf{i}_\mathbf{r} \tag{13.920}$$

In addition to the N forces $\mathbf{F}_{ele}$, $\mathbf{F}_{diamagnetic}$, $\mathbf{F}_{mag\ 2}$, and $\mathbf{F}_{diamagnetic\ 2}$ of NO being the same as N_2 given by Eqs. (13.621-13.624), respectively, $\mathbf{F}_{ele}$, $\mathbf{F}_{mag\ 2}$, and $\mathbf{F}_{diamagnetic\ 2}$ are also the same as those of CN (Eqs. (13.820) and (13.822-13.823)). In the N_2 and CN cases, the contribution of a $2p$ electron from the N atom in the formation of the σ MO gives rise to an additional paramagnetic force on the remaining two $2p$ electrons that pair. However, the force, $\mathbf{F}_{mag\ 3}$, is absent in NO since the single outer electron is unpaired.

The radius of the $2p$ shell is calculated by equating the outward centrifugal force to the sum of the electric (Eq. (13.917)) and diamagnetic (Eqs. (13.918) and (13.920)), and paramagnetic (Eq. (13.919)) forces as follows:

$$\frac{m_e v_5^2}{r_5} = \left(\begin{array}{l}\frac{(Z-4)e^2}{4\pi\varepsilon_0 r_5^2} - \frac{\hbar^2}{12 m_e r_5^2 r_3}\sqrt{s(s+1)} + \frac{3\hbar^2}{Z m_e r_5^2 r_3}\sqrt{s(s+1)} \\ -\left[\frac{Z-5}{Z-4}\right]\left(1-\frac{\sqrt{2}}{2}\right)\frac{r_3\hbar^2}{r_5^4 m_e}10\sqrt{s(s+1)}\end{array}\right) \tag{13.921}$$

Substitution of $v_5 = \frac{\hbar}{m_e r_5}$ (Eq. (1.35)) and $s = \frac{1}{2}$ into Eq. (13.921) gives:

$$\frac{\hbar^2}{m_e r_5^3} = \frac{(Z-4)e^2}{4\pi\varepsilon_0 r_5^2} - \frac{\hbar^2}{12 m_e r_5^2 r_3}\sqrt{\frac{3}{4}} + \frac{3\hbar^2}{Z m_e r_5^2 r_3}\sqrt{\frac{3}{4}} - \left[\frac{Z-5}{Z-4}\right]\left(1-\frac{\sqrt{2}}{2}\right)\frac{r_3\hbar^2}{r_5^4 m_e}10\sqrt{\frac{3}{4}} \tag{13.922}$$

The quadratic equation corresponding to Eq. (13.922) is

$$r_5^2 - \frac{\frac{\hbar^2}{m_e}}{\left(\frac{(Z-4)e^2}{4\pi\varepsilon_0} - \left(\frac{1}{12}-\frac{3}{Z}\right)\frac{\hbar^2}{m_e r_3}\sqrt{\frac{3}{4}}\right)}r_5 - \frac{\frac{\hbar^2}{m_e}\left[\frac{Z-5}{Z-4}\right]\left(1-\frac{\sqrt{2}}{2}\right)r_3 10\sqrt{\frac{3}{4}}}{\left(\frac{(Z-4)e^2}{4\pi\varepsilon_0} - \left(\frac{1}{12}-\frac{3}{Z}\right)\frac{\hbar^2}{m_e r_3}\sqrt{\frac{3}{4}}\right)} = 0 \tag{13.923}$$

The solution of Eq. (13.923) using the quadratic formula is:

$$r_5 = \frac{\frac{a_0}{\left((Z-4) - \left(\frac{1}{12}-\frac{3}{Z}\right)\frac{\sqrt{3}}{2r_3}\right)} \pm a_0\sqrt{\left(\frac{1}{\left((Z-4) - \left(\frac{1}{12}-\frac{3}{Z}\right)\frac{\sqrt{3}}{2r_3}\right)}\right)^2 + \frac{20\sqrt{3}\left(\left[\frac{Z-5}{Z-4}\right]\left(1-\frac{\sqrt{2}}{2}\right)r_3\right)}{\left((Z-4) - \left(\frac{1}{12}-\frac{3}{Z}\right)\frac{\sqrt{3}}{2r_3}\right)}}}{2}, \; r_3 \text{ in units of } a_0 \tag{13.924}$$

The positive root of Eq. (13.924) must be taken in order that $r_5 > 0$. Substitution of $\frac{r_3}{a_0} = 0.69385$ (Eq. (10.62) with $Z = 7$) into Eq. (13.924) gives:

$$r_5 = 0.74841 a_0 \tag{13.925}$$

FORCE BALANCE OF THE $2p$ SHELL OF THE OXYGEN ATOM OF THE NITRIC OXIDE RADICAL

For the O atom, force balance for the outermost $2p$ electron of NO (electron 6) is achieved between the centrifugal force and the Coulombic and magnetic forces that arise due to interactions between electron 6 and the other $2p$ electron as well as the $2s$-shell electrons due to spin and orbital angular momentum. The forces used are derived in the Eight-Electron Atoms section. The central Coulomb force on the outer-most $2p$ shell electron of NO (electron 6) due to the nucleus and the inner five electrons is given by Eq. (10.70) with the appropriate charge and radius:

$$\mathbf{F}_{ele} = \frac{(Z-5)e^2}{4\pi\varepsilon_0 r_6^2}\mathbf{i}_\mathbf{r} \tag{13.926}$$

for $r > r_5$. The $2p$ shell possess an external electric field of +2 given by Eq. (10.92) for $r > r_6$. The energy is minimized with conservation of angular momentum. This condition is met when the diamagnetic force, $\mathbf{F}_{diamagnetic}$, of Eq. (10.82) due to the p-orbital contribution is given by:

$$\begin{aligned}\mathbf{F}_{diamagnetic} &= -\left(\frac{2}{3}\right)\frac{\hbar^2}{4m_e r_6^2 r_3}\sqrt{s(s+1)}\mathbf{i}_\mathbf{r} \\ &= -\frac{2\hbar^2}{12m_e r_6^2 r_3}\sqrt{\frac{3}{4}}\mathbf{i}_\mathbf{r}\end{aligned} \tag{13.927}$$

And, $\mathbf{F}_{mag\ 2}$ corresponding to the conserved spin and orbital angular momentum given by Eqs. (10.157) and (13.670) is:

$$\mathbf{F}_{mag\ 2} = \frac{1}{Z}\frac{2\hbar^2}{m_e r_6^2 r_3}\sqrt{s(s+1)}\mathbf{i}_\mathbf{r} \tag{13.928}$$

The electric field external to the $2p$ shell given by Eq. (10.92) for $r > r_6$ gives rise to a second diamagnetic force, $\mathbf{F}_{diamagnetic\ 2}$, given by Eq. (10.93). $\mathbf{F}_{diamagnetic\ 2}$ due to the binding of the p-orbital electron having an electric field of +2 outside of its radius is:

$$\mathbf{F}_{diamagnetic\ 2} = -\left[\frac{Z-6}{Z-5}\right]\left(1-\frac{\sqrt{2}}{2}\right)\frac{r_3\hbar^2}{m_e r_6^4}10\sqrt{s(s+1)}\mathbf{i}_\mathbf{r} \tag{13.929}$$

In addition, the contribution of two $2p$ electrons in the formation of the σ MO gives rise to a paramagnetic force on the remaining paired $2p$ electrons. The force $\mathbf{F}_{mag\ 3}$ is given by Eq. (13.625) wherein the radius is r_6:

$$\mathbf{F}_{mag\ 3} = \frac{\hbar^2}{4m_e r_6^3}\sqrt{s(s+1)}\mathbf{i}_\mathbf{r} \tag{13.930}$$

The radius of the $2p$ shell is calculated by equating the outward centrifugal force to the sum of the electric (Eq. (13.926)) and diamagnetic (Eqs. (13.927) and (13.929)), and paramagnetic (Eqs. (13.928) and (13.930)) forces as follows:

$$\frac{m_e v_6^2}{r_6} = \left(\begin{array}{l}\frac{(Z-5)e^2}{4\pi\varepsilon_0 r_6^2} - \frac{2\hbar^2}{12m_e r_6^2 r_3}\sqrt{s(s+1)} + \frac{2\hbar^2}{Zm_e r_6^2 r_3}\sqrt{s(s+1)} \\ -\left[\frac{Z-6}{Z-5}\right]\left(1-\frac{\sqrt{2}}{2}\right)\frac{r_3\hbar^2}{r_6^4 m_e}10\sqrt{s(s+1)} + \frac{\hbar^2}{4m_e r_6^3}\sqrt{s(s+1)}\end{array}\right) \tag{13.931}$$

Substitution of $v_6 = \frac{\hbar}{m_e r_6}$ (Eq. (1.35)) and $s = \frac{1}{2}$ into Eq. (13.931) gives:

$$\frac{\hbar^2}{m_e r_6^3} - \frac{\hbar^2}{4m_e r_6^3}\sqrt{\frac{3}{4}} = \frac{(Z-5)e^2}{4\pi\varepsilon_0 r_6^2} - \frac{2\hbar^2}{12m_e r_6^2 r_3}\sqrt{\frac{3}{4}} + \frac{2\hbar^2}{Zm_e r_6^2 r_3}\sqrt{\frac{3}{4}} - \left[\frac{Z-6}{Z-5}\right]\left(1-\frac{\sqrt{2}}{2}\right)\frac{r_3\hbar^2}{r_6^4 m_e}10\sqrt{\frac{3}{4}} \tag{13.932}$$

The quadratic equation corresponding to Eq. (13.932) is:

$$r_6^2 - \frac{\frac{\hbar^2}{m_e}\left(1-\frac{\sqrt{3}}{8}\right)}{\left(\frac{(Z-5)e^2}{4\pi\varepsilon_0} - \left(\frac{2}{12}-\frac{2}{Z}\right)\frac{\hbar^2}{m_e r_3}\sqrt{\frac{3}{4}}\right)}r_6 - \frac{\frac{\hbar^2}{m_e}\left[\frac{Z-6}{Z-5}\right]\left(1-\frac{\sqrt{2}}{2}\right)r_3 10\sqrt{\frac{3}{4}}}{\left(\frac{(Z-5)e^2}{4\pi\varepsilon_0} - \left(\frac{2}{12}-\frac{2}{Z}\right)\frac{\hbar^2}{m_e r_3}\sqrt{\frac{3}{4}}\right)} = 0 \tag{13.933}$$

The solution of Eq. (13.933) using the quadratic formula is:

$$r_6 = \frac{\dfrac{a_0\left(1-\dfrac{\sqrt{3}}{8}\right)}{\left((Z-5)-\left(\dfrac{2}{12}-\dfrac{2}{Z}\right)\dfrac{\sqrt{3}}{2r_3}\right)} \pm a_0\sqrt{\left(\dfrac{1-\dfrac{\sqrt{3}}{8}}{\left((Z-5)-\left(\dfrac{2}{12}-\dfrac{2}{Z}\right)\dfrac{\sqrt{3}}{2r_3}\right)}\right)^2 + \dfrac{20\sqrt{3}\left(\left[\dfrac{Z-6}{Z-5}\right]\left(1-\dfrac{\sqrt{2}}{2}\right)r_3\right)}{\left((Z-5)-\left(\dfrac{2}{12}-\dfrac{2}{Z}\right)\dfrac{\sqrt{3}}{2r_3}\right)}}}{2}, \; r_3 \text{ in units of } a_0 \tag{13.934}$$

The positive root of Eq. (13.934) must be taken in order that $r_6 > 0$. Substitution of $\frac{r_3}{a_0} = 0.59020$ (Eq. (10.62) with $Z = 8$) into Eq. (13.934) gives:

$$r_6 = 0.70460 a_0 \tag{13.935}$$

ENERGIES OF THE $2p$ SHELLS OF THE NITROGEN ATOM AND OXYGEN ATOM OF THE NITRIC OXIDE RADICAL

With the formation of the H_2-type MO by the contribution of two $2p$ electrons from each of the N and O atoms, the total energy of the NO molecule, which is subtracted from the sum of the energies of the nitrogen and oxygen atoms to determine the bond energy, is increased by the ionization energies of N^+ and O^+ given by Eqs. (10.132-10.133) and (10.152-10.153), respectively. Experimentally, the energies are [6] :

$$E(\textit{ionization};\ N^+) = 29.6013\ eV \tag{13.936}$$

$$E(\textit{ionization};\ O^+) = 35.11730\ eV \tag{13.937}$$

In addition, the central forces on the $2p$ shells of the N and O atoms are increased with the formation of the σ MO which reduces each shell's radius and increases its total energy. The Coulombic energy terms of the total energy of the N and O atoms at the new radii are calculated and added to the ionization energies of N^+ and O^+, and the energy of the σ MO to give the total energy of NO. Then, the bond energy is determined from the total NO energy.

The radius r_7 of the nitrogen atom before bonding is given by Eq. (10.142):

$$r_7 = 0.93084 a_0 \tag{13.938}$$

Using the initial radius r_7 of the N atom and the final radius r_5 of the $N2p$ shell (Eq. (13.925)) and by considering that the central Coulombic field decreases by an integer for each successive electron of the shell, the sum $E_T(N,2p)$ of the Coulombic energy change of the $N2p$ electrons of the N atom is determined using Eq. (10.102):

$$E_T(N,2p) = -\sum_{n=4}^{4}\frac{(Z-n)e^2}{8\pi\varepsilon_0}\left(\frac{1}{r_5}-\frac{1}{r_7}\right) = -(13.60580\ eV)(0.26186)(3) = -10.68853\ eV \tag{13.939}$$

The radius r_8 of the oxygen atom before bonding is given by Eq. (10.162):

$$r_8 = a_0 \tag{13.940}$$

Using the initial radius r_8 of the O atom and the final radius r_6 of the $O2p$ shell (Eq. (13.935)) and by considering that the central Coulombic field decreases by an integer for each successive electron of the shell, the sum $E_T(O,2p)$ of the Coulombic energy change of the $O2p$ electrons of the O atom is determined using Eq. (10.102):

$$E_T(O,2p) = -\sum_{n=4}^{5}\frac{(Z-n)e^2}{8\pi\varepsilon_0}\left(\frac{1}{r_6}-\frac{1}{r_8}\right) = -(13.60580\ eV)(0.41925)(3+4) = -39.92918\ eV \tag{13.941}$$

FORCE BALANCE OF THE σ MO OF THE NITRIC OXIDE RADICAL

The force balance can be considered due to a second pair of two electrons binding to a molecular ion having $+2e$ at each focus and a first bound pair. Then, the forces are the same as those of a molecule ion having $+e$ at each focus. The diamagnetic force $\mathbf{F}_{diamagneticMO1}$ for the σ-MO of the NO molecule due to the two paired electrons in the $O2p$ shell is given by Eq. (13.633) with: $n_e = 2$:

$$\mathbf{F}_{diamagneticMO1} = \frac{\hbar^2}{2m_e a^2 b^2} D\mathbf{i}_\xi \tag{13.942}$$

$\mathbf{F}_{diamagneticMO2}$ of the nitric oxide radical comprising nitrogen with charge $Z_1 = 7$ and $|L_1| = \hbar$ and $|L_2| = \sqrt{\frac{3}{4}}\hbar$ and oxygen with $Z_2 = 8$ and $|L_3| = \hbar$ is given by the corresponding sum of the contributions. Using Eq. (13.835), $\mathbf{F}_{diamagneticMO2}$ for NO is:

$$\mathbf{F}_{diamagneticMO2} = \left(\frac{1}{Z_1} + \frac{\sqrt{\frac{3}{4}}}{Z_1} + \frac{1}{Z_2} \right) \frac{\hbar^2}{2m_e a^2 b^2} D\mathbf{i}_\xi \tag{13.943}$$

The general force balance equation for the σ-MO of the nitric oxide radical given by Eqs. (11.200), (13.633-13.634), and (13.942-13.943) is the same as that of CN (Eq. (13.836)):

$$\frac{\hbar^2}{m_e a^2 b^2} D = \frac{e^2}{8\pi\varepsilon_0 a b^2} D + \frac{\hbar^2}{2m_e a^2 b^2} D - \left(1 + \frac{1}{Z_1} + \frac{\sqrt{\frac{3}{4}}}{Z_1} + \frac{1}{Z_2} \right) \frac{\hbar^2}{2m_e a^2 b^2} D \tag{13.944}$$

$$\frac{\hbar^2}{m_e a^2 b^2} D = \frac{e^2}{8\pi\varepsilon_0 a b^2} D - \left(\frac{1}{Z_1} + \frac{\sqrt{\frac{3}{4}}}{Z_1} + \frac{1}{Z_2} \right) \frac{\hbar^2}{2m_e a^2 b^2} D \tag{13.945}$$

$$\left(2 + \frac{1}{Z_1} + \frac{\sqrt{\frac{3}{4}}}{Z_1} + \frac{1}{Z_2} \right) \frac{\hbar^2}{2m_e a^2 b^2} D = \frac{e^2}{8\pi\varepsilon_0 a b^2} D \tag{13.946}$$

$$a = \left(2 + \frac{1}{Z_1} + \frac{\sqrt{\frac{3}{4}}}{Z_1} + \frac{1}{Z_2} \right) a_0 \tag{13.947}$$

Substitution of $Z_1 = 7$ and $Z_2 = 8$ into Eq. (13.947) gives:

$$a = 2.39158 a_0 = 1.26557\ X\ 10^{-10}\ m \tag{13.948}$$

Substitution of Eq. (13.948) into Eq. (11.79) is:

$$c' = 1.09352 a_0 = 5.78666\ X\ 10^{-11}\ m \tag{13.949}$$

The internuclear distance given by multiplying Eq. (13.949) by two is:

$$2c' = 2.18704 a_0 = 1.15733\ X\ 10^{-10}\ m \tag{13.950}$$

The experimental bond distance is [28]:

$$2c' = 1.15077\ X\ 10^{-10}\ m \tag{13.951}$$

Substitution of Eqs. (13.948-13.949) into Eq. (11.80) is:

$$b = c = 2.12693 a_0 = 1.12552\ X\ 10^{-10}\ m \tag{13.952}$$

Substitution of Eqs. (13.948-13.949) into Eq. (11.67) is:

$$e = 0.45724 \tag{13.953}$$

Using the electron configuration of NO (Eq. (13.916)), the radii of the $N1s = 0.14605 a_0$ (Eq. (10.51)), $N2s = 0.69385 a_0$ (Eq. (10.62)), $N2p = 0.74841 a_0$ (Eq. (13.925)), $O1s = 0.12739 a_0$ (Eq. (10.51)), $O2s = 0.59020 a_0$ (Eq. (10.62)), and $O2p = 0.70460 a_0$ (Eq. (13.935)) shells and the parameters of the σ MO of NO given by Eqs. (13.3-13.4), (13.948-13.950), and (13.952-13.953), the dimensional diagram and charge-density of the NO MO are shown in Figures 13.26 and 13.27, respectively.

Figure 13.26. The cross section of the NO MO showing the axes, σ MO (H_2-type ellipsoidal MO) with four paired electrons, with the N $1s$, $2s$, and $2p$ atomic orbitals (AOs) and the O $1s$, $2s$, and $2p$ AOs. Legend: a: semimajor axis, b: semiminor axis, c': internuclear distance, r_5: radius of the $N2p$ shell having two paired electrons, r_6: radius of the $O2p$ shell having two paired electrons.

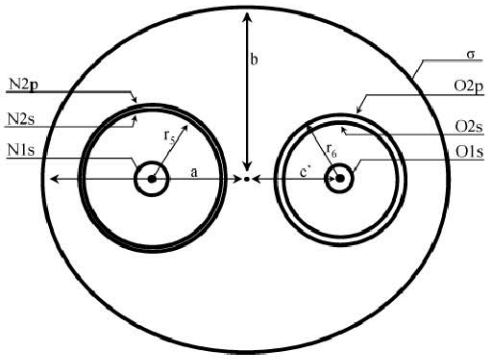

Figure 13.27. NO MO comprising the σ MO (H_2-type MO) with N and O atoms at the foci that have each donated two electrons to the σ MO and have smaller radii and higher binding energies as a consequence. (A) Color scale, translucent view of the charge-density of the NO MO. (B) Off-center cut-away view showing the complete inner most $N1s$ shell, and moving radially, the $N2s$ shell, the $N2p$ shell, and the σ prolate spheroidal MO that has the N atom as a focus. Moving radially from the oxygen-atom focus, the complete inner most $O1s$ shell, the $O2s$ shell, the $O2p$ shell, and the σ prolate spheroidal MO are shown.

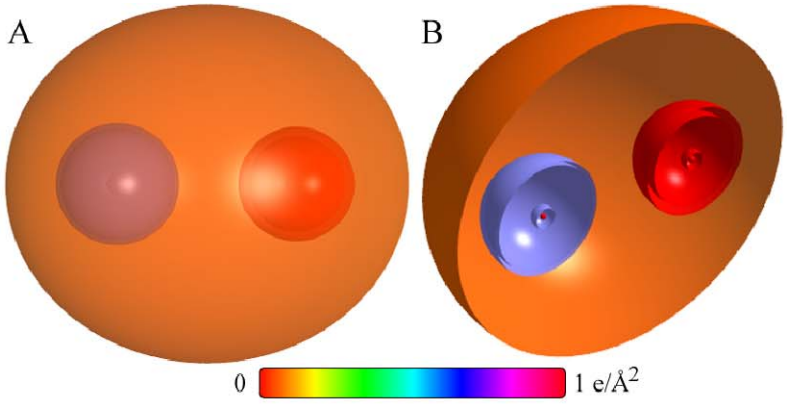

SUM OF THE ENERGIES OF THE σ MO AND THE AOs OF THE NITRIC OXIDE RADICAL

The energies of the NO σ MO are given by the substitution of the semiprincipal axes (Eqs. (13.948-13.949) and (13.952)) into the energy equations (Eqs. (11.207-11.212)) of H_2 except that the terms based on charge are multiplied by four and the kinetic energy term is multiplied by two due to the σ-MO double bond with two pairs of paired electrons:

$$V_e = 2^2 \frac{-2e^2}{8\pi\varepsilon_0\sqrt{a^2-b^2}} \ln\frac{a+\sqrt{a^2-b^2}}{a-\sqrt{a^2-b^2}} = -98.30623\ eV \tag{13.954}$$

$$V_p = 2^2 \frac{e^2}{8\pi\varepsilon_0\sqrt{a^2-b^2}} = 49.76880\ eV \tag{13.955}$$

$$T = 2\frac{\hbar^2}{2m_e a\sqrt{a^2-b^2}} \ln\frac{a+\sqrt{a^2-b^2}}{a-\sqrt{a^2-b^2}} = 10.27631\ eV \tag{13.956}$$

$$V_m = 2^2 \frac{-\hbar^2}{4m_e a\sqrt{a^2-b^2}} \ln\frac{a+\sqrt{a^2-b^2}}{a-\sqrt{a^2-b^2}} = -10.27631\ eV \tag{13.957}$$

$$E_T = V_e + T + V_m + V_p \tag{13.958}$$

Substitution of Eqs. (11.79) and (13.954-13.957) into Eq. (13.958) gives:

$$E_T(NO,\sigma) = \frac{-e^2}{8\pi\varepsilon_0\sqrt{\frac{aa_0}{2}}}\left(8\ln\frac{a+\sqrt{\frac{aa_0}{2}}}{a-\sqrt{\frac{aa_0}{2}}} - 4\right) = -48.53743\ eV \tag{13.959}$$

where $E_T(NO,\sigma)$ is the total energy of the σ MO of NO. The total energy of NO, $E_T(NO)$, is given by the sum of $E(ionization; N^+)$, the energy of the second electron of nitrogen (Eq. (13.936)) donated to the double bond, $E(ionization; O^+)$, the energy of the second electron of oxygen (Eq. (13.937)) donated to the double bond, $E_T(N,2p)$, the $N2p$ AO contribution

due to the decrease in radius with bond formation (Eq. (13.939)), $E_T\left(O,2p\right)$, the $O2p$ AO contribution due to the decrease in radius with bond formation (Eq. (13.941)), and $E_T\left(NO,\sigma\right)$, the σ MO contribution given by Eq. (13.959).

$$E_T\left(NO\right)=\begin{pmatrix}E(ionization;\ N^+)+E(ionization;\ O^+)\\+E_T\left(N,2p\right)+E_T\left(O,2p\right)+E_T\left(NO,\sigma\right)\end{pmatrix}=\begin{pmatrix}29.6013\ eV+35.11730\ eV\\-10.68853\ eV-39.92918\ eV-48.53743\ eV\end{pmatrix}$$
$$=-34.43653\ eV \tag{13.960}$$

VIBRATION OF *NO*

The vibrational energy levels of NO may be solved by determining the Morse potential curve from the energy relationships for the transition from a N atom and O atom whose parameters are given by Eqs. (10.134-10.143) and (10.154-10.163), respectively, to a N atom whose parameter r_5 is given by Eq. (13.925), an O atom whose parameter r_6 is given by Eq. (13.935), and the σ MO whose parameters are given by Eqs. (13.948-13.950) and (13.952-13.953). As shown in the Vibration of Hydrogen-type Molecular Ions section, the harmonic oscillator potential energy function can be expanded about the internuclear distance and expressed as a Maclaurin series corresponding to a Morse potential after Karplus and Porter (K&P) [15] and after Eq. (11.134). Treating the Maclaurin series terms as anharmonic perturbation terms of the harmonic states, the energy corrections can be found by perturbation methods.

THE DOPPLER ENERGY TERMS OF THE NITRIC OXIDE RADICAL

The equations of the radiation reaction force of nitric oxide are the same as those of H_2 with the substitution of the NO parameters except that there is a factor of four increase in the central force in Eq. (11.231) due to the double bond. Using Eqs. (11.231-11.233) and (13.901), the angular frequency of the reentrant oscillation in the transition state is

$$\omega=\sqrt{\frac{\frac{4e^2}{4\pi\varepsilon_0 a^3}}{m_e}}=2.23557\ X\ 10^{16}\ rad/s \tag{13.961}$$

where a is given by Eq. (13.948). The kinetic energy, E_K, is given by Planck's equation (Eq. (11.127)):

$$\bar{E}_K=\hbar\omega=\hbar 2.23557\ X\ 10^{16}\ rad/s=14.71493\ eV \tag{13.962}$$

In Eq. (11.181), substitution of $E_T\left(NO\right)$ for $E_{h\nu}$, the mass of the electron, m_e, for M, and the kinetic energy given by Eq. (13.962) for $\bar{E}_K$ gives the Doppler energy of the electrons of the reentrant orbit:

$$\bar{E}_D\cong E_{h\nu}\sqrt{\frac{2\bar{E}_K}{Mc^2}}=-34.43653\ eV\sqrt{\frac{2e\left(14.71493\ eV\right)}{m_e c^2}}=-0.26134\ eV \tag{13.963}$$

In addition to the electrons, the nuclei also undergo simple harmonic oscillation in the transition state at their corresponding frequency. The decrease in the energy of the NO MO due to the reentrant orbit in the transition state corresponding to simple harmonic oscillation of the electrons and nuclei, $\bar{E}_{osc}$, is given by the sum of the corresponding energies, $\bar{E}_D$ given by Eq. (13.963) and $\bar{E}_{Kvib}$, the average kinetic energy of vibration which is 1/2 of the vibrational energy. Using the experimental NO ω_e of 1904.20 cm^{-1} $\left(0.23609\ eV\right)$ [28] for $\bar{E}_{Kvib}$ of the transition state, $\bar{E}'_{osc}\left(NO\right)$ per bond is:

$$\bar{E}'_{osc}\left(NO\right)=\bar{E}_D+\bar{E}_{Kvib}=\bar{E}_D+\frac{1}{2}\hbar\sqrt{\frac{k}{\mu}} \tag{13.964}$$

$$\bar{E}'_{osc}\left(NO\right)=-0.26134\ eV+\frac{1}{2}\left(0.23609\ eV\right)=-0.14329\ eV \tag{13.965}$$

Since the σ MO bond is a double bond with twice a many electrons as a single bond, $\bar{E}'_{osc}\left(NO\right)$ is multiplied by two to give:

$$\bar{E}_{osc}\left(NO\right)=-0.28658\ eV \tag{13.966}$$

TOTAL AND BOND ENERGIES OF THE NITRIC OXIDE RADICAL

$E_{T+osc}(NO)$, the total energy of NO including the Doppler term, is given by the sum of $E_T(NO)$ (Eq. (13.960)) and $\bar{E}_{osc}(NO)$ given by Eq. (13.966).

$$\begin{aligned} E_{T+osc}(NO) &= \begin{pmatrix} V_e + T + V_m + V_p + E(ionization;\ N^+) + E(ionization;\ O^+) \\ + E_T(N,2p) + E_T(O,2p) + \bar{E}_{osc}(NO) \end{pmatrix} \\ &= \begin{pmatrix} E_T(NO,\sigma) + E(ionization;\ N^+) + E(ionization;\ O^+) \\ + E_T(N,2p) + E_T(O,2p) + \bar{E}_{osc}(NO) \end{pmatrix} \\ &= E_T(NO) + \bar{E}_{osc}(NO) \end{aligned} \tag{13.967}$$

$$E_{T+osc}(NO) = \left\{ \begin{pmatrix} \dfrac{-e^2}{8\pi\varepsilon_0\sqrt{\dfrac{aa_0}{2}}} \left(8\ln\dfrac{a+\sqrt{\dfrac{aa_0}{2}}}{a-\sqrt{\dfrac{aa_0}{2}}} - 4 \right) \\ + E(ionization;\ N^+) + E(ionization;\ O^+) \\ - \sum_{N,n=4}^{4} \dfrac{(Z-n)e^2}{8\pi\varepsilon_0}\left(\dfrac{1}{r_5} - \dfrac{1}{r_7}\right) - \sum_{O,n=4}^{5} \dfrac{(Z-n)e^2}{8\pi\varepsilon_0}\left(\dfrac{1}{r_6} - \dfrac{1}{r_8}\right) \end{pmatrix} \right\} \\ \left(1 + 2\sqrt{\dfrac{2\hbar\sqrt{\dfrac{4e^2}{4\pi\varepsilon_0 a^3 m_e}}}{m_e c^2}} \right) + 2\left(\frac{1}{2}\hbar\sqrt{\frac{k}{\mu}}\right) \\ = -34.43653\ eV - 2(0.26134\ eV) + 2\left(\frac{1}{2}\hbar\sqrt{\frac{k}{\mu}}\right) \end{aligned} \tag{13.968}$$

From Eqs. (13.966-13.968), the total energy of the NO MO is:

$$E_{T+osc}(NO) = -34.43653\ eV + \bar{E}_{osc}(NO) = -34.43653\ eV + (-0.28658) = -34.72312\ eV \tag{13.969}$$

where the experimental ω_e was used for the $\hbar\sqrt{\dfrac{k}{\mu}}$ term.

The NO bond dissociation energy, $E_D(NO)$, is given by the difference between the sum of the energies of the N and O atoms and $E_{T+osc}(NO)$:

$$E_D(NO) = E(N) + E(O) - E_{T+osc}(NO) \tag{13.970}$$

where the energy of a nitrogen atom is [6]:

$$E(N) = -14.53414\ eV \tag{13.971}$$

and the energy of an oxygen atom is [6]:

$$E(O) = -13.61806\ eV \tag{13.972}$$

Thus, the NO bond dissociation energy, $E_D(NO)$, given by Eqs. (13.969-13.972) is:

$$\begin{aligned} E_D(NO) &= -(14.53414\ eV + 13.61806\ eV) - E_{T+osc}(NO) \\ &= -28.15220\ eV - (-34.72312\ eV) \\ &= 6.57092\ eV \end{aligned} \tag{13.973}$$

The experimental NO bond dissociation energy is [49]:

$$E_{D298}(NO) = 6.5353\ eV \tag{13.974}$$

The results of the determination of bond parameters of NO are given in Table 13.1. The calculated results are based on first principles and given in closed-form, exact equations containing fundamental constants only. The agreement between the experimental and calculated results is excellent.

Table 13.1. The calculated and experimental bond parameters of H_3^+, D_3^+, OH, OD, H_2O, D_2O, NH, ND, NH_2, ND_2, NH_3, ND_3, CH, CD, CH_2, CH_3, CH_4, N_2, O_2, F_2, Cl_2, CN, CO, and NO.

Parameter	Calculated	Experimental	Ref. for Exp.
H_3^+ Bond Energy	4.373 eV	4.373 eV	8
D_3^+ Bond Energy	4.374 eV		
OH Bond Energy	4.4104 eV	4.4117 eV	22
OD Bond Energy	4.4687 eV	4.454 eV	23
OH Bond Length	0.971651 Å	0.971 Å	13
OD Bond Length	0.971651 Å	0.971 Å	13
OH Vibrational Energy	0.4367 eV	0.4424 eV	16-17
OD Vibrational Energy	0.3219 eV	0.3263 eV	16-17
OH ω_e	3696.38 cm^{-1}	3735.21 cm^{-1}	14
OD ω_e	2689.51 cm^{-1}	2720.9 cm^{-1}	14
OH $\omega_e x_e$	87.18 cm^{-1}	82.81 cm^{-1}	14
OD $\omega_e x_e$	46.75 cm^{-1}	44.2 cm^{-1}	14
OH B_e	18.835 cm^{-1}	18.871 cm^{-1}	14
OD B_e	9.971 cm^{-1}	10.01 cm^{-1}	14
H_2O Bond Energy	5.1059 eV	5.0991 eV	26
D_2O Bond Energy	5.178 eV	5.191 eV	31-32
H_2O $O-H$ Bond Length	0.971574 Å	0.970 ± 0.005 Å	23
D_2O $O-D$ Bond Length	0.971574 Å	0.970 ± 0.005 Å	23
H_2O $H-H$ Distance	1.552 Å	1.55 ± 0.01 Å	13
D_2O $D-D$ Distance	1.552 Å	1.55 ± 0.01 Å	13
H_2O Bond Angle	106°	106°	23
D_2O Bond Angle	106°	106°	23
NH Bond Energy	3.47530 eV	3.47 eV	30
ND Bond Energy	3.52556 eV	3.5134 eV	31
NH Bond Length	1.04262 Å	1.0362 Å	28
ND Bond Length	1.04262 Å	1.0361 Å	28
NH Vibrational Energy	0.38581 eV	0.38752 eV	28
ND Vibrational Energy	0.28583 eV	0.28690 eV	28
NH ω_e	3284.58 cm^{-1}	3282.3 cm^{-1}	28
ND ω_e	2398.72 cm^{-1}	2398 cm^{-1}	28
NH $\omega_e x_e$	86.37 cm^{-1}	78.4 cm^{-1}	28
ND $\omega_e x_e$	47.40 cm^{-1}	42 cm^{-1}	28
NH B_e	16.495 cm^{-1}	16.993 cm^{-1}	28
ND B_e	8.797 cm^{-1}	8.7913 cm^{-1}	28
NH_2 Bond Energy	3.9323 eV	3.9461 eV	35
ND_2 Bond Energy	3.9401 eV	3.9362 eV	33-35
NH_2 Bond Length	1.04262 Å	1.0240 Å	32
ND_2 Bond Length	1.04262 Å		
NH_2 Bond Angle	105.97°	103.3°	32
ND_2 Bond Angle	105.97°		
NH_3 Bond Energy	4.57913 eV	4.60155 eV	37
ND_3 Bond Energy	4.64499 eV	4.71252 eV	37
NH_3 Bond Length	1.0368 Å	1.012 Å	32
ND_3 Bond Length	1.0368 Å		
NH_3 Bond Angle	106.67°	106.67°	36
ND_3 Bond Angle	106.67°	106.70°	36
CH Bond Energy	3.47404 eV	3.47 eV	14

Parameter	Calculated	Experimental	Ref. for Exp.
CD Bond Energy	3.51673 eV	3.52 eV	14
CH Bond Length	1.1183 Å	1.1198 Å	14
CD Bond Length	1.1183 Å	1.118 Å	14
CH Vibrational Energy	0.33879 eV	0.33885 eV	14
CD Vibrational Energy	0.25173 eV	0.25189 eV	14
CH ω_e	2865.86 cm^{-1}	2861.6 cm^{-1}	14
CD ω_e	2102.97 cm^{-1}	2101.0 cm^{-1}	14
CH $\omega_e x_e$	66.624 cm^{-1}	64.3 cm^{-1}	14
CD $\omega_e x_e$	36.335 cm^{-1}	34.7 cm^{-1}	14
CH B_e	14.498 cm^{-1}	14.457 cm^{-1}	14
CD B_e	7.807 cm^{-1}	7.808 cm^{-1}	14
CH_2 Bond Energy	4.36968 eV	4.33064 eV	39
CH_2 Bond Length	1.1067 Å	1.111 Å	38
CH_2 Bond Angle	100.22°	102.4°	38
CH_3 Bond Energy	4.70075 eV	4.72444 eV	40
CH_3 Bond Length	1.1029 Å	1.079 Å	38
CH_3 Bond Angle	120°	120°	38
CH_4 Bond Energy	4.4900 eV	4.48464 eV	40
CH_4 Bond Length	1.1010 Å	1.087 Å	41
CH_4 Bond Angle	109.5°	109.5°	41
N_2 Bond Energy	9.71181 eV	9.756 eV	43
N_2 Bond Length	1.0955 Å	1.094 Å	43
O_2 Bond Energy	5.10711 eV	5.11665 eV	46
O_2 Bond Length	1.20862 Å	1.20752 Å	28
F_2 Bond Energy	1.62168 eV	1.606 eV	48
F_2 Bond Length	1.41114 Å	1.41193 Å	28
Cl_2 Bond Energy	2.52236 eV	2.51412 eV	49
Cl_2 Bond Length	1.988 Å	1.988 Å	28
Cl_2 ω_e	538.52 cm^{-1}	559.7 cm^{-1}	28
Cl_2 $\omega_e x_e$	3.41 cm^{-1}	2.68 cm^{-1}	28
Cl_2 B_e	0.2420 cm^{-1}	0.2440 cm^{-1}	28
CN Bond Energy	7.77526 eV	7.7731 eV	50
CN Bond Length	1.17231 Å	1.17181 Å	28
CO Bond Energy	11.16652 eV	11.15696 eV	49
CO Bond Length	1.13290 Å	1.12823 Å	28
NO Bond Energy	6.57092 eV	6.5353 eV	49
NO Bond Length	1.15733 Å	1.15077 Å	28

REFERENCES

1. G. C. Lie, D. Frye, "Vibrational analysis of a Hylleraas-configuration interaction potential for H_3^+," J. Chem. Phys., Vol. 96, No. 9, (1992), pp. 6784-6790.
2. G. R. Fowles, *Analytical Mechanics,* Third Edition, Holt, Rinehart, and Winston, New York, (1977), pp. 251-305.
3. N. V. Sidgwick, *The Chemical Elements and Their Compounds*, Volume I, Oxford, Clarendon Press, (1950), p.17.
4. D. A. McQuarrie, *Quantum Chemistry*, University Science Books, Mill Valley, CA, (1983), p. 172.
5. D. R. Lide, *CRC Handbook of Chemistry and Physics*, 79th Edition, CRC Press, Boca Raton, Florida, (1998-9), p. 10-181.
6. D. R. Lide, *CRC Handbook of Chemistry and Physics*, 79th Edition, CRC Press, Boca Raton, Florida, (1998-9), p. 10-175.
7. P. W. Atkins, *Physical Chemistry*, 2nd Edition, W. H. Freeman, San Francisco, (1982), p. 589.
8. P. C. Cosby, H. Helm, "Experimental determination of the H_3^+ bond dissociation energy," Vol. 152, No. 1, (1988), pp. 71-74.
9. K. P. Huber, G. Herzberg, *Molecular Spectra and Molecular Structure, IV. Constants of Diatomic Molecules*, Van Nostrand Reinhold Company, New York, (1979).
10. NIST Atomic Spectra Database, www.physics.nist.gov/cgi-bin/AtData/display.ksh.
11. G. R. Fowles, *Analytical Mechanics*, Third Edition, Holt, Rinehart, and Winston, New York, (1977), pp. 154-156
12. R. C. Weast, CRC Handbook of Chemistry and Physics, 58th Edition, CRC Press, West Palm Beach, Florida, (1977), p. E-68.
13. P. C. Hariharan, J. A. Pople, Accuracy of AH_n equilibrium geometries by single determinant molecular orbital theory, Mol. Phys., Vol. 27(1), (1974), pp. 209–214.
14. G. Herzberg, J. W. T. Spinks, *Molecular Spectra and Molecular Structure, I. Spectra of Diatomic Molecules*, 2nd Edition, Krieger Publishing Company, Malabar, FL, (1989), p. 560.
15. M. Karplus, R. N. Porter, *Atoms and Molecules an Introduction for Students of Physical Chemistry*, The Benjamin/Cummings Publishing, Menlo Park, CA, (1970), pp. 447-484.
16. K. P. Huber, G. Herzberg, *Molecular Spectra and Molecular Structure, IV. Constants of Diatomic Molecules*, Van Nostrand Reinhold Company, New York, (1979).
17. J. Crovisier, Molecular Database—Constants for molecules of astrophysical interest in the gas phase: photodissociation, microwave and infrared spectra, Ver. 4.2, Observatoire de Paris, Section de Meudon, Meudon, France, May 2002, pp. 34–37, available at http://wwwusr.obspm.fr/~crovisie/.
18. D. R. Lide, *CRC Handbook of Chemistry and Physics*, 79th Edition, CRC Press, Boca Raton, Florida, (1998-9), p. 10-175.
19. NIST Atomic Spectra Database, www.physics.nist.gov/cgi-bin/AtData/display.ksh.
20. J. A. Joens, The dissociation energy of OH($X^2\Pi_{3/2}$) and the enthalpy of formation of OH ($X^2\Pi_{3/2}$), ClOH, and BrOH from thermochemical cycles, J. Phys. Chem., Vol. 105, (2001), pp. 11041–11044.
21. Y.-M. Chen, D.E. Clemmer, P. B. Armentrout, Kinetic and electronic energy dependence of the reactions of Sc^+ and Ti^+ with D_2O, J. Phys. Chem., Vol. 98, (1994), pp. 11490–11498.
22. L. V. Gurvich, I. V. Veyts, C. B. Alcock, *Thermodynamic Properties of Individual Substances*, 4th ed., Hemisphere: New York, 1989, Vol. 1, Part 2.
23. K. Ichikawa, Y. Kameda, T. Yamaguchi, H. Wakita and M. Misawa, Neutron diffraction investigation of the intramolecular structure of a water molecule in the liquid phase at high temperatures, Mol. Phys. Vol. 73, (1991), pp. 79-86.
24. H. A. Haus, J. R. Melcher, *Electromagnetic Fields and Energy*, Department of Electrical Engineering and Computer Science, Massachusetts Institute of Technology, (1985), Sec. 5.4.
25. R. Lemus, "Vibrational excitations in H_2O in the framework of a local model," J. Mol. Spectrosc., Vol. 225, (2004), pp. 73–92.
26. B. Ruscic, A. F. Wagner, L. B. Harding, R. L. Asher, D. Feller, D. A. Dixon, K. A. Peterson, Y. Song, X. Qian, C.-Y. Ng, J. Liu, W. Chen, D. W. Schwenke, On the enthalpy of formation of hydroxyl radical and gas-phase bond dissociation energies of water and hydroxyl, J. Phys. Chem. A, Vol. 106, (2002), pp. 2727–2747.
27. X.-M. Qian, Y. Song, K.-C. Lau, C. Y. Ng, J. Liu, W. Chen, G. Z. He, A pulsed field ionization photoelectron–photoion coincidence study of the dissociative photoionization process $D_2O + h\nu \rightarrow OD^+ + D + e^-$, Chem. Phys. Letts., Vol. 353(1-2), (2002), pp. 19–26.
28. D. R. Lide, *CRC Handbook of Chemistry and Physics*, 79th Edition, CRC Press, Boca Raton, Florida, (1998-9), pp. 9-80 to 9-85.
29. J. B. Marquette, C. Rebrion, B. R. Rowe, "The reactions of $N^+\left(^3P\right)$ ions with normal, para, and deuterated hydrogens at low temperatures," J. Chem. Phys., Vol. 89, (4), (1988), pp. 2041-2047.
30. W. R. Graham, H. Lew, "Spectra of the $d\,^1\Sigma^+ - c^1\Pi$ and $d\,^1\Sigma^+ - b^1\Pi^+$ systems and dissociation energy of NH and ND," Can. J. Phys., Vol. 56, (1978), pp. 85-99.
31. D. R. Lide, *CRC Handbook of Chemistry and Physics*, 79th Edition, CRC Press, Boca Raton, Florida, (1998-9), p. 9-54.
32. D. R. Lide, *CRC Handbook of Chemistry and Physics*, 79th Edition, CRC Press, Boca Raton, Florida, (1998-9), p. 9-20.
33. T. Amano, P. F. Bernath, R. W. McKellar, "Direct observation of the ν_1 and ν_3 fundamental bands of NH_2 by difference frequency laser spectroscopy," J. Mol. Spectrosc., Vol. 94, (1982), pp. 100-113.\

34. A. P. Altshuller, "Heat of formation of $NH(g)$ and the bond dissociation energy of $D(NH-H)$," J. Chem. Phys., Vol. 22, No. 11, (1954), pp. 1947-1948.
35. J. Berkowitz, G. B. Ellison, D. Gutman, "Three methods to measure RH bond energies," J. Phys. Chem., Vol. 98, (1994), pp. 2744-2765.
36. W. S. Benedict, E. K. Plyler, "Vibration-rotation bands of ammonia," Can. J. Phys., Vol. 35, (1957), pp. 1235-1241.
37. D. H. Mordaunt, R. N. Dixon, M. N. R. Ashfold, "Photodissociation dynamics of the $\widetilde{A}$ state ammonia molecules. II. The isotopic dependence for partially and fully deuterated isotopomers," J. Chem. Phys., Vol. 104, (17), (1996), pp. 6472-6481.
38. D. J. DeFrees, B. A. Levi, S. K. Pollack, W. J. Hehre, J. S. Binkley, J. A. Pople, "Effect of correlation on theoretical equilibrium geometries," J. Am. Chem. Soc., 101:15, (1979), pp. 4085-4089.
39. A. G. Csaszar, M. L. Leininger, V. Szalay, "The standard enthalpy of formation of CH_2," J. Chem. Phys., Vol. 118, No. 23, (2003), pp. 10631-10642.
40. B. Ruscic, M. Litorja, R. L. Asher, "Ionization energy of methylene revisited: Improved values for the enthalpy of formation of CH_2 and the bond dissociation energy of CH_3 via simultaneous solution of the local thermodynamic network," J. Phys. Chem. A, Vol. 103, (1999), pp. 8625-8633.
41. D. R. Lide, *CRC Handbook of Chemistry and Physics*, 79th Edition, CRC Press, Boca Raton, Florida, (1998-9), p. 9-34.
42. D. R. Lide, *CRC Handbook of Chemistry and Physics*, 79th Edition, CRC Press, Boca Raton, Florida, (1998-9), pp. 4-130 to 4-135.
43. G. Herzberg, J. W. T. Spinks, *Molecular Spectra and Molecular Structure, I. Spectra of Diatomic Molecules*, 2nd Edition, Krieger Publishing Company, Malabar, FL, (1989), pp. 551-553.
44. 24. J. Itatani, J. Levesque, D. Zeidler, H. Niikura, H. Pepin, J. C. Kieffer, P. B. Corkum, D. M. Villeneuve, Tomographic imaging of molecular orbitals, Nature, Vol. 432, (2004), pp. 867-871.
45. R. H. Christian, R. E. Duff, F. L. Yarger, "Equation of state of gases by shock wave measurements. II. The dissociation energy of nitrogen," J. Chem. Phys., Vol. 23, No. 11, (1955), pp. 2045-2049.
46. K. M. Ervin, I. Anusiewicz, P. Skurski, J. Simons, W. C. Lineberger, The only stable state of O_2^- is the $X^2\Pi_g$ ground state and it (still!) has an adiabatic electron detachment energy of 0.45 eV, J. Phys. Chem. A, Vol. 107, (2003), pp. 8521-8529.
47. P. C. Cosby, D. L. Huestis, On the dissociation energy of O_2 and the energy of the O_2^+ $b\ ^4\Sigma_g^-$ state, J. Chem. Phys., Vol. 97, No. 9, (1992), pp. 6108-6112.
48. J. Yang, Y. Hao, J. Li, C. Zhou, Y. Mo, A combined zero electronic kinetic energy spectroscopy and ion-pair dissociation imaging study of the $F_2^+(X^2\Pi_g)$ structure, J. Chem. Phys., Vol. 122, No. 13, (2005), 134308-1–134308-7.
49. D. R. Lide, *CRC Handbook of Chemistry and Physics*, 79th Edition, CRC Press, Boca Raton, Florida, (1998-9), pp. 9-51 to 9-57.
50. D. R. Lide, *CRC Handbook of Chemistry and Physics*, 86th Edition, Taylor & Francis, Boca Raton, Florida, (2005-6), pp. 9-54 to 9-62.

Chapter 14

MORE POLYATOMIC MOLECULES AND HYDROCARBONS

Additional polyatomic molecules can be solved using similar principles as those used to solve hydrogen molecular ions and molecules wherein the hydrogen molecular orbitals (MOs) and hydrogen atomic orbitals serve as basis functions for the MOs. The MO must (1) be a solution of Laplace's equation to give a equipotential energy surface, (2) correspond to an orbital solution of the Newtonian equation of motion in an inverse-radius-squared central field having a constant total energy, (3) be stable to radiation, and (4) conserve the electron angular momentum of $\hbar$. Energy of the MO must be matched to that of the outermost atomic orbital of a bonding heteroatom in the case where a minimum energy is achieved with a direct bond to the AO. Alternatively, the MO is continuous with the AO containing paired electrons that do not particpate in the bond. Rather, they only provide a means for the energy matched MO to form a continuous equipotential energy surface. In the case that an independent MO is formed, the AO force balance causes the remaining electrons to be at lower energy and a smaller radius. In another case, the atomic orbital may hybridize in order to achieve a bond at an energy minimum, and the sharing of electrons between two or more such orbitals to form a MO permits the participating hybridized orbitals to decrease in energy through a decrease in the radius of one or more of the participating orbitals. Representative cases were solved. Specifically, the results of the determination of bond parameters of carbon dioxide (CO_2), nitrogen dioxide (NO_2), ethane (CH_3CH_3), ethylene (CH_2CH_2), acetylene ($CHCH$), benzene (C_6H_6), propane (C_3H_8), butane (C_4H_{10}), pentane (C_5H_{12}), hexane (C_6H_{14}), heptane (C_7H_{16}), octane (C_8H_{18}), nonane (C_9H_{20}), decane ($C_{10}H_{22}$), undecane ($C_{11}H_{24}$), dodecane ($C_{12}H_{26}$), and octadecane ($C_{18}H_{38}$) are given in Table 14.1. The calculated results are based on first principles and given in closed-form, exact equations containing fundamental constants only. The agreement between the experimental and calculated results is excellent.

CARBON DIOXIDE MOLECULE

The carbon dioxide molecule can be formed by the reaction of carbon monoxide and an oxygen atom:

$$CO + O \rightarrow CO_2 \tag{14.1}$$

Each equivalent bond in the carbon dioxide molecule comprises a double bond that is energy-matched to the filled $C2s$ orbital. Each such bond comprises 75% of a H_2-type MO with four paired electrons as a basis set such that three electrons can be assigned to each $C=O$ bond. Thus, the two $C2p$ electrons combine with the four $O2p$ electrons, two from each O, as a linear combination to form the two $C=O$ bonds of CO_2. The force balance equation and radius r_8 of the $2p$ shell of O is derived in the Eight-Electron Atoms section. With the formation of the H_2-type MOs by the contribution of two $2p$ electrons from each of the two O atoms, a factor of two increase of the central field on the remaining $O2p$ electrons arises. The resulting increased Coulombic as well as magnetic central forces decrease the radii of the $O2p$ shells such that the energy minimum is achieved that is lower than that of the reactant atoms. The resulting electron configuration of CO_2 is $C1s^2O_1 1s^2O_2 1s^2C2s^2O_1 2s^2O_2 2s^2O_1 2p^2O_2 2p^2\sigma^6_{O_2,C,O_1}$ where the subscripts designate the O atom, 1 or 2, σ designates the H_2-type MO, and the orbital arrangement is:

σ state

$\uparrow\downarrow \quad \uparrow\downarrow \quad \uparrow\downarrow$

2p state

$\uparrow\downarrow$ 0 $\qquad$ $\uparrow\downarrow$ 0

2s state

$\uparrow\downarrow \qquad \uparrow\downarrow \qquad \uparrow\downarrow$

1s state

$\uparrow\downarrow$ O $\qquad$ $\uparrow\downarrow$ C $\qquad$ $\uparrow\downarrow$ O (14.2)

Carbon dioxide is predicted to be diamagnetic in agreement with observations [1].

FORCE BALANCE OF THE $2p$ SHELL OF THE OXYGEN ATOM OF THE CARBON DIOXIDE MOLECULE

For each O atom, force balance for the outermost $2p$ electron of CO_2 (electron 6) is achieved between the centrifugal force and the Coulombic and magnetic forces that arise due to interactions between electron 6 and the other $2p$ electrons as well as the $2s$-shell electrons due to spin and orbital angular momentum. The forces used are derived in the Eight-Electron Atoms section. The central Coulomb force on the outer-most $2p$ shell electron of CO (electron 6) due to the nucleus and the inner five electrons is given by Eq. (10.70) with the appropriate charge and radius:

$$\mathbf{F}_{ele} = \frac{(Z-5)e^2}{4\pi\varepsilon_0 r_6^2}\mathbf{i}_\mathbf{r} \tag{14.3}$$

for $r > r_5$. The $2p$ shell possess a +2 external electric field given by Eq. (10.92) for $r > r_6$. The energy is minimized with conservation of angular momentum. This condition is met when the diamagnetic force, $\mathbf{F}_{diamagnetic}$, of Eq. (10.82) due to the p-orbital contribution is given by:

$$\mathbf{F}_{diamagnetic} = -\left(\frac{2}{3}\right)\frac{\hbar^2}{4m_e r_6^2 r_3}\sqrt{s(s+1)}\mathbf{i}_\mathbf{r} = -\frac{2\hbar^2}{12m_e r_6^2 r_3}\sqrt{\frac{3}{4}}\mathbf{i}_\mathbf{r} \tag{14.4}$$

where $s = 1/2$. And, $\mathbf{F}_{mag\ 2}$ corresponding to the conserved spin and orbital angular momentum given by Eq. (10.157) is:

$$\mathbf{F}_{mag\ 2} = \frac{1}{Z}\frac{2\hbar^2}{m_e r_6^2 r_3}\sqrt{s(s+1)}\mathbf{i}_\mathbf{r} \tag{14.5}$$

The electric field external to the $2p$ shell given by Eq. (10.92) for $r > r_6$ gives rise to a second diamagnetic force, $\mathbf{F}_{diamagnetic\ 2}$, given by Eq. (10.93). $\mathbf{F}_{diamagnetic\ 2}$ due to the binding of the p-orbital electron having an electric field of +2 outside of its radius is:

$$\mathbf{F}_{diamagnetic\ 2} = -\left[\frac{Z-6}{Z-5}\right]\left(1-\frac{\sqrt{2}}{2}\right)\frac{r_3\hbar^2}{m_e r_6^4}10\sqrt{s(s+1)}\mathbf{i}_\mathbf{r} \tag{14.6}$$

The radius of the $2p$ shell is calculated by equating the outward centrifugal force to the sum of the electric (Eq. (14.3)) and diamagnetic (Eqs. (14.4) and (14.6)), and paramagnetic (Eq. (14.5)) forces as follows:

$$\frac{m_e v_6^2}{r_6} = \frac{(Z-5)e^2}{4\pi\varepsilon_0 r_6^2} - \frac{2\hbar^2}{12m_e r_6^2 r_3}\sqrt{s(s+1)} + \frac{2\hbar^2}{Zm_e r_6^2 r_3}\sqrt{s(s+1)} - \left[\frac{Z-6}{Z-5}\right]\left(1-\frac{\sqrt{2}}{2}\right)\frac{r_3\hbar^2}{r_6^4 m_e}10\sqrt{s(s+1)} \tag{14.7}$$

Substitution of $v_6 = \frac{\hbar}{m_e r_6}$ (Eq. (1.35)) and $s = \frac{1}{2}$ into Eq. (14.7) gives:

$$\frac{\hbar^2}{m_e r_6^3} = \frac{(Z-5)e^2}{4\pi\varepsilon_0 r_6^2} - \frac{2\hbar^2}{12m_e r_6^2 r_3}\sqrt{\frac{3}{4}} + \frac{2\hbar^2}{Zm_e r_6^2 r_3}\sqrt{\frac{3}{4}} - \left[\frac{Z-6}{Z-5}\right]\left(1-\frac{\sqrt{2}}{2}\right)\frac{r_3\hbar^2}{r_6^4 m_e}10\sqrt{\frac{3}{4}} \tag{14.8}$$

The quadratic equation corresponding to Eq. (14.8) is:

$$r_6^2-\frac{\dfrac{\hbar^2}{m_e}}{\left(\dfrac{(Z-5)e^2}{4\pi\varepsilon_0}-\left(\dfrac{2}{12}-\dfrac{2}{Z}\right)\dfrac{\hbar^2}{m_e r_3}\sqrt{\dfrac{3}{4}}\right)}r_6-\frac{\dfrac{\hbar^2}{m_e}\left[\dfrac{Z-6}{Z-5}\right]\left(1-\dfrac{\sqrt{2}}{2}\right)r_3 10\sqrt{\dfrac{3}{4}}}{\left(\dfrac{(Z-5)e^2}{4\pi\varepsilon_0}-\left(\dfrac{2}{12}-\dfrac{2}{Z}\right)\dfrac{\hbar^2}{m_e r_3}\sqrt{\dfrac{3}{4}}\right)}=0 \tag{14.9}$$

The solution of Eq. (14.9) using the quadratic formula is:

$$r_6=\frac{\dfrac{a_0}{\left((Z-5)-\left(\dfrac{2}{12}-\dfrac{2}{Z}\right)\dfrac{\sqrt{3}}{2r_3}\right)}\pm a_0\sqrt{\left(\dfrac{1}{\left((Z-5)-\left(\dfrac{2}{12}-\dfrac{2}{Z}\right)\dfrac{\sqrt{3}}{2r_3}\right)}\right)^2+\dfrac{20\sqrt{3}\left(\left[\dfrac{Z-6}{Z-5}\right]\left(1-\dfrac{\sqrt{2}}{2}\right)r_3\right)}{\left((Z-5)-\left(\dfrac{2}{12}-\dfrac{2}{Z}\right)\dfrac{\sqrt{3}}{2r_3}\right)}}}{2},\ r_3\ \textit{in units of}\ a_0 \tag{14.10}$$

The positive root of Eq. (14.10) must be taken in order that $r_6>0$. Substitution of $\frac{r_3}{a_0}=0.59020$ (Eq. (10.62) with $Z=8$) into Eq. (14.10) gives:

$$r_6=0.74776a_0 \tag{14.11}$$

ENERGIES OF THE $2s$ AND $2p$ SHELLS OF THE CARBON ATOM AND THE $2p$ SHELL OF THE OXYGEN ATOMS OF THE CARBON DIOXIDE MOLECULE

Consider the determination of the total energy of CO_2 from the reaction of a carbon atom with two oxygen atoms. With the formation of the H_2-type MO by the contribution of two $2p$ electrons from the C atom, the remaining outer-shell atomic electrons comprise the $2s$ electrons which are unchanged by bonding with two oxygen atoms. However, the total energy of the CO_2 molecule, which is subtracted from the sum of the energies of the oxygen atom and carbon monoxide molecule to determine the $O-CO$ bond energy, is increased by the ionization energies of C, C^+, O, and $2O^+$ given by Eqs. (14.12-14.15), respectively. Experimentally, the energies are [2]:

$$E(\textit{ionization};\ C)=11.26030\ eV \tag{14.12}$$

$$E(\textit{ionization};\ C^+)=24.38332\ eV \tag{14.13}$$

$$E(\textit{ionization};\ O)=13.61806\ eV \tag{14.14}$$

$$E(\textit{ionization};\ O^+)=35.11730\ eV \tag{14.15}$$

In addition, the central forces on the $2p$ shell of the O atom are increased with the formation of the σ MO which reduces the shell's radius and increases its total energy. The Coulombic energy terms of the total energy of each O atom at the new radius are calculated and added to the ionization energies of C, C^+, O, and $2O^+$, and the energy of the σ MO to give the total energy of CO_2. Then, the bond energy is determined from the total CO_2 energy.

The radius r_8 of each oxygen atom before bonding is given by Eq. (10.162):

$$r_8=a_0 \tag{14.16}$$

Using the initial radius r_8 of each O atom and the final radius r_6 of the $O2p$ shell (Eq. (14.11)) and by considering that the central Coulombic field decreases by an integer for each successive electron of the shell, the sum $E_T(O,2p)$ of the Coulombic energy change of the $O2p$ electrons of each O atom is determined using Eq. (10.102):

$$E_T(O,2p)=-\sum_{n=4}^{5}\frac{(Z-n)e^2}{8\pi\varepsilon_0}\left(\frac{1}{r_6}-\frac{1}{r_8}\right)=-(13.60580\ eV)(0.33733)(3+4)=-32.12759\ eV \tag{14.17}$$

FORCE BALANCE OF THE σ MO OF THE CARBON DIOXIDE MOLECULE

As in the case of H_2, the σ MO is a prolate spheroid with the exception that the ellipsoidal MO surface cannot extend into the C atom for distances shorter than the radius of the $C2s$ shell; nor, can it extend into the O atom for distances shorter than the radius of the $O2p$ shell. Thus, the MO surface of each $C=O$ bond comprises a prolate spheroid that bridges and is continuous with the $2s$ and $2p$ shells of the O and C atoms whose nuclei serve as the foci. The energy of each prolate spheroid is matched to that of the $C2s$ and $O2p$ shells. As in the case of previous examples of energy-matched MOs such as OH and NH, the $C=O$-bond MO must comprise 75% of a H_2-type ellipsoidal MO in order to match potential, kinetic, and orbital

energy relationships. However, the paired electrons of the $C2s$ and $O2p$ shells are not involved in bonding. Rather, the AOs permit a continuous surface comprising the two $C=O$-bond MOs having six paired electrons, two from each of the C and the two O atoms:

$$2\left(0.75\ H_2\ MO\right)\rightarrow CO_2\ MO \tag{14.18}$$

The force balance of the CO_2 MO is determined by the boundary conditions that arise from the linear combination of orbitals according to Eq. (14.18) and the energy matching condition between the carbon and oxygen components of the MO.

Similar to the OH and H_2O cases given by Eqs. (13.57) and (13.162), the H_2-type ellipsoidal MO comprises 75% of the CO_2 MO; so, the electron charge density in Eq. (11.65) is given by $-0.75e$. Thus, k' of each H_2-type-ellipsoidal-MO component of the CO_2 MO is given by Eq. (13.59). The distance from the origin of each $C=O$-bond MO to each focus c' is given by Eq. (13.60). The internuclear distance is given by Eq. (13.61). The length of the semiminor axis of the prolate spheroidal $C=O$-bond MO $b=c$ is given by Eq. (13.62). The eccentricity, e, is given by Eq. (13.63). Then, the solution of the semimajor axis a allows for the solution of the other axes of the prolate spheroidal and eccentricity of the CO_2 MO.

The energy components of V_e, V_p, T, V_m, and E_T of the CO_2 σ MO are the same as those of OH given by Eqs. (13.67-13.73), except that the terms based on charge are multiplied by four and the kinetic energy term is multiplied by two due to each σ-MO double bond:

$$E_T\left(C=O,\sigma\right)=-\frac{4e^2}{8\pi\varepsilon_0 c'}\left[\left(\frac{3}{2}\right)\ln\frac{a+c'}{a-c'}-1\right] \tag{14.19}$$

where $E_T\left(C=O,\sigma\right)$ is the total energy of each $C=O$ σ MO of CO_2. The total energy of a H_2-type ellipsoidal MO is given by Eqs. (11.212) and (13.75). A minimum energy is obtained when each double bond of the σ MO of CO_2 comprises the energy equivalent of four H_2-type ellipsoidal MOs. For each $C=O$ bond to match the energy of the $C2s$ orbital, the ionization energy of C and C^+ (Eqs. (14.12-14.13)) must be added for each bond of the double bond. Thus, the total energy of each $C=O$-bond MOs is:

$$\begin{aligned}E_T\left(C=O,\sigma\right)&=2\left(\begin{array}{l}2\left(-\frac{e^2}{8\pi\varepsilon_0 a_0}\left[\left(2\sqrt{2}-\sqrt{2}+\frac{\sqrt{2}}{2}\right)\ln\frac{\sqrt{2}+1}{\sqrt{2}-1}-\sqrt{2}\right]\right)\\ +E(ionization;\ C)+E(ionization;\ C^+)\end{array}\right)\\&=2\left(2\left(-31.63536831\ eV\right)+11.26030\ eV+24.38332\ eV\right)\\&=-55.25423\ eV\end{aligned} \tag{14.20}$$

$E_T\left(C=O,\sigma\right)$ given by Eq. (14.19) is set equal to Eq. (14.20):

$$\frac{4e^2}{8\pi\varepsilon_0 c'}\left[\left(\frac{3}{2}\right)\ln\frac{a+c'}{a-c'}-1\right]=e55.25423\ eV \tag{14.21}$$

From the energy relationship given by Eq. (14.21) and the relationship between the axes given by Eqs. (13.60-13.63), the dimensions of the CO_2 MO can be solved.

Substitution of Eq. (13.60) into Eq. (14.21) gives:

$$E_T\left(C=O,\sigma\right)=\frac{4e^2}{8\pi\varepsilon_0\sqrt{\frac{2aa_0}{3}}}\left[\left(\frac{3}{2}\right)\ln\frac{a+\sqrt{\frac{2aa_0}{3}}}{a-\sqrt{\frac{2aa_0}{3}}}-1\right]=e55.25423\ eV \tag{14.22}$$

The most convenient way to solve Eq. (14.22) is by the reiterative technique using a computer. The result to within the round-off error with five-significant figures is

$$a=1.80703a_0=9.56239\ X\ 10^{-11}\ m \tag{14.23}$$

Substitution of Eq. (14.23) into Eq. (13.60) is:

$$c'=1.09758a_0=5.80815\ X\ 10^{-11}\ m \tag{14.24}$$

The internuclear distance given by multiplying Eq. (14.24) by two is:

$$2c'=2.19516a_0=1.16163\ X\ 10^{-10}\ m \tag{14.25}$$

The experimental bond distance is [3]

$$2c'=1.1600\ X\ 10^{-10}\ m \tag{14.26}$$

Substitution of Eqs. (14.23-14.24) into Eq. (13.62) is:

$$b=c=1.43550a_0=7.59636\ X\ 10^{-11}\ m \tag{14.27}$$

Substitution of Eqs. (14.23-14.24) into Eq. (13.63) is:

$$e=0.60740 \tag{14.28}$$

The C and O nuclei comprise the foci of each H_2-type ellipsoidal MO defined as $O=C=O$. Consider the left-hand $C=O$ bond of the two equivalent bonds in the absence of the right-hand bond. The parameters of the point of intersection of the H_2-type ellipsoidal MO and the $C2s$ AO are given by Eqs. (13.84-13.95) and (13.261-13.270). The polar intersection angle θ' is given by Eq. (13.261) where $r_n = r_4 = 0.84317a_0$ is the radius of the $C2s$ shell. Substitution of Eqs. (14.23-14.24) into Eq. (13.261) gives

$$\theta' = 54.53° \tag{14.29}$$

Then, the angle θ_{C2sAO} the radial vector of the $C2s$ AO makes with the internuclear axis is:

$$\theta_{C2sAO} = 180° - 54.53° = 125.47° \tag{14.30}$$

as shown in Figure 14.1. The Cartesian $\mathbf{i}$-coordinate of the interception point of the MO and the AO can be calculated using the MO ellipsoidal parameters by first calculating the parametric angle in Eq. (11.83) that matches Cartesian $\mathbf{j}$-coordinate components at the point of intersection. Thus, the matching elliptic parametric angle $\omega t = \theta_{H_2MO}$ satisfies the following relationship:

$$r_4 \sin\theta_{C2sAO} = 0.84317a_0 \sin\theta_{C2sAO} = b\sin\theta_{H_2MO} \tag{14.31}$$

such that

$$\theta_{H_2MO} = \sin^{-1}\frac{0.84317a_0 \sin\theta_{C2sAO}}{b} = \sin^{-1}\frac{0.84317a_0 \sin 125.47°}{b} \tag{14.32}$$

with the use of Eq. (14.30). Substitution of Eq. (14.27) into Eq. (14.32) gives:

$$\theta_{H_2MO} = 28.58° \tag{14.33}$$

Then, the distance d_{H_2MO} along the internuclear axis from the origin of H_2-type ellipsoidal MO to the point of intersection of the orbitals is given by

$$d_{H_2MO} = a\cos\theta_{H_2MO} \tag{14.34}$$

Substitution of Eqs. (14.23) and (14.33) into Eq. (14.34) gives:

$$d_{H_2MO} = 1.58687a_0 = 8.39737\ X\ 10^{-11}\ m \tag{14.35}$$

The distance d_{C2sAO} along the internuclear axis from the origin of the C atom to the point of intersection of the orbitals is given by

$$d_{C2sAO} = d_{H_2MO} - c' \tag{14.36}$$

Substitution of Eqs. (14.24) and (14.35) into Eq. (14.36) gives:

$$d_{C2sAO} = 0.48929a_0 = 2.58922\ X\ 10^{-11}\ m \tag{14.37}$$

The C and O nuclei comprise the foci of each H_2-type ellipsoidal MO defined as $O=C=O$. Consider the right-hand $C=O$ bond of the two equivalent bonds. The parameters of the point of intersection of the H_2-type ellipsoidal MO and the $O2p$ AO are given by Eqs. (13.84-13.95) and (13.261-13.270). The polar intersection angle θ' is given by Eq. (13.261) where $r_n = r_6 = 0.74776a_0$ is the radius of the $O2p$ shell. Substitution of Eqs. (14.23-14.24) into Eq. (13.261) gives

$$\theta' = 30.18° \tag{14.38}$$

Then, the angle θ_{O2pAO} the radial vector of the $O2p$ AO makes with the internuclear axis is:

$$\theta_{O2pAO} = 180° - 30.18° = 149.82° \tag{14.39}$$

as shown in Figure 14.1. The Cartesian $\mathbf{i}$-coordinate of the interception point of the MO and the AO can be calculated using the MO ellipsoidal parameters by first calculating the parametric angle in Eq. (11.83) that matches Cartesian $\mathbf{j}$-coordinate components at the point of intersection. Thus, the matching elliptic parametric angle $\omega t = \theta_{H_2MO}$ satisfies the following relationship:

$$r_6 \sin\theta_{O2pAO} = 0.74776a_0 \sin\theta_{O2pAO} = b\sin\theta_{H_2MO} \tag{14.40}$$

such that

$$\theta_{H_2MO} = \sin^{-1}\frac{0.74776a_0 \sin\theta_{O2pAO}}{b} = \sin^{-1}\frac{0.74776a_0 \sin 149.82°}{b} \tag{14.41}$$

with the use of Eq. (14.39). Substitution of Eq. (14.27) into Eq. (14.41) gives:

$$\theta_{H_2MO} = 15.18° \tag{14.42}$$

Then, the distance d_{H_2MO} along the internuclear axis from the origin of H_2-type ellipsoidal MO to the point of intersection of the orbitals is given by:

$$d_{H_2MO} = a\cos\theta_{H_2MO} \tag{14.43}$$

Substitution of Eqs. (14.23) and (14.42) into Eq. (14.43) gives:

$$d_{H_2MO} = 1.74396a_0 = 9.22862\ X\ 10^{-11}\ m \tag{14.44}$$

The distance d_{O2pAO} along the internuclear axis from the origin of each O atom to the point of intersection of the orbitals is given by:

$$d_{2pAO} = d_{H_2MO} - c' \tag{14.45}$$

Substitution of Eqs. (14.24) and (14.44) into Eq. (14.45) gives:

$$d_{O2pAO} = 0.64637a_0 = 3.42047\ X\ 10^{-11}\ m \tag{14.46}$$

As shown in Eq. (14.18), each $C=O$ bond comprises a factor of 0.75 of the charge-density of double that of the H_2-type ellipsoidal MO. Using the electron configuration of CO_2 (Eq. (14.2)), the radii of the $C1s = 0.17113a_0$ (Eq. (10.51)), $C2s = 0.84317a_0$ (Eq. (10.62)), $O1s = 0.12739a_0$ (Eq. (10.51)), $O2s = 0.59020a_0$ (Eq. (10.62)), and $O2p = 0.74776a_0$ (Eq. (14.11)) shells and the parameters of the σ MO of CO_2 given by Eqs. (13.3-13.4), (14.23-14.25), and (14.27-14.28), the dimensional diagram and charge-density of the CO_2 MO are shown in Figures 14.1 and 14.2, respectively.

Figure 14.1. The cross section of the CO_2 MO showing the axes, σ MO (two H_2-type ellipsoidal MOs) with six paired electrons, with the C $1s$ and $2s$ AOs and the O $1s$, $2s$, and $2p$ AOs. Legend: a: semimajor axis, b: semiminor axis, c': internuclear distance, r_4: radius of the $C2s$ shell having two paired electrons, r_6: radius of the $O2p$ shell having two paired electrons.

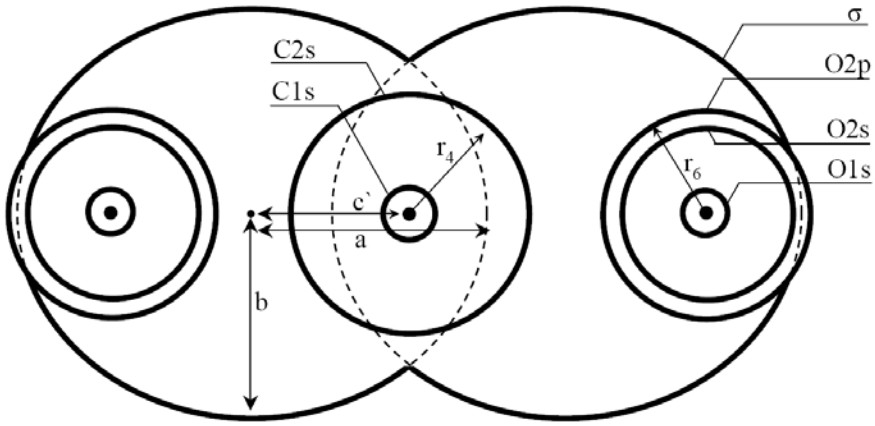

Figure 14.2. CO_2 MO comprising the σ MO (two H_2-type MOs) with C and two O atoms at the foci that have each donated two electrons to the σ MO. Consequently, the outer electrons of the carbon atom comprise the $C2s$ shell, and each $O2p$ shell has a smaller radius and a higher binding energy. (A) Color scale, translucent view of the charge-density of the CO_2 MO. (B) Off-center cut-away view showing each complete inner most $O1s$ shell, and moving radially, the $O2s$ shell, the $O2p$ shell, and the σ prolate spheroidal MO that has the corresponding O atom as a focus. Moving radially from the carbon-atom focus, the complete inner most $C1s$ shell, the $C2s$ shell, and the σ prolate spheroidal MOs are shown.

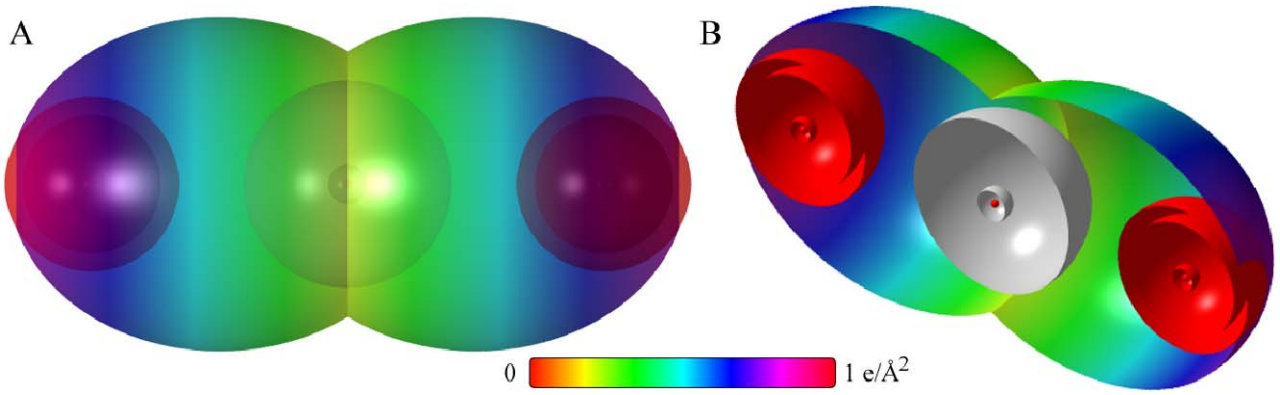

SUM OF THE ENERGIES OF THE σ MO AND THE AOS OF THE CARBON DIOXIDE MOLECULE

The energies of the CO_2 σ MO are given by the substitution of the semiprincipal axes (Eqs. (14.23-14.24) and (14.27)) into the energy equations of OH (Eqs. (13.67-13.73)), except that the terms based on charge are multiplied by four and the kinetic energy term is multiplied by two due to each σ-MO double bond:

$$V_e = 2^2\left(\frac{3}{4}\right)\frac{-2e^2}{8\pi\varepsilon_0\sqrt{a^2-b^2}}\ln\frac{a+\sqrt{a^2-b^2}}{a-\sqrt{a^2-b^2}} = -104.83940\ eV \tag{14.47}$$

$$V_p = 2^2\frac{e^2}{8\pi\varepsilon_0\sqrt{a^2-b^2}} = 49.58464\ eV \tag{14.48}$$

$$T = 2\left(\frac{3}{4}\right)\frac{\hbar^2}{2m_e a\sqrt{a^2-b^2}}\ln\frac{a+\sqrt{a^2-b^2}}{a-\sqrt{a^2-b^2}} = 14.50438\ eV \tag{14.49}$$

$$V_m = 2^2\left(\frac{3}{4}\right)\frac{-\hbar^2}{4m_e a\sqrt{a^2-b^2}}\ln\frac{a+\sqrt{a^2-b^2}}{a-\sqrt{a^2-b^2}} = -14.50438\ eV \tag{14.50}$$

$$E_T = V_e + T + V_m + V_p \tag{14.51}$$

Substitution of Eqs. (13.60) and (14.47-14.50) into Eq. (14.51) gives:

$$E_T\left(C=O,\sigma\right) = V_e + T + V_m + V_p = \frac{-4e^2}{8\pi\varepsilon_0\sqrt{\frac{2aa_0}{3}}}\left[\left(\frac{3}{2}\right)\ln\frac{a+\sqrt{\frac{2aa_0}{3}}}{a-\sqrt{\frac{2aa_0}{3}}}-1\right] = -55.25476\ eV \tag{14.52}$$

where $E_T\left(C=O,\sigma\right)$ is the total energy of each $C=O$ σ MO of CO_2 given by Eq. (14.19) which is reiteratively matched to Eq. (14.20) within five-significant-figure round off error.

The total energy of CO_2, $E_T\left(CO_2\right)$, is given by the sum of $E(ionization;\ C)$ and $E(ionization;\ C^+)$, the sum of the energies of the first and second electrons of carbon (Eqs. (14.12-14.13)) donated to each double bond, the sum of $E(ionization;\ O)$ and two times $E(ionization;\ O^+)$, the energies of the first and second electrons of oxygen (Eqs. (14.14-14.15)) donated to the double bonds, two times $E_T\left(O,2p\right)$, the $O2p$ AO contribution due to the decrease in radius with the formation of each bond (Eq. (14.17)), and two times $E_T\left(C=O,\sigma\right)$, the σ MO contribution given by Eq. (14.22):

$$\begin{aligned}E_T\left(CO_2\right) &= \begin{pmatrix}E(ionization;\ C)+E(ionization;\ C^+)+E(ionization;\ O)\\ +2E(ionization;\ O^+)+2E_T\left(O,2p\right)+2E_T\left(C=O,\sigma\right)\end{pmatrix}\\ &= \begin{pmatrix}11.26030\ eV+24.38332\ eV+13.61806\ eV\\ +2\left(35.11730\ eV\right)+2\left(-32.12759\ eV\right)\\ -2\left(\frac{4e^2}{8\pi\varepsilon_0\sqrt{\frac{2aa_0}{3}}}\left(\left(\frac{3}{2}\right)\ln\frac{a+\sqrt{\frac{2aa_0}{3}}}{a-\sqrt{\frac{2aa_0}{3}}}-1\right)\right)\end{pmatrix}\\ &= \begin{pmatrix}11.26030\ eV+24.38332\ eV+13.61806\ eV\\ +2\left(35.11730\ eV\right)+2\left(-32.12759\ eV\right)-2\left(55.25423\ eV\right)\end{pmatrix} = -55.26841\ eV\end{aligned} \tag{14.53}$$

VIBRATION OF CO_2

The vibrational energy levels of CO_2 may be solved by determining the Morse potential curve from the energy relationships for the transition from a C atom and two O atoms whose parameters are given by Eqs. (10.115-10.123) and (10.154-10.163), respectively, to a C atom whose parameter r_4 is given by Eq. (10.61), two O atoms whose parameter r_6 is given by Eq. (14.11), and the σ CO_2 MO whose parameters are given by Eqs. (14.23-14.25) and (14.27-14.28). As shown in the Vibration of Hydrogen-type Molecular Ions section, the harmonic oscillator potential energy function can be expanded about the internuclear distance and expressed as a Maclaurin series corresponding to a Morse potential after Karplus and Porter (K&P) [4] and after Eq. (11.134). Treating the Maclaurin series terms as anharmonic perturbation terms of the harmonic states, the energy corrections can be found by perturbation methods.

THE DOPPLER ENERGY TERMS OF THE CARBON DIOXIDE MOLECULE

The equations of the radiation reaction force of carbon dioxide are the same as those of OH with the substitution of the CO_2 parameters except that there is a factor of four increase in the central force in Eq. (13.140) due to the double bond. Using Eqs. (13.140-13.142), the angular frequency of the reentrant oscillation in the transition state is

$$\omega = \sqrt{\frac{\frac{4(0.75)e^2}{4\pi\varepsilon_0 b^3}}{m_e}} = 4.16331\ X\ 10^{16}\ rad/s \tag{14.54}$$

where b is given by Eq. (14.27). The kinetic energy, E_K, is given by Planck's equation (Eq. (11.127)).

$$\bar{E}_K = \hbar\omega = \hbar 4.16331\ X\ 10^{16}\ rad/s = 27.40365\ eV \tag{14.55}$$

In Eq. (11.181), substitution of $E_T(CO_2)/2$ for $E_{h\nu}$, the mass of the electron, m_e, for M, and the kinetic energy given by Eq. (14.55) for $\bar{E}_K$ gives the Doppler energy of the electrons of the reentrant orbit:

$$\bar{E}_D \cong E_{h\nu}\sqrt{\frac{2\bar{E}_K}{Mc^2}} = -27.63421\ eV\sqrt{\frac{2e(27.40365\ eV)}{m_e c^2}} = -0.28619\ eV \tag{14.56}$$

In addition to the electrons, the nuclei also undergo simple harmonic oscillation in the transition state at their corresponding frequency. The transition state comprises $O--CO$, oxygen binding to CO. Vibration of the linear XYZ-molecular transition state corresponds to υ_3 [5] with the maximum kinetic energy localized to the nascent $C-O$ bond. In this case, the kinetic energy of the nuclei is the maximum for this bond. Thus, $\bar{E}_{Kvib}$ is the vibrational energy. The decrease in the energy of the CO_2 MO due to the reentrant orbit in the transition state corresponding to simple harmonic oscillation of the electrons and nuclei, $\bar{E}_{osc}$, is given by the sum of the corresponding energies, $\bar{E}_D$ given by Eq. (14.56) and $\bar{E}_{Kvib}$, the vibrational energy. Using the experimental CO_2 $E_{vib}(\upsilon_3)$ of 2349 cm^{-1} $(0.29124\ eV)$ [6] for $\bar{E}_{Kvib}$ of the transition state, $\bar{E}_{osc}(CO_2)$ is:

$$\bar{E}_{osc}(CO_2) = \bar{E}_D + \bar{E}_{Kvib} = \bar{E}_D + E_{vib} \tag{14.57}$$

$$\bar{E}_{osc}(CO_2) = -0.28619\ eV + 0.29124\ eV = 0.00505\ eV \tag{14.58}$$

TOTAL AND BOND ENERGIES OF THE CARBON DIOXIDE MOLECULE

$E_{T+osc}(CO_2)$, the total energy of CO_2 including the Doppler term, is given by the sum of $E_T(CO_2)$ (Eq. (14.53)) and $\bar{E}_{osc}(CO_2)$ given by Eq. (14.58).

$$\begin{aligned}
E_{T+osc}(CO_2) &= \begin{pmatrix} 2(V_e + T + V_m + V_p) + E(ionization;\ C) \\ +E(ionization;\ C^+) + E(ionization;\ O) + 2E(ionization;\ O^+) \\ +2E_T(O,2p) + \bar{E}_{osc}(CO_2) \end{pmatrix} \\
&= \begin{pmatrix} 2E_T(C=O,\sigma) + E(ionization;\ C) + E(ionization;\ C^+) \\ +E(ionization;\ O) + 2E(ionization;\ O^+) \\ +2E_T(O,2p) + \bar{E}_{osc}(CO_2) \end{pmatrix} \\
&= E_T(CO_2) + \bar{E}_{osc}(CO_2)
\end{aligned} \tag{14.59}$$

$$\begin{aligned}
E_{T+osc}(CO_2) = \Bigg\{ & \begin{pmatrix} 2\left(\frac{-4e^2}{8\pi\varepsilon_0\sqrt{\frac{2aa_0}{3}}}\left(\left(\frac{3}{2}\right)\ln\frac{a+\sqrt{\frac{2aa_0}{3}}}{a-\sqrt{\frac{2aa_0}{3}}} - 1\right)\right) + E(ionization;\ C) \\ +E(ionization;\ C^+) + E(ionization;\ O) \\ +2E(ionization;\ O^+) - 2\sum_{O,n=4}^{5}\frac{(Z-n)e^2}{8\pi\varepsilon_0}\left(\frac{1}{r_6} - \frac{1}{r_8}\right) \end{pmatrix} \\
& \begin{pmatrix} 1 + \frac{1}{2}\sqrt{\frac{2\hbar\sqrt{\frac{\frac{4(0.75)e^2}{4\pi\varepsilon_0 b^3}}{m_e}}}{m_e c^2}} \end{pmatrix} + E_{vib} \Bigg\} \\
= & -55.26841\ eV - 0.28619\ eV + E_{vib}
\end{aligned} \tag{14.60}$$

From Eqs. (14.57-14.60), the total energy of the CO_2 MO is:

$$E_{T+osc}\left(CO_2\right) = -55.25476\ eV + \bar{E}_{osc}\left(CO_2\right) = -55.25476\ eV + 0.00505\ eV = -55.26336\ eV \tag{14.61}$$

where the experimental E_{vib} was used.

As in the case of the dissociation of the bond of the hydroxyl radical, an oxygen atom is formed with dissociation of CO_2. O has two unpaired electrons as shown in Eq. (13.55) which interact to stabilize the atom as shown by Eq. (10.161-10.162). The lowering of the energy of the reactants decreases the bond energy. Thus, the total energy of oxygen is reduced by the energy in the field of the two magnetic dipoles given by Eq. (7.46) and Eq. (13.101).

$$E(magnetic) = \frac{2\pi\mu_0 e^2\hbar^2}{m_e^2 a_0^3} = \frac{8\pi\mu_0\mu_B^2}{a_0^3} = 0.11441\ eV \tag{14.62}$$

The CO_2 bond dissociation energy, $E_D\left(CO_2\right)$, is given by the sum of the energies of the CO and the O atom minus the sum of $E_{T+osc}\left(CO_2\right)$ and $E(magnetic)$:

$$E_D\left(CO_2\right) = E\left(CO\right) + E\left(O\right) - \left(E(magnetic) + E_{T+osc}\left(CO_2\right)\right) \tag{14.63}$$

The energy of an oxygen atom is given by Eq. (14.14) and $E_T(CO)$ is given by the sum of the experimental energies of C (Eq. (14.12)), O (Eq. (14.14)), and the negative of the bond energy of CO (Eq. (13.914)):

$$E(CO) = -11.26030\ eV - 13.618060\ eV - 11.15696\ eV = -36.03532\ eV \tag{14.64}$$

The energy of O is given by the negative of the corresponding ionization energy given in Eq. (4.14). Thus, the CO_2 bond dissociation energy, $E_D\left(CO_2\right)$, given by the Eqs. (4.14) and (14.61-14.64) is:

$$\begin{aligned} E_D\left(CO_2\right) &= -\left(36.03532\ eV + 13.618060\ eV\right) - \left(E(magnetic) + E_{T+osc}\left(CO_2\right)\right) \\ &= -49.65338\ eV - \left(0.11441\ eV - 55.26336\ eV\right) \\ &= 5.49557\ eV \end{aligned} \tag{14.65}$$

The experimental CO_2 bond dissociation energy is [7]:

$$E_{D298}\left(CO_2\right) = 5.516\ eV \tag{14.66}$$

The results of the determination of bond parameters of CO_2 are given in Table 14.1. The calculated results are based on first principles and given in closed-form, exact equations containing fundamental constants only. The agreement between the experimental and calculated results is excellent.

NITROGEN DIOXIDE MOLECULE

The nitrogen dioxide molecule can be formed by the reaction of nitric oxide and an oxygen atom:

$$NO + O \rightarrow NO_2 \tag{14.67}$$

The bonding in the nitrogen dioxide molecule comprises two double bonds, each a H_2-type MO with four paired electrons wherein the central N atom is shared by both bonds such that six electrons can be assigned to the two $N=O$ bonds. Thus, two $N2p$ electrons combine with the four $O2p$ electrons, two from each O, as a linear combination to form the two overlapping $N=O$ bonds of NO_2. The force balance equation and radius r_7 of the $2p$ shell of N is derived in the Seven-Electron Atoms section. The force balance equation and radius r_8 of the $2p$ shell of O is derived in the Eight-Electron Atoms section. With the formation of each of the two H_2-type MOs by the contribution of two $2p$ electrons each from the N and O atoms, a diamagnetic force arises between the remaining outer shell atomic electrons, the $2s$ and $2p$ electrons of N and O, and the H_2-type MO. This force from N and O causes the H_2-type MO to move to greater principal axes than would result with the Coulombic force alone. But, the factor of two increase of the central field and the resulting increased Coulombic as well as magnetic central forces on the remaining N and O electrons decrease the radii of the corresponding shells such that the energy minimum is achieved that is lower than that of the reactant atoms. The resulting electron configuration of NO_2 is $N1s^2O_1 1s^2O_2 1s^2 N2s^2O_1 2s^2O_2 2s^2 N2p^1O_1 2p^2O_2 2p^2\sigma^6_{O_2,N,O_1}$ where the subscripts designate the O atom, 1 or 2, σ designates the H_2-type MO, and the orbital arrangement is:

σ state

$\underline{\uparrow\downarrow}\ \underline{\uparrow\downarrow}\ \underline{\uparrow\downarrow}$

2p state

$\underline{\uparrow\downarrow}$ $\underline{\uparrow}$ $\underline{\uparrow\downarrow}$

0 0 0

2s state

$\underline{\uparrow\downarrow}$ $\underline{\uparrow\downarrow}$ $\underline{\uparrow\downarrow}$ (14.68)

1s state

$\underline{\uparrow\downarrow}$ $\underline{\uparrow\downarrow}$ $\underline{\uparrow\downarrow}$

O N O

Nitrogen dioxide is predicted to be weakly paramagnetic in agreement with observations [1].

FORCE BALANCE OF THE $2p$ SHELL OF THE NITROGEN ATOM OF NITROGEN DIOXIDE

For the N atom, force balance for the outermost $2p$ electron of NO_2 (electron 5) is achieved between the centrifugal force and the Coulombic and magnetic forces that arise due to interactions between electron 5 and the $2s$-shell electrons due to spin and orbital angular momentum. The forces used are derived in the Seven-Electron Atoms section. The central Coulomb force on the outer-most $2p$ shell electron of NO (electron 5) due to the nucleus and the inner four electrons is given by Eq. (10.70) with the appropriate charge and radius:

$$\mathbf{F}_{ele} = \frac{(Z-4)e^2}{4\pi\varepsilon_0 r_5^2}\mathbf{i}_\mathbf{r} \tag{14.69}$$

for $r > r_4$. The $2p$ shell possess a +2 external electric field given by Eq. (10.92) for $r > r_5$. The energy is minimized with conservation of angular momentum. This condition is met when the magnetic forces of N in NO_2 are the same as those of N in NO. They are also the same as those of N in the nitrogen molecule with r_5 replacing r_6 and with an increase of the central field by an integer. The diamagnetic force, $\mathbf{F}_{diamagnetic}$, of Eq. (10.82) due to the p-orbital contribution is given by Eq. (13.918).

$$\mathbf{F}_{diamagnetic} = -\left(\frac{1}{3}\right)\frac{\hbar^2}{4m_e r_5^2 r_3}\sqrt{s(s+1)}\mathbf{i}_\mathbf{r} = -\frac{\hbar^2}{12m_e r_5^2 r_3}\sqrt{\frac{3}{4}}\mathbf{i}_\mathbf{r} \tag{14.70}$$

And, $\mathbf{F}_{mag\ 2}$ corresponding to the conserved orbital angular momentum of the three orbitals is also the same as that of NO_2 given by Eq. (13.919):

$$\mathbf{F}_{mag\ 2} = \frac{1}{Z}\frac{3\hbar^2}{m_e r_5^2 r_3}\sqrt{s(s+1)}\mathbf{i}_\mathbf{r} \tag{14.71}$$

The electric field external to the $2p$ shell given by Eq. (10.92) for $r > r_5$ gives rise to a second diamagnetic force, $\mathbf{F}_{diamagnetic\ 2}$, given by Eq. (10.93). $\mathbf{F}_{diamagnetic\ 2}$ due to the binding of the p-orbital electron having an electric field of +2 outside of its radius is given by Eq. (13.920):

$$\mathbf{F}_{diamagnetic\ 2} = -\left[\frac{Z-5}{Z-4}\right]\left(1-\frac{\sqrt{2}}{2}\right)\frac{r_3\hbar^2}{m_e r_5^4}10\sqrt{s(s+1)}\mathbf{i}_\mathbf{r} \tag{14.72}$$

The radius of the $2p$ shell is calculated by equating the outward centrifugal force to the sum of the electric (Eq. (14.69)) and diamagnetic (Eqs. (14.70) and (14.72)), and paramagnetic (Eq. (14.71)) forces as follows:

$$\frac{m_e v_5^2}{r_5} = \left(\begin{array}{l}\dfrac{(Z-4)e^2}{4\pi\varepsilon_0 r_5^2} - \dfrac{\hbar^2}{12m_e r_5^2 r_3}\sqrt{s(s+1)} + \dfrac{3\hbar^2}{Zm_e r_5^2 r_3}\sqrt{s(s+1)} \\ -\left[\dfrac{Z-5}{Z-4}\right]\left(1-\dfrac{\sqrt{2}}{2}\right)\dfrac{r_3\hbar^2}{r_5^4 m_e}10\sqrt{s(s+1)}\end{array}\right) \tag{14.73}$$

Substitution of $v_5 = \dfrac{\hbar}{m_e r_5}$ (Eq. (1.35)) and $s = \dfrac{1}{2}$ into Eq. (14.73) gives:

$$\frac{\hbar^2}{m_e r_5^3}=\frac{(Z-4)e^2}{4\pi\varepsilon_0 r_5^2}-\frac{\hbar^2}{12m_e r_5^2 r_3}\sqrt{\frac{3}{4}}+\frac{3\hbar^2}{Zm_e r_5^2 r_3}\sqrt{\frac{3}{4}}-\left[\frac{Z-5}{Z-4}\right]\left(1-\frac{\sqrt{2}}{2}\right)\frac{r_3\hbar^2}{r_5^4 m_e}10\sqrt{\frac{3}{4}} \tag{14.74}$$

The quadratic equation corresponding to Eq. (14.74) is:

$$r_5^2-\frac{\frac{\hbar^2}{m_e}}{\left(\frac{(Z-4)e^2}{4\pi\varepsilon_0}-\left(\frac{1}{12}-\frac{3}{Z}\right)\frac{\hbar^2}{m_e r_3}\sqrt{\frac{3}{4}}\right)}r_5-\frac{\frac{\hbar^2}{m_e}\left[\frac{Z-5}{Z-4}\right]\left(1-\frac{\sqrt{2}}{2}\right)r_3 10\sqrt{\frac{3}{4}}}{\left(\frac{(Z-4)e^2}{4\pi\varepsilon_0}-\left(\frac{1}{12}-\frac{3}{Z}\right)\frac{\hbar^2}{m_e r_3}\sqrt{\frac{3}{4}}\right)}=0 \tag{14.75}$$

The solution of Eq. (14.75) using the quadratic formula is:

$$r_5=\frac{\frac{a_0}{\left((Z-4)-\left(\frac{1}{12}-\frac{3}{Z}\right)\frac{\sqrt{3}}{2r_3}\right)}\pm a_0\sqrt{\left(\frac{1}{\left((Z-4)-\left(\frac{1}{12}-\frac{3}{Z}\right)\frac{\sqrt{3}}{2r_3}\right)}\right)^2+\frac{20\sqrt{3}\left(\left[\frac{Z-5}{Z-4}\right]\left(1-\frac{\sqrt{2}}{2}\right)r_3\right)}{\left((Z-4)-\left(\frac{1}{12}-\frac{3}{Z}\right)\frac{\sqrt{3}}{2r_3}\right)}}}{2},\ r_3 \text{ in units of } a_0 \tag{14.76}$$

The positive root of Eq. (14.76) must be taken in order that $r_5>0$. Substitution of $\frac{r_3}{a_0}=0.69385$ (Eq. (10.62) with $Z=7$) into Eq. (14.76) gives:

$$r_5=0.74841a_0 \tag{14.77}$$

FORCE BALANCE OF THE $2p$ SHELL OF EACH OXYGEN ATOM OF NITROGEN DIOXIDE

For each O atom, force balance for the outermost $2p$ electron of NO_2 (electron 6) is achieved between the centrifugal force and the Coulombic and magnetic forces that arise due to interactions between electron 6 and the other $2p$ electron as well as the $2s$-shell electrons due to spin and orbital angular momentum. The forces used are derived in the Eight-Electron Atoms section. The central Coulomb force on the outer-most $2p$ shell electron of NO_2 (electron 6) due to the nucleus and the inner five electrons is given by Eq. (10.70) with the appropriate charge and radius:

$$\mathbf{F}_{ele}=\frac{(Z-5)e^2}{4\pi\varepsilon_0 r_6^2}\mathbf{i}_\mathbf{r} \tag{14.78}$$

for $r>r_5$. The $2p$ shell possess an external electric field of +2 given by Eq. (10.92) for $r>r_6$. The energy is minimized with conservation of angular momentum. This condition is met when the magnetic forces of O in NO_2 are the same as those of O in NO. The diamagnetic force, $\mathbf{F}_{diamagnetic}$, of Eq. (10.82) due to the p-orbital contribution given by Eq. (13.927) is:

$$\mathbf{F}_{diamagnetic}=-\left(\frac{2}{3}\right)\frac{\hbar^2}{4m_e r_6^2 r_3}\sqrt{s(s+1)}\mathbf{i}_\mathbf{r}=-\frac{2\hbar^2}{12m_e r_6^2 r_3}\sqrt{\frac{3}{4}}\mathbf{i}_\mathbf{r} \tag{14.79}$$

And, $\mathbf{F}_{mag\ 2}$ corresponding to the conserved spin and orbital angular momentum given by Eq. (13.928) is:

$$\mathbf{F}_{mag\ 2}=\frac{1}{Z}\frac{2\hbar^2}{m_e r_6^2 r_3}\sqrt{s(s+1)}\mathbf{i}_\mathbf{r} \tag{14.80}$$

The electric field external to the $2p$ shell given by Eq. (10.92) for $r>r_6$ gives rise to a second diamagnetic force, $\mathbf{F}_{diamagnetic\ 2}$, given by Eq. (10.93). $\mathbf{F}_{diamagnetic\ 2}$ due to the binding of the p-orbital electron having an electric field of +2 outside of its radius given by Eq. (13.929) is:

$$\mathbf{F}_{diamagnetic\ 2}=-\left[\frac{Z-6}{Z-5}\right]\left(1-\frac{\sqrt{2}}{2}\right)\frac{r_3\hbar^2}{m_e r_6^4}10\sqrt{s(s+1)}\mathbf{i}_\mathbf{r} \tag{14.81}$$

In addition, the contribution of two $2p$ electrons in the formation of the σ MO gives rise to a paramagnetic force on the remaining paired $2p$ electrons. The force $\mathbf{F}_{mag\ 3}$ is given by Eq. (13.930) is:

$$\mathbf{F}_{mag\ 3}=\frac{\hbar^2}{4m_e r_6^3}\sqrt{s(s+1)}\mathbf{i}_{\mathbf{r}} \tag{14.82}$$

The radius of the $2p$ shell is calculated by equating the outward centrifugal force to the sum of the electric (Eq. (14.78)) and diamagnetic (Eqs. (14.79) and (14.81)), and paramagnetic (Eqs. (14.80) and (14.82)) forces as follows:

$$\frac{m_e v_6^2}{r_6}=\begin{pmatrix}\frac{(Z-5)e^2}{4\pi\varepsilon_0 r_6^2}-\frac{2\hbar^2}{12m_e r_6^2 r_3}\sqrt{s(s+1)}+\frac{2\hbar^2}{Zm_e r_6^2 r_3}\sqrt{s(s+1)}\\ -\left[\frac{Z-6}{Z-5}\right]\left(1-\frac{\sqrt{2}}{2}\right)\frac{r_3\hbar^2}{r_6^4 m_e}10\sqrt{s(s+1)}+\frac{\hbar^2}{4m_e r_6^3}\sqrt{s(s+1)}\end{pmatrix} \tag{14.83}$$

Substitution of $v_6=\frac{\hbar}{m_e r_6}$ (Eq. (1.35)) and $s=\frac{1}{2}$ into Eq. (14.83) gives:

$$\frac{\hbar^2}{m_e r_6^3}-\frac{\hbar^2}{4m_e r_6^3}\sqrt{\frac{3}{4}}=\frac{(Z-5)e^2}{4\pi\varepsilon_0 r_6^2}-\frac{2\hbar^2}{12m_e r_6^2 r_3}\sqrt{\frac{3}{4}}+\frac{2\hbar^2}{Zm_e r_6^2 r_3}\sqrt{\frac{3}{4}}-\left[\frac{Z-6}{Z-5}\right]\left(1-\frac{\sqrt{2}}{2}\right)\frac{r_3\hbar^2}{r_6^4 m_e}10\sqrt{\frac{3}{4}} \tag{14.84}$$

The quadratic equation corresponding to Eq. (14.84) is:

$$r_6^2-\frac{\frac{\hbar^2}{m_e}\left(1-\frac{\sqrt{3}}{8}\right)}{\left(\frac{(Z-5)e^2}{4\pi\varepsilon_0}-\left(\frac{2}{12}-\frac{2}{Z}\right)\frac{\hbar^2}{m_e r_3}\sqrt{\frac{3}{4}}\right)}r_6-\frac{\frac{\hbar^2}{m_e}\left[\frac{Z-6}{Z-5}\right]\left(1-\frac{\sqrt{2}}{2}\right)r_3 10\sqrt{\frac{3}{4}}}{\left(\frac{(Z-5)e^2}{4\pi\varepsilon_0}-\left(\frac{2}{12}-\frac{2}{Z}\right)\frac{\hbar^2}{m_e r_3}\sqrt{\frac{3}{4}}\right)}=0 \tag{14.85}$$

The solution of Eq. (14.85) using the quadratic formula is:

$$r_6=\frac{\frac{a_0\left(1-\frac{\sqrt{3}}{8}\right)}{\left((Z-5)-\left(\frac{2}{12}-\frac{2}{Z}\right)\frac{\sqrt{3}}{2r_3}\right)}\pm a_0\sqrt{\left(\frac{1-\frac{\sqrt{3}}{8}}{\left((Z-5)-\left(\frac{2}{12}-\frac{2}{Z}\right)\frac{\sqrt{3}}{2r_3}\right)}\right)^2+\frac{20\sqrt{3}\left(\left[\frac{Z-6}{Z-5}\right]\left(1-\frac{\sqrt{2}}{2}\right)r_3\right)}{\left((Z-5)-\left(\frac{2}{12}-\frac{2}{Z}\right)\frac{\sqrt{3}}{2r_3}\right)}}}{2},\ r_3\ \textit{in units of}\ a_0 \tag{14.86}$$

The positive root of Eq. (14.86) must be taken in order that $r_6>0$. Substitution of $\frac{r_3}{a_0}=0.59020$ (Eq. (10.62) with $Z=8$) into Eq. (14.86) gives:

$$r_6=0.70460a_0 \tag{14.87}$$

ENERGIES OF THE $2p$ SHELLS OF THE NITROGEN ATOM AND OXYGEN ATOMS OF NITROGEN DIOXIDE

Consider the determination of the total energy of NO_2 from the reaction of a nitrogen atom with two oxygen atoms. With the formation of each H_2-type MO by the contribution of two $2p$ electrons from each of the N and the two O atoms, the total energy of the NO_2 molecule, which is subtracted from the sum of the energies of the nitrogen and oxygen atoms to determine the bond energy, is increased by the ionization energies of N, N^+, O, and $2O^+$ given by Eqs. (14.88-14.91), respectively. Experimentally, the energies are [2]:

$$E(\textit{ionization};\ N)=14.53414\ eV \tag{14.88}$$

$$E(\textit{ionization};\ N^+)=29.6013\ eV \tag{14.89}$$

$$E(\textit{ionization};\ O)=13.61806\ eV \tag{14.90}$$

$$E(\textit{ionization};\ O^+)=35.11730\ eV \tag{14.91}$$

In addition, the central forces on the $2p$ shells of the N and O atoms are increased with the formation of the σ MOs which reduces each shell's radius and increases its total energy. The change per bond is the same as that of NO since the final radii given by Eq. (14.77) and (14.87) are the same for NO and NO_2. The Coulombic energy terms of the total energy of the N and O atoms at the new radii are calculated and added to the ionization energies of N, N^+, O, and $2O^+$, and the energy of the

σ MOs to give the total energy of NO_2. Then, the bond energy is determined from the total NO_2 energy.

The radius r_7 of the nitrogen atom before bonding is given by Eq. (10.142).

$$r_7 = 0.93084a_0 \tag{14.92}$$

Using the initial radius r_7 of the N atom and the final radius r_5 of the $N2p$ shell (Eq. (14.77)) and by considering that the central Coulombic field decreases by an integer for each successive electron of the shell, the sum $E_T(N,2p)$ of the Coulombic energy change of the $N2p$ electrons of the N atom is determined using Eq. (10.102):

$$E_T(N,2p) = -\sum_{n=4}^{4}\frac{(Z-n)e^2}{8\pi\varepsilon_0}\left(\frac{1}{r_5}-\frac{1}{r_7}\right) = -(13.60580\ eV)(0.26186)(3) = -10.68853\ eV \tag{14.93}$$

The radius r_8 of the oxygen atom before bonding is given by Eq. (10.162).

$$r_8 = a_0 \tag{14.94}$$

Using the initial radius r_8 of the O atom and the final radius r_6 of the $O2p$ shell (Eq. (14.87)) and by considering that the central Coulombic field decreases by an integer for each successive electron of the shell, the sum $E_T(O,2p)$ of the Coulombic energy change of the $O2p$ electrons of the O atom is determined using Eq. (10.102).

$$E_T(O,2p) = \sum_{n=4}^{5}\frac{(Z-n)e^2}{8\pi\varepsilon_0}\left(\frac{1}{r_6}-\frac{1}{r_8}\right) = (13.60580\ eV)\left(0.41925a_0^{-1}\right)(3+4) = -39.92918\ eV \tag{14.95}$$

FORCE BALANCE OF THE σ MO OF NITROGEN DIOXIDE

The force balance can be considered due to a second pair of two electrons binding to a molecular ion having $+2e$ at each focus and a first bound pair. Then, the forces are the same as those of a molecule ion having $+e$ at each focus. The diamagnetic force $\mathbf{F}_{diamagneticMO1}$ for each σ-MO of the NO_2 molecule due to the two, paired electrons in the $O2p$ shell is given by Eq. (13.633) with $n_e = 2$:

$$\mathbf{F}_{diamagneticMO1} = \frac{\hbar^2}{2m_e a^2 b^2} D\mathbf{i}_\xi \tag{14.96}$$

This is also the corresponding force of NO given by Eq. (13.942). $\mathbf{F}_{diamagneticMO2}$ of the nitrogen dioxide molecule comprising nitrogen with charge $Z_1 = 7$ and $|L_1| = \hbar$ and $|L_2| = \sqrt{\frac{3}{4}}\hbar$ and the two oxygen atoms, each with $Z_2 = 8$ and $|L_3| = \hbar$ is given by the corresponding sum of the contributions. Using Eq. (13.835), $\mathbf{F}_{diamagneticMO2}$ for NO_2 is:

$$\mathbf{F}_{diamagneticMO2} = \left(\frac{1}{Z_1}+\frac{\sqrt{\frac{3}{4}}}{Z_1}+\frac{2}{Z_2}\right)\frac{\hbar^2}{2m_e a^2 b^2} D\mathbf{i}_\xi \tag{14.97}$$

This is also the corresponding force of NO given by Eq. (13.943) except the term due to oxygen is twice that of NO due to the two oxygen atoms of NO_2. The general force balance equation for the σ-MO of the nitrogen dioxide molecule given by Eqs. (11.200), and (14.97-14.98) is also the same as that of CN (Eq. (14.836)) except for the doubling of the $\frac{2}{Z_2}$ term due to the two oxygen atoms:

$$\frac{\hbar^2}{m_e a^2 b^2} D = \frac{e^2}{8\pi\varepsilon_0 ab^2} D + \frac{\hbar^2}{2m_e a^2 b^2} D - \left(1+\frac{1}{Z_1}+\frac{\sqrt{\frac{3}{4}}}{Z_1}+\frac{2}{Z_2}\right)\frac{\hbar^2}{2m_e a^2 b^2} D \tag{14.98}$$

$$\frac{\hbar^2}{m_e a^2 b^2} D = \frac{e^2}{8\pi\varepsilon_0 ab^2} D - \left(\frac{1}{Z_1}+\frac{\sqrt{\frac{3}{4}}}{Z_1}+\frac{2}{Z_2}\right)\frac{\hbar^2}{2m_e a^2 b^2} D \tag{14.99}$$

$$\left(2+\frac{1}{Z_1}+\frac{\sqrt{\frac{3}{4}}}{Z_1}+\frac{2}{Z_2}\right)\frac{\hbar^2}{2m_e a^2 b^2} D = \frac{e^2}{8\pi\varepsilon_0 ab^2} D \tag{14.100}$$

$$a = \left(2 + \frac{1}{Z_1} + \frac{\sqrt{\frac{3}{4}}}{Z_1} + \frac{2}{Z_2} \right) a_0 \tag{14.101}$$

Substitution of $Z_1 = 7$ and $Z_2 = 8$ into Eq. (14.101) gives:

$$a = 2.51658 a_0 = 1.33171\ X\ 10^{-10}\ m \tag{14.102}$$

Substitution of Eq. (14.102) into Eq. (11.79) is:

$$c' = 1.12173 a_0 = 5.93596\ X\ 10^{-11}\ m \tag{14.103}$$

The internuclear distance given by multiplying Eq. (14.103) by two is:

$$2c' = 2.24347 a_0 = 1.18719\ X\ 10^{-10}\ m \tag{14.104}$$

The experimental bond distance is [3]:

$$2c' = 1.193\ X\ 10^{-10}\ m \tag{14.105}$$

Substitution of Eqs. (14.102-14.103) into Eq. (11.80) is:

$$b = c = 2.25275 a_0 = 1.19210\ X\ 10^{-10}\ m \tag{14.106}$$

Substitution of Eqs. (14.102-14.103) into Eq. (11.67) is:

$$e = 0.44574 \tag{14.107}$$

The bonding in the nitrogen dioxide molecule comprises two double bonds, each a H_2-type MO with four paired electrons wherein the central N atom is shared by both bonds such that six electrons can be assigned to the two $N = O$ bonds. Thus, two $N2p$ electrons combine with the four $O2p$ electrons, two from each O, as a linear combination to form the two overlapping $N = O$ bonds of NO_2. Using the electron configuration of NO_2 (Eq. (14.68)), the radii of the $N1s = 0.14605 a_0$ (Eq. (10.51)), $N2s = 0.69385 a_0$ (Eq. (10.62)), $N2p = 0.74841 a_0$ (Eq. (14.77)), $O1s = 0.12739 a_0$ (Eq. (10.51)), $O2s = 0.59020 a_0$ (Eq. (10.62)), and $O2p = 0.70460 a_0$ (Eq. (14.87)) shells and the parameters of the σ MOs of NO_2 given by Eqs. (13.3-13.4), (14.102-14.104), and (14.106-14.107), the dimensional diagram and charge-density of the NO_2 MO are shown in Figures 14.3 and 14.4, respectively.

Figure 14.3. The cross section of the NO_2 MO showing the axes, σ MOs (two H_2-type ellipsoidal MOs) with six paired electrons, with the N $1s$, $2s$, and $2p$ AOs and the O $1s$, $2s$, and $2p$ AOs. Legend: a: semimajor axis, b: semiminor axis, c': internuclear distance, r_5: radius of the $N2p$ shell having one unpaired electron, r_6: radius of each $O2p$ shell having two paired electrons.

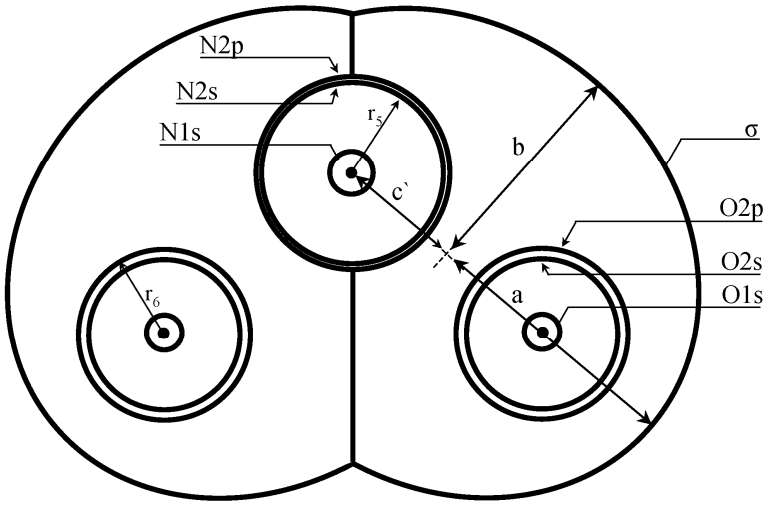

Figure 14.4. NO_2 MO comprising two σ MOs (H_2-type MOs) with N and O atoms at the foci that have each donated two electrons to the σ MOs and have smaller radii and higher binding energies as a consequence. (A)-(B) Top and side color scale, translucent views of the charge-density of the NO_2 MO. (C) Off-center cut-away view showing the complete inner most $N1s$ shell, and moving radially, the $N2s$ shell, the $N2p$ shell, and the σ prolate spheroidal MOs that each have the N atom as a focus. Moving radially from each oxygen-atom focus, the complete innermost $O1s$ shell, the $O2s$ shell, the $O2p$ shell, and the σ prolate spheroidal MOs are shown.

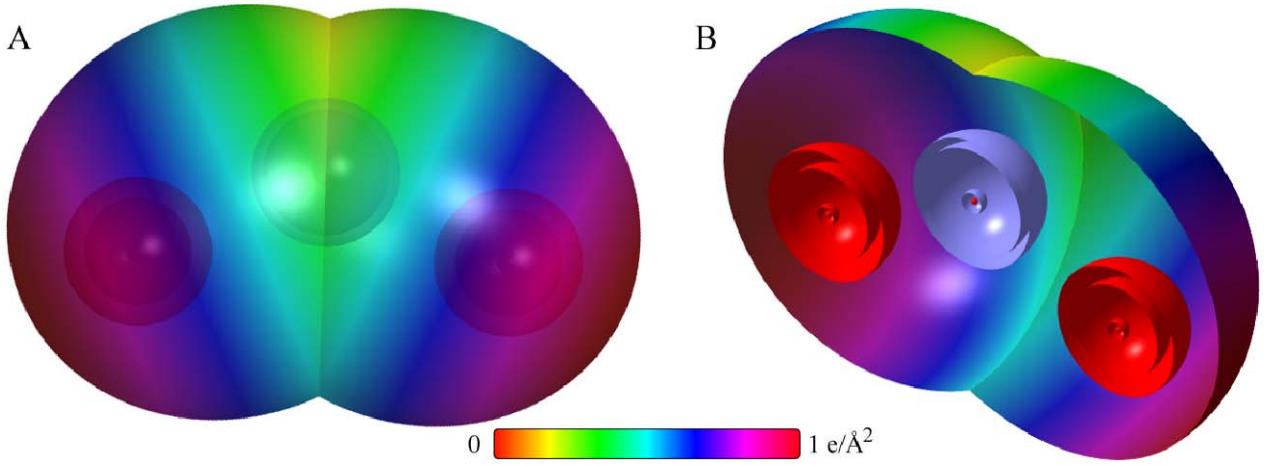

SUM OF THE ENERGIES OF THE σ MOS AND THE AOS OF NITROGEN DIOXIDE

The energies of each NO_2 σ MO are the same as those of NO (Eqs. (13.954-13.958)). They are given by the substitution of the semiprincipal axes (Eqs. (14.102-14.103) and (14.106)) into the energy equations (Eqs. (11.207-11.212)) of H_2 except that the terms based on charge are multiplied by four and the kinetic energy term is multiplied by two due to the σ-MO double bond with two pairs of paired electrons:

$$V_e = 2^2 \frac{-2e^2}{8\pi\varepsilon_0\sqrt{a^2-b^2}} \ln\frac{a+\sqrt{a^2-b^2}}{a-\sqrt{a^2-b^2}} = -93.03032\ eV \tag{14.108}$$

$$V_p = 2^2 \frac{e^2}{8\pi\varepsilon_0\sqrt{a^2-b^2}} = 48.51704\ eV \tag{14.109}$$

$$T = 2\frac{\hbar^2}{2m_e a\sqrt{a^2-b^2}} \ln\frac{a+\sqrt{a^2-b^2}}{a-\sqrt{a^2-b^2}} = 9.24176\ eV \tag{14.110}$$

$$V_m = 2^2 \frac{-\hbar^2}{4m_e a\sqrt{a^2-b^2}} \ln\frac{a+\sqrt{a^2-b^2}}{a-\sqrt{a^2-b^2}} = -9.24176\ eV \tag{14.111}$$

$$E_T = V_e + T + V_m + V_p \tag{14.112}$$

Substitution of Eqs. (11.79) and (14.108-14.111) into Eq. (14.112) gives:

$$E_T\left(N=O,\sigma\right) = \frac{-e^2}{8\pi\varepsilon_0\sqrt{\frac{aa_0}{2}}}\left(8\ln\frac{a+\sqrt{\frac{aa_0}{2}}}{a-\sqrt{\frac{aa_0}{2}}} - 4\right) = -44.51329\ eV \tag{14.113}$$

where $E_T\left(N=O,\sigma\right)$ is the total energy of each σ MO of NO_2. The total energy of NO_2, $E_T\left(NO_2\right)$, is given by the sum of $E(ionization; N)$ and $E(ionization; N^+)$, the sum of the energies of the first and second electrons of nitrogen (Eqs. (14.88-14.89)) donated to each double bond, the sum of $E(ionization; O)$ and two times $E(ionization; O^+)$, the energies of the first and second electrons of oxygen (Eqs. (14.90-14.91)) donated to the double bonds, $E_T\left(N,2p\right)$, the $N2p$ AO contribution due to the decrease in radius with the formation of each bond (Eq. (14.93)), two times $E_T\left(O,2p\right)$, the $O2p$ AO contribution due to the decrease in radius with the formation of each bond (Eq. (14.95)), and two times $E_T\left(N=O,\sigma\right)$, the σ MO contribution given by Eq. (14.113):

$$E_T\left(NO_2\right)=\begin{pmatrix} E(ionization;\ N)+E(ionization;\ N^+) \\ +E(ionization;\ O)+2E(ionization;\ O^+)+E_T\left(N,2p\right) \\ +2E_T\left(O,2p\right)+2E_T\left(N=O,\sigma\right) \end{pmatrix}$$
$$=\begin{pmatrix} 14.53414\ eV+29.6013\ eV+13.61806\ eV \\ +2\left(35.11730\ eV\right)+\left(-10.68853\ eV\right)+2\left(-39.92918\ eV\right) \\ +2\left(\dfrac{-e^2}{8\pi\varepsilon_0\sqrt{\dfrac{aa_0}{2}}}\left(8\ln\dfrac{a+\sqrt{\dfrac{aa_0}{2}}}{a-\sqrt{\dfrac{aa_0}{2}}}-4\right)\right) \end{pmatrix}$$
$$=\begin{pmatrix} 14.53414\ eV+29.6013\ eV+13.61806\ eV \\ +2\left(35.11730\ eV\right)+\left(-10.68853\ eV\right) \\ +2\left(-39.92918\ eV\right)+2\left(-44.51329\ eV\right) \end{pmatrix}=-51.58536\ eV \tag{14.114}$$

VIBRATION OF NO_2

The vibrational energy levels of NO_2 may be solved by determining the Morse potential curve from the energy relationships for the transition from a N atom and two O atoms whose parameters are given by Eqs. (10.134-10.143) and (10.154-10.163), respectively, to a N atom whose parameter r_5 is given by Eq. (14.77), two O atoms whose parameter r_6 is given by Eq. (14.87), and the σ MOs whose parameters are given by Eqs. (14.102-14.104) and (14.106-14.107). As shown in the Vibration of Hydrogen-type Molecular Ions section, the harmonic oscillator potential energy function can be expanded about the internuclear distance and expressed as a Maclaurin series corresponding to a Morse potential after Karplus and Porter (K&P) [4] and after Eq. (11.134). Treating the Maclaurin series terms as anharmonic perturbation terms of the harmonic states, the energy corrections can be found by perturbation methods.

THE DOPPLER ENERGY TERMS OF NITROGEN DIOXIDE

The equations of the radiation reaction force of nitrogen dioxide are the same as those of NO with the substitution of the NO_2 parameters. Using Eq. (13.961), the angular frequency of the reentrant oscillation in the transition state is:

$$\omega=\sqrt{\frac{4e^2}{4\pi\varepsilon_0 a^3 m_e}}=2.07110\ X\ 10^{16}\ rad/s \tag{14.115}$$

where a is given by Eq. (14.102). The kinetic energy, E_K, is given by Planck's equation (Eq. (11.127)).

$$\bar{E}_K=\hbar\omega=\hbar 2.07110\ X\ 10^{16}\ rad/s=13.63231\ eV \tag{14.116}$$

In Eq. (11.181), substitution of $E_T\left(NO_2\right)/2$ for $E_{h\nu}$, the mass of the electron, m_e, for M, and the kinetic energy given by Eq. (14.116) for $\bar{E}_K$ gives the Doppler energy of the electrons of the reentrant orbit:

$$\bar{E}_D\cong E_{h\nu}\sqrt{\frac{2\bar{E}_K}{Mc^2}}=-25.79268\ eV\sqrt{\frac{2e\left(13.63231\ eV\right)}{m_e c^2}}=-0.18840\ eV \tag{14.117}$$

In addition to the electrons, the nuclei also undergo simple harmonic oscillation in the transition state at their corresponding frequency. The transition state comprises $O--NO$, oxygen binding to NO. As in the case of CO_2 bond formation, vibration in the transition state corresponds to υ_3 [5] with the maximum kinetic energy localized to the nascent $N-O$ bond. In this case, the kinetic energy of the nuclei is the maximum for this bond. Thus, $\bar{E}_{Kvib}$ is the vibrational energy. The decrease in the energy of the NO_2 MO due to the reentrant orbit in the transition state corresponding to simple harmonic oscillation of the electrons and nuclei, $\bar{E}_{osc}$, is given by the sum of the corresponding energies, $\bar{E}_D$ given by Eq. (14.117) and $\bar{E}_{Kvib}$, the vibrational energy. Using the experimental NO_2 $E_{vib}\left(\upsilon_3\right)$ of 1618 cm^{-1} $\left(0.20061\ eV\right)$ [6] for $\bar{E}_{Kvib}$ of the transition state, $\bar{E}_{osc}\left(NO_2\right)$ is:

$$\bar{E}_{osc}\left(NO_2\right)=\bar{E}_D+\bar{E}_{Kvib}=\bar{E}_D+E_{vib} \tag{14.118}$$

$$\bar{E}_{osc}\left(NO_2\right)=-0.18840\ eV+0.20061\ eV=0.01221\ eV \tag{14.119}$$

TOTAL AND BOND ENERGIES OF NITROGEN DIOXIDE

$E_{T+osc}(NO_2)$, the total energy of NO_2 including the Doppler term, is given by the sum of $E_T(NO_2)$ (Eq. (14.114)) and $\bar{E}_{osc}(NO_2)$ given by Eq. (14.119).

$$\begin{aligned} E_{T+osc}(NO_2) &= \begin{pmatrix} 2\left(V_e+T+V_m+V_p\right)+E(ionization;\ N)+E(ionization;\ N^+) \\ +E(ionization;\ O)+2E(ionization;\ O^+) \\ +E_T(N,2p)+2E_T(O,2p)+\bar{E}_{osc}(NO_2) \end{pmatrix} \\ &= \begin{pmatrix} 2E_T(N=O,\sigma)+E(ionization;\ N)+E(ionization;\ N^+) \\ +E(ionization;\ O)+2E(ionization;\ O^+) \\ +E_T(N,2p)+2E_T(O,2p)+\bar{E}_{osc}(NO_2) \end{pmatrix} \\ &= E_T(NO_2)+\bar{E}_{osc}(NO_2) \end{aligned} \tag{14.120}$$

$$\begin{aligned} E_{T+osc}(NO_2) = \Bigg\{ & \Bigg(2\left(\frac{-e^2}{8\pi\varepsilon_0\sqrt{\frac{aa_0}{2}}} \left(8\ln\frac{a+\sqrt{\frac{aa_0}{2}}}{a-\sqrt{\frac{aa_0}{2}}}-4 \right) \right) \\ & E(ionization;\ N)+E(ionization;\ N^+) \\ & +E(ionization;\ O)+2E(ionization;\ O^+) \\ & -\sum_{N,n=4}^{4}\frac{(Z-n)e^2}{8\pi\varepsilon_0}\left(\frac{1}{r_5}-\frac{1}{r_7}\right)-2\sum_{O,n=4}^{5}\frac{(Z-n)e^2}{8\pi\varepsilon_0}\left(\frac{1}{r_6}-\frac{1}{r_8}\right) \Bigg) \\ & \left(1+\frac{1}{2}\sqrt{\frac{2\hbar\sqrt{\frac{4e^2}{4\pi\varepsilon_0 a^3}}}{m_e c^2}} \right)+E_{vib} \Bigg\} \\ = & -51.58536\ eV-0.18840\ eV+E_{vib} \end{aligned} \tag{14.121}$$

From Eqs. (14.119-14.121), the total energy of the NO_2 MO is:

$$\begin{aligned} E_{T+osc}(NO_2) &= -51.58536\ eV+\bar{E}_{osc}(NO_2) \\ &= -51.58536\ eV+0.01221\ eV \\ &= -51.57315\ eV \end{aligned} \tag{14.122}$$

where the experimental E_{vib} was used.

As in the case of the dissociation of the bond of the hydroxyl radical, an oxygen atom is formed with dissociation of NO_2. O has two unpaired electrons as shown in Eq. (13.55) which interact to stabilize the atom as shown by Eq. (10.161-10.162). The lowering of the energy of the reactants decreases the bond energy. Thus, the total energy of oxygen is reduced by the energy in the field of the two magnetic dipoles given by Eq. (7.46) and Eq. (13.101).

$$E(magnetic)=\frac{2\pi\mu_0 e^2\hbar^2}{m_e^2 a_0^3}=\frac{8\pi\mu_0\mu_B^2}{a_0^3}=0.11441\ eV \tag{14.123}$$

The NO_2 bond dissociation energy, $E_D(NO_2)$, is given by the sum of the energies of the NO and the O atom minus the sum of $E_{T+osc}(NO_2)$ and $E(magnetic)$:

$$E_D(NO_2)=E(NO)+E(O)-\left(E(magnetic)+E_{T+osc}(NO_2)\right) \tag{14.124}$$

The energy of an oxygen atom is given by the negative of Eq. (14.90), and $E_T(NO)$ is given by the sum of the experimental energies of N (negative of Eq. (14.88)), O, and the negative of the bond energy of NO (Eq. (13.974)).

$$E(NO)=-14.53414\ eV-13.618060\ eV-6.53529\ eV=-34.68749\ eV \tag{14.125}$$

Thus, the NO_2 bond dissociation energy, $E_D(NO_2)$, given by Eqs. (4.90) and (14.112-14.125) is:

$$\begin{aligned} E_D(NO_2) &= -(34.68749\ eV + 13.618060\ eV) - (E(magnetic) + E_{T+osc}(NO_2)) \\ &= -48.30555\ eV - (0.11441\ eV - 51.57315\ eV) = 3.15319\ eV \end{aligned} \tag{14.126}$$

The experimental NO_2 bond dissociation energy is [7]:

$$E_{D298}(NO_2) = 3.161\ eV \tag{14.127}$$

BOND ANGLE OF NO_2

The NO_2 MO comprises a linear combination of two $N=O$-bond MOs. A bond is also possible between the two O atoms of the $N=O$ bonds. Such $O=O$ bonding would decrease the $N=O$ bond strength since electron density would be shifted from the $N=O$ bonds to the $O=O$ bond. Thus, the bond angle between the two $N=O$ bonds is determined by the condition that the total energy of the H_2-type ellipsoidal MO between the terminal O atoms of the $N=O$ bonds is zero. From Eqs. (11.79) and (13.228), the distance from the origin to each focus of the $O=O$ ellipsoidal MO is:

$$c' = a\sqrt{\frac{\hbar^2 4\pi\varepsilon_0}{m_e e^2 2a}} = \sqrt{\frac{aa_0}{2}} \tag{14.128}$$

The internuclear distance from Eq. (13.229) is:

$$2c' = 2\sqrt{\frac{aa_0}{2}} \tag{14.129}$$

The length of the semiminor axis of the prolate spheroidal $O=O$ MO $b=c$ is given by Eq. (13.167).

The component energies and the total energy E_T of the $O=O$ bond are given by the energy equations (Eqs. (11.207-11.212), (11.213-11.217), and (11.239)) of H_2 except that the terms based on charge are multiplied by four and the kinetic energy term is multiplied by two due to the $O=O$ double bond with two pairs of paired electrons. Substitution of Eq. (14.128) into Eqs. (11.207-11.212) gives:

$$0 = \left[\frac{-e^2}{8\pi\varepsilon_0\sqrt{\frac{aa_0}{2}}} \left(8\ln\frac{a+\sqrt{\frac{aa_0}{2}}}{a-\sqrt{\frac{aa_0}{2}}} - 4 \right) \left[1 + \sqrt{\frac{2\hbar\sqrt{\frac{4e^2}{4\pi\varepsilon_0 a^3}}}{m_e c^2}} \right] \right. \\ \left. + \frac{1}{2}\hbar\sqrt{\frac{\frac{4e^2}{8\pi\varepsilon_0 a^3} - \frac{4e^2}{8\pi\varepsilon_0 (a+c')^3}}{8m_p}} \right] \tag{14.130}$$

From the energy relationship given by Eq. (14.130) and the relationship between the axes given by Eqs. (14.128-14.129) and (13.167-14.168), the dimensions of the $O=O$ MO can be solved.

The most convenient way to solve Eq. (14.130) is by the reiterative technique using a computer. The result to within the round-off error with five-significant figures is:

$$a = 8.3360a_0 = 4.4112\ X\ 10^{-10}\ m \tag{14.131}$$

Substitution of Eq. (14.131) into Eq. (14.128) gives:

$$c' = 2.0416a_0 = 1.0804\ X\ 10^{-10}\ m \tag{14.132}$$

The internuclear distance given by multiplying Eq. (14.132) by two is:

$$2c' = 4.0831a_0 = 2.1607\ X\ 10^{-10}\ m \tag{14.133}$$

Substitution of Eqs. (14.131-14.132) into Eq. (14.167) gives:

$$b = c = 8.0821a_0 = 4.2769\ X\ 10^{-10}\ m \tag{14.134}$$

Substitution of Eqs. (14.131-14.132) into Eq. (14.168) gives:

$$e = 0.2449 \tag{14.135}$$

From, $2c'_{C=C}$ (Eq. (14.133)), the distance between the two O atoms when the total energy of the corresponding MO is zero (Eq. (14.130)), and $2c'_{N=O}$ (Eq. (14.104)), the internuclear distance of each $N=O$ bond, the corresponding bond angle can be determined from the law of cosines. Using, Eqs. (13.240-13.242), the bond angle θ between the $N=O$ bonds is:

$$\theta = \cos^{-1}\left(\frac{2\left(2.24347\right)^2 - \left(4.0831\right)^2}{2\left(2.24347\right)^2}\right) = \cos^{-1}\left(-0.6562\right) = 131.012° \tag{14.136}$$

The experimental angle between the $N = O$ bonds is [3]:

$$\theta = 134.1° \tag{14.137}$$

The results of the determination of bond parameters of NO_2 are given in Table 14.1. The calculated results are based on first principles and given in closed-form, exact equations containing fundamental constants only. The agreement between the experimental and calculated results is excellent.

ETHANE MOLECULE (CH_3CH_3)

The ethane molecule CH_3CH_3 is formed by the reaction of two methyl radicals:

$$CH_3 + CH_3 \rightarrow CH_3CH_3 \tag{14.138}$$

CH_3CH_3 can be solved using the same principles as those used to solve CH_3, wherein the $2s$ and $2p$ shells of each C hybridize to form a single $2sp^3$ shell as an energy minimum, and the sharing of electrons between two $C2sp^3$ hybridized orbitals (HOs) to form a molecular orbital (MO) permits each participating hybridized orbital to decrease in radius and energy. First, two sets of three H atomic orbitals (AOs) combine with two sets of three carbon $2sp^3$ HOs to form two methyl groups comprising a linear combination of six diatomic H_2-type MOs developed in the Nature of the Chemical Bond of Hydrogen-Type Molecules and Molecular Ions section. Then, the two CH_3 groups bond by forming a H_2-type MO between the remaining $C2sp^3$ HO on each carbon.

FORCE BALANCE OF THE $C-C$-BOND MO OF ETHANE

CH_3CH_3 comprises a chemical bond between two CH_3 radicals wherein each methyl radical comprises three chemical bonds between carbon and hydrogen atoms. The solution of the parameters of CH_3 is given in the Methyl Radical (CH_3) section. Each $C-H$ bond of CH_3 having two spin-paired electrons, one from an initially unpaired electron of the carbon atom and the other from the hydrogen atom, comprises the linear combination of 75% H_2-type ellipsoidal MO and 25% $C2sp^3$ HO. The proton of the H atom and the nucleus of the C atom are along each internuclear axis and serve as the foci. As in the case of H_2, each of the three $C-H$-bond MOs is a prolate spheroid with the exception that the ellipsoidal MO surface cannot extend into $C2sp^3$ HO for distances shorter than the radius of the $C2sp^3$ shell since it is energetically unfavorable. Thus, each MO surface comprises a prolate spheroid at the H proton that is continuous with the $C2sp^3$ shell at the C atom whose nucleus serves as the other focus. The electron configuration and the energy, $E\left(C,2sp^3\right)$, of the $C2sp^3$ shell is given by Eqs. (13.422) and (13.428), respectively. The central paramagnetic force due to spin of each $C-H$ bond is provided by the spin-pairing force of the CH_3 MO that has the symmetry of an s orbital that superimposes with the $C2sp^3$ orbitals such that the corresponding angular momenta are unchanged.

Two CH_3 radicals bond to form CH_3CH_3 by forming a MO between the two remaining $C2sp^3$-HO electrons of the two carbon atoms. However, in this case, the sharing of electrons between two $C2sp^3$ HOs to form a molecular orbital (MO) comprising two spin-paired electrons permits each $C2sp^3$ HO to decrease in radius and energy.

As in the case of the $C-H$ bonds, the $C-C$-bond MO is a prolate-spheroidal-MO surface that cannot extend into $C2sp^3$ HO for distances shorter than the radius of the $C2sp^3$ shell of each atom. Thus, the MO surface comprises a partial prolate spheroid in between the carbon nuclei and is continuous with the $C2sp^3$ shell at each C atom. The energy of the H_2-type ellipsoidal MO is matched to that of the $C2sp^3$ shell. As in the case of previous examples of energy-matched MOs such as those of OH, NH, CH, and the $C=O$-bond MO of CO_2, the $C-C$-bond MO of ethane must comprise 75% of a H_2-type ellipsoidal MO in order to match potential, kinetic, and orbital energy relationships. Thus, the $C-C$-bond MO must comprise two $C2sp^3$ HOs and 75% of a H_2-type ellipsoidal MO divided between the two $C2sp^3$ HOs:

$$2\,C2sp^3 + 0.75\,H_2\ MO \rightarrow C-C-bond\ MO \tag{14.139}$$

The linear combination of the H_2-type ellipsoidal MO with each $C2sp^3$ HO further comprises an excess 25% charge-density contribution from each $C2sp^3$ HO to the $C-C$-bond MO to achieve an energy minimum. The force balance of the $C-C$-bond

MO is determined by the boundary conditions that arise from the linear combination of orbitals according to Eq. (14.139) and the energy matching condition between the $C2sp^3$-HO components of the MO.

Similarly, the energies of each CH_3 MO involve each $C2sp^3$ and each $H1s$ electron with the formation of each $C-H$ bond. The sum of the energies of the H_2-type ellipsoidal MOs is matched to that of the $C2sp^3$ shell. This energy is determined by the considering the effect of the donation of 25% electron density from the two $C2sp^3$ HOs to the $C-C$-bond MO. The $2sp^3$ hybridized orbital arrangement given by Eq. (13.422) is:

$$\begin{array}{cccc} & 2\text{sp}^3 \text{ state} & & \\ \uparrow & \uparrow & \uparrow & \uparrow \\ \hline 0,0 & 1,\text{-}1 & 1,0 & 1,1 \end{array} \tag{14.140}$$

where the quantum numbers (ℓ, m_ℓ) are below each electron. The total energy of the state is given by the sum over the four electrons. The sum $E_T\left(C,2sp^3\right)$ of calculated energies of C, C^+, C^{2+}, and C^{3+} from Eqs. (10.123), (10.113-10.114), (10.68), and (10.48), respectively, is:

$$E_T\left(C,2sp^3\right)=64.3921\ eV+48.3125\ eV+24.2762\ eV+11.27671\ eV=148.25751\ eV \tag{14.141}$$

which agrees well with the sum of 148.02532 eV from the experimental [2] values. Consider the case of the $C2sp^3$ HO of each methyl radical. The orbital-angular-momentum interactions cancel such that the energy of the $E_T\left(C,2sp^3\right)$ is purely Coulombic. By considering that the central field decreases by an integer for each successive electron of the shell, the radius r_{2sp^3} of the $C2sp^3$ shell may be calculated from the Coulombic energy using Eq. (10.102):

$$r_{2sp^3}=\sum_{n=2}^{5}\frac{(Z-n)e^2}{8\pi\varepsilon_0\left(e148.25751\ eV\right)}=\frac{10e^2}{8\pi\varepsilon_0\left(e148.25751\ eV\right)}=0.91771a_0 \tag{14.142}$$

where $Z=6$ for carbon. Using Eqs. (10.102) and (14.142), the Coulombic energy $E_{Coulomb}\left(C,2sp^3\right)$ of the outer electron of the $C2sp^3$ shell is:

$$E_{Coulomb}\left(C,2sp^3\right)=\frac{-e^2}{8\pi\varepsilon_0 r_{2sp^3}}=\frac{-e^2}{8\pi\varepsilon_0 0.91771a_0}=-14.82575\ eV \tag{14.143}$$

During hybridization, the spin-paired $2s$ electrons are promoted to the $C2sp^3$ shell as unpaired electrons. The energy for the promotion is the magnetic energy given by Eq. (13.152) at the initial radius of the $2s$ electrons. From Eq. (10.62) with $Z=6$, the radius r_3 of the $C2s$ shell is:

$$r_3=0.84317a_0 \tag{14.144}$$

Using Eqs. (13.152) and (14.144), the unpairing energy is:

$$E(magnetic)=\frac{2\pi\mu_0 e^2\hbar^2}{m_e^2\left(r_3\right)^3}=\frac{8\pi\mu_0\mu_B^2}{\left(0.84317a_0\right)^3}=0.19086\ eV \tag{14.145}$$

Using Eqs. (14.143) and (14.145), the energy $E\left(C,2sp^3\right)$ of the outer electron of the $C2sp^3$ shell is:

$$E\left(C,2sp^3\right)=\frac{-e^2}{8\pi\varepsilon_0 r_{2sp^3}}+\frac{2\pi\mu_0 e^2\hbar^2}{m_e^2\left(r_3\right)^3}=-14.82575\ eV+0.19086\ eV=-14.63489\ eV \tag{14.146}$$

Next, consider the formation of the $C-C$-bond MO of ethane from two methyl radicals, each having a $C2sp^3$ electron with an energy given by Eq. (14.146). The total energy of the state is given by the sum over the four electrons. The sum $E_T\left(C_{ethane},2sp^3\right)$ of calculated energies of $C2sp^3$, C^+, C^{2+}, and C^{3+} from Eqs. (10.123), (10.113-10.114), (10.68), and (10.48), respectively, is:

$$\begin{aligned} E_T\left(C_{ethane},2sp^3\right)&=-\left(64.3921\ eV+48.3125\ eV+24.2762\ eV+E\left(C,2sp^3\right)\right)\\ &=-\left(64.3921\ eV+48.3125\ eV+24.2762\ eV+14.63489\ eV\right)\\ &=-151.61569\ eV \end{aligned} \tag{14.147}$$

where $E\left(C,2sp^3\right)$ is the sum of the energy of C, $-11.27671\ eV$, and the hybridization energy. The orbital-angular-momentum

interactions also cancel such that the energy of the $E_T\left(C_{ethane},2sp^3\right)$ is purely Coulombic.

The sharing of electrons between two $C2sp^3$ HOs to form a $C-C$-bond MO permits each participating hybridized orbital to decrease in radius and energy. In order to further satisfy the potential, kinetic, and orbital energy relationships, each $C2sp^3$ HO donates an excess of 25% of its electron density to the $C-C$-bond MO to form an energy minimum. By considering this electron redistribution in the ethane molecule as well as the fact that the central field decreases by an integer for each successive electron of the shell, the radius $r_{ethane2sp^3}$ of the $C2sp^3$ shell of ethane may be calculated from the Coulombic energy using Eq. (10.102).

$$r_{ethane2sp^3}=\left(\sum_{n=2}^{5}(Z-n)-0.25\right)\frac{e^2}{8\pi\varepsilon_0\left(e151.61569\ eV\right)}=\frac{9.75e^2}{8\pi\varepsilon_0\left(e151.61569\ eV\right)}=0.87495a_0 \tag{14.148}$$

Using Eqs. (10.102) and (14.148), the Coulombic energy $E_{Coulomb}\left(C_{ethane},2sp^3\right)$ of the outer electron of the $C2sp^3$ shell is:

$$E_{Coulomb}\left(C_{ethane},2sp^3\right)=\frac{-e^2}{8\pi\varepsilon_0 r_{ethane2sp^3}}=\frac{-e^2}{8\pi\varepsilon_0 0.87495a_0}=-15.55033\ eV \tag{14.149}$$

During hybridization, the spin-paired $2s$ electrons are promoted to the $C2sp^3$ shell as unpaired electrons. The energy for the promotion is the magnetic energy given by Eq. (13.152). Using Eqs. (14.145) and (14.149), the energy $E\left(C_{ethane},2sp^3\right)$ of the outer electron of the $C2sp^3$ shell is:

$$E\left(C_{ethane},2sp^3\right)=\frac{-e^2}{8\pi\varepsilon_0 r_{ethane2sp^3}}+\frac{2\pi\mu_0 e^2\hbar^2}{m_e^2\left(r_3\right)^3}=-15.55033\ eV+0.19086\ eV=-15.35946\ eV \tag{14.150}$$

Thus, $E_T\left(C-C,2sp^3\right)$, the energy change of each $C2sp^3$ shell with the formation of the $C-C$-bond MO is given by the difference between Eq. (14.146) and Eq. (14.150).

$$E_T\left(C-C,2sp^3\right)=E\left(C_{ethane},2sp^3\right)-E\left(C,2sp^3\right)=-15.35946\ eV-\left(-14.63489\ eV\right)=-0.72457\ eV \tag{14.151}$$

The H_2-type ellipsoidal MO comprises 75% of the $C-C$-bond MO shared between two $C2sp^3$ HOs corresponding to the electron charge density in Eq. (11.65) of $\frac{-0.75e}{2}$. But, the additional 25% charge-density contribution to the $C-C$-bond MO causes the electron charge density in Eq. (11.65) to be $\frac{-e}{2}=-0.5e$. Thus, the force constant k' to determine the ellipsoidal parameter c' in terms of the central force of the foci given by Eq. (11.65) is:

$$k'=\frac{(0.5)2e^2}{4\pi\varepsilon_0} \tag{14.152}$$

The distance from the origin to each focus c' is given by substitution of Eq. (14.152) into Eq. (13.60). Thus, the distance from the origin of the $C-C$-bond MO to each focus c' is given by:

$$c'=a\sqrt{\frac{\hbar^2 4\pi\varepsilon_0}{m_e e^2 a}}=\sqrt{aa_0} \tag{14.153}$$

The internuclear distance from Eq. (14.153) is:

$$2c'=2\sqrt{aa_0} \tag{14.154}$$

The length of the semiminor axis of the prolate spheroidal $C-C$-bond MO $b=c$ is given by Eq. (13.62). The eccentricity, e, is given by Eq. (13.63). The solution of the semimajor axis a then allows for the solution of the other axes of each prolate spheroid and eccentricity of the $C-C$-bond MO. Since the $C-C$-bond MO comprises a H_2-type-ellipsoidal MO that transitions to the $C_{ethane}2sp^3$ HO of each carbon, the energy $E\left(C_{ethane},2sp^3\right)$ in Eq. (14.150) adds to that of the H_2-type ellipsoidal MO to give the total energy of the $C-C$-bond MO. From the energy equation and the relationship between the axes, the dimensions of the $C-C$-bond MO are solved. Similarly, $E\left(C_{ethane},2sp^3\right)$ is added to the energy of the H_2-type ellipsoidal MO of each $C-H$ bond of the methyl groups to give its total energy. From the energy equation and the relationship between the axes, the dimensions of the equivalent $C-H$-bond MOs of the methyl groups in ethane are solved.

The general equations for the energy components of V_e, V_p, T, V_m, and E_T of the $C-C$-bond MO are the same as those of the CH MO as well as each $C-H$-bond MO of the methyl groups except that energy of the $C_{ethane}2sp^3$ HO is used. Since the prolate spheroidal H_2-type MO transitions to the $C_{ethane}2sp^3$ HO of each carbon and the energy of the $C_{ethane}2sp^3$ shell must remain constant and equal to the $E\left(C_{ethane},2sp^3\right)$ given by Eq. (14.150), the total energy $E_T\left(C-C,\sigma\right)$ of the σ component of the $C-C$-bond MO is given by the sum of the energies of the orbitals corresponding to the composition of the linear combination of the $C_{ethane}2sp^3$ HO and the H_2-type ellipsoidal MO that forms the σ component of the $C-C$-bond MO as given by Eq. (14.139) with the electron charge redistribution. Using Eqs. (13.431) and (14.150), $E_T\left(C-C,\sigma\right)$ is given by:

$$E_T\left(C-C,\sigma\right)=E_T+E\left(C_{ethane},2sp^3\right)=-\frac{e^2}{8\pi\varepsilon_0 c'}\left[\left(0.91771\right)\left(2-\frac{1}{2}\frac{a_0}{a}\right)\ln\frac{a+c'}{a-c'}-1\right]-15.35946\ eV \tag{14.155}$$

To match the boundary condition that the total energy of the entire the H_2-type ellipsoidal MO is given by Eqs. (11.212) and (13.75), $E_T\left(C-C,\sigma\right)$ given by Eq. (14.155) is set equal to Eq. (13.75):

$$E_T\left(C-C,\sigma\right)=-\frac{e^2}{8\pi\varepsilon_0 c'}\left[\left(0.91771\right)\left(2-\frac{1}{2}\frac{a_0}{a}\right)\ln\frac{a+c'}{a-c'}-1\right]-15.35946\ eV=-31.63536831\ eV \tag{14.156}$$

From the energy relationship given by Eq. (14.156) and the relationship between the axes given by Eqs. (14.153-14.154) and (13.62-13.63), the dimensions of the $C-C$-bond MO can be solved.

Substitution of Eq. (14.153) into Eq. (14.156) gives:

$$\frac{e^2}{8\pi\varepsilon_0\sqrt{aa_0}}\left[\left(0.91771\right)\left(2-\frac{1}{2}\frac{a_0}{a}\right)\ln\frac{a+\sqrt{aa_0}}{a-\sqrt{aa_0}}-1\right]=e16.27589 \tag{14.157}$$

The most convenient way to solve Eq. (14.157) is by the reiterative technique using a computer. The result to within the round-off error with five-significant figures is

$$a=2.10725a_0=1.11511\ X\ 10^{-10}\ m \tag{14.158}$$

Substitution of Eq. (14.158) into Eq. (14.153) gives:

$$c'=1.45164a_0=7.68173\ X\ 10^{-11}\ m \tag{14.159}$$

The internuclear distance given by multiplying Eq. (14.159) by two is:

$$2c'=2.90327a_0=1.53635\ X\ 10^{-10}\ m \tag{14.160}$$

The experimental bond distance is [3]:

$$2c'=1.5351\ X\ 10^{-10}\ m \tag{14.161}$$

Substitution of Eqs. (14.158-14.159) into Eq. (13.62) gives:

$$b=c=1.52750a_0=8.08317\ X\ 10^{-11}\ m \tag{14.162}$$

Substitution of Eqs. (14.158-14.159) into Eq. (13.63) gives:

$$e=0.68888 \tag{14.163}$$

The nucleus of the C atoms comprise the foci of the H_2-type ellipsoidal MO. The parameters of the point of intersection of the H_2-type ellipsoidal MO and the $C_{ethane}2sp^3$ HO are given by Eqs. (13.84-13.95) and (13.261-13.270). The polar intersection angle θ' is given by Eq. (13.261) where $r_n=r_{ethane2sp^3}=0.87495a_0$ is the radius of the $C_{ethane}2sp^3$ shell. Substitution of Eqs. (14.158-14.159) into Eq. (13.261) gives:

$$\theta'=67.33° \tag{14.164}$$

Then, the angle $\theta_{C-C_{ethane}2sp^3HO}$ the radial vector of the $C2sp^3$ HO makes with the internuclear axis is:

$$\theta_{C-C_{ethane}2sp^3HO}=180°-67.33°=112.67° \tag{14.165}$$

as shown in Figure 14.5.

Figure 14.5. The cross section of the $C-C$-bond MO (σ MO) and one $C-H$-bond MO of ethane showing the axes, angles, and point of intersection of each H_2-type ellipsoidal MO with the corresponding $C_{ethane}2sp^3$ HO. The continuation of each H_2-type-ellipsoidal-MO basis element of the $C-C$ bond and the $C-H$-bond beyond the intersection point with each $C_{ethane}2sp^3$ shell and σ MO is shown as dashed since each only serves to solve the energy match with the $C_{ethane}2sp^3$ shell and does not represent charge density. Similarly, the vertical dashed line only designates the parameters of each intersection point. The actual charge density is shown by the solid lines. Legend: a: semimajor axis, b: semiminor axis, c': internuclear distance, $d_1 : d_{C-C_{ethane},H_2MO}$, $\theta_1 : \theta_{C-C_{ethane}2sp^3HO}$, $d_2 : d_{C-C_{ethane}2sp^3HO}$, $R : r_{ethaneC2sp^3}$, $d_3 : d_{C-H_{ethane},H_2MO}$, $\theta_2 : \theta_{C-H_{ethane}2sp^3HO}$, and $d_4 : d_{C-H_{ethane}2sp^3HO}$.

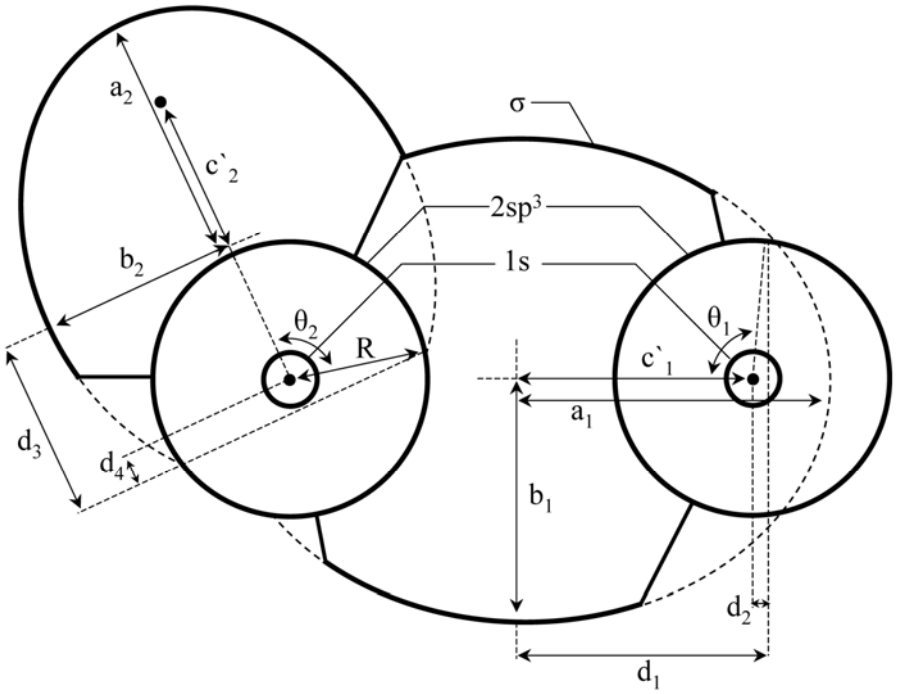

Consider the right-hand intersection point. The Cartesian **i**-coordinate of the interception point of the MO and the AO can be calculated using the MO ellipsoidal parameters by first calculating the parametric angle in Eq. (11.83) that matches Cartesian **j**-coordinate components at the point of intersection. Thus, the matching elliptic parametric angle $\omega t = \theta_{C-C_{ethane},H_2MO}$ satisfies the following relationship:

$$r_{ethane2sp^3} \sin\theta_{C-C_{ethane}2sp^3HO} = 0.87495a_0 \sin\theta_{C-C_{ethane}2sp^3HO} = b\sin\theta_{C-C_{ethane},H_2MO} \tag{14.166}$$

such that

$$\theta_{C-C_{ethane},H_2MO} = \sin^{-1}\frac{0.87495a_0 \sin\theta_{C-C_{ethane}2sp^3HO}}{b} = \sin^{-1}\frac{0.87495a_0 \sin 112.67°}{b} \tag{14.167}$$

with the use of Eq. (14.166). Substitution of Eq. (14.162) into Eq. (14.167) gives:

$$\theta_{C-C_{ethane},H_2MO} = 31.91° \tag{14.168}$$

Then, the distance d_{C-C_{ethane},H_2MO} along the internuclear axis from the origin of H_2-type ellipsoidal MO to the point of intersection of the orbitals is given by:

$$d_{C-C_{ethane},H_2MO} = a\cos\theta_{C-C_{ethane},H_2MO} \tag{14.169}$$

Substitution of Eqs. (14.158) and (14.168) into Eq. (14.169) gives:

$$d_{C-C_{ethane},H_2MO} = 1.78885a_0 = 9.46617\ X\ 10^{-11}\ m \tag{14.170}$$

The distance $d_{C-C_{ethane}2sp^3HO}$ along the internuclear axis from the origin of the C atom to the point of intersection of the orbitals is given by:

$$d_{C-C_{ethane}2sp^3HO} = d_{C-C_{ethane},H_2MO} - c' \tag{14.171}$$

Substitution of Eqs. (14.159) and (14.170) into Eq. (14.171) gives:

$$d_{C-C_{ethane}2sp^3HO} = 0.33721a_0 = 1.78444\ X\ 10^{-11}\ m \tag{14.172}$$

FORCE BALANCE OF THE CH_3 MOS OF ETHANE

Each of the two equivalent CH_3 MOs must comprise three $C-H$ bonds with each comprising 75% of a H_2-type ellipsoidal MO and a $C2sp^3$ HO as given by Eq. (13.540):

$$3\left[1\ C2sp^3 + 0.75\ H_2\ MO\right] \rightarrow CH_3\ MO \tag{14.173}$$

The force balance of the CH_3 MO is determined by the boundary conditions that arise from the linear combination of orbitals according to Eq. (13.540) and the energy matching condition between the hydrogen and $C2sp^3$ HO components of the MO.

The force constant k' to determine the ellipsoidal parameter c' of the each H_2-type-ellipsoidal-MO component of the CH_3 MO in terms of the central force of the foci is given by Eq. (13.59). The distance from the origin of each $C-H$-bond MO to each focus c' is given by Eq. (13.60). The internuclear distance is given by Eq. (13.61). The length of the semiminor axis of the prolate spheroidal $C-H$-bond MO $b=c$ is given by Eq. (13.62). The eccentricity, e, is given by Eq. (13.63). The solution of the semimajor axis a then allows for the solution of the other axes of each prolate spheroid and eccentricity of each $C-H$-bond MO. Since each of the three prolate spheroidal $C-H$-bond MOs comprises an H_2-type-ellipsoidal MO that transitions to the $C_{ethane}2sp^3$ HO of ethane, the energy $E\left(C_{ethane},2sp^3\right)$ of Eq. (14.150) adds to that of the three corresponding H_2-type ellipsoidal MOs to give the total energy of the CH_3 MO. From the energy equation and the relationship between the axes, the dimensions of the CH_3 MO are solved.

The energy components of V_e, V_p, T, and V_m are the same as those of methyl radical, three times those of CH corresponding to the three $C-H$ bonds except that energy of the $C_{ethane}2sp^3$ HO is used. Since each prolate spheroidal H_2-type MO transitions to the $C_{ethane}2sp^3$ HO and the energy of the $C_{ethane}2sp^3$ shell must remain constant and equal to the $E\left(C_{ethane},2sp^3\right)$ given by Eq. (14.150), the total energy $E_{T_{ethane}}\left(CH_3\right)$ of the CH_3 MO is given by the sum of the energies of the orbitals corresponding to the composition of the linear combination of the $C_{ethane}2sp^3$ HO and the three H_2-type ellipsoidal MOs that forms the CH_3 MO as given by Eq. (13.540). Using Eq. (13.431), $E_{T_{ethane}}\left(CH_3\right)$ is given by:

$$E_{T_{ethane}}\left(CH_3\right) = E_T + E\left(C_{ethane},2sp^3\right) = -\frac{3e^2}{8\pi\varepsilon_0 c'}\left[\left(0.91771\right)\left(2-\frac{1}{2}\frac{a_0}{a}\right)\ln\frac{a+c'}{a-c'}-1\right]-15.35946\ eV \tag{14.174}$$

$E_{T_{ethane}}\left(CH_3\right)$ given by Eq. (14.174) is set equal to three times the energy of the H_2-type ellipsoidal MO minus two times the Coulombic energy of H given by Eq. (13.542):

$$E_T\left(CH_3\right) = -\frac{3e^2}{8\pi\varepsilon_0 c'}\left[\left(0.91771\right)\left(2-\frac{1}{2}\frac{a_0}{a}\right)\ln\frac{a+c'}{a-c'}-1\right]-15.35946\ eV = -67.69450\ eV \tag{14.175}$$

From the energy relationship given by Eq. (14.175) and the relationship between the axes given by Eqs. (13.60-13.63), the dimensions of the CH_3 MO can be solved.

Substitution of Eq. (13.60) into Eq. (14.175) gives:

$$\frac{3e^2}{8\pi\varepsilon_0\sqrt{\frac{2aa_0}{3}}}\left[\left(0.91771\right)\left(2-\frac{1}{2}\frac{a_0}{a}\right)\ln\frac{a+\sqrt{\frac{2aa_0}{3}}}{a-\sqrt{\frac{2aa_0}{3}}}-1\right] = e52.33505 \tag{14.176}$$

The most convenient way to solve Eq. (14.176) is by the reiterative technique using a computer. The result to within the round-off error with five-significant figures is:

$$a = 1.64469a_0 = 8.70331\ X\ 10^{-11}\ m \tag{14.177}$$

Substitution of Eq. (14.177) into Eq. (14.60) gives:

$$c' = 1.04712a_0 = 5.54111\ X\ 10^{-11}\ m \tag{14.178}$$

The internuclear distance given by multiplying Eq. (14.178) by two is:

$$2c' = 2.09424a_0 = 1.10822\ X\ 10^{-10}\ m \tag{14.179}$$

The experimental bond distance is [3]:

$$2c' = 1.0940\ X\ 10^{-10}\ m \tag{14.180}$$

Substitution of Eqs. (14.177-14.178) into Eq. (14.62) gives:

$$b = c = 1.26828a_0 = 6.71145\ X\ 10^{-11}\ m \tag{14.181}$$

Substitution of Eqs. (14.177-14.178) into Eq. (13.63) gives:

$$e = 0.63667 \tag{14.182}$$

The nucleus of the H atom and the nucleus of the C atom comprise the foci of each H_2-type ellipsoidal MO. The parameters of the point of intersection of the H_2-type ellipsoidal MO and the $C_{ethane}2sp^3$ HO are given by Eqs. (13.84-13.95) and (13.261-13.270). The polar intersection angle θ' is given by Eq. (13.261) where $r_n = r_{ethane\,2sp^3} = 0.87495a_0$ is the radius of the $C_{ethane}2sp^3$ shell. Substitution of Eqs. (14.177-14.178) into Eq. (13.261) gives:

$$\theta' = 79.34° \tag{14.183}$$

Then, the angle $\theta_{C-H_{ethane}2sp^3HO}$ the radial vector of the $C2sp^3$ HO makes with the internuclear axis is:

$$\theta_{C-H_{ethane}2sp^3HO} = 180° - 79.34° = 100.66° \tag{14.184}$$

as shown in Figure 14.6.

Figure 14.6. The cross section of one $C-H$-bond MO of ethane showing the axes, angles, and point of intersection of the H_2-type ellipsoidal MO with the $C_{ethane}2sp^3$ HO. The continuation of the H_2-type-ellipsoidal-MO basis element beyond the intersection point with the $C_{ethane}2sp^3$ shell is shown as dashed since it only serves to solve the energy match with the $C_{ethane}2sp^3$ shell and does not represent charge density. Similarly, the vertical dashed line only designates the parameters of the intersection point. The actual charge density is shown by the solid lines. Legend: a: semimajor axis, b: semiminor axis, c': internuclear distance, $d_1 : d_{C-H_{ethane},H_2MO}$, $\theta_1 : \theta_{C-H_{ethane}2sp^3HO}$, $d_2 : d_{C-H_{ethane}2sp^3HO}$, and $R : r_{ethane2sp^3}$.

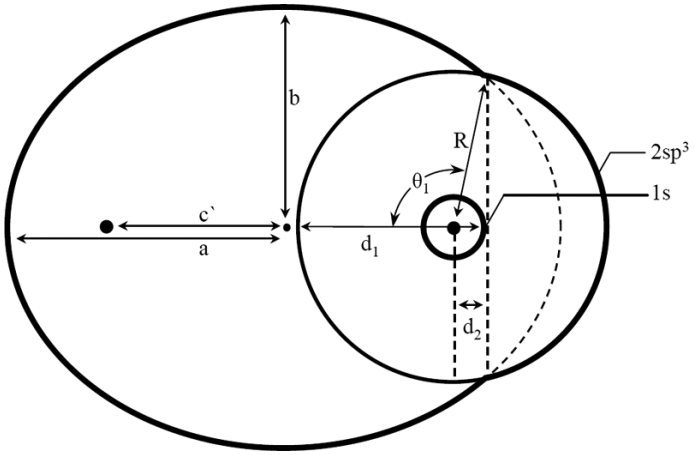

The Cartesian $\mathbf{i}$-coordinate of the interception point of the MO and the AO can be calculated using the MO ellipsoidal parameters by first calculating the parametric angle in Eq. (11.83) that matches Cartesian $\mathbf{j}$-coordinate components at the point of intersection. Thus, the matching elliptic parametric angle $\omega t = \theta_{C-H_{ethane},H_2MO}$ satisfies the following relationship:

$$r_{ethane2sp^3} \sin\theta_{C-H_{ethane}2sp^3HO} = 0.87495a_0 \sin\theta_{C-H_{ethane}2sp^3HO} = b\sin\theta_{C-H_{ethane},H_2MO} \tag{14.185}$$

such that

$$\theta_{C-H_{ethane},H_2MO} = \sin^{-1}\frac{0.87495a_0 \sin\theta_{C-H_{ethane}2sp^3HO}}{b} = \sin^{-1}\frac{0.87495a_0 \sin 100.66°}{b} \tag{14.186}$$

with the use of Eq. (14.184). Substitution of Eq. (14.181) into Eq. (14.186) gives:

$$\theta_{C-H_{ethane},H_2MO} = 42.68° \tag{14.187}$$

Then, the distance d_{C-H_{ethane},H_2MO} along the internuclear axis from the origin of H_2-type ellipsoidal MO to the point of intersection of the orbitals is given by:

$$d_{C-H_{ethane},H_2MO} = a\cos\theta_{C-H_{ethane},H_2MO} \tag{14.188}$$

Substitution of Eqs. (14.177) and (14.187) into Eq. (14.188) gives:

$$d_{C-H_{ethane},H_2MO} = 1.20901a_0 = 6.39780\ X\ 10^{-11}\ m \tag{14.189}$$

The distance $d_{C-H_{ethane}2sp^3HO}$ along the internuclear axis from the origin of the C atom to the point of intersection of the orbitals is given by

$$d_{C-H_{ethane}2sp^3HO} = d_{C-H_{ethane},H_2MO} - c' \tag{14.190}$$

Substitution of Eqs. (14.178) and (14.189) into Eq. (14.190) gives:

$$d_{C-H_{ethane}2sp^3HO} = 0.16189a_0 = 8.56687\ X\ 10^{-12}\ m \tag{14.191}$$

BOND ANGLE OF THE CH_3 GROUPS

Each CH_3 MO comprises a linear combination of three $C-H$-bond MOs. Each $C-H$-bond MO comprises the superposition of a H_2-type ellipsoidal MO and the $C_{ethane}2sp^3$ HO. A bond is also possible between the two H atoms of the $C-H$ bonds. Such $H-H$ bonding would decrease the $C-H$ bond strength since electron density would be shifted from the $C-H$ bonds to the $H-H$ bond. Thus, the bond angle between the two $C-H$ bonds is determined by the condition that the total energy of the H_2-type ellipsoidal MO between the terminal H atoms of the $C-H$ bonds is zero. From Eqs. (11.79) and (13.228), the distance from the origin to each focus of the $H-H$ ellipsoidal MO is:

$$c' = a\sqrt{\frac{\hbar^2 4\pi\varepsilon_0}{m_e e^2 2a}} = \sqrt{\frac{aa_0}{2}} \tag{14.192}$$

The internuclear distance from Eq. (13.229) is:

$$2c' = 2\sqrt{\frac{aa_0}{2}} \tag{14.193}$$

The length of the semiminor axis of the prolate spheroidal $H-H$ MO $b=c$ is given by Eq. (14.62).

The bond angle of the CH_3 groups of ethane is derived by using the orbital composition and an energy matching factor as in the case with the CH_3 radical. Since the two H_2-type ellipsoidal MOs initially comprise 75% of the H electron density of H_2 and the energy of each H_2-type ellipsoidal MO is matched to that of the $C_{ethane}2sp^3$ HO, the component energies and the total energy E_T of the $H-H$ bond are given by Eqs. (13.67-13.73) except that V_e, T, and V_m are corrected for the hybridization-energy-matching factor of 0.87495. Hybridization with 25% electron donation to the $C-C$-bond gives rise to the $C_{ethane}2sp^3$ HO-shell Coulombic energy $E_{Coulomb}\left(C_{ethane},2sp^3\right)$ given by Eq. (14.149). The corresponding normalization factor for determining the zero of the total $H-H$ bond energy is given by the ratio of $15.55033\,eV$, the magnitude of $E_{Coulomb}\left(C_{ethane},2sp^3\right)$ given by Eq. (14.149), and $13.605804\,eV$, the magnitude of the Coulombic energy between the electron and proton of H given by Eq. (1.264). The hybridization energy factor $C_{ethaneC2sp^3HO}$ is:

$$C_{ethaneC2sp^3HO} = \frac{\frac{e^2}{8\pi\varepsilon_0 a_0}}{\frac{e^2}{8\pi\varepsilon_0 r_{ethane2sp^3}}} = \frac{\frac{e^2}{8\pi\varepsilon_0 a_0}}{\frac{e^2}{8\pi\varepsilon_0 0.87495a_0}} = \frac{13.605804\ eV}{15.55033\ eV} = 0.87495 \tag{14.194}$$

Substitution of Eq. (14.152) into Eq. (13.233) with the hybridization factor of 0.87495 gives:

$$0 = \left[\frac{-e^2}{8\pi\varepsilon_0\sqrt{\frac{aa_0}{2}}}\left[\left(0.87495\right)^{-1}\left(\frac{3}{2}-\frac{3}{8}\frac{a_0}{a}\right)\ln\frac{a+\sqrt{\frac{aa_0}{2}}}{a-\sqrt{\frac{aa_0}{2}}}-1\right]\left[1+\sqrt{\frac{2\hbar\sqrt{\frac{0.75e^2}{4\pi\varepsilon_0 a^3}}}{m_e c^2}}\right]\right.$$
$$\left.+\hbar\sqrt{\frac{\frac{0.75e^2}{8\pi\varepsilon_0 a^3}-\frac{e^2}{8\pi\varepsilon_0\left(a+c'\right)^3}}{0.5m_p}}\right] \tag{14.195}$$

From the energy relationship given by Eq. (14.195) and the relationship between the axes given by Eqs. (14.192-14.193) and (14.62-14.63), the dimensions of the $H-H$ MO can be solved.

The most convenient way to solve Eq. (14.195) is by the reiterative technique using a computer. The result to within the round-off error with five-significant figures is

$$a = 5.7000a_0 = 3.0163\ X\ 10^{-10}\ m \tag{14.196}$$

Substitution of Eq. (14.196) into Eq. (14.192) gives:

$$c' = 1.6882a_0 = 8.9335\ X\ 10^{-11}\ m \tag{14.197}$$

The internuclear distance given by multiplying Eq. (14.197) by two is:

$$2c' = 3.3764a_0 = 1.7867\ X\ 10^{-10}\ m \tag{14.198}$$

Substitution of Eqs. (14.196-14.197) into Eq. (14.62) gives:

$$b = c = 5.4443a_0 = 2.8810\ X\ 10^{-10}\ m \tag{14.199}$$

Substitution of Eqs. (14.196-14.197) into Eq. (13.63) gives:

$$e = 0.2962 \tag{14.200}$$

From, $2c'_{H-H}$ (Eq. (14.198)), the distance between the two H atoms when the total energy of the corresponding MO is zero (Eq. (14.195)), and $2c'_{C-H}$ (Eq. (14.179)), the internuclear distance of each $C-H$ bond, the corresponding bond angle can be determined from the law of cosines. Using, Eq. (13.242), the bond angle θ between the $C-H$ bonds is

$$\theta = \cos^{-1}\left(\frac{2\left(2.09424\right)^2 - \left(3.3764\right)^2}{2\left(2.09424\right)^2}\right) = \cos^{-1}\left(-0.29964\right) = 107.44° \tag{14.201}$$

The experimental angle between the $C-H$ bonds is [8]:

$$\theta = 107.4° \tag{14.202}$$

The CH_3 radical has a pyramidal structure with the carbon atom along the z-axis at the apex and the hydrogen atoms at the base in the xy-plane. The distance $d_{origin-H}$ from the origin to the nucleus of a hydrogen atom given by Eqs. (14.198) and (13.412) is:

$$d_{origin-H} = 1.94936a_0 \tag{14.203}$$

The height along the z-axis of the pyramid from the origin to C nucleus d_{height} given by Eqs. (13.414), (14.179), and (14.203) is

$$d_{height} = 0.76540a_0 \tag{14.204}$$

The angle θ_v of each $C-H$ bond from the z-axis given by Eqs. (13.416), (14.203), and (14.204) is:

$$\theta_v = 68.563° \tag{14.205}$$

The $C-C$ bond is along the z-axis. Thus, the bond angle θ_{C-C-H} between the internuclear axis of the $C-C$ bond and a H atom of the methyl groups is given by:

$$\theta_{C-C-H} = 180 - \theta_v \tag{14.206}$$

Substitution of Eq. (14.205) into Eq. (14.206) gives:

$$\theta_{C-C-H} = 111.44° \tag{14.207}$$

The experimental angle between the $C-C-H$ bonds is [3]:

$$\theta_{C-C-H} = 111.17° \tag{14.208}$$

The CH_3CH_3 MO shown in Figure 14.7 was rendered using these parameters. A minimum energy is obtained with a staggered configuration consistent with observations [3].

The charge-density in the $C-C$-bond MO is increased by a factor of 0.25 with the formation of the $C_{ethane}2sp^3$ HOs each having a smaller radius. Using the orbital composition of the CH_3 groups (Eq. (14.173)) and the $C-C$-bond MO (Eq. (14.139)), the radii of $C1s = 0.17113a_0$ (Eq. (10.51)) and $C_{ethane}2sp^3 = 0.87495a_0$ (Eq. (14.148)) shells, and the parameters of the $C-C$-bond (Eqs. (13.3-13.4), (14.158-14.160), and (14.162-14.172)), the parameters of the $C-H$-bond MOs (Eqs. (13.3-13.4), (14.177-14.179), and (14.181-14.191)), and the bond-angle parameters (Eqs. (14.195-14.208)), the charge-density of the CH_3CH_3 MO comprising the linear combination of two sets of three $C-H$-bond MOs and a $C-C$-bond MO bridging the two methyl groups is shown in Figure 14.7. Each $C-H$-bond MO comprises a H_2-type ellipsoidal MO and a $C_{ethane}2sp^3$ HO

having the dimensional diagram shown in Figure 14.6. The $C-C$-bond MO comprises a H_2-type ellipsoidal MO bridging two $C_{ethane}2sp^3$ HOs having the dimensional diagram shown in Figure 14.5.

Figure 14.7. CH_3CH_3 MO comprising the linear combination of two sets of three $C-H$-bond MOs and a $C-C$-bond MO. (A) Color scale, translucent view of the charge-density of the $C-C$-bond MO with the $C_{ethane}2sp^3$ HOs shown transparently. The $C-C$-bond MO comprises a H_2-type ellipsoidal MO bridging two $C_{ethane}2sp^3$ HOs. For each $C-H$ and the $C-C$ bond, the ellipsoidal surface of the H_2-type ellipsoidal MO that transitions to the $C_{ethane}2sp^3$ HO, the $C_{ethane}2sp^3$ HO shell, inner most $C1s$ shell, and the nuclei (red, not to scale), are shown. (B)-(C) End-on view, translucent view high-lighting the $C-C$-bond MO, and opaque view of the charge-density of the CH_3CH_3 MO, respectively.

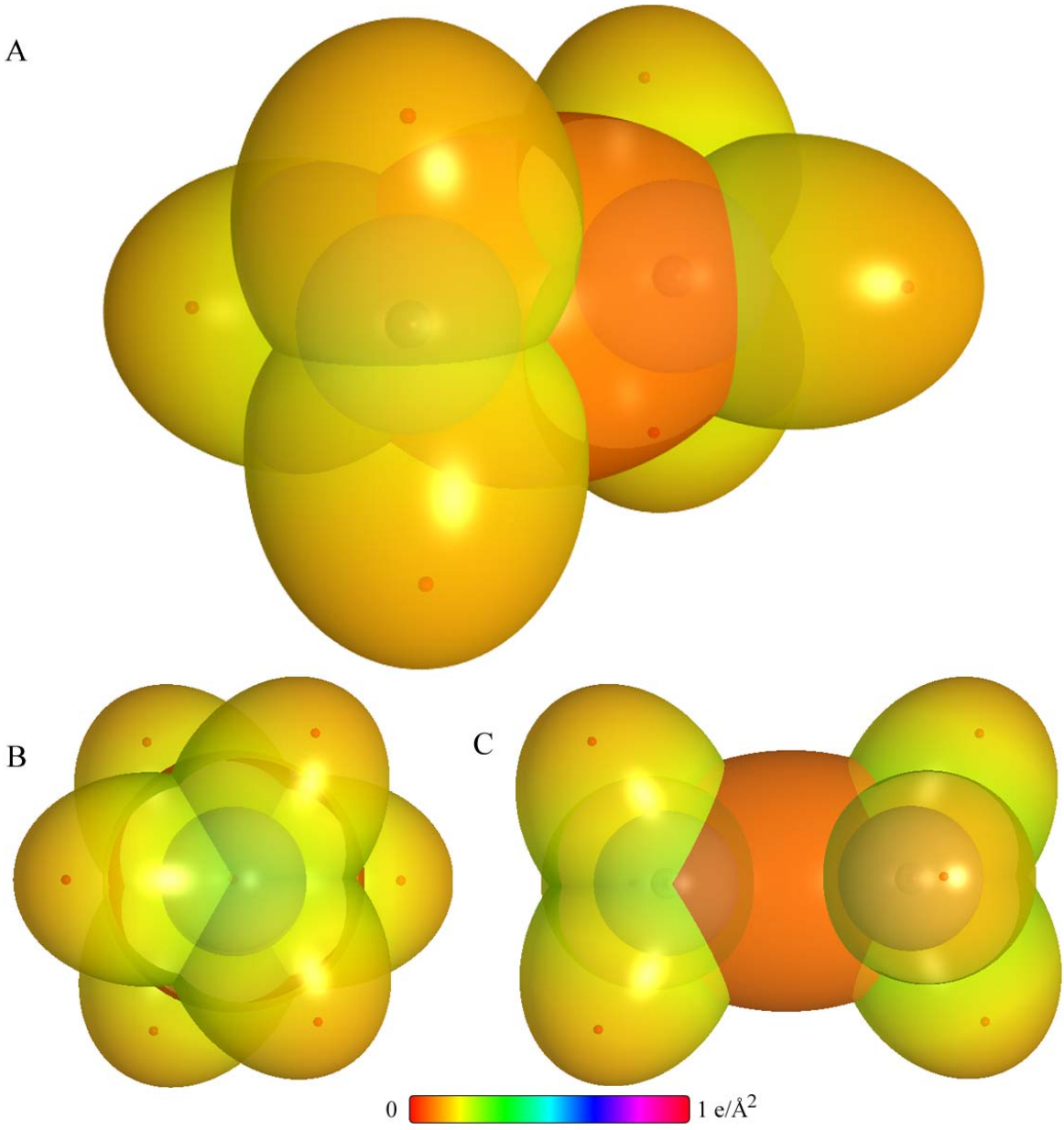

ENERGIES OF THE CH_3 GROUPS

The energies of each CH_3 group of ethane are given by the substitution of the semiprincipal axes (Eqs. (14.177-14.178) and (14.181)) into the energy equations of the methyl radical (Eqs. (13.556-13.560)), with the exception that $E\left(C_{ethane}, 2sp^3\right)$ replaces $E\left(C, 2sp^3\right)$ in Eq. (13.560):

$$V_e = 3\left(0.91771\right)\frac{-2e^2}{8\pi\varepsilon_0\sqrt{a^2-b^2}}\ln\frac{a+\sqrt{a^2-b^2}}{a-\sqrt{a^2-b^2}} = -107.68424\ eV \tag{14.209}$$

$$V_p = \frac{3e^2}{8\pi\varepsilon_0\sqrt{a^2-b^2}} = 38.98068\ eV \tag{14.210}$$

$$T = 3\left(0.91771\right)\frac{\hbar^2}{2m_e a\sqrt{a^2-b^2}}\ln\frac{a+\sqrt{a^2-b^2}}{a-\sqrt{a^2-b^2}} = 32.73700\ eV \tag{14.211}$$

$$V_m = 3\left(0.91771\right)\frac{-\hbar^2}{4m_e a\sqrt{a^2-b^2}}\ln\frac{a+\sqrt{a^2-b^2}}{a-\sqrt{a^2-b^2}} = -16.36850\ eV \tag{14.212}$$

$$E_{T_{ethane}}\left(CH_3\right) = -\frac{3e^2}{8\pi\varepsilon_0 c'}\left[\left(0.91771\right)\left(2-\frac{1}{2}\frac{a_0}{a}\right)\ln\frac{a+c'}{a-c'}-1\right] - 15.35946\ eV = -67.69451\ eV \tag{14.213}$$

where $E_{T_{ethane}}\left(CH_3\right)$ is given by Eq. (14.174) which is reiteratively matched to Eq. (13.542) within five-significant-figure round off error.

VIBRATION OF THE $^{12}CH_3$ GROUPS

The vibrational energy levels of CH_3 in ethane may be solved as three equivalent coupled harmonic oscillators by developing the Lagrangian, the differential equation of motion, and the eigenvalue solutions [9] wherein the spring constants are derived from the central forces as given in the Vibration of Hydrogen-Type Molecular Ions section and the Vibration of Hydrogen-Type Molecules section.

THE DOPPLER ENERGY TERMS OF THE $^{12}CH_3$ GROUPS

The equations of the radiation reaction force of the methyl groups in ethane are the same as those of the methyl radical with the substitution of the methyl-group parameters. Using Eq. (13.561), the angular frequency of the reentrant oscillation in the transition state is

$$\omega = \sqrt{\frac{0.75e^2}{4\pi\varepsilon_0 b^3}} = 2.50664\ X\ 10^{16}\ rad/s \tag{14.214}$$

where b is given by Eq. (14.181). The kinetic energy, E_K, is given by Planck's equation (Eq. (11.127)):

$$\overline{E}_K = \hbar\omega = \hbar 2.50664\ X\ 10^{16}\ rad/s = 16.49915\ eV \tag{14.215}$$

In Eq. (11.181), substitution of $E_T\left(H_2\right)$ (Eqs. (11.212) and (13.75)), the maximum total energy of each H_2-type MO, for E_{hv}, the mass of the electron, m_e, for M, and the kinetic energy given by Eq. (14.215) for $\overline{E}_K$ gives the Doppler energy of the electrons of each of the three bonds for the reentrant orbit:

$$\overline{E}_D \cong E_{hv}\sqrt{\frac{2\overline{E}_K}{Mc^2}} = -31.63537\ eV\sqrt{\frac{2e\left(16.49915\ eV\right)}{m_e c^2}} = -0.25422\ eV \tag{14.216}$$

In addition to the electrons, the nuclei also undergo simple harmonic oscillation in the transition state at their corresponding frequency. The decrease in the energy of CH_3 due to the reentrant orbit of each bond in the transition state corresponding to simple harmonic oscillation of the electrons and nuclei, $\overline{E}_{osc}$, is given by the sum of the corresponding energies, $\overline{E}_D$ given by Eq. (14.216) and $\overline{E}_{Kvib}$, the average kinetic energy of vibration which is 1/2 of the vibrational energy of each $C-H$ bond. Using ω_e given by Eq. (13.458) for $\overline{E}_{Kvib}$ of the transition state having three independent bonds, $\overline{E}'_{ethane\ osc}\left(^{12}CH_3\right)$ per bond is:

$$\overline{E}'_{ethane\ osc}\left(^{12}CH_3\right) = \overline{E}_D + \overline{E}_{Kvib} = \overline{E}_D + \frac{1}{2}\hbar\sqrt{\frac{k}{\mu}} \tag{14.217}$$

$$\overline{E}'_{ethane\ osc}\left(^{12}CH_3\right) = -0.25422\ eV + \frac{1}{2}\left(0.35532\ eV\right) = -0.07656\ eV \tag{14.218}$$

Given that the vibration and reentrant oscillation is for three $C-H$ bonds, $\bar{E}_{ethane\ osc}\left({}^{12}CH_3\right)$, is:

$$\bar{E}_{ethane\ osc}\left({}^{12}CH_3\right)=3\left(\bar{E}_D+\frac{1}{2}\hbar\sqrt{\frac{k}{\mu}}\right)=3\left(-0.25422\ eV+\frac{1}{2}\left(0.35532\ eV\right)\right)=-0.22967\ eV \tag{14.219}$$

TOTAL AND DIFFERENCE ENERGIES OF THE ${}^{12}CH_3$ GROUPS

$E_{ethaneT+osc}\left({}^{12}CH_3\right)$, the total energy of each ${}^{12}CH_3$ group including the Doppler term, is given by the sum of $E_{T_{ethane}}\left(CH_3\right)$ (Eq. (14.213)) and $\bar{E}_{ethane\ osc}\left({}^{12}CH_3\right)$ given by Eq. (14.219).

$$\begin{aligned}E_{ethaneT+osc}\left({}^{12}CH_3\right)&=V_e+T+V_m+V_p+E\left(C_{ethane},2sp^3\right)+\bar{E}_{ethane\ osc}\left({}^{12}CH_3\right)\\&=E_{T_{ethane}}\left(CH_3\right)+\bar{E}_{ethane\ osc}\left({}^{12}CH_3\right)\end{aligned} \tag{14.220}$$

$$E_{ethaneT+osc}\left({}^{12}CH_3\right)=\left\{\begin{array}{l}\left(\frac{-3e^2}{8\pi\varepsilon_0 c'}\left[\left(0.91771\right)\left(2-\frac{1}{2}\frac{a_0}{a}\right)\ln\frac{a+c'}{a-c'}-1\right]-15.359469\ eV\right)\\-3\left(\left(31.63536831\ eV\right)\sqrt{\frac{2\hbar\sqrt{\frac{3}{4}\frac{e^2}{4\pi\varepsilon_0 b^3}}}{m_e c^2}}-\frac{1}{2}\hbar\sqrt{\frac{k}{\mu}}\right)\end{array}\right\} \tag{14.221}$$

$$=-67.69450\ eV-3\left(0.25422\ eV-\frac{1}{2}\hbar\sqrt{\frac{k}{\mu}}\right)$$

From Eqs. (14.217-14.221), the total energy of each ${}^{12}CH_3$ is:

$$\begin{aligned}E_{ethaneT+osc}\left({}^{12}CH_3\right)&=-67.69450\ eV+\bar{E}_{ethane\ osc}\left({}^{12}CH_3\right)\\&=-67.69450\ eV-3\left(0.25422\ eV-\frac{1}{2}\left(0.35532\ eV\right)\right)=-67.92417\ eV\end{aligned} \tag{14.222}$$

where ω_e given by Eq. (13.458) was used for the $\hbar\sqrt{\frac{k}{\mu}}$ term.

The total energy for each methyl radical given by Eq. (13.569) is:

$$\begin{aligned}E_{radicalT+osc}\left({}^{12}CH_3\right)&=-67.69450\ eV+\bar{E}_{radical\ osc}\left({}^{12}CH_3\right)\\&=-67.69450\ eV-3\left(0.25670\ eV-\frac{1}{2}\left(0.35532\ eV\right)\right)=-67.93160\ eV\end{aligned} \tag{14.223}$$

The difference in energy between the methyl groups and the methyl radical $\Delta E_{T+osc}\left({}^{12}CH_3\right)$ is given by two times the difference between Eqs. (14.222) and (14.223):

$$\begin{aligned}\Delta E_{T+osc}\left({}^{12}CH_3\right)&=2\left(E_{ethaneT+osc}\left({}^{12}CH_3\right)-E_{radicalT+osc}\left({}^{12}CH_3\right)\right)\\&=2\left(-67.92417\ eV-\left(-67.93160\ eV\right)\right)=0.01487\ eV\end{aligned} \tag{14.224}$$

SUM OF THE ENERGIES OF THE $C-C$ σ MO AND THE HOS OF ETHANE

The energy components of V_e, V_p, T, V_m, and E_T of the $C-C$-bond MO are the same as those of the CH MO as well as each $C-H$-bond MO of the methyl groups except that energy of the $C_{ethane}2sp^3$ HO is used. The energies of each $C-C$-bond MO are given by the substitution of the semiprincipal axes (Eqs. (14.158-14.159) and (14.162)) into the energy equations of the CH MO (Eqs. (13.449-13.453)), with the exception that $E\left(C_{ethane},2sp^3\right)$ replaces $E\left(C,2sp^3\right)$ in Eq. (13.453).

$$V_e=\left(0.91771\right)\frac{-2e^2}{8\pi\varepsilon_0\sqrt{a^2-b^2}}\ln\frac{a+\sqrt{a^2-b^2}}{a-\sqrt{a^2-b^2}}=-29.101124\ eV \tag{14.225}$$

$$V_p=\frac{e^2}{8\pi\varepsilon_0\sqrt{a^2-b^2}}=9.37273\ eV \tag{14.226}$$

$$T=\left(0.91771\right)\frac{\hbar^2}{2m_e a\sqrt{a^2-b^2}}\ln\frac{a+\sqrt{a^2-b^2}}{a-\sqrt{a^2-b^2}}=6.90500\ eV \tag{14.227}$$

$$V_m = (0.91771)\frac{-\hbar^2}{4m_e a\sqrt{a^2-b^2}}\ln\frac{a+\sqrt{a^2-b^2}}{a-\sqrt{a^2-b^2}} = -3.45250\ eV \tag{14.228}$$

$$E_T(C-C,\sigma) = -\frac{e^2}{8\pi\varepsilon_0 c'}\left[(0.91771)\left(2-\frac{1}{2}\frac{a_0}{a}\right)\ln\frac{a+c'}{a-c'}-1\right]-15.35946\ eV = -31.63535\ eV \tag{14.229}$$

where $E_T(C-C,\sigma)$ is the total energy of the $C-C$ σ MO given by Eq. (14.155) which is reiteratively matched to Eq. (13.75) within five-significant-figure round off error.

The total energy of the $C-C$-bond MO, $E_T(C-C)$, is given by the sum of two times $E_T(C-C,2sp^3)$, the energy change of each $C2sp^3$ shell due to the decrease in radius with the formation of the $C-C$-bond MO (Eq. (14.151)), and $E_T(C-C,\sigma)$, the σ MO contribution given by Eq. (14.156).

$$\begin{aligned} E_T(C-C) &= 2E_T(C-C,2sp^3)+E_T(C-C,\sigma) \\ &= \left(\begin{array}{l} 2(-0.72457\ eV)+ \\ \left(-\frac{e^2}{8\pi\varepsilon_0\sqrt{aa_0}}\left[(0.91771)\left(2-\frac{1}{2}\frac{a_0}{a}\right)\ln\frac{a+\sqrt{aa_0}}{a-\sqrt{aa_0}}-1\right]-15.35946\ eV\right) \end{array}\right) \\ &= 2(-0.72457\ eV)+(-31.63537\ eV) = -33.08452\ eV \end{aligned} \tag{14.230}$$

VIBRATION OF ETHANE

The vibrational energy levels of CH_3CH_3 may be solved as two sets of three equivalent coupled harmonic oscillators with a bridging harmonic oscillator by developing the Lagrangian, the differential equation of motion, and the eigenvalue solutions [9] wherein the spring constants are derived from the central forces as given in the Vibration of Hydrogen-Type Molecular Ions section and the Vibration of Hydrogen-Type Molecules section.

THE DOPPLER ENERGY TERMS OF THE $C-C$-BOND MO OF ETHANE

The equations of the radiation reaction force of the symmetrical $C-C$-bond MO are given by Eqs. (11.231-11.233), except the force-constant factor is 0.5 based on the force constant k' of Eq. (14.152), and the $C-C$-bond MO parameters are used. The angular frequency of the reentrant oscillation in the transition state is

$$\omega = \sqrt{\frac{\frac{0.5e^2}{4\pi\varepsilon_0 a^3}}{m_e}} = 9.55643\ X\ 10^{15}\ rad/s \tag{14.231}$$

where a is given by Eq. (14.158). The kinetic energy, E_K, is given by Planck's equation (Eq. (11.127)).

$$\bar{E}_K = \hbar\omega = \hbar 9.55643\ X\ 10^{15}\ rad/s = 6.29021\ eV \tag{14.232}$$

In Eq. (11.181), substitution of $E_T(C-C)$ (Eq. (14.230)) for E_{hv}, the mass of the electron, m_e, for M, and the kinetic energy given by Eq. (14.232) for $\bar{E}_K$ gives the Doppler energy of the electrons of each of the three bonds for the reentrant orbit:

$$\bar{E}_D \cong E_{hv}\sqrt{\frac{2\bar{E}_K}{Mc^2}} = -33.08450\ eV\sqrt{\frac{2e(6.29021\ eV)}{m_e c^2}} = -0.16416\ eV \tag{14.233}$$

In addition to the electrons, the nuclei also undergo simple harmonic oscillation in the transition state at their corresponding frequency. The decrease in the energy of the $C-C$-bond MO due to the reentrant orbit of the bond in the transition state corresponding to simple harmonic oscillation of the electrons and nuclei, $\bar{E}_{osc}$, is given by the sum of the corresponding energies, $\bar{E}_D$ given by Eq. (14.233) and $\bar{E}_{Kvib}$, the average kinetic energy of vibration which is 1/2 of the vibrational energy of the $C-C$ bond. Using the experimental $C-C$ $E_{vib}(\upsilon_3)$ of 993 cm^{-1} $(0.12312\ eV)$ [10] for $\bar{E}_{Kvib}$ of the transition state, $\bar{E}_{osc}(C-C,\sigma)$ is:

$$\bar{E}_{osc}(C-C,\sigma) = \bar{E}_D + \bar{E}_{Kvib} = \bar{E}_D + \frac{1}{2}\hbar\sqrt{\frac{k}{\mu}} \tag{14.234}$$

$$\bar{E}_{osc}(C-C,\sigma) = -0.16416\ eV + \frac{1}{2}(0.12312\ eV) = -0.10260\ eV \tag{14.235}$$

TOTAL ENERGIES OF THE $C-C$-BOND MO OF ETHANE

$E_{T+osc}\left(C-C\right)$, the total energy of the $C-C$-bond MO including the Doppler term, is given by the sum of $E_T\left(C-C\right)$ (Eq. (14.230)) and $\bar{E}_{osc}\left(C-C,\sigma\right)$ given by Eq. (14.235).

$$\begin{aligned} E_{T+osc}\left(C-C\right) &= V_e+T+V_m+V_p+E\left(C_{ethane},2sp^3\right)+2E_T\left(C-C,2sp^3\right)+\bar{E}_{osc}\left(C-C,\sigma\right) \\ &= E_T\left(C-C,\sigma\right)+2E_T\left(C-C,2sp^3\right)+\bar{E}_{osc}\left(C-C,\sigma\right)=E_T\left(C-C\right)+\bar{E}_{osc}\left(C-C,\sigma\right) \end{aligned} \tag{14.236}$$

$$\begin{aligned} E_{T+osc}\left(C-C\right) &= \left\{\begin{array}{l}\left(\frac{-e^2}{8\pi\varepsilon_0 c'}\left[\left(0.91771\right)\left(2-\frac{1}{2}\frac{a_0}{a}\right)\ln\frac{a+c'}{a-c'}-1\right]-15.35946\ eV+2E_T\left(C-C,2sp^3\right)\right) \\ \left(1+\sqrt{\frac{2\hbar\sqrt{\frac{1}{2}\frac{e^2}{4\pi\varepsilon_0 a^3}}}{m_e c^2}}\right)+\frac{1}{2}\hbar\sqrt{\frac{k}{\mu}}\end{array}\right\} \\ &= -33.08452\ eV-0.16416\ eV+\frac{1}{2}\hbar\sqrt{\frac{k}{\mu}} \end{aligned} \tag{14.237}$$

From Eqs. (14.234-14.237), the total energy of the $C-C$-bond MO is:

$$\begin{aligned} E_{T+osc}\left(C-C\right) &= -31.63537\ eV+2E_T\left(C-C,2sp^3\right)+\bar{E}_{osc}\left(C-C,\sigma\right) \\ &= -31.63537\ eV+2\left(-0.72457\ eV\right)-0.16416\ eV+\frac{1}{2}\left(0.12312\ eV\right)=-33.18712\ eV \end{aligned} \tag{14.238}$$

where the experimental E_{vib} was used for the $\hbar\sqrt{\frac{k}{\mu}}$ term.

BOND ENERGY OF THE $C-C$ BOND OF ETHANE

The dissociation energy of the $C-C$ bond of CH_3CH_3, $E_D\left(H_3C-CH_3\right)$, is given by two times $E\left(C,2sp^3\right)$ (Eq. (14.146)), the initial energy of the $C2sp^3$ HO of each CH_3 radical that bond with a single $C-C$ bond, minus the sum of $\Delta E_{T+osc}\left({}^{12}CH_3\right)$ (Eq. (14.224)), the energy change going from the methyl radicals to the methyl groups of ethane, and $E_{T+osc}\left(C-C\right)$ (Eq. (14.238)). Thus, the dissociation energy of the $C-C$ bond of CH_3CH_3, is:

$$\begin{aligned} E_D\left(H_3C-CH_3\right) &= 2\left(E\left(C,2sp^3\right)\right)-\left(\Delta E_{T+osc}\left({}^{12}CH_3\right)+E_{T+osc}\left(C-C\right)\right) \\ &= 2\left(-14.63489\ eV\right)-\left(0.01487\ eV-33.18712\ eV\right) \\ &= 2\left(-14.63489\ eV\right)-\left(33.17225\ eV\right)=3.90247\ eV \end{aligned} \tag{14.239}$$

The experimental dissociation energy of the $C-C$ bond of CH_3CH_3 is [6]:

$$E_D\left(H_3C-CH_3\right)=3.89690\ eV \tag{14.240}$$

The results of the determination of bond parameters of CH_3CH_3 are given in Table 14.1. The calculated results are based on first principles and given in closed-form, exact equations containing fundamental constants only. The agreement between the experimental and calculated results is excellent.

ETHYLENE MOLECULE (CH_2CH_2)

The ethylene molecule CH_2CH_2 is formed by the reaction of two dihydrogen carbide radicals:

$$CH_2+CH_2\rightarrow CH_2CH_2 \tag{14.241}$$

CH_2CH_2 can be solved using the same principles as those used to solve the methane series $CH_{n=1,2,3,4}$, wherein the $2s$ and $2p$ shells of each C hybridize to form a single $2sp^3$ shell as an energy minimum, and the sharing of electrons between two $C2sp^3$ hybridized orbitals (HOs) to form a molecular orbital (MO) permits each participating hybridized orbital to decrease in radius and energy. First, two sets of two H atomic orbitals (AOs) combine with two sets of two carbon $2sp^3$ HOs to form two dihydrogen carbide groups comprising a linear combination of four diatomic H_2-type MOs developed in the Nature of the Chemical Bond of Hydrogen-Type Molecules and Molecular Ions section. Then, the two CH_2 groups bond by forming a H_2-type MO between the remaining two $C2sp^3$ HOs on each carbon atom.

FORCE BALANCE OF THE $C=C$-BOND MO OF ETHYLENE

CH_2CH_2 comprises a chemical bond between two CH_2 radicals wherein each radical comprises two chemical bonds between carbon and hydrogen atoms. The solution of the parameters of CH_2 is given in the Dihydrogen Carbide (CH_2) section. Each $C-H$ bond of CH_2 having two spin-paired electrons, one from an initially unpaired electron of the carbon atom and the other from the hydrogen atom, comprises the linear combination of 75% H_2-type ellipsoidal MO and 25% $C2sp^3$ HO. The proton of the H atom and the nucleus of the C atom are along each internuclear axis and serve as the foci. As in the case of H_2, each of the two $C-H$-bond MOs is a prolate spheroid with the exception that the ellipsoidal MO surface cannot extend into $C2sp^3$ HO for distances shorter than the radius of the $C2sp^3$ shell since it is energetically unfavorable. Thus, each MO surface comprises a prolate spheroid at the H proton that is continuous with the $C2sp^3$ shell at the C atom whose nucleus serves as the other focus. The electron configuration and the energy, $E\left(C,2sp^3\right)$, of the $C2sp^3$ shell is given by Eqs. (13.422) and (13.428), respectively. The central paramagnetic force due to spin of each $C-H$ bond is provided by the spin-pairing force of the CH_2 MO that has the symmetry of an s orbital that superimposes with the $C2sp^3$ orbitals such that the corresponding angular momenta are unchanged.

Two CH_2 radicals bond to form CH_2CH_2 by forming a MO between the two pairs of remaining $C2sp^3$-HO electrons of the two carbon atoms. However, in this case, the sharing of electrons between four $C2sp^3$ HOs to form a molecular orbital (MO) comprising four spin-paired electrons permits each $C2sp^3$ HO to decrease in radius and energy.

As in the case of the $C-H$ bonds, the $C=C$-bond MO is a prolate-spheroidal-MO surface that cannot extend into $C2sp^3$ HO for distances shorter than the radius of the $C2sp^3$ shell of each atom. Thus, the MO surface comprises a partial prolate spheroid in between the carbon nuclei and is continuous with the $C2sp^3$ shell at each C atom. The energy of the H_2-type ellipsoidal MO is matched to that of the $C2sp^3$ shell. As in the case of previous examples of energy-matched MOs such as those of OH, NH, CH, the $C=O$-bond MO of CO_2, and the $C-C$-bond MO of CH_3CH_3, the $C=C$-bond MO of ethylene must comprise 75% of a H_2-type ellipsoidal MO in order to match potential, kinetic, and orbital energy relationships. Thus, the $C=C$-bond MO must comprise a linear combination of two MOs wherein each comprises two $C2sp^3$ HOs and 75% of a H_2-type ellipsoidal MO divided between the $C2sp^3$ HOs:

$$2\left(2\ C2sp^3+0.75\ H_2\ MO\right)\rightarrow C=C-bond\ MO \tag{14.242}$$

The linear combination of each H_2-type ellipsoidal MO with each $C2sp^3$ HO further comprises an excess 25% charge-density contribution from each $C2sp^3$ HO to the $C=C$-bond MO to achieve an energy minimum. The force balance of the $C=C$-bond MO is determined by the boundary conditions that arise from the linear combination of orbitals according to Eq. (14.242) and the energy matching condition between the $C2sp^3$-HO components of the MO.

Similarly, the energies of each CH_2 MO involve each $C2sp^3$ and each $H1s$ electron with the formation of each $C-H$ bond. The sum of the energies of the H_2-type ellipsoidal MOs is matched to that of the $C2sp^3$ shell. This energy is determined by the considering the effect of the donation of 25% electron density from the two pairs of $C2sp^3$ HOs to the $C=C$-bond MO with the formation of the $C_{ethylene}2sp^3$ HOs each having a smaller radius. The $2sp^3$ hybridized orbital arrangement is given by Eq. (14.140). The sum $E_T\left(C,2sp^3\right)$ of calculated energies of C, C^+, C^{2+}, and C^{3+} is given by Eq. (14.141). The radius r_{2sp^3} of the $C2sp^3$ shell is given by Eq. (14.142). The Coulombic energy $E_{Coulomb}\left(C,2sp^3\right)$ and the energy $E\left(C,2sp^3\right)$ of the outer electron of the $C2sp^3$ shell are given by Eqs. (14.143) and (14.146), respectively.

Next, consider the formation of the $C=C$-bond MO of ethylene from two CH_2 radicals, each having a $C2sp^3$ electron with an energy given by Eq. (14.146). The total energy of the state is given by the sum over the four electrons. The sum $E_T\left(C_{ethylene},2sp^3\right)$ of calculated energies of $C2sp^3$, C^+, C^{2+}, and C^{3+} from Eqs. (10.123), (10.113-10.114), (10.68), and (10.48), respectively, is:

$$\begin{aligned}E_T\left(C_{ethylene},2sp^3\right)&=-\left(64.3921\ eV+48.3125\ eV+24.2762\ eV+E\left(C,2sp^3\right)\right)\\&=-\left(64.3921\ eV+48.3125\ eV+24.2762\ eV+14.63489\ eV\right)\\&=-151.61569\ eV\end{aligned} \tag{14.243}$$

where $E\left(C,2sp^3\right)$ (Eq. (14.146)) is the sum of the energy of C, $-11.27671\,eV$, and the hybridization energy. The orbital-angular-momentum interactions also cancel such that the energy of the $E_T\left(C_{ethylene},2sp^3\right)$ is purely Coulombic.

The sharing of electrons between two pairs of $C2sp^3$ HOs to form a $C=C$-bond MO permits each participating hybridized orbital to decrease in radius and energy. In order to further satisfy the potential, kinetic, and orbital energy relationships, each participating $C2sp^3$ HO donates an excess of 25% per bond of its electron density to the $C=C$-bond MO to form an energy minimum. By considering this electron redistribution in the ethylene molecule as well as the fact that the central field decreases by an integer for each successive electron of the shell, the radius $r_{ethylene\,2sp^3}$ of the $C2sp^3$ shell of ethylene may be calculated from the Coulombic energy using Eq. (10.102).

$$r_{ethylene\,2sp^3}=\left(\sum_{n=2}^{5}(Z-n)-0.5\right)\frac{e^2}{8\pi\varepsilon_0\left(e151.61569\ eV\right)}=\frac{9.5e^2}{8\pi\varepsilon_0\left(e151.61569\ eV\right)}=0.85252a_0 \tag{14.244}$$

where $Z=6$ for carbon. Using Eqs. (10.102) and (14.244), the Coulombic energy $E_{Coulomb}\left(C_{ethylene},2sp^3\right)$ of the outer electron of the $C2sp^3$ shell is:

$$E_{Coulomb}\left(C_{ethylene},2sp^3\right)=\frac{-e^2}{8\pi\varepsilon_0 r_{ethylene\,2sp^3}}=\frac{-e^2}{8\pi\varepsilon_0 0.85252a_0}=-15.95955\ eV \tag{14.245}$$

During hybridization, the spin-paired $2s$ electrons are promoted to the $C2sp^3$ shell as unpaired electrons. The energy for the promotion is the magnetic energy given by Eq. (13.152). Using Eqs. (14.145) and (14.245), the energy $E\left(C_{ethylene},2sp^3\right)$ of the outer electron of the $C2sp^3$ shell is

$$E\left(C_{ethylene},2sp^3\right)=\frac{-e^2}{8\pi\varepsilon_0 r_{ethylene\,2sp^3}}+\frac{2\pi\mu_0 e^2\hbar^2}{m_e^2\left(r_3\right)^3}=-15.95955\ eV+0.19086\ eV=-15.76868\ eV \tag{14.246}$$

Thus, $E_T\left(C=C,2sp^3\right)$, the energy change of each $C2sp^3$ shell with the formation of the $C=C$-bond MO is given by the difference between Eq. (14.146) and Eq. (14.246):

$$E_T\left(C=C,2sp^3\right)=E\left(C_{ethylene},2sp^3\right)-E\left(C,2sp^3\right)=-15.76868\ eV-\left(-14.63489\ eV\right)=-1.13380\ eV \tag{14.247}$$

As in the case of Cl_2, each H_2-type ellipsoidal MO comprises 75% of the $C=C$-bond MO shared between two $C2sp^3$ HOs corresponding to the electron charge density in Eq. (11.65) of $\frac{-0.75e}{2}$. But, the additional 25% charge-density contribution to each bond of the $C=C$-bond MO causes the electron charge density in Eq. (11.65) to be $\frac{-e}{2}=-0.5e$. The corresponding force constant k' is given by Eq. (14.152). In addition, the energy matching at both $C2sp^3$ HOs further requires that k' be corrected by the hybridization factor given by Eq. (13.430). Thus, the force constant k' to determine the ellipsoidal parameter c' in terms of the central force of the foci (Eq. (11.65)) is given by:

$$k'=C_{C2sp^3HO}\frac{(0.5)2e^2}{4\pi\varepsilon_0}=0.91771\frac{(0.5)2e^2}{4\pi\varepsilon_0} \tag{14.248}$$

The distance from the origin to each focus c' is given by substitution of Eq. (14.248) into Eq. (13.60). Thus, the distance from the origin of the component of the double $C=C$-bond MO to each focus c' is given by:

$$c'=a\sqrt{\frac{\hbar^2 4\pi\varepsilon_0}{(0.91771)m_e e^2 a}}=\sqrt{\frac{aa_0}{0.91771}} \tag{14.249}$$

The internuclear distance from Eq. (14.249) is:

$$2c'=2\sqrt{\frac{aa_0}{0.91771}} \tag{14.250}$$

The length of the semiminor axis of the prolate spheroidal $C=C$-bond MO $b=c$ is given by Eq. (13.62). The eccentricity, e, is given by Eq. (13.63). The solution of the semimajor axis a then allows for the solution of the other axes of each prolate spheroid and eccentricity of the $C=C$-bond MO. From the energy equation and the relationship between the axes, the dimensions of the $C=C$-bond MO are solved.

The general equations for the energy components of V_e, V_p, T, V_m, and E_T of the $C=C$-bond MO are the same as those of the CH MO except that energy of the $C_{ethylene}2sp^3$ HO is used and the double-bond nature is considered. In the case of a single bond, the prolate spheroidal H_2-type MO transitions to the $C_{ethylene}2sp^3$ HO of each carbon, and the energy of the $C_{ethylene}2sp^3$ shell must remain constant and equal to the $E\left(C_{ethylene},2sp^3\right)$ given by Eq. (14.246). Thus, the energy $E\left(C_{ethylene},2sp^3\right)$ in Eq. (14.246) adds to that of the energies of the corresponding H_2-type ellipsoidal MO. The second bond of the double $C=C$-bond MO also transitions to the $C_{ethylene}2sp^3$ HO of each C. The energy of a second H_2-type ellipsoidal MO

adds to the first energy component, and the two bonds achieve an energy minimum as a linear combination of the two H_2-type ellipsoidal MOs each having the carbon nuclei as the foci. Each $C-C$-bond MO comprises the same $C_{ethylene}2sp^3$ HO shells of constant energy given by Eq. (14.246). As in the case of the water, NH_2, and ammonia molecules given by Eqs. (13.180), (13.320), and (13.372), respectively, the energy of the redundant shell is subtracted from the total energy of the linear combination of the σ MO. Thus, the total energy $E_T\left(C=C,\sigma\right)$ of the σ component of the $C=C$-bond MO is given by the sum of the energies of the two bonds each comprising the linear combination of the $C_{ethylene}2sp^3$ HO and the H_2-type ellipsoidal MO as given by Eq. (14.242) wherein the E_T terms add positively, the $E\left(C_{ethylene},2sp^3\right)$ terms cancel, and the energy matching condition between the components is provided by Eq. (14.248). Using Eqs. (13.431) and (14.246), $E_T\left(C=C,\sigma\right)$ is given by:

$$\begin{aligned} E_T\left(C=C,\sigma\right) &= E_T + E\left(C_{ethylene},2sp^3\right) - E\left(C_{ethylene},2sp^3\right) \\ &= -\frac{2e^2}{8\pi\varepsilon_0 c'}\left[\left(0.91771\right)\left(2-\frac{1}{2}\frac{a_0}{a}\right)\ln\frac{a+c'}{a-c'}-1\right] \end{aligned} \tag{14.251}$$

The total energy term of the double $C=C$-bond MO is given by the sum of the two H_2-type ellipsoidal MOs given by Eq. (11.212). To match this boundary condition, $E_T\left(C=C,\sigma\right)$ given by Eq. (14.251) is set equal to two times Eq. (13.75).

$$E_T\left(C=C,\sigma\right) = -\frac{2e^2}{8\pi\varepsilon_0 c'}\left[\left(0.91771\right)\left(2-\frac{1}{2}\frac{a_0}{a}\right)\ln\frac{a+c'}{a-c'}-1\right] = -63.27074\ eV \tag{14.252}$$

From the energy relationship given by Eq. (14.252) and the relationship between the axes given by Eqs. (14.249-14.250) and (13.62-13.63), the dimensions of the $C=C$-bond MO can be solved.

Substitution of Eq. (14.249) into Eq. (14.252) gives:

$$\frac{2e^2}{8\pi\varepsilon_0\sqrt{\frac{aa_0}{0.91771}}}\left[\left(0.91771\right)\left(2-\frac{1}{2}\frac{a_0}{a}\right)\ln\frac{a+\sqrt{\frac{aa_0}{0.91771}}}{a-\sqrt{\frac{aa_0}{0.91771}}}-1\right] = e63.27074 \tag{14.253}$$

The most convenient way to solve Eq. (14.253) is by the reiterative technique using a computer. The result to within the round-off error with five-significant figures is:

$$a = 1.47228a_0 = 7.79098\ X\ 10^{-11}\ m \tag{14.254}$$

Substitution of Eq. (14.254) into Eq. (14.249) gives

$$c' = 1.26661a_0 = 6.70259\ X\ 10^{-11}\ m \tag{14.255}$$

The internuclear distance given by multiplying Eq. (14.255) by two is:

$$2c' = 2.53321a_0 = 1.34052\ X\ 10^{-10}\ m \tag{14.256}$$

The experimental bond distance is [3]:

$$2c' = 1.339\ X\ 10^{-10}\ m \tag{14.257}$$

Substitution of Eqs. (14.254-14.255) into Eq. (13.62) gives:

$$b = c = 0.75055a_0 = 3.97173\ X\ 10^{-11}\ m \tag{14.258}$$

Substitution of Eqs. (14.252-14.255) into Eq. (13.63) gives:

$$e = 0.86030 \tag{14.259}$$

The nucleus of the C atoms comprise the foci of the H_2-type ellipsoidal MO. The parameters of the point of intersection of the H_2-type ellipsoidal MO and the $C_{ethylene}2sp^3$ HO are given by Eqs. (13.84-13.95) and (13.261-13.270). The polar intersection angle θ' is given by Eq. (13.261) where $r_n = r_{ethylene2sp^3} = 0.85252a_0$ is the radius of the $C_{ethylene}2sp^3$ shell. Substitution of Eqs. (14.254-14.255) into Eq. (13.261) gives:

$$\theta' = 129.84° \tag{14.260}$$

Then, the angle $\theta_{C=C_{ethylene}2sp^3HO}$ the radial vector of the $C2sp^3$ HO makes with the internuclear axis is:

$$\theta_{C=C_{ethylene}2sp^3HO} = 180° - 129.84° = 50.16° \tag{14.261}$$

as shown in Figure 14.8.

Figure 14.8. The cross section of the $C=C$-bond MO (σ MO) and one $C-H$-bond MO of ethylene showing the axes, angles, and point of intersection of each H_2-type ellipsoidal MO with the corresponding $C_{ethylene}2sp^3$ HO. The continuation of each H_2-type-ellipsoidal-MO basis element of the $C=C$ bond and the $C-H$-bond beyond the intersection point with each $C_{ethylene}2sp^3$ shell and σ MO is shown as dashed since each only serves to solve the energy match with the $C_{ethylene}2sp^3$ shell and does not represent charge density. Similarly, the vertical dashed line only designates the parameters of each intersection point. The actual charge density is shown by the solid lines. Legend: a: semimajor axis, b: semiminor axis, c': internuclear distance, $d_1 : d_{C=C_{ethylene},H_2MO}$, $\theta_1 : \theta_{C=C_{ethylene}2sp^3HO}$, $d_2 : d_{C=C_{ethylene}2sp^3HO}$, $R : r_{ethyleneC2sp^3}$, $d_3 : d_{C-H_{ethylene},H_2MO}$, $\theta_2 : \theta_{C-H_{ethylene}2sp^3HO}$, and $d_4 : d_{C-H_{ethylene}2sp^3HO}$.

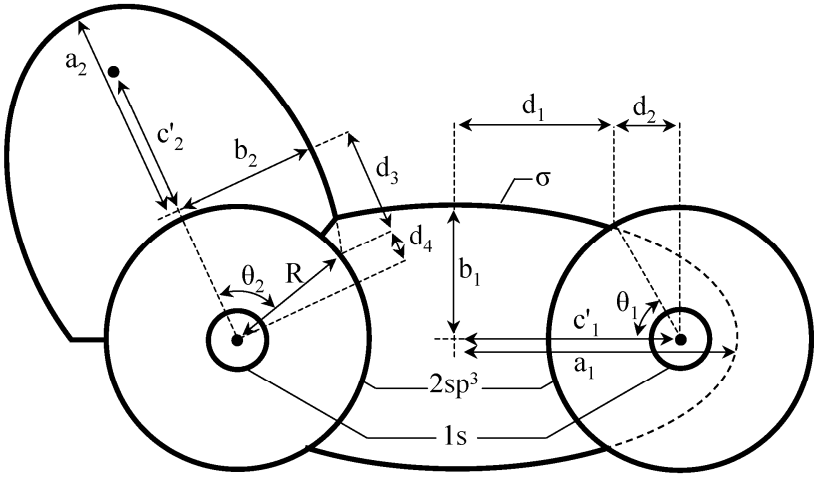

Consider the right-hand intersection point. The Cartesian $\mathbf{i}$-coordinate of the interception point of the MO and the AO can be calculated using the MO ellipsoidal parameters by first calculating the parametric angle in Eq. (11.83) that matches Cartesian $\mathbf{j}$-coordinate components at the point of intersection. Thus, the matching elliptic parametric angle $\omega t = \theta_{C=C_{ethylene},H_2MO}$ satisfies the following relationship:

$$r_{ethylene2sp^3} \sin\theta_{C=C_{ethylene}2sp^3HO} = 0.85252a_0 \sin\theta_{C=C_{ethylene}2sp^3HO} = b\sin\theta_{C=C_{ethylene},H_2MO} \tag{14.262}$$

such that

$$\theta_{C=C_{ethylene},H_2MO} = \sin^{-1}\frac{0.85252a_0 \sin\theta_{C=C_{ethylene}2sp^3HO}}{b} = \sin^{-1}\frac{0.85252a_0 \sin 50.16°}{b} \tag{14.263}$$

with the use of Eq. (14.261). Substitution of Eq. (14.258) into Eq. (14.263) gives:

$$\theta_{C=C_{ethylene},H_2MO} = 60.70° \tag{14.264}$$

Then, the distance $d_{C=C_{ethylene},H_2MO}$ along the internuclear axis from the origin of H_2-type ellipsoidal MO to the point of intersection of the orbitals is given by:

$$d_{C=C_{ethylene},H_2MO} = a\cos\theta_{C=C_{ethylene},H_2MO} \tag{14.265}$$

Substitution of Eqs. (14.254) and (14.264) into Eq. (14.265) gives:

$$d_{C=C_{ethylene},H_2MO} = 0.72040a_0 = 3.81221\ X\ 10^{-11}\ m \tag{14.266}$$

The distance $d_{C=C_{ethylene}2sp^3HO}$ along the internuclear axis from the origin of the C atom to the point of intersection of the orbitals is given by:

$$d_{C=C_{ethylene}2sp^3HO} = c' - d_{C=C_{ethylene},H_2MO} \tag{14.267}$$

Substitution of Eqs. (14.255) and (14.266) into Eq. (14.267) gives:

$$d_{C=C_{ethylene}2sp^3HO} = 0.54620a_0 = 2.89038\ X\ 10^{-11}\ m \tag{14.268}$$

FORCE BALANCE OF THE CH_2 MOS OF ETHYLENE

Each of the two equivalent CH_2 MOs must comprise two $C-H$ bonds with each comprising 75% of a H_2-type ellipsoidal MO and a $C2sp^3$ HO as given by Eq. (13.494):

$$2\left[1\,C2sp^3+0.75\,H_2\;MO\right]\rightarrow CH_2\;MO \tag{14.269}$$

The force balance of the CH_2 MO is determined by the boundary conditions that arise from the linear combination of orbitals according to Eq. (13.494) and the energy matching condition between the hydrogen and $C2sp^3$ HO components of the MO.

The force constant k' to determine the ellipsoidal parameter c' of each H_2-type-ellipsoidal-MO component of the CH_2 MO in terms of the central force of the foci is given by Eq. (13.59). The distance from the origin of each $C-H$-bond MO to each focus c' is given by Eq. (13.60). The internuclear distance is given by Eq. (13.61). The length of the semiminor axis of the prolate spheroidal $C-H$-bond MO $b=c$ is given by Eq. (13.62). The eccentricity, e, is given by Eq. (13.63). The solution of the semimajor axis a then allows for the solution of the other axes of each prolate spheroid and eccentricity of each $C-H$-bond MO. From the energy equation and the relationship between the axes, the dimensions of the CH_2 MO are solved.

Consider the formation of the double $C=C$-bond MO of ethylene from two CH_2 radicals, each having a $C2sp^3$ shell with an energy given by Eq. (14.146). The energy components of V_e, V_p, T, V_m, and E_T are the same as those of the dihydrogen carbide radical, two times those of CH corresponding to the two $C-H$ bonds, except that two times $E_T\left(C=C,2sp^3\right)$ is subtracted from $E_T\left(CH_2\right)$ of Eq. (13.495). The subtraction of the energy change of the $C2sp^3$ shells with the formation of the $C=C$-bond MO matches the energy of the $C-H$-bond MOs to the decrease in the energy of the $C2sp^3$ HOs. Using Eqs. (13.495) and (14.247), $E_{T_{ethylene}}\left(CH_2\right)$ is given by:

$$E_{T_{ethylene}}\left(CH_2\right)=E_T+E\left(C,2sp^3\right)-2E_T\left(C=C,2sp^3\right)=\begin{pmatrix}-\dfrac{2e^2}{8\pi\varepsilon_0 c'}\left[\left(0.91771\right)\left(2-\dfrac{1}{2}\dfrac{a_0}{a}\right)\ln\dfrac{a+c'}{a-c'}-1\right]\\-14.63489\;eV-\left(-2.26758\;eV\right)\end{pmatrix} \tag{14.270}$$

$E_{T_{ethylene}}\left(CH_2\right)$ given by Eq. (14.270) is set equal to two times the energy of the H_2-type ellipsoidal MO minus the Coulombic energy of H given by Eq. (13.496):

$$E_{T_{ethylene}}\left(CH_2\right)=\begin{pmatrix}-\dfrac{2e^2}{8\pi\varepsilon_0 c'}\left[\left(0.91771\right)\left(2-\dfrac{1}{2}\dfrac{a_0}{a}\right)\ln\dfrac{a+c'}{a-c'}-1\right]\\-14.63489\;eV-\left(-2.26758\;eV\right)\end{pmatrix}=-49.66493\;eV \tag{14.271}$$

From the energy relationship given by Eq. (14.271) and the relationship between the axes given by Eqs. (13.60-13.63), the dimensions of the CH_2 MO can be solved.

Substitution of Eq. (13.60) into Eq. (14.271) gives:

$$\frac{2e^2}{8\pi\varepsilon_0\sqrt{\dfrac{2aa_0}{3}}}\left[\left(0.91771\right)\left(2-\frac{1}{2}\frac{a_0}{a}\right)\ln\frac{a+\sqrt{\dfrac{2aa_0}{3}}}{a-\sqrt{\dfrac{2aa_0}{3}}}-1\right]=e37.29762 \tag{14.272}$$

The most convenient way to solve Eq. (14.272) is by the reiterative technique using a computer. The result to within the round-off error with five-significant figures is:

$$a=1.56946a_0=8.30521\;X\;10^{-11}\;m \tag{14.273}$$

Substitution of Eq. (14.273) into Eq. (13.60) gives:

$$c'=1.02289a_0=5.41290\;X\;10^{-11}\;m \tag{14.274}$$

The internuclear distance given by multiplying Eq. (14.274) by two is:

$$2c'=2.04578a_0=1.08258\;X\;10^{-10}\;m \tag{14.275}$$

The experimental bond distance is [3]:

$$2c'=1.087\;X\;10^{-10}\;m \tag{14.276}$$

Substitution of Eqs. (14.273-14.274) into Eq. (14.62) gives:

$$b=c=1.19033a_0=6.29897\;X\;10^{-11}\;m \tag{14.277}$$

Substitution of Eqs. (14.273-14.274) into Eq. (14.63) gives:

$$e=0.65175 \tag{14.278}$$

The nucleus of the H atom and the nucleus of the C atom comprise the foci of each H_2-type ellipsoidal MO. The parameters of the point of intersection of the H_2-type ellipsoidal MO and the $C_{ethylene}2sp^3$ HO are given by Eqs. (13.84-13.95)

and (13.261-13.270). The polar intersection angle θ' is given by Eq. (13.261) where $r_n = r_{ethylene2sp^3} = 0.85252a_0$ is the radius of the $C_{ethylene}2sp^3$ shell. Substitution of Eqs. (14.273-14.274) into Eq. (13.261) gives:

$$\theta' = 84.81° \tag{14.279}$$

Then, the angle $\theta_{C-H_{ethylene}2sp^3HO}$ the radial vector of the $C2sp^3$ HO makes with the internuclear axis is:

$$\theta_{C-H_{ethylene}2sp^3HO} = 180° - 84.81° = 95.19° \tag{14.280}$$

as shown in Figure 14.9.

Figure 14.9. The cross section of one $C-H$-bond MO of ethylene showing the axes, angles, and point of intersection of the H_2-type ellipsoidal MO with the $C_{ethylene}2sp^3$ HO. The continuation of the H_2-type-ellipsoidal-MO basis element beyond the intersection point with the $C_{ethylene}2sp^3$ shell is shown as dashed since it only serves to solve the energy match with the $C_{ethylene}2sp^3$ shell and does not represent charge density. Similarly, the vertical dashed line only designates the parameters of the intersection point. The actual charge density is shown by the solid lines. Legend: a: semimajor axis, b: semiminor axis, c': internuclear distance, $d_1 : d_{C-H_{ethylene},H_2MO}$, $\theta_1 : \theta_{C-H_{ethylene}2sp^3HO}$, $d_2 : d_{C-H_{ethylene}2sp^3HO}$, and $R : r_{ethylene2sp^3}$.

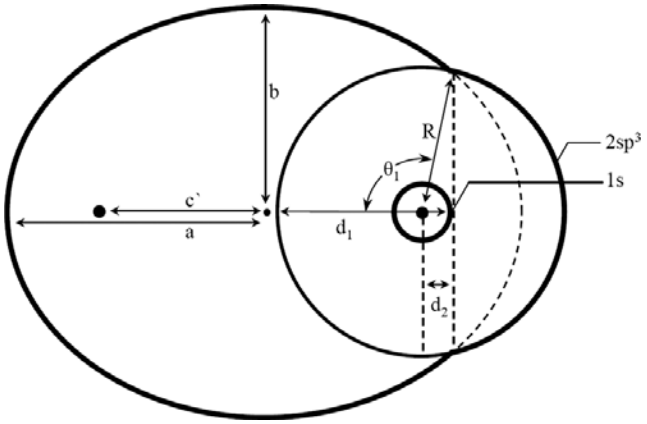

The Cartesian $\mathbf{i}$-coordinate of the interception point of the MO and the AO can be calculated using the MO ellipsoidal parameters by first calculating the parametric angle in Eq. (11.83) that matches Cartesian $\mathbf{j}$-coordinate components at the point of intersection. Thus, the matching elliptic parametric angle $\omega t = \theta_{C-H_{ethylene},H_2MO}$ satisfies the following relationship:

$$r_{ethylene2sp^3} \sin\theta_{C-H_{ethylene}2sp^3HO} = 0.85252a_0 \sin\theta_{C-H_{ethylene}2sp^3HO} = b\sin\theta_{C-H,H_2MO} \tag{14.281}$$

such that

$$\theta_{C-H_{ethylene},H_2MO} = \sin^{-1}\frac{0.85252a_0 \sin\theta_{C-H_{ethylene}2sp^3HO}}{b} = \sin^{-1}\frac{0.85252a_0 \sin 95.19°}{b} \tag{14.282}$$

with the use of Eq. (14.280). Substitution of Eq. (14.277) into Eq. (14.282) gives:

$$\theta_{C-H_{ethylene},H_2MO} = 45.50° \tag{14.283}$$

Then, the distance $d_{C-H_{ethylene},H_2MO}$ along the internuclear axis from the origin of H_2-type ellipsoidal MO to the point of intersection of the orbitals is given by:

$$d_{C-H_{ethylene},H_2MO} = a\cos\theta_{C-H_{ethylene},H_2MO} \tag{14.284}$$

Substitution of Eqs. (14.273) and (14.283) into Eq. (14.284) gives:

$$d_{C-H_{ethylene},H_2MO} = 1.10002a_0 = 5.82107\ X\ 10^{-11}\ m \tag{14.285}$$

The distance $d_{C-H_{ethylene}2sp^3HO}$ along the internuclear axis from the origin of the C atom to the point of intersection of the orbitals is given by:

$$d_{C-H_{ethylene}2sp^3HO} = d_{C-H_{ethylene},H_2MO} - c' \tag{14.286}$$

Substitution of Eqs. (14.274) and (14.285) into Eq. (14.286) gives:

$$d_{C-H_{ethylene}2sp^3HO} = 0.07713a_0 = 4.08171\ X\ 10^{-12}\ m \tag{14.287}$$

BOND ANGLE OF THE CH_2 GROUPS

Each CH_2 MO comprises a linear combination of two $C-H$-bond MOs. Each $C-H$-bond MO comprises the superposition of a H_2-type ellipsoidal MO and the $C_{ethylene}2sp^3$ HO. A bond is also possible between the two H atoms of the $C-H$ bonds. Such $H-H$ bonding would decrease the $C-H$ bond strength since electron density would be shifted from the $C-H$ bonds to the $H-H$ bond. Thus, the bond angle between the two $C-H$ bonds is determined by the condition that the total energy of the H_2-type ellipsoidal MO between the terminal H atoms of the $C-H$ bonds is zero. From Eqs. (11.79) and (13.228), the distance from the origin to each focus of the $H-H$ ellipsoidal MO is:

$$c' = a\sqrt{\frac{\hbar^2 4\pi\varepsilon_0}{m_e e^2 2a}} = \sqrt{\frac{aa_0}{2}} \tag{14.288}$$

The internuclear distance from Eq. (13.229) is:

$$2c' = 2\sqrt{\frac{aa_0}{2}} \tag{14.289}$$

The length of the semiminor axis of the prolate spheroidal $H-H$ MO $b=c$ is given by Eq. (14.62).

The bond angle of the CH_2 groups of ethane is derived by using the orbital composition and an energy matching factor as in the case with the dihydrogen carbide radical and the CH_3 groups of ethane. Since the two H_2-type ellipsoidal MOs initially comprise 75% of the H electron density of H_2 and the energy of each H_2-type ellipsoidal MO is matched to that of the $C_{ethylene}2sp^3$ HO, the component energies and the total energy E_T of the $H-H$ bond are given by Eqs. (13.67-13.73) except that V_e, T, and V_m are corrected for the hybridization-energy-matching factor of 0.85252. Hybridization with 25% electron donation to the $C=C$-bond gives rise to the $C_{ethylene}2sp^3$ HO-shell Coulombic energy $E_{Coulomb}\left(C_{ethylene}, 2sp^3\right)$ given by Eq. (14.245). The corresponding normalization factor for determining the zero of the total $H-H$ bond energy is given by the ratio of $15.95955\ eV$, the magnitude of $E_{Coulomb}\left(C_{ethylene}, 2sp^3\right)$ given by Eq. (14.245), and $13.605804\ eV$, the magnitude of the Coulombic energy between the electron and proton of H given by Eq. (1.264). The hybridization energy factor $C_{ethyleneC2sp^3HO}$ is:

$$C_{ethyleneC2sp^3HO} = \frac{\frac{e^2}{8\pi\varepsilon_0 a_0}}{\frac{e^2}{8\pi\varepsilon_0 r_{ethylene2sp^3}}} = \frac{\frac{e^2}{8\pi\varepsilon_0 a_0}}{\frac{e^2}{8\pi\varepsilon_0 0.85252 a_0}} = \frac{13.605804\ eV}{15.95955\ eV} = 0.85252 \tag{14.290}$$

Substitution of Eq. (14.290) into Eq. (13.233) or Eq. (14.195) with the hybridization factor of 0.85252 gives:

$$0 = \left[\frac{-e^2}{8\pi\varepsilon_0\sqrt{\frac{aa_0}{2}}}\left[(0.85252)^{-1}\left(\frac{3}{2}-\frac{3}{8}\frac{a_0}{a}\right)\ln\frac{a+\sqrt{\frac{aa_0}{2}}}{a-\sqrt{\frac{aa_0}{2}}}-1\right]\left[1+\sqrt{\frac{2\hbar\sqrt{\frac{0.75e^2}{4\pi\varepsilon_0 a^3}}}{m_e c^2}}\right]\right.$$
$$\left.+\hbar\sqrt{\frac{\frac{0.75e^2}{8\pi\varepsilon_0 a^3}-\frac{e^2}{8\pi\varepsilon_0\left(a+c'\right)^3}}{0.5m_p}}\right] \tag{14.291}$$

From the energy relationship given by Eq. (14.291) and the relationship between the axes given by Eqs. (14.192-14.193) and (14.62-14.63), the dimensions of the $H-H$ MO can be solved.

The most convenient way to solve Eq. (14.291) is by the reiterative technique using a computer. The result to within the round-off error with five-significant figures is:

$$a = 6.0400a_0 = 3.1962\ X\ 10^{-10}\ m \tag{14.292}$$

Substitution of Eq. (14.292) into Eq. (14.288) gives:

$$c' = 1.7378a_0 = 9.1961\ X\ 10^{-11}\ m \tag{14.293}$$

The internuclear distance given by multiplying Eq. (14.293) by two is:

$$2c' = 3.4756a_0 = 1.8392\ X\ 10^{-10}\ m \tag{14.294}$$

Substitution of Eqs. (14.292-14.293) into Eq. (14.62) gives:

$$b = c = 5.7846a_0 = 3.0611\ X\ 10^{-10}\ m \tag{14.295}$$

Substitution of Eqs. (14.292-14.293) into Eq. (14.63) gives:

$$e = 0.2877 \tag{14.296}$$

From, $2c'_{H-H}$ (Eq. (14.294)), the distance between the two H atoms when the total energy of the corresponding MO is zero (Eq. (14.291)), and $2c'_{C-H}$ (Eq. (14.275)), the internuclear distance of each $C-H$ bond, the corresponding bond angle can be determined from the law of cosines. Using, Eq. (13.242), the bond angle θ_{HCH} between the $C-H$ bonds is:

$$\theta_{HCH} = \cos^{-1}\left(\frac{2\left(2.04578\right)^2 - \left(3.4756\right)^2}{2\left(2.04578\right)^2}\right) = \cos^{-1}\left(-0.44318\right) = 116.31° \tag{14.297}$$

The experimental angle between the $C-H$ bonds is [11]:

$$\theta_{HCH} = 116.6° \tag{14.298}$$

The $C=C$ bond is along the z-axis. Thus, based on the symmetry of the equivalent bonds, the bond angle $\theta_{C=C-H}$ between the internuclear axis of the $C=C$ bond and a H atom of the CH_2 groups is given by:

$$\theta_{C=C-H} = \frac{\left(360° - \theta_{HCH}\right)}{2} \tag{14.299}$$

Substitution of Eq. (14.298) into Eq. (14.299) gives:

$$\theta_{C=C-H} = 121.85° \tag{14.300}$$

The experimental angle between the $C=C-H$ bonds is [11]:

$$\theta_{C=C-H} = 121.7° \tag{14.301}$$

and [3]

$$\theta_{C=C-H} = 121.3° \tag{14.302}$$

The $C=C$ bond and H atoms of ethylene line in a plane, and rotation about the $C=C$ is not possible due to conservation of angular momentum in the two sets of spin-paired electrons of the double bond. The CH_2CH_2 MO shown in Figure 14.10 was rendered using these parameters.

The charge-density in the $C=C$-bond MO is increased by a factor of 0.25 per bond with the formation of the $C_{ethylene}2sp^3$ HOs each having a smaller radius. Using the orbital composition of the CH_2 groups (Eq. (14.269)) and the $C=C$-bond MO (Eq. (14.242)), the radii of $C1s = 0.17113a_0$ (Eq. (10.51)) and $C_{ethylene}2sp^3 = 0.85252a_0$ (Eq. (14.244)) shells, and the parameters of the $C=C$-bond (Eqs. (13.3-13.4), (14.254-14.256), and (14.258-14.268)), the parameters of the $C-H$-bond MOs (Eqs. (13.3-13.4), (14.273-14.275), and (14.277-14.287)), and the bond-angle parameters (Eqs. (14.297-14.302)), the charge-density of the CH_2CH_2 MO comprising the linear combination of two sets of two $C-H$-bond MOs and a $C=C$-bond MO bridging the two CH_2 groups is shown in Figure 14.10. Each $C-H$-bond MO comprises a H_2-type ellipsoidal MO and a $C_{ethylene}2sp^3$ HO having the dimensional diagram shown in Figure 14.9. The $C=C$-bond MO comprises a H_2-type ellipsoidal MO bridging two $C_{ethylene}2sp^3$ HOs having the dimensional diagram shown in Figure 14.8.

Figure 14.10. CH_2CH_2 MO comprising the linear combination of two sets of two $C-H$ -bond MOs and a $C=C$ -bond MO. (A) Color scale, translucent view of the charge-density of the $C=C$ -bond MO with the $C_{ethylene}2sp^3$ HOs shown transparently. The $C=C$ -bond MO comprises a H_2 -type ellipsoidal MO bridging two sets of two $C_{ethylene}2sp^3$ HOs. For each $C-H$ and the $C=C$ bond, the ellipsoidal surface of the H_2 -type ellipsoidal MO that transitions to the $C_{ethylene}2sp^3$ HO, the $C_{ethylene}2sp^3$ HO shell, inner most $C1s$ shell, and the nuclei (red, not to scale), are shown. (B)-(D) End-on view, translucent view high-lighting the $C=C$ -bond MO, and opaque view of the charge-density of the CH_2CH_2 MO, respectively.

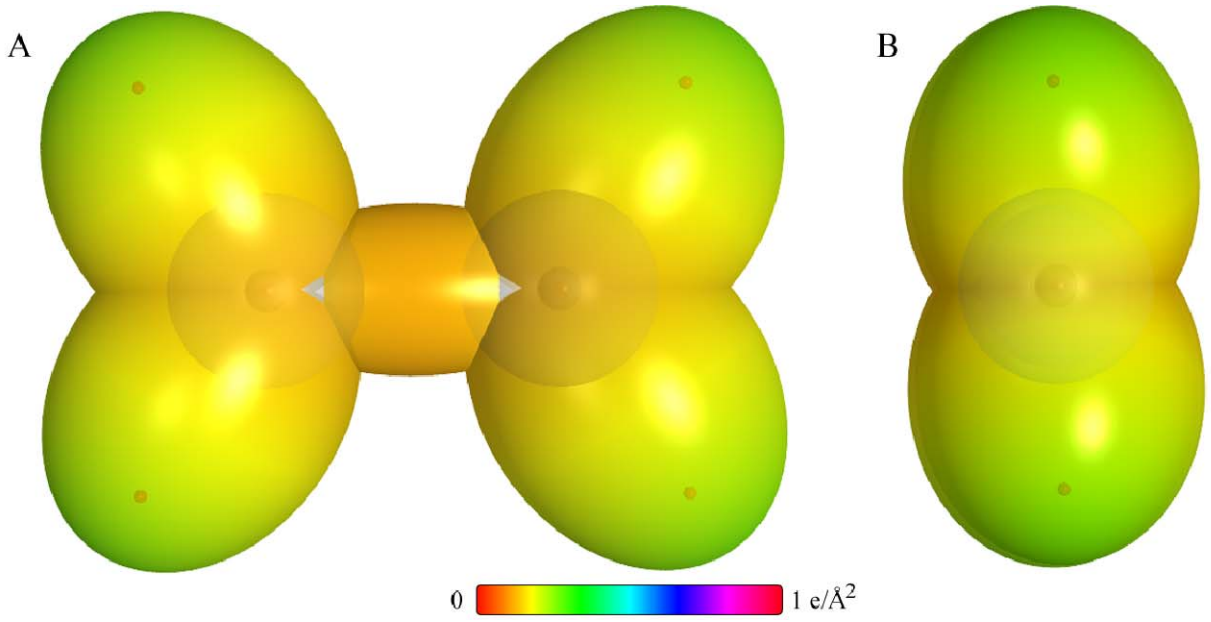

ENERGIES OF THE CH_2 GROUPS

The energies of each CH_2 group of ethylene are given by the substitution of the semiprincipal axes (Eqs. (14.273-14.274) and (14.277)) into the energy equations of dihydrogen carbide (Eqs. (13.510-13.514)), with the exception that two times $E_T\left(C=C,2sp^3\right)$ (Eq. (14.247)) is subtracted from $E_T\left(CH_2\right)$ in Eq. (13.514).

$$V_e = 2\left(0.91771\right)\frac{-2e^2}{8\pi\varepsilon_0\sqrt{a^2-b^2}}\ln\frac{a+\sqrt{a^2-b^2}}{a-\sqrt{a^2-b^2}} = -76.00757\ eV \tag{14.303}$$

$$V_p = \frac{2e^2}{8\pi\varepsilon_0\sqrt{a^2-b^2}} = 26.60266\ eV \tag{14.304}$$

$$T = 2\left(0.91771\right)\frac{\hbar^2}{2m_e a\sqrt{a^2-b^2}}\ln\frac{a+\sqrt{a^2-b^2}}{a-\sqrt{a^2-b^2}} = 24.21459\ eV \tag{14.305}$$

$$V_m = 2\left(0.91771\right)\frac{-\hbar^2}{4m_e a\sqrt{a^2-b^2}}\ln\frac{a+\sqrt{a^2-b^2}}{a-\sqrt{a^2-b^2}} = -12.10730\ eV \tag{14.306}$$

$$E_{T_{ethylene}}\left(CH_2\right) = \left(\begin{array}{l} -\dfrac{2e^2}{8\pi\varepsilon_0 c'}\left[\left(0.91771\right)\left(2-\dfrac{1}{2}\dfrac{a_0}{a}\right)\ln\dfrac{a+c'}{a-c'}-1\right] \\ -14.63489\ eV-\left(-2.26758\ eV\right)\end{array}\right) = -49.66493\ eV \tag{14.307}$$

where $E_{T_{ethylene}}\left(CH_2\right)$ is given by Eq. (14.270) which is reiteratively matched to Eq. (13.496) within five-significant-figure round off error.

VIBRATION OF THE $^{12}CH_2$ GROUPS

The vibrational energy levels of CH_2 in ethylene may be solved as two equivalent coupled harmonic oscillators by developing the Lagrangian, the differential equation of motion, and the eigenvalue solutions [9] wherein the spring constants are derived from the central forces as given in the Vibration of Hydrogen-Type Molecular Ions section and the Vibration of Hydrogen-Type Molecules section.

THE DOPPLER ENERGY TERMS OF THE $^{12}CH_2$ GROUPS

The equations of the radiation reaction force of the CH_2 groups in ethylene are the same as those of the dihydrogen carbide radical with the substitution of the CH_2-group parameters. Using Eq. (13.515), the angular frequency of the reentrant oscillation in the transition state is:

$$\omega = \sqrt{\frac{0.75e^2}{4\pi\varepsilon_0 b^3}} = 2.75685\ X\ 10^{16}\ rad/s \tag{14.308}$$

where b is given by Eq. (14.277). The kinetic energy, E_K, is given by Planck's equation (Eq. (11.127)):

$$\bar{E}_K = \hbar\omega = \hbar 2.75685\ X\ 10^{16}\ rad/s = 18.14605\ eV \tag{14.309}$$

In Eq. (11.181), substitution of $E_T\left(H_2\right)$ (Eqs. (11.212) and (13.75)), the maximum total energy of each H_2-type MO, for $E_{h\nu}$, the mass of the electron, m_e, for M, and the kinetic energy given by Eq. (14.309) for $\bar{E}_K$ gives the Doppler energy of the electrons of each of the two bonds for the reentrant orbit:

$$\bar{E}_D \cong E_{h\nu}\sqrt{\frac{2\bar{E}_K}{Mc^2}} = -31.63537\ eV\sqrt{\frac{2e(18.14605\ eV)}{m_e c^2}} = -0.26660\ eV \tag{14.310}$$

In addition to the electrons, the nuclei also undergo simple harmonic oscillation in the transition state at their corresponding frequency. The decrease in the energy of CH_2 due to the reentrant orbit of each bond in the transition state corresponding to simple harmonic oscillation of the electrons and nuclei, $\bar{E}_{osc}$, is given by the sum of the corresponding energies, $\bar{E}_D$ given by Eq. (14.310) and $\bar{E}_{Kvib}$, the average kinetic energy of vibration which is 1/2 of the vibrational energy of each $C-H$ bond. Using ω_e given by Eq. (13.458) for $\bar{E}_{Kvib}$ of the transition state having two independent bonds, $\bar{E}'_{ethylene\ osc}\left(^{12}CH_2\right)$ per bond is:

$$\bar{E}'_{ethylene\ osc}\left(^{12}CH_2\right) = \bar{E}_D + \bar{E}_{Kvib} = \bar{E}_D + \frac{1}{2}\hbar\sqrt{\frac{k}{\mu}} \tag{14.311}$$

$$\bar{E}'_{ethylene\ osc}\left(^{12}CH_2\right) = -0.26660\ eV + \frac{1}{2}(0.35532\ eV) = -0.08894\ eV \tag{14.312}$$

Given that the vibration and reentrant oscillation is for two $C-H$ bonds, $\bar{E}_{ethylene\ osc}\left(^{12}CH_2\right)$, is:

$$\bar{E}_{ethylene\ osc}\left(^{12}CH_2\right) = 2\left(\bar{E}_D + \frac{1}{2}\hbar\sqrt{\frac{k}{\mu}}\right) = 2\left(-0.26660\ eV + \frac{1}{2}(0.35532\ eV)\right) = -0.17788\ eV \tag{14.313}$$

TOTAL AND DIFFERENCE ENERGIES OF THE $^{12}CH_2$ GROUPS

$E_{ethyleneT+osc}\left(^{12}CH_2\right)$, the total energy of each $^{12}CH_2$ group including the Doppler term, is given by the sum of $E_{T_{ethylene}}\left(CH_2\right)$ (Eq. (14.307)) and $\bar{E}_{ethylene\ osc}\left(^{12}CH_2\right)$ given by Eq. (14.313):

$$\begin{aligned} E_{ethyleneT+osc}\left(^{12}CH_2\right) &= \begin{pmatrix} V_e + T + V_m + V_p + E\left(C, 2sp^3\right) \\ -2E_T\left(C=C, 2sp^3\right) + \bar{E}_{ethylene\ osc}\left(^{12}CH_2\right) \end{pmatrix} \\ &= E_{T_{ethylene}}\left(CH_2\right) + \bar{E}_{ethylene\ osc}\left(^{12}CH_2\right) \end{aligned} \tag{14.314}$$

$$E_{ethyleneT+osc}\left({}^{12}CH_2\right)=\left\{\begin{array}{l}\left(\begin{array}{l}\dfrac{-2e^2}{8\pi\varepsilon_0 c'}\left[(0.91771)\left(2-\dfrac{1}{2}\dfrac{a_0}{a}\right)\ln\dfrac{a+c'}{a-c'}-1\right]\\ -14.63489\ eV-(-2.26759\ eV)\end{array}\right)\\ -2\left((31.63536831\ eV)\sqrt{\dfrac{2\hbar\sqrt{\dfrac{3}{4}\dfrac{e^2}{4\pi\varepsilon_0 b^3}}}{m_e c^2}}-\dfrac{1}{2}\hbar\sqrt{\dfrac{k}{\mu}}\right)\end{array}\right\}$$
$$=-49.66493\ eV-2\left(0.26660\ eV-\frac{1}{2}\hbar\sqrt{\frac{k}{\mu}}\right) \tag{14.315}$$

From Eqs. (14.313-14.315), the total energy of each ${}^{12}CH_2$ is:

$$\begin{aligned}E_{ethyleneT+osc}\left({}^{12}CH_2\right)&=-49.66493\ eV+\bar{E}_{ethylene\ osc}\left({}^{12}CH_2\right)\\&=-49.66493\ eV-2\left(0.26660\ eV-\frac{1}{2}(0.35532\ eV)\right)\\&=-49.84282\ eV\end{aligned} \tag{14.316}$$

where ω_e given by Eq. (13.458) was used for the $\hbar\sqrt{\dfrac{k}{\mu}}$ term.

The total energy for each dihydrogen carbide radical given by Eq. (13.523) is:

$$\begin{aligned}E_{radicalT+osc}\left({}^{12}CH_2\right)&=-49.66493\ eV+\bar{E}_{radicalosc}\left({}^{12}CH_2\right)\\&=-49.66493\ eV-2\left(0.25493\ eV-\frac{1}{2}(0.35532\ eV)\right)\\&=-49.81948\ eV\end{aligned} \tag{14.317}$$

The difference in energy between the CH_2 groups and the dihydrogen carbide radical $\Delta E_{T+osc}\left({}^{12}CH_2\right)$ is given by two times the difference between Eqs. (14.316) and (14.317):

$$\begin{aligned}\Delta E_{T+osc}\left({}^{12}CH_2\right)&=2\left(E_{ethyleneT+osc}\left({}^{12}CH_2\right)-E_{radicalT+osc}\left({}^{12}CH_2\right)\right)\\&=2\left(-49.84282\ eV-(-49.81948\ eV)\right)\\&=-0.04667\ eV\end{aligned} \tag{14.318}$$

SUM OF THE ENERGIES OF THE $C=C$ σ MO AND THE HOS OF ETHYLENE

The energy components of V_e, V_p, T, V_m, and E_T of the $C=C$-bond MO are the same as those of the CH MO except that each term is multiplied by two corresponding to the double bond and the energy term corresponding to the $C_{ethylene}2sp^3$ HOs in the equation for E_T is zero. The energies of each $C=C$-bond MO are given by the substitution of the semiprincipal axes (Eqs. (14.254-14.255) and (14.258)) into two times the energy equations of the CH MO (Eqs. (13.449-13.453)), with the exception that zero replaces $E\left(C,2sp^3\right)$ in Eq. (13.453).

$$V_e=2(0.91771)\frac{-2e^2}{8\pi\varepsilon_0\sqrt{a^2-b^2}}\ln\frac{a+\sqrt{a^2-b^2}}{a-\sqrt{a^2-b^2}}=-102.08992\ eV \tag{14.319}$$

$$V_p=2\frac{e^2}{8\pi\varepsilon_0\sqrt{a^2-b^2}}=21.48386\ eV \tag{14.320}$$

$$T=2(0.91771)\frac{\hbar^2}{2m_e a\sqrt{a^2-b^2}}\ln\frac{a+\sqrt{a^2-b^2}}{a-\sqrt{a^2-b^2}}=34.67062\ eV \tag{14.321}$$

$$V_m=2(0.91771)\frac{-\hbar^2}{4m_e a\sqrt{a^2-b^2}}\ln\frac{a+\sqrt{a^2-b^2}}{a-\sqrt{a^2-b^2}}=-17.33531\ eV \tag{14.322}$$

$$E_T(C=C,\sigma)=-\frac{2e^2}{8\pi\varepsilon_0 c'}\left[(0.91771)\left(2-\frac{1}{2}\frac{a_0}{a}\right)\ln\frac{a+c'}{a-c'}-1\right]=-63.27075\ eV \tag{14.323}$$

where $E_T\left(C=C,\sigma\right)$ is the total energy of the $C=C$ σ MO given by Eq. (14.251) which is reiteratively matched to two times Eq. (13.75) within five-significant-figure round off error.

The total energy of the $C=C$-bond MO, $E_T\left(C=C\right)$, is given by the sum of two times $E_T\left(C=C,2sp^3\right)$, the energy change of each $C2sp^3$ shell due to the decrease in radius with the formation of the $C=C$-bond MO (Eq. (14.247)), and $E_T\left(C=C,\sigma\right)$, the σ MO contribution given by Eq. (14.252).

$$\begin{aligned} E_T\left(C=C\right) &= 2E_T\left(C=C,2sp^3\right)+E_T\left(C=C,\sigma\right) \\ &= \left(\begin{array}{l} 2\left(-1.13380\ eV\right)+ \\ \left(-\frac{2e^2}{8\pi\varepsilon_0 c'}\left[\left(0.91771\right)\left(2-\frac{1}{2}\frac{a_0}{a}\right)\ln\frac{a+c'}{a-c'}-1\right]\right) \end{array}\right) \\ &= 2\left(-1.13380\ eV\right)+\left(-63.27074\ eV\right) \\ &= -65.53833\ eV \end{aligned} \tag{14.324}$$

VIBRATION OF ETHYLENE

The vibrational energy levels of CH_2CH_2 may be solved as two sets of two equivalent coupled harmonic oscillators with a bridging harmonic oscillator by developing the Lagrangian, the differential equation of motion, and the eigenvalue solutions [9] wherein the spring constants are derived from the central forces as given in the Vibration of Hydrogen-Type Molecular Ions section and the Vibration of Hydrogen-Type Molecules section.

THE DOPPLER ENERGY TERMS OF THE $C=C$-BOND MO OF ETHYLENE

The equations of the radiation reaction force of the $C=C$-bond MO are given by Eq. (13.142), except the force-constant factor is $\left(0.93172\right)0.5$ based on the force constant k' of Eq. (14.248), and the $C=C$-bond MO parameters are used. The angular frequency of the reentrant oscillation in the transition state is:

$$\omega=\sqrt{\frac{0.91771\frac{\left(0.5\right)e^2}{4\pi\varepsilon_0 b^3}}{m_e}}=4.30680\ X\ 10^{16}\ rad/s \tag{14.325}$$

where b is given by Eq. (14.258). The kinetic energy, E_K, is given by Planck's equation (Eq. (11.127)).

$$\bar{E}_K=\hbar\omega=\hbar 4.30680\ X\ 10^{16}\ rad/s=28.34813\ eV \tag{14.326}$$

In Eq. (11.181), substitution of $E_T\left(C=C\right)/2$ (Eq. (14.324)) for E_{hv}, the mass of the electron, m_e, for M, and the kinetic energy given by Eq. (14.326) for $\bar{E}_K$ gives the Doppler energy of the electrons of each of the two bonds for the reentrant orbit:

$$\bar{E}_D\cong E_{hv}\sqrt{\frac{2\bar{E}_K}{Mc^2}}=-32.76916\ eV\sqrt{\frac{2e\left(28.34813\ eV\right)}{m_e c^2}}=-0.34517\ eV \tag{14.327}$$

In addition to the electrons, the nuclei also undergo simple harmonic oscillation in the transition state at their corresponding frequency. The decrease in the energy of the $C=C$-bond MO due to the reentrant orbit of the bond in the transition state corresponding to simple harmonic oscillation of the electrons and nuclei, $\bar{E}_{osc}$, is given by the sum of the corresponding energies, $\bar{E}_D$ given by Eq. (14.327) and $\bar{E}_{Kvib}$, the average kinetic energy of vibration which is 1/2 of the vibrational energy of the $C=C$ bond. Using the experimental $C=C$ $E_{vib}\left(\upsilon_3\right)$ of 1443.5 cm^{-1} $\left(0.17897\ eV\right)$ [12] for $\bar{E}_{Kvib}$ of the transition state having two bonds, $\bar{E}'_{osc}\left(C=C,\sigma\right)$ per bond is:

$$\bar{E}'_{osc}\left(C=C,\sigma\right)=\bar{E}_D+\bar{E}_{Kvib}=\bar{E}_D+\frac{1}{2}\hbar\sqrt{\frac{k}{\mu}} \tag{14.328}$$

$$\bar{E}'_{osc}\left(C=C,\sigma\right)=-0.34517\ eV+\frac{1}{2}\left(0.17897\ eV\right)=-0.25568\ eV \tag{14.329}$$

Given that the vibration and reentrant oscillation is for two $C-C$ bonds of the $C=C$ double bond, $\bar{E}_{ethylene\ osc}\left(C=C,\sigma\right)$, is:

$$\bar{E}_{ethylene\ osc}\left(C=C,\sigma\right)=2\left(\bar{E}_D+\frac{1}{2}\hbar\sqrt{\frac{k}{\mu}}\right)=2\left(-0.34517\ eV+\frac{1}{2}\left(0.17897\ eV\right)\right)=-0.51136\ eV \tag{14.330}$$

TOTAL ENERGIES OF THE $C=C$-BOND MO OF ETHYLENE

$E_{T+osc}\left(C=C\right)$, the total energy of the $C=C$-bond MO including the Doppler term, is given by the sum of $E_T\left(C=C\right)$ (Eq. (14.324)) and $\overline{E}_{ethylene\ osc}\left(C=C,\sigma\right)$ given by Eq. (14.330).

$$\begin{aligned}E_{T+osc}\left(C=C\right)&=V_e+T+V_m+V_p+2E_T\left(C=C,2sp^3\right)+\overline{E}_{ethylene\ osc}\left(C=C,\sigma\right)\\&=E_T\left(C=C,\sigma\right)+2E_T\left(C=C,2sp^3\right)+\overline{E}_{ethylene\ osc}\left(C=C,\sigma\right)\\&=E_T\left(C=C\right)+\overline{E}_{ethylene\ osc}\left(C=C,\sigma\right)\end{aligned}\tag{14.331}$$

$$\begin{aligned}E_{T+osc}\left(C=C\right)&=\left\{\begin{pmatrix}\dfrac{-2e^2}{8\pi\varepsilon_0 c'}\left[\left(0.91771\right)\left(2-\dfrac{1}{2}\dfrac{a_0}{a}\right)\ln\dfrac{a+c'}{a-c'}-1\right]+2E_T\left(C=C,2sp^3\right)\\ \\1+\left(2\right)\left(\dfrac{1}{2}\right)\sqrt{\dfrac{2\hbar\sqrt{\dfrac{\left(0.91771\right)\dfrac{1}{2}\dfrac{e^2}{4\pi\varepsilon_0 b^3}}{m_e}}}{m_e c^2}}\end{pmatrix}+2\left(\frac{1}{2}\hbar\sqrt{\frac{k}{\mu}}\right)\right\}\\&=-65.53833\ eV-2\left(0.34517\ eV-\frac{1}{2}\hbar\sqrt{\frac{k}{\mu}}\right)\end{aligned}\tag{14.332}$$

From Eqs. (14.330-14.332), the total energy of the $C=C$-bond MO is:

$$\begin{aligned}E_{T+osc}\left(C=C\right)&=-63.27074\ eV+2E_T\left(C=C,2sp^3\right)+\overline{E}_{ethylene\ osc}\left(C=C,\sigma\right)\\&=-63.27074\ eV+2\left(-1.13380\ eV\right)-2\left(0.34517\ eV-\frac{1}{2}\left(0.17897\ eV\right)\right)\\&=-66.04969\ eV\end{aligned}\tag{14.333}$$

where the experimental E_{vib} was used for the $\hbar\sqrt{\dfrac{k}{\mu}}$ term.

BOND ENERGY OF THE $C=C$ BOND OF ETHYLENE

The dissociation energy of the $C=C$ bond of CH_2CH_2, $E_D\left(H_2C=CH_2\right)$, is given by four times $E\left(C,2sp^3\right)$ (Eq. (14.146)), the initial energy of each $C2sp^3$ HO of each CH_2 radical that forms the double $C=C$ bond, minus the sum of $\Delta E_{T+osc}\left(^{12}CH_2\right)$ (Eq. (14.318)), the energy change going from the dihydrogen carbide radicals to the CH_2 groups of ethylene, and $E_{T+osc}\left(C=C\right)$ (Eq. (14.333)). Thus, the dissociation energy of the $C=C$ bond of CH_2CH_2, is:

$$\begin{aligned}E_D\left(H_2C=CH_2\right)&=4\left(E\left(C,2sp^3\right)\right)-\left(\Delta E_{T+osc}\left(^{12}CH_2\right)+E_{T+osc}\left(C=C\right)\right)\\&=4\left(-14.63489\ eV\right)-\left(-0.04667\ eV-66.04969\ eV\right)\\&=4\left(-14.63489\ eV\right)-\left(-66.09636\ eV\right)\\&=7.55681\ eV\end{aligned}\tag{14.334}$$

The experimental dissociation energy of the $C=C$ bond of CH_2CH_2 is [7]:

$$E_D\left(H_2C-CH_2\right)=7.5969\ eV\tag{14.335}$$

The results of the determination of bond parameters of CH_2CH_2 are given in Table 14.1. The calculated results are based on first principles and given in closed-form, exact equations containing fundamental constants only. The agreement between the experimental and calculated results is excellent.

ACETYLENE MOLECULE ($CHCH$)

The acetylene molecule $CHCH$ is formed by the reaction of two hydrogen carbide radicals:

$$CH + CH \rightarrow CHCH \tag{14.336}$$

$CHCH$ can be solved using the same principles as those used to solve the methane series $CH_{n=1,2,3,4}$ as well as ethane, wherein the $2s$ and $2p$ shells of each C hybridize to form a single $2sp^3$ shell as an energy minimum, and the sharing of electrons between two $C2sp^3$ hybridized orbitals (HOs) to form a molecular orbital (MO) permits each participating hybridized orbital to decrease in radius and energy. First, two sets of one H atomic orbital (AO) combine with two sets of one carbon $2sp^3$ HO to form two hydrogen carbide groups comprising a linear combination of two diatomic H_2-type MOs developed in the Nature of the Chemical Bond of Hydrogen-Type Molecules and Molecular Ions section. Then, the two CH groups bond by forming a H_2-type MO between the remaining three $C2sp^3$ HOs on each carbon atom.

FORCE BALANCE OF THE $C \equiv C$-BOND MO OF ACETYLENE

$CHCH$ comprises a chemical bond between two CH radicals wherein each radical comprises a chemical bond between a carbon and a hydrogen atom. The solution of the parameters of CH is given in the Hydrogen Carbide (CH) section. The $C-H$ bond of CH having two spin-paired electrons, one from an initially unpaired electron of the carbon atom and the other from the hydrogen atom, comprises the linear combination of 75% H_2-type ellipsoidal MO and 25% $C2sp^3$ HO. The proton of the H atom and the nucleus of the C atom are along each internuclear axis and serve as the foci. As in the case of H_2, the $C-H$-bond MOs is a prolate spheroid with the exception that the ellipsoidal MO surface cannot extend into $C2sp^3$ HO for distances shorter than the radius of the $C2sp^3$ shell since it is energetically unfavorable. Thus, the MO surface comprises a prolate spheroid at the H proton that is continuous with the $C2sp^3$ shell at the C atom whose nucleus serves as the other focus. The electron configuration and the energy, $E\left(C,2sp^3\right)$, of the $C2sp^3$ shell is given by Eqs. (13.422) and (13.428), respectively. The central paramagnetic force due to spin of the $C-H$ bond is provided by the spin-pairing force of the CH MO that has the symmetry of an s orbital that superimposes with the $C2sp^3$ orbitals such that the corresponding angular momenta are unchanged.

Two CH radicals bond to form $CHCH$ by forming a MO between the two pairs of three remaining $C2sp^3$-HO electrons of the two carbon atoms. However, in this case, the sharing of electrons between two $C2sp^3$ HOs to form a MO comprising six spin-paired electrons permits each $C2sp^3$ HO to decrease in radius and energy.

As in the case of the $C-H$ bonds, the $C \equiv C$-bond MO is a prolate-spheroidal-MO surface that cannot extend into $C2sp^3$ HO for distances shorter than the radius of the $C2sp^3$ shell of each atom. Thus, the MO surface comprises a partial prolate spheroid in between the carbon nuclei and is continuous with the $C2sp^3$ shell at each C atom. The energy of the H_2-type ellipsoidal MO is matched to that of the $C2sp^3$ shell. As in the case of previous examples of energy-matched MOs such as those of OH, NH, CH, the $C=O$-bond MO of CO_2, the $C-C$-bond MO of CH_3CH_3, and the $C=C$-bond MO of CH_2CH_2, the $C \equiv C$-bond MO of acetylene must comprise 75% of a H_2-type ellipsoidal MO in order to match potential, kinetic, and orbital energy relationships. Thus, the $C \equiv C$-bond MO must comprise a linear combination of three MOs wherein each comprises two $C2sp^3$ HOs and 75% of a H_2-type ellipsoidal MO divided between the $C2sp^3$ HOs:

$$3\left(2C2sp^3 + 0.75\ H_2\ MO\right) \rightarrow C \equiv C - bond\ MO \tag{14.337}$$

The linear combination of each H_2-type ellipsoidal MO with each $C2sp^3$ HO further comprises an excess 25% charge-density contribution from each $C2sp^3$ HO to the $C \equiv C$-bond MO to achieve an energy minimum. The force balance of the $C \equiv C$-bond MO is determined by the boundary conditions that arise from the linear combination of orbitals according to Eq. (14.337) and the energy matching condition between the $C2sp^3$-HO components of the MO.

Similarly, the energies of each CH MO involve each $C2sp^3$ and each $H1s$ electron with the formation of each $C-H$ bond. The sum of the energies of the H_2-type ellipsoidal MOs is matched to that of the $C2sp^3$ shell. This energy is determined by the considering the effect of the donation of 25% electron density from the three pairs of $C2sp^3$ HOs to the $C \equiv C$-bond MO with the formation of the $C_{acetylene}2sp^3$ HOs each having a smaller radius. The $2sp^3$ hybridized orbital arrangement is given by Eq. (14.140). The sum $E_T\left(C,2sp^3\right)$ of calculated energies of C, C^+, C^{2+}, and C^{3+} is given by Eq. (14.141). The radius r_{2sp^3} of the $C2sp^3$ shell is given by Eq. (14.142). The Coulombic energy $E_{Coulomb}\left(C,2sp^3\right)$ and the energy $E\left(C,2sp^3\right)$ of the outer electron of the $C2sp^3$ shell are given by Eqs. (14.143) and (14.146), respectively.

Next, consider the formation of the $C \equiv C$-bond MO of acetylene from two CH radicals, each having a $C2sp^3$ electron with an energy given by Eq. (14.146). The total energy of the state is given by the sum over the four electrons. The sum $E_T\left(C_{acetylene}, 2sp^3\right)$ of calculated energies of $C2sp^3$, C^+, C^{2+}, and C^{3+} from Eqs. (10.123), (10.113-10.114), (10.68), and (10.48), respectively, is

$$\begin{aligned} E_T\left(C_{acetylene}, 2sp^3\right) &= -\left(64.3921\ eV + 48.3125\ eV + 24.2762\ eV + E\left(C, 2sp^3\right)\right) \\ &= -\left(64.3921\ eV + 48.3125\ eV + 24.2762\ eV + 14.63489\ eV\right) \\ &= -151.61569\ eV \end{aligned} \tag{14.338}$$

where $E\left(C, 2sp^3\right)$ (Eq. (14.146)) is the sum of the energy of C, $-11.27671\ eV$, and the hybridization energy. The orbital-angular-momentum interactions also cancel such that the energy of the $E_T\left(C_{acetylene}, 2sp^3\right)$ is purely Coulombic.

The sharing of electrons between three pairs of $C2sp^3$ HOs to form a $C \equiv C$-bond MO permits each participating hybridized orbital to decrease in radius and energy. In order to further satisfy the potential, kinetic, and orbital energy relationships, each participating $C2sp^3$ HO donates an excess of 25% of its electron density to the $C \equiv C$-bond MO to form an energy minimum. By considering this electron redistribution in the acetylene molecule as well as the fact that the central field decreases by an integer for each successive electron of the shell, the radius $r_{acetylene\,2sp^3}$ of the $C2sp^3$ shell of acetylene may be calculated from the Coulombic energy using Eq. (10.102).

$$r_{acetylene\,2sp^3} = \left(\sum_{n=2}^{5}(Z-n) - 0.75\right)\frac{e^2}{8\pi\varepsilon_0\left(e151.61569\ eV\right)} = \frac{9.25e^2}{8\pi\varepsilon_0\left(e151.61569\ eV\right)} = 0.83008a_0 \tag{14.339}$$

where $Z = 6$ for carbon. Using Eqs. (10.102) and (14.339), the Coulombic energy $E_{Coulomb}\left(C_{acetylene}, 2sp^3\right)$ of the outer electron of the $C2sp^3$ shell is:

$$E_{Coulomb}\left(C_{acetylene}, 2sp^3\right) = \frac{-e^2}{8\pi\varepsilon_0 r_{acetylene\,2sp^3}} = \frac{-e^2}{8\pi\varepsilon_0 0.83008a_0} = -16.39089\ eV \tag{14.340}$$

During hybridization, the spin-paired $2s$ electrons are promoted to the $C2sp^3$ shell as unpaired electrons. The energy for the promotion is the magnetic energy given by Eq. (13.152). Using Eqs. (14.145) and (14.340), the energy $E\left(C_{acetylene}, 2sp^3\right)$ of the outer electron of the $C2sp^3$ shell is

$$E\left(C_{acetylene}, 2sp^3\right) = \frac{-e^2}{8\pi\varepsilon_0 r_{acetylene\,2sp^3}} + \frac{2\pi\mu_0 e^2\hbar^2}{m_e^2\left(r_3\right)^3} = -16.39089\ eV + 0.19086\ eV = -16.20002\ eV \tag{14.341}$$

Thus, $E_T\left(C \equiv C, 2sp^3\right)$, the energy change of each $C2sp^3$ shell with the formation of the $C \equiv C$-bond MO is given by the difference between Eq. (14.146) and Eq. (14.341):

$$E_T\left(C \equiv C, 2sp^3\right) = E\left(C_{acetylene}, 2sp^3\right) - E\left(C, 2sp^3\right) = -16.20002\ eV - \left(-14.63489\ eV\right) = -1.56513\ eV \tag{14.342}$$

As in the case of Cl_2, each H_2-type ellipsoidal MO comprises 75% of the $C \equiv C$-bond MO shared between two $C2sp^3$ HOs corresponding to the electron charge density in Eq. (11.65) of $\frac{-0.75e}{2}$. But, the additional 25% charge-density contribution to each bond of the $C \equiv C$-bond MO causes the electron charge density in Eq. (11.65) to be $\frac{-e}{2} = -0.5e$. The corresponding force constant k' to determine the ellipsoidal parameter c' in terms of the central force of the foci (Eq. (11.65)) is given by Eq. (14.152). The distance from the origin to each focus c' is given by Eq. (14.153). The internuclear distance is given by Eq. (14.154). The length of the semiminor axis of the prolate spheroidal $C \equiv C$-bond MO $b = c$ is given by Eq. (13.62). The eccentricity, e, is given by Eq. (13.63). The solution of the semimajor axis a then allows for the solution of the other axes of each prolate spheroid and eccentricity of the $C \equiv C$-bond MO. From the energy equation and the relationship between the axes, the dimensions of the $C \equiv C$-bond MO are solved.

The general equations for the energy components of V_e, V_p, T, V_m, and E_T of the $C \equiv C$-bond MO are the same as those of the CH MO except that energy of the $C_{acetylene}2sp^3$ HO is used and the triple-bond nature is considered. In the case of a single bond, the prolate spheroidal H_2-type MO transitions to the $C_{acetylene}2sp^3$ HO of each carbon, and the energy of the $C_{acetylene}2sp^3$ shell must remain constant and equal to the $E\left(C_{acetylene}, 2sp^3\right)$ given by Eq. (14.391). Thus, the energy $E\left(C_{acetylene}, 2sp^3\right)$ in Eq. (14.391) adds to that of the energies of the corresponding H_2-type ellipsoidal MO. The second and third bonds of the triple $C \equiv C$-bond MO also transition to each $C_{acetylene}2sp^3$ HO of each C. The energy of a second and a third

H_2-type ellipsoidal MO adds to the first energy component, and the three bonds achieve an energy minimum as a linear combination of the three H_2-type ellipsoidal MOs each having the carbon nuclei as the foci. Each $C-C$-bond MO comprises the same $C_{acetylene}2sp^3$ HO shells of constant energy given by Eq. (14.391). As in the case of the water, NH_2, ammonia, and ethylene molecules given by Eqs. (13.180), (13.320), (13.372), and (14.251), respectively, the energy of the redundant shell is subtracted from the total energy of the linear combination of the σ MO. Thus, the total energy $E_T\left(C\equiv C,\sigma\right)$ of the σ component of the $C\equiv C$-bond MO is given by the sum of the energies of the three bonds each comprising the linear combination of the $C_{acetylene}2sp^3$ HO and the H_2-type ellipsoidal MO as given by Eq. (14.337) wherein the E_T terms add positively and the $E\left(C_{acetylene},2sp^3\right)$ term is positive due to the sum over a negative and two positive terms. Using Eqs. (13.431) and (14.341), $E_T\left(C\equiv C,\sigma\right)$ is given by:

$$\begin{aligned}E_T\left(C\equiv C,\sigma\right)&=E_T+E\left(C_{acetylene},2sp^3\right)-E\left(C_{acetylene},2sp^3\right)-E\left(C_{acetylene},2sp^3\right)\\&=-\frac{3e^2}{8\pi\varepsilon_0 c'}\left[\left(0.91771\right)\left(2-\frac{1}{2}\frac{a_0}{a}\right)\ln\frac{a+c'}{a-c'}-1\right]-E\left(C_{acetylene},2sp^3\right)\\&=-\frac{3e^2}{8\pi\varepsilon_0 c'}\left[\left(0.91771\right)\left(2-\frac{1}{2}\frac{a_0}{a}\right)\ln\frac{a+c'}{a-c'}-1\right]+16.20002\ eV\end{aligned}\tag{14.343}$$

The total energy term of the triple $C\equiv C$-bond MO is given by the sum of the three H_2-type ellipsoidal MOs given by Eq. (11.212). To match this boundary condition, $E_T\left(C\equiv C,\sigma\right)$ given by Eq. (14.343) is set equal to three times Eq. (13.75):

$$E_T\left(C\equiv C,\sigma\right)=-\frac{3e^2}{8\pi\varepsilon_0 c'}\left[\left(0.91771\right)\left(2-\frac{1}{2}\frac{a_0}{a}\right)\ln\frac{a+c'}{a-c'}-1\right]+16.20002\ eV=-94.90610\ eV\tag{14.344}$$

From the energy relationship given by Eq. (14.344) and the relationship between the axes given by Eqs. (14.153-14.154) and (13.62-13.63), the dimensions of the $C\equiv C$-bond MO can be solved.

Substitution of Eq. (14.153) into Eq. (14.344) gives:

$$\frac{3e^2}{8\pi\varepsilon_0\sqrt{aa_0}}\left[\left(0.91771\right)\left(2-\frac{1}{2}\frac{a_0}{a}\right)\ln\frac{a+\sqrt{aa_0}}{a-\sqrt{aa_0}}-1\right]=e111.10613\tag{14.345}$$

The most convenient way to solve Eq. (14.345) is by the reiterative technique using a computer. The result to within the round-off error with five-significant figures is

$$a=1.28714a_0=6.81122\ X\ 10^{-11}\ m\tag{14.346}$$

Substitution of Eq. (14.346) into Eq. (14.153) gives:

$$c'=1.13452a_0=6.00362\ X\ 10^{-11}\ m\tag{14.347}$$

The internuclear distance given by multiplying Eq. (14.347) by two is:

$$2c'=2.26904a_0=1.20072\ X\ 10^{-10}\ m\tag{14.348}$$

The experimental bond distance is [3]:

$$2c'=1.203\ X\ 10^{-10}\ m\tag{14.349}$$

Substitution of Eqs. (14.346-14.347) into Eq. (13.62) gives:

$$b=c=0.60793a_0=3.21704\ X\ 10^{-11}\ m\tag{14.350}$$

Substitution of Eqs. (14.346-14.347) into Eq. (13.63) gives:

$$e=0.88143\tag{14.351}$$

The nucleus of the C atoms comprise the foci of the H_2-type ellipsoidal MO. The parameters of the point of intersection of the H_2-type ellipsoidal MO and the $C_{acetylene}2sp^3$ HO are given by Eqs. (13.84-13.95) and (13.261-13.270). The polar intersection angle θ' is given by Eq. (13.261) where $r_n=r_{acetylene2sp^3}=0.83008a_0$ is the radius of the $C_{acetylene}2sp^3$ shell. Substitution of Eqs. (14.346-14.347) into Eq. (13.261) gives:

$$\theta'=137.91°\tag{14.352}$$

Then, the angle $\theta_{C\equiv C_{acetylene}2sp^3HO}$ the radial vector of the $C2sp^3$ HO makes with the internuclear axis is:

$$\theta_{C\equiv C_{acetylene}2sp^3HO}=180°-137.91°=42.09°\tag{14.353}$$

as shown in Figure 14.11.

Figure 14.11. The cross section of the $C \equiv C$-bond MO (σ MO) and one $C-H$-bond MO of acetylene showing the axes, angles, and point of intersection of each H_2-type ellipsoidal MO with the corresponding $C_{acetylene}2sp^3$ HO. The continuation of each H_2-type-ellipsoidal-MO basis element of the $C \equiv C$ bond and the $C-H$-bond beyond the intersection point with each $C_{acetylene}2sp^3$ shell and σ MO is shown as dashed since each only serves to solve the energy match with the $C_{acetylene}2sp^3$ shell and does not represent charge density. Similarly, the vertical dashed line only designates the parameters of each intersection point. The actual charge density is shown by the solid lines. Legend: a: semimajor axis, b: semiminor axis, c': internuclear distance, $d_1 : d_{C\equiv C_{acetylene},H_2MO}$, $\theta_1 : \theta_{C\equiv C_{acetylene}2sp^3HO}$, $d_2 : d_{C\equiv C_{acetylene}2sp^3HO}$, $R : r_{acetylene2sp^3}$, $\theta_2 : \theta_{C-H_{acetylene}2sp^3HO}$, $d_3 : d_{C-H_{acetylene},H_2MO}$, and $d_4 : d_{C-H_{acetylene}2sp^3HO}$.

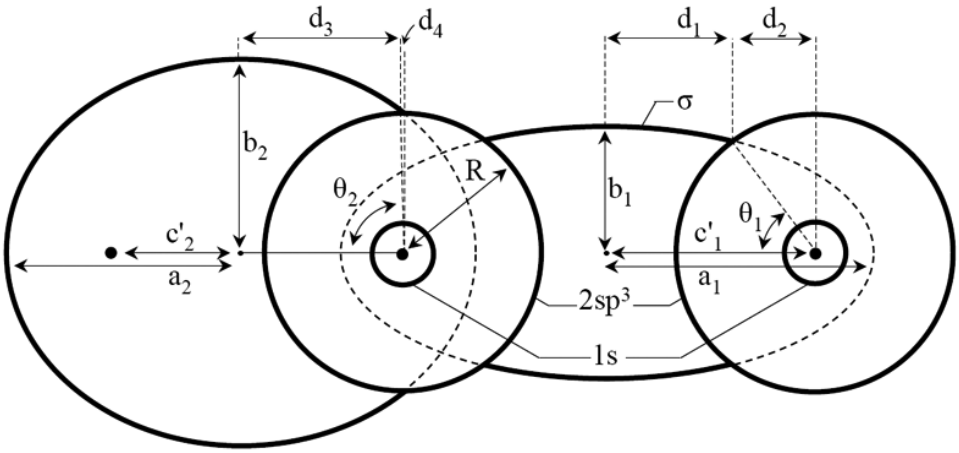

Consider the right-hand intersection point. The Cartesian $\mathbf{i}$-coordinate of the interception point of the MO and the AO can be calculated using the MO ellipsoidal parameters by first calculating the parametric angle in Eq. (11.83) that matches Cartesian $\mathbf{j}$-coordinate components at the point of intersection. Thus, the matching elliptic parametric angle $\omega t = \theta_{C\equiv C_{acetylene},H_2MO}$ satisfies the following relationship:

$$r_{acetylene2sp^3} \sin\theta_{C\equiv C_{acetylene}2sp^3HO} = 0.83008a_0 \sin\theta_{C\equiv C_{acetylene}2sp^3HO} = b\sin\theta_{C\equiv C_{acetylene},H_2MO} \tag{14.354}$$

such that

$$\theta_{C\equiv C_{acetylene},H_2MO} = \sin^{-1}\frac{0.83008a_0 \sin\theta_{C\equiv C_{acetylene}2sp^3HO}}{b} = \sin^{-1}\frac{0.83008a_0 \sin 42.09°}{b} \tag{14.355}$$

with the use of Eq. (14.353). Substitution of Eq. (14.350) into Eq. (14.355) gives:

$$\theta_{C\equiv C_{acetylene},H_2MO} = 66.24° \tag{14.356}$$

Then, the distance $d_{C\equiv C_{acetylene},H_2MO}$ along the internuclear axis from the origin of H_2-type ellipsoidal MO to the point of intersection of the orbitals is given by:

$$d_{C\equiv C_{acetylene},H_2MO} = a\cos\theta_{C\equiv C_{acetylene},H_2MO} \tag{14.357}$$

Substitution of Eqs. (14.346) and (14.356) into Eq. (14.357) gives:

$$d_{C\equiv C_{acetylene},H_2MO} = 0.51853a_0 = 2.74396\ X\ 10^{-11}\ m \tag{14.358}$$

The distance $d_{C\equiv C_{acetylene}2sp^3HO}$ along the internuclear axis from the origin of the C atom to the point of intersection of the orbitals is given by:

$$d_{C\equiv C_{acetylene}2sp^3HO} = c' - d_{C\equiv C_{acetylene},H_2MO} \tag{14.359}$$

Substitution of Eqs. (14.347) and (14.358) into Eq. (14.359) gives:

$$d_{C\equiv C_{acetylene}2sp^3HO} = 0.61599a_0 = 3.25966\ X\ 10^{-11}\ m \tag{14.360}$$

FORCE BALANCE OF THE CH MOS OF ACETYLENE

The $C-H$ bond of each of the two equivalent CH MOs must comprise 75% of a H_2-type ellipsoidal MO and a $C2sp^3$ HO as given by Eq. (13.429):

$$1\,C2sp^3 + 0.75\,H_2\ MO \rightarrow CH\ MO \tag{14.361}$$

The force balance of the CH MO is determined by the boundary conditions that arise from the linear combination of orbitals according to Eq. (13.429) and the energy matching condition between the hydrogen and $C2sp^3$ HO components of the MO.

The force constant k' to determine the ellipsoidal parameter c' of the each H_2-type-ellipsoidal-MO component of the CH MO in terms of the central force of the foci is given by Eq. (13.59). The distance from the origin of each $C-H$-bond MO to each focus c' is given by Eq. (13.60). The internuclear distance is given by Eq. (13.61). The length of the semiminor axis of the prolate spheroidal $C-H$-bond MO $b=c$ is given by Eq. (13.62). The eccentricity, e, is given by Eq. (13.63). The solution of the semimajor axis a then allows for the solution of the other axes of each prolate spheroid and eccentricity of each $C-H$-bond MO. From the energy equation and the relationship between the axes, the dimensions of the CH MO are solved.

Consider the formation of the triple $C\equiv C$-bond MO of acetylene from two CH radicals, each having a $C2sp^3$ shell with an energy given by Eq. (14.146). The energy components of V_e, V_p, T, V_m, and E_T are the same as those of the hydrogen carbide radical, except that two times $E_T\left(C\equiv C,2sp^3\right)$ is subtracted from $E_T\left(CH\right)$ of Eq. (13.495). The subtraction of the energy change of the $C2sp^3$ shells with the formation of the $C\equiv C$-bond MO matches the energy of the $C-H$-bond MOs to the decrease in the energy of the $C2sp^3$ HOs. Using Eqs. (13.495) and (14.342), $E_{T_{acetylene}}\left(CH\right)$ is given by:

$$E_{T_{acetylene}}\left(CH\right)=E_T+E\left(C,2sp^3\right)-2E_T\left(C\equiv C,2sp^3\right)=\begin{pmatrix}-\dfrac{e^2}{8\pi\varepsilon_0 c'}\left[\left(0.91771\right)\left(2-\dfrac{1}{2}\dfrac{a_0}{a}\right)\ln\dfrac{a+c'}{a-c'}-1\right]\\ -14.63489\ eV-\left(-3.13026\ eV\right)\end{pmatrix} \tag{14.362}$$

$E_{T_{acetylene}}\left(CH\right)$ given by Eq. (14.362) is set equal to the energy of the H_2-type ellipsoidal MO given by Eq. (13.75).

$$E_{T_{acetylene}}\left(CH\right)=\begin{pmatrix}-\dfrac{e^2}{8\pi\varepsilon_0 c'}\left[\left(0.91771\right)\left(2-\dfrac{1}{2}\dfrac{a_0}{a}\right)\ln\dfrac{a+c'}{a-c'}-1\right]\\ -14.63489\ eV-\left(-3.13026\ eV\right)\end{pmatrix}=-31.63537\ eV \tag{14.363}$$

From the energy relationship given by Eq. (14.363) and the relationship between the axes given by Eqs. (13.60-13.63), the dimensions of the CH MO can be solved.

Substitution of Eq. (13.60) into Eq. (14.363) gives:

$$\frac{e^2}{8\pi\varepsilon_0\sqrt{\dfrac{2aa_0}{3}}}\left[\left(0.91771\right)\left(2-\frac{1}{2}\frac{a_0}{a}\right)\ln\frac{a+\sqrt{\dfrac{2aa_0}{3}}}{a-\sqrt{\dfrac{2aa_0}{3}}}-1\right]=e20.13074 \tag{14.364}$$

The most convenient way to solve Eq. (14.364) is by the reiterative technique using a computer. The result to within the round-off error with five-significant figures is

$$a=1.48719a_0=7.86987\ X\ 10^{-11}\ m \tag{14.365}$$

Substitution of Eq. (14.365) into Eq. (14.60) gives:

$$c'=0.99572a_0=5.26913\ X\ 10^{-11}\ m \tag{14.366}$$

The internuclear distance given by multiplying Eq. (14.366) by two is:

$$2c'=1.99144a_0=1.05383\ X\ 10^{-10}\ m \tag{14.367}$$

The experimental bond distance is [3]:

$$2c'=1.060\ X\ 10^{-10}\ m \tag{14.368}$$

Substitution of Eqs. (14.365-14.366) into Eq. (14.62) gives:

$$b=c=1.10466a_0=5.84561\ X\ 10^{-11}\ m \tag{14.369}$$

Substitution of Eqs. (14.365-14.366) into Eq. (14.63) gives:

$$e=0.66953 \tag{14.370}$$

The nucleus of the H atom and the nucleus of the C atom comprise the foci of each H_2-type ellipsoidal MO. The parameters of the point of intersection of the H_2-type ellipsoidal MO and the $C_{acetylene}2sp^3$ HO are given by Eqs. (13.84-13.95) and (13.261-13.270). The polar intersection angle θ' is given by Eq. (13.261) where $r_n=r_{acetylene\,2sp^3}=0.83008a_0$ is the radius of the $C_{acetylene}2sp^3$ shell. Substitution of Eqs. (14.365-14.366) into Eq. (13.261) gives:

$$\theta'=90.99^\circ \tag{14.371}$$

Then, the angle $\theta_{C-H_{acetylene}2sp^3HO}$ the radial vector of the $C2sp^3$ HO makes with the internuclear axis is

$$\theta_{C-H_{acetylene}2sp^3HO} = 180° - 90.99° = 89.01° \tag{14.372}$$

as shown in Figure 14.11. The Cartesian $\mathbf{i}$-coordinate of the interception point of the MO and the AO can be calculated using the MO ellipsoidal parameters by first calculating the parametric angle in Eq. (11.83) that matches Cartesian $\mathbf{j}$-coordinate components at the point of intersection. Thus, the matching elliptic parametric angle $\omega t = \theta_{C-H_{acetylene},H_2MO}$ satisfies the following relationship:

$$r_{acetylene2sp^3} \sin\theta_{C-H_{acetylene}2sp^3HO} = 0.83008a_0 \sin\theta_{C-H_{acetylene}2sp^3HO} = b\sin\theta_{C-H_{acetylene},H_2MO} \tag{14.373}$$

such that

$$\theta_{C-H_{acetylene},H_2MO} = \sin^{-1}\frac{0.83008a_0 \sin\theta_{C-H_{acetylene}2sp^3HO}}{b} = \sin^{-1}\frac{0.83008a_0 \sin 89.01°}{b} \tag{14.374}$$

with the use of Eq. (14.372). Substitution of Eq. (14.369) into Eq. (14.374) gives:

$$\theta_{C-H_{acetylene},H_2MO} = 48.71° \tag{14.375}$$

Then, the distance $d_{C-H_{acetylene},H_2MO}$ along the internuclear axis from the origin of H_2-type ellipsoidal MO to the point of intersection of the orbitals is given by

$$d_{C-H_{acetylene},H_2MO} = a\cos\theta_{C-H_{acetylene},H_2MO} \tag{14.376}$$

Substitution of Eqs. (14.365) and (14.375) into Eq. (14.376) gives:

$$d_3 : d_{C-H_{acetylene},H_2MO} = 0.98145a_0 = 5.19359\ X\ 10^{-11}\ m \tag{14.377}$$

The distance $d_{C-H_{acetylene}2sp^3HO}$ along the internuclear axis from the origin of the C atom to the point of intersection of the orbitals is given by

$$d_{C-H_{acetylene}2sp^3HO} = c' - d_{C-H_{acetylene},H_2MO} \tag{14.378}$$

Substitution of Eqs. (14.366) and (14.377) into Eq. (14.378) gives:

$$d_4 : d_{C-H_{acetylene}2sp^3HO} = 0.01427a_0 = 7.55329\ X\ 10^{-13}\ m \tag{14.379}$$

with the $C \equiv C$ triple bond along one axis, the minimum energy is obtained with the $C-H$-bond MO at a maximum separation. Thus, the bond angle $\theta_{C\equiv C-H}$ between the internuclear axis of the $C \equiv C$ bond and the H atom of the CH groups is

$$\theta_{C\equiv C-H} = 180° \tag{14.380}$$

The experimental angle between the $C \equiv C-H$ bonds is [6]:

$$\theta_{C\equiv C-H} = 180° \tag{14.381}$$

The $CHCH$ MO shown in Figure 14.12 was rendered using these parameters.

The charge-density in the $C \equiv C$-bond MO is increased by a factor of 0.25 per bond with the formation of the $C_{acetylene}2sp^3$ HOs each having a smaller radius. Using the orbital composition of the CH groups (Eq. (14.361)) and the $C \equiv C$-bond MO (Eq. (14.337)), the radii of $C1s = 0.17113a_0$ (Eq. (10.51)) and $C_{acetylene}2sp^3 = 0.83008a_0$ (Eq. (14.339)) shells, and the parameters of the $C \equiv C$-bond (Eqs. (13.3-13.4), (14.346-14.348), and (14.350-14.360)), the parameters of the $C-H$-bond MOs (Eqs. (13.3-13.4), (14.365-14.367), and (14.369-14.379)), and the bond-angle parameter (Eqs. (14.380-14.381)), the charge-density of the $CHCH$ MO comprising the linear combination of two $C-H$-bond MOs and a $C \equiv C$-bond MO bridging the two CH groups is shown in Figure 14.12. Each $C-H$-bond MO comprises a H_2-type ellipsoidal MO and a $C_{acetylene}2sp^3$ HO having the dimensional diagram shown in Figure 14.11. The $C \equiv C$-bond MO comprises a H_2-type ellipsoidal MO bridging two $C_{acetylene}2sp^3$ HOs having the dimensional diagram also shown in Figure 14.11.

Figure 14.12. $CHCH$ MO comprising the linear combination of two $C-H$ -bond MOs and a $C\equiv C$ -bond MO. (A) Color scale, translucent view of the charge-density of the $C\equiv C$ -bond MO with the $C_{acetylene}2sp^3$ HOs shown transparently. The $C\equiv C$ -bond MO comprises a H_2 -type ellipsoidal MO bridging two sets of three $C_{acetylene}2sp^3$ HOs. For each $C-H$ and the $C\equiv C$ bond, the ellipsoidal surface of the H_2 -type ellipsoidal MO that transitions to the $C_{acetylene}2sp^3$ HO, the $C_{acetylene}2sp^3$ HO shell, inner most $C1s$ shell, and the nuclei (red, not to scale), are shown. (B)-(D) Translucent view high-lighting the $C\equiv C$ -bond MO and end-on view of the charge-density of the $CHCH$ MO, respectively.

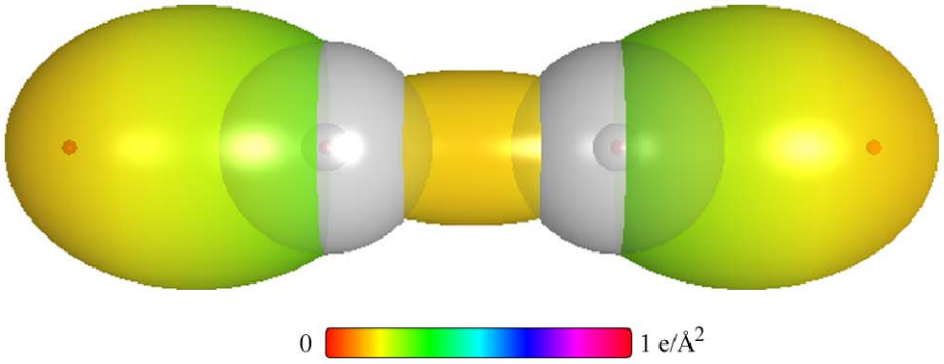

ENERGIES OF THE CH GROUPS

The energies of each CH group of acetylene are given by the substitution of the semiprincipal axes (Eqs. (14.365-14.366) and (14.369)) into the energy equations of hydrogen carbide (Eqs. (13.510-13.514)), with the exception that two times $E_T\left(C\equiv C,2sp^3\right)$ (Eq. (14.342)) is subtracted from $E_T\left(CH\right)$ in Eq. (13.514).

$$V_e=\left(0.91771\right)\frac{-2e^2}{8\pi\varepsilon_0\sqrt{a^2-b^2}}\ln\frac{a+\sqrt{a^2-b^2}}{a-\sqrt{a^2-b^2}}=-40.62396\ eV \tag{14.382}$$

$$V_p=\frac{e^2}{8\pi\varepsilon_0\sqrt{a^2-b^2}}=13.66428\ eV \tag{14.383}$$

$$T=\left(0.91771\right)\frac{\hbar^2}{2m_e a\sqrt{a^2-b^2}}\ln\frac{a+\sqrt{a^2-b^2}}{a-\sqrt{a^2-b^2}}=13.65796\ eV \tag{14.384}$$

$$V_m=\left(0.91771\right)\frac{-\hbar^2}{4m_e a\sqrt{a^2-b^2}}\ln\frac{a+\sqrt{a^2-b^2}}{a-\sqrt{a^2-b^2}}=-6.82898\ eV \tag{14.385}$$

$$E_{T_{acetylene}}\left(CH\right)=\left(\begin{array}{l}-\dfrac{e^2}{8\pi\varepsilon_0 c'}\left[\left(0.91771\right)\left(2-\dfrac{1}{2}\dfrac{a_0}{a}\right)\ln\dfrac{a+c'}{a-c'}-1\right]\\ -14.63489\ eV-\left(-3.13026\ eV\right)\end{array}\right)=-31.63532\ eV \tag{14.386}$$

where $E_{T_{acetylene}}\left(CH\right)$ is given by Eq. (14.362) which is reiteratively matched to Eq. (13.75) within five-significant-figure round off error.

VIBRATION OF THE ^{12}CH GROUPS

The vibrational energy levels of CH in acetylene may be solved using the methods given in the Vibration and Rotation of CH section.

THE DOPPLER ENERGY TERMS OF THE ^{12}CH GROUPS

The equations of the radiation reaction force of the CH groups in acetylene are the same as those of the hydrogen carbide radical with the substitution of the CH -group parameters. Using Eq. (13.477), the angular frequency of the reentrant oscillation in the transition state is:

$$\omega = \sqrt{\frac{0.75e^2}{4\pi\varepsilon_0 b^3}} = 3.08370\ X\ 10^{16}\ rad/s \tag{14.387}$$

where b is given by Eq. (14.369). The kinetic energy, E_K, is given by Planck's equation (Eq. (11.127)):

$$\overline{E}_K = \hbar\omega = \hbar 3.08370\ X\ 10^{16}\ rad/s = 20.29747\ eV \tag{14.388}$$

In Eq. (11.181), substitution of $E_T\left(H_2\right)$ (Eqs. (11.212) and (13.75)), the maximum total energy of each H_2-type MO, for $E_{h\nu}$, the mass of the electron, m_e, for M, and the kinetic energy given by Eq. (14.388) for $\overline{E}_K$ gives the Doppler energy of the electrons for the reentrant orbit:

$$\overline{E}_D \cong E_{h\nu}\sqrt{\frac{2\overline{E}_K}{Mc^2}} = -31.63537\ eV\sqrt{\frac{2e(20.29747\ eV)}{m_e c^2}} = -0.28197\ eV \tag{14.389}$$

In addition to the electrons, the nuclei also undergo simple harmonic oscillation in the transition state at their corresponding frequency. The decrease in the energy of CH due to the reentrant orbit of each bond in the transition state corresponding to simple harmonic oscillation of the electrons and nuclei, $\overline{E}_{osc}$, is given by the sum of the corresponding energies, $\overline{E}_D$ given by Eq. (14.389) and $\overline{E}_{Kvib}$, the average kinetic energy of vibration which is 1/2 of the vibrational energy of each $C-H$ bond. Using ω_e given by Eq. (13.458) for $\overline{E}_{Kvib}$ of the transition state, $\overline{E}_{acetylene\ osc}\left({}^{12}CH\right)$ is:

$$\overline{E}_{acetylene\ osc}\left({}^{12}CH\right) = \overline{E}_D + \overline{E}_{Kvib} = \overline{E}_D + \frac{1}{2}\hbar\sqrt{\frac{k}{\mu}} \tag{14.390}$$

$$\overline{E}_{acetylene\ osc}\left({}^{12}CH\right) = -0.28197\ eV + \frac{1}{2}(0.35532\ eV) = -0.10430\ eV \tag{14.391}$$

TOTAL AND DIFFERENCE ENERGIES OF THE ${}^{12}CH$ GROUPS

$E_{acetyleneT+osc}\left({}^{12}CH\right)$, the total energy of each ${}^{12}CH$ group including the Doppler term, is given by the sum of $E_{T_{acetylene}}(CH)$ (Eq. (14.386)) and $\overline{E}_{acetylene\ osc}\left({}^{12}CH\right)$ given by Eq. (14.391).

$$\begin{aligned} E_{acetyleneT+osc}\left({}^{12}CH\right) &= \begin{pmatrix} V_e + T + V_m + V_p + E\left(C, 2sp^3\right) \\ -2E_T\left(C \equiv C, 2sp^3\right) + \overline{E}_{acetylene\ osc}\left({}^{12}CH\right) \end{pmatrix} \\ &= E_{T_{acetylene}}(CH) + \overline{E}_{acetylene\ osc}\left({}^{12}CH\right) \end{aligned} \tag{14.392}$$

$$\begin{aligned} E_{acetyleneT+osc}\left({}^{12}CH\right) &= \left\{ \begin{pmatrix} \left(\frac{-e^2}{8\pi\varepsilon_0 c'}\right)\left[(0.91771)\left(2 - \frac{1}{2}\frac{a_0}{a}\right)\ln\frac{a+c'}{a-c'} - 1\right] \\ -14.63489\ eV - (-3.13026\ eV) \end{pmatrix} \right. \\ &\quad \left. - \left((31.63536831\ eV)\sqrt{\frac{2\hbar\sqrt{\frac{3}{4}\frac{e^2}{4\pi\varepsilon_o b^3}}}{m_e c^2}} - \frac{1}{2}\hbar\sqrt{\frac{k}{\mu}} \right) \right\} \\ &= -31.63537\ eV - \left(0.28197\ eV - \frac{1}{2}\hbar\sqrt{\frac{k}{\mu}}\right) \end{aligned} \tag{14.393}$$

From Eqs. (14.391-14.393), the total energy of each ${}^{12}CH$ is:

$$\begin{aligned} E_{acetyleneT+osc}\left({}^{12}CH\right) &= -31.63537\ eV + \overline{E}_{acetylene\ osc}\left({}^{12}CH\right) \\ &= -31.63537\ eV - \left(0.28197\ eV - \frac{1}{2}(0.35532\ eV)\right) = -31.73967\ eV \end{aligned} \tag{14.394}$$

where ω_e given by Eq. (13.458) was used for the $\hbar\sqrt{\frac{k}{\mu}}$ term.

The total energy for each hydrogen carbide radical given by Eq. (13.485) is:

$$\begin{aligned} E_{radicalT+osc}\left({}^{12}CH\right) &= -31.63537\ eV + \bar{E}_{radicalosc}\left({}^{12}CH\right) \\ &= -31.63537\ eV - 0.24966\ eV + \frac{1}{2}\left(0.35532\ eV\right) \\ &= -31.70737\ eV \end{aligned} \tag{14.395}$$

The difference in energy between the CH groups and the hydrogen carbide radical $\Delta E_{T+osc}\left({}^{12}CH\right)$ is given by two times the difference between Eqs. (14.394) and (14.395).

$$\begin{aligned} \Delta E_{T+osc}\left({}^{12}CH\right) &= 2\left(E_{acetyleneT+osc}\left({}^{12}CH\right) - E_{radicalT+osc}\left({}^{12}CH\right)\right) \\ &= 2\left(-31.73967\ eV - \left(-31.70737\ eV\right)\right) \\ &= -0.06460\ eV \end{aligned} \tag{14.396}$$

SUM OF THE ENERGIES OF THE $C \equiv C$ σ MO AND THE HOS OF ACETYLENE

The energy components of V_e, V_p, T, V_m, and E_T of the $C \equiv C$-bond MO are the same as those of the CH MO except that each term is multiplied by three corresponding to the triple bond and the energy term corresponding to the $C_{acetylene}2sp^3$ HOs in the equation for E_T is positive. The energies of each $C \equiv C$-bond MO are given by the substitution of the semiprincipal axes (Eqs. (14.346-14.347) and (14.350)) into three times the energy equations of the CH MO (Eqs. (13.449-13.453)), with the exception that $E\left(C, 2sp^3\right)$ in Eq. (13.453) is positive and given by Eq. (14.341).

$$V_e = 3\left(0.91771\right)\frac{-2e^2}{8\pi\varepsilon_0\sqrt{a^2-b^2}}\ln\frac{a+\sqrt{a^2-b^2}}{a-\sqrt{a^2-b^2}} = -182.53826\ eV \tag{14.397}$$

$$V_p = 3\frac{e^2}{8\pi\varepsilon_0\sqrt{a^2-b^2}} = 35.97770\ eV \tag{14.398}$$

$$T = 3\left(0.91771\right)\frac{\hbar^2}{2m_e a\sqrt{a^2-b^2}}\ln\frac{a+\sqrt{a^2-b^2}}{a-\sqrt{a^2-b^2}} = 70.90876\ eV \tag{14.399}$$

$$V_m = 3\left(0.91771\right)\frac{-\hbar^2}{4m_e a\sqrt{a^2-b^2}}\ln\frac{a+\sqrt{a^2-b^2}}{a-\sqrt{a^2-b^2}} = -35.45438\ eV \tag{14.400}$$

$$E_T\left(C \equiv C, \sigma\right) = -\frac{3e^2}{8\pi\varepsilon_0 c'}\left[\left(0.91771\right)\left(2 - \frac{1}{2}\frac{a_0}{a}\right)\ln\frac{a+c'}{a-c'} - 1\right] + 16.20002\ eV = -94.90616\ eV \tag{14.401}$$

where $E_T\left(C \equiv C, \sigma\right)$ is the total energy of the $C \equiv C$ σ MO given by Eq. (14.343) which is reiteratively matched to three times Eq. (13.75) within five-significant-figure round off error.

The total energy of the $C \equiv C$-bond MO, $E_T\left(C \equiv C\right)$, is given by the sum of two times $E_T\left(C \equiv C, 2sp^3\right)$, the energy change of each $C2sp^3$ shell due to the decrease in radius with the formation of the $C \equiv C$-bond MO (Eq. (14.342)), and $E_T\left(C \equiv C, \sigma\right)$, the σ MO contribution given by Eq. (14.344).

$$\begin{aligned} E_T\left(C \equiv C\right) &= 2E_T\left(C \equiv C, 2sp^3\right) + E_T\left(C \equiv C, \sigma\right) \\ &= \left(\begin{array}{l} 2\left(-1.56513\ eV\right) + \\ \left(-\frac{2e^2}{8\pi\varepsilon_0 c'}\left[\left(0.91771\right)\left(2 - \frac{1}{2}\frac{a_0}{a}\right)\ln\frac{a+c'}{a-c'} - 1\right] + 16.20002\ eV\right) \end{array}\right) \\ &= 2\left(-1.56513\ eV\right) + \left(-94.90610\ eV\right) \\ &= -98.03637\ eV \end{aligned} \tag{14.402}$$

VIBRATION OF ACETYLENE

The vibrational energy levels of $CHCH$ may be solved as two equivalent coupled harmonic oscillators with a bridging harmonic oscillator by developing the Lagrangian, the differential equation of motion, and the eigenvalue solutions [9] wherein the spring constants are derived from the central forces as given in the Vibration of Hydrogen-Type Molecular Ions section and the Vibration of Hydrogen-Type Molecules section.

THE DOPPLER ENERGY TERMS OF THE $C \equiv C$-BOND MO OF ACETYLENE

The equations of the radiation reaction force of the $C \equiv C$-bond MO are given by Eq. (14.231), except that the $C \equiv C$-bond MO parameters are used. The angular frequency of the reentrant oscillation in the transition state is:

$$\omega = \sqrt{\frac{0.5e^2}{4\pi\varepsilon_0 a^3}} = 2.00186\ X\ 10^{16}\ rad/s \tag{14.403}$$

where a is given by Eq. (14.346). The kinetic energy, E_K, is given by Planck's equation (Eq. (11.127)).

$$\bar{E}_K = \hbar\omega = \hbar 2.00186\ X\ 10^{16}\ rad/s = 13.17659\ eV \tag{14.404}$$

In Eq. (11.181), substitution of $E_T(C \equiv C)/3$ (Eq. (14.402)) for E_{hv}, the mass of the electron, m_e, for M, and the kinetic energy given by Eq. (14.404) for $\bar{E}_K$ gives the Doppler energy of the electrons of each of the three bonds for the reentrant orbit:

$$\bar{E}_D \cong E_{hv}\sqrt{\frac{2\bar{E}_K}{Mc^2}} = -32.67879\ eV\sqrt{\frac{2e(13.17659\ eV)}{m_e c^2}} = -0.23468\ eV \tag{14.405}$$

In addition to the electrons, the nuclei also undergo simple harmonic oscillation in the transition state at their corresponding frequency. The decrease in the energy of the $C \equiv C$-bond MO due to the reentrant orbit of the bond in the transition state corresponding to simple harmonic oscillation of the electrons and nuclei, $\bar{E}_{osc}$, is given by the sum of the corresponding energies, $\bar{E}_D$ given by Eq. (14.405) and $\bar{E}_{Kvib}$, the average kinetic energy of vibration which is 1/2 of the vibrational energy of the $C \equiv C$ bond. Using the experimental $C \equiv C$ $E_{vib}(\upsilon_3)$ of 3374 cm^{-1} $(0.41833\ eV)$ [6] for $\bar{E}_{Kvib}$ of the transition state having three bonds, $\bar{E}'_{osc}(C \equiv C, \sigma)$ per bond is:

$$\bar{E}'_{osc}(C \equiv C, \sigma) = \bar{E}_D + \bar{E}_{Kvib} = \bar{E}_D + \frac{1}{2}\hbar\sqrt{\frac{k}{\mu}} \tag{14.406}$$

$$\bar{E}'_{osc}(C \equiv C, \sigma) = -0.23468\ eV + \frac{1}{2}(0.41833\ eV) = -0.02551\ eV \tag{14.407}$$

Given that the vibration and reentrant oscillation is for three $C-C$ bonds of the $C \equiv C$ triple bond, $\bar{E}_{acetylene\ osc}(C \equiv C, \sigma)$, is:

$$\begin{aligned}\bar{E}_{acetylene\ osc}(C \equiv C, \sigma) &= 3\left(\bar{E}_D + \frac{1}{2}\hbar\sqrt{\frac{k}{\mu}}\right)\\ &= 3\left(-0.23468\ eV + \frac{1}{2}(0.41833\ eV)\right)\\ &= -0.07654\ eV\end{aligned} \tag{14.408}$$

TOTAL ENERGIES OF THE $C \equiv C$-BOND MO OF ACETYLENE

$E_{T+osc}(C \equiv C)$, the total energy of the $C \equiv C$-bond MO including the Doppler term, is given by the sum of $E_T(C \equiv C)$ (Eq. (14.402)) and $\bar{E}_{acetylene\ osc}(C \equiv C, \sigma)$ given by Eq. (14.408).

$$\begin{aligned}E_{T+osc}(C \equiv C) &= \begin{pmatrix} V_e + T + V_m + V_p - E(C_{acetylene}, 2sp^3) \\ +2E_T(C \equiv C, 2sp^3) + \bar{E}_{acetylene\ osc}(C \equiv C, \sigma)\end{pmatrix}\\ &= E_T(C \equiv C, \sigma) + 2E_T(C \equiv C, 2sp^3) + \bar{E}_{acetylene\ osc}(C \equiv C, \sigma)\\ &= E_T(C \equiv C) + \bar{E}_{acetylene\ osc}(C \equiv C, \sigma)\end{aligned} \tag{14.409}$$

$$E_{T+osc}(C \equiv C) = \left\{\begin{pmatrix} \left(\frac{-3e^2}{8\pi\varepsilon_0 c'}\right)\left[(0.91771)\left(2 - \frac{1}{2}\frac{a_0}{a}\right)\ln\frac{a+c'}{a-c'} - 1\right] \\ -E(C_{acetylene}, 2sp^3) + 2E_T(C \equiv C, 2sp^3)\end{pmatrix}\right\}$$
$$\left\{\begin{pmatrix} 1 + (3)\left(\frac{1}{3}\right)\sqrt{\frac{2\hbar\sqrt{\frac{1}{2}\frac{e^2}{4\pi\varepsilon_0 a^3}}}{m_e c^2}} \end{pmatrix} + 3\left(\frac{1}{2}\hbar\sqrt{\frac{k}{\mu}}\right)\right\} \tag{14.410}$$

$$= -98.03637\ eV - 3\left(0.23468\ eV - \frac{1}{2}\hbar\sqrt{\frac{k}{\mu}}\right)$$

From Eqs. (14.408-14.410), the total energy of the $C \equiv C$ -bond MO is:

$$\begin{aligned} E_{T+osc}\left(C \equiv C\right) &= -94.90610\ eV + 2E_T\left(C \equiv C, 2sp^3\right) + \bar{E}_{acetylene\ osc}\left(C \equiv C, \sigma\right) \\ &= -94.90610\ eV + 2\left(-1.56513\ eV\right) - 3\left(0.23468\ eV - \frac{1}{2}\left(0.41833\ eV\right)\right) \\ &= -98.11291\ eV \end{aligned} \tag{14.411}$$

where the experimental E_{vib} was used for the $\hbar\sqrt{\frac{k}{\mu}}$ term.

BOND ENERGY OF THE $C \equiv C$ BOND OF ACETYLENE

As in the case of $^{12}CH_2$ and ^{14}NH, the dissociation of the $C \equiv C$ bond forms three unpaired electrons per central atom wherein the magnetic moments cannot all cancel. The energy per atom $E(magnetic)$ is given by Eq. (13.524). Thus, the dissociation energy of the $C \equiv C$ bond of $CHCH$, $E_D\left(HC \equiv CH\right)$, is given by six times $E\left(C, 2sp^3\right)$ (Eq. (14.146)), the initial energy of each $C2sp^3$ HO of each CH radical that forms the triple $C \equiv C$ bond, minus the sum of $\Delta E_{T+osc}\left(^{12}CH\right)$ (Eq. (14.396)), the energy change going from the hydrogen carbide radicals to the CH groups of acetylene, $E_{T+osc}\left(C \equiv C\right)$ (Eq. (14.411)), and two times $E(magnetic)$ given by Eq. (13.524). Thus, the dissociation energy of the $C \equiv C$ bond of $CHCH$, is:

$$\begin{aligned} E_D\left(HC \equiv CH\right) &= 6\left(E\left(C, 2sp^3\right)\right) - \left(\Delta E_{T+osc}\left(^{12}CH\right) + E_{T+osc}\left(C \equiv C\right) + 2E(magnetic)\right) \\ &= 6\left(-14.63489\ eV\right) - \left(-0.06460\ eV - 98.11291\ eV + 0.29606\ eV\right) \\ &= 6\left(-14.63489\ eV\right) - \left(-97.88145\ eV\right) = 10.07212\ eV \end{aligned} \tag{14.412}$$

The experimental dissociation energy of the $C \equiv C$ bond of $CHCH$ is [7]:

$$E_D\left(HC \equiv CH\right) = 10.0014\ eV \tag{14.413}$$

The results of the determination of bond parameters of $CHCH$ are given in Table 14.1. The calculated results are based on first principles and given in closed-form, exact equations containing fundamental constants only. The agreement between the experimental and calculated results is excellent.

BENZENE MOLECULE (C_6H_6)

The benzene molecule C_6H_6 is formed by the reaction of three ethylene molecules:

$$3CH_2CH_2 \rightarrow C_6H_6 + 3H_2 \tag{14.414}$$

C_6H_6 can be solved using the same principles as those used to solve ethylene wherein the $2s$ and $2p$ shells of each C hybridize to form a single $2sp^3$ shell as an energy minimum, and the sharing of electrons between two $C2sp^3$ hybridized orbitals (HOs) to form a molecular orbital (MO) permits each participating hybridized orbital to decrease in radius and energy. Each $2sp^3$ HO of each carbon atom initially has four unpaired electrons. Thus, the $6H$ atomic orbitals (AOs) of benzene contribute six electrons and the six sp^3-hybridized carbon atoms contribute twenty-four electrons to form six $C-H$ bonds and six $C=C$ bonds. Each $C-H$ bond has two paired electrons with one donated from the H AO and the other from the $C2sp^3$ HO. Each $C=C$ bond comprises a linear combination of a factor of 0.75 of four paired electrons (three electrons) from two sets of two $C2sp^3$ HOs of the participating carbon atoms. Each $C-H$ and each $C=C$ bond comprises a linear combination of one and two diatomic H_2-type MOs developed in the Nature of the Chemical Bond of Hydrogen-Type Molecules and Molecular Ions section, respectively.

FORCE BALANCE OF THE $C=C$-BOND MO OF BENZENE

C_6H_6 can be considered a linear combination of three ethylene molecules wherein a $C-H$ bond of each CH_2 group of $H_2C=CH_2$ is replaced by a $C=C$ bond to form a six-member ring of carbon atoms. The solution of the ethylene molecule is given in the Ethylene Molecule (CH_2CH_2) section. Before forming ethylene groups, the $2sp^3$ hybridized orbital arrangement of each carbon atom is given by Eq. (14.140). The sum $E_T\left(C, 2sp^3\right)$ of calculated energies of C, C^+, C^{2+}, and C^{3+} is given by Eq. (14.141). The radius r_{2sp^3} of the $C2sp^3$ shell is given by Eq. (14.142). The Coulombic energy $E_{Coulomb}\left(C, 2sp^3\right)$ and the energy $E\left(C, 2sp^3\right)$ of the outer electron of the $C2sp^3$ shell are given by Eqs. (14.143) and (14.146), respectively. Two CH_2 radicals bond to form CH_2CH_2 by forming a MO between the two pairs of remaining $C2sp^3$-HO electrons of the two carbon

atoms. However, in this case, the sharing of electrons between four $C2sp^3$ HOs to form a MO comprising four spin-paired electrons permits each $C2sp^3$ HO to decrease in radius and energy. The $C=C$-bond MO is a prolate-spheroidal-MO surface that cannot extend into $C2sp^3$ HO for distances shorter than the radius of the $C2sp^3$ shell of each atom. Thus, the MO surface comprises a partial prolate spheroid in between the carbon nuclei and is continuous with the $C2sp^3$ shell at each C atom. The energy of the H_2-type ellipsoidal MO is matched to that of each $C2sp^3$ shell. As in the case of previous examples of energy-matched MOs such as those of OH, NH, CH, the $C=O$-bond MO of CO_2, and the $C-C$-bond MO of CH_3CH_3, the $C=C$-bond MO of ethylene must comprise 75% of a H_2-type ellipsoidal MO in order to match potential, kinetic, and orbital energy relationships. Thus, the $C=C$-bond MO must comprise a linear combination of two MOs wherein each comprises two $C2sp^3$ HOs and 75% of a H_2-type ellipsoidal MO divided between the $C2sp^3$ HOs:

$$2\left(2\ C2sp^3 + 0.75\ H_2\ MO\right) \rightarrow C=C-bond\ MO \tag{14.415}$$

The linear combination of each H_2-type ellipsoidal MO with each $C2sp^3$ HO further comprises an excess 25% charge-density contribution from each $C2sp^3$ HO to the $C=C$-bond MO to achieve an energy minimum. The force balance of the $C=C$-bond MO is determined by the boundary conditions that arise from the linear combination of orbitals according to Eq. (14.415) and the energy matching condition between the $C2sp^3$-HO components of the MO.

The sharing of electrons between two pairs of $C2sp^3$ HOs to form a $C=C$-bond MO permits each participating hybridized orbital to decrease in radius and energy. The sum $E_T\left(C_{ethylene}, 2sp^3\right)$ of calculated energies of $C2sp^3$, C^+, C^{2+}, and C^{3+} is given by Eq. (14.243). In order to further satisfy the potential, kinetic, and orbital energy relationships, each participating $C2sp^3$ HO donates an excess of 25% of its electron density to the $C=C$-bond MO to form an energy minimum. By considering this electron redistribution in the ethylene molecule as well as the fact that the central field decreases by an integer for each successive electron of the shell, the radius $r_{ethylene\,2sp^3}$ of the $C2sp^3$ shell of ethylene calculated from the Coulombic energy is given by Eq. (14.244). The Coulombic energy $E_{Coulomb}\left(C_{ethylene}, 2sp^3\right)$ of the outer electron of the $C2sp^3$ shell is given by Eq. (14.245). The energy $E\left(C_{ethylene}, 2sp^3\right)$ of the outer electron of the $C2sp^3$ shell is given by Eq. (14.246). $E_T\left(C=C, 2sp^3\right)$ (Eq. (14.247)), the energy change of each $C2sp^3$ shell with the formation of the $C=C$-bond MO is given by the difference between $E\left(C_{ethylene}, 2sp^3\right)$ and $E\left(C, 2sp^3\right)$.

Consider the case where three sets of $C=C$-bond MOs form bonds between the two carbon atoms of each molecule to form a six-member ring such that the six resulting bonds comprise eighteen paired electrons. Each bond comprises a linear combination of two MOs wherein each comprises two $C2sp^3$ HOs and 75% of a H_2-type ellipsoidal MO divided between the $C2sp^3$ HOs:

$$\begin{pmatrix} 3\left(2\ C2sp^3 + 0.75\ H_2\ MO\right) \rightarrow 3\left(C \overset{4e}{=} C\right) - ethylene-type-bond\ MO \\ \rightarrow 6\left(C \overset{3e}{=} C\right) - bond\ MO\ of\ benzene \end{pmatrix} \tag{14.416}$$

The linear combination of each H_2-type ellipsoidal MO with each $C2sp^3$ HO further comprises an excess 25% charge-density contribution per bond from each $C2sp^3$ HO to the $C=C$-bond MO to achieve an energy minimum. Thus, the dimensional parameters of each bond $C=C$-bond are determined using the same equations as those used to determine the same parameters of the $C=C$-bond MO of ethylene (Eqs. (14.242-14.268)) while matching the boundary conditions of the structure of benzene. The energies of each $C=C$ bond of benzene are also determined using the same equations as those of ethylene with the parameters of benzene. The result is that the energies are essentially given as 0.75 times the energies of the $C=C$-bond MO of ethylene (Eqs. (14.251-14.253) and (14.319-14.333)).

The derivation of the dimensional parameters of benzene follows the same procedure as the determination of those of ethylene. As in the case of ethylene, each H_2-type ellipsoidal MO comprises 75% of the $C=C$-bond MO shared between two $C2sp^3$ HOs corresponding to the electron charge density in Eq. (11.65) of $\frac{-0.75e}{2}$. But, the additional 25% charge-density contribution to each bond of the $C=C$-bond MO causes the electron charge density in Eq. (11.65) to be $\frac{-e}{2} = -0.5e$. The corresponding force constant k' is given by Eq. (14.152). In addition, the energy matching at all six $C2sp^3$ HOs further requires that k' be corrected by a hybridization factor (Eq. (13.430)) as in the case of ethylene, expect that the constraint that the bonds connect a six-member ring of $C=C$ bonds of benzene rather two $C2sp^3$ HOs of ethylene decreases the hybridization factor of benzene compared to that of ethylene (Eq. (14.248)).

Since the energy of each H_2-type ellipsoidal MO is matched to that of all the continuously connected $C_{benzene}2sp^3$ HOs, the hybridization-energy-matching factor is 0.85252. Hybridization with 25% electron donation to each $C=C$-bond gives rise to the $C_{benzene}2sp^3$ HO-shell Coulombic energy $E_{Coulomb}\left(C_{benzene},2sp^3\right)$ given by Eq. (14.245). The corresponding hybridization factor is given by the ratio of $15.95955\ eV$, the magnitude of $E_{Coulomb}\left(C_{benzene},2sp^3\right)$ given by Eq. (14.245), and $13.605804\ eV$, the magnitude of the Coulombic energy between the electron and proton of H given by Eq. (1.264). The hybridization energy factor $C_{benzeneC2sp^3HO}$ is:

$$C_{benzeneC2sp^3HO}=\frac{\frac{e^2}{8\pi\varepsilon_0 a_0}}{\frac{e^2}{8\pi\varepsilon_0 r_{benzene2sp^3}}}=\frac{\frac{e^2}{8\pi\varepsilon_0 a_0}}{\frac{e^2}{8\pi\varepsilon_0 0.85252a_0}}=\frac{13.605804\ eV}{15.95955\ eV}=0.85252 \tag{14.417}$$

Thus, the force constant k' to determine the ellipsoidal parameter c' in terms of the central force of the foci (Eq. (11.65)) is given by:

$$k'=C_{benzeneC2sp^3HO}\frac{(0.5)2e^2}{4\pi\varepsilon_0}=0.85252\frac{(0.5)2e^2}{4\pi\varepsilon_0} \tag{14.418}$$

The distance from the origin to each focus c' is given by substitution of Eq. (14.418) into Eq. (13.60). Thus, the distance from the origin of the component of the double $C=C$-bond MO to each focus c' is given by

$$c'=a\sqrt{\frac{\hbar^2 4\pi\varepsilon_0}{(0.85252)m_e e^2 a}}=\sqrt{\frac{aa_0}{0.85252}} \tag{14.419}$$

The internuclear distance from Eq. (14.419) is:

$$2c'=2\sqrt{\frac{aa_0}{0.85252}} \tag{14.420}$$

The length of the semiminor axis of the prolate spheroidal $C=C$-bond MO $b=c$ is given by Eq. (13.62). The eccentricity, e, is given by Eq. (13.63). The solution of the semimajor axis a then allows for the solution of the other axes of each prolate spheroid and eccentricity of the $C=C$-bond MO. From the energy equation and the relationship between the axes, the dimensions of the $C=C$-bond MO are solved.

The general equations for the energy components of V_e, V_p, T, V_m, and E_T of the $C=C$-bond MO of benzene are the same as those of the CH_2CH_2 MO except that energy of the $C_{benzene}2sp^3$ HO is used and the hybridization factor is given by Eq. (14.417). Using Eqs. (14.251) and (14.417), $E_T\left(C=C,\sigma\right)$ is given by:

$$E_T\left(C=C,\sigma\right)=E_T+E\left(C_{benzene},2sp^3\right)-E\left(C_{benzene},2sp^3\right)=-\frac{2e^2}{8\pi\varepsilon_0 c'}\left[(0.85252)\left(2-\frac{1}{2}\frac{a_0}{a}\right)\ln\frac{a+c'}{a-c'}-1\right] \tag{14.421}$$

The total energy term of the double $C=C$-bond MO is given by the sum of the two H_2-type ellipsoidal MOs given by Eq. (11.212). To match this boundary condition, $E_T\left(C=C,\sigma\right)$ given by Eq. (14.421) is set equal to two times Eq. (13.75):

$$E_T\left(C=C,\sigma\right)=-\frac{2e^2}{8\pi\varepsilon_0 c'}\left[(0.85252)\left(2-\frac{1}{2}\frac{a_0}{a}\right)\ln\frac{a+c'}{a-c'}-1\right]=-63.27074\ eV \tag{14.422}$$

From the energy relationship given by Eq. (14.422) and the relationship between the axes given by Eqs. (14.419-14.420) and (13.62-13.63), the dimensions of the $C=C$-bond MO can be solved.

Substitution of Eq. (14.419) into Eq. (14.422) gives:

$$\frac{2e^2}{8\pi\varepsilon_0\sqrt{\frac{aa_0}{0.85252}}}\left[(0.85252)\left(2-\frac{1}{2}\frac{a_0}{a}\right)\ln\frac{a+\sqrt{\frac{aa_0}{0.85252}}}{a-\sqrt{\frac{aa_0}{0.85252}}}-1\right]=e63.27074 \tag{14.423}$$

The most convenient way to solve Eq. (14.423) is by the reiterative technique using a computer. The result to within the round-off error with five-significant figures is:

$$a=1.47348a_0=7.79733\ X\ 10^{-11}\ m \tag{14.424}$$

Substitution of Eq. (14.424) into Eq. (14.4129) gives:

$$c'=1.31468a_0=6.95699\ X\ 10^{-11}\ m \tag{14.425}$$

The internuclear distance given by multiplying Eq. (14.425) by two is:

$$2c'=2.62936a_0=1.39140\ X\ 10^{-10}\ m \tag{14.426}$$

The experimental bond distance is [3] :

$$2c' = 1.339\ X\ 10^{-10}\ m \tag{14.427}$$

Substitution of Eqs. (14.424-14.425) into Eq. (13.62) gives:

$$b = c = 0.66540a_0 = 3.52116\ X\ 10^{-11}\ m \tag{14.428}$$

Substitution of Eqs. (14.424-14.425) into Eq. (13.63) gives:

$$e = 0.89223 \tag{14.429}$$

The nucleus of the C atoms comprise the foci of the H_2-type ellipsoidal MO. The parameters of the point of intersection of the H_2-type ellipsoidal MO and the $C_{benzene}2sp^3$ HO are given by Eqs. (13.84-13.95) and (13.261-13.270). Each benzene carbon atom contributes $(0.75)(-1.13380\ eV) = -0.85035\ eV$ (Eqs. (14.483) and (14.493)) to each of the two $C \overset{3e}{=} C$-bond MOs and $(0.5)(-1.13380\ eV) = -0.56690\ eV$ (Eq. (14.467)) to the corresponding $C-H$-bond MO. The energy contribution due to the charge donation at each carbon superimposes linearly. The radius of $r_{benzene2sp^3} = 0.79597a_0$ is calculated using Eq. (14.518) using the total energy donation to each bond with which it is participates in bonding. The polar intersection angle θ' is given by Eq. (13.261) where $r_n = r_{benzene2sp^3} = 0.79597a_0$ is the radius of the $C_{benzene}2sp^3$ shell. Substitution of Eqs. (14.424-14.425) into Eq. (13.261) gives:

$$\theta' = 134.24° \tag{14.430}$$

Then, the angle $\theta_{C=C_{benzene}2sp^3HO}$ the radial vector of the $C2sp^3$ HO makes with the internuclear axis is:

$$\theta_{C=C_{benzene}2sp^3HO} = 180° - 134.24° = 45.76° \tag{14.431}$$

as shown in Figure 14.13.

Figure 14.13. The cross section of one $C=C$-bond MO (σ MO) and one $C-H$-bond MO of benzene showing the axes, angles, and point of intersection of each H_2-type ellipsoidal MO with the corresponding $C_{benzene}2sp^3$ HO. The continuation of each H_2-type-ellipsoidal-MO basis element of the $C=C$ bond and the $C-H$-bond beyond the intersection point with each $C_{benzene}2sp^3$ shell and σ MO is shown as dashed since each only serves to solve the energy match with the $C_{benzene}2sp^3$ shell and does not represent charge density. Similarly, the vertical dashed line only designates the parameters of each intersection point. The actual charge density is shown by the solid lines. Legend: a: semimajor axis, b: semiminor axis, c': internuclear distance, $d_1 : d_{C=C_{benzene},H_2MO}$, $\theta_1 : \theta_{C=C_{benzene}2sp^3HO}$, $d_2 : d_{C=C_{benzene}2sp^3HO}$, $R : r_{benzeneC2sp^3}$, $d_3 : d_{C-H_{benzene},H_2MO}$, $\theta_2 : \theta_{C-H_{benzene}2sp^3HO}$, and $d_4 : d_{C-H_{benzene}2sp^3HO}$.

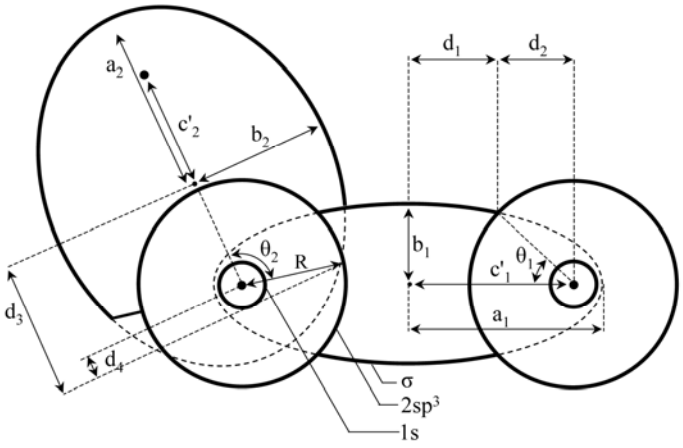

Consider the right-hand intersection point. The Cartesian **i**-coordinate of the interception point of the MO and the AO can be calculated using the MO ellipsoidal parameters by first calculating the parametric angle in Eq. (11.83) that matches Cartesian **j**-coordinate components at the point of intersection. Thus, the matching elliptic parametric angle $\omega t = \theta_{C=C_{benzene},H_2MO}$ satisfies the following relationship:

$$r_{benzene2sp^3} \sin\theta_{C=C_{benzene}2sp^3HO} = 0.79597a_0 \sin\theta_{C=C_{benzene}2sp^3HO} = b\sin\theta_{C=C_{benzene},H_2MO} \tag{14.432}$$

such that

$$\theta_{C=C_{benzene},H_2MO} = \sin^{-1}\frac{0.79597a_0 \sin\theta_{C=C_{benzene}2sp^3HO}}{b} = \sin^{-1}\frac{0.79597a_0 \sin 45.76°}{b} \tag{14.433}$$

with the use of Eq. (14.431). Substitution of Eq. (14.428) into Eq. (14.433) gives:

$$\theta_{C=C_{benzene},H_2MO} = 58.98° \tag{14.434}$$

Then, the distance $d_{C=C_{benzene},H_2MO}$ along the internuclear axis from the origin of H_2-type ellipsoidal MO to the point of intersection of the orbitals is given by:

$$d_{C=C_{benzene},H_2MO} = a\cos\theta_{C=C_{benzene},H_2MO} \tag{14.435}$$

Substitution of Eqs. (14.424) and (14.434) into Eq. (14.435) gives:

$$d_{C=C_{benzene},H_2MO} = 0.75935a_0 = 4.01829\ X\ 10^{-11}\ m \tag{14.436}$$

The distance $d_{C=C_{benzene}2sp^3HO}$ along the internuclear axis from the origin of the C atom to the point of intersection of the orbitals is given by

$$d_{C=C_{benzene}2sp^3HO} = c' - d_{C=C_{benzene},H_2MO} \tag{14.437}$$

Substitution of Eqs. (14.425) and (14.436) into Eq. (14.437) gives:

$$d_{C=C_{benzene}2sp^3HO} = 0.55533a_0 = 2.93870\ X\ 10^{-11}\ m \tag{14.438}$$

FORCE BALANCE OF THE CH MOS OF BENZENE

Benzene can also be considered as comprising chemical bonds between six CH radicals wherein each radical comprises a chemical bond between carbon and hydrogen atoms. The solution of the parameters of CH is given in the Hydrogen Carbide (CH) section. Each $C-H$ bond of CH having two spin-paired electrons, one from an initially unpaired electron of the carbon atom and the other from the hydrogen atom, comprises the linear combination of 75% H_2-type ellipsoidal MO and 25% $C2sp^3$ HO as given by Eq. (13.439):

$$1\ C2sp^3 + 0.75\ H_2\ MO \rightarrow CH\ MO \tag{14.439}$$

The proton of the H atom and the nucleus of the C atom are along each internuclear axis and serve as the foci. As in the case of H_2, the $C-H$-bond MO is a prolate spheroid with the exception that the ellipsoidal MO surface cannot extend into $C2sp^3$ HO for distances shorter than the radius of the $C2sp^3$ shell since it is energetically unfavorable. Thus, each MO surface comprises a prolate spheroid at the H proton that is continuous with the $C2sp^3$ shell at the C atom whose nucleus serves as the other focus.

The force balance of the CH MO is determined by the boundary conditions that arise from the linear combination of orbitals according to Eq. (14.439) and the energy matching condition between the hydrogen and $C2sp^3$ HO components of the MO. The force constant k' to determine the ellipsoidal parameter c' of each H_2-type-ellipsoidal-MO component of the CH MO in terms of the central force of the foci is given by Eq. (13.59). The distance from the origin of each $C-H$-bond MO to each focus c' is given by Eq. (13.60). The internuclear distance is given by Eq. (13.61). The length of the semiminor axis of the prolate spheroidal $C-H$-bond MO $b=c$ is given by Eq. (13.62). The eccentricity, e, is given by Eq. (13.63). The solution of the semimajor axis a then allows for the solution of the other axes of each prolate spheroid and eccentricity of each $C-H$-bond MO. From the energy equation and the relationship between the axes, the dimensions of the CH MO are solved.

Consider the formation of the double $C=C$-bond MOs of benzene wherein ethylene formed from two CH_2 radicals, each having a $C2sp^3$ shell with an energy given by Eq. (14.146), serves as a basis element. The energy components of V_e, V_p, T, V_m, and E_T are the same as those of the hydrogen carbide radical, except that $E_T\left(C=C,2sp^3\right)$ is subtracted from $E_T\left(CH\right)$ of Eq. (13.495). As in the case of the CH_2 groups of ethylene (Eq. (14.270)), the subtraction of the energy change of the $C2sp^3$ shell per H with the formation of the $C=C$-bond MO matches the energy of each $C-H$-bond MO to the decrease in the energy of the corresponding $C2sp^3$ HO. Using Eqs. (13.431) and (14.247), $E_{T_{benzene}}\left(CH\right)$ is given by:

$$E_{T_{benzene}}\left(CH\right) = E_T + E\left(C,2sp^3\right) - E_T\left(C=C,2sp^3\right) = \begin{pmatrix} -\frac{e^2}{8\pi\varepsilon_0 c'}\left[\left(0.91771\right)\left(2-\frac{1}{2}\frac{a_0}{a}\right)\ln\frac{a+c'}{a-c'}-1\right] \\ -14.63489\ eV-\left(-1.13379\ eV\right)\end{pmatrix} \tag{14.440}$$

$E_{T_{benzene}}\left(CH\right)$ given by Eq. (14.440) is set equal to the energy of the H_2-type ellipsoidal MO given by Eq. (13.75).

$$E_{T_{benzene}}\left(CH\right) = \begin{pmatrix} -\frac{e^2}{8\pi\varepsilon_0 c'}\left[\left(0.91771\right)\left(2-\frac{1}{2}\frac{a_0}{a}\right)\ln\frac{a+c'}{a-c'}-1\right] \\ -14.63489\ eV-\left(-1.13379\ eV\right)\end{pmatrix} = -31.63537\ eV \tag{14.441}$$

From the energy relationship given by Eq. (14.441) and the relationship between the axes given by Eqs. (13.60-13.63), the dimensions of the CH MO can be solved.

Substitution of Eq. (13.60) into Eq. (14.441) gives:

$$\frac{e^2}{8\pi\varepsilon_0\sqrt{\frac{2aa_0}{3}}}\left[(0.91771)\left(2-\frac{1}{2}\frac{a_0}{a}\right)\ln\frac{a+\sqrt{\frac{2aa_0}{3}}}{a-\sqrt{\frac{2aa_0}{3}}}-1\right]=e18.13427 \tag{14.442}$$

The most convenient way to solve Eq. (14.442) is by the reiterative technique using a computer. The result to within the round-off error with five-significant figures is

$$a=1.60061a_0=8.47006\ X\ 10^{-11}\ m \tag{14.443}$$

Substitution of Eq. (14.443) into Eq. (14.60) gives:

$$c'=1.03299a_0=5.46636\ X\ 10^{-11}\ m \tag{14.444}$$

The internuclear distance given by multiplying Eq. (14.444) by two is:

$$2c'=2.06598a_0=1.09327\ X\ 10^{-10}\ m \tag{14.445}$$

The experimental bond distance is [3]:

$$2c'=1.101\ X\ 10^{-10}\ m \tag{14.446}$$

Substitution of Eqs. (14.443-14.444) into Eq. (14.62) gives:

$$b=c=1.22265a_0=6.47000\ X\ 10^{-11}\ m \tag{14.447}$$

Substitution of Eqs. (14.443-14.444) into Eq. (14.63) gives:

$$e=0.64537 \tag{14.448}$$

The nucleus of the H atom and the nucleus of the C atom comprise the foci of each H_2-type ellipsoidal MO. The parameters of the point of intersection of the H_2-type ellipsoidal MO and the $C_{benzene}2sp^3$ HO are given by Eqs. (13.84-13.95) and (13.261-13.270). The polar intersection angle θ' is given by Eq. (13.261) where $r_n=r_{benzene2sp^3}=0.79597a_0$ is the radius of the $C_{benzene}2sp^3$ shell. Substitution of Eqs. (14.443-14.444) into Eq. (13.261) gives:

$$\theta'=74.42° \tag{14.449}$$

Then, the angle $\theta_{C-H_{benzene}2sp^3HO}$ the radial vector of the $C2sp^3$ HO makes with the internuclear axis is:

$$\theta_{C-H_{benzene}2sp^3HO}=180°-74.42°=105.58° \tag{14.450}$$

as shown in Figure 14.14.

Figure 14.14. The cross section of one $C-H$-bond MO of benzene showing the axes, angles, and point of intersection of the H_2-type ellipsoidal MO with the $C_{benzene}2sp^3$ HO. The continuation of the H_2-type-ellipsoidal-MO basis element beyond the intersection point with the $C_{benzene}2sp^3$ shell is shown as dashed since it only serves to solve the energy match with the $C_{benzene}2sp^3$ shell and does not represent charge density. Similarly, the vertical dashed line only designates the parameters of the intersection point. The actual charge density is shown by the solid lines. Legend: a: semimajor axis, b: semiminor axis, c': internuclear distance, $d_1:d_{C-H_{benzene},H_2MO}$, $\theta_1:\theta_{C-H_{benzene}2sp^3HO}$, $d_2:d_{C-H_{benzene}2sp^3HO}$, and $R:r_{benzene2sp^3}$

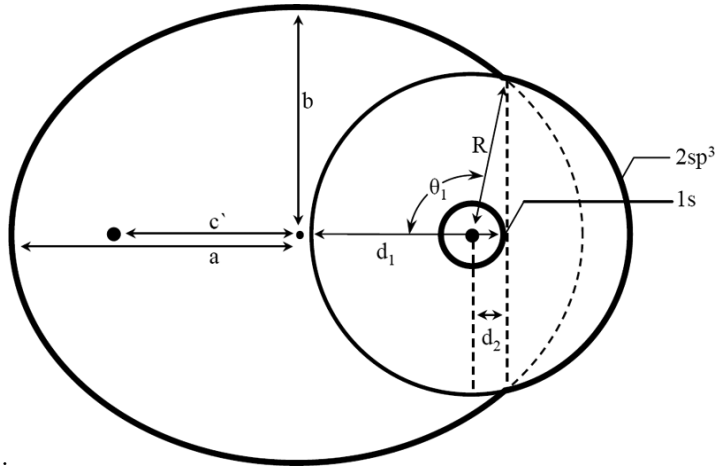

The Cartesian $\mathbf{i}$-coordinate of the interception point of the MO and the AO can be calculated using the MO ellipsoidal parameters by first calculating the parametric angle in Eq. (11.83) that matches Cartesian $\mathbf{j}$-coordinate components at the point of intersection. Thus, the matching elliptic parametric angle $\omega t = \theta_{C-H_{benzene},H_2MO}$ satisfies the following relationship:

$$r_{benzene\,2sp^3} \sin\theta_{C-H_{benzene}\,2sp^3HO} = 0.79597a_0 \sin\theta_{C-H_{benzene}\,2sp^3HO} = b\sin\theta_{C-H_{benzene},H_2MO} \tag{14.451}$$

such that

$$\theta_{C-H_{benzene},H_2MO} = \sin^{-1}\frac{0.79597a_0 \sin\theta_{C-H_{benzene}\,2sp^3HO}}{b} = \sin^{-1}\frac{0.79597a_0 \sin 105.58°}{b} \tag{14.452}$$

with the use of Eq. (14.450). Substitution of Eq. (14.447) into Eq. (14.452) gives:

$$\theta_{C-H_{benzene},H_2MO} = 38.84° \tag{14.453}$$

Then, the distance $d_{C-H_{benzene},H_2MO}$ along the internuclear axis from the origin of H_2-type ellipsoidal MO to the point of intersection of the orbitals is given by:

$$d_{C-H_{benzene},H_2MO} = a\cos\theta_{C-H_{benzene},H_2MO} \tag{14.454}$$

Substitution of Eqs. (14.443) and (14.453) into Eq. (14.454) gives:

$$d_{C-H_{benzene},H_2MO} = 1.24678a_0 = 6.59767\ X\ 10^{-11}\ m \tag{14.455}$$

The distance $d_{C-H_{benzene}\,2sp^3HO}$ along the internuclear axis from the origin of the C atom to the point of intersection of the orbitals is given by:

$$d_{C-H_{benzene}\,2sp^3HO} = d_{C-H_{benzene},H_2MO} - c' \tag{14.456}$$

Substitution of Eqs. (14.444) and (14.455) into Eq. (14.456) gives:

$$d_{C-H_{benzene}\,2sp^3HO} = 0.21379a_0 = 1.13131\ X\ 10^{-11}\ m \tag{14.457}$$

The basis set of benzene, the ethylene molecule, is planar with bond angles of approximately 120° (Eqs. (14.298-14.302)). To form a closed ring of equivalent planar bonds, the $C=C$ bonds of benzene form a planar hexagon. The bond angle $\theta_{C=C=C}$ between the internuclear axis of any two adjacent $C=C$ bonds is:

$$\theta_{C=C=C} = 120° \tag{14.458}$$

The bond angle $\theta_{C=C-H}$ between the internuclear axis of each $C=C$ bond and the corresponding H atom of each CH group is

$$\theta_{C=C-H} = 120° \tag{14.459}$$

The experimental angle between the $C=C=C$ bonds is [13-15]:

$$\theta_{C=C=C} = 120° \tag{14.460}$$

The experimental angle between the $C=C-H$ bonds is [13-15]:

$$\theta_{C=C-H} = 120° \tag{14.461}$$

The C_6H_6 MO shown in Figure 14.15 was rendered using these parameters.

The charge-density in the $C=C$-bond MO is increased by a factor of 0.25 per bond with the formation of the $C_{benzene}\,2sp^3$ HOs each having a smaller radius. Using the orbital composition of the CH groups (Eq. (14.439)) and the $C=C$-bond MO (Eq. (14.416)), the radii of $C1s = 0.17113a_0$ (Eq. (10.51)) and $C_{benzene}\,2sp^3 = 0.79597a_0$ (Eq. (14.520)) shells, and the parameters of the $C=C$-bond (Eqs. (13.3-13.4), (14.424-14.426), and (14.428-14.438)), the parameters of the $C-H$-bond MOs (Eqs. (13.3-13.4), (14.443-14.445), and (14.447-14.457)), and the bond-angle parameters (Eqs. (14.458-14.459)), the charge-density of the C_6H_6 MO comprising the linear combination of six sets of $C-H$-bond MOs with bridging $C\overset{3e}{=}C$-bond MOs is shown in Figure 14.15. Each $C-H$-bond MO comprises a H_2-type ellipsoidal MO and a $C_{benzene}\,2sp^3$ HO having the dimensional diagram shown in Figure 14.14. The $C=C$-bond MO comprises a H_2-type ellipsoidal MO bridging two sets of two $C_{benzene}\,2sp^3$ HOs having the dimensional diagram shown in Figure 14.13.

Figure 14.15. C_6H_6 MO comprising the linear combination of six sets of $C-H$ -bond MOs bridged by $C=C$ -bond MOs. (A) Color scale, translucent view of the charge-density of the C_6H_6 -bond MO with each $C_{benzene}2sp^3$ HOs shown transparently. Each $C=C$ -bond MO comprises a H_2 -type ellipsoidal MO bridging two pairs of $C_{benzene}2sp^3$ HOs. For each $C-H$ and $C=C$ bond, the ellipsoidal surface of the H_2 -type ellipsoidal MO that transitions to the $C_{benzene}2sp^3$ HO, the $C_{benzene}2sp^3$ HO shell, inner most $C1s$ shell, and the nuclei (red, not to scale), are shown. (B)-(D) End-on view, translucent view high-lighting each $C=C$ -bond MO, and opaque view of the charge-density of the C_6H_6 MO, respectively.

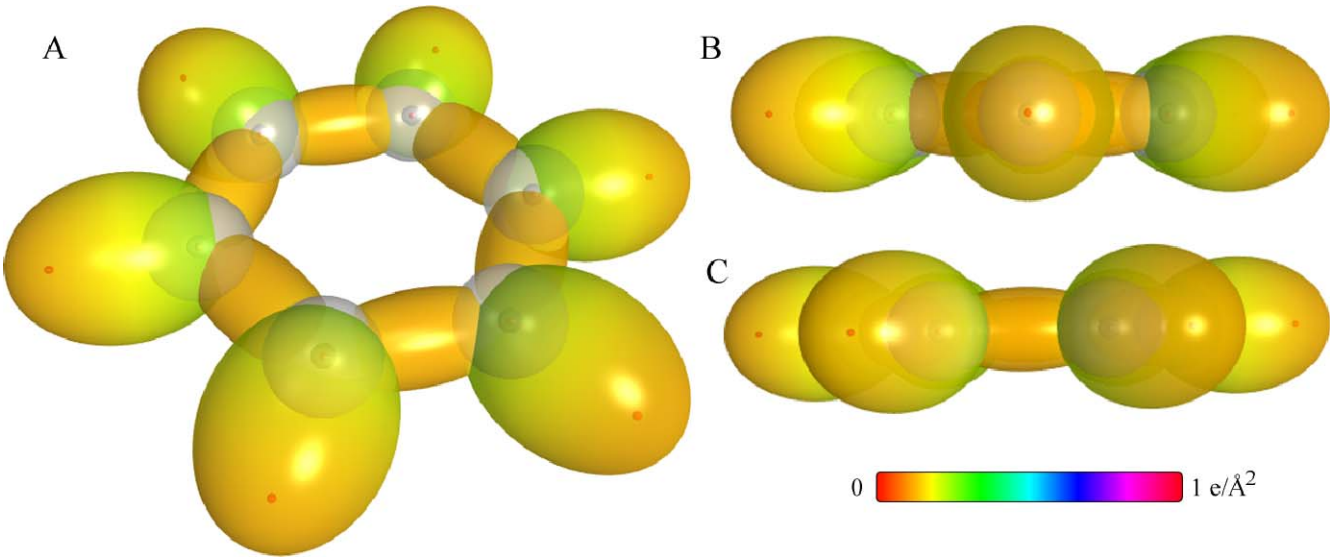

ENERGIES OF THE *CH* GROUPS

The energies of each CH group of benzene are given by the substitution of the semiprincipal axes (Eqs. (14.443-14.444) and (14.447)) into the energy equations of hydrogen carbide (Eqs. (13.449-13.453)), with the exception that $E_T\left(C=C,2sp^3\right)$ (Eq. (14.247)) is subtracted from $E_T\left(CH\right)$ in Eq. (13.453).

$$V_e=\left(0.91771\right)\frac{-2e^2}{8\pi\varepsilon_0\sqrt{a^2-b^2}}\ln\frac{a+\sqrt{a^2-b^2}}{a-\sqrt{a^2-b^2}}=-37.10024\ eV \tag{14.462}$$

$$V_p=\frac{e^2}{8\pi\varepsilon_0\sqrt{a^2-b^2}}=13.17125\ eV \tag{14.463}$$

$$T=\left(0.91771\right)\frac{\hbar^2}{2m_e a\sqrt{a^2-b^2}}\ln\frac{a+\sqrt{a^2-b^2}}{a-\sqrt{a^2-b^2}}=11.58941\ eV \tag{14.464}$$

$$V_m=\left(0.91771\right)\frac{-\hbar^2}{4m_e a\sqrt{a^2-b^2}}\ln\frac{a+\sqrt{a^2-b^2}}{a-\sqrt{a^2-b^2}}=-5.79470\ eV \tag{14.465}$$

$$E_{T_{benzene}}\left(CH\right)=\begin{pmatrix}-\frac{e^2}{8\pi\varepsilon_0 c'}\left[\left(0.91771\right)\left(2-\frac{1}{2}\frac{a_0}{a}\right)\ln\frac{a+c'}{a-c'}-1\right]\\ -14.63489\ eV-\left(-1.13379\ eV\right)\end{pmatrix}=-31.63539\ eV \tag{14.466}$$

where $E_{T_{benzene}}\left(CH\right)$ is given by Eq. (14.440) which is reiteratively matched to Eq. (13.75) within five-significant-figure round off error.

The total energy of the $C-H$ -bond MO, $E_{T_{benzene}}\left(C-H\right)$, is given by the sum of $0.5E_T\left(C=C,2sp^3\right)$, the energy change of each $C2sp^3$ shell per single bond due to the decrease in radius with the formation of the corresponding $C=C$ -bond MO (Eq. (14.247)), and $E_{T_{benzene}}\left(CH\right)$, the σ MO contribution given by Eq. (14.441).

$$\begin{aligned} E_{T_{benzene}}(C-H) &= (0.5)E_T\left(C=C,2sp^3\right)+E_{T_{benzene}}(CH) \\ &= \left(\begin{array}{l}(0.5)(-1.13379\ eV)+ \\ \left(-\frac{e^2}{8\pi\varepsilon_0 c'}\left[(0.91771)\left(2-\frac{1}{2}\frac{a_0}{a}\right)\ln\frac{a+c'}{a-c'}-1\right]\right) \\ -14.63489\ eV-(-1.13379\ eV)\end{array}\right) \\ &= (0.5)(-1.13379\ eV)+(-31.63537\ eV) \\ &= -32.20226\ eV \end{aligned} \tag{14.467}$$

VIBRATION OF THE ^{12}CH GROUPS

The vibrational energy levels of CH in benzene may be solved using the methods given in the Vibration and Rotation of CH section.

THE DOPPLER ENERGY TERMS OF THE ^{12}CH GROUPS

The equations of the radiation reaction force of the CH groups in benzene are the same as those of the hydrogen carbide radical with the substitution of the CH -group parameters. Using Eq. (13.477), the angular frequency of the reentrant oscillation in the transition state is

$$\omega = \sqrt{\frac{0.75e^2}{4\pi\varepsilon_0 b^3}} = 2.64826\ X\ 10^{16}\ rad/s \tag{14.468}$$

where b is given by Eq. (14.447). The kinetic energy, E_K, is given by Planck's equation (Eq. (11.127)).

$$\bar{E}_K = \hbar\omega = \hbar 2.64826\ X\ 10^{16}\ rad/s = 17.43132\ eV \tag{14.469}$$

In Eq. (11.181), substitution of $E_T(H_2)$ (Eqs. (11.212) and (13.75)), the maximum total energy of each H_2-type MO, for $E_{h\nu}$, the mass of the electron, m_e, for M, and the kinetic energy given by Eq. (14.469) for $\bar{E}_K$ gives the Doppler energy of the electrons for the reentrant orbit:

$$\bar{E}_D \cong E_{h\nu}\sqrt{\frac{2\bar{E}_K}{Mc^2}} = -31.63537\ eV\sqrt{\frac{2e(17.43132\ eV)}{m_e c^2}} = -0.26130\ eV \tag{14.470}$$

In addition to the electrons, the nuclei also undergo simple harmonic oscillation in the transition state at their corresponding frequency. The decrease in the energy of CH due to the reentrant orbit of each bond in the transition state corresponding to simple harmonic oscillation of the electrons and nuclei, $\bar{E}_{osc}$, is given by the sum of the corresponding energies, $\bar{E}_D$ given by Eq. (14.470) and $\bar{E}_{Kvib}$, the average kinetic energy of vibration which is 1/2 of the vibrational energy of the $C-H$ bond. Using ω_e given by Eq. (13.458) for $\bar{E}_{Kvib}$ of the transition, $\bar{E}_{benzene\ osc}(^{12}CH)$ per bond is:

$$\bar{E}_{benzene\ osc}(^{12}CH) = \bar{E}_D + \bar{E}_{Kvib} = \bar{E}_D + \frac{1}{2}\hbar\sqrt{\frac{k}{\mu}} \tag{14.471}$$

$$\bar{E}_{benzene\ osc}(^{12}CH) = -0.26130\ eV + \frac{1}{2}(0.35532\ eV) = -0.08364\ eV \tag{14.472}$$

TOTAL AND BOND ENERGIES OF THE ^{12}CH GROUPS

$E_{benzeneT+osc}(^{12}CH)$, the total energy of each ^{12}CH group including the Doppler term, is given by the sum of $E_{T_{benzene}}(C-H)$ (Eq. (14.467)) and $\bar{E}_{benzene\ osc}(^{12}CH)$ given by Eq. (14.472).

$$\begin{aligned} E_{benzeneT+osc}(^{12}CH) &= \left(\begin{array}{l}\left(V_e+T+V_m+V_p+E\left(C,2sp^3\right)-E_T\left(C=C,2sp^3\right)\right) \\ +0.5E_T\left(C=C,2sp^3\right)+\bar{E}_{benzene\ osc}(^{12}CH)\end{array}\right) \\ &= E_{T_{benzene}}(C-H)+\bar{E}_{benzene\ osc}(^{12}CH) \end{aligned} \tag{14.473}$$

$$E_{benzeneT+osc}\left({}^{12}CH\right)=\left\{\begin{array}{l}\left(\begin{array}{l}\dfrac{-e^2}{8\pi\varepsilon_0 c'}\left[(0.91771)\left(2-\dfrac{1}{2}\dfrac{a_0}{a}\right)\ln\dfrac{a+c'}{a-c'}-1\right]\\ -14.63489\ eV-(-1.13379\ eV)\end{array}\right)-0.5(1.13379\ eV)\\ -\left((31.63536831\ eV)\sqrt{\dfrac{2\hbar\sqrt{\dfrac{3}{4}\dfrac{e^2}{4\pi\varepsilon_0 b^3}}}{m_e c^2}}-\dfrac{1}{2}\hbar\sqrt{\dfrac{k}{\mu}}\right)\end{array}\right\}$$
$$=-32.20226\ eV-\left(0.26130\ eV-\frac{1}{2}\hbar\sqrt{\frac{k}{\mu}}\right) \tag{14.474}$$

From Eqs. (14.472-14.474), the total energy of each ${}^{12}CH$ is:

$$\begin{aligned}E_{benzeneT+osc}\left({}^{12}CH\right)&=-32.20226\ eV+\bar{E}_{benzene\ osc}\left({}^{12}CH_2\right)\\&=-32.20226\ eV-\left(0.26130\ eV-\frac{1}{2}(0.35532\ eV)\right)\\&=-32.28590\ eV\end{aligned} \tag{14.475}$$

where ω_e given by Eq. (13.458) was used for the $\hbar\sqrt{\dfrac{k}{\mu}}$ term.

As in the case of ${}^{12}CH_2$, ${}^{14}NH$, and acetylene, the dissociation of the $C=C$ bonds forms three unpaired electrons per central atom wherein the magnetic moments cannot all cancel. The energy per atom $E(magnetic)$ is given by Eq. (13.524). Thus, the bond dissociation energy of each CH group of the linear combination to form benzene, $E_{D_{benzene}}\left({}^{12}CH\right)$, is given by the sum of the total energies of the $C2sp^3$ HO and the hydrogen atom minus the sum of $E_{benzeneT+osc}\left({}^{12}CH\right)$ and $E(magnetic)$ given by Eq. (13.524):

$$E_{D_{benzene}}\left({}^{12}CH\right)=E\left(C,2sp^3\right)+E(H)-\left(E_{benzeneT+osc}\left({}^{12}CH\right)+E(magnetic)\right) \tag{14.476}$$

$E\left(C,2sp^3\right)$ is given by Eq. (13.428), $E_D(H)$ is given by Eq. (13.154), and $E(magnetic)$ is given by Eq. (13.524). Thus, $E_{D_{benzene}}\left({}^{12}CH\right)$ given by Eqs. (13.154), (13.428), (13.524), (14.475), and (14.476) is:

$$\begin{aligned}E_{D_{benzene}}\left({}^{12}CH\right)&=-(14.63489\ eV+13.59844\ eV)-\left(E_{benzeneT+osc}(CH)+E(magnetic)\right)\\&=-28.23333\ eV-(-32.28590\ eV+0.14803\ eV)\\&=3.90454\ eV\end{aligned} \tag{14.477}$$

SUM OF THE ENERGIES OF THE $C=C$ σ MO ELEMENT AND THE HOs OF BENZENE

The energy components of V_e, V_p, T, V_m, and E_T of the $C=C$-bond MO of benzene are the same as those of the CH_2CH_2 MO except that the hybridization factor is given by Eq. (14.417). The energies of each $C=C$-bond MO are given by the substitution of the semiprincipal axes (Eqs. (14.424-14.425) and (14.428)) into energy equations of the CH_2CH_2 MO (Eqs. (14.319-14.323)), with the exception that the hybridization factor is 0.85252 (Eq. (14.417)).

$$V_e=2(0.85252)\frac{-2e^2}{8\pi\varepsilon_0\sqrt{a^2-b^2}}\ln\frac{a+\sqrt{a^2-b^2}}{a-\sqrt{a^2-b^2}}=-101.12679\ eV \tag{14.478}$$

$$V_p=2\frac{e^2}{8\pi\varepsilon_0\sqrt{a^2-b^2}}=20.69825\ eV \tag{14.479}$$

$$T=2(0.85252)\frac{\hbar^2}{2m_e a\sqrt{a^2-b^2}}\ln\frac{a+\sqrt{a^2-b^2}}{a-\sqrt{a^2-b^2}}=34.31559\ eV \tag{14.480}$$

$$V_m=2(0.85252)\frac{-\hbar^2}{4m_e a\sqrt{a^2-b^2}}\ln\frac{a+\sqrt{a^2-b^2}}{a-\sqrt{a^2-b^2}}=-17.15779\ eV \tag{14.481}$$

$$E_T(C=C,\sigma)=-\frac{2e^2}{8\pi\varepsilon_0 c'}\left[(0.85252)\left(2-\frac{1}{2}\frac{a_0}{a}\right)\ln\frac{a+c'}{a-c'}-1\right]=-63.27075\ eV \tag{14.482}$$

where $E_T\left(C=C,\sigma\right)$ is the total energy of the $C=C$ σ MO given by Eq. (14.421) which is reiteratively matched to two times Eq. (13.75) within five-significant-figure round off error.

The total energy of the $C=C$-bond MO, $E_T\left(C=C\right)$, is given by the sum of two times $E_T\left(C=C,2sp^3\right)$, the energy change of each $C2sp^3$ shell due to the decrease in radius with the formation of the $C=C$-bond MO (Eq. (14.247)), and $E_T\left(C=C,\sigma\right)$, the σ MO contribution given by Eq. (14.422).

$$\begin{aligned} E_T\left(C=C\right) &= 2E_T\left(C=C,2sp^3\right)+E_T\left(C=C,\sigma\right) \\ &= \left(\begin{array}{l} 2(-1.13380\ eV)+ \\ \left(-\dfrac{2e^2}{8\pi\varepsilon_0 c'}\left[(0.85252)\left(2-\dfrac{1}{2}\dfrac{a_0}{a}\right)\ln\dfrac{a+c'}{a-c'}-1\right]\right) \end{array}\right) \\ &= 2(-1.13380\ eV)+(-63.27074\ eV)=-65.53833\ eV \end{aligned} \tag{14.483}$$

which is the same $E_T\left(C=C,\sigma\right)$ of ethylene given by Eq. (14.324).

VIBRATION OF BENZENE

The $C=C$ vibrational energy levels of C_6H_6 may be solved as six sets of equivalent coupled harmonic oscillators where each C is further coupled to the corresponding $C-H$ oscillator by developing the Lagrangian, the differential equation of motion, and the eigenvalue solutions [9] wherein the spring constants are derived from the central forces as given in the Vibration of Hydrogen-Type Molecular Ions section and the Vibration of Hydrogen-Type Molecules section.

THE DOPPLER ENERGY TERMS OF THE $C=C$-BOND MO ELEMENT OF BENZENE

The equations of the radiation reaction force of the $C=C$-bond MO of benzene are given by Eq. (13.142), except the force-constant factor is $\left(0.85252\right)0.5$ based on the force constant k' of Eq. (14.418), and the $C=C$-bond MO parameters are used. The angular frequency of the reentrant oscillation in the transition state is:

$$\omega=\sqrt{\frac{0.85252\dfrac{(0.5)e^2}{4\pi\varepsilon_0 b^3}}{m_e}}=4.97272\ X\ 10^{16}\ rad/s \tag{14.484}$$

where b is given by Eq. (14.428). The kinetic energy, E_K, is given by Planck's equation (Eq. (11.127)).

$$\bar{E}_K=\hbar\omega=\hbar 4.97272\ X\ 10^{16}\ rad/s=32.73133\ eV \tag{14.485}$$

In Eq. (11.181), substitution of $E_T\left(H_2\right)$ (Eqs. (11.212) and (13.75)), the maximum total energy of each H_2-type MO, for E_{hv}, the mass of the electron, m_e, for M, and the kinetic energy given by Eq. (14.485) for $\bar{E}_K$ gives the Doppler energy of the electrons for the reentrant orbit:

$$\bar{E}_D\cong E_{hv}\sqrt{\frac{2\bar{E}_K}{Mc^2}}=-31.63536831\ eV\sqrt{\frac{2e\left(32.73133\ eV\right)}{m_e c^2}}=-0.35806\ eV \tag{14.486}$$

In addition to the electrons, the nuclei also undergo simple harmonic oscillation in the transition state at their corresponding frequency. The decrease in the energy of the $C=C$-bond MO due to the reentrant orbit of the bond in the transition state corresponding to simple harmonic oscillation of the electrons and nuclei, $\bar{E}_{osc}$, is given by the sum of the corresponding energies, $\bar{E}_D$ given by Eq. (14.486) and $\bar{E}_{Kvib}$, the average kinetic energy of vibration which is 1/2 of the vibrational energy of the $C=C$ bond. Using the experimental $C=C$ $E_{vib}\left(\upsilon_{16}\right)$ of 1584.8 cm^{-1} $\left(0.19649\ eV\right)$ [16] for $\bar{E}_{Kvib}$ of the transition state having two bonds, $\bar{E}'_{osc}\left(C=C,\sigma\right)$ per bond is:

$$\bar{E}'_{osc}\left(C=C,\sigma\right)=\bar{E}_D+\bar{E}_{Kvib}=\bar{E}_D+\frac{1}{2}\hbar\sqrt{\frac{k}{\mu}} \tag{14.487}$$

$$\bar{E}'_{osc}\left(C=C,\sigma\right)=-0.35806\ eV+\frac{1}{2}\left(0.19649\ eV\right)=-0.25982\ eV \tag{14.488}$$

Given that the vibration and reentrant oscillation is for two $C-C$ bonds of each $C=C$ double bond, $\bar{E}_{benzene\ osc}\left(C=C,\sigma\right)$, is:

$$\bar{E}_{benzene\ osc}\left(C=C,\sigma\right)=2\left(\bar{E}_D+\frac{1}{2}\hbar\sqrt{\frac{k}{\mu}}\right)=2\left(-0.35806\ eV+\frac{1}{2}\left(0.19649\ eV\right)\right)=-0.51963\ eV \tag{14.489}$$

TOTAL ENERGIES OF THE $C=C$-BOND MO ELEMENT OF BENZENE

$E_{T+osc}(C=C)$, the total energy of the $C=C$-bond MO of benzene including the Doppler term, is given by the sum of $E_T(C=C)$ (Eq. (14.483)) and $\bar{E}_{benzene\ osc}(C=C,\sigma)$ given by Eq. (14.489).

$$\begin{aligned} E_{T+osc}(C=C) &= V_e + T + V_m + V_p + 2E_T\left(C=C,2sp^3\right) + \bar{E}_{benzene\ osc}(C=C,\sigma) \\ &= E_T(C=C,\sigma) + 2E_T\left(C=C,2sp^3\right) + \bar{E}_{benzene\ osc}(C=C,\sigma) \\ &= E_T(C=C) + \bar{E}_{benzene\ osc}(C=C,\sigma) \end{aligned} \tag{14.490}$$

$$\begin{aligned} E_{T+osc}(C=C) &= \left\{ \begin{array}{l} \left(\dfrac{-2e^2}{8\pi\varepsilon_0 c'} \left[(0.85252)\left(2-\dfrac{1}{2}\dfrac{a_0}{a}\right)\ln\dfrac{a+c'}{a-c'} - 1 \right] + 2E_T\left(C=C,2sp^3\right) \right) \\ -2\left((31.63536831\ eV)\sqrt{\dfrac{2\hbar\sqrt{\dfrac{(0.85252)\dfrac{1}{2}\dfrac{e^2}{4\pi\varepsilon_0 b^3}}{m_e}}}{m_e c^2}} - \dfrac{1}{2}\hbar\sqrt{\dfrac{k}{\mu}} \right) \end{array} \right\} \\ &= -65.53833\ eV - 2\left(0.35806\ eV - \frac{1}{2}\hbar\sqrt{\frac{k}{\mu}} \right) \end{aligned} \tag{14.491}$$

From Eqs. (14.489-14.491), the total energy of the $C=C$-bond MO is:

$$\begin{aligned} E_{T+osc}(C=C) &= -63.27074\ eV + 2E_T\left(C=C,2sp^3\right) + \bar{E}_{benzene\ osc}(C=C,\sigma) \\ &= -63.27074\ eV + 2(-1.13380\ eV) - 2\left(0.35806\ eV - \frac{1}{2}(0.19649\ eV) \right) \\ &= -66.05796\ eV \end{aligned} \tag{14.492}$$

where the experimental E_{vib} was used for the $\hbar\sqrt{\dfrac{k}{\mu}}$ term.

TOTAL BOND DISSOCIATION ENERGY OF BENZENE

Ethylene serves as a basis element for the $C=C$ bonding of benzene wherein each of the six $C\overset{3e}{=}C$ bonds of benzene comprises $(0.75)(4)=3$ electrons according to Eq. (14.416). The total energy of the bonds of the eighteen electrons of the $C\overset{3e}{=}C$ bonds of benzene, $E_T\left(C_6H_6,C\overset{3e}{=}C\right)$, is given by $(6)(0.75)$ times $E_{T+osc}(C=C)$ (Eq. (14.492)), the total energy of the $C=C$-bond MO of benzene including the Doppler term, minus eighteen times $E\left(C,2sp^3\right)$ (Eq. (14.146)), the initial energy of each $C2sp^3$ HO of each C that forms the double $C=C$ bonds. Thus, the total energy of the six $C\overset{3e}{=}C$ bonds of benzene is:

$$\begin{aligned} E_T\left(C_6H_6,C\overset{3e}{=}C\right) &= (6)(0.75)E_{T+osc}(C=C) - 18E\left(C,2sp^3\right) \\ &= (6)(0.75)(-66.05796\ eV) - 18(-14.63489\ eV) \\ &= -297.26081\ eV - (-263.42798\ eV) \\ &= -33.83284\ eV \end{aligned} \tag{14.493}$$

Each of the $C-H$ bonds of benzene comprises two electrons according to Eq. (14.439). From the energy of each $C-H$ bond, $-E_{D_{benzene}}\left({}^{12}CH\right)$ (Eq. (14.477)), the total energy of the twelve electrons of the six $C-H$ bonds of benzene, $E_T\left(C_6H_6,C-H\right)$, is given by:

$$E_T\left(C_6H_6,C-H\right) = (6)\left(-E_{D_{benzene}}\left({}^{12}CH\right)\right) = 6(-3.90454\ eV) = -23.42724\ eV \tag{14.494}$$

The total bond dissociation energy of benzene, $E_D\left(C_6H_6\right)$, is given by the negative sum of $E_T\left(C_6H_6,C\overset{3e}{=}C\right)$ (Eq. (14.493)) and $E_T\left(C_6H_6,C-H\right)$ (Eq. (14.494)):

$$\begin{aligned} E_D\left(C_6H_6\right) &= -\left(E_T\left(C_6H_6,C\overset{3e}{=}C\right) + E_T\left(C_6H_6,C-H\right) \right) \\ &= -\left((-33.83284\ eV) + (-23.42724\ eV) \right) = 57.2601\ eV \end{aligned} \tag{14.495}$$

The experimental total bond dissociation energy of benzene, $E_T\left(C_6H_6\right)$, is given by the negative difference between the enthalpy of its formation ($\Delta H_f\left(benzene\left(gas\right)\right)$) and the sum of the enthalpy of the formation of the gaseous carbons ($\Delta H_f\left(C\left(gas\right)\right)$) and hydrogen ($\Delta H_f\left(H\left(gas\right)\right)$) atoms. The heats of formation are [17-18]:

$$\Delta H_f\left(benzene\left(gas\right)\right)=82.9\ kJ/mole\ \left(0.8592\ eV/molecule\right) \tag{14.496}$$

$$\Delta H_f\left(C\left(gas\right)\right)=716.68\ kJ/mole\ \left(7.42774\ eV/atom\right) \tag{14.497}$$

$$\Delta H_f\left(H\left(gas\right)\right)=217.998\ kJ/mole\ \left(2.259353\ eV/atom\right) \tag{14.498}$$

thus, the total bond dissociation energy of benzene, $E_D\left(C_6H_6\right)$, is:

$$\begin{aligned} E_D\left(C_6H_6\right)-E_T\left(C_6H_6\right) &= -\left(\Delta H_f\left(benzene\left(gas\right)\right)-\left(6\Delta H_f\left(C\left(gas\right)\right)+6\Delta H_f\left(H\left(gas\right)\right)\right)\right) \\ &= -\left(0.8592\ eV-6\left(7.42774\ eV+2.259353\ eV\right)\right) \\ &= 57.26\ eV \end{aligned} \tag{14.499}$$

where $E_T\left(C_6H_6\right)$ is the total energy of the bonds. The results of the determination of bond parameters of C_6H_6 are given in Table 14.1. The calculated results are based on first principles and given in closed-form, exact equations containing fundamental constants only. The agreement between the experimental and calculated results is excellent.

CONTINUOUS-CHAIN ALKANES ($C_nH_{2n+2},\ n=3,4,5...\infty$)

The continuous chain alkanes, C_nH_{2n+2}, are the homologous series comprising terminal methyl groups at each end of the chain with $n-2$ methylene (CH_2) groups in between:

$$CH_3\left(CH_2\right)_{n-2}CH_3 \tag{14.500}$$

C_nH_{2n+2} can be solved using the same principles as those used to solve ethane and ethylene wherein the $2s$ and $2p$ shells of each C hybridize to form a single $2sp^3$ shell as an energy minimum, and the sharing of electrons between two $C2sp^3$ hybridized orbitals (HOs) to form a molecular orbital (MO) permits each participating hybridized orbital to decrease in radius and energy. Three H AOs combine with three carbon $2sp^3$ HOs and two H AOs combine with two carbon $2sp^3$ HOs to form each methyl and methylene group, respectively, where each bond comprises a H_2-type MO developed in the Nature of the Chemical Bond of Hydrogen-Type Molecules and Molecular Ions section. The CH_3 and CH_2 groups bond by forming H_2-type MOs between the remaining $C2sp^3$ HOs on the carbons such that each carbon forms four bonds involving its four $C2sp^3$ HOs.

FORCE BALANCE OF THE $C-C$-BOND MOs OF CONTINUOUS-CHAIN ALKANES

C_nH_{2n+2} comprises a chemical bond between two terminal CH_3 radicals and $n-2$ CH_2 radicals wherein each methyl and methylene radical comprises three and two chemical bonds, respectively, between carbon and hydrogen atoms. The solution of the parameters of CH_3 is given in the Methyl Radical (CH_3) section. The solution of the parameters of CH_2 is given in the Dihydrogen Carbide Radical (CH_2) section and follows the same procedure. Each $C-H$ bond having two spin-paired electrons, one from an initially unpaired electron of the carbon atom and the other from the hydrogen atom, comprises the linear combination of 75% H_2-type ellipsoidal MO and 25% $C2sp^3$ HO as given by Eq. (13.429):

$$1\ C2sp^3+0.75\ H_2\ MO\rightarrow C-H\ MO \tag{14.501}$$

The proton of the H atom and the nucleus of the C atom are along each internuclear axis and serve as the foci. As in the case of H_2, each of the $C-H$-bond MOs is a prolate spheroid with the exception that the ellipsoidal MO surface cannot extend into $C2sp^3$ HO for distances shorter than the radius of the $C2sp^3$ shell since it is energetically unfavorable. Thus, each MO surface comprises a prolate spheroid at the H proton that is continuous with the $C2sp^3$ shell at the C atom whose nucleus serves as the other focus. The electron configuration and the energy, $E\left(C,2sp^3\right)$, of the $C2sp^3$ shell is given by Eqs. (13.422) and (13.428), respectively. The central paramagnetic force due to spin of each $C-H$ bond is provided by the spin-pairing force of the CH_3 or CH_2 MO that has the symmetry of an s orbital that superimposes with the $C2sp^3$ orbitals such that the corresponding angular momenta are unchanged. The energies of each CH_3 and CH_2 MO involve each $C2sp^3$ and each $H1s$ electron with the formation of each $C-H$ bond. The sum of the energies of the H_2-type ellipsoidal MOs is matched to that of the $C2sp^3$ shell.

The force balance of the $C-H$-bond MO is determined by the boundary conditions that arise from the linear combination of orbitals according to Eq. (14.139) and the energy matching condition between the $C2sp^3$-HO components of the MO.

The CH_3 and CH_2 groups form $C-C$ bonds comprising H_2-type MOs between the remaining $C2sp^3$ HOs on the carbons such that each carbon forms four bonds involving its four $C2sp^3$ HOs. The sharing of electrons between any two $C2sp^3$ HOs to form a molecular orbital (MO) comprising two spin-paired electrons permits each $C2sp^3$ HO to decrease in radius and energy. As in the case of the $C-H$ bonds, each $C-C$-bond MO is a prolate-spheroidal-MO surface that cannot extend into $C2sp^3$ HO for distances shorter than the radius of the $C2sp^3$ shell of each atom. Thus, the MO surface comprises a partial prolate spheroid in between the carbon nuclei and is continuous with the $C2sp^3$ shell at each C atom. The energy of the H_2-type ellipsoidal MO is matched to that of the $C2sp^3$ shell. As in the case of previous examples of energy-matched MOs such as the $C-C$-bond MO of ethane, each $C-C$-bond MO of C_nH_{2n+2} must comprise 75% of a H_2-type ellipsoidal MO in order to match potential, kinetic, and orbital energy relationships. Thus, the $C-C$-bond MO must comprise two $C2sp^3$ HOs and 75% of a H_2-type ellipsoidal MO divided between the two $C2sp^3$ HOs:

$$2\ C2sp^3 + 0.75\ H_2\ MO \rightarrow C-C-bond\ MO \tag{14.502}$$

The linear combination of the H_2-type ellipsoidal MO with each $C2sp^3$ HO further comprises an excess 25% charge-density contribution from each $C2sp^3$ HO to the $C-C$-bond MO to achieve an energy minimum. The force balance of the $C-C$-bond MO is determined by the boundary conditions that arise from the linear combination of orbitals according to Eq. (14.502) and the energy matching condition between the $C2sp^3$-HO components of the MO.

Before bonding, the $2sp^3$ hybridized orbital arrangement of each carbon atom is given by Eq. (14.140). The sum $E_T\left(C,2sp^3\right)$ of calculated energies of C, C^+, C^{2+}, and C^{3+} is given by Eq. (14.141). The radius r_{2sp^3} of the $C2sp^3$ shell is given by Eq. (14.142). The Coulombic energy $E_{Coulomb}\left(C,2sp^3\right)$ and the energy $E\left(C,2sp^3\right)$ of the outer electron of the $C2sp^3$ shell are given by Eqs. (14.143) and (14.146), respectively.

The formation of each $C-C$ bond of C_nH_{2n+2} further requires that the energy of all H_2-type prolate spheroidal MOs (σ MOs) be matched at all $C2sp^3$ HOs since they are continuous throughout the molecule. Thus, the energy of each $C2sp^3$ HO must be a linear combination of that of the CH_3 and CH_2 groups that serve as basis elements. Each CH_3 forms one $C-C$ bond, and each CH_2 group forms two. Thus, the energy of each $C2sp^3$ HO of each CH_3 and CH_2 group alone is given by that in ethane and ethylene, respectively. The parameters of ethane and ethylene are given by Eqs. (14.147-14.151) and (14.244-14.247), respectively. The alkane parameters can be determined by first reviewing those of ethane and ethylene.

With the formation of the $C-C$-bond MO of ethane from two methyl radicals, each having a $C2sp^3$ electron with an energy given by Eq. (14.146), the total energy of the state is given by the sum over the four electrons. The sum $E_T\left(C_{ethane},2sp^3\right)$ of calculated energies of $C2sp^3$, C^+, C^{2+}, and C^{3+} given by Eq. (14.147), is:

$$\begin{aligned} E_T\left(C_{ethane},2sp^3\right) &= -\left(64.3921\ eV + 48.3125\ eV + 24.2762\ eV + E\left(C,2sp^3\right)\right) \\ &= -\left(64.3921\ eV + 48.3125\ eV + 24.2762\ eV + 14.63489\ eV\right) \\ &= -151.61569\ eV \end{aligned} \tag{14.503}$$

where $E\left(C,2sp^3\right)$ is the sum of the energy of C, $-11.27671\ eV$, and the hybridization energy. The orbital-angular-momentum interactions also cancel such that the energy of the $E_T\left(C_{ethane},2sp^3\right)$ is purely Coulombic.

The sharing of electrons between two $C2sp^3$ HOs to form a $C-C$-bond MO permits each participating hybridized orbital to decrease in radius and energy. In order to further satisfy the potential, kinetic, and orbital energy relationships, each $C2sp^3$ HO donates an excess of 25% of its electron density to the $C-C$-bond MO to form an energy minimum. By considering this electron redistribution in the ethane molecule as well as the fact that the central field decreases by an integer for each successive electron of the shell, the radius $r_{ethane\,2sp^3}$ of the $C2sp^3$ shell of ethane may be calculated from the Coulombic energy using Eq. (10.102).

$$r_{ethane\,2sp^3} = \left(\sum_{n=2}^{5}(Z-n) - 0.25\right)\frac{e^2}{8\pi\varepsilon_0\left(e151.61569\ eV\right)} = \frac{9.75e^2}{8\pi\varepsilon_0\left(e151.61569\ eV\right)} = 0.87495a_0 \tag{14.504}$$

using Eqs. (10.102) and (14.504), the Coulombic energy $E_{Coulomb}\left(C_{ethane},2sp^3\right)$ of the outer electron of the $C2sp^3$ shell is:

$$E_{Coulomb}\left(C_{ethane},2sp^3\right) = \frac{-e^2}{8\pi\varepsilon_0 r_{ethane\,2sp^3}} = \frac{-e^2}{8\pi\varepsilon_0 0.87495a_0} = -15.55033\ eV \tag{14.505}$$

During hybridization, one of the spin-paired $2s$ electrons is promoted to the $C2sp^3$ shell as an unpaired electron. The energy for the promotion is the magnetic energy given by Eq. (14.145). Using Eqs. (14.145) and (14.505), the energy $E\left(C_{ethane},2sp^3\right)$ of the outer electron of the $C2sp^3$ shell is:

$$E\left(C_{ethane},2sp^3\right)=\frac{-e^2}{8\pi\varepsilon_0 r_{ethane\,2sp^3}}+\frac{2\pi\mu_0 e^2\hbar^2}{m_e^2\left(r_3\right)^3}=-15.55033\ eV+0.19086\ eV=-15.35946\ eV \tag{14.506}$$

thus, $E_T\left(C-C,2sp^3\right)$, the energy change of each $C2sp^3$ shell with the formation of the $C-C$-bond MO is given by the difference between Eq. (14.146) and Eq. (14.506).

$$E_T\left(C-C,2sp^3\right)=E\left(C_{ethane},2sp^3\right)-E\left(C,2sp^3\right)=-15.35946\ eV-\left(-14.63489\ eV\right)=-0.72457\ eV \tag{14.507}$$

Next, consider the formation of the $C=C$-bond MO of ethylene from two CH_2 radicals, each having a $C2sp^3$ electron with an energy given by Eq. (14.146). The sum $E_T\left(C_{ethylene},2sp^3\right)$ of calculated energies of $C2sp^3$, C^+, C^{2+}, and C^{3+} is given by Eq. (14.147). The sharing of electrons between two pairs of $C2sp^3$ HOs to form a $C=C$-bond MO permits each participating HO to decrease in radius and energy. In order to further satisfy the potential, kinetic, and orbital energy relationships, each participating $C2sp^3$ HO donates an excess of 25% of its electron density to the $C=C$-bond MO to form an energy minimum. By considering this electron redistribution in the ethylene molecule as well as the fact that the central field decreases by an integer for each successive electron of the shell, the radius $r_{ethylene\,2sp^3}$ of the $C2sp^3$ shell of ethylene may be calculated from the Coulombic energy using Eqs. (10.102) and (14.147):

$$\begin{aligned} r_{ethylene\,2sp^3} &= \left(\sum_{n=2}^{5}(Z-n)-0.5\right)\frac{e^2}{8\pi\varepsilon_0\left(e151.61569\ eV\right)} \\ &= \frac{9.5e^2}{8\pi\varepsilon_0\left(e151.61569\ eV\right)} \\ &= 0.85252a_0 \end{aligned} \tag{14.508}$$

where $Z=6$ for carbon. Using Eqs. (10.102) and (14.508), the Coulombic energy $E_{Coulomb}\left(C_{ethylene},2sp^3\right)$ of the outer electron of the $C2sp^3$ shell is:

$$E_{Coulomb}\left(C_{ethylene},2sp^3\right)=\frac{-e^2}{8\pi\varepsilon_0 r_{ethylene\,2sp^3}}=\frac{-e^2}{8\pi\varepsilon_0 0.85252a_0}=-15.95955\ eV \tag{14.509}$$

During hybridization, one of the spin-paired $2s$ electrons is promoted to the $C2sp^3$ shell as an unpaired electron. The energy for the promotion is the magnetic energy given by Eq. (14.145). Using Eqs. (14.145) and (14.509), the energy $E\left(C_{ethylene},2sp^3\right)$ of the outer electron of the $C2sp^3$ shell is:

$$E\left(C_{ethylene},2sp^3\right)=\frac{-e^2}{8\pi\varepsilon_0 r_{ethylene\,2sp^3}}+\frac{2\pi\mu_0 e^2\hbar^2}{m_e^2\left(r_3\right)^3}=-15.95955\ eV+0.19086\ eV=-15.76868\ eV \tag{14.510}$$

thus, $E_T\left(C=C,2sp^3\right)$, the energy change of each $C2sp^3$ shell with the formation of the $C=C$-bond MO is given by the difference between Eq. (14.146) and Eq. (14.510):

$$\begin{aligned} E_T\left(C=C,2sp^3\right) &= E\left(C_{ethylene},2sp^3\right)-E\left(C,2sp^3\right) \\ &= -15.76868\ eV-\left(-14.63489\ eV\right) \\ &= -1.13380\ eV \end{aligned} \tag{14.511}$$

To meet the energy matching condition for all σ MOs at all $C2sp^3$ HOs, the energy $E\left(C_{alkane},2sp^3\right)$ of the outer electron of the $C2sp^3$ shell of each alkane carbon atom must be the average of $E\left(C_{ethane},2sp^3\right)$ (Eq. (14.506)) and $E\left(C_{ethylene},2sp^3\right)$ (Eq. (14.510)).

$$\begin{aligned} E\left(C_{alkane},2sp^3\right) &= \frac{E\left(C_{ethane},2sp^3\right)+E\left(C_{ethylene},2sp^3\right)}{2} \\ &= \frac{\left(-15.35946\ eV\right)+\left(-15.76868\ eV\right)}{2} \\ &= -15.56407\ eV \end{aligned} \tag{14.512}$$

And, $E_{T_{alkane}}\left(C-C,2sp^3\right)$, the energy change of each $C2sp^3$ shell with the formation of each $C-C$-bond MO, must be the average of $E_T\left(C-C,2sp^3\right)$ (Eq. (14.507)) and $E_T\left(C=C,2sp^3\right)$ (Eq. (14.511)).

$$\begin{aligned} E_{T_{alkane}}\left(C-C,2sp^3\right) &= \frac{E_T\left(C-C,2sp^3\right)+E_T\left(C=C,2sp^3\right)}{2} \\ &= \frac{\left(-0.72457\ eV\right)+\left(-1.13379\ eV\right)}{2} \\ &= -0.92918\ eV \end{aligned} \tag{14.513}$$

using Eq. (10.102), the radius $r_{alkane2sp^3}$ of the $C2sp^3$ shell of each carbon atom of C_nH_{2n+2} may be calculated from the Coulombic energy using the initial energy $E_{Coulomb}\left(C,2sp^3\right)=-14.82575\ eV$ (Eq. (14.143)) and $E_{T_{alkane}}\left(C-C,2sp^3\right)$ Eq. (14.513)), the energy change of each $C2sp^3$ shell with the formation of each $C-C$-bond MO. Consider the case of a methyl carbon which donates $E_{T_{alkane}}\left(C-C,2sp^3\right)$ Eq. (14.513)) to a single $C-C$ bond:

$$\begin{aligned} r_{alkane2sp^3} &= \frac{-e^2}{8\pi\varepsilon_0\left(E_{Coulomb}\left(C,2sp^3\right)+E_{T_{alkane}}\left(C-C,2sp^3\right)\right)} \\ &= \frac{e^2}{8\pi\varepsilon_0\left(e14.825751\ eV+e0.92918\ eV\right)} \\ &= 0.86359a_0 \end{aligned} \tag{14.514}$$

using Eqs. (10.102) and (14.514), the Coulombic energy $E_{Coulomb}\left(C_{alkane},2sp^3\right)$ of the outer electron of the $C2sp^3$ shell is:

$$E_{Coulomb}\left(C_{alkane},2sp^3\right)=\frac{-e^2}{8\pi\varepsilon_0 r_{alkane2sp^3}}=\frac{-e^2}{8\pi\varepsilon_0 0.86359a_0}=-15.75493\ eV \tag{14.515}$$

During hybridization, one of the spin-paired $2s$ electrons is promoted to the $C2sp^3$ shell as an unpaired electron. The energy for the promotion is the magnetic energy given by Eq. (14.145). Using Eqs. (14.145) and (14.515), the energy $E\left(C_{alkane},2sp^3\right)$ of the outer electron of the $C2sp^3$ shell is:

$$E\left(C_{alkane},2sp^3\right)=\frac{-e^2}{8\pi\varepsilon_0 r_{alkane2sp^3}}+\frac{2\pi\mu_0 e^2\hbar^2}{m_e^2\left(r_3\right)^3}=-15.75493\ eV+0.19086\ eV=-15.56407\ eV \tag{14.516}$$

thus, $E_{T_{alkane}}\left(C-C,2sp^3\right)$, the energy change of each $C2sp^3$ shell with the formation of each $C-C$-bond MO is given by the difference between Eq. (14.146) and Eq. (14.516):

$$E_{T_{alkane}}\left(C-C,2sp^3\right)=E\left(C_{alkane},2sp^3\right)-E\left(C,2sp^3\right)=-15.56407\ eV-\left(-14.63489\ eV\right)=-0.92918\ eV \tag{14.517}$$

which agrees with Eq. (14.513).

The energy contribution due to the charge donation at each carbon superimposes linearly. In general, the radius r_{mol2sp^3} of the $C2sp^3$ HO of a carbon atom of a group of a given molecule is calculated using Eq. (14.514) by considering $\sum E_{T_{mol}}\left(MO,2sp^3\right)$, the total energy donation to each bond with which it participates in bonding. The general equation for the radius is given by:

$$\begin{aligned} r_{mol2sp^3} &= \frac{-e^2}{8\pi\varepsilon_0\left(E_{Coulomb}\left(C,2sp^3\right)+\sum E_{T_{mol}}\left(MO,2sp^3\right)\right)} \\ &= \frac{e^2}{8\pi\varepsilon_0\left(e14.825751\ eV+\sum\left|E_{T_{mol}}\left(MO,2sp^3\right)\right|\right)} \end{aligned} \tag{14.518}$$

The $C2sp^3$ HO of each methyl group of an alkane contributes $-0.92918\ eV$ to the corresponding single $C-C$ bond; thus, the corresponding $C2sp^3$ HO radius is given by Eq. (14.514). The $C2sp^3$ HO of each methylene group of C_nH_{2n+2} contributes $-0.92918\ eV$ to each of the two corresponding $C-C$ bond MOs. Thus, the radius of each methylene group of an alkane is given by:

$$r_{alkaneC_{methylene}2sp^3} = \frac{-e^2}{8\pi\varepsilon_0\left(E_{Coulomb}\left(C,2sp^3\right)+\sum E_{T_{alkane}}\left(methylene\ C-C,2sp^3\right)\right)}$$
$$= \frac{e^2}{8\pi\varepsilon_0\left(e14.825751\ eV + e0.92918\ eV + e0.92918\ eV\right)} \tag{14.519}$$
$$= 0.81549a_0$$

As in the case with ethane, the H_2-type ellipsoidal MO comprises 75% of the $C-C$-bond MO shared between two $C2sp^3$ HOs corresponding to the electron charge density in Eq. (11.65) of $\frac{-0.75e}{2}$. But, the additional 25% charge-density contribution to the $C-C$-bond MO causes the electron charge density in Eq. (11.65) to be $\frac{-e}{2} = -0.5e$. Thus, the force constant k' to determine the ellipsoidal parameter c' in terms of the central force of the foci is given by Eq. (14.152). The distance from the origin of the $C-C$-bond MO to each focus c' is given by Eq. (14.153). The internuclear distance from is given by Eq. (14.154). The length of the semiminor axis of the prolate spheroidal $C-C$-bond MO $b=c$ is given by Eq. (13.62). The eccentricity, e, is given by Eq. (13.63). The solution of the semimajor axis a then allows for the solution of the other axes of each prolate spheroid and eccentricity of the $C-C$-bond MO. Since the $C-C$-bond MO comprises a H_2-type-ellipsoidal MO that transitions to the $C_{alkane}2sp^3$ HO of each carbon, the energy $E\left(C_{alkane},2sp^3\right)$ in Eq. (14.512) adds to that of the H_2-type ellipsoidal MO to give the total energy of the $C-C$-bond MO. From the energy equation and the relationship between the axes, the dimensions of the $C-C$-bond MO are solved. Similarly, $E\left(C_{alkane},2sp^3\right)$ is added to the energy of the H_2-type ellipsoidal MO of each $C-H$ bond of the methyl and methylene groups to give their total energy. From the energy equation and the relationship between the axes, the dimensions of the equivalent $C-H$-bond MOs of the methyl and methylene groups in the alkane are solved.

The general equations for the energy components of V_e, V_p, T, V_m, and E_T of each $C-C$-bond MO are the same as those of the CH MO except that energy of the $C_{alkane}2sp^3$ HO is used. The energy components at each carbon atom superimpose linearly and may be treated independently. Since each prolate spheroidal H_2-type MO transitions to the $C_{alkane}2sp^3$ HO of each corresponding carbon of the bond and the energy of the $C_{alkane}2sp^3$ shell treated independently must remain constant and equal to the $E\left(C_{alkane},2sp^3\right)$ given by Eq. (14.512), the total energy $E'_{T_{alkane}}\left(C-C,\sigma\right)$ of the σ component of each $C-C$-bond MO is given by the sum of the energies of the orbitals corresponding to the composition of the linear combination of the $C_{alkane}2sp^3$ HO and the H_2-type ellipsoidal MO that forms the σ component of the $C-C$-bond MO as given by Eq. (14.502) with the electron charge redistribution. The total number of $C-C$ bonds in C_nH_{2n+2} is $n-1$. Using Eqs. (13.431) and (14.512), $E_{T_{alkane}}\left(C-C,\sigma\right)$ of the $n-1$ bonds is given by:

$$E_{T_{alkane}}\left(C-C,\sigma\right) = \left(n-1\right)\left(E_T + E\left(C_{alkane},2sp^3\right)\right)$$
$$= \left(n-1\right)\left(-\frac{e^2}{8\pi\varepsilon_0 c'}\left[\left(0.91771\right)\left(2-\frac{1}{2}\frac{a_0}{a}\right)\ln\frac{a+c'}{a-c'}-1\right]-15.56407\ eV\right) \tag{14.520}$$

To match the boundary condition that the total energy of each H_2-type ellipsoidal MO is given by Eqs. (11.212) and (13.75), $E_{T_{alkane}}\left(C-C,\sigma\right)$ given by Eq. (14.520) is set equal to $\left(n-1\right)$ times Eq. (13.75).

$$E_{T_{alkane}}\left(C-C,\sigma\right) = \left(n-1\right)\left(\begin{array}{l}-\frac{e^2}{8\pi\varepsilon_0 c'}\left[\left(0.91771\right)\left(2-\frac{1}{2}\frac{a_0}{a}\right)\ln\frac{a+c'}{a-c'}-1\right]\\ -15.56407\ eV\end{array}\right) = \left(n-1\right)\left(-31.63536831\ eV\right) \tag{14.521}$$

From the energy relationship given by Eq. (14.521) and the relationship between the axes given by Eqs. (14.153-14.154) and (13.62-13.63), the dimensions of the $C-C$-bond MO can be solved.

Substitution of Eq. (14.153) into Eq. (14.521) gives:

$$\frac{e^2}{8\pi\varepsilon_0\sqrt{aa_0}}\left[\left(0.91771\right)\left(2-\frac{1}{2}\frac{a_0}{a}\right)\ln\frac{a+\sqrt{aa_0}}{a-\sqrt{aa_0}}-1\right] = e16.07130 \tag{14.522}$$

The most convenient way to solve Eq. (14.522) is by the reiterative technique using a computer. The result to within the round-off error with five-significant figures is:

$$a = 2.12499a_0 = 1.12450\ X\ 10^{-10}\ m \tag{14.523}$$

Substitution of Eq. (14.523) into Eq. (14.155) gives:

$$c' = 1.45774a_0 = 7.71400\ X\ 10^{-11}\ m \tag{14.524}$$

The internuclear distance given by multiplying Eq. (14.524) by two is:

$$2c' = 2.91547a_0 = 1.54280\ X\ 10^{-10}\ m \tag{14.525}$$

The experimental $C-C$ bond distance of propane is [3]:

$$2c' = 1.532\ X\ 10^{-10}\ m \tag{14.526}$$

The experimental $C-C$ bond distance of butane is [3]:

$$2c' = 1.531\ X\ 10^{-10}\ m \tag{14.527}$$

Substitution of Eqs. (14.523-14.524) into Eq. (13.62) gives:

$$b = c = 1.54616a_0 = 8.18192\ X\ 10^{-11}\ m \tag{14.528}$$

Substitution of Eqs. (14.523-14.524) into Eq. (13.63) gives:

$$e = 0.68600 \tag{14.529}$$

The nucleus of the C atoms comprise the foci of each H_2-type ellipsoidal MO. The parameters of the point of intersection of the H_2-type ellipsoidal MO and the $C_{alkane}2sp^3$ HO are given by Eqs. (13.84-13.95) and (13.261-13.270). The polar intersection angle θ' is given by Eq. (13.261) where for methylene bonds $r_n = r_{alkane2sp^3} = r_{methylene2sp^3} = 0.81549a_0$ is the radius of the $C_{alkane}2sp^3$ shell given by Eq. (14.519). Substitution of Eqs. (14.523-14.524) into Eq. (13.261) gives:

$$\theta' = 56.41° \tag{14.530}$$

Then, the angle $\theta_{C-C_{alkane}2sp^3HO}$ the radial vector of the $C2sp^3$ HO makes with the internuclear axis is:

$$\theta_{C-C_{alkane}2sp^3HO} = 180° - 56.41° = 123.59° \tag{14.531}$$

as shown in Figure 14.16.

Figure 14.16. The cross section of one $C-C$-bond MO (σ MO) and one $C-H$-bond MO of C_nH_{2n+2} showing the axes, angles, and point of intersection of each H_2-type ellipsoidal MO with the corresponding $C_{alkane}2sp^3$ HO. The continuation of each H_2-type-ellipsoidal-MO basis element of the $C-C$ bond and the $C-H$-bond beyond the intersection point with each $C_{alkane}2sp^3$ shell and σ MO is shown as dashed since each only serves to solve the energy match with the $C_{alkane}2sp^3$ shell and does not represent charge density. Similarly, the vertical dashed line only designates the parameters of each intersection point. The actual charge density is shown by the solid lines. Legend: a: semimajor axis, b: semiminor axis, c': internuclear distance, $d_1 : d_{C-C_{alkane},H_2MO}$, $\theta_1 : \theta_{C-C_{alkane}2sp^3HO}$, $d_2 : d_{C-C_{alkane}2sp^3HO}$, $R : r_{alkaneC2sp^3}$, $d_3 : d_{C-H_{alkane},H_2MO}$, $\theta_2 : \theta_{C-H_{alkane}2sp^3HO}$, and $d_4 : d_{C-H_{alkane}2sp^3HO}$.

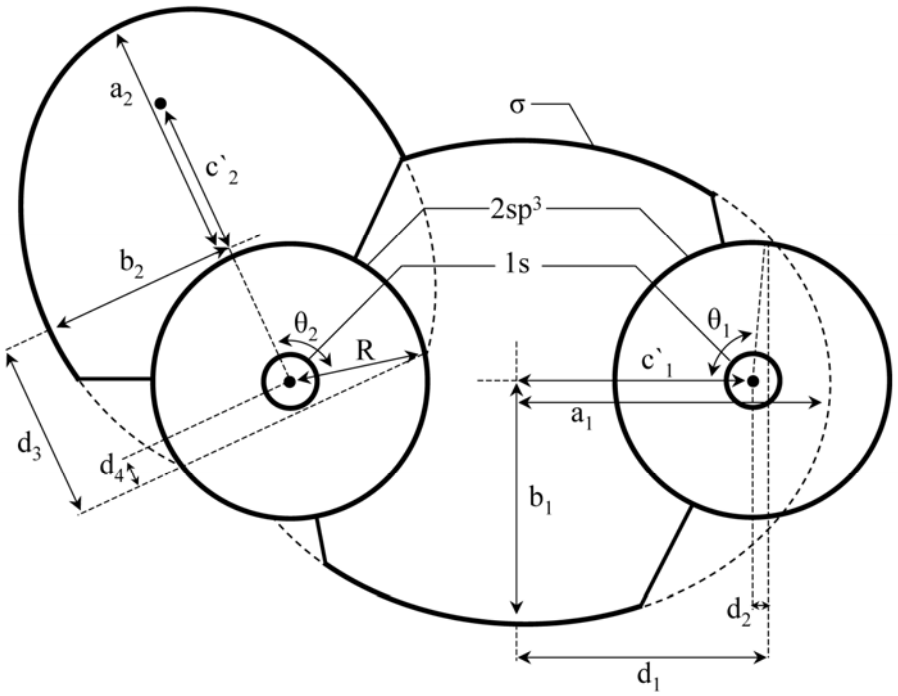

Consider the right-hand intersection point. The Cartesian $\mathbf{i}$-coordinate of the interception point of the MO and the AO can be calculated using the MO ellipsoidal parameters by first calculating the parametric angle in Eq. (11.83) that matches Cartesian $\mathbf{j}$-coordinate components at the point of intersection. Thus, the matching elliptic parametric angle $\omega t = \theta_{C-C_{alkane},H_2MO}$ satisfies the following relationship:

$$r_{alkane2sp^3}\sin\theta_{C-C_{alkane}2sp^3HO} = 0.81549a_0\sin\theta_{C-C_{alkane}2sp^3HO} = b\sin\theta_{C-C_{alkane},H_2MO} \tag{14.532}$$

such that

$$\theta_{C-C_{alkane},H_2MO} = \sin^{-1}\frac{0.81549a_0\sin\theta_{C-C_{alkane}2sp^3HO}}{b} = \sin^{-1}\frac{0.81549a_0\sin 123.59°}{b} \tag{14.533}$$

with the use of Eq. (14.531). Substitution of Eq. (14.528) into Eq. (14.533) gives:

$$\theta_{C-C_{alkane},H_2MO} = 26.06° \tag{14.534}$$

Then, the distance d_{C-C_{alkane},H_2MO} along the internuclear axis from the origin of H_2-type ellipsoidal MO to the point of intersection of the orbitals is given by

$$d_{C-C_{alkane},H_2MO} = a\cos\theta_{C-C_{alkane},H_2MO} \tag{14.535}$$

Substitution of Eqs. (14.523) and (14.534) into Eq. (14.535) gives:

$$d_{C-C_{alkane},H_2MO} = 1.90890a_0 = 1.01015\ X\ 10^{-10}\ m \tag{14.536}$$

The distance $d_{C-C_{alkane}2sp^3HO}$ along the internuclear axis from the origin of the C atom to the point of intersection of the orbitals is given by:

$$d_{C-C_{alkane}2sp^3HO} = d_{C-C_{alkane},H_2MO} - c' \tag{14.537}$$

Substitution of Eqs. (14.524) and (14.536) into Eq. (14.537) gives:

$$d_{C-C_{alkane}2sp^3HO} = 0.45117a_0 = 2.38748\ X\ 10^{-11}\ m \tag{14.538}$$

FORCE BALANCE OF THE CH_3 MOs OF CONTINUOUS-CHAIN ALKANES

Each of the two CH_3 MOs must comprise three equivalent $C-H$ bonds with each comprising 75% of a H_2-type ellipsoidal MO and a $C2sp^3$ HO as given by Eq. (13.540).

$$3\left[1\ C2sp^3 + 0.75\ H_2\ MO\right] \rightarrow CH_3\ MO \tag{14.539}$$

The force balance of the CH_3 MO is determined by the boundary conditions that arise from the linear combination of orbitals according to Eq. (14.539) and the energy matching condition between the hydrogen and $C2sp^3$ HO components of the MO.

The force constant k' to determine the ellipsoidal parameter c' of the each H_2-type-ellipsoidal-MO component of the CH_3 MO in terms of the central force of the foci is given by Eq. (13.59). The distance from the origin of each $C-H$-bond MO to each focus c' is given by Eq. (13.60). The internuclear distance is given by Eq. (13.61). The length of the semiminor axis of the prolate spheroidal $C-H$-bond MO $b=c$ is given by Eq. (13.62). The eccentricity, e, is given by Eq. (13.63). The solution of the semimajor axis a then allows for the solution of the other axes of each prolate spheroid and eccentricity of each $C-H$-bond MO. Since each of the three prolate spheroidal $C-H$-bond MOs comprises an H_2-type-ellipsoidal MO that transitions to the $C_{alkane}2sp^3$ HO of C_nH_{2n+2}, the energy $E\left(C_{alkane},2sp^3\right)$ of Eq. (14.512) adds to that of the three corresponding H_2-type ellipsoidal MOs to give the total energy of the CH_3 MO. From the energy equation and the relationship between the axes, the dimensions of the CH_3 MO are solved.

The energy components of V_e, V_p, T, and V_m are the same as those of methyl radical, three times those of CH corresponding to the three $C-H$ bonds except that energy of the $C_{alkane}2sp^3$ HO is used. Since each prolate spheroidal H_2-type MO transitions to the $C_{alkane}2sp^3$ HO and the energy of the $C_{alkane}2sp^3$ shell must remain constant and equal to the $E\left(C_{alkane},2sp^3\right)$ given by Eq. (14.512), the total energy $E_{T_{alkane}}\left(CH_3\right)$ of the CH_3 MO is given by the sum of the energies of the orbitals corresponding to the composition of the linear combination of the $C_{alkane}2sp^3$ HO and the three H_2-type ellipsoidal MOs that forms the CH_3 MO as given by Eq. (14.539). Using Eq. (13.431) or Eq. (13.541), $E_{T_{alkane}}\left(CH_3\right)$ is given by:

$$E_{T_{alkane}}\left(CH_3\right) = E_T + E\left(C_{alkane},2sp^3\right) = -\frac{3e^2}{8\pi\varepsilon_0 c'}\left[\left(0.91771\right)\left(2-\frac{1}{2}\frac{a_0}{a}\right)\ln\frac{a+c'}{a-c'}-1\right] - 15.56407\ eV \tag{14.540}$$

$E_{T_{alkane}}\left(CH_3\right)$ given by Eq. (14.540) is set equal to three times the energy of the H_2-type ellipsoidal MO minus two times the Coulombic energy of H given by Eq. (13.542):

$$E_T\left(CH_3\right) = -\frac{3e^2}{8\pi\varepsilon_0 c'}\left[\left(0.91771\right)\left(2-\frac{1}{2}\frac{a_0}{a}\right)\ln\frac{a+c'}{a-c'}-1\right] - 15.56407\ eV = -67.69450\ eV \tag{14.541}$$

From the energy relationship given by Eq. (14.541) and the relationship between the axes given by Eqs. (13.60-13.63), the dimensions of the CH_3 MO can be solved.

Substitution of Eq. (13.60) into Eq. (14.541) gives:

$$\frac{3e^2}{8\pi\varepsilon_0\sqrt{\frac{2aa_0}{3}}}\left[(0.91771)\left(2-\frac{1}{2}\frac{a_0}{a}\right)\ln\frac{a+\sqrt{\frac{2aa_0}{3}}}{a-\sqrt{\frac{2aa_0}{3}}}-1\right]=e52.13044 \tag{14.542}$$

The most convenient way to solve Eq. (14.542) is by the reiterative technique using a computer. The result to within the round-off error with five-significant figures is:

$$a=1.64920a_0=8.72720\ X\ 10^{-11}\ m \tag{14.543}$$

Substitution of Eq. (14.543) into Eq. (14.60) gives:

$$c'=1.04856a_0=5.54872\ X\ 10^{-11}\ m \tag{14.544}$$

The internuclear distance given by multiplying Eq. (14.544) by two is:

$$2c'=2.09711a_0=1.10974\ X\ 10^{-10}\ m \tag{14.545}$$

The experimental $C-H$ bond distance of propane is [3]:

$$2c'=1.107\ X\ 10^{-10}\ m \tag{14.546}$$

Substitution of Eqs. (14.543-14.544) into Eq. (14.62) gives:

$$b=c=1.27295a_0=6.73616\ X\ 10^{-11}\ m \tag{14.547}$$

Substitution of Eqs. (14.543-14.544) into Eq. (14.63) gives:

$$e=0.63580 \tag{14.548}$$

The nucleus of the H atom and the nucleus of the C atom comprise the foci of each H_2-type ellipsoidal MO. The parameters of the point of intersection of the H_2-type ellipsoidal MO and the $C_{alkane}2sp^3$ HO are given by Eqs. (13.84-13.95) and (13.261-13.270). The polar intersection angle θ' is given by Eq. (13.261) where $r_n=r_{alkane2sp^3}=0.86359a_0$ is the radius of the $C_{alkane}2sp^3$ shell. Substitution of Eqs. (14.543-14.544) into Eq. (13.261) gives:

$$\theta'=77.49° \tag{14.549}$$

Then, the angle $\theta_{C-H_{alkane}2sp^3HO}$ the radial vector of the $C2sp^3$ HO makes with the internuclear axis is:

$$\theta_{C-H_{alkane}2sp^3HO}=180°-77.49°=102.51° \tag{14.550}$$

as shown in Figure 14.17.

Figure 14.17. The cross section of one $C-H$-bond MO of C_nH_{2n+2} showing the axes, angles, and point of intersection of the H_2-type ellipsoidal MO with the $C_{alkane}2sp^3$ HO. The continuation of the H_2-type-ellipsoidal-MO basis element beyond the intersection point with the $C_{alkane}2sp^3$ shell is shown as dashed since it only serves to solve the energy match with the $C_{alkane}2sp^3$ shell and does not represent charge density. Similarly, the vertical dashed line only designates the parameters of the intersection point. The actual charge density is shown by the solid lines. Legend: a: semimajor axis, b: semiminor axis, c': internuclear distance, $d_1:d_{C-H_{alkane},H_2MO}$, $\theta_1:\theta_{C-H_{alkane}2sp^3HO}$, $d_2:d_{C-H_{alkane}2sp^3HO}$, and $R:r_{alkane2sp^3}$.

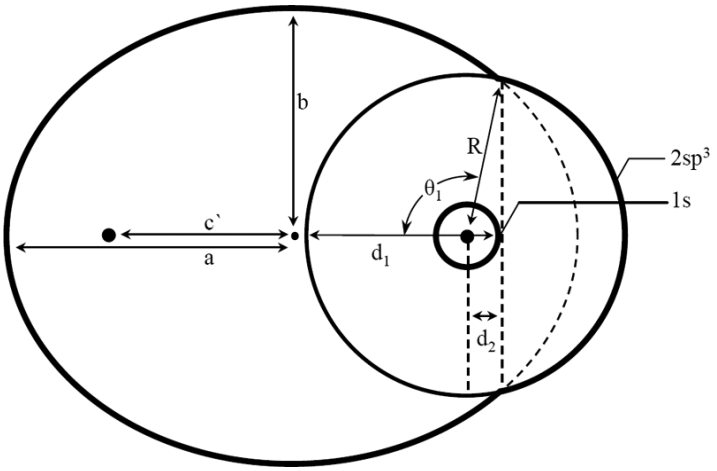

The Cartesian $\mathbf{i}$-coordinate of the interception point of the MO and the AO can be calculated using the MO ellipsoidal parameters by first calculating the parametric angle in Eq. (11.83) that matches Cartesian $\mathbf{j}$-coordinate components at the point of intersection. Thus, the matching elliptic parametric angle $\omega t = \theta_{C-H_{alkane},H_2MO}$ satisfies the following relationship:

$$r_{alkane2sp^3}\sin\theta_{C-H_{alkane}2sp^3HO} = 0.86359a_0\sin\theta_{C-H_{alkane}2sp^3HO} = b\sin\theta_{C-H_{alkane},H_2MO} \tag{14.551}$$

such that

$$\theta_{C-H_{alkane},H_2MO} = \sin^{-1}\frac{0.86359a_0\sin\theta_{C-H_{alkane}2sp^3HO}}{b} = \sin^{-1}\frac{0.86359a_0\sin 102.51°}{b} \tag{14.552}$$

with the use of Eq. (14.550). Substitution of Eq. (14.547) into Eq. (14.552) gives:

$$\theta_{C-H_{alkane},H_2MO} = 41.48° \tag{14.553}$$

Then, the distance d_{C-H_{alkane},H_2MO} along the internuclear axis from the origin of H_2-type ellipsoidal MO to the point of intersection of the orbitals is given by:

$$d_{C-H_{alkane},H_2MO} = a\cos\theta_{C-H_{alkane},H_2MO} \tag{14.554}$$

Substitution of Eqs. (14.543) and (14.553) into Eq. (14.554) gives:

$$d_{C-H_{alkane},H_2MO} = 1.23564a_0 = 6.53871\ X\ 10^{-11}\ m \tag{14.555}$$

The distance $d_{C-H_{alkane}2sp^3HO}$ along the internuclear axis from the origin of the C atom to the point of intersection of the orbitals is given by

$$d_{C-H_{alkane}2sp^3HO} = d_{C-H_{alkane},H_2MO} - c' \tag{14.556}$$

Substitution of Eqs. (14.544) and (14.555) into Eq. (14.556) gives:

$$d_{C-H_{alkane}2sp^3HO} = 0.18708a_0 = 9.89999\ X\ 10^{-12}\ m \tag{14.557}$$

BOND ANGLE OF THE CH_3 AND CH_2 GROUPS

Each CH_3 MO comprises a linear combination of three $C-H$-bond MOs. Each $C-H$-bond MO comprises the superposition of a H_2-type ellipsoidal MO and the $C_{alkane}2sp^3$ HO. A bond is also possible between the two H atoms of the $C-H$ bonds. Such $H-H$ bonding would decrease the $C-H$ bond strength since electron density would be shifted from the $C-H$ bonds to the $H-H$ bond. Thus, the bond angle between the two $C-H$ bonds is determined by the condition that the total energy of the H_2-type ellipsoidal MO between the terminal H atoms of the $C-H$ bonds is zero. From Eqs. (11.79) and (13.228), the distance from the origin to each focus of the $H-H$ ellipsoidal MO is:

$$c' = a\sqrt{\frac{\hbar^2 4\pi\varepsilon_0}{m_e e^2 2a}} = \sqrt{\frac{aa_0}{2}} \tag{14.558}$$

The internuclear distance from Eq. (14.558) is:

$$2c' = 2\sqrt{\frac{aa_0}{2}} \tag{14.559}$$

The length of the semiminor axis of the prolate spheroidal $H-H$ MO $b=c$ is given by Eq. (14.62).

The bond angle of the CH_3 groups of C_nH_{2n+2} is derived by using the orbital composition and an energy matching factor as in the case with the CH_3 radical. Since each pair of H_2-type ellipsoidal MOs initially comprise 75% of the H electron density of H_2 and the energy of each H_2-type ellipsoidal MO is matched to that of the $C_{alkane}2sp^3$ HO, the component energies and the total energy E_T of the $H-H$ bond are given by Eqs. (13.67-13.73) except that V_e, T, and V_m are corrected for the hybridization-energy-matching factor of 0.86359. Hybridization with 25% electron donation to the $C-C$-bond gives rise to the $C_{alkane}2sp^3$ HO-shell Coulombic energy $E_{Coulomb}\left(C_{alkane},2sp^3\right)$ given by Eq. (14.515). The corresponding normalization factor for determining the zero of the total $H-H$ bond energy is given by the ratio of $15.75493\ eV$, the magnitude of $E_{Coulomb}\left(C_{alkane},2sp^3\right)$ given by Eq. (14.515), and $13.605804\ eV$, the magnitude of the Coulombic energy between the electron and proton of H given by Eq. (1.264). The hybridization energy factor $C_{alkaneC2sp^3HO}$ is:

$$C_{alkaneC2sp^3HO} = \frac{\frac{e^2}{8\pi\varepsilon_0 a_0}}{\frac{e^2}{8\pi\varepsilon_0 r_{alkane2sp^3}}} = \frac{\frac{e^2}{8\pi\varepsilon_0 a_0}}{\frac{e^2}{8\pi\varepsilon_0 0.86359a_0}} = \frac{13.605804\ eV}{15.75493\ eV} = 0.86359 \tag{14.560}$$

Substitution of Eq. (14.558) into Eq. (13.233) with the hybridization factor of 0.86359 gives:

$$0=\left[\begin{array}{l}\dfrac{-e^2}{8\pi\varepsilon_0\sqrt{\dfrac{aa_0}{2}}}\left[(0.86359)^{-1}\left(\dfrac{3}{2}-\dfrac{3}{8}\dfrac{a_0}{a}\right)\ln\dfrac{a+\sqrt{\dfrac{aa_0}{2}}}{a-\sqrt{\dfrac{aa_0}{2}}}-1\right]\left[1+\sqrt{\dfrac{2\hbar\sqrt{\dfrac{0.75e^2}{4\pi\varepsilon_0 a^3}}}{m_e c^2}}\right] \\ +\hbar\sqrt{\dfrac{\dfrac{0.75e^2}{8\pi\varepsilon_0 a^3}-\dfrac{e^2}{8\pi\varepsilon_0\left(a+c'\right)^3}}{0.5m_p}}\end{array}\right] \tag{14.561}$$

From the energy relationship given by Eq. (14.561) and the relationship between the axes given by Eqs. (14.558-14.559) and (14.62-14.63), the dimensions of the $H-H$ MO can be solved.

The most convenient way to solve Eq. (14.561) is by the reiterative technique using a computer. The result to within the round-off error with five-significant figures is:

$$a=5.8660a_0=3.1042\ X\ 10^{-10}\ m \tag{14.562}$$

Substitution of Eq. (14.562) into Eq. (14.558) gives:

$$c'=1.7126a_0=9.0627\ X\ 10^{-11}\ m \tag{14.563}$$

The internuclear distance given by multiplying Eq. (14.563) by two is:

$$2c'=3.4252a_0=1.8125\ X\ 10^{-10}\ m \tag{14.564}$$

Substitution of Eqs. (14.562-14.563) into Eq. (14.62) gives:

$$b=c=5.6104a_0=2.9689\ X\ 10^{-10}\ m \tag{14.565}$$

Substitution of Eqs. (14.562-14.563) into Eq. (14.63) gives:

$$e=0.2920 \tag{14.566}$$

Using $2c'_{H-H}$ (Eq. (14.564)), the distance between the two H atoms when the total energy of the corresponding MO is zero (Eq. (14.561)), and $2c'_{C-H}$, the internuclear distance of each $C-H$ bond, the corresponding bond angle can be determined from the law of cosines. Since the internuclear distance of each $C-H$ bond of CH_3 (Eq. (14.545)) and CH_2 (Eq. (14.597)) are sufficiently equivalent, the bond angle determined with either is within experimental error of being the same. Using, Eqs. (13.242), (14.545), and (14.564), the bond angle θ between the $C-H$ bonds is:

$$\theta=\cos^{-1}\left(\frac{2\left(2.09711\right)^2-\left(3.4252\right)^2}{2\left(2.09711\right)^2}\right)=\cos^{-1}\left(-0.33383\right)=109.50° \tag{14.567}$$

The experimental angle between the $C-H$ bonds is [19]:

$$\theta=109.3° \tag{14.568}$$

The CH_3 radical has a pyramidal structure with the carbon atom along the z-axis at the apex and the hydrogen atoms at the base in the xy-plane. The distance $d_{origin-H}$ from the origin to the nucleus of a hydrogen atom given by Eqs. (14.564) and (13.412) is:

$$d_{origin-H}=1.97754a_0 \tag{14.569}$$

The height along the z-axis of the pyramid from the origin to C nucleus d_{height} given by Eqs. (13.414), (14.545), and (14.569) is

$$d_{height}=0.69800a_0 \tag{14.570}$$

The angle θ_v of each $C-H$ bond from the z-axis given by Eqs. (13.416), (14.569), and (14.570) is:

$$\theta_v=70.56° \tag{14.571}$$

The $C-C$ bond is along the z-axis. Thus, the bond angle θ_{C-C-H} between the internuclear axis of the $C-C$ bond and a H atom of the methyl groups is given by:

$$\theta_{C-C-H}=180-\theta_v \tag{14.572}$$

Substitution of Eq. (14.571) into Eq. (14.572) gives:

$$\theta_{C-C-H}=109.44° \tag{14.573}$$

The experimental angle between the $C-C-H$ bonds is [19]:

$$\theta_{C-C-H}=109.3° \tag{14.574}$$

The C_nH_{2n+2} MOs shown in Figures 14.18-14.28 were rendered using these parameters. A minimum energy is obtained with a staggered configuration consistent with observations [3].

ENERGIES OF THE CH_3 GROUPS

The energies of each CH_3 group of C_nH_{2n+2} are given by the substitution of the semiprincipal axes (Eqs. (14.543-14.544) and (14.547)) into the energy equations of methyl radical (Eqs. (13.556-13.560)), with the exception that $E\left(C_{alkane},2sp^3\right)$ (Eq. (14.514)) replaces $E\left(C,2sp^3\right)$ in Eq. (13.560).

$$V_e = 3\left(0.91771\right)\frac{-2e^2}{8\pi\varepsilon_0\sqrt{a^2-b^2}}\ln\frac{a+\sqrt{a^2-b^2}}{a-\sqrt{a^2-b^2}} = -107.32728\ eV \tag{14.575}$$

$$V_p = \frac{3e^2}{8\pi\varepsilon_0\sqrt{a^2-b^2}} = 38.92728\ eV \tag{14.576}$$

$$T = 3\left(0.91771\right)\frac{\hbar^2}{2m_e a\sqrt{a^2-b^2}}\ln\frac{a+\sqrt{a^2-b^2}}{a-\sqrt{a^2-b^2}} = 32.53914\ eV \tag{14.577}$$

$$V_m = 3\left(0.91771\right)\frac{-\hbar^2}{4m_e a\sqrt{a^2-b^2}}\ln\frac{a+\sqrt{a^2-b^2}}{a-\sqrt{a^2-b^2}} = -16.26957\ eV \tag{14.578}$$

$$E_{T_{alkane}}\left(CH_3\right) = \begin{pmatrix} -\frac{3e^2}{8\pi\varepsilon_0 c'}\left[\left(0.91771\right)\left(2-\frac{1}{2}\frac{a_0}{a}\right)\ln\frac{a+c'}{a-c'}-1\right] \\ -15.56407\ eV \end{pmatrix} = -67.69451\ eV \tag{14.579}$$

where $E_{T_{alkane}}\left(CH_3\right)$ is given by Eq. (14.540) which is reiteratively matched to Eq. (13.542) within five-significant-figure round off error.

VIBRATION OF THE $^{12}CH_3$ GROUPS

The vibrational energy levels of the $C-H$ bonds of CH_3 in C_nH_{2n+2} may be solved as three equivalent coupled harmonic oscillators by developing the Lagrangian, the differential equation of motion, and the eigenvalue solutions [9] wherein the spring constants are derived from the central forces as given in the Vibration of Hydrogen-Type Molecular Ions section and the Vibration of Hydrogen-Type Molecules section.

THE DOPPLER ENERGY TERMS OF THE $^{12}CH_3$ GROUPS

The equations of the radiation reaction force of the methyl groups in C_nH_{2n+2} are the same as those of the methyl radical with the substitution of the methyl-group parameters. Using Eq. (13.561), the angular frequency of the reentrant oscillation in the transition state is:

$$\omega = \sqrt{\frac{\frac{0.75e^2}{4\pi\varepsilon_0 b^3}}{m_e}} = 2.49286\ X\ 10^{16}\ rad/s \tag{14.580}$$

where b is given by Eq. (14.547). The kinetic energy, E_K, is given by Planck's equation (Eq. (11.127)).

$$\overline{E}_K = \hbar\omega = \hbar 2.49286\ X\ 10^{16}\ rad/s = 16.40846\ eV \tag{14.581}$$

In Eq. (11.181), substitution of $E_T\left(H_2\right)$ (Eqs. (11.212) and (13.75)), the maximum total energy of each H_2-type MO, for E_{hv}, the mass of the electron, m_e, for M, and the kinetic energy given by Eq. (14.581) for $\overline{E}_K$ gives the Doppler energy of the electrons of each of the three bonds for the reentrant orbit:

$$\overline{E}_D \cong E_{hv}\sqrt{\frac{2\overline{E}_K}{Mc^2}} = -31.63537\ eV\sqrt{\frac{2e\left(16.40846\ eV\right)}{m_e c^2}} = -0.25352\ eV \tag{14.582}$$

In addition to the electrons, the nuclei also undergo simple harmonic oscillation in the transition state at their corresponding frequency. The decrease in the energy of CH_3 due to the reentrant orbit of each bond in the transition state corresponding to simple harmonic oscillation of the electrons and nuclei, $\overline{E}_{osc}$, is given by the sum of the corresponding energies, $\overline{E}_D$ given by Eq. (14.582) and $\overline{E}_{Kvib}$, the average kinetic energy of vibration which is 1/2 of the vibrational energy of each $C-H$ bond. Using ω_e given by Eq. (13.458) for $\overline{E}_{Kvib}$ of the *transition* state having three independent bonds, $\overline{E}'_{alkane\ osc}\left(^{12}CH_3\right)$ per bond is:

$$\overline{E}'_{alkane\ osc}\left(^{12}CH_3\right) = \overline{E}_D + \overline{E}_{Kvib} = \overline{E}_D + \frac{1}{2}\hbar\sqrt{\frac{k}{\mu}} \tag{14.583}$$

$$\overline{E}'_{alkane\ osc}\left(^{12}CH_3\right) = -0.25352\ eV + \frac{1}{2}\left(0.35532\ eV\right) = -0.07586\ eV \tag{14.584}$$

Given that the vibration and reentrant oscillation is for three $C-H$ bonds, $\bar{E}_{alkane\ osc}\left({}^{12}CH_3\right)$, is:

$$\bar{E}_{alkane\ osc}\left({}^{12}CH_3\right)=3\left(\bar{E}_D+\frac{1}{2}\hbar\sqrt{\frac{k}{\mu}}\right)=3\left(-0.25352\ eV+\frac{1}{2}\left(0.35532\ eV\right)\right)=-0.22757\ eV \tag{14.585}$$

TOTAL BOND ENERGIES OF THE ${}^{12}CH_3$ GROUPS

$E_{alkaneT+osc}\left({}^{12}CH_3\right)$, the total energy of each ${}^{12}CH_3$ group including the Doppler term, is given by the sum of $E_{T_{alkane}}\left(CH_3\right)$ (Eq. (14.579)) and $\bar{E}_{alkane\ osc}\left({}^{12}CH_3\right)$ given by Eq. (14.585).

$$E_{alkaneT+osc}\left({}^{12}CH_3\right)=V_e+T+V_m+V_p+E\left(C_{alkane},2sp^3\right)+\bar{E}_{alkane\ osc}\left({}^{12}CH_3\right)=E_{T_{alkane}}\left(CH_3\right)+\bar{E}_{alkane\ osc}\left({}^{12}CH_3\right) \tag{14.586}$$

$$\begin{aligned}E_{alkaneT+osc}\left({}^{12}CH_3\right)&=\left\{\begin{array}{l}\left(\frac{-3e^2}{8\pi\varepsilon_0 c'}\left[\left(0.91771\right)\left(2-\frac{1}{2}\frac{a_0}{a}\right)\ln\frac{a+c'}{a-c'}-1\right]-15.56407\ eV\right)\\ -3\left(\left(31.63536831\ eV\right)\sqrt{\frac{2\hbar\sqrt{\frac{3}{4}\frac{e^2}{4\pi\varepsilon_0 b^3}}}{m_e c^2}}-\frac{1}{2}\hbar\sqrt{\frac{k}{\mu}}\right)\end{array}\right\}\\&=-67.69450\ eV-3\left(0.25352\ eV-\frac{1}{2}\hbar\sqrt{\frac{k}{\mu}}\right)\end{aligned} \tag{14.587}$$

From Eqs. (14.585-14.587), the total energy of each ${}^{12}CH_3$ is:

$$\begin{aligned}E_{alkaneT+osc}\left({}^{12}CH_3\right)&=-67.69450\ eV+\bar{E}_{alkane\ osc}\left({}^{12}CH_3\right)\\&=-67.69450\ eV-3\left(0.25352\ eV-\frac{1}{2}\left(0.35532\ eV\right)\right)=-67.92207\ eV\end{aligned} \tag{14.588}$$

where ω_e given by Eq. (13.458) was used for the $\hbar\sqrt{\frac{k}{\mu}}$ term.

The total CH_3 bond dissociation energy, $E_{D_{alkane}}\left({}^{12}CH_3\right)$ is given by the sum of the initial $C2sp^3$ HO energy, $E\left(C,2sp^3\right)$ (Eq. (14.146)), and three times the energy of the hydrogen atom, $E_D\left(H\right)$ (Eq. (13.154)), minus $E_{alkaneT+osc}\left({}^{12}CH_3\right)$ (Eq. (14.588)).

$$E_{D_{alkane}}\left({}^{12}CH_3\right)=E\left(C,2sp^3\right)+3E(H)-E_{alkaneT+osc}\left({}^{12}CH_3\right) \tag{14.589}$$

Thus, the total ${}^{12}CH_3$ bond dissociation energy, $E_{D_{alkane}}\left({}^{12}CH_3\right)$ is:

$$\begin{aligned}E_{D_{alkane}}\left({}^{12}CH_3\right)&=-\left(14.63489\ eV+3\left(13.59844\ eV\right)\right)-\left(E_{alkaneT+osc}\left({}^{12}CH_2\right)\right)\\&=-55.43021\ eV-\left(-67.92207\ eV\right)=12.49186\ eV\end{aligned} \tag{14.590}$$

FORCE BALANCE OF THE CH_2 MOs OF CONTINUOUS-CHAIN ALKANES

Each of the CH_2 MOs must comprise two equivalent $C-H$ bonds with each comprising 75% of a H_2-type ellipsoidal MO and a $C2sp^3$ HO as given by Eq. (13.494).

$$2\left[1\ C2sp^3+0.75\ H_2\ MO\right]\rightarrow CH_2\ MO \tag{14.591}$$

The force balance of each CH_2 MO is determined by the boundary conditions that arise from the linear combination of orbitals according to Eq. (14.591) and the energy matching condition between the hydrogen and $C2sp^3$ HO components of the MO.

The force constant k' to determine the ellipsoidal parameter c' of the each H_2-type-ellipsoidal-MO component of the CH_2 MO in terms of the central force of the foci is given by Eq. (13.59). The distance from the origin of each $C-H$-bond MO to each focus c' is given by Eq. (13.60). The internuclear distance is given by Eq. (13.61). The length of the semiminor axis of the prolate spheroidal $C-H$-bond MO $b=c$ is given by Eq. (13.62). The eccentricity, e, is given by Eq. (13.63). The solution of the semimajor axis a then allows for the solution of the other axes of each prolate spheroid and eccentricity of each $C-H$-bond MO. Since each of the two prolate spheroidal $C-H$-bond MOs comprises an H_2-type-ellipsoidal MO that transitions to the $C_{alkane}2sp^3$ HO of C_nH_{2n+2}, the energy $E\left(C_{alkane},2sp^3\right)$ of Eq. (14.512) adds to that of the two corresponding H_2-type ellipsoidal

MOs to give the total energy of the CH_2 MO. From the energy equation and the relationship between the axes, the dimensions of the CH_2 MO are solved.

The energy components of V_e, V_p, T, and V_m are the same as those of dihydrogen carbide radical, two times those of CH corresponding to the two $C-H$ bonds except that energy of the $C_{alkane}2sp^3$ HO is used. Since each prolate spheroidal H_2-type MO transitions to the $C_{alkane}2sp^3$ HO and the energy of the $C_{alkane}2sp^3$ shell treated independently must remain constant and equal to the $E\left(C_{alkane},2sp^3\right)$ given by Eq. (14.512), the total energy $E_{T_{alkane}}\left(CH_2\right)$ of the CH_2 MO is given by the sum of the energies of the orbitals corresponding to the composition of the linear combination of the $C_{alkane}2sp^3$ HO and the two H_2-type ellipsoidal MOs that forms the CH_2 MO as given by Eq. (14.591). Using Eq. (13.431) or Eq. (13.495), $E_{T_{alkane}}\left(CH_2\right)$ is given by:

$$E_{T_{alkane}}\left(CH_2\right)=E_T+E\left(C_{alkane},2sp^3\right)=-\frac{2e^2}{8\pi\varepsilon_0 c'}\left[\left(0.91771\right)\left(2-\frac{1}{2}\frac{a_0}{a}\right)\ln\frac{a+c'}{a-c'}-1\right]-15.56407\ eV \tag{14.592}$$

$E_{T_{alkane}}\left(CH_2\right)$ given by Eq. (14.592) is set equal to two times the energy of the H_2-type ellipsoidal MO minus the Coulombic energy of H given by Eq. (13.496).

$$E_T\left(CH_2\right)=-\frac{2e^2}{8\pi\varepsilon_0 c'}\left[\left(0.91771\right)\left(2-\frac{1}{2}\frac{a_0}{a}\right)\ln\frac{a+c'}{a-c'}-1\right]-15.56407\ eV=-49.66493\ eV \tag{14.593}$$

From the energy relationship given by Eq. (14.593) and the relationship between the axes given by Eqs. (13.60-13.63), the dimensions of the CH_2 MO can be solved.

Substitution of Eq. (13.60) into Eq. (14.593) gives:

$$\frac{2e^2}{8\pi\varepsilon_0\sqrt{\frac{2aa_0}{3}}}\left[\left(0.91771\right)\left(2-\frac{1}{2}\frac{a_0}{a}\right)\ln\frac{a+\sqrt{\frac{2aa_0}{3}}}{a-\sqrt{\frac{2aa_0}{3}}}-1\right]=e34.10086 \tag{14.594}$$

The most convenient way to solve Eq. (14.594) is by the reiterative technique using a computer. The result to within the round-off error with five-significant figures is

$$a=1.67122a_0=8.84370\ X\ 10^{-11}\ m \tag{14.595}$$

Substitution of Eq. (14.595) into Eq. (14.60) gives:

$$c'=1.05553a_0=5.58563\ X\ 10^{-11}\ m \tag{14.596}$$

The internuclear distance given by multiplying Eq. (14.596) by two is:

$$2c'=2.11106a_0=1.11713\ X\ 10^{-10}\ m \tag{14.597}$$

The experimental $C-H$ bond distance of butane is [3]:

$$2c'=1.117\ X\ 10^{-10}\ m \tag{14.598}$$

Substitution of Eqs. (14.595-14.596) into Eq. (14.62) gives:

$$b=c=1.29569a_0=6.85652\ X\ 10^{-11}\ m \tag{14.599}$$

Substitution of Eqs. (14.595-14.596) into Eq. (14.63) gives:

$$e=0.63159 \tag{14.600}$$

The nucleus of the H atom and the nucleus of the C atom comprise the foci of each H_2-type ellipsoidal MO. The parameters of the point of intersection of the H_2-type ellipsoidal MO and the $C_{alkane}2sp^3$ HO are given by Eqs. (13.84-13.95) and (13.261-13.270). The polar intersection angle θ' is given by Eq. (13.261) where $r_n=r_{methylene2sp^3}=0.81549a_0$ is the radius of the $C_{methylene}2sp^3$ shell (Eq. (14.521)). Substitution of Eqs. (14.595-14.596) into Eq. (13.261) gives:

$$\theta'=68.47° \tag{14.601}$$

Then, the angle $\theta_{C-H_{alkane}2sp^3HO}$ the radial vector of the $C2sp^3$ HO makes with the internuclear axis is:

$$\theta_{C-H_{alkane}2sp^3HO}=180°-68.47°=111.53° \tag{14.602}$$

as shown in Figure 14.17. The Cartesian **i**-coordinate of the interception point of the MO and the AO can be calculated using the MO ellipsoidal parameters by first calculating the parametric angle in Eq. (11.83) that matches Cartesian **j**-coordinate components at the point of intersection. Thus, the matching elliptic parametric angle $\omega t=\theta_{C-H_{alkane},H_2MO}$ satisfies the following relationship:

$$r_{alkane2sp^3}\sin\theta_{C-H_{alkane}2sp^3HO}=0.81549a_0\sin\theta_{C-H_{alkane}2sp^3HO}=b\sin\theta_{C-H_{alkane},H_2MO} \tag{14.603}$$

such that

$$\theta_{C-H_{alkane},H_2MO} = \sin^{-1}\frac{0.81549a_0\sin\theta_{C-H_{alkane}2sp^3HO}}{b} = \sin^{-1}\frac{0.81549a_0\sin 111.53°}{b} \tag{14.604}$$

with the use of Eq. (14.602). Substitution of Eq. (14.599) into Eq. (14.604) gives:

$$\theta_{C-H_{alkane},H_2MO} = 35.84° \tag{14.605}$$

Then, the distance d_{C-H_{alkane},H_2MO} along the internuclear axis from the origin of H_2-type ellipsoidal MO to the point of intersection of the orbitals is given by:

$$d_{C-H_{alkane},H_2MO} = a\cos\theta_{C-H_{alkane},H_2MO} \tag{14.606}$$

Substitution of Eqs. (14.595) and (14.605) into Eq. (14.606) gives:

$$d_{C-H_{alkane},H_2MO} = 1.35486a_0 = 7.16963\ X\ 10^{-11}\ m \tag{14.607}$$

The distance $d_{C-H_{alkane}2sp^3HO}$ along the internuclear axis from the origin of the C atom to the point of intersection of the orbitals is given by:

$$d_{C-H_{alkane}2sp^3HO} = d_{C-H_{alkane},H_2MO} - c' \tag{14.608}$$

Substitution of Eqs. (14.596) and (14.605) into Eq. (14.608) gives:

$$d_{C-H_{alkane}2sp^3HO} = 0.29933a_0 = 1.58400\ X\ 10^{-11}\ m \tag{14.609}$$

The charge-density in each $C-C$-bond MO is increased by a factor of 0.25 with the formation of the $C_{alkane}2sp^3$ HOs each having a smaller radius. Using the orbital composition of the $C-C$-bond MOs (Eq. (14.504)), CH_3 groups (Eq. (14.539)), and the CH_2 groups (Eq. (14.591)), the radii of $C1s = 0.17113a_0$ (Eq. (10.51)), $C_{alkane}2sp^3 = 0.86359a_0$ (Eq. (14.514)), and $C_{alkane}2sp^3 = C_{methylene}2sp^3 = 0.81549a_0$ (Eq. (14.521)) shells, the parameters of the $C-C$-bonds (Eqs. (13.3-13.4), (14.523-14.525), and (14.528-14.538)), the parameters of the $C-H$-bond MOs of the CH_3 groups (Eqs. (13.3-13.4), (14.544-14.545), and (14.547-14.557)), the parameters of the $C-H$-bond MOs of the CH_2 groups (Eqs. (13.3-13.4), (14.595-14.597), and (14.599-14.609)), and the bond-angle parameters (Eqs. (14.562-14.574)), the charge-density of the C_nH_{2n+2} MO comprising the linear combination $2n+2$ $C-H$-bond MOs and $n-1$ $C-C$-bond MOs, each bridging one or more methyl or methylene groups is shown for representative cases where data was available [17-18]. Propane, butane, pentane, hexane, heptane, octane, nonane, decane, undecane, dodecane, and octadecane are shown in Figures 14.18-14.28, respectively. Each $C-H$-bond MO comprises a H_2-type ellipsoidal MO and a $C_{alkane}2sp^3$ HO having the dimensional diagram shown in Figure 14.16. Each $C-C$-bond MO comprises a H_2-type ellipsoidal MO bridging two $C_{alkane}2sp^3$ HOs having the dimensional diagram shown in Figure 14.17.

ENERGIES OF THE CH_2 GROUPS

The energies of each CH_2 group of C_nH_{2n+2} are given by the substitution of the semiprincipal axes (Eqs. (14.595-14.596) and (14.599)) into the energy equations of dihydrogen carbide radical (Eqs. (13.510-13.514)), with the exception that $E\left(C_{alkane},2sp^3\right)$ (Eq. (14.512)) replaces $E\left(C,2sp^3\right)$ in Eq. (13.514):

$$V_e = 2\left(0.91771\right)\frac{-2e^2}{8\pi\varepsilon_0\sqrt{a^2-b^2}}\ln\frac{a+\sqrt{a^2-b^2}}{a-\sqrt{a^2-b^2}} = -70.41425\ eV \tag{14.610}$$

$$V_p = \frac{2e^2}{8\pi\varepsilon_0\sqrt{a^2-b^2}} = 25.78002\ eV \tag{14.611}$$

$$T = 2\left(0.91771\right)\frac{\hbar^2}{2m_e a\sqrt{a^2-b^2}}\ln\frac{a+\sqrt{a^2-b^2}}{a-\sqrt{a^2-b^2}} = 21.06675\ eV \tag{14.612}$$

$$V_m = 2\left(0.91771\right)\frac{-\hbar^2}{4m_e a\sqrt{a^2-b^2}}\ln\frac{a+\sqrt{a^2-b^2}}{a-\sqrt{a^2-b^2}} = -10.53337\ eV \tag{14.613}$$

$$E_{T_{alkane}}\left(CH_2\right) = -\frac{2e^2}{8\pi\varepsilon_0 c'}\left[\left(0.91771\right)\left(2-\frac{1}{2}\frac{a_0}{a}\right)\ln\frac{a+c'}{a-c'}-1\right] - 15.56407\ eV = -49.66493\ eV \tag{14.614}$$

where $E_{T_{alkane}}\left(CH_2\right)$ is given by Eq. (14.592) which is reiteratively matched to Eq. (13.496) within five-significant-figure round off error.

VIBRATION OF THE $^{12}CH_2$ GROUPS

The vibrational energy levels of the $C-H$ bonds of CH_2 in C_nH_{2n+2} may be solved as two equivalent coupled harmonic oscillators by developing the Lagrangian, the differential equation of motion, and the eigenvalue solutions [9] wherein the spring constants are derived from the central forces as given in the Vibration of Hydrogen-Type Molecular Ions section and the Vibration of Hydrogen-Type Molecules section.

THE DOPPLER ENERGY TERMS OF THE $^{12}CH_2$ GROUPS

The equations of the radiation reaction force of the methylene groups in C_nH_{2n+2} are the same as those of the dihydrogen carbide radical with the substitution of the methylene-group parameters. Using Eq. (13.515), the angular frequency of the reentrant oscillation in the transition state is:

$$\omega = \sqrt{\frac{0.75e^2}{\frac{4\pi\varepsilon_0 b^3}{m_e}}} = 2.42751\ X\ 10^{16}\ rad/s \tag{14.615}$$

where b is given by Eq. (14.599). The kinetic energy, E_K, is given by Planck's equation (Eq. (11.127)).

$$\bar{E}_K = \hbar\omega = \hbar 2.42751\ X\ 10^{16}\ rad/s = 15.97831\ eV \tag{14.616}$$

In Eq. (11.181), substitution of $E_T(H_2)$ (Eqs. (11.212) and (13.75)), the maximum total energy of each H_2-type MO, for $E_{h\nu}$, the mass of the electron, m_e, for M, and the kinetic energy given by Eq. (14.616) for $\bar{E}_K$ gives the Doppler energy of the electrons of each of the three bonds for the reentrant orbit:

$$\bar{E}_D \cong E_{h\nu}\sqrt{\frac{2\bar{E}_K}{Mc^2}} = -31.63537\ eV\sqrt{\frac{2e(15.97831\ eV)}{m_e c^2}} = -0.25017\ eV \tag{14.617}$$

In addition to the electrons, the nuclei also undergo simple harmonic oscillation in the transition state at their corresponding frequency. The decrease in the energy of CH_2 due to the reentrant orbit of each bond in the transition state corresponding to simple harmonic oscillation of the electrons and nuclei, $\bar{E}_{osc}$, is given by the sum of the corresponding energies, $\bar{E}_D$ given by Eq. (14.617) and $\bar{E}_{Kvib}$, the average kinetic energy of vibration which is 1/2 of the vibrational energy of each $C-H$ bond. Using ω_e given by Eq. (13.458) for $\bar{E}_{Kvib}$ of the transition state having two independent bonds, $\bar{E}'_{alkane\ osc}(^{12}CH_2)$ per bond is:

$$\bar{E}'_{alkane\ osc}(^{12}CH_2) = \bar{E}_D + \bar{E}_{Kvib} = \bar{E}_D + \frac{1}{2}\hbar\sqrt{\frac{k}{\mu}} \tag{14.618}$$

$$\bar{E}'_{alkane\ osc}(^{12}CH_2) = -0.25017\ eV + \frac{1}{2}(0.35532\ eV) = -0.07251\ eV \tag{14.619}$$

Given that the vibration and reentrant oscillation is for two $C-H$ bonds, $\bar{E}_{alkane\ osc}(^{12}CH_2)$, is:

$$\bar{E}_{alkane\ osc}(^{12}CH_2) = 2\left(\bar{E}_D + \frac{1}{2}\hbar\sqrt{\frac{k}{\mu}}\right) = 2\left(-0.25017\ eV + \frac{1}{2}(0.35532\ eV)\right) = -0.14502\ eV \tag{14.620}$$

TOTAL BOND ENERGIES OF THE $^{12}CH_2$ GROUPS

$E_{alkaneT+osc}(^{12}CH_2)$, the total energy of each $^{12}CH_2$ group including the Doppler term, is given by the sum of $E_{T_{alkane}}(CH_2)$ (Eq. (14.614)) and $\bar{E}_{alkane\ osc}(^{12}CH_2)$ given by Eq. (14.620).

$$\begin{aligned} E_{alkaneT+osc}(^{12}CH_2) &= V_e + T + V_m + V_p + E(C_{alkane}, 2sp^3) + \bar{E}_{alkane\ osc}(^{12}CH_2) \\ &= E_{T_{alkane}}(CH_2) + \bar{E}_{alkane\ osc}(^{12}CH_2) \end{aligned} \tag{14.621}$$

$$E_{alkaneT+osc}(^{12}CH_2) = \left\{ \begin{array}{l} \left(\frac{-2e^2}{8\pi\varepsilon_0 c'}\left[(0.91771)\left(2-\frac{1}{2}\frac{a_0}{a}\right)\ln\frac{a+c'}{a-c'}-1\right]-15.56407\ eV\right) \\ -2\left((31.63536831\ eV)\sqrt{\frac{2\hbar\sqrt{\frac{3}{4}\frac{e^2}{4\pi\varepsilon_0 b^3}}}{m_e c^2}}-\frac{1}{2}\hbar\sqrt{\frac{k}{\mu}}\right) \end{array} \right\} \tag{14.622}$$

$$= -49.66493\ eV - 2\left(0.25017\ eV - \frac{1}{2}\hbar\sqrt{\frac{k}{\mu}}\right)$$

From Eqs. (14.620-14.622), the total energy of each $^{12}CH_2$ is:

$$\begin{aligned} E_{alkaneT+osc}\left(^{12}CH_2\right) &= -49.66493\ eV + \bar{E}_{alkane\ osc}\left(^{12}CH_2\right) \\ &= -49.66493\ eV - 2\left(0.25017\ eV - \frac{1}{2}\left(0.35532\ eV\right)\right) = -49.80996\ eV \end{aligned} \tag{14.623}$$

where ω_e given by Eq. (13.458) was used for the $\hbar\sqrt{\frac{k}{\mu}}$ term.

The derivation of the total CH_2 bond dissociation energy, $E_{D_{alkane}}\left(^{12}CH_2\right)$ follows from that of the bond dissociation energy of dihydrogen carbide radical, $E_D\left(^{12}CH_2\right)$, given by Eqs. (13.524-13.527). $E_{D_{alkane}}\left(^{12}CH_2\right)$ is given by the sum of the initial $C2sp^3$ HO energy, $E\left(C,2sp^3\right)$ (Eq. (14.146)), and two times the energy of the hydrogen atom, $E(H)$ (Eq. (13.154)), minus the sum of $E_{alkaneT+osc}\left(^{12}CH_2\right)$ (Eq. (14.623)) and $E(magnetic)$ (Eq. (13.524)):

$$E_{D_{alkane}}\left(^{12}CH_2\right) = E\left(C,2sp^3\right) + 2E(H) - E_{alkaneT+osc}\left(^{12}CH_2\right) - E\left(magnetic\right) \tag{14.624}$$

Thus, the total $^{12}CH_2$ bond dissociation energy, $E_{D_{alkane}}\left(^{12}CH_2\right)$ is:

$$\begin{aligned} E_{D_{alkane}}\left(^{12}CH_2\right) &= -\left(14.63489\ eV + 2\left(13.59844\ eV\right)\right) - \left(E_{alkaneT+osc}\left(^{12}CH_2\right) + E\left(magnetic\right)\right) \\ &= -41.83177\ eV - \left(-49.80996\ eV + 0.14803\ eV\right) = 7.83016\ eV \end{aligned} \tag{14.625}$$

SUM OF THE ENERGIES OF THE $C-C$ σ MOs AND THE HOs OF CONTINUOUS-CHAIN ALKANES

The energy components of V_e, V_p, T, V_m, and E_T of the $C-C$-bond MOs are the same as those of the CH MO except that energy of the $C_{alkane}2sp^3$ HO is used. The energies of each $C-C$-bond MO are given by the substitution of the semiprincipal axes (Eqs. (14.523-14.524) and (14.528)) into the energy equations of the CH MO (Eqs. (13.449-13.453)), with the exception that $E\left(C_{alkane},2sp^3\right)$ (Eq. (14.512)) replaces $E\left(C,2sp^3\right)$ in Eq. (13.453). The total number of $C-C$ bonds of C_nH_{2n+2} is $n-1$. Thus, the energies of the $n-1$ bonds is given by:

$$V_e = (n-1)(0.91771)\frac{-2e^2}{8\pi\varepsilon_0\sqrt{a^2-b^2}}\ln\frac{a+\sqrt{a^2-b^2}}{a-\sqrt{a^2-b^2}} = -(n-1)28.79214\ eV \tag{14.626}$$

$$V_p = \frac{(n-1)e^2}{8\pi\varepsilon_0\sqrt{a^2-b^2}} = (n-1)9.33352\ eV \tag{14.627}$$

$$T = (n-1)(0.91771)\frac{\hbar^2}{2m_e a\sqrt{a^2-b^2}}\ln\frac{a+\sqrt{a^2-b^2}}{a-\sqrt{a^2-b^2}} = (n-1)6.77464\ eV \tag{14.628}$$

$$V_m = (n-1)(0.91771)\frac{-\hbar^2}{4m_e a\sqrt{a^2-b^2}}\ln\frac{a+\sqrt{a^2-b^2}}{a-\sqrt{a^2-b^2}} = -(n-1)3.38732\ eV \tag{14.629}$$

$$E_{T_{alkane}}(C-C,\sigma) = -\frac{(n-1)e^2}{8\pi\varepsilon_0 c'}\left[(0.91771)\left(2-\frac{1}{2}\frac{a_0}{a}\right)\ln\frac{a+c'}{a-c'}-1\right] - 15.56407\ eV = -(n-1)31.63537\ eV \tag{14.630}$$

where $E_{T_{alkane}}\left(C-C,\sigma\right)$ is the total energy of the $C-C$ σ MOs given by Eq. (14.520) which is reiteratively matched to Eq. (13.75) within five-significant-figure round off error.

Since there are two carbon atoms per bond, the number of $C-C$ bonds is $n-1$, and the energy change of each $C2sp^3$ shell due to the decrease in radius with the formation of each $C-C$-bond MO is $E_{T_{alkane}}\left(C-C,2sp^3\right)$ (Eq. (14.517)), the total energy of the $C-C$-bond MOs, $E_{T_{alkane}}(C-C)$, is given by the sum of $2(n-1)E_{T_{alkane}}\left(C-C,2sp^3\right)$ and $E_{T_{alkane}}\left(C-C,\sigma\right)$, the σ MO contribution given by Eq. (14.630).

$$E_{T_{alkane}}(C-C) = 2(n-1)E_{T_{alkane}}(C-C,2sp^3) + E_{T_{alkane}}(C-C,\sigma)$$
$$= (n-1)\left(\begin{array}{l} 2(-0.92918\ eV) \\ +\left(\begin{array}{l} -\dfrac{e^2}{8\pi\varepsilon_0\sqrt{aa_0}}\left[(0.91771)\left(2-\dfrac{1}{2}\dfrac{a_0}{a}\right)\ln\dfrac{a+\sqrt{aa_0}}{a-\sqrt{aa_0}}-1\right] \\ -15.56407\ eV \end{array}\right) \end{array}\right) \quad (14.631)$$
$$= (n-1)\left(2(-0.92918\ eV)+(-31.63537\ eV)\right) = -(n-1)33.49373\ eV$$

VIBRATION OF CONTINUOUS-CHAIN ALKANES

The vibrational energy levels of the $C-C$ bonds of C_nH_{2n+2} may be solved as $n-1$ sets of coupled carbon harmonic oscillators wherein each carbon is further coupled to two or three equivalent H harmonic oscillators by developing the Lagrangian, the differential equation of motion, and the eigenvalue solutions [9] wherein the spring constants are derived from the central forces as given in the Vibration of Hydrogen-Type Molecular Ions section and the Vibration of Hydrogen-Type Molecules section.

THE DOPPLER ENERGY TERMS OF THE $C-C$-BOND MOs OF CONTINUOUS-CHAIN ALKANES

The equations of the radiation reaction force of each symmetrical $C-C$-bond MO are given by Eqs. (11.231-11.233), except the force-constant factor is 0.5 based on the force constant k' of Eq. (14.152), and the $C-C$-bond MO parameters are used. The angular frequency of the reentrant oscillation in the transition state is:

$$\omega = \sqrt{\frac{0.5e^2}{4\pi\varepsilon_0 a^3}} = 9.43699\ X\ 10^{15}\ rad/s \quad (14.632)$$

where a is given by Eq. (14.523). The kinetic energy, E_K, is given by Planck's equation (Eq. (11.127)).

$$\bar{E}_K = \hbar\omega = \hbar 9.43699\ X\ 10^{15}\ rad/s = 6.21159\ eV \quad (14.633)$$

In Eq. (11.181), substitution of $E_{T_{alkane}}(C-C)$ (Eq. (14.631)) with $n=2$ for $E_{h\nu}$, the mass of the electron, m_e, for M, and the kinetic energy given by Eq. (14.633) for $\bar{E}_K$ gives the Doppler energy of the electrons of each of the bonds for the reentrant orbit:

$$\bar{E}_D \cong E_{h\nu}\sqrt{\frac{2\bar{E}_K}{Mc^2}} = -33.49373\ eV\sqrt{\frac{2e(6.21159\ eV)}{m_e c^2}} = -0.16515\ eV \quad (14.634)$$

In addition to the electrons, the nuclei also undergo simple harmonic oscillation in the transition state at their corresponding frequency. The decrease in the energy of each $C-C$-bond MO due to the reentrant orbit of the bond in the transition state corresponding to simple harmonic oscillation of the electrons and nuclei, $\bar{E}_{osc}$, is given by the sum of the corresponding energies, $\bar{E}_D$ given by Eq. (14.634) and $\bar{E}_{Kvib}$, the average kinetic energy of vibration which is 1/2 of the vibrational energy of each $C-C$ bond. Using the ethane experimental $C-C$ $E_{vib}(\upsilon_3)$ of 993 cm^{-1} $(0.12312\ eV)$ [10] for $\bar{E}_{Kvib}$ of the transition state having $n-1$ independent bonds, $\bar{E}'_{alkane\ osc}(C-C,\sigma)$ per bond is:

$$\bar{E}'_{alkane\ osc}(C-C,\sigma) = \bar{E}_D + \bar{E}_{Kvib} = \bar{E}_D + \frac{1}{2}\hbar\sqrt{\frac{k}{\mu}} \quad (14.635)$$

$$\bar{E}'_{alkane\ osc}(C-C,\sigma) = -0.16515\ eV + \frac{1}{2}(0.12312\ eV) = -0.10359\ eV \quad (14.636)$$

Given that the vibration and reentrant oscillation is for $n-1$ $C-C$ bonds, $\bar{E}_{alkane\ osc}(C-C,\sigma)$, is:

$$\bar{E}_{alkane\ osc}(C-C,\sigma) = (n-1)\left(\bar{E}_D + \frac{1}{2}\hbar\sqrt{\frac{k}{\mu}}\right)$$
$$= (n-1)\left(-0.16515\ eV + \frac{1}{2}(0.12312\ eV)\right) = -(n-1)0.10359\ eV \quad (14.637)$$

TOTAL ENERGIES OF THE $C-C$-BOND MOs OF CONTINUOUS-CHAIN ALKANES

$E_{alkaneT+osc}(C-C)$, the total energy of the $n-1$ bonds of the $C-C$-bond MOs including the Doppler term, is given by the sum of $E_{T_{alkane}}(C-C)$ (Eq. (14.631)) and $\bar{E}_{alkane\ osc}(C-C,\sigma)$ given by Eq. (14.637).

$$
\begin{aligned}
E_{alkaneT+osc}(C-C) &= \left((n-1)\begin{pmatrix} V_e+T+V_m+V_p+E\left(C_{alkane},2sp^3\right) \\ +2E_{T_{alkane}}\left(C-C,2sp^3\right) \end{pmatrix} + \bar{E}_{alkane\ osc}(C-C,\sigma) \right) \\
&= E_{T_{alkane}}(C-C,\sigma) + 2(n-1)E_{T_{alkane}}\left(C-C,2sp^3\right) + \bar{E}_{alkane\ osc}(C-C,\sigma) \\
&= E_{T_{alkane}}(C-C) + \bar{E}_{alkane\ osc}(C-C,\sigma)
\end{aligned} \tag{14.638}
$$

$$
E_{alkaneT+osc}(C-C) = (n-1)\left\{ \begin{pmatrix} \frac{-e^2}{8\pi\varepsilon_0 c'}\left[(0.91771)\left(2-\frac{1}{2}\frac{a_0}{a}\right)\ln\frac{a+c'}{a-c'}-1 \right] \\ -15.56407\ eV + 2E_{T_{alkane}}\left(C-C,2sp^3\right) \end{pmatrix} \right\}
$$

$$
\left\{ \begin{pmatrix} 1+\sqrt{\dfrac{2\hbar\sqrt{\dfrac{1}{2}\dfrac{e^2}{4\pi\varepsilon_0 a^3}}}{m_e c^2}} \end{pmatrix} + \frac{1}{2}\hbar\sqrt{\frac{k}{\mu}} \right\} \tag{14.639}
$$

$$
= (n-1)\left(-33.49373\ eV - 0.16515\ eV + \frac{1}{2}\hbar\sqrt{\frac{k}{\mu}} \right)
$$

From Eqs. (14.637-14.639), the total energy of the $n-1$ bonds of the $C-C$ -bond MOs is:

$$
\begin{aligned}
E_{alkaneT+osc}(C-C) &= (n-1)\left(-31.63537\ eV + 2E_{T_{alkane}}\left(C-C,2sp^3\right)\right) + \bar{E}_{alkane\ osc}(C-C,\sigma) \\
&= (n-1)\begin{pmatrix} -31.63537\ eV + 2(-0.92918\ eV) \\ -0.16515\ eV + \frac{1}{2}(0.12312\ eV) \end{pmatrix} = -(n-1)33.59732\ eV
\end{aligned} \tag{14.640}
$$

where the experimental E_{vib} was used for the $\hbar\sqrt{\frac{k}{\mu}}$ term.

TOTAL BOND ENERGY OF THE $C-C$ BONDS OF CONTINUOUS-CHAIN ALKANES

Since there are two carbon atoms per bond and the number of $C-C$ bonds is $n-1$, the total bond energy of the $C-C$ bonds of C_nH_{2n+2}, $E_D(C-C)_{n-1}$, is given by $2(n-1)E\left(C,2sp^3\right)$ minus $E_{alkaneT+osc}(C-C)$ (Eq. (14.640)) where $E\left(C,2sp^3\right)$ (Eq. (14.146)) is the initial energy of each $C2sp^3$ HO of the CH_3 and CH_2 groups that bond to the $C-C$ bonds. Thus, the total dissociation energy of the $C-C$ bonds of C_nH_{2n+2}, is:

$$
\begin{aligned}
E_D(C-C)_{n-1} &= 2(n-1)\left(E\left(C,2sp^3\right)\right) - \left(E_{alakneT+osc}(C-C)\right) \\
&= 2(n-1)(-14.63489\ eV) - (n-1)(-33.59732\ eV) \\
&= (n-1)\left(2(-14.63489\ eV) - (-33.59732\ eV)\right) = (n-1)(4.32754\ eV)
\end{aligned} \tag{14.641}
$$

TOTAL ENERGY OF CONTINUOUS-CHAIN ALKANES

$E_D\left(C_nH_{2n+2}\right)$, the total bond dissociation energy of C_nH_{2n+2}, is given as the sum of the energy components due to the two methyl groups, $n-2$ methylene groups, and $n-1$ $C-C$ bonds where each energy component is given by Eqs. (14.590), (14.625), and (14.641), respectively. Thus, the total bond dissociation energy of C_nH_{2n+2} is:

$$
\begin{aligned}
E_D\left(C_nH_{2n+2}\right) &= E_D(C-C)_{n-1} + 2E_{D_{alkane}}\left({}^{12}CH_3\right) + (n-2)E_{D_{alkane}}\left({}^{12}CH_2\right) \\
&= (n-1)(4.32754\ eV) + 2(12.49186\ eV) + (n-2)(7.83016\ eV)
\end{aligned} \tag{14.642}
$$

The experimental total bond dissociation energy of C_nH_{2n+2}, $E_{D_{\exp}}\left(C_nH_{2n+2}\right)$, is given by the negative difference between the enthalpy of its formation ($\Delta H_f\left(C_nH_{2n+2}(gas)\right)$) and the sum of the enthalpy of the formation of the reactant gaseous carbons ($\Delta H_f\left(C(gas)\right)$) and hydrogen ($\Delta H_f\left(H(gas)\right)$) atoms:

$$
\begin{aligned}
E_{D_{\exp}}\left(C_nH_{2n+2}\right) &= -\left\{\Delta H_f\left(C_nH_{2n+2}(gas)\right) - \left[n\Delta H_f\left(C(gas)\right) + (2n+2)\Delta H_f\left(H(gas)\right)\right]\right\} \\
&= -\left\{\Delta H_f\left(C_nH_{2n+2}(gas)\right) - \left[n7.42774\ eV + (2n+2)2.259353\ eV\right]\right\}
\end{aligned} \tag{14.643}
$$

where the heats of formation atomic carbon and hydrogen gas are given by [17-18]:

$$
\Delta H_f\left(C(gas)\right) = 716.68\ kJ/mole\ \left(7.42774\ eV/atom\right) \tag{14.644}
$$

$$\Delta H_f\left(H\left(gas\right)\right)=217.998\ kJ/mole\ \left(2.259353\ eV/atom\right) \tag{14.645}$$

Using the corresponding experimental $\Delta H_f\left(C_nH_{2n+2}\left(gas\right)\right)$ [18], $E_D\left(C_nH_{2n+2}\right)$ was determined for propane, butane, pentane, hexane, heptane, octane, nonane, decane, undecane, dodecane, and octadecane in the corresponding sections, and the results of the determination of the total energies are given in Table 14.1. The calculated results are based on first principles and given in closed-form, exact equations containing fundamental constants only. The agreement between the experimental and calculated results is excellent.

Using the results for C_nH_{2n+2} and the functional groups as basis sets that are linearly combined, the exact solution for the dimensional parameters, charge density functions, and energies of all molecules can be obtained. For example, one or more of the hydrogen atoms of the solution for C_nH_{2n+2} can be substituted with one or more of the previously solved functional groups or derivative functional groups to give a desired molecule. The solution is given by energy matching each group to C_nH_{2n+2}. Substitution of one or more H's of C_nH_{2n+2} with functional groups from the list of CH_3, other C_nH_{2n+2} groups, $H_2C=CH_2$, $HC\equiv CH$, F, Cl, O, OH, NH, NH_2, CN, NO, NO_2, CO, CO_2, and C_6H_6 give the solutions of branched alkanes, alkenes, and alkynes, alkyl halides, ethers, alcohols, amides, amines, nitriles, alkyl nitrosos, alkyl nitrates, aldehydes, ketones, carbolylic acids, esters, and substituted aromatics.

PROPANE (C_3H_8)

Using Eq. (14.642) with $n=3$, the total bond dissociation energy of C_3H_8 is:

$$\begin{aligned}E_D\left(C_3H_8\right)&=E_D\left(C-C\right)_2+2E_{D_{alkane}}\left(^{12}CH_3\right)+E_{D_{alkane}}\left(^{12}CH_2\right)\\&=\left(2\right)\left(4.32754\ eV\right)+\left(2\right)\left(12.49186\ eV\right)+\left(1\right)\left(7.83016\ eV\right)=41.46896\ eV\end{aligned} \tag{14.646}$$

Using Eq. (14.643), the experimental total bond dissociation energy of C_3H_8, $E_{D_{\exp}}\left(C_3H_8\right)$, given by the negative difference between the enthalpy of its formation ($\Delta H_f\left(C_3H_8\left(gas\right)=-1.0758\ eV\right)$) [18] and the sum of the enthalpy of the formation of the gaseous carbons ($\Delta H_f\left(C\left(gas\right)\right)$) and hydrogen ($\Delta H_f\left(H\left(gas\right)\right)$) atoms is:

$$\begin{aligned}E_{D_{\exp}}\left(C_3H_8\right)&=-\left\{\Delta H_f\left(C_3H_8\left(gas\right)\right)-\left[3\Delta H_f\left(C\left(gas\right)\right)+8\Delta H_f\left(H\left(gas\right)\right)\right]\right\}\\&=-\left\{-1.0758\ eV-\left[\left(3\right)7.42774\ eV+\left(8\right)2.259353\ eV\right]\right\}=41.434\ eV\end{aligned} \tag{14.647}$$

The charge-density of the C_3H_8 molecular orbital (MO) comprising a linear combination of two methyl groups and one methylene group is shown in Figure 14.18.

Figure 14.18. C_3H_8 MO comprising a linear combination of $C-H$-bond MOs and $C-C$-bond MOs of the two methyl groups and one methylene group. (A) Color scale, translucent view of the charge-density of the $C-C$-bond and $C-H$-bond MOs and the $C_{\text{propane}}2sp^3$ HOs. Each $C-C$-bond MO comprises a H_2-type ellipsoidal MO bridging two $C_{propane}2sp^3$ HOs. For each $C-H$ and the $C-C$ bond, the ellipsoidal surface of the H_2-type ellipsoidal MO that transitions to the $C_{propane}2sp^3$ HO, the $C_{propane}2sp^3$ HO shell, inner most $C1s$ shell, and the nuclei (red, not to scale), are shown. (B) Opaque view highlighting the $C-C$-bond MOs of the charge-density of the C_3H_8 MO.

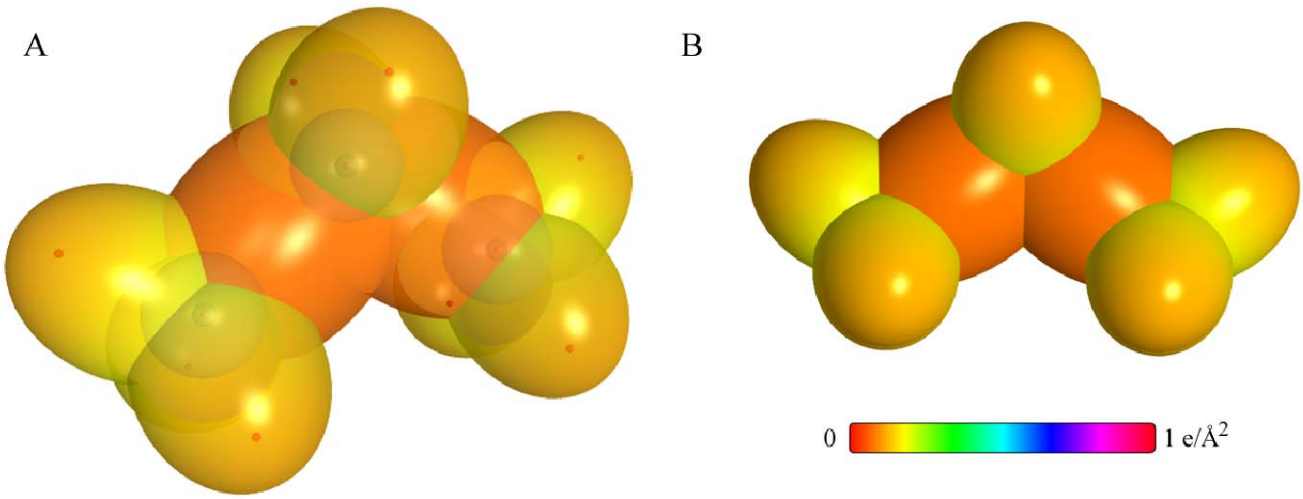

BUTANE (C_4H_{10})

Using Eq. (14.642) with $n=4$, the total bond dissociation energy of C_4H_{10} is:

$$\begin{aligned} E_D\left(C_4H_{10}\right) &= E_D\left(C-C\right)_3 + 2E_{D_{alkane}}\left({}^{12}CH_3\right) + 2E_{D_{alkane}}\left({}^{12}CH_2\right) \\ &= (3)(4.32754\ eV) + (2)(12.49186\ eV) + (2)(7.83016\ eV) \\ &= 53.62666\ eV \end{aligned} \tag{14.648}$$

Using Eq. (14.643), the experimental total bond dissociation energy of C_4H_{10}, $E_{D_{exp}}\left(C_4H_{10}\right)$, given by the negative difference between the enthalpy of its formation ($\Delta H_f\left(C_4H_{10}\left(gas\right)\right) = -1.3028\ eV$) [18] and the sum of the enthalpy of the formation of the gaseous carbons ($\Delta H_f\left(C\left(gas\right)\right)$) and hydrogen ($\Delta H_f\left(H\left(gas\right)\right)$) atoms is:

$$\begin{aligned} E_{D_{exp}}\left(C_4H_{10}\right) &= -\left\{\Delta H_f\left(C_4H_{10}\left(gas\right)\right) - \left[4\Delta H_f\left(C\left(gas\right)\right) + 10\Delta H_f\left(H\left(gas\right)\right)\right]\right\} \\ &= -\left\{-1.3028\ eV - \left[(4)7.42774\ eV + (10)2.259353\ eV\right]\right\} \\ &= 53.61\ eV \end{aligned} \tag{14.649}$$

The charge-density of the C_4H_{10} molecular orbital (MO) comprising a linear combination of two methyl and two methylene groups is shown in Figure 14.19.

Figure 14.19. C_4H_{10} MO comprising a linear combination of $C-H$-bond MOs and $C-C$-bond MOs of the two methyl and two methylene groups. (A) Color scale, translucent view of the charge-density of the $C-C$-bond and $C-H$-bond MOs and the $C_{\text{butane}}2sp^3$ HOs. Each $C-C$-bond MO comprises a H_2-type ellipsoidal MO bridging two $C_{\text{butane}}2sp^3$ HOs. For each $C-H$ and the $C-C$ bond, the ellipsoidal surface of the H_2-type ellipsoidal MO that transitions to the $C_{\text{butane}}2sp^3$ HO, the $C_{\text{butane}}2sp^3$ HO shell, inner most $C1s$ shell, and the nuclei (red, not to scale), are shown. (B) Opaque view highlighting the $C-C$-bond MOs of the charge-density of the C_4H_{10} MO.

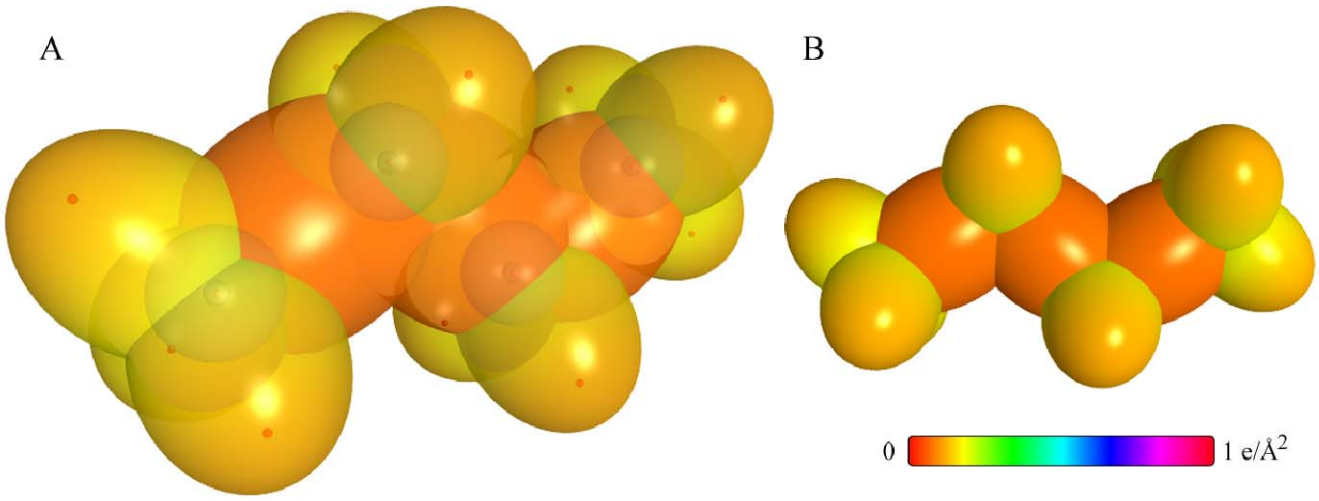

PENTANE (C_5H_{12})

Using Eq. (14.642) with $n=5$, the total bond dissociation energy of C_5H_{12} is:

$$\begin{aligned} E_D\left(C_5H_{12}\right) &= E_D\left(C-C\right)_4 + 2E_{D_{alkane}}\left({}^{12}CH_3\right) + 3E_{D_{alkane}}\left({}^{12}CH_2\right) \\ &= (4)(4.32754\ eV) + (2)(12.49186\ eV) + (3)(7.83016\ eV) \\ &= 65.78436\ eV \end{aligned} \tag{14.650}$$

Using Eq. (14.643), the experimental total bond dissociation energy of C_5H_{12}, $E_{D_{\exp}}\left(C_5H_{12}\right)$, given by the negative difference between the enthalpy of its formation ($\Delta H_f\left(C_5H_{12}\left(gas\right)=-1.5225\ eV\right)$) [18] and the sum of the enthalpy of the formation of the gaseous carbons ($\Delta H_f\left(C\left(gas\right)\right)$) and hydrogen ($\Delta H_f\left(H\left(gas\right)\right)$) atoms is:

$$\begin{aligned} E_{D_{\exp}}\left(C_5H_{12}\right) &= -\left\{\Delta H_f\left(C_5H_{12}\left(gas\right)\right) - \left[5\Delta H_f\left(C\left(gas\right)\right) + 12\Delta H_f\left(H\left(gas\right)\right)\right]\right\} \\ &= -\left\{-1.5225\ eV - \left[(5)7.42774\ eV + (12)2.259353\ eV\right]\right\} \\ &= 65.77\ eV \end{aligned} \tag{14.651}$$

The charge-density of the C_5H_{12} molecular orbital (MO) comprising a linear combination of two methyl and three methylene groups is shown in Figure 14.20.

Figure 14.20. C_5H_{12} MO comprising a linear combination of $C-H$-bond MOs and $C-C$-bond MOs of the two methyl and three methylene groups. (A) Color scale, translucent view of the charge-density of the $C-C$-bond and $C-H$-bond MOs and the $C_{\text{pentane}}2sp^3$ HOs. Each $C-C$-bond MO comprises a H_2-type ellipsoidal MO bridging two $C_{\text{pentane}}2sp^3$ HOs. For each $C-H$ and the $C-C$ bond, the ellipsoidal surface of the H_2-type ellipsoidal MO that transitions to the $C_{\text{pentane}}2sp^3$ HO, the $C_{\text{pentane}}2sp^3$ HO shell, inner most $C1s$ shell, and the nuclei (red, not to scale), are shown. (B) Opaque view highlighting the $C-C$-bond MOs of the charge-density of the C_5H_{12} MO.

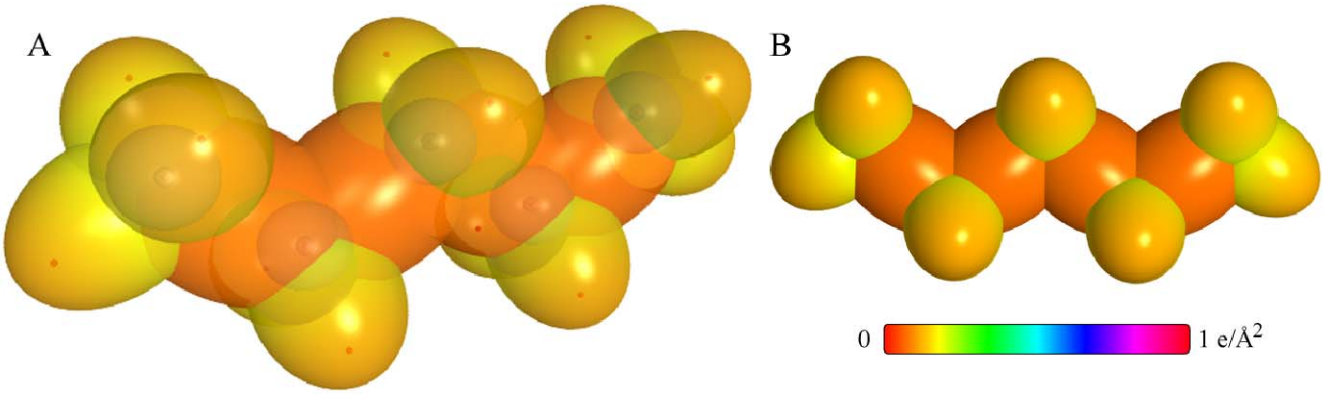

HEXANE (C_6H_{14})

Using Eq. (14.642) with $n=6$, the total bond dissociation energy of C_6H_{14} is:

$$\begin{aligned} E_D\left(C_6H_{14}\right) &= E_D\left(C-C\right)_5 + 2E_{D_{alkane}}\left({}^{12}CH_3\right) + 4E_{D_{alkane}}\left({}^{12}CH_2\right) \\ &= (5)(4.32754\ eV) + (2)(12.49186\ eV) + (4)(7.83016\ eV) \\ &= 77.94206\ eV \end{aligned} \tag{14.652}$$

Using Eq. (14.643), the experimental total bond dissociation energy of C_6H_{14}, $E_{D_{exp}}\left(C_6H_{14}\right)$, given by the negative difference between the enthalpy of its formation ($\Delta H_f\left(C_6H_{14}\left(gas\right)=-1.7298\ eV\right)$) [18] and the sum of the enthalpy of the formation of the gaseous carbons ($\Delta H_f\left(C\left(gas\right)\right)$) and hydrogen ($\Delta H_f\left(H\left(gas\right)\right)$) atoms is:

$$\begin{aligned} E_{D_{exp}}\left(C_6H_{14}\right) &= -\left\{\Delta H_f\left(C_6H_{14}\left(gas\right)\right) - \left[6\Delta H_f\left(C\left(gas\right)\right) + 14\Delta H_f\left(H\left(gas\right)\right)\right]\right\} \\ &= -\left\{-1.7298\ eV - \left[(6)7.42774\ eV + (14)2.259353\ eV\right]\right\} \\ &= 77.93\ eV \end{aligned} \tag{14.653}$$

The charge-density of the C_6H_{14} molecular orbital (MO) comprising a linear combination of two methyl and four methylene groups is shown in Figure 14.21.

Figure 14.21. C_6H_{14} MO comprising a linear combination of $C-H$-bond MOs and $C-C$-bond MOs of the two methyl and four methylene groups. (A) Opaque view of the charge-density of the $C-C$-bond and $C-H$-bond MOs. Each $C-C$-bond MO comprises a H_2-type ellipsoidal MO bridging two $C_{\text{hexane}}2sp^3$ HOs. (B) Translucent view high-lighting the $C-C$-bond MOs of the charge-density of the C_6H_{14} MO. For each $C-H$ and the $C-C$ bond, the ellipsoidal surface of the H_2-type ellipsoidal MO that transitions to the $C_{\text{hexane}}2sp^3$ HO, the $C_{\text{hexane}}2sp^3$ HO shell, inner most $C1s$ shell, and the nuclei (red, not to scale), are shown.

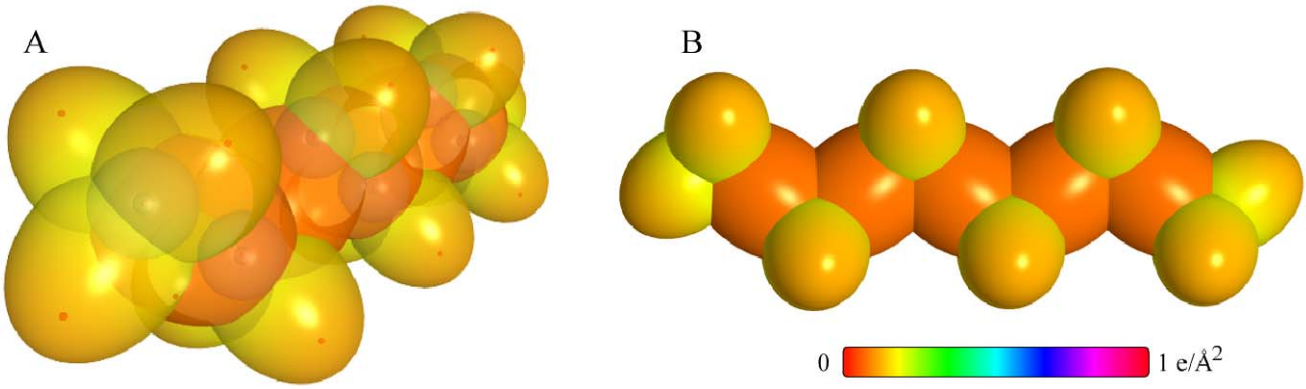

HEPTANE (C_7H_{16})

Using Eq. (14.642) with $n=7$, the total bond dissociation energy of C_7H_{16} is:

$$\begin{aligned} E_D\left(C_7H_{16}\right) &= E_D\left(C-C\right)_6 + 2E_{D_{alkane}}\left({}^{12}CH_3\right) + 5E_{D_{alkane}}\left({}^{12}CH_2\right) \\ &= (6)(4.32754\ eV) + (2)(12.49186\ eV) + (5)(7.83016\ eV) \\ &= 90.09976\ eV \end{aligned} \tag{14.654}$$

Using Eq. (14.643), the experimental total bond dissociation energy of C_7H_{16}, $E_{D_{exp}}\left(C_7H_{16}\right)$, given by the negative difference between the enthalpy of its formation ($\Delta H_f\left(C_7H_{16}\left(gas\right)=-1.9443\ eV\right)$) [18] and the sum of the enthalpy of the formation of the gaseous carbons ($\Delta H_f\left(C\left(gas\right)\right)$) and hydrogen ($\Delta H_f\left(H\left(gas\right)\right)$) atoms is:

$$\begin{aligned} E_{D_{\exp}}\left(C_7H_{16}\right) &= -\left\{\Delta H_f\left(C_7H_{16}\left(gas\right)\right) - \left[7\Delta H_f\left(C\left(gas\right)\right) + 16\Delta H_f\left(H\left(gas\right)\right)\right]\right\} \\ &= -\left\{-1.9443\ eV - \left[(7)7.42774\ eV + (16)2.259353\ eV\right]\right\} \\ &= 90.09\ eV \end{aligned} \tag{14.655}$$

The charge-density of the C_7H_{16} MO comprising a linear combination of two methyl and five methylene groups is shown in Figure 14.22.

Figure 14.22. C_7H_{16} MO comprising a linear combination of $C-H$-bond MOs and $C-C$-bond MOs of the two methyl and five methylene groups. (A) Opaque view of the charge-density of the $C-C$-bond and $C-H$-bond MOs. Each $C-C$-bond MO comprises a H_2-type ellipsoidal MO bridging two $C_{\text{heptane}}2sp^3$ HOs. (B) Translucent view high-lighting the $C-C$-bond MOs of the charge-density of the C_7H_{16} MO. For each $C-H$ and the $C-C$ bond, the ellipsoidal surface of the H_2-type ellipsoidal MO that transitions to the $C_{\text{heptane}}2sp^3$ HO, the $C_{\text{heptane}}2sp^3$ HO shell, inner most $C1s$ shell, and the nuclei (red, not to scale), are shown.

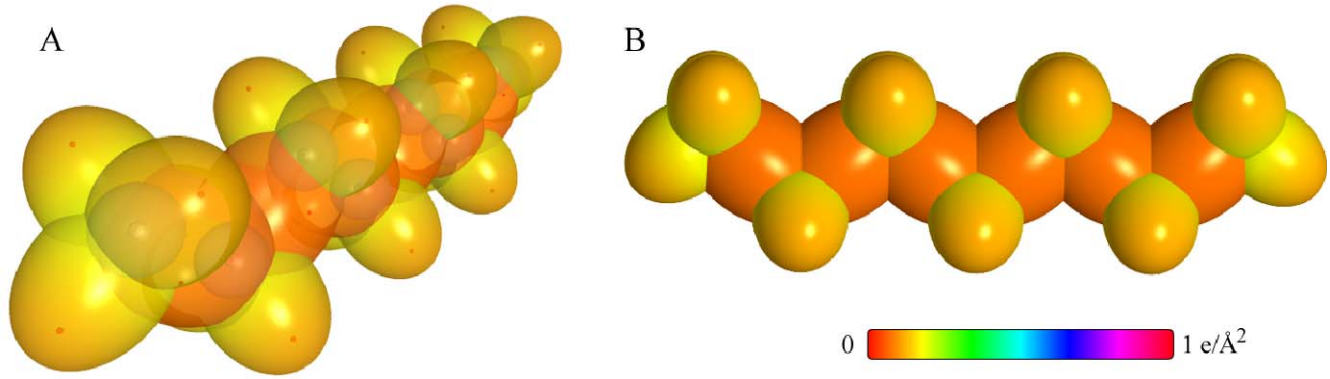

OCTANE (C_8H_{18})

Using Eq. (14.642) with $n=8$, the total bond dissociation energy of C_8H_{18} is:

$$\begin{aligned} E_D\left(C_8H_{18}\right) &= E_D\left(C-C\right)_7 + 2E_{D_{alkane}}\left({}^{12}CH_3\right) + 6E_{D_{alkane}}\left({}^{12}CH_2\right) \\ &= (7)(4.32754\ eV) + (2)(12.49186\ eV) + (6)(7.83016\ eV) \\ &= 102.25746\ eV \end{aligned} \tag{14.656}$$

Using Eq. (14.643), the experimental total bond dissociation energy of C_8H_{18}, $E_{D_{\exp}}\left(C_8H_{18}\right)$, given by the negative difference between the enthalpy of its formation ($\Delta H_f\left(C_8H_{18}\left(gas\right)\right) = -2.1609\ eV$) [18] and the sum of the enthalpy of the formation of the gaseous carbons ($\Delta H_f\left(C\left(gas\right)\right)$) and hydrogen ($\Delta H_f\left(H\left(gas\right)\right)$) atoms is:

$$\begin{aligned} E_{D_{\exp}}\left(C_8H_{18}\right) &= -\left\{\Delta H_f\left(C_8H_{18}\left(gas\right)\right) - \left[8\Delta H_f\left(C\left(gas\right)\right) + 18\Delta H_f\left(H\left(gas\right)\right)\right]\right\} \\ &= -\left\{-2.1609\ eV - \left[(8)7.42774\ eV + (18)2.259353\ eV\right]\right\} \\ &= 102.25\ eV \end{aligned} \tag{14.657}$$

The charge-density of the C_8H_{18} MO comprising a linear combination of two methyl and six methylene groups is shown in Figure 14.23.

Figure 14.23. C_8H_{18} MO comprising a linear combination of $C-H$-bond MOs and $C-C$-bond MOs of the two methyl and six methylene groups. (A) Opaque view of the charge-density of the $C-C$-bond and $C-H$-bond MOs. Each $C-C$-bond MO comprises a H_2-type ellipsoidal MO bridging two $C_{\text{octane}}2sp^3$ HOs. (B) Translucent view high-lighting the $C-C$-bond MOs of the charge-density of the C_8H_{18} MO. For each $C-H$ and the $C-C$ bond, the ellipsoidal surface of the H_2-type ellipsoidal MO that transitions to the $C_{\text{octane}}2sp^3$ HO, the $C_{\text{octane}}2sp^3$ HO shell, inner most $C1s$ shell, and the nuclei (red, not to scale), are shown.

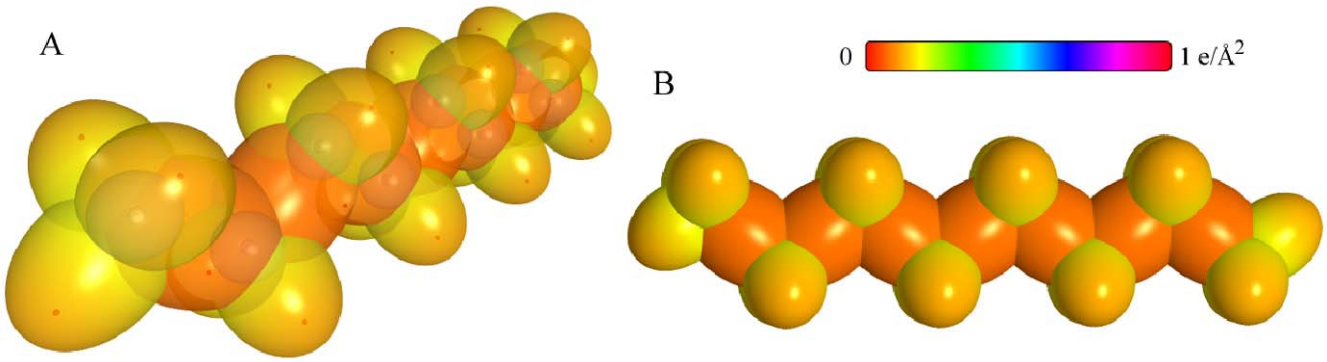

NONANE (C_9H_{20})

Using Eq. (14.642) with $n=9$, the total bond dissociation energy of C_9H_{20} is:

$$\begin{aligned} E_D\left(C_9H_{20}\right) &= E_D\left(C-C\right)_8 + 2E_{D_{alkane}}\left({}^{12}CH_3\right) + 7E_{D_{alkane}}\left({}^{12}CH_2\right) \\ &= (8)(4.32754\ eV) + (2)(12.49186\ eV) + (7)(7.83016\ eV) \\ &= 114.41516\ eV \end{aligned} \tag{14.658}$$

Using Eq. (14.643), the experimental total bond dissociation energy of C_9H_{20}, $E_{D_{\exp}}\left(C_9H_{20}\right)$, given by the negative difference between the enthalpy of its formation ($\Delta H_f\left(C_9H_{20}\left(gas\right)\right) = -2.3651\ eV$) [18] and the sum of the enthalpy of the formation of the gaseous carbons ($\Delta H_f\left(C\left(gas\right)\right)$) and hydrogen ($\Delta H_f\left(H\left(gas\right)\right)$) atoms is:

$$\begin{aligned} E_{D_{\exp}}\left(C_9H_{20}\right) &= -\left\{\Delta H_f\left(C_9H_{20}\left(gas\right)\right) - \left[9\Delta H_f\left(C\left(gas\right)\right) + 20\Delta H_f\left(H\left(gas\right)\right)\right]\right\} \\ &= -\left\{-2.3651\ eV - \left[(9)7.42774\ eV + (20)2.259353\ eV\right]\right\} \\ &= 114.40\ eV \end{aligned} \tag{14.659}$$

The charge-density of the C_9H_{20} MO comprising a linear combination of two methyl and seven methylene groups is shown in Figure 14.24.

Figure 14.24. C_9H_{20} MO comprising a linear combination of $C-H$-bond MOs and $C-C$-bond MOs of the two methyl and seven methylene groups. (A) Opaque view of the charge-density of the $C-C$-bond and $C-H$-bond MOs. Each $C-C$-bond MO comprises a H_2-type ellipsoidal MO bridging two $C_{\text{nonane}}2sp^3$ HOs. (B) Translucent view high-lighting the $C-C$-bond MOs of the charge-density of the C_9H_{20} MO. For each $C-H$ and the $C-C$ bond, the ellipsoidal surface of the H_2-type ellipsoidal MO that transitions to the $C_{\text{nonane}}2sp^3$ HO, the $C_{\text{nonane}}2sp^3$ HO shell, inner most $C1s$ shell, and the nuclei (red, not to scale), are shown.

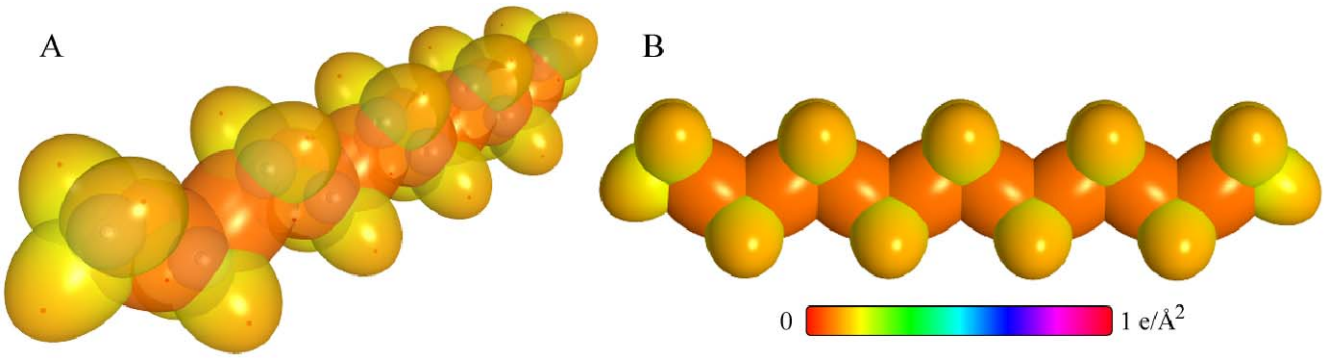

DECANE ($C_{10}H_{22}$)

Using Eq. (14.642) with $n=10$, the total bond dissociation energy of $C_{10}H_{22}$ is:

$$\begin{aligned} E_D\left(C_{10}H_{22}\right) &= E_D\left(C-C\right)_9 + 2E_{D_{alkane}}\left({}^{12}CH_3\right) + 8E_{D_{alkane}}\left({}^{12}CH_2\right) \\ &= (9)(4.32754\ eV) + (2)(12.49186\ eV) + (8)(7.83016\ eV) \\ &= 126.57286\ eV \end{aligned} \tag{14.660}$$

Using Eq. (14.643), the experimental total bond dissociation energy of $C_{10}H_{22}$, $E_{D_{\exp}}\left(C_{10}H_{22}\right)$, given by the negative difference between the enthalpy of its formation ($\Delta H_f\left(C_{10}H_{22}\left(gas\right)\right) = -2.5858\ eV$) [18] and the sum of the enthalpy of the formation of the gaseous carbons ($\Delta H_f\left(C\left(gas\right)\right)$) and hydrogen ($\Delta H_f\left(H\left(gas\right)\right)$) atoms is:

$$\begin{aligned} E_{D_{\exp}}\left(C_{10}H_{22}\right) &= -\left\{\Delta H_f\left(C_{10}H_{22}\left(gas\right)\right) - \left[10\Delta H_f\left(C\left(gas\right)\right) + 22\Delta H_f\left(H\left(gas\right)\right)\right]\right\} \\ &= -\left\{-2.5858\ eV - \left[(10)7.42774\ eV + (22)2.259353\ eV\right]\right\} \\ &= 126.57\ eV \end{aligned} \tag{14.661}$$

The charge-density of the $C_{10}H_{22}$ molecular orbital (MO) comprising a linear combination of two methyl and eight methylene groups is shown in Figure 14.25.

Figure 14.25. $C_{10}H_{22}$ MO comprising a linear combination of $C-H$-bond MOs and $C-C$-bond MOs of the two methyl and eight methylene groups. (A) Opaque view of the charge-density of the $C-C$-bond and $C-H$-bond MOs. Each $C-C$-bond MO comprises a H_2-type ellipsoidal MO bridging two $C_{\text{decane}}2sp^3$ HOs. (B) Translucent view high-lighting the $C-C$-bond MOs of the charge-density of the $C_{10}H_{22}$ MO. For each $C-H$ and the $C-C$ bond, the ellipsoidal surface of the H_2-type ellipsoidal MO that transitions to the $C_{\text{decane}}2sp^3$ HO, the $C_{\text{decane}}2sp^3$ HO shell, inner most $C1s$ shell, and the nuclei (red, not to scale), are shown.

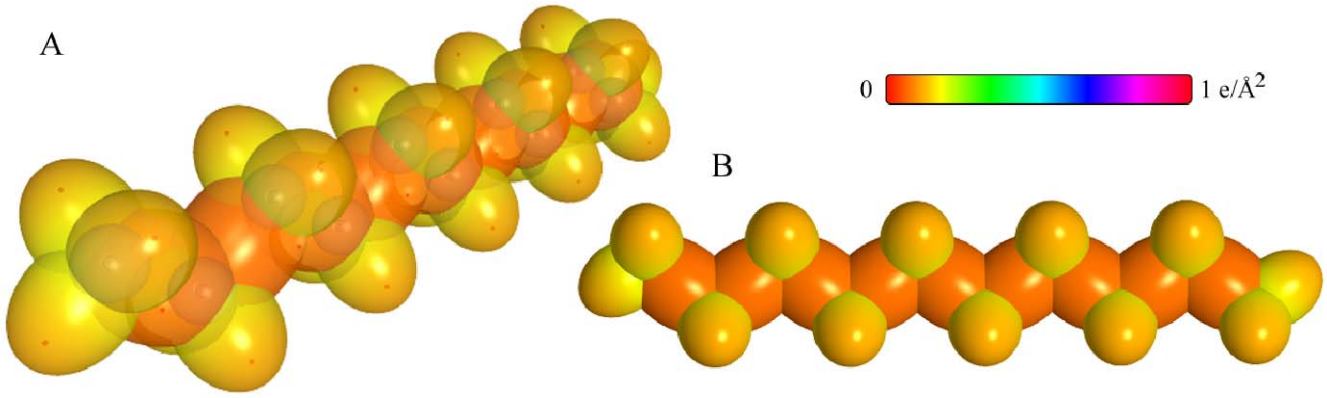

UNDECANE ($C_{11}H_{24}$)

Using Eq. (14.642) with $n=11$, the total bond dissociation energy of $C_{11}H_{24}$ is:

$$\begin{aligned} E_D\left(C_{11}H_{24}\right) &= E_D\left(C-C\right)_{10} + 2E_{D_{alkane}}\left({}^{12}CH_3\right) + 9E_{D_{alkane}}\left({}^{12}CH_2\right) \\ &= (10)(4.32754\ eV) + (2)(12.49186\ eV) + (9)(7.83016\ eV) \\ &= 138.73056\ eV \end{aligned} \tag{14.662}$$

Using Eq. (14.643), the experimental total bond dissociation energy of $C_{11}H_{24}$, $E_{D_{\exp}}\left(C_{11}H_{24}\right)$, given by the negative difference between the enthalpy of its formation ($\Delta H_f\left(C_{11}H_{24}\left(gas\right)\right) = -2.8066\ eV$) [18] and the sum of the enthalpy of the formation of the gaseous carbons ($\Delta H_f\left(C\left(gas\right)\right)$) and hydrogen ($\Delta H_f\left(H\left(gas\right)\right)$) atoms is:

$$\begin{aligned} E_{D_{\exp}}\left(C_{11}H_{24}\right) &= -\left\{\Delta H_f\left(C_{11}H_{24}\left(gas\right)\right) - \left[11\Delta H_f\left(C\left(gas\right)\right) + 24\Delta H_f\left(H\left(gas\right)\right)\right]\right\} \\ &= -\left\{-2.8066\ eV - \left[(11)7.42774\ eV + (24)2.259353\ eV\right]\right\} \\ &= 138.736\ eV \end{aligned} \tag{14.663}$$

The charge-density of the $C_{11}H_{24}$ MO comprising a linear combination of two methyl and nine methylene groups is shown in Figure 14.26.

Figure 14.26. $C_{11}H_{24}$ MO comprising a linear combination of $C-H$-bond MOs and $C-C$-bond MOs of the two methyl and nine methylene groups. (A) Opaque view of the charge-density of the $C-C$-bond and $C-H$-bond MOs. Each $C-C$-bond MO comprises a H_2-type ellipsoidal MO bridging two $C_{\text{undecane}}2sp^3$ HOs. (B) Translucent view high-lighting the $C-C$-bond MOs of the charge-density of the $C_{11}H_{24}$ MO. For each $C-H$ and the $C-C$ bond, the ellipsoidal surface of the H_2-type ellipsoidal MO that transitions to the $C_{\text{undecane}}2sp^3$ HO, the $C_{\text{undecane}}2sp^3$ HO shell, inner most $C1s$ shell, and the nuclei (red, not to scale), are shown.

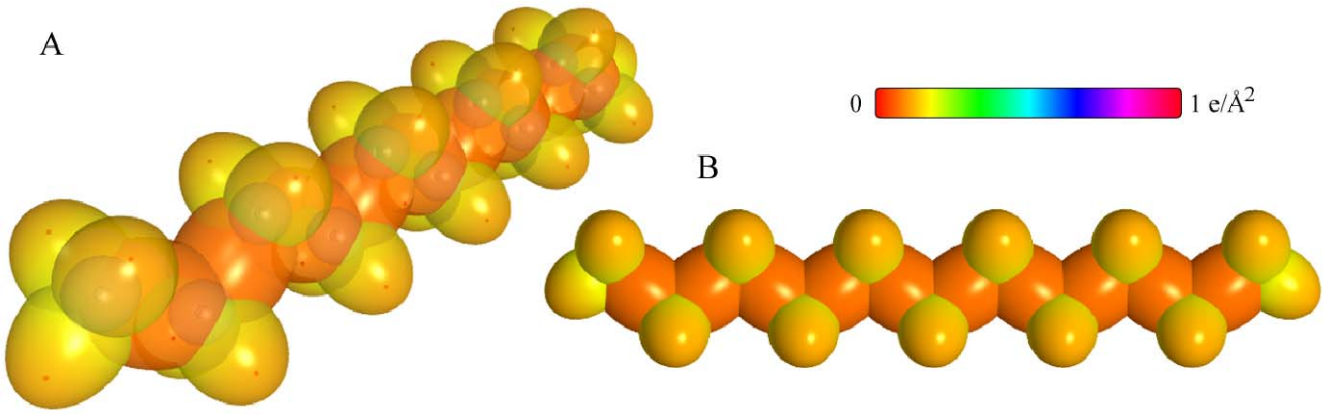

DODECANE ($C_{12}H_{26}$)

Using Eq. (14.642) with $n=12$, the total bond dissociation energy of $C_{12}H_{26}$ is:

$$\begin{aligned} E_D\left(C_{12}H_{26}\right) &= E_D\left(C-C\right)_{11} + 2E_{D_{alkane}}\left({}^{12}CH_3\right) + 10E_{D_{alkane}}\left({}^{12}CH_2\right) \\ &= (11)(4.32754\ eV) + (2)(12.49186\ eV) + (10)(7.83016\ eV) \\ &= 150.88826\ eV \end{aligned} \tag{14.664}$$

Using Eq. (14.643), the experimental total bond dissociation energy of $C_{12}H_{26}$, $E_{D_{\exp}}\left(C_{12}H_{26}\right)$, given by the negative difference between the enthalpy of its formation ($\Delta H_f\left(C_{12}H_{26}\left(gas\right)\right) = -2.9994\ eV$) [18] and the sum of the enthalpy of the formation of the gaseous carbons ($\Delta H_f\left(C\left(gas\right)\right)$) and hydrogen ($\Delta H_f\left(H\left(gas\right)\right)$) atoms is:

$$\begin{aligned} E_{D_{\exp}}\left(C_{12}H_{26}\right) &= -\left\{\Delta H_f\left(C_{12}H_{26}\left(gas\right)\right) - \left[12\Delta H_f\left(C\left(gas\right)\right) + 26\Delta H_f\left(H\left(gas\right)\right)\right]\right\} \\ &= -\left\{-2.9994\ eV - \left[(12)7.42774\ eV + (26)2.259353\ eV\right]\right\} \\ &= 150.88\ eV \end{aligned} \tag{14.665}$$

The charge-density of the $C_{12}H_{26}$ MO comprising a linear combination of two methyl and ten methylene groups is shown in Figure 14.27.

Figure 14.27. $C_{12}H_{26}$ MO comprising a linear combination of $C-H$-bond MOs and $C-C$-bond MOs of the two methyl and ten methylene groups. (A) Opaque view of the charge-density of the $C-C$-bond and $C-H$-bond MOs. Each $C-C$-bond MO comprises a H_2-type ellipsoidal MO bridging two $C_{\text{dodecane}}2sp^3$ HOs. (B) Translucent view high-lighting the $C-C$-bond MOs of the charge-density of the $C_{12}H_{26}$ MO. For each $C-H$ and the $C-C$ bond, the ellipsoidal surface of the H_2-type ellipsoidal MO that transitions to the $C_{\text{dodecane}}2sp^3$ HO, the $C_{\text{dodecane}}2sp^3$ HO shell, inner most $C1s$ shell, and the nuclei (red, not to scale), are shown.

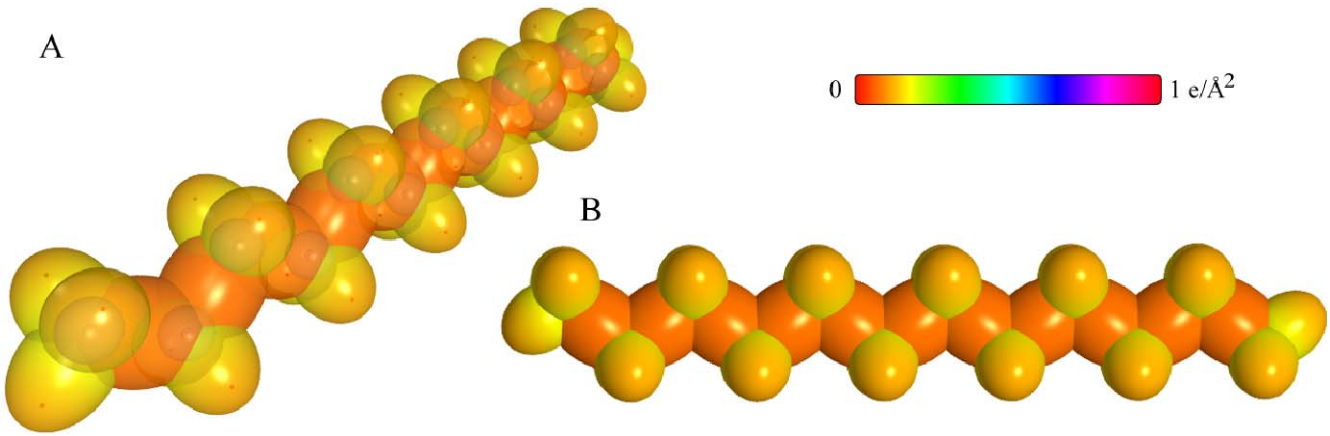

OCTADECANE ($C_{18}H_{38}$)

Using Eq. (14.642) with $n=18$, the total bond dissociation energy of $C_{18}H_{38}$ is:

$$\begin{aligned} E_D\left(C_{18}H_{38}\right) &= E_D\left(C-C\right)_{17} + 2E_{D_{alkane}}\left({}^{12}CH_3\right) + 16E_{D_{alkane}}\left({}^{12}CH_2\right) \\ &= (17)(4.32754\ eV) + (2)(12.49186\ eV) + (16)(7.83016\ eV) \\ &= 223.83446\ eV \end{aligned} \tag{14.666}$$

Using Eq. (14.643), the experimental total bond dissociation energy of $C_{18}H_{38}$, $E_{D_{\exp}}\left(C_{18}H_{38}\right)$, given by the negative difference between the enthalpy of its formation ($\Delta H_f\left(C_{18}H_{38}\left(gas\right)\right) = -4.2970\ eV$) [18] and the sum of the enthalpy of the formation of the gaseous carbons ($\Delta H_f\left(C\left(gas\right)\right)$) and hydrogen ($\Delta H_f\left(H\left(gas\right)\right)$) atoms is:

$$\begin{aligned} E_{D_{\exp}}\left(C_{18}H_{38}\right) &= -\left\{\Delta H_f\left(C_{18}H_{38}\left(gas\right)\right) - \left[18\Delta H_f\left(C\left(gas\right)\right) + 38\Delta H_f\left(H\left(gas\right)\right)\right]\right\} \\ &= -\left\{-4.2970\ eV - \left[(18)7.42774\ eV + (38)2.259353\ eV\right]\right\} \\ &= 223.85\ eV \end{aligned} \tag{14.667}$$

The charge-density of the $C_{18}H_{38}$ molecular orbital (MO) comprising a linear combination of two methyl and sixteen methylene groups is shown in Figure 14.28.

Figure 14.28. $C_{18}H_{38}$ MO comprising a linear combination of $C-H$-bond MOs and $C-C$-bond MOs of the two methyl and sixteen methylene groups. (A) Opaque view of the charge-density of the $C-C$-bond and $C-H$-bond MOs. Each $C-C$-bond MO comprises a H_2-type ellipsoidal MO bridging two $C_{\text{octadecane}}2sp^3$ HOs. (B) Translucent view high-lighting the $C-C$-bond MOs of the charge-density of the $C_{18}H_{38}$ MO. For each $C-H$ and the $C-C$ bond, the ellipsoidal surface of the H_2-type ellipsoidal MO that transitions to the $C_{\text{octadecane}}2sp^3$ HO, the $C_{\text{octadecane}}2sp^3$ HO shell, inner most $C1s$ shell, and the nuclei (red, not to scale), are shown.

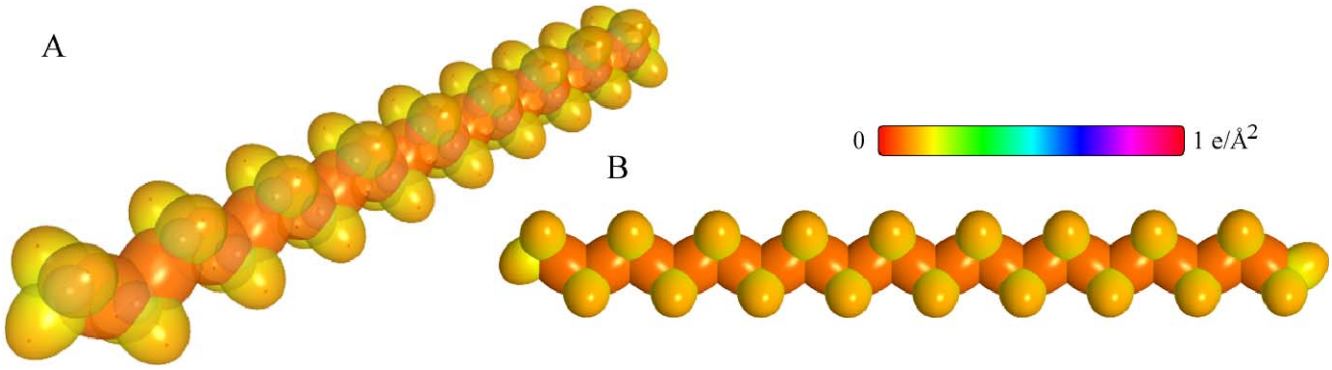

Table 14.1. The calculated and experimental bond parameters of CO_2, NO_2, CH_3CH_3, CH_2CH_2, $CHCH$, benzene, propane, butane, pentane, hexane, heptane, octane, nonane, decane, undecane, dodecane, and octadecane.

Parameter	Calculated	Experimental	Ref. for Exp.
CO_2 Bond Energy	5.49553 eV	5.51577 eV	7
CO_2 Bond Length	1.1616 Å	1.1600 Å	3
NO_2 Bond Energy	3.1532 eV	3.161 eV	7
NO_2 Bond Length	1.1872 Å	1.193 Å	3
NO_2 Bond Angle	131.012°	134.1°	3
H_3C-CH_3 Bond Energy	3.90245 eV	3.8969 eV	7
H_3C-CH_3 Bond Length	1.53635 Å	1.5351 Å	3
$H-CH_2CH_3$ Bond Length	1.10822 Å	1.0940 Å	3
Ethane $H-C-H$ Bond Angle	107.44°	107.4°	8
Ethane $C-C-H$ Bond Angle	111.44°	111.17°	3
$H_2C=CH_2$ Bond Energy	7.55681 eV	7.597 eV	7
$H_2C=CH_2$ Bond Length	1.3405 Å	1.339 Å	3
$H-CHCH_2$ Bond Length	1.0826 Å	1.087 Å	3
Ethylene $H-C-H$ Bond Angle	116.31°	116.6°	11
Ethylene $C=C-H$ Bond Angle	121.85°	121.7°	11
$HC\equiv CH$ Bond Energy	10.07212 eV	10.0014 eV	7
$HC\equiv CH$ Bond Length	1.2007 Å	1.203 Å	3
$H-CCH$ Bond Length	1.0538 Å	1.060 Å	3
Acetylene $C\equiv C-H$ Bond Angle	180°	180°	6
C_6H_6 Total Bond Energy	57.2601 eV	57.26 eV	17-18
Benzene $C=C$ Bond Length	1.3914 Å	1.399 Å	3
$H-C_6H_5$ Bond Length	1.0933 Å	1.101 Å	3
C_6H_6 $C=C=C$ Bond Angle	120°	120°	13-15
C_6H_6 $C=C-H$ Bond Angle	120°	120°	13-15
C_3H_8 Total Bond Energy	41.46896 eV	41.434 eV	17-18
Propane $C-C$ Bond Length	1.5428 Å	1.532 Å	3
Propane $C-H$ Bond Length	1.1097 Å	1.107 Å	3
Alkane $H-C-H$ Bond Angle	109.50°	109.3°	19
Alkane $C-C-H$ Bond Angle	109.44°	109.3°	19
C_4H_{10} Total Bond Energy	53.62666 eV	53.61 eV	17-18
Butane $C-C$ Bond Length	1.5428 Å	1.531 Å	3
Butane $C-H$ Bond Length	1.11713 Å	1.117 Å	3
C_5H_{12} Total Bond Energy	65.78436 eV	65.77 eV	17-18
C_6H_{14} Total Bond Energy	77.94206 eV	77.93 eV	17-18
C_7H_{16} Total Bond Energy	90.09976 eV	90.09 eV	17-18
C_8H_{18} Total Bond Energy	102.25746 eV	102.25 eV	17-18
C_9H_{20} Total Bond Energy	114.41516 eV	114.40 eV	17-18
$C_{10}H_{22}$ Total Bond Energy	126.57286 eV	126.57 eV	17-18
$C_{11}H_{24}$ Total Bond Energy	138.73056 eV	138.736 eV	17-18
$C_{12}H_{26}$ Total Bond Energy	150.88826 eV	150.88 eV	17-18
$C_{18}H_{38}$ Total Bond Energy	223.83446 eV	223.85 eV	17-18

REFERENCES

1. D. R. Lide, *CRC Handbook of Chemistry and Physics*, 79th Edition, CRC Press, Boca Raton, Florida, (1998-9), pp. 4-130 to 4-135.
2. D. R. Lide, *CRC Handbook of Chemistry and Physics*, 79th Edition, CRC Press, Boca Raton, Florida, (1998-9), p. 10-175.
3. D. R. Lide, *CRC Handbook of Chemistry and Physics*, 79th Edition, CRC Press, Boca Raton, Florida, (1998-9), pp. 9-15 to 9-41.
4. M. Karplus, R. N. Porter, *Atoms and Molecules an Introduction for Students of Physical Chemistry*, The Benjamin/Cummings Publishing Company, Menlo Park, California, (1970), pp. 447-484.
5. G. Herzberg, *Molecular Spectra and Molecular Structure II. Infrared and Raman Spectra of Polyatomic Molecules*, Krieger Publishing Company, Malabar, FL, (1945), p. 174.
6. D. R. Lide, *CRC Handbook of Chemistry and Physics*, 79th Edition, CRC Press, Boca Raton, Florida, (1998-9), pp. 9-76 to 9-79.
7. D. R. Lide, *CRC Handbook of Chemistry and Physics*, 79th Edition, CRC Press, Boca Raton, Florida, (1998-9), pp. 9-63 to 9-69.
8. R. L. DeKock, H. B. Gray, *Chemical Structure and Bonding*, The Benjamin/Cummings Publishing Company, Menlo Park, CA, (1980), p. 162.
9. G. R. Fowles, *Analytical Mechanics,* Third Edition, Holt, Rinehart, and Winston, New York, (1977), pp. 251-305.
10. G. Herzberg, *Molecular Spectra and Molecular Structure II. Infrared and Raman Spectra of Polyatomic Molecules*, Van Nostrand Reinhold Company, New York, New York, (1945), p. 344.
11. R. L. DeKock, H. B. Gray, *Chemical Structure and Bonding*, The Benjamin/Cummings Publishing Company, Menlo Park, CA, (1980), p. 179.
12. G. Herzberg, *Molecular Spectra and Molecular Structure II. Infrared and Raman Spectra of Polyatomic Molecules*, Van Nostrand Reinhold Company, New York, New York, (1945), p. 326.
13. W. I. F. David, R. M. Ibberson, G. A. Jeffrey, J. R. Ruble, "The structure analysis of deuterated benzene and deuterated nitromethane by pulsed-neutron powder diffraction: a comparison with single crystal neutron analysis," Physica B (1992), 180 & 181, pp. 597-600.
14. G. A. Jeffrey, J. R. Ruble, R. K. McMullan, J. A. Pople, "The crystal structure of deuterated benzene," Proceedings of the Royal Society of London. Series A, Mathematical and Physical Sciences, Vol. 414, No. 1846, (Nov. 9, 1987), pp. 47-57.
15. H. B. Burgi, S. C. Capelli, "Getting more out of crystal-structure analyses," Helvetica Chimica Acta, Vol. 86, (2003), pp. 1625-1640.
16. G. Herzberg, *Molecular Spectra and Molecular Structure II. Infrared and Raman Spectra of Polyatomic Molecules*, Van Nostrand Reinhold Company, New York, New York, (1945), pp. 362-369.
17. D. R. Lide, *CRC Handbook of Chemistry and Physics*, 79th Edition, CRC Press, Boca Raton, Florida, (1998-9), pp. 9-63.
18. D. R. Lide, *CRC Handbook of Chemistry and Physics*, 79th Edition, CRC Press, Boca Raton, Florida, (1998-9), pp. 5-1 to 5-60.
19. R. J. Fessenden, J. S. Fessenden, *Organic Chemistry*, Willard Grant Press. Boston, Massachusetts, (1979), pp. 46-48.

Chapter 15

ORGANIC MOLECULAR FUNCTIONAL GROUPS AND MOLECULES

DERIVATION OF THE GENERAL GEOMETRICAL AND ENERGY EQUATIONS OF ORGANIC CHEMISTRY

Organic molecules comprising an arbitrary number of atoms can be solved using similar principles and procedures as those used to solve alkanes of arbitrary length. Alkanes can be considered to be comprised of the functional groups of CH_3, CH_2, and $C-C$. These groups with the corresponding geometrical parameters and energies can be added as a linear sum to give the solution of any straight chain alkane as shown in the Continuous-Chain Alkanes section. Similarly, the geometrical parameters and energies of all functional groups such as alkanes, branched alkanes, alkenes, branched alkenes, alkynes, alkyl fluorides, alkyl chlorides, alkyl bromides, alkyl iodides, alkene halides, primary alcohols, secondary alcohols, tertiary alcohols, ethers, primary amines, secondary amines, tertiary amines, aldehydes, ketones, carboxylic acids, carboxylic esters, amides, N-alkyl amides, N,N-dialkyl amides, urea, acid halides, acid anhydrides, nitriles, thiols, sulfides, disulfides, sulfoxides, sulfones, sulfites, sulfates, nitro alkanes, nitrites, nitrates, conjugated polyenes, aromatics, heterocyclic aromatics, substituted aromatics, and others can be solved. The functional-group solutions can be made into a linear superposition and sum, respectively, to give the solution of any organic molecule. The solutions of the functional groups can be conveniently obtained by using generalized forms of the geometrical and energy equations. The total bond energies of exemplary organic molecules calculated using the functional group composition and the corresponding energies derived in the following sections compared to the experimental values are given in Tables 15.410.1–15.410.43.

Consider the case wherein at least two atomic orbitals hybridize as a linear combination of electrons at the same energy in order to achieve a bond at an energy minimum, and the sharing of electrons between two or more such orbitals to form a MO permits the participating hybridized orbitals to decrease in energy through a decrease in the radius of one or more of the participating orbitals. The force-generalized constant k' of a H_2-type ellipsoidal MO due to the equivalent of two point charges at the foci is given by:

$$k' = \frac{C_1 C_2 2e^2}{4\pi\varepsilon_0} \tag{15.1}$$

where C_1 is the fraction of the H_2-type ellipsoidal MO basis function of a chemical bond of the molecule or molecular ion which is 0.75 (Eq. (13.59)) in the case of H bonding to a central atom and 0.5 (Eq. (14.152)) otherwise, and C_2 is the factor that results in an equipotential energy match of the participating at least two molecular or atomic orbitals of the chemical bond. From Eqs. (13.58-13.63), the distance from the origin of the MO to each focus c' is given by:

$$c' = a\sqrt{\frac{\hbar^2 4\pi\varepsilon_0}{m_e e^2 2C_1 C_2 a}} = \sqrt{\frac{aa_0}{2C_1 C_2}} \tag{15.2}$$

The internuclear distance is

$$2c' = 2\sqrt{\frac{aa_0}{2C_1 C_2}} \tag{15.3}$$

The length of the semiminor axis of the prolate spheroidal MO $b = c$ is given by:

$$b = \sqrt{a^2 - c'^2} \tag{15.4}$$

And, the eccentricity, e, is

$$e = \frac{c'}{a} \tag{15.5}$$

From Eqs. (11.207-11.212), the potential energy of the two electrons in the central field of the nuclei at the foci is:

$$V_e = n_1 c_1 c_2 \frac{-2e^2}{8\pi\varepsilon_0\sqrt{a^2-b^2}} \ln\frac{a+\sqrt{a^2-b^2}}{a-\sqrt{a^2-b^2}} \tag{15.6}$$

The potential energy of the two nuclei is:

$$V_p = n_1 \frac{e^2}{8\pi\varepsilon_0\sqrt{a^2-b^2}} \tag{15.7}$$

The kinetic energy of the electrons is

$$T = n_1 c_1 c_2 \frac{\hbar^2}{2m_e a\sqrt{a^2-b^2}} \ln\frac{a+\sqrt{a^2-b^2}}{a-\sqrt{a^2-b^2}} \tag{15.8}$$

And, the energy, V_m, of the magnetic force between the electrons is:

$$V_m = n_1 c_1 c_2 \frac{-\hbar^2}{4m_e a\sqrt{a^2-b^2}} \ln\frac{a+\sqrt{a^2-b^2}}{a-\sqrt{a^2-b^2}} \tag{15.9}$$

The total energy of the H_2-type prolate spheroidal MO, $E_T(_{H_2MO})$, is given by the sum of the energy terms:

$$E_T(_{H_2MO}) = V_e + T + V_m + V_p \tag{15.10}$$

$$E_T(_{H_2MO}) = -\frac{n_1 e^2}{8\pi\varepsilon_0\sqrt{a^2-b^2}}\left[c_1 c_2\left(2-\frac{a_0}{a}\right)\ln\frac{a+\sqrt{a^2-b^2}}{a-\sqrt{a^2-b^2}} - 1\right] = -\frac{n_1 e^2}{8\pi\varepsilon_0 c'}\left[c_1 c_2\left(2-\frac{a_0}{a}\right)\ln\frac{a+c'}{a-c'} - 1\right] \tag{15.11}$$

where n_1 is the number of equivalent bonds of the MO and applies in the case of functional groups. In the case of independent MOs not in contact with the bonding atoms, the terms based on charge are multiplied by c_{BO}, the bond-order factor. It is 1 for a single bond, 4 for an independent double bond as in the case of the CO_2 and NO_2 molecules, and 9 for an independent triplet bond. Then, the kinetic energy term is multiplied by c'_{BO} which is 1 for a single bond, 2 for a double bond, and 9/2 for a triple bond. c_1 is the fraction of the H_2-type ellipsoidal MO basis function of an MO which is 0.75 (Eqs. (13.67-13.73)) in the case of H bonding to an unhybridized central atom and 1 otherwise, and c_2 is the factor that results in an equipotential energy match of the participating MO and at least two atomic orbitals of the chemical bond. Specifically, to meet the equipotential condition and energy matching conditions for the union of the H_2-type-ellipsoidal-MO and the HOs or AOs of the bonding atoms, the factor c_2 of a H_2-type ellipsoidal MO may given by (i) one, (ii) the ratio of the Coulombic or valence energy of the AO or HO of at least one atom of the bond and 13.605804 eV, the Coulombic energy between the electron and proton of H, (iii) the ratio of the valence energy of the AO or HO of one atom and the Coulombic energy of another, (iv) the ratio of the valence energies of the AOs or HOs of two atoms, (v) the ratio of two c_2 factors corresponding to any of cases (ii)-(iv), and (vi) the product of two different c_2 factors corresponding to any of the cases (i)-(v). Specific examples of the factor c_2 of a H_2-type ellipsoidal MO given in previous sections are:

0.936127, the ratio of the ionization energy of N 14.53414 eV and 13.605804 eV, the Coulombic energy between the electron and proton of H;

0.91771, the ratio of 14.82575 eV, $-E_{Coulomb}\left(C, 2sp^3\right)$, and 13.605804 eV;

0.87495, the ratio of 15.55033 eV, $-E_{Coulomb}\left(C_{ethane}, 2sp^3\right)$, and 13.605804 eV;

0.85252, the ratio of 15.95955 eV, $-E_{Coulomb}\left(C_{ethylene}, 2sp^3\right)$, and 13.605804 eV;

0.85252, the ratio of 15.95955 eV, $-E_{Coulomb}\left(C_{benzene}, 2sp^3\right)$, and 13.605804 eV, and

0.86359, the ratio of 15.55033 eV, $-E_{Coulomb}\left(C_{alkane}, 2sp^3\right)$, and 13.605804 eV.

In the generalization of the hybridization of at least two atomic-orbital shells to form a shell of hybrid orbitals, the hybridized shell comprises a linear combination of the electrons of the atomic-orbital shells. The radius of the hybridized shell is calculated from the total Coulombic energy equation by considering that the central field decreases by an integer for each successive electron of the shell and that the total energy of the shell is equal to the total Coulombic energy of the initial AO electrons. The total energy $E_T\left(atom, msp^3\right)$ (m is the integer of the valence shell) of the AO electrons and the hybridized shell is given by the sum of energies of successive ions of the atom over the n electrons comprising total electrons of the at least one AO shell.

$$E_T\left(atom, msp^3\right) = -\sum_{m=1}^{n} IP_m \tag{15.12}$$

where IP_m is the m th ionization energy (positive) of the atom. The radius r_{msp^3} of the hybridized shell is given by:

$$r_{msp^3} = \sum_{q=Z-n}^{Z-1} \frac{-(Z-q)e^2}{8\pi\varepsilon_0 E_T\left(atom, msp^3\right)} \tag{15.13}$$

Then, the Coulombic energy $E_{Coulomb}\left(atom, msp^3\right)$ of the outer electron of the *atom* msp^3 shell is given by:

$$E_{Coulomb}\left(atom, msp^3\right) = \frac{-e^2}{8\pi\varepsilon_0 r_{msp^3}} \tag{15.14}$$

In the case that during hybridization at least one of the spin-paired AO electrons is unpaired in the hybridized orbital (HO), the energy change for the promotion to the unpaired state is the magnetic energy $E(magnetic)$ at the initial radius r of the AO electron:

$$E(magnetic) = \frac{2\pi\mu_0 e^2\hbar^2}{m_e^2 r^3} = \frac{8\pi\mu_0\mu_B^2}{r^3} \tag{15.15}$$

Then, the energy $E\left(atom, msp^3\right)$ of the outer electron of the *atom* msp^3 shell is given by the sum of $E_{Coulomb}\left(atom, msp^3\right)$ and $E(magnetic)$:

$$E\left(atom, msp^3\right) = \frac{-e^2}{8\pi\varepsilon_0 r_{msp^3}} + \frac{2\pi\mu_0 e^2\hbar^2}{m_e^2 r^3} \tag{15.16}$$

Consider next that the at least two atomic orbitals hybridize as a linear combination of electrons at the same energy in order to achieve a bond at an energy minimum with another atomic orbital or hybridized orbital. As a further generalization of the basis of the stability of the MO, the sharing of electrons between two or more such hybridized orbitals to form a MO permits the participating hybridized orbitals to decrease in energy through a decrease in the radius of one or more of the participating orbitals. In this case, the total energy of the hybridized orbitals is given by the sum of $E\left(atom, msp^3\right)$ and the next energies of successive ions of the atom over the n electrons comprising the total electrons of the at least two initial AO shells. Here, $E\left(atom, msp^3\right)$ is the sum of the first ionization energy of the atom and the hybridization energy. An example of $E\left(atom, msp^3\right)$ for $E\left(C, 2sp^3\right)$ is given in Eq. (14.503) where the sum of the negative of the first ionization energy of C, $-11.27671\ eV$, plus the hybridization energy to form the $C2sp^3$ shell given by Eq. (14.146) is $E\left(C, 2sp^3\right) = -14.63489\ eV$.

Thus, the sharing of electrons between two *atom* msp^3 HOs to form an atom-atom-bond MO permits each participating hybridized orbital to decrease in radius and energy. In order to further satisfy the potential, kinetic, and orbital energy relationships, each *atom* msp^3 HO donates an excess of 25% per bond of its electron density to the atom-atom-bond MO to form an energy minimum wherein the atom-atom bond comprises one of a single, double, or triple bond. In each case, the radius of the hybridized shell is calculated from the Coulombic energy equation by considering that the central field decreases by an integer for each successive electron of the shell and the total energy of the shell is equal to the total Coulombic energy of the initial AO electrons plus the hybridization energy. The total energy $E_T\left(mol.atom, msp^3\right)$ (m is the integer of the valence shell) of the HO electrons is given by the sum of energies of successive ions of the atom over the n electrons comprising total electrons of the at least one initial AO shell and the hybridization energy:

$$E_T\left(mol.atom, msp^3\right) = E\left(atom, msp^3\right) - \sum_{m=2}^{n} IP_m \tag{15.17}$$

where IP_m is the m th ionization energy (positive) of the atom and the sum of $-IP_1$ plus the hybridization energy is $E\left(atom, msp^3\right)$. Thus, the radius r_{msp^3} of the hybridized shell due to its donation of a total charge $-Qe$ to the corresponding MO is given by:

$$r_{msp^3} = \left(\sum_{q=Z-n}^{Z-1} (Z-q) - Q\right)\frac{-e^2}{8\pi\varepsilon_0 E_T\left(mol.atom, msp^3\right)} = \left(\sum_{q=Z-n}^{Z-1} (Z-q) - s(0.25)\right)\frac{-e^2}{8\pi\varepsilon_0 E_T\left(mol.atom, msp^3\right)} \tag{15.18}$$

where $-e$ is the fundamental electron charge and $s = 1, 2, 3$ for a single, double, and triple bond, respectively. The Coulombic energy $E_{Coulomb}\left(mol.atom, msp^3\right)$ of the outer electron of the *atom* msp^3 shell is given by:

$$E_{Coulomb}\left(mol.atom, msp^3\right) = \frac{-e^2}{8\pi\varepsilon_0 r_{msp^3}} \tag{15.19}$$

In the case that during hybridization at least one of the spin-paired AO electrons is unpaired in the hybridized orbital (HO), the energy change for the promotion to the unpaired state is the magnetic energy $E(magnetic)$ at the initial radius r of the AO electron given by Eq. (15.15). Then, the energy $E\left(mol.atom, msp^3\right)$ of the outer electron of the *atom* msp^3 shell is given by the sum of $E_{Coulomb}\left(mol.atom, msp^3\right)$ and $E(magnetic)$:

$$E\left(mol.atom, msp^3\right) = \frac{-e^2}{8\pi\varepsilon_0 r_{msp^3}} + \frac{2\pi\mu_0 e^2\hbar^2}{m_e^2 r^3} \tag{15.20}$$

$E_T\left(atom-atom, msp^3\right)$, the energy change of each *atom* msp^3 shell with the formation of the atom-atom-bond MO is given by: the difference between $E\left(mol.atom, msp^3\right)$ and $E\left(atom, msp^3\right)$:

$$E_T\left(atom-atom, msp^3\right) = E\left(mol.atom, msp^3\right) - E\left(atom, msp^3\right) \tag{15.21}$$

As examples from prior sections, $E_{Coulomb}\left(mol.atom, msp^3\right)$ is one of:

$E_{Coulomb}\left(C_{ethylene}, 2sp^3\right)$, $E_{Coulomb}\left(C_{ethane}, 2sp^3\right)$, $E_{Coulomb}\left(C_{acetylene}, 2sp^3\right)$, and $E_{Coulomb}\left(C_{alkane}, 2sp^3\right)$;

$E_{Coulomb}\left(atom, msp^3\right)$ is one of $E_{Coulomb}\left(C, 2sp^3\right)$ and $E_{Coulomb}\left(Cl, 3sp^3\right)$;

$E\left(mol.atom, msp^3\right)$ is one of $E\left(C_{ethylene}, 2sp^3\right)$, $E\left(C_{ethane}, 2sp^3\right)$, $E\left(C_{acetylene}, 2sp^3\right)$ and $E\left(C_{alkane}, 2sp^3\right)$;

$E\left(atom, msp^3\right)$ is one of $E\left(C, 2sp^3\right)$ and $E\left(Cl, 3sp^3\right)$;

$E_T\left(atom-atom, msp^3\right)$ is one of $E\left(C-C, 2sp^3\right)$, $E\left(C=C, 2sp^3\right)$, and $E\left(C\equiv C, 2sp^3\right)$;

atom msp^3 is one of $C2sp^3$, and $Cl3sp^3$

$E_T\left(atom-atom(s_1), msp^3\right)$ is $E_T\left(C-C, 2sp^3\right)$ and $E_T\left(atom-atom(s_2), msp^3\right)$ is $E_T\left(C=C, 2sp^3\right)$, and

r_{msp^3} is one of r_{C2sp^3}, $r_{ethane2sp^3}$, $r_{ethylene2sp^3}$, $r_{acetylene2sp^3}$, $r_{alkane2sp^3}$, and r_{Cl3sp^3}.

In the case of the $C2sp^3$ HO, the initial parameters (Eqs. (14.142-14.146)) are:

$$r_{2sp^3} = \sum_{n=2}^{5} \frac{(Z-n)e^2}{8\pi\varepsilon_0\left(e148.25751\ eV\right)} = \frac{10e^2}{8\pi\varepsilon_0\left(e148.25751\ eV\right)} = 0.91771a_0 \tag{15.22}$$

$$E_{Coulomb}\left(C, 2sp^3\right) = \frac{-e^2}{8\pi\varepsilon_0 r_{2sp^3}} = \frac{-e^2}{8\pi\varepsilon_0 0.91771a_0} = -14.82575\ eV \tag{15.23}$$

$$E(magnetic) = \frac{2\pi\mu_0 e^2\hbar^2}{m_e^2\left(r_3\right)^3} = \frac{8\pi\mu_0\mu_B^2}{\left(0.84317a_0\right)^3} = 0.19086\ eV \tag{15.24}$$

$$E\left(C, 2sp^3\right) = \frac{-e^2}{8\pi\varepsilon_0 r_{2sp^3}} + \frac{2\pi\mu_0 e^2\hbar^2}{m_e^2\left(r_3\right)^3} = -14.82575\ eV + 0.19086\ eV = -14.63489\ eV \tag{15.25}$$

In Eq. (15.18),

$$\sum_{q=Z-n}^{Z-1}(Z-q) = 10 \tag{15.26}$$

Eqs. (14.147) and (15.17) gives:

$$E_T\left(mol.atom, msp^3\right) = E_T\left(C_{ethane}, 2sp^3\right) = -151.61569\ eV \tag{15.27}$$

Using Eqs. (15.18-15.28), the final values of r_{C2sp^3}, $E_{Coulomb}\left(C2sp^3\right)$, and $E\left(C2sp^3\right)$, and the resulting $E_T\left(C\overset{BO}{-}C, C2sp^3\right)$ of the MO due to charge donation from the HO to the MO where $C\overset{BO}{-}C$ refers to the bond order of the carbon-carbon bond for different values of the parameter s are given in Table 15.1.

Table 15.1. The final values of r_{C2sp^3}, $E_{Coulomb}(C2sp^3)$, and $E(C2sp^3)$ and the resulting $E_T(C\overset{BO}{-}C,C2sp^3)$ of the MO due to charge donation from the HO to the MO where $C\overset{BO}{-}C$ refers to the bond order of the carbon-carbon bond.

MO Bond Order (BO)	s_1	s_2	$r_{C2sp^3}(a_0)$ Final	$E_{Coulomb}\left(C2sp^3\right)$ (eV) Final	$E\left(C2sp^3\right)$ (eV) Final	$E_T\left(C\overset{BO}{-}C,C2sp^3\right)$ (eV)
I	1	0	0.87495	-15.55033	-15.35946	-0.72457
II	2	0	0.85252	-15.95955	-15.76868	-1.13379
III	3	0	0.83008	-16.39089	-16.20002	-1.56513
IV	4	0	0.80765	-16.84619	-16.65532	-2.02043

In another generalized case of the basis of forming a minimum-energy bond with the constraint that it must meet the energy matching condition for all MOs at all HOs or AOs, the energy $E\left(mol.atom,msp^3\right)$ of the outer electron of the *atom* msp^3 shell of each bonding atom must be the average of $E\left(mol.atom,msp^3\right)$ for two different values of s:

$$E\left(mol.atom,msp^3\right)=\frac{E\left(mol.atom\left(s_1\right),msp^3\right)+E\left(mol.atom\left(s_2\right),msp^3\right)}{2} \tag{15.28}$$

In this case, $E_T\left(atom-atom,msp^3\right)$, the energy change of each *atom* msp^3 shell with the formation of each atom-atom-bond MO, is average for two different values of s:

$$E_T\left(atom-atom,msp^3\right)=\frac{E_T\left(atom-atom\left(s_1\right),msp^3\right)+E_T\left(atom-atom\left(s_2\right),msp^3\right)}{2} \tag{15.29}$$

Consider an aromatic molecule such as benzene given in the Benzene Molecule section. Each $C=C$ double bond comprises a linear combination of a factor of 0.75 of four paired electrons (three electrons) from two sets of two $C2sp^3$ HOs of the participating carbon atoms. Each $C-H$ bond of CH having two spin-paired electrons, one from an initially unpaired electron of the carbon atom and the other from the hydrogen atom, comprises the linear combination of 75% H_2-type ellipsoidal MO and 25% $C2sp^3$ HO as given by Eq. (13.439). However, $E_T\left(atom-atom,msp^3\right)$ of the $C-H$-bond MO is given by $0.5E_T\left(C=C,2sp^3\right)$ (Eq. (14.247)) corresponding to one half of a double bond that matches the condition for a single-bond order for $C-H$ that is lowered in energy due to the aromatic character of the bond.

A further general possibility is that a minimum-energy bond is achieved with satisfaction of the potential, kinetic, and orbital energy relationships by the formation of an MO comprising an allowed multiple of a linear combination of H_2-type ellipsoidal MOs and corresponding HOs or AOs that contribute a corresponding allowed multiple (e.g. 0.5, 0.75, 1) of the bond order given in Table 15.1. For example, the alkane MO given in the Continuous-Chain Alkanes section comprises a linear combination of factors of 0.5 of a single bond and 0.5 of a double bond.

Consider a first MO and its HOs comprising a linear combination of bond orders and a second MO that shares a HO with the first. In addition to the mutual HO, the second MO comprises another AO or HO having a single bond order or a mixed bond order. Then, in order for the two MOs to be energy matched, the bond order of the second MO and its HOs or its HO and AO is a linear combination of the terms corresponding to the bond order of the mutual HO and the bond order of the independent HO or AO. Then, in general, $E_T\left(atom-atom,msp^3\right)$, the energy change of each *atom* msp^3 shell with the formation of each atom-atom-bond MO, is a weighted linear sum for different values of s that matches the energy of the bonded MOs, HOs, and AOs:

$$E_T\left(atom-atom,msp^3\right)=\sum_{n=1}^{N}c_{s_n}E_T\left(atom-atom\left(s_n\right),msp^3\right) \tag{15.30}$$

where c_{s_n} is the multiple of the BO of s_n. The radius r_{msp^3} of the *atom* msp^3 shell of each bonding atom is given by the Coulombic energy using the initial energy $E_{Coulomb}\left(atom,msp^3\right)$ and $E_T\left(atom-atom,msp^3\right)$, the energy change of each *atom* msp^3 shell with the formation of each atom-atom-bond MO:

$$r_{msp^3}=\frac{-e^2}{8\pi\varepsilon_0 a_0\left(E_{Coulonb}\left(atom,msp^3\right)+E_T\left(atom-atom,msp^3\right)\right)} \tag{15.31}$$

where $E_{Coulomb}\left(C2sp^3\right)=-14.825751\,eV$. The Coulombic energy $E_{Coulomb}\left(mol.atom,msp^3\right)$ of the outer electron of the *atom* msp^3 shell is given by Eq. (15.19). In the case that during hybridization, at least one of the spin-paired AO electrons is unpaired in the hybridized orbital (HO), the energy change for the promotion to the unpaired state is the magnetic energy $E(magnetic)$ (Eq. (15.15)) at the initial radius r of the AO electron. Then, the energy $E\left(mol.atom,msp^3\right)$ of the outer electron

of the *atom* msp^3 shell is given by the sum of $E_{Coulomb}\left(mol.atom,msp^3\right)$ and $E(magnetic)$ (Eq. (15.20)). $E_T\left(atom-atom,msp^3\right)$, the energy change of each *atom* msp^3 shell with the formation of the atom-atom-bond MO is given by the difference between $E\left(mol.atom,msp^3\right)$ and $E\left(atom,msp^3\right)$ given by Eq. (15.21). Using Eq. (15.23) for $E_{Coulomb}\left(C,2sp^3\right)$ in Eq. (15.31), the single bond order energies given by Eqs. (15.18-15.27) and shown in Table 15.1, and the linear combination energies (Eqs. (15.28-15.30)), the parameters of linear combinations of bond orders and linear combinations of mixed bond orders are given in Table 15.2.

Table 15.2. The final values of r_{C2sp3}, $E_{Coulomb}(C2sp^3)$, and $E(C2sp^3)$ and the resulting $E_T(\overset{BO}{C-C},C2sp^3)$ of the MO comprising a linear combination of H_2-type ellipsoidal MOs and corresponding HOs of single or mixed bond order where c_{s_n} is the multiple of the bond order parameter $E_T(atom-atom\ (s_n), msp^3)$ given in Table 15.1.

MO Bond Order (BO)	s_1	c_{s_1}	s_2	c_{s_2}	s_3	c_{s_3}	$r_{C2sp^3}(a_0)$ Final	$E_{Coulomb}\left(C2sp^3\right)$ (eV) Final	$E\left(C2sp^3\right)$ (eV) Final	$E_T\left(\overset{BO}{C-C},C2sp^3\right)$ (eV)
1/2I	1	0.5	0	0	0	0	0.89582	-15.18804	-14.99717	-0.36228
1/2II	2	0.5	0	0	0	0	0.88392	-15.39265	-15.20178	-0.56689
1/2I + 1/4II	1	0.5	2	0.25	0	0	0.87941	-15.47149	-15.28062	-0.64573
1/4II + 1/4(I + II)	2	0.25	1	0.25	2	0.25	0.87363	-15.57379	-15.38293	-0.74804
3/4II	2	0.75	0	0	0	0	0.86793	-15.67610	-15.48523	-0.85034
1/2I + 1/2II	1	0.5	2	0.5	0	0	0.86359	-15.75493	-15.56407	-0.92918
1/2I + 1/2III	1	0.5	3	0.5	0	0	0.85193	-15.97060	-15.77974	-1.14485
1/2I + 1/2IV	1	0.5	4	0.5	0	0	0.83995	-16.19826	-16.00739	-1.37250
1/2II + 1/2III	2	0.5	3	0.5	0	0	0.84115	-16.17521	-15.98435	-1.34946
1/2II + 1/2IV	2	0.5	4	0.5	0	0	0.82948	-16.40286	-16.21200	-1.57711
I+1/2(I + II)	1	1	1	0.5	2	0.5	0.82562	-16.47951	-16.28865	-1.65376
1/2III + 1/2IV	3	0.5	4	0.5	0	0	0.81871	-16.61853	-16.42767	-1.79278
1/2IV + 1/2IV	4	0.5	4	0.5	0	0	0.80765	-16.84619	-16.65532	-2.02043
1/2(I + II)+II	1	0.5	2	0.5	2	1	0.80561	-16.88873	-16.69786	-2.06297

Consider next the radius of the AO or HO due to the contribution of charge to more than one bond. The energy contribution due to the charge donation at each atom such as carbon superimposes linearly. In general, the radius r_{mol2sp^3} of the $C2sp^3$ HO of a carbon atom of a given molecule is calculated using Eq. (14.514) by considering $\sum E_{T_{mol}}\left(MO,2sp^3\right)$, the total energy donation to all bonds with which it participates in bonding. The general equation for the radius is given by:

$$r_{mol2sp^3}=\frac{-e^2}{8\pi\varepsilon_0\left(E_{Coulomb}\left(C,2sp^3\right)+\sum E_{T_{mol}}\left(MO,2sp^3\right)\right)}=\frac{e^2}{8\pi\varepsilon_0\left(e14.825751\ eV+\sum\left|E_{T_{mol}}\left(MO,2sp^3\right)\right|\right)} \tag{15.32}$$

The Coulombic energy $E_{Coulomb}\left(mol.atom,msp^3\right)$ of the outer electron of the *atom* msp^3 shell is given by Eq. (15.19). In the case that during hybridization, at least one of the spin-paired AO electrons is unpaired in the hybridized orbital (HO), the energy change for the promotion to the unpaired state is the magnetic energy $E(magnetic)$ (Eq. (15.15)) at the initial radius r of the AO electron. Then, the energy $E\left(mol.atom,msp^3\right)$ of the outer electron of the *atom* msp^3 shell is given by the sum of $E_{Coulomb}\left(mol.atom,msp^3\right)$ and $E(magnetic)$ (Eq. (15.20)).

For example, the $C2sp^3$ HO of each methyl group of an alkane contributes $-0.92918\ eV$ (Eq. (14.513)) to the corresponding single $C-C$ bond; thus, the corresponding $C2sp^3$ HO radius is given by Eq. (14.514). The $C2sp^3$ HO of each methylene group of C_nH_{2n+2} contributes $-0.92918\ eV$ to each of the two corresponding $C-C$ bond MOs. Thus, the radius (Eq. (15.32)), the Coulombic energy (Eq. (15.19)), and the energy (Eq. (15.20)) of each alkane methylene group are:

$$\begin{aligned}r_{alkaneC_{methylene}2sp^3}&=\frac{-e^2}{8\pi\varepsilon_0\left(E_{Coulomb}\left(C,2sp^3\right)+\sum E_{T_{alkane}}\left(methylene\ C-C,2sp^3\right)\right)}\\&=\frac{e^2}{8\pi\varepsilon_0\left(e14.825751\ eV+e0.92918\ eV+e0.92918\ eV\right)}=0.81549a_0\end{aligned} \tag{15.33}$$

$$E_{Coulomb}\left(C_{methylene}2sp^3\right)=\frac{-e^2}{8\pi\varepsilon_0\left(0.81549a_0\right)}=-16.68412\ eV \tag{15.34}$$

$$E\left(C_{methylene}2sp^3\right)=\frac{-e^2}{8\pi\varepsilon_0\left(0.81549a_0\right)}+\frac{2\pi\mu_0 e^2\hbar^2}{m_e^2\left(0.84317a_0\right)^3}=-16.49325\ \ eV \tag{15.35}$$

In the determination of the parameters of functional groups, heteroatoms bonding to $C2sp^3$ HOs to form MOs are energy matched to the $C2sp^3$ HOs. Thus, the radius and the energy parameters of a bonding heteroatom are given by the same equations as those for $C2sp^3$ HOs. Using Eqs. (15.15), (15.19-15.20), (15.24), and (15.32) in a generalized fashion, the final values of the radius of the HO or AO, $r_{Atom.HO.AO}$, $E_{Coulomb}\left(mol.atom,msp^3\right)$, and $E\left(C_{mol}2sp^3\right)$ are calculated using $\sum E_{T_{group}}\left(MO,2sp^3\right)$, the total energy donation to each bond with which an atom participates in bonding corresponding to the values of $E_T\left(C\overset{BO}{-}C,C2sp^3\right)$ of the MO due to charge donation from the AO or HO to the MO given in Tables 15.1 and 15.2.

Table 15.3.A. The final values of $r_{Atom.HO.AO}$, $E_{Coulomb}$ ($mol.atom$,msp^3), and $E(C_{mol}C2sp^3)$ calculated using the values of $E_T(C\overset{BO}{-}C,C2sp^3)$ given in Tables 15.1 and 15.2.

Atom Hybridization Designation	$E_T\left(C\overset{BO}{-}C,C2sp^3\right)$	$E_T\left(C\overset{BO}{-}C,C2sp^3\right)$	$E_T\left(C\overset{BO}{-}C,C2sp^3\right)$	$E_T\left(C\overset{BO}{-}C,C2sp^3\right)$	$E_T\left(C\overset{BO}{-}C,C2sp^3\right)$	$r_{Atom.HO.AO}$ Final (a_0)	$E_{Coulomb}\left(mol.atom,msp^3\right)$ (eV) Final	$E\left(C_{mol}2sp^3\right)$ (eV) Final
1	0	0	0	0	0	0.91771	-14.82575	-14.63489
2	-0.56690	0	0	0	0	0.88392	-15.39265	-15.20178
3	-0.72457	0	0	0	0	0.87495	-15.55033	-15.35946
4	-0.92918	0	0	0	0	0.86359	-15.75493	-15.56407
5	-0.54343	-0.54343	0	0	0	0.85503	-15.91261	-15.72175
6	-1.13379	0	0	0	0	0.85252	-15.95954	-15.76868
7	-0.60631	-0.60631	0	0	0	0.84833	-16.03838	-15.84752
8	-1.34946	0	0	0	0	0.84115	-16.17521	-15.98435
9	-0.46459	-0.92918	0	0	0	0.83885	-16.21953	-16.02866
10	-0.72457	-0.72457	0	0	0	0.83600	-16.27490	-16.08404
11	0	-0.92918	-0.56690	0	0	0.83360	-16.32183	-16.13097
12	-0.92918	-0.60631	0	0	0	0.83159	-16.36125	-16.17038
13	0	-1.13379	-0.46459	0	0	0.82840	-16.42413	-16.23327
14	-0.92918	-0.72457	0	0	0	0.82562	-16.47951	-16.28864
15	-0.85035	-0.85035	0	0	0	0.82327	-16.52644	-16.33558
16	-0.82688	0	0	0	0	0.86924	-16.58181	-16.39095
17	-0.92918	-0.92918	0	0	0	0.81549	-16.68411	-16.49325
18	-1.13379	-0.72457	0	0	0	0.81549	-16.68412	-16.49325
19	-0.92918	-0.56690	-0.46459	0	0	0.81052	-16.78642	-16.59556
20	-1.13379	-0.92918	0	0	0	0.80561	-16.88873	-16.69786
21	-0.85035	-0.85035	-0.46459	0	0	0.80076	-16.99103	-16.80017
22	0	-1.34946	-0.82688	0	0	0.80024	-17.00209	-16.81123
23	-0.85034	-0.85034	-0.56690	0	0	0.79597	-17.09334	-16.90247
24	-1.13379	-1.13380	0	0	0	0.79597	-17.09334	-16.90248
25	-1.34946	-0.92918	0	0	0	0.79546	-17.10440	-16.91353
26	-0.85035	-0.54343	0	-0.92918	0	0.79340	-17.14871	-16.95785
27	-0.85035	-0.56690	-0.92918	0	0	0.79232	-17.17218	-16.98132
28	-0.56690	-0.92918	-0.92918	0	0	0.78870	-17.25101	-17.06015
29	-0.46459	-1.13380	-0.92918	0	0	0.78405	-17.35332	-17.16246
30	-0.54343	-0.54343	-0.56690	-0.92918	0	0.78155	-17.40869	-17.21783
31	-0.85034	-0.28345	-0.54343	-0.92918	0	0.78050	-17.43216	-17.24130
32	-0.92918	-0.92918	-0.92918	0	0	0.77247	-17.61330	-17.42243
33	-0.85034	-0.54343	-0.56690	-0.92918	0	0.76801	-17.71560	-17.52474
34	-0.85034	-0.54343	-0.60631	-0.92918	0	0.76631	-17.75502	-17.56416
35	-1.13379	-0.92918	-0.92918	0	0	0.76360	-17.81791	-17.62704
36	-1.13379	-1.13380	-0.72457	0	0	0.76360	-17.81791	-17.62705
37	-0.46459	-0.85035	-0.85035	-0.92918	0	0.75924	-17.92022	-17.72935
38	-0.92918	-1.34946	-0.82688	0	0	0.75878	-17.93127	-17.74041
39	-0.85034	-0.54343	-0.60631	-1.13379	0	0.75758	-17.95963	-17.76877
40	-1.13380	-1.13379	-0.92918	0	0	0.75493	-18.02252	-17.83166
41	-1.13379	-1.13379	-1.13379	0	0	0.74646	-18.22713	-18.03627

Table 15.3.B. The final values of $r_{Atom.HO.AO}$, $E_{Coulomb}$ ($mol.atom,msp^3$), and $E(C_{mol}C2sp^3)$ calculated for heterocyclic groups using the values of $E_T(\overset{BO}{C-C},C2sp^3)$ given in Tables 15.1 and 15.2.

Atom Hybridization Designation	$E_T\left(\overset{BO}{C-C},C2sp^3\right)$	$E_T\left(\overset{BO}{C-C},C2sp^3\right)$	$E_T\left(\overset{BO}{C-C},C2sp^3\right)$	$E_T\left(\overset{BO}{C-C},C2sp^3\right)$	$E_T\left(\overset{BO}{C-C},C2sp^3\right)$	$r_{Atom.HO.AO}$ Final (a_o)	$E_{Coulomb}\left(mol.atom,msp^3\right)$ (eV) Final	$E\left(C_{mol}2sp^3\right)$ (eV) Final
1	0	0	0	0	0	0.91771	-14.82575	-14.63489
2	-0.56690	0	0	0	0	0.88392	-15.39265	-15.20178
3	-0.72457	0	0	0	0	0.87495	-15.55033	-15.35946
4	-0.92918	0	0	0	0	0.86359	-15.75493	-15.56407
5	-0.54343	-0.54343	0	0	0	0.85503	-15.91261	-15.72175
6	-1.13379	0	0	0	0	0.85252	-15.95954	-15.76868
7	-0.60631	-0.60631	0	0	0	0.84833	-16.03838	-15.84752
8	-1.34946	0	0	0	0	0.84115	-16.17521	-15.98435
9	-0.46459	-0.92918	0	0	0	0.83885	-16.21953	-16.02866
10	-0.72457	-0.72457	0	0	0	0.83600	-16.27490	-16.08404
11	0	-0.92918	-0.56690	0	0	0.83360	-16.32183	-16.13097
12	-0.92918	-0.60631	0	0	0	0.83159	-16.36125	-16.17038
13	0	-1.13379	-0.46459	0	0	0.82840	-16.42413	-16.23327
14	-0.92918	-0.72457	0	0	0	0.82562	-16.47951	-16.28864
15	-0.85035	-0.85035	0	0	0	0.82327	-16.52644	-16.33558
16	-0.82688	0	0	0	0	0.86924	-16.58181	-16.39095
17	-0.92918	-0.92918	0	0	0	0.81549	-16.68411	-16.49325
18	-1.13379	-0.72457	0	0	0	0.81549	-16.68412	-16.49325
19	-0.92918	-0.56690	-0.46459	0	0	0.81052	-16.78642	-16.59556
20	-1.13379	-0.92918	0	0	0	0.80561	-16.88873	-16.69786
21	-0.85035	-0.85035	-0.46459	0	0	0.80076	-16.99103	-16.80017
22	0	-1.34946	-0.82688	0	0	0.80024	-17.00209	-16.81123
23	-0.85034	-0.85034	-0.56690	0	0	0.79597	-17.09334	-16.90247
24	-1.13379	-1.13380	0	0	0	0.79597	-17.09334	-16.90248
25	-1.34946	-0.92918	0	0	0	0.79546	-17.10440	-16.91353
26	-0.85035	-0.54343	0	-0.92918	0	0.79340	-17.14871	-16.95785
27	-0.85035	-0.56690	-0.92918	0	0	0.79232	-17.17218	-16.98132
28	-0.56690	-0.92918	-0.92918	0	0	0.78870	-17.25101	-17.06015
29	-0.46459	-1.13380	-0.92918	0	0	0.78405	-17.35332	-17.16246
30	-0.54343	-0.54343	-0.56690	-0.92918	0	0.78155	-17.40869	-17.21783
31	-0.85034	-0.28345	-0.54343	-0.92918	0	0.78050	-17.43216	-17.24130
32	-0.92918	-0.92918	-0.92918	0	0	0.77247	-17.61330	-17.42243
33	-0.85034	-0.54343	-0.56690	-0.92918	0	0.76801	-17.71560	-17.52474
34	-0.85034	-0.54343	-0.60631	-0.92918	0	0.76631	-17.75502	-17.56416
35	-1.13379	-0.92918	-0.92918	0	0	0.76360	-17.81791	-17.62704
36	-1.13379	-1.13380	-0.72457	0	0	0.76360	-17.81791	-17.62705
37	-0.46459	-0.85035	-0.85035	-0.92918	0	0.75924	-17.92022	-17.72935
38	-0.92918	-1.34946	-0.82688	0	0	0.75878	-17.93127	-17.74041
39	-0.85034	-0.54343	-0.60631	-1.13379	0	0.75758	-17.95963	-17.76877
40	-1.13380	-1.13379	-0.92918	0	0	0.75493	-18.02252	-17.83166
41	-1.13379	-1.13379	-1.13379	0	0	0.74646	-18.22713	-18.03627

From Eq. (15.18), the general equation for the radius due to a total charge $-Qe$ of an AO or a HO that participates in bonding to form a MO is given by:

$$r_{msp^3}=\left(\sum_{q=Z-n}^{Z-1}(Z-q)-Q\right)\frac{-e^2}{8\pi\varepsilon_0 E_T\left(mol.atom,msp^3\right)} \tag{15.36}$$

By equating the radii of Eqs. (15.36) and (15.32), the total charge parameter Q of the AO or HO can be calculated wherein the excess charge is on the MO:

$$Q=\left(\sum_{q=Z-n}^{Z-1}(Z-q)\right)-\frac{\left|E_T\left(mol.atom,msp^3\right)\right|}{\left(e14.825751\ eV+\sum\left|E_{T_{mol}}\left(MO,2sp^3\right)\right|\right)} \tag{15.37}$$

The modulation of the constant function by the time and spherically harmonic functions as given in Eq. (1.29) time-averages to zero such that the charge density of any HO or AO is determined by the constant function. The charge density σ is then given by the fundamental charge $-e$ times the number of electrons n divided by the area of the spherical shell of radius r_{mol2sp^3} given by Eq. (15.32):

$$\sigma=\frac{(n-Q)(-e)}{\frac{4}{3}\pi r_{mol2sp^3}^2} \tag{15.38}$$

The charge density of an ellipsoidal MO in rectangular coordinates (Eqs. (11.42-11.45)) is:

$$\sigma = \frac{q}{4\pi abc}\frac{1}{\sqrt{\frac{x^2}{a^4}+\frac{y^2}{b^4}+\frac{z^2}{c^4}}} = \frac{q}{4\pi abc}D \tag{15.39}$$

where D is the distance from the origin to the tangent plane. The charge q is given by the fundamental electron charge $-e$ times the sum of parameter n_1 of Eqs. (15.51) and (15.61) and the charge donation parameter Q (Eq. (15.37)) of each AO or HO to the MO. Thus, the charge density of the MO is given by:

$$\sigma = \frac{-e\left(n_1+Q\right)}{4\pi abc}D \tag{15.40}$$

The charge density of the MO that is continuous with the surface of the AO or HO and any radial bisector current resulting from the intersection of two or more MOs as given in the Methane Molecule (CH_4) section is determined by the current continuity condition. Consider the continuity of the current due to the intersection of an MO with a corresponding AO or HO. The parameters of each point of intersection of each H_2-type ellipsoidal MO and the corresponding atom AO or HO determined from the polar equation of the ellipse are given by Eqs. (15.80-15.87). The overlap charge Δq is given by the total charge of the prolate-spheroidal MO minus the integral of the charge density of the MO over the area between curves of intersection with the AOs or HOs that forms the MO:

$$\Delta q = -e\left(n_1+Q\right) - \int \sigma dA = -e\left(n_1+Q\right)\left(1-\int \frac{D}{4\pi abc}dA\right) \tag{15.41}$$

The overlap charge of the prolate-spheroidal MO Δq is uniformly distributed on the external spherical surface of the AO or HO of radius $r^3_{mol2sp^3}$ such that the charge density σ from Eq. (15.41) is:

$$\sigma = \frac{\Delta q}{A} \tag{15.42}$$

where A is the external surface area of the AO or HO between the curves of intersection with the MO surface.

At the curves of intersection of two or more MOs where they occur, the current between the AO or HO shell and curves of mutual contact is projected onto and flows in the direction of the radial vector to the surface of the AO or HO shell. This current designated the bisector current (BC) meets the AO or HO surface and does not travel to distances shorter than its radius. Due to symmetry, a radial axis through the AO or HO exists such that current travels from the MOs to the AO or HO along the radial vector in one direction and returns to the MO along the radial vector in the opposite direction from the AO or HO surface to conserve current flow. The MO current onto the bisector currents and the connecting current on the external surface of the AO or HO must be continuously maintained. Given the corresponding constant MO ω (Eq. (11.24)), the continuity condition requires that the charge density on these surfaces times the area ($\propto r^{-2}$) must be a constant corresponding to constant current, and this current must be matched at the inflow from the MO to the inflow bisector current, the HO or AO external surface, the outflow bisector current, and the return current on the opposite surface of the MO. Thus, σ on each surface s having charge Δq_s is given by Eq. (15.42) wherein $\Delta q = \sum \Delta q_s$ and Δq is given by Eq. (15.41) with the integral over the MO area between curves of intersection of the MOs. A is surface area corresponding to each Δq_s of the bisector currents and the external surface of the AO or HO between the curves of intersection of the bisector current with the AO or HO surface. Since the potential of an MO is that of a point charge at infinity (Eq. (11.36)), an asymmetry in the distribution of charge between nonequivalent HOs or AOs of the MO occurs to maintain an energy match of the MO with the bridged orbitals. The charge must redistribute between the spherical orbitals to achieve a corresponding current-density that maintains constant current at the equivalent-energy condition according to the energy-matching factor such as c_2 or C_2 of Eqs. (15.51) and (15.61). Since the orbital energy and radius are reciprocally related, the contribution scales as the square of the ratio (over unity) of the energy of the resultant net positively-charged orbital and the initial matched energy of the resultant net negatively-charged orbital of the bond multiplied by the energy-matching factor (e.g. c_2 or C_2). The partial charges on the HOs or AOs corresponding to the charge contribution are equivalent to point charges centered on the nuclei. Due to symmetry, the bond moment μ of each functional group is along the internuclear axis and is calculated from the partial changes at the separation distance, the internuclear distance. The dipole moment of a given molecule is then given by the vector sum of the bond moments in the molecule. Thus, the dipole moment is given by taking into account the magnitude and direction of the bond moment of each functional group wherein the function-group bond moment stays constant from molecule to molecule and is in the vector direction of the internuclear axis as given in the Bonds and Dipole Moments section.

The angles at which any two prolate spheroidal $A-C$ and $B-C$-bond MOs intersect can be determined using Eq. (13.85) by equating the radii of the elliptic cross sections of the MOs:

$$\left(a_1-c_1'\right)\frac{1+\frac{c_1'}{a_1}}{1+\frac{c_1'}{a_1}\cos\theta_1'} = \left(a_2-c_2'\right)\frac{1+\frac{c_2'}{a_2}}{1+\frac{c_2'}{a_2}\cos\theta_2'} \tag{15.43}$$

and by using the following relationship between the polar angles θ_1' and θ_2':

$$\theta_{\angle ACB} = \theta_1' + \theta_2' - 360° \tag{15.44}$$

where $\theta_{\angle ACB}$ is the bond angle of atoms A and B with central atom C. From either angle, the polar radius of intersection can be determined using Eq. (13.85). An example for methane is shown in Eqs. (13.597-13.600). Using these coordinates and the radius of the AO or HO, the limits of the integrals for the determination of the charge densities as well as the regions of each charge density are determined.

The energy of the MO is matched to each of the participating outermost atomic or hybridized orbitals of the bonding atoms wherein the energy match includes the energy contribution due to the AO or HO's donation of charge to the MO. The force constant k' (Eq. (15.1)) is used to determine the ellipsoidal parameter c' (Eq. (15.2)) of each H_2-type-ellipsoidal-MO in terms of the central force of the foci. Then, c' is substituted into the energy equation (from Eq. (15.11)) which is set equal to n_1 times the total energy of H_2 where n_1 is the number of equivalent bonds of the MO and the energy of H_2, $-31.63536831\ eV$, Eq. (11.212) is the minimum energy possible for a prolate spheroidal MO. From the energy equation and the relationship between the axes, the dimensions of the MO are solved. The energy equation has the semimajor axis a as its only parameter. The solution of the semimajor axis a then allows for the solution of the other axes of each prolate spheroid and eccentricity of each MO (Eqs. (15.3-15.5)). The parameter solutions then allow for the component and total energies of the MO to be determined.

The total energy, $E_{T\,(H_2MO)}$, is given by the sum of the energy terms (Eqs. (15.6-15.11)) plus $E_T(AO/HO)$:

$$E_{T\,(H_2MO)} = V_e + T + V_m + V_p + E_T(AO/HO) \tag{15.45}$$

$$\begin{aligned} E_{T\,(H_2MO)} &= -\frac{n_1 e^2}{8\pi\varepsilon_0\sqrt{a^2-b^2}}\left[c_1c_2\left(2-\frac{a_0}{a}\right)\ln\frac{a+\sqrt{a^2-b^2}}{a-\sqrt{a^2-b^2}}-1\right]+E_T(AO/HO) \\ &= -\frac{n_1 e^2}{8\pi\varepsilon_0 c'}\left[c_1c_2\left(2-\frac{a_0}{a}\right)\ln\frac{a+c'}{a-c'}-1\right]+E_T(AO/HO) \end{aligned} \tag{15.46}$$

where n_1 is the number of equivalent bonds of the MO, c_1 is the fraction of the H_2-type ellipsoidal MO basis function of a chemical bond of the group, c_2 is the factor that results in an equipotential energy match of the participating at least two atomic orbitals of each chemical bond, and $E_T(AO/HO)$ is the total energy comprising the difference of the energy $E(AO/HO)$ of at least one atomic or hybrid orbital to which the MO is energy matched and any energy component $\Delta E_{H_2MO}(AO/HO)$ due to the AO or HO's charge donation to the MO.

$$E_T(AO/HO) = E(AO/HO) - \Delta E_{H_2MO}(AO/HO) \tag{15.47}$$

As specific examples given in previous sections, $E_T(AO/HO)$ is one from the group of:

$E_T(AO/HO) = E(O2p\ shell) = -E(ionization;\ O) = -13.6181\ eV$;

$E_T(AO/HO) = E(N2p\ shell) = -E(ionization;\ N) = -14.53414\ eV$;

$E_T(AO/HO) = E(C, 2sp^3) = -14.63489\ eV$;

$E_T(AO/HO) = E_{Coulomb}(Cl, 3sp^3) = -14.60295\ eV$;

$E_T(AO/HO) = E(ionization;\ C) + E(ionization;\ C^+)$;

$E_T(AO/HO) = E(C_{ethane}, 2sp^3) = -15.35946\ eV$;

$E_T(AO/HO) = E(C_{ethylene}, 2sp^3) - E(C_{ethylene}, 2sp^3)$;

$E_T(AO/HO) = E(C, 2sp^3) - 2E_T(C=C, 2sp^3) = -14.63489\ eV - (-2.26758\ eV)$;

$E_T(AO/HO) = E(C_{acetylene}, 2sp^3) - E(C_{acetylene}, 2sp^3) - E(C_{acetylene}, 2sp^3) = 16.20002\ eV$;

$E_T(AO/HO) = E(C, 2sp^3) - 2E_T(C\equiv C, 2sp^3) = -14.63489\ eV - (-3.13026\ eV)$;

$E_T(AO/HO) = E(C_{benzene}, 2sp^3) - E(C_{benzene}, 2sp^3)$;

$E_T(AO/HO) = E(C, 2sp^3) - E_T(C=C, 2sp^3) = -14.63489\ eV - (-1.13379\ eV)$, and

$E_T(AO/HO) = E(C_{alkane}, 2sp^3) = -15.56407\ eV$.

To solve the bond parameters and energies, $c' = a\sqrt{\frac{\hbar^2 4\pi\varepsilon_0}{m_e e^2 2C_1C_2 a}} = \sqrt{\frac{aa_0}{2C_1C_2}}$ (Eq. (15.2)) is substituted into $E_{T\,(H_2MO)}$ to:

give

$$E_{T\,(H_2MO)} = -\frac{n_1 e^2}{8\pi\varepsilon_0\sqrt{a^2-b^2}}\left[c_1c_2\left(2-\frac{a_0}{a}\right)\ln\frac{a+\sqrt{a^2-b^2}}{a-\sqrt{a^2-b^2}}-1\right]+E_T\left(AO/HO\right)$$
$$= -\frac{n_1 e^2}{8\pi\varepsilon_0 c'}\left[c_1c_2\left(2-\frac{a_0}{a}\right)\ln\frac{a+c'}{a-c'}-1\right]+E_T\left(AO/HO\right) \quad (15.48)$$
$$= -\frac{n_1 e^2}{8\pi\varepsilon_0\sqrt{\frac{aa_0}{2C_1C_2}}}\left[c_1c_2\left(2-\frac{a_0}{a}\right)\ln\frac{a+\sqrt{\frac{aa_0}{2C_1C_2}}}{a-\sqrt{\frac{aa_0}{2C_1C_2}}}-1\right]+E_T\left(AO/HO\right)$$

The total energy is set equal to $E(basis\ energies)$ which in the most general case is given by the sum of a first integer n_1 times the total energy of H_2 minus a second integer n_2 times the total energy of H, minus a third integer n_3 times the valence energy of $E(AO)$ (e.g. $E(N) = -14.53414\ eV$) where the first integer can be $1,2,3...$, and each of the second and third integers can be $0,1,2,3....$

$$E(basis\ energies) = n_1\left(-31.63536831\ eV\right) - n_2\left(-13.605804\ eV\right) - n_3E\left(AO\right) \quad (15.49)$$

In the case that the MO bonds two atoms other than hydrogen, $E(basis\ energies)$ is n_1 times the total energy of H_2 where n_1 is the number of equivalent bonds of the MO and the energy of H_2, $-31.63536831\ eV$, Eq. (11.212) is the minimum energy possible for a prolate spheroidal MO:

$$E(basis\ energies) = n_1\left(-31.63536831\ eV\right) \quad (15.50)$$

$E_{T\,(H_2MO)}$, is set equal to $E(basis\ energies)$, and the semimajor axis a is solved. Thus, the semimajor axis a is solved from the equation of the form:

$$-\frac{n_1 e^2}{8\pi\varepsilon_0\sqrt{\frac{aa_0}{2C_1C_2}}}\left[c_1c_2\left(2-\frac{a_0}{a}\right)\ln\frac{a+\sqrt{\frac{aa_0}{2C_1C_2}}}{a-\sqrt{\frac{aa_0}{2C_1C_2}}}-1\right]+E_T\left(AO/HO\right) = E(basis\ energies) \quad (15.51)$$

The distance from the origin of the H_2-type-ellipsoidal-MO to each focus c', the internuclear distance $2c'$, and the length of the semiminor axis of the prolate spheroidal H_2-type MO $b = c$ are solved from the semimajor axis a using Eqs. (15.2-15.4). Then, the component energies are given by Eqs. (15.6-15.9) and (15.48).

The total energy of the MO of the functional group, $E_{T\,(MO)}$, is the sum of the total energy of the components comprising the energy contribution of the MO formed between the participating atoms and $E_T\left(atom-atom, msp^3.AO\right)$, the change in the energy of the AOs or HOs upon forming the bond. From Eqs. (15.48-15.49), $E_{T\,(MO)}$ is:

$$E_{T\,(MO)} = E(basis\ energies) + E_T\left(atom-atom, msp^3.AO\right) \quad (15.52)$$

During bond formation, the electrons undergo a reentrant oscillatory orbit with vibration of the nuclei, and the corresponding energy $\overline{E}_{osc}$ is the sum of the Doppler, $\overline{E}_D$, and average vibrational kinetic energies, $\overline{E}_{Kvib}$:

$$\overline{E}_{osc} = n_1\left(\overline{E}_D + \overline{E}_{Kvib}\right) = n_1\left(E_{h\nu}\sqrt{\frac{2\overline{E}_K}{m_e c^2}} + \frac{1}{2}\hbar\sqrt{\frac{k}{\mu}}\right) \quad (15.53)$$

where n_1 is the number of equivalent bonds of the MO, k is the spring constant of the equivalent harmonic oscillator, and μ is the reduced mass. The angular frequency of the reentrant oscillation in the transition state corresponding to $\overline{E}_D$ is determined by the force between the central field and the electrons in the transition state. The force and its derivative are given by:

$$f\left(R\right) = -c_{BO}\frac{C_{1o}C_{2o}e^2}{4\pi\varepsilon_0 R^3} \quad (15.54)$$

and

$$f'\left(a\right) = 2c_{BO}\frac{C_{1o}C_{2o}e^2}{4\pi\varepsilon_0 R^3} \quad (15.55)$$

such that the angular frequency of the oscillation in the transition state is given by:

$$\omega = \sqrt{\frac{\left[\frac{-3}{a}f\left(a\right) - f'\left(a\right)\right]}{m_e}} = \sqrt{\frac{k}{m_e}} = \sqrt{\frac{c_{BO}\frac{C_{1o}C_{2o}e^2}{4\pi\varepsilon_0 R^3}}{m_e}} \quad (15.56)$$

where R is the semimajor axis a or the semiminor axis b depending on the eccentricity of the bond that is most representative of the oscillation in the transition state, c_{BO} is the bond-order factor which is 1 for a single bond and when the MO comprises n_1 equivalent single bonds as in the case of functional groups. c_{BO} is 4 for an independent double bond as in the case of the CO_2 and NO_2 molecules and 9 for an independent triple bond. C_{1o} is the fraction of the H_2-type ellipsoidal MO basis function of the oscillatory transition state of a chemical bond of the group, and C_{2o} is the factor that results in an equipotential energy match of the participating at least two atomic orbitals of the transition state of the chemical bond. Typically, $C_{1o} = C_1$ and $C_{2o} = C_2$. The kinetic energy, E_K, corresponding to $\bar{E}_D$ is given by Planck's equation for functional groups:

$$\bar{E}_K = \hbar\omega = \hbar\sqrt{\frac{\frac{C_{1o}C_{2o}e^2}{4\pi\varepsilon_0 R^3}}{m_e}} \tag{15.57}$$

The Doppler energy of the electrons of the reentrant orbit is:

$$\bar{E}_D \cong E_{h\nu}\sqrt{\frac{2\bar{E}_K}{m_e c^2}} = E_{h\nu}\sqrt{\frac{2\hbar\sqrt{\frac{\frac{C_{1o}C_{2o}e^2}{4\pi\varepsilon_0 R^3}}{m_e}}}{m_e c^2}} \tag{15.58}$$

$\bar{E}_{osc}$ given by the sum of $\bar{E}_D$ and $\bar{E}_{Kvib}$ is:

$$\bar{E}_{osc\,(group)} = n_1\left(\bar{E}_D + \bar{E}_{Kvib}\right) = n_1\left(E_{h\nu}\sqrt{\frac{2\hbar\sqrt{\frac{\frac{C_{1o}C_{2o}e^2}{4\pi\varepsilon_0 R^3}}{m_e}}}{m_e c^2}} + E_{vib}\right) \tag{15.59}$$

$E_{h\nu}$ of a group having n_1 bonds is given by $E_{T\,(MO)}/n_1$ such that:

$$\bar{E}_{osc} = n_1\left(\bar{E}_D + \bar{E}_{Kvib}\right) = n_1\left(E_{T\,(MO)}/n_1\sqrt{\frac{2\bar{E}_K}{Mc^2}} + \frac{1}{2}\hbar\sqrt{\frac{k}{\mu}}\right) \tag{15.60}$$

$E_{T+osc\,(Group)}$ is given by the sum of $E_{T\,(MO)}$ (Eq. (15.51)) and $\bar{E}_{osc}$ (Eq. (15.60)).

$$\begin{aligned} E_{T+osc\,(Group)} = E_{T\,(MO)} + \bar{E}_{osc} &= \left(\begin{array}{l} \left(-\frac{n_1 e^2}{8\pi\varepsilon_0\sqrt{\frac{aa_0}{2C_1C_2}}}\left[c_1c_2\left(2-\frac{a_0}{a}\right)\ln\frac{a+\sqrt{\frac{aa_0}{2C_1C_2}}}{a-\sqrt{\frac{aa_0}{2C_1C_2}}}-1\right]\right) \\ +E_T\left(AO/HO\right)+E_T\left(atom-atom, msp^3.AO\right) \end{array}\right) \\ &\left(\left[1+\sqrt{\frac{2\hbar\sqrt{\frac{\frac{C_{1o}C_{2o}e^2}{4\pi\varepsilon_0 R^3}}{m_e}}}{m_e c^2}}\right]+n_1\frac{1}{2}\hbar\sqrt{\frac{k}{\mu}}\right) \\ &= \left(E(basis\ energies)+E_T\left(atom-atom, msp^3.AO\right)\right)\left[1+\sqrt{\frac{2\hbar\sqrt{\frac{\frac{C_{1o}C_{2o}e^2}{4\pi\varepsilon_0 R^3}}{m_e}}}{m_e c^2}}\right]+n_1\frac{1}{2}\hbar\sqrt{\frac{k}{\mu}} \end{aligned} \tag{15.61}$$

The total energy of the functional group $E_{T\,(group)}$ is the sum of the total energy of the components comprising the energy contribution of the MO formed between the participating atoms, $E(basis\ energies)$, the change in the energy of the AOs or HOs upon forming the bond ($E_T\left(atom-atom, msp^3.AO\right)$), the energy of oscillation in the transition state, and the change in magnetic energy with bond formation, E_{mag}. From Eq. (15.61), the total energy of the group $E_{T\,(Group)}$ is:

$$E_T\left(_{Group}\right)=\left(\begin{array}{l}\left(E(basis\ energies)+E_T\left(atom-atom,msp^3.AO\right)\right)\left[1+\sqrt{\dfrac{2\hbar\sqrt{\dfrac{\dfrac{C_{1o}C_{2o}e^2}{4\pi\varepsilon_0R^3}}{m_e}}}{m_ec^2}}\right]\\ +n_1\overline{E}_{Kvib}+E_{mag}\end{array}\right) \tag{15.62}$$

The change in magnetic energy E_{mag} which arises due to the formation of unpaired electrons in the corresponding fragments relative to the bonded group is given by:

$$E_{mag}=c_3\frac{2\pi\mu_0e^2\hbar^2}{m_e^2r^3}=c_3\frac{8\pi\mu_0\mu_B^2}{r^3} \tag{15.63}$$

where *r* is the radius of the atom that reacts to form the bond and c_3 is the number of electron pairs.

$$E_T\left(_{Group}\right)=\left(\begin{array}{l}\left(E(basis\ energies)+E_T\left(atom-atom,msp^3.AO\right)\right)\left[1+\sqrt{\dfrac{2\hbar\sqrt{\dfrac{\dfrac{C_{1o}C_{2o}e^2}{4\pi\varepsilon_0R^3}}{m_e}}}{m_ec^2}}\right]\\ +n_1\overline{E}_{Kvib}+c_3\dfrac{8\pi\mu_0\mu_B^2}{r^3}\end{array}\right) \tag{15.64}$$

The total bond energy of the group $E_D\left(_{Group}\right)$ is the negative difference of the total energy of the group (Eq. (15.64)) and the total energy of the two starting orbitals given by the sum of $c_4E_{initial}\left(c_4\ AO/HO\right)$ and $c_5E_{initial}\left(c_5\ AO/HO\right)$:

$$E_D\left(_{Group}\right)=-\left(\begin{array}{l}\left(E(basis\ energies)+E_T\left(atom-atom,msp^3.AO\right)\right)\left[1+\sqrt{\dfrac{2\hbar\sqrt{\dfrac{\dfrac{C_{1o}C_{2o}e^2}{4\pi\varepsilon_0R^3}}{m_e}}}{m_ec^2}}\right]\\ +n_1\overline{E}_{Kvib}+c_3\dfrac{8\pi\mu_0\mu_B^2}{r^3}-\left(c_4E_{initial}\left(c_4AO/HO\right)+c_5E_{initial}\left(c_5\ AO/HO\right)\right)\end{array}\right) \tag{15.65}$$

In the case of organic molecules, the atoms of the functional groups are energy matched to the $C2sp^3$ HO such that:

$$E\left(AO/HO\right)=-14.63489\ eV \tag{15.66}$$

For examples of E_{mag} from previous sections:

$$E_{mag}\left(C2sp^3\right)=c_3\frac{8\pi\mu_0\mu_B^2}{r^3}=c_3\frac{8\pi\mu_0\mu_B^2}{\left(0.91771a_0\right)^3}=c_30.14803\ eV \tag{15.67}$$

$$E_{mag}\left(O2p\right)=c_3\frac{8\pi\mu_0\mu_B^2}{r^3}=c_3\frac{8\pi\mu_0\mu_B^2}{a_0^3}=c_30.11441\ eV \tag{15.68}$$

$$E_{mag}\left(N2p\right)=c_3\frac{8\pi\mu_0\mu_B^2}{r^3}=c_3\frac{8\pi\mu_0\mu_B^2}{\left(0.93084a_0\right)^3}=c_30.14185\ eV \tag{15.69}$$

In the general case of the solution of an organic functional group, the geometric bond parameters are solved from the semimajor axis and the relationships between the parameters by first using Eq. (15.51) to arrive at a. Then, the remaining parameters are determined using Eqs. (15.1-15.5). Next, the energies are given by Eqs. (15.61-15.68). To meet the equipotential condition for the union of the H_2-type-ellipsoidal-MO and the HO or AO of the atom of a functional group, the factor c_2 of a H_2-type ellipsoidal MO in principal Eqs. (15.51) and (15.61) may given by:

(i) one:

$$c_2=1 \tag{15.70}$$

(ii) the ratio that is less than one of 13.605804 eV, the magnitude of the Coulombic energy between the electron and proton of H given by Eq. (1.264), and the magnitude of the Coulombic energy of the participating AO or HO of the atom, $E_{Coulomb}\left(MO.atom,msp^3\right)$ given by Eqs. (15.19) and (15.31-15.32). For $\left|E_{Coulomb}\left(MO.atom,msp^3\right)\right|$>13.605804 eV:

$$c_2 = \frac{\frac{e^2}{8\pi\varepsilon_0 a_0}}{\frac{e^2}{8\pi\varepsilon_0 r_{A-B\ AorBsp^3}}} = \frac{13.605804\ eV}{\left|E_{Coulomb}\left(MO.atom, msp^3\right)\right|} \tag{15.71}$$

For $\left|E_{Coulomb}\left(MO.atom, msp^3\right)\right| < 13.605804\ eV$:

$$c_2 = \frac{\frac{e^2}{8\pi\varepsilon_0 r_{A-B\ AorBsp^3}}}{\frac{e^2}{8\pi\varepsilon_0 a_0}} = \frac{\left|E_{Coulomb}\left(MO.atom, msp^3\right)\right|}{13.605804\ eV} \tag{15.72}$$

(iii) the ratio that is less than one of 13.605804 eV, the magnitude of the Coulombic energy between the electron and proton of H given by Eq. (1.264), and the magnitude of the valence energy, $E(valence)$, of the participating AO or HO of the atom where $E(valence)$ is the ionization energy or $E\left(MO.atom, msp^3\right)$ given by Eqs. (15.20) and (15.31-15.32). For $\left|E(valence)\right| > 13.605804\ eV$:

$$c_2 = \frac{\frac{e^2}{8\pi\varepsilon_0 a_0}}{\frac{e^2}{8\pi\varepsilon_0 r_{A-B\ AorBsp^3}}} = \frac{13.605804\ eV}{\left|E(valence)\right|} \tag{15.73}$$

For $\left|E(valence)\right| < 13.605804\ eV$:

$$c_2 = \frac{\frac{e^2}{8\pi\varepsilon_0 r_{A-B\ AorBsp^3}}}{\frac{e^2}{8\pi\varepsilon_0 a_0}} = \frac{\left|E(valence)\right|}{13.605804\ eV} \tag{15.74}$$

(iv) the ratio that is less than one of the magnitude of the Coulombic energy of the participating AO or HO of a first atom, $E_{Coulomb}\left(MO.atom, msp^3\right)$ given by Eqs. (15.19) and (15.31-15.32), and the magnitude of the valence energy, $E(valence)$, of the participating AO or HO of a second atom to which the first is energy matched where $E(valence)$ is the ionization energy or $E\left(MO.atom, msp^3\right)$ given by Eqs. (15.20) and (15.31-15.32). For $\left|E_{Coulomb}\left(MO.atom, msp^3\right)\right| > E(valence)$:

$$c_2 = \frac{\left|E(valence)\right|}{\left|E_{Coulomb}\left(MO.atom, msp^3\right)\right|} \tag{15.75}$$

For $\left|E_{Coulomb}\left(MO.atom, msp^3\right)\right| < E(valence)$:

$$c_2 = \frac{\left|E_{Coulomb}\left(MO.atom, msp^3\right)\right|}{\left|E(valence)\right|} \tag{15.76}$$

(v) the ratio of the magnitude of the valence-level energies, $E_n(valence)$, of the AO or HO of the nth participating atom of two that are energy matched where $E(valence)$ is the ionization energy or $E\left(MO.atom, msp^3\right)$ given by Eqs. (15.20) and (15.31-15.32):

$$c_2 = \frac{E_1(valence)}{E_2(valence)} \tag{15.77}$$

(vi) the factor that is the ratio of the hybridization factor $c_2(1)$ of the valence AO or HO of a first atom and the hybridization factor $c_2(2)$ of the valence AO or HO of a second atom to which the first is energy matched where $c_2(n)$ is given by Eqs. (15.71-15.77); alternatively c_2 is the hybridization factor $c_2(1)$ of the valence AOs or HOs a first pair of atoms and the hybridization factor $c_2(2)$ of the valence AO or HO a third atom or second pair to which the first two are energy matched:

$$c_2 = \frac{c_2(1)}{c_2(2)} \tag{15.78}$$

(vii) the factor that is the product of the hybridization factor $c_2(1)$ of the valence AO or HO of a first atom and the hybridization factor $c_2(2)$ of the valence AO or HO of a second atom to which the first is energy matched where $c_2(n)$ is given by Eqs. (15.71-15.78); alternatively c_2 is the hybridization factor $c_2(1)$ of the valence AOs or HOs a first pair of atoms and the hybridization factor $c_2(2)$ of the valence AO or HO a third atom or second pair to which the first two are energy matched:

$$c_2 = c_2(1)c_2(2) \tag{15.79}$$

The hybridization factor c_2 corresponds to the force constant k (Eqs. (11.65) and (13.58)). In the case that the valence or Coulombic energy of the AO or HO is less than $13.605804\ eV$, the magnitude of the Coulombic energy between the electron and proton of H given by Eq. (1.264), then C_2 corresponding to k' (Eq. (15.1)) is given by Eqs. (15.71-15.79).

Specific examples of the factors c_2 and C_2 of a H_2-type ellipsoidal MO of Eq. (15.60) given in following sections are:

$$c_2\left(C2sp^3HO\ to\ F\right) = \frac{E\left(C,2sp^3\right)}{E(F)}c_2\left(C2sp^3HO\right) = \frac{-14.63489\ eV}{-17.42282\ eV}(0.91771) = 0.77087;$$

$$C_2\left(C2sp^3HO\ to\ Cl\right) = \frac{E(Cl)}{E\left(C,2sp^3\right)}c_2\left(C2sp^3HO\right) = \frac{-12.96764\ eV}{-14.63489\ eV}(0.91771) = 0.81317;$$

$$C_2\left(C2sp^3HO\ to\ Br\right) = \frac{E(Br)}{E\left(C,2sp^3\right)}c_2\left(C2sp^3HO\right) = \frac{-11.81381\ eV}{-14.63489\ eV}(0.91771) = 0.74081;$$

$$C_2\left(C2sp^3HO\ to\ I\right) = \frac{E(I)}{E\left(C,2sp^3\right)}c_2\left(C2sp^3HO\right) = \frac{-10.45126\ eV}{-14.63489\ eV}(0.91771) = 0.65537;$$

$$c_2\left(C2sp^3HO\ to\ O\right) = \frac{E(O)}{E\left(C,2sp^3\right)}c_2\left(C2sp^3HO\right) = \frac{-13.61806\ eV}{-14.63489\ eV}(0.91771) = 0.85395;$$

$$c_2\left(H\ to\ 1°N\right) = \frac{E(N)}{E\left(C,2sp^3\right)} = \frac{-14.53414\ eV}{-15.35946\ eV} = 0.94627;$$

$$c_2\left(C2sp^3HO\ to\ N\right) = \frac{E(N)}{E\left(C,2sp^3\right)}c_2\left(C2sp^3HO\right) = \frac{-14.53414\ eV}{-14.63489\ eV}(0.91771) = 0.91140;$$

$$c_2\left(H\ to\ 2°N\right) = \frac{E(N)}{E\left(C,2sp^3\right)} = \frac{-14.53414\ eV}{-15.56407\ eV} = 0.93383;$$

$$C_2\left(S3p\ to\ H\right) = \frac{E(S,3p)}{E(H)} = \frac{-10.36001\ eV}{-13.60580\ eV} = 0.76144;$$

$$C_2\left(C2sp^3HO\ to\ \mathrm{S}\right) = \frac{E(S)}{E\left(C,2sp^3\right)}c_2\left(C2sp^3HO\right) = \frac{-10.36001\ eV}{-14.63489\ eV}(0.91771) = 0.64965;$$

$$c_2\left(O\ to\ S3sp^3\ to\ C2sp^3HO\right) = \frac{E(O)}{E(S)}c_2\left(C2sp^3HO\right) = \frac{-13.61806\ eV}{-10.36001\ eV}(0.91771) = 1.20632;$$

$$c_2\left(S3sp^3\right) = \frac{E_{Coulomb}\left(S3sp^3\right)}{E(H)} = \frac{-11.57099\ eV}{-13.60580\ eV} = 0.85045;$$

$$C_2\left(C2sp^3HO\ to\ S3sp^3\right) = \frac{E\left(S3sp^3\right)}{E\left(C,2sp^3\right)}c_2\left(S3sp^3\right) = \frac{-11.52126\ eV}{-14.63489\ eV}(0.85045) = 0.66951;$$

$$C_2\left(S3sp^3\ to\ O\ to\ C2sp^3HO\right) = \frac{E\left(S,3sp^3\right)}{E(O,2p)}c_2\left(C2sp^3HO\right) = \frac{-11.52126\ eV}{-13.61806\ eV}(0.91771) = 0.77641;$$

$$c_2\left(O\ to\ N2p\ to\ C2sp^3HO\right) = \frac{E(O)}{E(N)}c_2\left(C2sp^3HO\right) = \frac{-13.61806\ eV}{-14.53414\ eV}(0.91771) = 0.85987;$$

$$c_2\left(N2p\ to\ O2p\right)=\frac{c_2\left(C2sp^3HO\ to\ N\right)}{c_2\left(C2sp^3HO\ to\ O\right)}=\frac{0.91140}{0.85395}=1.06727\,;$$

$$C_2\left(benzeneC2sp^3HO\right)=c_2\left(benzeneC2sp^3HO\right)=\frac{13.605804\ eV}{15.95955\ eV}=0.85252\,;$$

$$c_2\left(arylC2sp^3HO\ to\ O\right)=\frac{E\left(O\right)}{E\left(C,2sp^3\right)}c_2\left(arylC2sp^3HO\right)=\frac{-13.61806\ eV}{-14.63489\ eV}\left(0.85252\right)=0.79329\,;$$

$$c_2\left(H\ to\ aniline\ N\right)=\frac{E\left(N\right)}{E\left(C,2sp^3\right)}=\frac{-14.53414\ eV}{-15.76868\ eV}=0.92171;$$

$$c_2\left(arylC2sp^3HO\ to\ N\right)=\frac{E\left(N\right)}{E\left(C,2sp^3\right)}c_2\left(arylC2sp^3HO\right)=\frac{-14.53414\ eV}{-14.63489\ eV}\left(0.85252\right)=0.84665\text{, and}$$

$$C_2\left(S3p\ to\ aryl\text{-}type\ C2sp^3HO\right)=\frac{E\left(S,3p\right)}{E\left(C,2sp^3\right)}=\frac{-10.36001\ eV}{-15.76868\ eV}=0.65700\,.$$

MO INTERCEPT ANGLES AND DISTANCES

Consider the general case of Eqs. (13.84-13.95), wherein the nucleus of a B atom and the nucleus of a A atom comprise the foci of each H_2-type ellipsoidal MO of an $A-B$ bond. The parameters of the point of intersection of each H_2-type ellipsoidal MO and the A-atom AO are determined from the polar equation of the ellipse:

$$r=r_0\frac{1+e}{1+e\cos\theta'} \tag{15.80}$$

The radius of the A shell is r_A, and the polar radial coordinate of the ellipse and the radius of the A shell are equal at the point of intersection such that:

$$r_A=\left(a-c'\right)\frac{1+\frac{c'}{a}}{1+\frac{c'}{a}\cos\theta'} \tag{15.81}$$

The polar angle θ' at the intersection point is given by:

$$\theta'=\cos^{-1}\left(\frac{a}{c'}\left(\left(a-c'\right)\frac{1+\frac{c'}{a}}{r_A}-1\right)\right) \tag{15.82}$$

Then, the angle $\theta_{A\,AO}$ the radial vector of the A AO makes with the internuclear axis is:

$$\theta_{A\,AO}=180°-\theta' \tag{15.83}$$

The Cartesian $\mathbf{i}$-coordinate of the interception point of the MO and the AO can be calculated using the MO ellipsoidal parameters by first calculating the parametric angle in Eq. (11.83) that matches Cartesian $\mathbf{j}$-coordinate components at the point of intersection. Thus, the matching elliptic parametric angle $\omega t=\theta_{H_2MO}$ satisfies the following relationship:

$$r_A\sin\theta_{A\,AO}=b\sin\theta_{H_2MO} \tag{15.84}$$

such that

$$\theta_{H_2MO}=\sin^{-1}\frac{r_a\sin\theta_{A\,AO}}{b} \tag{15.85}$$

The distance d_{H_2MO} along the internuclear axis from the origin of H_2-type ellipsoidal MO to the point of intersection of the orbitals is given by:

$$d_{H_2MO}=a\cos\theta_{H_2MO} \tag{15.86}$$

The distance $d_{A\,AO}$ along the internuclear axis from the origin of the A atom to the point of intersection of the orbitals is given by:

$$d_{A\,AO}=c'-d_{H_2MO} \tag{15.87}$$

BOND ANGLES

Further consider an ACB MO comprising a linear combination of $C-A$-bond and $C-B$-bond MOs where C is the general central atom. A bond is also possible between the A and B atoms of the $C-A$ and $C-B$ bonds. Such $A-B$ bonding would decrease the $C-A$ and $C-B$ bond strengths since electron density would be shifted from the latter bonds to the former bond. Thus, the $\angle ACB$ bond angle is determined by the condition that the total energy of the H_2-type ellipsoidal MO between the

terminal A and B atoms is zero. The force constant k' of a H_2-type ellipsoidal MO due to the equivalent of two point charges at the foci is given by:

$$k' = \frac{C_1 C_2 2e^2}{4\pi\varepsilon_0} \tag{15.88}$$

where C_1 is the fraction of the H_2-type ellipsoidal MO basis function of a chemical bond of the molecule which is 0.75 (Eq. (13.59)) for a terminal $A-H$ (A is H or other atom) and 1 otherwise and C_2 is the factor that results in an equipotential energy match of the participating at least two atomic orbitals of the chemical bond and is equal to the corresponding factor of Eqs. (15.51) and (15.61). The distance from the origin of the MO to each focus c' of the $A-B$ ellipsoidal MO is given by:

$$c' = a\sqrt{\frac{\hbar^2 4\pi\varepsilon_0}{m_e e^2 2C_1 C_2 a}} = \sqrt{\frac{aa_0}{2C_1 C_2}} \tag{15.89}$$

The internuclear distance is:

$$2c' = 2\sqrt{\frac{aa_0}{2C_1 C_2}} \tag{15.90}$$

The length of the semiminor axis of the prolate spheroidal $A-B$ MO $b=c$ is given by Eq. (15.4).

The component energies and the total energy, $E_T(_{H_2MO})$, of the $A-B$ bond are given by the energy equations (Eqs. (11.207-11.212), (11.213-11.217), and (11.239)) of H_2 except that the terms based on charge are multiplied by c_{BO}, the bond-order factor which is 1 for a single bond and when the MO comprises n_1 equivalent single bonds as in the case of functional groups. c_{BO} is 4 for an independent double bond as in the case of the CO_2 and NO_2 molecules. The kinetic energy term is multiplied by c'_{BO} which is 1 for a single bond, 2 for a double bond, and 9/2 for a triple bond. The electron energy terms are multiplied by c_1, the fraction of the H_2-type ellipsoidal MO basis function of a terminal chemical bond, which is 0.75 (Eq. (13.233)) for a terminal $A-H$ (A is H or other atom) and 1 otherwise. The electron energy terms are further multiplied by c_2', the hybridization or energy-matching factor that results in an equipotential energy match of the participating at least two atomic orbitals of each terminal bond. Furthermore, when $A-B$ comprises atoms other than H, $E_T\left(atom-atom, msp^3.AO\right)$, the energy component due to the AO or HO's charge donation to the terminal MO, is added to the other energy terms to give $E_T(_{H_2MO})$:

$$E_T(_{H_2MO}) = \frac{-e^2}{8\pi\varepsilon_0 c'}\left[c_1 c_2'\left(2c_{BO} - c'_{BO}\frac{a_0}{a}\right)\ln\frac{a+c'}{a-c'} - 1\right] + E_T\left(atom-atom, msp^3.AO\right) \tag{15.91}$$

The radiation reaction force in the case of the vibration of $A-B$ in the transition state corresponds to the Doppler energy, E_D, given by Eq. (11.181) that is dependent on the motion of the electrons and the nuclei. The total energy that includes the radiation reaction of the $A-B$ MO is given by the sum of $E_T(_{H_2MO})$ (Eq. (15.91)) and $\overline{E}_{osc}$ given by Eqs. (11.213-11.220), (11.231-11.236), and (11.239-11.240). Thus, the total energy $E_T\left(A-B\right)$ of the $A-B$ MO including the Doppler term is:

$$E_T\left(A-B\right) = \left[\left(\frac{-e^2}{8\pi\varepsilon_0 c'}\left[c_1 c_2'\left(2c_{BO} - c'_{BO}\frac{a_0}{a}\right)\ln\frac{a+c'}{a-c'} - 1\right] + E_T\left(atom-atom, msp^3.AO\right)\right)\right.$$
$$\left.\left[1 + \sqrt{\frac{2\hbar\sqrt{\frac{c_{BO}\frac{C_{1o}C_{2o}e^2}{4\pi\varepsilon_0 a^3}}{m_e}}}{m_e c^2}}\right] + \frac{1}{2}\hbar\sqrt{\frac{c_{BO}\frac{c_1 c_2' e^2}{8\pi\varepsilon_0 a^3} - \frac{c_{BO}e^2}{8\pi\varepsilon_0\left(a+c'\right)^3}}{\mu}}\right] \tag{15.92}$$

where C_{1o} is the fraction of the H_2-type ellipsoidal MO basis function of the oscillatory transition state of the $A-B$ bond which is 0.75 (Eq. (13.233)) in the case of H bonding to a central atom and 1 otherwise, C_{2o} is the factor that results in an equipotential energy match of the participating at least two atomic orbitals of the transition state of the chemical bond, and $\mu = \frac{m_1 m_2}{m_1 + m_2}$ is the reduced mass of the nuclei given by Eq. (11.154). To match the boundary condition that the total energy of the $A-B$ ellipsoidal MO is zero, $E_T\left(A-B\right)$ given by Eq. (15.92) is set equal to zero. Substitution of Eq. (15.90) into Eq. (15.92) gives:

$$0=\left[\left(\frac{-e^2}{8\pi\varepsilon_0\sqrt{\frac{aa_0}{2C_1C_2}}}\left[c_1c_2'\left(2c_{BO}-c'_{BO}\frac{a_0}{a}\right)\ln\frac{a+\sqrt{\frac{aa_0}{2C_1C_2}}}{a-\sqrt{\frac{aa_0}{2C_1C_2}}}-1\right]+E_T\left(atom-atom,msp^3.AO\right)\right)\left[1+\sqrt{\frac{2\hbar\sqrt{\frac{c_{BO}\frac{C_{1o}C_{2o}e^2}{4\pi\varepsilon_0a^3}}{m_e}}}{m_ec^2}}\right]+\frac{1}{2}\hbar\sqrt{\frac{c_{BO}\frac{c_1c_2'e^2}{8\pi\varepsilon_0a^3}-\frac{c_{BO}e^2}{8\pi\varepsilon_0\left(a+\sqrt{\frac{aa_0}{2C_1C_2}}\right)^3}}{\mu}}\right] \tag{15.93}$$

The vibrational energy-term of Eq. (15.93) is determined by the forces between the central field and the electrons and those between the nuclei (Eqs. (11.141-11.145)). The electron-central-field force and its derivative are given by:

$$f\left(a\right)=-c_{BO}\frac{c_1c_2'e^2}{4\pi\varepsilon_0a^3} \tag{15.94}$$

and

$$f'\left(a\right)=2c_{BO}\frac{c_1c_2'e^2}{4\pi\varepsilon_0a^3} \tag{15.95}$$

The nuclear repulsion force and its derivative are given by:

$$f\left(a+c'\right)=\frac{e^2}{8\pi\varepsilon_0\left(a+c'\right)^2} \tag{15.96}$$

and

$$f'\left(a+c'\right)=-\frac{e^2}{4\pi\varepsilon_0\left(a+c'\right)^3} \tag{15.97}$$

such that the angular frequency of the oscillation is given by:

$$\omega=\sqrt{\frac{\left[\frac{-3}{a}f\left(a\right)-f'\left(a\right)\right]}{\mu}}=\sqrt{\frac{k}{m_e}}=\sqrt{\frac{c_{BO}\frac{c_1c_2'e^2}{4\pi\varepsilon_0a^3}-\frac{e^2}{8\pi\varepsilon_0\left(a+c'\right)^2}}{\mu}} \tag{15.98}$$

Since both terms of $\overline{E}_{osc}=\overline{E}_D+\overline{E}_{Kvib}$ are small due to the large values of a and c', to very good approximation, a convenient form of Eq. (15.93) which is evaluated to determine the bond angles of functional groups is given by:

$$0=\left[\left(\frac{-e^2}{8\pi\varepsilon_0\sqrt{\frac{aa_0}{2C_1C_2}}}\left[c_1c_2'\left(2-\frac{a_0}{a}\right)\ln\frac{a+\sqrt{\frac{aa_0}{2C_1C_2}}}{a-\sqrt{\frac{aa_0}{2C_1C_2}}}-1\right]+E_T\left(atom-atom,msp^3.AO\right)\right)\left[1+\sqrt{\frac{2\hbar\sqrt{\frac{c_1e^2}{4\pi\varepsilon_0a^3}}}{m_ec^2}}\right]+\frac{1}{2}\hbar\sqrt{\frac{\frac{c_1e^2}{8\pi\varepsilon_0a^3}-\frac{e^2}{8\pi\varepsilon_0\left(a+\sqrt{\frac{aa_0}{2C_1C_2}}\right)^3}}{\mu}}\right] \tag{15.99}$$

From the energy relationship given by Eq. (15.99) and the relationship between the axes given by Eqs. (15.2-15.5), the dimensions of the $A-B$ MO can be solved. The most convenient way to solve Eq. (15.99) is by the reiterative technique using a computer.

A factor c_2 of a given atom in the determination of c_2' for calculating the zero of the total $A-B$ bond energy is typically given by Eqs. (15.71-15.74). In the case of a $H-H$ terminal bond of an alkyl or alkenyl group, c_2' is typically the ratio of c_2 of Eq. (15.71) for the $H-H$ bond which is one and c_2 of the carbon of the corresponding $C-H$ bond:

$$c_2'=\frac{1}{c_2(C2sp^3)}=\frac{E_{Coulomb}\left(C-H\ C2sp^3\right)}{13.605804\ eV} \tag{15.100}$$

In the case of the determination of the bond angle of the ACH MO comprising a linear combination of $C-A$-bond and $C-H$-bond MOs where A and C are general, C is the central atom, and c_2 for an atom is given by Eqs. (15.71-15.79), c_2' of the

$A-H$ terminal bond is typically the ratio of c_2 of the A atom for the $A-H$ terminal bond and c_2 of the C atom of the corresponding $C-H$ bond:

$$c_2' = \frac{c_2(A(A-H)msp^3)}{c_2(C(C-H)msp^3)} \tag{15.101}$$

In the case of the determination of the bond angle of the COH MO of an alcohol comprising a linear combination of $C-O$-bond and $O-H$ -bond MOs where C, O, and H are carbon, oxygen, and hydrogen, respectively, c_2' of the $C-H$ terminal bond is typically 0.91771 since the oxygen and hydrogen atoms are at the Coulomb potential of a proton and an electron (Eqs. (1.257) and (10.162), respectively) that is energy matched to the $C2sp^3$ HO.

In the determination of the hybridization factor c_2' of Eq. (15.99) from Eqs. (15.71-15.79), the Coulombic energy, $E_{Coulomb}\left(MO.atom, msp^3\right)$, or the energy, $E\left(MO.atom, msp^3\right)$, the radius $r_{A-B\ AorBsp^3}$ of the A or B AO or HO of the heteroatom of the $A-B$ terminal bond MO such as the $C2sp^3$ HO of a terminal $C-C$ bond is calculated using Eq. (15.32) by considering $\sum E_{T_{mol}}\left(MO, 2sp^3\right)$, the total energy donation to each bond with which it participates in bonding as it forms the terminal bond. The Coulombic energy $E_{Coulomb}\left(MO.atom, msp^3\right)$ of the outer electron of the *atom* msp^3 shell is given by Eq. (15.19). In the case that during hybridization, at least one of the spin-paired AO electrons is unpaired in the hybridized orbital (HO), the energy change for the promotion to the unpaired state is the magnetic energy $E(magnetic)$ (Eq. (15.15)) at the initial radius r of the AO electron. Then, the energy $E\left(MO.atom, msp^3\right)$ of the outer electron of the *atom* msp^3 shell is given by the sum of $E_{Coulomb}\left(MO.atom, msp^3\right)$ and $E(magnetic)$ (Eq. (15.20)).

In the specific case of the terminal bonding of two carbon atoms, the c_2 factor of each carbon given by Eq. (15.71) is determined using the Coulombic energy $E_{Coulomb}\left(C-C\ C2sp^3\right)$ of the outer electron of the $C2sp^3$ shell given by Eq. (15.19) with the radius $r_{C-C\ C2sp^3}$ of each $C2sp^3$ HO of the terminal $C-C$ bond calculated using Eq. (15.32) by considering $\sum E_{T_{mol}}\left(MO, 2sp^3\right)$, the total energy donation to each bond with which it participates in bonding as it forms the terminal bond including the contribution of the methylene energy, $0.92918\ eV$ (Eq. (14.513)), corresponding to the terminal $C-C$ bond. The corresponding $E_T\left(atom-atom, msp^3.AO\right)$ in Eq. (15.99) is $E_T\left(C-C\ C2sp^3\right) = -1.85836\ eV$.

In the case that the terminal atoms are carbon or other heteroatoms, the terminal bond comprises a linear combination of the HOs or AOs; thus, c_2' is the average of the hybridization factors of the participating atoms corresponding to the normalized linear sum:

$$c_2' = \frac{1}{2}\left(c_2'\left(atom\ 1\right) + c_2'\left(atom\ 2\right)\right) \tag{15.102}$$

In the exemplary cases of $C-C$, $O-O$, and $N-N$ where C is carbon:

$$\begin{aligned} c_2' &= \frac{1}{2}\left(\frac{\dfrac{e^2}{8\pi\varepsilon_0 a_0}}{\dfrac{e^2}{8\pi\varepsilon_0 r_{A-A\ A_1AO/HO}}} + \frac{\dfrac{e^2}{8\pi\varepsilon_0 a_0}}{\dfrac{e^2}{8\pi\varepsilon_0 r_{A-A\ A_2AO/HO}}}\right) \\ &= \frac{1}{2}\left(\frac{13.605804\ eV}{E_{Coulomb}\left(A-A.A_1AO/HO\right)} + \frac{13.605804\ eV}{E_{Coulomb}\left(A-A.A_2AO/HO\right)}\right) \end{aligned} \tag{15.103}$$

In the exemplary cases of $C-N$, $C-O$, and $C-S$,

$$c_2' = \frac{1}{2}\left(\frac{13.605804\ eV}{E_{Coulomb}\left(C-B\ C2sp^3\right)} + c_2\left(C\ to\ B\right)\right) \tag{15.104}$$

where C is carbon and $c_2\left(C\ to\ B\right)$ is the hybridization factor of Eqs. (15.61) and (15.93) that matches the energy of the atom B to that of the atom C in the group. For these cases, the corresponding $E_T\left(atom-atom, msp^3.AO\right)$ term in Eq. (15.99) depends on the hybridization and bond order of the terminal atoms in the molecule, but typical values matching those used in the determination of the bond energies (Eq. (15.65)) are:

$E_T\left(C-O\ C2sp^3.O2p\right) = -1.44915\ eV$; $E_T\left(C-O\ C2sp^3.O2p\right) = -1.65376\ eV$; $E_T\left(C-N\ C2sp^3.N2p\right) = -1.44915\ eV$;

$E_T\left(C-S\ C2sp^3.S2p\right) = -0.72457\ eV$; $E_T\left(O-O\ O2p.O2p\right) = -1.44915\ eV$; $E_T\left(O-O\ O2p.O2p\right) = -1.65376\ eV$;

$E_T\left(N-N\ N2p.N2p\right) = -1.44915\ eV$; $E_T\left(N-O\ N2p.O2p\right) = -1.44915\ eV$; $E_T\left(F-F\ F2p.F2p\right) = -1.44915\ eV$;

$E_T\left(Cl-Cl\ Cl3p.Cl3p\right) = -0.92918\ eV$; $E_T\left(Br-Br\ Br4p.Br4p\right) = -0.92918\ eV$; $E_T\left(I-I\ I5p.I5p\right) = -0.36229\ eV$;

$E_T\left(C-F\ C2sp^3.F2p\right)=-1.85836\ eV$; $E_T\left(C-Cl\ C2sp^3.Cl3p\right)=-0.92918\ eV$; $E_T\left(C-Br\ C2sp^3.Br4p\right)=-0.72457\ eV$; $E_T\left(C-I\ C2sp^3.I5p\right)=-0.36228\ eV$, and $E_T\left(O-Cl\ O2p.Cl3p\right)=-0.92918\ eV$.

In the case that the terminal bond is $X-X$ where X is a halogen atom, c_1 is one, and c_2' is the average (Eq. (15.102)) of the hybridization factors of the participating halogen atoms given by Eqs. (15.71-15.72) where $E_{Coulomb}\left(MO.atom,msp^3\right)$ is determined using Eq. (15.32) and $E_{Coulomb}\left(MO.atom,msp^3\right)=13.605804\ eV$ for $X=I$. The factor C_1 of Eq. (15.99) is one for all halogen atoms. The factor C_2 of fluorine is one since it is the only halogen wherein the ionization energy is greater than $13.605804\ eV$, the magnitude of the Coulombic energy between the electron and proton of H given by Eq. (1.264). For each of the other halogens, Cl, Br, and I, C_2 is the hybridization factor of Eq. (15.61) given by Eq. (15.79) with $c_2(1)$ being that of the halogen given by Eq. (15.77) that matches the valence energy of X ($E_1\left(valence\right)$) to that of the $C2sp^3$ HO ($E_2\left(valence\right)=-14.63489\ eV$, Eq. (15.25)) and to the hybridization of $C2sp^3$ HO ($c_2(2)=0.91771$, Eq. (13.430)). $E_T\left(atom-atom,msp^3.AO\right)$ of Eq. (15.99) is the maximum for the participating atoms which is $-1.44915\ eV$, $-0.92918\ eV$, $-0.92918\ eV$, and $-0.33582\ eV$ for F, Cl, Br, and I, respectively.

Consider the case that the terminal bond is $C-X$ where C is a carbon atom and X is a halogen atom. The factors c_1 and C_1 of Eq. (15.99) are one for all halogen atoms. For $X=F$, c_2' is the average (Eq. (15.104)) of the hybridization factors of the participating carbon and F atoms where c_2 for carbon is given by Eq. (15.71) and c_2 for fluorine matched to carbon is given by Eq. (15.79) with $c_2(1)$ for the fluorine atom given by Eq. (15.77) that matches the valence energy of F ($E_1\left(valence\right)=-17.42282\ eV$) to that of the $C2sp^3$ HO ($E_2\left(valence\right)=-14.63489\ eV$, Eq. (15.25)) and to the hybridization of $C2sp^3$ HO ($c_2(2)=0.91771$, Eq. (13.430)). The factor C_2 of fluorine is one since it is the only halogen wherein the ionization energy is greater than $13.605804\ eV$, the magnitude of the Coulombic energy between the electron and proton of H given by Eq. (1.264). For each of the other halogens, Cl, Br, and I, c_2' is the hybridization factor of the participating carbon atom since the halogen atom is energy matched to the carbon atom. C_2 of the terminal-atom bond matches that used to determine the energies of the corresponding $C-X$-bond MO. Then, C_2 is the hybridization factor of Eq. (15.61) given by Eq. (15.79) with $c_2(1)$ for the halogen atom given by Eq. (15.77) that matches the valence energy of X ($E_1\left(valence\right)$) to that of the $C2sp^3$ HO ($E_2\left(valence\right)=-14.63489\ eV$, Eq. (15.25)) and to the hybridization of $C2sp^3$ HO ($c_2(2)=0.91771$, Eq. (13.430)). $E_T\left(atom-atom,msp^3.AO\right)$ of Eq. (15.99) is the maximum for the participating atoms which is $-1.85836\ eV$, $-0.92918\ eV$, $-0.72457\ eV$, and $-0.33582\ eV$ for F, Cl, Br, and I, respectively.

Consider the case that the terminal bond is $H-X$ corresponding to the angle of the atoms HCX where C is a carbon atom and X is a halogen atom. The factors c_1 and C_1 of Eq. (15.99) are 0.75 for all halogen atoms. For $X=F$, c_2' is given by Eq. (15.78) with c_2 of the participating carbon and F atoms given by Eq. (15.71) and Eq. (15.74), respectively. The factor C_2 of fluorine is one since it is the only halogen wherein the ionization energy is greater than $13.605804\ eV$, the magnitude of the Coulombic energy between the electron and proton of H given by Eq. (1.264). For each of the other halogens, Cl, Br, and I, c_2' is also given by Eq. (15.78) with c_2 of the participating carbon given by Eq. (15.71) and c_2 of the participating X atom given by $c_2=0.91771$ (Eq. (13.430)) since the X atom is energy matched to the $C2sp^3$ HO. In these cases, C_2 is given by Eq. (15.74) for the corresponding atom X where C_2 matches the energy of the atom X to that of H.

Using the distance between the two atoms A and B of the general molecular group ACB when the total energy of the corresponding $A-B$ MO is zero, the corresponding bond angle can be determined from the law of cosines:

$$s_1^{\,2}+s_2^{\,2}-2s_1s_2\cos\theta=s_3^{\,2} \tag{15.105}$$

With $s_1=2c'_{C-A}$, the internuclear distance of the $C-A$ bond, $s_2=2c'_{C-B}$, the internuclear distance of each $C-B$ bond, and $s_3=2c'_{A-B}$, the internuclear distance of the two terminal atoms, the bond angle $\theta_{\angle ACB}$ between the $C-A$ and $C-B$ bonds is given by:

$$\left(2c'_{C-A}\right)^2+\left(2c'_{C-B}\right)^2-2\left(2c'_{C-A}\right)\left(2c'_{C-B}\right)\cos\theta=\left(2c'_{A-B}\right)^2 \tag{15.106}$$

$$\theta_{\angle ACB}=\cos^{-1}\left(\frac{\left(2c'_{C-A}\right)^2+\left(2c'_{C-B}\right)^2-\left(2c'_{A-B}\right)^2}{2\left(2c'_{C-A}\right)\left(2c'_{C-B}\right)}\right) \tag{15.107}$$

Consider the exemplary structure $C_bC_a(O_a)O_b$ wherein C_a is bound to C_b, O_a, and O_b. In the general case that the three bonds are coplanar and two of the angles are known, say θ_1 and θ_2, then the third θ_3 can be determined geometrically:

$$\theta_3 = 360 - \theta_1 - \theta_2 \tag{15.108}$$

In the general case that two of the three coplanar bonds are equivalent and one of the angles is known, say θ_1, then the second and third can be determined geometrically:

$$\theta_2 = \theta_3 = \frac{(360 - \theta_1)}{2} \tag{15.109}$$

ANGLES AND DISTANCES FOR AN MO THAT FORMS AN ISOSCELES TRIANGLE

In the general case where the group comprises three $A-B$ bonds having B as the central atom at the apex of a pyramidal structure formed by the three bonds with the A atoms at the base in the xy-plane, the C_{3v} axis centered on B is defined as the vertical or z-axis, and any two $A-B$ bonds form an isosceles triangle. Then, the angle of the bonds and the distances from and along the z-axis are determined from the geometrical relationships given by Eqs. (13.412-13.416).

the distance $d_{origin-B}$ from the origin to the nucleus of a terminal B atom is given by

$$d_{origin-B} = \frac{2c'_{B-B}}{2\sin 60°} \tag{15.110}$$

the height along the z-axis from the origin to the A nucleus d_{height} is given by:

$$d_{height} = \sqrt{\left(2c'_{A-B}\right)^2 - \left(d_{origin-B}\right)^2}\text{, and} \tag{15.111}$$

the angle θ_v of each $A-B$ bond from the z-axis is given by:

$$\theta_v = \tan^{-1}\left(\frac{d_{origin-B}}{d_{height}}\right) \tag{15.112}$$

Consider the case where the central atom B is further bound to a fourth atom C and the $B-C$ bond is along the z-axis. Then, the bond $\theta_{\angle ABC}$ given by Eq. (14.206) is:

$$\theta_{\angle ABC} = 180 - \theta_v \tag{15.113}$$

DIHEDRAL ANGLE

Consider the plane defined by a general ACA MO comprising a linear combination of two $C-A$-bond MOs where C is the central atom. The dihedral angle $\theta_{\angle BC/ACA}$ between the ACA-plane and a line defined by a third bond with C, specifically that corresponding to a $C-B$-bond MO, is calculated from the bond angle $\theta_{\angle ACA}$ and the distances between the A, B, and C atoms. The distance d_1 along the bisector of $\theta_{\angle ACA}$ from C to the internuclear-distance line between A and A, $2c'_{A-A}$, is given by:

$$d_1 = 2c'_{C-A}\cos\frac{\theta_{\angle ACA}}{2} \tag{15.114}$$

where $2c'_{C-A}$ is the internuclear distance between A and C. The atoms A, A, and B define the base of a pyramid. Then, the pyramidal angle $\theta_{\angle ABA}$ can be solved from the internuclear distances between A and A, $2c'_{A-A}$, and between A and B, $2c'_{A-B}$, using the law of cosines (Eq. (15.107)):

$$\theta_{\angle ABA} = \cos^{-1}\left(\frac{\left(2c'_{A-B}\right)^2 + \left(2c'_{A-B}\right)^2 - \left(2c'_{A-A}\right)^2}{2\left(2c'_{A-B}\right)\left(2c'_{A-B}\right)}\right) \tag{15.115}$$

Then, the distance d_2 along the bisector of $\theta_{\angle ABA}$ from B to the internuclear-distance line $2c'_{A-A}$, is given by:

$$d_2 = 2c'_{A-B}\cos\frac{\theta_{\angle ABA}}{2} \tag{15.116}$$

The lengths d_1, d_2, and $2c'_{C-B}$ define a triangle wherein the angle between d_1 and the internuclear distance between B and C, $2c'_{C-B}$, is the dihedral angle $\theta_{\angle BC/ACA}$ that can be solved using the law of cosines (Eq. (15.107)):

$$\theta_{\angle BC/ACA} = \cos^{-1}\left(\frac{d_1^2 + \left(2c'_{C-B}\right)^2 - d_2^2}{2d_1\left(2c'_{C-B}\right)}\right) \tag{15.117}$$

GENERAL DIHEDRAL ANGLE

Consider the plane defined by a general ACB MO comprising a linear combination of $C-A$ and $C-B$-bond MOs where C is the central atom. The dihedral angle $\theta_{\angle CD/ACB}$ between the ACB-plane and a line defined by a third bond of C with D, specifically that corresponding to a $C-D$-bond MO, is calculated from the bond angle $\theta_{\angle ACB}$ and the distances between the A, B, C, and D atoms. The distance d_1 from C to the bisector of the internuclear-distance line between A and B, $2c'_{A-B}$, is

given by two equations involving the law of cosines (Eq. (15.105)). One with $s_1 = 2c'_{C-A}$, the internuclear distance of the $C-A$ bond, $s_2 = d_1$, $s_3 = \frac{2c'_{A-B}}{2}$, half the internuclear distance between A and B, and $\theta = \theta_{\angle ACd_1}$, the angle between d_1 and the $C-A$ bond is given by:

$$\left(2c'_{C-A}\right)^2 + \left(d_1\right)^2 - 2\left(2c'_{C-A}\right)\left(d_1\right)\text{cosine}\,\theta_{\angle ACd_1} = \left(\frac{2c'_{A-B}}{2}\right)^2 \tag{15.118}$$

The other with $s_1 = 2c'_{C-B}$, the internuclear distance of the $C-B$ bond, $s_2 = d_1$, $s_3 = \frac{2c'_{A-B}}{2}$, and $\theta = \theta_{\angle ACB} - \theta_{\angle ACd_1}$ where $\theta_{\angle ACB}$ is the bond angle between the $C-A$ and $C-B$ bonds is given by:

$$\left(2c'_{C-B}\right)^2 + \left(d_1\right)^2 - 2\left(2c'_{C-B}\right)\left(d_1\right)\text{cosine}\left(\theta_{\angle ACB} - \theta_{\angle ACd_1}\right) = \left(\frac{2c'_{A-B}}{2}\right)^2 \tag{15.119}$$

Subtraction of Eq. (15.119) from Eq. (15.118) gives:

$$d_1 = \frac{\left(2c'_{C-A}\right)^2 - \left(2c'_{C-B}\right)^2}{2\left(\left(2c'_{C-A}\right)\text{cosine}\,\theta_{\angle ACd_1} - \left(2c'_{C-B}\right)\text{cosine}\left(\theta_{\angle ACB} - \theta_{\angle ACd_1}\right)\right)} \tag{15.120}$$

Substitution of Eq. (15.120) into Eq. (15.118) gives

$$\left(\begin{array}{l} \left(2c'_{C-A}\right)^2 + \left(\frac{\left(2c'_{C-A}\right)^2 - \left(2c'_{C-B}\right)^2}{2\left(\left(2c'_{C-A}\right)\text{cosine}\,\theta_{\angle ACd_1} - \left(2c'_{C-B}\right)\text{cosine}\left(\theta_{\angle ACB} - \theta_{\angle ACd_1}\right)\right)}\right)^2 \\ -2\left(2c'_{C-A}\right)\left(\frac{\left(2c'_{C-A}\right)^2 - \left(2c'_{C-B}\right)^2}{2\left(\left(2c'_{C-A}\right)\text{cosine}\,\theta_{\angle ACd_1} - \left(2c'_{C-B}\right)\text{cosine}\left(\theta_{\angle ACB} - \theta_{\angle ACd_1}\right)\right)}\right)\text{cosine}\,\theta_{\angle ACd_1} \\ -\left(\frac{2c'_{A-B}}{2}\right)^2 \end{array}\right) = 0 \tag{15.121}$$

The angle between d_1 and the $C-A$ bond, $\theta_{\angle ACd_1}$, can be solved reiteratively using Eq. (15.121), and the result can be substituted into Eq. (15.120) to give d_1.

The atoms A, B, and D define the base of a pyramid. Then, the pyramidal angle $\theta_{\angle ADB}$ can be solved from the internuclear distances between A and D, $2c'_{A-D}$, between B and D, $2c'_{B-D}$, and between A and B, $2c'_{A-B}$, using the law of cosines (Eq. (15.107)):

$$\theta_{\angle ADB} = \cos^{-1}\left(\frac{\left(2c'_{A-D}\right)^2 + \left(2c'_{B-D}\right)^2 - \left(2c'_{A-B}\right)^2}{2\left(2c'_{A-D}\right)\left(2c'_{B-D}\right)}\right) \tag{15.122}$$

Then, the distance d_2 from D to the bisector of the internuclear-distance line between A and B, $2c'_{A-B}$, is given by two equations involving the law of cosines (Eq. (15.105)). One with $s_1 = 2c'_{A-D}$, the internuclear distance between A and D, $s_2 = d_2$, $s_3 = \frac{2c'_{A-B}}{2}$, half the internuclear distance between A and B, and $\theta = \theta_{\angle ADd_2}$, the angle between d_2 and the $A-D$ axis is given by:

$$\left(2c'_{A-D}\right)^2 + \left(d_2\right)^2 - 2\left(2c'_{A-D}\right)\left(d_2\right)\text{cosine}\,\theta_{\angle ADd_2} = \left(\frac{2c'_{A-B}}{2}\right)^2 \tag{15.123}$$

The other with $s_1 = 2c'_{B-D}$, the internuclear distance between B and D, $s_2 = d_2$, and $\theta = \theta_{\angle ADB} - \theta_{\angle ADd_2}$ where $\theta_{\angle ADB}$ is the bond angle between the $A-D$ and $B-D$ axes is given by:

$$\left(2c'_{B-D}\right)^2 + \left(d_2\right)^2 - 2\left(2c'_{B-D}\right)\left(d_2\right)\text{cosine}\left(\theta_{\angle ADB} - \theta_{\angle ADd_2}\right) = \left(\frac{2c'_{A-B}}{2}\right)^2 \tag{15.124}$$

Subtraction of Eq. (15.124) from Eq. (15.123) gives:

$$d_2 = \frac{\left(2c'_{A-D}\right)^2 - \left(2c'_{B-D}\right)^2}{2\left(\left(2c'_{A-D}\right)\text{cosine}\,\theta_{\angle ADd_2} - \left(2c'_{B-D}\right)\text{cosine}\left(\theta_{\angle ADB} - \theta_{\angle ADd2}\right)\right)} \tag{15.125}$$

Substitution of Eq. (15.125) into Eq. (15.123) gives:

$$\left(\begin{array}{l}\left(2c'_{A-D}\right)^2+\left(\dfrac{\left(2c'_{A-D}\right)^2-\left(2c'_{B-D}\right)^2}{2\left(\left(2c'_{A-D}\right)\text{cosine}\theta_{\angle ADd_2}-\left(2c'_{B-D}\right)\text{cosine}\left(\theta_{\angle ADB}-\theta_{\angle ADd_2}\right)\right)}\right)^2 \\ -2\left(2c'_{A-D}\right)\left(\dfrac{\left(2c'_{A-D}\right)^2-\left(2c'_{B-D}\right)^2}{2\left(\left(2c'_{A-D}\right)\text{cosine}\theta_{\angle ADd_2}-\left(2c'_{B-D}\right)\text{cosine}\left(\theta_{\angle ADB}-\theta_{\angle ADd_2}\right)\right)}\right)\text{cosine}\theta_{\angle ADd_2} \\ -\left(\dfrac{2c'_{A-B}}{2}\right)^2\end{array}\right)=0 \tag{15.126}$$

The angle between d_2 and the $A-D$ axis, $\theta_{\angle ADd_2}$, can be solved reiteratively using Eq. (15.126), and the result can be substituted into Eq. (15.125) to give d_2.

The lengths d_1, d_2, and $2c'_{C-B}$ define a triangle wherein the angle between d_1 and the internuclear distance between C and D, $2c'_{C-D}$, is the dihedral angle $\theta_{\angle CD/ACB}$ that can be solved using the law of cosines (Eq. (15.107)):

$$\theta_{\angle CD/ACB}=\cos^{-1}\left(\frac{d_1^2+\left(2c'_{C-D}\right)^2-d_2^2}{2d_1\left(2c'_{C-D}\right)}\right) \tag{15.127}$$

SOLUTION OF GEOMETRICAL AND ENERGY PARAMETERS OF MAJOR FUNCTIONAL GROUPS AND CORRESPONDING ORGANIC MOLECULES

The exemplary molecules given in the following sections were solved using the solutions of organic chemical functional groups as basis elements wherein the structures and energies where linearly added to achieve the molecular solutions. Each functional group can be treated as a building block to form any desired molecular solution from the corresponding linear combination. Each functional group element was solved using the atomic orbital and hybrid orbital spherical atomic orbital solutions bridged by molecular orbitals comprised of the H_2-type prolate spheroidal solution given in the Nature of the Chemical Bond of Hydrogen-Type Molecules section. The energy of each MO was matched at the HO or AO by matching the hybridization and total energy of the MO to the AOs and HOs. The energy E_{mag} (e.g. given by Eq. (15.67) for a $C2sp^3$ HO and Eq. (15.68) for an $O2p$ AO) was subtracted for each set of unpaired electrons created by bond breakage.

The bond energy is not equal to the component energy of each bond as it exists in the molecule, although, they are close. The total energy of each group is its contribution to the total energy of the molecule as a whole. The determination of the bond energies for the creation of the separate parts must take into account the energy of the formation of any radicals and any redistribution of charge density within the pieces and the corresponding energy change with bond cleavage. Also, the vibrational energy in the transition state is dependent on the other groups that are bound to a given functional group. This will affect the functional-group energy. But, because the variations in the energy based on the balance of the molecular composition are typically of the order of a few hundreds of electron volts at most, they were neglected.

The energy of each functional-group MO bonding to a given carbon HO is independently matched to the HO by subtracting the contribution to the change in the energy of the HO from the total MO energy given by the sum of the MO contributions and $E\left(C,2sp^3\right)=-14.63489\,eV$ (Eq. (13.428)). The intercept angles are determined from Eqs. (15.80-15.87) using the final radius of the HO of each atom. The final carbon-atom radius is determined using Eqs. (15.32) wherein the sum of the energy contributions of each atom to all the MOs in which it participates in bonding is determined. This final radius is used in Eqs. (15.19) and (15.20) to calculate the final valence energy of the HO of each atom at the corresponding final radius. The radius of any bonding heteroatom that contributes to a MO is calculated in the same manner, and the energy of its outermost shell is matched to that of the MO by the hybridization factor between the carbon-HO energy and the energy of the heteroatomic shell. The donation of electron density to the AOs and HOs reduces the energy. The donation of the electron density to the MO's at each AO or HO is that which causes the resulting energy to be divided equally between the participating AOs or HOs to achieve energy matching.

The molecular solutions can be used to design synthetic pathways and predict product yields based on equilibrium constants calculated from the heats of formation. New stable compositions of matter can be predicted as well as the structures of combinatorial chemistry reactions. Further important pharmaceutical applications include the ability to graphically or computationally render the structures of drugs that permit the identification of the biologically active parts of the molecules to be identified from the common spatial charge-density functions of a series of active molecules. Drugs can be designed according to geometrical parameters and bonding interactions with the data of the structure of the active site of the drug.

To calculate conformations, folding, and physical properties, the exact solutions of the charge distributions in any given molecule are used to calculate the fields, and from the fields, the interactions between groups of the same molecule or between groups on different molecules are calculated wherein the interactions are distance and relative orientation dependent. The fields and interactions can be determined using a finite-element-analysis approach of Maxwell's equations.

CONTINUOUS-CHAIN ALKANES ($C_nH_{2n+2},\ n=3,4,5...\infty$)

The continuous-chain alkanes, C_nH_{2n+2}, are the homologous series comprising terminal methyl groups at each end of the chain with $n-2$ methylene (CH_2) groups in between:

$$CH_3(CH_2)_{n-2}CH_3 \tag{15.128}$$

C_nH_{2n+2} can be solved using the same principles as those used to solve ethane and ethylene wherein the $2s$ and $2p$ shells of each C hybridize to form a single $2sp^3$ shell as an energy minimum, and the sharing of electrons between two $C2sp^3$ hybridized orbitals (HOs) to form a molecular orbital (MO) permits each participating hybridized orbital to decrease in radius and energy. Three H AOs combine with three carbon $2sp^3$ HOs and two H AOs combine with two carbon $2sp^3$ HOs to form each methyl and methylene group, respectively, where each bond comprises a H_2-type MO developed in the Nature of the Chemical Bond of Hydrogen-Type Molecules and Molecular Ions section. The CH_3 and CH_2 groups bond by forming H_2-type MOs between the remaining $C2sp^3$ HOs on the carbons such that each carbon forms four bonds involving its four $C2sp^3$ HOs. For the alkyl $C-C$ group, $E_T\left(atom-atom,msp^3.AO\right)$ is $-1.85836\,eV$ where both energy contributions are given by Eq. (14.513). It is based on the energy match between the $C2sp^3$ HOs of the chain comprising methylene groups and terminal methyl groups.

The geometrical (Eqs. (15.1-15.5) and (15.51)), intercept (Eqs. (15.80-15.87)), and energy (Eqs. (15.6-15.11) and (15.17-15.65)) parameters of straight-chain alkanes are given in Tables 15.4, 15.5, and 15.6, respectively. The total energy of each straight-chain alkane given in Table 15.7 was calculated as the sum over the integer multiple of each $E_{D\,(Group)}$ of Table 15.6 corresponding to functional-group composition of the molecule. The bond angle parameters of straight-chain alkanes determined using Eqs. (15.88-15.117) are given in Table 15.8. In this angle table and those given in subsequent sections when c_2' is given as the ratio of two values of c_2 designated to Atom 1 and Atom 2 and corresponding to $E_{Coulombic}$ of Atom 1 and Atom 2, respectively, then $c_2'=\dfrac{c_2(Atom\ 2)}{c_2(Atom\ 1)}$. The color scale, translucent view of the charge-density of exemplary alkane, butane comprising the concentric shells of atoms with the outer shell bridged by one or more H_2-type ellipsoidal MOs or joined with one or more hydrogen MOs is shown in Figure 15.1.

Figure 15.1. (A-B) Color scale, translucent and opaque views of the charge-density of butane. Each representation shows the orbitals of the atoms at their radii, the ellipsoidal surface of each H or H_2-type ellipsoidal MO that transitions to the corresponding outer shell of the atom(s) participating in each bond, and the hydrogen nuclei (red, not to scale).

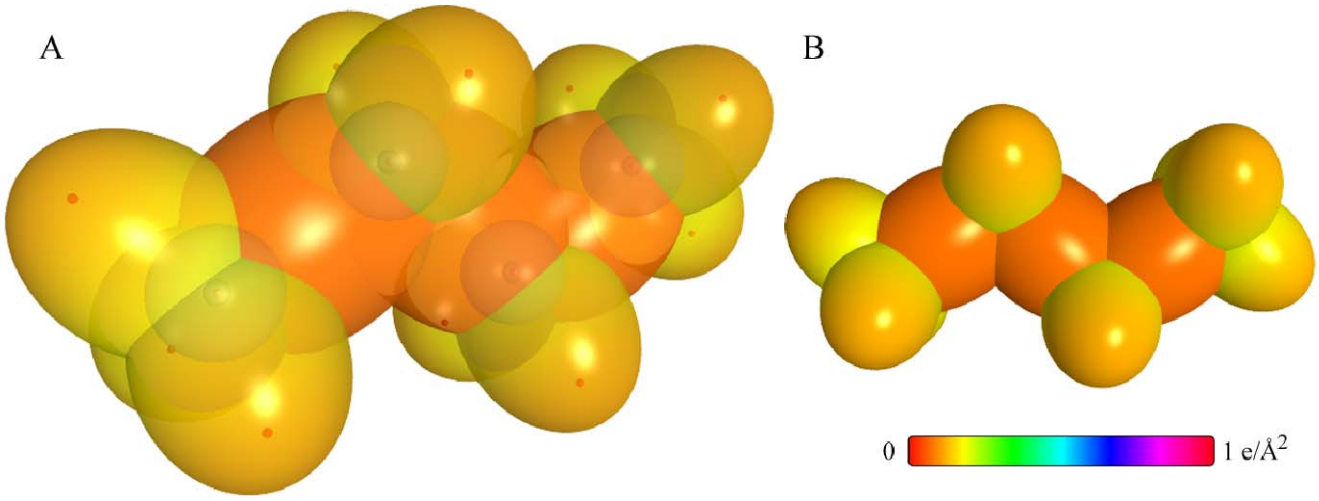

Table 15.4. The geometrical bond parameters of straight-chain alkanes and experimental values [1].

Parameter	$C-C$ Group	$C-H\ (CH_3)$ Group	$C-H\ (CH_2)$ Group
$a\ (a_0)$	2.12499	1.64920	1.67122
$c'\ (a_0)$	1.45744	1.04856	1.05553
Bond Length $2c'\ (\mathring{A})$	1.54280	1.10974	1.11713
Exp. Bond Length $(\mathring{A})$	1.532 (propane) 1.531 (butane)	1.107 ($C-H$ propane) 1.117 ($C-H$ butane)	1.107 ($C-H$ propane) 1.117 ($C-H$ butane)
$b,c\ (a_0)$	1.54616	1.27295	1.29569
e	0.68600	0.63580	0.63159

Table 15.5. The MO to HO intercept geometrical bond parameters of straight-chain alkanes. E_T is E_T (*atom – atom, msp*^{3}*.AO*).

Bond	Atom	E_T (eV) Bond 1	E_T (eV) Bond 2	E_T (eV) Bond 3	E_T (eV) Bond 4	Final Total Energy $C2sp^3$ (eV)	$r_{initial}$ (a_0)	r_{final} (a_0)	$E_{Coulomb}(C2sp^3)$ (eV) Final	$E(C2sp^3)$ (eV) Final	θ' $(^\circ)$	θ_1 $(^\circ)$	θ_2 $(^\circ)$	d_1 (a_0)	d_2 (a_0)
$C-H\ (CH_3)$	C	-0.92918	0	0	0	-152.54487	0.91771	0.86359	-15.75493	-15.56407	77.49	102.51	41.48	1.23564	0.18708
$C-H\ (CH_2)$	C	-0.92918	-0.92918	0	0	-153.47406	0.91771	0.81549	-16.68412	-16.49325	68.47	111.53	35.84	1.35486	0.29933
$H_3C_a-C_bH_2CH_2$	C_a	-0.92918	0	0	0	-152.54487	0.91771	0.86359	-15.75493	-15.56407	63.82	116.18	30.08	1.83879	0.38106
$H_3C_a-C_bH_2CH_2$	C_b	-0.92918	-0.92918	0	0	-153.47406	0.91771	0.81549	-16.68412	-16.49325	56.41	123.59	26.06	1.90890	0.45117

Table 15.6. The energy parameters (eV) of functional groups of straight-chain alkanes.

Parameters	$C-C$ Group	CH_3 Group	CH_2 Group
n_1	1	3	2
n_2	0	2	1
n_3	0	0	0
C_1	0.5	0.75	0.75
C_2	1	1	1
c_1	1	1	1
c_2	0.91771	0.91771	0.91771
c_3	0	0	1
c_4	2	1	1
c_5	0	3	2
C_{1o}	0.5	0.75	0.75
C_{2o}	1	1	1
$V_e\ (eV)$	-28.79214	-107.32728	-70.41425
$V_p\ (eV)$	9.33352	38.92728	25.78002
$T\ (eV)$	6.77464	32.53914	21.06675
$V_m\ (eV)$	-3.38732	-16.26957	-10.53337
$E_{(AO/HO)}\ (eV)$	-15.56407	-15.56407	-15.56407
$\Delta E_{H_2MO\,(AO/HO)}\ (eV)$	0	0	0
$E_{T\,(AO/HO)}\ (eV)$	-15.56407	-15.56407	-15.56407
$E_{T\,(H_2MO)}\ (eV)$	-31.63537	-67.69451	-49.66493
$E_T\left(atom-atom, msp^3.AO\right)\ (eV)$	-1.85836	0	0
$E_{T\,(MO)}\ (eV)$	-33.49373	-67.69450	-49.66493
$\omega\ \left(10^{15}\ rad/s\right)$	9.43699	24.9286	24.2751
$E_K\ (eV)$	6.21159	16.40846	15.97831
$\overline{E}_D\ (eV)$	-0.16515	-0.25352	-0.25017
$\overline{E}_{Kvib}\ (eV)$	0.12312 [2]	0.35532 (Eq. (13.458))	0.35532 (Eq. (13.458))
$\overline{E}_{osc}\ (eV)$	-0.10359	-0.22757	-0.14502
$E_{mag}\ (eV)$	0.14803	0.14803	0.14803
$E_{T\,(Group)}\ (eV)$	-33.59732	-67.92207	-49.80996
$E_{initial\,(c_4\ AO/HO)}\ (eV)$	-14.63489	-14.63489	-14.63489
$E_{initial\,(c_5\ AO/HO)}\ (eV)$	0	-13.59844	-13.59844
$E_{D\,(Group)}\ (eV)$	4.32754	12.49186	7.83016

Table 15.7. The total bond energies of n-alkanes calculated using the functional group composition and the energies of Table 15.6 compared to the experimental values [3].

Formula	Name	$C-C$	CH_3	CH_2	Calculated Total Bond Energy (eV)	Experimental Total Bond Energy (eV)	Relative Error
C_3H_8	Propane	2	2	1	41.46896	41.434	-0.00085
C_4H_{10}	Butane	3	2	2	53.62666	53.61	-0.00036
C_5H_{12}	Pentane	4	2	3	65.78436	65.77	-0.00017
C_6H_{14}	Hexane	5	2	4	77.94206	77.93	-0.00019
C_7H_{16}	Heptane	6	2	5	90.09976	90.09	-0.00013
C_8H_{18}	Octane	7	2	6	102.25746	102.25	-0.00006
C_9H_{20}	Nonane	8	2	7	114.41516	114.40	-0.00012
$C_{10}H_{22}$	Decane	9	2	8	126.57286	126.57	-0.00003
$C_{11}H_{24}$	Undecane	10	2	9	138.73056	138.736	0.00004
$C_{12}H_{26}$	Dodecane	11	2	10	150.88826	150.88	-0.00008
$C_{18}H_{38}$	Octadecane	17	2	16	223.83446	223.85	0.00008

Table 15.8. The bond angle parameters of straight-chain alkanes and experimental values [1]. In the calculation of θ_v, the parameters from the preceding angle were used. E_T is $E_T(atom-atom, msp^3.AO)$.

Atoms of Angle	2c' Bond 1 (a_0)	2c' Bond 2 (a_0)	2c' Terminal Atoms (a_0)	$E_{Coulombic}$ Atom 1	Atom 1 Hybridization Designation (Table 15.3.A)	$E_{Coulombic}$ Atom 2	Atom 2 Hybridization Designation (Table 15.3.A)	c_2 Atom 1	c_2 Atom 2	C_1	C_2	c_1	c_2'	E_T (eV)	θ_v (°)	θ_1 (°)	θ_2 (°)	Cal. θ (°)	Exp. θ (°)
Methylene $\angle HC_aH$	2.11106	2.11106	3.4252	-15.75493 C_a	7	H	H	0.86359	1	1	1	0.75	1.15796	0				108.44	107 (propane)
$\angle C_aC_bC_c$															69.51			110.49	112 (propane) 113.8 (butane)
$\angle C_aC_bH$															69.51			110.49	111.0 (butane)
Methyl $\angle HC_aH$	2.09711	2.09711	3.4252	-15.75493 C_a	7	H	H	0.86359	1	1	1	0.75	1.15796	0				109.50	
$\angle C_aC_bC_c$															70.56			109.44	
$\angle C_aC_bH$															70.56			109.44	

BRANCHED ALKANES ($C_nH_{2n+2},\ n=3,4,5...\infty$)

The branched-chain alkanes, C_nH_{2n+2}, comprise at least two terminal methyl groups (CH_3) at each end of the chain, and may comprise methylene (CH_2), and methylyne (CH) functional groups as well as C bound by carbon-carbon single bonds. The methyl and methylene functional groups are equivalent to those of straight-chain alkanes. Six types of $C-C$ bonds can be identified. The n-alkane $C-C$ bond is the same as that of straight-chain alkanes. In addition, the $C-C$ bonds within isopropyl ($(CH_3)_2CH$) and t-butyl ($(CH_3)_3C$) groups and the isopropyl to isopropyl, isopropyl to t-butyl, and t-butyl to t-butyl $C-C$ bonds comprise functional groups. The branched-alkane groups are solved using the same principles as those used to solve the methyl and methylene functional groups wherein the $2s$ and $2p$ AOs of each C hybridize to form a single $2sp^3$ shell as an energy minimum, and the sharing of electrons between two $C2sp^3$ HOs to form a MO permits each participating hybridized orbital to decrease in radius and energy. $E_T\left(atom-atom,msp^3.AO\right)$ of each $C-C$-bond MO in Eq. (15.61) due to the charge donation from the C atoms to the MO is $-1.85836\,eV$ or $-1.44915\,eV$ based on the energy match between the $C2sp^3$ HOs corresponding to the energy contributions equivalent to those of methylene, $-0.92918\,eV$ (Eq. (14.513)), or methyl, $-0.72457\,eV$ (Eq. (14.151)), groups, respectively.

The symbols of the functional groups of branched-chain alkanes are given in Table 15.9. The geometrical (Eqs. (15.1-15.5) and (15.51)), intercept (Eqs. (15.80-15.87)), and energy (Eqs. (15.6-15.11) and (15.17-15.65)) parameters of branched-chain alkanes are given in Tables 15.10, 15.11, and 15.12, respectively. The total energy of each branched-chain alkane given in Table 15.13 was calculated as the sum over the integer multiple of each $E_D(Group)$ of Table 15.12 corresponding to functional-group composition of the molecule. The bond angle parameters of branched-chain alkanes determined using Eqs. (15.88-15.117) are given in Table 15.14. The color scale, translucent view of the charge-density of exemplary alkane, isobutane, comprising the concentric shells of atoms with the outer shell bridged by one or more H_2-type ellipsoidal MOs or joined with one or more hydrogen MOs is shown in Figure 15.2.

Figure 15.2. Color scale, translucent view of the charge-density of isobutane showing the orbitals of the atoms at their radii, the ellipsoidal surface of each H or H_2-type ellipsoidal MO that transitions to the corresponding outer shell of the atom(s) participating in each bond, and the hydrogen nuclei (red, not to scale). (A) Top view. (B) Side view.

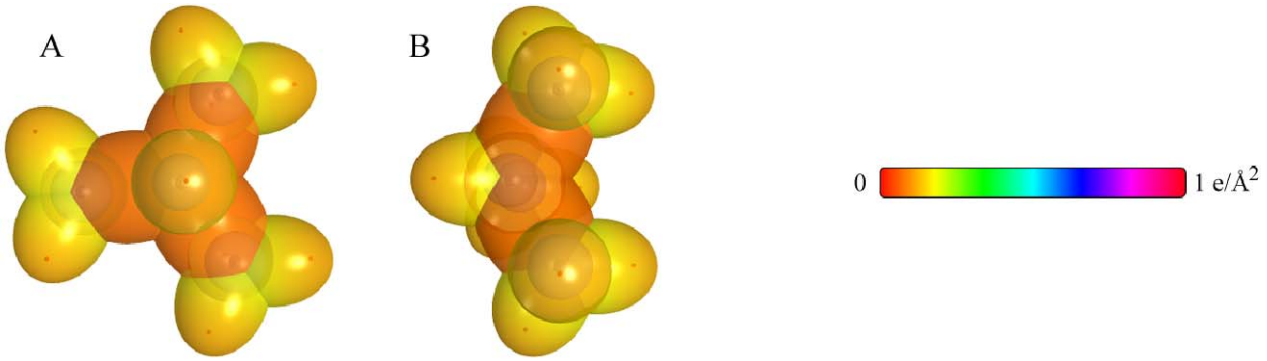

Table 15.9. The symbols of functional groups of branched alkanes.

Functional Group	Group Symbol
CH_3 group	$C-H\ (CH_3)$
CH_2 group	$C-H\ (CH_2)$
CH	$C-H$
CC bond (*n-C*)	$C-C$ (a)
CC bond (*iso-C*)	$C-C$ (b)
CC bond (*tert-C*)	$C-C$ (c)
CC (*iso* to *iso-C*)	$C-C$ (d)
CC (*t* to *t-C*)	$C-C$ (e)
CC (*t* to *iso-C)*	$C-C$ (f)

Table 15.10. The geometrical bond parameters of branched alkanes and experimental values [1].

Parameter	$C-H$ (CH_3) Group	$C-H$ (CH_2) Group	$C-H$ Group	$C-C$ (a) Group	$C-C$ (b) Group	$C-C$ (c) Group	$C-C$ (d) Group	$C-C$ (e) Group	$C-C$ (f) Group
a (a_0)	1.64920	1.67122	1.67465	2.12499	2.12499	2.10725	2.12499	2.10725	2.10725
c' (a_0)	1.04856	1.05553	1.05661	1.45744	1.45744	1.45164	1.45744	1.45164	1.45164
Bond Length $2c'$ (A)	1.10974	1.11713	1.11827	1.54280	1.54280	1.53635	1.54280	1.53635	1.53635
Exp. Bond Length (A)	1.107 ($C-H$ propane) 1.117 ($C-H$ butane)	1.107 ($C-H$ propane) 1.117 ($C-H$ butane)	1.122 (isobutane)	1.532 (propane) 1.531 (butane)	1.532 (propane) 1.531 (butane)	1.532 (propane) 1.531 (butane)	1.532 (propane) 1.531 (butane)	1.532 (propane) 1.531 (butane)	1.532 (propane) 1.531 (butane)
b,c (a_0)	1.27295	1.29569	1.29924	1.54616	1.54616	1.52750	1.54616	1.52750	1.52750
e	0.63580	0.63159	0.63095	0.68600	0.68600	0.68888	0.68600	0.68888	0.68888

Table 15.11. The MO to HO intercept geometrical bond parameters of branched-chain alkanes. *R, R′, R″* are *H* or alkyl groups. E_T is E_T $(atom-atom,\ msp^3.AO)$.

Bond	Atom	E_T (eV) Bond 1	E_T (eV) Bond 2	E_T (eV) Bond 3	E_T (eV) Bond 4	Final Total Energy $C2sp^3$ (eV)	$r_{initial}$ (a_0)	r_{final} (a_0)	$E_{Coulomb}(C2sp^3)$ (eV) Final	$E(C2sp^3)$ (eV) Final	θ' (°)	θ_1 (°)	θ_2 (°)	d_1 (a_0)	d_2 (a_0)
$C-H$ (CH_3)	C	-0.92918	0	0	0	-152.54487	0.91771	0.86359	-15.75493	-15.56407	77.49	102.51	41.48	1.23564	0.18708
$C-H$ (CH_2)	C	-0.92918	-0.92918	0	0	-153.47406	0.91771	0.81549	-16.68412	-16.49325	68.47	111.53	35.84	1.35486	0.29933
$C-H$ (CH)	C	-0.92918	-0.92918	-0.92918	0	-154.40324	0.91771	0.77247	-17.61330	-17.42244	61.10	118.90	31.37	1.42988	0.37326
$H_3C_aC_bH_2CH_2-$ $(C-C$ (a))	C_a	-0.92918	0	0	0	-152.54487	0.91771	0.86359	-15.75493	-15.56407	63.82	116.18	30.08	1.83879	0.38106
$H_3C_aC_bH_2CH_2-$ $(C-C$ (a))	C_b	-0.92918	-0.92918	0	0	-153.47406	0.91771	0.81549	-16.68412	-16.49325	56.41	123.59	26.06	1.90890	0.45117
$R-H_2C_aC_b(H_2C_c-R')HCH_2-$ $(C-C$ (b))	C_b	-0.92918	-0.92918	-0.92918	0	-154.40324	0.91771	0.77247	-17.61330	-17.42244	48.30	131.70	21.90	1.97162	0.51388
$R-H_2C_a(R'-H_2C_d)C_b(R''-H_2C_c)CH_2-$ $(C-C$ (e))	C_b	-0.92918	-0.72457	-0.72457	-0.72457	-154.71860	0.91771	0.75889	-17.92866	-17.73779	48.21	131.79	21.74	1.95734	0.50570
$isoC_aC_b(H_2C_c-R')HCH_2-$ $(C-C$ (d))	C_b	-0.92918	-0.92918	-0.92918	0	-154.40324	0.91771	0.77247	-17.61330	-17.42244	48.30	131.70	21.90	1.97162	0.51388
$tertC_a(R'-H_2C_d)C_b(R''-H_2C_c)CH_2-$ $(C-C$ (e))	C_b	-0.72457	-0.72457	-0.72457	-0.72457	-154.51399	0.91771	0.76765	-17.92866	-17.73779	50.04	129.96	22.66	1.94462	0.49298
$tertC_aC_b(H_2C_c-R')HCH_2-$ $(C-C$ (f))	C_b	-0.72457	-0.92918	-0.92918	0	-154.19863	0.91771	0.78155	-17.40869	-17.21783	52.78	127.22	24.04	1.92443	0.47279
$isoC_a(R'-H_2C_d)C_b(R''-H_2C_c)CH_2-$ $(C-C$ (f))	C_b	-0.72457	-0.72457	-0.72457	-0.72457	-154.51399	0.91771	0.76765	-17.92866	-17.73779	50.04	129.96	22.66	1.94462	0.49298

Table 15.12. The energy parameters (eV) of functional groups of branched-chain alkanes.

Parameters	CH_3 Group	CH_2 Group	$C-H$ Group	$C-C$ (a) Group	$C-C$ (b) Group	$C-C$ (c) Group	$C-C$ (d) Group	$C-C$ (e) Group	$C-C$ (f) Group
n_1	3	2	1	1	1	1	1	1	1
n_2	2	1	0	0	0	0	0	0	0
n_3	0	0	0	0	0	0	0	0	0
C_1	0.75	0.75	0.75	0.5	0.5	0.5	0.5	0.5	0.5
C_2	1	1	1	1	1	1	1	1	1
c_1	1	1	1	1	1	1	1	1	1
c_2	0.91771	0.91771	0.91771	0.91771	0.91771	0.91771	0.91771	0.91771	0.91771
c_3	0	1	1	0	0	0	1	1	0
c_4	1	1	1	2	2	2	2	2	2
c_5	3	2	1	0	0	0	0	0	0
C_{1o}	0.75	0.75	0.75	0.5	0.5	0.5	0.5	0.5	0.5
C_{2o}	1	1	1	1	1	1	1	1	1
V_e (eV)	-107.32728	-70.41425	-35.12015	-28.79214	-28.79214	-29.10112	-28.79214	-29.10112	-29.10112
V_p (eV)	38.92728	25.78002	12.87680	9.33352	9.33352	9.37273	9.33352	9.37273	9.37273
T (eV)	32.53914	21.06675	10.48582	6.77464	6.77464	6.90500	6.77464	6.90500	6.90500
V_m (eV)	-16.26957	-10.53337	-5.24291	-3.38732	-3.38732	-3.45250	-3.38732	-3.45250	-3.45250
$E_{(AO/HO)}$ (eV)	-15.56407	-15.56407	-14.63489	-15.56407	-15.56407	-15.35946	-15.56407	-15.35946	-15.35946
$\Delta E_{H_2MO(AO/HO)}$ (eV)	0	0	0	0	0	0	0	0	0
$E_{T(AO/HO)}$ (eV)	-15.56407	-15.56407	-14.63489	-15.56407	-15.56407	-15.35946	-15.56407	-15.35946	-15.35946
$E_{T(H_2MO)}$ (eV)	-67.69451	-49.66493	-31.63533	-31.63537	-31.63537	-31.63535	-31.63537	-31.63535	-31.63535
$E_T\left(atom-atom, msp^3.AO\right)$ (eV)	0	0	0	-1.85836	-1.85836	-1.44915	-1.85836	-1.44915	-1.44915
$E_{T(MO)}$ (eV)	-67.69450	-49.66493	-31.63537	-33.49373	-33.49373	-33.08452	-33.49373	-33.08452	-33.08452
$\omega\ \left(10^{15}\ rad/s\right)$	24.9286	24.2751	24.1759	9.43699	9.43699	15.4846	9.43699	9.55643	9.55643
E_K (eV)	16.40846	15.97831	15.91299	6.21159	6.21159	10.19220	6.21159	6.29021	6.29021
$\overline{E}_D$ (eV)	-0.25352	-0.25017	-0.24966	-0.16515	-0.16515	-0.20896	-0.16515	-0.16416	-0.16416
$\overline{E}_{Kvib}$ (eV)	0.35532 (Eq. (13.458))	0.35532 (Eq. (13.458))	0.35532 (Eq. (13.458))	0.12312 [2]	0.17978 [4]	0.09944 [5]	0.12312 [2]	0.12312 [2]	0.12312 [2]
$\overline{E}_{osc}$ (eV)	-0.22757	-0.14502	-0.07200	-0.10359	-0.07526	-0.15924	-0.10359	-0.10260	-0.10260
E_{mag} (eV)	0.14803	0.14803	0.14803	0.14803	0.14803	0.14803	0.14803	0.14803	0.14803
$E_{T(Group)}$ (eV)	-67.92207	-49.80996	-31.70737	-33.59732	-33.49373	-33.24376	-33.59732	-33.18712	-33.18712
$E_{initial(c_4\ AO/HO)}$ (eV)	-14.63489	-14.63489	-14.63489	-14.63489	-14.63489	-14.63489	-14.63489	-14.63489	-14.63489
$E_{initial(c_5\ AO/HO)}$ (eV)	-13.59844	-13.59844	-13.59844	0	0	0	0	0	0
$E_{D(Group)}$ (eV)	12.49186	7.83016	3.32601	4.32754	4.29921	3.97398	4.17951	3.62128	3.91734

Table 15.13. The total bond energies of branched alkanes calculated using the functional group composition and the energies of Table 15.12 compared to the experimental values [3].

Formula	Name	CH_3	CH_2	CH	$C-C$ (a)	$C-C$ (b)	$C-C$ (c)	$C-C$ (d)	$C-C$ (e)	$C-C$ (f)	Calculated Total Bond Energy (eV)	Experimental Total Bond Energy (eV)	Relative Error
C_4H_{10}	Isobutane	3	0	1	0	3	0	0	0	0	53.69922	53.695	-0.00007
C_5H_{12}	Isopentane	3	1	1	1	3	0	0	0	0	65.85692	65.843	-0.00021
C_5H_{12}	Neopentane	4	0	0	0	0	4	0	0	0	65.86336	65.992	0.00195
C_6H_{14}	2-Methylpentane	3	2	1	2	3	0	0	0	0	78.01462	78.007	-0.00010
C_6H_{14}	3-Methylpentane	3	2	1	2	3	0	0	0	0	78.01462	77.979	-0.00046
C_6H_{14}	2,2-Dimethylbutane	4	1	0	1	0	4	0	0	0	78.02106	78.124	0.00132
C_6H_{14}	2,3-Dimethylbutane	4	0	2	0	4	0	1	0	0	77.99581	78.043	0.00061
C_7H_{16}	2-Methylhexane	3	3	1	3	3	0	0	0	0	90.17232	90.160	-0.00014
C_7H_{16}	3-Methylhexane	3	3	1	3	3	0	0	0	0	90.17232	90.127	-0.00051
C_7H_{16}	3-Ethylpentane	3	3	1	3	3	0	0	0	0	90.17232	90.108	-0.00072
C_7H_{16}	2,2-Dimethylpentane	4	2	0	2	0	4	0	0	0	90.17876	90.276	0.00107
C_7H_{16}	2,2,3-Trimethylbutane	5	0	1	0	2	3	0	0	1	90.22301	90.262	0.00044
C_7H_{16}	2,4-Dimethylpentane	4	1	2	0	6	0	0	0	0	90.24488	90.233	-0.00013
C_7H_{16}	3,3-Dimethylpentane	4	2	0	2	0	4	0	0	0	90.17876	90.227	0.00054
C_8H_{18}	2-Methylheptane	3	4	1	4	3	0	0	0	0	102.33002	102.322	-0.00008
C_8H_{18}	3-Methylheptane	3	4	1	4	3	0	0	0	0	102.33002	102.293	-0.00036
C_8H_{18}	4-Methylheptane	3	4	1	4	3	0	0	0	0	102.33002	102.286	-0.00043
C_8H_{18}	3-Ethylhexane	3	4	1	3	4	0	0	0	0	102.33002	102.274	-0.00055
C_8H_{18}	2,2-Dimethylhexane	4	3	0	3	0	4	0	0	0	102.33646	102.417	0.00079
C_8H_{18}	2,3-Dimethylhexane	4	2	2	2	4	0	1	0	0	102.31121	102.306	-0.00005
C_8H_{18}	2,4-Dimethylhexane	4	2	2	1	6	0	0	0	0	102.40258	102.362	-0.00040
C_8H_{18}	2,5-Dimethylhexane	4	2	2	1	6	0	0	0	0	102.40258	102.396	-0.00006
C_8H_{18}	3,3-Dimethylhexane	4	3	0	3	0	4	0	0	0	102.33646	102.369	0.00032
C_8H_{18}	3,4-Dimethylhexane	4	2	2	2	4	0	1	0	0	102.31121	102.296	-0.00015
C_8H_{18}	3-Ethyl-2-methylpentane	4	2	2	2	4	0	1	0	0	102.31121	102.277	-0.00033
C_8H_{18}	3-Ethyl-3-methylpentane	4	3	0	3	0	4	0	0	0	102.33646	102.317	-0.00019
C_8H_{18}	2,2,3-Trimethylpentane	5	1	1	1	2	3	0	0	1	102.38071	102.370	-0.00010
C_8H_{18}	2,2,4-Trimethylpentane	5	1	1	0	3	4	0	0	0	102.40902	102.412	0.00003
C_8H_{18}	2,3,3-Trimethylpentane	5	1	1	1	2	3	0	0	1	102.38071	102.332	-0.00048
C_8H_{18}	2,3,4-Trimethylpentane	5	0	3	0	5	0	2	0	0	102.29240	102.342	0.00049
C_8H_{18}	2,2,3,3-Tetramethylbutane	6	0	0	0	0	6	0	1	0	102.41632	102.433	0.00016
C_9H_{20}	2,3,5-Trimethylhexane	5	1	3	0	7	0	1	0	0	114.54147	114.551	0.00008
C_9H_{20}	3,3-Diethylpentane	4	4	0	4	0	4	0	0	0	114.49416	114.455	-0.00034
C_9H_{20}	2,2,3,3-Tetramethylpentane	6	1	0	1	0	6	0	1	0	114.57402	114.494	-0.00070
C_9H_{20}	2,2,3,4-Tetramethylpentane	6	0	2	0	3	3	1	0	1	114.51960	114.492	-0.00024
C_9H_{20}	2,2,4,4-Tetramethylpentane	6	1	0	0	0	8	0	0	0	114.57316	114.541	-0.00028
C_9H_{20}	2,3,3,4-Tetramethylpentane	6	0	2	0	4	2	0	0	2	114.58266	114.484	-0.00086
$C_{10}H_{22}$	2-Methylnonane	3	6	1	6	3	0	0	0	0	126.64542	126.680	0.00027
$C_{10}H_{22}$	5-Methylnonane	3	6	1	6	3	0	0	0	0	126.64542	126.663	0.00014

Table 15.14. The bond angle parameters of branched-chain alkanes and experimental values [1]. In the calculation of θ_v, the parameters from the preceding angle were used. E_T is E_T (*atom – atom, msp*^{3}*.AO*).

Atoms of Angle	2c' Bond 1 (a_0)	2c' Bond 2 (a_0)	2c' Terminal Atoms (a_0)	$E_{Coulombic}$ Atom 1	Atom 1 Hybridization Designation (Table 15.3.A)	$E_{Coulombic}$ Atom 2	Atom 2 Hybridization Designation (Table 15.3.A)	c_2 Atom 1	c_2 Atom 2	C_1	C_2	c_1	c_2'	E_T (eV)	θ_v (°)	θ_1 (°)	θ_2 (°)	Cal. θ (°)	Exp. θ (°)
Methylene $\angle HC_aH$	2.11106	2.11106	3.4252	-15.75493	7	H	H	0.86359	1	1	1	0.75	1.15796	0				108.44	107 (propane)
$\angle C_aC_bC_c$															69.51			110.49	112 (propane) 113.8 (butane) 110.8 (isobutane)
$\angle C_aC_bH$															69.51			110.49	111.0 (butane) 111.4 (isobutane)
Methyl $\angle HC_aH$	2.09711	2.09711	3.4252	-15.75493	7	H	H	0.86359	1	1	1	0.75	1.15796	0				109.50	
$\angle C_aC_bC_c$															70.56			109.44	
$\angle C_aC_bH$															70.56			109.44	
$\angle C_bC_aC_c$ iso C_a	2.91547	2.91547	4.7958	-16.68412 C_b	26	-16.68412 C_c	26	0.81549	0.81549	1	1	1	0.81549	-1.85836				110.67	110.8 (isobutane)
$\angle C_bC_aH$ iso C_a	2.91547	2.11323	4.1633	-15.55033 C_a	5	-14.82575 C_b	1	0.87495	0.91771	0.75	1	0.75	1.04887	0				110.76	
$\angle C_aC_bH$ iso C_a	2.91547	2.09711	4.1633	-15.55033 C_b	5	-14.82575 C_a	1	0.87495	0.91771	0.75	1	0.75	1.04887	0				111.27	111.4 (isobutane)
$\angle C_bC_aC_b$ tert C_a	2.90327	2.90327	4.7958	-16.68412 C_b	26	-16.68412 C_b	26	0.81549	0.81549	1	1	1	0.81549	-1.85836				111.37	110.8 (isobutane)
$\angle C_bC_aC_d$															72.50			107.50	

ALKENES (C_nH_{2n}, $n=3,4,5...\infty$)

The straight and branched-chain alkenes, C_nH_{2n}, comprise at least one carbon-carbon double bond comprising a functional group that is solved equivalently to the double bond of ethylene. The double bond may be bound to one, two, three, or four carbon single bonds that substitute for the hydrogen atoms of ethylene. Based on the condition of energy matching of the orbital, any magnetic energy due to unpaired electrons in the constituent fragments, and differences in oscillation in the transition state, three distinct functional groups can be identified: C vinyl single bond to $-C(C)=C$, C vinyl single bond to $-C(H)=C$, and C vinyl single bond to $-C(C)=CH_2$. In addition, CH_2 of the $-C=CH_2$ moiety is an alkene functional group.

The alkyl portion of the alkene may comprise at least two terminal methyl groups (CH_3) at each end of the chain, and may comprise methylene (CH_2), and methylyne (CH) functional groups as well as C bound by carbon-carbon single bonds. The methyl and methylene functional groups are equivalent to those of straight-chain alkanes. Six types of $C-C$ bonds can be identified. The n-alkane $C-C$ bond is the same as that of straight-chain alkanes. In addition, the $C-C$ bonds within isopropyl ($(CH_3)_2CH$) and t-butyl ($(CH_3)_3C$) groups and the isopropyl to isopropyl, isopropyl to t-butyl, and t-butyl to t-butyl $C-C$ bonds comprise functional groups. The branched-chain-alkane groups in alkenes are equivalent to those in branched-chain alkanes. The solution of the functional groups comprises the hybridization of the $2s$ and $2p$ AOs of each C to form a single $2sp^3$ shell as an energy minimum, and the sharing of electrons between two $C2sp^3$ HOs to form a MO permits each participating hybridized orbital to decrease in radius and energy. $E_T\left(atom-atom,msp^3.AO\right)$ of the $C=C$-bond MO in Eq. (15.61) due to the charge donation from the C atoms to the MO is equivalent to that of ethylene, $-2.26759\ eV$, given by Eq. (14.247). $E_T\left(atom-atom,msp^3.AO\right)$ of each $C-C$-bond MO in Eq. (15.61) is $-1.85836\ eV$ or $-1.44915\ eV$ based on the energy match between the $C2sp^3$ HOs corresponding to the energy contributions equivalent to those of methylene, $-0.92918\ eV$ (Eq. (14.513)), or methyl, $-0.72457\ eV$ (Eq. (14.151)), groups, respectively.

The symbols of the functional groups of alkenes are given in Table 15.15. The geometrical (Eqs. (15.1-15.5) and (15.41)), intercept (Eqs. (15.80-15.87)), and energy (Eqs. (15.6-15.11) and (15.17-15.56)) parameters of alkenes are given in Tables 15.16, 15.17, and 15.18, respectively. The total energy of each alkene given in Table 15.19 was calculated as the sum over the integer multiple of each $E_{D(Group)}$ of Table 15.18 corresponding to functional-group composition of the molecule. For each set of unpaired electrons created by bond breakage, the $C2sp^3$ HO magnetic energy E_{mag} that is subtracted from the weighted sum of the $E_{D(Group)}$ (eV) values based on composition is given by Eq. (15.67). The bond angle parameters of alkenes, determined using Eqs. (15.88-15.117), are given in Table 15.20. The color scale, translucent view of the charge-density of exemplary alkene, propene, comprising the concentric shells of atoms with the outer shell bridged by one or more H_2-type ellipsoidal MOs or joined with one or more hydrogen MOs is shown in Figure 15.3.

Figure 15.3. Color scale, translucent view of the charge-density of propene showing the orbitals of the atoms at their radii, the ellipsoidal surface of each H or H_2-type ellipsoidal MO that transitions to the corresponding outer shell of the atom(s) participating in each bond, and the hydrogen nuclei (red, not to scale). (A) Top view. (B) Side view.

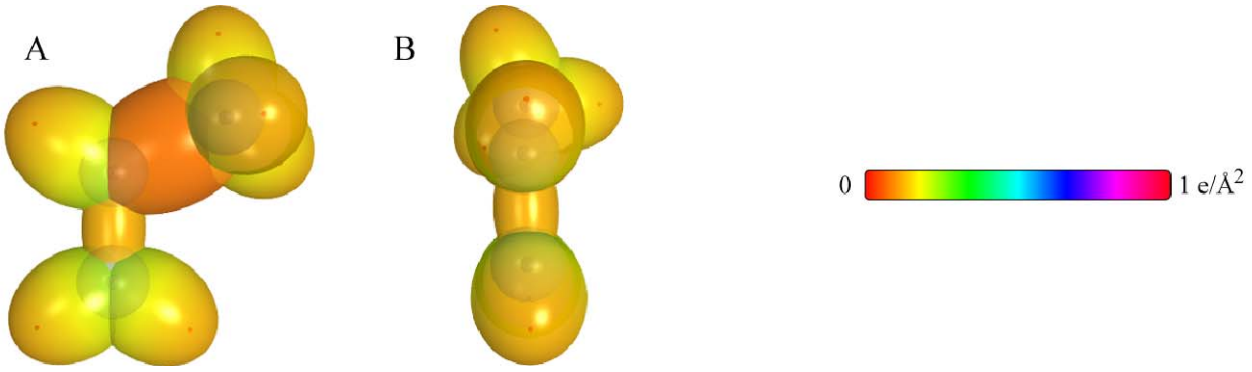

Table 15.15. The symbols of functional groups of alkenes.

Functional Group	Group Symbol
CC double bond	$C = C$
C vinyl single bond to -*C(C)=C*	$C - C$ (i)
C vinyl single bond to -*C(H)=C*	$C - C$ (ii)
C vinyl single bond to -*C(C)=CH₂*	$C - C$ (iii)
CH₂ alkenyl group	$C - H\ \left(CH_2\right)$ (i)
CH₃ group	$C - H\ \left(CH_3\right)$
CH₂ alkyl group	$C - H\ \left(CH_2\right)$ (ii)
CH	$C - H$
CC bond (*n*-*C*)	$C - C$ (a)
CC bond (*iso*-*C*)	$C - C$ (b)
CC bond (*tert*-*C*)	$C - C$ (c)
CC (*iso* to *iso*-*C*)	$C - C$ (d)
CC (*t* to *t*-*C*)	$C - C$ (e)
CC (*t* to *iso*-*C*)	$C - C$ (f)

Table 15.16. The geometrical bond parameters of alkenes and experimental values [1].

Parameter	$C=C$ Group	$C-C$ (i) Group	$C-C$ (ii) Group	$C-C$ (iii) Group	$C-H\ (CH_2)$ (i) Group	$C-H\ (CH_3)$ Group	$C-H\ (CH_2)$ (ii) Group	$C-H$ Group	$C-C$ (a) Group	$C-C$ (b) Group	$C-C$ (c) Group	$C-C$ (d) Group	$C-C$ (e) Group	$C-C$ (f) Group
$a\ (a_0)$	1.47228	2.04740	2.04740	2.04740	1.64010	1.64920	1.67122	1.67465	2.12499	2.12499	2.10725	2.12499	2.10725	2.10725
$c'\ (a_0)$	1.26661	1.43087	1.43087	1.43087	1.04566	1.04856	1.05553	1.05661	1.45744	1.45744	1.45164	1.45744	1.45164	1.45164
Bond Length $2c'\ (\text{Å})$	1.34052	1.51437	1.51437	1.51437	1.10668	1.10974	1.11713	1.11827	1.54280	1.54280	1.53635	1.54280	1.53635	1.53635
Exp. Bond Length (Å)	1.342 (2-methylpropene) 1.346 (2-butene) 1.349 (1,3-butadiene)		1.508 (2-butene)	1.508 (2-methylpropene)	1.10 (2-methylpropene) 1.108 (avg.) (1,3-butadiene)	1.107 ($C-H$ propane) 1.117 ($C-H$ butane)	1.107 ($C-H$ propane) 1.117 ($C-H$ butane)	1.122 (isobutane)	1.532 (propane) 1.531 (butane)	1.532 (propane) 1.531 (butane)	1.532 (propane) 1.531 (butane)	1.532 (propane) 1.531 (butane)	1.532 (propane) 1.531 (butane)	1.532 (propane) 1.531 (butane)
$b,c\ (a_0)$	0.75055	1.46439	1.46439	1.46439	1.26354	1.27295	1.29569	1.29924	1.54616	1.54616	1.52750	1.54616	1.52750	1.52750
e	0.86030	0.69887	0.69887	0.69887	0.63756	0.63580	0.63159	0.63095	0.68600	0.68600	0.68888	0.68600	0.68888	0.68888

Table 15.17. The MO to HO intercept geometrical bond parameters of alkenes. R_1 is an alkyl group and *R, R′, R″* are *H* or alkyl groups. E_T is E_T (*atom – atom, msp*^{3}*.AO*).

Bond	Atom	E_T (eV) Bond 1	E_T (eV) Bond 2	E_T (eV) Bond 3	E_T (eV) Bond 4	Final Total Energy $C2sp^3$ (eV)	$r_{initial}$ (a_0)	r_{final} (a_0)	$E_{Coulomb}\left(C2sp^3\right)$ (eV) Final	$E\left(C2sp^3\right)$ (eV) Final	θ' (°)	θ_1 (°)	θ_2 (°)	d_1 (a_0)	d_2 (a_0)
$C_c(H)C_a=C_a(H)C_d$	C_a	-1.13380	-0.92918	0	0	-153.67867	0.91771	0.80561	-16.88873	-16.69786	127.61	52.39	58.24	0.77492	0.49168
$C_c(H)C_a=C_bH_2$	C_b	-1.13380	0	0	0	-152.74949	0.91771	0.85252	-15.95955	-15.76868	129.84	50.16	60.70	0.72040	0.54620
$C_c(C_d)C_a=C_bH,C_e$	C_a	-1.13380	-0.72457	-0.72457	0	-154.19863	0.91771	0.78155	-17.40869	-17.21783	126.39	53.61	56.95	0.80289	0.46371
$R_1C_bH_2-C_a(C)=C$ ($C-C$ (i))	C_a	-1.13380	-0.72457	-0.72457	0	-154.19863	0.91771	0.78155	-17.40869	-17.21783	60.88	119.12	27.79	1.81127	0.38039
$R_1C_bH_2-C_a(C)=C$ ($C-C$ (i)) $R_1C_bH_2-C_a(C)=CH_2$ ($C-C$ (iii))	C_b	-0.72457	-0.92918	0	0	-153.26945	0.91771	0.82562	-16.47951	-16.28864	67.40	112.60	31.36	1.74821	0.31734
$R_1C_bH_2-C_a(H)=C$ ($C-C$ (ii))	C_a	-1.13380	-0.92918	0	0	-153.67866	0.91771	0.80561	-16.88873	-16.69786	64.57	115.43	29.79	1.77684	0.34596
$R_1C_bH_2-C_a(H)=C$ ($C-C$ (i))	C_b	-0.92918	-0.92918	0	0	-153.47405	0.91771	0.81549	-16.68411	-16.49325	65.99	114.01	30.58	1.76270	0.33183
$C-H\ (CH_2)$ (i)	C	-1.13380	0	0	0	-152.74949	0.91771	0.85252	-15.95955	-15.76868	77.15	102.85	41.13	1.23531	0.18965
$C-H\ (CH_3)$	C	-0.92918	0	0	0	-152.54487	0.91771	0.86359	-15.75493	-15.56407	77.49	102.51	41.48	1.23564	0.18708
$C-H\ (CH_2)$ (ii)	C	-0.92918	-0.92918	0	0	-153.47406	0.91771	0.81549	-16.68412	-16.49325	68.47	111.53	35.84	1.35486	0.29933
$C-H\ (CH)$	C	-0.92918	-0.92918	-0.92918	0	-154.40324	0.91771	0.77247	-17.61330	-17.42244	61.10	118.90	31.37	1.42988	0.37326
$H_3C_aC_bH_2CH_2-$ ($C-C$ (a))	C_a	-0.92918	0	0	0	-152.54487	0.91771	0.86359	-15.75493	-15.56407	63.82	116.18	30.08	1.83879	0.38106
$H_3C_aC_bH_2CH_2-$ ($C-C$ (a))	C_b	-0.92918	-0.92918	0	0	-153.47406	0.91771	0.81549	-16.68412	-16.49325	56.41	123.59	26.06	1.90890	0.45117
$R-H_2C_cC_b(H_2C_c-R')HCH_2-$ ($C-C$ (b))	C_b	-0.92918	-0.92918	-0.92918	0	-154.40324	0.91771	0.77247	-17.61330	-17.42244	48.30	131.70	21.90	1.97162	0.51388
$R-H_2C_c(R'-H_2C_d)C_b(R''-H_2C_c)CH_2-$ ($C-C$ (e))	C_b	-0.92918	-0.72457	-0.72457	-0.72457	-154.71860	0.91771	0.75889	-17.92866	-17.73779	48.21	131.79	21.74	1.95734	0.50570
$isoC_aC_b(H_2C_c-R')HCH_2-$ ($C-C$ (d))	C_b	-0.92918	-0.92918	-0.92918	0	-154.40324	0.91771	0.77247	-17.61330	-17.42244	48.30	131.70	21.90	1.97162	0.51388
$tertC_a(R'-H_2C_d)C_b(R''-H_2C_c)CH_2-$ ($C-C$ (e))	C_b	-0.72457	-0.72457	-0.72457	-0.72457	-154.51399	0.91771	0.76765	-17.92866	-17.73779	50.04	129.96	22.66	1.94462	0.49298
$tertC_aC_b(H_2C_c-R')HCH_2-$ ($C-C$ (f))	C_b	-0.72457	-0.92918	-0.92918	0	-154.19863	0.91771	0.78155	-17.40869	-17.21783	52.78	127.22	24.04	1.92443	0.47279
$isoC_a(R-H_2C_d)C_b(R''-H_2C_c)CH_2-$ ($C-C$ (f))	C_b	-0.72457	-0.72457	-0.72457	-0.72457	-154.51399	0.91771	0.76765	-17.92866	-17.73779	50.04	129.96	22.66	1.94462	0.49298

Table 15.18. The energy parameters (eV) of functional groups of alkenes.

Parameters	$C=C$ Group	$C-C$ (i) Group	$C-C$ (ii) Group	$C-C$ (iii) Group	CH_2 (i) Group	CH_3 Group	CH_2 (ii) Group	$C-H$ Group	$C-C$ (a) Group	$C-C$ (b) Group	$C-C$ (c) Group	$C-C$ (d) Group	$C-C$ (e) Group	$C-C$ (f) Group
n_1	2	1	1	1	2	3	2	1	1	1	1	1	1	1
n_2	0	0	0	0	1	2	1	0	0	0	0	0	0	0
n_3	0	0	0	0	0	0	0	0	0	0	0	0	0	0
C_1	0.5	0.5	0.5	0.5	0.75	0.75	0.75	0.75	0.5	0.5	0.5	0.5	0.5	0.5
C_2	0.91771	1	1	1	1	1	1	1	1	1	1	1	1	1
c_1	1	1	1	1	1	1	1	1	1	1	1	1	1	1
c_2	0.91771	0.91771	0.91771	0.91771	0.91771	0.91771	0.91771	0.91771	0.91771	0.91771	0.91771	0.91771	0.91771	0.91771
c_3	0	1	0	1	1	0	1	1	0	0	0	1	1	0
c_4	4	2	2	2	1	1	1	1	2	2	2	2	2	2
c_5	0	0	0	0	2	3	2	1	0	0	0	0	0	0
C_{1o}	0.5	0.5	0.5	0.5	0.75	0.75	0.75	0.75	0.5	0.5	0.5	0.5	0.5	0.5
C_{2o}	0.91771	1	1	1	1	1	1	1	1	1	1	1	1	1
V_e (eV)	-102.08992	-30.19634	-30.19634	-30.19634	-72.03287	-107.32728	-70.41425	-35.12015	-28.79214	-28.79214	-29.10112	-28.79214	-29.10112	-29.10112
V_p (eV)	21.48386	9.50874	9.50874	9.50874	26.02344	38.92728	25.78002	12.87680	9.33352	9.33352	9.37273	9.33352	9.37273	9.37273
T (eV)	34.67062	7.37432	7.37432	7.37432	21.95990	32.53914	21.06675	10.48582	6.77464	6.77464	6.90500	6.77464	6.90500	6.90500
V_m (eV)	-17.33531	-3.68716	-3.68716	-3.68716	-10.97995	-16.26957	-10.53337	-5.24291	-3.38732	-3.38732	-3.45250	-3.38732	-3.45250	-3.45250
$E_{(AO/HO)}$ (eV)	0	-14.63489	-14.63489	-14.63489	-14.63489	-15.56407	-15.56407	-14.63489	-15.56407	-15.56407	-15.35946	-15.56407	-15.35946	-15.35946
$\Delta E_{H_2MO(AO/HO)}$ (eV)	0	0	0	0	0	0	0	0	0	0	0	0	0	0
$E_T(_{AO/HO})$ (eV)	0	-14.63489	-14.63489	-14.63489	-14.63489	-15.56407	-15.56407	-14.63489	-15.56407	-15.56407	-15.35946	-15.56407	-15.35946	-15.35946
$E_T(_{H_2MO})$ (eV)	-63.27075	-31.63534	-31.63534	-31.63534	-49.66437	-67.69451	-49.66493	-31.63533	-31.63537	-31.63537	-31.63535	-31.63537	-31.63535	-31.63535
$E_T\left(atom-atom, msp^3.AO\right)$ (eV)	-2.26759	-1.44915	-1.85836	-1.44915	0	0	0	0	-1.85836	-1.85836	-1.44915	-1.85836	-1.44915	-1.44915
$E_T(_{MO})$ (eV)	-65.53833	-33.08452	-33.49373	-33.08452	-49.66493	-67.69450	-49.66493	-31.63537	-33.49373	-33.49373	-33.08452	-33.49373	-33.08452	-33.08452
$\omega\left(10^{15}\ rad/s\right)$	43.0680	9.97851	16.4962	9.97851	25.2077	24.9286	24.2751	24.1759	9.43699	9.43699	15.4846	9.43699	9.55643	9.55643
E_K (eV)	28.34813	6.56803	10.85807	6.56803	16.59214	16.40846	15.97831	15.91299	6.21159	6.21159	10.19220	6.21159	6.29021	6.29021
$\bar{E}_D$ (eV)	-0.34517	-0.16774	-0.21834	-0.16774	-0.25493	-0.25352	-0.25017	-0.24966	-0.16515	-0.16515	-0.20896	-0.16515	-0.16416	-0.16416
$\bar{E}_{Kvib}$ (eV)	0.17897 [6]	0.15895 [7]	0.09931 [8]	0.09931 [8]	0.35532 Eq. (13.458)	0.35532 Eq. (13.458)	0.35532 Eq. (13.458)	0.35532 Eq. (13.458)	0.12312 [2]	0.17978 [4]	0.09944 [5]	0.12312 [2]	0.12312 [2]	0.12312 [2]
$\bar{E}_{osc}$ (eV)	-0.25568	-0.08827	-0.16869	-0.11809	-0.07727	-0.22757	-0.14502	-0.07200	-0.10359	-0.07526	-0.15924	-0.10359	-0.10260	-0.10260
E_{mag} (eV)	0.14803	0.14803	0.14803	0.14803	0.14803	0.14803	0.14803	0.14803	0.14803	0.14803	0.14803	0.14803	0.14803	0.14803
$E_T(_{Group})$ (eV)	-66.04969	-33.17279	-33.66242	-33.20260	-49.81948	-67.92207	-49.80996	-31.70737	-33.59732	-33.49373	-33.24376	-33.59732	-33.18712	-33.18712
$E_{initial(c_4\ AO/HO)}$ (eV)	-14.63489	-14.63489	-14.63489	-14.63489	-14.63489	-14.63489	-14.63489	-14.63489	-14.63489	-14.63489	-14.63489	-14.63489	-14.63489	-14.63489
$E_{initial(c_5\ AO/HO)}$ (eV)	0	0	0	0	-13.59844	-13.59844	-13.59844	-13.59844	0	0	0	0	0	0
$E_{D(Group)}$ (eV)	7.51014	3.75498	4.39264	3.78480	7.83968	12.49186	7.83016	3.32601	4.32754	4.29921	3.97398	4.17951	3.62128	3.91734

Table 15.19. The total bond energies of alkenes calculated using the functional group composition and the energies of Table 15.18 compared to the experimental values [3]. The magnetic energy E_{mag} that is subtracted from the weighted sum of the $E_{D\,(Group)}$ (eV) values based on composition is given by (15.58).

Formula	Name	$C=C$	$C-C$ (i)	$C-C$ (ii)	$C-C$ (iii)	CH_2 (i)	CH_3	CH_2 (ii)	CH	$C-C$ (a)	$C-C$ (b)	$C-C$ (c)	$C-C$ (d)	$C-C$ (e)	$C-C$ (f)	E_{mag}	Calculated Total Bond Energy (eV)	Experimental Total Bond Energy (eV)	Relative Error
C_3H_6	Propene	1	0	1	0	1	1	0	1	0	0	0	0	0	0	0	35.56033	35.63207	0.00201
C_4H_8	1-Butene	1	0	1	0	1	1	1	1	1	0	0	0	0	0	0	47.71803	47.78477	0.00140
C_4H_8	trans-2-Butene	1	0	2	0	0	2	0	2	0	0	0	0	0	0	0	47.93116	47.90395	-0.00057
C_4H_8	Isobutene	1	0	0	2	1	2	0	0	0	0	0	0	0	0	0	47.90314	47.96096	0.00121
C_5H_{10}	1-Pentene	1	0	1	0	1	1	2	1	2	0	0	0	0	0	0	59.87573	59.95094	0.00125
C_5H_{10}	trans-2-Pentene	1	0	2	0	0	2	1	2	1	0	0	0	0	0	0	60.08886	60.06287	-0.00043
C_5H_{10}	2-Methyl-1-butene	1	0	0	2	1	2	1	0	1	0	0	0	0	0	0	60.06084	60.09707	0.00060
C_5H_{10}	2-Methyl-2-butene	1	2	1	0	0	3	0	1	0	0	0	0	0	0	0	60.21433	60.16444	-0.00083
C_5H_{10}	3-Methyl-1-butene	1	0	1	0	1	2	0	2	0	2	0	0	0	0	0	59.97662	60.01727	0.00068
C_6H_{12}	1-Hexene	1	0	1	0	1	1	3	1	3	0	0	0	0	0	0	72.03343	72.12954	0.00133
C_6H_{12}	trans-2-Hexene	1	0	2	0	0	2	2	2	2	0	0	0	0	0	0	72.24656	72.23733	-0.00013
C_6H_{12}	trans-3-Hexene	1	0	2	0	0	2	2	2	2	0	0	0	0	0	0	72.24656	72.24251	-0.00006
C_6H_{12}	2-Methyl-1-pentene	1	0	0	2	1	2	2	0	2	0	0	0	0	0	0	72.21854	72.29433	0.00105
C_6H_{12}	2-Methyl-2-pentene	1	2	1	0	0	3	1	1	1	0	0	0	0	0	0	72.37203	72.37206	0.00000
C_6H_{12}	3-Methyl-1-pentene	1	0	1	0	1	2	1	2	1	2	0	0	0	0	0	72.13432	72.19173	0.00080
C_6H_{12}	4-Methyl-1-pentene	1	0	1	0	1	2	1	2	0	3	0	0	0	0	0	72.10599	72.21038	0.00145
C_6H_{12}	3-Methyl-trans-2-pentene	1	2	1	0	0	3	1	1	1	0	0	0	0	0	0	72.37203	72.33268	-0.00054
C_6H_{12}	4-Methyl-trans-2-pentene	1	0	2	0	0	3	0	3	0	2	0	0	0	0	0	72.34745	72.31610	-0.00043
C_6H_{12}	2-Ethyl-1-butene	1	0	0	2	1	2	2	0	2	0	0	0	0	0	0	72.21854	72.25909	0.00056
C_6H_{12}	2,3-Dimethyl-1-butene	1	0	0	2	1	3	0	1	0	2	0	0	0	0	0	72.31943	72.32543	0.00008
C_6H_{12}	3,3-Dimethyl-1-butene	1	0	1	0	1	3	0	1	0	0	3	0	0	0	-1	72.31796	72.30366	-0.00020
C_6H_{12}	2,3-Dimethyl-2-butene	1	4	0	0	0	4	0	0	0	0	0	0	0	0	0	72.49750	72.38450	-0.00156
C_7H_{14}	1-Heptene	1	0	1	0	1	1	4	1	4	0	0	0	0	0	0	84.19113	84.27084	0.00095
C_7H_{14}	5-Methyl-1-hexene	1	0	1	0	1	2	2	2	1	3	0	0	0	0	0	84.26369	84.30608	0.00050
C_7H_{14}	trans-3-Methyl-3-hexene	1	2	1	0	0	3	2	1	2	0	0	0	0	0	0	84.52973	84.42112	-0.00129
C_7H_{14}	2,4-Dimethyl-1-pentene	1	0	0	2	1	3	1	1	0	3	0	0	0	0	0	84.44880	84.49367	0.00053
C_7H_{14}	4,4-Dimethyl-1-pentene	1	0	1	0	1	3	1	1	0	0	4	0	0	0	0	84.27012	84.47087	0.00238
C_7H_{14}	2,4-Dimethyl-2-pentene	1	2	1	0	0	4	0	2	0	2	0	0	0	0	0	84.63062	84.54445	-0.00102
C_7H_{14}	trans-4,4-Dimethyl-2-pentene	1	0	2	0	0	4	0	2	0	0	3	0	0	0	-2	84.54076	84.54549	0.00006
C_7H_{14}	2-Ethyl-3-methyl-1-butene	1	0	0	2	1	3	1	1	1	2	0	0	0	0	0	84.47713	84.44910	-0.00033
C_7H_{14}	2,3,3-Trimethyl-1-butene	1	0	0	2	1	4	0	0	0	0	3	0	0	0	-2	84.51274	84.51129	-0.00002
C_8H_{16}	1-Octene	1	0	1	0	1	1	5	1	5	0	0	0	0	0	0	96.34883	96.41421	0.00068
C_8H_{16}	trans-2,2-Dimethyl-3-hexene	1	0	2	0	0	4	1	2	1	0	3	0	0	0	-2	96.69846	96.68782	-0.00011
C_8H_{16}	3-Ethyl-2-methyl-1-pentene	1	0	0	2	1	3	2	1	2	2	0	0	0	0	0	96.63483	96.61113	-0.00025
C_8H_{16}	2,4,4-Trimethyl-1-pentene	1	0	0	2	1	4	1	0	0	0	4	0	0	0	0	96.61293	96.71684	0.00107
C_8H_{16}	2,4,4-Trimethyl-2-pentene	1	2	1	0	0	5	0	1	0	0	3	0	0	0	-3	96.67590	96.65880	-0.00018
$C_{10}H_{20}$	1-Decene	1	0	1	0	1	1	7	1	7	0	0	0	0	0	0	120.66423	120.74240	0.00065
$C_{12}H_{24}$	1-Dodecene	1	0	1	0	1	1	9	1	9	0	9	0	0	0	0	144.97963	145.07163	0.00063
$C_{16}H_{32}$	1-Hexadecene	1	0	1	0	1	1	13	1	13	0	0	0	0	0	0	193.61043	193.71766	0.00055

Table 15.20. The bond angle parameters of alkenes and experimental values [1]. In the calculation of θ_v, the parameters from the preceding angle were used. E_T is E_T $(atom-atom,\ msp^3.AO)$.

Atoms of Angle	2c' Bond 1 (a_0)	2c' Bond 2 (a_0)	2c' Terminal Atoms (a_0)	$E_{Coulombic}$ Atom 1	Atom 1 Hybridization Designation (Table 15.3.A)	$E_{Coulombic}$ Atom 2	Atom 2 Hybridization Designation (Table 15.3.A)	c_2 Atom 1	c_2 Atom 2	C_1	C_2	c_1	c_2'	E_T (eV)	θ_v (°)	θ_1 (°)	θ_2 (°)	Cal. θ (°)	Exp. θ (°)
$\angle HC_cC_c$ $(C_c(H)C_a=C_*)$	2.11323	2.86175	4.2895	-15.95955 C_a	10	-14.82575 C_c	1	0.85252	0.91771	0.75	1	0.75	1.07647	0				118.36	
$\angle C_cC_aC_c$ $(C_c(C_c)C_a=C_b)$	2.86175	2.86175	4.7958	-16.68411 C_c	25	-16.68411 C_c	25	0.81549	0.81549	1	1	1	0.81549	-1.85836				113.84	
$\angle C_bC_aC_c$ $(C_b=C_aC_c)$	2.53321	2.86175	4.7539	-16.88873 C_b	29	-16.68411 C_c	25	0.80561	0.81549	1	1	1	0.81055	-1.85836				123.46	124.4 (1,3,5-hexatriene CbCcCc) 121.7 (1,3,5-hexatriene CaCbCc) 124.4 (1,3-butadiene CCC) 125.3 (2-butene CbCaCc)
$\angle HC_cC_b$																118.36	123.46	118.19	
$\angle HC_aH$ $(H_2C_a=C_bC_c)$	2.04578	2.04578	3.4756	-15.95955	10	H	H	0.85252	1	1	1	0.75	1.17300	0				116.31	118.5 (2-methylpropene)
$\angle C_bC_aH$ $(H_2C_a=C_bC_c)$																116.31		121.85	121 (2-methylpropene)
Methylene $\angle HC_cH$	2.11106	2.11106	3.4252	-15.75493	7	H	H	0.86359	1	1	1	0.75	1.15796	0				108.44	107 (propane)
$\angle C_aC_bC_c$															69.51			110.49	112 (propane) 113.8 (butane) 110.8 (isobutane)
$\angle C_aC_bH$															69.51			110.49	111.0 (butane) 111.4 (isobutane)
Methyl $\angle HC_aH$	2.09711	2.09711	3.4252	-15.75493	7	H	H	0.86359	1	1	1	0.75	1.15796	0				109.50	
$\angle C_aC_bC_c$															70.56			109.44	
$\angle C_aC_bH$															70.56			109.44	
$\angle C_bC_aC_c$ iso C_a	2.91547	2.91547	4.7958	-16.68412 C_b	26	-16.68412 C_c	26	0.81549	0.81549	1	1	1	0.81549	-1.85836				110.67	110.8 (isobutane)
$\angle C_bC_aH$ iso C_a	2.91547	2.11323	4.1633	-15.55033 C_a	5	-14.82575 C_b	1	0.87495	0.91771	0.75	1	0.75	1.04887	0				110.76	
$\angle C_aC_bH$ iso C_a	2.91547	2.09711	4.1633	-15.55033 C_b	5	-14.82575 C_a	1	0.87495	0.91771	0.75	1	0.75	1.04887	0				111.27	111.4 (isobutane)
$\angle C_bC_aC_b$ tert C_a	2.90327	2.90327	4.7958	-16.68412 C_b	26	-16.68412 C_b	26	0.81549	0.81549	1	1	1	0.81549	-1.85836				111.37	110.8 (isobutane)
$\angle C_bC_aC_d$															72.50			107.50	

ALKYNES (C_nH_{2n-2}, $n=3,4,5...\infty$)

The straight and branched-chain alkynes, C_nH_{2n-2}, have at least one carbon-carbon triple bond comprising a functional group that is solved equivalently to the triple bond of acetylene. The triple bond may be bound to one or two carbon single bonds that substitute for the hydrogen atoms of acetylene. Based on the energy matching of the mutually bound C, these $C-C$-bond MOs are defined as primary and secondary $C-C$ functional groups, respectively, that are unique to alkynes. In addition, the corresponding terminal CH of a primary alkyne comprises a functional group that is solved equivalently to the methylyne group of acetylene as given in the Acetylene Molecule section.

The alkyl portion of the alkyne may comprise at least two terminal methyl groups (CH_3) at each end of the chain, and may comprise methylene (CH_2), and methylyne (CH) functional groups as well as C bound by carbon-carbon single bonds. The methyl and methylene functional groups are equivalent to those of straight-chain alkanes. Six types of $C-C$ bonds can be identified. The n-alkane $C-C$ bond is the same as that of straight-chain alkanes. In addition, the $C-C$ bonds within isopropyl ($(CH_3)_2CH$) and t-butyl ($(CH_3)_3C$) groups and the isopropyl to isopropyl, isopropyl to t-butyl, and t-butyl to t-butyl $C-C$ bonds comprise functional groups. The branched-chain-alkane groups in alkynes are equivalent to those in branched-chain alkanes.

The solution of the functional groups comprises the hybridization of the $2s$ and $2p$ AOs of each C to form a single $2sp^3$ shell as an energy minimum, and the sharing of electrons between two $C2sp^3$ HOs to form a MO permits each participating hybridized orbital to decrease in radius and energy. $E_T\left(atom-atom,msp^3.AO\right)$ of the $C\equiv C$-bond MO in Eq. (15.61) due to the charge donation from the C atoms to the MO is equivalent to that of acetylene, $-3.13026\,eV$, given by Eq. (14.342). $E_T\left(atom-atom,msp^3.AO\right)$ of each -alkyl-bond MO in Eq. (15.61) is $-1.85836\,eV$ or $-1.44915\,eV$ based on the energy match between the $C2sp^3$ HOs corresponding to the energy contributions equivalent to those of methylene, $-0.92918\,eV$ (Eq. (14.513)), or methyl, $-0.72457\,eV$ (Eq. (14.151)), groups, respectively. For the $C-C$ groups each comprising a C single bond to $C\equiv C$, $E_T\left(atom-atom,msp^3.AO\right)$ is $-0.72457\,eV$ based on the energy match between the $C2sp^3$ HOs for the mutually bound C of the single and triple bonds. The parameter ω of each group is matched for oscillation in the transition state based on the group being primary or secondary.

The symbols of the functional groups of alkynes are given in Table 15.21. The geometrical (Eqs. (15.1-15.5) and (15.51)), intercept (Eqs. (15.80-15.87)), and energy (Eqs. (15.6-15.11) and (15.17-15.65)) parameters of alkynes are given in Tables 15.22, 15.23, and 15.24, respectively. The total energy of each alkyne given in Table 15.25 is calculated as the sum over the integer multiple of each $E_{D(Group)}$ of Table 15.24 corresponding to functional-group composition of the molecule. The bond angle parameters of alkynes determined using Eqs. (15.88-15.117) are given in Table 15.26. Each C of the $C\equiv C$ group can further bond with only one atom, and the bond is linear as a minimum of energy as in the case of acetylene. The color scale, translucent view of the charge-density of exemplary alkyne, propyne, comprising the concentric shells of atoms with the outer shell bridged by one or more H_2-type ellipsoidal MOs or joined with one or more hydrogen MOs is shown in Figure 15.4.

Figure 15.4. Color scale, translucent view of the charge-density of propyne showing the orbitals of the atoms at their radii, the ellipsoidal surface of each H or H_2-type ellipsoidal MO that transitions to the corresponding outer shell of the atom(s) participating in each bond, and the hydrogen nuclei (red, not to scale).

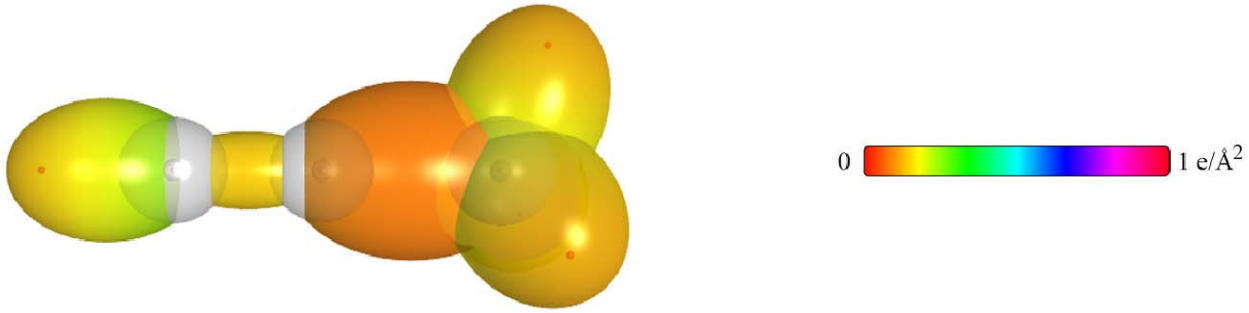

Table 15.21. The symbols of functional groups of alkynes.

Functional Group	Group Symbol
CC triple bond	$C \equiv C$
C single bond to $C \equiv C$ (1°)	$C - C$ (i)
C single bond to $C \equiv C$ (2°)	$C - C$ (ii)
CH (terminal)	$C - H$ (i)
CH_3 group	$C - H\ \left(CH_3\right)$
CH_2 group	$C - H\ \left(CH_2\right)$
CH (alkyl)	$C - H$ (ii)
CC bond (*n-C*)	$C - C$ (a)
CC bond (*iso-C*)	$C - C$ (b)
CC bond (*tert-C*)	$C - C$ (c)
CC (*iso* to *iso-C*)	$C - C$ (d)
CC (*t* to *t-C)*	$C - C$ (e)
CC (*t* to *iso-C*)	$C - C$ (f)

Table 15.22. The geometrical bond parameters of alkynes and experimental values [1].

Parameter	$C \equiv C$ Group	$C-C$ (i) Group	$C-C$ (ii) Group	$C-H$ (i) Group	$C-H\ (CH_3)$ Group	$C-H\ (CH_2)$ Group	$C-H$ (ii) Group	$C-C$ (a) Group	$C-C$ (b) Group	$C-C$ (c) Group	$C-C$ (d) Group	$C-C$ (e) Group	$C-C$ (f) Group
$a\ (a_0)$	1.28714	1.99185	1.99185	1.48719	1.64920	1.67122	1.67465	2.12499	2.12499	2.10725	2.12499	2.10725	2.10725
$c'\ (a_0)$	1.13452	1.41133	1.41133	0.99572	1.04856	1.05553	1.05661	1.45744	1.45744	1.45164	1.45744	1.45164	1.45164
Bond Length $2c'\ (\AA)$	1.20072	1.49369	1.49369	1.05383	1.10974	1.11713	1.11827	1.54280	1.54280	1.53635	1.54280	1.53635	1.53635
Exp. Bond Length $(\AA)$	1.203 (acetylene) 1.208 (2,4-hexadiyne)	1.450 (2,4-hexadiyne)	1.450 (2,4-hexadiyne)	1.060 (acetylene)	1.107 ($C-H$ propane) 1.117 ($C-H$ butane)	1.107 ($C-H$ propane) 1.117 ($C-H$ butane)	1.122 (isobutane)	1.532 (propane) 1.531 (butane)	1.532 (propane) 1.531 (butane)	1.532 (propane) 1.531 (butane)	1.532 (propane) 1.531 (butane)	1.532 (propane) 1.531 (butane)	1.532 (propane) 1.531 (butane)
$b,c\ (a_0)$	0.60793	1.40557	1.40557	1.10466	1.27295	1.29569	1.29924	1.54616	1.54616	1.52750	1.54616	1.52750	1.52750
e	0.88143	0.70855	0.70855	0.66953	0.63580	0.63159	0.63095	0.68600	0.68600	0.68888	0.68600	0.68888	0.68888

Table 15.23. The MO to HO intercept geometrical bond parameters of alkynes. E_T is $E_T\,(atom-atom,\ msp^3.AO)$.

Bond	Atom	E_T (eV) Bond 1	E_T (eV) Bond 2	E_T (eV) Bond 3	E_T (eV) Bond 4	Final Total Energy $C2sp^3$ (eV)	$r_{initial}\ (a_0)$	$r_{final}\ (a_0)$	$E_{Coulomb}\left(C2sp^3\right)$ (eV) Final	$E\left(C2sp^3\right)$ (eV) Final	θ' (°)	θ_1 (°)	θ_2 (°)	$d_1\ (a_0)$	$d_2\ (a_0)$
$RC_cC_bC_a-H$	C_a	-1.56513	0	0	0	-153.18082	0.91771	0.83008	-16.39088	-16.20002	90.99	89.01	48.71	0.98144	0.01428
$C_cC_a \equiv C_bH$	C_a	-1.56513	-0.36229	0	0	-153.54311	0.91771	0.81213	-16.75317	-16.56231	137.17	42.83	65.25	0.53890	0.59562
$C_cC_a \equiv C_bH$	C_b	-1.56513	0	0	0	-153.18082	0.91771	0.83008	-16.39088	-16.20002	137.91	42.09	66.24	0.51853	0.61599
$C_c-C_a \equiv C_bH$	C_c	-0.36229	-0.92918	0	0	-152.90716	0.91771	0.84418	-16.11722	-15.92636	75.71	104.29	35.59	1.61974	0.20841
$C-H\ (CH_3)$	C	-0.92918	0	0	0	-152.54487	0.91771	0.86359	-15.75493	-15.56407	77.49	102.51	41.48	1.23564	0.18708
$C-H\ (CH_2)$	C	-0.92918	-0.92918	0	0	-153.47406	0.91771	0.81549	-16.68412	-16.49325	68.47	111.53	35.84	1.35486	0.29933
$C-H\ (CH)$	C	-0.92918	-0.92918	-0.92918	0	-154.40324	0.91771	0.77247	-17.61330	-17.42244	61.10	118.90	31.37	1.42988	0.37326
$H_3C_aC_bH_2CH_2-$ $(C-C$ (a))	C_a	-0.92918	0	0	0	-152.54487	0.91771	0.86359	-15.75493	-15.56407	63.82	116.18	30.08	1.83879	0.38106
$H_3C_aC_bH_2CH_2-$ $(C-C$ (a))	C_b	-0.92918	-0.92918	0	0	-153.47406	0.91771	0.81549	-16.68412	-16.49325	56.41	123.59	26.06	1.90890	0.45117
$R-H_2C_aC_b(H_2C_c-R')HCH_2-$ $(C-C$ (b))	C_b	-0.92918	-0.92918	-0.92918	0	-154.40324	0.91771	0.77247	-17.61330	-17.42244	48.30	131.70	21.90	1.97162	0.51388
$R-H_2C_a(R'-H_2C_d)C_b(R''-H_2C_c)CH_2-$ $(C-C$ (c))	C_b	-0.92918	-0.72457	-0.72457	-0.72457	-154.71860	0.91771	0.75889	-17.92866	-17.73779	48.21	131.79	21.74	1.95734	0.50570
$isoC_aC_b(H_2C_c-R')HCH_2-$ $(C-C$ (d))	C_b	-0.92918	-0.92918	-0.92918	0	-154.40324	0.91771	0.77247	-17.61330	-17.42244	48.30	131.70	21.90	1.97162	0.51388
$tertC_a(R'-H_2C_d)C_b(R''-H_2C_c)CH_2-$ $(C-C$ (e))	C_b	-0.72457	-0.72457	-0.72457	-0.72457	-154.51399	0.91771	0.76765	-17.92866	-17.73779	50.04	129.96	22.66	1.94462	0.49298
$tertC_aC_b(H_2C_c-R')HCH_2-$ $(C-C$ (f))	C_b	-0.72457	-0.92918	-0.92918	0	-154.19863	0.91771	0.78155	-17.40869	-17.21783	52.78	127.22	24.04	1.92443	0.47279
$isoC_a(R'-H_2C_d)C_b(R''-H_2C_c)CH_2-$ $(C-C$ (f))	C_b	-0.72457	-0.72457	-0.72457	-0.72457	-154.51399	0.91771	0.76765	-17.92866	-17.73779	50.04	129.96	22.66	1.94462	0.49298

Table 15.24. The energy parameters (eV) of functional groups of alkynes.

Parameters	$C \equiv C$ Group	$C-C$ (i) Group	$C-C$ (ii) Group	$C-H$ (i) Group	CH_3 Group	CH_2 Group	$C-H$ (ii) Group	$C-C$ (a) Group	$C-C$ (b) Group	$C-C$ (c) Group	$C-C$ (d) Group	$C-C$ (e) Group	$C-C$ (f) Group
n_1	3	1	1	1	3	2	1	1	1	1	1	1	1
n_2	0	0	0	0	2	1	0	0	0	0	0	0	0
n_3	0	0	0	0	0	0	0	0	0	0	0	0	0
C_1	0.5	0.5	0.5	0.75	0.75	0.75	0.75	0.5	0.5	0.5	0.5	0.5	0.5
C_2	1	1	1	1	1	1	1	1	1	1	1	1	1
c_1	1	1	1	1	1	1	1	1	1	1	1	1	1
c_2	0.91771	0.91771	0.91771	0.91771	0.91771	0.91771	0.91771	0.91771	0.91771	0.91771	0.91771	0.91771	0.91771
c_3	2	1	1	0	0	1	1	0	0	0	1	1	0
c_4	6	2	2	1	1	1	1	2	2	2	2	2	2
c_5	0	0	0	1	3	2	1	0	0	0	0	0	0
C_{1o}	0.5	0.5	0.5	0.75	0.75	0.75	0.75	0.5	0.5	0.5	0.5	0.5	0.5
C_{2c}	1	1	1	1	1	1	1	1	1	1	1	1	1
V_e (eV)	-182.53826	-31.29307	-31.29307	-40.62396	-107.32728	-70.41425	-35.12015	-28.79214	-28.79214	-29.10112	-28.79214	-29.10112	-29.10112
V_p (eV)	35.97770	9.64042	9.64042	13.66428	38.92728	25.78002	12.87680	9.33352	9.33352	9.37273	9.33352	9.37273	9.37273
T (eV)	70.90876	7.85528	7.85528	13.65796	32.53914	21.06675	10.48582	6.77464	6.77464	6.90500	6.77464	6.90500	6.90500
V_m (eV)	-35.45438	-3.92764	-3.92764	-6.82898	-16.26957	-10.53337	-5.24291	-3.38732	-3.38732	-3.45250	-3.38732	-3.45250	-3.45250
$E_{(AO/HO)}$ (eV)	-16.20002	-14.63489	-14.63489	-14.63489	-15.56407	-15.56407	-14.63489	-15.56407	-15.56407	-15.35946	-15.56407	-15.35946	-15.35946
$\Delta E_{(H_2MO)(AO/HO)}$ (eV)	0	-0.72457	-0.72457	-3.130269	0	0	0	0	0	0	0	0	0
$E_{T(AO/HO)}$ (eV)	-16.20002	-13.91032	-13.91032	-11.50462	-15.56407	-15.56407	-14.63489	-15.56407	-15.56407	-15.35946	-15.56407	-15.35946	-15.35946
$E_{T(H_2MO)}$ (eV)	-94.90616	-31.63533	-31.63533	-31.63532	-67.69451	-49.66493	-31.63533	-31.63537	-31.63537	-31.63535	-31.63537	-31.63535	-31.63535
$E_T\left(atom-atom,msp^3.AO\right)$ (eV)	-3.13026	-0.72457	-0.72457	0	0	0	0	-1.85836	-1.85836	-1.44915	-1.85836	-1.44915	-1.44915
$E_{T(MO)}$ (eV)	-98.03637	-32.35994	-32.35994	-31.63537	-67.69450	-49.66493	-31.63537	-33.49373	-33.49373	-33.08452	-33.49373	-33.08452	-33.08452
$\omega\ \left(10^{15}\ rad/s\right)$	20.0186	10.3988	17.5426	30.8370	24.9286	24.2751	24.1759	9.43699	9.43699	15.4846	9.43699	9.55643	9.55643
E_K (eV)	13.17659	6.84470	11.54682	20.29747	16.40846	15.97831	15.91299	6.21159	6.21159	10.19220	6.21159	6.29021	6.29021
$\bar{E}_D$ (eV)	-0.23468	-0.16749	-0.21754	-0.28197	-0.25352	-0.25017	-0.24966	-0.16515	-0.16515	-0.20896	-0.16515	-0.16416	-0.16416
$\bar{E}_{Knb}$ (eV)	0.27773 [9]	0.08989 [9]	0.08989 [9]	0.35532 Eq. (13.458)	0.35532 Eq. (13.458)	0.35532 Eq. (13.458)	0.35532 Eq. (13.458)	0.12312 [2]	0.17978 [4]	0.09944 [5]	0.12312 [2]	0.12312 [2]	0.12312 [2]
$\bar{E}_{osc}$ (eV)	-0.09581	-0.12255	-0.17260	-0.10430	-0.22757	-0.14502	-0.07200	-0.10359	-0.07526	-0.15924	-0.10359	-0.10260	-0.10260
E_{mag} (eV)	0.14803	0.14803	0.14803	0.14803	0.14803	0.14803	0.14803	0.14803	0.14803	0.14803	0.14803	0.14803	0.14803
$E_{T(Group)}$ (eV)	-98.02775	-32.48249	-32.53254	-31.73967	-67.92207	-49.80996	-31.70737	-33.59732	-33.49373	-33.24376	-33.59732	-33.18712	-33.18712
$E_{initial\ (c_4\ AO/HO)}$ (eV)	-14.63489	-14.63489	-14.63489	-14.63489	-14.63489	-14.63489	-14.63489	-14.63489	-14.63489	-14.63489	-14.63489	-14.63489	-14.63489
$E_{initial\ (c_5\ AO/HO)}$ (eV)	0	0	0	-13.59844	-13.59844	-13.59844	-13.59844	0	0	0	0	0	0
$E_{D(Group)}$ (eV)	10.21841	3.21271	3.26276	3.50634	12.49186	7.83016	3.32601	4.32754	4.29921	3.97398	4.17951	3.62128	3.91734

Table 15.25. The total bond energies of alkynes calculated using the functional group composition and the energies of Table 15.24 compared to the experimental values [3].

Formula	Name	$C \equiv C$	$C-C$ (i)	$C-C$ (ii)	CH (i)	CH_3	CH_2	CH (ii)	$C-C$ (a)	$C-C$ (b)	$C-C$ (c)	$C-C$ (d)	$C-C$ (e)	$C-C$ (f)	Calculated Total Bond Energy (eV)	Experimental Total Bond Energy (eV)	Relative Error
C_3H_4	Propyne	1	1	0	1	1	0	0	0	0	0	0	0	0	29.42932	29.40432	-0.00085
C_4H_6	1-Butyne	1	1	0	1	1	1	0	1	0	0	0	0	0	41.58702	41.55495	-0.00077
C_4H_6	2-Butyne	1	0	2	0	2	0	0	0	0	0	0	0	0	41.72765	41.75705	0.00070
C_9H_{16}	1-Nonyne	1	1	0	1	1	6	0	6	0	0	0	0	0	102.37552	102.35367	-0.00021

Table 15.26. The bond angle parameters of alkynes and experimental values [1]. In the calculation of θ_v, the parameters from the preceding angle were used. E_T is $E_\pi(atom-atom.\ msp^3.AO)$.

Atoms of Angle	2c' Bond 1 (a_0)	2c' Bond 2 (a_0)	2c' Terminal Atoms (a_0)	$E_{Coulombic}$ Atom 1	Atom 1 Hybridization Designation (Table 15.3.A)	$E_{Coulombic}$ Atom 2	Atom 2 Hybridization Designation (Table 15.3.A)	c_2 Atom 1	c_2 Atom 2	C_1	C_2	c_1	c_2'	E_T (eV)	θ_v (°)	θ_1 (°)	θ_2 (°)	Cal. θ (°)	Exp. θ (°)
$\angle C_cC_aC_b$ $(C_cC_a \equiv C_bH)$																		180	
Methylene $\angle HC_aH$	2.11106	2.11106	3.4252	-15.75493	7	H	H	0.86359	1	1	1	0.75	1.15796	0				108.44	107 (propane)
$\angle C_aC_bC_c$															69.51			110.49	112 (propane) 113.8 (butane) 110.8 (isobutane)
$\angle C_aC_bH$															69.51			110.49	111.0 (butane) 111.4 (isobutane)
Methyl $\angle HC_aH$	2.09711	2.09711	3.4252	-15.75493	7	H	H	0.86359	1	1	1	0.75	1.15796	0				109.50	
$\angle C_aC_bC_c$															70.56			109.44	
$\angle C_aC_bH$															70.56			109.44	
$\angle C_bC_aC_c$ iso C_a	2.91547	2.91547	4.7958	-16.68412 C_b	26	-16.68412 C_c	26	0.81549	0.81549	1	1	1	0.81549	-1.85836				110.67	110.8 (isobutane)
$\angle C_bC_aH$ iso C_a	2.91547	2.11323	4.1633	-15.55033 C_a	5	-14.82575 C_b	1	0.87495	0.91771	0.75	1	0.75	1.04887	0				110.76	
$\angle C_aC_bH$ iso C_a	2.91547	2.09711	4.1633	-15.55033 C_b	5	-14.82575 C_c	1	0.87495	0.91771	0.75	1	0.75	1.04887	0				111.27	111.4 (isobutane)
$\angle C_bC_aC_b$ tert C_a	2.90327	2.90327	4.7958	-16.68412 C_b	26	-16.68412 C_b	26	0.81549	0.81549	1	1	1	0.81549	-1.85836				111.37	110.8 (isobutane)
$\angle C_bC_aC_d$															72.50			107.50	

ALKYL FLUORIDES ($C_nH_{2n+2-m}F_m,\ n=1,2,3,4,5...\infty\ m=1,2,3...\infty$)

The branched-chain alkyl fluorides, $C_nH_{2n+2-m}F_m$, may comprise at least two terminal methyl groups (CH_3) at each end of the chain, and may comprise methylene (CH_2), and methylyne (CH) functional groups as well as C bound by carbon-carbon single bonds wherein at least one H is replaced by a fluorine. The $C-F$ bond comprises a functional group for each case of F replacing a H of methane in the series $H_{4-m}C-F_m$, $m=1,2,3,4$, and F replacing a H of an alkane. The methyl, methylene, methylyne functional groups are equivalent to those of branched-chain alkanes. Six types of $C-C$ bonds can be identified. The n-alkane $C-C$ bond is the same as that of straight-chain alkanes. In addition, the $C-C$ bonds within isopropyl ($(CH_3)_2CH$) and t-butyl ($(CH_3)_3C$) groups and the isopropyl to isopropyl, isopropyl to t-butyl, and t-butyl to t-butyl $C-C$ bonds comprise functional groups that are equivalent to those of branched-chain alkanes.

The solution of the $C-F$ functional groups comprises the hybridization of the $2s$ and $2p$ AOs of each C to form a single $2sp^3$ shell as an energy minimum, and the sharing of electrons between the $C2sp^3$ HO and the F AO to form a molecular orbital (MO) permits each participating orbital to decrease in radius and energy. In alkyl fluorides, the $C2sp^3$ HO has a hybridization factor of 0.91771 (Eq. (13.430)) with a corresponding energy of $E\left(C,2sp^3\right)=-14.63489\ eV$ (Eq. (15.25)), and the F AO has an energy of $E(F)=-17.42282\ eV$. To meet the equipotential condition of the union of the $C-F$ H_2-type-ellipsoidal-MO with these orbitals, the hybridization factor c_2 of Eq. (15.61) for the $C-F$-bond MO given by Eqs. (15.77) and (15.79) is:

$$c_2\left(C2sp^3HO\ to\ F\right)=\frac{E\left(C,2sp^3\right)}{E(F)}c_2\left(C2sp^3HO\right)=\frac{-14.63489\ eV}{-17.42282\ eV}(0.91771)=0.77087 \tag{15.129}$$

$E_T\left(atom-atom,msp^3.AO\right)$ of the $C-F$-bond MO in Eq. (15.61) based on the charge donation from F to the MO is determined by the linear combination that results in a energy that is a minimum which does not exceed the energy of the AO of the F atom to which it is energy matched.

The symbols of the functional groups of branched-chain alkyl fluorides are given in Table 15.27. The geometrical (Eqs. (15.1-15.5) and (15.51)), intercept (Eqs. (15.80-15.87)), and energy (Eqs. (15.6-15.11) and (15.17-15.65)) parameters of branched-chain alkyl fluorides are given in Tables 15.28, 15.29, and 15.30, respectively. The total energy of each branched-chain alkyl fluoride given in Table 15.31 was calculated as the sum over the integer multiple of each $E_D(Group)$ of Table 15.30 corresponding to functional-group composition of the molecule. For each set of unpaired electrons created by bond breakage, the $C2sp^3$ HO magnetic energy E_{mag} that is subtracted from the weighted sum of the $E_D(Group)$ (eV) values based on composition is given by Eq. (15.67). In the case of trifluoromethane, E_{mag} is positive since the term due to the fluorine atoms cancels that of the CH group. The $C-C$ bonds to the CHF group (one H bond to C) were each treated as an iso $C-C$ bond. The $C-C$ bonds to the CF group (no H bonds to C) were each treated as a tert-butyl $C-C$. E_{mag} was subtracted for each t-butyl group. The bond angle parameters of branched-chain alkyl fluorides determined using Eqs. (15.70-15.79), (15.87-15.117) and (15.129) are given in Table 15.32. The color scale, translucent view of the charge-density of exemplary alkyl fluoride, 1-fluoropropane, comprising the concentric shells of atoms with the outer shell bridged by one or more H_2-type ellipsoidal MOs or joined with one or more hydrogen MOs is shown in Figure 15.5.

Figure 15.5. Color scale, translucent view of the charge-density of 1-fluoropropane showing the orbitals of the atoms at their radii, the ellipsoidal surface of each H or H_2-type ellipsoidal MO that transitions to the corresponding outer shell of the atom(s) participating in each bond, and the hydrogen nuclei (red, not to scale).

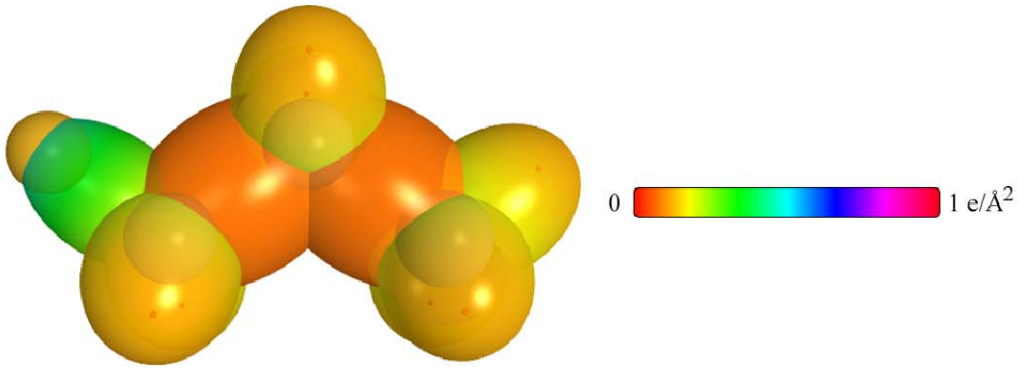

Table 15.27. The symbols of functional groups of branched-chain alkyl fluorides.

Functional Group	Group Symbol
CF of CF_mH_{4-m}	$C-F$ (i)
CF of $C_nH_{2n+2-m}F_m$	$C-F$ (ii)
CH_3 group	$C-H\ (CH_3)$
CH_2 group	$C-H\ (CH_2)$
CH	$C-H$
CC bond (*n*-*C*)	$C-C$ (a)
CC bond (*iso*-*C*)	$C-C$ (b)
CC bond (*tert*-*C*)	$C-C$ (c)
CC (*iso* to *iso*-*C*)	$C-C$ (d)
CC (*t* to *t*-*C*)	$C-C$ (e)
CC (*t* to *iso*-*C*)	$C-C$ (f)

Table 15.28. The geometrical bond parameters of branched-chain alkyl fluorides and experimental values [1].

Parameter	$C-F$ (i) Group	$C-F$ (ii) Group	$C-H\ (CH_3)$ Group	$C-H\ (CH_2)$ Group	$C-H$ Group	$C-C$ (a) Group	$C-C$ (b) Group	$C-C$ (c) Group	$C-C$ (d) Group	$C-C$ (e) Group	$C-C$ (f) Group
$a\ (a_0)$	1.72139	1.72139	1.64920	1.67122	1.67465	2.12499	2.12499	2.10725	2.12499	2.10725	2.10725
$c'\ (a_0)$	1.31202	1.31202	1.04856	1.05553	1.05661	1.45744	1.45744	1.45164	1.45744	1.45164	1.45164
Bond Length $2c'\ (A)$	1.38858	1.38858	1.10974	1.11713	1.11827	1.54280	1.54280	1.53635	1.54280	1.53635	1.53635
Exp. Bond Length (A)	1.382 (methyl fluoride)	1.382 (methyl fluoride)	1.107 ($C-H$ propane) 1.117 ($C-H$ butane)	1.107 ($C-H$ propane) 1.117 ($C-H$ butane)	1.122 (isobutane)	1.532 (propane) 1.531 (butane)	1.532 (propane) 1.531 (butane)	1.532 (propane) 1.531 (butane)	1.532 (propane) 1.531 (butane)	1.532 (propane) 1.531 (butane)	1.532 (propane) 1.531 (butane)
$b,c\ (a_0)$	1.11435	1.11435	1.27295	1.29569	1.29924	1.54616	1.54616	1.52750	1.54616	1.52750	1.52750
e	0.76219	0.76219	0.63580	0.63159	0.63095	0.68600	0.68600	0.68888	0.68600	0.68888	0.68888

Table 15.29. The MO to HO intercept geometrical bond parameters of branched-chain alkyl fluorides. R, R', R'' are H or alkyl groups. E_T is E_T ($atom-atom$, $msp^3.AO$).

Bond	Atom	E_T (eV) Bond 1	E_T (eV) Bond 2	E_T (eV) Bond 3	E_T (eV) Bond 4	Final Total Energy $C2sp^3$ (eV)	$r_{initial}\ (a_0)$	$r_{final}\ (a_0)$	$E_{Coulomb}$ (eV) Final	$E(C2sp^3)$ (eV) Final	θ' (°)	θ_1 (°)	θ_2 (°)	$d_1\ (a_0)$	$d_2\ (a_0)$
$H_{4-m}C_a-F_m$ (C_a-F (i))	C_a	-1.34946	0	0	0	-152.96515	0.91771	0.84115	-16.17521	-15.98435	100.77	79.23	47.86	1.15488	0.15714
$H_{4-m}C_a-F_m$ (C_a-F (i))	F	-1.34946	0	0	0		0.78069	0.84115	-16.17521		100.77	79.23	47.86	1.15488	0.15714
$-H_2C_bC_aF$ (C_a-F (ii))	C_a	-1.34946	-0.92918	0	0	-153.89433	0.91771	0.79546	-17.10440	-16.91353	97.02	82.98	45.11	1.21483	0.09718
$-H_2C_bC_aF$ (C_a-F (ii))	F	-1.34946	0	0	0		0.78069	0.84115	-16.17521		100.77	79.23	47.86	1.15488	0.15714
$C-H\ (CH_3)$	C	-0.92918	0	0	0	-152.54487	0.91771	0.86359	-15.75493	-15.56407	77.49	102.51	41.48	1.23564	0.18708
$C-H\ (CH_2)$	C	-0.92918	-0.92918	0	0	-153.47406	0.91771	0.81549	-16.68412	-16.49325	68.47	111.53	35.84	1.35486	0.29933
$C-H\ (CH)$	C	-0.92918	-0.92918	-0.92918	0	-154.40324	0.91771	0.77247	-17.61330	-17.42244	61.10	118.90	31.37	1.42988	0.37326
$H_3C_aC_bH_2CH_2-$ ($C-C$ (a))	C_a	-0.92918	0	0	0	-152.54487	0.91771	0.86359	-15.75493	-15.56407	63.82	116.18	30.08	1.83879	0.38106
$H_3C_aC_bH_2CH_2-$ ($C-C$ (a))	C_b	-0.92918	-0.92918	0	0	-153.47406	0.91771	0.81549	-16.68412	-16.49325	56.41	123.59	26.06	1.90890	0.45117
$R-H_2C_aC_b(H_2C_c-R')HCH_2-$ ($C-C$ (b))	C_b	-0.92918	-0.92918	-0.92918	0	-154.40324	0.91771	0.77247	-17.61330	-17.42244	48.30	131.70	21.90	1.97162	0.51388
$R-H_2C_a(R'-H_2C_d)C_b(R''-H_2C_c)CH_2-$ ($C-C$ (e))	C_b	-0.92918	-0.72457	-0.72457	-0.72457	-154.71860	0.91771	0.75889	-17.92866	-17.73779	48.21	131.79	21.74	1.95734	0.50570
$isoC_aC_b(H_2C_c-R')HCH_2-$ ($C-C$ (d))	C_b	-0.92918	-0.92918	-0.92918	0	-154.40324	0.91771	0.77247	-17.61330	-17.42244	48.30	131.70	21.90	1.97162	0.51388
$iertC_a(R'-H_2C_d)C_b(R''-H_2C_c)CH_2-$ ($C-C$ (e))	C_b	-0.72457	-0.72457	-0.72457	-0.72457	-154.51399	0.91771	0.76765	-17.92866	-17.73779	50.04	129.96	22.66	1.94462	0.49298
$iertC_aC_b(H_2C_c-R')HCH_2-$ ($C-C$ (f))	C_b	-0.72457	-0.92918	-0.92918	0	-154.19863	0.91771	0.78155	-17.40869	-17.21783	52.78	127.22	24.04	1.92443	0.47279
$isoC_a(R'-H_2C_d)C_b(R''-H_2C_c)CH_2-$ ($C-C$ (f))	C_b	-0.72457	-0.72457	-0.72457	-0.72457	-154.51399	0.91771	0.76765	-17.92866	-17.73779	50.04	129.96	22.66	1.94462	0.49298

Table 15.30. The energy parameters (eV) of functional groups of branched-chain alkyl fluorides.

Parameters	$C-F$ (i) Group	$C-F$ (ii) Group	CH_3 Group	CH_2 Group	$C-H$ Group	$C-C$ (a) Group	$C-C$ (b) Group	$C-C$ (c) Group	$C-C$ (d) Group	$C-C$ (e) Group	$C-C$ (f) Group
n_1	1	1	3	2	1	1	1	1	1	1	1
n_2	0	0	2	1	0	0	0	0	0	0	0
n_3	0	0	0	0	0	0	0	0	0	0	0
C_1	0.5	0.5	0.75	0.75	0.75	0.5	0.5	0.5	0.5	0.5	0.5
C_2	1	1	1	1	1	1	1	1	1	1	1
c_1	1	1	1	1	1	1	1	1	1	1	1
c_2	0.77087	0.77087	0.91771	0.91771	0.91771	0.91771	0.91771	0.91771	0.91771	0.91771	0.91771
c_3	0	0	0	1	1	0	0	0	1	1	0
c_4	2	2	1	1	1	2	2	2	2	2	2
c_5	0	0	3	2	1	0	0	0	0	0	0
C_{1o}	0.5	0.5	0.75	0.75	0.75	0.5	0.5	0.5	0.5	0.5	0.5
C_{2o}	1	1	1	1	1	1	1	1	1	1	1
V_e (eV)	-32.02108	-32.02108	-107.32728	-70.41425	-35.12015	-28.79214	-28.79214	-29.10112	-28.79214	-29.10112	-29.10112
V_p (eV)	10.37015	10.37015	38.92728	25.78002	12.87680	9.33352	9.33352	9.37273	9.33352	9.37273	9.37273
T (eV)	9.30097	9.30097	32.53914	21.06675	10.48582	6.77464	6.77464	6.90500	6.77464	6.90500	6.90500
V_m (eV)	-4.65048	-4.65048	-16.26957	-10.53337	-5.24291	-3.38732	-3.38732	-3.45250	-3.38732	-3.45250	-3.45250
$E_{(AO/HO)}$ (eV)	-14.63489	-14.63489	-15.56407	-15.56407	-14.63489	-15.56407	-15.56407	-15.35946	-15.56407	-15.35946	-15.35946
$\Delta E_{H_2MO\,(AO/HO)}$ (eV)	0	0	0	0	0	0	0	0	0	0	0
$E_T{}_{(AO/HO)}$ (eV)	-14.63489	-14.63489	-15.56407	-15.56407	-14.63489	-15.56407	-15.56407	-15.35946	-15.56407	-15.35946	-15.35946
$E_T{}_{(H_2MO)}$ (eV)	-31.63534	-31.63534	-67.69451	-49.66493	-31.63533	-31.63537	-31.63537	-31.63535	-31.63537	-31.63535	-31.63535
$E_T\left(atom-atom, msp^3.AO\right)$ (eV)	-2.69892	-2.69892	0	0	0	-1.85836	-1.85836	-1.44915	-1.85836	-1.44915	-1.44915
$E_T{}_{(HO)}$ (eV)	-34.33429	-34.33429	-67.69450	-49.66493	-31.63537	-33.49373	-33.49373	-33.08452	-33.49373	-33.08452	-33.08452
$\omega\ \left(10^{15}\ rad/s\right)$	24.8506	12.9435	24.9286	24.2751	24.1759	9.43699	9.43699	15.4846	9.43699	9.55643	9.55643
E_K (eV)	16.35707	8.51966	16.40846	15.97831	15.91299	6.21159	6.21159	10.19220	6.21159	6.29021	6.29021
$\bar{E}_D$ (eV)	-0.27472	-0.19826	-0.25352	-0.25017	-0.24966	-0.16515	-0.16515	-0.20896	-0.16515	-0.16416	-0.16416
$\bar{E}_{Kvib}$ (eV)	0.13849 [10]	0.10911 [11]	0.35532 (Eq. (13.458))	0.35532 (Eq. (13.458))	0.35532 (Eq. (13.458))	0.12312 [2]	0.17978 [4]	0.09944 [5]	0.12312 [2]	0.12312 [2]	0.12312 [2]
$\bar{E}_{osc}$ (eV)	-0.20547	-0.14371	-0.22757	-0.14502	-0.07200	-0.10359	-0.07526	-0.15924	-0.10359	-0.10260	-0.10260
E_{mag} (eV)	0.14803	0.14803	0.14803	0.14803	0.14803	0.14803	0.14803	0.14803	0.14803	0.14803	0.14803
$E_{T\,(Group)}$ (eV)	-34.53976	-34.47800	-67.92207	-49.80996	-31.70737	-33.59732	-33.49373	-33.24376	-33.59732	-33.18712	-33.18712
$E_{initial\,(c_4\,AO/HO)}$ (eV)	-14.63489	-14.63489	-14.63489	-14.63489	-14.63489	-14.63489	-14.63489	-14.63489	-14.63489	-14.63489	-14.63489
$E_{initial\,(c_5\,AO/HO)}$ (eV)	0	0	-13.59844	-13.59844	-13.59844	0	0	0	0	0	0
$E_{D\,(Group)}$ (eV)	5.26998	5.20822	12.49186	7.83016	3.32601	4.32754	4.29921	3.97398	4.17951	3.62128	3.91734

Table 15.31. The total bond energies of branched-chain alkyl fluorides calculated using the functional group composition and the energies of Table 15.30 compared to the experimental values [3]. The magnetic energy E_{mag} that is subtracted from the weighted sum of the $E_{D\,(Group)}$ (eV) values based on composition is given by (15.58).

Formula	Name	$C-F$ (i)	$C-F$ (ii)	CH_3	CH_2	CH	$C-C$ (a)	$C-C$ (b)	$C-C$ (c)	$C-C$ (d)	$C-C$ (e)	$C-C$ (f)	E_{mag}	Calculated Total Bond Energy (eV)	Experimental Total Bond Energy (eV)	Relative Error
CF_4	Tetrafluoromethane	4	0	0	0	0	0	0	0	0	0	0	0	21.07992	21.016	-0.00303
CHF_3	Trifluoromethane	3	0	0	0	1	0	0	0	0	0	0	0	19.28398	19.362	0.00405
CH_2F_2	Difluoromethane	2	0	0	1	0	0	0	0	0	0	0	0	18.37012	18.280	-0.00496
C_3H_7F	1-Fluoropropane	0	1	1	2	0	2	0	0	0	0	0	-1	41.86745	41.885	0.00041
C_3H_7F	2-Fluoropropane	0	1	2	0	1	0	2	0	0	0	0	-1	41.96834	41.963	-0.00012

Table 15.32. The bond angle parameters of branched-chain alkyl fluorides and experimental values [1]. In the calculation of θ_v, the parameters from the preceding angle were used. E_T is E_T (*atom – atom, msp*^{3}*.AO*).

Atoms of Angle	2c' Bond 1 (a_0)	2c' Bond 2 (a_0)	2c' Terminal Atoms (a_0)	$E_{Coulombic}$ Atom 1	Atom 1 Hybridization Designation (Table 15.3.A)	$E_{Coulombic}$ Atom 2	Atom 2 Hybridization Designation (Table 15.3.A)	c_2 Atom 1	c_2 Atom 2	C_1	C_2	c	c'_2	E_T (eV)	θ_v (°)	θ_1 (°)	θ_2 (°)	Cal. θ (°)	Exp. θ (°)
$\angle FC_aF$ (C_a-F (i))	2.62403	2.62403	4.3128	-16.17521 *F*	13	-16.17521 *F*	13	0.84115	0.84115	1	1	1	0.84115	-1.44915				110.53	108.8 (fluoroform)
$\angle HC_aF$ (C_a-F (i))	2.11106	2.62403	3.8987	-17.10440 C_a	35	-17.42282 *F*	F	0.79546	0.78092 (Eq. (15.73))	0.75	1	0.75	0.98172	0				110.38	
$\angle C_bC_aF$ (C_a-F (ii))	2.91547	2.62403	4.5826	-16.68412 C_b	26	-17.42282 *F*	F	0.81549	0.77087 (Eq. (15.129))	1	1	1	0.79318	-1.85836				111.53	110.3 (1,2-difluoroethane)
$\angle C_bC_aH$ (C_a-F (ii))	2.91547	2.11106	4.1633	-15.55033 C_a	5	-14.82575 C_b	1	0.87495	0.91771	0.75	1	0.75	1.04887	0				110.83	111.0 (1,1-difluoroethane)
Methylene $\angle HC_aH$	2.11106	2.11106	3.4252	-15.75493	7	H	H	0.86359	1	1	1	0.75	1.15796	0				108.44	107 (propane)
$\angle C_aC_bC_c$															69.51			110.49	112 (propane) 113.8 (butane) 110.8 (isobutane)
$\angle C_aC_bH$															69.51			110.49	111.0 (butane) 111.4 (isobutane)
Methyl $\angle HC_aH$	2.09711	2.09711	3.4252	-15.75493	7	H	H	0.86359	1	1	1	0.75	1.15796	0				109.50	
$\angle C_aC_bC_c$															70.56			109.44	
$\angle C_aC_bH$															70.56			109.44	
$\angle C_bC_aC_c$ iso C_a	2.91547	2.91547	4.7958	-16.68412 C_b	26	-16.68412 C_c	26	0.81549	0.81549	1	1	1	0.81549	-1.85836				110.67	110.8 (isobutane)
$\angle C_bC_aH$ iso C_a	2.91547	2.11323	4.1633	-15.55033 C_a	5	-14.82575 C_b	1	0.87495	0.91771	0.75	1	0.75	1.04887	0				110.76	
$\angle C_aC_bH$ iso C_a	2.91547	2.09711	4.1633	-15.55033 C_b	5	-14.82575 C_a	1	0.87495	0.91771	0.75	1	0.75	1.04887	0				111.27	111.4 (isobutane)
$\angle C_bC_aC_b$ tert C_a	2.90327	2.90327	4.7958	-16.68412 C_b	26	-16.68412 C_b	26	0.81549	0.81549	1	1	1	0.81549	-1.85836				111.37	110.8 (isobutane)
$\angle C_bC_aC_d$															72.50			107.50	

ALKYL CHLORIDES ($C_nH_{2n+2-m}Cl_m,\ n=1,2,3,4,5...\infty\ m=1,2,3...\infty$)

The branched-chain alkyl chlorides, $C_nH_{2n+2-m}Cl_m$, may comprise at least two terminal methyl groups (CH_3) at each end of the chain, and may comprise methylene (CH_2), and methylyne (CH) functional groups as well as C bound by carbon-carbon single bonds wherein at least one H is replaced by a chlorine. The $C-Cl$ bond comprises a functional group for each case of Cl replacing a H of methane for the series $H_{4-m}C-Cl_m$, $m=1,2,3$, with the $C-Cl$ bond of CCl_4 comprising another functional group due to the limitation of the minimum energy of Cl matched to that of the $C2sp^3$ HO. In addition, the $C-Cl$ bond due to Cl replacing an H of an alkane is a functional group. The methyl, methylene, methylyne functional groups are equivalent to those of branched-chain alkanes. Six types of $C-C$ bonds can be identified. The n-alkane $C-C$ bond is the same as that of straight-chain alkanes. In addition, the $C-C$ bonds within isopropyl ($(CH_3)_2CH$) and t-butyl ($(CH_3)_3C$) groups and the isopropyl to isopropyl, isopropyl to t-butyl, and t-butyl to t-butyl $C-C$ bonds comprise functional groups that are equivalent to those of branched-chain alkanes.

The solution of the $C-Cl$ functional groups comprises the hybridization of the $2s$ and $2p$ AOs of each C to form a single $2sp^3$ shell as an energy minimum, and the sharing of electrons between the $C2sp^3$ HO and the Cl AO to form a MO permits each participating orbital to decrease in radius and energy. In alkyl chlorides, the energy of chlorine is less than the Coulombic energy between the electron and proton of H given by Eq. (1.264). Thus, c_2 in Eq. (15.61) is one, and the energy matching condition is determined by the C_2 parameter. Then, $C2sp^3$ HO has a hybridization factor of 0.91771 (Eq. (13.430)) with a corresponding energy of $E\left(C,2sp^3\right)=-14.63489\ eV$ (Eq. (15.25)), and the Cl AO has an energy of $E\left(Cl\right)=-12.96764\ eV$. To meet the equipotential condition of the union of the $C-Cl$ H_2-type-ellipsoidal-MO with these orbitals, the hybridization factor C_2 of Eq. (15.61) for the $C-Cl$-bond MO given by Eqs. (15.77) and (15.79) is:

$$C_2\left(C2sp^3HO\ to\ Cl\right)=\frac{E\left(Cl\right)}{E\left(C,2sp^3\right)}c_2\left(C2sp^3HO\right)=\frac{-12.96764\ eV}{-14.63489\ eV}\left(0.91771\right)=0.81317 \tag{15.130}$$

The valence energy of the carbon $2p$ is $-11.2603\ eV$ and that of the Cl AO is $-12.96764\ eV$. The energy difference is more than that of $2E_T\left(C-C,2sp^3\right)$ given by Eq. (14.151) for a single bond. Thus, $E_T\left(atom-atom,msp^3.AO\right)$ of the $C-Cl$-bond MO of CCl_mH_{4-m} and $C_nH_{2n+2-m}Cl_m$ in Eq. (15.61) due to the charge donation from the C and Cl atoms to the MO is $-1.44915\ eV$ based on the energy match between the $C2sp^3$ HO and the Cl AO corresponding to the energy contributions equivalent to those of methyl groups, $-0.72457\ eV$ (Eq. (14.151)). $E_T\left(atom-atom,msp^3.AO\right)$ of the $C-Cl$-bond MO of chloroform with four $C-Cl$ bonds is $-0.92918\ eV$ (Eq. (14.513)) based on the maximum single-bond-energy contribution of the $C2sp^3$ HO.

The symbols of the functional groups of branched-chain alkyl chlorides are given in Table 15.33. The geometrical (Eqs. (15.1-15.5) and (15.51)), intercept (Eqs. (15.80-15.87)), and energy (Eqs. (15.6-15.11) and (15.17-15.65)) parameters of branched-chain alkyl chlorides are given in Tables 15.34, 15.35, and 15.36, respectively. The total energy of each branched-chain alkyl chloride given in Table 15.37 was calculated as the sum over the integer multiple of each $E_D(Group)$ of Table 15.36 corresponding to functional-group composition of the molecule. For each set of unpaired electrons created by bond breakage, the $C2sp^3$ HO magnetic energy E_{mag} that was subtracted from the weighted sum of the $E_D(Group)$ (eV) values based on composition is given by Eq. (15.67). The $C-C$ bonds to the $CHCl$ group (one H bond to C) were each treated as an iso $C-C$ bond. The $C-C$ bonds to the CCl group (no H bonds to C) were each treated as a tert-butyl $C-C$. E_{mag} was subtracted for each t-butyl group. The bond angle parameters of branched-chain alkyl chlorides determined using Eqs. (15.70-15.79), (15.88-15.117) and (15.130) are given in Table 15.38. The color scale, translucent view of the charge-density of exemplary alkyl chloride, 1-chloropropane, comprising the concentric shells of atoms with the outer shell bridged by one or more H_2-type ellipsoidal MOs or joined with one or more hydrogen MOs is shown in Figure 15.6.

Figure 15.6. Color scale, translucent view of the charge-density of 1-chloropropane showing the orbitals of the atoms at their radii, the ellipsoidal surface of each H or H_2-type ellipsoidal MO that transitions to the corresponding outer shell of the atom(s) participating in each bond, and the hydrogen nuclei (red, not to scale).

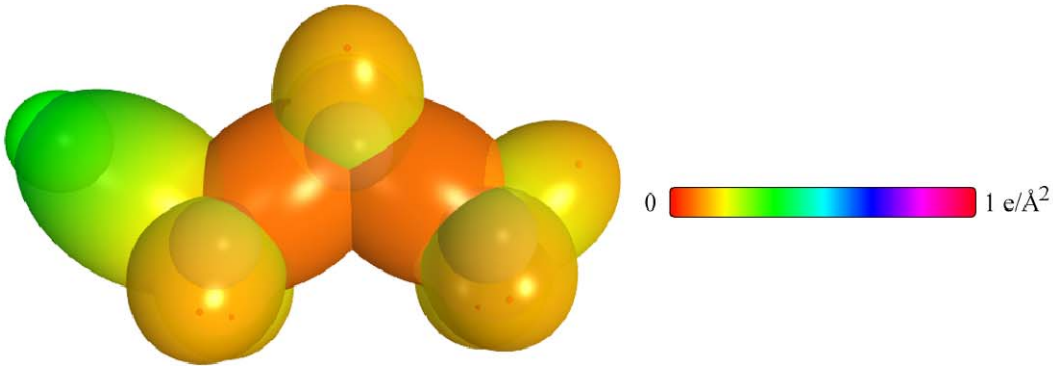

Table 15.33. The symbols of functional groups of branched-chain alkyl chlorides.

Functional Group	Group Symbol
CCl of CCl_mH_{4-m}	$C-Cl$ (i)
CCl of CCl_4	$C-Cl$ (ii)
CCl of $C_nH_{2n+2-m}Cl_m$	$C-Cl$ (iii)
CH_3 group	$C-H\ (CH_3)$
CH_2 group	$C-H\ (CH_2)$
CH	$C-H$
CC bond (*n*-*C*)	$C-C$ (a)
CC bond (*iso*-*C*)	$C-C$ (b)
CC bond (*tert*-*C*)	$C-C$ (c)
CC (*iso* to *iso*-*C*)	$C-C$ (d)
CC (*t* to *t*-*C*)	$C-C$ (e)
CC (*t* to *iso*-*C*)	$C-C$ (f)

Table 15.34. The geometrical bond parameters of branched-chain alkyl chlorides and experimental values [1].

Parameter	$C-Cl$ (i) Group	$C-Cl$ (ii) Group	$C-Cl$ (iii) Group	$C-H\ (CH_3)$ Group	$C-H\ (CH_2)$ Group	$C-H$ Group	$C-C$ (a) Group	$C-C$ (b) Group	$C-C$ (c) Group	$C-C$ (d) Group	$C-C$ (e) Group	$C-C$ (f) Group
$a\ (a_0)$	2.32621	2.37026	2.32621	1.64920	1.67122	1.67465	2.12499	2.12499	2.10725	2.12499	2.10725	2.10725
$c'\ (a_0)$	1.69136	1.70729	1.69136	1.04856	1.05553	1.05661	1.45744	1.45744	1.45164	1.45744	1.45164	1.45164
Bond Length $2c'\ (\AA)$	1.79005	1.80692	1.79005	1.10974	1.11713	1.11827	1.54280	1.54280	1.53635	1.54280	1.53635	1.53635
Exp. Bond Length $(\AA)$	1.785 (methyl chloride)	1.767 (carbon tetrachloride)	1.802 (ethyl chloride) 1.790 (1,2-dichloroethane)	1.107 ($C-H$ propane) 1.117 ($C-H$ butane)	1.107 ($C-H$ propane) 1.117 ($C-H$ butane)	1.122 (isobutane)	1.532 (propane) 1.531 (butane)	1.532 (propane) 1.531 (butane)	1.532 (propane) 1.531 (butane)	1.532 (propane) 1.531 (butane)	1.532 (propane) 1.531 (butane)	1.532 (propane) 1.531 (butane)
$b,c\ (a_0)$	1.59705	1.64416	1.59705	1.27295	1.29569	1.29924	1.54616	1.54616	1.52750	1.54616	1.52750	1.52750
e	0.72709	0.72030	0.72709	0.63580	0.63159	0.63095	0.68600	0.68600	0.68888	0.68600	0.68888	0.68888

Table 15.35. The MO to HO intercept geometrical bond parameters of branched-chain alkyl chlorides. R, R', R'' are H or alkyl groups. E_T is E_T ($atom-atom$, $msp^3.AO$).

Bond	Atom	E_T (eV) Bond 1	E_T (eV) Bond 2	E_T (eV) Bond 3	E_T (eV) Bond 4	Final Total Energy $C2sp^3$ (eV)	$r_{initial}$ (a_0)	r_{final} (a_0)	$E_{Coulomb}$ (eV) Final	$E(C2sp^3)$ (eV) Final	θ' (°)	θ_1 (°)	θ_2 (°)	d_1 (a_0)	d_2 (a_0)
$H_{4-m}C_a-Cl_m$, $m=1,2,3$, (C_a-Cl (i))	C_a	-0.72457	0	0	0	-152.34026	0.91771	0.87495	-15.55033	-15.35946	69.62	110.38	30.90	1.99599	0.30463
$H_{4-m}C_a-Cl_m$, $m=1,2,3$, (C_a-Cl (i))	Cl	-0.72457	0	0	0		1.05158	0.87495	-15.55033		69.62	110.38	30.90	1.99599	0.30463
C_aCl_4 (C_a-Cl (ii))	C_a	-0.46459	0	0	0	-152.08028	0.91771	0.88983	-15.29034	-15.09948	66.98	113.02	29.87	2.05530	0.34801
C_aCl_4 (C_a-Cl (ii))	Cl	-0.46459	0	0	0		1.05158	0.88983	-15.29034		66.98	113.02	29.87	2.05530	0.34801
$-H_2C_bC_a-Cl$ (C_a-Cl (iii))	C_a	-0.72457	-0.92918	0	0	-153.26945	0.91771	0.82562	-16.47951	-16.28864	63.18	116.82	27.48	2.06384	0.37248
$-H_2C_bC_a-Cl$ (C_a-Cl (iii))	Cl	-0.72457	0	0	0		1.05158	0.87495	-15.55033		69.62	110.38	30.90	1.99599	0.30463
$C-H\ (CH_3)$	C	-0.92918	0	0	0	-152.54487	0.91771	0.86359	-15.75493	-15.56407	77.49	102.51	41.48	1.23564	0.18708
$C-H\ (CH_2)$	C	-0.92918	-0.92918	0	0	-153.47406	0.91771	0.81549	-16.68412	-16.49325	68.47	111.53	35.84	1.35486	0.29933
$C-H\ (CH)$	C	-0.92918	-0.92918	-0.92918	0	-154.40324	0.91771	0.77247	-17.61330	-17.42244	61.10	118.90	31.37	1.42988	0.37326
$H_3C_aC_bH_2CH_2-$ ($C-C$ (a))	C_a	-0.92918	0	0	0	-152.54487	0.91771	0.86359	-15.75493	-15.56407	63.82	116.18	30.08	1.83879	0.38106
$H_3C_aC_bH_2CH_2-$ ($C-C$ (a))	C_b	-0.92918	-0.92918	0	0	-153.47406	0.91771	0.81549	-16.68412	-16.49325	56.41	123.59	26.06	1.90890	0.45117
$R-H_2C_aC_b(H_2C_c-R')HCH_2-$ ($C-C$ (b))	C_b	-0.92918	-0.92918	-0.92918	0	-154.40324	0.91771	0.77247	-17.61330	-17.42244	48.30	131.70	21.90	1.97162	0.51388
$R-H_2C_a(R'-H_2C_d)C_b(R''-H_2C_c)CH_2-$ ($C-C$ (c))	C_b	-0.92918	-0.72457	-0.72457	-0.72457	-154.71860	0.91771	0.75889	-17.92866	-17.73779	48.21	131.79	21.74	1.95734	0.50570
$isoC_aC_b(H_2C_c-R')HCH_2-$ ($C-C$ (d))	C_b	-0.92918	-0.92918	-0.92918	0	-154.40324	0.91771	0.77247	-17.61330	-17.42244	48.30	131.70	21.90	1.97162	0.51388
$tertC_a(R'-H_2C_d)C_b(R''-H_2C_c)CH_2-$ ($C-C$ (e))	C_b	-0.72457	-0.72457	-0.72457	-0.72457	-154.51399	0.91771	0.76765	-17.92866	-17.73779	50.04	129.96	22.66	1.94462	0.49298
$tertC_aC_b(H_2C_c-R')HCH_2-$ ($C-C$ (f))	C_b	-0.72457	-0.92918	-0.92918	0	-154.19863	0.91771	0.78155	-17.40869	-17.21783	52.78	127.22	24.04	1.92443	0.47279
$isoC_a(R'-H_2C_d)C_b(R''-H_2C_c)CH_2-$ ($C-C$ (f))	C_b	-0.72457	-0.72457	-0.72457	-0.72457	-154.51399	0.91771	0.76765	-17.92866	-17.73779	50.04	129.96	22.66	1.94462	0.49298

Table 15.36. The energy parameters (eV) of functional groups of branched-chain alkyl chlorides.

Parameters	$C-Cl$ (i) Group	$C-Cl$ (ii) Group	$C-Cl$ (iii) Group	CH_3 Group	CH_2 Group	$C-H$ Group	$C-C$ (a) Group	$C-C$ (b) Group	$C-C$ (c) Group	$C-C$ (d) Group	$C-C$ (e) Group	$C-C$ (f) Group
n_1	1	1	1	3	2	1	1	1	1	1	1	1
n_2	0	0	0	2	1	0	0	0	0	0	0	0
n_3	0	0	0	0	0	0	0	0	0	0	0	0
C_1	0.5	0.5	0.5	0.75	0.75	0.75	0.5	0.5	0.5	0.5	0.5	0.5
C_2	0.81317	0.81317	0.81317	1	1	1	1	1	1	1	1	1
c_1	1	1	1	1	1	1	1	1	1	1	1	1
c_2	1	1	1	0.91771	0.91771	0.91771	0.91771	0.91771	0.91771	0.91771	0.91771	0.91771
c_3	1	1	1	0	1	1	0	0	0	1	1	0
c_4	2	2	2	1	1	1	2	2	2	2	2	2
c_5	0	0	0	3	2	1	0	0	0	0	0	0
C_{1o}	0.5	0.5	0.5	0.75	0.75	0.75	0.5	0.5	0.5	0.5	0.5	0.5
C_{2o}	0.81317	0.81317	0.81317	1	1	1	1	1	1	1	1	1
V_e (eV)	-29.68411	-28.95265	-29.68411	-107.32728	-70.41425	-35.12015	-28.79214	-28.79214	-29.10112	-28.79214	-29.10112	-29.10112
V_p (eV)	8.04432	7.96922	8.04432	38.92728	25.78002	12.87680	9.33352	9.33352	9.37273	9.33352	9.37273	9.37273
T (eV)	6.38036	6.10748	6.38036	32.53914	21.06675	10.48582	6.77464	6.77464	6.90500	6.77464	6.90500	6.90500
V_m (eV)	-3.19018	-3.05374	-3.19018	-16.26957	-10.53337	-5.24291	-3.38732	-3.38732	-3.45250	-3.38732	-3.45250	-3.45250
$E_{(AO/HO)}$ (eV)	-14.63489	-14.63489	-14.63489	-15.56407	-15.56407	-14.63489	-15.56407	-15.56407	-15.35946	-15.56407	-15.35946	-15.35946
$\Delta E_{H_2MO\,(AO/HO)}$ (eV)	-1.44915	-0.92918	-1.44915	0	0	0	0	0	0	0	0	0
$E_{T\,(AO/HO)}$ (eV)	-13.18574	-13.70571	-13.18574	-15.56407	-15.56407	-14.63489	-15.56407	-15.56407	-15.35946	-15.56407	-15.35946	-15.35946
$E_{T\,(H_2MO)}$ (eV)	-31.63536	-31.63540	-31.63536	-67.69451	-49.66493	-31.63533	-31.63537	-31.63537	-31.63535	-31.63537	-31.63535	-31.63535
$E_T\left(atom-atom, msp^3.AO\right)$ (eV)	-1.44915	-0.92918	-1.44915	0	0	0	-1.85836	-1.85836	-1.44915	-1.85836	-1.44915	-1.44915
$E_{T\,(MO)}$ (eV)	-33.08452	-32.56455	-33.08452	-67.69450	-49.66493	-31.63537	-33.49373	-33.49373	-33.08452	-33.49373	-33.08452	-33.08452
ω $\left(10^{15}\ rad/s\right)$	7.42995	7.22380	13.0612	24.9286	24.2751	24.1759	9.43699	9.43699	15.4846	9.43699	9.55643	9.55643
E_K (eV)	4.89052	4.75483	8.59708	16.40846	15.97831	15.91299	6.21159	6.21159	10.19220	6.21159	6.29021	6.29021
$\overline{E}_D$ (eV)	-0.14475	-0.14048	-0.19191	-0.25352	-0.25017	-0.24966	-0.16515	-0.16515	-0.20896	-0.16515	-0.16416	-0.16416
$\overline{E}_{Kvib}$ (eV)	0.08059 [12]	0.08059 [12]	0.09113 [13]	0.35532 (Eq. (13.458))	0.35532 (Eq. (13.458))	0.35532 (Eq. (13.458))	0.12312 [2]	0.17978 [4]	0.09944 [5]	0.12312 [2]	0.12312 [2]	0.12312 [2]
$\overline{E}_{osc}$ (eV)	-0.10445	-0.10019	-0.14635	-0.22757	-0.14502	-0.07200	-0.10359	-0.07526	-0.15924	-0.10359	-0.10260	-0.10260
E_{mag} (eV)	0.14803	0.14803	0.14803	0.14803	0.14803	0.14803	0.14803	0.14803	0.14803	0.14803	0.14803	0.14803
$E_{T\,(Group)}$ (eV)	-33.18897	-32.66473	-33.23086	-67.92207	-49.80996	-31.70737	-33.59732	-33.49373	-33.24376	-33.59732	-33.18712	-33.18712
$E_{initial\,(c_4\,AO/HO)}$ (eV)	-14.63489	-14.63489	-14.63489	-14.63489	-14.63489	-14.63489	-14.63489	-14.63489	-14.63489	-14.63489	-14.63489	-14.63489
$E_{initial\,(c_5\,AO/HO)}$ (eV)	0	0	0	-13.59844	-13.59844	-13.59844	0	0	0	0	0	0
$E_{D\,(Group)}$ (eV)	3.77116	3.39496	3.96108	12.49186	7.83016	3.32601	4.32754	4.29921	3.97398	4.17951	3.62128	3.91734

Table 15.37. The total bond energies of branched-chain alkyl chlorides calculated using the functional group composition and the energies of Table 15.36 compared to the experimental values [3]. The magnetic energy E_{mag} that is subtracted from the weighted sum of the $E_{D\,(Group)}$ (eV) values based on composition is given by (15.58).

Formula	Name	$C-Cl$ (i)	$C-Cl$ (ii)	$C-Cl$ (iii)	CH_3	CH_2	CH	$C-C$ (a)	$C-C$ (b)	$C-C$ (c)	$C-C$ (d)	$C-C$ (e)	$C-C$ (f)	E_{mag}	Calculated Total Bond Energy (eV)	Experimental Total Bond Energy (eV)	Relative Error
CCl_4	Tetrachloromethane	0	4	0	0	0	0	0	0	0	0	0	0	-1	13.43181	13.448	0.00123
$CHCl_3$	Trichloromethane	3	0	0	0	0	1	0	0	0	0	0	0	-1	14.49146	14.523	0.00217
CH_2Cl_2	Dichloromethane	2	0	0	0	1	0	0	0	0	0	0	0	0	15.37248	15.450	0.00499
CH_3Cl	Chloromethane	1	0	0	1	0	0	0	0	0	0	0	0	0	16.26302	16.312	0.00299
C_2H_5Cl	Chloroethane	0	0	1	1	1	0	1	0	0	0	0	0	0	28.61064	28.571	-0.00138
C_3H_7Cl	1-Chloropropane	0	0	1	1	2	0	2	0	0	0	0	0	0	40.76834	40.723	-0.00112
C_3H_7Cl	2-Chloropropane	0	0	1	2	0	1	0	2	0	0	0	0	0	40.86923	40.858	-0.00028
C_4H_9Cl	1-Chlorobutane	0	0	1	1	3	0	3	0	0	0	0	0	0	52.92604	52.903	-0.00044
C_4H_9Cl	2-Chlorobutane	0	0	1	2	1	1	1	2	0	0	0	0	0	52.02693	52.972	-0.00104
C_4H_9Cl	1-Chloro-2-methylpropane	0	0	1	2	1	1	0	3	0	0	0	0	0	52.99860	52.953	-0.00085
C_4H_9Cl	2-Chloro-2-methylpropane	0	0	1	3	0	0	0	0	3	0	0	0	-1	53.21057	53.191	-0.00037
$C_5H_{11}Cl$	1-Chloropentane	0	0	1	1	4	0	4	0	0	0	0	0	0	65.08379	65.061	0.00034
$C_5H_{11}Cl$	1-Chloro-3-methylbutane	0	0	1	2	2	1	1	3	0	0	0	0	0	65.15630	65.111	-0.00069
$C_5H_{11}Cl$	2-Chloro-2-methylbutane	0	0	1	3	1	0	1	0	3	0	0	0	-1	65.36827	65.344	-0.00037
$C_5H_{11}Cl$	2-Chloro-3-methylbutane	0	0	1	3	0	2	0	3	0	1	0	0	0	65.16582	65.167	0.00002
$C_6H_{13}Cl$	2-Chlorohexane	0	0	1	2	3	1	3	2	0	0	0	0	0	77.34233	77.313	-0.00038
$C_8H_{17}Cl$	1-Chlorooctane	0	0	1	1	7	0	7	0	0	0	0	0	0	101.55684	101.564	0.00007
$C_{12}H_{25}Cl$	1-Chlorododecane	0	0	1	1	11	0	11	0	0	0	0	0	0	150.18764	150.202	0.00009
$C_{18}H_{37}Cl$	1-Chlorooctadecane	0	0	1	1	17	0	17	0	0	0	0	0	0	223.13384	223.175	0.00018

Table 15.38. The bond angle parameters of branched-chain alkyl chlorides and experimental values [1]. In the calculation of θ_v, the parameters from the preceding angle were used. E_T is $E_T(atom-atom,\ msp^3.AO)$.

Atoms of Angle	2c' Bond 1 (a_0)	2c' Bond 2 (a_0)	2c' Terminal Atoms (a_0)	$E_{Coulombic}$ Atom 1	Atom 1 Hybridization Designation (Table 15.3.A)	$E_{Coulombic}$ Atom 2	Atom 2 Hybridization Designation (Table 15.3.A)	c_2 Atom 1	c_2 Atom 2	C_1	C_2	c_1	c_2'	E_T (eV)	θ_v (°)	θ_1 (°)	θ_2 (°)	Cal. θ (°)	Exp. θ (°)
$\angle ClC_aCl$ (C_a-Cl (i))	3.38271	3.38271	5.5889	-14.82575 Cl	1	-14.82575 Cl	1	0.91771	0.91771	1	0.81317 (Eq. (15.130))	1	0.91771	-0.92918				111.40	112.0 (dichloromethane) 111.3 (chloroform)
$\angle HC_aCi$ (C_a-Cl (iii))	2.11106	3.38271	4.5961	-16.27490 C_a	16	-12.96764 Cl	Cl	0.83600	0.91771	0.75	0.95310 (Eq. (15.74))	0.75	1.09775	0				111.46	
$\angle HC_aH$ $\angle HC_bH$ (C_a-Cl (iii))	2.09711	2.09711	3.4252	-15.75493	7	H	H	0.86359	1	1	1	0.75	1.15796	0				109.50	109.2 ($\angle HC_aH$ ethyl chloride) 109.8 ($\angle HC_aH$ ethyl chloride)
$\angle C_aC_bH_b$ (C_a-Cl (iii))															70.56			109.44	
$\angle C_bC_aCl$ (C_a-Cl (iii))	2.91547	3.38271	5.1539	-15.75493 C_b	7	-12.96764 Cl	Cl	0.86359	0.86359	1	0.81317 (Eq. (15.130))	1	0.86359	-0.92918				109.61	110.7 (ethyl chloride) 111.0 (1,1-dichloroethane) 109.0 (1,2-dichloroethane) 109.6 (1,1,1-trichloroethane) 110.0 (hexachloroethane)
$\angle C_bC_aH_a$ (C_a-Cl (iii))	2.91547	2.11106	4.1633	-15.55033 C_a	5	-14.82575 C_b	1	0.87495	0.91771	0.75	1	0.75	1.04887	0				110.83	110.6 (ethyl chloride)
Methylene $\angle HC_aH$	2.11106	2.11106	3.4252	-15.75493	7	H	H	0.86359	1	1	1	0.75	1.15796	0				108.44	107 (propane)
$\angle C_aC_bC_c$															69.51			110.49	112 (propane) 113.8 (butane) 110.8 (isobutane)
$\angle C_aC_bH$															69.51			110.49	111.0 (butane) 111.4 (isobutane)
Methyl $\angle HC_aH$	2.09711	2.09711	3.4252	-15.75493	7	H	H	0.86359	1	1	1	0.75	1.15796	0				109.50	
$\angle C_aC_bC_c$															70.56			109.44	
$\angle C_aC_bH$															70.56			109.44	
$\angle C_bC_aC_c$ iso C_a	2.91547	2.91547	4.7958	-16.68412 C_b	26	-16.68412 C_c	26	0.81549	0.81549	1	1	1	0.81549	-1.85836				110.67	110.8 (isobutane)
$\angle C_bC_aH$ iso C_a	2.91547	2.11323	4.1633	-15.55033 C_a	5	-14.82575 C_b	1	0.87495	0.91771	0.75	1	0.75	1.04887	0				110.76	
$\angle C_aC_bH$ iso C_a	2.91547	2.09711	4.1633	-15.55033 C_b	5	-14.82575 C_a	1	0.87495	0.91771	0.75	1	0.75	1.04887	0				111.27	111.4 (isobutane)
$\angle C_bC_aC_b$ tert C_a	2.90327	2.90327	4.7958	-16.68412 C_b	26	-16.68412 C_b	26	0.81549	0.81549	1	1	1	0.81549	-1.85836				111.37	110.8 (isobutane)
$\angle C_bC_aC_d$															72.50			107.50	

ALKYL BROMIDES ($C_nH_{2n+2-m}Br_m,\ n=1,2,3,4,5...\infty\ \ m=1,2,3...\infty$)

The branched-chain alkyl bromides, $C_nH_{2n+2-m}Br_m$, may comprise at least two terminal methyl groups (CH_3) at each end of the chain, and may comprise methylene (CH_2), and methylyne (CH) functional groups as well as C bound by carbon-carbon single bonds wherein at least one H is replaced by a bromine. The $C-Br$ bond comprises a functional group for each case of Br replacing a H of methane for the series $H_{4-m}C-Br_m,\ m=1,2,3,$ with the $C-Br$ bond of CBr_4 comprising another functional group due to the limitation of the minimum energy of Br matched to that of the $C2sp^3$ HO. In addition, the $C-Br$ bond due to Br replacing a H of an alkane is a functional group. The methyl, methylene, methylyne functional groups are equivalent to those of branched-chain alkanes. Six types of $C-C$ bonds can be identified. The n-alkane $C-C$ bond is the same as that of straight-chain alkanes. In addition, the $C-C$ bonds within isopropyl ($(CH_3)_2CH$) and t-butyl ($(CH_3)_3C$) groups and the isopropyl to isopropyl, isopropyl to t-butyl, and t-butyl to t-butyl $C-C$ bonds comprise functional groups that are equivalent to those of branched-chain alkanes.

The solution of the $C-Br$ functional groups comprises the hybridization of the $2s$ and $2p$ shells of each C to form a single $2sp^3$ shell as an energy minimum, and the sharing of electrons between the $C2sp^3$ hybridized orbital (HO) and the Br AO to form a molecular orbital (MO) permits each participating orbital to decrease in radius and energy. In alkyl bromides, the energy of bromine is less than the Coulombic energy between the electron and proton of H given by Eq. (1.264). Thus, c_2 in Eq. (15.61) is one, and the energy matching condition is determined by the C_2 parameter. Then, the $C2sp^3$ HO has a hybridization factor of 0.91771 (Eq. (13.430)) with a corresponding energy of $E\left(C,2sp^3\right)=-14.63489\ eV$ (Eq. (15.25)), and the Br AO has an energy of $E\left(Br\right)=-11.81381\ eV$. To meet the equipotential condition of the union of the $C-Br$ H_2-type-ellipsoidal-MO with these orbitals, the hybridization factor C_2 of Eq. (15.61) for the $C-Br$-bond MO given by Eqs. (15.77) and (15.79) is:

$$C_2\left(C2sp^3HO\ to\ Br\right)=\frac{E\left(Br\right)}{E\left(C,2sp^3\right)}c_2\left(C2sp^3HO\right)=\frac{-11.81381\ eV}{-14.63489\ eV}\left(0.91771\right)=0.74081 \tag{15.131}$$

The valence energy of the carbon $2p$ is $-11.2603\ eV$ and that of the Br AO is $-11.81381\ eV$. The energy difference is less than that of $E_T\left(C-C,2sp^3\right)$ given by Eq. (14.151) for a single bond. Thus, $E_T\left(atom-atom,msp^3.AO\right)$ of the alkyl $C-Br$-bond MO in Eq. (15.61) due to the charge donation from the C and Br atoms to the MO is $-0.92918\ eV$ (Eq. (14.513)) based on the maximum single-bond-energy contribution of the $C2sp^3$ HO. $E_T\left(atom-atom,msp^3.AO\right)$ of the series $CBr_mH_{4-m}\ m=1,2,3$ is equivalent to those of methyl groups, $-0.72457\ eV$ (Eq. (14.151)). For CBr_4, $E_T\left(atom-atom,msp^3.AO\right)$ of the $C-Br$-bond MO in Eq. (15.61) due to the charge donation from the C and Br atoms to the MO is $-0.36229\ eV$ based on the maximum charge density on the $C2sp^3$ HO. It is given by Eqs. (15.18-15.20) and Eq. (15.29) with a linear combination of $s=1$ corresponding to $E_T\left(atom-atom,msp^3.AO\right)=-0.72457\ eV$ and $s=0$ corresponding to: $E_T\left(atom-atom,msp^3.AO\right)=0$.

The symbols of the functional groups of branched-chain alkyl bromides are given in Table 15.39. The geometrical (Eqs. (15.1-15.5) and (15.51)), intercept (Eqs. (15.80-15.87)), and energy (Eqs. (15.6-15.11) and (15.17-15.65)) parameters of branched-chain alkyl bromides are given in Tables 15.49, 15.50, and 15.51, respectively. The total energy of each branched-chain alkyl bromide given in Table 15.52 was calculated as the sum over the integer multiple of each $E_{D\,(Group)}$ of Table 15.51 corresponding to functional-group composition of the molecule. For each set of unpaired electrons created by bond breakage, the $C2sp^3$ HO magnetic energy E_{mag} that was subtracted from the weighted sum of the $E_{D\,(Group)}$ (eV) values based on composition is given by Eq. (15.67). The $C-C$ bonds to the $CHBr$ group (one H bond to C) were each treated as an iso $C-C$ bond. The $C-C$ bonds to the CBr group (no H bonds to C) were each treated as a tert-butyl $C-C$. The bond angle parameters of branched-chain alkyl bromides determined using Eqs. (15.70-15.79), (15.88-15.117) and (15.131) are given in Table 15.44. The color scale, translucent view of the charge-density of exemplary alkyl bromide, 1-bromopropane, comprising the concentric shells of atoms with the outer shell bridged by one or more H_2-type ellipsoidal MOs or joined with one or more hydrogen MOs is shown in Figure 15.7.

Figure 15.7. Color scale, translucent view of the charge-density of 1-bromopropane showing the orbitals of the atoms at their radii, the ellipsoidal surface of each H or H_2-type ellipsoidal MO that transitions to the corresponding outer shell of the atom(s) participating in each bond, and the hydrogen nuclei (red, not to scale).

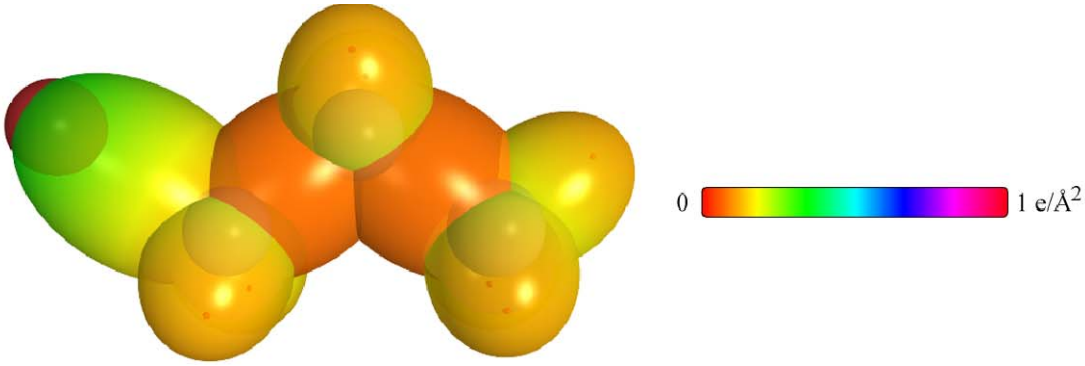

Table 15.39. The symbols of functional groups of branched-chain alkyl bromides.

Functional Group	Group Symbol
CBr of CBr_mH_{4-m}	$C-Br$ (i)
CBr of CBr_4	$C-Br$ (ii)
CBr of $C_nH_{2n+2-m}Br_m$	$C-Br$ (iii)
CH_3 group	$C-H\ (CH_3)$
CH_2 group	$C-H\ (CH_2)$
CH	$C-H$
CC bond (*n-C*)	$C-C$ (a)
CC bond (*iso-C*)	$C-C$ (b)
CC bond (*tert-C*)	$C-C$ (c)
CC (*iso* to *iso-C*)	$C-C$ (d)
CC (*t* to *t-C*)	$C-C$ (e)
CC (*t* to *iso-C*)	$C-C$ (f)

Table 15.40. The geometrical bond parameters of branched-chain alkyl bromides and experimental values [1].

Parameter	$C-Br$ (i) Group	$C-Br$ (ii) Group	$C-Br$ (iii) Group	$C-H\left(CH_3\right)$ Group	$C-H\left(CH_2\right)$ Group	$C-H$ Group	$C-C$ (a) Group	$C-C$ (b) Group	$C-C$ (c) Group	$C-C$ (d) Group	$C-C$ (e) Group	$C-C$ (f) Group
$a\left(a_0\right)$	2.49163	2.52509	2.47329	1.64920	1.67122	1.67465	2.12499	2.12499	2.10725	2.12499	2.10725	2.10725
$c'\left(a_0\right)$	1.83395	1.84622	1.82719	1.04856	1.05553	1.05661	1.45744	1.45744	1.45164	1.45744	1.45164	1.45164
Bond Length $2c'\left(\AA\right)$	1.94097	1.95396	1.93381	1.10974	1.11713	1.11827	1.54280	1.54280	1.53635	1.54280	1.53635	1.53635
Exp. Bond Length $\left(\AA\right)$	1.933 (methyl bromide)	1.935 (carbon tetrabromide)	1.93 (1,1,1-tribromoethane) 1.950 (1,2-dibromoethane)	1.107 ($C-H$ propane) 1.117 ($C-H$ butane)	1.107 ($C-H$ propane) 1.117 ($C-H$ butane)	1.122 (isobutane)	1.532 (propane) 1.531 (butane)	1.532 (propane) 1.531 (butane)	1.532 (propane) 1.531 (butane)	1.532 (propane) 1.531 (butane)	1.532 (propane) 1.531 (butane)	1.532 (propane) 1.531 (butane)
$b,c\left(a_0\right)$	1.68667	1.72265	1.66689	1.27295	1.29569	1.29924	1.54616	1.54616	1.52750	1.54616	1.52750	1.52750
e	0.73604	0.73115	0.73877	0.63580	0.63159	0.63095	0.68600	0.68600	0.68888	0.68600	0.68888	0.68888

Table 15.41. The MO to HO intercept geometrical bond parameters of branched-chain alkyl bromides. R, R', R'' are H or alkyl groups. E_T is $E_T(atom-atom,msp^3.AO)$.

Bond	Atom	E_T (eV) Bond 1	E_T (eV) Bond 2	E_T (eV) Bond 3	E_T (eV) Bond 4	Final Total Energy $C2sp^3$ (eV)	$r_{initial}\left(a_0\right)$	$r_{final}\left(a_0\right)$	$E_{Coulomb}$ (eV) Final	$E\left(C2sp^3\right)$ (eV) Final	θ' (°)	θ_1 (°)	θ_2 (°)	$d_1\left(a_0\right)$	$d_2\left(a_0\right)$
$H_{4-m}C_a-Br_m,\ m=1,2,3,$ (C_a-Br (i))	C_a	-0.36229	0	0	0	-151.97798	0.91771	0.89582	-15.18804	-14.99717	68.10	111.90	29.52	2.16808	0.33413
$H_{4-m}C_a-Br_m,\ m=1,2,3,$ (C_a-Br (i))	Br	-0.36229	0	0	0		1.15169	0.89582	-15.18804		68.10	111.90	29.52	2.16808	0.33413
C_aBr_4 (C_a-Br (ii))	C_a	-0.18114	0	0	0	-151.79683	0.91771	0.90664	-15.00589	-14.81603	66.10	113.90	28.76	2.21357	0.36734
C_aBr_4 (C_a-Br (ii))	Br	-0.18114	0	0	0		1.15169	0.90664	-15.00589		66.10	113.90	28.76	2.21357	0.36734
$-H_2C_bC_aBr$ (C_a-Br (iii))	C_a	-0.46459	-0.92918	0	0	-153.00946	0.91771	0.83885	-16.21952	-16.02866	62.67	117.33	26.55	2.21237	0.38518
$-H_2C_bC_aBr$ (C_a-Br (iii))	Br	-0.46459	0	0	0		1.15169	0.88983	-15.29034		69.19	110.81	29.93	2.14337	0.31618
$C-H\left(CH_3\right)$	C	-0.92918	0	0	0	-152.54487	0.91771	0.86359	-15.75493	-15.56407	77.49	102.51	41.48	1.23564	0.18708
$C-H\left(CH_2\right)$	C	-0.92918	-0.92918	0	0	-153.47406	0.91771	0.81549	-16.68412	-16.49325	68.47	111.53	35.84	1.35486	0.29933
$C-H\left(CH\right)$	C	-0.92918	-0.92918	-0.92918	0	-154.40324	0.91771	0.77247	-17.61330	-17.42244	61.10	118.90	31.37	1.42988	0.37326
$H_3C_aC_bH_2CH_2-$ ($C-C$ (a))	C_a	-0.92918	0	0	0	-152.54487	0.91771	0.86359	-15.75493	-15.56407	63.82	116.18	30.08	1.83879	0.38106
$H_3C_aC_bH_2CH_2-$ ($C-C$ (a))	C_b	-0.92918	-0.92918	0	0	-153.47406	0.91771	0.81549	-16.68412	-16.49325	56.41	123.59	26.06	1.90890	0.45117
$R-H_2C_aC_b\left(H_2C_c-R'\right)HCH_2-$ ($C-C$ (b))	C_b	-0.92918	-0.92918	-0.92918	0	-154.40324	0.91771	0.77247	-17.61330	-17.42244	48.30	131.70	21.90	1.97162	0.51388
$R-H_2C_a\left(R'-H_2C_d\right)C_b\left(R''-H_2C_c\right)CH_2-$ ($C-C$ (c))	C_b	-0.92918	-0.72457	-0.72457	-0.72457	-154.71860	0.91771	0.75889	-17.92866	-17.73779	48.21	131.79	21.74	1.95734	0.50570
$isoC_aC_b\left(H_2C_c-R'\right)HCH_2-$ ($C-C$ (d))	C_b	-0.92918	-0.92918	-0.92918	0	-154.40324	0.91771	0.77247	-17.61330	-17.42244	48.30	131.70	21.90	1.97162	0.51388
$tertC_a\left(R'-H_2C_d\right)C_b\left(R''-H_2C_c\right)CH_2-$ ($C-C$ (e))	C_b	-0.72457	-0.72457	-0.72457	-0.72457	-154.51399	0.91771	0.76765	-17.92866	-17.73779	50.04	129.96	22.66	1.94462	0.49298
$tertC_aC_b\left(H_2C_c-R'\right)HCH_2-$ ($C-C$ (f))	C_b	-0.72457	-0.92918	-0.92918	0-	-154.19863	0.91771	0.78155	-17.40869	-17.21783	52.78	127.22	24.04	1.92443	0.47279
$isoC_a\left(R'-H_2C_d\right)C_b\left(R''-H_2C_c\right)CH_2-$ ($C-C$ (f))	C_b	-0.72457	-0.72457	-0.72457	-0.72457	-154.51399	0.91771	0.76765	-17.92866	-17.73779	50.04	129.96	22.66	1.94462	0.49298

Table 15.42. The energy parameters (eV) of functional groups of branched-chain alkyl bromides.

Parameters	$C-Br$ (i) Group	$C-Br$ (ii) Group	$C-Br$ (iii) Group	CH_3 Group	CH_2 Group	$C-H$ Group	$C-C$ (a) Group	$C-C$ (b) Group	$C-C$ (c) Group	$C-C$ (d) Group	$C-C$ (e) Group	$C-C$ (f) Group
n_1	1	1	1	3	2	1	1	1	1	1	1	1
n_2	0	0	0	2	1	0	0	0	0	0	0	0
n_3	0	0	0	0	0	0	0	0	0	0	0	0
C_1	0.5	0.5	0.5	0.75	0.75	0.75	0.5	0.5	0.5	0.5	0.5	0.5
C_2	0.74081	0.74081	0.74081	1	1	1	1	1	1	1	1	1
c_1	1	1	1	1	1	1	1	1	1	1	1	1
c_2	1	1	1	0.91771	0.91771	0.91771	0.91771	0.91771	0.91771	0.91771	0.91771	0.91771
c_3	0	0	0	0	1	1	0	0	0	1	1	0
c_4	2	2	2	1	1	1	2	2	2	2	2	2
c_5	0	0	0	3	2	1	0	0	0	0	0	0
C_{1o}	0.5	0.5	0.5	0.75	0.75	0.75	0.5	0.5	0.5	0.5	0.5	0.5
C_{2o}	0.74081	0.74081	0.74081	1	1	1	1	1	1	1	1	1
V_e (eV)	-27.94806	-27.44996	-28.22940	-107.32728	-70.41425	-35.12015	-28.79214	-28.79214	-29.10112	-28.79214	-29.10112	-29.10112
V_p (eV)	7.41885	7.36953	7.44631	38.92728	25.78002	12.87680	9.33352	9.33352	9.37273	9.33352	9.37273	9.37273
T (eV)	5.60839	5.43544	5.70686	32.53914	21.06675	10.48582	6.77464	6.77464	6.90500	6.77464	6.90500	6.90500
V_m (eV)	-2.80419	-2.71772	-2.85343	-16.26957	-10.53337	-5.24291	-3.38732	-3.38732	-3.45250	-3.38732	-3.45250	-3.45250
$E_{(AO/HO)}$ (eV)	-14.63489	-14.63489	-14.63489	-15.56407	-15.56407	-14.63489	-15.56407	-15.56407	-15.35946	-15.56407	-15.35946	-15.35946
$\Delta E_{H_2MO_{(AO/HO)}}$ (eV)	-0.72457	-0.36229	-0.92918	0	0	0	0	0	0	0	0	0
$E_T{}_{(AO/HO)}$ (eV)	-13.91032	-14.27260	-13.70571	-15.56407	-15.56407	-14.63489	-15.56407	-15.56407	-15.35946	-15.56407	-15.35946	-15.35946
$E_T{}_{(H_2MO)}$ (eV)	-31.63533	-31.63531	-31.63537	-67.69451	-49.66493	-31.63533	-31.63537	-31.63537	-31.63535	-31.63537	-31.63535	-31.63535
$E_T\left(atom-atom.msp^3.AO\right)(eV)$	-0.72457	-0.36229	-0.92918	0	0	0	-1.85836	-1.85836	-1.44915	-1.85836	-1.44915	-1.44915
$E_T{}_{(MO)}$ (eV)	-32.35994	-31.99766	-32.56455	-67.69450	-49.66493	-31.63537	-33.49373	-33.49373	-33.08452	-33.49373	-33.08452	-33.08452
$\omega\ \left(10^{15}\ rad/s\right)$	6.39733	6.27059	6.46864	24.9286	24.2751	24.1759	9.43699	9.43699	15.4846	9.43699	9.55643	9.55643
E_K (eV)	4.21083	4.12741	4.25777	16.40846	15.97831	15.91299	6.21159	6.21159	10.19220	6.21159	6.29021	6.29021
$\bar{E}_{ED}$ (eV)	-0.13137	-0.12861	-0.13293	-0.25352	-0.25017	-0.24966	-0.16515	-0.16515	-0.20896	-0.16515	-0.16416	-0.16416
$\bar{E}_{Kvib}$ (eV)	0.07575 [14]	0.08332 [15]	0.07575 [14]	0.35532 (Eq. (13.458))	0.35532 (Eq. (13.458))	0.35532 (Eq. (13.458))	0.12312 [2]	0.17978 [4]	0.09944 [5]	0.12312 [2]	0.12312 [2]	0.12312 [2]
$\bar{E}_{osc}$ (eV)	-0.09349	-0.08695	-0.09506	-0.22757	-0.14502	-0.07200	-0.10359	-0.07526	-0.15924	-0.10359	-0.10260	-0.10260
E_{mag} (eV)	0.14803	0.14803	0.14803	0.14803	0.14803	0.14803	0.14803	0.14803	0.14803	0.14803	0.14803	0.14803
$E_T{}_{(Group)}$ (eV)	-32.45343	-32.08460	-32.65961	-67.92207	-49.80996	-31.70737	-33.59732	-33.49373	-33.24376	-33.59732	-33.18712	-33.18712
$E_{initial_{(x\ AO/HO)}}$ (eV)	-14.63489	-14.63489	-14.63489	-14.63489	-14.63489	-14.63489	-14.63489	-14.63489	-14.63489	-14.63489	-14.63489	-14.63489
$E_{initial_{(x\ AO/HO)}}$ (eV)	0	0	0	-13.59844	-13.59844	-13.59844	0	0	0	0	0	0
$E_D{}_{(Group)}$ (eV)	3.18365	2.81482	3.38983	12.49186	7.83016	3.32601	4.32754	4.29921	3.97398	4.17951	3.62128	3.91734

Table 15.43. The total bond energies of branched-chain alkyl bromides calculated using the functional group composition and the energies of Table 15.42 compared to the experimental values [3]. The magnetic energy E_{mag} that is subtracted from the weighted sum of the E_D $(Group)$ (eV) values based on composition is given by (15.58).

Formula	Name	$C-Br$ (i)	$C-Br$ (ii)	$C-Br$ (iii)	CH_3	CH_2	CH (i)	CH (ii)	$C-C$ (a)	$C-C$ (b)	$C-C$ (c)	$C-C$ (d)	$C-C$ (e)	$C-C$ (f)	Calculated Total Bond Energy (eV)	Experimental Total Bond Energy (eV)	Relative Error
CBr_4	Tetrabromomethane	0	4	0	0	0	0	0	0	0	0	0	0	0	11.25929	11.196	-0.00566
$CHBr_3$	Tribromomethane	3	0	0	0	0	1	0	0	0	0	0	0	0	12.87698	12.919	0.00323
CH_3Br	Bromomethane	1	0	0	1	0	0	0	0	0	0	0	0	0	15.67551	15.732	0.00360
C_2H_5Br	Bromoethane	0	0	1	1	1	0	0	1	0	0	0	0	0	28.03939	27.953	-0.00308
C_3H_7Br	1-Bromopropane	0	0	1	1	2	0	0	2	0	0	0	0	0	40.19709	40.160	-0.00093
C_3H_7Br	2-Bromopropane	0	0	1	2	0	1	0	0	2	0	0	0	0	40.29798	40.288	-0.00024
$C_5H_{10}Br_2$	2,3-Dibromo-2-methylbutane	1	0	1	3	0	1	0	0	1	2	0	0	1	63.53958	63.477	-0.00098
$C_6H_{13}Br$	1-Bromohexane	0	0	1	1	5	0	0	5	0	0	0	0	0	76.67019	76.634	-0.00047
$C_7H_{15}Br$	1-Bromoheptane	0	0	1	1	6	0	0	6	0	0	0	0	0	88.82789	88.783	0.00051
$C_8H_{17}Br$	1-Bromooctane	0	0	1	1	7	0	0	7	0	0	0	0	0	100.98559	100.952	-0.00033
$C_{12}H_{25}Br$	1-Bromododecane	0	0	1	1	11	0	0	11	0	0	0	0	0	149.61639	149.573	-0.00029
$C_{16}H_{33}Br$	1-Bromohexadecane	0	0	1	1	15	0	0	15	0	0	0	0	0	198.24719	198.192	-0.00028

Table 15.44. The bond angle parameters of branched-chain alkyl bromides and experimental values [1]. In the calculation of θ_v, the parameters from the preceding angle were used. E_T is $E_T(atom-atom,msp^3.AO)$.

Atoms of Angle	2c' Bond 1 (a_0)	2c' Bond 2 (a_0)	2c' Terminal Atoms (a_0)	$E_{Coulombic}$ Atom 1	Atom 1 Hybridization Designation (Table 15.3.A)	$E_{Coulombic}$ Atom 2	Atom 2 Hybridization Designation (Table 15.3.A)	c_2 Atom 1	c_2 Atom 2	C_1	C_2	c_1	c_2'	E_T (eV)	θ_v (°)	θ_1 (°)	θ_2 (°)	Cal. θ (°)	Exp. θ (°)
$\angle BrC_aBr$ (C_a-Br (i))	3.66790	3.66790	6.0816	-15.18804 Br	2	-15.18804 Br	2	0.89582	0.89582	1	0.74081 (Eq. (15.131))	1	0.89582	-0.92918				112.00	111.2 (methyl bromide) 113.2 (dibromomethane) 111.7 (bromoform)
$\angle HC_aBr$ (C_a-Br (iii))	2.11106	3.66790	4.8312	-15.55033 C_a	5	-11.81381 Br	Br	0.87495	0.91771	0.75	0.86829 (Eq. (15.74))	0.75	1.04887	0				110.53	109 (dibromomethane)
$\angle HC_aH$ $\angle HC_bH$ (C_a-Br (iii))	2.09711	2.09711	3.4252	-15.75493	7	H	H	0.86359	1	1	1	0.75	1.15796	0				109.50	
$\angle C_aC_bH_b$ (C_a-Br (iii))															70.56			109.44	110 (1,2-dibromoethane) 109.0 (1,1,1-tribromoethane)
$\angle C_bC_aBr$ (C_a-Br (iii))	2.91547	3.65437	5.4247	-15.75493 C_b	7	-11.81381 Br	Br	0.86359	0.86359	1	0.74081 (Eq. (15.131))	1	0.86359	-0.72457				110.82	109.5 (1,1-dibromoethane)
Methylene $\angle HC_aH$	2.11106	2.11106	3.4252	-15.75493	7	H	H	0.86359	1	1	1	0.75	1.15796	0				108.44	107 (propane)
$\angle C_aC_bC_c$															69.51			110.49	112 (propane) 113.8 (butane) 110.8 (isobutane)
$\angle C_aC_bH$															69.51			110.49	111.0 (butane) 111.4 (isobutane)
Methyl $\angle HC_aH$	2.09711	2.09711	3.4252	-15.75493	7	H	H	0.86359	1	1	1	0.75	1.15796	0				109.50	
$\angle C_aC_bC_c$															70.56			109.44	
$\angle C_aC_bH$															70.56			109.44	
$\angle C_bC_aC_c$ iso C_a	2.91547	2.91547	4.7958	-16.68412 C_b	26	-16.68412 C_c	26	0.81549	0.81549	1	1	1	0.81549	-1.85836				110.67	110.8 (isobutane)
$\angle C_bC_aH$ iso C_a	2.91547	2.11323	4.1633	-15.55033 C_a	5	-14.82575 C_b	1	0.87495	0.91771	0.75	1	0.75	1.04887	0				110.76	
$\angle C_aC_bH$ iso C_a	2.91547	2.09711	4.1633	-15.55033 C_b	5	-14.82575 C_a	1	0.87495	0.91771	0.75	1	0.75	1.04887	0				111.27	111.4 (isobutane)
$\angle C_bC_aC_b$ tert C_a	2.90327	2.90327	4.7958	-16.68412 C_b	26	-16.68412 C_b	26	0.81549	0.81549	1	1	1	0.81549	-1.85836				111.37	110.8 (isobutane)
$\angle C_bC_aC_d$															72.50			107.50	

ALKYL IODIDES ($C_nH_{2n+2-m}I_m,\ n=1,2,3,4,5...\infty\ m=1,2,3...\infty$)

The branched-chain alkyl iodides, $C_nH_{2n+2-m}I_m$, may comprise at least two terminal methyl groups (CH_3) at each end of the chain, and may comprise methylene (CH_2), and methylyne (CH) functional groups as well as C bound by carbon-carbon single bonds wherein at least one H is replaced by an iodine atom. The $C-I$ bond comprises a functional group for I replacing a H of methane (CH_3I) or for I replacing a H of an alkane corresponding to the series $C_nH_{2n+2-m}I_m$. The $C-I$ bond of each of CH_2I_2 and CHI_3 comprise separate functional groups due to the limitation of the minimum energy of I matched to that of the $C2sp^3$ HO. The methyl, methylene, methylyne functional groups are equivalent to those of branched-chain alkanes. Six types of $C-C$ bonds can be identified. The n-alkane $C-C$ bond is the same as that of straight-chain alkanes. In addition, the $C-C$ bonds within isopropyl ($(CH_3)_2CH$) and t-butyl ($(CH_3)_3C$) groups and the isopropyl to isopropyl, isopropyl to t-butyl, and t-butyl to t-butyl $C-C$ bonds comprise functional groups that are equivalent to those of branched-chain alkanes.

The solution of the $C-I$ functional groups comprises the hybridization of the $2s$ and $2p$ AOs of each C to form a single $2sp^3$ shell as an energy minimum, and the sharing of electrons between the $C2sp^3$ HO and the I AO to form a MO permits each participating orbital to decrease in radius and energy. In alkyl iodides, the energy of iodine is less than the Coulombic energy between the electron and proton of H given by Eq. (1.264). Thus, c_2 in Eq. (15.61) is one, and the energy matching condition is determined by the C_2 parameter. Then, the $C2sp^3$ HO has a hybridization factor of 0.91771 (Eq. (13.430)) with a corresponding energy of $E\left(C,2sp^3\right)=-14.63489\ eV$ (Eq. (15.25)). The I AO has an energy of $E(I)=-10.45126\ eV$. To meet the equipotential condition of the union of the $C-I$ H_2-type-ellipsoidal-MO with these orbitals, the hybridization factor C_2 of Eq. (15.60) for the $C-I$-bond MO given by Eqs. (15.77) and (15.79) is:

$$C_2\left(C2sp^3HO\ to\ I\right)=\frac{E(I)}{E\left(C,2sp^3\right)}c_2\left(C2sp^3HO\right)=\frac{-10.45126\ eV}{-14.63489\ eV}(0.91771)=0.65537 \tag{15.132}$$

The valence energy of the carbon $2p$ is $-11.2603\ eV$ and that of the I AO is $-10.45126\ eV$. The energy difference is positive. Thus, based on the maximum charge density on the $C2sp^3$ HO $E_T\left(atom-atom,msp^3.AO\right)$ of the $C-I$-bond MO in Eq. (15.61) due to the charge donation from the C and I atoms to the MO is $-0.36229\ eV$ (Eqs. (15.18-15.20 and Eq. (15.29) with a linear combination of $s=1$, $E_T\left(atom-atom,msp^3.AO\right)=-0.72457\ eV$ and $E_T\left(atom-atom,msp^3.AO\right)=0$) for methyl and alkyl iodides, $-0.18114\ eV$ for diiodomethane, and 0 for CHI_3.

The symbols of the functional groups of branched-chain alkyl iodides are given in Table 15.45. The geometrical (Eqs. (15.1-15.5) and (15.51)), intercept (Eqs. (15.80-15.87)), and energy (Eqs. (15.6-15.11) and (15.17-15.65)) parameters of branched-chain alkyl iodides are given in Tables 15.55, 15.56, and 15.57, respectively. The total energy of each branched-chain alkyl iodide given in Table 15.49 was calculated as the sum over the integer multiple of each $E_{D(Group)}$ of Table 15.48 corresponding to functional-group composition of the molecule. For each set of unpaired electrons created by bond breakage, the $C2sp^3$ HO magnetic energy E_{mag} that was subtracted from the weighted sum of the $E_{D(Group)}$ (eV) values based on composition is given by Eq. (15.67). The $C-C$ bonds to the CHI group (one H bond to C) were each treated as an iso $C-C$ bond. The $C-C$ bonds to the CI group (no H bonds to C) were each treated as a tert-butyl $C-C$. E_{mag} is subtracted for each t-butyl group. The bond angle parameters of branched-chain alkyl iodides determined using Eqs. (15.70-15.79), (15.88-15.117) and (15.132) are given in Table 15.50. The color scale, translucent view of the charge-density of exemplary alkyl iodide, 1-iodopropane, comprising the concentric shells of atoms with the outer shell bridged by one or more H_2-type ellipsoidal MOs or joined with one or more hydrogen MOs is shown in Figure 15.8.

Figure 15.8. Color scale, translucent view of the charge-density of 1-iodopropane showing the orbitals of the atoms at their radii, the ellipsoidal surface of each H or H_2-type ellipsoidal MO that transitions to the corresponding outer shell of the atom(s) participating in each bond, and the hydrogen nuclei (red, not to scale).

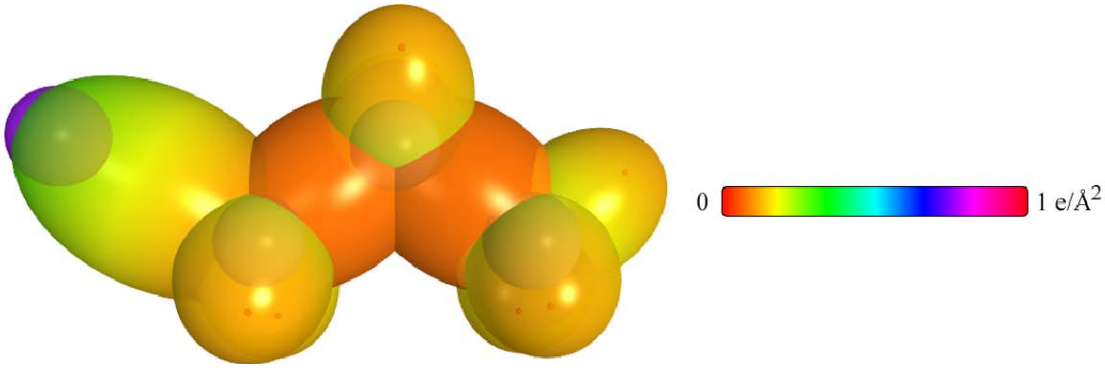

Table 15.45. The symbols of functional groups of branched-chain alkyl iodides.

Functional Group	Group Symbol
CI of CH_3I and $C_nH_{2n+2-m}I_m$	$C-I$ (i)
CI of CH_2I_2	$C-I$ (ii)
CI of CHI_3	$C-I$ (iii)
CH_3 group	$C-H\ (CH_3)$
CH_2 group	$C-H\ (CH_2)$
CH	$C-H$
CC bond (*n-C*)	$C-C$ (a)
CC bond (*iso-C*)	$C-C$ (b)
CC bond (*tert-C*)	$C-C$ (c)
CC (*iso* to *iso-C*)	$C-C$ (d)
CC (*t* to *t-C*)	$C-C$ (e)
CC (*t* to *iso-C*)	$C-C$ (f)

Table 15.46. The geometrical bond parameters of branched-chain alkyl iodides and experimental values [1].

Parameter	$C-I$ (i) Group	$C-I$ (ii) Group	$C-I$ (iii) Group	$C-H\ (CH_3)$ Group	$C-H\ (CH_2)$ Group	$C-H$ Group	$C-C$ (a) Group	$C-C$ (b) Group	$C-C$ (c) Group	$C-C$ (d) Group	$C-C$ (e) Group	$C-C$ (f) Group
$a\ (a_0)$	2.67103	2.68865	2.70662	1.64920	1.67122	1.67465	2.12499	2.12499	2.10725	2.12499	2.10725	2.10725
$c'\ (a_0)$	2.01881	2.02546	2.03222	1.04856	1.05553	1.05661	1.45744	1.45744	1.45164	1.45744	1.45164	1.45164
Bond Length $2c'\ (A)$	2.13662	2.14365	2.15081	1.10974	1.11713	1.11827	1.54280	1.54280	1.53635	1.54280	1.53635	1.53635
Exp. Bond Length (A)	2.132 (methyl iodide)	2.132 (methyl iodide)	2.15 (carbon tetraiodide)	1.107 ($C-H$ propane) 1.117 ($C-H$ butane)	1.107 ($C-H$ propane) 1.117 ($C-H$ butane)	1.122 (isobutane)	1.532 (propane) 1.531 (butane)	1.532 (propane) 1.531 (butane)	1.532 (propane) 1.531 (butane)	1.532 (propane) 1.531 (butane)	1.532 (propane) 1.531 (butane)	1.532 (propane) 1.531 (butane)
$b,c\ (a_0)$	1.74894	1.76815	1.78770	1.27295	1.29569	1.29924	1.54616	1.54616	1.52750	1.54616	1.52750	1.52750
e	0.75582	0.75334	0.75083	0.63580	0.63159	0.63095	0.68600	0.68600	0.68888	0.68600	0.68888	0.68888

Table 15.47. The MO to HO intercept geometrical bond parameters of branched-chain alkyl iodides. R, R', R'' are H or alkyl groups. E_T is $E_T(atom - atom, msp^3.AO)$.

Bond	Atom	E_T (eV) Bond 1	E_T (eV) Bond 2	E_T (eV) Bond 3	E_T (eV) Bond 4	Final Total Energy $C2sp^3$ (eV)	$r_{initial}$ (a_0)	r_{final} (a_0)	$E_{Coulomb}$ (eV) Final	$E(C2sp^3)$ (eV) Final	θ' (°)	θ_1 (°)	θ_2 (°)	d_1 (a_0)	d_2 (a_0)
CH_3I $(C_a - I$ (i))	C_a	-0.18114	0	0	0	-151.79683	0.91771	0.90664	-15.00689	-14.81603	69.63	110.37	29.08	2.33442	0.31560
CH_3I $(C_a - I$ (i))	I	-0.18114	0	0	0		1.30183	0.90664	-15.00689		69.63	110.37	29.08	2.33442	0.31560
$-H_2C_bC_aI$ $(C_a - I$ (i))	C_a	-0.18114	-0.92918	0	0	-152.72602	0.91771	0.85377	-15.93608	-15.74521	63.16	116.84	25.82	2.40436	0.38554
$-H_2C_bC_aI$ $(C_a - I$ (i))	I	-0.18114	0	0	0		1.30183	0.90664	-15.00689		69.63	110.37	29.08	2.33442	0.31560
$C_aH_2I_2$ $(C_a - I$ (ii))	C_a	-0.09057	0	0	0	-151.70626	0.91771	0.91214	-14.91632	-14.72546	68.61	111.39	28.71	2.35818	0.33272
$C_aH_2I_2$ $(C_a - I$ (ii))	I	-0.09057	0	0	0		1.30183	0.91214	-14.91632		68.61	111.39	28.71	2.35818	0.33272
C_aHI_3 $(C_a - I$ (iii))	C_a	0	0	0	0	-151.61569	0.91771	0.91771	-14.82575	-14.63489	67.56	112.44	28.32	2.38256	0.35035
C_aHI_3 $(C_a - I$ (iii))	I	0	0	0	0		1.30183	0.91771	-14.82575	-14.63489	67.56	112.44	28.32	2.38256	0.35035
$C - H$ (CH_3)	C	-0.92918	0	0	0	-152.54487	0.91771	0.86359	-15.75493	-15.56407	77.49	102.51	41.48	1.23564	0.18708
$C - H$ (CH_2)	C	-0.92918	-0.92918	0	0	-153.47406	0.91771	0.81549	-16.68412	-16.49325	68.47	111.53	35.84	1.35486	0.29933
$C - H$ (CH)	C	-0.92918	-0.92918	-0.92918	0	-154.40324	0.91771	0.77247	-17.61330	-17.42244	61.10	118.90	31.37	1.42988	0.37326
$H_3C_aC_bH_2CH_2 -$ $(C - C$ (a))	C_a	-0.92918	0	0	0	-152.54487	0.91771	0.86359	-15.75493	-15.56407	63.82	116.18	30.08	1.83879	0.38106
$H_3C_aC_bH_2CH_2 -$ $(C - C$ (a))	C_b	-0.92918	-0.92918	0	0	-153.47406	0.91771	0.81549	-16.68412	-16.49325	56.41	123.59	26.06	1.90890	0.45117
$R - H_2C_aC_b(H_2C_c - R')HCH_2 -$ $(C - C$ (b))	C_b	-0.92918	-0.92918	-0.92918	0	-154.40324	0.91771	0.77247	-17.61330	-17.42244	48.30	131.70	21.90	1.97162	0.51388
$R - H_2C_a(R' - H_2C_d)C_b(R'' - H_2C_c)CH_2 -$ $(C - C$ (c))	C_b	-0.92918	-0.72457	-0.72457	-0.72457	-154.71860	0.91771	0.75889	-17.92866	-17.73779	48.21	131.79	21.74	1.95734	0.50570
$isoC_aC_b(H_2C_c - R')HCH_2 -$ $(C - C$ (d))	C_b	-0.92918	-0.92918	-0.92918	0	-154.40324	0.91771	0.77247	-17.61330	-17.42244	48.30	131.70	21.90	1.97162	0.51388
$tertC_a(R' - H_2C_d)C_b(R'' - H_2C_c)CH_2 -$ $(C - C$ (e))	C_b	-0.72457	-0.72457	-0.72457	-0.72457	-154.51399	0.91771	0.76765	-17.92866	-17.73779	50.04	129.96	22.66	1.94462	0.49298
$tertC_aC_b(H_2C_c - R')HCH_2 -$ $(C - C$ (f))	C_b	-0.72457	-0.92918	-0.92918	0-	-154.19863	0.91771	0.78155	-17.40869	-17.21783	52.78	127.22	24.04	1.92443	0.47279
$isoC_a(R' - H_2C_d)C_b(R'' - H_2C_c)CH_2 -$ $(C - C$ (f))	C_b	-0.72457	-0.72457	-0.72457	-0.72457	-154.51399	0.91771	0.76765	-17.92866	-17.73779	50.04	129.96	22.66	1.94462	0.49298

Table 15.48. The energy parameters (eV) of functional groups of branched-chain alkyl iodides.

Parameters	$C-I$ (i) Group	$C-I$ (ii) Group	$C-I$ (iii) Group	CH_3 Group	CH_2 Group	$C-H$ Group	$C-C$ (a) Group	$C-C$ (b) Group	$C-C$ (c) Group	$C-C$ (d) Group	$C-C$ (e) Group	$C-C$ (f) Group
n_1	1	1	1	3	2	1	1	1	1	1	1	1
n_2	0	0	0	2	1	0	0	0	0	0	0	0
n_3	0	0	0	0	0	0	0	0	0	0	0	0
C_1	0.5	0.5	0.5	0.75	0.75	0.75	0.5	0.5	0.5	0.5	0.5	0.5
C_2	0.65537	0.65537	0.65537	1	1	1	1	1	1	1	1	1
c_1	1	1	1	1	1	1	1	1	1	1	1	1
c_2	1	1	1	0.91771	0.91771	0.91771	0.91771	0.91771	0.91771	0.91771	0.91771	0.91771
c_3	1	0	1	0	1	1	0	0	0	1	1	0
c_4	2	2	2	1	1	1	2	2	2	2	2	2
c_5	0	0	0	3	2	1	0	0	0	0	0	0
C_{1o}	0.5	0.5	0.5	0.75	0.75	0.75	0.5	0.5	0.5	0.5	0.5	0.5
C_{2o}	0.65537	0.65537	0.65537	1	1	1	1	1	1	1	1	1
V_e (eV)	-26.59109	-26.34902	-26.10696	-107.32728	-70.41425	-35.12015	-28.79214	-28.79214	-29.10112	-28.79214	-29.10112	-29.10112
V_p (eV)	6.73951	6.71739	6.69505	38.92728	25.78002	12.87680	9.33352	9.33352	9.37273	9.33352	9.37273	9.37273
T (eV)	4.97768	4.90005	4.82280	32.53914	21.06675	10.48582	6.77464	6.77464	6.90500	6.77464	6.90500	6.90500
V_m (eV)	-2.48884	-2.45002	-2.41140	-16.26957	-10.53337	-5.24291	-3.38732	-3.38732	-3.45250	-3.38732	-3.45250	-3.45250
$E_{(AO/HO)}$ (eV)	-14.63489	-14.63489	-14.63489	-15.56407	-15.56407	-14.63489	-15.56407	-15.56407	-15.35946	-15.56407	-15.35946	-15.35946
$\Delta E_{H_2MO\,(AO/HO)}$ (eV)	-0.36229	-0.18114	0	0	0	0	0	0	0	0	0	0
$E_{T(AO/HO)}$ (eV)	-14.29907	-14.45375	-14.63489	-15.56407	-15.56407	-14.63489	-15.56407	-15.56407	-15.35946	-15.56407	-15.35946	-15.35946
$E_{T(H_2MO)}$ (eV)	-31.63534	-31.63535	-31.63540	-67.69451	-49.66493	-31.63533	-31.63537	-31.63537	-31.63535	-31.63537	-31.63535	-31.63535
$E_T\left(atom-atom, msp^3.AO\right)(eV)$	-0.36229	-0.18114	0	0	0	0	-1.85836	-1.85836	-1.44915	-1.85836	-1.44915	-1.44915
$E_{T(MO)}$ (eV)	-31.99766	-31.81651	-31.63537	-67.69450	-49.66493	-31.63537	-33.49373	-33.49373	-33.08452	-33.49373	-33.08452	-33.08452
$\omega\ \left(10^{15}\ rad/s\right)$	10.2318	5.36799	9.90080	24.9286	24.2751	24.1759	9.43699	9.43699	15.4846	9.43699	9.55643	9.55643
E_K (eV)	6.73472	3.53331	6.51688	16.40846	15.97831	15.91299	6.21159	6.21159	10.19220	6.21159	6.29021	6.29021
$\bar{E}_D$ (eV)	-0.16428	-0.11832	-0.15977	-0.25352	-0.25017	-0.24966	-0.16515	-0.16515	-0.20896	-0.16515	-0.16416	-0.16416
$\bar{E}_{Kvib}$ (eV)	0.06608 [16]	0.06608 [16]	0.06608 [16]	0.35532 (Eq. (13.458))	0.35532 (Eq. (13.458))	0.35532 (Eq. (13.458))	0.12312 [2]	0.17978 [4]	0.09944 [5]	0.12312 [2]	0.12312 [2]	0.12312 [2]
$\bar{E}_{osc}$ (eV)	-0.13124	-0.08527	-0.12673	-0.22757	-0.14502	-0.07200	-0.10359	-0.07526	-0.15924	-0.10359	-0.10260	-0.10260
E_{mag} (eV)	0.14803	0.14803	0.14803	0.14803	0.14803	0.14803	0.14803	0.14803	0.14803	0.14803	0.14803	0.14803
$E_{T(Group)}$ (eV)	-32.12889	-31.90179	-31.76210	-67.92207	-49.80996	-31.70737	-33.59732	-33.49373	-33.24376	-33.59732	-33.18712	-33.18712
$E_{initial\,(s_A\,AO/HO)}$ (eV)	-14.63489	-14.63489	-14.63489	-14.63489	-14.63489	-14.63489	-14.63489	-14.63489	-14.63489	-14.63489	-14.63489	-14.63489
$E_{initial\,(s_S\,AO/HO)}$ (eV)	0	0	0	-13.59844	-13.59844	-13.59844	0	0	0	0	0	0
$E_{D(Group)}$ (eV)	2.71108	2.63201	2.34429	12.49186	7.83016	3.32601	4.32754	4.29921	3.97398	4.17951	3.62128	3.91734

Table 15.49. The total bond energies of branched-chain alkyl iodides calculated using the functional group composition and the energies of Table 15.48 compared to the experimental values [3]. The magnetic energy E_{mag} that is subtracted from the weighted sum of the E_D $(Group)$ (eV) values based on composition is given by (15.58).

Formula	Name	$C-I$ (i)	$C-I$ (ii)	$C-I$ (iii)	CH_3	CH_2	CH (i)	CH (ii)	$C-C$ (a)	$C-C$ (b)	$C-C$ (c)	$C-C$ (d)	$C-C$ (e)	$C-C$ (f)	E_{mag}	Calculated Total Bond Energy (eV)	Experimental Total Bond Energy (eV)	Relative Error
CHI_3	Triiodomethane	0	0	3	0	0	1	0	0	0	0	0	0	0	0	10.35888	10.405	0.00444
CH_2I_2	Diiodomethane	0	2	0	0	1	0	0	0	0	0	0	0	0	-1	12.94614	12.921	-0.00195
CH_3I	Iodomethane	1	0	0	1	0	0	0	0	0	0	0	0	0	0	15.20294	15.163	-0.00263
C_2H_5I	Iodoethane	1	0	0	1	1	0	0	1	0	0	0	0	0	0	27.36064	27.343	-0.00066
C_3H_7I	1-Iodopropane	1	0	0	1	2	0	0	2	0	0	0	0	0	0	39.51834	39.516	-0.00006
C_3H_7I	2-Iodopropane	1	0	0	2	0	1	0	0	2	0	0	0	0	0	39.61923	39.623	0.00009
C_4H_9I	2-Iodo-2-methylpropane	1	0	0	3	0	0	0	0	0	3	0	0	0	-1	51.96057	51.899	-0.00119

Table 15.50. The bond angle parameters of branched-chain alkyl iodides and experimental values [1]. In the calculation of θ_v, the parameters from the preceding angle were used. E_T is $E_T(atom - atom, msp^3.AO)$.

Atoms of Angle	2c' Bond 1 (a_0)	2c' Bond 2 (a_0)	2c' Terminal Atoms (a_0)	$E_{Coulombic}$ Atom 1	Atom 1 Hybridization Designation (Table 15.3.A)	$E_{Coulombic}$ Atom 2	Atom 2 Hybridization Designation (Table 15.3.A)	c_2 Atom 1	c_2 Atom 2	C_1	C_2	c_1	c_2'	E_T (eV)	θ_v (°)	θ_1 (°)	θ_2 (°)	Cal. θ (°)	Exp. θ (°)
$\angle IC_aI$ ($C_a - I$ (ii))	4.05092	4.05092	6.7205	-10.45126 I	I	-10.45126 I	I	1	1	1	0.65537 (Eq. (15.132))	1	1	-0.36228				112.10	
$\angle HC_aI$ ($C_a - I$ (i))	2.11106	4.03763	5.2203	-14.82575 C_a	1	-10.45126 I	I	0.91771	0.91771	0.75	0.76815 (Eq. (15.74))	0.75	1.00000	0				112.39	
$\angle HC_aH$ $\angle HC_bH$ ($C_a - I$ (i))	2.09711	2.09711	3.4252	-15.75493	7	H	H	0.86359	1	1	1	0.75	1.15796	0				109.50	111.2 (methyl iodide)
$\angle C_aC_bH_b$ ($C_a - I$ (i))															70.56			109.44	
$\angle C_bC_aI$ ($C_a - I$ (i))	2.91547	4.03763	5.7939	-15.55033 C_b	5	-10.45126 I	I	0.87495	0.87495	1	0.65537 (Eq. (15.132))	1	0.87495	-0.36228				111.86	
Methylene $\angle HC_aH$	2.11106	2.11106	3.4252	-15.75493	7	H	H	0.86359	1	1	1	0.75	1.15796	0				108.44	107 (propane)
$\angle C_aC_bC_c$															69.51			110.49	112 (propane) 113.8 (butane) 110.8 (isobutane)
$\angle C_aC_bH$															69.51			110.49	111.0 (butane) 111.4 (isobutane)
Methyl $\angle HC_aH$	2.09711	2.09711	3.4252	-15.75493	7	H	H	0.86359	1	1	1	0.75	1.15796	0				109.50	
$\angle C_aC_bC_c$															70.56			109.44	
$\angle C_aC_bH$															70.56			109.44	
$\angle C_bC_aC_c$ iso C_a	2.91547	2.91547	4.7958	-16.68412 C_b	26	-16.68412 C_c	26	0.81549	0.81549	1	1	1	0.81549	-1.85836				110.67	110.8 (isobutane)
$\angle C_bC_aH$ iso C_a	2.91547	2.11323	4.1633	-15.55033 C_a	5	-14.82575 C_b	1	0.87495	0.91771	0.75	1	0.75	1.04887	0				110.76	
$\angle C_aC_bH$ iso C_a	2.91547	2.09711	4.1633	-15.55033 C_b	5	-14.82575 C_a	1	0.87495	0.91771	0.75	1	0.75	1.04887	0				111.27	111.4 (isobutane)
$\angle C_bC_aC_b$ tert C_a	2.90327	2.90327	4.7958	-16.68412 C_b	26	-16.68412 C_b	26	0.81549	0.81549	1	1	1	0.81549	-1.85836				111.37	110.8 (isobutane)
$\angle C_bC_aC_d$															72.50			107.50	

ALKENYL HALIDES ($C_nH_{2n-m}X_m,\ n=3,4,5...\infty\ m=1,2,3...\infty$)

The branched-chain alkenyl halides, $C_nH_{2n+2-m}X_m$ with $X=F,Cl,Br,I$, may comprise alkyl and alkenyl functional groups wherein at least one H is replaced by a halogen atom. In the case that a halogen atom replaces an alkyl H, the $C-X$ bond comprises the alkyl-halogen functional groups given in their respective sections. The alkenyl halogen $C-X$ bond comprises a separate functional group for each case of X bonding to the $C=C$-bond functional group given in the Alkenes section. In addition the CH group of the moiety $XCH=C$ comprises a functional group unique to alkenyl halides. The straight and branched-chain alkenes, C_nH_{2n}, comprise at least one carbon-carbon double bond comprising a functional group that is solved equivalently to the double bond of ethylene. The double bond may be bound to one, two, three, or four carbon single bonds that substitute for the hydrogen atoms of ethylene. The three distinct functional groups given in the Alkenes section are C vinyl single bond to $-C(C)=C$, C vinyl single bond to $-C(H)=C$, and C vinyl single bond to $-C(C)=CH_2$. In addition, CH_2 of the $-C=CH_2$ moiety is also an alkene functional group solved in the Alkenes section.

Consider the case where $X=Cl$ substitutes for a carbon single bond or a hydrogen atom. Based on the condition of energy matching of the orbital, any magnetic energy due to unpaired electrons in the constituent fragments, and differences in oscillation in the transition state, two distinct $C-Cl$ functional groups can be identified: Cl vinyl single bond to $-C(C)=C$ and Cl vinyl single bond to $-C(H)=C$. The alkenyl-halide CH group is equivalent to that solved in the Hydrogen Carbide (CH) section except that $\Delta E_{H_2MO}\left(AO/HO\right)=-1.13379\ eV$ in order to energy match to the $C-Cl$ and $C=C$ bonds.

The alkyl portion of the alkenyl halide may comprise at least two terminal methyl groups (CH_3) at each end of the chain, and may comprise methylene (CH_2), and methylyne (CH) functional groups as well as C bound by carbon-carbon single bonds. The methyl and methylene functional groups are equivalent to those of straight-chain alkanes. Six types of $C-C$ bonds can be identified. The n-alkane $C-C$ bond is the same as that of straight-chain alkanes. In addition, the $C-C$ bonds within isopropyl ($\left(CH_3\right)_2CH$) and t-butyl ($\left(CH_3\right)_3C$) groups and the isopropyl to isopropyl, isopropyl to t-butyl, and t-butyl to t-butyl $C-C$ bonds comprise functional groups. The branched-chain-alkane groups in alkene halides are equivalent to those in branched-chain alkanes.

$E_T\left(atom-atom,msp^3.AO\right)$ of the $C=C$-bond MO in Eq. (15.61) due to the charge donation from the C atoms to the MO is equivalent to that of ethylene, $-2.26759\ eV$, given by Eq. (14.247). $E_T\left(atom-atom,msp^3.AO\right)$ of each $C-C$-bond MO in Eq. (15.61) is $-1.85836\ eV$ or $-1.44915\ eV$ based on the energy match between the $C2sp^3$ HOs corresponding to the energy contributions equivalent to those of methylene, $-0.92918\ eV$ (Eq. (14.513), or methyl, $-0.72457\ eV$ (Eq. (14.151)), groups, respectively.

The solution of each $C-X$ functional group comprises the hybridization of the $2s$ and $2p$ AOs of the C atom to form a single $2sp^3$ shell as an energy minimum, and the sharing of electrons between the $C2sp^3$ HO and the X AO to form a MO permits each participating orbital to decrease in radius and energy. The alkenyl $C-X$-bond functional groups comprise single bonds and are equivalent to those of the corresponding alkyl halides except that the halogen AO and the $C-X$-bond MO are each energy matched to the alkene $C2sp^3$ HO. In alkenyl halides with $X=Cl,Br,\ or\ I$, the energy of the halogen atom is less than the Coulombic energy between the electron and proton of H given by Eq. (1.264)). Thus, c_2 in Eq. (15.61) is one, and the energy matching condition is determined by the C_2 parameter. For example, the hybridization factor C_2 of Eq. (15.61) for the alkenyl $C-Cl$-bond MO given by Eq. (15.130) is $C_2\left(C2sp^3HO\ to\ \mathrm{Cl}\right)=0.81317$.

$E_T\left(atom-atom,msp^3.AO\right)$ of the alkenyl $C-Cl$-bond MO in Eq. (15.61) due to the charge donation from the C and Cl atoms to the MO is $-1.44915\ eV$ for the Cl vinyl single bond to $-C(H)=C\ \ C-Cl$ group and $-0.92918\ eV$ for the Cl vinyl single bond to $-C(C)=C\ \ C-Cl$ group. It is based on the energy match between the Cl atom and the $C2sp^3$ HO of an unsubstituted vinyl group and a substituted vinyl group given by Eqs. (14.151) and (14.513), respectively.

The symbols of the functional groups of branched-chain alkenyl chlorides are given in Table 15.51. The geometrical (Eqs. (15.1-15.5) and (15.51)), intercept (Eqs. (15.80-15.87)), and energy (Eqs. (15.6-15.11) and (15.17-15.65)) parameters of branched-chain alkenyl chlorides are given in Tables 15.52, 15.53, and 15.54, respectively. The total energy of each branched-chain alkenyl chloride given in Table 15.55 was calculated as the sum over the integer multiple of each $E_D(Group)$ of Table 15.54 corresponding to functional-group composition of the molecule. The bond angle parameters of branched-chain alkenyl chlorides determined using Eqs. (15.70-15.79), (15.88-15.117) and (15.130) are given in Table 15.56. The color scale, translucent view of the charge-density of exemplary alkenyl halide, 2-chloropropene, comprising the concentric shells of atoms with the outer shell bridged by one or more H_2-type ellipsoidal MOs or joined with one or more hydrogen MOs is shown in Figure 15.9.

Figure 15.9. Color scale, translucent view of the charge-density of 2-chloropropene showing the orbitals of the atoms at their radii, the ellipsoidal surface of each H or H_2-type ellipsoidal MO that transitions to the corresponding outer shell of the atom(s) participating in each bond, and the hydrogen nuclei (red, not to scale).

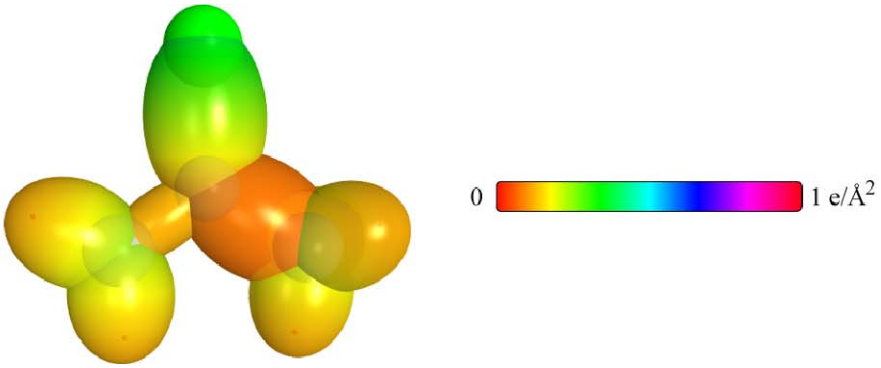

Table 15.51. The symbols of functional groups of branched-chain alkenyl chlorides.

Functional Group	Group Symbol
Cl vinyl single bond to -*C*(*H*)=*C*	$C-Cl$ (i)
Cl vinyl single bond to -*C*(*C*)=*C*	$C-Cl$ (ii)
CC double bond	$C=C$
C vinyl single bond to -*C*(*C*)=*C*	$C-C$ (i)
C vinyl single bond to -*C*(*H*)=*C*	$C-C$ (ii)
C vinyl single bond to -*C*(*C*))=CH_2	$C-C$ (iii)
CH (alkenyl halide)	$C-H$ (i)
CH_2 alkenyl group	$C-H\ (CH_2)$ (i)
CH_3 group	$C-H\ (CH_3)$
CH_2 alkyl group	$C-H\ (CH_2)$ (ii)
CH (alkyl)	$C-H$ (ii)
CC bond (*n*-*C*)	$C-C$ (a)
CC bond (*iso*-*C*)	$C-C$ (b)
CC bond (*tert*-*C*)	$C-C$ (c)
CC (*iso* to *iso*-*C*)	$C-C$ (d)
CC (*t* to *t*-*C*)	$C-C$ (e)
CC (*t* to *iso*-*C*)	$C-C$ (f)

Table 15.52. The geometrical bond parameters of branched-chain alkenyl chlorides and experimental values [1].

Parameter	$C-Cl$ (i) Group	$C-Cl$ (ii) Group	$C=C$ Group	$C-C$ (i) Group	$C-C$ (ii) Group	$C-C$ (iii) Group	$C-H\ (CH_2)$ (i) Group	$C-H$ (i) Group	$C-H\ (CH_3)$ Group	$C-H\ (CH_2)$ (ii) Group	$C-H$ (ii) Group	$C-C$ (a) Group	$C-C$ (b) Group	$C-C$ (c) Group	$C-C$ (d) Group	$C-C$ (e) Group	$C-C$ (f) Group
$a\ (a_0)$	2.15818	2.19358	1.47228	2.04740	2.04740	2.04740	1.64010	1.60061	1.64920	1.67122	1.67465	2.12499	2.12499	2.10725	2.12499	2.10725	2.10725
$c'\ (a_0)$	1.62912	1.64243	1.26661	1.43087	1.43087	1.43087	1.04566	1.03299	1.04856	1.05553	1.05661	1.45744	1.45744	1.45164	1.45744	1.45164	1.45164
Bond Length $2c'\ (\text{Å})$	1.72419	1.73827	1.34052	1.51437	1.51437	1.51437	1.10668	1.09327	1.10974	1.11713	1.11827	1.54280	1.54280	1.53635	1.54280	1.53635	1.53635
Exp. Bond Length (Å)	1.730 (vinyl chloride) 1.73 (1,1-dichloroethylene)	1.730 (vinyl chloride) 1.73 (1,1-dichloroethylene)	1.342 (2-methylpropene) 1.346 (2-butene) 1.349 (1,3-butadiene)		1.508 (2-butene)	1.508 (2-methylpropene)	1.10 (2-methylpropene) 1.108 (avg.) (1,3-butadiene)	1.09 (vinyl chloride)	1.107 ($C-H$ propane) 1.117 ($C-H$ butane)	1.107 ($C-H$ propane) 1.117 ($C-H$ butane)	1.122 (isobutane)	1.532 (propane) 1.531 (butane)	1.532 (propane) 1.531 (butane)	1.532 (propane) 1.531 (butane)	1.532 (propane) 1.531 (butane)	1.532 (propane) 1.531 (butane)	1.532 (propane) 1.531 (butane)
$b,c\ (a_0)$	1.41552	1.45403	0.75055	1.46439	1.46439	1.46439	1.26354	1.22265	1.27295	1.29569	1.29924	1.54616	1.54616	1.52750	1.54616	1.52750	1.52750
e	0.75486	0.74874	0.86030	0.69887	0.69887	0.69887	0.63756	0.64537	0.63580	0.63159	0.63095	0.68600	0.68600	0.68888	0.68600	0.68888	0.68888

Table 15.53. The MO to HO intercept geometrical bond parameters of branched-chain alkenyl chlorides. R, R', R'' are H or alkyl groups. E_T is $E_T(atom - atom, msp^3.AO)$.

Bond	Atom	E_T (eV) Bond 1	E_T (eV) Bond 2	E_T (eV) Bond 3	E_T (eV) Bond 4	Final Total Energy $C2sp^3$ (eV)	$r_{initial}$ (a_0)	r_{final} (a_0)	$E_{Coulomb}(C2sp^3)$ (eV) Final	$E(C2sp^3)$ (eV) Final	θ' (°)	θ_1 (°)	θ_2 (°)	d_1 (a_0)	d_2 (a_0)
$C_b = C_a(Cl) - H\ (CH)$ (i)	C_a	-1.34946	-0.72457	0	0	-153.47406	0.91771	0.81549	-16.68412	-16.49325	76.99	103.01	40.53	1.21653	0.18354
$-C_b = C_a(H)Cl$ $(C_a - Cl$ (i))	C_a	-1.13379	-0.72457	0	0	-153.47406	0.91771	0.81549	-16.68412	-16.49325	79.43	100.57	34.49	1.77872	0.14960
$-C_b = C_a(H)Cl$ $(C_a - Cl$ (i))	Cl	-0.72457	0	0	0		1.05158	0.87495	-15.55033		85.36	94.64	38.03	1.69995	0.07083
$-C_b = C_a(C)Cl$ $(C_a - Cl$ (ii))	C_a	1.13379	-0.46459	-0.92918	0	-154.14326	0.91771	0.78405	-17.35332	-17.16245	72.17	107.83	30.88	1.88253	0.24010
$-C_b = C_a(C)Cl$ $(C_a - Cl$ (ii))	Cl	-0.46459	0	0	0		1.05158	0.88983	-15.29034		83.62	96.38	37.46	1.74125	0.09882
$C_c(H)C_a = C_aH, C_d$	C_a	-1.13380	-0.92918	0	0	-153.67867	0.91771	0.80561	-16.88873	-16.69786	127.61	52.39	58.24	0.77492	0.49168
$C_c(H)C_a = C_bH_2$	C_b	-1.13380	0	0	0	-152.74949	0.91771	0.85252	-15.95955	-15.76868	129.84	50.16	60.70	0.72040	0.54620
$C_c(C_d)C_a = C_bH, C_e$	C_a	-1.13380	-0.72457	-0.72457	0	-154.19863	0.91771	0.78155	-17.40869	-17.21783	126.39	53.61	56.95	0.80289	0.46371
$R_1C_bH_2 - C_a(C) = C$ $(C - C$ (i))	C_a	-1.13380	-0.72457	-0.72457	0	-154.19863	0.91771	0.78155	-17.40869	-17.21783	60.88	119.12	27.79	1.81127	0.38039
$R_1C_bH_2 - C_a(C) = C$ $(C - C$ (i)) $R_1C_bH_2 - C_a(C) = CH_2$ $(C - C$ (iii))	C_b	-0.72457	-0.92918	0	0	-153.26945	0.91771	0.82562	-16.47951	-16.28864	67.40	112.60	31.36	1.74821	0.31734
$R_1C_bH_2 - C_a(H) = C$ $(C - C$ (ii))	C_a	-1.13380	-0.92918	0	0	-153.67866	0.91771	0.80561	-16.88873	-16.69786	64.57	115.43	29.79	1.77684	0.34596
$R_1C_bH_2 - C_a(H) = C$ $(C - C$ (i))	C_b	-0.92918	-0.92918	0	0	-153.47405	0.91771	0.81549	-16.68411	-16.49325	65.99	114.01	30.58	1.76270	0.33183
$C - H\ (CH_2)$ (i)	C	-1.13380	0	0	0	-152.74949	0.91771	0.85252	-15.95955	-15.76868	77.15	102.85	41.13	1.23531	0.18965
$C - H\ (CH_3)$	C	-0.92918	0	0	0	-152.54487	0.91771	0.86359	-15.75493	-15.56407	77.49	102.51	41.48	1.23564	0.18708
$C - H\ (CH_2)$ (ii)	C	-0.92918	-0.92918	0	0	-153.47406	0.91771	0.81549	-16.68412	-16.49325	68.47	111.53	35.84	1.35486	0.29933
$C - H\ (CH)$ (ii)	C	-0.92918	-0.92918	-0.92918	0	-154.40324	0.91771	0.77247	-17.61330	-17.42244	61.10	118.90	31.37	1.42988	0.37326
$H_3C_aC_bH_2CH_2 -$ $(C - C$ (a))	C_a	-0.92918	0	0	0	-152.54487	0.91771	0.86359	-15.75493	-15.56407	63.82	116.18	30.08	1.83879	0.38106
$H_3C_aC_bH_2CH_2 -$ $(C - C$ (a))	C_b	-0.92918	-0.92918	0	0	-153.47406	0.91771	0.81549	-16.68412	-16.49325	56.41	123.59	26.06	1.90890	0.45117
$R - H_2C_aC_b(H_2C_c - R')HCH_2 -$ $(C - C$ (b))	C_b	-0.92918	-0.92918	-0.92918	0	-154.40324	0.91771	0.77247	-17.61330	-17.42244	48.30	131.70	21.90	1.97162	0.51388
$R - H_2C_a(R' - H_2C_d)C_b(R'' - H_2C_c)CH_2 -$ $(C - C$ (c))	C_b	-0.92918	-0.72457	-0.72457	-0.72457	-154.71860	0.91771	0.75889	-17.92866	-17.73779	48.21	131.79	21.74	1.95734	0.50570
$isoC_aC_b(H_2C_c - R')HCH_2 -$ $(C - C$ (d))	C_b	-0.92918	-0.92918	-0.92918	0	-154.40324	0.91771	0.77247	-17.61330	-17.42244	48.30	131.70	21.90	1.97162	0.51388
$tertC_a(R' - H_2C_d)C_b(R'' - H_2C_c)CH_2 -$ $(C - C$ (e))	C_b	-0.72457	-0.72457	-0.72457	-0.72457	-154.51399	0.91771	0.76765	-17.92866	-17.73779	50.04	129.96	22.66	1.94462	0.49298
$tertC_aC_b(H_2C_c - R')HCH_2 -$ $(C - C$ (f))	C_b	-0.72457	-0.92918	-0.92918	0	-154.19863	0.91771	0.78155	-17.40869	-17.21783	52.78	127.22	24.04	1.92443	0.47279
$isoC_a(R' - H_2C_d)C_b(R'' - H_2C_c)CH_2 -$ $(C - C$ (f))	C_b	-0.72457	-0.72457	-0.72457	-0.72457	-154.51399	0.91771	0.76765	-17.92866	-17.73779	50.04	129.96	22.66	1.94462	0.49298

Table 15.54. The energy parameters (eV) of functional groups of branched-chain alkenyl chlorides.

Parameters	$C-Cl$ (i) Group	$C-Cl$ (ii) Group	$C=C$ Group	$C-C$ (i) Group	$C-C$ (ii) Group	$C-C$ (iii) Group	CH_2 (i) Group	$C-H$ (i) Group	CH_3 Group	CH_2 (ii) Group	$C-H$ (ii) Group	$C-C$ (a) Group	$C-C$ (b) Group	$C-C$ (c) Group	$C-C$ (d) Group	$C-C$ (e) Group	$C-C$ (f) Group
n_1	1	1	2	1	1	1	2	1	3	2	1	1	1	1	1	1	1
n_2	0	0	0	0	0	0	1	0	2	1	0	0	0	0	0	0	0
n_3	0	0	0	0	0	0	0	0	0	0	0	0	0	0	0	0	0
C_1	0.5	0.5	0.5	0.5	0.5	0.5	0.75	0.75	0.75	0.75	0.75	0.5	0.5	0.5	0.5	0.5	0.5
C_2	0.81317	0.81317	0.91771	1	1	1	1	1	1	1	1	1	1	1	1	1	1
c_1	1	1	1	1	1	1	1	1	1	1	1	1	1	1	1	1	1
c_2	1	1	0.91771	0.91771	0.91771	0.91771	0.91771	0.91771	0.91771	0.91771	0.91771	0.91771	0.91771	0.91771	0.91771	0.91771	0.91771
c_3	1	0	0	1	0	1	1	1	0	1	1	0	0	0	1	1	0
c_4	2	2	4	2	2	2	1	1	1	1	1	2	2	2	2	2	2
c_5	0	0	0	0	0	0	2	1	3	2	1	0	0	0	0	0	0
C_{1o}	0.5	0.5	0.5	0.5	0.5	0.5	0.75	0.75	0.75	0.75	0.75	0.5	0.5	0.5	0.5	0.5	0.5
C_{2o}	0.81317	0.81317	0.91771	1	1	1	1	1	1	1	1	1	1	1	1	1	1
V_e (eV)	-32.87721	-32.14474	-102.08992	-30.19634	-30.19634	-30.19634	-72.03287	-37.10024	-107.32728	-70.41425	-35.12015	-28.79214	-28.79214	-29.10112	-28.79214	-29.10112	-29.10112
V_p (eV)	8.35160	8.28394	21.48386	9.50874	9.50874	9.50874	26.02344	13.17125	38.92728	25.78002	12.87680	9.33352	9.33352	9.37273	9.33352	9.37273	9.37273
T (eV)	7.61688	7.32700	34.67062	7.37432	7.37432	7.37432	21.95990	11.58941	32.53914	21.06675	10.48582	6.77464	6.77464	6.90500	6.77464	6.90500	6.90500
V_m (eV)	-3.80844	-3.66350	-17.33531	-3.68716	-3.68716	-3.68716	-10.97995	-5.79470	-16.26957	-10.53337	-5.24291	-3.38732	-3.38732	-3.45250	-3.38732	-3.45250	-3.45250
$E_{(AO/HO)}$ (eV)	-14.63489	-14.63489	0	-14.63489	-14.63489	-14.63489	-14.63489	-14.63489	-15.56407	-15.56407	-14.63489	-15.56407	-15.56407	-15.35946	-15.56407	-15.35946	-15.35946
$\Delta E_{H_2MO_{(AO/HO)}}$ (eV)	-3.71674	-3.19677	0	0	0	0	0	-1.13379	0	0	0	0	0	0	0	0	0
$E_{T_{(AO/HO)}}$ (eV)	-10.91815	-10.97139	0	-14.63489	-14.63489	-14.63489	-14.63489	-13.50110	-15.56407	-15.56407	-14.63489	-15.56407	-15.56407	-15.35946	-15.56407	-15.35946	-15.35946
$E_{T_{(H_2MO)}}$ (eV)	-31.63531	-31.63541	-63.27075	-31.63534	-31.63534	-31.63534	-49.66437	-31.63539	-67.69451	-49.66493	-31.63533	-31.63537	-31.63537	-31.63535	-31.63537	-31.63535	-31.63535
$E_T\left(aiom-atom,msp^3.AO\right)$ (eV)	-1.44915	-0.92918	-2.26759	-1.44915	-1.85836	-1.44915	0	0	0	0	0	-1.85836	-1.85836	-1.44915	-1.85836	-1.44915	-1.44915
$E_{T_{(MO)}}$ (eV)	-33.08452	-32.56455	-65.53833	-33.08452	-33.49373	-33.08452	-49.66493	-31.63537	-67.69450	-49.66493	-31.63537	-33.49373	-33.49373	-33.08452	-33.49373	-33.08452	-33.08452
$\omega\ \left(10^{15}\ rad/s\right)$	8.31434	8.11389	43.0680	9.97851	16.4962	9.97851	25.2077	26.4826	24.9286	24.2751	24.1759	9.43699	9.43699	15.4846	9.43699	9.55643	9.55643
E_K (eV)	5.47264	5.34070	28.34813	6.56803	10.85807	6.56803	16.59214	17.43132	16.40846	15.97831	15.91299	6.21159	6.21159	10.19220	6.21159	6.29021	6.29021
$\bar{E}_D$ (eV)	-0.15312	-0.14888	-0.34517	-0.16774	-0.21834	-0.16774	-0.25493	-0.26130	-0.25352	-0.25017	-0.24966	-0.16515	-0.16515	-0.20896	-0.16515	-0.16416	-0.16416
$\bar{E}_{Kvib}$ (eV)	0.08059 [12]	0.08059 [12]	0.17897 [6]	0.15895 [7]	0.09931 [8]	0.09931 [8]	0.35532 Eq. (13.458)	0.35532 Eq. (13.458)	0.35532 Eq. (13.458)	0.35532 Eq. (13.458)	0.35532 Eq. (13.458)	0.12312 [2]	0.17978 [4]	0.09944 [5]	0.12312 [2]	0.12312 [2]	0.12312 [2]
$\bar{E}_{osc}$ (eV)	-0.11282	-0.10859	-0.25568	-0.08827	-0.16869	-0.11809	-0.07727	-0.08364	-0.22757	-0.14502	-0.07200	-0.10359	-0.07526	-0.15924	-0.10359	-0.10260	-0.10260
E_{mag} (eV)	0.14803	0.14803	0.14803	0.14803	0.14803	0.14803	0.14803	0.14803	0.14803	0.14803	0.14803	0.14803	0.14803	0.14803	0.14803	0.14803	0.14803
$E_{T_{(Group)}}$ (eV)	-33.19734	-32.67314	-66.04969	-33.17279	-33.66242	-33.20260	-49.81948	-31.71901	-67.92207	-49.80996	-31.70737	-33.59732	-33.49373	-33.24376	-33.59732	-33.18712	-33.18712
$E_{initial\ (c_4\ AO/HO)}$ (eV)	-14.63489	-14.63489	-14.63489	-14.63489	-14.63489	-14.63489	-14.63489	-14.63489	-14.63489	-14.63489	-14.63489	-14.63489	-14.63489	-14.63489	-14.63489	-14.63489	-14.63489
$E_{initial\ (c_5\ AO/HO)}$ (eV)	0	0	0	0	0	0	-13.59844	-13.59844	-13.59844	-13.59844	-13.59844	0	0	0	0	0	0
$E_{D_{(Group)}}$ (eV)	3.77953	3.40336	7.51014	3.75498	4.39264	3.78480	7.83968	3.33765	12.49186	7.83016	3.32601	4.32754	4.29921	3.97398	4.17951	3.62128	3.91734

Table 15.55. The total bond energies of branched-chain alkenyl chlorides calculated using the functional group composition and the energies of Table 15.54 compared to the experimental values [3].

Formula	Name	$C-Cl$ (i)	$C-Cl$ (ii)	$C=C$	$C-C$ (i)	$C-C$ (ii)	$C-C$ (iii)	CH_2 (i)	CH (i)	CH_3	CH_2 (ii)	CH (ii)	$C-C$ (a)	$C-C$ (b)	$C-C$ (c)	$C-C$ (d)	$C-C$ (e)	$C-C$ (f)	Calculated Total Bond Energy (eV)	Experimental Total Bond Energy (eV)	Relative Error
C_2H_3Cl	Chloroethene	1	0	1	0	0	0	1	1	0	0	0	0	0	0	0	0	0	22.46700	22.505	0.00170
C_3H_5Cl	2-Chloropropene	0	1	1	0	0	1	1	0	1	0	0	0	0	0	0	0	0	35.02984	35.05482	0.00071

Table 15.56. The bond angle parameters of branched-chain alkenyl chlorides and experimental values [1]. In the calculation of θ_v, the parameters from the preceding angle were used. E_T is $E_T(atom-atom,msp^3.AO)$.

Atoms of Angle	2c' Bond 1 (a_0)	2c' Bond 2 (a_0)	2c' Terminal Atoms (a_0)	$E_{Coulombic}$ Atom 1	Atom 1 Hybridization Designation (Table 15.3.A)	$E_{Coulombic}$ Atom 2	Atom 2 Hybridization Designation (Table 15.3.A)	c_2 Atom 1	c_2 Atom 2	C_1	C_2	c_1	c_2'	E_T (eV)	θ_v (°)	θ_1 (°)	θ_2 (°)	Cal. θ (°)	Exp. θ (°)
$\angle HC_aCl$ (C_a-Cl (i))	2.06598	3.25825	4.5809	-16.27490 C_a	16	-12.96764 Cl	Cl	0.83600	0.91771	0.75	0.95310 (Eq. (15.65))	0.75	1.09775	0				116.94	
$\angle C_b=C_aH$ (C_a-Cl (i))																116.94		121.53	124 (vinyl chloride)
$\angle C_b=C_aCl$ (C_a-Cl (i))																116.94		121.53	122.5 (vinyl chloride) 123.8 (1,1-dichloroethylene)
$\angle C_b=C_aCl$ (C_a-Cl (i))	2.53321	3.25825	5.1060	-15.75493 C_b	7	-12.96764 Cl	Cl	0.86359	0.86359	1	0.81317 (Eq. (15.111))	1	0.86359	-0.92918				123.19	123.8 (1,1-dichloroethylene) 122.5 (vinyl chloride)
$\angle HC_aC_c$ $(C_c(H)C_a=C_b)$	2.11323	2.86175	4.2895	-15.95955 C_a	10	-14.82575 C_c	1	0.85252	0.91771	0.75	1	0.75	1.07647	0				118.36	
$\angle C_cC_aC_c$ $(C_c(C_c)C_a=C_b)$	2.86175	2.86175	4.7958	-16.68411 C_c	25	-16.68411 C_c	25	0.81549	0.81549	1	1	1	0.81549	-1.85836				113.84	
$\angle C_bC_aC_c$ $(C_b=C_aC_c)$	2.53321	2.86175	4.7539	-16.88873 C_b	30	-16.68411 C_c	25	0.80561	0.81549	1	1	1	0.81055	-1.85836				123.46	124.4 (1,3,5-hexatriene CbCcCc) 121.7 (1,3,5-hexatriene CaCbCc) 124.4 (1,3-butadiene CCC) 125.3 (2-butene CbCaCc)
$\angle HC_aC_b$																118.36	123.46	118.19	
$\angle HC_aH$ $(H_2C_a=C_bC_c)$	2.04578	2.04578	3.4756	-15.95955	10	H	H	0.85252	1	1	1	0.75	1.17300	0				116.31	118.5 (2-methylpropene)
$\angle C_bC_aH$ $(H_2C_a=C_bC_c)$																116.31		121.85	121 (2-methylpropene)
Methylene $\angle HC_aH$	2.11106	2.11106	3.4252	-15.75493	7	H	H	0.86359	1	1	1	0.75	1.15796	0				108.44	107 (propane)
$\angle C_aC_bC_c$															69.51			110.49	112 (propane) 113.8 (butane) 110.8 (isobutane)
$\angle C_aC_bH$															69.51			110.49	111.0 (butane) 111.4 (isobutane)
Methyl $\angle HC_aH$	2.09711	2.09711	3.4252	-15.75493	7	H	H	0.86359	1	1	1	0.75	1.15796	0				109.50	
$\angle C_aC_bC_c$															70.56			109.44	
$\angle C_aC_bH$															70.56			109.44	
$\angle C_bC_aC_c$ iso C_a	2.91547	2.91547	4.7958	-16.68412 C_b	26	-16.68412 C_c	26	0.81549	0.81549	1	1	1	0.81549	-1.85836				110.67	110.8 (isobutane)
$\angle C_bC_aH$ iso C_a	2.91547	2.11323	4.1633	-15.55033 C_a	5	-14.82575 C_b	1	0.87495	0.91771	0.75	1	0.75	1.04887	0				110.76	
$\angle C_aC_bH$ iso C_a	2.91547	2.09711	4.1633	-15.55033 C_b	5	-14.82575 C_a	1	0.87495	0.91771	0.75	1	0.75	1.04887	0				111.27	111.4 (isobutane)
$\angle C_bC_aC_b$ tert C_a	2.90327	2.90327	4.7958	-16.68412 C_b	26	-16.68412 C_b	26	0.81549	0.81549	1	1	1	0.81549	-1.85836				111.37	110.8 (isobutane)
$\angle C_bC_aC_d$															72.50			107.50	

ALCOHOLS ($C_nH_{2n+2}O_m,\ n=1,2,3,4,5...\infty$)

The alkyl alcohols, $C_nH_{2n+2}O_m$, comprise an OH functional group and two types of $C-O$ functional groups, one for methyl alcohol and the other for general alkyl alcohols. The alkyl portion of the alkyl alcohol may comprise at least two terminal methyl groups (CH_3) at each end of the chain, and may comprise methylene (CH_2), and methylyne (CH) functional groups as well as C bound by carbon-carbon single bonds. The methyl and methylene functional groups are equivalent to those of straight-chain alkanes. Six types of $C-C$ bonds can be identified. The n-alkane $C-C$ bond is the same as that of straight-chain alkanes. In addition, the $C-C$ bonds within isopropyl ($(CH_3)_2CH$) and t-butyl ($(CH_3)_3C$) groups and the isopropyl to isopropyl, isopropyl to t-butyl, and t-butyl to t-butyl $C-C$ bonds comprise functional groups. The branched-chain-alkane groups in alcohols are equivalent to those in branched-chain alkanes.

The OH functional group was solved in the Hydroxyl Radical (OH) section. Each $C-O$ group is solved by hybridizing the $2s$ and $2p$ AOs of the C atom to form a single $2sp^3$ shell as an energy minimum, and the sharing of electrons between the $C2sp^3$ HO and the O AO to form a MO permits each participating orbital to decrease in radius and energy. In alkyl alcohols, the $C2sp^3$ HO has a hybridization factor of 0.91771 (Eq. (13.430)) with a corresponding energy of $E(C,2sp^3)=-14.63489\ eV$ (Eq. (15.25)) and the O AO has an energy of $E(O)=-13.61806\ eV$. To meet the equipotential condition of the union of the $C-O$ H_2-type-ellipsoidal-MO with these orbitals, the hybridization factor c_2 of Eq. (15.61) for the $C-O$-bond MO given by Eqs. (15.77) and (15.79) is:

$$c_2\left(C2sp^3HO\ to\ O\right)=\frac{E(O)}{E\left(C,2sp^3\right)}c_2\left(C2sp^3HO\right)=\frac{-13.61806\ eV}{-14.63489\ eV}(0.91771)=0.85395 \tag{15.133}$$

$E_T\left(atom-atom,msp^3.AO\right)$ of the $C-O$-bond MO in Eq. (15.61) due to the charge donation from the C and O atoms to the MO is $-1.65376\ eV$ for the CH_3-OH $C-O$ group. It is based on the energy match between the OH group and the $C2sp^3$ HO of a methyl group and is given by the linear combination of $-0.92918\ eV$ (Eq. (14.513)) and $-0.72457\ eV$ (Eq. (14.151)), respectively. For the alkyl $C-O$ group, $E_T\left(atom-atom,msp^3.AO\right)$ is $-1.85836\ eV$. It is based on the energy match between the O AO and the $C2sp^3$ HO of a methylene group where both energy contributions are given by Eq. (14.513).

The symbols of the functional groups of branched-chain alkyl alcohols are given in Table 15.66. The geometrical (Eqs. (15.1-15.5) and (15.51)), intercept (Eqs. (15.80-15.87)), and energy (Eqs. (15.6-15.11) and (15.17-15.65)) parameters of alkyl alcohols are given in Tables 15.58, 15.59, and 15.60, respectively. The total energy of each alkyl alcohol given in Table 15.61 was calculated as the sum over the integer multiple of each $E_D(Group)$ of Table 15.60 corresponding to functional-group composition of the molecule. The bond angle parameters of alkyl alcohols determined using Eqs. (15.88-15.117) are given in Table 15.62. The color scale, translucent view of the charge-density of exemplary alcohol, 1-propanol, comprising the concentric shells of atoms with the outer shell bridged by one or more H_2-type ellipsoidal MOs or joined with one or more hydrogen MOs is shown in Figure 15.10.

Figure 15.10. Color scale, translucent view of the charge-density of 1-propanol showing the orbitals of the atoms at their radii, the ellipsoidal surface of each H or H_2-type ellipsoidal MO that transitions to the corresponding outer shell of the atom(s) participating in each bond, and the hydrogen nuclei (red, not to scale). (A) Side view. (B) Front view.

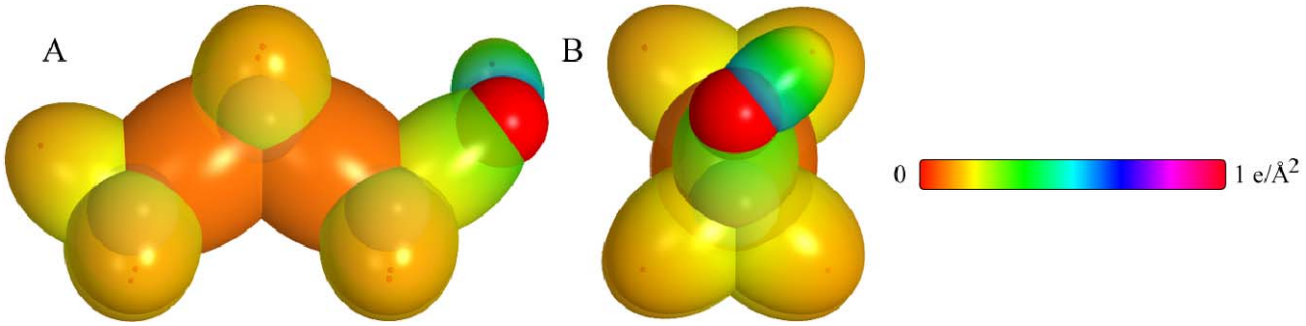

Table 15.57. The symbols of functional groups of alkyl alcohols.

Functional Group	Group Symbol
OH group	*OH*
CH_3OH *C-O*	$C-O$ (i)
Alkyl *C-O*	$C-O$ (ii)
CH_3 group	$C-H\ (CH_3)$
CH_2 group	$C-H\ (CH_2)$
CH	$C-H$
CC bond (*n-C*)	$C-C$ (a)
CC bond (*iso-C*)	$C-C$ (b)
CC bond (*tert-C*)	$C-C$ (c)
CC (*iso* to *iso-C*)	$C-C$ (d)
CC (*t* to *t-C*)	$C-C$ (e)
CC (*t* to iso-*C*)	$C-C$ (f)

Table 15.58. The geometrical bond parameters of alkyl alcohols and experimental values [1].

Parameter	OH Group	$C-O$ (i) Group	$C-O$ (ii) Group	$C-H\ (CH_3)$ Group	$C-H\ (CH_2)$ Group	$C-H$ Group	$C-C$ (a) Group	$C-C$ (b) Group	$C-C$ (c) Group	$C-C$ (d) Group	$C-C$ (e) Group	$C-C$ (f) Group
$a\ (a_0)$	1.26430	1.79473	1.78255	1.64920	1.67122	1.67465	2.12499	2.12499	2.10725	2.12499	2.10725	2.10725
$c'\ (a_0)$	0.91808	1.33968	1.33512	1.04856	1.05553	1.05661	1.45744	1.45744	1.45164	1.45744	1.45164	1.45164
Bond Length $2c'\ (\AA)$	0.971651	1.41785	1.41303	1.10974	1.11713	1.11827	1.54280	1.54280	1.53635	1.54280	1.53635	1.53635
Exp. Bond Length $(\AA)$	0.971 (ethanol) 0.9451 (methanol)	1.4246 (methanol)	1.431 (ethanol)	1.107 ($C-H$ propane) 1.117 ($C-H$ butane)	1.107 ($C-H$ propane) 1.117 ($C-H$ butane)	1.122 (isobutane)	1.532 (propane) 1.531 (butane)	1.532 (propane) 1.531 (butane)	1.532 (propane) 1.531 (butane)	1.532 (propane) 1.531 (butane)	1.532 (propane) 1.531 (butane)	1.532 (propane) 1.531 (butane)
$b,c\ (a_0)$	0.86925	1.19429	1.18107	1.27295	1.29569	1.29924	1.54616	1.54616	1.52750	1.54616	1.52750	1.52750
e	0.72615	0.74645	0.74900	0.63580	0.63159	0.63095	0.68600	0.68600	0.68888	0.68600	0.68888	0.68888

Table 15.59. The MO to HO intercept geometrical bond parameters of alkyl alcohols. R, R', R'' are H or alkyl groups. E_T is $E_T(atom-atom,msp^3.AO)$.

Bond	Atom	E_T (eV) Bond 1	E_T (eV) Bond 2	E_T (eV) Bond 3	E_T (eV) Bond 4	Final Total Energy $C2sp^3$ (eV)	$r_{initial}\ (a_0)$	$r_{final}\ (a_0)$	$E_{Coulomb}$ (eV) Final	$E(C2sp^3)$ (eV) Final	θ' (°)	θ_1 (°)	θ_2 (°)	$d_1\ (a_0)$	$d_2\ (a_0)$
H_3CO-H	O	-0.82688	0	0	0		1.00000	0.86923	-15.65263		115.49	64.51	64.51	0.54405	0.37403
$-H_2C_aO-H$	O	-0.92918	0	0	0		1.00000	0.86359	-15.75493		115.09	64.91	64.12	0.55182	0.36625
H_3C-OH ($C-O$ (i))	C	-0.82688	0	0	0	-152.44257	0.91771	0.86923	-15.65263	-15.46177	96.59	83.41	46.30	1.23986	0.09981
H_3C-OH ($C-O$ (i))	O	-0.82688	0	0	0		1.00000	0.86923	-15.65263		96.59	83.41	46.30	1.23986	0.09981
$-H_2C_a-OH$ ($C-O$ (ii))	C_a	-0.92918	-0.92918	0	0	-153.47405	0.91771	0.81549	-16.68411	-16.49325	93.09	86.91	43.59	1.29114	0.04398
$-H_2C_a-OH$ ($C-O$ (ii))	O	-0.92918	0	0	0		1.00000	0.86359	-15.75493		97.20	82.80	46.50	1.22692	0.10820
$C-H\ (CH_3)$	C	-0.92918	0	0	0	-152.54487	0.91771	0.86359	-15.75493	-15.56407	77.49	102.51	41.48	1.23564	0.18708
$C-H\ (CH_2)$	C	-0.92918	-0.92918	0	0	-153.47406	0.91771	0.81549	-16.68412	-16.49325	68.47	111.53	35.84	1.35486	0.29933
$C-H\ (CH)$	C	-0.92918	-0.92918	-0.92918	0	-154.40324	0.91771	0.77247	-17.61330	-17.42244	61.10	118.90	31.37	1.42988	0.37326
$H_3C_aC_bH_2CH_2-$ ($C-C$ (a))	C_a	-0.92918	0	0	0	-152.54487	0.91771	0.86359	-15.75493	-15.56407	63.82	116.18	30.08	1.83879	0.38106
$H_3C_aC_bH_2CH_2-$ ($C-C$ (a))	C_b	-0.92918	-0.92918	0	0	-153.47406	0.91771	0.81549	-16.68412	-16.49325	56.41	123.59	26.06	1.90890	0.45117
$R-H_2C_aC_b(H_2C_c-R')HCH_2-$ ($C-C$ (b))	C_b	-0.92918	-0.92918	-0.92918	0	-154.40324	0.91771	0.77247	-17.61330	-17.42244	48.30	131.70	21.90	1.97162	0.51388
$R-H_2C_a(R'-H_2C_d)C_b(R''-H_2C_c)CH_2-$ ($C-C$ (c))	C_b	-0.92918	-0.72457	-0.72457	-0.72457	-154.71860	0.91771	0.75889	-17.92866	-17.73779	48.21	131.79	21.74	1.95734	0.50570
$isoC_aC_b(H_2C_c-R')HCH_2-$ ($C-C$ (d))	C_b	-0.92918	-0.92918	-0.92918	0	-154.40324	0.91771	0.77247	-17.61330	-17.42244	48.30	131.70	21.90	1.97162	0.51388
$tertC_a(R'-H_2C_d)C_b(R''-H_2C_c)CH_2-$ ($C-C$ (e))	C_b	-0.72457	-0.72457	-0.72457	-0.72457	-154.51399	0.91771	0.76765	-17.92866	-17.73779	50.04	129.96	22.66	1.94462	0.49298
$tertC_aC_b(H_2C_c-R')HCH_2-$ ($C-C$ (f))	C_b	-0.72457	-0.92918	-0.92918	0	-154.19863	0.91771	0.78155	-17.40869	-17.21783	52.78	127.22	24.04	1.92443	0.47279
$isoC_a(R'-H_2C_d)C_b(R''-H_2C_c)CH_2-$ ($C-C$ (f))	C_b	-0.72457	-0.72457	-0.72457	-0.72457	-154.51399	0.91771	0.76765	-17.92866	-17.73779	50.04	129.96	22.66	1.94462	0.49298

Table 15.60. The energy parameters (eV) of functional groups of alkyl alcohols.

Parameters	OH Group	$C-O$ (i) Group	$C-O$ (ii) Group	CH_3 Group	CH_2 Group	$C-H$ Group	$C-C$ (a) Group	$C-C$ (b) Group	$C-C$ (c) Group	$C-C$ (d) Group	$C-C$ (e) Group	$C-C$ (f) Group
n_1	1	1	1	3	2	1	1	1	1	1	1	1
n_2	0	0	0	2	1	0	0	0	0	0	0	0
n_3	0	0	0	0	0	0	0	0	0	0	0	0
C_1	0.75	0.5	0.5	0.75	0.75	0.75	0.5	0.5	0.5	0.5	0.5	0.5
C_2	1	1	1	1	1	1	1	1	1	1	1	1
c_1	0.75	1	1	1	1	1	1	1	1	1	1	1
c_2	1	0.85395	0.85395	0.91771	0.91771	0.91771	0.91771	0.91771	0.91771	0.91771	0.91771	0.91771
c_3	1	0	0	0	1	1	0	0	0	1	1	0
c_4	1	2	2	1	1	1	2	2	2	2	2	2
c_5	1	0	0	3	2	1	0	0	0	0	0	0
C_{1o}	0.75	0.5	0.5	0.75	0.75	0.75	0.5	0.5	0.5	0.5	0.5	0.5
C_{2o}	1	1	1	1	1	1	1	1	1	1	1	1
V_e (eV)	-40.92709	-33.47304	-33.78820	-107.32728	-70.41425	-35.12015	-28.79214	-28.79214	-29.10112	-28.79214	-29.10112	-29.10112
V_p (eV)	14.81988	10.15605	10.19068	38.92728	25.78002	12.87680	9.33352	9.33352	9.37273	9.33352	9.37273	9.37273
T (eV)	16.18567	9.32537	9.47749	32.53914	21.06675	10.48582	6.77464	6.77464	6.90500	6.77464	6.90500	6.90500
V_m (eV)	-8.09284	-4.66268	-4.73874	-16.26957	-10.53337	-5.24291	-3.38732	-3.38732	-3.45250	-3.38732	-3.45250	-3.45250
$E_{(AO/HO)}$ (eV)	-13.6181	-14.63489	-14.63489	-15.56407	-15.56407	-14.63489	-15.56407	-15.56407	-15.35946	-15.56407	-15.35946	-15.35946
$\Delta E_{H_2MO(AO/HO)}$ (eV)	0	-1.65376	-1.85836	0	0	0	0	0	0	0	0	0
$E_T(_{AO/HO})$ (eV)	-13.6181	-12.98113	-12.77653	-15.56407	-15.56407	-14.63489	-15.56407	-15.56407	-15.35946	-15.56407	-15.35946	-15.35946
$E_T(_{H_2MO})$ (eV)	-31.63247	-31.63544	-31.63529	-67.69451	-49.66493	-31.63533	-31.63537	-31.63537	-31.63535	-31.63537	-31.63535	-31.63535
$E_T\left(atom-atom, msp^3.AO\right)(eV)$	0	-1.65376	-1.85836	0	0	0	-1.85836	-1.85836	-1.44915	-1.85836	-1.44915	-1.44915
$E_T(_{MO})$ (eV)	-31.63537	-33.28912	-33.49373	-67.69450	-49.66493	-31.63537	-33.49373	-33.49373	-33.08452	-33.49373	-33.08452	-33.08452
$\omega\left(10^{15}\ rad/s\right)$	44.1776	22.3978	12.2831	24.9286	24.2751	24.1759	9.43699	9.43699	15.4846	9.43699	9.55643	9.55643
E_K (eV)	29.07844	14.74264	8.08494	16.40846	15.97831	15.91299	6.21159	6.21159	10.19220	6.21159	6.29021	6.29021
$\bar{E}_D$ (eV)	-0.33749	-0.25287	-0.18841	-0.25352	-0.25017	-0.24966	-0.16515	-0.16515	-0.20896	-0.16515	-0.16416	-0.16416
$\bar{E}_{Kvib}$ (eV)	0.46311 [17-18]	0.12808 [19]	0.13328 [20]	0.35532 (Eq. (13.458))	0.35532 (Eq. (13.458))	0.35532 (Eq. (13.458))	0.12312 [2]	0.17978 [4]	0.09944 [5]	0.12312 [2]	0.12312 [2]	0.12312 [2]
$\bar{E}_{osc}$ (eV)	-0.10594	-0.18883	-0.12177	-0.22757	-0.14502	-0.07200	-0.10359	-0.07526	-0.15924	-0.10359	-0.10260	-0.10260
E_{mag} (eV)	0.11441	0.14803	0.14803	0.14803	0.14803	0.14803	0.14803	0.14803	0.14803	0.14803	0.14803	0.14803
$E_T(_{Group})$ (eV)	-31.74130	-33.47795	-33.61550	-67.92207	-49.80996	-31.70737	-33.59732	-33.49373	-33.24376	-33.59732	-33.18712	-33.18712
$E_{initial}(_{c_4\ AO/HO})$ (eV)	-13.6181	-14.63489	-14.63489	-14.63489	-14.63489	-14.63489	-14.63489	-14.63489	-14.63489	-14.63489	-14.63489	-14.63489
$E_{initial}(_{c_5\ AO/HO})$ (eV)	-13.59844	0	0	-13.59844	-13.59844	-13.59844	0	0	0	0	0	0
$E_D(_{Group})$ (eV)	4.41035	4.20817	4.34572	12.49186	7.83016	3.32601	4.32754	4.29921	3.97398	4.17951	3.62128	3.91734

Table 15.61. The total bond energies of alkyl alcohols calculated using the functional group composition and the energies of Table 15.60 compared to the experimental values [3].

Formula	Name	*OH* Group	*C – O* (i) Group	*C – O* (ii) Group	CH_3	CH_2	*CH*	*C – C* (a)	*C – C* (b)	*C – C* (c)	*C – C* (d)	*C – C* (e)	*C – C* (f)	Calculated Total Bond Energy (eV)	Experimental Total Bond Energy (eV)	Relative Error
CH_4O	Methanol	1	0	1	1	0	0	0	0	0	0	0	0	21.11038	21.131	0.00097
C_2H_6O	Ethanol	1	0	1	1	1	0	1	0	0	0	0	0	33.40563	33.428	0.00066
C_3H_8O	1-Propanol	1	0	1	1	2	0	2	0	0	0	0	0	45.56333	45.584	0.00046
C_3H_8O	2-Propanol	1	0	1	2	0	1	2	0	0	0	0	0	45.72088	45.766	0.00098
$C_4H_{10}O$	1-Butanol	1	0	1	1	3	0	3	0	0	0	0	0	57.72103	57.736	0.00026
$C_4H_{10}O$	2-Butanol	1	0	1	2	1	1	3	0	0	0	0	0	57.87858	57.922	0.00074
$C_4H_{10}O$	2-Methyl-1-propananol	1	0	1	2	1	1	0	3	0	0	0	0	57.79359	57.828	0.00060
$C_4H_{10}O$	2-Methyl-2-propananol	1	0	1	3	0	0	0	0	3	0	0	0	58.15359	58.126	-0.00048
$C_5H_{12}O$	1-Pentanol	1	0	1	1	4	0	4	0	0	0	0	0	69.87873	69.887	0.00011
$C_5H_{12}O$	2-Pentanol	1	0	1	2	2	1	4	0	0	0	0	0	70.03628	70.057	0.00029
$C_5H_{12}O$	3-Pentanol	1	0	1	2	2	1	2	2	0	0	0	0	69.97962	70.097	0.00168
$C_5H_{12}O$	2-Methyl-1-butananol	1	0	1	2	2	1	1	3	0	0	0	0	69.95129	69.957	0.00008
$C_5H_{12}O$	3-Methyl-1-butananol	1	0	1	2	2	1	1	3	0	0	0	0	69.95129	69.950	-0.00002
$C_5H_{12}O$	2-Methyl-2-butananol	1	0	1	3	1	0	1	0	3	0	0	0	70.31129	70.246	-0.00092
$C_5H_{12}O$	3-Methyl-2-butananol	1	0	1	3	0	2	0	3	0	1	0	0	69.96081	70.083	0.00174
$C_6H_{14}O$	1-Hexanol	1	0	1	1	5	0	5	0	0	0	0	0	82.03643	82.054	0.00021
$C_6H_{14}O$	2-Hexanol	1	0	1	2	3	1	5	0	0	0	0	0	82.19398	82.236	0.00052
$C_7H_{15}O$	1-Heptanol	1	0	1	1	6	0	6	0	0	0	0	0	94.19413	94.214	0.00021
$C_8H_{18}O$	1-Octanol	1	0	1	1	7	0	7	0	0	0	0	0	106.35183	106.358	0.00006
$C_8H_{18}O$	2-Ethyl-1-hexananol	1	0	1	2	5	1	4	3	0	0	0	0	106.42439	106.459	0.00032
$C_9H_{20}O$	1-Nonanol	1	0	1	1	8	0	8	0	0	0	0	0	118.50953	118.521	0.00010
$C_{10}H_{22}O$	1-Decanol	1	0	1	1	9	0	9	0	0	0	0	0	130.66723	130.676	0.00007
$C_{12}H_{26}O$	1-Dodecanol	1	0	1	1	11	0	11	0	0	0	0	0	154.98263	154.984	0.00001
$C_{16}H_{34}O$	1-Hexadecanol	1	0	1	1	15	0	15	0	0	0	0	0	203.61343	203.603	-0.00005

Table 15.62. The bond angle parameters of alkyl alcohols and experimental values [1]. In the calculation of θ_V, the parameters from the preceding angle were used. E_T is $E_T(atom-atom,msp^3.AO)$.

Atoms of Angle	2c' Bond 1 (a_0)	2c' Bond 2 (a_0)	2c' Terminal Atoms (a_0)	$E_{Coulombic}$ Atom 1	Atom 1 Hybridization Designation (Table 15.3.A)	$E_{Coulombic}$ Atom 2	Atom 2 Hybridization Designation (Table 15.3.A)	c_2 Atom 1	c_2 Atom 2	C_1	C_2	c_1	c_2'	E_T (eV)	θ_v (°)	θ_1 (°)	θ_2 (°)	Cal. θ (°)	Exp. θ (°)
$\angle C_aOH$ (C_a-O (i))	2.67935	1.83616	3.6697	-14.82575	1	-14.82575	1	1	0.91771	0.75	1	0.75	0.91771	0				107.24	108.53 (methanol)
$\angle C_aOH$ (C_a-O (ii))	2.67024	1.83616	3.6515	-14.82575	1	-14.82575	1	1	0.91771	0.75	1	0.75	0.91771	0				106.78	105 (ethanol)
$\angle C_bC_aO$ (C_a-O (ii))	2.91547	2.67024	4.5826	-16.68412	26	-13.61806	O	0.81549	0.85395 (Eq. (15.114))	1	1	1	0.83472	-1.65376				110.17	107.8 (ethanol)
Methylene $\angle HC_aH$	2.11106	2.11106	3.4252	-15.75493	7	H	H	0.86359	1	1	1	0.75	1.15796	0				108.44	107 (propane)
$\angle C_aC_bC_c$															69.51			110.49	112 (propane) 113.8 (butane) 110.8 (isobutane)
$\angle C_aC_bH$															69.51			110.49	111.0 (butane) 111.4 (isobutane)
Methyl $\angle HC_aH$	2.09711	2.09711	3.4252	-15.75493	7	H	H	0.86359	1	1	1	0.75	1.15796	0				109.50	
$\angle C_aC_bC_c$															70.56			109.44	
$\angle C_aC_bH$															70.56			109.44	
$\angle C_bC_aC_c$ iso C_a	2.91547	2.91547	4.7958	-16.68412 C_b	26	-16.68412 C_c	26	0.81549	0.81549	1	1	1	0.81549	-1.85836				110.67	110.8 (isobutane)
$\angle C_bC_aH$ iso C_a	2.91547	2.11323	4.1633	-15.55033 C_a	5	-14.82575 C_b	1	0.87495	0.91771	0.75	1	0.75	1.04887	0				110.76	
$\angle C_aC_bH$ iso C_a	2.91547	2.09711	4.1633	-15.55033 C_b	5	-14.82575 C_a	1	0.87495	0.91771	0.75	1	0.75	1.04887	0				111.27	111.4 (isobutane)
$\angle C_bC_aC_b$ tert C_a	2.90327	2.90327	4.7958	-16.68412 C_b	26	-16.68412 C_b	26	0.81549	0.81549	1	1	1	0.81549	-1.85836				111.37	110.8 (isobutane)
$\angle C_bC_aC_d$															72.50			107.50	

ETHERS ($C_nH_{2n+2}O_m,\ n=2,3,4,5...\infty$)

The alkyl ethers, $C_nH_{2n+2}O_m$, comprise two types of $C-O$ functional groups, one for methyl or t-butyl groups corresponding to the C and the other for general alkyl groups. The alkyl portion of the alkyl ether may comprise at least two terminal methyl groups (CH_3) at each end of the chain, and may comprise methylene (CH_2), and methylyne (CH) functional groups as well as C bound by carbon-carbon single bonds. The methyl and methylene functional groups are equivalent to those of straight-chain alkanes. Six types of $C-C$ bonds can be identified. The n-alkane $C-C$ bond is the same as that of straight-chain alkanes. In addition, the $C-C$ bonds within isopropyl ($(CH_3)_2CH$) and t-butyl ($(CH_3)_3C$) groups and the isopropyl to isopropyl, isopropyl to t-butyl, and t-butyl to t-butyl $C-C$ bonds comprise functional groups. The branched-chain-alkane groups in ethers are equivalent to those in branched-chain alkanes.

Each $C-O$ group is solved by hybridizing the $2s$ and $2p$ AOs of the C atom to form a single $2sp^3$ shell as an energy minimum, and the sharing of electrons between the $C2sp^3$ HO and the O AO to form a MO permits each participating orbital to decrease in radius and energy. In alkyl ethers, the $C2sp^3$ HO has a hybridization factor of 0.91771 (Eq. (13.430)) and an energy of $E(C,2sp^3)=-14.63489\,eV$ (Eq. (15.25)) and the O AO has an energy of $E(O)=-13.61806\,eV$. To meet the equipotential condition of the union of the $C-O$ H_2-type-ellipsoidal-MO with these orbitals, the hybridization factor c_2 of Eq. (15.61) for the $C-O$-bond MO given by Eq. (15.133) is $c_2(C2sp^3HO\ to\ O)=0.85395$. $E_T(atom-atom,msp^3.AO)$ of the $C-O$-bond MO in Eq. (15.52) due to the charge donation from the C and O atoms to the MO is $-1.44915\,eV$ for the CH_3-O- and $(CH_3)_3C-O-$ $C-O$ groups. It is based on the energy match between the O AO, initially at the Coulomb potential of a proton and an electron (Eqs. (1.257) and (10.162), respectively), and the $C2sp^3$ HO of a methyl group as given by Eq. (14.151). For the alkyl $C-O$ group, $E_T(atom-atom,msp^3.AO)$ is $-1.65376\,eV$. It is based on the energy match between the O AO and the $C2sp^3$ HO of a methylene group and is given by the linear combination of $-0.72457\,eV$ (Eq. (14.151)) and $-0.92918\,eV$ (Eq. (14.513)), respectively.

The symbols of the functional groups of branched-chain alkyl ethers are given in Table 15.63. The geometrical (Eqs. (15.1-15.5) and (15.51)), intercept (Eqs. (15.80-15.87)), and energy (Eqs. (15.6-15.11) and (15.17-15.65)) parameters of alkyl ethers are given in Tables 15.64, 15.65, and 15.66, respectively. The total energy of each alkyl ether given in Table 15.67 was calculated as the sum over the integer multiple of each $E_{D(Group)}$ of Table 15.66 corresponding to functional-group composition of the molecule. The bond angle parameters of alkyl ethers determined using Eqs. (15.88-15.117) are given in Table 15.68. The color scale, translucent view of the charge-density of exemplary ether, diethyl ether, comprising the concentric shells of atoms with the outer shell bridged by one or more H_2-type ellipsoidal MOs or joined with one or more hydrogen MOs is shown in Figure 15.11.

Figure 15.11. Color scale, translucent view of the charge-density of diethyl ether showing the orbitals of the atoms at their radii, the ellipsoidal surface of each H or H_2-type ellipsoidal MO that transitions to the corresponding outer shell of the atom(s) participating in each bond, and the hydrogen nuclei (red, not to scale). (A) Oblique view. (B) View along the nitrogen atom.

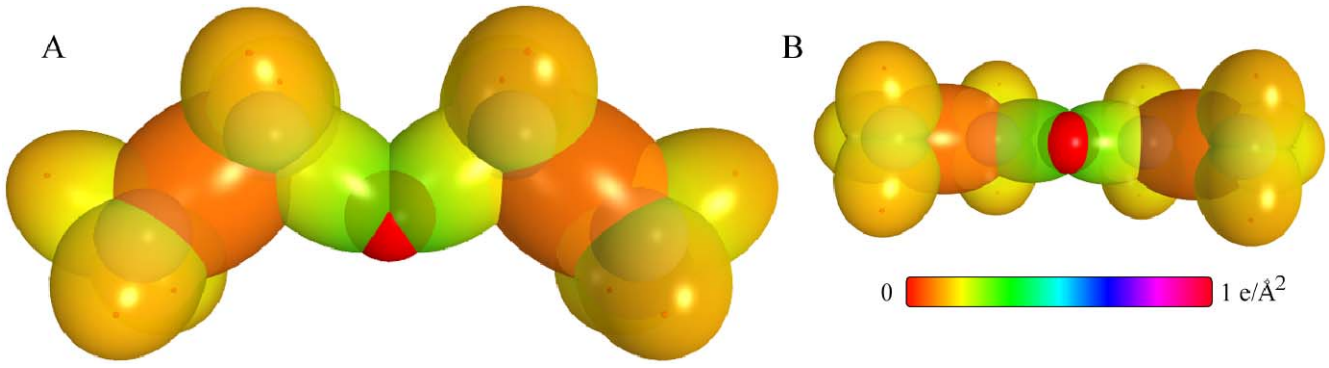

Table 15.63. The symbols of functional groups of alkyl ethers.

Functional Group	Group Symbol
C-*O* (CH_3-O- and $(CH_3)_3C-O-$)	$C-O$ (i)
C-*O* (alkyl)	$C-O$ (ii)
CH_3 group	$C-H\ (CH_3)$
CH_2 group	$C-H\ (CH_2)$
CH	$C-H$
CC bond (*n*-*C*)	$C-C$ (a)
CC bond (*iso*-*C*)	$C-C$ (b)
CC bond (*tert*-*C*)	$C-C$ (c)
CC (*iso to iso*-*C*)	$C-C$ (d)
CC (*t* to *t*-*C*)	$C-C$ (e)
CC (*t* to *iso*-*C*)	$C-C$ (f)

Table 15.64. The geometrical bond parameters of alkyl ethers and experimental values [1].

Parameter	$C-O$ (i) Group	$C-O$ (ii) Group	$C-H\ (CH_3)$ Group	$C-H\ (CH_2)$ Group	$C-H$ Group	$C-C$ (a) Group	$C-C$ (b) Group	$C-C$ (c) Group	$C-C$ (d) Group	$C-C$ (e) Group	$C-C$ (f) Group
$a\ (a_0)$	1.80717	1.79473	1.64920	1.67122	1.67465	2.12499	2.12499	2.10725	2.12499	2.10725	2.10725
$c'\ (a_0)$	1.34431	1.33968	1.04856	1.05553	1.05661	1.45744	1.45744	1.45164	1.45744	1.45164	1.45164
Bond Length $2c'\ (A)$	1.42276	1.41785	1.10974	1.11713	1.11827	1.54280	1.54280	1.53635	1.54280	1.53635	1.53635
Exp. Bond Length (A)	1.416 (dimethyl ether)	1.418 (ethyl methyl ether (avg.))	1.107 ($C-H$ propane) 1.117 ($C-H$ butane)	1.107 ($C-H$ propane) 1.117 ($C-H$ butane)	1.122 (isobutane)	1.532 (propane) 1.531 (butane)	1.532 (propane) 1.531 (butane)	1.532 (propane) 1.531 (butane)	1.532 (propane) 1.531 (butane)	1.532 (propane) 1.531 (butane)	1.532 (propane) 1.531 (butane)
$b,c\ (a_0)$	1.20776	1.19429	1.27295	1.29569	1.29924	1.54616	1.54616	1.52750	1.54616	1.52750	1.52750
e	0.74388	0.74645	0.63580	0.63159	0.63095	0.68600	0.68600	0.68888	0.68600	0.68888	0.68888

Table 15.65. The MO to HO intercept geometrical bond parameters of alkyl ethers. R, R', R'' are H or alkyl groups. E_T is $E_T(atom - atom, msp^3.AO)$.

Bond	Atom	E_T (eV) Bond 1	E_T (eV) Bond 2	E_T (eV) Bond 3	E_T (eV) Bond 4	Final Total Energy $C2sp^3$ (eV)	$r_{initial}$ (a_0)	r_{final} (a_0)	$E_{Coulomb}$ (eV) Final	$E(C2sp^3)$ (eV) Final	θ' (°)	θ_1 (°)	θ_2 (°)	d_1 (a_0)	d_2 (a_0)
$C-H\ (OC_aH_3)$	C_a	-0.72457	0	0	0	-152.34026	0.91771	0.87495	-15.55033	-15.35946	78.85	101.15	42.40	1.21777	0.16921
$H_3C_a-O-C_aH_3$ $(CH_3)_3C_a-O-C_bH_3$ $(CH_3)_3C_a-O-C_a(CH_3)_3$ $(C-O$ (i))	$C_{a,b}$	-0.72457	0	0	0	-152.34026	0.91771	0.87495	-15.55033	-15.35946	95.98	84.02	46.10	1.25319	0.09112
$H_3C_a-O-C_aH_3$ $(CH_3)_3C_a-O-C_bH_3$ $(CH_3)_3C_a-O-C_a(CH_3)_3$ $(C-O$ (i))	O	-0.72457	-0.72457	0	0		1.00000	0.83600	-16.27490		92.66	87.34	43.74	1.30555	0.03876
$-H_2C_a-OC_b(CH_3)_3$ $-H_2C_a-OC_bH_3$ $(C-O$ (ii))	C_a	-0.82688	-0.92918	0	0	-153.37175	0.91771	0.82053	-16.58181	-16.39095	92.41	87.59	43.35	1.30512	0.03456
$-H_2C_a-OC_b(CH_3)_3$ $-H_2C_a-OC_bH_3$ $(C-O$ (ii))	O	-0.72457	-0.82688	0	0		1.00000	0.83078	-16.37720		93.33	86.67	43.98	1.29138	0.04829
$-H_2C_a-O-H_2C_a-$ $(C-O$ (ii))	O	-0.82688	-0.82688	0	0		1.00000	0.82562	-16.47951		92.87	87.13	43.66	1.29829	0.04138
$C-H\ (CH_3)$	C	-0.92918	0	0	0	-152.54487	0.91771	0.86359	-15.75493	-15.56407	77.49	102.51	41.48	1.23564	0.18708
$C-H\ (CH_2)$	C	-0.92918	-0.92918	0	0	-153.47406	0.91771	0.81549	-16.68412	-16.49325	68.47	111.53	35.84	1.35486	0.29933
$C-H\ (CH)$	C	-0.92918	-0.92918	-0.92918	0	-154.40324	0.91771	0.77247	-17.61330	-17.42244	61.10	118.90	31.37	1.42988	0.37326
$H_3C_aC_bH_2CH_2-$ $(C-C$ (a))	C_a	-0.92918	0	0	0	-152.54487	0.91771	0.86359	-15.75493	-15.56407	63.82	116.18	30.08	1.83879	0.38106
$H_3C_aC_bH_2CH_2-$ $(C-C$ (a))	C_b	-0.92918	-0.92918	0	0	-153.47406	0.91771	0.81549	-16.68412	-16.49325	56.41	123.59	26.06	1.90890	0.45117
$R-H_2C_aC_b(H_2C_c-R')HCH_2-$ $(C-C$ (b))	C_b	-0.92918	-0.92918	-0.92918	0	-154.40324	0.91771	0.77247	-17.61330	-17.42244	48.30	131.70	21.90	1.97162	0.51388
$R-H_2C_a(R'-H_2C_d)C_b(R''-H_2C_c)CH_2-$ $(C-C$ (c))	C_b	-0.92918	-0.72457	-0.72457	-0.72457	-154.71860	0.91771	0.75889	-17.92866	-17.73779	48.21	131.79	21.74	1.95734	0.50570
$isoC_aC_b(H_2C_c-R')HCH_2-$ $(C-C$ (d))	C_b	-0.92918	-0.92918	-0.92918	0	-154.40324	0.91771	0.77247	-17.61330	-17.42244	48.30	131.70	21.90	1.97162	0.51388
$tertC_a(R'-H_2C_d)C_b(R''-H_2C_c)CH_2-$ $(C-C$ (e))	C_b	-0.72457	-0.72457	-0.72457	-0.72457	-154.51399	0.91771	0.76765	-17.92866	-17.73779	50.04	129.96	22.66	1.94462	0.49298
$tertC_aC_b(H_2C_c-R')HCH_2-$ $(C-C$ (f))	C_b	-0.72457	-0.92918	-0.92918	0	-154.19863	0.91771	0.78155	-17.40869	-17.21783	52.78	127.22	24.04	1.92443	0.47279
$isoC_a(R'-H_2C_d)C_b(R''-H_2C_c)CH_2-$ $(C-C$ (f))	C_b	-0.72457	-0.72457	-0.72457	-0.72457	-154.51399	0.91771	0.76765	-17.92866	-17.73779	50.04	129.96	22.66	1.94462	0.49298

Table 15.66. The energy parameters (eV) of functional groups of alkyl ethers.

Parameters	$C-O$ (i) Group	$C-O$ (ii) Group	CH_3 Group	CH_2 Group	$C-H$ Group	$C-C$ (a) Group	$C-C$ (b) Group	$C-C$ (c) Group	$C-C$ (d) Group	$C-C$ (e) Group	$C-C$ (f) Group
n_1	1	1	3	2	1	1	1	1	1	1	1
n_2	0	0	2	1	0	0	0	0	0	0	0
n_3	0	0	0	0	0	0	0	0	0	0	0
C_1	0.5	0.5	0.75	0.75	0.75	0.5	0.5	0.5	0.5	0.5	0.5
C_2	1	1	1	1	1	1	1	1	1	1	1
c_1	1	1	1	1	1	1	1	1	1	1	1
c_2	0.85395	0.85395	0.91771	0.91771	0.91771	0.91771	0.91771	0.91771	0.91771	0.91771	0.91771
c_3	0	0	0	1	1	0	0	0	1	1	0
c_4	2	2	1	1	1	2	2	2	2	2	2
c_5	0	0	3	2	1	0	0	0	0	0	0
C_{1o}	0.5	0.5	0.75	0.75	0.75	0.5	0.5	0.5	0.5	0.5	0.5
C_{2o}	1	1	1	1	1	1	1	1	1	1	1
V_e (eV)	-33.15757	-33.47304	-107.32728	-70.41425	-35.12015	-28.79214	-28.79214	-29.10112	-28.79214	-29.10112	-29.10112
V_p (eV)	10.12103	10.15605	38.92728	25.78002	12.87680	9.33352	9.33352	9.37273	9.33352	9.37273	9.37273
T (eV)	9.17389	9.32537	32.53914	21.06675	10.48582	6.77464	6.77464	6.90500	6.77464	6.90500	6.90500
V_m (eV)	-4.58695	-4.66268	-16.26957	-10.53337	-5.24291	-3.38732	-3.38732	-3.45250	-3.38732	-3.45250	-3.45250
$E_{(AO/HO)}$ (eV)	-14.63489	-14.63489	-15.56407	-15.56407	-14.63489	-15.56407	-15.56407	-15.35946	-15.56407	-15.35946	-15.35946
$\Delta E_{H_2sAO(AO/HO)}$ (eV)	-1.44915	-1.65376	0	0	0	0	0	0	0	0	0
$E_J{}_{(AO/HO)}$ (eV)	-13.18574	-12.98113	-15.56407	-15.56407	-14.63489	-15.56407	-15.56407	-15.35946	-15.56407	-15.35946	-15.35946
$E_J{}_{(H_2MO)}$ (eV)	-31.63533	-31.63544	-67.69451	-49.66493	-31.63533	-31.63537	-31.63537	-31.63535	-31.63537	-31.63535	-31.63535
$E_J\left(atom-atom, msp^3.AO\right)(eV)$	-1.44915	-1.65376	0	0	0	-1.85836	-1.85836	-1.44915	-1.85836	-1.44915	-1.44915
$E_J{}_{(MO)}$ (eV)	-33.08452	-33.28912	-67.69450	-49.66493	-31.63537	-33.49373	-33.49373	-33.08452	-33.49373	-33.08452	-33.08452
$\omega\ \left(10^{15}\ rad/s\right)$	12.0329	12.1583	24.9286	24.2751	24.1759	9.43699	9.43699	15.4846	9.43699	9.55643	9.55643
E_K (eV)	7.92028	8.00277	16.40846	15.97831	15.91299	6.21159	6.21159	10.19220	6.21159	6.29021	6.29021
$\bar{E}_D$ (eV)	-0.18420	-0.18631	-0.25352	-0.25017	-0.24966	-0.16515	-0.16515	-0.20896	-0.16515	-0.16416	-0.16416
$\bar{E}_{Kvib}$ (eV)	0.13663 [21]	0.16118 [4]	0.35532 (Eq. (13.458))	0.35532 (Eq. (13.458))	0.35532 (Eq. (13.458))	0.12312 [2]	0.17978 [4]	0.09944 [5]	0.12312 [2]	0.12312 [2]	0.12312 [2]
$\bar{E}_{osc}$ (eV)	-0.11589	-0.10572	-0.22757	-0.14502	-0.07200	-0.10359	-0.07526	-0.15924	-0.10359	-0.10260	-0.10260
E_{mag} (eV)	0.14803	0.14803	0.14803	0.14803	0.14803	0.14803	0.14803	0.14803	0.14803	0.14803	0.14803
$E_J{}_{(Group)}$ (eV)	-33.20040	-33.39484	-67.92207	-49.80996	-31.70737	-33.59732	-33.49373	-33.24376	-33.59732	-33.18712	-33.18712
$E_{initial(\varepsilon_4\ AO/HO)}$ (eV)	-14.63489	-14.63489	-14.63489	-14.63489	-14.63489	-14.63489	-14.63489	-14.63489	-14.63489	-14.63489	-14.63489
$E_{initial(\varepsilon_5\ AO/HO)}$ (eV)	0	0	-13.59844	-13.59844	-13.59844	0	0	0	0	0	0
$E_{D(Group)}$ (eV)	3.93062	4.12506	12.49186	7.83016	3.32601	4.32754	4.29921	3.97398	4.17951	3.62128	3.91734

Table 15.67. The total bond energies of alkyl ethers calculated using the functional group composition and the energies of Table 15.66 compared to the experimental values [3].

Formula	Name	$C-O$ (i) Group	$C-O$ (ii) Group	CH_3	CH_2	CH	$C-C$ (a)	$C-C$ (b)	$C-C$ (c)	$C-C$ (d)	$C-C$ (e)	$C-C$ (f)	Calculated Total Bond Energy (eV)	Experimental Total Bond Energy (eV)	Relative Error
C_2H_6O	Dimethyl ether	2	0	2	0	0	0	0	0	0	0	0	32.84496	32.902	0.00174
C_3H_8O	Ethyl methyl ether	1	1	2	1	0	1	0	0	0	0	0	45.19710	45.183	-0.00030
$C_4H_{10}O$	Diethyl ether	0	2	2	2	0	2	0	0	0	0	0	57.54924	57.500	-0.00086
$C_4H_{10}O$	Methyl propyl ether	1	1	2	2	0	2	0	0	0	0	0	57.35480	57.355	0.00000
$C_4H_{10}O$	Isopropyl methyl ether	1	1	3	0	1	0	2	0	0	0	0	57.45569	57.499	0.00075
$C_6H_{14}O$	Dipropyl ether	0	2	2	4	0	4	0	0	0	0	0	81.86464	81.817	-0.00059
$C_6H_{14}O$	Diisopropyl ether	0	2	4	0	2	0	4	0	0	0	0	82.06642	82.088	0.00026
$C_6H_{14}O$	t-Butyl ethyl ether	1	1	4	1	0	1	0	3	0	0	0	82.10276	82.033	-0.00085
$C_7H_{16}O$	t-Butyl isopropyl ether	1	1	5	0	1	0	2	3	0	0	0	94.36135	94.438	0.00081
$C_8H_{18}O$	Dibutyl ether	0	2	2	6	0	6	0	0	0	0	0	106.18004	106.122	-0.00055
$C_8H_{18}O$	Di-sec-butyl ether	0	2	4	2	2	2	4	0	0	0	0	106.38182	106.410	0.00027
$C_8H_{18}O$	Di-t-butyl ether	2	0	6	0	0	0	0	6	0	0	0	106.65628	106.425	-0.00218
$C_8H_{18}O$	t-Butyl isobutyl ether	1	1	5	1	1	0	3	3	0	0	0	106.49072	106.497	0.00006

Table 15.68. The bond angle parameters of alkyl ethers and experimental values [1]. In the calculation of θ_v, the parameters from the preceding angle were used. E_T is $E_T(atom-atom,msp^3.AO)$.

Atoms of Angle	$2c'$ Bond 1 (a_0)	$2c'$ Bond 2 (a_0)	$2c'$ Terminal Atoms (a_0)	$E_{Coulombic}$ Atom 1	Atom 1 Hybridization Designation (Table 15.3.A)	$E_{Coulombic}$ Atom 2	Atom 2 Hybridization Designation (Table 15.3.A)	c_2 Atom 1	c_2 Atom 2	C_1	C_2	c_1	c_2'	E_T (eV)	θ_v (°)	θ_1 (°)	θ_2 (°)	Cal. θ (°)	Exp. θ (°)
$\angle C_aOC_a$ (C_a-O (i))	2.68862	2.68862	4.4721	-17.40869	44	-17.40869	44	0.78155	0.78155	1	1	1	0.78155	-1.85836				112.54	112 (dimethyl ether)
$\angle C_aOC_b$ (C_a-O (i)) (C_b-O (ii))	2.68862	2.67935	4.4385	-17.51099	46	-17.51099	46	0.77699	0.77699	1	1	1	0.77699	-1.85836				111.55	111.9 (ethyl methyl ether)
$\angle C_bC_aO$ (C_a-O (ii))	2.91547	2.67935	4.5607	-16.68412	26	-13.61806	O	0.81549	0.85395 (Eq. (15.133))	1	1	1	0.83472	-1.65376				109.13	109.4 (ethyl methyl ether)
Methylene $\angle HC_aH$	2.11106	2.11106	3.4252	-15.75493	7	H	H	0.86359	1	1	1	0.75	1.15796	0				108.44	107 (propane)
$\angle C_aC_bC_c$															69.51			110.49	112 (propane) 113.8 (butane) 110.8 (isobutane)
$\angle C_aC_bH$															69.51			110.49	111.0 (butane) 111.4 (isobutane)
Methyl $\angle HC_aH$	2.09711	2.09711	3.4252	-15.75493	7	H	H	0.86359	1	1	1	0.75	1.15796	0				109.50	
$\angle C_aC_bC_c$															70.56			109.44	
$\angle C_aC_bH$															70.56			109.44	
$\angle C_bC_aC_c$ iso C_a	2.91547	2.91547	4.7958	-16.68412 C_b	26	-16.68412 C_c	26	0.81549	0.81549	1	1	1	0.81549	-1.85836				110.67	110.8 (isobutane)
$\angle C_bC_aH$ iso C_a	2.91547	2.11323	4.1633	-15.55033 C_a	5	-14.82575 C_b	1	0.87495	0.91771	0.75	1	0.75	1.04887	0				110.76	
$\angle C_aC_bH$ iso C_a	2.91547	2.09711	4.1633	-15.55033 C_b	5	-14.82575 C_a	1	0.87495	0.91771	0.75	1	0.75	1.04887	0				111.27	111.4 (isobutane)
$\angle C_bC_aC_b$ tert C_a	2.90327	2.90327	4.7958	-16.68412 C_b	26	-16.68412 C_b	26	0.81549	0.81549	1	1	1	0.81549	-1.85836				111.37	110.8 (isobutane)
$\angle C_bC_aC_d$															72.50			107.50	

PRIMARY AMINES ($C_nH_{2n+2+m}N_m,\ n=1,2,3,4,5...\infty$)

The primary amines, $C_nH_{2n+2+m}N_m$, comprise an NH_2 functional group and a $C-N$ functional group. The alkyl portion of the primary amine may comprise at least two terminal methyl groups (CH_3) at each end of the chain, and may comprise methylene (CH_2), and methylyne (CH) functional groups as well as C bound by carbon-carbon single bonds. The methyl and methylene functional groups are equivalent to those of straight-chain alkanes. Six types of $C-C$ bonds can be identified. The n-alkane $C-C$ bond is the same as that of straight-chain alkanes. In addition, the $C-C$ bonds within isopropyl ($(CH_3)_2CH$) and t-butyl ($(CH_3)_3C$) groups and the isopropyl to isopropyl, isopropyl to t-butyl, and t-butyl to t-butyl $C-C$ bonds comprise functional groups. The branched-chain-alkane groups in primary amines are equivalent to those in branched-chain alkanes.

The primary amino (NH_2) functional group was solved using the procedure given in the Dihydrogen Nitride (NH_2) section. Using the results of Eqs. (13.245-13.368), the primary amino parameters in Eq. (15.61) are $n_1=2$, $C_1=0.75$, $C_2=0.93613$ (Eqs. (13.248-13.249)), $C_{1o}=1.5$, and $c_1=0.75$. In primary amines, the $C2sp^3$ HO of the $C-NH_2$-bond MO has an energy of $E\left(C,2sp^3\right)=-15.35946\ eV$ (Eq. (15.18) with $s=1$ and Eqs. (15.19-15.20)) and the N AO has an energy of $E(N)=-14.53414\ eV$. To meet the equipotential condition of the union of the $N-H$ H_2-type-ellipsoidal-MO with the $C2sp^3$ HO, the hybridization factor c_2 of Eq. (15.61) for the $N-H$-bond MO given by Eq. (15.77) is:

$$c_2\left(H\ to\ 1°N\right)=\frac{E(N)}{E\left(C,2sp^3\right)}=\frac{-14.53414\ eV}{-15.35946\ eV}=0.94627 \tag{15.134}$$

The $C-N$ group is solved by hybridizing the $2s$ and $2p$ AOs of the C atom to form a single $2sp^3$ shell as an energy minimum, and the sharing of electrons between the $C2sp^3$ HO and the N AO to form a MO permits each participating orbital to decrease in radius and energy. In primary amines, the $C2sp^3$ HO has a hybridization factor of 0.91771 (Eq. (13.430)) with a corresponding energy of $E\left(C,2sp^3\right)=-14.63489\ eV$ (Eq. (15.25)), and the N AO has an energy of $E(N)=-14.53414\ eV$. To meet the equipotential condition of the union of the $C-N$ H_2-type-ellipsoidal-MO with these orbitals, the hybridization factor c_2 of Eq. (15.61) for the $C-N$-bond MO given by Eqs. (15.77) and (15.79) is:

$$c_2\left(C2sp^3HO\ to\ N\right)=\frac{E(N)}{E\left(C,2sp^3\right)}c_2\left(C2sp^3HO\right)=\frac{-14.53414\ eV}{-14.63489\ eV}(0.91771)=0.91140 \tag{15.135}$$

$E_T\left(atom-atom,msp^3.AO\right)$ of the $C-N$-bond MO in Eq. (15.61) due to the charge donation from the C and N atoms to the MO is $-1.44915\ eV$. It is based on the energy match between the N of the NH_2 group and the $C2sp^3$ HO corresponding to the energy contributions to the single bond that are equivalent to those of methyl groups, $-0.72457\ eV$ (Eq. (14.151)), where the $N-H$ bonds are also energy matched to the $C-N$ bond.

The symbols of the functional groups of branched-chain primary amines are given in Table 15.69. The geometrical (Eqs. (15.1-15.5) and (15.51)), intercept (Eqs. (15.80-15.87)), and energy (Eqs. (15.6-15.11) and (15.17-15.65)) parameters of primary amines are given in Tables 15.70, 15.71, and 15.72, respectively. The total energy of each primary amine given in Table 15.73 was calculated as the sum over the integer multiple of each $E_{D(Group)}$ of Table 15.72 corresponding to functional-group composition of the molecule. The bond angle parameters of primary amines determined using Eqs. (15.88-15.117) are given in Table 15.74. The color scale, translucent view of the charge-density of exemplary primary amine, propylamine, comprising the concentric shells of atoms with the outer shell bridged by one or more H_2-type ellipsoidal MOs or joined with one or more hydrogen MOs is shown in Figure 15.12.

Figure 15.12. (A)-(B) Color scale, translucent views of the charge-density of propylamine showing the orbitals of the atoms at their radii, the ellipsoidal surface of each H or H_2-type ellipsoidal MO that transitions to the corresponding outer shell of the atom(s) participating in each bond, and the hydrogen nuclei (red, not to scale).

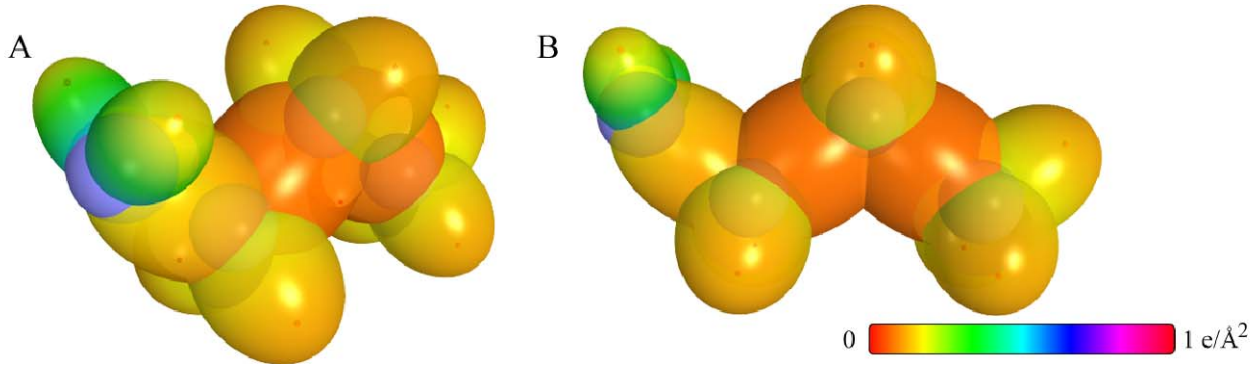

Table 15.69. The symbols of functional groups of primary amines.

Functional Group	Group Symbol
NH_2 group	NH_2
C-N	$C-N$
CH_3 group	$C-H\ (CH_3)$
CH_2 group	$C-H\ (CH_2)$
CH	$C-H$
CC bond (*n-C*)	$C-C$ (a)
CC bond (*iso-C*)	$C-C$ (b)
CC bond (*tert-C*)	$C-C$ (c)
CC (iso to *iso-C*)	$C-C$ (d)
CC (*t* to *t-C*)	$C-C$ (e)
CC (*t* to *iso-C*)	$C-C$ (f)

Table 15.70. The geometrical bond parameters of primary amines and experimental values [1].

Parameter	NH_2 Group	$C-N$ Group	$C-H\ (CH_3)$ Group	$C-H\ (CH_2)$ Group	$C-H$ Group	$C-C$ (a) Group	$C-C$ (b) Group	$C-C$ (c) Group	$C-C$ (d) Group	$C-C$ (e) Group	$C-C$ (f) Group
$a\ (a_0)$	1.28083	1.92682	1.64920	1.67122	1.67465	2.12499	2.12499	2.10725	2.12499	2.10725	2.10725
$c'\ (a_0)$	0.95506	1.38810	1.04856	1.05553	1.05661	1.45744	1.45744	1.45164	1.45744	1.45164	1.45164
Bond Length $2c'\ (\AA)$	1.0108	1.46910	1.10974	1.11713	1.11827	1.54280	1.54280	1.53635	1.54280	1.53635	1.53635
Exp. Bond Length $(\AA)$	1.010 (methylamine)	1.471 (methylamine)	1.107 ($C-H$ propane) 1.117 ($C-H$ butane)	1.107 ($C-H$ propane) 1.117 ($C-H$ butane)	1.122 (isobutane)	1.532 (propane) 1.531 (butane)	1.532 (propane) 1.531 (butane)	1.532 (propane) 1.531 (butane)	1.532 (propane) 1.531 (butane)	1.532 (propane) 1.531 (butane)	1.532 (propane) 1.531 (butane)
$b,c\ (a_0)$	0.85345	1.33634	1.27295	1.29569	1.29924	1.54616	1.54616	1.52750	1.54616	1.52750	1.52750
e	0.74566	0.72041	0.63580	0.63159	0.63095	0.68600	0.68600	0.68888	0.68600	0.68888	0.68888

Table 15.71. The MO to HO intercept geometrical bond parameters of primary amines. R, R', R'' are H or alkyl groups. E_T is $E_T(atom-atom,msp^3.AO)$.

Bond	Atom	E_T (eV) Bond 1	E_T (eV) Bond 2	E_T (eV) Bord 3	E_T (eV) Bond 4	Final Total Energy $C2sp^3$ (eV)	$r_{initial}\ (a_0)$	$r_{final}\ (a_0)$	$E_{Coulomb}$ (eV) Final	$E(C2sp^3)$ (eV) Final	θ' (°)	θ_1 (°)	θ_2 (°)	$d_1\ (a_0)$	$d_2\ (a_0)$
$H_3CN(H)-H$	N	-0.72457	0	0	0		0.93084	0.87495	-15.55033		118.00	62.00	64.85	0.54432	0.41075
$-H_2C_aN(H)-H$	N	-0.72457	0	0	0		0.93084	0.87495	-15.55033		118.00	62.00	64.85	0.54432	0.41075
H_3C-NH_2	C	-0.72457	0	0	0	-152.34026	0.91771	0.87495	-15.55033	-15.35946	85.28	94.72	40.73	1.46010	0.07200
H_3C-NH_2	N	-0.72457	0	0	0		0.93084	0.87495	-15.55033		85.28	94.72	40.73	1.46010	0.07200
$-H_2C_a-NH_2$	C_a	-0.72457	-0.92918	0	0	-153.26945	0.91771	0.82562	-16.47951	-16.28864	80.20	99.80	37.50	1.52858	0.14048
$-H_2C_a-NH_2$	N	-0.72457	0	0	0		0.93084	0.87495	-15.55033		85.28	94.72	40.73	1.46010	0.07200
$C-H\ (CH_3)$	C	-0.92918	0	0	0	-152.54487	0.91771	0.86359	-15.75493	-15.56407	77.49	102.51	41.48	1.23564	0.18708
$C-H\ (CH_2)$	C	-0.92918	-0.92918	0	0	-153.47406	0.91771	0.81549	-16.68412	-16.49325	68.47	111.53	35.84	1.35486	0.29933
$C-H\ (CH)$	C	-0.92918	-0.92918	-0.92918	0	-154.40324	0.91771	0.77247	-17.61330	-17.42244	61.10	118.90	31.37	1.42988	0.37326
$H_3C_aC_bH_2CH_2-$ ($C-C$ (a))	C_a	-0.92918	0	0	0	-152.54487	0.91771	0.86359	-15.75493	-15.56407	63.82	116.18	30.08	1.83879	0.38106
$H_3C_aC_bH_2CH_2-$ ($C-C$ (a))	C_b	-0.92918	-0.92918	0	0	-153.47406	0.91771	0.81549	-16.68412	-16.49325	56.41	123.59	26.06	1.90890	0.45117
$R-H_2C_aC_b(H_2C_c-R')HCH_2-$ ($C-C$ (b))	C_b	-0.92918	-0.92918	-0.92918	0	-154.40324	0.91771	0.77247	-17.61330	-17.42244	48.30	131.70	21.90	1.97162	0.51388
$R-H_2C_a(R'-H_2C_d)C_b(R''-H_2C_c)CH_2-$ ($C-C$ (c))	C_b	-0.92918	-0.72457	-0.72457	-0.72457	-154.71860	0.91771	0.75889	-17.92866	-17.73779	48.21	131.79	21.74	1.95734	0.50570
$isoC_aC_b(H_2C_c-R')HCH_2-$ ($C-C$ (d))	C_b	-0.92918	-0.92918	-0.92918	0	-154.40324	0.91771	0.77247	-17.61330	-17.42244	48.30	131.70	21.90	1.97162	0.51388
$tertC_a(R'-H_2C_d)C_b(R''-H_2C_c)CH_2-$ ($C-C$ (e))	C_b	-0.72457	-0.72457	-0.72457	-0.72457	-154.51399	0.91771	0.76765	-17.92866	-17.73779	50.04	129.96	22.66	1.94462	0.49298
$tertC_aC_b(H_2C_c-R')HCH_2-$ ($C-C$ (f))	C_b	-0.72457	-0.92918	-0.92918	0	-154.19863	0.91771	0.78155	-17.40869	-17.21783	52.78	127.22	24.04	1.92443	0.47279
$isoC_a(R'-H_2C_d)C_b(R''-H_2C_c)CH_2-$ ($C-C$ (f))	C_b	-0.72457	-0.72457	-0.72457	-0.72457	-154.51399	0.91771	0.76765	-17.92866	-17.73779	50.04	129.96	22.66	1.94462	0.49298

Table 15.72. The energy parameters (eV) of functional groups of primary amines.

Parameters	NH_2 Group	$C-N$ Group	CH_3 Group	CH_2 Group	$C-H$ Group	$C-C$ (a) Group	$C-C$ (b) Group	$C-C$ (c) Group	$C-C$ (d) Group	$C-C$ (e) Group	$C-C$ (f) Group
n_1	2	1	3	2	1	1	1	1	1	1	1
n_2	0	0	2	1	0	0	0	0	0	0	0
n_3	1	0	0	0	0	0	0	0	0	0	0
C_1	0.75	0.5	0.75	0.75	0.75	0.5	0.5	0.5	0.5	0.5	0.5
C_2	0.93613	1	1	1	1	1	1	1	1	1	1
c_1	0.75	1	1	1	1	1	1	1	1	1	1
c_2	0.94627	0.91140	0.91771	0.91771	0.91771	0.91771	0.91771	0.91771	0.91771	0.91771	0.91771
c_3	0	0	0	1	1	0	0	0	1	1	0
c_4	1	2	1	1	1	2	2	2	2	2	2
c_5	2	0	3	2	1	0	0	0	0	0	0
C_{1o}	1.5	0.5	0.75	0.75	0.75	0.5	0.5	0.5	0.5	0.5	0.5
C_{2o}	1	1	1	1	1	1	1	1	1	1	1
$V_e\ (eV)$	-77.89897	-32.46339	-107.32728	-70.41425	-35.12015	-28.79214	-28.79214	-29.10112	-28.79214	-29.10112	-29.10112
$V_p\ (eV)$	28.49191	9.80175	38.92728	25.78002	12.87680	9.33352	9.33352	9.37273	9.33352	9.37273	9.37273
$T\ (eV)$	30.40957	8.42409	32.53914	21.06675	10.48582	6.77464	6.77464	6.90500	6.77464	6.90500	6.90500
$V_m\ (eV)$	-15.20478	-4.21204	-16.26957	-10.53337	-5.24291	-3.38732	-3.38732	-3.45250	-3.38732	-3.45250	-3.45250
$E_{(AO/HO)}\ (eV)$	-14.53414	-14.63489	-15.56407	-15.56407	-14.63489	-15.56407	-15.56407	-15.35946	-15.56407	-15.35946	-15.35946
$\Delta E_{H_2MO(AO/HO)}\ (eV)$	0	-1.44915	0	0	0	0	0	0	0	0	0
$E_{T(AO/HO)}\ (eV)$	-14.53414	-13.18574	-15.56407	-15.56407	-14.63489	-15.56407	-15.56407	-15.35946	-15.56407	-15.35946	-15.35946
$E_{(n_1\ AO/HO)}\ (eV)$	-14.53414	0	0	0	0	0	0	0	0	0	0
$E_{T(H_2MO)}\ (eV)$	-48.73642	-31.63534	-67.69451	-49.66493	-31.63533	-31.63537	-31.63537	-31.63535	-31.63537	-31.63535	-31.63535
$E_T\left(atom-atom, msp^3.AO\right)(eV)$	0	-1.44915	0	0	0	-1.85836	-1.85836	-1.44915	-1.85836	-1.44915	-1.44915
$E_{T(MO)}\ (eV)$	-48.73660	-33.08452	-67.69450	-49.66493	-31.63537	-33.49373	-33.49373	-33.08452	-33.49373	-33.08452	-33.08452
$\omega\ \left(10^{15}\ rad/s\right)$	64.2189	18.9231	24.9286	24.2751	24.1759	9.43699	9.43699	15.4846	9.43699	9.55643	9.55643
$E_K\ (eV)$	42.27003	12.45552	16.40846	15.97831	15.91299	6.21159	6.21159	10.19220	6.21159	6.29021	6.29021
$\bar{E}_D\ (eV)$	-0.40690	-0.23100	-0.25352	-0.25017	-0.24966	-0.16515	-0.16515	-0.20896	-0.16515	-0.16416	-0.16416
$\bar{E}_{Kvib}\ (eV)$	0.40929 [22]	0.12944 [23]	0.35532 (Eq. (13.458))	0.35532 (Eq. (13.458))	0.35532 (Eq. (13.458))	0.12312 [2]	0.17978 [4]	0.09944 [5]	0.12312 [2]	0.12312 [2]	0.12312 [2]
$\bar{E}_{osc}\ (eV)$	-0.20226	-0.16628	-0.22757	-0.14502	-0.07200	-0.10359	-0.07526	-0.15924	-0.10359	-0.10260	-0.10260
$E_{mag}\ (eV)$	0.14803	0.14803	0.14803	0.14803	0.14803	0.14803	0.14803	0.14803	0.14803	0.14803	0.14803
$E_{T(Group)}\ (eV)$	-49.14112	-33.25079	-67.92207	-49.80996	-31.70737	-33.59732	-33.49373	-33.24376	-33.59732	-33.18712	-33.18712
$E_{initial\ (c_1\ AO/HO)}\ (eV)$	-14.53414	-14.63489	-14.63489	-14.63489	-14.63489	-14.63489	-14.63489	-14.63489	-14.63489	-14.63489	-14.63489
$E_{initial\ (c_5\ AO/HO)}\ (eV)$	-13.59844	0	-13.59844	-13.59844	-13.59844	0	0	0	0	0	0
$E_{D(Group)}\ (eV)$	7.41010	3.98101	12.49186	7.83016	3.32601	4.32754	4.29921	3.97398	4.17951	3.62128	3.91734

Table 15.73. The total bond energies of primary amines calculated using the functional group composition and the energies of Table 15.72 compared to the experimental values [3].

Formula	Name	NH_2 Group	$C-N$ Group	CH_3	CH_2	CH	$C-C$ (a)	$C-C$ (b)	$C-C$ (c)	$C-C$ (d)	$C-C$ (e)	$C-C$ (f)	Calculated Total Bond Energy (eV)	Experimental Total Bond Energy (eV)	Relative Error
CH_5N	Methylamine	1	1	1	0	0	0	0	0	0	0	0	23.88297	23.857	-0.00110
C_2H_7N	Ethylamine	1	1	1	1	0	1	0	0	0	0	0	36.04067	36.062	0.00060
C_3H_9N	Propylamine	1	1	1	2	0	2	0	0	0	0	0	48.19837	48.243	0.00092
$C_4H_{11}N$	Butylamine	1	1	1	3	0	3	0	0	0	0	0	60.35607	60.415	0.00098
$C_4H_{11}N$	sec-Butylamine	1	1	2	1	1	1	2	0	0	0	0	60.45596	60.547	0.00148
$C_4H_{11}N$	t-Butylamine	1	1	3	0	0	0	0	3	0	0	0	60.78863	60.717	-0.00118
$C_4H_{11}N$	Isobutylamine	1	1	2	1	1	0	3	0	0	0	0	60.42863	60.486	0.00094

Table 15.74. The bond angle parameters of primary amines and experimental values [1]. In the calculation of θ_v, the parameters from the preceding angle were used. E_T is $E_T(atom-atom,msp^3.AO)$.

Atoms of Angle	$2c'$ Bond 1 (a_0)	$2c'$ Bond 2 (a_0)	$2c'$ Terminal Atoms (a_0)	$E_{Coulombic}$ or E Atom 1	Atom 1 Hybridization Designation (Table 15.3.A)	$E_{Coulombic}$ Atom 2	Atom 2 Hybridization Designation (Table 15.3.A)	c_2 Atom 1	c_2 Atom 2	C_1	C_2	c_1	c_2'	E_T (eV)	θ_v (°)	θ_1 (°)	θ_2 (°)	Cal. θ (°)	Exp. θ (°)
$\angle HNH$	1.91013	1.91013	3.0984	-14.53414	N	H	H	0.94627 Eq. (15.134))	1	1	1	0.75	1.05679	0				108.40	107.1 (methylamine)
$\angle HNC_a$	1.91013	2.77620	3.8816	-14.53414	N	-15.35946	5	0.91140 (Eq. (15.135))	0.88583	0.75	1	0.75	0.97194	0				110.48	110.3 (methylamine)
Methylene $\angle HC_aH$	2.11106	2.11106	3.4252	-15.75493	7	H	H	0.86359	1	1	1	0.75	1.15796	0				108.44	108.0 (methylamine) 107 (propane)
$\angle C_aC_bC_c$															69.51			110.49	112 (propane) 113.8 (butane) 110.8 (isobutane)
$\angle C_aC_bH$															69.51			110.49	111.0 (butane) 111.4 (isobutane)
Methyl $\angle HC_aH$	2.09711	2.09711	3.4252	-15.75493	7	H	H	0.86359	1	1	1	0.75	1.15796	0				109.50	
$\angle C_aC_bC_c$															70.56			109.44	
$\angle C_aC_bH$															70.56			109.44	
$\angle C_bC_aC_c$ iso C_a	2.91547	2.91547	4.7958	-16.68412 C_a	26	-16.68412 C_c	26	0.81549	0.81549	1	1	1	0.81549	-1.85836				110.67	110.8 (isobutane)
$\angle C_bC_aH$ iso C_a	2.91547	2.11323	4.1633	-15.55033 C_a	5	-14.82575 C_b	1	0.87495	0.91771	0.75	1	0.75	1.04887	0				110.76	
$\angle C_aC_bH$ iso C_a	2.91547	2.09711	4.1633	-15.55033 C_b	5	-14.82575 C_a	1	0.87495	0.91771	0.75	1	0.75	1.04887	0				111.27	111.4 (isobutane)
$\angle C_bC_aC_b$ tert C_a	2.90327	2.90327	4.7958	-16.68412 C_a	26	-16.68412 C_b	26	0.81549	0.81549	1	1	1	0.81549	-1.85836				111.37	110.8 (isobutane)
$\angle C_bC_aC_d$															72.50			107.50	

SECONDARY AMINES ($C_nH_{2n+2+m}N_m,\ n=2,3,4,5...\infty$)

The secondary amines, $C_nH_{2n+2+m}N_m$, comprise an NH functional group and two types of $C-N$ functional groups, one for the methyl group corresponding to the C of $C-N$ and the other for general alkyl secondary amines. The alkyl portion of the secondary amine may comprise at least two terminal methyl groups (CH_3) at each end of the chain, and may comprise methylene (CH_2), and methylyne (CH) functional groups as well as C bound by carbon-carbon single bonds. The methyl and methylene functional groups are equivalent to those of straight-chain alkanes. Six types of $C-C$ bonds can be identified. The n-alkane $C-C$ bond is the same as that of straight-chain alkanes. In addition, the $C-C$ bonds within isopropyl ($(CH_3)_2CH$) and t-butyl ($(CH_3)_3C$) groups and the isopropyl to isopropyl, isopropyl to t-butyl, and t-butyl to t-butyl $C-C$ bonds comprise functional groups. The branched-chain-alkane groups in secondary amines are equivalent to those in branched-chain alkanes.

The secondary amino (NH) functional group was solved using the procedure given in the Hydrogen Nitride (NH) section. Using the results of Eqs. (13.245-13.316), the secondary amino parameters in Eq. (15.61) are $n_1=1$, $C_1=0.75$, $C_2=0.93613$ (Eqs. (13.248-13.249)), $C_{1o}=0.75$, and $c_1=0.75$. In secondary amines, the $C2sp^3$ HO of the $C-NH$ -bond MO has an energy of $E\left(C,2sp^3\right)=-15.56407\ eV$ (Eqs. (14.514-14.516)); Eq. (15.29) with $s=1$ and $s=2$, Eq. (15.31), and Eqs. (15.19-15.20)) and the N AO has an energy of $E(N)=-14.53414\ eV$ (Eq. (13.251)). To meet the equipotential condition of the union of the $N-H$ H_2-type-ellipsoidal-MO with the $C2sp^3$ HO, the hybridization factor c_2 of Eq. (15.61) for the $N-H$ -bond MO given by Eq. (15.77) is:

$$c_2\left(H\ to\ 2°N\right)=\frac{E(N)}{E\left(C,2sp^3\right)}=\frac{-14.53414\ eV}{-15.56407\ eV}=0.93383 \tag{15.136}$$

The $C-N$ group is solved by hybridizing the $2s$ and $2p$ AOs of the C atom to form a single $2sp^3$ shell as an energy minimum, and the sharing of electrons between the $C2sp^3$ HO and the N AO to form a MO permits each participating orbital to decrease in radius and energy. In secondary amines, the $C2sp^3$ HO has a hybridization factor of 0.91771 (Eq. (13.430)) with a corresponding energy of $E\left(C,2sp^3\right)=-14.63489\ eV$ (Eq. (15.25)), and the N AO has an energy of $E(N)=-14.53414\ eV$. To meet the equipotential condition of the union of the $C-N$ H_2-type-ellipsoidal-MO with these orbitals, the hybridization factor c_2 of Eq. (15.61) for the $C-N$ -bond MO given by Eq. (15.135) is $c_2\left(C2sp^3HO\ to\ N\right)=0.91140$.

As given in the Continuous-Chain Alkanes ($C_nH_{2n+2},\ n=3,4,5...\infty$) section, each methylene group forms two single bonds, and the energy of each $C2sp^3$ HO of each CH_2 group alone is given by that in ethylene, $-1.13379\ eV$ (Eq. (14.511)). In secondary amines, the N of the NH group also binds to two $C2sp^3$ HOs and the corresponding $E_T\left(atom-atom,msp^3.AO\right)$ of each $C-N$ -bond MO in Eq. (15.61) due to the charge donation from the C and N atoms to the MO is $-1.13379\ eV$. It is based on the energy match between the N of the NH group to the two $C2sp^3$ HOs corresponding to the energy contributions to each of the two single bonds that are equivalent to those of independent methylene groups, $-1.13379\ eV$ (Eq. (14.511)), where the $N-H$ bond is also energy matched to the $C-N$ bonds. $E_T\left(atom-atom,msp^3.AO\right)$ of the $C-N$ -bond MO in Eq. (15.61) due to the charge donation from the C and N atoms to the MO is $-1.13379\ eV$. It is based on the energy match between the N of the NH group to two $C2sp^3$ HOs corresponding to the energy contributions to the single bond that are equivalent to those of methyl groups, $-0.72457\ eV$ (Eq. (14.151)), where the $N-H$ bonds are also energy matched to the $C-N$ bond.

The symbols of the functional groups of branched-chain secondary amines are given in Table 15.75. The geometrical (Eqs. (15.1-15.5) and (15.51)), intercept (Eqs. (15.80-15.87)), and energy (Eqs. (15.6-15.11) and (15.17-15.65)) parameters of secondary amines are given in Tables 15.76, 15.77, and 15.78, respectively. As in the case of NH_2 (Eq. (13.339)), $C_{1o}=2C_1$ rather than $C_{1o}=C_1$ in Eq. (15.61) for the $C-N$ bond. The total energy of each secondary amine given in Table 15.79 was calculated as the sum over the integer multiple of each $E_{D(Group)}$ of Table 15.78 corresponding to functional-group composition of the molecule. The bond angle parameters of secondary amines determined using Eqs. (15.88-15.117) are given in Table 15.80. The color scale, translucent view of the charge-density of exemplary secondary amine, dimenthylamine, comprising the concentric shells of atoms with the outer shell bridged by one or more H_2-type ellipsoidal MOs or joined with one or more hydrogen MOs is shown in Figure 15.13.

Figure 15.13. (A)-(B) Color scale, translucent views of the charge-density of dimethylamine showing the orbitals of the atoms at their radii, the ellipsoidal surface of each H or H_2-type ellipsoidal MO that transitions to the corresponding outer shell of the atom(s) participating in each bond, and the hydrogen nuclei (red, not to scale).

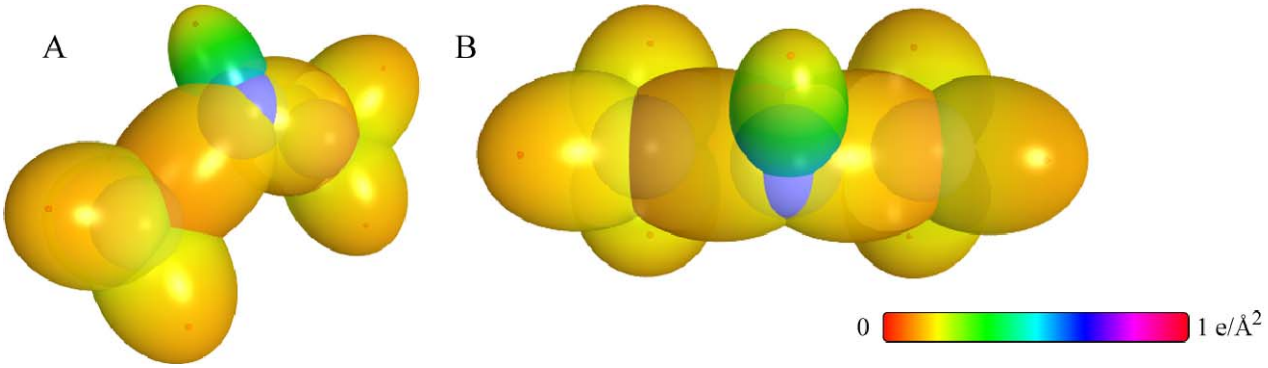

Table 15.75. The symbols of functional groups of secondary amines.

Functional Group	Group Symbol
NH group	*NH*
C-N (methyl)	$C-N$ (i)
C-N (alkyl)	$C-N$ (ii)
CH₃ group	$C-H\ (CH_3)$
CH₂ group	$C-H\ (CH_2)$
CH	$C-H$
CC bond (*n-C*)	$C-C$ (a)
CC bond (*iso-C*)	$C-C$ (b)
CC bond (*tert-C*)	$C-C$ (c)
CC (*iso* to *iso-C*)	$C-C$ (d)
CC (*t* to *t-C*)	$C-C$ (e)
CC (*t* to *iso-C*)	$C-C$ (f)

Table 15.76. The geometrical bond parameters of secondary amines and experimental values [1].

Parameter	NH Group	$C-N$ (i) Group	$C-N$ (ii) Group	$C-H\ (CH_3)$ Group	$C-H\ (CH_2)$ Group	$C-H$ Group	$C-C$ (a) Group	$C-C$ (b) Group	$C-C$ (c) Group	$C-C$ (d) Group	$C-C$ (e) Group	$C-C$ (f) Group
$a\ (a_0)$	1.26224	1.94862	1.94862	1.64920	1.67122	1.67465	2.12499	2.12499	2.10725	2.12499	2.10725	2.10725
$c'\ (a_0)$	0.94811	1.39593	1.39593	1.04856	1.05553	1.05661	1.45744	1.45744	1.45164	1.45744	1.45164	1.45164
Bond Length $2c'\ (\AA)$	1.00343	1.47739	1.47739	1.10974	1.11713	1.11827	1.54280	1.54280	1.53635	1.54280	1.53635	1.53635
Exp. Bond Length $(\AA)$	1.00 (dimethylamine)	1.455 (dimethylamine)		1.107 ($C-H$ propane) 1.117 ($C-H$ butane)	1.107 ($C-H$ propane) 1.117 ($C-H$ butane)	1.122 (isobutane)	1.532 (propane) 1.531 (butane)	1.532 (propane) 1.531 (butane)	1.532 (propane) 1.531 (butane)	1.532 (propane) 1.531 (butane)	1.532 (propane) 1.531 (butane)	1.532 (propane) 1.531 (butane)
$b,c\ (a_0)$	0.83327	1.35960	1.35960	1.27295	1.29569	1.29924	1.54616	1.54616	1.52750	1.54616	1.52750	1.52750
e	0.75113	0.71637	0.71637	0.63580	0.63159	0.63095	0.68600	0.68600	0.68888	0.68600	0.68888	0.68888

Table 15.77. The MO to HO intercept geometrical bond parameters of secondary amines. R, R', R'' are H or alkyl groups. E_T is $E_T(atom-atom, msp^3.AO)$.

Bond	Atom	E_T (eV) Bond 1	E_T (eV) Bond 2	E_T (eV) Bond 3	E_T (eV) Bond 4	Final Total Energy $C2sp^3$ (eV)	$r_{initial}\ (a_0)$	$r_{final}\ (a_0)$	$E_{Coulomb}$ (eV) Final	$E(C2sp^3)$ (eV) Final	θ' (°)	θ_1 (°)	θ_2 (°)	$d_1\ (a_0)$	$d_2\ (a_0)$
$H_3C_aN(C_bH_3)-H$	N	-0.56690	-0.56690	0	0		0.93084	0.85252	-15.95954		118.18	61.82	64.40	0.54546	0.40264
$-H_2C_aN(R_{alkyl})-H$	N	-0.56690	-0.56690	0	0		0.93084	0.85252	-15.95954		118.18	61.82	64.40	0.54546	0.40264
$H_3C_a-NH-C_aH_3$	C_a	-0.56690	0	0	0	-152.18259	0.91771	0.88392	-15.39265	-15.20178	84.14	95.86	40.30	1.48625	0.09032
$H_3C_a-NH-C_aH_3$	N	-0.56690	-0.56690	0	0		0.93084	0.85252	-15.95954		80.95	99.05	38.26	1.53008	0.13415
$-H_2C_a-NH-C_bR$	C_a	-0.56690	-0.92918	0	0	-153.11177	0.91771	0.83360	-16.32183	-16.13097	78.89	101.11	36.99	1.55650	0.16057
$-H_2C_a-NH-C_bH_2-$	N	-0.56690	-0.56690	0	0		0.93084	0.85252	-15.95954		80.95	99.05	38.26	1.53008	0.13415
$C-H\ (CH_3)$	C	-0.92918	0	0	0	-152.54487	0.91771	0.86359	-15.75493	-15.56407	77.49	102.51	41.48	1.23564	0.18708
$C-H\ (CH_2)$	C	-0.92918	-0.92918	0	0	-153.47406	0.91771	0.81549	-16.68412	-16.49325	68.47	111.53	35.84	1.35486	0.29933
$C-H\ (CH)$	C	-0.92918	-0.92918	-0.92918	0	-154.40324	0.91771	0.77247	-17.61330	-17.42244	61.10	118.90	31.37	1.42988	0.37326
$H_3C_aC_bH_2CH_2-$ ($C-C$ (a))	C_a	-0.92918	0	0	0	-152.54487	0.91771	0.86359	-15.75493	-15.56407	63.82	116.18	30.08	1.83879	0.38106
$H_3C_aC_bH_2CH_2-$ ($C-C$ (a))	C_b	-0.92918	-0.92918	0	0	-153.47406	0.91771	0.81549	-16.68412	-16.49325	56.41	123.59	26.06	1.90890	0.45117
$R-H_2C_aC_b(H_2C_c-R')HCH_2-$ ($C-C$ (b))	C_b	-0.92918	-0.92918	-0.92918	0	-154.40324	0.91771	0.77247	-17.61330	-17.42244	48.30	131.70	21.90	1.97162	0.51388
$R-H_2C_a(R'-H_2C_d)C_b(R''-H_2C_c)CH_2-$ ($C-C$ (c))	C_b	-0.92918	-0.72457	-0.72457	-0.72457	-154.71860	0.91771	0.75889	-17.92866	-17.73779	48.21	131.79	21.74	1.95734	0.50570
$isoC_aC_b(H_2C_c-R')HCH_2-$ ($C-C$ (d))	C_b	-0.92918	-0.92918	-0.92918	0	-154.40324	0.91771	0.77247	-17.61330	-17.42244	48.30	131.70	21.90	1.97162	0.51388
$tertC_c(R'-H_2C_d)C_b(R''-H_2C_c)CH_2-$ ($C-C$ (e))	C_b	-0.72457	-0.72457	-0.72457	-0.72457	-154.51399	0.91771	0.76765	-17.92866	-17.73779	50.04	129.96	22.66	1.94462	0.49298
$tertC_cC_b(H_2C_c-R')HCH_2-$ ($C-C$ (f))	C_b	-0.72457	-0.92918	-0.92918	0	-154.19863	0.91771	0.78155	-17.40869	-17.21783	52.78	127.22	24.04	1.92443	0.47279
$isoC_a(R'-H_2C_d)C_b(R''-H_2C_c)CH_2-$ ($C-C$ (f))	C_b	-0.72457	-0.72457	-0.72457	-0.72457	-154.51399	0.91771	0.76765	-17.92866	-17.73779	50.04	129.96	22.66	1.94462	0.49298

Table 15.78. The energy parameters (eV) of functional groups of secondary amines.

Parameters	NH Group	$C-N$ (i) Group	$C-N$ (ii) Group	CH_3 Group	CH_2 Group	$C-H$ Group	$C-C$ (a) Group	$C-C$ (b) Group	$C-C$ (c) Group	$C-C$ (d) Group	$C-C$ (e) Group	$C-C$ (f) Group
n_1	1	1	1	3	2	1	1	1	1	1	1	1
n_2	0	0	0	2	1	0	0	0	0	0	0	0
n_3	0	0	0	0	0	0	0	0	0	0	0	0
C_1	0.75	0.5	0.5	0.75	0.75	0.75	0.5	0.5	0.5	0.5	0.5	0.5
C_2	0.93613	1	1	1	1	1	1	1	1	1	1	1
c_1	0.75	1	1	1	1	1	1	1	1	1	1	1
c_2	0.93383	0.91140	0.91140	0.91771	0.91771	0.91771	0.91771	0.91771	0.91771	0.91771	0.91771	0.91771
c_3	1	0	0	0	1	1	0	0	0	1	1	0
c_4	1	2	2	1	1	1	2	2	2	2	2	2
c_5	1	0	0	3	2	1	0	0	0	0	0	0
C_{1o}	0.75	1	1	0.75	0.75	0.75	0.5	0.5	0.5	0.5	0.5	0.5
C_{2o}	1	1	1	1	1	1	1	1	1	1	1	1
V_e (eV)	-39.21967	-31.98456	-31.98456	-107.32728	-70.41425	-35.12015	-28.79214	-28.79214	-29.10112	-28.79214	-29.10112	-29.10112
V_p (eV)	14.35050	9.74677	9.74677	38.92728	25.78002	12.87680	9.33352	9.33352	9.37273	9.33352	9.37273	9.37273
T (eV)	15.53581	8.20698	8.20698	32.53914	21.06675	10.48582	6.77464	6.77464	6.90500	6.77464	6.90500	6.90500
V_m (eV)	-7.76790	-4.10349	-4.10349	-16.26957	-10.53337	-5.24291	-3.38732	-3.38732	-3.45250	-3.38732	-3.45250	-3.45250
$E_{(AO/HO)}$ (eV)	-14.53414	-14.63489	-14.63489	-15.56407	-15.56407	-14.63489	-15.56407	-15.56407	-15.35946	-15.56407	-15.35946	-15.35946
$\Delta E_{H_2MO_{(AO/HO)}}$ (eV)	0	-1.13379	-1.13379	0	0	0	0	0	0	0	0	0
$E_{T_{(AO/HO)}}$ (eV)	-14.53414	-13.50110	-13.50110	-15.56407	-15.56407	-14.63489	-15.56407	-15.56407	-15.35946	-15.56407	-15.35946	-15.35946
$E_{T_{(H_2MO)}}$ (eV)	-31.63541	-31.63540	-31.63540	-67.69451	-49.66493	-31.63533	-31.63537	-31.63537	-31.63535	-31.63537	-31.63535	-31.63535
$E_T\left(atom-atom, msp^3.AO\right)(eV)$	0	-1.13379	-1.13379	0	0	0	-1.85836	-1.85836	-1.44915	-1.85836	-1.44915	-1.44915
$E_{T_{(MO)}}$ (eV)	-31.63537	-32.76916	-32.76916	-67.69450	-49.66493	-31.63537	-33.49373	-33.49373	-33.08452	-33.49373	-33.08452	-33.08452
$\omega\left(10^{15}\ rad/s\right)$	47.0696	15.1983	26.0778	24.9286	24.2751	24.1759	9.43699	9.43699	15.4846	9.43699	9.55643	9.55643
E_K (eV)	30.98202	10.00377	17.16484	16.40846	15.97831	15.91299	6.21159	6.21159	10.19220	6.21159	6.29021	6.29021
$\bar{E}_D$ (eV)	-0.34836	-0.20505	-0.26859	-0.25352	-0.25017	-0.24966	-0.16515	-0.16515	-0.20896	-0.16515	-0.16416	-0.16416
$\bar{E}_{Kvib}$ (eV)	0.40696 [24]	0.12944 [23]	0.11159 [25]	0.35532 (Eq. (13.458))	0.35532 (Eq. (13.458))	0.35532 (Eq. (13.458))	0.12312 [2]	0.17978 [4]	0.09944 [5]	0.12312 [2]	0.12312 [2]	0.12312 [2]
$\bar{E}_{osc}$ (eV)	-0.14488	-0.14033	-0.21280	-0.22757	-0.14502	-0.07200	-0.10359	-0.07526	-0.15924	-0.10359	-0.10260	-0.10260
E_{mag} (eV)	0.14803	0.14803	0.14803	0.14803	0.14803	0.14803	0.14803	0.14803	0.14803	0.14803	0.14803	0.14803
$E_{T_{(Group)}}$ (eV)	-31.78025	-32.90949	-32.98196	-67.92207	-49.80996	-31.70737	-33.59732	-33.49373	-33.24376	-33.59732	-33.18712	-33.18712
$E_{initial_{(s\ AO/HO)}}$ (eV)	-14.53414	-14.63489	-14.63489	-14.63489	-14.63489	-14.63489	-14.63489	-14.63489	-14.63489	-14.63489	-14.63489	-14.63489
$E_{initial_{(s\ AO/HO)}}$ (eV)	-13.59844	0	0	-13.59844	-13.59844	-13.59844	0	0	0	0	0	0
$E_{D_{(Group)}}$ (eV)	3.50582	3.63971	3.71218	12.49186	7.83016	3.32601	4.32754	4.29921	3.97398	4.17951	3.62128	3.91734

Table 15.79. The total bond energies of secondary amines calculated using the functional group composition and the energies of Table 15.78 compared to the experimental values [3].

Formula	Name	NH Group	$C-N$ (i) Group	$C-N$ (ii) Group	CH_3	CH_2	CH	$C-C$ (a)	$C-C$ (b)	$C-C$ (c)	$C-C$ (d)	$C-C$ (e)	$C-C$ (f)	Calculated Total Bond Energy (eV)	Experimental Total Bond Energy (eV)	Relative Error
C_2H_7N	Dimethylamine	1	2	0	2	0	0	0	0	0	0	0	0	35.76895	35.765	-0.00012
$C_4H_{11}N$	Diethylamine	1	0	2	2	2	0	2	0	0	0	0	0	60.22930	60.211	-0.00030
$C_6H_{15}N$	Dipropylamine	1	0	2	2	4	0	4	0	0	0	0	0	84.54470	84.558	0.00016
$C_6H_{15}N$	Diisopropylamine	1	0	2	4	0	2	0	4	0	0	0	0	84.74648	84.846	0.00117
$C_8H_{19}N$	Dibutylamine	1	0	2	2	6	0	6	0	0	0	0	0	108.86010	108.872	0.00011
$C_8H_{19}N$	Diisobutylamine	1	0	2	4	2	2	0	6	0	0	0	0	109.00522	109.106	0.00092

Table 15.80. The bond angle parameters of secondary amines and experimental values [1]. In the calculation of θ_v, the parameters from the preceding angle were used. E_T is $E_T(atom-atom,msp^3.AO)$.

Atoms of Angle	2c' Bond 1 (a_0)	2c' Bond 2 (a_0)	2c' Terminal Atoms (a_0)	$E_{Coulombic}$ or E Atom 1	Atom 1 Hybridization Designation (Table 15.3.A)	$E_{Coulombic}$ Atom 2	Atom 2 Hybridization Designation (Table 15.3.A)	c_2 Atom 1	c_2 Atom 2	C_1	C_2	c_1	c_2'	E_T (eV)	θ_v (°)	θ_1 (°)	θ_2 (°)	Cal. θ (°)	Exp. θ (°)
$\angle HCN$ ($C-N$ (i) & (ii))	2.09711	2.79186	4.0661	-14.82575	1	-14.53414	N	0.91771	0.93383 (Eq. (15.136))	0.75	1	0.75	1.01756	0				111.76	112 (dimethylamine)
$\angle HNC_a$ ($C-N$ (i) & (ii))	1.89621	2.79186	3.8123	-14.53414	N	-15.56407 (Eq. (15.136))	7	0.91140 (Eq. (15.135))	0.87418	0.75	1	0.75	0.95917	0				107.27	107 (dimethylamine)
$\angle CNC$ ($C-N$ (i) & (ii))	2.79186	2.79186	4.6260	-17.04641	33	-17.04641	33	0.79816	0.79816	1	1	1	0.79816	-1.85836				111.89	111.8 (dimethylamine)
Methylene $\angle HC_aH$	2.11106	2.11106	3.4252	-15.75493	7	H	H	0.86359	1	1	1	0.75	1.15796	0				108.44	107 (dimethylamine) 107 (propane)
$\angle C_aC_bC_c$															69.51			110.49	112 (propane) 113.8 (butane) 110.8 (isobutane)
$\angle C_aC_bH$															69.51			110.49	111.0 (butane) 111.4 (isobutane)
Methyl $\angle HC_aH$	2.09711	2.09711	3.4252	-15.75493	7	H	H	0.86359	1	1	1	0.75	1.15796	0				109.50	
$\angle C_aC_bC_c$															70.56			109.44	
$\angle C_aC_bH$															70.56			109.44	
$\angle C_bC_aC_c$ iso C_a	2.91547	2.91547	4.7958	-16.68412 C_b	26	-16.68412 C_c	26	0.81549	0.81549	1	1	1	0.81549	-1.85836				110.67	110.8 (isobutane)
$\angle C_bC_aH$ iso C_a	2.91547	2.11323	4.1633	-15.55033 C_a	5	-14.82575 C_b	1	0.87495	0.91771	0.75	1	0.75	1.04887	0				110.76	
$\angle C_aC_bH$ iso C_a	2.91547	2.09711	4.1633	-15.55033 C_b	5	-14.82575 C_a	1	0.87495	0.91771	0.75	1	0.75	1.04887	0				111.27	111.4 (isobutane)
$\angle C_bC_aC_b$ tert C_a	2.90327	2.90327	4.7958	-16.68412 C_b	26	-16.68412 C_b	26	0.81549	0.81549	1	1	1	0.81549	-1.85836				111.37	110.8 (isobutane)
$\angle C_bC_aC_d$															72.50			107.50	

TERTIARY AMINES ($C_nH_{2n+3}N,\ n=3,4,5...\infty$)

The tertiary amines, $C_nH_{2n+3}N$, have three $C-N$ bonds to methyl or alkyl groups wherein $C-N$ comprises a functional group. The alkyl portion of the tertiary amine may comprise at least two terminal methyl groups (CH_3) at each end of the chain, and may comprise methylene (CH_2), and methylyne (CH) functional groups as well as C bound by carbon-carbon single bonds. The methyl and methylene functional groups are equivalent to those of straight-chain alkanes. Six types of $C-C$ bonds can be identified. The n-alkane $C-C$ bond is the same as that of straight-chain alkanes. In addition, the $C-C$ bonds within isopropyl ($(CH_3)_2CH$) and t-butyl ($(CH_3)_3C$) groups and the isopropyl to isopropyl, isopropyl to t-butyl, and t-butyl to t-butyl $C-C$ bonds comprise functional groups. The branched-chain-alkane groups in tertiary amines are equivalent to those in branched-chain alkanes.

The $C-N$ group is solved by hybridizing the $2s$ and $2p$ AOs of the C atom to form a single $2sp^3$ shell as an energy minimum, and the sharing of electrons between the $C2sp^3$ HO and the N AO to form a MO permits each participating orbital to decrease in radius and energy. In tertiary amines, the $C2sp^3$ HO has a hybridization factor of 0.91771 (Eq. (13.430)) with a corresponding energy of $E(C,2sp^3)=-14.63489\ eV$ (Eq. (15.25)), and the N AO has an energy of $E(N)=-14.53414\ eV$. To meet the equipotential condition of the union of the $C-N$ H_2-type-ellipsoidal-MO with these orbitals, the hybridization factor c_2 of Eq. (15.61) for the $C-N$-bond MO given by Eq. (15.135) is $c_2(C2sp^3 HO\ to\ \mathrm{N})=0.91140$.

As given in the Continuous-Chain Alkanes ($C_nH_{2n+2},\ n=3,4,5...\infty$) section, the energy of each $C2sp^3$ HO must be a linear combination of that of the CH_3 and CH_2 groups that serve as basis elements. Each CH_3 forms one $C-C$ bond, and each CH_2 group forms two. Thus, the energy of each $C2sp^3$ HO of each CH_3 and CH_2 group alone is given by that in ethane, $-0.72457\ eV$ (Eq. (14.151)), and ethylene, $-1.13379\ eV$ (Eq. (14.511)), respectively. In order to match the energy of the component HOs and MOs for the entire molecule, the energy $E_{T_{alkane}}(C-C,2sp^3)$ given as a linear combination of these basis elements is $-0.92918\ eV$ (Eq. (14.513)). In tertiary amines, the N binds to three $C2sp^3$ HOs and the corresponding $E_T(atom-atom,msp^3.AO)$ of each $C-N$-bond MO in Eq. (15.61) due to the charge donation from the C and N atoms to the MO is $-0.92918\ eV$. It comprises a linear combination of the energy for a primary amine, $-0.72457\ eV$ and a secondary amine, $-1.13379\ eV$.

The symbols of the functional groups of branched-chain tertiary amines are given in Table 15.81. The geometrical (Eqs. (15.1-15.5) and (15.51)), intercept (Eqs. (15.80-15.87)), and energy (Eqs. (15.6-15.11) and (15.17-15.65)) parameters of tertiary amines are given in Tables 15.82, 15.83, and 15.84, respectively. The total energy of each tertiary amine given in Table 15.85 was calculated as the sum over the integer multiple of each $E_D(Group)$ of Table 15.84 corresponding to functional-group composition of the molecule. The bond angle parameters of tertiary amines determined using Eqs. (15.88-15.117) are given in Table 15.86. The color scale, translucent view of the charge-density of exemplary tertiary amine, trimethylamine, comprising the concentric shells of atoms with the outer shell bridged by one or more H_2-type ellipsoidal MOs or joined with one or more hydrogen MOs is shown in Figure 15.14.

Figure 15.14. Color scale, translucent view of the charge-density of trimethylamine showing the orbitals of the atoms at their radii, the ellipsoidal surface of each H or H_2-type ellipsoidal MO that transitions to the corresponding outer shell of the atom(s) participating in each bond, and the hydrogen nuclei (red, not to scale). (A) Top view. (B) Side view.

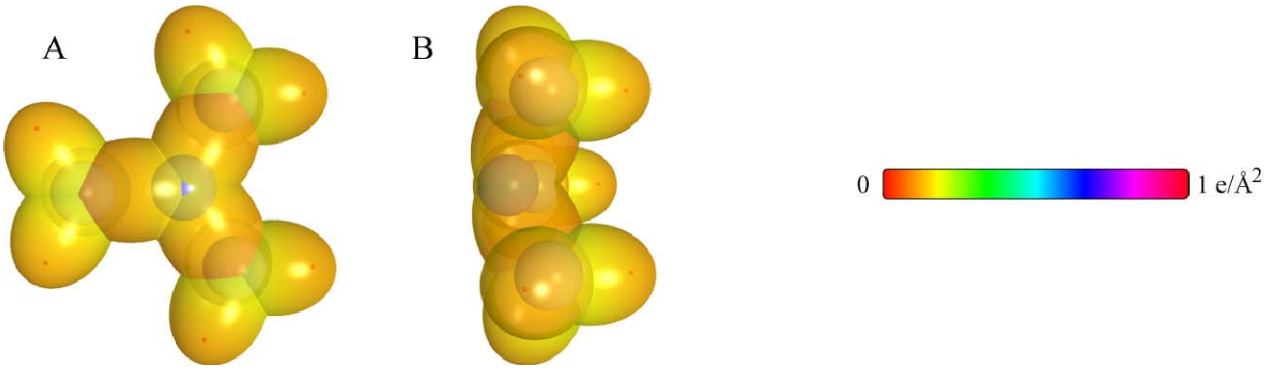

Table 15.81. The symbols of functional groups of tertiary amines.

Functional Group	Group Symbol
C-N	$C-N$
CH_3 group	$C-H\ (CH_3)$
CH_2 group	$C-H\ (CH_2)$
CH	$C-H$
CC bond (*n-C*)	$C-C$ (a)
CC bond (*iso-C*)	$C-C$ (b)
CC bond (*tert-C*)	$C-C$ (c)
CC (*iso* to *iso-C*)	$C-C$ (d)
CC (*t* to *t-C*)	$C-C$ (e)
CC (*t* to *iso-C*)	$C-C$ (f)

Table 15.82. The geometrical bond parameters of tertiary amines and experimental values [1].

Parameter	$C-N$ Group	$C-H\ (CH_3)$ Group	$C-H\ (CH_2)$ Group	$C-H$ Group	$C-C$ (a) Group	$C-C$ (b) Group	$C-C$ (c) Group	$C-C$ (d) Group	$C-C$ (e) Group	$C-C$ (f) Group
$a\ (a_0)$	1.96313	1.64920	1.67122	1.67465	2.12499	2.12499	2.10725	2.12499	2.10725	2.10725
$c'\ (a_0)$	1.40112	1.04856	1.05553	1.05661	1.45744	1.45744	1.45164	1.45744	1.45164	1.45164
Bond Length $2c'\ (\AA)$	1.48288	1.10974	1.11713	1.11827	1.54280	1.54280	1.53635	1.54280	1.53635	1.53635
Exp. Bond Length $(\AA)$	1.458 (trimethylamine)	1.107 ($C-H$ propane) 1.117 ($C-H$ butane)	1.107 ($C-H$ propane) 1.117 ($C-H$ butane)	1.122 (isobutane)	1.532 (propane) 1.531 (butane)	1.532 (propane) 1.531 (butane)	1.532 (propane) 1.531 (butane)	1.532 (propane) 1.531 (butane)	1.532 (propane) 1.531 (butane)	1.532 (propane) 1.531 (butane)
$b,c\ (a_0)$	1.37505	1.27295	1.29569	1.29924	1.54616	1.54616	1.52750	1.54616	1.52750	1.52750
e	0.71372	0.63580	0.63159	0.63095	0.68600	0.68600	0.68888	0.68600	0.68888	0.68888

Table 15.83. The MO to HO intercept geometrical bond parameters of tertiary amines. R, R', R'' are H or alkyl groups. E_T is $E_T(atom-atom,msp^3.AO)$.

Bond	Atom	E_T (eV) Bond 1	E_T (eV) Bond 2	E_T (eV) Bond 3	E_T (eV) Bond 4	Final Total Energy $C2sp^3$ (eV)	$r_{initial}\ (a_0)$	$r_{final}\ (a_0)$	$E_{Coulomb}$ (eV) Final	$E(C2sp^3)$ (eV) Final	$\theta'\ (^\circ)$	$\theta_1\ (^\circ)$	$\theta_2\ (^\circ)$	$d_1\ (a_0)$	$d_2\ (a_0)$
$N-(C_aH_3)_3$	C_a	-0.46459		0	0	-152.08028	0.91771	0.88983	-15.29034	-15.09948	83.37	96.63	40.00	1.50383	0.10271
$N-(C_aH_3)_3$	N	-0.46459	-0.46459	-0.46459	0		0.93084	0.83885	-16.21953		78.02	101.98	36.64	1.57525	0.17413
$N-(C_aH_2-)_2$	C_a	-0.46459	-0.92918	0	0	-153.00946	0.91771	0.83885	-16.21953	-16.02866	78.02	101.98	36.64	1.57525	0.17413
$N-(C_aH_2-)_2$	N	-0.46459	-0.46459	-0.46459	0		0.93084	0.83885	-16.21953		78.02	101.98	36.64	1.57525	0.17413
$C-H\ (CH_3)$	C	-0.92918	0	0	0	-152.54487	0.91771	0.86359	-15.75493	-15.56407	77.49	102.51	41.48	1.23564	0.18708
$C-H\ (CH_2)$	C	-0.92918	-0.92918	0	0	-153.47406	0.91771	0.81549	-16.68412	-16.49325	68.47	111.53	35.84	1.35486	0.29933
$C-H\ (CH)$	C	-0.92918	-0.92918	-0.92918	0	-154.40324	0.91771	0.77247	-17.61330	-17.42244	61.10	118.90	31.37	1.42988	0.37326
$H_3C_aC_bH_2CH_2-$ ($C-C$ (a))	C_a	-0.92918	0	0	0	-152.54487	0.91771	0.86359	-15.75493	-15.56407	63.82	116.18	30.08	1.83879	0.38106
$H_3C_aC_bH_2CH_2-$ ($C-C$ (a))	C_b	-0.92918	-0.92918	0	0	-153.47406	0.91771	0.81549	-16.68412	-16.49325	56.41	123.59	26.06	1.90890	0.45117
$R-H_2C_aC_b(H_2C_c-R')HCH_2-$ ($C-C$ (b))	C_b	-0.92918	-0.92918	-0.92918	0	-154.40324	0.91771	0.77247	-17.61330	-17.42244	48.30	131.70	21.90	1.97162	0.51388
$R-H_2C_a(R'-H_2C_d)C_b(R''-H_2C_c)CH_2-$ ($C-C$ (c))	C_b	-0.92918	-0.72457	-0.72457	-0.72457	-154.71860	0.91771	0.75889	-17.92866	-17.73779	48.21	131.79	21.74	1.95734	0.50570
$isoC_aC_b(H_2C_c-R')HCH_2-$ ($C-C$ (d))	C_b	-0.92918	-0.92918	-0.92918	0	-154.40324	0.91771	0.77247	-17.61330	-17.42244	48.30	131.70	21.90	1.97162	0.51388
$tertC_a(R'-H_2C_d)C_b(R''-H_2C_c)CH_2-$ ($C-C$ (e))	C_b	-0.72457	-0.72457	-0.72457	-0.72457	-154.51399	0.91771	0.76765	-17.92866	-17.73779	50.04	129.96	22.66	1.94462	0.49298
$tertC_aC_b(H_2C_c-R')HCH_2-$ ($C-C$ (f))	C_b	-0.72457	-0.92918	-0.92918	0	-154.19863	0.91771	0.78155	-17.40869	-17.21783	52.78	127.22	24.04	1.92443	0.47279
$isoC_a(R'-H_2C_d)C_b(R''-H_2C_c)CH_2-$ ($C-C$ (f))	C_b	-0.72457	-0.72457	-0.72457	-0.72457	-154.51399	0.91771	0.76765	-17.92866	-17.73779	50.04	129.96	22.66	1.94462	0.49298

Table 15.84. The energy parameters (eV) of functional groups of tertiary amines.

Parameters	$C-N$ Group	CH_3 Group	CH_2 Group	$C-H$ Group	$C-C$ (a) Group	$C-C$ (b) Group	$C-C$ (c) Group	$C-C$ (d) Group	$C-C$ (e) Group	$C-C$ (f) Group
n_1	1	3	2	1	1	1	1	1	1	1
n_2	0	2	1	0	0	0	0	0	0	0
n_3	0	0	0	0	0	0	0	0	0	0
C_1	0.5	0.75	0.75	0.75	0.5	0.5	0.5	0.5	0.5	0.5
C_2	1	1	1	1	1	1	1	1	1	1
c_1	1	1	1	1	1	1	1	1	1	1
c_2	0.91140	0.91771	0.91771	0.91771	0.91771	0.91771	0.91771	0.91771	0.91771	0.91771
c_3	0	0	1	1	0	0	0	1	1	0
c_4	2	1	1	1	2	2	2	2	2	2
c_5	0	3	2	1	0	0	0	0	0	0
C_{1o}	0.5	0.75	0.75	0.75	0.5	0.5	0.5	0.5	0.5	0.5
C_{2o}	1	1	1	1	1	1	1	1	1	1
V_e (eV)	-31.67393	-107.32728	-70.41425	-35.12015	-28.79214	-28.79214	-29.10112	-28.79214	-29.10112	-29.10112
V_p (eV)	9.71067	38.92728	25.78002	12.87680	9.33352	9.33352	9.37273	9.33352	9.37273	9.37273
T (eV)	8.06719	32.53914	21.06675	10.48582	6.77464	6.77464	6.90500	6.77464	6.90500	6.90500
V_m (eV)	-4.03359	-16.26957	-10.53337	-5.24291	-3.38732	-3.38732	-3.45250	-3.38732	-3.45250	-3.45250
$E_{(AO/HO)}$ (eV)	-14.63489	-15.56407	-15.56407	-14.63489	-15.56407	-15.56407	-15.35946	-15.56407	-15.35946	-15.35946
$\Delta E_{H_2MO(AO/HO)}$ (eV)	-0.92918	0	0	0	0	0	0	0	0	0
$E_{1(AO/HO)}$ (eV)	-13.70571	-15.56407	-15.56407	-14.63489	-15.56407	-15.56407	-15.35946	-15.56407	-15.35946	-15.35946
$E_{1(H_2MO)}$ (eV)	-31.63537	-67.69451	-49.66493	-31.63533	-31.63537	-31.63537	-31.63535	-31.63537	-31.63535	-31.63535
$E_1(atom-atom, msp^3.AO)$ (eV)	-0.92918	0	0	0	-1.85836	-1.85836	-1.44915	-1.85836	-1.44915	-1.44915
$E_{1(MO)}$ (eV)	-32.56455	-67.69450	-49.66493	-31.63537	-33.49373	-33.49373	-33.08452	-33.49373	-33.08452	-33.08452
ω $(10^{15}\ rad/s)$	18.1298	24.9286	24.2751	24.1759	9.43699	9.43699	15.4846	9.43699	9.55643	9.55643
E_K (eV)	11.93333	16.40846	15.97831	15.91299	6.21159	6.21159	10.19220	6.21159	6.29021	6.29021
$\bar{E}_D$ (eV)	-0.22255	-0.25352	-0.25017	-0.24966	-0.16515	-0.16515	-0.20896	-0.16515	-0.16416	-0.16416
$\bar{E}_{Kvib}$ (eV)	0.12944 [23]	0.35532 (Eq. (13.458))	0.35532 (Eq. (13.458))	0.35532 (Eq. (13.458))	0.12312 [2]	0.17978 [4]	0.09944 [5]	0.12312 [2]	0.12312 [2]	0.12312 [2]
$\bar{E}_{osc}$ (eV)	-0.15783	-0.22757	-0.14502	-0.07200	-0.10359	-0.07526	-0.15924	-0.10359	-0.10260	-0.10260
E_{mag} (eV)	0.14803	0.14803	0.14803	0.14803	0.14803	0.14803	0.14803	0.14803	0.14803	0.14803
$E_{1(Group)}$ (eV)	-32.72238	-67.92207	-49.80996	-31.70737	-33.59732	-33.49373	-33.24376	-33.59732	-33.18712	-33.18712
$E_{initial(4\ AO/HO)}$ (eV)	-14.63489	-14.63489	-14.63489	-14.63489	-14.63489	-14.63489	-14.63489	-14.63489	-14.63489	-14.63489
$E_{initial(5\ AO/HO)}$ (eV)	0	-13.59844	-13.59844	-13.59844	0	0	0	0	0	0
$E_{1(Group)}$ (eV)	3.45260	12.49186	7.83016	3.32601	4.32754	4.29921	3.97398	4.17951	3.62128	3.91734

Table 15.85. The total bond energies of tertiary amines calculated using the functional group composition and the energies of Table 15.84 compared to the experimental values [3].

Formula	Name	$C-N$ Group	CH_3	CH_2	CH	$C-C$ (a)	$C-C$ (b)	$C-C$ (c)	$C-C$ (d)	$C-C$ (e)	$C-C$ (f)	Calculated Total Bond Energy (eV)	Experimental Total Bond Energy (eV)	Relative Error
C_3H_9N	Trimethylamine	3	3	0	0	0	0	0	0	0	0	47.83338	47.761	-0.00152
$C_6H_{15}N$	Triethylamine	3	3	3	0	3	0	0	0	0	0	84.30648	84.316	0.00012
$C_9H_{21}N$	Tripropylamine	3	3	6	0	6	0	0	0	0	0	120.77958	120.864	0.00070

Table 15.86. The bond angle parameters of tertiary amines and experimental values [1]. In the calculation of θ_v, the parameters from the preceding angle were used. E_T is $E_T(atom-atom,msp^3.AO)$.

Atoms of Angle	2c' Bond 1 (a_0)	2c' Bond 2 (a_0)	2c' Terminal Atoms (a_0)	$E_{Coulombic}$ or E Atom 1	Atom 1 Hybridization Designation (Table 15.3.A)	$E_{Coulombic}$ Atom 2	Atom 2 Hybridization Designation (Table 15.3.A)	c_2 Atom 1	c_2 Atom 2	C_1	C_2	c_1	c_2'	E_T (eV)	θ_v (°)	θ_1 (°)	θ_2 (°)	Cal. θ (°)	Exp. θ (°)
$\angle CNC$	2.80224	2.80224	4.6043	-17.14871	36	-17.14871	36	0.79340	0.79340	1	1	1	0.79340	-1.85836				110.48	110.9 (trimethylamine)
Methylene $\angle HC_aH$	2.11106	2.11106	3.4252	-15.75493	7	H	H	0.86359	1	1	1	0.75	1.15796	0				108.44	107 (dimethylamine) 107 (propane)
$\angle C_aC_bC_c$															69.51			110.49	112 (propane) 113.8 (butane) 110.8 (isobutane)
$\angle C_aC_bH$															69.51			110.49	111.0 (butane) 111.4 (isobutane)
Methyl $\angle HC_aH$	2.09711	2.09711	3.4252	-15.75493	7	H	H	0.86359	1	1	1	0.75	1.15796	0				109.50	
$\angle C_aC_bC_c$															70.56			109.44	
$\angle C_aC_bH$															70.56			109.44	
$\angle C_bC_aC_c$ iso C_a	2.91547	2.91547	4.7958	-16.68412 C_b	26	-16.68412 C_c	26	0.81549	0.81549	1	1	1	0.81549	-1.85836				110.67	110.8 (isobutane)
$\angle C_bC_aH$ iso C_a	2.91547	2.11323	4.1633	-15.55033 C_a	5	-14.82575 C_b	1	0.87495	0.91771	0.75	1	0.75	1.04887	0				110.76	
$\angle C_aC_bH$ iso C_a	2.91547	2.09711	4.1633	-15.55033 C_b	5	-14.82575 C_a	1	0.87495	0.91771	0.75	1	0.75	1.04887	0				111.27	111.4 (isobutane)
$\angle C_bC_aC_b$ tert C_a	2.90327	2.90327	4.7958	-16.68412 C_b	26	-16.68412 C_b	26	0.81549	0.81549	1	1	1	0.81549	-1.85836				111.37	110.8 (isobutane)
$\angle C_bC_aC_d$															72.50			107.50	

ALDEHYDES ($C_nH_{2n}O,\ n=1,2,3,4,5...\infty$)

The alkyl aldehydes, $C_nH_{2n}O$, each have a $HC=O$ moiety that comprises a $C=O$ functional group and a CH functional group. The single bond of carbon to the carbonyl carbon atom, $C-C(O)H$, is a functional group. In addition to the $C=O$ functional group, formaldehyde comprises a CH_2 functional group. The alkyl portion of the alkyl aldehyde may comprise at least two terminal methyl groups (CH_3) at each end of the chain, and may comprise methylene (CH_2), and methylyne (CH) functional groups as well as C bound by carbon-carbon single bonds. The methyl and methylene functional groups are equivalent to those of straight-chain alkanes. Six types of $C-C$ bonds can be identified. The n-alkane $C-C$ bond is the same as that of straight-chain alkanes. In addition, the $C-C$ bonds within isopropyl ($(CH_3)_2CH$) and t-butyl ($(CH_3)_3C$) groups and the isopropyl to isopropyl, isopropyl to t-butyl, and t-butyl to t-butyl $C-C$ bonds comprise functional groups. The branched-chain-alkane groups in aldehydes are equivalent to those in branched-chain alkanes.

The CH functional group was solved in the Hydrogen Carbide (CH) section except that E_{mag} is not subtracted since unpaired electrons are not created with fragmentation of the CH functional group of aldehydes. The CH_2 functional group of formaldehyde is solved in the Dihydrogen Carbide (CH_2) section except that the energy of each $C-H$ MO is matched to the initial energy of the $C2sp^3$ HO (Eq. (15.25)). The $C=O$ and $C-C(O)H$ groups are solved by hybridizing the $2s$ and $2p$ AOs of each C atom to form a single $2sp^3$ shell as an energy minimum, and the sharing of electrons between the $C2sp^3$ HO and the O AO or between two $C2sp^3$ HOs, respectively, to form a MO permits each participating orbital to decrease in radius and energy. In alkyl aldehydes, the $C2sp^3$ HO has a hybridization factor of 0.91771 (Eq. (13.430)) with a corresponding energy of $E\left(C,2sp^3\right)=-14.63489\,eV$ (Eq. (15.25)) and the O AO has an energy of $E(O)=-13.61806\,eV$. To meet the equipotential condition of the union of the $C=O$ H_2-type-ellipsoidal-MO with these orbitals, the hybridization factor c_2 of Eq. (15.61) for the $C=O$-bond MO given by Eq. (15.133) is $c_2\left(C2sp^3HO\ to\ O\right)=0.85395$. The unpaired electrons created by bond breakage of the double $C=O$ bond requires that two times the $O2p$ AO magnetic energy E_{mag} (Eq. (15.69)) be subtracted from the total energy to give $E_{D(Group)}$ (eV) for $C=O$.

$E_T\left(atom-atom,msp^3.AO\right)$ of the $C=O$-bond MO in Eq. (15.61) due to the charge donation from the C and O atoms to the MO is $-2.69893\,eV$ which is an energy minimum for the double bond between the pair of $C2sp^3$ HO electrons of the C atom and the pair of AO electrons of the O atom. It is given as a linear combination of the energy contributions corresponding to a double bond, $-1.13379\,eV$ (Eq. (14.247)), and a triple bond, $-1.56513\,eV$ (Eq. (14.342)). The triple bond contribution includes the $C2sp^3$ HO electron of the $C-H$ bond in addition to the pair involved directly in the double bond with O. $E_T\left(atom-atom,msp^3.AO\right)$ of the $C-C(O)H$ group is equivalent to that of an alkane, $-1.85836\,eV$, where both energy contributions are given by Eq. (14.513). It is based on the energy match between the $C2sp^3$ HOs of the aldehyde. In order to match energy between the groups bonded to the $C=O$, electron-density is shared. Due to the interaction in the transition state between the groups based on the sharing, $C_{1o}=2C_1$ rather than $C_{1o}=C_1$ in Eq. (15.61) for the $C-C(O)H$ bond.

The symbols of the functional groups of alkyl aldehydes are given in Table 15.87. The geometrical (Eqs. (15.1-15.5) and (15.51)), intercept (Eqs. (15.80-15.87)), and energy (Eqs. (15.6-15.11) and (15.17-15.65)) parameters of alkyl aldehydes are given in Tables 15.88, 15.89, and 15.90, respectively. The total energy of each alkyl aldehyde given in Table 15.91 was calculated as the sum over the integer multiple of each $E_{D(Group)}$ of Table 15.90 corresponding to functional-group composition of the molecule. The bond angle parameters of alkyl aldehydes determined using Eqs. (15.88-15.117) are given in Table 15.92. The color scale, translucent view of the charge-density of exemplary aldehyde, Propanal, comprising the concentric shells of atoms with the outer shell bridged by one or more H_2-type ellipsoidal MOs or joined with one or more hydrogen MOs is shown in Figure 15.15.

Figure 15.15. (A)-(B) Color scale, translucent views of the charge-density of propanal showing the orbitals of the atoms at their radii, the ellipsoidal surface of each H or H_2-type ellipsoidal MO that transitions to the corresponding outer shell of the atom(s) participating in each bond, and the hydrogen nuclei (red, not to scale).

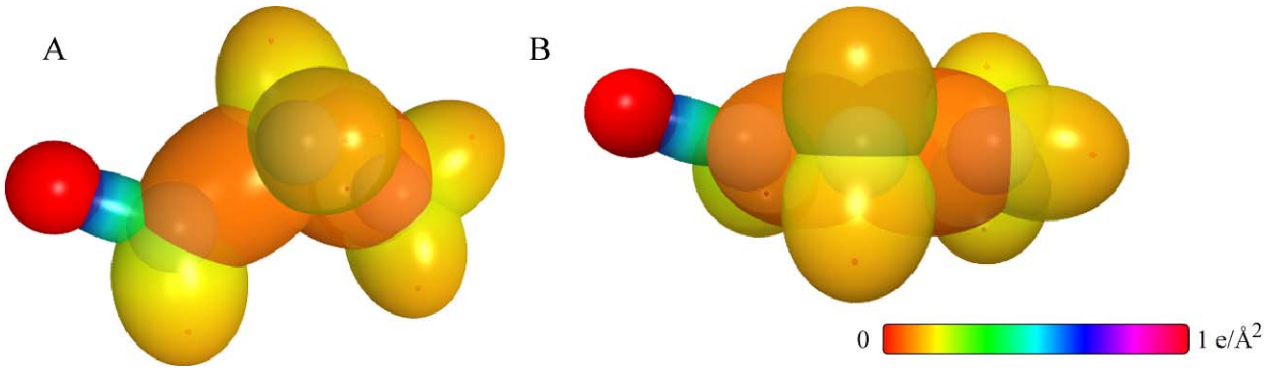

Table 15.87. The symbols of functional groups of alkyl aldehydes.

Functional Group	Group Symbol
CH_2 (formaldehyde) group	$C-H\ (CH_2)$ (i)
CH (aldehyde) group	CH (i)
C=O	$C=O$ (i)
C-C(O)H	$C-C(O)H$
CH_3 group	$C-H\ (CH_3)$
CH_2 (alkyl) group	$C-H\ (CH_2)$ (ii)
CH (alkyl)	$C-H$ (ii)
CC bond (*n-C)*	$C-C$ (a)
CC bond (*iso-C*)	$C-C$ (b)
CC bond (*tert-C*)	$C-C$ (c)
CC (*iso* to *iso-C*)	$C-C$ (d)
CC (*t* to *t-C*)	$C-C$ (e)
CC (*t* to *iso-C*)	$C-C$ (f)

Table 15.88. The geometrical bond parameters of alkyl aldehydes and experimental values [1].

Parameter	$C-H\ (CH_2)$ (i)	CH (i) Group	$C=O$ Group	$C-C(O)H$ Group	$C-H\ (CH_3)$ Group	$C-H\ (CH_2)$ (ii) Group	$C-H$ (ii) Group	$C-C$ (a) Group	$C-C$ (b) Group	$C-C$ (c) Group	$C-C$ (d) Group	$C-C$ (e) Group	$C-C$ (f) Group
$a\ (a_0)$	1.64010	1.67465	1.29907	2.04740	1.64920	1.67122	1.67465	2.12499	2.12499	2.10725	2.12499	2.10725	2.10725
$c'\ (a_0)$	1.04566	1.05661	1.13977	1.43087	1.04856	1.05553	1.05661	1.45744	1.45744	1.45164	1.45744	1.45164	1.45164
Bond Length $2c'\ (\text{Å})$	1.10668	1.11827	1.20628	1.51437	1.10974	1.11713	1.11827	1.54280	1.54280	1.53635	1.54280	1.53635	1.53635
Exp. Bond Length (Å)	1.116 (formaldehyde)	1.128 (acetaldehyde)	1.208 (formaldehyde) 1.210 (acetaldehyde)	1.515 (acetaldehyde)	1.107 ($C-H$ propane) 1.117 ($C-H$ butane)	1.107 ($C-H$ propane) 1.117 ($C-H$ butane)	1.122 (isobutane)	1.532 (propane) 1.531 (butane)	1.532 (propane) 1.531 (butane)	1.532 (propane) 1.531 (butane)	1.532 (propane) 1.531 (butane)	1.532 (propane) 1.531 (butane)	1.532 (propane) 1.531 (butane)
$b,c\ (a_0)$	1.26354	1.29924	0.62331	1.46439	1.27295	1.29569	1.29924	1.54616	1.54616	1.52750	1.54616	1.52750	1.52750
e	0.63756	0.63095	0.87737	0.69887	0.63580	0.63159	0.63095	0.68600	0.68600	0.68888	0.68600	0.68888	0.68888

Table 15.89. The MO to HO intercept geometrical bond parameters of alkyl aldehydes. R, R', R'' are H or alkyl groups. E_T is $E_T\,(atom-atom,msp^3.AO)$.

Bond	Atom	E_T (eV) Bond 1	E_T (eV) Bond 2	E_T (eV) Bond 3	E_T (eV) Bond 4	Final Total Energy $C2sp^3$ (eV)	$r_{initial}\ (a_0)$	$r_{final}\ (a_0)$	$E_{Coulomb}$ (eV) Final	$E(C2sp^3)$ (eV) Final	ϑ' (°)	θ_1 (°)	θ_2 (°)	$d_1\ (a_0)$	$d_2\ (a_0)$
$HC(O)-H\ (CH_2)$ (i)	C	-1.34946	0	0	0	-152.96515	0.91771	0.84115	-16.17521	-15.98435	75.72	104.28	40.18	1.25314	0.20748
$-C_bH_2C_a(O)-H\ (CH)$ (i)	C_a	-1.34946	-0.92918	0	0	-153.89434	0.91771	0.79546	-17.10440	-16.91353	64.95	115.05	33.69	1.39345	0.33684
$H_2C=O$	O	-1.34946	0	0	0		1.00000	0.84115	-16.17521		137.27	42.73	66.31	0.52193	0.61784
$-C_bH_2C_a(H)=O$	O	-1.34946	0	0	0		1.00000	0.84115	-16.17521		137.27	42.73	66.31	0.52193	0.61784
$RH_2C_b-C_a(H)(O)$	C_a	-1.34946	-0.92918	0	0	-153.89434	0.91771	0.79546	-17.10440	-16.91353	135.34	44.66	63.78	0.57401	0.56576
$H_3C_b-C_a(H)(O)$	C_b	-0.92918	0	0	0	-152.54487	0.91771	0.86359	-15.75493	-15.56407	72.27	107.73	34.17	1.69388	0.26301
$-C_bH_2-C_a(H)(O)$	C_b	-0.92918	-0.92918	0	0	-153.47405	0.91771	0.81549	-16.68411	-16.49325	65.99	114.01	30.58	1.76270	0.33183
$C-H\ (CH_3)$	C	-0.92918	0	0	0	-152.54487	0.91771	0.86359	-15.75493	-15.56407	77.49	102.51	41.48	1.23564	0.18708
$C-H\ (CH_2)$ (ii)	C	-0.92918	-0.92918	0	0	-153.47406	0.91771	0.81549	-16.68412	-16.49325	68.47	111.53	35.84	1.35486	0.29933
$C-H\ (CH)$ (ii)	C	-0.92918	-0.92918	-0.92918	0	-154.40324	0.91771	0.77247	-17.61330	-17.42244	61.10	118.90	31.37	1.42988	0.37326
$H_3C_aC_bH_2CH_2-$ ($C-C$ (a))	C_a	-0.92918	0	0	0	-152.54487	0.91771	0.86359	-15.75493	-15.56407	63.82	116.18	30.08	1.83879	0.38106
$H_3C_aC_bH_2CH_2-$ ($C-C$ (a))	C_b	-0.92918	-0.92918	0	0	-153.47406	0.91771	0.81549	-16.68412	-16.49325	56.41	123.59	26.06	1.90890	0.45117
$R-H_2C_aC_b(H_2C_c-R')HCH_2-$ ($C-C$ (b))	C_b	-0.92918	-0.92918	-0.92918	0	-154.40324	0.91771	0.77247	-17.61330	-17.42244	48.30	131.70	21.90	1.97162	0.51388
$R-H_2C_a(R'-H_2C_d)C_b(R''-H_2C_c)CH_2-$ ($C-C$ (c))	C_b	-0.92918	-0.72457	-0.72457	-0.72457	-154.71860	0.91771	0.75889	-17.92866	-17.73779	48.21	131.79	21.74	1.95734	0.50570
$isoC_aC_b(H_2C_c-R')HCH_2-$ ($C-C$ (d))	C_b	-0.92918	-0.92918	-0.92918	0	-154.40324	0.91771	0.77247	-17.61330	-17.42244	48.30	131.70	21.90	1.97162	0.51388
$tertC_a(R'-H_2C_d)C_b(R''-H_2C_c)CH_2-$ ($C-C$ (e))	C_b	-0.72457	-0.72457	-0.72457	-0.72457	-154.51399	0.91771	0.76765	-17.92866	-17.73779	50.04	129.96	22.66	1.94462	0.49298
$tertC_aC_b(H_2C_c-R')HCH_2-$ ($C-C$ (f))	C_b	-0.72457	-0.92918	-0.92918	0	-154.19863	0.91771	0.78155	-17.40869	-17.21783	52.78	127.22	24.04	1.92443	0.47279
$isoC_a(R'-H_2C_d)C_b(R''-H_2C_c)CH_2-$ ($C-C$ (f))	C_b	-0.72457	-0.72457	-0.72457	-0.72457	-154.51399	0.91771	0.76765	-17.92866	-17.73779	50.04	129.96	22.66	1.94462	0.49298

Table 15.90. The energy parameters (eV) of functional groups of alkyl aldehydes.

Parameters	CH_2 (i) Group	CH (i) Group	$C=O$ Group	$C-C(O)H$ Group	CH_3 Group	CH_2 (ii) Group	$C-H$ (ii) Group	$C-C$ (a) Group	$C-C$ (b) Group	$C-C$ (c) Group	$C-C$ (d) Group	$C-C$ (e) Group	$C-C$ (f) Group
n_1	2	1	2	1	3	2	1	1	1	1	1	1	1
n_2	1	0	0	0	2	1	0	0	0	0	0	0	0
n_3	0	0	0	0	0	0	0	0	0	0	0	0	0
C_1	0.75	0.75	0.5	0.5	0.75	0.75	0.75	0.5	0.5	0.5	0.5	0.5	0.5
C_2	1	1	1	1	1	1	1	1	1	1	1	1	1
c_1	1	1	1	1	1	1	1	1	1	1	1	1	1
c_2	0.91771	0.91771	0.85395	0.91771	0.91771	0.91771	0.91771	0.91771	0.91771	0.91771	0.91771	0.91771	0.91771
c_3	1	0	2	0	0	1	1	0	0	0	1	1	0
c_4	1	1	4	2	1	1	1	2	2	2	2	2	2
c_5	2	1	0	0	3	2	1	0	0	0	0	0	0
$C_{1\sigma}$	0.75	0.75	0.5	1	0.75	0.75	0.75	0.5	0.5	0.5	0.5	0.5	0.5
$C_{2\sigma}$	1	1	1	1	1	1	1	1	1	1	1	1	1
V_e (eV)	-72.03287	-35.12015	-111.25473	-30.19634	-107.32728	-70.41425	-35.12015	-28.79214	-28.79214	-29.10112	-28.79214	-29.10112	-29.10112
V_p (eV)	26.02344	12.87680	23.87467	9.50874	38.92728	25.78002	12.87680	9.33352	9.33352	9.37273	9.33352	9.37273	9.37273
T (eV)	21.95990	10.48582	42.82081	7.37432	32.53914	21.06675	10.48582	6.77464	6.77464	6.90500	6.77464	6.90500	6.90500
V_m (eV)	-10.97995	-5.24291	-21.41040	-3.68716	-16.26957	-10.53337	-5.24291	-3.38732	-3.38732	-3.45250	-3.38732	-3.45250	-3.45250
$E_{(AO/HO)}$ (eV)	-14.63489	-14.63489	0	-14.63489	-15.56407	-15.56407	-14.63489	-15.56407	-15.56407	-15.35946	-15.56407	-15.35946	-15.35946
$\Delta E_{H_2MO(AO/HO)}$ (eV)	0	0	-2.69893	0	0	0	0	0	0	0	0	0	0
$E_T(_{AO/HO})$ (eV)	-14.63489	-14.63489	2.69893	-14.63489	-15.56407	-15.56407	-14.63489	-15.56407	-15.56407	-15.35946	-15.56407	-15.35946	-15.35946
$E_T(_{H_2MO})$ (eV)	-49.66437	-31.63533	-63.27074	-31.63534	-67.69451	-49.66493	-31.63533	-31.63537	-31.63537	-31.63535	-31.63537	-31.63535	-31.63535
$E_T\left(atom-atom, msp^3.AO\right)(eV)$	0	0	-2.69893	-1.85836	0	0	0	-1.85836	-1.85836	-1.44915	-1.85836	-1.44915	-1.44915
$E_T(_{MO})$ (eV)	-49.66493	-31.63537	-65.96966	-33.49373	-67.69450	-49.66493	-31.63537	-33.49373	-33.49373	-33.08452	-33.49373	-33.08452	-33.08452
$\omega\ \left(10^{15}\ rad/s\right)$	25.2077	24.1759	59.4034	23.3291	24.9286	24.2751	24.1759	9.43699	9.43699	15.4846	9.43699	9.55643	9.55643
E_K (eV)	16.59214	15.91299	39.10034	15.35563	16.40846	15.97831	15.91299	6.21159	6.21159	10.19220	6.21159	6.29021	6.29021
$\bar{E}_D$ (eV)	-0.25493	-0.24966	-0.40804	-0.25966	-0.25352	-0.25017	-0.24966	-0.16515	-0.16515	-0.20896	-0.16515	-0.16416	-0.16416
$\bar{E}_{Kvib}$ (eV)	0.35532 (Eq. (13.458))	0.35532 (Eq. (13.458))	0.21077 [12]	0.13800 [26]	0.35532 (Eq. (13.458))	0.35532 (Eq. (13.458))	0.35532 (Eq. (13.458))	0.12312 [2]	0.17978 [4]	0.09944 [5]	0.12312 [2]	0.12312 [2]	0.12312 [2]
$\bar{E}_{osc}$ (eV)	-0.07727	-0.07200	-0.30266	-0.19066	-0.22757	-0.14502	-0.07200	-0.10359	-0.07526	-0.15924	-0.10359	-0.10260	-0.10260
E_{mag} (eV)	0.14803	0.14803	0.11441	0.14803	0.14803	0.14803	0.14803	0.14803	0.14803	0.14803	0.14803	0.14803	0.14803
$E_T(_{Group})$ (eV)	-49.81948	-31.70737	-66.57498	-33.68439	-67.92207	-49.80996	-31.70737	-33.59732	-33.49373	-33.24376	-33.59732	-33.18712	-33.18712
$E_{initial}(_{c_4\ AO/HO})$ (eV)	-14.63489	-14.63489	-14.63489	-14.63489	-14.63489	-14.63489	-14.63489	-14.63489	-14.63489	-14.63489	-14.63489	-14.63489	-14.63489
$E_{initial}(_{c_5\ AO/HO})$ (eV)	-13.59844	-13.59844	0	0	-13.59844	-13.59844	-13.59844	0	0	0	0	0	0
$E_D(_{Group})$ (eV)	7.83968	3.47404	7.80660	4.41461	12.49186	7.83016	3.32601	4.32754	4.29921	3.97398	4.17951	3.62128	3.91734

Table 15.91. The total bond energies of alkyl aldehydes calculated using the functional group composition and the energies of Table 15.90 compared to the experimental values [3].

Formula	Name	CH_2 (i) Group	CH (i) Group	$C=O$ Group	$C-C(O)H$ Group	CH_3	CH_2 (ii)	CH (ii)	$C-C$ (a)	$C-C$ (b)	$C-C$ (c)	$C-C$ (d)	$C-C$ (e)	$C-C$ (f)	Calculated Total Bond Energy (eV)	Experimental Total Bond Energy (eV)	Relative Error
CH_2O	Formaldehyde	1	0	1	0	0	0	0	0	0	0	0	0	0	15.64628	15.655	0.00056
C_2H_4O	Acetaldehyde	0	1	1	1	1	0	0	0	0	0	0	0	0	28.18711	28.198	0.00039
C_3H_6O	Propanal	0	1	1	1	1	1	0	1	0	0	0	0	0	40.34481	40.345	0.00000
C_4H_8O	Butanal	0	1	1	1	1	2	0	2	0	0	0	0	0	52.50251	52.491	-0.00022
C_4H_8O	Isobutanal	0	1	1	1	2	0	1	0	2	0	0	0	0	52.60340	52.604	0.00001
$C_5H_{10}O$	Pentanal	0	1	1	1	1	3	0	3	0	0	0	0	0	64.66021	64.682	0.00034
$C_7H_{14}O$	Heptanal	0	1	1	1	1	5	0	5	0	0	0	0	0	88.97561	88.942	-0.00038
$C_8H_{16}O$	Octanal	0	1	1	1	1	6	0	6	0	0	0	0	0	101.13331	101.179	0.00045
$C_8H_{16}O$	2-Ethylhexanal	0	1	1	1	2	4	1	4	2	0	0	0	0	101.23420	101.259	0.00025

Table 15.92. The bond angle parameters of alkyl aldehydes and experimental values [1]. In the calculation of θ_v, the parameters from the preceding angle were used. E_T is $E_T(atom-atom,msp^3.AO)$.

Atoms of Angle	2c' Bond 1 (a_0)	2c' Bond 2 (a_0)	2c' Terminal Atoms (a_0)	$E_{Coulombic}$ Atom 1	Atom 1 Hybridization Designation (Table 15.3.A)	$E_{Coulombic}$ Atom 2	Atom 2 Hybridization Designation (Table 15.3.A)	c_2 Atom 1	c_2 Atom 2	C_1	C_2	c_1	c_2'	E_T (eV)	θ_v (°)	θ_1 (°)	θ_2 (°)	Cal. θ (°)	Exp. θ (°)
$\angle HC_aH$ ($C_aH_3(O)$ (i))	2.09132	2.09132	3.5637	-16.39089	19	H	H	0.83008	1	1	1	0.75	1.20470	0				116.87	116.5 (formaldehyde)
$\angle C_bC_aH$ $RC_a(H)=O$	2.86175	2.11323	4.2269	-15.75493 C_a	7	-14.82575 C_b	1	0.86359	0.91771	0.75	1	0.75	1.06267	0				115.52	115.3 (acetaldehyde)
$\angle C_bC_aO$	2.86175	2.27954	4.5826	-16.68412	26	-13.61806	O	0.81549	0.85395 (Eq. (15.133))	1	1	1	0.83472	-1.65376				125.70	124.1 (acetaldehyde)
Methylene $\angle HC_aH$	2.11106	2.11106	3.4252	-15.75493	7	H	H	0.86359	1	1	1	0.75	1.15796	0				108.44	107 (propane)
$\angle C_aC_bC_c$															69.51			110.49	112 (propane) 113.8 (butane) 110.8 (isobutane)
$\angle C_aC_bH$															69.51			110.49	111.0 (butane) 111.4 (isobutane)
Methyl $\angle HC_aH$	2.09711	2.09711	3.4252	-15.75493	7	H	H	0.86359	1	1	1	0.75	1.15796	0				109.50	
$\angle C_aC_bC_c$															70.56			109.44	
$\angle C_aC_bH$															70.56			109.44	
$\angle C_bC_aC_c$ iso C_a	2.91547	2.91547	4.7958	-16.68412 C_b	26	-16.68412 C_c	26	0.81549	0.81549	1	1	1	0.81549	-1.85836				110.67	110.8 (isobutane)
$\angle C_bC_aH$ iso C_a	2.91547	2.11323	4.1633	-15.55033 C_a	5	-14.82575 C_b	1	0.87495	0.91771	0.75	1	0.75	1.04887	0				110.76	
$\angle C_aC_bH$ iso C_a	2.91547	2.09711	4.1633	-15.55033 C_b	5	-14.82575 C_a	1	0.87495	0.91771	0.75	1	0.75	1.04887	0				111.27	111.4 (isobutane)
$\angle C_bC_aC_b$ tert C_a	2.90327	2.90327	4.7958	-16.68412 C_b	26	-16.68412 C_b	26	0.81549	0.81549	1	1	1	0.81549	-1.85836				111.37	110.8 (isobutane)
$\angle C_bC_aC_d$															72.50			107.50	

KETONES ($C_nH_{2n}O,\ n=1,2,3,4,5...\infty$)

The alkyl ketones, $C_nH_{2n}O$, each have a $C=O$ moiety that comprises a functional group. Each of the two single bonds of carbon to the carbonyl carbon atom, $C-C(O)$, is also a functional group. The alkyl portion of the alkyl ketone may comprise at least two terminal methyl groups (CH_3) at each end of the chain, and may comprise methylene (CH_2), and methylyne (CH) functional groups as well as C bound by carbon-carbon single bonds. The methyl and methylene functional groups are equivalent to those of straight-chain alkanes. Six types of $C-C$ bonds can be identified. The n-alkane $C-C$ bond is the same as that of straight-chain alkanes. In addition, the $C-C$ bonds within isopropyl ($(CH_3)_2CH$) and t-butyl ($(CH_3)_3C$) groups and the isopropyl to isopropyl, isopropyl to t-butyl, and t-butyl to t-butyl $C-C$ bonds comprise functional groups. The branched-chain-alkane groups in ketones are equivalent to those in branched-chain alkanes.

The $C=O$ and $C-C(O)$ groups are solved by hybridizing the $2s$ and $2p$ AOs of each C atom to form a single $2sp^3$ shell as an energy minimum, and the sharing of electrons between the $C2sp^3$ HO and the O AO or between two $C2sp^3$ HOs, respectively, to form a MO permits each participating orbital to decrease in radius and energy. In alkyl ketones, the $C2sp^3$ HO has a hybridization factor of 0.91771 (Eq. (13.430)) with a corresponding energy of $E\left(C,2sp^3\right)=-14.63489\ eV$ (Eq. (15.25)) and the O AO has an energy of $E(O)=-13.61806\ eV$. To meet the equipotential condition of the union of the $C=O$ H_2-type-ellipsoidal-MO with these orbitals, the hybridization factor c_2 of Eq. (15.61) for the $C=O$-bond MO given by Eq. (15.133) is $c_2\left(C2sp^3HO\ to\ O\right)=0.85395$. The unpaired electrons created by bond breakage of the double $C=O$ bond requires that two times the $O2p$ AO magnetic energy E_{mag} (Eq. (15.69)) be subtracted from the total energy to give $E_{D\,(Group)}$ (eV) for $C=O$.

As in the case with aldehydes, $E_T\left(atom-atom,msp^3.AO\right)$ of the $C=O$-bond MO in Eq. (15.61) due to the charge donation from the C and O atoms to the MO is $-2.69893\ eV$ which is an energy minimum for the double bond between the pair of $C2sp^3$ HO electrons of the C atom and the pair of AO electrons of the O atom. It is given as a linear combination of the energy contributions corresponding to a double bond, $-1.13379\ eV$ (Eq. (14.247)), and a triple bond, $-1.56513\ eV$ (Eq. (14.342)). The triple bond contribution includes the $C2sp^3$ HO electron of the $C-C(O)$ bond in addition to the pair involved directly in the double bond with O. Consequently, $E_T\left(atom-atom,msp^3.AO\right)$ of the $C-C(O)$-bond MO is $-1.44915\ eV$, corresponding to the energy contributions of the two $C2sp^3$ HOs to the single bond that are equivalent to those of methyl groups, $-0.72457\ eV$ (Eq. (14.151)). Since there are two $C-C(O)$ bonds in ketones versus one in aldehydes, $C_{1o}=C_1$ in Eq. (15.61) for each $C-C(O)$ ketone bond.

The symbols of the functional groups of alkyl ketones are given in Table 15.93. The geometrical (Eqs. (15.1-15.5) and (15.51)), intercept (Eqs. (15.80-15.87)), and energy (Eqs. (15.6-15.11) and (15.17-15.64)) parameters of alkyl ketones are given in Tables 15.94, 15.95, and 15.96, respectively. The total energy of each alkyl ketone given in Table 15.97 was calculated as the sum over the integer multiple of each $E_{D\,(Group)}$ of Table 15.96 corresponding to functional-group composition of the molecule. For each set of unpaired electrons created by bond breakage , the $C2sp^3$ HO magnetic energy E_{mag} that is subtracted from the weighted sum of the $E_{D\,(Group)}$ (eV) values based on composition is given by Eq. (15.67). The bond angle parameters of alkyl ketones determined using Eqs. (15.88-15.117) are given in Table 15.98. The color scale, translucent view of the charge-density of exemplary ketone, methyl ethyl ketone, comprising the concentric shells of atoms with the outer shell bridged by one or more H_2-type ellipsoidal MOs or joined with one or more hydrogen MOs is shown in Figure 15.16.

Figure 15.16. (A)-(B) Color scale, translucent views of the charge-density of methyl ethyl ketone showing the orbitals of the atoms at their radii, the ellipsoidal surface of each H or H_2-type ellipsoidal MO that transitions to the corresponding outer shell of the atom(s) participating in each bond, and the hydrogen nuclei (red, not to scale).

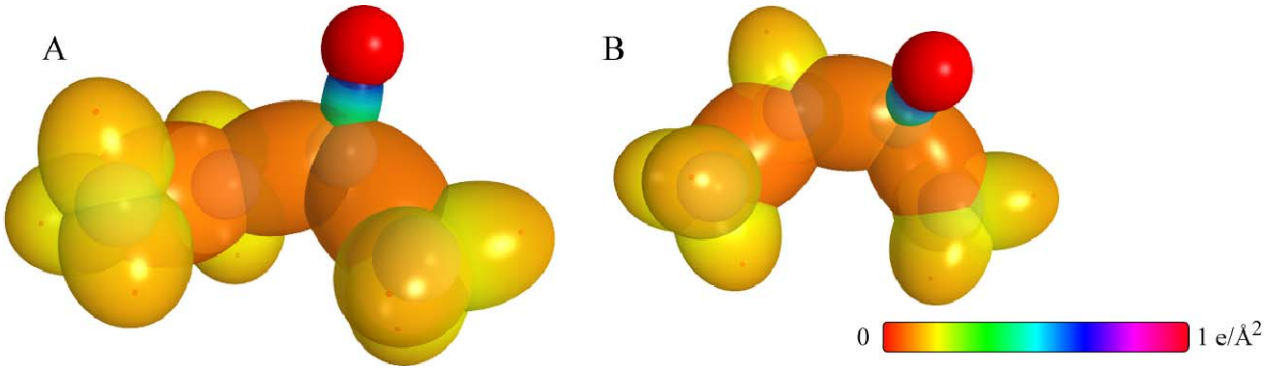

Table 15.93. The symbols of functional groups of alkyl ketones.

Functional Group	Group Symbol
C=O	$C=O$
C-C(O)	$C-C(O)$
CH_3 group	$C-H\ (CH_3)$
CH_2 group	$C-H\ (CH_2)$
CH	$C-H$
CC bond (*n-C*)	$C-C$ (a)
CC bond (*iso-C*)	$C-C$ (b)
CC bond (*tert-C*)	$C-C$ (c)
CC (*iso* to *iso-C*)	$C-C$ (d)
CC (*t* to *t-C*)	$C-C$ (e)
CC (*t* to *iso-C*)	$C-C$ (f)

Table 15.94. The geometrical bond parameters of alkyl ketones and experimental values [1].

Parameter	$C=O$ Group	$C-C(O)$ Group	$C-H\left(CH_3\right)$ Group	$C-H\left(CH_2\right)$ Group	$C-H$ Group	$C-C$ (a) Group	$C-C$ (b) Group	$C-C$ (c) Group	$C-C$ (d) Group	$C-C$ (e) Group	$C-C$ (f) Group
$a\left(a_0\right)$	1.312172	2.04740	1.64920	1.67122	1.67465	2.12499	2.12499	2.10725	2.12499	2.10725	2.10725
$c'\left(a_0\right)$	1.14550	1.43087	1.04856	1.05553	1.05661	1.45744	1.45744	1.45164	1.45744	1.45164	1.45164
Bond Length $2c'\left(A\right)$	1.21235	1.51437	1.10974	1.11713	1.11827	1.54280	1.54280	1.53635	1.54280	1.53635	1.53635
Exp. Bond Length $\left(A\right)$	1.213 (acetone) 1.219 (2-butanone)	1.520 (acetone) 1.518 (2-butanone)	1.107 ($C-H$ propane) 1.117 ($C-H$ butane)	1.107 ($C-H$ propane) 1.117 ($C-H$ butane)	1.122 (isobutane)	1.532 (propane) 1.531 (butane)	1.532 (propane) 1.531 (butane)	1.532 (propane) 1.531 (butane)	1.532 (propane) 1.531 (butane)	1.532 (propane) 1.531 (butane)	1.532 (propane) 1.531 (butane)
$b,c\left(a_0\right)$	0.64002	1.46439	1.27295	1.29569	1.29924	1.54616	1.54616	1.52750	1.54616	1.52750	1.52750
e	0.87298	0.69887	0.63580	0.63159	0.63095	0.68600	0.68600	0.68888	0.68600	0.68888	0.68888

Table 15.95. The MO to HO intercept geometrical bond parameters of alkyl ketones. R, R', R'' are H or alkyl groups. E_T is $E_T\left(atom-atom,msp^3.AO\right)$.

Bond	Atom	E_T (eV) Bond 1	E_T (eV) Bond 2	E_T (eV) Bond 3	E_T (eV) Bond 4	Final Total Energy $C2sp^3$ (eV)	$r_{initial}\left(a_0\right)$	$r_{final}\left(a_0\right)$	$E_{Coulomb}$ (eV) Final	$E\left(C2sp^3\right)$ (eV) Final	θ' $\left(^\circ\right)$	θ_1 $\left(^\circ\right)$	θ_2 $\left(^\circ\right)$	d_1 $\left(a_0\right)$	d_2 $\left(a_0\right)$
$R'C_cH_2\left(RC_bH_2\right)C_a=O$	O	-1.34946	0	0	0		1.00000	0.84115	-16.17521		136.09	43.91	65.72	0.53955	0.60595
$R'C_cH_2\left(RC_bH_2\right)C_a=O$	C_a	-1.34946	-0.72458	-0.72458	0	-154.41430	0.91771	0.77199	-17.62437	-17.43350	133.02	46.98	61.86	0.61878	0.52672
$H_3C_b-C_a(O)(R')$	C_b	-0.72458	0	0	0	-152.34026	0.91771	0.87495	-15.55033	-15.35946	73.62	106.38	34.98	1.67762	0.246675
$RH_2C_c-H_2C_b-C_a(O)(R')$	C_b	-0.72458	-0.92918	0	0	-153.26945	0.91771	0.82562	-16.47951	-16.28865	67.40	112.60	31.36	1.74821	0.31734
$C-H\left(CH_3\right)$	C	-0.92918	0	0	0	-152.54487	0.91771	0.86359	-15.75493	-15.56407	77.49	102.51	41.48	1.23564	0.18708
$C-H\left(CH_2\right)$	C	-0.92918	-0.92918	0	0	-153.47406	0.91771	0.81549	-16.68412	-16.49325	68.47	111.53	35.84	1.35486	0.29933
$C-H\left(CH\right)$	C	-0.92918	-0.92918	-0.92918	0	-154.40324	0.91771	0.77247	-17.61330	-17.42244	61.10	118.90	31.37	1.42988	0.37326
$H_3C_aC_bH_2CH_2-$ $(C-C$ (a))	C_a	-0.92918	0	0	0	-152.54487	0.91771	0.86359	-15.75493	-15.56407	63.82	116.18	30.08	1.83879	0.38106
$H_3C_aC_bH_2CH_2-$ $(C-C$ (a))	C_b	-0.92918	-0.92918	0	0	-153.47406	0.91771	0.81549	-16.68412	-16.49325	56.41	123.59	26.06	1.90890	0.45117
$R-H_2C_aC_b\left(H_2C_c-R'\right)HCH_2-$ $(C-C$ (b))	C_b	-0.92918	-0.92918	-0.92918	0	-154.40324	0.91771	0.77247	-17.61330	-17.42244	48.30	131.70	21.90	1.97162	0.51388
$R-H_2C_a\left(R'-H_2C_d\right)C_b\left(R''-H_2C_c\right)CH_2-$ $(C-C$ (c))	C_b	-0.92918	-0.72457	-0.72457	-0.72457	-154.71860	0.91771	0.75889	-17.92866	-17.73779	48.21	131.79	21.74	1.95734	0.50570
$isoC_aC_b\left(H_2C_c-R'\right)HCH_2-$ $(C-C$ (d))	C_b	-0.92918	-0.92918	-0.92918	0	-154.40324	0.91771	0.77247	-17.61330	-17.42244	48.30	131.70	21.90	1.97162	0.51388
$tertC_a\left(R'-H_2C_d\right)C_b\left(R''-H_2C_c\right)CH_2-$ $(C-C$ (e))	C_b	-0.72457	-0.72457	-0.72457	-0.72457	-154.51399	0.91771	0.76765	-17.92866	-17.73779	50.04	129.96	22.66	1.94462	0.49298
$tertC_aC_b\left(H_2C_c-R'\right)HCH_2-$ $(C-C$ (f))	C_b	-0.72457	-0.92918	-0.92918	0	-154.19863	0.91771	0.78155	-17.40869	-17.21783	52.78	127.22	24.04	1.92443	0.47279
$isoC_a\left(R'-H_2C_a\right)C_b\left(R''-H_2C_c\right)CH_2-$ $(C-C$ (f))	C_b	-0.72457	-0.72457	-0.72457	-0.72457	-154.51399	0.91771	0.76765	-17.92866	-17.73779	50.04	129.96	22.66	1.94462	0.49298

Table 15.96. The energy parameters (eV) of functional groups of alkyl ketones.

Parameters	$C=O$ Group	$C-C(O)$ Group	CH_3 Group	CH_2 Group	$C-H$ Group	$C-C$ (a) Group	$C-C$ (b) Group	$C-C$ (c) Group	$C-C$ (d) Group	$C-C$ (e) Group	$C-C$ (f) Group
n_1	2	1	3	2	1	1	1	1	1	1	1
n_2	0	0	2	1	0	0	0	0	0	0	0
n_3	0	0	0	0	0	0	0	0	0	0	0
C_1	0.5	0.5	0.75	0.75	0.75	0.5	0.5	0.5	0.5	0.5	0.5
C_2	1	1	1	1	1	1	1	1	1	1	1
c_1	1	1	1	1	1	1	1	1	1	1	1
c_2	0.85395	0.91771	0.91771	0.91771	0.91771	0.91771	0.91771	0.91771	0.91771	0.91771	0.91771
c_3	2	0	0	1	1	0	0	0	1	1	0
c_4	4	2	1	1	1	2	2	2	2	2	2
c_5	0	0	3	2	1	0	0	0	0	0	0
C_{1o}	0.5	1	0.75	0.75	0.75	0.5	0.5	0.5	0.5	0.5	0.5
C_{2o}	1	1	1	1	1	1	1	1	1	1	1
$V_e\ (eV)$	-109.17602	-30.19634	-107.32728	-70.41425	-35.12015	-28.79214	-28.79214	-29.10112	-28.79214	-29.10112	-29.10112
$V_p\ (eV)$	23.75521	9.50874	38.92728	25.78002	12.87680	9.33352	9.33352	9.37273	9.33352	9.37273	9.37273
$T\ (eV)$	41.60126	7.37432	32.53914	21.06675	10.48582	6.77464	6.77464	6.90500	6.77464	6.90500	6.90500
$V_m\ (eV)$	-20.80063	-3.68716	-16.26957	-10.53337	-5.24291	-3.38732	-3.38732	-3.45250	-3.38732	-3.45250	-3.45250
$E(_{AO/HO})\ (eV)$	0	-14.63489	-15.56407	-15.56407	-14.63489	-15.56407	-15.56407	-15.35946	-15.56407	-15.35946	-15.35946
$\Delta E_{H_2MO}(_{AO/HO})\ (eV)$	-1.34946	0	0	0	0	0	0	0	0	0	0
$E_J(_{AO/HO})\ (eV)$	1.34946	-14.63489	-15.56407	-15.56407	-14.63489	-15.56407	-15.56407	-15.35946	-15.56407	-15.35946	-15.35946
$E_J(_{H_2MO})\ (eV)$	-63.27071	-31.63534	-67.69451	-49.66493	-31.63533	-31.63537	-31.63537	-31.63535	-31.63537	-31.63535	-31.63535
$E_J\left(atom-atom,msp^3.AO\right)(eV)$	-2.69893	-1.44915	0	0	0	-1.85836	-1.85836	-1.44915	-1.85836	-1.44915	-1.44915
$E_J(_{MO})\ (eV)$	-65.96966	-33.08452	-67.69450	-49.66493	-31.63537	-33.49373	-33.49373	-33.08452	-33.49373	-33.08452	-33.08452
$\omega\ \left(10^{15}\ rad/s\right)$	57.0928	16.4962	24.9286	24.2751	24.1759	9.43699	9.43699	15.4846	9.43699	9.55643	9.55643
$E_K\ (eV)$	37.57947	10.85807	16.40846	15.97831	15.91299	6.21159	6.21159	10.19220	6.21159	6.29021	6.29021
$\bar{E}_D\ (eV)$	-0.40003	-0.21568	-0.25352	-0.25017	-0.24966	-0.16515	-0.16515	-0.20896	-0.16515	-0.16416	-0.16416
$\bar{E}_{Kvib}\ (eV)$	0.21462 [27]	0.14655 [28]	0.35532 (Eq. (13.458))	0.35532 (Eq. (13.458))	0.35532 (Eq. (13.458))	0.12312 [2]	0.17978 [4]	0.09944 [5]	0.12312 [2]	0.12312 [2]	0.12312 [2]
$\bar{E}_{osc}\ (eV)$	-0.29272	-0.14240	-0.22757	-0.14502	-0.07200	-0.10359	-0.07526	-0.15924	-0.10359	-0.10260	-0.10260
$E_{mag}\ (eV)$	0.11441	0.14803	0.14803	0.14803	0.14803	0.14803	0.14803	0.14803	0.14803	0.14803	0.14803
$E_J(_{Group})\ (eV)$	-66.55510	-33.22692	-67.92207	-49.80996	-31.70737	-33.59732	-33.49373	-33.24376	-33.59732	-33.18712	-33.18712
$E_{initial}(_{c_4\ AO/HO})\ (eV)$	-14.63489	-14.63489	-14.63489	-14.63489	-14.63489	-14.63489	-14.63489	-14.63489	-14.63489	-14.63489	-14.63489
$E_{initial}(_{c_5\ AO/HO})\ (eV)$	0	0	-13.59844	-13.59844	-13.59844	0	0	0	0	0	0
$E_D(_{Group})\ (eV)$	7.78672	3.95714	12.49186	7.83016	3.32601	4.32754	4.29921	3.97398	4.17951	3.62128	3.91734

Table 15.97. The total bond energies of alkyl ketones calculated using the functional group composition and the energies of Table 15.96 compared to the experimental values [3]. The magnetic energy E_{mag} that is subtracted from the weighted sum of the E_D $(_{Group})$ (eV) values based on composition is given by (15.57).

Formula	Name	$C=O$ Group	$C-C(O)$ Group	CH_3	CH_2	CH	$C-C$ (a)	$C-C$ (b)	$C-C$ (c)	$C-C$ (d)	$C-C$ (e)	$C-C$ (f)	E_{mag}	Calculated Total Bond Energy (eV)	Experimental Total Bond Energy (eV)	Relative Error
C_3H_6O	Acetone	1	2	2	0	0	0	0	0	0	0	0	0	40.68472	40.672	-0.00031
C_4H_8O	2-Butanone	1	2	2	1	0	1	0	0	0	0	0	0	52.84242	52.84	-0.00005
$C_5H_{10}O$	2-Pentanone	1	2	2	2	0	2	0	0	0	0	0	0	65.00012	64.997	-0.00005
$C_5H_{10}O$	3-Pentanone	1	2	2	2	0	2	0	0	0	0	0	0	65.00012	64.997	-0.00005
$C_5H_{10}O$	3-Methyl-2-butanone	1	2	3	0	1	0	2	0	0	0	0	0	65.10101	65.036	-0.00099
$C_6H_{12}O$	2-Hexanone	1	2	2	3	0	3	0	0	0	0	0	0	77.15782	77.152	-0.00008
$C_6H_{12}O$	3-Hexanone	1	2	2	3	0	3	0	0	0	0	0	0	77.15782	77.138	-0.00025
$C_6H_{12}O$	2-Methyl-3-pentanone	1	2	3	1	1	1	2	0	0	0	0	0	77.25871	77.225	-0.00043
$C_6H_{12}O$	3,3-Dimethyl-2-butanone	1	2	4	0	0	0	0	3	0	0	0	-2	77.29432	77.273	-0.00028
$C_7H_{14}O$	3-Heptanone	1	2	2	4	0	4	0	0	0	0	0	0	89.31552	89.287	-0.00032
$C_7H_{14}O$	4-Heptanone	1	2	2	4	0	4	0	0	0	0	0	0	89.31552	89.299	-0.00018
$C_7H_{14}O$	2,2-Dimethyl-3-pentanone	1	2	4	1	0	1	0	3	0	0	0	-2	89.45202	89.458	0.00007
$C_7H_{14}O$	2,4-Dimethyl-3-pentanone	1	2	4	0	2	0	4	0	0	0	0	0	89.51730	89.434	-0.00093
$C_8H_{16}O$	2,2,4-Trimethyl-3-pentanone	1	2	5	0	1	0	2	3	0	0	0	-2	101.71061	101.660	-0.00049
$C_9H_{18}O$	2-Nonanone	1	2	2	6	0	6	0	0	0	0	0	0	113.63092	113.632	0.00001
$C_9H_{18}O$	5-Nonanone	1	2	2	6	0	6	0	0	0	0	0	0	113.63092	113.675	0.00039
$C_9H_{18}O$	2,6-Dimethyl-4-heptanone	1	2	4	2	2	0	6	0	0	0	0	0	113.77604	113.807	0.00027

Table 15.98. The bond angle parameters of alkyl ketones and experimental values [1]. In the calculation of θ_v, the parameters from the preceding angle were used. E_T is $E_T(atom - atom, msp^3.AO)$.

Atoms of Angle	$2c'$ Bond 1 (a_0)	$2c'$ Bond 2 (a_0)	$2c'$ Terminal Atoms (a_0)	$E_{Coulombic}$ Atom 1	Atom 1 Hybridization Designation (Table 15.3.A)	$E_{Coulombic}$ Atom 2	Atom 2 Hybridization Designation (Table 15.3.A)	c_2 Atom 1	c_2 Atom 2	C_1	C_2	c_1	c_2'	E_T (eV)	θ_v (°)	θ_1 (°)	θ_2 (°)	Cal. θ (°)	Exp. θ (°)
$\angle C_bC_a(O)C_c$	2.86175	2.86175	4.8477	-16.68412 C_b	26	-16.68412 C_c	26	0.81549	0.81549	1	1	1	0.81549	-1.85836				115.77	116.0 (acetone)
$\angle C_dC_bC_a(O)$	2.91547	2.86175	4.8374	-16.68412 C_d	26	-16.68412 C_a	26	0.81549	0.81549	1	1	1	0.81549	-1.85836				113.71	113.5 (2-butanaone)
$\angle C_bC_aO$	2.86175	2.29100	4.5166	-15.55033	5	-13.61806	O	0.87495	0.85395 (Eq. (15.133))	1	1	1	0.86445	-1.44915				122.07	121.9 (2-butanaone)
Methylene $\angle HC_aH$	2.11106	2.11106	3.4252	-15.75493	7	H	H	0.86359	1	1	1	0.75	1.15796	0				108.44	107 (propane)
$\angle C_aC_bC_c$															69.51			110.49	112 (propane) 113.8 (butane) 110.8 (isobutane)
$\angle C_aC_bH$															69.51			110.49	111.0 (butane) 111.4 (isobutane)
Methyl $\angle HC_aH$	2.09711	2.09711	3.4252	-15.75493	7	H	H	0.86359	1	1	1	0.75	1.15796	0				109.50	
$\angle C_aC_bC_c$															70.56			109.44	
$\angle C_aC_bH$															70.56			109.44	
$\angle C_bC_aC_c$ isc C_a	2.91547	2.91547	4.7958	-16.68412 C_b	26	-16.68412 C_c	26	0.81549	0.81549	1	1	1	0.81549	-1.85836				110.67	110.8 (isobutane)
$\angle C_bC_aH$ isc C_a	2.91547	2.11323	4.1633	-15.55033 C_a	5	-14.82575 C_b	1	0.87495	0.91771	0.75	1	0.75	1.04887	0				110.76	
$\angle C_aC_bH$ isc C_a	2.91547	2.09711	4.1633	-15.55033 C_b	5	-14.82575 C_a	1	0.87495	0.91771	0.75	1	0.75	1.04887	0				111.27	111.4 (isobutane)
$\angle C_bC_aC_b$ tert C_a	2.90327	2.90327	4.7958	-16.68412 C_b	26	-16.68412 C_b	26	0.81549	0.81549	1	1	1	0.81549	-1.85836				111.37	110.8 (isobutane)
$\angle C_bC_aC_d$															72.50			107.50	

CARBOXYLIC ACIDS ($C_nH_{2n}O_2,\ n=1,2,3,4,5...\infty$)

The alkyl carboxylic acids, $C_nH_{2n}O_2$, comprise a $C=O$ functional group, and the single bond of carbon to the carbonyl carbon atom, $C-C(O)$, is also a functional group. Formic acid has a $HC=O$ moiety that comprises a more stable $C=O$ functional group and a CH functional group. All carboxylic acids further comprise a $C-OH$ moiety that comprises $C-O$ and OH functional groups. The alkyl portion of the alkyl carboxylic acid may comprise at least two terminal methyl groups (CH_3) at each end of the chain, and may comprise methylene (CH_2), and methylyne (CH) functional groups as well as C bound by carbon-carbon single bonds. The methyl and methylene functional groups are equivalent to those of straight-chain alkanes. Six types of $C-C$ bonds can be identified. The n-alkane $C-C$ bond is the same as that of straight-chain alkanes. In addition, the $C-C$ bonds within isopropyl ($(CH_3)_2CH$) and t-butyl ($(CH_3)_3C$) groups and the isopropyl to isopropyl, isopropyl to t-butyl, and t-butyl to t-butyl $C-C$ bonds comprise functional groups. The branched-chain-alkane groups in carboxylic acids are equivalent to those in branched-chain alkanes.

The CH functional group was solved in the Hydrogen Carbide (CH) section except that the energy of the $C-H$ MO is matched to the carbon-atom contribution to $\Delta E_{H_2MO}(AO/HO)$ and $E_T\left(atom-atom,msp^3.AO\right)$ of the $C-O$ group. The alkyl carboxylic acid $C=O$ and $C-C(O)$ groups are equivalent to those given in the Aldehydes section except that $\overline{E}_{Kvib}$ is that of a carboxylic acid, and $C-C(O)$ is equivalent to the n-alkane $C-C$ bond group in the case of conjugated carbonyls wherein the alkene groups when present such as the $C=C$ group are equivalent to those of the corresponding alkene. The formic acid $C=O$ group is solved equivalently to that of the alkyl carboxylic acid group, except that $\Delta E_{H_2MO}(AO/HO)$ and $E_T\left(atom-atom,msp^3.AO\right)$ correspond to a 25% increase in the donation of charge density from the orbitals of the atoms to the $C=O$ MO due to the presence of a H bound to the carbonyl carbon. Also, $\overline{E}_{Kvib}$ is that corresponding to formic acid. The $C-O$ and OH groups are equivalent to those of alkyl alcohols given in the corresponding section except that the energy of the $C-O$ MO is matched to that of the $C=O$ group and $\overline{E}_{Kvib}$ is that of a carboxylic acid. $\Delta E_{H_2MO}(AO/HO)$ of the $C-O$ group is equal to $E_T\left(atom-atom,msp^3.AO\right)$ of the alkyl $C=O$ group in order to match the energies of the corresponding MOs.

As in the case with aldehydes and ketones, $E_T\left(atom-atom,msp^3.AO\right)$ of the $C=O$-bond MO in Eq. (15.61) of alkyl carboxylic acids due to the charge donation from the C and O atoms to the MO is $-2.69893\ eV$ which is an energy minimum for the double bond between the pair of $C2sp^3$ HO electrons of the C atom and the pair of AO electrons of the carbonyl O atom. It is given as a linear combination of the energy contributions corresponding to a double bond, $-1.13379\ eV$ (Eq. (14.247)), and a triple bond, $-1.56513\ eV$ (Eq. (14.342)). The triple bond contribution includes the energy match of the carbonyl $C2sp^3$ HO electron with the O of the $C-O$-bond MO in addition to the pair involved directly in the double bond with the carbonyl O.

$E_T\left(atom-atom,msp^3.AO\right)$ of the formic acid $C=O$-bond MO in Eq. (15.61) due to the charge donation from the C and O atoms to the MO is $-3.58557\ eV$. This is also an energy minimum for the double bond between the pair of $C2sp^3$ HO electrons of the C atom and the pair of AO electrons of the carbonyl O atom. It is given as a linear combination of the energy contributions corresponding to a triple bond, $-1.56513\ eV$ (Eq. (14.342)), and a quadruple bond, $-2.02043\ eV$ (Eqs. (15.18-15.21) with $s=4$)) where the bond order components are increased by an integer over that of alkyl carboxylic acids due to the presence of a H bound to the carbonyl carbon.

$E_T\left(atom-atom,msp^3.AO\right)$ of the carboxylic acid $C-C(O)$ group is equivalent to that of alkanes and aldehydes, $-1.85836\ eV$, where both energy contributions are given by Eq. (14.513). It is based on the energy match between the $C2sp^3$ HOs of the carboxylic acid. As in the case of aldehydes, $C_{1o}=2C_1$ in Eq. (15.52).

$E_T\left(atom-atom,msp^3.AO\right)$ of the carboxylic acid $C-O$ group is equivalent to that of alkyl alcohols, $-1.85836\ eV$. It is based on the energy match between the O AO and the $C2sp^3$ HO of a methylene group (the maximum hybridization for a single bond) where both energy contributions are given by Eq. (14.513). $E_T\left(atom-atom,msp^3.AO\right)$ of the $C-O$ group matches that of the $C-C(O)$ group.

The symbols of the functional groups of alkyl carboxylic acids are given in Table 15.99. The geometrical (Eqs. (15.1-15.5) and (15.51)), intercept (Eqs. (15.80-15.87)), and energy (Eqs. (15.6-15.11) and (15.17-15.65)) parameters of alkyl carboxylic acids are given in Tables 15.100, 15.101, and 15.102, respectively. The total energy of each alkyl carboxylic acid given in Table 15.103 was calculated as the sum over the integer multiple of each $E_{D(Group)}$ of Table 15.102 corresponding to functional-group composition of the molecule. For each set of unpaired electrons created by bond breakage, the $C2sp^3$ HO magnetic energy E_{mag} that is subtracted from the weighted sum of the $E_{D(Group)}$ (eV) values based on composition is given by Eq. (15.67). The bond angle parameters of alkyl carboxylic acids determined using Eqs. (15.79-15.108) are given in Table

15.104. The color scale, translucent view of the charge-density of exemplary carboxylic acid, Propanoic acid, comprising the concentric shells of atoms with the outer shell bridged by one or more H_2-type ellipsoidal MOs or joined with one or more hydrogen MOs is shown in Figure 15.17.

Figure 15.17. (A)-(B) Color scale, translucent views of the charge-density of propanoic acid showing the orbitals of the atoms at their radii, the ellipsoidal surface of each H or H_2-type ellipsoidal MO that transitions to the corresponding outer shell of the atom(s) participating in each bond, and the hydrogen nuclei (red, not to scale).

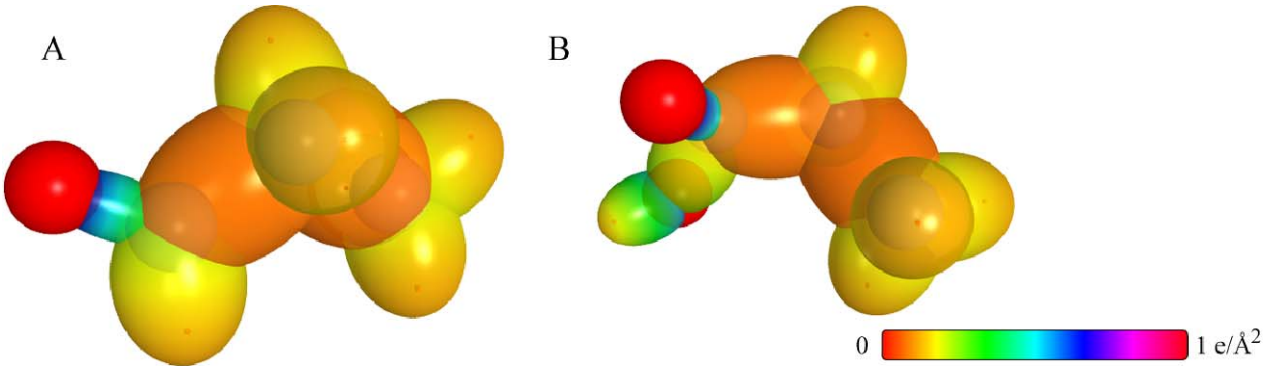

Table 15.99. The symbols of functional groups of alkyl carboxylic acids.

Functional Group	Group Symbol
CH (formic acid) group	$C-H$ (i)
C-C(O)	$C-C(O)$
C=O (formic acid)	$C=O$ (i)
C=O (alkyl carboxylic acid)	$C=O$ (ii)
(O)C-O	$C-O$
OH group	OH
CH_3 group	$C-H\ (CH_3)$
CH_2 group	$C-H\ (CH_2)$
CH (alkyl) group	$C-H$ (ii)
CC bond (*n-C*)	$C-C$ (a)
CC bond (*iso-C*)	$C-C$ (b)
CC bond (*tert-C*)	$C-C$ (c)
CC (*iso* to *iso-C*)	$C-C$ (d)
CC (*t* to *t-C*)	$C-C$ (e)
CC (*t* to *iso-C*)	$C-C$ (f)
CC double bond	$C=C$

Table 15.100. The geometrical bond parameters of alkyl carboxylic acids and experimental values [1].

Parameter	$C-H$ (i) Group	$C-C(O)$ Group	$C=O$ (i) Group	$C=O$ (ii) Group	$C-O$ Group	OH Group	$C-H\ (CH_3)$ Group	$C-H\ (CH_2)$ Group	$C-H$ (ii) Group	$C-C$ (a) Group	$C-C$ (b) Group	$C-C$ (c) Group	$C-C$ (d) Group	$C-C$ (e) Group	$C-C$ (f) Group	$C=C$ Group
$a\ (a_0)$	1.61341	2.04740	1.290799	1.29907	1.73490	1.26430	1.64920	1.67122	1.67465	2.12499	2.12499	2.10725	2.12499	2.10725	2.10725	1.47228
$c'\ (a_0)$	1.03711	1.43087	1.13613	1.13977	1.31716	0.91808	1.04856	1.05553	1.05661	1.45744	1.45744	1.45164	1.45744	1.45164	1.45164	1.26661
Bond Length $2c'\ (\AA)$	1.09763	1.51437	1.20243	1.20628	1.39402	0.971651	1.10974	1.11713	1.11827	1.54280	1.54280	1.53635	1.54280	1.53635	1.53635	1.34052
Exp. Bond Length $(\AA)$	1.097 (formic acid)	1.520 (acetic acid)	1.202 (formic acid)	1.214 (acetic acid)	1.393 (methyl formate)	0.972 (formic acid)	1.107 ($C-H$ propane) 1.117 ($C-H$ butane)	1.107 ($C-H$ propane) 1.117 ($C-H$ butane)	1.122 (isobutane)	1.532 (propane) 1.531 (butane)	1.532 (propane) 1.531 (butane)	1.532 (propane) 1.531 (butane)	1.532 (propane) 1.531 (butane)	1.532 (propane) 1.531 (butane)	1.532 (propane) 1.531 (butane)	1.342 (2-methylpropene) 1.346 (2-butene) 1.349 (1,3-butadiene)
$b,c\ (a_0)$	1.23591	1.46439	0.61267	0.62331	1.12915	0.86925	1.27295	1.29569	1.29924	1.54616	1.54616	1.52750	1.54616	1.52750	1.52750	0.75055
e	0.64281	0.69887	0.88018	0.87737	0.75921	0.72615	0.63580	0.63159	0.63095	0.68600	0.68600	0.68888	0.68600	0.68888	0.68888	0.86030

Table 15.101. The MO to HO intercept geometrical bond parameters of alkyl carboxylic acids. R, R', R'' are H or alkyl groups. E_T is E_T ($atom - atom, msp^3.AO$).

Bond	Atom	E_T (eV) Bond 1	E_T (eV) Bond 2	E_T (eV) Bond 3	E_T (eV) Bond 4	Final Total Energy $C2sp^3$ (eV)	$r_{initial}$ (a_0)	r_{final} (a_0)	$E_{Coulomb}$ (eV) Final	$E(C2sp^3)$ (eV) Final	θ' (°)	θ_1 (°)	θ_2 (°)	d_1 (a_0)	d_2 (a_0)
$RC_a(O)O-H$	O	-0.92918	0	0	0		1.00000	0.86359	-15.75493		115.09	64.91	64.12	0.55182	0.36625
$HC_a(O)-OH$ ($C=O$ (i))	O	-0.92918	0	0	0		1.00000	0.86359	-15.75493		101.32	78.68	48.58	1.14765	0.16950
$HC_a(O)-OH$ ($C=O$ (i))	C_a	-0.92918	-1.79278	0	0	-154.33765	0.91771	0.77536	-17.54772	-17.35685	93.94	86.06	43.24	1.26386	0.05329
$RH_2C_bC_a(O)-OH$	O	-0.92918	0	0	0		1.00000	0.86359	-15.75493		101.32	78.68	48.58	1.14765	0.16950
$RH_2C_bC_a(O)-OH$	C_a	-0.92918	-1.34946	-0.92918	0	-154.82352	0.91771	0.75447	-18.03358	-17.84271	91.96	88.04	41.90	1.29138	0.02578
$HC_a(OH)=O$ ($C=O$ (i))	O	-1.79278	0	0	0		1.00000	0.81871	-16.61853		137.10	42.90	65.45	0.53635	0.59978
$HC_a(OH)=O$ ($C=O$ (i))	C_a	-1.79278	-0.92918	0	0	-154.33766	0.91771	0.77536	-17.54772	-17.35685	135.24	44.76	63.02	0.58561	0.55053
$RC_bH_2C_a(OH)=O$ ($C=O$ (ii))	O	-1.34946	0	0	0		1.00000	0.84115	-16.17521		137.27	42.73	66.31	0.52193	0.61784
$RC_bH_2C_a(OH)=O$ ($C=O$ (ii))	C_a	-1.34946	-0.92918	-0.92918	0	-154.82352	0.91771	0.75447	-18.03358	-17.84271	133.47	46.53	61.46	0.62072	0.51905
$H-C(O)OH$ (CH (i))	C	-1.79278	-0.92918	0	0	-154.33766	0.91771	0.77536	-17.54772	-17.35685	69.89	110.11	36.09	1.30373	0.26662
$RH_2C_b-C_a(O)OH$	C_a	-0.92918	-1.34946	-0.92918	0	-154.82352	0.91771	0.75447	-18.03358	-17.84271	56.25	123.75	25.37	1.85002	0.41915
$H_3C_b-C_a(O)OH$	C_b	-0.92918	0	0	0	-152.54487	0.91771	0.86359	-15.75493	-15.56407	72.27	107.73	34.17	1.69388	0.26301
$RH_2C_cH_2C_b-C_a(O)OH$	C_b	-0.92918	-0.92918	0	0	-153.47405	0.91771	0.81549	-16.68411	-16.49325	65.99	114.01	30.58	1.76270	0.33183
$C-H$ (CH_3)	C	-0.92918	0	0	0	-152.54487	0.91771	0.86359	-15.75493	-15.56407	77.49	102.51	41.48	1.23564	0.18708
$C-H$ (CH_2)	C	-0.92918	-0.92918	0	0	-153.47406	0.91771	0.81549	-16.68412	-16.49325	68.47	111.53	35.84	1.35486	0.29933
$C-H$ (CH) (ii)	C	-0.92918	-0.92918	-0.92918	0	-154.40324	0.91771	0.77247	-17.61330	-17.42244	61.10	118.90	31.37	1.42988	0.37326
$H_3C_aC_bH_2CH_2-$ ($C-C$ (a))	C_a	-0.92918	0	0	0	-152.54487	0.91771	0.86359	-15.75493	-15.56407	63.82	116.18	30.08	1.83879	0.38106
$H_3C_aC_bH_2CH_2-$ ($C-C$ (a))	C_b	-0.92918	-0.92918	0	0	-153.47406	0.91771	0.81549	-16.68412	-16.49325	56.41	123.59	26.06	1.90890	0.45117
$R-H_2C_bC_b(H_2C_c-R')HCH_2-$ ($C-C$ (b))	C_b	-0.92918	-0.92918	-0.92918	0	-154.40324	0.91771	0.77247	-17.61330	-17.42244	48.30	131.70	21.90	1.97162	0.51388
$R-H_2C_a(R'-H_2C_d)C_b(R''-H_2C_c)CH_2-$ ($C-C$ (c))	C_b	-0.92918	-0.72457	-0.72457	-0.72457	-154.71860	0.91771	0.75889	-17.92866	-17.73779	48.21	131.79	21.74	1.95734	0.50570
$isoC_aC_b(H_2C_c-R')HCH_2-$ ($C-C$ (d))	C_b	-0.92918	-0.92918	-0.92918	0	-154.40324	0.91771	0.77247	-17.61330	-17.42244	48.30	131.70	21.90	1.97162	0.51388
$tertC_a(R'-H_2C_d)C_b(R''-H_2C_c)CH_2-$ ($C-C$ (e))	C_b	-0.72457	-0.72457	-0.72457	-0.72457	-154.51399	0.91771	0.76765	-17.92866	-17.73779	50.04	129.96	22.66	1.94462	0.49298
$tertC_aC_b(H_2C_c-R')HCH_2-$ ($C-C$ (f))	C_b	-0.72457	-0.92918	-0.92918	0	-154.19863	0.91771	0.78155	-17.40869	-17.21783	52.78	127.22	24.04	1.92443	0.47279
$isoC_a(R'-H_2C_d)C_b(R''-H_2C_c)CH_2-$ ($C-C$ (f))	C_b	-0.72457	-0.72457	-0.72457	-0.72457	-154.51399	0.91771	0.76765	-17.92866	-17.73779	50.04	129.96	22.66	1.94462	0.49298

Table 15.102. The energy parameters (eV) of functional groups of alkyl carboxylic acids.

Parameters	$C-H$ (i) Group	$C-C(O)$ Group	$C=O$ (i) Group	$C=O$ (ii) Group	$C-O$ Group	OH Group	CH_3 Group	CH_2 Group	$C-H$ (ii) Group	$C-C$ (a) Group	$C-C$ (b) Group	$C-C$ (c) Group	$C-C$ (d) Group	$C-C$ (e) Group	$C-C$ (f) Group	$C=C$ Group
n_1	1	1	2	2	1	1	3	2	1	1	1	1	1	1	1	2
n_2	0	0	0	0	0	0	2	1	0	0	0	0	0	0	0	0
n_3	0	0	0	0	0	0	0	0	0	0	0	0	0	0	0	0
C_1	0.75	0.5	0.5	0.5	0.5	0.75	0.75	0.75	0.75	0.5	0.5	0.5	0.5	0.5	0.5	0.5
C_2	1	1	1	1	1	1	1	1	1	1	1	1	1	1	1	0.91771
c_1	1	1	1	1	1	0.75	1	1	1	1	1	1	1	1	1	1
c_2	0.91771	0.91771	0.85395	0.85395	0.85395	1	0.91771	0.91771	0.91771	0.91771	0.91771	0.91771	0.91771	0.91771	0.91771	0.91771
c_3	0	0	2	2	0	1	0	1	1	0	0	0	1	1	0	0
c_4	1	2	4	4	2	1	1	1	1	2	2	2	2	2	2	4
c_5	1	0	0	0	0	1	3	2	1	0	0	0	0	0	0	0
C_{1o}	0.75	1	0.5	0.5	0.5	0.75	0.75	0.75	0.75	0.5	0.5	0.5	0.5	0.5	0.5	0.5
C_{2o}	1	1	1	1	1	1	1	1	1	1	1	1	1	1	1	0.91771
V_e (eV)	-36.74167	-30.19634	-112.61934	-111.25473	-35.08488	-40.92709	-107.32728	-70.41425	-35.12015	-28.79214	-28.79214	-29.10112	-28.79214	-29.10112	-29.10112	-102.08992
V_p (eV)	13.11890	9.50874	23.95107	23.87467	10.32968	14.81988	38.92728	25.78002	12.87680	9.33352	9.33352	9.37273	9.33352	9.37273	9.37273	21.48386
T (eV)	11.38634	7.37432	43.62389	42.82081	10.11150	16.18567	32.53914	21.06675	10.48582	6.77464	6.77464	6.90500	6.77464	6.90500	6.90500	34.67062
V_m (eV)	-5.69317	-3.68716	-21.81195	-21.41040	-5.05575	-8.09284	-16.26957	-10.53337	-5.24291	-3.38732	-3.38732	-3.45250	-3.38732	-3.45250	-3.45250	-17.33531
$E_{(AO/HO)}$ (eV)	-14.63489	-14.63489	0	0	-14.63489	-13.6181	-15.56407	-15.56407	-14.63489	-15.56407	-15.56407	-15.35946	-15.56407	-15.35946	-15.35946	0
$\Delta E_{H_2MO(AO/HO)}$ (eV)	-0.92918	0	-3.58557	-2.69893	-2.69893	0	0	0	0	0	0	0	0	0	0	0
$E_T{}_{(AO/HO)}$ (eV)	-13.70571	-14.63489	3.58557	2.69893	-11.93596	-13.6181	-15.56407	-15.56407	-14.63489	-15.56407	-15.56407	-15.35946	-15.56407	-15.35946	-15.35946	0
$E_T{}_{(H_2MO)}$ (eV)	-31.63530	-31.63534	-63.27075	-63.27074	-31.63541	-31.63247	-67.69451	-49.66493	-31.63533	-31.63537	-31.63537	-31.63535	-31.63537	-31.63535	-31.63535	-63.27075
$E_T\left(atom-atom, msp^3.AO\right)$ (eV)	0	-1.85836	-3.58557	-2.69893	-1.85836	0	0	0	0	-1.85836	-1.85836	-1.44915	-1.85836	-1.44915	-1.44915	-2.26759
$E_T{}_{(MO)}$ (eV)	-31.63537	-33.49373	-66.85630	-65.96966	-33.49373	-31.63537	-67.69450	-49.66493	-31.63537	-33.49373	-33.49373	-33.08452	-33.49373	-33.08452	-33.08452	-65.53833
$\omega\left(10^{15}\ rad/s\right)$	26.0575	23.3291	60.9581	59.4034	24.3637	44.1776	24.9286	24.2751	24.1759	9.43699	9.43699	15.4846	9.43699	9.55643	9.55643	43.0680
E_K (eV)	17.15150	15.35563	40.12366	39.10034	16.03660	29.07844	16.40846	15.97831	15.91299	6.21159	6.21159	10.19220	6.21159	6.29021	6.29021	28.34813
$\bar{E}_D$ (eV)	-0.25920	-0.25966	-0.41891	-0.40804	-0.26535	-0.33749	-0.25352	-0.25017	-0.24966	-0.16515	-0.16515	-0.20896	-0.16515	-0.16416	-0.16416	-0.34517
$\bar{E}_{Kvib}$ (eV)	0.35532 (Eq. (13.458))	0.10502 [29]	0.21945 [30]	0.21077 [12]	0.14010 [31]	0.46311 [17-18]	0.35532 (Eq. (13.458))	0.35532 (Eq. (13.458))	0.35532 (Eq. (13.458))	0.12312 [2]	0.17978 [4]	0.09944 [5]	0.12312 [2]	0.12312 [2]	0.12312 [2]	0.17897 [6]
$\bar{E}_{osc}$ (eV)	-0.08153	-0.20715	-0.30918	-0.30266	-0.19530	-0.10594	-0.22757	-0.14502	-0.07200	-0.10359	-0.07526	-0.15924	-0.10359	-0.10260	-0.10260	-0.25568
E_{mag} (eV)	0.14803	0.14803	0.11441	0.11441	0.14803	0.11441	0.14803	0.14803	0.14803	0.14803	0.14803	0.14803	0.14803	0.14803	0.14803	0.14803
$E_{T(Group)}$ (eV)	-31.71690	-33.70088	-67.47466	-66.57498	-33.68903	-31.74130	-67.92207	-49.80996	-31.70737	-33.59732	-33.49373	-33.24376	-33.59732	-33.18712	-33.18712	-66.04969
$E_{initial(c_4\ AO/HO)}$ (eV)	-14.63489	-14.63489	-14.63489	-14.63489	-14.63489	-13.6181	-14.63489	-14.63489	-14.63489	-14.63489	-14.63489	-14.63489	-14.63489	-14.63489	-14.63489	-14.63489
$E_{initial(c_5\ AO/HO)}$ (eV)	-13.59844	0	0	0	0	-13.59844	-13.59844	-13.59844	-13.59844	0	0	0	0	0	0	0
$E_{D(Group)}$ (eV)	3.48357	4.43110	8.70628	7.80660	4.41925	4.41035	12.49186	7.83016	3.32601	4.32754	4.29921	3.97398	4.17951	3.62128	3.91734	7.51014

Table 15.103. The total bond energies of alkyl carboxylic acids calculated using the functional group composition and the energies of Table 15.102 compared to the experimental values [3]. The magnetic energy E_{mag} that is subtracted from the weighted sum of the E_D $(_{Group})$ (eV) values based on composition is given by (15.57).

Formula	Name	$C-H$ (i) Group	$C-C(O)$ Group	$C=O$ (i) Group	$C=O$ (ii) Group	$C-O$ Group	OH Group	CH_3	CH_2	CH (ii)	$C-C$ (a)	$C-C$ (b)	$C-C$ (c)	$C-C$ (d)	$C-C$ (e)	$C-C$ (f)	$C=C$	E_{mag}	Calculated Total Bond Energy (eV)	Experimental Total Bond Energy (eV)	Relative Error
CH_2O_2	Formic acid	1	0	1	0	1	1	0	0	0	0	0	0	0	0	0	0	0	21.01945	21.036	0.00079
$C_2H_4O_2$	Acetic acid	0	1	0	1	1	1	1	0	0	0	0	0	0	0	0	0	0	33.55916	33.537	-0.00066
$C_3H_6O_2$	Propanoic acid	0	1	0	1	1	1	1	1	0	1	0	0	0	0	0	0	0	45.71686	45.727	0.00022
$C_4H_8O_2$	Butanoic acid	0	1	0	1	1	1	1	2	0	2	0	0	0	0	0	0	0	57.87456	57.883	0.00015
$C_4H_4O_4$	Maleic acid	0	0	0	2	2	2	0	0	2	2	0	0	0	0	0	1	0	56.08964	56.120	0.00054
$C_4H_4O_4$	Fumaric acid	0	0	0	2	2	2	0	0	2	2	0	0	0	0	0	1	0	56.08964	56.083	-0.00013
$C_5H_{10}O_2$	Pentanoic acid	0	1	0	1	1	1	1	3	0	3	0	0	0	0	0	0	0	70.03226	69.995	-0.00053
$C_5H_{10}O_2$	3-Methylbutanoic acid	0	1	0	1	1	1	2	1	1	0	3	0	0	0	0	0	0	70.10482	70.183	0.00111
$C_5H_{10}O_2$	2,2-Dimethylpropanoic acid	0	1	0	1	1	1	3	0	0	0	0	3	0	0	0	0	-1	70.31679	69.989	-0.00468
$C_6H_{12}O_2$	Hexanoic acid	0	1	0	1	1	1	1	4	0	4	0	0	0	0	0	0	0	82.18996	82.149	-0.00050
$C_7H_{14}O_2$	Heptanoic acid	0	1	0	1	1	1	1	5	0	5	0	0	0	0	0	0	0	94.34766	94.347	0.00000
$C_8H_{16}O_2$	Octanoic acid	0	1	0	1	1	1	1	6	0	6	0	0	0	0	0	0	0	106.50536	106.481	-0.00022
$C_9H_{18}O_2$	Nonanoic acid	0	1	0	1	1	1	1	7	0	7	0	0	0	0	0	0	0	118.66306	118.666	0.00003
$C_{10}H_{20}O_2$	Decanoic acid	0	1	0	1	1	1	1	8	0	8	0	0	0	0	0	0	0	130.82076	130.795	-0.00020
$C_{12}H_{24}O_2$	Dodecanoic acid	0	1	0	1	1	1	1	10	0	10	0	0	0	0	0	0	0	155.13616	155.176	0.00026
$C_{14}H_{28}O_2$	Tetradecanoic acid	0	1	0	1	1	1	1	12	0	12	0	0	0	0	0	0	0	179.45156	179.605	0.00085
$C_{15}H_{30}O_2$	Pentadecanoic acid	0	1	0	1	1	1	1	13	0	13	0	0	0	0	0	0	0	191.60926	191.606	-0.00002
$C_{16}H_{32}O_2$	Hexadecanoic acid	0	1	0	1	1	1	1	14	0	14	0	0	0	0	0	0	0	203.76696	203.948	0.00089
$C_{18}H_{36}O_2$	Stearic acid	0	1	0	1	1	1	1	16	0	16	0	0	0	0	0	0	0	228.08236	228.298	0.00094
$C_{20}H_{40}O_2$	Eicosanoic acid	0	1	0	1	1	1	1	18	0	18	0	0	0	0	0	0	0	252.39776	252.514	0.00046

Table 15.104. The bond angle parameters of alkyl carboxylic acids and experimental values [1]. In the calculation of θ_v, the parameters from the preceding angle were used. E_T is $E_T(atom-atom,msp^3.AO)$.

Atoms of Angle	2c' Bond 1 (a_0)	2c' Bond 2 (a_0)	2c' Terminal Atoms (a_0)	$E_{Coulombic}$ Atom 1	Atom 1 Hybridization Designation (Table 15.3.A)	$E_{Coulombic}$ Atom 2	Atom 2 Hybridization Designation (Table 15.3.A)	c_2 Atom 1	c_2 Atom 2	C_1	C_2	c_1	c_2'	E_T (eV)	θ_v (°)	θ_1 (°)	θ_2 (°)	Cal. θ (°)	Exp. θ (°)
$\angle HC_aO_a$ (CH (i); $C=O$ (i))	2.06598	2.27227	3.8816	-15.55033 C_a	5	-13.61806	O	0.87495	0.85395 (Eq. (15.133))	0.75	1	0.75	0.97600	0				126.88	124.1 (formic acid)
$\angle HC_aO_b$ (CH (i))	2.06598	2.63431	3.8816	-15.55033 C_a	5	-13.61806	O	0.87495	0.85395 (Eq. (15.133))	0.75	1	0.75	0.97600	0				110.76	
$\angle O_aC_aO_b$	2.27227	2.63431	4.3243	-16.61853 O_a	24	-15.75493 O_b	7	0.81871	0.86359	1	1	1	0.84115	-1.44915				123.44	124.9 (formic acid)
$\angle C_aO_bH$ (CH (i); $C=O$ (i))	2.63431	1.83616	3.6405	-14.82575	1	-14.82575	1	1	0.91771	0.75	1	0.75	0.91771	0				107.71	106.3 (formic acid)
$\angle C_bC_aO_a$	2.86175	2.27954	4.5826	-16.68411	25	-13.61806	O	0.81549	0.85395 (Eq. (15.133))	1	1	1	0.83472	-1.65376				125.70	126.6 (acetic acid)
$\angle C_bC_aO_b$	2.86175	2.63431	4.4944	-15.75493	7	-13.61806	O	0.86359	0.85395 (Eq. (15.133))	1	1	1	0.85877	-1.44915				109.65	110.6 (acetic acid)
$\angle O_aC_aO_b$	2.27954	2.63431	4.3818	-16.17521 O_a	13	-15.75493 O_b	7	0.84115	0.86359	1	1	1	0.85237	-1.44915				126.03	
Methylene $\angle HC_aH$	2.11106	2.11106	3.4252	-15.75493	7	H	H	0.86359	1	1	1	0.75	1.15796	0				108.44	107 (propane)
$\angle C_aC_bC_c$															69.51			110.49	112 (propane) 113.8 (butane) 110.8 (isobutane)
$\angle C_aC_bH$															69.51			110.49	111.0 (butane) 111.4 (isobutane)
Methyl $\angle HC_aH$	2.09711	2.09711	3.4252	-15.75493	7	H	H	0.86359	1	1	1	0.75	1.15796	0				109.50	
$\angle C_aC_bC_c$															70.56			109.44	
$\angle C_aC_bH$															70.56			109.44	
$\angle C_bC_aC_c$ iso C_a	2.91547	2.91547	4.7958	-16.68412 C_b	26	-16.68412 C_c	26	0.81549	0.81549	1	1	1	0.81549	-1.85836				110.67	110.8 (isobutane)
$\angle C_bC_aH$ iso C_a	2.91547	2.11323	4.1633	-15.55033 C_a	5	-14.82575 C_b	1	0.87495	0.91771	0.75	1	0.75	1.04887	0				110.76	
$\angle C_aC_bH$ iso C_a	2.91547	2.09711	4.1633	-15.55033 C_b	5	-14.82575 C_a	1	0.87495	0.91771	0.75	1	0.75	1.04887	0				111.27	111.4 (isobutane)
$\angle C_bC_aC_b$ tert C_a	2.90327	2.90327	4.7958	-16.68412 C_b	26	-16.68412 C_b	26	0.81549	0.81549	1	1	1	0.81549	-1.85836				111.37	110.8 (isobutane)
$\angle C_bC_aC_d$															72.50			107.50	

CARBOXYLIC ACID ESTERS ($C_nH_{2n}O_2,\ n=1,2,3,4,5...\infty$)

The alkyl carboxylic acid esters, $C_nH_{2n}O_2$, comprise a $C=O$ functional group, and the single bond of carbon to the carbonyl carbon atom, $C-C(O)$, is also a functional group. Formic acid ester has a $HC=O$ moiety that comprises a more stable $C=O$ functional group and a CH functional group. All carboxylic acid esters further comprise a COR moiety that comprises a $C-O$ functional group and three types of $O-R$ functional groups, one for R comprising methyl, one for R comprising an alkyl ester group of a formate, and one for R comprising an alkyl ester group of an alkyl carboxylate. The alkyl portion of the alkyl carboxylic acid ester may comprise at least two terminal methyl groups (CH_3) at each end of the chain, and may comprise methylene (CH_2), and methylyne (CH) functional groups as well as C bound by carbon-carbon single bonds. The methyl and methylene functional groups are equivalent to those of straight-chain alkanes. Six types of $C-C$ bonds can be identified. The n-alkane $C-C$ bond is the same as that of straight-chain alkanes. In addition, the $C-C$ bonds within isopropyl ($(CH_3)_2CH$) and t-butyl ($(CH_3)_3C$) groups and the isopropyl to isopropyl, isopropyl to t-butyl, and t-butyl to t-butyl $C-C$ bonds comprise functional groups. The branched-chain-alkane groups in carboxylic acid esters are equivalent to those in branched-chain alkanes.

The CH functional group is equivalent to that of formic acid. The alkyl carboxylic acid ester $C=O$ and $C-C(O)$ groups are equivalent to those given in the Carboxylic Acids section. The formic acid ester $C=O$ group is equivalent to that given in the Carboxylic Acids section except that $\overline{E}_{Kvib}$ is that corresponding to a formic acid ester. The $C-O$ group is equivalent to that given in the Carboxylic Acids section except that the parameters corresponding to oscillation of the bond in the transition state, $\overline{E}_D\ (eV)$ and $\overline{E}_{Kvib}$, are those of a carboxylic acid ester. As in the case with the alkyl ethers, each $O-C$ group is solved by hybridizing the $2s$ and $2p$ AOs of the C atom to form a single $2sp^3$ shell as an energy minimum, and the sharing of electrons between the $C2sp^3$ HO and the O AO to form a MO permits each participating orbital to decrease in radius and energy. To meet the equipotential condition of the union of the $O-C$ H_2-type-ellipsoidal-MO with other orbitals of the molecule, the hybridization factor c_2 of Eq. (15.60) for the $O-C$-bond MO given by Eq. (15.133) is: $c_2\left(C2sp^3 HO\ to\ O\right)=0.85395$.

$E_T\left(atom-atom, msp^3.AO\right)$ (Eq. (15.61)) of (1) the $C=O$ group of alkyl carboxylic acid esters, (2) the $C=O$ group of formic acid esters, (3) the alkyl carboxylic acid ester $C-C(O)$ group, and (4) the carboxylic acid ester $C-O$ group are equivalent to those of the corresponding carboxylic acids. The values given in the Carboxylic Acids section are $-2.69893\ eV$, $-3.58557\ eV$, $-1.85836\ eV$, and $-1.85836\ eV$, respectively. $E_T\left(atom-atom, msp^3.AO\right)$ of the $C-O$ group matches that of the $C-C(O)$ group. Also, as in the case of aldehydes, $C_{1o}=2C_1$ in Eq. (15.61) for the $C-C(O)$ group.

$E_T\left(atom-atom, msp^3.AO\right)$ of the $O-C$-bond MO in Eq. (15.61) due to the charge donation from the C and O atoms to the MO is $-1.13379\ eV$ for the $O-CH_3$ group of formate and alkyl carboxylates, $-1.44915\ eV$ for the $O-R$ group of alkyl carboxylates, and $-1.85836\ eV$ for the $O-R$ group of alkyl formates, where R is an alkyl group. Each is based on the energy match between the O AO, initially at the Coulomb potential of a proton and an electron (Eqs. (1.257) and (10.162), respectively), the $C2sp^3$ HO of the methyl or alkyl ester group, and the carbonyl carbon. The increasing energy contributions to the single bond correspond to the increasing hybridization of linear combinations of increasing bond order. The energy contributions corresponding to one half of a double bond and those of the methyl-methyl and methylene-methylene bonds are $-1.13379\ eV$ (Eq. (14.247)), two times $-0.72457\ eV$ (Eq. (14.151)), and two times $-0.92918\ eV$ (Eq. (14.513)), respectively.

The symbols of the functional groups of alkyl carboxylic acid esters are given in Table 15.105. The geometrical (Eqs. (15.1-15.5) and (15.51)), intercept (Eqs. (15.80-15.87)), and energy (Eqs. (15.6-15.11) and (15.17-15.65)) parameters of alkyl carboxylic acid esters are given in Tables 15.106, 15.107, and 15.108, respectively. The total energy of each alkyl carboxylic acid ester given in Table 15.109 was calculated as the sum over the integer multiple of each $E_{D\,(Group)}$ of Table 15.108 corresponding to functional-group composition of the molecule. For each set of unpaired electrons created by bond breakage , the $C2sp^3$ HO magnetic energy E_{mag} that is subtracted from the weighted sum of the $E_{D\,(Group)}\ (eV)$ values based on composition is given by Eq. (15.67). The bond angle parameters of alkyl carboxylic acid esters determined using Eqs. (15.88-15.117) are given in Table 15.110. The color scale, translucent view of the charge-density of exemplary carboxylic acid ester, methyl acetate, comprising the concentric shells of atoms with the outer shell bridged by one or more H_2-type ellipsoidal MOs or joined with one or more hydrogen MOs is shown in Figure 15.18.

Figure 15.18. Color scale, translucent view of the charge-density of methyl acetate showing the orbitals of the atoms at their radii, the ellipsoidal surface of each H or H_2-type ellipsoidal MO that transitions to the corresponding outer shell of the atom(s) participating in each bond, and the hydrogen nuclei (red, not to scale).

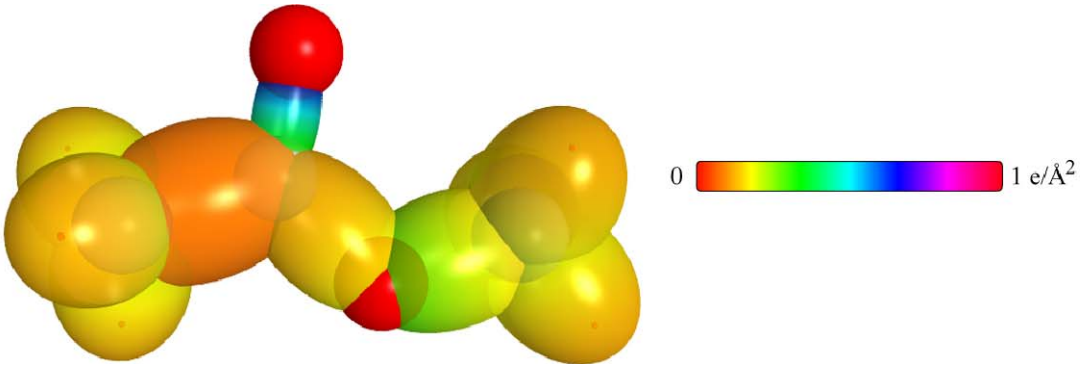

Table 15.105. The symbols of functional groups of alkyl carboxylic acid esters.

Functional Group	Group Symbol
CH (formic acid ester) group	$C-H$ (i)
C-C(O)	$C-C(O)$
C=O (formic acid ester)	$C=O$ (i)
C=O (alkyl carboxylic acid ester)	$C=O$ (ii)
(O)C-O	$C-O$
O-CH₃	$O-C$ (i)
O-R (formic acid ester)	$O-C$ (ii)
O-R (alkyl acid ester)	$O-C$ (iii)
OH group	*OH*
CH₃ group	$C-H\ (CH_3)$
CH₂ group	$C-H\ (CH_2)$
CH (alkyl) group	$C-H$ (ii)
CC bond (*n-C*)	$C-C$ (a)
CC bond (*iso-C*)	$C-C$ (b)
CC bond (*tert-C*)	$C-C$ (c)
CC (*iso* to *iso-C*)	$C-C$ (d)
CC (*t* to *t-C*)	$C-C$ (e)
CC (*t* to *iso-C*)	$C-C$ (f)

Table 15.106. The geometrical bond parameters of alkyl carboxylic acid esters and experimental values [1].

Parameter	$C-H$ (i) Group	$C-C(O)$ Group	$C=O$ (i) Group	$C=O$ (ii) Group	$C-O$ Group	$O-C$ (i) Group	$O-C$ (ii) Group	$O-C$ (iii) Group	$C-H\ (CH_3)$ Group	$C-H\ (CH_2)$ Group	$C-H$ (ii) Group	$C-C$ (a) Group	$C-C$ (b) Group	$C-C$ (c) Group	$C-C$ (d) Group	$C-C$ (e) Group	$C-C$ (f) Group
$a\ (a_0)$	1.61341	2.04740	1.290799	1.29907	1.73490	1.82683	1.78255	1.80717	1.64920	1.67122	1.67465	2.12499	2.12499	2.10725	2.12499	2.10725	2.10725
$c'\ (a_0)$	1.03711	1.43087	1.13613	1.13977	1.31716	1.35160	1.33512	1.34431	1.04856	1.05553	1.05661	1.45744	1.45744	1.45164	1.45744	1.45164	1.45164
Bond Length $2c'\ (\AA)$	1.09763	1.51437	1.20243	1.20628	1.39402	1.43047	1.41303	1.42276	1.10974	1.11713	1.11827	1.54280	1.54280	1.53635	1.54280	1.53635	1.53635
Exp. Bond Length $(\AA)$	1.101 (methyl formate)	1.520 (acetic acid)	1.206 (methyl formate)	1.214 (acetic acid)	1.393 (avg. methyl formate)	1.393 (avg. methyl formate)	1.393 (avg. methyl formate)	1.393 (avg. methyl formate)	1.08 (methyl formate) 1.107 ($C-H$ propane) 1.117 ($C-H$ butane)	1.107 ($C-H$ propane) 1.117 ($C-H$ butane)	1.122 (isobutane)	1.532 (propane) 1.531 (butane)	1.532 (propane) 1.531 (butane)	1.532 (propane) 1.531 (butane)	1.532 (propane) 1.531 (butane)	1.532 (propane) 1.531 (butane)	1.532 (propane) 1.531 (butane)
$b,c\ (a_0)$	1.23591	1.46439	0.61267	0.62331	1.12915	1.22901	1.18107	1.20776	1.27295	1.29569	1.29924	1.54616	1.54616	1.52750	1.54616	1.52750	1.52750
e	0.64281	0.69887	0.88018	0.87737	0.75921	0.73986	0.74900	0.74388	0.63580	0.63159	0.63095	0.68600	0.68600	0.68888	0.68600	0.68888	0.68888

Table 15.107. The MO to HO intercept geometrical bond parameters of alkyl carboxylic acid esters. R, R', R'' are H or alkyl groups. E_T is E_T ($atom - atom, msp^3.AO$).

Bond	Atom	E_T (eV) Bond 1	E_T (eV) Bond 2	E_T (eV) Bond 3	E_T (eV) Bond 4	Final Total Energy $C2sp^3$ (eV)	$r_{initial}$ (a_0)	r_{final} (a_0)	$E_{Coulomb}$ (eV) Final	$E(C2sp^3)$ (eV) Final	θ' (°)	θ_1 (°)	θ_2 (°)	d_1 (a_0)	d_2 (a_0)
$RC_a(O)O-C_bH_3$ $(O-C$ (i))	O	-0.92918	-0.56690	0	0		1.00000	0.83360	-16.32183		90.63	89.37	42.70	1.34246	0.00914
$RC_a(O)O-C_bH_3$ $(O-C$ (i))	C_b	-0.56690	0	0	0	-152.18259	0.91771	0.88392	-15.39265	-15.20178	95.01	84.99	45.76	1.27445	0.07716
$HC_a(O)O-C_bH_2C_cH_2R$ $(O-C$ (ii))	O	-0.92918	-0.92918	0	0		1.00000	0.81549	-16.68412		93.09	86.91	43.59	1.29113	0.04399
$HC_a(O)O-C_bH_2C_cH_2R$ $(O-C$ (ii))	C_b	-0.92918	-0.92918	0	0	-153.47405	0.91771	0.81549	-16.68411	-16.49325	93.09	86.91	43.59	1.29113	0.04399
$R'C_a(O)O-C_bH_2C_cH_2R$ $(O-C$ (iii))	O	-0.92918	-0.72457	0	0		1.00000	0.82562	-16.47951		91.72	88.28	43.10	1.31951	0.02480
$R'C_a(O)O-C_bH_2C_cH_2R$ $(O-C$ (iii))	C_b	-0.72457	-0.92918	0	0	-153.26945	0.91771	0.82562	-16.47951	-16.28864	91.72	88.28	43.10	1.31951	0.02480
$HC_a(O)-OC_bH_3$ $(C=O$ (i)) $(O-C$ (i))	O	-0.92918	-0.56690	0	0		1.00000	0.83360	-16.32183		98.97	81.03	46.82	1.18716	0.13000
$HC_a(O)-OC_bH_3$ $(C=O$ (i)) $(O-C$ (i))	C_a	-0.92918	-1.79278	0	0	-154.33765	0.91771	0.77536	-17.54772	-17.35685	93.94	86.06	43.24	1.26386	0.05329
$HC_a(O)-OR$ $(C=O$ (i)) $(O-C$ (ii))	O	-0.92918	-0.92918	0	0		1.00000	0.81549	-16.68412		97.48	82.52	45.73	1.21100	0.10616
$HC_a(O)-OR$ $(C=O$ (i)) $(O-C$ (ii))	C_a	-1.79278	-0.92918	0	0	-154.33765	0.91771	0.77536	-17.54772	-17.35685	93.94	86.06	43.24	1.26386	0.05329
$R'H_2C_bC_a(O)-OC_bH_3$ $(C=O$ (ii)) $(O-C$ (i))	O	-0.92918	-0.56690	0	0		1.00000	0.83360	-16.32183		98.97	81.03	46.82	1.18716	0.13000
$R'H_2C_bC_a(O)-OC_bH_3$ $(C=O$ (ii)) $(O-C$ (i))	C_a	-0.92918	-1.34946	-0.92918	0	-154.82352	0.91771	0.75447	-18.03358	-17.84271	91.96	88.04	41.90	1.29138	0.02578
$R'H_2C_bC_a(O)-OC_bH_2C_cH_2R$ $(C=O$ (ii)) $(O-C$ (iii))	O	-0.92918	-0.72457	0	0		1.00000	0.82562	-16.47951		98.32	81.68	46.34	1.19766	0.11949
$R'H_2C_bC_a(O)-OC_bH_2C_cH_2R$ $(C=O$ (ii)) $(O-C$ (iii))	C_a	-0.92918	-1.34946	-0.92918	0	-154.82352	0.91771	0.75447	-18.03358	-17.84271	91.96	88.04	41.90	1.29138	0.02578
$HC_a(OR)=O$ $(C=O$ (i))	O	-1.79278	0	0	0		1.00000	0.81871	-16.61853		137.10	42.90	65.45	0.53635	0.59978

Table 15.107 Cont' d. The MO to HO intercept geometrical bond parameters of alkyl carboxylic acid esters. R, R', R'' are H or alkyl groups. E_T is E_T ($atom - atom, msp^3.AO$).

Bond	Atom	E_T (eV) Bond 1	E_T (eV) Bond 2	E_T (eV) Bond 3	E_T (eV) Bond 4	Final Total Energy $C2sp^3$ (eV)	$r_{initial}$ (a_0)	r_{final} (a_0)	$E_{Coulomb}$ (eV) Final	$E(C2sp^3)$ (eV) Final	θ' (°)	θ_1 (°)	θ_2 (°)	d_1 (a_0)	d_2 (a_0)
$HC_a(OR)=O$ ($C=O$ (i))	C_a	-1.79278	-0.92918	0	0	-154.33766	0.91771	0.77536	-17.54772	-17.35685	135.24	44.76	63.02	0.58561	0.55053
$R'C_bH_2C_a(OR)=O$ ($C=O$ (ii))	O	-1.34946	0	0	0		1.00000	0.84115	-16.17521		137.27	42.73	66.31	0.52193	0.61784
$R'C_bH_2C_a(OR)=O$ ($C=O$ (ii))	C_a	-1.34946	-0.92918	-0.92918	0	-154.82352	0.91771	0.75447	-18.03358	-17.84272	133.47	46.53	61.46	0.62072	0.51905
$H-C(O)OR$ (CH (i))	C	-1.79278	-0.92918	0	0	-154.33766	0.91771	0.77536	-17.54772	-17.35685	69.89	110.11	36.09	1.30373	0.26662
$R'H_2C_b-C_a(O)OR$	C_a	-0.92918	-1.34946	-0.92918	0	-154.82352	0.91771	0.75447	-18.03358	-17.84272	56.25	123.75	25.37	1.85002	0.41915
$H_3C_b-C_a(O)OR$	C_b	-0.92918	0	0	0	-152.54487	0.91771	0.86359	-15.75493	-15.56407	72.27	107.73	34.17	1.69388	0.26301
$R'H_2C_cH_2C_b-C_a(O)OR$	C_b	-0.92918	-0.92918	0	0	-153.47405	0.91771	0.81549	-16.68411	-16.49325	65.99	114.01	30.58	1.76270	0.33183
$C-H\ (CH_3)$	C	-0.92918	0	0	0	-152.54487	0.91771	0.86359	-15.75493	-15.56407	77.49	102.51	41.48	1.23564	0.18708
$C-H\ (CH_2)$	C	-0.92918	-0.92918	0	0	-153.47406	0.91771	0.81549	-16.68412	-16.49325	68.47	111.53	35.84	1.35486	0.29933
$C-H\ (CH)$ (ii)	C	-0.92918	-0.92918	-0.92918	0	-154.40324	0.91771	0.77247	-17.61330	-17.42244	61.10	118.90	31.37	1.42988	0.37326
$H_3C_aC_bH_2CH_2-$ ($C-C$ (a))	C_a	-0.92918	0	0	0	-152.54487	0.91771	0.86359	-15.75493	-15.56407	63.82	116.18	30.08	1.83879	0.38106
$H_3C_aC_bH_2CH_2-$ ($C-C$ (a))	C_b	-0.92918	-0.92918	0	0	-153.47406	0.91771	0.81549	-16.68412	-16.49325	56.41	123.59	26.06	1.90890	0.45117
$R-H_2C_aC_b(H_2C_c-R')HCH_2-$ ($C-C$ (b))	C_b	-0.92918	-0.92918	-0.92918	0	-154.40324	0.91771	0.77247	-17.61330	-17.42244	48.30	131.70	21.90	1.97162	0.51388
$R-H_2C_a(R'-H_2C_d)C_b(R''-H_2C_c)CH_2-$ ($C-C$ (c))	C_b	-0.92918	-0.72457	-0.72457	-0.72457	-154.71860	0.91771	0.75889	-17.92866	-17.73779	48.21	131.79	21.74	1.95734	0.50570
$isoC_aC_b(H_2C_c-R')HCH_2-$ ($C-C$ (d))	C_b	-0.92918	-0.92918	-0.92918	0	-154.40324	0.91771	0.77247	-17.61330	-17.42244	48.30	131.70	21.90	1.97162	0.51388
$tertC_a(R'-H_2C_d)C_b(R''-H_2C_c)CH_2-$ ($C-C$ (e))	C_b	-0.72457	-0.72457	-0.72457	-0.72457	-154.51399	0.91771	0.76765	-17.92866	-17.73779	50.04	129.96	22.66	1.94462	0.49298
$tertC_aC_b(H_2C_c-R')HCH_2-$ ($C-C$ (f))	C_b	-0.72457	-0.92918	-0.92918	0	-154.19863	0.91771	0.78155	-17.40869	-17.21783	52.78	127.22	24.04	1.92443	0.47279
$isoC_a(R'-H_2C_d)C_b(R''-H_2C_c)CH_2-$ ($C-C$ (f))	C_b	-0.72457	-0.72457	-0.72457	-0.72457	-154.51399	0.91771	0.76765	-17.92866	-17.73779	50.04	129.96	22.66	1.94462	0.49298

Table 15.108. The energy parameters (eV) of functional groups of alkyl carboxylic acid esters.

Parameters	$C-H$ (i) Group	$C-C(O)$ Group	$C=O$ (i) Group	$C=O$ (ii) Group	$C-O$ Group	$O-C$ (i) Group	$O-C$ (ii) Group	$O-C$ (iii) Group	CH_3 Group	CH_2 Group	$C-H$ (ii) Group	$C-C$ (a) Group	$C-C$ (b) Group	$C-C$ (c) Group	$C-C$ (d) Group	$C-C$ (e) Group	$C-C$ (f) Group
n_1	1	1	2	2	1	1	1	1	3	2	1	1	1	1	1	1	1
n_2	0	0	0	0	0	0	0	0	2	1	0	0	0	0	0	0	0
n_3	0	0	0	0	0	0	0	0	0	0	0	0	0	0	0	0	0
C_1	0.75	0.5	0.5	0.5	0.5	0.5	0.5	0.5	0.75	0.75	0.75	0.5	0.5	0.5	0.5	0.5	0.5
C_2	1	1	1	1	1	1	1	1	1	1	1	1	1	1	1	1	1
c_1	1	1	1	1	1	1	1	1	1	1	1	1	1	1	1	1	1
c_2	0.91771	0.91771	0.85395	0.85395	0.85395	0.85395	0.85395	0.85395	0.91771	0.91771	0.91771	0.91771	0.91771	0.91771	0.91771	0.91771	0.91771
c_3	0	0	2	2	0	0	0	0	0	1	1	0	0	0	1	1	0
c_4	1	2	4	4	2	2	2	2	1	1	1	2	2	2	2	2	2
c_5	1	0	0	0	0	0	0	0	3	2	1	0	0	0	0	0	0
C_{1o}	0.75	1	0.5	0.5	0.5	0.5	0.5	0.5	0.75	0.75	0.75	0.5	0.5	0.5	0.5	0.5	0.5
C_{2o}	1	1	1	1	1	1	1	1	1	1	1	1	1	1	1	1	1
V_e (eV)	-36.74167	-30.19634	-112.61934	-111.25473	-35.08488	-32.67173	-33.78830	-33.15757	-107.32728	-70.41425	-35.12015	-28.79214	-28.79214	-29.10112	-28.79214	-29.10112	-29.10112
V_p (eV)	13.11890	9.50874	23.95107	23.87467	10.32968	10.06642	10.19070	10.12103	38.92728	25.78002	12.87680	9.33352	9.33352	9.37273	9.33352	9.37273	9.37273
T (eV)	11.38634	7.37432	43.62389	42.82081	10.11150	8.94219	9.47754	9.17389	32.53914	21.06675	10.48582	6.77464	6.77464	6.90500	6.77464	6.90500	6.90500
V_m (eV)	-5.69317	-3.68716	-21.81195	-21.41040	-5.05575	-4.47110	-4.73877	-4.58695	-16.26957	-10.53337	-5.24291	-3.38732	-3.38732	-3.45250	-3.38732	-3.45250	-3.45250
$E_{(AO/HO)}$ (eV)	-14.63489	-14.63489	0	0	-14.63489	-14.63489	-14.63489	-14.63489	-15.56407	-15.56407	-14.63489	-15.56407	-15.56407	-15.35946	-15.56407	-15.35946	-15.35946
$\Delta E_{H_2MO(AO/HO)}$ (eV)	-0.92918	0	-3.58557	-2.69893	-2.69893	-1.13379	-1.85836	-1.44915	0	0	0	0	0	0	0	0	0
$E_T(_{AO/HO})$ (eV)	-13.70571	-14.63489	3.58557	2.69893	-11.93596	-13.50110	-12.77653	-13.18574	-15.56407	-15.56407	-14.63489	-15.56407	-15.56407	-15.35946	-15.56407	-15.35946	-15.35946
$E_T(_{H_2MO})$ (eV)	-31.63530	-31.63534	-63.27075	-63.27074	-31.63541	-31.63531	-31.63536	-31.63533	-67.69451	-49.66493	-31.63533	-31.63537	-31.63537	-31.63535	-31.63537	-31.63535	-31.63535
$E_T(atom-atom, msp^3.AO)$ (eV)	0	-1.85836	-3.58557	-2.69893	-1.85836	-1.13379	-1.85836	-1.44915	0	0	0	-1.85836	-1.85836	-1.44915	-1.85836	-1.44915	-1.44915
$E_T(_{MO})$ (eV)	-31.63537	-33.49373	-66.85630	-65.96966	-33.49373	-32.76916	-33.49373	-33.08452	-67.69450	-49.66493	-31.63537	-33.49373	-33.49373	-33.08452	-33.49373	-33.08452	-33.08452
ω $(10^{15}\ rad/s)$	26.0575	23.3291	60.9581	59.4034	12.7926	21.4553	22.7749	12.0329	24.9286	24.2751	24.1759	9.43699	9.43699	15.4846	9.43699	9.55643	9.55643
E_K (eV)	17.15150	15.35563	40.12366	39.10034	8.42030	14.12224	14.99085	7.92028	16.40846	15.97831	15.91299	6.21159	6.21159	10.19220	6.21159	6.29021	6.29021
$\bar{E}_D$ (eV)	-0.25920	-0.25966	-0.41891	-0.40804	-0.19228	-0.24362	-0.25655	-0.18420	-0.25352	-0.25017	-0.24966	-0.16515	-0.16515	-0.20896	-0.16515	-0.16416	-0.16416
$\bar{E}_{Kvib}$ (eV)	0.35532 (Eq. (13.458))	0.10502 [29]	0.21747 [32]	0.21077 [12]	0.14965 [32]	0.11469 [32]	0.11469 [32]	0.16118 [4]	0.35532 (Eq. (13.458))	0.35532 (Eq. (13.458))	0.35532 (Eq. (13.458))	0.12312 [2]	0.17978 [4]	0.09944 [5]	0.12312 [2]	0.12312 [2]	0.12312 [2]
$\bar{E}_{osc}$ (eV)	-0.08153	-0.20715	-0.31017	-0.30266	-0.11745	-0.18628	-0.19921	-0.10361	-0.22757	-0.14502	-0.07200	-0.10359	-0.07526	-0.15924	-0.10359	-0.10260	-0.10260
E_{mag} (eV)	0.14803	0.14803	0.11441	0.11441	0.14803	0.14803	0.14803	0.14803	0.14803	0.14803	0.14803	0.14803	0.14803	0.14803	0.14803	0.14803	0.14803
$E_T(_{Group})$ (eV)	-31.71690	-33.70088	-67.47664	-66.57498	-33.61118	-32.95544	-33.69294	-33.18813	-67.92207	-49.80996	-31.70737	-33.59732	-33.49373	-33.24376	-33.59732	-33.18712	-33.18712
$E_{initial}(_{c_4\ AO/HO})$ (eV)	-14.63489	-14.63489	-14.63489	-14.63489	-14.63489	-14.63489	-14.63489	-14.63489	-14.63489	-14.63489	-14.63489	-14.63489	-14.63489	-14.63489	-14.63489	-14.63489	-14.63489
$E_{initial}(_{c_5\ AO/HO})$ (eV)	-13.59844	0	0	0	0	0	0	0	-13.59844	-13.59844	-13.59844	0	0	0	0	0	0
$E_D(_{Group})$ (eV)	3.48357	4.43110	8.70826	7.80660	4.34141	3.68566	4.42316	3.91835	12.49186	7.83016	3.32601	4.32754	4.29921	3.97398	4.17951	3.62128	3.91734

Table 15.109. The total bond energies of alkyl carboxylic acid esters calculated using the functional group composition and the energies of Table 15.108 compared to the experimental values [3]. The magnetic energy E_{mag} that is subtracted from the weighted sum of the E_D $(Group)$ (eV) values based on composition is given by (15.57).

Formula	Name	$C-H$ (i) Group	$C-C(O)$ Group	$C=O$ (i) Group	$C=O$ (ii) Group	$C-O$ Group	$O-C$ (i) Group	$O-C$ (ii) Group	$O-C$ (iii) Group	CH_3	CH_2	CH (ii)	$C-C$ (a)	$C-C$ (b)	$C-C$ (c)	$C-C$ (d)	$C-C$ (e)	$C-C$ (f)	E_{mag}	Calculated Total Bond Energy (eV)	Experimental Total Bond Energy (eV)	Relative Error
$C_2H_4O_2$	Methyl formate	1	0	1	0	1	1	0	0	1	0	0	0	0	0	0	0	0	0	32.71076	32.762	0.00156
$C_3H_6O_2$	Methyl acetate	0	1	0	1	1	1	0	0	2	0	0	0	0	0	0	0	0	0	45.24849	45.288	0.00087
$C_6H_{12}O_2$	Methyl pentanoate	0	1	0	1	1	1	0	0	2	3	0	3	0	0	0	0	0	0	81.72159	81.726	0.00005
$C_7H_{14}O_2$	Methyl hexanoate	0	1	0	1	1	1	0	0	2	4	0	4	0	0	0	0	0	0	93.87929	93.891	0.00012
$C_8H_{16}O_2$	Methyl heptanoate	0	1	0	1	1	1	0	0	2	5	0	5	0	0	0	0	0	0	106.03699	106.079	0.00040
$C_9H_{18}O_2$	Methyl octanoate	0	1	0	1	1	1	0	0	2	6	0	6	0	0	0	0	0	0	118.19469	118.217	0.00018
$C_{10}H_{20}O_2$	Methyl nonanoate	0	1	0	1	1	1	0	0	2	7	0	7	0	0	0	0	0	0	130.35239	130.373	0.00016
$C_{11}H_{22}O_2$	Methyl decanoate	0	1	0	1	1	1	0	0	2	8	0	8	0	0	0	0	0	0	142.51009	142.523	0.00009
$C_{12}H_{24}O_2$	Methyl undecancate	0	1	0	1	1	1	0	0	2	9	0	9	0	0	0	0	0	0	154.66779	154.677	0.00006
$C_{13}H_{26}O_2$	Methyl dodecancate	0	1	0	1	1	1	0	0	2	10	0	10	0	0	0	0	0	0	166.82549	166.842	0.00010
$C_{14}H_{28}O_2$	Methyl tridecanoate	0	1	0	1	1	1	0	0	2	11	0	11	0	0	0	0	0	0	178.98319	179.000	0.00009
$C_{15}H_{30}O_2$	Methyl tetradecanoate	0	1	0	1	1	1	0	0	2	12	0	12	0	0	0	0	0	0	191.14089	191.170	0.00015
$C_{16}H_{32}O_2$	Methyl pentadecanoate	0	1	0	1	1	1	0	0	2	13	0	13	0	0	0	0	0	0	203.29859	203.356	0.00028
$C_4H_8O_2$	Propyl formate	1	0	1	0	1	0	1	0	1	2	0	2	0	0	0	0	0	0	57.76366	57.746	-0.00030
$C_4H_8O_2$	Ethyl acetate	0	1	0	1	1	0	0	1	2	1	0	1	0	0	0	0	0	0	57.63888	57.548	-0.00157
$C_5H_{10}O_2$	Isopropyl acetate	0	1	0	1	1	0	0	1	3	0	1	0	2	0	0	0	0	0	69.89747	69.889	-0.00013
$C_5H_{10}O_2$	Ethyl propanoate	0	1	0	1	1	0	0	1	2	2	0	2	0	0	0	0	0	0	69.79658	69.700	-0.00139
$C_6H_{12}O_2$	Butyl acetate	0	1	0	1	1	0	0	1	2	3	0	3	0	0	0	0	0	0	81.95428	81.873	-0.00099
$C_6H_{12}O_2$	t-Butyl acetate	0	1	0	1	1	0	0	1	4	0	0	0	0	3	0	0	0	-1	82.23881	82.197	-0.00051
$C_6H_{12}O_2$	Methyl 2,2-dimethylpropanoate	0	1	0	1	1	1	0	0	4	0	0	0	0	3	0	0	0	-1	82.00612	81.935	-0.00087
$C_7H_{14}O_2$	Ethyl pentanoate	0	1	0	1	1	0	0	1	2	4	0	4	0	0	0	0	0	0	94.11198	94.033	-0.00084
$C_7H_{14}O_2$	Ethyl 3-methylbutanoate	0	1	0	1	1	0	0	1	3	2	1	1	3	0	0	0	0	0	94.18454	94.252	0.00072
$C_7H_{14}O_2$	Ethyl 2,2-dimethylpropanoate	0	1	0	1	1	0	0	1	4	1	0	1	0	3	0	0	0	-1	94.39651	94.345	-0.00054
$C_8H_{16}O_2$	Isobutyl isobutanoate	0	1	0	1	1	0	0	1	4	1	2	0	5	0	0	0	0	0	106.44313	106.363	-0.00075
$C_8H_{16}O_2$	Propyl pentanoate	0	1	0	1	1	0	0	1	2	5	0	5	0	0	0	0	0	0	106.26968	106.267	-0.00003
$C_8H_{16}O_2$	Isopropyl pentanoate	0	1	0	1	1	0	0	1	3	3	1	3	2	0	0	0	0	0	106.37057	106.384	0.00013
$C_9H_{18}O_2$	Butyl pentanoate	0	1	0	1	1	0	0	1	2	6	0	6	0	0	0	0	0	0	118.42738	118.489	0.00052
$C_9H_{18}O_2$	sec-Butyl pentanoate	0	1	0	1	1	0	0	1	3	4	1	4	2	0	0	0	0	0	118.52827	118.624	0.00081
$C_9H_{18}O_2$	Isobutyl pentanoate	0	1	0	1	1	0	0	1	3	4	1	3	3	0	0	0	0	0	118.49994	118.576	0.00064

Table 15.110. The bond angle parameters of alkyl carboxylic acid esters and experimental values [1]. In the calculation of θ_v, the parameters from the preceding angle were used. E_T is $E_T(atom - atom, msp^3.AO)$.

Atoms of Angle	2c' Bond 1 (a_0)	2c' Bond 2 (a_0)	2c' Terminal Atoms (a_0)	$E_{Coulombic}$ Atom 1	Atom 1 Hybridization Designation (Table 15.3.A)	$E_{Coulombic}$ Atom 2	Atom 2 Hybridization Designation (Table 15.3.A)	c_2 Atom 1	c_2 Atom 2	C_1	C_2	c_1	c'_2	E_T (eV)	θ_v (°)	θ_1 (°)	θ_2 (°)	Cal. θ (°)	Exp. θ (°)
$\angle HC_bO_b$ (CH (i); $C=O$ (i))	2.09711	2.70321	3.9463	-15.75493 C_b	7	-13.61806	O	0.86359	0.85395 (Eq. (15.133))	0.75	1	0.75	0.98884	0				109.95	110 (methyl formate)
$\angle O_aC_aO_b$ (CH (i); $C=O$ (i))	2.27227	2.63431	4.4045	-16.61853 O_a	24	-16.68412 O_b	26	0.81871	0.81549	1	1	1	0.81710	-1.65376				127.56	127 (methyl formate)
$\angle C_bO_bC_a$ (CH (i); $C=O$ (i))	2.70321	2.63431	4.4833	-16.32183 C_b	17	-18.47690 C_a	58	0.83360	0.73637	1	1	1	0.78498	-1.85836				114.27	114 (methyl formate)
Methylene $\angle HC_aH$	2.11106	2.11106	3.4252	-15.75493	7	H	H	0.86359	1	1	1	0.75	1.15796	0				108.44	107 (propane)
$\angle C_aC_bC_c$															69.51			110.49	112 (propane) 113.8 (butane) 110.8 (isobutane)
$\angle C_aC_bH$															69.51			110.49	111.0 (butane) 111.4 (isobutane)
Methyl $\angle HC_aH$	2.09711	2.09711	3.4252	-15.75493	7	H	H	0.86359	1	1	1	0.75	1.15796	0				109.50	
$\angle C_aC_bC_c$															70.56			109.44	
$\angle C_aC_bH$															70.56			109.44	
$\angle C_aC_aC_c$ isc C_a	2.91547	2.91547	4.7958	-16.68412 C_b	26	-16.68412 C_c	26	0.81549	0.81549	1	1	1	0.81549	-1.85836				110.67	110.8 (isobutane)
$\angle C_aC_aH$ isc C_a	2.91547	2.11323	4.1633	-15.55033 C_a	5	-14.82575 C_b	1	0.87495	0.91771	0.75	1	0.75	1.04887	0				110.76	
$\angle C_aC_bH$ isc C_a	2.91547	2.09711	4.1633	-15.55033 C_b	5	-14.82575 C_a	1	0.87495	0.91771	0.75	1	0.75	1.04887	0				111.27	111.4 (isobutane)
$\angle C_aC_aC_b$ tert C_a	2.90327	2.90327	4.7958	-16.68412 C_b	26	-16.68412 C_b	26	0.81549	0.81549	1	1	1	0.81549	-1.85836				111.37	110.8 (isobutane)
$\angle C_iC_aC_d$															72.50			107.50	

AMIDES ($C_nH_{2n+1}NO,\ n=1,2,3,4,5...\infty$)

The alkyl amides, $C_nH_{2n+1}NO$, comprise a $C=O$ functional group, and the single bond of carbon to the carbonyl carbon atom, $C-C(O)$, is also a functional group. Formamide has a $HC=O$ moiety that comprises a more stable $C=O$ functional group and a CH functional group that is equivalent to that of the CH (i) of aldehydes given in the corresponding section. It is also equivalent to that of the iso-CH group of branched-chain-alkyl portion of the alkyl amide except that E_{mag} (Eq. (15.47)) is not subtracted from $E_D(Group)$. All amides further comprise a $C-NH_2$ moiety that comprises a NH_2 functional group and two types of $C-N$ functional groups, one for formamide and the other for alkyl amides ($RC(O)NH_2$ where R is alkyl). The alkyl portion of the alkyl amide may comprise at least two terminal methyl groups (CH_3) at each end of the chain, and may comprise methylene (CH_2), and methylyne (CH) functional groups as well as C bound by carbon-carbon single bonds. The methyl and methylene functional groups are equivalent to those of straight-chain alkanes. Six types of $C-C$ bonds can be identified. The n-alkane $C-C$ bond is the same as that of straight-chain alkanes. In addition, the $C-C$ bonds within isopropyl ($(CH_3)_2CH$) and t-butyl ($(CH_3)_3C$) groups and the isopropyl to isopropyl, isopropyl to t-butyl, and t-butyl to t-butyl $C-C$ bonds comprise functional groups. The branched-chain-alkane groups in amides are equivalent to those in branched-chain alkanes.

The NH_2 functional group was solved in the Dihydrogen Nitride (NH_2) section except that the energy of the $N-H$ MO is matched to the nitrogen-atom contribution to $\Delta E_{H_2MO}(AO/HO)$ and $E_T\left(atom-atom,msp^3.AO\right)$ of the $C-N$ group. Both alkyl amide $C=O$ groups and the $C-C(O)$ group are equivalent to those given in the Carboxylic Acid Esters section except that $\bar{E}_{Kvib}$ of the $C-C(O)$ group is matched to that of an amide. The $C-N$ groups are equivalent to those of alkyl amines given in the corresponding section except that the energy of the $C-N$ MO is matched to that of the $C=O$ group and $\bar{E}_{Kvib}$ is that of a amide. $\Delta E_{H_2MO}(AO/HO)$ of the $C-N$ group is equal to $E_T\left(atom-atom,msp^3.AO\right)$ of the alkyl $C=O$ and $C-N$ groups in order to match the energies of the corresponding MOs.

As in the case of primary amines, each $C-N$ group is solved by hybridizing the $2s$ and $2p$ AOs of the C atom to form a single $2sp^3$ shell as an energy minimum, and the sharing of electrons between the $C2sp^3$ HO and the N AO to form a MO permits each participating orbital to decrease in radius and energy. To meet the equipotential condition of the union of the $C-N$ H_2-type-ellipsoidal-MO with other orbitals of the molecule, the hybridization factor c_2 of Eq. (15.52) for the $C-N$-bond MO given by Eq. (15.133) is $c_2\left(C2sp^3HO\ to\ N\right)=0.91140$.

$E_T\left(atom-atom,msp^3.AO\right)$ (Eq. (15.52)) of the $C=O$ group of alkyl amides and the $C=O$ group of formamide are equivalent to those of the corresponding carboxylic acids and esters. The values given in the Carboxylic Acids section are $-2.69893\ eV$ and $-3.58557\ eV$, respectively.

$E_T\left(atom-atom,msp^3.AO\right)$ of the amide $C-C(O)$ group is the same as alkanes, aldehydes, carboxylic acids, and carboxylic acid esters, $-1.85836\ eV$, where both energy contributions are given by Eq. (14.513). Also, as in the case of aldehydes, $C_{1o}=2C_1$ in Eq. (15.61).

In order to match energy throughout the chain of the amide molecule, $E_T\left(atom-atom,msp^3.AO\right)$ of the $C-N$-bond MO in Eq. (15.61) due to the charge donation from the C and N atoms to the MO is $-1.65376\ eV$. It is based on the energy match between the $C2sp^3$ HO of the carbonyl and the primary amino group NH_2. It is given by the linear combination of $-0.92918\ eV$ (Eq. (14.513)) which matches the contiguous $C-C(O)$ or $HC(O)$ group and $-0.72457\ eV$ (Eq. (14.151)), the contribution of a primary amino group given in the Primary Amines section.

The symbols of the functional groups of alkyl amides are given in Table 15.111. The geometrical (Eqs. (15.1-15.5) and (15.51)), intercept (Eqs. (15.80-15.87)), and energy (Eqs. (15.6-15.11) and (15.17-15.65)) parameters of alkyl amides are given in Tables 15.112, 15.113, and 15.114, respectively. The total energy of each alkyl amide given in Table 15.115 was calculated as the sum over the integer multiple of each $E_D(Group)$ of Table 15.114 corresponding to functional-group composition of the molecule. The bond angle parameters of alkyl amides determined using Eqs. (15.88-15.117) are given in Table 15.116. The color scale, translucent view of the charge-density of exemplary amide, propionamide, comprising the concentric shells of atoms with the outer shell bridged by one or more H_2-type ellipsoidal MOs or joined with one or more hydrogen MOs is shown in Figure 15.19.

Figure 15.19. (A)-(B) Color scale, translucent views of the charge-density of propionamide showing the orbitals of the atoms at their radii, the ellipsoidal surface of each H or H_2-type ellipsoidal MO that transitions to the corresponding outer shell of the atom(s) participating in each bond, and the hydrogen nuclei (red, not to scale).

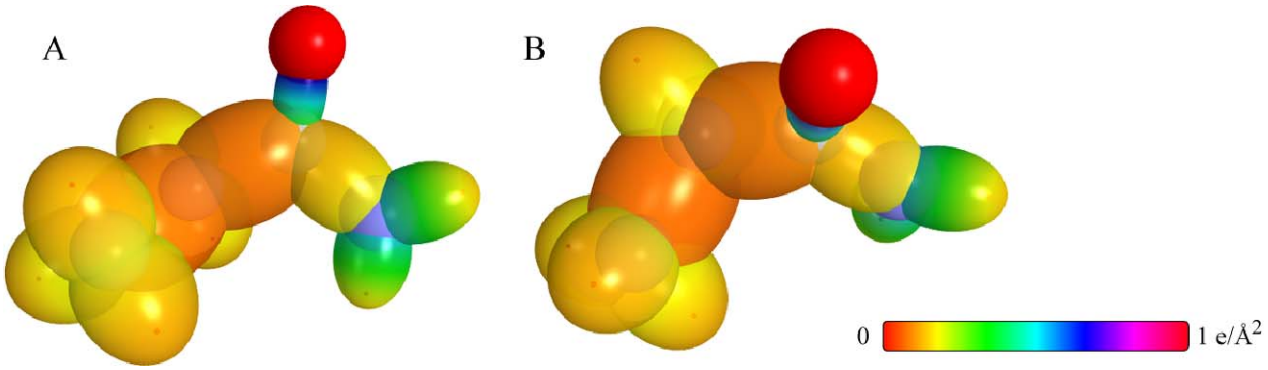

Table 15.111. The symbols of functional groups of alkyl amides.

Functional Group	Group Symbol
CH (formamide) group	$C-H$ (i)
C-C(O)	$C-C(O)$
C=O (formamide)	$C=O$ (i)
C=O (alkyl amide)	$C=O$ (ii)
(O)C-N (formamide)	$C-N$ (i)
(*O)C-N* (alkyl amide)	$C-N$ (ii)
NH_2 group	NH_2
CH_3 group	$C-H\ (CH_3)$
CH_2 group	$C-H\ (CH_2)$
CH (alkyl) group	$C-H$ (ii)
CC bond (*n-C*)	$C-C$ (a)
CC bond (*iso-C*)	$C-C$ (b)
CC bond (*tert-C*)	$C-C$ (c)
CC (*iso* to *iso-C*)	$C-C$ (d)
CC (*t* to *t-C*)	$C-C$ (e)
CC (*t* to *iso-C*)	$C-C$ (f)

Table 15.112. The geometrical bond parameters of alkyl amides and experimental values [1].

Parameter	$C-H$ (i) Group	$C-C(O)$ Group	$C=O$ (i) Group	$C=O$ (ii) Group	$C-N$ (i) Group	$C-N$ (ii) Group	NH_2 Group	$C-H\ (CH_3)$ Group	$C-H\ (CH_2)$ Group	$C-H$ (ii) Group	$C-C$ (a) Group	$C-C$ (b) Group	$C-C$ (c) Group	$C-C$ (d) Group	$C-C$ (e) Group	$C-C$ (f) Group
$a\ (a_0)$	1.67465	2.04740	1.290799	1.29907	1.70920	1.75370	1.32297	1.64920	1.67122	1.67465	2.12499	2.12499	2.10725	2.12499	2.10725	2.10725
$c'\ (a_0)$	1.05661	1.43087	1.13613	1.13977	1.30736	1.32427	0.97065	1.04856	1.05553	1.05661	1.45744	1.45744	1.45164	1.45744	1.45164	1.45164
Bond Length $2c'\ (\AA)$	1.11827	1.51437	1.20243	1.20628	1.38365	1.40155	1.02729	1.10974	1.11713	1.11827	1.54280	1.54280	1.53635	1.54280	1.53635	1.53635
Exp. Bond Length $(\AA)$	1.125 (formamide)	1.519 (acetamide) 1.520 (N-methylacetamide)	1.212 (formamide)	1.220 (acetamide) 1.225 (N-methylacetamide)	1.368 (formamide)	1.380 (acetamide)	1.027 (formamide) 1.022 (acetamide)	1.107 ($C-H$ propane) 1.117 ($C-H$ butane)	1.107 ($C-H$ propane) 1.117 ($C-H$ butane)	1.122 (isobutane)	1.532 (propane) 1.531 (butane)	1.532 (propane) 1.531 (butane)	1.532 (propane) 1.531 (butane)	1.532 (propane) 1.531 (butane)	1.532 (propane) 1.531 (butane)	1.532 (propane) 1.531 (butane)
$b,c\ (a_0)$	1.29924	1.46439	0.61267	0.62331	1.10098	1.14968	0.89894	1.27295	1.29569	1.29924	1.54616	1.54616	1.52750	1.54616	1.52750	1.52750
e	0.63095	0.69887	0.88018	0.87737	0.76490	0.75513	0.73369	0.63580	0.63159	0.63095	0.68600	0.68600	0.68888	0.68600	0.68888	0.68888

Table 15.113. The MO to HO intercept geometrical bond parameters of alkyl amides. R, R', R'' are H or alkyl groups. E_T is E_T ($atom - atom, msp^3.AO$).

Bond	Atom	E_T (eV) Bond 1	E_T (eV) Bond 2	E_T (eV) Bond 3	E_T (eV) Bond 4	Final Total Energy $C2sp^3$ (eV)	$r_{initial}$ (a_0)	r_{final} (a_0)	$E_{Coulomb}$ (eV) Final	$E(C2sp^3)$ (eV) Final	θ' (°)	θ_1 (°)	θ_2 (°)	d (a_c)	d_2 (a_c)
$RC(O)N(H)-H$ ($C=O$ (i) and (ii))	N	-0.82688	0	0	0		0.93084	0.86923	-15.65263		113.90	66.10	62.13	0.61843	0.35222
$HC(O)-NH_2$ ($C=O$ (i)) ($C-N$ (i))	N	-0.82688	0	0	0		0.93084	0.86923	-15.65263		103.93	76.07	50.02	1.09814	0.20922
$HC(O)-NH_2$ ($C=O$ (i)) ($C-N$ (i))	C	-0.82688	-1.79278	0	0	-154.23535	0.91771	0.77991	-17.44541	-17.25455	96.81	83.19	44.70	1.21492	0.09244
$RH_2C_bC_a(O)-NH_2$ ($C=O$ (ii)) ($C-N$ (ii))	N	-0.82688	0	0	0		0.93084	0.86923	-15.65263		100.14	79.86	48.10	1.17127	0.15300
$RH_2C_bC_a(O)-NH_2$ ($C=O$ (ii)) ($C-N$ (ii))	C_a	-0.82688	-1.34946	-0.92918	0	-154.72121	0.91771	0.75878	-17.93127	-17.74041	90.51	89.49	41.30	1.31755	0.00672
$HC_a(NH_2)=O$ ($C=O$ (i))	O	-1.79278	0	0	0		1.00000	0.81871	-16.61853		137.10	42.90	65.45	0.53635	0.59978
$HC_a(NH_2)=O$ ($C=O$ (i))	C_a	-1.79278	--0.82688	0	0	-154.23535	0.91771	0.77991	-17.44541	-17.25455	135.44	44.56	63.28	0.58044	0.55569
$RC_bH_2C_a(NH_2)=O$ ($C=O$ (ii))	O	-1.34946	0	0	0		1.00000	0.84115	-16.17521		137.27	42.73	66.31	0.52193	0.61784
$RC_bH_2C_a(NH_2)=O$ ($C=O$ (ii))	C_a	-1.34946	-0.82688	-0.92918	0	-154.72121	0.91771	0.75878	-17.93127	-17.74041	133.67	46.33	61.70	0.61582	0.52395
$H-C(O)NH_2$ (CH (i))	C	-1.79278	-0.82688	0	0	-154.23535	0.91771	0.77991	-17.44541	-17.25455	62.39	117.61	32.13	1.41810	0.36148
$RH_2C_b-C_a(O)NH_2$	C_a	-0.92918	-1.34946	-0.82688	0	-154.72121	0.91771	0.75878	-17.93127	-17.74041	57.02	122.98	25.76	1.84386	0.41299
$H_3C_b-C_a(O)NH_2$	C_b	-0.92918	0	0	0	-152.54487	0.91771	0.86359	-15.75493	-15.56407	72.27	107.73	34.17	1.69388	0.26301
$RH_2C_cH_2C_b-C_a(O)NH_2$	C_b	-0.92918	-0.92918	0	0	-153.47405	0.91771	0.81549	-16.68411	-16.49325	65.99	114.01	30.58	1.76270	0.33183
$C-H$ (CH_3)	C	-0.92918	0	0	0	-152.54487	0.91771	0.86359	-15.75493	-15.56407	77.49	102.51	41.48	1.23564	0.18708
$C-H$ (CH_2)	C	-0.92918	-0.92918	0	0	-153.47406	0.91771	0.81549	-16.68412	-16.49325	68.47	111.53	35.84	1.35486	0.29933
$C-H$ (CH) (ii)	C	-0.92918	-0.92918	-0.92918	0	-154.40324	0.91771	0.77247	-17.61330	-17.42244	61.10	118.90	31.37	1.42988	0.37326
$H_3C_aC_bH_2CH_2-$ ($C-C$ (a))	C_a	-0.92918	0	0	0	-152.54487	0.91771	0.86359	-15.75493	-15.56407	63.82	116.18	30.08	1.83879	0.38106
$H_3C_aC_bH_2CH_2-$ ($C-C$ (a))	C_b	-0.92918	-0.92918	0	0	-153.47406	0.91771	0.81549	-16.68412	-16.49325	56.41	123.59	26.06	1.90890	0.45117
$R-H_2C_aC_b(H_2C_c-R')HCH_2-$ ($C-C$ (b))	C_b	-0.92918	-0.92918	-0.92918	0	-154.40324	0.91771	0.77247	-17.61330	-17.42244	48.30	131.70	21.90	1.97162	0.51388
$R-H_2C_a(R'-H_2C_d)C_b(R''-H_2C_c)CH_2-$ ($C-C$ (c))	C_b	-0.92918	-0.72457	-0.72457	-0.72457	-154.71860	0.91771	0.75889	-17.92866	-17.73779	48.21	131.79	21.74	1.95734	0.50570
$isoC_aC_b(H_2C_c-R')HCH_2-$ ($C-C$ (d))	C_b	-0.92918	-0.92918	-0.92918	0	-154.40324	0.91771	0.77247	-17.61330	-17.42244	48.30	131.70	21.90	1.97162	0.51388
$tertC_a(R'-H_2C_d)C_b(R''-H_2C_c)CH_2-$ ($C-C$ (e))	C_b	-0.72457	-0.72457	-0.72457	-0.72457	-154.51399	0.91771	0.76765	-17.92866	-17.73779	50.04	129.96	22.66	1.94462	0.49298
$tertC_aC_b(H_2C_c-R')HCH_2-$ ($C-C$ (f))	C_b	-0.72457	-0.92918	-0.92918	0-	-154.19863	0.91771	0.78155	-17.40869	-17.21783	52.78	127.22	24.04	1.92443	0.47279
$isoC_a(R'-H_2C_d)C_b(R''-H_2C_c)CH_2-$ ($C-C$ (f))	C_b	-0.72457	-0.72457	-0.72457	-0.72457	-154.51399	0.91771	0.76765	-17.92866	-17.73779	50.04	129.96	22.66	1.94462	0.49298

Table 15.114. The energy parameters (eV) of functional groups of alkyl amides.

Parameters	$C-H$ (i) Group	$C-C(O)$ Group	$C=O$ (i) Group	$C=O$ (ii) Group	$C-N$ (i) Group	$C-N$ (ii) Group	NH_2 Group	CH_3 Group	CH_2 Group	$C-H$ (ii) Group	$C-C$ (a) Group	$C-C$ (b) Group	$C-C$ (c) Group	$C-C$ (d) Group	$C-C$ (e) Group	$C-C$ (f) Group
n	1	1	2	2	1	1	2	3	2	1	1	1	1	1	1	1
n_2	0	0	0	0	0	0	0	2	1	0	0	0	0	0	0	0
n_3	0	0	0	0	0	0	1	0	0	0	0	0	0	0	0	0
C_1	0.75	0.5	0.5	0.5	0.5	0.5	0.75	0.75	0.75	0.75	0.5	0.5	0.5	0.5	0.5	0.5
C_2	1	1	1	1	1	1	0.93613	1	1	1	1	1	1	1	1	1
c_1	1	1	1	1	1	1	0.75	1	1	1	1	1	1	1	1	1
c_2	0.91771	0.91771	0.85395	0.85395	0.91140	0.91140	1	0.91771	0.91771	0.91771	0.91771	0.91771	0.91771	0.91771	0.91771	0.91771
c_3	0	0	2	2	0	0	0	0	1	1	0	0	0	1	1	0
c_4	1	2	4	4	2	2	1	1	1	1	2	2	2	2	2	2
c_5	1	0	0	0	0	0	2	3	2	1	0	0	0	0	0	0
C_{1o}	0.75	1	0.5	0.5	0.5	0.5	1.5	0.75	0.75	0.75	0.5	0.5	0.5	0.5	0.5	0.5
C_{2o}	1	1	1	1	1	1	1	1	1	1	1	1	1	1	1	1
V_c (eV)	-35.12015	-30.19634	-112.61934	-111.25473	-38.24008	-36.88558	-78.77719	-107.32728	-70.41425	-35.12015	-28.79214	-28.79214	-29.10112	-28.79214	-29.10112	-29.10112
V_n (eV)	12.87680	9.50874	23.95107	23.87467	10.40705	10.27417	28.03446	38.92728	25.78002	12.87680	9.33352	9.33352	9.37273	9.33352	9.37273	9.37273
T (eV)	10.48582	7.37432	43.62389	42.82081	11.18655	10.51650	29.77286	32.53914	21.06675	10.48582	6.77464	6.77464	6.90500	6.77464	6.90500	6.90500
V_{ni} (eV)	-5.24291	-3.68716	-21.81195	-21.41040	-5.59327	-5.25825	-14.88643	-16.26957	-10.53337	-5.24291	-3.38732	-3.38732	-3.45250	-3.38732	-3.45250	-3.45250
$E_{(AO/HO)}$ (eV)	-14.63489	-14.63489	0	0	-14.63489	-14.63489	-14.53414	-15.56407	-15.56407	-14.63489	-15.56407	-15.56407	-15.35946	-15.56407	-15.35946	-15.35946
$\Delta E_{H_2MO}(_{AO/HO})$ (eV)	0	0	-3.58557	-2.69893	-5.23932	-4.35268	-1.65376	0	0	0	0	0	0	0	0	0
$E_T(_{AO/HO})$ (eV)	-14.63489	-14.63489	3.58557	2.69893	-9.39557	-10.28221	-12.88038	-15.56407	-15.56407	-14.63489	-15.56407	-15.56407	-15.35946	-15.56407	-15.35946	-15.35946
$E(_{n,\ AO/HO})$ (eV)	0	0	0	0	0	0	-14.53414	0	0	0	0	0	0	0	0	0
$E_T(_{H_2MO})$ (eV)	-31.63533	-31.63534	-63.27075	-63.27074	-31.63533	-31.63537	-48.73668	-67.69451	-49.66493	-31.63533	-31.63537	-31.63537	-31.63535	-31.63537	-31.63535	-31.63535
$E_T\left(aiom-atom,msp^3,AO\right)$ (eV)	0	-1.85836	-3.58557	-2.69893	-1.65376	-1.65376	0	0	0	0	-1.85836	-1.85836	-1.44915	-1.85836	-1.44915	-1.44915
$E_T(_{MO})$ (eV)	-31.63537	-33.49373	-66.85630	-65.96966	-33.28912	-33.28912	-48.73660	-67.69450	-49.66493	-31.63537	-33.49373	-33.49373	-33.08452	-33.49373	-33.08452	-33.08452
$\omega\left(10^{15}\ rad/s\right)$	24.1759	14.1117	60.9581	59.4034	13.0822	12.5874	59.4067	24.9286	24.2751	24.1759	9.43699	9.43699	15.4846	9.43699	9.55643	9.55643
E_K (eV)	15.91299	9.28860	40.12366	39.10034	8.61093	8.28526	39.10250	16.40846	15.97831	15.91299	6.21159	6.21159	10.19220	6.21159	6.29021	6.29021
$\bar{E}_D$ (eV)	-0.24966	-0.20195	-0.41891	-0.40804	-0.19325	-0.18957	-0.39136	-0.25352	-0.25017	-0.24966	-0.16515	-0.16515	-0.20896	-0.16515	-0.16416	-0.16416
$\bar{E}_{Kvib}$ (eV)	0.35532 (Eq. (13.458))	0.14655 [28]	0.21747 [32]	0.21077 [12]	0.17358 [33]	0.17358 [33]	0.40929 [22]	0.35532 (Eq. (13.458))	0.35532 (Eq. (13.458))	0.35532 (Eq. (13.458))	0.12312 [2]	0.17978 [4]	0.09944 [5]	0.12312 [2]	0.12312 [2]	0.12312 [2]
$\bar{E}_{osc}$ (eV)	-0.07200	-0.12867	-0.31017	-0.30266	-0.10647	-0.10278	-0.18672	-0.22757	-0.14502	-0.07200	-0.10359	-0.07526	-0.15924	-0.10359	-0.10260	-0.10260
E_{mag} (eV)	0.14803	0.14803	0.11441	0.11441	0.14803	0.14803	0.14185	0.14803	0.14803	0.14803	0.14803	0.14803	0.14803	0.14803	0.14803	0.14803
$E_T(_{Group})$ (eV)	-31.70737	-33.62241	-67.47664	-66.57498	-33.39559	-33.39190	-49.11003	-67.92207	-49.80996	-31.70737	-33.59732	-33.49373	-33.24376	-33.59732	-33.18712	-33.18712
$E_{initial}(_{s_4\ AO/HO})$ (eV)	-14.63489	-14.63489	-14.63489	-14.63489	-14.63489	-14.63489	-14.53414	-14.63489	-14.63489	-14.63489	-14.63489	-14.63489	-14.63489	-14.63489	-14.63489	-14.63489
$E_{initial}(_{s_5\ AO/HO})$ (eV)	-13.59844	0	0	0	0	0	-13.59844	-13.59844	-13.59844	-13.59844	0	0	0	0	0	0
$E_D(_{Group})$ (eV)	3.47404	4.35263	8.70826	7.80660	4.12581	4.12212	7.37901	12.49186	7.83016	3.32601	4.32754	4.29921	3.97398	4.17951	3.62128	3.91734

Table 15.115. The total bond energies of alkyl amides calculated using the functional group composition and the energies of Table 15.114 compared to the experimental values [3].

Formula	Name	$C-H$ (i) Group	$C-C(O)$ Group	$C=O$ (i) Group	$C=O$ (ii) Group	$C-N$ (i) Group	$C-N$ (ii) Group	NH_2 Group	CH_3	CH_1	CH (ii)	$C-C$ (a)	$C-C$ (b)	$C-C$ (c)	$C-C$ (d)	$C-C$ (e)	$C-C$ (f)	Calculated Total Bond Energy (eV)	Experimental Total Bond Energy (eV)	Relative Error
CH_3NO	Formamide	1	0	1	0	1	0	1	0	0	0	0	0	0	0	0	0	23.68712	23.697	0.00041
C_2H_5NO	Acetamide	0	1	0	1	0	1	1	1	0	0	0	0	0	0	0	0	36.15222	36.103	-0.00135
C_3H_7NO	Propanamide	0	1	0	1	0	1	1	1	1	0	1	0	0	0	0	0	48.30992	48.264	-0.00094
C_4H_9NO	Butanamide	0	1	0	1	0	1	1	1	2	0	2	0	0	0	0	0	60.46762	60.449	-0.00030
C_4H_9NO	2-Methylpropanamide	0	0	0	1	0	1	1	2	0	1	0	3	0	0	0	0	60.51509	60.455	-0.00099
$C_5H_{11}NO$	Pentanamide	0	1	0	1	0	1	1	1	3	0	3	0	0	0	0	0	72.65232	72.481	-0.00200
$C_5H_{11}NO$	2,2-Dimethylpropanamide	0	0	0	1	0	1	1	3	0	0	0	0	3	0	0	0	72.67890	72.718	0.00054
$C_6H_{13}NO$	Hexanamide	0	1	0	1	0	1	1	1	4	0	4	0	0	0	0	0	84.78302	84.780	-0.00004
$C_8H_{17}NO$	Octanamide	0	1	0	1	0	1	1	1	6	0	6	0	0	0	0	0	109.09842	109.071	-0.00025

Table 15.116. The bond angle parameters of alkyl amides and experimental values [1]. In the calculation of θ_v, the parameters from the preceding angle were used. E_T is $E_T(atom - atom, msp^3.AO)$.

Atoms of Angle	2c' Bond 1 (a_0)	2c' Bond 2 (a_0)	2c' Terminal Atoms (a_0)	$E_{Coulombic}$ Atom 1	Atom 1 Hybridization Designation (Table 15.3.A)	$E_{Coulombic}$ Atom 2	Atom 2 Hybridization Designation (Table 15.3.A)	c_2 Atom 1	c_2 Atom 2	C_1	C_2	c_1	c_2'	E_T (eV)	θ_v (°)	θ_1 (°)	θ_2 (°)	Cal. θ (°)	Exp. θ (°)
$\angle HNH$	1.94130	1.94130	3.1464	-14.53414	N	H	H	0.93613 Eq. (15.71))	1	1	1	0.75	1.06823	0				108.27	
$\angle C_aNH$ (CH (i); $C_a = O$ (i))	2.61473	1.94130	3.9328	-14.53414 N	N	-14.82575 C_a	1	0.93613 (Eq. (15.71))	0.91771	0.75	1	0.75	0.98033	0				118.61	119.2 (formamide)
$\angle HC_aN$ (CH (i); $C_a = O$ (i))	2.11323	2.61473	4.0825	-14.82575 C_a	1	-14.53414 N	N	0.91771	0.93613 (Eq. (15.71))	0.75	1	0.75	1.02006	0				119.04	
$\angle HC_aO_a$ (CH (i))	2.11323	2.27227	3.7238	-14.82575 C_a	1	-13.61806	O	0.91771	0.85395 (Eq. (15.133))	0.75	1	0.75	0.93052	0				116.18	
$\angle OC_aN$ ($C_a = O$ (i))	2.27227	2.61473	4.3359	16.17521 O	13	-16.37721 N	18	0.84115	0.83078	1	1	1	0.83596	-1.44915				124.91	125.0 (formamide)
$\angle C_bC_aN$ ($C_a = O$ (ii))	2.86175	2.64855	4.6904	-15.75493 C_b	7	-14.53414 N	N	0.86359	0.91140 (Eq. (15.135))	1	1	1	0.88749	-1.44915				116.63	115.1 (acetamide)
$\angle C_bC_aO$ ($C_a = O$ (ii))	2.86175	2.27954	4.5607	-16.68411	25	-13.61806	O	0.81549	0.85395 (Eq. (15.133))	1	1	1	0.83472	-1.65376				124.63	
$\angle OC_aN$ ($C_a = O$ (ii))	2.27954	2.64855	4.3128	16.17521 O	13	-16.37721 N	18	0.84115	0.83078	1	1	1	0.83596	-1.44915				121.95	122.0 (acetamide)
Methylene $\angle HC_aH$	2.11106	2.11106	3.4252	-15.75493	7	H	H	0.86359	1	1	1	0.75	1.15796	0				108.44	107 (propane)
$\angle C_aC_bC_c$															69.51			110.49	112 (propane) 113.8 (butane) 110.8 (isobutane)
$\angle C_aC_bH$															69.51			110.49	111.0 (butane) 111.4 (isobutane)
Methyl $\angle HC_aH$	2.09711	2.09711	3.4252	-15.75493	7	H	H	0.86359	1	1	1	0.75	1.15796	0				109.50	
$\angle C_aC_bC_c$															70.56			109.44	
$\angle C_aC_bH$															70.56			109.44	
$\angle C_bC_aC_c$ iso C_c	2.91547	2.91547	4.7958	-16.68412 C_b	26	-16.68412 C_c	26	0.81549	0.81549	1	1	1	0.81549	-1.85836				110.67	110.8 (isobutane)
$\angle C_bC_aH$ iso C_c	2.91547	2.11323	4.1633	-15.55033 C_a	5	-14.82575 C_b	1	0.87495	0.91771	0.75	1	0.75	1.04887	0				110.76	
$\angle C_aC_bH$ iso C_c	2.91547	2.09711	4.1633	-15.55033 C_b	5	-14.82575 C_a	1	0.87495	0.91771	0.75	1	0.75	1.04887	0				111.27	111.4 (isobutane)
$\angle C_bC_aC_b$ tert C_a	2.90327	2.90327	4.7958	-16.68412 C_b	26	-16.68412 C_b	26	0.81549	0.81549	1	1	1	0.81549	-1.85836				111.37	110.8 (isobutane)
$\angle C_bC_aC_d$															72.50			107.50	

N-ALKYL AND N,N-DIALKYL-AMIDES ($C_nH_{2n+1}NO,\ n=2,3,4,5...\infty$)

The N-alkyl and N,N-dialkyl amides, $C_nH_{2n+1}NO$, comprise a $C=O$ functional group, and the single bond of carbon to the carbonyl carbon atom, $C-C(O)$, is also a functional group. Formamide has a $HC=O$ moiety that comprises a more stable $C=O$ functional group and a CH functional group that is equivalent to that of the iso-CH group of branched-chain-alkyl portion of the N-alkyl or N,N-dialkyl amide. All amides further comprise a $C-N\left(R_1\right)R_2$ moiety that comprises two types of $C-N$ functional groups, one for formamide and the other for alkyl amides ($RC(O)N\left(R_1\right)R_2$ where R is alkyl). The N or N,N-dialkyl moiety comprises three additional groups depending on the alkyl substitution of the nitrogen. In the case of a single methyl or alkyl substitution, the $NH-C$ bond and NH are functional groups, and the $N-C$ bond of a di-substituted nitrogen is the third.

The alkyl portion of the N-alkyl or N,N-dialkyl amide may comprise at least two terminal methyl groups (CH_3) at each end of the chain, and may comprise methylene (CH_2), and methylyne (CH) functional groups as well as C bound by carbon-carbon single bonds. The methyl and methylene functional groups are equivalent to those of straight-chain alkanes. Six types of $C-C$ bonds can be identified. The n-alkane $C-C$ bond is the same as that of straight-chain alkanes. In addition, the $C-C$ bonds within isopropyl ($\left(CH_3\right)_2CH$) and t-butyl ($\left(CH_3\right)_3C$) groups and the isopropyl to isopropyl, isopropyl to t-butyl, and t-butyl to t-butyl $C-C$ bonds comprise functional groups. The branched-chain-alkane groups in N-alkyl or N,N-dialkyl amides are equivalent to those in branched-chain alkanes.

The NH functional group was solved in the Hydrogen Nitride (NH) section except that the energy of the $N-H$ MO is matched to the nitrogen-atom contribution to $\Delta E_{H_2MO}\left(AO/HO\right)$ and $E_T\left(atom-atom,msp^3.AO\right)$ of the $C-N$ group. The $C-C(O)$ group, both N-alkyl or N,N-dialkyl amide $C=O$ groups, and both $C-N$ groups are equivalent to those given in the Amides section.

As in the case of primary amines, each $N-C$ group is solved by hybridizing the $2s$ and $2p$ AOs of the C atom to form a single $2sp^3$ shell as an energy minimum, and the sharing of electrons between the $C2sp^3$ HO and the N AO to form a MO permits each participating orbital to decrease in radius and energy. To meet the equipotential condition of the union of the $N-C$ H_2-type-ellipsoidal-MO with other orbitals of the molecule, the hybridization factor c_2 of Eq. (15.61) for the $N-C$-bond MO given by Eq. (15.133) is $c_2\left(C2sp^3HO\ to\ N\right)=0.91140$.

$E_T\left(atom-atom,msp^3.AO\right)$ of the N-substituted amide $C-C(O)$ group is the same as alkanes, aldehydes, carboxylic acids, carboxylic acid esters, and amides, $-1.85836\ eV$, where both energy contributions are given by Eq. (14.513). Also, as in the case of aldehydes, $C_{1o}=2C_1$ in Eq. (15.61).

$E_T\left(atom-atom,msp^3.AO\right)$ (Eq. (15.61)) of the $C=O$ group of N-substituted alkyl amides and the $C=O$ group of N-substituted formamide are equivalent to those of the corresponding carboxylic acids, carboxylic esters, and amides. The values given in the Carboxylic Acids section are $-2.69893\ eV$ and $-3.58557\ eV$, respectively.

$E_T\left(atom-atom,msp^3.AO\right)$ of both $C-N$ functional groups are the same as those of the corresponding groups of amides, $-1.65376\ eV$. $E_T\left(atom-atom,msp^3.AO\right)$ of the singly-substituted $NH-C$-bond MO in Eq. (15.61) due to the charge donation from the N and C atoms to the MO is $-0.92918\ eV$. It is equivalent to that of tertiary amines and matches the energy of the $NH-C$ group to that of the $C-N$ group wherein $E_T\left(atom-atom,msp^3.AO\right)$ of the latter is a linear combination of $-0.92918\ eV$ (Eq. (14.513)) and $-0.72457\ eV$ (Eq. (14.151)). $E_T\left(atom-atom,msp^3.AO\right)$ of the doubly-substituted $N-C$-bond MO is $-0.72457\ eV$. It is equivalent to that of the contribution of each atom of a primary amine and also matches the energy of the $N-C$ group to that of the $C-N$ group by matching one of the components of $E_T\left(atom-atom,msp^3.AO\right)$ of the latter.

The symbols of the functional groups of N-alkyl and N,N-dialkyl amides are given in Table 15.117. The geometrical (Eqs. (15.1-15.5) and (15.51)), intercept (Eqs. (15.80-15.87)), and energy (Eqs. (15.6-15.11) and (15.17-15.65)) parameters of N-alkyl and N,N-dialkyl amides are given in Tables 15.118, 15.119, and 15.120, respectively. The total energy of each N-alkyl or N,N-dialkyl amide given in Table 15.121 was calculated as the sum over the integer multiple of each $E_{D\,(Group)}$ of Table 15.120 corresponding to functional-group composition of the molecule. The bond angle parameters of N-alkyl and N,N-dialkyl amides determined using Eqs. (15.79-15.108) are given in Table 15.122. The color scale, translucent view of the charge-density of exemplary alkyl-amide, N,N-dimethylacetamide, comprising the concentric shells of atoms with the outer shell bridged by one or more H_2-type ellipsoidal MOs or joined with one or more hydrogen MOs is shown in Figure 15.20.

Figure 15.20. Color scale, translucent view of the charge-density of N,N-dimethylacetamide showing the orbitals of the atoms at their radii, the ellipsoidal surface of each H or H_2-type ellipsoidal MO that transitions to the corresponding outer shell of the atom(s) participating in each bond, and the hydrogen nuclei (red, not to scale).

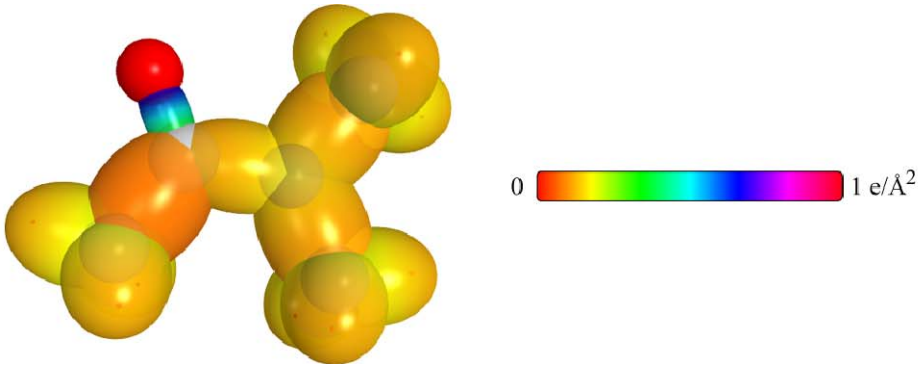

Table 15.117. The symbols of functional groups of N-alkyl and N,N-dialkyl amides.

Functional Group	Group Symbol
CH (formamide) group	$C-H$ (i)
C-C(O)	$C-C(O)$
C=O (N-alkyl and N,N-dialkyl formamide)	$C=O$ (i)
C=O (N-alkyl and N,N-dialkyl amide)	$C=O$ (ii)
(O)C-N (N-alkyl and N,N-dialkyl formamide)	$C-N$ (i)
(O)C-N (N-alkyl and N,N-dialkyl amide)	$C-N$ (ii)
NH group	*NH*
N-C (*N*-alkyl)	$N-C$ (i)
N-C (N,N,-dialkyl)	$N-C$ (ii)
CH_3 group	$C-H\ (CH_3)$
CH_2 group	$C-H\ (CH_2)$
CH (alkyl) group	$C-H$ (ii)
CC bond (*n-C*)	$C-C$ (a)
CC bond (*iso-C*)	$C-C$ (b)
CC bond (*tert-C*)	$C-C$ (c)
CC (*iso* to *iso-C*)	$C-C$ (d)
CC (*t* to *t-C*)	$C-C$ (e)
CC (*t* to *iso-C*)	$C-C$ (f)

Table 15.118. The geometrical bond parameters of N-alkyl and N,N-dialkyl amides and experimental values [1].

Parameter	$C-H$ (i) Group	$C-C(O)$ Group	$C=O$ (i) Group	$C=O$ (ii) Group	$C-N$ (i) Group	$C-N$ (ii) Group	NH Group	$N-C$ (i) Group	$N-C$ (ii) Group	$C-H\ (CH_3)$ Group	$C-H\ (CH_2)$ Group	$C-H$ (ii) Group	$C-C$ (a) Group	$C-C$ (b) Group	$C-C$ (c) Group	$C-C$ (d) Group	$C-C$ (e) Group	$C-C$ (f) Group
$a\ (a_0)$	1.67465	2.04740	1.290799	1.29907	1.70920	1.75370	1.28620	1.96313	1.97794	1.64920	1.67122	1.67465	2.12499	2.12499	2.10725	2.12499	2.10725	2.10725
$c'\ (a_0)$	1.05661	1.43087	1.13613	1.13977	1.30736	1.32427	0.95706	1.40112	1.40639	1.04856	1.05553	1.05661	1.45744	1.45744	1.45164	1.45744	1.45164	1.45164
Bond Length $2c'\ (\AA)$	1.11827	1.51437	1.20243	1.20628	1.38365	1.40155	1.01291	1.48288	1.48846	1.10974	1.11713	1.11827	1.54280	1.54280	1.53635	1.54280	1.53635	1.53635
Exp. Bond Length $(\AA)$	1.125 (formamide)	1.520 (N-methyl-acetamide)	1.212 (formamide)	1.225 (N-methyl-acetamide)	1.368 (formamide)	1.380 (acetamide)		1.469 (N-methyl-acetamide)		1.107 ($C-H$ propane) 1.117 ($C-H$ butane)	1.107 ($C-H$ propane) 1.117 ($C-H$ butane)	1.122 (isobutane)	1.532 (propane) 1.531 (butane)	1.532 (propane) 1.531 (butane)	1.532 (propane) 1.531 (butane)	1.532 (propane) 1.531 (butane)	1.532 (propane) 1.531 (butane)	1.532 (propane) 1.531 (butane)
$b,c\ (a_0)$	1.29924	1.46439	0.61267	0.62331	1.10098	1.14968	0.85927	1.37505	1.39079	1.27295	1.29569	1.29924	1.54616	1.54616	1.52750	1.54616	1.52750	1.52750
e	0.63095	0.69887	0.88018	0.87737	0.76490	0.75513	0.74410	0.71372	0.71104	0.63580	0.63159	0.63095	0.68600	0.68600	0.68888	0.68600	0.68888	0.68888

Table 15.119. The MO to HO intercept geometrical bond parameters of N-alkyl and N,N-dialkyl amides. *R*, *R′*, *R″* are *H* or alkyl groups. E_T is E_T (*atom – atom,msp³.AO*).

Bond	Atom	E_T (eV) Bond 1	E_T (eV) Bond 2	E_T (eV) Bond 3	E_T (eV) Bond 4	Final Total Energy $C2sp^3$ (eV)	$r_{initial}$ (a_0)	r_{final} (a_0)	$E_{Coulomb}$ (eV) Final	$E(C2sp^3)$ (eV) Final	θ' (°)	θ_1 (°)	θ_2 (°)	d_1 (a_0)	d_2 (a_0)
$R'C_a(O)N(C_bR)-H$ (C = O (i) and (ii)) (C – N (i) and (ii))	N	-0.82688	-0.46459	0	0		0.93084	0.84418	-16.11722		115.47	64.53	62.49	0.59403	0.36303
$RC_a(O)N(H)-C_bH_3$ (C = O (i) and (ii)) (C – N (i) and (ii)) (N – C (i))	N	-0.82688	-0.46459	0	0		0.93084	0.84418	-16.11722		78.61	101.39	37.00	1.56779	0.16667
$RC_a(O)N(H)-C_bH_3$ (C = O (i) and (ii)) (C – N (i) and (ii)) (N – C (i))	C_b	-0.46459	0	0	0	-152.08028	0.91771	0.88983	-15.29034	-15.09948	83.37	96.63	40.00	1.50383	0.10271
$R'C_a(O)N(H)-C_bH_2C_cH_2R$ (C = O (i) and (ii)) (C – N (i) and (ii)) (N – C (i))	N	-0.82688	-0.46459	0	0		0.93084	0.84418	-16.11722		78.61	101.39	37.00	1.56779	0.16667
$R'C_a(O)N(H)-C_bH_2C_cH_2R$ (C = O (i) and (ii)) (C – N (i) and (ii)) (N – C (i))	C_b	-0.46459	-0.92918	0	0	-153.00946	0.91771	0.83885	-16.21952	-16.02866	78.02	101.39	36.64	1.57525	0.17413
$R'C_a(O)N(C_cH_2)-C_bH_3$ (C = O (i) and (ii)) (C – N (i) and (ii)) (N – C (ii))	N	-0.82688	-0.36229	-0.36229	0		0.93084	0.83078	-16.37720		75.57	104.43	35.35	1.61336	0.20697
$R'C_a(O)N(C_cH_2)-C_bH_3$ (C = O (i) and (ii)) (C – N (i) and (ii)) (N – C (ii))	C_b	-0.36229	0	0	0	-151.97798	0.91771	0.89582	-15.18804	-14.99717	82.59	97.41	39.70	1.52188	0.11549
$R'C_a(O)N(C_cH_2C_dH_2R)-C_bH_3$ (C = O (i) and (ii)) (C – N (i) and (ii)) (N – C (ii))	N	-0.82688	-0.36229	-0.36229	0		0.93084	0.83078	-16.37720		75.57	104.43	35.35	1.61336	0.20697
$R'C_a(O)N(C_cH_2C_dH_2R)-C_bH_3$ (C = O (i) and (ii)) (C – N (i) and (ii)) (N – C (ii))	C_b	-0.36229	0	0	0	-151.97798	0.91771	0.89582	-15.18804	-14.99717	82.59	97.41	39.70	1.52188	0.11549
$R''C_a(O)N(R')-C_bH_2C_cH_2R$ (C = O (i) and (ii)) (C – N (i) and (ii)) (N – C (ii))	N	-0.82688	-0.36229	-0.36229	0		0.93084	0.83078	-16.37720		75.57	104.43	35.35	1.61336	0.20697
$R''C_a(O)N(R')-C_bH_2C_cH_2R$ (C = O (i) and (ii)) (C – N (i) and (ii)) (N – C (ii))	C_b	-0.36229	-0.92918	0	0	-152.90716	0.91771	0.84418	-16.11722	-15.92636	77.12	102.88	36.28	1.59451	0.18812
$HC_a(O)-N(H)R$ (C = O (i)) (C – N (i)) (N – C (i)) *R = methyl or alkyl*	N	-0.82688	-0.46459	0	0		0.93084	0.84418	-16.11722		102.07	77.93	48.57	1.13090	0.17647
$HC_a(O)-N(H)R$ (C = O (i)) (C – N (i)) (N – C (i)) *R = methyl or alkyl*	C_a	-0.82688	-1.79278	0	0	-154.23535	0.91771	0.77991	-17.44541	-17.25455	96.81	83.19	44.70	1.21492	0.09244
$HC_a(O)-N(R')R$ (C = O (i)) (C – N (i)) (N – C (ii)) *R, R' = methyl or alkyl*	N	-0.82688	-0.36229	-0.36229	0		0.93084	0.83078	-16.37720		101.03	78.97	47.79	1.14842	0.15895
$HC_a(O)-N(R')R$ (C = O (i)) (C – N (i)) (N – C (ii)) *R, R' = methyl or alkyl*	C_a	-0.82688	-1.79278	0	0	-154.23535	0.91771	0.77991	-17.44541	-17.25455	96.81	83.19	44.70	1.21492	0.09244

Table 15.119 cont' d. The MO to HO intercept geometrical bond parameters of N-alkyl and N,N-dialkyl amides. R, R', R'' are H or alkyl groups. E_T is E_T (*atom atom,msp³.AO*).

Bond	Atom	E_T (eV) Bond 1	E_T (eV) Bond 2	E_T (eV) Bond 3	E_T (eV) Bond 4	Final Total Energy $C2sp^3$ (eV)	$r_{initial}$ (a_0)	r_{final} (a_0)	$E_{Coulomb}$ (eV) Final	$E(C2sp^3)$ (eV) Final	θ' (°)	θ_1 (°)	θ_2 (°)	d_1 (a_0)	d_2 (a_0)
$R'H_2C_bC_a(O)-N(H)R$ $(C=O$ (ii)) $(C-N$ (ii)) $(N-C$ (i)) *R = methyl or alkyl*	C_a	-0.82688	-1.34946	-0.92918	0	-154.72121	0.91771	0.75878	-17.93127	-17.74041	90.51	89.49	41.30	1.31755	0.00672
$R''H_2C_bC_a(O)-N(R')R$ $(C=O$ (ii)) $(C-N$ (ii)) $(N-C$ (ii)) *R,R' = methyl or alkyl*	N	-0.82688	-0.36229	-0.36229	0		0.93084	0.83078	-16.37720		97.06	82.94	45.82	1.22220	0.10207
$R''H_2C_bC_a(O)-N(R')R$ $(C=O$ (ii)) $(C-N$ (ii)) $(N-C$ (ii)) *R,R' = methyl or alkyl*	C_a	-0.82688	-1.34946	-0.92918	0	-154.72121	0.91771	0.75878	-17.93127	-17.74041	90.51	89.49	41.30	1.31755	0.00672
$HC_a(N(R'')R')=O$ $(C=O$ (i)) *R',R'' = H, methyl, or alkyl*	O	-1.79278	0	0	0		1.00000	0.81871	-16.61853		137.10	42.90	65.45	0.53635	0.59978
$HC_a(N(R'')R')=O$ $(C=O$ (i)) *R',R'' = H, methyl, or alkyl*	C_a	-1.79278	--0.82688	0	0	-154.23535	0.91771	0.77991	-17.44541	-17.25455	135.44	44.56	63.28	0.58044	0.55569
$RC_bH_2C_a(N(R'')R')=O$ $(C=O$ (ii)) *R',R'' = H, methyl, or alkyl*	O	-1.34946	0	0	0		1.00000	0.84115	-16.17521		137.27	42.73	66.31	0.52193	0.61784
$RC_bH_2C_a(N(R'')R')=O$ $(C=O$ (ii)) *R',R'' = H, methyl, or alkyl*	C_a	-1.34946	-0.82688	-0.92918	0	-154.72121	0.91771	0.75878	-17.93127	-17.74041	133.67	46.33	61.70	0.61582	0.52395
$H-C(O)N(R'')R'$ *R',R'' = H, methyl, or alkyl*	C	-1.79278	-0.82688	0	0	-154.23535	0.91771	0.77991	-17.44541	-17.25455	62.39	117.61	32.13	1.41810	0.36148
$RH_2C_b-C_a(O)N(R'')R'$ *R',R'' = H, methyl, or alkyl*	C_a	-0.92918	-1.34946	-0.82688	0	-154.72121	0.91771	0.75878	-17.93127	-17.74041	57.02	122.98	25.76	1.84386	0.41299
$H_3C_b-C_a(O)N(R'')R'$ *R',R'' = H, methyl, or alkyl*	C_b	-0.92918	0	0	0	-152.54487	0.91771	0.86359	-15.75493	-15.56407	72.27	107.73	34.17	1.69388	0.26301
$RH_2C_bH_2C_b-C_a(O)N(R'')R'$ *R',R'' = H, methyl, or alkyl*	C_b	-0.92918	-0.92918	0	0	-153.47405	0.91771	0.81549	-16.68411	-16.49325	65.99	114.01	30.58	1.76270	0.33183
$C-H$ (CH_3)	C	-0.92918	0	0	0	-152.54487	0.91771	0.86359	-15.75493	-15.56407	77.49	102.51	41.48	1.23564	0.18708
$C-H$ (CH_2)	C	-0.92918	-0.92918	0	0	-153.47406	0.91771	0.81549	-16.68412	-16.49325	68.47	111.53	35.84	1.35486	0.29933
$C-H$ (CH) (ii)	C	-0.92918	-0.92918	-0.92918	0	-154.40324	0.91771	0.77247	-17.61330	-17.42244	61.10	118.90	31.37	1.42988	0.37326
$H_3C_aC_bH_2CH_2-$ $(C-C$ (a))	C_a	-0.92918	0	0	0	-152.54487	0.91771	0.86359	-15.75493	-15.56407	63.82	116.18	30.08	1.83879	0.38106
$H_3C_aC_bH_2CH_2-$ $(C-C$ (a))	C_b	-0.92918	-0.92918	0	0	-153.47406	0.91771	0.81549	-16.68412	-16.49325	56.41	123.59	26.06	1.90890	0.45117
$R-H_2C_aC_b(H_2C_c-R')HCH_2-$ $(C-C$ (b))	C_b	-0.92918	-0.92918	-0.92918	0	-154.40324	0.91771	0.77247	-17.61330	-17.42244	48.30	131.70	21.90	1.97162	0.51388
$R-H_2C_a(R'-H_2C_d)C_b(R''-H_2C_c)CH_2-$ $(C-C$ (c))	C_b	-0.92918	-0.72457	-0.72457	-0.72457	-154.71860	0.91771	0.75889	-17.92866	-17.73779	48.21	131.79	21.74	1.95734	0.50570
$isoC_aC_b(H_2C_c-R')HCH_2-$ $(C-C$ (d))	C_b	-0.92918	-0.92918	-0.92918	0	-154.40324	0.91771	0.77247	-17.61330	-17.42244	48.30	131.70	21.90	1.97162	0.51388
$tertC_a(R'-H_2C_d)C_b(R''-H_2C_c)CH_2-$ $(C-C$ (e))	C_b	-0.72457	-0.72457	-0.72457	-0.72457	-154.51399	0.91771	0.76765	-17.92866	-17.73779	50.04	129.96	22.66	1.94462	0.49298
$tertC_aC_b(H_2C_c-R')HCH_2-$ $(C-C$ (f))	C_b	-0.72457	-0.92918	-0.92918	0	-154.19863	0.91771	0.78155	-17.40869	-17.21783	52.78	127.22	24.04	1.92443	0.47279
$isoC_a(R'-H_2C_d)C_b(R''-H_2C_c)CH_2-$ $(C-C$ (f))	C_b	-0.72457	-0.72457	-0.72457	-0.72457	-154.51399	0.91771	0.76765	-17.92866	-17.73779	50.04	129.96	22.66	1.94462	0.49298

Table 15.120. The energy parameters (eV) of functional groups of N-alkyl and N,N-dialkyl amides.

Parameters	$C-H$ (i) Group	$C-C(O)$ Group	$C=O$ (i) Group	$C=O$ (ii) Group	$C-N$ (i) Group	$C-N$ (ii) Group	NH Group	$N-C$ (i)	$N-C$ (ii)	CH_3 Group	CH_2 Group	$C-H$ (ii) Group	$C-C$ (a) Group	$C-C$ (b) Group	$C-C$ (c) Group	$C-C$ (d) Group	$C-C$ (e) Group	$C-C$ (f) Group
n_1	1	1	2	2	1	1	1	1	1	3	2	1	1	1	1	1	1	1
n_2	0	0	0	0	0	0	0	0	0	2	1	0	0	0	0	0	0	0
n_3	0	0	0	0	0	0	0	0	0	0	0	0	0	0	0	0	0	0
C_1	0.75	0.5	0.5	0.5	0.5	0.5	0.75	0.5	0.5	0.75	0.75	0.75	0.5	0.5	0.5	0.5	0.5	0.5
C_2	1	1	1	1	1	1	0.93613	1	1	1	1	1	1	1	1	1	1	1
c_1	1	1	1	1	1	1	0.75	1	1	1	1	1	1	1	1	1	1	1
c_2	0.91771	0.91771	0.85395	0.85395	0.91140	0.91140	1	0.91140	0.91140	0.91771	0.91771	0.91771	0.91771	0.91771	0.91771	0.91771	0.91771	0.91771
c_3	0	0	2	2	0	0	1	0	0	0	1	1	0	0	0	1	1	0
c_4	1	2	4	4	2	2	1	2	2	1	1	1	2	2	2	2	2	2
c_5	1	0	0	0	0	0	1	0	0	3	2	1	0	0	0	0	0	0
C_{1o}	0.75	1	0.5	0.5	0.5	0.5	0.75	0.5	0.5	0.75	0.75	0.75	0.5	0.5	0.5	0.5	0.5	0.5
C_{2o}	1	1	1	1	1	1	1	1	1	1	1	1	1	1	1	1	1	1
V_e (eV)	-35.12015	-30.19634	-112.61934	-111.25473	-38.24008	-36.88558	-40.92593	-31.67393	-31.36351	-107.32728	-70.41425	-35.12015	-28.79214	-28.79214	-29.10112	-28.79214	-29.10112	-29.10112
V_p (eV)	12.87680	9.50874	23.95107	23.87467	10.40705	10.27417	14.21618	9.71067	9.67426	38.92728	25.78002	12.87680	9.33352	9.33352	9.37273	9.33352	9.37273	9.37273
T (eV)	10.48582	7.37432	43.62389	42.82081	11.18655	10.51650	15.90963	8.06719	7.92833	32.53914	21.06675	10.48582	6.77464	6.77464	6.90500	6.77464	6.90500	6.90500
V_m (eV)	-5.24291	-3.68716	-21.81195	-21.41040	-5.59327	-5.25825	-7.95482	-4.03359	-3.96416	-16.26957	-10.53337	-5.24291	-3.38732	-3.38732	-3.45250	-3.38732	-3.45250	-3.45250
$E_{(AO/HO)}$ (eV)	-14.63489	-14.63489	0	0	-14.63489	-14.63489	-14.53414	-14.63489	-14.63489	-15.56407	-15.56407	-14.63489	-15.56407	-15.56407	-15.35946	-15.56407	-15.35946	-15.35946
$\Delta E_{H_2MG(AO/HO)}$ (eV)	0	0	-3.58557	-2.69893	-5.23932	-4.35268	-1.65376	-0.92918	-0.72457	0	0	0	0	0	0	0	0	0
$E_T(AO/HO)$ (eV)	-14.63489	-14.63489	3.58557	2.69893	-9.39557	-10.28221	-12.88038	-13.70571	-13.91032	-15.56407	-15.56407	-14.63489	-15.56407	-15.56407	-15.35946	-15.56407	-15.35946	-15.35946
$E_T(H_2MO)$ (eV)	0	-31.63534	-63.27075	-63.27074	-31.63533	-31.63537	-31.63531	-31.63537	-31.63540	-67.69451	-49.66493	-31.63533	-31.63537	-31.63537	-31.63535	-31.63537	-31.63535	-31.63535
$E_T\left(atom-atom, msp^3.AO\right)$ (eV)	-31.63533	-1.85836	-3.58557	-2.69893	-1.65376	-1.65376	0	-0.92918	-0.72457	0	0	0	-1.85836	-1.85836	-1.44915	-1.85836	-1.44915	-1.44915
$E_T(MO)$ (eV)	0	-33.49373	-66.85630	-65.96966	-33.28912	-33.28912	-31.63537	-32.56455	-32.35994	-67.69450	-49.66493	-31.63537	-33.49373	-33.49373	-33.08452	-33.49373	-33.08452	-33.08452
$\omega\left(10^{15}\ rad/s\right)$	-31.63537	14.1117	60.9581	59.4034	13.0822	12.5874	44.9494	10.6278	10.5087	24.9286	24.2751	24.1759	9.43699	9.43699	15.4846	9.43699	9.55643	9.55643
E_K (eV)	24.1759	9.28860	40.12366	39.10034	8.61093	8.28526	29.58649	6.99543	6.91703	16.40846	15.97831	15.91299	6.21159	6.21159	10.19220	6.21159	6.29021	6.29021
$\bar{E}_{El}$ (eV)	15.91299	-0.20195	-0.41891	-0.40804	-0.19325	-0.18957	-0.34043	-0.17039	-0.16837	-0.25352	-0.25017	-0.24966	-0.16515	-0.16515	-0.20896	-0.16515	-0.16416	-0.16416
$\bar{E}_{Kvib}$ (eV)	-0.24966	0.14655 [28]	0.21747 [32]	0.21077 [12]	0.17358 [33]	0.17358 [33]	0.40696 [24]	0.12944 [23]	0.12944 [23]	0.35532 (Eq. (13.458))	0.35532 (Eq. (13.458))	0.35532 (Eq. (13.458))	0.12312 [2]	0.17978 [4]	0.09944 [5]	0.12312 [2]	0.12312 [2]	0.12312 [2]
$\bar{E}_{osc}$ (eV)	0.35532 (Eq. (13.458))	-0.12867	-0.31017	-0.30266	-0.10647	-0.10278	-0.13695	-0.10567	-0.10365	-0.22757	-0.14502	-0.07200	-0.10359	-0.07526	-0.15924	-0.10359	-0.10260	-0.10260
E_{mag} (eV)	-0.07200	0.14803	0.11441	0.11441	0.14803	0.14803	0.14185	0.14803	0.14803	0.14803	0.14803	0.14803	0.14803	0.14803	0.14803	0.14803	0.14803	0.14803
$E_T(Group)$ (eV)	0.14803	-33.62241	-67.47664	-66.57498	-33.39559	-33.39190	-31.77232	-32.67022	-32.46359	-67.92207	-49.80996	-31.70737	-33.59732	-33.49373	-33.24376	-33.59732	-33.18712	-33.18712
$E_{initial(c_4\ AO/HO)}$ (eV)	-31.70737	-14.63489	-14.63489	-14.63489	-14.63489	-14.63489	-14.53414	-14.63489	-14.63489	-14.63489	-14.63489	-14.63489	-14.63489	-14.63489	-14.63489	-14.63489	-14.63489	-14.63489
$E_{initial(c_5\ AO/HO)}$ (eV)	-14.63489	0	0	0	0	0	-13.59844	0	0	-13.59844	-13.59844	-13.59844	0	0	0	0	0	0
$E_{El}(Group)$ (eV)	-13.59844	4.35263	8.70826	7.80660	4.12581	4.12212	3.49788	3.40044	3.19381	12.49186	7.83016	3.32601	4.32754	4.29921	3.97398	4.17951	3.62128	3.91734

Table 15.121. The total bond energies of N-alkyl and N,N-dialkyl amides calculated using the functional group composition and the energies of Table 15.120 compared to the experimental values [3].

Formula	Name	$C-H$ (i) Group	$C-C(O)$ Group	$C=O$ (i) Group	$C=O$ (ii) Group	$C-N$ (i) Group	$C-N$ (ii) Group	NH Group	$N-C$ (i)	$N-C$ (ii)	CH_3	CH_2	CH (ii)	$C-C$ (a)	$C-C$ (b)	$C-C$ (c)	$C-C$ (d)	$C-C$ (e)	$C-C$ (f)	Calculated Total Bond Energy (eV)	Experimental Total Bond Energy (eV)	Relative Error
C_3H_7NO	N,N-Dimethylformamide	1	0	1	0	1	0	0	0	2	2	0	0	0	0	0	0	0	0	47.67945	47.574	0.00221
C_4H_9NO	N,N-Dimethylacetamide	0	1	0	1	0	1	0	0	2	3	0	0	0	0	0	0	0	0	60.14455	59.890	-0.00426
$C_6H_{13}NO$	N-Butylacetamide	0	1	0	1	0	1	1	1	0	2	3	0	3	0	0	0	0	0	84.63649	84.590	-0.00055

Table 15.122. The bond angle parameters of N-alkyl and N,N-dialkyl amides and experimental values [1]. In the calculation of θ_v, the parameters from the preceding angle were used. E_T is $E_T(atom-atom,msp^3.AO)$.

Atoms of Angle	2c' Bond 1 (a_0)	2c' Bond 2 (a_0)	2c' Terminal Atoms (a_0)	$E_{Coulombic}$ Atom 1	Atom 1 Hybridization Designation (Table 15.3.A)	$E_{Coulombic}$ Atom 2	Atom 2 Hybridization Designation (Table 15.3.A)	c_2 Atom 1	c_2 Atom 2	C_1	C_2	c_1	c_2'	E_T (eV)	θ_v (°)	θ_1 (°)	θ_2 (°)	Cal. θ (°)	Exp. θ (°)
$\angle OC_aN$ ($C_a=O$ (ii))	2.27954	2.64855	4.3243	16.17521 *O*	13	-16.11722 *N*	12	0.84115	0.84418	1	1	1	0.84266	-1.44915				122.51	121.8 (N-methylacetamide)
$\angle C_bC_aN$ ($C_a=O$ (ii))	2.86175	2.64855	4.6904	-15.75493 C_b	7	-14.53414 *N*	N	0.86359	0.91140 (Eq. (15.135))	1	1	1	0.88749	-1.44915				116.63	114.1 (N-methylacetamide)
$\angle C_bC_aO$ ($C_a=O$ (ii))	2.86175	2.27954	4.5607	-16.68411	25	-13.61806	O	0.81549	0.85395 (Eq. (15.133))	1	1	1	0.83472	-1.65376				124.63	
$\angle C_aNC_c$ ($C_a=O$ (ii))	2.64855	2.80224	4.6904	-17.93127 C_a	55	-16.21952 C_c	15	0.75878	0.83885	1	1	1	0.79881	-1.85836				118.72	119.7 (N-methylacetamide)
Methylene $\angle HC_aH$	2.11106	2.11106	3.4252	-15.75493	7	H	H	0.86359	1	1	1	0.75	1.15796	0				108.44	107 (propane)
$\angle C_aC_bC_c$															69.51			110.49	112 (propane) 113.8 (butane) 110.8 (isobutane)
$\angle C_aC_bH$															69.51			110.49	111.0 (butane) 111.4 (isobutane)
Methyl $\angle HC_aH$	2.09711	2.09711	3.4252	-15.75493	7	H	H	0.86359	1	1	1	0.75	1.15796	0				109.50	
$\angle C_aC_bC_c$															70.56			109.44	
$\angle C_aC_bH$															70.56			109.44	
$\angle C_bC_aC_c$ iso C_a	2.91547	2.91547	4.7958	-16.68412 C_b	26	-16.68412 C_c	26	0.81549	0.81549	1	1	1	0.81549	-1.85836				110.67	110.8 (isobutane)
$\angle C_bC_aH$ iso C_a	2.91547	2.11323	4.1633	-15.55033 C_a	5	-14.82575 C_b	1	0.87495	0.91771	0.75	1	0.75	1.04887	0				110.76	
$\angle C_aC_bH$ iso C_a	2.91547	2.09711	4.1633	-15.55033 C_b	5	-14.82575 C_a	1	0.87495	0.91771	0.75	1	0.75	1.04887	0				111.27	111.4 (isobutane)
$\angle C_bC_aC_b$ tert C_c	2.90327	2.90327	4.7958	-16.68412 C_b	26	-16.68412 C_b	26	0.81549	0.81549	1	1	1	0.81549	-1.85836				111.37	110.8 (isobutane)
$\angle C_bC_aC_d$															72.50			107.50	

UREA (CH_4N_2O)

Urea, CH_4N_2O, comprises a $C=O$ functional group and two $C-NH_2$ moieties that each comprise a NH_2 functional group and a $C-N$ functional group. The $C=O$ group is equivalent to that given for formamide in the Amides section except that the energy terms due to oscillation in the transition state are matched to that of urea. The NH_2 and $C-N$ functional groups are also equivalent to those given in the Amides section. $E_T\left(atom-atom,msp^3.AO\right)$ (Eq. (15.61)) of the $C=O$ and $C-N$ groups are equivalent to those of formamide. The values given in the Amides section are $-3.58557\,eV$, and $-1.65376\,eV$, respectively.

The symbols of the functional groups of urea are given in Table 15.123. The geometrical (Eqs. (15.1-15.5) and (15.51)), intercept (Eqs. (15.80-15.87)), and energy (Eqs. (15.6-15.11) and (15.17-15.65)) parameters of urea are given in Tables 15.124, 15.125, and 15.126, respectively. The total energy of urea given in Table 15.127 was calculated as the sum over the integer multiple of each $E_D(Group)$ of Table 15.126 corresponding to functional-group composition of the molecule. The bond angle parameters of urea determined using Eqs. (15.88-15.117) are given in Table 15.128. The color scale, translucent view of the charge-density of urea comprising the concentric shells of atoms with the outer shell bridged by one or more H_2-type ellipsoidal MOs or joined with one or more hydrogen MOs is shown in Figure 15.21.

Figure 15.21. Color scale, translucent view of the charge-density of urea showing the orbitals of the atoms at their radii, the ellipsoidal surface of each H or H_2-type ellipsoidal MO that transitions to the corresponding outer shell of the atom(s) participating in each bond, and the hydrogen nuclei (red, not to scale).

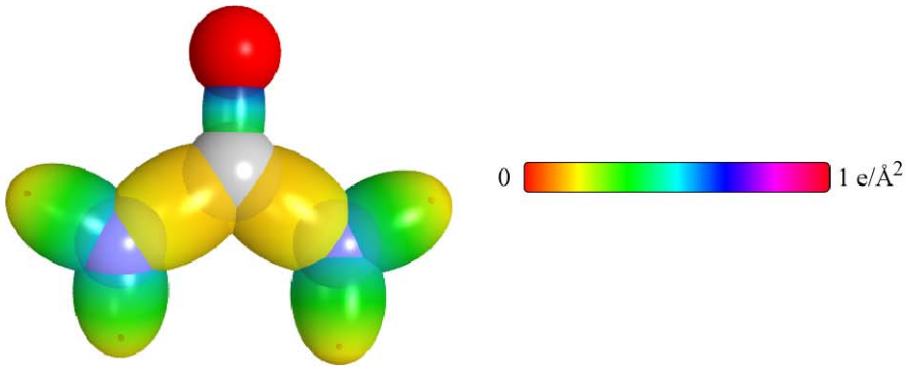

Table 15.123. The symbols of functional groups of urea.

Functional Group	Group Symbol
C=*O* (urea)	$C=O$
(*O*)*C*-*N* (urea)	$C-N$
NH$_2$ *group*	NH_2

Table 15.124. The geometrical bond parameters of urea and experimental values [1].

Parameter	$C=O$ Group	$C-N$ Group	NH_2 Group
$a\ (a_0)$	1.290799	1.70920	1.32297
$c'\ (a_0)$	1.13613	1.30736	0.97065
Bond Length $2c'\ (\text{Å})$	1.20243	1.38365	1.02729
Exp. Bond Length (Å)	1.212 (formamide)	1.368 (formamide)	1.027 (formamide) 1.022 (acetamide)
$b,c\ (a_0)$	0.61267	1.10098	0.89894
e	0.88018	0.76490	0.73369

Table 15.125. The MO to HO intercept geometrical bond parameters of urea. E_T is $E_T(atom-atom,msp^3.AO)$.

Bond	Atom	E_T (eV) Bond 1	E_T (eV) Bond 2	E_T (eV) Bond 3	E_T (eV) Bond 4	Final Total Energy $C2sp^3$ (eV)	$r_{initial}$ (a_0)	r_{final} (a_0)	$E_{Coulomb}$ (eV) Final	$E(C2sp^3)$ (eV) Final	θ' (°)	θ_1 (°)	θ_2 (°)	d_1 (a_0)	d_2 (a_0)
$H_2NC(O)N(H)-H$	N	-0.82688	0	0	0		0.93084	0.86923	-15.65263		113.90	66.10	62.13	0.61843	0.35222
$H_2NC(O)-NH_2$	N	-0.82688	0	0	0		0.93084	0.86923	-15.65263		103.93	76.07	50.02	1.09814	0.20922
$H_2NC(O)-NH_2$	C	-0.82688	-1.79278	-0.82688	0	-155.06223	0.91771	0.74461	-18.27229	-18.08143	93.56	86.44	42.45	1.26106	0.04630
$H_2NC_a(NH_2)=O$	O	-1.79278	0	0	0		1.00000	0.81871	-16.61853		137.10	42.90	65.45	0.53635	0.59978
$H_2NC_a(NH_2)=O$	C	-1.79278	--0.82688	-0.82688	0	-155.06223	0.91771	0.74461	-18.27229	-18.08143	133.82	46.18	61.27	0.62054	0.51559

Table 15.126. The energy parameters (eV) of functional groups of urea.

Parameters	$C=O$ Group	$C-N$ Group	NH_2 Group
n_1	2	1	2
n_2	0	0	0
n_3	0	0	1
C_1	0.5	0.5	0.75
C_2	1	1	0.93613
c_1	1	1	0.75
c_2	0.85395	0.91140	1
c_3	2	0	0
c_4	4	2	1
c_5	0	0	2
C_{1o}	0.5	0.5	1.5
C_{2o}	1	1	1
$V_e\ (eV)$	-112.61934	-38.24008	-78.77719
$V_p\ (eV)$	23.95107	10.40705	28.03446
$T\ (eV)$	43.62389	11.18655	29.77286
$V_m\ (eV)$	-21.81195	-5.59327	-14.88643
$E(_{AO/HO})\ (eV)$	0	-14.63489	-14.53414
$\Delta E_{H_2MO}(_{AO/HO})\ (eV)$	-3.58557	-5.23932	-1.65376
$E_T(_{AO/HO})\ (eV)$	3.58557	-9.39557	-12.88038
$E(_{n_3\ AO/HO})\ (eV)$	0	0	-14.53414
$E_J(_{H_2MO})\ (eV)$	-63.27075	-31.63533	-48.73668
$E_T(atom-atom, msp^3.AO)\ (eV)$	-3.58557	-1.65376	0
$E_J(_{MO})\ (eV)$	-66.85630	-33.28912	-48.73660
$\omega\ (10^{15}\ rad/s)$	19.9334	13.0822	59.4067
$E_K\ (eV)$	13.12053	8.61093	39.10250
$\bar{E}_D\ (eV)$	-0.23955	-0.19325	-0.39136
$\bar{E}_{Kvib}\ (eV)$	0.21747 [32]	0.17358 [33]	0.40929 [22]
$\bar{E}_{osc}\ (eV)$	-0.13081	-0.10647	-0.18672
$E_{mag}\ (eV)$	0.11441	0.14803	0.14185
$E_J(_{Group})\ (eV)$	-67.11793	-33.39559	-49.11003
$E_{initial}(_{n_4\ AO/HO})\ (eV)$	-14.63489	-14.63489	-14.53414
$E_{initial}(_{n_5\ AO/HO})\ (eV)$	0	0	-13.59844
$E_D(_{Group})\ (eV)$	8.34955	4.12581	7.37901

Table 15.127. The total bond energies of urea calculated using the functional group composition and the energies of Table 15.126 compared to the experimental values [3].

Formula	Name	$C=O$ Group	$C-N$ Group	NH_2 Group	Calculated Total Bond Energy (eV)	Experimental Total Bond Energy (eV)	Relative Error
CH_4N_2O	Urea	1	2	2	31.35919	31.393	0.00108

Table 15.128. The bond angle parameters of urea and experimental values [1]. In the calculation of θ_v, the parameters from the preceding angle were used. E_T is $E_T(atom-atom,msp^3.AO)$.

Atoms of Angle	$2c'$ Bond 1 (a_0)	$2c'$ Bond 2 (a_0)	$2c'$ Terminal Atoms (a_0)	$E_{Coulombic}$ Atom 1	Atom 1 Hybridization Designation (Table 15.3.A)	$E_{Coulombic}$ Atom 2	Atom 2 Hybridization Designation (Table 15.3.A)	c_2 Atom 1	c_2 Atom 2	C_1	C_2	c_1	c_2'	E_T (eV)	θ_v (°)	θ_1 (°)	θ_2 (°)	Cal. θ (°)	Exp. θ (°)
$\angle HNH$	1.94130	1.94130	3.1464	-14.53414	N	H	H	0.93613 Eq. (15.71))	1	1	1	0.75	1.06823	0				108.27	
$\angle C_aNH$	2.61473	1.94130	3.9328	-14.53414 N	N	-14.82575 C_a	1	0.93613 (Eq. (15.71))	0.91771	0.75	1	0.75	0.98033	0				118.61	119.2 (formamide)
$\angle OC_aN$	2.27227	2.61473	4.3359	16.17521 O	13	-16.37720 N	19	0.84115	0.83078	1	1	1	0.83596	-1.44915				124.91	125.0 (formamide)

CARBOXYLIC ACID HALIDES ($C_nH_{2n-1}OX,\ X=F,Cl,Br,I;\ n=1,2,3,4,5...\infty$)

The alkyl carboxylic acid halides, $C_nH_{2n-1}OX$, comprise a $C=O$ functional group, and the single bond of carbon to the carbonyl carbon atom, $C-C(O)$, is also a functional group. All carboxylic acid halides further comprise a $C-X$ functional group where X is a halogen atom. The alkyl portion of the alkyl carboxylic acid halide may comprise at least two terminal methyl groups (CH_3) at each end of the chain, and may comprise methylene (CH_2), and methylyne (CH) functional groups as well as C bound by carbon-carbon single bonds. The methyl and methylene functional groups are equivalent to those of straight-chain alkanes. Six types of $C-C$ bonds can be identified. The n-alkane $C-C$ bond is the same as that of straight-chain alkanes. In addition, the $C-C$ bonds within isopropyl ($(CH_3)_2CH$) and t-butyl ($(CH_3)_3C$) groups and the isopropyl to isopropyl, isopropyl to t-butyl, and t-butyl to t-butyl $C-C$ bonds comprise functional groups. The branched-chain-alkane groups in carboxylic acids are equivalent to those in branched-chain alkanes.

The alkyl carboxylic acid halide $C=O$ and $C-C(O)$ groups are equivalent to those given in the Aldehydes section and the Ketones section, respectively. The values of $E_T\left(atom-atom,msp^3.AO\right)$ given in these sections are $-2.69893\ eV$ and $-1.44915\ eV$, respectively.

As in the case of alkyl halides, each $(O)C-X$ group is solved by hybridizing the $2s$ and $2p$ AOs of the C atom to form a single $2sp^3$ shell as an energy minimum, and the sharing of electrons between the $C2sp^3$ HO and the X AO to form a MO permits each participating orbital to decrease in radius and energy. For example, to meet the equipotential condition of the union of the $(O)C-Cl$ H_2-type-ellipsoidal-MO with other orbitals of the molecule, the hybridization factor C_2 of Eq. (15.61) for the $(O)C-Cl$-bond MO given by Eq. (15.130) is $C_2\left(C2sp^3HO\ to\ Cl\right)=0.81317$. The solution is equivalent to that of the alkyl chloride bond except that the energy parameters corresponding to oscillation in the transition state are matched to those of a carboxylic acid chloride.

As in the case with the $C-Cl$ group of alkyl chlorides, $E_T\left(atom-atom,msp^3.AO\right)$ of the $(O)C-Cl$-bond MO in Eq. (15.61) of alkyl carboxylic acid chlorides due to the charge donation from the C and Cl atoms to the MO is $-1.44915\ eV$ where both energy contributions are given by Eq. (14.511). This matches the energy of the $C-C(O)$ functional group with that of the $(O)C-Cl$ group within the carboxylic acid chloride molecule.

The symbols of the functional groups of alkyl carboxylic acid chlorides are given in Table 15.129. The geometrical (Eqs. (15.1-15.5) and (15.51)), intercept (Eqs. (15.80-15.87)), and energy (Eqs. (15.6-15.11) and (15.17-15.65)) parameters of alkyl carboxylic acid chlorides are given in Tables 15.130, 15.131, and 15.132, respectively. The total energy of each alkyl carboxylic acid chloride given in Table 15.133 was calculated as the sum over the integer multiple of each $E_{D\,(Group)}$ of Table 15.132 corresponding to functional-group composition of the molecule. The bond angle parameters of alkyl carboxylic acid chlorides determined using Eqs. (15.88-15.117) are given in Table 15.134. The color scale, translucent view of the charge-density of exemplary carboxylic acid halide, acetyl chloride, comprising the concentric shells of atoms with the outer shell bridged by one or more H_2-type ellipsoidal MOs or joined with one or more hydrogen MOs is shown in Figure 15.22.

Figure 15.22. Color scale, translucent view of the charge-density of acetyl chloride showing the orbitals of the atoms at their radii, the ellipsoidal surface of each H or H_2-type ellipsoidal MO that transitions to the corresponding outer shell of the atom(s) participating in each bond, and the hydrogen nuclei (red, not to scale).

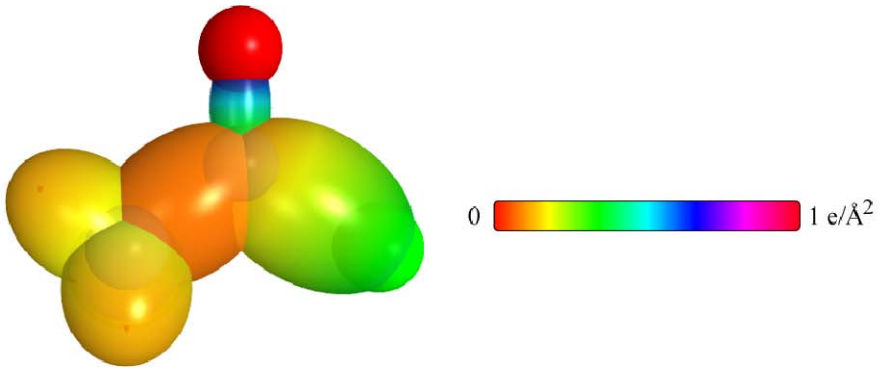

Table 15.129. The symbols of functional groups of alkyl carboxylic acid chlorides.

Functional Group	Group Symbol
C-*C*(*O*)	$C-C(O)$
C=*O* (alkyl carboxylic acid chloride)	$C=O$
(*O*)*C*-*Cl*	$C-Cl$
CH_3 group	$C-H\ (CH_3)$
CH_2 group	$C-H\ (CH_2)$
CH (alkyl) group	$C-H$
CC bond (*n*-*C*)	$C-C$ (a)
CC bond (*iso*-*C*)	$C-C$ (b)
CC bond (*tert*-*C*)	$C-C$ (c)
CC (*iso* to *iso*-*C*)	$C-C$ (d)
CC (*t* to *t*-*C*)	$C-C$ (e)
CC (*t* to *iso*-*C*)	$C-C$ (f)

Table 15.130. The geometrical bond parameters of alkyl carboxylic acid chlorides and experimental values [1].

Parameter	$C-C(O)$ Group	$C=O$ Group	$C-Cl$ Group	$C-H\left(CH_3\right)$ Group	$C-H\left(CH_2\right)$ Group	$C-H$ Group	$C-C$ (a) Group	$C-C$ (b) Group	$C-C$ (c) Group	$C-C$ (d) Group	$C-C$ (e) Group	$C-C$ (f) Group
$a\left(a_0\right)$	2.04740	1.29907	2.32621	1.64920	1.67122	1.67465	2.12499	2.12499	2.10725	2.12499	2.10725	2.10725
$c'\left(a_0\right)$	1.43087	1.13977	1.69136	1.04856	1.05553	1.05661	1.45744	1.45744	1.45164	1.45744	1.45164	1.45164
Bond Length $2c'\left(\AA\right)$	1.51437	1.20628	1.79005	1.10974	1.11713	1.11827	1.54280	1.54280	1.53635	1.54280	1.53635	1.53635
Exp. Bond Length $\left(\AA\right)$	1.520 (acetone) 1.518 (2-butanone)	1.187 (acetyl chloride) 1.214 (acetic acid)	1.798 (acetyl chloride)	1.107 ($C-H$ propane) 1.117 ($C-H$ butane)	1.107 ($C-H$ propane) 1.117 ($C-H$ butane)	1.122 (isobutane)	1.532 (propane) 1.531 (butane)	1.532 (propane) 1.531 (butane)	1.532 (propane) 1.531 (butane)	1.532 (propane) 1.531 (butane)	1.532 (propane) 1.531 (butane)	1.532 (propane) 1.531 (butane)
$b,c\left(a_0\right)$	1.46439	0.62331	1.59705	1.27295	1.29569	1.29924	1.54616	1.54616	1.52750	1.54616	1.52750	1.52750
e	0.69887	0.87737	0.72709	0.63580	0.63159	0.63095	0.68600	0.68600	0.68888	0.68600	0.68888	0.68888

Table 15.131. The MO to HO intercept geometrical bond parameters of alkyl carboxylic acid chlorides. R, R', R'' are H or alkyl groups. E_T is $E_T\left(atom-atom,msp^3.AO\right)$.

Bond	Atom	E_T (eV) Bond 1	E_T (eV) Bond 2	E_T (eV) Bond 3	E_T (eV) Bond 4	Final Total Energy $C2sp^3$ (eV)	$r_{initial}\left(a_0\right)$	$r_{final}\left(a_0\right)$	$E_{Coulomb}$ (eV) Final	$E\left(C2sp^3\right)$ (eV) Final	θ' (°)	θ_1 (°)	θ_2 (°)	$d_1\left(a_0\right)$	$d_2\left(a_0\right)$
$H_3C_bC_a(O)-Cl$	Cl	-0.72457	0	0	0		1.05158	0.87495	-15.55033		69.62	110.38	30.90	1.99599	0.30463
$H_3C_bC_a(O)-Cl$	C_a	-1.34946	-0.72457	-0.72457	0	-154.41430	0.91771	0.77199	-17.62436	-17.43350	54.69	125.31	23.23	2.13760	0.44625
$H_3C_bC_a(Cl)=O$	O	-1.34946	0	0	0		1.00000	0.84115	-16.17521		137.27	42.73	66.31	0.52193	0.61784
$H_3C_bC_a(Cl)=O$	C_a	-1.34946	-0.72457	-0.72457	0	-154.41430	0.91771	0.77199	-17.62436	-17.43350	134.28	45.72	62.45	0.60076	0.53901
$H_3C_b-C_a(O)-Cl$	C_a	-0.72457	-1.34946	-0.72457	0	-154.41430	0.91771	0.77199	-17.62436	-17.43350	59.30	120.70	26.96	1.82495	0.39408
$H_3C_b-C_a(O)-Cl$	C_b	-0.72457	0	0	0	-152.34026	0.91771	0.87495	-15.55033	-15.35946	73.62	106.38	34.98	1.67762	0.24675
$C-H\left(CH_3\right)$	C	-0.92918	0	0	0	-152.54487	0.91771	0.86359	-15.75493	-15.56407	77.49	102.51	41.48	1.23564	0.18708
$C-H\left(CH_2\right)$	C	-0.92918	-0.92918	0	0	-153.47406	0.91771	0.81549	-16.68412	-16.49325	68.47	111.53	35.84	1.35486	0.29933
$C-H\left(CH\right)$(ii)	C	-0.92918	-0.92918	-0.92918	0	-154.40324	0.91771	0.77247	-17.61330	-17.42244	61.10	118.90	31.37	1.42988	0.37326
$H_3C_aC_bH_2CH_2-$ ($C-C$ (a))	C_a	-0.92918	0	0	0	-152.54487	0.91771	0.86359	-15.75493	-15.56407	63.82	116.18	30.08	1.83879	0.38106
$H_3C_aC_bH_2CH_2-$ ($C-C$ (a))	C_b	-0.92918	-0.92918	0	0	-153.47406	0.91771	0.81549	-16.68412	-16.49325	56.41	123.59	26.06	1.90890	0.45117
$R-H_2C_aC_b\left(H_2C_c-R'\right)HCH_2-$ ($C-C$ (b))	C_b	-0.92918	-0.92918	-0.92918	0	-154.40324	0.91771	0.77247	-17.61330	-17.42244	48.30	131.70	21.90	1.97162	0.51388
$R-H_2C_a\left(R'-H_2C_d\right)C_b\left(R''-H_2C_c\right)CH_2-$ ($C-C$ (c))	C_b	-0.92918	-0.72457	-0.72457	-0.72457	-154.71860	0.91771	0.75889	-17.92866	-17.73779	48.21	131.79	21.74	1.95734	0.50570
$isoC_aC_b\left(H_2C_c-R'\right)HCH_2-$ ($C-C$ (d))	C_b	-0.92918	-0.92918	-0.92918	0	-154.40324	0.91771	0.77247	-17.61330	-17.42244	48.30	131.70	21.90	1.97162	0.51388
$tertC_a\left(R'-H_2C_d\right)C_b\left(R''-H_2C_c\right)CH_2-$ ($C-C$ (e))	C_b	-0.72457	-0.72457	-0.72457	-0.72457	-154.51399	0.91771	0.76765	-17.92866	-17.73779	50.04	129.96	22.66	1.94462	0.49298
$tertC_aC_b\left(H_2C_c-R'\right)HCH_2-$ ($C-C$ (f))	C_b	-0.72457	-0.92918	-0.92918	0	-154.19863	0.91771	0.78155	-17.40869	-17.21783	52.78	127.22	24.04	1.92443	0.47279
$isoC_a\left(R'-H_2C_d\right)C_b\left(R''-H_2C_c\right)CH_2-$ ($C-C$ (f))	C_b	-0.72457	-0.72457	-0.72457	-0.72457	-154.51399	0.91771	0.76765	-17.92866	-17.73779	50.04	129.96	22.66	1.94462	0.49298

Table 15.132. The energy parameters (*eV*) of functional groups of alkyl carboxylic acid chlorides.

Parameters	$C-C(O)$ Group	$C=O$ Group	$C-Cl$ Group	CH_3 Group	CH_2 Group	$C-H$ (ii) Group	$C-C$ (a) Group	$C-C$ (b) Group	$C-C$ (c) Group	$C-C$ (d) Group	$C-C$ (e) Group	$C-C$ (f) Group
n_1	1	2	1	3	2	1	1	1	1	1	1	1
n_2	0	0	0	2	1	0	0	0	0	0	0	0
n_3	0	0	0	0	0	0	0	0	0	0	0	0
C_1	0.5	0.5	0.5	0.75	0.75	0.75	0.5	0.5	0.5	0.5	0.5	0.5
C_2	1	1	0.81317	1	1	1	1	1	1	1	1	1
c_1	1	1	1	1	1	1	1	1	1	1	1	1
c_2	0.91771	0.85395	1	0.91771	0.91771	0.91771	0.91771	0.91771	0.91771	0.91771	0.91771	0.91771
c_3	0	2	1	0	1	1	0	0	0	1	1	0
c_4	2	4	2	1	1	1	2	2	2	2	2	2
c_5	0	0	0	3	2	1	0	0	0	0	0	0
$C_{1\sigma}$	1	0.5	0.5	0.75	0.75	0.75	0.5	0.5	0.5	0.5	0.5	0.5
$C_{2\sigma}$	1	1	0.81317	1	1	1	1	1	1	1	1	1
$V_s\ (eV)$	-30.19634	-111.25473	-29.68411	-107.32728	-70.41425	-35.12015	-28.79214	-28.79214	-29.10112	-28.79214	-29.10112	-29.10112
$V_p\ (eV)$	9.50874	23.87467	8.04432	38.92728	25.78002	12.87680	9.33352	9.33352	9.37273	9.33352	9.37273	9.37273
$T\ (eV)$	7.37432	42.82081	6.38036	32.53914	21.06675	10.48582	6.77464	6.77464	6.90500	6.77464	6.90500	6.90500
$V_m\ (eV)$	-3.68716	-21.41040	-3.19018	-16.26957	-10.53337	-5.24291	-3.38732	-3.38732	-3.45250	-3.38732	-3.45250	-3.45250
$E_{(AO/HO)}\ (eV)$	-14.63489	0	-14.63489	-15.56407	-15.56407	-14.63489	-15.56407	-15.56407	-15.35946	-15.56407	-15.35946	-15.35946
$\Delta E_{H_2MO(AO/HO)}\ (eV)$	0	-2.69893	-1.44915	0	0	0	0	0	0	0	0	0
$E_{T(AO/HO)}\ (eV)$	-14.63489	2.69893	-13.18574	-15.56407	-15.56407	-14.63489	-15.56407	-15.56407	-15.35946	-15.56407	-15.35946	-15.35946
$E_{T(H_2MO)}\ (eV)$	-31.63534	-63.27074	-31.63536	-67.69451	-49.66493	-31.63533	-31.63537	-31.63537	-31.63535	-31.63537	-31.63535	-31.63535
$E_T\left(atom-atom,msp^3.AO\right)\ (eV)$	-1.44915	-2.69893	-1.44915	0	0	0	-1.85836	-1.85836	-1.44915	-1.85836	-1.44915	-1.44915
$E_{T(MO)}\ (eV)$	-33.08452	-65.96966	-33.08452	-67.69450	-49.66493	-31.63537	-33.49373	-33.49373	-33.08452	-33.49373	-33.08452	-33.08452
$\omega\left(10^{15}\ rad/s\right)$	16.4962	59.4034	7.42995	24.9286	24.2751	24.1759	9.43699	9.43699	15.4846	9.43699	9.55643	9.55643
$E_E\ (eV)$	10.85807	39.10034	4.89052	16.40846	15.97831	15.91299	6.21159	6.21159	10.19220	6.21159	6.29021	6.29021
$\bar{E}_D\ (eV)$	-0.21568	-0.40804	-0.14475	-0.25352	-0.25017	-0.24966	-0.16515	-0.16515	-0.20896	-0.16515	-0.16416	-0.16416
$\bar{E}_{Evib}\ (eV)$	0.14655 [28]	0.21077 [12]	0.09063 [34]	0.35532 (Eq. (13.458))	0.35532 (Eq. (13.458))	0.35532 (Eq. (13.458))	0.12312 [2]	0.17978 [4]	0.09944 [5]	0.12312 [2]	0.12312 [2]	0.12312 [2]
$\bar{E}_{osc}\ (eV)$	-0.14240	-0.30266	-0.09943	-0.22757	-0.14502	-0.07200	-0.10359	-0.07526	-0.15924	-0.10359	-0.10260	-0.10260
$E_{magg}\ (eV)$	0.14803	0.11441	0.14803	0.14803	0.14803	0.14803	0.14803	0.14803	0.14803	0.14803	0.14803	0.14803
$E_{T(Group)}\ (eV)$	-33.22692	-66.57498	-33.18395	-67.92207	-49.80996	-31.70737	-33.59732	-33.49373	-33.24376	-33.59732	-33.18712	-33.18712
$E_{initial(4\ AO/HO)}\ (eV)$	-14.63489	-14.63489	-14.63489	-14.63489	-14.63489	-14.63489	-14.63489	-14.63489	-14.63489	-14.63489	-14.63489	-14.63489
$E_{initial(5\ AO/HO)}\ (eV)$	0	0	0	-13.59844	-13.59844	-13.59844	0	0	0	0	0	0
$E_{D(Group)}\ (eV)$	3.95714	7.80660	3.76614	12.49186	7.83016	3.32601	4.32754	4.29921	3.97398	4.17951	3.62128	3.91734

Table 15.133. The total bond energies of alkyl carboxylic acid chlorides calculated using the functional group composition and the energies of Table 15.132 compared to the experimental values [3].

Formula	Name	$C-C(O)$ Group	$C=O$ Group	$C-Cl$ Group	CH_3	CH_2	CH	$C-C$ (a)	$C-C$ (b)	$C-C$ (c)	$C-C$ (d)	$C-C$ (e)	$C-C$ (f)	Calculated Total Bond Energy (eV)	Experimental Total Bond Energy (eV)	Relative Error
C_2H_3ClO	Acetyl chloride	1	1	1	1	0	0	0	0	0	0	0	0	28.02174	27.990	-0.00115

Table 15.134. The bond angle parameters of alkyl carboxylic acid chlorides and experimental values [1]. In the calculation of θ_v, the parameters from the preceding angle were used. E_T is $E_T(atom-atom,msp^3.AO)$.

Atoms of Angle	2c' Bond 1 (a_0)	2c' Bond 2 (a_0)	2c' Terminal Atoms (a_0)	$E_{Coulombic}$ Atom 1	Atom 1 Hybridization Designation (Table 15.3.A)	$E_{Coulombic}$ Atom 2	Atom 2 Hybridization Designation (Table 15.3.A)	c_2 Atom 1	c_2 Atom 2	C_1	C_2	c_1	c_2'	E_T (eV)	θ_v (°)	θ_1 (°)	θ_2 (°)	Cal. θ (°)	Exp. θ (°)
$\angle C_bC_aO$	2.86175	2.27954	4.5826	-16.68411	25	-13.61806	O	0.81549	0.85395 (Eq. (15.132))	1	1	1	0.83472	-1.65376				125.70	
$\angle C_bC_aCl$	2.86175	3.38271	5.1539	-15.75493 C_b	7	-12.96764 Cl	Cl	0.86359	0.86359	1	0.81317 (Eq. (15.130))	1	0.86359	-0.92918				110.98	111.6 (acetyl chloride)
$\angle OC_aCl$	2.27954	3.38271	4.9841	-16.68412 O	26	-15.55033 Cl	5	0.81549	0.87495	1	0.81317 (Eq. (15.130))	1	0.84522	-0.92918				122.13	121.2 (acetyl chloride)
Methylene $\angle HC_aH$	2.11106	2.11106	3.4252	-15.75493	7	H	H	0.86359	1	1	1	0.75	1.15796	0				108.44	107 (propane)
$\angle C_aC_bC_c$															69.51			110.49	112 (propane) 113.8 (butane) 110.8 (isobutane)
$\angle C_aC_bH$															69.51			110.49	111.0 (butane) 111.4 (isobutane)
Methyl $\angle HC_aH$	2.09711	2.09711	3.4252	-15.75493	7	H	H	0.86359	1	1	1	0.75	1.15796	0				109.50	
$\angle C_aC_bC_c$															70.56			109.44	
$\angle C_aC_bH$															70.56			109.44	
$\angle C_bC_aC_c$ iso C_a	2.91547	2.91547	4.7958	-16.68412 C_b	26	-16.68412 C_b	26	0.81549	0.81549	1	1	1	0.81549	-1.85836				110.67	110.8 (isobutane)
$\angle C_bC_aH$ iso C_a	2.91547	2.11323	4.1633	-15.55033 C_a	5	-14.82575 C_b	1	0.87495	0.91771	0.75	1	0.75	1.04887	0				110.76	
$\angle C_aC_bH$ iso C_a	2.91547	2.09711	4.1633	-15.55033 C_b	5	-14.82575 C_a	1	0.87495	0.91771	0.75	1	0.75	1.04887	0				111.27	111.4 (isobutane)
$\angle C_bC_aC_b$ tert C_a	2.90327	2.90327	4.7958	-16.68412 C_b	26	-16.68412 C_b	26	0.81549	0.81549	1	1	1	0.81549	-1.85836				111.37	110.8 (isobutane)
$\angle C_bC_aC_d$															72.50			107.50	

CARBOXYLIC ACID ANHYDRIDES ($C_nH_{2n-2}O_3,\ n=2,3,4,5...\infty$)

The alkyl carboxylic acid anhydrides, $C_nH_{2n-2}O_3$, have two $(O)C-O$ moieties that each comprise $C=O$ and $C-O$ functional groups. The single bond of carbon to the carbonyl carbon atom, $C-C(O)$, is also a functional group. The alkyl portion of the alkyl carboxylic acid anhydride may comprise at least two terminal methyl groups (CH_3) at each end of the chain, and may comprise methylene (CH_2), and methylyne (CH) functional groups as well as C bound by carbon-carbon single bonds. The methyl and methylene functional groups are equivalent to those of straight-chain alkanes. Six types of $C-C$ bonds can be identified. The n-alkane $C-C$ bond is the same as that of straight-chain alkanes. In addition, the $C-C$ bonds within isopropyl ($(CH_3)_2CH$) and t-butyl ($(CH_3)_3C$) groups and the isopropyl to isopropyl, isopropyl to t-butyl, and t-butyl to t-butyl $C-C$ bonds comprise functional groups. The branched-chain-alkane groups in carboxylic acid anhydrides are equivalent to those in branched-chain alkanes.

The alkyl carboxylic acid anhydride $C=O$ and $C-C(O)$ groups are equivalent to those given in the Carboxylic Acid Esters section and the Ketones section, respectively. The values of $E_T\left(atom-atom,msp^3.AO\right)$ given in these sections are $-2.69893\ eV$ and $-1.44915\ eV$, respectively. The $C-O$ group is also equivalent to that given in the Carboxylic Acid Esters section except that $E_T\left(atom-atom,msp^3.AO\right)$ is equivalent to that of an alkyl ether as given in the corresponding section and the energy terms due to oscillation in the transition state are matched to that of a carboxylic acid anhydride.

For the $C-O$ group, $E_T\left(atom-atom,msp^3.AO\right)$ is $-1.65376\ eV$. It is based on the energy match between the O AO and the $C2sp^3$ HO of each $C-C(O)$ group and is given by the linear combination of $-0.72457\ eV$ (Eq. (14.151)) and $-0.92918\ eV$ (Eq. (14.513)), respectively. This matches $-0.72457\ eV$, the energy contribution of each of the $C2sp^3$ HOs to each $C-C(O)$ functional group, with that of the corresponding energy component of the $C-O$ group and gives a minimum energy within the carboxylic acid anhydride molecule.

The symbols of the functional groups of alkyl carboxylic acid anhydrides are given in Table 15.135. The geometrical (Eqs. (15.1-15.5) and (15.51)), intercept (Eqs. (15.80-15.87)), and energy (Eqs. (15.6-15.11) and (15.17-15.65)) parameters of alkyl carboxylic acid anhydrides are given in Tables 15.136, 15.137, and 15.138, respectively. The total energy of each alkyl carboxylic acid anhydride given in Table 15.139 was calculated as the sum over the integer multiple of each $E_D(Group)$ of Table 15.138 corresponding to functional-group composition of the molecule. The bond angle parameters of alkyl carboxylic acid anhydrides determined using Eqs. (15.88-15.117) are given in Table 15.140. The color scale, translucent view of the charge-density of exemplary carboxylic acid anhydride, acetic anhydride, comprising the concentric shells of atoms with the outer shell bridged by one or more H_2-type ellipsoidal MOs or joined with one or more hydrogen MOs is shown in Figure 15.23.

Figure 15.23. (A)-(B), color scale, translucent views of the charge-density of acetic anhydride showing the orbitals of the atoms at their radii, the ellipsoidal surface of each H or H_2-type ellipsoidal MO that transitions to the corresponding outer shell of the atom(s) participating in each bond, and the hydrogen nuclei (red, not to scale).

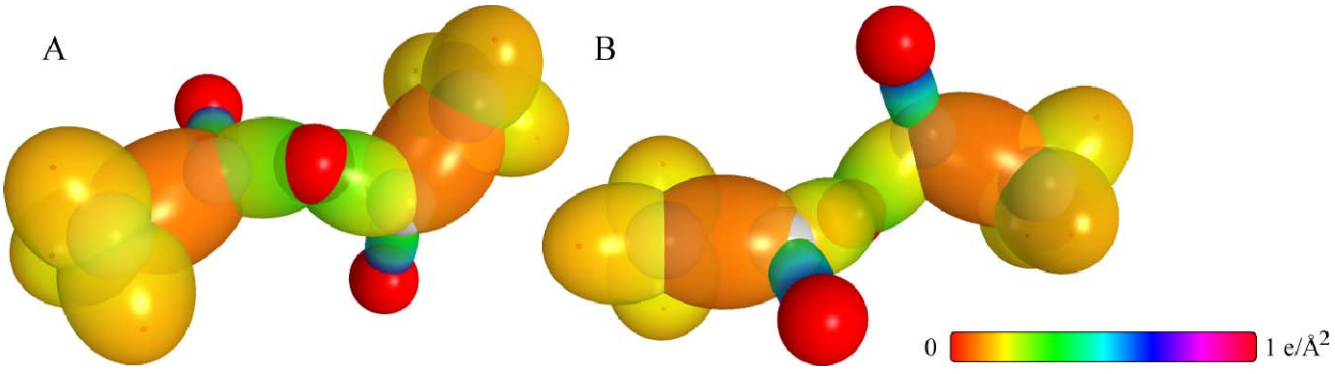

Table 15.135. The symbols of functional groups of alkyl carboxylic acid anhydrides.

Functional Group	Group Symbol
C-*C*(*O*)	$C-C(O)$
C=*O* (alkyl carboxylic acid anhydride)	$C=O$
(O)C-*O*	$C-O$
CH_3 group	$C-H\ (CH_3)$
CH_2 group	$C-H\ (CH_2)$
CH (alkyl) group	$C-H$
CC bond (*n*-*C*)	$C-C$ (a)
CC bond (*iso*-*C*)	$C-C$ (b)
CC bond (*tert*-*C*)	$C-C$ (c)
CC (*iso* to *iso*-*C*)	$C-C$ (d)
CC (*t* to *t*-*C*)	$C-C$ (e)
CC (*t* to *iso*-*C*)	$C-C$ (f)

Table 15.136. The geometrical bond parameters of alkyl carboxylic acid anhydrides and experimental values [1].

Parameter	$C-C(O)$ Group	$C=O$ Group	$C-O$ Group	$C-H\,(CH_3)$ Group	$C-H\,(CH_2)$ Group	$C-H$ Group	$C-C$ (a) Group	$C-C$ (b) Group	$C-C$ (c) Group	$C-C$ (d) Group	$C-C$ (e) Group	$C-C$ (f) Group
$a\,(a_0)$	2.04740	1.29907	1.73490	1.64920	1.67122	1.67465	2.12499	2.12499	2.10725	2.12499	2.10725	2.10725
$c'\,(a_0)$	1.43087	1.13977	1.31716	1.04856	1.05553	1.05661	1.45744	1.45744	1.45164	1.45744	1.45164	1.45164
Bond Length $2c'\,(\AA)$	1.51437	1.20628	1.39402	1.10974	1.11713	1.11827	1.54280	1.54280	1.53635	1.54280	1.53635	1.53635
Exp. Bond Length $(\AA)$	1.520 (acetone) 1.518 (2-butanone)	1.214 (acetic acid)	1.393 (avg. methyl formate)	1.107 ($C-H$ propane) 1.117 ($C-H$ butane)	1.107 ($C-H$ propane) 1.117 ($C-H$ butane)	1.122 (isobutane)	1.532 (propane) 1.531 (butane)	1.532 (propane) 1.531 (butane)	1.532 (propane) 1.531 (butane)	1.532 (propane) 1.531 (butane)	1.532 (propane) 1.531 (butane)	1.532 (propane) 1.531 (butane)
$b,c\,(a_0)$	1.46439	0.62331	1.12915	1.27295	1.29569	1.29924	1.54616	1.54616	1.52750	1.54616	1.52750	1.52750
e	0.69887	0.87737	0.75921	0.63580	0.63159	0.63095	0.68600	0.68600	0.68888	0.68600	0.68888	0.68888

Table 15.137. The MO to HO intercept geometrical bond parameters of alkyl carboxylic acid anhydrides. R, R', R'' are H or alkyl groups. E_T is $E_T(atom-atom,msp^3.AO)$.

Bond	Atom	E_T (eV) Bond 1	E_T (eV) Bond 2	E_T (eV) Bond 3	E_T (eV) Bond 4	Final Total Energy $C2sp^3$ (eV)	$r_{initial}$ (a_0)	r_{final} (a_0)	$E_{Coulomb}$ (eV) Final	$E(C2sp^3)$ (eV) Final	θ' $(^\circ)$	θ_1 $(^\circ)$	θ_2 $(^\circ)$	d_1 (a_0)	d_2 (a_0)
$RC_bH_2C_a(O)-O_a-C_a(O)C_cH_2R'$	O_a	-0.82688	-0.82688	0	0		1.00000	0.82562	-16.47951		98.32	81.68	46.34	1.19766	0.11949
$RC_bH_2C_a(O)-O_a-C_a(O)C_cH_2R'$	C_a	-0.82688	-1.34946	-0.82688	0	-154.51660	0.91771	0.76753	-17.72667	-17.53580	93.21	86.79	42.74	1.27417	0.04298
$RC_bH_2(R'C_cH_2C_a(O_a)O)C_a=O_a$	O_a	-1.34946	0	0	0		1.00000	0.84115	-16.17521		137.27	42.73	66.31	0.52193	0.61784
$RC_bH_2(R'C_cH_2C_a(O_a)O)C_a=O_a$	C_a	-1.34946	-0.72457	-0.82688	0	-154.51660	0.91771	0.76753	-17.72667	-17.53580	134.08	45.92	62.20	0.60583	0.53394
$RH_2C_b-C_a(O)OC_a(O)C_cH_2R'$	C_a	-0.72457	-1.34946	-0.82688	0	-154.51660	0.91771	0.76753	-17.72667	-17.53580	58.55	121.45	26.56	1.83133	0.40045
$H_3C_b-C_a(O)OC_a(O)C_cH_2R'$	C_b	-0.72457	0	0	0	-152.34026	0.91771	0.87495	-15.55033	-15.35946	73.62	106.38	34.98	1.67762	0.24675
$RH_2C_b-C_a(O)OC_a(O)C_cH_2R'$ R = alkyl	C_b	-0.72457	-0.92918	0	0	-153.26945	0.91771	0.82562	-16.47951	-16.28865	67.40	112.60	31.36	1.74821	0.31734
$C-H\,(CH_3)$	C	-0.92918	0	0	0	-152.54487	0.91771	0.86359	-15.75493	-15.56407	77.49	102.51	41.48	1.23564	0.18708
$C-H\,(CH_2)$	C	-0.92918	-0.92918	0	0	-153.47406	0.91771	0.81549	-16.68412	-16.49325	68.47	111.53	35.84	1.35486	0.29933
$C-H\,(CH)$ (ii)	C	-0.92918	-0.92918	-0.92918	0	-154.40324	0.91771	0.77247	-17.61330	-17.42244	61.10	118.90	31.37	1.42988	0.37326
$H_3C_aC_bH_2CH_2-$ ($C-C$ (a))	C_a	-0.92918	0	0	0	-152.54487	0.91771	0.86359	-15.75493	-15.56407	63.82	116.18	30.08	1.83879	0.38106
$H_3C_aC_bH_2CH_2-$ ($C-C$ (a))	C_b	-0.92918	-0.92918	0	0	-153.47406	0.91771	0.81549	-16.68412	-16.49325	56.41	123.59	26.06	1.90890	0.45117
$R-H_2C_aC_b(H_2C_c-R')HCH_2-$ ($C-C$ (b))	C_b	-0.92918	-0.92918	-0.92918	0	-154.40324	0.91771	0.77247	-17.61330	-17.42244	48.30	131.70	21.90	1.97162	0.51388
$R-H_2C_a(R''-H_2C_d)C_b(R''-H_2C_c)CH_2-$ ($C-C$ (c))	C_b	-0.92918	-0.72457	-0.72457	-0.72457	-154.71860	0.91771	0.75889	-17.92866	-17.73779	48.21	131.79	21.74	1.95734	0.50570
$isoC_aC_b(H_2C_c-R')HCH_2-$ ($C-C$ (d))	C_b	-0.92918	-0.92918	-0.92918	0	-154.40324	0.91771	0.77247	-17.61330	-17.42244	48.30	131.70	21.90	1.97162	0.51388
$tertC_a(R'-H_2C_d)C_b(R''-H_2C_c)CH_2-$ ($C-C$ (e))	C_b	-0.72457	-0.72457	-0.72457	-0.72457	-154.51399	0.91771	0.76765	-17.92866	-17.73779	50.04	129.96	22.66	1.94462	0.49298
$tertC_aC_b(H_2C_c-R')HCH_2-$ ($C-C$ (f))	C_b	-0.72457	-0.92918	-0.92918	0	-154.19863	0.91771	0.78155	-17.40869	-17.21783	52.78	127.22	24.04	1.92443	0.47279
$isoC_a(R'-H_2C_d)C_b(R''-H_2C_c)CH_2-$ ($C-C$ (f))	C_b	-0.72457	-0.72457	-0.72457	-0.72457	-154.51399	0.91771	0.76765	-17.92866	-17.73779	50.04	129.96	22.66	1.94462	0.49298

Table 15.138. The energy parameters (eV) of functional groups of alkyl carboxylic acid anhydrides.

Parameters	$C-C(O)$ Group	$C=O$ Group	$C-O$ Group	CH_3 Group	CH_2 Group	$C-H$ (ii) Group	$C-C$ (a) Group	$C-C$ (b) Group	$C-C$ (c) Group	$C-C$ (d) Group	$C-C$ (e) Group	$C-C$ (f) Group
n_1	1	2	1	3	2	1	1	1	1	1	1	1
n_2	0	0	0	2	1	0	0	0	0	0	0	0
n_3	0	0	0	0	0	0	0	0	0	0	0	0
C_1	0.5	0.5	0.5	0.75	0.75	0.75	0.5	0.5	0.5	0.5	0.5	0.5
C_2	1	1	1	1	1	1	1	1	1	1	1	1
c_1	1	1	1	1	1	1	1	1	1	1	1	1
c_2	0.91771	0.85395	0.85395	0.91771	0.91771	0.91771	0.91771	0.91771	0.91771	0.91771	0.91771	0.91771
c_3	0	2	0	0	1	1	0	0	0	1	1	0
c_4	2	4	2	1	1	1	2	2	2	2	2	2
c_5	0	0	0	3	2	1	0	0	0	0	0	0
C_{1o}	1	0.5	0.5	0.75	0.75	0.75	0.5	0.5	0.5	0.5	0.5	0.5
C_{2o}	1	1	1	1	1	1	1	1	1	1	1	1
$V_e\ (eV)$	-30.19634	-111.25473	-35.08488	-107.32728	-70.41425	-35.12015	-28.79214	-28.79214	-29.10112	-28.79214	-29.10112	-29.10112
$V_p\ (eV)$	9.50874	23.87467	10.32968	38.92728	25.78002	12.87680	9.33352	9.33352	9.37273	9.33352	9.37273	9.37273
$T\ (eV)$	7.37432	42.82081	10.11150	32.53914	21.06675	10.48582	6.77464	6.77464	6.90500	6.77464	6.90500	6.90500
$V_m\ (eV)$	-3.68716	-21.41040	-5.05575	-16.26957	-10.53337	-5.24291	-3.38732	-3.38732	-3.45250	-3.38732	-3.45250	-3.45250
$E_{(AO/HO)}\ (eV)$	-14.63489	0	-14.63489	-15.56407	-15.56407	-14.63489	-15.56407	-15.56407	-15.35946	-15.56407	-15.35946	-15.35946
$\Delta E_{H_2MO(AO/HO)}\ (eV)$	0	-2.69893	-2.69893	0	0	0	0	0	0	0	0	0
$E_T(_{AO/HO})\ (eV)$	-14.63489	2.69893	-11.93596	-15.56407	-15.56407	-14.63489	-15.56407	-15.56407	-15.35946	-15.56407	-15.35946	-15.35946
$E_T(_{H_2MO})\ (eV)$	-31.63534	-63.27074	-31.63541	-67.69451	-49.66493	-31.63533	-31.63537	-31.63537	-31.63535	-31.63537	-31.63535	-31.63535
$E_T\left(atom-atom, msp^3.AO\right)(eV)$	-1.44915	-2.69893	-1.65376	0	0	0	-1.85836	-1.85836	-1.44915	-1.85836	-1.44915	-1.44915
$E_J(_{MO})\ (eV)$	-33.08452	-65.96966	-33.28912	-67.69450	-49.66493	-31.63537	-33.49373	-33.49373	-33.08452	-33.49373	-33.08452	-33.08452
$\omega\ \left(10^{15}\ rad/s\right)$	16.4962	59.4034	24.3637	24.9286	24.2751	24.1759	9.43699	9.43699	15.4846	9.43699	9.55643	9.55643
$E_K\ (eV)$	10.85807	39.10034	16.03660	16.40846	15.97831	15.91299	6.21159	6.21159	10.19220	6.21159	6.29021	6.29021
$\bar{E}_D\ (eV)$	-0.21568	-0.40804	-0.26373	-0.25352	-0.25017	-0.24966	-0.16515	-0.16515	-0.20896	-0.16515	-0.16416	-0.16416
$\bar{E}_{Kvib}\ (eV)$	0.14655 [28]	0.21077 [12]	0.13638 [35]	0.35532 (Eq. (13.458))	0.35532 (Eq. (13.458))	0.35532 (Eq. (13.458))	0.12312 [2]	0.17978 [4]	0.09944 [5]	0.12312 [2]	0.12312 [2]	0.12312 [2]
$\bar{E}_{osc}\ (eV)$	-0.14240	-0.30266	-0.19554	-0.22757	-0.14502	-0.07200	-0.10359	-0.07526	-0.15924	-0.10359	-0.10260	-0.10260
$E_{mag}\ (eV)$	0.14803	0.11441	0.14803	0.14803	0.14803	0.14803	0.14803	0.14803	0.14803	0.14803	0.14803	0.14803
$E_T(_{Group})\ (eV)$	-33.22692	-66.57498	-33.48466	-67.92207	-49.80996	-31.70737	-33.59732	-33.49373	-33.24376	-33.59732	-33.18712	-33.18712
$E_{initial}(_{4\ AO/HO})\ (eV)$	-14.63489	-14.63489	-14.63489	-14.63489	-14.63489	-14.63489	-14.63489	-14.63489	-14.63489	-14.63489	-14.63489	-14.63489
$E_{initial}(_{5\ AO/HO})\ (eV)$	0	0	0	-13.59844	-13.59844	-13.59844	0	0	0	0	0	0
$E_D(_{Group})\ (eV)$	3.95714	7.80660	4.21488	12.49186	7.83016	3.32601	4.32754	4.29921	3.97398	4.17951	3.62128	3.91734

Table 15.139. The total bond energies of alkyl carboxylic acid anhydrides calculated using the functional group composition and the energies of Table 15.138 compared to the experimental values [3].

Formula	Name	$C-C(O)$ Group	$C=O$ Group	$C-O$ Group	CH_3	CH_2	CH	$C-C$ (a)	$C-C$ (b)	$C-C$ (c)	$C-C$ (d)	$C-C$ (e)	$C-C$ (f)	Calculated Total Bond Energy (eV)	Experimental Total Bond Energy (eV)	Relative Error
$C_4H_6O_3$	Acetic anhydride	2	2	2	2	0	0	0	0	0	0	0	0	56.94096	56.948	0.00013
$C_6H_{10}O_3$	Propanoic anhydride	2	2	2	2	2	0	2	0	0	0	0	0	81.25636	81.401	0.00177

Table 15.140. The bond angle parameters of alkyl carboxylic acid anhydrides and experimental values [1]. In the calculation of θ_v, the parameters from the preceding angle were used. E_T is $E_T(atom-atom,msp^3.AO)$.

Atoms of Angle	$2c'$ Bond 1 (a_0)	$2c'$ Bond 2 (a_0)	$2c'$ Terminal Atoms (a_0)	$E_{Coulombic}$ Atom 1	Atom 1 Hybridization Designation (Table 15.3.A)	$E_{Coulombic}$ Atom 2	Atom 2 Hybridization Designation (Table 15.3.A)	c_2 Atom 1	c_2 Atom 2	C_1	C_2	c_1	c_2'	E_T (eV)	θ_v (°)	θ_1 (°)	θ_2 (°)	Cal. θ (°)	Exp. θ (°)
$\angle O_aC_aO_b$	2.27954	2.63431	4.3012	-16.17521 O_a	13	-16.47951 O_b	22	0.84115	0.82562	1	1	1	0.83339	-1.44915				122.00	121.7 [36] (acetic anhydride)
$\angle C_aO_bC_a$	2.63431	2.63431	4.4944	-17.30638 C_b	42	-17.30638 C_a	42	0.78617	0.78617	1	1	1	0.78617	-1.85836				117.09	115.8 [36] (acetic anhydride)
$\angle C_bC_aO_b$	2.86175	2.63431	4.4944	-15.55033	5	-13.61806	O	0.87495	0.85395 (Eq. (15.133))	1	1	1	0.86445	-1.44915				109.65	108.3 [36] (acetic anhydride)
$\angle C_bC_aO_a$	2.86175	2.27954	4.6368	-16.47951	22	-13.61806	O	0.82562	0.85395 (Eq. (15.133))	1	1	1	0.83979	-1.65376				128.46	
Methylene $\angle HC_aH$	2.11106	2.11106	3.4252	-15.75493	7	H	H	0.86359	1	1	1	0.75	1.15796	0				108.44	107 (propane)
$\angle C_aC_bC_c$															69.51			110.49	112 (propane) 113.8 (butane) 110.8 (isobutane)
$\angle C_aC_bH$															69.51			110.49	111.0 (butane) 111.4 (isobutane)
Methyl $\angle HC_aH$	2.09711	2.09711	3.4252	-15.75493	7	H	H	0.86359	1	1	1	0.75	1.15796	0				109.50	
$\angle C_aC_bC_c$															70.56			109.44	
$\angle C_aC_bH$															70.56			109.44	
$\angle C_bC_aC_c$ iso C_a	2.91547	2.91547	4.7958	-16.68412 C_b	26	-16.68412 C_c	26	0.81549	0.81549	1	1	1	0.81549	-1.85836				110.67	110.8 (isobutane)
$\angle C_bC_aH$ iso C_a	2.91547	2.11323	4.1633	-15.55033 C_a	5	-14.82575 C_b	1	0.87495	0.91771	0.75	1	0.75	1.04887	0				110.76	
$\angle C_aC_bH$ iso C_a	2.91547	2.09711	4.1633	-15.55033 C_b	5	-14.82575 C_a	1	0.87495	0.91771	0.75	1	0.75	1.04887	0				111.27	111.4 (isobutane)
$\angle C_bC_aC_b$ tert C_a	2.90327	2.90327	4.7958	-16.68412 C_b	26	-16.68412 C_b	26	0.81549	0.81549	1	1	1	0.81549	-1.85836				111.37	110.8 (isobutane)
$\angle C_bC_aC_d$															72.50			107.50	

NITRILES ($C_nH_{2n-1}N,\ n=2,3,4,5...\infty$)

The nitriles, $C_nH_{2n-1}N$, comprise a $C\equiv N$ functional group, and the single bond of carbon to the nitrile carbon atom, $C-CN$, is also a functional group. The alkyl portion of the nitrile may comprise at least two terminal methyl groups (CH_3) at each end of the chain, and may comprise methylene (CH_2), and methylyne (CH) functional groups as well as C bound by carbon-carbon single bonds. The methyl and methylene functional groups are equivalent to those of straight-chain alkanes. Six types of $C-C$ bonds can be identified. The n-alkane $C-C$ bond is the same as that of straight-chain alkanes. In addition, the $C-C$ bonds within isopropyl ($(CH_3)_2CH$) and t-butyl ($(CH_3)_3C$) groups and the isopropyl to isopropyl, isopropyl to t-butyl, and t-butyl to t-butyl $C-C$ bonds comprise functional groups. The branched-chain-alkane groups in nitriles are equivalent to those in branched-chain alkanes.

The nitrile $C\equiv N$ is solved equivalently to acetylene as given in the Acetylene Molecule section except that the energy for $E_{(AO/HO)}$ is two times that given in Eq. (14.343), 16.20002 eV, in order to match the N AOs to that of the nitrile $C2sp^3$ HO having a bond order of three. $E_T\left(atom-atom,msp^3.AO\right)$ of the $C\equiv N$ functional group is $-1.56513\,eV$ (Eq. (14.342)) corresponding to the third-order bonded $C2sp^3$ HO.

The $C-CN$ functional group is equivalent to that of an alkyl $C-C$ group given in the Continuous-Chain Alkanes section except that $E_{T(H_2MO)}$ and $\bar{E}_{Kvib}$ are those corresponding to a nitrile. As given in the Continuous-Chain Alkanes section, $E_T\left(atom-atom,msp^3.AO\right)$ of the alkyl $C-C$ group is $-1.85836\,eV$ where both energy contributions are given by Eq. (14.513). It is based on energy matching within the nitrile. It corresponds to the maximum-magnitude energy contributions of a single-bonded and a third-order bonded $C2sp^3$ HO.

The symbols of the functional groups of nitriles are given in Table 15.141. The geometrical (Eqs. (15.1-15.5) and (15.51)), intercept (Eqs. (15.80-15.87)), and energy (Eqs. (15.6-15.11) and (15.17-15.65)) parameters of nitriles are given in Tables 15.142, 15.143, and 15.144, respectively. The total energy of each nitrile given in Table 15.139 was calculated as the sum over the integer multiple of each $E_{D(Group)}$ of Table 15.144 corresponding to functional-group composition of the molecule. For each set of unpaired electrons created by bond breakage, the $C2sp^3$ HO magnetic energy E_{mag} that is subtracted from the weighted sum of the $E_{D(Group)}$ (eV) values based on composition is given by Eq. (15.67). The bond angle parameters of nitriles determined using Eqs. (15.88-15.117) are given in Table 15.146. The C of the $C\equiv N$ group can further bond with only one atom, and the bond is linear as a minimum of energy as in the case of acetylene and alkynes. The color scale, translucent view of the charge-density of exemplary nitrile, propanenitrile, comprising the concentric shells of atoms with the outer shell bridged by one or more H_2-type ellipsoidal MOs or joined with one or more hydrogen MOs is shown in Figure 15.24.

Figure 15.24. Color scale, translucent view of the charge-density of propanenitrile showing the orbitals of the atoms at their radii, the ellipsoidal surface of each H or H_2-type ellipsoidal MO that transitions to the corresponding outer shell of the atom(s) participating in each bond, and the hydrogen nuclei (red, not to scale).

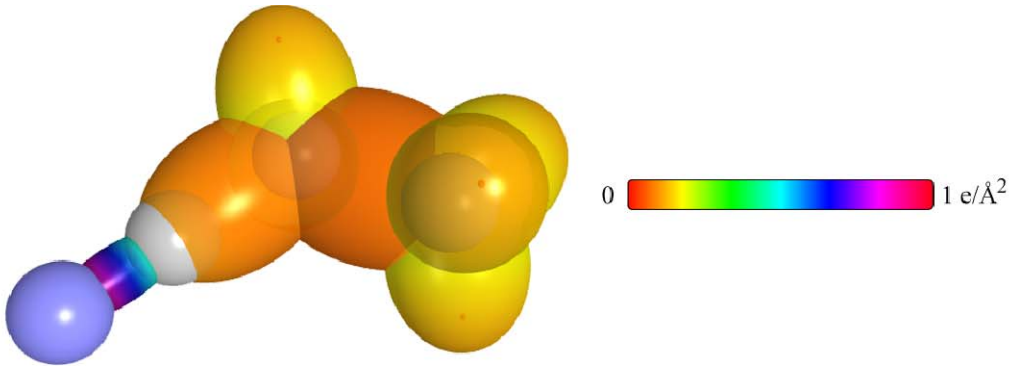

Table 15.141. The symbols of functional groups of nitriles.

Functional Group	Group Symbol
C-*CN*	$C-C$ (i)
CN	$C \equiv N$
CH_3 group	$C-H\ (CH_3)$
CH_2 group	$C-H\ (CH_2)$
CH (*alkyl*) group	$C-H$
CC bond (*n*-*C*)	$C-C$ (a)
CC bond (*iso*-*C*)	$C-C$ (b)
CC bond (*tert*-*C)*	$C-C$ (c)
CC (*iso* to *iso*-*C*)	$C-C$ (d)
CC (*t* to *t*-*C*)	$C-C$ (e)
CC (*t* to iso-*C*)	$C-C$ (f)

Table 15.142. The geometrical bond parameters of nitriles and experimental values [1].

Parameter	$C-C$ (i) Group	$C \equiv N$ Group	$C-H\ (CH_3)$ Group	$C-H\ (CH_2)$ Group	$C-H$ Group	$C-C$ (a) Group	$C-C$ (b) Group	$C-C$ (c) Group	$C-C$ (d) Group	$C-C$ (e) Group	$C-C$ (f) Group
$a\ (a_0)$	1.91255	1.20590	1.64920	1.67122	1.67465	2.12499	2.12499	2.10725	2.12499	2.10725	2.10725
$c'\ (a_0)$	1.38295	1.09813	1.04856	1.05553	1.05661	1.45744	1.45744	1.45164	1.45744	1.45164	1.45164
Bond Length $2c'\ (A)$	1.46365	1.16221	1.10974	1.11713	1.11827	1.54280	1.54280	1.53635	1.54280	1.53635	1.53635
Exp. Bond Length (A)	1.468 (acetonitrile)	1.159 (acetonitrile)	1.107 ($C-H$ propane) 1.117 ($C-H$ butane)	1.107 ($C-H$ propane) 1.117 ($C-H$ butane)	1.122 (isobutane)	1.532 (propane) 1.531 (butane)	1.532 (propane) 1.531 (butane)	1.532 (propane) 1.531 (butane)	1.532 (propane) 1.531 (butane)	1.532 (propane) 1.531 (butane)	1.532 (propane) 1.531 (butane)
$b,c\ (a_0)$	1.382110	0.49828	1.27295	1.29569	1.29924	1.54616	1.54616	1.52750	1.54616	1.52750	1.52750
e	0.72309	0.91064	0.63580	0.63159	0.63095	0.68600	0.68600	0.68888	0.68600	0.68888	0.68888

Table 15.143. The MO to HO intercept geometrical bond parameters of nitriles. R, R', R'' are H or alkyl groups. E_T is $E_T(atom-atom, msp^3.AO)$.

Bond	Atom	E_T (eV) Bond 1	E_T (eV) Bond 2	E_T (eV) Bond 3	E_T (eV) Bond 4	Final Total Energy $C2sp^3$ (eV)	$r_{initial}\ (a_0)$	$r_{final}\ (a_0)$	$E_{Coulomb}$ (eV) Final	$E(C2sp^3)$ (eV) Final	θ' (°)	θ_1 (°)	θ_2 (°)	$d_1\ (a_0)$	$d_2\ (a_0)$
$RH_2C_bC_a \equiv N$	N	-0.78257	0	0	0		0.93084	0.87170	-15.60832		147.01	32.99	72.28	0.36699	0.73114
$RH_2C_bC_a \equiv N$	C_a	-0.78257	-0.92918	0	0	-153.32744	0.91771	0.82272	-16.53750	-16.34664	145.42	34.58	69.58	0.42077	0.67736
$RH_2C_b - C_aN$	C_a	-0.92918	-0.78257	0	0	-153.32744	0.91771	0.82272	-16.53750	-16.34664	81.32	98.68	38.00	1.50718	0.12423
$H_3C_b - C_aN$	C_b	-0.92918	0	0	0	-152.54487	0.91771	0.86359	-15.75493	-15.56407	85.50	94.50	40.67	1.45066	0.06771
$RH_2C_cH_2C_b - C_aN$ R = alkyl	C_b	-0.92918	-0.92918	0	0	-153.47406	0.91771	0.81549	-16.68412	-16.49325	80.53	99.47	37.51	1.51718	0.13423
$C-H\ (CH_3)$	C	-0.92918	0	0	0	-152.54487	0.91771	0.86359	-15.75493	-15.56407	77.49	102.51	41.48	1.23564	0.18708
$C-H\ (CH_2)$	C	-0.92918	-0.92918	0	0	-153.47406	0.91771	0.81549	-16.68412	-16.49325	68.47	111.53	35.84	1.35486	0.29933
$C-H\ (CH)$ (ii)	C	-0.92918	-0.92918	-0.92918	0	-154.40324	0.91771	0.77247	-17.61330	-17.42244	61.10	118.90	31.37	1.42988	0.37326
$H_3C_aC_bH_2CH_1 -$ ($C-C$ (a))	C_a	-0.92918	0	0	0	-152.54487	0.91771	0.86359	-15.75493	-15.56407	63.82	116.18	30.08	1.83879	0.38106
$H_3C_aC_bH_2CH_1 -$ ($C-C$ (a))	C_b	-0.92918	-0.92918	0	0	-153.47406	0.91771	0.81549	-16.68412	-16.49325	56.41	123.59	26.06	1.90890	0.45117
$R-H_2C_aC_b(H_2C_c-R')HCH_2 -$ ($C-C$ (b))	C_b	-0.92918	-0.92918	-0.92918	0	-154.40324	0.91771	0.77247	-17.61330	-17.42244	48.30	131.70	21.90	1.97162	0.51388
$R-H_2C_a(R'-H_2C_d)C_b(R''-H_2C_c)CH_2 -$ ($C-C$ (c))	C_b	-0.92918	-0.72457	-0.72457	-0.72457	-154.71860	0.91771	0.75889	-17.92866	-17.73779	48.21	131.79	21.74	1.95734	0.50570
$isoC_aC_b(H_2C_c-R')HCH_2 -$ ($C-C$ (d))	C_b	-0.92918	-0.92918	-0.92918	0	-154.40324	0.91771	0.77247	-17.61330	-17.42244	48.30	131.70	21.90	1.97162	0.51388
$teriC_a(R'-H_2C_d)C_b(R''-H_2C_c)CH_2 -$ ($C-C$ (e))	C_b	-0.72457	-0.72457	-0.72457	-0.72457	-154.51399	0.91771	0.76765	-17.92866	-17.73779	50.04	129.96	22.66	1.94462	0.49298
$teriC_aC_b(H_2C_c-R')HCH_2 -$ ($C-C$ (f))	C_b	-0.72457	-0.92918	-0.92918	0	-154.19863	0.91771	0.78155	-17.40869	-17.21783	52.78	127.22	24.04	1.92443	0.47279
$isoC_a(R'-H_2C_d)C_b(R''-H_2C_c)CH_2 -$ ($C-C$ (f))	C_b	-0.72457	-0.72457	-0.72457	-0.72457	-154.51399	0.91771	0.76765	-17.92866	-17.73779	50.04	129.96	22.66	1.94462	0.49298

Table 15.144. The energy parameters (eV) of functional groups of nitriles.

Parameters	$C-C$ (i) Group	$C\equiv N$ Group	CH_3 Group	CH_2 Group	$C-H$ Group	$C-C$ (a) Group	$C-C$ (b) Group	$C-C$ (c) Group	$C-C$ (d) Group	$C-C$ (e) Group	$C-C$ (f) Group
n_1	1	3	3	2	1	1	1	1	1	1	1
n_2	0	0	2	1	0	0	0	0	0	0	0
n_3	0	0	0	0	0	0	0	0	0	0	0
C_1	0.5	0.5	0.75	0.75	0.75	0.5	0.5	0.5	0.5	0.5	0.5
C_2	1	1	1	1	1	1	1	1	1	1	1
c_1	1	1	1	1	1	1	1	1	1	1	1
c_2	0.91771	0.91140	0.91771	0.91771	0.91771	0.91771	0.91771	0.91771	0.91771	0.91771	0.91771
c_3	0	1	0	1	1	0	0	0	1	1	0
c_4	2	6	1	1	1	2	2	2	2	2	2
c_5	0	0	3	2	1	0	0	0	0	0	0
C_{1o}	0.5	0.5	0.75	0.75	0.75	0.5	0.5	0.5	0.5	0.5	0.5
C_{2o}	1	1	1	1	1	1	1	1	1	1	1
V_e (eV)	-33.01231	-207.49229	-107.32728	-70.41425	-35.12015	-28.79214	-28.79214	-29.10112	-28.79214	-29.10112	-29.10112
V_p (eV)	9.83824	37.16984	38.92728	25.78002	12.87680	9.33352	9.33352	9.37273	9.33352	9.37273	9.37273
T (eV)	8.63043	86.03250	32.53914	21.06675	10.48582	6.77464	6.77464	6.90500	6.77464	6.90500	6.90500
V_m (eV)	-4.31522	-43.01625	-16.26957	-10.53337	-5.24291	-3.38732	-3.38732	-3.45250	-3.38732	-3.45250	-3.45250
$E_{(AO/HO)}$ (eV)	-14.63489	32.40004	-15.56407	-15.56407	-14.63489	-15.56407	-15.56407	-15.35946	-15.56407	-15.35946	-15.35946
$\Delta E_{H_2MO(AO/HO)}$ (eV)	-1.85837	0	0	0	0	0	0	0	0	0	0
$E_T(_{AO/HO})$ (eV)	-12.77652	32.40004	-15.56407	-15.56407	-14.63489	-15.56407	-15.56407	-15.35946	-15.56407	-15.35946	-15.35946
$E_T(_{H_2MO})$ (eV)	-31.63537	-94.90616	-67.69451	-49.66493	-31.63533	-31.63537	-31.63537	-31.63535	-31.63537	-31.63535	-31.63535
$E_T\left(atom-atom,msp^3.AO\right)(eV)$	-1.85836	-1.56513	0	0	0	-1.85836	-1.85836	-1.44915	-1.85836	-1.44915	-1.44915
$E_T(_{MO})$ (eV)	-33.49374	-96.47124	-67.69450	-49.66493	-31.63537	-33.49373	-33.49373	-33.08452	-33.49373	-33.08452	-33.08452
$\omega\left(10^{15}\ rad/s\right)$	19.2516	22.0753	24.9286	24.2751	24.1759	9.43699	9.43699	15.4846	9.43699	9.55643	9.55643
$\bar{E}_K$ (eV)	12.67172	14.53031	16.40846	15.97831	15.91299	6.21159	6.21159	10.19220	6.21159	6.29021	6.29021
$\bar{E}_D$ (eV)	-0.23588	-0.24250	-0.25352	-0.25017	-0.24966	-0.16515	-0.16515	-0.20896	-0.16515	-0.16416	-0.16416
$\bar{E}_{Kvib}$ (eV)	0.11407 [37]	0.28107 [37]	0.35532 (Eq. (13.458))	0.35532 (Eq. (13.458))	0.35532 (Eq. (13.458))	0.12312 [2]	0.17978 [4]	0.09944 [5]	0.12312 [2]	0.12312 [2]	0.12312 [2]
$\bar{E}_{osc}$ (eV)	-0.17884	-0.10197	-0.22757	-0.14502	-0.07200	-0.10359	-0.07526	-0.15924	-0.10359	-0.10260	-0.10260
E_{mag} (eV)	0.14803	0.14185	0.14803	0.14803	0.14803	0.14803	0.14803	0.14803	0.14803	0.14803	0.14803
$E_T(_{Group})$ (eV)	-33.67258	-96.77713	-67.92207	-49.80996	-31.70737	-33.59732	-33.49373	-33.24376	-33.59732	-33.18712	-33.18712
$E_{initial}(_{s\ AO/HO})$ (eV)	-14.63489	-14.63489	-14.63489	-14.63489	-14.63489	-14.63489	-14.63489	-14.63489	-14.63489	-14.63489	-14.63489
$E_{initial}(_{s\ AO/HO})$ (eV)	0	0	-13.59844	-13.59844	-13.59844	0	0	0	0	0	0
$E_D(_{Group})$ (eV)	4.40280	8.82594	12.49186	7.83016	3.32601	4.32754	4.29921	3.97398	4.17951	3.62128	3.91734

Table 15.145. The total bond energies of nitriles calculated using the functional group composition and the energies of Table 15.144 compared to the experimental values [3]. The magnetic energy E_{mag} that is subtracted from the weighted sum of the E_D ($Group$) (eV) values based on composition is given by (15.58).

Formula	Name	$C-C$ (i) Group	$C\equiv N$ Group	CH_3	CH_2	CH	$C-C$ (a)	$C-C$ (b)	$C-C$ (c)	$C-C$ (d)	$C-C$ (e)	$C-C$ (f)	E_{mag}	Calculated Total Bond Energy (eV)	Experimental Total Bond Energy (eV)	Relative Error
C_2H_3N	Acetonitrile	1	1	1	0	0	0	0	0	0	0	0	0	25.72060	25.77	0.00174
C_3H_5N	Propanenitrile	1	1	1	1	0	1	0	0	0	0	0	0	37.87830	37.94	0.00171
C_4H_7N	Butanenitrile	1	1	1	2	0	2	0	0	0	0	0	0	50.03600	50.08	0.00082
C_4H_7N	2-Methylpropanenitrile	1	1	2	0	1	0	2	0	0	0	0	0	50.13689	50.18	0.00092
C_5H_9N	Pentanenitrile	1	1	1	3	0	3	0	0	0	0	0	0	62.19370	62.26	0.00111
C_5H_9N	2,2-Dimethylpropanenitrile	1	1	3	0	0	0	0	3	0	0	0	-1	62.47823	62.40	-0.00132
$C_7H_{13}N$	Heptanenitrile	1	1	1	5	0	5	0	0	0	0	0	0	86.50910	86.59	0.00089
$C_8H_{15}N$	Octanenitrile	1	1	1	6	0	6	0	0	0	0	0	0	98.66680	98.73	0.00069
$C_{10}H_{19}N$	Decanenitrile	1	1	1	8	0	8	0	0	0	0	0	0	122.98220	123.05	0.00057
$C_{14}H_{27}N$	Tetradecanenitrile	1	1	1	12	0	12	0	0	0	0	0	0	171.61300	171.70	0.00052

Table 15.146. The bond angle parameters of nitriles and experimental values [1]. In the calculation of θ_v, the parameters from the preceding angle were used. E_T is $E_T(atom-atom,msp^3.AO)$.

Atoms of Angle	$2c'$ Bond 1 (a_0)	$2c'$ Bond 2 (a_0)	$2c'$ Terminal Atoms (a_0)	$E_{Coulombic}$ Atom 1	Atom 1 Hybridization Designation (Table 15.3.A)	$E_{Coulombic}$ Atom 2	Atom 2 Hybridization Designation (Table 15.3.A)	c_2 Atom 1	c_2 Atom 2	C_1	C_2	c_1	c_2'	E_T (eV)	θ_v (°)	θ_1 (°)	θ_2 (°)	Cal. θ (°)	Exp. θ (°)
$\angle C_bC_aN$																		180	
$\angle HC_bH$	2.09711	2.09711	3.4252	-15.75493	7	H	H	0.86359	1	1	1	0.75	1.15796	0				109.50	
$\angle HC_bC_a$															70.56			109.44	109.7 (acetonitrile)
Methylene $\angle HC_aH$	2.11106	2.11106	3.4252	-15.75493	7	H	H	0.86359	1	1	1	0.75	1.15796	0				108.44	107 (propane)
$\angle C_aC_bC_c$															69.51			110.49	112 (propane) 113.8 (butane) 110.8 (isobutane)
$\angle C_aC_bH$															69.51			110.49	111.0 (butane) 111.4 (isobutane)
Methyl $\angle HC_aH$	2.09711	2.09711	3.4252	-15.75493	7	H	H	0.86359	1	1	1	0.75	1.15796	0				109.50	
$\angle C_aC_bC_c$															70.56			109.44	
$\angle C_aC_bH$															70.56			109.44	
$\angle C_bC_aC_c$ iso C_a	2.91547	2.91547	4.7958	-16.68412 C_t	26	-16.68412 C_c	26	0.81549	0.81549	1	1	1	0.81549	-1.85836				110.67	110.8 (isobutane)
$\angle C_bC_aH$ iso C_a	2.91547	2.11323	4.1633	-15.55033 C_a	5	-14.82575 C_b	1	0.87495	0.91771	0.75	1	0.75	1.04887	0				110.76	
$\angle C_aC_bH$ iso C_a	2.91547	2.09711	4.1633	-15.55033 C_t	5	-14.82575 C_a	1	0.87495	0.91771	0.75	1	0.75	1.04887	0				111.27	111.4 (isobutane)
$\angle C_bC_aC_b$ tert C_a	2.90327	2.90327	4.7958	-16.68412 C_t	26	-16.68412 C_b	26	0.81549	0.81549	1	1	1	0.81549	-1.85836				111.37	110.8 (isobutane)
$\angle C_bC_aC_d$															72.50			107.50	

THIOLS ($C_nH_{2n+2}S_m,\ n=1,2,3,4,5...\infty$)

The alkyl thiols, $C_nH_{2n+2}S_m$, comprise a SH functional group and a $C-S$ functional group. The alkyl portion of the alkyl thiol may comprise at least two terminal methyl groups (CH_3) at each end of the chain, and may comprise methylene (CH_2), and methylyne (CH) functional groups as well as C bound by carbon-carbon single bonds. The methyl and methylene functional groups are equivalent to those of straight-chain alkanes. Six types of $C-C$ bonds can be identified. The n-alkane $C-C$ bond is the same as that of straight-chain alkanes. In addition, the $C-C$ bonds within isopropyl ($(CH_3)_2CH$) and t-butyl ($(CH_3)_3C$) groups and the isopropyl to isopropyl, isopropyl to t-butyl, and t-butyl to t-butyl $C-C$ bonds comprise functional groups. The branched-chain-alkane groups in thiols are equivalent to those in branched-chain alkanes.

The parameters of the SH functional group is solved using Eq. (15.41). As in the case of the $C-H$ bonds of CH_n $n=1,2,3$, the $S-H$-bond MO is a partial prolate spheroid in between the sulfur and hydrogen nuclei and is continuous with the $S3p$ shell. The energy of the H_2-type ellipsoidal MO is matched to that of the $S3p$ shell and comprises 75% of a H_2-type ellipsoidal MO in order to match potential, kinetic, and orbital energy relationships. Since the energy of S, $E(S)=-10.36001\ eV$, is less that that of H, the linear combination of the H_2-type ellipsoidal MO with the $S3p$ shell further comprises an excess 50% charge-density donation from H to the $S3p$ shell of the $S-H$-bond MO to achieve an energy minimum. The initial total energy of the shell is given by the sum over the four $3p$ electrons. From Eq. (15.12), the sum $E_T(S,3p)$ of the energies of S, S^+, S^{2+}, and S^{3+} [38] is:

$$E_T(S,3p)=10.36001\ eV+23.33788\ eV+34.79\ eV+47.222\ eV=115.70989\ eV \tag{15.137}$$

By considering that the central field decreases by an integer for each successive electron of the shell, the radius r_{3p} of the $S3p$ shell may be calculated from the Coulombic energy using Eqs. (15.13) and (15.137).

$$r_{3p}=\sum_{q=12}^{15}\frac{(Z-q)e^2}{8\pi\varepsilon_0\left(e115.70989\ eV\right)}=\frac{10e^2}{8\pi\varepsilon_0\left(e115.70989\ eV\right)}=1.17585a_0 \tag{15.138}$$

where $Z=16$ for sulfur. Using Eqs. (15.14) and (15.138), the Coulombic energy $E_{Coulomb}(S,3p)$ of the outer electron of the $S3p$ shell is:

$$E_{Coulomb}(S,3p)=\frac{-e^2}{8\pi\varepsilon_0 r_{3p}}=\frac{-e^2}{8\pi\varepsilon_0 1.17585a_0}=-11.57099\ eV \tag{15.139}$$

The sharing of the electrons between the S and H atoms permits the formation an $S-H$-bond MO that is lowered more in energy than the participating $S3p$ orbital which consequently increases in energy. By considering the 50% electron redistribution in the $S-H$ group as well as the fact that the central field decreases by an integer for each successive electron of the shell, the radius r_{S-H3p} of the $S3p$ shell may be calculated from the Coulombic energy using Eq. (15.18).

$$r_{S-H3p}=\left(\sum_{n=12}^{15}(Z-n)+2(0.25)\right)\frac{e^2}{8\pi\varepsilon_0\left(e115.70989\ eV\right)}=\frac{10.5e^2}{8\pi\varepsilon_0\left(e115.70989\ eV\right)}=1.23465a_0 \tag{15.140}$$

where the $s=-2$ in Eq. (15.18) due to the charge donation from H to S. Using Eqs. (15.19) and (15.121), the Coulombic energy $E_{Coulomb}(S_{S-H},3p)$ of the outer electron of the $S3p$ shell is:

$$E_{Coulomb}(S_{S-H},3p)=\frac{-e^2}{8\pi\varepsilon_0 r_{S-H3p}}=\frac{-e^2}{8\pi\varepsilon_0 1.23465a_0}=-11.01999\ eV \tag{15.141}$$

Thus, $E_T(S-H,3p)$, the energy change of each $S3p$ shell with the formation of the $S-H$-bond MO is given by the difference between Eq. (15.139) and Eq. (15.141):

$$E_T(S-H,3p)=E(S_{S-H},3p)-E(S,3p)=-11.01999\ eV-(-11.57099\ eV)=0.55100\ eV \tag{15.142}$$

Then, in Eq. (15.51):

$$E_T(AO/HO)=E(S)-E_T(S-H,3p)=-10.36001\ eV-0.55100\ eV=-10.91101\ eV \tag{15.143}$$

And, in Eq. (15.65),

$$E_T(atom-atom,msp^3.AO)=0.55100\ eV \tag{15.144}$$

Due to the charge donation from H to S, $c_1 = 1$ in both Eqs. (15.51) and (15.65). As in the case of the $C-H$-bond MO, $C_1 = 0.75$ based on the orbital composition. In alkyl thiols, the energy of sulfur is less than the Coulombic energy between the electron and proton of H given by Eq. (1.264). Thus, c_2 in Eq. (15.61) is also one, and the energy matching condition is determined by the C_2 parameter. Using the energy of S, $E(S) = -10.36001\ eV$ in Eq. (15.74), the hybridization factor C_2 of Eq. (15.61) for the $S-H$-bond MO is:

$$C_2(S3p\ to\ H) = \frac{E(S,3p)}{E(H)} = \frac{-10.36001\ eV}{-13.60580\ eV} = 0.76144 \tag{15.145}$$

Since the energy of S is matched to the Coulombic energy between the electron and proton of H, $E(H(a_0))$, $E_{initial}(c_4 AO/HO) = E(H(a_0)) = -13.60580\ eV$, $E_{initial}(c_5 AO/HO) = E(H) = -13.59844\ eV$, and E_{mag} is that corresponding to $E(H(a_0))$ given by Eq. (15.67). $E_D(Group)$ for hydrogen sulfide is equivalent to that of the SH functional group, and the $E_D(Group)$ (eV) for dihydrogen sulfide follows the same derivation as that for the SH functional group except that the parameters correspond to $n_1 = 2$ rather than $n_1 = 1$ in Eqs. (15.51) and (15.65).

Furthermore, with the energy of S matched to the Coulombic energy between the electron and proton of H, the energy of the $C-S$-bond MO is the sum of the component energies of the H_2-type ellipsoidal MO given in Eq. (15.51) with $E(AO/HO) = 0$ and $E_T(AO/HO) = \Delta E_{H_2 MO}(AO/HO)$. Then, the solution of the $C-S$ functional group comprises the hybridization of the $2s$ and $2p$ AOs of C to form a single $2sp^3$ shell as an energy minimum, and the sharing of electrons between the $C2sp^3$ HO and the S AO to form a MO permits each participating orbital to decrease in radius and energy. Since the energy of sulfur is less than the Coulombic energy between the electron and proton of H given by Eq. (1.264), c_2 in Eq. (15.61) is one, and the energy matching condition is determined by the C_2 parameter. Then, $C2sp^3$ HO has a hybridization factor of 0.91771 (Eq. (13.430)) with a corresponding energy of $E(C,2sp^3) = -14.63489\ eV$ (Eq. (15.25)), and the S AO has an energy of $E(S) = -10.36001\ eV$. To meet the equipotential condition of the union of the $C-S$ H_2-type-ellipsoidal-MO with these orbitals, the hybridization factor C_2 of Eq. (15.60) for the $C-S$-bond MO given by Eqs. (15.77) and (15.79) is:

$$C_2(C2sp^3 HO\ to\ \mathrm{S}) = \frac{E(S)}{E(C,2sp^3)} c_2(C2sp^3 HO) = \frac{-10.36001\ eV}{-14.63489\ eV}(0.91771) = 0.64965 \tag{15.146}$$

Since the sulfur is energy matched to $E(H(a_0))$ in the $S-H$-bond MO, $E_T(atom-atom, msp^3.AO)$ of the $C-S$-bond MO in Eq. (15.61) due to the charge donation from the C and S atoms to the MO is $-0.72457\ eV$ corresponding to the energy contribution equivalent to that of a methyl group (Eq. (14.151)).

The symbols of the functional groups of branched-chain alkyl thiols are given in Table 15.147. The geometrical (Eqs. (15.1-15.5) and (15.51)), intercept (Eqs. (15.80-15.87)), and energy (Eqs. (15.6-15.11) and (15.17-15.65)) parameters of alkyl thiols are given in Tables 15.148, 15.149, and 15.150, respectively. The total energy of each alkyl thiol given in Table 15.151 was calculated as the sum over the integer multiple of each $E_D(Group)$ of Table 15.150 corresponding to functional-group composition of the molecule. For each set of unpaired electrons created by bond breakage, the $C2sp^3$ HO magnetic energy E_{mag} that is subtracted from the weighted sum of the $E_D(Group)$ (eV) values based on composition is given by Eq. (15.67). The $C-C$ bonds to the $HCSH$ group (one H bond to C) were each treated as an iso $C-C$ bond. The $C-C$ bonds to the CSH group (no H bonds to C) were each treated as a tert-butyl $C-C$. E_{mag} was subtracted for each t-butyl group. The bond angle parameters of alkyl thiols determined using Eqs. (15.88-15.117) are given in Table 15.152. The color scale, translucent view of the charge-density of exemplary thiol, ethanethiol, comprising the concentric shells of atoms with the outer shell bridged by one or more H_2-type ellipsoidal MOs or joined with one or more hydrogen MOs is shown in Figure 15.25.

Figure 15.25. Color scale, translucent view of the charge-density of ethanethiol showing the orbitals of the atoms at their radii, the ellipsoidal surface of each H or H_2-type ellipsoidal MO that transitions to the corresponding outer shell of the atom(s) participating in each bond, and the hydrogen nuclei (red, not to scale).

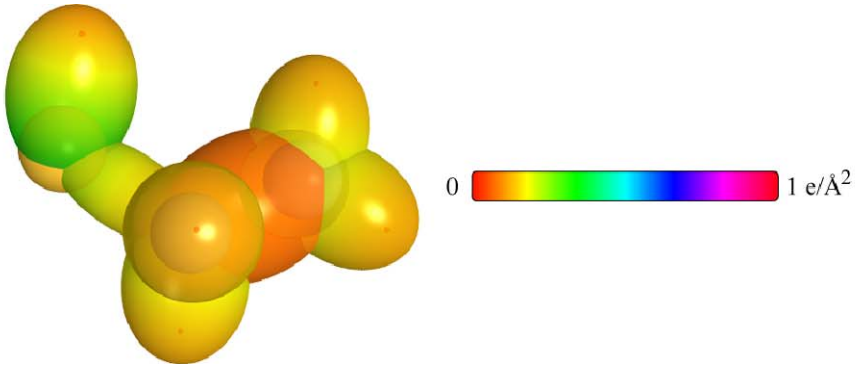

Table 15.147. The symbols of functional groups of alkyl thiols.

Functional Group	Group Symbol
SH group	*SH*
H_2S	H_2S
C-S	$C-S$
CH_3 group	$C-H\ (CH_3)$
CH_2 group	$C-H\ (CH_2)$
CH	$C-H$
CC bond (*n-C*)	$C-C$ (a)
CC bond (*iso-C*)	$C-C$ (b)
CC bond (*tert-C*)	$C-C$ (c)
CC (*iso* to *iso-C*)	$C-C$ (d)
CC (*t* to *t-C*)	$C-C$ (e)
CC (*t* to *iso-C*)	$C-C$ (f)

Table 15.148. The geometrical bond parameters of alkyl thiols and experimental values [1].

Parameter	$S-H\ (H_2S)$	SH Group	$C-S$ Group	$C-H\ (CH_3)$ Group	$C-H\ (CH_2)$ Group	$C-H$ Group	$C-C$ (a) Group	$C-C$ (b) Group	$C-C$ (c) Group	$C-C$ (d) Group	$C-C$ (e) Group	$C-C$ (f) Group
$a\ (a_0)$	1.83762	1.83762	1.90975	1.64920	1.67122	1.67465	2.12499	2.12499	2.10725	2.12499	2.10725	2.10725
$c'\ (a_0)$	1.26842	1.26842	1.71455	1.04856	1.05553	1.05661	1.45744	1.45744	1.45164	1.45744	1.45164	1.45164
Bond Length $2c'\ (\AA)$	1.34244	1.34244	1.81460	1.10974	1.11713	1.11827	1.54280	1.54280	1.53635	1.54280	1.53635	1.53635
Exp. Bond Length $(\AA)$	1.3356	1.34066 (hydrogen sulfide) 1.34 (methanethiol)	1.819 (methanethiol) 1.829 (ethanethiol)	1.107 ($C-H$ propane) 1.117 ($C-H$ butane)	1.107 ($C-H$ propane) 1.117 ($C-H$ butane)	1.122 (isobutane)	1.532 (propane) 1.531 (butane)	1.532 (propane) 1.531 (butane)	1.532 (propane) 1.531 (butane)	1.532 (propane) 1.531 (butane)	1.532 (propane) 1.531 (butane)	1.532 (propane) 1.531 (butane)
$b,c\ (a_0)$	1.32964	1.32964	0.84112	1.27295	1.29569	1.29924	1.54616	1.54616	1.52750	1.54616	1.52750	1.52750
e	0.69025	0.69025	0.89778	0.63580	0.63159	0.63095	0.68600	0.68600	0.68888	0.68600	0.68888	0.68888

Table 15.149. The MO to HO intercept geometrical bond parameters of alkyl thiols. R, R', R'' are H or alkyl groups. E_T is $E_T(atom-atom,msp^3.AO)$.

Bond	Atom	E_T (eV) Bond 1	E_T (eV) Bond 2	E_T (eV) Bond 3	E_T (eV) Bond 4	Final Total Energy $C2sp^3$ (eV)	$r_{initial}\ (a_0)$	$r_{final}\ (a_0)$	$E_{Coulomb}$ (eV) Final	$E(C2sp^3)$ (eV) Final	θ' (°)	θ_1 (°)	θ_2 (°)	$d_1\ (a_0)$	$d_2\ (a_0)$
$S-H$ (hydrogen sulfide) (dihydrogen sulfide)	S	0.55100	0	0	0		1.32010	1.23465	-11.01999		108.65	71.35	61.62	0.87355	0.39487
$RS-H$	S	-0.36229	0.55100	0	0		1.32010	0.92955	-14.63704		87.09	92.91	44.28	1.31557	0.04714
C_aH_3-SH	S	-0.36229	0.55100	0	0		1.32010	0.92955	-14.63704		132.06	47.94	55.13	1.09181	0.62274
C_aH_3-SH	C_a	-0.36229	0	0	0	-151.97798	0.91771	0.89582	-15.18804	-14.99717	69.84	110.16	88.87	0.03762	1.67692
$RC_cH_2C_bH_2-C_aH_3SH$	C_a	-0.36229	-0.92918	0	0	-152.90716	0.91771	0.84418	-16.11722	-15.92636	128.69	51.31	51.57	1.18689	0.52765
$C-H\ (CH_3)$	C	-0.92918	0	0	0	-152.54487	0.91771	0.86359	-15.75493	-15.56407	77.49	102.51	41.48	1.23564	0.18708
$C-H\ (CH_2)$	C	-0.92918	-0.92918	0	0	-153.47406	0.91771	0.81549	-16.68412	-16.49325	68.47	111.53	35.84	1.35486	0.29933
$C-H\ (CH)$	C	-0.92918	-0.92918	-0.92918	0	-154.40324	0.91771	0.77247	-17.61330	-17.42244	61.10	118.90	31.37	1.42988	0.37326
$H_3C_aC_bH_2CH_2-$ ($C-C$ (a))	C_a	-0.92918	0	0	0	-152.54487	0.91771	0.86359	-15.75493	-15.56407	63.82	116.18	30.08	1.83879	0.38106
$H_3C_aC_bH_2CH_2-$ ($C-C$ (a))	C_b	-0.92918	-0.92918	0	0	-153.47406	0.91771	0.81549	-16.68412	-16.49325	56.41	123.59	26.06	1.90890	0.45117
$R-H_2C_aC_b(H_2C_c-R')HCH_2-$ ($C-C$ (b))	C_b	-0.92918	-0.92918	-0.92918	0	-154.40324	0.91771	0.77247	-17.61330	-17.42244	48.30	131.70	21.90	1.97162	0.51388
$R-H_2C_a(R'-H_2C_d)C_b(R''-H_2C_c)CH_2-$ ($C-C$ (c))	C_b	-0.92918	-0.72457	-0.72457	-0.72457	-154.71860	0.91771	0.75889	-17.92866	-17.73779	48.21	131.79	21.74	1.95734	0.50570
$isoC_aC_b(H_2C_c-R')HCH_2-$ ($C-C$ (d))	C_b	-0.92918	-0.92918	-0.92918	0	-154.40324	0.91771	0.77247	-17.61330	-17.42244	48.30	131.70	21.90	1.97162	0.51388
$tertC_a(R'-H_2C_d)C_b(R''-H_2C_c)CH_2-$ ($C-C$ (e))	C_b	-0.72457	-0.72457	-0.72457	-0.72457	-154.51399	0.91771	0.76765	-17.92866	-17.73779	50.04	129.96	22.66	1.94462	0.49298
$tertC_aC_b(H_2C_c-R')HCH_2-$ ($C-C$ (f))	C_b	-0.72457	-0.92918	-0.92918	0	-154.19863	0.91771	0.78155	-17.40869	-17.21783	52.78	127.22	24.04	1.92443	0.47279
$isoC_a(R'-H_2C_d)C_b(R''-H_2C_c)CH_2-$ ($C-C$ (f))	C_b	-0.72457	-0.72457	-0.72457	-0.72457	-154.51399	0.91771	0.76765	-17.92866	-17.73779	50.04	129.96	22.66	1.94462	0.49298

Table 15.150. The energy parameters (eV) of functional groups of alkyl thiols.

Parameters	H_2S	SH Group	$C-S$ Group	CH_3 Group	CH_2 Group	$C-H$ Group	$C-C$ (a) Group	$C-C$ (b) Group	$C-C$ (c) Group	$C-C$ (d) Group	$C-C$ (e) Group	$C-C$ (f) Group
n_1	2	1	1	3	2	1	1	1	1	1	1	1
n_2	0	0	0	2	1	0	0	0	0	0	0	0
n_3	0	0	0	0	0	0	0	0	0	0	0	0
C_1	0.75	0.75	0.5	0.75	0.75	0.75	0.5	0.5	0.5	0.5	0.5	0.5
C_2	0.76144	0.76144	0.64965	1	1	1	1	1	1	1	1	1
c_1	1	1	1	1	1	1	1	1	1	1	1	1
c_2	1	1	1	0.91771	0.91771	0.91771	0.91771	0.91771	0.91771	0.91771	0.91771	0.91771
c_3	2	1	0	0	1	1	0	0	0	1	1	0
c_4	1	1	2	1	1	1	2	2	2	2	2	2
c_5	1	1	0	3	2	1	0	0	0	0	0	0
C_{1o}	0.75	0.75	0.5	0.75	0.75	0.75	0.5	0.5	0.5	0.5	0.5	0.5
C_{2o}	0.76144	0.76144	0.64965	1	1	1	1	1	1	1	1	1
$V_e\ (eV)$	-72.80662	-36.40331	-46.36495	-107.32728	-70.41425	-35.12015	-28.79214	-28.79214	-29.10112	-28.79214	-29.10112	-29.10112
$V_p\ (eV)$	21.45310	10.72655	7.93551	38.92728	25.78002	12.87680	9.33352	9.33352	9.37273	9.33352	9.37273	9.37273
$T\ (eV)$	19.81003	9.90502	12.13899	32.53914	21.06675	10.48582	6.77464	6.77464	6.90500	6.77464	6.90500	6.90500
$V_m\ (eV)$	-9.90502	-4.95251	-6.06949	-16.26957	-10.53337	-5.24291	-3.38732	-3.38732	-3.45250	-3.38732	-3.45250	-3.45250
$E(_{AO/HO})\ (eV)$	-20.72002	-10.36001	0	-15.56407	-15.56407	-14.63489	-15.56407	-15.56407	-15.35946	-15.56407	-15.35946	-15.35946
$\Delta E_{H_2MO}(_{AO/HO})\ (eV)$	1.10200	0.55100	-0.72457	0	0	0	0	0	0	0	0	0
$E_T(_{AO/HO})\ (eV)$	-19.61802	-10.91101	0.72457	-15.56407	-15.56407	-14.63489	-15.56407	-15.56407	-15.35946	-15.56407	-15.35946	-15.35946
$E_T(_{H_2MO})\ (eV)$	-63.27052	-31.63526	-31.63537	-67.69451	-49.66493	-31.63533	-31.63537	-31.63537	-31.63535	-31.63537	-31.63535	-31.63535
$E_T\left(atom-atom, msp^3.AO\right)(eV)$	1.10200	0.55100	-0.72457	0	0	0	-1.85836	-1.85836	-1.44915	-1.85836	-1.44915	-1.44915
$E_T(_{MO})\ (eV)$	-62.16874	-31.08437	-32.35994	-67.69450	-49.66493	-31.63537	-33.49373	-33.49373	-33.08452	-33.49373	-33.08452	-33.08452
$\omega\ \left(10^{15}\ rad/s\right)$	12.5415	12.5415	30.5436	24.9286	24.2751	24.1759	9.43699	9.43699	15.4846	9.43699	9.55643	9.55643
$E_K\ (eV)$	8.25504	8.25504	20.10434	16.40846	15.97831	15.91299	6.21159	6.21159	10.19220	6.21159	6.29021	6.29021
$\bar{E}_D\ (eV)$	-0.17669	-0.17669	-0.28705	-0.25352	-0.25017	-0.24966	-0.16515	-0.16515	-0.20896	-0.16515	-0.16416	-0.16416
$\bar{E}_{Kvib}\ (eV)$	0.32422 [39]	0.33620 [40]	0.08146 [41]	0.35532 (Eq. (13.458))	0.35532 (Eq. (13.458))	0.35532 (Eq. (13.458))	0.12312 [2]	0.17978 [4]	0.09944 [5]	0.12312 [2]	0.12312 [2]	0.12312 [2]
$\bar{E}_{osc}\ (eV)$	-0.01458	-0.00859	-0.24632	-0.22757	-0.14502	-0.07200	-0.10359	-0.07526	-0.15924	-0.10359	-0.10260	-0.10260
$E_{mag}\ (eV)$	0.11441	0.11441	0.14803	0.14803	0.14803	0.14803	0.14803	0.14803	0.14803	0.14803	0.14803	0.14803
$E_T(_{Group})\ (eV)$	-31.10493[a]	-31.09296	-32.60626	-67.92207	-49.80996	-31.70737	-33.59732	-33.49373	-33.24376	-33.59732	-33.18712	-33.18712
$E_{initial}(_{4\ AO/HO})\ (eV)$	-13.60580	-13.60580	-14.63489	-14.63489	-14.63489	-14.63489	-14.63489	-14.63489	-14.63489	-14.63489	-14.63489	-14.63489
$E_{initial}(_{5\ AO/HO})\ (eV)$	-13.59844	-13.59844	0	-13.59844	-13.59844	-13.59844	0	0	0	0	0	0
$E_D(_{Group})\ (eV)$	3.78628	3.77430	3.33648	12.49186	7.83016	3.32601	4.32754	4.29921	3.97398	4.17951	3.62128	3.91734

[a] $E_T(_{H-S,H_2S}) = E_T(_{H_2S}) - E_T(_{HS}) = 62.19789\ eV - (-31.09296\ eV)$.

Table 15.151. The total bond energies of alkyl thiols calculated using the functional group composition and the energies of Table 15.150 compared to the experimental values [3]. The magnetic energy E_{mag} that is subtracted from the weighted sum of the E_D ($Group$) (eV) values based on composition is given by (15.58).

Formula	Name	H_2S Group	SH Group	$C-S$ Group	CH_3	CH_2	CH	$C-C$ (a)	$C-C$ (b)	$C-C$ (c)	$C-C$ (d)	$C-C$ (e)	$C-C$ (f)	E_{mag}	Calculated Total Bond Energy (eV)	Experimental Total Bond Energy (eV)	Relative Error
HS	Hydrogen Sulfide	0	1	0	0	0	0	0	0	0	0	0	0	0	3.77430	3.653	-0.03320
H_2S	Dihydrogen Sulfide	1	1	0	0	0	0	0	0	0	0	0	0	0	7.56058	7.605	0.00582
CH_4S	Methanethiol	0	1	1	1	0	0	0	0	0	0	0	0	0	19.60264	19.575	-0.00141
C_2H_6S	Ethanethiol	0	1	1	1	1	0	1	0	0	0	0	0	0	31.76034	31.762	0.00005
C_3H_8S	1-Propanethiol	0	1	1	1	2	0	2	0	0	0	0	0	0	43.91804	43.933	0.00035
C_3H_8S	2-Propanethiol	0	1	1	2	0	1	0	2	0	0	0	0	0	44.01893	44.020	0.00003
$C_4H_{10}S$	1-Butanethiol	0	1	1	1	3	0	3	0	0	0	0	0	0	56.07574	56.089	0.00024
$C_4H_{10}S$	2-Butanethiol	0	1	1	2	1	1	1	2	0	0	0	0	0	56.17663	56.181	0.00009
$C_4H_{10}S$	2-Methyl-1-propanethiol	0	1	1	2	1	1	0	3	0	0	0	0	0	56.14830	56.186	0.00066
$C_4H_{10}S$	2-Methyl-2-propanethiol	0	1	1	3	0	0	0	0	3	0	0	0	-1	56.36027	56.313	-0.00084
$C_5H_{12}S$	2-Methyl-1-butanethiol	0	1	1	2	2	1	1	3	0	0	0	0	0	68.30600	68.314	0.00012
$C_5H_{12}S$	1-Pentanethiol	0	1	1	1	4	0	4	0	0	0	0	0	0	68.23344	68.264	0.00044
$C_5H_{12}S$	2-Methyl-2-butanethiol	0	1	1	3	1	0	1	0	3	0	0	0	-1	68.51797	68.441	-0.00113
$C_5H_{12}S$	3-Methyl-2-butanethiol	0	1	1	3	0	2	0	3	0	1	0	0	0	68.31552	68.381	0.00095
$C_5H_{12}S$	2,2-Dimethyl-1-propanethiol	0	1	1	3	1	0	1	0	3	0	0	0	-1	68.16441	68.461	0.00433
$C_6H_{14}S$	1-Hexanethiol	0	1	1	1	5	0	5	0	0	0	0	0	0	80.39114	80.416	0.00031
$C_6H_{14}S$	2-Methyl-2-pentanethiol	0	1	1	3	2	0	2	0	3	0	0	0	-1	80.67567	80.607	-0.00085
$C_6H_{14}S$	2,3-Dimethyl-2-butanethiol	0	1	1	4	0	1	0	2	2	0	0	1	-1	80.71992	80.603	-0.00145
$C_7H_{16}S$	1-Heptanethiol	0	1	1	1	6	0	6	0	0	0	0	0	0	92.54884	92.570	0.00023
$C_{10}H_{22}S$	1-Decanethiol	0	1	1	1	9	0	9	0	0	0	0	0	0	129.02194	129.048	0.00020

Table 15.152. The bond angle parameters of alkyl thiols and experimental values [1]. In the calculation of θ_v, the parameters from the preceding angle were used. E_T is E_T ($atom - atom, msp^3.AO$).

Atoms of Argle	2c' Bond 1 (a_0)	2c' Bond 2 (a_0)	2c' Terminal Atoms (a_0)	$E_{Coulombic}$ Atom 1	Atom 1 Hybridization Designation (Table 15.3.A)	$E_{Coulombic}$ Atom 2	Atom 2 Hybridization Designation (Table 15.3.A)	c_2 Atom 1	c_2 Atom 2	C_1	C_2	c_1	c_2'	E_T (eV)	θ_v (°)	θ_1 (°)	θ_2 (°)	Cal. θ (°)	Exp. θ (°)
$\angle HSC_a$	2.53685	3.42910	4.5166	-10.36001 S	S	-15.75493 C_a	7	0.76144 (Eq. 15.144))	0.86359	0.75	1	0.75	1.13415	0				97.28	96.5 (methanethiol) 96.4 (ethanethiol)
$\angle C_bC_aS$	2.91547	3.42910	5.2344	-16.68412 C_b	26	-10.36001 S	S	0.81549	0.64965 (Eq. (15.146))	1	0.64965 (Eq. (15.146))	1	0.73257	-0.72457				110.92	108.3 (ethanethiol)
Methylene $\angle HC_aH$	2.11106	2.11106	3.4252	-15.75493	7	H	H	0.86359	1	1	1	0.75	1.15796	0				108.44	107 (propane)
$\angle C_cC_bC_c$															69.51			110.49	112 (propane) 113.8 (butane) 110.8 (isobutane)
$\angle C_aC_bH$															69.51			110.49	111.0 (butane) 111.4 (isobutane)
Methyl $\angle HC_aH$	2.09711	2.09711	3.4252	-15.75493	7	H	H	0.86359	1	1	1	0.75	1.15796	0				109.50	
$\angle C_cC_bC_c$															70.56			109.44	
$\angle C_aC_bH$															70.56			109.44	
$\angle C_tC_aC_c$ iso C_a	2.91547	2.91547	4.7958	-16.68412 C_b	26	-16.68412 C_c	26	0.81549	0.81549	1	1	1	0.81549	-1.85836				110.67	110.8 (isobutane)
$\angle C_tC_aH$ iso C_a	2.91547	2.11323	4.1633	-15.55033 C_a	5	-14.82575 C_b	1	0.87495	0.91771	0.75	1	0.75	1.04887	0				110.76	
$\angle C_aC_bH$ iso C_a	2.91547	2.09711	4.1633	-15.55033 C_b	5	-14.82575 C_a	1	0.87495	0.91771	0.75	1	0.75	1.04887	0				111.27	111.4 (isobutane)
$\angle C_tC_aC_b$ tert C_a	2.90327	2.90327	4.7958	-16.68412 C_b	26	-16.68412 C_b	26	0.81549	0.81549	1	1	1	0.81549	-1.85836				111.37	110.8 (isobutane)
$\angle C_bC_aC_d$															72.50			107.50	

SULFIDES ($C_nH_{2n+2}S_m,\ n=2,3,4,5...\infty$)

The alkyl sulfides, $C_nH_{2n+2}S_m$, comprise two types of $C-S$ functional groups, one for t-butyl groups corresponding to the C and the other for the remaining general alkyl groups including methyl. The alkyl portion of the alkyl sulfide may comprise at least two terminal methyl groups (CH_3) at each end of the chain, and may comprise methylene (CH_2), and methylyne (CH) functional groups as well as C bound by carbon-carbon single bonds. The methyl and methylene functional groups are equivalent to those of straight-chain alkanes. Six types of $C-C$ bonds can be identified. The n-alkane $C-C$ bond is the same as that of straight-chain alkanes. In addition, the $C-C$ bonds within isopropyl ($(CH_3)_2CH$) and t-butyl ($(CH_3)_3C$) groups and the isopropyl to isopropyl, isopropyl to t-butyl, and t-butyl to t-butyl $C-C$ bonds comprise functional groups. The branched-chain-alkane groups in sulfides are equivalent to those in branched-chain alkanes.

Each $C-S$ group is solved by hybridizing the $2s$ and $2p$ AOs of the C atom to form a single $2sp^3$ shell as an energy minimum, and the sharing of electrons between the $C2sp^3$ HO and the S AO to form a MO permits each participating orbital to decrease in radius and energy. Since the energy of sulfur is less than the Coulombic energy between the electron and proton of H given by Eq. (1.264), c_2 in Eq. (15.61) is one, and the energy matching condition is determined by the C_2 parameter. As in the case of thiols, C_2 of Eq. (15.61) for the $C-S$-bond MO given by Eq. (15.146) is $C_2\left(C2sp^3HO\ to\ \mathrm{S}\right)=0.64965$.

The $C-S$ group of alkyl sulfides is equivalent to that of thiols where $E_T\left(atom-atom,msp^3.AO\right)$ is $-0.72457\ eV$ (Eq. (14.151)). The t-butyl-$C-S$ group is also equivalent to that of thiols except that the energy parameters corresponding to the oscillation in the transition state are matched to those of the t-butyl group.

The symbols of the functional groups of branched-chain alkyl sulfides are given in Table 15.153. The geometrical (Eqs. (15.1-15.5) and (15.51)), intercept (Eqs. (15.80-15.87)), and energy (Eqs. (15.6-15.11) and (15.17-15.65)) parameters of alkyl sulfides are given in Tables 15.154, 15.155, and 15.156, respectively. Consider that the $C-S$ bond is along the x axis in the xy-plane. The S nucleus is at the focus +c and the C nucleus is at the focus –c. The elliptic angle θ' is taken as counterclockwise from the x-axis for S and as clockwise from the –x-axis for C. The total energy of each alkyl sulfide given in Table 15.157 was calculated as the sum over the integer multiple of each $E_D(Group)$ of Table 15.156 corresponding to functional-group composition of the molecule. E_{mag} given by Eq. (15.67) was subtracted for each t-butyl group. The bond angle parameters of alkyl sulfides determined using Eqs. (15.88-15.117) are given in Table 15.158. The color scale, translucent view of the charge-density of exemplary sulfide, dimethyl sulfide, comprising the concentric shells of atoms with the outer shell bridged by one or more H_2-type ellipsoidal MOs or joined with one or more hydrogen MOs is shown in Figure 15.26.

Figure 15.26. Color scale, translucent view of the charge-density of dimethyl sulfide showing the orbitals of the atoms at their radii, the ellipsoidal surface of each H or H_2-type ellipsoidal MO that transitions to the corresponding outer shell of the atom(s) participating in each bond, and the hydrogen nuclei (red, not to scale).

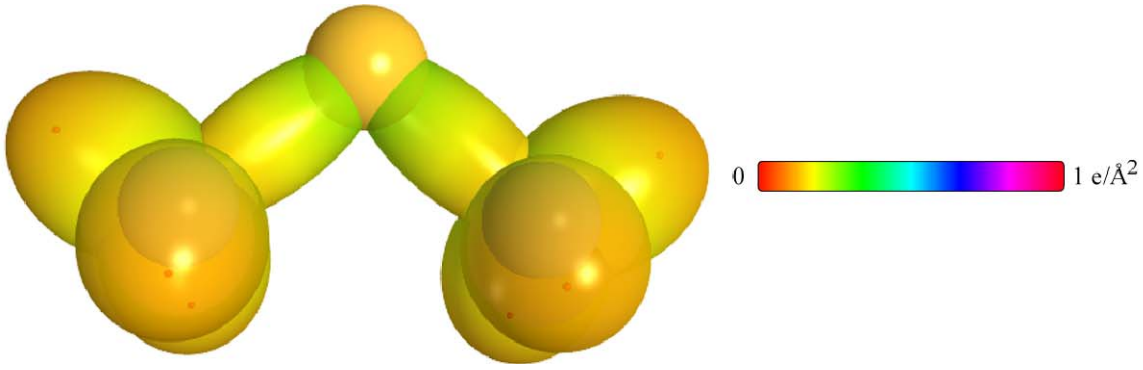

Table 15.153. The symbols of functional groups of alkyl sulfides.

Functional Group	Group Symbol
C-S (*methyl, alkyl*)	$C-S$ (i)
C-S ($(CH_3)_3 C-S-$)	$C-S$ (ii)
CH_3 group	$C-H\ (CH_3)$
CH_2 group	$C-H\ (CH_2)$
CH	$C-H$
CC bond (*n-C*)	$C-C$ (a)
CC bond (*iso-C*)	$C-C$ (b)
CC bond (*tert-C*)	$C-C$ (c)
CC (*iso* to *iso-C*)	$C-C$ (d)
CC (*t* to *t-C*)	$C-C$ (e)
CC (*t* to *iso-C*)	$C-C$ (f)

Table 15.154. The geometrical bond parameters of alkyl sulfides and experimental values [1].

Parameter	$C-S$ (i) Group	$C-S$ (ii) Group	$C-H\left(CH_3\right)$ Group	$C-H\left(CH_2\right)$ Group	$C-H$ Group	$C-C$ (a) Group	$C-C$ (b) Group	$C-C$ (c) Group	$C-C$ (d) Group	$C-C$ (e) Group	$C-C$ (f) Group
$a\left(a_0\right)$	1.90975	1.90975	1.64920	1.67122	1.67465	2.12499	2.12499	2.10725	2.12499	2.10725	2.10725
$c'\left(a_0\right)$	1.71455	1.71455	1.04856	1.05553	1.05661	1.45744	1.45744	1.45164	1.45744	1.45164	1.45164
Bond Length $2c'\left(\AA\right)$	1.81460	1.81460	1.10974	1.11713	1.11827	1.54280	1.54280	1.53635	1.54280	1.53635	1.53635
Exp. Bond Length $\left(\AA\right)$	1.807 (dimethyl sulfide) 1.813 (ethyl methyl sulfide, avg.)	1.807 (dimethyl sulfide) 1.813 (ethyl methyl sulfide, avg.)	1.107 ($C-H$ propane) 1.117 ($C-H$ butane)	1.107 ($C-H$ propane) 1.117 ($C-H$ butane)	1.122 (isobutane)	1.532 (propane) 1.531 (butane)	1.532 (propane) 1.531 (butane)	1.532 (propane) 1.531 (butane)	1.532 (propane) 1.531 (butane)	1.532 (propane) 1.531 (butane)	1.532 (propane) 1.531 (butane)
$b,c\left(a_0\right)$	0.84112	0.84112	1.27295	1.29569	1.29924	1.54616	1.54616	1.52750	1.54616	1.52750	1.52750
e	0.89778	0.89778	0.63580	0.63159	0.63095	0.68600	0.68600	0.68888	0.68600	0.68888	0.68888

Table 15.155. The MO to HO intercept geometrical bond parameters of alkyl sulfides. R, R', R'' are H or alkyl groups. E_T is $E_T(atom-atom,msp^3.AO)$.

Bond	Atom	E_T (eV) Bond 1	E_T (eV) Bond 2	E_T (eV) Bond 3	E_T (eV) Bond 4	Final Total Energy $C2sp^3$ (eV)	$r_{initial}\left(a_0\right)$	$r_{final}\left(a_0\right)$	$E_{Coulomb}$ (eV) Final	$E\left(C2sp^3\right)$ (eV) Final	$\theta'\left(^\circ\right)$	$\theta_1\left(^\circ\right)$	$\theta_2\left(^\circ\right)$	$d_1\left(a_0\right)$	$d_2\left(a_0\right)$
$R-S-R$ ($C-S$ (i) and (ii))	S	-0.36229	-0.36229	0	0		1.32010	0.87495	-15.55033		129.96	50.04	52.88	1.15262	0.56193
$H_3C_a-S-C_bH_2CH_2R$ ($C-S$ (i))	C_a	-0.36229	0	0	0	-151.97798	0.91771	0.89582	-15.18804	-14.99717	130.79	49.21	53.75	1.12937	0.58518
$H_3C_a-S-C_bH_2CH_2R$ ($C-S$ (i))	C_b	-0.36229	-0.92918	0	0	-152.90716	0.91771	0.84418	-16.11722	-15.92636	128.69	51.31	51.57	1.18689	0.52765
$H_3C_a-S-C_c\left(CH_3\right)_3$ ($C-S$ (i) and (ii))	C_c	-0.36229	-0.72457	-0.72457	-0.72457	-154.15170	0.91771	0.78367	-17.36176	-17.17090	125.97	54.03	48.94	1.25430	0.46025
$C-H\left(CH_3\right)$	C	-0.92918	0	0	0	-152.54487	0.91771	0.86359	-15.75493	-15.56407	77.49	102.51	41.48	1.23564	0.18708
$C-H\left(CH_2\right)$	C	-0.92918	-0.92918	0	0	-153.47406	0.91771	0.81549	-16.68412	-16.49325	68.47	111.53	35.84	1.35486	0.29933
$C-H\left(CH\right)$	C	-0.92918	-0.92918	-0.92918	0	-154.40324	0.91771	0.77247	-17.61330	-17.42244	61.10	118.90	31.37	1.42988	0.37326
$H_3C_aC_bH_2CH_2-$ ($C-C$ (a))	C_a	-0.92918	0	0	0	-152.54487	0.91771	0.86359	-15.75493	-15.56407	63.82	116.18	30.08	1.83879	0.38106
$H_3C_aC_bH_2CH_2-$ ($C-C$ (a))	C_b	-0.92918	-0.92918	0	0	-153.47406	0.91771	0.81549	-16.68412	-16.49325	56.41	123.59	26.06	1.90890	0.45117
$R-H_2C_aC_b\left(H_2C_c-R'\right)HCH_2-$ ($C-C$ (b))	C_b	-0.92918	-0.92918	-0.92918	0	-154.40324	0.91771	0.77247	-17.61330	-17.42244	48.30	131.70	21.90	1.97162	0.51388
$R-H_2C_a\left(R'-H_2C_d\right)C_b\left(R''-H_2C_c\right)CH_2-$ ($C-C$ (c))	C_b	-0.92918	-0.72457	-0.72457	-0.72457	-154.71860	0.91771	0.75889	-17.92866	-17.73779	48.21	131.79	21.74	1.95734	0.50570
$isoC_aC_b\left(H_2C_c-R'\right)HCH_2-$ ($C-C$ (d))	C_b	-0.92918	-0.92918	-0.92918	0	-154.40324	0.91771	0.77247	-17.61330	-17.42244	48.30	131.70	21.90	1.97162	0.51388
$tertC_a\left(R'-H_2C_d\right)C_b\left(R''-H_2C_c\right)CH_2-$ ($C-C$ (e))	C_b	-0.72457	-0.72457	-0.72457	-0.72457	-154.51399	0.91771	0.76765	-17.92866	-17.73779	50.04	129.96	22.66	1.94462	0.49298
$tertC_aC_b\left(H_2C_c-R'\right)HCH_2-$ ($C-C$ (f))	C_b	-0.72457	-0.92918	-0.92918	0	-154.19863	0.91771	0.78155	-17.40869	-17.21783	52.78	127.22	24.04	1.92443	0.47279
$isoC_a\left(R'-H_2C_d\right)C_b\left(R''-H_2C_c\right)CH_2-$ ($C-C$ (f))	C_b	-0.72457	-0.72457	-0.72457	-0.72457	-154.51399	0.91771	0.76765	-17.92866	-17.73779	50.04	129.96	22.66	1.94462	0.49298

Table 15.156. The energy parameters (eV) of functional groups of alkyl sulfides.

Parameters	$C-S$ (i) Group	$C-S$ (ii) Group	CH_3 Group	CH_2 Group	$C-H$ Group	$C-C$ (a) Group	$C-C$ (b) Group	$C-C$ (c) Group	$C-C$ (d) Group	$C-C$ (e) Group	$C-C$ (f) Group
n_1	1	1	3	2	1	1	1	1	1	1	1
n_2	0	0	2	1	0	0	0	0	0	0	0
n_3	0	0	0	0	0	0	0	0	0	0	0
C_1	0.5	0.5	0.75	0.75	0.75	0.5	0.5	0.5	0.5	0.5	0.5
C_2	0.64965	0.64965	1	1	1	1	1	1	1	1	1
c_1	1	1	1	1	1	1	1	1	1	1	1
c_2	1	1	0.91771	0.91771	0.91771	0.91771	0.91771	0.91771	0.91771	0.91771	0.91771
c_3	0	0	0	1	1	0	0	0	1	1	0
c_4	2	2	1	1	1	2	2	2	2	2	2
c_5	0	0	3	2	1	0	0	0	0	0	0
C_{1o}	0.5	0.5	0.75	0.75	0.75	0.5	0.5	0.5	0.5	0.5	0.5
C_{2o}	0.64965	0.64965	1	1	1	1	1	1	1	1	1
$V_e\ (eV)$	-46.36495	-46.36495	-107.32728	-70.41425	-35.12015	-28.79214	-28.79214	-29.10112	-28.79214	-29.10112	-29.10112
$V_p\ (eV)$	7.93551	7.93551	38.92728	25.78002	12.87680	9.33352	9.33352	9.37273	9.33352	9.37273	9.37273
$T\ (eV)$	12.13899	12.13899	32.53914	21.06675	10.48582	6.77464	6.77464	6.90500	6.77464	6.90500	6.90500
$V_m\ (eV)$	-6.06949	-6.06949	-16.26957	-10.53337	-5.24291	-3.38732	-3.38732	-3.45250	-3.38732	-3.45250	-3.45250
$E_{(AO/HO)}\ (eV)$	0	0	-15.56407	-15.56407	-14.63489	-15.56407	-15.56407	-15.35946	-15.56407	-15.35946	-15.35946
$\Delta E_{H_2MO(AO/HO)}\ (eV)$	-0.72457	-0.72457	0	0	0	0	0	0	0	0	0
$E_{T(AO/HO)}\ (eV)$	0.72457	0.72457	-15.56407	-15.56407	-14.63489	-15.56407	-15.56407	-15.35946	-15.56407	-15.35946	-15.35946
$E_{T(H_2MO)}\ (eV)$	-31.63537	-31.63537	-67.69451	-49.66493	-31.63533	-31.63537	-31.63537	-31.63535	-31.63537	-31.63535	-31.63535
$E_T\left(atom-atom, msp^3.AO\right)(eV)$	-0.72457	-0.72457	0	0	0	-1.85836	-1.85836	-1.44915	-1.85836	-1.44915	-1.44915
$E_{T(MO)}\ (eV)$	-32.35994	-32.35994	-67.69450	-49.66493	-31.63537	-33.49373	-33.49373	-33.08452	-33.49373	-33.08452	-33.08452
$\omega\ \left(10^{15}\ rad/s\right)$	30.5436	8.92777	24.9286	24.2751	24.1759	9.43699	9.43699	15.4846	9.43699	9.55643	9.55643
$E_K\ (eV)$	20.10434	5.87641	16.40846	15.97831	15.91299	6.21159	6.21159	10.19220	6.21159	6.29021	6.29021
$\bar{E}_D\ (eV)$	-0.28705	-0.15519	-0.25352	-0.25017	-0.24966	-0.16515	-0.16515	-0.20896	-0.16515	-0.16416	-0.16416
$\bar{E}_{Kvib}\ (eV)$	0.08146 [41]	0.08146 [41]	0.35532 (Eq. (13.458))	0.35532 (Eq. (13.458))	0.35532 (Eq. (13.458))	0.12312 [2]	0.17978 [4]	0.09944 [5]	0.12312 [2]	0.12312 [2]	0.12312 [2]
$\bar{E}_{osc}\ (eV)$	-0.24632	-0.11446	-0.22757	-0.14502	-0.07200	-0.10359	-0.07526	-0.15924	-0.10359	-0.10260	-0.10260
$E_{mag}\ (eV)$	0.14803	0.14803	0.14803	0.14803	0.14803	0.14803	0.14803	0.14803	0.14803	0.14803	0.14803
$E_{T(group)}\ (eV)$	-32.60626	-32.47440	-67.92207	-49.80996	-31.70737	-33.59732	-33.49373	-33.24376	-33.59732	-33.18712	-33.18712
$E_{initial(A\ AO/HO)}\ (eV)$	-14.63489	-14.63489	-14.63489	-14.63489	-14.63489	-14.63489	-14.63489	-14.63489	-14.63489	-14.63489	-14.63489
$E_{initial(S\ AO/HO)}\ (eV)$	0	0	-13.59844	-13.59844	-13.59844	0	0	0	0	0	0
$E_{D(group)}\ (eV)$	3.33648	3.20462	12.49186	7.83016	3.32601	4.32754	4.29921	3.97398	4.17951	3.62128	3.91734

Table 15.157. The total bond energies of alkyl sulfides calculated using the functional group composition and the energies of Table 15.156 compared to the experimental values [3]. The magnetic energy E_{mag} that is subtracted from the weighted sum of the E_D $(_{Group})$ (eV) values based on composition is given by (15.58).

Formula	Name	$C-S$ (i) Group	$C-S$ (ii) Group	CH_3	CH_2	CH	$C-C$ (a)	$C-C$ (b)	$C-C$ (c)	$C-C$ (d)	$C-C$ (e)	$C-C$ (f)	E_{mag}	Calculated Total Bond Energy (eV)	Experimental Total Bond Energy (eV)	Relative Error
C_2H_6S	Dimethyl sulfide	2	0	2	0	0	0	0	0	0	0	0	0	31.65668	31.672	0.00048
C_3H_8S	Ethyl methyl sulfide	2	0	2	1	0	1	0	0	0	0	0	0	43.81438	43.848	0.00078
$C_4H_{10}S$	Diethyl sulfide	2	0	2	2	0	2	0	0	0	0	0	0	55.97208	56.043	0.00126
$C_4H_{10}S$	Methyl propyl sulfide	2	0	2	2	0	2	0	0	0	0	0	0	55.97208	56.029	0.00102
$C_4H_{10}S$	Isopropyl methyl sulfide	2	0	3	0	1	0	2	0	0	0	0	0	56.07297	56.115	0.00075
$C_5H_{12}S$	Butyl methyl sulfide	2	0	2	3	0	3	0	0	0	0	0	0	68.12978	68.185	0.00081
$C_5H_{12}S$	t-Butyl methyl sulfide	1	1	4	0	0	0	0	3	0	0	0	-1	68.28245	68.381	0.00144
$C_5H_{12}S$	Ethyl propyl sulfide	2	0	2	3	0	3	0	0	0	0	0	0	68.12978	68.210	0.00117
$C_5H_{12}S$	Ethyl isopropyl sulfide	2	0	3	1	1	1	2	0	0	0	0	0	68.23067	68.350	0.00174
$C_6H_{14}S$	Diisopropyl sulfide	2	0	4	0	2	0	4	0	0	0	0	0	80.48926	80.542	0.00065
$C_6H_{14}S$	Butyl ethyl sulfide	2	0	2	4	0	4	0	0	0	0	0	0	80.28748	80.395	0.00133
$C_6H_{14}S$	Methyl pentyl sulfide	2	0	2	4	0	4	0	0	0	0	0	0	80.28748	80.332	0.00056
$C_8H_{18}S$	Dibutyl sulfide	2	0	2	6	0	6	0	0	0	0	0	0	104.60288	104.701	0.00094
$C_8H_{18}S$	Di-sec-butyl sulfide	2	0	4	2	2	2	4	0	0	0	0	0	104.80466	104.701	-0.00099
$C_8H_{18}S$	Di-t-butyl sulfide	0	2	6	0	0	0	0	6	0	0	0	-2	104.90822	104.920	0.00011
$C_8H_{18}S$	Diisobutyl sulfide	2	0	4	2	2	0	6	0	0	0	0	0	104.74800	104.834	0.00082
$C_{10}H_{22}S$	Dipentyl sulfide	2	0	2	8	0	8	0	0	0	0	0	0	128.91828	128.979	0.00047
$C_{10}H_{22}S$	Diisopentyl sulfide	2	0	4	4	2	2	6	0	0	0	0	0	129.06340	129.151	0.00068

Table 15.158. The bond angle parameters of alkyl sulfides and experimental values [1]. In the calculation of θ_v, the parameters from the preceding angle were used. E_T is $E_T(atom - atom, msp^3.AO)$.

Atoms of Angle	2c' Bond 1 (a_0)	2c' Bond 2 (a_0)	2c' Terminal Atoms (a_0)	$E_{Coulombic}$ Atom 1	Atom 1 Hybridization Designation (Table 15.3.A)	$E_{Coulombic}$ Atom 2	Atom 2 Hybridization Designation (Table 15.3.A)	c_2 Atom 1	c_2 Atom 2	C_1	C_2	c_1	c_2'	E_T (eV)	θ_v (°)	θ_1 (°)	θ_2 (°)	Cal. θ (°)	Exp. θ (°)
$\angle C_aSC_a$ ($C-S$ (i))	3.42910	3.42910	5.2173	-16.11722	12	-16.11722	12	0.84418	0.84418	1	1	1	0.84418	-1.85836				99.06	99.05 (dimethyl sulfide)
$\angle C_aSC_b$ ($C-S$ (i))	3.42910	3.42910	5.1381	-15.75493 methyl C_a	7	-16.68412 methylene C_b	26	0.86359	0.81549	1	1	1	0.83954	-1.85836				97.04	97 (ethyl methyl sulfide)
$\angle SC_aC_b$ ($C-S$ (ii))	3.42910	2.91547	5.3364	-10.36001	S	-16.27490	16	0.64965 (Eq. (15.146))	0.83600	1	0.64965 (Eq. (15.146))	1	0.74282	-0.72457				114.27	114.0 (ethyl methyl sulfide)
Methylene $\angle HC_aH$	2.11106	2.11106	3.4252	-15.75493	7	H	H	0.86359	1	1	1	0.75	1.15796	0				108.44	107 (propane)
$\angle C_aC_bC_c$															69.51			110.49	112 (propane) 113.8 (butane) 110.8 (isobutane)
$\angle C_aC_bH$															69.51			110.49	111.0 (butane) 111.4 (isobutane)
Methyl $\angle HC_aH$	2.09711	2.09711	3.4252	-15.75493	7	H	H	0.86359	1	1	1	0.75	1.15796	0				109.50	109.3 (dimethyl sulfide) 110 (ethyl methyl sulfide)
$\angle C_aC_bC_c$															70.56			109.44	
$\angle C_aC_bH$															70.56			109.44	
$\angle C_bC_aC_c$ iso C_a	2.91547	2.91547	4.7958	-16.68412 C_b	26	-16.68412 C_c	26	0.81549	0.81549	1	1	1	0.81549	-1.85836				110.67	110.8 (isobutane)
$\angle C_bC_aH$ iso C_a	2.91547	2.11323	4.1633	-15.55033 C_a	5	-14.82575 C_b	1	0.87495	0.91771	0.75	1	0.75	1.04887	0				110.76	
$\angle C_aC_bH$ iso C_a	2.91547	2.09711	4.1633	-15.55033 C_b	5	-14.82575 C_a	1	0.87495	0.91771	0.75	1	0.75	1.04887	0				111.27	111.4 (isobutane)
$\angle C_bC_aC_b$ tert C_a	2.90327	2.90327	4.7958	-16.68412 C_b	26	-16.68412 C_b	26	0.81549	0.81549	1	1	1	0.81549	-1.85836				111.37	110.8 (isobutane)
$\angle C_bC_aC_d$															72.50			107.50	

DISULFIDES ($C_nH_{2n+2}S_{2m},\ n=2,3,4,5...\infty$)

The alkyl disulfides, $C_nH_{2n+2}S_{2m}$, comprise $C-S$ and $S-S$ functional groups. The alkyl portion of the alkyl disulfide may comprise at least two terminal methyl groups (CH_3) at each end of the chain, and may comprise methylene (CH_2), and methylyne (CH) functional groups as well as C bound by carbon-carbon single bonds. The methyl and methylene functional groups are equivalent to those of straight-chain alkanes. Six types of $C-C$ bonds can be identified. The n-alkane $C-C$ bond is the same as that of straight-chain alkanes. In addition, the $C-C$ bonds within isopropyl ($(CH_3)_2CH$) and t-butyl ($(CH_3)_3C$) groups and the isopropyl to isopropyl, isopropyl to t-butyl, and t-butyl to t-butyl $C-C$ bonds comprise functional groups. The branched-chain-alkane groups in disulfides are equivalent to those in branched-chain alkanes.

Each $C-S$ group is equivalent to that of general alkyl sulfides given in the corresponding section. As in the case of thiols and sulfides, C_2 of Eq. (15.61) for the $C-S$-bond MO given by Eq. (15.146) is $C_2\left(C2sp^3HO\ to\ \mathrm{S}\right)=0.64965$ and $E_T\left(atom-atom,msp^3.AO\right)$ is $-0.72457\ eV$ (Eq. (14.151)).

The $S-S$ group is solved as an H_2-type-ellipsoidal-MO that is energy matched to the energy of sulfur, $E(S)=-10.36001\ eV$, such that $E(AO/HO)=-10.36001\ eV$ in Eq. (15.51) with $E_T(AO/HO)=E(AO/HO)$. The $S-S$-bond MO is further energy matched to the $C2sp^3$ HO of the $C-S$-bond MO. C_2 of Eq. (15.61) for the $S-S$-bond MO given by Eq. (15.146) is also $C_2\left(C2sp^3HO\ to\ \mathrm{S}\right)=0.64965$. In order to match $E_T\left(atom-atom,msp^3.AO\right)$ of the $C-S$ group ($-0.72457\ eV$ (Eq. (14.151))), $E_T\left(atom-atom,msp^3.AO\right)$ of the $S-S$-bond MO is determined using a linear combination of the AOs corresponding to $-0.72457\ eV$ and $0\ eV$ in Eq. (15.29), Eq. (15.31), and Eqs. (15.19-15.20). The result corresponding to bond order 1/2I in Table 15.2 is $E_T\left(atom-atom,msp^3.AO\right)=-0.36229\ eV$.

The symbols of the functional groups of branched-chain alkyl disulfides are given in Table 15.159. The geometrical (Eqs. (15.1-15.5) and (15.51)), intercept (Eqs. (15.80-15.87)), and energy (Eqs. (15.6-15.11) and (15.17-15.65)) parameters of alkyl disulfides are given in Tables 15.160, 15.161, and 15.162, respectively. The total energy of each alkyl disulfide given in Table 15.163 was calculated as the sum over the integer multiple of each $E_{D\,(Group)}$ of Table 15.162 corresponding to functional-group composition of the molecule. E_{mag} given by Eq. (15.67) was subtracted for each t-butyl group. The bond angle parameters of alkyl disulfides determined using Eqs. (15.88-15.117) are given in Table 15.164. The color scale, translucent view of the charge-density of exemplary disulfide, dimethyl disulfide, comprising the concentric shells of atoms with the outer shell bridged by one or more H_2-type ellipsoidal MOs or joined with one or more hydrogen MOs is shown in Figure 15.27.

Figure 15.27. Color scale, translucent view of the charge-density of dimethyl disulfide showing the orbitals of the atoms at their radii, the ellipsoidal surface of each H or H_2-type ellipsoidal MO that transitions to the corresponding outer shell of the atom(s) participating in each bond, and the hydrogen nuclei (red, not to scale).

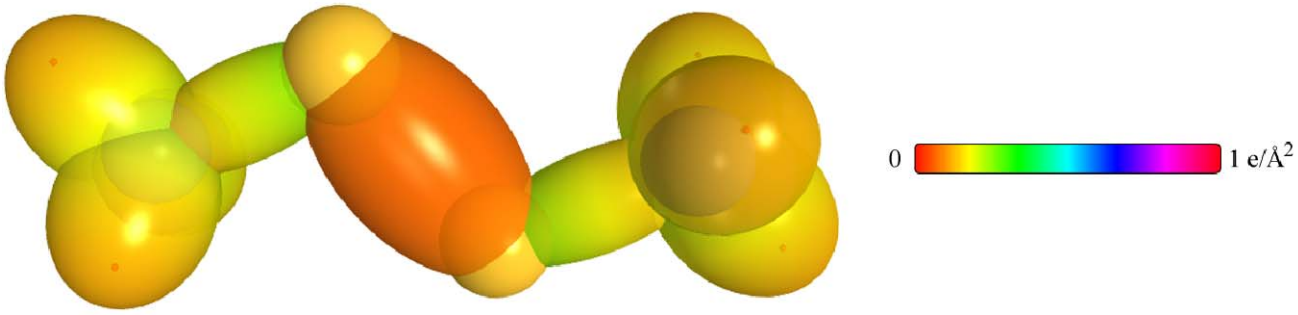

Table 15.159. The symbols of functional groups of alkyl disulfides.

Functional Group	Group Symbol
C-S	$C-S$
S-S	$S-S$
CH_3 group	$C-H\ (CH_3)$
CH_2 group	$C-H\ (CH_2)$
CH	$C-H$
CC bond (*n-C*)	$C-C$ (a)
CC bond (*iso-C*)	$C-C$ (b)
CC bond (*tert-C*)	$C-C$ (c)
CC (*iso* to *iso-C*)	$C-C$ (d)
CC (*t* to *t-C*)	$C-C$ (e)
CC (*t* to *iso-C*)	$C-C$ (f)

Table 15.160. The geometrical bond parameters of alkyl disulfides and experimental values [1].

Parameter	$C-S$ (i) Group	$S-S$ Group	$C-H\ (CH_3)$ Group	$C-H\ (CH_2)$ Group	$C-H$ Group	$C-C$ (a) Group	$C-C$ (b) Group	$C-C$ (c) Group	$C-C$ (d) Group	$C-C$ (e) Group	$C-C$ (f) Group
$a\ (a_0)$	1.90975	2.37173	1.64920	1.67122	1.67465	2.12499	2.12499	2.10725	2.12499	2.10725	2.10725
$c'\ (a_0)$	1.71455	1.91070	1.04856	1.05553	1.05661	1.45744	1.45744	1.45164	1.45744	1.45164	1.45164
Bond Length $2c'\ (\AA)$	1.81460	2.02220	1.10974	1.11713	1.11827	1.54280	1.54280	1.53635	1.54280	1.53635	1.53635
Exp. Bond Length $(\AA)$	1.816 (dimethyl disulfide)	2.029 (dimethyl disulfide)	1.107 ($C-H$ propane) 1.117 ($C-H$ butane)	1.107 ($C-H$ propane) 1.117 ($C-H$ butane)	1.122 (isobutane)	1.532 (propane) 1.531 (butane)	1.532 (propane) 1.531 (butane)	1.532 (propane) 1.531 (butane)	1.532 (propane) 1.531 (butane)	1.532 (propane) 1.531 (butane)	1.532 (propane) 1.531 (butane)
$b,c\ (a_0)$	0.84112	1.40510	1.27295	1.29569	1.29924	1.54616	1.54616	1.52750	1.54616	1.52750	1.52750
e	0.89778	0.80562	0.63580	0.63159	0.63095	0.68600	0.68600	0.68888	0.68600	0.68888	0.68888

Table 15.161. The MO to HO intercept geometrical bond parameters of alkyl disulfides. R, R', R'' are H or alkyl groups. E_T is $E_T(atom-atom,msp^3.AO)$.

Bond	Atom	E_T (eV) Bond 1	E_T (eV) Bond 2	E_T (eV) Bond 3	E_T (eV) Bond 4	Final Total Energy $C2sp^3$ (eV)	$r_{initial}\ (a_0)$	$r_{final}\ (a_0)$	$E_{Coulomb}$ (eV) Final	$E(C2sp^3)$ (eV) Final	θ' (°)	θ_1 (°)	θ_2 (°)	$d_1\ (a_0)$	$d_2\ (a_0)$
$RS-SR$ ($C-S$ (i) and (ii))	S	-0.36229	-0.18114	0	0		1.32010	0.88527	-15.36918		94.25	85.75	38.93	1.84513	0.06558
$H_3C_a-SS-C_bH_2CH_2R$	C_a	-0.36229	0	0	0	-151.97798	0.91771	0.89582	-15.18804	-14.99717	130.79	49.21	53.75	1.12937	0.58518
$H_3C_a-SS-C_bH_2CH_2R$ ($C-S$ (i))	C_b	-0.36229	-0.92918	0	0	-152.90716	0.91771	0.84418	-16.11722	-15.92636	128.69	51.31	51.57	1.18689	0.52765
	C_c	-0.36229	-0.72457	-0.72457	-0.72457	-154.15170	0.91771	0.78367	-17.36176	-17.17090	125.97	54.03	48.94	1.25430	0.46025
$C-H\ (CH_3)$	C	-0.92918	0	0	0	-152.54487	0.91771	0.86359	-15.75493	-15.56407	77.49	102.51	41.48	1.23564	0.18708
$C-H\ (CH_2)$	C	-0.92918	-0.92918	0	0	-153.47406	0.91771	0.81549	-16.68412	-16.49325	68.47	111.53	35.84	1.35486	0.29933
$C-H\ (CH)$	C	-0.92918	-0.92918	-0.92918	0	-154.40324	0.91771	0.77247	-17.61330	-17.42244	61.10	118.90	31.37	1.42988	0.37326
$H_3C_aC_bH_2CH_2-$ ($C-C$ (a))	C_a	-0.92918	0	0	0	-152.54487	0.91771	0.86359	-15.75493	-15.56407	63.82	116.18	30.08	1.83879	0.38106
$H_3C_aC_bH_2CH_2-$ ($C-C$ (a))	C_b	-0.92918	-0.92918	0	0	-153.47406	0.91771	0.81549	-16.68412	-16.49325	56.41	123.59	26.06	1.90890	0.45117
$R-H_2C_aC_b(H_2C_c-R')HCH_2-$ ($C-C$ (b))	C_b	-0.92918	-0.92918	-0.92918	0	-154.40324	0.91771	0.77247	-17.61330	-17.42244	48.30	131.70	21.90	1.97162	0.51388
$R-H_2C_a(R'-H_2C_d)C_b(R''-H_2C_c)CH_2-$ ($C-C$ (c))	C_b	-0.92918	-0.72457	-0.72457	-0.72457	-154.71860	0.91771	0.75889	-17.92866	-17.73779	48.21	131.79	21.74	1.95734	0.50570
$isoC_aC_b(H_2C_c-R')HCH_2-$ ($C-C$ (d))	C_b	-0.92918	-0.92918	-0.92918	0	-154.40324	0.91771	0.77247	-17.61330	-17.42244	48.30	131.70	21.90	1.97162	0.51388
$tertC_a(R'-H_2C_d)C_b(R''-H_2C_c)CH_2-$ ($C-C$ (e))	C_b	-0.72457	-0.72457	-0.72457	-0.72457	-154.51399	0.91771	0.76765	-17.92866	-17.73779	50.04	129.96	22.66	1.94462	0.49298
$tertC_aC_b(H_2C_c-R')HCH_2-$ ($C-C$ (f))	C_b	-0.72457	-0.92918	-0.92918	0	-154.19863	0.91771	0.78155	-17.40869	-17.21783	52.78	127.22	24.04	1.92443	0.47279
$isoC_a(R'-H_2C_d)C_b(R''-H_2C_c)CH_2-$ ($C-C$ (f))	C_b	-0.72457	-0.72457	-0.72457	-0.72457	-154.51399	0.91771	0.76765	-17.92866	-17.73779	50.04	129.96	22.66	1.94462	0.49298

Table 15.162. The energy parameters (eV) of functional groups of alkyl disulfides.

Parameters	$C-S$ (i) Group	$S-S$ Group	CH_3 Group	CH_2 Group	$C-H$ Group	$C-C$ (a) Group	$C-C$ (b) Group	$C-C$ (c) Group	$C-C$ (d) Group	$C-C$ (e) Group	$C-C$ (f) Group
n_1	1	1	3	2	1	1	1	1	1	1	1
n_2	0	0	2	1	0	0	0	0	0	0	0
n_3	0	0	0	0	0	0	0	0	0	0	0
C_1	0.5	0.5	0.75	0.75	0.75	0.5	0.5	0.5	0.5	0.5	0.5
C_2	0.64965	0.64965	1	1	1	1	1	1	1	1	1
c_1	1	1	1	1	1	1	1	1	1	1	1
c_2	1	1	0.91771	0.91771	0.91771	0.91771	0.91771	0.91771	0.91771	0.91771	0.91771
c_3	0	0	0	1	1	0	0	0	1	1	0
c_4	2	2	1	1	1	2	2	2	2	2	2
c_5	0	0	3	2	1	0	0	0	0	0	0
C_{1o}	0.5	0.5	0.75	0.75	0.75	0.5	0.5	0.5	0.5	0.5	0.5
C_{2o}	0.64965	0.64965	1	1	1	1	1	1	1	1	1
$V_e\ (eV)$	-46.36495	-31.74215	-107.32728	-70.41425	-35.12015	-28.79214	-28.79214	-29.10112	-28.79214	-29.10112	-29.10112
$V_p\ (eV)$	7.93551	7.12083	38.92728	25.78002	12.87680	9.33352	9.33352	9.37273	9.33352	9.37273	9.37273
$T\ (eV)$	12.13899	6.69177	32.53914	21.06575	10.48582	6.77464	6.77464	6.90500	6.77464	6.90500	6.90500
$V_m\ (eV)$	-6.06949	-3.34589	-16.26957	-10.53337	-5.24291	-3.38732	-3.38732	-3.45250	-3.38732	-3.45250	-3.45250
$E_{(AO/HO)}\ (eV)$	0	-10.36001	-15.56407	-15.56407	-14.63489	-15.56407	-15.56407	-15.35946	-15.56407	-15.35946	-15.35946
$\Delta E_{H_2MO\ (AO/HO)}\ (eV)$	-0.72457	0	0	0	0	0	0	0	0	0	0
$E_T{}_{(AO/HO)}\ (eV)$	0.72457	-10.36001	-15.56407	-15.56407	-14.63489	-15.56407	-15.56407	-15.35946	-15.56407	-15.35946	-15.35946
$E_T{}_{(H_2MO)}\ (eV)$	-31.63537	-31.63544	-67.69451	-49.66493	-31.63533	-31.63537	-31.63537	-31.63535	-31.63537	-31.63535	-31.63535
$E_T\left(atom-atom, msp^3.AO\right)\ (eV)$	-0.72457	-0.36229	0	0	0	-1.85836	-1.85836	-1.44915	-1.85836	-1.44915	-1.44915
$E_T{}_{(MO)}\ (eV)$	-32.35994	-31.99766	-67.69450	-49.66493	-31.63537	-33.49373	-33.49373	-33.08452	-33.49373	-33.08452	-33.08452
$\omega\ \left(10^{15}\ rad/s\right)$	30.5436	6.45076	24.9286	24.2751	24.1759	9.43699	9.43699	15.4846	9.43699	9.55643	9.55643
$E_K\ (eV)$	20.10434	4.24600	16.40846	15.97831	15.91299	6.21159	6.21159	10.19220	6.21159	6.29021	6.29021
$\bar{E}_D\ (eV)$	-0.28705	-0.13044	-0.25352	-0.25017	-0.24966	-0.16515	-0.16515	-0.20896	-0.16515	-0.16416	-0.16416
$\bar{E}_{Kvib}\ (eV)$	0.08146 [41]	0.06745 []	0.35532 (Eq. (13.458))	0.35532 (Eq. (13.458))	0.35532 (Eq. (13.458))	0.12312 [2]	0.17978 [4]	0.09944 [5]	0.12312 [2]	0.12312 [2]	0.12312 [2]
$\bar{E}_{esc}\ (eV)$	-0.24632	-0.09672	-0.22757	-0.14502	-0.07200	-0.10359	-0.07526	-0.15924	-0.10359	-0.10260	-0.10260
$E_{mag}\ (eV)$	0.14803	0.14803	0.14803	0.14803	0.14803	0.14803	0.14803	0.14803	0.14803	0.14803	0.14803
$E_T{}_{(Group)}\ (eV)$	-32.60526	-32.09437	-67.92207	-49.80996	-31.70737	-33.59732	-33.49373	-33.24376	-33.59732	-33.18712	-33.18712
$E_{initial\ (C_4\ AO/HO)}\ (eV)$	-14.63489	-14.63489	-14.63489	-14.63489	-14.63489	-14.63489	-14.63489	-14.63489	-14.63489	-14.63489	-14.63489
$E_{initial\ (C_5\ AO/HO)}\ (eV)$	0	0	-13.59844	-13.59844	-13.59844	0	0	0	0	0	0
$E_{D\ (Group)}\ (eV)$	3.33648	2.82459	12.49186	7.83016	3.32601	4.32754	4.29921	3.97398	4.17951	3.62128	3.91734

Table 15.163. The total bond energies of alkyl disulfides calculated using the functional group composition and the energies of Table 15.162 compared to the experimental values [3]. The magnetic energy E_{mag} that is subtracted from the weighted sum of the E_D ($Group$) (eV) values based on composition is given by (15.58).

Formula	Name	$C-S$ Group	$S-S$ Group	CH_3	CH_2	CH	$C-C$ (a)	$C-C$ (b)	$C-C$ (c)	$C-C$ (d)	$C-C$ (e)	$C-C$ (f)	E_{mag}	Calculated Total Bond Energy (eV)	Experimental Total Bond Energy (eV)	Relative Error
$C_2H_6S_2$	Dimethyl disulfide	2	1	2	0	0	0	0	0	0	0	0	0	34.48127	34.413	-0.00199
$C_4H_{10}S_2$	Diethyl disulfide	2	1	2	2	0	2	0	0	0	0	0	0	58.79667	58.873	0.00129
$C_6H_{14}S_2$	Dipropyl disulfide	2	1	2	4	0	4	0	0	0	0	0	0	83.11207	83.169	0.00068
$C_8H_{18}S_2$	Di-t-butyl disulfide	2	1	6	0	0	0	0	6	0	0	0	-2	107.99653	107.919	-0.00072

Table 15.164. The bond angle parameters of alkyl disulfides and experimental values [1]. In the calculation of θ_v, the parameters from the preceding angle were used. E_T is $E_T(atom-atom,msp^3.AO)$.

Atoms of Angle	$2c'$ Bond 1 (a_0)	$2c'$ Bond 2 (a_0)	$2c'$ Terminal Atoms (a_0)	$E_{Coulombic}$ Atom 1	Atom 1 Hybridization Designation (Table 15.3.A)	$E_{Coulombic}$ Atom 2	Atom 2 Hybridization Designation (Table 15.3.A)	c_2 Atom 1	c_2 Atom 2	C_1	C_2	c_1	c_2'	E_T (eV)	θ_v (°)	θ_1 (°)	θ_2 (°)	Cal. θ (°)	Exp. θ (°)
$\angle HC_aH$	2.09711	2.09711	3.4252	-15.75493	7	H	H	0.86359	1	1	1	0.75	1.15796	0				109.50	
$\angle SC_aH$															70.56			109.44	111.3 (dimethyl disulfide)
$\angle HC_aS$	2.09711	3.42910	4.6220	-15.55033 C_c	5	-10.36001 S	S	0.87495	0.76144 (Eq. (15.145))	0.75	0.76144 (Eq. 15.145))	0.75	0.87026	0				111.22	111.3 (dimethyl disulfide)
$\angle SSC_a$	3.82141	3.42910	5.7017	-10.36001 S	S	-14.82575 C_a	1	0.64965 (Eq. (15.146))	0.91771	1	0.64965 (Eq. (15.146))	1	0.78368	-0.72457				103.57	103.2 (dimethyl disulfide)
Methylene $\angle HC_aH$	2.11106	2.11106	3.4252	-15.75493	7	H	H	0.86359	1	1	1	0.75	1.15796	0				108.44	107 (propane)
$\angle C_aC_bC_c$															69.51			110.49	112 (propane) 113.8 (butane) 110.8 (isobutane)
$\angle C_aC_bH$															69.51			110.49	111.0 (butane) 111.4 (isobutane)
Methyl $\angle HC_aH$	2.09711	2.09711	3.4252	-15.75493	7	H	H	0.86359	1	1	1	0.75	1.15796	0				109.50	
$\angle C_aC_bC_c$															70.56			109.44	
$\angle C_aC_bH$															70.56			109.44	
$\angle C_bC_aC_c$ iso C_a	2.91547	2.91547	4.7958	-16.68412 C_t	26	-16.68412 C_c	26	0.81549	0.81549	1	1	1	0.81549	-1.85836				110.67	110.8 (isobutane)
$\angle C_bC_aH$ iso C_a	2.91547	2.11323	4.1633	-15.55033 C_c	5	-14.82575 C_b	1	0.87495	0.91771	0.75	1	0.75	1.04887	0				110.76	
$\angle C_aC_bH$ iso C_a	2.91547	2.09711	4.1633	-15.55033 C_t	5	-14.82575 C_a	1	0.87495	0.91771	0.75	1	0.75	1.04887	0				111.27	111.4 (isobutane)
$\angle C_bC_aC_b$ tert C_a	2.90327	2.90327	4.7958	-16.68412 C_t	26	-16.68412 C_b	26	0.81549	0.81549	1	1	1	0.81549	-1.85836				111.37	110.8 (isobutane)
$\angle C_bC_aC_d$															72.50			107.50	

SULFOXIDES ($C_nH_{2n+2}\left(SO\right)_m$, $n=2,3,4,5...\infty$)

The alkyl sulfoxides, $C_nH_{2n+2}\left(SO\right)_m$, comprise a $C-SO-C$ moiety that comprises $C-S$ and SO functional groups. The alkyl portion of the alkyl sulfoxide may comprise at least two terminal methyl groups (CH_3) at each end of the chain, and may comprise methylene (CH_2), and methylyne (CH) functional groups as well as C bound by carbon-carbon single bonds. The methyl and methylene functional groups are equivalent to those of straight-chain alkanes. Six types of $C-C$ bonds can be identified. The n-alkane $C-C$ bond is the same as that of straight-chain alkanes. In addition, the $C-C$ bonds within isopropyl ($\left(CH_3\right)_2CH$) and t-butyl ($\left(CH_3\right)_3C$) groups and the isop.ropyl to isopropyl, isopropyl to t-butyl, and t-butyl to t-butyl $C-C$ bonds comprise functional groups. The branched-chain-alkane groups in sulfoxides are equivalent to those in branched-chain alkanes.

The electron configuration of oxygen is $1s^22s^22p^4$, and the orbital arrangement given by Eq. (10.154) has two unpaired electrons corresponding to the ground state ${}^3P_2$. The SO functional group comprises a double bond between the two unpaired electrons of O. The sulfur atom is energy matched to the $C2sp^3$ HO. In alkyl sulfoxides, the $C2sp^3$ HO has a hybridization factor of 0.91771 (Eq. (13.430)) with a corresponding energy of $E\left(C,2sp^3\right)=-14.63489\ eV$ (Eq. (15.25)), and the S AO has an initial energy of $E\left(S\right)=-10.36001\ eV$ [38]. To meet the equipotential condition of the union of the $S=O$ H_2-type-ellipsoidal-MO with these orbitals, the hybridization factor c_2 of Eq. (15.61) for the $S=O$-bond MO given by Eqs. (15.77) and (15.79) is:

$$c_2\left(O\ to\ S3sp^3\ to\ C2sp^3HO\right)=\frac{E\left(O\right)}{E\left(S\right)}c_2\left(C2sp^3HO\right)=\frac{-13.61806\ eV}{-10.36001\ eV}\left(0.91771\right)=1.20632 \tag{15.147}$$

The S atom also forms a single bond with each of the $C2sp^3$ HOs of the two $C-S$ groups. The formation of these bonds is permitted by the hybridization of the four electrons of the $S3p$ shell to give the orbital arrangement:

$3sp^3$ state

$$\underset{0,0}{\uparrow}\quad\underset{1,-1}{\uparrow}\quad\underset{1,0}{\uparrow}\quad\underset{1,1}{\uparrow} \tag{15.148}$$

where the quantum numbers (ℓ,m_ℓ) are below each electron. The $3s$ shell remains unchanged. Then, the Coulombic energy $E_{Coulomb}\left(S,3sp^3\right)$ of the outer electron of the $S3sp^3$ shell given by Eq. (15.137) with $r_{3sp^3}=1.17585a_0$ (Eq. (15.138)) is $-11.57099\ eV$. Using Eq. (15.16) with the radius of the sulfur atom $r_{16}=1.32010a_0$ given by Eq. (10.341), the energy $E\left(S3sp^3\right)$ of the outer electron of the $S3sp^3$ shell is given by the sum of $E_{Coulomb}\left(S3sp^3\right)$ and $E(magnetic)$:

$$\begin{aligned}E\left(S3sp^3\right)&=\frac{-e^2}{8\pi\varepsilon_0r_{3sp^3}}+\frac{2\pi\mu_0e^2\hbar^2}{m_e^2r_{16}^3}=\frac{-e^2}{8\pi\varepsilon_01.17585a_0}+\frac{2\pi\mu_0e^2\hbar^2}{m_e^2\left(1.32010a_0\right)^3}\\&=-11.57099\ eV+0.04973=-11.52126\ eV\end{aligned} \tag{15.149}$$

Then, the hybridization energy $E_{hybridization}\left(S3sp^3\right)$ of the $S3sp^3$ HO is

$$E_{hybridization}\left(S3sp^3\right)=E\left(S3sp^3\right)-E\left(S\right)=-11.52126\ eV-10.36001\ eV=-1.16125\ eV \tag{15.150}$$

The SO group is matched to the $C-S$ group with which it shares the common hybridized S atom. Consequently, $E_{hybridization}\left(S3sp^3\right)$ is subtracted from $E_T\left(Group\right)$ in the determination of $E_D\left(Group\right)$ (Eq. (15.65)). Furthermore, the energy of the $S=O$-bond MO is the sum of the component energies of the H_2-type ellipsoidal MO given in Eq. (15.51) with the energy matched to the final energy of the hybridized S atom such that $E\left(AO/HO\right)=E\left(S3sp^3\right)=-11.52126\ eV$ and $\Delta E_{H_2MO}\left(AO/HO\right)=E_{hybridization}\left(S3sp^3\right)=-1.16125\ eV$. Then, $E_T\left(AO/HO\right)=E\left(S\right)=-10.36001\ eV$. Also, $E_T\left(atom-atom,msp^3.AO\right)$ of the $S=O$ bond is zero since there are no bonds with a $C2sp^3$ HO.

The $C-S$ group is solved as an energy minimum by hybridizing the $2s$ and $2p$ AOs of the C atom to form a single $2sp^3$ shell and by hybridizing the four $S3p$ electrons to form a $S3sp^3$ shell, and the sharing of electrons between the $C2sp^3$ HO and the $S3sp^3$ HO to form a MO permits each participating orbital to decrease in radius and energy. Using the Coulombic energy of the $S3sp^3$ shell, $E_{Coulomb}\left(S3sp^3\right)$ given by Eq. (15.139) in Eq. (15.72), the $S3sp^3$-shell hybridization factor, $c_2\left(S3sp^3\right)$, is:

$$c_2\left(S3sp^3\right)=\frac{E_{Coulomb}\left(S3sp^3\right)}{E\left(H\right)}=\frac{-11.57099\ eV}{-13.60580\ eV}=0.85045 \tag{15.151}$$

As in the case of thiols, sulfides, and disulfides, the energy of sulfur is less than the Coulombic energy between the electron and proton of H given by Eq. (1.264). Thus, c_1 and c_2 are equal to one in Eq. (15.61), and the energy matching condition is determined by the C_2 parameter. In alkyl sulfoxides, the $C2sp^3$ HO has a hybridization factor of 0.91771 (Eq. (13.430)) with a corresponding energy of $E\left(C,2sp^3\right)=-14.63489\ eV$ (Eq. (15.25)) and the $S3sp^3$ HO has an energy of $E\left(S3sp^3\right)=-11.52126\ eV$ (Eq. (15.149)). To meet the equipotential condition of the union of the $C-S$ H_2-type-ellipsoidal-MO with these orbitals, the hybridization factor C_2 of Eq. (15.61) for the $C-S$-bond MO given by Eqs. (15.77) and (15.79) is:

$$C_2\left(C2sp^3HO\ to\ S3sp^3\right)=\frac{E\left(S3sp^3\right)}{E\left(C,2sp^3\right)}c_2\left(S3sp^3\right)=\frac{-11.52126\ eV}{-14.63489\ eV}\left(0.85045\right)=0.66951 \tag{15.152}$$

As in the case of thiols, sulfides, and disulfides, with the energy of S matched to the Coulombic energy between the electron and proton of H, the energy of the $C-S$-bond MO is the sum of the component energies of the H_2-type ellipsoidal MO given in Eq. (15.51) with $E_{(AO/HO)}=0$ and $E_T\left(AO/HO\right)=\Delta E_{H_2MO}\left(AO/HO\right)$. For sulfoxides, $\Delta E_{H_2MO}\left(AO/HO\right)=-0.72457\ eV$. Further equivalently, $E_T\left(atom-atom,msp^3.AO\right)=-0.72457\ eV$ (Eq. (14.151)).

The symbols of the functional groups of branched-chain alkyl sulfoxides are given in Table 15.165. The geometrical (Eqs. (15.1-15.5) and (15.51)), intercept (Eqs. (15.80-15.87)), and energy (Eqs. (15.6-15.11) and (15.17-15.65)) parameters of alkyl sulfoxides are given in Tables 15.166, 15.167, and 15.168, respectively. Consider that the $C-S$ bond is along the x axis in the xy-plane. The S nucleus is at the focus +c and the C nucleus is at the focus –c. The elliptic angle θ' is taken as counterclockwise from the x-axis for S and as clockwise from the –x-axis for C. The total energy of each alkyl sulfoxide given in Table 15.169 was calculated as the sum over the integer multiple of each $E_{D\,(Group)}$ of Table 15.168 corresponding to functional-group composition of the molecule. The bond angle parameters of alkyl sulfoxides determined using Eqs. (15.88-15.117) are given in Table 15.170. The color scale, translucent view of the charge-density of exemplary sulfoxide, dimethyl sulfoxide, comprising the concentric shells of atoms with the outer shell bridged by one or more H_2-type ellipsoidal MOs or joined with one or more hydrogen MOs is shown in Figure 15.28.

Figure 15.28. (A)-(B) Color scale, translucent views of the charge-density of dimethyl sulfoxide showing the orbitals of the atoms at their radii, the ellipsoidal surface of each H or H_2-type ellipsoidal MO that transitions to the corresponding outer shell of the atom(s) participating in each bond, and the hydrogen nuclei (red, not to scale).

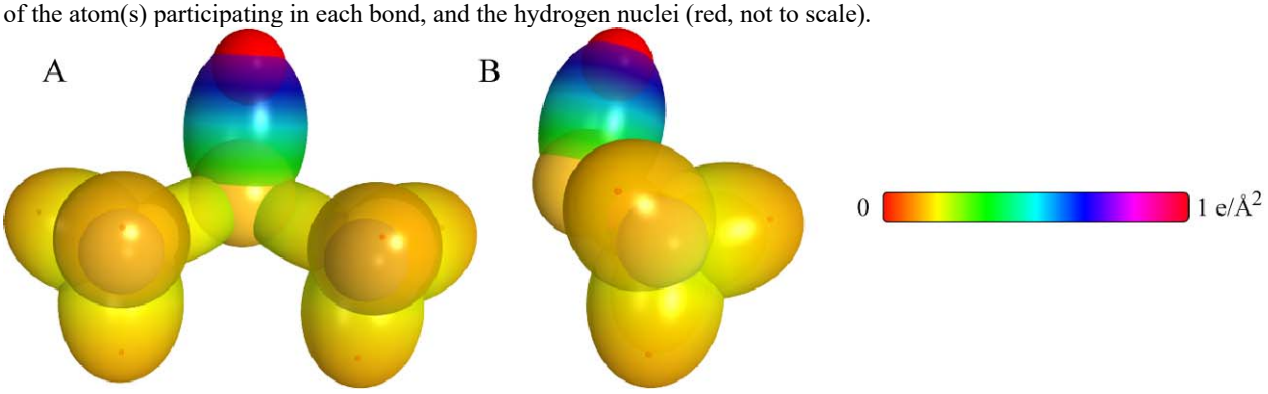

Table 15.165. The symbols of functional groups of alkyl sulfoxides.

Functional Group	Group Symbol
C-S	$C-S$
SO	*SO*
CH_3 group	$C-H\ \left(CH_3\right)$
CH_2 group	$C-H\ \left(CH_2\right)$
CH	$C-H$
CC bond (*n-C*)	$C-C$ (a)
CC bond (*iso-C*)	$C-C$ (b)
CC bond (*tert-C*)	$C-C$ (c)
CC (*iso* to *iso-C*)	$C-C$ (d)
CC (*t* to *t-C*)	$C-C$ (e)
CC (*t* to *iso-C*)	$C-C$ (f)

Table 15.166. The geometrical bond parameters of alkyl sulfoxides and experimental values [1].

Parameter	$C-S$ Group	SO Group	$C-H\ (CH_3)$ Group	$C-H\ (CH_2)$ Group	$C-H$ Group	$C-C$ (a) Group	$C-C$ (b) Group	$C-C$ (c) Group	$C-C$ (d) Group	$C-C$ (e) Group	$C-C$ (f) Group
$a\ (a_0)$	1.87325	1.98517	1.64920	1.67122	1.67465	2.12499	2.12499	2.10725	2.12499	2.10725	2.10725
$c'\ (a_0)$	1.67271	1.40896	1.04856	1.05553	1.05661	1.45744	1.45744	1.45164	1.45744	1.45164	1.45164
Bond Length $2c'\ (\AA)$	1.77031	1.49118	1.10974	1.11713	1.11827	1.54280	1.54280	1.53635	1.54280	1.53635	1.53635
Exp. Bond Length $(\AA)$	1.799 (dimethyl sulfoxide)	1.485 (dimethyl sulfoxide)	1.107 ($C-H$ propane) 1.117 ($C-H$ butane)	1.107 ($C-H$ propane) 1.117 ($C-H$ butane)	1.122 (isobutane)	1.532 (propane) 1.531 (butane)	1.532 (propane) 1.531 (butane)	1.532 (propane) 1.531 (butane)	1.532 (propane) 1.531 (butane)	1.532 (propane) 1.531 (butane)	1.532 (propane) 1.531 (butane)
$b,c\ (a_0)$	0.84328	1.39847	1.27295	1.29569	1.29924	1.54616	1.54616	1.52750	1.54616	1.52750	1.52750
e	0.89294	0.70974	0.63580	0.63159	0.63095	0.68600	0.68600	0.68888	0.68600	0.68888	0.68888

Table 15.167. The MO to HO intercept geometrical bond parameters of alkyl sulfoxides. R, R', R'' are H or alkyl groups. E_T is $E_T(atom-atom,msp^3.AO)$.

Bond	Atom	E_T (eV) Bond 1	E_T (eV) Bond 2	E_T (eV) Bond 3	E_T (eV) Bond 4	Final Total Energy $C2sp^3$ (eV)	$r_{initial}\ (a_0)$	$r_{final}\ (a_0)$	$E_{Coulomb}$ (eV) Final	$E(C2sp^3)$ (eV) Final	θ' (°)	θ_1 (°)	θ_2 (°)	$d_1\ (a_0)$	$d_2\ (a_0)$
$R_2S=O$	S	0	-0.36229	-0.36229	0		1.32010	0.87495	-15.55033		79.78	100.22	38.00	1.56425	0.15529
$R_2S=O$	O	0	0	0	0		1.00000	0.91771	-14.82575		84.06	95.94	40.75	1.50400	0.09504
R_2-SO	S	-0.36229	-0.36229	0	0		1.32010	0.87495	-15.55033		129.35	50.65	53.36	1.11799	0.55472
$H_3C_a-S(O)-C_bH_2CH_2R$	C_a	-0.36229	0	0	0	-151.97798	0.91771	0.89582	-15.18804	-14.99717	130.19	49.81	54.24	1.09461	0.57809
$H_3C_a-S(O)-C_bH_2CH_2R$	C_b	-0.36229	-0.92918	0	0	-152.90716	0.91771	0.84418	-16.11722	-15.92636	128.05	51.95	52.03	1.15245	0.52026
$C-H\ (CH_3)$	C	-0.92918	0	0	0	-152.54487	0.91771	0.86359	-15.75493	-15.56407	77.49	102.51	41.48	1.23564	0.18708
$C-H\ (CH_2)$	C	-0.92918	-0.92918	0	0	-153.47406	0.91771	0.81549	-16.68412	-16.49325	68.47	111.53	35.84	1.35486	0.29933
$C-H\ (CH)$	C	-0.92918	-0.92918	-0.92918	0	-154.40324	0.91771	0.77247	-17.61330	-17.42244	61.10	118.90	31.37	1.42988	0.37326
$H_3C_aC_bH_2CH_2-$ ($C-C$ (a))	C_a	-0.92918	0	0	0	-152.54487	0.91771	0.86359	-15.75493	-15.56407	63.82	116.18	30.08	1.83879	0.38106
$H_3C_aC_bH_2CH_2-$ ($C-C$ (a))	C_b	-0.92918	-0.92918	0	0	-153.47406	0.91771	0.81549	-16.68412	-16.49325	56.41	123.59	26.06	1.90890	0.45117
$R-H_2C_aC_b(H_2C_c-R')HCH_2-$ ($C-C$ (b))	C_b	-0.92918	-0.92918	-0.92918	0	-154.40324	0.91771	0.77247	-17.61330	-17.42244	48.30	131.70	21.90	1.97162	0.51388
$R-H_2C_a(R'-H_2C_d)C_b(R''-H_2C_c)CH_2-$ ($C-C$ (c))	C_b	-0.92918	-0.72457	-0.72457	-0.72457	-154.71860	0.91771	0.75889	-17.92866	-17.73779	48.21	131.79	21.74	1.95734	0.50570
$isoC_aC_b(H_2C_c-R')HCH_2-$ ($C-C$ (d))	C_b	-0.92918	-0.92918	-0.92918	0	-154.40324	0.91771	0.77247	-17.61330	-17.42244	48.30	131.70	21.90	1.97162	0.51388
$tertC_a(R'-H_2C_d)C_b(R''-H_2C_c)CH_2-$ ($C-C$ (e))	C_b	-0.72457	-0.72457	-0.72457	-0.72457	-154.51399	0.91771	0.76765	-17.92866	-17.73779	50.04	129.96	22.66	1.94462	0.49298
$tertC_aC_b(H_2C_c-R')HCH_2-$ ($C-C$ (f))	C_b	-0.72457	-0.92918	-0.92918	0	-154.19863	0.91771	0.78155	-17.40869	-17.21783	52.78	127.22	24.04	1.92443	0.47279
$isoC_a(R'-H_2C_d)C_b(R''-H_2C_c)CH_2-$ ($C-C$ (f))	C_b	-0.72457	-0.72457	-0.72457	-0.72457	-154.51399	0.91771	0.76765	-17.92866	-17.73779	50.04	129.96	22.66	1.94462	0.49298

Table 15.168. The energy parameters (eV) of functional groups of alkyl sulfoxides.

Parameters	$C-S$ Group	SO Group	CH_3 Group	CH_2 Group	$C-H$ Group	$C-C$ (a) Group	$C-C$ (b) Group	$C-C$ (c) Group	$C-C$ (d) Group	$C-C$ (e) Group	$C-C$ (f) Group
n_1	1	2	3	2	1	1	1	1	1	1	1
n_2	0	0	2	1	0	0	0	0	0	0	0
n_3	0	0	0	0	0	0	0	0	0	0	0
C_1	0.5	0.5	0.75	0.75	0.75	0.5	0.5	0.5	0.5	0.5	0.5
C_2	0.66951	1	1	1	1	1	1	1	1	1	1
c_1	1	1	1	1	1	1	1	1	1	1	1
c_2	1	1.20632	0.91771	0.91771	0.91771	0.91771	0.91771	0.91771	0.91771	0.91771	0.91771
c_3	0	0	0	1	1	0	0	0	1	1	0
c_4	2	4	1	1	1	2	2	2	2	2	2
c_5	0	1	3	2	1	0	0	0	0	0	0
C_{1o}	0.5	0.5	0.75	0.75	0.75	0.5	0.5	0.5	0.5	0.5	0.5
C_{2o}	0.66951	1	1	1	1	1	1	1	1	1	1
V_e (eV)	-46.73032	-82.63003	-107.32728	-70.41425	-35.12015	-28.79214	-28.79214	-29.10112	-28.79214	-29.10112	-29.10112
V_p (eV)	8.13401	19.31325	38.92728	25.78002	12.87680	9.33352	9.33352	9.37273	9.33352	9.37273	9.37273
T (eV)	12.47306	20.81183	32.53914	21.06675	10.48582	6.77464	6.77464	6.90500	6.77464	6.90500	6.90500
V_m (eV)	-6.23653	-10.40592	-16.26957	-10.53337	-5.24291	-3.38732	-3.38732	-3.45250	-3.38732	-3.45250	-3.45250
$E_{(AO/HO)}$ (eV)	0	-11.52126	-15.56407	-15.56407	-14.63489	-15.56407	-15.56407	-15.35946	-15.56407	-15.35946	-15.35946
$\Delta E_{H_2MO(AO/HO)}$ (eV)	-0.72457	-1.16125	0	0	0	0	0	0	0	0	0
$E_{T(AO/HO)}$ (eV)	0.72457	-10.36001	-15.56407	-15.56407	-14.63489	-15.56407	-15.56407	-15.35946	-15.56407	-15.35946	-15.35946
$E_{T(H_2MO)}$ (eV)	-31.63521	-63.27088	-67.69451	-49.66493	-31.63533	-31.63537	-31.63537	-31.63535	-31.63537	-31.63535	-31.63535
$E_T\left(atom-atom, msp^3.AO\right)(eV)$	-0.72457	0	0	0	0	-1.85836	-1.85836	-1.44915	-1.85836	-1.44915	-1.44915
$E_{T(MO)}$ (eV)	-32.35994	-63.27074	-67.69450	-49.66493	-31.63537	-33.49373	-33.49373	-33.08452	-33.49373	-33.08452	-33.08452
$\omega\ \left(10^{15}\ rad/s\right)$	30.8880	17.6762	24.9286	24.2751	24.1759	9.43699	9.43699	15.4846	9.43699	9.55643	9.55643
E_K (eV)	20.33104	11.63476	16.40846	15.97831	15.91299	6.21159	6.21159	10.19220	6.21159	6.29021	6.29021
$\bar{E}_D$ (eV)	-0.28866	-0.21348	-0.25352	-0.25017	-0.24966	-0.16515	-0.16515	-0.20896	-0.16515	-0.16416	-0.16416
$\bar{E}_{Kvib}$ (eV)	0.08543 [42]	0.12832 [43]	0.35532 (Eq. (13.458))	0.35532 (Eq. (13.458))	0.35532 (Eq. (13.458))	0.12312 [2]	0.17978 [4]	0.09944 [5]	0.12312 [2]	0.12312 [2]	0.12312 [2]
$\bar{E}_{osc}$ (eV)	-0.24595	-0.14932	-0.22757	-0.14502	-0.07200	-0.10359	-0.07526	-0.15924	-0.10359	-0.10260	-0.10260
E_{mag} (eV)	0.14803	0.11441	0.14803	0.14803	0.14803	0.14803	0.14803	0.14803	0.14803	0.14803	0.14803
$E_{T(Group)}$ (eV)	-32.60589	-63.56937	-67.92207	-49.80996	-31.70737	-33.59732	-33.49373	-33.24376	-33.59732	-33.18712	-33.18712
$E_{initial(s_4,AO/HO)}$ (eV)	-14.63489	-14.63489	-14.63489	-14.63489	-14.63489	-14.63489	-14.63489	-14.63489	-14.63489	-14.63489	-14.63489
$E_{initial(s_5,AO/HO)}$ (eV)	0	-1.16125	-13.59844	-13.59844	-13.59844	0	0	0	0	0	0
$E_{D(Group)}$ (eV)	3.33611	3.86856	12.49186	7.83016	3.32601	4.32754	4.29921	3.97398	4.17951	3.62128	3.91734

Table 15.169. The total bond energies of alkyl sulfoxides calculated using the functional group composition and the energies of Table 15.168 compared to the experimental values [3].

Formula	Name	$C-S$ Group	SO Group	CH_3	CH_2	CH	$C-C$ (a)	$C-C$ (b)	$C-C$ (c)	$C-C$ (d)	$C-C$ (e)	$C-C$ (f)	Calculated Total Bond Energy (eV)	Experimental Total Bond Energy (eV)	Relative Error
C_2H_6SO	Dimethyl sulfoxide	2	1	2	0	0	0	0	0	0	0	0	35.52450	35.435	-0.00253
$C_4H_{10}SO$	Diethyl sulfoxide	2	1	2	2	0	2	0	0	0	0	0	59.83990	59.891	0.00085
$C_6H_{14}SO$	Dipropyl sulfoxide	2	1	2	4	0	4	0	0	0	0	0	84.15530	84.294	0.00165

Table 15.170. The bond angle parameters of alkyl sulfoxides and experimental values [1]. In the calculation of θ_v, the parameters from the preceding angle were used. E_T is E_T ($atom-atom$,msp^3.AO).

Atoms of Angle	$2c'$ Bond 1 (a_0)	$2c'$ Bond 2 (a_0)	$2c'$ Terminal Atoms (a_0)	$E_{Coulombic}$ Atom 1	Atom 1 Hybridization Designation (Table 15.3.A)	$E_{Coulombic}$ Atom 2	Atom 2 Hybridization Designation (Table 15.3.A)	c_2 Atom 1	c_2 Atom 2	C_1	C_2	c_1	c_2'	E_T (eV)	θ_v (°)	θ_1 (°)	θ_2 (°)	Cal. θ (°)	Exp. θ (°)
$\angle C_aSC_a$	3.34541	3.34541	4.9800	-16.47951	22	-16.47951	22	0.82562	0.82562	1	1	1	0.82562	-1.85836				96.20	96.6 (dimethyl sulfoxide)
$\angle C_aSO$	3.34541	2.81792	4.9598	-15.18804 C_a	2	-13.61806 O	O	0.89582	0.85395 (Eq. (15.133))	1	1	1	0.87489	-1.65376				106.88	106.7 (dimethyl sulfoxide)
Methylene $\angle HC_aH$	2.11106	2.11106	3.4252	-15.75493	7	H	H	0.86359	1	1	1	0.75	1.15796	0				108.44	107 (propane)
$\angle C_aC_bC_c$															69.51			110.49	112 (propane) 113.8 (butane) 110.8 (isobutane)
$\angle C_aC_bH$															69.51			110.49	111.0 (butane) 111.4 (isobutane)
Methyl $\angle HC_aH$	2.09711	2.09711	3.4252	-15.75493	7	H	H	0.86359	1	1	1	0.75	1.15796	0				109.50	110.3 (dimethyl sulfoxide)
$\angle C_aC_bC_c$															70.56			109.44	
$\angle C_aC_bH$															70.56			109.44	
$\angle C_bC_aC_c$ iso C_a	2.91547	2.91547	4.7958	-16.68412 C_b	26	-16.68412 C_c	26	0.81549	0.81549	1	1	1	0.81549	-1.85836				110.67	110.8 (isobutane)
$\angle C_bC_aH$ iso C_a	2.91547	2.11323	4.1633	-15.55033 C_a	5	-14.82575 C_b	1	0.87495	0.91771	0.75	1	0.75	1.04887	0				110.76	
$\angle C_aC_bH$ iso C_a	2.91547	2.09711	4.1633	-15.55033 C_b	5	-14.82575 C_a	1	0.87495	0.91771	0.75	1	0.75	1.04887	0				111.27	111.4 (isobutane)
$\angle C_bC_aC_b$ tert C_a	2.90327	2.90327	4.7958	-16.68412 C_b	26	-16.68412 C_b	26	0.81549	0.81549	1	1	1	0.81549	-1.85836				111.37	110.8 (isobutane)
$\angle C_bC_aC_d$															72.50			107.50	

DIMETHYL SULFOXIDE DIHEDRAL ANGLE

The dihedral angle $\theta_{\angle S=O/CSC}$ between the plane defined by the CSC MO comprising a linear combination of two $S-C$-bond MOs and a line defined by the $S=O$-bond MO where S is the central atom is calculated using the results given in Table 15.170 and Eqs. (15.114-15.117). The distance d_1 along the bisector of $\theta_{\angle CSC}$ from S to the internuclear-distance line between C and C, $2c'_{C-C}$, is given by:

$$d_1 = 2c'_{S-C}\cos\frac{\theta_{\angle CSC}}{2} = 4.9800a_0\cos\frac{96.20°}{2} = 2.23423a_0 \tag{15.153}$$

where $2c'_{S-C}$ is the internuclear distance between S and C. The atoms C, C, and O define the base of a pyramid. Then, the pyramidal angle $\theta_{\angle COC}$ can be solved from the internuclear distances between C and C, $2c'_{C-C}$, and between C and O, $2c'_{C-O}$, using the law of cosines (Eq. (15.115)):

$$\theta_{\angle COC} = \cos^{-1}\left(\frac{\left(2c'_{C-O}\right)^2+\left(2c'_{C-O}\right)^2-\left(2c'_{C-C}\right)^2}{2\left(2c'_{C-O}\right)\left(2c'_{C-O}\right)}\right) = \cos^{-1}\left(\frac{(4.95984)^2+(4.95984)^2-(4.9800)^2}{2(4.95984)(4.95984)}\right) = 60.27° \tag{15.154}$$

Then, the distance d_2 along the bisector of $\theta_{\angle COC}$ from O to the internuclear-distance line $2c'_{C-C}$, is given by:

$$d_2 = 2c'_{C-O}\cos\frac{\theta_{\angle COC}}{2} = 4.95984a_0\cos\frac{60.27°}{2} = 4.28952a_0 \tag{15.155}$$

The lengths d_1, d_2, and $2c'_{S=O}$ define a triangle wherein the angle between d_1 and the internuclear distance between O and S, $2c'_{S=O}$, is the dihedral angle $\theta_{\angle S=O/CSC}$ that can be solved using the law of cosines (Eq. (15.117)).

$$\theta_{\angle S=O/CSC} = \cos^{-1}\left(\frac{d_1^2+\left(2c'_{S=O}\right)^2-d_2^2}{2d_1\left(2c'_{S=O}\right)}\right) = \cos^{-1}\left(\frac{(2.23423)^2+(2.81792)^2-(4.28952)^2}{2(2.23423)(2.81792)}\right) = 115.74° \tag{15.156}$$

The experimental [1] dihedral angle $\theta_{\angle S=O/CSC}$ is

$$\theta_{\angle S=O/CSC} = 115.5° \tag{15.157}$$

SULFONES ($C_nH_{2n+2}\left(SO_2\right)_m$, $n=2,3,4,5...\infty$)

The alkyl sulfones, $C_nH_{2n+2}\left(SO_2\right)_m$, comprise a $C-SO_2-C$ moiety that comprises $C-S$ and SO_2 functional groups. The alkyl portion of the alkyl sulfone may comprise at least two terminal methyl groups (CH_3) at each end of the chain, and may comprise methylene (CH_2), and methylyne (CH) functional groups as well as C bound by carbon-carbon single bonds. The methyl and methylene functional groups are equivalent to those of straight-chain alkanes. Six types of $C-C$ bonds can be identified. The n-alkane $C-C$ bond is the same as that of straight-chain alkanes. In addition, the $C-C$ bonds within isopropyl ($\left(CH_3\right)_2CH$) and t-butyl ($\left(CH_3\right)_3C$) groups and the isopropyl to isopropyl, isopropyl to t-butyl, and t-butyl to t-butyl $C-C$ bonds comprise functional groups. The branched-chain-alkane groups in sulfones are equivalent to those in branched-chain alkanes.

The two unpaired electrons of each O atom form a MO with two unpaired electrons of the sulfur atom such that the MO comprises a linear combination of two bonds, each of bond order two involving the sulfur HOs and oxygen AOs of both oxygen atoms. Due to the bonding between unpaired electrons of different oxygen atoms E_{mag} (Eq. (15.68)) is subtracted from the total energy. Otherwise, the SO_2-bond MO of sulfones is solved in the same manner as the SO-bond MO of sulfoxides given in the corresponding section wherein n_1 in Eqs. (15.51) and (15.61) is four versus two. Also, the $C-S$-bond MO is equivalent to that of sulfoxides having $E_T\left(atom-atom,msp^3.AO\right)=-0.72457\ eV$ (Eq. (14.151)).

The symbols of the functional groups of branched-chain alkyl sulfones are given in Table 15.171. The geometrical (Eqs. (15.1-15.5) and (15.51)), intercept (Eqs. (15.80-15.87)), and energy (Eqs. (15.6-15.11) and (15.17-15.65)) parameters of alkyl sulfones are given in Tables 15.172, 15.173, and 15.174, respectively. The total energy of each alkyl sulfone given in Table 15.165 was calculated as the sum over the integer multiple of each $E_{D\,(Group)}$ of Table 15.174 corresponding to functional-group composition of the molecule. The bond angle parameters of alkyl sulfones determined using Eqs. (15.88-15.117) are given in Table 15.176. The color scale, translucent view of the charge-density of exemplary sulfone, dimethyl sulfone, comprising the concentric shells of atoms with the outer shell bridged by one or more H_2-type ellipsoidal MOs or joined with one or more hydrogen MOs is shown in Figure 15.29.

Figure 15.29. (A)-(B) Color scale, translucent views of the charge-density of dimethyl sulfone showing the orbitals of the atoms at their radii, the ellipsoidal surface of each H or H_2-type ellipsoidal MO that transitions to the corresponding outer shell of the atom(s) participating in each bond, and the hydrogen nuclei (red, not to scale).

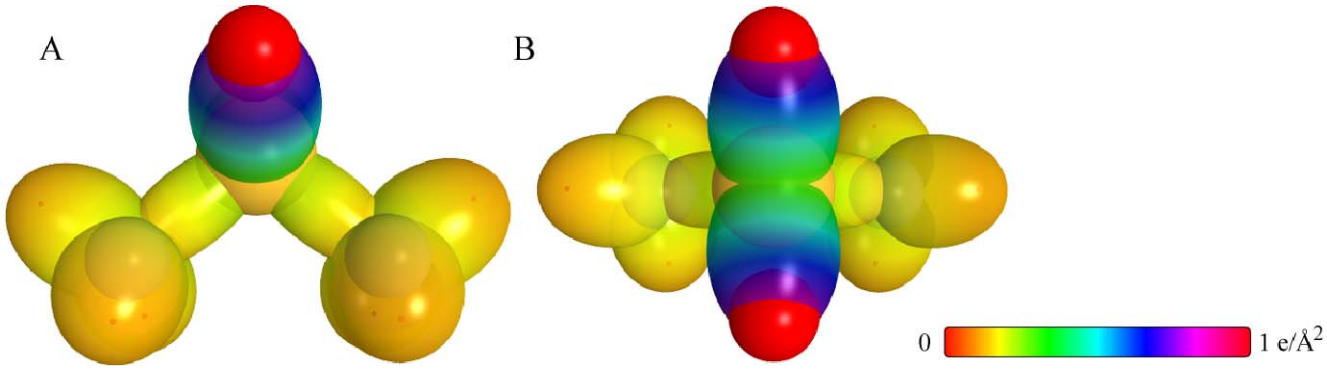

Table 15.171. The symbols of functional groups of alkyl sulfones.

Functional Group	Group Symbol
C-S	$C-S$
SO2	SO_2
CH3 group	$C-H\ \left(CH_3\right)$
CH2 group	$C-H\ \left(CH_2\right)$
CH	$C-H$
CC bond (*n-C*)	$C-C$ (a)
CC bond (*iso-C*)	$C-C$ (b)
CC bond (*tert-C*)	$C-C$ (c)
CC (*iso* to *iso-C*)	$C-C$ (d)
CC (*t* to *t-C*)	$C-C$ (e)
CC (*t* to *iso-C*)	$C-C$ (f)

Table 15.172. The geometrical bond parameters of alkyl sulfones and experimental values [1].

Parameter	$C-S$ Group	SO_2 Group	$C-H\ (CH_3)$ Group	$C-H\ (CH_2)$ Group	$C-H$ Group	$C-C$ (a) Group	$C-C$ (b) Group	$C-C$ (c) Group	$C-C$ (d) Group	$C-C$ (e) Group	$C-C$ (f) Group
$a\ (a_0)$	1.87325	1.85851	1.64920	1.67122	1.67465	2.12499	2.12499	2.10725	2.12499	2.10725	2.10725
$c'\ (a_0)$	1.67271	1.36327	1.04856	1.05553	1.05661	1.45744	1.45744	1.45164	1.45744	1.45164	1.45164
Bond Length $2c'\ (\AA)$	1.77031	1.44282	1.10974	1.11713	1.11827	1.54280	1.54280	1.53635	1.54280	1.53635	1.53635
Exp. Bond Length $(\AA)$	1.771 (dimethyl sulfone)	1.435 (dimethyl sulfone)	1.107 ($C-H$ propane) 1.117 ($C-H$ butane)	1.107 ($C-H$ propane) 1.117 ($C-H$ butane)	1.122 (isobutane)	1.532 (propane) 1.531 (butane)	1.532 (propane) 1.531 (butane)	1.532 (propane) 1.531 (butane)	1.532 (propane) 1.531 (butane)	1.532 (propane) 1.531 (butane)	1.532 (propane) 1.531 (butane)
$b,c\ (a_0)$	0.84328	1.26315	1.27295	1.29569	1.29924	1.54616	1.54616	1.52750	1.54616	1.52750	1.52750
e	0.89294	0.73353	0.63580	0.63159	0.63095	0.68600	0.68600	0.68888	0.68600	0.68888	0.68888

Table 15.173. The MO to HO intercept geometrical bond parameters of alkyl sulfones. R, R', R'' are H or alkyl groups. E_T is $E_T(atom-atom,msp^3.AO)$.

Bond	Atom	E_T (eV) Bond 1	E_T (eV) Bond 2	E_T (eV) Bond 3	E_T (eV) Bond 4	Final Total Energy $C2sp^3$ (eV)	$r_{initial}\ (a_0)$	$r_{final}\ (a_0)$	$E_{Coulomb}$ (eV) Final	$E(C2sp^3)$ (eV) Final	θ' (°)	θ_1 (°)	θ_2 (°)	$d_1\ (a_0)$	$d_2\ (a_0)$
$R_2(O)S=O$	S	0	0	-0.36229	-0.36229		1.32010	0.87495	-15.55033		91.47	88.53	43.82	1.34086	0.02242
$R_2(O)S=O$	O	0	0	0	0		1.00000	0.91771	-14.82575		95.05	84.95	46.36	1.28256	0.08071
R_2-SO	S	-0.36229	-0.36229	0	0		1.32010	0.87495	-15.55033		129.35	50.65	53.36	1.11799	0.55472
$H_3C_a-S(O)-C_bH_2CH_2R$	C_a	-0.36229	0	0	0	-151.97798	0.91771	0.89582	-15.18804	-14.99717	130.19	49.81	54.24	1.09461	0.57809
$H_3C_a-S(O)-C_bH_2CH_2R$	C_b	-0.36229	-0.92918	0	0	-152.90716	0.91771	0.84418	-16.11722	-15.92636	128.05	51.95	52.03	1.15245	0.52026
$C-H\ (CH_3)$	C	-0.92918	0	0	0	-152.54487	0.91771	0.86359	-15.75493	-15.56407	77.49	102.51	41.48	1.23564	0.18708
$C-H\ (CH_2)$	C	-0.92918	-0.92918	0	0	-153.47406	0.91771	0.81549	-16.68412	-16.49325	68.47	111.53	35.84	1.35486	0.29933
$C-H\ (CH)$	C	-0.92918	-0.92918	-0.92918	0	-154.40324	0.91771	0.77247	-17.61330	-17.42244	61.10	118.90	31.37	1.42988	0.37326
$H_3C_aC_bH_2CH_2-$ ($C-C$ (a))	C_a	-0.92918	0	0	0	-152.54487	0.91771	0.86359	-15.75493	-15.56407	63.82	116.18	30.08	1.83879	0.38106
$H_3C_aC_bH_2CH_2-$ ($C-C$ (a))	C_b	-0.92918	-0.92918	0	0	-153.47406	0.91771	0.81549	-16.68412	-16.49325	56.41	123.59	26.06	1.90890	0.45117
$R-H_2C_aC_b(H_2C_c-R')HCH_2-$ ($C-C$ (b))	C_b	-0.92918	-0.92918	-0.92918	0	-154.40324	0.91771	0.77247	-17.61330	-17.42244	48.30	131.70	21.90	1.97162	0.51388
$R-H_2C_a(R'-H_2C_d)C_b(R''-H_2C_c)CH_2-$ ($C-C$ (e))	C_b	-0.92918	-0.72457	-0.72457	-0.72457	-154.71860	0.91771	0.75889	-17.92866	-17.73779	48.21	131.79	21.74	1.95734	0.50570
$isoC_aC_b(H_2C_c-R')HCH_2-$ ($C-C$ (d))	C_b	-0.92918	-0.92918	-0.92918	0	-154.40324	0.91771	0.77247	-17.61330	-17.42244	48.30	131.70	21.90	1.97162	0.51388
$tertC_a(R'-H_2C_d)C_b(R''-H_2C_c)CH_2-$ ($C-C$ (e))	C_b	-0.72457	-0.72457	-0.72457	-0.72457	-154.51399	0.91771	0.76765	-17.92866	-17.73779	50.04	129.96	22.66	1.94462	0.49298
$tertC_aC_b(H_2C_c-R')HCH_2-$ ($C-C$ (f))	C_b	-0.72457	-0.92918	-0.92918	0	-154.19863	0.91771	0.78155	-17.40869	-17.21783	52.78	127.22	24.04	1.92443	0.47279
$isoC_a(R'-H_2C_d)C_b(R''-H_2C_c)CH_2-$ ($C-C$ (f))	C_b	-0.72457	-0.72457	-0.72457	-0.72457	-154.51399	0.91771	0.76765	-17.92866	-17.73779	50.04	129.96	22.66	1.94462	0.49298

Table 15.174. The energy parameters (eV) of functional groups of alkyl sulfones.

Parameters	$C-S$ Group	SO_2 Group	CH_3 Group	CH_2 Group	$C-H$ Group	$C-C$ (a) Group	$C-C$ (b) Group	$C-C$ (c) Group	$C-C$ (d) Group	$C-C$ (e) Group	$C-C$ (f) Group
n_1	1	4	3	2	1	1	1	1	1	1	1
n_2	0	0	2	1	0	0	0	0	0	0	0
n_3	0	0	0	0	0	0	0	0	0	0	0
C_1	0.5	0.5	0.75	0.75	0.75	0.5	0.5	0.5	0.5	0.5	0.5
C_2	0.66951	1	1	1	1	1	1	1	1	1	1
c_1	1	1	1	1	1	1	1	1	1	1	1
c_2	1	1.20632	0.91771	0.91771	0.91771	0.91771	0.91771	0.91771	0.91771	0.91771	0.91771
c_3	0	1	0	1	1	0	0	0	1	1	0
c_4	2	8	1	1	1	2	2	2	2	2	2
c_5	0	1	3	2	1	0	0	0	0	0	0
C_{1o}	0.5	0.5	0.75	0.75	0.75	0.5	0.5	0.5	0.5	0.5	0.5
C_{2o}	0.66951	1	1	1	1	1	1	1	1	1	1
$V_e\ (eV)$	-46.73032	-180.36454	-107.32728	-70.41425	-35.12015	-28.79214	-28.79214	-29.10112	-28.79214	-29.10112	-29.10112
$V_p\ (eV)$	8.13401	39.92103	38.92728	25.78002	12.87680	9.33352	9.33352	9.37273	9.33352	9.37273	9.37273
$T\ (eV)$	12.47306	48.52397	32.53914	21.06675	10.48582	6.77464	6.77464	6.90500	6.77464	6.90500	6.90500
$V_m\ (eV)$	-6.23653	-24.26198	-16.26957	-10.53337	-5.24291	-3.38732	-3.38732	-3.45250	-3.38732	-3.45250	-3.45250
$E_{(AO/HO)}\ (eV)$	0	-11.52126	-15.56407	-15.56407	-14.63489	-15.56407	-15.56407	-15.35946	-15.56407	-15.35946	-15.35946
$\Delta E_{H_2MO\,(AO/HO)}\ (eV)$	-0.72457	-1.16125	0	0	0	0	0	0	0	0	0
$E_{\gamma\,(AO/HO)}\ (eV)$	0.72457	-10.36001	-15.56407	-15.56407	-14.63489	-15.56407	-15.56407	-15.35946	-15.56407	-15.35946	-15.35946
$E_{\gamma\,(H_2MO)}\ (eV)$	-31.63521	-126.54154	-67.69451	-49.66493	-31.63533	-31.63537	-31.63537	-31.63535	-31.63537	-31.63535	-31.63535
$E_{\gamma}\left(atom-atom, msp^3.AO\right)\ (eV)$	-0.72457	0	0	0	0	-1.85836	-1.85836	-1.44915	-1.85836	-1.44915	-1.44915
$E_{\gamma\,(MO)}\ (eV)$	-32.35994	-126.54147	-67.69450	-49.66493	-31.63537	-33.49373	-33.49373	-33.08452	-33.49373	-33.08452	-33.08452
$\omega\ \left(10^{15}\ rad/s\right)$	30.8880	11.5378	24.9286	24.2751	24.1759	9.43699	9.43699	15.4846	9.43699	9.55643	9.55643
$E_K\ (eV)$	20.33104	7.59437	16.40846	15.97831	15.91299	6.21159	6.21159	10.19220	6.21159	6.29021	6.29021
$\bar{E}_D\ (eV)$	-0.28866	-0.17247	-0.25352	-0.25017	-0.24966	-0.16515	-0.16515	-0.20896	-0.16515	-0.16416	-0.16416
$\bar{E}_{Kvib}\ (eV)$	0.08543 [42]	0.12832 [43]	0.35532 (Eq. (13.458))	0.35532 (Eq. (13.458))	0.35532 (Eq. (13.458))	0.12312 [2]	0.17978 [4]	0.09944 [5]	0.12312 [2]	0.12312 [2]	0.12312 [2]
$\bar{E}_{osc}\ (eV)$	-0.24595	-0.10831	-0.22757	-0.14502	-0.07200	-0.10359	-0.07526	-0.15924	-0.10359	-0.10260	-0.10260
$E_{wag}\ (eV)$	0.14803	0.11441	0.14803	0.14803	0.14803	0.14803	0.14803	0.14803	0.14803	0.14803	0.14803
$E_{\gamma\,(Group)}\ (eV)$	-32.60589	-126.97472	-67.92207	-49.80996	-31.70737	-33.59732	-33.49373	-33.24376	-33.59732	-33.18712	-33.18712
$E_{lattital\,(4\ AO/HO)}\ (eV)$	-14.63489	-14.63489	-14.63489	-14.63489	-14.63489	-14.63489	-14.63489	-14.63489	-14.63489	-14.63489	-14.63489
$E_{lattital\,(5\ AO/HO)}\ (eV)$	0	-1.16125	-13.59844	-13.59844	-13.59844	0	0	0	0	0	0
$E_{D\,(Group)}\ (eV)$	3.33611	8.61994	12.49186	7.83016	3.32601	4.32754	4.29921	3.97398	4.17951	3.62128	3.91734

Table 15.175. The total bond energies of alkyl sulfones calculated using the functional group composition and the energies of Table 15.174 compared to the experimental values [3].

Formula	Name	$C-S$ Group	SO_2 Group	CH_3	CH_2	CH	$C-C$ (a)	$C-C$ (b)	$C-C$ (c)	$C-C$ (d)	$C-C$ (e)	$C-C$ (f)	Calculated Total Bond Energy (eV)	Experimental Total Bond Energy (eV)	Relative Error
$C_2H_6SO_2$	Dimethyl sulfone	2	1	2	0	0	0	0	0	0	0	0	40.27588	40.316	0.00100

Table 15.176. The bond angle parameters of alkyl sulfones and experimental values [1]. In the calculation of θ_v, the parameters from the preceding angle were used. E_T is E_T (*atom – atom,msp³.AO*).

Atoms of Angle	2c' Bond 1 (a_0)	2c' Bond 2 (a_0)	2c' Terminal Atoms (a_0)	$E_{Coulombic}$ Atom 1	Atom 1 Hybridization Designation (Table 15.3.A)	$E_{Coulombic}$ Atom 2	Atom 2 Hybridization Designation (Table 15.3.A)	c_2 Atom 1	c_2 Atom 2	C_1	C_2	c_1	c'_2	E_T (eV)	θ_r (°)	θ_1 (°)	θ_2 (°)	Cal. θ (°)	Exp. θ (°)
$\angle O_a S O_b$	2.72654	2.72654	4.7539	-15.95954 O_a	10	-15.95954 O_b	10	0.85252	0.85252	1	1	1	0.85252	-1.65376				121.33	121 (dimethyl sulfone)
$\angle C_a S C_a$	3.34541	3.34541	5.2154	-16.11722	12	-16.11722	12	0.84418	0.84418	1	1	1	0.84418	-1.85836				102.43	102 (dimethyl sulfone)
$\angle C_a S O$	3.34541	2.72654	4.9193	-15.55033 C_a	5	-13.61806 O	O	0.87495	0.85395 (Eq. (15.133))	1	1	1	0.86445	-1.65376				107.79	
Methylene $\angle H C_a H$	2.11106	2.11106	3.4252	-15.75493	7	H	H	0.86359	1	1	1	0.75	1.15796	0				108.44	107 (propane)
$\angle C_a C_b C_c$															69.51			110.49	112 (propane) 113.8 (butane) 110.8 (isobutane)
$\angle C_a C_b H$															69.51			110.49	111.0 (butane) 111.4 (isobutane)
Methyl $\angle H C_a H$	2.09711	2.09711	3.4252	-15.75493	7	H	H	0.86359	1	1	1	0.75	1.15796	0				109.50	
$\angle C_a C_b C_c$															70.56			109.44	
$\angle C_a C_b H$															70.56			109.44	
$\angle C_b C_a C_c$ iso C_a	2.91547	2.91547	4.7958	-16.68412 C_b	26	-16.68412 C_c	26	0.81549	0.81549	1	1	1	0.81549	-1.85836				110.67	110.8 (isobutane)
$\angle C_b C_a H$ iso C_a	2.91547	2.11323	4.1633	-15.55033 C_a	5	-14.82575 C_b	1	0.87495	0.91771	0.75	1	0.75	1.04887	0				110.76	
$\angle C_a C_b H$ iso C_a	2.91547	2.09711	4.1633	-15.55033 C_b	5	-14.82575 C_a	1	0.87495	0.91771	0.75	1	0.75	1.04887	0				111.27	111.4 (isobutane)
$\angle C_b C_a C_b$ tert C_a	2.90327	2.90327	4.7958	-16.68412 C_b	26	-16.68412 C_b	26	0.81549	0.81549	1	1	1	0.81549	-1.85836				111.37	110.8 (isobutane)
$\angle C_b C_a C_d$															72.50			107.50	

SULFITES ($C_nH_{2n+2}\left(SO_3\right)_m$, $n=2,3,4,5...\infty$)

The alkyl sulfites, $C_nH_{2n+2}\left(SO_3\right)_m$, comprise a $C-O-SO-O-C$ moiety that comprises two types $C-O$ functional groups, one for methyl and one for alkyl, and $O-S$ and SO functional groups. The alkyl portion of the alkyl sulfite may comprise at least two terminal methyl groups (CH_3) at each end of the chain, and may comprise methylene (CH_2), and methylyne (CH) functional groups as well as C bound by carbon-carbon single bonds. The methyl and methylene functional groups are equivalent to those of straight-chain alkanes. Six types of $C-C$ bonds can be identified. The n-alkane $C-C$ bond is the same as that of straight-chain alkanes. In addition, the $C-C$ bonds within isopropyl ($\left(CH_3\right)_2CH$) and t-butyl ($\left(CH_3\right)_3C$) groups and the isopropyl to isopropyl, isopropyl to t-butyl, and t-butyl to t-butyl $C-C$ bonds comprise functional groups. The branched-chain-alkane groups in sulfites are equivalent to those in branched-chain alkanes.

The SO functional group is equivalent to that of sulfoxides with $E_T\left(atom-atom,msp^3.AO\right)=0$ as given in the Sulfoxides section. The methyl and alkyl $C-O$ functional groups having $E_T\left(atom-atom,msp^3.AO\right)=-1.44915\,eV$ and $E_T\left(atom-atom,msp^3.AO\right)=-1.65376\,eV$, respectively, are equivalent to the corresponding ether groups given in the Ethers section except for the energy terms corresponding to oscillation of the bond in the transition state.

The electron configuration of oxygen is $1s^22s^22p^4$, and the orbital arrangement given by Eq. (10.154) has two unpaired electrons corresponding to the ground state ${}^3P_2$. The SO functional group comprises a double bond between the S atom and the two unpaired electrons of O. The S atom also forms single bonds with two additional oxygen atoms that are each further bound to methyl or alkyl groups. The first bond-order bonding in the $O-S$ groups is between the sulfur atom and a $O2p$ AO of each oxygen of the two bonds. The formation of these four bonds with the sulfur atom is permitted by the hybridization of the four electrons of the $S3p$ shell to give the orbital arrangement given by Eq. (15.148). Then, the Coulombic energy $E_{Coulomb}\left(S,3sp^3\right)$ of the outer electron of the $S3sp^3$ shell given by Eq. (15.139) with $r_{3sp^3}=1.17585a_0$ (Eq. (15.138)) is $-11.57099\,eV$. Using Eq. (15.16) with the radius of the sulfur atom $r_{16}=1.32010a_0$ given by Eq. (10.341), the energy $E\left(S3sp^3\right)$ of the outer electron of the $S3sp^3$ shell given by the sum of $E_{Coulomb}\left(S3sp^3\right)$ and $E(magnetic)$ is $E\left(S3sp^3\right)=-11.52126\,eV$ (Eq. (15.149)).

Thus, the $O-S$ group is solved as an energy minimum by hybridizing the four $S3p$ electrons to form a $S3sp^3$ shell, and the sharing of electrons between the $O2p$ AO and the $S3sp^3$ HO to form a MO permits each participating orbital to decrease in radius and energy. As in the case of thiols, sulfides, disulfides, and sulfoxides, the energy of sulfur is less than the Coulombic energy between the electron and proton of H given by Eq. (1.264). Thus, c_1 and c_2 are equal to one in Eq. (15.61), and the energy matching condition is determined by the C_2 parameter. Each $C2sp^3$ HO has a hybridization factor of 0.91771 (Eq. (13.430)) with a corresponding energy of $E\left(C,2sp^3\right)=-14.63489\,eV$ (Eq. (15.25)), and the S HO has an energy of $E\left(S3sp^3\right)=-11.52126\,eV$. To meet the equipotential condition of the union of the $O-S$ H_2-type-ellipsoidal-MO with these orbitals with the oxygen that further bonds to a $C2sp^3$ HO, the hybridization factor C_2 of Eq. (15.61) for the $O-S$-bond MO given by Eqs. (15.77) and (15.79) is:

$$C_2\left(S3sp^3\ to\ O\ to\ C2sp^3HO\right)=\frac{E\left(S,3sp^3\right)}{E\left(O,2p\right)}c_2\left(C2sp^3HO\right)=\frac{-11.52126\,eV}{-13.61806\,eV}\left(0.91771\right)=0.77641 \tag{15.158}$$

As in the case of thiols, sulfides, disulfides, and sulfoxides, with the energy of S matched to the Coulombic energy between the electron and proton of H, the energy of the $O-S$-bond MO is the sum of the component energies of the H_2-type ellipsoidal MO given in Eq. (15.51) with $E\left(AO/HO\right)=0$ and $E_T\left(AO/HO\right)=\Delta E_{H_2MO}\left(AO/HO\right)$. For sulfites, $\Delta E_{H_2MO}\left(AO/HO\right)=-0.92918\,eV$ and equivalently, $E_T\left(atom-atom,msp^3.AO\right)=-0.92918\,eV$ (Eq. (14.513)) due to the maximum energy match with the oxygen AO as in the case with carboxylic acid esters.

The symbols of the functional groups of branched-chain alkyl sulfites are given in Table 15.177. The geometrical (Eqs. (15.1-15.5) and (15.51)), intercept (Eqs. (15.80-15.87)), and energy (Eqs. (15.6-15.11) and (15.17-15.65)) parameters of alkyl sulfites are given in Tables 15.178, 15.179, and 15.180, respectively. The total energy of each alkyl sulfite given in Table 15.175 was calculated as the sum over the integer multiple of each $E_{D\,(Group)}$ of Table 15.180 corresponding to functional-group composition of the molecule. The bond angle parameters of alkyl sulfites determined using Eqs. (15.88-15.117) are given in Table 15.182. The color scale, translucent view of the charge-density of sulfite, dimethyl sulfite, comprising the concentric shells of atoms with the outer shell bridged by one or more H_2-type ellipsoidal MOs or joined with one or more hydrogen MOs is shown in Figure 15.30.

Figure 15.30. Color scale, translucent view of the charge-density of dimethyl sulfite showing the orbitals of the atoms at their radii, the ellipsoidal surface of each H or H_2-type ellipsoidal MO that transitions to the corresponding outer shell of the atom(s) participating in each bond, and the hydrogen nuclei (red, not to scale).

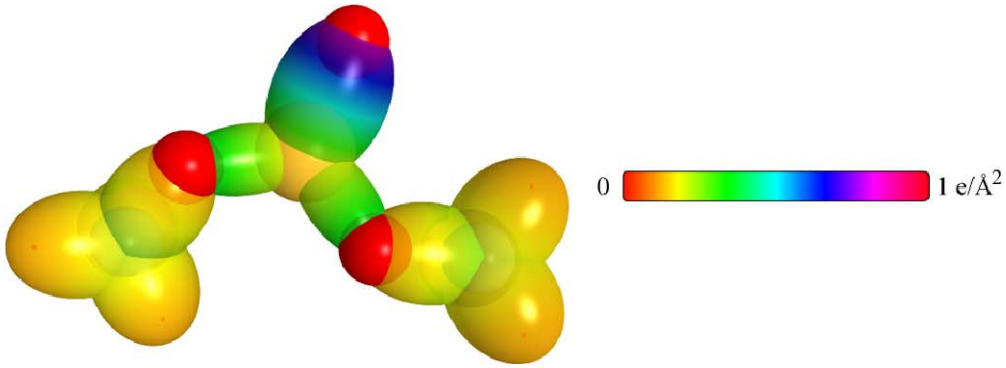

Table 15.177. The symbols of functional groups of alkyl sulfites.

Functional Group	Group Symbol
C-O (*methyl*)	$C-O$ (i)
C-O (*alkyl*)	$C-O$ (ii)
O-SO$_2$	$O-S$
SO	*SO*
CH$_3$ group	$C-H\ (CH_3)$
CH$_2$ group	$C-H\ (CH_2)$
CH	$C-H$
CC bond (*n-C*)	$C-C$ (a)
CC bond (*iso-C*)	$C-C$ (b)
CC bond (*tert-C*)	$C-C$ (c)
CC (*iso* to *iso-C*)	$C-C$ (d)
CC (*t* to *t-C*)	$C-C$ (e)
CC (*t* to *iso-C*)	$C-C$ (f)

Table 15.178. The geometrical bond parameters of alkyl sulfites and experimental values [1].

Parameter	$C-O$ (i) Group	$C-O$ (ii) Group	$O-S$	SO	$C-H\ (CH_3)$ Group	$C-H\ (CH_2)$ Group	$C-H$ Group	$C-C$ (a) Group	$C-C$ (b) Group	$C-C$ (c) Group	$C-C$ (d) Group	$C-C$ (e) Group	$C-C$ (f) Group
$a\ (a_0)$	1.80717	1.79473	1.70299	1.98517	1.64920	1.67122	1.67465	2.12499	2.12499	2.10725	2.12499	2.10725	2.10725
$c'\ (a_0)$	1.34431	1.33968	1.48102	1.40896	1.04856	1.05553	1.05661	1.45744	1.45744	1.45164	1.45744	1.45164	1.45164
Bond Length $2c'\ (A)$	1.42276	1.41785	1.56744	1.49118	1.10974	1.11713	1.11827	1.54280	1.54280	1.53635	1.54280	1.53635	1.53635
Exp. Bond Length (A)			1.574 (H_2SO_4)	1.485 (dimethyl sulfoxide)	1.107 ($C-H$ propane) 1.117 ($C-H$ butane)	1.107 ($C-H$ propane) 1.117 ($C-H$ butane)	1.122 (isobutane)	1.532 (propane) 1.531 (butane)	1.532 (propane) 1.531 (butane)	1.532 (propane) 1.531 (butane)	1.532 (propane) 1.531 (butane)	1.532 (propane) 1.531 (butane)	1.532 (propane) 1.531 (butane)
$b,c\ (a_0)$	1.20776	1.19429	0.84069	1.39847	1.27295	1.29569	1.29924	1.54616	1.54616	1.52750	1.54616	1.52750	1.52750
e	0.74388	0.74645	0.86966	0.70974	0.63580	0.63159	0.63095	0.68500	0.68600	0.68888	0.68600	0.68888	0.68888

Table 15.179. The MO to HO intercept geometrical bond parameters of alkyl sulfites. R, R', R'' are H or alkyl groups. E_T is $E_T(atom-atom,msp^3.AO)$.

Bond	Atom	E_T (eV) Bond 1	E_T (eV) Bond 2	E_T (eV) Bond 3	E_T (eV) Bond 4	Final Total Energy $C2sp^3$ (eV)	$r_{initial}$ (a_0)	r_{final} (a_0)	$E_{Coulomb}$ (eV) Final	$E(C2sp^3)$ (eV) Final	θ' (°)	θ_1 (°)	θ_2 (°)	d_1 (a_0)	d_2 (a_0)
$(RO)_2S=O_a$	S	0	-0.46459	-0.46459	0		1.32010	0.86359	-15.75493		78.56	101.44	37.25	1.58026	0.17130
$(RO)_2S=O_a$	O_a	0	0	0	0		1.00000	0.91771	-14.82575		84.06	95.94	40.75	1.50400	0.09504
$CH_3O_a-S(O)OR'$	S	-0.46459	-0.46459	0	0		1.32010	0.86359	-15.75493		126.68	53.32	55.47	0.96521	0.51581
$CH_3O_a-S(O)OR'$ $(C-O$ (i))	O_a	-0.46459	-0.72457	0	0		1.00000	0.84957	-16.01492		126.03	53.97	54.81	0.98133	0.49969
$RCH_2O_a-S(O)OR'$ $(C-O$ (ii))	O_a	-0.46459	-0.82688	0	0		1.00000	0.84418	-16.11722		125.77	54.23	54.56	0.98753	0.49349
$H_3C_a-O_aS(O)OR$ $(C-O$ (i))	O_a	-0.72457	-0.46459	0	0		1.00000	0.84957	-16.01492		93.85	86.15	44.57	1.28731	0.05700
$H_3C_a-O_aS(O)OR$ $(C-O$ (i))	C_a	-0.72457	0	0	0	-152.34026	0.91771	0.87495	-15.55033	-15.35946	95.98	84.02	46.10	1.25319	0.09112
$RH_2C_a-O_aS(O)OR'$ $(C-O$ (ii))	O_a	-0.82688	-0.46459	0	0		1.00000	0.84418	-16.11722		94.50	85.50	44.80	1.27343	0.06624
$RH_2C_a-O_aS(O)OR'$ $(C-O$ (ii))	C_a	-0.82688	-0.92918	0	0	-153.37175	0.91771	0.82053	-16.58181	-16.39095	92.41	87.59	43.35	1.30512	0.03456
$C-H\ (CH_3)$	C	-0.92918	0	0	0	-152.54487	0.91771	0.86359	-15.75493	-15.56407	77.49	102.51	41.48	1.23564	0.18708
$C-H\ (CH_2)$	C	-0.92918	-0.92918	0	0	-153.47406	0.91771	0.81549	-16.68412	-16.49325	68.47	111.53	35.84	1.35486	0.29933
$C-H\ (CH)$	C	-0.92918	-0.92918	-0.92918	0	-154.40324	0.91771	0.77247	-17.61330	-17.42244	61.10	118.90	31.37	1.42988	0.37326
$H_3C_aC_bH_2CH_2-$ $(C-C$ (a))	C_a	-0.92918	0	0	0	-152.54487	0.91771	0.86359	-15.75493	-15.56407	63.82	116.18	30.08	1.83879	0.38106
$H_3C_aC_bH_2CH_2-$ $(C-C$ (a))	C_b	-0.92918	-0.92918	0	0	-153.47406	0.91771	0.81549	-16.68412	-16.49325	56.41	123.59	26.06	1.90890	0.45117
$R-H_2C_aC_b(H_2C_c-R')HCH_2-$ $(C-C$ (b))	C_b	-0.92918	-0.92918	-0.92918	0	-154.40324	0.91771	0.77247	-17.61330	-17.42244	48.30	131.70	21.90	1.97162	0.51388
$R-H_2C_d(R'-H_2C_d)C_b(R''-H_2C_c)CH_2-$ $(C-C$ (c))	C_b	-0.92918	-0.72457	-0.72457	-0.72457	-154.71860	0.91771	0.75889	-17.92866	-17.73779	48.21	131.79	21.74	1.95734	0.50570
$isoC_aC_b(H_2C_c-R')HCH_2-$ $(C-C$ (d))	C_b	-0.92918	-0.92918	-0.92918	0	-154.40324	0.91771	0.77247	-17.61330	-17.42244	48.30	131.70	21.90	1.97162	0.51388
$tertC_a(R'-H_2C_d)C_b(R''-H_2C_c)CH_2-$ $(C-C$ (e))	C_b	-0.72457	-0.72457	-0.72457	-0.72457	-154.51399	0.91771	0.76765	-17.92866	-17.73779	50.04	129.96	22.66	1.94462	0.49298
$tertC_aC_b(H_2C_c-R')HCH_2-$ $(C-C$ (f))	C_b	-0.72457	-0.92918	-0.92918	0	-154.19863	0.91771	0.78155	-17.40869	-17.21783	52.78	127.22	24.04	1.92443	0.47279
$isoC_a(R'-H_2C_d)C_b(R''-H_2C_c)CH_2-$ $(C-C$ (f))	C_b	-0.72457	-0.72457	-0.72457	-0.72457	-154.51399	0.91771	0.76765	-17.92866	-17.73779	50.04	129.96	22.66	1.94462	0.49298

Table 15.180. The energy parameters (eV) of functional groups of alkyl sulfites.

Parameters	$C-O$ (i) Group	$C-O$ (ii) Group	$O-S$ Group	SO Group	CH_3 Group	CH_2 Group	$C-H$ Group	$C-C$ (a) Group	$C-C$ (b) Group	$C-C$ (c) Group	$C-C$ (d) Group	$C-C$ (e) Group	$C-C$ (f) Group
n_1	1	1	1	2	3	2	1	1	1	1	1	1	1
n_2	0	0	0	0	2	1	0	0	0	0	0	0	0
n_3	0	0	0	0	0	0	0	0	0	0	0	0	0
C_1	0.5	0.5	0.5	0.5	0.75	0.75	0.75	0.5	0.5	0.5	0.5	0.5	0.5
C_2	1	1	0.77641	1	1	1	1	1	1	1	1	1	1
c_1	1	1	1	1	1	1	1	1	1	1	1	1	1
c_2	0.85395	0.85395	1	1.20632	0.91771	0.91771	0.91771	0.91771	0.91771	0.91771	0.91771	0.91771	0.91771
c_3	0	0	0	0	0	1	1	0	0	0	1	1	0
c_4	2	2	2	4	1	1	1	2	2	2	2	2	2
c_5	0	0	0	1	3	2	1	0	0	0	0	0	0
C_{1o}	0.5	0.5	0.5	0.5	0.75	0.75	0.75	0.5	0.5	0.5	0.5	0.5	0.5
C_{2o}	1	1	0.77641	1	1	1	1	1	1	1	1	1	1
V_e (eV)	-33.15757	-33.47304	-48.93512	-82.63003	-107.32728	-70.41425	-35.12015	-28.79214	-28.79214	-29.10112	-28.79214	-29.10112	-29.10112
V_p (eV)	10.12103	10.15605	9.18680	19.31325	38.92728	25.78002	12.87680	9.33352	9.33352	9.37273	9.33352	9.37273	9.37273
T (eV)	9.17389	9.32537	14.36741	20.81183	32.53914	21.06675	10.48582	6.77464	6.77464	6.90500	6.77464	6.90500	6.90500
V_m (eV)	-4.58695	-4.66268	-7.18371	-10.40592	-16.26957	-10.53337	-5.24291	-3.38732	-3.38732	-3.45250	-3.38732	-3.45250	-3.45250
$E(_{AO/HO})$ (eV)	-14.63489	-14.63489	0	-11.52126	-15.56407	-15.56407	-14.63489	-15.56407	-15.56407	-15.35946	-15.56407	-15.35946	-15.35946
$\Delta E_{H_2MO}(_{AO/HO})$ (eV)	-1.44915	-1.65376	-0.92918	-1.16125	0	0	0	0	0	0	0	0	0
$E_T(_{AO/HO})$ (eV)	-13.18574	-12.98113	0.92918	-10.36001	-15.56407	-15.56407	-14.63489	-15.56407	-15.56407	-15.35946	-15.56407	-15.35946	-15.35946
$E_T(_{H_2MO})$ (eV)	-31.63533	-31.63544	-31.63543	-63.27088	-67.69451	-49.66493	-31.63533	-31.63537	-31.63537	-31.63535	-31.63537	-31.63535	-31.63535
$E_T(atom-atom, msp^3.AO)$ (eV)	-1.44915	-1.65376	-0.92918	0	0	0	0	-1.85836	-1.85836	-1.44915	-1.85836	-1.44915	-1.44915
$E_T(_{MO})$ (eV)	-33.08452	-33.28912	-32.56455	-63.27074	-67.69450	-49.66493	-31.63537	-33.49373	-33.49373	-33.08452	-33.49373	-33.08452	-33.08452
ω $(10^{15}\ rad/s)$	22.0240	12.1583	33.4164	17.6762	24.9286	24.2751	24.1759	9.43699	9.43699	15.4846	9.43699	9.55643	9.55643
E_K (eV)	14.49660	8.00277	21.99527	11.63476	16.40846	15.97831	15.91299	6.21159	6.21159	10.19220	6.21159	6.29021	6.29021
E_D (eV)	-0.24921	-0.18631	-0.30214	-0.21348	-0.25352	-0.25017	-0.24966	-0.16515	-0.16515	-0.20896	-0.16515	-0.16416	-0.16416
$\bar{E}_{Kvib}$ (eV)	0.13663 [21]	0.13663 [21]	0.08679 [42]	0.12832 [43]	0.35532 (Eq. (13.458))	0.35532 (Eq. (13.458))	0.35532 (Eq. (13.458))	0.12312 [2]	0.17978 [4]	0.09944 [5]	0.12312 [2]	0.12312 [2]	0.12312 [2]
$\bar{E}_{osc}$ (eV)	-0.18089	-0.11799	-0.25875	-0.14932	-0.22757	-0.14502	-0.07200	-0.10359	-0.07526	-0.15924	-0.10359	-0.10260	-0.10260
$\bar{E}_{mag}$ (eV)	0.14803	0.14803	0.11441	0.11441	0.14803	0.14803	0.14803	0.14803	0.14803	0.14803	0.14803	0.14803	0.14803
$E_T(_{Group})$ (eV)	-33.26541	-33.40711	-32.82330	-63.56937	-67.92207	-49.80996	-31.70737	-33.59732	-33.49373	-33.24376	-33.59732	-33.18712	-33.18712
$E_{initial}(_{\varepsilon_A\ AO/HO})$ (eV)	-14.63489	-14.63489	-14.63489	-14.63489	-14.63489	-14.63489	-14.63489	-14.63489	-14.63489	-14.63489	-14.63489	-14.63489	-14.63489
$E_{initial}(_{\varepsilon_S\ AO/HO})$ (eV)	0	0	0	-1.16125	-13.59844	-13.59844	-13.59844	0	0	0	0	0	0
$E_D(_{Group})$ (eV)	3.99563	4.13733	3.55352	3.86856	12.49186	7.83016	3.32601	4.32754	4.29921	3.97398	4.17951	3.62128	3.91734

Table 15.181. The total bond energies of alkyl sulfites calculated using the functional group composition and the energies of Table 15.180 compared to the experimental values [3].

Formula	Name	$C-O$ (i) Group	$C-O$ (ii) Group	$O-S$ Group	SO Group	CH_3	CH_2	CH	$C-C$ (a)	$C-C$ (b)	$C-C$ (c)	$C-C$ (d)	$C-C$ (e)	$C-C$ (f)	Calculated Total Bond Energy (eV)	Experimental Total Bond Energy (eV)	Relative Error
$C_2H_6SO_3$	Dimethyl sulfite	2	0	2	1	2	0	0	0	0	0	0	0	0	43.95058	44.042	0.00207
$C_4H_{10}SO_3$	Diethyl sulfite	0	2	2	1	2	2	0	2	0	0	0	0	0	68.54939	68.648	0.00143
$C_8H_{18}SO_3$	Dibutyl sulfite	0	2	2	1	2	6	0	6	0	0	0	0	0	117.18019	117.191	0.00009

Table 15.182. The bond angle parameters of alkyl sulfites and experimental values [1]. In the calculation of θ_v, the parameters from the preceding angle were used. E_T is $E_T(atom-atom,msp^3.AO)$.

Atoms of Angle	$2c'$ Bond 1 (a_0)	$2c'$ Bond 2 (a_0)	$2c'$ Terminal Atoms (a_0)	$E_{Coulombic}$ Atom 1	Atom 1 Hybridization Designation (Table 15.3.A)	$E_{Coulombic}$ Atom 2	Atom 2 Hybridization Designation (Table 15.3.A)	c_2 Atom 1	c_2 Atom 2	C_1	C_2	c_1	c_2'	E_T (eV)	θ_v (°)	θ_1 (°)	θ_2 (°)	Cal. θ (°)	Exp. θ (°)
$\angle O_aSO_b$	2.81792	2.96203	4.6904	-15.95954 O_a	10	-16.11722 O_c	12	0.85252	0.84418	1	1	1	0.84835	-1.65376				108.46	
$\angle O_bSO_c$	2.96203	2.96203	4.6476	-16.11722 O_b	12	-16.11722 O_c	12	0.84418	0.84418	1	1	1	0.84418	-1.65376				103.35	
$\angle C_aO_bS$	2.68862	2.96203	4.8416	-15.75493 C_a	7	-10.36001 S	S	0.86359	0.77641 (Eq. (15.158))	1	0.77641 (Eq. (15.158))	1	0.82000	-0.72457				117.84	
Methylene $\angle HC_aH$	2.11106	2.11106	3.4252	-15.75493	7	H	H	0.86359	1	1	1	0.75	1.15796	0				108.44	107 (propane)
$\angle C_aC_bC_c$															69.51			110.49	112 (propane) 113.8 (butane) 110.8 (isobutane)
$\angle C_cC_bH$															69.51			110.49	111.0 (butane) 111.4 (isobutane)
Methyl $\angle HC_aH$	2.09711	2.09711	3.4252	-15.75493	7	H	H	0.86359	1	1	1	0.75	1.15796	0				109.50	
$\angle C_aC_bC_c$															70.56			109.44	
$\angle C_cC_bH$															70.56			109.44	
$\angle C_bC_aC_c$ iso C_a	2.91547	2.91547	4.7958	-16.68412 C_b	26	-16.68412 C_c	26	0.81549	0.81549	1	1	1	0.81549	-1.85836				110.67	110.8 (isobutane)
$\angle C_bC_aH$ iso C_a	2.91547	2.11323	4.1633	-15.55033 C_a	5	-14.82575 C_b	1	0.87495	0.91771	0.75	1	0.75	1.04887	0				110.76	
$\angle C_cC_bH$ iso C_a	2.91547	2.09711	4.1633	-15.55033 C_b	5	-14.82575 C_a	1	0.87495	0.91771	0.75	1	0.75	1.04887	0				111.27	111.4 (isobutane)
$\angle C_bC_aC_b$ tert C_a	2.90327	2.90327	4.7958	-16.68412 C_b	26	-16.68412 C_b	26	0.81549	0.81549	1	1	1	0.81549	-1.85836				111.37	110.8 (isobutane)
$\angle C_bC_aC_d$															72.50			107.50	

SULFATES ($C_nH_{2n+2}(SO_4)_m$, $n=2,3,4,5...\infty$)

The alkyl sulfates, $C_nH_{2n+2}(SO_4)_m$, comprise a $C-O-SO_2-O-C$ moiety that comprises two types $C-O$ functional groups, one for methyl and one for alkyl, and $O-S$ and SO_2 functional groups. The alkyl portion of the alkyl sulfate may comprise at least two terminal methyl groups (CH_3) at each end of the chain, and may comprise methylene (CH_2), and methylyne (CH) functional groups as well as C bound by carbon-carbon single bonds. The methyl and methylene functional groups are equivalent to those of straight-chain alkanes. Six types of $C-C$ bonds can be identified. The n-alkane $C-C$ bond is the same as that of straight-chain alkanes. In addition, the $C-C$ bonds within isopropyl ($(CH_3)_2CH$) and t-butyl ($(CH_3)_3C$) groups and the isopropyl to isopropyl, isopropyl to t-butyl, and t-butyl to t-butyl $C-C$ bonds comprise functional groups. The branched-chain-alkane groups in sulfates are equivalent to those in branched-chain alkanes.

The methyl and alkyl $C-O$ functional groups having $E_T(atom-atom, msp^3.AO) = -1.44915\ eV$ and $E_T(atom-atom, msp^3.AO) = -1.65376\ eV$, respectively, are equivalent to the corresponding groups given in the Sulfites section. The $O-S$ functional group having $E_T(atom-atom, msp^3.AO) = -0.92918\ eV$ is equivalent to that given in the Sulfites section. The SO_2 functional group is equivalent to that of sulfones with $E_T(atom-atom, msp^3.AO) = 0$ as given in the Sulfones section.

The symbols of the functional groups of branched-chain alkyl sulfates are given in Table 15.183. The geometrical (Eqs. (15.1-15.5) and (15.51)), intercept (Eqs. (15.80-15.87)), and energy (Eqs. (15.6-15.11) and (15.17-15.65)) parameters of alkyl sulfates are given in Tables 15.184, 15.185, and 15.186, respectively. The total energy of each alkyl sulfate given in Table 15.187 was calculated as the sum over the integer multiple of each $E_{D(Group)}$ of Table 15.186 corresponding to functional-group composition of the molecule. The bond angle parameters of alkyl sulfates determined using Eqs. (15.88-15.117) are given in Table 15.188. The color scale, translucent view of the charge-density of exemplary sulfate, dimethyl sulfate, comprising the concentric shells of atoms with the outer shell bridged by one or more H_2-type ellipsoidal MOs or joined with one or more hydrogen MOs is shown in Figure 15.31.

Figure 15.31. (A)-(B) Color scale, translucent views of the charge-density of dimethyl sulfate showing the orbitals of the atoms at their radii, the ellipsoidal surface of each H or H_2-type ellipsoidal MO that transitions to the corresponding outer shell of the atom(s) participating in each bond, and the hydrogen nuclei (red, not to scale).

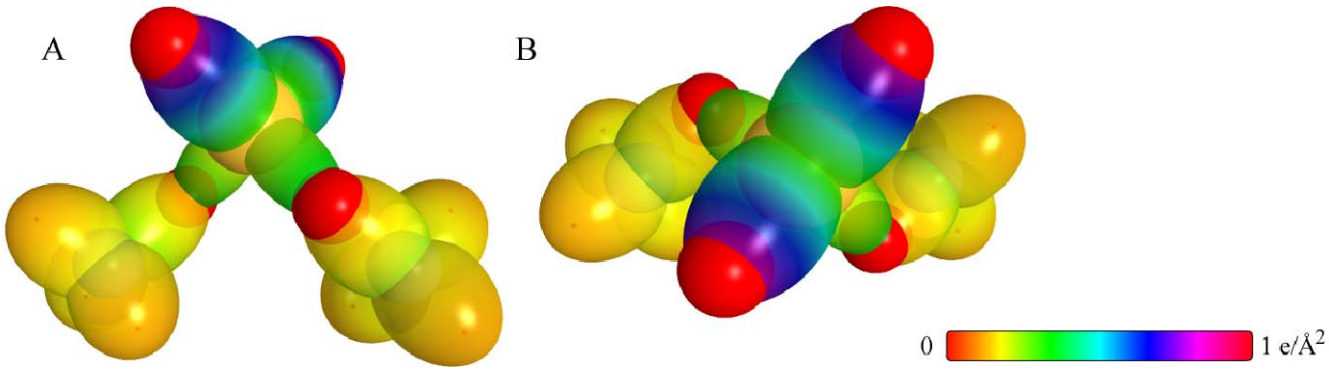

Table 15.183. The symbols of functional groups of alkyl sulfates.

Functional Group	Group Symbol
C-O (*methyl*)	$C-O$ (i)
C-O (*alkyl*)	$C-O$ (ii)
O-SO₃	$O-S$
SO₂	SO_2
CH₃ group	$C-H\ (CH_3)$
CH₂ group	$C-H\ (CH_2)$
CH	$C-H$
CC bond (*n-C*)	$C-C$ (a)
CC bond (*iso-C*)	$C-C$ (b)
CC bond (*tert-C*)	$C-C$ (c)
CC (*iso* to *iso-C*)	$C-C$ (d)
CC (*t* to *t-C*)	$C-C$ (e)
CC (*t* to *iso-C*)	$C-C$ (f)

Table 15.184. The geometrical bond parameters of alkyl sulfates and experimental values [1].

Parameter	$C-O$ (i) Group	$C-O$ (ii) Group	$O-S$	SO_2	$C-H\,(CH_3)$ Group	$C-H\,(CH_2)$ Group	$C-H$ Group	$C-C$ (a) Group	$C-C$ (b) Group	$C-C$ (c) Group	$C-C$ (d) Group	$C-C$ (e) Group	$C-C$ (f) Group
$a\,(a_0)$	1.80717	1.79473	1.70299	1.85851	1.64920	1.67122	1.67465	2.12499	2.12499	2.10725	2.12499	2.10725	2.10725
$c'\,(a_0)$	1.34431	1.33968	1.48102	1.36327	1.04856	1.05553	1.05661	1.45744	1.45744	1.45164	1.45744	1.45164	1.45164
Bond Length $2c'\,(\AA)$	1.42276	1.41785	1.56744	1.44282	1.10974	1.11713	1.11827	1.54280	1.54280	1.53635	1.54280	1.53635	1.53635
Exp. Bond Length $(\AA)$			1.574 (H_2SO_4)	1.435 (dimethyl sulfone)	1.107 ($C-H$ propane) 1.117 ($C-H$ butane)	1.107 ($C-H$ propane) 1.117 ($C-H$ butane)	1.122 (isobutane)	1.532 (propane) 1.531 (butane)	1.532 (propane) 1.531 (butane)	1.532 (propane) 1.531 (butane)	1.532 (propane) 1.531 (butane)	1.532 (propane) 1.531 (butane)	1.532 (propane) 1.531 (butane)
$b,c\,(a_0)$	1.20776	1.19429	0.84069	1.26315	1.27295	1.29569	1.29924	1.54616	1.54616	1.52750	1.54616	1.52750	1.52750
e	0.74388	0.74645	0.86966	0.73353	0.63580	0.63159	0.63095	0.68600	0.68600	0.68888	0.68600	0.68888	0.68888

Table 15.185. The MO to HO intercept geometrical bond parameters of alkyl sulfates. R, R', R'' are H or alkyl groups. E_T is $E_T(atom-atom,msp^3.AO)$.

Bond	Atom	E_T (eV) Bond 1	E_T (eV) Bond 2	E_T (eV) Bond 3	E_T (eV) Bond 4	Final Total Energy $C2sp^3$ (eV)	$r_{initial}$ (a_0)	r_{final} (a_0)	$E_{Coulomb}$ (eV) Final	$E(C2sp^3)$ (eV) Final	θ' (°)	θ_1 (°)	θ_2 (°)	d_1 (a_0)	d_2 (a_0)
$(RO)_2(O_a)S=O_a$	S	0	0	-0.46459	-0.46459		1.32010	0.86359	-15.75493		90.46	89.54	43.13	1.35635	0.00693
$(RO)_2(O_a)S=O_a$	O_a	0	0	0	0		1.00000	0.91771	-14.82575		95.05	84.95	46.36	1.28256	0.08071
$CH_3O_a-S(O_2)OR'$	S	-0.46459	-0.46459	0	0		1.32010	0.86359	-15.75493		126.68	53.32	55.47	0.96521	0.51581
$CH_3O_a-S(O_2)OR'$ $(C-O$ (i))	O_a	-0.46459	-0.72457	0	0		1.00000	0.84957	-16.01492		126.03	53.97	54.81	0.98133	0.49969
$RCH_2O_a-S(O_2)OR'$ $(C-O$ (ii))	O_a	-0.46459	-0.82688	0	0		1.00000	0.84418	-16.11722		125.77	54.23	54.56	0.98753	0.49349
$H_3C_a-O_aS(O_2)OR$ $(C-O$ (i))	O_a	-0.72457	-0.46459	0	0		1.00000	0.84957	-16.01492		93.85	86.15	44.57	1.28731	0.05700
$H_3C_a-O_aS(O_2)OR$ $(C-O$ (i))	C_a	-0.72457	0	0	0	-152.34026	0.91771	0.87495	-15.55033	-15.35946	95.98	84.02	46.10	1.25319	0.09112
$RH_2C_a-O_aS(O_2)OR'$ $(C-O$ (ii))	O_a	-0.82688	-0.46459	0	0		1.00000	0.84418	-16.11722		94.50	85.50	44.80	1.27343	0.06624
$RH_2C_a-O_aS(O_2)OR'$ $(C-O$ (ii))	C_a	-0.82688	-0.92918	0	0	-153.37175	0.91771	0.82053	-16.58181	-16.39095	92.41	87.59	43.35	1.30512	0.03456
$C-H\ (CH_3)$	C	-0.92918	0	0	0	-152.54487	0.91771	0.86359	-15.75493	-15.56407	77.49	102.51	41.48	1.23564	0.18708
$C-H\ (CH_2)$	C	-0.92918	-0.92918	0	0	-153.47406	0.91771	0.81549	-16.68412	-16.49325	68.47	111.53	35.84	1.35486	0.29933
$C-H\ (CH)$	C	-0.92918	-0.92918	-0.92918	0	-154.40324	0.91771	0.77247	-17.61330	-17.42244	61.10	118.90	31.37	1.42988	0.37326
$H_3C_aC_bH_2CH_2-$ $(C-C$ (a))	C_a	-0.92918	0	0	0	-152.54487	0.91771	0.86359	-15.75493	-15.56407	63.82	116.18	30.08	1.83879	0.38106
$H_3C_aC_bH_2CH_2-$ $(C-C$ (a))	C_b	-0.92918	-0.92918	0	0	-153.47406	0.91771	0.81549	-16.68412	-16.49325	56.41	123.59	26.06	1.90890	0.45117
$R-H_2C_aC_b(H_2C_c-R')HCH_2-$ $(C-C$ (b))	C_b	-0.92918	-0.92918	-0.92918	0	-154.40324	0.91771	0.77247	-17.61330	-17.42244	48.30	131.70	21.90	1.97162	0.51388
$R-H_2C_a(R'-H_2C_d)C_b(R''-H_2C_c)CH_2-$ $(C-C$ (e))	C_b	-0.92918	-0.72457	-0.72457	-0.72457	-154.71860	0.91771	0.75889	-17.92866	-17.73779	48.21	131.79	21.74	1.95734	0.50570
$isoC_aC_b(H_2C_c-R')HCH_2-$ $(C-C$ (d))	C_b	-0.92918	-0.92918	-0.92918	0	-154.40324	0.91771	0.77247	-17.61330	-17.42244	48.30	131.70	21.90	1.97162	0.51388
$tertC_a(R'-H_2C_d)C_b(R''-H_2C_c)CH_2-$ $(C-C$ (e))	C_b	-0.72457	-0.72457	-0.72457	-0.72457	-154.51399	0.91771	0.76765	-17.92866	-17.73779	50.04	129.96	22.66	1.94462	0.49298
$tertC_aC_b(H_2C_c-R')HCH_2-$ $(C-C$ (f))	C_b	-0.72457	-0.92918	-0.92918	0	-154.19863	0.91771	0.78155	-17.40869	-17.21783	52.78	127.22	24.04	1.92443	0.47279
$isoC_a(R'-H_2C_d)C_b(R''-H_2C_c)CH_2-$ $(C-C$ (f))	C_b	-0.72457	-0.72457	-0.72457	-0.72457	-154.51399	0.91771	0.76765	-17.92866	-17.73779	50.04	129.96	22.66	1.94462	0.49298

Table 15.186. The energy parameters (eV) of functional groups of alkyl sulfates.

Parameters	$C-O$ (i) Group	$C-O$ (ii) Group	$O-S$ Group	SO_2 Group	CH_3 Group	CH_2 Group	$C-H$ Group	$C-C$ (a) Group	$C-C$ (b) Group	$C-C$ (c) Group	$C-C$ (d) Group	$C-C$ (e) Group	$C-C$ (f) Group
n_1	1	1	1	4	3	2	1	1	1	1	1	1	1
n_2	0	0	0	0	2	1	0	0	0	0	0	0	0
n_3	0	0	0	0	0	0	0	0	0	0	0	0	0
C_1	0.5	0.5	0.5	0.5	0.75	0.75	0.75	0.5	0.5	0.5	0.5	0.5	0.5
C_2	1	1	0.77641	1	1	1	1	1	1	1	1	1	1
c_1	1	1	1	1	1	1	1	1	1	1	1	1	1
c_2	0.85395	0.85395	1	1.20632	0.91771	0.91771	0.91771	0.91771	0.91771	0.91771	0.91771	0.91771	0.91771
c_3	0	0	0	1	0	1	1	0	0	0	1	1	0
c_4	2	2	2	8	1	1	1	2	2	2	2	2	2
c_5	0	0	0	1	3	2	1	0	0	0	0	0	0
C_{1o}	0.5	0.5	0.5	0.5	0.75	0.75	0.75	0.5	0.5	0.5	0.5	0.5	0.5
C_{2o}	1	1	0.77641	1	1	1	1	1	1	1	1	1	1
$V_e\ (eV)$	-33.15757	-33.47304	-48.93512	-180.36454	-107.32728	-70.41425	-35.12015	-28.79214	-28.79214	-29.10112	-28.79214	-29.10112	-29.10112
$V_p\ (eV)$	10.12103	10.15605	9.18680	39.92103	38.92728	25.78002	12.87680	9.33352	9.33352	9.37273	9.33352	9.37273	9.37273
$T\ (eV)$	9.17389	9.32537	14.36741	48.52397	32.53914	21.06675	10.48582	6.77464	6.77464	6.90500	6.77464	6.90500	6.90500
$V_m\ (eV)$	-4.58695	-4.66268	-7.18371	-24.26198	-16.26957	-10.53337	-5.24291	-3.38732	-3.38732	-3.45250	-3.38732	-3.45250	-3.45250
$E_{(AO/HO)}\ (eV)$	-14.63489	-14.63489	0	-11.52126	-15.56407	-15.56407	-14.63489	-15.56407	-15.56407	-15.35946	-15.56407	-15.35946	-15.35946
$\Delta E_{H_2MO(AO/HO)}\ (eV)$	-1.44915	-1.65376	-0.92918	-1.16125	0	0	0	0	0	0	0	0	0
$E_T\ (_{AO/HO})\ (eV)$	-13.18574	-12.98113	0.92918	-10.36001	-15.56407	-15.56407	-14.63489	-15.56407	-15.56407	-15.35946	-15.56407	-15.35946	-15.35946
$E_T\ (_{H_2MO})\ (eV)$	-31.63533	-31.63544	-31.63543	-126.54154	-67.69451	-49.66493	-31.63533	-31.63537	-31.63537	-31.63535	-31.63537	-31.63535	-31.63535
$E_T\left(atom-atom, msp^3.AO\right)(eV)$	-1.44915	-1.65376	-0.92918	0	0	0	0	-1.85836	-1.85836	-1.44915	-1.85836	-1.44915	-1.44915
$E_T\ (_{MO})\ (eV)$	-33.08452	-33.28912	-32.56455	-126.54147	-67.69450	-49.66493	-31.63537	-33.49373	-33.49373	-33.08452	-33.49373	-33.08452	-33.08452
$\omega\ \left(10^{15}\ rad/s\right)$	22.0240	12.1583	33.4164	11.5378	24.9286	24.2751	24.1759	9.43699	9.43699	15.4846	9.43699	9.55643	9.55643
$E_K\ (eV)$	14.49660	8.00277	21.99527	7.59437	16.40846	15.97831	15.91299	6.21159	6.21159	10.19220	6.21159	6.29021	6.29021
$\bar{E}_D\ (eV)$	-0.24921	-0.18631	-0.30214	-0.17247	-0.25352	-0.25017	-0.24966	-0.16515	-0.16515	-0.20896	-0.16515	-0.16416	-0.16416
$\bar{E}_{Kvib}\ (eV)$	0.13663 [21]	0.13663 [21]	0.08679 [42]	0.12832 [43]	0.35532 (Eq. (13.458))	0.35532 (Eq. (13.458))	0.35532 (Eq. (13.458))	0.12312 [2]	0.17978 [4]	0.09944 [5]	0.12312 [2]	0.12312 [2]	0.12312 [2]
$\bar{E}_{osc}\ (eV)$	-0.18089	-0.11799	-0.25875	-0.10831	-0.22757	-0.14502	-0.07200	-0.10359	-0.07526	-0.15924	-0.10359	-0.10260	-0.10260
$E_{mag}\ (eV)$	0.14803	0.14803	0.11441	0.11441	0.14803	0.14803	0.14803	0.14803	0.14803	0.14803	0.14803	0.14803	0.14803
$E_T\ (_{Group})\ (eV)$	-33.26541	-33.40711	-32.82330	-126.97472	-67.92207	-49.80996	-31.70737	-33.59732	-33.49373	-33.24376	-33.59732	-33.18712	-33.18712
$E_{initial}\ (_{c_4\ AO/HO})\ (eV)$	-14.63489	-14.63489	-14.63489	-14.63489	-14.63489	-14.63489	-14.63489	-14.63489	-14.63489	-14.63489	-14.63489	-14.63489	-14.63489
$E_{initial}\ (_{c_5\ AO/HO})\ (eV)$	0	0	0	-1.16125	-13.59844	-13.59844	-13.59844	0	0	0	0	0	0
$E_D\ (_{Group})\ (eV)$	3.99563	4.13733	3.55352	8.61994	12.49186	7.83016	3.32601	4.32754	4.29921	3.97398	4.17951	3.62128	3.91734

Table 15.187. The total bond energies of alkyl sulfates calculated using the functional group composition and the energies of Table 15.186 compared to the experimental values [3].

Formula	Name	$C-O$ (i) Group	$C-O$ (ii) Group	$O-S$ Group	SO_2 Group	CH_3	CH_2	CH	$C-C$ (a)	$C-C$ (b)	$C-C$ (c)	$C-C$ (d)	$C-C$ (e)	$C-C$ (f)	Calculated Total Bond Energy (eV)	Experimental Total Bond Energy (eV)	Relative Error
$C_2H_6SO_4$	Dimethyl sulfate	2	0	2	1	2	0	0	0	0	0	0	0	0	48.70196	48.734	0.00067
$C_4H_{10}SO_4$	Diethyl sulfate	0	2	2	1	2	2	0	2	0	0	0	0	0	73.30077	73.346	0.00061
$C_6H_{14}SO_4$	Dipropyl sulfate	0	2	2	1	2	4	0	4	0	0	0	0	0	97.61617	97.609	-0.00008

Table 15.188. The bond angle parameters of alkyl sulfates and experimental values [1]. In the calculation of θ_v, the parameters from the preceding angle were used. E_T is E_T ($atom-atom$,$msp^3.AO$).

Atoms of Angle	2c' Bond 1 (a_0)	2c' Bond 2 (a_0)	2c' Terminal Atoms (a_0)	$E_{Coulombic}$ Atom 1	Atom 1 Hybridization Designation (Table 15.3.A)	$E_{Coulombic}$ Atom 2	Atom 2 Hybridization Designation (Table 15.3.A)	c_2 Atom 1	c_2 Atom 2	C_1	C_2	c_1	c_2'	E_T (eV)	θ_v (°)	θ_1 (°)	θ_2 (°)	Cal. θ (°)	Exp. θ (°)
$\angle O_aSO_b$	2.72654	2.72654	4.7329	-15.95954 O_a	10	-15.95954 O_b	10	0.85252	0.85252	1	1	1	0.85252	-1.65376				120.44	120.9 [44] (dimethyl sulfate)
$\angle O_aSO_c$	2.72654	2.96203	4.6690	-15.95954 O_a	10	-16.11722 O_c	12	0.85252	0.84418	1	1	1	0.84835	-1.65376				110.26	109.67 [44] (dimethyl sulfate)
$\angle O_cSO_d$	2.96203	2.96203	4.6476	-16.11722 O_c	12	-16.11722 O_d	12	0.84418	0.84418	1	1	1	0.84418	-1.65376				103.35	103.85 [44] (dimethyl sulfate)
$\angle C_aO_cS$	2.68862	2.96203	4.8416	-15.75493 C_a	7	-10.36001 S	S	0.86359	0.77641 (Eq. (15.158))	1	0.77641 (Eq. (15.158))	1	0.82000	-0.72457				117.84	117.43[44] (dimethyl sulfate)
Methylene $\angle HC_aH$	2.11106	2.11106	3.4252	-15.75493	7	H	H	0.86359	1	1	1	0.75	1.15796	0				108.44	107 (propane)
$\angle C_aC_bC_c$															69.51			110.49	112 (propane) 113.8 (butane) 110.8 (isobutane)
$\angle C_aC_bH$															69.51			110.49	111.0 (butane) 111.4 (isobutane)
Methyl $\angle HC_aH$	2.09711	2.09711	3.4252	-15.75493	7	H	H	0.86359	1	1	1	0.75	1.15796	0				109.50	
$\angle C_aC_bC_c$															70.56			109.44	
$\angle C_aC_bH$															70.56			109.44	
$\angle C_bC_aC_c$ iso C_a	2.91547	2.91547	4.7958	-16.68412 C_b	26	-16.68412 C_c	26	0.81549	0.81549	1	1	1	0.81549	-1.85836				110.67	110.8 (isobutane)
$\angle C_bC_aH$ iso C_a	2.91547	2.11323	4.1633	-15.55033 C_a	5	-14.82575 C_b	1	0.87495	0.91771	0.75	1	0.75	1.04887	0				110.76	
$\angle C_aC_bH$ iso C_a	2.91547	2.09711	4.1633	-15.55033 C_b	5	-14.82575 C_a	1	0.87495	0.91771	0.75	1	0.75	1.04887	0				111.27	111.4 (isobutane)
$\angle C_bC_aC_b$ tert C_a	2.90327	2.90327	4.7958	-16.68412 C_b	26	-16.68412 C_b	26	0.81549	0.81549	1	1	1	0.81549	-1.85836				111.37	110.8 (isobutane)
$\angle C_bC_aC_d$															72.50			107.50	

NITROALKANES ($C_nH_{2n+2-m}\left(NO_2\right)_m$, $n=1,2,3,4,5...\infty$)

The nitroalkanes, $C_nH_{2n+2-m}\left(NO_2\right)_m$, comprise a NO_2 functional group and a $C-N$ functional group. The alkyl portion of the nitroalkane may comprise at least two terminal methyl groups (CH_3) at each end of the chain, and may comprise methylene (CH_2), and methylyne (CH) functional groups as well as C bound by carbon-carbon single bonds. The methyl and methylene functional groups are equivalent to those of straight-chain alkanes. Six types of $C-C$ bonds can be identified. The n-alkane $C-C$ bond is the same as that of straight-chain alkanes. In addition, the $C-C$ bonds within isopropyl ($\left(CH_3\right)_2CH$) and t-butyl ($\left(CH_3\right)_3C$) groups and the isopropyl to isopropyl, isopropyl to t-butyl, and t-butyl to t-butyl $C-C$ bonds comprise functional groups. The branched-chain-alkane groups in nitroalkanes are equivalent to those in branched-chain alkanes.

The electron configuration of oxygen is $1s^22s^22p^4$, and the orbital arrangement given by Eq. (10.154) has two unpaired electrons corresponding to the ground state ${}^3P_2$. The electron configuration of nitrogen is $1s^22s^22p^3$, and the orbital arrangement given by Eq. (10.134) has three unpaired electrons corresponding to the ground state ${}^4S^0_{3/2}$. The bonding in the nitro (NO_2) functional group is similar to that in the SO_2 group given previously. It also has similarities to the bonding in the carbonyl functional group. In the NO_2 group, the two unpaired electrons of the O atoms form a MO with two unpaired electrons of the nitrogen atom such that the MO comprises a linear combination of two bonds, each of bond order two involving the nitrogen AOs and oxygen AOs of both oxygen atoms. The nitrogen atom is then energy matched to the $C2sp^3$ HO. In nitroalkanes, the $C2sp^3$ HO has a hybridization factor of 0.91771 (Eq. (13.430)) with a corresponding energy of $E\left(C,2sp^3\right)=-14.63489\ eV$ (Eq. (15.25)), the N AO has an energy of $E\left(N\right)=-14.53414\ eV$, and the O AO has an energy of $E\left(O\right)=-13.61806\ eV$ [38]. To meet the equipotential condition of the union of the $N=O$ H_2-type-ellipsoidal-MO with these orbitals, the hybridization factor c_2 of Eq. (15.61) for the $N=O$-bond MO given by Eqs. (15.77) and (15.79) is:

$$c_2\left(O\ to\ N2p\ to\ C2sp^3HO\right)=\frac{E\left(O\right)}{E\left(N\right)}c_2\left(C2sp^3HO\right)=\frac{-13.61806\ eV}{-14.53414\ eV}\left(0.91771\right)=0.85987 \tag{15.159}$$

Since there are two O atoms in a linear combination that comprises the bonding of the NO_2 group, the unpaired electrons of each O cancel each others effect such that E_{mag} is not subtracted from the total energy of NO_2. Additionally, $E_T\left(atom-atom,msp^3.AO\right)=-3.71673\ eV=4\left(-0.92918\ eV\right)$ (Eq. (14.513)) is the maximum given the bonding involves four electrons comprising two bonds, each having a bond order of one.

The $C-N$ group is equivalent to that of primary amines except that the energies corresponding to vibration in the transition state are matched to a nitroalkane and $\Delta E_{H_2MO}\left(AO/HO\right)=-0.72457\ eV$ for nitroalkane and $\Delta E_{H_2MO}\left(AO/HO\right)=-1.44915\ eV$ for primary amines. Whereas, $E_T\left(atom-atom,msp^3.AO\right)=-1.44915\ eV$ for both functional groups. This condition matches the energy of the $C-N$ group with the NO_2 having $\Delta E_{H_2MO}\left(AO/HO\right)=0$.

The symbols of the functional groups of branched-chain nitroalkanes are given in Table 15.189. The geometrical (Eqs. (15.1-15.5) and (15.51)), intercept (Eqs. (15.80-15.87)), and energy (Eqs. (15.6-15.11) and (15.17-15.65)) parameters of nitroalkanes are given in Tables 15.190, 15.191, and 15.192, respectively. The total energy of each nitroalkane given in Table 15.193 was calculated as the sum over the integer multiple of each $E_{D\,(Group)}$ of Table 15.192 corresponding to functional-group composition of the molecule. E_{mag} given by Eq. (15.67) was subtracted for each t-butyl group. The bond angle parameters of nitroalkanes determined using Eqs. (15.88-15.117) are given in Table 15.194. The color scale, translucent view of the charge-density of exemplary nitroalkane, nitroethane, comprising the concentric shells of atoms with the outer shell bridged by one or more H_2-type ellipsoidal MOs or joined with one or more hydrogen MOs is shown in Figure 15.32.

Figure 15.32. Color scale, translucent view of the charge-density of nitroethane showing the orbitals of the atoms at their radii, the ellipsoidal surface of each H or H_2-type ellipsoidal MO that transitions to the corresponding outer shell of the atom(s) participating in each bond, and the hydrogen nuclei (red, not to scale).

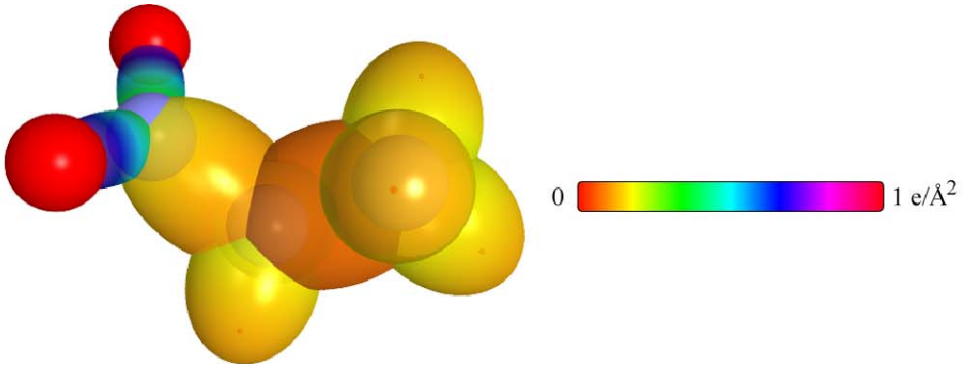

Table 15.189. The symbols of functional groups of nitroalkanes.

Functional Group	Group Symbol
NO_2 group	NO_2
C-N	$C-N$
CH_3 group	$C-H\ (CH_3)$
CH_2 group	$C-H\ (CH_2)$
CH	$C-H$
CC bond (*n-C*)	$C-C$ (a)
CC bond (*iso-C*)	$C-C$ (b)
CC bond (*tert-C*)	$C-C$ (c)
CC (*iso* to *iso-C*)	$C-C$ (d)
CC (*t* to *t-C*)	$C-C$ (e)
CC (*t* to *iso-C*)	$C-C$ (f)

Table 15.190. The geometrical bond parameters of nitroalkanes and experimental values [1].

Parameter	NO_2 Group	$C-N$ Group	$C-H\ (CH_3)$ Group	$C-H\ (CH_2)$ Group	$C-H$ Group	$C-C$ (a) Group	$C-C$ (b) Group	$C-C$ (c) Group	$C-C$ (d) Group	$C-C$ (e) Group	$C-C$ (f) Group
$a\ (a_0)$	1.33221	1.97794	1.64920	1.67122	1.67465	2.12499	2.12499	2.10725	2.12499	2.10725	2.10725
$c'\ (a_0)$	1.15421	1.40639	1.04856	1.05553	1.05661	1.45744	1.45744	1.45164	1.45744	1.45164	1.45164
Bond Length $2c'\ (A)$	1.22157	1.48846	1.10974	1.11713	1.11827	1.54280	1.54280	1.53635	1.54280	1.53635	1.53635
Exp. Bond Length (A)	1.224 (nitromethane)	1.489 (nitromethane)	1.107 ($C-H$ propane) 1.117 ($C-H$ butane)	1.107 ($C-H$ propane) 1.117 ($C-H$ butane)	1.122 (isobutane)	1.532 (propane) 1.531 (butane)	1.532 (propane) 1.531 (butane)	1.532 (propane) 1.531 (butane)	1.532 (propane) 1.531 (butane)	1.532 (propane) 1.531 (butane)	1.532 (propane) 1.531 (butane)
$b,c\ (a_0)$	0.66526	1.39079	1.27295	1.29569	1.29924	1.54616	1.54616	1.52750	1.54616	1.52750	1.52750
e	0.86639	0.71104	0.63580	0.63159	0.63095	0.68600	0.68600	0.68888	0.68600	0.68888	0.68888

Table 15.191. The MO to HO intercept geometrical bond parameters of nitroalkanes. R, R', R'' are H or alkyl groups. E_T is $E_T(atom-atom,msp^3.AO)$.

Bond	Atom	E_T (eV) Bond 1	E_T (eV) Bond 2	E_T (eV) Bond 3	E_T (eV) Bond 4	Final Total Energy $C2sp^3$ (eV)	$r_{initial}\ (a_0)$	$r_{final}\ (a_0)$	$E_{Coulomb}$ (eV) Final	$E(C2sp^3)$ (eV) Final	θ' (°)	θ_1 (°)	θ_2 (°)	$d_1\ (a_0)$	$d_2\ (a_0)$
$RN(O)=O$	O	-0.92918	0	0	0		1.00000	0.86359	-15.75493		135.25	44.75	66.05	0.54089	0.61333
$RN(O)=O$	N	-0.92918	-0.92918	-0.72457	0		0.93084	0.78155	-17.40869		131.57	48.43	61.50	0.63558	0.51864
H_3C-NO_2	C	-0.72457	0	0	0	-152.34026	0.91771	0.87495	-15.55033	-15.35946	80.47	99.53	38.35	1.55123	0.14484
RH_2C-NO_2 $R=H,alkyl$	N	-0.92918	-0.92918	-0.72457	0		0.93084	0.78155	-17.40869		69.30	110.70	31.71	1.68259	0.27620
$-H_2C_a-NO_2$	C_a	-0.72457	-0.92918	0	0	-153.26945	0.91771	0.82562	-16.47951	-16.28864	74.96	105.04	34.98	1.62061	0.21422
$C-H\ (CH_3)$	C	-0.92918	0	0	0	-152.54487	0.91771	0.86359	-15.75493	-15.56407	77.49	102.51	41.48	1.23564	0.18708
$C-H\ (CH_2)$	C	-0.92918	-0.92918	0	0	-153.47406	0.91771	0.81549	-16.68412	-16.49325	68.47	111.53	35.84	1.35486	0.29933
$C-H\ (CH)$	C	-0.92918	-0.92918	-0.92918	0	-154.40324	0.91771	0.77247	-17.61330	-17.42244	61.10	118.90	31.37	1.42988	0.37326
$H_3C_aC_bH_2CH_2-$ ($C-C$ (a))	C_a	-0.92918	0	0	0	-152.54487	0.91771	0.86359	-15.75493	-15.56407	63.82	116.18	30.08	1.83879	0.38106
$H_3C_aC_bH_2CH_2-$ ($C-C$ (a))	C_b	-0.92918	-0.92918	0	0	-153.47406	0.91771	0.81549	-16.68412	-16.49325	56.41	123.59	26.06	1.90890	0.45117
$R-H_2C_aC_b(H_2C_c-R')HCH_2-$ ($C-C$ (b))	C_b	-0.92918	-0.92918	-0.92918	0	-154.40324	0.91771	0.77247	-17.61330	-17.42244	48.30	131.70	21.90	1.97162	0.51388
$R-H_2C_a(R'-H_2C_d)C_b(R''-H_2C_e)CH_2-$ ($C-C$ (c))	C_b	-0.92918	-0.72457	-0.72457	-0.72457	-154.71860	0.91771	0.75889	-17.92866	-17.73779	48.21	131.79	21.74	1.95734	0.50570
$isoC_aC_b(H_2C_c-R')HCH_2-$ ($C-C$ (d))	C_b	-0.92918	-0.92918	-0.92918	0	-154.40324	0.91771	0.77247	-17.61330	-17.42244	48.30	131.70	21.90	1.97162	0.51388
$tertC_a(R'-H_2C_d)C_b(R''-H_2C_e)CH_2-$ ($C-C$ (e))	C_b	-0.72457	-0.72457	-0.72457	-0.72457	-154.51399	0.91771	0.76765	-17.92866	-17.73779	50.04	129.96	22.66	1.94462	0.49298
$tertC_aC_b(H_2C_c-R')HCH_3-$ ($C-C$ (f))	C_b	-0.72457	-0.92918	-0.92918	0-	-154.19863	0.91771	0.78155	-17.40869	-17.21783	52.78	127.22	24.04	1.92443	0.47279
$isoC_a(R'-H_2C_d)C_b(R''-H_2C_c)CH_2-$ ($C-C$ (f))	C_b	-0.72457	-0.72457	-0.72457	-0.72457	-154.51399	0.91771	0.76765	-17.92866	-17.73779	50.04	129.96	22.66	1.94462	0.49298

Table 15.192. The energy parameters (eV) of functional groups of nitroalkanes.

Parameters	NO_2 Group	$C-N$ Group	CH_3 Group	CH_2 Group	$C-H$ Group	$C-C$ (a) Group	$C-C$ (b) Group	$C-C$ (c) Group	$C-C$ (d) Group	$C-C$ (e) Group	$C-C$ (f) Group
n_1	2	1	3	2	1	1	1	1	1	1	1
n_2	0	0	2	1	0	0	0	0	0	0	0
n_3	0	0	0	0	0	0	0	0	0	0	0
C_1	0.5	0.5	0.75	0.75	0.75	0.5	0.5	0.5	0.5	0.5	0.5
C_2	1	1	1	1	1	1	1	1	1	1	1
c_1	1	1	1	1	1	1	1	1	1	1	1
c_2	0.85987	0.91140	0.91771	0.91771	0.91771	0.91771	0.91771	0.91771	0.91771	0.91771	0.91771
c_3	0	0	0	1	1	0	0	0	1	1	0
c_4	4	2	1	1	1	2	2	2	2	2	2
c_5	0	0	3	2	1	0	0	0	0	0	0
C_{1o}	0.5	0.5	0.75	0.75	0.75	0.5	0.5	0.5	0.5	0.5	0.5
C_{2o}	1	1	1	1	1	1	1	1	1	1	1
V_e (eV)	-106.90919	-31.36351	-107.32728	-70.41425	-35.12015	-28.79214	-28.79214	-29.10112	-28.79214	-29.10112	-29.10112
V_p (eV)	23.57588	9.67426	38.92728	25.78002	12.87680	9.33352	9.33352	9.37273	9.33352	9.37273	9.37273
T (eV)	40.12475	7.92833	32.53914	21.06675	10.48582	6.77464	6.77464	6.90500	6.77464	6.90500	6.90500
V_m (eV)	-20.06238	-3.96416	-16.26957	-10.53337	-5.24291	-3.38732	-3.38732	-3.45250	-3.38732	-3.45250	-3.45250
$E_{(AO/HO)}$ (eV)	0	-14.63489	-15.56407	-15.56407	-14.63489	-15.56407	-15.56407	-15.35946	-15.56407	-15.35946	-15.35946
$\Delta E_{H_2MO(AO/HO)}$ (eV)	0	-0.72457	0	0	0	0	0	0	0	0	0
$\bar{E}_{I(AO/HO)}$ (eV)	0	-13.91032	-15.56407	-15.56407	-14.63489	-15.56407	-15.56407	-15.35946	-15.56407	-15.35946	-15.35946
$\bar{E}_{I(H_2MO)}$ (eV)	-63.27093	-31.63540	-67.69451	-49.66493	-31.63533	-31.63537	-31.63537	-31.63535	-31.63537	-31.63535	-31.63535
$\bar{E}_{I}(atom-atom,msp^3.AO)$ (eV)	-3.71673	-1.44915	0	0	0	-1.85836	-1.85836	-1.44915	-1.85836	-1.44915	-1.44915
$\bar{E}_{I(MO)}$ (eV)	-66.98746	-33.08452	-67.69450	-49.66493	-31.63537	-33.49373	-33.49373	-33.08452	-33.49373	-33.08452	-33.08452
ω $(10^{15}\ rad/s)$	19.0113	10.5087	24.9286	24.2751	24.1759	9.43699	9.43699	15.4846	9.43699	9.55643	9.55643
$\bar{E}_K$ (eV)	12.51354	6.91703	16.40846	15.97831	15.91299	6.21159	6.21159	10.19220	6.21159	6.29021	6.29021
$\bar{E}_D$ (eV)	-0.23440	-0.17214	-0.25352	-0.25017	-0.24966	-0.16515	-0.16515	-0.20896	-0.16515	-0.16416	-0.16416
$\bar{E}_{Kvib}$ (eV)	0.19342 [45]	0.10539 [45]	0.35532 (Eq. (13.458))	0.35532 (Eq. (13.458))	0.35532 (Eq. (13.458))	0.12312 [2]	0.17978 [4]	0.09944 [5]	0.12312 [2]	0.12312 [2]	0.12312 [2]
$\bar{E}_{esc}$ (eV)	-0.13769	-0.11945	-0.22757	-0.14502	-0.07200	-0.10359	-0.07526	-0.15924	-0.10359	-0.10260	-0.10260
$\bar{E}_{mag}$ (eV)	0.11441	0.14803	0.14803	0.14803	0.14803	0.14803	0.14803	0.14803	0.14803	0.14803	0.14803
$\bar{E}_{I(Group)}$ (eV)	-67.26284	-33.20397	-67.92207	-49.80996	-31.70737	-33.59732	-33.49373	-33.24376	-33.59732	-33.18712	-33.18712
$\bar{E}_{initial(c_4\ AO/HO)}$ (eV)	-14.63489	-14.63489	-14.63489	-14.63489	-14.63489	-14.63489	-14.63489	-14.63489	-14.63489	-14.63489	-14.63489
$\bar{E}_{initial(c_5\ AO/HO)}$ (eV)	0	0	-13.59844	-13.59844	-13.59844	0	0	0	0	0	0
$\bar{E}_{D(Group)}$ (eV)	8.72329	3.93419	12.49186	7.83016	3.32601	4.32754	4.29921	3.97398	4.17951	3.62128	3.91734

Table 15.193. The total bond energies of nitroalkanes calculated using the functional group composition and the energies of Table 15.192 compared to the experimental values [3]. The magnetic energy E_{mag} that is subtracted from the weighted sum of the E_D $(_{Group})$ (eV) values based on composition is given by (15.58).

Formula	Name	NO_2 Group	$C-N$ Group	CH_3	CH_2	CH	$C-C$ (a)	$C-C$ (b)	$C-C$ (c)	$C-C$ (d)	$C-C$ (e)	$C-C$ (f)	E_{mag}	Calculated Total Bond Energy (eV)	Experimental Total Bond Energy (eV)	Relative Error
CH_3NO_2	Nitromethane	1	1	1	0	0	0	0	0	0	0	0	0	25.14934	25.107	-0.00168
$C_2H_5NO_2$	Nitroethane	1	1	1	1	0	1	0	0	0	0	0	0	37.30704	37.292	-0.00040
$C_3H_7NO_2$	1-Nitropropane	1	1	1	2	0	2	0	0	0	0	0	0	49.46474	49.451	-0.00028
$C_3H_7NO_2$	2-Nitropropane	1	1	2	0	1	0	2	0	0	0	0	0	49.56563	49.602	0.00074
$C_4H_9NO_2$	1-Nitrobutane	1	1	1	3	0	3	0	0	0	0	0	0	61.62244	61.601	-0.00036
$C_4H_9NO_2$	2-Nitroisobutane	1	1	3	0	0	0	0	3	0	0	0	-1	61.90697	61.945	0.00061
$C_5H_{11}NO_2$	1-Nitropentane	1	1	1	4	0	4	0	0	0	0	0	0	73.78014	73.759	-0.00028

Table 15.194. The bond angle parameters of nitroalkanes and experimental values [1]. In the calculation of θ_v, the parameters from the preceding angle were used. E_T is $E_T(atom-atom,msp^3.AO)$.

Atoms of Angle	$2c'$ Bond 1 (a_0)	$2c'$ Bond 2 (a_0)	$2c'$ Terminal Atoms (a_0)	$E_{Coulombic}$ or E Atom 1	Atom 1 Hybridization Designation (Table 15.3.A)	$E_{Coulombic}$ Atom 2	Atom 2 Hybridization Designation (Table 15.3.A)	c_2 Atom 1	c_2 Atom 2	C_1	C_2	c_1	c_2'	E_T (eV)	θ_v (°)	θ_1 (°)	θ_2 (°)	Cal. θ (°)	Exp. ϑ (°)
$\angle NC_aH$	2.81279	2.09711	3.9665	-14.82575	1	-14.53414	N	0.91771	0.91140 (Eq. (15.135))	0.75	1	0.75	0.99312	0				106.87	107 (nitromethane)
$\angle O_aNO_b$	2.30843	2.30843	4.1231	-16.68411 O_a	25	-16.68411 O_b	25	0.81549	0.81549	1	1	1	0.81549	-1.44915				126.52	125.3 (nitromethane)
Methylene $\angle HC_aH$	2.11106	2.11106	3.4252	-15.75493	7	H	H	0.86359	1	1	1	0.75	1.15796	0				108.44	107 (propane)
$\angle C_aC_bC_c$															69.51			110.49	112 (propane) 113.8 (butane) 110.8 (isobutane)
$\angle C_aC_bH$															69.51			110.49	111.0 (butane) 111.4 (isobutane)
Methyl $\angle HC_aH$	2.09711	2.09711	3.4252	-15.75493	7	H	H	0.86359	1	1	1	0.75	1.15796	0				109.50	
$\angle C_aC_bC_c$															70.56			109.44	
$\angle C_aC_bH$															70.56			109.44	
$\angle C_bC_aC_c$ iso C_a	2.91547	2.91547	4.7958	-16.68412 C_b	26	-16.68412 C_c	26	0.81549	0.81549	1	1	1	0.81549	-1.85836				110.67	110.8 (isobutane)
$\angle C_bC_aH$ iso C_a	2.91547	2.11323	4.1633	-15.55033 C_a	5	-14.82575 C_b	1	0.87495	0.91771	0.75	1	0.75	1.04887	0				110.76	
$\angle C_aC_bH$ iso C_a	2.91547	2.09711	4.1633	-15.55033 C_b	5	-14.82575 C_a	1	0.87495	0.91771	0.75	1	0.75	1.04887	0				111.27	111.4 (isobutane)
$\angle C_bC_aC_b$ tert C_a	2.90327	2.90327	4.7958	-16.68412 C_b	26	-16.68412 C_b	26	0.81549	0.81549	1	1	1	0.81549	-1.85836				111.37	110.8 (isobutane)
$\angle C_bC_aC_d$															72.50			107.50	

ALKYL NITRITES ($C_nH_{2n+2-m}\left(NO_2\right)_m$, $n=1,2,3,4,5...\infty$)

The alkyl nitrites, $C_nH_{2n+2-m}\left(NO_2\right)_m$, comprise a $RC-O-NO$ moiety that comprises $C-O$, $O-N$, and NO functional groups. The alkyl portion of the alkyl nitrite may comprise at least two terminal methyl groups (CH_3) at each end of the chain, and may comprise methylene (CH_2), and methylyne (CH) functional groups as well as C bound by carbon-carbon single bonds. The methyl and methylene functional groups are equivalent to those of straight-chain alkanes. Six types of $C-C$ bonds can be identified. The n-alkane $C-C$ bond is the same as that of straight-chain alkanes. In addition, the $C-C$ bonds within isopropyl ($\left(CH_3\right)_2CH$) and t-butyl ($\left(CH_3\right)_3C$) groups and the isopropyl to isopropyl, isopropyl to t-butyl, and t-butyl to t-butyl $C-C$ bonds comprise functional groups. The branched-chain-alkane groups in alkyl nitrites are equivalent to those in branched-chain alkanes.

The electron configuration of oxygen is $1s^22s^22p^4$, and the orbital arrangement given by Eq. (10.154) has two unpaired electrons corresponding to the ground state ${}^3P_2$. The electron configuration of nitrogen is $1s^22s^22p^3$, and the orbital arrangement given by Eq. (10.134) has three unpaired electrons corresponding to the ground state ${}^4S^0_{3/2}$. The bonding in the nitro (NO) functional group is similar to that in the SO group given previously. It also has similarities to the bonding in the carbonyl functional group. In the NO group, the two unpaired electrons of the O atom form a MO with two unpaired electrons of the nitrogen atom such that the MO comprises a double bond. The nitrogen atom is then energy matched to the $O-N$ functional group that is further energy matched to the $C2sp^3$ HO of the $C-O$ functional group. To meet the equipotential condition of the union of the $N=O$ H_2-type-ellipsoidal-MO with other orbitals of the molecule, the hybridization factor c_2 of Eq. (15.60) for the $N=O$-bond MO given by Eq. (15.159) is $c_2\left(O\ to\ N2p\ to\ C2sp^3HO\right)=0.85987$.

As in the case of the carbonyl group, two unpaired O electrons result upon bond breakage of the $N=O$ bond which requires that two times E_{mag} of oxygen (Eq. (15.68)) be subtracted from the total energy of NO. Additionally, $E_T\left(atom-atom,msp^3.AO\right)$ and $\Delta E_{H_2MO}\left(AO/HO\right)$ are equal to $-0.92918\ eV$ (Eq. (14.513)) which matches the energy of the $N=O$ bond with the contiguous $O-N$ bond and matches the energy contribution of an oxygen atom.

The $O-N$ functional group comprise a single-bond, H_2-type-ellipsoidal-MO between the remaining unpaired nitrogen electron and an unpaired electron of the second oxygen atom which further forms a single bond with the $C2sp^3$ HO of the $C-O$ functional group. In alkyl nitrites, the hybridization factor c_2 of Eq. (15.61) for the $C-O$-bond MO given by Eq. (15.133) is $c_2\left(C2sp^3HO\ to\ O\right)=0.85395$. The hybridization factor c_2 of Eq. (15.61) for a $C-N$-bond MO given by Eq. (15.135) is $c_2\left(C2sp^3HO\ to\ N\right)=0.91140$. Thus, the hybridization factor c_2 of Eq. (15.61) for $O-N$ that bridges the $C-O$ and $N=O$ bonds given by Eq. (15.78) is:

$$c_2\left(N2p\ to\ O2p\right)=\frac{c_2\left(C2sp^3HO\ to\ N\right)}{c_2\left(C2sp^3HO\ to\ O\right)}=\frac{0.91140}{0.85395}=1.06727 \tag{15.160}$$

$E_T\left(atom-atom,msp^3.AO\right)=-0.92918\ eV$ in order to match the energy of the NO group and $E\left(AO/HO\right)=-15.35946\ eV$ in order to match the $C-O$ functional group.

The $C-O$ functional group is equivalent to that of an ether as given in the corresponding section except that $E_T\left(atom-atom,msp^3.AO\right)$ and $\Delta E_{H_2MO}\left(AO/HO\right)$ are both $-0.72457\ eV$ which matches the energy contribution of an independent $C2sp^3$ HO (Eq. (14.151)). Also, the energy terms corresponding to the oscillation of the bond in the transition state are matched to a nitrite.

The symbols of the functional groups of branched-chain alkyl nitrites are given in Table 15.195. The geometrical (Eqs. (15.1-15.5) and (15.51)), intercept (Eqs. (15.80-15.87)), and energy (Eqs. (15.6-15.11) and (15.17-15.65)) parameters of alkyl nitrites are given in Tables 15.196, 15.197, and 15.198, respectively. The total energy of each alkyl nitrite given in Table 15.199 was calculated as the sum over the integer multiple of each $E_{D\,(Group)}$ of Table 15.198 corresponding to functional-group composition of the molecule. The bond angle parameters of alkyl nitrites determined using Eqs. (15.88-15.117) are given in Table 15.200. The color scale, translucent view of the charge-density of exemplary alkyl nitrite, methyl nitrite, comprising the concentric shells of atoms with the outer shell bridged by one or more H_2-type ellipsoidal MOs or joined with one or more hydrogen MOs is shown in Figure 15.33.

Figure 15.33. (A)-(B) Color scale, translucent views of the charge-density of methyl nitrite showing the orbitals of the atoms at their radii, the ellipsoidal surface of each H or H_2-type ellipsoidal MO that transitions to the corresponding outer shell of the atom(s) participating in each bond, and the hydrogen nuclei (red, not to scale).

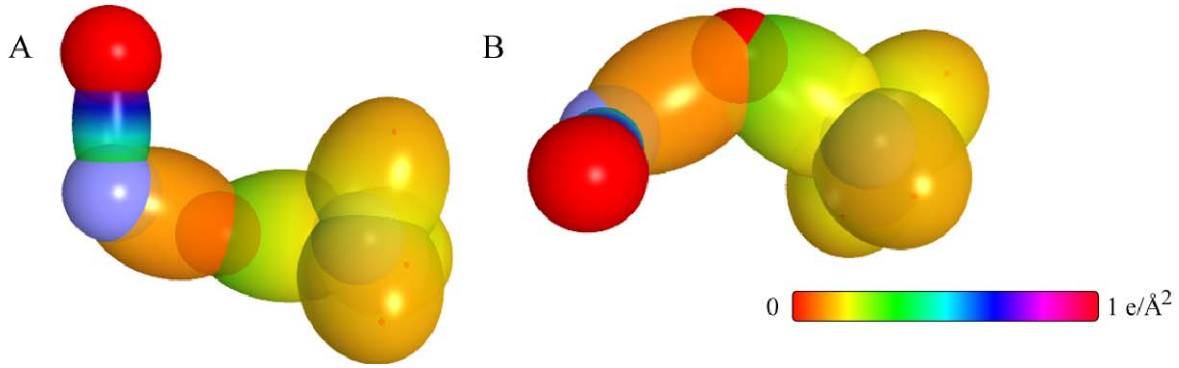

Table 15.195. The symbols of functional groups of alkyl nitrites.

Functional Group	Group Symbol
NO group	*NO*
O-N	$O-N$
C-O	$C-O$
CH_3 group	$C-H\ (CH_3)$
CH_2 group	$C-H\ (CH_2)$
CH	$C-H$
CC bond (*n-C*)	$C-C$ (a)
CC bond (*iso-C*)	$C-C$ (b)
CC bond (*tert-C*)	$C-C$ (c)
CC (*iso* to *iso-C*)	$C-C$ (d)
CC (*t* to *t-C*)	$C-C$ (e)
CC (*t* to *iso-C*)	$C-C$ (f)

Table 15.196. The geometrical bond parameters of alkyl nitrites and experimental values [1].

Parameter	NO Group	$O-N$ Group	$C-O$ Group	$C-H\ (CH_3)$ Group	$C-H\ (CH_2)$ Group	$C-H$ Group	$C-C$ (a) Group	$C-C$ (b) Group	$C-C$ (c) Group	$C-C$ (d) Group	$C-C$ (e) Group	$C-C$ (f) Group
$a\ (a_0)$	1.32255	1.76440	1.85327	1.64920	1.67122	1.67465	2.12499	2.12499	2.10725	2.12499	2.10725	2.10725
$c'\ (a_0)$	1.15002	1.32831	1.36135	1.04856	1.05553	1.05661	1.45744	1.45744	1.45164	1.45744	1.45164	1.45164
Bond Length $2c$ (Å)	1.21713	1.40582	1.44079	1.10974	1.11713	1.11827	1.54280	1.54280	1.53635	1.54280	1.53635	1.53635
Exp. Bond Length (Å)	1.205 (methyl nitrate) 1.2 (HNO_2)	1.402 (methyl nitrate) 1.432 (HNO_2)	1.437 (methyl nitrate)	1.107 ($C-H$ propane) 1.117 ($C-H$ butane)	1.107 ($C-H$ propane) 1.117 ($C-H$ butane)	1.122 (isobutane)	1.532 (propane) 1.531 (butane)	1.532 (propane) 1.531 (butane)	1.532 (propane) 1.531 (butane)	1.532 (propane) 1.531 (butane)	1.532 (propane) 1.531 (butane)	1.532 (propane) 1.531 (butane)
$b,c\ (a_0)$	0.65314	1.16134	1.25751	1.27295	1.29569	1.29924	1.54616	1.54616	1.52750	1.54616	1.52750	1.52750
e	0.86955	0.75284	0.73457	0.63580	0.63159	0.63095	0.68600	0.68600	0.68888	0.68600	0.68888	0.68888

Table 15.197. The MO to HO intercept geometrical bond parameters of alkyl nitrites. R, R', R'' are H or alkyl groups. E_T is $E_T(atom-atom,msp^3.AO)$.

Bond	Atom	E_T (eV) Bond 1	E_T (eV) Bond 2	E_T (eV) Bond 3	E_T (eV) Bond 4	Final Total Energy $C2sp^3$ (eV)	$r_{initial}\ (a_0)$	$r_{final}\ (a_0)$	$E_{Coulomb}$ (eV) Final	$E(C2sp^3)$ (eV) Final	θ' (°)	θ_1 (°)	θ_2 (°)	$d_1\ (a_0)$	$d_2\ (a_0)$
$RON=O$	O	-0.46459	0	0	0		1.00000	0.88983	-15.29034		137.15	42.85	67.90	0.49764	0.65238
$RON=O$	N	-0.46459	-0.46459	0	0		0.93084	0.86359	-15.75493		136.09	43.91	66.48	0.52781	0.62221
RO_b-NO_a	O_b	-0.46459	-0.36229	0	0		1.00000	0.86923	-15.65263		99.22	80.78	47.63	1.18905	0.13925
RO_b-NO_a	N	-0.46459	-0.46459	0	0		0.93084	0.86359	-15.75493		98.78	81.22	47.30	1.19655	0.13175
$RH_2C_a-O_bNO_a$ $R=H,alkyl$	O_b	-0.36229	-0.46459	0	0		1.00000	0.86923	-15.65263		91.43	88.57	43.71	1.33962	0.02173
$H_3C_a-O_bNO_a$	C_a	-0.36229	0	0	0	-151.97798	0.91771	0.89582	-15.18804	-14.99717	93.71	86.29	45.31	1.30342	0.05793
$-CH_2H_2C_a-O_bNO_a$	C_a	-0.36229	-0.92918	0	0	-152.90716	0.91771	0.84418	-16.11722	-15.92636	89.16	90.84	42.16	1.37373	0.01238
$C-H\ (CH_3)$	C	-0.92918	0	0	0	-152.54487	0.91771	0.86359	-15.75493	-15.56407	77.49	102.51	41.48	1.23564	0.18708
$C-H\ (CH_2)$	C	-0.92918	-0.92918	0	0	-153.47406	0.91771	0.81549	-16.68412	-16.49325	68.47	111.53	35.84	1.35486	0.29933
$C-H\ (CH)$	C	-0.92918	-0.92918	-0.92918	0	-154.40324	0.91771	0.77247	-17.61330	-17.42244	61.10	118.90	31.37	1.42988	0.37326
$H_3C_aC_bH_2CH_2-$ ($C-C$ (a))	C_a	-0.92918	0	0	0	-152.54487	0.91771	0.86359	-15.75493	-15.56407	63.82	116.18	30.08	1.83879	0.38106
$H_3C_aC_bH_2CH_2-$ ($C-C$ (a))	C_b	-0.92918	-0.92918	0	0	-153.47406	0.91771	0.81549	-16.68412	-16.49325	56.41	123.59	26.06	1.90890	0.45117
$R-H_2C_aC_b(H_2C_c-R')HCH_2-$ ($C-C$ (b))	C_b	-0.92918	-0.92918	-0.92918	0	-154.40324	0.91771	0.77247	-17.61330	-17.42244	48.30	131.70	21.90	1.97162	0.51388
$R-H_2C_a(R'-H_2C_d)C_b(R''-H_2C_c)CH_2-$ ($C-C$ (c))	C_b	-0.92918	-0.72457	-0.72457	-0.72457	-154.71860	0.91771	0.75889	-17.92866	-17.73779	48.21	131.79	21.74	1.95734	0.50570
$isoC_aC_b(H_2C_c-R')HCH_2-$ ($C-C$ (d))	C_b	-0.92918	-0.92918	-0.92918	0	-154.40324	0.91771	0.77247	-17.61330	-17.42244	48.30	131.70	21.90	1.97162	0.51388
$tertC_a(R'-H_2C_d)C_b(R''-H_2C_c)CH_2-$ ($C-C$ (e))	C_b	-0.72457	-0.72457	-0.72457	-0.72457	-154.51399	0.91771	0.76765	-17.92866	-17.73779	50.04	129.96	22.66	1.94462	0.49298
$tertC_aC_b(H_2C_c-R')HCH_2-$ ($C-C$ (f))	C_b	-0.72457	-0.92918	-0.92918	0	-154.19863	0.91771	0.78155	-17.40869	-17.21783	52.78	127.22	24.04	1.92443	0.47279
$isoC_a(R'-H_2C_d)C_b(R''-H_2C_c)CH_2-$ ($C-C$ (f))	C_b	-0.72457	-0.72457	-0.72457	-0.72457	-154.51399	0.91771	0.76765	-17.92866	-17.73779	50.04	129.96	22.66	1.94462	0.49298

Table 15.198. The energy parameters (eV) of functional groups of alkyl nitrites.

Parameters	NO Group	$O-N$ Group	$C-O$ Group	CH_3 Group	CH_2 Group	$C-H$ Group	$C-C$ (a) Group	$C-C$ (b) Group	$C-C$ (c) Group	$C-C$ (d) Group	$C-C$ (e) Group	$C-C$ (f) Group
n_1	2	1	1	3	2	1	1	1	1	1	1	1
n_2	0	0	0	2	1	0	0	0	0	0	0	0
n_3	0	0	0	0	0	0	0	0	0	0	0	0
C_1	0.5	0.5	0.5	0.75	0.75	0.75	0.5	0.5	0.5	0.5	0.5	0.5
C_2	1	1	1	1	1	1	1	1	1	1	1	1
c_1	1	1	1	1	1	1	1	1	1	1	1	1
c_2	0.85987	1.06727	0.85395	0.91771	0.91771	0.91771	0.91771	0.91771	0.91771	0.91771	0.91771	0.91771
c_3	2	0	0	0	1	1	0	0	0	1	1	0
c_4	4	2	2	1	1	1	2	2	2	2	2	2
c_5	0	0	0	3	2	1	0	0	0	0	0	0
C_{1o}	0.5	0.5	0.5	0.75	0.75	0.75	0.5	0.5	0.5	0.5	0.5	0.5
C_{2o}	1	1	1	1	1	1	1	1	1	1	1	1
$V_e\ (eV)$	-108.34117	-42.83043	-32.04173	-107.32728	-70.41425	-35.12015	-28.79214	-28.79214	-29.10112	-28.79214	-29.10112	-29.10112
$V_p\ (eV)$	23.66182	20.48593	9.99436	38.92728	25.78002	12.87680	9.33352	9.33352	9.37273	9.33352	9.37273	9.37273
$T\ (eV)$	40.95920	12.13739	8.64465	32.53914	21.06675	10.48582	6.77464	6.77464	6.90500	6.77464	6.90500	6.90500
$V_m\ (eV)$	-20.47960	-6.06870	-4.32232	-16.26957	-10.53337	-5.24291	-3.38732	-3.38732	-3.45250	-3.38732	-3.45250	-3.45250
$E_{(AO/HO)}\ (eV)$	0	-15.35946	-14.63489	-15.56407	-15.56407	-14.63489	-15.56407	-15.56407	-15.35946	-15.56407	-15.35946	-15.35946
$\Delta E_{H_2MO(AO/HO)}\ (eV)$	-0.92918	0	-0.72457	0	0	0	0	0	0	0	0	0
$E_{T(AO/HO)}\ (eV)$	0.92918	-15.35946	-13.91032	-15.56407	-15.56407	-14.63489	-15.56407	-15.56407	-15.35946	-15.56407	-15.35946	-15.35946
$E_{T(H_2MO)}\ (eV)$	-63.27057	-31.63527	-31.63537	-67.69451	-49.66493	-31.63533	-31.63537	-31.63537	-31.63535	-31.63537	-31.63535	-31.63535
$E_{T(atom-atom,msp^3.AO)}\ (eV)$	-0.92918	-0.92918	-0.72457	0	0	0	-1.85836	-1.85836	-1.44915	-1.85836	-1.44915	-1.44915
$E_{T(MO)}\ (eV)$	-64.19992	-32.56455	-32.35994	-67.69450	-49.66493	-31.63537	-33.49373	-33.49373	-33.08452	-33.49373	-33.08452	-33.08452
$\omega\ (10^{15}\ rad/s)$	19.2199	23.3578	20.7301	24.9286	24.2751	24.1759	9.43699	9.43699	15.4845	9.43699	9.55643	9.55643
$E_K\ (eV)$	12.65089	15.37450	13.64490	16.40846	15.97831	15.91299	6.21159	6.21159	10.19220	6.21159	6.29021	6.29021
$\bar{E}_D\ (eV)$	-0.22587	0.25261	-0.23648	-0.25352	-0.25017	-0.24966	-0.16515	-0.16515	-0.20896	-0.16515	-0.16416	-0.16416
$\bar{E}_{Kvib}\ (eV)$	0.20396 [46]	0.10725 [47]	0.13663 [21]	0.35532 (Eq. (13.458))	0.35532 (Eq. (13.458))	0.35532 (Eq. (13.458))	0.12312 [2]	0.17978 [4]	0.09944 [5]	0.12312 [2]	0.12312 [2]	0.12312 [2]
$\bar{E}_{osc}\ (eV)$	-0.12390	0.19899	-0.16817	-0.22757	-0.14502	-0.07200	-0.10359	-0.07526	-0.15924	-0.10359	-0.10260	-0.10260
$E_{mag}\ (eV)$	0.11441	0.11441	0.14803	0.14803	0.14803	0.14803	0.14803	0.14803	0.14803	0.14803	0.14803	0.14803
$E_{T(group)}\ (eV)$	-64.44771	32.76354	-32.52811	-67.92207	-49.80996	-31.70737	-33.59732	-33.49373	-33.24376	-33.59732	-33.18712	-33.18712
$E_{initial(s\ AO/HO)}\ (eV)$	-14.63489	-14.63489	-14.63489	-14.63489	-14.63489	-14.63489	-14.63489	-14.63489	-14.63489	-14.63489	-14.63489	-14.63489
$E_{initial(s\ AO/HO)}\ (eV)$	0	0	0	-13.59844	-13.59844	-13.59844	0	0	0	0	0	0
$E_{D(group)}\ (eV)$	5.67933	3.49376	3.25833	12.49186	7.83016	3.32601	4.32754	4.29921	3.97398	4.17951	3.62128	3.91734

Table 15.199. The total bond energies of alkyl nitrites calculated using the functional group composition and the energies of Table 15.198 compared to the experimental values [3].

Formula	Name	NO Group	$O-N$ Group	$C-O$ Group	CH_3	CH_2	CH	$C-C$ (a)	$C-C$ (b)	$C-C$ (c)	$C-C$ (d)	$C-C$ (e)	$C-C$ (f)	Calculated Total Bond Energy (eV)	Experimental Total Bond Energy (eV)	Relative Error
CH_3NO_2	Methyl nitrite	1	1	1	1	0	0	0	0	0	0	0	0	24.92328	24.955	0.00126

Table 15.200. The bond angle parameters of alkyl nitrites and experimental values [1]. In the calculation of $\square_v$, the parameters from the preceding angle were used. E_T is $E_T(atom-atom,\ msp^3.AO)$.

Atoms of Angle	$2c'$ Bond 1 (a_0)	$2c'$ Bond 2 (a_0)	$2c'$ Terminal Atoms (a_0)	$E_{Coulombic}$ or E Atom 1	Atom 1 Hybridization Designation (Table 15.3.A)	$E_{Coulombic}$ Atom 2	Atom 2 Hybridization Designation (Table 15.3.A)	c_2 Atom 1	c_2 Atom 2	C_1	C_2	c_1	c_2'	E_T (eV)	θ_v (°)	θ_1 (°)	θ_2 (°)	Cal. θ (°)	Exp. θ (°)
$\angle CO_bN$	2.72270	2.65661	4.4944	-16.68412 C_b	26	-14.53414 N	N	0.81549	0.91140 (Eq. (15.135))	1	1	1	0.86345	-1.44915				113.33	
$\angle O_aNO_b$	2.30004	2.65661	4.1231	-16.68411 O_a	25	-16.68411 O_b	25	0.81549	0.81549	1	1	1	0.81549	-1.44915				112.38	110.7 (HNO_3)
Methylene $\angle HC_aH$	2.11106	2.11106	3.4252	-15.75493	7	H	H	0.86359	1	1	1	0.75	1.15796	0				108.44	107 (propane)
$\angle C_aC_bC_c$															69.51			110.49	112 (propane) 113.8 (butane) 110.8 (isobutane)
$\angle C_aC_bH$															69.51			110.49	111.0 (butane) 111.4 (isobutane)
Methyl $\angle HC_aH$	2.09711	2.09711	3.4252	-15.75493	7	H	H	0.86359	1	1	1	0.75	1.15796	0				109.50	
$\angle C_aC_bC_c$															70.56			109.44	
$\angle C_aC_bH$															70.56			109.44	
$\angle C_bC_aC_c$ iso C_a	2.91547	2.91547	4.7958	-16.68412 C_b	26	-16.68412 C_c	26	0.81549	0.81549	1	1	1	0.81549	-1.85836				110.67	110.8 (isobutane)
$\angle C_bC_aH$ iso C_a	2.91547	2.11323	4.1633	-15.55033 C_a	5	-14.82575 C_b	1	0.87495	0.91771	0.75	1	0.75	1.04887	0				110.76	
$\angle C_aC_bH$ iso C_a	2.91547	2.09711	4.1633	-15.55033 C_b	5	-14.82575 C_a	1	0.87495	0.91771	0.75	1	0.75	1.04887	0				111.27	111.4 (isobutane)
$\angle C_bC_aC_b$ tert C_a	2.90327	2.90327	4.7958	-16.68412 C_b	26	-16.68412 C_b	26	0.81549	0.81549	1	1	1	0.81549	-1.85836				111.37	110.8 (isobutane)
$\angle C_bC_aC_d$															72.50			107.50	

ALKYL NITRATES ($C_nH_{2n+2-m}\left(NO_3\right)_m$, $n=1,2,3,4,5...\infty$)

The alkyl nitrates, $C_nH_{2n+2-m}\left(NO_3\right)_m$, comprise a $RC-O-NO_2$ moiety that comprises $C-O$, $O-N$, and NO_2 functional groups. The alkyl portion of the alkyl nitrate may comprise at least two terminal methyl groups (CH_3) at each end of the chain, and may comprise methylene (CH_2), and methylyne (CH) functional groups as well as C bound by carbon-carbon single bonds. The methyl and methylene functional groups are equivalent to those of straight-chain alkanes. Six types of $C-C$ bonds can be identified. The n-alkane $C-C$ bond is the same as that of straight-chain alkanes. In addition, the $C-C$ bonds within isopropyl ($\left(CH_3\right)_2CH$) and t-butyl ($\left(CH_3\right)_3C$) groups and the isopropyl to isopropyl, isopropyl to t-butyl, and t-butyl to t-butyl $C-C$ bonds comprise functional groups. The branched-chain-alkane groups in alkyl nitrates are equivalent to those in branched-chain alkanes.

The NO_2 functional group is equivalent to that of nitro alkanes with the exception that $\Delta E_{H_2MO}\left(AO/HO\right)$ as well as $E_T\left(atom-atom,msp^3.AO\right)$ is equal to $-3.71673\,eV$ in order to match the group energy to that of the contiguous $O-N$ bond. Furthermore, the $O-N$ group with $E_T\left(atom-atom,msp^3.AO\right)=-0.92918\,eV$ is equivalent to that of nitrites as given in the corresponding section.

The $C-O$ functional group is equivalent to that of an ether as given in the corresponding section except that $E_T\left(atom-atom,msp^3.AO\right)$ and $\Delta E_{H_2MO}\left(AO/HO\right)$ are both $-0.92918\,eV$ which matches the energy contribution of an independent $C2sp^3$ HO (Eq. (14.513)). Also, the energy terms corresponding to the oscillation of the bond in the transition state are matched to a nitrate.

The symbols of the functional groups of branched-chain alkyl nitrates are given in Table 15.201. The geometrical (Eqs. (15.1-15.5) and (15.51)), intercept (Eqs. (15.80-15.87)), and energy (Eqs. (15.6-15.11) and (15.17-15.65)) parameters of alkyl nitrates are given in Tables 15.202, 15.203, and 15.204, respectively. The total energy of each alkyl nitrate given in Table 15.205 was calculated as the sum over the integer multiple of each $E_{D\,(Group)}$ of Table 15.204 corresponding to functional-group composition of the molecule. The bond angle parameters of alkyl nitrates determined using Eqs. (15.88-15.117) are given in Table 15.206. The color scale, translucent view of the charge-density of exemplary alkyl nitrate, ethyl nitrate, comprising the concentric shells of atoms with the outer shell bridged by one or more H_2-type ellipsoidal MOs or joined with one or more hydrogen MOs is shown in Figure 15.34.

Figure 15.34. (A)-(B) Color scale, translucent views of the charge-density of ethyl nitrate showing the orbitals of the atoms at their radii, the ellipsoidal surface of each H or H_2-type ellipsoidal MO that transitions to the corresponding outer shell of the atom(s) participating in each bond, and the hydrogen nuclei (red, not to scale).

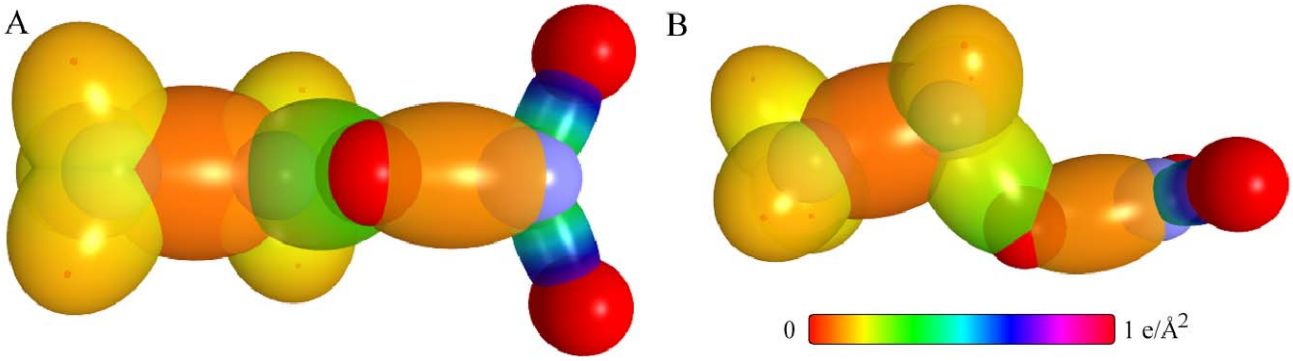

Table 15.201. The symbols of functional groups of alkyl nitrates.

Functional Group	Group Symbol
NO_2 group	NO_2
O-N	$O-N$
C-O	$C-O$
CH_3 group	$C-H\ (CH_3)$
CH_2 group	$C-H\ (CH_2)$
CH	$C-H$
CC bond (*n-C*)	$C-C$ (a)
CC bond (*iso-C*)	$C-C$ (b)
CC bond (*tert-C*)	$C-C$ (c)
CC (*iso* to *iso-C*)	$C-C$ (d)
CC (*t* to *t-C*)	$C-C$ (e)
CC (*t* to *iso-C*)	$C-C$ (f)

Table 15.202. The geometrical bond parameters of alkyl nitrates and experimental values [1].

Parameter	NO_2 Group	$O-N$ Group	$C-O$ Group	$C-H\ (CH_3)$ Group	$C-H\ (CH_2)$ Group	$C-H$ Group	$C-C$ (a) Group	$C-C$ (b) Group	$C-C$ (c) Group	$C-C$ (d) Group	$C-C$ (e) Group	$C-C$ (f) Group
$a\ (a_0)$	1.29538	1.76440	1.83991	1.64920	1.67122	1.67465	2.12499	2.12499	2.10725	2.12499	2.10725	2.10725
$c'\ (a_0)$	1.13815	1.32831	1.35643	1.04856	1.05553	1.05661	1.45744	1.45744	1.45164	1.45744	1.45164	1.45164
Bond Length $2c'\ (\AA)$	1.20456	1.40582	1.43559	1.10974	1.11713	1.11827	1.54280	1.54280	1.53635	1.54280	1.53635	1.53635
Exp. Bond Length $(\AA)$	1.205 (methyl nitrate) 1.2 (HNO_2)	1.402 (methyl nitrate) 1.432 (HNO_2)	1.437 (methyl nitrate)	1.107 $(C-H$ propane) 1.117 $(C-H$ butane)	1.107 $(C-H$ propane) 1.117 $(C-H$ butane)	1.122 (isobutane)	1.532 (propane) 1.531 (butane)	1.532 (propane) 1.531 (butane)	1.532 (propane) 1.531 (butane)	1.532 (propane) 1.531 (butane)	1.532 (propane) 1.531 (butane)	1.532 (propane) 1.531 (butane)
$b,c\ (a_0)$	0.61857	1.16134	1.24312	1.27295	1.29569	1.29924	1.54616	1.54616	1.52750	1.54616	1.52750	1.52750
e	0.87862	0.75284	0.73723	0.63580	0.63159	0.63095	0.68600	0.68600	0.68888	0.68600	0.68888	0.68888

Table 15.203. The MO to HO intercept geometrical bond parameters of alkyl nitrates. R, R', R'' are H or alkyl groups. E_T is E_T $(atom-atom,msp^3.AO)$.

Bond	Atom	E_T (eV) Bond 1	E_T (eV) Bond 2	E_T (eV) Bond 3	E_T (eV) Bond 4	Final Total Energy $C2sp^3$ (eV)	$r_{initial}\ (a_0)$	$r_{final}\ (a_0)$	$E_{Coulomb}$ (eV) Final	$E(C2sp^3)$ (eV) Final	θ' (°)	θ_1 (°)	θ_2 (°)	$d_1\ (a_0)$	$d_2\ (a_0)$
$RON(O)=O$	O	-0.92918	0	0	0		1.00000	0.86359	-15.75493		138.49	41.51	67.70	0.49144	0.64671
$RON(O)=O$	N	-0.92918	-0.92918	-0.46459	0		0.93084	0.79340	-17.14870		135.60	44.40	63.83	0.57133	0.56682
$RO_b-N(O_a)_2$	O_b	-0.46459	-0.46459	0	0		1.00000	0.86359	-15.75493		98.78	81.22	47.30	1.19655	0.13175
$RO_b-N(O_a)_2$	N	-0.46459	-0.92918	-0.92918	0		0.93084	0.79340	-17.14870		92.78	87.22	43.03	1.28978	0.03852
$RH_2C_a-O_bN(O_a)_2$ $R=H,alkyl$	O_b	-0.46459	-0.46459	0	0		1.00000	0.86359	-15.75493		92.13	87.87	43.96	1.32431	0.03212
$H_3C_a-O_bN(O_a)_2$	C_a	-0.46459	0	0	o	-152.08028	0.91771	0.88983	-15.29034	-15.09948	94.36	85.64	45.54	1.28872	0.06771
$-CH_2H_2C_a-O_bN(O_a)_2$	C_a	-0.46459	-0.92918	0	o	-153.00946	0.91771	0.83885	-16.21952	-16.02866	89.90	90.10	42.44	1.35787	0.00143
$C-H\ (CH_3)$	C	-0.92918	0	0	0	-152.54487	0.91771	0.86359	-15.75493	-15.56407	77.49	102.51	41.48	1.23564	0.18708
$C-H\ (CH_2)$	C	-0.92918	-0.92918	0	0	-153.47406	0.91771	0.81549	-16.68412	-16.49325	68.47	111.53	35.84	1.35486	0.29933
$C-H\ (CH)$	C	-0.92918	-0.92918	-0.92918	0	-154.40324	0.91771	0.77247	-17.61330	-17.42244	61.10	118.90	31.37	1.42988	0.37326
$H_3C_aC_bH_2CH_2-$ $(C-C$ (a))	C_a	-0.92918	0	0	0	-152.54487	0.91771	0.86359	-15.75493	-15.56407	63.82	116.18	30.08	1.83879	0.38106
$H_3C_aC_bH_2CH_2-$ $(C-C$ (a))	C_b	-0.92918	-0.92918	0	0	-153.47406	0.91771	0.81549	-16.68412	-16.49325	56.41	123.59	26.06	1.90890	0.45117
$R-H_2C_aC_b(H_2C_c-R')HCH_2-$ $(C-C$ (b))	C_b	-0.92918	-0.92918	-0.92918	0	-154.40324	0.91771	0.77247	-17.61330	-17.42244	48.30	131.70	21.90	1.97162	0.51388
$R-H_2C_a(R'-H_2C_d)C_b(R''-H_2C_c)CH_2-$ $(C-C$ (c))	C_b	-0.92918	-0.72457	-0.72457	-0.72457	-154.71860	0.91771	0.75889	-17.92866	-17.73779	48.21	131.79	21.74	1.95734	0.50570
$isoC_aC_b(H_2C_c-R')HCH_2-$ $(C-C$ (d))	C_b	-0.92918	-0.92918	-0.92918	0	-154.40324	0.91771	0.77247	-17.61330	-17.42244	48.30	131.70	21.90	1.97162	0.51388
$tertC_a(R'-H_2C_d)C_b(R''-H_2C_c)CH_2-$ $(C-C$ (e))	C_b	-0.72457	-0.72457	-0.72457	-0.72457	-154.51399	0.91771	0.76765	-17.92866	-17.73779	50.04	129.96	22.66	1.94462	0.49298
$tertC_aC_b(H_2C_c-R')HCH_2-$ $(C-C$ (f))	C_b	-0.72457	-0.92918	-0.92918	0	-154.19863	0.91771	0.78155	-17.40869	-17.21783	52.78	127.22	24.04	1.92443	0.47279
$isoC_a(R'-H_2C_d)C_b(R''-H_2C_c)CH_2-$ $(C-C$ (f))	C_b	-0.72457	-0.72457	-0.72457	-0.72457	-154.51399	0.91771	0.76765	-17.92866	-17.73779	50.04	129.96	22.66	1.94462	0.49298

Table 15.204. The energy parameters (eV) of functional groups of alkyl nitrates.

Parameters	NO_2 Group	$O-N$ Group	$C-O$ Group	CH_3 Group	CH_2 Group	$C-H$ Group	$C-C$ (a) Group	$C-C$ (b) Group	$C-C$ (c) Group	$C-C$ (d) Group	$C-C$ (e) Group	$C-C$ (f) Group
n_1	2	1	1	3	2	1	1	1	1	1	1	1
n_2	0	0	0	2	1	0	0	0	0	0	0	0
n_3	0	0	0	0	0	0	0	0	0	0	0	0
C_1	0.5	0.5	0.5	0.75	0.75	0.75	0.5	0.5	0.5	0.5	0.5	0.5
C_2	1	1	1	1	1	1	1	1	1	1	1	1
c_1	1	1	1	1	1	1	1	1	1	1	1	1
c_2	0.85987	1.06727	0.85395	0.91771	0.91771	0.91771	0.91771	0.91771	0.91771	0.91771	0.91771	0.91771
c_3	0	0	0	0	1	1	0	0	0	1	1	0
c_4	4	2	2	1	1	1	2	2	2	2	2	2
c_5	0	0	0	3	2	1	0	0	0	0	0	0
C_{1o}	0.5	0.5	0.5	0.75	0.75	0.75	0.5	0.5	0.5	0.5	0.5	0.5
C_{2o}	1	1	1	1	1	1	1	1	1	1	1	1
V_e (eV)	-112.63415	-42.83043	-32.35681	-107.32728	-70.41425	-35.12015	-28.79214	-28.79214	-29.10112	-28.79214	-29.10112	-29.10112
V_p (eV)	23.90868	20.48593	10.03058	38.92728	25.78002	12.87680	9.33352	9.33352	9.37273	9.33352	9.37273	9.37273
T (eV)	43.47534	12.13739	8.79304	32.53914	21.06675	10.48582	6.77464	6.77464	6.90500	6.77464	6.90500	6.90500
V_{ee} (eV)	-21.73767	-6.06870	-4.39652	-16.26957	-10.53337	-5.24291	-3.38732	-3.38732	-3.45250	-3.38732	-3.45250	-3.45250
$E_{(AO/HO)}$ (eV)	0	-15.35946	-14.63489	-15.56407	-15.56407	-14.63489	-15.56407	-15.56407	-15.35946	-15.56407	-15.35946	-15.35946
$\Delta E_{H_2MO(AO/HO)}$ (eV)	-3.71673	0	-0.92918	0	0	0	0	0	0	0	0	0
$E_T(_{AO/HO})$ (eV)	3.71673	-15.35946	-13.70571	-15.56407	-15.56407	-14.63489	-15.56407	-15.56407	-15.35946	-15.56407	-15.35946	-15.35946
$E_T(_{H_2MO})$ (eV)	-63.27107	-31.63527	-31.63542	-67.69451	-49.66493	-31.63533	-31.63537	-31.63537	-31.63535	-31.63537	-31.63535	-31.63535
$E_T\left(atom-atom,msp^3.AO\right)(eV)$	-3.71673	-0.92918	-0.92918	0	0	0	-1.85836	-1.85836	-1.44915	-1.85836	-1.44915	-1.44915
$E_T(_{MO})$ (eV)	-66.98746	-32.56455	-32.56455	-67.69450	-49.66493	-31.63537	-33.49373	-33.49373	-33.08452	-33.49373	-33.08452	-33.08452
$\omega\left(10^{15}\ rad/s\right)$	19.8278	23.3578	21.0910	24.9286	24.2751	24.1759	9.43699	9.43699	15.4846	9.43699	9.55643	9.55643
E_K (eV)	13.05099	15.37450	13.88249	16.40846	15.97831	15.91299	6.21159	6.21159	10.19220	6.21159	6.29021	6.29021
$\bar{E}_D$ (eV)	-0.23938	0.25261	-0.24004	-0.25352	-0.25017	-0.24966	-0.16515	-0.16515	-0.20896	-0.16515	-0.16416	-0.16416
$\bar{E}_{Kvib}$ (eV)	0.19342 [45]	0.10725 [47]	0.13663 [21]	0.35532 (Eq. (13.458))	0.35532 (Eq. (13.458))	0.35532 (Eq. (13.458))	0.12312 [2]	0.17978 [4]	0.09944 [5]	0.12312 [2]	0.12312 [2]	0.12312 [2]
$\bar{E}_{osc}$ (eV)	-0.14267	0.19899	-0.17172	-0.22757	-0.14502	-0.07200	-0.10359	-0.07526	-0.15924	-0.10359	-0.10260	-0.10260
E_{mag} (eV)	0.11441	0.11441	0.14803	0.14803	0.14803	0.14803	0.14803	0.14803	0.14803	0.14803	0.14803	0.14803
$E_T(_{Group})$ (eV)	-67.27281	32.76354	-32.73627	-67.92207	-49.80996	-31.70737	-33.59732	-33.49373	-33.24376	-33.59732	-33.18712	-33.18712
$E_{initial}(_{s\ AO/HO})$ (eV)	-14.63489	-14.63489	-14.63489	-14.63489	-14.63489	-14.63489	-14.63489	-14.63489	-14.63489	-14.63489	-14.63489	-14.63489
$E_{initial}(_{s\ AO/HO})$ (eV)	0	0	0	-13.59844	-13.59844	-13.59844	0	0	0	0	0	0
$E_D(_{Group})$ (eV)	8.73325	3.49376	3.46649	12.49186	7.83016	3.32601	4.32754	4.29921	3.97398	4.17951	3.62128	3.91734

Table 15.205. The total bond energies of alkyl nitrates calculated using the functional group composition and the energies of Table 15.204 compared to the experimental values [3].

Formula	Name	NO_2 Group	$O-N$ Group	$C-O$ Group	CH_3	CH_2	CH	$C-C$ (a)	$C-C$ (b)	$C-C$ (c)	$C-C$ (d)	$C-C$ (e)	$C-C$ (f)	Calculated Total Bond Energy (eV)	Experimental Total Bond Energy (eV)	Relative Error
CH_3NO_3	Methyl nitrate	1	1	1	1	0	0	0	0	0	0	0	0	28.18536	28.117	-0.00244
$C_2H_5NO_3$	Ethyl nitrate	1	1	1	1	1	0	1	0	0	0	0	0	40.34306	40.396	0.00131
$C_3H_7NO_3$	Propyl nitrate	1	1	1	1	2	1	2	0	0	0	0	0	52.50076	52.550	0.00093
$C_3H_7NO_3$	Isopropyl nitrate	1	1	1	2	0	1	0	2	0	0	0	0	52.60165	52.725	0.00233

Table 15.206. The bond angle parameters of alkyl nitrates and experimental values [1]. In the calculation of θ_v, the parameters from the preceding angle were used. E_T is $E_T(atom - atom, msp^3.AO)$.

Atoms of Angle	2c' Bond 1 (a_0)	2c' Bond 2 (a_0)	2c' Terminal Atoms (a_0)	$E_{Coulombic}$ or E Atom 1	Atom 1 Hybridization Designation (Table 15.3.A)	$E_{Coulombic}$ Atom 2	Atom 2 Hybridization Designation (Table 15.3.A)	c_2 Atom 1	c_2 Atom 2	C_1	C_2	c_1	c_2'	E_T (eV)	θ_v (°)	θ_1 (°)	θ_2 (°)	Cal. θ (°)	Exp. θ (°)
Methyl $\angle HC_aH$	2.09711	2.09711	3.4252	-15.75493	7	H	H	0.86359	1	1	1	0.75	1.15796	0				109.50	
$\angle H_aC_aO_c$															70.56			109.44	110 (methyl nitrate)
$\angle H_bC_aO_c$	2.09711	2.71287	3.7238	-14.82575 C_a	1	-13.61806	O	0.91771	0.85395 (Eq. (15.133))	0.75	1	0.75	0.93052	0				100.68	103 (methyl nitrate)
$\angle O_aNO_b$	2.27630	2.27630	4.1231	-16.68411 O_a	25	-16.68411 O_b	25	0.81549	0.81549	1	1	1	0.81549	-1.44915				129.83	
$\angle O_aNO_c$																129.83		115.09 (Eq. (15.108))	118.1 (methyl nitrate)
$\angle O_bNO_c$																129.83		115.09 (Eq. (15.108))	112.4 (methyl nitrate)
$\angle CO_cN$	2.71287	2.65661	4.4721	-16.68412 C_b	26	-14.53414 N	N	0.81549	0.91140 (Eq. (15.135))	1	1	1	0.86345	-1.44915				112.79	112.7 (methyl nitrate)
Methylene $\angle HC_aH$	2.11106	2.11106	3.4252	-15.75493	7	H	H	0.86359	1	1	1	0.75	1.15796	0				108.44	107 (propane)
$\angle C_aC_bC_c$															69.51			110.49	112 (propane) 113.8 (butane) 110.8 (isobutane)
$\angle C_aC_bH$															69.51			110.49	111.0 (butane) 111.4 (isobutane)
Methyl $\angle HC_aH$	2.09711	2.09711	3.4252	-15.75493	7	H	H	0.86359	1	1	1	0.75	1.15796	0				109.50	
$\angle C_aC_bC_c$															70.56			109.44	
$\angle C_aC_bH$															70.56			109.44	
$\angle C_bC_aC_c$ iso C_a	2.91547	2.91547	4.7958	-16.68412 C_b	26	-16.68412 C_c	26	0.81549	0.81549	1	1	1	0.81549	-1.85836				110.67	110.8 (isobutane)
$\angle C_bC_aH$ iso C_a	2.91547	2.11323	4.1633	-15.55033 C_a	5	-14.82575 C_b	1	0.87495	0.91771	0.75	1	0.75	1.04887	0				110.76	
$\angle C_aC_bH$ iso C_a	2.91547	2.09711	4.1633	-15.55033 C_b	5	-14.82575 C_a	1	0.87495	0.91771	0.75	1	0.75	1.04887	0				111.27	111.4 (isobutane)
$\angle C_bC_aC_b$ tert C_a	2.90327	2.90327	4.7958	-16.68412 C_b	26	-16.68412 C_b	26	0.81549	0.81549	1	1	1	0.81549	-1.85836				111.37	110.8 (isobutane)
$\angle C_bC_aC_d$															72.50			107.50	

CYCLIC AND CONJUGATED ALKENES ($C_nH_{2n+2-2m-2c}$, $n=3,4,5...\infty$, $m=1,2,3...$, $c=0$ *or* 1)

The cyclic and conjugated alkenes are represented by the general formula $C_nH_{2n+2-2m-2c}$, $n=3,4,5...\infty$, $m=1,2,3...$, $c=0$ *or* 1 where m is the number of double bonds and $c=0$ for a straight-chain alkene and $c=1$ for a cyclic alkene. They have at least one carbon-carbon double bond comprising a functional group that is solved equivalently to the double bond of ethylene. Consider the cyclic and conjugated alkenes 1,3-butadiene, 1,3-pentadiene, 1,4-pentadiene, 1,3-cyclopentadiene, and cyclopentene. Based on the condition of energy matching of the orbital, any magnetic energy due to unpaired electrons in the constituent fragments, and differences in oscillation in the transition state, five distinct $C-C$ functional groups can be identified as given in Table 15.208. The designation of the structure of the groups are shown in Figures 15.35A-E. In addition, CH_2 of any $-C=CH_2$ moiety is a conjugated alkene functional group. The alkyl portion of the cyclic or conjugated alkene may comprise at least one terminal methyl group (CH_3), and may comprise methylene (CH_2), and methylyne (CH) functional groups that are equivalent to those of branched-chain alkanes.

The solution of the functional groups comprises the hybridization of the $2s$ and $2p$ AOs of each C to form a single $2sp^3$ shell as an energy minimum, and the sharing of electrons between two $C2sp^3$ HOs to form a MO permits each participating hybridized orbital to decrease in radius and energy. The $C-C$ groups are solved in the same manner as those of the branched-chain alkanes given in the corresponding section. For example, the cyclopentene C_a-C_b group is equivalent to the n-$C-C$ alkane group. Many of the corresponding energies of the molecules of this class are similar, and they can be related to one another based on the structure. For example, cyclopentadiene is formed by ring closure of 1,3-pentadiene with the elimination of H from the terminal methyl and methylene groups. Thus, the energy of each of the corresponding carbon-carbon bonds in cyclopentadiene is the same as that in 1,3-pentadiene except that the difference between the energies of the 1,3-pentadiene C_c-C_d and the cyclopentadiene C_a-C_b groups is the magnetic energy (Eq. (15.67)) which is subtracted from the C_a-C_b total bond energy according to Eqs. (13.524-13.527) due to the formation of a CH group from the methylene group. The color scale, translucent view of the charge-density of exemplary cyclic and conjugated alkene, 1,3-butadiene, comprising the concentric shells of atoms with the outer shell bridged by one or more H_2-type ellipsoidal MOs or joined with one or more hydrogen MOs is shown in Figure 15.35.

Figure 15.35. Color scale, translucent view of the charge-density of 1,3-butadiene showing the orbitals of the atoms at their radii, the ellipsoidal surface of each H or H_2-type ellipsoidal MO that transitions to the corresponding outer shell of the atom(s) participating in each bond, and the hydrogen nuclei (red, not to scale).

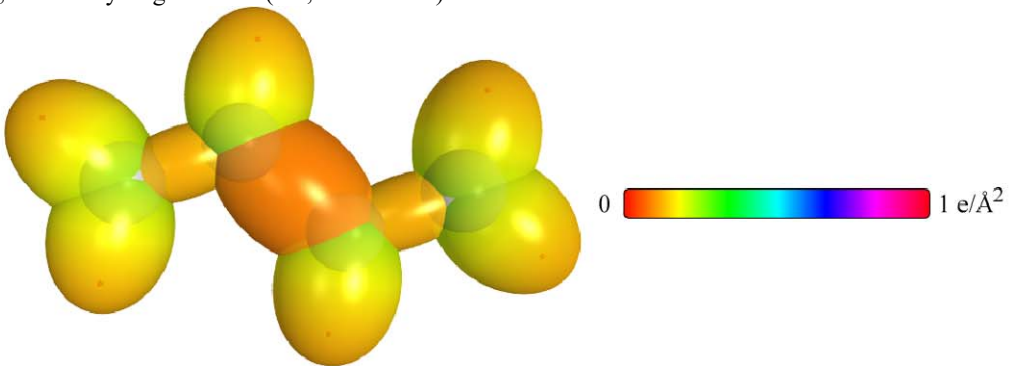

$E_T\left(atom-atom,msp^3.AO\right)$ of the $C=C$-bond MO in Eq. (15.61) due to the charge donation from the C atoms to the MO is equivalent to that of ethylene, $-2.26759\,eV$, given by Eq. (14.247). $E_T\left(atom-atom,msp^3.AO\right)$ of each $C-C$-bond MO in Eq. (15.61) is $-2.26759\,eV$ or $-1.85836\,eV$ based on the energy match between the $C2sp^3$ HOs corresponding to the energy contributions equivalent to those of alkene, $-1.13379\,eV$ (Eq. (14.247)), or methylene, $-0.92918\,eV$ (Eq. (14.513)), groups, respectively, that are contiguous with the $C-C$-bond carbons. In the former case, the total energy of the $C-C$ bond MO is matched to that of the alkane energy in the determination of the bond length. The charge density of 0.5e must be donated to the $C-C$ bond in order to match the energy of the adjacent flanking double bonds. This further lowers the total energy of the $C-C$-bond MO and increases the $C-C$ bond energy. This additional lowering of the $C-C$-bond energy by additional charge donation over that of an alkane bond due to adjacent double bonds is called *conjugation*.

The symbols of the functional groups of cyclic and conjugated alkenes are given in Table 15.207. The structures of 1,3-butadiene, 1,3-pentadiene, 1,4-pentadiene, 1,3-cyclopentadiene, and cyclopentene are shown in Figures 15.35A-E, respectively. The geometrical (Eqs. (15.1-15.5) and (15.51)), intercept (Eqs. (15.80-15.87)), and energy (Eqs. (15.6-15.11) and (15.17-15.65)) parameters of cyclic and conjugated alkenes are given in Tables 15.208, 15.209, and 15.210, respectively. The total energy of each cyclic or conjugated alkenes given in Table 15.211 was calculated as the sum over the integer multiple of each $E_D(Group)$ of

Table 15.210 corresponding to functional-group composition of the molecule. For each set of unpaired electrons created by bond breakage, the $C2sp^3$ HO magnetic energy E_{mag} that is subtracted from the weighted sum of the $E_D\,(Group)$ (eV) values based on composition is given by Eq. (15.67). The bond angle parameters of cyclic and conjugated alkenes determined using Eqs. (15.88-15.117) are given in Table 15.212.

Figure 15.35A. 1,3 Butadiene

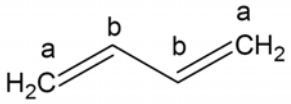

Figure 15.35B. 1,3 Pentadiene

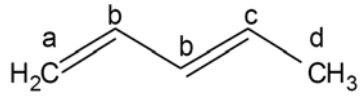

Figure 15.35C. 1,4 Pentadiene

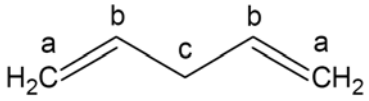

Figure 15.35D. 1,3 Cyclopentadiene

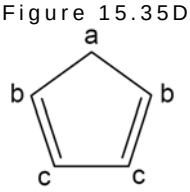

Figure 15.35E. Cyclopentene

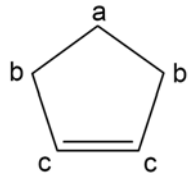

Table 15.207. The symbols of functional groups of cyclic and conjugated alkenes.

Functional Group	Group Symbol
CC double bond	$C=C$
1,3-butadiene, 1,3-pentadiene C_b-C_b 1,3-cyclopentadiene C_c-C_c	$C-C$ (a)
1,3-pentadiene C_c-C_d cyclopentene C_b-C_c	$C-C$ (b)
1,4-pentadiene C_b-C_c	$C-C$ (c)
1,3-cyclopentadiene C_a-C_b	$C-C$ (d)
cyclopentene C_a-C_b	$C-C$ (e)
CH_2 alkenyl group	$C-H\ (CH_2)$ (i)
CH_3 group	$C-H\ (CH_3)$
CH_2 alkyl group	$C-H\ (CH_2)$ (ii)
CH	$C-H$

Table 15.208. The geometrical bond parameters of cyclic and conjugated alkenes and experimental values [1].

Parameter	$C=C$ Group	$C-C$ (a) Group	$C-C$ (b) Group	$C-C$ (c) Group	$C-C$ (d) Group	$C-C$ (e) Group	$C-H\ (CH_2)$ (i) Group	$C-H\ (CH_3)$ Group	$C-H\ (CH_2)$ (ii) Group	$C-H$ Group
$a\ (a_0)$	1.47228	1.91256	2.04740	2.04740	2.04740	2.12499	1.64010	1.64920	1.67122	1.67465
$c'\ (a_0)$	1.26661	1.38295	1.43087	1.43087	1.43087	1.45773	1.04566	1.04856	1.05553	1.05661
Bond Length $2c'\ (\AA)$	1.34052	1.46365	1.51437	1.51437	1.51437	1.54280	1.10668	1.10974	1.11713	1.11827
Exp. Bond Length $(\AA)$	1.349 (1,3-butadiene) 1.342 (1,3-cyclopentadiene) 1.342 (cyclopentene)	1.467 (1,3-butadiene) 1.469 (1,3-cyclopentadiene)	1.519 (cyclopentene)		1.509 (1,3-cyclopentadiene)	1.546 (cyclopentene)	1.10 (2-methylpropene) 1.108 (avg.) (1,3-butadiene)	1.107 ($C-H$ propane) 1.117 ($C-H$ butane)	1.107 ($C-H$ propane) 1.117 ($C-H$ butane)	1.122 (isobutane)
$b,c\ (a_0)$	0.75055	1.32110	1.46439	1.46439	1.46439	1.54615	1.26354	1.27295	1.29569	1.29924
e	0.86030	0.72309	0.69887	0.69887	0.69887	0.68600	0.63756	0.63580	0.63159	0.63095

Table 15.209. The MO to HO intercept geometrical bond parameters of cyclic and conjugated alkenes. R_1 is an alkyl group and R, R', R'' are H or alkyl groups. E_T *is* E_T $(atom-atom, msp^3.AO)$.

Bond	Atom	E_T (eV) Bond 1	E_T (eV) Bond 2	E_T (eV) Bond 3	E_T (eV) Bond 4	Final Total Energy $C2sp^3$ (eV)	$r_{initial}$ (a_0)	r_{final} (a_0)	$E_{Coulomb}(C2sp^3)$ (eV) Final	$E(C2sp^3)$ (eV) Final	θ' (°)	θ_1 (°)	θ_2 (°)	d_1 (a_0)	d_2 (a_0)
$H_2C_a=C_b(H)(H)C=CR$ (1,3-butadiene, 1,3-pentadiene) $H_2C_a=C_b(H)C_cH_2C_b(H)=C_aH_2$ (1,4-pentadiene)	C_a	-1.13380	0	0	0	-152.74949	0.91771	0.85252	-15.95955	-15.76868	129.84	50.16	60.70	0.72040	0.54620
$H_2C_a=C_b(H)(H)C=CR$ (1,3-butadiene, 1,3-pentadiene) $-HC_b=C_c(H)(H)C_c=C_bH-$ (1,3-cyclopentadiene)	C_b C_c	-1.13380	-1.13380	0	0	-153.88328	0.91771	0.79597	-17.09334	-16.90248	127.13	52.87	57.73	0.78613	0.48047
$H_2C_a=C_b(H)(H)C_b=C_c(H)C_dH_3$ (1,3-pentadiene) $H_2C_a=C_b(H)C_cH_2C_b(H)=C_aH_2$ (1,4-pentadiene) $-HC_b=C_c(H)(H)C_c=C_bH-$ (1,3-cyclopentadiene) $-H_2C_bC_c(H)=(H)C_cC_bH_2-$ (cyclopentene)	C_c C_b C_b C_c	-1.13380	-0.92918	0	0	-153.67867	0.91771	0.80561	-16.88873	-16.69786	127.61	52.39	58.24	0.77492	0.49168
$RC=C_{b,c}(H)-(H)C_{b,c}=CR'$ $(C-C$ (a))	$C_{b,c}$	-1.13380	-1.13380	0	0	-153.88328	0.91771	0.79597	-17.09334	-16.90248	78.31	101.69	36.16	1.54418	0.16123
$H_2C_a=C_b(H)(H)C_b=C_c(H)-C_dH_3$ (1,3-pentadiene) $-H_2C_b-C_c(H)=(H)C_c-C_bH_2-$ (cyclopentene) $(C-C$ (b))	C_c C_c	-1.13380	-0.92918	0	0	-153.67867	0.91771	0.80561	-16.88873	-16.69786	64.57	115.43	29.79	1.77684	0.34596
$H_2C_a=C_b(H)(H)C_b=C_c(H)-C_dH_3$ (1,3-pentadiene) $(C-C$ (b))	C_d	-0.92918	0	0	0	-152.54487	0.91771	0.86359	-15.75493	-15.56407	72.27	107.73	34.17	1.69388	0.26301
$-H_2C_b-C_c(H)=(H)C_c-C_bH_2-$ (cyclopentene) $(C-C$ (b))	C_b	-0.92918	-0.92918	0	0	-153.47405	0.91771	0.81549	-16.68411	-16.49325	65.99	114.01	30.58	1.76270	0.33183
$H_2C_a=C_b(H)-C_cH_2C_b(H)=C_aH_2$ (1,4-pentadiene) $(C-C$ (c)) $-H_2C_a-HC_b=C_c(H)(H)C_c=C_bH-$ (1,3-cyclopentadiene) $(C-C$ (d))	C_b C_b	-1.13380	-0.92918	0	0	-153.67866	0.91771	0.80561	-16.88873	-16.69786	64.57	115.43	29.79	1.77684	0.34596
$H_2C_a=C_b(H)-C_cH_2C_b(H)=C_aH_2$ (1,4-pentadiene) $(C-C$ (c)) $-H_2C_a-HC_b=C_c(H)(H)C_c=C_bH-$ (1,3-cyclopentadiene) $(C-C$ (d))	C_c C_a	-0.92918	-0.92918	0	0	-153.47405	0.91771	0.81549	-16.68411	-16.49325	65.99	114.01	30.58	1.76270	0.33183
$-H_2C_a-H_2C_bC_c(H)=(H)C_cC_bH_2-$ (cyclopentene) $(C-C$ (e))	C_a, C_b	-0.92918	-0.92918	0	0	-153.47405	0.91771	0.81549	-16.68411	-16.49325	56.41	123.59	26.06	1.90890	0.45116
$C-H$ (CH_2) (i)	C	-1.13380	0	0	0	-152.74949	0.91771	0.85252	-15.95955	-15.76868	77.15	102.85	41.13	1.23531	0.18965
$C-H$ (CH_3)	C	-0.92918	0	0	0	-152.54487	0.91771	0.86359	-15.75493	-15.56407	77.49	102.51	41.48	1.23564	0.18708
$C-H$ (CH_2) (ii)	C	-0.92918	-0.92918	0	0	-153.47406	0.91771	0.81549	-16.68412	-16.49325	68.47	111.53	35.84	1.35486	0.29933
$C-H$ (CH)	C	-0.92918	-0.92918	-0.92918	0	-154.40324	0.91771	0.77247	-17.61330	-17.42244	61.10	118.90	31.37	1.42988	0.37326

Table 15.210. The energy parameters (eV) of functional groups of cyclic and conjugated alkenes.

Parameters	$C=C$ Group	$C-C$ (a) Group	$C-C$ (b) Group	$C-C$ (c) Group	$C-C$ (d) Group	$C-C$ (e) Group	CH_2 (i) Group	CH_3 Group	CH_2 (ii) Group	$C-H$ Group
n_1	2	1	1	1	1	1	2	3	2	1
n_2	0	0	0	0	0	0	1	2	1	0
n_3	0	0	0	0	0	0	0	0	0	0
C_1	0.5	0.5	0.5	0.5	0.5	0.5	0.75	0.75	0.75	0.75
C_2	0.91771	1	1	1	1	1	1	1	1	1
c_1	1	1	1	1	1	1	1	1	1	1
c_2	0.91771	0.91771	0.91771	0.91771	0.91771	0.91771	0.91771	0.91771	0.91771	0.91771
c_3	0	0	0	0	1	0	1	0	1	1
c_4	4	2	2	2	2	2	1	1	1	1
c_5	0	0	0	0	0	0	2	3	2	1
C_{1o}	0.5	0.5	0.5	0.5	0.5	0.5	0.75	0.75	0.75	0.75
C_{2o}	0.91771	1	1	1	1	1	1	1	1	1
$V_e\ (eV)$	-102.08992	-33.01226	-30.19634	-30.19634	-30.19634	-28.79214	-72.03287	-107.32728	-70.41425	-35.12015
$V_p\ (eV)$	21.48386	9.83824	9.50874	9.50874	9.50874	9.33352	26.02344	38.92728	25.78002	12.87680
$T\ (eV)$	34.67062	8.63041	7.37432	7.37432	7.37432	6.77464	21.95990	32.53914	21.06675	10.48582
$V_{ne}\ (eV)$	-17.33531	-4.31520	-3.68716	-3.68716	-3.68716	-3.38732	-10.97995	-16.26957	-10.53337	-5.24291
$E_{(AO/HO)}\ (eV)$	0	-14.63489	-14.63489	-14.63489	-14.63489	-15.56407	-14.63489	-15.56407	-15.56407	-14.63489
$\Delta E_{H_2MO\,(AO/HO)}\ (eV)$	0	-1.85836	0	0	0	0	0	0	0	0
$E_{I\,(AO/HO)}\ (eV)$	0	-12.77653	-14.63489	-14.63489	-14.63489	-15.56407	-14.63489	-15.56407	-15.56407	-14.63489
$E_{I\,(H_2MO)}\ (eV)$	-63.27075	-31.63535	-31.63534	-31.63534	-31.63534	-31.63537	-49.66437	-67.69451	-49.66493	-31.63533
$E_I\left(atom-atom,msp^3.AO\right)\ (eV)$	-2.26759	-2.26759	-1.85836	-1.85836	-1.85836	-1.85836	0	0	0	0
$E_{I\,(MO)}\ (eV)$	-65.53833	-33.90295	-33.49373	-33.49373	-33.49373	-33.49373	-49.66493	-67.69450	-49.66493	-31.63537
$\omega\ \left(10^{15}\ rad/s\right)$	43.0680	11.0522	9.97851	23.3291	9.97851	9.43699	25.2077	24.9286	24.2751	24.1759
$E_K\ (eV)$	28.34813	7.27475	6.56803	15.35563	6.56803	6.21159	16.59214	16.40846	15.97831	15.91299
$\bar{E}_D\ (eV)$	-0.34517	-0.18090	-0.16982	-0.25966	-0.16982	-0.16515	-0.25493	-0.25352	-0.25017	-0.24966
$\bar{E}_{Kvib}\ (eV)$	0.17897 [6]	0.14829 [48]	0.11159 [12]	0.11159 [12]	0.11159 [12]	0.12312 [2]	0.35532 Eq. (13.458)	0.35532 Eq. (13.458)	0.35532 Eq. (13.458)	0.35532 Eq. (13.458)
$\bar{E}_{osc}\ (eV)$	-0.25568	-0.10676	-0.11402	-0.20386	-0.11402	-0.10359	-0.07727	-0.22757	-0.14502	-0.07200
$E_{mag}\ (eV)$	0.14803	0.14803	0.14803	0.14803	0.14803	0.14803	0.14803	0.14803	0.14803	0.14803
$E_{I\,(Group)}\ (eV)$	-66.04969	-34.00972	-33.60776	-33.69760	-33.60776	-33.59732	-49.81948	-67.92207	-49.80996	-31.70737
$E_{mitial\,(\varepsilon_4\ AO/HO)}\ (eV)$	-14.63489	-14.63489	-14.63489	-14.63489	-14.63489	-14.63489	-14.63489	-14.63489	-14.63489	-14.63489
$E_{mitial\,(\varepsilon_5\ AO/HO)}\ (eV)$	0	0	0	0	0	0	-13.59844	-13.59844	-13.59844	-13.59844
$E_{D\,(Group)}\ (eV)$	7.51014	4.73994	4.33798	4.42782	4.18995	4.32754	7.83968	12.49186	7.83016	3.32601

Table 15.211. The total bond energies of cyclic and conjugated alkenes calculated using the functional group composition and the energies of Table 15.210 compared to the experimental values [3]. The magnetic energy E_{mag} that is subtracted from the weighted sum of the $E_D\ (Group)\ (eV)$ values based on composition is given by (15.58).

Formula	Name	$C=C$	$C-C$ (a)	$C-C$ (b)	$C-C$ (c)	$C-C$ (d)	$C-C$ (e)	CH_2 (i)	CH_3	CH_2 (ii)	CH	E_{mag}	Calculated Total Bond Energy (eV)	Experimental Total Bond Energy (eV)	Relative Error
C_4H_6	1,3 Butadiene	2	1	0	0	0	0	2	0	0	2	0	42.09159	42.12705	0.00084
C_5H_8	1,3 Pentadiene	2	1	1	0	0	0	1	1	0	3	0	54.40776	54.42484	0.00031
C_5H_8	1,4 Pentadiene	2	0	0	2	0	0	2	0	1	2	0	54.03745	54.11806	0.00149
C_5H_6	1,3 Cyclopentadiene	2	1	0	0	2	0	0	0	1	4	0	49.27432	49.30294	0.00058
C_5H_8	Cyclopentene	1	0	2	0	0	2	0	0	3	2	-1	54.83565	54.86117	0.00047

Table 15.212. The bond angle parameters of cyclic and conjugated alkenes and experimental values [1]. In the calculation of θ_v, the parameters from the preceding angle were used. E_T is $E_T(atom-atom,\ msp^3.AO)$.

Atoms of Angle	2c' Bond 1 (a_0)	2c' Bond 2 (a_0)	2c' Terminal Atoms (a_0)	$E_{Coulombic}$ Atom 1	Atom 1 Hybridization Designation (Table 15.3.A)	$E_{Coulombic}$ Atom 2	Atom 2 Hybridization Designation (Table 15.3.A)	c_2 Atom 1	c_2 Atom 2	C_1	C_2	c_1	c_2'	E_T (eV)	θ_v (°)	θ_1 (°)	θ_2 (°)	Cal. θ (°)	Exp. θ (°)
$\angle HC_aH$ $H_2C_a=C_b$ 1,3-butadiene	2.09132	2.09132	3.4928	-15.95955	10	H	H	0.85252	1	1	1	0.75	1.17300	0				113.25	
$\angle C_bC_aH_a$ $H_2C_a=C_b$ 1,3-butadiene																113.25		123.38	120.9 (1,3-butadiene)
$\angle C_bC_aH_a$ $H_2C_a=C_b$ 1,3-butadiene	2.53321	2.09132	4.0000	-15.95954 C_a	10	-15.95954 C_b	10	0.85252	0.85252	0.75	1	0.75	1.00000	0				119.45	120.9 (1,3-butadiene)
$\angle C_aC_bC_b$ $C_a=C_bC_b$ 1,3-butadiene	2.53321	2.76590	4.6904	-16.88873 C_a	29	-17.09334 C_b	34	0.80561	0.79597	1	1	1	0.85395	-1.85836				124.48	124.4 (1,3-butadiene CCC) 124.4 (1,3,5-hexatriene CbCcCc) 121.7 (1,3,5-hexatriene CaCbCc) 125.3 (2-butene CbCaCc)
$\angle C_bC_cC_c$ $C_b=C_cC_c$ 1,3-cyclopentadiene	2.53321	2.76590	4.3012	-17.81791 C_b	53	-17.81791 C_c	53	0.76360	0.76360	1	1	1	0.76360	-1.85836				108.44	109.4 (1,3-cyclopentadiene)
$\angle C_aC_bC_c$ $C_aC_b=C_c$ 1,3-cyclopentadiene	2.86175	2.53321	4.3818	-17.61330 C_a	49	-17.61330 C_c	49	0.77247	0.77247	1	1	1	0.77247	-1.85836				108.47	109.3 (1,3-cyclopentadiene)
$\angle C_bC_aC_b$ $=C_bHC_cH_2C_b(H)=$ 1,3-cyclopentadiene	2.86175	2.86175	4.4609	-17.40869 C_b	44	-17.40869 C_b	44	0.78155	0.78155	1	1	1	0.78155	-1.85836				102.41	102.8 (1,3-cyclopentadiene)
$\angle C_bC_cC_c$ $-H_2C_bHC_c=C_cHC_bH_2-$ cyclopentene	2.86175	2.53321	4.4272	-17.40869 C_b	44	-17.61330 C_b	49	0.78155	0.77247	1	1	1	0.77701	-1.85836				110.14	110.0 (cyclopentene)
$\angle C_aC_bC_c$ $-H_2C_aH_2C_bHC_c=C_cH-$ cyclopentene	2.91548	2.86175	4.5166	-17.20408 C_a	39	-17.40869 C_c	44	0.79085	0.78155	1	1	1	0.78620	-1.85836				102.85	103.0 (cyclopentene)
$\angle C_bC_aC_b$ $-C_bH_2C_aH_2C_bH_2-$ cyclopentene	2.91548	2.91548	4.5826	-17.20408 C_b	39	-17.20408 C_b	39	0.79085	0.79085	1	1	1	0.79085	-1.85836				103.61	104.0 (cyclopentene)

AROMATIC AND HETEROCYCLIC COMPOUNDS

Aromatic and heterocyclic molecules comprise at least one of an aromatic or a cyclic conjugated alkene functional group. The latter was described in the Cyclic and Conjugated Alkenes section. The aromatic bond is uniquely stable and requires the sharing of the electrons of multiple H_2-type MOs. The results of the derivation of the parameters of the benzene molecule given in the Benzene Molecule (C_6H_6) section can be generalized to any aromatic functional group(s) of aromatic and heterocyclic compounds.

C_6H_6 can be considered a linear combination of three ethylene molecules wherein a $C-H$ bond of each CH_2 group of $H_2C=CH_2$ is replaced by a $C=C$ bond to form a six-member ring of carbon atoms. The solution of the ethylene molecule is given in the Ethylene Molecule (CH_2CH_2) section. The radius $r_{ethylene\,2sp^3}$ ($0.85252a_0$) of the $C2sp^3$ shell of ethylene calculated from the Coulombic energy is given by Eq. (14.244). The Coulombic energy $E_{Coulomb}\left(C_{ethylene},2sp^3\right)$ ($-15.95955\,eV$) of the outer electron of the $C2sp^3$ shell is given by Eq. (14.245). The energy $E\left(C_{ethylene},2sp^3\right)$ ($-15.76868\,eV$) of the outer electron of the $C2sp^3$ shell is given by Eq. (14.246). $E_T\left(C=C,2sp^3\right)$ ($-1.13380\,eV$) (Eq. (14.247)), the energy change of each $C2sp^3$ shell with the formation of the $C=C$-bond MO is given by the difference between $E\left(C_{ethylene},2sp^3\right)$ and $E\left(C,2sp^3\right)$. C_6H_6 can be solved using the same principles as those used to solve ethylene wherein the $2s$ and $2p$ shells of each C hybridize to form a single $2sp^3$ shell as an energy minimum, and the sharing of electrons between two $C2sp^3$ hybridized orbitals (HOs) to form a molecular orbital (MO) permits each participating hybridized orbital to decrease in radius and energy. Each $2sp^3$ HO of each carbon atom initially has four unpaired electrons. Thus, the $6H$ atomic orbitals (AOs) of benzene contribute six electrons and the six sp^3-hybridized carbon atoms contribute twenty-four electrons to form six $C-H$ bonds and six $C=C$ bonds. Each $C-H$ bond has two paired electrons with one donated from the H AO and the other from the $C2sp^3$ HO. Each $C=C$ bond comprises a linear combination of a factor of 0.75 of four paired electrons (three electrons) from two sets of two $C2sp^3$ HOs of the participating carbon atoms. Each $C-H$ and each $C=C$ bond comprises a linear combination of one and two diatomic H_2-type MOs developed in the Nature of the Chemical Bond of Hydrogen-Type Molecules and Molecular Ions section, respectively.

Consider the case where three sets of $C=C$-bond MOs form bonds between the two carbon atoms of each molecule to form a six-member ring such that the six resulting bonds comprise eighteen paired electrons. Each bond comprises a linear combination of two MOs wherein each comprises two $C2sp^3$ HOs and 75% of a H_2-type ellipsoidal MO divided between the $C2sp^3$ HOs:

$$\begin{pmatrix} 3\left(2\;C2sp^3+0.75\;H_2\;MO\right)\rightarrow 3\left(C\overset{4e}{=}C\right)-ethylene-type-bond\;MO \\ \rightarrow 6\left(C\overset{3e}{=}C\right)-bond\;MO\;of\;benzene \end{pmatrix} \tag{15.161}$$

The linear combination of each H_2-type ellipsoidal MO with each $C2sp^3$ HO further comprises an excess of 25% charge-density contribution per bond from each $C2sp^3$ HO to the $C=C$-bond MO to achieve an energy minimum. Thus, the dimensional parameters of each bond $C=C$-bond are determined using Eqs. (15.51) and (15.1-15.5) in a form that are the same equations as those used to determine the same parameters of the $C=C$-bond MO of ethylene (Eqs. (14.242-14.268)) while matching the boundary conditions of the structure of benzene.

Hybridization with 25% electron donation to each $C=C$-bond gives rise to the $C_{benzene}2sp^3$ HO-shell Coulombic energy $E_{Coulomb}\left(C_{benzene},2sp^3\right)$ given by Eq. (14.245). To meet the equipotential condition of the union of the six $C2sp^3$ HOs, c_2 and C_2 of Eq. (15.51) for the aromatic $C\overset{3e}{=}C$-bond MO is given by Eq. (15.71) as the ratio of $15.95955\,eV$, the magnitude of $E_{Coulomb}\left(C_{benzene},2sp^3\right)$ (Eq. (14.245)), and $13.605804\,eV$, the magnitude of the Coulombic energy between the electron and proton of H (Eq. (1.264)):

$$C_2\left(benzeneC2sp^3HO\right)=c_2\left(benzeneC2sp^3HO\right)=\frac{13.605804\;eV}{15.95955\;eV}=0.85252 \tag{15.162}$$

The energies of each $C\overset{3e}{=}C$ bond of benzene are also determined using the same equations as those of ethylene (Eqs. (14.251-14.253) and (14.319-14.333)) with the parameters of benzene. Ethylene serves as a basis element for the $C\overset{3e}{=}C$ bonding of benzene wherein each of the six $C\overset{3e}{=}C$ bonds of benzene comprises (0.75)(4) = 3 electrons according to Eq. (15.161). The total energy of the bonds of the eighteen electrons of the $C\overset{3e}{=}C$ bonds of benzene, $E_T\left(C_6H_6,C\overset{3e}{=}C\right)$, is given by (6)(0.75) times $E_{T+osc}(C=C)$ (Eq. (14.492)), the total energy of the $C\overset{3e}{=}C$-bond MO of benzene including the Doppler term, minus eighteen times $E\left(C,2sp^3\right)$ (Eq. (14.146)), the initial energy of each $C2sp^3$ HO of each C that forms the $C\overset{3e}{=}C$ bonds of bond order two.

Thus, the total energy of the six $C\overset{3e}{=}C$ bonds of benzene with three electron per aromatic bond given by Eq. (14.493) is:

$$\begin{aligned} E_T\left(C_6H_6, C\overset{3e}{=}C\right) &= (6)(0.75)E_{T+osc}\left(C=C\right)-(6)(3)E\left(C,2sp^3\right) \\ &= (6)(0.75)(-66.05796\ eV)-18(-14.63489\ eV) \\ &= -297.26081\ eV-(-263.42798\ eV) = -33.83284\ eV \end{aligned} \tag{15.163}$$

The results of benzene can be generalized to the class of aromatic and heterocyclic compounds. $E_{h\nu}$ of an aromatic bond is given by $E_T\left(H_2\right)$ (Eqs. (11.212) and (14.486)), the maximum total energy of each H_2-type MO such that:

$$\bar{E}_{osc} = n_1\left(\bar{E}_D+\bar{E}_{Kvib}\right) = n_1\left(-31.63536831\ eV\sqrt{\frac{2\bar{E}_K}{Mc^2}}+\frac{1}{2}\hbar\sqrt{\frac{k}{\mu}}\right) \tag{15.164}$$

The factor of 0.75 corresponding to the three electrons per aromatic bond of bond order two given in the Benzene Molecule (C_6H_6) section modifies Eqs. (15.61-15.65). Multiplication of the total energy given by Eq. (15.64) by $f_1=0.75$ with the substitution of Eq. (15.164) gives the total energy of the aromatic bond:

$$E_T\left(Group\right) = f_1\begin{pmatrix} E(basis\ energies)+E_T\left(atom-atom, msp^3.AO\right) \\ -31.63536831\ eV\sqrt{\dfrac{2\hbar\sqrt{\dfrac{C_{1o}C_{2o}e^2}{4\pi\varepsilon_0R^3}}}{m_ec^2}}+n_1\bar{E}_{Kvib}+c_3\dfrac{8\pi\mu_0\mu_B^2}{r^3} \end{pmatrix} \tag{15.165}$$

The total bond energy of the aromatic group $E_D\left(Group\right)$ is the negative difference of the total energy of the group (Eq. (15.165)) and the total energy of the starting species given by the sum of $c_4E_{initial}\left(c_4\ AO/HO\right)$ and $c_5E_{initial}\left(c_5\ AO/HO\right)$:

$$E_D\left(Group\right) = -\begin{pmatrix} f_1\begin{pmatrix} E(basis\ energies)+E_T\left(atom-atom, msp^3.AO\right) \\ -31.63536831\ eV\sqrt{\dfrac{2\hbar\sqrt{\dfrac{C_{1o}C_{2o}e^2}{4\pi\varepsilon_0R^3}}}{m_ec^2}}+n_1\bar{E}_{Kvib}+c_3\dfrac{8\pi\mu_0\mu_B^2}{r^3} \end{pmatrix} \\ -\left(c_4E_{initial}\left(AO/HO\right)+c_5E_{initial}\left(c_5\ AO/HO\right)\right) \end{pmatrix} \tag{15.166}$$

Since there are three electrons per aromatic bond, c_4 is three times the number of aromatic bonds.

Benzene can also be considered as comprising chemical bonds between six *CH* radicals wherein each radical comprises a chemical bond between carbon and hydrogen atoms. The solution of the parameters of *CH* is given in the Hydrogen Carbide (CH) section. Those of the benzene are given in the Benzene Molecule (C_6H_6) section. The energy components of V_e, V_p, T, V_m, and E_T are the same as those of the hydrogen carbide radical, except that $E_T\left(C=C,2sp^3\right)=-1.13379\ eV$ (Eq. (14.247)) is subtracted from $E_T\left(CH\right)$ of Eq. (13.495) to match the energy of each $C-H$-bond MO to the decrease in the energy of the corresponding $C2sp^3$ HO. In the corresponding generalization of the aromatic CH group, the geometrical parameters are determined using Eq. (15.51) and Eqs. (15.1-15.5) with $E_T\left(atom-atom, msp^3.AO\right)=-1.13379\ eV$.

The total energy of the benzene $C-H$-bond MO, $E_{T_{benzene}}\left(C-H\right)$, given by Eq. (14.467) is the sum of $0.5E_T\left(C=C,2sp^3\right)$, the energy change of each $C2sp^3$ shell per single bond due to the decrease in radius with the formation of the corresponding $C\overset{3e}{=}C$-bond MO (Eq. (14.247)), and $E_{T_{benzene}}\left(CH\right)$, the σ MO contribution given by Eq. (14.441). In the corresponding generalization of the aromatic *CH* group, the energy parameters are determined using Eqs. (15.165-15.166) with $f_1=1$ and $E_T\left(atom-atom, msp^3.AO\right)=\dfrac{-1.13379\ eV}{2}$. Thus, the energy contribution to the single aromatic CH bond is one half that of the $C\overset{3e}{=}C$ double bond contribution. This matches the energies of the CH and $C\overset{3e}{=}C$ aromatic groups, conserves the electron number with the equivalent charge density as that of $s=1$ in Eqs. (15.18-15.21), and further gives a minimum energy for the molecule. Breakage of the aromatic $C\overset{3e}{=}C$ bonds to give CH groups creates unpaired electrons in these fragments that corresponds to $c_3=1$ in Eq. (15.65) with E_{mag} given by Eq. (15.67).

Each of the $C-H$ bonds of benzene comprises two electrons according to Eq. (14.439). From the energy of each $C-H$ bond, $-E_{D_{benzene}}\left({}^{12}CH\right)$ (Eq. (14.477)), the total energy of the twelve electrons of the six $C-H$ bonds of benzene, $E_T\left(C_6H_6,C-H\right)$, given by Eq. (14.494) is:

$$E_T\left(C_6H_6,C-H\right)=(6)\left(-E_{D_{benzene}}\left({}^{12}CH\right)\right)=6\left(-3.90454\ eV\right)=-23.42724\ eV \tag{15.167}$$

The total bond dissociation energy of benzene, $E_D\left(C_6H_6\right)$, given by Eq. (14.495) is the negative sum of $E_T\left(C_6H_6,C\overset{3e}{=}C\right)$ (Eq. (14.493)) and $E_T\left(C_6H_6,C-H\right)$ (Eq. (14.494)):

$$E_D\left(C_6H_6\right)=-\left(E_T\left(C_6H_6,C\overset{3e}{=}C\right)+E_T\left(C_6H_6,C-H\right)\right)=-\left(\left(-33.83284\ eV\right)+\left(-23.42724\ eV\right)\right)=57.2601\ eV \tag{15.168}$$

Using the parameters given in Tables 15.214 and 15.216 in the general equations (Eqs. (15.51), (15.1-15.5), and (15.165-15.166)) reproduces the results for benzene given in the Benzene Molecule (C_6H_6) section as shown in Tables 15.214 and 15.216.

The symbols of the functional groups of aromatics and heterocyclics are given in Table 15.213. The geometrical (Eqs. (15.1-15.5) and (15.51)), intercept (Eqs. (15.80-15.87)), and energy (Eqs. (15.6-15.11), (15.17-15.65), and (15.165-15.166)) parameters of aromatics and heterocyclics are given in Tables 15.214, 15.215, and 15.216, respectively. The total energy of benzene given in Table 15.217 was calculated as the sum over the integer multiple of each $E_D(Group)$ of Table 15.216 corresponding to functional-group composition of the molecule. The bond angle parameters of benzene determined using Eqs. (15.88-15.117) are given in Table 15.218. The color scale, translucent view of the charge-density of exemplary aromatic, benzene, comprising the concentric shells of atoms with the outer shell bridged by one or more H_2-type ellipsoidal MOs or joined with one or more hydrogen MOs is shown in Figure 15.36.

Figure 15.36. Color scale, translucent view of the charge-density of benzene showing the orbitals of the atoms at their radii, the ellipsoidal surface of each H or H_2-type ellipsoidal MO that transitions to the corresponding outer shell of the atom(s) participating in each bond, and the hydrogen nuclei (red, not to scale).

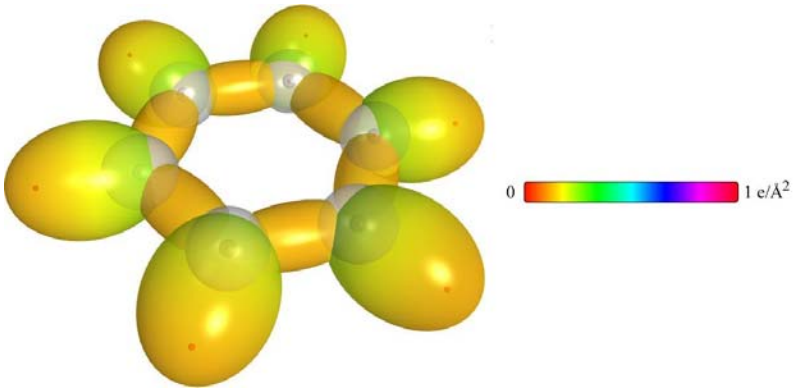

Table 15.213. The symbols of functional groups of aromatics and heterocyclics.

Functional Group	Group Symbol
CC (aromatic bond)	$C\overset{3e}{=}C$
CH (aromatic)	CH (i)

Table 15.214. The geometrical bond parameters of aromatics and heterocyclics and experimental values [1].

Parameter	$C\overset{3e}{=}C$ Group	CH Group
$a\ (a_0)$	1.47348	1.60061
$c'\ (a_0)$	1.31468	1.03299
Bond Length $2c'\ (\text{Å})$	1.39140	1.09327
Exp. Bond Length (Å)	1.399 (benzene)	1.101 (benzene)
$b,c\ (a_0)$	0.66540	1.22265
e	0.89223	0.64537

Table 15.215. The MO to HO intercept geometrical bond parameters of benzene. E_T is E_T (*atom – atom,msp³.AO*).

Bond	Atom	E_T (eV) Bond 1	E_T (eV) Bond 2	E_T (eV) Bond 3	E_T (eV) Bond 4	Final Total Energy $C2sp^3$ (eV)	$r_{initial}$ (a_0)	r_{final} (a_0)	$E_{Coulomb}(C2sp^3)$ (eV) Final	$E(C2sp^3)$ (eV) Final	θ' (°)	θ_1 (°)	θ_2 (°)	d_1 (a_0)	d_2 (a_0)
$C-H\ (CH)$	C	-0.85035	-0.85035	-0.56690	0	-153.88327	0.91771	0.79597	-17.09334	-16.90248	74.42	105.58	38.84	1.24678	0.21379
$C \overset{3e}{=} HC_a \overset{3e}{=} C$	C_a	-0.85035	-0.85035	-0.56690	0	-153.88327	0.91771	0.79597	-17.09334	-16.90248	134.24	45.76	58.98	0.75935	0.55533

Table 15.216. The energy parameters (eV) of functional groups of aromatics and heterocyclics.

Parameters	$C\overset{3e}{=}C$ Group	CH Group
f_1	0.75	1
n_1	2	1
n_2	0	0
n_3	0	0
C_1	0.5	0.75
C_2	0.85252	1
c_1	1	1
c_2	0.85252	0.91771
c_3	0	1
c_4	3	1
c_5	0	1
C_{1o}	0.5	0.75
C_{2o}	0.85252	1
$V_e\ (eV)$	-101.12679	-37.10024
$V_p\ (eV)$	20.69825	13.17125
$T\ (eV)$	34.31559	11.58941
$V_m\ (eV)$	-17.15779	-5.79470
$E_{(AO/HO)}\ (eV)$	0	-14.63489
$\Delta E_{\Pi_2 MO\ (AO/HO)}\ (eV)$	0	-1.13379
$E_{I_{(AO/HO)}}\ (eV)$	0	-13.50110
$E_{I_{(H_2MO)}}\ (eV)$	-63.27075	-31.63539
$E_{I_{(atom-atom,msp^3.AO)}}\ (eV)$	-2.26759	-0.56690
$E_{I_{(MO)}}\ (eV)$	-65.53833	-32.20226
$\omega\ (10^{15}\ rad/s)$	49.7272	26.4826
$E_K\ (eV)$	32.73133	17.43132
$\bar{E}_D\ (eV)$	-0.35806	-0.26130
$\bar{E}_{Kvib}\ (eV)$	0.19649 [49]	0.35532 Eq. (13.458)
$\bar{E}_{osc}\ (eV)$	-0.25982	-0.08364
$E_{mag}\ (eV)$	0.14803	0.14803
$E_{I_{(Group)}}\ (eV)$	-49.54347	-32.28590
$E_{initial\ (c_4\ AO/HO)}\ (eV)$	-14.63489	-14.63489
$E_{initial\ (c_3\ AO/HO)}\ (eV)$	0	-13.59844
$E_{D_{(Group)}}\ (eV)$	5.63881	3.90454

Table 15.217. The total bond energies of benzene calculated using the functional group composition and the energies of Table 15.216 compared to the experimental values [3].

Formula	Name	$C\overset{3e}{=}C$	CH	Calculated Total Bond Energy (eV)	Experimental Total Bond Energy (eV)	Relative Error
C_6H_6	Benzene	6	6	57.26008	57.26340	0.00006

Table 15.218. The bond angle parameters of benzene and experimental values [1]. E_T is E_T ($atom-atom$,$msp^3.AO$).

Atoms of Angle	$2c'$ Bond 1 (a_0)	$2c'$ Bond 2 (a_0)	$2c'$ Terminal Atoms (a_0)	$E_{Conlombic}$ Atom 1	Atom 1 Hybridization Designation (Table 15.3.A)	$E_{Coulambic}$ Atom 2	Atom 2 Hybridization Designation (Table 15.3.A)	c_2 Atom 1	c_2 Atom 2	C_1	C_2	c_1	c_2'	E_T (eV)	θ_v (°)	θ_1 (°)	θ_2 (°)	Cal. θ (°)	Exp. θ (°)
$\angle CCC$ (aromatic)	2.62936	2.62936	4.5585	-17.17218	38	-17.17218	38	0.79232	0.79232	1	1	1	0.79232	-1.85836				120.19	120 [50-52] (benzene)
$\angle CCH$ (aromatic)																120.19		119.91	120 [50-52] (benzene)

NAPHTHALENE

Naphthalene has the formula $C_{10}H_8$ and comprises a planar molecule with two aromatic rings that share a common $C-C$ group. In order to be aromatic, the total number of bonding electrons must be a multiple of 3 since the number of electrons of the aromatic bond is $(0.75)(4)=3$ as shown in the Benzene section. In the case of naphthalene, the peripheral 10 carbons form the aromatic MO with the center bridged by a $C-C$ single bond. Then, 30 electrons of the 48 available form aromatic bonds, two electrons form the bridging $C-C$ single bond, and 16 electrons form the eight $C-H$ single bonds. The energies of the aromatic carbons are given by the same equations as those of benzene (Eqs. (15.51), (15.1-15.5), and (15.165-15.166)), except that there are 10 in naphthalene versus six in benzene. Since there are three electrons per aromatic bond, c_4 is three times ten, the number of aromatic bonds. Similarly, the aromatic $C-H$ group of naphthalene is equivalent to that of benzene.

To meet the equipotential condition of the union of the ten $C2sp^3$ HOs bridged by the $C-C$ single bond, the parameters c_1, C_2, and C_{2o} of Eq. (15.51) are one for the $C-C$ group, C_{1o} and C_1 are 0.5, and c_2 given by Eq. (15.161) is $c_2\left(C2sp^3HO\right)=0.85252$. Otherwise, the solutions of the $C-C$ bond parameters are equivalent to those of the replaced $C-H$ groups with $E\left(AO/HO\right)=-14.63489\ eV$ and $\Delta E_{H_2MO}\left(AO/HO\right)=-1.13379\ eV$ per carbon in Eq. (15.51). Similarly, the energy parameters are determined using Eqs. (15.61-15.65) with $E_T\left(atom-atom,msp^3.AO\right)=\dfrac{-1.13379\ eV}{2}$.

The symbols of the functional groups of naphthalene are given in Table 15.219. The corresponding designation of the structure is shown in Figure 15.37B. The geometrical (Eqs. (15.1-15.5) and (15.51)), intercept (Eqs. (15.80-15.87)), and energy (Eqs. (15.6-15.11), (15.17-15.65), and (15.165-15.166)) parameters of naphthalene are given in Tables 15.220, 15.221, and 15.222, respectively. The total energy of naphthalene given in Table 15.223 was calculated as the sum over the integer multiple of each $E_{D\,(Group)}$ of Table 15.222 corresponding to functional-group composition of the molecule. The bond angle parameters of naphthalene determined using Eqs. (15.88-15.117) are given in Table 15.224. The color scale, translucent view of the charge-density of naphthalene, comprising the concentric shells of atoms with the outer shell bridged by one or more H_2-type ellipsoidal MOs or joined with one or more hydrogen MOs is shown in Figure 15.37A. The polycyclic aromatic hydrocarbon pentacene was imaged by atomic force microscopy using a single CO molecule as the probe [53]. The resulting breakthrough in resolution revealed that in contrast to the fuzzy images touted by quantum theoreticians as proof of the cloud model of the electron, the images showed localized bonding MOs and AOs in agreement with the classical solution as shown in Figure 15.38.

Figure 15.37. (A) Color scale, translucent view of the charge-density of naphthalene showing the orbitals of the atoms at their radii, the ellipsoidal surface of each H or H_2-type ellipsoidal MO that transitions to the corresponding outer shell of the atom(s) participating in each bond, and the hydrogen nuclei (red, not to scale). (B) Chemical structure and atom designation of naphthalene.

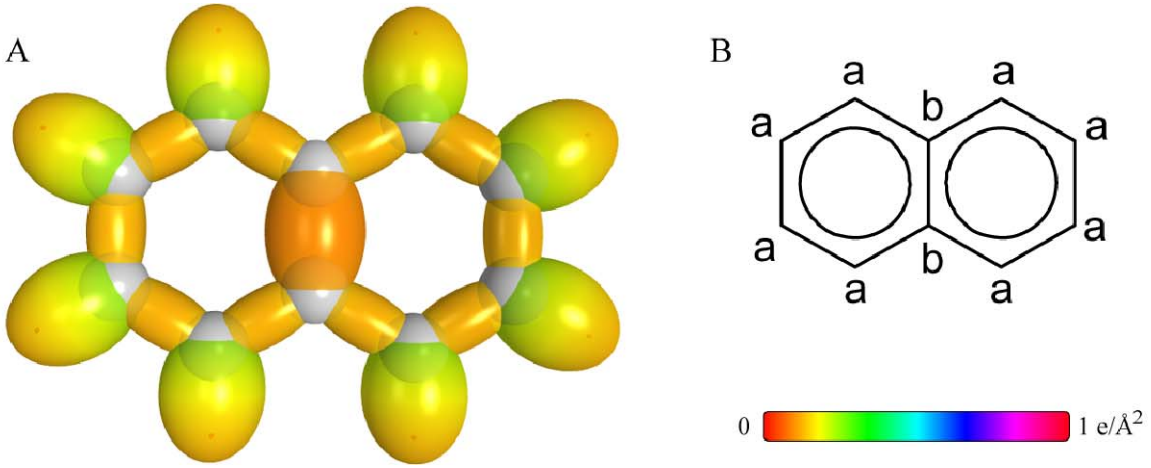

Figure 15.38. Atomic force microscopy image of pentacene by Gross et al. [53] and the superimposed analytical classical solution that matches the physical structure.

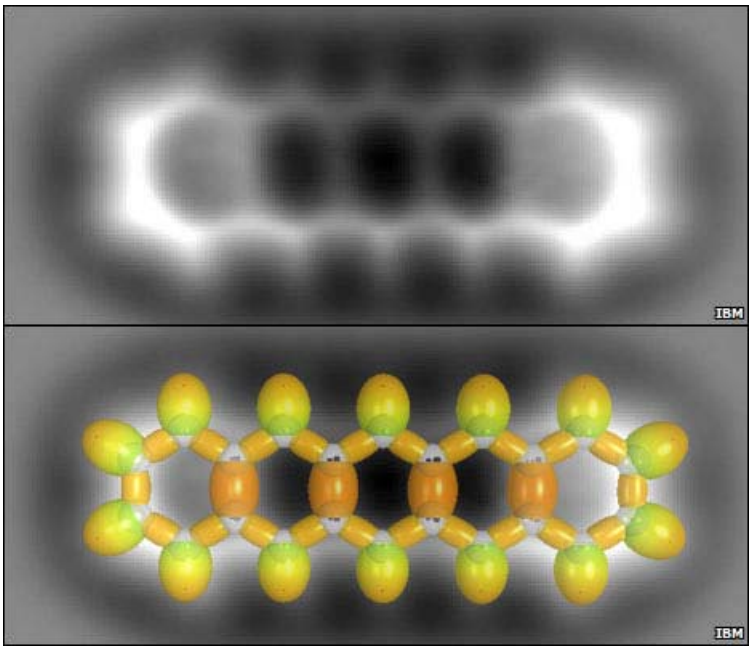

Table 15.219. The symbols of functional groups of naphthalene.

Functional Group	Group Symbol
C_aC_a (aromatic bond)	$C \overset{3e}{=} C$
CH (aromatic)	CH (i)
$C_b - C_b$ (bridging bond)	$C - C$

Table 15.220. The geometrical bond parameters of naphthalene and experimental values [1].

Parameter	$C \overset{3e}{=} C$ Group	CH Group	$C-C$ Group
$a\ (a_0)$	1.47348	1.60061	1.75607
$c'\ (a_0)$	1.31468	1.03299	1.32517
Bond Length $2c'\ (\text{Å})$	1.39140	1.09327	1.40250
Exp. Bond Length (Å)	1.40 (avg.) (naphthalene)	1.101 (benzene)	1.42 (naphthalene)
$b,c\ (a_0)$	0.66540	1.22265	1.15226
e	0.89223	0.64537	0.75462

Table 15.221. The MO to HO intercept geometrical bond parameters of naphthalene. E_T is E_T ($atom-atom$,$msp^3.AO$).

Bond	Atom	E_T (eV) Bond 1	E_T (eV) Bond 2	E_T (eV) Bond 3	E_T (eV) Bond 4	Final Total Energy $C2sp^3$ (eV)	$r_{initial}$ (a_0)	r_{final} (a_0)	$E_{Coulomb}(C2sp^3)$ (eV) Final	$E(C2sp^3)$ (eV) Final	θ' (°)	θ_1 (°)	θ_2 (°)	d_1 (a_0)	d_2 (a_0)
$C-H\ (CH)$	C	-0.85035	-0.85035	-0.56690	0	-153.88327	0.91771	0.79597	-17.09334	-16.90248	74.42	105.58	38.84	1.24678	0.21379
$C \overset{3e}{=} HC_a \overset{3e}{=} C$	C_a	-0.85035	-0.85035	-0.56690	0	-153.88327	0.91771	0.79597	-17.09334	-16.90248	134.24	45.76	58.98	0.75935	0.55533
$C \overset{3e}{=} C_b(C_b) \overset{3e}{=} C$	C_b	-0.85035	-0.85035	-0.28345	0	-153.59983	0.91771	0.80939	-16.80989	-16.61903	134.81	45.19	59.66	0.74430	0.57038
$(C_a)_2 C_b - C_b (C_a)_2$	C_b	-0.85035	-0.85035	-0.28345	0	-153.59983	0.91771	0.80939	-16.80989	-16.61903	99.50	80.50	47.66	1.18269	0.14248

Table 15.222. The energy parameters (eV) of functional groups of naphthalene.

Parameters	$C\overset{3e}{=}C$ Group	CH Group	$C-C$ Group
f_1	0.75	1	1
n_1	2	1	1
n_2	0	0	0
n_3	0	0	0
C_1	0.5	0.75	0.5
C_2	0.85252	1	1
c_1	1	1	1
c_2	0.85252	0.91771	0.85252
c_3	0	1	0
c_4	3	1	2
c_5	0	1	0
C_{1o}	0.5	0.75	0.5
C_{2o}	0.85252	1	1
$V_e\ (eV)$	-101.12679	-37.10024	-34.43791
$V_p\ (eV)$	20.69825	13.17125	10.26723
$T\ (eV)$	34.31559	11.58941	9.80539
$V_m\ (eV)$	-17.15779	-5.79470	-4.90270
$E_{(AO/HO)}\ (eV)$	0	-14.63489	-14.63489
$\Delta E_{H_2MO\,(AO/HO)}\ (eV)$	0	-1.13379	-1.13379
$E_{T\,(AO/HO)}\ (eV)$	0	-13.50110	-13.50110
$E_{T\,(H_2MO)}\ (eV)$	-63.27075	-31.63539	-31.63529
$E_T\left(atom-atom, msp^3.AO\right)(eV)$	-2.26759	-0.56690	-0.56690
$E_{T\,(MO)}\ (eV)$	-65.53833	-32.20226	-32.20226
$\omega\ \left(10^{15}\ rad/s\right)$	49.7272	26.4826	23.6343
$E_K\ (eV)$	32.73133	17.43132	15.55648
$\bar{E}_D\ (eV)$	-0.35806	-0.26130	-0.25127
$\bar{E}_{Kvib}\ (eV)$	0.19649 [49]	0.35532 Eq. (13.458)	0.12312 [2]
$\bar{E}_{osc}\ (eV)$	-0.25982	-0.08364	-0.18971
$E_{mag}\ (eV)$	0.14803	0.14803	0.14803
$E_{T\,(Group)}\ (eV)$	-49.54347	-32.28590	-32.39198
$E_{initial\,(c_4\ AO/HO)}\ (eV)$	-14.63489	-14.63489	-14.63489
$E_{initial\,(c_5\ AO/HO)}\ (eV)$	0	-13.59844	0
$E_{D\,(Group)}\ (eV)$	5.63881	3.90454	3.12220

Table 15.223. The total bond energies of naphthalene calculated using the functional group composition and the energies of Table 15.222 compared to the experimental values [3].

Formula	Name	$C \overset{3e}{=} C$	CH	$C-C$ Group	Calculated Total Bond Energy (eV)	Experimental Total Bond Energy (eV)	Relative Error
$C_{10}H_8$	Naphthalene	10	8	1	90.74658	90.79143	0.00049

Table 15.224. The bond angle parameters of naphthalene and experimental values [1]. E_T is $E_T(atom-atom,msp^3.AO)$.

Atoms of Angle	$2c'$ Bond 1 (a_0)	$2c'$ Bond 2 (a_0)	$2c'$ Terminal Atoms (a_0)	$E_{Coulombic}$ Atom 1	Atom 1 Hybridization Designation (Table 15.3.A)	$E_{Coulombic}$ Atom 2	Atom 2 Hybridization Designation (Table 15.3.A)	c_2 Atom 1	c_2 Atom 2	C_1	C_2	c_1	c_2'	E_T (eV)	θ_v (°)	θ_1 (°)	θ_2 (°)	Cal. θ (°)	Exp. θ (°)
$\angle C_aC_cC_c$ (naphthalene)	2.62936	2.65034	4.5585	-17.17218	38	-17.17218	38	0.79232	0.79232	1	1	1	0.79232	-1.85836				119.40	119.4 (naphthalene)
$\angle C_cC_aH$ (naphthalene)																119.40		120.30	
$\angle CCC$ (aromatic)	2.62936	2.62936	4.5585	-17.17218	38	-17.17218	38	0.79232	0.79232	1	1	1	0.79232	-1.85836				120.19	120 [50-52] (benzene)
$\angle CCH$ (aromatic)																120.19		119.91	120 [50-52] (benzene)

TOLUENE

Toluene has the formula C_7H_8 and comprises the benzene molecule with one hydrogen atom replaced by a methyl group corresponding to a CH_3 functional group and a $C-C$ functional group. The aromatic $C\overset{3e}{=}C$ and $C-H$ functional groups are equivalent to those of benzene given in the Aromatic and Heterocyclic Compounds section. The CH_3 functional group is the same as that of continuous and branched-chain alkanes given in the corresponding sections.

The bond between the methyl and aromatic ring comprises a $C-C$ functional group that is solved using the same principles as those used to solve the alkane functional groups wherein the $2s$ and $2p$ AOs of each C hybridize to form a single $2sp^3$ shell as an energy minimum, and the sharing of electrons between two $C2sp^3$ HOs to form a MO permits each participating hybridized orbital to decrease in radius and energy. To match energies within the MO that bridges methyl and aromatic carbons, $E(AO/HO)$ and $\Delta E_{H_2MO}(AO/HO)$ in Eq. (15.50) are $-15.35946\ eV$ (Eq. (14.155)) and $\frac{-1.13379\ eV}{2}$, respectively.

To meet the equipotential condition of the union of the aromatic and methyl $C2sp^3$ HOs of the $C-C$ single bond, the parameters c_1, C_2, and C_{2o} of Eq. (15.51) are one for the $C-C$ group, C_{1o} and C_1 are 0.5, and c_2 given by Eq. (13.430) is $c_2\left(C2sp^3HO\right)=0.91771$. To match the energies of the functional groups, $E_T\left(atom-atom,msp^3.AO\right)$ of the $C-C$-bond MO in Eq. (15.61) due to the charge donation from the C atoms to the MO is $-1.13379\ eV$ which is the same energy per $C2sp^3$ HO as that of the replaced $C-H$ group.

The symbols of the functional groups of toluene are given in Table 15.225. The corresponding designation of the structure is shown in Figure 15.39B. The geometrical (Eqs. (15.1-15.5) and (15.51)), intercept (Eqs. (15.80-15.87)), and energy (Eqs. (15.6-15.11), (15.17-15.65), and (15.165-15.166)) parameters of toluene are given in Tables 15.226, 15.227, and 15.228, respectively. The total energy of toluene given in Table 15.229 was calculated as the sum over the integer multiple of each $E_D(Group)$ of Table 15.228 corresponding to functional-group composition of the molecule. The bond angle parameters of toluene determined using Eqs. (15.88-15.117) are given in Table 15.230. The color scale, translucent view of the charge-density of toluene comprising the concentric shells of atoms with the outer shell bridged by one or more H_2-type ellipsoidal MOs or joined with one or more hydrogen MOs is shown in Figure 15.39A.

Figure 15.39. (A) Color scale, translucent view of the charge-density of toluene showing the orbitals of the atoms at their radii, the ellipsoidal surface of each H or H_2-type ellipsoidal MO that transitions to the corresponding outer shell of the atom(s) participating in each bond, and the hydrogen nuclei (red, not to scale). (B) Chemical structure and atom designation of toluene.

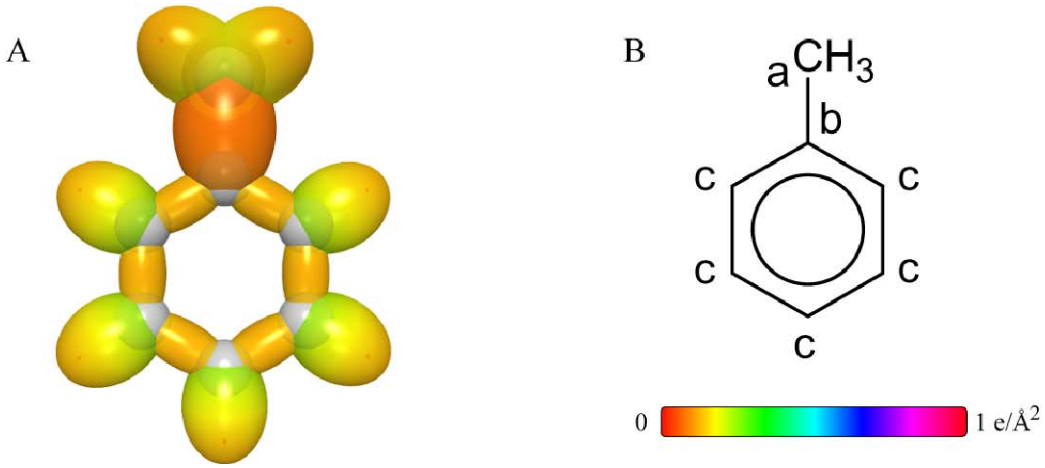

Table 15.225. The symbols of functional groups of toluene.

Functional Group	Group Symbol
CC (aromatic bond)	$C \overset{3e}{=} C$
CH (aromatic)	CH (i)
$C_a - C_b$ (CH_3 to aromatic bond)	$C - C$
CH_3 group	$C - H\ (CH_3)$

Table 15.226. The geometrical bond parameters of toluene and experimental values [1].

Parameter	$C \overset{3e}{=} C$ Group	CH (i) Group	$C - C$ Group	$C - H\ (CH_3)$ Group
$a\ (a_0)$	1.47348	1.60061	2.06004	1.64920
$c'\ (a_0)$	1.31468	1.03299	1.43528	1.04856
Bond Length $2c'\ (\text{Å})$	1.39140	1.09327	1.51904	1.10974
Exp. Bond Length (Å)	1.399 (toluene)	1.11 (avg.) (toluene)	1.524 (toluene)	1.11 (avg.) (toluene)
$b,c\ (a_0)$	0.66540	1.22265	1.47774	1.27295
e	0.89223	0.64537	0.69673	0.63580

Table 15.227. The MO to HO intercept geometrical bond parameters of toluene. E_T is E_T (*atom – atom,msp³.AO*).

Bond	Atom	E_T (eV) Bond 1	E_T (eV) Bond 2	E_T (eV) Bond 3	E_T (eV) Bond 4	Final Total Energy $C2sp^3$ (eV)	$r_{initial}$ (a_0)	r_{final} (a_0)	$E_{Conlomb}(C2sp^3)$ (eV) Final	$E(C2sp^3)$ (eV) Final	θ' (°)	θ_1 (°)	θ_2 (°)	d_1 (a_0)	d_2 (a_0)
$C-H\ (C_aH_3)$	C_a	-0.56690	0	0	0	-152.18259	0.91771	0.88392	-15.39265	-15.20178	79.89	101.11	43.13	1.20367	0.15511
$C-H\ (C_cH)$	C_c	-0.85035	-0.85035	-0.56690	0	-153.88327	0.91771	0.79597	-17.09334	-16.90248	74.42	105.58	38.84	1.24678	0.21379
$C^{3e}=HC_c^{3e}=C$ $C^{3e}=(H_2C_a)C_b^{3e}=C$	C_c C_b	-0.85035	-0.85035	-0.56690	0	-153.88327	0.91771	0.79597	-17.09334	-16.90248	134.24	45.76	58.98	0.75935	0.55533
$\left(C^{3e}=\right)_2 C_b-C_aH_3$	C_a	-0.56690	0	0	0	-152.18259	0.91771	0.88392	-15.39265	-15.20178	73.38	106.62	34.97	1.68807	0.25279
$\left(C^{3e}=\right)_2 C_b-C_aH_3$	C_b	-0.56690	-0.85035	-0.85035	0	-153.88328	0.91771	0.79597	-17.09334	-16.90247	61.56	118.44	28.27	1.81430	0.37901

Table 15.228. The energy parameters (eV) of functional groups of toluene.

Parameters	$C=C$ Group	CH (i) Group	$C-C$ Group	CH_3 Group
f_1	0.75	1		
n_1	2	1	1	3
n_2	0	0	0	2
n_3	0	0	0	0
C_1	0.5	0.75	0.5	0.75
C_2	0.85252	1	1	1
c_1	1	1	1	1
c_2	0.85252	0.91771	0.91771	0.91771
c_3	0	1	0	0
c_4	3	1	2	1
c_5	0	1	0	3
C_{1o}	0.5	0.75	0.5	0.75
C_{2o}	0.85252	1	1	1
$V_e\ (eV)$	-101.12679	-37.10024	-29.95792	-107.32728
$V_p\ (eV)$	20.69825	13.17125	9.47952	38.92728
$T\ (eV)$	34.31559	11.58941	7.27120	32.53914
$V_m\ (eV)$	-17.15779	-5.79470	-3.63560	-16.26957
$E_{(AO/HO)}\ (eV)$	0	-14.63489	-15.35946	-15.56407
$\Delta E_{H_2MO\,(AO/HO)}\ (eV)$	0	-1.13379	-0.56690	0
$E_{T\,(AO/HO)}\ (eV)$	0	-13.50110	-14.79257	-15.56407
$E_{T\,(H_2MO)}\ (eV)$	-63.27075	-31.63539	-31.63537	-67.69451
$E_I\left(atom-atom, msp^3.AO\right)\ (eV)$	-2.26759	-0.56690	-1.13379	0
$E_{T\,(MO)}\ (eV)$	-65.53833	-32.20226	-32.76916	-67.69450
$\omega\ \left(10^{15}\ rad/s\right)$	49.7272	26.4826	16.2731	24.9286
$E_K\ (eV)$	32.73133	17.43132	10.71127	16.40846
$\overline{E}_D\ (eV)$	-0.35806	-0.26130	-0.21217	-0.25352
$\overline{E}_{Kvib}\ (eV)$	0.19649 [49]	0.35532 Eq. (13.458)	0.14940 [54]	0.35532 (Eq. (13.458))
$\overline{E}_{osc}\ (eV)$	-0.25982	-0.08364	-0.13747	-0.22757
$E_{mag}\ (eV)$	0.14803	0.14803	0.14803	0.14803
$E_{T\,(Group)}\ (eV)$	-49.54347	-32.28590	-32.90663	-67.92207
$E_{initial\,(c_1\ AO/HO)}\ (eV)$	-14.63489	-14.63489	-14.63489	-14.63489
$E_{initial\,(c_5\ AO/HO)}\ (eV)$	0	-13.59844	0	-13.59844
$E_{D\,(Group)}\ (eV)$	5.63881	3.90454	3.63685	12.49186

Table 15.229. The total bond energies of toluene calculated using the functional group composition and the energies of Table 15.228 compared to the experimental values [3].

Formula	Name	$C^{3e}=C$	CH (i)	$C-C$ Group	CH_3	Calculated Total Bond Energy (eV)	Experimental Total Bond Energy (eV)	Relative Error
C_7H_8	Toluene	6	5	1	1	69.48425	69.546	0.00088

Table 15.230. The bond angle parameters of toluene and experimental values [1]. E_T is E_T ($atom-atom,msp^3.AO$).

Atoms of Angle	$2c'$ Bond 1 (a_0)	$2c'$ Bond 2 (a_0)	$2c'$ Terminal Atoms (a_0)	$E_{Coulombic}$ Atom 1	Atom 1 Hybridization Designation (Table 15.3.A)	$E_{Coulombic}$ Atom 2	Atom 2 Hybridization Designation (Table 15.3.A)	c_2 Atom 1	c_2 Atom 2	C_1	C_2	c_1	c_2'	E_T (eV)	θ_v (°)	θ_1 (°)	θ_2 (°)	Cal. θ (°)	Exp. θ (°)
$\angle CCC$ (aromatic)	2.62936	2.62936	4.5585	-17.17218	38	-17.17218	38	0.79232	0.79232	1	1	1	0.79232	-1.85836				120.19	120 [50-52] (benzene)
$\angle CCH$ (aromatic)																120.19		119.91	120 [50-52] (benzene)

HALOBENZENES

Halobenzenes have the formula $C_6H_{6-m}X_m$ $X=F,Cl,Br,I$ and comprise the benzene molecule with at least one hydrogen atom replaced by a halogen atom corresponding to a $C-X$ functional group. The aromatic $C\overset{3e}{=}C$ and $C-H$ functional groups are equivalent to those of benzene given in the Aromatic and Heterocyclic Compounds section. The hybridization factors of the aryl $C-X$ functional groups are equivalent to those of the corresponding alkyl halides as given in Tables 15.30, 15.36, 15.42, and 15.48, and are solved using the same principles as those used to solve the alkyl halide functional groups as given in the corresponding sections. In each case, the $2s$ and $2p$ AOs of each C hybridize to form a single $2sp^3$ shell as an energy minimum, and the sharing of electrons between the $C2sp^3$ HO and X AO to form a MO permits each participating hybridized orbital to decrease in radius and energy. Therefore, the MO is energy matched to the $C2sp^3$ HO such that $E\left(AO/HO\right)$ in Eq. (15.51) is $-14.63489\,eV$. $E_T\left(atom-atom,msp^3.AO\right)$ of each $C-X$ functional group given in Table 15.234 that achieves matching of the energies of the AOs and HOs within the functional groups of the MOs are those of alkanes and alkenes given in Tables 15.1 and 15.2. To further match energies within each MO that bridges the halogen AO and aromatic carbon $C2sp^3$ HO, $\Delta E_{H_2MO}\left(AO/HO\right)$ in Eq. (15.51) is $E_T\left(atom-atom,msp^3.AO\right)$ of the alkene $C=C$ functional group, $-2.26759\,eV$ given by Eq. (14.247), plus the maximum possible contribution of $E_T\left(atom-atom,msp^3.AO\right)$ of the $C-X$ functional group to minimize the energy of the MO as given in Table 15.234. $E_{initial}\left(c_4\ AO/HO\right)$ is $-14.63489\,eV$ (Eq. (15.25)), except for $C-I$ due to the low ionization potential of the I AO. In order to achieve an energy minimum with energy matching within iodo-aryl molecules, $E_{initial}\left(c_4\ AO/HO\right)$ of the $C-I$ functional group is $-15.76868\,eV$ (Eq. (14.246)), and $E_T\left(atom-atom,msp^3.AO\right)$ is $-1.65376\,eV$ given by the linear combination of $-0.72457\,eV$ (Eq. (14.151)) and $-0.92918\,eV$ (Eq. (14.513)), respectively.

The small differences between energies of ortho, meta, and para-dichlorobenzene is due to differences in the energies of vibration in the transition state that contribute to E_{osc}. Two types of $C-Cl$ functional groups can be identified based on symmetry that determine the parameter R in Eq. (15.57). One corresponds to the special case of 1,3,5 substitution and the other corresponds to other cases of single or multiple substitutions of Cl for H. P-dichlorobenzene is representative of the bonding with $R=a$. 1,2,3-trichlorobenzene is the particular case wherein $R=b$. Also, beyond the binding of three chlorides E_{mag} is subtracted for each additional Cl due to the formation of an unpaired electrons on each $C-Cl$ bond.

The symbols of the functional groups of halobenzenes are given in Table 15.231. The geometrical (Eqs. (15.1-15.5) and (15.51)), intercept (Eqs. (15.80-15.87)), and energy (Eqs. (15.6-15.11), (15.17-15.65), and (15.165-15.166)) parameters of halobenzenes are given in Tables 15.232, 15.233, and 15.234, respectively. The total energy of each halobenzene given in Table 15.235 was calculated as the sum over the integer multiple of each $E_{D\,(Group)}$ of Table 15.234 corresponding to functional-group composition of the molecule. For each set of unpaired electrons created by bond breakage, the $C2sp^3$ HO magnetic energy E_{mag} that is subtracted from the weighted sum of the $E_{D\,(Group)}$ (eV) values based on composition is given by Eq. (15.67). The bond angle parameters of halobenzenes determined using Eqs. (15.88-15.117) are given in Table 15.236. The color scale, translucent view of the charge-density of chlorobenzene comprising the concentric shells of atoms with the outer shell bridged by one or more H_2-type ellipsoidal MOs or joined with one or more hydrogen MOs is shown in Figure 15.40.

Figure 15.40. Color scale, translucent view of the charge-density of chlorobenzene showing the orbitals of the atoms at their radii, the ellipsoidal surface of each H or H_2-type ellipsoidal MO that transitions to the corresponding outer shell of the atom(s) participating in each bond, and the hydrogen nuclei (red, not to scale).

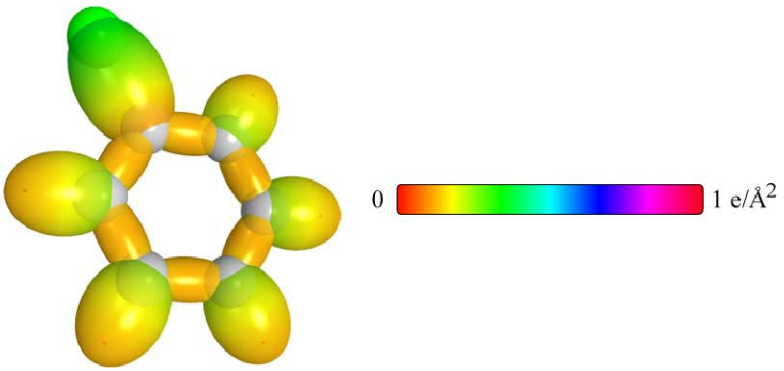

Table 15.231. The symbols of functional groups of halobenzenes.

Functional Group	Group Symbol
CC (aromatic bond)	$C \overset{3e}{=} C$
CH (aromatic)	CH (i)
$F-C$ (F to aromatic bond)	$C-F$
$Cl-C$ (Cl to aromatic bond)	$C-Cl$ (a)
$Cl-C$ (Cl to aromatic bond of 1,3,5-trichlorobenzene)	$C-Cl$ (b)
$Br-C$ (Br to aromatic bond)	$C-Br$
$I-C$ (I to aromatic bond)	$C-I$

Table 15.232. The geometrical bond parameters of halobenzenes and experimental values [1].

Parameter	$C \overset{3e}{=} C$ Group	CH (i) Group	$C-F$ Group	$C-Cl$ (a) Group	$C-Cl$ (b) Group	$C-Br$ Group	$C-I$ Group
$a\ (a_0)$	1.47348	1.60061	1.60007	2.20799	2.20799	2.30810	2.50486
$c'\ (a_0)$	1.31468	1.03299	1.26494	1.64782	1.64782	1.76512	1.95501
Bond Length $2c'\ (\AA)$	1.39140	1.09327	1.33875	1.74397	1.74397	1.86812	2.06909
Exp. Bond Length $(\AA)$	1.400 (chlorobenzene)	1.083 (chlorobenzene)	1.356 [55] (fluorobenzene)	1.737 (chlorobenzene)	1.737 (chlorobenzene)	1.8674 [56] (bromobenzene)	2.08 [57] (iodobenzene)
$b,c\ (a_0)$	0.66540	1.22265	0.97987	1.46967	1.46967	1.48718	1.56597
e	0.89223	0.64537	0.79055	0.74630	0.74630	0.76475	0.78049

Table 15.233. The MO to HO intercept geometrical bond parameters of halobenzenes. E_T is $E_T(atom-atom, msp^3.AO)$.

Bond	Atom	E_T (eV) Bond 1	E_T (eV) Bond 2	E_T (eV) Bond 3	E_T (eV) Bond 4	Final Total Energy $C2sp^3$ (eV)	$r_{initial}$ (a_0)	r_{final} (a_0)	$E_{Coulomb}(C2sp^3)$ (eV) Final	$E(C2sp^3)$ (eV) Final	θ' (°)	θ_1 (°)	θ_2 (°)	d_1 (a_0)	d_2 (a_0)
$C-H\ (C_bH)$	C_b	-0.85035	-0.85035	-0.56690	0	-153.88327	0.91771	0.79597	-17.09334	-16.90248	74.42	105.58	38.84	1.24678	0.21379
$C \overset{3e}{=} HC_b \overset{3e}{=} C$	C_b	-0.85035	-0.85035	-0.56690	0	-153.88327	0.91771	0.79597	-17.09334	-16.90248	134.24	45.76	58.98	0.75935	0.55533
$\left(C \overset{3e}{=}\right)_2 C_a - F$	C_a	-1.03149	-0.85035	-0.85035	0	-154.34787	0.91771	0.77491	-17.55793	-17.36707	106.58	73.42	49.28	1.04378	0.22116
$\left(C \overset{3e}{=}\right)_2 C_a - F$	F	-1.03149	0	0	0		0.78069	0.85802	-15.85724		112.35	67.65	54.08	0.93865	0.32629
$\left(C \overset{3e}{=}\right)_2 C_a - Cl$	C_a	-0.36229	-0.85035	-0.85035	0	-153.67867	0.91771	0.80561	-16.88873	-16.69786	73.32	106.68	31.67	1.87911	0.23129
$\left(C \overset{3e}{=}\right)_2 C_a - Cl$	Cl	-0.36229	0	0	0		1.05158	0.89582	15.18804		82.92	97.08	37.22	1.75824	0.11042
$C_b \overset{3e}{=} (Cl) C_a \overset{3e}{=} C_b$ (C_b bound to Cl)	C_b	-0.36229	-0.85035	-0.85035	0	-153.67867	0.91771	0.80561	-16.88873	-16.69786	134.65	45.35	59.47	0.74854	0.56614
$\left(C \overset{3e}{=}\right)_2 C_a - Br$	C_a	-0.18114	-0.85035	-0.85035	0	-153.49753	0.91771	0.81435	-16.70759	-16.51672	76.64	103.36	32.19	1.95326	0.18814
$\left(C \overset{3e}{=}\right)_2 C_a - Br$	Br	-0.18114	0	0	0		1.15169	0.90664	-15.00689		85.73	94.27	37.44	1.83258	0.06746
$\left(C \overset{3e}{=}\right)_2 C_a - I$	C_a	-0.82688	-0.85035	-0.85035	0	-154.14326	0.91771	0.78405	-17.35332	-17.16246	71.42	108.58	28.33	2.20480	0.24979
$\left(C \overset{3e}{=}\right)_2 C_a - I$	I	-0.82688	0	0	0		1.30183	0.86923	-15.65263		80.69	99.31	33.21	2.09565	0.14064

Table 15.234. The energy parameters (eV) of functional groups of halobenzenes.

Parameters	$C\overset{3e}{=}C$ Group	CH (i) Group	$C-F$ Group	$C-Cl$ (a) Group	$C-Cl$ (b) Group	$C-Br$ Group	$C-I$ Group
f_1	0.75	1	1	1	1	1	1
n_1	2	1	1	1	1	2	2
n_2	0	0	0	0	0	0	0
n_3	0	0	0	0	0	0	0
C_1	0.5	0.75	0.5	0.5	0.5	0.5	0.5
C_2	0.85252	1	1	0.81317	0.81317	0.74081	0.65537
c_1	1	1	1	1	1	1	1
c_2	0.85252	0.91771	0.77087	1	1	1	1
c_3	0	1	0	0	0	0	0
c_4	3	1	2	2	2	2	2
c_5	0	1	0	0	0	0	0
C_{1o}	0.5	0.75	1	0.5	0.5	0.5	0.5
C_{2o}	0.85252	1	0.5	0.81317	0.81317	0.74081	0.65537
V_e (eV)	-101.12679	-37.10024	-35.58388	-31.85648	-31.85648	-31.06557	-29.13543
V_p (eV)	20.69825	13.17125	10.75610	8.25686	8.25686	7.70816	6.95946
T (eV)	34.31559	11.58941	11.11948	7.21391	7.21391	6.72969	5.81578
V_m (eV)	-17.15779	-5.79470	-5.55974	-3.60695	-3.60695	-3.36484	-2.90789
$E_{(AO/HO)}$ (eV)	0	-14.63489	-14.63489	-14.63489	-14.63489	-2.99216	-2.26759
$\Delta E_{H_2MO(AO/HO)}$ (eV)	0	-1.13379	-2.26759	-2.99216	-2.99216	-14.63489	-14.63489
$E_{T(AO/HO)}$ (eV)	0	-13.50110	-12.36730	-11.64273	-11.64273	-11.64273	-12.36730
$E_{T(H_2MO)}$ (eV)	-63.27075	-31.63539	-31.63535	-31.63539	-31.63539	-31.63530	-31.63538
$E_T\left(atom-atom,msp^3.AO\right)$ (eV)	-2.26759	-0.56690	-2.06297	-0.72457	-0.72457	-0.36229	-1.65376
$E_{T(MO)}$ (eV)	-65.53833	-32.20226	-33.69834	-32.35994	-32.35994	-31.99766	-33.28912
ω $\left(10^{15}\ rad/s\right)$	49.7272	26.4826	14.4431	8.03459	14.7956	7.17533	12.0764
E_K (eV)	32.73133	17.43132	9.50672	5.28851	9.73870	4.72293	7.94889
$\overline{E}_D$ (eV)	-0.35806	-0.26130	-0.20555	-0.14722	-0.19978	-0.13757	-0.18568
$\overline{E}_{Kvib}$ (eV)	0.19649 [49]	0.35532 Eq. (13.458)	0.10911 [11]	0.08059 [12]	0.08059 [12]	0.08332 [15]	0.06608 [16]
$\overline{E}_{osc}$ (eV)	-0.25982	-0.08364	-0.15100	-0.10693	-0.15949	-0.09591	-0.15264
E_{meg} (eV)	0.14803	0.14803	0.14803	0.14803	0.14803	0.14803	0.14803
$E_{T(Group)}$ (eV)	-49.54347	-32.28590	-33.84934	-32.46687	-32.51943	-32.09357	-33.44176
$E_{intial(c_4\ AO/HO)}$ (eV)	-14.63489	-14.63489	-14.63489	-14.63489	-14.63489	-14.63489	-15.76868
$E_{intial(c_5\ AO/HO)}$ (eV)	0	-13.59844	0	0	0	0	0
$E_{D(Group)}$ (eV)	5.63881	3.90454	4.57956	3.19709	3.24965	2.82379	1.90439

Table 15.235. The total bond energies of halobenzenes calculated using the functional group composition and the energies of Table 15.234 compared to the experimental values [3]. The magnetic energy E_{mag} that is subtracted from the weighted sum of the E_D $(Group)$ (eV) values based on composition is given by (15.58).

Formula	Name	$C=C$	CH (i)	$C-F$ Group	$C-Cl$ (a) Group	$C-Cl$ (b) Group	$C-Br$ Group	$C-I$ Group	E_{mag}	Calculated Total Bond Energy (eV)	Experimental Total Bond Energy (eV)	Relative Error
C_6H_5Cl	Fluorobenzene	6	5	1	0	0	0	0	0	57.93510	57.887	-0.00083
C_6H_5Cl	Chlorobenzene	6	5		1	0			0	56.55263	56.581	0.00051
$C_6H_4Cl_2$	m-dichlorobenzene	6	4		2	0			0	55.84518	55.852	0.00012
$C_6H_3Cl_3$	1,2,3-trichlorobenzene	6	3		3	0			0	55.13773	55.077	-0.00111
$C_6H_3Cl_3$	1,3,5-trichlorobenzene	6	3		0	3			0	55.29542	55.255	-0.00073
C_6Cl_6	Hexachlorobenzene	6	0		6	0			3	52.57130	52.477	-0.00179
C_6H_5Br	Bromobenzene	6	5	0	0	0	1	0	0	56.17932	56.391[a]	0.00376
C_6H_5I	Iodobenzene	6	5	0	0	0	0	1	0	55.25993	55.261	0.00001

[a] Liquid.

Table 15.236. The bond angle parameters of halobenzenes and experimental values [1]. E_T is E_T $(atom-atom, msp^3.AO)$.

Atoms of Angle	$2c'$ Bond 1 (a_0)	$2c'$ Bond 2 (a_3)	$2c'$ Terminal Atoms (a_0)	$E_{Coulombic}$ Atom 1	Atom 1 Hybridization Designation (Table 15.3.A)	$E_{Coulombic}$ Atom 2	Atom 2 Hybridization Designation (Table 15.3.A)	c_2 Atom 1	c_2 Atom 2	C_1	C_2	c_1	c_2'	E_T (eV)	θ_v (°)	θ_1 (°)	θ_2 (°)	Cal. θ (°)	Exp. θ (°)
$\angle CCC$ (aromatic)	2.62936	2.62936	4.5585	-17.17218	38	-17.17218	38	0.79232	0.79232	1	1	1	0.79232	-1.85836				120.19	120 ($\angle CC(H)C$ chlorobenzene) 121.7 ($\angle CC(Cl)C$ chlorobenzene) 120 [50-52] (benzene)
$\angle CCH$ $\angle CCX$ (aromatic)																120.19		119.91	120 [50-52] (benzene)

PHENOL

Phenol has the formula C_6H_6O and comprises the benzene molecule with one hydrogen atom replaced by a hydroxyl corresponding to an OH functional group and a $C-O$ functional group. The aromatic $C\overset{3e}{=}C$ and $C-H$ functional groups are equivalent to those of benzene given in the Aromatic and Heterocyclic Compounds section. The OH functional group is the same as that of alcohols given in the corresponding section.

The bond between the hydroxyl and aromatic ring comprises a $C-O$ functional group that is solved using the same principles as those used to solve the alcohol functional groups wherein the $2s$ and $2p$ AOs of each C hybridize to form a single $2sp^3$ shell as an energy minimum, and the sharing of electrons between the $C2sp^3$ HO and O AO to form a MO permits each participating hybridized orbital to decrease in radius and energy. In aryl alcohols, the aromatic $C2sp^3$ HO has a hybridization factor of 0.85252 (Eq. (15.162)) with an initial energy of $E\left(C,2sp^3\right)=-14.63489\,eV$ (Eq. (15.25)) and the O AO has an energy of $E(O)=-13.61806\,eV$. To meet the equipotential condition of the union of the $C-O$ H_2-type-ellipsoidal-MO with these orbitals, the hybridization factor c_2 of Eq. (15.61) for the $C-O$-bond MO given by Eqs. (15.77) and (15.79) is:

$$c_2\left(arylC2sp^3HO\ to\ O\right)=\frac{E(O)}{E\left(C,2sp^3\right)}c_2\left(arylC2sp^3HO\right)=\frac{-13.61806\,eV}{-14.63489\,eV}(0.85252)=0.79329 \tag{15.169}$$

$E_T\left(atom-atom,msp^3.AO\right)$ of the $C-O$-bond MO in Eq. (15.61) due to the charge donation from the C and O atoms to the MO is $-1.49608\,eV$. It is based on the energy match between the OH group and the $C2sp^3$ HO of an aryl group and is given by the linear combination of $-0.92918\,eV$ (Eq. (14.513)) and $-1.13379\,eV$ (Eq. (14.247)), respectively.

The symbols of the functional groups of phenol are given in Table 15.237. The geometrical (Eqs. (15.1-15.5) and (15.51)), intercept (Eqs. (15.80-15.87)), and energy (Eqs. (15.6-15.11), (15.17-15.65), and (15.165-15.166)) parameters of phenol are given in Tables 15.238, 15.239, and 15.240, respectively. The total energy of phenol given in Table 15.241 was calculated as the sum over the integer multiple of each $E_D(Group)$ of Table 15.240 corresponding to functional-group composition of the molecule. The bond angle parameters of phenol determined using Eqs. (15.88-15.117) are given in Table 15.242. The color scale, translucent view of the charge-density of phenol comprising the concentric shells of atoms with the outer shell bridged by one or more H_2-type ellipsoidal MOs or joined with one or more hydrogen MOs is shown in Figure 15.41.

Figure 15.41. Color scale, translucent view of the charge-density of phenol showing the orbitals of the atoms at their radii, the ellipsoidal surface of each H or H_2-type ellipsoidal MO that transitions to the corresponding outer shell of the atom(s) participating in each bond, and the hydrogen nuclei (red, not to scale).

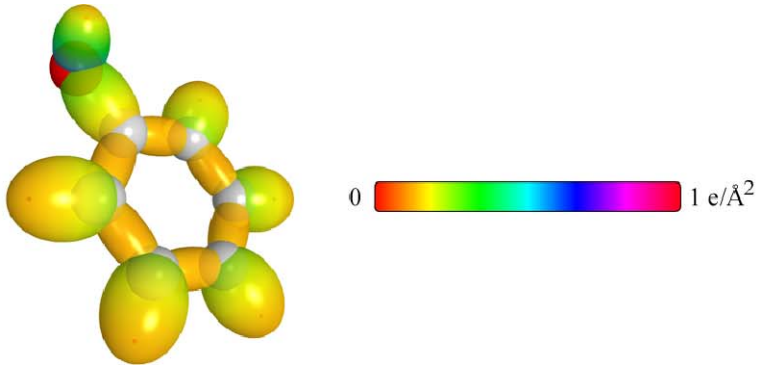

Table 15.237. The symbols of functional groups of phenol.

Functional Group	Group Symbol
CC (aromatic bond)	$C\overset{3e}{=}C$
CH (aromatic)	CH (i)
Aryl C-O	$C-O$ (a)
OH group	OH

Table 15.238. The geometrical bond parameters of phenol and experimental values [1].

Parameter	$C \overset{3e}{=} C$ Group	CH (i) Group	$C-O$ (a) Group	OH Group
$a\ (a_0)$	1.47348	1.60061	1.68220	1.26430
$c'\ (a_0)$	1.31468	1.03299	1.29700	0.91808
Bond Length $2c'\ (\AA)$	1.39140	1.09327	1.37268	0.971651
Exp. Bond Length $(\AA)$	1.397 avg. (phenol)	1.084 (phenol)	1.364 (phenol)	0.956 (phenol)
$b,c\ (a_0)$	0.66540	1.22265	1.07126	0.86925
e	0.89223	0.64537	0.77101	0.72615

Table 15.239. The MO to HO intercept geometrical bond parameters of phenol. E_T is $E_T\,(atom-atom, msp^3.AO)$.

Bond	Atom	E_T (eV) Bond 1	E_T (eV) Bond 2	E_T (eV) Bond 3	E_T (eV) Bond 4	Final Total Energy $C2sp^3$ (eV)	$r_{initial}$ (a_0)	r_{final} (a_0)	$E_{Coulomb}(C2sp^3)$ (eV) Final	$E(C2sp^3)$ (eV) Final	θ' (°)	θ_1 (°)	θ_2 (°)	d_1 (a_0)	d_2 (a_0)
$C-H\ (C_bH)$	C_b	-0.85035	-0.85035	-0.56690	0	-153.88327	0.91771	0.79597	-17.09334	-16.90248	74.42	105.58	38.84	1.24678	0.21379
$\left(C_b \overset{3e}{=}\right)_2 C_aO-H$	O	-0.74804	0	0	0		1.00000	0.87363	-15.57379		115.79	64.21	64.82	0.53799	0.38009
$\left(C_b \overset{3e}{=}\right)_2 C_a-OH$	C_a	-0.74804	-0.85035	-0.85035	0	-154.06442	0.91771	0.78762	-17.27448	-17.08362	100.00	80.00	46.39	1.16026	0.13674
$\left(C_b \overset{3e}{=}\right)_2 C_a-OH$	O	-0.74804	0	0	0		1.00000	0.87363	15.57379		106.51	73.49	51.43	1.04871	0.24829
$\left(C_b \overset{3e}{=}\right)_2 C_aOH$	C_a	-0.74804	-0.85035	-0.85035	0	-154.06442	0.91771	0.78762	-17.27448	-17.08362	133.88	46.12	58.55	0.76870	0.54598
$\left(\overset{3e}{=}(H)C_b\right)_2 C_aOH$	C_b	-0.85035	-0.85035	-0.56690	0	-153.88327	0.91771	0.79597	-17.09334	-16.90248	134.24	45.76	58.98	0.75935	0.55533

Table 15.240. The energy parameters (eV) of functional groups of phenol.

Parameters	$C\overset{3e}{=}C$ Group	CH (i) Group	$C-O$ (a) Group	OH Group
f_1	0.75	1		
n_1	2	1	1	1
n_2	0	0	0	0
n_3	0	0	0	0
C_1	0.5	0.75	0.5	0.75
C_2	0.85252	1	1	1
c_1	1	1	1	0.75
c_2	0.85252	0.91771	0.79329	1
c_3	0	1	0	1
c_4	3	1	2	1
c_5	0	1	0	1
C_{1o}	0.5	0.75	0.5	0.75
C_{2o}	0.85252	1	1	1
$V_e\ (eV)$	-101.12679	-37.10024	-34.04658	-40.92709
$V_p\ (eV)$	20.69825	13.17125	10.49024	14.81988
$T\ (eV)$	34.31559	11.58941	10.11966	16.18567
$V_m\ (eV)$	-17.15779	-5.79470	-5.05983	-8.09284
$E(_{AO/HO})\ (eV)$	0	-14.63489	-14.63489	-13.6181
$\Delta E_{H_2MO}(_{AO/HO})\ (eV)$	0	-1.13379	-1.49608	0
$E_T(_{AO/HO})\ (eV)$	0	-13.50110	-13.13881	-13.6181
$E_T(_{H_2MO})\ (eV)$	-63.27075	-31.63539	-31.63532	-31.63247
$E_T\left(atom-atom, msp^3.AO\right)(eV)$	-2.26759	-0.56690	-1.49608	0
$E_T(_{MO})\ (eV)$	-65.53833	-32.20226	-33.13145	-31.63537
$\omega\ \left(10^{15}\ rad/s\right)$	49.7272	26.4826	13.3984	44.1776
$E_K\ (eV)$	32.73133	17.43132	8.81907	29.07844
$\bar{E}_D\ (eV)$	-0.35806	-0.26130	-0.19465	-0.33749
$\bar{E}_{Kvib}\ (eV)$	0.19649 [49]	0.35532 Eq. (13.458)	0.12808 [19]	0.46311 [17-18]
$\bar{E}_{osc}\ (eV)$	-0.25982	-0.08364	-0.13061	-0.10594
$E_{mag}\ (eV)$	0.14803	0.14803	0.14803	0.11441
$E_T(_{Group})\ (eV)$	-49.54347	-32.28590	-33.26206	-31.74130
$E_{initial}(_{\epsilon_4\ AO/HO})\ (eV)$	-14.63489	-14.63489	-14.63489	-13.6181
$E_{initial}(_{\epsilon_5\ AO/HO})\ (eV)$	0	-13.59844	0	-13.59844
$E_D(_{Group})\ (eV)$	5.63881	3.90454	3.99228	4.41035

Table 15.241. The total bond energies of phenol calculated using the functional group composition and the energies of Table 15.240 compared to the experimental values [3].

Formula	Name	$C \overset{3e}{=} C$	CH (i)	$C-O$ (a) Group	OH Group	Calculated Total Bond Energy (eV)	Experimental Total Bond Energy (eV)	Relative Error
C_6H_6O	Phenol	6	5	1	1	61.75817	61.704	-0.00087

Table 15.242. The bond angle parameters of phenol and experimental values [1]. E_T is E_T ($atom-atom,msp^3.AO$).

Atoms of Angle	$2c'$ Bond 1 (a_0)	$2c'$ Bond 2 (a_0)	$2c'$ Terminal Atoms (a_0)	$E_{Coulombic}$ Atom 1	Atom 1 Hybridization Designation (Table 15.3.A)	$E_{Coulombic}$ Atom 2	Atom 2 Hybridization Designation (Table 15.3.A)	c_2 Atom 1	c_2 Atom 2	C_1	C_2	c_1	c_2'	E_T (eV)	θ_v (°)	θ_1 (°)	θ_2 (°)	Cal. θ (°)	Exp. θ (°)
$\angle CCC$ (aromatic)	2.62936	2.62936	4.5585	-17.17218	38	-17.17218	38	0.79232	0.79232	1	1	1	0.79232	-1.85836				120.19	120 [50-52] (benzene)
$\angle CCH$ (aromatic)																120.19		119.91	120 [50-52] (benzene)
$\angle C_aOH$	2.59399	1.83616	3.6515	-14.82575	1	-14.82575	1	1	0.91771	0.75	1	0.75	0.91771	0				109.84	109.0 (phenol)

ANILINE

Aniline and methyl aniline have the formula C_6H_7N and C_7H_9N, respectively. They comprise the benzene and toluene molecules with one hydrogen atom replaced by an amino group corresponding to an NH_2 functional group and a $C-N$ functional group. The aromatic $C\overset{3e}{=}C$ and $C-H$ functional groups are equivalent to those of benzene given in the Aromatic and Heterocyclic Compounds section. The $C-C$ and CH_3 functional groups of methyl anilines are equivalent to those of toluene given in the corresponding section.

The aryl amino (NH_2) functional group was solved using the procedure given in the Dihydrogen Nitride (NH_2) section. Using the results of Eqs. (13.245-13.368), the aryl amino parameters in Eq. (15.60) are $n_1=2$, $C_1=0.75$, $C_2=0.93613$ (Eqs. (13.248-13.249)), $C_{1o}=1.5$, and $c_1=0.75$. In the determination of the hybridization factor c_2 of Eq. (15.61) for the $N-H$ -bond MO of aryl amines, the $C2sp^3$ HO of the $C-NH_2$ -bond MO has an energy of $E\left(C,2sp^3\right)=-15.76868\ eV$ (Eq. (15.18)) corresponding to $s=2$ in Eqs. (15.18-15.20), and the N AO has an energy of $E(N)=-14.53414\ eV$. To meet the equipotential condition of the union of the $N-H$ H_2-type-ellipsoidal-MO with the $C2sp^3$ HO, the hybridization factor c_2 given by Eq. (15.77) is:

$$c_2\left(H\ to\ aniline\ N\right)=\frac{E(N)}{E\left(C,2sp^3\right)}=\frac{-14.53414\ eV}{-15.76868\ eV}=0.92171 \tag{15.170}$$

The bond between the amino and aromatic ring comprises a $C-N$ functional group that is the same as that of 2° amines (methylene) except that the energies corresponding to oscillation in the transition state are those of aniline. The group is solved using the same principles as those used to solve the primary and secondary-amine functional groups wherein the $2s$ and $2p$ AOs of each C hybridize to form a single $2sp^3$ shell as an energy minimum, and the sharing of electrons between the $C2sp^3$ HO and N AO to form a MO permits each participating hybridized orbital to decrease in radius and energy. The hybridization is determined in a similar manner to that of the $C-O$ group of phenol. In anilines, the aromatic $C2sp^3$ HO has a hybridization factor of 0.85252 (Eq. (15.162)) with an initial energy of $E\left(C,2sp^3\right)=-14.63489\ eV$ (Eq. (15.25)) and the N AO has an energy of $E(N)=-14.53414\ eV$. To meet the equipotential condition of the union of the $C-N$ H_2-type-ellipsoidal-MO with these orbitals, the hybridization factor c_2 of Eq. (15.60) for the $C-N$ -bond MO given by Eqs. (15.77) and (15.79) is:

$$\begin{aligned} c_2\left(arylC2sp^3HO\ to\ N\right)&=\frac{E(N)}{E\left(C,2sp^3\right)}c_2\left(arylC2sp^3HO\right)\\ &=\frac{-14.53414\ eV}{-14.63489\ eV}(0.85252)\\ &=0.84665 \end{aligned} \tag{15.171}$$

$E_T\left(atom-atom,msp^3.AO\right)$ of the $C-N$ -bond MO in Eq. (15.61) due to the charge donation from the C and N atoms to the MO is $-1.13379\ eV$ (Eq. (14.247)). It is based on the energy match between the NH_2 group and the $C2sp^3$ HO of the aryl group and is twice that of the aryl $C-H$ group that it replaces.

The symbols of the functional groups of aniline and methyl-substituted anilines are given in Table 15.243. The geometrical (Eqs. (15.1-15.5) and (15.51)), intercept (Eqs. (15.80-15.87)), and energy (Eqs. (15.6-15.11), (15.17-15.65), and (15.165-15.166)) parameters of aniline and methyl-substituted anilines are given in Tables 15.244, 15.245, and 15.246, respectively. The total energy of each aniline and methyl-substituted aniline given in Table 15.247 was calculated as the sum over the integer multiple of each $E_{D\,(Group)}$ of Table 15.246 corresponding to functional-group composition of the molecule. The bond angle parameters of aniline and methyl-substituted anilines determined using Eqs. (15.88-15.117) are given in Table 15.248. The color scale, translucent view of the charge-density of aniline comprising the concentric shells of atoms with the outer shell bridged by one or more H_2-type ellipsoidal MOs or joined with one or more hydrogen MOs is shown in Figure 15.42.

Figure 15.42. Color scale, translucent view of the charge-density of aniline showing the orbitals of the atoms at their radii, the ellipsoidal surface of each H or H_2-type ellipsoidal MO that transitions to the corresponding outer shell of the atom(s) participating in each bond, and the hydrogen nuclei (red, not to scale).

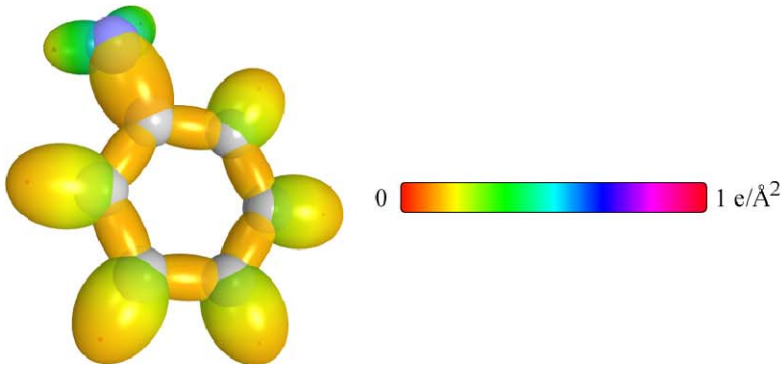

Table 15.243. The symbols of functional groups of aniline and methyl-substituted anilines.

Functional Group	Group Symbol
CC (aromatic bond)	$C \overset{3e}{=} C$
CH (aromatic)	CH (i)
Aryl C-N	$C-N$ (a)
NH_2 group	NH_2
$C_a - C_b$ (CH_3 to aromatic bond)	$C-C$ (a)
CH_3 group	$C-H$ (CH_3)

Table 15.244. The geometrical bond parameters of aniline and methyl-substituted anilines and experimental values [1].

Parameter	$C \overset{3e}{=} C$ Group	CH (i) Group	$C-N$ (a) Group	NH_2 Group	$C-C$ (a) Group	$C-H\ (CH_3)$ Group
$a\ (a_0)$	1.47348	1.60061	1.81158	1.24428	2.06004	1.64920
$c'\ (a_0)$	1.31468	1.03299	1.34595	0.94134	1.43528	1.04856
Bond Length $2c'\ (\text{Å})$	1.39140	1.09327	1.42449	0.99627	1.51904	1.10974
Exp. Bond Length (Å)	1.397 avg. (phenol)	1.084 (phenol)	1.431 (aniline)	0.998 (aniline)	1.524 (toluene)	1.11 (avg.) (toluene)
$b,c\ (a_0)$	0.66540	1.22265	1.21254	0.81370	1.47774	1.27295
e	0.89223	0.64537	0.74297	0.75653	0.69673	0.63580

Table 15.245. The MO to HO intercept geometrical bond parameters of aniline and methyl-substituted anilines. E_T is $E_T\,(atom-atom,msp^3.AO)$.

Bond	Atom	E_T (eV) Bond 1	E_T (eV) Bond 2	E_T (eV) Bond 3	E_T (eV) Bond 4	Final Total Energy $C2sp^3$ (eV)	$r_{initial}\ (a_0)$	$r_{final}\ (a_0)$	$E_{Coulomb}\left(C2sp^3\right)$ (eV) Final	$E\left(C2sp^3\right)$ (eV) Final	θ' (°)	θ_1 (°)	θ_2 (°)	$d_1\ (a_0)$	$d_2\ (a_0)$
$C-H\ (C_bH)$	C_b	-0.85035	-0.85035	-0.56690	0	-153.88328	0.91771	0.79597	-17.09334	-16.90248	74.42	105.58	38.84	1.24678	0.21379
$C-H\ (C_aH_3)$	C_a	-0.56690	0	0	0	-152.18259	0.91771	0.88392	-15.39265	-15.20178	79.89	101.11	43.13	1.20367	0.15511
$\left(C_b \overset{3e}{=}\right)_2 C_aNH-H$	N	-0.56690	0	0	0		0.93084	0.88392	-15.39265		121.74	58.26	67.49	0.47634	0.46500
$\left(C_b \overset{3e}{=}\right)_2 C_a-NH_2$	C_a	-0.56690	-0.85035	-0.85035	0	-153.88328	0.91771	0.79597	-17.09334	-16.90248	88.49	91.51	41.01	1.36696	0.02101
$\left(C_b \overset{3e}{=}\right)_2 C_a-NH_2$	N	-0.56690	0	0	0		0.93084	0.88392	-15.39265		96.32	83.68	46.43	1.24859	0.09736
$\left(C \overset{3e}{=}\right)_2 C_b-C_aH_3$	C_a	-0.56690	0	0	0	-152.18259	0.91771	0.88392	-15.39265	-15.20178	73.38	106.62	34.97	1.68807	0.25279
$\left(C \overset{3e}{=}\right)_2 C_b-C_aH_3$	C_b	-0.56690	-0.85035	-0.85035	0	-153.88328	0.91771	0.79597	-17.09334	-16.90247	61.56	118.44	28.27	1.81430	0.37901
$C \overset{3e}{=} HC_c \overset{3e}{=} C$ $C \overset{3e}{=} (H_2N) C_a \overset{3e}{=} C$ $C \overset{3e}{=} (H_3C_a) C_b \overset{3e}{=} C$	C_c C_a C_b	-0.85035	-0.85035	-0.56690	0	-153.88327	0.91771	0.79597	-17.09334	-16.90248	134.24	45.76	58.98	0.75935	0.55533

Table 15.246. The energy parameters (eV) of functional groups of aniline and methyl-substituted anilines.

Parameters	$C=C$ Group	CH (i) Group	$C-N$ (a) Group	NH_2 Group	$C-C$ (a) Group	CH_3 Group
f_1	0.75	1				
n_1	2	1	1	2	1	3
n_2	0	0	0	0	0	2
n_3	0	0	0	1	0	0
C_1	0.5	0.75	0.5	0.75	0.5	0.75
C_2	0.85252	1	1	0.93613	1	1
c_1	1	1	1	0.75	1	1
c_2	0.85252	0.91771	0.84665	0.92171	0.91771	0.91771
c_3	0	1	0	0	0	0
c_4	3	1	2	1	2	1
c_5	0	1	0	2	0	3
C_{1o}	0.5	0.75	0.5	1.5	0.5	0.75
C_{2o}	0.85252	1	1	1	1	1
$V_e\ (eV)$	-101.12679	-37.10024	-32.76465	-78.97795	-29.95792	-107.32728
$V_p\ (eV)$	20.69825	13.17125	10.10870	28.90735	9.47952	38.92728
$T\ (eV)$	34.31559	11.58941	9.04312	31.73641	7.27120	32.53914
$V_m\ (eV)$	-17.15779	-5.79470	-4.52156	-15.86820	-3.63560	-16.26957
$E_{(AO/HO)}\ (eV)$	0	-14.63489	-14.63489	-14.53414	-15.35946	-15.56407
$\Delta E_{H_2MO\,(AO/HO)}\ (eV)$	0	-1.13379	-1.13379	0	-0.56690	0
$E_{T\,(AO/HO)}\ (eV)$	0	-13.50110	-13.50110	-14.53414	-14.79257	-15.56407
$E_{(n_3\,AO/HO)}\ (eV)$	0	0	0	-14.53414	0	0
$E_{T\,(H_2MO)}\ (eV)$	-63.27075	-31.63539	-31.63549	-48.73654	-31.63537	-67.69451
$E_T\left(atom-atom, msp^3.AO\right)\ (eV)$	-2.26759	-0.56690	-1.13379	0	-1.13379	0
$E_{T\,(MO)}\ (eV)$	-65.53833	-32.20226	-32.76916	-48.73660	-32.76916	-67.69450
$\omega\ \left(10^{15}\ rad/s\right)$	49.7272	26.4826	11.9890	68.9812	16.2731	24.9286
$E_K\ (eV)$	32.73133	17.43132	7.89138	45.40465	10.71127	16.40846
$\overline{E}_D\ (eV)$	-0.35806	-0.26130	-0.18211	-0.42172	-0.21217	-0.25352
$\overline{E}_{Kvib}\ (eV)$	0.19649 [49]	0.35532 Eq. (13.458)	0.15498 [58]	0.40929 [22]	0.14940 [54]	0.35532 (Eq. (13.458))
$\overline{E}_{osc}\ (eV)$	-0.25982	-0.08364	-0.10462	-0.21708	-0.13747	-0.22757
$E_{mag}\ (eV)$	0.14803	0.14803	0.14803	0.14803	0.14803	0.14803
$E_{T\,(Group)}\ (eV)$	-49.54347	-32.28590	-32.87379	-49.17075	-32.90663	-67.92207
$E_{initial\,(c_4\,AO/HO)}\ (eV)$	-14.63489	-14.63489	-14.63489	-14.53414	-14.63489	-14.63489
$E_{initial\,(c_5\,AO/HO)}\ (eV)$	0	-13.59844	0	-13.59844	0	-13.59844
$E'_{D\,(Group)}\ (eV)$	5.63881	3.90454	3.60401	7.43973	3.63685	12.49186

Table 15.247. The total bond energies of aniline and methyl-substituted anilines calculated using the functional group composition and the energies of Table 15.246 compared to the experimental values [3].

Formula	Name	$C=C$	CH (i)	$C-N$ (a) Group	NH_2 Group	$C-C$ (a) Group	CH_3	Calculated Total Bond Energy (eV)	Experimental Total Bond Energy (eV)	Relative Error
C_6H_7N	Aniline	6	5	1	1	0	0	64.43373	64.374	-0.00093
C_7H_9N	2-methylaniline	6	4	1	1	1	1	76.62345	76.643	-0.00025
C_7H_9N	3-methylaniline	6	4	1	1	1	1	76.62345	76.661	0.00050
C_7H_9N	4-methylaniline	6	4	1	1	1	1	76.62345	76.654	0.00040

Table 15.248. The bond angle parameters of aniline and methyl-substituted anilines and experimental values [1]. E_T is $E_T(atom-atom, msp^3.AO)$.

Atoms of Angle	$2c'$ Bond 1 (a_0)	$2c'$ Bond 2 (a_0)	$2c'$ Terminal Atoms (a_0)	$E_{Coulombic}$ Atom 1	Atom 1 Hybridization Designation (Table 15.3.A)	$E_{Coulombic}$ Atom 2	Atom 2 Hybridization Designation (Table 15.3.A)	c_2 Atom 1	c_2 Atom 2	C_1	C_2	c_1	c_2'	E_T (eV)	θ_v (°)	θ_1 (°)	θ_2 (°)	Cal. θ (°)	Exp. θ (°)
$\angle CCC$ (aromatic)	2.62936	2.62936	4.5585	-17.17218	38	-17.17218	38	0.79232	0.79232	1	1	1	0.79232	-1.85836				120.19	120 [50-52] (benzene)
$\angle CCH$ (aromatic)																120.19		119.91	120 [50-52] (benzene)
$\angle HNH$	1.88268	1.88268	3.1559	-14.53414	N	H	H	0.93613 Eq. (13.248))	1	1	1	0.75	1.06823	0				113.89	113.9 (aniline)
$\angle HNC_a$	1.88268	2.69190	4.0332	-14.53414	N	-15.95955	10	0.84665 (Eq. (15.171))	0.86284 (Eq. (15.73))	0.75	1	0.75	1.01912	0				122.70	

ARYL NITRO COMPOUNDS

Aryl nitro compounds have a hydrogen of an aryl group replaced by a nitro corresponding to an NO_2 functional group and a $C-N$ functional group. Examples include nitrobenzene, nitrophenol, and nitroaniline with formulas $C_6H_5NO_2$, $C_6H_5NO_3$, and $C_6H_6N_2O_2$, respectively. The aromatic $C\overset{3e}{=}C$ and $C-H$ functional groups are equivalent to those of benzene given in the Aromatic and Heterocyclic Compounds section. The OH and $C-O$ functional groups of nitrophenols are the same as those of phenol given in the corresponding section. The NH_2 and $C-N$ functional groups of nitroanilines are the same as those of aniline given in the corresponding section. The differences between the total bond energies of the nitroanilines given in Table 15.252 are due to differences in the E_{osc} term. For simplicity and since the differences are small, the E_{osc} terms for nitroanilines were taken as the same.

The NO_2 group is the same as that given in the Nitroalkanes section. The bond between the nitro and aromatic ring comprises a $C-N$ functional group that is the same as that of nitroalkanes given in the corresponding section except that $E_T\left(atom-atom, msp^3.AO\right)$ is $-0.72457\ eV$, one half of that of the $C-N$ -bond MO of nitroalkanes and equivalent to that of methyl (Eq. (14.151)) in order to maintain the independence and aromaticity of the benzene functional group. In addition, the energy terms due to oscillation in the transition state correspond to those of an aryl nitro compound.

The symbols of the functional groups of aryl nitro compounds are given in Table 15.249. The geometrical (Eqs. (15.1-15.5) and (15.42)), intercept (Eqs. (15.80-15.87)), and energy (Eqs. (15.6-15.11), (15.17-15.65), and (15.165-15.166)) parameters of aryl nitro compounds are given in Tables 15.250, 15.251, and 15.252, respectively. The total energy of each aryl nitro compound given in Table 15.253 was calculated as the sum over the integer multiple of each $E_D(Group)$ of Table 15.252 corresponding to functional-group composition of the molecule. For each set of unpaired electrons created by bond breakage, the $C2sp^3$ HO magnetic energy E_{mag} that is subtracted from the weighted sum of the $E_D(Group)$ (eV) values based on composition is given by Eq. (15.67). The bond angle parameters of aryl nitro compounds determined using Eqs. (15.88-15.117) are given in Table 15.254. The color scale, translucent view of the charge-density of exemplary aryl nitro, nitrobenzene, comprising the concentric shells of atoms with the outer shell bridged by one or more H_2-type ellipsoidal MOs or joined with one or more hydrogen MOs is shown in Figure 15.43.

Figure 15.43. Color scale, translucent view of the charge-density of nitrobenzene showing the orbitals of the atoms at their radii, the ellipsoidal surface of each H or H_2-type ellipsoidal MO that transitions to the corresponding outer shell of the atom(s) participating in each bond, and the hydrogen nuclei (red, not to scale).

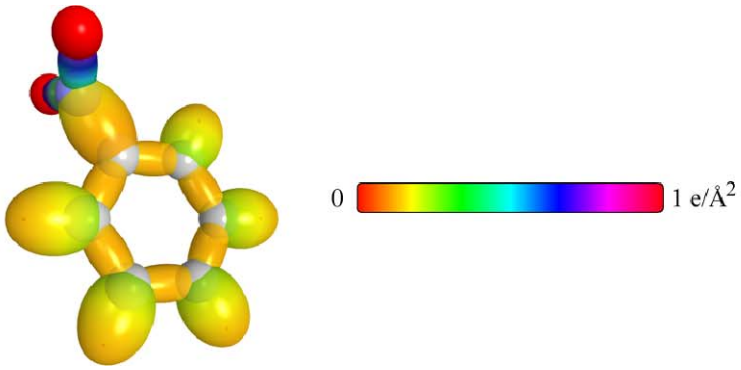

Table 15.249. The symbols of functional groups of aryl nitro compounds.

Functional Group	Group Symbol
CC (aromatic bond)	$C\overset{3e}{=}C$
CH (aromatic)	CH (i)
Aryl C-N (aniline)	$C-N$ (a)
Aryl C-N (nitro)	$C-N$ (b)
Aryl C-O	$C-O$ (a)
NO_2 group	NO_2
NH_2 group	NH_2
OH group	OH

Table 15.250. The geometrical bond parameters of aryl nitro compounds and experimental values [1].

Parameter	$C^{3e}=C$ Group	CH (i) Group	$C-N$ (a) Group	$C-N$ (b) Group	$C-O$ (a) Group	NO_2 Group	NH_2 Group	OH Group
$a\ (a_0)$	1.47348	1.60061	1.81158	1.97794	1.68220	1.33221	1.24428	1.26430
$c'\ (a_0)$	1.31468	1.03299	1.34595	1.40639	1.29700	1.15421	0.94134	0.91808
Bond Length $2c'\ (\AA)$	1.39140	1.09327	1.42449	1.48846	1.37268	1.22157	0.99627	0.971651
Exp. Bond Length $(\AA)$	1.397 avg. (phenol)	1.084 (phenol)	1.431 (aniline)		1.364 (phenol)	1.224 (nitromethane)	0.998 (aniline)	0.956 (phenol)
$b,c\ (a_0)$	0.66540	1.22265	1.21254	1.39079	1.07126	0.66526	0.81370	0.86925
e	0.89223	0.64537	0.74297	0.71104	0.77101	0.86639	0.75653	0.72615

Table 15.251. The MO to HO intercept geometrical bond parameters of aryl nitro compounds. E_T is $E_T(atom-atom,msp^3.AO)$.

Bond	Atom	E_T (eV) Bond 1	E_T (eV) Bond 2	E_T (eV) Bond 3	E_T (eV) Bond 4	Final Total Energy $C2sp^3$ (eV)	$r_{initial}$ (a_0)	r_{final} (a_0)	$E_{Coulomb}(C2sp^3)$ (eV) Final	$E(C2sp^3)$ (eV) Final	θ' (°)	θ_1 (°)	θ_2 (°)	d_1 (a_0)	d_2 (a_0)
$C-H\ (C_bH)$	C_b	-0.85035	-0.85035	-0.56690	0	-153.88327	0.91771	0.79597	-17.09334	-16.90248	74.42	105.58	38.84	1.24678	0.21379
$\left(C_b^{3e}=\right)_2 C_aO-H$	O	-0.74804	0	0	0		1.00000	0.87363	-15.57379		115.79	64.21	64.82	0.53799	0.38009
$\left(C_b^{3e}=\right)_2 C_a-OH$	C_a	-0.74804	-0.85035	-0.85035	0	-154.06442	0.91771	0.78762	-17.27448	-17.08362	100.00	80.00	46.39	1.16026	0.13674
$\left(C_b^{3e}=\right)_2 C_a-OH$	O	-0.74804	0	0	0		1.00000	0.87363	15.57379		106.51	73.49	51.43	1.04871	0.24829
$\left(C_b^{3e}=\right)_2 C_aOH$	C_a	-0.74804	-0.85035	-0.85035	0	-154.06442	0.91771	0.78762	-17.27448	-17.08362	133.88	46.12	58.55	0.76870	0.54598
$C^{3e}=HC_c^{3e}=C$ $C^{3e}=(H_2N)C_a^{3e}=C$ $\left(^{3e}=(H)C_b\right)_2 C_aOH$ $C^{3e}=(H_3C_a)C_b^{3e}=C$	C_c C_a C_b C_b	-0.85035	-0.85035	-0.56690	0	-153.88327	0.91771	0.79597	-17.09334	-16.90248	134.24	45.76	58.98	0.75935	0.55533
$\left(C_b^{3e}=\right)_2 C_aNH-H$	N	-0.56690	0	0	0		0.93084	0.88392	-15.39265		121.74	58.26	67.49	0.47634	0.46500
$\left(C_b^{3e}=\right)_2 C_a-NH_2$	C_a	-0.56690	-0.85035	-0.85035	0	-153.88328	0.91771	0.79597	-17.09334	-16.90248	88.49	91.51	41.01	1.36696	0.02101
$\left(C_b^{3e}=\right)_2 C_a-NH_2$	N	-0.56690	0	0	0		0.93084	0.88392	-15.39265		96.32	83.68	46.43	1.24859	0.09736
$\left(C^{3e}=\right)_2 C_b-C_aH_3$	C_a	-0.56690	0	0	0	-152.18259	0.91771	0.88392	-15.39265	-15.20178	73.38	106.62	34.97	1.68807	0.25279
$\left(C^{3e}=\right)_2 C_b-C_aH_3$	C_b	-0.56690	-0.85035	-0.85035	0	-153.88328	0.91771	0.79597	-17.09334	-16.90247	61.56	118.44	28.27	1.81430	0.37901
$RN(O)=O$	O	-0.92918	0	0	0		1.00000	0.86359	-15.75493		135.25	44.75	66.05	0.54089	0.61333
$RN(O)=O$	N	-0.92918	-0.92918	-0.36229	0		0.93084	0.79816	-17.04640		132.36	47.64	62.44	0.61640	0.53781
$\left(C^{3e}=\right)_2 C_a-NO_2$	C_a	-0.36229	-0.85035	-0.85035	0	-153.67867	0.91771	0.80561	-16.88873	-16.69786	72.49	107.51	33.53	1.64875	0.24236
$\left(C^{3e}=\right)_2 C_a-NO_2$	N	-0.92918	-0.92918	-0.36229	0		0.93084	0.79816	-17.04640		71.53	108.47	32.98	1.65923	0.25284
$C^{3e}=(O_2N)C_a^{3e}=C$	C_a	-0.36229	-0.85035	-0.85035	0	-153.67867	0.91771	0.80561	-16.88873	-16.69786	134.65	45.35	59.47	0.74854	0.56614

Table 15.252. The energy parameters (eV) of functional groups of aryl nitro compounds.

Parameters	$C\overset{3e}{=}C$ Group	CH (i) Group	$C-N$ (a) Group	$C-N$ (b) Group	$C-O$ (a) Group	NO_2 Group	NH_2 Group	OH Group
f_1	0.75	1						
n_1	2	1	1	1	1	2	2	1
n_2	0	0	0	0	0	0	0	0
n_3	0	0	0	0	0	0	1	0
C_1	0.5	0.75	0.5	0.5	0.5	0.5	0.75	0.75
C_2	0.85252	1	1	1	1	1	0.93613	1
c_1	1	1	1	1	1	1	0.75	0.75
c_2	0.85252	0.91771	0.84665	0.91140	0.79329	0.85987	0.92171	1
c_3	0	1	0	0	0	0	0	1
c_4	3	1	2	2	2	4	1	1
c_5	0	1	0	0	0	0	2	1
C_{1o}	0.5	0.75	0.5	0.5	0.5	0.5	1.5	0.75
C_{2o}	0.85252	1	1	1	1	1	1	1
$V_e\ (eV)$	-101.12679	-37.10024	-32.76465	-31.36351	-34.04658	-106.90919	-78.97795	-40.92709
$V_p\ (eV)$	20.69825	13.17125	10.10870	9.67426	10.49024	23.57588	28.90735	14.81988
$T\ (eV)$	34.31559	11.58941	9.04312	7.92833	10.11966	40.12475	31.73641	16.18567
$V_m\ (eV)$	-17.15779	-5.79470	-4.52156	-3.96416	-5.05983	-20.06238	-15.86820	-8.09284
$E_{(AO/HO)}\ (eV)$	0	-14.63489	-14.63489	-14.63489	-14.63489	0	-14.53414	-13.6181
$\Delta E_{H_2MO\ (AO/HO)}\ (eV)$	0	-1.13379	-1.13379	-0.72457	-1.49608	0	0	0
$E_{T\ (AO/HO)}\ (eV)$	0	-13.50110	-13.50110	-13.91032	-13.13881	0	-14.53414	-13.6181
$E_{(n_3\ AO/HO)}\ (eV)$	0	0	0	0	0	0	-14.53414	0
$E_{T\ (H_2MO)}\ (eV)$	-63.27075	-31.63539	-31.63549	-31.63540	-31.63532	-63.27093	-48.73654	-31.63247
$E_T\left(atom-atom, msp^3.AO\right)\ (eV)$	-2.26759	-0.56690	-1.13379	-0.72457	-1.49608	-3.71673	0	0
$E_{T\ (MO)}\ (eV)$	-65.53833	-32.20226	-32.76916	-32.35994	-33.13145	-66.98746	-48.73660	-31.63537
$\omega\ \left(10^{15}\ rad/s\right)$	49.7272	26.4826	11.9890	17.8228	13.3984	19.0113	68.9812	44.1776
$E_K\ (eV)$	32.73133	17.43132	7.89138	11.73128	8.81907	12.51354	45.40465	29.07844
$\overline{E}_D\ (eV)$	-0.35806	-0.26130	-0.18211	-0.21927	-0.19465	-0.23440	-0.42172	-0.33749
$\overline{E}_{Kvib}\ (eV)$	0.19649 [49]	0.35532 Eq. (13.458)	0.15498 [58]	0.10539 [45]	0.12808 [19]	0.19342 [45]	0.40929 [22]	0.46311 [17-18]
$\overline{E}_{osc}\ (eV)$	-0.25982	-0.08364	-0.10462	-0.16658	-0.13061	-0.13769	-0.21708	-0.10594
$E_{mag}\ (eV)$	0.14803	0.14803	0.14803	0.14803	0.14803	0.11441	0.14803	0.11441
$E_{T\ (Group)}\ (eV)$	-49.54347	-32.28590	-32.87379	-32.52652	-33.26206	-67.26284	-49.17075	-31.74130
$E_{initial\ (c_4\ AO/HO)}\ (eV)$	-14.63489	-14.63489	-14.63489	-14.63489	-14.63489	-14.63489	-14.53414	-13.6181
$E_{initial\ (c_5\ AO/HO)}\ (eV)$	0	-13.59844	0	0	0	0	-13.59844	-13.59844
$E_{D\ (Group)}\ (eV)$	5.63881	3.90454	3.60401	3.25674	3.99228	8.72329	7.43973	4.41035

Table 15.253. The total bond energies of aryl nitro compounds calculated using the functional group composition and the energies of Table 15.252 compared to the experimental values [3]. The magnetic energy E_{mag} that is subtracted from the weighted sum of the E_D $(_{Group})$ (eV) values based on composition is given by (15.58).

Formula	Name	$C=C^{3e}$	CH (i)	$C-N$ (a) Group	$C-N$ (b) Group	$C-O$ (a) Group	NO_2 Group	NH_2 Group	OH Group	E_{mag}	Calculated Total Bond Energy (eV)	Experimental Total Bond Energy (eV)	Relative Error
$C_6H_5NO_2$	Nitrobenzene	6	5	0	1	0	1	0	0	1	65.18754	65.217	0.00046
$C_6H_4N_2O_5$	2,4-dinitrophenol	6	4	0	2	1	2	0	1	2	77.61308	77.642	0.00037
$C_6H_6N_2O_2$	2-nitroaniline	6	4	1	1	0	1	1	0	0	72.47476	72.424	-0.00070
$C_6H_6N_2O_2$	3-nitroaniline	6	4	1	1	0	1	1	0	0	72.47476	72.481	-0.00009
$C_6H_6N_2O_2$	4-nitroaniline	6	4	1	1	0	1	1	0	0	72.47476	72.476	-0.00002

Table 15.254. The bond angle parameters of aryl nitro compounds and experimental values [1]. E_T is E_T $(atom-atom,msp^3.AO)$.

Atoms of Angle	$2c'$ Bond 1 (a_0)	$2c'$ Bond 2 (a_0)	$2c'$ Terminal Atoms (a_0)	$E_{Coulombic}$ Atom 1	Atom 1 Hybridization Designation (Table 15.3.A)	$E_{Coulombic}$ Atom 2	Atom 2 Hybridization Designation (Table 15.3.A)	c_2 Atom 1	c_2 Atom 2	C_1	C_2	c_1	c_2'	E_T (eV)	θ_v (°)	θ_1 (°)	θ_2 (°)	Cal. θ (°)	Exp. θ (°)
$\angle CCC$ (aromatic)	2.62936	2.62936	4.5585	-17.17218	38	-17.17218	38	0.79232	0.79232	1	1	1	0.79232	-1.85836				120.19	120 [50-52] (benzene)
$\angle CCH$ (aromatic)																120.19		119.91	120 [50-52] (benzene)
$\angle O_aNO_b$	2.30843	2.30843	4.1231	-16.68411 O_a	25	-16.68411 O_b	25	0.81549	0.81549	1	1	1	0.81549	-1.44915				126.52	123.2 [57] (nitrobenzene) 125.3 (nitromethane)
$\angle CNO$	2.81279	2.30843	4.4159	-17.45562	46	-13.61806	O	0.77945	0.85395 (Eq. (15.133))	1	1	1	0.81670	-1.65376				118.82	118.5 [57] (nitrobenzene)
$\angle C_aOH$	2.59399	1.83616	3.6515	-14.82575	1	-14.82575	1	1	0.91771	0.75	1	0.75	0.91771	0				109.84	109.0 (phenol)
$\angle HNH$	1.88268	1.88268	3.1559	-14.53414	N	H	H	0.93613 Eq. (13.248))	1	1	1	0.75	1.06823	0				113.89	113.9 (aniline)
$\angle C_aNH$	2.69190	1.88268	3.9833	-15.95955	10	-14.53414	N	0.84665 (Eq. (15.171))	0.84665 (Eq. (15.171))	0.75	1	0.75	1.00000	0				120.05	

BENZOIC ACID COMPOUNDS

Benzoic acid compounds have a hydrogen of an aryl group replaced by a carboxylic acid group corresponding to an $C-C(O)-OH$ moiety that comprises $C=O$ and OH functional groups that are the same as those of carboxylic acids given in the corresponding section. The single bond of aryl carbon to the carbonyl carbon atom, $C-C(O)$, is also a functional group. This group is also equivalent to the same group of carboxylic acids except that $\Delta E_{H_2MO}\left(AO/HO\right)$ in Eq. (15.51) and $E_T\left(atom-atom,msp^3.AO\right)$ in Eq. (15.61) are both $-1.29147\,eV$ which is a linear combination of $\frac{-1.13379\,eV}{2}$, $E_T\left(atom-atom,msp^3.AO\right)$ of the $C-H$ group that the $C-C(O)$ group replaces, and that of an independent $C2sp^3$ HO, $-0.72457\,eV$ (Eq. (14.151)).

Examples include benzoic acid, chlorobenzoic acid, and aniline carboxylic acid with formulas $C_7H_6O_2$, $C_7H_5O_2Cl$, and $C_7H_7NO_2$, respectively. The aromatic $C\overset{3e}{=}C$ and $C-H$ functional groups are equivalent to those of benzene given in Aromatic and Heterocyclic Compounds section. The NH_2 and $C-N$ functional groups of aniline carboxylic acids are the same as those of aniline given in the corresponding section. The $C-Cl$ functional group of 2-chlorobenzoic acids corresponding to meta substitution is equivalent to that of chlorobenzene given in the corresponding section. The $C-Cl$ functional group of 3 or 4-chlorobenzoic acids corresponding to ortho and para substitution is also equivalent to that of chlorobenzene, except that $E_T\left(atom-atom,msp^3.AO\right)$ in Eq. (15.61) is $-0.92918\,eV$ (Eq. (14.513)) for both cases since each of these positions can form a resonance structure with the carboxylic acid group which is permissive of greater charge donation from the $C2sp^3$ HO.

The symbols of the functional groups of benzoic acid compounds are given in Table 15.255. The corresponding designations of benzoic acid is shown in Figure 15.44B. The geometrical (Eqs. (15.1-15.5) and (15.51)), intercept (Eqs. (15.80-15.87)), and energy (Eqs. (15.6-15.11), (15.17-15.65), and (15.165-15.166)) parameters of benzoic acid compounds are given in Tables 15.256, 15.257, and 15.258, respectively. The total energy of each benzoic acid compound given in Table 15.259 was calculated as the sum over the integer multiple of each $E_D\left(Group\right)$ of Table 15.258 corresponding to functional-group composition of the molecule. The bond angle parameters of benzoic acid compounds determined using Eqs. (15.88-15.117) are given in Table 15.260. The color scale, translucent view of the charge-density of benzoic acid comprising the concentric shells of atoms with the outer shell bridged by one or more H_2-type ellipsoidal MOs or joined with one or more hydrogen MOs is shown in Figure 15.44A.

Figure 15.44. (A) Color scale, translucent view of the charge-density of benzoic acid showing the orbitals of the atoms at their radii, the ellipsoidal surface of each H or H_2-type ellipsoidal MO that transitions to the corresponding outer shell of the atom(s) participating in each bond, and the hydrogen nuclei (red, not to scale). (B) Chemical structure and atom designation of benzoic acid.

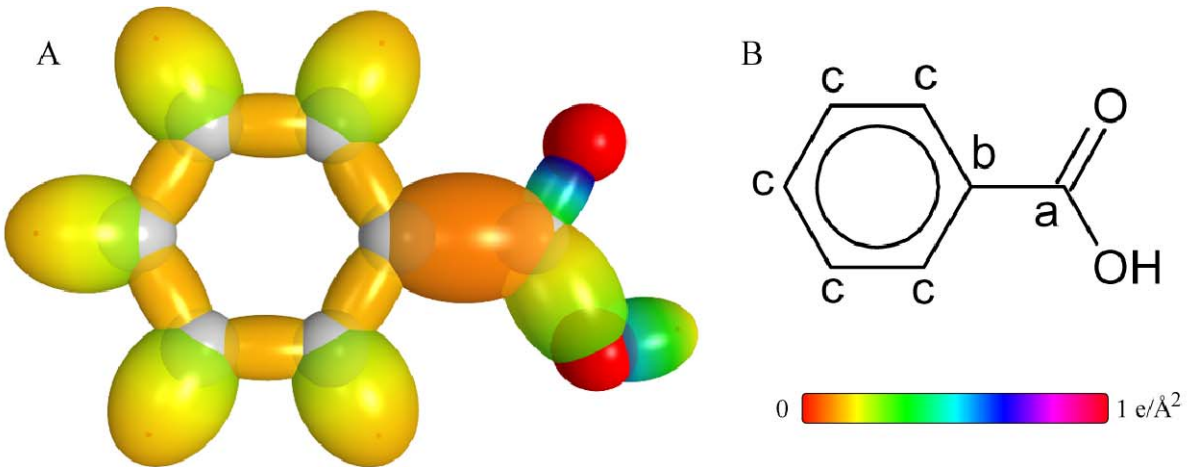

Table 15.255. The symbols of functional groups of benzoic acid compounds.

Functional Group	Group Symbol
CC (aromatic bond)	$C\overset{3e}{=}C$
CH (aromatic)	*CH* (i)
C-*C*(*O*)	$C-C(O)$
C=*O* (aryl carboxylic acid)	$C=O$
(*O*)*C*-*O*	$C-O$
OH group	OH
$Cl-C$ (*Cl* to aromatic bond of 2-chlorobenzoic acid)	$C-Cl$ (i)
$Cl-C$ (*Cl* to aromatic bond of 3 or 4-chlorobenzoic acid)	$C-Cl$ (ii)
Aryl *C*-*N* (aniline)	$C-N$
NH_2 group	NH_2

Table 15.256. The geometrical bond parameters of benzoic acid compounds and experimental values [1].

Parameters	$C \overset{3e}{=} C$ Group	CH (i) Group	$C-C(O)$ Group	$C=O$ Group	$C-O$ Group	OH Group	$C-Cl$ (i) Group	$C-Cl$ (ii) Group	$C-N$ Group	NH_2 Group
f_1	0.75	1								
n_1	2	1	1	2	1	1	1	1	1	2
n_2	0	0	0	0	0	0	0	0	0	0
n_3	0	0	0	0	0	0	0	0	0	1
C_1	0.5	0.75	0.5	0.5	0.5	0.75	0.5	0.5	0.5	0.75
C_2	0.85252	1	1	1	1	1	0.81317	0.81317	1	0.93613
c_1	1	1	1	1	1	0.75	1	1	1	0.75
c_2	0.85252	0.91771	0.91771	0.85395	0.85395	1	1	1	0.84665	0.92171
c_3	0	1	0	2	0	1	0	0	0	0
c_4	3	1	2	4	2	1	2	2	2	1
c_5	0	1	0	0	0	1	0	0	0	2
C_{1o}	0.5	0.75	0.5	0.5	0.5	0.75	0.5	0.5	0.5	1.5
C_{2o}	0.85252	1	1	1	1	1	0.81317	0.81317	1	1
V_e (eV)	-101.12679	-37.10024	-32.15216	-111.25473	-35.08488	-40.92709	-31.85648	-32.14474	-32.76465	-78.97795
V_p (eV)	20.69825	13.17125	9.74055	23.87467	10.32968	14.81988	8.25686	8.28394	10.10870	28.90735
T (eV)	34.31559	11.58941	8.23945	42.82081	10.11150	16.18567	7.21391	7.32700	9.04312	31.73641
V_m (eV)	-17.15779	-5.79470	-4.11973	-21.41040	-5.05575	-8.09284	-3.60695	-3.66350	-4.52156	-15.86820
$E_{(AO/HO)}$ (eV)	0	-14.63489	-14.63489	0	-14.63489	-13.6181	-14.63489	-14.63489	-14.63489	-14.53414
$\Delta E_{H_2MO\,(AO/HO)}$ (eV)	0	-1.13379	-1.29147	-2.69893	-2.69893	0	-2.99216	-2.99216	-1.13379	0
$E_{T\,(AO/HO)}$ (eV)	0	-13.50110	-13.34342	2.69893	-11.93596	-13.6181	-11.64273	-11.64273	-13.50110	-14.53414
$E_{(n_5\,AO/HO)}$ (eV)	0	0	0	0	0	0	0	0	0	-14.53414
$E_{T\,(H_2MO)}$ (eV)	-63.27075	-31.63539	-31.63530	-63.27074	-31.63541	-31.63247	-31.63539	-31.63542	-31.63549	-48.73654
$E_T\left(atom-atom, msp^3.AO\right)$ (eV)	-2.26759	-0.56690	-1.29147	-2.69893	-1.85836	0	-0.72457	-0.92918	-1.13379	0
$E_{T\,(MO)}$ (eV)	-65.53833	-32.20226	-32.92684	-65.96966	-33.49373	-31.63537	-32.35994	-32.56455	-32.76916	-48.73660
$\omega\ \left(10^{15}\ rad/s\right)$	49.7272	26.4826	10.7262	59.4034	24.3637	44.1776	8.03459	8.11389	11.9890	68.9812
E_K (eV)	32.73133	17.43132	7.06019	39.10034	16.03660	29.07844	5.28851	5.34070	7.89138	45.40465
$\overline{E}_D$ (eV)	-0.35806	-0.26130	-0.17309	-0.40804	-0.26535	-0.33749	-0.14722	-0.14888	-0.18211	-0.42172
$\overline{E}_{Kvib}$ (eV)	0.19649 [49]	0.35532 Eq. (13.458)	0.10502 [29]	0.21077 [12]	0.14010 [31]	0.46311 [17-18]	0.08059 [12]	0.08059 [12]	0.15498 [58]	0.40929 [22]
$\overline{E}_{osc}$ (eV)	-0.25982	-0.08364	-0.12058	-0.30266	-0.19530	-0.10594	-0.10693	-0.10859	-0.10462	-0.21708
E_{mag} (eV)	0.14803	0.14803	0.14803	0.11441	0.14803	0.11441	0.14803	0.14803	0.14803	0.14803
$E_{T\,(Group)}$ (eV)	-49.54347	-32.28590	-33.04742	-66.57498	-33.68903	-31.74130	-32.46687	-32.67314	-32.87379	-49.17075
$E_{initial\,(c_4\,AO/HO)}$ (eV)	-14.63489	-14.63489	-14.63489	-14.63489	-14.63489	-13.6181	-14.63489	-14.63489	-14.63489	-14.53414
$E_{initial\,(c_5\,AO/HO)}$ (eV)	0	-13.59844	0	0	0	-13.59844	0	0	0	-13.59844
$E_{D\,(Group)}$ (eV)	5.63881	3.90454	3.77764	7.80660	4.41925	4.41035	3.19709	3.40336	3.60401	7.43973

Table 15.257. The MO to HO intercept geometrical bond parameters of benzoic acid compounds. E_T is E_T ($atom - atom, msp^3.AO$).

Bond	Atom	E_T (eV) Bond 1	E_T (eV) Bond 2	E_T (eV) Bond 3	E_T (eV) Bond 4	Final Total Energy $C2sp^3$ (eV)	$r_{initial}$ (a_0)	r_{final} (a_0)	$E_{Coulomb}(C2sp^3)$ (eV) Final	$E(C2sp^3)$ (eV) Final	θ' (°)	θ_1 (°)	θ_2 (°)	d_1 (a_0)	d_2 (a_0)
Aryl $C-H$	C_b	-0.85035	-0.85035	-0.56690	0	-153.88327	0.91771	0.79597	-17.09334	-16.90248	74.42	105.58	38.84	1.24678	0.21379
$C^{3e}=HC_b^{3e}=C$ $C^{3e}=(HOOC_a)C_b^{3e}=C_c(H)$ $C^{3e}=(Cl)C_a^{3e}=C_b(H)$ $C^{3e}=(H_2N)C_a^{3e}=C_b(H)$	C_b C_c C_b C_b	-0.85035	-0.85035	-0.56690	0	-153.88327	0.91771	0.79597	-17.09334	-16.90248	134.24	45.76	58.98	0.75935	0.55533
$C_bC_a(O)O-H$	O	-0.92918	0	0	0		1.00000	0.86359	-15.75493		115.09	64.91	64.12	0.55182	0.36625
$C_bC_a(O)-OH$	O	-0.92918	0	0	0		1.00000	0.86359	-15.75493		101.32	78.68	48.58	1.14765	0.16950
$C_bC_a(O)-OH$	C_a	-0.92918	-1.34946	-0.64574	0	-154.54007	0.91771	0.76652	-17.75013	-17.55927	93.11	86.89	42.68	1.27551	0.04165
$C_bC_a(OH)=O$	O	-1.34946	0	0	0		1.00000	0.84115	-16.17521		137.27	42.73	66.31	0.52193	0.61784
$C_bC_a(OH)=O$	C_a	-1.34946	-0.64574	-0.92918	0	-154.54007	0.91771	0.76652	-17.75013	-17.55927	134.03	45.97	62.14	0.60699	0.53278
$C_b-C_a(O)OH$	C_a	-0.64574	-1.34946	-0.92918	0	-154.54007	0.91771	0.76652	-17.75013	-17.55927	70.34	109.66	32.00	1.65466	0.25784
$C_b-C_a(O)OH$	C_b	-0.64574	-0.85035	-0.85035	0	-153.96212	0.91771	0.79232	-17.17218	-16.98131	73.74	106.26	33.94	1.61863	0.22181
$C_c^{3e}=(HOOC_a)C_b^{3e}=C_c$ (C_c bound to H, Cl, or NH_2)	C_b	-0.64574	-0.85035	-0.85035	0	-153.96212	0.91771	0.79232	-17.17218	-16.98132	134.09	45.91	58.79	0.76344	0.55124
$\left(C^{3e}=\right)_2 C_a-Cl$	Cl	-0.36229	0	0	0		1.05158	0.89582	15.18804		82.92	97.08	37.22	1.75824	0.11042
$\left(C^{3e}=\right)_2 C_a-Cl$	C_a	-0.36229	-0.85035	-0.85035	0	-153.67867	0.91771	0.80561	-16.88873	-16.69786	73.32	106.68	31.67	1.87911	0.23129
$C_b^{3e}=(Cl)C_a^{3e}=C_b$ (C_b bound to H or Cl)	C_a	-0.36229	-0.85035	-0.85035	0	-153.67867	0.91771	0.80561	-16.88873	-16.69786	134.65	45.35	59.47	0.74854	0.56614
$\left(C_b^{3e}=\right)_2 C_aNH-H$	N	-0.56690	0	0	0		0.93084	0.88392	-15.39265		121.74	58.26	67.49	0.47634	0.46500
$\left(C_b^{3e}=\right)_2 C_a-NH_2$	C_a	-0.56690	-0.85035	-0.85035	0	-153.88328	0.91771	0.79597	-17.09334	-16.90248	88.49	91.51	41.01	1.36696	0.02101
$\left(C_b^{3e}=\right)_2 C_a-NH_2$	N	-0.56690	0	0	0		0.93084	0.88392	-15.39265		96.32	83.68	46.43	1.24859	0.09736
$C^{3e}=(H_2N)C_c^{3e}=C$	C_a	-0.85035	-0.85035	-0.56690	0	-153.88327	0.91771	0.79597	-17.09334	-16.90248	134.24	45.76	58.98	0.75935	0.55533

Table 15.258. The energy parameters (eV) of functional groups of benzoic acid compounds.

Parameters	$C=C$ Group	CH (i) Group	$C-C(O)$ Group	$C=O$ Group	$C-O$ Group	OH Group	$C-Cl$ (i) Group	$C-Cl$ (ii) Group	$C-N$ Group	NH_2 Group
f_1	0.75	1								
n_1	2	1	1	2	1	1	1	1	1	2
n_2	0	0	0	0	0	0	0	0	0	0
n_3	0	0	0	0	0	0	0	0	0	1
C_1	0.5	0.75	0.5	0.5	0.5	0.75	0.5	0.5	0.5	0.75
C_2	0.85252	1	1	1	1	1	0.81317	0.81317	1	0.93613
c_1	1	1	1	1	1	0.75	1	1	1	0.75
c_2	0.85252	0.91771	0.91771	0.85395	0.85395	1	1	1	0.84665	0.92171
c_3	0	1	0	2	0	1	0	0	0	0
c_4	3	1	2	4	2	1	2	2	2	1
c_5	0	1	0	0	0	1	0	0	0	2
C_{1o}	0.5	0.75	0.5	0.5	0.5	0.75	0.5	0.5	0.5	1.5
C_{2o}	0.85252	1	1	1	1	1	0.81317	0.81317	1	1
V_e (eV)	-101.12679	-37.10024	-32.15216	-111.25473	-35.08488	-40.92709	-31.85648	-32.14474	-32.76465	-78.97795
V_p (eV)	20.69825	13.17125	9.74055	23.87467	10.32968	14.81988	8.25686	8.28394	10.10870	28.90735
T (eV)	34.31559	11.58941	8.23945	42.82081	10.11150	16.18567	7.21391	7.32700	9.04312	31.73641
V_m (eV)	-17.15779	-5.79470	-4.11973	-21.41040	-5.05575	-8.09284	-3.60695	-3.66350	-4.52156	-15.86820
$E_{(AO/HO)}$ (eV)	0	-14.63489	-14.63489	0	-14.63489	-13.6181	-14.63489	-14.63489	-14.63489	-14.53414
$\Delta E_{H_2MO(AO/HO)}$ (eV)	0	-1.13379	-1.29147	-2.69893	-2.69893	0	-2.99216	-2.99216	-1.13379	0
E_T $_{(AO/HO)}$ (eV)	0	-13.50110	-13.34342	2.69893	-11.93596	-13.6181	-11.64273	-11.64273	-13.50110	-14.53414
$E_{(n_5\ AO/HO)}$ (eV)	0	0	0	0	0	0	0	0	0	-14.53414
E_T $_{(H_2MO)}$ (eV)	-63.27075	-31.63539	-31.63530	-63.27074	-31.63541	-31.63247	-31.63539	-31.63542	-31.63549	-48.73654
$E_T\left(atom-atom, msp^3.AO\right)$ (eV)	-2.26759	-0.56690	-1.29147	-2.69893	-1.85836	0	-0.72457	-0.92918	-1.13379	0
E_T $_{(MO)}$ (eV)	-65.53833	-32.20226	-32.92684	-65.96966	-33.49373	-31.63537	-32.35994	-32.56455	-32.76916	-48.73660
$\omega\ \left(10^{15}\ rad/s\right)$	49.7272	26.4826	10.7262	59.4034	24.3637	44.1776	8.03459	8.11389	11.9890	68.9812
E_K (eV)	32.73133	17.43132	7.06019	39.10034	16.03660	29.07844	5.28851	5.34070	7.89138	45.40465
$\overline{E}_D$ (eV)	-0.35806	-0.26130	-0.17309	-0.40804	-0.26535	-0.33749	-0.14722	-0.14888	-0.18211	-0.42172
$\overline{E}_{Kvib}$ (eV)	0.19649 [49]	0.35532 Eq. (13.458)	0.10502 [29]	0.21077 [12]	0.14010 [31]	0.46311 [17-18]	0.08059 [12]	0.08059 [12]	0.15498 [58]	0.40929 [22]
$\overline{E}_{osc}$ (eV)	-0.25982	-0.08364	-0.12058	-0.30266	-0.19530	-0.10594	-0.10693	-0.10859	-0.10462	-0.21708
E_{mag} (eV)	0.14803	0.14803	0.14803	0.11441	0.14803	0.11441	0.14803	0.14803	0.14803	0.14803
E_T $_{(Group)}$ (eV)	-49.54347	-32.28590	-33.04742	-66.57498	-33.68903	-31.74130	-32.46687	-32.67314	-32.87379	-49.17075
$E_{initial(c_4\ AO/HO)}$ (eV)	-14.63489	-14.63489	-14.63489	-14.63489	-14.63489	-13.6181	-14.63489	-14.63489	-14.63489	-14.53414
$E_{initial(c_5\ AO/HO)}$ (eV)	0	-13.59844	0	0	0	-13.59844	0	0	0	-13.59844
E_D $_{(Group)}$ (eV)	5.63881	3.90454	3.77764	7.80660	4.41925	4.41035	3.19709	3.40336	3.60401	7.43973

Table 15.259. The total bond energies of benzoic acid compounds calculated using the functional group composition and the energies of Table 15.258 compared to the experimental values [3].

Formula	Name	$C^{3e}=C$ Group	CH (i) Group	$C-C(O)$ Group	$C=O$ Group	$C-O$ Group	OH Group	$C-Cl$ (i) Group	$C-Cl$ (ii) Group	$C-N$ Group	NH_2 Group	Calculated Total Bond Energy (eV)	Experimental Total Bond Energy (eV)	Relative Error
$C_7H_6O_2$	Benzoic acid	6	5	1	1	1	1	0	0	0	0	73.76938	73.762	-0.00009
$C_7H_5ClO_2$	2-chlorobenzoic acid	6	4	1	1	1	1	1	0	0	0	73.06193	73.082	0.00027
$C_7H_5ClO_2$	3-chlorobenzoic acid	6	4	1	1	1	1	0	1	0	0	73.26820	73.261	-0.00010
$C_7H_5ClO_2$	4-chlorobenzoic acid	6	4	1	1	1	1	0	1	0	0	73.26820	73.247	-0.00028
$C_7H_7NO_2$	Aniline-2-carboxylic acid	6	4	1	1	1	1	0	0	1	1	80.90857	80.941	0.00041
$C_7H_7NO_2$	Aniline-3-carboxylic acid	6	4	1	1	1	1	0	0	1	1	80.90857	80.813	-0.00118
$C_7H_7NO_2$	Aniline-4-carboxylic acid	6	4	1	1	1	1	0	0	1	1	80.90857	80.949	0.00050

Table 15.260. The bond angle parameters of benzoic acid compounds and experimental values [1]. E_T is E_T ($atom-atom$,$msp^3.AO$).

Atoms of Angle	$2c'$ Bond 1 (a_0)	$2c'$ Bond 2 (a_0)	$2c'$ Terminal Atoms (a_0)	$E_{Coulombic}$ Atom 1	Atom 1 Hybridization Designation (Table 15.3.A)	$E_{Coulombic}$ Atom 2	Atom 2 Hybridization Designation (Table 15.3.A)	c_2 Atom 1	c_2 Atom 2	C_1	C_2	c_1	c_2'	E_T (eV)	θ_v (°)	θ_1 (°)	θ_2 (°)	Cal. θ (°)	Exp. θ (°)
$\angle CCC$ (aromatic)	2.62936	2.62936	4.5585	-17.17218	38	-17.17218	38	0.79232	0.79232	1	1	1	0.79232	-1.85836				120.19	120 [50-52] (benzene)
$\angle CCH$ (aromatic)																120.19		119.91	120 [50-52] (benzene)
$\angle C_aO_bH$	2.63431	1.83616	3.6405	-14.82575	1	-14.82575	1	1	0.91771	0.75	1	0.75	0.91771	0				107.71	
$\angle C_bC_aO_a$	2.82796	2.27954	4.4721	-17.17218	38	-13.61806	O	0.79232	0.85395 (Eq. (15.33))	1	1	1	0.82313	-1.65376				121.86	122 [59] (benzoic acid)
$\angle C_bC_aO_b$	2.82796	2.63431	4.6690	-16.40067	20	-13.61806	O	0.82959	0.85395 (Eq. (15.133))	1	1	1	0.84177	-1.65376				117.43	118 [59] (benzoic acid)
$\angle O_aC_aO_b$	2.27954	2.63431	4.3818	-16.17521 O_a	13	-15.75493 O_b	7	0.84115	0.86359	1	1	1	0.85237	-1.44915				126.03	122 [59] (benzoic acid)
$\angle CCC$ (aromatic)	2.62936	2.62936	4.5585	-17.17218	38	-17.17218	38	0.79232	0.79232	1	1	1	0.79232	-1.85836				120.19	120 ($\angle CC(H)C$ chlorobenzene) 121.7 ($\angle CC(Cl)C$ chlorobenzene) 120 [50-52] (benzene)
$\angle CCH$ $\angle CCCl$ (aromatic)																120.19		119.91	120 [50-52] (benzene)
$\angle HNH$	1.88268	1.88268	3.1559	-14.53414	N	H	H	0.93613 Eq. (13.248))	1	1	1	0.75	1.06823	0				113.89	113.9 (aniline)
$\angle C_aNH$	2.69190	1.88268	3.9833	-15.95955	10	-14.53414	N	0.84665 (Eq. (15.171))	0.84665 (Eq. (15.171))	0.75	1	0.75	1.00000	0				120.05	

ANISOLE

Anisole has the formula C_7H_8O and comprises the phenol molecule with the hydroxyl hydrogen atom replaced by the moiety $-O-CH_3$ to form an ether comprising aromatic and methyl functional groups as well as two types of $C-O$ functional groups, one for aryl carbon to oxygen and one for methyl carbon to oxygen. The aromatic $C\overset{3e}{=}C$ and $C-H$ functional groups are equivalent to those of benzene given in the Aromatic and Heterocyclic Compounds section. The CH_3 and methyl $C-O$ functional groups are the same as those of the corresponding ether groups given in the corresponding section.

The $C-O$ functional group comprising the bond between the ether oxygen and aromatic ring is equivalent to that of the methyl ether $C-O$ functional group except that $\Delta E_{H_2MO}\left(AO/HO\right)$ in Eq. (15.51) and $E_T\left(atom-atom,msp^3.AO\right)$ in Eq. (15.61) are both $-1.13379\,eV$ (Eq. (14.247)). $E_T\left(atom-atom,msp^3.AO\right)$ is based on the energy match between the OCH_3 group and the $C2sp^3$ HO of the aryl group and is twice that of the aryl $C-H$ group that it replaces.

The symbols of the functional groups of anisole are given in Table 15.261. The geometrical (Eqs. (15.1-15.5) and (15.51)), intercept (Eqs. (15.80-15.87)), and energy (Eqs. (15.6-15.11), (15.17-15.65), and (15.165-15.166)) parameters of anisole are given in Tables 15.262, 15.263, and 15.264, respectively. The total energy of anisole given in Table 15.265 was calculated as the sum over the integer multiple of each $E_{D\,(Group)}$ of Table 15.264 corresponding to functional-group composition of the molecule. The bond angle parameters of anisole determined using Eqs. (15.88-15.117) are given in Table 15.266. The color scale, translucent view of the charge-density of anisole comprising the concentric shells of atoms with the outer shell bridged by one or more H_2-type ellipsoidal MOs or joined with one or more hydrogen MOs is shown in Figure 15.45.

Figure 15.45. Color scale, translucent view of the charge-density of anisole showing the orbitals of the atoms at their radii, the ellipsoidal surface of each H or H_2-type ellipsoidal MO that transitions to the corresponding outer shell of the atom(s) participating in each bond, and the hydrogen nuclei (red, not to scale).

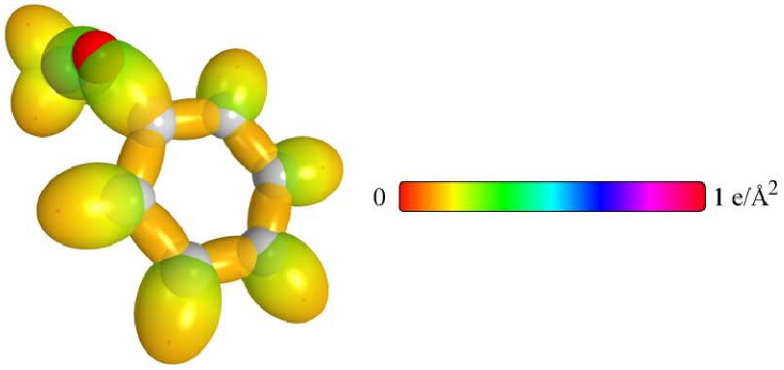

Table 15.261. The symbols of functional groups of anisole.

Functional Group	Group Symbol
CC (aromatic bond)	$C\overset{3e}{=}C$
CH (aromatic)	CH (i)
Aryl C-O	$C-O$ (a)
Methyl C-O	$C-O$ (b)
CH_3 group	$C-H\ \left(CH_3\right)$

Table 15.262. The geometrical bond parameters of anisole and experimental values [1].

Parameter	$C \overset{3e}{=} C$ Group	CH (i) Group	$C-O$ (a) Group	$C-O$ (b) Group	$C-H\ (CH_3)$ Group
$a\ (a_0)$	1.47348	1.60061	1.82682	1.80717	1.64920
$c'\ (a_0)$	1.31468	1.03299	1.35160	1.34431	1.04856
Bond Length $2c'\ (\AA)$	1.39140	1.09327	1.43047	1.42276	1.10974
Exp. Bond Length $(\AA)$	1.397 avg. (phenol)	1.084 (phenol)			1.11 (avg.) (toluene)
$b,c\ (a_0)$	0.66540	1.22265	1.22900	1.20776	1.27295
e	0.89223	0.64537	0.73986	0.74388	0.63580

Table 15.263. The MO to HO intercept geometrical bond parameters of anisole. E_T is E_T ($atom-atom$,$msp^3.AO$).

Bond	Atom	E_T (eV) Bond 1	E_T (eV) Bond 2	E_T (eV) Bond 3	E_T (eV) Bond 4	Final Total Energy $C2sp^3$ (eV)	$r_{initial}$ (a_0)	r_{final} (a_c)	$E_{Coulomb}(C2sp^3)$ (eV) Final	$E(C2sp^3)$ (eV) Final	θ' (°)	θ_1 (°)	θ_2 (°)	d_1 (a_0)	d_2 (a_0)
$C-H\ (C_bH)$	C_b	-0.85035	-0.85035	-0.56690	0	-153.88327	0.91771	0.79597	-17.09334	-16.90248	74.42	105.58	38.84	1.24678	0.21379
$C-H\ (OC_cH_3)$	C_c	-0.72457	0	0	0	-152.34026	0.91771	0.87495	-15.55033	-15.35946	78.85	101.15	42.40	1.21777	0.16921
$\left(C_b \overset{3e}{=}\right)_2 C_aO-C_cH_3$	C_c	-0.72457	0	0	0	-152.34026	0.91771	0.87495	-15.55033	-15.35946	95.98	84.02	46.10	1.25319	0.09112
$\left(C_b \overset{3e}{=}\right)_2 C_aO-C_cH_3$	O	-0.72457	-0.56690	0	0		1.00000	0.84418	-16.11722		93.38	86.62	44.25	1.29456	0.04975
$\left(C_b \overset{3e}{=}\right)_2 C_a-OC_cH_3$	C_a	-0.56690	-0.85035	-0.85035	0	-153.88327	0.91771	0.79597	-17.09334	-16.90248	87.00	93.00	40.30	1.39329	0.04170
$\left(C_b \overset{3e}{=}\right)_2 C_a-OC_cH_3$	O	-0.56690	-0.72457	0	0		1.00000	0.84418	-16.11722		91.59	88.41	43.36	1.32814	0.02346
$\left(C_b \overset{3e}{=}\right)_2 C_aOC_cH_3$	C_a	-0.56690	-0.85035	-0.85035	0	-153.88327	0.91771	0.79597	-17.09334	-16.90248	134.24	45.76	58.98	0.75935	0.55533
$\left(\overset{3e}{=}(H)C_b\right)_2 C_aOC_cH_3$	C_b	-0.85035	-0.85035	-0.56690	0	-153.88327	0.91771	0.79597	-17.09334	-16.90248	134.24	45.76	58.98	0.75935	0.55533

Table 15.264. The energy parameters (eV) of functional groups of anisole.

Parameters	$C \overset{3e}{=} C$ Group	CH (i) Group	$C-O$ (a) Group	$C-O$ (b) Group	CH_3 Group
f_1	0.75	1			
n_1	2	1	1	1	3
n_2	0	0	0	0	2
n_3	0	0	0	0	0
C_1	0.5	0.75	0.5	0.5	0.75
C_2	0.85252	1	1	1	1
c_1	1	1	1	1	1
c_2	0.85252	0.91771	0.85395	0.85395	0.91771
c_3	0	1	0	0	0
c_4	3	1	2	2	1
c_5	0	1	0	0	3
C_{1o}	0.5	0.75	0.5	0.5	0.75
C_{2o}	0.85252	1	1	1	1
$V_e\ (eV)$	-101.12679	-37.10024	-32.67197	-33.15757	-107.32728
$V_p\ (eV)$	20.69825	13.17125	10.06645	10.12103	38.92728
$T\ (eV)$	34.31559	11.58941	8.94231	9.17389	32.53914
$V_m\ (eV)$	-17.15779	-5.79470	-4.47115	-4.58695	-16.26957
$E_{(AO/HO)}\ (eV)$	0	-14.63489	-14.63489	-14.63489	-15.56407
$\Delta E_{H_2MO(AO/HO)}\ (eV)$	0	-1.13379	-1.13379	-1.44915	0
$E_{T(AO/HO)}\ (eV)$	0	-13.50110	-13.50110	-13.18574	-15.56407
$E_{T(H_2MO)}\ (eV)$	-63.27075	-31.63539	-31.63547	-31.63533	-67.69451
$E_T\left(atom-atom, msp^3.AO\right)(eV)$	-2.26759	-0.56690	-1.13379	-1.44915	0
$E_{T(MO)}\ (eV)$	-65.53833	-32.20226	-32.76916	-33.08452	-67.69450
$\omega\ \left(10^{15}\ rad/s\right)$	49.7272	26.4826	11.8393	12.0329	24.9286
$E_K\ (eV)$	32.73133	17.43132	7.79284	7.92028	16.40846
$\bar{E}_D\ (eV)$	-0.35806	-0.26130	-0.18097	-0.18420	-0.25352
$\bar{E}_{Kvib}\ (eV)$	0.19649 [49]	0.35532 Eq. (13.458)	0.13663 [21]	0.13663 [21]	0.35532 (Eq. (13.458))
$\bar{E}_{osc}\ (eV)$	-0.25982	-0.08364	-0.11266	-0.11589	-0.22757
$E_{mag}\ (eV)$	0.14803	0.14803	0.14803	0.14803	0.14803
$E_{T(Group)}\ (eV)$	-49.54347	-32.28590	-32.88182	-33.20040	-67.92207
$E_{initial(s\ AO/HO)}\ (eV)$	-14.63489	-14.63489	-14.63489	-14.63489	-14.63489
$E_{initial(s\ AO/HO)}\ (eV)$	0	-13.59844	0	0	-13.59844
$E_{D(Group)}\ (eV)$	5.63881	3.90454	3.61204	3.93062	12.49186

Table 15.265. The total bond energies of anisole calculated using the functional group composition and the energies of Table 15.264 compared to the experimental values [3].

Formula	Name	$C^{3e}=C$	CH (i)	$C-O$ (a) Group	$C-O$ (b) Group	CH_3 Group	Calculated Total Bond Energy (eV)	Experimental Total Bond Energy (eV)	Relative Error
C_7H_8O	Anisole	6	5	1	1	1	73.39006	73.355	-0.00047

Table 15.266. The bond angle parameters of anisole and experimental values [1]. E_T is E_T ($atom-atom,msp^3.AO$).

Atoms of Angle	2c' Bond 1 (a_0)	2c' Bond 2 (a_0)	2c' Terminal Atoms (a_0)	$E_{Coulombic}$ Atom 1	Atom 1 Hybridization Designation (Table 15.3.A)	$E_{Coulombic}$ Atom 2	Atom 2 Hybridization Designation (Table 15.3.A)	c_2 Atom 1	c_2 Atom 2	C_1	C_2	c_1	c_2'	E_T (eV)	θ_v (°)	θ_1 (°)	θ_2 (°)	Cal. θ (°)	Exp. θ (°)
$\angle CCC$ (aromatic)	2.62936	2.62936	4.5585	-17.17218	38	-17.17218	38	0.79232	0.79232	1	1	1	0.79232	-1.85836				120.19	120 [50-52] (benzene)
$\angle CCH$ (aromatic)																120.19		119.91	120 [50-52] (benzene)

PYRROLE

Pyrrole having the formula C_4H_5N comprises the conjugated alkene 1,3-butadiene that forms a cyclic structure by terminal-atom bonding to a NH functional group. The two symmetrical carbon-to-nitrogen bonds comprise the $C-N-C$ functional group. The 1,3-butadiene moiety comprises $C-C$, $C=C$, and CH functional groups. The $C-C$ and $C=C$ groups are equivalent to the corresponding groups of 1,3-butadiene given in the Cyclic and Conjugated Alkenes section except that the energy terms corresponding to oscillation in the transition state match pyrrole. Furthermore, the conjugated double bonds have the same bonding as in 1,3-butadiene except that the hybridization terms c_2 of the $C-C$ and $C=C$ groups and C_2 and C_{2o} of the $C=C$ group in Eqs. (15.51) and (15.61) become that of benzene given by Eq. (15.162), $(C_2\left(benzeneC2sp^3HO\right)=c_2\left(benzeneC2sp^3HO\right)=0.85252)$, in the cyclic pyrrole MO which has aromatic character. The bonding in pyrrole, furan, and thiophene are the same except for the energy match to the corresponding heteroatoms. The hybridization permits double-bond character in the carbon-heteroatom bonding.

The NH group is solved equivalently to that of a secondary amine as given in the corresponding section except that the hybridization term c_2 is that of the amino group of aniline in order provide double-bond character to match the group to the other orbitals of the molecule. Similarly, the CH functional group is equivalent to that of 1,3-butadiene, except that $\Delta E_{H_2MO}\left(AO/HO\right)=-2.26758\ eV$ (Eq. (14.247)) in Eq. (15.51) in order to provide matching double-bond character.

The solution of the $C-N-C$ functional group comprises the hybridization of the $2s$ and $2p$ AOs of each C to form a single $2sp^3$ shell as an energy minimum, and the sharing of electrons between two $C2sp^3$ HOs and the nitrogen atom to form a MO permits each participating hybridized orbital to decrease in radius and energy. Thus, the $C-N-C$ -bond MO comprising a linear combination of two single bonds is solved in the same manner as a double bond with $n_1=2$ in Eqs. (15.51) and (15.61). The hybridization factor $c_2\left(arylC2sp^3HO\ to\ N\right)=0.84665$ (Eq. (15.171)) matches the double-bond character of the $C2sp^3$ HOs to the N atom of the NH group, and C_2 and C_{2o} in Eqs. (15.51) and (15.61) become that of benzene given by Eq. (15.162), $C_2\left(benzeneC2sp^3HO\right)=0.85252$. Furthermore, $\Delta E_{H_2MO}\left(AO/HO\right)$ in Eq. (15.51) and $E_T\left(atom-atom,msp^3.AO\right)$ in Eq. (15.61) are both $-0.92918\ eV$ (Eq. (14.513)) per atom corresponding to $-3.71673\ eV$ in total. This is the maximum energy for a single bond and corresponds to methylene character as given in the Continuous-Chain Alkanes section.

The symbols of the functional groups of pyrrole are given in Table 15.267. The structure of pyrrole is shown in Figure 15.46B. The geometrical (Eqs. (15.1-15.5) and (15.51)), intercept (Eqs. (15.80-15.87)), and energy (Eqs. (15.6-15.11) and (15.17-15.65)) parameters of pyrrole are given in Tables 15.268, 15.269, and 15.270, respectively. The total energy of pyrrole given in Table 15.271 was calculated as the sum over the integer multiple of each $E_D(Group)$ of Table 15.270 corresponding to functional-group composition of the molecule. The bond angle parameters of pyrrole determined using Eqs. (15.88-15.117) are given in Table 15.272. The color scale, translucent view of the charge-density of pyrrole comprising the concentric shells of atoms with the outer shell bridged by one or more H_2-type ellipsoidal MOs or joined with one or more hydrogen MOs is shown in Figure 15.46A.

Figure 15.46. (A) Color scale, translucent view of the charge-density of pyrrole showing the orbitals of the atoms at their radii, the ellipsoidal surface of each H or H_2-type ellipsoidal MO that transitions to the corresponding outer shell of the atom(s) participating in each bond, and the hydrogen nuclei (red, not to scale). (B) Chemical structure and atom designation of pyrrole.

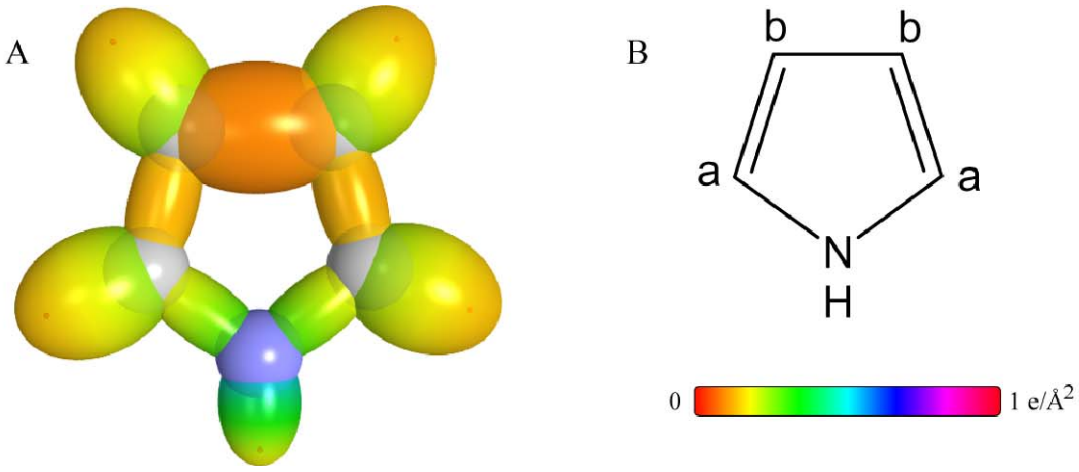

Table 15.267. The symbols of functional groups of pyrrole.

Functional Group	Group Symbol
$C_a = C_b$ double bond	$C = C$
$C_b - C_b$	$C - C$
$C_a - N - C_a$	$C - N - C$
NH group	*NH*
CH	*CH*

Table 15.268. The geometrical bond parameters of pyrrole and experimental values [1].

Parameter	$C=C$ Group	$C-C$ Group	$C-N-C$ Group	NH Group	CH Group
$a\ (a_0)$	1.45103	1.77965	1.43222	1.24428	1.53380
$c'\ (a_0)$	1.30463	1.33404	1.29614	0.94134	1.01120
Bond Length $2c'\ (\text{Å})$	1.38076	1.41188	1.37178	0.996270	1.07021
Exp. Bond Length (Å)	1.382 (pyrrole)	1.417 (pyrrole)	1.370 (pyrrole)	0.996 (pyrrole)	1.076 (pyrrole)
$b,c\ (a_0)$	0.63517	1.17792	0.60931	0.81370	1.15326
e	0.89910	0.74961	0.90499	0.75653	0.65928

Table 15.269. The MO to HO intercept geometrical bond parameters of pyrrole. R_1 is an alkyl group and R, R', R'' are H or alkyl groups. E_T is E_T ($atom-atom$,$msp^3.AO$).

Bond	Atom	E_T (eV) Bond 1	E_T (eV) Bond 2	E_T (eV) Bond 3	E_T (eV) Bond 4	Final Total Energy $C2sp^3$ (eV)	$r_{initial}\ (a_0)$	$r_{final}\ (a_0)$	$E_{Coulomb}(C2sp^3)$ (eV) Final	$E(C2sp^3)$ (eV) Final	θ' (°)	θ_1 (°)	θ_2 (°)	$d_1\ (a_0)$	$d_2\ (a_0)$
$C-H\ (C_aH)$	C_a	-1.13380	-0.92918	0	0	-153.67867	0.91771	0.80561	-16.88873	-16.69786	83.35	96.65	43.94	1.10452	0.09331
$C-H\ (C_bH)$	C_b	-1.13380	-1.13380	0	0	-153.88328	0.91771	0.79597	-17.09334	-16.90248	82.21	97.79	43.14	1.11914	0.10794
$C_a=(H)C_b-C_b(H)=C_a$	C_b	-1.13380	-1.13380	0	0	-153.88328	0.91771	0.79597	-17.09334	-16.90248	91.57	88.43	42.49	1.31226	0.02177
$C_a=C_b(H)(H)C_b=C_a$	C_b	-1.13380	-1.13380	0	0	-153.88328	0.91771	0.79597	-17.09334	-16.90248	136.36	43.64	59.86	0.72857	0.57606
$HNC_a=C_b(H)$	C_a	-1.13380	-0.92918	0	0	-153.67867	0.91771	0.80561	-16.88873	-16.69786	136.75	43.25	60.35	0.71784	0.58678
$C_a(H)N-C_a=C_b(H)$	C_a	-1.13380	-0.92918	0	0	-153.67867	0.91771	0.80561	-16.88873	-16.69786	138.54	41.46	61.09	0.69238	0.60376
$C_a(H)N-C_a=C_b(H)$	N	-0.92918	-0.92918	0	0		0.93084	0.81549	-16.68411		138.92	41.08	61.59	0.68147	0.61467
$N-H\ (NH)$	N	-0.92918	-0.92918	0	0		0.93084	0.81549	-16.68411		117.34	62.66	62.90	0.56678	0.37456

Table 15.270. The energy parameters (eV) of functional groups of pyrrole.

Parameters	$C=C$ Group	$C-C$ Group	$C-N-C$ Group	NH Group	CH Group
n_1	2	1	2	1	1
n_2	0	0	0	0	0
n_3	0	0	0	0	0
C_1	0.5	0.5	0.5	0.75	0.75
C_2	0.85252	1	0.85252	0.93613	1
c_1	1	1	1	0.75	1
c_2	0.85252	0.85252	0.84665	0.92171	0.91771
c_3	0	0	0	1	1
c_4	4	2	4	1	1
c_5	0	0	0	1	1
C_{1o}	0.5	0.5	0.5	0.75	0.75
C_{2o}	0.85252	1	0.85252	1	1
$V_e\ (eV)$	-104.37986	-33.80733	-106.58684	-39.48897	-39.09538
$V_p\ (eV)$	20.85777	10.19898	20.99432	14.45367	13.45505
$T\ (eV)$	35.96751	9.49831	37.21047	15.86820	12.74462
$V_m\ (eV)$	-17.98376	-4.74915	-18.60523	-7.93410	-6.37231
$E_{(AO/HO)}\ (eV)$	0	-14.63489	0	-14.53414	-14.63489
$\Delta E_{H_2MO\,(AO/HO)}\ (eV)$	-2.26759	-1.85836	-3.71673	0	-2.26758
$E_{T\,(AO/HO)}\ (eV)$	2.26759	-12.77653	3.71673	-14.53414	-12.36731
$E_{T\,(H_2MO)}\ (eV)$	-63.27075	-31.63572	-63.27056	-31.63534	-31.63533
$E_{I}\left(atom-atom, msp^3.AO\right)\ (eV)$	-2.26759	-2.26759	-3.71673	0	0
$E_{T\,(MO)}\ (eV)$	-65.53833	-33.90295	-66.98746	-31.63537	-31.63537
$\omega\ \left(10^{15}\ rad/s\right)$	15.4421	12.3131	15.7474	48.7771	28.9084
$E_K\ (eV)$	10.16428	8.10471	10.36521	32.10594	19.02803
$\overline{E}_D\ (eV)$	-0.20668	-0.19095	-0.21333	-0.35462	-0.27301
$\overline{E}_{Kvib}\ (eV)$	0.17897 [6]	0.14829 [48]	0.11159 [12]	0.40696 [24]	0.39427 [59]
$\overline{E}_{osc}\ (eV)$	-0.11720	-0.11680	-0.15754	-0.15115	-0.07587
$E_{mag}\ (eV)$	0.14803	0.14803	0.14803	0.14803	0.14803
$E_{T\,(Group)}\ (eV)$	-65.77272	-34.01976	-67.30254	-31.78651	-31.71124
$E_{initial\,(e_4\ AO/HO)}\ (eV)$	-14.63489	-14.63489	-14.63489	-14.53414	-14.63489
$E_{initial\,(e_5\ AO/HO)}\ (eV)$	0	0	0	-13.59844	-13.59844
$E_{D\,(Group)}\ (eV)$	7.23317	4.74998	8.76298	3.51208	3.32988

Table 15.271. The total bond energies of pyrrole calculated using the functional group composition and the energies of Table 15.270 compared to the experimental values [3].

Formula	Name	$C=C$	$C-C$	$C-N-C$	NH	CH	Calculated Total Bond Energy (eV)	Experimental Total Bond Energy (eV)	Relative Error
C_4H_5N	Pyrrole	2	1	1	1	4	44.81090	44.785	-0.00057

Table 15.272. The bond angle parameters of pyrrole and experimental values [1]. In the calculation of θ_v, the parameters from the preceding angle were used. E_T is E_T ($atom-atom$,$msp^3.AO$).

Atoms of Angle	2c' Bond 1 (a_0)	2c' Bond 2 (a_0)	2c' Terminal Atoms (a_0)	$E_{Coulombic}$ Atom 1	Atom 1 Hybridization Designation (Table 15.3.B)	$E_{Coulombic}$ Atom 2	Atom 2 Hybridization Designation (Table 15.3.B)	c_2 Atom 1	c_2 Atom 2	C_1	C_2	c_1	c'_2	E_T (eV)	θ_v (°)	θ_1 (°)	θ_2 (°)	Cal. θ (°)	Exp. θ (°)
$\angle HC_aN$	2.02241	2.59228	4.0166	-14.82575	1	-14.53414	N	0.91771	0.92171 Eq. (15.170))	0.75	1	0.75	1.00435	0				120.51	121.5 (pyrrole)
$\angle C_bC_aH_a$																120.51	107.52	131.97	
$\angle HNC_a$	1.88268	2.59228	3.8987	-14.53414	N	-16.49325	6	0.84665 (Eq. (15.171))	0.82493 (Eq. (15.73))	0.75	1	0.75	0.97435	0				120.37	
$\angle H_bC_bC_b$	2.02241	2.66807	4.2111	-16.88873 C_b	20	-15.95954 C_b	6	0.80561	0.85252	0.75	1	0.75	1.05822	0				127.20	127.1 (pyrrole)
$\angle H_aC_aC_b$	2.02241	2.60925	4.2111	-16.88873 C_a	20	-15.95954 C_b	6	0.80561	0.85252	0.75	1	0.75	1.05822	0				130.36	
$\angle H_bC_bC_a$	2.02241	2.60925	4.1312	-17.09334 C_b	24	-16.47951 C_a	14	0.79597	0.82562	0.75	1	0.75	1.03725	0				125.76	
$\angle C_4C_bH_b$																125.76	107.01	127.23	127.1 (pyrrole)
$\angle NC_aC_b$	2.59228	2.60925	4.1952	-14.53414	N	-17.09334 C_b	24	0.84665 (Eq. (15.171))	0.79597	1	1	1	0.82131	-1.44915				107.52	107.7 (pyrrole)
$\angle C_aNC_a$	2.59228	2.59228	4.2426	-17.81791	35	-17.81791	35	0.76360	0.76360	1	1	1	0.76360	-1.85836				109.83	109.8 (pyrrole)
$\angle C_aC_bC_b$	2.60925	2.66807	4.2426	-17.81791	35	-18.02252	40	0.76360	0.75493	1	1	1	0.75927	-1.85836				107.01	107.4 (pyrrole)

FURAN

Furan having the formula C_4H_4O comprises the conjugated alkene 1,3-butadiene that forms a cyclic structure by terminal-atom bonding to an oxygen atom. The two symmetrical carbon-to-oxygen bonds comprise the $C-O-C$ functional group. The 1,3-butadiene moiety comprises $C-C$, $C=C$, and CH functional groups. The CH, $C-C$, and $C=C$ groups are equivalent to the corresponding groups of pyrrole given in the corresponding section.

The $C-O-C$ functional group of furan is solved in a similar manner as that of the $C-N-C$ group of pyrrole. The solution of the $C-O-C$ functional group comprises the hybridization of the $2s$ and $2p$ AOs of each C to form a single $2sp^3$ shell as an energy minimum, and the sharing of electrons between two $C2sp^3$ HOs and the oxygen atom to form a MO permits each participating hybridized orbital to decrease in radius and energy. Thus, the $C-O-C$-bond MO comprising a linear combination of two single bonds is solved in the same manner as a double bond with $n_1=2$ in Eqs. (15.51) and (15.61). The hybridization factor $c_2\left(arylC2sp^3HO\ to\ O\right)=0.79329$ (Eq. (15.169)) matches the double-bond character of the $C2sp^3$ HOs to the O atom, and C_2 and C_{2o} in Eqs. (15.51) and (15.61) become that of benzene given by Eq. (15.162), $C_2\left(benzeneC2sp^3HO\right)=0.85252$. Furthermore, $E_T\left(atom-atom,msp^3.AO\right)$ in Eq. (15.61) is $-0.92918\ eV$ (Eq. (14.513)) per atom corresponding to $-3.71673\ eV$ in total.

The symbols of the functional groups of furan are given in Table 15.273. The structure of furan is shown in Figure 15.47B. The geometrical (Eqs. (15.1-15.5) and (15.51)), intercept (Eqs. (15.80-15.87)), and energy (Eqs. (15.6-15.11) and (15.17-15.65)) parameters of furan are given in Tables 15.274, 15.275, and 15.276, respectively. The total energy of furan given in Table 15.277 was calculated as the sum over the integer multiple of each $E_{D\,(Group)}$ of Table 15.276 corresponding to functional-group composition of the molecule. The bond angle parameters of furan determined using Eqs. (15.88-15.117) are given in Table 15.278. The color scale, translucent view of the charge-density of furan comprising the concentric shells of atoms with the outer shell bridged by one or more H_2-type ellipsoidal MOs or joined with one or more hydrogen MOs is shown in Figure 15.47A.

Figure 15.47. (A) Color scale, translucent view of the charge-density of furan showing the orbitals of the atoms at their radii, the ellipsoidal surface of each H or H_2-type ellipsoidal MO that transitions to the corresponding outer shell of the atom(s) participating in each bond, and the hydrogen nuclei (red, not to scale). (B) Chemical structure and atom designation of furan.

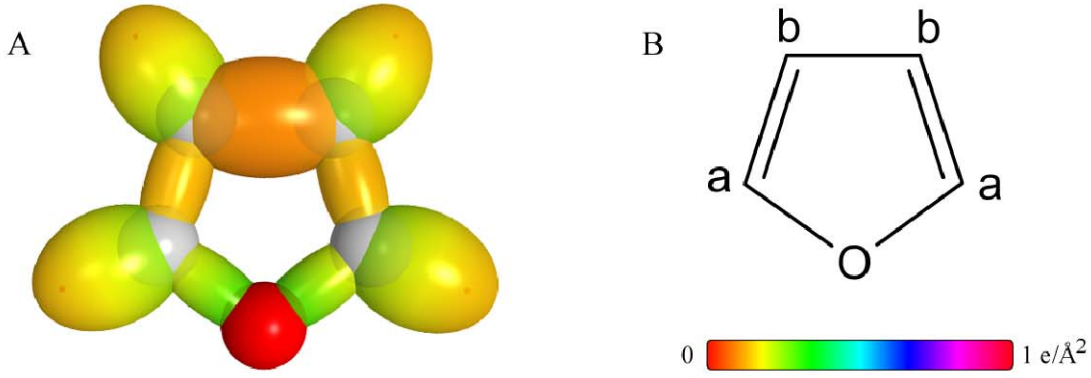

Table 15.273. The symbols of functional groups of furan.

Functional Group	Group Symbol
$C_a=C_b$ double bond	$C=C$
C_b-C_b	$C-C$
C_a-O-C_a	$C-O-C$
CH	CH

Table 15.274. The geometrical bond parameters of furan and experimental values [1].

Parameter	$C=C$ Group	$C-C$ Group	$C-O-C$ Group	CH Group
$a\ (a_0)$	1.45103	1.77965	1.41546	1.53380
$c'\ (a_0)$	1.30463	1.33404	1.28854	1.01120
Bond Length $2c'\ (\AA)$	1.38076	1.41188	1.36373	1.07021
Exp. Bond Length $(\AA)$	1.361 (furan)	1.431 (furan)	1.362 (furan)	1.075 (furan)
$b,c\ (a_0)$	0.63517	1.17792	0.58583	1.15326
e	0.89910	0.74961	0.91033	0.65928

Table 15.275. The MO to HO intercept geometrical bond parameters of furan. R_1 is an alkyl group and R, R', R'' are H or alkyl groups. E_T is E_T ($atom-atom$,$msp^3.AO$).

Bond	Atom	E_T (eV) Bond 1	E_T (eV) Bond 2	E_T (eV) Bond 3	E_T (eV) Bond 4	Final Total Energy $C2sp^3$ (eV)	$r_{initial}$ (a_0)	r_{final} (a_0)	$E_{Coulomb}(C2sp^3)$ (eV) Final	$E(C2sp^3)$ (eV) Final	θ' (°)	θ_1 (°)	θ_2 (°)	d_1 (a_0)	d_2 (a_0)
$C-H\ (C_aH)$	C_a	-1.13380	-0.92918	0	0	-153.67867	0.91771	0.80561	-16.88873	-16.69786	83.35	96.65	43.94	1.10452	0.09331
$C-H\ (C_bH)$	C_b	-1.13380	-1.13380	0	0	-153.88328	0.91771	0.79597	-17.09334	-16.90248	82.21	97.79	43.14	1.11914	0.10794
$C_a=(H)C_b-C_b(H)=C_a$	C_b	-1.13380	-1.13380	0	0	-153.88328	0.91771	0.79597	-17.09334	-16.90248	91.57	88.43	42.49	1.31226	0.02177
$C_a=C_b(H)(H)C_b=C_a$	C_b	-1.13380	-1.13380	0	0	-153.88328	0.91771	0.79597	-17.09334	-16.90248	136.36	43.64	59.86	0.72857	0.57606
$OC_a=C_a(H)$	C_a	-1.13380	-0.92918	0	0	-153.67867	0.91771	0.80561	-16.88873	-16.69786	136.75	43.25	60.35	0.71784	0.58678
$C_aO-C_a=C_b(H)$	C_a	-1.13380	-0.92918	0	0	-153.67867	0.91771	0.80561	-16.88873	-16.69786	140.16	39.84	61.75	0.66992	0.61862
$C_aO-C_a=C_b(H)$	O	-0.92918	-0.92918	0	0		1.00000	0.81549	-16.68411		140.52	39.48	62.25	0.65906	0.62947

Table 15.276. The energy parameters (eV) of functional groups of furan.

Parameters	$C=C$ Group	$C-C$ Group	$C-O-C$ Group	CH Group
n_1	2	1	2	1
n_2	0	0	0	0
n_3	0	0	0	0
C_1	0.5	0.5	0.5	0.75
C_2	0.85252	1	0.85252	1
c_1	1	1	1	1
c_2	0.85252	0.85252	0.79329	0.91771
c_3	0	0	0	1
c_4	4	2	4	1
c_5	0	0	0	1
C_{1o}	0.5	0.5	0.5	0.75
C_{2o}	0.85252	1	0.85252	1
$V_e\ (eV)$	-104.37986	-33.80733	-102.49036	-39.09538
$V_p\ (eV)$	20.85777	10.19898	21.11822	13.45505
$T\ (eV)$	35.96751	9.49831	36.20391	12.74462
$V_m\ (eV)$	-17.98376	-4.74915	-18.10196	-6.37231
$E_{(AO/HO)}\ (eV)$	0	-14.63489	0	-14.63489
$\Delta E_{H_2MO\ (AO/HO)}\ (eV)$	-2.26759	-1.85836	0	-2.26758
$E_{T\ (AO/HO)}\ (eV)$	2.26759	-12.77653	0	-12.36731
$E_{T\ (H_2MO)}\ (eV)$	-63.27075	-31.63572	-63.27019	-31.63533
$E_T\left(atom-atom, msp^3.AO\right)\ (eV)$	-2.26759	-2.26759	-3.71673	0
$E_{T\ (MO)}\ (eV)$	-65.53833	-33.90295	-66.98746	-31.63537
$\omega\ \left(10^{15}\ rad/s\right)$	15.4421	12.3131	58.0664	28.9084
$E_K\ (eV)$	10.16428	8.10471	38.22034	19.02803
$\overline{E}_D\ (eV)$	-0.20668	-0.19095	-0.40965	-0.27301
$\overline{E}_{Kvib}\ (eV)$	0.17897 [6]	0.14829 [48]	0.12523 [60	0.39427 [59]
$\overline{E}_{osc}\ (eV)$	-0.11720	-0.11680	-0.34704	-0.07587
$E_{mag}\ (eV)$	0.14803	0.14803	0.14803	0.14803
$E_{T\ (Group)}\ (eV)$	-65.77272	-34.01976	-67.68154	-31.71124
$E_{initial\ (c_4\ AO/HO)}\ (eV)$	-14.63489	-14.63489	-14.63489	-14.63489
$E_{initial\ (c_5\ AO/HO)}\ (eV)$	0	0	0	-13.59844
$E_{D\ (Group)}\ (eV)$	7.23317	4.74998	9.14198	3.32988

Table 15.277. The total bond energies of furan calculated using the functional group composition and the energies of Table 15.276 compared to the experimental values [3].

Formula	Name	$C=C$	$C-C$	$C-O-C$	CH	Calculated Total Bond Energy (eV)	Experimental Total Bond Energy (eV)	Relative Error
C_4H_4O	Furan	2	1	1	4	41.67782	41.692	0.00033

Table 15.278. The bond angle parameters of furan and experimental values [1]. In the calculation of θ_v, the parameters from the preceding angle were used. E_T is $_T(atom-atom,msp^3.AO)$.

Atoms of Angle	$2c'$ Bond 1 (a_0)	$2c'$ Bond 2 (a_0)	$2c'$ Terminal Atoms (a_0)	$E_{Coulombic}$ Atom 1	Atom 1 Hybridization Designation (Table 15.3.B)	$E_{Coulombic}$ Atom 2	Atom 2 Hybridization Designation (Table 15.3.B)	c_2 Atom 1	c_2 Atom 2	C_1	C_2	c_1	c_2'	E_T (eV)	θ_v (°)	θ_1 (°)	θ_2 (°)	Cal. θ (°)	Exp. θ (°)
$\angle HC_aO$	2.02241	2.57707	3.9328	-16.88873	20	-13.61806	O	0.80561	0.79329 Eq. (15.169))	0.75	1	0.75	0.98470	0				117.02	115.9 (furan)
$\angle C_bC_aH_a$																117.02	110.69	132.29	
$\angle H_bC_bC_b$	2.02241	2.66807	4.2269	-16.88873 C_b	20	-15.95954 C_b	6	0.80561	0.85252	0.75	1	0.75	1.05822	0				128.09	128.0 (furan)
$\angle H_aC_aC_b$	2.02241	2.60925	4.2269	-16.88873 C_a	20	-15.95954 C_b	6	0.80561	0.85252	0.75	1	0.75	1.05822	0				131.32	
$\angle H_bC_bC_a$	2.02241	2.60925	4.1312	-17.09334 C_b	24	-16.47951 C_a	14	0.79597	0.82562	0.75	1	0.75	1.03725	0				125.76	
$\angle C_bC_bH_b$																125.76	107.01	127.23	128.0 (furan)
$\angle C_bC_aO$	2.60925	2.57707	4.2661	-17.09334 C_b	24	-13.61806	O	0.79597	0.79329 Eq. (15.169))	1	1	1	0.79463	-1.65376				110.69	110.7 (furan)
$\angle C_aOC_a$	2.57707	2.57707	4.1231	-18.22713	41	-18.22713	41	0.74646	0.74646	1	1	1	0.74646	-1.85836				106.25	106.6 (furan)
$\angle C_aC_bC_b$	2.60925	2.66807	4.2426	-17.81791	35	-18.02252	40	0.76360	0.75493	1	1	1	0.75927	-1.85836				107.01	106.1 (furan)

THIOPHENE

Thiophene having the formula C_4H_4S comprises the conjugated alkene 1,3-butadiene that forms a cyclic structure by terminal-atom bonding to an oxygen atom. The two symmetrical carbon-to-sulfur bonds comprise the $C-S-C$ functional group. The 1,3-butadiene moiety comprises $C-C$, $C=C$, and CH functional groups. The CH, $C-C$, and $C=C$ groups are equivalent to the corresponding groups of pyrrole and furan given in the corresponding sections.

The $C-S-C$ functional group of thiophene is solved in a similar manner as that of the $C-N-C$ group of pyrrole and the $C-O-C$ group of furan. The solution of the $C-S-C$ functional group comprises the hybridization of the $2s$ and $2p$ AOs of each C to form a single $2sp^3$ shell as an energy minimum, and the sharing of electrons between two $C2sp^3$ HOs and the sulfur atom to form a MO permits each participating hybridized orbital to decrease in radius and energy. Thus, the $C-S-C$-bond MO comprising a linear combination of two single bonds is solved in the same manner as a double bond with $n_1=2$ in Eqs. (15.51) and (15.61).

In thiophene, the energy of sulfur is less than the Coulombic energy between the electron and proton of H given by Eq. (1.264). Thus, c_2 in Eq. (15.61) is $c_2\left(benzeneC2sp^3HO\right)=0.85252$ to match the double-bond character of the $C2sp^3$ HOs, and the energy matching condition is further determined by the C_2 parameter. Using the energy of S, $E\left(S\right)=-10.36001\ eV$ in Eq. (15.77) and the $C2sp^3$ HO energy of $E\left(C,2sp^3\right)=-15.76868\ eV$ (Eq. (15.18)) corresponding to $s=2$ in Eqs. (15.18-15.20), the hybridization factor C_2 of Eq. (15.61) for the $C-S-C$-bond MO is:

$$C_2\left(S3p\ to\ \text{aryl-type}\ C2sp^3HO\right)=\frac{E\left(S,3p\right)}{E\left(C,2sp^3\right)}=\frac{-10.36001\ eV}{-15.76868\ eV}=0.65700 \tag{15.172}$$

C_{1o} is also given by Eq. (15.172). Furthermore, $\Delta E_{H_2MO}\left(AO/HO\right)$ of the $C-S-C$-bond MO in Eq. (15.51) and $E_T\left(atom-atom,msp^3.AO\right)$ in Eq. (15.61) are both $-0.72457\ eV$ per atom corresponding to $-2.89830\ eV$ in total. The energy contribution equivalent to that of a methyl group (Eq. (14.151)) and that of the $C-S$-bond MO of thiols given in the corresponding section matches the energy of the sulfur atom to the $C2sp^3$ HOs.

The symbols of the functional groups of thiophene are given in Table 15.279. The structure of thiophene is shown in Figure 15.48B. The geometrical (Eqs. (15.1-15.5) and (15.51)), intercept (Eqs. (15.80-15.87)), and energy (Eqs. (15.6-15.11) and (15.17-15.65)) parameters of thiophene are given in Tables 15.280, 15.281, and 15.282, respectively. The total energy of thiophene given in Table 15.283 was calculated as the sum over the integer multiple of each $E_{D\,(Group)}$ of Table 15.282 corresponding to functional-group composition of the molecule. The bond angle parameters of thiophene determined using Eqs. (15.88-15.117) are given in Table 15.284. The color scale, translucent view of the charge-density of thiophene comprising the concentric shells of atoms with the outer shell bridged by one or more H_2-type ellipsoidal MOs or joined with one or more hydrogen MOs is shown in Figure 15.48A.

Figure 15.48. (A) Color scale, translucent view of the charge-density of thiophene showing the orbitals of the atoms at their radii, the ellipsoidal surface of each H or H_2-type ellipsoidal MO that transitions to the corresponding outer shell of the atom(s) participating in each bond, and the hydrogen nuclei (red, not to scale). (B) Chemical structure and atom designation of thiophene.

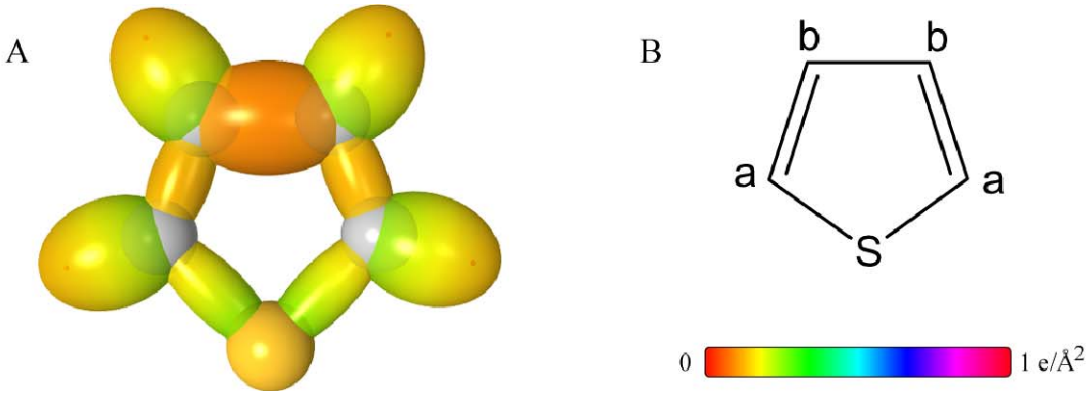

Table 15.279. The symbols of functional groups of thiophene.

Functional Group	Group Symbol
$C_a = C_b$ double bond	$C = C$
$C_b - C_b$	$C - C$
$C_a - S - C_a$	$C - S - C$
CH	CH

Table 15.280. The geometrical bond parameters of thiophene and experimental values [1].

Parameter	$C = C$ Group	$C - C$ Group	$C - S - C$ Group	CH Group
$a\ (a_0)$	1.45103	1.77965	1.74058	1.53380
$c'\ (a_0)$	1.30463	1.33404	1.62766	1.01120
Bond Length $2c'\ (\AA)$	1.38076	1.41188	1.72264	1.07021
Exp. Bond Length $(\AA)$	1.370 (thiophene)	1.423 (thiophene)	1.714 (thiophene)	1.078 (thiophene)
$b,c\ (a_0)$	0.63517	1.17792	0.61671	1.15326
e	0.89910	0.74961	0.93513	0.65928

Table 15.281. The MO to HO intercept geometrical bond parameters of thiophene. R_1 is an alkyl group and *R, R′, R″* are *H* or alkyl groups. E_T is E_T (*atom – atom,msp³.AO*).

Bond	Atom	E_T (eV) Bond 1	E_T (eV) Bond 2	E_T (eV) Bond 3	E_T (eV) Bond 4	Final Total Energy $C2sp^3$ (eV)	$r_{initial}$ (a_0)	r_{final} (a_0)	$E_{Coulomb}(C2sp^3)$ (eV) Final	$E(C2sp^3)$ (eV) Final	θ' (°)	θ_1 (°)	θ_2 (°)	d_1 (a_0)	d_2 (a_0)
$C-H\ (C_aH)$	C_a	-1.13380	-0.72457	0	0	-153.47406	0.91771	0.81549	-16.68412	-16.49326	84.49	95.51	44.74	1.08953	0.07833
$C-H\ (C_bH)$	C_b	-1.13380	-1.13380	0	0	-153.88328	0.91771	0.79597	-17.09334	-16.90248	82.21	97.79	43.14	1.11914	0.10794
$C_a=(H)C_b-C_b(H)=C_a$	C_b	-1.13380	-1.13380	0	0	-153.88328	0.91771	0.79597	-17.09334	-16.90248	91.57	88.43	42.49	1.31226	0.02177
$C_a=C_b(H)(H)C_b=C_a$	C_b	-1.13380	-1.13380	0	0	-153.88328	0.91771	0.79597	-17.09334	-16.90248	136.36	43.64	59.86	0.72857	0.57606
$SC_a=C_b(H)$	C_a	-1.13380	-0.72457	0	0	-153.47406	0.91771	0.81549	-16.68412	-16.49326	137.14	42.86	60.85	0.70685	0.59777
$C_aS-C_a=C_b(H)$	C_a	-1.13380	-0.72457	0	0	-153.47406	0.91771	0.81549	-16.68412	-16.49326	141.52	38.48	55.36	0.98926	0.63840
$C_aS-C_a=C_b(H)$	S	-0.72457	-0.72457	0	0		1.3201	0.83600	-16.27490		142.17	37.83	56.24	0.96733	0.66033

Table 15.282. The energy parameters (eV) of functional groups of thiophene.

Parameters	$C=C$ Group	$C-C$ Group	$C-S-C$ Group	CH Group
n_1	2	1	2	1
n_2	0	0	0	0
n_3	0	0	0	0
C_1	0.5	0.5	0.5	0.75
C_2	0.85252	1	0.65700	1
c_1	1	1	1	1
c_2	0.85252	0.85252	0.85252	0.91771
c_3	0	0	0	1
c_4	4	2	4	1
c_5	0	0	0	1
C_{1o}	0.5	0.5	0.5	0.75
C_{2o}	0.85252	1	0.65700	1
$V_e\ (eV)$	-104.37986	-33.80733	-96.78916	-39.09538
$V_p\ (eV)$	20.85777	10.19898	16.71820	13.45505
$T\ (eV)$	35.96751	9.49831	27.80371	12.74462
$V_m\ (eV)$	-17.98376	-4.74915	-13.90186	-6.37231
$E_{(AO/HO)}\ (eV)$	0	-14.63489	0	-14.63489
$\Delta E_{H_2MO\,(AO/HO)}\ (eV)$	-2.26759	-1.85836	-2.89830	-2.26758
$E_{T\,(AO/HO)}\ (eV)$	2.26759	-12.77653	2.89830	-12.36731
$E_{T\,(H_2MO)}\ (eV)$	-63.27075	-31.63572	-63.27080	-31.63533
$E_T\left(atom-atom, msp^3.AO\right)\ (eV)$	-2.26759	-2.26759	-2.89830	0
$E_{T\,(MO)}\ (eV)$	-65.53833	-33.90295	-66.16903	-31.63537
$\omega\ \left(10^{15}\ rad/s\right)$	15.4421	12.3131	10.3184	28.9084
$E_K\ (eV)$	10.16428	8.10471	6.79173	19.02803
$\overline{E}_D\ (eV)$	-0.20668	-0.19095	-0.17058	-0.27301
$\overline{E}_{Kvib}\ (eV)$	0.17897 [6]	0.14829 [48]	0.08146 [41]	0.39427 [59]
$\overline{E}_{osc}\ (eV)$	-0.11720	-0.11680	-0.12985	-0.07587
$E_{mag}\ (eV)$	0.14803	0.14803	0.14803	0.14803
$E_{T\,(Group)}\ (eV)$	-65.77272	-34.01976	-66.42873	-31.71124
$E_{initial\,(c_4\,AO/HO)}\ (eV)$	-14.63489	-14.63489	-14.63489	-14.63489
$E_{initial\,(c_5\,AO/HO)}\ (eV)$	0	0	0	-13.59844
$E_{D\,(Group)}\ (eV)$	7.23317	4.74998	7.88917	3.32988

Table 15.283. The total bond energies of thiophene calculated using the functional group composition and the energies of Table 15.282 compared to the experimental values [3].

Formula	Name	$C=C$	$C-C$	$C-S-C$	CH	Calculated Total Bond Energy (eV)	Experimental Total Bond Energy (eV)	Relative Error
C_4H_4S	Thiophene	2	1	1	4	40.42501	40.430	0.00013

Table 15.284. The bond angle parameters of thiophene and experimental values [1]. In the calculation of θ_v, the parameters from the preceding angle were used. E_T is E_T ($atom-atom,msp^3.AO$).

Atoms of Angle	$2c'$ Bond 1 (a_0)	$2c'$ Bond 2 (a_0)	$2c'$ Terminal Atoms (a_0)	$E_{Coulombic}$ Atom 1	Atom 1 Hybridization Designation (Table 15.3.B)	$E_{Coulombic}$ Atom 2	Atom 2 Hybridization Designation (Table 15.3.B)	c_2 Atom 1	c_2 Atom 2	C_1	C_2	c_1	c_2'	E_T (eV)	θ_v (°)	θ_1 (°)	θ_2 (°)	Cal. θ (°)	Exp. θ (°)
$\angle HC_aS$	2.02241	3.25533	4.6030	-15.55033	3	-10.36001	S	0.87495 Eq. (15.74))	0.76144 (Eq. 15.145))	0.75	0.76144 (Eq. 15.145))	0.75	0.87495	0				119.58	119.9 (thiophene)
$\angle C_bC_aH_a$																119.58	115.84	124.58	
$\angle H_bC_bC_b$	2.02241	2.66807	4.1633	-16.68412 C_b	18	-15.95954 C_b	6	0.81549	0.85252	0.75	1	0.75	1.04540	0				124.58	124.3 (thiophene)
$\angle H_aC_aC_b$	2.02241	2.60925	4.1633	-16.68412 C_a	18	-15.95954 C_b	6	0.81549	0.85252	0.75	1	0.75	1.04540	0				127.57	
$\angle H_bC_bC_a$	2.02241	2.60925	4.0825	-17.09334 C_b	24	-16.68412 C_a	18	0.79597	0.81549	0.75	1	0.75	1.02453	0				123.13	
$\angle C_bC_sH_b$																123.13	113.60	123.27	124.3 (thiophene)
$\angle C_bC_aS$	2.60925	3.25533	4.9809	-17.81791 C_b	36	-10.36001	S	0.76360	0.65700 Eq. (15.172))	1	0.65700 Eq. (15.172))	1	0.71030	-0.72457				115.84	115.5 (thiophene)
$\angle C_aSC_a$	3.25533	3.25533	4.7958	-16.68412	18	-16.68412	18	0.81549	0.81549	1	1	1	0.81549	-1.85836				94.89	92.2 (thiophene)
$\angle C_aC_bC_b$	2.60925	2.66807	4.4159	-16.88873	20	-18.02252	40	0.80561	0.75493	1	1	1	0.78027	-1.85836				113.60	112.5 (thiophene)

IMIDAZOLE

Imidazole having the formula $C_3H_4N_2$ comprises a conjugated system that is equivalent to pyrrole with one of the conjugated CH groups replaced by a nitrogen atom. The CH, NH, and $C=C$ groups are equivalent to the corresponding groups of pyrrole, furan, and thiophene where present. In addition, the nitrogen substitution creates a $C-N=C$ moiety comprising $C-N$ and $N=C$ functional groups. The $C-N$ bonding is the same as that of a tertiary amine except that the hybridization term c_2 in Eqs. (15.51) and (15.61) is that of the amino group of aniline, $c_2\left(arylC2sp^3HO\ to\ N\right)=0.84665$ (Eq. (15.171)). The hybridization factor provides double-bond character to match the group to the other orbitals of the molecule. $\Delta E_{H_2MO}\left(AO/HO\right)$ in Eq. (15.51) and $E_T\left(atom-atom,msp^3.AO\right)$ in Eq. (15.61) are both $-0.92918\ eV$ (Eq. (14.513)). This matches the energy of the group to that of the contiguous $N=C$ group wherein $\Delta E_{H_2MO}\left(AO/HO\right)$ in Eq. (15.51) and $E_T\left(atom-atom,msp^3.AO\right)$ in Eq. (15.61) are both $-0.92918\ eV$ (Eq. (14.513)) per atom of the double bond with aromatic character as in the case of the prior heterocyclic compounds. As in the prior cases of pyrrole, furan, and thiophene, $n_1=2$ and C_2 and C_{2o} are the same as $C_2\left(benzeneC2sp^3HO\right)=0.85252$ (Eq. (15.162)) in Eqs. (15.51) and (15.61). To match the energy of the nitrogen to the $C2sp^3$ HO, c_2 of the $N=C$-bond MO is also given by Eq. (15.171). These parameters also provide an energy match to the $C-N-C$ group.

As in the case of pyrrole, the $C-N-C$-bond MO comprising a linear combination of two single bonds is solved in the same manner as a double bond with $n_1=2$ in Eqs. (15.51) and (15.61). The hybridization factor $c_2\left(arylC2sp^3HO\ to\ N\right)=0.84665$ (Eq. (15.171)) matches the double-bond character of the $C2sp^3$ HOs to the N atom of the NH group, and C_2 and C_{2o} in Eqs. (15.51) and (15.61) become that of benzene given by Eq. (15.162), $C_2\left(benzeneC2sp^3HO\right)=0.85252$. Furthermore, $\Delta E_{H_2MO}\left(AO/HO\right)$ in Eq. (15.51) and $E_T\left(atom-atom,msp^3.AO\right)$ in Eq. (15.61) are both $-0.92918\ eV$ (Eq. (14.513)) per atom corresponding to $-3.71673\ eV$ in total.

The symbols of the functional groups of imidazole are given in Table 15.285. The structure of imidazole is shown in Figure 15.49B. The geometrical (Eqs. (15.1-15.5) and (15.51)), intercept (Eqs. (15.80-15.87)), and energy (Eqs. (15.6-15.11) and (15.17-15.65)) parameters of imidazole are given in Tables 15.286, 15.287, and 15.288, respectively. The total energy of imidazole given in Table 15.289 was calculated as the sum over the integer multiple of each $E_D(Group)$ of Table 15.288 corresponding to functional-group composition of the molecule. The bond angle parameters of imidazole determined using Eqs. (15.88-15.117) are given in Table 15.290. The color scale, translucent view of the charge-density of imidazole, comprising the concentric shells of atoms with the outer shell bridged by one or more H_2-type ellipsoidal MOs or joined with one or more hydrogen MOs is shown in Figure 15.49A.

Figure 15.49. (A) Color scale, translucent view of the charge-density of imidazole showing the orbitals of the atoms at their radii, the ellipsoidal surface of each H or H_2-type ellipsoidal MO that transitions to the corresponding outer shell of the atom(s) participating in each bond, and the hydrogen nuclei (red, not to scale). (B) Chemical structure and atom designation of imidizole.

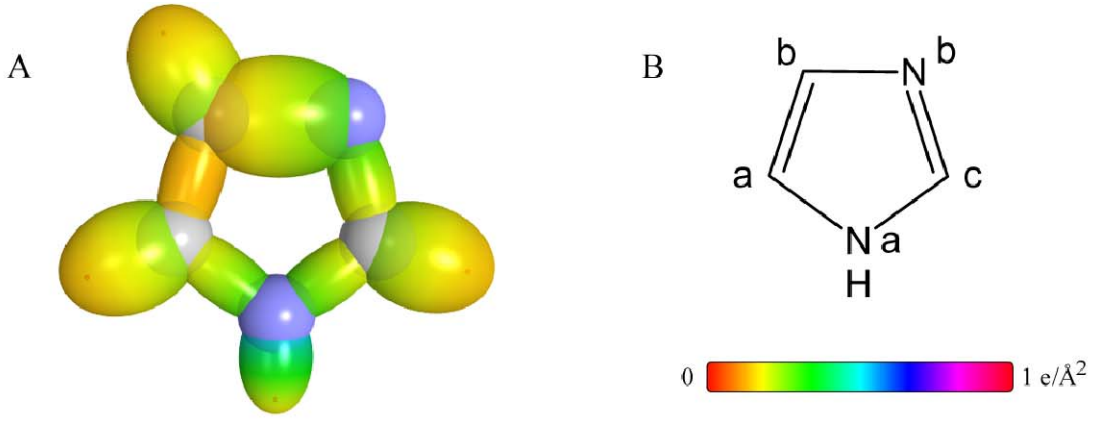

Table 15.285. The symbols of functional groups of imidazole.

Functional Group	Group Symbol
$C_a = C_b$ double bond	$C = C$
$N_b = C_c$ double bond	$N = C$
$C_b - N_b$	$C - N$
$C_a - N_a - C_c$	$C - N - C$
$N_a H$ group	NH
CH	CH

Table 15.286. The geometrical bond parameters of imidazole and experimental values [1].

Parameter	$C = C$ Group	$N = C$ Group	$C - N$ Group	$C - N - C$ Group	NH Group	CH Group
$a\ (a_0)$	1.45103	1.44926	1.82450	1.43222	1.24428	1.53380
$c'\ (a_0)$	1.30463	1.30383	1.35074	1.29614	0.94134	1.01120
Bond Length $2c'\ (\text{Å})$	1.38076	1.37991	1.42956	1.37178	0.996270	1.07021
Exp. Bond Length (Å)	1.382 (pyrrole)			1.370 (pyrrole)	0.996 (pyrrole)	1.076 (pyrrole)
$b,c\ (a_0)$	0.63517	0.63276	1.22650	0.60931	0.81370	1.15326
e	0.89910	0.89965	0.74033	0.90499	0.75653	0.65928

Table 15.287. The MO to HO intercept geometrical bond parameters of imidazole. R_1 is an alkyl group and *R, R′, R″* are *H* or alkyl groups. E_T is E_T(*atom – atom,msp³.AO*).

Bond	Atom	E_T (eV) Bond 1	E_T (eV) Bond 2	E_T (eV) Bond 3	E_T (eV) Bond 4	Final Total Energy $C2sp^3$ (eV)	$r_{initial}$ (a_0)	r_{final} (a_0)	$E_{Coulomb}\left(C2sp^3\right)$ (eV) Final	$E\left(C2sp^3\right)$ (eV) Final	θ' (°)	θ_1 (°)	θ_2 (°)	d_1 (a_0)	d_2 (a_0)
$C-H\ (C_aH)$	C_a	-1.13380	-0.92918	0	0	-153.67867	0.91771	0.80561	-16.88873	-16.69786	83.35	96.65	43.94	1.10452	0.09331
$C-H\ (C_bH)$	C_b	-1.13380	-0.46459	0	0	-153.21408	0.91771	0.82840	-16.42414	-16.23327	85.93	94.07	45.77	1.06995	0.05875
$C-H\ (C_cH)$	C_c	-0.92918	-0.92918	0	0	-153.47405	0.91771	0.81549	-16.68411	-16.49325	84.49	95.51	44.47	1.08953	0.07833
$C_a=(H)C_b-N_b=C_c$	C_b	-0.46459	-1.13380	0	0	-153.21408	0.91771	0.82840	-16.42414	-16.23327	90.36	89.64	42.49	1.34547	0.00527
$C_a=(H)C_b-N_b=C_c$	N_b	-0.46459	-0.92918	0	0		0.93084	0.83885	-16.21953		91.32	88.68	43.14	1.33135	0.01939
$C_a=C_b(H)N_b=C_c$	C_b	-1.13380	-0.46459	0	0	-153.21408	0.91771	0.82840	-16.42414	-16.23327	137.64	42.36	61.49	0.69250	0.61213
$HN_aC_a=C_b(H)$	C_a	-1.13380	-0.92918	0	0	-153.67867	0.91771	0.80561	-16.88873	-16.69786	136.75	43.25	60.35	0.71784	0.58678
$C_c(H)N_a-C_a=C_b(H)$	C_a	-1.13380	-0.92918	0	0	-153.67867	0.91771	0.80561	-16.88873	-16.69786	138.54	41.46	61.09	0.69238	0.60376
$C_c(H)N_a-C_a=C_b(H)$	N_a	-0.92918	-0.92918	0	0		0.93084	0.81549	-16.68411		138.92	41.08	61.59	0.68147	0.61467
$N-H\ (N_aH)$	N_a	-0.92918	-0.92918	0	0		0.93084	0.81549	-16.68411		117.34	62.66	62.90	0.56678	0.37456
$(H)C_c-N_aC_a=C_b(H)$	C_c	-0.92918	-0.92918	0	0	-153.47405	0.91771	0.81549	-16.68411	-16.49325	138.92	41.08	61.59	0.68147	0.61467
$C_a=(H)C_bN_b=C_c$	C_c	-0.92918	-0.92918	0	0	-153.47405	0.91771	0.81549	-16.68411	-16.49325	137.31	42.69	60.92	0.70446	0.59938
$C_a=(H)C_bN_b=C_c$	N_b	-0.92918	-0.46459	0	0		0.93084	0.83885	-16.21953		138.20	41.80	62.08	0.67849	0.62534

Table 15.288. The energy parameters (eV) of functional groups of imidazole.

Parameters	$C=C$ Group	$N=C$ Group	$C-N$ Group	$C-N-C$ Group	NH Group	CH Group
n_1	2	2	1	2	1	1
n_2	0	0	0	0	0	0
n_3	0	0	0	0	0	0
C_1	0.5	0.5	0.5	0.5	0.75	0.75
C_2	0.85252	0.85252	1	0.85252	0.93613	1
c_1	1	1	1	1	0.75	1
c_2	0.85252	0.84665	0.84665	0.84665	0.92171	0.91771
c_3	0	0	0	0	1	1
c_4	4	4	2	4	1	1
c_5	0	0	0	0	1	1
C_{1o}	0.5	0.5	0.5	0.5	0.75	0.75
C_{2o}	0.85252	0.85252	1	0.85252	1	1
$V_e\ (eV)$	-104.37986	-103.92756	-32.44864	-106.58684	-39.48897	-39.09538
$V_p\ (eV)$	20.85777	20.87050	10.07285	20.99432	14.45367	13.45505
$T\ (eV)$	35.96751	35.85539	8.89248	37.21047	15.86820	12.74462
$V_m\ (eV)$	-17.98376	-17.92770	-4.44624	-18.60523	-7.93410	-6.37231
$E_{(AO/HO)}\ (eV)$	0	0	-14.63489	0	-14.53414	-14.63489
$\Delta E_{H_2MO\ (AO/HO)}\ (eV)$	-2.26759	-1.85836	-0.92918	-3.71673	0	-2.26758
$E_{T\ (AO/HO)}\ (eV)$	2.26759	1.85836	-13.70571	3.71673	-14.53414	-12.36731
$E_{T\ (H_2MO)}\ (eV)$	-63.27075	-63.27100	-31.63527	-63.27056	-31.63534	-31.63533
$E_T\left(atom-atom, msp^3.AO\right)\ (eV)$	-2.26759	-1.85836	-0.92918	-3.71673	0	0
$E_{T\ (MG)}\ (eV)$	-65.53833	-65.12910	-32.56455	-66.98746	-31.63537	-31.63537
$\omega\ \left(10^{15}\ rad/s\right)$	15.4421	15.4704	21.5213	15.7474	48.7771	28.9084
$E_K\ (eV)$	10.16428	10.18290	14.16571	10.36521	32.10594	19.02803
$\overline{E}_D\ (eV)$	-0.20668	-0.20558	-0.24248	-0.21333	-0.35462	-0.27301
$\overline{E}_{Kvib}\ (eV)$	0.17897 [6]	0.20768 [62]	0.12944 [23]	0.11159 [12]	0.40696 [24]	0.39427 [60]
$\overline{E}_{osc}\ (eV)$	-0.11720	-0.10174	-0.17775	-0.15754	-0.15115	-0.07587
$E_{mag}\ (eV)$	0.14803	0.14803	0.14803	0.14803	0.14803	0.14803
$E_{T\ (Group)}\ (eV)$	-65.77272	-65.33259	-32.74230	-67.30254	-31.78651	-31.71124
$E_{initial\ (c_4\ AO/HO)}\ (eV)$	-14.63489	-14.63489	-14.63489	-14.63489	-14.53414	-14.63489
$E_{initial\ (c_5\ AO/HO)}\ (eV)$	0	0	0	0	-13.59844	-13.59844
$E_{D\ (Group)}\ (eV)$	7.23317	6.79303	3.47253	8.76298	3.51208	3.32988

Table 15.289. The total bond energies of imidazole calculated using the functional group composition and the energies of Table 15.288 compared to the experimental values [3].

Formula	Name	$C=C$	$N=C$	$C-N$	$C-N-C$	NH	CH	Calculated Total Bond Energy (eV)	Experimental Total Bond Energy (eV)	Relative Error
$C_3H_4N_2$	Imidazole	1	1	1	1	1	3	39.76343	39.74106	-0.00056

Table 15.290. The bond angle parameters of imidazole and experimental values [62]. In the calculation of θ_v, the parameters from the preceding angle were used. E_T is $E_T(atom-atom,msp^3.AO)$.

Atoms of Angle	2c' Bond 1 (a_0)	2c' Bond 2 (a_0)	2c' Terminal Atoms (a_0)	$E_{Coulombic}$ Atom 1	Atom 1 Hybridization Designation (Table 15.3B)	$E_{Coulombic}$ Atom 2	Atom 2 Hybridization Designation (Table 15.3B)	c_2 Atom 1	c_2 Atom 2	C_1	C_2	c_1	c_2'	E_T (eV)	θ_v (°)	θ_1 (°)	θ_2 (°)	Cal. θ (°)	Exp. θ (°)
$\angle HC_aN_a$	2.02241	2.59228	4.0166	-14.82575	1	-14.53414	N	0.91771	0.92171 Eq. (15.170))	0.75	1	0.75	1.00435	0				120.51	117.4 (imidazole)
$\angle C_bC_aH_a$																120.51	106.63	132.86	136.3 (imidazole)
$\angle HN_aC_a$	1.88268	2.59228	3.8987	-14.53414	N	-16.49325	25 (Table 15.3A)	0.84665 (Eq. (15.170))	0.82493 (Eq. (15.73))	0.75	1	0.75	0.97435	0				120.37	122.9 (imidazole)
$\angle H_aC_aC_b$	2.02241	2.60925	4.2895	-16.88873 C_a	20	-15.75493 C_b	4	0.80561	0.86359	0.75	1	0.75	1.07196	0				135.30	136.3 (imidazole)
$\angle H_bC_bC_a$	2.02241	2.60925	4.2740	-15.95954 C_b	6	-14.82575 C_a	1	0.85252	0.91771	0.75	1	0.75	1.07647	0				134.28	133.2 (imidazole)
$\angle N_bC_bH_b$																134.28	111.18	114.54	115.8 (imidazole)
$\angle H_cC_cN_a$	2.02241	2.59228	3.8471	-15.95954 C_c	6	-14.53414	N	0.87495	0.84665 (Eq. (15.171))	0.75	1	0.75	0.96765					112.37	110.4 (imidazole)
$\angle N_bC_cH_c$																112.37	109.83	137.80	138.2 (imidazole)
$\angle HN_aC_c$	1.88268	2.59228	4.0661	-14.53414	N	-15.76868	6	0.84665 (Eq. (15.170))	0.86284 (Eq. (15.73))	0.75	1	0.75	1.01912	0				129.96	129.1 (imidazole)
$\angle N_aC_aC_b$	2.59228	2.60925	4.1952	-14.53414	N	-17.09334 C_b	24	0.84665 (Eq. (15.171))	0.79597	1	1	1	0.82131	-1.44915				107.52	106.3 (imidazole)
$\angle C_aN_aC_c$	2.59228	2.59228	4.2426	-17.81791	35	-17.81791	35	0.76360	0.76360	1	1	1	0.76360	-1.85836				109.83	107.2 (imidazole)
$\angle C_cN_bC_b$	2.60766	2.70148	4.3128	-17.61330	32	-17.61330	32	0.77247	0.77247	1	1	1	0.77247	-1.85836				108.64	105.4 (imidazole)
$\angle C_aC_bN_b$	2.60925	2.70148	4.3818	-15.95955	6	-14.53414	N	0.85252	0.84665 (Eq. (15.171))	1	1	1	0.84958	-1.85836				111.18	109.8 (imidazole)
$\angle N_aC_cN_b$	2.59228	2.60766	4.2544	-16.68411	17	-16.21953	9	0.81549	0.83885	1	1	1	0.82717	-1.44915				109.80	111.3 (imidazole)

PYRIDINE

Pyridine has the formula C_5H_5N and comprises the benzene molecule with one CH group replaced by a nitrogen atom which gives rise to a $\overset{3e}{C=N}$ functional group. The aromatic $\overset{3e}{C=C}$ and $C-H$ functional groups are equivalent to those of benzene given in the Aromatic and Heterocyclic Compounds section with the aromaticity maintained by the electrons from nitrogen in the $\overset{3e}{C=N}$ group, which is also aromatic.

As in the case of the aromatic carbons of benzene, each pyridine $C2sp^3$ HO initially has four unpaired electrons. Each $C-H$ bond has two paired electrons with one donated from the H AO and the other from the $C2sp^3$ HO. In pyridine the three $N2p$ electrons are donated to the aromatic bond. Thus, as in the case of the $\overset{3e}{C=C}$ group, each $\overset{3e}{C=N}$ bond comprises a linear combination of a factor of 0.75 of four paired electrons (three electrons) from the $C2sp^3$ HO and the $N2p$ AO of the participating carbon and nitrogen atoms, respectively.

The solution of the $\overset{3e}{C=N}$ functional group comprises the hybridization of the $2s$ and $2p$ AOs of each C to form a single $2sp^3$ shell as an energy minimum, and the sharing of electrons between the $C2sp^3$ HO and the nitrogen atom to form a MO permits each participating hybridized orbital to decrease in radius and energy. The $\overset{3e}{C=N}$-bond MO is solved as a double bond with $n_1=2$ in Eqs. (15.51) and (15.166). The hybridization factor $c_2\left(C2sp^3 HO\ to\ N\right)=0.91140$ (Eq. (15.135)) matches the double-bond character of the $C2sp^3$ HO to the N atom, and C_2 and C_{2o} in Eqs. (15.51) and (15.166) are also given by Eq. (15.135) in order to match the nitrogen to the aromatic $C2sp^3$ HO such that $\Delta E_{H_2MO}\left(AO/HO\right)=0$ in Eq. (15.51). Furthermore, $E_T\left(atom-atom, msp^3.AO\right)$ of the $\overset{3e}{C=N}$-bond MO in Eq. (15.166) due to the charge donation from the C and N atoms to the MO is $-1.44915\ eV$ corresponding to an energy contribution from each atom that is equivalent to that of an independent methyl group, $-0.72457\ eV$ (Eq. (14.151)). The contributions are also the same as those for a primary amine group as given in the corresponding section. As in the case of benzene, the aromatic $E_T(Group)$ and $E_D(Group)$ are given by Eqs. (15.165) and (15.166), respectively, with $f_1=0.75$. The breakage of the CNC bonds results in three unpaired electrons on the N atom. Thus, the corresponding E_{mag} given by Eq. (15.69) was normalized for the two bonds per atom and for $f_1=0.75$ and was subtracted from the total energy of the $\overset{3e}{C=N}$-bond MO in Eq. (15.166). The pyridine vibrational energies are similar to those of benzene [63]; thus, the value for benzene was used.

The symbols of the functional groups of pyridine are given in Table 15.291. The corresponding designation of the structure is shown in Figure 15.50B. The geometrical (Eqs. (15.1-15.5) and (15.51)), intercept (Eqs. (15.80-15.87)), and energy (Eqs. (15.6-15.11), (15.17-15.65), and (15.165-15.166)) parameters of pyridine are given in Tables 15.292, 15.293, and 15.294, respectively. The total energy of pyridine given in Table 15.295 was calculated as the sum over the integer multiple of each $E_D(Group)$ of Table 15.294 corresponding to functional-group composition of the molecule. The bond angle parameters of pyridine determined using Eqs. (15.88-15.117) are given in Table 15.296. The color scale, translucent view of the charge-density of pyridine comprising the concentric shells of atoms with the outer shell bridged by one or more H_2-type ellipsoidal MOs or joined with one or more hydrogen MOs is shown in Figure 15.50A.

Figure 15.50. (A) Color scale, translucent view of the charge-density of pyridine showing the orbitals of the atoms at their radii, the ellipsoidal surface of each H or H_2-type ellipsoidal MO that transitions to the corresponding outer shell of the atom(s) participating in each bond, and the hydrogen nuclei (red, not to scale). (B) Chemical structure and atom designation of pyridine.

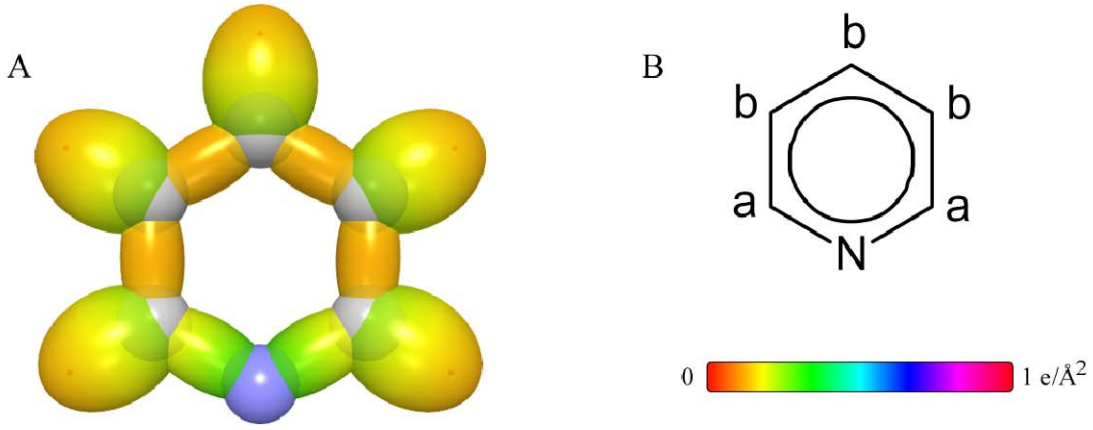

Table 15.291. The symbols of functional groups of pyridine.

Functional Group	Group Symbol
CC (aromatic bond)	$C\overset{3e}{=}C$
CH (aromatic)	CH
$C_a\overset{3e}{=}N$	$C\overset{3e}{=}N$

Table 15.292. The geometrical bond parameters of pyridine and experimental values [1].

Parameter	$C\overset{3e}{=}C$ Group	CH Group	$C\overset{3e}{=}N$ Group
$a\ (a_0)$	1.47348	1.60061	1.47169
$c'\ (a_0)$	1.31468	1.03299	1.27073
Bond Length $2c'\ (\text{Å})$	1.39140	1.09327	1.34489
Exp. Bond Length (Å)	1.394 (pyridine)	1.084 (pyridine)	1.340 (pyridine)
$b,c\ (a_0)$	0.66540	1.22265	0.74237
e	0.89223	0.64537	0.86345

Table 15.293. The MO to HO intercept geometrical bond parameters of pyridine. E_T is E_T (*atom – atom,msp³.AO*).

Bond	Atom	E_T (eV) Bond 1	E_T (eV) Bond 2	E_T (eV) Bond 3	E_T (eV) Bond 4	Final Total Energy $C2sp^3$ (eV)	$r_{initial}$ (a_0)	r_{final} (a_0)	$E_{Coulomb}(C2sp^3)$ (eV) Final	$E(C2sp^3)$ (eV) Final	θ' (°)	θ_1 (°)	θ_2 (°)	d_1 (a_0)	d_2 (a_0)
$C-H\ (C_aH)$	C_a	-0.54343	-0.85035	-0.56690	0	-153.57636	0.91771	0.81052	-16.78642	-16.59556	76.35	103.65	40.11	1.22423	0.19124
$C-H\ (C_bH)$	C_b	-0.85035	-0.85035	-0.56690	0	-153.88327	0.91771	0.79597	-17.09334	-16.90248	74.42	105.58	38.84	1.24678	0.21379
$(H)C_b(H)C_a \overset{3e}{=} NC_a$	C_a	-0.85035	-0.54343	-0.56690	0	-153.57636	0.91771	0.81052	-16.78642	-16.59556	128.54	51.46	58.65	0.76572	0.50501
$(H)C_b(H)C_a \overset{3e}{=} NC_a$	N	-0.54343	-0.54343	0	0		0.93084	0.85503	-15.91261		130.61	49.39	60.97	0.71418	0.55656
$(H)C_b \overset{3e}{=} C_a(H)N$	C_a	-0.54343	-0.85035	-0.56690	0	-153.57636	0.91771	0.81052	-16.78642	-16.59556	134.85	45.15	59.72	0.74304	0.57165
$(H)C_b \overset{3e}{=} C_a(H)N$ $(H)C_b \overset{3e}{=} C_b(H)C_a(H)$	C_b	-0.85035	-0.85035	-0.56690	0	-153.88327	0.91771	0.79597	-17.09334	-16.90248	134.24	45.76	58.98	0.75935	0.55533

Table 15.294. The energy parameters (eV) of functional groups of pyridine.

Parameters	$C \overset{3e}{=} C$ Group	CH Group	$C \overset{3e}{=} N$ Group
f_1	0.75	1	0.75
n_1	2	1	2
n_2	0	0	0
n_3	0	0	0
C_1	0.5	0.75	0.5
C_2	0.85252	1	0.91140
c_1	1	1	1
c_2	0.85252	0.91771	0.91140
c_3	0	1	0
c_4	3	1	3
c_5	0	1	0
C_{1o}	0.5	0.75	0.5
C_{2o}	0.85252	1	0.91140
$V_e\ (eV)$	-101.12679	-37.10024	-102.01431
$V_p\ (eV)$	20.69825	13.17125	21.41410
$T\ (eV)$	34.31559	11.58941	34.65890
$V_m\ (eV)$	-17.15779	-5.79470	-17.32945
$E_{(AO/HO)}\ (eV)$	0	-14.63489	0
$\Delta E_{H_2MO_{(AO/HO)}}\ (eV)$	0	-1.13379	0
$E_{J_{(AO/HO)}}\ (eV)$	0	-13.50110	0
$E_{T_{(H_2MO)}}\ (eV)$	-63.27075	-31.63539	-63.27076
$E_T\left(atom-atom, msp^3.AO\right)\ (eV)$	-2.26759	-0.56690	-1.44915
$E_{T_{(MO)}}\ (eV)$	-65.53833	-32.20226	-64.71988
$\omega\ \left(10^{15}\ rad/s\right)$	49.7272	26.4826	43.6311
$E_K\ (eV)$	32.73133	17.43132	28.71875
$\bar{E}_D\ (eV)$	-0.35806	-0.26130	-0.33540
$\bar{E}_{Kvib}\ (eV)$	0.19649 [49]	0.35532 Eq. (13.458)	0.19649 [49]
$\bar{E}_{osc}\ (eV)$	-0.25982	-0.08364	-0.23715
$E_{mag}\ (eV)$	0.14803	0.14803	0.09457
$E_{J_{(Group)}}\ (eV)$	-49.54347	-32.28590	-48.82472
$E_{initial_{(c_4\ AO/HO)}}\ (eV)$	-14.63489	-14.63489	-14.63489
$E_{initial_{(c_5\ AO/HO)}}\ (eV)$	0	-13.59844	0
$E_{D_{(Group)}}\ (eV)$	5.63881	3.90454	4.92005

Table 15.295. The total bond energies of pyridine calculated using the functional group composition and the energies of Table 15.294 compared to the experimental values [3].

Formula	Name	$C^{3e}=C$	CH	$C^{3e}=N$ Group	Calculated Total Bond Energy (eV)	Experimental Total Bond Energy (eV)	Relative Error
C_5H_5N	Pyridine	4	5	2	51.91802	51.87927	-0.00075

Table 15.296. The bond angle parameters of pyridine and experimental values [1]. E_T is E_T ($atom - atom, msp^3.AO$).

Atoms of Angle	2c' Bond 1 (a_0)	2c' Bond 2 (a_0)	2c' Terminal Atoms (a_0)	$E_{Coulombic}$ Atom 1	Atom 1 Hybridization Designation (Table 15.3B)	$E_{Coulombic}$ Atom 2	Atom 2 Hybridization Designation (Table 15.3B)	c_2 Atom 1	c_2 Atom 2	C_1	C_2	c_1	c_2'	E_T (eV)	θ_v (°)	θ_1 (°)	θ_2 (°)	Cal. θ (°)	Exp. θ (°)
$\angle CCC$ (aromatic)	2.62936	2.62936	4.5585	-17.17218	27	-17.17218	27	0.79232	0.79232	1	1	1	0.79232	-1.85836				120.19	120 [50-52] (benzene) 118.3 (pyridine) 118.5 (pyridine)
$\angle CCH$ (aromatic)																120.19		119.91	120 [50-52] (benzene) 121.3 (pyridine)
$\angle HC_aN$	2.06598	2.54147	3.9497	-14.82575	1	-14.53414	N	0.91771	0.91140 Eq. (15.135))	0.75	1	0.75	0.99312	0				117.65	115.9 (pyridine)
$\angle NC_cC_b$	2.54147	2.62936	4.5607	-14.53414	N	-16.52644 C_b	15	0.91140 Eq. (15.135))	0.82327	1	1	1	0.86734	-1.44915				123.76	123.9 (pyridine)
$\angle C_aNC_a$	2.54147	2.54147	4.3359	-17.71560	33	-17.71560	33	0.76801	0.76801	1	1	1	0.76801	-1.85836				117.09	116.8 (pyridine)

PYRIMIDINE

Pyrimidine has the formula $C_4H_4N_2$ and comprises the pyridine molecule with one additional CH group replaced by a nitrogen atom, which gives rise to a second $C^{3e}{=}N$ functional group that is equivalent to that of pyridine given in the corresponding section. The aromatic $C^{3e}{=}C$ and $C-H$ functional groups are also equivalent to those of pyridine and benzene given in the Aromatic and Heterocyclic Compounds section with the aromaticity maintained by the electrons from nitrogen in the $C^{3e}{=}N$ group which is also aromatic.

The symbols of the functional groups of pyrimidine are given in Table 15.297. The corresponding designation of the structure is shown in Figure 15.51B. The geometrical (Eqs. (15.1-15.5) and (15.51)), intercept (Eqs. (15.80-15.87)), and energy (Eqs. (15.6-15.11), (15.17-15.65), and (15.165-15.166)) parameters of pyrimidine are given in Tables 15.298, 15.299, and 15.300, respectively. The total energy of pyrimidine given in Table 15.301 was calculated as the sum over the integer multiple of each $E_D(Group)$ of Table 15.300 corresponding to functional-group composition of the molecule. The bond angle parameters of pyrimidine determined using Eqs. (15.88-15.117) are given in Table 15.302. The color scale, translucent view of the charge-density of pyrimidine comprising the concentric shells of atoms with the outer shell bridged by one or more H_2-type ellipsoidal MOs or joined with one or more hydrogen MOs is shown in Figure 15.51A.

Figure 15.51. (A) Color scale, translucent view of the charge-density of pyrimidine showing the orbitals of the atoms at their radii, the ellipsoidal surface of each H or H_2-type ellipsoidal MO that transitions to the corresponding outer shell of the atom(s) participating in each bond, and the hydrogen nuclei (red, not to scale). (B) Chemical structure and atom designation of pyrimidine.

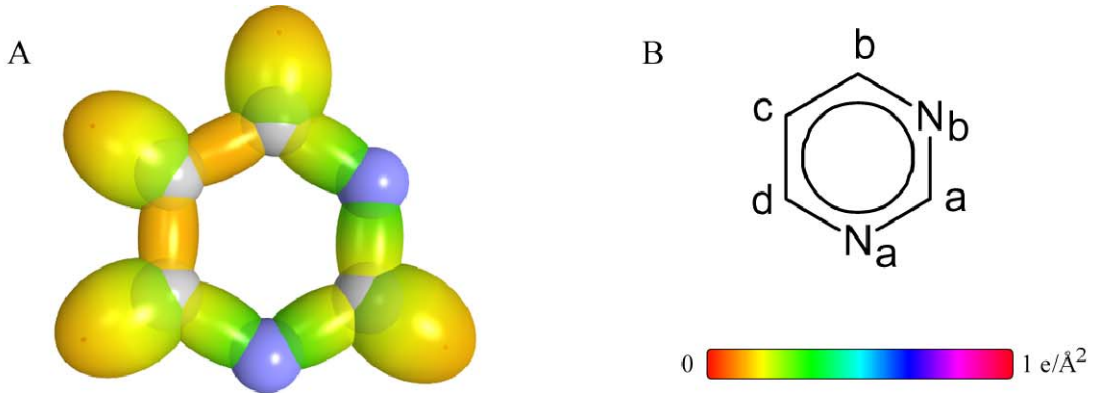

Table 15.297. The symbols of functional groups of pyrimidine.

Functional Group	Group Symbol
CC (aromatic bond)	$C^{3e}{=}C$
CH (aromatic)	CH
$C_{a,b,d}{}^{3e}{=}N$	$C^{3e}{=}N$

Table 15.298. The geometrical bond parameters of pyrimidine and experimental values [1].

Parameter	$C^{3e}{=}C$ Group	CH Group	$C^{3e}{=}N$ Group
$a\ (a_0)$	1.47348	1.60061	1.47169
$c'\ (a_0)$	1.31468	1.03299	1.27073
Bond Length $2c'\ (\text{Å})$	1.39140	1.09327	1.34489
Exp. Bond Length (Å)	1.393 (pyrimidine)	1.084 (pyridine)	1.340 (pyrimidine)
$b,c\ (a_0)$	0.66540	1.22265	0.74237
e	0.89223	0.64537	0.86345

Table 15.299. The MO to HO intercept geometrical bond parameters of pyrimidine. E_T is E_T ($atom - atom, msp^3.AO$).

Bond	Atom	E_T (eV) Bond 1	E_T (eV) Bond 2	E_T (eV) Bond 3	E_T (eV) Bond 4	Final Total Energy $C2sp^3$ (eV)	$r_{initial}$ (a_0)	r_{final} (a_0)	$E_{Coulomb}\left(C2sp^3\right)$ (eV) Final	$E\left(C2sp^3\right)$ (eV) Final	θ' (°)	θ_1 (°)	θ_2 (°)	d_1 (a_0)	d_2 (a_0)
$C-H\ (C_aH)$	C_a	-0.54343	-0.54343	-0.56690	0	-153.26945	0.91771	0.82562	-16.47951	-16.28864	78.27	101.73	41.39	1.20084	0.16785
$C-H\ (C_{b,d}H)$	C_b C_d	-0.54343	-0.85035	-0.56690	0	-153.57636	0.91771	0.81052	-16.78642	-16.59556	76.35	103.65	40.11	1.22423	0.19124
$C-H\ (C_cH)$	C_c	-0.85035	-0.85035	-0.56690	0	-153.88327	0.91771	0.79597	-17.09334	-16.90248	74.42	105.58	38.84	1.24678	0.21379
$(H)C_c(H)C_b \overset{3e}{=} N_bC_a$ $(H)C_c(H)C_d \overset{3e}{=} N_aC_a$	C_b C_d	-0.85035	-0.54343	-0.56690	0	-153.57636	0.91771	0.81052	-16.78642	-16.59556	128.54	51.46	58.65	0.76572	0.50501
$(H)C_c(H)C_b \overset{3e}{=} N_bC_a$ $(H)C_c(H)C_d \overset{3e}{=} N_aC_a$	N_b N_a	-0.54343	-0.54343	0	0		0.93084	0.85503	-15.91261		130.61	49.39	60.97	0.71418	0.55656
$(H)C_c(H)C_bN_b \overset{3e}{=} C_a(H)$ $(H)C_c(H)C_aN_a \overset{3e}{=} C_a(H)$	C_a	-0.54343	-0.54343	-0.56690	0	-153.26945	0.91771	0.82562	-16.47951	-16.28865	129.26	50.74	59.44	0.74824	0.52249
$(H)C_c(H)C_bN_b \overset{3e}{=} C_a(H)$ $(H)C_c(H)C_aN_a \overset{3e}{=} C_a(H)$	N_b N_a	-0.54343	-0.54343	0	0		0.93084	0.85503	-15.91261		130.61	49.39	60.97	0.71418	0.55656
$N_a(H)C_d \overset{3e}{=} C_c(H)C_b$ $N_b(H)C_b \overset{3e}{=} C_c(H)C_d$	C_c	-0.85035	-0.85035	-0.56690	0	-153.88327	0.91771	0.79597	-17.09334	-16.90248	134.24	45.76	58.98	0.75935	0.55533
$N_a(H)C_d \overset{3e}{=} C_c(H)C_b$ $N_b(H)C_b \overset{3e}{=} C_c(H)C_d$	C_b C_d	-0.85035	-0.54343	-0.56690	0	-153.57636	0.91771	0.81052	-16.78642	-16.59556	134.85	45.15	59.72	0.74304	0.57165

Table 15.300. The energy parameters (eV) of functional groups of pyrimidine.

Parameters	$C\overset{3e}{=}C$ Group	CH Group	$C\overset{3e}{=}N$ Group
f_1	0.75	1	0.75
n_1	2	1	2
n_2	0	0	0
n_3	0	0	0
C_1	0.5	0.75	0.5
C_2	0.85252	1	0.91140
c_1	1	1	1
c_2	0.85252	0.91771	0.91140
c_3	0	1	0
c_4	3	1	3
c_5	0	1	0
C_{1o}	0.5	0.75	0.5
C_{2o}	0.85252	1	0.91140
$V_e\ (eV)$	-101.12679	-37.10024	-102.01431
$V_p\ (eV)$	20.69825	13.17125	21.41410
$T\ (eV)$	34.31559	11.58941	34.65890
$V_m\ (eV)$	-17.15779	-5.79470	-17.32945
$E\left(_{AO/HO}\right)(eV)$	0	-14.63489	0
$\Delta E_{_{H_2MO}}\left(_{AO/HO}\right)(eV)$	0	-1.13379	0
$E_{_T}\left(_{AO/HO}\right)(eV)$	0	-13.50110	0
$E_{_T}\left(_{H_2MO}\right)(eV)$	-63.27075	-31.63539	-63.27076
$E_{_T}\left(atom-atom,msp^3.AO\right)(eV)$	-2.26759	-0.56690	-1.44915
$E_{_T}\left(_{MO}\right)(eV)$	-65.53833	-32.20226	-64.71988
$\omega\ \left(10^{15}\ rad/s\right)$	49.7272	26.4826	43.6311
$E_{_K}\ (eV)$	32.73133	17.43132	28.71875
$\bar{E}_{_D}\ (eV)$	-0.35806	-0.26130	-0.33540
$\bar{E}_{Kvib}\ (eV)$	0.19649 [49]	0.35532 Eq. (13.458)	0.19649 [49]
$\bar{E}_{osc}\ (eV)$	-0.25982	-0.08364	-0.23715
$E_{mag}\ (eV)$	0.14803	0.14803	0.09457
$E_{_T}\left(_{group}\right)(eV)$	-49.54347	-32.28590	-48.82472
$E_{initial}\left(_{3\ AO/HO}\right)(eV)$	-14.63489	-14.63489	-14.63489
$E_{initial}\left(_{5\ AO/HO}\right)(eV)$	0	-13.59844	0
$E_{_D}\left(_{group}\right)(eV)$	5.63881	3.90454	4.92005

Table 15.301. The total bond energies of pyrimidine calculated using the functional group composition and the energies of Table 15.300 compared to the experimental values [3].

Formula	Name	$C=C$	CH	$C=N$ Group	Calculated Total Bond Energy (eV)	Experimental Total Bond Energy (eV)	Relative Error
$C_4H_4N_2$	Pyrimidine	2	4	4	46.57597	46.51794	-0.00125

Table 15.302. The bond angle parameters of pyrimidine and experimental values [1]. E_T is E_T $(atom-atom,msp^3.AO)$.

Atoms of Angle	$2c'$ Bond 1 (a_0)	$2c'$ Bond 2 (a_0)	$2c'$ Terminal Atoms (a_0)	$E_{Coulombic}$ Atom 1	Atom 1 Hybridization Designation (Table 15.3B)	$E_{Coulombic}$ Atom 2	Atom 2 Hybridization Designation (Table 15.3B)	c_2 Atom 1	c_2 Atom 2	C_1	C_2	c_1	c_2'	E_T (eV)	θ_v (°)	θ_1 (°)	θ_2 (°)	Cal. θ (°)	Exp. θ (°)
$\angle CCC$ (aromatic)	2.62936	2.62936	4.5585	-17.17218	27	-17.17218	27	0.79232	0.79232	1	1	1	0.79232	-1.85836				120.19	120 [50-52] (benzene) 118.3 (pyridine) 118.5 (pyridine)
$\angle CCH$ (aromatic)																120.19		119.91	120 [50-52] (benzene) 121.3 (pyridine)
$\angle HCN$	2.06598	2.54147	3.9497	-14.82575	1	-14.53414	N	0.91771	0.91140 Eq. (15.135))	0.75	1	0.75	0.99312	0				117.65	115.9 (pyridine)
$\angle NCC$	2.54147	2.62936	4.5607	-14.53414	N	-16.52644	15	0.91140 Eq. (15.135))	0.82327	1	1	1	0.86734	-1.44915				123.76	123.9 (pyridine)
$\angle CNC$	2.54147	2.54147	4.3359	-17.71560	33	-17.71560	33	0.76801	0.76801	1	1	1	0.76801	-1.85836				117.09	115.5 (pyrimidine)
$\angle NCN$	2.54147	2.54147	4.5826	-15.55033	3	-15.55033	3	0.87495	0.87495	1	1	1	0.87495	-1.85836				128.73	127.6 (pyrimidine)

PYRAZINE

Pyrazine has the formula $C_4H_4N_2$ and comprises the pyrimidine molecule with para rather than ortho aromatic nitrogen atoms. The $C\overset{3e}{=}N$ functional group is equivalent to that of pyrimidine and pyridine given in the corresponding sections. The aromatic $C\overset{3e}{=}C$ and $C-H$ functional groups are also equivalent to those of pyrimidine, pyridine, and benzene given in the Aromatic and Heterocyclic Compounds section with the aromaticity maintained by the electrons from nitrogen in the $C\overset{3e}{=}N$ group, which is also aromatic.

The symbols of the functional groups of pyrazine are given in Table 15.303. The corresponding designation of the structure is shown in Figure 15.52B. The geometrical (Eqs. (15.1-15.5) and (15.51)), intercept (Eqs. (15.80-15.87)), and energy (Eqs. (15.6-15.11), (15.17-15.65), and (15.165-15.166)) parameters of pyrazine are given in Tables 15.304, 15.305, and 15.306, respectively. The total energy of pyrazine given in Table 15.307 was calculated as the sum over the integer multiple of each $E_D(Group)$ of Table 15.306 corresponding to functional-group composition of the molecule. The bond angle parameters of pyrazine determined using Eqs. (15.88-15.117) are given in Table 15.308. The color scale, translucent view of the charge-density of pyrazine comprising the concentric shells of atoms with the outer shell bridged by one or more H_2-type ellipsoidal MOs or joined with one or more hydrogen MOs is shown in Figure 15.52A.

Figure 15.52. (A) Color scale, translucent view of the charge-density of pyrazine showing the orbitals of the atoms at their radii, the ellipsoidal surface of each H or H_2-type ellipsoidal MO that transitions to the corresponding outer shell of the atom(s) participating in each bond, and the hydrogen nuclei (red, not to scale). (B) Chemical structure and atom designation of pyrazine.

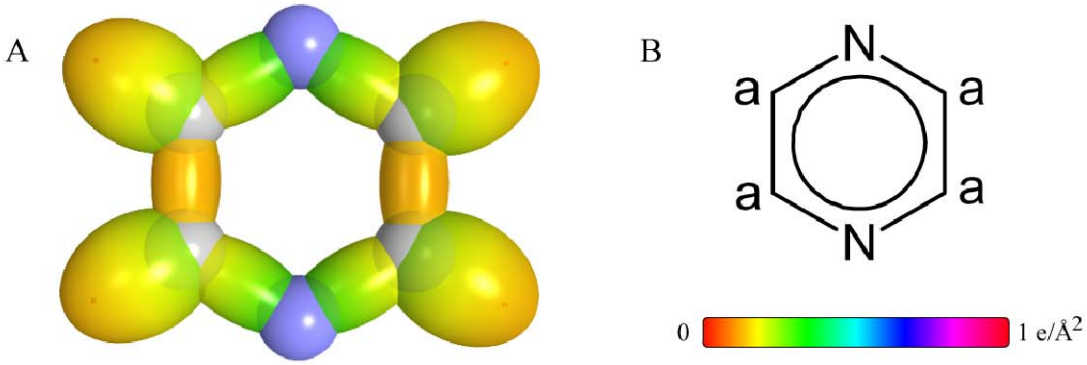

Table 15.303. The symbols of functional groups of pyrazine.

Functional Group	Group Symbol
CC (aromatic bond)	$C\overset{3e}{=}C$
CH (aromatic)	CH
$C_a\overset{3e}{=}N$	$C\overset{3e}{=}N$

Table 15.304. The geometrical bond parameters of pyrazine and experimental values [1].

Parameter	$C\overset{3e}{=}C$ Group	CH Group	$C\overset{3e}{=}N$ Group
$a\ (a_0)$	1.47348	1.60061	1.47169
$c'\ (a_0)$	1.31468	1.03299	1.27073
Bond Length $2c'\ (\text{Å})$	1.39140	1.09327	1.34489
Exp. Bond Length (Å)	1.339 (pyrazine)	1.115 (pyrazine)	1.403 (pyrazine)
$b,c\ (a_0)$	0.66540	1.22265	0.74237
e	0.89223	0.64537	0.86345

Table 15.305. The MO to HO intercept geometrical bond parameters of pyrazine. E_T is E_T (*atom – atom,msp³.AO*).

Bond	Atom	E_T (eV) Bond 1	E_T (eV) Bond 2	E_T (eV) Bond 3	E_T (eV) Bond 4	Final Total Energy $C2sp^3$ (eV)	$r_{initial}$ (a_0)	r_{final} (a_0)	$E_{Coulomb}(C2sp^3)$ (eV) Final	$E(C2sp^3)$ (eV) Final	θ' (°)	θ_1 (°)	θ_2 (°)	d_1 (a_0)	d_2 (a_0)
$C-H\ (C_aH)$	C_a	-0.54343	-0.85035	-0.56690	0	-153.57636	0.91771	0.81052	-16.78642	-16.59556	76.35	103.65	40.11	1.22423	0.19124
$(H)C_a(H)C_a^{3e}=NC_a$	C_a	-0.85035	-0.54343	-0.56690	0	-153.57636	0.91771	0.81052	-16.78642	-16.59556	128.54	51.46	58.65	0.76572	0.50501
$(H)C_a(H)C_a^{3e}=NC_a$	N	-0.54343	-0.54343	0	0		0.93084	0.85503	-15.91261		130.61	49.39	60.97	0.71418	0.55656
$N(H)C_a^{3e}=C_a(H)N$	C_a	-0.85035	-0.54343	-0.56690	0	-153.57636	0.91771	0.81052	-16.78642	-16.59556	134.85	45.15	59.72	0.74304	0.57165

Table 15.306. The energy parameters (eV) of functional groups of pyrazine.

Parameters	$C\overset{3e}{=}C$ Group	CH Group	$C\overset{3e}{=}N$ Group
f_1	0.75	1	0.75
n_1	2	1	2
n_2	0	0	0
n_3	0	0	0
C_1	0.5	0.75	0.5
C_2	0.85252	1	0.91140
c_1	1	1	1
c_2	0.85252	0.91771	0.91140
c_3	0	1	0
c_4	3	1	3
c_5	0	1	0
C_{1o}	0.5	0.75	0.5
C_{2o}	0.85252	1	0.91140
$V_e\ (eV)$	-101.12679	-37.10024	-102.01431
$V_p\ (eV)$	20.69825	13.17125	21.41410
$T\ (eV)$	34.31559	11.58941	34.65890
$V_m\ (eV)$	-17.15779	-5.79470	-17.32945
$E_{(AO/HO)}\ (eV)$	0	-14.63489	0
$\Delta E_{H_2MO\ (AO/HO)}\ (eV)$	0	-1.13379	0
$E_{T_1\ (AO/HO)}\ (eV)$	0	-13.50110	0
$E_{I_1\ (H_2MO)}\ (eV)$	-63.27075	-31.63539	-63.27076
$E_{I_1\ (atom-atom,msp^3.AO)}\ (eV)$	-2.26759	-0.56690	-1.44915
$E_{I_1\ (MO)}\ (eV)$	-65.53833	-32.20226	-64.71988
$\omega\ (10^{15}\ rad/s)$	49.7272	26.4826	43.6311
$E_K\ (eV)$	32.73133	17.43132	28.71875
$\bar{E}_D\ (eV)$	-0.35806	-0.26130	-0.33540
$\bar{E}_{Kvib}\ (eV)$	0.19649 [49]	0.35532 Eq. (13.458)	0.19649 [49]
$\bar{E}_{osc}\ (eV)$	-0.25982	-0.08364	-0.23715
$E_{mag}\ (eV)$	0.14803	0.14803	0.09457
$E_{I_1\ (Group)}\ (eV)$	-49.54347	-32.28590	-48.82472
$E_{initial\ (c_4\ AO/HO)}\ (eV)$	-14.63489	-14.63489	-14.63489
$E_{initial\ (c_5\ AO/HO)}\ (eV)$	0	-13.59844	0
$E_{D\ (Group)}\ (eV)$	5.63881	3.90454	4.92005

Table 15.307. The total bond energies of pyrazine calculated using the functional group composition and the energies of Table 15.306 compared to the experimental values [3].

Formula	Name	$C=C^{3e}$	CH	$C=N^{3e}$ Group	Calculated Total Bond Energy (eV)	Experimental Total Bond Energy (eV)	Relative Error
$C_4H_4N_2$	Pyrazine	2	4	4	46.57597	46.51380	0.00095

Table 15.308. The bond angle parameters of pyrazine and experimental values [1]. E_T is $E_T(atom-atom,msp^3.AO)$.

Atoms of Angle	$2c'$ Bond 1 (a_0)	$2c'$ Bond 2 (a_0)	$2c'$ Terminal Atoms (a_0)	$E_{Coulombic}$ Atom 1	Atom 1 Hybridization Designation (Table 15.3B)	$E_{Coulombic}$ Atom 2	Atom 2 Hybridization Designation (Table 15.3B)	c_2 Atom 1	c_2 Atom 2	C_1	C_2	c_1	c_2'	E_T (eV)	θ_v (°)	θ_1 (°)	θ_2 (°)	Cal. θ (°)	Exp. θ (°)
$\angle CCC$ (aromatic)	2.62936	2.62936	4.5585	-17.17218	27	-17.17218	27	0.79232	0.79232	1	1	1	0.79232	-1.85836				120.19	120 [50-52] (benzene) 118.3 (pyridine) 118.5 (pyridine)
$\angle CCH$ (aromatic)																120.19		119.91	120 [50-52] (benzene) 121.3 (pyridine)
$\angle HCN$	2.06598	2.54147	3.9497	-14.82575	1	-14.53414	N	0.91771	0.91140 Eq. (15.135))	0.75	1	0.75	0.99312	0				117.65	115.9 (pyridine)
$\angle CCH$																117.65	116.81	125.54	123.9 (pyrazine)
$\angle NCC$	2.54147	2.62936	4.4045	-14.53414	N	-17.09334	23	0.91140 Eq. (15.135))	0.79597	1	1	1	0.85368	-1.44915				116.81	115.6 (pyrazine
$\angle CNC$	2.54147	2.54147	4.3359	-17.71560	33	-17.71560	33	0.76801	0.76801	1	1	1	0.76801	-1.85836				117.09	116.8 (pyrimidine)

QUINOLINE

Quinoline has the formula C_9H_7N and comprises the naphthalene molecule with one CH group replaced by a nitrogen atom which gives rise to a $C\overset{3e}{=}N$ functional group. The aromatic $C\overset{3e}{=}C$ and $C-H$ functional groups are equivalent to those of naphthalene given in the corresponding section with the aromaticity maintained by the electrons from nitrogen in the $C\overset{3e}{=}N$ group, which is also aromatic. The $C-C$ functional group is also equivalent to that of naphthalene. The bonding in quinoline can be further considered as a linear combination of the naphthalene and pyridine groups wherein the $C\overset{3e}{=}N$ group is equivalent to that of pyridine, pyrimidine, and pyrazine as given in the corresponding sections.

The symbols of the functional groups of quinoline are given in Table 15.309. The corresponding designation of the structure is shown in Figure 15.53B. The geometrical (Eqs. (15.1-15.5) and (15.51)), intercept (Eqs. (15.80-15.87)), and energy (Eqs. (15.6-15.11), (15.17-15.65), and (15.165-15.166)) parameters of quinoline are given in Tables 15.310, 15.311, and 15.312, respectively. The total energy of quinoline given in Table 15.313 was calculated as the sum over the integer multiple of each $E_D(Group)$ of Table 15.312 corresponding to functional-group composition of the molecule. The bond angle parameters of quinoline determined using Eqs. (15.88-15.117) are given in Table 15.314. The color scale, translucent view of the charge-density of quinoline comprising the concentric shells of atoms with the outer shell bridged by one or more H_2-type ellipsoidal MOs or joined with one or more hydrogen MOs is shown in Figure 15.53A.

Figure 15.53. (A) Color scale, translucent view of the charge-density of quinoline showing the orbitals of the atoms at their radii, the ellipsoidal surface of each H or H_2-type ellipsoidal MO that transitions to the corresponding outer shell of the atom(s) participating in each bond, and the hydrogen nuclei (red, not to scale). (B) Chemical structure and atom designation of quinoline.

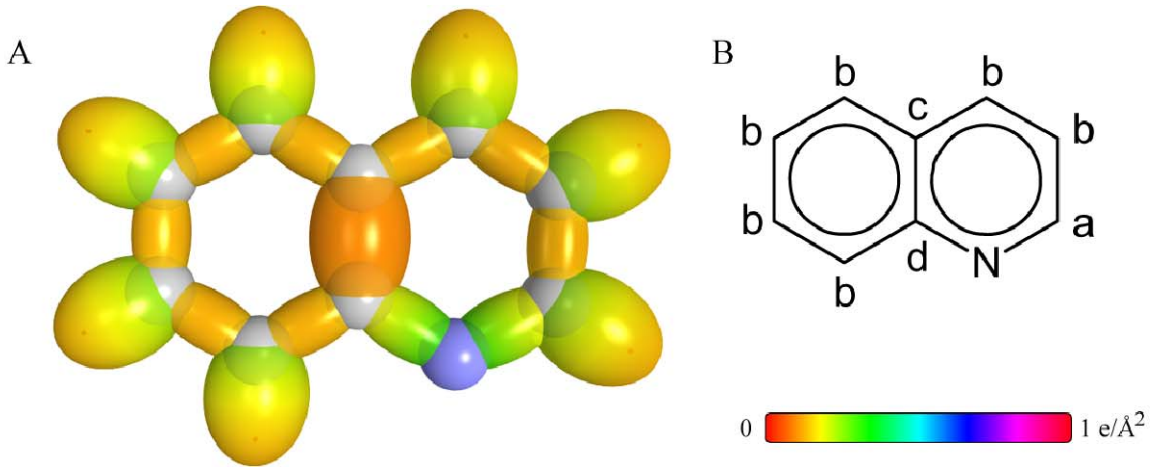

Table 15.309. The symbols of functional groups of quinoline.

Functional Group	Group Symbol
CC (aromatic bond)	$C \overset{3e}{=} C$
CH (aromatic)	CH
$C_b - C_b$ (bridging bond)	$C - C$
$C_{a,d} \overset{3e}{=} N$	$C \overset{3e}{=} N$

Table 15.310. The geometrical bond parameters of quinoline and experimental values [1].

Parameter	$C \overset{3e}{=} C$ Group	CH Group	$C - C$ Group	$C \overset{3e}{=} N$ Group
$a\ (a_0)$	1.47348	1.60061	1.75607	1.47169
$c'\ (a_0)$	1.31468	1.03299	1.32517	1.27073
Bond Length $2c'\ (\AA)$	1.39140	1.09327	1.40250	1.34489
Exp. Bond Length $(\AA)$	1.40 (avg.) (naphthalene)	1.101 (benzene)	1.42 (naphthalene)	1.340 (pyridine)
$b,c\ (a_0)$	0.66540	1.22265	1.15226	0.74237
e	0.89223	0.64537	0.75462	0.86345

Table 15.311. The MO to HO intercept geometrical bond parameters of quinoline. E_T is E_T (*atom – atom,msp³.AO*).

Bond	Atom	E_T (eV) Bond 1	E_T (eV) Bond 2	E_T (eV) Bond 3	E_T (eV) Bond 4	Final Total Energy $C2sp^3$ (eV)	$r_{initial}$ (a_0)	r_{final} (a_0)	$E_{Coulomb}(C2sp^3)$ (eV) Final	$E(C2sp^3)$ (eV) Final	θ' (°)	θ_1 (°)	θ_2 (°)	d_1 (a_0)	d_2 (a_0)
$C-H\ (C_aH)$	C_a	-0.85035	-0.54343	-0.56690	0	-153.57636	0.91771	0.81052	-16.78642	-16.59556	76.35	103.65	40.11	1.22423	0.19124
$C-H\ (C_bH)$	C_b	-0.85035	-0.85035	-0.56690	0	-153.88327	0.91771	0.79597	-17.09334	-16.90248	74.42	105.58	38.84	1.24678	0.21379
$N(H)C_a \overset{3e}{=} C_b(H)$	C_a	-0.85035	-0.54343	-0.56690	0	-153.57636	0.91771	0.81052	-16.78642	-16.59556	134.85	45.15	59.72	0.74304	0.57165
$(H)C_b \overset{3e}{=} C_{a,b,c,d}(H)$	C_b	-0.85035	-0.85035	-0.56690	0	-153.88327	0.91771	0.79597	-17.09334	-16.90248	134.24	45.76	58.98	0.75935	0.55533
$(H)C_b(C_d)C_c \overset{3e}{=} C_b$	C_c	-0.85035	-0.85035	-0.28345	0	-153.59983	0.91771	0.80939	-16.80989	-16.61903	134.81	45.19	59.66	0.74430	0.57038
$N(C_c)C_d \overset{3e}{=} C_b$	C_d	-0.85035	-0.54343	-0.28345	0	-153.29292	0.91771	0.82445	-16.50298	-16.31211	135.42	44.58	60.42	0.72743	0.58725
$C_b(H)C_a \overset{3e}{=} N$	C_a	-0.85035	-0.54343	-0.56690	0	-153.57636	0.91771	0.81052	-16.78642	-16.59556	128.54	51.46	58.65	0.76572	0.50501
$C_b(H)C_a \overset{3e}{=} N$ $C_b(C_c)C_d \overset{3e}{=} N$	N	-0.54343	-0.54343	0	0		0.93084	0.85503	-15.91261		130.61	49.39	60.97	0.71418	0.55656
$C_b(C_c)C_d \overset{3e}{=} N$	C_d	-0.85035	-0.54343	-0.28345	0	-153.29291	0.91771	0.82445	-16.50297	-16.31211	129.21	50.79	59.38	0.74960	0.52113
$\left((H)C_b \overset{3e}{=}\right)_2 C_c - C_d$	C_c	-0.85035	-0.85035	-0.28345	0	-153.59983	0.91771	0.80939	-16.80989	-16.61903	95.01	84.99	44.41	1.25451	0.07066
$N(C_b)C_d - C_c$	C_d	-0.85035	-0.54343	-0.28345	0	-153.29292	0.91771	0.82445	-16.50298	-16.31211	96.31	83.69	45.33	1.23456	0.09061

Table 15.312. The energy parameters (eV) of functional groups of quinoline.

Parameters	$C\overset{3e}{=}C$ Group	CH Group	$C-C$ Group	$C\overset{3e}{=}N$ Group
f_1	0.75	1	1	0.75
n_1	2	1	1	2
n_2	0	0	0	0
n_3	0	0	0	0
C_1	0.5	0.75	0.5	0.5
C_2	0.85252	1	1	0.91140
c_1	1	1	1	1
c_2	0.85252	0.91771	0.85252	0.91140
c_3	0	1	0	0
c_4	3	1	2	3
c_5	0	1	0	0
C_{1o}	0.5	0.75	0.5	0.5
C_{2o}	0.85252	1	1	0.91140
$V_e\ (eV)$	-101.12679	-37.10024	-34.43791	-102.01431
$V_p\ (eV)$	20.69825	13.17125	10.26723	21.41410
$T\ (eV)$	34.31559	11.58941	9.80539	34.65890
$V_m\ (eV)$	-17.15779	-5.79470	-4.90270	-17.32945
$E_{(AO/HO)}\ (eV)$	0	-14.63489	-14.63489	0
$\Delta E_{H_2MO(AO/HO)}\ (eV)$	0	-1.13379	-1.13379	0
$E_{T(AO/HO)}\ (eV)$	0	-13.50110	-13.50110	0
$E_{J(H_2MO)}\ (eV)$	-63.27075	-31.63539	-31.63529	-63.27076
$E_J\left(atom-atom, msp^3.AO\right)(eV)$	-2.26759	-0.56690	-0.56690	-1.44915
$E_{J(MO)}\ (eV)$	-65.53833	-32.20226	-32.20226	-64.71988
$\omega\ \left(10^{15}\ rad/s\right)$	49.7272	26.4826	23.6343	43.6311
$E_K\ (eV)$	32.73133	17.43132	15.55648	28.71875
$\bar{E}_D\ (eV)$	-0.35806	-0.26130	-0.25127	-0.33540
$\bar{E}_{Kvib}\ (eV)$	0.19649 [49]	0.35532 Eq. (13.458)	0.12312 [2]	0.19649 [49]
$\bar{E}_{osc}\ (eV)$	-0.25982	-0.08364	-0.18971	-0.23715
$E_{mag}\ (eV)$	0.14803	0.14803	0.14803	0.09457
$E_{J(Group)}\ (eV)$	-49.54347	-32.28590	-32.39198	-48.82472
$E_{initial(4\ AO/HO)}\ (eV)$	-14.63489	-14.63489	-14.63489	-14.63489
$E_{initial(3\ AO/HO)}\ (eV)$	0	-13.59844	0	0
$E_{D(Group)}\ (eV)$	5.63881	3.90454	3.12220	4.92005

Table 15.313. The total bond energies of quinoline calculated using the functional group composition and the energies of Table 15.312 compared to the experimental values [3].

Formula	Name	$C^{3e}=C$	CH	$C-C$ Group	$C^{3e}=N$ Group	Calculated Total Bond Energy (eV)	Experimental Total Bond Energy (eV)	Relative Error
C_9H_7N	Quinoline	8	7	1	2	85.40453	85.48607	0.00178

Table 15.314. The bond angle parameters of quinoline and experimental values [1]. E_T is E_T ($atom-atom,msp^3.AO$).

Atoms of Angle	2c' Bond 1 (a_0)	2c' Bond 2 (a_0)	2c' Terminal Atoms (a_0)	$E_{Coulombic}$ Atom 1	Atom 1 Hybridization Designation (Table 15.3B)	$E_{Coulombic}$ Atom 2	Atom 2 Hybridization Designation (Table 15.3B)	c_2 Atom 1	c_2 Atom 2	C_1	C_2	c_1	c_2'	E_T (eV)	θ_v (°)	θ_1 (°)	θ_2 (°)	Cal. θ (°)	Exp. θ (°)
$\angle CCC$	2.62936	2.65034	4.5585	-17.17218	27	-17.17218	27	0.79232	0.79232	1	1	1	0.79232	-1.85836				119.40	119.4 (naphthalene)
$\angle CCH$																119.40		120.30	
$\angle C_dNC_a$	2.54147	2.54147	4.3818	-17.43216	31	-17.71560	33	0.78050	0.76801	1	1	1	0.77426	-1.85836				119.10	

ISOQUINOLINE

Isoquinoline has the formula C_9H_7N and comprises the naphthalene molecule with one CH group replaced by a nitrogen atom which gives rise to a $C\overset{3e}{=}N$ functional group. Isoquinoline is also equivalent to quinoline with the nitrogen in the meta rather than the ortho position relative to the benzene ring of the molecule. The aromatic $C\overset{3e}{=}C$ and $C-H$ functional groups are equivalent to those of naphthalene given in the corresponding section with the aromaticity maintained by the electrons from nitrogen in the $C\overset{3e}{=}N$ group which is also aromatic. The $C-C$ functional group is also equivalent to that of naphthalene. The bonding in isoquinoline can be further considered as a linear combination of the naphthalene and pyridine groups wherein the $C\overset{3e}{=}N$ group is equivalent to that of pyridine, pyrimidine, pyrazine, and quinoline as given in the corresponding sections.

The symbols of the functional groups of isoquinoline are given in Table 15.315. The corresponding designation of the structure is shown in Figure 15.54B. The geometrical (Eqs. (15.1-15.5) and (15.51)), intercept (Eqs. (15.80-15.87)), and energy (Eqs. (15.6-15.11), (15.17-15.65), and (15.165-15.166)) parameters of isoquinoline are given in Tables 15.316, 15.317, and 15.318, respectively. The total energy of isoquinoline given in Table 15.319 was calculated as the sum over the integer multiple of each $E_D(Group)$ of Table 15.318 corresponding to functional-group composition of the molecule. The bond angle parameters of isoquinoline determined using Eqs. (15.88-15.117) are given in Table 15.320. The color scale, translucent view of the charge-density of isoquinoline comprising the concentric shells of atoms with the outer shell bridged by one or more H_2-type ellipsoidal MOs or joined with one or more hydrogen MOs is shown in Figure 15.54A.

Figure 15.54. (A) Color scale, translucent view of the charge-density of isoquinoline showing the orbitals of the atoms at their radii, the ellipsoidal surface of each H or H_2-type ellipsoidal MO that transitions to the corresponding outer shell of the atom(s) participating in each bond, and the hydrogen nuclei (red, not to scale). (B) Chemical structure and atom designation of isoquinoline.

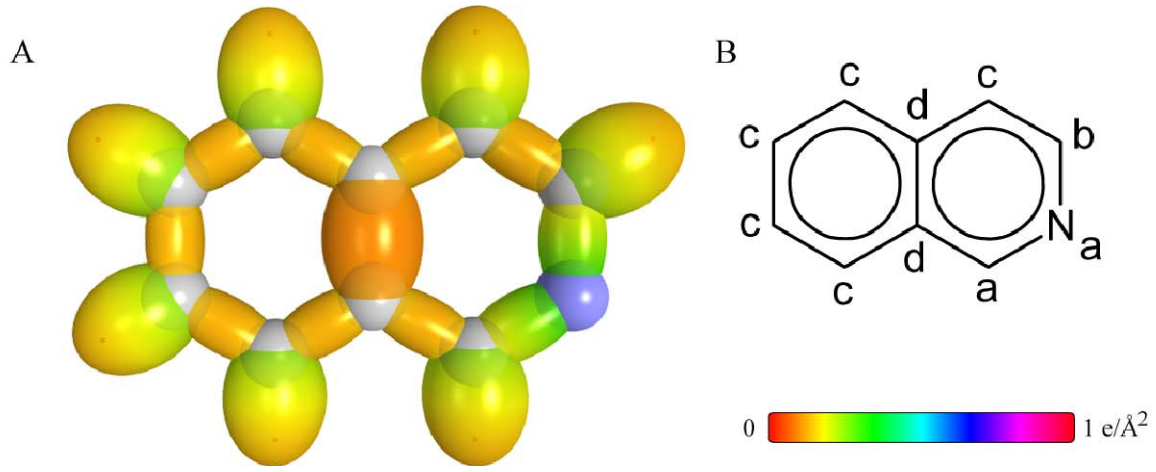

Table 15.315. The symbols of functional groups of isoquinoline.

Functional Group	Group Symbol
CC (aromatic bond)	$C \overset{3e}{=} C$
CH (aromatic)	CH
$C_b - C_b$ (bridging bond)	$C - C$
$C_{a,d} \overset{3e}{=} N$	$C \overset{3e}{=} N$

Table 15.316. The geometrical bond parameters of isoquinoline and experimental values [1].

Parameter	$C \overset{3e}{=} C$ Group	CH Group	$C - C$ Group	$C \overset{3e}{=} N$ Group
$a\ (a_0)$	1.47348	1.60061	1.75607	1.47169
$c'\ (a_0)$	1.31468	1.03299	1.32517	1.27073
Bond Length $2c'\ (\text{Å})$	1.39140	1.09327	1.40250	1.34489
Exp. Bond Length (Å)	1.40 (avg.) (naphthalene)	1.101 (benzene)	1.42 (naphthalene)	1.340 (pyridine)
$b,c\ (a_0)$	0.66540	1.22265	1.15226	0.74237
e	0.89223	0.64537	0.75462	0.86345

Table 15.317. The MO to HO intercept geometrical bond parameters of isoquinoline. E_T is E_T (*atom – atom,msp³.AO*).

Bond	Atom	E_T (eV) Bond 1	E_T (eV) Bond 2	E_T (eV) Bond 3	E_T (eV) Bond 4	Final Total Energy $C2sp^3$ (eV)	$r_{initial}$ (a_0)	r_{final} (a_0)	$E_{Coulomb}(C2sp^3)$ (eV) Final	$E(C2sp^3)$ (eV) Final	θ' (°)	θ_1 (°)	θ_2 (°)	d_1 (a_0)	d_2 (a_0)
$C-H\ (C_aH)$	C_a	-0.85035	-0.54343	-0.56690	0	-153.57636	0.91771	0.81052	-16.78642	-16.59556	76.35	103.65	40.11	1.22423	0.19124
$C-H\ (C_bH)$	C_b	-0.85035	-0.54343	-0.56690	0	-153.57636	0.91771	0.81052	-16.78642	-16.59556	76.35	103.65	40.11	1.22423	0.19124
$C-H\ (C_cH)$	C_c	-0.85035	-0.85035	-0.56690	0	-153.88327	0.91771	0.79597	-17.09334	-16.90248	74.42	105.58	38.84	1.24678	0.21379
$N(H)C_a^{3e}=C_1$ $N(H)C_b^{3e}=C_c$	C_a C_b	-0.85035	-0.54343	-0.56690	0	-153.57636	0.91771	0.81052	-16.78642	-16.59556	134.85	45.15	59.72	0.74304	0.57165
$(H)C_c^{3e}=C_{b,c,d}(H)$	C_c	-0.85035	-0.85035	-0.56690	0	-153.88327	0.91771	0.79597	-17.09334	-16.90248	134.24	45.76	58.98	0.75935	0.55533
$(H)C_c(C_d)C_d^{3e}=C_{a,c}$	C_d	-0.85035	-0.85035	-0.28345	0	-153.59983	0.91771	0.80939	-16.80989	-16.61903	134.81	45.19	59.66	0.74430	0.57038
$C_d(H)C_a^{3e}=N$ $C_c(H)C_b^{3e}=N$	C_a C_b	-0.85035	-0.54343	-0.56690	0	-153.57636	0.91771	0.81052	-16.78642	-16.59556	128.54	51.46	58.65	0.76572	0.50501
$C_d(H)C_a^{3e}=N$ $C_c(H)C_b^{3e}=N$	N	-0.54343	-0.54343	0	0		0.93084	0.85503	-15.91261		130.61	49.39	60.97	0.71418	0.55656
$C_{a,c}(C_c)C_d-C_d$	C_d	-0.85035	-0.85035	-0.28345	0	-153.59983	0.91771	0.80939	-16.80989	-16.61903	95.01	84.99	44.41	1.25451	0.07066

Table 15.318. The energy parameters (eV) of functional groups of isoquinoline.

Parameters	$C \overset{3e}{=} C$ Group	CH Group	$C-C$ Group	$C \overset{3e}{=} N$ Group
f_1	0.75	1	1	0.75
n_1	2	1	1	2
n_2	0	0	0	0
n_3	0	0	0	0
C_1	0.5	0.75	0.5	0.5
C_2	0.85252	1	1	0.91140
c_1	1	1	1	1
c_2	0.85252	0.91771	0.85252	0.91140
c_3	0	1	0	0
c_4	3	1	2	3
c_5	0	1	0	0
C_{1o}	0.5	0.75	0.5	0.5
C_{2o}	0.85252	1	1	0.91140
$V_e\ (eV)$	-101.12679	-37.10024	-34.43791	-102.01431
$V_p\ (eV)$	20.69825	13.17125	10.26723	21.41410
$T\ (eV)$	34.31559	11.58941	9.80539	34.65890
$V_m\ (eV)$	-17.15779	-5.79470	-4.90270	-17.32945
$E_{(AO/HO)}\ (eV)$	0	-14.63489	-14.63489	0
$\Delta E_{H_2MO\ (AO/HO)}\ (eV)$	0	-1.13379	-1.13379	0
$E_{T\ (AO/HO)}\ (eV)$	0	-13.50110	-13.50110	0
$E_{T\ (H_2MO)}\ (eV)$	-63.27075	-31.63539	-31.63529	-63.27076
$E_{T}\left(atom-atom, msp^3.AO\right)(eV)$	-2.26759	-0.56690	-0.56690	-1.44915
$E_{T\ (MO)}\ (eV)$	-65.53833	-32.20226	-32.20226	-64.71988
$\omega\ \left(10^{15}\ rad/s\right)$	49.7272	26.4826	23.6343	43.6311
$E_K\ (eV)$	32.73133	17.43132	15.55648	28.71875
$\bar{E}_D\ (eV)$	-0.35806	-0.26130	-0.25127	-0.33540
$\bar{E}_{Kvib}\ (eV)$	0.19649 [49]	0.35532 Eq. (13.458)	0.12312 [2]	0.19649 [49]
$\bar{E}_{osc}\ (eV)$	-0.25982	-0.08364	-0.18971	-0.23715
$E_{mag}\ (eV)$	0.14803	0.14803	0.14803	0.09457
$E_{T\ (Group)}\ (eV)$	-49.54347	-32.28590	-32.39198	-48.82472
$E_{initial\ (c_4\ AO/HO)}\ (eV)$	-14.63489	-14.63489	-14.63489	-14.63489
$E_{initial\ (c_5\ AO/HO)}\ (eV)$	0	-13.59844	0	0
$E_{D\ (Group)}\ (eV)$	5.63881	3.90454	3.12220	4.92005

Table 15.319. The total bond energies of isoquinoline calculated using the functional group composition and the energies of Table 15.318 compared to the experimental values [3].

Formula	Name	$C=^{3e}C$	CH	$C-C$ Group	$C=^{3e}N$ Group	Calculated Total Bond Energy (eV)	Experimental Total Bond Energy (eV)	Relative Error
C_9H_7N	Isoquinoline	8	7	1	2	85.40453	85.44358	0.00046

Table 15.320. The bond angle parameters of isoquinoline and experimental values [1]. E_T is E_T ($atom-atom,msp^3.AO$).

Atoms of Angle	$2c'$ Bond 1 (a_0)	$2c'$ Bond 2 (a_0)	$2c'$ Terminal Atoms (a_0)	$E_{Coulombic}$ Atom 1	Atom 1 Hybridization Designation (Table 15.3B)	$E_{Coulombic}$ Atom 2	Atom 2 Hybridization Designation (Table 15.3B)	c_2 Atom 1	c_2 Atom 2	C_1	C_2	c_1	c_2'	E_T (eV)	θ_v (°)	θ_1 (°)	θ_2 (°)	Cal. θ (°)	Exp. θ (°)
$\angle CCC$	2.62936	2.65034	4.5585	-17.17218	27	-17.17218	27	0.79232	0.79232	1	1	1	0.79232	-1.85836				119.40	119.4 (naphthalene)
$\angle CCH$																119.40		120.30	
$\angle C_aNC_b$	2.54147	2.54147	4.3818	-17.43216	31	-17.71560	33	0.78050	0.76801	1	1	1	0.77426	-1.85836				119.10	

INDOLE

Indole having the formula C_8H_7N comprises a phenyl moiety with a conjugated five-membered ring which comprises pyrrole except that one of the double bonds is part of the aromatic ring. The structure is shown in Figure 15.55B. The aromatic $C\overset{3e}{=}C$ and $C-H$ functional groups of the phenyl moiety are equivalent to those of benzene given in the Aromatic and Heterocyclic Compounds section. The CH, NH, and $C_d=C_e$ groups of the pyrrole-type ring are equivalent to the corresponding groups of pyrrole, furan, and thiophene where present as given in the corresponding sections. The C_b-C_d single bond of aryl carbon to the $C_d=C_e$ bond is also a functional group. This group is equivalent to the $C-C(O)$ group of benzoic acids with regard to $\Delta E_{H_2MO}\left(AO/HO\right)$ in Eq. (15.51) and $E_T\left(atom-atom,msp^3.AO\right)$ in Eq. (15.61) both being $-1.29147\,eV$. This energy is a linear combination of $\frac{-1.13379\,eV}{2}$, $E_T\left(atom-atom,msp^3.AO\right)$ of the $C-H$ group that the C_b-C_d and $C-C(O)$ groups replace, and that of an independent $C2sp^3$ HO, $-0.72457\,eV$ (Eq. (14.151)). However, as in the case of pyrrole, the indole hybridization term c_2 is the aromatic $c_2\left(benzeneC2sp^3HO\right)=0.85252$ to match the aryl $C2sp^3$ HO, and the energy terms corresponding to oscillation in the transition state correspond to indole.

As in the case of pyrrole, the $C-N-C$-bond MO comprising a linear combination of two single bonds is solved in the same manner as a double bond with $n_1=2$ in Eqs. (15.51) and (15.61). The hybridization factor $c_2\left(arylC2sp^3HO\ to\ N\right)=0.84665$ (Eq. (15.171)) matches the aromatic character of the $C2sp^3$ HOs to the N atom of the NH group, and C_2 and C_{2o} in Eqs. (15.51) and (15.61) become that of benzene given by Eq. (15.162), $C_2\left(benzeneC2sp^3HO\right)=0.85252$. Furthermore, $\Delta E_{H_2MO}\left(AO/HO\right)$ in Eq. (15.51) and $E_T\left(atom-atom,msp^3.AO\right)$ in Eq. (15.61) are both $-2.42526\,eV$ which is a linear combination of $\frac{-1.13379\,eV}{2}$, $E_T\left(atom-atom,msp^3.AO\right)$ of the $C-H$ group that the C_c-N bond replaces, and $-1.85836\,eV$ (Eq. (14.513)) which is equivalent to the corresponding component of the $C-N-C$-bond of pyrrole.

The symbols of the functional groups of indole are given in Table 15.321. The geometrical (Eqs. (15.1-15.5) and (15.51)), intercept (Eqs. (15.80-15.87)), and energy (Eqs. (15.6-15.11) and (15.17-15.65)) parameters of indole are given in Tables 15.322, 15.323, and 15.324, respectively. The total energy of indole given in Table 15.325 was calculated as the sum over the integer multiple of each $E_{D\,(Group)}$ of Table 15.324 corresponding to functional-group composition of the molecule. The bond angle parameters of indole determined using Eqs. (15.88-15.117) are given in Table 15.326. The color scale, translucent view of the charge-density of indole comprising the concentric shells of atoms with the outer shell bridged by one or more H_2-type ellipsoidal MOs or joined with one or more hydrogen MOs is shown in Figure 15.55A.

Figure 15.55. (A) Color scale, translucent view of the charge-density of indole showing the orbitals of the atoms at their radii, the ellipsoidal surface of each H or H_2-type ellipsoidal MO that transitions to the corresponding outer shell of the atom(s) participating in each bond, and the hydrogen nuclei (red, not to scale). (B) Chemical structure and atom designation of indole.

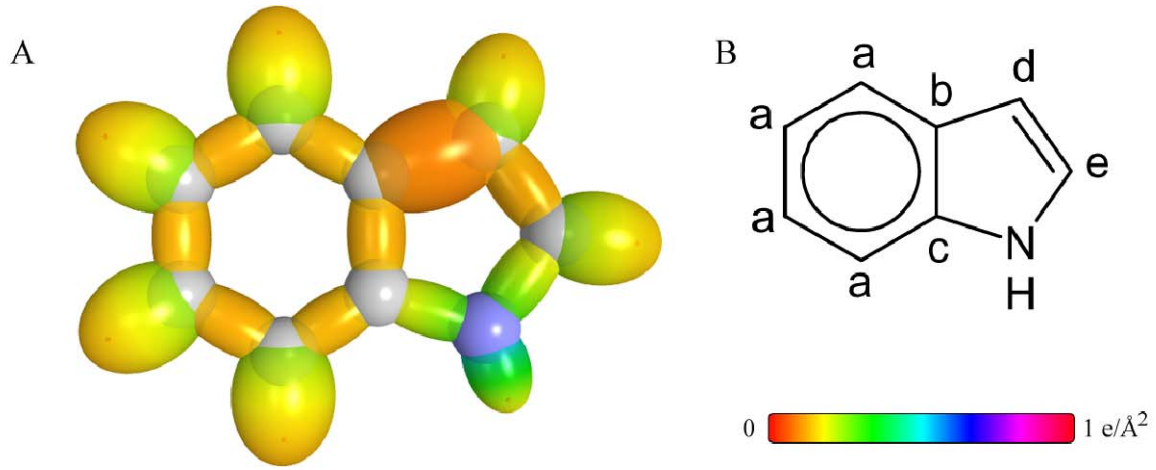

Table 15.321. The symbols of functional groups of indole.

Functional Group	Group Symbol
CC (aromatic bond)	$C\overset{3e}{=}C$
CH (aromatic)	CH (i)
$C_d = C_e$ double bond	$C = C$
$C_b - C_d$	$C - C$
CH	CH (ii)
$C_c - N - C_e$	$C - N - C$
NH group	NH

Table 15.322. The geometrical bond parameters of indole and experimental values [1].

Parameter	$C^{3e}=C$ Group	CH (i) Group	$C=C$ Group	CH (ii) Group	$C-C$ Group	$C-N-C$ Group	NH Group
$a\ (a_0)$	1.47348	1.60061	1.45103	1.53380	1.81395	1.44394	1.24428
$c'\ (a_0)$	1.31468	1.03299	1.30463	1.01120	1.34683	1.30144	0.94134
Bond Length $2c'\ (\AA)$	1.39140	1.09327	1.38076	1.07021	1.42542	1.37738	0.996270
Exp. Bond Length $(\AA)$	1.399 (benzene)	1.101 (benzene)	1.382 (pyrrole)	1.076 (pyrrole	1.417 (pyrrole)	1.370 (pyrrole)	0.996 (pyrrole)
$b,c\ (a_0)$	0.66540	1.22265	0.63517	1.15326	1.21510	0.62548	0.81370
e	0.89223	0.64537	0.89910	0.65928	0.74248	0.90131	0.75653

Table 15.323. The MO to HO intercept geometrical bond parameters of indole. R_1 is an alkyl group and R, R', R'' are H or alkyl groups. E_T is E_T ($atom-atom,msp^3.AO$).

Bond	Atom	E_T (eV) Bond 1	E_T (eV) Bond 2	E_T (eV) Bond 3	E_T (eV) Bond 4	Final Total Energy $C2sp^3$ (eV)	$r_{initial}\ (a_0)$	$r_{final}\ (a_0)$	$E_{Coulomb}(C2sp^3)$ (eV) Final	$E(C2sp^3)$ (eV) Final	θ' (°)	θ_1 (°)	θ_2 (°)	$d_1\ (a_0)$	$d_2\ (a_0)$
$C-H\ (C_aH)$	C_a	-0.85035	-0.85035	-0.56690	0	-153.88327	0.91771	0.79597	-17.09334	-16.90248	74.42	105.58	38.84	1.24678	0.21379
$C_a=^{3e}HC_a=^{3e}C_{a,b,c}$	C_a	-0.85035	-0.85035	-0.56690	0	-153.88327	0.91771	0.79597	-17.09334	-16.90248	134.24	45.76	58.98	0.75935	0.55533
$C_a=^{3e}(C_d)C_b=^{3e}C_c$ $C_c=^{3e}(C_d)C_b=^{3e}C_a$	C_b	-0.85035	-0.64574	-0.85035	0	-153.96212	0.91771	0.79232	-17.17218	-16.98132	134.09	45.91	58.79	0.76344	0.55124
$C_a=^{3e}C_c(N)C_b$ $C_b=^{3e}C_c(N)C_a$	C_c	-0.60631	-0.85035	-0.85035	0	-153.92270	0.91771	0.79414	-17.13276	-16.94190	134.16	45.84	58.89	0.76140	0.55328
$C_a(H)C_b-C_d(H)C_e$	C_b	-0.85035	-0.85035	-0.64574	0	-153.96212	0.91771	0.79232	-17.17218	-16.98132	87.89	92.11	40.66	1.37597	0.02914
$C_a(H)C_b-C_d(H)C_e$	C_d	-0.64574	-1.13379	0	0	-153.39522	0.91771	0.81937	-16.60528	-16.41442	90.51	89.49	42.40	1.33953	0.00729
$C_b(H)C_d=C_eN$	C_d	-0.64574	-1.13379	0	0	-153.39522	0.91771	0.81937	-16.60528	-16.41442	137.29	42.71	61.04	0.70255	0.60208
$C_b(H)C_d=C_eN$	C_e	-1.13379	-0.60631	0	0	-153.35580	0.91771	0.82132	-16.56586	-16.37500	137.37	42.63	61.14	0.70038	0.60425
$C_dC_e-NC_e$	C_e	-1.13379	-0.60631	0	0	-153.35580	0.91771	0.82132	-16.56586	-16.37500	138.03	41.97	61.42	0.69080	0.61064
$C_dC_e-NC_e$ $C_aC_c-NC_c$	N	-0.60631	-0.60631	0	0		0.93084	0.84833	-16.03838		139.04	40.96	62.76	0.66083	0.64061
$N-H\ (NH)$	N	-0.60631	-0.60631	0	0		0.93084	0.84833	-16.03838		119.52	60.48	65.13	0.52338	0.41796
$C_aC_c-NC_c$	C_c	-0.85035	-0.85035	-0.60631	0	-153.92269	0.91771	0.79414	-17.13276	-16.94189	136.97	43.03	60.05	0.72095	0.58048

Table 15.324. The energy parameters (eV) of functional groups of indole.

Parameters	$C \overset{3e}{=} C$ Group	CH (i) Group	$C=C$ Group	$C-C$ Group	CH (ii) Group	$C-N-C$ Group	NH Group
f_1	0.75	1	1	1	1	1	1
n_1	2	1	2	1	1	2	1
n_2	0	0	0	0	0	0	0
n_3	0	0	0	0	0	0	0
C_1	0.5	0.75	0.5	0.5	0.75	0.5	0.75
C_2	0.85252	1	0.85252	1	1	0.85252	0.93613
c_1	1	1	1	1	1	1	0.75
c_2	0.85252	0.91771	0.85252	0.85252	0.91771	0.84665	0.92171
c_3	0	1	0	0	1	0	1
c_4	3	1	4	2	1	4	1
c_5	0	1	0	0	1	0	1
C_{1o}	0.5	0.75	0.5	0.5	0.75	0.5	0.75
C_{2o}	0.85252	1	0.85252	1	1	0.85252	1
V_e (eV)	-101.12679	-37.10024	-104.37986	-32.93291	-39.09538	-104.73877	-39.48897
V_p (eV)	20.69825	13.17125	20.85777	10.10210	13.45505	20.90891	14.45367
T (eV)	34.31559	11.58941	35.96751	9.07768	12.74462	36.26840	15.86820
V_{ee} (eV)	-17.15779	-5.79470	-17.98376	-4.53884	-6.37231	-18.13420	-7.93410
$E_{(AO/HO)}$ (eV)	0	-14.63489	0	-14.63489	-14.63489	0	-14.53414
$\Delta E_{(H_2MO)\,(AO/HO)}$ (eV)	0	-1.13379	-2.26759	-1.29147	-2.26758	-2.42526	0
$E_{T\,(AO/HO)}$ (eV)	0	-13.50110	2.26759	-13.34342	-12.36731	2.42526	-14.53414
$E_{T\,(H_2MO)}$ (eV)	-63.27075	-31.63539	-63.27075	-31.63539	-31.63533	-63.27040	-31.63534
$E_T\left(atom-atom, msp^3.AO\right)$ (eV)	-2.26759	-0.56690	-2.26759	-1.29147	0	-2.42526	0
$E_{T\,(MO)}$ (eV)	-65.53833	-32.20226	-65.53833	-32.92684	-31.63537	-65.69600	-31.63537
$\omega\left(10^{15}\ rad/s\right)$	49.7272	26.4826	15.4421	21.8249	28.9084	54.5632	48.7771
E_K (eV)	32.73133	17.43132	10.16428	14.36554	19.02803	35.91442	32.10594
$\bar{E}_D$ (eV)	-0.35806	-0.26130	-0.20668	-0.24690	-0.27301	-0.38945	-0.35462
$\bar{E}_{Kvib}$ (eV)	0.19649 [49]	0.35532 Eq. (13.458)	0.17897 [6]	0.12312 [2]	0.39427 [57]	0.11159 [12]	0.40696 [24]
$\bar{E}_{osc}$ (eV)	-0.25982	-0.08364	-0.11720	-0.18534	-0.07587	-0.33365	-0.15115
E_{mag} (eV)	0.14803	0.14803	0.14803	0.14803	0.14803	0.14803	0.14803
$E_{T\,(Group)}$ (eV)	-49.54347	-32.28590	-65.77272	-33.11218	-31.71124	-66.36330	-31.78651
$E_{initial\,(c_4\ AO/HO)}$ (eV)	-14.63489	-14.63489	-14.63489	-14.63489	-14.63489	-14.63489	-14.53414
$E_{initial\,(c_5\ AO/HO)}$ (eV)	0	-13.59844	0	0	-13.59844	0	-13.59844
$E_{D\,(Group)}$ (eV)	5.63881	3.90454	7.23317	3.84240	3.32988	7.82374	3.51208

Table 15.325. The total bond energies of indole calculated using the functional group composition and the energies of Table 15.324 compared to the experimental values [3].

Formula	Name	$C^{3e}=C$	CH (i)	$C=C$	$C-C$	CH (ii)	$C-N-C$	NH	Calculated Total Bond Energy (eV)	Experimental Total Bond Energy (eV)	Relative Error
C_8H_7N	Indole	6	4	1	1	2	1	1	78.52215	78.514	-0.00010

Table 15.326. The bond angle parameters of indole and experimental values [1]. In the calculation of θ_v, the parameters from the preceding angle were used. E_T is E_T ($atom-atom,msp^3.AO$).

Atoms of Angle	$2c'$ Bond 1 (a_0)	$2c'$ Bond 2 (a_0)	$2c'$ Terminal Atoms (a_0)	$E_{Coulombic}$ Atom 1	Atom 1 Hybridization Designation (Table 15.3B)	$E_{Coulombic}$ Atom 2	Atom 2 Hybridization Designation (Table 15.3B)	c_2 Atom 1	c_2 Atom 2	C_1	C_2	c_1	c_2'	E_T (eV)	θ_v (°)	θ_1 (°)	θ_2 (°)	Cal. θ (°)	Exp. θ (°)
$\angle CCC$ (aromatic)	2.62936	2.62936	4.5585	-17.17218	27	-17.17218	27	0.79232	0.79232	1	1	1	0.79232	-1.85836				120.19	120 [50-52] (benzene)
$\angle CCH$ (aromatic)																120.19		119.91	120 [50-52] (benzene)

ADENINE

Adenine having the formula $C_5H_5N_5$ comprises a pyrimidine moiety with an aniline-type moiety and a conjugated five-membered ring, which comprises imidazole except that one of the double bonds is part of the aromatic ring. The structure is shown in Figure 15.56B. The aromatic $C\overset{3e}{=}C$, $C-H$, and $C\overset{3e}{=}N$ functional groups of the pyrimidine moiety are equivalent to those of pyrimidine as given in the corresponding section. The CH, NH, C_d-N_e, and $N_e=C_e$ groups of the imidazole-type ring are equivalent to the corresponding groups of imidazole as given in the corresponding section. The $C-N-C$ functional group of the imidazole-type ring is equivalent to the corresponding group of indole having the same structure with the $C-N-C$ group bonding to aryl and alkenyl groups. The NH_2 and C_a-N_a functional groups of the aniline-type moiety are equivalent to those of aniline as given in the corresponding section except that $\Delta E_{H_2MO}\left(AO/HO\right)$ of the C_a-N_a group is equal to twice $E_T\left(atom-atom,msp^3.AO\right)$, and to meet the equipotential condition of the union of the $C-N$ H_2-type-ellipsoidal-MO with these orbitals, the hybridization factor c_2 of Eq. (15.60) for the $C-N$-bond MO given by Eqs. (15.77), (15.79), and (15.162) is:

$$c_2\left(arylC2sp^3HO\ to\ N\right)=\frac{E\left(N\right)}{E\left(C,2sp^3\right)}c_2\left(arylC2sp^3HO\right)=\frac{-14.53414\ eV}{-15.95955\ eV}\left(0.85252\right)=0.77638 \tag{15.173}$$

The symbols of the functional groups of adenine are given in Table 15.327. The geometrical (Eqs. (15.1-15.5) and (15.51)), intercept (Eqs. (15.80-15.87)), and energy (Eqs. (15.6-15.11) and (15.17-15.65)) parameters of adenine are given in Tables 15.328, 15.329, and 15.330, respectively. The total energy of adenine given in Table 15.331 was calculated as the sum over the integer multiple of each $E_D\left(Group\right)$ of Table 15.330 corresponding to functional-group composition of the molecule. The bond angle parameters of adenine determined using Eqs. (15.88-15.117) are given in Table 15.332. The color scale, charge-density of adenine comprising atoms with the outer shell bridged by one or more H_2-type ellipsoidal MOs or joined with one or more hydrogen MOs is shown in Figure 15.56A.

Figure 15.56. (A) Color scale, charge-density of adenine showing the orbitals of the atoms at their radii, the ellipsoidal surface of each H or H_2-type ellipsoidal MO that transitions to the corresponding outer shell of the atom(s) participating in each bond, and the hydrogen nuclei. (B) Chemical structure and atomic designation of adenine.

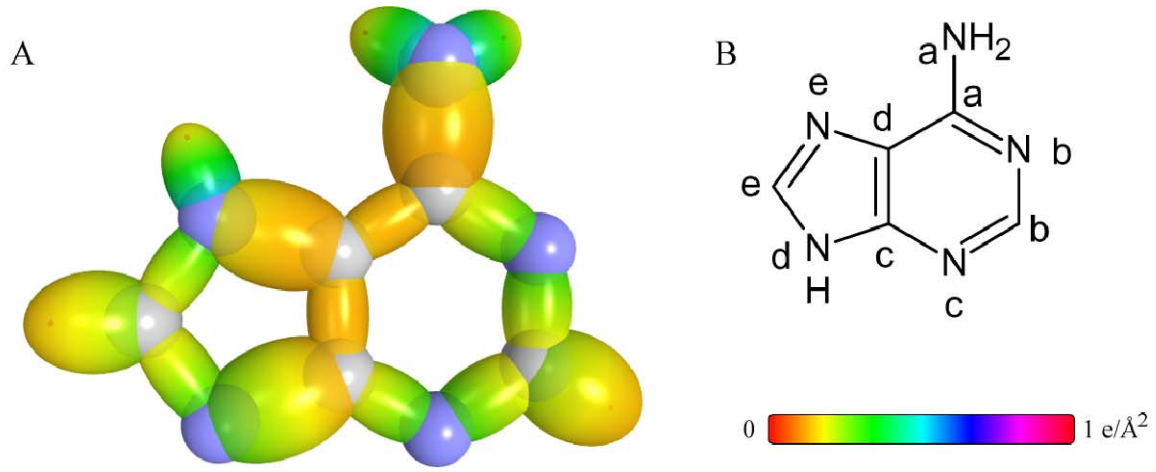

Table 15.327. The symbols of functional groups of adenine.

Functional Group	Group Symbol
CC (aromatic bond)	$C \overset{3e}{=} C$
CH (aromatic)	CH (i)
$C_{b,c} \overset{3e}{=} N_c \qquad C_{a,b} \overset{3e}{=} N_b$	$C \overset{3e}{=} N$
$C_a - N_a$	$C - N$ (a)
NH_2 group	NH_2
$N_e = C_e$ double bond	$N = C$
$C_d - N_e$	$C - N$ (b)
$N_d H$ group	NH
CH	CH (ii)
$C_c - N_d - C_e$	$C - N - C$

Table 15.328. The geometrical bond parameters of adenine and experimental values [1].

Parameter	$C \overset{3e}{=} C$ Group	CH (i) Group	$C \overset{3e}{=} N$ Group	$C-N$ (a) Group	NH_2 Group	$N=C$ Group	$C-N$ (b) Group	NH Group	CH (ii) Group	$C-N-C$ Group
$a\ (a_0)$	1.47348	1.60061	1.47169	1.61032	1.24428	1.44926	1.82450	1.24428	1.53380	1.44394
$c'\ (a_0)$	1.31468	1.03299	1.27073	1.26898	0.94134	1.30383	1.35074	0.94134	1.01120	1.30144
Bond Length $2c'\ (\text{Å})$	1.39140	1.09327	1.34489	1.34303	0.99627	1.37991	1.42956	0.996270	1.07021	1.37738
Exp. Bond Length (Å)	1.393 (pyrimidine)	1.084 (pyridine)	1.340 (pyrimidine)	1.34 [64] (adenine)	0.998 (aniline)			0.996 (pyrrole)	1.076 (pyrrole)	1.370 (pyrrole)
$b,c\ (a_0)$	0.66540	1.22265	0.74237	0.99137	0.81370	0.63276	1.22650	0.81370	1.15326	0.62548
e	0.89223	0.64537	0.86345	0.78803	0.75653	0.89965	0.74033	0.75653	0.65928	0.90131

Table 15.329. The MO to HO intercept geometrical bond parameters of adenine. R_1 is an alkyl group and R, R', R'' are H or alkyl groups. E_T is E_T (*atom – atom,msp*^{3}*.AO*).

Bond	Atom	E_T (eV) Bond 1	E_T (eV) Bond 2	E_T (eV) Bond 3	E_T (eV) Bond 4	Final Total Energy $C2sp^3$ (eV)	$r_{initial}\ (a_0)$	$r_{final}\ (a_0)$	$E_{Coulomb}(C2sp^3)$ (eV) Final	$E(C2sp^3)$ (eV) Final	θ' (°)	θ_1 (°)	θ_2 (°)	$d_1\ (a_0)$	$d_2\ (a_0)$
$C_d(N_b)C_aN_aH-H$	N_a	-0.56690	0	0	0		0.93084	0.88392	-15.39265		121.74	58.26	67.49	0.47634	0.46500
$C_d(N_b)C_a-N_aH_2$	C_a	-0.56690	-0.54343	-0.85035	0	-153.57636	0.91771	0.81052	-16.78642	-16.59556	108.27	71.73	50.93	1.01493	0.25406
$C_d(N_b)C_a-N_aH_2$	N_a	-0.56690	0	0	0		0.93084	0.88392	-15.39265		113.13	66.87	55.08	0.92180	0.34719
$C-H\ (C_bH)$	C_b	-0.54343	-0.54343	-0.56690	0	-153.26945	0.91771	0.82562	-16.47951	-16.28864	78.27	101.73	41.39	1.20084	0.16785
$C-H\ (C_eH)$	C_e	-0.92918	-0.60631	0	0	-153.15119	0.91771	0.83159	-16.36125	-16.17038	86.28	93.72	46.02	1.06512	0.05392
$N-H\ (N_dH)$	N	-0.60631	-0.60631	0	0		0.93084	0.84833	-16.03838		119.52	60.48	65.13	0.52338	0.41796
$C_d(NH_2)C_a \overset{3e}{=} N_bC_b$	C_a	-0.85035	-0.54343	-0.56690	0	-153.57636	0.91771	0.81052	-16.78642	-16.59556	128.54	51.46	58.65	0.76572	0.50501
$C_d(NH_2)C_a \overset{3e}{=} N_bC_b$ $N_bC_b \overset{3e}{=} N_cC_c$	N_b N_c	-0.54343	-0.54343	0	0		0.93084	0.85503	-15.91261		130.61	49.39	60.97	0.71418	0.55656
$N_bC_b \overset{3e}{=} N_cC_c$ $C_aN_b \overset{3e}{=} C_bN_c$	C_b	-0.54343	-0.54343	-0.56690	0	-153.26945	0.91771	0.82562	-16.47951	-16.28865	129.26	50.74	59.44	0.74824	0.52249
$C_d(N_dH)C_c \overset{3e}{=} N_cC_b$	C_c	-0.85035	-0.54343	-0.60631	0	-153.61578	0.91771	0.80863	-16.82584	-16.63498	128.45	51.55	58.55	0.76792	0.50281
$N_b(N_aH_2)C_a \overset{3e}{=} C_d(N_e)C_c$	C_a	-0.85035	-0.54343	-0.56690	0	-153.57636	0.91771	0.81052	-16.78642	-16.59556	134.85	45.15	59.72	0.74304	0.57165
$N_b(N_aH_2)C_a \overset{3e}{=} C_d(N_e)C_c$ $C_a(N_e)C_d \overset{3e}{=} C_c(N_dH)N_c$	C_d	-0.85035	-0.85035	-0.46459	0	-153.78097	0.91771	0.80076	-16.99103	-16.80017	134.44	45.56	59.22	0.75398	0.56071
$C_a(N_e)C_d \overset{3e}{=} C_c(N_dH)N_c$	C_c	-0.85035	-0.54343	-0.60631	0	-153.61578	0.91771	0.80863	-16.82584	-16.63498	134.77	45.23	59.62	0.74516	0.56952
$C_d(N_c)C_c-N_dH$	C_c	-0.85035	-0.54343	-0.60631	0	-153.61578	0.91771	0.80863	-16.82584	-16.63498	137.54	42.46	60.78	0.70488	0.59656
$C_e(H)N_d-C_c(N_c)C_d$ $N_e(H)C_e-N_d(H)C_c$	N_d	-0.60631	-0.60631	0	0		0.93084	0.84833	-16.03838		139.04	40.96	62.76	0.66083	0.64061
$N_e(H)C_e-N_d(H)C_c$	C_e	-0.60631	-0.92918	0	0	-153.15119	0.91771	0.83159	-16.36125	-16.17039	138.42	41.58	61.93	0.67940	0.62203
$C_dN_c-C_e(H)N_dH$	C_e	-0.92918	-0.60631	0	0	-153.15119	0.91771	0.83159	-16.36125	-16.17039	137.93	42.07	61.72	0.68657	0.61726
$C_dN_c-C_e(H)N_dH$	N_e	-0.92918	-0.46459	0	0		0.93084	0.83885	-16.21952		138.20	41.80	62.08	0.67849	0.62534
$C_a(C_c)C_d-N_eC_e$	N_e	-0.46459	-0.92918	0	0		0.93084	0.83885	-16.21952		91.32	88.68	43.14	1.33135	0.01939
$C_a(C_c)C_d-N_eC_e$	C_d	-0.46459	-0.85035	-0.85035	0	-153.78097	0.91771	0.80076	-16.99103	-16.80017	87.71	92.29	40.72	1.38280	0.03206

Table 15.330. The energy parameters (eV) of functional groups of adenine.

Parameters	$C^{3e}=C$ Group	CH (i) Group	$C^{3e}=N$ Group	$C-N$ (a) Group	NH_2 Group	$N=C$ Group	$C-N$ (b) Group	NH Group	CH (ii) Group	$C-N-C$ Group
f_1	0.75	1	0.75	1	1	1	1	1	1	1
n_1	2	1	2	1	2	2	1	1	1	2
n_2	0	0	0	0	0	0	0	0	0	0
n_3	0	0	0	0	1	0	0	0	0	0
C_1	0.5	0.75	0.5	0.5	0.75	0.5	0.5	0.75	0.75	0.5
C_2	0.85252	1	0.91140	1	0.93613	0.85252	1	0.93613	1	0.85252
c_1	1	1	1	1	0.75	1	1	0.75	1	1
c_2	0.85252	0.91771	0.91140	0.84665	0.92171	0.84665	0.84665	0.92171	0.91771	0.84665
c_3	0	1	0	0	0	0	0	1	1	0
c_4	3	1	3	2	1	4	2	1	1	4
c_5	0	1	0	0	2	0	0	1	1	0
C_{1o}	0.5	0.75	0.5	0.5	1.5	0.5	0.5	0.75	0.75	0.5
C_{2o}	0.85252	1	0.91140	1	1	0.85252	1	1	1	0.85252
$V_r\ (eV)$	-101.12679	-37.10024	-102.01431	-35.50149	-78.97795	-103.92756	-32.44864	-39.48897	-39.09538	-104.73877
$V_p\ (eV)$	20.69825	13.17125	21.41410	10.72181	28.90735	20.87050	10.07285	14.45367	13.45505	20.90891
$T\ (eV)$	34.31559	11.58941	34.65890	11.02312	31.73641	35.85539	8.89248	15.86820	12.74462	36.26840
$V_w\ (eV)$	-17.15779	-5.79470	-17.32945	-5.51156	-15.86820	-17.92770	-4.44624	-7.93410	-6.37231	-18.13420
$E_{(AO/HO)}\ (eV)$	0	-14.63489	0	-14.63489	-14.53414	0	-14.63489	-14.53414	-14.63489	0
$\Delta E_{H_2MO\ (AO/HO)}\ (eV)$	0	-1.13379	0	-2.26759	0	-1.85836	-0.92918	0	-2.26758	-2.42526
$E_{I\ (AO/HO)}\ (eV)$	0	-13.50110	0	-12.36730	-14.53414	1.85836	-13.70571	-14.53414	-12.36731	2.42526
$E_{\vert n_1\ AO/HO\rangle}\ (eV)$	0	0	0	0	-14.53414	0	0	0	0	0
$E_{T\ (H_2MO)}\ (eV)$	-63.27075	-31.63539	-63.27076	-31.63543	-48.73654	-63.27100	-31.63527	-31.63534	-31.63533	-63.27040
$E_{I}\left(atom-atom, msp^3.AO\right)\ (eV)$	-2.26759	-0.56690	-1.44915	-1.13379	0	-1.85836	-0.92918	0	0	-2.42526
$E_{T\ (MO)}\ (eV)$	-65.53833	-32.20226	-64.71988	-32.76916	-48.73660	-65.12910	-32.56455	-31.63537	-31.63537	-65.69600
$\omega\left(10^{15}\ rad/s\right)$	49.7272	26.4826	43.6311	14.3055	68.9812	15.4704	21.5213	48.7771	28.9084	54.5632
$E_K\ (eV)$	32.73133	17.43132	28.71875	9.41610	45.40465	10.18290	14.16571	32.10594	19.02803	35.91442
$\bar{E}_D\ (eV)$	-0.35806	-0.26130	-0.33540	-0.19893	-0.42172	-0.20558	-0.24248	-0.35462	-0.27301	-0.38945
$\bar{E}_{Evib}\ (eV)$	0.19649 [49]	0.35532 Eq. (13.458)	0.19649 [49]	0.15498 [58]	0.40929 [22]	0.20768 [62]	0.12944 [23]	0.40696 [24]	0.39427 [60]	0.11159 [12]
$\bar{E}_{inc}\ (eV)$	-0.25982	-0.08364	-0.23715	-0.12144	-0.21708	-0.10174	-0.17775	-0.15115	-0.07587	-0.33365
$E_{rag}\ (eV)$	0.14803	0.14803	0.09457	0.14803	0.14803	0.14803	0.14803	0.14803	0.14803	0.14803
$E_{I\ (Group)}\ (eV)$	-49.54347	-32.28590	-48.82472	-32.89060	-49.17075	-65.33259	-32.74230	-31.78651	-31.71124	-66.36330
$E_{initial\ (c_4\ AO/HO)}\ (eV)$	-14.63489	-14.63489	-14.63489	-14.63489	-14.53414	-14.63489	-14.63489	-14.53414	-14.63489	-14.63489
$E_{initial\ (c_5\ AO/HO)}\ (eV)$	0	-13.59844	0	0	-13.59844	0	0	-13.59844	-13.59844	0
$E_{D\ (Group)}\ (eV)$	5.63881	3.90454	4.92005	3.62082	7.43973	6.79303	3.47253	3.51208	3.32988	7.82374

Table 15.331. The total bond energies of adenine calculated using the functional group composition and the energies of Table 15.330 compared to the experimental values [3].

Formula	Name	$C^{3e}=C$	CH (i)	$C^{3e}=N$ Group	$C-N$ (a) Group	NH_2 Group	$N=C$	$C-N$ (b)	NH	CH (ii)	$C-N-C$	Calculated Total Bond Energy (eV)	Experimental Total Bond Energy (eV)	Relative Error
$C_5H_5N_5$	Adenine	2	1	4	1	1	1	1	1	1	1	70.85416	70.79811	-0.00079

Table 15.332. The bond angle parameters of adenine and experimental values [66]. In the calculation of θ_v, the parameters from the preceding angle were used. E_T is E_T ($atom-atom,msp^3.AO$).

Atoms of Angle	2c' Bond 1 (a_c)	2c' Bond 2 (a_0)	2c' Terminal Atoms (a_0)	$E_{Coulombic}$ Atom 1	Atom 1 Hybridization Designation (Table 15.3B)	$E_{Coulombic}$ Atom 2	Atom 2 Hybridization Designation (Table 15.3B)	c_2 Atom 1	c_2 Atom 2	C_1	C_2	c_1	c_2'	E_T (eV)	θ_v (°)	θ_1 (°)	θ_2 (°)	Cal. θ (°)	Exp. θ (°)
$\angle HNH$	1.88268	1.88268	3.1559	-14.53414	N	H	H	0.93613 Eq. (13.248)	1	1	1	0.75	1.06823	0				113.89	113.9 [1] (aniline)
$\angle C_aNH$	2.53797	1.88268	3.8123	-16.78642	19	-14.53414	N	0.81052 Eq. (15.71)	0.77638 Eq. (15.173)	0.75	1	0.75	0.95787	0				118.42	118
$\angle N_bC_bN_c$	2.54147	2.54147	4.5826	-15.55033	3	-15.55033	3	0.87495	0.87495	1	1	1	0.87495	-1.44915				128.73	128.9
$\angle H_bC_bN_b$ $\angle H_bC_bN_c$																	128.73	115.64 Eq. (15.109)	115 116
$\angle H_cC_cN_e$	2.02241	2.60766	4.0661	-16.36125	12	-14.53414	N	0.83159	0.84665 Eq. (15.171)	0.75	1	0.75	1.01811	0				122.35	126
$\angle N_cC_cN_d$	2.60766	2.60287	4.3359	-16.21952	9	-16.03838	7	0.83885	0.84833	1	1	1	0.84359	-1.44915				112.64	114.4
$\angle N_cC_cN_d$	2.54147	2.60287	4.6260	-14.53414	N	-14.53414	N	0.91140 Eq. (15.135)	0.84665 Eq. (15.171)	1	1	1	0.87902	-1.44915				128.11	127.8
$\angle H_cC_cN_d$																122.35	112.64	125.02	119
$\angle H_dN_dC_e$	1.88268	2.60287	4.0166	-14.53414	N	-15.95955	6	0.84665 Eq. (15.171)	0.85252 Eq. (15.162)	0.75	1	0.75	1.00693	0				126.39	127
$\angle C_eN_dC_e$	2.60287	2.60287	4.1952	-17.95963	39	-17.95963	39	0.75758	0.75758	1	1	1	0.75758	-1.85836				107.39	106.1
$\angle H_dN_dC_c$																126.39	107.39	126.22	127
$\angle N_aC_aC_d$	2.53797	2.62936	4.5387	-14.53414	N	-16.52644 C_d	15	0.91140 Eq. (15.135)	0.82327	1	1	1	0.86734	-1.44915				122.88	122.1
$\angle N_bC_aC_d$	2.54147	2.62936	4.4272	-14.53414	N	-16.99103 C_d	21	0.91140 Eq. (15.135)	0.80076	1	1	1	0.85608	-1.44915				117.77	118.2
$\angle N_bC_aN_a$																122.88	117.77	119.35	119.4
$\angle N_eC_dC_c$	2.70148	2.62936	4.3818	-14.53414	N	-15.95955 C_c	6	0.84665 Eq. (15.171)	0.85252	1	1	1	0.84958	-1.44915				110.56	110.4
$\angle N_dC_cC_d$	2.60287	2.62936	4.1952	-14.53414	N	-16.99103 C_d	21	0.84665 Eq. (15.171)	0.80076	1	1	1	0.82371	-1.44915				106.60	105.9
$\angle N_cC_cC_d$	2.54147	2.62936	4.6043	-14.53414	N	-16.52644 C_d	15	0.84665 Eq. (15.171)	0.82327	1	1	1	0.83496	-1.65376				125.85	126.4
$\angle N_eC_dC_a$	2.70148	2.62936	4.8580	-14.53414	N	-16.78642 C_a	1	0.91140 Eq. (15.135)	0.81052	1	1	1	0.86096	-1.65376				131.37	132.8
$\angle C_dN_eC_e$	2.70148	2.60766	4.2661	-17.92022	37	-17.92022	37	0.75924	0.75924	1	1	1	0.75924	-1.85836				106.93	103.3
$\angle C_bN_cC_c$	2.54147	2.54147	4.1952	-17.95963	39	-17.95963	39	0.75758	0.75758	1	1	1	0.75758	-1.85836				111.25	111.3
$\angle C_aN_bC_b$	2.54147	2.54147	4.3704	-17.71560	33	-17.40869	30	0.76801	0.78155	1	1	1	0.77478	-1.85836				118.59	118.6
$\angle C_aC_dC_c$	2.62936	2.62936	4.4721	-17.71560	33	-17.14871	26	0.76801	0.79340	1	1	1	0.78071	-1.85836				116.52	116.7

THYMINE

Thymine having the formula $C_5H_6N_2O_2$ is a pyrimidine with carbonyl substitutions at positions C_a and C_b and a methyl substitution at position C_d further comprising a vinyl group as shown in Figure 15.57B. Each $C=O$, adjacent $C-N$, and NH functional group is equivalent to the corresponding group of alkyl amides. The methyl-vinyl moiety is equivalent to the CH_3, $-C(C)=C$, CH, and $C=C$ functional groups of alkenes. Thymine further comprises N_bH and $C_b-N_c-C_c$ groups that are equivalent to the corresponding groups of imidazole as given in the corresponding section. The C_a-C_d bond comprises another functional group that is equivalent to the C_a-C_d group of guanine.

The symbols of the functional groups of thymine are given in Table 15.333. The geometrical (Eqs. (15.1-15.5) and (15.51)), intercept (Eqs. (15.80-15.87)), and energy (Eqs. (15.6-15.11) and (15.17-15.65)) parameters of thymine are given in Tables 15.334, 15.335, and 15.336, respectively. The total energy of thymine given in Table 15.337 was calculated as the sum over the integer multiple of each $E_D(Group)$ of Table 15.336 corresponding to functional-group composition of the molecule. The bond angle parameters of thymine determined using Eqs. (15.88-15.117) are given in Table 15.338. The color scale, charge-density of thymine comprising atoms with the outer shell bridged by one or more H_2-type ellipsoidal MOs or joined with one or more hydrogen MOs is shown in Figure 15.57A.

Figure 15.57. (A) Color scale, charge-density of thymine showing the orbitals of the atoms at their radii, the ellipsoidal surface of each H or H_2-type ellipsoidal MO that transitions to the corresponding outer shell of the atom(s) participating in each bond, and the hydrogen nuclei. (B) Chemical structure and atom designation of thyamine.

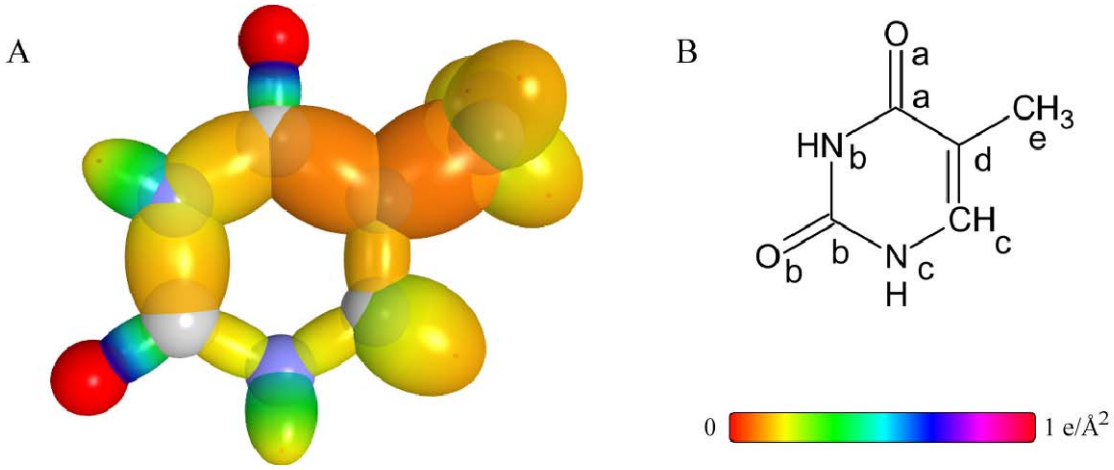

Table 15.333. The symbols of functional groups of thymine.

Functional Group	Group Symbol
$C_a=O$ $C_b=O$ (alkyl amide)	$C=O$
C_a-N_b C_b-N_b amide	$C-N$
N_bH amide group	NH (i)
CH_3 group	$C-H$ (CH_3)
$C_c=C_d$ double bond	$C=C$
C_d-C_e	$C-C$ (i)
C_a-C_d	$C-C$ (ii)
$C_b-N_c-C_c$	$C-N-C$
N_cH *group*	NH (ii)
C_cH	CH

Table 15.334. The geometrical bond parameters of thymine and experimental values [1].

Parameter	$C=O$ Group	$C-N$ Group	NH (i) Group	$C-H\ (CH_3)$ Group	$C=C$ Group	$C-C$ (i) Group	$C-C$ (ii) Group	$C-N-C$ Group	NH (ii) Group	CH Group
$a\ (a_0)$	1.29907	1.75370	1.28620	1.64920	1.47228	2.04740	1.88599	1.43222	1.24428	1.53380
$c'\ (a_0)$	1.13977	1.32427	0.95706	1.04856	1.26661	1.43087	1.37331	1.29614	0.94134	1.01120
Bond Length $2c'\ (\AA)$	1.20628	1.40155	1.01291	1.10974	1.34052	1.51437	1.45345	1.37178	0.996270	1.07021
Exp. Bond Length $(\AA)$	1.220 (acetamide) 1.225 (N-methylacetamide)	1.380 (acetamide)		1.107 ($C-H$ propane) 1.117 ($C-H$ butane)	1.34 [64] (thymine) 1.342 (2-methylpropene) 1.346 (2-butene) 1.349 (1,3-butadiene)		1.43 [65] (thymine)	1.370 (pyrrole)	0.996 (pyrrole)	1.076 (pyrrole)
$b,c\ (a_0)$	0.62331	1.14968	0.85927	1.27295	0.75055	1.46439	1.29266	0.60931	0.81370	1.15326
e	0.87737	0.75513	0.74410	0.63580	0.86030	0.69887	0.72817	0.90499	0.75653	0.65928

Table 15.335. The MO to HO intercept geometrical bond parameters of thymine. R_1 is an alkyl group and R, R', R'' are H or alkyl groups. E_T is E_T ($atom-atom, msp^3.AO$).

Bond	Atom	E_T (eV) Bond 1	E_T (eV) Bond 2	E_T (eV) Bond 3	E_T (eV) Bond 4	Final Total Energy $C2sp^3$ (eV)	$r_{initial}$ (a_0)	r_{final} (a_0)	$E_{Coulomb}(C2sp^3)$ (eV) Final	$E(C2sp^3)$ (eV) Final	θ' (°)	θ_1 (°)	θ_2 (°)	d_1 (a_0)	d_2 (a_0)
$N_b(C_d)C_a=O$	O_a	-1.34946	0	0	0		1.00000	0.84115	-16.17521		137.27	42.73	66.31	0.52193	0.61784
$N_b(C_d)C_a=O$	C_a	-1.34946	-0.82688	0	0	-153.79203	0.91771	0.80024	-17.00209	-16.81123	135.55	44.45	64.05	0.56855	0.57122
$N-H\ (N_bH)$	N_b	-0.82688	-0.82688	0	0		0.93084	0.82562	-16.47951		118.03	61.97	63.59	0.55339	0.38795
$C_d(O)C_a-N_bH(C_b)$	N_b	-0.82688	-0.82688	0	0		0.93084	0.82562	-16.47951		96.62	83.38	45.51	1.22903	0.09524
$C_d(O)C_a-N_bH(C_b)$	C_a	-0.82688	-1.34946	0	0	-153.79203	0.91771	0.80024	-17.00209	-16.81123	94.42	85.58	43.95	1.26264	0.06164
$C_aN_bH-C_b(O)N_cH$	N_b	-0.82688	-0.82688	0	0		0.93084	0.82562	-16.47951		96.62	83.38	45.51	1.22903	0.09524
$C_aN_bH-C_b(O)N_cH$	C_b	-0.82688	-1.34946	-0.82688	0	-154.61891	0.91771	0.76313	-17.82897	-17.63811	90.94	89.06	41.58	1.31179	0.01249
$(HN_c)(HN_b)C_b=O$	O_b	-1.34946	0	0	0		1.00000	0.84115	-16.17521		137.27	42.73	66.31	0.52193	0.61784
$(HN_c)(HN_b)C_b=O$	C_b	-1.34946	-0.82688	-0.92918	0	-154.72121	0.91771	0.75878	-17.93127	-17.74041	133.67	46.33	61.70	0.61582	0.52395
$N-H\ (N_cH)$	N_c	-0.92918	-0.92918	0	0		0.93084	0.81549	-16.68411		117.34	62.66	62.90	0.56678	0.37456
$N_b(O)C_b-N_cHC_c$	N_c	-0.92918	-0.92918	0	0		0.93084	0.81549	-16.68411		138.92	41.08	61.59	0.68147	0.61467
$N_b(O)C_b-N_cHC_c$	C_b	-0.92918	-1.34946	-0.82688	0	-154.72121	0.91771	0.75878	-17.93127	-17.74041	136.68	43.32	58.70	0.74414	0.55200
$C_bHN_c-HC_cC_d$	N_c	-0.92918	-0.92918	0	0		0.93084	0.81549	-16.68411		138.92	41.08	61.59	0.68147	0.61467
$C_bHN_c-HC_cC_d$	C_c	-0.92918	-1.13379	0	0	-153.67866	0.91771	0.80561	-16.88873	-16.69786	138.54	41.46	61.09	0.69238	0.60376
$C-H\ (C_cH)$	C_c	-1.13380	-0.92918	0	0	-153.67867	0.91771	0.80561	-16.88873	-16.69786	83.35	96.65	43.94	1.10452	0.09331
$N_cHC_c=C_dC_a(C_e)$	C_c	-1.13380	-0.92918	-0.72457	0	-154.40324	0.91771	0.77247	-17.61330	-17.42244	125.92	54.08	56.46	0.81345	0.45316
$N_cHC_c=C_dC_a(C_e)$	C_d	-1.13380	0	-0.72457	0	-153.47406	0.91771	0.81549	-16.68412	-16.49326	128.10	51.90	58.77	0.76344	0.50317
$C-H\ (CH_3)$	C_e	-0.72457	0	0	0	-152.34026	0.91771	0.87495	-15.55033	-15.35946	78.85	101.15	42.40	1.21777	0.16921
$(C_a)C_cC_d-C_eH_3$	C_e	-0.72457	0	0	0	-152.34026	0.91771	0.87495	-15.55033	-15.35946	73.62	106.38	34.98	1.67762	0.24675
$(C_a)C_cC_d-C_eH_3$	C_d	-0.72457	-1.13379	0	0	-153.47406	0.91771	0.81549	-16.68412	-16.49325	65.99	114.01	30.58	1.76270	0.33183
$(C_e)C_cC_d-C_a(O)N_b$	C_a	0	-1.34946	-0.82688	0	-153.79203	0.91771	0.80024	-17.00209	-16.81123	81.54	98.46	37.76	1.49107	0.11776
$(C_e)C_cC_d-C_a(O)N_b$	C_d	0	-1.13379	-0.72457	0	-153.47406	0.91771	0.81549	-16.68412	-16.49325	92.72	87.28	45.17	1.32975	0.04357

Table 15.336. The energy parameters (eV) of functional groups of thymine.

Parameters	$C=O$ Group	$C-N$ Group	NH (i) Group	$C=C$ Group	CH_3 Group	$C-C$ (i) Group	$C-C$ (ii) Group	$C-N-C$ Group	NH (ii) Group	CH Group
n_1	2	1	1	2	3	1	1	2	1	1
n_2	0	0	0	0	2	0	0	0	0	0
n_3	0	0	0	0	0	0	0	0	0	0
C_1	0.5	0.5	0.75	0.5	0.75	0.5	0.5	0.5	0.75	0.75
C_2	1	1	0.93613	0.91771	1	1	1	0.85252	0.93613	1
c_1	1	1	0.75	1	1	1	1	1	0.75	1
c_2	0.85395	0.91140	1	0.91771	0.91771	0.91771	0.91771	0.84665	0.92171	0.91771
c_3	2	0	1	0	0	1	0	0	1	1
c_4	4	2	1	4	1	2	2	4	1	1
c_5	0	0	1	0	3	0	0	0	1	1
C_{1o}	0.5	0.5	0.75	0.5	0.75	0.5	0.5	0.5	0.75	0.75
C_{2o}	1	1	1	0.91771	1	1	1	0.85252	1	1
V_e (eV)	-111.25473	-36.88558	-40.92593	-102.08992	-107.32728	-30.19634	-33.63376	-106.58684	-39.48897	-39.09538
V_p (eV)	23.87467	10.27417	14.21618	21.48386	38.92728	9.50874	9.90728	20.99432	14.45367	13.45505
T (eV)	42.82081	10.51650	15.90963	34.67062	32.53914	7.37432	8.91674	37.21047	15.86820	12.74462
V_m (eV)	-21.41040	-5.25825	-7.95482	-17.33531	-16.26957	-3.68716	-4.45837	-18.60523	-7.93410	-6.37231
$E_{(AO/HO)}$ (eV)	0	-14.63489	-14.53414	0	-15.56407	-14.63489	-14.63489	0	-14.53414	-14.63489
$\Delta E_{H_2MO(AO/HO)}$ (eV)	-2.69893	-4.35268	-1.65376	0	0	0	-2.26759	-3.71673	0	-2.26758
$E_{T(AO/HO)}$ (eV)	2.69893	-10.28221	-12.88038	0	-15.56407	-14.63489	-12.36730	3.71673	-14.53414	-12.36731
$E_{(n_3\ AO/HO)}$ (eV)	0	0	0	0	0	0	0	0	0	0
$E_{T(H_2MO)}$ (eV)	-63.27074	-31.63537	-31.63531	-63.27075	-67.69451	-31.63534	-31.63541	-63.27056	-31.63534	-31.63533
$E_T\left(atom-atom, msp^3.AO\right)$ (eV)	-2.69893	-1.65376	0	-2.26759	0	-1.44915	0.00000	-3.71673	0	0
$E_{T(MO)}$ (eV)	-65.96966	-33.28912	-31.63537	-65.53833	-67.69450	-33.08452	-31.63537	-66.98746	-31.63537	-31.63537
$\omega\ \left(10^{15}\ rad/s\right)$	59.4034	12.5874	44.9494	43.0680	24.9286	9.97851	19.8904	15.7474	48.7771	28.9084
E_K (eV)	39.10034	8.28526	29.58649	28.34813	16.40846	6.56803	13.09221	10.36521	32.10594	19.02803
$\overline{E}_D$ (eV)	-0.40804	-0.18957	-0.34043	-0.34517	-0.25352	-0.16774	-0.22646	-0.21333	-0.35462	-0.27301
$\overline{E}_{Kvib}$ (eV)	0.21077 [12]	0.17358 [33]	0.40696 [24]	0.17897 [6]	0.35532 Eq. (13.458)	0.15895 [7]	0.14667 [67]	0.11159 [12]	0.40696 [24]	0.39427 [60]
$\overline{E}_{osc}$ (eV)	-0.30266	-0.10278	-0.13695	-0.25568	-0.22757	-0.08827	-0.15312	-0.15754	-0.15115	-0.07587
E_{mag} (eV)	0.11441	0.14803	0.14185	0.14803	0.14803	0.14803	0.14803	0.14803	0.14803	0.14803
$E_{T(Group)}$ (eV)	-66.57498	-33.39190	-31.77232	-66.04969	-67.92207	-33.17279	-31.64046	-67.30254	-31.78651	-31.71124
$E_{initial\ (c_4\ AO/HO)}$ (eV)	-14.63489	-14.63489	-14.53414	-14.63489	-14.63489	-14.63489	-14.63489	-14.63489	-14.53414	-14.63489
$E_{initial\ (c_5\ AO/HO)}$ (eV)	0	0	-13.59844	0	-13.59844	0	0	0	-13.59844	-13.59844
$E_{D(Group)}$ (eV)	7.80660	4.12212	3.49788	7.51014	12.49186	3.75498	2.37068	8.76298	3.51208	3.32988

Table 15.337. The total gaseous bond energies of thymine calculated using the functional group composition and the energies of Table 15.336 compared to the experimental values [3].

Formula	Name	$C=O$ Group	$C-N$ Group	NH (i) Group	$C=C$ Group	CH_3 Group	$C-C$ (i) Group	$C-C$ (ii) Group	$C-N-C$ Group	NH (ii) Group	CH Group	Calculated Total Bond Energy (eV)	Experimental Total Bond Energy (eV)	Relative Error
$C_5H_5N_2O_2$	Thymine	2	2	1	1	1	1	1	1	1	1	69.08792	69.06438	-0.00034

Table 15.338. The bond angle parameters of thymine and experimental values [64]. In the calculation of θ_v, the parameters from the preceding angle were used. E_T is $E_T\,(atom-atom, msp^3.AO)$.

Atoms of Angle	$2c'$ Bond 1 (a_0)	$2c'$ Bond 2 (a_0)	$2c'$ Terminal Atoms (a_0)	$E_{Coulombic}$ Atom 1	Atom 1 Hybridization Designation (Table 15.3B)	$E_{Coulombic}$ Atom 2	Atom 2 Hybridization Designation (Table 15.3B)	c_2 Atom 1	c_2 Atom 2	C_1	C_2	c_1	c_2'	E_T (eV)	θ_v (°)	θ_1 (°)	θ_2 (°)	Cal. θ (°)	Exp. θ (°)
$\angle N_bC_aC_d$	2.64855	2.74663	4.5277	-14.53414	N	-16.68412 C_d	18	0.91140 Eq. (15.135)	0.81549	1	1	1	0.86345	-1.44915				114.10	115.7
$\angle N_bC_aO$	2.64855	2.27954	4.2661	-16.47951	14	-16.17521	8	0.82562	0.84115	1	1	1	0.83339	-1.44915				119.73	119.5
$\angle OC_aC_d$																114.10	119.73	126.17	124.8
$\angle C_bN_bC_a$	2.64855	2.64855	4.6904	-17.40869	30	-16.58181	16	0.78155	0.82053	1	1	1	0.80104	-1.85836				124.62	126.1
$\angle N_bC_bN_c$	2.64855	2.59228	4.4497	-16.47951	14	-16.68411	17	0.82562	0.81549	1	1	1	0.82056	-1.65376				116.21	115.1
$\angle H_bN_bC_a$	1.88268	2.64855	3.9158	-14.53414	N	-14.82575 C_a	1	0.93613 Eq. (13.248)	0.91771	0.75	1	0.75	0.98033	0				118.60	
$\angle C_bN_bH_b$																124.62	118.60	116.78	
$\angle C_bN_cC_c$	2.59228	2.59228	4.4944	-17.93127	38	-16.88873	20	0.75878	0.80561	1	1	1	0.78219	-1.85836				120.20	120.7
$\angle N_cC_bO_b$	2.59228	2.27954	4.2661	-16.68411	18	-16.17521	8	0.81549	0.84115	1	1	1	0.82832	-1.44915				122.12	123.7
$\angle N_bC_bO_b$																116.21	122.12	121.67	121.2
$\angle N_cC_cC_d$	2.59228	2.53321	4.5387	-14.53414	N	-16.68412	18	0.84665 Eq. (15.171)	0.81549	1	1	1	0.83107	-1.65376				124.63	122.9
$\angle H_cN_cC_c$	1.88268	2.59228	3.8644	-14.53414	N	-16.68412	18	0.84665 Eq. (15.171)	0.81549	0.75	1	0.75	0.96320	0				118.58	
$\angle H_cN_cC_b$																120.20	118.58	121.23	
$\angle H_cC_cC_d$	2.02241	2.53321	3.9833	-15.95955	6	-15.95955	6	0.85252	0.85252	0.75	1	0.75	1.00000	0				121.54	
$\angle H_cC_cN_c$																124.63	121.54	113.84	
$\angle C_dC_dC_c$	2.74663	2.53321	4.5387	-17.00209	22	-17.61330	32	0.80024	0.77247	1	1	1	0.78636	-1.85836				118.49	118.5
$\angle C_cC_dC_c$	2.86175	2.53321	4.7117	-16.47951	14	-17.40869	30	0.82562	0.78155	1	1	1	0.80359	-1.85836				121.58	123.3
$\angle C_cC_dC_a$																118.49	121.58	119.93	118.2
Methyl $\angle HC_cH$	2.09711	2.09711	3.4252	-15.75493 C_c	4	H	H	0.86359	1	1	1	0.75	1.15796	0				109.50	

GUANINE

Guanine having the formula $C_5H_5N_5O$ is a purine with a carbonyl substitution at position C_a, and a primary amine moiety is at position C_b as shown in Figure 15.58B. The carbonyl functional group is equivalent to that of alkyl amides and the NH_2 and C_b-N_a functional groups of the primary amine moiety are equivalent to the NH_2 and C_a-N_a functional groups of adenine. Guanine further comprises an imidazole moiety wherein the CH, N_dH, $C_d=C_c$, C_d-N_e, $N_e=C_e$, and $C_c-N_d-C_e$ groups of the imidazole-type ring are equivalent to the corresponding groups of imidazole as given in the corresponding section. The six-membered ring also comprises the groups $C_a-N_b-C_b$, N_bH, $N_c=C_c$, and C_c-N_d that are equivalent to the corresponding imidazole and adenine functional groups. The C_a-C_d bond comprises another functional group that is the C_{60}-single-bond functional group except that $E_T\left(atom-atom, msp^3.AO\right)=0$ in order to match the energies of the single and double-bonded moieties within the molecule.

The symbols of the functional groups of guanine are given in Table 15.339. The geometrical (Eqs. (15.1-15.5) and (15.51)), intercept (Eqs. (15.80-15.87)), and energy (Eqs. (15.6-15.11) and (15.17-15.65)) parameters of guanine are given in Tables 15.340, 15.341, and 15.342, respectively. The total energy of guanine given in Table 15.343 was calculated as the sum over the integer multiple of each $E_D(Group)$ of Table 15.342 corresponding to functional-group composition of the molecule. The bond angle parameters of guanine determined using Eqs. (15.88-15.117) are given in Table 15.344. The color scale, charge-density of guanine comprising atoms with the outer shell bridged by one or more H_2-type ellipsoidal MOs or joined with one or more hydrogen MOs is shown in Figure 15.58A.

Figure 15.58. (A) Color scale, charge-density of guanine showing the orbitals of the atoms at their radii, the ellipsoidal surface of each H or H_2-type ellipsoidal MO that transitions to the corresponding outer shell of the atom(s) participating in each bond, and the hydrogen nuclei. (B) Chemical structure and atomic designation of guanine.

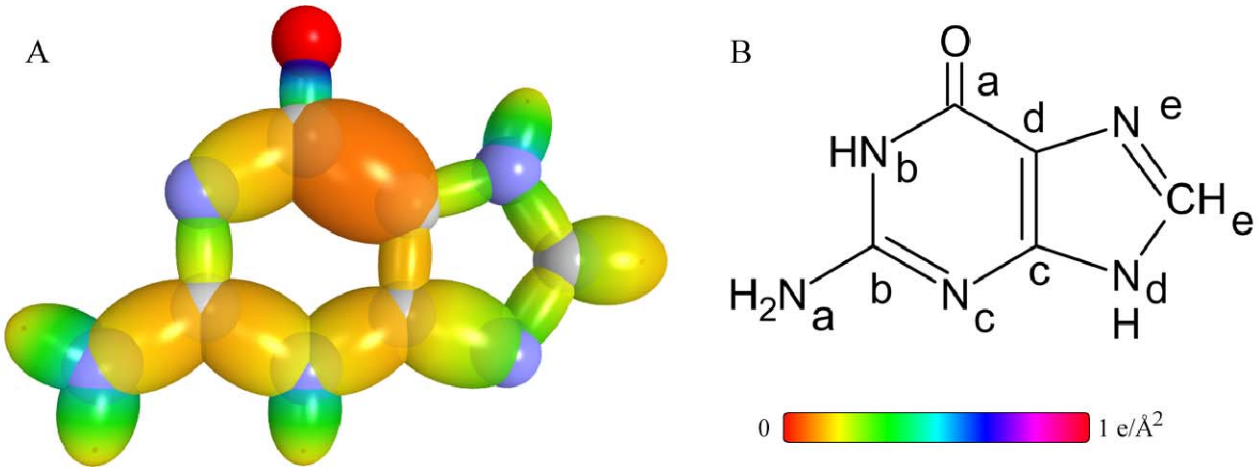

Table 15.339. The symbols of functional groups of guanine.

Functional Group	Group Symbol
$C_a = O$ (alkyl amide)	$C = O$
$C_b - N_a$	$C - N$ (a)
NH_2 group	NH_2
$C_c = C_d$ double bond	$C = C$
$C_a - C_d$	$C - C$
$N_e = C_e$ $N_c = C_b$ double bond	$N = C$
$C_d - N_e$ $C_c - N_c$	$C - N$ (b)
$C_c - N_d - C_e$ $C_a - N_b - C_b$	$C - N - C$
N_dH N_bH *group*	NH
C_eH	CH

Table 15.340. The geometrical bond parameters of guanine and experimental values [1].

Parameter	$C=O$ Group	$C-N$ (a) Group	NH_2 Group	$C=C$ Group	$C-C$ Group	$N=C$ Group	$C-N$ (b) Group	$C-N-C$ Group	NH Group	CH Group
$a\ (a_0)$	1.29907	1.61032	1.24428	1.45103	1.88599	1.44926	1.82450	1.43222	1.24428	1.53380
$c\ (a_0)$	1.13977	1.26898	0.94134	1.30463	1.37331	1.30383	1.35074	1.29614	0.94134	1.01120
Bond Length $2c'\ (\AA)$	1.20628	1.34303	0.99627	1.38076	1.45345	1.37991	1.42956	1.37178	0.996270	1.07021
Exp. Bond Length $(\AA)$	1.220 (acetamide) 1.225 (N-methylacetamide)	1.34 [64] (guanine)	0.998 (aniline)	1.382 (pyrrole)	1.42 [64] (guanine)			1.370 (pyrrole)	0.996 (pyrrole)	1.076 (pyrrole)
$b,c\ (a_0)$	0.62331	0.99137	0.81370	0.63517	1.29266	0.63276	1.22650	0.60931	0.81370	1.15326
e	0.87737	0.78803	0.75653	0.89910	0.72817	0.89965	0.74033	0.90499	0.75653	0.65928

Table 15.341. The MO to HO intercept geometrical bond parameters of guanine. R_1 is an alkyl group and R, R', R'' are H or alkyl groups. E_T is E_T ($atom-atom,msp^3.AO$).

Bond	Atom	E_T (eV) Bond 1	E_T (eV) Bond 2	E_T (eV) Bond 3	E_T (eV) Bond 4	Final Total Energy $C2sp^3$ (eV)	$r_{initial}$ (a_0)	r_{final} (a_0)	$E_{Coulomb}(C2sp^3)$ (eV) Final	$E(C2sp^3)$ (eV) Final	θ' (°)	θ_1 (°)	θ_2 (°)	d_1 (a_0)	d_2 (a_0)
$N_b(C_d)C_a=O$	O	-1.34946	0	0	0		1.00000	0.84115	-16.17521		137.27	42.73	66.31	0.52193	0.61784
$N_b(C_d)C_a=O$	C_c	-1.34946	-0.92918	0	0	-153.89433	0.91771	0.79546	-17.10440	-16.91353	135.34	44.66	63.78	0.57401	0.56576
$N-H\ (N_bH)$	N_b	-0.92918	-0.92918	0	0		0.93084	0.81549	-16.68411		117.34	62.66	62.90	0.56678	0.37456
$C_d(O)C_a-N_bH(C_b)$	N_b	-0.92918	-0.92918	0	0		0.93084	0.81549	-16.68411		138.92	41.08	61.59	0.68147	0.61467
$C_d(O)C_a-N_bH(C_b)$	C_c	-1.34946	-0.92918	0	0	-153.89433	0.91771	0.79546	-17.10440	-16.91353	138.15	41.85	60.58	0.70361	0.59253
$C_d(O)C_aN_bH-C_bN_c(N_aH_2)$	N_b	-0.92918	-0.92918	0	0		0.93084	0.81549	-16.68411		138.92	41.08	61.59	0.68147	0.61467
$C_d(O)C_aN_bH-C_bN_c(N_aH_2)$	C_t	-0.56690	-0.92918	-0.92918	0	-154.04095	0.91771	0.78870	-17.25101	-17.06015	137.89	42.11	60.23	0.71108	0.58506
$N_c(N_b)C_bN_aH-H$	N_a	-0.56690	0	0	0		0.93084	0.88392	-15.39265		121.74	58.26	67.49	0.47634	0.46500
$HN_bC_b-N_aH_2(N_c)$	N_a	-0.56690	0	0	0		0.93084	0.88392	-15.39265		113.13	66.87	55.08	0.92180	0.34719
$HN_bC_b-N_aH_2(N_c)$	C_t	-0.56690	-0.92918	-0.92918	0	-154.04095	0.91771	0.78870	-17.25101	-17.06015	106.68	73.32	49.65	1.04263	0.22636
$HN_bC_b=N_cC_c(N_aH_2)$	N_c	-0.92918	-0.46459	0	0		0.93084	0.83885	-16.21952		138.20	41.80	62.08	0.67849	0.62534
$HN_bC_b=N_cC_c(N_aH_2)$	C_t	-0.92918	-0.92918	-0.56690	0	-154.04095	0.91771	0.78870	-17.25101	-17.06015	136.24	43.76	59.56	0.73424	0.56959
$C_bN_c-C_cC_d(N_dH)$	N_c	-0.46459	-0.92918	0	0		0.93084	0.83885	-16.21953		91.32	88.68	43.14	1.33135	0.01939
$C_bN_c-C_cC_d(N_dH)$	C_c	-0.46459	-1.13380	-0.92918	0	-154.14326	0.91771	0.78405	-17.35332	-17.16246	86.00	94.00	39.62	1.40538	0.05464
$N_c(N_dH)C_c=C_dN_e(C_a)$	C_c	-1.13380	-0.92918	-0.46459	0	-154.14326	0.91771	0.78405	-17.35332	-17.16246	135.87	44.13	59.25	0.74183	0.56280
$N_c(N_dH)C_c=C_dN_e(C_a)$	C_d	-1.13380	-0.46459	0	0	-153.21408	0.91771	0.82840	-16.42414	-16.23327	137.64	42.36	61.49	0.69250	0.61213
$N-H\ (N_dH)$	N_d	-0.92918	-0.92918	0	0		0.93084	0.81549	-16.68411		117.34	62.66	62.90	0.56678	0.37456
$(N_c)C_dC_c-N_dH(C_e)$	N_d	-0.92918	-0.92918	0	0		0.93084	0.81549	-16.68411		138.92	41.08	61.59	0.68147	0.61467
$(N_c)C_dC_c-N_dH(C_e)$	C_c	-1.13379	-0.92918	-0.46459	0	-154.14326	0.91771	0.78405	-17.35332	-17.16245	137.70	42.30	59.99	0.71622	0.57992
$C-H\ (C_eH)$	C_e	-0.92918	-0.92918	0	0	-153.47405	0.91771	0.81549	-16.68411	-16.49325	84.49	95.51	44.47	1.08953	0.07833
$C_eHN_dH-C_eH(N_e)$	N_d	-0.92918	-0.92918	0	0		0.93084	0.81549	-16.68411		138.92	41.08	61.59	0.68147	0.61467
$C_eHN_dH-C_eH(N_e)$	C_e	-0.92918	-0.92918	0	0	-153.47405	0.91771	0.81549	-16.68411	-16.49325	138.92	41.08	61.59	0.68147	0.61467
$N_d(H)C_e=N_eC_d$	N_e	-0.92918	-0.46459	0	0		0.93084	0.83885	-16.21952		138.20	41.80	62.08	0.67849	0.62534
$N_d(H)C_e=N_eC_d$	C_e	-0.92918	-0.92918	0	0	-153.47405	0.91771	0.81549	-16.68411	-16.49325	137.31	42.69	60.92	0.70446	0.59938
$C_eN_e-C_dC_a(C_c)$	N_e	-0.46459	-0.92918	0	0		0.93084	0.83885	-16.21953		91.32	88.68	43.14	1.33135	0.01939
$C_eN_e-C_dC_a(C_c)$	C_d	-0.46459	-1.13380	0	0	-153.21408	0.91771	0.82840	-16.42414	-16.23327	90.36	89.64	42.49	1.34547	0.00527
$(N_e)C_cC_d-C_a(O)N_b$	C_c	0.00000	-1.34946	-0.92918	0	-153.89433	0.91771	0.79546	-17.10440	-16.91353	81.01	98.99	37.43	1.49764	0.12433
$(N_e)C_cC_d-C_a(O)N_b$	C_d	0.00000	-1.13379	-0.46459	0	-153.21407	0.91771	0.82840	-16.42413	-16.23327	92.72	87.28	45.17	1.32975	0.04357

Table 15.342. The energy parameters (eV) of functional groups of guanine.

Parameters	$C=O$ Group	$C-N$ (a) Group	NH_2 Group	$C=C$ Group	$C-C$ Group	$N=C$ Group	$C-N$ (b) Group	$C-N-C$ Group	NH Group	CH Group
n_1	2	1	2	2	1	2	1	2	1	1
n_2	0	0	0	0	0	0	0	0	0	0
n_3	0	0	1	0	0	0	0	0	0	0
C_1	0.5	0.5	0.75	0.5	0.5	0.5	0.5	0.5	0.75	0.75
C_2	1	1	0.93613	0.85252	1	0.85252	1	0.85252	0.93613	1
c_1	1	1	0.75	1	1	1	1	1	0.75	1
c_2	0.85395	0.84665	0.92171	0.85252	0.91771	0.84665	0.84665	0.84665	0.92171	0.91771
c_3	2	0	0	0	0	0	0	0	1	1
c_4	4	2	1	4	2	4	2	4	1	1
c_5	0	0	2	0	0	0	0	0	1	1
C_{1o}	0.5	0.5	1.5	0.5	0.5	0.5	0.5	0.5	0.75	0.75
C_{2o}	1	1	1	0.85252	1	0.85252	1	0.85252	1	1
V_e (eV)	-111.25473	-35.50149	-78.97795	-104.37986	-33.63376	-103.92756	-32.44864	-106.58684	-39.48897	-39.09538
V_p (eV)	23.87467	10.72181	28.90735	20.85777	9.90728	20.87050	10.07285	20.99432	14.45367	13.45505
T (eV)	42.82081	11.02312	31.73641	35.96751	8.91674	35.85539	8.89248	37.21047	15.86820	12.74462
V_n (eV)	-21.41040	-5.51156	-15.86820	-17.98376	-4.45837	-17.92770	-4.44624	-18.60523	-7.93410	-6.37231
$E_{(AO/HO)}$ (eV)	0	-14.63489	-14.53414	0	-14.63489	0	-14.63489	0	-14.53414	-14.63489
$\Delta E_{H_2MO(AO/HO)}$ (eV)	-2.69893	-2.26759	0	-2.26759	-2.26759	-1.85836	-0.92918	-3.71673	0	-2.26758
E_T $_{(AO/HO)}$ (eV)	2.69893	-12.36730	-14.53414	2.26759	-12.36730	1.85836	-13.70571	3.71673	-14.53414	-12.36731
$E_{(n_3 AO/HO)}$ (eV)	0	0	-14.53414	0	0	0	0	0	0	0
E_T $_{(H_2MO)}$ (eV)	-63.27074	-31.63543	-48.73654	-63.27075	-31.63541	-63.27100	-31.63527	-63.27056	-31.63534	-31.63533
$E_T\left(atom-atom, msp^3.AO\right)$ (eV)	-2.69893	-1.13379	0	-2.26759	0.00000	-1.85836	-0.92918	-3.71673	0	0
E_T $_{(MO)}$ (eV)	-65.96966	-32.76916	-48.73660	-65.53833	-31.63537	-65.12910	-32.56455	-66.98746	-31.63537	-31.63537
$\omega\left(10^5\ rad/s\right)$	59.4034	14.3055	68.9812	15.4421	19.8904	15.4704	21.5213	15.7474	48.7771	28.9084
E_K (eV)	39.10034	9.41610	45.40465	10.16428	13.09221	10.18290	14.16571	10.36521	32.10594	19.02803
$\bar{E}_D$ (eV)	-0.40804	-0.19893	-0.42172	-0.20668	-0.22646	-0.20558	-0.24248	-0.21333	-0.35462	-0.27301
$\bar{E}_{Kvib}$ (eV)	0.21077 [12]	0.15498 [58]	0.40929 [22]	0.17897 [6]	0.14667 [67]	0.20768 [62]	0.12944 [23]	0.11159 [12]	0.40696 [24]	0.39427 [60]
$\bar{E}_{osc}$ (eV)	-0.30266	-0.12144	-0.21708	-0.11720	-0.15312	-0.10174	-0.17775	-0.15754	-0.15115	-0.07587
E_{mag} (eV)	0.11441	0.14803	0.14803	0.14803	0.14803	0.14803	0.14803	0.14803	0.14803	0.14803
E_T $_{(Group)}$ (eV)	-66.57498	-32.89060	-49.17075	-65.77272	-31.64046	-65.33259	-32.74230	-67.30254	-31.78651	-31.71124
$E_{initial\ (c_4\ AO/HO)}$ (eV)	-14.63489	-14.63489	-14.53414	-14.63489	-14.63489	-14.63489	-14.63489	-14.63489	-14.53414	-14.63489
$E_{initial\ (c_5\ AO/HO)}$ (eV)	0	0	-13.59844	0	0	0	0	0	-13.59844	-13.59844
$E_{D\ (Group)}$ (eV)	7.80660	3.62082	7.43973	7.23317	2.37068	6.79303	3.47253	8.76298	3.51208	3.32988

Table 15.343. The total gaseous bond energies of guanine calculated using the functional group composition and the energies of Table 15.342 compared to the experimental values [3].

Formula	Name	$C=O$ Group	$C-N$ (a) Group	NH_2 Group	$C=C$ Group	$C-C$ Group	$N=C$ Group	$C-N$ (b) Group	$C-N-C$ Group	NH Group	CH Group	Calculated Total Bond Energy (eV)	Experimental Total Bond Energy (eV)	Relative Error
$C_5H_5N_5O$	Guanine	1	1	1	1	1	2	2	2	2	1	76.88212	77.41849[a]	0.00693

[a] Crystal.

Table 15.344. The bond angle parameters of guanine and experimental values [65]. In the calculation of θ_v, the parameters from the preceding angle were used. E_T is E_T (*atom – atom,msp*^{3}*.AO*).

Atoms of Angle	2c' Bond 1 (a_0)	2c' Bond 2 (a_0)	2c' Terminal Atoms (a_0)	$E_{Coulombic}$ Atom 1	Atom 1 Hybridization Designation (Table 15.3B)	$E_{Coulombic}$ Atom 2	Atom 2 Hybridization Designation (Table 15.3B)	c_2 Atom 1	c_2 Atom 2	C_1	C_2	c_1	c_2'	E_T (eV)	θ_v (°)	θ_1 (°)	θ_2 (°)	Cal. θ (°)	Exp. θ (°)
$\angle N_b C_a C_d$	2.59228	2.74663	4.3359	-14.53414	N	-16.42413 C_d	13	0.84665 Eq. (15.171)	0.82840	1	1	1	0.83753	-1.44915				108.57	110.8
$\angle N_b C_a O$	2.59228	2.27954	4.2426	-16.68411	18	-16.17521	8	0.81549	0.84115	1	1	1	0.82832	-1.44915				120.98	120.4
$\angle OC_a C_d$																108.57	120.98	130.44	128.8
$\angle C_b N_b C_a$	2.59228	2.59228	4.5826	-17.25101	28	-17.10440	25	0.78870	0.79546	1	1	1	0.79208	-1.85836				124.23	125.6
$\angle N_b C_b N_c$	2.59228	2.60766	4.5166	-15.75493	4	-15.75493	4	0.86359	0.86359	1	1	1	0.86359	-1.44915				120.59	123.3
$\angle H_b N_b C_a$	1.88268	2.64855	3.9158	-14.53414	N	-14.82575 C_a	1	0.93613 Eq. (13.248)	0.91771	0.75	1	0.75	0.98033	0				118.60	
$\angle C_b N_b H_b$																124.23	118.60	117.17	
$\angle N_b C_b N_a$	2.59228	2.53797	4.3818	-16.68411	18	-15.39265	2	0.81549	0.88392	1	1	1	0.84971	-1.44915				117.32	115.8
$\angle N_a C_b N_c$	2.53797	2.60766	4.4721	-15.39265	2	-16.21952	9	0.88392	0.83885	1	1	1	0.86138	-1.44915				120.71	120.9
$\angle HN_a C_b$	1.88268	2.53797	3.8987	-14.53414	N	-16.32183	11	0.93613 Eq. (13.248)	0.83360	0.75	1	0.75	0.98458	0				123.07	118 [66]
$\angle HN_a H$	1.88268	1.88268	3.1559	-14.53414	N	H	H	0.93613 Eq. (13.248)	1	1	1	0.75	1.06823	0				113.89	113.9 [1] (aniline)
$\angle C_b N_c C_c$	2.60766	2.70148	4.4721	-17.25101	28	-17.35332	29	0.78870	0.78405	1	1	1	0.78637	-1.85836				114.77	112.6
$\angle N_c C_c N_d$	2.70148	2.59228	4.7117	-14.53414	N	-14.53414	N	0.84665 Eq. (15.171)	0.84665 Eq. (15.171)	1	1	1	0.84665	-1.65376				125.75	125.8
$\angle N_c C_c C_d$	2.70148	2.60925	4.7539	-14.53414	N	-15.95955	6	0.84665 Eq. (15.171)	0.85252	1	1	1	0.84958	-1.65376				127.05	128.3
$\angle C_a C_d C_c$	2.74663	2.60925	4.6476	-17.10440	25	-16.88873	20	0.79546	0.80561	1	1	1	0.80054	-1.85836				120.38	119.4
$\angle C_c N_d C_e$	2.59228	2.59228	4.2071	-17.95963	39	-17.95963	39	0.75758	0.75758	1	1	1	0.75758	-1.85836				108.48	108.2
$\angle N_a C_c C_d$	2.59228	2.60925	4.1473	-14.53414	N	-17.35332	29	0.84665 Eq. (15.171)	0.78405	1	1	1	0.81535	-1.44915				105.75	105.9
$\angle N_e C_e N_d$	2.60766	2.60287	4.3359	-16.21952	9	-16.03838	7	0.83885	0.84833	1	1	1	0.84359	-1.44915				112.64	110.0
$\angle C_e N_d H$	2.59228	1.88268	4.0166	-14.53414	N	-15.95954	6	0.84665 Eq. (15.171)	0.85252	0.75	1	0.75	1.00693	0				126.96	127 [66]
$\angle C_c N_d H$																108.48	126.96	124.56	127
$\angle HC_e N_e$	2.02241	2.60766	4.1312	-16.68411	18	-14.53414	N	0.81549	0.84665 Eq. (15.171)	0.75	1	0.75	1.03820	0				125.85	126 [66]
$\angle N_a C_e H$																112.64	125.85	121.52	119 [66]
$\angle C_a N_e C_e$	2.70148	2.60766	4.2661	-17.92022	37	-17.92022	37	0.75924	0.75924	1	1	1	0.75924	-1.85836				106.93	108.0°
$\angle N_e C_d C_c$	2.70148	2.60925	4.2895	-14.53414	N	-16.42414	13	0.84665 Eq. (15.171)	0.82840	1	1	1	0.83753	-1.44915				107.73	107.9
$\angle C_a C_d N_e$	2.74663	2.70148	4.9396	-17.10440	25	-14.53414	N	0.79546	0.84665 Eq. (15.171)	1	1	1	0.82105	-1.85836				130.10	133.6

CYTOSINE

Cytosine having the formula $C_4H_5N_3O$ is a pyrimidine with a carbonyl substitution at position C_b, and a primary amine moiety is at position C_a as shown in Figure 15.59B. The carbonyl and adjacent $C_b - N_b$ functional groups are equivalent to the corresponding groups of alkyl amides. The NH_2 and $C_a - N_a$ functional groups of the primary amine moiety are equivalent to the NH_2 and $C_a - N_a$ functional groups of adenine. The vinyl moiety, $HC_c = C_dH$, comprises $C = C$ and CH functional groups that are equivalent to the corresponding alkene groups. Cytosine further comprises $N_b = C_a$, N_cH, and $C_b - N_c - C_c$ groups that are equivalent to the corresponding groups of imidazole as given in the corresponding section. The $C_a - C_d$ bond comprises another functional group that is equivalent to the $C_a - C_d$ group of guanine and thymine except that $E_T\left(atom - atom, msp^3.AO\right)$ is equivalent to the contribution of a $C2sp^3$ HO of an alkane, $-0.92918\ eV$ (Eq. (14.513)), in order to match the energies of the single and double-bonded moieties within the molecule.

The symbols of the functional groups of cytosine are given in Table 15.345. The geometrical (Eqs. (15.1-15.5) and (15.51)), intercept (Eqs. (15.80-15.87)), and energy (Eqs. (15.6-15.11) and (15.17-15.65)) parameters of cytosine are given in Tables 15.346, 15.347, and 15.348, respectively. The total energy of cytosine given in Table 15.349 was calculated as the sum over the integer multiple of each $E_D(Group)$ of Table 15.348 corresponding to functional-group composition of the molecule. The bond angle parameters of cytosine determined using Eqs. (15.88-15.117) are given in Table 15.350. The color scale, charge-density of cytosine comprising atoms with the outer shell bridged by one or more H_2-type ellipsoidal MOs or joined with one or more hydrogen MOs is shown in Figure 15.59A.

Figure 15.59. (A) Color scale, charge-density of cytosine showing the orbitals of the atoms at their radii, the ellipsoidal surface of each H or H_2-type ellipsoidal MO that transitions to the corresponding outer shell of the atom(s) participating in each bond, and the hydrogen nuclei. (B) Chemical structure and atomic designation of cytosine.

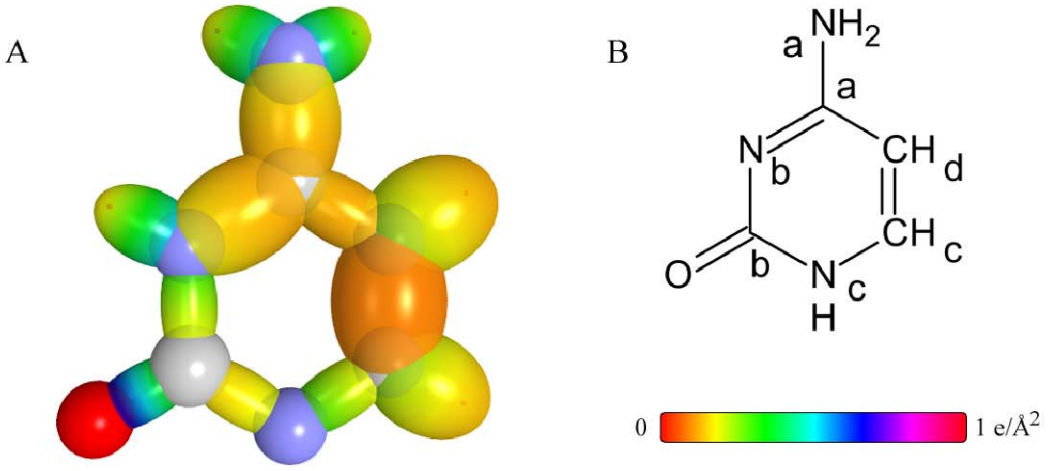

Table 15.345. The symbols of functional groups of cytosine.

Functional Group	Group Symbol
$C_a - N_a$	$C - N$ (a)
NH_2 group	NH_2
$N_b = C_a$ double bond	$N = C$
$C_b = O$ (alkyl amide)	$C = O$
$C_b - N_b$ amide	$C - N$ (b)
$C_c = C_d$ double bond	$C = C$
$C_cH \quad C_dH$	CH
$C_a - C_d$	$C - C$
$C_b - N_c - C_c$	$C - N - C$
N_cH group	NH

Table 15.346. The geometrical bond parameters of cytosine and experimental values [1].

Parameter	$C-N$ (a) Group	NH_2 Group	$N=C$ Group	$C=O$ Group	$C-N$ (b) Group	$C=C$ Group	CH Group	$C-C$ Group	$C-N-C$ Group	NH Group
$a\ (a_0)$	1.61032	1.24428	1.44926	1.29907	1.75370	1.47228	1.53380	1.88599	1.43222	1.24428
$c'\ (a_0)$	1.26898	0.94134	1.30383	1.13977	1.32427	1.26661	1.01120	1.37331	1.29614	0.94134
Bond Length $2c'\ (\AA)$	1.34303	0.99627	1.37991	1.20628	1.40155	1.34052	1.07021	1.45345	1.37178	0.996270
Exp. Bond Length $(\AA)$	1.34 [64] (adenine)	0.998 (aniline)		1.220 (acetamide) 1.225 (N-methylacetamide)	1.380 (acetamide)	1.34 [65] (cytosine) 1.342 (2-methylpropene) 1.346 (2-butene) 1.349 (1,3-butadiene)	1.076 (pyrrole)	1.43 [65] (cytosine)	1.370 (pyrrole)	0.996 (pyrrole)
$b,c\ (a_0)$	0.99137	0.81370	0.63276	0.62331	1.14968	0.75055	1.15326	1.29266	0.60931	0.81370
e	0.78803	0.75653	0.89965	0.87737	0.75513	0.86030	0.65928	0.72817	0.90499	0.75653

Table 15.347. The MO to HO intercept geometrical bond parameters of cytosine. R_1 is an alkyl group and R, R', R'' are H or alkyl groups. E_T is E_T ($atom-atom,msp^3.AO$).

Bond	Atom	E_T (eV) Bond 1	E_T (eV) Bond 2	E_T (eV) Bond 3	E_T (eV) Bond 4	Final Total Energy $C2sp^3$ (eV)	$r_{initial}$ (a_0)	r_{final} (a_0)	$E_{Coulomb}(C2sp^3)$ (eV) Final	$E(C2sp^3)$ (eV) Final	θ' (°)	θ_1 (°)	θ_2 (°)	d_1 (a_0)	d_2 (a_0)
$C_d(N_b)C_aN_aH-H$	N_a	-0.56690	0	0	0		0.93084	0.88392	-15.39265		121.74	58.26	67.49	0.47634	0.46500
$C_d(N_b)C_a-N_aH_2$	N_a	-0.56690	0	0	0		0.93084	0.88392	-15.39265		113.13	66.87	55.08	0.92180	0.34719
$C_d(N_b)C_a-N_aH_2$	C_a	-0.56690	-0.92918	-0.46459	0	-153.57636	0.91771	0.81052	-16.78642	-16.59556	108.27	71.73	50.93	1.01493	0.25406
$C_d(N_a)C_a=N_bC_b$	N_b	-0.92918	-0.82688	0	0		0.93084	0.82053	-16.58181		137.50	42.50	61.17	0.69886	0.60497
$C_d(N_a)C_a=N_bC_b$	C_a	-0.92918	-0.56690	-0.46459	0	-153.57636	0.91771	0.81052	-16.78642	-16.59556	137.11	42.89	60.67	0.70998	0.59385
$C_aN_b-C_b(O)N_c$	N_b	-0.82688	-0.92918	0	0		0.93084	0.82053	-16.58181		96.19	83.81	45.20	1.23578	0.08850
$C_aN_b-C_b(O)N_c$	C_b	-0.82688	-1.34946	-0.92918	0	-154.72121	0.91771	0.75878	-17.93127	-17.74041	90.51	89.49	41.30	1.31755	0.00672
$N_b(N_c)C_b=O$	O_a	-1.34946	0	0	0		1.00000	0.84115	-16.17521		137.27	42.73	66.31	0.52193	0.61784
$N_b(N_c)C_b=O$	C_b	-1.34946	-0.82688	-0.92918	0	-154.72121	0.91771	0.75878	-17.93127	-17.74041	133.67	46.33	61.70	0.61582	0.52395
$N-H\ (N_cH)$	N_c	-0.92918	-0.92918	0	0		0.93084	0.81549	-16.68411		117.34	62.66	62.90	0.56678	0.37456
$C-H\ (C_cH)$	C_c	-1.13380	-0.92918	0	0	-153.67867	0.91771	0.80561	-16.88873	-16.69786	83.35	96.65	43.94	1.10452	0.09331
$C-H\ (C_dH)$	C_d	-1.13380	-0.46459	0	0	-153.21408	0.91771	0.82840	-16.42414	-16.23327	85.93	94.07	45.77	1.06995	0.05875
$N_b(O)C_b-N_cHC_c$	N_c	-0.92918	-0.92918	0	0		0.93084	0.81549	-16.68411		138.92	41.08	61.59	0.68147	0.61467
$N_b(O)C_b-N_cHC_c$	C_b	-0.92918	-1.34946	-0.82688	0	-154.72121	0.91771	0.75878	-17.93127	-17.74041	136.68	43.32	58.70	0.74414	0.55200
$C_bHN_c-C_cHC_d$	N_c	-0.92918	-0.92918	0	0		0.93084	0.81549	-16.68411		138.92	41.08	61.59	0.68147	0.61467
$C_bHN_c-C_cHC_d$	C_d	-0.92918	-1.13379	0	0	-153.67866	0.91771	0.80561	-16.88873	-16.69786	138.54	41.46	61.09	0.69238	0.60376
$N_cHC_c=C_dHC_a$	C_c	-1.13380	-0.92918	0.00000	0	-153.67867	0.91771	0.80561	-16.88873	-16.69786	127.61	52.39	58.24	0.77492	0.49168
$N_cHC_c=C_dHC_a$	C_d	-1.13380	-0.46459	0.00000	0	-153.21408	0.91771	0.82840	-16.42414	-16.23327	128.72	51.28	59.45	0.74844	0.51817
$HC_cC_d-C_a(N_a)N_b$	C_a	-0.46459	-0.56690	-0.92918	0	-153.57636	0.91771	0.81052	-16.78642	-16.59556	82.65	97.35	38.45	1.47695	0.10364
$HC_cC_d-C_a(N_a)N_b$	C_d	-0.46459	-1.13379	0	0	-153.21407	0.91771	0.82840	-16.42414	-16.23327	84.52	95.48	39.64	1.45240	0.07908

Table 15.348. The energy parameters (eV) of functional groups of cytosine.

Parameters	$C-N$ (a) Group	NH_2 Group	$N=C$ Group	$C=O$ Group	$C-N$ (b) Group	$C=C$ Group	CH Group	$C-C$ Group	$C-N-C$ Group	NH Group
n_1	1	2	2	2	1	2	1	1	2	1
n_2	0	0	0	0	0	0	0	0	0	0
n_3	0	1	0	0	0	0	0	0	0	0
C_1	0.5	0.75	0.5	0.5	0.5	0.5	0.75	0.5	0.5	0.75
C_2	1	0.93613	0.85252	1	1	0.91771	1	1	0.85252	0.93613
c_1	1	0.75	1	1	1	1	1	1	1	0.75
c_2	0.84665	0.92171	0.84665	0.85395	0.91140	0.91771	0.91771	0.91771	0.84665	0.92171
c_3	0	0	0	2	0	0	1	0	0	1
c_4	2	1	4	4	2	4	1	2	4	1
c_5	0	2	0	0	0	0	1	0	0	1
C_{1v}	0.5	1.5	0.5	0.5	0.5	0.5	0.75	0.5	0.5	0.75
C_{2v}	1	1	0.85252	1	1	0.91771	1	1	0.85252	1
V_e (eV)	-35.50149	-78.97795	-103.92756	-111.25473	-36.88558	-102.08992	-39.09538	-33.63376	-106.58684	-39.48897
V_p (eV)	10.72181	28.90735	20.87050	23.87467	10.27417	21.48386	13.45505	9.90728	20.99432	14.45367
T (eV)	11.02312	31.73641	35.85539	42.82081	10.51650	34.67062	12.74462	8.91674	37.21047	15.86820
V_m (eV)	-5.51156	-15.86820	-17.92770	-21.41040	-5.25825	-17.33531	-6.37231	-4.45837	-18.60523	-7.93410
$E_{(AO/HO)}$ (eV)	-14.63489	-14.53414	0	0	-14.63489	0	-14.63489	-14.63489	0	-14.53414
$\Delta E_{H_2MO_{(AO/HO)}}$ (eV)	-2.26759	0	-1.85836	-2.69893	-4.35268	0	-2.26758	-2.26759	-3.71673	0
$E_{T_{(AO/HO)}}$ (eV)	-12.36730	-14.53414	1.85836	2.69893	-10.28221	0	-12.36731	-12.36730	3.71673	-14.53414
$E_{(n_3\ AO/HO)}$ (eV)	0	-14.53414	0	0	0	0	0	0	0	0
$E_{T_{(H_2MO)}}$ (eV)	-31.63543	-48.73654	-63.27100	-63.27074	-31.63537	-63.27075	-31.63533	-31.63541	-63.27056	-31.63534
$E_{T}\left(atom-atom, msp^3.AO\right)$ (eV)	-1.13379	0	-1.85836	-2.69893	-1.65376	-2.26759	0	-0.92918	-3.71673	0
$E_{T_{(MO)}}$ (eV)	-32.76916	-48.73660	-65.12910	-65.96966	-33.28912	-65.53833	-31.63537	-32.56455	-66.98746	-31.63537
$\omega\ \left(10^{15}\ rad/s\right)$	14.3055	68.9812	15.4704	59.4034	12.5874	43.0680	28.9084	19.8904	15.7474	48.7771
E_K (eV)	9.41610	45.40465	10.18290	39.10034	8.28526	28.34813	19.02803	13.09221	10.36521	32.10594
$\overline{E}_D$ (eV)	-0.19893	-0.42172	-0.20558	-0.40804	-0.18957	-0.34517	-0.27301	-0.23311	-0.21333	-0.35462
$\overline{E}_{Kvib}$ (eV)	0.15498 [58]	0.40929 [22]	0.20768 [62]	0.21077 [12]	0.17358 [33]	0.17897 [6]	0.39427 [60]	0.14667 [67]	0.11159 [12]	0.40696 [24]
$\overline{E}_{osc}$ (eV)	-0.12144	-0.21708	-0.10174	-0.30266	-0.10278	-0.25568	-0.07587	-0.15977	-0.15754	-0.15115
E_{mag} (eV)	0.14803	0.14803	0.14803	0.11441	0.14803	0.14803	0.14803	0.14803	0.14803	0.14803
$E_{T_{(Group)}}$ (eV)	-32.89060	-49.17075	-65.33259	-66.57498	-33.39190	-66.04969	-31.71124	-32.57629	-67.30254	-31.78651
$E_{initial\ (c_4\ AO/HO)}$ (eV)	-14.63489	-14.53414	-14.63489	-14.63489	-14.63489	-14.63489	-14.63489	-14.63489	-14.63489	-14.53414
$E_{initial\ (c_5\ AO/HO)}$ (eV)	0	-13.59844	0	0	0	0	-13.59844	0	0	-13.59844
$E_{D_{(Group)}}$ (eV)	3.62082	7.43973	6.79303	7.80660	4.12212	7.51014	3.32988	3.30651	8.76298	3.51208

Table 15.349. The total gaseous bond energies of cytosine calculated using the functional group composition and the energies of Table 15.348 compared to the experimental values [3].

Formula	Name	$C-N$ (a) Group	NH_2 Group	$N=C$ Group	$C=O$ Group	$C-N$ (b) Group	$C=C$ Group	CH Group	$C-C$ Group	$C-N-C$ Group	NH Group	Calculated Total Bond Energy (eV)	Experimental Total Bond Energy (eV)	Relative Error
$C_4H_5N_3O$	Cytosine	1	1	1	1	1	1	2	1	1	1	59.53378	60.58056	0.01728

Table 15.350. The bond angle parameters of cytosine and experimental values [64]. In the calculation of θ_v, the parameters from the preceding angle were used. E_T is E_T $(atom-atom,msp^3.AO)$.

Atoms of Angle	2c' Bond 1 (a_0)	2c' Bond 2 (a_0)	2c' Terminal Atoms (a_0)	$E_{Coulombic}$ Atom 1	Atom 1 Hybridization Designation (Table 15.3B)	$E_{Coulombic}$ Atom 2	Atom 2 Hybridization Designation (Table 15.3B)	c_2 Atom 1	c_2 Atom 2	C_1	C_2	c_1	c_2'	E_T (eV)	θ_v (°)	θ_1 (°)	θ_2 (°)	Cal. θ (°)	Exp. θ (°)
$\angle HNH$	1.88268	1.88268	3.1559	-14.53414	N	H	H	0.93613 Eq. (13.248)	1	1	1	0.75	1.06823	0				113.89	113.9 [1] (aniline)
$\angle C_aNH$	2.53797	1.88268	3.8123	-16.78642	19	-14.53414	N	0.81052 Eq. (15.71)	0.77638 Eq. (15.173)	0.75	1	0.75	0.95787	0				118.42	118 [66]
$\angle N_bC_aC_d$	2.60766	2.74663	4.6476	-14.53414	N	-16.42414	13	0.84665 Eq. (15.171)	0.82840	1	1	1	0.83753	-1.65376				120.43	121.4
$\angle N_bC_aN_a$	2.60766	2.53797	4.4272	-15.39265	2	-16.58181	16	0.88392	0.82053	1	1	1	0.85222	-1.44915				118.71	117.5
$\angle C_dC_aN_a$																120.43	118.71	120.85	121.1
$\angle C_bN_bC_a$	2.64855	2.60766	4.4944	-17.93127	38	-16.78642	19	0.75878	0.81052	1	1	1	0.78465	-1.85836				117.53	120.3
$\angle N_bC_bN_c$	2.64855	2.59228	4.4721	-16.58181	16	-16.68411	17	0.82053	0.81549	1	1	1	0.81801	-1.65376				117.15	118.9
$\angle N_cC_bO$	2.59228	2.27954	4.2426	-16.68411	17	-16.17521	8	0.81549	0.84115	1	1	1	0.82832	-1.44915				120.98	119.8
$\angle N_bC_bO$																117.15	120.98	121.87	121.3
$\angle C_bN_cC_c$	2.59228	2.59228	4.4944	-17.93127	38	-16.88873	20	0.75878	0.80561	1	1	1	0.78219	-1.85836				120.20	121.7
$\angle N_cC_cC_d$	2.59228	2.53321	4.4272	-14.53414	N	-15.95955	6	0.84665 Eq. (15.171)	0.85252	1	1	1	0.84958	-1.44915				119.48	121.4
$\angle H_cN_cC_c$	1.88268	2.59228	3.8644	-14.53414	N	-16.68411	17	0.84665 Eq. (15.171)	0.81549	0.75	1	0.75	0.96320	0				118.58	
$\angle H_cN_cC_b$																120.20	118.58	121.23	
$\angle C_aC_dC_c$	2.74663	2.53321	4.5166	-16.78642	19	-17.81791	36	0.81052	0.76360	1	1	1	0.78706	-1.85836				117.56	116.4
$\angle H_cC_cC_d$	2.02241	2.53321	3.9833	-15.95955	6	-15.95955	6	0.85252	0.85252	0.75	1	0.75	1.00000	0				121.54	
$\angle H_cC_cN_c$																119.48	121.54	118.99	
$\angle H_dC_dC_c$	2.02241	2.53321	3.9833	-15.95955	6	-15.95955	6	0.85252	0.85252	0.75	1	0.75	1.00000	0				121.54	
$\angle H_dC_dC_a$																117.56	121.54	120.90	

ALKYL PHOSPHINES ($\left(C_nH_{2n+1}\right)_3P,\ n=1,2,3,4,5...\infty$)

The alkyl phosphines, $\left(C_nH_{2n+1}\right)_3P$, comprise a $P-C$ functional group. The alkyl portion of the alkyl phosphine may comprise at least two terminal methyl groups (CH_3) at each end of each chain, and may comprise methylene (CH_2), and methylyne (CH) functional groups as well as C bound by carbon-carbon single bonds. The methyl and methylene functional groups are equivalent to those of straight-chain alkanes. Six types of $C-C$ bonds can be identified. The n-alkane $C-C$ bond is the same as that of straight-chain alkanes. In addition, the $C-C$ bonds within isopropyl ($\left(CH_3\right)_2CH$) and t-butyl ($\left(CH_3\right)_3C$) groups and the isopropyl to isopropyl, isopropyl to t-butyl, and t-butyl to t-butyl $C-C$ bonds comprise functional groups. The branched-chain-alkane groups in alkyl phosphines are equivalent to those in branched-chain alkanes. The $P-C$ group may further join the $P3sp^3$ HO to an aryl HO.

As in the case of carbon, the bonding in the phosphorous atom involves sp^3 hybridized orbitals formed, in this case, from the $3p$ and $3s$ electrons of the outer shells with five $P3sp^3$ HOs rather than four $C2sp^3$ HOs. The $P-C$ bond forms between $P3sp^3$ and $C2sp^3$ HOs to yield phosphines. The semimajor axis a of the $P-C$ functional group is solved using Eq. (15.51). Using the semimajor axis and the relationships between the prolate spheroidal axes, the geometric and energy parameters of the MO are calculated using Eqs. (15.1-15.117) in the same manner as the organic functional groups given in Organic Molecular Functional Groups and Molecules section.

The energy of phosphorous is less than the Coulombic energy between the electron and proton of H given by Eq. (1.264). A minimum energy is achieved while matching the potential, kinetic, and orbital energy relationships given in the Hydroxyl Radical (OH) section with hybridization of the phosphorous atom such that in Eqs. (15.51) and (15.61), the sum of the energies of the H_2-type ellipsoidal MOs is matched to that of the $P3sp^3$ shell as in the case of the corresponding carbon and silicon molecules.

The P electron configuration is $[Ne]3s^23p^3$ corresponding to the ground state ${}^4S_{3/2}$, and the $3sp^3$ hybridized orbital arrangement after Eq. (13.422) is:

$$\begin{array}{cccc} & 3\text{sp}^3 \text{ state} & & \\ \uparrow\downarrow & \uparrow & \uparrow & \uparrow \\ \hline 0,0 & 1,\text{-}1 & 1,0 & 1,1 \end{array} \tag{15.174}$$

where the quantum numbers (ℓ, m_ℓ) are below each electron. The total energy of the state is given by the sum over the five electrons. The sum $E_T\left(P,3sp^3\right)$ of experimental energies [38] of P, P^+, P^{2+}, P^{3+}, and P^{4+} is:

$$\begin{aligned} E_T\left(P,3sp^3\right) &= 65.0251\ eV + 51.4439\ eV + 30.2027\ eV + 19.7695\ eV + 10.48669\ eV \\ &= 176.92789\ eV \end{aligned} \tag{15.175}$$

By considering that the central field decreases by an integer for each successive electron of the shell, the radius r_{3sp^3} of the $P3sp^3$ shell may be calculated from the Coulombic energy using Eq. (15.13).

$$r_{3sp^3} = \sum_{n=10}^{14} \frac{(Z-n)e^2}{8\pi\varepsilon_0\left(e176.92789\ eV\right)} = \frac{15e^2}{8\pi\varepsilon_0\left(e176.92789\ eV\right)} = 1.15350a_0 \tag{15.176}$$

where $Z=15$ for phosphorous. Using Eq. (15.14), the Coulombic energy $E_{Coulomb}\left(P,3sp^3\right)$ of the outer electron of the $P3sp^3$ shell is:

$$E_{Coulomb}\left(P,3sp^3\right) = \frac{-e^2}{8\pi\varepsilon_0 r_{3sp^3}} = \frac{-e^2}{8\pi\varepsilon_0 1.15350a_0} = -11.79519\ eV \tag{15.177}$$

During hybridization, the spin-paired $3s$ electrons are promoted to the $P3sp^3$ shell as paired electrons at the radius r_{3sp^3} of the $P3sp^3$ shell. The energy for the promotion is the difference in the magnetic energy given by Eq. (15.15) at the initial radius of the $3s$ electrons and the final radius of the $P3sp^3$ electrons. From Eq. (10.255) with $Z=15$, the radius r_{12} of $P3s$ shell is

$$r_{12} = 1.09443a_0 \tag{15.178}$$

Using Eqs. (15.15) and (15.178), the unpairing energy is:

$$E(magnetic) = \frac{2\pi\mu_0 e^2\hbar^2}{m_e^2}\left(\frac{1}{\left(r_{12}\right)^3} - \frac{1}{\left(r_{3sp^3}\right)^3}\right) = 8\pi\mu_o\mu_B^2\left(\frac{1}{\left(1.09443a_0\right)^3} - \frac{1}{\left(1.15350a_0\right)^3}\right) = 0.01273\ eV \tag{15.179}$$

Using Eqs. (15.177) and (15.179), the energy $E\left(P,3sp^3\right)$ of the outer electron of the $P3sp^3$ shell is:

$$E\left(P,3sp^3\right)=\frac{-e^2}{8\pi\varepsilon_0 r_{3sp^3}}+\frac{2\pi\mu_0 e^2\hbar^2}{m_e^2}\left(\frac{1}{\left(r_{12}\right)^3}-\frac{1}{\left(r_{3sp^3}\right)^3}\right)=-11.79519\ eV+0.01273\ eV=-11.78246\ eV \tag{15.180}$$

For the $P-C$ functional group, hybridization of the $2s$ and $2p$ AOs of each C and the $3s$ and $3p$ AOs of each P to form single $2sp^3$ and $3sp^3$ shells, respectively, forms an energy minimum, and the sharing of electrons between the $C2sp^3$ and $P3sp^3$ HOs to form a MO permits each participating orbital to decrease in radius and energy. In branched-chain alkyl phosphines, the energy of phosphorous is less than the Coulombic energy between the electron and proton of H given by Eq. (1.264). Thus, c_2 in Eq. (15.61) is one, and the energy matching condition is determined by the C_2 parameter. Then, the $C2sp^3$ HO has an energy of $E\left(C,2sp^3\right)=-14.63489\ eV$ (Eq. (15.25)), and the $P3sp^3$ HO has an energy of $E\left(P,3sp^3\right)=-11.78246\ eV$ (Eq. (15.180)). To meet the equipotential condition of the union of the $P-C$ H_2-type-ellipsoidal-MO with these orbitals, the hybridization factor C_2 of Eq. (15.61) for the $P-C$-bond MO given by Eqs. (15.77), (15.79), and (13.430) is:

$$C_2\left(C2sp^3HO\ to\ P3sp^3HO\right)=\frac{E\left(P,3sp^3\right)}{E\left(C,2sp^3\right)}c_2\left(C2sp^3HO\right)=\frac{-11.78246\ eV}{-14.63489\ eV}\left(0.91771\right)=0.73885 \tag{15.181}$$

The energy of the $P-C$-bond MO is the sum of the component energies of the H_2-type ellipsoidal MO given in Eq. (15.51) with $E\left(AO/HO\right)=E\left(P,3sp^3\right)$ given by Eq. (15.180), and $E_T\left(atom-atom,msp^3.AO\right)$ is one half $-0.72457\ eV$ given by Eq. (14.151) in order to match the energies of the carbon and phosphorous HOs.

The symbols of the functional groups of branched-chain alkyl phosphines are given in Table 15.351. The geometrical (Eqs. (15.1-15.5) and (15.51)), intercept (Eqs. (15.80-15.87)), and energy (Eqs. (15.6-15.11) and (15.17-15.65)) parameters of alkyl phosphines are given in Tables 15.352, 15.353, and 15.354, respectively. The total energy of each alkyl phosphine given in Table 15.355 was calculated as the sum over the integer multiple of each $E_D\left(Group\right)$ of Table 15.354 corresponding to functional-group composition of the molecule. The bond angle parameters of alkyl phosphines determined using Eqs. (15.88-15.117) are given in Table 15.356. The color scale, charge-density of exemplary alkyl phosphine, triphenylphosphine, comprising atoms with the outer shell bridged by one or more H_2-type ellipsoidal MOs or joined with one or more hydrogen MOs is shown in Figure 15.60.

Figure 15.60. Color scale, charge-density of triphenylphosphine showing the orbitals of the atoms at their radii, the ellipsoidal surface of each H or H_2-type ellipsoidal MO that transitions to the corresponding outer shell of the atom(s) participating in each bond, and the hydrogen nuclei. (A) Top view. (B) Side view.

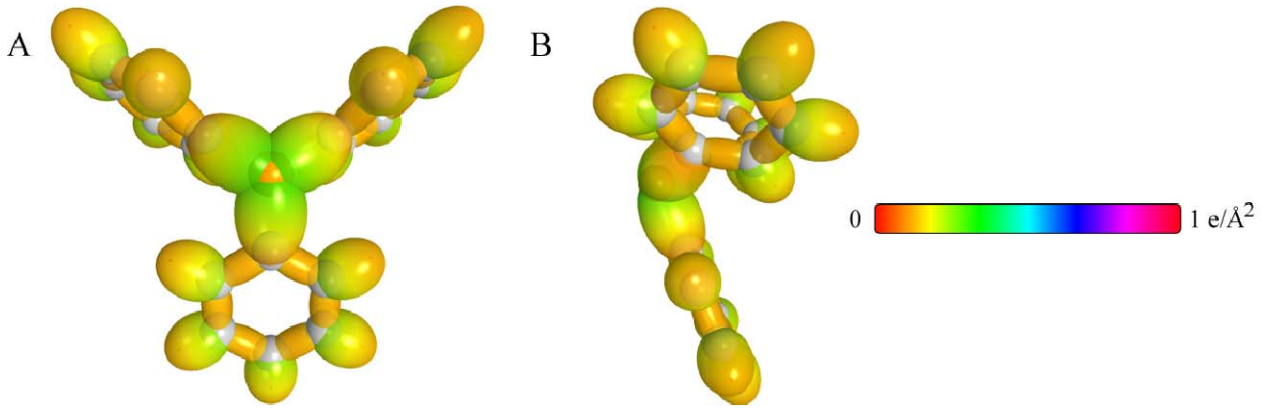

Table 15.351. The symbols of functional groups of alkyl phosphines.

Functional Group	Group Symbol
P-C	$P-C$
CH_3 group	$C-H\ (CH_3)$
CH_2 group	$C-H\ (CH_2)$
CH	$C-H$ (i)
CC bond (*n-C*)	$C-C$ (a)
CC bond (*iso-C*)	$C-C$ (b)
CC bond (*tert-C*)	$C-C$ (c)
CC (*iso* to *iso-C*)	$C-C$ (d)
CC (*t* to *t-C*)	$C-C$ (e)
CC (*t* to *iso-C*)	$C-C$ (f)
CC (aromatic bond)	$C\overset{3e}{=}C$
CH (aromatic)	CH (ii)

Table 15.352. The geometrical bond parameters of alkyl phosphines and experimental values [1].

Parameter	$P-C$ Group	$C-H\ (CH_3)$ Group	$C-H\ (CH_2)$ Group	$C-H$ (i) Group	$C-C$ (a) Group	$C-C$ (b) Group	$C-C$ (c) Group	$C-C$ (d) Group	$C-C$ (e) Group	$C-C$ (f) Group	$C \overset{3e}{=} C$ Group	CH (ii) Group
$a\ (a_0)$	2.29513	1.64920	1.67122	1.67465	2.12499	2.12499	2.10725	2.12499	2.10725	2.10725	1.47348	1.60061
$c'\ (a_0)$	1.76249	1.04856	1.05553	1.05661	1.45744	1.45744	1.45164	1.45744	1.45164	1.45164	1.31468	1.03299
Bond Length $2c'\ (\AA)$	1.86534	1.10974	1.11713	1.11827	1.54280	1.54280	1.53635	1.54280	1.53635	1.53635	1.39140	1.09327
Exp. Bond Length $(\AA)$	1.847 $((CH_3)_2PCH_3)$ 1.858 (H_2PCH_3)	1.107 $(C-H$ propane) 1.117 $(C-H$ butane)	1.107 $(C-H$ propane) 1.117 $(C-H$ butane)	1.122 (isobutane)	1.532 (propane) 1.531 (butane)	1.532 (propane) 1.531 (butane)	1.532 (propane) 1.531 (butane)	1.532 (propane) 1.531 (butane)	1.532 (propane) 1.531 (butane)	1.532 (propane) 1.531 (butane)	1.399 (benzene)	1.101 (benzene)
$b,c\ (a_0)$	1.47012	1.27295	1.29569	1.29924	1.54616	1.54616	1.52750	1.54616	1.52750	1.52750	0.66540	1.22265
e	0.76793	0.63580	0.63159	0.63095	0.68600	0.68600	0.68888	0.68600	0.68888	0.68888	0.89223	0.64537

Table 15.353. The MO to HO intercept geometrical bond parameters of alkyl phosphines. R_1 is an alkyl group and R, R', R'' are H or alkyl groups. E_T is E_T ($atom-atom,msp^3.AO$).

Bond	Atom	E_T (eV) Bond 1	E_T (eV) Bond 2	E_T (eV) Bond 3	E_T (eV) Bond 4	Final Total Energy $C2sp^3$ (eV)	$r_{initial}$ (a_0)	r_{final} (a_0)	$E_{Coulomb}$ (eV) Final	$E(C2sp^3)$ (eV) Final	θ' (°)	θ_1 (°)	θ_2 (°)	d_1 (a_0)	d_2 (a_0)
$C-H\ (CH_3)$	C	-0.36229	0	0	0	-151.97798	0.91771	0.89582	-15.18804	-14.99717	81.24	98.76	44.07	1.18494	0.13638
$(CH_3)_2P-CH_3$	C	-0.18114	0	0	0		0.91771	0.90654	-15.00689	-14.81603	87.12	92.88	38.02	1.80811	0.04562
$(CH_3)_2P-CH_3$	P	-0.18114	-0.18114	-0.18114	0		1.15350	0.88527	-15.36918		85.24	94.76	36.88	1.83594	0.07345
$C-H\ (CH_3)$	C	-0.92918	0	0	0	-152.54487	0.91771	0.86359	-15.75493	-15.56407	77.49	102.51	41.48	1.23564	0.18708
$C-H\ (CH_2)$	C	-0.92918	-0.92918	0	0	-153.47406	0.91771	0.81549	-16.68412	-16.49325	68.47	111.53	35.84	1.35486	0.29933
$C-H\ (CH)$	C	-0.92918	-0.92918	-0.92918	0	-154.40324	0.91771	0.77247	-17.61330	-17.42244	61.10	118.90	31.37	1.42988	0.37326
$H_3C_aC_bH_2CH_2-$ $(C-C$ (a))	C_a	-0.92918	0	0	0	-152.54487	0.91771	0.86359	-15.75493	-15.56407	63.82	116.18	30.08	1.83879	0.38106
$H_3C_aC_bH_2CH_2-$ $(C-C$ (a))	C_b	-0.92918	-0.92918	0	0	-153.47406	0.91771	0.81549	-16.68412	-16.49325	56.41	123.59	26.06	1.90890	0.45117
$R-H_2C_aC_b(H_2C_c-R')HCH_2-$ $(C-C$ (b))	C_b	-0.92918	-0.92918	-0.92918	0	-154.40324	0.91771	0.77247	-17.61330	-17.42244	48.30	131.70	21.90	1.97162	0.51388
$R-H_2C_a(R'-H_2C_d)C_b(R''-H_2C_c)CH_2-$ $(C-C$ (c))	C_b	-0.92918	-0.72457	-0.72457	-0.72457	-154.71860	0.91771	0.75889	-17.92866	-17.73779	48.21	131.79	21.74	1.95734	0.50570
$isoC_aC_b(H_2C_c-R')HCH_2-$ $(C-C$ (d))	C_b	-0.92918	-0.92918	-0.92918	0	-154.40324	0.91771	0.77247	-17.61330	-17.42244	48.30	131.70	21.90	1.97162	0.51388
$tertC_a(R'-H_2C_d)C_b(R''-H_2C_c)CH_2-$ $(C-C$ (e))	C_b	-0.72457	-0.72457	-0.72457	-0.72457	-154.51399	0.91771	0.76765	-17.92866	-17.73779	50.04	129.96	22.66	1.94462	0.49298
$tertC_aC_b(H_2C_c-R')HCH_2-$ $(C-C$ (f))	C_b	-0.72457	-0.92918	-0.92918	0	-154.19863	0.91771	0.78155	-17.40869	-17.21783	52.78	127.22	24.04	1.92443	0.47279
$isoC_a(R'-H_2C_d)C_b(R''-H_2C_c)CH_2-$ $(C-C$ (f))	C_b	-0.72457	-0.72457	-0.72457	-0.72457	-154.51399	0.91771	0.76765	-17.92866	-17.73779	50.04	129.96	22.66	1.94462	0.49298

Table 15.354. The energy parameters (eV) of functional groups of alkyl phosphines.

Parameters	$P-C$ Group	CH_3 Group	CH_2 Group	CH (i) Group	$C-C$ (a) Group	$C-C$ (b) Group	$C-C$ (c) Group	$C-C$ (d) Group	$C-C$ (e) Group	$C-C$ (f) Group	$C=C$ Group	CH (ii) Group
f_1	1	1	1	1	1	1	1	1	1	1	0.75	1
n_1	1	3	2	1	1	1	1	1	1	1	2	1
n_2	0	2	1	0	0	0	0	0	0	0	0	0
n_3	0	0	0	0	0	0	0	0	0	0	0	0
C_1	0.5	0.75	0.75	0.75	0.5	0.5	0.5	0.5	0.5	0.5	0.5	0.75
C_2	0.73885	1	1	1	1	1	1	1	1	1	0.85252	1
c_1	1	1	1	1	1	1	1	1	1	1	1	1
c_2	1	0.91771	0.91771	0.91771	0.91771	0.91771	0.91771	0.91771	0.91771	0.91771	0.85252	0.91771
c_3	0	0	1	1	0	0	0	1	1	0	0	1
c_4	2	1	1	1	2	2	2	2	2	2	3	1
c_5	0	3	2	1	0	0	0	0	0	0	0	1
C_{1o}	0.5	0.75	0.75	0.75	0.5	0.5	0.5	0.5	0.5	0.5	0.5	0.75
C_{2o}	0.73885	1	1	1	1	1	1	1	1	1	0.85252	1
V_e (eV)	-31.34959	-107.32728	-70.41425	-35.12015	-28.79214	-28.79214	-29.10112	-28.79214	-29.10112	-29.10112	-101.12679	-37.10024
V_p (eV)	7.71965	38.92728	25.78002	12.87680	9.33352	9.33352	9.37273	9.33352	9.37273	9.37273	20.69825	13.17125
T (eV)	6.82959	32.53914	21.06675	10.48582	6.77464	6.77464	6.90500	6.77464	6.90500	6.90500	34.31559	11.58941
V_m (eV)	-3.41479	-16.26957	-10.53337	-5.24291	-3.38732	-3.38732	-3.45250	-3.38732	-3.45250	-3.45250	-17.15779	-5.79470
$E_{(AO/HO)}$ (eV)	-11.78246	-15.56407	-15.56407	-14.63489	-15.56407	-15.56407	-15.35946	-15.56407	-15.35946	-15.35946	0	-14.63489
$\Delta E_{H_2MO\,(AO/HO)}$ (eV)	-0.36229	0	0	0	0	0	0	0	0	0	0	-1.13379
$E_{T\,(AO/HO)}$ (eV)	-11.42017	-15.56407	-15.56407	-14.63489	-15.56407	-15.56407	-15.35946	-15.56407	-15.35946	-15.35946	0	-13.50110
$E_{T\,(H_2MO)}$ (eV)	-31.63532	-67.69451	-49.66493	-31.63533	-31.63537	-31.63537	-31.63535	-31.63537	-31.63535	-31.63535	-63.27075	-31.63539
$E_T\left(atom-atom, msp^3.AO\right)$ (eV)	-0.36229	0	0	0	-1.85836	-1.85836	-1.44915	-1.85836	-1.44915	-1.44915	-2.26759	-0.56690
$E_{T\,(MO)}$ (eV)	-31.99766	-67.69450	-49.66493	-31.63537	-33.49373	-33.49373	-33.08452	-33.49373	-33.08452	-33.08452	-65.53833	-32.20226
$\omega\ \left(10^{15}\ rad/s\right)$	7.22663	24.9286	24.2751	24.1759	9.43699	9.43699	15.4846	9.43699	9.55643	9.55643	49.7272	26.4826
E_K (eV)	4.75669	16.40846	15.97831	15.91299	6.21159	6.21159	10.19220	6.21159	6.29021	6.29021	32.73133	17.43132
$\overline{E}_D$ (eV)	-0.13806	-0.25352	-0.25017	-0.24956	-0.16515	-0.16515	-0.20896	-0.16515	-0.16416	-0.16416	-0.35806	-0.26130
$\overline{E}_{Kvib}$ (eV)	0.17606 [68]	0.35532 (Eq. (13.458))	0.35532 (Eq. (13.458))	0.35532 (Eq. (13.458))	0.12312 [2]	0.17978 [4]	0.09944 [5]	0.12312 [2]	0.12312 [2]	0.12312 [2]	0.19649 [49]	0.35532 Eq. (13.458)
$\overline{E}_{osc}$ (eV)	-0.05003	-0.22757	-0.14502	-0.07200	-0.10359	-0.07526	-0.15924	-0.10359	-0.10260	-0.10260	-0.25982	-0.08364
E_{mag} (eV)	0.14803	0.14803	0.14803	0.14803	0.14803	0.14803	0.14803	0.14803	0.14803	0.14803	0.14803	0.14803
$E_{T\,(Group)}$ (eV)	-32.04769	-67.92207	-49.80996	-31.70737	-33.59732	-33.49373	-33.24376	-33.59732	-33.18712	-33.18712	-49.54347	-32.28590
$E_{initial\,(c_4\ AO/HO)}$ (eV)	-14.63489	-14.63489	-14.63489	-14.63489	-14.63489	-14.63489	-14.63489	-14.63489	-14.63489	-14.63489	-14.63489	-14.63489
$E_{initial\,(c_5\ AO/HO)}$ (eV)	0	-13.59844	-13.59844	-13.59844	0	0	0	0	0	0	0	-13.59844
$E_{D\,(Group)}$ (eV)	2.77791	12.49186	7.83016	3.32601	4.32754	4.29921	3.97398	4.17951	3.62128	3.91734	5.63881	3.90454

Table 15.355. The total bond energies of alkyl phosphines calculated using the functional group composition and the energies of Table 15.354 compared to the experimental values [69].

Formula	Name	$P-C$	CH_3	CH_2	CH (i)	$C-C$ (a)	$C-C$ (b)	$C-C$ (c)	$C-C$ (d)	$C-C$ (e)	$C-C$ (f)	$C\overset{3e}{=}C$	CH (ii)	Calculated Total Bond Energy (eV)	Experimental Total Bond Energy (eV)	Relative Error
C_3H_9P	Trimethylphosphine	3	3	0	0	0	0	0	0	0	0	0	0	45.80930	46.87333	0.02270
$C_6H_{15}P$	Triethylphosphine	3	3	3	0	3	0	0	0	0	0	0	0	82.28240	82.24869	-0.00041
$C_{18}H_{15}P$	Triphenylphosphine	3	0	0	0	0	0	0	0	0	0	18	15	168.40033	167.46591	-0.00558

Table 15.356. The bond angle parameters of alkyl phosphines and experimental values [1]. In the calculation of θ_v, the parameters from the preceding angle were used. E_T is E_T ($atom-atom,msp^3.AO$).

Atoms of Angle	2c' Bond 1 (a_0)	2c' Bond 2 (a_0)	2c' Terminal Atoms (a_0)	$E_{Coulombic}$ or E Atom 1	Atom 1 Hybridization Designation (Table 15.3.A)	$E_{Coulombic}$ Atom 2	Atom 2 Hybridization Designation (Table 15.3.A)	c_2 Atom 1	c_2 Atom 2	C_1	C_2	c_1	c_2'	E_T (eV)	θ_v (°)	θ_1 (°)	θ_2 (°)	Cal. θ (°)	Exp. θ (°)
Methyl $\angle HC_aH$	2.09711	2.09711	3.4252	-15.75493	7	H	H	0.86359	1	1	1	0.75	1.15796	0				109.50	
$\angle H_aC_aP$															70.56			109.44	110.7 (trimethyl phosphine)
$\angle C_aPC_b$	3.52498	3.52498	5.3479	-15.93607	9	-15.93607	9	0.85377	0.85377	1	1	1	0.85377	-1.85836				98.68	98.6 (trimethyl phosphine)
Methylene $\angle HC_aH$	2.11106	2.11106	3.4252	-15.75493	7	H	H	0.86359	1	1	1	0.75	1.15796	0				108.44	107 (propane)
$\angle C_aC_bC_c$															69.51			110.49	112 (propane) 113.8 (butane) 110.8 (isobutane)
$\angle C_aC_bH$															69.51			110.49	111.0 (butane) 111.4 (isobutane)
Methyl $\angle HC_aH$	2.09711	2.09711	3.4252	-15.75493	7	H	H	0.86359	1	1	1	0.75	1.15796	0				109.50	
$\angle C_aC_bC_c$															70.56			109.44	
$\angle C_aC_bH$															70.56			109.44	
$\angle C_bC_aC_c$ iso C_a	2.91547	2.91547	4.7958	-16.68412 C_b	26	-16.68412 C_c	26	0.81549	0.81549	1	1	1	0.81549	-1.85836				110.67	110.8 (isobutane)
$\angle C_bC_aH$ iso C_a	2.91547	2.11323	4.1633	-15.55033 C_a	5	-14.82575 C_b	1	0.87495	0.91771	0.75	1	0.75	1.04887	0				110.76	
$\angle C_aC_bH$ iso C_a	2.91547	2.09711	4.1633	-15.55033 C_b	5	-14.82575 C_a	1	0.87495	0.91771	0.75	1	0.75	1.04887	0				111.27	111.4 (isobutane)
$\angle C_bC_aC_b$ tert C_a	2.90327	2.90327	4.7958	-16.68412 C_b	26	-16.68412 C_b	26	0.81549	0.81549	1	1	1	0.81549	-1.85836				111.37	110.8 (isobutane)
$\angle C_bC_aC_d$															72.50			107.50	

ALKYL PHOSPHITES ($\left(C_nH_{2n+1}O\right)_3P,\ \ n=1,2,3,4,5...\infty$)

The alkyl phosphites, $\left(C_nH_{2n+1}O\right)_3P$, comprise $P-O$ and $C-O$ functional groups. The alkyl portion of the alkyl phosphite may comprise at least two terminal methyl groups (CH_3) at each end of each chain, and may comprise methylene (CH_2), and methylyne (CH) functional groups as well as C bound by carbon-carbon single bonds. The methyl and methylene functional groups are equivalent to those of straight-chain alkanes. Six types of $C-C$ bonds can be identified. The n-alkane $C-C$ bond is the same as that of straight-chain alkanes. In addition, the $C-C$ bonds within isopropyl ($\left(CH_3\right)_2CH$) and t-butyl ($\left(CH_3\right)_3C$) groups and the isopropyl to isopropyl, isopropyl to t-butyl, and t-butyl to t-butyl $C-C$ bonds comprise functional groups. The branched-chain-alkane groups in alkyl phosphites are equivalent to those in branched-chain alkanes.

The ether portion comprises two types of $C-O$ functional groups, one for methyl or t-butyl groups corresponding to the C, and the other for general alkyl groups that are equivalent to those in the Ethers section. The $P-O$ bond forms between the $P3sp^3$ HO and an $O2p$ AO to yield phosphites. The semimajor axis a of the $P-O$ functional group is solved using Eq. (15.51). Using the semimajor axis and the relationships between the prolate spheroidal axes, the geometric and energy parameters of the MO are calculated using Eqs. (15.1-15.117) in the same manner as the organic functional groups given in Organic Molecular Functional Groups and Molecules section.

For the $P-O$ functional group, hybridization the $3s$ and $3p$ AOs of each to form a single $3sp^3$ shell forms an energy minimum, and the sharing of electrons between the $O2p$ AOs and $P3sp^3$ HOs to form a MO permits each participating orbital to decrease in radius and energy. The O AO has an energy of $E\left(O\right)=-13.61805\ eV$, and the $P3sp^3$ HO has an energy of $E\left(P,3sp^3\right)=-11.78246\ eV$ (Eq. (15.180)). In branched-chain alkyl phosphites, the energy matching condition is determined by the c_2 and C_2 parameters of Eq. (15.51) given by Eqs. (15.77), (15.79), and (13.430).

$$c_2\ and\ C_2\left(O2pAO\ to\ P3sp^3HO\right)=\frac{E\left(P,3sp^3\right)}{E\left(O,2p\right)}c_2\left(C2sp^3HO\right)=\frac{-11.78246\ eV}{-13.61805\ eV}\left(0.91771\right)=0.79401 \tag{15.182}$$

The energy of the $P-O$-bond MO is the sum of the component energies of the H_2-type ellipsoidal MO given in Eq. (15.51) with $E\left(AO/HO\right)$ being $E\left(P,3sp^3\right)$ given by Eq. (23.180), and $E_T\left(atom-atom,msp^3.AO\right)$ is equivalent to that of single bond, $-1.44914\ eV$, given by twice Eq. (14.151) in order to match the energies of the oxygen AO with the phosphorous and carbon HOs.

The symbols of the functional groups of branched-chain alkyl phosphites are given in Table 15.357. The geometrical (Eqs. (15.1-15.5) and (15.51)), intercept (Eqs. (15.80-15.87)), and energy (Eqs. (15.6-15.11) and (15.17-15.65)) parameters of alkyl phosphites are given in Tables 15.358, 15.359, and 15.360, respectively. The total energy of each alkyl phosphite given in Table 15.361 was calculated as the sum over the integer multiple of each $E_{D\,(Group)}$ of Table 15.360 corresponding to functional-group composition of the molecule. The bond angle parameters of alkyl phosphites determined using Eqs. (15.88-15.117) are given in Table 15.362. The color scale, charge-density of exemplary alkyl phosphite, tri-isopropyl phosphite, comprising atoms with the outer shell bridged by one or more H_2-type ellipsoidal MOs or joined with one or more hydrogen MOs is shown in Figure 15.61.

Figure 15.61. Color scale, charge-density of tri-isopropyl phosphite showing the orbitals of the atoms at their radii, the ellipsoidal surface of each H or H_2-type ellipsoidal MO that transitions to the corresponding outer shell of the atom(s) participating in each bond, and the hydrogen nuclei.

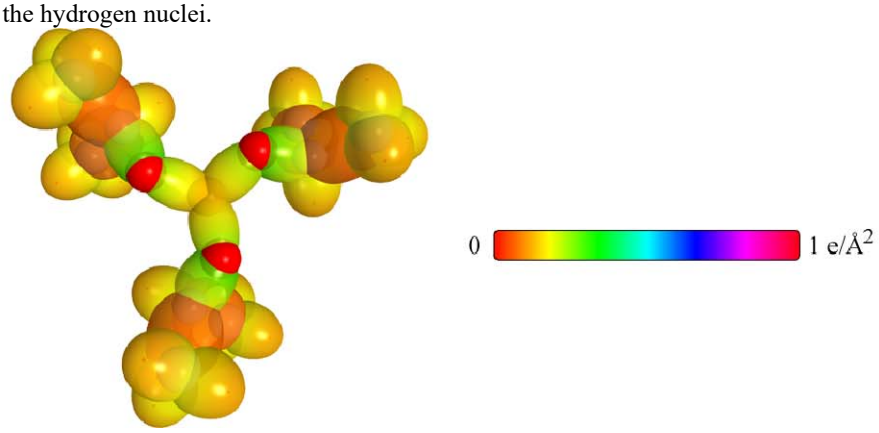

Table 15.357. The symbols of functional groups of alkyl phosphites.

Functional Group	Group Symbol
P-O	$P-O$
C-O (CH_3-O- and $(CH_3)_3C-O-$)	$C-O$ (i)
C-O (alkyl)	$C-O$ (ii)
CH_2 group	$C-H$ (CH_2)
CH	$C-H$
CC bond (*n-C*)	$C-C$ (a)
CC bond (*iso-C*)	$C-C$ (b)
CC bond (*tert-C*)	$C-C$ (c)
CC (*iso* to *iso-C*)	$C-C$ (d)
CC (*t* to *t-C*)	$C-C$ (e)
CC (*t* to *iso-C*)	$C-C$ (f)

Table 15.358. The geometrical bond parameters of alkyl phosphites and experimental values [1].

Parameter	$P-O$ Group	$C-O$ (i) Group	$C-O$ (ii) Group	$C-H$ (CH_3) Group	$C-H$ (CH_2) Group	$C-H$ Group	$C-C$ (a) Group	$C-C$ (b) Group	$C-C$ (c) Group	$C-C$ (d) Group	$C-C$ (e) Group	$C-C$ (f) Group
$a\ (a_0)$	1.84714	1.80717	1.79473	1.64920	1.67122	1.67465	2.12499	2.12499	2.10725	2.12499	2.10725	2.10725
$c'\ (a_0)$	1.52523	1.34431	1.33968	1.04856	1.05553	1.05661	1.45744	1.45744	1.45164	1.45744	1.45164	1.45164
Bond Length $2c'\ (\AA)$	1.61423	1.42276	1.41785	1.10974	1.11713	1.11827	1.54280	1.54280	1.53635	1.54280	1.53635	1.53635
Exp. Bond Length $(\AA)$	1.631 [70] (MHP) 1.60 [65] (DNA)	1.416 (dimethyl ether)	1.418 (ethyl methyl ether (avg.))	1.107 ($C-H$ propane) 1.117 ($C-H$ butane)	1.107 ($C-H$ propane) 1.117 ($C-H$ butane)	1.122 (isobutane)	1.532 (propane) 1.531 (butane)	1.532 (propane) 1.531 (butane)	1.532 (propane) 1.531 (butane)	1.532 (propane) 1.531 (butane)	1.532 (propane) 1.531 (butane)	1.532 (propane) 1.531 (butane)
$b,c\ (a_0)$	1.04192	1.20776	1.19429	1.27295	1.29569	1.29924	1.54616	1.54616	1.52750	1.54616	1.52750	1.52750
e	0.82573	0.74388	0.74645	0.63580	0.63159	0.63095	0.68600	0.68600	0.68888	0.68600	0.68888	0.68888

Table 15.359. The MO to HO intercept geometrical bond parameters of alkyl phosphites. R, R', R'' are H or alkyl groups. E_T is E_T ($atom-atom,msp^3.AO$).

Bond	Atom	E_T (eV) Bond 1	E_T (eV) Bond 2	E_T (eV) Bond 3	E_T (eV) Bond 4	Final Total Energy $C2sp^3$ (eV)	$r_{initial}$ (a_0)	r_{final} (a_0)	$E_{Coulomb}$ (eV) Final	$E(C2sp^3)$ (eV) Final	θ' (°)	θ_1 (°)	θ_2 (°)	d_1 (a_0)	d_2 (a_0)
$(CH_3O)_2P-OCH_3$ $(CH_3O)_2P-OC(CH_3)_3$ $(C-O$ (i))	O	-0.72457	-0.72457	0	0		1.00000	0.83600	-16.27489		111.08	68.92	48.48	1.22455	0.30068
$(CH_3O)_2P-OCH_3$ $(CH_3O)_2P-OC(CH_3)_3$ $(CH_3O)_2P-OCH_2R$ $(C-O$ (i)) and $(C-O$ (ii))	P	-0.72457	-0.72457	-0.72457	0		1.15350	0.80037	-16.99947		108.77	71.23	46.66	1.26770	0.25753
$(CH_3O)_2P-OCH_2R$ $(C-O$ (ii))	O	-0.72457	-0.82688	0	0		1.00000	0.83078	-16.37720		110.75	69.25	48.21	1.23087	0.29436
$C-H(OC_aH_3)$	C_a	-0.72457	0	0	0	-152.34026	0.91771	0.87495	-15.55033	-15.35946	78.85	101.15	42.40	1.21777	0.16921
$(CH_3O)_2PO-C_aH_3$	C_a	-0.72457	0	0	0	-152.34026	0.91771	0.87495	-15.55033	-15.35946	95.98	84.02	46.10	1.25319	0.09112
$(CH_3O)_2PO-C_a(CH_3)_3$ $(C-O$ (i))	C_a	-0.72457	-0.72457	-0.72457	-0.72457	-154.51399	0.91771	0.76765	-17.72405		86.03	93.97	39.35	1.39744	0.05313
$(H_3CO)_2PO-C_cH_3$ $(CH_3)_3C_c-OP(OC_bH_3)_2$ $(C-O$ (i))	O	-0.72457	-0.72457	0	0		1.00000	0.83600	-16.27490		92.66	87.34	43.74	1.30555	0.03876
$-H_2C_a-OP(OCH_3)_2$ $(C-O$ (ii))	C_a	-0.82688	-0.92918	0	0	-153.37175	0.91771	0.82053	-16.58181	-16.39095	92.41	87.59	43.35	1.30512	0.03456
$(CH_3O)_2PO-C_aH(CH_3)_2$ $(C-O$ (ii))	C_a	-0.82688	-0.92918	-0.92918	0	-154.30093	0.91771	0.77699	-17.51099	-17.32013	88.25	91.75	40.56	1.36345	0.02377
$-H_2C_a-OP(OCH_3)_2$ $(H_3C)_2HC_a-OP(OCH_3)_2$ $(C-O$ (ii))	O	-0.72457	-0.82688	0	0		1.00000	0.83078	-16.37720		93.33	86.67	43.98	1.29138	0.04829
$C-H(CH_3)$	C	-0.92918	0	0	0	-152.54487	0.91771	0.86359	-15.75493	-15.56407	77.49	102.51	41.48	1.23564	0.18708
$C-H(CH_2)$	C	-0.92918	-0.92918	0	0	-153.47406	0.91771	0.81549	-16.68412	-16.49325	68.47	111.53	35.84	1.35486	0.29933
$C-H(CH)$	C	-0.92918	-0.92918	-0.92918	0	-154.40324	0.91771	0.77247	-17.61330	-17.42244	61.10	118.90	31.37	1.42988	0.37326
$H_3C_aC_bH_2CH_2-$ $(C-C$ (a))	C_a	-0.92918	0	0	0	-152.54487	0.91771	0.86359	-15.75493	-15.56407	63.82	116.18	30.08	1.83879	0.38106
$H_3C_aC_bH_2CH_2-$ $(C-C$ (a))	C_b	-0.92918	-0.92918	0	0	-153.47406	0.91771	0.81549	-16.68412	-16.49325	56.41	123.59	26.06	1.90890	0.45117
$R-H_2C_aC_b(H_2C_c-R')HCH_2-$ $(C-C$ (b))	C_b	-0.92918	-0.92918	-0.92918	0	-154.40324	0.91771	0.77247	-17.61330	-17.42244	48.30	131.70	21.90	1.97162	0.51388
$R-H_2C_a(R'-H_2C_d)C_b(R''-H_2C_c)CH_2-$ $(C-C$ (c))	C_b	-0.92918	-0.72457	-0.72457	-0.72457	-154.71860	0.91771	0.75889	-17.92866	-17.73779	48.21	131.79	21.74	1.95734	0.50570
$isoC_aC_b(H_2C_c-R')HCH_2-$ $(C-C$ (d))	C_b	-0.92918	-0.92918	-0.92918	0	-154.40324	0.91771	0.77247	-17.61330	-17.42244	48.30	131.70	21.90	1.97162	0.51388
$tertC_a(R'-H_2C_d)C_b(R''-H_2C_c)CH_2-$ $(C-C$ (e))	C_b	-0.72457	-0.72457	-0.72457	-0.72457	-154.51399	0.91771	0.76765	-17.92866	-17.73779	50.04	129.96	22.66	1.94462	0.49298
$tertC_aC_b(H_2C_c-R')HCH_2-$ $(C-C$ (f))	C_b	-0.72457	-0.92918	-0.92918	0	-154.19863	0.91771	0.78155	-17.40869	-17.21783	52.78	127.22	24.04	1.92443	0.47279
$isoC_a(R'-H_2C_d)C_b(R''-H_2C_c)CH_2-$ $(C-C$ (f))	C_b	-0.72457	-0.72457	-0.72457	-0.72457	-154.51399	0.91771	0.76765	-17.92866	-17.73779	50.04	129.96	22.66	1.94462	0.49298

Table 15.360. The energy parameters (eV) of functional groups of alkyl phosphites.

Parameters	$P-O$ Group	$C-O$ (i) Group	$C-O$ (ii) Group	CH_3 Group	CH_2 Group	CH (i) Group	$C-C$ (a) Group	$C-C$ (b) Group	$C-C$ (c) Group	$C-C$ (d) Group	$C-C$ (e) Group	$C-C$ (f) Group
n_1	1	1	1	3	2	1	1	1	1	1	1	1
n_2	0	0	0	2	1	0	0	0	0	0	0	0
n_3	0	0	0	0	0	0	0	0	0	0	0	0
C_1	0.5	0.5	0.5	0.75	0.75	0.75	0.5	0.5	0.5	0.5	0.5	0.5
C_2	1	1	1	1	1	1	1	1	1	1	1	1
c_1	1	1	1	1	1	1	1	1	1	1	1	1
c_2	0.79401	0.85395	0.85395	0.91771	0.91771	0.91771	0.91771	0.91771	0.91771	0.91771	0.91771	0.91771
c_3	0	0	0	0	1	1	0	0	0	1	1	0
c_4	2	2	2	1	1	1	2	2	2	2	2	2
c_5	0	0	0	3	2	1	0	0	0	0	0	0
C_{1o}	0.5	0.5	0.5	0.75	0.75	0.75	0.5	0.5	0.5	0.5	0.5	0.5
C_{2o}	0.79401	1	1	1	1	1	1	1	1	1	1	1
V_e (eV)	-33.27738	-33.15757	-33.47304	-107.32728	-70.41425	-35.12015	-28.79214	-28.79214	-29.10112	-28.79214	-29.10112	-29.10112
V_p (eV)	8.92049	10.12103	10.15605	38.92728	25.78002	12.87680	9.33352	9.33352	9.37273	9.33352	9.37273	9.37273
T (eV)	9.00781	9.17389	9.32537	32.53914	21.06675	10.48582	6.77464	6.77464	6.90500	6.77464	6.90500	6.90500
V_m (eV)	-4.50391	-4.58695	-4.66268	-16.26957	-10.53337	-5.24291	-3.38732	-3.38732	-3.45250	-3.38732	-3.45250	-3.45250
$E_{(AO/HO)}$ (eV)	-11.78246	-14.63489	-14.63489	-15.56407	-15.56407	-14.63489	-15.56407	-15.56407	-15.35946	-15.56407	-15.35946	-15.35946
$\Delta E_{H_2MO\,(AG/HO)}$ (eV)	0	-1.44915	-1.65376	0	0	0	0	0	0	0	0	0
$E_{T\,(AG/HO)}$ (eV)	-11.78246	-13.18574	-12.98113	-15.56407	-15.56407	-14.63489	-15.56407	-15.56407	-15.35946	-15.56407	-15.35946	-15.35946
$E_{T\,(H_2MO)}$ (eV)	-31.63544	-31.63533	-31.63544	-67.69451	-49.66493	-31.63533	-31.63537	-31.63537	-31.63535	-31.63537	-31.63535	-31.63535
$E_T\left(atom-atom, msp^3.AO\right)$ (eV)	-1.44914	-1.44915	-1.65376	0	0	0	-1.85836	-1.85836	-1.44915	-1.85836	-1.44915	-1.44915
$E_{T\,(MO)}$ (eV)	-33.08451	-33.08452	-33.28912	-67.69450	-49.66493	-31.63537	-33.49373	-33.49373	-33.08452	-33.49373	-33.08452	-33.08452
$\omega\ \left(10^{15}\ rad/s\right)$	10.3761	12.0329	12.1583	24.9286	24.2751	24.1759	9.43699	9.43699	15.4846	9.43699	9.55643	9.55643
E_K (eV)	6.82973	7.92028	8.00277	16.40846	15.97831	15.91299	6.21159	6.21159	10.19220	6.21159	6.29021	6.29021
$\overline{E}_D$ (eV)	-0.17105	-0.18420	-0.18631	-0.25352	-0.25017	-0.24966	-0.16515	-0.16515	-0.20896	-0.16515	-0.16416	-0.16416
$\overline{E}_{Kvib}$ (eV)	0.10477 [71]	0.13663 [21]	0.16118 [4]	0.35532 (Eq. (13.458))	0.35532 (Eq. (13.458))	0.35532 (Eq. (13.458))	0.12312 [2]	0.17978 [4]	0.09944 [5]	0.12312 [2]	0.12312 [2]	0.12312 [2]
$\overline{E}_{osc}$ (eV)	-0.11867	-0.11589	-0.10572	-0.22757	-0.14502	-0.07200	-0.10359	-0.07526	-0.15924	-0.10359	-0.10260	-0.10260
E_{mag} (eV)	0.14803	0.14803	0.14803	0.14803	0.14803	0.14803	0.14803	0.14803	0.14803	0.14803	0.14803	0.14803
$E_{T\,(Group)}$ (eV)	-33.20318	-33.20040	-33.39484	-67.92207	-49.80996	-31.70737	-33.59732	-33.49373	-33.24376	-33.59732	-33.18712	-33.18712
$E_{initial\,(c_4\ AO/HO)}$ (eV)	-14.63489	-14.63489	-14.63489	-14.63489	-14.63489	-14.63489	-14.63489	-14.63489	-14.63489	-14.63489	-14.63489	-14.63489
$E_{initial\,(c_5\ AO/HO)}$ (eV)	0	0	0	-13.59844	-13.59844	-13.59844	0	0	0	0	0	0
$E_{D\,(Group)}$ (eV)	3.93340	3.93062	4.12506	12.49186	7.83016	3.32601	4.32754	4.29921	3.97398	4.17951	3.62128	3.91734

Table 15.361. The total bond energies of alkyl phosphites calculated using the functional group composition and the energies of Table 15.360 compared to the experimental values [69].

Formula	Name	$P-O$	$C-O$ (i)	$C-O$ (ii)	CH_3	CH_2	CH (i)	$C-C$ (a)	$C-C$ (b)	$C-C$ (c)	$C-C$ (d)	$C-C$ (e)	$C-C$ (f)	Calculated Total Bond Energy (eV)	Experimental Total Bond Energy (eV)	Relative Error
$C_3H_9O_3P$	Trimethyl phosphite	3	3	0	3	0	0	0	0	0	0	0	0	61.06764	60.94329	-0.00204
$C_6H_{15}O_3P$	Triethyl phosphite	3	0	3	3	3	0	3	0	0	0	0	0	98.12406	97.97947	-0.00148
$C_9H_{21}O_3P$	Tri-isopropyl phosphite	3	0	3	6	0	3	0	6	0	0	0	0	134.89983	135.00698	0.00079

Table 15.362. The bond angle parameters of alkyl phosphites and experimental values [1]. In the calculation of θ_v, the parameters from the preceding angle were used. E_T is E_T ($atom-atom,msp^3.AO$).

Atoms of Angle	$2c'$ Bond 1 (a_0)	$2c'$ Bond 2 (a_0)	$2c'$ Terminal Atoms (a_0)	$E_{Coulombic}$ or E Atom 1	Atom 1 Hybridization Designation (Table 15.3.A)	$E_{Coulombic}$ Atom 2	Atom 2 Hybridization Designation (Table 15.3.A)	c_2 Atom 1	c_2 Atom 2	C_1	C_2	c_1	c_2'	E_T (eV)	θ_v (°)	θ_1 (°)	θ_2 (°)	Cal. θ (°)	Exp. θ (°)
$\angle OPO$	3.05046	3.05046	4.5826	-16.27489	16	-16.27489	16	0.83600	0.83600	1	1	1	0.83600	-1.65376				97.38	96 [72] (triethyl phosphite)
$\angle POC$	3.05046	2.68862	4.9768	-11.78246	Psp^3	-15.75493	7	0.73885 Eq. (23.181)	0.86359	1	0.73885	1	0.80122	-0.72457				120.13	120 [72] (triethyl phosphite)
$\angle C_bC_aO$	2.91547	2.67935	4.5607	-16.68412	26	-13.61806	O	0.81549	0.85395 (Eq. (15.133))	1	1	1	0.83472	-1.65376				109.13	109.4 (ethyl methyl ether)
Methylene $\angle HC_aH$	2.11106	2.11106	3.4252	-15.75493	7	H	H	0.86359	1	1	1	0.75	1.15796	0				108.44	107 (propane)
$\angle C_aC_bC_c$															69.51			110.49	112 (propane) 113.8 (butane) 110.8 (isobutane)
$\angle C_aC_bH$															69.51			110.49	111.0 (butane) 111.4 (isobutane)
Methyl $\angle HC_aH$	2.09711	2.09711	3.4252	-15.75493	7	H	H	0.86359	1	1	1	0.75	1.15796	0				109.50	
$\angle C_aC_bC_c$															70.56			109.44	
$\angle C_aC_bH$															70.56			109.44	
$\angle C_bC_aC_c$ iso C_a	2.91547	2.91547	4.7958	-16.68412 C_b	26	-16.68412 C_c	26	0.81549	0.81549	1	1	1	0.81549	-1.85836				110.67	110.8 (isobutane)
$\angle C_bC_aH$ iso C_a	2.91547	2.11323	4.1633	-15.55033 C_a	5	-14.82575 C_b	1	0.87495	0.91771	0.75	1	0.75	1.04887	0				110.76	
$\angle C_aC_bH$ iso C_a	2.91547	2.09711	4.1633	-15.55033 C_b	5	-14.82575 C_a	1	0.87495	0.91771	0.75	1	0.75	1.04887	0				111.27	111.4 (isobutane)
$\angle C_bC_aC_b$ tert C_a	2.90327	2.90327	4.7958	-16.68412 C_b	26	-16.68412 C_b	26	0.81549	0.81549	1	1	1	0.81549	-1.85836				111.37	110.8 (isobutane)
$\angle C_bC_aC_d$															72.50			107.50	

ALKYL PHOSPHINE OXIDES ($\left(C_nH_{2n+1}\right)_3 P=O,\ n=1,2,3,4,5...\infty$)

The alkyl phosphine oxides, $\left(C_nH_{2n+1}\right)_3 P=O$, comprise $P-C$ and $P=O$ functional groups. The alkyl portion of the alkyl phosphine oxide may comprise at least two terminal methyl groups (CH_3) at each end of each chain, and may comprise methylene (CH_2), and methylyne (CH) functional groups as well as C bound by carbon-carbon single bonds. The methyl and methylene functional groups are equivalent to those of straight-chain alkanes. Six types of $C-C$ bonds can be identified. The n-alkane $C-C$ bond is the same as that of straight-chain alkanes. In addition, the $C-C$ bonds within isopropyl ($\left(CH_3\right)_2 CH$) and t-butyl ($\left(CH_3\right)_3 C$) groups and the isopropyl to isopropyl, isopropyl to t-butyl, and t-butyl to t-butyl $C-C$ bonds comprise functional groups. The branched-chain-alkane groups in alkyl phosphine oxides are equivalent to those in branched-chain alkanes.

The $P-C$ functional group is equivalent to that of alkyl phosphines. The $P=O$ bond forms between the $P3sp^3$ HO and an $O2p$ AO to yield phosphine oxides. The semimajor axis a of the $P=O$ functional group is solved using Eq. (15.51). Using the semimajor axis and the relationships between the prolate spheroidal axes, the geometric and energy parameters of the MO are calculated using Eqs. (15.1-15.117) in the same manner as the organic functional groups given in Organic Molecular Functional Groups and Molecules section.

For the $P=O$ functional group, hybridization the $3s$ and $3p$ AOs of each P to form a single $3sp^3$ shells forms an energy minimum, and the sharing of electrons between the $O2p$ AOs and $P3sp^3$ HOs to form a MO permits each participating orbital to decrease in radius and energy. In branched-chain alkyl phosphine oxides, the energy of phosphorous is less than the Coulombic energy between the electron and proton of H given by Eq. (1.264). The energy matching condition is determined by the c_2 parameter given by Eq. (15.182). The energy of the $P=O$-bond MO is the sum of the component energies of the H_2-type ellipsoidal MO given in Eq. (15.51) with $E\left(AO/HO\right)$ being twice $E\left(P,3sp^3\right)$ given by Eq. (15.180) corresponding to the double bond, and $E_T\left(atom-atom,msp^3.AO\right)$ is equivalent to that of an alkene double bond, $-2.26758\,eV$, given by Eq. (14.247) in order to match the energies of the carbon and phosphorous HOs and the oxygen AO.

The symbols of the functional groups of branched-chain alkyl phosphine oxides are given in Table 15.363. The geometrical (Eqs. (15.1-15.5) and (15.51)), intercept (Eqs. (15.80-15.87)), and energy (Eqs. (15.6-15.11) and (15.17-15.65)) parameters of alkyl phosphine oxides are given in Tables 15.364, 15.365, and 15.366, respectively. The total energy of each alkyl phosphine oxide given in Table 15.367 was calculated as the sum over the integer multiple of each $E_{D\,(Group)}$ of Table 15.366 corresponding to functional-group composition of the molecule. The bond angle parameters of alkyl phosphine oxides determined using Eqs. (15.88-15.117) are given in Table 15.368. The color scale, charge-density of exemplary alkyl phosphine oxide, trimethylphosphine oxide, comprising atoms with the outer shell bridged by one or more H_2-type ellipsoidal MOs or joined with one or more hydrogen MOs is shown in Figure 15.62.

Figure 15.62. Color scale, charge-density of trimethylphosphine oxide showing the orbitals of the atoms at their radii, the ellipsoidal surface of each H or H_2-type ellipsoidal MO that transitions to the corresponding outer shell of the atom(s) participating in each bond, and the hydrogen nuclei. (A) Top view. (B) Side view.

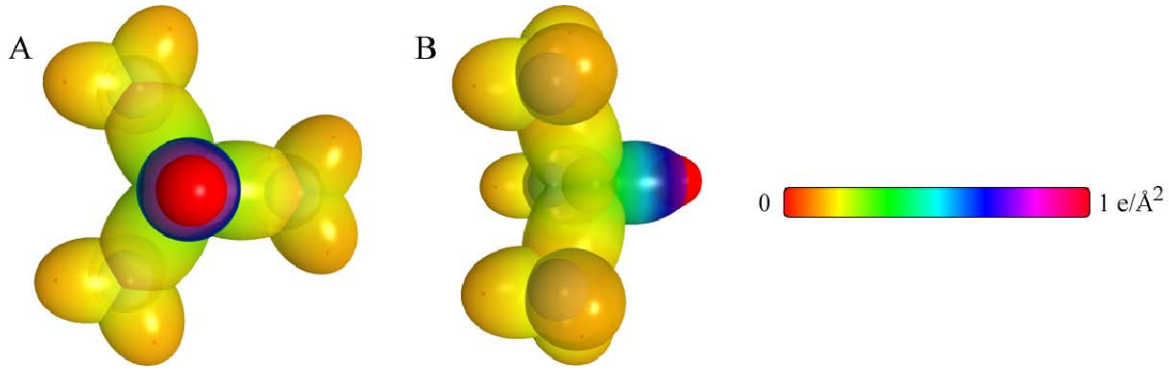

Table 15.363. The symbols of functional groups of alkyl phosphine oxides.

Functional Group	Group Symbol
P=O	$P=O$
P-C	$P-C$
CH_3 group	$C-H\ (CH_3)$
CH_2 group	$C-H\ (CH_2)$
CH	$C-H$ (i)
CC bond (*n-C*)	$C-C$ (a)
CC bond (*iso-C*)	$C-C$ (b)
CC bond (*tert-C*)	$C-C$ (c)
CC (*iso* to *iso-C*)	$C-C$ (d)
CC (*t* to *t-C*)	$C-C$ (e)
CC (*t* to *iso-C*)	$C-C$ (f)
CC (aromatic bond)	$C\overset{3e}{=}C$
CH (aromatic)	*CH* (ii)

Table 15.364. The geometrical bond parameters of alkyl phosphine oxides and experimental values [1].

Parameter	$P=O$ Group	$P-C$ Group	$C-H\ (CH_3)$ Group	$C-H\ (CH_2)$ Group	$C-H$ (i) Group	$C-C$ (a) Group	$C-C$ (b) Group	$C-C$ (c) Group	$C-C$ (d) Group	$C-C$ (e) Group	$C-C$ (f) Group	$^{3a}C=C$ Group	CH (ii) Group
$a\ (a_0)$	1.91663	2.29513	1.64920	1.67122	1.67465	2.12499	2.12499	2.10725	2.12499	2.10725	2.10725	1.47348	1.60061
$c'\ (a_0)$	1.38442	1.76249	1.04856	1.05553	1.05661	1.45744	1.45744	1.45164	1.45744	1.45164	1.45164	1.31468	1.03299
Bond Length $2c'\ (\AA)$	1.46521E-10	1.86534	1.10974	1.11713	1.11827	1.54280	1.54280	1.53635	1.54280	1.53635	1.53635	1.39140	1.09327
Exp. Bond Length $(\AA)$	1.48 [65] (DNA) 1.4759 (PO)	1.847 $((CH3)_2PCH_3)$ 1.858 (H_2PCH_3)	1.107 $(C-H$ propane) 1.117 $(C-H$ butane)	1.107 $(C-H$ propane) 1.117 $(C-H$ butane)	1.122 (isobutane)	1.532 (propane) 1.531 (butane)	1.532 (propane) 1.531 (butane)	1.532 (propane) 1.531 (butane)	1.532 (propane) 1.531 (butane)	1.532 (propane) 1.531 (butane)	1.532 (propane) 1.531 (butane)	1.399 (benzene)	1.101 (benzene)
$b,c\ (a_0)$	1.32546	1.47012	1.27295	1.29569	1.29924	1.54616	1.54616	1.52750	1.54616	1.52750	1.52750	0.66540	1.22265
e	0.72232	0.76793	0.63580	0.63159	0.63095	0.68600	0.68600	0.68888	0.68600	0.68888	0.68888	0.89223	0.64537

Table 15.365. The MO to HO intercept geometrical bond parameters of alkyl phosphine oxides. R, R', R'' are H or alkyl groups. E_T is $E_T\,(atom-atom,msp^3.AO)$.

Bond	Atom	E_T (eV) Bond 1	E_T (eV) Bond 2	E_T (eV) Bond 3	E_T (eV) Bond 4	Final Total Energy $C2sp^3$ (eV)	$r_{initial}\ (a_0)$	$r_{final}\ (a_0)$	$E_{Coulomb}$ (eV) Final	$E(C2sp^3)$ (eV) Final	θ' (°)	θ_1 (°)	θ_2 (°)	$d_1\ (a_0)$	$d_2\ (a_0)$
$(CH_3)_3P=O$	O	-1.13379	0	0	0		1.00000	0.85252	-15.95954		84.02	95.98	39.77	1.47318	0.08876
$(CH_3)_3P=O$	P	-1.13379	-0.18114	-0.18114	-0.18114		1.15350	0.82445	-16.50297		81.09	98.91	37.92	1.51205	0.12762
$(CH_3)_2(O)P-CH_3$	C	-0.18114	0	0	0		0.91771	0.90664	-15.00689	-14.81603	87.12	92.88	38.02	1.80811	0.04562
$(CH_3)_2(O)P-CH_3$	P	-0.18114	-0.18114	-0.18114	-1.13379		1.15350	0.82445	-16.50297		79.33	100.67	33.44	1.91514	0.15265
$C-H\ (CH_3)$	C	-0.92918	0	0	0	-152.54487	0.91771	0.86359	-15.75493	-15.56407	77.49	102.51	41.48	1.23564	0.18708
$C-H\ (CH_2)$	C	-0.92918	-0.92918	0	0	-153.47406	0.91771	0.81549	-16.68412	-16.49325	68.47	111.53	35.84	1.35486	0.29933
$C-H\ (CH)$	C	-0.92918	-0.92918	-0.92918	0	-154.40324	0.91771	0.77247	-17.61330	-17.42244	61.10	118.90	31.37	1.42988	0.37326
$H_3C_aC_bH_2CH_2-$ $(C-C$ (a))	C_a	-0.92918	0	0	0	-152.54487	0.91771	0.86359	-15.75493	-15.56407	63.82	116.18	30.08	1.83879	0.38106
$H_3C_aC_bH_2CH_2-$ $(C-C$ (a))	C_b	-0.92918	-0.92918	0	0	-153.47406	0.91771	0.81549	-16.68412	-16.49325	56.41	123.59	26.06	1.90890	0.45117
$R-H_2C_aC_b(H_2C_c-R')HCH_2-$ $(C-C$ (b))	C_b	-0.92918	-0.92918	-0.92918	0	-154.40324	0.91771	0.77247	-17.61330	-17.42244	48.30	131.70	21.90	1.97162	0.51388
$R-H_2C_a(R'-H_2C_d)C_b(R''-H_2C_c)CH_2-$ $(C-C$ (c))	C_b	-0.92918	-0.72457	-0.72457	-0.72457	-154.71860	0.91771	0.75889	-17.92866	-17.73779	48.21	131.79	21.74	1.95734	0.50570
$isoC_aC_b(H_2C_c-R')HCH_2-$ $(C-C$ (d))	C_b	-0.92918	-0.92918	-0.92918	0	-154.40324	0.91771	0.77247	-17.61330	-17.42244	48.30	131.70	21.90	1.97162	0.51388
$iertC_a(R'-H_2C_d)C_b(R''-H_2C_c)CH_2-$ $(C-C$ (e))	C_b	-0.72457	-0.72457	-0.72457	-0.72457	-154.51399	0.91771	0.76765	-17.92866	-17.73779	50.04	129.96	22.66	1.94462	0.49298
$iertC_aC_b(H_2C_c-R')HCH_2-$ $(C-C$ (f))	C_b	-0.72457	-0.92918	-0.92918	0	-154.19863	0.91771	0.78155	-17.40869	-17.21783	52.78	127.22	24.04	1.92443	0.47279
$isoC_a(R'-H_2C_d)C_b(R''-H_2C_c)CH_2-$ $(C-C$ (f))	C_b	-0.72457	-0.72457	-0.72457	-0.72457	-154.51399	0.91771	0.76765	-17.92866	-17.73779	50.04	129.96	22.66	1.94462	0.49298

Table 15.366. The energy parameters (eV) of functional groups of alkyl phosphine oxides.

Parameters	$P=O$ Group	$P-C$ Group	CH_3 Group	CH_2 Group	CH (i) Group	$C-C$ (a) Group	$C-C$ (b) Group	$C-C$ (c) Group	$C-C$ (d) Group	$C-C$ (e) Group	$C-C$ (f) Group	$C^{3e}=C$ Group	CH (ii) Group
f_1	1	1	1	1	1	1	1	1	1	1	1	0.75	1
n_1	2	1	3	2	1	1	1	1	1	1	1	2	1
n_2	0	0	2	1	0	0	0	0	0	0	0	0	0
n_3	0	0	0	0	0	0	0	0	0	0	0	0	0
C_1	0.5	0.5	0.75	0.75	0.75	0.5	0.5	0.5	0.5	0.5	0.5	0.5	0.75
C_2	1	0.73885	1	1	1	1	1	1	1	1	1	0.85252	1
c_1	1	1	1	1	1	1	1	1	1	1	1	1	1
c_2	0.79401	1	0.91771	0.91771	0.91771	0.91771	0.91771	0.91771	0.91771	0.91771	0.91771	0.85252	0.91771
c_3	0	0	0	1	1	0	0	0	1	1	0	0	1
c_4	4	2	1	1	1	2	2	2	2	2	2	3	1
c_5	0	0	3	2	1	0	0	0	0	0	0	0	1
C_{1o}	0.5	0.5	0.75	0.75	0.75	0.5	0.5	0.5	0.5	0.5	0.5	0.5	0.75
C_{2o}	1	0.73885	1	1	1	1	1	1	1	1	1	0.85252	1
V_e (eV)	-56.96374	-31.34959	-107.32728	-70.41425	-35.12015	-28.79214	-28.79214	-29.10112	-28.79214	-29.10112	-29.10112	-101.12679	-37.10024
V_p (eV)	9.82777	7.71965	38.92728	25.78002	12.87680	9.33352	9.33352	9.37273	9.33352	9.37273	9.37273	20.69825	13.17125
T (eV)	14.86039	6.82959	32.53914	21.06675	10.48582	6.77464	6.77464	6.90500	6.77464	6.90500	6.90500	34.31559	11.58941
V_m (eV)	-7.43020	-3.41479	-16.26957	-10.53337	-5.24291	-3.38732	-3.38732	-3.45250	-3.38732	-3.45250	-3.45250	-17.15779	-5.79470
$E_{(AO/HO)}$ (eV)	-23.56492	-11.78246	-15.56407	-15.56407	-14.63489	-15.56407	-15.56407	-15.35946	-15.56407	-15.35946	-15.35946	0	-14.63489
$\Delta E_{H_2MO\,(AO/HO)}$ (eV)	0	-0.36229	0	0	0	0	0	0	0	0	0	0	-1.13379
$E_T{}_{(AO/HO)}$ (eV)	-23.56492	-11.42017	-15.56407	-15.56407	-14.63489	-15.56407	-15.56407	-15.35946	-15.56407	-15.35946	-15.35946	0	-13.50110
$E_T{}_{(H_2MO)}$ (eV)	-63.27069	-31.63532	-67.69451	-49.66493	-31.63533	-31.63537	-31.63537	-31.63535	-31.63537	-31.63535	-31.63535	-63.27075	-31.63539
$E_T\left(atom-atom,msp^3.AO\right)$ (eV)	-2.26758	-0.36229	0	0	0	-1.85836	-1.85836	-1.44915	-1.85836	-1.44915	-1.44915	-2.26759	-0.56690
$E_T{}_{(MO)}$ (eV)	-65.53832	-31.99766	-67.69450	-49.66493	-31.63537	-33.49373	-33.49373	-33.08452	-33.49373	-33.08452	-33.08452	-65.53833	-32.20226
$\omega\ \left(10^{15}\ rad/s\right)$	11.0170	7.22663	24.9286	24.2751	24.1759	9.43699	9.43699	15.4846	9.43699	9.55643	9.55643	49.7272	26.4826
E_K (eV)	7.25157	4.75669	16.40846	15.97831	15.91299	6.21159	6.21159	10.19220	6.21159	6.29021	6.29021	32.73133	17.43132
$\bar{E}_D$ (eV)	-0.17458	-0.13806	-0.25352	-0.25017	-0.24966	-0.16515	-0.16515	-0.20896	-0.16515	-0.16416	-0.16416	-0.35806	-0.26130
$\bar{E}_{Kvib}$ (eV)	0.15292 [24]	0.17606 [68]	0.35532 (Eq. (13.458))	0.35532 (Eq. (13.458))	0.35532 (Eq. (13.458))	0.12312 [2]	0.17978 [4]	0.09944 [5]	0.12312 [2]	0.12312 [2]	0.12312 [2]	0.19649 [49]	0.35532 Eq. (13.458)
$\bar{E}_{osc}$ (eV)	-0.09812	-0.05003	-0.22757	-0.14502	-0.07200	-0.10359	-0.07526	-0.15924	-0.10359	-0.10260	-0.10260	-0.25982	-0.08364
E_{mag} (eV)	0.14803	0.14803	0.14803	0.14803	0.14803	0.14803	0.14803	0.14803	0.14803	0.14803	0.14803	0.14803	0.14803
$E_T{}_{(Group)}$ (eV)	-65.73455	-32.04769	-67.92207	-49.80996	-31.70737	-33.59732	-33.49373	-33.24376	-33.59732	-33.18712	-33.18712	-49.54347	-32.28590
$E_{initial\,(e_4\ AO/HO)}$ (eV)	-14.63489	-14.63489	-14.63489	-14.63489	-14.63489	-14.63489	-14.63489	-14.63489	-14.63489	-14.63489	-14.63489	-14.63489	-14.63489
$E_{initial\,(e_5\ AO/HO)}$ (eV)	0	0	-13.59844	-13.59844	-13.59844	0	0	0	0	0	0	0	-13.59844
$E_{D\,(Group)}$ (eV)	7.19500	2.77791	12.49186	7.83016	3.32601	4.32754	4.29921	3.97398	4.17951	3.62128	3.91734	5.63881	3.90454

Table 15.367. The total bond energies of alkyl phosphine oxides calculated using the functional group composition and the energies of Table 15.366 compared to the experimental values [69].

Formula	Name	$P=O$	$P-C$	CH_3	CH_2	CH (i)	$C-C$ (a)	$C-C$ (b)	$C-C$ (c)	$C-C$ (d)	$C-C$ (e)	$C-C$ (f)	$C^{3e}=C$	CH (ii)	Calculated Total Bond Energy (eV)	Experimental Total Bond Energy (eV)	Relative Error
C_3H_9PO	Trimethylphosphine oxide	1	3	3	0	0	0	0	0	0	0	0	0	0	53.00430	52.91192	-0.00175

Table 15.368. The bond angle parameters of alkyl phosphine oxides and experimental values [1]. In the calculation of θ_v, the parameters from the preceding angle were used. E_T is $E_T(atom-atom, msp^3.AO)$.

Atoms of Angle	2c' Bond 1 (a_0)	2c' Bond 2 (a_0)	2c' Terminal Atoms (a_0)	$E_{Coulombic}$ or E Atom 1	Atom 1 Hybridization Designation (Table 15.3.A)	$E_{Coulombic}$ Atom 2	Atom 2 Hybridization Designation (Table 15.3.A)	c_2 Atom 1	c_2 Atom 2	C_1	C_2	c_1	c_2'	E_T (eV)	θ_v (°)	θ_1 (°)	θ_2 (°)	Cal. θ (°)	Exp. θ (°)
Methyl $\angle HC_aH$	2.09711	2.09711	3.4252	-15.75493	7	H	H	0.86359	1	1	1	0.75	1.15796	0				109.50	
$\angle H_aC_aP$															70.56			109.44	110.7 (trimethyl phosphine)
$\angle C_aPC_b$	3.52498	3.52498	5.4955	-15.75493	7	-15.75493	7	0.86359	0.86359	1	1	1	0.86359	-1.85836				102.43	104.31 [73] ($Ph_2P(O)CH_2OH$)
$\angle C_aPO$	3.52498	2.76885	5.3104	-15.95954	10	-15.95954	10	0.85252	0.85252	1	1	1	0.85252	-1.85836				114.54	114.03 [73] ($Ph_2P(O)CH_2OH$)
Methylene $\angle HC_aH$	2.11106	2.11106	3.4252	-15.75493	7	H	H	0.86359	1	1	1	0.75	1.15796	0				108.44	107 (propane)
$\angle C_aC_bC_c$															69.51			110.49	112 (propane) 113.8 (butane) 110.8 (isobutane)
$\angle C_aC_bH$															69.51			110.49	111.0 (butane) 111.4 (isobutane)
Methyl $\angle HC_aH$	2.09711	2.09711	3.4252	-15.75493	7	H	H	0.86359	1	1	1	0.75	1.15796	0				109.50	
$\angle C_aC_bC_c$															70.56			109.44	
$\angle C_aC_bH$															70.56			109.44	
$\angle C_bC_aC_c$ iso C_a	2.91547	2.91547	4.7958	-16.68412 C_b	26	-16.68412 C_c	26	0.81549	0.81549	1	1	1	0.81549	-1.85836				110.67	110.8 (isobutane)
$\angle C_bC_aH$ iso C_a	2.91547	2.11323	4.1633	-15.55033 C_a	5	-14.82575 C_b	1	0.87495	0.91771	0.75	1	0.75	1.04887	0				110.76	
$\angle C_aC_bH$ iso C_a	2.91547	2.09711	4.1633	-15.55033 C_b	5	-14.82575 C_a	1	0.87495	0.91771	0.75	1	0.75	1.04887	0				111.27	111.4 (isobutane)
$\angle C_bC_aC_b$ tert C_a	2.90327	2.90327	4.7958	-16.68412 C_b	26	-16.68412 C_b	26	0.81549	0.81549	1	1	1	0.81549	-1.85836				111.37	110.8 (isobutane)
$\angle C_bC_aC_d$															72.50			107.50	

ALKYL PHOSPHATES ($\left(C_nH_{2n+1}O\right)_3P=O,\ n=1,2,3,4,5...\infty$)

The alkyl phosphates, $\left(C_nH_{2n+1}O\right)_3P=O$, comprise $P=O$, $P-O$, and $C-O$ functional groups. The $P=O$ functional group is equivalent to that of alkyl phosphine oxides. The $P-O$ and $C-O$ functional groups are equivalent to those of alkyl phosphites. The alkyl portion of the alkyl phosphate may comprise at least two terminal methyl groups (CH_3) at each end of each chain, and may comprise methylene (CH_2), and methylyne (CH) functional groups as well as C bound by carbon-carbon single bonds. The methyl and methylene functional groups are equivalent to those of straight-chain alkanes. Six types of $C-C$ bonds can be identified. The n-alkane $C-C$ bond is the same as that of straight-chain alkanes. In addition, the $C-C$ bonds within isopropyl ($\left(CH_3\right)_2CH$) and t-butyl ($\left(CH_3\right)_3C$) groups and the isopropyl to isopropyl, isopropyl to t-butyl, and t-butyl to t-butyl $C-C$ bonds comprise functional groups. The branched-chain-alkane groups in alkyl phosphates are equivalent to those in branched-chain alkanes.

The symbols of the functional groups of branched-chain alkyl phosphates are given in Table 15.369. The geometrical (Eqs. (15.1-15.5) and (15.51)), intercept (Eqs. (15.80-15.87)), and energy (Eqs. (15.6-15.11) and (15.17-15.65)) parameters of alkyl phosphates are given in Tables 15.370, 15.371, and 15.372, respectively. The total energy of each alkyl phosphate given in Table 15.373 was calculated as the sum over the integer multiple of each $E_D(Group)$ of Table 15.372 corresponding to functional-group composition of the molecule. The bond angle parameters of alkyl phosphates determined using Eqs. (15.88-15.117) are given in Table 15.374. The color scale, charge-density of exemplary alkyl phosphate, tri-isopropyl phosphate, comprising of atoms with the outer shell bridged by one or more H_2-type ellipsoidal MOs or joined with one or more hydrogen MOs is shown in Figure 15.63.

Figure 15.63. Color scale, charge-density of tri-isopropyl phosphate showing the orbitals of the atoms at their radii, the ellipsoidal surface of each H or H_2-type ellipsoidal MO that transitions to the corresponding outer shell of the atom(s) participating in each bond, and the hydrogen nuclei.

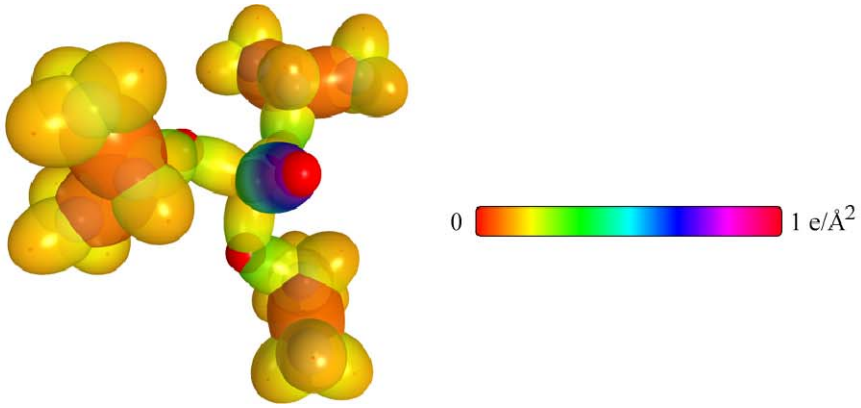

Table 15.369. The symbols of functional groups of alkyl phosphates.

Functional Group	Group Symbol
P=O	$P=O$
P-O	$P-O$
C-O (CH_3-O- and $\left(CH_3\right)_3C-O-$)	$C-O$ (i)
C-O (alkyl)	$C-O$ (ii)
CH_2 group	$C-H\ \left(CH_2\right)$
CH	$C-H$
CC bond (*n-C*)	$C-C$ (a)
CC bond (*iso-C*)	$C-C$ (b)
CC bond (*tert-C*)	$C-C$ (c)
CC (*iso* to *iso-C*)	$C-C$ (d)
CC (*t* to *t-C*)	$C-C$ (e)
CC (*t* to *iso-C*)	$C-C$ (f)

Table 15.370. The geometrical bond parameters of alkyl phosphates and experimental values [1].

Parameter	$P=O$ Group	$P-O$ Group	$C-O$ (i) Group	$C-O$ (ii) Group	$C-H$ (CH_2) Group	$C-H$ (CH_3) Group	$C-H$ Group	$C-C$ (a) Group	$C-C$ (b) Group	$C-C$ (c) Group	$C-C$ (d) Group	$C-C$ (e) Group	$C-C$ (f) Group
$a\ (a_0)$	1.91663	1.84714	1.80717	1.79473	1.64920	1.67122	1.67465	2.12499	2.12499	2.10725	2.12499	2.10725	2.10725
$c'\ (a_0)$	1.38442	1.52523	1.34431	1.33968	1.04856	1.05553	1.05661	1.45744	1.45744	1.45164	1.45744	1.45164	1.45164
Bond Length $2c'\ (\AA)$	1.46521E-10	1.61423	1.42276	1.41785	1.10974	1.11713	1.11827	1.54280	1.54280	1.53635	1.54280	1.53635	1.53635
Exp. Bond Length $(\AA)$	1.48 [65] (DNA) 1.4759 (PO)	1.631 [70] (MHP) 1.60 [65] (DNA)	1.416 (dimethyl ether)	1.418 (ethyl methyl ether (avg.))	1.107 $(C-H$ propane) 1.117 $(C-H$ butane)	1.107 $(C-H$ propane) 1.117 $(C-H$ butane)	1.122 (isobutane)	1.532 (propane) 1.531 (butane)	1.532 (propane) 1.531 (butane)	1.532 (propane) 1.531 (butane)	1.532 (propane) 1.531 (butane)	1.532 (propane) 1.531 (butane)	1.532 (propane) 1.531 (butane)
$b,c\ (a_0)$	1.32546	1.04192	1.20776	1.19429	1.27295	1.29569	1.29924	1.54616	1.54616	1.52750	1.54616	1.52750	1.52750
e	0.72232	0.82573	0.74388	0.74645	0.63580	0.63159	0.63095	0.68600	0.68600	0.68888	0.68600	0.68888	0.68888

Table 15.371. The MO to HO intercept geometrical bond parameters of alkyl phosphates. R, R', R'' are H or alkyl groups. E_T is E_T $(atom-atom, msp^3.AO)$.

Bond	Atom	E_T (eV) Bond 1	E_T (eV) Bond 2	E_T (eV) Bond 3	E_T (eV) Bond 4	Final Total Energy $C2sp^3$ (eV)	$r_{initial}$ (a_0)	r_{final} (a_0)	$E_{Coulomb}$ (eV) Final	$E(C2sp^3)$ (eV) Final	θ' (°)	θ_1 (°)	θ_2 (°)	d_1 (a_0)	d_2 (a_0)
$(CH_3)_3P=O$	O	-1.13379	0	0	0		1.00000	0.85252	-15.95954		84.02	95.98	39.77	1.47318	0.08876
$(CH_3O)_3P=O$	P	-1.13379	-0.72457	-0.72457	-0.72457		1.15350	0.75032	-18.13326		72.13	107.87	32.60	1.61466	0.23024
$(CH_3O)_2(O)P-OCH_3$ $(CH_3O)_2(O)P-OC(CH_3)_3$ $(C-O$ (i))	O	-0.72457	-0.72457	0	0		1.00000	0.83600	-16.27489		111.08	68.92	48.48	1.22455	0.30068
$(CH_3O)_2(O)P-OCH_3$ $(CH_3O)_2(O)P-OC(CH_3)_3$ $(CH_3O)_2(O)P-OCH_2R$ $(C-O$ (i)) and $(C-O$ (ii))	P	-0.72457	-0.72457	-0.72457	-1.13379		1.15350	0.75032	-18.13326		105.22	74.78	44.02	1.32831	0.19692
$(CH_3O)_2(O)P-OCH_2R$ $(C-O$ (ii))	O	-0.72457	-0.82688	0	0		1.00000	0.83078	-16.37720		110.75	69.25	48.21	1.23087	0.29436
$C-H$ (OC_aH_3)	C_a	-0.72457	0	0	0	-152.34026	0.91771	0.87495	-15.55033	-15.35946	78.85	101.15	42.40	1.21777	0.16921
$(CH_3O)_2(O)PO-C_aH_3$	C_a	-0.72457	0	0	0	-152.34026	0.91771	0.87495	-15.55033	-15.35946	95.98	84.02	46.10	1.25319	0.09112
$(CH_3O)_2(O)PO-C_a(CH_3)_3$ $(C-O$ (i))	C_a	-0.72457	-0.72457	-0.72457	-0.72457	-154.51399	0.91771	0.76765	-17.72405		86.03	93.97	39.35	1.39744	0.05313
$(H_3CO)_2(O)PO-C_aH_3$ $(CH_3)_3C_a-OP(O)(OC_bH_3)_2$ $(C-O$ (i))	O	-0.72457	-0.72457	0	0		1.00000	0.83600	-16.27490		92.66	87.34	43.74	1.30555	0.03876
$-H_2C_a-OP(O)(OCH_3)_2$ $(C-O$ (ii))	C_a	-0.82688	-0.92918	0	0	-153.37175	0.91771	0.82053	-16.58181	-16.39095	92.41	87.59	43.35	1.30512	0.03456
$(CH_3O)_2(O)PO-C_aH(CH_3)_2$ $(C-O$ (ii))	C_a	-0.82688	-0.92918	-0.92918	0	-154.30093	0.91771	0.77699	-17.51099	-17.32013	88.25	91.75	40.56	1.36345	0.02377
$-H_2C_a-OP(O)(OCH_3)_2$ $(H_3C)_2HC_a-OP(O)(OCH_3)_2$ $(C-O$ (ii))	O	-0.72457	-0.82688	0	0		1.00000	0.83078	-16.37720		93.33	86.67	43.98	1.29138	0.04829
$C-H$ (CH_3)	C	-0.92918	0	0	0	-152.54487	0.91771	0.86359	-15.75493	-15.56407	77.49	102.51	41.48	1.23564	0.18708
$C-H$ (CH_2)	C	-0.92918	-0.92918	0	0	-153.47406	0.91771	0.81549	-16.68412	-16.49325	68.47	111.53	35.84	1.35486	0.29933
$C-H$ (CH)	C	-0.92918	-0.92918	-0.92918	0	-154.40324	0.91771	0.77247	-17.61330	-17.42244	61.10	118.90	31.37	1.42988	0.37326
$H_3C_aC_bH_2CH_2-$ $(C-C$ (a))	C_a	-0.92918	0	0	0	-152.54487	0.91771	0.86359	-15.75493	-15.56407	63.82	116.18	30.08	1.83879	0.38106
$H_3C_aC_bH_2CH_2-$ $(C-C$ (a))	C_b	-0.92918	-0.92918	0	0	-153.47406	0.91771	0.81549	-16.68412	-16.49325	56.41	123.59	26.06	1.90890	0.45117
$R-H_2C_aC_b(H_2C_c-R')HCH_2-$ $(C-C$ (b))	C_b	-0.92918	-0.92918	-0.92918	0	-154.40324	0.91771	0.77247	-17.61330	-17.42244	48.30	131.70	21.90	1.97162	0.51388
$R-H_2C_a(R'-H_2C_d)C_b(R''-H_2C_c)CH_2-$ $(C-C$ (c))	C_b	-0.92918	-0.72457	-0.72457	-0.72457	-154.71860	0.91771	0.75889	-17.92866	-17.73779	48.21	131.79	21.74	1.95734	0.50570
$isoC_aC_b(H_2C_c-R')HCH_2-$ $(C-C$ (d))	C_b	-0.92918	-0.92918	-0.92918	0	-154.40324	0.91771	0.77247	-17.61330	-17.42244	48.30	131.70	21.90	1.97162	0.51388
$tertC_a(R'-H_2C_d)C_b(R''-H_2C_c)CH_2-$ $(C-C$ (e))	C_b	-0.72457	-0.72457	-0.72457	-0.72457	-154.51399	0.91771	0.76765	-17.92866	-17.73779	50.04	129.96	22.66	1.94462	0.49298
$tertC_aC_b(H_2C_c-R')HCH_2-$ $(C-C$ (f))	C_b	-0.72457	-0.92918	-0.92918	0	-154.19863	0.91771	0.78155	-17.40869	-17.21783	52.78	127.22	24.04	1.92443	0.47279
$isoC_a(R'-H_2C_d)C_b(R''-H_2C_c)CH_2-$ $(C-C$ (f))	C_b	-0.72457	-0.72457	-0.72457	-0.72457	-154.51399	0.91771	0.76765	-17.92866	-17.73779	50.04	129.96	22.66	1.94462	0.49298

Table 15.372. The energy parameters (eV) of functional groups of alkyl phosphates.

Parameters	$P=O$ Group	$P-O$ Group	$C-O$ (i) Group	$C-O$ (ii) Group	CH_3 Group	CH_2 Group	CH (i) Group	$C-C$ (a) Group	$C-C$ (b) Group	$C-C$ (c) Group	$C-C$ (d) Group	$C-C$ (e) Group	$C-C$ (f) Group
n_1	2	1	1	1	3	2	1	1	1	1	1	1	1
n_2	0	0	0	0	2	1	0	0	0	0	0	0	0
n_3	0	0	0	0	0	0	0	0	0	0	0	0	0
C_1	0.5	0.5	0.5	0.5	0.75	0.75	0.75	0.5	0.5	0.5	0.5	0.5	0.5
C_2	1	1	1	1	1	1	1	1	1	1	1	1	1
c_1	1	1	1	1	1	1	1	1	1	1	1	1	1
c_2	0.79401	0.79401	0.85395	0.85395	0.91771	0.91771	0.91771	0.91771	0.91771	0.91771	0.91771	0.91771	0.91771
c_3	0	0	0	0	0	1	1	0	0	0	1	1	0
c_4	4	2	2	2	1	1	1	2	2	2	2	2	2
c_5	0	0	0	0	3	2	1	0	0	0	0	0	0
C_{1o}	0.5	0.5	0.5	0.5	0.75	0.75	0.75	0.5	0.5	0.5	0.5	0.5	0.5
C_{2o}	1	0.79401	1	1	1	1	1	1	1	1	1	1	1
V_e (eV)	-56.96374	-33.27738	-33.15757	-33.47304	-107.32728	-70.41425	-35.12015	-28.79214	-28.79214	-29.10112	-28.79214	-29.10112	-29.10112
V_p (eV)	9.82777	8.92049	10.12103	10.15605	38.92728	25.78002	12.87680	9.33352	9.33352	9.37273	9.33352	9.37273	9.37273
T (eV)	14.86039	9.00781	9.17389	9.32537	32.53914	21.06675	10.48582	6.77464	6.77464	6.90500	6.77464	6.90500	6.90500
V_w (eV)	-7.43020	-4.50391	-4.58695	-4.66268	-16.26957	-10.53337	-5.24291	-3.38732	-3.38732	-3.45250	-3.38732	-3.45250	-3.45250
$E_{(AO/BO)}$ (eV)	-23.56492	-11.78246	-14.63489	-14.63489	-15.56407	-15.56407	-14.63489	-15.56407	-15.56407	-15.35946	-15.56407	-15.35946	-15.35946
$\Delta E_{H_2MO\,(AO/BO)}$ (eV)	0	0	-1.44915	-1.65376	0	0	0	0	0	0	0	0	0
$E_T{}_{(AO/BO)}$ (eV)	-23.56492	-11.78246	-13.18574	-12.98113	-15.56407	-15.56407	-14.63489	-15.56407	-15.56407	-15.35946	-15.56407	-15.35946	-15.35946
$E_T{}_{(H_2MO)}$ (eV)	-63.27069	-31.63544	-31.63533	-31.63544	-67.69451	-49.66493	-31.63533	-31.63537	-31.63537	-31.63535	-31.63537	-31.63535	-31.63535
$E_T\left(atom-atom, msp^3.AO\right)$ (eV)	-2.26758	-1.44914	-1.44915	-1.65376	0	0	0	-1.85836	-1.85836	-1.44915	-1.85836	-1.44915	-1.44915
$E_T{}_{(MO)}$ (eV)	-65.53832	-33.08451	-33.08452	-33.28912	-67.69450	-49.66493	-31.63537	-33.49373	-33.49373	-33.08452	-33.49373	-33.08452	-33.08452
$\omega\left(10^5\ rad/s\right)$	11.0170	10.3761	12.0329	12.1583	24.9286	24.2751	24.1759	9.43699	9.43699	15.4846	9.43699	9.55643	9.55643
E_K (eV)	7.25157	6.82973	7.92028	8.00277	16.40846	15.97831	15.91299	6.21159	6.21159	10.19220	6.21159	6.29021	6.29021
$\vec{E}_D$ (eV)	-0.17458	-0.17105	-0.18420	-0.18631	-0.25352	-0.25017	-0.24966	-0.16515	-0.16515	-0.20896	-0.16515	-0.16416	-0.16416
$\vec{E}_{Kvib}$ (eV)	0.15292 [24]	0.10477 [71]	0.13663 [21]	0.16118 [4]	0.35532 (Eq. (13.458))	0.35532 (Eq. (13.458))	0.35532 (Eq. (13.458))	0.12312 [2]	0.17978 [4]	0.09944 [5]	0.12312 [2]	0.12312 [2]	0.12312 [2]
$\vec{E}_{osc}$ (eV)	-0.09812	-0.11867	-0.11589	-0.10572	-0.22757	-0.14502	-0.07200	-0.10359	-0.07526	-0.15924	-0.10359	-0.10260	-0.10260
E_{mag} (eV)	0.14803	0.14803	0.14803	0.14803	0.14803	0.14803	0.14803	0.14803	0.14803	0.14803	0.14803	0.14803	0.14803
$E_T{}_{(Group)}$ (eV)	-65.73455	-33.20318	-33.20040	-33.39484	-67.92207	-49.80996	-31.70737	-33.59732	-33.49373	-33.24376	-33.59732	-33.18712	-33.18712
$E_{initial\,(s_4\ AO/BO)}$ (eV)	-14.63489	-14.63489	-14.63489	-14.63489	-14.63489	-14.63489	-14.63489	-14.63489	-14.63489	-14.63489	-14.63489	-14.63489	-14.63489
$E_{initial\,(s_5\ AO/BO)}$ (eV)	0	0	0	0	-13.59844	-13.59844	-13.59844	0	0	0	0	0	0
$E_{D\,(Group)}$ (eV)	7.19500	3.93340	3.93062	4.12506	12.49186	7.83016	3.32601	4.32754	4.29921	3.97398	4.17951	3.62128	3.91734

Table 15.373. The total bond energies of alkyl phosphates calculated using the functional group composition and the energies of Table 15.372 compared to the experimental values [69].

Formula	Name	$P=O$	$P-O$	$C-O$ (i)	$C-O$ (ii)	CH_3	CH_2	CH (i)	$C-C$ (a)	$C-C$ (b)	$C-C$ (c)	$C-C$ (d)	$C-C$ (e)	$C-C$ (f)	Calculated Total Bond Energy (eV)	Experimental Total Bond Energy (eV)	Relative Error
$C_6H_{15}O_4P$	Triethyl phosphate	1	3	0	3	3	3	0	3	0	0	0	0	0	105.31906	104.40400	-0.00876
$C_9H_{21}O_4P$	Tri-n-propyl phosphate	1	3	0	3	3	6	0	6	0	0	0	0	0	141.79216	140.86778	-0.00656
$C_9H_{21}O_4P$	Tri-isopropyl phosphate	1	3	0	3	6	0	3	0	6	0	0	0	0	142.09483	141.42283	-0.00475
$C_9H_{27}O_4P$	Tri-n-butyl phosphate	1	3	0	3	3	9	0	9	0	0	0	0	0	178.26526	178.07742	-0.00105

Table 15.374. The bond angle parameters of alkyl phosphates and experimental values [1]. In the calculation of θ_v, the parameters from the preceding angle were used. E_T is E_T (*atom* – *atom*,msp^3.*AO*).

Atoms of Angle	2c' Bond 1 (a_0)	2c' Bond 2 (a_0)	2c' Terminal Atoms (a_0)	$E_{Coulombic}$ or E Atom 1	Atom 1 Hybridization Designation (Table 15.3.A)	$E_{Coulombic}$ Atom 2	Atom 2 Hybridization Designation (Table 15.3.A)	c_2 Atom 1	c_2 Atom 2	C_1	C_2	c_1	c_2'	E_T (eV)	θ_v (°)	θ_1 (°)	θ_2 (°)	Cal. θ (°)	Exp. θ (°)
$\angle POC$	3.05046	2.67935	4.9904	-11.78246	Psp^3	-15.75493	7	0.73885 Eq. (15.181)	0.86359	1	0.73885	1	0.80122	-0.72457				121.00	122.2 [70] (MHPO)
$\angle O_a PO_a$	3.05046	3.05046	4.7539	-15.95954	10	-15.95954	10	0.85252	0.85252	1	1	1	0.85252	-1.65376				102.38	101.4 [65] (DNA)
$\angle O_a PO_b$	3.05046	2.76885	4.7539	-15.95954	10	-15.95954	10	0.85252	0.85252	1	1	1	0.85395	-1.65376				109.46	109.7 [65] (DNA)
$\angle C_b C_a O$ ($C_a - O$ (ii))	2.91547	2.67935	4.5607	-16.68412	26	-13.61806	O	0.81549	0.85395 (Eq. (15.133))	1	1	1	0.83472	-1.65376				109.13	109.4 (ethyl methyl ether)
Methylene $\angle HC_a H$	2.11106	2.11106	3.4252	-15.75493	7	H	H	0.86359	1	1	1	0.75	1.15796	0				108.44	107 (propane)
$\angle C_a C_b C_c$															69.51			110.49	112 (propane) 113.8 (butane) 110.8 (isobutane)
$\angle C_a C_b H$															69.51			110.49	111.0 (butane) 111.4 (isobutane)
Methyl $\angle HC_a H$	2.09711	2.09711	3.4252	-15.75493	7	H	H	0.86359	1	1	1	0.75	1.15796	0				109.50	
$\angle C_a C_b C_c$															70.56			109.44	
$\angle C_a C_b H$															70.56			109.44	
$\angle C_b C_a C_c$ iso C_a	2.91547	2.91547	4.7958	-16.68412 C_b	26	-16.68412 C_c	26	0.81549	0.81549	1	1	1	0.81549	-1.85836				110.67	110.8 (isobutane)
$\angle C_b C_a H$ iso C_a	2.91547	2.11323	4.1633	-15.55033 C_a	5	-14.82575 C_b	1	0.87495	0.91771	0.75	1	0.75	1.04887	0				110.76	
$\angle C_a C_b H$ iso C_a	2.91547	2.09711	4.1633	-15.55033 C_b	5	-14.82575 C_a	1	0.87495	0.91771	0.75	1	0.75	1.04887	0				111.27	111.4 (isobutane)
$\angle C_b C_a C_b$ tert C_a	2.90327	2.90327	4.7958	-16.68412 C_b	26	-16.68412 C_b	26	0.81549	0.81549	1	1	1	0.81549	-1.85836				111.37	110.8 (isobutane)
$\angle C_b C_a C_d$															72.50			107.50	

ORGANIC AND RELATED IONS (RCO_2^-, $ROSO_3^-$, NO_3^-, $(RO)_2PO_2^-$, $(RO)_3SiO^-$, $(R)_2Si(O^-)_2$, RNH_3^+, $R_2NH_2^+$)

Proteins comprising amino acids with amino and carboxylic acid groups are charged at physiological pH. Deoxyribonucleic acid (DNA), the genetic material of living organisms also comprises negatively charged phosphate groups. Thus, the bonding of organic ions is considered next. The molecular ions also comprise functional groups that have an additional electron or are deficient by an electron in the cases of monovalent molecular anions and cations, respectively. The molecular chemical bond typically comprises an even integer number of paired electrons, but with an excess of deficiency, the bonding may involve an odd number of electrons, and the electrons may be distributed over multiple bonds, solved as a linear combination of standard bonds. As given in the Benzene Molecule section and other sections on aromatic molecules such as naphthalene, toluene, chlorobenzene, phenol, aniline, nitrobenzene, benzoic acid, pyridine, pyrimidine, pyrazine, quinoline, isoquinoline, indole, and adenine, the paired electrons of MOs may be distributed over a linear combination of bonds such that the bonding between two atoms involves less than an integer multiple of two electrons. Specifically, the results of the derivation of the parameters of the benzene molecule given in the Benzene Molecule (C_6H_6) section was generalized to any aromatic functional group of aromatic and heterocyclic compounds in the Aromatic and Heterocyclic Compounds section. Ethylene serves as a basis element for the $C\overset{3e}{=}C$ bonding of the aromatic bond wherein each of the $C\overset{3e}{=}C$ aromatic bonds comprises $(0.75)(4)=3$ electrons according to Eq. (15.161). Thus, in these aromatic cases, three electrons can be assigned to a given bond between two atoms wherein the electrons of the linear combination of bonded atoms are paired and comprise an integer multiple of two.

In graphite, the minimum energy structure with equivalent carbon atoms wherein each carbon forms bonds with three other such carbons requires a redistribution of charge within an aromatic system of bonds. Considering that each carbon contributes four bonding electrons, the sum of electrons of a vertex-atom group is four from the vertex atom plus two from each of the two atoms bonded to the vertex atom where the latter also contribute two each to the juxtaposed group. These eight electrons are distributed equivalently over the three bonds of the group such that the electron number assignable to each bond is $\frac{8}{3}$. Thus, the $C\overset{8/3e}{=}C$ functional group of graphite comprises the aromatic bond with the exception that the electron-number per bond is $\frac{8}{3}$.

As given in the Bridging Bonds of Boranes section and the Bridging Bonds of Organoaluminum Hydrides section, other examples of electron deficient bonding involving two paired electrons centered on three atoms are *three-center bonds* as opposed to the typical single bond, a *two-center bond*. The $B2sp^3$ HOs comprise four orbitals containing three electrons as given by Eq. (23.1) that can form three-center as well as two-center bonds. The designation for a three-center bond involving two $B2sp^3$ HOs and a $H1s$ AO is $B-H-B$, and the designation for a three-center bond involving three $B2sp^3$ HOs is $B-B-B$. In the aluminum case, each $Al-H-Al$-bond MO and $Al-C-Al$-bond MO comprises the corresponding single bond and forms with further sharing of electrons between each $Al3sp^3$ HO and each $H1s$ AO and $C2sp^3$ HO, respectively. Thus, the geometrical and energy parameters of the three-center bond are equivalent to those of the corresponding two-center bonds except that the bond energy is increased in the former case since the donation of electron density from the unoccupied $Al3sp^3$ HO to each $Al-H-Al$-bond MO and $Al-C-Al$-bond MO permits the participating orbital to decrease in size and energy.

To match the energies of the AOs and MOs of the ionic functional group with the others within the molecular ion, the bonding in organic ions comprises a standard bond that serves as basis element and retains the same geometrical characteristics as that standard bond. In the case of organic oxyanions, the $A-O^-$ ($A=C,S,N,P,Si$) bond is intermediate between a single and double bond, and the latter serves as a basis element. Similar to the case of the $C\overset{3e}{=}C$ aromatic bond wherein ethylene is the basis element, the $A=O$-bond functional group serves as the basis element for the $A-O^-$ functional group of the oxyanion of carboxylates, sulfates, nitrates, phosphates, silanolates, and siloxanolates. This oxyanion group designated by $A\overset{3e}{=}O^-$ comprises $(0.75)(4)=3$ electrons after Eq. (15.161). Thus, the energy parameters of the $A\overset{3e}{=}O^-$ functional group are given by the factor of $(0.75)(4)=3$ times those of the corresponding $A=O$ functional group, and the geometric parameters are the same. The $C=O$, $S=O$, $N=O_2$, $P=O$, and $Si=O$ basis elements are given in the Carboxylic Acids, Sulfates, Alkyl Nitrates, Phosphates, and Silicon Oxides, Silicic Acids, Silanols, Siloxanes and Disiloxanes sections, respectively. A convenient means to obtain the final group energy parameters of $E_T(Group)$ and $E_D(Group)$ is by using Eqs. (15.165-15.166) with $f_1=0.75$:

$$E_T\,(Group) = f_1\left(\begin{array}{l} E(basis\ energies) + E_T\left(atom - atom, msp^3.AO\right) \\ -31.63536831\ eV\sqrt{\dfrac{2\hbar\sqrt{\dfrac{C_{1o}C_{2o}e^2}{4\pi\varepsilon_o R^3}}}{m_e c^2}} + n_1\bar{E}_{Kvib} + c_3\dfrac{8\pi\mu_o\mu_B^2}{r^3} \end{array}\right) \tag{15.183}$$

$$E_D\,(Group) = -\left(\begin{array}{l} f_1\left(\begin{array}{l} E(basis\ energies) + E_T\left(atom - atom, msp^3.AO\right) \\ -31.63536831\ eV\sqrt{\dfrac{2\hbar\sqrt{\dfrac{C_{1o}C_{2o}e^2}{4\pi\varepsilon_o R^3}}}{m_e c^2}} + n_1\bar{E}_{Kvib} + c_3\dfrac{8\pi\mu_o\mu_B^2}{r^3} \end{array}\right) \\ -\left(c_4 E_{initial}\left(AO/HO\right) + c_5 E_{initial}\left(c_5\ AO/HO\right)\right) \end{array}\right) \tag{15.184}$$

where c_4 is $(0.75)(4) = 3$ when $c_5 = 0$ and otherwise c_4 is $(0.75)(2) = 1.5$ and c_5 is $(0.75)(2) = 1.5$.

The nature of the bonding of the amino functional group of protonated amines is similar to that in H_3^+. As given in the Triatomic Molecular Hydrogen-type Ion (H_3^+) section, H_3^+ comprises two indistinguishable spin-paired electrons bound by three protons. The ellipsoidal molecular orbital (MO) satisfies the boundary constraints as shown in the Nature of the Chemical Bond of Hydrogen-Type Molecules section. Since the protons are indistinguishable, ellipsoidal MOs about each pair of protons taken one at a time are indistinguishable. H_3^+ is then given by a superposition or linear combinations of three equivalent ellipsoidal MOs that form an equilateral triangle where the points of contact between the prolate spheroids are equivalent in energy and charge density. Due to the equivalence of the H_2-type ellipsoidal MOs and the linear superposition of their energies, the energy components defined previously for the H_2 molecule, Eqs. (11.207-11.212) apply in the case of the corresponding H_3^+ molecular ion. And, each molecular energy component is given by the integral of corresponding force in Eq. (13.5). Each energy component is the total for the two equivalent electrons with the exception that the total charge of the two electrons is normalized over the three basis set H_2-type ellipsoidal MOs. Thus, the energies (Eqs. (13.12-13.17)) are those given in the Energies of Hydrogen-Type Molecules section with the electron charge, where it appears, multiplied by a factor of $3/2$, and the three sets of equivalent proton-proton pairs give rise to a factor of three times the proton-proton repulsion energy given by Eq. (11.208).

With the protonation of the imidogen (NH) functional group, the minimum energy structure with equivalent hydrogen atoms comprises two protons bound to N by two paired electrons, one from H and one from N with the MO matched to the $N2p$ AO. These two electrons are distributed equivalently over the two $H-N$ bonds of the group such that the electron number assignable to each bond is $\frac{2}{2}$. Thus, the NH_2^+ functional group has the imidogen energy parameters with the exception that each energy term is multiplied by the factor 2 due to the two bonds with electron-number per bond of $\frac{2}{2}$ and has the same geometric parameters as the NH functional group given in the Secondary Amines section. A convenient means to obtain the final group energy parameters of $E_T\,(Group)$ and $E_D\,(Group)$ is by using Eqs. (15.165-15.166) (Eqs. (15.183-15.184)) with $f_1 = 2$ and c_4 and c_5 multiplied by two.

With the protonation of the amidogen (NH_2) functional group, the minimum energy structure with equivalent hydrogen atoms comprises three protons bound to N by four paired electrons, two from $2H$ and two from N with the MO matched to the $N2p$ AO. These four electrons are distributed equivalently over the three $H-N$ bonds of the group such that the electron number assignable to each bond is $\frac{4}{3}$. Thus, the NH_3^+ functional group has the amidogen energy parameters with the exception that each energy term is multiplied by the factor $\frac{3}{2}$ due to the three bonds with electron-number per bond of $\frac{4}{3}$ and has the same geometric parameters as the NH_2 functional group given in the Primary Amines section. A convenient means to obtain the final group energy parameters of $E_T\,(Group)$ and $E_D\,(Group)$ is by using Eqs. (15.165-15.166) (Eqs. (15.183-15.184)) with $f_1 = 3/2$ and c_4 and c_5 multiplied by 3/2.

The symbols of the functional groups of organic and related ions are given in Table 15.375. The geometrical (Eqs. (15.1-15.5) and (15.51)), intercept (Eqs. (15.80-15.87)), and energy (Eqs. (15.6-15.11) and (15.17-15.65)) parameters are given in Tables 15.376, 15.377, and 15.378, respectively. Due to its charge, the bond angles of the organic and related ions that minimize the total energy are those that maximize the separation of the groups. For ions having three bonds to the central atom, the angles are 120°, and ions having four bonds are tetrahedral. The color scale, charge-density of exemplary organic ion, protonated lysine, comprising atoms with the outer shell bridged by one or more H_2-type ellipsoidal MOs or joined with one or more hydrogen MOs is shown in Figure 15.64.

Figure 15.64. Color scale, charge-density of protonated lysine ion showing the orbitals of the atoms at their radii, the ellipsoidal surface of each H or H_2-type ellipsoidal MO that transitions to the corresponding outer shell of the atom(s) participating in each bond, and the hydrogen nuclei.

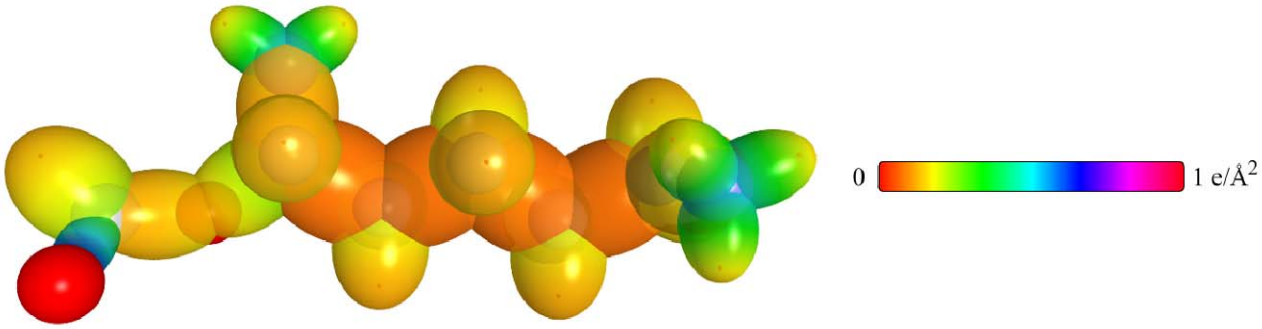

Table 15.375. The symbols of functional groups of organic and related ions.

Functional Group	Group Symbol
$(O)C\text{-}O^-$ (alkyl carboxylate)	$C-O^-$
$(RO)(O)_2S\text{-}O^-$ (alkyl sulfate)	$S-O^-$
$(O)_2N\text{-}O^-$ (nitrate)	$N-O^-$
$(RO)_2(O)P\text{-}O^-$ (alkyl phosphate)	$P-O^-$
$(RO)_3Si\text{-}O^-$ (alkyl siloxanolate) $(R)_2Si(\text{-}O^-)_2$ (alkyl silanolate)	$Si-O^-$
NH_2^+ group	NH_2^+
NH_3^+ group	NH_3^+

Table 15.376. The geometrical bond parameters of organic and related ions and experimental values of corresponding basis elements [1].

Parameter	$C-O^-$ Group	$S-O^-$ Group	$N-O^-$ Group	$P-O^-$ Group	$Si-O^-$ Group	NH_2^+ Group	NH_3^+ Group
$a\ (a_0)$	1.29907	1.98517	1.29538	1.91663	2.24744	1.26224	1.28083
$c'\ (a_0)$	1.13977	1.40896	1.13815	1.38442	1.41056	0.94811	0.95506
Bond Length $2c'\ (\AA)$	1.20628	1.49118	1.20456	1.46521	1.49287	1.00343	1.0108
Exp. Bond Length $(\AA)$	1.214 (acetic acid)	1.485 (dimethyl sulfoxide)	1.205 (methyl nitrate) 1.2 (HNO_2)	1.48 [65] (DNA)	1.509 (silicon oxide) [74]	1.00 (dimethylamine)	1.010 (methylamine)
$b,c\ (a_0)$	0.62331	1.39847	0.61857	1.32546	1.74966	0.83327	0.85345
e	0.87737	0.70974	0.87862	0.72232	0.62763	0.75113	0.74566

Table 15.377. The MO to HO intercept geometrical bond parameters of organic and related ions. E_T is E_T ($atom-atom$,$msp^3.AO$).

Bond	Atom	E_T (eV) Bond 1	E_T (eV) Bond 2	E_T (eV) Bond 3	E_T (eV) Bond 4	Final Total Energy $C2sp^3$ (eV)	$r_{initial}\ (a_0)$	$r_{final}\ (a_0)$	$E_{Coulomb}(C2sp^3)$ (eV) Final	$E(C2sp^3)$ (eV) Final	θ' (°)	θ_1 (°)	θ_2 (°)	$d_1\ (a_0)$	$d_2\ (a_0)$
$RH_2C_bC_a(O)-O^-$	O	-1.01210	0	0	0		1.00000	0.85907	-15.83785		137.99	42.01	67.29	0.50150	0.63827
$RH_2C_bC_a(O)-O^-$	C_a	-1.01210	-0.92918	-0.92918	0	-154.48615	0.91771	0.76885	-17.69621	-17.50535	134.14	45.86	62.28	0.60433	0.53544
$(RO)_2(O)S-O^-$	S	0	-0.46459	-0.46459	0		1.32010	0.86359	-15.75493		78.56	101.44	37.25	1.58026	0.17130
$(RO)_2(O)S-O^-$	O	0	0	0	0		1.00000	0.91771	-14.82575		84.06	95.94	40.75	1.50400	0.09504
O_2N-O^-	O	-0.69689	0	0	0		1.00000	0.87651	-15.52264		135.13	44.87	63.23	0.58339	0.55475
O_2N-O^-	N	-0.92918	-0.92918	-0.69689	0		0.93084	0.78280	-17.38100		138.99	41.01	68.41	0.47673	0.66142
$(RO)_2(O)P-O^-$	P	-0.72457	-0.72457	-1.13379	-0.85034		1.15350	0.74515	-18.25903		71.42	108.58	32.20	1.62182	0.23739
$(RO)_2(O)P-O^-$	O	-0.85034	0	0	0		1.00000	0.86793	-15.67609		85.55	94.45	40.76	1.45184	0.06742
$(RO)_3Si-O^-$	Si	-1.55205	-0.62217	-0.62217	-0.62217		1.31926	0.99082	-13.73181		53.34	126.66	27.02	2.00216	0.59160
$(RO)_3Si-O^-$	O	-1.55205	0	0	0		1.00000	0.89688	-15.17010		34.26	145.74	16.77	2.15183	0.74128
$-H_2C_aNH(R_{alkyl})-H^+$	N	-0.56690	-0.56690	0	0		0.93084	0.85252	-15.95954		118.18	61.82	64.40	0.54546	0.40264
$-H_2C_aN(H_2)-H^+$	N	-0.72457	0	0	0		0.93084	0.87495	-15.55033		118.00	62.00	64.85	0.54432	0.41075

Table 15.378. The energy parameters (eV) of functional groups of organic and related ions.

Parameters	$C-O^-$ Group	$S-O^-$ Group	$N-O^-$ Group	$P-O^-$ Group	$Si-O^-$ Group	NH_2^+ Group	NH_3^+ Group
f_1	0.75	0.75	0.75	0.75	0.75	2	3/2
n_1	2	2	2	2	2	1	2
n_2	0	0	0	0	0	0	0
n_3	0	0	0	0	0	0	1
C_1	0.5	0.5	0.5	0.5	0.75	0.75	0.75
C_2	1	1	1	1	0.75304	0.93613	0.93613
c_1	1	1	1	1	1	0.75	0.75
c_2	0.85395	1.20632	0.85987	0.78899	1	0.93383	0.94627
c_3	2	0	0	0	0	1	0
c_4	4	4	4	4	2	1	1
c_5	0	1	0	0	2	1	2
C_{1o}	0.5	0.5	0.5	0.5	0.75	0.75	1.5
C_{2o}	1	1	1	1	0.75304	1	1
V_e (eV)	-111.25473	-82.63003	-112.63415	-56.96374	-56.90923	-39.21967	-77.89897
V_p (eV)	23.87467	19.31325	23.90868	9.82777	19.29141	14.35050	28.49191
T (eV)	42.82081	20.81183	43.47534	14.86039	12.66092	15.53581	30.40957
V_m (eV)	-21.41040	-10.40592	-21.73767	-7.43020	-6.33046	-7.76790	-15.20478
$E_{(AO/HO)}$ (eV)	0	-11.52126	0	-11.78246	-20.50975	-14.53414	-14.53414
$\Delta E_{H_2MO\,(AO/HO)}$ (eV)	-2.69893	-1.16125	-3.71673	0	0	0	0
$E_{(n_3\,AO/HO)}$ (eV)	0	0	0	0	0	0	-14.53414
$E_{T\,(AO/HO)}$ (eV)	2.69893	-10.36001	3.71673	-11.78246	-20.50975	-14.53414	-14.53414
$E_{T\,(H_2MO)}$ (eV)	-63.27074	-63.27088	-63.27107	-63.27069	-51.79710	-31.63541	-48.73642
$E_T\left(atom-atom, msp^3.AO\right)$ (eV)	-2.69893	0	-3.71673	-2.26758	-4.13881	0	0
$E_{T\,(MO)}$ (eV)	-65.96966	-63.27074	-66.98746	-65.53832	-55.93591	-31.63537	-48.73660
$\omega\ \left(10^{15}\ rad/s\right)$	59.4034	17.6762	19.8278	11.0170	9.22130	47.0696	64.2189
E_K (eV)	39.10034	11.63476	13.05099	7.25157	6.06962	30.98202	42.27003
$\overline{E}_D$ (eV)	-0.40804	-0.21348	-0.23938	-0.17458	-0.13632	-0.34836	-0.40690
$\overline{E}_{Kvib}$ (eV)	0.21077 [12]	0.12832 [43]	0.19342 [45]	0.12337 [75]	0.15393 [24]	0.40696 [24]	0.40929 [22]
$\overline{E}_{osc}$ (eV)	-0.30266	-0.14932	-0.14267	-0.11289	-0.05935	-0.14488	-0.20226
E_{mag} (eV)	0.11441	0.11441	0.11441	0.14803	0.04983	0.14803	0.14803
$E_{T\,(Group)}$ (eV)	-49.93123	-47.67703	-50.45460	-49.32308	-42.04096	-63.56050	-73.71167
$E_{initial\,(\varepsilon_4\,AO/HO)}$ (eV)	-14.63489	-14.63489	-14.63489	-14.63489	-10.25487	-14.53414	-14.53414
$E_{initial\,(\varepsilon_5\,AO/HO)}$ (eV)	0	-1.16125	0	0	-13.61805	-13.59844	-13.59844
$E_{D\,(Group)}$ (eV)	6.02656	2.90142	6.54994	5.41841	6.23157	7.01164	11.11514

MONOSACCHARIDES OF DNA AND RNA

The simple sugar moiety of DNA and RNA comprises the alpha forms of 2-deoxy-D-ribose and D-ribose, respectively. The sugars comprise the alkyl CH_2, CH, and $C-C$ functional groups and the alkyl alcohol $C-O$ and OH functional groups given in the Alcohols section. In addition, the alpha form of the sugars comprise the $C-O$ ether functional group given in the Ethers section, and the open-chain forms further comprise the carbon to carbonyl $C-C$, the methylyne carbon of the aldehyde carbonyl CH, and the aldehyde carbonyl $C=O$ functional groups given in the Aldehydes section. The total energy of each sugar given in Tables 15.379-15.382 was calculated as the sum over the integer multiple of each $E_D(Group)$ corresponding to the functional-group composition wherein the group identity and energy $E_D(Group)$ are given in each table. The color scale, charge-density of the monosaccharides, each comprising atoms with the outer shell bridged by one or more H_2-type ellipsoidal MOs or joined with one or more hydrogen MOs are shown in Figure 15.65.

Figure 15.65. Color scale, charge-density of riboses showing the orbitals of the atoms at their radii, the ellipsoidal surface of each H or H_2-type ellipsoidal MO that transitions to the corresponding outer shell of the atom(s) participating in each bond, and the hydrogen nuclei. (A) 2-deoxy-D-ribose. (B) D-ribose. (C) Alpha-2-deoxy-D-ribose. (D) Alpha-D-ribose.

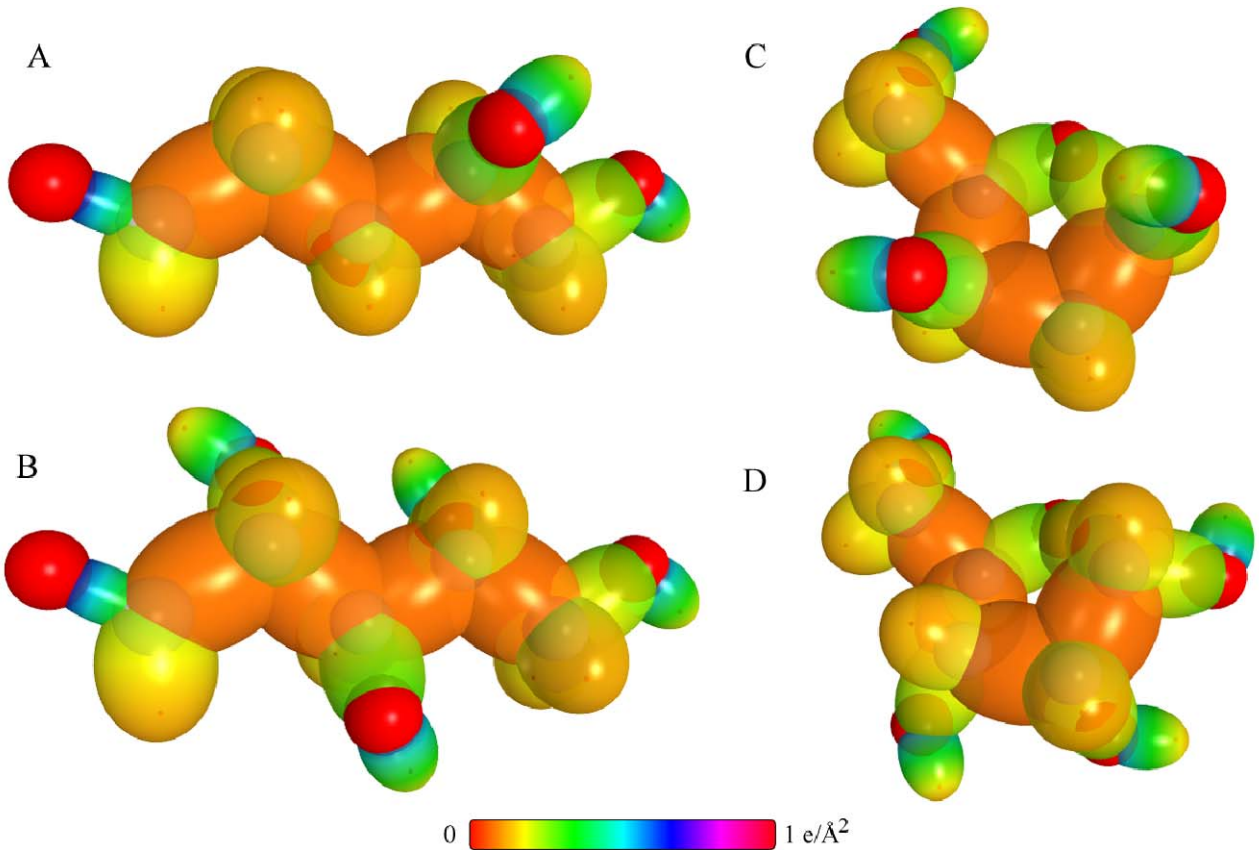

Table 15.379. The total gaseous bond energy of 2-deoxy-D-ribose ($C_5H_{10}O_4$) calculated using the functional group composition and the energies given *supra*.

Formula	CH_2 Group	CH (alkyl) Group	CH ($HC{=}O$) Group	$C-C$ (n-C) Group	$C-C(O)$ (aldehyde) Group	$C=O$ (aldehyde) Group	$C-O$ (C-OH) Group	OH Group	Calculated Total Bond Energy (eV)	Experimental Total Bond Energy (eV)	Relative Error
Energies $E_{D\,(Group)}$ of Functional Groups (eV)	7.83016	3.32601	3.47404	4.32754	4.41461	7.80660	4.34572	4.41035			
Composition	2	2	1	3	1	1	3	3	77.25842		

Table 15.380. The total gaseous bond energy of D-ribose ($C_5H_{10}O_5$) calculated using the functional group composition and the energies given *supra*. compared to the experimental values [3].

Formula	CH_2 Group	CH (alkyl) Group	CH ($HC{=}O$) Group	$C-C$ (n-C) Group	$C-C(O)$ (aldehyde) Group	$C=O$ (aldehyde) Group	$C-O$ (C-OH) Group	OH Group	Calculated Total Bond Energy (eV)	Experimental Total Bond Energy (eV)	Relative Error
Energies $E_{D\,(Group)}$ of Functional Groups (eV)	7.83016	3.32601	3.47404	4.32754	4.41461	7.80660	4.34572	4.41035			
Composition	1	3	1	3	1	1	4	4	81.51034	83.498[a]	0.02381

[a] Crystal.

Table 15.381. The total gaseous bond energy of alpha-2-deoxy-D-ribose ($C_5H_{10}O_4$) calculated using the functional group composition and the energies given *supra*.

Formula	CH_2 Group	CH (alkyl) Group	$C-C$ (n-C) Group	$C-O$ (alkyl ether) Group	$C-O$ (C-OH) Group	OH Group	Calculated Total Bond Energy (eV)	Experimental Total Bond Energy (eV)	Relative Error
Energies $E_{D\,(Group)}$ of Functional Groups (eV)	7.83016	3.32601	4.32754	4.12506	4.34572	4.41035			
Composition	2	3	4	2	3	3	77.46684		

Table 15.382. The total gaseous bond energy of alpha-D-ribose ($C_5H_{10}O_5$) calculated using the functional group composition and the energies given *supra*.

Formula	CH_2 Group	CH (alkyl) Group	$C-C$ (n-C) Group	$C-O$ (alkyl ether) Group	$C-O$ (C-OH) Group	OH Group	Calculated Total Bond Energy (eV)	Experimental Total Bond Energy (eV)	Relative Error
Energies $E_{D\,(Group)}$ of Functional Groups (eV)	7.83016	3.32601	4.32754	4.12506	4.34572	4.41035			
Composition	1	4	4	2	4	4	82.31088		

NUCLEOTIDE BONDS OF DNA AND RNA

DNA and RNA comprise a backbone of alpha-2-deoxy-D-ribose and alpha-D-ribose, respectively, with a charged phosphate moiety at the 3' and 5' positions of two consecutive ribose units in the chain and a base bound at the 1' position wherein the ribose H of each of the corresponding 3' or 5' $O-H$ and 1' $C-H$ bonds is replaced by P and the base N, respectively. For the base, the H of the $N-H$ at the pyrimidine 1 position or the purine 9 position is replaced by the sugar C. The basic repeating unit of DNA or RNA is a nucleotide that comprises a monosaccharide, a phosphate moiety and a base. The structure of the nucleotide bond is shown in Figure 15.66 with the designation of the corresponding atoms. The phosphate moiety comprises the $P=O$, $P-O$, and $C-O$ functional groups given in the Phosphates section as well as the $P-O^-$ group given in the Organic and Related Ions section. The nucleoside bond (sugar C to base N) comprises the tertiary amine $C-N$ functional group given in the corresponding section. The bases, adenine, guanine, thymine, and cytosine are equivalent to those given in the corresponding sections. The symbols of the functional groups of the nucleotide bond are given in Table 15.383. The geometrical (Eqs. (15.1-15.5) and (15.51)), intercept (Eqs. (15.80-15.87)), and energy (Eqs. (15.6-15.11) and (15.17-15.65)) parameters are given in Tables 15.384, 15.385, and 15.386, respectively. The functional group composition and the corresponding energy $E_D(Group)$ of each group of the nucleotide bond of DNA and RNA are given in Table 15.387. The bond angle parameters of the nucleoside bond determined using Eqs. (15.88-15.117) are given in Table 15.388. The color scale rendering of the charge-density of the exemplary tetra-nucleotide, (deoxy)adenosine 3'-monophosphate—5'-(deoxy)thymidine 3'-monophosphate—5'-(deoxy)guanosine 3'-monophosphate—5'-(deoxy)cytidine monophosphate (ATGC) comprising the concentric shells of atoms with the outer shell bridged by one or more H_2-type ellipsoidal MOs or joined with one or more hydrogen MOs is shown in Figure 15.67. Figure 15.68 shows the color scale rendering of the charge-density of the exemplary DNA fragment $\begin{matrix}\text{ACTGACTGACTG}\\ \text{TGACTGACTGAC}\end{matrix}$ wherein each complementary strand comprises a dodeca-nucleotide of the form (base (1)—deoxyribose) monophosphate—(base(2)—deoxyribose) monophosphate— with the phosphates bridging the 3' and 5' ribose carbons with the opposite order for the complementary stands. Figure 15.68 shows the color scale rendering of the charge-density of an exemplary double-stranded DNA helix.

Figure 15.66. Designation of the atoms of the nucleotide bond.

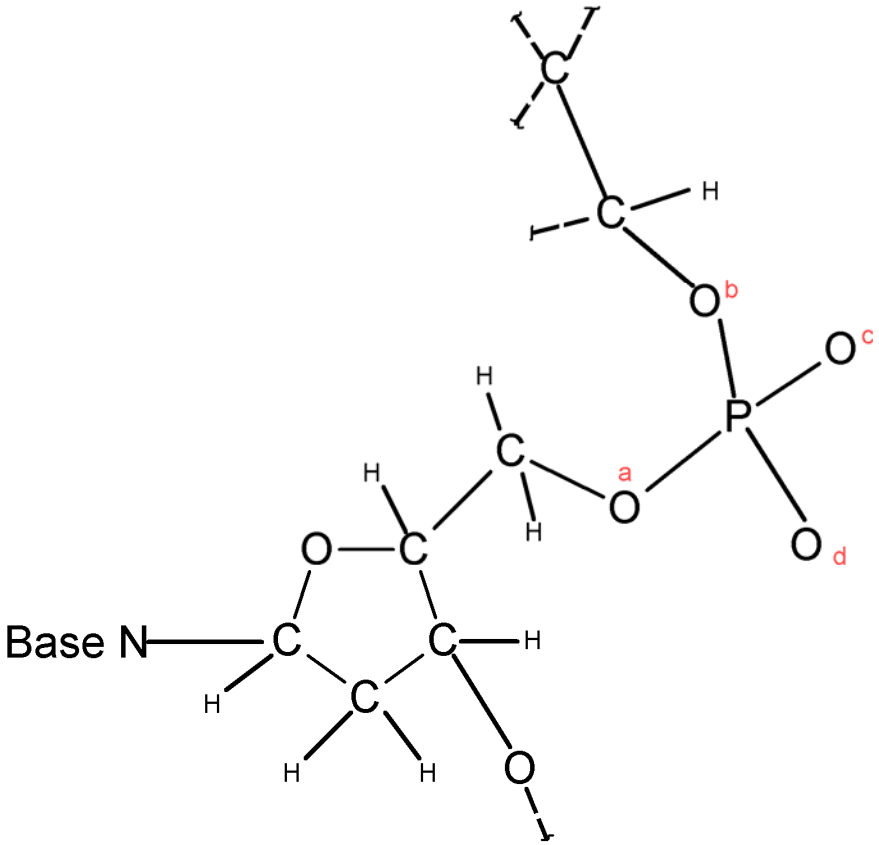

Figure 15.67. The color scale rendering of the charge-density of the exemplary tetra-nucleotide, (deoxy)adenosine monophosphate—(deoxy)thymidine monophosphate—(deoxy)guanosine monophosphate—(deoxy)cytidine monophosphate (ATGC) showing the orbitals of the atoms at their radii and the ellipsoidal surface of each H or H_2-type ellipsoidal MO that transitions to the corresponding outer shell of the atom(s) participating in each bond.

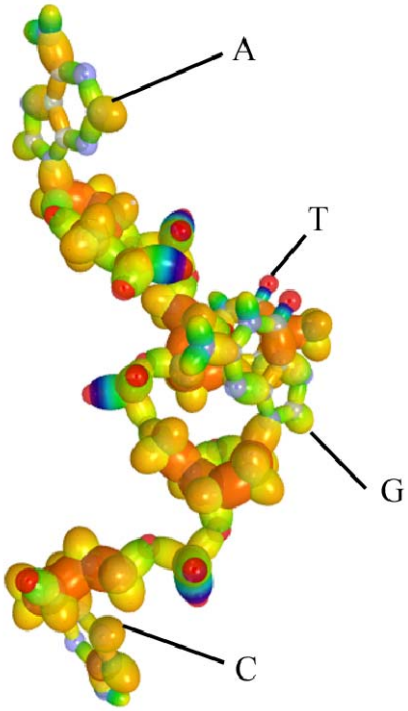

Figure 15.68. Color scale rendering of the charge-density of the DNA fragment ACTGACTGACTG TGACTGACTGAC showing the orbitals of the atoms at their radii and the ellipsoidal surface of each H or H_2-type ellipsoidal MO that transitions to the corresponding outer shell of the atom(s) participating in each bond.

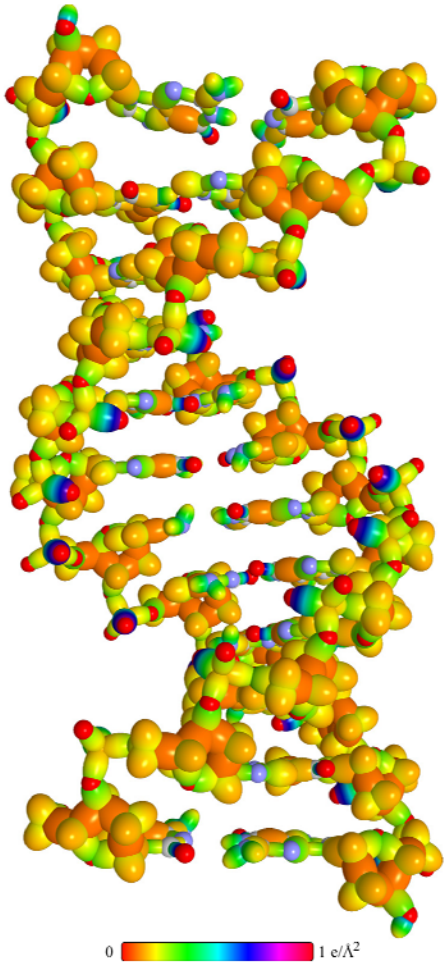

Figure 15.69. Color scale, opaque view of the charge density of a double-stranded DNA helix created and modeled using Millsian 2.0.

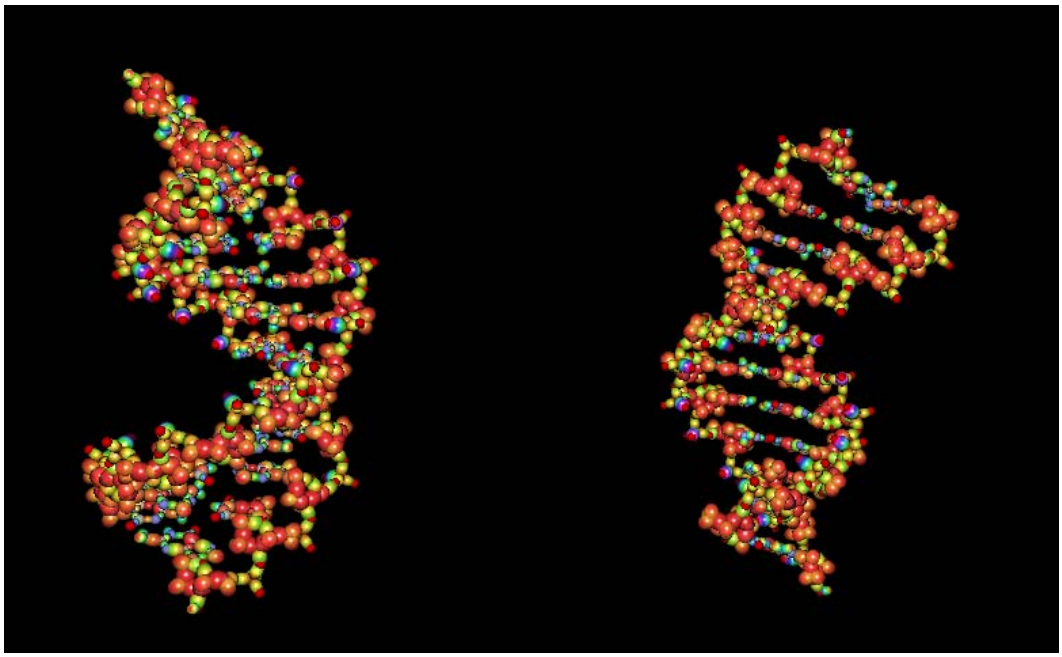

Table 15.383. The symbols of functional groups of the nucleotide bond.

Functional Group	Group Symbol
C-N	$C-N$
C-O (alkyl)	$C-O$
P=O	$P=O$
P-O	$P-O$
(RO)2(O)P-O⁻ (alkyl phosphate)	$P-O^{-}$

Table 15.384. The geometrical bond parameters of the nucleotide bond and experimental values [1].

Parameter	$C-N$ Group	$C-O$ Group	$P=O$ Group	$P-O$ Group	$P-O^{-}$ Group
$a\ (a_0)$	1.96313	1.79473	1.91663	1.84714	1.91663
$c'\ (a_0)$	1.40112	1.33968	1.38442	1.52523	1.38442
Bond Length $2c'\ (\text{Å})$	1.48288	1.41785	1.46521E-10	1.61423	1.46521
Exp. Bond Length (Å)	1.458 (trimethylamine)	1.418 (ethyl methyl ether (avg.))	1.48 [65] (DNA) 1.4759 (PO)	1.631 [70] (MHP) 1.60 [65] (DNA)	1.48 [65] (DNA)
$b,c\ (a_0)$	1.37505	1.19429	1.32546	1.04192	1.32546
e	0.71372	0.74645	0.72232	0.82573	0.72232

Table 15.385. The MO to HO intercept geometrical bond parameters of the nucleotide bond. E_T is E_T ($atom - atom, msp^3.AO$).

Bond	Atom	E_T (eV) Bond 1	E_T (eV) Bond 2	E_T (eV) Bond 3	E_T (eV) Bond 4	Final Total Energy $C2sp^3$ (eV)	$r_{initial}$ (a_0)	r_{final} (a_0)	$E_{Coulomb}(C2sp^3)$ (eV) Final	$E(C2sp^3)$ (eV) Final	θ' (°)	θ_1 (°)	θ_2 (°)	d_1 (a_0)	d_2 (a_0)
$C_z(H)N_d - C_c(N_e)C_d$ $N_e(H)C_e - N_d(H)C_c$ (adenine nucleoside)	N_d	-0.60631	-0.60631	-0.46459	0		0.93084	0.82445	-16.50297		138.15	41.85	61.57	0.68733	0.61411
$C_z(H)N_d - C_c(N_e)C_d$ $N_e(H)C_e - N_d(H)C_c$ (guanine nucleoside)	N_d	-0.92918	-0.92918	-0.46459	0		0.93084	0.79340	-17.14871		138.07	41.93	60.47	0.70588	0.59026
$N_b(O)C_b - N_cHC_c$ $C_bHN_c - HC_cC_d$ (thymine nucleoside)	N_c	-0.92918	-0.92918	-0.46459	0		-0.93084	-0.79340	-17.14871		138.07	41.93	60.47	0.70588	0.59026
$N_b(O)C_b - N_cHC_c$ $C_bHN_c - HC_cC_d$ (cytosine nucleoside)	N_c	-0.92918	-0.92918	-0.46459	0		-0.93084	-0.79340	-17.14871		138.07	41.93	60.47	0.70588	0.59026
$N_d - C$ *ribose* (adenine nucleoside)	N_d	-0.46459	-0.60631	-0.60631	0		0.93084	0.82445	-16.50297		76.37	103.63	35.64	1.59544	0.19432
$N_d - C$ *ribose* (adenine nucleoside)	*C ribose*	-0.46459	-0.92918	-0.82688	0	-153.83634	-0.91771	-0.79816	-17.04640	-16.85554	73.17	106.83	33.75	1.63226	0.23114
$N_d - C$ *ribose* (guanine nucleoside)	N_d	-0.46459	-0.92918	-0.92918	0		0.93084	0.79340	-17.14871		72.56	107.44	33.40	1.63893	0.23782
$N_d - C$ *ribose* (guanine nucleoside)	*C ribose*	-0.46459	-0.92918	-0.82688	0	-153.83634	-0.91771	-0.79816	-17.04640	-16.85554	73.17	106.83	33.75	1.63226	0.23114
$N_c - C$ *ribose* (thymine nucleoside)	N_c	-0.46459	-0.92918	-0.92918	0		0.93084	0.79340	-17.14871		72.56	107.44	33.40	1.63893	0.23782
$N_c - C$ *ribose* (thymine nucleoside)	*C ribose*	-0.46459	-0.92918	-0.82688	0	-153.83634	-0.91771	-0.79816	-17.04640	-16.85554	73.17	106.83	33.75	1.63226	0.23114
$N_c - C$ *ribose* (cytosine nucleoside)	N_c	-0.46459	-0.92918	-0.92918	0		0.93084	0.79340	-17.14871		72.56	107.44	33.40	1.63893	0.23782
$N_c - C$ *ribose* (cytosine nucleoside)	*C ribose*	-0.46459	-0.92918	-0.82688	0	-153.83634	-0.91771	-0.79816	-17.04640	-16.85554	73.17	106.83	33.75	1.63226	0.23114

Table 15.386. The energy parameters (eV) of functional groups of the nucleotide bond.

Parameters	$C-N$ Group	$C-O$ Group	$P=O$ Group	$P-O$ Group	$P-O^-$ Group
n_1	1	1	2	1	2
n_2	0	0	0	0	0
n_3	0	0	0	0	0
C_1	0.5	0.5	0.5	0.5	0.5
C_2	1	1	1	1	1
c_1	1	1	1	1	1
c_2	0.91140	0.85395	0.79401	0.79401	0.78899
c_3	0	0	0	0	0
c_4	2	2	4	2	4
c_5	0	0	0	0	0
C_{1o}	0.5	0.5	0.5	0.5	0.5
C_{2o}	1	1	1	0.79401	1
$V_e\ (eV)$	-31.67393	-33.47304	-56.96374	-33.27738	-56.96374
$V_p\ (eV)$	9.71067	10.15605	9.82777	8.92049	9.82777
$T\ (eV)$	8.06719	9.32537	14.86039	9.00781	14.86039
$V_m\ (eV)$	-4.03359	-4.66268	-7.43020	-4.50391	-7.43020
$E_{(AO/HO)}\ (eV)$	-14.63489	-14.63489	-23.56492	-11.78246	-11.78246
$\Delta E_{H_2MO\ (AO/HO)}\ (eV)$	-0.92918	-1.65376	0	0	0
$E_{I\ (AO/HO)}\ (eV)$	-13.70571	-12.98113	-23.56492	-11.78246	-11.78246
$E_{T\ (H_2MO)}\ (eV)$	-31.63537	-31.63544	-63.27069	-31.63544	-63.27069
$E_T\left(atom-atom, msp^3.AO\right)\ (eV)$	-0.92918	-1.65376	-2.26758	-1.44914	-2.26758
$E_{T\ (MO)}\ (eV)$	-32.56455	-33.28912	-65.53832	-33.08451	-65.53832
$\omega\ \left(10^{15}\ rad/s\right)$	18.1298	12.1583	11.0170	10.3761	11.0170
$E_K\ (eV)$	11.93333	8.00277	7.25157	6.82973	7.25157
$\overline{E}_D\ (eV)$	-0.22255	-0.18631	-0.17458	-0.17105	-0.17458
$\overline{E}_{Kvib}\ (eV)$	0.12944 [23]	0.16118 [4]	0.15292 [24]	0.10477 [71]	0.12337 [75]
$\overline{E}_{osc}\ (eV)$	-0.15783	-0.10572	-0.09812	-0.11867	-0.11289
$E_{mag}\ (eV)$	0.14803	0.14803	0.14803	0.14803	0.14803
$E_{T\ (Group)}\ (eV)$	-32.72238	-33.39484	-65.73455	-33.20318	-49.32308
$E_{initial\ (c_4\ AO/HO)}\ (eV)$	-14.63489	-14.63489	-14.63489	-14.63489	-14.63489
$E_{initial\ (c_5\ AO/HO)}\ (eV)$	0	0	0	0	0
$E_{D\ (Group)}\ (eV)$	3.45260	4.12506	7.19500	3.93340	5.41841

Table 15.387. The functional group composition and the energy $E_{D(Group)}$ of each group of the nucleotide bond.

Formula	$C-N$ (3° amine) Group	$C-O$ (alkyl ether) Group	$P=O$ (phosphate) Group	$P-O$ (phosphate) Group	$P-O^-$ (organic ions) Group
Energies $E_{D\ (Group)}$ of Functional Groups (eV)	3.45260	4.12506	7.19500	3.93340	5.41841
Composition	1	2	1	2	1

Table 15.388. The bond angle parameters of the nucleotide bond and experimental values [1]. In the calculation of θ_v, the parameters from the preceding angle were used. E_T is E_T ($atom - atom, msp^3.AO$).

Atoms of Angle	2c' Bond 1 (a_0)	2c' Bond 2 (a_0)	2c' Terminal Atoms (a_0)	$E_{Coulombic}$ Atom 1	Atom 1 Hybridization Designation (Table 15.3A)	$E_{Coulombic}$ Atom 2	Atom 2 Hybridization Designation (Table 15.3A)	c_2 Atom 1	c_2 Atom 2	C_1	C_2	c_1	c_2'	E_T (eV)	θ_v (°)	θ_1 (°)	θ_2 (°)	Cal. θ (°)	Exp. θ (°)
$\angle(P)OCN$	2.67935	2.80224	4.5277	-16.47951	22	-16.47951	22	0.82562	0.82562	1	1	1	0.82562	-1.65376				111.36	111.3 [65]
$\angle POC$	3.05046	2.67935	4.9904	-11.78246	Psp^3	-15.75493	7	0.73885 Eq. (15.181)	0.86359	1	0.73885	1	0.80122	-0.72457				121.00	121.3 [65]
$\angle O_aPO_b$	3.05046	3.05046	4.7539	-15.95954	10	-15.95954	10	0.85252	0.85252	1	1	1	0.85252	-1.65376				102.38	101.4 [65]
$\angle O_bPO_c$	3.05046	2.76885	4.7539	-15.95954	10	-15.95954	10	0.85252	0.85252	1	1	1	0.85395	-1.65376				109.46	109.7 [65]
$\angle O_cPO_d$	2.76885	2.76885	4.7539	-15.95954	10	-15.95954	10	0.85252	0.85252	1	1	1	0.85252	-1.65376				118.29	116.0 [65]
$\angle C_aOC_b$ (C_a-O (i)) (C_b-O (ii))	2.68862	2.67935	4.4385	-17.51099	48	-17.51099	48	0.77699	0.77699	1	1	1	0.77699	-1.85836				111.55	111.9 (ethyl methyl ether)
$\angle C_bC_aO$ (C_a-O (ii))	2.91547	2.67935	4.5607	-16.68412	26	-13.61806	O	0.81549	0.85395 (Eq. (15.133))	1	1	1	0.83472	-1.65376				109.13	109.4 (ethyl methyl ether)
$\angle C_aOH$ (C_a-O (ii))	2.67024	1.83616	3.6515	-14.82575	1	-14.82575	1	1	0.91771	0.75	1	0.75	0.91771	0				106.78	105 (ethanol)
$\angle C_bC_aO$ (C_a-O (ii))	2.91547	2.67024	4.5826	-16.68412	26	-13.61806	O	0.81549	0.85395 (Eq. (15.114))	1	1	1	0.83472	-1.65376				110.17	107.8 (ethanol)
$\angle CNC$ (3° amine)	2.80224	2.80224	4.6043	-17.14871	36	-17.14871	36	0.79340	0.79340	1	1	1	0.79340	-1.85836				110.48	110.9 (trimethyl amine)
Methylene $\angle HC_aH$	2.11106	2.11106	3.4252	-15.75493	7	H	H	0.86359	1	1	1	0.75	1.15796	0				108.44	107 (propane)
$\angle C_aC_bC_c$															69.51			110.49	112 (propane) 113.8 (butane) 110.8 (isobutane)
$\angle C_aC_bH$															69.51			110.49	111.0 (butane) 111.4 (isobutane)
Methyl $\angle HC_aH$	2.09711	2.09711	3.4252	-15.75493	7	H	H	0.86359	1	1	1	0.75	1.15796	0				109.50	
$\angle C_aC_bC_c$															70.56			109.44	
$\angle C_aC_bH$															70.56			109.44	
$\angle C_bC_aC_c$ iso C_a	2.91547	2.91547	4.7958	-16.68412 C_b	26	-16.68412 C_c	26	0.81549	0.81549	1	1	1	0.81549	-1.85836				110.67	110.8 (isobutane)
$\angle C_bC_aH$ iso C_a	2.91547	2.11323	4.1633	-15.55033 C_a	5	-14.82575 C_b	1	0.87495	0.91771	0.75	1	0.75	1.04887	0				110.76	
$\angle C_aC_bH$ iso C_a	2.91547	2.09711	4.1633	-15.55033 C_b	5	-14.82575 C_a	1	0.87495	0.91771	0.75	1	0.75	1.04887	0				111.27	111.4 (isobutane)

AMINO ACIDS ($H_2N-CH(R)-COOH$)

The amino acids, $H_2NCH(R)COOH$, each have a primary amine moiety comprised of NH_2 and $C-N$ functional groups, an alkyl carboxylic acid moiety comprised of a $C=O$ functional group, and the single bond of carbon to the carbonyl carbon atom, $C-C(O)$, is also a functional group. The carboxylic acid moiety further comprises a $C-OH$ moiety that comprises $C-O$ and OH functional groups. The alpha carbon comprises a methylyne (CH) functional group bound to a side chain R group by an isopropyl $C-C$ bond functional group. These groups common to all amino acids are given in the Primary Amines section, the Carboxylic Acids section, and the Branched Alkanes section, respectively. The R group is unique for each amino acid and determines its characteristic hydrophilic, hydrophobic, acidic, and basic properties. These characteristic functional groups are given in the prior organic functional group sections. The total energy of each amino acid given in Tables 15.389-15.408 was calculated as the sum over the integer multiple of each $E_D(Group)$ corresponding to the functional-group composition of the amino acid wherein the group identity and energy $E_D(Group)$ are given in each table. The structure and the color scale, charge-density of the amino acids, each comprising atoms with the outer shell bridged by one or more H_2-type ellipsoidal MOs or joined with one or more hydrogen MOs are shown in Figures 15.70-15.89.

ASPARTIC ACID

Figure 15.70. (A) Color scale, charge-density of aspartic acid showing the orbitals of the atoms at their radii, the ellipsoidal surface of each H or H_2-type ellipsoidal MO that transitions to the corresponding outer shell of the atom(s) participating in each bond, and the hydrogen nuclei. (B) Chemical structure of aspartic acid.

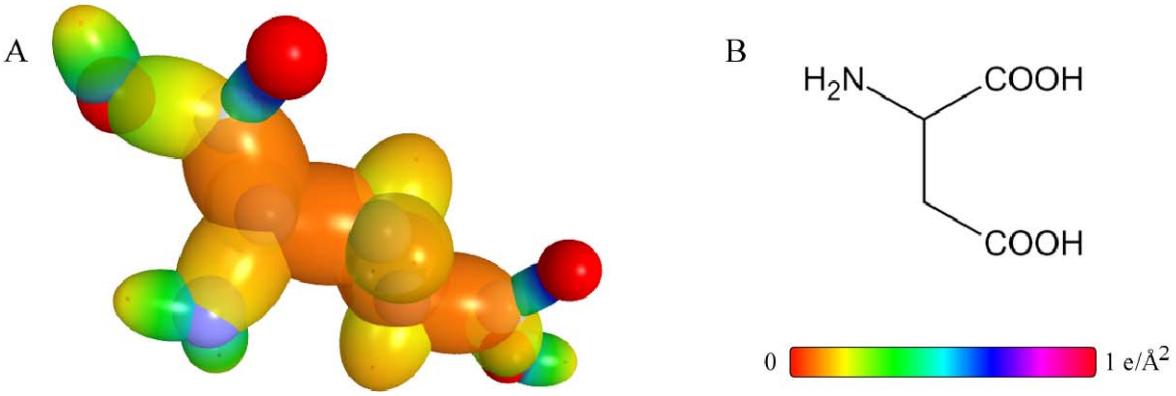

GLUTAMIC ACID

Figure 15.71. (A) Color scale, charge-density of glutamic acid showing the orbitals of the atoms at their radii, the ellipsoidal surface of each H or H_2-type ellipsoidal MO that transitions to the corresponding outer shell of the atom(s) participating in each bond, and the hydrogen nuclei. (B) Chemical structure of glutamic acid.

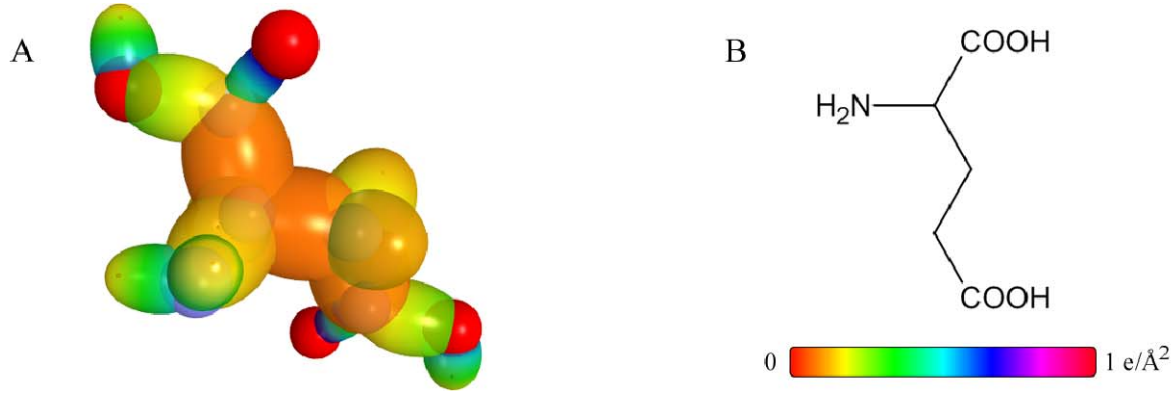

CYSTEINE

Figure 15.72. (A) Color scale, charge-density of cysteine showing the orbitals of the atoms at their radii, the ellipsoidal surface of each H or H_2-type ellipsoidal MO that transitions to the corresponding outer shell of the atom(s) participating in each bond, and the hydrogen nuclei. (B) Chemical structure of cysteine.

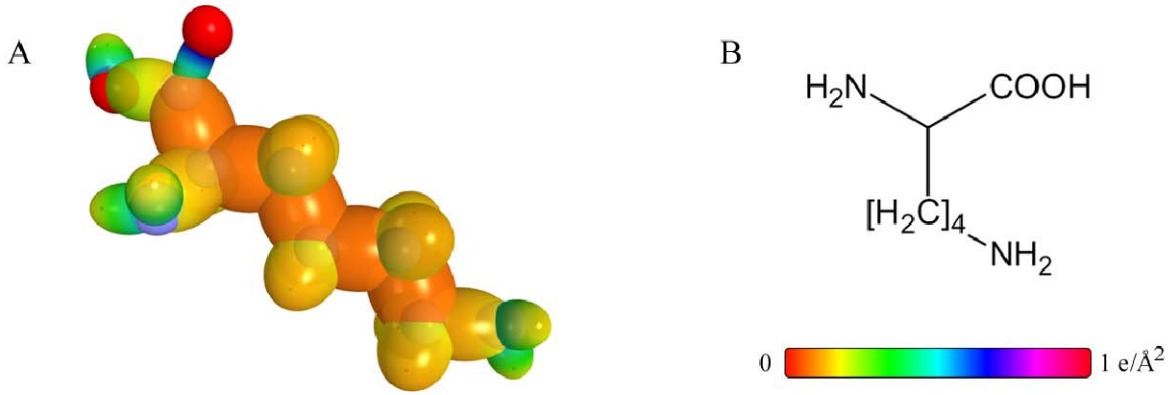

LYSINE

Figure 15.73. (A) Color scale, charge-density of lysine showing the orbitals of the atoms at their radii, the ellipsoidal surface of each H or H_2-type ellipsoidal MO that transitions to the corresponding outer shell of the atom(s) participating in each bond, and the hydrogen nuclei. (B) Chemical structure of lysine.

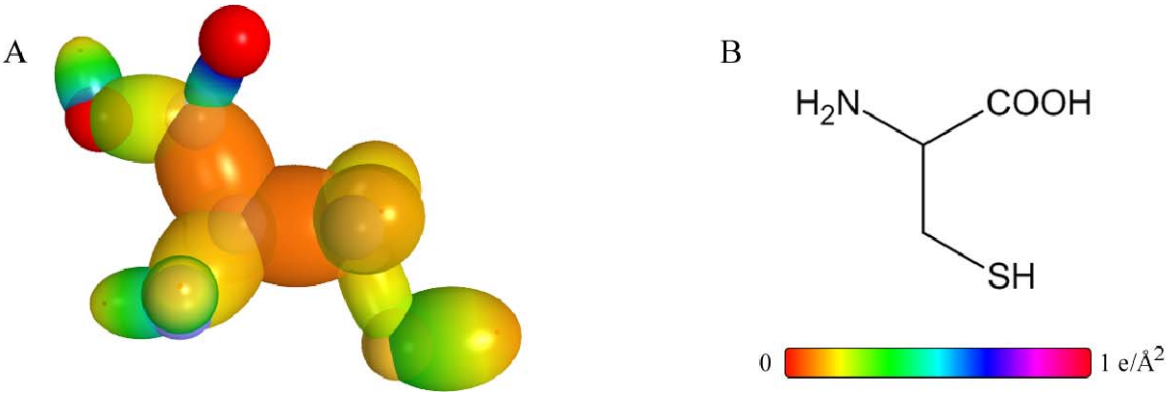

Table 15.389. The total bond energy of aspartic acid ($C_4H_7NO_4$) calculated using the functional group composition and the energies given *supra*. compared to the experimental values [3].

Formula	CH_2 Group	CH Group	$C-C$ (iso-C) Group	$C-C(O)$ (alkyl carboxylic acid) Group	$C=O$ (alkyl carboxylic acid) Group	$C-O$ ($(O)C$-O) Group	OH Group	NH_2 Group	$C-N$ (1° amine)	Calculated Total Bond Energy (eV)	Experimental Total Bond Energy (eV)	Relative Error
Energies $E_{D(Group)}$ of Functional Groups (eV)	7.83016	3.32601	4.29921	4.43110	7.80660	4.41925	4.41035	7.41010	3.98101			
Composition	1	1	1	2	2	2	2	1	1	68.98109	70.843[a]	0.02628

[a] Crystal.

Table 15.390. The total bond energy of glutamic acid ($C_5H_9NO_4$) calculated using the functional group composition and the energies given *supra*. compared to the experimental values [3].

Formula	CH_2 Group	CH Group	$C-C$ (n-C) Group	$C-C$ (iso-C) Group	$C-C(O)$ (alkyl carboxylic acid) Group	$C=O$ (alkyl carboxylic acid) Group	$C-O$ ($(O)C$-O) Group	OH Group	NH_2 Group	$C-N$ (1° amine)	Calculated Total Bond Energy (eV)	Experimental Total Bond Energy (eV)	Relative Error
Energies $E_{D(Group)}$ of Functional Groups (eV)	7.83016	3.32601	4.32754	4.29921	4.43110	7.80660	4.41925	4.41035	7.41010	3.98101			
Composition	2	1	1	1	2	2	2	2	1	1	81.13879	83.167[a]	0.02438

[a] Crystal.

Table 15.391. The total bond energy of cysteine ($C_3H_7NO_4S$) calculated using the functional group composition and the energies given *supra*. compared to the experimental values [3].

Formula	CH_2 Group	CH Group	$C-C$ (iso-C) Group	$C-C(O)$ (alkyl carboxylic acid) Group	$C=O$ (alkyl carboxylic acid) Group	$C-O$ ($(O)C$-O) Group	OH Group	NH_2 Group	$C-N$ (1° amine)	SH Group	$C-S$ (thiol) Group	Calculated Total Bond Energy (eV)	Experimental Total Bond Energy (eV)	Relative Error
Energies $E_{D(Group)}$ of Functional Groups (eV)	7.83016	3.32601	4.29921	4.43110	7.80660	4.41925	4.41035	7.41010	3.98101	3.77430	3.33648			
Composition	1	1	1	1	1	1	1	1	1	1	1	55.02457	56.571[a]	0.02733

Table 15.392. The total bond energy of lysine ($C_6H_{14}N_2O_2$) calculated using the functional group composition and the energies given *supra*. compared to the experimental values [3].

Formula	CH_2 Group	CH Group	$C-C$ (n-C) Group	$C-C$ (iso-C) Group	$C-C(O)$ (alkyl carboxylic acid) Group	$C=O$ (alkyl carboxylic acid) Group	$C-O$ ($(O)C$-O) Group	OH Group	NH_2 Group	$C-N$ (1° amine)	Calculated Total Bond Energy (eV)	Experimental Total Bond Energy (eV)	Relative Error
Energies $E_{D(Group)}$ of Functional Groups (eV)	7.83016	3.32601	4.32754	4.29921	4.43110	7.80660	4.41925	4.41035	7.41010	3.98101			
Composition	4	1	3	1	1	1	1	1	2	2	95.77799	98.194[a]	0.02461

ARGININE

Figure 15.74. (A) Color scale, charge-density of arginine showing the orbitals of the atoms at their radii, the ellipsoidal surface of each H or H_2-type ellipsoidal MO that transitions to the corresponding outer shell of the atom(s) participating in each bond, and the hydrogen nuclei. (B) Chemical structure of arginine.

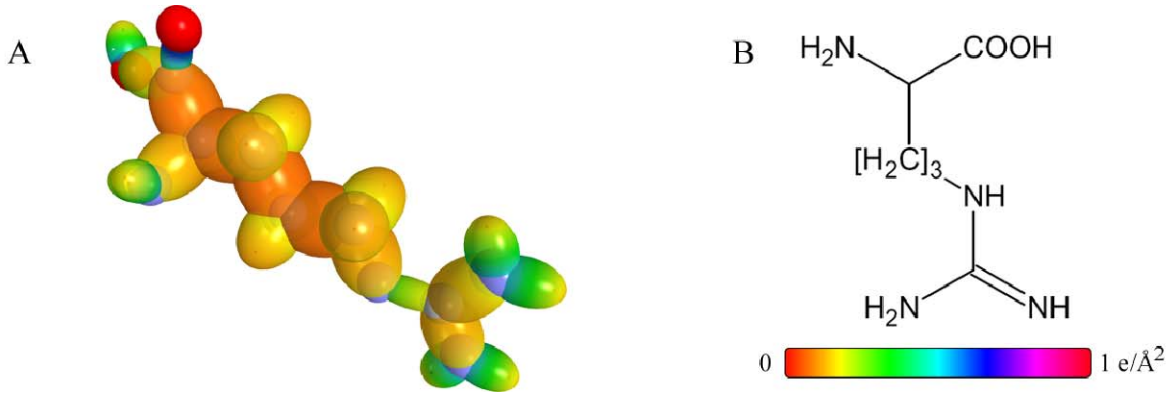

HISTIDINE

Figure 15.75. (A) Color scale, charge-density of histidine showing the orbitals of the atoms at their radii, the ellipsoidal surface of each H or H_2-type ellipsoidal MO that transitions to the corresponding outer shell of the atom(s) participating in each bond, and the hydrogen nuclei. (B) Chemical structure of histidine.

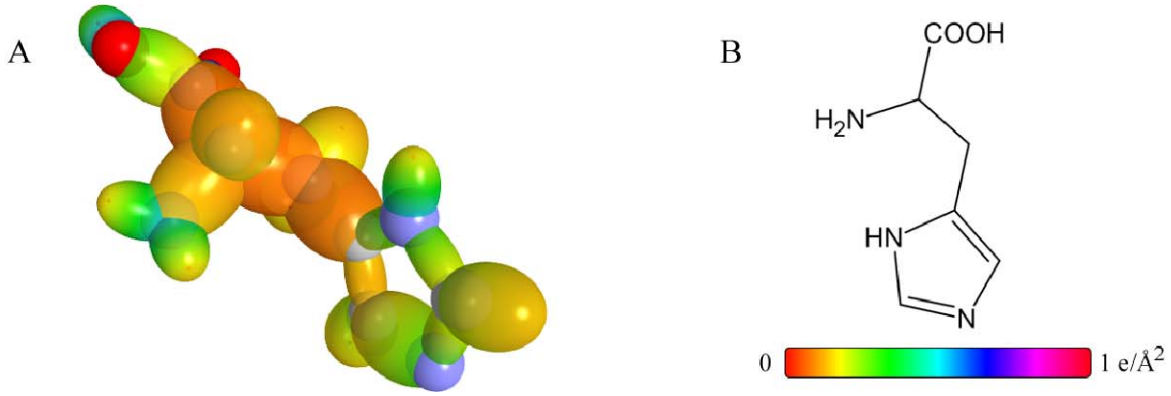

ASPARAGINE

Figure 15.76. (A) Color scale, charge-density of asparagine showing the orbitals of the atoms at their radii, the ellipsoidal surface of each H or H_2-type ellipsoidal MO that transitions to the corresponding outer shell of the atom(s) participating in each bond, and the hydrogen nuclei. (B) Chemical structure of asparagine.

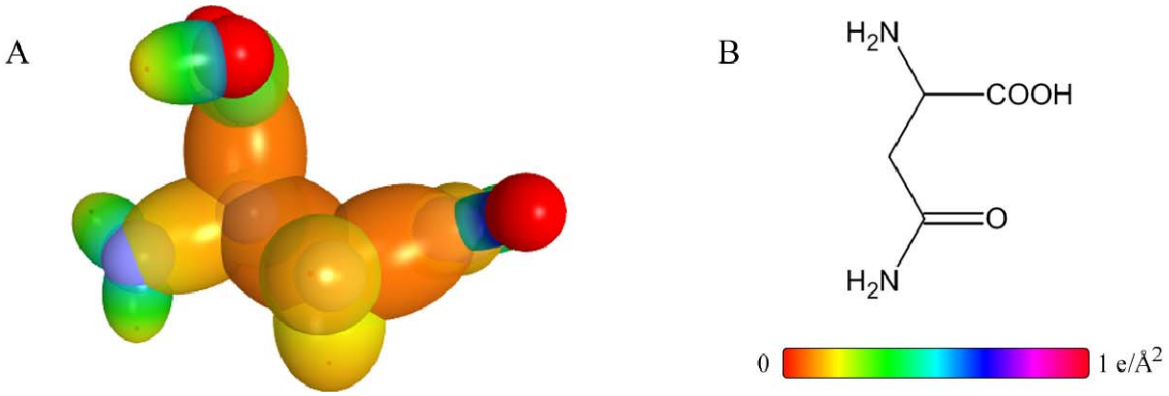

GLUTAMINE

Figure 15.77. (A) Color scale, charge-density of glutamine showing the orbitals of the atoms at their radii, the ellipsoidal surface of each H or H_2-type ellipsoidal MO that transitions to the corresponding outer shell of the atom(s) participating in each bond, and the hydrogen nuclei. (B) Chemical structure of Glutamine.

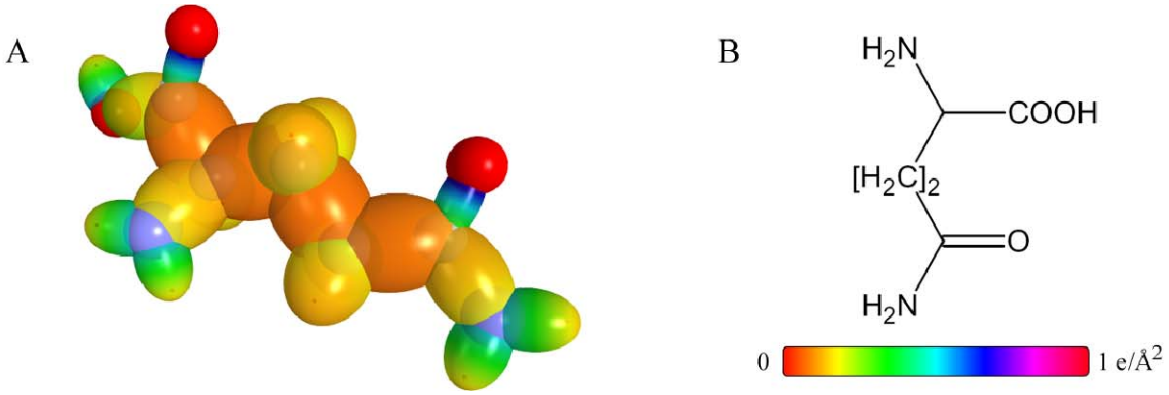

Table 15.393. The total bond energy of arginine ($C_6H_{14}N_2O_2$) calculated using the functional group composition and the energies given *supra*. compared to the experimental values [3].

Formula	CH_2 Group	CH Group	$C-C$ (n-C) Group	$C-C$ (iso-C) Group	$C-C(O)$ (alkyl carboxylic acid) Group	$C=O$ (alkyl carboxylic acid) Group	$C-O$ ($(O)C$-O) Group	OH Group	NH_2 Group	$C-N$ (1° amine)	$N=C$ ($N_b=C_c$ imidazole) Group	NH (heterocyclic imidazole) Group	$C-N$ (N alkyl amide) Group	$C-N$ ($(O)C$-N alkyl amide) Group	NH_2 (amide) Group	Calculated Total Bond Energy (eV)	Experimental Total Bond Energy (eV)	Relative Error
Energies $E_{D\,(Group)}$ of Functional Groups (eV)	7.83016	3.32601	4.32754	4.29921	4.43110	7.80660	4.41925	4.41035	7.41010	3.98101	6.79303	3.51208	3.40044	4.12212	7.37901			
Composition	3	1	2	1	1	1	1	1	1	1	1	2	1	2	1	105.07007	107.420[a]	0.02188

Table 15.394. The total bond energy of histidine ($C_6H_9N_3O_2$) calculated using the functional group composition and the energies given *supra*. compared to the experimental values [3].

Formula	CH_2 Group	CH Group	$C-C$ (iso-C) Group	$C-C(O)$ (alkyl carboxylic acid) Group	$C=O$ (alkyl carboxylic acid) Group	$C-O$ ($(O)C$-O) Group	OH Group	NH_2 Group	$C-N$ (1° amine)	$C-C$ ($-C(C)=C$) Group	CH (imidazole) Group	$C=C$ ($C_a=C_b$ imidazole) Group	$N=C$ ($N_b=C_c$ imidazole) Group	$C-N$ (C_b-N_b imidazole) Group	NH (heterocyclic imidazole) Group	$C-N-C$ ($C_a-N_a-C_c$ imidazole) Group	Calculated Total Bond Energy (eV)	Experimental Total Bond Energy (eV)	Relative Error
Energies $E_{D\,(Group)}$ of Functional Groups (eV)	7.83016	3.32601	4.29921	4.43110	7.80660	4.41925	4.41035	7.41010	3.98101	3.75498	3.32988	7.23317	6.79303	3.47253	3.51208	8.76298			
Composition	1	1	1	1	1	1	1	1	1	1	2	1	1	1	1	1	88.10232	89.599[a]	0.01671

Table 15.395. The total bond energy of asparagine ($C_4H_8N_2O_2$) calculated using the functional group composition and the energies given *supra*. compared to the experimental values [3].

Formula	CH_2 Group	CH Group	$C-C$ (iso-C) Group	$C-C(O)$ (alkyl carboxylic acid) Group	$C=O$ (alkyl carboxylic acid) Group	$C-O$ ($(O)C$-O) Group	OH Group	NH_2 Group	$C-N$ (1° amine)	$C-C(O)$ (alkyl amide) Group	$C-N$ ($(O)C$-N alkyl amide) Group	NH_2 (amide) Group	Calculated Total Bond Energy (eV)	Experimental Total Bond Energy (eV)	Relative Error
Energies $E_{D\,(Group)}$ of Functional Groups (eV)	7.83016	3.32601	4.29921	4.43110	7.80660	4.41925	4.41035	7.41010	3.98101	4.35263	4.12212	7.37901			
Composition	1	1	1	1	2	1	1	1	1	1	1	1	71.57414	73.513[a]	0.02637

Table 15.396. The total bond energy of glutamine ($C_5H_{10}N_2O_2$) calculated using the functional group composition and the energies given *supra*. compared to the experimental values [3].

Formula	CH_2 Group	CH Group	$C-C$ (n-C) Group	$C-C$ (iso-C) Group	$C-C(O)$ (alkyl carboxylic acid) Group	$C=O$ (alkyl carboxylic acid) Group	$C-O$ ($(O)C$-O) Group	OH Group	NH_2 Group	$C-N$ (1° amine)	$C-C(O)$ (alkyl amide) Group	$C-N$ ($(O)C$-N alkyl amide) Group	NH_2 (amide) Group	Calculated Total Bond Energy (eV)	Experimental Total Bond Energy (eV)	Relative Error
Energies $E_{D\,(Group)}$ of Functional Groups (eV)	7.83016	3.32601	4.32754	4.29921	4.43110	7.80660	4.41925	4.41035	7.41010	3.98101	4.35263	4.12212	7.37901			
Composition	2	1	1	1	1	2	1	1	1	1	1	1	1	83.73184	85.843[a]	0.02459

[a] Crystal

THREONINE

Figure 15.78. (A) Color scale, charge-density of threonine showing the orbitals of the atoms at their radii, the ellipsoidal surface of each H or H_2-type ellipsoidal MO that transitions to the corresponding outer shell of the atom(s) participating in each bond, and the hydrogen nuclei. (B) Chemical structure of threonine.

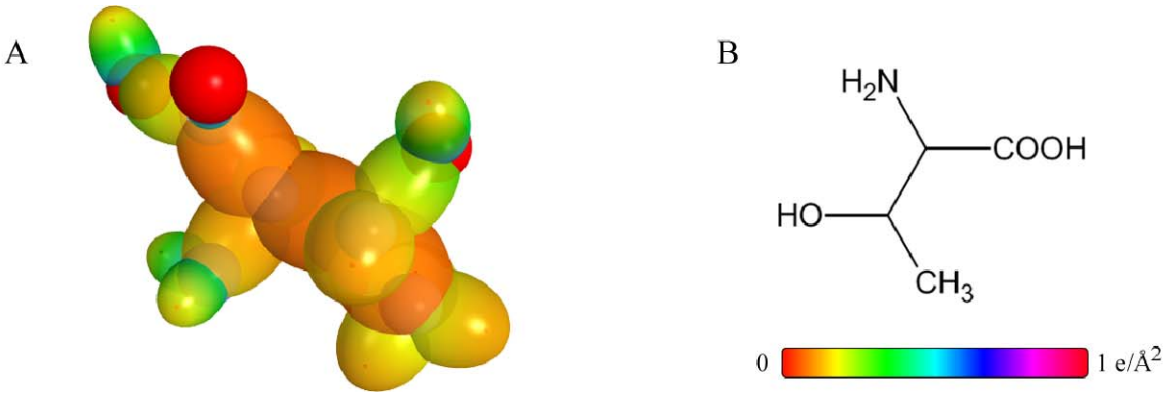

TYROSINE

Figure 15.79. (A) Color scale, charge-density of tyrosine showing the orbitals of the atoms at their radii, the ellipsoidal surface of each H or H_2-type ellipsoidal MO that transitions to the corresponding outer shell of the atom(s) participating in each bond, and the hydrogen nuclei. (B) Chemical structure of tyrosine.

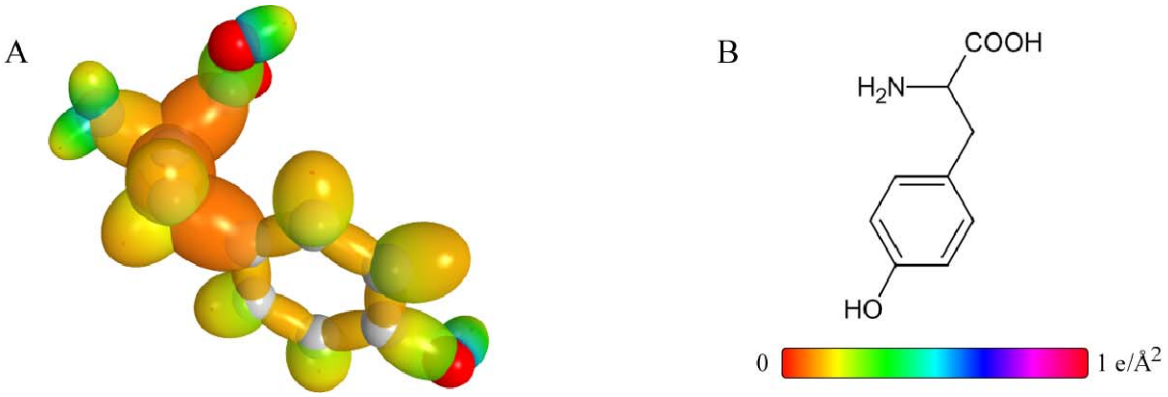

SERINE

Figure 15.80. (A) Color scale, charge-density of serine showing the orbitals of the atoms at their radii, the ellipsoidal surface of each H or H_2-type ellipsoidal MO that transitions to the corresponding outer shell of the atom(s) participating in each bond, and the hydrogen nuclei. (B) Chemical structure of serine.

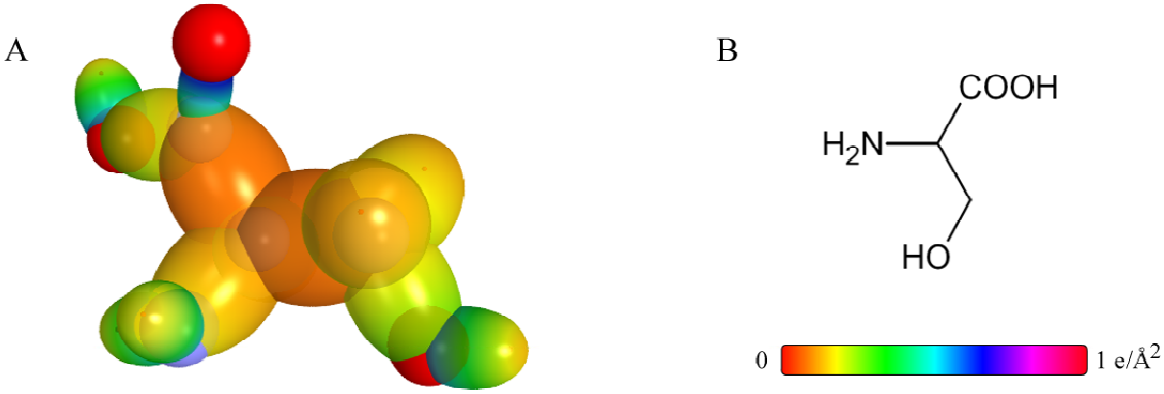

TRYPTOPHAN

Figure 15.81. (A) Color scale, charge-density of tryptophan showing the orbitals of the atoms at their radii, the ellipsoidal surface of each H or H_2-type ellipsoidal MO that transitions to the corresponding outer shell of the atom(s) participating in each bond, and the hydrogen nuclei. (B) Chemical structure of tryptophan.

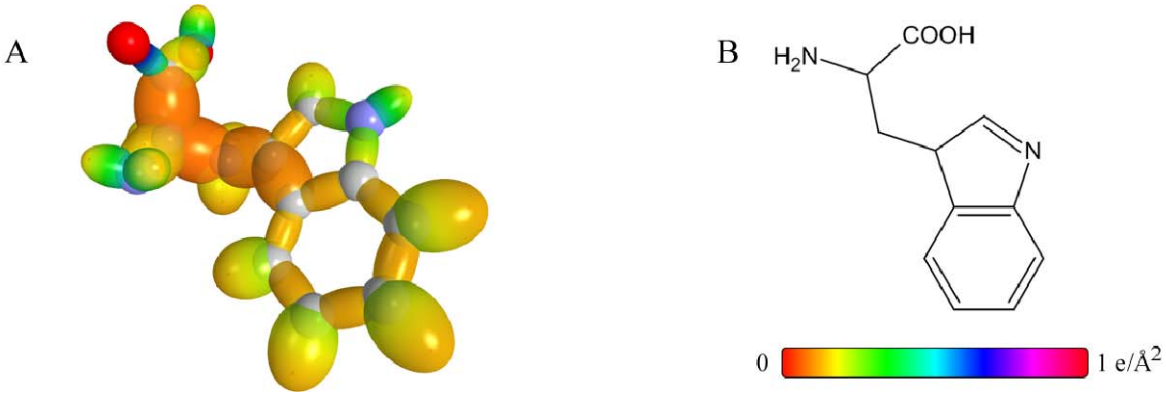

Table 15.397. The total bond energy of threonine ($C_4H_9NO_3$) calculated using the functional group composition and the energies given *supra*. compared to the experimental values [3].

Formula	CH_3 Group	CH Group	$C-C$ (iso-C) Group	$C-C(O)$ (alkyl carboxylic acid) Group	$C=O$ (alkyl carboxylic acid) Group	$C-O$ ($(O)C-O$) Group	OH Group	NH_2 Group	$C-N$ (1° amine)	$C-O$ (alkyl alcohol) Group	Calculated Total Bond Energy (eV)	Experimental Total Bond Energy (eV)	Relative Error
Energies $E_D(Group)$ of Functional Groups (eV)	12.49186	3.32601	4.29921	4.43110	7.80660	4.41925	4.41035	7.41010	3.98101	4.34572			
Composition	1	2	2	1	1	1	2	1	1	1	68.95678	71.058[a]	0.02956

Table 15.398. The total bond energy of tyrosine ($C_9H_{11}NO_3$) calculated using the functional group composition and the energies given *supra*. compared to the experimental values [3].

Formula	CH_2 Group	CH Group	$C-C$ (iso-C) Group	$C-C(O)$ (alkyl carboxylic acid) Group	$C=O$ (alkyl carboxylic acid) Group	$C-O$ ($(O)C-O$) Group	OH Group	NH_2 Group	$C-N$ (1° amine)	$C^{3e}=C$ (CC aromatic bond) Group	CH (CH aromatic) Group	$C-C$ (C alkyl to aryl toluene) Group	$C-O$ (Aryl C-O phenol) Group	Calculated Total Bond Energy (eV)	Experimental Total Bond Energy (eV)	Relative Error
Energies $E_D(Group)$ of Functional Groups (eV)	7.83016	3.32601	4.29921	4.43110	7.80660	4.41925	4.41035	7.41010	3.98101	5.63881	3.90454	3.63685	3.99228			
Composition	1	1	1	1	1	1	2	1	1	6	4	1	1	109.40427	111.450[a]	0.01835

Table 15.399. The total bond energy of serine ($C_3H_7NO_3$) calculated using the functional group composition and the energies given *supra*. compared to the experimental values [3].

Formula	CH_2 Group	CH Group	$C-C$ (iso-C) Group	$C-C(O)$ (alkyl carboxylic acid) Group	$C=O$ (alkyl carboxylic acid) Group	$C-O$ ($(O)C-O$) Group	OH Group	NH_2 Group	$C-N$ (1° amine)	$C-O$ (alkyl alcohol) Group	Calculated Total Bond Energy (eV)	Experimental Total Bond Energy (eV)	Relative Error
Energies $E_D(Group)$ of Functional Groups (eV)	7.83016	3.32601	4.29921	4.43110	7.80660	4.41925	4.41035	7.41010	3.98101	4.34572			
Composition	1	1	1	1	1	1	2	1	1	1	56.66986	58.339[a]	0.02861

Table 15.400. The total bond energy of tryptophan ($C_{11}H_{12}N_2O_2$) calculated using the functional group composition and the energies given *supra*. compared to the experimental values [3].

Formula	CH_2 Group	CH Group	$C-C$ (iso-C) Group	$C-C(O)$ (alkyl carboxylic acid) Group	$C=O$ (alkyl carboxylic acid) Group	$C-O$ ($(O)C-O$) Group	OH Group	NH_2 Group	$C-N$ (1° amine)	$C^{3e}=C$ (CC aromatic bond) Group	CH (CH aromatic) Group	$C-C$ (C_b-C_d indole) Group	$C=C$ ($C_d=C_e$ indole) Group	CH (CH indole) Group	$C-N-C$ (indole) Group	NH (indole) Group	$C-C$ (C alkyl to aryl toluene) Group	Calculated Total Bond Energy (eV)	Experimental Total Bond Energy (eV)	Relative Error
Energies $E_D(Group)$ of Functional Groups (eV)	7.83016	3.32601	4.29921	4.43110	7.80660	4.41925	4.41035	7.41010	3.98101	5.63881	3.90454	3.47253	6.79303			3.63685	3.63685			
Composition	1	1	2	1	1	1	2	1	1	6	4	1	1	1	1	1	1	126.74291	128.084[a]	0.01047

[a] Crystal

PHENYLALANINE

Figure 15.82. (A) Color scale, charge-density of phenylalanine showing the orbitals of the atoms at their radii, the ellipsoidal surface of each H or H_2-type ellipsoidal MO that transitions to the corresponding outer shell of the atom(s) participating in each bond, and the hydrogen nuclei. (B) Chemical structure of phenylalanine.

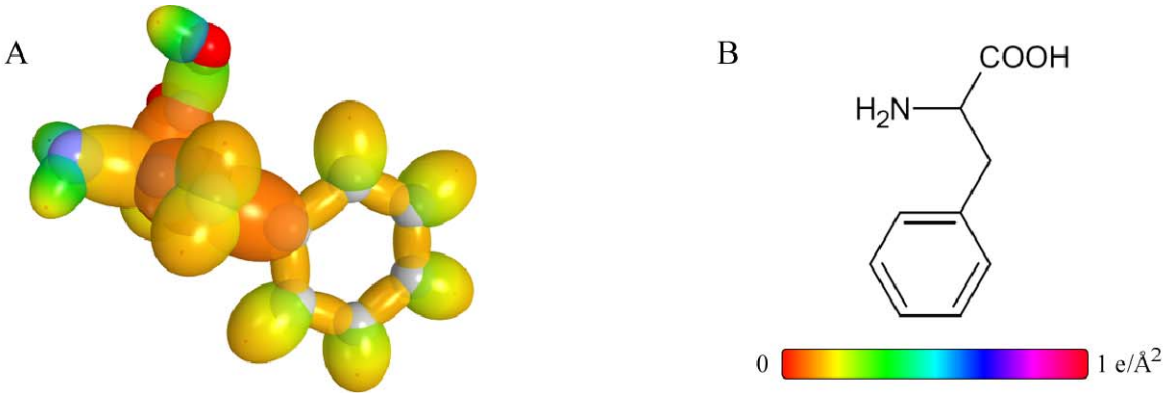

PROLINE

Figure 15.83. (A) Color scale, charge-density of proline showing the orbitals of the atoms at their radii, the ellipsoidal surface of each H or H_2-type ellipsoidal MO that transitions to the corresponding outer shell of the atom(s) participating in each bond, and the hydrogen nuclei. (B) Chemical structure of proline.

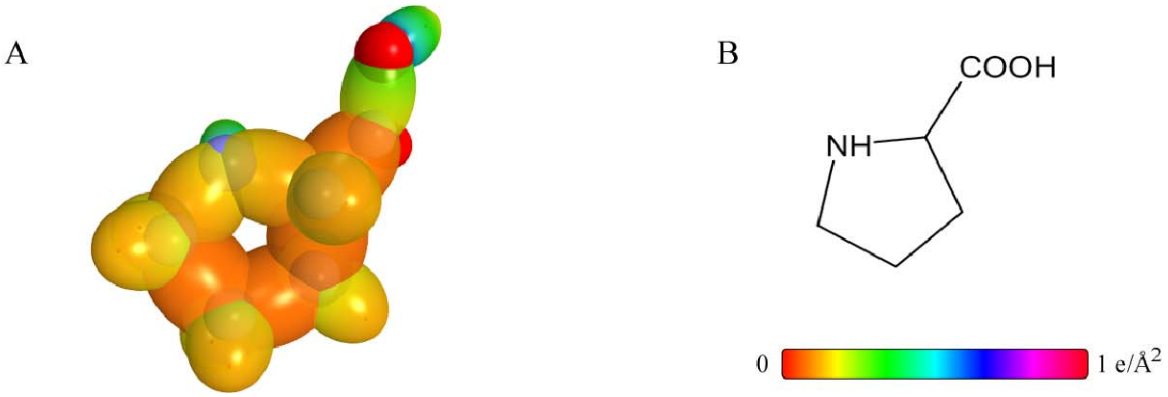

METHIONINE

Figure 15.84. (A) Color scale, charge-density of methionine showing the orbitals of the atoms at their radii, the ellipsoidal surface of each H or H_2-type ellipsoidal MO that transitions to the corresponding outer shell of the atom(s) participating in each bond, and the hydrogen nuclei. (B) Chemical structure of methionine.

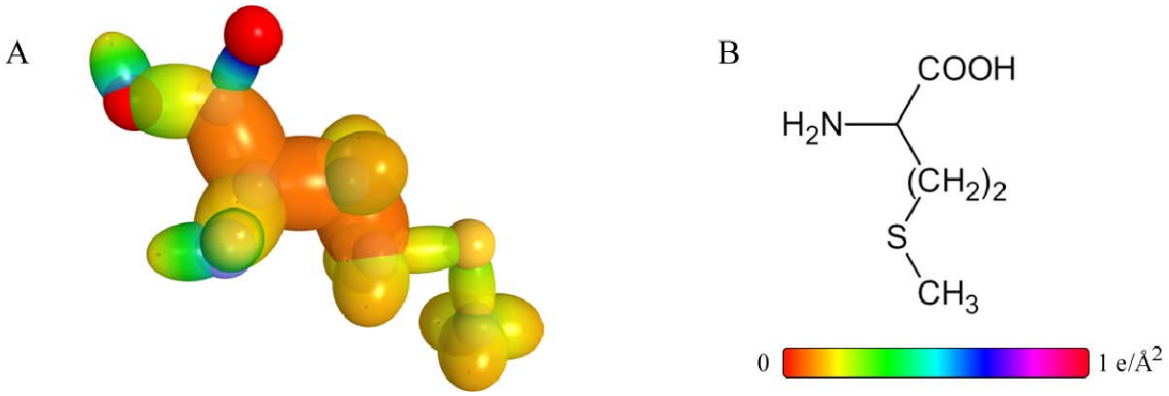

LEUCINE

Figure 15.85. (A) Color scale, charge-density of leucine showing the orbitals of the atoms at their radii, the ellipsoidal surface of each H or H_2-type ellipsoidal MO that transitions to the corresponding outer shell of the atom(s) participating in each bond, and the hydrogen nuclei. (B) Chemical structure of leucine.

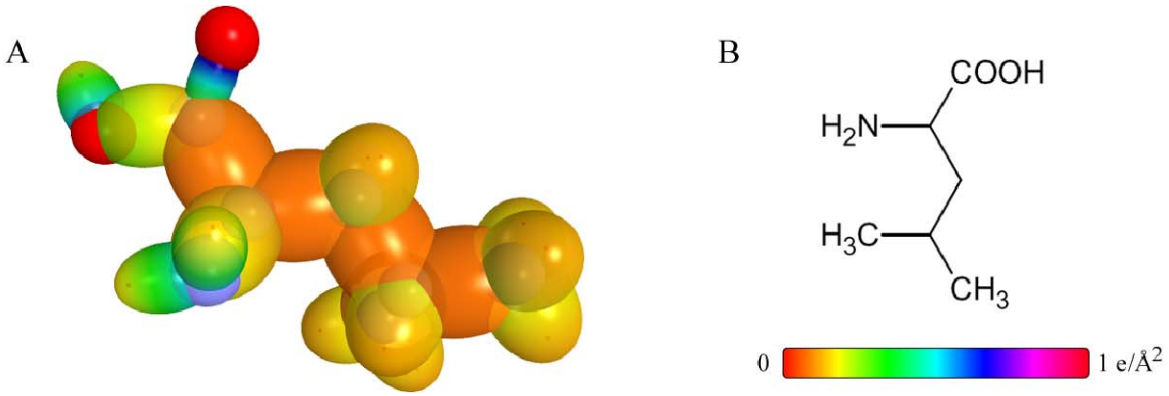

Table 15.401. The total bond energy of phenylalanine ($C_9H_{11}NO_2$) calculated using the functional group composition and the energies given *supra*. compared to the experimental values [3].

Formula	CH_2 Group	CH Group	$C-C$ (iso-C) Group	$C-C(O)$ (alkyl carboxylic acid) Group	$C=O$ (alkyl carboxylic acid) Group	$C-O$ ($(O)C$-O) Group	OH Group	NH_2 Group	$C-N$ (1° amine)	$C^{3e}=C$ (CC aromatic bond) Group	CH (CH aromatic) Group	$C-C$ (C alkyl to aryl toluene) Group	Calculated Total Bond Energy (eV)	Experimental Total Bond Energy (eV)	Relative Error
Energies $E_{D(Group)}$ of Functional Groups (eV)	7.83016	3.32601	4.29921	4.43110	7.80660	4.41925	4.41035	7.41010	3.98101	5.63881	3.90454	3.63685			
Composition	1	1	1	1	1	1	2	1	1	6	5	1	104.90618	105.009	0.00098

Table 15.402. The total bond energy of proline ($C_5H_9NO_2$) calculated using the functional group composition and the energies given *supra*. compared to the experimental values [3].

Formula	CH_2 Group	CH Group	$C-C$ (n-C) Group	$C-C$ (iso-C) Group	$C-C(O)$ (alkyl carboxylic acid) Group	$C=O$ (alkyl carboxylic acid) Group	$C-O$ ($(O)C$-O) Group	OH Group	NH (2° amine)	$C-N$ (2° amine)	Calculated Total Bond Energy (eV)	Experimental Total Bond Energy (eV)	Relative Error
Energies $E_{D(Group)}$ of Functional Groups (eV)	7.83016	3.32601	4.32754	4.29921	4.43110	7.80660	4.41925	4.41035	3.50582	3.71218			
Composition	3	1	2	1	1	1	1	1	1	2	71.76826	71.332	-0.00611

Table 15.403. The total bond energy of methionine ($C_5H_{11}NO_2S$) calculated using the functional group composition and the energies given *supra*. compared to the experimental values [3].

Formula	CH_3 Group	CH_2 Group	CH Group	$C-C$ (n-C) Group	$C-C$ (iso-C) Group	$C-C(O)$ (alkyl carboxylic acid) Group	$C=O$ (alkyl carboxylic acid) Group	$C-O$ ($(O)C$-O) Group	OH Group	NH_2 Group	$C-N$ (1° amine)	$C-S$ (alkyl sulfide)	Calculated Total Bond Energy (eV)	Experimental Total Bond Energy (eV)	Relative Error
Energies $E_{D(Group)}$ of Functional Groups (eV)	12.49186	7.83016	3.32601	4.32754	4.29921	4.43110	7.80660	4.41925	4.41035	7.41010	3.98101	3.33648			
Composition	1	2	1	1	1	1	1	1	1	1	1	2	79.23631	79.214	-0.00028

Table 15.404. The total bond energy of leucine ($C_6H_{13}NO_2$) calculated using the functional group composition and the energies given *supra*. compared to the experimental values [3].

Formula	CH_3 Group	CH_2 Group	CH Group	$C-C$ (iso-C) Group	$C-C(O)$ (alkyl carboxylic acid) Group	$C=O$ (alkyl carboxylic acid) Group	$C-O$ ($(O)C$-O) Group	OH Group	NH_2 Group	$C-N$ (1° amine)	Calculated Total Bond Energy (eV)	Experimental Total Bond Energy (eV)	Relative Error
Energies $E_{D(Group)}$ of Functional Groups (eV)	12.49186	7.83016	3.32601	4.29921	4.43110	7.80660	4.41925	4.41035	7.41010	3.98101			
Composition	2	1	2	4	1	1	1	1	1	1	89.12115	89.047	-0.00083

ISOLEUCINE

Figure 15.86. (A) Color scale, charge-density of isoleucine showing the orbitals of the atoms at their radii, the ellipsoidal surface of each H or H_2-type ellipsoidal MO that transitions to the corresponding outer shell of the atom(s) participating in each bond, and the hydrogen nuclei. (B) Chemical structure of isoleucine.

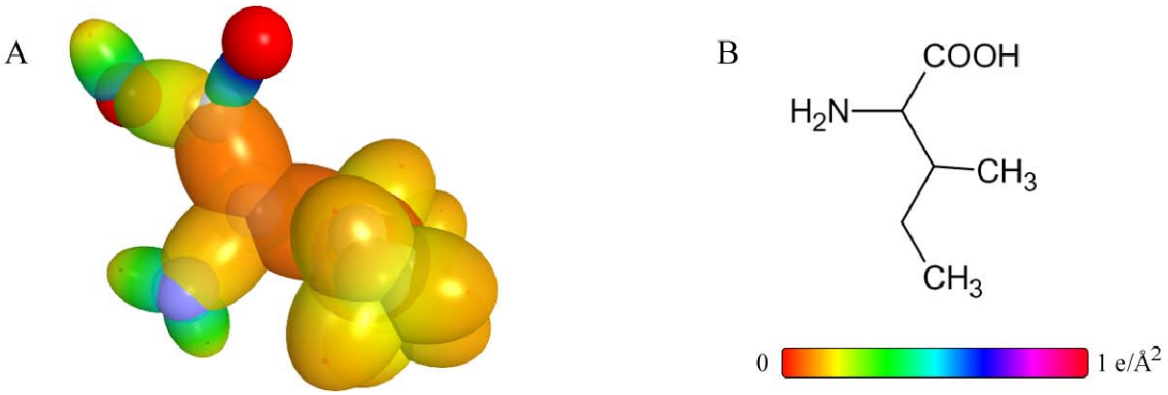

VALINE

Figure 15.87. (A) Color scale, charge-density of valine showing the orbitals of the atoms at their radii, the ellipsoidal surface of each H or H_2-type ellipsoidal MO that transitions to the corresponding outer shell of the atom(s) participating in each bond, and the hydrogen nuclei. (B) Chemical structure of valine.

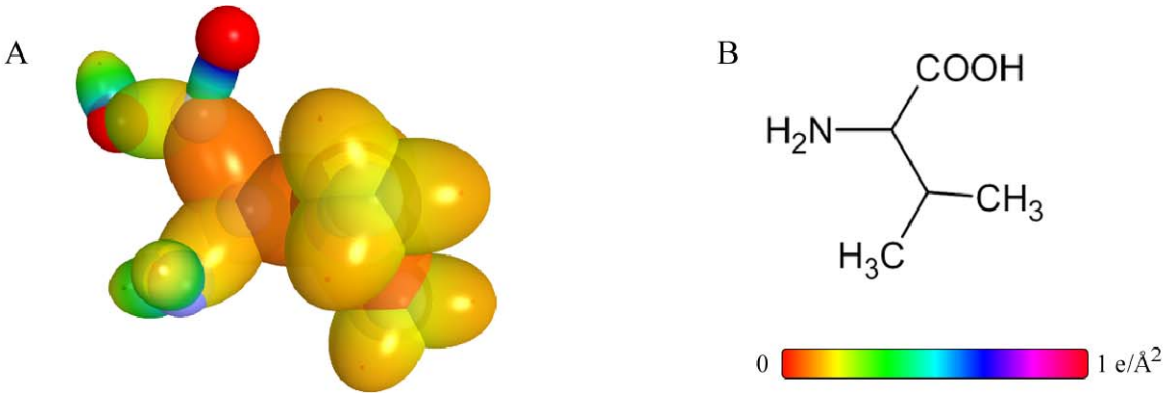

ALANINE

Figure 15.88. (A) Color scale, charge-density of alanine showing the orbitals of the atoms at their radii, the ellipsoidal surface of each H or H_2-type ellipsoidal MO that transitions to the corresponding outer shell of the atom(s) participating in each bond, and the hydrogen nuclei. (B) Chemical structure of alanine.

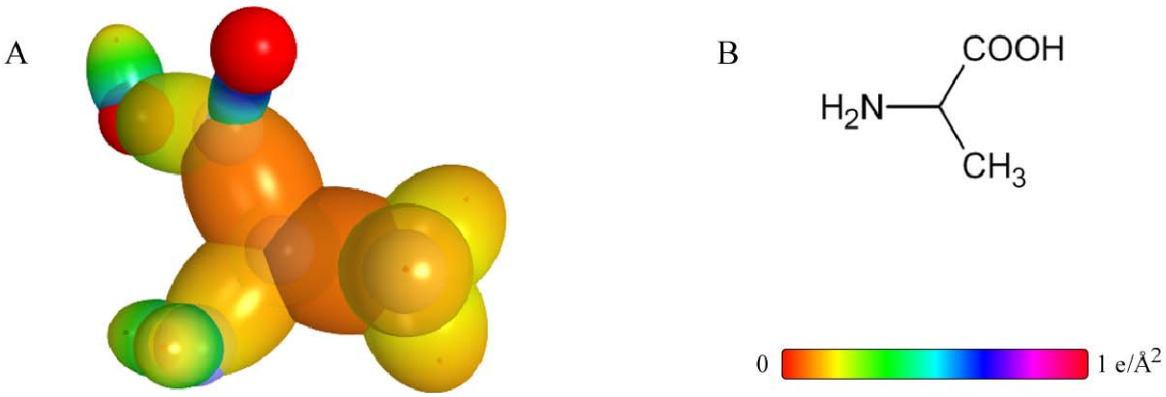

GLYCINE

Figure 15.89. (A) Color scale, charge-density of glycine showing the orbitals of the atoms at their radii, the ellipsoidal surface of each H or H_2-type ellipsoidal MO that transitions to the corresponding outer shell of the atom(s) participating in each bond, and the hydrogen nuclei. (B) Chemical structure of glycine.

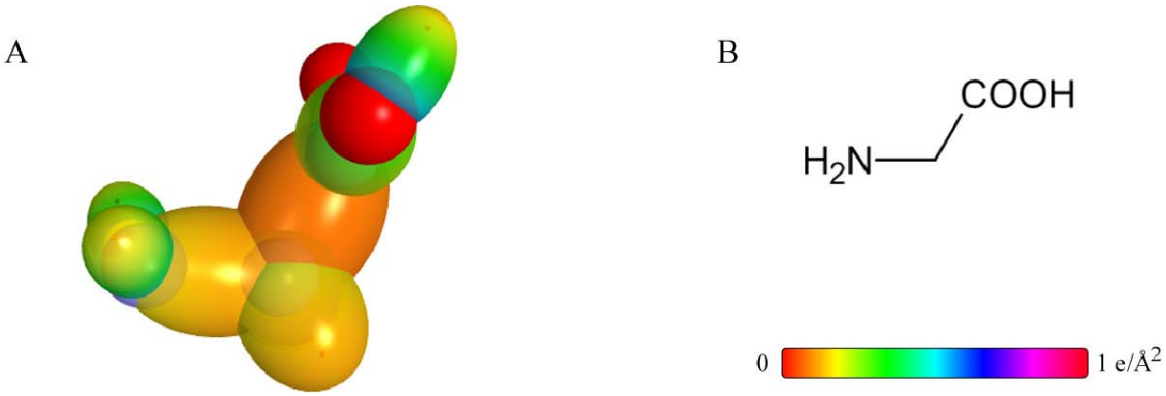

Table 15.405. The total bond energy of isoleucine ($C_6H_{13}NO_2$) calculated using the functional group composition and the energies given *supra*. compared to the experimental values [3].

Formula	CH_3 Group	CH_2 Group	CH Group	$C-C$ (n-C) Group	$C-C$ (iso-C) Group	$C-C(O)$ (alkyl carboxylic acid) Group	$C-C$ (iso to iso-C) Group	$C=O$ (alkyl carboxylic acid) Group	$C-O$ ($(O)C$-O) Group	OH Group	NH_2 Group	$C-N$ (1° amine)	Calculated Total Bond Energy (eV)	Experimental Total Bond Energy (eV)	Relative Error
Energies $E_D(Group)$ of Functional Groups (eV)	12.49186	7.83016	3.32601	4.32754	4.29921	4.43110	4.17951	7.80660	4.41925	4.41035	7.41010	3.98101			
Composition	2	1	2	1	2	1	1	1	1	1	1	1	89.02978	90.612	0.01746

Table 15.406. The total bond energy of valine ($C_5H_{11}NO_2$) calculated using the functional group composition and the energies given *supra*. compared to the experimental values [3].

Formula	CH_3 Group	CH Group	$C-C$ (iso-C) Group	$C-C$ (iso to iso-C) Group	$C-C(O)$ (alkyl carboxylic acid) Group	$C=O$ (alkyl carboxylic acid) Group	$C-O$ ($(O)C$-O) Group	OH Group	NH_2 Group	$C-N$ (1° amine)	Calculated Total Bond Energy (eV)	Experimental Total Bond Energy (eV)	Relative Error
Energies $E_D(Group)$ of Functional Groups (eV)	12.49186	3.32601	4.29921	4.17951	4.43110	7.80660	4.41925	4.41035	7.41010	3.98101			
Composition	2	2	2	1	1	1	1	1	1	1	76.87208	76.772	-0.00130

Table 15.407. The total bond energy of alanine ($C_3H_7NO_2$) calculated using the functional group composition and the energies given *supra*. compared to the experimental values [3].

Formula	CH_3 Group	CH Group	$C-C$ (iso-C) Group	$C-C(O)$ (alkyl carboxylic acid) Group	$C=O$ (alkyl carboxylic acid) Group	$C-O$ ($(O)C$-O) Group	OH Group	NH_2 Group	$C-N$ (1° amine)	Calculated Total Bond Energy (eV)	Experimental Total Bond Energy (eV)	Relative Error
Energies $E_D(Group)$ of Functional Groups (eV)	12.49186	3.32601	4.2992 1	4.43110	7.80660	4.41925	4.41035	7.41010	3.98101			
Composition	1	1	1	1	1	1	1	1	1	52.57549	52.991	0.00785

Table 15.408. The total bond energy of glycine ($C_2H_5NO_2$) calculated using the functional group composition and the energies given *supra*. compared to the experimental values [3].

Formula	CH_2 Group	$C-C(O)$ (alkyl carboxylic acid) Group	$C=O$ (alkyl carboxylic acid) Group	$C-O$ ($(O)C$-O) Group	OH Group	NH_2 Group	$C-N$ (1° amine)	Calculated Total Bond Energy (eV)	Experimental Total Bond Energy (eV)	Relative Error
Energies $E_D(Group)$ of Functional Groups (eV)	7.83016	4.43110	7.80660	4.41925	4.41035	7.41010	3.98101			
Composition	1	1	1	1	1	1	1	40.28857	40.280	-0.00021

POLYPEPTIDES $(-\left[HN-CH(R)-C(O)\right]_n-)$

The amino acids can be polymerized by reaction of the OH group from the carboxylic acid moiety of one amino acid with H from the alpha-carbon NH_2 of another amino acid to form H_2O and an amide bond as part of a polyamide chain of a polypeptide or protein. Each amide bond that forms by the condensation of two amino acids is called a peptide bond. It comprises a $C=O$ functional group, and the single bond of carbon to the carbonyl carbon atom, $C-C(O)$, is also a functional group. The peptide bond further comprises a $C-NH\left(R\right)$ moiety that comprises NH and $C-N$ functional groups where R is the characteristic side chain of each amino acid that is unchanged in terms of its functional group composition upon the formation of the peptide bond. From the N-Alkyl and N,N-Dialkyl-Amides section, the functional group composition and the corresponding energy $E_D\,(Group)$ of each group of the peptide bond is given in Table 15.409. The color scale, charge-density of the exemplary polypeptide, phenylalanine-leucine-glutamine-asparic acid (phe-leu-gln-asp) comprising the atoms with the outer shell bridged by one or more H_2-type ellipsoidal MOs or joined with one or more hydrogen MOs is shown in Figure 15.90. The color scale, opaque view of the charge-density of the exemplary protein bovine pancreatic trypsin inhibitor (BPTI) is shown in Figure 15.91.

Figure 15.90. Color scale, charge-density of the polypeptide phenylalanine-leucine-glutamine-aspartic acid (phe-leu-gln-asp) showing the orbitals of the atoms at their radii and the ellipsoidal surface of each H or H_2-type ellipsoidal MO that transitions to the corresponding outer shell of the atom(s) participating in each bond.

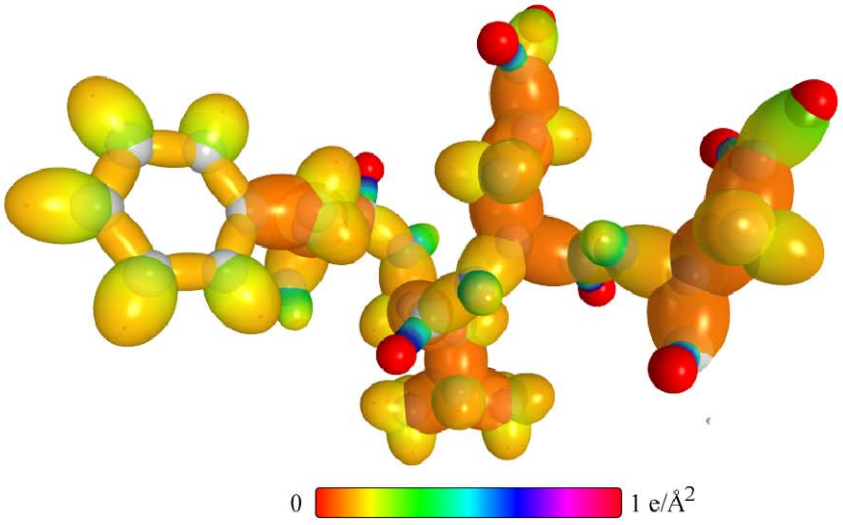

Figure 15.91. Color scale, opaque view of the charge-density of bovine pancreatic trypsin inhibitor (BPTI) protein created and modeled using Millsian 2.0. BPTI has been used as a medication administered by injection to reduce bleeding during complex surgery, such as heart and liver surgery. Its main effect is the inhibition of fibrinolysis, the process that leads to the breakdown of blood clots. The aim in its use is to decrease the need for blood transfusions during surgery, as well as end-organ damage due to hypotension (low blood pressure) as a result of marked blood loss. However, this drug was temporarily withdrawn worldwide in 2007 after studies suggested that its use increased the risk of complications or death. This protein is usually used as the benchmark for bimolecular modeling method and with accurate knowledge of its structure, it is possible to engineer it to avoid its prior side effects.

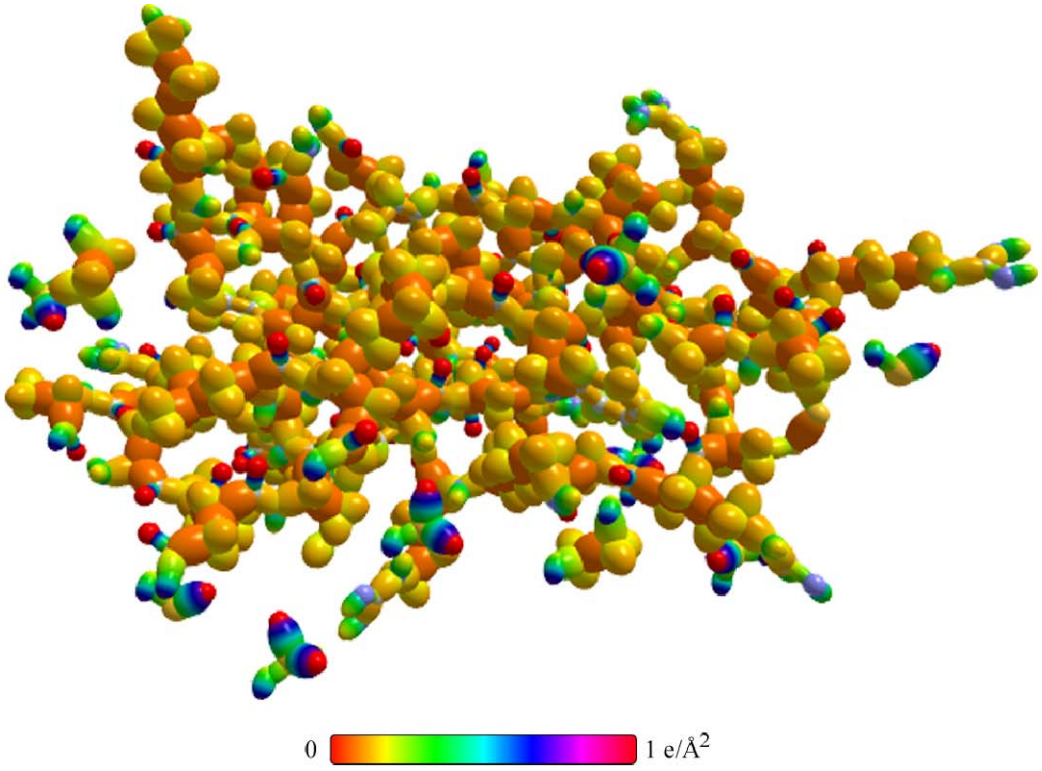

Table 15.409. The functional group composition and the energy $E_D(Group)$ of each group of the peptide bond.

Formula	$C-C(O)$ (alkyl amide) Group	$C-N$ ($(O)C$-N alkyl amide) Group	$C-N$ (N alkyl amide) Group	NH (N alkyl amide) Group
Energies $E_D(Group)$ of Functional Groups (eV)	4.35263	4.12212	3.40044	3.49788
Composition	1	1	1	1

SUMMARY TABLES OF ORGANIC MOLECULES

The bond energies, calculated using closed-form equations having integers and fundamental constants only for classes of molecules whose designation is based on the main functional group, are given in the following tables with the experimental values.

Table 15.410.1. Summary results of n-alkanes.

Formula	Name	Calculated Total Bond Energy (eV)	Experimental Total Bond Energy (eV)	Relative Error
C_3H_8	propane	41.46896	41.434	-0.00085
C_4H_{10}	butane	53.62666	53.61	-0.00036
C_5H_{12}	pentane	65.78436	65.77	-0.00017
C_6H_{14}	hexane	77.94206	77.93	-0.00019
C_7H_{16}	heptane	90.09976	90.09	-0.00013
C_8H_{18}	octane	102.25746	102.25	-0.00006
C_9H_{20}	nonane	114.41516	114.40	-0.00012
$C_{10}H_{22}$	decane	126.57286	126.57	-0.00003
$C_{11}H_{24}$	undecane	138.73056	138.736	0.00004
$C_{12}H_{26}$	dodecane	150.88826	150.88	-0.00008
$C_{18}H_{38}$	octadecane	223.83446	223.85	0.00008

Table 15.410.2. Summary results of branched alkanes.

Formula	Name	Calculated Total Bond Energy (eV)	Experimental Total Bond Energy (eV)	Relative Error
C_4H_{10}	isobutane	53.69922	53.695	-0.00007
C_5H_{12}	isopentane	65.85692	65.843	-0.00021
C_5H_{12}	neopentane	65.86336	65.992	0.00195
C_6H_{14}	2-methylpentane	78.01462	78.007	-0.00010
C_6H_{14}	3-methylpentane	78.01462	77.979	-0.00046
C_6H_{14}	2,2-dimethylbutane	78.02106	78.124	0.00132
C_6H_{14}	2,3-dimethylbutane	77.99581	78.043	0.00061
C_7H_{16}	2-methylhexane	90.17232	90.160	-0.00014
C_7H_{16}	3-methylhexane	90.17232	90.127	-0.00051
C_7H_{16}	3-ethylpentane	90.17232	90.108	-0.00072
C_7H_{16}	2,2-dimethylpentane	90.17876	90.276	0.00107
C_7H_{16}	2,2,3-trimethylbutane	90.22301	90.262	0.00044
C_7H_{16}	2,4-dimethylpentane	90.24488	90.233	-0.00013
C_7H_{16}	3,3-dimethylpentane	90.17876	90.227	0.00054
C_8H_{18}	2-methylheptane	102.33002	102.322	-0.00008
C_8H_{18}	3-methylheptane	102.33002	102.293	-0.00036
C_8H_{18}	4-methylheptane	102.33002	102.286	-0.00043
C_8H_{18}	3-ethylhexane	102.33002	102.274	-0.00055
C_8H_{18}	2,2-dimethylhexane	102.33646	102.417	0.00079
C_8H_{18}	2,3-dimethylhexane	102.31121	102.306	-0.00005
C_8H_{18}	2,4-dimethylhexane	102.40258	102.362	-0.00040
C_8H_{18}	2,5-dimethylhexane	102.40258	102.396	-0.00006
C_8H_{18}	3,3-dimethylhexane	102.33646	102.369	0.00032
C_8H_{18}	3,4-dimethylhexane	102.31121	102.296	-0.00015
C_8H_{18}	3-ethyl-2-methylpentane	102.31121	102.277	-0.00033
C_8H_{18}	3-ethyl-3-methylpentane	102.33646	102.317	-0.00019
C_8H_{18}	2,2,3-trimethylpentane	102.38071	102.370	-0.00010
C_8H_{18}	2,2,4-trimethylpentane	102.40902	102.412	0.00003
C_8H_{18}	2,3,3-trimethylpentane	102.38071	102.332	-0.00048
C_8H_{18}	2,3,4-trimethylpentane	102.29240	102.342	0.00049
C_8H_{18}	2,2,3,3-tetramethylbutane	102.41632	102.433	0.00016
C_9H_{20}	2,3,5-trimethylhexane	114.54147	114.551	0.00008
C_9H_{20}	3,3-diethylpentane	114.49416	114.455	-0.00034
C_9H_{20}	2,2,3,3-tetramethylpentane	114.57402	114.494	-0.00070
C_9H_{20}	2,2,3,4-tetramethylpentane	114.51960	114.492	-0.00024
C_9H_{20}	2,2,4,4-tetramethylpentane	114.57316	114.541	-0.00028

Formula	Name	Calculated Total Bond Energy (eV)	Experimental Total Bond Energy (eV)	Relative Error
C_9H_{20}	2,3,3,4-tetramethylpentane	114.58266	114.484	-0.00086
$C_{10}H_{22}$	2-methylnonane	126.64542	126.680	0.00027
$C_{10}H_{22}$	5-methylnonane	126.64542	126.663	0.00014

Table 15.410.3. Summary results of alkenes.

Formula	Name	Calculated Total Bond Energy (eV)	Experimental Total Bond Energy (eV)	Relative Error
C_3H_6	propene	35.56033	35.63207	0.00201
C_4H_8	1-butene	47.71803	47.78477	0.00140
C_4H_8	trans-2-butene	47.93116	47.90395	-0.00057
C_4H_8	isobutene	47.90314	47.96096	0.00121
C_5H_{10}	1-pentene	59.87573	59.95094	0.00125
C_5H_{10}	trans-2-pentene	60.08886	60.06287	-0.00043
C_5H_{10}	2-methyl-1-butene	60.06084	60.09707	0.00060
C_5H_{10}	2-methyl-2-butene	60.21433	60.16444	-0.00083
C_5H_{10}	3-methyl-1-butene	59.97662	60.01727	0.00068
C_6H_{12}	1-hexene	72.03343	72.12954	0.00133
C_6H_{12}	trans-2-hexene	72.24656	72.23733	-0.00013
C_6H_{12}	trans-3-hexene	72.24656	72.24251	-0.00006
C_6H_{12}	2-methyl-1-pentene	72.21854	72.29433	0.00105
C_6H_{12}	2-methyl-2-pentene	72.37203	72.37206	0.00000
C_6H_{12}	3-methyl-1-pentene	72.13432	72.19173	0.00080
C_6H_{12}	4-methyl-1-pentene	72.10599	72.21038	0.00145
C_6H_{12}	3-methyl-trans-2-pentene	72.37203	72.33268	-0.00054
C_6H_{12}	4-methyl-trans-2-pentene	72.34745	72.31610	-0.00043
C_6H_{12}	2-ethyl-1-butene	72.21854	72.25909	0.00056
C_6H_{12}	2,3-dimethyl-1-butene	72.31943	72.32543	0.00008
C_6H_{12}	3,3-dimethyl-1-butene	72.31796	72.30366	-0.00020
C_6H_{12}	2,3-dimethyl-2-butene	72.49750	72.38450	-0.00156
C_7H_{14}	1-heptene	84.19113	84.27084	0.00095
C_7H_{14}	5-methyl-1-hexene	84.26369	84.30608	0.00050
C_7H_{14}	trans-3-methyl-3-hexene	84.52973	84.42112	-0.00129
C_7H_{14}	2,4-dimethyl-1-pentene	84.44880	84.49367	0.00053
C_7H_{14}	4,4-dimethyl-1-pentene	84.27012	84.47087	0.00238
C_7H_{14}	2,4-dimethyl-2-pentene	84.63062	84.54445	-0.00102
C_7H_{14}	trans-4,4-dimethyl-2-pentene	84.54076	84.54549	0.00006
C_7H_{14}	2-ethyl-3-methyl-1-butene	84.47713	84.44910	-0.00033
C_7H_{14}	2,3,3-trimethyl-1-butene	84.51274	84.51129	-0.00002
C_8H_{16}	1-octene	96.34883	96.41421	0.00068
C_8H_{16}	trans-2,2-dimethyl-3-hexene	96.69846	96.68782	-0.00011
C_8H_{16}	3-ethyl-2-methyl-1-pentene	96.63483	96.61113	-0.00025
C_8H_{16}	2,4,4-trimethyl-1-pentene	96.61293	96.71684	0.00107
C_8H_{16}	2,4,4-trimethyl-2-pentene	96.67590	96.65880	-0.00018
$C_{10}H_{20}$	1-decene	120.66423	120.74240	0.00065
$C_{12}H_{24}$	1-dodecene	144.97963	145.07163	0.00063
$C_{16}H_{32}$	1-hexadecene	193.61043	193.71766	0.00055

Table 15.410.4. Summary results of alkynes.

Formula	Name	Calculated Total Bond Energy (eV)	Experimental Total Bond Energy (eV)	Relative Error
C_3H_4	propyne	29.42932	29.40432	-0.00085
C_4H_6	1-butyne	41.58702	41.55495	-0.00077
C_4H_6	2-butyne	41.72765	41.75705	0.00070
C_9H_{16}	1-nonyne	102.37552	102.35367	-0.00021

Table 15.410.5. Summary results of alkyl fluorides.

Formula	Name	Calculated Total Bond Energy (eV)	Experimental Total Bond Energy (eV)	Relative Error
CF_4	tetrafluoromethane	21.07992	21.016	-0.00303
CHF_3	trifluoromethane	19.28398	19.362	0.00405
CH_2F_2	difluoromethane	18.22209	18.280	0.00314
C_3H_7F	1-fluoropropane	41.86745	41.885	0.00041
C_3H_7F	2-fluoropropane	41.96834	41.963	-0.00012

Table 15.410.6. Summary results of alkyl chlorides.

Formula	Name	Calculated Total Bond Energy (eV)	Experimental Total Bond Energy (eV)	Relative Error
CCl_4	tetrachloromethane	13.43181	13.448	0.00123
$CHCl_3$	trichloromethane	14.49146	14.523	0.00217
CH_2Cl_2	dichloromethane	15.37248	15.450	0.00499
CH_3Cl	chloromethane	16.26302	16.312	0.00299
C_2H_5Cl	chloroethane	28.61064	28.571	-0.00138
C_3H_7Cl	1-chloropropane	40.76834	40.723	-0.00112
C_3H_7Cl	2-chloropropane	40.86923	40.858	-0.00028
C_4H_9Cl	1-chlorobutane	52.92604	52.903	-0.00044
C_4H_9Cl	2-chlorobutane	53.02693	52.972	-0.00104
C_4H_9Cl	1-chloro-2-methylpropane	52.99860	52.953	-0.00085
C_4H_9Cl	2-chloro-2-methylpropane	53.21057	53.191	-0.00037
$C_5H_{11}Cl$	1-chloropentane	65.08374	65.061	-0.00034
$C_5H_{11}Cl$	1-chloro-3-methylbutane	65.15630	65.111	-0.00069
$C_5H_{11}Cl$	2-chloro-2-methylbutane	65.36827	65.344	-0.00037
$C_5H_{11}Cl$	2-chloro-3-methylbutane	65.16582	65.167	0.00002
$C_6H_{13}Cl$	2-chlorohexane	77.34233	77.313	-0.00038
$C_8H_{17}Cl$	1-chlorooctane	101.55684	101.564	0.00007
$C_{12}H_{25}Cl$	1-chlorododecane	150.18764	150.202	0.00009
$C_{18}H_{37}Cl$	1-chlorooctadecane	223.13384	223.175	0.00018

Table 15.410.7. Summary results of alkyl bromides.

Formula	Name	Calculated Total Bond Energy (eV)	Experimental Total Bond Energy (eV)	Relative Error
CBr_4	tetrabromomethane	11.25929	11.196	-0.00566
$CHBr_3$	tribromomethane	12.87698	12.919	0.00323
CH_3Br	bromomethane	15.67551	15.732	0.00360
C_2H_5Br	bromoethane	28.03939	27.953	-0.00308
C_3H_7Br	1-bromopropane	40.19709	40.160	-0.00093
C_3H_7Br	2-bromopropane	40.29798	40.288	-0.00024
$C_5H_{10}Br_2$	2,3-dibromo-2-methylbutane	63.53958	63.477	-0.00098
$C_6H_{13}Br$	1-bromohexane	76.67019	76.634	-0.00047
$C_7H_{15}Br$	1-bromoheptane	88.82789	88.783	-0.00051
$C_8H_{17}Br$	1-bromooctane	100.98559	100.952	-0.00033
$C_{12}H_{25}Br$	1-bromododecane	149.61639	149.573	-0.00029
$C_{16}H_{33}Br$	1-bromohexadecane	198.24719	198.192	-0.00028

Table 15.410.8. Summary results of alkyl iodides.

Formula	Name	Calculated Total Bond Energy (eV)	Experimental Total Bond Energy (eV)	Relative Error
CHI_3	triiodomethane	10.35888	10.405	0.00444
CH_2I_2	diiodomethane	12.94614	12.921	-0.00195
CH_3I	iodomethane	15.20294	15.163	-0.00263
C_2H_5I	iodoethane	27.36064	27.343	-0.00066
C_3H_7I	1-iodopropane	39.51834	39.516	-0.00006
C_3H_7I	2-iodopropane	39.61923	39.623	0.00009
C_4H_9I	2-iodo-2-methylpropane	51.96057	51.899	-0.00119

Table 15.410.9. Summary results of alkene halides.

Formula	Name	Calculated Total Bond Energy (eV)	Experimental Total Bond Energy (eV)	Relative Error
C_2H_3Cl	chloroethene	22.46700	22.505	0.00170
C_3H_5Cl	2-chloropropene	35.02984	35.05482	0.00071

Table 15.410.10. Summary results of alcohols.

Formula	Name	Calculated Total Bond Energy (eV)	Experimental Total Bond Energy (eV)	Relative Error
CH_4O	methanol	21.11038	21.131	0.00097
C_2H_6O	ethanol	33.40563	33.428	0.00066
C_3H_8O	1-propanol	45.56333	45.584	0.00046
C_3H_8O	2-propanol	45.72088	45.766	0.00098
$C_4H_{10}O$	1-butanol	57.72103	57.736	0.00026
$C_4H_{10}O$	2-butanol	57.87858	57.922	0.00074
$C_4H_{10}O$	2-methyl-1-propananol	57.79359	57.828	0.00060
$C_4H_{10}O$	2-methyl-2-propananol	58.15359	58.126	-0.00048
$C_5H_{12}O$	1-pentanol	69.87873	69.887	0.00011
$C_5H_{12}O$	2-pentanol	70.03628	70.057	0.00029
$C_5H_{12}O$	3-pentanol	70.03628	70.097	0.00087
$C_5H_{12}O$	2-methyl-1-butananol	69.95129	69.957	0.00008
$C_5H_{12}O$	3-methyl-1-butananol	69.95129	69.950	-0.00002
$C_5H_{12}O$	2-methyl-2-butananol	70.31129	70.246	-0.00092
$C_5H_{12}O$	3-methyl-2-butananol	69.96081	70.083	0.00174
$C_6H_{14}O$	1-hexanol	82.03643	82.054	0.00021
$C_6H_{14}O$	2-hexanol	82.19398	82.236	0.00052
$C_7H_{16}O$	1-heptanol	94.19413	94.214	0.00021
$C_8H_{18}O$	1-octanol	106.35183	106.358	0.00006
$C_8H_{18}O$	2-ethyl-1-hexananol	106.42439	106.459	0.00032
$C_9H_{20}O$	1-nonanol	118.50953	118.521	0.00010
$C_{10}H_{22}O$	1-decanol	130.66723	130.676	0.00007
$C_{12}H_{26}O$	1-dodecanol	154.98263	154.984	0.00001
$C_{16}H_{34}O$	1-hexadecanol	203.61343	203.603	-0.00005

Table 15.410.11. Summary results of ethers.

Formula	Name	Calculated Total Bond Energy (eV)	Experimental Total Bond Energy (eV)	Relative Error
C_2H_6O	dimethyl ether	32.84496	32.902	0.00174
C_3H_8O	ethyl methyl ether	45.19710	45.183	-0.00030
$C_4H_{10}O$	diethyl ether	57.54924	57.500	-0.00086
$C_4H_{10}O$	methyl propyl ether	57.35480	57.355	0.00000
$C_4H_{10}O$	isopropyl methyl ether	57.45569	57.499	0.00075
$C_6H_{14}O$	dipropyl ether	81.86464	81.817	-0.00059
$C_6H_{14}O$	diisopropyl ether	82.06642	82.088	0.00026
$C_6H_{14}O$	t-butyl ethyl ether	82.10276	82.033	-0.00085
$C_7H_{16}O$	t-butyl isopropyl ether	94.36135	94.438	0.00081
$C_8H_{18}O$	dibutyl ether	106.18004	106.122	-0.00055
$C_8H_{18}O$	di-sec-butyl ether	106.38182	106.410	0.00027
$C_8H_{18}O$	di-t-butyl ether	106.36022	106.425	0.00061
$C_8H_{18}O$	t-butyl isobutyl ether	106.65628	106.497	-0.00218

Table 15.410.12. Summary results of 1° amines.

Formula	Name	Calculated Total Bond Energy (eV)	Experimental Total Bond Energy (eV)	Relative Error
CH_5N	methylamine	23.88297	23.857	-0.00110
C_2H_7N	ethylamine	36.04067	36.062	0.00060
C_3H_9N	propylamine	48.19837	48.243	0.00092
$C_4H_{11}N$	butylamine	60.35607	60.415	0.00098
$C_4H_{11}N$	sec-butylamine	60.45696	60.547	0.00148
$C_4H_{11}N$	t-butylamine	60.78863	60.717	-0.00118
$C_4H_{11}N$	isobutylamine	60.42863	60.486	0.00094

Table 15.410.13. Summary results of 2° amines.

Formula	Name	Calculated Total Bond Energy (eV)	Experimental Total Bond Energy (eV)	Relative Error
C_2H_7N	dimethylamine	35.76895	35.765	-0.00012
$C_4H_{11}N$	diethylamine	60.22930	60.211	-0.00030
$C_6H_{15}N$	dipropylamine	84.54470	84.558	0.00016
$C_6H_{15}N$	diisopropylamine	84.74648	84.846	0.00117
$C_8H_{19}N$	dibutylamine	108.86010	108.872	0.00011
$C_8H_{19}N$	diisobutylamine	109.00522	109.106	0.00092

Table 15.410.14. Summary results of 3° amines.

Formula	Name	Calculated Total Bond Energy (eV)	Experimental Total Bond Energy (eV)	Relative Error
C_3H_9N	trimethylamine	47.83338	47.761	-0.00152
$C_6H_{15}N$	triethylamine	84.30648	84.316	0.00012
$C_9H_{21}N$	tripropylamine	120.77958	120.864	0.00070

Table 15.410.15. Summary results of aldehydes.

Formula	Name	Calculated Total Bond Energy (eV)	Experimental Total Bond Energy (eV)	Relative Error
CH_2O	formaldehyde	15.64628	15.655	0.00056
C_2H_4O	acetaldehyde	28.18711	28.198	0.00039
C_3H_6O	propanal	40.34481	40.345	0.00000
C_4H_8O	butanal	52.50251	52.491	-0.00022
C_4H_8O	isobutanal	52.60340	52.604	0.00001
$C_5H_{10}O$	pentanal	64.66021	64.682	0.00034
$C_7H_{14}O$	heptanal	88.97561	88.942	-0.00038
$C_8H_{16}O$	octanal	101.13331	101.179	0.00045
$C_8H_{16}O$	2-ethylhexanal	101.23420	101.259	0.00025

Table 15.410.16. Summary results of ketones.

Formula	Name	Calculated Total Bond Energy (eV)	Experimental Total Bond Energy (eV)	Relative Error
C_3H_6O	acetone	40.68472	40.672	-0.00031
C_4H_8O	2-butanone	52.84242	52.84	-0.00005
$C_5H_{10}O$	2-pentanone	65.00012	64.997	-0.00005
$C_5H_{10}O$	3-pentanone	65.00012	64.988	-0.00005
$C_5H_{10}O$	3-methyl-2-butanone	65.10101	65.036	-0.00099
$C_6H_{12}O$	2-hexanone	77.15782	77.152	-0.00008
$C_6H_{12}O$	3-hexanone	77.15782	77.138	-0.00025
$C_6H_{12}O$	2-methyl-3-pentanone	77.25871	77.225	-0.00043
$C_6H_{12}O$	3,3-dimethyl-2-butanone	77.29432	77.273	-0.00028
$C_7H_{14}O$	3-heptanone	89.31552	89.287	-0.00032
$C_7H_{14}O$	4-heptanone	89.31552	89.299	-0.00018
$C_7H_{14}O$	2,2-dimethyl-3-pentanone	89.45202	89.458	0.00007

Formula	Name	Calculated Total Bond Energy (eV)	Experimental Total Bond Energy (eV)	Relative Error
$C_7H_{14}O$	2,4-dimethyl-3-pentanone	89.51730	89.434	-0.00093
$C_8H_{16}O$	2,2,4-trimethyl-3-pentanone	101.71061	101.660	-0.00049
$C_9H_{18}O$	2-nonanone	113.63092	113.632	0.00001
$C_9H_{18}O$	5-nonanone	113.63092	113.675	0.00039
$C_9H_{18}O$	2,6-dimethyl-4-heptanone	113.77604	113.807	0.00027

Table 15.410.17. Summary results of carboxylic acids.

Formula	Name	Calculated Total Bond Energy (eV)	Experimental Total Bond Energy (eV)	Relative Error
CH_2O_2	formic acid	21.01945	21.036	0.00079
$C_2H_4O_2$	acetic acid	33.55916	33.537	-0.00066
$C_3H_6O_2$	propanoic acid	45.71686	45.727	0.00022
$C_4H_8O_2$	butanoic acid	57.87456	57.883	0.00015
$C_5H_{10}O_2$	pentanoic acid	70.03226	69.995	-0.00053
$C_5H_{10}O_2$	3-methylbutanoic acid	70.10482	70.183	0.00111
$C_5H_{10}O_2$	2,2-dimethylpropanoic acid	70.31679	69.989	-0.00468
$C_6H_{12}O_2$	hexanoic acid	82.18996	82.149	-0.00050
$C_7H_{14}O_2$	heptanoic acid	94.34766	94.347	0.00000
$C_8H_{16}O_2$	octanoic acid	106.50536	106.481	-0.00022
$C_9H_{18}O_2$	nonanoic acid	118.66306	118.666	0.00003
$C_{10}H_{20}O_2$	decanoic acid	130.82076	130.795	-0.00020
$C_{12}H_{24}O_2$	dodecanoic acid	155.13616	155.176	0.00026
$C_{14}H_{28}O_2$	tetradecanoic acid	179.45156	179.605	0.00085
$C_{15}H_{30}O_2$	pentadecanoic acid	191.60926	191.606	-0.00002
$C_{16}H_{32}O_2$	hexadecanoic acid	203.76696	203.948	0.00089
$C_{18}H_{36}O_2$	stearic acid	228.08236	228.298	0.00094
$C_{20}H_{40}O_2$	eicosanoic acid	252.39776	252.514	0.00046

Table 15.410.18. Summary results of carboxylic acid esters.

Formula	Name	Calculated Total Bond Energy (eV)	Experimental Total Bond Energy (eV)	Relative Error
$C_2H_4O_2$	methyl formate	32.71076	32.762	0.00156
$C_3H_6O_2$	methyl acetate	45.24849	45.288	0.00087
$C_6H_{12}O_2$	methyl pentanoate	81.72159	81.726	0.00005
$C_7H_{14}O_2$	methyl hexanoate	93.87929	93.891	0.00012
$C_8H_{16}O_2$	methyl heptanoate	106.03699	106.079	0.00040
$C_9H_{18}O_2$	methyl octanoate	118.19469	118.217	0.00018
$C_{10}H_{20}O_2$	methyl nonanoate	130.35239	130.373	0.00016
$C_{11}H_{22}O_2$	methyl decanoate	142.51009	142.523	0.00009
$C_{12}H_{24}O_2$	methyl undecanoate	154.66779	154.677	0.00006
$C_{13}H_{26}O_2$	methyl dodecanoate	166.82549	166.842	0.00010
$C_{14}H_{28}O_2$	methyl tridecanoate	178.98319	179.000	0.00009
$C_{15}H_{30}O_2$	methyl tetradecanoate	191.14089	191.170	0.00015
$C_{16}H_{32}O_2$	methyl pentadecanoate	203.29859	203.356	0.00028
$C_4H_8O_2$	propyl formate	57.76366	57.746	-0.00030
$C_4H_8O_2$	ethyl acetate	57.63888	57.548	-0.00157
$C_5H_{10}O_2$	isopropyl acetate	69.89747	69.889	-0.00013
$C_5H_{10}O_2$	ethyl propanoate	69.79658	69.700	-0.00139
$C_6H_{12}O_2$	butyl acetate	81.95428	81.873	-0.00099
$C_6H_{12}O_2$	t-butyl acetate	82.23881	82.197	-0.00051
$C_6H_{12}O_2$	methyl 2,2-dimethylpropanoate	82.00612	81.935	-0.00087
$C_7H_{14}O_2$	ethyl pentanoate	94.11198	94.033	-0.00084
$C_7H_{14}O_2$	ethyl 3-methylbutanoate	94.18454	94.252	0.00072
$C_7H_{14}O_2$	ethyl 2,2-dimethylpropanoate	94.39651	94.345	-0.00054
$C_8H_{16}O_2$	isobutyl isobutanoate	106.44313	106.363	-0.00075
$C_8H_{16}O_2$	propyl pentanoate	106.26968	106.267	-0.00003

Formula	Name	Calculated Total Bond Energy (eV)	Experimental Total Bond Energy (eV)	Relative Error
$C_8H_{16}O_2$	isopropyl pentanoate	106.37057	106.384	0.00013
$C_9H_{18}O_2$	butyl pentanoate	118.42738	118.489	0.00052
$C_9H_{18}O_2$	sec-butyl pentanoate	118.52827	118.624	0.00081
$C_9H_{18}O_2$	isobutyl pentanoate	118.49994	118.576	0.00064

Table 15.410.19. Summary results of amides.

Formula	Name	Calculated Total Bond Energy (eV)	Experimental Total Bond Energy (eV)	Relative Error
CH_3NO	formamide	23.68712	23.697	0.00041
C_2H_5NO	acetamide	36.15222	36.103	-0.00135
C_3H_7NO	propanamide	48.30992	48.264	-0.00094
C_4H_9NO	butanamide	60.46762	60.449	-0.00030
C_4H_9NO	2-methylpropanamide	60.51509	60.455	-0.00099
$C_5H_{11}NO$	pentanamide	72.62532	72.481	-0.00200
$C_5H_{11}NO$	2,2-dimethylpropanamide	72.67890	72.718	0.00054
$C_6H_{13}NO$	hexanamide	84.78302	84.780	-0.00004
$C_8H_{17}NO$	octanamide	109.09842	109.071	-0.00025

Table 15.410.20. Summary results of N-alkyl and N,N-dialkyl amides.

Formula	Name	Calculated Total Bond Energy (eV)	Experimental Total Bond Energy (eV)	Relative Error
C_3H_7NO	N,N-dimethylformamide	47.679454	47.574	0.00221
C_4H_9NO	N,N-dimethylacetamide	60.14455	59.890	-0.00426
$C_6H_{13}NO$	N-butylacetamide	84.63649	84.590	-0.00055

Table 15.410.21. Summary results of urea.

Formula	Name	Calculated Total Bond Energy (eV)	Experimental Total Bond Energy (eV)	Relative Error
CH_4N_2O	urea	31.35919	31.393	0.00108

Table 15.410.22. Summary results of acid halide.

Formula	Name	Calculated Total Bond Energy (eV)	Experimental Total Bond Energy (eV)	Relative Error
C_2H_3ClO	acetyl chloride	28.02174	27.990	-0.00115

Table 15.410.23. Summary results of acid anhydrides.

Formula	Name	Calculated Total Bond Energy (eV)	Experimental Total Bond Energy (eV)	Relative Error
$C_4H_6O_3$	acetic anhydride	56.94096	56.948	0.00013
$C_6H_{10}O_3$	propanoic anhydride	81.25636	81.401	0.00177

Table 15.410.24. Summary results of nitriles.

Formula	Name	Calculated Total Bond Energy (eV)	Experimental Total Bond Energy (eV)	Relative Error
C_2H_3N	acetonitrile	25.72060	25.77	0.00174
C_3H_5N	propanenitrile	37.87830	37.94	0.00171
C_4H_7N	butanenitrile	50.03600	50.08	0.00082
C_4H_7N	2-methylpropanenitrile	50.13689	50.18	0.00092
C_5H_9N	pentanenitrile	62.19370	62.26	0.00111
C_5H_9N	2,2-dimethylpropanenitrile	62.47823	62.40	-0.00132
$C_7H_{13}N$	heptanenitrile	86.50910	86.59	0.00089
$C_8H_{15}N$	octanenitrile	98.66680	98.73	0.00069
$C_{10}H_{19}N$	decanenitrile	122.98220	123.05	0.00057
$C_{14}H_{27}N$	tetradecanenitrile	171.61300	171.70	0.00052

Table 15.410.25. Summary results of thiols.

Formula	Name	Calculated Total Bond Energy (eV)	Experimental Total Bond Energy (eV)	Relative Error
HS	hydrogen sulfide	3.77430	3.653	-0.03320
H_2S	dihydrogen sulfide	7.56058	7.605	0.00582
CH_4S	methanethiol	19.60264	19.575	-0.00141
C_2H_6S	ethanethiol	31.76034	31.762	0.00005
C_3H_8S	1-propanethiol	43.91804	43.933	0.00035
C_3H_8S	2-propanethiol	44.01893	44.020	0.00003
$C_4H_{10}S$	1-butanethiol	56.07574	56.089	0.00024
$C_4H_{10}S$	2-butanethiol	56.17663	56.181	0.00009
$C_4H_{10}S$	2-methyl-1-propanethiol	56.14830	56.186	0.00066
$C_4H_{10}S$	2-methyl-2-propanethiol	56.36027	56.313	-0.00084
$C_5H_{12}S$	2-methyl-1-butanethiol	68.30600	68.314	0.00012
$C_5H_{12}S$	1-pentanethiol	68.23344	68.264	0.00044
$C_5H_{12}S$	2-methyl-2-butanethiol	68.51797	68.441	-0.00113
$C_5H_{12}S$	3-methyl-2-butanethiol	68.31552	68.381	0.00095
$C_5H_{12}S$	2,2-dimethyl-1-propanethiol	68.16441	68.461	0.00433
$C_6H_{14}S$	1-hexanethiol	80.39114	80.416	0.00031
$C_6H_{14}S$	2-methyl-2-pentanethiol	80.67567	80.607	-0.00085
$C_7H_{16}S$	1-heptanethiol	92.54884	92.570	0.00023
$C_{10}H_{22}S$	1-decanethiol	129.02194	129.048	0.00020

Table 15.410.26. Summary results of sulfides.

Formula	Name	Calculated Total Bond Energy (eV)	Experimental Total Bond Energy (eV)	Relative Error
C_2H_6S	dimethyl sulfide	31.65668	31.672	0.00048
C_3H_8S	ethyl methyl sulfide	43.81438	43.848	0.00078
$C_4H_{10}S$	diethyl sulfide	55.97208	56.043	0.00126
$C_4H_{10}S$	methyl propyl sulfide	55.97208	56.029	0.00102
$C_4H_{10}S$	isopropyl methyl sulfide	56.07297	56.115	0.00075
$C_5H_{12}S$	butyl methyl sulfide	68.12978	68.185	0.00081
$C_5H_{12}S$	t-butyl methyl sulfide	68.28245	68.381	0.00144
$C_5H_{12}S$	ethyl propyl sulfide	68.12978	68.210	0.00117
$C_5H_{12}S$	ethyl isopropyl sulfide	68.23067	68.350	0.00174
$C_6H_{14}S$	diisopropyl sulfide	80.48926	80.542	0.00065
$C_6H_{14}S$	butyl ethyl sulfide	80.28748	80.395	0.00133
$C_6H_{14}S$	methyl pentyl sulfide	80.28748	80.332	0.00056
$C_8H_{18}S$	dibutyl sulfide	104.60288	104.701	0.00094
$C_8H_{18}S$	di-sec-butyl sulfide	104.80466	104.701	-0.00099
$C_8H_{18}S$	di-t-butyl sulfide	104.90822	104.920	0.00011
$C_8H_{18}S$	diisobutyl sulfide	104.74800	104.834	0.00082
$C_{10}H_{22}S$	dipentyl sulfide	128.91828	128.979	0.00047
$C_{10}H_{22}S$	diisopentyl sulfide	129.06340	129.151	0.00068

Table 15.410.27. Summary results of disulfides.

Formula	Name	Calculated Total Bond Energy (eV)	Experimental Total Bond Energy (eV)	Relative Error
$C_2H_6S_2$	dimethyl disulfide	34.48127	34.413	-0.00199
$C_4H_{10}S_2$	diethyl disulfide	58.79667	58.873	0.00129
$C_6H_{14}S_2$	dipropyl disulfide	83.11207	83.169	0.00068
$C_8H_{18}S_2$	di-t-butyl disulfide	107.99653	107.919	-0.00072

Table 15.410.28. Summary results of sulfoxides.

Formula	Name	Calculated Total Bond Energy (eV)	Experimental Total Bond Energy (eV)	Relative Error
C_2H_6SO	dimethyl sulfoxide	35.52450	35.435	-0.00253
$C_4H_{10}SO$	diethyl sulfoxide	59.83990	59.891	0.00085
$C_6H_{14}SO$	dipropyl sulfoxide	84.15530	84.294	0.00165

Table 15.410.29. Summary results of sulfones.

Formula	Name	Calculated Total Bond Energy (eV)	Experimental Total Bond Energy (eV)	Relative Error
$C_2H_6SO_2$	dimethyl sulfone	40.27588	40.316	0.00100

Table 15.410.30. Summary results of sulfites.

Formula	Name	Calculated Total Bond Energy (eV)	Experimental Total Bond Energy (eV)	Relative Error
$C_2H_6SO_3$	dimethyl sulfite	43.95058	44.042	0.00207
$C_4H_{10}SO_3$	diethyl sulfite	68.54939	68.648	0.00143
$C_8H_{18}SO_3$	dibutyl sulfite	117.18019	117.191	0.00009

Table 15.410.31. Summary results of sulfates.

Formula	Name	Calculated Total Bond Energy (eV)	Experimental Total Bond Energy (eV)	Relative Error
$C_2H_6SO_4$	dimethyl sulfate	48.70196	48.734	0.00067
$C_4H_{10}SO_4$	diethyl sulfate	73.30077	73.346	0.00061
$C_6H_{14}SO_4$	dipropyl sulfate	97.61617	97.609	-0.00008

Table 15.410.32. Summary results of nitro alkanes.

Formula	Name	Calculated Total Bond Energy (eV)	Experimental Total Bond Energy (eV)	Relative Error
CH_3NO_2	nitromethane	25.14934	25.107	-0.00168
$C_2H_5NO_2$	nitroethane	37.30704	37.292	-0.00040
$C_3H_7NO_2$	1-nitropropane	49.46474	49.451	-0.00028
$C_3H_7NO_2$	2-nitropropane	49.56563	49.602	0.00074
$C_4H_9NO_2$	1-nitrobutane	61.62244	61.601	-0.00036
$C_4H_9NO_2$	2-nitroisobutane	61.90697	61.945	0.00061
$C_5H_{11}NO_2$	1-nitropentane	73.78014	73.759	-0.00028

Table 15.410.33. Summary results of nitrite.

Formula	Name	Calculated Total Bond Energy (eV)	Experimental Total Bond Energy (eV)	Relative Error
CH_3NO_2	methyl nitrite	24.92328	24.955	0.00126

Table 15.410.34. Summary results of nitrate.

Formula	Name	Calculated Total Bond Energy (eV)	Experimental Total Bond Energy (eV)	Relative Error
CH_3NO_3	methyl nitrate	28.18536	28.117	-0.00244
$C_2H_5NO_3$	ethyl nitrate	40.34306	40.396	0.00131
$C_3H_7NO_3$	propyl nitrate	52.50076	52.550	0.00093
$C_3H_7NO_3$	isopropyl nitrate	52.60165	52.725	0.00233

Table 15.410.35. Summary results of conjugated alkenes.

Formula	Name	Calculated Total Bond Energy (eV)	Experimental Total Bond Energy (eV)	Relative Error
C_5H_8	cyclopentene	54.83565	54.86117	0.00047
C_4H_6	1,3 butadiene	42.09159	42.12705	0.00084
C_5H_8	1,3 pentadiene	54.40776	54.42484	0.00031
C_5H_8	1,4 pentadiene	54.03745	54.11806	0.00149
C_5H_6	1,3 cyclopentadiene	49.27432	49.30294	0.00058

Table 15.410.36. Summary results of aromatics and heterocyclic aromatics.

Formula	Name	Calculated Total Bond Energy (eV)	Experimental Total Bond Energy (eV)	Relative Error
C_6H_6	benzene	57.26008	57.26340	0.00006
C_6H_5Cl	fluorobenzene	57.93510	57.887	-0.00083
C_6H_5Cl	chlorobenzene	56.55263	56.581	0.00051
$C_6H_4Cl_2$	m-dichlorobenzene	55.84518	55.852	0.00012
$C_6H_3Cl_3$	1,2,3-trichlorobenzene	55.13773	55.077	-0.00111
$C_6H_3Cl_3$	1,3,5-trichlorobenzene	55.29542	55.255	-0.00073
C_6Cl_6	hexachlorobenzene	52.57130	52.477	-0.00179
C_6H_5Br	bromobenzene	56.17932	56.391[a]	0.00376
C_6H_5I	iodobenzene	55.25993	55.261	0.00001
$C_6H_5NO_2$	nitrobenzene	65.18754	65.217	0.00046
C_7H_8	toluene	69.48425	69.546	0.00088
$C_7H_6O_2$	benzoic acid	73.76938	73.762	-0.00009
$C_7H_5ClO_2$	2-chlorobenzoic acid	73.06193	73.082	0.00027
$C_7H_5ClO_2$	3-chlorobenzoic acid	73.26820	73.261	-0.00010
C_6H_7N	aniline	64.43373	64.374	-0.00093
C_7H_9N	2-methylaniline	76.62345	76.643	-0.00025
C_7H_9N	3-methylaniline	76.62345	76.661	0.00050
C_7H_9N	4-methylaniline	76.62345	76.654	0.00040
$C_6H_6N_2O_2$	2-nitroaniline	72.47476	72.424	-0.00070
$C_6H_6N_2O_2$	3-nitroaniline	72.47476	72.481	-0.00009
$C_6H_6N_2O_2$	4-nitroaniline	72.47476	72.476	-0.00002
$C_7H_7NO_2$	aniline-2-carboxylic acid	80.90857	80.941	0.00041
$C_7H_7NO_2$	aniline-3-carboxylic acid	80.90857	80.813	-0.00118
$C_7H_7NO_2$	aniline-4-carboxylic acid	80.90857	80.949	0.00050
C_6H_6O	phenol	61.75817	61.704	-0.00087
$C_6H_4N_2O_5$	2,4-dinitrophenol	77.61308	77.642	0.00037
C_6H_8O	anisole	73.39006	73.355	-0.00047
$C_{10}H_8$	naphthalene	90.74658	90.79143	0.00049
C_4H_5N	pyrrole	44.81090	44.785	-0.00057
C_4H_4O	furan	41.67782	41.692	0.00033
C_4H_4S	thiophene	40.42501	40.430	0.00013
$C_3H_4N_2$	imidazole	39.76343	39.74106	-0.00056
C_5H_5N	pyridine	51.91802	51.87927	-0.00075
$C_4H_4N_2$	pyrimidine	46.57597	46.51794	-0.00125
$C_4H_4N_2$	pyrazine	46.57597	46.51380	0.00095
C_9H_7N	quinoline	85.40453	85.48607	0.00178
C_9H_7N	isoquinoline	85.40453	85.44358	0.00046
C_8H_7N	indole	78.52215	78.514	-0.00010

[a] Liquid.

Table 15.410.37. Summary results of DNA bases.

Formula	Name	Calculated Total Bond Energy (eV)	Experimental Total Bond Energy (eV)	Relative Error
$C_5H_5N_5$	adenine	70.85416	70.79811	-0.00079
$C_5H_6N_2O_2$	thymine	69.08792	69.06438	-0.00034
$C_5H_5N_5O$	guanine	76.88212	77.41849	-0.00055
$C_4H_5N_3O$	cytosine	59.53378	60.58056	0.01728

Table 15.410.38. Summary results of alkyl phosphines.

Formula	Name	Calculated Total Bond Energy (eV)	Experimental Total Bond Energy (eV)	Relative Error
C_3H_9P	trimethylphosphine	45.80930	46.87333	0.02270
$C_6H_{15}P$	triethylphosphine	82.28240	82.24869	-0.00041
$C_{18}H_{15}P$	triphenylphosphine	168.40033	167.46591	-0.00558

Table 15.410.39. Summary results of alkyl phosphites.

Formula	Name	Calculated Total Bond Energy (eV)	Experimental Total Bond Energy (eV)	Relative Error
$C_3H_9O_3P$	trimethyl phosphite	61.06764	60.94329	-0.00204
$C_6H_{15}O_3P$	triethyl phosphite	98.12406	97.97947	-0.00148
$C_9H_{21}O_3P$	tri-isopropyl phosphite	134.89983	135.00698	0.00079

Table 15.410.40. Summary results of alkyl phosphine oxides.

Formula	Name	Calculated Total Bond Energy (eV)	Experimental Total Bond Energy (eV)	Relative Error
C_3H_9PO	trimethylphosphine oxide	53.00430	52.91192	-0.00175

Table 15.410.41. Summary results of alkyl phosphates.

Formula	Name	Calculated Total Bond Energy (eV)	Experimental Total Bond Energy (eV)	Relative Error
$C_6H_{15}O_4P$	triethyl phosphate	105.31906	104.40400	-0.00876
$C_9H_{21}O_4P$	tri-n-propyl phosphate	141.79216	140.86778	-0.00656
$C_9H_{21}O_4P$	tri-isopropyl phosphate	142.09483	141.42283	-0.00475
$C_9H_{27}O_4P$	tri-n-butyl phosphate	178.26526	178.07742	-0.00105

Table 15.410.42. Summary results of monosaccharides of DNA and RNA.

Formula	Name	Calculated Total Bond Energy (eV)	Experimental Total Bond Energy (eV)	Relative Error
$C_5H_{10}O_4$	2-deoxy-D-ribose	77.25842		
$C_5H_{10}O_5$	D-ribose	81.51034	83.498[a]	0.02381
$C_5H_{10}O_4$	alpha-2-deoxy-D-ribose	77.46684		
$C_5H_{10}O_5$	alpha-D-ribose	82.31088		

[a] Crystal

Table 15.410.43. Summary results of amino acids.

Formula	Name	Calculated Total Bond Energy (eV)	Experimental Total Bond Energy (eV)	Relative Error
$C_4H_7NO_4$	aspartic acid	68.98109	70.843[a]	0.02628
$C_5H_9NO_4$	glutamic acid	81.13879	83.167[a]	0.02438
$C_3H_7NO_4S$	cysteine	55.02457	56.571[a]	0.02733
$C_6H_{14}N_2O_2$	lysine	95.77799	98.194[a]	0.02461
$C_6H_{14}N_2O_2$	arginine	105.07007	107.420[a]	0.02188
$C_6H_9N_3O_2$	histidine	88.10232	89.599[a]	0.01671
$C_4H_8N_2O_2$	asparagine	71.57414	73.513[a]	0.02637
$C_5H_{10}N_2O_2$	glutamine	83.73184	85.843[a]	0.02459
$C_4H_9NO_3$	threonine	68.95678	71.058[a]	0.02956
$C_9H_{11}NO_3$	tyrosine	109.40427	111.450[a]	0.01835
$C_3H_7NO_3$	serine	56.66986	58.339[a]	0.02861
$C_{11}H_{12}N_2O_2$	tryptophan	126.74291	128.084[a]	0.01047
$C_9H_{11}NO_2$	phenylalanine	104.90618	105.009	0.00098
$C_5H_9NO_2$	proline	71.76826	71.332	-0.00611
$C_5H_9NO_2$	methionine	79.23631	79.214	-0.00028
$C_6H_{13}NO_2$	leucine	89.12115	89.047	-0.00083
$C_6H_{13}NO_2$	isoleucine	89.02978	90.612	0.01746
$C_6H_{13}NO_2$	valine	76.87208	76.772	-0.00130
$C_3H_7NO_2$	alanine	52.57549	52.991	0.00785
$C_2H_5NO_2$	glycine	40.28857	40.280	-0.00021

[a] Crystal

REFERENCES

1. D. R. Lide, *CRC Handbook of Chemistry and Physics*, 86th Edition, CRC Press, Taylor & Francis, Boca Raton, (2005-6), pp. 9-19 to 9-45.
2. G. Herzberg, *Molecular Spectra and Molecular Structure II. Infrared and Raman Spectra of Polyatomic Molecules*, Van Nostrand Reinhold Company, New York, New York, (1945), p. 344.
3. D. R. Lide, *CRC Handbook of Chemistry and Physics*, 86th Edition, CRC Press, Taylor & Francis, Boca Raton, (2005-6), pp. 9-63; 5-18 to 5-42.
4. R. J. Fessenden, J. S. Fessenden, *Organic Chemistry*, Willard Grant Press. Boston, Massachusetts, (1979), p. 320.
5. cyclohexane at http://webbook.nist.gov/.
6. G. Herzberg, *Molecular Spectra and Molecular Structure II. Infrared and Raman Spectra of Polyatomic Molecules*, Van Nostrand Reinhold Company, New York, New York, (1945), p. 326.
7. b1 2-methyl-1-propene at http://webbook.nist.gov/.
8. a1 2-methyl-1-propene at http://webbook.nist.gov/.
9. 2-butyne at http://webbook.nist.gov/.
10. trifluoromethane at http://webbook.nist.gov/.
11. fluoroethane at http://webbook.nist.gov/.
12. G. Herzberg, *Molecular Spectra and Molecular Structure II. Infrared and Raman Spectra of Polyatomic Molecules*, Krieger Publishing Company, Malabar, FL, (1991), p. 195.
13. chloromethane at http://webbook.nist.gov/.
14. methyl bromide at http://webbook.nist.gov/.
15. tetrabromomethane at http://webbook.nist.gov/.
16. methyl iodide at http://webbook.nist.gov/.
17. K. P. Huber, G. Herzberg, *Molecular Spectra and Molecular Structure, IV. Constants of Diatomic Molecules*, Van Nostrand Reinhold Company, New York, (1979).
18. J. Crovisier, Molecular Database—Constants for molecules of astrophysical interest in the gas phase: photodissociation, microwave and infrared spectra, Ver. 4.2, Observatoire de Paris, Section de Meudon, Meudon, France, May 2002, pp. 34–37, available at http://wwwusr.obspm.fr/~crovisie/.
19. methanol at http://webbook.nist.gov/.
20. D. Lin-Vien. N. B. Colthup, W. G. Fateley, J. G. Grasselli, The *Handbook of Infrared and Raman Frequencies of Organic Molecules*, Academic Press, Inc., Harcourt Brace Jovanovich, Boston, (1991), p. 46.
21. dimethyl ether at http://webbook.nist.gov/.
22. T. Amano, P. F. Bernath, R. W. McKellar, "Direct observation of the ν_1 and ν_3 fundamental bands of NH_2 by difference frequency laser spectroscopy," J. Mol. Spectrosc., Vol. 94, (1982), pp. 100-113.
23. methylamine at http://webbook.nist.gov/.
24. D. R. Lide, *CRC Handbook of Chemistry and Physics*, 79th Edition, CRC Press, Boca Raton, Florida, (1998-9), pp. 9-80 to 9-86.
25. D. Lin-Vien. N. B. Colthup, W. G. Fateley, J. G. Grasselli, The *Handbook of Infrared and Raman Frequencies of Organic Molecules*, Academic Press, Inc., Harcourt Brace Jovanovich, Boston, (1991), p. 482.
26. acetaldehyde at http://webbook.nist.gov/.
27. acetone at http://webbook.nist.gov/.
28. 2-butanone at http://webbook.nist.gov/.
29. acetic acid at http://webbook.nist.gov/.
30. formic acid at http://webbook.nist.gov/.
31. D. Lin-Vien. N. B. Colthup, W. G. Fateley, J. G. Grasselli, The *Handbook of Infrared and Raman Frequencies of Organic Molecules*, Academic Press, Inc., Harcourt Brace Jovanovich, Boston, (1991), p. 138.
32. methyl formate at http://webbook.nist.gov/.
33. D. Lin-Vien. N. B. Colthup, W. G. Fateley, J. G. Grasselli, The *Handbook of Infrared and Raman Frequencies of Organic Molecules*, Academic Press, Inc., Harcourt Brace Jovanovich, Boston, (1991), p. 144.
34. D. Lin-Vien. N. B. Colthup, W. G. Fateley, J. G. Grasselli, The *Handbook of Infrared and Raman Frequencies of Organic Molecules*, Academic Press, Inc., Harcourt Brace Jovanovich, Boston, (1991), p. 147.
35. D. Lin-Vien. N. B. Colthup, W. G. Fateley, J. G. Grasselli, The *Handbook of Infrared and Raman Frequencies of Organic Molecules*, Academic Press, Inc., Harcourt Brace Jovanovich, Boston, (1991), p. 143.
36. H. J. Vledder, F. C. Mijlhoff, J. C. Leyte, C. Romers, "An electron diffraction investigation of the molecular structure of gaseous acetic anhydride," Journal of Molecular Structure, Vol. 7, Issues 3-4, (1971), pp. 421-429.
37. acetonitrile at http://webbook.nist.gov/.
38. D. R. Lide, *CRC Handbook of Chemistry and Physics*, 86th Edition, CRC Press, Taylor & Francis, Boca Raton, (2005-6), pp. 10-202 to 10-204.
39. D. R. Lide, *CRC Handbook of Chemistry and Physics*, 86th Edition, CRC Press, Taylor & Francis, Boca Raton, (2005-6), p. 9-79.

40. D. R. Lide, *CRC Handbook of Chemistry and Physics*, 86th Edition, CRC Press, Taylor & Francis, Boca Raton, (2005-6), pp. 9-82 to 9-86.
41. thiirane at http://webbook.nist.gov/.
42. D. Lin-Vien. N. B. Colthup, W. G. Fateley, J. G. Grasselli, The *Handbook of Infrared and Raman Frequencies of Organic Molecules*, Academic Press, Inc., Harcourt Brace Jovanovich, Boston, (1991), p. 242.
43. D. Lin-Vien. N. B. Colthup, W. G. Fateley, J. G. Grasselli, The *Handbook of Infrared and Raman Frequencies of Organic Molecules*, Academic Press, Inc., Harcourt Brace Jovanovich, Boston, (1991), p. 241.
44. R. M. Ibberson, M. T. F. Telling, S. Parsons, "Structural determination and phase transition behavior of dimethyl sulfate," Acta. Cryst., Vol. B62, (2006), pp. 280-286.
45. D. Lin-Vien. N. B. Colthup, W. G. Fateley, J. G. Grasselli, The *Handbook of Infrared and Raman Frequencies of Organic Molecules*, Academic Press, Inc., Harcourt Brace Jovanovich, Boston, (1991), p. 187.
46. D. Lin-Vien. N. B. Colthup, W. G. Fateley, J. G. Grasselli, The *Handbook of Infrared and Raman Frequencies of Organic Molecules*, Academic Press, Inc., Harcourt Brace Jovanovich, Boston, (1991), p. 480.
47. D. Lin-Vien. N. B. Colthup, W. G. Fateley, J. G. Grasselli, The *Handbook of Infrared and Raman Frequencies of Organic Molecules*, Academic Press, Inc., Harcourt Brace Jovanovich, Boston, (1991), p. 187.
48. 1,3-butadiene at http://webbook.nist.gov/.
49. G. Herzberg, *Molecular Spectra and Molecular Structure II. Infrared and Raman Spectra of Polyatomic Molecules*, Van Nostrand Reinhold Company, New York, New York, (1945), pp. 362-369.
50. W. I. F. David, R. M. Ibberson, G. A. Jeffrey, J. R. Ruble, "The structure analysis of deuterated benzene and deuterated nitromethane by pulsed-neutron powder diffraction: a comparison with single crystal neutron analysis," Physica B (1992), 180 & 181, pp. 597-600.
51. G. A. Jeffrey, J. R. Ruble, R. K. McMullan, J. A. Pople, "The crystal structure of deuterated benzene," Proceedings of the Royal Society of London. Series A, Mathematical and Physical Sciences, Vol. 414, No. 1846, (Nov. 9, 1987), pp. 47-57.
52. H. B. Burgi, S. C. Capelli, "Getting more out of crystal-structure analyses," Helvetica Chimica Acta, Vol. 86, (2003), pp. 1625-1640.
53. L. Gross, F. Mohn, N. Moll, P. Liljeroth, G. Meyer, "The chemical structure of a molecule resolved by atomic force microscopy", Science, Vol. 325, (2009), pp. 1110-1114.
54. D. Lin-Vien. N. B. Colthup, W. G. Fateley, J. G. Grasselli, The *Handbook of Infrared and Raman Frequencies of Organic Molecules*, Academic Press, Inc., Harcourt Brace Jovanovich, Boston, (1991), p. 481.
55. E. Csakvari, I. Hargittai, "Molecular structure of 2,6-difluorobenzamine and 2-fluorobenzamine from gas-phase electron diffraction," J. Phys. Chem., Vol. 96, (1992), pp. 5837-5842.
56. E. Rosenthal, B. P. Dailey, "Microwave spectrum of bromobenzene, its structure, quadrupole coupling constants, and carbon-bromine bond," Journal of Chemical Physics, Vol. 43, No. 6, (1965), pp. 2093-2110.
57. H. J. M. Bowen, *Tables of Interatomic Distances and Configuration in Molecules and Ions*, L. Sutton, Editor, Special Publication No. 11, The Chemical Society, Burlington House, London (1958).
58. R. Boese, D. Blaser, M. Nussbaumer, T. M. Krygowski, "Low temperature crystal and molecular structure of nitrobenzene," Structural Chemistry, Vol. 3, No. 5, (1992), pp. 363-368.
59. G. A. Sim, J. M. Robertson, T. H. Goodwin, "The crystal and molecular structure of benzoic acid," Acta Cryst., Vol. 8, (1955), pp.157-164.
60. D. Lin-Vien. N. B. Colthup, W. G. Fateley, J. G. Grasselli, The *Handbook of Infrared and Raman Frequencies of Organic Molecules*, Academic Press, Inc., Harcourt Brace Jovanovich, Boston, (1991), p. 301.
61. D. Lin-Vien. N. B. Colthup, W. G. Fateley, J. G. Grasselli, The *Handbook of Infrared and Raman Frequencies of Organic Molecules*, Academic Press, Inc., Harcourt Brace Jovanovich, Boston, (1991), p. 303.
62. D. Lin-Vien. N. B. Colthup, W. G. Fateley, J. G. Grasselli, The *Handbook of Infrared and Raman Frequencies of Organic Molecules*, Academic Press, Inc., Harcourt Brace Jovanovich, Boston, (1991), p. 207.
63. S. Martinez-Carrera, "The crystal structure of Imidazole at -150°C," Acta. Cryst., Vol. 20, (1966), pp. 783-789.
64. D. Lin-Vien. N. B. Colthup, W. G. Fateley, J. G. Grasselli, The *Handbook of Infrared and Raman Frequencies of Organic Molecules*, Academic Press, Inc., Harcourt Brace Jovanovich, Boston, (1991), pp. 296-297.
65. S. Arnott, S. D. Dover, A. J. Wonacott, "Least-squares refinement of the crystal and molecular structures of DNA and RNA from X-ray data and standard bond lengths and angles," Acta. Cryst., Vol. B-25, (1969), pp. 2192-2206.
66. H. Sternglanz, C. E. Bugg, "Conformations of N^6-monosubstituted adenine derivatives crystal structure of N^6-methyladenine," Biochimica et Biophysica Acta, Vol. 308, (1973), pp. 1-8.
67. B. Chase, N. Herron, E. Holler, "Vibrational spectroscopy of C_{60} and C_{70} temperature-dependent studies," J. Phys. Chem., Vol. 96, (1992), pp. 4262-4266.
68. D. Lin-Vien. N. B. Colthup, W. G. Fateley, J. G. Grasselli, The *Handbook of Infrared and Raman Frequencies of Organic Molecules*, Academic Press, Inc., Harcourt Brace Jovanovich, Boston, (1991), p. 272.
69. J. D. Cox, G. Pilcher, *Thermochemistry of Organometallic Compounds*, Academic Press, New York, (1970), pp. 478-485.
70. M. G. Newton, B. S. Campbell, "Preparation and crystal structures of trans-methyl meso-hydrobenzoin phosphite and phosphate," JACS, Vol. 96, No. 25, (1974), pp. 7790-7797.

71. D. Lin-Vien. N. B. Colthup, W. G. Fateley, J. G. Grasselli, The *Handbook of Infrared and Raman Frequencies of Organic Molecules*, Academic Press, Inc., Harcourt Brace Jovanovich, Boston, (1991), p. 271.
72. J. C. J. Bart, G. Favini, R. Todeschini, "Conformational analysis of trimethylphoshite and its metal complexes," *Phosphorous and Sulfur*, Gordon and Breach Scientific Publishers, Inc. USA, Vol. 17, (1983), pp. 205-220.
73. N. J. Goodwin, W. Henderson, B. K. Nicholson, "Hydrogen bonding in hydroxymethylphosphine chalcogenides," Inorganica Chimica Acta, Vol. 335, (2002), pp. 113-118.
74. M. W. Chase, Jr., C. A. Davies, J. R. Downey, Jr., D. J. Frurip, R. A. McDonald, A. N. Syverud, JANAF Thermochemical Tables, Third Edition, Part II, Cr-Zr, J. Phys. Chem. Ref. Data, Vol. 14, Suppl. 1, (1985), p. 1728.
75. D. Lin-Vien. N. B. Colthup, W. G. Fateley, J. G. Grasselli, The *Handbook of Infrared and Raman Frequencies of Organic Molecules*, Academic Press, Inc., Harcourt Brace Jovanovich, Boston, (1991), p. 269.

The Grand Unified Theory of Classical Physics

Dr. Randell L. Mills

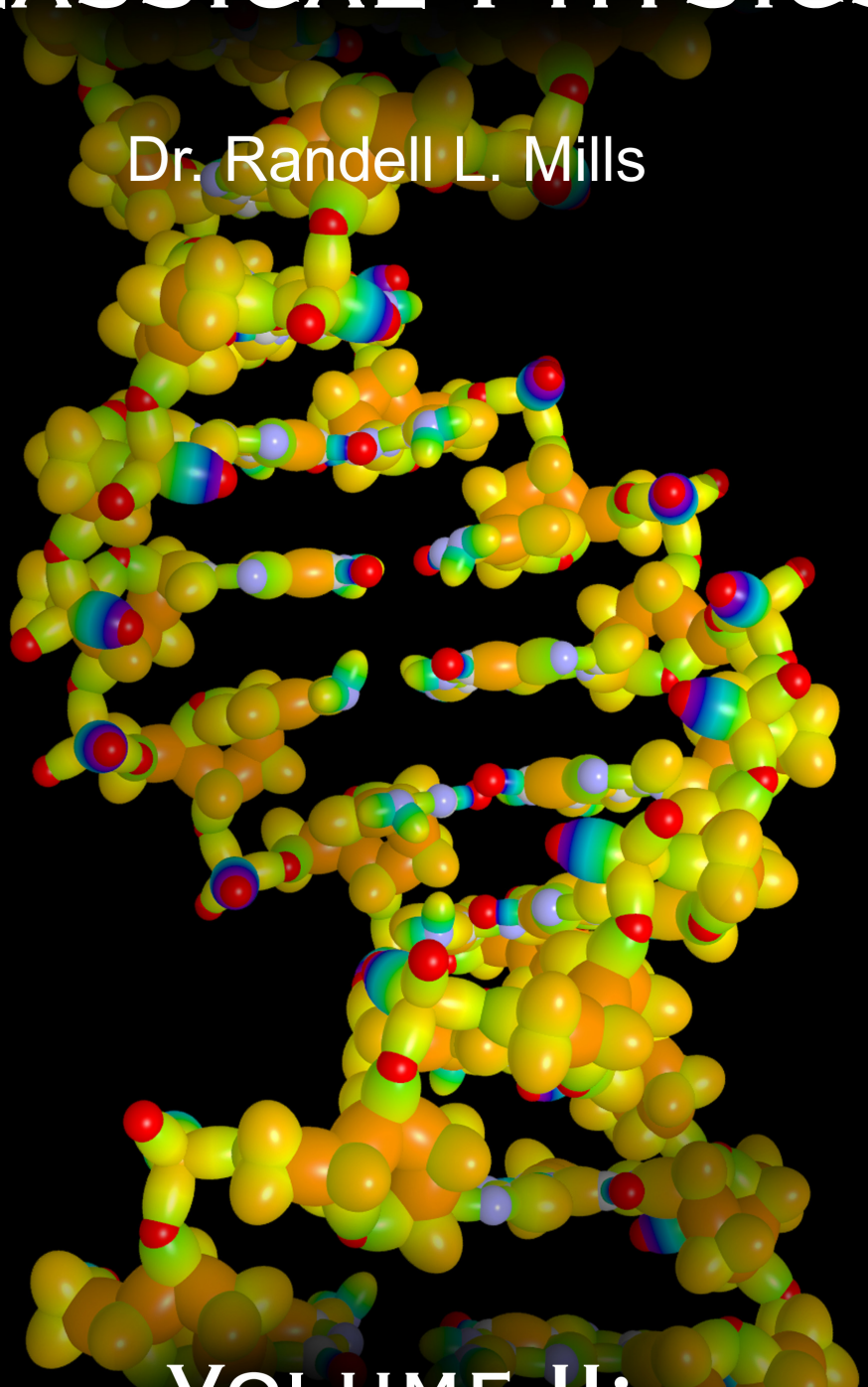

Volume II:

Part B

Molecular Physics

THE GRAND UNIFIED THEORY
OF CLASSICAL PHYSICS

Volume 2B of 3

THE GRAND UNIFIED THEORY OF CLASSICAL PHYSICS

BY

Dr. Randell L. Mills

April 2023 Edition
Volume 2B of 3

ISBN 979-8-218-17988-5
Library of Congress Control Number 2023905641

TABLE OF CONTENTS

VOLUME 2 MOLECULAR PHYSICS Part B

Chapter 16

APPLICATIONS: PHARMACEUTICALS, SPECIALTY MOLECULAR FUNCTIONAL GROUPS AND MOLECULES, DIPOLE MOMENTS AND INTERACTIONS

GENERAL CONSIDERATIONS OF THE BONDING IN PHARMACEUTICALS AND SPECIALTY MOLECULES

Pharmaceutical and specialty molecules comprising an arbitrary number of atoms can be solved using similar principles and procedures as those used to solve general organic molecules of arbitrary length and complexity. Pharmaceuticals and specialty molecules can be considered to be comprised of functional groups such as those of alkanes, branched alkanes, alkenes, branched alkenes, alkynes, alkyl fluorides, alkyl chlorides, alkyl bromides, alkyl iodides, alkene halides, primary alcohols, secondary alcohols, tertiary alcohols, ethers, primary amines, secondary amines, tertiary amines, aldehydes, ketones, carboxylic acids, carboxylic esters, amides, N-alkyl amides, N,N-dialkyl amides, ureas, acid halides, acid anhydrides, nitriles, thiols, sulfides, disulfides, sulfoxides, sulfones, sulfites, sulfates, nitro alkanes, nitrites, nitrates, conjugated polyenes, aromatics, heterocyclic aromatics, substituted aromatics, and others given in the Organic Molecular Functional Groups and Molecules section. The solutions of the functional groups can be conveniently obtained by using generalized forms of the geometrical and energy equations. The functional-group solutions can be made into a linear superposition and sum, respectively, to give the solution of any pharmaceutical or specialty molecule comprising these groups. The total bond energies of exemplary pharmaceutical or specialty molecules such as aspirin, RDX, and NaH are calculated using the functional group composition and the corresponding energies derived in the previous sections as well as those of any new component functional groups derived herein.

ASPIRIN (ACETYLSALICYLIC ACID)

Aspirin comprises salicylic acid (ortho-hydroxybenzoic acid) with the H of the phenolic OH group replaced by an acetyl group. Thus, aspirin comprises the benzoic acid $C-C(O)-OH$ moiety that comprises $C=O$ and OH functional groups that are the same as those of carboxylic acids given in the corresponding section. The single bond of aryl carbon to the carbonyl carbon atom, $C-C(O)$, is also a functional group given in the Benzoic Acid Compounds section. The aromatic $C\overset{3e}{=}C$ and $C-H$ functional groups are equivalent to those of benzene given in the Aromatic and Heterocyclic Compounds section. The phenolic ester $C-O$ functional group is equivalent to that given in the Phenol section. The acetyl $O-C(O)-CH_3$ moiety comprises (i) $C=O$ and $C-C$ functional groups that are the same as those of carboxylic acids and esters given in the corresponding sections, (ii) a CH_3 group that is equivalent to that of alkanes given in the corresponding sections, (iii) and a $C-O$ bridging the carbonyl carbon and the phenolic ester which is equivalent to that of esters given in the corresponding section.

The symbols of the functional groups of aspirin are given in Table 16.1.

The corresponding designations of aspirin are shown in Figure 16.1B. The geometrical (Eqs. (15.1-15.5) and (15.51)), intercept (Eqs. (15.80-15.87)), and energy (Eqs. (15.6-15.11) and (15.17-15.65)) parameters of aspirin are given in Tables 16.2, 16.3, and 16.4, respectively. The total energy of aspirin given in Table 16.5 was calculated as the sum over the integer multiple of each $E_D(Group)$ of Table 16.4 corresponding to functional-group composition of the molecule. The bond angle parameters of aspirin determined using Eqs. (15.88-15.117) are given in Table 16.6. The color scale, translucent view of the charge density of aspirin comprising the concentric shells of atoms with the outer shell bridged by one or more H_2-type ellipsoidal MOs or joined with one or more hydrogen MOs is shown in Figure 16.1A.

Figure 16.1. (A) Color scale, translucent view of the charge density of aspirin showing the orbitals of the atoms at their radii, the ellipsoidal surface of each H or H_2-type ellipsoidal MO that transitions to the corresponding outer shell of the atom(s) participating in each bond, and the hydrogen nuclei (red, not to scale). (B) Chemical structure and designation of aspirin.

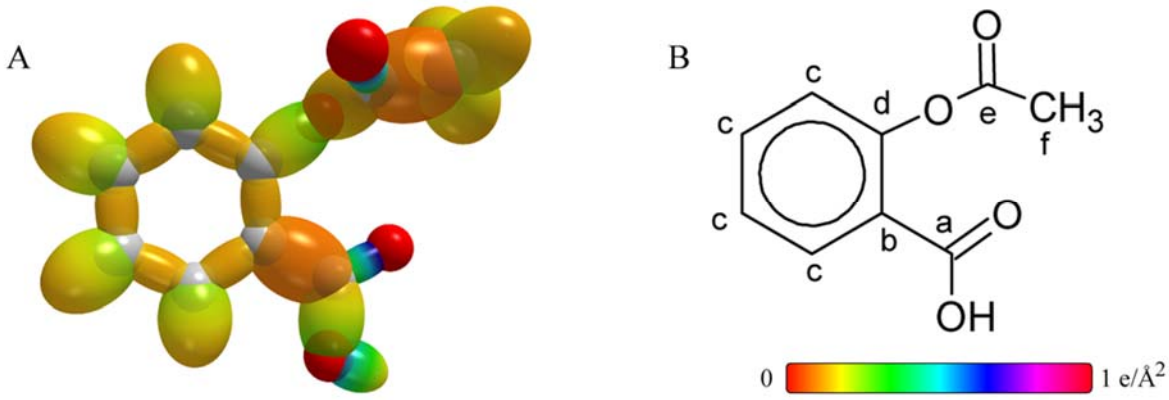

Table 16.1. The symbols of functional groups of aspirin.

Functional Group	Group Symbol
CC (aromatic bond)	$C\overset{3e}{=}C$
CH (aromatic)	*CH*
Aryl *C*-*C*(*O*)	$C-C(O)$ (i)
Alkyl *C*-*C*(*O*)	$C-C(O)$ (ii)
C=*O* (aryl carboxylic acid)	$C=O$
Aryl (*O*)*C*-*O*	$C-O$ (i)
Alkyl (*O*)*C*-*O*	$C-O$ (ii)
Aryl *C*-*O*	$C-O$ (iii)
OH group	*OH*
CH_3 group	CH_3

Table 16.2. The geometrical bond parameters of aspirin and experimental values of similar molecules [1].

Parameter	$C^{3\varepsilon}=C$ Group	CH Group	$C-C(O)$ (i) Group	$C-C(O)$ (ii) Group	$C=O$ Group	$C-O$ (i) Group	$C-O$ (ii) Group	$C-O$ (iii) Group	OH Group	$C-H\ (CH_3)$ Group
$a\ (a_0)$	1.47348	1.60061	1.95111	2.04740	1.29907	1.73490	1.73490	1.68220	1.26430	1.64920
$c'\ (a_0)$	1.31468	1.03299	1.39682	1.43087	1.13977	1.31716	1.31716	1.29700	0.91808	1.04856
Bond Length $2c'\ (\AA)$	1.39140	1.09327	1.47833	1.51437	1.20628	1.39402	1.39402	1.37268	0.971651	1.10974
Exp. Bond Length $(\AA)$	1.399 (benzene)	1.101 (benzene)	1.48 [2] (benzoic acid)	1.520 (acetic acid)	1.214 (acetic acid)	1.393 (methyl formate)	1.393 (avg. methyl formate)	1.364 (phenol)	0.972 (formic acid)	1.08 (methyl formate) 1.107 ($C-H$ propane) 1.117 ($C-H$ butane)
$b,c\ (a_0)$	0.66540	1.22265	1.36225	1.46439	0.62331	1.12915	1.12915	1.07126	0.86925	1.27295
e	0.89223	0.64537	0.71591	0.69887	0.87737	0.75921	0.75921	0.77101	0.72615	0.63580

Table 16.3. The MO to HO intercept geometrical bond parameters of aspirin. E_T is E_T (*atom – atom* msp^3.*AO*).

Bond	Atom	E_T (eV) Bond 1	E_T (eV) Bond 2	E_T (eV) Bond 3	E_T (eV) Bond 4	Final Total Energy $C2sp^3$ (eV)	$r_{initial}$ (a_0)	r_{final} (a_0)	$E_{Coulomb}(C2sp^3)$ (eV) Final	$E(C2sp^3)$ (eV) Final	θ' (°)	θ_1 (°)	θ_2 (°)	d_1 (a_0)	d_2 (a_0)
$C-H\ (C_cH)$	C_c	-0.85035	-0.85035	-0.56690	0	-153.88327	0.91771	0.79597	-17.09334	-16.90248	74.42	105.58	38.84	1.24678	0.21379
$C^{3\varepsilon}=(HOOC_a)C_b^{3\varepsilon}=C_c(H)$	C_c	-0.85035	-0.85035	-0.56690	0	-153.88327	0.91771	0.79597	-17.09334	-16.90248	134.24	45.76	58.98	0.75935	0.55533
$C_bC_a(O)O-H$	O	-0.92918	0	0	0		1.00000	0.86359	-15.75493		115.09	64.91	64.12	0.55182	0.36625
$C_bC_a(O)-OH$	O	-0.92918	0	0	0		1.00000	0.86359	-15.75493		101.32	78.68	48.58	1.14765	0.16950
$C_bC_a(O)-OH$	C_a	-0.92918	-1.34946	-0.64574	0	-154.54007	0.91771	0.76652	-17.75013	-17.55927	93.11	86.89	42.68	1.27551	0.04165
$C_bC_a(OH)=O$ $OC_e(C_fH_3)=O$	O	-1.34946	0	0	0		1.00000	0.84115	-16.17521		137.27	42.73	66.31	0.52193	0.61784
$C_bC_a(OH)=O$	C_a	-1.34946	-0.64574	-0.92918	0	-154.54007	0.91771	0.76652	-17.75013	-17.55927	134.03	45.97	62.14	0.60699	0.53278
$C_b-C_a(O)OH$	C_a	-0.64574	-1.34946	-0.92918	0	-154.54007	0.91771	0.76652	-17.75013	-17.55927	70.34	109.66	32.00	1.65466	0.25784
$C_b-C_a(O)OH$	C_b	-0.64574	-0.85035	-0.85035	0	-153.96212	0.91771	0.79232	-17.17218	-16.98131	73.74	106.26	33.94	1.61863	0.22181
$C_c^{3\varepsilon}=(HOOC_a)C_b^{3\varepsilon}=C_c$	C_b	-0.64574	-0.85035	-0.85035	0	-153.96212	0.91771	0.79232	-17.17218	-16.98132	134.09	45.91	58.79	0.76344	0.55124
$C_c^{3\varepsilon}=(CH_3(O)CO)C_d^{3\varepsilon}=C_b$	C_d	-0.74804	-0.85035	-0.85035	0	-154.06442	0.91771	0.78762	-17.27448	-17.08362	100.00	80.00	46.39	1.16026	0.13674
$C_c^{3\varepsilon}=(C_b^{3\varepsilon}=)C_d-OC(O)CH_3$	O	-0.74804	-0.92918	0	0		1.00000	0.82445	-16.50297		102.93	77.02	48.60	1.11250	0.18449
$C_c^{3\varepsilon}=(C_b^{3\varepsilon}=)C_dO-C(O)CH_3$	O	-0.92918	-0.74804	0	0		1.00000	0.82445	-16.50297		98.22	81.78	46.27	1.19921	0.11795
$O-C_e(O)C_fH_3$	C_e	-0.92918	-1.34946	-0.92918	0	-154.82352	0.91771	0.75447	-18.03358	-17.84271	91.96	88.04	41.90	1.29138	0.02578
$OC_e(C_fH_3)=O$	C_e	-1.34946	-0.92918	-0.92918	0	-154.82352	0.91771	0.75447	-18.03358	-17.84271	133.47	46.53	61.46	0.62072	0.51905
$O(O)C_e-C_fH_3$	C_e	-0.92918	-1.34946	-0.92918	0	-154.82352	0.91771	0.75447	-18.03358	-17.84272	56.25	123.75	25.37	1.85002	0.41915
$OC_e(O)-C_fH_3$	C_f	-0.92918	0	0	0	-152.54487	0.91771	0.86359	-15.75493	-15.56407	72.27	107.73	34.17	1.69388	0.26301

Table 16.4. The energy parameters (eV) of functional groups of aspirin.

Parameters	$C\overset{>}{=}C$ Group	CH Group	$C-C(O)$ (i) Group	$C-C(O)$ (ii) Group	$C=O$ Group	$C-O$ (i) Group	$C-O$ (ii) Group	$C-O$ (iii) Group	OH Group	CH_3 Group
f_1	0.75	1								
n_1	2	1	1	1	2	1	1	1	1	3
n_2	0	0	0	0	0	0	0	0	0	2
n_3	0	0	0	0	0	0	0	0	0	0
C_1	0.5	0.75	0.5	0.5	0.5	0.5	0.5	0.5	0.75	0.75
C_2	0.85252	1	1	1	1	1	1	1	1	1
c_1	1	1	1	1	1	1	1	1	0.75	1
c_2	0.85252	0.91771	0.91771	0.91771	0.85395	0.85395	0.85395	0.79329	1	0.91771
c_3	0	1	0	0	2	0	0	0	1	0
c_4	3	1	2	2	4	2	2	2	1	1
c_5	0	1	0	0	0	0	0	0	1	3
C_{1o}	0.5	0.75	0.5	1	0.5	0.5	0.5	0.5	0.75	0.75
C_{2o}	0.85252	1	1	1	1	1	1	1	1	1
V_s (eV)	-101.12679	-37.10024	-32.15216	-30.19634	-111.25473	-35.08488	-35.08488	-34.04658	-40.92709	-107.32728
V_p (eV)	20.69825	13.17125	9.74055	9.50874	23.87467	10.32968	10.32968	10.49024	14.81988	38.92728
T (eV)	34.31559	11.58941	8.23945	7.37432	42.82081	10.11150	10.11150	10.11966	16.18567	32.53914
V_{ss} (eV)	-17.15779	-5.79470	-4.11973	-3.68716	-21.41040	-5.05575	-5.05575	-5.05983	-8.09284	-16.26957
$E_{(AO:HO)}$ (eV)	0	-14.63489	-14.63489	-14.63489	0	-14.63489	-14.63489	-14.63489	-13.6181	-15.56407
$\Delta E_{H_2(AO:HO)}$ (eV)	0	-1.13379	-1.29147	0	-2.69893	-2.69893	-2.69893	-1.49608	0	0
E_T $(AO:HO)$ (eV)	0	-13.50110	-13.34342	-14.63489	2.69893	-11.93596	-11.93596	-13.13881	-13.6181	-15.56407
E_T (H_2AO) (eV)	-63.27075	-31.63539	-31.63530	-31.63534	-63.27074	-31.63541	-31.63541	-31.63532	-31.63247	-67.69451
$E_I\left(atom-atom, msp^3.AO\right)$ (eV)	-2.26759	-0.56690	-1.29147	-1.85836	-2.69893	-1.85836	-1.85836	-1.49608	0	0
E_I (MO) (eV)	-65.53833	-32.20226	-32.92684	-33.49373	-65.96966	-33.49373	-33.49373	-33.13145	-31.63537	-67.69450
$\omega\left(10^{15}\ rad/s\right)$	49.7272	26.4826	10.7262	23.3291	59.4034	24.3637	12.7926	13.3984	44.1776	24.9286
E_K (eV)	32.73133	17.43132	7.06019	15.35563	39.10034	16.03660	8.42030	8.81907	29.07844	16.40846
$\overline{E}_D$ (eV)	-0.35806	-0.26130	-0.17309	-0.25966	-0.40804	-0.26535	-0.19228	-0.19465	-0.33749	-0.25352
$\overline{E}_{Keith}$ (eV)	0.19649 [3]	0.35532 Eq. (13.458)	0.10502 [4]	0.10502 [4]	0.21077 [5]	0.14010 [6]	0.14965 [7]	0.12808 [8]	0.46311 [9-10]	0.35532 (Eq. (13.458))
$\overline{E}_{exc}$ (eV)	-0.25982	-0.08364	-0.12058	-0.20715	-0.30266	-0.19530	-0.11745	-0.13061	-0.10594	-0.22757
E_{mag} (eV)	0.14803	0.14803	0.14803	0.14803	0.11441	0.14803	0.14803	0.14803	0.11441	0.14803
E_T $(Group)$ (eV)	-49.54347	-32.28590	-33.04742	-33.70088	-66.57498	-33.68903	-33.61118	-33.26206	-31.74130	-67.92207
E_{antiad} $(s_4:AO:HO)$ (eV)	-14.63489	-14.63489	-14.63489	-14.63489	-14.63489	-14.63489	-14.63489	-14.63489	-13.6181	-14.63489
E_{antiad} $(s_5:AO:HO)$ (eV)	0	-13.59844	0	0	0	0	0	0	-13.59844	-13.59844
E_D $(Group)$ (eV)	5.63881	3.90454	3.77764	4.43110	7.80660	4.41925	4.34141	3.99228	4.41035	12.49186

Table 16.5. The total bond energies of salicylic acid and aspirin calculated using the functional group composition and the energies of Table 16.4.

Formula	Name	$C\overset{3e}{=}C$ Group	CH Group	$C-C(O)$ (i) Group	$C-C(O)$ (ii) Group	$C=O$ Group	$C-O$ (i) Group	$C-O$ (ii) Group	$C-O$ (iii) Group	OH Group	$C-H\ (CH_3)$ Group	Calculated Total Bond Energy (eV)	Experimental Total Bond Energy (eV)	Relative Error
$C_7H_6O_3$	Salicylic acid	6	4	1	0	1	1	0	1	2	0	78.26746 [11]	78.426	0.00202
$C_9H_8O_4$	Aspirin	6	4	1	1	2	1	1	1	1	1	102.92809		

Table 16.6. The bond angle parameters of aspirin and experimental values [1]. E_T is E_T ($atom - atom\ msp^3.AO$).

Atoms of Angle	$2c'$ Bond 1 (a_0)	$2c'$ Bond 2 (a_0)	$2c'$ Terminal Atoms (a_0)	$E_{Coulombic}$ Atom 1	Atom 1 Hybridization Designation (Table 15.3.A)	$E_{Coulombic}$ Atom 2	Atom 2 Hybridization Designation (Table 15.3.A)	c_2 Atom 1	c_2 Atom 2	C_1	C_2	c_1	c_2'	E_T (eV)	θ_e (°)	θ_1 (°)	θ_2 (°)	Cal. θ (°)	Exp. θ (°)
$\angle CCC$ (aromatic)	2.62936	2.62936	4.5585	-17.17218	38	-17.17218	38	0.79232	0.79232	1	1	1	0.79232	-1.85836				120.19	120 [12-14] (benzene)
$\angle CCH$ $\angle CCO$ (aromatic)																120.19		119.91	120 [12-14] (benzene)
$\angle C_aO_bH$	2.63431	1.83616	3.6405	-14.82575	1	-14.82575	1	1	0.91771	0.75	1	0.75	0.91771	0				107.71	
$\angle C_bC_a(O)$	2.82796	2.27954	4.4721	-17.17218	38	-13.61806	O	0.79232	0.85395 (Eq. (15.114))	1	1	1	0.82313	-1.65376				121.86	122 [2] (benzoic acid)
$\angle C_bC_aO$	2.82796	2.63431	4.6690	-16.40067	20	-13.61806	O	0.82959	0.85395 (Eq. (15.114))	1	1	1	0.84177	-1.65376				117.43	118 [2] (benzoic acid)
$\angle(O)C_aO$	2.27954	2.63431	4.3818	-16.17521 (O)	13	-15.75493 O	7	0.84115	0.86359	1	1	1	0.85237	-1.44915				126.03	122 [2] (benzoic acid)
$\angle C_fC_e(O)$	2.86175	2.27954	4.5826	-16.68411	25	-13.61806	O	0.81549	0.85395 (Eq. (15.133))	1	1	1	0.83472	-1.65376				125.70	126.6 [1] (acetic acid)
$\angle C_fC_eO$	2.86175	2.63431	4.4944	-15.75493	7	-13.61806	O	0.86359	0.85395 (Eq. (15.133))	1	1	1	0.85877	-1.44915				109.65	110.6 [1] (acetic acid)
$\angle OC_eO$	2.27954	2.63431	4.3818	-16.17521 (O)	13	-15.75493 O	7	0.84115	0.86359	1	1	1	0.85237	-1.44915				126.03	
$\angle C_dOC_e$	2.59399	2.63431	4.3589	-17.27448 C_d	41	-18.03358 C_e	56	0.78762	0.75447	1	1	1	0.77105	-1.85836				112.96	114 [1] (methyl formate)
Methyl $\angle HC_fH$	2.09711	2.09711	3.4252	-15.75493	7	H	H	0.86359	1	1	1	0.75	1.15796	0				109.50	

CYCLOTRIMETHYLENE-TRINITRAMINE ($C_3H_6N_6O_6$)

The compound cyclotrimethylene-trinitramine, commonly referred to as Cyclonite or by the code designation RDX, is a well-known explosive. RDX comprises three methylene (CH_2) groups joined by six alkyl $C-N$ secondary amine functional groups given in the corresponding section. Each of the three N's of the six-membered ring shown in Figure 16.2B is bonded to a NO_2 functional group given in the Nitroalkanes section by a $N-N$ functional group. The latter requires hybridization of the nitrogen atoms in order to match the energies of the bridged groups.

Similar to the case of carbon, silicon, and aluminum, the bonding in the nitrogen of the $N-N$ functional group involves four sp^3 hybridized orbitals formed from the outer $2p$ and $2s$ shells. In RDX, bonds form between two $N2sp^3$ HOs ($N-N$ functional group), between a $N2sp^3$ HO and a $C2sp^3$ HO ($C-N$ functional group), and between a $N2sp^3$ HO and a $O2p$ AO (each $N-O$ bond of the NO_2 functional group). The geometrical and energy equations of the $N-N$ functional group are given in the Derivation of the General Geometrical and Energy Equations of Organic Chemistry section wherein the energy is matched to $E\left(C,2sp^3\right)=-14.63489\ eV$ (Eq. (15.25)).

The $2sp^3$ hybridized orbital arrangement after Eq. (13.422) is:

$$\begin{array}{cccc} & 2\text{sp}^3 \text{ state} & & \\ \uparrow\downarrow & \uparrow & \uparrow & \uparrow \\ \hline 0,0 & 1,-1 & 1,0 & 1,1 \end{array} \tag{16.1}$$

where the quantum numbers (ℓ,m_ℓ) are below each electron. The total energy of the state is given by the sum over the five electrons. The sum $E_T\left(N,2sp^3\right)$ of experimental energies [15] of N, N^+, N^{2+}, N^{3+}, and N^{4+} is:

$$\begin{aligned} E_T\left(N,2sp^3\right) &= -\begin{pmatrix} 97.8902\ eV+77.4735\ eV+47.44924\ eV \\ +29.6013\ eV+14.53414\ eV \end{pmatrix} \\ &= -266.94838\ eV \end{aligned} \tag{16.2}$$

By considering that the central field decreases by an integer for each successive electron of the shell, the radius r_{2sp^3} of the $N2sp^3$ shell may be calculated from the Coulombic energy using Eq. (15.13).

$$r_{2sp^3}=\sum_{n=2}^{6}\frac{(Z-n)e^2}{8\pi\varepsilon_0\left(e266.94838\ eV\right)}=\frac{15e^2}{8\pi\varepsilon_0\left(e266.94838\ eV\right)}=0.76452a_0 \tag{16.3}$$

where $Z=7$ for nitrogen. Using Eq. (15.14), the Coulombic energy $E_{Coulomb}\left(N,2sp^3\right)$ of the outer electron of the $N2sp^3$ shell is:

$$E_{Coulomb}\left(N,2sp^3\right)=\frac{-e^2}{8\pi\varepsilon_0 r_{2sp^3}}=\frac{-e^2}{8\pi\varepsilon_0 0.76452a_0}=-17.79656\ eV \tag{16.4}$$

In RDX, the $C2sp^3$ HO has a hybridization factor of 0.91771 (Eq. (13.430)) with a corresponding energy of $E\left(C,2sp^3\right)=-14.63489\ eV$ (Eq. (15.25)), and the N HO has an energy of $E\left(N,2sp^3\right)=-17.79656\ eV$ (Eq. (16.4)). To meet the equipotential, minimum-energy condition of the union of the $N2sp^3$ and $C2sp^3$ HOs, $C_2=1$ in Eqs. (15.2-15.5), (15.51), and (15.61) for the $N-N$-bond MO, and c_2 given by Eqs. (15.77) and (15.79) is:

$$c_2\left(C2sp^3HO\ to\ N_b2sp^3HO\ to\ N_a2sp^3HO\right)=\frac{E\left(C,2sp^3\right)}{E\left(N,2sp^3\right)}c_2\left(C2sp^3HO\right)=\frac{-14.63489\ eV}{-17.79656\ eV}\left(0.91771\right)=0.75468 \tag{16.5}$$

The energy of the $N-N$-bond MO is the sum of the component energies of the H_2-type ellipsoidal MO given in Eq. (15.51). Since the energy of the MO is matched to that of the $C2sp^3$ HO, $E\left(AO/HO\right)$ in Eqs. (15.51) and (15.61) is: $E\left(C,2sp^3\right)=-14.63489\ eV$ given by Eq. (15.25) and $E_T\left(atom-atom,msp^3.AO\right)$ is $0\ eV$.

The symbols of the functional groups of RDX are given in Table 16.7. The geometrical (Eqs. (15.1-15.5) and (15.51)), intercept (Eqs. (15.80-15.87)), and energy (Eqs. (15.6-15.11) and (15.17-15.65)) parameters of RDX are given in Tables 16.8, 16.9, and 16.10, respectively. The total energy of RDX given in Table 16.11 was calculated as the sum over the integer multiple of each $E_{D(Group)}$ of Table 16.10 corresponding to functional-group composition of the molecule. The bond angle parameters of RDX determined using Eqs. (15.88-15.117) are given in Table 16.12. The color scale charge density of RDX comprising atoms with the outer shell bridged by one or more H_2-type ellipsoidal MOs or joined with one or more hydrogen MOs is shown in Figure 16.2A.

Figure 16.2. (A) Color scale charge density of RDX showing the outer orbitals of the atoms at their radii and the ellipsoidal surface of each H or H_2-type ellipsoidal MO that transitions to the corresponding outer shell of the atom(s) participating in each bond. (B) Chemical structure and atom designation of RDX.

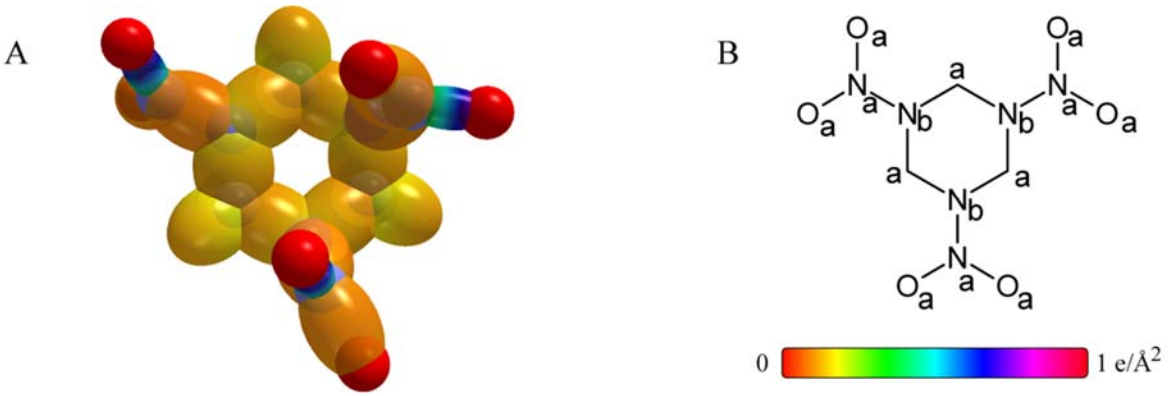

Table 16.7. The symbols of functional groups of RDX.

Functional Group	Group Symbol
NO_2 group	NO_2
N-N	$N-N$
C-N (alkyl)	$C-N$
CH_2 group	$C-H\ (CH_2)$

Table 16.8. The geometrical bond parameters of RDX and experimental values [1].

Parameter	NO_2 Group	$N-N$ Group	$C-N$ Group	$C-H\ (CH_2)$ Group
$a\ (a_0)$	1.33221	1.68711	1.94862	1.67122
$c'\ (a_0)$	1.15421	1.29889	1.39593	1.05553
Bond Length $2c'\ (Å)$	1.22157	1.37468	1.47739	1.11713
Exp. Bond Length	1.224 (nitromethane) 1.22 avg. [16] (RDX)	1.390 [16] (RDX)	1.468 [16] (RDX)	1.107 ($C-H$ propane) 1.117 ($C-H$ butane) 1.092 [16] (RDX)
$b,c\ (a_0)$	0.66526	1.07668	1.35960	1.29569
e	0.86639	0.76989	0.71637	0.63159

Table 16.9. The MO to HO intercept geometrical bond parameters of RDX. E_T is E_T ($atom - atom, msp^3.AO$).

Bond	Atom	E_T (eV) Bond 1	E_T (eV) Bond 2	E_T (eV) Bond 3	E_T (eV) Bond 4	Final Total Energy $C2sp^3$ (eV)	$r_{initial}$ (a_0)	r_{final} (a_0)	$E_{Coulomb}$ (eV) Final	$E(C2sp^3)$ (eV) Final	θ' (°)	θ_1 (°)	θ_2 (°)	d_1 (a_0)	d_2 (a_0)
$N_bN_a(O)=O$	O_a	-0.92918	0	0	0		1.00000	0.86359	-15.75493		135.25	44.75	66.05	0.54089	0.61333
$N_bN_a(O)=O$	N_a	-0.92918	-0.92918	0	0		0.93084	0.81549	-16.68411		133.16	46.84	63.41	0.59640	0.55781
$CH_2N_b-N_aO_2$	N_a	-0.92918	-0.92918	0	0		0.93084	0.81549	-16.68411		101.80	78.20	47.85	1.13213	0.16676
$CH_2N_b-N_aO_2$	N_b	-0.56690	-0.56690	0	0		0.93084	0.85252	-15.95954		104.60	75.40	50.02	1.08404	0.21485
$C-H\ (CH_2)$	C_a	-0.56690	-0.56690	0	0	-152.74948	0.91771	0.85252	-15.95954	-15.76868	73.60	106.40	39.14	1.29624	0.24071
$-H_2C_a-N_bN_a$	N_b	-0.56690	-0.56690	0	0		0.93084	0.85252	-15.95954		80.95	99.05	38.26	1.53008	0.13415
$-H_2C_a-N_bN_a$	C_a	-0.56690	-0.56690	0	0	-152.74948	0.91771	0.85252	-15.95954	-15.76868	80.95	99.05	38.26	1.53008	0.13415

Table 16.10. The energy parameters (eV) of functional groups of RDX.

Parameters	NO_2 Group	$N-N$ Group	$C-N$ Group	CH_2 Group
n_1	2	1	1	2
n_2	0	0	0	1
n_3	0	0	0	0
C_1	0.5	0.5	0.5	0.75
C_2	1	1	1	1
c_1	1	1	1	1
c_2	0.85987	0.75468	0.91140	0.91771
c_3	0	0	0	1
c_4	4	2	2	1
c_5	0	0	0	2
C_{1o}	0.5	0.5	1	0.75
C_{2o}	1	1	1	1
$V_e\ (eV)$	-106.90919	-32.25503	-31.98456	-70.41425
$V_p\ (eV)$	23.57588	10.47496	9.74677	25.78002
$T\ (eV)$	40.12475	9.55926	8.20698	21.06675
$V_m\ (eV)$	-20.06238	-4.77963	-4.10349	-10.53337
$E_{(AO/HO)}\ (eV)$	0	-14.63489	-14.63489	-15.56407
$\Delta E_{H_2MO\,(AO/HO)}\ (eV)$	0	0	-1.13379	0
$E_{T\,(AO/HO)}\ (eV)$	0	-14.63489	-13.50110	-15.56407
$E_{T\,(H_2MO)}\ (eV)$	-63.27093	-31.63533	-31.63540	-49.66493
$E_T\left(atom-atom, msp^3.AO\right)\ (eV)$	-3.71673	0	-1.13379	0
$E_{T\,(MO)}\ (eV)$	-66.98746	-31.63537	-32.76916	-49.66493
$\omega\ \left(10^{15}\ rad/s\right)$	19.0113	26.1663	26.0778	24.2751
$E_K\ (eV)$	12.51354	17.22313	17.16484	15.97831
$\bar{E}_D\ (eV)$	-0.23440	-0.25974	-0.26859	-0.25017
$\bar{E}_{Kvib}\ (eV)$	0.19342 [17]	0.12770 [18]	0.11159 [19]	0.35532 (Eq. (13.458))
$\bar{E}_{osc}\ (eV)$	-0.13769	-0.19588	-0.21280	-0.14502
$E_{mag}\ (eV)$	0.11441	0.14803	0.14803	0.14803
$E_{T\,(Group)}\ (eV)$	-67.26284	-31.83125	-32.98196	-49.80996
$E_{initial\,(c_4\ AO/HO)}\ (eV)$	-14.63489	-14.63489	-14.63489	-14.63489
$E_{initial\,(c_5\ AO/HO)}\ (eV)$	0	0	0	-13.59844
$E_{D\,(Group)}\ (eV)$	8.72329	2.56147	3.71218	7.83016
Exp. $E_{D\,(Group)}\ (eV)$		Est. 2.86, 2.08 [20]	3.69 [20]	

Table 16.11. The total bond energy of gaseous-state RDX calculated using the functional group composition and the energies of Table 16.10.

Formula	Name	NO_2 Group	$N-N$ Group	$C-N$ Group	CH_2 Group	Calculated Total Bond Energy (eV)	Experimental Total Bond Energy (eV)	Relative Error
$C_3H_6N_6O_6$	RDX	3	3	6	3	79.61783		

Table 16.12. The bond angle parameters of RDX and experimental values [1]. E_T is E_T (*atom – atom,msp*^{3}*.AO*).

Atoms of Angle	2c' Bond 1 (a_0)	2c' Bond 2 (a_0)	2c' Terminal Atoms (a_0)	$E_{Coulombic}$ Atom 1	Atom 1 Hybridization Designation (Table 15.3A)	$E_{Coulombic}$ Atom 2	Atom 2 Hybridization Designation (Table 15.3A)	c_2 Atom 1	c_2 Atom 2	C_1	C_2	c_1	c_2'	E_T (eV)	θ_v (°)	θ_1 (°)	θ_2 (°)	Cal. θ (°)	Exp. θ (°)
$\angle O_a N O_b$	2.30843	2.30843	4.1231	-16.68411 O_a	25	-16.68411 O_b	25	0.81549	0.81549	1	1	1	0.81549	-1.44915				126.52	125.3 (nitromethane)
$\angle N_b N_a O_a$	2.59778	2.27630	4.0988	-17.79656 N_b (Eq. (16.4))		-13.61806 O_a		0.75468 (Eq. (16.5))	0.85987 (Eq. (15.159))	1	1	1	0.80727	-1.44915				114.32	116.8 [16] (RDX)
$\angle C N_b N_a$	2.79186	2.59778	4.5826	-16.32183	17	-14.53414		0.83360	0.91140 (Eq. (15.135))	1	1	1	0.87250	-1.44915				116.43	116.6 [16] (RDX)
$\angle CNC$	2.79186	2.79186	4.6260	-17.04640	33	-17.04640	33	0.79816	0.79816	1	1	1	0.79816	-1.85836				111.89	111.8 (dimethylamine)
Methylene $\angle HC_a H$	2.11106	2.11106	3.4252	-15.75493	7	H	H	0.86359	1	1	1	0.75	1.15796	0				108.44	107 (propane)
$\angle HCN$	2.09711	2.79186	4.0661	-14.82575	1	-14.53414	N	0.91771	0.93383 (Eq. (15.136))	0.75	1	0.75	1.01756	0				111.76	112 (dimethylamine)

SODIUM HYDRIDE MOLECULE (NaH)

Alkali hydride molecules each comprising an alkali metal atom and a hydrogen atom can be solved using similar principles and procedures as those used to solve organic molecules. The solutions of these molecules can be conveniently obtained by using generalized forms of the force balance equation given in the Force Balance of the σ MO of the Carbon Nitride Radical section and the geometrical and energy equations given in the Derivation of the General Geometrical and Energy Equations of Organic Chemistry section.

The bonding in the sodium atom involves the outer $3s$ atomic orbital (AO), and the $Na-H$ bond forms between the $Na3s$ AO and the $H1s$ AO. The energy of the reactive outer electron of the sodium atom is significantly less than the Coulombic energy between the electron and proton of H given by Eq. (1.276). Consequently, the outer electron comprising the $Na3s$ AO and the $H1s$ AO form a σ-MO, and the inner AOs of Na remain unaltered. The MO semimajor axis of molecular sodium hydride is determined from the force balance equation of the centrifugal, Coulombic, and magnetic forces as given in the Polyatomic Molecular Ions and Molecules section and the More Polyatomic Molecules and Hydrocarbons section. Then, the geometric and energy parameters of the MO are calculated using Eqs. (15.1-15.117) wherein the distance from the origin of the H_2-type-ellipsoidal-MO to each focus c', the internuclear distance $2c'$, and the length of the semiminor axis of the prolate spheroidal H_2-type MO $b=c$ are solved from the semimajor axis a.

The force balance of the centrifugal force equated to the Coulombic and magnetic forces is solved for the length of the semimajor axis. The Coulombic force on the pairing electron of the MO is:

$$\mathbf{F}_{Coulomb}=\frac{e^2}{8\pi\varepsilon_0 ab^2}D\mathbf{i}_\xi \tag{16.6}$$

The spin pairing force is

$$\mathbf{F}_{spin-pairing}=\frac{\hbar^2}{2m_e a^2b^2}D\mathbf{i}_\xi \tag{16.7}$$

The diamagnetic force is:

$$\mathbf{F}_{diamagneticMO1}=-\frac{n_e\hbar^2}{4m_e a^2b^2}D\mathbf{i}_\xi \tag{16.8}$$

where n_e is the total number of electrons that interact with the binding σ-MO electron. The diamagnetic force $\mathbf{F}_{diamagneticMO2}$ on the pairing electron of the σ MO is given by the sum of the contributions over the components of angular momentum:

$$\mathbf{F}_{diamagneticMO2}=-\sum_{i,j}\frac{|L_i|\hbar}{Z_j 2m_e a^2b^2}D\mathbf{i}_\xi \tag{16.9}$$

where $|L|$ is the magnitude of the angular momentum of each atom at a focus that is the source of the diamagnetism at the σ-MO. The centrifugal force is:

$$\mathbf{F}_{centrifugalMO}=-\frac{\hbar^2}{m_e a^2b^2}D\mathbf{i}_\xi \tag{16.10}$$

The force balance equation for the σ-MO of the $Na-H$-bond MO with $n_e=2$ and $|L|=\left(2+\sqrt{\frac{3}{4}}\right)\hbar$ is:

$$\frac{\hbar^2}{m_e a^2b^2}D=\frac{e^2}{8\pi\varepsilon_0 ab^2}D+\frac{\hbar^2}{2m_e a^2b^2}D-\left(\frac{2}{2}+\frac{2}{Z}+\frac{\sqrt{\frac{3}{4}}}{Z}\right)\frac{\hbar^2}{2m_e a^2b^2}D \tag{16.11}$$

$$a=\left(2+\frac{2}{Z}+\frac{\sqrt{\frac{3}{4}}}{Z}\right)a_0 \tag{16.12}$$

With $Z=11$, the semimajor axis of the $Na-H$-bond MO is:

$$a=2.26055a_0 \tag{16.13}$$

Using the semimajor axis, the geometric and energy parameters of the MO are calculated using Eqs. (15.1-15.117) in the same manner as the organic functional groups given in the Organic Molecular Functional Groups and Molecules section. For the $Na-H$-bond MO of the NaH, $c_1=1$, $c_2=1$ and $C_2=1$ in both the geometry relationships (Eqs. (15.2-15.5)) and the energy equation (Eq. (15.61)). In NaH the molecule, the $Na3s$ AO has an energy of $E(Na3s)=-5.139076\ eV$ [15] and the H AO has an energy of $E(H)=-13.59844\ eV$ [15]. To meet the equipotential condition of the union of the $Na3s$ AO and the $H1s$ AO, c_2 and C_2 of Eqs. (15.2-15.5) and Eq. (15.61) for the $Na-H$-bond MO given by Eq. (15.77) is:

$$C_2\left(Na3s\ AO\ to\ H1s\ AO\right)=c_2\left(Na3s\ AO\ to\ H1s\ AO\right)=\frac{-5.139076\ eV}{-13.59844\ eV}=0.37792 \tag{16.14}$$

The energy of the MO is matched to that of the $Na2p$ AO with which it intersects such that $E\left(AO/HO\right)$ is $E\left(Na2p\right)=-47.2864\ eV$ [15]; thus, $E_{initial}\left(c_4\ AO/HO\right)\ (eV)$ is given by the sum of $E\left(Na2p\right)=-47.2864\ eV$ and $E\left(Na3s\right)=-5.139076\ eV$.

The symbol of the functional group of molecular NaH is given in Table 16.13. The geometrical (Eqs. (15.1-15.5) and (16.11-16.14)), intercept (Eqs. (15.80-15.87)), and energy (Eqs. (15.61-15.65) and (16.13-16.14)) parameters of molecular NaH are given in Tables 16.14, 16.15, and 16.16, respectively. The color scale, translucent view of the charge-densities of molecular NaH comprising the concentric shells of the inner AOs of the Na atom and an outer MO formed from the outer $Na3s$ AO and the $H1s$ AO are shown in Figure 16.3.

Figure 16.3. Color scale, translucent view of the charge-densities of molecular NaH showing the inner orbitals of the Na atom at their radii, the ellipsoidal surface of the H_2-type ellipsoidal MO formed from the outer $Na3s$ AO and the $H1s$ AO H, and the hydrogen nucleus (red, not to scale).

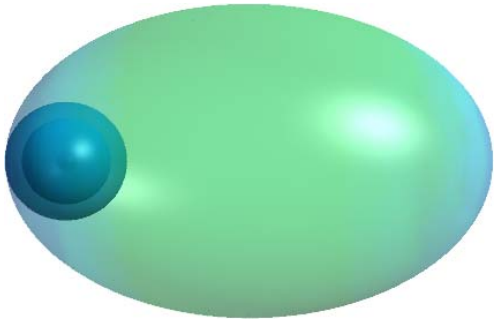

Table 16.13. The symbol of the functional group of molecular NaH.

Functional Group	Group Symbol
NaH group	$Na-H$

Table 16.14. The geometrical bond parameters of molecular NaH and experimental values [20].

Parameter	$Na-H$ Group
$a\ (a_0)$	2.26055
$c'\ (a_0)$	1.72939
Bond Length $2c'\ (\text{Å})$	1.83031
Exp. Bond Length (Å)	1.88654 (NaH)
$b,c\ (a_0)$	1.45577
e	0.76503

Table 16.15. The MO to *Na2p* AO intercept geometrical bond parameters of *NaH*. E_T is E_T (*atom – atom,msp³.AO*).

Bond	Atom	E_T (eV) Bond 1	E_T (eV) Bond 2	E_T (eV) Bond 3	E_T (eV) Bond 4	Final Total Energy *Na2p* (eV)	$r_{initial}$ (a_0)	r_{final} (a_0)	$E_{Coulomb}(Na2p)$ (eV) Final	$E(Na2p)$ (eV) Final	θ' (°)	θ_1 (°)	θ_2 (°)	d_1 (a_0)	d_2 (a_0)
Na – H (NaH)	*Na*	0	0	0	0		2.65432	0.56094		-47.2864	28.66	151.34	10.65	2.22161	0.49221

Table 16.16. The energy parameters (eV) of the *Na–H* functional group of molecular *NaH*.

Parameters	$Na-H$ Group
n_1	1
n_2	0
n_3	0
C_1	0.37792
C_2	1
c_1	1
c_2	1
c_3	0
c_4	1
c_5	1
C_{1o}	0.37792
C_{2o}	1
$V_e\ (eV)$	-31.72884
$V_p\ (eV)$	7.86738
$T\ (eV)$	7.01795
$V_m\ (eV)$	-3.50898
$E_{(AO/HO)}\ (eV)$	-47.2864
$\Delta E_{H_2MO(AO/HO)}\ (eV)$	0
$E_{T(AO/HO)}\ (eV)$	-47.2864
$E_{T(H_2MO)}\ (eV)$	-67.63888
$E_T\left(atom-atom, msp^3.AO\right)\ (eV)$	0
$E_{T(MO)}\ (eV)$	-67.63888
$\omega\ \left(10^{15}\ rad/s\right)$	14.4691 [20]
$E_K\ (eV)$	9.52384
$\overline{E}_D\ (eV)$	-0.41296
$\overline{E}_{Kvib}\ (eV)$	0.14534
$\overline{E}_{osc}\ (eV)$	-0.34029
$E_{mag}\ (eV)$	0.11441
$E_{T(Group)}\ (eV)$	-67.97917
$E_{initial(c_4\ AO/HO)}\ (eV)$	-52.425476
$E_{initial(c_5\ AO/HO)}\ (eV)$	-13.59844
$E_{D(Group)}\ (eV)$	1.95525
Exp. $E_{D(Group)}\ (eV)$	1.92451 ($Na-H$ [21])

BOND AND DIPOLE MOMENTS

The bond moment of a functional group may be calculated by considering the charge donation between atoms of the functional group. Since the potential of an MO is that of a point charge at infinity (Eq. (11.36)), an asymmetry in the distribution of charge between nonequivalent HOs or AOs of the MO occurs to maintain an energy match of the MO with the bridged orbitals. The charge must redistribute between the spherical orbitals to achieve a corresponding current-density that maintains constant current at the equivalent-energy condition according to the energy-matching factor such as c_2 or C_2 of Eqs. (15.51) and (15.61). Since the orbital energy and radius are reciprocally related, the contribution scales as the square of the ratio (over unity) of the energy of the resultant net positively-charged orbital and the initial matched energy of the resultant net negatively-charged orbital of the bond multiplied by the energy-matching factor (e.g. c_2 or C_2). The partial charges on the HOs or AOs corresponding to the charge contribution are equivalent to point charges centered on the nuclei. Due to symmetry, the bond moment μ of each functional group is along the internuclear axis and is calculated from the partial charges at the separation distance, the internuclear distance.

Using the reciprocal relationship between the orbital energies and radii, the dependence of the orbital area on the radius squared, and the relationship of the partial charge q to the areas with energy matching for each electron of the MO, the bond moment μ along the internuclear axis of $A-B$ wherein A is the net positively-charged atom is given by:

$$\mu = qd = n_1 ce\left(1-\left(\frac{E_A(valence)}{E_B(valence)}\right)^2\right)2c' \tag{16.15}$$

wherein n_1 is the number of equivalent bonds of the MO, c is energy-matching factor such as c_1, c_2, C_1, or C_2 of Eqs. (15.51) and (15.61) where c_1 and C_2 may correspond to both electrons of a MO localized on one AO or HO such as when the magnitude of the valence or Coulombic energy of the AO or HO is less than that of $E_{Coulomb}(H) = -13.605804\ eV$ or when the orbital may contain paired or shared electrons in a linear combination with the partner orbital, and d is the charge-separation distance, the internuclear distance $2c'$. $E_B(valence)$ is the initial matched energy of the resultant net negatively-charged orbital of the bond that is further lowered by bonding (Eqs. (15.32) and (15.16)) to atom A having an energy $E_A(valence)$. Typically, $E_B(valence)$ of a carbon-heteroatom bond is $-14.63489\ eV$, the initial $C2sp^3$ HO (Eq. (15.25)) energy to which the heteroatom is energy matched. Functional group bond moments determined using Eq. (16.15) are given in Table 16.17.

Table 16.17. The bond moments of functional groups compared to experimental values [22–87] wherein the parameters correspond to those given previously except as indicated.

Functional Group [a]	n_1	$(c_1)c_2$	$(C_1)C_2$	$E_B(valence)$	$E_A(valence)$	$\frac{q}{e}$	Bond Length $2c'$ (Å)	Bond Moment μ (D)	Exp. Bond Moment μ (D)
$H-C$ (alkyl)	1	0.91771	1	14.63489	15.35946	0.070	1.11713	0.37	0.4
$H-C$ (aromatic)	1	0.91771	1	15.95955	15.95955	0	1.09327	0	0
$H-N$ [b] (amine)	1	0.78896	1	13.59844	15.81768	0.279	1.00343	1.34	1.31
$H-N$ [c] (ammonia)	1	0.74230	1	13.59844	15.81768	0.262	1.03677	1.30	1.31
$H-O$ [d] (alcohol)	1	0.91771	1	13.59844	15.81768	0.324	0.97165	1.51	1.51
$H-O$ [e] (water)	1	0.91419	1	13.59844	15.81768	0.323	0.97157	1.51	1.51
$C-N$	1	0.91140	1	14.53414	14.82575	0.037	1.46910	0.26	0.22
$C-O$	1	0.85395	1	14.63489	15.56407	0.112	1.41303	0.76	0.74
$C-F$ [f]	1	1.09254[b]	1	14.63489	15.98435	0.211	1.38858	1.41	1.41
$C-Cl$	1	1	(2)0.81317	14.63489	15.35946	0.165	1.79005	1.42	1.46
$C-Br$	1	1	(2)0.74081	14.63489	15.35946	0.150	1.93381	1.40	1.38
$C-I$ [g]	1	1	(2)0.65537	14.63489	15.28545	0.119	2.13662	1.22	1.19
$C=O$	2	0.85395	1	14.63489	16.20002	0.385	1.20628	2.23	2.3
$C\equiv N$	3	0.91140	1	14.63489	16.20002	0.616	1.16221	3.44	3.5
$H-S$ [h]	1	0.69878	1	14.63489	15.81768	0.118	1.34244	0.76	0.69
$C-S$	1	1	0.91771	14.63489	15.35946	0.093	1.81460	0.81	0.9
$S-O$	1	1	0.77641	14.63489	15.76868	0.125	1.56744	0.94	1.0
$S=O$ [i]	2	0.82897	1	10.36001	11.57099	0.410	1.49118	2.94	2.93
$N-O$	1	1.06727	1	14.53414	14.82575	0.043	1.40582	0.29	0.30
$N=O$ (nitro)	2	0.91140	1	14.63489	15.95955	0.345	1.22157	2.02	2.01
$C-P$	1	1	0.73885	14.63489	15.35946	0.075	1.86534	0.67	0.69
$P-O$	1	0.79401	1	14.63489	15.35946	0.081	1.61423	0.62	0.60
$P=O$ [j]	2	1.25942	1	14.63489	15.76868	0.405	1.46521	2.85	2.825
$Si-H$	1	1	0.75800	10.25487	11.37682	0.131	1.48797	0.94	0.99
$Si-C$	1	1	0.70071	14.63489	15.35946	0.071	1.87675	0.64	0.60
$Si-O$ [k]	1	1	1.32796	10.25487	10.87705	0.166	1.72480	1.38	1.38
$B-H$ [l]	1	1.14361	1	11.80624	12.93364	0.172	1.20235	0.99	1.0
$B-C$	1	0.80672	1	14.63489	15.35946	0.082	1.57443	0.62	0.69
$B-O$ (alkoxy)	1	1	0.79562	11.80624	12.93364	0.159	1.37009	1.05	0.93
$B-N$	1	1	0.81231	11.89724	14.53414	0.400	1.36257	2.62	2.68
$B-F$ [m]	1	0.85447	1	14.88734	17.42282	0.316	1.29621	1.97	1.903
$B-Cl$	1	1	0.91044	11.80624	12.93364	0.182	1.76065	1.54	1.58

[a] The more positive atom is on the left.

[b] c_2 from Eqs. (15.77), (15.79), and Eq. (13.430) and $E_A(valence)$ is given by 1/2 two H_2-type ellipsoidal MOs (Eq. (11.212)).

[c] c_2 from Eqs. (15.77), (15.79), and the product of 0.936127 (Eq. (13.248)) and 0.92235 given by $13.59844\ eV / (13.59844\ eV + 0.25 \cdot E_D)$ where E_D is the $N-H$ bond energy $E_D\left({}^{14}NH_3\right) = 4.57913\ eV$ given by Eq. (13.404) and the energy of H is $13.59844\ eV$; $E_A(valence)$ is given by 1/2 two H_2-type ellipsoidal MOs (Eq. (11.212)).

[d] $E_A(valence)$ is given by 1/2 two H_2-type ellipsoidal MOs (Eq. (11.212)).

[e] c_2 from Eqs. (15.77) given by $13.59844\ eV / (13.59844\ eV + 0.25 \cdot E_D)$ where E_D is the $O-H$ bond energy $E_D(H^{16}OH) = 5.1059\ eV$ given by Eq. (13.222) and the energy of H is $13.59844\ eV$; $E_A(valence)$ is given by 1/2 two H_2-type ellipsoidal MOs (Eq. (11.212)).

[f] Eq. (15.129) with the inverse energy ratio of $E(F) = -17.42282\ eV$ and $E(C, 2sp^3) = -14.63489\ eV$ corresponding to the higher binding energy of the former.

[g] $E_A(valence)$ is given by $15.35946\ eV - 1/2E_{mag}$ (Eqs. (14.150) and (15.67)).

[h] c_1 from Eqs. (15.79), (15.145), and (13.430); $E_A(valence)$ is given by 1/2 two H_2-type ellipsoidal MOs (Eq. (11.212)).

[i] c_2 from the reciprocal of Eq. (15.147), $E_A(valence)$ is given by Eq. (15.139), and $E_B(valence)$ is $E(S) = -10.36001\ eV$.

[j] c_2 from the reciprocal of Eq. (15.182).

[k] c_2 from the reciprocal of Eq. (20.49).

[l] c_2 from the reciprocal of Eq. (22.29).

[m] c_2 from Eq. (15.77) using $E(F) = -17.42282\ eV$ and $E\left(B_{B-Fborane}, 2sp^3\right) = -14.88734\ eV$ (Eq. (22.61)).

The dipole moment of a given molecule is then given by the vector sum of the bond moments in the molecule. Thus, the dipole moment is given by taking into account the magnitude and direction of the bond moment of each functional group wherein the functional group bond moment stays constant from molecule to molecule and is in the vector direction of the internuclear axis. The dipole moments of water and ammonia to compare to the experimental values are given from the corresponding moments in Table 16.17. The calculated dipole moment of H_2O is:

$$\mu_{H_2O} = 2(1.51)\cos\left(\frac{106°}{2}\right) = 1.8128D \tag{16.16}$$

where the angle between the $O-H$ bond is 106° given by Eq. (13.242). The experimental dipole moment of H_2O is [23] :

$$\mu_{H_2O} = 1.8546D \tag{16.17}$$

The calculated dipole moment of NH_3 is:

$$\mu_{NH_3} = 3(1.30)\cos(68°) = 1.467D \tag{16.18}$$

where the angle between each $N-H$ bond and the z-axis is 68° given by Eq. (13.417). The experimental dipole moment of NH_3 is [23]:

$$\mu_{NH_3} = 1.4718D \tag{16.19}$$

The charge distributions of the functional groups given in Table 16.17 facilitate the rendering of the charge distribution of molecules of unlimited complexity comprised of these functional groups. What was previously impossible to achieve using supercomputers can be readily accomplished on a personal computer (PC). The rendering of the true charge densities of the exemplary proteins insulin and lysozyme are shown in color scale, opaque view in Figures 16.4 and 16.5, respectively. The color scale, opaque view of the charge density of an exemplary double-stranded RNA helix is shown in Figure 16.6.

Figure 16.4. Color scale, opaque view of the charge density of insulin created and modeled using Millsian 2.0 on a PC.

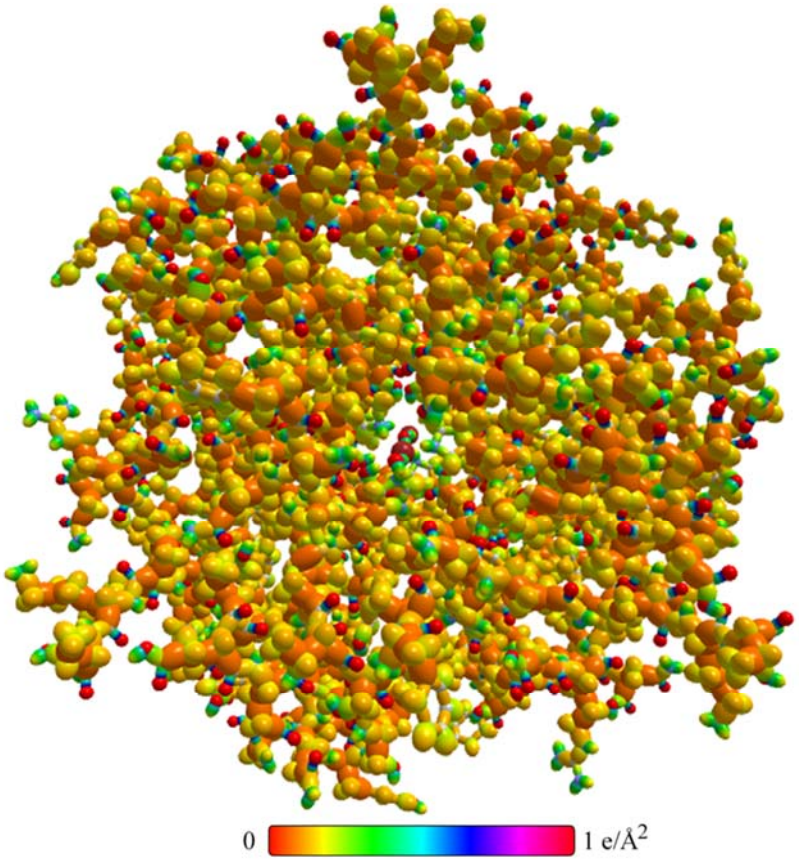

Figure 16.5. Color scale, opaque view of the charge density of lysozyme created and modeled using Millsian 2.0 on a PC.

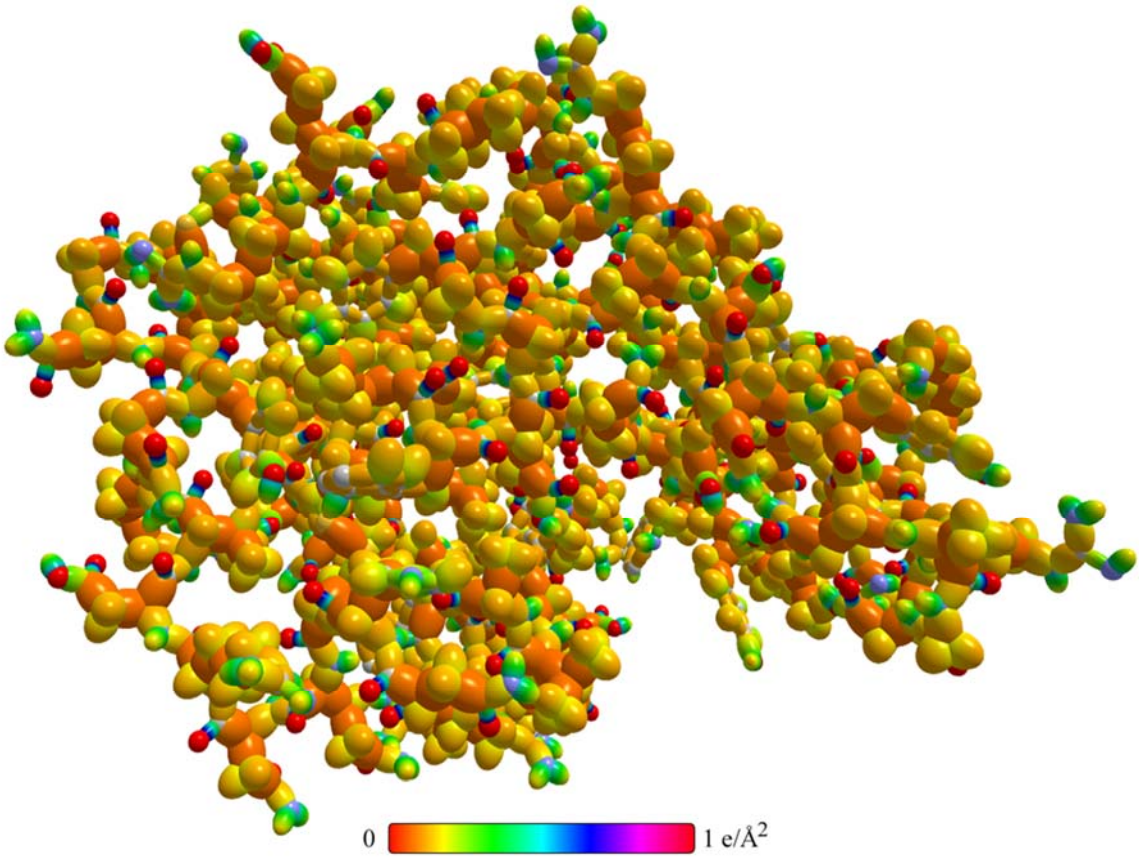

Figure 16.6. Color scale, opaque view of the charge density of a double-stranded DNA helix created and modeled using Millsian 2.0 on a PC.

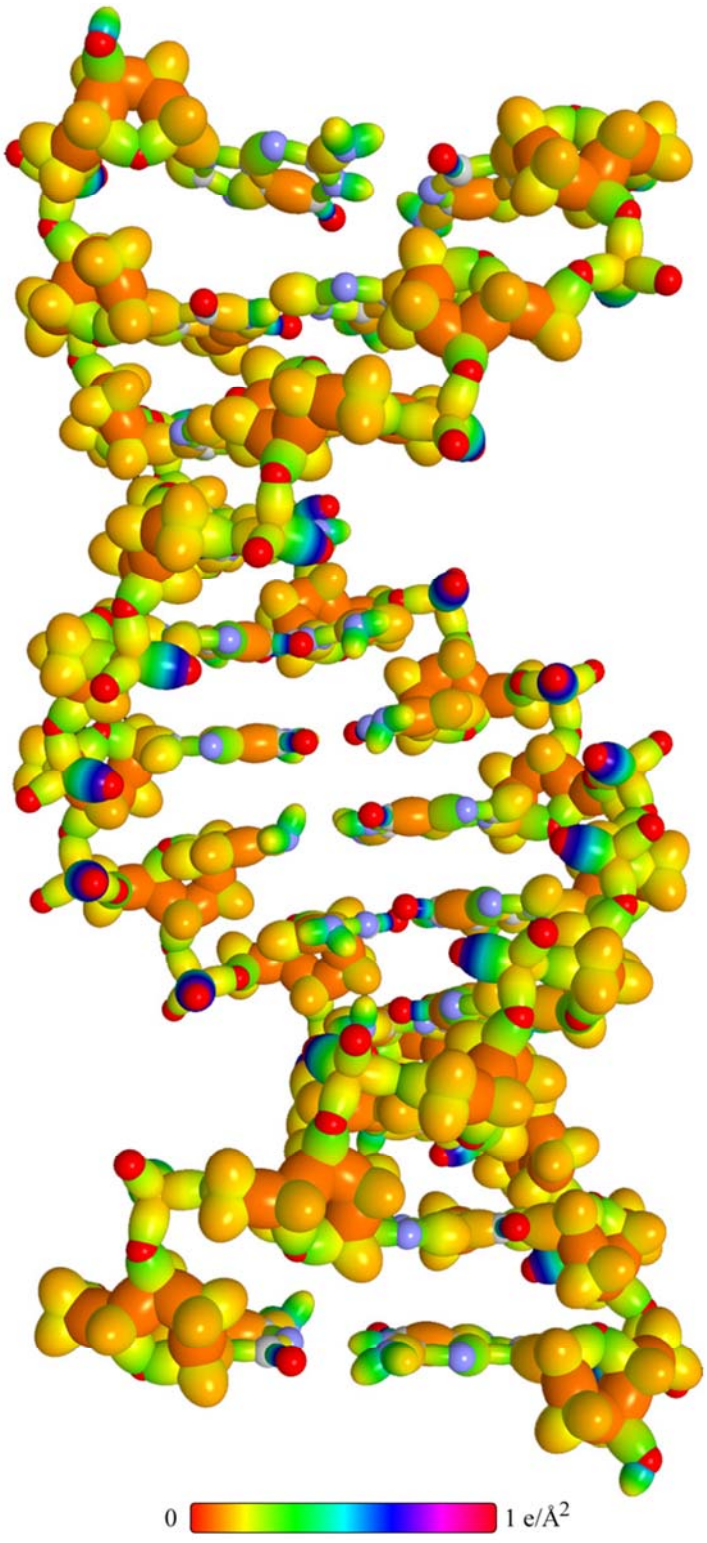

NATURE OF THE DIPOLE BOND: DIPOLE-DIPOLE, HYDROGEN, AND VAN DER WAALS BONDING

The boundless number and length of permutations of the functional groups can form a correspondingly infinite number of molecules. The intermolecular forces instill upon molecules their inherent properties such as state—being solid, liquid, or gas, the temperatures at which phase transitions occur, and the energy content change required to change the state. However, the types of bonding are relatively few even though the breadth of molecular compositions is infinite. Since all molecules comprise nuclei that behave on the scale of molecules as electrostatic point charges, and electrically charged electrons exist as charge and current densities that obey Maxwell's equations, the binding is determined by electrical and electrodynamics forces. These typically dominate over any magnetic forces since the latter is a relativistic effect of the former and is thus negligible as the norm. Thus, essentially all molecular bonding is Coulombic in nature. The extreme case involves ions, and ionic bonding between charged functional groups of molecules obeys the same physical principles as inorganic ions as given in the Nature of the Solid Ionic Bond of Alkali Hydrides and Halides section. Similarly, the charge-density distributions of negatively-charged electrons relative to the positively-charged nuclei of neutral molecules gives rise to Coulombic-based bonding that can be grouped into two main categories, bonding that comprises permanent dipole-dipole interactions further including an extreme case, hydrogen bonding, and bonding regarding reversible mutually induced dipole fields in near-neighbor molecules called van der Waals bonding.

The H bond is exemplary of the extreme of dipole-dipole interactions as the source of bond energy and rises from the extremely high dipole moments of H bound to F, O, or N as shown in the Bond and Dipole Moments section. The bond energies of these types of bonds are large due to the very high Coulombic energy associated with the dipole-dipole interaction between H-bonded molecules compared to those having much lower dipole moments. Still H-bond energies are typically small by the standards of covalent bonds. The differences are also reflected in the relative bond lengths. In water for example, the $O-H$ bond distance and energy are $2c' = 0.970 \pm .005\ \mathring{A}$ (Eq. (13.186)) and $E_D(H^{16}OH) = 5.1059\ eV$ (Eq. (13.222), respectively; whereas, those of the hydrogen bond of water are $2c'_{O\sim H} = 1.78\ \mathring{A}$ (Eq. (16.27) and $E_{vapor,0°C} = 0.233\ eV\ /\ H-bond$ (Eq. (16.57)), respectively. On the other end of the spectrum, van der Waals bonds are also Coulombic in nature and are between dipoles. However, the dipoles are mutually induced rather than permanent, and the mutual induction is typically small. Thus, the bond distances are on the order of angstroms and the energies in the 10's of meV's range. The bonding between molecules gives rise to condensed matter, and the classical theory of condensed matter based on these forms of bonding is treated next.

CONDENSED MATTER PHYSICS

Condensed matter comprises liquids and solids of atoms and molecules. It is shown *infra* that the geometrical parameters, energies, and properties of the latter can be solved using the same equations as those used to solve the geometrical parameters and component energies of the individual molecules as given in the Organic Molecular Functional Groups and Molecules section.

The structure and properties of liquids can be solved by first solving the unit cell of the corresponding condensed solid. The unit cell may be solved by first determining the packing that minimizes the lattice energy. In nature, there are a small, finite number of packing arrangements. The particular arrangement relates to the most efficient one giving the most objects packed into a given space with the size and shape limitations. The water molecule, for example, is small compared to the unit cell of ice; so, it will naturally assume a tetrahedral structure and hexagonal packing given the geometry of its electric dipoles with a partial positive on the H's and partial negative on the O. In general, a reiterative algorithm is used that optimizes the packing of the molecules and tests that packing against the unit cell parameters and lattice energy until an optimum is found. The lattice parameters can be verified by X-ray crystallography and neutron diffraction. The lattice energy can be measured using calorimetry; so, the model can be directly tested.

Bonding in neutral condensed solids and liquids arises from interactions between molecules wherein the molecules of the lattice have multipoles that give rise to corresponding Coulombic or magnetic interactions. Typically, the multipoles are electric or magnetic dipoles. Consider the former case. Since the separated partial charges that give rise to bond moments are equivalent to point charges centered on the bond nuclei as given in the Bond and Dipole Moments section, the maximum interaction energy between interacting species can be calculated using Coulomb's law with the corresponding partial monopole charges and separation distance. The energy from the interaction of the partial charges increases as the separation decreases, but concomitantly, the energy of a bond that may form between the interacting species increases as well. The equilibrium separation distance corresponds to the occurrence of the balance between the Coulombic potential energy of the interacting atoms and the energy of the bond whose formation involves the interacting atoms. Thus, the balance is at the energy threshold for the formation of a nascent bond that would replace the interacting partial charges while also destabilizing the standard bonds of the interacting molecules. Then, an optimal lattice structure corresponds to an energy minimum with an associated energy. The minimum energy structure corresponds to the highest density of interacting dipoles in their minimum energy state. A convenient method to calculate the lattice energy is to determine the electric or magnetic field in the material having an electric or magnetic polarization density, and in turn, the energy can be calculated from the energy of each dipole in the corresponding field using the electrostatic or magnetostatic form of Gauss' or Amperes' equation, respectively.

Once the a, b, and c parameters of the unit cell are solved from the energy (force) balance between the electric monopoles and the nascent bond energy, the unit cell is determined. Then, the unit cell can be proliferated to arbitrary scale to

render the solid. Typically, only one lattice parameter needs to be determined since the additional distances can be determined from geometrical relations based on the unit cell structure. The lattice energy may be calculated from the potential between dipoles using the cell parameters. The dielectric constant and other properties may also be calculated using Maxwell's equations and other first principles.

The structures of liquids can be modeled as linear combinations of unit cells comprising perturbations of the solid unit cell. In one approach, increasing disorder is added to the solid structure in the transition from solid to liquid to gas. Complete disorder or statistical gas behavior applies in the ideal gas limit. Thus, liquid states may be modeled by adding more cells with increasing loss of order of the solid unit cell as the temperature of the liquid is increased. The disorder is due to population of translational, rotational, and vibrational levels to match the internal energy at a given temperature. Consider thermodynamics. In principle, it is possible to classically calculate the fields over all space, the exact field interactions, and the position, trajectory, momentum, and energy of every particle of a material at each instance. Then, the material properties can be determined from these parameters. However, in practice, it is impossible computationally. For the same reason, simple underlying physical principles are applied to derive statistical properties for large ensembles of particles as given in the Statistical Mechanics section. The same statistical thermodynamic methods may be applied to modeling liquids and gases using the exact solutions of the individual molecules. Using the molecular geometrical parameters, charge distributions, and corresponding interactions as input, unit cells can be computed based on the solid unit cell. Working with increasing numbers of unit cells of increasing randomness and populating the unit cells based on appropriate statistical models such as Boltzmann statistics for increasing enthalpy input and temperature, accurate models of liquids are provided. The corresponding liquid properties can be solved from each liquid structure.

A preferred approach to solving the energy and geometric parameters of ice, considered next, is to solve the separation distance of the electric monopoles comprising a partial positive on each H and a partial negative charge on each O as the balance between the Coulombic attraction energy between the partial charges and the repulsion energy due to the formation of a nascent $H-O$ bond between the hydrogen-bonded atoms. The nascent bond substitutes for the hydrogen bond while also removing electron density and stability from the standard water molecule bonds. Thus, it offsets the Coulombic energy and establishes the equilibrium minimum approach distance of the interacting atoms of the water molecules. Then, using Gauss's law, the energy per water molecule is calculated as the dipole energy in the electric field of the lattice of electric dipoles.

GEOMETRICAL PARAMETERS AND ENERGIES OF THE HYDROGEN BOND OF H_2O IN THE ICE PHASE

The extraordinary properties of water are determined by hydrogen (H) bonds, designated by the dotted bond $O-H\cdots O$, each between a participating H of one water molecule and an O of another. The structure of each phase of water is then determined by the number of H bonds on average per water molecule. As shown in the Bond and Dipole Moments section, the $O-H$ bond has a bond moment μ of 1.51 D corresponding to a partial charge on each H of $+0.323e$ and a component of partial charge on each O per bond moment of $-0.323e$. The thermodynamic basis of the H bond is the minimization of the Coulombic energy between the H and O of the hydrogen bond, limited by the formation of a nascent bond between these atoms that destabilizes the initial $O-H$ bond. The sum of the torques and forces are zero at force balance to achieve a hexagonal crystal structure that is an energy minimum. The maximum electrostatic energy of the partial charges is calculated for the components along the H-bond axis. This energy is balanced by the total energy of the nascent bond that can form between the $H\cdots O$ atoms of the H bond. The bond length of the H bond, the internuclear distance between the H and O of the $H\cdots O$ bond, is calculated by a similar method as that used to determine the bond angle given in the Bond Angle of H_2O section.

The H_2O MO comprises a linear combination of two $O-H$-bond MOs. Each $O-H$-bond MO comprises the superposition of a H_2-type ellipsoidal MO and the $O2p_z$ AO or the $O2p_y$ AO with a relative H partial orbital contribution to the MO of 0.75; otherwise, the $O2p$ orbitals are the same as those of the oxygen atom. The solution of the geometrical parameters and component energies are given in the Water Molecule (H_2O) section and the color scale charge density of the H_2O MO is shown in Figure 16.7.

Figure 16.7. H_2O MO comprising the linear combination of two $O-H$ -bond MOs. Each $O-H$ -bond MO comprises the superposition of a H_2 -type ellipsoidal MO and the $O2p_z$ AO or the $O2p_y$ AO with a relative charge-density of 0.75 to 1.25; otherwise, the $O2p$ orbitals are the same as those of the oxygen atom. The internuclear axis of one $O-H$ bond is perpendicular to the bonding p_y orbital, and the internuclear axis of the other $O-H$ bond is perpendicular to the bonding p_z orbital. (A) Color scale, translucent view of the charge-density of the H_2O MO from the top. For each $O-H$ bond, the ellipsoidal surface of each H_2 -type ellipsoidal MO transitions to the $O2p$ AO. The $O2p$ shell, the $O2s$ shell, the $O1s$ shell, and the nuclei (red, not to scale) are shown. (B) Cut-away view showing the innermost $O1s$ shell, and moving radially, the $O2s$ shell, the $O2p$ shell, and the H_2 -type ellipsoidal MO that transitions to the $O2p$ AO for each $O-H$ bond. Bisector current not shown.

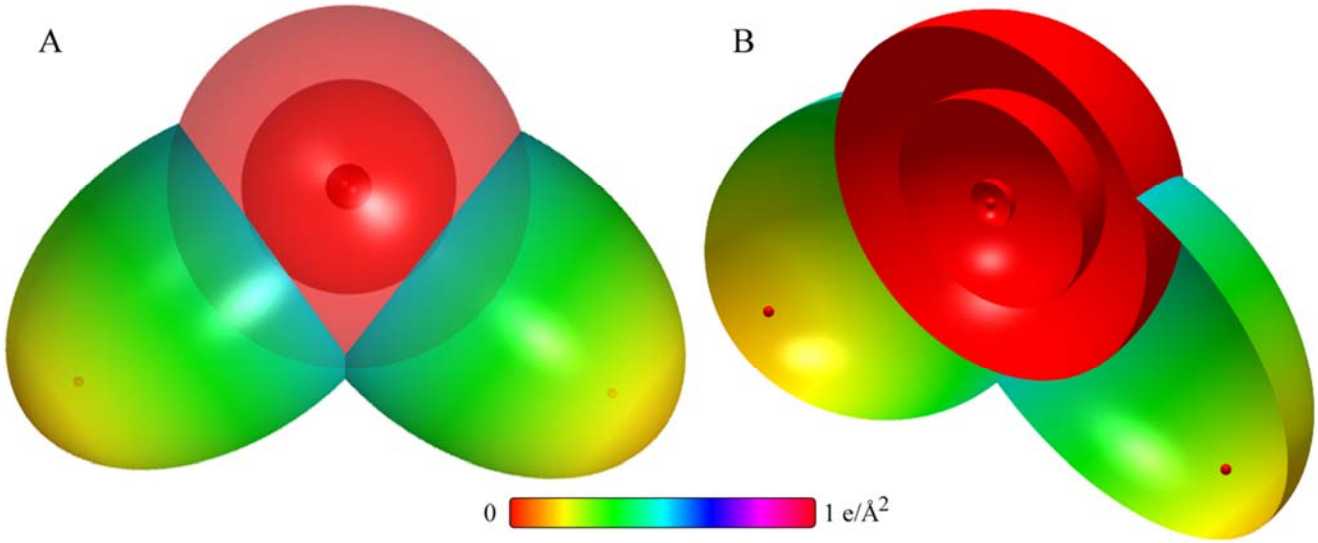

Rather than consider the possible bond between the two H atoms of the $O-H$ bonds in the determination of the bond angle, consider that the hydrogen bond may achieve a partial bond order or partial three-centered $O-H-O$ bond as given in the Bridging Bonds of Organoaluminum Hydrides ($Al-H-Al$ and $Al-C-Al$) and Bridging Bonds of Boranes ($B-H-B$ and $B-B-B$) sections, and the H can become mobile between water molecules corresponding to H exchange. Such exchange of $O\cdots H-O$ to $O-H\cdots O$ bonding would decrease the initial $O-H$ -bond strength since electron density would be shifted from the $O-H$ bonds to the $O\cdots H$ bond. Concomitantly, the Coulombic energy of the H bond would be eliminated. Thus, the equilibrium distance r_e or internuclear bond distance of $O\cdots H$ designated as $2c'_{O\cdots H}=r_e$ is determined by the condition that the total energy of the nascent H_2 -type ellipsoidal MO formed from the atoms of the $O\cdots H$ bond is equal to the maximum Coulombic energy between the partial charges of the H and O atoms of the H bond.

The $O-H$ bond moments superimpose at the central O. The minimum energy corresponds to the maximum separation of the δ^- of each bond moment on the O atom that occurs in space and time with π phase. The corresponding distance is the hypotenuse of the right triangle having the distance $2c'_{O\cdots H}$ between the H and O nuclei of the $H\cdots O$ bond as one side and the radius of the oxygen atom, $r_{O2p}=a_0$ (Eq. (10.162)), as the other. Then, the maximum Coulomb energy $E_{Coulomb}(H-bond)$ between the atoms of the $O\cdots H$ bond due to the two separated δ^-'s on the oxygen atom with the δ^+ centered on the nucleus of hydrogen is:

$$E_{Coulomb}(H-bond)=\frac{-2\delta^2e^2}{4\pi\varepsilon_0\sqrt{\left(2c'_{O\cdots H}\right)^2+\left(r_{O2p}\right)^2}} \tag{16.20}$$

Since each H bond is between two H_2O molecules and there are four H bonds per H_2O molecule, the Coulomb energy per H_2O $E_{Coulomb}(H_2O)$ is equivalent to two times $E_{Coulomb}(H-bond)$ (Eq. (16.20)):

$$E_{Coulomb}(H_2O)=\frac{-4\delta^2e^2}{4\pi\varepsilon_0\sqrt{\left(2c'_{O\cdots H}\right)^2+\left(r_{O2p}\right)^2}} \tag{16.21}$$

Eq. (16.21) is the energy to be equated to that of the nascent covalent bonds involving the atoms of the H bonds of the water molecule. Using Eq. (15.3), the internuclear distance of this bond, $2c'_{O\cdots H} = r_e$, in terms of the corresponding semimajor axis $a_{O\cdots H}$ is:

$$2c'_{O\cdots H} = 2\sqrt{\frac{a_{O\cdots H}a_0}{2C_1C_2}} \tag{16.22}$$

The length of the semiminor axis of the prolate spheroidal MO $b = c$ is given by:

$$b_{O\cdots H} = \sqrt{\left(a_{O\cdots H}\right)^2 - \left(c'_{O\cdots H}\right)^2} \tag{16.23}$$

And, the eccentricity, e, is:

$$e_{O\cdots H} = \frac{c'_{O\cdots H}}{a_{O\cdots H}} \tag{16.24}$$

The semimajor axis $a_{O\cdots H}$ of the $O\cdots H$ bond is determined using the general equation for determination of the bond angle between terminal atoms given by Eqs. (15.93) and (15.99) with Eqs. (15.46-15.47) except that the MO energy is matched to the Coulombic energy of the H bond (Eq. (16.21) with substitution of Eq. (15.3)) rather than being set equal to zero for zero interaction energy in the case of the bond-angle determination:

$$\frac{-4\delta^2e^2}{4\pi\varepsilon_0\sqrt{\left(2\sqrt{\frac{a_{O\cdots H}a_0}{2C_1C_2}}\right)^2 + \left(r_{O2p}\right)^2}} = \left[\begin{array}{l} \left(\begin{array}{l} -\frac{n_1e^2}{8\pi\varepsilon_0\sqrt{\frac{aa_0}{2C_1C_2}}}\left[c_1c_2\left(2-\frac{a_0}{a}\right)\ln\frac{a+\sqrt{\frac{aa_0}{2C_1C_2}}}{a-\sqrt{\frac{aa_0}{2C_1C_2}}} - 1\right] + E_T\left(AO/HO\right) \\ +E_T\left(atom-atom, msp^3.AO\right) \end{array}\right) \\ \left[1+\sqrt{\frac{2\hbar\sqrt{\frac{\frac{C_{1o}C_{2o}e^2}{4\pi\varepsilon_oR^3}}{m_e}}{m_ec^2}}\right] + n_1\frac{1}{2}\hbar\sqrt{\frac{\frac{c_1c_2e^2}{8\pi\varepsilon_oa^3} - \frac{e^2}{8\pi\varepsilon_o\left(a+\sqrt{\frac{aa_0}{2C_1C_2}}\right)^3}}{\mu}}\end{array}\right] \tag{16.25}$$

where n_1 is the number of equivalent bonds of the MO, c_1 is the fraction of the H_2-type ellipsoidal MO basis function, c_2 is the factor that results in an equipotential energy match of the participating at least two atomic orbitals of each chemical bond, C_{1o} is the fraction of the H_2-type ellipsoidal MO basis function of the oscillatory transition state of a chemical bond of the group, and C_{2o} is the factor that results in an equipotential energy match of the participating at least two atomic orbitals of the transition state of the chemical bond, $E_T\left(AO/HO\right)$ is the total energy comprising the difference of the energy $E\left(AO/HO\right)$ of at least one atomic or hybrid orbital to which the MO is energy matched and any energy component $\Delta E_{H_2MO}\left(AO/HO\right)$ due to the AO or HO's charge donation to the MO, $E_T\left(atom-atom, msp^3.AO\right)$ is the change in the energy of the AOs or HOs upon forming the bond, and μ is the reduced mass.

For the determination of the H-bond distance, the energy parameters are the same as those of water given in the Water Molecule $\left(H_2O\right)$ section except that any parameters due to matching AO's, $E_T\left(AO/HO\right)$ and $E_T\left(atom-atom, msp^3.AO\right)$, is zero since only the energies of the MO electrons to form the $O\cdots H$ MO are considered. The partial charge $\delta = q/e$ from Table 16.17 is 0.323, and the reduced mass is $\mu = \frac{16}{17}$. The parameters are summarized in Table 16.18 and Eq. (16.26).

Table 16.18. The energy parameters (eV) of the $O\cdots H$ functional group of the hydrogen bond of Type I ice.

Parameters	$O\cdots H$ Group
δ	0.323
n_1	2
C_1	0.75
C_2	1
c_1	0.75
c_2	1
C_{1o}	1.5
C_{2o}	1
$V_e\ (eV)$	-20.30177
$V_p\ (eV)$	16.15958
$T\ (eV)$	2.38652
$V_m\ (eV)$	-1.19326
$E_{(AO/HO)}\ (eV)$	0
$\Delta E_{H_2MO(AO/HO)}\ (eV)$	0
$E_{T(AO/HO)}\ (eV)$	0
$E_{T(H_2MO)}\ (eV)$	-2.94892
$E_T\left(atom-atom, msp^3.AO\right)\ (eV)$	0
$E_{T(MO)}\ (eV)$	-2.94892
$\omega\ \left(10^{15}\ rad/s\right)$	6.55917
$E_K\ (eV)$	4.31736
$\bar{E}_D\ (eV)$	-0.012122
$\bar{E}_{Kvib}\ (eV)$	0.03263
$\bar{E}_{osc}\ (eV)$	0.004191
$E_{T(Group)}\ (eV)$	-2.94054

Substitution of the parameters of Table 16.18, the internuclear distance $2c'_{O-H}$ given by Eq. (13.185), and R given by Eq. (16.23) and (16.22) into Eq. (16.25) gives:

$$\frac{-4(0.323)^2 e^2}{4\pi\varepsilon_0\sqrt{\left(2\sqrt{\frac{a_{O\cdots H}a_0}{2(0.75)}}\right)^2+\left(5.2917706\,X\,10^{-11}\ m\right)^2}}=\left\{\begin{array}{l}\left(\frac{-e^2}{4\pi\varepsilon_0\sqrt{\frac{a_{O\cdots H}a_0}{2(0.75)}}}\left(\left(\frac{3}{2}-\frac{3}{8}\frac{a_0}{a_{O\cdots H}}\right)\ln\frac{a_{O\cdots H}+\sqrt{\frac{a_{O\cdots H}a_0}{2(0.75)}}}{a_{O\cdots H}-\sqrt{\frac{a_{O\cdots H}a_0}{2(0.75)}}}-1\right)\right)\\ \left(1+2\sqrt{\frac{2\hbar\sqrt{\frac{\frac{3}{2}\frac{e^2}{4\pi\varepsilon_0\left(\sqrt{\left(a_{O\cdots H}\right)^2-\left(2\sqrt{\frac{a_{O\cdots H}a_0}{2(0.75)}}\right)^2}\right)^3}}{m_e}}{m_e c^2}}\right)\\ +2\left(\frac{1}{2}\right)\hbar\sqrt{\frac{\frac{0.75e^2}{8\pi\varepsilon_o\left(a_{O\cdots H}\right)^3}-\frac{e^2}{8\pi\varepsilon_o\left(a+\sqrt{\frac{a_{O\cdots H}a_0}{2(0.75)}}\right)^3}}{\frac{16}{17}}}\end{array}\right\} \tag{16.26}$$

From the energy relationship given by Eq. (16.26) and the relationships between the axes given by Eqs. (16.22-16.24), the dimensions of the $O\cdots H$ MO can be solved.

The most convenient way to solve Eq. (16.26) is by the reiterative technique using a computer. The result to within the round-off error with five-significant figures is:

$$a_{O\cdots H}=4.25343a_0=2.25082\,X\,10^{-10}\ m \tag{16.27}$$

The component energy parameters at this condition are given in Table 16.18. Substitution of Eq. (16.27) into Eq. (16.22) gives

$$c'_{O\cdots H}=1.68393a_0=8.91097\,X\,10^{-11}\ m \tag{16.28}$$

and internuclear distance of the H bond:

$$2c'_{O\cdots H}=3.36786a_0=1.78219\,X\,10^{-10}\ m=1.78219\ \text{Å} \tag{16.29}$$

The internuclear distance of the $O-H$ given by Eq. (13.185) is:

$$2c'=1.83601a_0=9.71574\,X\,10^{-11}\ m \tag{16.30}$$

The internuclear distance $2c'_{O\text{-}H}$ of the $O-H$ bond added to $2c'_{O\cdots H}$ gives the internuclear distance $2c'_{O\cdots HO}$ between the oxygen atoms of the group $O-H\cdots O$:

$$2c'_{O\cdots HO}=2c'_{O\cdots H}+2c'_{O\text{-}H} \tag{16.31}$$

Substitution of $2c'_{O\cdots H}$ (Eq. (16.29)) and $2c'_{O\text{-}H}$ (Eq. (13.185)) into Eq. (16.31) gives the nearest-neighbor separation, the internuclear distance $2c'_{O\cdots HO}$ between the oxygen atoms of the $O-H\cdots O$ bond in Type I ice:

$$2c'_{O\cdots HO}=2c'_{O\cdots H}+2c'_{O\text{-}H}=1.78219\,X\,10^{-10}\ m+9.71574\,X\,10^{-11}\ m=2.75377\,X\,10^{-10}\ m=2.75377\ \text{Å} \tag{16.32}$$

The experimental oxygen nearest-neighbor separation distance $2c'_{O\cdots HO}$ is [88]:

$$2c'_{O\cdots HO}=2.75\ \text{Å} \tag{16.33}$$

The experimental internuclear distance of the $O-H$ bond of H_2O is [89]:

$$2c'=9.70\pm.005\,X\,10^{-11}\ m \tag{16.34}$$

Using Eqs. (16.33) and (16.34), the experimental H bond distance $2c'_{O\cdots H}$ in Type I ice is [88, 89]:

$$2c'_{O\cdots H}=1.78\ \text{Å} \tag{16.35}$$

The other H-bond MO parameters can also be determined by the relationships among the parameters. Substitution of Eqs. (16.27) and (16.28) into Eq. (16.23) gives:

$$b_{O\cdots H}=c_{O\cdots H}=3.90590a_0=2.06691\,X\,10^{-10}\ m \tag{16.36}$$

Substitution of Eqs. (16.27) and (16.28) into Eq. (16.24) gives:

$$e_{O\cdots H}=0.39590 \tag{16.37}$$

Since water is a hexagonal crystal system in common with the carbon allotrope diamond, the internuclear distance of the two terminal O atoms of a set of three H_2O's corresponding to the hexagonal lattice parameter a_l is calculated using the same approach as that given by Eqs. (17.1-17.3) using the law of cosines:

$$s_1^{\,2} + s_2^{\,2} - 2s_1 s_2 \text{cosine}\theta = s_3^{\,2} \tag{16.38}$$

where $s_3 = a_l$ is the hypotenuse of the isosceles triangle having equivalent sides of length equal to $2c'_{O\cdots HO}$. With the bond angle between three water molecules formed by the two corresponding H bonds given by $\theta_{\angle H_2O,H_2O,H_2O} = 109.5°$ [90] and $s_1 = s_2 = 2c'_{O\cdots HO}$ given by Eq. (16.32), the distance between the oxygen atoms of the terminal water molecules along the hypotenuse, $s_3 = 2c'_{H_2O\cdots H_2O} = a_l$, is:

$$a_l = 2c'_{H_2O\cdots H_2O} = \sqrt{2\left(2c'_{O\cdots HO}\right)^2\left(1-\cos ine(109.5°)\right)} = \sqrt{2\left(2.75377\ \text{Å}\right)^2\left(1-\cos ine(109.5°)\right)} = 4.49768\ \text{Å} \tag{16.39}$$

Due to the tetrahedral structure shown in Figure 16.8, four water molecules form a pyramidal structure with a central $H_2O(1)$ at the apex designated as on the z-axis, and the three other water molecules, $H_2O(n)$ $n = 2,3,4$, form the base in the xy-plane. As further shown in Figure 16.8, a fifth $H_2O(5)$ is positioned a distance $2c'_{O\cdots HO}$ along the z-axis. Twice the height along the z-axis from the base of the pyramid to the fifth H_2O comprises the Type I ice unit cell parameter c which is determined next using Eqs. (13.412-13.417).

Since any two $O-H\cdots O$ bonds having the internuclear distance $2c'_{O\cdots HO}$ between the oxygen atoms of Type I ice form an isosceles triangle having the hypotenuse a_l between the terminal oxygens, the distance $d_{origin-O}$ from the origin of the pyramidal base to the nucleus of a terminal oxygen atom is given by:

$$d_{origin-O} = \frac{a_l}{2\sin 60°} \tag{16.40}$$

Substitution of Eq. (16.39) into Eq. (16.40) gives

$$d_{origin-O} = 2.59674 a_0 \tag{16.41}$$

The height d_{height} along the z-axis of the pyramid from the origin to the O nucleus of $H_2O(1)$ is given by:

$$d_{height} = \sqrt{\left(2c'_{O\cdots HO}\right)^2 - \left(d_{origin-O}\right)^2} \tag{16.42}$$

Substitution of Eqs. (16.32) and (16.41) into Eq. (16.42) gives:

$$d_{height} = 0.91662 a_0 \tag{16.43}$$

The angle θ_v of each $O-H\cdots O$ bond from the z-axis is given by:

$$\theta_v = \tan^{-1}\left(\frac{d_{origin-O}}{d_{height}}\right) \tag{16.44}$$

Substitution of Eqs. (16.41) and (16.43) into Eq. (16.44) gives:

$$\theta_v = 70.56° \tag{16.45}$$

Using Eqs. (16.32) and (16.43), the hexagonal lattice parameter c_l for Type I ice given by twice the height along the z-axis from the base of the pyramid to the fifth water, $H_2O(5)$, is

$$c_l = 2\left(2c'_{O\cdots HO} + d_{height}\right) = 2\left(2.75377\ \text{Å} + 0.91662\ \text{Å}\right) = 7.34077\ \text{Å} \tag{16.46}$$

The experimental lattice parameters a_l and c_l for Type I ice are [90, 91]:

$$\begin{aligned} a_l &= 4.49\ \text{Å} \\ a_l &= 4.5212\ \text{Å} \end{aligned} \tag{16.47}$$

and [91, 92] :

$$\begin{aligned} c_l &= 7.31\ \text{Å} \\ c_l &= 7.3666\ \text{Å} \end{aligned} \tag{16.48}$$

The tetrahedral unit cell and the ideal hexagonal lattice structure of Type I ice are shown in Figures 16.8–16.10, using the color scale charge density of each water molecule.

Figure 16.8. Tetrahedral unit cell structure of Type I ice using the transparent color scale charge density of each H_2O MO comprising the linear combination of two $O-H$ -bond MOs. (A) Each dipole-dipole bond that is Coulombic in nature is depicted by connecting sticks. (B) Bond representation removed.

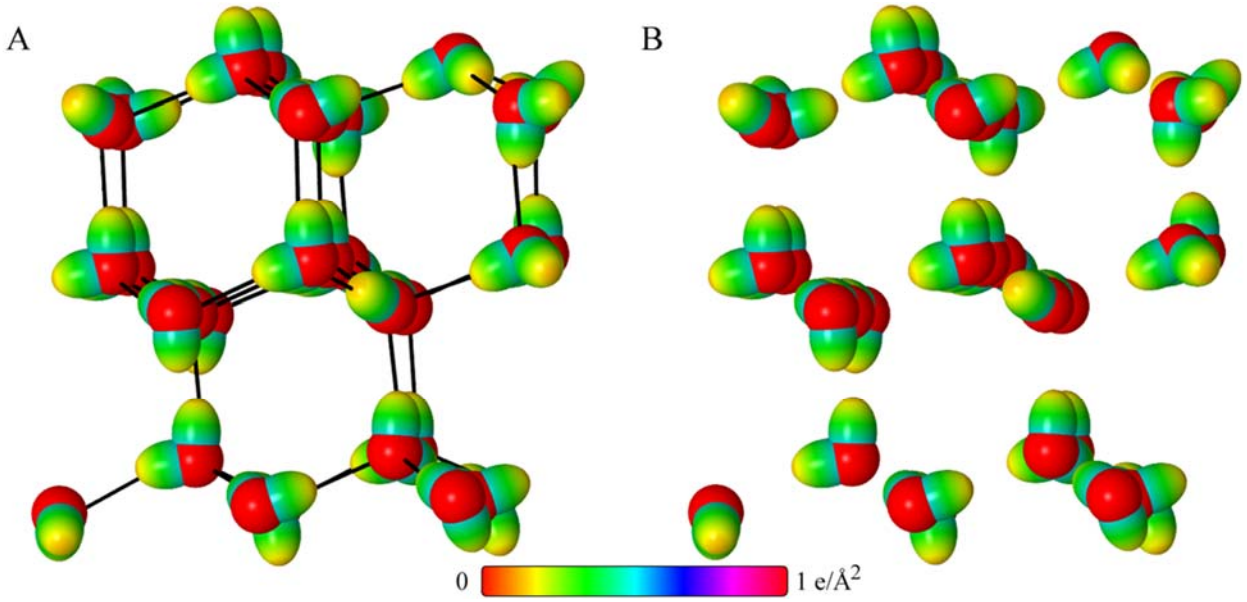

Figure 16.9. C-axis view of the ideal hexagonal lattice structure of Type I ice using the opaque color scale charge density of each H_2O MO comprising the linear combination of two $O-H$ -bond MOs. Each dipole-dipole bond that is Coulombic in nature is depicted by connecting sticks.

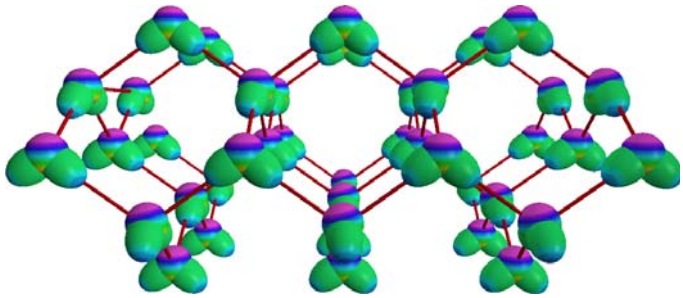

Figure 16.10. An off-angle view of the ideal hexagonal lattice structure of Type I ice using the opaque color scale charge density of each H_2O MO comprising the linear combination of two $O-H$ -bond MOs. Each dipole-dipole bond that is Coulombic in nature is depicted by connecting sticks.

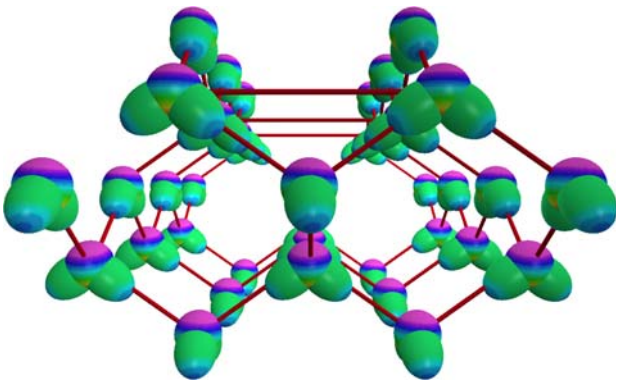

A convenient method to calculate the lattice energy is to determine the electric field in ice having an electric polarization density corresponding to the aligned molecular water dipoles moments, and in turn, the energy can be calculated from the energy of each dipole in the corresponding field using the electrostatic form of Gauss' equation. The electric field inside of a material having a uniform polarization density P_0 given by Eq. (6.3.3.15) of Haus and Melcher [93] is:

$$\mathbf{E}\left(H_2O\right)=\frac{P_0}{3\varepsilon_0}\left(-\cos\theta\mathbf{i}_r+\sin\theta\mathbf{i}_\theta\right) \tag{16.49}$$

The polarization density P_0 given by Eq. (6.3.3.3) of Haus and Melcher [93] is:

$$P_0=N\mu_{H_2O} \tag{16.50}$$

where μ_{H_2O} is the dipole moment of water and N is the number density of water dipoles given by the density ρ_{ice} divided by the molecular weight MW and multiplied by the Avogadro constant N_A:

$$N=\frac{\rho_{ice}}{MW}N_A \tag{16.51}$$

Substitution of Eqs. (16.50) and (16.51) into Eq. (16.49) gives:

$$\mathbf{E}\left(H_2O\right)=\frac{\mu_{H_2O}\dfrac{\rho_{ice}}{MW}N_A}{3\varepsilon_0}\left(-\cos\theta\mathbf{i}_r+\sin\theta\mathbf{i}_\theta\right) \tag{16.52}$$

The energy of forming the condensed phase is that of the alignment of the water dipoles each comprised of two $O-H$ component dipoles where the angular dependence along the z-axis in ice is unity, and this condition applies even in the case of the local order in water. The corresponding energy $U\left(H_2O\right)$ per water dipole due to the polarization electric field of the lattice of hexagonal dipoles is given by**:**

$$U\left(H_2O\right)=2\mu_{H_2O}\cdot\mathbf{E}\left(H_2O\right)=\frac{-2\left(\mu_{H_2O}\right)^2\dfrac{\rho_{ice}}{MW}N_A}{3\varepsilon_0} \tag{16.53}$$

Substitution of the density of ice $\rho=\dfrac{0.92\ g}{1\ X\ 10^{-6}\ m^3}$ [90], the $MW=18g/mole$, $N_A=6.0221415\ X\ 10^{23}\ molecules/mole$, and the water dipole moment given by Eq. (16.16) with the predicted and experimental hexagonal bond angle of ice, $\theta_{\angle H_2O}=109.5°$ [90]:

$$\mu_{H_2O}=2\left(1.51\right)\cos\left(109.5/2°\right)=5.79898\ X\ 10^{-30}C\cdot m \tag{16.54}$$

into Eq. (16.53) gives

$$\begin{aligned}U\left(H_2O\right)&=\frac{-2\left(5.79898\ X\ 10^{-30}C\cdot m\right)^2\dfrac{0.92\ g}{1\ X\ 10^{-6}\ m^3}6.0221415\ X\ 10^{23}\ molecules/mole}{18g/mole}\\&=-0.48643\ eV\ \left(-46.934\ kJ/mole\right)\end{aligned} \tag{16.55}$$

$U\left(H_2O\right)$ is also the negative of $E_{vapor,0°C}$, the energy of water initially at 0 °C or the energy of vaporization of water at 0 °C:

$$E_{vapor,0°C}=-U\left(H_2O\right)=0.48643\ eV\ \left(46.934\ kJ/mole\right) \tag{16.56}$$

The experimental energy of vaporization of water at 0 °C (Type I ice) is [94] :

$$E_{vapor,0°C}=45.054\ kJ/mole \tag{16.57}$$

The calculated results based on first principles and given analytical equations are summarized in Table 16.19.

Table 16.19. The calculated and experimental geometrical and energy parameters of the H bond of water of Type I ice.

Parameter	Calculated	Experimental	Ref. for Exp.
H Bond Length $2c'_{O\text{-}H}$	1.78219 Å	1.78 Å	88, 89
Nearest Neighbor Separation Distance $2c'_{O\text{-}HO}$	2.75377 Å	2.75 Å	88
H_2O Lattice Parameter a_l	4.49768 Å	4.49 Å 4.5212 Å	90 91
H_2O Lattice Parameter c_l	7.34077 Å	7.31 Å 7.3666 Å	92 91
Energy of Vaporization of Water at 0 °C	46.934 kJ/mole	45.054 kJ/mole	94

As the temperature increases, the corresponding molecular kinetic energy can excite a vibrational mode along the H bond axis. Concomitantly, the $O-H$ bond elongates and decreases in energy. As a consequence, the hydrogen bond achieves a partial bond order or partial three-centered $O-H-O$ bond, and the H can undergo exchange between water molecules. The time-average effect of exchange is to decrease the statistical equilibrium separation distance of water molecules. In competition with the separation-distance decreasing effect of exchange is the increasing effect due to collisional impact and recoil as a function of increasing temperature. The former effect dominates from the temperature of ice to 4°C at which point water assumes a maximum density. Thereafter, the momentum imparted with water-water collisions overwhelms the decrease due to exchange, and the molecular separation statistically increases with temperature until a totally gaseous state is achieved at atmospheric pressure at 100°C. Unit cells with increasing entropy can be derived from the ice unit cell by populating translational, rotational, and vibrational levels of molecules within the cells to match the internal energy at a given temperature. Using statistical mechanical models such as Boltzmann statistics to populate an increasing number of basis units cells of increasing disorder and based on the ice unit cell, the behavior of water as a function of temperature can be modeled over the range of states from ice to liquid to steam. The structure of each phase of water is then determined by the number of H bonds on average per water molecule. Based on the 10% energy change in the heat of vaporization in going from ice at 0°C to water at 100°C [94], the average number of H bonds per water molecule in boiling water is 3.6. The H bond distance is calculated next using the enthalpy to form steam from boiling water.

GEOMETRICAL PARAMETERS AND ENERGIES OF THE HYDROGEN BOND OF H_2O IN THE VAPOR PHASE

Two or more water molecules can interact along the $O\cdots H$ or H bond axis. In the gas phase, the maximum energy of interaction between water molecules of steam is equivalent to the negative of the heat of vaporization of water at the boiling point, 100°C; otherwise, water vapor would form the corresponding condensed state. For the determination of the H-bond distance, the energy parameters, partial charge, and reduced mass are the same as those of the water molecules of ice given in Eq. (16.26) except that the negative of the experimental $E_{vapor,100°C}=0.42137\,eV\ \left(40.657\,kJ/mole\right)$ [94] is equated to the nascent covalent bond energy. The parameters are summarized in Table 16.20 and Eq. (16.58).

Table 16.20. The energy parameters (eV) of the $O\cdots H$ functional group of the hydrogen bond of water vapor.

Parameters	$O\cdots H$ Group
δ	0.323
n_1	2
C_1	0.75
C_2	1
c_1	0.75
c_2	1
C_{1o}	1.5
C_{2o}	1
$V_e\ (eV)$	-15.20020
$V_p\ (eV)$	14.08285
$T\ (eV)$	1.35707
$V_m\ (eV)$	-0.67853
$E_{(AO/HO)}\ (eV)$	0
$\Delta E_{H_2MO(AO/HO)}\ (eV)$	0
$E_{T(AO/HO)}\ (eV)$	0
$E_{T(H_2MO)}\ (eV)$	-0.43882
$E_T\left(atom-atom, msp^3.AO\right)\ (eV)$	0
$E_{T(MO)}\ (eV)$	-0.43882
$\omega\ \left(10^{15}\ rad/s\right)$	4.20131
$E_K\ (eV)$	2.76538
$\bar{E}_D\ (eV)$	-0.001444
$\bar{E}_{Kvib}\ (eV)$	0.02033
$\bar{E}_{osc}\ (eV)$	0.008724
$E_{T(Group)}\ (eV)$	-0.42137

Substitution of the parameters of Table 16.20 and $-E_{vapor,0°C}$ (Eq. (16.57)) into Eq. (16.26) gives:

$$e\left(0.42137\ eV\right)=\left\{\left(\frac{-e^2}{4\pi\varepsilon_0\sqrt{\frac{a_{O\cdots H}a_0}{2(0.75)}}}\left(\left(\frac{3}{2}-\frac{3}{8}\frac{a_0}{a_{O\cdots H}}\right)\ln\frac{a_{O\cdots H}+\sqrt{\frac{a_{O\cdots H}a_0}{2(0.75)}}}{a_{O\cdots H}-\sqrt{\frac{a_{O\cdots H}a_0}{2(0.75)}}}-1\right)\right)\right\}$$
$$\left\{\left(1+2\sqrt{\frac{2\hbar\sqrt{\frac{\frac{3}{2}\frac{e^2}{4\pi\varepsilon_0\left(\sqrt{\left(a_{O\cdots H}\right)^2-\left(2\sqrt{\frac{a_{O\cdots H}a_0}{2(0.75)}}\right)^2}\right)^3}}{m_e}}{m_e c^2}}\right)\right.$$
$$\left.+2\left(\frac{1}{2}\right)\hbar\sqrt{\frac{\frac{0.75e^2}{8\pi\varepsilon_o\left(a_{O\cdots H}\right)^3}-\frac{e^2}{8\pi\varepsilon_o\left(a_{O\cdots H}+\sqrt{\frac{a_{O\cdots H}a_0}{2(0.75)}}\right)^3}}{\frac{16}{17}}}\right\} \tag{16.58}$$

From the energy relationship given by Eq. (16.58) and the relationships between the axes given by Eqs. (16.22-16.24), the dimensions of the $O\cdots H$ MO can be solved.

The most convenient way to solve Eq. (16.58) is by the reiterative technique using a computer. The result to within the round-off error with five-significant figures is:

$$a_{O\cdots H}=5.60039a_0=2.96360\,X\,10^{-10}\ m \tag{16.59}$$

The component energy parameters at this condition are given in Table 16.20. Substitution of Eq. (16.59) into Eq. (16.22) gives

$$c'_{O\cdots H}=1.93225a_0=1.02250\,X\,10^{-10}\ m \tag{16.60}$$

and internuclear distance of the H bond:

$$2c'_{O\cdots H}=3.86450a_0=2.04501\,X\,10^{-10}\ m \tag{16.61}$$

The experimental H bond distance $2c'_{O\cdots H}$ in the gas phase is [95]:

$$2c'_{O\cdots H}=2.02\,X\,10^{-10}\ m \tag{16.62}$$

and [96]

$$2c'_{O\cdots H}=2.05\,X\,10^{-10}\ m \tag{16.63}$$

The other H-bond MO parameters can also be determined by the relationships among the parameters. Substitution of Eqs. (16.59) and (16.60) into Eq. (16.23) gives:

$$b_{O\cdots H}=c_{O\cdots H}=5.25650a_0=2.78162\,X\,10^{-10}\ m \tag{16.64}$$

Substitution of Eqs. (16.59) and (16.60) into Eq. (16.24) gives:

$$e_{O\cdots H}=0.34502 \tag{16.65}$$

Substitution of $2c'_{O\cdots H}$ (Eq. (16.61)) and $2c'_{O\cdots H}$ (Eq. (13.185)) into Eq. (16.31) gives the nearest neighbor separation, the internuclear distance $2c'_{O\cdots HO}$ between the oxygen atoms of the $O-H\cdots O$ bond of water vapor:

$$2c'_{O\cdots HO}=2c'_{O\cdots H}+2c'_{O-H}=2.04501\,X\,10^{-10}\ m+9.71574\,X\,10^{-11}\ m=3.01658\,X\,10^{-10}\ m=3.01658\,\text{Å} \tag{16.66}$$

Using Eqs. (16.31), (16.34), and (16.63), the experimental nearest neighbor separation $2c'_{O\cdots HO}$ is [89, 96]:

$$2c'_{O\cdots HO}=2c'_{O\cdots H}+2c'_{O-H}=2.05\,X\,10^{-10}\ m+9.70\,X\,10^{-11}\ m=3.02\,X\,10^{-10}\ m=3.02\,\text{Å} \tag{16.67}$$

H-bonded water vapor molecules in steam are shown in Figure 16.11 using the color scale charge density of each water molecule.

Figure 16.11. Structure of steam. (A). Ensemble of gaseous water molecules undergoing elastic hard-sphere collisions. (B). H-bonded water vapor molecules using the color scale charge density of each H_2O MO comprising the linear combination of two $O-H$ -bond MOs.

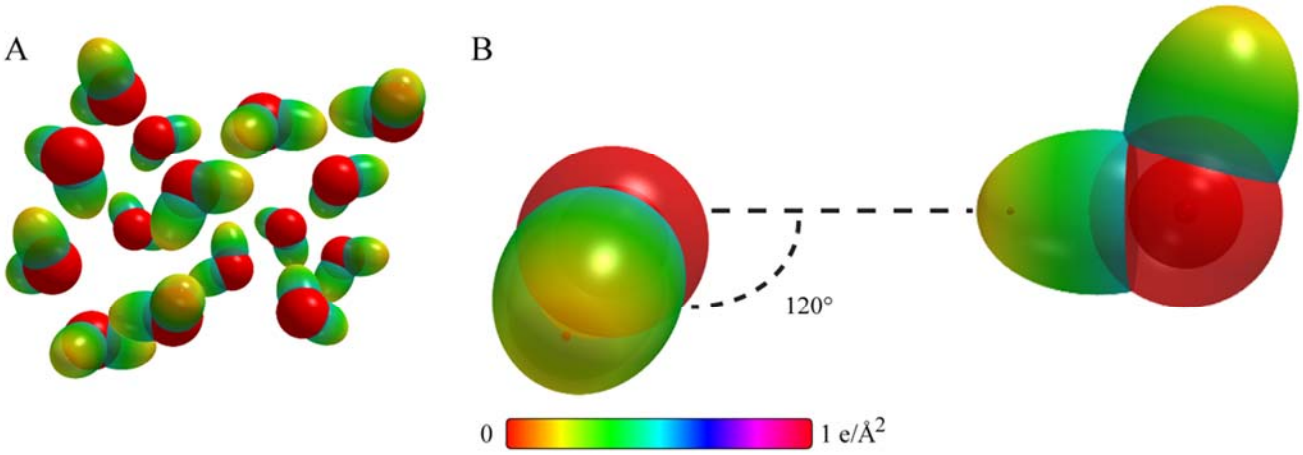

The calculated results based on first principles and given by analytical equations are summarized in Table 16.21.

Table 16.21. The calculated and experimental geometrical and energy parameters of the H bond of steam.

Parameter	Calculated	Experimental	Ref. for Exp.
H Bond Length $2c'_{O\cdots H}$	2.04501 Å	2.02 Å 2.05 Å	95, 96
Nearest Neighbor Separation Distance $2c'_{O\cdots HO}$	3.01658 Å	3.02 Å	89, 96

GEOMETRICAL PARAMETERS AND ENERGIES OF THE HYDROGEN BOND OF H_2O AND NH_3

Similar to the water molecule, the ammonia molecule has a strong dipole moment along each of its $N-H$ -bonds. The NH_3 MO comprises the linear combination of three $N-H$ -bond MOs. Each $N-H$ -bond MO comprises the superposition of a H_2-type ellipsoidal MO and the $N2p_x$, $N2p_y$, or $N2p_z$ AO with a relative H partial orbital contribution to the MO of 0.75. The solution of the geometrical parameters and component energies are given in the Ammonia (NH_3) section, and the color scale charge density of the NH_3 MO is shown in Figure 16.12.

Figure 16.12. NH_3 MO comprising the linear combination of three $N-H$ -bonds. Each $N-H$ -bond MO comprises the superposition of a H_2-type ellipsoidal MO and the $N2p_x$, $N2p_y$, or $N2p_z$ AO. (A) Color scale, translucent view of the charge density of the NH_3 MO shown obliquely from the top. For each $N-H$ bond, the ellipsoidal surface of each H_2-type ellipsoidal MO transitions to a $N2p$ AO. The $N2p$ shell, the $N2s$ shell, the $N1s$ shell, and the nuclei (red, not to scale) are shown. (B) Off-center cut-away view showing the complete inner most $N1s$ shell, and moving radially, the cross section of the $N2s$ shell, the $N2p$ shell, and the H_2-type ellipsoidal MO that transitions to a $N2p$ AO for each $N-H$ bond. (C)-(E) Color scale, side-on, top, and bottom translucent views of the charge density of the NH_3 MO, respectively.

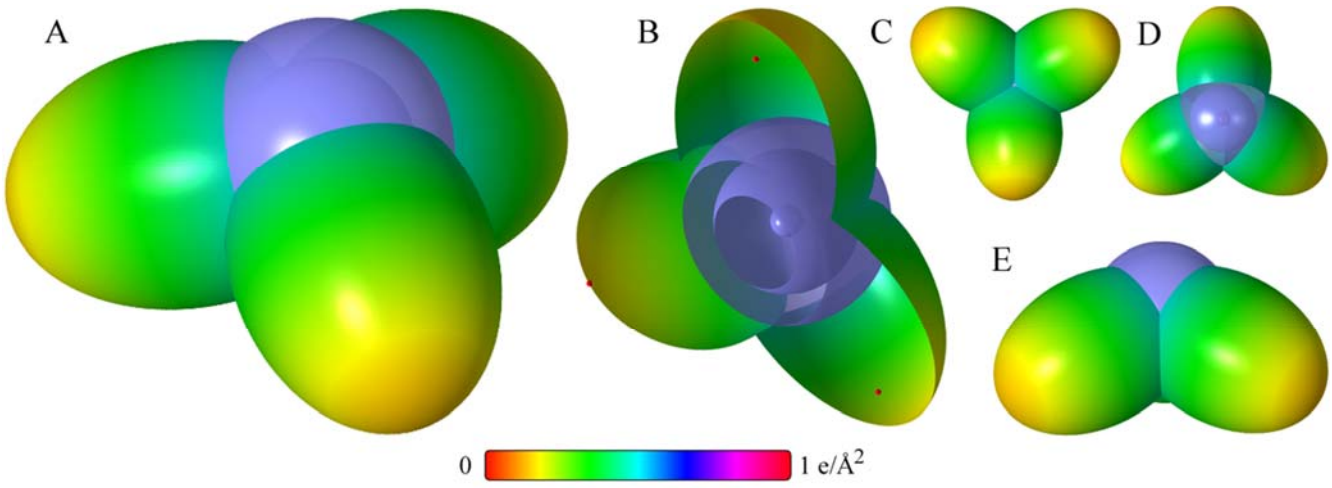

Due to the interacting dipoles, hydrogen bonds also form between the nitrogen of ammonia and the hydrogen of water molecules. Water hydrogen bonds to ammonia molecules by interaction along the $N\cdots HO$ or H bond axis. As shown in the Bond and Dipole Moments section, each $N-H$ bond of ammonia has a bond moment μ of 1.30 D corresponding to a N component of partial charge of $-0.262e$, and the $O-H$ bond has a bond moment μ of 1.51 D corresponding to a H partial charge of $+0.323e$. The thermodynamic basis of the H bond is the minimization of the Coulombic energy between the hydrogen bonded H of H_2O and N of ammonia, limited by the formation of a nascent $N-H$ bond between these atoms that destabilizes the initial $O-H$ bond of the water molecule partner. As in the case of ice, the maximum electrostatic energy of the partial charges is calculated for the components along the H-bond axis. This energy is balanced by the total energy of the nascent bond that can form between the $N\cdots H$ atoms of the H bond. The bond length of the H bond, the internuclear distance between the N and H of the $N\cdots H$ bond, is calculated using Eq. (16.25) by a similar method as that used to calculate the $O\cdots H$ bond distance of ice. According to the method given in the Geometrical Parameters and Energies of the Hydrogen Bond of H_2O section, the equilibrium distance r_e or internuclear bond distance of $N\cdots H$ designated as $2c'_{N\cdots H}=r_e$ is determined by the condition that the total energy of the nascent H_2-type ellipsoidal MO formed from the atoms of the $N\cdots H$ bond is equal to the maximum Coulombic energy between the partial charges of the N and H atoms of the H bond.

The maximum Coulumbic energy corresponds to the minimum separation distance of N and H atoms corresponding to the alignment along the $N\cdots H$ bond axis. The corresponding distance from the δ^+ of the H_2O H and the NH_3 N is the

distance $2c'_{N\cdots H}$ between the N and H nuclei of the $N\cdots H$ bond. Then, the maximum Coulomb energy $E_{Coulomb}(H-bond)$ between the atoms of the $N\cdots H$ bond due to the δ^- on the nitrogen atom with the δ^+ centered on the nucleus of hydrogen is:

$$E_{Coulomb}(H-bond)=\frac{-\delta_N^-\delta_H^+e^2}{4\pi\varepsilon_0 2c'_{N\cdots H}} \tag{16.68}$$

Eq. (16.68) is the energy to be equated to that of the nascent bonds involving the atoms of the H bond.

For the determination of the H-bond distance, the energy parameters of the nascent $N-H$ bond are the same as those of ammonia given in the Ammonia (NH_3) section except that any parameter due to matching AO's, $E_T(AO/HO)$ and $E_T(atom-atom,msp^3.AO)$, is zero since only the energies of the MO electrons to form the $N\cdots H$ MO are considered. The energy of Eq. (16.68) is multiplied by three to match the total energy of the three $N-H$ bond MOs of ammonia. The partial charges $\delta=q/e$ from Table 16.17 are –0.262 and +0.323, and the reduced mass is $\mu=\frac{14}{15}$. The parameters are summarized in Table 16.22 and Eq. (16.69).

Table 16.22. The energy parameters (eV) of the $N\cdots H$ functional group of the hydrogen bond of the ammonia-water molecular dimer.

Parameters	$N\cdots H$ Group
δ_N^-	0.262
δ_H^+	0.323
n_1	3
C_1	0.75
C_2	0.93613
c_1	0.75
c_2	1
C_{1o}	1.5
C_{2o}	1
$V_e\ (eV)$	-23.60741
$V_p\ (eV)$	20.75035
$T\ (eV)$	2.17246
$V_m\ (eV)$	-1.08623
$E_{(AO/HO)}\ (eV)$	0
$\Delta E_{H_2MO(AO/HO)}\ (eV)$	0
$E_{T(AO/HO)}\ (eV)$	0
$E_{T(H_2MO)}\ (eV)$	-1.77083
$E_T\left(atom-atom, msp^3.AO\right)\ (eV)$	0
$E_{T(MO)}\ (eV)$	-1.77083
$\omega\ \left(10^{15}\ rad/s\right)$	4.44215
$E_K\ (eV)$	2.92390
$\bar{E}_D\ (eV)$	-0.00599
$\bar{E}_{Kvib}\ (eV)$	0.021843
$\bar{E}_{osc}\ (eV)$	0.00493
$E_{T(Group)}\ (eV)$	1.75603
$E_{T(Group)}\ (eV)$ per $N-H$	0.58534

Substitution of the parameters of Table 16.22 into Eq. (16.25) with $R=a_{N\cdots H}$ gives:

$$\frac{-3(0.262)(0.323)e^2}{4\pi\varepsilon_0\left(2\sqrt{\frac{a_{N\cdots H}a_0}{2(0.75)(0.93613)}}\right)}=\left\{\begin{array}{l}\left(\frac{-3e^2}{8\pi\varepsilon_0\sqrt{\frac{a_{N\cdots H}a_0}{2(0.75)(0.93613)}}}\left(\left(\frac{3}{2}-\frac{3}{8}\frac{a_0}{a_{N\cdots H}}\right)\ln\frac{a_{N\cdots H}+\sqrt{\frac{a_{N\cdots H}a_0}{2(0.75)(0.93613)}}}{a_{N\cdots H}-\sqrt{\frac{a_{N\cdots H}a_0}{2(0.75)(0.93613)}}}-1\right)\right)\\ \left(1+3\sqrt{\frac{2\hbar\sqrt{\frac{\frac{3}{2}\frac{e^2}{4\pi\varepsilon_0\left(\sqrt{(a_{N\cdots H})^2-\left(2\sqrt{\frac{a_{N\cdots H}a_0}{2(0.75)}}\right)^2}\right)^3}}{m_e}}{m_ec^2}}\right)\\ +3\left(\frac{1}{2}\right)\hbar\sqrt{\frac{\frac{0.75e^2}{8\pi\varepsilon_o(a_{N\cdots H})^3}-\frac{e^2}{8\pi\varepsilon_o\left(a_{N\cdots H}+\sqrt{\frac{a_{N\cdots H}a_0}{2(0.75)(0.93613)}}\right)^3}}{\frac{14}{15}}}\end{array}\right\} \tag{16.69}$$

From the energy relationship given by Eq. (16.69) and the relationships between the axes given by Eqs. (16.22-16.24), the dimensions of the $N\cdots H$ MO can be solved.

The most convenient way to solve Eq. (16.69) is by the reiterative technique using a computer. The result to within the round-off error with five-significant figures is:

$$a_{N\cdots H}=5.43333a_0=2.87519\,X\,10^{-10}\ m \tag{16.70}$$

The component energy parameters at this condition are given in Table 16.22. Substitution of Eq. (16.70) into Eq. (16.22) gives

$$c'_{N\cdots H}=1.96707a_0=1.04093\,X\,10^{-10}\ m \tag{16.71}$$

and internuclear distance of the H bond:

$$2c'_{N\cdots H}=3.93414a_0=2.08186\,X\,10^{-10}\ m=2.08186\,\text{Å} \tag{16.72}$$

The experimental H bond distance $2c'_{N\cdots H}$ in the gas phase is [96, 97]:

$$2c'_{N\cdots HO}=2.02\,X\,10^{-10}\ m \tag{16.73}$$

The other H-bond MO parameters can also be determined by the relationships among the parameters. Substitution of Eqs. (16.70) and (16.71) into Eq. (16.23) gives

$$b_{N\cdots H}=c_{N\cdots H}=5.06475a_0=2.68015\,X\,10^{-10}\ m \tag{16.74}$$

Substitution of Eqs. (16.70) and (16.71) into Eq. (16.24) gives:

$$e_{N\cdots H}=0.36204 \tag{16.75}$$

The addition of $2c'_{N\cdots H}$ (Eq. (16.72)) and $2c'_{O\cdots H}$ (Eq. (13.185)) gives the nearest neighbor separation, the internuclear distance $2c'_{N\cdots HO}$ between the nitrogen and oxygen atoms of the $N\cdots H-O$ bond of the ammonia-water molecular dimer:

$$\begin{aligned}2c'_{N\cdots HO}&=2c'_{N\cdots H}+2c'_{O\cdots H}=2.08186\,X\,10^{-10}\ m+9.71574\,X\,10^{-11}\ m\\&=3.05343\,X\,10^{-10}\ m=3.05343\,\text{Å}\end{aligned} \tag{16.76}$$

The addition of the experimental $2c'_{N\cdots H}$ (Eq. (16.73)) and $2c'_{O\cdots H}$ (Eq. (13.185)) gives the experimental nearest neighbor separation $2c'_{N\cdots HO}$ [96, 89]:

$$\begin{aligned}2c'_{N\cdots HO}&=2c'_{N\cdots H}+2c'_{O\cdots H}=2.02\,X\,10^{-10}\ m+9.70\,X\,10^{-11}\ m\\&=2.99\,X\,10^{-10}\ m=2.99\,\text{Å}\end{aligned} \tag{16.77}$$

H-bonded ammonia-water molecular dimer is shown in Figure 16.13 using the color scale charge density of each molecule.

Figure 16.13. Structure of the $H_3N\cdots H-OH$ H bond. The H-bonded ammonia-water vapor molecular dimer using the color scale charge density of each NH_3 and H_2O MO comprising the linear combination of three $N-H$ and two $O-H$ -bond MOs, respectively.

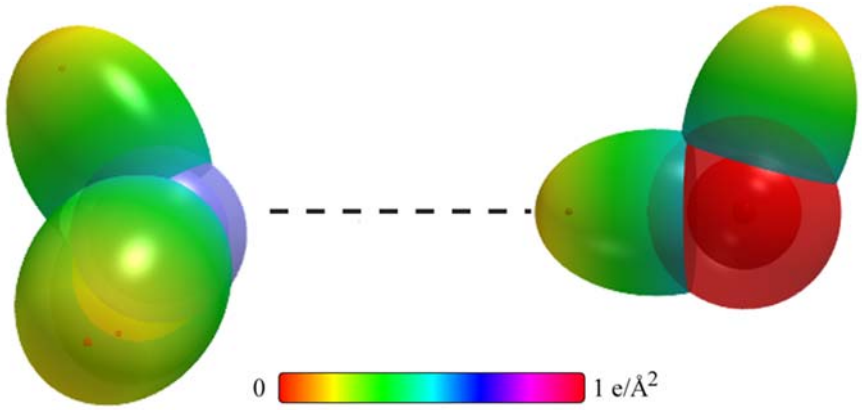

The energy of forming the dimer in the gas phase is that of the alignment of the ammonia dipole moment in the electric field of the $H-O$ water dipole. Using $\mu_{H_3N}=1.467\ D=4.89196\ X\ 10^{-30}C\cdot m$ Eq. (16.18), $\mu_{H-O,H_2O}=1.51\ D=5.02385\ X\ 10^{-30}C\cdot m$ (Table 16.17), and the $N\cdots H$ distance, $2c'_{N\cdots H}=2.08186\ X\ 10^{-10}\ m$ (Eq. (16.72)), the $N\cdots H$ bond dissociation energy $E_D(N\cdots H)$ of the ammonia-water molecular dimer is:

$$E_D(N\cdots H)=\mu_{H_3N}\cdot\frac{2\mu_{H-O,H_2O}}{4\pi\varepsilon_0\left(2c'_{N\cdots H}\right)^3}$$
$$=\frac{\left(4.89196\ X\ 10^{-30}C\cdot m\right)\left(5.02385\ X\ 10^{-30}C\cdot m\right)}{4\pi\varepsilon_0\left(2.08186\ X\ 10^{-10}\ m\right)^2}=29.48\ kJ \tag{16.78}$$

The experimental $N\cdots H$ bond dissociation energy between amino N and hydroxyl H is approximately [98] :

$$E_D(N\cdots H)=29\ kJ \tag{16.79}$$

The calculated results based on first principles and given by analytical equations are summarized in Table 16.23.

Table 16.23. The calculated and experimental geometrical and energy parameters of the H-bonded ammonia-water vapor molecular dimer.

Parameter	Calculated	Experimental	Ref. for Exp.
H Bond Length $2c'_{N\cdots H}$	2.08186 Å	2.02 Å	96, 97
Nearest Neighbor Separation Distance $2c'_{N\cdots HO}$	3.05343 Å	2.99 Å	96, 89
$N\cdots H$ Bond Dissociation Energy	29.48 kJ/mole	29 kJ/mole	98

GEOMETRICAL PARAMETERS DUE TO THE INTERPLANE VAN DER WAALS COHESIVE ENERGY OF GRAPHITE

Eq. (16.25) can be applied to other solids such as graphite. Graphite is an allotrope of carbon that comprises planar sheets of covalently bound carbon atoms arranged in hexagonal aromatic rings of a macromolecule of indefinite size. The structure of graphite is shown in Figures 16.14A and B. The structure shown in Figure 16.14 has been confirmed directly by TEM imaging, and the Pi cloud predicted by quantum mechanics has been dispatched [99].

Figure 16.14. The structure of graphite. (A) Single plane of macromolecule of indefinite size. (B) Layers of graphitic planes.

(A) **(B)**

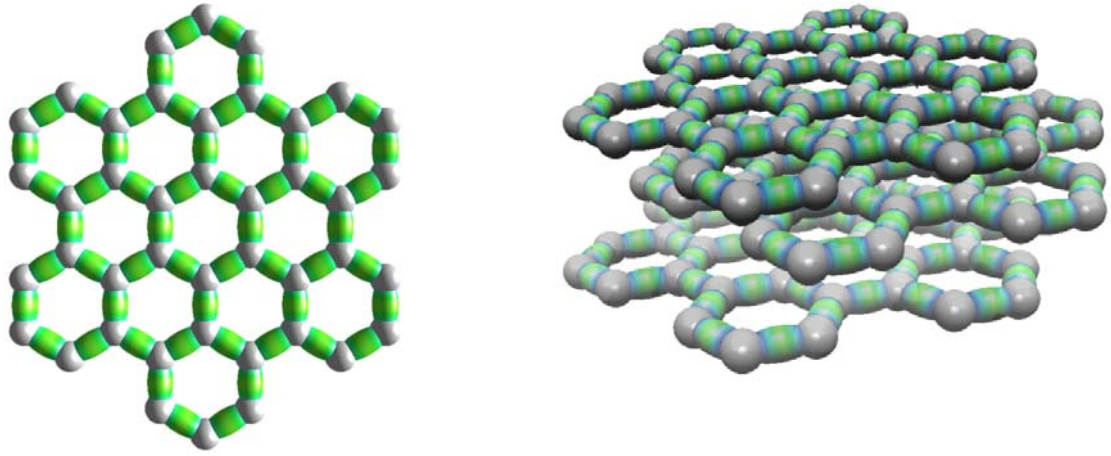

As given in the Graphite section, the structure of the indefinite network of aromatic hexagons of a sheet of graphite is solved using a linear combination of aromatic $C\overset{3e}{=}C$ aromatic bonds comprising $(0.75)(4)=3$ electrons according to Eq. (15.161). In graphite, the minimum energy structure with equivalent carbon atoms wherein each carbon forms bonds with three other such carbons requires a redistribution of charge within an aromatic system of bonds. Considering that each carbon contributes four bonding electrons, the sum of electrons of graphite at a vertex-atom comprises four from the vertex atom plus two from each of the two atoms bonded to the vertex atom where the latter also contribute two each to the juxtaposed bond. These eight electrons are distributed equivalently over the three bonds of the group such that the electron number assignable to each bond is $\frac{8}{3}$. Thus, the $C\overset{8/3e}{=}C$ functional group of graphite comprises the aromatic bond with the exception that the electron-number per bond is $\frac{8}{3}$. The sheets, in turn, are bound together by weaker intermolecular van der Waals forces. The geometrical and energy parameters of graphite are calculated using Eq. (16.25) with the van der Waals energy equated to the nascent bond energy.

The van der Waals energy is due to mutually induced nonpermanent dipoles in near-neighbor bonds. Albeit, the $C\overset{8/3e}{=}C$ functional group is symmetrical such that it lacks a permanent dipole moment, a reversible dipole can be induced upon van der Waals bonding. The parameters of the $C\overset{8/3e}{=}C$ functional group are the same as those of the aromatic $C\overset{3e}{=}C$ functional group, the basis functional group of aromatics, except that the bond order is 8/3 (e.g. $2c'_{C\overset{8/3e}{=}C}=2c'_{C\overset{3e}{=}C}$). Using Eq. (16.15) wherein C_2 of Eq. (15.51) for the aromatic $C\overset{3e}{=}C$-bond MO is $C_2\left(aromaticC2sp^3HO\right)=c_2\left(aromaticC2sp^3HO\right)=0.85252$ (Eq. (15.162)) and $E_{Coulomb}\left(C_{benzene},2sp^3\right)$ is 15.95955 eV (Eq. (14.245)), $E\left(C,2sp^3\right)=-14.63489\ eV$ (Eq. (14.143)) and $2c'=1.39140\ X\ 10^{-10}\ m$ (Table 15.214), the van der Waals dipole of graphite is given in Table 16.24.

Table 16.24. The parameters and van der Waals dipole bond moment of the $C\overset{8/3e}{=}C$ functional group of graphite.

Functional Group	n_1	$(c_1)c_2$	(C_1) C_2	$E_B(valence)$	$E_A(valence)$	$\frac{q}{e}$	Bond Length $2c'$ $(\AA)$	Bond Moment μ (D)

$C \overset{8/3e}{=} C$	$\frac{8}{3}$	0.85252	1	14.82575	15.95955	0.36101	1.3914	2.41270

The interaction between a dipole in one plane with the nearest neighbor in another plane is zero in the case that the aromatic rings of one layer are aligned such that they would superimpose as the interlayer separation goes to zero. But, the energy of interaction is nonzero when one plane is translated relative to a neighboring plane. A minimum equal-energy is achieved throughout the graphite structure when each layer is displaced by $2c'_{C\overset{3e}{=}C}$, the bond length of $C \overset{8/3e}{=} C$, along an intra-planar C_2 axis relative to the next as shown in Figure 16.14B. Then, a pair of dipoles exists for each dipole of a given plane with one dipole above and one below in neighboring planes such that all planes can be equivalently bound by van der Waals forces. In this case, the distance $r_{\mu_1\cdots\mu_2}$ between dipole μ_1 in one plane and its nearest neighbor μ_2 above or below on a neighboring and $2c'_{C\overset{3e}{=}C}$-displaced plane is**:**

$$r_{\mu_1\cdots\mu_2} = \sqrt{\left(2c'_{C\overset{3e}{=}C}\right)^2 + \left(2c'_{C\cdots C}\right)^2} \tag{16.80}$$

where $2c'_{C\cdots C}$ is the interplane distance. The alignment angle $\theta_{\mu_1\cdots\mu_2}$ between the dipoles is**:**

$$\theta_{\mu_1\cdots\mu_2} = \sin^{-1}\frac{2c'_{C\cdots C}}{r_{\mu_1\cdots\mu_2}} = \sin^{-1}\frac{2c'_{C\cdots C}}{\sqrt{\left(2c'_{C\overset{3e}{=}C}\right)^2 + \left(2c'_{C\cdots C}\right)^2}} \tag{16.81}$$

The van der Waals energy is the potential energy between interacting neighboring pairs of $C \overset{8/3e}{=} C$ induced dipoles. Using Eqs. (16.80-16.81), $\mu_{C\overset{8/3e}{=}C} = 2.41270\ D = 8.04790\ X\ 10^{-30} C\cdot m$ (Table 16.24), and the $C \overset{8/3e}{=} C$ distance, $2c'_{C\overset{8/3e}{=}C} = 1.39140\ X\ 10^{-10}\ m$ (Table 15.214), the van der Waals energy of graphite between two planes at a vertex atom is**:**

$$E_{van\ der\ Waals}(graphite) = (3)\frac{2\left(\mu_{C\overset{8/3e}{=}C}\right)^2}{4\pi\varepsilon_0\left(r_{\mu_1\cdots\mu_2}\right)^3}\cos\theta_{\mu_1\cdots\mu_2}$$

$$= \left(\frac{6\left(8.04790\ X\ 10^{-30} C\cdot m\right)^2}{4\pi\varepsilon_0\left(\left(1.39140\ X\ 10^{-10}\ m\right)^2 + \left(2\sqrt{\frac{a_{C\cdots C}a_0}{2C_1C_2}}\right)^2\right)^{1.5}}\right)\left(\cos\sin^{-1}\frac{2\sqrt{\frac{a_{C\cdots C}a_0}{2C_1C_2}}}{\sqrt{\left(1.39140\ X\ 10^{-10}\ m\right)^2 + \left(2\sqrt{\frac{a_{C\cdots C}a_0}{2C_1C_2}}\right)^2}}\right) \tag{16.82}$$

where there are three bonds at each vertex atom.

The graphite inter-plane distance of 3.5Å [100] is calculated using Eq. (16.25) with the van der Waals energy (Eq. (16.82)) between dipoles of two neighboring planes equated to the nascent bond energy. The energy matching parameter c_2 is the same that of the graphite sheet corresponding to the aromatic carbons as given in the Graphite section, and the reduced mass is $\mu = 6$. The parameters are summarized in Table 16.25 and Eq. (16.83).

Table 16.25. The energy parameters (eV) of the graphite interplanar functional group ($C_{aromatic}\cdots C_{aromatic}$).

Parameters	$C_{aromatic}\cdots C_{aromatic}$ Group
n_1	1
C_1	0.5
C_2	1
c_1	1
c_2	0.85252
C_{1o}	0.5
C_{2o}	1
$V_e\ (eV)$	-4.35014
$V_p\ (eV)$	4.10093
$T\ (eV)$	0.19760
$V_m\ (eV)$	-0.09880
$E_{(AO/HO)}\ (eV)$	0
$\Delta E_{H_2MO(AO/HO)}\ (eV)$	0
$E_{T(AO/HO)}\ (eV)$	0
$E_{T(H_2MO)}\ (eV)$	-0.15042
$E_T\left(atom-atom, msp^3.AO\right)\ (eV)$	0
$E_{T(MO)}\ (eV)$	-0.15042
$\omega\ \left(10^{15}\ rad/s\right)$	0.800466
$E_K\ (eV)$	0.52688
$\bar{E}_D\ (eV)$	-0.00022
$\bar{E}_{Kvib}\ (eV)$	0.00317
$\bar{E}_{osc}\ (eV)$	0.00137
$E_{T(Group)}\ (eV)$	-0.14905

Substitution of the parameters of Table 16.25 and the interlayer cohesive energy of graphite (Eq. (16.82)) into Eq. (16.25) with $R=a_{C\text{-}C}$ gives:

$$\frac{-6\left(8.04790\,X\,10^{-30}\,C\cdot m\right)^2}{4\pi\varepsilon_0\left(\left(1.39140\,X\,10^{-10}\,m\right)^2+\left(2\sqrt{\frac{a_{C\cdots C}a_0}{2(0.5)}}\right)^2\right)^{1.5}}\cos\sin^{-1}\frac{2\sqrt{\frac{a_{C\cdots C}a_0}{2(0.5)}}}{\sqrt{\left(1.39140\,X\,10^{-10}\,m\right)^2+\left(2\sqrt{\frac{a_{C\cdots C}a_0}{2(0.5)}}\right)^2}}$$

$$=\left\{\left(\frac{-e^2}{8\pi\varepsilon_0\sqrt{\frac{a_{C\cdots C}a_0}{2(0.5)}}}\left((0.85252)\left(2-\frac{1}{2}\frac{a_0}{a_{C\cdots C}}\right)\ln\frac{a+\sqrt{\frac{a_{C\cdots C}a_0}{2(0.5)}}}{a-\sqrt{\frac{a_{C\cdots C}a_0}{2(0.5)}}}-1\right)\right)\left(1+2\sqrt{\frac{2\hbar\sqrt{\frac{(0.5)\frac{e^2}{4\pi\varepsilon_o\left(a_{C\cdots C}\right)^3}}{m_e}}}{m_ec^2}}\right)\right.$$
$$\left.+\left(\frac{1}{2}\right)\hbar\sqrt{\frac{\frac{(0.85252)e^2}{8\pi\varepsilon_o\left(a_{C\cdots C}\right)^3}-\frac{e^2}{8\pi\varepsilon_o\left(a_{C\cdots C}+\sqrt{\frac{a_{C\cdots C}a_0}{2(0.5)}}\right)^3}}{6}}\right\} \tag{16.83}$$

From the energy relationship given by Eq. (16.83) and the relationships between the axes given by Eqs. (16.22-16.24), the dimensions of the $C\cdots C$ MO can be solved.

The most convenient way to solve Eq. (16.83) is by the reiterative technique using a computer. The result to within the round-off error with five-significant figures is:

$$a_{C\cdots C}=11.00740a_0=5.82486\,X\,10^{-10}\,m \tag{16.84}$$

The component energy parameters at this condition are given in Table 16.25. Substitution of Eq. (16.84) into Eq. (16.22) gives:

$$c'_{C\cdots C}=3.31774a_0=1.75567\,X\,10^{-10}\,m \tag{16.85}$$

and internuclear distance of the graphite interplane bond at vacuum ambient pressure:

$$2c'_{C\cdots C}=6.63548a_0=3.51134\,X\,10^{-10}\,m=3.51134\,\text{Å} \tag{16.86}$$

The experimental graphite interplane distance $2c'_{C\cdots C}$ is [100]:

$$2c'_{C\cdots C}=3.5\,X\,10^{-10}\,m=3.5\,\text{Å} \tag{16.87}$$

The other interplane bond MO parameters can also be determined by the relationships among the parameters. Substitution of Eqs. (16.84) and (16.85) into Eq. (16.23) gives:

$$b_{C\cdots C}=c_{C\cdots C}=10.49550a_0=5.55398\,X\,10^{-10}\,m \tag{16.88}$$

Substitution of Eqs. (16.84) and (16.85) into Eq. (16.25) gives:

$$e_{C\cdots C}=0.30141 \tag{16.89}$$

Using Eqs. (16.80) and (16.86), the distance $r_{\mu_1\cdots\mu_2}$ between dipole μ_1 on one plane and its nearest neighbor μ_2 above or below on a juxtaposed and $2c'_{\substack{3e\\C=C}}$-displaced plane is:

$$r_{\mu_1\cdots\mu_2}=3.77697\,X\,10^{-10}\,m \tag{16.90}$$

Using Eqs. (16.81) and (16.86), the alignment angle $\theta_{\mu_1\cdots\mu_2}$ between the dipoles is**:**

$$\theta_{\mu_1\cdots\mu_2}=68.38365\,^\circ \tag{16.91}$$

Using Eqs. (16.82) and (16.90-91), the van der Waals energy per carbon atom is:

$$E_{van\ der\ Waals}\left(graphite/C\right)=0.04968\,eV \tag{16.92}$$

The experimental van der Waals energy per carbon atom is [101]:

$$E_{van\ der\ Waals}\left(graphite/C\right)=0.052\,eV \tag{16.93}$$

The calculated results based on first principles and given by analytical equations are summarized in Table 16.26.

Table 16.26. The calculated and experimental geometrical parameters and interplane van der Waals cohesive energy of graphite.

Parameter	Calculated	Experimental	Ref. for Exp.
Graphite Interplane Distance $2c'_{C-C}$	3.51134 Å	3.5 Å	100
van der Waals Energy per Carbon Atom	0.04968 eV	0.052 eV	101

Graphite has a high cohesive energy due to its significant van der Waals dipole bond moment of 2.41270D. Other species such as atoms and molecules having mirror symmetry and consequently no permanent dipole moment also form reversible van der Waals dipole bond moments. Different phases can be achieved according to the extent of the van der Waals dipole bonding as the internal energy as a function of temperature and pressure changes analogously to the H-bonded system water that can exist as ice, water, and steam. Thus, the factors in the van der Waals bonding can give rise to numerous material behaviors. In the case of atoms such as noble gas atoms and certain diatomic molecules such as hydrogen, the moments, their interaction energies, and the corresponding nascent bond energies are much smaller. Thus, except at cryogenic temperatures, these elements exist as gases, and even at temperatures approaching absolute zero, solidification of helium has not been achieved in the absence of high pressure. This is due to the nature of the induced dipoles and van der Waals phenomena in helium. Since this system is a good example of van der Waals forces in atoms, it will be treated next.

GEOMETRICAL PARAMETERS AND ENERGIES DUE TO THE INTERATOMIC VAN DER WAALS COHESIVE ENERGY OF LIQUID HELIUM

Noble gases such as helium are typically gaseous and comprised of non-interacting atoms having no electric or magnetic multipoles. But, at very low temperatures it is possible to form diffuse diatomic molecules, or alternatively, these gases may be condensed with the formation of mutually induced van der Waals dipole interactions. As a measure of the nascent bond between two noble gas atoms used to calculate the limiting separation for condensation, consider that the experimental bond energies of diatomic molecules of helium and argon, for example, are only 49.7 meV and 49 meV, respectively [21]. This is a factor of about 100 smaller than the bond energy of a carbon-carbon bond that is the form of nascent bond in graphite. Thus, the corresponding energy of the interspecies interaction is smaller and the van der Waals spacing is larger, except wherein the nascent bond energy as a function of separation distance mitigates this relationship to some extent. The nature of the helium bonding is solved using the same approach as that of other functional groups given in the Organic Molecular Functional Groups and Molecules section.

Helium is a two-electron neutral atom with both electrons paired as mirror-image current densities in a shell of radius $0.566987a_0$ (Eq. (7.35)). Thus, in isolation or at sufficient separation, there is no energy between helium atoms. The absence of any force such as so-called long-range London forces having a $r^{-n};n>2$ dependency is confirmed by elastic electron scattering from helium atoms as shown in the Electron Scattering Equation for the Helium Atom Based on the Atomic Orbital Model section. However, reversible mutual van der Waals dipoles may be induced by collisions when the atoms are in close proximity such that helium gas can condense into a liquid. The physics is similar to the case of graphite except that the dipoles are atomic rather than molecular, and in both cases the limiting separation is based on the formation of a nascent bond to replace the dipole-dipole interaction. Thus, Eq. (16.25) can also be applied to atoms such as helium.

The van der Waals bonding in the helium atom involves hybridizing the one $1s$ AO into $1s^1$ HO orbitals containing two electrons. The total energy of the state is given by the sum over the two electrons. The sum $E_T\left(He,1s^1\right)$ of experimental energies [15] of He and He^+ is:

$$\begin{aligned} E_T\left(He,1s^1\right) &= 54.41776\ eV + 24.587387\ eV \\ &= 79.005147\ eV \end{aligned} \tag{16.94}$$

By considering that the central field decreases by an integer for each successive electron of the shell, the radius r_{1s^1} of the $He1s^1$ shell may be calculated from the Coulombic energy using Eq. (15.13):

$$r_{1s^1} = \sum_{n=0}^{1} \frac{(Z-n)e^2}{8\pi\varepsilon_0\left(e79.005147\ eV\right)} = \frac{3e^2}{8\pi\varepsilon_0\left(e79.005147\ eV\right)} = 0.51664a_0 \tag{16.95}$$

where $Z=2$ for helium. Using Eq. (15.14), the Coulombic energy $E_{Coulomb}\left(He,1s^1\right)$ of the outer electron of the van der Waals bound $He1s^1$ shell is:

$$E_{Coulomb}\left(He,1s^1\right) = \frac{-e^2}{8\pi\varepsilon_0 r_{1s^1}} = \frac{-e^2}{8\pi\varepsilon_0 0.51664a_0} = -26.335049\ eV \tag{16.96}$$

To meet the equipotential condition of the union of the two $He1s^1$ HOs in a nascent bond, c_2 of Eqs. (15.2-15.5) and Eq. (15.61) for the nascent $He-He$-bond MO is given by Eq. (15.75) as the ratio of the valance energy of the He AO, $E\left(He\right)=-24.587387\ eV$ and the magnitude of $E_{Coulomb}\left(He,1s^1\right)$ (Eq. (16.96)):

$$c_2\left(He-He, He1s^1HO\right)=\frac{24.587387\ eV}{26.33505\ eV}=0.93364 \tag{16.97}$$

The opposite charge distributions act as symmetrical point charges at the point of maximum separation, each being centered at 1/2 the He-atom radius from the origin. Using the parameters of Eq. (16.97) and $2c'=0.51664a_0=2.73395\ X\ 10^{-11}\ m$ (Eq. (16.95)), the van der Waals dipole of helium is given in Table 16.27.

Table 16.27. The parameters and van der Waals dipole bond moment of the He functional group of liquid helium.

Functional Group	n_1	$(c_1)c_2$	$(C_1)C_2$	$E_B(valence)$	$E_A(valence)$	$\frac{q}{e}$	Bond Length $2c'\ (\AA)$	Bond Moment μ (D)
He	1	0.93364	1	24.587387	26.33505	0.13744	0.273395	0.18049

As in the case with graphite, the van der Waals energy is the potential energy between interacting neighboring induced dipoles. Using $\mu_{He}=0.18049\ D=6.02040\ X\ 10^{-31}C\cdot m$ (Table 16.27), the van der Waals energy is:

$$E_{van\ der\ Waals}\left(He\right)=2\frac{2\left(\mu_{He}\right)^2}{4\pi\varepsilon_0\left(r_{He...He}\right)^3}=\left(\frac{2\left(6.02040\ X\ 10^{-31}C\cdot m\right)^2}{4\pi\varepsilon_0\left(2\sqrt{\frac{a_{He\text{-}He}a_0}{2C_1C_2}}\right)^3}\right) \tag{16.98}$$

where there are two bonds at each vertex atom.

The helium interatomic distance is calculated using Eq. (16.25) with the van der Waals energy (Eq. (16.98)) between neighboring dipoles equated to the nascent bond energy. The energy matching parameter c_2 is the same as that of the helium dipole, and the reduced mass is $\mu=2$. The parameters are summarized in Table 16.28 and Eq. (16.99).

Table 16.28. The energy parameters (eV) of the helium functional group ($He\cdots He$).

Parameters	$He\cdots He$ Group
n_1	1
C_1	0.5
C_2	0.93364^{-1}
c_1	1
c_2	0.93364
C_{1o}	0.5
C_{2o}	0.93364^{-1}
$V_e\ (eV)$	-3.96489
$V_p\ (eV)$	3.88560
$T\ (eV)$	0.15095
$V_m\ (eV)$	-0.07548
$E_{(AO/HO)}\ (eV)$	0
$\Delta E_{H_2MO(AO/HO)}\ (eV)$	0
$E_{T(AO/HO)}\ (eV)$	0
$E_{T(H_2MO)}\ (eV)$	-0.00382
$E_T\left(atom-atom, msp^3.AO\right)\ (eV)$	0
$E_{T(MO)}\ (eV)$	-0.00382
$\omega\ \left(10^{15}\ rad/s\right)$	0.635696
$E_K\ (eV)$	0.41843
$\bar{E}_D\ (eV)$	0.00000
$\bar{E}_{Kvib}\ (eV)$	0.00443
$\bar{E}_{osc}\ (eV)$	0.00221
$E_{T(Group)}\ (eV)$	-0.00160

Substitution of the parameters of Table 16.28 and the interatomic cohesive energy of helium (Eq. (16.98)) into Eq. (16.25) with $R = a_{He\cdots He}$ gives:

$$\frac{-4\left(6.02040\ X\ 10^{-31} C\cdot m\right)^2}{4\pi\varepsilon_0\left(2\sqrt{\frac{a_{He\cdots He}a_0}{2(0.5)(0.93364)^{-1}}}\right)^3} = \left\{\left(\frac{-e^2}{8\pi\varepsilon_0\sqrt{\frac{a_{He\cdots He}a_0}{2(0.5)(0.93364)^{-1}}}}\left((0.93364)\left(2-\frac{1}{2}\frac{a_0}{a_{He\cdots He}}\right)\ln\frac{a+\sqrt{\frac{a_{He\cdots He}a_0}{2(0.5)(0.93364)^{-1}}}}{a-\sqrt{\frac{a_{He\cdots He}a_0}{2(0.5)(0.93364)^{-1}}}}-1\right)\right)\right\}$$

$$= \left\{\left(1+2\sqrt{\frac{2\hbar\sqrt{\frac{(0.5)(0.93364)^{-1}\frac{e^2}{4\pi\varepsilon_o\left(a_{He\cdots He}\right)^3}}{m_e}}{m_e c^2}}\right)\right.$$

$$\left.+\left(\frac{1}{2}\right)\hbar\sqrt{\frac{\frac{(0.93364)e^2}{8\pi\varepsilon_o\left(a_{He\cdots He}\right)^3}-\frac{e^2}{8\pi\varepsilon_o\left(a_{He\cdots He}+\sqrt{\frac{a_{He\cdots He}a_0}{2(0.5)(0.93364)^{-1}}}\right)^3}}{2}}\right\} \tag{16.99}$$

From the energy relationship given by Eq. (16.99) and the relationships between the axes given by Eqs. (16.22-16.24), the dimensions of the $He\cdots He$ MO can be solved.

The most convenient way to solve Eq. (16.99) is by the reiterative technique using a computer. The result to within the round-off error with five-significant figures is:

$$a_{He\cdots He} = 13.13271 a_0 = 6.94953\ X\ 10^{-10}\ m \tag{16.100}$$

The component energy parameters at this condition are given in Table 16.28. Substitution of Eq. (16.100) into Eq. (16.22) gives

$$c'_{He\cdots He} = 3.50160 a_0 = 1.85297\ X\ 10^{-10}\ m \tag{16.101}$$

and internuclear distance between neighboring helium atoms:

$$2c'_{He\cdots He} = 7.00320 a_0 = 3.70593\ X\ 10^{-10}\ m = 3.70593\ \text{Å} \tag{16.102}$$

The experimental helium interatomic distance $2c'_{C\cdots C}$ at 4.24K and <2.25 K are [102]:

$$\begin{aligned} 2c'_{He\cdots He}(4.24K) &= 3.72\ X\ 10^{-10}\ m = 3.72\ \text{Å} \\ 2c'_{He\cdots He}(<2.25K) &= 3.70\ X\ 10^{-10}\ m = 3.70\ \text{Å} \end{aligned} \tag{16.103}$$

The other interatomic bond MO parameters can also be determined by the relationships among the parameters. Substitution of Eqs. (16.100) and (16.101) into Eq. (16.23) gives

$$b_{He\cdots He} = c_{He\cdots He} = 12.65729 a_0 = 6.69795\ X\ 10^{-10}\ m \tag{16.104}$$

Substitution of Eqs. (16.100) and (16.101) into Eq. (16.25) gives:

$$e_{He\cdots He} = 0.26663 \tag{16.105}$$

Using Eqs. (16.99) and (16.102) and the relationship that there are two van der Waals bonds per helium atom and two atoms per bond, the van der Waals energy per helium atom is:

$$E_{van\ der\ Waals}(liquid\ He/He) = 0.000799\ eV \tag{16.106}$$

The experimental van der Waals energy calculated from the heat of vaporization per helium atom is [103]:

$$E_{van\ der\ Waals}(liquid\ He) = E_{vapor,4.221K} = 0.0829\ kJ/mole = 0.000859\ eV/He \tag{16.107}$$

At 1.7 K, the viscosity of liquid helium is close to zero, and a characteristic roton scattering dominates over phonon scattering at this temperature and below [104]. The van der Waals bond energy is also equivalent to the roton energy [105, 106]

$$E_{roton}(liquid\ He) = 8.7\ K = 0.00075\ eV \tag{16.108}$$

and the roton is localized within a region of radius $\approx 3.7-4.0$ Å [104, 106-108] that matches the $He\cdots He$ van der Waals bond distance (Eq. (16.102)). The origin of the roton energy and its cross section as belonging to the van der Waals bond resolves its nature. Independent of this result, the modern view of the roton is that it is not considered associated with the excitation of

vorticity as it was historically; rather it is considered to be due to short-wavelength phonon excitations [105]. Its role in scattering free electrons in superfluid helium is discussed in the Free Electrons in Superfluid Helium are Real in the Absence of Measurement Requiring a Connection of ψ to Physical Reality section. The calculated results based on first principles and given by analytical equations are summarized in Table 16.29.

Table 16.29. The calculated and experimental geometrical parameters and interatomic van der Waals cohesive energy of liquid helium.

Parameter	Calculated	Experimental	Ref. for Exp.
Liquid Helium Interatomic Distance $2c'_{C\text{-}C}$	3.70593 Å	3.72 Å (T=4.24 K) 3.70 (T<2.25K)	102
Roton Length Scale	3.70593 Å	3.7-4.0 Å	104, 106-108
van der Waals Energy per Helium Atom (4.221 K)	0.000799 eV	0.000859 eV	103
Roton Energy	0.000799 eV	0.00075 eV	105, 106

Helium exhibits unique behavior due to its possible phases based on the interplay of the factors that determine the van der Waals bonding at a given temperature and pressure to achieve an energy minimum. In extreme cases of sufficient ultra-low temperatures with the atoms driven in phase with an external excitation field such that the formation of a van der Waals-dipole-bound macromolecular state or other forms of bonding, such as metallic bonding in the case of alkali metals or van der Waals bonding in meta-stable helium atoms, are suppressed, a pure statistical thermodynamic state called a Bose-Einstein condensate [109] (BEC)[1] can form having a predominant population of the atoms in a single, lowest-energy translational state in the trap. Since helium has only two electrons in an outer s-shell having a small diameter, the dipole moment is too weak to form transverse dipoles associated with packing. Specifically, with the angular dependence of packed dipoles interactions, the van der Waals energy $E_{van\ der\ Waals}(He)$ (Eqs. (16.98) and (16.99)) between neighboring dipoles becomes less than the vibrational energy in the transition state ($\bar{E}_{Kvib}$ term of Eq. (16.99) from Eq. (15.53)). Consequently, helium can only mutually induce and form linear dipole-dipole bonds having end-to-end interactions as an energy minimum. Interposed atoms can form a non-bonded phase having correlated translational motion and obeying Bose-Einstein statistics. This phase forms a Bose-Einstein condensate (BEC) as an energy minimum wherein the translations are synchronous. Since a phase comprised of linearly ordered unit cells held together by dipole interactions, specifically van der Waals dipole interactions, can exist with a BEC phase, super-fluidity can arise wherein the lines of bound dipoles move without friction relative to the BEC phase having correlated-translational motion. The linear bonding is also the origin of quantized vortex rings that enter as quantized vortex lines to form rings.

The van der Waals bonds undergo breakage and formation and exist on a time-average basis depending on the internal energy and pressure as in the case of liquid water. The van der Waals bonding exhibits a maximum extent as the temperature is lowered below the boiling point, and the BEC phase comprises the balance of the atoms as the temperature is further lowered to absolute zero. Helium cannot form a solid without application of high pressure to decrease the interatomic separation and permit energetically favorable transverse dipole interactions as well as linear ones. In contrast, other noble gases such as Ne, Ar, Kr, and Xe each possess additional shells including an outer p-shell having a relatively larger radius that gives rise to a significant bond moment supportive of dipole packing interactions; thus, these gases can form solids without the application of high pressure.

GEOMETRICAL PARAMETERS AND ENERGIES DUE TO THE INTERATOMIC VAN DER WAALS COHESIVE ENERGY OF SOLID NEON

Neon is a ten-electron neutral atom having the electron configuration $1s^2 2s^2 2p^6$ with the electrons of each shell paired as mirror-image current densities in a shell wherein the radius of the outer shell is $r_{10} = 0.63659 a_0$ (Eq. (10.202)). Thus, in isolation or at sufficient separation, there is no energy between neon atoms. However, reversible mutual van der Waals dipoles may be induced by collisions when the atoms are in close proximity such that neon gas can condense into a liquid and further solidify at sufficiently low temperatures due to the strong dipole moment that accommodates close packing. As in the case of helium, the dipoles are atomic rather than molecular, and the limiting separation is based on the formation of a nascent bond to replace the dipole-dipole interaction. Thus, Eq. (16.25) can also be applied to neon atoms.

[1] The BEC is incorrectly interpreted as a single large atom having a corresponding probability wave function of quantum mechanics. Since excitation occurs in units of $\hbar$ in order of to conserve angular momentum as shown previously for electronic (Chapter 2), vibrational (Chapter 11), rotational (Chapter 12), and translational excitation (Chapter 3) and Bose-Einstein statistics arise from an underlying deterministic physics (Chapter 24), this state comprised of an ensemble of individual atoms is predicted classically using known equations [110]. As in the case of the coherent state of photons in a laser cavity (Chapter 4), the coherency of the BEC actually disproves the inherent Heisenberg Uncertainty Principle (HUP) of quantum mechanics since the atomic positions and energies are precisely determined simultaneously. Furthermore, it is possible to form a BEC comprising molecules in addition to atoms [111] wherein the molecules lack zero-order vibration in contradiction to the HUP. The classical physics underlying Bose-Einstein statistics was covered in the Statistical Mechanics section.

The van der Waals bonding in the neon atom involves hybridizing the three $2p$ AOs into $2p^3$ HO orbitals containing six electrons. The total energy of the state is given by the sum over the six electrons. The sum $E_T\left(Ne,2p^3\right)$ of experimental energies [15] of Ne, Ne^+, Ne^{2+}, Ne^{3+}, Ne^{4+}, and Ne^{5+} is

$$E_T\left(Ne,2p^3\right)=\begin{pmatrix}157.93\ eV+126.21\ eV+97.12\ eV\\ +63.45\ eV+40.96296\ eV+21.56454\ eV\end{pmatrix}=507.2375\ eV \tag{16.109}$$

By considering that the central field decreases by an integer for each successive electron of the shell, the radius r_{2p^3} of the $Ne2p^3$ shell may be calculated from the Coulombic energy using Eq. (15.13).

$$r_{2p^3}=\sum_{n=4}^{9}\frac{(Z-n)e^2}{8\pi\varepsilon_0\left(e507.2375\ eV\right)}=\frac{21e^2}{8\pi\varepsilon_0\left(e507.2375\ eV\right)}=0.56329a_0 \tag{16.110}$$

where $Z=10$ for neon. Using Eq. (15.14), the Coulombic energy $E_{Coulomb}\left(Ne,2p^3\right)$ of the outer electron of the van der Waals bound $Ne2p^3$ shell is:

$$E_{Coulomb}\left(Ne,2p^3\right)=\frac{-e^2}{8\pi\varepsilon_0 r_{2p^3}}=\frac{-e^2}{8\pi\varepsilon_0 0.56329a_0}=-24.154167\ eV \tag{16.111}$$

To meet the equipotential condition of the union of the two $Ne2p^3$ HOs in a nascent bond, c_2 of Eqs. (15.2-15.5) and Eq. (15.61) for the nascent $Ne-Ne$-bond MO is given by Eq. (15.75) as the ratio of the valance energy of the Ne AO, $E\left(Ne\right)=-21.56454\ eV$ and the magnitude of $E_{Coulomb}\left(Ne,2p^3\right)$ (Eq. (16.111)).

$$c_2\left(Ne-Ne,Ne2p^3HO\right)=\frac{21.56454\ eV}{24.154167\ eV}=0.89279 \tag{16.112}$$

The opposite charge distributions act as symmetrical point charges at the point of maximum separation, each being centered at 1/2 the Ne-atom radius from the origin. Using the parameters of Eq. (16.112) and $2c'=0.56329a_0=2.98080\ X\ 10^{-11}\ m$ (Eq. (16.110)), the van der Waals dipole of neon is given in Table 16.30.

Table 16.30. The parameters and van der Waals dipole bond moment of the Ne functional group of solid neon.

Functional Group	n_1	$(c_1)c_2$	$(C_1)C_2$	$E_B\left(valence\right)$	$E_A\left(valence\right)$	$\frac{q}{e}$	Bond Length $2c'\ \left(\AA\right)$	Bond Moment μ (D)
Ne	1	0.89279	1	21.56454	24.15417	0.22730	0.298080	0.32544

The minimum-energy packing of neon dipoles is face-centered cubic also called cubic close packing. In this case, each neon atom has 12 nearest neighbors and the angle between the aligned dipoles is $\frac{\pi}{4}$ radians. As in the case with graphite, the van der Waals energy is the potential energy between interacting neighboring induced dipoles. Using $\mu_{Ne}=0.32544\ D=1.08554\ X\ 10^{-30}C\cdot m$ (Table 16.30), the van der Waals energy is**:**

$$E_{van\ der\ Waals}\left(Ne\right)=12\frac{2\left(\mu_{Ne}\right)^2}{4\pi\varepsilon_0\left(r_{Ne\cdots Ne}\right)^3}\cos\left(\frac{\pi}{4}\right)=\left(\frac{24\left(1.08554\ X\ 10^{-30}C\cdot m\right)^2}{4\pi\varepsilon_0\left(2\sqrt{\frac{a_{Ne\cdots Ne}a_0}{2C_1C_2}}\right)^3}\right)\cos\left(\frac{\pi}{4}\right) \tag{16.113}$$

The neon interatomic distance is calculated using Eq. (16.25) with the van der Waals energy (Eq. (16.113)) between neighboring dipoles equated to the nascent bond energy. The energy matching parameter c_2 is the same as that of the neon dipole, and the reduced mass is $\mu=10$. The parameters are summarized in Table 16.31 and Eq. (16.114).

Table 16.31. The energy parameters (eV) of the neon functional group ($Ne\cdots Ne$).

Parameters	$Ne\cdots Ne$ Group
n_1	1
C_1	0.5
C_2	0.89279^{-1}
c_1	1
c_2	0.89279
C_{1o}	0.5
C_{2o}	0.89279^{-1}
$V_e\ (eV)$	-4.40464
$V_p\ (eV)$	4.27694
$T\ (eV)$	0.19429
$V_m\ (eV)$	-0.09714
$E_{(AO/HO)}\ (eV)$	0
$\Delta E_{H_2MO(AO/HO)}\ (eV)$	0
$E_{T(AO/HO)}\ (eV)$	0
$E_{T(H_2MO)}\ (eV)$	-0.03055
$E_T\left(atom-atom, msp^3.AO\right)\ (eV)$	0
$E_{T(MO)}\ (eV)$	-0.03055
$\omega\ \left(10^{15}\ rad/s\right)$	0.810674
$E_K\ (eV)$	0.53360
$\bar{E}_D\ (eV)$	-0.00004
$\bar{E}_{Kvib}\ (eV)$	0.00240
$\bar{E}_{osc}\ (eV)$	0.00116
$E_{T(Group)}\ (eV)$	-0.02939

Substitution of the parameters of Table 16.31 and the interatomic cohesive energy of neon (Eq. (16.113)) into Eq. (16.25) with $R = a_{Ne\cdots Ne}$ gives:

$$\frac{-24\left(1.08554\ X\ 10^{-30} C\cdot m\right)^2}{4\pi\varepsilon_0\left(2\sqrt{\frac{a_{Ne\cdots Ne}a_0}{2(0.5)(0.89279)^{-1}}}\right)^3}\cos\left(\frac{\pi}{4}\right)$$

$$= \left\{\left(\frac{-e^2}{8\pi\varepsilon_0\sqrt{\frac{a_{Ne\cdots Ne}a_0}{2(0.5)(0.89279)^{-1}}}}\left((0.89279)\left(2-\frac{1}{2}\frac{a_0}{a_{Ne\cdots Ne}}\right)\ln\frac{a+\sqrt{\frac{a_{Ne\cdots Ne}a_0}{2(0.5)(0.89279)^{-1}}}}{a-\sqrt{\frac{a_{Ne\cdots Ne}a_0}{2(0.5)(0.89279)^{-1}}}}-1\right)\right)\right.$$

$$\left.+\left(1+2\sqrt{\frac{2\hbar\sqrt{\frac{(0.5)(0.89279)^{-1}\frac{e^2}{4\pi\varepsilon_o\left(a_{Ne\cdots Ne}\right)^3}}{m_e}}{m_e c^2}}\right)+\left(\frac{1}{2}\right)\hbar\sqrt{\frac{\frac{(0.89279)e^2}{8\pi\varepsilon_o\left(a_{Ne\cdots Ne}\right)^3}-\frac{e^2}{8\pi\varepsilon_o\left(a_{Ne\cdots Ne}+\sqrt{\frac{a_{Ne\cdots Ne}a_0}{2(0.5)(0.89279)^{-1}}}\right)^3}}{10}}\right\} \tag{16.114}$$

From the energy relationship given by Eq. (16.114) and the relationships between the axes given by Eqs. (16.22-16.24), the dimensions of the $Ne\cdots Ne$ MO can be solved.

The most convenient way to solve Eq. (16.114) is by the reiterative technique using a computer. The result to within the round-off error with five-significant figures is:

$$a_{Ne\cdots Ne} = 11.33530 a_0 = 5.99838\ X\ 10^{-10}\ m \tag{16.115}$$

The component energy parameters at this condition are given in Table 16.31. Substitution of Eq. (16.115) into Eq. (16.22) gives

$$c'_{Ne\cdots Ne} = 3.18120 a_0 = 1.68342\ X\ 10^{-10}\ m \tag{16.116}$$

and internuclear distance between neighboring neon atoms:

$$2c'_{Ne\cdots Ne} = 6.36239 a_0 = 3.36683\ X\ 10^{-10}\ m = 3.36683\ \text{Å} \tag{16.117}$$

The experimental neon interatomic distance $2c'_{C\cdots C}$ at the melting point of 24.48 K is [112, 113]:

$$2c'_{Ne\cdots Ne}(24.48K) = 3.21\ X\ 10^{-10}\ m = 3.21\ \text{Å} \tag{16.118}$$

The other interatomic bond MO parameters can also be determined by the relationships among the parameters. Substitution of Eqs. (16.115) and (16.116) into Eq. (16.23) gives:

$$b_{Ne\cdots Ne} = c_{Ne\cdots Ne} = 10.87975 a_0 = 5.75732\ X\ 10^{-10}\ m \tag{16.119}$$

Substitution of Eqs. (16.115) and (16.116) into Eq. (16.25) gives:

$$e_{Ne\cdots Ne} = 0.28065 \tag{16.120}$$

A convenient method to calculate the lattice energy is to determine the electric field in solid neon having an electric polarization density corresponding to the aligned dipoles moments, and in turn, the energy can be calculated from the energy of each dipole in the corresponding field using the electrostatic form of Gauss' equation. Substitution of the density of solid neon at the melting point $\rho = \frac{1.433\ g}{1\ X\ 10^{-6}\ m^3}$ [113], the $MW = 20.179 g/mole$, $N_A = 6.0221415\ X\ 10^{23}\ molecules/mole$, and the neon dipole moment given in Table 16.30 into Eq. (16.53) gives:

$$U(Ne) = \frac{-2(\mu_{Ne})^2\frac{\rho_{solid\ Ne}}{MW}N_A}{3\varepsilon_0} = \frac{-2\left(1.08554\ X\ 10^{-30} C\cdot m\right)^2\frac{\frac{1.433\ g}{1\ X\ 10^{-6}\ m^3}}{20.179 g/mole}6.0221415\ X\ 10^{23}\ molecules/mole}{3\varepsilon_0} \tag{16.121}$$

$$= -0.02368\ eV\ \ (-2.285\ kJ/mole)$$

$U(Ne)$ is also the negative of $E_{van\ der\ Waals}$, the van der Waals energy per neon atom:

$$E_{van\ der\ Waals}\left(solid\ Ne/Ne\right)=0.02368\ eV=2.285\ kJ/mole \tag{16.122}$$

The experimental van der Waals energy calculated from the heat of vaporization and fusion per neon atom at the boiling point and triple point, respectively, is [103] :

$$E_{van\ der\ Waals}\left(solid\ Ne\right)=E_{vapor}+E_{fusion}=0.02125\ eV/Ne=2.0502\ kJ/mole \tag{16.123}$$

The calculated results based on first principles and given by analytical equations are summarized in Table 16.32. Using neon the atomic radius (Eq. (16.110)) and the nearest-neighbor distance (Eq. (16.117)), the lattice structure of neon is shown in Figure 16.17A. The charge density of the van der Waals dipoles of the crystalline lattice is shown in Figure 16.18A.

Table 16.32. The calculated and experimental geometrical parameters and interatomic van der Waals cohesive energy of solid neon.

Parameter	Calculated	Experimental	Ref. for Exp.
Solid Neon Interatomic Distance $2c'_{C-C}$	3.36683 Å	3.21 Å (T=24.48 K)	113
van der Waals Energy per Neon Atom	0.02368 eV	0.02125 eV	103

GEOMETRICAL PARAMETERS AND ENERGIES DUE TO THE INTERATOMIC VAN DER WAALS COHESIVE ENERGY OF SOLID ARGON

Argon is an eighteen-electron neutral atom having the electron configuration $1s^2 2s^2 2p^6 3s^2 3p^6$ with the electrons of each shell paired as mirror-image current densities in a shell wherein the radius of the outer shell is $r_{18}=0.86680a_0$ (Eq. (10.386)). Thus, in isolation or at sufficient separation, there is no energy between argon atoms. However, reversible mutual van der Waals dipoles may be induced by collisions when the atoms are in close proximity such that argon gas can condense into a liquid and further solidify at sufficiently low temperatures due to the strong dipole moment that accommodates close packing. As in the case of helium, the dipoles are atomic rather than molecular, and the limiting separation is based on the formation of a nascent bond to replace the dipole-dipole interaction. Thus, Eq. (16.25) can also be applied to argon atoms.

The van der Waals bonding in the argon atom involves hybridizing the three $3p$ AOs into $3p^3$ HO orbitals containing six electrons. The total energy of the state is given by the sum over the six electrons. The sum $E_T\left(Ar,3p^3\right)$ of experimental energies [15] of Ar, Ar^+, Ar^{2+}, Ar^{3+}, Ar^{4+}, and Ar^{5+} is:

$$E_T\left(Ar,3p^3\right)=\begin{pmatrix}91.009\ eV+75.02\ eV+59.81\ eV\\ +40.74\ eV+27.62966\ eV+15.75961\ eV\end{pmatrix}=309.96827\ eV \tag{16.124}$$

By considering that the central field decreases by an integer for each successive electron of the shell, the radius r_{3p^3} of the $Ar3p^3$ shell may be calculated from the Coulombic energy using Eq. (15.13).

$$r_{3p^3}=\sum_{n=12}^{17}\frac{(Z-n)e^2}{8\pi\varepsilon_0\left(e309.96827\ eV\right)}=\frac{21e^2}{8\pi\varepsilon_0\left(e309.96827\ eV\right)}=0.92178a_0 \tag{16.125}$$

where $Z=18$ for argon. Using Eq. (15.14), the Coulombic energy $E_{Coulomb}\left(Ar,3p^3\right)$ of the outer electron of the van der Waals bound $Ar3p^3$ shell is

$$E_{Coulomb}\left(Ar,3p^3\right)=\frac{-e^2}{8\pi\varepsilon_0 r_{3p^3}}=\frac{-e^2}{8\pi\varepsilon_0 0.92178a_0}=-14.760394\ eV \tag{16.126}$$

To meet the equipotential condition of the union of the two $Ar3p^3$ HOs in a nascent bond, c_2 of Eqs. (15.2-15.5) and Eq. (15.61) for the nascent $Ar-Ar$-bond MO is given by Eq. (15.75) as the ratio of the valance energy of the Ar AO, $E\left(Ar\right)=-15.75961\ eV$ and the magnitude of $E_{Coulomb}\left(Ar,3p^3\right)$ (Eq. (16.126)).

$$c_2\left(Ar-Ar,Ar3p^3HO\right)=\frac{14.760394\ eV}{15.75961\ eV}=0.93660 \tag{16.127}$$

Since the outer $Ar3p^3$ HO shell is at a lower energy and greater radius than the non-polarized $3p$ shell, the inner shells are polarized as well. The dipole of the outer shell can polarize the inner shells to the limit that the sum of the primary and secondary dipoles is twice the primary scaled by the energy matching factors of the van der Waals bond given in Eq. (16.15). Thus, the limiting dipole due to polarization of the inner shells is given by:

$$\begin{aligned}\mu_{Ar}<2c_1^{-1}qC_2 2c' &= 2\left(0.93660\right)^{-1}\left(0.13110\right)e\left(0.93660\right)^{-1}\left(4.87784\ X\ 10^{-11}\ m\right)\\ &=2.49410\ X\ 10^{-30}C\cdot m=0.74771\ D\end{aligned} \tag{16.128}$$

The condition of Eq. (16.128) is matched by the participation of the outer four shells as given in Table 16.33. At each shell, opposite charge distributions act as symmetrical point charges at the point of maximum separation, each being centered at 1/2 the shell radius from the origin. Using the parameters of Eq. (16.127) and $2c' = 0.92178a_0 = 4.87784\ X\ 10^{-11}\ m$ (Eq. (16.125)) as well as the radii of the inner shells of argon (Table 10.17), the van der Waals dipole of argon is given in Table 16.33 as the sum of the moments of each participating shell.

Table 16.33. The parameters and van der Waals dipole bond moment of the Ar functional group of solid argon.

Functional Group	n_1	(c_1) c_2	(C_1) C_2	$E_B(valence)$	$E_A(valence)$	$\frac{q}{e}$	Bond Length $2c'$ (Å)	Bond Moment μ (D)
Ar	1	0.93660	1	14.76039	15.75961	0.13110	$Ar3p^3$ HO 0.48778 $Ar3s$ AO 0.41422 $Ar2p$ AO 0.15282 $Ar2s$ AO 0.12615	0.74366

The minimum-energy packing of argon dipoles is face-centered cubic also called cubic close packing. In this case, each argon atom has 12 nearest neighbors and the angle between the aligned dipoles is $\frac{\pi}{4}$ radians. As in the case with graphite, the van der Waals energy is the potential energy between interacting neighboring induced dipoles. Using $\mu_{Ar} = 0.74366\ D = 2.48058\ X\ 10^{-30} C \cdot m$ (Table 16.33), the van der Waals energy is**:**

$$E_{van\ der\ Waals}(Ar) = 12\frac{2(\mu_{Ar})^2}{4\pi\varepsilon_0 (r_{Ar\ldots Ar})^3}\cos\left(\frac{\pi}{4}\right) = \left(\frac{24\left(2.48058\ X\ 10^{-30} C \cdot m\right)^2}{4\pi\varepsilon_0\left(2\sqrt{\frac{a_{Ar\ldots Ar}a_0}{2C_1C_2}}\right)^3}\right)\cos\left(\frac{\pi}{4}\right) \tag{16.129}$$

The argon interatomic distance is calculated using Eq. (16.25) with the van der Waals energy (Eq. (16.129)) between neighboring dipoles equated to the nascent bond energy. The energy matching parameter c_2 is the same as that of the argon dipole, and the reduced mass is $\mu = 20$. The parameters are summarized in Table 16.34 and Eq. (16.130).

Table 16.34. The energy parameters (eV) of the argon functional group ($Ar\cdots Ar$).

Parameters	$Ar\cdots Ar$ Group
n_1	1
C_1	0.5
C_2	0.93660^{-1}
c_1	1
c_2	0.93660
C_{1o}	0.5
C_{2o}	0.93660^{-1}
$V_e\ (eV)$	-4.18356
$V_p\ (eV)$	3.97600
$T\ (eV)$	0.16731
$V_m\ (eV)$	-0.08365
$E_{(AO/HO)}\ (eV)$	0
$\Delta E_{H_2MO(AO/HO)}\ (eV)$	0
$E_{T(AO/HO)}\ (eV)$	0
$E_{T(H_2MO)}\ (eV)$	-0.12391
$E_T\left(atom-atom, msp^3.AO\right)\ (eV)$	0
$E_{T(MO)}\ (eV)$	-0.12391
$\omega\ \left(10^{15}\ rad/s\right)$	0.683262
$E_K\ (eV)$	0.44974
$\bar{E}_D\ (eV)$	-0.00016
$\bar{E}_{Kvib}\ (eV)$	0.00153
$\bar{E}_{osc}\ (eV)$	0.00060
$E_{T(Group)}\ (eV)$	-0.12331

Substitution of the parameters of Table 16.34 and the interatomic cohesive energy of argon (Eq. (16.129)) into Eq. (16.25) with $R=a_{Ar...Ar}$ gives:

$$\frac{-24\left(2.48058\ X\ 10^{-30} C\cdot m\right)^2}{4\pi\varepsilon_0\left(2\sqrt{\frac{a_{Ar\cdots Ar}a_0}{2(0.5)(0.93660)^{-1}}}\right)^3}\cos\left(\frac{\pi}{4}\right)$$

$$= \left\{\left(\frac{-e^2}{8\pi\varepsilon_0\sqrt{\frac{a_{Ar\cdots Ar}a_0}{2(0.5)(0.93660)^{-1}}}}\left((0.93660)\left(2-\frac{1}{2}\frac{a_0}{a_{Ar\cdots Ar}}\right)\ln\frac{a+\sqrt{\frac{a_{Ar\cdots Ar}a_0}{2(0.5)(0.93660)^{-1}}}}{a-\sqrt{\frac{a_{Ar\cdots Ar}a_0}{2(0.5)(0.93660)^{-1}}}}-1\right)\right)\right\}$$

$$= \left\{\begin{array}{l}\left(1+2\sqrt{\frac{2\hbar\sqrt{\frac{(0.5)(0.93660)^{-1}\frac{e^2}{4\pi\varepsilon_o\left(a_{Ar\cdots Ar}\right)^3}}{m_e}}{m_e c^2}}\right) \\ +\left(\frac{1}{2}\right)\hbar\sqrt{\frac{\frac{(0.93660)e^2}{8\pi\varepsilon_o\left(a_{Ar\cdots Ar}\right)^3}-\frac{e^2}{8\pi\varepsilon_o\left(a_{Ar\cdots Ar}+\sqrt{\frac{a_{Ar\cdots Ar}a_0}{2(0.5)(0.93660)^{-1}}}\right)^3}}{20}}\end{array}\right\} \quad (16.130)$$

From the energy relationship given by Eq. (16.130) and the relationships between the axes given by Eqs. (16.22-16.24), the dimensions of the $Ar\cdots Ar$ MO can be solved.

The most convenient way to solve Eq. (16.130) is by the reiterative technique using a computer. The result to within the round-off error with five-significant figures is:

$$a_{Ar\cdots Ar} = 12.50271 a_0 = 6.61615\ X\ 10^{-10}\ m \quad (16.131)$$

The component energy parameters at this condition are given in Table 16.34. Substitution of Eq. (16.131) into Eq. (16.22) gives

$$c'_{Ar\cdots Ar} = 3.42199 a_0 = 1.81084\ X\ 10^{-10}\ m \quad (16.132)$$

and internuclear distance between neighboring argon atoms:

$$2c'_{Ar\cdots Ar}(0\ K) = 6.84397 a_0 = 3.62167\ X\ 10^{-10}\ m = 3.62167\ \text{Å} \quad (16.133)$$

The experimental argon interatomic distance $2c'_{C\cdots C}$ is [114]

$$2c'_{Ar\cdots Ar}(4.2\ K) = 3.71\ X\ 10^{-10}\ m = 3.71\ \text{Å} \quad (16.134)$$

The other interatomic bond MO parameters can also be determined by the relationships among the parameters. Substitution of Eqs. (16.131) and (16.132) into Eq. (16.23) gives:

$$b_{Ar\cdots Ar} = c_{Ar\cdots Ar} = 12.02530 a_0 = 6.36351\ X\ 10^{-10}\ m \quad (16.135)$$

Substitution of Eqs. (16.131) and (16.132) into Eq. (16.25) gives:

$$e_{Ar\cdots Ar} = 0.27370 \quad (16.136)$$

A convenient method to calculate the lattice energy is to determine the electric field in solid argon having an electric polarization density corresponding to the aligned dipoles moments, and in turn, the energy can be calculated from the energy of each dipole in the corresponding field using the electrostatic form of Gauss' equation. Substitution of the density of solid argon at 4.2 K $\rho = \frac{1.83\ g}{1\ X\ 10^{-6}\ m^3}$ [114], the $MW = 39.948 g/mole$, $N_A = 6.0221415\ X\ 10^{23}\ molecules/mole$, and the argon dipole moment given in Table 16.33 into Eq. (16.53) gives:

$$U(Ar) = \frac{-2(\mu_{Ar})^2\frac{\rho_{solid\ Ar}}{MW}N_A}{3\varepsilon_0}$$

$$= \frac{-2\left(2.48058\ X\ 10^{-30} C\cdot m\right)^2\frac{\frac{1.83\ g}{1\ X\ 10^{-6}\ m^3}}{39.948 g/mole}6.0221415\ X\ 10^{23}\ molecules/mole}{3\varepsilon_0} \quad (16.137)$$

$$= -0.07977\ eV\ \ (-7.697\ kJ/mole)$$

$U(Ar)$ is also the negative of $E_{van\ der\ Waals}$, the van der Waals energy per argon atom:

$$E_{van\ der\ Waals}\left(solid\ Ar, 4.2\ K / Ar\right) = 0.07977\ eV = 7.697\ kJ / mole \tag{16.138}$$

The experimental van der Waals energy is the cohesive energy [115]:

$$E_{van\ der\ Waals}\left(solid\ Ar, 0\ K\right) = 0.08022\ eV / Ar = 7.74\ kJ / mole \tag{16.139}$$

The calculated results based on first principles and given by analytical equations are summarized in Table 16.35. Using argon the atomic radius (Eq. (16.125)) and the nearest-neighbor distance (Eq. (16.133)), the lattice structure of argon is shown in Figure 16.17B. The charge density of the van der Waals dipoles of the crystalline lattice is shown in Figure 16.18B.

Table 16.35. The calculated and experimental geometrical parameters and interatomic van der Waals cohesive energy of solid argon.

Parameter	Calculated	Experimental	Ref. for Exp.
Solid Argon Interatomic Distance $2c'_{C\text{-}C}$	3.62167 Å (T=0 K)	3.71 Å (T=4.2 K)	114
van der Waals Energy per Argon Atom	0.07977 eV (T=4.2 K)	0.08022 eV (T=0 K)	115

GEOMETRICAL PARAMETERS AND ENERGIES DUE TO THE INTERATOMIC VAN DER WAALS COHESIVE ENERGY OF SOLID KRYPTON

Krypton is a thirty-six-electron neutral atom having the electron configuration $1s^2 2s^2 2p^6 3s^2 3p^6 3d^{10} 4s^2 4p^6$ with the electrons of each shell paired as mirror-image current densities in a shell wherein the radius of the outer shell is $r_{36} = 0.97187 a_0$ (Eq. (10.102)). Thus, in isolation or at sufficient separation, there is no energy between krypton atoms. However, reversible mutual van der Waals dipoles may be induced by collisions when the atoms are in close proximity such that krypton gas can condense into a liquid and further solidify at sufficiently low temperatures due to the strong dipole moment that accommodates close packing. As in the case of helium, the dipoles are atomic rather than molecular, and the limiting separation is based on the formation of a nascent bond to replace the dipole-dipole interaction. Thus, Eq. (16.25) can also be applied to krypton atoms.

The van der Waals bonding in the krypton atom involves hybridizing the three $4p$ AOs into $4p^3$ HO orbitals containing six electrons. The total energy of the state is given by the sum over the six electrons. The sum $E_T\left(Kr, 4p^3\right)$ of experimental energies [15, 116-119] of Kr, Kr^+, Kr^{2+}, Kr^{3+}, Kr^{4+}, and Kr^{5+} is:

$$E_T\left(Kr, 4p^3\right) = \begin{pmatrix} 78.5\ eV + 64.7\ eV + 52.5\ eV \\ +36.950\ eV + 24.35984\ eV + 13.99961\ eV \end{pmatrix} = 271.00945\ eV \tag{16.140}$$

By considering that the central field decreases by an integer for each successive electron of the shell, the radius r_{4p^3} of the $Kr4p^3$ shell may be calculated from the Coulombic energy using Eq. (15.13).

$$r_{4p^3} = \sum_{n=30}^{35} \frac{(Z-n)e^2}{8\pi\varepsilon_0\left(e271.00945\ eV\right)} = \frac{21e^2}{8\pi\varepsilon_0\left(e271.00945\ eV\right)} = 1.05429 a_0 \tag{16.141}$$

where $Z = 36$ for krypton. Using Eq. (15.14), the Coulombic energy $E_{Coulomb}\left(Kr, 4p^3\right)$ of the outer electron of the van der Waals bound $Kr4p^3$ shell is:

$$E_{Coulomb}\left(Kr, 4p^3\right) = \frac{-e^2}{8\pi\varepsilon_0 r_{4p^3}} = \frac{-e^2}{8\pi\varepsilon_0 1.05429 a_0} = -12.905212\ eV \tag{16.142}$$

To meet the equipotential condition of the union of the two $Kr4p^3$ HOs in a nascent bond, c_2 of Eqs. (15.2-15.5) and Eq. (15.61) for the nascent $Kr-Kr$-bond MO is given by Eq. (15.75) as the ratio of the valance energy of the Kr AO, $E\left(Kr\right) = -13.99961\ eV$ and the magnitude of $E_{Coulomb}\left(Kr, 4p^3\right)$ (Eq. (16.142)).

$$c_2\left(Kr - Kr, Kr4p^3 HO\right) = \frac{12.905212\ eV}{13.99961\ eV} = 0.92183 \tag{16.143}$$

Since the outer $Kr4p^3$ HO shell is at a lower energy and greater radius than the non-polarized $4p$ shell, the inner shells are polarized as well. The dipole of the outer shell can polarize the inner shells to the limit that the sum of the primary and secondary dipoles is twice the primary scaled by the energy matching factors of the van der Waals bond given in Eq. (16.15). Thus, the limiting dipole due to polarization of the inner shells is given by:

$$\begin{aligned} \mu_{Kr} &< 2c_1^{-1} q C_2 2c' = 2\left(0.16298\right) e \left(0.92183\right)^{-1} \left(5.57905\ X\ 10^{-11}\ m\right) \\ &= 3.42870\ X\ 10^{-30} C \cdot m = 1.02790\ D \end{aligned} \tag{16.144}$$

The condition of Eq. (16.144) is matched by the participation of the outer three shells as given in Table 16.36. At each shell, opposite charge distributions act as symmetrical point charges at the point of maximum separation, each being centered at 1/2 the

shell radius from the origin. Using the parameters of Eq. (16.143) and $2c' = 1.05429a_0 = 5.57905\,X\,10^{-11}\,m$ (Eq. (16.141)) as well as the radii of the inner shells of krypton (Eq. (10.102)), the van der Waals dipole of krypton is given in Table 16.36 as the sum of the moments of each participating shell.

Table 16.36. The parameters and van der Waals dipole bond moment of the Kr functional group (FG) of solid krypton.

FG	n_1	(c_1) c_2	(C_1) C_2	$E_B(valence)$	$E_A(valence)$	$\frac{q}{e}$	*Ion / IP / Z* [116-119]	Bond Length $2c'$ (Å) (Eqs. (16.141) and (10.102))	Bond Moment μ (D)
Kr	1	0.92183	1	12.90521	13.99961	0.16298	Kr^{6+} 111.0 7 Kr^{8+} 231.5 9	$Kr4p^3$ HO 0.55790 $Kr4s$ AO 0.45405 $Kr3d$ AO 0.27991	1.01129

The minimum-energy packing of krypton dipoles is face-centered cubic also called cubic close packing. In this case, each krypton atom has 12 nearest neighbors and the angle between the aligned dipoles is $\frac{\pi}{4}$ radians. As in the case with graphite, the van der Waals energy is the potential energy between interacting neighboring induced dipoles. Using $\mu_{Kr} = 1.01129\,D = 3.37329\,X\,10^{-30} C \cdot m$ (Table 16.36), the van der Waals energy is**:**

$$E_{van\ der\ Waals}(Kr) = 12\frac{2(\mu_{Kr})^2}{4\pi\varepsilon_0 (r_{Kr\ldots Kr})^3}\cos\left(\frac{\pi}{4}\right) = \left(\frac{24\left(3.37329\,X\,10^{-30} C \cdot m\right)^2}{4\pi\varepsilon_0\left(2\sqrt{\frac{a_{Kr\ldots Kr}a_0}{2C_1C_2}}\right)^3}\right)\cos\left(\frac{\pi}{4}\right) \tag{16.145}$$

The krypton interatomic distance is calculated using Eq. (16.25) with the van der Waals energy (Eq. (16.145)) between neighboring dipoles equated to the nascent bond energy. The energy matching parameter c_2 is the same as that of the krypton dipole, and the reduced mass is $\mu = 42$. The parameters are summarized in Table 16.37 and Eq. (16.146).

Table 16.37. The energy parameters (eV) of the krypton functional group ($Kr\cdots Kr$).

Parameters	$Kr\cdots Kr$ Group
n_1	1
C_1	0.5
C_2	0.92183
c_1	1
c_2	0.92183
C_{1o}	0.5
C_{2o}	0.92183
$V_e\ (eV)$	-3.75058
$V_p\ (eV)$	3.52342
$T\ (eV)$	0.13643
$V_m\ (eV)$	-0.06821
$E_{(AO/HO)}\ (eV)$	0
$\Delta E_{H_2MO(AO/HO)}\ (eV)$	0
$E_{T(AO/HO)}\ (eV)$	0
$E_{T(H_2MO)}\ (eV)$	-0.15895
$E_T\left(atom-atom, msp^3.AO\right)\ (eV)$	0
$E_{T(MO)}\ (eV)$	-0.15895
$\omega\ \left(10^{15}\ rad/s\right)$	0.550731
$E_K\ (eV)$	0.36250
$\bar{E}_D\ (eV)$	-0.00019
$\bar{E}_{Kvib}\ (eV)$	0.00091
$\bar{E}_{osc}\ (eV)$	0.00026
$E_{T(Group)}\ (eV)$	-0.15869

Substitution of the parameters of Table 16.37 and the interatomic cohesive energy of krypton (Eq. (16.145)) into Eq. (16.25) with $R=a_{Kr\ldots Kr}$ gives:

$$\frac{-24\left(3.37329\ X\ 10^{-31} C\cdot m\right)^2}{4\pi\varepsilon_0\left(2\sqrt{\frac{a_{Kr\cdots Kr}a_0}{2(0.5)(0.92183)}}\right)^3}\cos\left(\frac{\pi}{4}\right)$$

$$= \left\{\left(\frac{-e^2}{8\pi\varepsilon_0\sqrt{\frac{a_{Kr\cdots Kr}a_0}{2(0.5)(0.92183)}}}\left((0.92183)\left(2-\frac{1}{2}\frac{a_0}{a_{Kr\cdots Kr}}\right)\ln\frac{a+\sqrt{\frac{a_{Kr\cdots Kr}a_0}{2(0.5)(0.92183)}}}{a-\sqrt{\frac{a_{Kr\cdots Kr}a_0}{2(0.5)(0.92183)}}}-1\right)\right)\right.$$

$$\left.+\left(1+2\sqrt{\frac{2\hbar\sqrt{\frac{(0.5)(0.92183)\frac{e^2}{4\pi\varepsilon_o\left(a_{Kr\cdots Kr}\right)^3}}{m_e}}{m_e c^2}}\right)\right.$$

$$\left.+\left(\frac{1}{2}\right)\hbar\sqrt{\frac{\frac{(0.92183)e^2}{8\pi\varepsilon_o\left(a_{Kr\cdots Kr}\right)^3}-\frac{e^2}{8\pi\varepsilon_o\left(a_{Kr\cdots Kr}+\sqrt{\frac{a_{Kr\cdots Kr}a_0}{2(0.5)(0.92183)}}\right)^3}}{42}}\right\} \tag{16.146}$$

From the energy relationship given by Eq. (16.146) and the relationships between the axes given by Eqs. (16.22-16.24), the dimensions of the $Kr\cdots Kr$ MO can be solved.

The most convenient way to solve Eq. (16.146) is by the reiterative technique using a computer. The result to within the round-off error with five-significant figures is:

$$a_{Kr\cdots Kr} = 13.74580 a_0 = 7.27396\ X\ 10^{-10}\ m \tag{16.147}$$

The component energy parameters at this condition are given in Table 16.37. Substitution of Eq. (16.147) into Eq. (16.22) gives

$$c'_{Kr\cdots Kr} = 3.86154 a_0 = 2.04344\ X\ 10^{-10}\ m \tag{16.148}$$

and internuclear distance between neighboring krypton atoms:

$$2c'_{Kr\cdots Kr}\left(0\ K\right) = 7.72308 a_0 = 4.08688\ X\ 10^{-10}\ m = 4.08688\ \mathring{A} \tag{16.149}$$

The experimental krypton interatomic distance $2c'_{C\cdots C}$ is [113]

$$2c'_{Kr\cdots Kr}\left(0\ K\right) = 3.992\ \ X\ 10^{-10}\ m = 3.992\ \ \mathring{A} \tag{16.150}$$

The other interatomic bond MO parameters can also be determined by the relationships among the parameters. Substitution of Eqs. (16.147) and (16.148) into Eq. (16.23) gives:

$$b_{Kr\cdots Kr} = c_{Kr\cdots Kr} = 13.19225 a_0 = 6.98104\ X\ 10^{-10}\ m \tag{16.151}$$

Substitution of Eqs. (16.147) and (16.148) into Eq. (16.25) gives:

$$e_{Kr\cdots Kr} = 0.28092 \tag{16.152}$$

A convenient method to calculate the lattice energy is to determine the electric field in solid krypton having an electric polarization density corresponding to the aligned dipoles moments, and in turn, the energy can be calculated from the energy of each dipole in the corresponding field using the electrostatic form of Gauss' equation. Substitution of the density of solid krypton at 4.2 K $\rho = \frac{3.094\ g}{1\ X\ 10^{-6}\ m^3}$ [113], the $MW = 83.80 g/mole$, $N_A = 6.0221415\ X\ 10^{23}\ molecules/mole$, and the krypton dipole moment given in Table 16.36 into Eq. (16.53) gives:

$$U\left(Kr\right) = \frac{-2\left(\mu_{Kr}\right)^2\frac{\rho_{solid\ Kr}}{MW}N_A}{3\varepsilon_0}$$

$$= \frac{-2\left(3.37329\ X\ 10^{-30} C\cdot m\right)^2\frac{\frac{3.094\ g}{1\ X\ 10^{-6}\ m^3}}{83.80 g/mole}6.0221415\ X\ 10^{23}\ molecules/mole}{3\varepsilon_0} \tag{16.153}$$

$$= -0.11890\ eV\ \ \left(-11.472\ kJ/mole\right)$$

$[U\left(Kr\right)]$ is also the negative of $E_{van\ der\ Waals}$, the van der Waals energy per krypton atom:

$$E_{van\ der\ Waals}\left(solid\ Kr, 0\ K / Kr\right) = 0.11890\ eV = 11.472\ kJ / mole \tag{16.154}$$

The experimental van der Waals energy is the cohesive energy [120]:

$$E_{van\ der\ Waals}\left(solid\ Kr, 0\ K / Kr\right) = 0.11561\ eV = 11.15454\ kJ / mole \tag{16.155}$$

The calculated results based on first principles and given by analytical equations (0 K) are summarized in Table 16.38. Using krypton the atomic radius (Eq. (16.141)) and the nearest-neighbor distance (Eq. (16.149)), the lattice structure of krypton is shown in Figure 16.15C. The charge density of the van der Waals dipoles of the crystalline lattice is shown in Figure 16.16C.

Table 16.38. The calculated and experimental geometrical parameters and interatomic van der Waals cohesive energy (0 K) of solid krypton.

Parameter	Calculated	Experimental	Ref. for Exp.
Solid Krypton Interatomic Distance $2c'_{C-C}$	4.08688 Å	3.992 Å	113
van der Waals Energy per Krypton Atom	0.11890 eV	0.11561 eV	120

GEOMETRICAL PARAMETERS AND ENERGIES DUE TO THE INTERATOMIC VAN DER WAALS COHESIVE ENERGY OF SOLID XENON

Xenon is a fifty-four-electron neutral atom having the electron configuration $1s^2 2s^2 2p^6 3s^2 3p^6 3d^{10} 4s^2 4p^6 4d^{10} 5s^2 5p^6$ with the electrons of each shell paired as mirror-image current densities in a shell wherein the radius of the outer shell is $r_{54} = 1.12168 a_0$ (Eq. (10.102)). Thus, in isolation or at sufficient separation, there is no energy between xenon atoms. However, reversible mutual van der Waals dipoles may be induced by collisions when the atoms are in close proximity such that xenon gas can condense into a liquid and further solidify at sufficiently low temperatures due to the strong dipole moment that accommodates close packing. As in the case of helium, the dipoles are atomic rather than molecular, and the limiting separation is based on the formation of a nascent bond to replace the dipole-dipole interaction. Thus, Eq. (16.25) can also be applied to xenon atoms.

The van der Waals bonding in the xenon atom involves hybridizing the three $5p$ AOs into $5p^3$ HO orbitals containing six electrons. The total energy of the state is given by the sum over the six electrons. The sum $E_T\left(Xe, 5p^3\right)$ of experimental energies [15, 121-122] of Xe, Xe^+, Xe^{2+}, Xe^{3+}, Xe^{4+}, and Xe^{5+} is:

$$E_T\left(Xe, 5p^3\right) = \begin{pmatrix} 66.703\ eV + 54.14\ eV + 40.9\ eV \\ +31.050\ eV + 20.975\ eV + 12.129842\ eV \end{pmatrix} = 225.89784\ eV \tag{16.156}$$

By considering that the central field decreases by an integer for each successive electron of the shell, the radius r_{5p^3} of the $Xe5p^3$ shell may be calculated from the Coulombic energy using Eq. (15.13).

$$r_{5p^3} = \sum_{n=48}^{53} \frac{(Z-n)e^2}{8\pi\varepsilon_0\left(e225.897842\ eV\right)} = \frac{21e^2}{8\pi\varepsilon_0\left(e225.897842\ eV\right)} = 1.26483 a_0 \tag{16.157}$$

where $Z = 54$ for xenon. Using Eq. (15.14), the Coulombic energy $E_{Coulomb}\left(Xe, 5p^3\right)$ of the outer electron of the van der Waals bound $Xe5p^3$ shell is:

$$E_{Coulomb}\left(Xe, 5p^3\right) = \frac{-e^2}{8\pi\varepsilon_0 r_{5p^3}} = \frac{-e^2}{8\pi\varepsilon_0 1.26483 a_0} = -10.757040\ eV \tag{16.158}$$

To meet the equipotential condition of the union of the two $Xe5p^3$ HOs in a nascent bond, c_2 of Eqs. (15.2-15.5) and Eq. (15.61) for the nascent $Xe-Xe$-bond MO is given by Eq. (15.75) as the ratio of the valance energy of the Xe AO, $E\left(Xe\right) = -12.129842\ eV$ and the magnitude of $E_{Coulomb}\left(Xe, 5p^3\right)$ (Eq. (16.158)).

$$c_2\left(Xe - Xe, Xe5p^3 HO\right) = \frac{10.75704\ eV}{12.129842\ eV} = 0.88682 \tag{16.159}$$

Since the outer $Xe5p^3$ HO shell is at a lower energy and greater radius than the non-polarized $5p$ shell, the inner shells are polarized as well. The dipole of the outer shell can polarize the inner shells to the limit that the sum of the primary and secondary dipoles is twice the primary scaled by the energy matching factors of the van der Waals bond given in Eq. (16.15). Thus, the limiting dipole due to polarization of the inner shells is given by:

$$\mu_{Xe} < 2c_1^{-1} q C_2 2c' = 2\left(0.24079\right)e\left(0.88682\right)\left(6.69318\ X\ 10^{-11}\ m\right) = 5.16444\ X\ 10^{-30} C \cdot m = 1.54826\ D \tag{16.160}$$

The condition of Eq. (16.160) is matched by the participation of the outer two shells as given in Table 16.39. At each shell, opposite charge distributions act as symmetrical point charges at the point of maximum separation, each being centered at 1/2 the shell radius from the origin. Using the parameters of Eq. (16.159) and $2c' = 1.26483 a_0 = 6.69318\ X\ 10^{-11}\ m$ (Eq. (16.157)) as

well as the radius of the inner $5s$ shell of xenon (Eq. (10.102)), the van der Waals dipole of xenon is given in Table 16.39 as the sum of the moments of each participating shell.

Table 16.39. The parameters and van der Waals dipole bond moment of the *Xe* functional group (FG) of solid xenon.

FG	n_1	(c_1) c_2	(C_1) C_2	$E_B(valence)$	$E_A(valence)$	$\frac{q}{e}$	*Ion* / *IP* / *Z* [121-122]	Bond Length $2c'$ $(\mathring{A})$ (Eqs. (16.157) and (10.102))	Bond Moment μ (D)
Xe	1	0.88682	1	10.75704	12.12984	0.24079	Xe^{6+} 91.6 7	$Xe5p^3$ HO 0.66932 $Xe5s$ AO 0.55021	1.41050

The minimum-energy packing of xenon dipoles is face-centered cubic also called cubic close packing. In this case, each xenon atom has 12 nearest neighbors and the angle between the aligned dipoles is $\frac{\pi}{4}$ radians. As in the case with graphite, the van der Waals energy is the potential energy between interacting neighboring induced dipoles. Using $\mu_{Xe} = 1.41050\ D = 4.70492\ X\ 10^{-30} C \cdot m$ (Table 16.39), the van der Waals energy is**:**

$$E_{van\ der\ Waals}(Xe) = 12\frac{2(\mu_{Xe})^2}{4\pi\varepsilon_0 (r_{Xe\ldots Xe})^3}\cos\left(\frac{\pi}{4}\right) = \left(\frac{24\left(4.70492\ X\ 10^{-30} C \cdot m\right)^2}{4\pi\varepsilon_0\left(2\sqrt{\frac{a_{Xe\ldots Xe}a_0}{2C_1C_2}}\right)^3}\right)\cos\left(\frac{\pi}{4}\right) \tag{16.161}$$

The xenon interatomic distance is calculated using Eq. (16.25) with the van der Waals energy (Eq. (16.161)) between neighboring dipoles equated to the nascent bond energy. The energy matching parameter c_2 is the same that of the xenon dipole, and the reduced mass is $\mu = 65$. The parameters are summarized in Table 16.40 and Eq. (16.162).

Table 16.40. The energy parameters (eV) of the xenon functional group ($Xe\cdots Xe$).

Parameters	$Xe\cdots Xe$ Group
n_1	1
C_1	0.5
C_2	0.88682
c_1	1
c_2	1
C_{1o}	0.5
C_{2o}	0.88682
$V_e\ (eV)$	-3.49612
$V_p\ (eV)$	3.20821
$T\ (eV)$	0.10960
$V_m\ (eV)$	-0.05480
$E_{(AO/HO)}\ (eV)$	0
$\Delta E_{H_2MO(AO/HO)}\ (eV)$	0
$E_{T(AO/HO)}\ (eV)$	0
$E_{T(H_2MO)}\ (eV)$	-0.23311
$E_T\left(atom-atom, msp^3.AO\right)\ (eV)$	0
$E_{T(MO)}\ (eV)$	-0.23311
$\omega\ \left(10^{15}\ rad/s\right)$	0.432164
$E_K\ (eV)$	0.28446
$\bar{E}_D\ (eV)$	-0.00025
$\bar{E}_{Kvib}\ (eV)$	0.00062
$\bar{E}_{osc}\ (eV)$	0.00006
$E_{T(Group)}\ (eV)$	-0.23305

Substitution of the parameters of Table 16.40 and the interatomic cohesive energy of xenon (Eq. (16.161)) into Eq. (16.25) with $R=a_{Xe...Xe}$ gives:

$$\frac{-24\left(4.70492\ X\ 10^{-31} C\cdot m\right)^2}{4\pi\varepsilon_0\left(2\sqrt{\frac{a_{Xe\cdots Xe}a_0}{2(0.5)(0.88682)}}\right)^3}\cos\left(\frac{\pi}{4}\right)$$

$$= \left\{\left(\frac{-e^2}{8\pi\varepsilon_0\sqrt{\frac{a_{Xe\cdots Xe}a_0}{2(0.5)(0.88682)}}}\left(\left(2-\frac{1}{2}\frac{a_0}{a_{Xe\cdots Xe}}\right)\ln\frac{a+\sqrt{\frac{a_{Xe\cdots Xe}a_0}{2(0.5)(0.88682)}}}{a-\sqrt{\frac{a_{Xe\cdots Xe}a_0}{2(0.5)(0.88682)}}}-1\right)\right)\right.$$

$$\left.\left(1+2\sqrt{\frac{2\hbar\sqrt{\frac{(0.5)(0.88682)\frac{e^2}{4\pi\varepsilon_o\left(a_{Xe\cdots Xe}\right)^3}}{m_e}}{m_e c^2}}\right)\right\} \tag{16.162}$$

$$\left.+\left(\frac{1}{2}\right)\hbar\sqrt{\frac{\frac{e^2}{8\pi\varepsilon_o\left(a_{Xe\cdots Xe}\right)^3}-\frac{e^2}{8\pi\varepsilon_o\left(a_{Xe\cdots Xe}+\sqrt{\frac{a_{Xe\cdots Xe}a_0}{2(0.5)(0.88682)}}\right)^3}}{65}}\right\}$$

From the energy relationship given by Eq. (16.162) and the relationships between the axes given by Eqs. (16.22-16.24), the dimensions of the $Xe\cdots Xe$ MO can be solved.

The most convenient way to solve Eq. (16.162) is by the reiterative technique using a computer. The result to within the round-off error with five-significant figures is:

$$a_{Xe\cdots Xe} = 15.94999 a_0 = 8.44037\ X\ 10^{-10}\ m \tag{16.163}$$

The component energy parameters at this condition are given in Table 16.40. Substitution of Eq. (16.163) into Eq. (16.22) gives

$$c'_{Xe\cdots Xe} = 4.24093 a_0 = 2.24420\ X\ 10^{-10}\ m \tag{16.164}$$

and internuclear distance between neighboring xenon atoms:

$$2c'_{Xe\cdots Xe}\left(0\ K\right) = 8.48187 a_0 = 4.48841\ X\ 10^{-10}\ m = 4.48841\ \mathring{A} \tag{16.165}$$

The experimental xenon interatomic distance $2c'_{C\cdots C}$ at the melting point of 161.35 K is [112, 113]:

$$2c'_{Xe\cdots Xe}\left(161.35\ K\right) = 4.492\ \ X\ 10^{-10}\ m = 4.492\ \ \mathring{A} \tag{16.166}$$

The other interatomic bond MO parameters can also be determined by the relationships among the parameters. Substitution of Eqs. (16.163) and (16.164) into Eq. (16.23) gives:

$$b_{Xe\cdots Xe} = c_{Xe\cdots Xe} = 15.37585 a_0 = 8.13655\ X\ 10^{-10}\ m \tag{16.167}$$

Substitution of Eqs. (16.163) and (16.164) into Eq. (16.25) gives:

$$e_{Xe\cdots Xe} = 0.26589 \tag{16.168}$$

A convenient method to calculate the lattice energy is to determine the electric field in solid xenon having an electric polarization density corresponding to the aligned dipoles moments, and in turn, the energy can be calculated from the energy of each dipole in the corresponding field using the electrostatic form of Gauss' equation. Substitution of the density of solid xenon at 0 K $\rho = \frac{3.780\ g}{1\ X\ 10^{-6}\ m^3}$ [113], the $MW = 131.29 g/mole$, $N_A = 6.0221415\ X\ 10^{23}\ molecules/mole$, and the xenon dipole moment given in Table 16.39 into Eq. (16.53) gives:

$$U\left(Xe\right) = \frac{-2\left(\mu_{Xe}\right)^2\frac{\rho_{solid\ Xe}}{MW}N_A}{3\varepsilon_0}$$

$$= \frac{-2\left(4.70492\ X\ 10^{-30} C\cdot m\right)^2\frac{\frac{3.780\ g}{1\ X\ 10^{-6}\ m^3}}{131.29 g/mole}6.0221415\ X\ 10^{23}\ molecules/mole}{3\varepsilon_0} \tag{16.169}$$

$$= -0.18037\ eV\ \ \left(-17.403\ kJ/mole\right)$$

$U(Xe)$ is also the negative of $E_{van\ der\ Waals}$, the van der Waals energy per xenon atom:

$$E_{van\ der\ Waals}(solid\ Xe, 0\ K / Xe) = 0.18037\ eV = 17.403\ kJ / mole \tag{16.170}$$

The experimental van der Waals energy is the cohesive energy [123]:

$$E_{van\ der\ Waals}(solid\ Xe, 0\ K) = 0.16608\ eV / Xe = 16.02472\ kJ / mole \tag{16.171}$$

The calculated results based on first principles and given by analytical equations are summarized in Table 16.41. Using xenon the atomic radius (Eq. (16.157)) and the nearest-neighbor distance (Eq. (16.165)), the lattice structure of xenon is shown in Figure 16.15D. The charge density of the van der Waals dipoles of the crystalline lattice is shown in Figure 16.16D.

Table 16.41. The calculated and experimental geometrical parameters and interatomic van der Waals cohesive energy of solid xenon.

Parameter	Calculated	Experimental	Ref. for Exp.
Solid Xenon Interatomic Distance $2c'_{C-C}$	4.4884 Å (T=0 K)	4.492 Å (T=161.35K)	113
van der Waals Energy per Xenon Atom (0 K)	0.18037 eV	0.16608 eV	123

Figure 16.15. The face-centered cubic crystal structures of noble gas condensates, all to the same scale. (A) The crystal structure of neon. (B) The crystal structure of argon. (C) The crystal structure of krypton. (D) The crystal structure of xenon.

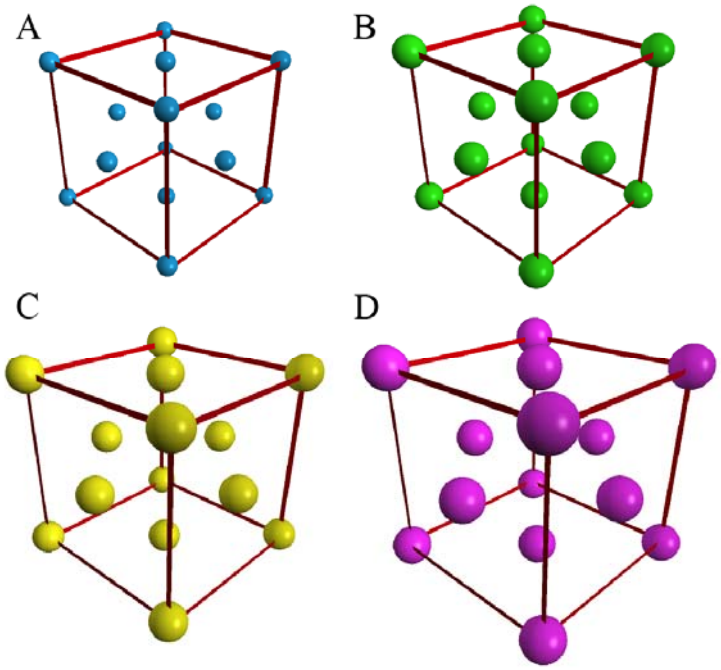

Figure 16.16. The charge densities of the van der Waals dipoles and face-centered cubic crystal structures of noble gas condensates, all to the same scale. (A) The charge density and crystal structure of neon. (B) The charge density and crystal structure of argon. (C) The charge density and crystal structure of krypton. (D) The charge density and crystal structure of xenon.

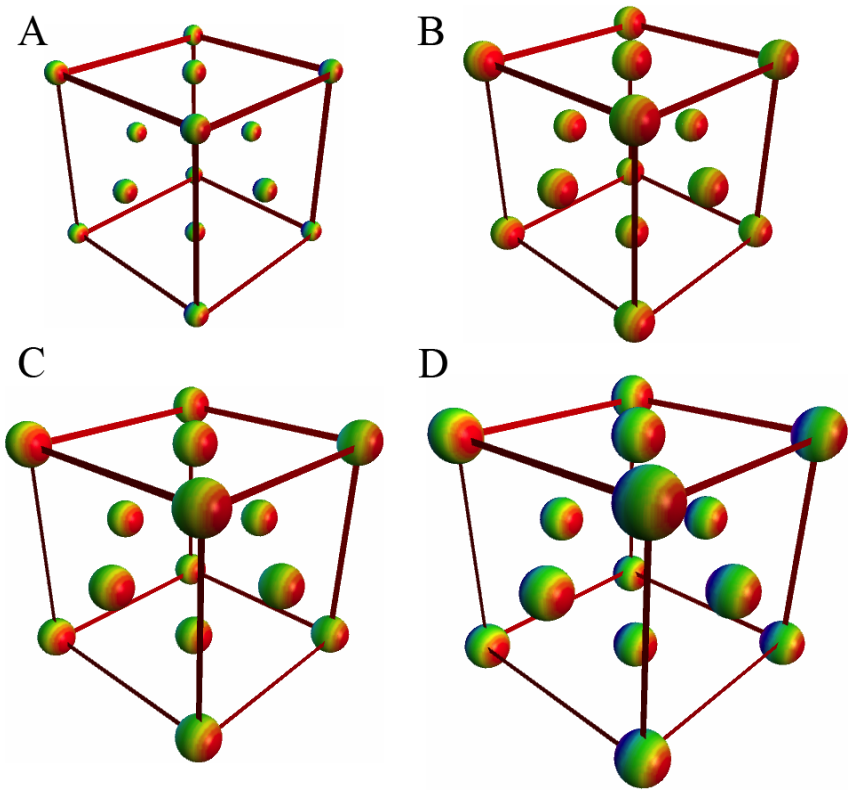

GEOMETRICAL PARAMETERS AND ENERGIES DUE TO THE INTERMOLECULAR VAN DER WAALS COHESIVE ENERGIES OF H_2 DIMER, SOLID H_2, $H_2(1/p)$ DIMER, AND SOLID $H_2(1/p)$

Molecular hydrogen and molecular hydrino are typically gaseous molecules having no net electric field. But, at very low temperatures it is possible to form diffuse dimers, or alternatively, these gases may be condensed with the formation of mutually induced van der Waals dipole interactions. The nature of the van der Waals bonding of molecular hydrogen and molecular hydrino is solved using the same approach as that of condensed helium atoms, except analogously with the comparison of isoelectronic helium and H_2 excited states, the prolate spherical coordinate equations replace the spherical coordinate equations of the two-electron system.

Molecular hydrogen and molecular hydrino are each a two-electron neutral molecule with both electrons paired as mirror-image current densities in a prolate spheroidal shell of semimajor and minor axes given by Eqs. (11.202) and (11.205), respectively. Thus, in isolation or at sufficient separation, there is no energy between hydrogen-type molecules. However, reversible mutual van der Waals dipoles may be induced by collisions when the atoms are in close proximity such that hydrogen-type gas can condense into dimers, liquid, and solid states depending on the temperature and pressure. The limiting separation of the corresponding van der Waals bonding between molecular dipoles is based on the formation of a nascent bond to replace the dipole-dipole interaction. Thus, the isoelectronic helium case of general van der Waals Eq. (16.25) given by Eq. (16.99) also applies to hydrogen-type molecules. Based on symmetry, the molecules at aligned along their semimajor axes, the induces charges act the position of the nuclei at the foci, and the dipole separation is in the direction of the semimajor axes given by the internuclear distance (Eq. (11.204)).

The van der Waals bonding in the hydrogen-type molecules involves hybridizing the $1s$ molecular orbitals (MO) into a $1s^1$ hybridized molecular orbital (HMO) containing two electrons. The total energy of the state is given by the sum over the two electrons given by Eq. (11.241). The sum $E_T\left(H_2\left(1/p\right),1s^1\right)$ is:

$$E_T = -p^2 31.351\, eV - p^3 0.326469\, eV \tag{16.172}$$

The HMO electron energy is equally distributed to each equivalent electron to give the Coulombic energy $E_{Coulomb}\left(H_2(1/p),1s^1\right)$ of the outer electron of the van der Waals bound $H_2(1/p)1s^1$ shell:

$$E_{Coulomb}\left(H_2(1/p),1s^1\right)=\frac{-p^2 31.351\ eV-p^3 0.326469\ eV}{2}$$
$$=-p^2 15.6755\ eV-p^3 0.16323\ eV \tag{16.173}$$

To meet the equipotential condition of the union of the two $H_2(1/p)1s^1$ HOs in a nascent bond, c_2 of Eqs. (15.2-15.5) and Eq. (15.61) for the nascent $H_2(1/p)-H_2(1/p)$-bond MO is given by Eq. (15.75) as the ratio of the valance energy of the $H_2(1/p)$ MO, $E_{IP_1}\left(H_2(1/p)\right)=p^2 15.2171\ eV+p^3 0.207714\ eV$ given by Eq. (11. 244) and the magnitude of $E_{Coulomb}\left(H_2(1/p),1s^1\right)$ (Eq. (16.173)):

$$c_2\left(H_2(1/p)-H_2(1/p),H_2(1/p)1s^1 HMO\right)=\frac{p^2 15.2171\ eV+p^3 0.207714\ eV}{p^2 15.6755\ eV+p^3 0.16323\ eV} \tag{16.174}$$

The opposite charge distributions act as point charges at the foci, the position of the nuclei such that the separation distance is the internuclear distance given by Eq. (11.204).

The van der Waals dipole of $H_2(1/p)$ is calculated by the same method as that of helium using the parameters of Eq. (16.174) and $2c'=\frac{a_0\sqrt{2}}{p}$ (Eq. (11.204)). As in the case with helium, the van der Waals energy is the potential energy between interacting neighboring induced dipoles. Using the van der Waals dipole of $H_2(1/p)$, the van der Waals energy for a hydrogen type dimer is:

$$E_{van\ der\ Waals}\left(H_2(1/p)\right)=\frac{2\left(\mu_{H_2(1/p)}\right)^2}{4\pi\varepsilon_0\left(r_{H_2(1/p)\cdots H_2(1/p)}\right)^3} \tag{16.175}$$

The dimer interatomic distance is calculated using Eq. (16.25) with the van der Waals energy (Eq. (16.175)) between neighboring dipoles equated to the nascent bond energy. From the energy relationship given by Eq. (16.25) and the relationships between the axes given by Eqs. (16.22-16.24), the dimensions of the $H_2(1/p)\cdots H_2(1/p)$ MO can be solved.

PARAMETERS AND ENERGIES DUE TO THE INTERMOLECULAR VAN DER WAALS COHESIVE ENERGIES OF H_2 DIMER

In the case of H_2, $p=1$ such that the parameter c_2 is given by

$$c_2\left(H_2-H_2,H_2 1s^1 HMO\right)=\frac{1^2 15.2171\ eV+1^3 0.207714\ eV}{1^2 15.6755\ eV+1^3 0.16323\ eV}=0.9739 \tag{16.176}$$

Using the parameters of Eq. (16.176) and $2c'=a_0\sqrt{2}$ (Eq. (11.204)), the van der Waals dipole of H_2 is given in Table 16.42.

Table 16.42. The parameters and van der Waals dipole bond moment of the H_2 functional group of hydrogen dimer.

Functional Group	n_1	$(c_1)c_2$	$(C_1)C_2$	$E_B(valence)$	$E_A(valence)$	$\frac{q}{e}$	Bond Length $2c'$ $(\AA)$	Bond Moment μ (D)
H_2	1	0.9739	1	15.4248	15.83901	0.05300	0.748369	0.19053

The van der Waals energy is the potential energy between interacting neighboring induced dipoles. Using $\mu_{H_2}=0.19053\ D=6.35524\ X\ 10^{-31} C\cdot m$ (Table 16.42), the van der Waals energy is:

$$E_{van\ der\ Waals}\left(H_2\right)=\frac{2\left(\mu_{H_2}\right)^2}{4\pi\varepsilon_0\left(r_{H_2\cdots H_2}\right)^3}=\frac{2\left(6.35524\ X\ 10^{-31} C\cdot m\right)^2}{4\pi\varepsilon_0\left(2\sqrt{\frac{a_{H_2\cdots H_2}a_0}{2C_1C_2}}\right)^3} \tag{16.177}$$

The hydrogen dimer intermolecular distance is calculated using Eq. (16.25) with the van der Waals energy (Eq. (16.177)) between neighboring dipoles equated to the nascent bond energy. The energy matching parameter c_2 of $H_2 \cdots H_2$ is the same as that of the H_2 dipole, and the reduced mass is $\mu = 1$. The parameters are summarized in Table 16.43 and Eq. (16.178).

Table 16.43. The energy parameters (eV) of the hydrogen dimer functional group ($H_2 \cdots H_2$).

Parameters	$H_2 \cdots H_2$ Group
n_1	1
C_1	0.5
C_2	0.97385^{-1}
c_1	1
c_2	0.97385
C_{1o}	0.5
C_{2o}	0.97385^{-1}
$V_e\ (eV)$	-3.64208
$V_p\ (eV)$	3.57387
$T\ (eV)$	0.12236
$V_m\ (eV)$	-0.06118
$E_{(AO/HO)}\ (eV)$	0
$\Delta E_{H_2MO(AO/HO)}\ (eV)$	0
$E_{T(AO/HO)}\ (eV)$	0
$E_{T(H_2MO)}\ (eV)$	-0.00703
$E_T\left(atom-atom, msp^3.AO\right)\ (eV)$	0
$E_{T(MO)}\ (eV)$	-0.00703
$\omega\ \left(10^{15}\ rad/s\right)$	0.515948
$E_K\ (eV)$	0.33961
$\bar{E}_D\ (eV)$	0.00001
$\bar{E}_{Kvib}\ (eV)$	0.00028
$\bar{E}_{osc}\ (eV)$	-0.00013
$E_{T(Group)}\ (eV)$	-0.00069

Substitution of the parameters of Table 16.43 and the interatomic cohesive energy of hydrogen dimer (Eq. (16.177)) into Eq. (16.25) with $R = a_{H_2 \cdots H_2}$ gives:

$$\frac{-2\left(6.35524\ X\ 10^{-31} C\cdot m\right)^2}{4\pi\varepsilon_0\left(2\sqrt{\frac{a_{H_2\cdots H_2}a_0}{2(0.5)(0.97385)^{-1}}}\right)^3}$$

$$=\left\{\left(\frac{-e^2}{8\pi\varepsilon_0\sqrt{\frac{a_{H_2\cdots H_2}a_0}{2(0.5)(0.97385)^{-1}}}}\left((0.97385)\left(2-\frac{1}{2}\frac{a_0}{a_{H_2\cdots H_2}}\right)\ln\frac{a+\sqrt{\frac{a_{H_2\cdots H_2}a_0}{2(0.5)(0.97385)^{-1}}}}{a-\sqrt{\frac{a_{H_2\cdots H_2}a_0}{2(0.5)(0.97385)^{-1}}}}-1\right)\right)\right.$$

$$\left.\left(1+2\sqrt{\frac{2\hbar\sqrt{(0.5)(0.97385)^{-1}\frac{e^2}{4\pi\varepsilon_o\left(a_{H_2\cdots H_2}\right)^3}}}{m_e c^2}}\right)+\left(\frac{1}{2}\right)\hbar\sqrt{\frac{\frac{(0.97385)(0.05300e)^2}{8\pi\varepsilon_o\left(a_{H_2\cdots H_2}\right)^3}-\frac{(0.05300e)^2}{8\pi\varepsilon_o\left(a_{H_2\cdots H_2}+\sqrt{\frac{a_{H_2\cdots H_2}a_0}{2(0.5)(0.97385)^{-1}}}\right)^3}}{1}}\right\}$$

(16.178)

wherein (0.05300) is q/e the induced charge from Table 16.42. From the energy relationship given by Eq. (16.178) and the relationships between the axes given by Eqs. (16.22-16.24), the dimensions of the $H_2\cdots H_2$ MO can be solved.

The most convenient way to solve Eq. (16.178) is by the reiterative technique using a computer. The result to within the round-off error with five-significant figures is:

$$a_{H_2\cdots H_2}=14.88260a_0=7.87553\ X\ 10^{-10}\ m \tag{16.179}$$

The component energy parameters at this condition are given in Table 16.43. Substitution of Eq. (16.179) into Eq. (16.22) gives

$$c'_{H_2\cdots H_2}=3.80702a_0=2.01459\ X\ 10^{-10}\ m \tag{16.180}$$

and internuclear distance between neighboring H_2 nuclei:

$$2c'_{H_2\cdots H_2}=7.61404a_0=4.02918\ X\ 10^{-10}\ m=4.02918\ \mathring{A} \tag{16.181}$$

The other intermolecular bond MO parameters can also be determined by the relationships among the parameters. Substitution of Eqs. (16.179) and (16.180) into Eq. (16.23) gives

$$b_{H_2\cdots H_2}=c_{H_2\cdots H_2}=14.38744a_0=7.61350\ X\ 10^{-10}\ m \tag{16.182}$$

Substitution of Eqs. (16.179) and (16.180) into Eq. (16.25) gives:

$$e_{H_2\cdots H_2}=0.25580 \tag{16.183}$$

Using Eqs. (16.177) and (16.181), the van der Waals energy of the hydrogen dimer is:

$$E_{van\ der\ Waals}\left([H_2]_2\right)=0.00069\ eV\left(5.59\ cm^{-1}\right) \tag{16.184}$$

The experimental D_0 is shown in Figure of Ref. [124], [125] is:

$$D_0=5.6\ cm^{-1} \tag{16.185}$$

From Table 16.43, the hydrogen dimer vibrational energy $\bar{E}_{Kvib}\ (eV)$ that matches the experimental dimer spectrum [126] is

$$\bar{E}_{Kvib}\ (eV)=0.00028\ eV\left(2.3\ cm^{-1}\right) \tag{16.186}$$

PARAMETERS AND ENERGIES DUE TO THE INTERMOLECULAR VAN DER WAALS COHESIVE ENERGIES OF SOLID H_2

The minimum-energy packing of H_2 dipoles is face-centered cubic also called cubic close packing. In this case, each H_2 molecule has 12 nearest neighbors and the angle between the aligned dipoles is $\frac{\pi}{4}$ radians. As in the case with hydrogen dimer, the van der Waals energy is the potential energy between interacting neighboring induced dipoles. Using $\mu_{H_2}=0.19053\ D=6.35524\ X\ 10^{-31} C\cdot m$ (Table 16.42), the van der Waals energy is:

$$E_{van\ der\ Waals}\left(H_2\right)=12\frac{2\left(\mu_{H_2}\right)^2}{4\pi\varepsilon_0\left(r_{H_2\cdots H_2}\right)^3}\cos\left(\frac{\pi}{4}\right)=\frac{24\left(6.35524\ X\ 10^{-31}C\cdot m\right)^2}{4\pi\varepsilon_0\left(2\sqrt{\frac{a_{H_2\cdots H_2}a_0}{2C_1C_2}}\right)^3}\cos\left(\frac{\pi}{4}\right) \tag{16.187}$$

The hydrogen dimer intermolecular distance is calculated using Eq. (16.25) with the van der Waals energy (Eq. (16.187)) between neighboring dipoles equated to the nascent bond energy. The energy matching parameter c_2 of $H_2\cdots H_2$ is the same as that of the H_2 dipole, and the reduced mass is $\mu=1$. The parameters are summarized in Table 16.44 and Eq. (16.188).

Table 16.44. The energy parameters (eV) of the solid hydrogen functional group ($H_2\cdots H_2$).

Parameters	$H_2\cdots H_2$ Group
n_1	1
C_1	0.5
C_2	0.97385^{-1}
c_1	1
c_2	0.97385
C_{1o}	0.5
C_{2o}	0.97385^{-1}
$V_e\ (eV)$	-3.63998
$V_p\ (eV)$	3.57286
$T\ (eV)$	0.12222
$V_m\ (eV)$	-0.06111
$E_{(AO/HO)}\ (eV)$	0
$\Delta E_{H_2MO(AO/HO)}\ (eV)$	0
$E_{T(AO/HO)}\ (eV)$	0
$E_{T(H_2MO)}\ (eV)$	-0.00601
$E_T\left(atom-atom, msp^3.AO\right)\ (eV)$	0
$E_{T(MO)}\ (eV)$	-0.00601
$\omega\ \left(10^{15}\ rad/s\right)$	0.515511
$E_K\ (eV)$	0.33932
$\bar{E}_D\ (eV)$	0.00001
$\bar{E}_{Kvib}\ (eV)$	0.00028
$\bar{E}_{osc}\ (eV)$	-0.00013
$E_{T(Group)}\ (eV)$	-0.00587

Substitution of the parameters of Table 16.43 and the interatomic cohesive energy of solid hydrogen (Eq. (16.187)) into Eq. (16.25) with $R=a_{H_2\cdots H_2}$ gives:

$$\frac{-24\left(6.35524\ X\ 10^{-31} C\cdot m\right)^2}{4\pi\varepsilon_0\left(2\sqrt{\frac{a_{H_2\cdots H_2}a_0}{2(0.5)(0.97385)^{-1}}}\right)^3}\cos\left(\frac{\pi}{4}\right)$$

$$=\left\{\left(\frac{-e^2}{8\pi\varepsilon_0\sqrt{\frac{a_{H_2\cdots H_2}a_0}{2(0.5)(0.97385)^{-1}}}}\left((0.97385)\left(2-\frac{1}{2}\frac{a_0}{a_{H_2\cdots H_2}}\right)\ln\frac{a+\sqrt{\frac{a_{H_2\cdots H_2}a_0}{2(0.5)(0.97385)^{-1}}}}{a-\sqrt{\frac{a_{H_2\cdots H_2}a_0}{2(0.5)(0.97385)^{-1}}}}-1\right)\right)\right.$$

$$\left.\left(1+2\sqrt{\frac{2\hbar\sqrt{\frac{(0.5)(0.97385)^{-1}\frac{e^2}{4\pi\varepsilon_o\left(a_{H_2\cdots H_2}\right)^3}}{m_e}}{m_e c^2}}\right)+\left(\frac{1}{2}\right)\hbar\sqrt{\frac{\frac{(0.97385)(0.05300e)^2}{8\pi\varepsilon_o\left(a_{H_2\cdots H_2}\right)^3}-\frac{(0.05300e)^2}{8\pi\varepsilon_o\left(a_{H_2\cdots H_2}+\sqrt{\frac{a_{H_2\cdots H_2}a_0}{2(0.5)(0.97385)^{-1}}}\right)^3}}{1}}\right\}$$

(16.188)

wherein (0.05300) is q/e the induced charge from Table 16.42. From the energy relationship given by Eq. (16.188) and the relationships between the axes given by Eqs. (16.22-16.24), the dimensions of the $H_2\cdots H_2$ MO can be solved.

The most convenient way to solve Eq. (16.188) is by the reiterative technique using a computer. The result to within the round-off error with five-significant figures is:

$$a_{H_2\cdots H_2}=14.89100a_0=7.87998\ X\ 10^{-10}\ m \tag{16.189}$$

The component energy parameters at this condition are given in Table 16.44. Substitution of Eq. (16.189) into Eq. (16.22) gives

$$c'_{H_2\cdots H_2}=3.80810a_0=2.01516\ X\ 10^{-10}\ m \tag{16.190}$$

and internuclear distance between neighboring H_2 nuclei:

$$2c'_{H_2\cdots H_2}=7.61619a_0=4.03031\ X\ 10^{-10}\ m=4.03031\ \mathring{A} \tag{16.191}$$

The other intermolecular bond MO parameters can also be determined by the relationships among the parameters. Substitution of Eqs. (16.189) and (16.190) into Eq. (16.23) gives

$$b_{H_2\cdots H_2}=c_{H_2\cdots H_2}=14.39584a_0=7.61795\ X\ 10^{-10}\ m \tag{16.192}$$

Substitution of Eqs. (16.189) and (16.190) into Eq. (16.25) gives:

$$e_{H_2\cdots H_2}=0.25573 \tag{16.193}$$

A convenient method to calculate the lattice energy is to determine the electric field in solid molecular hydrogen having an electric polarization density corresponding to the aligned dipoles moments, and in turn, the energy can be calculated from the energy of each dipole in the corresponding field using the electrostatic form of Gauss' equation. Substitution of the density of solid hydrogen $\rho=\frac{0.086\ g}{1\ X\ 10^{-6}\ m^3}$ [127], the $MW=2.016\ g/mole$, $N_A=6.0221415\ X\ 10^{23}\ molecules/mole$, and the H_2 dipole moment given in Table 16.42 into Eq. (16.53) gives:

$$U(H_2)=\frac{-2\left(\mu_{H_2}\right)^2\frac{\rho_{solid\ H_2}}{MW}N_A}{3\varepsilon_0}$$

$$=\frac{-2\left(6.35524\ X\ 10^{-31} C\cdot m\right)^2\frac{\frac{0.086\ g}{1\ X\ 10^{-6}\ m^3}}{2.016 g/mole}6.0221415\ X\ 10^{23}\ molecules/mole}{3\varepsilon_0}$$

$$=-0.00488\ eV\ \left(-0.470\ kJ/mole\right)$$

$$U(Ne)=\frac{-2(\mu_{Ne})^2\frac{\rho_{solid\ Ne}}{MW}N_A}{3\varepsilon_0}$$

$$=\frac{-2\left(1.08554\ X\ 10^{-30}C\cdot m\right)^2\frac{\frac{1.433\ g}{1\ X\ 10^{-6}\ m^3}}{20.179 g/mole}6.0221415\ X\ 10^{23}\ molecules/mole}{3\varepsilon_0} \tag{16.194}$$

$$=-0.02368\ eV\ \ (-2.285\ kJ/mole)$$

$U(H_2)$ is also the negative of $E_{van\ der\ Waals}$, the van der Waals energy per H_2 molecule:

$$E_{van\ der\ Waals}(solid\ H_2/H_2)=0.00488\ eV=0.470\ kJ/mole \tag{16.195}$$

The experimental van der Waals energy calculated from the heat of vaporization and fusion per hydrogen molecule [128] is

$$\begin{aligned}E_{van\ der\ Waals}(solid\ H_2)&=E_{vapor}+E_{fusion}\\&=0.44936\ kJ/mole+0.05868\ kJ/mole\\&=0.50804\ kJ/mole\end{aligned} \tag{16.196}$$

PARAMETERS AND ENERGIES DUE TO THE INTERMOLECULAR VAN DER WAALS COHESIVE ENERGIES OF $H_2(1/4)$ DIMER

In the case of H_2, $p=4$ such that the parameter c_2 is given by

$$\begin{aligned}c_2\left(H_2(1/4)-H_2(1/4),H_2(1/4)1s^1HMO\right)&=\frac{4^2 15.2171\ eV+4^3 0.207714\ eV}{4^2 15.6755\ eV+4^3 0.16323\ eV}\\&=0.9828\end{aligned} \tag{16.197}$$

Using the parameters of Eq. (16.197) and $2c'=a_0\frac{\sqrt{2}}{4}$ (Eq. (11.204)), the van der Waals dipole of $H_2(1/4)$ is given in Table 16.45.

Table 16.45. The parameters and van der Waals dipole bond moment of the $H_2(1/4)$ functional group of hydrogen dimer.

Functional Group	n_1	(c_1) c_2	(C_1) C_2	$E_B(valence)$	$E_A(valence)$	$\frac{q}{e}$	Bond Length $2c'$ (Å)	Bond Moment μ (D)
$H_2(1/4)$	1	0.9828	1	256.767	261.255	0.03466	0.187092	0.03114

The van der Waals energy is the potential energy between interacting neighboring induced dipoles. Using $\mu_{H_2(1/4)}=0.03114\ D=1.03885\ X\ 10^{-31}C\cdot m$ (Table 16.45), the van der Waals energy is:

$$E_{van\ der\ Waals}\left(H_2(1/4)\right)=\frac{2\left(\mu_{H_2(1/4)}\right)^2}{4\pi\varepsilon_0\left(r_{H_2(1/4)\cdots H_2(1/4)}\right)^3}=\frac{2\left(1.03885\ X\ 10^{-31}C\cdot m\right)^2}{4\pi\varepsilon_0\left(2\sqrt{\frac{a_{H_2(1/4)\cdots H_2(1/4)}a_0}{2C_1C_2}}\right)^3} \tag{16.198}$$

The molecular hydrino dimer intermolecular distance is calculated using Eq. (16.25) with the van der Waals energy (Eq. (16.198)) between neighboring dipoles equated to the nascent bond energy. The energy matching parameter c_2 of $H_2(1/4)\cdots H_2(1/4)$ is the same as that of the $H_2(1/4)$ dipole, and the reduced mass is $\mu=1$. The parameters are summarized in Table 16.46 and Eq. (16.199).

Table 16.46. The energy parameters (eV) of the hydrogen dimer functional group ($H_2(1/4)\cdots H_2(1/4)$).

Parameters	$H_2(1/4)\cdots H_2(1/4)$ Group
n_1	1
C_1	0.5
C_2	0.9828^{-1}
c_1	1
c_2	0.9828
C_{1o}	0.5
C_{2o}	0.9828^{-1}
$V_e\ (eV)$	-56.96364
$V_p\ (eV)$	56.03381
$T\ (eV)$	1.85462
$V_m\ (eV)$	-0.92731
$E_{(AO/HO)}\ (eV)$	0
$\Delta E_{H_2MO(AO/HO)}\ (eV)$	0
$E_{T(AO/HO)}\ (eV)$	0
$E_{T(H_2MO)}\ (eV)$	-0.00253
$E_T\left(atom-atom, msp^3.AO\right)\ (eV)$	0
$E_{T(MO)}\ (eV)$	-0.00253
$\omega\ \left(10^{15}\ rad/s\right)$	7.83940
$E_K\ (eV)$	5.16003
$\bar{E}_D\ (eV)$	0.00001
$\bar{E}_{Kvib}\ (eV)$	0.00285
$\bar{E}_{osc}\ (eV)$	-0.00141
$E_{T(Group)}\ (eV)$	-0.00111

Substitution of the parameters of Table 16.46 and the interatomic cohesive energy of hydrogen dimer (Eq. (16.198)) into Eq. (16.25) with $R = a_{H_2(1/4)\cdots H_2(1/4)}$ gives:

$$\frac{-2\left(1.03885\ X\ 10^{-31} C\cdot m\right)^2}{4\pi\varepsilon_0\left(2\sqrt{\frac{a_{H_2(1/4)\cdots H_2(1/4)}a_0}{2(0.5)(0.9828)^{-1}}}\right)^3} = \left\{\left(\frac{-e^2}{8\pi\varepsilon_0\sqrt{\frac{a_{H_2(1/4)\cdots H_2(1/4)}a_0}{2(0.5)(0.9828)^{-1}}}}\right)\left((0.9828)\left(2-\frac{1}{2}\frac{a_0}{a_{H_2(1/4)\cdots H_2(1/4)}}\right)\right)\left(\ln\frac{a+\sqrt{\frac{a_{H_2(1/4)\cdots H_2(1/4)}a_0}{2(0.5)(0.9828)^{-1}}}}{a-\sqrt{\frac{a_{H_2(1/4)\cdots H_2(1/4)}a_0}{2(0.5)(0.9828)^{-1}}}}-1\right)\right\}$$
$$\left\{\left(1+2\sqrt{\frac{2\hbar\sqrt{\frac{(0.5)(0.9828)^{-1}\frac{e^2}{4\pi\varepsilon_o\left(a_{H_2(1/4)\cdots H_2(1/4)}\right)^3}}{m_e}}}{m_e c^2}}\right)+\left(\frac{1}{2}\right)\hbar\sqrt{\frac{\frac{(0.9828)(0.03466e)^2}{8\pi\varepsilon_o\left(a_{H_2(1/4)\cdots H_2(1/4)}\right)^3}-\frac{(0.03466e)^2}{8\pi\varepsilon_o\left(a_{H_2(1/4)\cdots H_2(1/4)}+\sqrt{\frac{a_{H_2(1/4)\cdots H_2(1/4)}a_0}{2(0.5)(0.9828)^{-1}}}\right)^3}}{1}}\right\} \quad (16.199)$$

wherein (0.03466) is q/e the induced charge from Table 16.45. From the energy relationship given by Eq. (16.199) and the relationships between the axes given by Eqs. (16.22-16.24), the dimensions of the $H_2(1/4)\cdots H_2(1/4)$ MO can be solved.

The most convenient way to solve Eq. (16.199) is by the reiterative technique using a computer. The result to within the round-off error with five-significant figures is:

$$a_{H_2(1/4)\cdots H_2(1/4)_2} = 3.83931 a_0 = 2.03168\ X\ 10^{-10}\ m \quad (16.200)$$

The component energy parameters at this condition are given in Table 16.46. Substitution of Eq. (16.200) into Eq. (16.22) gives

$$c'_{H_2(1/4)\cdots H_2(1/4)_2} = 0.97126 a_0 = 5.13967\ X\ 10^{-11}\ m \quad (16.201)$$

and internuclear distance between neighboring H_2 nuclei:

$$2c'_{H_2(1/4)\cdots H_2(1/4)_2} = 1.94251 a_0 = 1.02793\ X\ 10^{-10}\ m = 1.02793\ \text{Å} \quad (16.202)$$

The other intermolecular bond MO parameters can also be determined by the relationships among the parameters. Substitution of Eqs. (16.200) and (16.201) into Eq. (16.23) gives

$$b_{H_2(1/4)\cdots H_2(1/4)_2} = c_{H_2(1/4)\cdots H_2(1/4)_2} = 3.71443 a_0 = 1.96559\ X\ 10^{-10}\ m \quad (16.203)$$

Substitution of Eqs. (16.200) and (16.201) into Eq. (16.25) gives:

$$e_{H_2(1/4)\cdots H_2(1/4)_2} = 0.25298 \quad (16.204)$$

Using Eqs. (16.198) and (16.202), the van der Waals energy of the hydrogen dimer is:

$$E_{van\ der\ Waals}\left([H_2(1/4)]_2\right) = 0.00111\ eV\left(8.991\ cm^{-1}\right) \quad (16.205)$$

PARAMETERS AND ENERGIES DUE TO THE INTERMOLECULAR VAN DER WAALS COHESIVE ENERGIES OF SOLID $H_2(1/4)$

The minimum-energy packing of $H_2(1/4)$ dipoles is face-centered cubic also called cubic close packing. In this case, each $H_2(1/4)$ molecule has 12 nearest neighbors and the angle between the aligned dipoles is $\frac{\pi}{4}$ radians. As in the case with $H_2(1/4)$ dimer, the van der Waals energy is the potential energy between interacting neighboring induced dipoles. Using $\mu_{H_2(1/4)} = 0.03114\ D = 1.03885\ X\ 10^{-31} C\cdot m$ (Table 16.45), the van der Waals energy is:

$$E_{van\ der\ Waals}\left(H_2(1/4)\right)=12\frac{2\left(\mu_{H_2(1/4)}\right)^2}{4\pi\varepsilon_0\left(r_{H_2(1/4)\cdots H_2(1/4)}\right)^3}\cos\left(\frac{\pi}{4}\right)$$
$$=\frac{24\left(1.03885\ X\ 10^{-31}C\cdot m\right)^2}{4\pi\varepsilon_0\left(2\sqrt{\frac{a_{H_2(1/4)\cdots H_2(1/4)}a_0}{2C_1C_2}}\right)^3}\cos\left(\frac{\pi}{4}\right) \quad (16.206)$$

The hydrogen dimer intermolecular distance is calculated using Eq. (16.25) with the van der Waals energy (Eq. (16.206)) between neighboring dipoles equated to the nascent bond energy. The energy matching parameter c_2 of $H_2(1/4)\cdots H_2(1/4)$ is the same as that of the $H_2(1/4)$ dipole, and the reduced mass is $\mu=1$. The parameters are summarized in Table 16.47 and Eq. (16.207).

Table 16.47. The energy parameters (eV) of the solid hydrogen functional group ($H_2(1/4)\cdots H_2(1/4)$).

Parameters	$H_2(1/4)\cdots H_2(1/4)$ Group
n_1	1
C_1	0.5
C_2	0.9828^{-1}
c_1	1
c_2	0.9828
C_{1o}	0.5
C_{2o}	0.9828^{-1}
$V_e\ (eV)$	-56.98072
$V_p\ (eV)$	56.04202
$T\ (eV)$	1.85572
$V_m\ (eV)$	-0.92786
$E_{(AO/HO)}\ (eV)$	0
$\Delta E_{H_2MO(AO/HO)}\ (eV)$	0
$E_{T(AO/HO)}\ (eV)$	0
$E_{T(H_2MO)}\ (eV)$	-0.01084
$E_T\left(atom-atom, msp^3.AO\right)\ (eV)$	0
$E_{T(MO)}\ (eV)$	-0.01084
$\omega\ \left(10^{15}\ rad/s\right)$	7.84284
$E_K\ (eV)$	5.16229
$\bar{E}_D\ (eV)$	0.00005
$\bar{E}_{Kvib}\ (eV)$	0.00285
$\bar{E}_{osc}\ (eV)$	-0.00138
$E_{T(Group)}\ (eV)$	-0.00946

Substitution of the parameters of Table 16.47 and the interatomic cohesive energy of solid hydrogen (Eq. (16.206)) into Eq. (16.25) with $R = a_{H_2(1/4)\cdots H_2(1/4)}$ gives:

$$\frac{-24\left(1.03885\ X\ 10^{-31} C\cdot m\right)^2}{4\pi\varepsilon_0\left(2\sqrt{\frac{a_{H_2(1/4)\cdots H_2(1/4)}a_0}{2(0.5)(0.9828)^{-1}}}\right)^3}\cos\left(\frac{\pi}{4}\right)$$

$$= \left\{ \left(\frac{-e^2}{8\pi\varepsilon_0\sqrt{\frac{a_{H_2(1/4)\cdots H_2(1/4)}a_0}{2(0.5)(0.9828)^{-1}}}} \left((0.9828)\left(2-\frac{1}{2}\frac{a_0}{a_{H_2(1/4)\cdots H_2(1/4)}}\right) \right) \right) \right.$$

$$\left. \left(1+2\sqrt{\frac{2\hbar\sqrt{(0.5)(0.9828)^{-1}\frac{e^2}{4\pi\varepsilon_o\left(a_{H_2(1/4)\cdots H_2(1/4)}\right)^3}}}{m_e c^2}} \right) + \left(\frac{1}{2}\right)\hbar\sqrt{\frac{\frac{(0.9828)(0.03466e)^2}{8\pi\varepsilon_o\left(a_{H_2(1/4)\cdots H_2(1/4)}\right)^3} - \frac{(0.03466e)^2}{8\pi\varepsilon_o\left(a_{H_2(1/4)\cdots H_2(1/4)}+\sqrt{\frac{a_{H_2(1/4)\cdots H_2(1/4)}a_0}{2(0.5)(0.9828)^{-1}}}\right)^3}}{1}} \right\} \tag{16.207}$$

wherein (0.03466) is q/e the induced charge from Table 16.42. From the energy relationship given by Eq. (16.207) and the relationships between the axes given by Eqs. (16.22-16.24), the dimensions of the $H_2(1/4)\cdots H_2(1/4)$ MO can be solved.

The most convenient way to solve Eq. (16.207) is by the reiterative technique using a computer. The result to within the round-off error with five-significant figures is:

$$a_{H_2(1/4)\cdots H_2(1/4)} = 3.83819 a_0 = 2.03108\ X\ 10^{-10}\ m \tag{16.208}$$

The component energy parameters at this condition are given in Table 16.47. Substitution of Eq. (16.208) into Eq. (16.22) gives

$$c'_{H_2(1/4)\cdots H_2(1/4)_2} = 0.97111 a_0 = 5.13891\ X\ 10^{-11}\ m \tag{16.209}$$

and internuclear distance between neighboring $H_2(1/4)$ nuclei:

$$2c'_{H_2(1/4)\cdots H_2(1/4)} = 1.94223 a_0 = 1.02778\ X\ 10^{-10}\ m = 1.02778\ \mathring{A} \tag{16.210}$$

The other intermolecular bond MO parameters can also be determined by the relationships among the parameters. Substitution of Eqs. (16.208) and (16.209) into Eq. (16.23) gives

$$b_{H_2(1/4)\cdots H_2(1/4)_2} = c_{H_2(1/4)\cdots H_2(1/4)_2} = 3.71330 a_0 = 1.96499\ X\ 10^{-10}\ m \tag{16.211}$$

Substitution of Eqs. (16.208) and (16.209) into Eq. (16.25) gives:

$$e_{H_2(1/4)\cdots H_2(1/4)_2} = 0.25301 \tag{16.212}$$

A convenient method to calculate the lattice energy is to determine the electric field in solid molecular hydrogen having an electric polarization density corresponding to the aligned dipoles moments, and in turn, the energy can be calculated from the energy of each dipole in the corresponding field using the electrostatic form of Gauss' equation. The $H_2(1/4)$ number density of solid $H_2(1/4)$ $\tilde{N}$ is given by the 4, the number of $H_2(1/4)$ molecules per unit cell divided by the volume of the face centered cubic cell. Using the neighbor internuclear distance $2c'_{H_2(1/4)\cdots H_2(1/4)}$ (Eq. (16.210)) as the length of the unit cell, $\tilde{N}$ can be approximated by

$$\tilde{N} = \frac{4}{\left(2c'_{H_2(1/4)\cdots H_2(1/4)}\right)^3} = \frac{4}{\left(1.02778\ X\ 10^{-10}\ m\right)^3} = 3.684\ X\ 10^{30}\ H_2(1/4) m^{-3} \tag{16.213}$$

Substitution of number density of solid $H_2(1/4)$ $\tilde{N}$ given by Eq. (16.213) and the $H_2(1/4)$ dipole moment given in Table 16.45 into Eq. (16.53) gives:

$$U\left(H_2(1/4)\right) = \frac{-2\left(\mu_{H_2(1/4)}\right)^2 \tilde{N}}{3\varepsilon_0}$$
$$= \frac{-2\left(1.03885\ X\ 10^{-31} C\cdot m\right)^2 3.684\ X\ 10^{30}\ H_2(1/4) m^{-3}}{3\varepsilon_0} \quad (16.214)$$
$$= -0.01869\ eV\ \left(-1.803\ kJ/mole\right)$$

$U\left(H_2(1/4)\right)$ is also the negative of $E_{van\ der\ Waals}$, the van der Waals energy per $H_2(1/4)$ molecule:

$$E_{van\ der\ Waals}\left(solid\ H_2(1/4)/H_2(1/4)\right) = 0.01869\ eV\ \left(1.803\ kJ/mole\right) \quad (16.215)$$

PARAMETERS AND MAGNETIC ENERGIES DUE TO THE SPIN MAGNETIC MOMENT OF $H_2(1/4)$

Molecular hydrino $H_2(1/p)$ comprises (i) two electrons bound in a minimum energy, equipotential, prolate spheroidal, two-dimensional current membrane comprising a molecular orbital (MO), (ii) two $Z=1$ nuclei such as two protons at the foci of the prolate spheroid, and (iii) a photon wherein the photon equation of each state is different from that of an excited H_2 state given in the Excited States of the Hydrogen Molecule section, in that the photon increases the central field by an integer rather than decreasing the central prolate spheroidal field to that of a reciprocal integer of the fundamental charge at each nucleus centered on the foci of the spheroid, and the electrons of $H_2(1/p)$ are paired in the same shell at the same position ξ versus being in separate ξ positions. The interaction of the hydrino state photon electric field with each electron gives rise to a nonradiative radial monopole such that the state is stable. In contrast, by the same mechanism, the excited H_2 state photon gives rise to a radiative radial dipole at the outer excited state electron resulting in the state being unstable to radiation. For exited states, the photon electric field comprises a prolate spheroidal harmonic in space and time that modulates the constant prolate spheroidal current of the outer electron in-phase. The former corresponds to orbital angular momentum and the latter corresponds to spin angular momentum. Due to the unique stable state of molecular hydrino comprising two nonradiative electrons in a single MO, the nature of the trapped photon field, the nature of the vector photon propagation inside the molecular hydrino serving as a resonator cavity, and the nature of the electron currents are unique.

Consider the formation of a nonradiative state H_2 molecule from two non-radiative $n=1$ state H atoms requiring the bond energy to be removed by a third body collision:

$$H + H + M \rightarrow H_2 + M^* \quad (16.216a)$$

wherein M^* denotes the third body in an energetic state[2]. Molecular hydrino may form by the same nonradiative mechanism wherein, hydrino atoms and hydrino molecules comprise an additional photon component of the central field that is nonradiative by virtue of being equivalent to an integer multiple of the central field of a proton at the origin and at each focus of the prolate spheroid MO, respectively. The combination of two electrons into a single molecular orbital while maintaining the radiationless integer photonic central field gives rise to the special case of a doublet MO state in molecular hydrino rather than a singlet state. The singlet state is nonmagnetic; whereas, the doublet state has a net magnetic moment of a Bohr magneton μ_B.

Specifically, the basis element of the current of each hydrogen-type atom is a great circle as shown in the Generation of the Atomic Orbital-CVFS section, and the great circle current basis elements transition to elliptic current basis elements in hydrogen-type molecules as shown in the Force Balance of Hydrogen-Type Molecules section. As shown in the Equation of the Electric Field inside the Atomic Orbital section, (i) photons carry electric field and comprise closed field line loops, (ii) a hydrino or a molecular hydrino each comprises a trapped photon wherein the photon field-line loops each travel along a mated great circle or elliptic current loop basis element in the same vector direction, (iii) the direction of each field line increases in the direction perpendicular to the propagation direction with relative motion as required by special relativity, and (iv) since the linear velocity of each point along a field line loop of a trapped photon is light speed c, the electric field direction relative to the laboratory frame is purely perpendicular to its mated current loop and it exists only at $\delta(r-r_n)$. The paired electrons of the hydrogen molecular orbital comprise a singlet state having no net magnetic moment. However, the photon field lines of two

---

[2] The hydrino molecule comprises two hydrogen isotope nuclei and two electrons in a single molecular orbital (MO). Uniquely the MO comprises a paired and unpaired electron (Parameters and Magnetic Energies Due to the Spin Magnetic Moment of $H_2(1/4)$ section). To conserve spin angular momentum during the formation of a bond between two hydrino atoms, the bond energy must be released as a neutrino such as an electron neutrino of spin ½ that serves the function of the third body of M^* Eq. (16.216a):

$$H(1/p) + H(1/p) \rightarrow H_2(1/p) + \upsilon_e \quad (16.216b)$$

Specifically, a neutrino comprises a photon having $\frac{\hbar}{2}$ angular momentum in its electric and magnetic fields (Neutrinos section). During the reaction of Eq. (16.216b), the angular momentum of the reactants is conserved in the products wherein each of the two reacting hydrino atoms are electron spin ½, and the product molecular hydrino and electron neutrino are also each spin ½. The neutrino emission reaction (Eq. (16.216b)) may be exploited for communication (e.g. a neutrino telecommunication system).

hydrino atoms that superimpose during the formation of a molecular hydrino can only propagate in one direction to avoid cancellation and give rise to a central field to provide force balance between the centrifugal and central forces (Eq. (11.200)). This special case gives rise to a doublet state in molecular hydrino.

The MO may be treated as a linear combination of the great ellipses that comprise the current density function of each electron as given in the Generation of the Orbitsphere-CVFS section and the Force Balance of Hydrogen-Type Molecules section. To meet the boundary conditions that each corresponding photon is matched in direction with each electron current and that the electron angular momentum is $\hbar$ are satisfied, one half of electron 1 and one half of electron 2 may be spin up and matched with the two photons of the two electrons on the MO, and the other half of electron 1 may be spin up and the other half of electron 2 may be spin down such that one half of the currents are paired and one half of the currents are unpaired. Thus, the spin of the MO is $\frac{1}{2}\left(\uparrow\uparrow+\downarrow\uparrow\right)$ where each arrow designates the spin vector of one electron. The two photons that bind the two electrons in the molecular hydrino state are phase-locked to the electron currents and circulate in opposite directions. Given the indivisibility of each electron and the condition that the MO comprises two identical electrons, the force of the two photons is transferred to the totality of the electron MO comprising a linear combination of the two identical electrons to satisfy Eq. (11.200). The resulting angular momentum and magnetic moment of the unpaired current density are $\hbar$ and a Bohr magneton μ_B, respectively.

Due to its unpaired electron, molecular hydrino is electron paramagnetic resonance (EPR) spectroscopy active. Moreover, due to the unpaired electron in a common molecular orbital with a paired electron, the EPR spectrum is uniquely characteristic of and identifies molecular hydrino as shown *infra*. As given in the Electron g Factor section, flux is linked by an unpaired electron in quantized units of the fluxon or magnetic flux quantum $\frac{h}{2e}$. The electric energy, the magnetic energy, and the dissipated energy of a fluxon treading the atomic orbital given by Eqs. (1.226 -1.227) is

$$\Delta E_{mag\ g}^{spin}=2\left(1+\frac{\alpha}{2\pi}+\frac{2}{3}\alpha^2\left(\frac{\alpha}{2\pi}\right)-\frac{4}{3}\left(\frac{\alpha}{2\pi}\right)^2\right)\mu_B B=g\mu_B B \tag{16.217}$$

In the case of the molecular hydrino, the unpaired electron is a linear combination of two electrons of the MO wherein one half of the current density is paired, and one half is unpaired. The fluxon links both interlocked electrons such that the contribution of the flux linkage terms are doubled. The corresponding g factor is

$$g_{H_2(1/p)}=2\left(1+2\left(\frac{\alpha}{2\pi}+\frac{2}{3}\alpha^2\left(\frac{\alpha}{2\pi}\right)-\frac{4}{3}\left(\frac{\alpha}{2\pi}\right)^2\right)\right)=2.0046386 \tag{16.218}$$

The energy between parallel and antiparallel levels of the unpaired electron in an applied magnetic field is

$$\Delta E_{mag\ 2.0046}^{spin}=g_{H_2(1/p)}\mu_B B=2.0046386\mu_B B \tag{16.219}$$

The result of Eq. (16.218) was confirmed wherein the electron paramagnetic resonance peak was observed with g factor of 2.00445 [131].

Molecular hydrino comprises a linear combination of an unpaired and a paired electron in a common prolate spheroidal molecular orbital (MO) wherein ellipsoidal current elements alternate in pairs of contiguous parallel and antiparallel currents. Consider the designation of the prolate spheroidal MO wherein the y and z-axes are semiminor axes and the x-axis is the semimajor axis. The resulting current density comprises a prolate spheroid possessing $\frac{\hbar}{2}$ of angular momentum along either the +z-axis or –z-axis and $\frac{\hbar}{4}$ along each of the +y and –y-axes as shown in Figure 11.4 wherein the unpaired-paired intrinsic current density may occupy two degenerate distributions about either the +z-axis or –z-axis. The application of a magnetic field lifts the degeneracy. The semimajor or x-axis of the molecular hydrino aligns parallel or antiparallel to an applied magnetic field with capture of a photon of the Larmor frequency corresponding to the applied field-electron spin interaction energy $E_{\uparrow\uparrow/\downarrow\uparrow}$ given by the Bohr magneton μ_B times the applied flux B:

$$E_{\uparrow\uparrow/\downarrow\uparrow}=\mu_B B \tag{16.220}$$

The resulting cylindrical rotation of the MO current about the semimajor axis gives rise to $\hbar$ of angular momentum along either the +x or –x-axis (Figure 11.4) and causes the spin current vectors in the transverse plane containing the semiminor axes to average to zero. A 180° electron spin flip transition along the semimajor axis may occur with the absorption of a resonant microwave photon having the energy given by Eqs. (16.217-16.219). The $\hbar$ of angular momentum of the spin flip photon aligns along either the +z or –z-axis in the transverse plane wherein the unpaired current $\frac{\hbar}{2}$ of angular momentum along the either the +z-axis or –z-axis quantizes the orientation of spin flip photon angular momentum. In the case that the angular momentum of the spin flip photon is opposite that of the unpaired current, the unpaired current also flips its orientation with a concomitant flip of the corresponding angular momentum by 180° in the transverse plane. The semiminor axis spin flip transition lifts the degeneracy of the semimajor axis spin flip transition due to an interaction of the paired and unpaired current of the MO. The

three sources of splitting of the spin flip transition are considered: (i) the energy of interaction of the internal magnetic field of the electron MO on the proton magnetic moments, (ii) the energy of interaction of the transition between nuclear spin isomer states on the spin of the electron MO, and (iii) the coupling energy between the spin unpaired electro and the spin paired electron of the $H_2(1/4)$ electron MO.

Hydrogen-type molecules comprise a proton at each focus of the prolate spheroid molecular orbital, each with nuclear spin and a corresponding magnetic dipole moment of μ_P. Consider that effect on the protons when a magnetic field is applied along the semimajor axis, the x-axis, that excites the Larmor precession of the unpaired electron of $H_2(1/p)$ to give rise to an electron spin magnetic moment of a Bohr magneton also aligned along the semimajor axis. The intrinsic electron spin vectors along the two transverse semiminor axes, the y-axis and the z-axis, as shown in Figure 11.4 rotate around the applied magnetic field and the electron spin magnetic moment at the Larmor frequency given by Eq. (1.227). The magnetic field inside the ellipsoidal MO, $\mathbf{H}_x^-$, (Eq. (12.31)) is:

$$B_x^- = \mu_0 \frac{e\hbar}{2m_e} \frac{1}{a^3\left(1-\frac{b^2}{a^2}\right)^{3/2}} \left(2\sqrt{1-\frac{b^2}{a^2}} + \ln \frac{1+\sqrt{1-\frac{b^2}{a^2}}}{1-\sqrt{1-\frac{b^2}{a^2}}} \right) \tag{16.221}$$

Substitution of the $H_2(1/4)$ semimajor axis a (Eq. (11.202)) and the $H_2(1/4)$ semiminor axis b (Eq. (11.205)) into Eq. (16.221) gives

$$B_x^- = 4.52\,X10^4\ T \tag{16.222}$$

This large electrodynamic field aligns parallel or antiparallel to the applied field corresponding to the direction of the Larmor electron magnetic moment. However, this electrodynamic field is transverse to the vector direction of the proton magnetic moments that must align along the direction of the magnetostatic intrinsic spin as a condition of the formation and energy stability of the $H_2(1/4)$ molecule. Thus, the nuclear magnetic moments align in the transverse plane, the yz-plane that is perpendicular to three-semimajor axis magnetic components: (i) the applied magnetic field that excites the Larmor rotation, (ii) the electron spin magnetic moment, and (iii) the electrodynamic magnetic field of the electron's Larmor rotation. The intrinsic electron spin vectors along the transverse two semiminor axes, the y-axis and the z-axis, (Figure 11.4) rotate around these three-semimajor axis magnetic components at the Larmor frequency given by Eq. (1.227). Since the nuclear magnetic moments are transverse to the three-semimajor axis magnetic components, and the Larmor-frequency rotation causes the intrinsic electron spin magnetic interaction with the nuclear spins to average to zero, the nuclear magnetic moments do not interact with the three-semimajor axis magnetic components. Then, the energy contribution of the nuclear magnetic moments to an electron spin transition depends only on the mutual interaction of the nuclear magnetic moments.

Next, the interaction between the proton nuclear magnetic moments resulting in the splitting of the quantized energy levels of the electron spin transition by the energy corresponding to the interaction is considered. In general, the potential energy of interaction $E_{mag\ dipole}$ of two quantized magnetic dipoles $\mathbf{m}_1$ and $\mathbf{m}_2$ separated by a distance $|\mathbf{r}|$ is given by

$$E_{mag\ dipole} = -\frac{\mu_0}{4\pi|\mathbf{r}|^3}\left(3(\mathbf{m}_1\cdot\hat{\mathbf{r}})(\mathbf{m}_2\cdot\hat{\mathbf{r}}) - \mathbf{m}_1\cdot\mathbf{m}_2\right) \tag{16.223}$$

where μ_0 is the permeability of free space and $\hat{\mathbf{r}}$ is a unit vector parallel to the line joining the centers of the two dipoles. The energy is decreased in the case of antiparallel interacting magnetic moments, and the energy is increased in the case of parallel magnetic moments. Consider the splitting energy of interaction with two parallel-aligned nuclear magnetic moments. With the substitution of the proton magnetic moment μ_P for each parallel-aligned nuclear magnetic moment and the $H_2(1/4)$ internuclear separation given by Eq. (11.204) for $|\mathbf{r}|$ into Eq. (16.223), the energy $E_{P\ mag\ e\text{-}dipole}$ to flip the spin direction of one proton magnetic moment of $H_2(1/4)$ relative to the other is

$$E_{P\ mag\ e\text{-}dipole} = \frac{2\mu_0\mu_P^2}{4\pi r^3} = \frac{\mu_0\left(1.41060671X10^{-26}JT^{-1}\right)^2}{2\pi\left(2\frac{a_0}{4\sqrt{2}}\right)^3} = \frac{\mu_0\left(1.41060671X10^{-26}JT^{-1}\right)^2}{2\pi\left(1.870924X10^{-11}m\right)^3} \tag{16.224}$$

$$= 6.077X10^{-27}\ J = 3.793X10^{-8}\ eV = 9.171X10^{-3}\ GHz$$

In order for this ortho-para nuclear spin isomer energy of Eq. (16.224) to split the electron spin transition, there must be a coupling mechanism between the nuclear and electron spins. Since the electron spin vector is along the semimajor axis, and the proton spins are transversely oriented in the plane containing the semiminor axes, there is no direct coupling mechanism. Moreover, the flux change inside of the electron MO due to the transition of the nuclear spin isomer state corresponding to Eq. (16.224) has an insignificant effect on the spin transition energy as shown by flux linkage terms of Eq. (16.217). Since the spin

transition is independent of the nuclear spin transition, the electron spin transition leaves the ortho or para nuclear spin state of $H_2(1/4)$ unchanged, and there is no nuclear spin state energy splitting.

Consider the third electron spin splitting mechanism regarding the coupling energy of the spin unpaired and paired electrons of the electron MO. The semiminor axis spin flip transition lifts the degeneracy of the semimajor axis spin flip transition due to an interaction of the paired and unpaired current of the MO. The magnetic field of the unpaired electron induces a diamagnetic current in the paired electron. The resulting magnetic moment that shifts the spin flip transition energy is opposite that of the spin magnetic moment and proportionally much smaller. In addition to the intrinsic relative motion of the linear combination of the paired and unpaired electron currents of $H_2(1/4)$ and the rotation of the electron MO about the semimajor axis corresponding to electron spin along this axis, the paired and unpaired electrons may rotate relative to each other during a spin transition similar to the case of excited-state H_2 as given in the Excited States of the Hydrogen Molecule section. The relative rotation is quantized in terms of m integer units of $\hbar$ in opposite directions wherein the magnetic moments cancel, but the relativistic effect gives rise to a corresponding electron spin-orbital coupling quantum number m. The unpaired-paired coupling or spin-orbital coupling energy is given as the diamagnetic moment times the magnetic flux of the unpaired electron. Since flux is linked by an unpaired electron in units of the magnetic flux quantum, the spin-orbital coupling energy $E_{S/O}$ between two magnetic moments of $H_2(1/4)$ given by Eq. (2.194) can be expressed as:

$$E_{S/O} = \chi_m m\left[\frac{1}{\left(4\sqrt{2}\right)^{-3}}\alpha^5(2\pi)^2 m_e c^2\sqrt{\frac{3}{4}}\right] \tag{16.225}$$

wherein the semiminor radius of the $H_2(1/4)$ MO is given by Eq. (11.205) with $p=4$ and χ_m is the magnitude of the diamagnetic susceptibility of the paired electron given by Eq. (11.416):

$$\begin{aligned}\chi_m &= \alpha\frac{\Delta B_T}{B}\sqrt{\frac{3}{4}} = \alpha\mu_0\left(4-\sqrt{2}\ln\frac{\sqrt{2}+1}{\sqrt{2}-1}\right)\frac{pe^2}{36a_0 m_e}\left(1+p\alpha^2\right)\sqrt{\frac{3}{4}}\\ &= \alpha\left(p28.01+p^2 1.49\ X\ 10^{-3}\right)\sqrt{\frac{3}{4}}ppm = 7.0821\ X\ 10^{-7}\end{aligned} \tag{16.226}$$

In the case of spin-orbital coupling involving the intrinsic spin of $\frac{\hbar}{2}$, the electron spin-orbital coupling quantum number m is $m = 1/2$. Additional states arise due to the relative motion of the two electrons of the $H_2(1/4)$ MO. Consider the case of H_2 excited states given in the Excited States of the Hydrogen Molecule section wherein the relative rotational motion of the two excited state electrons corresponds to the quantum number m being a positive or negative integer such that net relative motion obeys the condition $\ell = 0$. The quantum number m also applies to the molecular hydrino electron spin flip split by electron spin-orbital coupling wherein m is a positive integer. With the substitution of Eq. (16.226) into Eq. (16.225), the unpaired-paired coupling is

$$E_{s/o} = m7.0821X10^{-7}\left(64(2)^{1.5}\alpha^5(2\pi)^2\right)m_e c^2\sqrt{\frac{3}{4}} = m7.426\ X\ 10^{-27}\ J \tag{16.227}$$

The electron paramagnetic resonance (EPR) comprises a peak at the energy equivalent position given by Eq. (16.219), that is symmetrically split into a series of pairs of peaks, one shifted downfield by the energy of Eq. (16.227), and the other shifted upfield by the energy of Eq. (16.227), wherein downfield and upfield denote lower and higher magnetic flux for a resonant transition at fixed EPR frequency, respectively.

Consider the case that the EPR frequency is 9.820295 GHz, the resonance magnetic flux B for the principal peak given by Eq. (16.219) is

$$B = \frac{h9.820295GHz}{2.0046386\mu_B} = 0.35001\ T \tag{16.228}$$

where h is Planck's constant and μ_B is the Bohr magneton. The resonance magnetic flux shift ΔB_C of a principal peak at position B_1 due to a splitting energy E_C is given by

$$\Delta B_C = B_1\frac{E_C}{h9.820295GHz} \tag{16.229}$$

Using Eqs. (16.227-16.229), the downfield and upfield shifts $\Delta B_{S/O}$ with quantized spin-orbital splitting energies $E_{S/O}$ (Eq. (16.227) and electron spin-orbital coupling quantum numbers $m = 0.5, 1, 2, 3, 5....$ are given in units of Gauss by

$$\Delta B_{S/O} = m0.35001\left[\frac{7.426\ X\ 10^{-27}\ J}{h9.820295GHz}\right]T = m3.99427\ G \tag{16.230}$$

The spin-orbital splitting shift of $m7.426\ X\ 10^{-27} J$ is independent of the applied EPR field/frequency combination for both downfield and upfield shifted peaks.

The potential energy of a superconducting quantum interference device (SQUID) given by Eq. (42.115) comprises the sum of the Josephson coupling energy of the junction and the equivalent of the magnetic energy of the loop. The free electron of $H_2(1/4)$ behaves equivalently to a superconducting quantum interference device (SQUID). In addition to the flux linked by the unpaired electron during the spin flip transition corresponding to the energy terms of the $g_{H_2(1/p)}$ (Eqs. (16.218) and (16.219)), a free electron of $H_2(1/4)$ must link the magnetic flux component corresponding to spin-orbital coupling. This flux contribution increases the magnetic energy and the energy of the combined spin flip (Eq. (16.228)) and spin-orbital coupling (Eq. (16.227)) transition energy for a given spin-orbital quantum number m. Thus, the downfield spin-orbital splitting peaks are shifted further downfield by the corresponding magnetic energies; whereas, the upfield spin-orbital splitting peaks are not shifted since the upfield peaks correspond to emission of the spin-orbital coupling transition energies alone, and the magnetic energies thermalize. The Josephson coupling energies due to fluxon linkage during spin-orbital transitions are given by Eq. (16.227), and the magnetic energies $U_{S/OMag}$ arising from the absorption of the corresponding spin-orbital coupling transitional flux are given by

$$\begin{aligned} U_{S/OMag} &= \frac{1}{2}U_0\left(\frac{2\pi(\Delta\Phi)}{\Phi_0}\right)^2 = (0.5)\frac{0.5\Delta E^{spin}_{mag\ 2.0046}}{g_{H_2(1/p)}\mu_B}\left(\frac{2\pi(\Delta B_{S/O})}{\frac{0.5\Delta E^{spin}_{mag\ 2.0046}}{g_{H_2(1/p)}\mu_B}}\right)^2 \\ &= (0.5)\frac{\left(2\pi m 0.35001\left[\frac{7.426\ X\ 10^{-27}\ J}{h9.820295GHz}\right]\right)^2}{\frac{0.5\Delta E^{spin}_{mag\ 2.0046}}{g_{H_2(1/p)}\mu_B}} = (0.5)\frac{\left(2\pi m 3.99427 X\ 10^{-4}\right)^2}{0.5\frac{h9.820295GHz}{2.0046386\mu_B}} \\ &= (0.5)\frac{\left(2\pi m 3.99427 X\ 10^{-4}\right)^2}{0.1750} X\ 10^4 G \end{aligned} \tag{16.231}$$

wherein m is the spin-orbital quantum number, ½ the spin flip transition energy corresponds to the terms U_0 and Φ_0 as given by Eqs. (16.217), (16.218), and (16.228) in units of magnetic flux (i.e. the equivalent SQUID parameters of $H_2(1/4)$ are $U_0 = \Phi_0 = \frac{0.5\Delta E^{spin}_{mag\ 2.0046}}{g_{H_2(1/p)}\mu_B}$), and the flux change due to the transition $\Delta\Phi$ is the spin-orbital splitting energy of quantum number m given in units of magnetic flux by Eqs. (16.227) and (16.230). The corresponding magnetic energies $U_{S/OMag}$ given by Eqs. (16.231), (16.217), and (16.218) in units of Joules are

$$U_{S/OMag} = g_{H_2(1/p)}\mu_B(0.5)\frac{\left(2\pi m 3.99427 X\ 10^{-4}\right)^2}{0.1750} J \tag{16.232}$$

The downfield magnetic energy shifts $U_{S/OMag}$ given by Eq. (16.232) are added to the quantized spin-orbital splitting energies $E_{S/O}$ ($\Delta B_{S/O}$) (Eq. (16.227)) to given combined quantized spin-orbital splitting energies $E_{S/Ocombined}$ in units of Joules:

$$E_{S/Ocombined} = g_{H_2(1/p)}\mu_B(0.5)\frac{\left(2\pi m 3.99427 X\ 10^{-4}\right)^2}{0.1750} J + m7.426\ X\ 10^{-27}\ J \tag{16.233}$$

The downfield magnetic energy shifts $U_{S/OMag}$ given by Eq. (16.231) are added to the quantized spin-orbital splitting energies $E_{S/O}$ (Eq. (16.230)) to given combined quantized spin-orbital downfield shift energies $\Delta B^{downfield}_{S/Ocombined}$ in units of Gauss:

$$\Delta B^{downfield}_{S/Ocombined} = -\left(m3.99427 X\ 10^{-4} + (0.5)\frac{\left(2\pi m 3.99427 X\ 10^{-4}\right)^2}{0.1750}\right) X\ 10^4 G \tag{16.234}$$

The downfield peak positions $B^{downfield}_{S/Ocombined}$ due to the combined shifts due to the magnetic energy and the spin-orbital coupling energy given by Eq. (16.228) and (16.234) are:

$$B^{downfield}_{S/Ocombined} = \left(0.35001 - m3.99427 X\ 10^{-4} - (0.5)\frac{\left(2\pi m 3.99427 X\ 10^{-4}\right)^2}{0.1750}\right) T \tag{16.235}$$

There is no magnetic energy shift for upfield shift peaks corresponding to the emission of the spin-orbital coupling energy given by Eq. (16.230). Using Eq. (16.228) and Eqs. (16.227-16.230), the upfield peak positions $B^{upfield}_{S/O}$ with quantized spin-orbital

splitting energies $E_{S/O}$ (Eq. (16.227)) and electron spin-orbital coupling quantum numbers $m = 0.5,1,2,3,5....$ are given by

$$B_{S/O}^{upfield} = 0.35001\left(1+m\left[\frac{7.426\,X\,10^{-27}\,J}{h9.820295GHz}\right]\right)T = \left(0.35001+m3.99427\,X\,10^{-4}\right)T \tag{16.236}$$

The downfield shifts due to the magnetic energies in units of Joules (Eq. (16.232)) and Gauss (Eq. (16.231)), the downfield shifts due to spin-orbital coupling energies in units of Joules (Eq. (16.227) and Gauss (Eq. (16.230)) for spin-orbital coupling quantum numbers $m = 0.5,1,2,3,5....$ are given in Table 16.48.

Table 16.48. The 9.820295 GHz $H_2(1/4)$ EPR downfield shifts due to the magnetic energies and the downfield shifts due to spin-orbital coupling energies for spin-orbital coupling quantum numbers $m = 0.5,1,2,3,5$.

m	Downfield Magnetic Energy Shift (J)	Downfield Magnetic Energy Shift (G)	Spin-Orbital Shift (J)	Spin-Orbital Shift (G)
0.5	8.36376E-29	0.04499	3.71288E-27	1.99714
1	3.34550E-28	0.17995	7.42576E-27	3.99427
2	1.33820E-27	0.71981	1.48515E-26	7.98854
3	3.01095E-27	1.61957	2.22773E-26	11.98281
4	5.35280E-27	2.87924	2.97030E-26	15.97708
5	8.36376E-27	4.49881	3.71288E-26	19.97135

The combined downfield shifts due to the magnetic and spin-orbital coupling energies in units of Joules (Eq. (16.233) and Gauss (Eq. (16.234)), the resulting downfield peak positions (Eq. (16.235), and the upfield peak positions (Eq. (16.236)) shifted only by the spin-orbital coupling energies (Eqs. (16.227) and (16.230)), for spin-orbital coupling quantum numbers $m = 0.5,1,2,3,5....$ wherein the principal peak with the g-factor of 2.0046386 (Eq. (16.218)) is observed at 0.35001 T (Eq. (16.228) are given in Table 16.49.

Table 16.49. The 9.820295 GHz $H_2(1/4)$ EPR combined downfield shifts due to the magnetic and spin-orbital coupling, the resulting downfield peak positions, and the upfield peak positions shifted only by the spin-orbital coupling energies for spin-orbital coupling quantum numbers $m = 0.5,1,2,3,5$.

m	Combined Downfield Magnetic Energy Shift (J)	Combined Downfield Magnetic Energy Shift (G)	Downfield Peak Position (T)	Upfield Peak Position (T)
0.5	3.79652E-27	2.04212	0.34980	0.35021
1	7.76031E-27	4.17422	0.34959	0.35041
2	1.61897E-26	8.70835	0.34914	0.35081
3	2.52882E-26	13.60238	0.34865	0.35121
4	3.50559E-26	18.85632	0.34812	0.35160
5	4.54926E-26	24.47016	0.34756	0.35200

As given in the Electron g Factor section, magnetic flux is linked by an unpaired electron in quantized units of the fluxon or the magnetic flux quantum $\frac{h}{2e}$. As shown in the Hydrino Hydride Ion Hyperfine Lines section, hydrino hydride ion $H^-(1/p)$ also possesses a linear combination of two electrons with one paired and the other unpaired in a common atomic orbital versus a MO. The emission spectrum of the binding of a free electron to a hydrino atom to form the corresponding hydrino hydride ion results in a series of evenly spaced emission peaks wherein the energy spacing matches that predicted for the binding electron to link the magnetic flux of the hydrino atom in units of the magnetic flux quantum in the bound-free emission spectral region. The flat intensity profile matches that of Josephson junctions such as ones of superconducting quantum interference devices (SQUIDs) that also link magnetic flux in quantized units of the magnetic flux quantum or fluxon $\frac{h}{2e}$. The same behavior is predicted for the linkage of magnetic flux by molecular hydrino during a spin transition and the derivation of the corresponding fluxon linkage energies follows that of Eq. (7.93) of the Hydrino Hydride Ion Hyperfine Lines section.

As given by Eq. (16.218), the fluxon links both correlated electrons such that the energy contribution of the flux linkage of a fluxon by molecular hydrino is

$$g_{H_2(1/p)} - 2 = 2\left(1+2\left(\frac{\alpha}{2\pi}+\frac{2}{3}\alpha^2\left(\frac{\alpha}{2\pi}\right)-\frac{4}{3}\left(\frac{\alpha}{2\pi}\right)^2\right)\right)-2 = 0.0046386 \tag{16.237}$$

Using the energy of MO due to an applied flux given by Eq. (16.220), wherein (i) both the magnetic moments due to spin and the corresponding induced diamagnetic moment are corrected for the vector projection of $\sqrt{\frac{3}{4}}$ (Eqs. (16.226-16.227) corresponding to an increase of the energy for resonant flux linkage, (ii) the magnetic flux density B is given by the ratio of the flux and the area, and (iii) the flux is linked in units of the fluxon $\Phi_0 = \frac{h}{2e}$, the fluxon linkage energies E_Φ by molecular hydrino $H_2(1/4)$ during a spin transition are

$$\begin{aligned} E_\Phi &= m_\Phi 4\left(\frac{\alpha}{2\pi}+\frac{2}{3}\alpha^2\left(\frac{\alpha}{2\pi}\right)-\frac{4}{3}\left(\frac{\alpha}{2\pi}\right)^2\right)\chi_{m\Phi}\frac{\mu_B}{\sqrt{s(s+1)}}B = m_\Phi 0.0046386\frac{\chi_{m\Phi}\mu_B}{\sqrt{s(s+1)}}\left(\frac{j\Phi_0}{A}\right) \\ &= m_\Phi\left(j0.0046386\frac{\chi_{m\Phi}\mu_B}{\sqrt{s(s+1)}}\frac{\mu_0}{r^3}\left(\frac{e\hbar}{2m_e}\right)\right) \end{aligned} \tag{16.238}$$

In Eq. (16.238), the energy of flux linkage is an integer function of the components of angular moment involved in the splitting of the principal transition corresponding to the electron fluxon quantum number m_Φ. Therefore, the electron fluxon quantum number m_Φ has the following integer values: (i) the electron fluxon quantum number m_Φ corresponding to the spin-orbital coupling involving the intrinsic spin of $\frac{\hbar}{2}$ is $m_\Phi = 1$, (ii) the electron fluxon quantum number m_Φ corresponding to the spin with $m = 1$ involving the semimajor axis spin is $m_\Phi = 2$, and (iii) the electron fluxon quantum number m_Φ corresponding to the spin with $m > 1$; $|\Delta m| = 1$ involving the semimajor axis spin and relative motion of the two electrons of the $H_2(1/4)$ MO is $m_\Phi = 3$. In addition, j is an integer corresponding to the number of fluxons linked having fluxion linkage quantum number m_Φ, $s = 1/2$, A is the area of the continuous distribution of current element loops (Force Balance of Hydrogen-Type Molecules section and Figure 11.2) linked by the integer number of fluxons as given in the Electron g Factor section, and the magnitude of the diamagnetic susceptibility $\chi_{m\Phi}$ is given by

$$\chi_{m\Phi} = \alpha\left(p28.01 + p^2 1.49\ X\ 10^{-3}\right) ppm = 8.1777\ X\ 10^{-7} \tag{16.239}$$

With the substitution of Eq. (16.239) into Eq. (16.238), E_Φ is

$$E_\Phi = m_\Phi\left(j(0.0046386)\frac{\mu_0\left(8.1777\ X\ 10^{-7}\right)\mu_B^2}{\sqrt{\frac{3}{4}}\left(\frac{a_0}{4\sqrt{2}}\right)^3}\right) = m_\Phi\left(j5.7830\ X\ 10^{-28}\ J\right) \tag{16.240}$$

wherein the semiminor radius of the $H_2(1/4)$ MO is given by Eq. (11.205) with $p = 4$. Using Eq. (16.229) with the E_Φ, the fluxon linkage energy of $H_2(1/4)$ (Eq. (16.240)), and the spin-orbital peak positions (Eqs. (16.235) and (16.236)), the separation ΔB_Φ of the integer series of peaks at each spin-orbital peak position (Table 16.49) for an EPR frequency of 9.820295 GHz is given by

$$\Delta B_\Phi^{downfield} = \left(0.35001 - m3.99427X\ 10^{-4} - (0.5)\frac{\left(2\pi m3.99427X\ 10^{-4}\right)^2}{0.1750}\right)\left[\frac{m_\Phi 5.7830\ X\ 10^{-28}\ J}{h9.820295GHz}\right]X\ 10^4 G \tag{16.241}$$

and

$$\Delta B_\Phi^{upfield} = \left(0.35001 + m3.99427X\ 10^{-4}\right)\left[\frac{m_\Phi 5.7830\ X\ 10^{-28}\ J}{h9.820295GHz}\right]X\ 10^4 G \tag{16.242}$$

The 9.820295 GHz $H_2(1/4)$ EPR spectral separations ΔB_Φ (Eqs. (16.235) and (16.236)) of each integer series of the peaks comprising sub-splitting of the downfield and upfield peaks of Table 16.49 corresponding to the principal peak having a g-factor of 2.0046386 (Eq. (16.218)) split by quantized spin-orbital coupling energies $E_{S/O}$ (Eqs. (16.227) and (16.230)) and magnetic energies $U_{S/OMag}$ (Eqs. (16.231) and (16.232)) for electron spin-orbital coupling quantum numbers $m = 0.5, 1, 2, 3, 4, 5$ and electron fluxon quantum numbers $m_\Phi = 1, 2, 3$ (Eq. (16.240) are given in Table 16.50.

Table 16.50. The 9.820295 GHz $H_2(1/4)$ EPR spectral separation ΔB_Φ of each integer series of the peaks comprising sub-splitting of the downfield and upfield peaks of Table 16.49 for electron spin-orbital coupling quantum numbers $m = 0.5,1,2,3,4,5$ and electron fluxon quantum numbers $m_\Phi = 1,2,3$.

m	m_Φ	Downfield Peak Position (T)	ΔB_Φ (G)	Upfield Peak Position (T)	ΔB_Φ (G)
0.5	1	0.34980	0.3109	0.35021	0.3112
1	2	0.34959	0.6214	0.35041	0.6228
2	3	0.34914	0.9309	0.35081	0.9353
3	3	0.34865	0.9296	0.35121	0.9364
4	3	0.34812	0.9282	0.35160	0.9375
5	3	0.34756	0.9267	0.35200	0.9385

The spin-orbital splitting peak intensity for electron spin-orbital coupling quantum number $m = 0.5$ is predicted to be dominant due to the high cross section of the spin flip transition to involve a torque about the intrinsic angular moment vector as shown in Resonant Precession of the Spin-1/2-Current-Density Function Gives Rise to the Bohr Magneton section. For integer electron spin-orbital coupling quantum number m spin-orbital splitting peaks, the relative intensities are predicted to decrease with integer electron spin-orbital coupling quantum number m. In the case that the statistical population obeys the rules of multipole transitions, the relative peak intensities according to Eqs. (1.7-1.8) and Eq. (1.19) go as

$$\frac{I_{m+1}}{I_m} = \frac{m(m+1)}{(m+1)(m+2)} = \frac{m}{(m+2)}; m = 2,3,4.. \tag{16.243}$$

Furthermore, consider the relative intensities of fluxon peaks within an integer series. If the cross-sectional area of the flux linker is constant relative to the flux source, then the line intensities for the sub-splitting would be equal. However, the cross-sectional area of the electron current relative to the applied field changes as the current comprising a continuous ensemble of current loops flips orientation by 180°. The current flowing over the surface of the prolate spheroidal to reverse the spin direction by 180° is a mechanism whereby the relative intensities of the sub-splitting is higher for the center lines compared to those at the extrema. The line intensities and widths reflect the electron MO geometrical form factor in the case of $m = 0.5$.

In summary, the predicted $H_2(1/4)$ EPR spectrum comprises a principal peak with a theoretical g-factor of 2.0046386 (Eq. (16.218)) that is split by spin-orbital coupling energies $E_{S/O}$ and corresponding magnetic energies $U_{S/OMag}$ on the downfield side into a series of pairs of peaks with members separated by the sum of $E_{S/O}$ (Eqs. (16.227) and (16.230)) and $U_{S/OMag}$ (Eqs. (16.231) and (16.232)) that is a function of electron spin-orbital coupling quantum number m. Each spin-orbital splitting peak is further sub-split into a series of equally spaced peaks of integer fluxon energy ΔB_Φ (Eqs. (16.241) and (16.242)) that is a function of electron fluxon quantum number m_Φ. As given in the Hydrino Hydride Ion Hyperfine Lines section, the pattern of integer-spaced peaks predicted for the EPR spectrum of $H_2(1/4)$ is very similar to that experimentally observed on the hydrino hydride ion that also comprises a paired and unpaired electron in a common orbital, except that the orbital is an atomic orbital [132-135]. The peak separations and sub-splitting due to spin-orbital splitting energies, spin-orbital splitting magnetic energies, and fluxon energies may deviate from the values given in Tables 16.49 and 16.50. Interactions may exist with the matrix surrounding the hydrino molecule. For example, protons of water molecules absorbed as waters of hydration of a crystalline matrix having trapped hydrino molecules could cause and external nuclear splitting effect.

The predicted EPR spectrum was confirmed experimentally [131]. The 9.820295 GHz EPR spectrum was performed on a white polymeric compound (WPC) identified by X-ray diffraction (XRD), energy-dispersive X-ray spectroscopy (EDS), transmission electron spectroscopy (TEM), scanning electron microscopy (SEM), time-of-flight secondary ionization mass spectroscopy (ToF-SIMs), Rutherford backscattering spectroscopy (RBS), and X-ray photoelectron spectroscopy (XPS) as GaOOH:H_2(1/4). The WPC was formed by dissolving Ga_2O_3 collected from a hydrino reaction run in a SunCell® in 4M aqueous KOH, allowing fibers to grow, and float to the surface where they were collected by filtration. The white fibers were not solution in concentrated acid or base; whereas control GaOOH is. No white fibers formed in control solutions. Control GaOOH showed no EPR spectrum. The experimental EPR was acquired by Professor Fred Hagen, TU Delft, with a high sensitivity resonator at a microwave power of -28 dB and a modulation amplitude of 0.02 G, that can be changed to 0.1 G since Dr. Hagen rigorously determined that the minimum line width is 0.15 to 0.2 G. The average error between the EPR spectrum and theory for peak positions given in Tables 16.49-16.50 was 0.097 G. The EPR spectrum was replicated by Bruker using two instruments on two samples.

Specifically, the observed principal peak at g = 2.0045(5)) was assigned to the theoretical peak having a g-factor of 2.0046386 (Eq. (16.218)). This principal peak was split into a series of pairs of peaks with members separated by energies

matching $E_{S/O}$ (Eqs. (16.227) and (16.230)) corresponding to each electron spin-orbital coupling quantum number m. The results confirmed the spin-orbital coupling between the spin magnetic moment of the unpaired electron and an orbital diamagnetic moment induced in the paired electron alone or in combination with rotational current motion about the semimajor molecular axis that shifted the flip energy of the spin magnetic moment. The data further matched the theoretically predicted one-sided tilt of the spin-orbital splitting energies wherein the downfield shift was observed to increase with quantum number m due to the magnetic energies $U_{S/OMag}$ (Eqs. (16.231) and (16.232)) of the corresponding magnetic flux linked during a spin-orbital transition. Each spin-orbital splitting peak was further sub-split into a series of equally spaced peaks that matched the integer fluxon energies ΔB_Φ (Eqs. (16.241) and (16.242)) dependent on electron fluxon quantum number m_Φ corresponding to the number of angular momentum components involved in the transition. The evenly spaced series of sub-splitting peaks was assigned to flux linkage during the coupling between the paired and unpaired magnetic moments in units of the magnetic flux quantum $\frac{h}{2e}$ while a spin flip transition occurs. The EPR spectrum recorded at different frequencies showed that the peak assigned the g factor of 2.0046386 (Eq. (16.218)) remained at constant g factor. Moreover, the peaks, shifted by the fixed spin-orbital splitting energies relative to this true g-factor peak, exactly maintained the separation of the spin-orbital splitting energies independent of frequency as predicted.

Another consideration is that molecular hydrino can also form dimers that would alter the EPR spectrum. Consider the splitting energy of interaction with two axially aligned magnetic moments of a $H_2(1/4)$ dimer. With the substitution of a Bohr magneton μ_B for each axially aligned magnetic moment and the $H_2(1/4)$ dimer separation given by Eq. (16.202) for $|\mathbf{r}|$ into Eq. (16.223), the energy $E_{mag\ [H_2(1/4)]_2\ e\text{-}dipole}$ to flip the spin direction of two electron magnetic moments of $\left[H_2(1/4)\right]_2$ is

$$\begin{aligned} E_{mag\ [H_2(1/4)]_2\ e\text{-}dipole} &= -\frac{2\mu_0\mu_B^2}{4\pi r^3} \\ &= -\frac{\mu_0\left(9.27400949X10^{-24}JT^{-1}\right)^2}{2\pi\left(1.028X10^{-10}m\right)^3} \\ &= -1.584X10^{-23}\ J = -9.885X10^{-5}\ eV = 23.90\ GHz = 0.7972\ cm^{-1} \end{aligned} \tag{16.244}$$

ROTATIONAL ENERGIES DUE TO THE SPIN MAGNETIC MOMENT OF $H_2(1/4)$

Molecular hydrino $H_2(1/p)$ possesses an unpaired electron that causes rotational transitions to be forbidden. This selection rule barrier to observing infrared and Raman spectra may be circumvented by application of an external magnetic field or by recording the spectrum on a compound or material with intrinsic magnetization such as one being ferromagnetic or paramagnetic. An example of the former is molecular hydrino bonded or absorbed on the surface of a nickel or iron foil. An example of the latter is a paramagnetic compound that cages the molecular hydrino such as FeOOH, Fe_2O_3 or a compound that may be diamagnetic but possess paramagnetic ions in proximity to $H_2(1/p)$ such as Ga^{3+} ions in the case of $GaOOH$ that serves as a cage for $H_2(1/p)$.

The presence of molecular hydrino in strong matrix magnetic field may result in the alignment of the free electron angular moment of $\frac{\hbar}{2}$ along the magnetic field vector direction in either the z-axis or the y-axis direction of the coordinates of $H_2(1/p)$ shown in Figure 11.4. The alignment permits the excitation of a concerted transition of a rotational molecular hydrino transition coupling to the spin-orbital splitting and fluxon linkage sub-splitting of the free electron energy levels. The spin flip energy given by Eq. (16.219) with an exemplary intrinsic field of 1 T is

$$\Delta E_{mag\ 2.0046}^{spin} = g_{H_2(1/p)}\mu_B B = 2.0046386\mu_B B = 1.85910\ X\ 10^{-23} J\ (0.93588\ cm^{-1}) \tag{16.245}$$

To conserve the photon's angular momentum of $\hbar$, rotational excitation requires $\hbar$ of angular momentum along the axis of molecular rotation, a semiminor axis being either the z-axis or y-axis. The $\hbar$ of angular momentum gives rise to a corresponding magnet moment of a Bohr magneton along this rotational angular momentum axis. Typically, the unpaired electron of $H_2(1/p)$ gives rise to a Bohr magneton of magnetic moment along the internuclear axis when a magnetic field is applied. However, the molecular rotation of the hydrino molecule about one of the semiminor axes causes the excitation of the semimajor-axis Bohr magneton of magnetic moment to be forbidden. The rotational transition energy may be split by the spin-orbital energy given by Eq. (16.225), except that the orbital component of spin-orbital splitting is not diamagnetically induced such that $\chi_m = 1$ and the spin-orbital energy $E_{S/O,rot}$ due to rotational excitation is:

$$E_{S/O,rot} = m\left[\frac{1}{\left(4\sqrt{2}\right)^{-3}}\alpha^5\left(2\pi\right)^2 m_e c^2\sqrt{\frac{3}{4}}\right] \tag{16.246}$$
$$= m1.04853X\ 10^{-20}\ J \quad (m6.54434X\ 10^{-2}eV,\ m527.83\ cm^{-1})$$

wherein $m = 0.5,1,2,3,\ldots$. The spin-orbital splitting energies due to rotation are given in Table 16.51.

The energies of the concerted excitation of the rotational and spin-orbital coupling transitions are sub-split by the energy corresponding to flux linkage in units of the magnetic flux quantum $\frac{h}{2e}$. The free electron angular momentum of $\frac{\hbar}{2}$ and the rotational angular momentum of $\hbar$ add when the corresponding vectors are aligned along a common z-axis to give a resultant angular momentum of $L=\frac{3}{2}\hbar$. The energy contribution of the flux linkage of a fluxon by molecular hydrino is given by Eq. (16.238) with $\chi_{m\Phi}=1$ since the orbital component of spin-orbital coupling is not diamagnetically induced. In the case of $L=\frac{3}{2}\hbar$, the $H_2\left(1/4\right)$ fluxon linkage energies $E_{\Phi,rot,concerted}$ for fluxon sub-splitting quantum numbers $m_{\Phi 3/2}=0.5,1,2,3...$ due to spin-orbital coupling to a molecular rotational transition are

$$E_{\Phi,rot,concerted} = m_{\Phi 3/2}4\left(\frac{\alpha}{2\pi}+\frac{2}{3}\alpha^2\left(\frac{\alpha}{2\pi}\right)-\frac{4}{3}\left(\frac{\alpha}{2\pi}\right)^2\right)\frac{3}{2}\mu_B B$$
$$= m_{\Phi 3/2}j\frac{3}{2}\left(j0.0046386\frac{\mu_0\mu_B}{r^3}\left(\frac{e\hbar}{2m_e}\right)\right) \tag{16.247}$$
$$= m_{\Phi 3/2}46.24\ cm^{-1}$$

wherein j is an integer corresponding to the number of fluxons linked having fluxon linkage quantum number $m_{\Phi 3/2}$ and the semiminor radius of the $H_2\left(1/4\right)$ MO is given by Eq. (11.205) with $p=4$ ($r=\frac{a_0}{4\sqrt{2}}$). As in the case with spin flip transitions observable by EPR spectroscopy, the fluxon sub-splitting quantum number is determined by the number of angular momentum components active during the transition. Due to the nature of the rotation transition wherein the rotational quantum number J may be arbitrarily large, the upper range of the fluxon sub-splitting quantum number is not bounded.

Alternatively, the spin component of $\frac{\hbar}{2}$ may align perpendicular to the rotational angular momentum of $\hbar$ to give a resultant z-axis angular momentum of $L=\hbar$ wherein the spin component averages to zero since it rotates about the z-axis due to molecular rotation. In the case of $L=\hbar$, the $H_2\left(1/4\right)$ fluxon linkage energies $E_{\Phi,rot}$ for fluxon sub-splitting quantum numbers $m_\Phi=0.5,1,2,3,...$ due to spin-orbital coupling to a molecular rotational transition are

$$E_{\Phi,rot} = m_\Phi\left(j0.0046386\frac{\mu_B^2\mu_0}{r^3}\right) \tag{16.248}$$
$$= m_\Phi j30.83\ cm^{-1}$$

wherein j is an integer corresponding to the number of fluxons linked having fluxon linkage quantum number m_Φ and the semiminor radius of the $H_2\left(1/4\right)$ MO is given by Eq. (11.205) with $p=4$ ($r=\frac{a_0}{4\sqrt{2}}$). The fluxon linkage energies $E_{\Phi,rot}$ due to spin-orbital coupling to molecular rotation transition are given in Table 16.51.

The absorption of fluxons increases the magnetic energy of $H_2\left(1/p\right)$. Using Eq. (16.231), the Josephson coupling energies due to fluxon linkage during concerted rotational-spin rotational and spin-orbital transitions are given by Eq. (16.247), and the magnetic energies $U_{S/OMag,concerted}$ arising from the absorption of the integer number of fluxons j having fluxon linkage quantum number $m_{\Phi 3/2}$ are given by

$$U_{S/OMag,concerted} = \frac{1}{2}U_0\left(\frac{2\pi\left(\Delta\Phi\right)}{\Phi_0}\right)^2$$
$$= 46.24\ cm^{-1}\left(0.5\right)\left(\frac{jm_{\Phi 3/2}46.24\ cm^{-1}}{1950\ cm^{-1}}\right)^2 \tag{16.249}$$
$$= m_{\Phi 3/2}^2 0.0130 j^2\ cm^{-1}$$

wherein $U_0 = 46.24\ cm^{-1}; \Delta\Phi = E_{\Phi,rot,concerted} = m_{\Phi 3/2} 46.24\ cm^{-1}$ (Eq. (16.247)), and the energy between rotational transitions corresponds to the term Φ_0 (Eq. (16.256, $p = 4$)). The fluxon peak spacing increases as the energy of the concerted rotation-fluxon absorption transition increases and decreases in the case of emission.

Using Eq. (16.231), the magnetic energies $U_{S/OMag}$ arising from the absorption of the integer number of fluxons j having fluxon linkage quantum number m_Φ during concerted rotational and spin-orbital transitions are given by

$$\begin{aligned} U_{S/OMag} &= \frac{1}{2} U_0 \left(\frac{2\pi(\Delta\Phi)}{\Phi_0} \right)^2 \\ &= 30.83\ cm^{-1} (0.5) \left(\frac{j m_{\Phi 3/2} 30.83\ cm^{-1}}{1950\ cm^{-1}} \right)^2 \\ &= m_{\Phi 3/2}^2 0.00385 j^2\ cm^{-1} \end{aligned} \tag{16.250}$$

wherein $U_0 = 30.83\ cm^{-1}; \Delta\Phi = E_{\Phi,rot} = m_{\Phi 3/2} 30.83\ cm^{-1}$ (Eq. (16.248)), and the energy between rotational transitions corresponds to the term Φ_0 (Eq. (16.256, $p = 4$)). The fluxon peak spacing increases as the energy of the concerted rotation-fluxon absorption transition increases and decreases in the case of emission.

Table 16.51. . The electron spin-orbital coupling splitting energies and fluxon sub-splitting energies of molecular rotational transitions for spin-orbital coupling quantum numbers $m = 0.5,1,2,3,...,10$ and for electron fluxon quantum numbers $m_\Phi = 1,2,3,...,10$ and $m_{\Phi 3/2} = 1,2,3,...,10$.

m	Spin-Orbital Splitting Energy (cm^{-1})	m_Φ	Fluxon Sub-Splitting Energy (cm^{-1})	$m_{\Phi 3/2}$	Fluxon Sub-Splitting Energy (cm^{-1})
0.5	264	0.5	15.4	0.5	23.1
1	528	1	30.8	1	46.2
2	1056	2	61.7	2	92.5
3	1583	3	92.5	3	138.7
4	2111	4	123.3	4	185.0
5	2639	5	154.1	5	231.2
6	3167	6	185.0	6	277.5
7	3695	7	215.8	7	323.7
8	4223	8	246.6	8	370.0
9	4750	9	277.5	9	416.2
10	5278	10	308.3	10	462.4

The observation of spin-orbital transitions by Raman spectroscopy may be greatly enhanced by the deposition of molecular hydrinos on a metal surface to enhance the Raman spectrum. Surface enhanced Raman (SER) is very sensitive because of the surface plasmon waves set up by the stimulating wavelength. The surface plasmon field may extend about 40-60 nm below the surface, providing some depth sensitivity in the material.

The moment of inertia may be measured using rotational energy spectroscopy such as Raman spectroscopy, and using the known nuclear masses, the moment of inertia gives the nuclear separation which is characteristic of and identifies molecular hydrino of a given quantum state p. Specifically, for a diatomic molecule having atoms of masses m_1 and m_2, the moment of inertia is (Eq. (12.66)):

$$I = \mu r^2 \tag{16.251}$$

where μ is the reduced mass given by (Eq. (12.67)):

$$\mu = \frac{m_1 m_2}{m_1 + m_2} \tag{16.252}$$

and where r is the distance between the centers of the atoms, the internuclear distance. The rotational energy levels follow from Eq. (1.71) and are given by (Eq. (12.68)):

$$E_{rotational} = \frac{\hbar^2}{2I} J(J+1) \tag{16.253}$$

where J is an integer. The pure rotational energies of hydrogen type molecules for transition from the J to the quantized J'

rotational state are given by (Eq. (12.77)):

$$\begin{aligned}\Delta E_{J\to J'} &= E_{J'} - E_J \\ &= \frac{p^2\hbar^2}{2\left(0.5m_p\left(7.411X10^{-11}m\right)^2\right)}\left(J'\left(J'+1\right)-J\left(J+1\right)\right) \\ &= \frac{\left(J'\left(J'+1\right)-J\left(J+1\right)\right)}{2}p^2 121.89\ cm^{-1}\end{aligned} \tag{16.254}$$

wherein m_p is the mass of the proton, the moment of inertia $I = 0.5m_p\left(\frac{7.411X10^{-11}m}{p}\right)^2$, and the integer-squared dependence is due to the reciprocal integer dependence of the internuclear distance given by (Eq. (12.76)):

$$2c' = \frac{0.7411}{p}\ \text{Å} \tag{16.255}$$

For example, the predicted rotational energy of $H_2\left(1/4\right)$ is four squared or 16 times that of H_2 due to the internuclear distance being one fourth that of H_2 (Eq. (16.254)). At ambient laboratory temperature, molecules overwhelmingly populate the rotational state $J = 0$. Then, Eq. (16.253) becomes

$$\Delta E_{J=0\to J'} = \frac{J'\left(J'+1\right)}{2}p^2 121.89\ cm^{-1} \tag{16.256}$$

Molecular hydrino $H_2\left(1/p\right)$ is a diatomic molecule comprising two protons and two electrons, except that it is unique from molecular hydrogen in that it has an unpaired electron having an intrinsic angular momentum of $\frac{\hbar}{2}$. This electron spin angular momentum may align along the same axis as the rotational angular of $\hbar$ or transverse to it. Consider that the rotational energy $E_{rotational}$ of $H_2\left(1/p\right)$ about z-axis which is the common axis of the intrinsic electron angular momentum of $\frac{\hbar}{2}$ and rotational angular momentum of $\hbar$. The rotational energy due to the concerted double excitation of rotation due to spin and diatomic rotation is given by the sum of the diatomic molecular rotational energy given by Eq. (16.253) and the spin rotational energy also given by Eq. (16.253) with the exception that the rotational quantum number J can only change by ± 1:

$$\begin{aligned}E_{rotational+spin} &= \frac{\hbar^2}{2I}\left(J'\left(J'+1\right)-J\left(J+1\right)\right)+\frac{\hbar^2}{I}\left(J+1\right) \\ &= \left(\frac{J'^2+J'-J^2+J+2}{2}\right)p^2 121.89\ cm^{-1}\end{aligned} \tag{16.257}$$

In the case that the initial rotational state is $J = 0$, Eq. (16.256) becomes

$$\begin{aligned}E_{rotational+spin} &= \frac{\hbar^2}{2I}\left(J'\left(J'+1\right)-J\left(J+1\right)\right)+\frac{\hbar^2}{I}\left(J+1\right) \\ &= \left(\frac{J'^2+J'+2}{2}\right)p^2 121.89\ cm^{-1}\end{aligned} \tag{16.258}$$

Consider that the diatomic molecular rotation is about the z-axis such that the corresponding rotational angular momentum of $\hbar$ is aligned along the z-axis. In the case that the axis of the intrinsic electron spin angular momentum of $\frac{\hbar}{2}$ is along the orthogonal semiminor axis, the y-axis, the rotation energy $E_{rotational}$ of $H_2\left(1/p\right)$ is given by Eq. (16.255).

The radiation of a multipole of order (ℓ, m_ℓ) carries $m\hbar$ units of the z component of angular momentum per photon of energy $\hbar\omega$. Thus, the z component of the angular momentum of the corresponding excited rotational state is (Eq. (12.69)):

$$L_z = m\hbar \tag{16.259}$$

Thus, the selection rule for dipole and quadrupole rotational transitions are (Eq. (12.70)):

$$\Delta J = \pm 1 \tag{16.260}$$

and

$$\Delta J = \pm 2 \tag{12.261}$$

Not only are the lowest energy Raman transitions for pure rotational transitions (Eq.(16.255)) and for concerted rotational-spin transition (Eq. (16.257)) allowed by each of the selection rules given by Eqs. (16.259) and (16.260), but coupling of allowed dipole and quadrupole transitions permit excitation of higher rotational energy levels. Isotopic substitution and ortho-para state occupancy also determines the section rules of Raman transitions. Exemplary transitions are given in Table 16.52.

Due to the equivalence of the two semiminor axes, a double rotational excitation comprising the superposition of the independent rotations about each may occur. The energy of the double excitation of these two rotational modes is the sum of the individual pure and concerted rotational transitions. Using Eqs. (16.256) and (16.258), the energies $E_{double\ rotation}$ of the combined rotational excitations are

$$E_{double\ rotational} = \left(\frac{J_c'^2 + J_c'^2 + 2}{2} \right) + \frac{J_p' \left(J_p' + 1 \right)}{2} p^2 121.89\ cm^{-1} \tag{16.262}$$

Exemplary transitions are given in Table 16.52.

Table 16.52. H_2(1/4) Raman energies for (i) pure $J = 0$ to $J' = 1,2,3,...$ rotational transitions, (ii) concerted $J = 0$ to $J' = 0,1,2,3,...$ molecular rotational transition involving a spin rotation transition having the spin rotational state quantum number change from $J = 0$ to $J = 1$, and double transition having energies given by the sum of the independent transitions.

J'	Pure Rotational Transition (cm^{-1})	Concerted Molecular Rotational-Spin Rotation Transition (cm^{-1})	J_p' / J_c'	Double Rotational Transition (cm^{-1})
0	0	1950	1/0	3900
1	1950	3900	2/0	7801
2	5851	7801	2/1	9751
3	11701	13652	3/0	13652
4	19502	21453	3/1	15602
5	29254	31204	3/2	19502
6	40955	42905	4/0	21453
7	54607	56557	4/1	23403
8	70209	72159	4/2	27303
9	87761	89711	4/3	33154
10	107263	109213	5/0	31204

The rotation energies shown in Table 16.52 with spin-orbital splitting and fluxon linkage sub-splitting energy shifts were observed by Raman spectroscopy [136]. Moreover, some of the observed lines matched those of the Diffuse Interstellar Bands (DIBs) [136, 137].

END-OVER-END ROTATION OF HYDROGEN-TYPE MOLECULAR DIMERS

The reduced masses of hydrogen-type molecular dimers having two protons μ_{H_2} or deuterons μ_{D_2} are given by Eqs. (12.67) and (12.72) where $m_1 = m_2 = m_p$ and $m_1 = m_2 = 2m_p$, respectively:

$$\mu_{H_2} = \frac{m_p m_p}{m_p + m_p} = \frac{1}{2} m_p \tag{16.263}$$

$$\mu_{D_2} = \frac{2m_p 2m_p}{2m_p + 2m_p} = m_p \tag{16.264}$$

where m_p is the mass of the proton. The moment of inertia of hydrogen-type molecular dimers is given by summation of the moments of inertial for two sets of nuclei, each equidistant from the center of rotation along the x-axis. The moment of inertia of the nearest neighbor nuclei is given by substitution of the reduced mass (Eqs. (16.263) or (16.264)) for μ of Eq. (12.66) and substitution of the internuclear distance $2c'_{dimer}$ (Eq. (16.181) or (16.202))for r of Eq. (12.66). The moment of inertia of the farthest neighbor nuclei is given by substitution of the reduced mass (Eqs. (16.263) or (16.264)) for μ of Eq. (12.66) and substitution of the internuclear distance $2c'_{dimer}$ (Eq. (16.181) or (16.202))) plus the internuclear distance $2c'$ (Eq. (11.204) for r of Eq. (12.66).

$$I\left([H_2]_2\right)=\frac{m_p}{2}\left[\left(7.61404a_0\right)^2+\left(7.61404a_0+\sqrt{2}a_0\right)^2\right] \tag{16.265}$$

$$I\left([D_2]_2\right)=m_p\left[\left(7.61404a_0\right)^2+\left(7.61404a_0+\sqrt{2}a_0\right)^2\right] \tag{16.266}$$

$$I\left([H_2(1/4)]_2\right)=\frac{m_p}{2}\left[\left(1.94251a_0\right)^2+\left(1.94251a_0+\frac{\sqrt{2}}{4}a_0\right)^2\right] \tag{16.267}$$

$$I\left([H_2(1/4)]_2\right)=m_p\left[\left(1.94251a_0\right)^2+\left(1.94251a_0+\frac{\sqrt{2}}{4}a_0\right)^2\right] \tag{16.268}$$

Using Eqs. (12.71), (12.67), and (12.74), the rotational energies absorbed by a hydrogen-type molecular dimer with the transition from the state with the rotational quantum number J to one with the rotational quantum number $J+1$ are:

$$\begin{aligned}\Delta E\left([H_2]_2\right)&=E_{J+1}-E_J\\&=\frac{\hbar^2}{I\left([H_2]_2\right)}\left[J+1\right]\\&=\frac{\hbar^2}{\frac{m_p}{2}\left[\left(7.61404a_0\right)^2+\left(7.61404a_0+\sqrt{2}a_0\right)^2\right]}\\&=\left[J+1\right]1.71\ cm^{-1}\end{aligned} \tag{16.269}$$

$$\begin{aligned}\Delta E\left([D_2]_2\right)&=E_{J+1}-E_J\\&=\frac{\hbar^2}{I\left([D_2]_2\right)}\left[J+1\right]\\&=\frac{\hbar^2}{m_p\left[\left(7.61404a_0\right)^2+\left(7.61404a_0+\sqrt{2}a_0\right)^2\right]}\\&=\left[J+1\right]0.86\ cm^{-1}\end{aligned} \tag{16.270}$$

$$\begin{aligned}\Delta E\left([H_2(1/4)]_2\right)&=E_{J+1}-E_J\\&=\frac{\hbar^2}{I\left([H_2(1/4)]_2\right)}\left[J+1\right]\\&=\frac{\hbar^2}{\frac{m_p}{2}\left[\left(1.94251a_0\right)^2+\left(1.94251a_0+\frac{\sqrt{2}}{4}a_0\right)^2\right]}\\&=\left[J+1\right]44.30\ cm^{-1}\end{aligned} \tag{16.271}$$

$$\begin{aligned}\Delta E\left([D_2(1/4)]_2\right)&=E_{J+1}-E_J\\&=\frac{\hbar^2}{I\left([D_2(1/4)]_2\right)}\left[J+1\right]\\&\frac{\hbar^2}{m_p\left[\left(1.94251a_0\right)^2+\left(1.94251a_0+\frac{\sqrt{2}}{4}a_0\right)^2\right]}\\&=\left[J+1\right]22.15\ cm^{-1}\end{aligned} \tag{16.272}$$

The results for H_2 and D_2 dimers (Eqs. (16.269) and (16.270)) match experimental observations [138].

REACTION KINETICS AND THERMODYNAMICS

Reaction kinetics may be modeled using the classical solutions of reacting species and their interactions during collisions wherein the bond order of the initial and final bonds undergo a decreasing and increasing bond order, respectively, with conservation of charge and energy. Collisions can be modeled starting with the simple hard sphere model with conservation of energy and momentum. The energy distribution may be modeled using the appropriate statistical thermodynamics model such as

Maxwell-Boltzmann statistics. Low-energy collisions are elastic, but for sufficiently high energy, a reaction may occur. Hot reacting species such as molecules at the extreme of the kinetic energy distribution can achieve the transition state, the intermediate species at the cross over point in time and energy between the reactants and products. The rate function to form the transition state may depend on the collisional orientation as well as the collisional energy. Bond distortion conserves the energy and momentum of the collision from the trajectories of the reactants. For sufficient distortion due to a sufficiently energetic collision at an appropriate relative orientation, a reaction occurs wherein the products exiting the collision event are different from the reactants entering the collision. The initial reactant energy and momentum as well as those arising from any bonding energy changes are conserved in the translational, rotational, and vibrational energies of the products. The bond energy changes are given by the differences in the energies of the product and reactants molecules wherein the geometrical parameters, energies, and properties of the latter can be solved using the same equations as those used to solve the geometrical parameters and component energies of the individual molecules as given in the Organic Molecular Functional Groups and Molecules section. The bond energy changes at equilibrium determine the extent of a reaction according to the Gibbs free energy of reaction. Whereas, the corresponding dynamic reaction-trajectory parameters of translational, rotational, and vibrational energies as well as the time dependent electronic energy components such as the electron potential and kinetic energies of intermediates correspond to the reaction kinetics. Each aspect will be treated next in turn.

Consider the gas-phase reaction of two species A and B comprising the reactants that form one or more products C_n where n is an integer:

$$A+B \rightleftarrows C_1+\cdots+C_n \tag{16.273}$$

Arising from collisional probabilities, the concentrations (denoted $[A],[B],...$) as a function of time can be fitted to a second-order rate law

$$-\frac{d[A]}{dt}=k[A][B]-k'\prod_{i=1}^{n}[C_i] \tag{16.274}$$

where k and k' are the forward and reverse rate constants. The equilibrium constant K corresponding to the balance between the forward and reverse reactions is given by the quotient of the forward and reverse rate constants:

$$K=\frac{k}{k'} \tag{16.275}$$

The relationship between the temperature-dependent equilibrium constant and the standard Gibbs free energy of reaction $\Delta G_T^0(T)$ at temperature T is**:**

$$K=Q_K(T)e^{\frac{-\Delta G_T^0(T)}{RT}} \tag{16.276}$$

where R is the ideal gas constant,

$$Q_K(T)=\frac{\prod_{i=1}^{n}[C_i]}{[A][B]} \tag{16.277}$$

is the reaction quotient at the standard state, and

$$\Delta G_T^0(T)=\Delta H_T^0(T)-T\Delta S_T^0 \tag{16.278}$$

where $\Delta H_T^0(T)$ and ΔS_T^0 are the standard-state enthalpy and entropy of reaction, respectively. Rearranging Eq. (16.276) gives the free energy change upon reaction:

$$\Delta G=RTln\frac{Q_K}{K} \tag{16.279}$$

If the instantaneous free energy change is zero, then the reaction is at equilibrium. An exergonic or work-producing reaction corresponds to the cases with $\Delta G_T^0(T)$ or ΔG negative, and endergonic or work consuming reactions corresponds to positive values. The enthalpy of reaction or heat of reaction at constant pressure is negative for an exothermic (heat releasing) reaction, and is positive for an endothermic (heat absorbing) reaction. The enthalpy of reaction may be calculated by Hess's law as the difference of the sum of the heats of formation of the products minus the sum of the heats of formation of the reactants wherein the individual heats of the molecules are solved using the equations given in the Organic Molecular Functional Groups and Molecules section.

TRANSITION STATE THEORY

Transition state theory (TST) has been widely validated experimentally. It entails the application of classical trajectory calculations that allow the study of the dynamics at the microscopic level such as differential cross sections, total cross sections, and product energy distributions, as well as at the macroscopic level for the determination of thermal rate constants by solving the classical equations of motion with the formation of the transition state. The reaction trajectory parameters give rise to terms of a classical thermodynamic kinetics equation discovered in 1889 by Arrhenius and named after him. The data of the variation of the rate constant k with temperature of many reactions fit the Arrhenius equation given by

$$k = Ae^{\frac{-E_a}{RT}} \tag{16.280}$$

where E_a is the activation energy and A is a preexponential or frequency factor that may have a relatively small temperature dependence compared to the exponential term of Eq. (16.244). For reactions that obey the Arrhenius equation, when $\ln k$ is plotted versus $1/T$ in a so-called Arrhenius plot, the slope is the constant $-E_a/R$, and the intercept is A. Eq. (16.280) confirms that typically two colliding molecules require a certain minimum kinetic energy of relative motion to sufficiently distort initial reactant bonds and concomitantly allow nascent bonds to form. The crossover species from reactants to products called the transition state will proceed through the minimum energy complex involving the reactants. Thus, the activation energy can be interpreted as the minimum energy that the reactants must have in order to form the transition state and transform to product molecules. E_a can be calculated from the total energy of the transition state relative to that of the reactants and is achieved when the thermal energy of the reactants overcomes the energy deficit between the energy of the reactants and that of the transition state. The preexponential factor corresponds to the collision frequency and energy of collisions upon which the formation of the transition state is dependent.

For bimolecular reactions, transition state theory yields [139]:

$$k(T) = \frac{1}{(k_B T)h}\gamma(T)K^{\circ}\exp\left(-\Delta G_T^{\ddagger\circ}/RT\right) \tag{16.281}$$

where $\Delta G_T^{\ddagger\circ}$ is the quasi-thermodynamic free energy of activation, $\gamma(T)$ is a transmission coefficient, K° is the reciprocal of the concentration, h is Planck's constant, and k_B is the Boltzmann constant. The factor $\frac{1}{(k_B T)h}$ is obtained by dynamical classical equations of motion involving species trajectories having a statistical mechanical distribution. Specifically, the reactant molecular distribution is typically a Maxwell-Boltzmann distribution. The classical derivation of the preexponential term of the Arrhenius equation can be found in textbooks and review articles such as section 2.4 of Ref. [139]. Typically the A term can be accurately determined from the Maxwell-Boltzmann-distribution-constrained classical equations of motion by sampling or by using Monte Carlo methods on many sets (usually more than ten thousand) of initial conditions for the coordinates and momenta involving the trajectories. The translational levels are a continuous distribution, and the rotational and vibrational levels are quantized according to the classical equations given, for example, in the Vibration of the Hydrogen Molecular Ion section and the Diatomic Molecular Rotation section.

S_N2 REACTION OF Cl^- WITH CH_3Cl

Consider the S_N2 (bimolecular nucleophilic substitution) gas-phase reaction of Cl^- with chloromethane through a transition state:

$$Cl^- + CH_3Cl \rightarrow ClCH_3 + Cl^- \tag{16.282}$$

The corresponding Arrhenius equation for the reaction given by Eq. (16.280) is:

$$k(T) = \frac{k_B T}{h}\frac{Q^{\ddagger}}{\Phi^R}e^{\frac{-\Delta E^{\ddagger}}{k_B T}} \tag{16.283}$$

where k_B is the Boltzmann constant, h is Planck's constant, $\Delta E^{\ddagger}$ is the activation energy of the transition state ‡, T is the temperature, Φ^R is the reaction partition per unit volume, and $Q^{\ddagger}$ is the coordinate independent transition-state partition function. The preexponential factor $\frac{k_B T}{h}\frac{Q^{\ddagger}}{\Phi^R}$ has previously been calculated classically and shown to be in agreement with the experimental rate constant [140]. Then, only the transition state need be calculated and its geometry and energy compared to observations to confirm that classical physics is predictive of reaction kinetics. The activation energy can be calculated by determining the energy at the point that the nascent bond with the chloride ion is the same as that of the leaving chlorine wherein the negative charge is equally distributed on the chlorines. The rearrangement of bonds and the corresponding electron MOs of the reactants and products can be modeled as a continuous transition of the bond orders of the participating bonds from unity to zero and vice versa, respectively, wherein the transition state is a minimum-energy molecule having bonds between all of the reactants, Cl^- and CH_3Cl

TRANSITION STATE

The reaction proceeds by back-side attack of Cl^- on CH_3Cl. Based on symmetry, the reaction pathway passes through a D_{3h} configuration having $Cl^{\delta-}-C-Cl^{\delta-}$ on the C_3 axis. The hydrogen atoms are in the σ_h plane with the bond distances the same as those of the CH_3 functional group given in the Alkyl Chlorides section, since this group is not involved in the substitution reaction. The transition-state group $Cl^{\delta-}-C-Cl^{\delta-}$ is treated as a three-centered-bond functional group that comprises a linear

combination of Cl^- and the $C-Cl$ group of chloromethane ($C-Cl$ (i) given in Table 15.33). It is solved using the Eq. (15.51) with the total energy matched to the sum of the H_2-type ellipsoidal MO total energy, $-31.63536831\ eV$ given by Eq. (11.212) as in the case of chloromethane, and the energy of the two outer electrons of Cl^-, $E\left(Cl^-\right)=-IP_1-IP_2=-12.96764\ eV-3.612724\ eV=-16.58036\ eV$ [15, 141]. These electrons are contributed to form the back-side-attack bond. Then, the corresponding parameter $E_{T(AO/HO)}\ (eV)$ is $-14.63489\ eV-16.58036\ eV=-31.21525\ eV$ due to the match of the MO energy to both $E\left(C,2sp^3\right)=-14.63489\ eV$ (Eq. (15.25)) and $E\left(Cl^-\right)$, and $E_{initial\ (C_5\ AO/HO)}\ (eV)$ is $-16.58036\ eV$ corresponding to the initial energy of the Cl^- electrons. Also, due to the two $C-Cl$ bonds of the $Cl^{\delta-}-C-Cl^{\delta-}$ functional group $n_1=2$. Otherwise all of the parameters of Eq. (15.51) remain the same as those of chloromethane given in Table 15.36. The geometrical (Eqs. (15.1-15.5) and (15.51)), intercept (Eqs. (15.80-15.87)), and energy (Eqs. (15.6-15.11) and (15.17-15.65)) parameters are given in Tables 16.53, 16.54, and 16.55, respectively. The color scale, translucent view of the charge density of the chloride-ion-chloromethane transition state comprising the $Cl^{\delta-}-C-Cl^{\delta-}$ functional group is shown in Figure 16.17. The transition state bonding comprises two paired electrons in each $Cl^{\delta-}-C$ MO with two from Cl^-, one from Cl and one from CH_3. As a symmetrical three-centered bond, the central bonding species are two Cl bound to a central CH_3^+ per $Cl^{\delta-}-C$ MO with a continuous current onto the $C-H$ MO at the intersection of each $Cl^{\delta-}-C$ MO with the CH_3^+ group. Due to the four electrons and the valence of the chlorines, the latter possess a partial negative charge of $-0.5e$ distributed on each $Cl^{\delta-}-C$ MO such that the far field is equivalent to that of the corresponding point charge at each Cl nucleus.

Figure 16.17. Color scale, translucent view of the chloride-ion-chloromethane transition state comprising the $Cl^{\delta-}-C-Cl^{\delta-}$ functional group showing the orbitals of the atoms at their radii, the ellipsoidal surface of each H or H_2-type ellipsoidal MO that transitions to the corresponding outer shell of the atom(s) participating in each bond, and the hydrogen nuclei (red, not to scale).

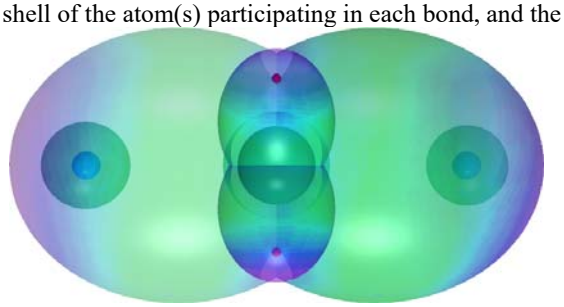

Table 16.53. The geometrical bond parameters of the $Cl^{\delta-}-C-Cl^{\delta-}$ and CH_3 functional groups of the chloride-ion-chloromethane transition state.

Parameter	$Cl^{\delta-}-C-Cl^{\delta-}$ Group	$C-H\ (CH_3)$ Group
$a\ (a_0)$	3.70862	1.64920
$c'\ (a_0)$	2.13558	1.04856
Bond Length $2c'\ (\text{Å})$	2.26020	1.10974
Literature Bond Length (Å)	2.3-2.4 [140,142]	1.06-1.07 [140]
$b,c\ (a_0)$	3.03202	1.27295
e	0.57584	0.63580

Table 16.54. The MO to HO and AO intercept geometrical bond parameters of the $-Cl^{\delta-}-C-Cl^{\delta-}$ and CH_3 functional groups of the chloride-ion-chloromethane transition state. E_T is $E_T(atom-atom, msp^3.AO)$.

Bond	Atom	E_T (eV) Bond 1	E_T (eV) Bond 2	E_T (eV) Bond 3	E_T (eV) Bond 4	Final Total Energy $C2sp^3$ (eV)	$r_{initial}$ (a_0)	r_{final} (a_0)	$E_{C\,radicals}(C2sp$ (eV) Final	$E(C2sp^3)$ (eV) Final	θ' (°)	θ_1 (°)	θ_2 (°)	d_1 (a_0)	d_2 (a_0)
$Cl^{\delta-}-C-Cl^{\delta-}$	C	-0.36229	-0.36229	0	0	-152.34026	0.91771	0.87495	-15.55033	-15.35946					
$Cl_a^{\delta-}-C-Cl_b^{\delta-}$	$Cl_a^{\delta-}$	-0.36229	0	0	0		2.68720	0.89582	-15.18804						
$Cl_a^{\delta-}-C-Cl_b^{\delta-}$	$Cl_b^{\delta-}$	-0.36229	0	0	0		1.05158	0.89582	-15.18804						
$C-H\ (CH_3)$	C	-0.36229	-0.36229	0	0	-152.34026	0.91771	0.87495	-15.55033	-15.35946	78.85	101.15	42.40	1.21777	0.16921

Table 16.55. The energy parameters (eV) of the $Cl^{\delta^-}-C-Cl^{\delta^-}$ and CH_3 functional groups of the chloride-ion-chloromethane transition state.

Parameters	$Cl^{\delta^-}-C-Cl^{\delta^-}$ Group	CH_3 Group
n_1	2	3
n_2	0	2
n_3	1	0
C_1	0.5	0.75
C_2	0.81317	1
c_1	1	1
c_2	1	0.91771
c_3	1	0
c_4	2	1
c_5	1	3
C_{1o}	0.5	0.75
C_{2o}	0.81317	1
$V_e\ (eV)$	-33.44629	-107.32728
$V_p\ (eV)$	12.74200	38.92728
$T\ (eV)$	4.50926	32.53914
$V_m\ (eV)$	-2.25463	-16.26957
$E_{(AO/HO)}\ (eV)$	-31.21525	-15.56407
$\Delta E_{H_2MO(AO/HO)}\ (eV)$	-1.44915	0
$E_{T(AO/HO)}\ (eV)$	-29.76611	-15.56407
$E_{(n_3\ AO/HO)}\ (eV)$	-16.58036	0
$E_{T(H_2MO)}\ (eV)$	-48.21577	-67.69451
$E_T\left(atom-atom, msp^3.AO\right)\ (eV)$	-1.44915	0
$E_{T(MO)}\ (eV)$	-49.66491	-67.69450
$\omega\ \left(10^{15}\ rad/s\right)$	3.69097	24.9286
$E_K\ (eV)$	2.42946	16.40846
$\bar{E}_D\ (eV)$	-0.07657	-0.25352
$\bar{E}_{Kvib}\ (eV)$	0.08059 [5]	0.35532 (Eq. (13.458))
$\bar{E}_{osc}\ (eV)$	-0.03628	-0.22757
$E_{mag}\ (eV)$	0.14803	0.14803
$E_{T(Group)}\ (eV)$	-49.73747	-67.92207
$E_{initial(c_4\ AO/HO)}\ (eV)$	-14.63489	-14.63489
$E_{initial(c_5\ AO/HO)}\ (eV)$	-16.58036	-13.59844
$E_{D(Group)}\ (eV)$	3.73930	12.49186

The bond energy of the $C-Cl$ group of chloromethane from Table 15.36 is $E_{D(Group)}\ (eV)=3.77116\,eV$ compared to the bond energy of the $Cl^{\delta^-}-C-Cl^{\delta^-}$ functional group of the chloride-ion-chloromethane transition state of

$E_{D(Group)}\ (eV) = 3.73930\ eV$ (Table 16.55). Since the energies of the CH_3 functional groups are unchanged, the chloride-ion-chloromethane transition state is $\Delta E = +0.03186\ eV\ (+0.73473\ kcal/mole)$ higher in energy than chloromethane. Experimentally, the transition state is about $1 \pm 1\ kcal/mole$ higher [137]. Using this energy as the corresponding activation energy $\Delta E^{\ddagger}$ of Eq. (16.283) with the classically determined preexponential factor $\frac{k_B T}{h}\frac{Q^{\ddagger}}{\Phi^R}$ predicts the experimental reaction rate very well [140].

NEGATIVELY-CHARGED MOLECULAR ION COMPLEX $\mathbb{C}$

In addition to the nature and energy of the transition state designated by ‡, experimental gas-phase rate constants indicate that the reaction of Cl^- with CH_3Cl passes through a bound state comprising the attachment of Cl^- to the positive dipole of CH_3Cl [140, 142, 143] (the dipole moment of the $C-Cl$ functional group is given in the Bond and Dipole Moments section). This negatively-charged molecular ion complex designated $\mathbb{C}$ exists as a more stable state in between the reactants and the transition state, and by equivalence of the chlorines, it also exists between the transition state and the products. Experimentally $\mathbb{C}$ is $12.2 \pm 2\ kcal/mole$ more stable than the isolated reactants and products, Cl^- and CH_3Cl. Thus, an energy well corresponding to $\mathbb{C}$ occurs on either side of the energy barrier of the transition state ‡ that is about $1 \pm 1\ kcal/mole$ above the reactants and products [140, 143]. Thus, the combination of the depth of this well and the barrier height yields an intrinsic barrier to nucleophilic substitution given by the reaction of Eq. (16.282) of $13.2 \pm 2.2\ kcal/mole$ [140, 143].

The negatively-charged molecular ion complex $\mathbb{C}$ comprises the functional groups of CH_3Cl ($C-Cl$ (i) and CH_3 given in Table 15.33 of the Alkyl Chlorides section) and a $Cl^-\cdot C^{\delta+}$ functional group wherein Cl^- is bound to the CH_3Cl moiety by an ion-dipole bond. As given in the case of the dipole-dipole bonding of ice, liquid water, and water vapor as well as the van der Waals bonding in graphite and noble gases given in the Condensed Matter Physics section, the bond energy and bond distance of the $Cl^-\cdot C^{\delta+}$ functional group are determined by the limiting energy and distance of the formation of a corresponding nascent $Cl^- - CH_3Cl$ covalent bond that destabilizes the $C-Cl$ bond of the CH_3Cl moiety by involving charge density of its electrons in the formation the nascent bond. Subsequently, the higher energy $Cl^{\delta-} - C - Cl^{\delta-}$ functional group of the transition state is formed.

The energy and geometric parameters of the $Cl^-\cdot C^{\delta+}$ functional group are solved using Eq. (15.51) with the total energy matched to the H_2-type ellipsoidal MO total energy, $-31.63536831\ eV$. The parameter $E_{T(AO/HO)}\ (eV)$ is $-14.63489\ eV - 3.612724\ eV = -18.24761\ eV$ due to the match of the MO energy to both $E\left(C, 2sp^3\right) = -14.63489\ eV$ (Eq. (15.25)) and the outer electron of $E\left(Cl^-\right)$ ($-IP_1 = -3.612724\ eV$) [141] that forms the nascent bond by the involving the electrons of the $C-Cl$ group of the CH_3Cl moiety. Then, $E_{initial(c_5\ AO/HO)}\ (eV)$ is $-3.612724\ eV$ corresponding to the initial energy of the outer Cl^- electron. Also, $E_T\left(atom-atom, msp^3.AO\right)$ in Eq. (15.61) is $-1.85836\ eV$ due to the charge donation from the C HO to the MO based on the energy match between the $C2sp^3$ HOs corresponding to the energy contribution of methylene, $-0.92918\ eV$ (Eq. (14.513)). $E_{mag} = 0$ since the Cl^- electrons are paired upon dissociation, and the vibrational energy of the transition state is appropriate for $Cl^-\cdot C^{\delta+}$. Otherwise, all of the parameters of Eq. (15.51) remain the same as those of chloromethane given in Table 15.36. The geometrical (Eqs. (15.1-15.5) and (15.51)), intercept (Eqs. (15.80-15.87)), and energy (Eqs. (15.6-15.11) and (15.17-15.65)) parameters are given in Tables 16.56, 16.57, and 16.58, respectively. The color scale, translucent view of the charge density of the negatively-charged molecular ion complex $\mathbb{C}$ comprising the $Cl^-\cdot C^{\delta+}$ functional group is shown in Figure 16.18. The bonding in the $\mathbb{C}$ complex comprises two paired electrons in the $Cl^-\cdot C^{\delta+}$ MO with 1/2 of the charge density from Cl^- and the other half from CH_3. The central bonding species are a Cl bound to a central CH_3^+ with a continuous current onto the $C-H$ MO at the intersection of the $Cl^-\cdot C^{\delta+}$ MO with the CH_3^+ group. Due to the two electrons and the valence of the chlorine, the latter possess a negative charge of $-e$ distributed on the $Cl^-\cdot C^{\delta+}$ MO such that the far field is equivalent to that of the corresponding point charge at the Cl nucleus. The bonding in the CH_3Cl moiety is equivalent to that of chloromethane except that the $C-H$ bonds are in a plane to accommodate the $Cl^-\cdot C^{\delta+}$ MO.

Figure 16.18. Color scale, translucent view of the negatively-charged molecular ion complex $\mathbb{C}$ comprising the $Cl^{-}\cdot C^{\delta+}$ functional group showing the orbitals of the atoms at their radii, the ellipsoidal surface of each H or H_2-type ellipsoidal MO that transitions to the corresponding outer shell of the atom(s) participating in each bond, and the hydrogen nuclei (red, not to scale).

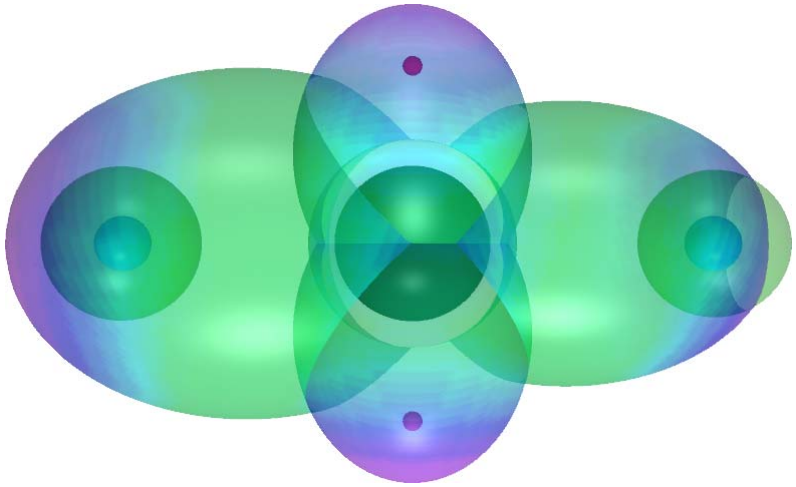

Table 16.56. The geometrical bond parameters of the $Cl^{-}\cdot C^{\delta+}$, $C-Cl$, and CH_3 functional groups of the negatively-charged molecular ion complex $\mathbb{C}$.

Parameter	$Cl^{-}\cdot C^{\delta+}$ Group	$C-H$ (CH_3) Group	$C-Cl$ (i) Group
a (a_0)	2.66434	1.64920	2.32621
c' (a_0)	1.81011	1.04856	1.69136
Bond Length $2c'$ (Å)	1.91574	1.10974	1.79005
Literature Bond Length (Å)	>1.80 curve fit [136]	1.06-1.07 [1]	1.785 [1] (methyl chloride)
b,c (a_0)	1.95505	1.27295	1.59705
e	0.67938	0.63580	0.72709

Table 16.57. The MO to HO and AO intercept geometrical bond parameters of the $Cl^- \cdot Cl^{\delta+}$, $C-Cl$, and CH_3 functional groups of the negatively-charged molecular ion complex C. E_T is $E_T(atom-atom, msp^3.AO)$.

Bond	Atom	E_T (eV) Bond 1	E_T (eV) Bond 2	E_T (eV) Bond 3	E_T (eV) Bond 4	Final Total Energy $C2sp^3$ (eV)	$r_{initial}$ (a_0)	r_{final} (a_0)	$E_{Coulomb}(C2sp^3)$ (eV) Final	$E(C2sp^3)$ (eV) Final	θ' (°)	θ_1 (°)	θ_2 (°)	d_1 (a_0)	d_2 (a_0)
$Cl^- \cdot C^{\delta+}$	C	-0.82688	-0.72457	0	0		0.91771	0.83078	-16.37720	-16.18634					
$Cl^- \cdot C^{\delta+}$	Cl^-	-0.82688	0	0	0		2.68720	0.86923	-15.65263		16.80	163.20	7.38	2.64225	0.83214
$C-Cl$	C	-0.82688	-0.72457	0	0	-153.16714	0.91771	0.83078	-16.37720	-16.18634	63.91	116.09	27.85	2.05675	0.36539
$C-Cl$	Cl	-0.72457	0	0	0		1.05158	0.87495	-15.55033		69.62	110.38	30.90	1.99599	0.30463
$C-H$ (CH_3)	C	-0.82688	-0.72457	0	0	-153.16714	0.91771	0.83078	-16.37720	-16.18634	73.30	106.70	38.69	1.28725	0.23869

Table 16.58. The energy parameters (eV) of the $Cl^{-}\cdot C^{\delta+}$, $C-Cl$, and CH_3 functional groups of the negatively-charged molecular ion complex $\mathbb{C}$.

Parameters	$Cl^{-}\cdot C^{\delta+}$ Group	CH_3 Group	$C-Cl$ (i) Group
n_1	1	3	1
n_2	0	2	0
n_3	0	0	0
C_1	0.5	0.75	0.5
C_2	0.81317	1	0.81317
c_1	1	1	1
c_2	1	0.91771	1
c_3	0	0	1
c_4	2	1	2
c_5	1	3	0
C_{1o}	0.5	0.75	0.5
C_{2o}	0.81317	1	0.81317
$V_e\ (eV)$	-24.89394	-107.32728	-29.68411
$V_p\ (eV)$	7.51656	38.92728	8.04432
$T\ (eV)$	4.67169	32.53914	6.38036
$V_m\ (eV)$	-2.33584	-16.26957	-3.19018
$E_{(AO/HO)}\ (eV)$	-18.24761	-15.56407	-14.63489
$\Delta E_{H_2MO(AO/HO)}\ (eV)$	-1.65376	0	-1.44915
$E_{T(AO/HO)}\ (eV)$	-16.59386	-15.56407	-13.18574
$E_{T(H_2MO)}\ (eV)$	-31.63537	-67.69451	-31.63536
$E_T\left(atom-atom, msp^3.AO\right)\ (eV)$	-1.65376	0	-1.44915
$E_{T(MO)}\ (eV)$	-33.28913	-67.69450	-33.08452
$\omega\ \left(10^{15}\ rad/s\right)$	6.06143	24.9286	7.42995
$E_K\ (eV)$	3.98974	16.40846	4.89052
$\bar{E}_D\ (eV)$	-0.13155	-0.25352	-0.14475
$\bar{E}_{Kvib}\ (eV)$	0.02790 [144]	0.35532 (Eq. (13.458))	0.08059 [5]
$\bar{E}_{osc}\ (eV)$	-0.11760	-0.22757	-0.10445
$E_{mag}\ (eV)$	0	0.14803	0.14803
$E_{T(Group)}\ (eV)$	-33.40672	-67.92207	-33.18897
$E_{initial(c_4\ AO/HO)}\ (eV)$	-14.63489	-14.63489	-14.63489
$E_{initial(c_5\ AO/HO)}\ (eV)$	-3.612724	-13.59844	0
$E_{D(Group)}\ (eV)$	0.52422	12.49186	3.77116

The bond energies of the CH_3Cl moiety are unchanged to the limit of the formation of the $Cl^{-}\cdot C^{\delta+}$ functional group of the negatively-charged molecular ion complex $\mathbb{C}$. Thus, the energy of stabilization of forming the ion-dipole complex is

equivalent to the bond energy of the $Cl^{-}\cdot C^{\delta+}$ functional group. Experimentally $\mathbb{C}$ is $12.2\pm 2\ kcal/mole$ more stable than the isolated reactants and products [134, 136, 137], Cl^{-} and CH_3Cl. The bond energy of the $Cl^{-}\cdot C^{\delta+}$ functional group of the negatively-charged molecular ion complex $\mathbb{C}$ of $E_D(Group)=12.08900\ kcal/mole\ (0.52422\ eV)$ given in Table 16.58 matches the experimental stabilization energy very well. A simulation of the reaction of Eq. (16.282) is available on the internet [145].

REFERENCES

1. D. R. Lide, *CRC Handbook of Chemistry and Physics*, 86th Edition, CRC Press, Taylor & Francis, Boca Raton, (2005-6), pp. 9-19 to 9-45.
2. G. A. Sim, J. M. Robertson, T. H. Goodwin, "The crystal and molecular structure of benzoic acid," Acta Cryst., Vol. 8, (1955), pp.157-164.
3. G. Herzberg, *Molecular Spectra and Molecular Structure II. Infrared and Raman Spectra of Polyatomic Molecules*, Van Nostrand Reinhold Company, New York, New York, (1945), pp. 362-369.
4. "Acetic acid," *NIST Chemistry Handbook.* http://webbook.nist.gov/.
5. G. Herzberg, *Molecular Spectra and Molecular Structure II. Infrared and Raman Spectra of Polyatomic Molecules*, Krieger Publishing Company, Malabar, FL, (1991), p. 195.
6. D. Lin-Vien. N. B. Colthup, W. G. Fateley, J. G. Grasselli, The *Handbook of Infrared and Raman Frequencies of Organic Molecules*, Academic Press, Inc., Harcourt Brace Jovanovich, Boston, (1991), p. 138.
7. "Methyl formate," *NIST Chemistry Handbook.* http://webbook.nist.gov/.
8. "Methanol," *NIST Chemistry Handbook.* http://webbook.nist.gov/.
9. K. P. Huber, G. Herzberg, *Molecular Spectra and Molecular Structure, IV. Constants of Diatomic Molecules*, Van Nostrand Reinhold Company, New York, (1979).
10. J. Crovisier, Molecular Database—Constants for molecules of astrophysical interest in the gas phase: photodissociation, microwave and infrared spectra, Ver. 4.2, Observatoire de Paris, Section de Meudon, Meudon, France, May 2002, pp. 34–37, available at http://www.usr.obspm.fr/~crovisie/.
11. J. D. Cox, G. Pilcher, *Thermochemistry of Organometallic Compounds*, Academic Press, New York, (1970), pp. 254-255.
12. W. I. F. David, R. M. Ibberson, G. A. Jeffrey, J. R. Ruble, "The structure analysis of deuterated benzene and deuterated nitromethane by pulsed-neutron powder diffraction: a comparison with single crystal neutron analysis," Physica B (1992), 180 & 181, pp. 597-600.
13. G. A. Jeffrey, J. R. Ruble, R. K. McMullan, J. A. Pople, "The crystal structure of deuterated benzene," Proceedings of the Royal Society of London. Series A, Mathematical and Physical Sciences, Vol. 414, No. 1846, (Nov. 9, 1987), pp. 47-57.
14. H. B. Burgi, S. C. Capelli, "Getting more out of crystal-structure analyses," Helvetica Chimica Acta, Vol. 86, (2003), pp. 1625-1640.
15. D. R. Lide, *CRC Handbook of Chemistry and Physics*, 86th Edition, CRC Press, Taylor & Francis, Boca Raton, (2005-6), pp. 10-202 to 10-204.
16. C. S. Choi, E. Prince, "The crystal structure of cyclotrimethylene-trinitramine," Acta Cryst., Vol. B28, (1972), pp. 2857-2862.
17. D. Lin-Vien. N. B. Colthup, W. G. Fateley, J. G. Grasselli, The *Handbook of Infrared and Raman Frequencies of Organic Molecules*, Academic Press, Inc., Harcourt Brace Jovanovich, Boston, (1991), p. 187.
18. D. Lin-Vien. N. B. Colthup, W. G. Fateley, J. G. Grasselli, The *Handbook of Infrared and Raman Frequencies of Organic Molecules*, Academic Press, Inc., Harcourt Brace Jovanovich, Boston, (1991), p. 194.
19. D. Lin-Vien. N. B. Colthup, W. G. Fateley, J. G. Grasselli, The *Handbook of Infrared and Raman Frequencies of Organic Molecules*, Academic Press, Inc., Harcourt Brace Jovanovich, Boston, (1991), p. 482.
20. D. R. Lide, *CRC Handbook of Chemistry and Physics*, 86th Edition, CRC Press, Taylor & Francis, Boca Raton, (2005-6), pp. 9-82 to 9-86.
21. D. R. Lide, *CRC Handbook of Chemistry and Physics*, 86th Edition, CRC Press, Taylor & Francis, Boca Raton, (2005-6), pp. 9-54 to 9-59.
22. R. J. Fessenden, J. S. Fessenden, *Organic Chemistry*, Willard Grant Press. Boston, Massachusetts, (1979), p. 20.
23. D. R. Lide, *CRC Handbook of Chemistry and Physics*, 86th Edition, CRC Press, Taylor & Francis, Boca Raton, (2005-6), pp. 9-47 to 9-53.
24. D. R. Lide, *CRC Handbook of Chemistry and Physics*, 89th Edition (Internet Version, 2009), CRC Press, Taylor and Francis, Boca Raton, (2009), 9-Dipole Moments.
25. V. H. J. Becher, "Über den Bindungszustand in Bor—Stickstoff-Verbindungen. II. Bindungsmomente in Borazanen und Borazenen," Zeitschrift für anorganische und allgemeine Chemie, Vol. 270, No. 5-6, (1952), pp. 273-286.
26. V. V. Kuznetsov, A. I. Gren, A. V. Bogatskii, S. P. Egorova, V. I. Sidorov, "Stereochemistry of heterocycles," XLIX. "Investigation of the conformation of alkyl-1,3,2-dioxaborinanes by PMR spectroscopy," Chemistry of Heterocyclic Compounds, Vol. 14, No. 1, (1978), pp. 19-22.

27. É. A. Ishmaeva, A. N. Vereshchagin, N. G. Khusainova, Z. A. Bredikhina, A. N. Pudovik, "Dipole moments of organophosphorous compounds. 15. Polarities and polarizabilities of some acetylenic compounds," Russian Chemical Bulletin, Vol. 27, No. 2, (1978), pp. 310-313.
28. O. A. Varnavskaya-Samarina, É. A. Ishmaeva, G.V. Romanov, R. Ya. Nazmutdinov, A. B. Remizov, A. N. Pudovik, "Dipole moments of organophosphorous compounds. 16. Conformations of trimethylsilyl groups in some phosphites, phosphates, and phosphonates," Russian Chemical Bulletin, Vol. 27, No. 2, (1978), pp. 313-318.
29. A. I. Echeistova, Ya. K. Syrkin, V. I. Stanko, and A. I. Klimova, "Dipole moments of halogen derivatives of ortho- and meta- carboranes," Journal of Structural Chemistry, Vol. 8, No. 5, (1967), p. 833-834.
30. V. I. Stanko, A. I. Echeistova, I. S. Astakhova, A. I. Klimova, Y. T. Struchkov, Y. K. Syrkin, "Use of dipole moments to determine the structure of halogen derivates of ortho and metacarboranes," J. Struct. Chem., Vol. 8, No. 5, (1967), pp. 829-832.
31. G. J. Moody, J. D. R. Thomas, *Dipole Moments in Inorganic Chemistry*, Edward Arnold, London, (1971), p. 43.
32. V. I. Minkin, O. A. Osipov, Y. A. Zhdanovv, *Dipole Moments in Organic Chemistry,* Plenum, (1970).
33. J. G. Speight, *Lange's Handbook of Chemistry*, Sixteenth Edition, McGraw-Hill Professional, New York, (2004), pp. 1.171 to 1.172.
34. J. A. Dean, *Lange's Handbook of Chemistry*, Fifteenth Edition, McGraw-Hill Professional, New York, (1998), pp. 4.53-4.54.
35. V. I. Minkin, O. A. Osipov, Y. A. Zhdanov, *Dipole Moments in Organic Chemistry*, Plenum Press, New York, (1956), p. 88.
36. J. M. Bellama, A. G. MacDiarmid, "An electric dipole moment study of methylsilyl and silylmethyl halides," J. Organomet. Chem., Vol. 24, No. 1, (1970), pp. 91-95.
37. R. Varma, A. G. MacDiarmid, J. G. Miller, "Nature of the silicon-phenyl and silicon-oxygen bond in hexaphenyldisiloxane: an electric dipole moment study," J. Organomet. Chem., Vol. 9, No. 1, (1967), pp. 77-81.
38. R. Varma, A. G. MacDiarmid, J. G. Miller, "The dipole moments and structures of disiloxane and methoxysilane," Inorg. Chem., Vol. 3, No. 12, (1964), pp. 1754-1757.
39. A. L. McClellan, *Tables of Experimental Dipole Moments*, W. H. Freeman and Company, San Fransico, (1963), p. 44.
40. A. L. McClellan, *Tables of Experimental Dipole Moments*, Volume 2, Rahara Enterprises, California, (1974).
41. A. L. McClellan, *Tables of Experimental Dipole Moments*, Volume 3, Rahara Enterprises, California, (1989), p. 39.
42. T. Kasuya, W. J. Lafferty, D.R. Lide, J Chem Phys., Vol. 48, (1968), pp. 1-4.
43. J. H. Hand, R. H. Schwendeman, "Microwave spectrum, molecular structure, dipole moment, and ring-bending vibration of 1,3,2-dioxaborolane," J. Chem. Phys., Vol. 45, (1966), pp. 3349-3354.
44. J. R. Weaver, R. W. Perry, "Dipole moment studies. III. The dipole moments of the methylamine boranes," Inorg. Chem., Vol. 5, No. 5, (1966), pp. 713-718.
45. NIST, "Listing of experimental data for H_2S (hydrogen sulfide)," http://cccbdb.nist.gov/exp2.asp?casno=7783064.
46. NIST, "Listing of experimental data for $N(CH_3)_3$ (trimethylamine)," http://cccbdb.nist.gov/exp2.asp?casno=75503.
47. NIST, "Listing of experimental data for CH_3SCH_3 (dimethyl sulfide)," http://cccbdb.nist.gov/exp2.asp?casno=75183.
48. http://en.wikipedia.org/wiki/Trimethylphosphine.
49. Springer, http://www.springerlink.com/content/t585467172mp2263/fulltext.pdf?page=1.
50. NIST, "Listing of experimental data for CH_3SiCH_3 (dimethyl silane)," http://cccbdb.nist.gov/exp2.asp?casno=75183.
51. NIST, "Listing of experimental data for SiH_4 (silane)," http://cccbdb.nist.gov/exp2.asp?casno=7803625.
52. NIST, "Listing of experimental data for BHF_2 (difluoroborane)," http://cccbdb.nist.gov/exp2.asp?casno=13709836.
53. Hand, J.H., Schwendeman, R.H., J. Chem Phys., Vol. 45, (1966), p. 3349. Available at http://www.springerlink.com/content/l825370723216k35/fulltext.pdf?page=1.
54. S. D. Hubbard, A. P. Cox, J. Mol. Spectrosc., Vol. 115, (1986), pp. 188. Available at, http://www.springerlink.com/content/n135855181p714r6/fulltext.pdf?page=1.
55. P. R. R. Langridge-Smith, R. Stevens, A. P. Cox, J. Chem. Soc., Faraday Trans. II, Vol. 75, (1979), p. 1620. Available at, http://www.springerlink.com/content/qh12341h1p157424/fulltext.pdf?page=1.
56. R. D. Nelson Jr., D. R. Lide, A. A. Maryott, "Selected Values of electric dipole moments for molecules in the gas phase," NSRDS-NBS10, (1967), p. 13.
57. R. D. Nelson Jr., D. R. Lide, A. A. Maryott, "Selected Values of electric dipole moments for molecules in the gas phase," NSRDS-NBS10, (1967), p. 26.
58. R. D. Nelson Jr., D. R. Lide, A. A. Maryott, "Selected Values of electric dipole moments for molecules in the gas phase," NSRDS-NBS10, (1967), p. 23.
59. K. K. Chatterjee, J. R. Durig, S. Bell, J. Mol. Struct., Vol. 265, (1992), p. 25.
60. J. L. Duncan, J. L. Harvie, D. C. McKean, S. Cradock, J. Mol. Struct., Vol. 145, (1986), p. 225.
61. M. Wong, I. Ozier, W. L. Meerts, J. Mol. Spectrosc., Vol. 102, (1983), p. 89.
62. S. D. Hubbard, A. P. Cox, J. Mol. Spectrosc., Vol. 115, (1986), pp. 188.
63. P. R. R. Langridge-Smith, R. Stevens, A. P. Cox, J. Chem. Soc., Faraday Trans. II, Vol. 75, (1979), p. 1620.
64. G. Kodama, J. R. Weaver, J. LaRochelle, R. W. Parry, "Dipole moment studies II. The dipole moments of the ethylphosphines," Inorg. Chem., Vol. 5, No. 5, (1966), pp. 710-713.
65. J. R. Weaver, R. W. Parry, "Dipole moment studies III. The dipole moments of the methylamine boranes," Inorg. Chem., Vol. 5, No. 5, (1966), pp. 713-718.
66. S. Bohm, O. Exner, "Prediction of molecular dipole moments from bond moments: testing of the method by DFT

calculations on isolated molecules," Phys. Chem. Chem. Phys., Vol. 6, No. 3, (2004), pp. 510-514.
67. C. W. N. Cumper, "Electric bond and group dipole moments," Tetrahedron, Vol. 25, No. 15, (1969), pp. 3131-3138.
68. O. A. Raevskii, F. G. Khalitov, "The inductive effect in a series of phosphines," Russ. Chem. Bull., Vol. 19, No. 10, (1970), pp. 2222-2224. http://www.springerlink.com/content/uw673505v7064355/.
69. E. Fluck, *The Chemistry of Phosphine*, Topics in Current Chemistry, Vol. 35, (1973). Available at http://www.springerlink.com/content/ y17151p8tqnq5772/.
70. M. J. S. Dewar, C. Jie, E. G. Zoebisch, "AM1 calculations for compounds containing boron," J. Organometallics, Vol. 7, No. 2, (1988), pp. 513-521.
71. J. R. Weaver, R. W. Parry, "Dipole moment studies IV. Trends in dipole moments," Inorg. Chem., Vol. 5, No. 5, (1966), pp. 718-723.
72. G. Zhou, W. Chen, *Fundamentals of Structural Chemistry*, World Scientific, (1993), p. 175.
73. B. A. Arbuzov, O. D. Zolova, L. K. Yuldasheva, "Dipole moments and conformation of cyclic compounds. III. Sulfites," J. Struct. Chem., Vol. 8, No. 2, (1967), pp. 249-252.
74. O. Exner, D. N. Harpp, J. G. Gleason, "Dipole moments and conformation of sultones, thiosultones and sultines," Can. J. Chem., Vol. 50, (1972), pp. 548-552.
75. O. Exner, Z. Fidlerova and V. Jehlicka, Collect. Czech. Chem. Commun., Vol. 33, (1968), pp. 2019.
76. O. Exner, P. Dembech, P. Vivarelli, "Dipole moments and conformation of sulphinic acid esters," J. Chem. Soc. B, (1970), pp. 278-281.
77. A. P. Altshuller, L. Rosenblum, "Dielectric properties of some alkylsilanes," J. Am. Chem. Soc., Vol. 77, No. 2, (1955), pp. 272-274.
78. V. A. Chetverikova, V. A. Kogan, G. I. Zelchan, M. G. Voronkov, O. A. Osipov, "Dipole moments of Si-substituted silatranes," Chem. Heterocycl. Compd., Vol. 5, No. 3, (1969), pp. 332-334.
79. J. M. Bellama, R. S. Evans, J. E. Huheey, "Bond moments, molecular moments, electronegativity, and the dipole moment of methylsilane," J. Am. Chem. Soc., Vol. 95, No. 22, (1973), pp 7242-7244.
80. L. K. Yuldasheva, R. P. Arshinova, Y. Y. Samitov, Y. P. Romadan, M. G. Voronkov, "Steric structure of 5-substituted 2,2-dimethyl-1,3,2-dioxasilanes," Russ. Chem. Bull., Vol. 23, No. 2, (1974), pp. 294-299.
81. M. G. Voronkov, T. N. Aksamentova, V. B. Modonov, L. I. Gubanova, Y. L. Frolov, V. M. Dyakov, "Dipole moments and molecular structure of (aroyloxymethyl)-trifluorosilanes and methyl(aroyloxymethyl)fluorosilanes," Russ. Chem. Bull., Vol. 33, No. 3, (1984), pp. 635-637.
82. L. K. Yuldasheva, R. P. Arshinova, S. G. Vulfson, "Dipole moments of the bonds and the unshared electron pair in sulfites and sulfoxides," Russ. Chem. Bull., Vol. 18, No. 3, (1969), pp. 495-498.
83. Y. Y. Borovikov, V. V. Pirozhenko, "Scale of additive group and bond dipole moments and dipole moments of lone pairs," Theor. Exp. Chem., Vol. 17, No. 2, (1981), pp. 136-146.
84. A. Borba, A. Gómez-Zavaglia, P. N. N. L. Simões, R. Fausto, "Matrix-isolation FT-IR spectra and theoretical study of dimethyl sulfate," Spectrochim. Acta Part A, Vol. 61, (2005), pp. 1461-1470.
85. E. N. Klimovitskii, L. K. Yuldasheva, A. N. Vereshchagin, G. N. Sergeeva, S. G. Vulfson, B. A. Arbuzov, "Sulfate group polarization and polarizability and the conformations of the dimethyl sulfates," Russ. Chem. Bull., Vol. 26, No. 1, (1977), pp. 83-85.
86. G. Wood, J. M. McIntosh, M. H. Miskow, "Conformational analysis of trimethylene sulfites. The vital importance of vicinal unshared electron pairs," Can. J. Chem., Vol. 49, (1971), pp. 1202-1208.
87. B. J. Lindberg, K. Hamrin, G. Johansson, U. Gelius, A. Fahlman, C. Nordling, K. Siegbahn, "Molecular spectroscopy by means of ESCA," Phys. Scr., Vol. 1, (1970), pp. 286-298.
88. D. Eisenberg, W. Kauzmann, *The Structure and Properties of Water*, Oxford University Press, London, (1969), p. 74.
89. K. Ichikawa, Y. Kameda, T. Yamaguchi, H. Wakita and M. Misawa, Neutron diffraction investigation of the intramolecular structure of a water molecule in the liquid phase at high temperatures, Mol. Phys. Vol. 73, (1991), pp. 79-86.
90. D. Eisenberg, W. Kauzmann, *The Structure and Properties of Water*, Oxford University Press, London, (1969), p. 85.
91. D. R. Lide, *CRC Handbook of Chemistry and Physics*, 86th Edition, CRC Press, Taylor & Francis, Boca Raton, (2005-6), p. 4-151.
92. D. Eisenberg, W. Kauzmann, *The Structure and Properties of Water*, Oxford University Press, London, (1969), p. 83.
93. H. A. Haus, J. R. Melcher, *Electromagnetic Fields and Energy*, Department of Electrical Engineering and Computer Science, Massachusetts Institute of Technology, (1985), Sec. 6.3.
94. D. R. Lide, *CRC Handbook of Chemistry and Physics*, 79th Edition, CRC Press, Boca Raton, Florida, (1998-9), p. 6.2.
95. R. L. DeKock, H. B. Gray, *Chemical Structure and Bonding*, The Benjamin/Cummings Publishing Company, Menlo Park, CA, (1980), pp. 436-439.
96. G. L. Miessler, D. A. Tarr, *Inorganic Chemistry*, Third Edition, Pearson Prentice Hall, Upper Saddle River, New Jersey, (2004), pp. 69-71.
97. D. D. Nelson, Jr., G. T. Fraser, W. Klemperer, "Does ammonia hydrogen bond?," Science, Vol. 238, (1987), pp. 1670-674.
98. R. J. Fessenden, J. S. Fessenden, *Organic Chemistry*, Willard Grant Press. Boston, Massachusetts, (1979), p. 25.
99. P. F. Harris, Z. Lheng, K. Suenaga, "Imaging the atomic structure of activated carbon," J. Phys.: Condens. Matter, Vol. 20, (2008), pp. 362201-362205.
100. R. J. Fessenden, J. S. Fessenden, *Organic Chemistry*, Willard Grant Press. Boston, Massachusetts, (1979), pp. 744-745.

101. R. Zacharia, H. Ulbricht, T. Hertel, "Interlayer cohesive energy of graphite from thermal desorption of polyaromatic hydrocarbons," Phys. Rev. B, Vol. 69, Issue 15, (2004), pp. 155406-155412.
102. D. G. Hurst, D. G. Henshaw, "Atomic distribution in liquid helium by neutron diffraction," Phys. Rev., Vol. 100, No. 4, (1955), pp. 994-1002.
103. D. R. Lide, *CRC Handbook of Chemistry and Physics*, 86th Edition, CRC Press, Taylor & Francis, Boca Raton, (2005-6), pp. 6-119 to 9-120.
104. K. W. Schwarz, R. W. Stark, Phys. Rev. Lett., Vol. 22, No. 24, (1969), pp. 1278-1280.
105. C. J. Pethick, H. Smith, *Bose-Einstein Condensation in Dilute Gases*, Second Edition, Cambridge University Press, Cambridge, UK, (2008), p. 8.
106. D. G. Henshaw, A. D. B. Woods, Phys. Rev. Lett., Vol. 121, (1961), p. 1266.
107. G. Baym, R. G. Barrera, C. J. Pethick, Phys. Rev. Letters, Vol. 22, No. 1, (1969), pp. 20-23.
108. F. London, *Superfluids* (Dover Publications, New York, 1964), Vol. III.
109. C. Pethick, H. Smith, *Bose-Einstein Condensation in Dilute Gases*, Cambridge University Press, Cambridge, (2008).
110. C. J. Pethick, H. Smith, *Bose-Einstein Condensation in Dilute Gases*, Second Edition, Cambridge University Press, Cambridge, UK, (2008), pp. 1-40.
111. R. Wynar, R. S. Freeland, D. J. Han, C. Ryu, and D. J. Heinzen, "Molecules in a Bose-Einstein condensate," Science, Vol. 287, February, 11, (2000), pp. 1016-1019.
112. J. A. Dean, *Lange's Handbook of Chemistry*, Fifteenth Edition, McGraw-Hill Professional, New York, (1998).
113. G. L. Pollack, "The solid state of rare gases," Rev. Mod. Phys., Vol. 36, (1964), pp. 748-791.
114. D. G. Henshaw, "Atomic distribution in liquid and solid neon and solid argon by neutron diffraction," Phys. Rev., Vol. 111, No. 6, (1958), pp. 1470-1475.
115. M. L. Klein, J. A. Venables, *Rare Gas Solids*, Volume 1, Academic Press, New York, (1977), p. 242.
116. J. Sugar and A. Musgrove, "Energy levels of krypton, Kr I through Kr XXXVI," J. Phys. Chem. Ref. Data, Vol. 20, No. 5, (1991), pp. 859-915. Available at http://www.nist.gov/srd/PDFfiles/jpcrd422.pdf.
117. J. Sugar and A. Musgrove, "Energy levels of krypton, Kr I through Kr XXXVI," J. Phys. Chem. Ref. Data, Vol. 20, No. 5, (1991), pp. 859-915. Available at http://www.nist.gov/srd/PDFfiles/jpcrd422.pdf.
118. E. B. Saloman, "Energy Levels and Observed Spectral Lines of Krypton, Kr I through Kr XXXVI," J. Phys. Chem. Ref. Data, Vol. 36, No. 1, (2007), pp. 215-386.
119. http://link.aip.org/link/?JPCRBU/36/215/1.
120. M. L. Klein, J. A. Venables, *Rare Gas Solids*, Volume 1, Academic Press, New York, (1977), p. 245.
121. E. B. Saloman, "Energy levels and observed spectral lines of xenon, Xe I through Xe LIV," J. Phys. Chem. Ref. Data, Vol. 33, No. 3, (2004), pp. 765-921. Available at http://www.nist.gov/srd/PDFfiles/jpcrd661.pdf.
122. E. B. Saloman, "Energy levels and observed spectral lines of xenon, Xe I through Xe LIV," J. Phys. Chem. Ref. Data, Vol. 33, No. 3, (2004), pp. 765-921. Available at http://www.nist.gov/srd/PDFfiles/jpcrd661.pdf.
123. M. L. Klein, J. A. Venables, *Rare Gas Solids*, Volume 1, Academic Press, New York, (1977), p. 250.
124. L. N. Fletcher, M. Gustafsson, G. S. Orton, "Hydrogen dimers in giant-planet infrared spectra", December 11, 2017, pp. 1-13, https://arxiv.org/pdf/1712.02813.pdf.
125. M. Gustafsson, "Hydrogen dimer features in low temperature collision-induced spectra," XXIII International Conference on Spectral Line Shapes, IOP Conf. Series: Journal of Physics: Conf. Series 810 (2017) 012017, doi:10.1088/1742-6596/810/1/012017, http://iopscience.iop.org/article/10.1088/1742-6596/810/1/012017/pdf.
126. A. R. W. McKellar," Infrared spectra of hydrogen dimers", J. Chem. Phys., Vol. 92, (1990), pp. 3261–3277.
127. https://en.wikipedia.org/wiki/Solid_hydrogen
128. https://www.nuclear-power.net/hydrogen-specific-heat-latent-heat-vaporization-fusion/.
129. D. A. McQuarrie, Quantum Chemistry, University Science Books, Mill Valley, CA, (1983), pp. 238-241.
130. J. D. Jackson, *Classical Electrodynamics*, Second Edition, John Wiley & Sons, New York, (1975), pp. 739-752.
131. W. R.. Hagen, R. L. Mills, " Distinguishing Electron Paramagnetic Resonance signature of molecular hydrino ", (2020), https://assets.researchsquare.com/files/rs-144403/v1_stamped.pdf.
132. R. L. Mills, P. Ray, "A Comprehensive Study of Spectra of the Bound-Free Hyperfine Levels of Novel Hydride Ion $H^-(1/2)$, Hydrogen, Nitrogen, and Air", Int. J. Hydrogen Energy, Vol. 28, No. 8, (2003), pp. 825-871.
133. R. Mills, W. Good, P. Jansson, J. He, "Stationary Inverted Lyman Populations and Free-Free and Bound-Free Emission of Lower-Energy State Hydride Ion formed by and Exothermic Catalytic Reaction of Atomic Hydrogen and Certain Group I Catalysts," Cent. Eur. J. Phys., Vol. 8, (2010), 7–16, doi: 10.2478/s11534-009-0052-6.
134. R. L. Mills, P. Ray, "Stationary Inverted Lyman Population and a Very Stable Novel Hydride Formed by a Catalytic Reaction of Atomic Hydrogen and Certain Catalysts," J. Opt. Mat., 27, (2004), 181–186.
135. R. L. Mills, P. C. Ray, R. M. Mayo, M. Nansteel, W. Good, P. Jansson, B. Dhandapani, J. He, "Hydrogen Plasmas Generated Using Certain Group I Catalysts Show Stationary Inverted Lyman Populations and Free-Free and Bound-Free Emission of Lower-Energy State Hydride," Res. J. Chem Env., Vol. 12(2), (2008), 42–72.
136. R. Mills, Z. Dong, J. Jenkins, R. Gandhi, N. S. Mehta, S. Mhatre, P. Sharma, "Hydrino states of hydrogen", https://brilliantlightpower.com/pdf/Hydrino_States_of_Hydrogen.pdf.

137. L. M. Hobbs, D. G. York, T. P. Snow, T. Oka, J. A. Thorburn, M. Bishof, S. D. Friedman, B. J. McCall, B. Rachford, P. Sonnentrucker, D. E. Welty, A Catalog of Diffuse Interstellar Bands in the Spectrum of HD 204827", Astrophysical Journal, Vol. 680, No. 2, (2008), pp. 1256-1270, http://dibdata.org/HD204827.pdf, https://iopscience.iop.org/article/10.1086/587930/pdf.

138. G. Danby, D. R. Flower, "Theoretical studies of van der Waals molecules: the H_2-H_2 dimer", J. Phys. B: At. Mol. Phys., Vol. 16, (1983), pp. 3411-3422.
139. A. Fernández-Ramos, J. A. Miller, S. J. Klipperstein, D. G. Truhlar, "Modeling the Kinetics of Bimolecular Reactions," Chem. Rev., Vol. 106, (2006), pp.4518-4584.
140. S. C. Tucker, D. G. Truhlar, "Ab initio calculations of the transition-state geometry and vibrational frequencies of the SN2 reaction of chloride with chloromethane," J. Phys. Chem, Vol. 93, No. 25, (1989), pp. 8138-8142.
141. D. R. Lide, *CRC Handbook of Chemistry and Physics*, 86th Edition, CRC Press, Taylor & Francis, Boca Raton, (2005-6), p. 10-156.
142. S. C. Tucker, D. G. Truhlar, "A six-body potential energy surface for the SN2 reaction Cl^- (g) + CH_3Cl (g) and a variational transition-state-theory calculation of the rate constant," J. Am. Chem. Soc., Vol. 112, No. 9, (1990), pp. 3338-3347.
143. S. E. Barlow, J. M. Van Doren, V. M. Bierbaum, "The gas phase displacement reaction of chloride ion with methyl chloride as a function of kinetic energy," J. Am. Chem. Soc., Vol. 110, No. 21, (1988), pp. 7240-7242.
144. "Cl_3^-," *NIST Chemistry Handbook.* http://webbook.nist.gov/.
145. "Simulation of the gas phase displacement reaction of chloride ion with methyl chloride," at http://www.brilliantlightpower.com/, at http://www.brilliantlightpower.com/molecular-physics/.

Chapter 17

NATURE OF THE SOLID MOLECULAR BOND OF THE THREE ALLOTROPES OF CARBON

GENERAL CONSIDERATIONS OF THE SOLID MOLECULAR BOND

The solid molecular bond of a material comprising an arbitrary number of atoms can be solved using similar principles and procedures as those used to solve organic molecules of arbitrary length. Molecular solids are also comprised of functional groups. Depending on the material, exemplary groups are $C-C$, $C=C$, $C-O$, $C-N$, $C-S$, and others given in the Organic Molecular Functional Groups and Molecules section. The solutions of these functional groups or any others corresponding to the particular solid can be conveniently obtained by using generalized forms of the geometrical and energy equations given in the Derivation of the General Geometrical and Energy Equations of Organic Chemistry section. The appropriate functional groups with their geometrical parameters and energies can be added as a linear sum to give the solution of any molecular solid.

DIAMOND

It is demonstrated in this Diamond section as well as the Fullerene (C_{60}) and Graphite sections, that very complex macromolecules can be simply solved from the groups at each vertex carbon atom of the structure. Specifically, for fullerene a $C=C$ group is bound to two $C-C$ bonds at each vertex carbon atom of C_{60}. The solution of the macromolecule is given by superposition of the geometrical and energy parameters of the corresponding two groups. In graphite, each sheet of joined hexagons can be constructed with a $C=C$ group bound to two $C-C$ bonds at each vertex carbon atom that hybridize to an aromatic-like functional group, $C \overset{8/3e}{=} C$, with $\frac{8}{3}$ electron-number per bond compared to the pure aromatic functional group, $C \overset{3e}{=} C$, with 3 electron-number per bond as given in the Aromatics section. Similarly, diamond comprising, in principle, an infinite network of carbons can be solved using the functional group solutions where the task is also simple since diamond has only one functional group, the diamond $C-C$ functional group.

The diamond $C-C$ bonds are all equivalent, and each $C-C$ bond can be considered bound to a t-butyl group at the corresponding vertex carbon. Thus, the parameters of the diamond $C-C$ functional group are equivalent to those of the t-butyl $C-C$ group of branched alkanes given in the Branched Alkanes section. Based on symmetry, the parameter R in Eqs. (15.56) and (15.61) is the semimajor axis a, and the vibrational energy in the $\bar{E}_{osc}$ term is that of diamond. Also, the $C2sp^3$ HO magnetic energy E_{mag} given by Eq. (15.67) was subtracted for each t-butyl group of alkyl fluorides, alkyl chlorides, alkyl iodides, thiols, sulfides, disulfides, and nitroalkanes as given in the corresponding sections of Chapter 15 due to a set of unpaired electrons being created by bond breakage. Since each $C-C$ group of diamond bonds with a t-butyl group at each vertex carbon, c_3 of Eq. (15.65) is one, and E_{mag} is given by Eq. (15.67).

The symbol of the functional group of diamond is given in Table 17.1. The geometrical (Eqs. (15.1-15.5) and (15.51)) parameters of diamond are given in Table 17.2. The lattice parameter a_l was calculated from the bond distance using the law of cosines:

$$s_1^2 + s_2^2 - 2s_1 s_2 \text{cosine}\theta = s_3^2 \tag{17.1}$$

With the bond angle $\theta_{\angle CCC} = 109.5°$ [1] and $s_1 = s_2 = 2c'_{C-C}$, the internuclear distance of the $C-C$ bond, $s_3 = 2c'_{C_t-C_t}$, the internuclear distance of the two terminal C atoms is given by:

$$2c'_{C_t-C_t} = \sqrt{2\left(2c'_{C-C}\right)^2\left(1-\text{cosine}\left(109.5°\right)\right)} \tag{17.2}$$

Two times the distance $2c'_{C_t-C_t}$ is the hypotenuse of the isosceles triangle having equivalent sides of length equal to the lattice parameter a_l. Using Eq. (17.2) and $2c'_{C-C} = 1.53635\ \text{Å}$ from Table 17.2, the lattice parameter a_l for the cubic diamond structure is given by:

$$a_l = \frac{2\left(2c'_{C_t-C_t}\right)}{\sqrt{2}} = \sqrt{2}\sqrt{2\left(2c'_{C-C}\right)^2\left(1-\text{cosine}\left(109.5°\right)\right)} = 3.54867\ \text{Å} \tag{17.3}$$

The intercept (Eqs. (15.80-15.87)) and energy (Eqs. (15.6-15.11) and (15.17-15.65)) parameters of diamond are given in Tables 17.2, 17.3, and 17.4, respectively. The total energy of diamond given in Table 17.5 was calculated as the sum over the integer multiple of each $E_{D\,(Group)}$ of Table 17.4 corresponding to functional-group composition of the molecular solid. The experimental $C-C$ bond energy of diamond, $E_{D_{\exp}}(C-C)$ at 298 K, is given by the difference between the enthalpy of formation of gaseous carbon atoms from graphite $\left(\Delta H_f\left(C_{graphite}\left(gas\right)\right)\right)$ and the heat of formation of diamond $\left(\Delta H_f\left(C(diamond)\right)\right)$ wherein graphite has a defined heat of formation of zero $\left(\Delta H_f\left(C\left(graphite\right)=0\right)\right)$:

$$E_{D_{\exp}}(C-C) = \frac{1}{2}\left[\Delta H_f\left(C_{graphite}\left(gas\right)\right) - \Delta H_f\left(C(diamond)\right)\right] \tag{17.4}$$

where the heats of formation of atomic carbon and diamond are [2]:

$$\Delta H_f\left(C_{graphite}\left(gas\right)\right) = 716.68\ kJ/mole\ \left(7.42774\ eV/atom\right) \tag{17.5}$$

$$\Delta H_f\left(C(diamond)\right) = 1.9\ kJ/mole\ \left(0.01969\ eV/atom\right) \tag{17.6}$$

Using Eqs. (17.4-17.6), $E_{D_{\exp}}(C-C)$ is:

$$E_{D_{\exp}}(C-C) = \frac{1}{2}\left[7.42774\ eV - 0.01969\ eV\right] = 3.704\ eV \tag{17.7}$$

where the factor of one half corresponds to the ratio of two electrons per bond and four electrons per carbon atom. The bond angle parameters of diamond determined using Eqs. (15.88-15.117) are given in Table 17.6. The structure of diamond is shown in Figure 17.1.

Figure 17.1. (A-B) The structure of diamond.

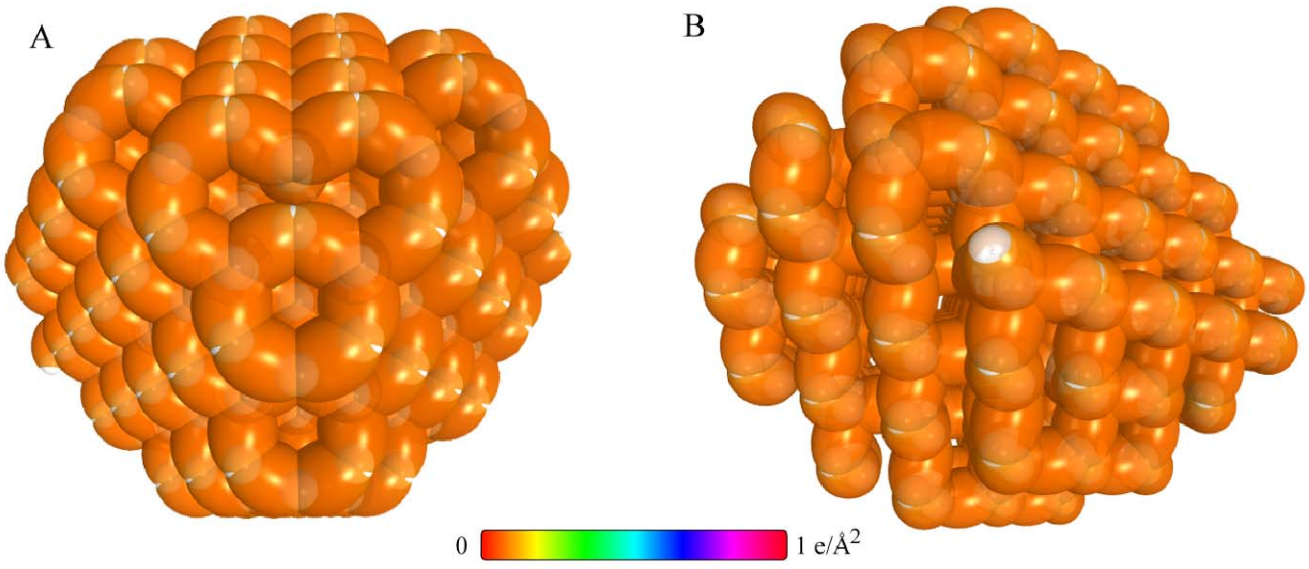

Table 17.1. The symbols of the functional group of diamond.

Functional Group	Group Symbol
CC bond (diamond-*C*)	$C-C$

Table 17.2. The geometrical bond parameters of diamond and experimental values [1, 3].

Parameter	$C-C$ Group
$a\ (a_0)$	2.10725
$c'\ (a_0)$	1.45164
Bond Length $2c'\ (\text{Å})$	1.53635
Exp. Bond Length (Å)	1.54428
$b, c\ (a_0)$	1.52750
e	0.68888
Lattice Parameter $a_l\ (\text{Å})$	3.54867
Exp. Lattice Parameter $a_l\ (\text{Å})$	3.5670

Table 17.3. The MO to HO intercept geometrical bond parameters of diamond. E_T is E_T (*atom - atom msp³.AO*).

Bond	Atom	E_T (eV) Bond 1	E_T (eV) Bond 2	E_T (eV) Bond 3	E_T (eV) Bond 4	Final Total Energy $C2sp^3$ (eV)	$r_{initial}$ (a_0)	r_{final} (a_0)	$E_{Coulomb}(C2sp^3)$ (eV) Final	$E(C2sp^3)$ (eV) Final	θ' $(^\circ)$	θ_1 $(^\circ)$	θ_2 $(^\circ)$	d_1 (a_0)	d_2 (a_0)
$C-C$	C	-0.72457	-0.72457	-0.72457	-0.72457	-154.51399	0.91771	0.76765	-17.92866	-17.73779	50.04	129.96	22.66	1.94462	0.49298

Table 17.4. The energy parameters (eV) of the functional group of diamond.

Parameters	$C-C$ Group
n_1	1
n_2	0
n_3	0
C_1	0.5
C_2	1
c_1	1
c_2	0.91771
c_3	1
c_4	2
c_5	0
C_{1o}	0.5
C_{2o}	1
$V_e\ (eV)$	-29.10112
$V_p\ (eV)$	9.37273
$T\ (eV)$	6.90500
$V_m\ (eV)$	-3.45250
$E_{(AO/HO)}\ (eV)$	-15.35946
$\Delta E_{H_2MO(AO/HO)}\ (eV)$	0
$E_{T(AO/HO)}\ (eV)$	-15.35946
$E_{T(H_2MO)}\ (eV)$	-31.63535
$E_T\left(atom-atom, msp^3.AO\right)\ (eV)$	-1.44915
$E_{T(MO)}\ (eV)$	-33.08452
$\omega\ \left(10^{15}\ rad/s\right)$	9.55643
$E_K\ (eV)$	6.29021
$\bar{E}_D\ (eV)$	-0.16416
$\bar{E}_{Kvib}\ (eV)$	0.16515 [4]
$\bar{E}_{osc}\ (eV)$	-0.08158
$E_{mag}\ (eV)$	0.14803
$E_{T(Group)}\ (eV)$	-33.16610
$E_{initial(c_4\ AO/HO)}\ (eV)$	-14.63489
$E_{initial(c_5\ AO/HO)}\ (eV)$	0
$E_{D(Group)}\ (eV)$	3.74829

Table 17.5. The total bond energy of diamond calculated using the functional group composition and the energy of Table 17.4 compared to the experimental value [1-2].

Formula	Name	$C-C$	Calculated Total Bond Energy (eV)	Experimental Total Bond Energy (eV)	Relative Error
C_n	Diamond	1	3.74829	3.704	-0.01

Table 17.6. The bond angle parameters of diamond and experimental values [1]. In the calculation of θ_v, the parameters from the preceding angle were used. E_T is E_T (*atom - atom msp³.AO*). The law of cosines was used to calculate the angle.

Atoms of Angle	2c' Bond 1 (a_0)	2c' Bond 2 (a_0)	2c' Terminal Atoms (a_0)	$E_{Coulombic}$ Atom 1	Atom 1 Hybridization Designation (Table 15.3.A)	$E_{Coulombic}$ Atom 2	Atom 2 Hybridization Designation (Table 15.3.A)	c_2 Atom 1	c_2 Atom 2	C_1	C_2	c_1	c_2'	E_T (eV)	θ_v (°)	θ_1 (°)	θ_2 (°)	Cal. θ (°)	Exp. θ (°)
$\angle CCC$ (aromatic)	2.62936	2.62936	4.5585	-17.17218	38	-17.17218	38	0.79232	0.79232	1	1	1	0.79232	-1.85836				120.19	120 [12-14] (benzene)
$\angle CCH$ $\angle CCO$ (aromatic)																120.19		119.91	120 [12-14] (benzene)
$\angle C_aO_bH$	2.63431	1.83616	3.6405	-14.82575	1	-14.82575	1	1	0.91771	0.75	1	0.75	0.91771	0				107.71	
$\angle C_bC_a(O)$	2.82796	2.27954	4.4721	-17.17218	38	-13.61806	O	0.79232	0.85395 (Eq. (15.114))	1	1	1	0.82313	-1.65376				121.86	122 [2] (benzoic acid)
$\angle C_bC_aO$	2.82796	2.63431	4.6690	-16.40067	20	-13.61806	O	0.82959	0.85395 (Eq. (15.114))	1	1	1	0.84177	-1.65376				117.43	118 [2] (benzoic acid)
$\angle(O)C_aO$	2.27954	2.63431	4.3818	-16.17521 (O)	13	-15.75493 O	7	0.84115	0.86359	1	1	1	0.85237	-1.44915				126.03	122 [2] (benzoic acid)
$\angle C_fC_e(O)$	2.86175	2.27954	4.5826	-16.68411	25	-13.61806	O	0.81549	0.85395 (Eq. (15.133))	1	1	1	0.83472	-1.65376				125.70	126.6 [1] (acetic acid)
$\angle C_fC_eO$	2.86175	2.63431	4.4944	-15.75493	7	-13.61806	O	0.86359	0.85395 (Eq. (15.133))	1	1	1	0.85877	-1.44915				109.65	110.6 [1] (acetic acid)
$\angle OC_eO$	2.27954	2.63431	4.3818	-16.17521 (O)	13	-15.75493 O	7	0.84115	0.86359	1	1	1	0.85237	-1.44915				126.03	
$\angle C_dOC_e$	2.59399	2.63431	4.3589	-17.27448 C_d	41	-18.03358 C_e	56	0.78762	0.75447	1	1	1	0.77105	-1.85836				112.96	114 [1] (methyl formate)
Methyl $\angle HC_fH$	2.09711	2.09711	3.4252	-15.75493	7	H	H	0.86359	1	1	1	0.75	1.15796	0				109.50	

FULLERENE (C_{60})

C_{60} comprises 60 equivalent carbon atoms that are bound as 60 single bonds and 30 double bonds in the geometric form of a truncated icosahedron: twelve pentagons and twenty hexagons joined such that no two pentagons share an edge. To achieve this minimum energy structure each equivalent carbon atom serves as a vertex incident with one double and two single bonds. Each type of bond serves as a functional group which has aromatic character. The aromatic bond is uniquely stable and requires the sharing of the electrons of multiple H_2-type MOs. The results of the derivation of the parameters of the benzene molecule given in the Benzene Molecule (C_6H_6) section was generalized to any aromatic functional group of aromatic and heterocyclic compounds in the Aromatic and Heterocyclic Compounds section. Ethylene serves as a basis element for the $C\overset{3e}{=}C$ bonding of the aromatic bond wherein each of the $C\overset{3e}{=}C$ aromatic bonds comprises $(0.75)(4)=3$ electrons according to Eq. (15.161) wherein C_2 of Eq. (15.51) for the aromatic $C\overset{3e}{=}C$-bond MO given by Eq. (15.162) is $C_2\left(aromaticC2sp^3HO\right)=c_2\left(aromaticC2sp^3HO\right)=0.85252$ and $E_T\left(atom-atom,msp^3.AO\right)=-2.26759\ eV$. In C_{60}, the minimum energy structure with equivalent carbon atoms wherein each carbon forms bonds with three other such carbons requires a redistribution of charge within an aromatic system of bonds. The $C=C$ functional group of C_{60} comprises the aromatic bond with the exception that it comprises four electrons. Thus, $E_T\,(Group)$ and $E_D\,(Group)$ are given by Eqs. (15.165) and (15.166), respectively, with $f_1=1$, $c_4=4$, and $\bar{E}_{Kvib}\ (eV)$ is that of C_{60}.

In addition to the $C=C$ bond, each vertex carbon atom of C_{60} is bound to two $C-C$ bonds that substitute for the aromatic $C\overset{3e}{=}C$ and $C-H$ bonds. As in the case of the $C-C$-bond MO of naphthalene, to match energies within the MO that bridges single and double-bond MOs, $E\left(AO/HO\right)$ and $\Delta E_{H_2MO}\left(AO/HO\right)$ in Eq. (15.51) are $-14.63489\ eV$ and $-2.26759\ eV$, respectively.

To meet the equipotential condition of the union of the $C2sp^3$ HOs of the $C-C$ single bond bridging double bonds, the parameters c_1, C_2, and C_{2o} of Eq. (15.51) are one for the $C-C$ group, C_{1o} and C_1 are 0.5, and c_2 given by Eq. (13.430) is $c_2\left(C2sp^3HO\right)=0.91771$. To match the energies of the functional groups with the electron-density shift to the double bond, $E_T\left(atom-atom,msp^3.AO\right)$ of each of the equivalent $C-C$-bond MOs in Eq. (15.61) due to the charge donation from the C atoms to the MO can be considered a linear combination of that of $C-C$-bond MO of toluene, $-1.13379\ eV$ and that of the aromatic $C-H$-bond MO, $\frac{-1.13379\ eV}{2}$. Thus, $E_T\left(atom-atom,msp^3.AO\right)$ of each $C-C$-bond MO of C_{60} is $\frac{-1.13379\ eV+0.5\left(-1.13379\ eV\right)}{2}=0.75\left(-1.13379\ eV\right)=-0.85034\ eV$. As in the case of the aromatic $C-H$ bond, $c_3=1$ in Eq. (15.65) with E_{mag} given by Eq. (15.67), and $\bar{E}_{Kvib}\ (eV)$ is that of C_{60}.

The symbols of the functional groups of C_{60} are given in Table 17.7. The geometrical (Eqs. (15.1-15.5) and (15.51)), intercept (Eqs. (15.80-15.87)), and energy (Eqs. (15.6-15.11), (15.17-15.65), and (15.165-15.166)) parameters of C_{60} are given in Tables 17.8, 17.9, and 17.10, respectively. The total energy of C_{60} given in Table 17.11 was calculated as the sum over the integer multiple of each $E_D\,(Group)$ of Table 17.10 corresponding to functional-group composition of the molecule. The bond angle parameters of C_{60} determined using Eqs. (15.87-15.117) are given in Table 17.12. The structure of C_{60} is shown in Figures 17.2A and B. The fullerene vertex-atom group comprising a double and two single bonds can serve as a basis element to form other higher-order fullerene-type macromolecules, hyperfullerenes, and complex hybrid conjugated carbon and aromatic structures comprising a mixture of elements from the group of fullerene, graphitic, and diamond carbon described in the corresponding sections.

Figure 17.2. C_{60} MO comprising a hollow cage of sixty carbon atoms bound with the linear combination of sixty sets of $C-C$-bond MOs bridged by 30 sets of $C=C$-bond MOs. A $C=C$ group is bound to two $C-C$ groups at each vertex carbon atom of C_{60}. Color scale, translucent pentagonal view (A), and hexagonal view (B), of the charge-density of the C_{60}-bond MO with each $C2sp^3$ HO shown transparently. For each $C-C$ and $C=C$ bond, the ellipsoidal surface of the H_2-type ellipsoidal MO that transitions to the $C2sp^3$ HO, the $C2sp^3$ HO shell, inner most $C1s$ shell, and the nuclei (red, not to scale), are shown.

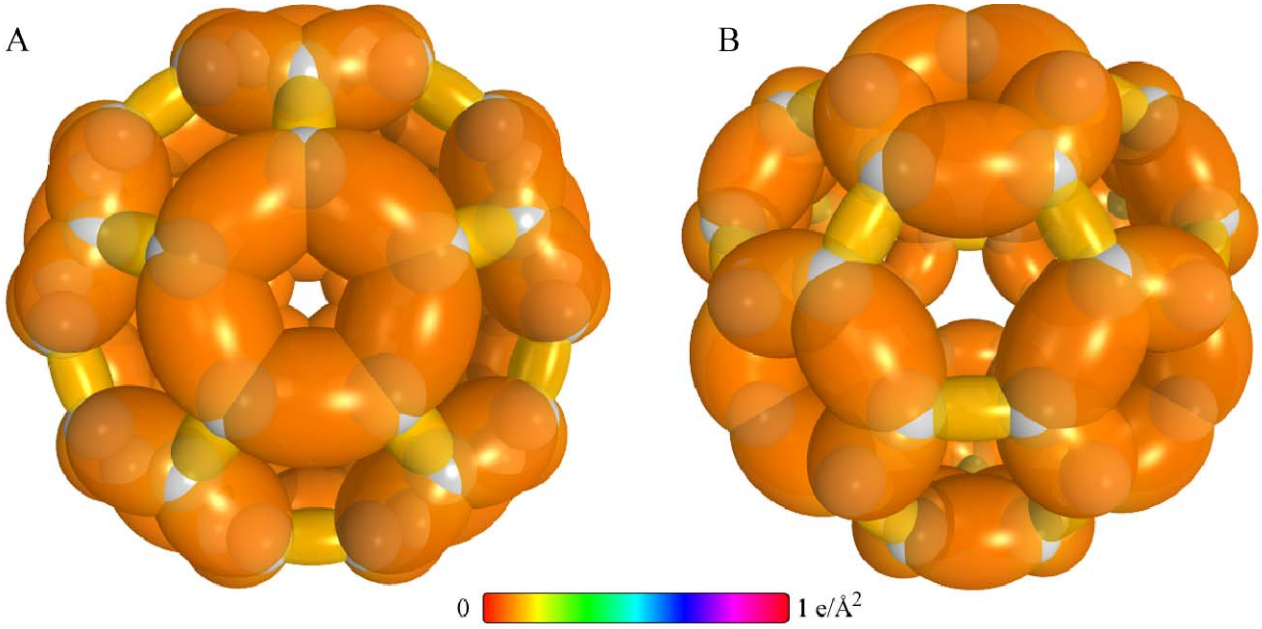

Table 17.7. The symbols of functional groups of C_{60}.

Functional Group	Group Symbol
$C=C$ (aromatic-type)	$C=C$
$C-C$ (bound to $C=C$ aromatic-type)	$C-C$

Table 17.8. The geometrical bond parameters of C_{60} and experimental values [5].

Parameter	$C=C$ Group	$C-C$ Group
$a\ (a_0)$	1.47348	1.88599
$c'\ (a_0)$	1.31468	1.37331
Bond Length $2c'\ (Å)$	1.39140	1.45345
Exp. Bond Length $(Å)$	1.391 (C_{60})	1.455 (C_{60})
$b,c\ (a_0)$	0.66540	1.29266
e	0.89223	0.72817

Table 17.9. The MO to HO intercept geometrical bond parameters of C_{60}. E_T is E_T (*atom - atom msp³.AO*).

Bond	Atom	E_T (eV) Bond 1	E_T (eV) Bond 2	E_T (eV) Bond 3	E_T (eV) Bond 4	Final Total Energy $C2sp^3$ (eV)	$r_{initial}$ (a_0)	r_{final} (a_0)	$E_{Coulomb}(C2sp^3)$ (eV) Final	$E(C2sp^3)$ (eV) Final	θ' $(^\circ)$	θ_1 $(^\circ)$	θ_2 $(^\circ)$	d_1 (a_0)	d_2 (a_0)
$C=C$	C	-1.13380	-0.42517	-0.42517	0	-153.59983	0.91771	0.80939	-16.80989	-16.61903	134.81	45.19	59.66	0.74430	0.57038
$C-C$	C	-0.42517	-0.42517	-1.13380	0	-153.59983	0.91771	0.80939	-16.80989	-16.61903	82.53	97.47	38.38	1.47851	0.10519

Table 17.10. The energy parameters (eV) of functional groups of C_{60}.

Parameters	$C=C$ Group	$C-C$ Group
f_1	1	1
n_1	2	1
n_2	0	0
n_3	0	0
C_1	0.5	0.5
C_2	0.85252	1
c_1	1	1
c_2	0.85252	0.91771
c_3	0	1
c_4	4	2
c_5	0	0
C_{1o}	0.5	0.5
C_{2o}	0.85252	1
$V_e\ (eV)$	-101.12679	-33.63376
$V_p\ (eV)$	20.69825	9.90728
$T\ (eV)$	34.31559	8.91674
$V_m\ (eV)$	-17.15779	-4.45837
$E_{(AO/HO)}\ (eV)$	0	-14.63489
$\Delta E_{H_2MO(AO/HO)}\ (eV)$	0	-2.26759
$E_{T(AO/HO)}\ (eV)$	0	-12.36730
$E_{T(H_2MO)}\ (eV)$	-63.27075	-31.63541
$E_T\left(atom-atom,msp^3.AO\right)\ (eV)$	-2.26759	-0.85034
$E_{T(MO)}\ (eV)$	-65.53833	-32.48571
$\omega\ \left(10^{15}\ rad/s\right)$	49.7272	19.8904
$E_K\ (eV)$	32.73133	13.09221
$\bar{E}_D\ (eV)$	-0.35806	-0.23254
$\bar{E}_{Kvib}\ (eV)$	0.17727 [6]	0.14667 [6]
$\bar{E}_{osc}\ (eV)$	-0.26942	-0.15921
$E_{mag}\ (eV)$	0.14803	0.14803
$E_{T(Group)}\ (eV)$	-66.07718	-32.49689
$E_{initial(c_4\ AO/HO)}\ (eV)$	-14.63489	-14.63489
$E_{initial(c_5\ AO/HO)}\ (eV)$	0	0
$E_{D(Group)}\ (eV)$	7.53763	3.22711

Table 17.11. The total bond energies of C_{60} calculated using the functional group composition and the energies of Table 17.10 compared to the experimental values [7].

Formula	Name	$C=C$	$C-C$	Calculated Total Bond Energy (eV)	Experimental Total Bond Energy (eV)	Relative Error
C_{60}	Fullerene	30	60	419.75539	419.73367	-0.00005

Table 17.12. The bond angle parameters of C_{60} and experimental values [8]. E_T is E_T (*atom - atom msp³.AO*). The law of cosines was used to calculate the angle.

Atoms of Angle	$2c'$ Bond 1 (a_0)	$2c'$ Bond 2 (a_0)	$2c'$ Terminal Atoms (a_0)	$E_{Coulombic}$ Atom 1	Atom 1 Hybridization Designation (Table 15.3.A)	$E_{Coulombic}$ Atom 2	Atom 2 Hybridization Designation (Table 15.3.A)	c_2 Atom 1	c_2 Atom 2	C_1	C_2	c_1	c_2'	E_T (eV)	θ_v (°)	θ_1 (°)	θ_2 (°)	Cal. θ (°)	Exp. θ (°)
$\angle C=C-C$	2.62936	2.74663	4.6562	-17.03045	32	-17.03045	32	0.79891	0.79891	1	1	1	0.79891	-1.85836				120.00	120.00
$\angle C-C-C$	2.74663	2.74663	4.4441	-17.45563	47	-17.45563	47	0.77945	0.77945	1	1	1	0.77945	-1.85836				108.00	108.00

FULLERENE DIHEDRAL ANGLES

For C_{60}, the bonding at each vertex atom C_b comprises two single bonds, $C_a - C_b - C_a$, and a double bond, $C_b = C_c$. The dihedral angle $\theta_{\angle C=C/C-C-C}$ between the plane defined by the $C_a - C_b - C_a$ moiety and the line defined by the corresponding $C_b = C_c$ moiety is calculated using the results given in Table 17.12 and Eqs. (15.114-15.117). The distance d_1 along the bisector of $\theta_{\angle C_a - C_b - Ca}$ from C_b to the internuclear-distance line between one C_a and the other C_a, $2c'_{C_a - C_a}$, is given by:

$$d_1 = 2c'_{C_b - C_a} \cos\frac{\theta_{\angle C_a - C_b - Ca}}{2} = 2.74663a_0 \cos\frac{108.00°}{2} = 1.61443a_0 \tag{17.8}$$

where $2c'_{C_b - C_a}$ is the internuclear distance between C_b and C_a. The atoms C_a, C_a, and C_c define the base of a pyramid. Then, the pyramidal angle $\theta_{\angle C_a C_c C_a}$ can be solved from the internuclear distances between C_c and C_a, $2c'_{C_c - C_a}$, and between C_a and C_a, $2c'_{C_a - C_a}$, using the law of cosines (Eq. (15.115)).

$$\begin{aligned}\theta_{\angle C_a C_b C_a} &= \cos^{-1}\left(\frac{\left(2c'_{C_c - C_a}\right)^2 + \left(2c'_{C_c - C_a}\right)^2 - \left(2c'_{C_a - C_a}\right)^2}{2\left(2c'_{C_c - C_a}\right)\left(2c'_{C_c - C_a}\right)}\right) = \cos^{-1}\left(\frac{\left(4.65618\mathrm{a}_0\right)^2 + \left(4.65618\mathrm{a}_0\right)^2 - \left(4.4441\mathrm{a}_0\right)^2}{2\left(4.65618\mathrm{a}_0\right)\left(4.65618\mathrm{a}_0\right)}\right) \\ &= 57.01°\end{aligned} \tag{17.9}$$

Then, the distance d_2 along the bisector of $\theta_{\angle C_a C_c C_a}$ from C_c to the internuclear-distance line $2c'_{C_a - C_a}$, is given by:

$$d_2 = 2c'_{C_c - C_a} \cos\frac{\theta_{\angle C_a C_c C_a}}{2} = 4.65618a_0 \cos\frac{57.01°}{2} = 4.09176a_0 \tag{17.10}$$

The lengths d_1, d_2, and $2c'_{C_b = C_c}$ define a triangle wherein the angle between d_1 and the internuclear distance between C_b and C_c, $2c'_{C_b = C_c}$, is the dihedral angle $\theta_{\angle C=C/C-C-C}$ that can be solved using the law of cosines (Eq. (15.117)).

$$\begin{aligned}\theta_{\angle C=C/C-C-C} &= \cos^{-1}\left(\frac{d_1^2 + \left(2c'_{C_b = C_c}\right)^2 - d_2^2}{2d_1\left(2c'_{C_b = C_c}\right)}\right) = \cos^{-1}\left(\frac{\left(1.61443\mathrm{a}_0\right)^2 + \left(2.62936\mathrm{a}_0\right)^2 - \left(4.09176\mathrm{a}_0\right)^2}{2\left(1.61443\mathrm{a}_0\right)\left(2.62936\mathrm{a}_0\right)}\right) \\ &= 148.29°\end{aligned} \tag{17.11}$$

The dihedral angle for a truncated icosahedron corresponding to $\theta_{\angle C=C/C-C-C}$ is:

$$\theta_{\angle C=C/C-C-C} = 148.28° \tag{17.12}$$

The dihedral angle $\theta_{\angle C-C/C-C=C}$ between the plane defined by the $C_a - C_b = C_c$ moiety and the line defined by the corresponding $C_b - C_a$ moiety is calculated using the results given in Table 17.12 and Eqs. (15.118-15.127). The parameter d_1 is the distance from C_b to the internuclear-distance line between C_a and C_c, $2c'_{C_a - C_c}$. The angle between d_1 and the $C_b - C_a$ bond, $\theta_{\angle C_a C_b d_1}$, can be solved reiteratively using Eq. (15.121).

$$\begin{aligned}&\left(2c'_{C_b - C_a}\right)^2 + \left(\frac{\left(2c'_{C_b - C_a}\right)^2 - \left(2c'_{C_b - C_c}\right)^2}{2\left(\left(2c'_{C_b - C_a}\right)\mathrm{cosine}\,\theta_{\angle C_a C_b d_1} - \left(2c'_{C_b - C_c}\right)\mathrm{cosine}\left(\theta_{\angle C_a C_b C_c} - \theta_{\angle C_a C_b d_1}\right)\right)}\right)^2 \\ &-2\left(2c'_{C_b - C_a}\right)\left(\frac{\left(2c'_{C_b - C_a}\right)^2 - \left(2c'_{C_b - C_c}\right)^2}{2\left(\begin{array}{l}\left(2c'_{C_b - C_a}\right)\mathrm{cosine}\,\theta_{\angle C_a C_b d_1} \\ -\left(2c'_{C_b - C_c}\right)\mathrm{cosine}\left(\theta_{\angle C_a C_b C_c} - \theta_{\angle C_a C_b d_1}\right)\end{array}\right)}\right)\mathrm{cosine}\,\theta_{\angle C_a C_b d_1} \\ &-\left(\frac{2c'_{C_a - C_c}}{2}\right)^2 = 0 \\ &\left(2.74663\mathrm{a}_0\right)^2 + \left(\frac{\left(2.74663\mathrm{a}_0\right)^2 - \left(2.62936\mathrm{a}_0\right)^2}{2\left(\left(2.74663\mathrm{a}_0\right)\mathrm{cosine}\,\theta_{\angle C_a C_b d_1} - \left(2.62936\mathrm{a}_0\right)\mathrm{cosine}\left(120.00° - \theta_{\angle C_a C_b d_1}\right)\right)}\right)^2 \\ &-\left(\begin{array}{l}2\left(2.74663\mathrm{a}_0\right)\left(\frac{\left(2.74663\mathrm{a}_0\right)^2 - \left(2.62936\mathrm{a}_0\right)^2}{2\left(\begin{array}{l}\left(2.74663\mathrm{a}_0\right)\mathrm{cosine}\,\theta_{\angle C_a C_b d_1} \\ -\left(2.62936\mathrm{a}_0\right)\mathrm{cosine}\left(120.00° - \theta_{\angle C_a C_b d_1}\right)\end{array}\right)}\right)\mathrm{cosine}\,\theta_{\angle C_a C_b d_1}\end{array}\right) = 0 \\ &-\left(\frac{4.6562\mathrm{a}_0}{2}\right)^2\end{aligned} \tag{17.13}$$

The solution of Eq. (17.13) is:

$$\theta_{\angle C_aC_ad_2} = 57.810° \tag{17.14}$$

Eq. (17.14) can be substituted into Eq. (15.120) to give d_1:

$$\begin{aligned} d_1 &= \frac{\left(2c'_{C_b-C_a}\right)^2 - \left(2c'_{C_b-C_c}\right)^2}{2\left(\left(2c'_{C_b-C_a}\right)\text{cosine}\,\theta_{\angle C_aC_bd_1} - \left(2c'_{C_b-C_c}\right)\text{cosine}\left(\theta_{\angle C_aC_bC_c} - \theta_{\angle C_aC_bd_1}\right)\right)} \\ &= \frac{\left(2.74663\text{a}_0\right)^2 - \left(2.62936\text{a}_0\right)^2}{2\left(\left(2.74663\text{a}_0\right)\text{cosine}\left(57.810°\right) - \left(2.62936\text{a}_0\right)\text{cosine}\left(120.00° - 57.810°\right)\right)} = 1.33278\text{a}_0 \end{aligned} \tag{17.15}$$

The atoms C_a, C_a, and C_c define the base of a pyramid. Then, the pyramidal angle $\theta_{\angle C_aC_aC_c}$ can be solved from the internuclear distances between C_a and C_a, $2c'_{C_a-C_a}$, and between C_a and C_c, $2c'_{C_a-C_c}$, using the law of cosines (Eq. (15.115)).

$$\begin{aligned} \theta_{\angle C_aC_aC_c} &= \cos^{-1}\left(\frac{\left(2c'_{C_a-C_a}\right)^2 + \left(2c'_{C_a-C_c}\right)^2 - \left(2c'_{C_a-C_c}\right)^2}{2\left(2c'_{C_a-C_a}\right)\left(2c'_{C_a-C_c}\right)}\right) \\ &= \cos^{-1}\left(\frac{\left(4.44410\text{a}_0\right)^2 + \left(4.65618\text{a}_0\right)^2 - \left(4.65618\text{a}_0\right)^2}{2\left(4.44410\text{a}_0\right)\left(4.65618\text{a}_0\right)}\right) = 61.50° \end{aligned} \tag{17.16}$$

The parameter d_2 is the distance from C_a to the bisector of the internuclear-distance line between C_a and C_c, $2c'_{C_a-C_c}$. The angle between d_2 and the $C_a - C_a$ axis, $\theta_{\angle C_aC_ad_2}$, can be solved reiteratively using Eq. (15.126).

$$\begin{aligned} &\left(2c'_{C_a-C_a}\right)^2 + \left(\frac{\left(2c'_{C_a-C_a}\right)^2 - \left(2c'_{C_a-C_c}\right)^2}{2\left(\left(2c'_{C_a-C_a}\right)\text{cosine}\,\theta_{\angle C_aC_ad_2} - \left(2c'_{C_a-C_c}\right)\text{cosine}\left(\theta_{\angle C_aC_aC_c} - \theta_{\angle C_aC_ad_2}\right)\right)}\right)^2 \\ &-2\left(2c'_{C_b-C_a}\right)\left(\frac{\left(2c'_{C_a-C_a}\right)^2 - \left(2c'_{C_a-C_c}\right)^2}{2\left(\begin{array}{l}\left(2c'_{C_a-C_a}\right)\text{cosine}\,\theta_{\angle C_aC_ad_2} \\ -\left(2c'_{C_a-C_c}\right)\text{cosine}\left(\theta_{\angle C_aC_aC_c} - \theta_{\angle C_aC_ad_2}\right)\end{array}\right)}\right)\text{cosine}\,\theta_{\angle C_aC_bd_1} \\ &-\left(\frac{2c'_{C_a-C_c}}{2}\right)^2 = 0 \\ &\left(4.44410\text{a}_0\right)^2 + \left(\frac{\left(4.44410\text{a}_0\right)^2 - \left(4.65618\text{a}_0\right)^2}{2\left(\left(4.44410\text{a}_0\right)\text{cosine}\,\theta_{\angle C_aC_ad_2} - \left(4.65618\text{a}_0\right)\text{cosine}\left(61.50° - \theta_{\angle C_aC_ad_2}\right)\right)}\right)^2 \\ &-\left(2\left(4.44410\text{a}_0\right)\left(\frac{\left(4.44410\text{a}_0\right)^2 - \left(4.65618\text{a}_0\right)^2}{2\left(\begin{array}{l}\left(4.44410\text{a}_0\right)\text{cosine}\,\theta_{\angle C_aC_ad_2} \\ -\left(4.65618\text{a}_0\right)\text{cosine}\left(61.50° - \theta_{\angle C_aC_ad_2}\right)\end{array}\right)}\right)\text{cosine}\,\theta_{\angle C_aC_ad_2}\right) \\ &-\left(\frac{4.6562\text{a}_0}{2}\right)^2 = 0 \end{aligned} \tag{17.17}$$

The solution of Eq. (17.17) is:

$$\theta_{\angle C_aC_ad_2} = 31.542° \tag{17.18}$$

Eq. (17.18) can be substituted into Eq. (15.125) to give d_2:

$$\begin{aligned} d_2 &= \frac{\left(2c'_{C_a-C_a}\right)^2 - \left(2c'_{C_a-C_c}\right)^2}{2\left(\left(2c'_{C_a-C_a}\right)\text{cosine}\,\theta_{\angle C_aC_ad_2} - \left(2c'_{C_a-C_c}\right)\text{cosine}\left(\theta_{\angle C_aC_aC_c} - \theta_{\angle C_aC_ad_2}\right)\right)} \\ &= \frac{\left(4.44410\text{a}_0\right)^2 - \left(4.65618\text{a}_0\right)^2}{2\left(\left(4.44410\text{a}_0\right)\text{cosine}\left(31.542°\right) - \left(4.65618\text{a}_0\right)\text{cosine}\left(61.50° - 31.542°\right)\right)} = 3.91101\text{a}_0 \end{aligned} \tag{17.19}$$

The lengths d_1, d_2, and $2c'_{C_b-C_a}$ define a triangle wherein the angle between d_1 and the internuclear distance between C_b and C_a, $2c'_{C_b-C_a}$, is the dihedral angle $\theta_{\angle C-C/C-C=C}$ that can be solved using the law of cosines (Eq. (15.117)).

$$\theta_{\angle C-C/C-C=C} = \cos^{-1}\left(\frac{d_1^2+\left(2c'_{C_b-C_a}\right)^2-d_2^2}{2d_1\left(2c'_{C_b-C_a}\right)}\right) = \cos^{-1}\left(\frac{\left(1.33278a_0\right)^2+\left(2.74663a_0\right)^2-\left(3.91101a_0\right)^2}{2\left(1.33278a_0\right)\left(2.74663a_0\right)}\right)=144.71^\circ \tag{17.20}$$

The dihedral angle for a truncated icosahedron corresponding to $\theta_{\angle C-C/C-C=C}$ is:

$$\theta_{\angle C-C/C-C=C}=144.24^\circ \tag{17.21}$$

GRAPHENE AND GRAPHITE

In addition to fullerene and diamond described in the corresponding sections, graphite is the third allotrope of carbon. It comprises planar sheets of covalently bound carbon atoms arranged in hexagonal aromatic rings of a macromolecule of indefinite size. Each sheet comprises graphene. The sheets, in turn, are bound together by weaker intermolecular forces. It was demonstrated in the Fullerene (C_{60}) section, that a very complex macromolecule, fullerene, could be simply solved from the groups at each vertex carbon atom of the structure. Specifically, a $C=C$ group is bound to two $C-C$ bonds at each vertex carbon atom of C_{60}. The solution of the macromolecule is given by superposition of the geometrical and energy parameters of the corresponding two groups. Similarly, diamond comprising, in principle, an infinite network of carbons was also solved in the Diamond section using the functional group solutions, the diamond $C-C$ functional group which is the only functional group of diamond.

The structure of the indefinite network of aromatic hexagons of a sheet of graphite can also be solved by considering the vertex atom. As in the case of fullerene, each sheet of joined hexagons can be constructed with a $C=C$ group bound to two $C-C$ bonds at each vertex carbon atom of graphite. However, an alternative bonding to that of C_{60} is possible for graphite due to the structure comprising repeating hexagonal units. In this case, the lowest energy structure is achieved with a single functional group, one which has aromatic character. The aromatic bond is uniquely stable and requires the sharing of the electrons of multiple H_2-type MOs. The results of the derivation of the parameters of the benzene molecule given in the Benzene Molecule (C_6H_6) section was generalized to any aromatic functional group of aromatic and heterocyclic compounds in the Aromatic and Heterocyclic Compounds section. Ethylene serves as a basis element for the $C\overset{3e}{=}C$ bonding of the aromatic bond wherein each of the $C\overset{3e}{=}C$ aromatic bonds comprises $(0.75)(4)=3$ electrons according to Eq. (15.161) wherein C_2 of Eq. (15.51) for the aromatic $C\overset{3e}{=}C$-bond MO given by Eq. (15.162) is $C_2\left(aromaticC2sp^3HO\right)=c_2\left(aromaticC2sp^3HO\right)=0.85252$ and $E_T\left(atom-atom,msp^3.AO\right)=-2.26759\ eV$.

In graphite, the minimum energy structure with equivalent carbon atoms wherein each carbon forms bonds with three other such carbons requires a redistribution of charge within an aromatic system of bonds. Considering that each carbon contributes four bonding electrons, the sum of electrons of a vertex-atom group is four from the vertex atom plus two from each of the two atoms bonded to the vertex atom where the latter also contribute two each to the juxtaposed group. These eight electrons are distributed equivalently over the three bonds of the group such that the electron number assignable to each bond is $\frac{8}{3}$. Thus, the $C\overset{8/3e}{=}C$ functional group of graphite comprises the aromatic bond with the exception that the electron-number per bond is $\frac{8}{3}$. $E_T(Group)$ and $E_D(Group)$ are given by Eqs. (15.165) and (15.166), respectively, with $f_1=\frac{2}{3}$ and $c_4=\frac{8}{3}$. As in the case of diamond comprising equivalent carbon atoms, the $C2sp^3$ HO magnetic energy E_{mag} given by Eq. (15.67) was subtracted due to a set of unpaired electrons being created by bond breakage such that c_3 of Eqs. (15.165) and (15.166) is one.

The symbol of the functional group of graphite is given in Table 17.13. The geometrical (Eqs. (15.1-15.5) and (15.51)), intercept (Eqs. (15.80-15.87)), and energy (Eqs. (15.6-15.11), (15.17-15.65), and (15.165-15.166)) parameters of graphite are given in Tables 17.14, 17.15, and 17.16, respectively. The total energy of graphite given in Table 17.17 was calculated as the sum over the integer multiple of each $E_D(Group)$ of Table 17.16 corresponding to functional-group composition of the molecular solid. The experimental $C\overset{8/3e}{=}C$ bond energy of graphite at 0 K, $E_{D_{\exp}}\left(C\overset{8/3e}{=}C\right)$, is given by the difference between the enthalpy of formation of gaseous carbon atoms from graphite, $\Delta H_f\left(C_{graphite}(gas)\right)$, and the interplanar binding energy, E_x, wherein graphite solid has a defined heat of formation of zero ($\Delta H_f\left(C(graphite)\right)=0$):

$$E_{D_{\exp}}\left(C\overset{8/3e}{=}C\right)=\frac{2}{3}\left[\Delta H_f\left(C_{graphite}(gas)\right)-E_x\right] \tag{17.22}$$

The factor of $\frac{2}{3}$ corresponds to the ratio of $\frac{8}{3}$ electrons per bond and 4 electrons per carbon atom. The heats of formation of atomic carbon from graphite [9] and E_x [10] are:

$$\Delta H_f\left(C_{graphite}\left(gas\right)\right) = 711.185\ kJ/mole\ \left(7.37079\ eV/atom\right) \tag{17.23}$$

$$E_x = 0.0228\ eV/atom \tag{17.24}$$

Using Eqs. (17.21-17.23), $E_{D_{\exp}}\left(C \overset{8/3e}{=} C\right)$ is:

$$E_{D_{\exp}}\left(C \overset{8/3e}{=} C\right) = \frac{2}{3}\left[7.37079\ eV - 0.0228\ eV\right] = 4.89866\ eV \tag{17.25}$$

The bond angle parameters of graphite determined using Eqs. (15.87-15.117) are given in Table 17.18. The inter-plane distance for graphite of 3.5Å is calculated in the Geometrical Parameters Due to the Interplane van der Waals Cohesive Energy of Graphite section. The structure of graphite is shown in Figure 17.3A and B. The graphite $C \overset{8/3e}{=} C$ functional group can serve as a basis element to form additional complex polycyclic aromatic carbon structures such as nanotubes [11-15].

Figure 17.3. The structure of graphite. (A) Single plane of macromolecule of indefinite size. (B) Layers of graphitic planes.

(A)

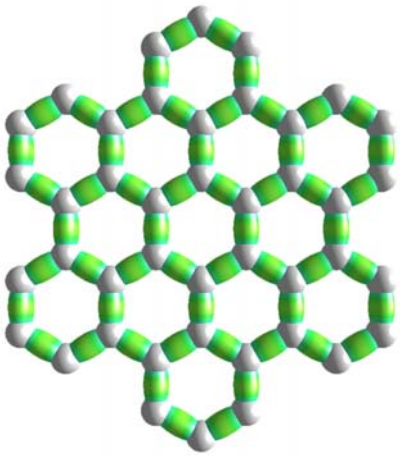

(B)

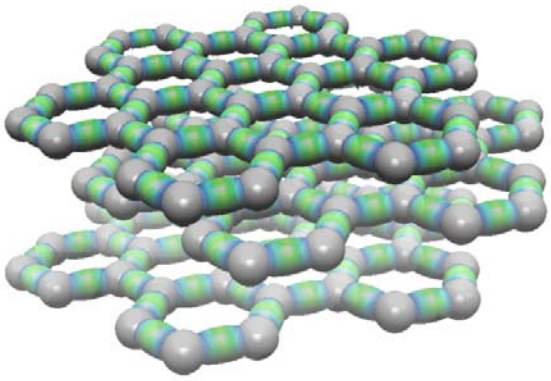

Table 17.13. The symbols of the functional group of graphite.

Functional Group	Group Symbol
CC bond (graphite-*C*)	$C \overset{8/3e}{=} C$

Table 17.14. The geometrical bond parameters of graphite and experimental values.

Parameter	$C \overset{8/3e}{=} C$ Group
$a\ (a_0)$	1.47348
$c'\ (a_0)$	1.31468
Bond Length $2c'\ (Å)$	1.39140
Exp. Bond Length $(Å)$	1.42 (graphite) [11] 1.399 (benzene) [16]
$b, c\ (a_0)$	0.66540
e	0.89223

Table 17.15. The MO to HO intercept geometrical bond parameters of graphite. E_T is E_T (*atom - atom msp³.AO*).

Bond	Atom	E_T (eV) Bond 1	E_T (eV) Bond 2	E_T (eV) Bond 3	E_T (eV) Bond 4	Final Total Energy $C2sp^3$ (eV)	$r_{initial}$ (a_0)	r_{final} (a_0)	$E_{Coulomb}(C2sp^3)$ (eV) Final	$E(C2sp^3)$ (eV) Final	θ' (°)	θ_1 (°)	θ_2 (°)	d_1 (a_0)	d_2 (a_0)
$C \overset{8/3e}{=} C$	C	-0.75586	-0.75586	-0.75586	0	-153.88328	0.91771	0.79597	-17.09334	-16.90248	134.24	45.76	58.98	0.75935	0.55533

Table 17.16. The energy parameters (eV) of the functional group of graphite.

Parameters	$C \overset{8/3e}{=} C$ Group
f_1	2/3
n_1	2
n_2	0
n_3	0
C_1	0.5
C_2	0.85252
c_1	1
c_2	0.85252
c_3	1
c_4	8/3
c_5	0
C_{1o}	0.5
C_{2o}	0.85252
$V_e\ (eV)$	-101.12679
$V_p\ (eV)$	20.69825
$T\ (eV)$	34.31559
$V_m\ (eV)$	-17.15779
$E_{(AO/HO)}\ (eV)$	0
$\Delta E_{H_2MO(AO/HO)}\ (eV)$	0
$E_{T(AO/HO)}\ (eV)$	0
$E_{T(H_2MO)}\ (eV)$	-63.27075
$E_T\left(atom-atom, msp^3.AO\right)\ (eV)$	-2.26759
$E_{T(MO)}\ (eV)$	-65.53833
$\omega\ \left(10^{15}\ rad/s\right)$	49.7272
$E_K\ (eV)$	32.73133
$\bar{E}_D\ (eV)$	-0.35806
$\bar{E}_{Kvib}\ (eV)$	0.19649 [17]
$\bar{E}_{osc}\ (eV)$	-0.25982
$E_{mag}\ (eV)$	0.14803
$E_{T(Group)}\ (eV)$	-43.93995
$E_{initial(c_4\ AO/HO)}\ (eV)$	-14.63489
$E_{initial(c_5\ AO/HO)}\ (eV)$	0
$E_{D(Group)}\ (eV)$	4.91359

Table 17.17. The total bond energy of graphite calculated using the functional group composition and the energy of Table 17.16 compared to the experimental value [9-10].

Formula	Name	$C \overset{8/3e}{=} C$	Calculated Total Bond Energy (eV)	Experimental Total Bond Energy (eV)	Relative Error
C_n	Graphite	1	4.91359	4.89866	-0.00305

Table 17.18. The bond angle parameters of graphite and experimental values. E_T is E_T (*atom - atom* msp^3*.AO*). The law of cosines was used to calculate the angle.

Atoms of Angle	2*c'* Bond 1 (a_0)	2*c'* Bond 2 (a_0)	2*c'* Terminal Atoms (a_0)	$E_{Coulombic}$ Atom 1	Atom 1 Hybridization Designation (Table 15.3.A)	$E_{Coulomtic}$ Atom 2	Atom 2 Hybridization Designation (Table 15.3.A)	c_2 Atom 1	c_2 Atom 2	C_1	C_2	c_1	c_2'	E_T (eV)	θ_π (°)	θ_1 (°)	θ_2 (°)	Cal. θ (°)	Exp. θ (°)
$\angle CCC$ (aromatic)	2.62936	2.62936	4.5387	-17.26666	40	-17.26666	40	0.78798	0.78798	1	1	1	0.78798	-1.85836				119.33	120 (graphite) [18] 120 (benzene) [19-21]

Table 17.19. The calculated and experimental total bond energies of allotropes of carbon using closed-form equations having integers and fundamental constants only.

Formula	Name	Calculated Total Bond Energy (eV)	Experimental Total Bond Energy (eV)	Relative Error
C_n	diamond	3.74829	3.704	-0.01
C_{60}	fullerene	419.75539	419.73367	-0.00005
C_n	graphite	4.91359	4.89866	-0.00305

REFERENCES

1. http://newton.ex.ac.uk/research/qsystems/people/sque/diamond/.
2. D. R. Lide, *CRC Handbook of Chemistry and Physics*, 86th Edition, CRC Press, Taylor & Francis, Boca Raton, (2005-6), pp. 5-18; 5-45.
3. D. R. Lide, *CRC Handbook of Chemistry and Physics*, 86th Edition, CRC Press, Taylor & Francis, Boca Raton, (2005-6), p. 4-150.
4. J. Wagner, Ch. Wild, P. Koidl, "Resonance effects in scattering from polycrystalline diamond films," Appl. Phys. Lett. Vol. 59, (1991), pp. 779-781.
5. W. I. F. David, R. M. Ibberson, J. C. Matthewman, K. Prassides, T. J. S. Dennis, J. P. Hare, H. W. Kroto, R. Taylor, D. R. M. Walton, "Crystal structure and bonding of C_{60}," Nature, Vol. 353, (1991), pp. 147-149.
6. B. Chase, N. Herron, E. Holler, "Vibrational spectroscopy of C_{60} and C_{70} temperature-dependent studies," J. Phys. Chem., Vol. 96, (1992), pp. 4262-4266.
7. D. R. Lide, *CRC Handbook of Chemistry and Physics*, 86th Edition, CRC Press, Taylor & Francis, Boca Raton, (2005-6), pp. 9-63; 5-18 to 5-42.
8. J. M. Hawkins, "Osmylation of C_{60}: proof and characterization of the soccer-ball framework," Acc. Chem. Res., (1992), Vol. 25, pp. 150-156.
9. M. W. Chase, Jr., C. A. Davies, J. R. Downey, Jr., D. J. Frurip, R. A. McDonald, A. N. Syverud, JANAF Thermochemical Tables, Third Edition, Part II, Cr-Zr, J. Phys. Chem. Ref. Data, Vol. 14, Suppl. 1, (1985), p. 536.
10. M. C. Schabel, J. L. Martins, "Energetics of interplanar binding in graphite," Phys. Rev. B, Vol. 46, No. 11, (1992), pp. 7185-7188.
11. J. -C. Charlier, J. -P. Michenaud, "Energetics of multilayered carbon tubules," Phys. Rev. Ltts., Vol. 70, No. 12, (19930, pp. 1858-1861.
12. J. P. Lu, "Elastic properties of carbon nanotubes and nanoropes," Phys. Rev. Letts., (1997), Vol. 79, No. 7, pp. 1297–1300.
13. G. Zhang, X. Jiang, E. Wang, "Tubular graphite cones," Science, (2003), vol. 300, pp. 472–474.
14. A. N. Kolmogorov, V. H. Crespi, M. H. Schleier-Smith, J. C. Ellenbogen, "Nanotube-substrate interactions: Distinguishing carbon nanotubes by the helical angle," Phys. Rev. Letts., (2004), Vol. 92, No. 8, pp. 085503-1–085503-4.
15. J.W. Jiang, H. Tang, B.S. Wang, Z.B. Su, "A lattice dynamical treatment for the total potential of single-walled carbon nanontubes and its applications: Relaxed equilibrium structure, elastic properties, and vibrational modes of ultra-narrow tubes," J. Phys. Condens. Matter, Vol. 20, (2008), p. 045228.
16. D. R. Lide, *CRC Handbook of Chemistry and Physics*, 86th Edition, CRC Press, Taylor & Francis, Boca Raton, (2005-6), p. 9-29.
17. G. Herzberg, *Molecular Spectra and Molecular Structure II. Infrared and Raman Spectra of Polyatomic Molecules*, Van Nostrand Reinhold Company, New York, New York, (1945), pp. 362-369.
18. D. R. McKenzie, D. Muller, B. A. Pailthorpe, "Compressive-stress-induced formation of thin-film tetrahedral amorphous carbon," Phys. Rev. Lett., (1991), Vol. 67, No. 6, pp. 773-776.
19. W. I. F. David, R. M. Ibberson, G. A. Jeffrey, J. R. Ruble, "The structure analysis of deuterated benzene and deuterated nitromethane by pulsed-neutron powder diffraction: a comparison with single crystal neutron analysis," Physica B (1992), 180 & 181, pp. 597-600.
20. G. A. Jeffrey, J. R. Ruble, R. K. McMullan, J. A. Pople, "The crystal structure of deuterated benzene," Proceedings of the Royal Society of London. Series A, Mathematical and Physical Sciences, Vol. 414, No. 1846, (Nov. 9, 1987), pp. 47-57.
21. H. B. Burgi, S. C. Capelli, "Getting more out of crystal-structure analyses," Helvetica Chimica Acta, Vol. 86, (2003), pp. 1625-1640.

Chapter 18

NATURE OF THE IONIC BOND OF ALKALI HYDRIDES AND HALIDES

ALKALI-HYDRIDE CRYSTAL STRUCTURES

The alkali hydrides are lithium hydride (LiH), sodium hydride (NaH), potassium hydride (KH), rubidium hydride (RbH), and cesium hydride (CsH). These saline or salt-like alkali-metal hydrides each comprise an equal number of alkali cations and hydride ions [1] in unit cells of a crystalline lattice. The crystal structure of these ionic compounds is the face-centered cubic $NaCl$ structure [2]. This close-packed structure is expected since it gives the optimal approach of the positive and negative ions [3]. The structure comprises face-centered cubes of both M^+ and H^- ions combined, but offset by half a unit cell length in one direction so that M^+ ions are centered in the edges of the H^- lattice and vice versa. Each M^+ is surrounded by six nearest neighbor H^- ions and vice versa. The resulting unit cell consists of anions (or cations) at the midpoint of each edge and at the center of the cell such that the unit cell contains four cations and four anions.

The interionic radius of each hydride can be derived by considering the radii of the alkali ion and the hydride ion, the electron energies at these radii, and the conditions for stability of the ions as the internuclear distance changes and the ions are mutually influenced by Coulombic forces. Then, the lattice energy is given by the sum over the crystal of the minimum energy of the interacting ion pairs at the radius of minimum approach for which the ions are stable. The sum is further over all Coulombic interactions of the ions of the crystal.

Each hydride MH ($M = Li, Na, K, Rb, Cs$) is comprised of M^+ and H^- ions. From Coulomb's Law, the lattice energy ΔU for point charges is given by the Born-Mayer equation [3]

$$\Delta U = NM_c Z_+ Z_- \frac{e^2}{4\pi\varepsilon_0 r_0}\left(1-\frac{\rho}{r_0}\right) \tag{18.1}$$

where N is Avogadro's number, M_c is the Madelung constant (the convergent sum of all Coulombic interactions of any given ion with the lattice of ions), Z_+ and Z_- are the ionic charges in elementary charge units, r_0 is the distance between ion centers, and ρ is a constant that corrects for higher-order terms (e.g. $1/r_0^6$ to $1/r_0^{12}$ terms) in repulsion between close neighbor ions. The $M\text{—}H$ distance can be calculated from the minimum energy packing of the ions, which is stable. Each ion is surrounded in a symmetrical octahedral field of six counterions. From Eq. (18.1), the lattice energy increases as the interionic distance decreases. But, the interionic distance cannot be the sum of the contact radii. This is easily appreciated by considering that the energies of the outer electron of M^+ and the outer two electrons of H^- are very different. For sufficiently small interionic distances, the most energetic reaction that can occur which eliminates the cation and consequently the lattice energy is the following :

$$M^+ + e^- \rightarrow M \tag{18.2}$$

For shorter distances, the spherically symmetrical ${}^1S_0$ state of the hydride ion is distorted by M^+, and it is not stable in the ionic crystal when the $M\text{—}H$ distance is given by the condition that the total Coulombic energy of attractive terms of H^- in the field of M^+ as well as the repulsive terms between like-charged ions is equal to the binding energy of M, $BE(M)$, for the cations of the crystal. Then, the lattice energy is given by the product of Avogadro's number, $BE(M)$, and the Madelung constant which takes into account all inverse r_0 (point-like) Coulombic interactions of the crystal:

$$\Delta U = NM_c BE(M) \tag{18.3}$$

Thus, M_c is the factor of stability of forming the crystal from M^+ and H^- ions. The value for the $NaCl$ structure is $M_c = 1.74756$ [3].

Since the Coulombic potential of the ions is equivalent to that of point charges with some higher order ion-ion-interaction repulsive terms, the $M — H$ distance $r_0(MH)$ given using Eq. (18.1), Eq. (18.3), and $BE(M)$ is:

$$r_0(MH) = \frac{\frac{Z_+Z_-e^2}{BE(M)4\pi\varepsilon_0} + \sqrt{\left(\frac{Z_+Z_-e^2}{BE(M)4\pi\varepsilon_0}\right)^2 - \frac{4\rho Z_+Z_-e^2}{BE(M)4\pi\varepsilon_0}}}{2} \tag{18.4}$$

wherein $\rho = 0.4\ X\ 10^{-10}\ m$ for alkali hydrides [4-5]. The parameters of the hydride ion are given in the corresponding section.

LITHIUM HYDRIDE

The calculated ionic radii for Li^+ and H^- ions given in Tables 7.1 and 7.2 are $0.35566a_0$ and $1.8660a_0$, respectively. But, the interionic distance cannot be the sum of the contact radii since the calculated ionization energies of Li^+ (Eqs. (7.35), (7.45-7.46), and (7.63)) and H^- (Eq. (7.69)) are $75.665\ eV$ and $0.75471\ eV$, respectively. Furthermore, since the calculated ionization energy (Eq. (10.25)) of Li to Li^+ is $5.40381\ eV$ as shown in Table 10.1 and the ionization energy (Eq. (7.69)) of H^- to H is $0.75471\ eV$ $(1.20836\ X\ 10^{-19}\ J)$, for sufficiently small interionic distances, the lithium ion may be reduced.

Substitution of $BE(Li) = 8.65786\ X\ 10^{-19}\ J$ into Eq. (18.3) gives the calculated lattice energy of

$$\Delta U = NM_cBE(Li) = 1.74756N8.65786\ X\ 10^{-19}\ J = 911.1\ kJ/mole\ (217.8\ kcal/mole) \tag{18.5}$$

This agrees well with the experimental lattice energy of $\Delta U = 217.95\ kcal/mole$ [1] and confirms that the ionic compound LiH comprises a precise packing of discrete ions.

The calculated radius of Li (Eq. (10.13)) given in Table 10.1 is $2.55606a_0$, and the calculated binding energy is $5.40381\ eV$ $(8.65786\ X\ 10^{-19}\ J)$ (Eq. (10.25)). The $Li — H$ distance, $r_0(LiH)$, calculated using Eq. (18.4) with the substitution of $BE(Li) = 8.65786\ X\ 10^{-19}\ J$ is:

$$r_0(LiH) = 2.17\ X\ 10^{-10}\ m \tag{18.6}$$

The calculated $Li — H$ is in reasonable agreement with the experimental distance of $r_0(LiH) = 2.04\ X\ 10^{-10}\ m$ [1] given the experimental difficulty of performing X-ray diffraction on lithium and hydrogen due to the low electron densities. Furthermore, there is a 15% variation in experimental measurements of the density of LiH [1] that affects the internuclear spacing. Using the $Li — H$ distance and the calculated ionic radii, the lattice structure of LiH is shown in Figure 18.1A.

SODIUM HYDRIDE

The calculated ionic radii for Na^+ and H^- ions given in Tables 10.8 and 7.2 are $0.560945a_0$ and $1.8660a_0$, respectively. But, the interionic distance can not be the sum of the contact radii since the calculated ionization energies of Na^+ (Eqs. (10.212-10.213)) and H^- (Eq. (7.69)) are $48.5103\ eV$ and $0.75471\ eV$, respectively. Furthermore, since the calculated ionization energy (Eqs. (10.226-10.227)) of Na to Na^+ is $5.12592\ eV$ as shown in Table 10.10 and the ionization energy (Eq. (7.69)) of H^- to H is $0.75471\ eV$ $(1.20836\ X\ 10^{-19}\ J)$, for sufficiently small interionic distances, the sodium ion may be reduced.

Substitution of $BE(Na) = 8.21263\ X\ 10^{-19}\ J$ into Eq. (18.3) gives the calculated lattice energy of

$$\Delta U = NM_cBE(Na) = 1.74756N8.21263\ X\ 10^{-19}\ J = 864.3\ kJ/mole\ (206.6\ kcal/mole) \tag{18.7}$$

This agrees well with the experimental lattice energy of $\Delta U = 202.0\ kcal/mole$ [2] and confirms that the ionic compound NaH comprises a precise packing of discrete ions.

The calculated radius of Na (Eq. (10.226)) given in Table 10.10 is $2.65432a_0$, and the calculated binding energy is $5.12592\ eV$ $(8.21263\ X\ 10^{-19}\ J)$ (Eqs. (10.226-10.227)). The $Na — H$ distance, $r_0(NaH)$, calculated using Eq. (18.4) with the substitution of $BE(Na) = 8.21263\ X\ 10^{-19}\ J$ is:

$$r_0(NaH) = 2.33\ X\ 10^{-10}\ m \tag{18.8}$$

The calculated $Na — H$ is in good agreement with the experimental distance of $r_0(NaH) = 2.44\ X\ 10^{-10}\ m$ [2]. Using the $Na — H$ distance and the calculated ionic radii, the lattice structure of NaH is shown in Figure 18.1B.

Figure 18.1. The crystal structures of MH all to the same scale. (Li^+ = green, Na^+ = yellow, K^+ = purple, and H^- and $H^-\left(\frac{1}{4}\right)$ = blue). (A) The crystal structure of LiH. (B) The crystal structure of NaH. (C) The crystal structure of KH. (D) The crystal structure of $KH\left(\frac{1}{4}\right)$.

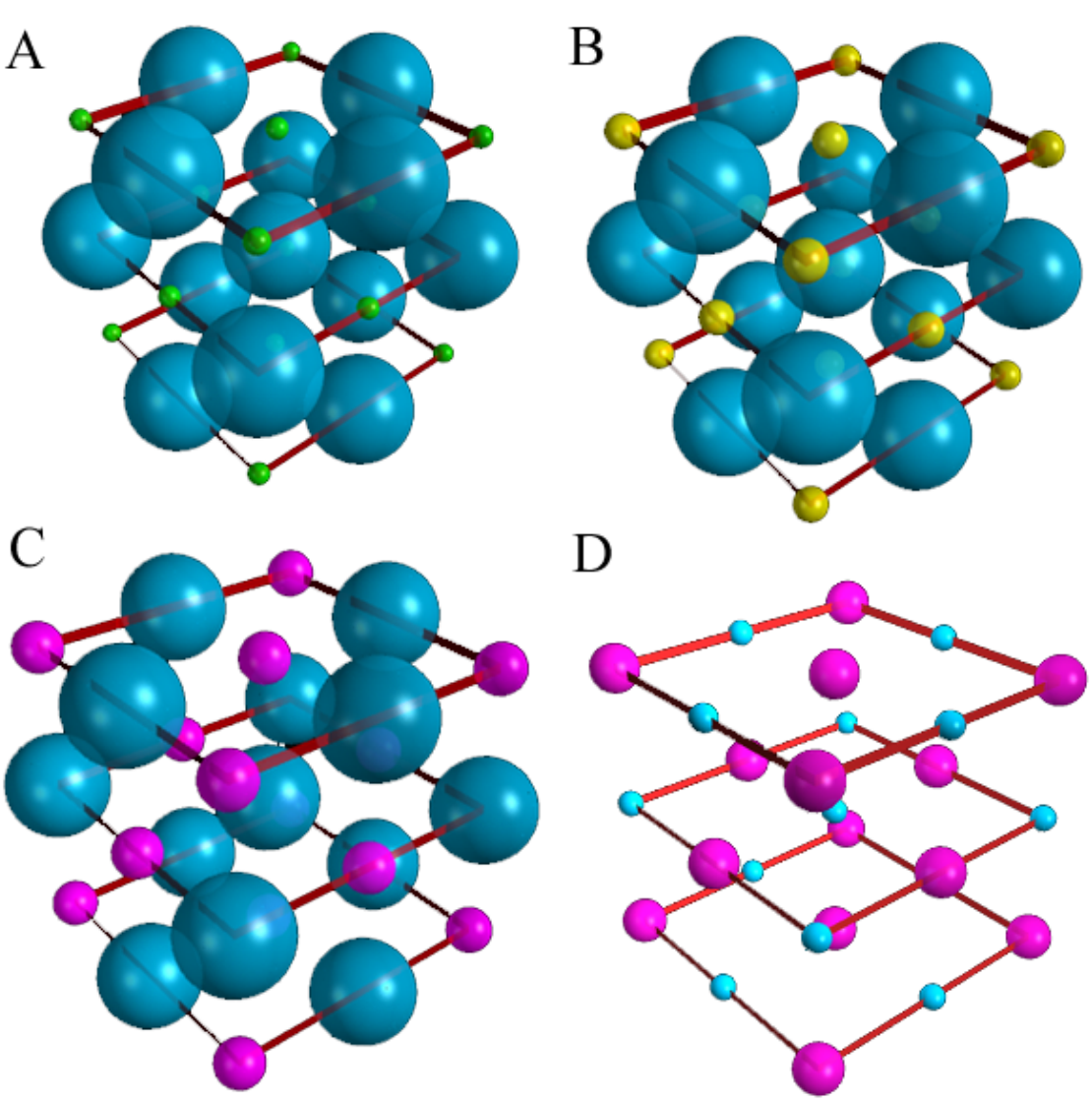

POTASSIUM HYDRIDE

The calculated ionic radii for K^+ and H^- ions given in Tables 10.17 and 7.2 are $0.85215a_0$ and $1.8660a_0$, respectively. But, the interionic distance cannot be the sum of the contact radii since the calculated ionization energies of K^+ (Eqs. (10.399-10.400)) and H^- (Eq. (7.69)) are $31.9330\ eV$ and $0.75471\ eV$, respectively. Furthermore, since the calculated ionization energy (Eqs. (10.414-10.415)) of K to K^+ is $4.33\ eV$ as shown in Table 10.19 and the ionization energy (Eq. (7.69)) of H^- to H is $0.75471\ eV$ $(1.20836\ X\ 10^{-19}\ J)$, for sufficiently small interionic distances, the potassium ion may be reduced.

Substitution of $BE(K) = 6.93095\ X\ 10^{-19}\ J$ into Eq. (18.3) gives the calculated lattice energy of:

$$\Delta U = NM_c BE(K) = 1.74756N6.93095\ X\ 10^{-19}\ J = 729.4\ kJ/mole\ (174.3\ kcal/mole) \tag{18.9}$$

This agrees well with the experimental lattice energy of $\Delta U = 177.2\ kcal/mole$ [2] and confirms that the ionic compound KH comprises a precise packing of discrete ions.

The calculated radius of K (Eq. (10.414)) given in Table 10.19 is $3.14515a_0$, and the calculated binding energy is $4.32596\ eV$ $(6.93095\ X\ 10^{-19}\ J)$ (Eqs. (10.414-10.415)). The $K-H$ distance, $r_0(KH)$, calculated using Eq. (18.4) with the substitution of $BE(K) = 6.93095\ X\ 10^{-19}\ J$ is:

$$r_0(KH) = 2.86\ X\ 10^{-10}\ m \tag{18.10}$$

The calculated $K-H$ is in good agreement with the experimental distance of $r_0(KH) = 2.85\ X\ 10^{-10}\ m$ [2]. Using the $K-H$ distance and the calculated ionic radii, the lattice structure of KH is shown in Figure 18.1C. An aggregate crystal of unit cells is shown in Figure 18.2.

Figure 18.2. The crystal structure of KH. (K^+= purple and H^-= blue). (A) Opaque view showing the external geometrical crystal structure of an aggregate of unit cells of KH. (B) The crystal structure of KH showing an aggregate of units cells.

A **B**

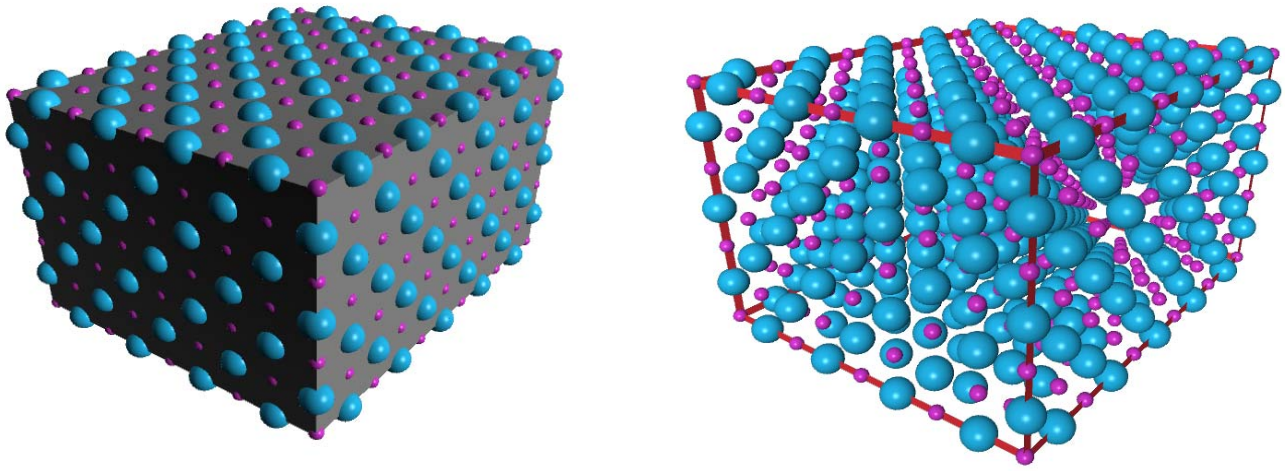

RUBIDIUM AND CESIUM HYDRIDE

As further tests of the boundary condition, the lattice energies of RbH and CsH are given by the product of Avogadro's number, the Madelung constant of $M_c = 1.74756$, and the binding energy of Rb and Cs of $4.17713\ eV$ and $3.89390\ eV$ [6], respectively. Using Eq. (18.3), the calculated lattice energy of RbH is:

$$\Delta U = 1.74756N(e4.17713\ eV) = 704.3\ kJ/mole = 168.3\ kcal/mole \tag{18.11}$$

This agrees well with the experimental lattice energy of $\Delta U = 168.6\ kcal/mole$ [2] and confirms that the ionic compound RbH comprises a precise packing of discrete ions.

Substitution of $BE(Rb) = 6.6925\ X\ 10^{-19}\ J$ into Eq. (18.4) gives the $Rb-H$ distance $r_0(RbH)$:

$$r_0(RbH) = 2.99\ X\ 10^{-10}\ m \tag{18.12}$$

The calculated $Rb-H$ is in good agreement with the experimental distance of $r_0(RbH) = 3.02\ X\ 10^{-10}\ m$ [2].

Using Eq. (18.3), the calculated lattice energy of CsH is:

$$\Delta U = 1.74756N\left(e3.89390\ eV\right) = 656.6\ kJ/mole = 156.9\ kcal/mole \tag{18.13}$$

This agrees well with the experimental lattice energy of $\Delta U = 154.46\ kcal/mole$ [1] and $\Delta U = 162.0\ kcal/mole$ [2] and confirms that the ionic compound CsH comprises a precise packing of discrete ions.

Substitution of $BE\left(Cs\right) = 6.23872\ X\ 10^{-19}\ J$ into Eq. (18.4) gives the $Cs — H$ distance $r_0\left(CsH\right)$:

$$r_0\left(CsH\right) = 3.24\ X\ 10^{-10}\ m \tag{18.14}$$

The calculated $Cs — H$ is in good agreement with the experimental distance of $r_0\left(CsH\right) = 3.19\ X\ 10^{-10}\ m$ [2].

POTASSIUM HYDRINO HYDRIDE ($KH\left(\frac{1}{4}\right)$)

The crystal structure of each alkali hydrino hydride $MH\left(\frac{1}{p}\right)$ is the same as that of the corresponding ordinary alkali hydride except that the radii of the hydride ions $H^-\left(\frac{1}{p}\right)$ are each a reciprocal integer times that of the ordinary hydride as given by Eq. (7.73). Thus, the lattice energy of $KH\left(\frac{1}{4}\right)$ is the same as that of KH given by Eq. (18.9), and the $K — H\left(\frac{1}{4}\right)$ distance $r_0\left(KH\left(\frac{1}{4}\right)\right)$ is the same as that of KH given by Eq. (18.10). Using the $K — H\left(\frac{1}{4}\right)$ distance (Eq. (18.10)), the radius of K^+ of $0.85215a_0$ (Eq. (10.399)) and the radius of $H^-\left(\frac{1}{4}\right)$ of $\frac{1.8660}{4}a_0 = 0.4665a_0$ (Eq. (7.73)), the lattice structure of $KH\left(\frac{1}{4}\right)$ is shown in Figure 18.1D.

ALKALI-HALIDE CRYSTAL STRUCTURES

The alkali halides (MX) are lithium, sodium, potassium, rubidium, and cesium cations, M^+, with fluoride, chloride, bromide, and iodide anions, X^-. These saline or salt-like alkali-metal halides each comprise an equal number of alkali cations and halide ions [3] in unit cells of a crystalline lattice. The crystal structure of these ionic compounds is the face-centered cubic $NaCl$ structure except for $CsCl$, $CsBr$, and CsI that have the $CsCl$ structure at ordinary temperatures and pressures [3]. These close-packed structures are expected since it gives the optimal approach of the positive and negative ions [3]. The $NaCl$ structure comprises face-centered cubes of both M^+ and X^- ions combined, but offset by half a unit cell length in one direction so that M^+ ions are centered in the edges of the X^- lattice and vice versa. Each M^+ is surrounded by six nearest neighbor X^- ions and vice versa. The resulting unit cell consists of anions (or cations) at the midpoint of each edge and at the center of the cell such that the unit cell contains four cations and four anions. The $CsCl$ structure comprises body-centered cubes of both M^+ and X^- ions wherein M^+ is in the center of cubes of X^- and vice versa.

ALKALI-HALIDE LATTICE PARAMETERS AND ENERGIES

The interionic radius of each alkali halide can be derived by considering the radii of the alkali ion and the halide ion, the electron energies at these radii, and the conditions for stability of the ions as the internuclear distance changes and the ions are mutually influenced by the Coulombic fields. Then, the lattice energy is given by the sum over the crystal of the minimum energy of the interacting ion pairs at the radius of minimum approach for which the ions are stable. The sum is further over all Coulombic interactions of the ions of the crystal.

As in the case with alkali hydrides, each alkali halide MX ($M = Li, Na, K, Rb, Cs$ and $X = F, Cl, Br, I$) is comprised of M^+ and X^- ions. From Coulomb's law, the lattice energy ΔU for point charges is given by Eq. (18.1), the Born-Mayer equation. The $M — X$ distance can be calculated from the minimum energy packing of the ions, which is stable. Each ion of the $NaCl$ and $CsCl$ structure is surrounded in a symmetrical octahedral or cubic field of six or four counterions, respectively. From Eq. (18.1), the lattice energy increases as the interionic distance decreases. But, the interionic distance cannot be the sum of the contact radii. This is easily appreciated by considering that the energies of the outer electron of M^+ and the outer electrons of X^- are very different. For sufficiently small interionic distances, the most energetic reaction that can occur which eliminates the cation and consequently the lattice energy is given by Eq. (18.2). For shorter distances, the spherically symmetrical ${}^1S_0$ state of the halide ion is distorted by M^+, and it is not stable in the ionic crystal when the $M — X$ distance is sufficiently small. To first order, this distance is given by the condition that the total Coulombic energy of attractive terms of X^- in the field of M^+ as well as the repulsive terms between like-charged ions is equal to the binding energy of M, $BE\left(M\right)$, for the cations of the crystal.

As in the case of the alkali hydrides, the lattice energies of alkali halides are determined by the binding energy of the corresponding metal atom. However, for each alkali halide an additional energy term arises corresponding to the effect of the electric field of the metal ion on the magnetic forces and energy of the halide ion. With the binding of the ions in both alkali hydrides and halides, the electric field lines of the metal ions end on those of the negative ions. But, each electron of the hydride ion occupies a symmetrically symmetrical s orbital, and the electrons collectively comprise a filled s shell only such that there is no dipole to interact with the external electric field of the positive ions. Whereas, the outer shell of the halide ions comprise p-orbital electrons having magnetic dipoles. These dipoles can interact with the external electric field having dipole components. Thus, the cation-anion separation in ionic compounds having electrons with magnetic dipole moments due to orbital angular momentum is dependent on the effect of the electric field on the magnetic forces of the anion.

Since the magnetic field is a relativistic effect of the electric field and the electron's charge, e, charge-to-mass ratio, $\frac{e}{m_e}$, angular momentum of $\hbar$, and the magnetic moment of μ_B are relativistically invariant, it is not surprising as shown in the Stark Effect section that the energy, E_{Stark}, of a one-electron atom in an electric field follows from that of a magnetic dipole in a magnetic field, Eqs. (2.68-2.69), with the magnetic dipole moment replaced by the electric dipole moment and the magnetic flux replaced by the electric field $\mathbf{E}_{applied}$. Thus, in alkali halides, the change in Coulombic lattice energy due to the Stark effect is given by the change in magnetic energy of the anion. The Stark-effect energy can be expressed in terms of the magnetic-dipole energy according to Eqs. (2.73-2.75):

$$E = \mu_B B \tag{18.15}$$

The corresponding force $\mathbf{F}_{Stark}$ on the outer nth electron of the anion is given by Eqs. (7.27-7.31).

$$\mathbf{F}_{Stark} = \frac{1}{Z}\frac{\hbar^2}{m_e r_n^3}\sqrt{s(s+1)}\mathbf{i}_r \tag{18.16}$$

From the radius change and the magnetic energy change, the Stark energy component $\Delta E(ionization;\ X^-)$ is calculated. Then, the lattice energy is given by the product of Avogadro's number, the Madelung constant which takes into account all inverse r_0 (point-like) Coulombic interactions of the crystal, and the sum of $BE(M)$, and $\Delta E(ionization;\ X^-)$:

$$\Delta U = NM_c\left(BE(M) + \Delta E(ionization;\ X^-)\right) \tag{18.17}$$

Thus, M_c is the factor of stability of forming the crystal from M^+ and X^- ions. The values for the *NaCl* and *CsCl* structures are $M_c = 1.74756$ and $M_c = 1.76267$ [3], respectively.

Since the Coulombic potential of the ions is equivalent to that of point charges with some higher order ion-ion-interaction repulsive terms, the $M - X$ distance $r_0(MX)$ given using Eq. (18.1), Eq. (18.3), $BE(M)$ and $\Delta E(ionization;\ X^-)$ is:

$$r_0(MX) = \frac{\dfrac{Z_+Z_-e^2}{\left(BE(M)+\Delta E(ionization;\ X^-)\right)4\pi\varepsilon_0} + \sqrt{\left(\dfrac{Z_+Z_-e^2}{\left(BE(M)+\Delta E(ionization;\ X^-)\right)4\pi\varepsilon_0}\right)^2 - \dfrac{4\rho Z_+Z_-e^2}{\left(BE(M)+\Delta E(ionization;\ X^-)\right)4\pi\varepsilon_0}}}{2} \tag{18.18}$$

wherein $\rho = 0.2\ X\ 10^{-10}\ m$ for alkali halides [5, 7]. The parameters of the gas-phase halide ions are derived next following the same procedure as that used to solve multielectron atoms.

RADIUS AND IONIZATION ENERGY OF THE OUTER ELECTRON OF THE FLUORIDE ION

The fluoride atom comprises a nine-electron atom having a central charge of $Z = 9$ times that of the proton. There are two indistinguishable spin-paired electrons in an atomic orbital with radii r_1 and r_2 both given by Eq. (7.35) (Eq. (10.51)), two indistinguishable spin-paired electrons in an atomic orbital with radii r_3 and r_4 both given by Eq. (10.62), and two sets of paired and an unpaired electron in an atomic orbital at r_9 given by Eq. (10.182). The next electron which binds to form the corresponding ten-electron fluoride ion is attracted by the net magnetic force between the pairing (electron 10) and unpaired (electron 9) to form three pairs of electrons of opposite spin in p_x, p_y, and p_z orbitals of an atomic orbital at the same radius r_{10}. The resulting electron configuration is $1s^2 2s^2 2p^6$, and the orbital arrangement is:

$$\begin{array}{c} \text{2p state} \\ \underline{\uparrow\downarrow}\ \ \underline{\uparrow\downarrow}\ \ \underline{\uparrow\downarrow} \\ 1 \quad 0 \quad -1 \end{array} \tag{18.19}$$

corresponding to the ground state $^1S_0$.

Unlike the case of the hydride ion comprising a filled s shell only, the outer shell of the fluoride ion comprises additional orbitals to the one filled by the electron which binds to form the negative ion. The forces are purely magnetic in order to maintain the boundary conditions of an equipotential minimum energy for electrons of the additional orbitals. Thus, the central Coulomb force acts on the outer electron to cause it to bind wherein this electric force on the outer-most electron due to the nucleus and the inner nine electrons is given by Eq. (10.70) with the appropriate charge and radius:

$$\mathbf{F}_{ele} = \frac{(Z-9)e^2}{4\pi\varepsilon_0 r_{10}^2}\mathbf{i}_\mathbf{r} = 0 \tag{18.20}$$

for $r > r_9$ with $Z = 9$.

As in the case with the closed-shell s orbitals, the spin-pairing force $\mathbf{F}_{mag}$ between electron 9 and electron 10 given by Eq. (7.24) is:

$$\mathbf{F}_{mag} = \frac{1}{Z}\frac{\hbar^2}{m_e r_{10}^3}\sqrt{s(s+1)}\mathbf{i}_\mathbf{r} \tag{18.21}$$

Due to the spin-pairing force the diamagnetic forces and paramagnetic forces are altered relative to those of the isoelectronic neon atom. The energy of the fluoride ion is minimized and the angular momentum is conserved with the pairing of electron ten to fill the 2 p_y orbital. Then, the orbital angular momentum of each set of the 2 p_x and p_z spin-paired electrons give rise to the diamagnetic force (Eq. (10.82)), $\mathbf{F}_{diamagnetic}$:

$$\mathbf{F}_{diamagnetic} = -\left(\frac{1}{3}+\frac{2}{3}\right)\frac{\hbar^2}{4m_e r_{10}^2 r_3}\sqrt{s(s+1)}\mathbf{i}_\mathbf{r} = -\frac{\hbar^2}{4m_e r_{10}^2 r_3}\sqrt{s(s+1)}\mathbf{i}_\mathbf{r} \tag{18.22}$$

From Eq. (10.84), $\mathbf{F}_{mag\ 2}$ due to spin and orbital angular momentum is:

$$\mathbf{F}_{mag\ 2} = \frac{1}{Z}\frac{4\hbar^2}{m_e r_{10}^2 r_3}\sqrt{s(s+1)}\mathbf{i}_\mathbf{r} \tag{18.23}$$

The outward centrifugal force on electron 10 is balanced by the electric force and the magnetic forces (on electron 10). The radius of the outer electron is calculated by equating the outward centrifugal force to the sum of the electric (Eq. (18.20)), diamagnetic (Eq. (18.22)), and paramagnetic (Eqs. (18.21) and (18.23)) forces as follows:

$$\frac{m_e v_{10}^2}{r_{10}} = \frac{(Z-9)e^2}{4\pi\varepsilon_0 r_{10}^2} - \frac{\hbar^2}{4m_e r_{10}^2 r_3}\sqrt{s(s+1)} + \frac{4\hbar^2}{Zm_e r_{10}^2 r_3}\sqrt{s(s+1)} + \frac{\hbar^2}{Zm_e r_{10}^3}\sqrt{s(s+1)} \tag{18.24}$$

Substitution of $v_{10} = \frac{\hbar}{m_e r_{10}}$ (Eq. (1.35)), $Z = 9$, and $s = \frac{1}{2}$ into Eq. (18.24) gives:

$$\frac{\hbar^2}{m_e r_{10}^3} = -\frac{\hbar^2}{4m_e r_{10}^2 r_3}\sqrt{\frac{3}{4}} + \frac{4\hbar^2}{9m_e r_{10}^2 r_3}\sqrt{\frac{3}{4}} + \frac{\hbar^2}{9m_e r_{10}^3}\sqrt{\frac{3}{4}} \tag{18.25}$$

$$r_{10} = \frac{\frac{\hbar^2}{m_e}\left(1-\frac{\sqrt{\frac{3}{4}}}{9}\right)}{-\frac{\hbar^2}{4m_e r_3}\sqrt{\frac{3}{4}} + \frac{4\hbar^2}{9m_e r_3}\sqrt{\frac{3}{4}}} \tag{18.26}$$

$$r_{10} = \frac{a_0\left(1-\frac{\sqrt{\frac{3}{4}}}{9}\right)}{\left(\frac{4}{9}-\frac{1}{4}\right)\frac{\sqrt{\frac{3}{4}}}{r_3}},\ r_3 \textit{ in units of } a_0 \tag{18.27}$$

Substitution of $\frac{r_3}{a_0} = 0.51382$ (Eq. (10.62)) into Eq. (18.27) gives:

$$r_{10} = 2.75769 a_0 \tag{18.28}$$

The ionization energy of the fluoride ion is given by the magnetic energy of the outer electron calculated by integrating the sum of the diamagnetic (Eq. (18.22)) and paramagnetic (Eqs. (18.21) and (18.23)) forces from r_{10} to ∞:

$$E_{magwork} = -\int_{r_{10}}^{\infty} -\frac{\hbar^2}{4m_e r_{10}^2 r_3}\sqrt{\frac{3}{4}} + \frac{4\hbar^2}{Zm_e r_{10}^2 r_3}\sqrt{\frac{3}{4}} + \frac{\hbar^2}{Zm_e r_{10}^3}\sqrt{\frac{3}{4}}dr = \frac{\hbar^2\sqrt{\frac{3}{4}}}{m_e r_{10}}\left(\left(\frac{4}{Z}-\frac{1}{4}\right)\frac{1}{r_3}+\frac{1}{2Zr_{10}}\right) \quad (18.29)$$

Eq. (18.29) with $r_3 = 0.51382a_0$ (Eq. (10.62)), $r_{10} = 2.75769a_0$ (Eq. (18.28)), and $Z = 9$ gives:

$$E(ionization;\ F^-) = 3.40603\ eV \quad (18.30)$$

The experimental ionization energy of the fluoride ion is [8] :

$$E(ionization;\ F^-) = 3.4011895\ eV \quad (18.31)$$

RADIUS AND IONIZATION ENERGY OF THE OUTER ELECTRON OF THE CHLORIDE ION

The chlorine atom comprises a seventeen-electron atom having a central charge of $Z = 17$ times that of the proton. There are two indistinguishable spin-paired electrons in an atomic orbital with radii r_1 and r_2 both given by Eq. (7.35) (Eq. (10.51)), two indistinguishable spin-paired electrons in an atomic orbital with radii r_3 and r_4 both given by Eq. (10.62), three sets of paired electrons in an atomic orbital at r_{10} given by Eq. (10.212), two indistinguishable spin-paired electrons in an atomic orbital with radii r_{11} and r_{12} both given by Eq. (10.255), and two sets of paired and an unpaired electron in an atomic orbital with radius r_{17} given by Eq. (10.363). The next electron which binds to form the corresponding eighteen-electron chloride ion is attracted by the net magnetic force between the pairing (electron 18) and unpaired (electron 17) to form three pairs of electrons of opposite spin in p_x, p_y, and p_z orbitals of an atomic orbital at the same radius r_{18}. The resulting electron configuration is $1s^2 2s^2 2p^6 3s^2 3p^6$, and the orbital arrangement is:

3p state

$$\underline{\uparrow\ \downarrow}\quad \underline{\uparrow\ \downarrow}\quad \underline{\uparrow\ \downarrow} \quad (18.32)$$

1 0 -1

corresponding to the ground state ${}^1S_0$.

Unlike the case of the hydride ion, the outer shell of the chloride ion comprises additional orbitals to the one filled by the electron which binds to form the negative ion. The forces are purely magnetic in order to maintain the boundary conditions of an equipotential minimum energy for electrons of the additional orbitals. Thus, the central Coulomb force acts on the outer electron to cause it to bind wherein this electric force on the outer-most electron due to the nucleus and the inner seventeen electrons is given by Eq. (10.70) with the appropriate charge and radius:

$$\mathbf{F}_{ele} = \frac{(Z-17)e^2}{4\pi\varepsilon_0 r_{18}^2}\mathbf{i}_\mathbf{r} = 0 \quad (18.33)$$

for $r > r_{17}$ with $Z = 17$.

As in the case with the closed-shell s orbitals, the spin-pairing force $\mathbf{F}_{mag}$ between electron 18 and electron 17 given by Eq. (7.24) is

$$\mathbf{F}_{mag} = \frac{1}{Z}\frac{\hbar^2}{m_e r_{18}^3}\sqrt{s(s+1)}\mathbf{i}_\mathbf{r} \quad (18.34)$$

Due to the spin-pairing force the diamagnetic forces and paramagnetic forces are altered relative to those of the isoelectronic argon atom. The energy of the chloride ion is minimized and the angular momentum is conserved with the pairing of electron eighteen to fill the 3 p_y orbital when the orbital angular momentum of each set of the p_x, p_y, and p_z spin-paired electrons add negatively to cancel. Then, the diamagnetic force (Eq. (10.82)), $\mathbf{F}_{diamagnetic}$, is zero as in the case of the closed-p-shell atom neon:

$$\mathbf{F}_{diamagnetic} = 0 \quad (18.35)$$

The orbital angular momentum of each set of the 3 p_x and p_z spin-paired electrons and the spin and orbital angular momentum of electrons 17 and 18 that pair upon the binding to fill the 3 p_y shell give rise to the magnetic force $\mathbf{F}_{mag\ 2}$ with the corresponding contributions given by Eqs. (10.83) and (10.84), respectively:

$$\mathbf{F}_{mag\ 2} = (1+1)\frac{1}{Z}\frac{\hbar^2}{m_e r_{18}^2 r_{12}}\sqrt{s(s+1)}\mathbf{i}_\mathbf{r} + \frac{1}{Z}\frac{4\hbar^2}{m_e r_{18}^2 r_{12}}\sqrt{s(s+1)}\mathbf{i}_\mathbf{r} = \frac{1}{Z}\frac{6\hbar^2}{m_e r_{18}^2 r_{12}}\sqrt{s(s+1)}\mathbf{i}_\mathbf{r} \quad (18.36)$$

The outward centrifugal force on electron 18 is balanced by the electric force and the magnetic forces (on electron 18). The radius of the outer electron is calculated by equating the outward centrifugal force to the sum of the electric (Eq. (18.33)), diamagnetic (Eq. (18.35)), and paramagnetic (Eqs. (18.34) and (18.36)) forces as follows:

$$\frac{m_e v_{18}^2}{r_{18}} = \frac{(Z-17)e^2}{4\pi\varepsilon_0 r_{18}^2} + \frac{6\hbar^2}{Zm_e r_{18}^2 r_{12}}\sqrt{s(s+1)} + \frac{\hbar^2}{Zm_e r_{18}^3}\sqrt{s(s+1)} \tag{18.37}$$

Substitution of $v_{18} = \frac{\hbar}{m_e r_{18}}$ (Eq. (1.35)), $Z = 17$, and $s = \frac{1}{2}$ into Eq. (18.37) gives:

$$\frac{\hbar^2}{m_e r_{18}^3} = \frac{6\hbar^2}{17m_e r_{18}^2 r_{12}}\sqrt{\frac{3}{4}} + \frac{\hbar^2}{17m_e r_{18}^3}\sqrt{\frac{3}{4}} \tag{18.38}$$

$$r_{18} = \frac{\frac{\hbar^2}{m_e}\left(1 - \frac{\sqrt{\frac{3}{4}}}{17}\right)}{\frac{6\hbar^2}{17m_e r_{12}}\sqrt{\frac{3}{4}}} \tag{18.39}$$

$$r_{18} = \frac{a_0\left(1 - \frac{\sqrt{\frac{3}{4}}}{17}\right)}{\frac{6\sqrt{\frac{3}{4}}}{17 r_{12}}},\ r_{12}\ \textit{in units of}\ a_0 \tag{18.40}$$

Substitution of $\frac{r_{12}}{a_0} = 0.86545$ (Eq. (10.255)) into Eq. (18.40) gives:

$$r_{18} = 2.68720 a_0 \tag{18.41}$$

The ionization energy of the chloride ion is given by the magnetic energy of the outer electron calculated by integrating the sum of the diamagnetic (Eq. (18.35)) and paramagnetic (Eqs. (18.34) and (18.36)) forces from r_{18} to ∞:

$$E_{magwork} = -\int_{r_{18}}^{\infty} \frac{6\hbar^2}{Zm_e r_{18}^2 r_{12}}\sqrt{\frac{3}{4}} + \frac{\hbar^2}{Zm_e r_{18}^3}\sqrt{\frac{3}{4}}dr = \frac{\hbar^2\sqrt{\frac{3}{4}}}{Zm_e r_{18}}\left(\frac{6}{r_{12}} + \frac{1}{2r_{18}}\right) \tag{18.42}$$

Eq. (18.42) with $r_{12} = 0.86545 a_0$ (Eq. (10.255)), $r_{18} = 2.68720 a_0$ (Eq. (18.41)), and $Z = 17$ gives:

$$E(\textit{ionization};\ Cl^-) = 3.67238\ eV \tag{18.43}$$

The experimental ionization energy of the chloride ion is [8]:

$$E(\textit{ionization};\ Cl^-) = 3.612724\ eV \tag{18.44}$$

CHANGE IN THE RADIUS AND IONIZATION ENERGY OF THE FLUORIDE ION DUE TO THE ION FIELD

As in the case of the alkali hydrides, the lattice energies of alkali halides are equivalent to the binding energy of the corresponding metal atom, except for an additional energy term corresponding to the Stark effect of the metal ion on the magnetic forces and energy of the halide ion. The corresponding force $\mathbf{F}_{Stark}$ on the outer electron of the fluoride ion given by Eq. (18.16) is

$$\mathbf{F}_{Stark} = \frac{1}{Z}\frac{\hbar^2}{m_e r_{10}^3}\sqrt{s(s+1)}\mathbf{i}_r \tag{18.45}$$

Then, the outward centrifugal force on electron 10 is balanced by the electric force and the magnetic forces (on electron 10). The radius of the outer electron is calculated by equating the outward centrifugal force to the sum of the electric (Eq. (18.20)), diamagnetic (Eq. (18.22)), and paramagnetic (Eqs. (18.21), (18.23), and (18.45)) forces as follows:

$$\frac{m_e v_{10}^2}{r_{10}} = \frac{(Z-9)e^2}{4\pi\varepsilon_0 r_{10}^2} - \frac{\hbar^2}{4m_e r_{10}^2 r_3}\sqrt{s(s+1)} + \frac{4\hbar^2}{Zm_e r_{10}^2 r_3}\sqrt{s(s+1)} + \frac{2\hbar^2}{Zm_e r_{10}^3}\sqrt{s(s+1)} \tag{18.46}$$

Substitution of $v_{10} = \frac{\hbar}{m_e r_{10}}$ (Eq. (1.35)), $Z = 9$, and $s = \frac{1}{2}$ into Eq. (18.46) gives:

$$r_{10} = \frac{a_0\left(1 - \frac{2\sqrt{\frac{3}{4}}}{9}\right)}{\left(\frac{4}{9} - \frac{1}{4}\right)\frac{\sqrt{\frac{3}{4}}}{r_3}},\ r_3\ \textit{in units of}\ a_0 \tag{18.47}$$

Substitution of $\frac{r_3}{a_0} = 0.51382$ (Eq. (10.62)) into Eq. (18.47) gives:

$$r_{10} = 2.46408 a_0 \tag{18.48}$$

The ionization energy of the fluoride ion is given by the magnetic energy of the outer electron calculated by integrating the sum of the diamagnetic (Eq. (18.22)) and paramagnetic (Eqs. (18.21), (18.23), and (18.45)) forces from r_{10} to ∞:

$$E_{magwork} = -\int_{r_{10}}^{\infty} -\frac{\hbar^2}{4m_e r_{10}^2 r_3}\sqrt{\frac{3}{4}} + \frac{4\hbar^2}{Zm_e r_{10}^2 r_3}\sqrt{\frac{3}{4}} + \frac{2\hbar^2}{Zm_e r_{10}^3}\sqrt{\frac{3}{4}} dr = \frac{\hbar^2\sqrt{\frac{3}{4}}}{m_e r_{10}}\left(\left(\frac{4}{Z} - \frac{1}{4}\right)\frac{1}{r_3} + \frac{1}{Zr_{10}}\right) \tag{18.49}$$

Eq. (18.49) with $r_3 = 0.51382 a_0$ (Eq. (10.62)), $r_{10} = 2.46408 a_0$ (Eq. (18.48)), and $Z = 9$ gives:

$$E(ionization;\ F^-) = 4.05046\ eV \tag{18.50}$$

The energy change of the fluoride ion $\Delta E(ionization;\ F^-)$ due to the Stark effect is given by the difference between Eqs. (18.50) and (18.30):

$$\Delta E(ionization;\ F^-) = 4.05046\ eV - 3.40603\ eV = 0.64444\ eV \tag{18.51}$$

CHANGE IN THE RADIUS AND IONIZATION ENERGY OF THE CHLORIDE ION DUE TO THE ION FIELD

Similar to the case of the alkali fluorides, the lattice energies of alkali chlorides are equivalent to the binding energy of the corresponding metal atom, except for those cases where there is an additional energy term corresponding to the Stark effect of the metal ion on the magnetic forces and energy of the chloride ion. The selection rules for the Stark effect in one-electron atoms given by Eq. (2.78) is:

$$\begin{aligned} &n = 1,2,3,4,... \\ &\ell = n-1 \\ &m_\ell = -\ell, -\ell+1, ..., 0, ..., +\ell \\ &m_s = \pm\frac{1}{2} \end{aligned} \tag{18.52}$$

The corresponding energies are given in Table 2.3. For fluoride having an outer 2p shell:

$$m_\ell = 1 \tag{18.53}$$

corresponding to the force $\mathbf{F}_{Stark}$ on the outer electron of the fluoride ion given by Eq. (18.45) and the binding energy change $\Delta E(ionization;\ F^-)$ given by Eq. (18.50).

In the case of the chloride ion, the outer shell is $3p$. For cations having an outer filled *ns or np*; $n < 3$ shell, the interaction of the $3p$ and $2p$ shells of Cl^- due to the field of the cation gives rise to a diamagnetic Stark force $\mathbf{F}_{Stark}$ corresponding to the selection rule:

$$m_\ell = -1 \tag{18.54}$$

wherein the cation's electrons cannot compensate for the diamagnetism by changing orientation. Thus, for Li^+ and Na^+

$$\mathbf{F}_{Stark} = -\frac{1}{Z}\frac{\hbar^2}{m_e r_{18}^3}\sqrt{s(s+1)}\mathbf{i}_r \tag{18.55}$$

and for K^+, Rb^+, and Cs^+ with *ns or np*; $n \geq 3$

$$\mathbf{F}_{Stark} = 0 \tag{18.56}$$

Then, the outward centrifugal force on electron 18 is balanced by the electric force and the magnetic forces (on electron 18). The radius of the outer electron is calculated by equating the outward centrifugal force to the sum of the electric (Eq. (18.33)), diamagnetic (Eq. (18.35)), and paramagnetic (Eqs. (18.34), (18.36), and (18.55)) forces as follows:

$$\frac{m_e v_{18}^2}{r_{18}} = \frac{(Z-17)e^2}{4\pi\varepsilon_0 r_{18}^2} + \frac{6\hbar^2}{Zm_e r_{18}^2 r_{12}}\sqrt{s(s+1)} \tag{18.57}$$

Substitution of $v_{18} = \frac{\hbar}{m_e r_{18}}$ (Eq. (1.35)), $Z = 17$, and $s = \frac{1}{2}$ into Eq. (18.57) gives:

$$r_{18} = \frac{a_0}{\frac{6\sqrt{\frac{3}{4}}}{17 r_{12}}},\ r_{12}\ in\ units\ of\ a_0 \tag{18.58}$$

Substitution of $\frac{r_{12}}{a_0} = 0.86545$ (Eq. (10.255)) into Eq. (18.58) gives:

$$r_{18} = 2.83145 a_0 \tag{18.59}$$

The ionization energy of the chloride ion is given by the magnetic energy of the outer electron calculated by integrating the sum of the diamagnetic (Eq. (18.35)) and paramagnetic (Eqs. (18.34), (18.36), and (18.55)) forces from r_{18} to ∞:

$$E_{magwork} = -\int_{r_{18}}^{\infty} \frac{6\hbar^2}{Z m_e r_{18}^2 r_{12}} \sqrt{\frac{3}{4}} dr = \frac{6\hbar^2 \sqrt{\frac{3}{4}}}{Z m_e r_{18} r_{12}} \tag{18.60}$$

Eq. (18.60) with $r_{12} = 0.86545 a_0$ (Eq. (10.255)), $r_{18} = 2.83145 a_0$ (Eq. (18.59)), and $Z = 17$ gives:

$$E(ionization;\ Cl^-) = 3.39420\ eV \tag{18.61}$$

For Li^+ and Na^+ chlorides, the energy change of the chloride ion $\Delta E(ionization;\ Cl^-)$ due to the Stark effect is given by the difference between Eqs. (18.61) and (18.43).

$$\Delta E(ionization;\ Cl^-) = 3.39420\ eV - 3.67238\ eV = -0.27818\ eV \tag{18.62}$$

LITHIUM FLUORIDE

The calculated ionic radii for Li^+ and F^- ions in LiF given by Eqs. (10.49) and (18.48) are $0.35566 a_0$ and $2.46408 a_0$, respectively. But, the interionic distance cannot be the sum of the contact radii since the calculated ionization energies of Li^+ (Eqs. (7.35), (7.45-7.46), and (7.63)) and F^- (Eq. (18.50)) are $75.665\ eV$ and $4.05046\ eV$, respectively. Furthermore, since the calculated ionization energy (Eq. (10.25)) of Li to Li^+ is $5.40381\ eV$ as shown in Table 10.1 and the ionization energy (Eq. (18.50)) of F^- to F is $4.05046\ eV$, for sufficiently small interionic distances, the lithium ion may be reduced.

Substitution of $BE(Li) = 8.65786\ X\ 10^{-19}\ J$ and $\Delta E(ionization;\ F^-) = 0.64444\ eV\ \left(1.03251\ X\ 10^{-19}\ J\right)$ (Eq. (18.51)) into Eq. (18.17) gives the calculated lattice energy of:

$$\begin{aligned} \Delta U &= N M_c \left(BE(Li) + \Delta E(ionization;\ F^-) \right) \\ &= 1.74756 N \left(8.65786\ X\ 10^{-19}\ J + 1.03251\ X\ 10^{-19}\ J \right) \\ &= 1019.8\ kJ/mole\ \left(243.7\ kcal/mole\right) \end{aligned} \tag{18.63}$$

This agrees well with the experimental lattice energy of $\Delta U = 250.7\ kcal/mole$ [9] and confirms that the ionic compound LiF comprises a precise packing of discrete ions.

The $Li — F$ distance, $r_0(LiF)$, calculated using Eq. (18.18) with the substitution of $BE(Li) = 8.65786\ X\ 10^{-19}\ J$ and $\Delta E(ionization;\ F^-) = 1.03251\ X\ 10^{-19}\ J$ is:

$$r_0(LiF) = 2.16\ X\ 10^{-10}\ m \tag{18.64}$$

The calculated $Li — F$ is in reasonable agreement with the experimental distance of $r_0(LiF) = 2.01\ X\ 10^{-10}\ m$ [10]. Using the $Li — F$ distance and the calculated ionic radii, the lattice structure of LiF is shown in Figure 18.3A.

SODIUM FLUORIDE

The calculated ionic radii for Na^+ and F^- ions in NaF given by Eqs. (10.212) and (18.48) are $0.560945 a_0$ and $2.46408 a_0$, respectively. But, the interionic distance cannot be the sum of the contact radii since the calculated ionization energies of Na^+ (Eqs. (10.212-10.213)) and F^- (Eq. (18.50)) are $48.5103\ eV$ and $4.05046\ eV$, respectively. Furthermore, since the calculated ionization energy (Eqs. (10.226-10.227)) of Na to Na^+ is $5.12592\ eV$ as shown in Table 10.10 and the ionization energy (Eq. (18.50)) of F^- to F is $4.05046\ eV$, for sufficiently small interionic distances, the sodium ion may be reduced.

Substitution of $BE(Na) = 8.21263\ X\ 10^{-19}\ J$ and $\Delta E(ionization;\ F^-) = 1.03251\ X\ 10^{-19}\ J$ (Eq. (18.51)) into Eq. (18.17) gives the calculated lattice energy of:

$$\begin{aligned} \Delta U &= N M_c \left(BE(Na) + \Delta E(ionization;\ F^-) \right) \\ &= 1.74756 N \left(8.21263\ X\ 10^{-19}\ J + 1.03251\ X\ 10^{-19}\ J \right) \\ &= 972.95\ kJ/mole\ \left(232.54\ kcal/mole\right) \end{aligned} \tag{18.65}$$

This agrees well with the experimental lattice energy of $\Delta U = 222\ kcal/mole$ [9] and confirms that the ionic compound NaF comprises a precise packing of discrete ions.

The $Na — F$ distance, $r_0(NaF)$, calculated using Eq. (18.18) with the substitution of $BE(Na) = 8.21263\ X\ 10^{-19}\ J$ and $\Delta E(ionization;\ F^-) = 1.03251\ X\ 10^{-19}\ J$ is:

$$r_0(NaF) = 2.28\ X\ 10^{-10}\ m \tag{18.66}$$

The calculated $Na — F$ is in reasonable agreement with the experimental distance of $r_0(NaF) = 2.32\ X\ 10^{-10}\ m$ [10]. Using the $Na — F$ distance and the calculated ionic radii, the lattice structure of NaF is shown in Figure 18.3B.

Figure 18.3. The crystal structures of MF all to the same scale. (Li^+ = green, Na^+ = yellow, K^+ = purple, Rb^+ = blue, Cs^+ = red, and F^- = gold). (A) The crystal structure of LiF. (B) The crystal structure of NaF. (C) The crystal structure of KF. (D) The crystal structure of RbF. (E) The crystal structure of CsF.

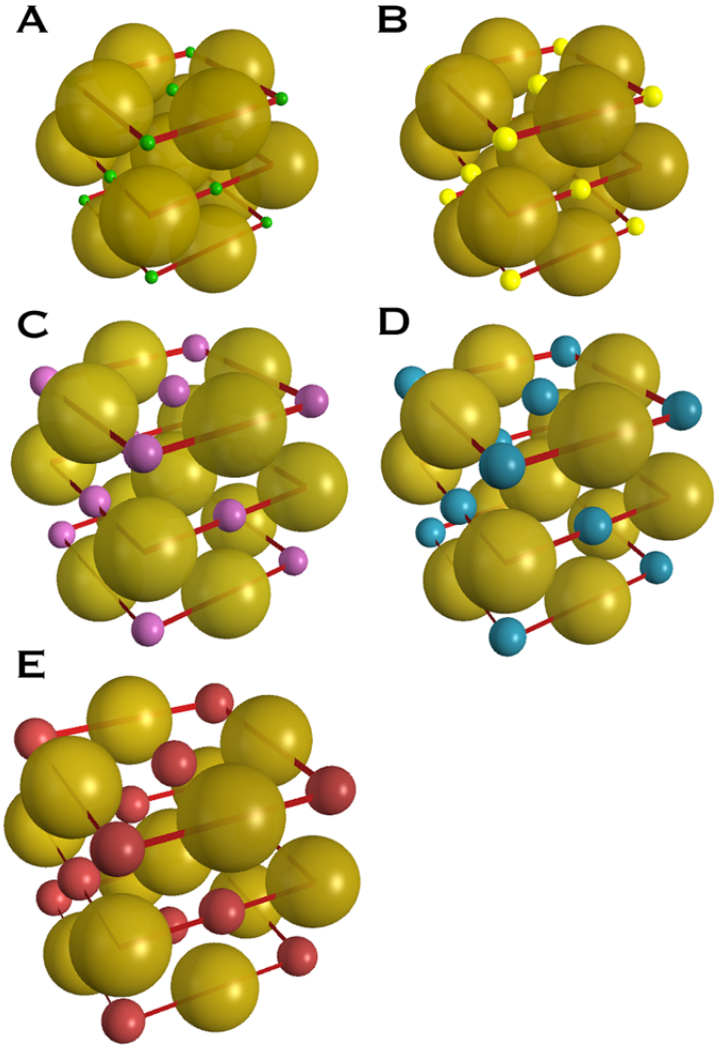

POTASSIUM FLUORIDE

The calculated ionic radii for K^+ and F^- ions in KF given by Eqs. (10.399) and (18.48) are $0.85215a_0$ and $2.46408a_0$, respectively. But, the interionic distance cannot be the sum of the contact radii since the calculated ionization energies of K^+ (Eqs. (10.399-10.400)) and F^- (Eq. (18.50)) are 31.9330 eV and 4.05046 eV, respectively. Furthermore, since the calculated ionization energy (Eqs. (10.414-10.415)) of K to K^+ is 4.33 eV as shown in Table 10.19 and the ionization energy (Eq. (18.50)) of F^- to F is 4.05046 eV, for sufficiently small interionic distances, the potassium ion may be reduced.

Substitution of $BE(K) = 6.93095\ X\ 10^{-19}\ J$ and $\Delta E(ionization;\ F^-) = 1.03251\ X\ 10^{-19}\ J$ (Eq. (18.51)) into Eq. (18.17) gives the calculated lattice energy of:

$$\begin{aligned} \Delta U &= NM_c\left(BE(K) + \Delta E(ionization;\ F^-)\right) \\ &= 1.74756N\left(6.93095\ X\ 10^{-19}\ J + 1.03251\ X\ 10^{-19}\ J\right) \\ &= 838.06\ kJ/mole\ \left(200.30\ kcal/mole\right) \end{aligned} \tag{18.67}$$

This agrees well with the experimental lattice energy of $\Delta U = 198\ kcal/mole$ [9] and confirms that the ionic compound KF comprises a precise packing of discrete ions.

The $K — F$ distance, $r_0(KF)$, calculated using Eq. (18.18) with the substitution of $BE(K) = 6.93095\ X\ 10^{-19}\ J$ and $\Delta E(ionization;\ F^-) = 1.03251\ X\ 10^{-19}\ J$ is:

$$r_0(KF) = 2.68\ X\ 10^{-10}\ m \tag{18.68}$$

The calculated $K — F$ is in reasonable agreement with the experimental distance of $r_0(KF) = 2.67\ X\ 10^{-10}\ m$ [10]. Using the $K — F$ distance and the calculated ionic radii, the lattice structure of KF is shown in Figure 18.3C.

RUBIDIUM FLUORIDE

The Rb^+ ionic radius calculated using Eq. (10.102) and the experimental ionization energy of Rb^+, $27.2895\ eV$ [6] is $0.99714a_0$ and the calculated ionic radius F^- ions in RbF given by Eq. (18.48) is $2.46408a_0$. But, the interionic distance cannot be the sum of the contact radii since the experimental and calculated ionization energies of Rb^+ [6] and F^- (Eq. (18.50)) are $27.2895\ eV$ and $4.05046\ eV$, respectively. Furthermore, since the experimental ionization energy of Rb to Rb^+ is $4.177128\ eV$ [6] and the ionization energy (Eq. (18.50)) of F^- to F is $4.05046\ eV$, for sufficiently small interionic distances, the rubidium ion may be reduced.

Substitution of $BE(Rb) = 6.6925\ X\ 10^{-19}\ J$ and $\Delta E(ionization;\ F^-) = 1.03251\ X\ 10^{-19}\ J$ (Eq. (18.51)) into Eq. (18.17) gives the calculated lattice energy of:

$$\begin{aligned}\Delta U &= NM_c\left(BE(Rb) + \Delta E(ionization;\ F^-)\right)\\ &= 1.74756N\left(6.6925\ X\ 10^{-19}\ J + 1.03251\ X\ 10^{-19}\ J\right)\\ &= 812.97\ kJ/mole\ \ (194.30\ kcal/mole)\end{aligned} \tag{18.69}$$

This agrees well with the experimental lattice energy of $\Delta U = 190\ kcal/mole$ [9] and confirms that the ionic compound RbF comprises a precise packing of discrete ions.

The $Rb — F$ distance, $r_0(RbF)$, calculated using Eq. (18.18) with the substitution of $BE(Rb) = 6.6925\ X\ 10^{-19}\ J$ and $\Delta E(ionization;\ F^-) = 1.03251\ X\ 10^{-19}\ J$ is:

$$r_0(RbF) = 2.77\ X\ 10^{-10}\ m \tag{18.70}$$

The calculated $Rb — F$ is in reasonable agreement with the experimental distance of $r_0(RbF) = 2.83\ X\ 10^{-10}\ m$ [10]. Using the $Rb — F$ distance and the ionic radii, the lattice structure of RbF is shown in Figure 18.3D.

CESIUM FLUORIDE

The Cs^+ ionic radius calculated using Eq. (10.102) and the experimental ionization energy of Cs^+, $23.15744\ eV$ [6] is $1.17506a_0$ and the calculated ionic radius F^- ions in CsF given by Eq. (18.48) is $2.46408a_0$. But, the interionic distance cannot be the sum of the contact radii since the experimental and calculated ionization energies of Cs^+ [6] and F^- (Eq. (18.50)) are $23.15744\ eV$ and $4.05046\ eV$, respectively. Furthermore, since the experimental ionization energy of Cs to Cs^+ is $3.893905\ eV$ [6] and the ionization energy (Eq. (18.50)) of F^- to F is $4.05046\ eV$, for sufficiently small interionic distances, the cesium ion may be reduced.

Substitution of $BE(Cs) = 6.23872\ X\ 10^{-19}\ J$ and $\Delta E(ionization;\ F^-) = 1.03251\ X\ 10^{-19}\ J$ (Eq. (18.51)) into Eq. (18.17) gives the calculated lattice energy of:

$$\begin{aligned}\Delta U &= NM_c\left(BE(Cs) + \Delta E(ionization;\ F^-)\right)\\ &= 1.74756N\left(6.23872\ X\ 10^{-19}\ J + 1.03251\ X\ 10^{-19}\ J\right)\\ &= 765.21\ kJ/mole\ \ (182.89\ kcal/mole)\end{aligned} \tag{18.71}$$

This agrees well with the experimental lattice energy of $\Delta U = 181\ kcal/mole$ [9] and confirms that the ionic compound CsF comprises a precise packing of discrete ions.

The $Cs — F$ distance, $r_0(CsF)$, calculated using Eq. (18.18) with the substitution of $BE(Cs) = 6.23872\ X\ 10^{-19}\ J$ and $\Delta E(ionization;\ F^-) = 1.03251\ X\ 10^{-19}\ J$ is:

$$r_0(CsF) = 2.96\ X\ 10^{-10}\ m \tag{18.72}$$

The calculated $Cs — F$ is in reasonable agreement with the experimental distance of $r_0(CsF) = 3.01\ X\ 10^{-10}\ m$ [10]. Using the $Cs — F$ distance and the ionic radii, the lattice structure of CsF is shown in Figure 18.3E.

LITHIUM CHLORIDE

The calculated ionic radii for Li^+ and Cl^- ions in $LiCl$ given by Eqs. (10.49) and (18.59) are $0.35566a_0$ and $2.83145a_0$, respectively. But, the interionic distance cannot be the sum of the contact radii since the calculated ionization energies of Li^+ (Eqs. (7.35), (7.45-7.46), and (7.63)) and Cl^- (Eq. (18.61)) are $75.665\ eV$ and $3.39420\ eV$, respectively. Furthermore, since the calculated ionization energy (Eq. (10.25)) of Li to Li^+ is $5.40381\ eV$ as shown in Table 10.1 and the ionization energy (Eq. (18.61)) of Cl^- to Cl is $3.39420\ eV$, for sufficiently small interionic distances, the lithium ion may be reduced.

Substitution of $BE\left(Li\right)=8.65786\ X\ 10^{-19}\ J$ and $\Delta E(ionization;\ Cl^-)=-0.27818\ eV\ \left(-4.45691\ X\ 10^{-20}\ J\right)$ (Eq. (18.62)) into Eq. (18.17) gives the calculated lattice energy of:

$$\begin{aligned}\Delta U &= NM_c\left(BE\left(Li\right)+\Delta E(ionization;\ Cl^-)\right)\\ &=1.74756N\left(8.65786\ X\ 10^{-19}\ J-4.45691\ X\ 10^{-20}\ J\right)\\ &=864.24\ kJ/mole\ \left(206.56\ kcal/mole\right)\end{aligned}\tag{18.73}$$

This agrees well with the experimental lattice energy of $\Delta U=207\ kcal/mole$ [9] and confirms that the ionic compound $LiCl$ comprises a precise packing of discrete ions.

The $Li\text{—}Cl$ distance, $r_0\left(LiCl\right)$, calculated using Eq. (18.18) with the substitution of $BE\left(Li\right)=8.65786\ X\ 10^{-19}\ J$ and $\Delta E(ionization;\ Cl^-)=-4.45691\ X\ 10^{-20}\ J$ is:

$$r_0\left(LiCl\right)=2.59\ X\ 10^{-10}\ m\tag{18.74}$$

The calculated $Li\text{—}Cl$ is in reasonable agreement with the experimental distance of $r_0\left(LiCl\right)=2.57\ X\ 10^{-10}\ m$ [10]. Using the $Li\text{—}Cl$ distance and the calculated ionic radii, the lattice structure of $LiCl$ is shown in Figure 18.4A.

Figure 18.4. The crystal structures of MCl all to the same scale. (Li^+ = green, Na^+ = yellow, K^+ = purple, Rb^+ = blue, Cs^+ = red, and Cl^- = brown). (A) The crystal structure of $LiCl$. (B) The crystal structure of $NaCl$. (C) The crystal structure of KCl. (D) The crystal structure of $RbCl$. (E) The crystal structure of $CsCl$.

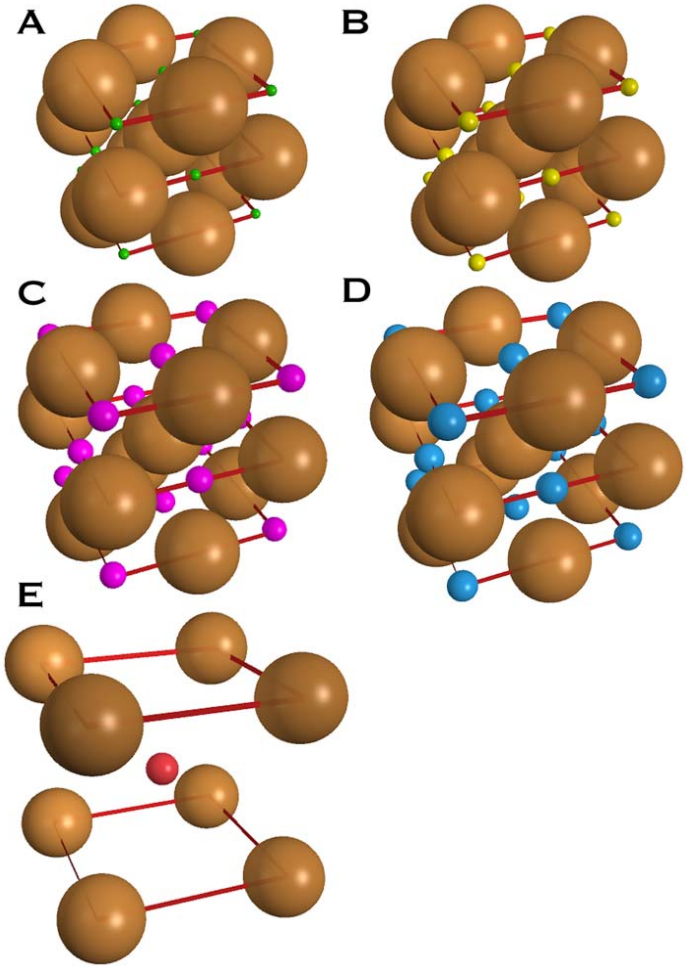

SODIUM CHLORIDE

The calculated ionic radii for Na^+ and Cl^- ions in $NaCl$ given by Eqs. (10.212) and (18.59) are $0.560945a_0$ and $2.83145a_0$, respectively. But, the interionic distance cannot be the sum of the contact radii since the calculated ionization energies of Na^+ (Eqs. (10.212-10.213)) and Cl^- (Eq. (18.61)) are $48.5103\ eV$ and $3.39420\ eV$, respectively. Furthermore, since the calculated ionization energy (Eqs. (10.226-10.227)) of Na to Na^+ is $5.12592\ eV$ as shown in Table 10.10 and the ionization energy (Eq. (18.61)) of Cl^- to Cl is $3.39420\ eV$, for sufficiently small interionic distances, the sodium ion may be reduced.

Substitution of $BE(Na) = 8.21263\ X\ 10^{-19}\ J$ and $\Delta E(ionization;\ Cl^-) = -4.45691\ X\ 10^{-20}\ J$ (Eq. (18.62)) into Eq. (18.17) gives the calculated lattice energy of:

$$\begin{aligned} \Delta U &= NM_c\left(BE(Na) + \Delta E(ionization;\ Cl^-)\right) \\ &= 1.74756N\left(8.21263\ X\ 10^{-19}\ J - 4.45691\ X\ 10^{-20}\ J\right) \\ &= 817.38\ kJ/mole\ \ (195.36\ kcal/mole) \end{aligned} \tag{18.75}$$

This agrees well with the experimental lattice energy of $\Delta U = 189\ kcal/mole$ [9] and confirms that the ionic compound $NaCl$ comprises a precise packing of discrete ions.

The $Na-Cl$ distance, $r_0(NaCl)$, calculated using Eq. (18.18) with the substitution of $BE(Na) = 8.21263\ X\ 10^{-19}\ J$ and $\Delta E(ionization;\ Cl^-) = -4.45691\ X\ 10^{-20}\ J$ is:

$$r_0(NaCl) = 2.75\ X\ 10^{-10}\ m \tag{18.76}$$

The calculated $Na-Cl$ is in reasonable agreement with the experimental distance of $r_0(NaCl) = 2.82\ X\ 10^{-10}\ m$ [10]. Using the $Na-Cl$ distance and the calculated ionic radii, the lattice structure of $NaCl$ is shown in Figure 18.4B.

POTASSIUM CHLORIDE

The calculated ionic radii for K^+ and Cl^- ions in KCl given by Eqs. (10.399) and (18.59) are $0.85215a_0$ and $2.83145a_0$, respectively. But, the interionic distance cannot be the sum of the contact radii since the calculated ionization energies of K^+ (Eqs. (10.399-10.400)) and Cl^- (Eq. (18.61)) are $31.9330\ eV$ and $3.39420\ eV$, respectively. Furthermore, since the calculated ionization energy (Eqs. (10.414-10.415)) of K to K^+ is $4.33\ eV$ as shown in Table 10.19 and the ionization energy (Eq. (18.61)) of Cl^- to Cl is $3.39420\ eV$, for sufficiently small interionic distances, the potassium ion may be reduced.

Substitution of $BE(K) = 6.93095\ X\ 10^{-19}\ J$ and $\Delta E(ionization;\ Cl^-) = -4.45691\ X\ 10^{-20}\ J$ (Eq. (18.62)) into Eq. (18.17) gives the calculated lattice energy of:

$$\begin{aligned} \Delta U &= NM_c\left(BE(K) + \Delta E(ionization;\ Cl^-)\right) \\ &= 1.74756N\left(6.93095\ X\ 10^{-19}\ J - 4.45691\ X\ 10^{-20}\ J\right) \\ &= 729.41\ kJ/mole\ \ (174.33\ kcal/mole) \end{aligned} \tag{18.77}$$

This agrees well with the experimental lattice energy of $\Delta U = 172\ kcal/mole$ [9] and confirms that the ionic compound KCl comprises a precise packing of discrete ions.

The $K-Cl$ distance, $r_0(KCl)$, calculated using Eq. (18.18) with the substitution of $BE(K) = 6.93095\ X\ 10^{-19}\ J$ and $\Delta E(ionization;\ Cl^-) = -4.45691\ X\ 10^{-20}\ J$ is:

$$r_0(KCl) = 3.11\ X\ 10^{-10}\ m \tag{18.78}$$

The calculated $K-Cl$ is in reasonable agreement with the experimental distance of $r_0(KCl) = 3.15\ X\ 10^{-10}\ m$ [10]. Using the $K-Cl$ distance and the calculated ionic radii, the lattice structure of KCl is shown in Figure 18.4C.

RUBIDIUM CHLORIDE

The Rb^+ ionic radius calculated using Eq. (10.102) and the experimental ionization energy of Rb^+, $27.2895\ eV$ [6] is $0.99714a_0$ and the calculated ionic radius Cl^- ions in $RbCl$ given by Eq. (18.59) is $2.83145a_0$. But, the interionic distance cannot be the sum of the contact radii since the experimental and calculated ionization energies of Rb^+ [6] and Cl^- (Eq. (18.61)) are $27.2895\ eV$ and $3.39420\ eV$, respectively. Furthermore, since the experimental ionization energy of Rb to Rb^+ is $4.177128\ eV$ [6] and the ionization energy (Eq. (18.61)) of Cl^- to Cl is $3.39420\ eV$, for sufficiently small interionic distances, the rubidium ion may be reduced.

Substitution of $BE(Rb) = 6.6925\ X\ 10^{-19}\ J$ and $\Delta E(ionization;\ Cl^-) = -4.45691\ X\ 10^{-20}\ J$ (Eq. (18.62)) into Eq. (18.17) gives the calculated lattice energy of:

$$\begin{aligned}\Delta U &= NM_c\left(BE\left(Rb\right)+\Delta E(ionization;\ Cl^-)\right)\\ &=1.74756N\left(6.6925\ X\ 10^{-19}\ J-4.45691\ X\ 10^{-20}\ J\right)\\ &=704.31\ kJ/mole\ \left(168.33\ kcal/mole\right)\end{aligned}\tag{18.79}$$

This agrees well with the experimental lattice energy of $\Delta U = 166\ kcal/mole$ [9] and confirms that the ionic compound $RbCl$ comprises a precise packing of discrete ions.

The $Rb\text{—}Cl$ distance, $r_0\left(RbCl\right)$, calculated using Eq. (18.18) with the substitution of $BE\left(Rb\right)=6.6925\ X\ 10^{-19}\ J$ and $\Delta E(ionization;\ Cl^-)=-4.45691\ X\ 10^{-20}\ J$ is:

$$r_0\left(RbCl\right)=3.23\ X\ 10^{-10}\ m\tag{18.80}$$

The calculated $Rb\text{—}Cl$ is in reasonable agreement with the experimental distance of $r_0\left(RbCl\right)=3.29\ X\ 10^{-10}\ m$ [10]. Using the $Rb\text{—}Cl$ distance and the ionic radii, the lattice structure of $RbCl$ is shown in Figure 18.4D.

CESIUM CHLORIDE

The Cs^+ ionic radius calculated using Eq. (10.102) and the experimental ionization energy of Cs^+, $23.15744\ eV$ [6] is $1.17506a_0$ and the calculated ionic radius Cl^- ions in $CsCl$ given by Eq. (18.59) is $2.83145a_0$. But, the interionic distance cannot be the sum of the contact radii since the experimental and calculated ionization energies of Cs^+ [6] and Cl^- (Eq. (18.61)) are $23.15744\ eV$ and $3.39420\ eV$, respectively. Furthermore, since the experimental ionization energy of Cs to Cs^+ is $3.893905\ eV$ [6] and the ionization energy (Eq. (18.61)) of Cl^- to Cl is $3.39420\ eV$, for sufficiently small interionic distances, the cesium ion may be reduced.

Substitution of $BE\left(Cs\right)=6.23872\ X\ 10^{-19}\ J$ and $\Delta E(ionization;\ Cl^-)=-4.45691\ X\ 10^{-20}\ J$ (Eq. (18.62)) into Eq. (18.17) gives the calculated lattice energy of:

$$\begin{aligned}\Delta U &= NM_c\left(BE\left(Cs\right)+\Delta E(ionization;\ Cl^-)\right)\\ &=1.76267N\left(6.23872\ X\ 10^{-19}\ J-4.45691\ X\ 10^{-20}\ J\right)\\ &=662.23\ kJ/mole\ \left(158.28\ kcal/mole\right)\end{aligned}\tag{18.81}$$

This agrees well with the experimental lattice energy of $\Delta U = 160\ kcal/mole$ [9] and confirms that the ionic compound $CsCl$ comprises a precise packing of discrete ions.

The $Cs\text{—}Cl$ distance, $r_0\left(CsCl\right)$, calculated using Eq. (18.18) with the substitution of $BE\left(Cs\right)=6.23872\ X\ 10^{-19}\ J$ and $\Delta E(ionization;\ Cl^-)=-4.45691\ X\ 10^{-20}\ J$ is:

$$r_0\left(CsCl\right)=3.49\ X\ 10^{-10}\ m\tag{18.82}$$

The calculated $Cs\text{—}Cl$ is in reasonable agreement with the experimental distance of $r_0\left(CsCl\right)=3.54\ X\ 10^{-10}\ m$ [10]. Using the $Cs\text{—}Cl$ distance and the ionic radii, the lattice structure of $CsCl$ is shown in Figure 18.4E.

REFERENCES

1. W. M. Muller, J. P. Blackledge, G. G. Libowitz, *Metal Hydrides*, Academic Press, New York, (1968), pp. 217-229.
2. J. C. Bailar, H. J. Emeleus, R. Nyholm, A. F. Trotman-Dickenson, (Editors), *Comprehensive Inorganic Chemistry*, Pergamon Press, (1973), p. 401.
3. G. L. Miessler, D. A. Tarr, *Inorganic Chemistry*, Third Edition, Pearson Prentice Hall, Upper Saddle River, New Jersey, (2004), pp. 207-222.
4. D. R. Stephens, E. M. Lilley, "Compressions of isotopic lithium hydrides," J. Appl. Phys. Vol. 39, (1968), pp. 177-180.
5. R. A. MacDonald, "Determination of the effective force constants between a substitutional impurity and its nearest neighbors in an alkali halide crystal," Phys. Rev., Vol. 150, No. 2, (1966), pp. 597-602.
6. D. R. Lide, *CRC Handbook of Chemistry and Physics*, 86th Edition, CRC Press, Taylor & Francis, Boca Raton, (2005-6), pp. 10-202 to 10-204.
7. K. G. Spears, "Repulsive potentials of atomic ions, atoms, and molecules," J. Chem. Phys., Vol. 57, No. 5, (1972), pp. 1842-1849.
8. D. R. Lide, *CRC Handbook of Chemistry and Physics*, 86th Edition, CRC Press, Taylor & Francis, Boca Raton, (2005-6), p. 10-156.
9. D. R. Lide, *CRC Handbook of Chemistry and Physics*, 86th Edition, CRC Press, Taylor & Francis, Boca Raton, (2005-6), p. 12-21.
10. D. B. Sirdeshmukh, L. Lirdeshmukh, K. G. Subhadra, *Alkali Halides: A Handbook of Physical Properties*, Academic Press, New York, (2001).

Chapter 19

THE NATURE OF THE METALLIC BOND OF ALKALI METALS

GENERALIZATION OF THE NATURE OF THE METALLIC BOND

Common metals comprise alkali, alkaline earth, and transition elements and have the properties of high electrical and thermal conductivity, opacity, surface luster, ductility, and malleability. From Maxwell's equations, the electric field inside of a metal conductor is zero. As shown in Appendix II, the bound electron exhibits this feature. The charge is confined to a two-dimensional layer and the field is normal and discontinuous at the surface. The relationship between the electric field equation and the electron source charge-density function is given by Maxwell's equation in two dimensions [1-3].

$$\mathbf{n} \bullet \left(\mathbf{E}_1 - \mathbf{E}_2 \right) = \frac{\sigma}{\varepsilon_0} \tag{19.1}$$

where $\mathbf{n}$ is the normal unit vector, $\mathbf{E}_1 = 0$ ($\mathbf{E}_1$ is the electric field inside of the MO), $\mathbf{E}_2$ is the electric field outside of the MO and σ is the surface charge density. The properties of metals can be accounted for by the existence of free electrons bound to the corresponding lattice of positive ions. Based on symmetry, the natural coordinates are Cartesian. Then, the problem of the solution of the nature of the metal bonds reduces to a familiar electrostatics problem—the fields and the two-dimensional surface charge density induced on a planar conductor by a point charge such that a zero potential inside of the conductor is maintained according to Maxwell's equations.

There are many examples of charges located near a conductor such as an electron emitted from a cathode or a power line suspended above the conducting earth. Consider a point charge $+e$ at a position $\left(0,0,d\right)$ near an infinite planar conductor as shown in Figure 19.1.

Figure 19.1. A point charge above an infinite planar conductor.

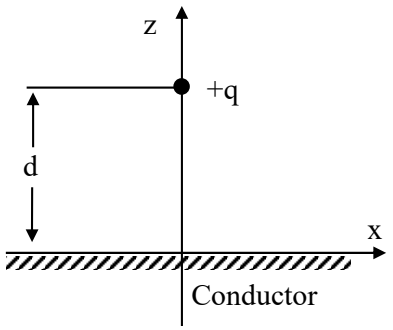

With the potential of the conductor set equal to zero, the potential Φ in the upper half space ($z > 0$) is given by Poisson's equation (Eq. (3.9)), subject to the boundary condition that $\Phi = 0$ at $z = 0$ and at $z = \infty$. The potential for the point charge in free space is:

$$\Phi\left(x,y,z\right) = \frac{e}{4\pi\varepsilon_0}\left(\frac{1}{\sqrt{x^2 + y^2 + \left(z-d\right)^2}} \right) \tag{19.2}$$

The Poisson solution that meets the boundary condition that the potential is zero at the surface of the infinite planar conductor is

that due to the point charge and an image charge of $-e$ at the position $(0,0,-d)$ as shown in Figure 19.2.

Figure 19.2. A point charge above an infinite planar conductor and the image charge to meet the boundary condition $\Phi = 0$ at $z = 0$.

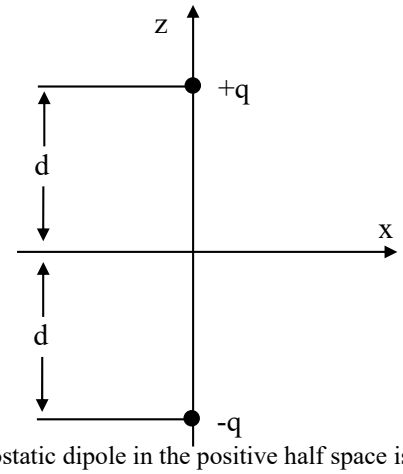

The potential for the corresponding electrostatic dipole in the positive half space is:

$$\Phi(x,y,z) = \begin{cases} \dfrac{e}{4\pi\varepsilon_0}\left(\dfrac{1}{\sqrt{x^2+y^2+(z-d)^2}} - \dfrac{1}{\sqrt{x^2+y^2+(z+d)^2}}\right) & \text{for } z > 0 \\ 0 & \text{for } z \le 0 \end{cases} \tag{19.3}$$

The electric field shown in Figure 19.3 is nonzero only in the positive half space and is given by:

$$\mathbf{E} = -\nabla\Phi = \frac{e}{4\pi\varepsilon_0}\left(\frac{x\mathbf{i}_x + y\mathbf{i}_y + (z-d)\mathbf{i}_z}{\left(x^2+y^2+(z-d)^2\right)^{3/2}} - \frac{x\mathbf{i}_x + y\mathbf{i}_y + (z+d)\mathbf{i}_z}{\left(x^2+y^2+(z+d)^2\right)^{3/2}}\right) \tag{19.4}$$

Figure 19.3. Electric field lines from a positive point charge near an infinite planar conductor.

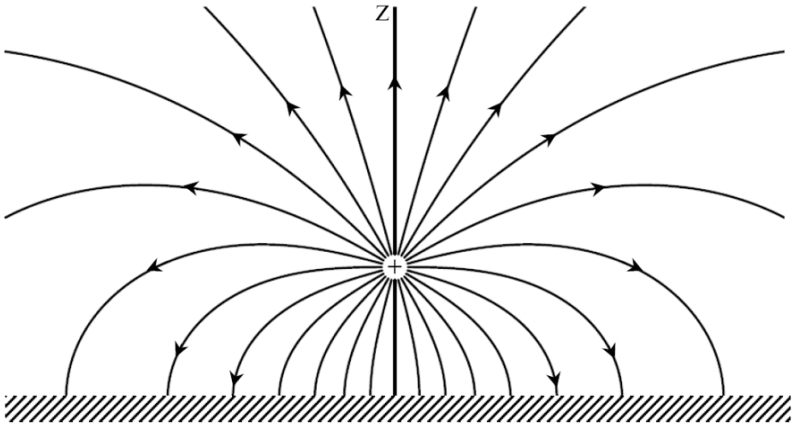

At the surface ($z = 0$), the electric field is normal to the conductor as required by Gauss' and Faraday's laws:

$$\mathbf{E}(x,y,0) = \frac{-ed\mathbf{i}_z}{2\pi\varepsilon_0\left(x^2+y^2+d^2\right)^{3/2}} \tag{19.5}$$

The surface charge density shown in Figure 19.4 is given by Eq. (19.1) with $\mathbf{n} = \mathbf{i}_z$ and $\mathbf{E}_2 = 0$:

$$\sigma = \frac{-ed}{2\pi\left(x^2+y^2+d^2\right)^{3/2}} = \frac{-ed}{2\pi\left(\rho^2+d^2\right)^{3/2}} \tag{19.6}$$

Figure 19.4. The surface charge density distribution on the surface of the conduction planar conductor induced by the point charge at the position $(0,0,d)$. (A) The surface charge density $-\sigma(\rho)$ (shown in color-scale relief). (B) The cross-sectional view of the surface charge density.

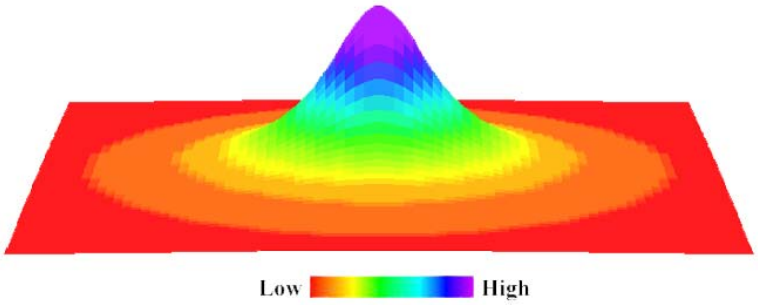

A

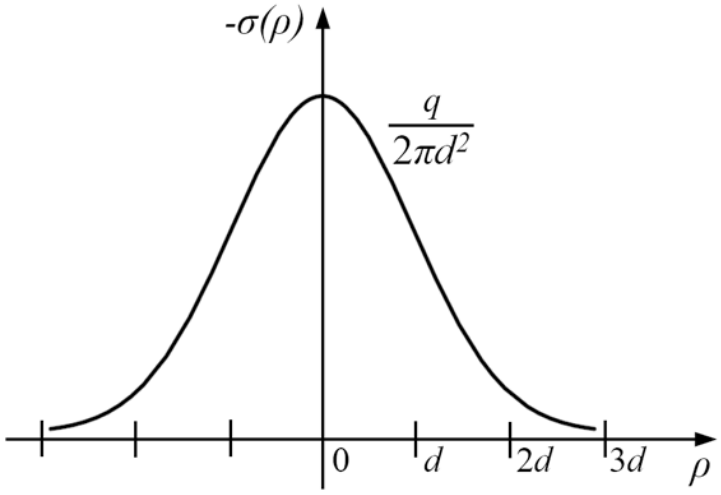

B

The total induced charge is given by the integral of the density over the surface:

$$
\begin{aligned}
q_{induced} &= \int \sigma ds \\
&= \int_{-\infty}^{\infty}\int_{-\infty}^{\infty} \frac{-ed}{2\pi\left(x^2+y^2+d^2\right)^{3/2}} dydx \\
&= \frac{-ed}{2\pi}\int_{-\infty}^{\infty}\int_{-\frac{\pi}{2}}^{\frac{\pi}{2}} \frac{\cos\theta}{x^2+d^2} d\theta dx \\
&= \frac{-ed}{\pi}\int_{-\infty}^{\infty} \frac{1}{x^2+d^2} dx \\
&= \frac{-ed}{\pi}\int_{-\frac{\pi}{2}}^{\frac{\pi}{2}} \frac{1}{d} d\theta' \\
&= -e
\end{aligned}
\tag{19.7}
$$

wherein the change of variables $y=\left(x^2+d^2\right)^{\frac{1}{2}}\tan\theta$ and $x=d\tan\theta'$ were used. The total surface charge induced on the surface of the conductor is exactly equal to the negative of the point charge located above the conductor.

Now consider the case where the infinite planar conductor is charged with a surface charge density σ corresponding to a total charge of a single electron, $-e$, and the point charge of $+e$ is due to a metal ion M^+. Then, according to Maxwell's

equations, the potential function of M^+ is given by Eq. (19.3), the electric field between M^+ and σ is given by Eqs. (19.4-19.5), and σ is given by Eq. (19.6). The field lines of M^+ end on σ, and the electric field is zero in the metal and in the negative half space. The potential energy between M^+ and σ at the surface ($z=0$) given by the product of Eq. (19.2) and Eq. (19.6) is

$$V=\int_{-\infty}^{\infty}\int_{-\infty}^{\infty}\frac{e}{4\pi\varepsilon_0}\left(\frac{1}{\sqrt{x^2+y^2+d^2}}\right)\left(\frac{-ed}{2\pi\left(x^2+y^2+d^2\right)^{3/2}}\right)dxdy \tag{19.8}$$

$$V=\frac{-e^2d}{8\pi^2\varepsilon_0}\int_{-\infty}^{\infty}\int_{-\infty}^{\infty}\frac{1}{\left(x^2+y^2+d^2\right)^2}dxdy \tag{19.9}$$

Using a change of coordinates to cylindrical and integral # 47 of Lide [4] gives:

$$V=\int_0^{\infty}\int_0^{2\pi}\frac{-e^2d}{8\pi^2\varepsilon_0\left(\rho^2+d^2\right)^2}\rho d\phi d\rho \tag{19.10}$$

$$V=\frac{-e^2d}{4\pi\varepsilon_0}\int_0^{\infty}\frac{\rho}{\left(\rho^2+d^2\right)^2}d\rho \tag{19.11}$$

$$V=\frac{-e^2d}{4\pi\varepsilon_0}\left(\frac{-1}{2\left(\rho^2+d^2\right)}\right)_0^{\infty} \tag{19.12}$$

$$V=\frac{-e^2}{4\pi\varepsilon_0(2d)} \tag{19.13}$$

The corresponding force from the negative gradient as well as the integral of the product of the electric field (Eq. (19.5)) and the charge density (Eq. (19.6)) is:

$$\begin{aligned}\mathbf{F}&=-\nabla V\\&=\int_A\mathbf{E}(x,y,0)\sigma dA\\&=\left(\frac{e^2d^2}{(2\pi)^2\varepsilon_0}\mathbf{i}_z\right)\int_0^{\infty}\int_0^{2\pi}\frac{\rho d\phi d\rho}{\left(\rho^2+d^2\right)^3}\\&=2\pi\left(\frac{e^2d^2}{(2\pi)^2\varepsilon_0}\mathbf{i}_z\right)\int_0^{\infty}\frac{\rho d\rho}{\left(\rho^2+d^2\right)^3}\\&=2\pi\left(\frac{e^2d^2}{(2\pi)^2\varepsilon_0}\mathbf{i}_z\right)\frac{1}{4d^4}\\&=\frac{e^2}{8\pi\varepsilon_0d^2}\mathbf{i}_z\end{aligned} \tag{19.14}$$

where d is treated as a variable to be solved as discussed below. The potential is equivalent to that of the charge and its image charge located a distance $2d$ apart. In addition, the potential and force are equivalent to those of the charge $+e$ and an image charge $\frac{-e}{2}$ located a distance d apart.

In addition to the infinite planar conductor at $z=0$ and the point charge $+e$ at a position $(0,0,d)$ near the infinite planar conductor as shown in Figure 19.1, next consider the introduction of a second infinite planar conductor located at position $z=2d$ as shown in Figure 19.5.

Figure 19.5. A point charge located between two infinite planar conductors.

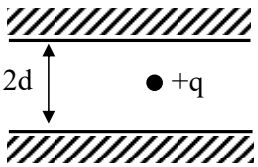

As shown, by Kong [5], an image charge at $(0,0,-d)$ meets the boundary condition of zero potential at the bottom plate, but it gives rise to a potential at the top. Similarly, an image charge at $(0,0,3d)$, meets the boundary condition of zero potential at the top plate, but it gives rise to a potential at the bottom. Satisfaction of the boundary condition of zero potential at both plates due to the presence of the initial real charge requires an infinite series of alternating positive and negative image charges spaced a distance d apart with the potential given by the summation over the real point source and its point-source image charges of $+e$ and $-e$. Since fields superimpose, by adding real charges in a periodic lattice, the image charges cancel except for one per each real charge at a distance $2d$ apart as in the original case considered in Figure 19.1.

In the real world, the idealized infinite planar conductor is a planar metal sheet experimentally comprised of an essentially infinite lattice of metal ions M^+ and free electrons that provide surface densities σ in response to an applied external field such as that due to an external charge of $+e$ due to a metal ion M^+. Then, it is required that the solutions of the external point charge at an infinite planar conductor are also those of the metal ions and free electrons of metals based on the uniqueness of solutions of Maxwell's equations and the constraint that the individual electrons in a metal conserve the classical physical laws of the macro-scale conductor. In metals, a superposition of planar free electrons given in the Electron in Free Space section replaces the infinite planar conductor. Then, the nature of the metal bond is a lattice of metal ions with field lines that end on the corresponding lattice of electrons wherein each has the two-dimensional charge density σ given by Eq. (19.6) to match the boundary conditions of equipotential, minimum energy, and conservation of charge and angular momentum for an ionized electron. Consider an infinite lattice of positive charges in the hollow Cartesian cavities whose walls are the intersecting planes of conductors and that each planar conductor comprises an electron. By Gauss' law, the field lines of each real charge end on each of the n planar-electron walls of the cavity wherein the surface charge density of contribution of each electron is that of image charge of $\frac{-e}{n}$ equidistant across each wall from a given charge $+e$. Then, each electron contributes the charge $\frac{-e}{n}$ to the corresponding ion where each is equivalent electrostatically to an image point charge at twice the distance from the point charge of $+e$ due to M^+.

Thus, the metallic bond is equivalent to the ionic bond given in the Alkali-Hydride Crystal Structures section with a Madelung constant of one with each negative ion at a position of one half the distance between the corresponding positive ions, but electrostatically equivalent to being positioned at twice this distance, the M^+-M^+-separation distance. The surface charge density of a planar electron having an electric field equivalent to that of image point charge for the corresponding positive ion of the lattice is shown in Figure 19.6.

Figure 19.6. The surface charge density $-\sigma(\rho)$ of a planar electron shown in color scale.

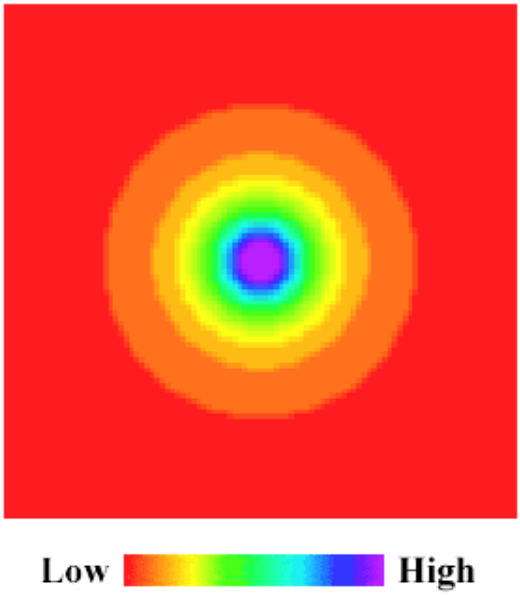

ALKALI-METAL CRYSTAL STRUCTURES

The alkali metals are lithium (*Li*), sodium (*Na*), potassium (*K*), rubidium (*Rb*), and cesium (*Cs*). These alkali metals each comprise an equal number of alkali cations and electrons in unit cells of a crystalline lattice. The crystal structure of these metals is the body-centered cubic *CsCl* structure [6-8]. This close-packed structure is expected since it gives the optimal approach of the positive ions and negative electrons. For a body-centered cell, there is an identical atom at $x+\frac{a}{2}, y+\frac{a}{2}, z+\frac{a}{2}$ for each atom at x, y, z. The structure of the ions with lattice parameters $a=b=c$ and electrons at the diagonal positions centered at $\left(x+\frac{a}{4}, y+\frac{a}{4}, z+\frac{a}{4}\right)$ are shown in Figure 19.7. In this case $n=8$ electron planes per body-centered ion are perpendicular to the four diagonal axes running from each corner of the cube through the center to the opposite corner. The planes intersect these diagonals at one half the distance from each corner to the center of the body-centered atom. The mutual intersection of the planes forms a hexagonal cavity about each ion of the lattice. The length l_1 to a perpendicular electron plane along the axis from a corner atom to a body-centered atom that is the midpoint of this axis is:

$$l_1=\sqrt{\left(\frac{a}{4}\right)^2+\left(\frac{a}{4}\right)^2+\left(\frac{a}{4}\right)^2}=\frac{a\sqrt{3}}{4} \tag{19.15}$$

The angle θ_d of each diagonal axis from the xy-plane of the unit cell is:

$$\theta_d=\tan^{-1}\left(\frac{\frac{1}{4}}{\frac{\sqrt{2}}{4}}\right)=35.26° \tag{19.16}$$

The angle θ_p from the horizontal to the electron plane that is perpendicular to the diagonal axis is:

$$\theta_p=180°-90°-35.26°=54.73° \tag{19.17}$$

The length l_3 along a diagonal axis in the xy-plane from a corner atom to another at which point an electron plane intersects the xy-plane is:

$$l_3=\frac{l_1}{\cos\theta_d}=\frac{\frac{a\sqrt{3}}{4}}{\cos(35.26°)}=\frac{\frac{a\sqrt{3}}{4}}{\sqrt{\frac{2}{3}}}=a\frac{3}{4\sqrt{2}} \tag{19.18}$$

The length l_2 of the octagonal edge of the electron plane from a body-centered atom to the xy-plane defined by four corner atoms is:

$$l_2=l_3\sin\theta_d=a\frac{3}{4\sqrt{2}}\sin(35.26°)=a\frac{3}{4\sqrt{2}}\frac{1}{\sqrt{3}}=\frac{a}{4}\sqrt{\frac{3}{2}} \tag{19.19}$$

The length l_4 along the edge of the unit cell in the xy-plane from a corner atom to another at which point an electron plane intersects the xy-plane at this axis is:

$$l_4=\frac{l_3}{\cos(45°)}=\frac{a\frac{3}{4\sqrt{2}}}{\cos(45°)}=\frac{3}{4}a \tag{19.20}$$

The dimensions and angles given by Eqs. (19.15-19.20) are shown in Figure 19.7.

Each M^+ is surrounded by six planar two-dimensional membranes that are comprised of electron density σ on which the electric field lines of the positive charges end. The resulting unit cell consists cations at the end of each edge and at the center of the cell with an electron membrane as the perpendicular bisector of the axis from an identical atom at $x+\frac{a}{2}, y+\frac{a}{2}, z+\frac{a}{2}$ for each atom at x, y, z such that the unit cell contains two cations and two electrons. The ions and electrons of the unit cell are also shown in Figure 19.7. The electron membranes exist throughout the metal, but they terminate on metal atomic orbitals or MOs of bonds between metal atoms and other reacted atoms such as the MOs of metal oxide bonds at the edges of the metal.

Figure 19.7. The body-centered cubic lithium metal lattice showing the electrons as planar two-dimensional membranes of zero thickness that are each an equipotential energy surface comprised of the superposition of multiple electrons. (A) and (B) The unit-cell component of the surface charge density of a planar electron having an electric field equivalent to that of an image point charge for each corresponding positive ion of the lattice. (C) Opaque view of the ions and electrons of a unit cell. (D) Transparent view of the ions and electrons of a unit cell.

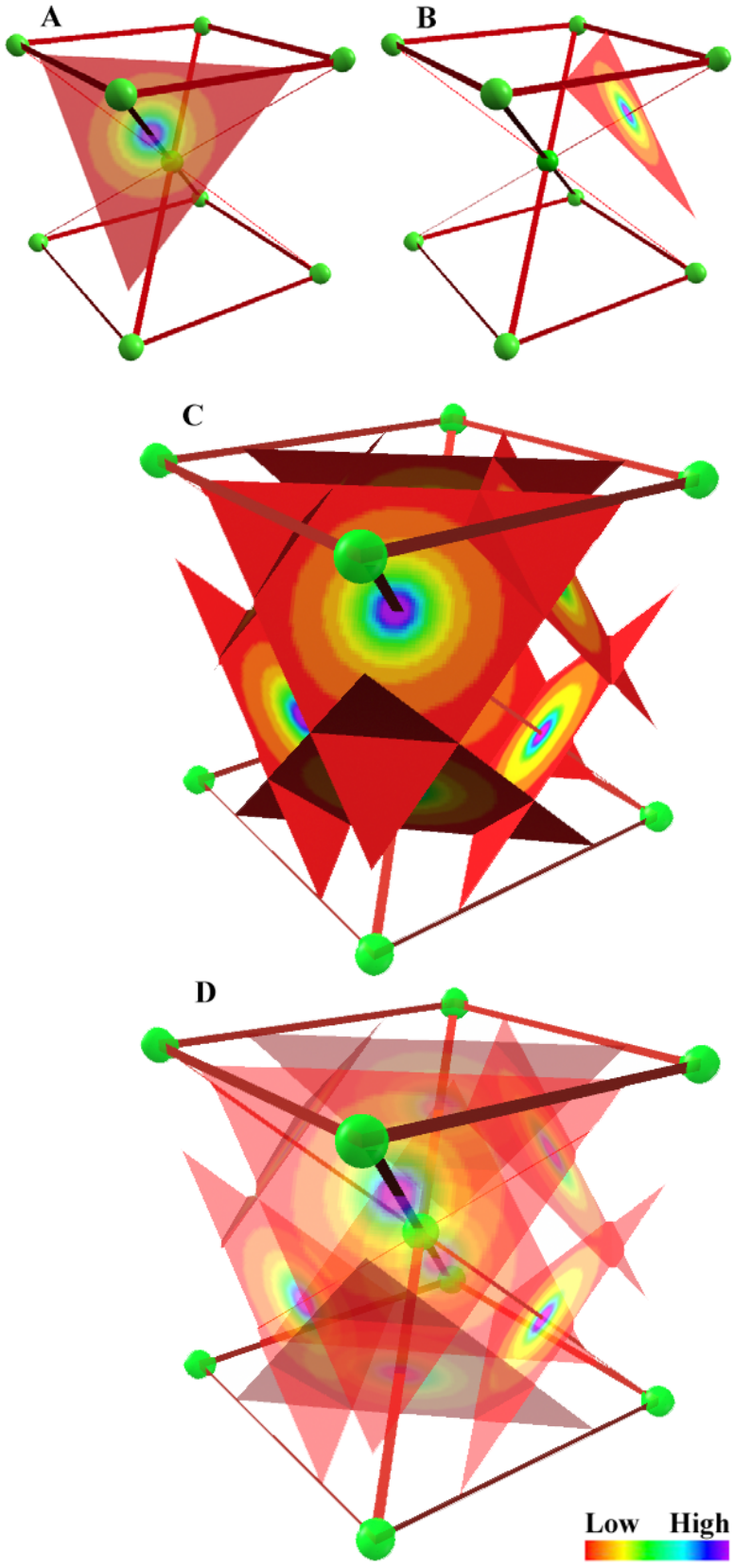

The interionic radius of each cation and electron membrane can be derived by considering the electron energies at these radii and by calculating the corresponding forces of the electrons with the ions. Then, the lattice energy is given by the sum over the crystal of the energy of the interacting ion and electron pairs at the radius of force balance between the electrons and ions.

For each point charge of $+e$ due to a metal ion M^+, the planar two-dimensional membrane comprised of electrons contributes a surface charge density σ given by Eq. (19.6) corresponding to that of a point image charge having a total charge of a single electron, $-e$. The potential of each electron is double that of Eq. (19.13) since there are two mirror-image M^+ ions per planar electron membrane:

$$V = \frac{-e^2}{4\pi\varepsilon_0 d} \tag{19.21}$$

where d is treated as a variable to be solved. The same result is obtained from considering the integral of the product of two times the electric field (Eq. (19.5)) and the charge density (Eq. (19.6)) according to Eq. (19.14). In order to conserve angular momentum and maintain current continuity, the kinetic energy has two components. Since the free electron of a metal behaves as a point mass, one component using Eq. (1.35) with $r = d$ is:

$$T = \frac{1}{2} m_e v^2 = \frac{1}{2} \frac{\hbar^2}{m_e d^2} \tag{19.22}$$

The other component of kinetic energy is given by integrating the mass density $\sigma_m(r)$ (Eq. (19.6)) with e replaced by m_e and velocity $v(r)$ (Eq. (1.35)) over their radial dependence ($r = \sqrt{x^2 + y^2 + z^2} = \sqrt{\rho^2 + d^2}$):

$$\begin{aligned} T &= \frac{1}{2}\int \sigma v^2 dA \\ &= \frac{1}{2}\int_0^\infty \int_0^{2\pi} \frac{m_e d}{2\pi\left(\rho^2 + d^2\right)^{3/2}} \frac{\hbar^2}{m_e^2\left(\rho^2 + d^2\right)} \rho d\phi d\rho \\ &= \frac{\hbar^2 d}{4\pi m_e}\int_0^\infty \int_0^{2\pi} \frac{\rho}{\left(\rho^2 + d^2\right)^{5/2}} d\phi d\rho \\ &= \frac{2\pi\hbar^2 d}{4\pi m_e}\left(\frac{-1}{2\left(\frac{3}{2}\right)\left(\rho^2 + d^2\right)^{3/2}}\right)_0^\infty \\ &= \left(\frac{1}{3}\right)\left(\frac{1}{2}\frac{\hbar^2}{m_e d^2}\right) \end{aligned} \tag{19.23}$$

where integral #47 of Lide [4] was used. Thus, the total kinetic energy given by the sum of Eqs. (19.22) and (19.23) is:

$$T = \left(1 + \frac{1}{3}\right)\left(\frac{1}{2}\frac{\hbar^2}{m_e d^2}\right) = \frac{4}{3}\left(\frac{1}{2}\frac{\hbar^2}{m_e d^2}\right) \tag{19.24}$$

Each metal M ($M = Li, Na, K, Rb, Cs$) is comprised of M^+ and e^- ions. The structure of the ions comprises lattice parameters $a = b = c$ and electrons at the diagonal positions centered at $\left(x + \frac{a}{4}, y + \frac{a}{4}, z + \frac{a}{4}\right)$. Thus, the separation distance d between each M^+ and the corresponding electron membrane is:

$$d = \sqrt{\left(\frac{\Delta x}{2}\right)^2 + \left(\frac{\Delta y}{2}\right)^2 + \left(\frac{\Delta z}{2}\right)^2} = \sqrt{\left(\frac{1}{4}a\right)^2 + \left(\frac{1}{4}a\right)^2 + \left(\frac{1}{4}a\right)^2} = \frac{\sqrt{3}}{4}a \tag{19.25}$$

where $\Delta x = \Delta y = \Delta z = \frac{a}{2}$. Thus, the lattice parameter a is given by:

$$a = \frac{4d}{\sqrt{3}} \tag{19.26}$$

The molar metal bond energy E_D is given by Avogadro's number N times the negative sum of the potential energy, kinetic energy, and ionization or binding energy ($BE(M)$) of M:

$$E_D = -N\left(V + T + BE(M)\right) = N\left(\frac{e^2}{4\pi\varepsilon_0 d} - \frac{4}{3}\left(\frac{1}{2}\frac{\hbar^2}{m_e d^2}\right) - BE(M)\right) \tag{19.27}$$

The separation distance d between each M^+ and the corresponding electron membrane is given by the force balance between the outward centrifugal force and the sum of the electric, paramagnetic and diamagnetic forces as given in the Three-Through Twenty-Electron Atoms section. The electric force $\mathbf{F}_{ele}$ corresponding to Eq. (19.21) given by its negative gradient is:

$$\mathbf{F}_{ele} = \frac{e^2}{4\pi\varepsilon_0 d^2}\mathbf{i}_z \tag{19.28}$$

where inward is taken as the positive direction. The centrifugal force $\mathbf{F}_{centrifugal}$ is given by the negative gradient of Eq. (19.24) times two since the charge and mass density are doubled due to the presence of mirror image M^+ ion pairs across the electron membrane at the origin for any given ion.

$$\mathbf{F}_{centrifugal} = -\frac{8}{3}\frac{\hbar^2}{m_e d^3}\mathbf{i}_z \tag{19.29}$$

where d is treated as a variable to be solved. In addition, there is an outward spin-pairing force $\mathbf{F}_{mag}$ between the electron density elements of two opposing ions that is given by Eqs. (7.24) and (10.52):

$$\mathbf{F}_{mag} = -\frac{1}{Z}\frac{\hbar^2}{m_e d^3}\sqrt{s(s+1)}\mathbf{i}_z \tag{19.30}$$

where $s = \frac{1}{2}$. The remaining magnetic forces are determined by the electron configuration of the particular atom as given for the examples of lithium, sodium, and potassium metals in the corresponding sections.

LITHIUM METAL

For Li^+, there are two spin-paired electrons in an atomic orbital with:

$$r_1 = r_2 = a_0\left[\frac{1}{2} - \frac{\sqrt{\frac{3}{4}}}{6}\right] \tag{19.31}$$

as given by Eq. (7.35) where r_n is the radius of electron n which has velocity v_n. For the next electron that contributes to the metal-electron membrane, the outward centrifugal force on electron 3 is balanced by the electric force and the magnetic forces (on electron 3). The radius of the metal-band electron is calculated by equating the outward centrifugal force (Eq. (19.29)) to the sum of the electric (Eq. (19.28)) and diamagnetic (Eq. (19.30)) forces as follows:

$$\frac{8}{3}\frac{\hbar^2}{m_e d^3} = \frac{e^2}{4\pi\varepsilon_0 d^2} - \frac{\hbar^2}{Z m_e d^3}\sqrt{\frac{3}{4}} \tag{19.32}$$

$$d = \left(\frac{8}{3} + \frac{\sqrt{\frac{3}{4}}}{3}\right)a_0 = 2.95534 a_0 = 1.56390\ X\ 10^{-10}\ m \tag{19.33}$$

where $Z = 3$. Using Eq. (19.26), the lattice parameter a is:

$$a = 6.82507 a_0 = 3.61167\ X\ 10^{-10}\ m \tag{19.34}$$

The experimental lattice parameter a [7] is:

$$a = 6.63162 a_0 = 3.5093\ X\ 10^{-10}\ m \tag{19.35}$$

The calculated $Li — Li$ distance is in reasonable agreement with the experimental distance given the experimental difficulty of performing X-ray diffraction on lithium due to the low electron densities.

Using Eq. (19.27) and the experimental binding energy of lithium, $BE(Li) = 5.39172\ eV = 8.63849\ X\ 10^{-19}\ J$ [9], the molar metal bond energy E_D is:

$$E_D = N\left(\frac{e^2}{4\pi\varepsilon_0 1.56390\ X\ 10^{-10}\ m} - \frac{4}{3}\left(\frac{1}{2}\frac{\hbar^2}{m_e\left(1.56390\ X\ 10^{-10}\ m\right)^2}\right) - 8.63849\ X\ 10^{-19}\ J\right) \tag{19.36}$$

$$= 167.76\ kJ/mole$$

This agrees well with the experimental lattice [10] energy of:

$$E_D = 159.3\ kJ/mole \tag{19.37}$$

and confirms that Li metal comprises a precise packing of discrete ions, Li^+ and e^-. Using the $Li — Li$ and $Li^+ — e^-$ distances and the calculated (Eq. (7.35)) Li^+ ionic radius of $0.35566 a_0 = 0.18821 Å$, the crystalline lattice structure of the unit cell of Li metal is shown in Figure 19.8 , a portion of the crystalline lattice of Li metal is shown in Figure 19.9, and the Li unit cell is shown relative to the other alkali metals in Figure 19.10.

Figure 19.8. The body-centered cubic metal lattice of lithium showing the unit cell of electrons and ions. (A) Diagonal view. (B) Top view.

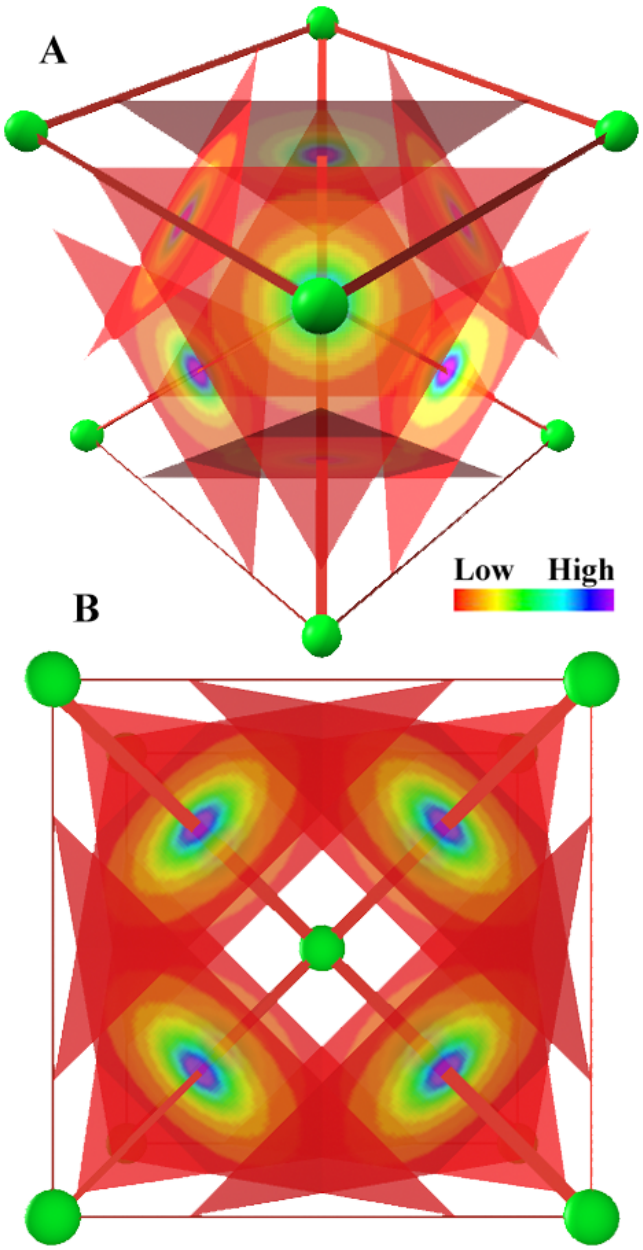

Figure 19.9. A portion of the crystalline lattice of *Li* metal comprising 3^3 body-centered cubic unit cells of electrons and ions. (A) Rotated diagonal opaque view. (B) Rotated diagonal transparent view. (C) Side transparent view.

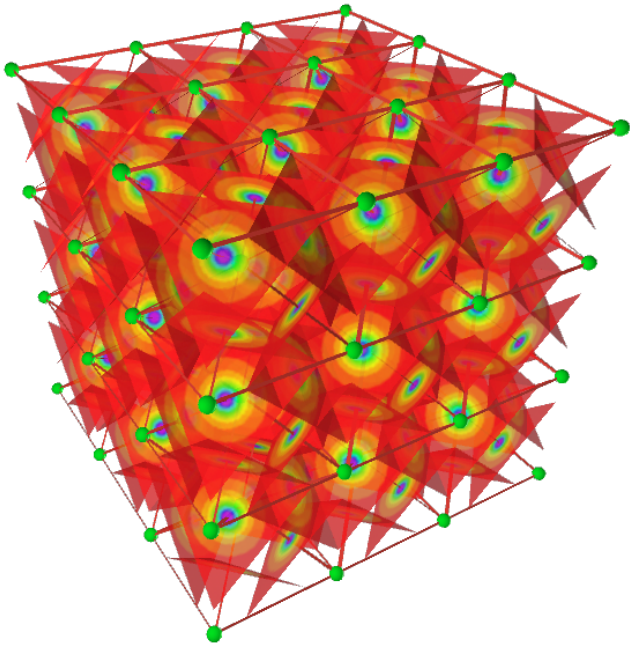

A

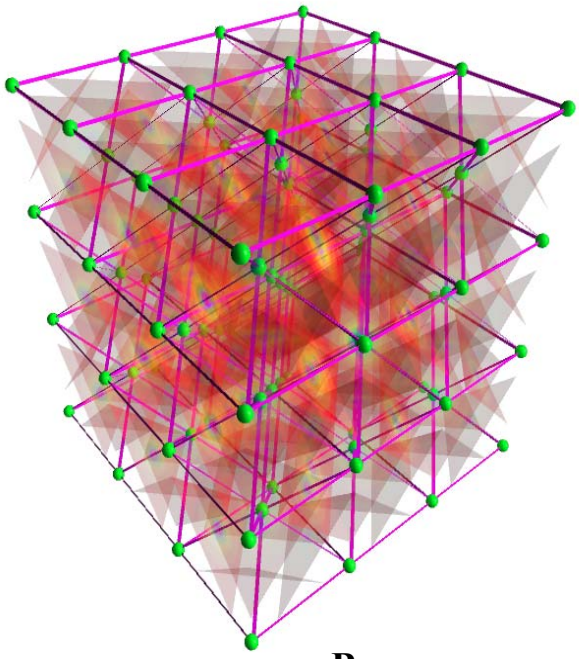

B

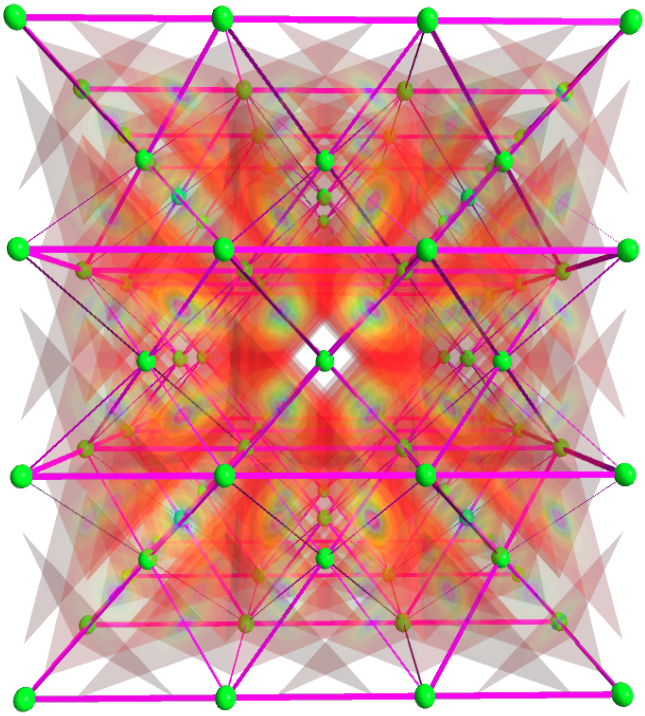

C

Figure 19.10. The crystalline unit cells of the alkali metals showing each lattice of ions and electrons to the same scale. (Li^+ = green, Na^+ = yellow, K^+ = purple, Rb^+ = blue, Cs^+ = red). (A) The crystal structure of Li. (B) The crystal structure of Na. (C) The crystal structure of K. (D) The crystal structure of Rb. (E) The crystal structure of Cs.

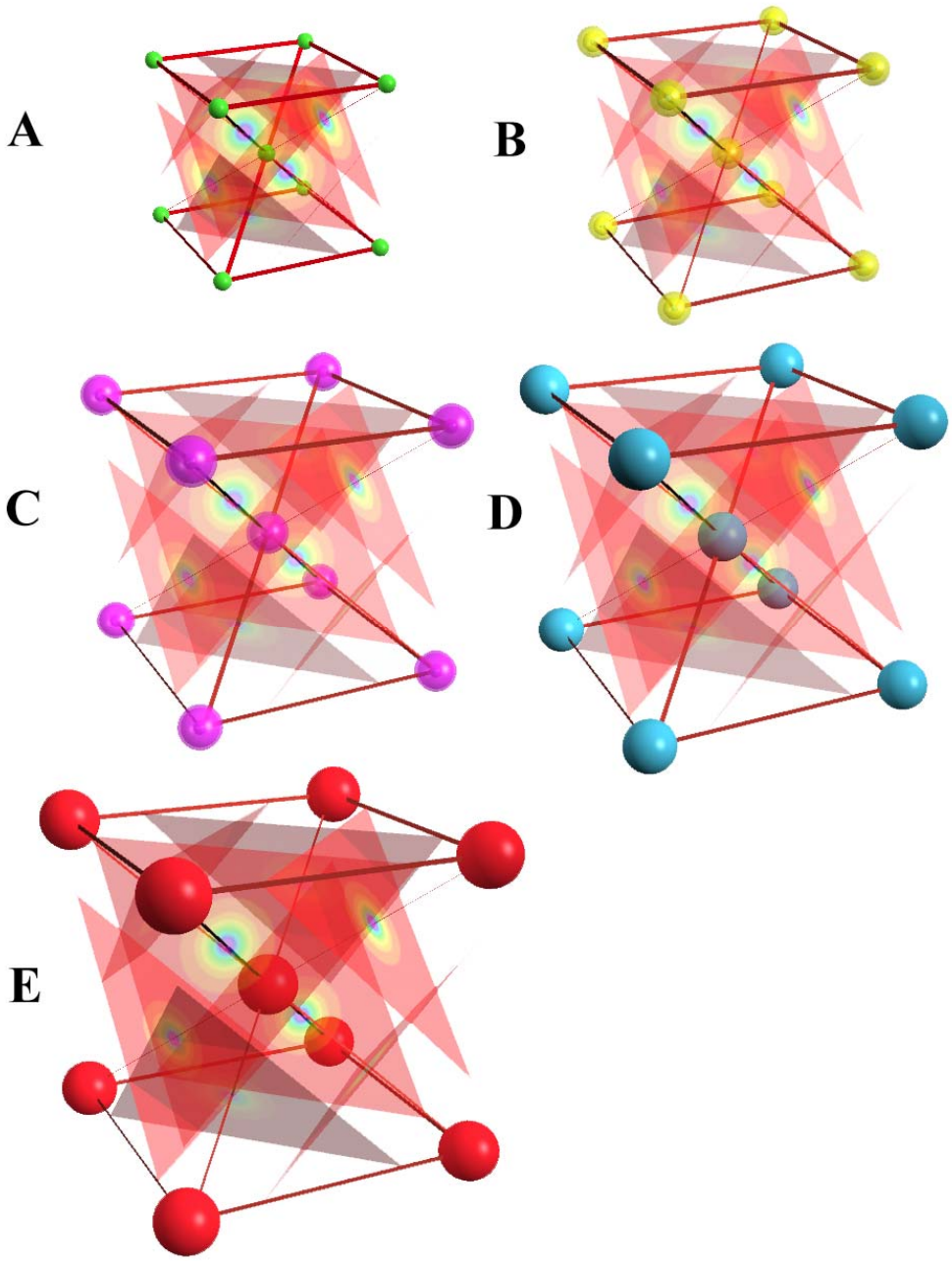

SODIUM METAL

For Na^+, there are two indistinguishable spin-paired electrons in an atomic orbital with radii r_1 and r_2 both given by Eq. (7.35) (Eq. (10.51)), two indistinguishable spin-paired electrons in an atomic orbital with radii r_3 and r_4 both given by Eq. (10.62), and three sets of paired electrons in an atomic orbital at r_{10} given by Eq. (10.212). For $Z = 11$, the next electron which binds to contribute to the metal electron membrane to form the metal bond is attracted by the central Coulomb field and is repelled by diamagnetic forces due to the 3 sets of spin-paired inner electrons.

In addition to the spin-spin interaction between electron pairs, the three sets of 2p electrons are orbitally paired. The metal electron of the sodium atom produces a magnetic field at the position of the three sets of spin-paired 2p electrons. In order for the electrons to remain spin and orbitally paired, a corresponding diamagnetic force, $\mathbf{F}_{diamagnetic\ 3}$, on electron eleven from the three sets of spin-paired electrons follows from Eqs. (10.83-10.84) and (10.220):

$$\mathbf{F}_{diamagnetic\ 3} = -\frac{1}{Z}\frac{10\hbar^2}{m_e d^3}\sqrt{s(s+1)}\mathbf{i}_z \tag{19.38}$$

corresponding to the p_x and p_y electrons with no spin-orbit coupling of the orthogonal p_z electrons (Eq. (10.84)). The outward centrifugal force on electron 11 is balanced by the electric force and the magnetic forces (on electron 11). The radius of the outer electron is calculated by equating the outward centrifugal force (Eq. (19.29)) to the sum of the electric (Eq. (19.28)) and diamagnetic (Eqs. (19.30) and (19.38)) forces as follows:

$$\frac{8}{3}\frac{\hbar^2}{m_e d^3} = \frac{e^2}{4\pi\varepsilon_0 d^2} - \frac{\hbar^2}{Z m_e d^3}\sqrt{\frac{3}{4}} - \frac{1}{Z}\frac{10\hbar^2}{m_e d^3}\sqrt{\frac{3}{4}} \tag{19.39}$$

$$d = \left(\frac{8}{3} + \frac{11\sqrt{\frac{3}{4}}}{11}\right)a_0 = 3.53269 a_0 = 1.86942\ X\ 10^{-10}\ m \tag{19.40}$$

where $Z = 11$ and $s = \frac{1}{2}$. Using Eq. (19.26), the lattice parameter a is:

$$a = 8.15840 a_0 = 4.31724\ X\ 10^{-10}\ m \tag{19.41}$$

The experimental lattice parameter a [7] is:

$$a = 8.10806 a_0 = 4.2906\ X\ 10^{-10}\ m \tag{19.42}$$

The calculated $Na — Na$ distance is in good agreement with the experimental distance.

Using Eq. (19.27) and the experimental binding energy of sodium, $BE(Na) = 5.13908\ eV = 8.23371\ X\ 10^{-19}\ J$ [9], the molar metal bond energy E_D is:

$$E_D = N\left(\frac{e^2}{4\pi\varepsilon_0 1.86942\ X\ 10^{-10}\ m} - \frac{4}{3}\left(\frac{1}{2}\frac{\hbar^2}{m_e\left(1.86942\ X\ 10^{-10}\ m\right)^2}\right) - 8.23371\ X\ 10^{-19}\ J\right) = 107.10\ kJ/mole \tag{19.43}$$

This agrees well with the experimental lattice [10] energy of:

$$E_D = 107.5\ kJ/mole \tag{19.44}$$

and confirms that Na metal comprises a precise packing of discrete ions, Na^+ and e^-. Using the $Na — Na$ and $Na^+ — e^-$ distances and the calculated (Eq. (10.212)) Na^+ ionic radius of $0.56094 a_0 = 0.29684 Å$, the crystalline lattice structure of Na metal is shown in Figure 19.10B.

POTASSIUM METAL

For K^+, there are two indistinguishable spin-paired electrons in an atomic orbital with radii r_1 and r_2 both given by Eq. (7.35) (Eq. (10.51)), two indistinguishable spin-paired electrons in an atomic orbital with radii r_3 and r_4 both given by Eq. (10.62), three sets of paired electrons in an atomic orbital at r_{10} given by Eq. (10.212), two indistinguishable spin-paired electrons in an atomic orbital with radii r_{11} and r_{12} both given by Eq. (10.255), and three sets of paired electrons in an atomic orbital with radius r_{18} given by Eq. (10.399). With $Z = 19$, the next electron which binds to contribute to the metal electron membrane to form the metal bond is attracted by the central Coulomb field and is repelled by diamagnetic forces due to the 3 sets of spin-paired inner 3p electrons.

The spherically symmetrical closed 3p shell of nineteen-electron atoms produces a diamagnetic force, $\mathbf{F}_{diamagnetic}$, that is equivalent to that of a closed s shell given by Eq. (10.11) with the appropriate radii. The inner electrons remain at their initial radii, but cause a diamagnetic force according to Lenz's law that is:

$$\mathbf{F}_{diamagnetic} = -\frac{\hbar^2}{4m_e d^2 r_{18}}\sqrt{s(s+1)}\mathbf{i}_z \tag{19.45}$$

The diamagnetic force, $\mathbf{F}_{diamagnetic\ 3}$, on electron nineteen from the three sets of spin-paired electrons given by Eq. (10.409) is

$$\mathbf{F}_{diamagnetic\ 3} = -\frac{1}{Z}\frac{12\hbar^2}{m_e d^3}\sqrt{s(s+1)}\mathbf{i}_z \tag{19.46}$$

corresponding to the 3 p_x, p_y, and p_z electrons.

The outward centrifugal force on electron 19 is balanced by the electric force and the magnetic forces (on electron 19). The radius of the outer electron is calculated by equating the outward centrifugal force (Eq. (19.29)) to the sum of the electric (Eq. (19.28)) and diamagnetic (Eqs. (19.30), (19.45), and (19.46)) forces as follows:

$$\frac{8}{3}\frac{\hbar^2}{m_e d^3} = \frac{e^2}{4\pi\varepsilon_0 d^2} - \frac{\hbar^2}{Zm_e d^3}\sqrt{\frac{3}{4}} - \frac{1}{Z}\frac{12\hbar^2}{m_e d^3}\sqrt{\frac{3}{4}} - \frac{\hbar^2}{4m_e d^2 r_{18}}\sqrt{\frac{3}{4}} \tag{19.47}$$

where $s = \frac{1}{2}$.

$$d = \frac{a_0\left(\frac{8}{3} + \frac{13}{Z}\sqrt{\frac{3}{4}}\right)}{(Z-18) - \frac{\sqrt{\frac{3}{4}}}{4\frac{r_{18}}{a_0}}} = \frac{a_0\left(\frac{8}{3} + \frac{13}{19}\sqrt{\frac{3}{4}}\right)}{1 - \frac{\sqrt{\frac{3}{4}}}{4\frac{r_{18}}{a_0}}} \tag{19.48}$$

Substitution of $\frac{r_{18}}{a_0} = 0.85215$ (Eq. (10.399) with $Z = 19$) into Eq. (19.48) gives:

$$d = 4.36934a_0 = 2.31215\ X\ 10^{-10}\ m \tag{19.49}$$

Using Eq. (19.26), the lattice parameter a is:

$$a = 10.09055a_0 = 5.33969\ X\ 10^{-10}\ m \tag{19.50}$$

The experimental lattice parameter a [7] is:

$$a = 10.05524a_0 = 5.321\ X\ 10^{-10}\ m \tag{19.51}$$

The calculated $K — K$ distance is in good agreement with the experimental distance.

Using Eq. (19.27) and the experimental binding energy of potassium, $BE(K) = 4.34066\ eV = 6.9545\ X\ 10^{-19}\ J$ [9], the molar metal bond energy E_D is:

$$E_D = N\left(\frac{e^2}{4\pi\varepsilon_0 2.31215\ X\ 10^{-10}\ m} - \frac{4}{3}\left(\frac{1}{2}\frac{\hbar^2}{m_e\left(2.31215\ X\ 10^{-10}\ m\right)^2}\right) - 6.9545\ X\ 10^{-19}\ J\right) = 90.40\ kJ/mole \tag{19.52}$$

This agrees well with the experimental lattice [10] energy of

$$E_D = 89\ kJ/mole \tag{19.53}$$

and confirms that K metal comprises a precise packing of discrete ions, K^+ and e^-. Using the $K — K$ and $K^+ — e^-$ distances and the calculated (Eq. (10.399)) K^+ ionic radius of $0.85215a_0 = 0.45094\text{Å}$, the crystalline lattice structure of K metal is shown in Figure 19.10C.

RUBIDIUM AND CESIUM METALS

Rubidium and cesium provide further examples of the nature of the bonding in alkali metals. The distance d between each metal ion M^+ and the corresponding electron membrane is calculated from the experimental parameter a, and then the molar metal bond energy E_D is calculated using Eq. (19.27).

The experimental lattice parameter a [7] for rubidium is:

$$a = 10.78089a_0 = 5.705\ X\ 10^{-10}\ m \tag{19.54}$$

Using Eq. (19.25), the lattice parameter d is:

$$d = 4.66826a_0 = 2.47034\ X\ 10^{-10}\ m \tag{19.55}$$

Using Eqs. (19.27) and (19.55) and the experimental binding energy of rubidium, $BE(Rb) = 4.17713\ eV = 6.6925\ X\ 10^{-19}\ J$ [9], the molar metal bond energy E_D is:

$$E_D = N\left(\frac{e^2}{4\pi\varepsilon_0 2.47034\ X\ 10^{-10}\ m} - \frac{4}{3}\left(\frac{1}{2}\frac{\hbar^2}{m_e\left(2.47034\ X\ 10^{-10}\ m\right)^2}\right) - 6.6925\ X\ 10^{-19}\ J\right) = 79.06\ kJ/mole \tag{19.56}$$

This agrees well with the experimental lattice [10] energy of:

$$E_D = 80.9\ kJ/mole \tag{19.57}$$

and confirms that Rb metal comprises a precise packing of discrete ions, Rb^+ and e^-. Using the $Rb — Rb$ and $Rb^+ — e^-$ distances and the Rb^+ ionic radius of 0.52766 Å calculated using Eq. (10.102) and the experimental ionization energy of Rb^+, $27.2895\ eV$ [9], the crystalline lattice structure of Rb metal is shown in Figure 19.10D.

The experimental lattice parameter a [7] for cesium is:

$$a = 11.60481a_0 = 6.141\ X\ 10^{-10}\ m \tag{19.58}$$

Using Eq. (19.25), the lattice parameter d is:

$$d = 5.02503a_0 = 2.65913\ X\ 10^{-10}\ m \tag{19.59}$$

Using Eqs. (19.27) and (19.59) and the experimental binding energy of cesium, $BE(Cs) = 3.8939\ eV = 6.23872\ X\ 10^{-19}\ J$ [9], the molar metal bond energy E_D is:

$$E_D = N\left(\frac{e^2}{4\pi\varepsilon_0 2.65913\ X\ 10^{-10}\ m} - \frac{4}{3}\left(\frac{1}{2}\frac{\hbar^2}{m_e\left(2.65913\ X\ 10^{-10}\ m\right)^2}\right) - 6.23872\ X\ 10^{-19}\ J\right) = 77.46\ kJ/mole \tag{19.60}$$

This agrees well with the experimental lattice [10] energy of:

$$E_D = 76.5\ kJ/mole \tag{19.61}$$

and confirms that Cs metal comprises a precise packing of discrete ions, Cs^+ and e^-. Using the $Cs — Cs$ and $Cs^+ — e^-$ distances and the Cs^+ ionic radius of 0.62182 Å calculated using Eq. (10.102) and the experimental ionization energy of Cs^+, $23.15744\ eV$ [9], the crystalline lattice structure of Cs metal is shown in Figure 19.10E.

Other metals can be solved in a similar manner. Iron, for example, is also a body-centered cubic lattice, and the solution of the lattice spacing and energies are given by Eqs. (19.21-19.30). The parameter d is given by the iron force balance which has a corresponding form to those of alkali metals such as that of lithium given by Eqs. (19.32-19.35). In addition, the changes in radius and energy of the second $4s$ electron due to the ionization of the first of the two $4s$ electrons to the metal band is calculated in the similar manner as those of the atoms of diatomic molecules such as N_2 given by Eqs. (13.621-13.632). This energy term is added to those of Eq. (19.27) to give the molar metal bond energy E_D.

PHYSICAL IMPLICATIONS OF THE NATURE OF FREE ELECTRONS IN METALS

The extension of the free-electron membrane throughout the crystalline lattice is the reason for the high thermal and electrical conductivity of metals. Electricity can be conducted on the extended electron membranes by the application of an electric field and a connection with a source of electrons to maintain current continuity. Heat can be transferred by radiation or by collisions, or by infrared-radiation-induced currents propagated through the crystal. The surface luster and opacity is due to the reflection of electromagnetic radiation by mirror currents on the surfaces of the free-planar electron membranes. Ductility and malleability result from the feature that the field lines of a given ion end on the induced electron surface charge of the planar, perfectly conducting electron membrane. Thus, layers of the metal lattice can slide over each other without juxtaposing charges of the same sign which causes ionic crystals to fracture.

The electrons in metals have surface-charge distributions that are merely equivalent to the image charges of the ions. When there is vibration of the ions, the thermal electron kinetic energy can be directed through channels of least resistance from collisions. The resulting kinetic energy distribution over the population of electrons can be modeled using Fermi Dirac statistics wherein the specific heat of a metal is dominated by the motion of the ions since the electrons behave as image charges. Based on the physical solution of the nature of the metallic bond, the small electron contribution to the specific heat of a metal is predicted to be proportional to the ratio of the temperature to the electron kinetic energy [11]. Based on Fermi-Dirac statistics, the electron contribution to the specific heat of a metal given by Eq. (23.68) is:

$$C_{Ve} = \frac{\pi^2}{2}\left(\frac{kT}{\varepsilon_F}\right)R \tag{19.62}$$

Now that the true structure of metals has been solved, it is interesting to relate the Fermi energy to the electron kinetic energy. The relationships between the electron velocity, the de Broglie wavelength, and the lattice spacing used to calculate the Fermi energy in the Electron-Energy Distribution section are also used in the kinetic energy derivation. The Fermi energy given by Eq. (23.61) is:

$$\varepsilon_F = \frac{h^2}{2m}\left(\frac{3N}{8\pi V}\right)^{2/3} = \frac{h^2}{2m_e}\left(\frac{3}{8\pi}\right)^{2/3} n^{2/3} \tag{19.63}$$

where the electron density parameter for alkali metals is two electrons per body-centered cubic cell of lattice spacing a. Since in the physical model, the field lines of two mirror-image ions M^+ end on opposite sides per section of the two-dimensional electron membrane, the kinetic energy equivalent to the Fermi energy is twice that given by Eq. (19.24). Then, the ratio $R_{\varepsilon_F/T}$ of the Fermi energy to the kinetic energy provides a comparison of the statistical model to the solution of the nature of the metallic bond in the determination of electron contribution to the specific heat:

$$R_{\varepsilon_F/T} = \frac{\varepsilon_F}{T} = \frac{\frac{h^2}{2m_e}\left(\frac{3}{8\pi}\right)^{2/3} n^{2/3}}{\frac{8}{3}\left(\frac{1}{2}\frac{\hbar^2}{m_e d^2}\right)} = \frac{\frac{h^2}{2m_e}\left(\frac{3}{8\pi}\right)^{2/3}\left(\frac{2}{a^3}\right)^{2/3}}{\frac{8}{3}\left(\frac{1}{2}\frac{\hbar^2}{m_e d^2}\right)} = \frac{\frac{h^2}{2m_e}\left(\frac{3}{8\pi}\right)^{2/3}\left(\frac{2}{\left(\frac{4d}{\sqrt{3}}\right)^3}\right)^{2/3}}{\left(\frac{8}{3}\right)\left(\frac{1}{2\pi}\right)^2\left(\frac{h^2}{2m_e d^2}\right)} = 1.068 \tag{19.64}$$

where Eq. (19.26) was used to convert the parameter a to d.

From the physical nature of the current, the electrical and thermal conductivities corresponding to the currents can be determined. The electrical current is classically given by

$$i = e\nu = \sigma\frac{\varepsilon_F}{he} \tag{19.65}$$

where the energy and angular momentum of the conduction electrons are quantized according to $\hbar$ and Planck's equation (Eq. (4.8)), respectively. From Eq. (19.65), the electrical conductivity is given by:

$$\sigma = \frac{e^2 h\nu}{\varepsilon_F} \tag{19.66}$$

where ν is the frequency of the unit current carried by each electron. The thermal current is also carried by the kinetic energy of the electron plane waves. Since there are two degrees of freedom in the plane of each electron rather than three, the thermal conductivity κ is given by:

$$\kappa = \frac{2}{3}\frac{C_{Ve}}{N_0 h} = \frac{\pi^2}{3}\left(\frac{k_B^2 T}{\varepsilon_F / h}\right) \tag{19.67}$$

The Wiedemann-Franz law gives the relationship of the thermal conductivity κ to the electrical conductivity σ and absolute temperature T. Thus, using Eqs. (19.66-19.67), the constant L_0 is given by:

$$L_0 = \frac{\kappa}{\sigma T} = \frac{\frac{\pi^2}{3}\left(\frac{hk_B^2}{\varepsilon_F}\right)}{\frac{he^2}{\varepsilon_F}} = \frac{\pi^2}{3}\left(\frac{k_B}{e}\right)^2 \tag{19.68}$$

From Eqs. (19.64) and (19.68), the statistical model is reasonably close to the physical model to be useful in modeling the specific-heat contribution of electrons in metals based on their inventory of thermal energy and the thermal-energy distribution in the crystal. However, the correct physical nature of the current carriers comprising two-dimensional electron planes is required in cases where the simplistic statistical model fails as in the case of the anisotropic violation of the Wiedemann-Franz law [12-13].

Semiconductors comprise covalent bonds wherein the electrons are of sufficiently high energy that excitation creates an ion and a free electron. The free electron forms a membrane as in the case of metals. This membrane has the same planar structure throughout the crystal. This feature accounts for the high conductivity of semiconductors when the electrons are excited by the application of external fields or electromagnetic energy that causes ion-pair ($M^+ — e^-$) formation.

Superconductors comprise free-electron membranes wherein current flows in a reduced dimensionality of two or one dimensions with the bonding being covalent along the remaining directions such that electron scattering from other planes does not interfere with the current flow. In addition, the spacing of the electrons along the membrane is such that the energy is band-passed with respect to magnetic interactions of conducting electrons as given in the superconductivity section.

REFERENCES

1. J. D. Jackson, Classical Electrodynamics, Second Edition, John Wiley & Sons, New York, (1975), pp. 17-22.
2. H. A. Haus, J. R. Melcher, "Electromagnetic Fields and Energy," Department of Electrical Engineering and Computer Science, Massachusetts Institute of Technology, (1985), Sec. 5.3.
3. J. A. Stratton, *Electromagnetic Theory*, McGraw-Hill Book Company, (1941), p. 195.
4. D. R. Lide, *CRC Handbook of Chemistry and Physics*, 86th Edition, CRC Press, Taylor & Francis, Boca Raton, (2005-6), p. A-23.
5. J. A. Kong, *Electromagnetic Wave Theory*, Second Edition, John Wiley & Sons, Inc., New York, (1990), pp. 330-331.
6. A. Beiser, *Concepts of Modern Physics*, Fourth Edition, McGraw-Hill, New York, (1987), p. 372.
7. D. R. Lide, *CRC Handbook of Chemistry and Physics*, 86th Edition, CRC Press, Taylor & Francis, Boca Raton, (2005-6), pp. 12-15 to 12-18.
8. A. K. Cheetham, P. Day, Editors, Solid State Chemistry Techniques, Clarendon Press, Oxford, (1987), pp. 52-57.
9. D. R. Lide, *CRC Handbook of Chemistry and Physics*, 86th Edition, CRC Press, Taylor & Francis, Boca Raton, (2005-6), pp. 10-202 to 10-204.
10. D. R. Lide, *CRC Handbook of Chemistry and Physics*, 86th Edition, CRC Press, Taylor & Francis, Boca Raton, (2005-6), pp. 5-4 to 5-18.
11. E. C. Stoner, "Collective electron specific heat and spin paramagnetism in metals," Proceedings of the Royal Society of London. Series A, Mathematical and Physical Sciences, Vol. 154, No. 883 (May 1, 1936), pp. 656-678.
12. M. A. Tanatar, J. Paglione, C. Petrovic, L. Taillefer, "Anisotropic violation of the Wiedemann-Franz law at a quantum critical point," Science, Vol. 316, (2007), pp. 1320-1322.
13. P. Coleman, "Watching electrons break up," Science, Vol. 316, (2007), pp. 1290-1291.

Chapter 20

SILICON MOLECULAR FUNCTIONAL GROUPS AND MOLECULES

GENERAL CONSIDERATIONS OF THE SILICON MOLECULAR BOND

Silane molecules comprising an arbitrary number of atoms can be solved using similar principles and procedures as those used to solve organic molecules of arbitrary length and complexity. Silanes can be considered to be comprised of functional groups such as SiH_3, SiH_2, SiH, $Si-Si$, and $C-Si$. The solutions of these functional groups or any others corresponding to the particular silane can be conveniently obtained by using generalized forms of the force balance equation given in the Force Balance of the σ MO of the Carbon Nitride Radical section for molecules comprised of silicon and hydrogen only and the geometrical and energy equations given in the Derivation of the General Geometrical and Energy Equations of Organic Chemistry section for silanes further comprised of heteroatoms such as carbon. The appropriate functional groups with their geometrical parameters and energies can be added as a linear sum to give the solution of any silane.

SILANES (Si_nH_{2n+2})

As in the case of carbon, the bonding in the silicon atom involves four sp^3 hybridized orbitals formed from the $3p$ and $3s$ electrons of the outer shells. $Si-Si$ and $Si-H$ bonds form between $Si3sp^3$ HOs and between a $Si3sp^3$ HO and a $H1s$ AO to yield silanes. The geometrical parameters of each $Si-Si$ and $SiH_{n=1,2,3}$ functional group is solved from the force balance equation of the electrons of the corresponding σ-MO and the relationships between the prolate spheroidal axes. Then, the sum of the energies of the H_2-type ellipsoidal MOs is matched to that of the $Si3sp^3$ shell as in the case of the corresponding carbon molecules. As in the case of ethane given in the Ethane Molecule section, the energy of the $Si-Si$ functional group is determined for the effect of the donation of 25% electron density from each participating $Si3sp^3$ HO to the $Si-Si$-bond MO.

The energy of silicon is less than the Coulombic energy between the electron and proton of H given by Eq. (1.264). A minimum energy is achieved while matching the potential, kinetic, and orbital energy relationships given in the Hydroxyl Radical (OH) section with the donation of 75% electron density from the participating $Si3sp^3$ HO to each $Si-H$-bond MO. As in the case of acetylene given in the Acetylene Molecule section, the energy of each $Si-H_n$ functional group is determined for the effect of the charge donation.

The $3sp^3$ hybridized orbital arrangement after Eq. (13.422) is:

$$\begin{array}{cccc} & 3\mathrm{sp}^3 \text{ state} & & \\ \underline{\uparrow} & \underline{\uparrow} & \underline{\uparrow} & \underline{\uparrow} \\ 0,0 & 1,-1 & 1,0 & 1,1 \end{array} \tag{20.1}$$

where the quantum numbers (ℓ, m_ℓ) are below each electron. The total energy of the state is given by the sum over the four electrons. The sum $E_T\left(Si,3sp^3\right)$ of experimental energies [1] of Si, Si^+, Si^{2+}, and Si^{3+} is:

$$E_T\left(Si,3sp^3\right)=45.14181\ eV+33.49302\ eV+16.34584\ eV+8.15168\ eV=103.13235\ eV \tag{20.2}$$

By considering that the central field decreases by an integer for each successive electron of the shell, the radius r_{3sp^3} of the $Si3sp^3$ shell may be calculated from the Coulombic energy using Eq. (15.13).

$$r_{3sp^3} = \sum_{n=10}^{13} \frac{(Z-n)e^2}{8\pi\varepsilon_0 \left(e103.13235\ eV\right)} = \frac{10e^2}{8\pi\varepsilon_0 \left(e103.13235\ eV\right)} = 1.31926a_0 \tag{20.3}$$

where $Z = 14$ for silicon. Using Eq. (15.14), the Coulombic energy $E_{Coulomb}\left(Si, 3sp^3\right)$ of the outer electron of the $Si3sp^3$ shell is:

$$E_{Coulomb}\left(Si, 3sp^3\right) = \frac{-e^2}{8\pi\varepsilon_0 r_{3sp^3}} = \frac{-e^2}{8\pi\varepsilon_0 1.31926a_0} = -10.31324\ eV \tag{20.4}$$

During hybridization, one of the spin-paired $3s$ electrons is promoted to the $Si3sp^3$ shell as an unpaired electron. The energy for the promotion is the magnetic energy given by Eq. (15.15) at the initial radius of the $3s$ electrons. From Eq. (10.255) with $Z = 14$, the radius r_{12} of the $Si3s$ shell is:

$$r_{12} = 1.25155a_0 \tag{20.5}$$

Using Eqs. (15.15) and (20.5), the unpairing energy is:

$$E(magnetic) = \frac{2\pi\mu_0 e^2\hbar^2}{m_e^2\left(r_{12}\right)^3} = \frac{8\pi\mu_o\mu_B^2}{\left(1.25155a_0\right)^3} = 0.05836\ eV \tag{20.6}$$

Using Eqs. (20.4) and (20.6), the energy $E(Si,3sp^3)$ of the outer electron of the $Si3sp^3$ shell is

$$E\left(Si, 3sp^3\right) = \frac{-e^2}{8\pi\varepsilon_0 r_{3sp^3}} + \frac{2\pi\mu_0 e^2\hbar^2}{m_e^2\left(r_{12}\right)^3} = -10.31324\ eV + 0.05836\ eV = -10.25487\ eV \tag{20.7}$$

Next, consider the formation of the *Si*–*Si*-bond MO of silanes wherein each silicon atom has a $Si3sp^3$ electron with an energy given by Eq. (20.7). The total energy of the state of each silicon atom is given by the sum over the four electrons. The sum $E_T\left(Si_{silane}, 3sp^3\right)$ of energies of $Si3sp^3$ (Eq. (20.7)), Si^+, Si^{2+}, and Si^{3+} is:

$$\begin{aligned} E_T\left(Si_{silane}, 3sp^3\right) &= -\left(45.14181\ eV + 33.49302\ eV + 16.34584\ eV + E\left(Si, 3sp^3\right)\right) \\ &= -\left(45.14181\ eV + 33.49302\ eV + 16.34584\ eV + 10.25487\ eV\right) = -105.23554\ eV \end{aligned} \tag{20.8}$$

where $E(Si,3sp^3)$ is the sum of the energy of *Si*, –8.15168 *eV*, and the hybridization energy.

The sharing of electrons between two $Si3sp^3$ HOs to form a *Si*–*Si*-bond MO permits each participating orbital to decrease in size and energy. In order to further satisfy the potential, kinetic, and orbital energy relationships, each $Si3sp^3$ HO donates an excess of 25% of its electron density to the *Si*–*Si*-bond MO to form an energy minimum. By considering this electron redistribution in the silane molecule as well as the fact that the central field decreases by an integer for each successive electron of the shell, the radius $r_{silane3sp^3}$ of the $Si3sp^3$ shell may be calculated from the Coulombic energy using Eq. (15.18):

$$r_{silane3sp^3} = \left(\sum_{n=10}^{13}(Z-n) - 0.25\right)\frac{e^2}{8\pi\varepsilon_0\left(e105.23554\ eV\right)} = \frac{9.75e^2}{8\pi\varepsilon_0\left(e105.23554\ eV\right)} = 1.26057a_0 \tag{20.9}$$

Using Eqs. (15.19) and (20.9), the Coulombic energy $E_{Coulomb}\left(Si_{silane}, 3sp^3\right)$ of the outer electron of the $Si3sp^3$ shell is:

$$E_{Coulomb}\left(Si_{silane}, 3sp^3\right) = \frac{-e^2}{8\pi\varepsilon_0 r_{silane3sp^3}} = \frac{-e^2}{8\pi\varepsilon_0 1.26057a_0} = -10.79339\ eV \tag{20.10}$$

During hybridization, one of the spin-paired $3s$ electrons is promoted to the $Si3sp^3$ shell as an unpaired electron. The energy for the promotion is the magnetic energy given by Eq. (20.6). Using Eqs. (20.6) and (20.10), the energy $E\left(Si_{silane}, 3sp^3\right)$ of the outer electron of the $Si3sp^3$ shell is:

$$E\left(Si_{silane}, 3sp^3\right) = \frac{-e^2}{8\pi\varepsilon_0 r_{silane3sp^3}} + \frac{2\pi\mu_0 e^2\hbar^2}{m_e^2\left(r_{12}\right)^3} = -10.79339\ eV + 0.05836\ eV = -10.73503\ eV \tag{20.11}$$

Thus, $E_T(Si–Si,3sp^3)$, the energy change of each $Si3sp^3$ shell with the formation of the *Si*–*Si*-bond MO is given by the difference between Eq. (20.11) and Eq. (20.7):

$$E_T\left(Si-Si, 3sp^3\right) = E\left(Si_{silane}, 3sp^3\right) - E\left(Si, 3sp^3\right) = -10.73503\ eV - \left(-10.25487\ eV\right) = -0.48015\ eV \tag{20.12}$$

Next, consider the formation of the $Si-H$ -bond MO of silanes wherein each silicon atom contributes a $Si3sp^3$ electron having the sum $E_T\left(Si_{silane}, 3sp^3\right)$ of energies of $Si3sp^3$ (Eq. (20.7)), Si^+, Si^{2+}, and Si^{3+} given by Eq. (20.8). Each $Si-H$ -bond MO of each functional group $SiH_{n=1,2,3}$ forms with the sharing of electrons between each $Si3sp^3$ HO and each $H1s$ AO. As in the case of $C-H$, the H_2-type ellipsoidal MO comprises 75% of the $Si-H$ -bond MO according to Eq. (13.429). Furthermore, the donation of electron density from each $Si3sp^3$ HO to each $Si-H$ -bond MO permits the participating orbital to decrease in size and energy. In order to further satisfy the potential, kinetic, and orbital energy relationships, each $Si3sp^3$ HO donates an excess of 75% of its electron density to the $Si-H$ -bond MO to form an energy minimum. By considering this electron redistribution in the silane molecule as well as the fact that the central field decreases by an integer for each successive

electron of the shell, the radius $r_{silane3sp^3}$ of the $Si3sp^3$ shell may be calculated from the Coulombic energy using Eq. (15.18).

$$r_{silane3sp^3} = \left(\sum_{n=10}^{13}(Z-n)-0.75\right)\frac{e^2}{8\pi\varepsilon_0\left(e105.23554\ eV\right)} = \frac{9.25e^2}{8\pi\varepsilon_0\left(e105.23554\ eV\right)} = 1.19592a_0 \tag{20.13}$$

Using Eqs. (15.19) and (20.13), the Coulombic energy $E_{Coulomb}\left(Si_{silane},3sp^3\right)$ of the outer electron of the $Si3sp^3$ shell is:

$$E_{Coulomb}\left(Si_{silane},3sp^3\right) = \frac{-e^2}{8\pi\varepsilon_0 r_{silane3sp^3}} = \frac{-e^2}{8\pi\varepsilon_0 1.19592a_0} = -11.37682\ eV \tag{20.14}$$

During hybridization, one of the spin-paired 3*s* electrons is promoted to the $Si3sp^3$ shell as an unpaired electron. The energy for the promotion is the magnetic energy given by Eq. (20.6). Using Eqs. (20.6) and (20.14), the energy $E\left(Si_{silane},3sp^3\right)$ of the outer electron of the $Si3sp^3$ shell is:

$$E\left(Si_{silane},3sp^3\right) = \frac{-e^2}{8\pi\varepsilon_0 r_{silane3sp^3}} + \frac{2\pi\mu_0 e^2\hbar^2}{m_e^2\left(r_{12}\right)^3} = -11.37682\ eV + 0.05836\ eV = -11.31845\ eV \tag{20.15}$$

Thus, $E_T\left(Si-H,3sp^3\right)$, the energy change of each $Si3sp^3$ shell with the formation of the $Si-H$ -bond MO is given by the difference between Eq. (20.15) and Eq. (20.7):

$$E_T\left(Si-H,3sp^3\right) = E\left(Si_{silane},3sp^3\right) - E\left(Si,3sp^3\right) = -11.31845\ eV - \left(-10.25487\ eV\right) = -1.06358\ eV \tag{20.16}$$

Silane (SiH_4) involves only $Si-H$ -bond MOs of equivalent tetrahedral structure to form a minimum energy surface involving a linear combination of all four hydrogen MOs. Here, the donation of electron density from the $Si3sp^3$ HO to each $Si-H$ -bond MO permits the participating orbital to decrease in size and energy as well. However, given the resulting continuous electron-density surface and the equivalent MOs, the $Si3sp^3$ HO donates an excess of 100% of its electron density to the $Si-H$ -bond MO to form an energy minimum. By considering this electron redistribution in the silane molecule as well as the fact that the central field decreases by an integer for each successive electron of the shell, the radius $r_{silane3sp^3}$ of the $Si3sp^3$ shell may be calculated from the Coulombic energy using Eq. (15.18):

$$r_{silane3sp^3} = \left(\sum_{n=10}^{13}(Z-n)-1\right)\frac{e^2}{8\pi\varepsilon_0\left(e105.23554\ eV\right)} = \frac{9e^2}{8\pi\varepsilon_0\left(e105.23554\ eV\right)} = 1.16360a_0 \tag{20.17}$$

Using Eqs. (15.19) and (20.17), the Coulombic energy $E_{Coulomb}\left(Si_{silane},3sp^3\right)$ of the outer electron of the $Si3sp^3$ shell is

$$E_{Coulomb}\left(Si_{silane},3sp^3\right) = \frac{-e^2}{8\pi\varepsilon_0 r_{silane3sp^3}} = \frac{-e^2}{8\pi\varepsilon_0 1.16360a_0} = -11.69284\ eV \tag{20.18}$$

During hybridization, one of the spin-paired 3*s* electrons is promoted to the $Si3sp^3$ shell as an unpaired electron. The energy for the promotion is the magnetic energy given by Eq. (20.6). Using Eqs. (20.6) and (20.18), the energy $E\left(Si_{silane},3sp^3\right)$ of the outer electron of the $Si3sp^3$ shell is:

$$E\left(Si_{silane},3sp^3\right) = \frac{-e^2}{8\pi\varepsilon_0 r_{silane3sp^3}} + \frac{2\pi\mu_0 e^2\hbar^2}{m_e^2\left(r_{12}\right)^3} = -11.69284\ eV + 0.05836\ eV = -11.63448\ eV \tag{20.19}$$

Thus, $E_T\left(Si-H,3sp^3\right)$, the energy change of each $Si3sp^3$ shell with the formation of the $Si-H$ -bond MO is given by the difference between Eq. (20.19) and Eq. (20.7):

$$E_T\left(Si-H,3sp^3\right) = E\left(Si_{silane},3sp^3\right) - E\left(Si,3sp^3\right) = -11.63448\ eV - \left(-10.25487\ eV\right) = -1.37960\ eV \tag{20.20}$$

Consider next the radius of the HO due to the contribution of charge to more than one bond. The energy contribution due to the charge donation at each silicon atom superimposes linearly. In general, the radius r_{mol3sp^3} of the $Si3sp^3$ HO of a silicon atom of a given silane molecule is calculated after Eq. (15.32) by considering $\sum E_{T_{mol}}\left(MO,3sp^3\right)$, the total energy donation to all bonds with which it participates in bonding. The general equation for the radius is given by:

$$r_{mol3sp^3} = \frac{-e^2}{8\pi\varepsilon_0\left(E_{Coulomb}\left(Si,3sp^3\right)+\sum E_{T_{mol}}\left(MO,3sp^3\right)\right)} = \frac{e^2}{8\pi\varepsilon_0\left(e10.31324\ eV+\sum\left|E_{T_{mol}}\left(MO,3sp^3\right)\right|\right)} \tag{20.21}$$

where $E_{Coulomb}\left(Si,3sp^3\right)$ is given by Eq. (20.4). The Coulombic energy $E_{Coulomb}\left(Si,3sp^3\right)$ of the outer electron of the *Si* sp^3 shell considering the charge donation to all participating bonds is given by Eq. (15.14) with Eq. (20.4). The energy E ($Si,3sp^3$) of the outer electron of the Si $3sp^3$ shell is given by the sum of $E_{Coulomb}\left(Si,3sp^3\right)$ and $E(magnetic)$ (Eq. (20.6)). The final values of the radius of the $Si3sp^3$ HO, r_{3sp^3}, $E_{Coulomb}\left(Si,3sp^3\right)$, and $E\left(Si_{silane}3sp^3\right)$ calculated using $\sum E_{T_{mol}}\left(MO,3sp^3\right)$, the total energy

donation to each bond with which an atom participates in bonding are given in Table 20.1. These hybridization parameters are used in Eqs. (15.88-15.117) for the determination of bond angles given in Table 20.7.

Table 20.1. Hybridization parameters of atoms for determination of bond angles with final values of r_{3sp^3}, $E_{Coulomb}\left(Si,3sp^3\right)$, and $E\left(Si_{silane}3sp^3\right)$ calculated using the appropriate values of $\sum E_{T_{mol}}\left(MO,3sp^3\right)$ ($E_{T_{mol}}\left(MO,3sp^3\right)$ designated as E_T) for each corresponding terminal bond spanning each angle.

Atom Hybridization Designation	E_T	E_T	E_T	E_T	E_T	r_{3sp^3} Final	$E_{Coulomb}\left(Si,3sp^3\right)$ (eV) Final	$E\left(Si,3sp^3\right)$ (eV) Final
1	0	0	0	0	0	1.31926	-10.31324	-10.25487
2	-0.48015	0	0	0	0	1.26057	-10.79339	-10.73503

The MO semimajor axis of each functional group of silanes is determined from the force balance equation of the centrifugal, Coulombic, and magnetic forces as given in the Polyatomic Molecular Ions and Molecules section and the More Polyatomic Molecules and Hydrocarbons section. The distance from the origin of the H_2-type-ellipsoidal-MO to each focus c', the internuclear distance $2c'$, and the length of the semiminor axis of the prolate spheroidal H_2-type MO $b = c$ are solved from the semimajor axis a. Then, the geometric and energy parameters of the MO are calculated using Eqs. (15.1-15.117).

The force balance of the centrifugal force equated to the Coulombic and magnetic forces is solved for the length of the semimajor axis. The Coulombic force on the pairing electron of the MO is:

$$\mathbf{F}_{Coulomb} = \frac{e^2}{8\pi\varepsilon_0 ab^2} D\mathbf{i}_\xi \tag{20.22}$$

The spin pairing force is

$$\mathbf{F}_{spin-pairing} = \frac{\hbar^2}{2m_e a^2 b^2} D\mathbf{i}_\xi \tag{20.23}$$

The diamagnetic force is:

$$\mathbf{F}_{diamagneticMO1} = -\frac{n_e \hbar^2}{4m_e a^2 b^2} D\mathbf{i}_\xi \tag{20.24}$$

where n_e is the total number of electrons that interact with the binding σ-MO electron. The diamagnetic force $\mathbf{F}_{diamagneticMO2}$ on the pairing electron of the σ MO is given by the sum of the contributions over the components of angular momentum:

$$\mathbf{F}_{diamagneticMO2} = -\sum_{i,j} \frac{|L_i|\hbar^2}{Z_j 2m_e a^2 b^2} D\mathbf{i}_\xi \tag{20.25}$$

where $|L|$ is the magnitude of the angular momentum of each atom at a focus that is the source of the diamagnetism at the σ-MO. The centrifugal force is:

$$\mathbf{F}_{centrifugalMO} = -\frac{\hbar^2}{m_e a^2 b^2} D\mathbf{i}_\xi \tag{20.26}$$

The force balance equation for the σ-MO of the $Si-Si$-bond MO with $n_e = 3$ and $|L| = 4\sqrt{\frac{3}{4}}\hbar$ corresponding to four electrons of the $Si3sp^3$ shell is**:**

$$\frac{\hbar^2}{m_e a^2 b^2} D = \frac{e^2}{8\pi\varepsilon_0 ab^2} D + \frac{\hbar^2}{2m_e a^2 b^2} D - \left(\frac{3}{2} + \frac{4\sqrt{\frac{3}{4}}}{Z}\right) \frac{\hbar^2}{2m_e a^2 b^2} D \tag{20.27}$$

$$a = \left(\frac{5}{2} + \frac{4\sqrt{\frac{3}{4}}}{Z}\right) a_0 \tag{20.28}$$

With $Z = 14$, the semimajor axis of the $Si-Si$-bond MO is:

$$a = 2.74744 a_0 \tag{20.29}$$

The force balance equation for each σ-MO of the $Si-H$-bond MO with $n_e = 2$ and $|L| = 4\sqrt{\frac{3}{4}}\hbar$ corresponding to four electrons of the $Si3sp^3$ shell is**:**

$$\frac{\hbar^2}{m_e a^2 b^2} D = \frac{e^2}{8\pi\varepsilon_0 a b^2} D + \frac{\hbar^2}{2m_e a^2 b^2} D - \left(1 + \frac{4\sqrt{\frac{3}{4}}}{Z}\right) \frac{\hbar^2}{2m_e a^2 b^2} D \tag{20.30}$$

$$a = \left(2 + \frac{4\sqrt{\frac{3}{4}}}{Z}\right) a_0 \tag{20.31}$$

With $Z = 14$, the semimajor axis of the $Si - H$-bond MO is:

$$a = 2.24744 a_0 \tag{20.32}$$

Using the semimajor axis, the geometric and energy parameters of the MO are calculated using Eqs. (15.1-15.117) in the same manner as the organic functional groups given in the Organic Molecular Functional Groups and Molecules section. For the $Si - Si$ functional group, the $Si3sp^3$ HOs are equivalent; thus, $c_1 = 1$ in both the geometry relationships (Eqs. (15.2-15.5)) and the energy equation (Eq. (15.61)). In order for the bridging MO to intersect the $Si3sp^3$ HOs while matching the potential, kinetic, and orbital energy relationships given in the Hydroxyl Radical (OH) section, for the $Si - Si$ functional group, $C_1 = \frac{0.75}{2}$ in both the geometry relationships (Eqs. (15.2-15.5)) and the energy equation (Eq. (15.61)). This is the same value as C_1 of the chlorine molecule given in the corresponding section. The hybridization factor gives the parameters c_2 and C_2 for both as well. To meet the equipotential condition of the union of the two $Si3sp^3$ HOs, c_2 and C_2 of Eqs. (15.2-15.5) and Eq. (15.61) for the $Si - Si$-bond MO is given by Eq. (15.72) as the ratio of 10.31324 eV, the magnitude of $E_{Coulomb}\left(Si_{silane}, 3sp^3\right)$ (Eq. (20.4)), and 13.605804 eV, the magnitude of the Coulombic energy between the electron and proton of H (Eq. (1.264)):

$$C_2\left(silaneSi3sp^3HO\right) = c_2\left(silaneSi3sp^3HO\right) = \frac{10.31324\ eV}{13.605804\ eV} = 0.75800 \tag{20.33}$$

The energy of the MO is matched to that of the $Si3sp^3$ HO such that $E\left(AO/HO\right)$ is $E\left(Si, 3sp^3\right)$ given by Eq. (20.7) and $E_T\left(atom - atom, msp^3.AO\right)$ is two times $E_T\left(Si - Si, 3sp^3\right)$ given by Eq. (20.12).

For the $Si - H$-bond MO of the $SiH_{n=1,2,3}$ functional groups, c_1 is one and $C_1 = 0.75$ based on the orbital composition as in the case of the $C - H$-bond MO. In silanes, the energy of silicon is less than the Coulombic energy between the electron and proton of H given by Eq. (1.264). Thus, c_2 in Eq. (15.61) is also one, and the energy matching condition is determined by the C_2 parameter, the hybridization factor for the $Si - H$-bond MO given by Eq. (20.33). Since the energy of the MO is matched to that of the $Si3sp^3$ HO, $E\left(AO/HO\right)$ is $E\left(Si, 3sp^3\right)$ given by Eq. (20.7) and $E_T\left(atom - atom, msp^3.AO\right)$ is $E_T\left(Si - H, 3sp^3\right)$ given by Eq. (20.16). The energy $E_D\left(SiH_{n=1,2,3}\right)$ of the functional groups $SiH_{n=1,2,3}$ is given by the integer *n* times that of $Si - H$:

$$E_D\left(SiH_{n=1,2,3}\right) = nE_D\left(SiH\right) \tag{20.34}$$

Similarly, for silane, $E_T\left(atom - atom, msp^3.AO\right)$ is $E_T\left(Si - H, 3sp^3\right)$ given by Eq. (20.20). The energy $E_D\left(SiH_4\right)$ of SiH_4 is given by the integer 4 times that of the $SiH_{n=4}$ functional group:

$$E_D\left(SiH_4\right) = 4E_D\left(SiH_{n=4}\right) \tag{20.35}$$

The symbols of the functional groups of silanes are given in Table 20.2. The geometrical (Eqs. (15.1-15.5), (20.1-20.16), (20.29), and (20.32-20.33)), intercept (Eqs. (15.80-15.87) and (20.21)), and energy (Eqs. (15.61), (20.1-20.16), and (20.33-20.35)) parameters of silanes are given in Tables 20.3, 20.4, and 20.5, respectively. The total energy of each silane given in Table 20.6 was calculated as the sum over the integer multiple of each $E_D(Group)$ of Table 20.5 corresponding to functional-group composition of the molecule. E_{mag} of Table 20.5 is given by Eqs. (15.15) and (20.3). The bond angle parameters of silanes determined using Eqs. (15.88-15.117) are given in Table 20.7. In particular for silanes, the bond angle $\angle HSiH$ is given by Eq. (15.99) wherein $E_T\left(atom - atom, msp^3.AO\right)$ is given by Eq. (20.16) in order to match the energy donated from the $Si3sp^3$ HO to the $Si - H$-bond MO due to the energy of silicon being less than the Coulombic energy between the electron and proton of H given by Eq. (1.264). The parameter c_2' is given by Eq. (15.100) as in the case of a $H - H$ terminal bond of an alkyl or alkenyl group, except that $c_2(Si3sp^3)$ is given by Eq. (15.63) such that c_2' is the ratio of c_2 of Eq. (15.72) for the $H - H$ bond which is one and c_2 of the silicon of the corresponding $Si - H$-bond considering the effect of the formation of the $H - H$ terminal bond:

$$c_2' = \frac{1}{c_2(Si3sp^3)} = \frac{13.605804\ eV}{E_{Coulomb}\left(Si - H\ Si3sp^3\right)} \tag{20.36}$$

The color scale, translucent view of the charge-densities of the series $SiH_{n=1,2,3,4}$ comprising the concentric shells of the central Si atom of each member with the outer shell joined with one or more hydrogen MOs are shown in Figures 20.1A-D. The

charge-density of disilane is shown in Figure 20.2.

Figure 20.1. (A)-(D) Color scale, translucent view of the charge-densities of the series $SiH_{n=1,2,3,4}$, showing the orbitals of each member Si atom at their radii, the ellipsoidal surface of each H_2-type ellipsoidal MO of H that transitions to the outer shell of the Si atom participating in each $Si-H$ bond, and the hydrogen nuclei (red, not to scale).

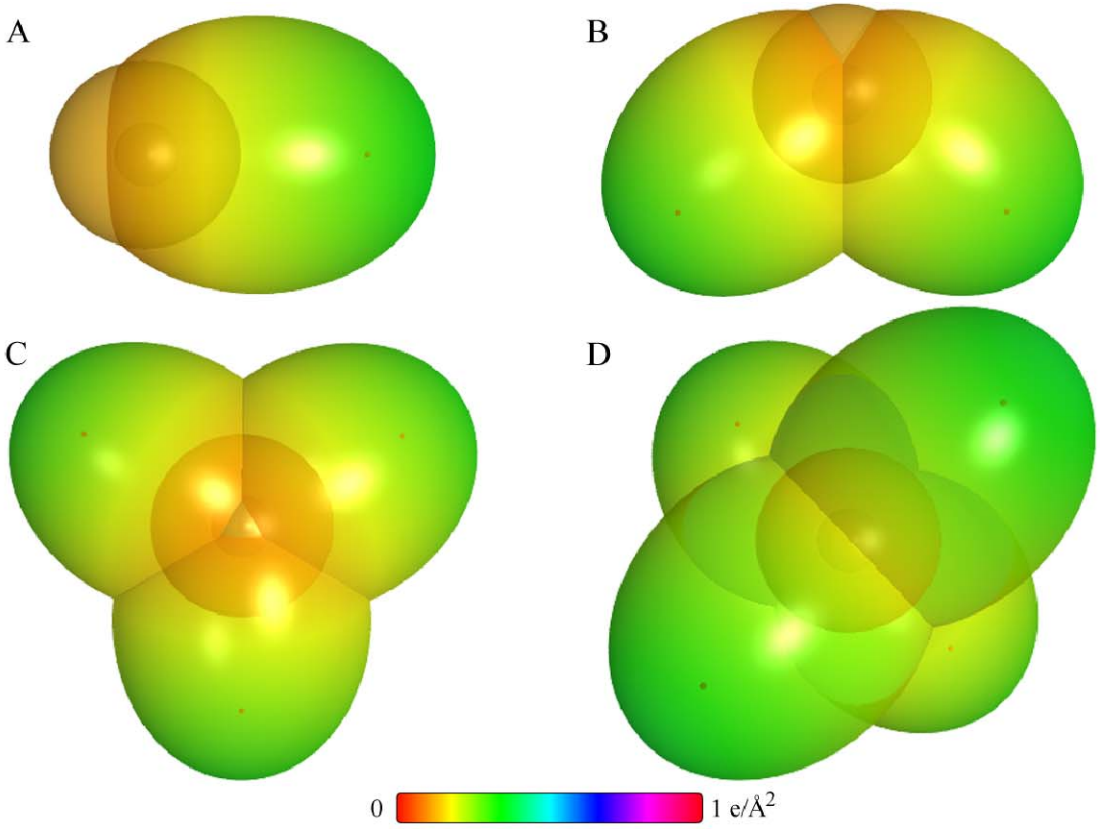

Figure 20.2. *Disilane.* Color scale, translucent view of the charge-density of H_3SiSiH_3 comprising the linear combination of two sets of three $Si-H$ -bond MOs and a $Si-Si$ -bond MO with the $Si_{silane}3sp^3$ HOs of the $Si-Si$ -bond MO shown transparently. The $Si-Si$ -bond MO comprises a H_2-type ellipsoidal MO bridging two $Si_{silane}3sp^3$ HOs. For each $Si-H$ and the $Si-Si$ bond, the ellipsoidal surface of the H_2-type ellipsoidal MO that transitions to the $Si_{silane}3sp^3$ HO, the $Si_{silane}3sp^3$ HO shell with radius $0.97295a_0$ (Eq. (20.21)), inner $Si1s$, $Si2s$, and $Si2p$ shells with radii of $Si1s = 0.07216a_0$ (Eq. (10.51)), $Si2s = 0.31274a_0$ (Eq. (10.62)), and $Si2p = 0.40978a_0$ (Eq. (10.212)), respectively, and the nuclei (red, not to scale), are shown.

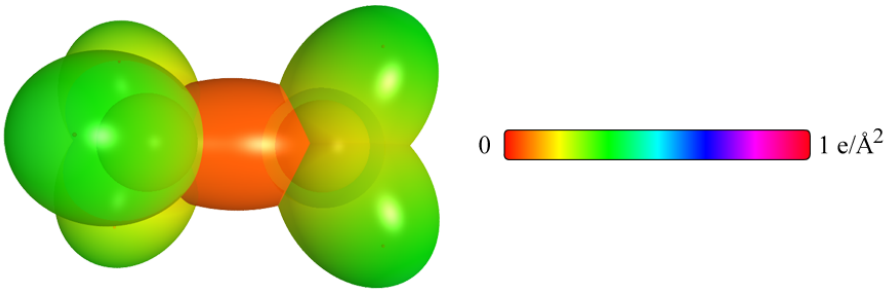

Table 20.2. The symbols of the functional groups of silanes.

Functional Group	Group Symbol
SiH group of $SiH_{n=1,2,3}$	$Si-H$ (i)
SiH group of $SiH_{n=4}$	$Si-H$ (ii)
SiSi bond (*n-Si*)	$Si-Si$

Table 20.3. The geometrical bond parameters of silanes and experimental values [2].

Parameter	$Si-H$ (i) and (ii) Group	$Si-Si$ Group
$a\ (a_0)$	2.24744	2.74744
$c'\ (a_0)$	1.40593	2.19835
Bond Length $2c'\ (\AA)$	1.48797	2.32664
Exp. Bond Length $(\AA)$	1.492 (Si_2H_6)	2.331 (Si_2H_6) 2.32 (Si_2Cl_6)
$b,c\ (a_0)$	1.75338	1.64792
e	0.62557	0.80015

Table 20.4. The MO to HO intercept geometrical bond parameters of silanes. E_T is E_T (*atom - atom* $msp^3.AO$).

Bond	Atom	E_T (eV) Bond 1	E_T (eV) Bond 2	E_T (eV) Bond 3	E_T (eV) Bond 4	Final Total Energy $C2sp^3$ (eV)	$r_{Initial}$ (a_0)	r_{final} (a_0)	$E_{Coulomb}\left(Si3sp^3\right)$ (eV) Final	$E\left(Si3sp^3\right)$ (eV) Final	θ' (°)	θ_1 (°)	θ_2 (°)	d_1 (a_0)	d_2 (a_0)
$Si-H\ (SiH)$	*Si*	-1.06358	0	0	0	-106.29912	1.31926	1.19592	-11.37682	-11.31845	76.71	103.29	41.59	1.68089	0.27496
$Si-H\ (SiH_2)$	*Si*	-1.06358	-1.06358	0	0	-107.36270	1.31926	1.09368	-12.44040	-12.38204	66.37	113.63	34.85	1.84433	0.43840
$Si-H\ (SiH_3)$	*Si*	-1.06358	-1.06358	-1.06358	0	-108.42628	1.31926	1.00754	-13.50398	-13.44562	55.12	124.88	28.13	1.98203	0.57610
$Si-H\ (SiH_4)$	*Si*	-1.37960	-1.37960	-1.37960	-1.37960	-110.75395	1.31926	0.85941	-15.83165	-15.77329	18.93	161.07	9.15	2.21883	0.81290
$H-(H_2)SiSi-$	*Si*	-1.06358	-1.06358	-1.06358	-0.48015	-108.90644	1.31926	0.97295	-13.98413	-13.92577	49.54	130.46	24.97	2.03733	0.63140
$H_3SiSi(H)-HSiH_2-$	*Si*	-1.06358	-1.06358	-0.48015	-0.48015	-108.32301	1.31926	1.01531	-13.40070	-13.34234	56.28	123.72	28.79	1.96962	0.56369
$H_3Si_a-Si_bH_2SiH_2$	Si_a	-0.48015	-1.06358	-1.06358	-1.06358	-108.90644	1.31926	0.97295	-13.98413	-13.92577	88.86	91.14	36.18	2.21770	0.01935
$H_3Si_a-Si_bH_2SiH_2$	Si_b	-0.48015	-0.48015	-1.06358	-1.06358	-108.32301	1.31926	1.01531	-13.40070	-13.34234	91.90	88.10	38.01	2.16476	0.03359

Table 20.5. The energy parameters (eV) of the functional groups of silanes.

Parameters	$Si-H$ (i) Group	$Si-H$ (ii) Group	$Si-Si$ Group
n_1	1	1	1
n_2	0	0	0
n_3	0	0	0
C_1	0.75	0.75	0.37500
C_2	0.75800	0.75800	0.75800
c_1	1	1	1
c_2	1	1	0.75800
c_3	0	0	0
c_4	1	1	2
c_5	1	1	0
C_{1o}	0.75	0.75	0.37500
C_{2o}	0.75800	0.75800	0.75800
$V_e\ (eV)$	-28.41703	-28.41703	-20.62357
$V_p\ (eV)$	9.67746	9.67746	6.18908
$T\ (eV)$	6.32210	6.32210	3.75324
$V_m\ (eV)$	-3.16105	-3.16105	-1.87662
$E_{(AO/HO)}\ (eV)$	-10.25487	-10.25487	-10.25487
$\Delta E_{H_2MO(AO/HO)}\ (eV)$	0	0	0
$E_{T(AO/HO)}\ (eV)$	-10.25487	-10.25487	-10.25487
$E_{T(H_2MO)}\ (eV)$	-25.83339	-25.83339	-22.81274
$E_T\left(atom-atom, msp^3.AO\right)\ (eV)$	-1.06358	-1.37960	-0.96031
$E_{T(MO)}\ (eV)$	-26.89697	-27.21299	-23.77305
$\omega\ \left(10^{15}\ rad/s\right)$	13.4257	13.4257	4.83999
$E_K\ (eV)$	8.83703	8.83703	3.18577
$\overline{E}_D\ (eV)$	-0.15818	-0.16004	-0.08395
$\overline{E}_{Kvib}\ (eV)$	0.25315 [3]	0.25315 [3]	0.06335 [3]
$\overline{E}_{osc}\ (eV)$	-0.03161	-0.03346	-0.05227
$E_{mag}\ (eV)$	0.04983	0.04983	0.04983
$E_{T(Group)}\ (eV)$	-26.92857	-27.24646	-23.82532
$E_{initial(c_4\ AO/HO)}\ (eV)$	-10.25487	-10.25487	-10.25487
$E_{initial(c_5\ AO/HO)}\ (eV)$	-13.59844	-13.59844	0
$E_{D(Group)}\ (eV)$	3.07526	3.39314	3.31557
Exp. $E_{D(Group)}\ (eV)$	3.0398 ($Si-H$ [4])		3.3269 ($H_3Si-SiH_3$ [5])

Table 20.6. The total bond energies of silanes calculated using the functional group composition and the energies of Table 20.5 compared to the experimental values.

Formula	Name	$Si-H$ (i) Group	$Si-H$ (ii) Group	$Si-Si$ Group	Calculated Total Bond Energy (eV)	Experimental Total Bond Energy (eV)	Relative Error
SiH	Silylidyne	1	0	0	3.07526	3.02008 [6]	-0.01827
SiH_2	Silylene	2	0	0	6.15052	6.35523 [7]	0.03221
SiH_3	Silyl	3	0	0	9.22578	9.36494 [7]	0.01486
SiH_4	Silane	0	4	0	13.57257	13.34577 [6]	-0.01699
Si_2H_6	Disilane	6	0	1	21.76713	22.05572 [7]	0.01308
Si_3H_8	Trisilane	8	0	2	31.23322	30.81334 [7]	-0.01363

Table 20.7. The bond angle parameters of silanes and experimental values [2]. In the calculation of θ_v (Eq. (15.112)), the parameters from the preceding angle were used. E_T is E_T (*atom - atom* msp^3*.AO*).

Atoms of Angle	2c' Bond 1 (a_0)	2c' Bond 2 (a_0)	2c' Terminal Atoms (a_0)	$E_{Coulombic}$ Atom 1	Atom 1 Hybridization terms (Table 20.1)	$E_{Coulombic}$ Atom 2	Atom 2 Hybridization terms (Table 20.1)	c_2 Atom 1	c_2 Atom 2	C_1	C_2	c_1	c_2'	E_T (eV)	θ_v (°)	θ_1 (°)	θ_2 (°)	Cal. θ (°)	Exp. θ (°)
Silyl $\angle HSi_aH$	2.81185	2.81185	4.5673	-10.79339 Si_a	2	H	H	0.79329	1	1	1	0.75	1.26057	-1.06358				108.61	108.6 (disilane)
$\angle HSi_aSi_b$															69.68			110.32	110.3 (disilane)

ALKYL SILANES AND DISILANES ($Si_mC_nH_{2(m+n)+2},\ m,n=1,2,3,4,5...\infty$)

The branched-chain alkyl silanes and disilanes, $Si_mC_nH_{2(m+n)+2}$, comprise at least a terminal methyl group (CH_3) and at least one Si bound by a carbon-silicon single bond comprising a $C-Si$ group, and may comprise methylene (CH_2), methylyne (CH), $C-C$, $SiH_{n=1,2,3}$, and $Si-Si$ functional groups. The methyl and methylene functional groups are equivalent to those of straight-chain alkanes. Six types of $C-C$ bonds can be identified. The n-alkane $C-C$ bond is the same as that of straight-chain alkanes. In addition, the $C-C$ bonds within isopropyl ($\left(CH_3\right)_2CH$) and t-butyl ($\left(CH_3\right)_3C$) groups and the isopropyl to isopropyl, isopropyl to t-butyl, and t-butyl to t-butyl $C-C$ bonds comprise functional groups. These groups in branched-chain alkyl silanes and disilanes are equivalent to those in branched-chain alkanes, and the $SiH_{n=1,2,3}$ functional groups of alkyl silanes are equivalent to those in silanes (Si_nH_{2n+2}). The $Si-Si$ functional group of alkyl silanes is equivalent to that in silanes; however, in dialkyl silanes, the $Si-Si$ functional group is different due to an energy matching condition with the $C-Si$ bond having a mutual silicon atom.

For the $C-Si$ functional group, hybridization of the $2s$ and $2p$ AOs of each C and the $3s$ and $3p$ AOs of each Si to form single $2sp^3$ and $3sp^3$ shells, respectively, forms an energy minimum, and the sharing of electrons between the $C2sp^3$ and $Si3sp^3$ HOs to form a MO permits each participating orbital to decrease in radius and energy. In branched-chain alkyl silanes, the energy of silane is less than the Coulombic energy between the electron and proton of H given by Eq. (1.264). Thus, c_2 in Eq. (15.61) is one, and the energy matching condition is determined by the C_2 parameter. Then, the $C2sp^3$ HO has an energy of $E\left(C,2sp^3\right)=-14.63489\ eV$ (Eq. (15.25)), and the $Si3sp^3$ HO has an energy of $E\left(Si,3sp^3\right)=-10.25487\ eV$ (Eq. (20.7)). To meet the equipotential condition of the union of the $C-Si$ H_2-type-ellipsoidal-MO with these orbitals, the hybridization factor C_2 of Eq. (15.61) for the $C-Si$-bond MO given by Eq. (15.77) is:

$$C_2\left(C2sp^3HO\ to\ Si3sp^3HO\right)=\frac{E\left(Si,3sp^3\right)}{E\left(C,2sp^3\right)}=\frac{-10.25487\ eV}{-14.63489\ eV}=0.70071 \tag{20.37}$$

For monosilanes, $E_T\left(atom-atom,msp^3.AO\right)$ of the $C-Si$-bond MO is $-1.20473\ eV$ corresponding to the single-bond contributions of carbon and silicon of $-0.72457\ eV$ given by Eq. (14.151) and $-0.48015\ eV$ given by Eq. (14.151) with $s=1$ in Eq. (15.18). The energy of the $C-Si$-bond MO is the sum of the component energies of the H_2-type ellipsoidal MO given in Eq. (15.51) with $E\left(AO/HO\right)=E\left(Si,3sp^3\right)$ given by Eq. (20.7) and $\Delta E_{H_2MO}\left(AO/HO\right)=E_T\left(atom-atom,msp^3.AO\right)$ in order to match the energies of the carbon and silicon HOs.

For the co-bonded $Si-Si$ group of the $C-Si$ group of disilanes, $E_T\left(atom-atom,msp^3.AO\right)$ is $-0.96031\ eV$, two times $E_T\left(Si-Si,3sp^3\right)$ given by Eq. (20.12). Thus, in order to match the energy between these groups, $E_T\left(atom-atom,msp^3.AO\right)$ of the $C-Si$-bond MO is $-0.92918\ eV$ corresponding to the single-bond methylene-type contribution of carbon given by Eq. (14.513). As in the case of monosilanes, $E\left(AO/HO\right)=E\left(Si,3sp^3\right)$ given by Eq. (20.7) and $\Delta E_{H_2MO}\left(AO/HO\right)=E_T\left(atom-atom,msp^3.AO\right)$ in order to match the energies of the carbon and silicon HOs.

The symbols of the functional groups of alkyl silanes and disilanes are given in Table 20.8. The geometrical (Eqs. (15.1-15.5), (20.1-20.16), (20.29), (20.32-20.33) and (20.37)) and intercept (Eqs. (15.80-15.87) and (20.21)) parameters of alkyl silanes and disilanes are given in Tables 20.9 and 20.10, respectively. Since the energy of the $Si3sp^3$ HO is matched to that of the $C2sp^3$ HO, the radius r_{mol2sp^3} of the $Si3sp^3$ HO of the silicon atom and the $C2sp^3$ HO of the carbon atom of a given $C-Si$-bond MO is calculated after Eq. (15.32) by considering $\sum E_{T_{mol}}\left(MO,2sp^3\right)$, the total energy donation to all bonds with which each atom participates in bonding. In the case that the MO does not intercept the Si HO due to the reduction of the radius from the donation of Si $3sp^3$ HO charge to additional MO's, the energy of each MO is energy matched as a linear sum to the Si HO by contacting it through the bisector current of the intersecting MOs as described in the Methane Molecule (CH_4) section. The energy (Eqs. (15.61), (20.1-20.16), and (20.33-20.37)) parameters of alkyl silanes and disilanes are given in Table 20.11. The total energy of each alkyl silane and disilane given in Table 20.12 was calculated as the sum over the integer multiple of each $E_D(Group)$ of Table 20.11 corresponding to functional-group composition of the molecule. The bond angle parameters of alkyl silanes and disilanes determined using Eqs. (15.88-15.117) and Eq. (20.36) are given in Table 20.13. The charge-densities of exemplary alkyl silane, dimethylsilane and alkyl disilane, hexamethyldisilane comprising the concentric shells of atoms with the outer shell bridged by one or more H_2-type ellipsoidal MOs or joined with one or more hydrogen MOs are shown in Figures 20.3A and B, respectively.

Figure 20.3. (A) *Dimethylsilane* and (B) *Hexamethyldisilane*, color scale, translucent views of the charge-density of each silane showing the orbitals of the Si and C atoms at their radii, the ellipsoidal surface of each H or H_2-type ellipsoidal MO that transitions to the corresponding outer shell of the atoms participating in each bond, and the hydrogen nuclei (red, not to scale).

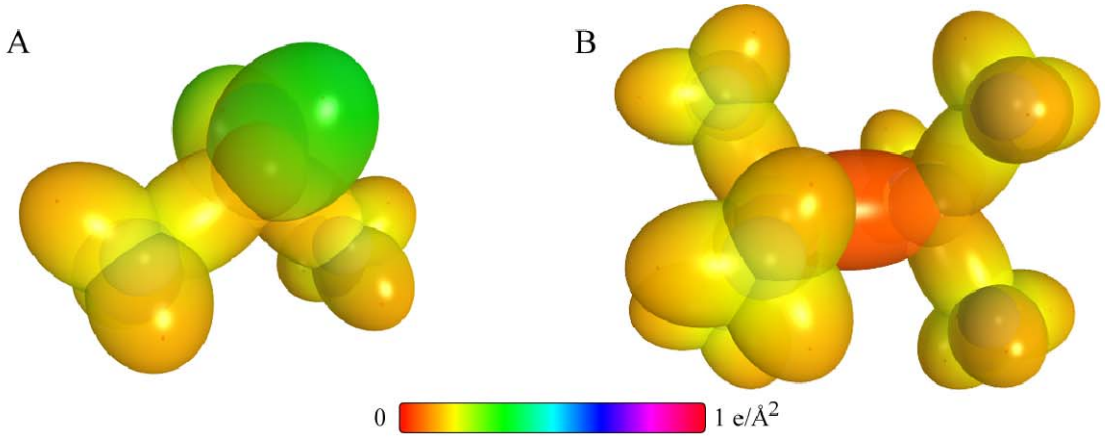

Table 20.8. The symbols of functional groups of alkyl silanes and disilanes.

Functional Group	Group Symbol
CSi bond (monosilanes)	$C-Si$ (i)
CSi bond (disilanes)	$C-Si$ (ii)
SiSi bond (*n-Si*)	$Si-Si$
SiH group of $SiH_{n=1,2,3}$	$Si-H$
CH_3 group	$C-H\ (CH_3)$
CH_2 group	$C-H\ (CH_2)$
CH	$C-H$
CC bond (*n-C*)	$C-C$ (a)
CC bond (*iso-C*)	$C-C$ (b)
CC bond (*tert-C*)	$C-C$ (c)
CC (*iso* to *iso-C*)	$C-C$ (d)
CC (*t* to *t-C*)	$C-C$ (e)
CC (*t* to *iso-C*)	$C-C$ (f)

Table 20.9. The geometrical bond parameters of alkyl silanes and disilanes and experimental values.

Parameter	$C-Si$ (i) Group	$C-Si$ (ii) Group	$Si-H$ Group	$Si-Si$ Group	$C-H\ (CH_3)$ Group	$C-H\ (CH_2)$ Group	$C-H$ Group	$C-C$ (a) Group	$C-C$ (b) Group	$C-C$ (c) Group	$C-C$ (d) Group	$C-C$ (e) Group	$C-C$ (f) Group
$a\ (a_0)$	2.20339	2.21935	2.24744	2.74744	1.64920	1.67122	1.67465	2.12499	2.12499	2.10725	2.12499	2.10725	2.10725
$c'\ (a_0)$	1.77327	1.77968	1.40593	2.19835	1.04856	1.05553	1.05661	1.45744	1.45744	1.45164	1.45744	1.45164	1.45164
Bond Length $2c'\ (\AA)$	1.87675	1.88353	1.48797	2.32664	1.10974	1.11713	1.11827	1.54280	1.54280	1.53635	1.54280	1.53635	1.53635
Exp. Bond Length $(\AA)$	1.867 (methylsilane) [8] 1.875 (tetramethylsilane) [8] 1.877 (methylsilane) [9] 1.871 (dimethylsilane) [9] 1.878 (trimethylsilane) [9]		1.485 (methylsilane) [8] 1.492 (Si_2H_6) [8] 1.489 (trimethylsilane) [9]	2.331 (Si_2H_6) [8] 2.32 (Si_2Cl_6) [8]	1.093 (methylsilane) [8] 1.115 (tetramethylsilane) [8] 1.107 ($C-H$ propane) [8] 1.117 ($C-H$ butane) [8]	1.107 ($C-H$ propane) [8] 1.117 ($C-H$ butane) [8]	1.122 (isobutane) [8]	1.532 (propane) [8] 1.531 (butane) [8]	1.532 (propane) [8] 1.531 (butane) [8]	1.532 (propane) [8] 1.531 (butane) [8]	1.532 (propane) [8] 1.531 (butane) [8]	1.532 (propane) [8] 1.531 (butane) [8]	1.532 (propane) [8] 1.531 (butane) [8]
$b,c\ (a_0)$	1.30783	1.32599	1.75338	1.64792	1.27295	1.29569	1.29924	1.54616	1.54616	1.52750	1.54616	1.52750	1.52750
e	0.80479	0.80189	0.62557	0.80015	0.63580	0.63159	0.63095	0.68600	0.68600	0.68888	0.68600	0.68888	0.68888

Table 20.10. The MO to HO intercept geometrical bond parameters of alkyl silanes and disilanes. *R, R', R"* are *H* or alkyl groups. E_T is E_T (*atom - atom msp³.AO*).

Bond	Atom	E_T (eV) Bond 1	E_T (eV) Bond 2	E_T (eV) Bond 3	E_T (eV) Bond 4	Final Total Energy $Si3sp^3$ $C2sp^3$ (eV)	$r_{initial}$ (a_0)	r_{final} (a_0)	$E_{Coulomb}(C2sp^3)$ (eV) Final	$E(Si3sp^3)$ $E(C2sp^3)$ (eV) Final	θ' (°)	θ_1 (°)	θ_2 (°)	d_1 (a_0)	d_2 (a_0)
$Si-H\ (RSiH_3)$	Si	-0.60236	-1.06358	-1.06358	-1.06358		1.31926	0.73075	-18.61886	-18.56050					
$Si-H\ (R_2SiH_2)$	Si	-0.60236	-0.60236	-1.06358	-1.06358		1.31926	0.74932	-18.15764	-18.09928					
$Si-H\ (R_3SiH)$	Si	-0.60236	-0.60236	-0.60236	-1.06358		1.31926	0.76884	-17.69642	-17.63806					
$H_3Si_a-C_aH_2-$ $(C-Si\ (i))$	Si_a	-0.60236	-1.06358	-1.06358	-1.06358		1.31926	0.73075	-18.61886	-18.56050	85.56	94.44	33.85	1.82982	0.05655
$H_2Si_a-(C_aH_2-)_2$ $(C-Si\ (i))$	Si_a	-0.60236	-0.60236	-1.06358	-1.06358		1.31926	0.74932	-18.15764	-18.09928	87.44	92.56	34.92	1.80676	0.03349
$HSi_a-(C_aH_2-)_3$ $(C-Si\ (i))$	Si_a	-0.60236	-0.60236	-0.60236	-1.06358		1.31926	0.76884	-17.69642	-17.63806	89.31	90.69	36.00	1.78249	0.00922
$Si_a-(C_aH_2-)_4$ $(C-Si\ (i))$	Si_a	-0.60236	-0.60236	-0.60236	-0.60236		1.31926	0.78942	-17.23521	-17.17685	91.19	88.81	37.12	1.75693	0.01634
$-Si_aH_2-CH_3$ $(C-Si\ (i))$	C	-0.60236	0	0	0	-152.21805	0.91771	0.88188	-15.42812	-15.23725	98.56	81.44	41.82	1.64204	0.13123
$-Si_aH_2-C_aH_2CH_2-$ $(C-Si\ (i))$	C_a	-0.60236	-0.92918	0	0	-153.14724	0.91771	0.83179	-16.35730	-16.16643	94.76	85.24	39.33	1.70428	0.06899
$Si-H\ (H_3Si_aSi)$	Si_a	-0.48015	-1.06358	-1.06358	-1.06358	-108.90644	1.31926	0.97295	-13.98413	-13.92577	49.54	130.46	24.97	2.03733	0.63140
$Si-H\ (R(H_2)Si_aSi)$	Si_a	-0.48015	-0.46459	-1.06358	-1.06358	-108.30745	1.31926	1.01649	-13.38514	-13.32678	56.45	123.55	28.89	1.96773	0.56180
$Si-H\ (R_2(H)Si_aSi)$	Si_a	-0.48015	-0.46459	-0.46459	-1.06358	-107.70846	1.31926	1.06410	-12.78615	-12.72779	62.84	117.16	32.68	1.89161	0.48568
$H_3Si_a-Si_bH_2CH_2-$	Si_a	-0.48015	-1.06358	-1.06358	-1.06358	-108.90644	1.31926	0.97295	-13.98413	-13.92577	88.86	91.14	36.18	2.21770	0.01935
$Si_a-Si_bH_2CH_2-$ $(C-Si\ (ii))$	Si_b	-0.48015	-0.46459	-1.06358	-1.06358	-108.30745	1.31926	1.01649	-13.38514	-13.32678	91.98	88.02	38.06	2.16329	0.03507
$Si_b-Si_aH(CH_2-)_2$ $(C-Si\ (ii))$	Si_b	-0.48015	-0.46459	-0.46459	-1.06358	-107.70846	1.31926	1.06410	-12.78615	-12.72779	95.10	84.90	40.03	2.10378	0.09458
$Si_a-Si_b(CH_2-)_3$ $(C-Si\ (ii))$	Si_b	-0.48015	-0.46459	-0.46459	-0.46459	-107.10947	1.31926	1.11640	-12.18716	-12.12880	98.24	81.76	42.10	2.03841	0.15994
$Si_bSi_aH_2-C_aH_2-$ $(C-Si\ (ii))$	Si_a	-0.46459	-0.48015	-1.06358	-1.06358		1.31926	0.76020	-17.89766	-17.83930	86.99	93.01	34.93	1.81963	0.03995
$Si_bSi_aH-(C_aH_2-)_2$ $(C-Si\ (ii))$	Si_a	-0.46459	-0.46459	-0.48015	-1.06358		1.31926	0.78652	-17.29867	-17.24031	89.48	90.52	36.38	1.78680	0.00712
$Si_bSi_a-(C_aH_2-)_3$ $(C-Si\ (ii))$	Si_a	-0.46459	-0.46459	-0.46459	-0.48015		1.31926	0.81473	-16.69968	-16.64132	91.97	88.03	37.88	1.75162	0.02806
$-Si_a-CH_3$ $(C-Si\ (ii))$	C	-0.46459	0	0	0	-152.08028	0.91771	0.88983	-15.29034	-15.09948	97.86	82.14	41.66	1.65798	0.12171
$-Si_a-C_aH_2CH_2-$ $(C-Si\ (ii))$	C_a	-0.46459	-0.92918	0	0	-153.00946	0.91771	0.83885	-16.21952	-16.02866	93.97	86.03	39.13	1.72155	0.05814
$C-H\ (CH_3)$	C	-0.92918	0	0	0	-152.54487	0.91771	0.86359	-15.75493	-15.56407	77.49	102.51	41.48	1.23564	0.18708
$C-H\ (CH_2)$	C	-0.92918	-0.92918	0	0	-153.47406	0.91771	0.81549	-16.68412	-16.49325	68.47	111.53	35.84	1.35486	0.29933
$C-H\ (CH)$	C	-0.92918	-0.92918	-0.92918	0	-154.40324	0.91771	0.77247	-17.61330	-17.42244	61.10	118.90	31.37	1.42988	0.37326
$H_3C_aC_bH_2CH_2-$ $(C-C\ (a))$	C_a	-0.92918	0	0	0	-152.54487	0.91771	0.86359	-15.75493	-15.56407	63.82	116.18	30.08	1.83879	0.38106
$H_3C_aC_bH_2CH_2-$ $(C-C\ (a))$	C_b	-0.92918	-0.92918	0	0	-153.47406	0.91771	0.81549	-16.68412	-16.49325	56.41	123.59	26.06	1.90890	0.45117
$R-H_2C_aC_b(H_2C_c-R')HCH_2-$ $(C-C\ (b))$	C_b	-0.92918	-0.92918	-0.92918	0	-154.40324	0.91771	0.77247	-17.61330	-17.42244	48.30	131.70	21.90	1.97162	0.51388
$R-H_2C_a(R'-H_2C_d)C_b(R''-H_2C_e)CH_2-$ $(C-C\ (c))$	C_b	-0.92918	-0.72457	-0.72457	-0.72457	-154.71860	0.91771	0.75889	-17.92866	-17.73779	48.21	131.79	21.74	1.95734	0.50570
$isoC_aC_b(H_2C_c-R')HCH_2-$ $(C-C\ (d))$	C_b	-0.92918	-0.92918	-0.92918	0	-154.40324	0.91771	0.77247	-17.61330	-17.42244	48.30	131.70	21.90	1.97162	0.51388
$tertC_a(R'-H_2C_d)C_b(R''-H_2C_e)CH_2-$ $(C-C\ (e))$	C_b	-0.72457	-0.72457	-0.72457	-0.72457	-154.51399	0.91771	0.76765	-17.72405	-17.53318	50.04	129.96	22.66	1.94462	0.49298
$tertC_aC_b(H_2C_c-R')HCH_2-$ $(C-C\ (f))$	C_b	-0.72457	-0.92918	-0.92918	0	-154.19863	0.91771	0.78155	-17.40869	-17.21783	52.78	127.22	24.04	1.92443	0.47279
$isoC_a(R'-H_2C_d)C_b(R''-H_2C_e)CH_2-$ $(C-C\ (f))$	C_b	-0.72457	-0.72457	-0.72457	-0.72457	-154.51399	0.91771	0.76765	-17.92866	-17.73779	50.04	129.96	22.66	1.94462	0.49298

Table 20.11. The energy parameters (eV) of functional groups of alkyl silanes and disilanes .

Parameters	$Si-H$ Group	$Si-Si$ Group	$C-Si$ (i) Group	$C-Si$ (ii) Group	CH_3 Group	CH_2 Group	$C-H$ Group	$C-C$ (a) Group	$C-C$ (b) Group	$C-C$ (c) Group	$C-C$ (d) Group	$C-C$ (e) Group	$C-C$ (f) Group
n_1	1	1	1	1	3	2	1	1	1	1	1	1	1
n_2	0	0	0	0	2	1	0	0	0	0	0	0	0
n_3	0	0	0	0	0	0	0	0	0	0	0	0	0
C_1	0.75	0.37500	0.5	0.5	0.75	0.75	0.75	0.5	0.5	0.5	0.5	0.5	0.5
C_2	0.75800	0.75800	0.70071	0.70071	1	1	1	1	1	1	1	1	1
c_1	1	1	1	1	1	1	1	1	1	1	1	1	1
c_2	1	0.75800	1	1	0.91771	0.91771	0.91771	0.91771	0.91771	0.91771	0.91771	0.91771	0.91771
c_3	0	0	0	0	0	1	1	0	0	0	1	1	0
c_4	1	2	2	2	1	1	1	2	2	2	2	2	2
c_5	1	0	0	0	3	2	1	0	0	0	0	0	0
C_{1o}	0.75	0.37500	0.5	0.5	0.75	0.75	0.75	0.5	0.5	0.5	0.5	0.5	0.5
C_{2o}	0.75800	0.75800	0.70071	0.70071	1	1	1	1	1	1	1	1	1
V_e (eV)	-28.41703	-20.62357	-34.13046	-33.75742	-107.32728	-70.41425	-35.12015	-28.79214	-28.79214	-29.10112	-28.79214	-29.10112	-29.10112
V_p (eV)	9.67746	6.18908	7.67272	7.64507	38.92728	25.78002	12.87680	9.33352	9.33352	9.37273	9.33352	9.37273	9.37273
T (eV)	6.32210	3.75324	7.74501	7.60525	32.53914	21.06675	10.48582	6.77464	6.77464	6.90500	6.77464	6.90500	6.90500
V_m (eV)	-3.16105	-1.87662	-3.87250	-3.80263	-16.26957	-10.53337	-5.24291	-3.38732	-3.38732	-3.45250	-3.38732	-3.45250	-3.45250
$E_{(AO/HO)}$ (eV)	-10.25487	-10.25487	-10.25487	-10.25487	-15.56407	-15.56407	-14.63489	-15.56407	-15.56407	-15.35946	-15.56407	-15.35946	-15.35946
$\Delta E_{H_2MO\,(AO/HO)}$ (eV)	0	0	-1.20473	-0.92918	0	0	0	0	0	0	0	0	0
$E_{T\,(AO/HO)}$ (eV)	-10.25487	-10.25487	-9.05014	-9.32569	-15.56407	-15.56407	-14.63489	-15.56407	-15.56407	-15.35946	-15.56407	-15.35946	-15.35946
$E_{T\,(H_2MO)}$ (eV)	-25.83339	-22.81274	-31.63538	-31.63541	-67.69451	-49.66493	-31.63533	-31.63537	-31.63537	-31.63535	-31.63537	-31.63535	-31.63535
$E_T\left(atom-atom,msp^3.AO\right)$ (eV)	-1.06358	-0.96031	-1.20473	-0.92918	0	0	0	-1.85836	-1.85836	-1.44915	-1.85836	-1.44915	-1.44915
$E_{T\,(MO)}$ (eV)	-26.89697	-23.77305	-32.84010	-32.56455	-67.69450	-49.66493	-31.63537	-33.49373	-33.49373	-33.08452	-33.49373	-33.08452	-33.08452
$\omega\left(10^{15}\ rad/s\right)$	13.4257	4.83999	7.48178	7.40119	24.9286	24.2751	24.1759	9.43699	9.43699	15.4846	9.43699	9.55643	9.55643
E_K (eV)	8.83703	3.18577	4.92463	4.87159	16.40846	15.97831	15.91299	6.21159	6.21159	10.19220	6.21159	6.29021	6.29021
$\bar{E}_D$ (eV)	-0.15818	-0.08395	-0.14418	-0.14219	-0.25352	-0.25017	-0.24966	-0.16515	-0.16515	-0.20896	-0.16515	-0.16416	-0.16416
$\bar{E}_{Kvib}$ (eV)	0.25315 [3]	0.06335 [3]	0.10663 [10]	0.10663 [10]	0.35532 (Eq. (13.458))	0.35532 (Eq. (13.458))	0.35532 (Eq. (13.458))	0.12312 [11]	0.17978 [12]	0.09944 [13]	0.12312 [11]	0.12312 [11]	0.12312 [11]
$\bar{E}_{osc}$ (eV)	-0.03161	-0.05227	-0.09086	-0.08888	-0.22757	-0.14502	-0.07200	-0.10359	-0.07526	-0.15924	-0.10359	-0.10260	-0.10260
E_{mag} (eV)	0.04983	0.04983	0.04983	0.04983	0.14803	0.14803	0.14803	0.14803	0.14803	0.14803	0.14803	0.14803	0.14803
$E_{T\,(Group)}$ (eV)	-26.92857	-23.82532	-32.93096	-32.65343	-67.92207	-49.80996	-31.70737	-33.59732	-33.49373	-33.24376	-33.59732	-33.18712	-33.18712
$E_{initial\,(c_4\,AO/HO)}$ (eV)	-10.25487	-10.25487	-14.63489	-14.63489	-14.63489	-14.63489	-14.63489	-14.63489	-14.63489	-14.63489	-14.63489	-14.63489	-14.63489
$E_{initial\,(c_5\,AO/HO)}$ (eV)	-13.59844	0	0	0	-13.59844	-13.59844	-13.59844	0	0	0	0	0	0
$E_{D\,(Group)}$ (eV)	3.07526	3.31557	3.56118	3.38365	12.49186	7.83016	3.32601	4.32754	4.29921	3.97398	4.17951	3.62128	3.91734

Table 20.12. The total bond energies of alkyl silanes and disilanes calculated using the functional group composition and the energies of Table 20.11 compared to the experimental values.

Formula	Name	*Si – H* Group	*Si – Si* Group	*C – Si* (i) Group	*C – Si* (ii) Group	CH_3	CH_2	*CH*	*C – C* (a)	*C – C* (b)	*C – C* (c)	*C – C* (d)	*C – C* (e)	*C – C* (f)	Calculated Total Bond Energy (eV)	Experimental Total Bond Energy (eV)	Relative Error
CH_6Si	Methylsilane	3	0	1	0	1	0	0	0	0	0	0	0	0	25.37882	25.99491 [9]	0.02370
C_2H_8Si	Dimethylsilane	2	0	2	0	2	0	0	0	0	0	0	0	0	38.45660	38.64819 [9]	0.00496
$C_3H_{10}Si$	Trimethylsilane	1	0	3	0	3	0	0	0	0	0	0	0	0	51.53438	51.33567 [9]	-0.00387
$C_4H_{12}Si$	Tetramethylsilane	0	0	4	0	4	0	0	0	0	0	0	0	0	64.61216	64.22319 [14]	-0.00606
$C_4H_{12}Si$	Diethylsilane	2	0	2	0	2	2	0	2	0	0	0	0	0	62.77200	63.37771 [15]	0.00956
$C_6H_{16}Si$	Triethylsilane	1	0	3	0	3	3	0	3	0	0	0	0	0	88.00748	87.46141 [15]	-0.00624
$C_8H_{20}Si$	Tetraethylsilane	0	0	4	0	4	4	0	4	0	0	0	0	0	113.24296	112.06547[15]	-0.01051
CH_8Si_2	Methyldisilane	5	1	0	1	1	0	0	0	0	0	0	0	0	34.56739	34.73920 [16]	0.00495
$C_2H_{10}Si_2$	1,1-dimethyldisilane	4	1	0	2	2	0	0	0	0	0	0	0	0	47.36764	47.42283 [16]	0.00116
$C_2H_{10}Si_2$	1,2-dimethyldisilane	4	1	0	2	2	0	0	0	0	0	0	0	0	47.36764	47.42283 [16]	0.00116
$C_3H_{12}Si_2$	1,1,1-trimethyldisilane	3	1	0	3	3	0	0	0	0	0	0	0	0	60.16789	60.10646 [16]	-0.00102
$C_3H_{12}Si_2$	1,1,2-trimethyldisilane	3	1	0	3	3	0	0	0	0	0	0	0	0	60.16789	60.10646 [16]	-0.00102
$C_4H_{14}Si_2$	1,1,1,2-tetramethyldisilane	2	1	0	4	4	0	0	0	0	0	0	0	0	72.96815	72.79442 [16]	-0.00239
$C_4H_{14}Si_2$	1,1,2,2-tetramethyldisilane	2	1	0	4	4	0	0	0	0	0	0	0	0	72.96815	72.79442 [16]	-0.00239
$C_5H_{16}Si_2$	1,1,1,2,2-pentamethyldisilane	1	1	0	5	5	0	0	0	0	0	0	0	0	85.76840	85.47805 [16]	-0.00340
$C_6H_{18}Si_2$	hexamethyldisilane	0	1	0	6	6	0	0	0	0	0	0	0	0	98.56865	98.32646 [16]	-0.00246

Table 20.13. The bond angle parameters of alkyl silanes and disilanes and experimental values. In the calculation of θ_v, the parameters from the preceding angle were used. E_T is E_T (*atom - atom msp³.AO*).

Atoms of Angle	2c' Bond 1 (a_0)	2c' Bond 2 (a_0)	2c' Terminal Atoms (a_0)	$E_{Coulombic}$ Atom 1	Atom 1 Hybridization Designation (Table)	$E_{Coulombic}$ Atom 2	Atom 2 Hybridization Designation (Table)	c_2 Atom 1	c_2 Atom 2	C_1	C_2	c_1	c_2'	E_T (eV)	θ_v (°)	θ_1 (°)	θ_2 (°)	Cal. θ (°)	Exp. θ (°)
Silyl $\angle HSi_aH$	2.81185	2.81185	4.5673	-10.79339 Si_a	2 (20.1)	H	H	0.79329	1	1	1	0.75	1.26057	-1.06358				108.61	108.3 (methylsilane) [8, 17] 108.6 (disilane) [8]
$\angle HSi_aSi_b$															69.68			110.32	110.3 (disilane) [8]
$\angle C_aSiC_b$	3.54654	3.54654	5.8310	-15.55033 C_a	5 (15.3A)	-15.55033 C_b	5 (15.3A)	0.87495	0.87495	1	1	1	0.87495	-1.85836				110.58	111.0 (dimethylsilane) [9] 110.2 (trimethylsilane) [9]
$\angle C_aSiH$															71.67			108.33	108.8 (trimethylsilane) [9]
Methyl $\angle HC_aH$	2.09711	2.09711	3.4252	-15.75493	7 (15.3A)	H	H	0.86359	1	1	1	0.75	1.15796	0				109.50	
$\angle HC_aSi$															70.56			109.44	
$\angle C_aC_bC_c$															70.56			109.44	
Methylene $\angle HC_aH$	2.11106	2.11106	3.4252	-15.75493	7 (15.3A)	H	H	0.86359	1	1	1	0.75	1.15796	0				108.44	107 (propane) [8]
$\angle C_aC_bC_c$															69.51			110.49	112 (propane) [8] 113.8 (butane) [8] 110.8 (isobutane) [8]
$\angle C_aC_bH$															69.51			110.49	111.0 (butane) [8] 111.4 (isobutane) [8]
Methyl $\angle HC_aH$	2.09711	2.09711	3.4252	-15.75493	7 (15.3A)	H	H	0.86359	1	1	1	0.75	1.15796	0				109.50	
$\angle C_aC_bC_c$															70.56			109.44	
$\angle C_aC_bH$															70.56			109.44	
$\angle C_bC_aC_c$ iso C_a	2.91547	2.91547	4.7958	-16.68412 C_b	26 (15.3A)	-16.68412 C_c	26 (15.3A)	0.81549	0.81549	1	1	1	0.81549	-1.85836				110.67	110.8 (isobutane) [8]
$\angle C_bC_aH$ iso C_a	2.91547	2.11323	4.1633	-15.55033 C_a	5 (15.3A)	-14.82575 C_b	1 (15.3A)	0.87495	0.91771	0.75	1	0.75	1.04887	0				110.76	
$\angle C_aC_bH$ iso C_a	2.91547	2.09711	4.1633	-15.55033 C_b	5 (15.3A)	-14.82575 C_a	1 (15.3A)	0.87495	0.91771	0.75	1	0.75	1.04887	0				111.27	111.4 (isobutane) [8]
$\angle C_bC_aC_b$ tert C_a	2.90327	2.90327	4.7958	-16.68412 C_b	26 (15.3A)	-16.68412 C_b	26 (15.3A)	0.81549	0.81549	1	1	1	0.81549	-1.85836				111.37	110.8 (isobutane) [8]
$\angle C_bC_aC_d$															72.50			107.50	

SILICON OXIDES, SILICIC ACIDS, SILANOLS, SILOXANES AND DISILOXANES

The silicon oxides, silicic acids, silanols, siloxanes, and disiloxanes each comprise at least one $Si-O$ group, and this group in disiloxanes is part of the $Si-O-Si$ moiety. Silicic acids may have up to three $Si-H$ bonds corresponding to the $SiH_{n=1,2,3}$ functional groups of alkyl silanes, and silicic acids and silanols further comprise at least one OH group equivalent to that of alcohols. In addition to the $SiH_{n=1,2,3}$ group of alkyl silanes, silanols, siloxanes, and disiloxanes may comprise the functional groups of organic molecules as well as the $C-Si$ group of alkyl silanes. The alkyl portion of the alkyl silanol, siloxane, or disiloxane may comprise at least one terminal methyl group (CH_3) the end of each alkyl chain, and may comprise methylene (CH_2), and methylyne (CH) functional groups as well as C bound by carbon-carbon single bonds. The methyl and methylene functional groups are equivalent to those of straight-chain alkanes. Six types of $C-C$ bonds can be identified. The n-alkane $C-C$ bond is the same as that of straight-chain alkanes. In addition, the $C-C$ bonds within isopropyl ($(CH_3)_2CH$) and t-butyl ($(CH_3)_3C$) groups and the isopropyl to isopropyl, isopropyl to t-butyl, and t-butyl to t-butyl $C-C$ bonds comprise functional groups. The branched-chain-alkane groups in silanols, siloxanes, and disiloxanes are equivalent to those in branched-chain alkanes. The alkene groups when present such as the $C=C$ group are equivalent to those of the corresponding alkene. Siloxanes further comprise two types of $C-O$ functional groups, one for methyl or t-butyl groups corresponding to the C and the other for general alkyl groups as given for ethers.

The distinguishing aspect of silicon oxides, silicic acids, silanols, siloxanes, and disiloxane is the nature of the corresponding $Si-O$ functional group. In general, the sharing of electrons between a $Si3sp^3$ HO and an $O2p$ AO to form a $Si-O$-bond MO permits each participating orbital to decrease in size and energy. Consider the case wherein the $Si3sp^3$ HO donates an excess of 50% of its electron density to the $Si-O$-bond MO to form an energy minimum while further satisfying the potential, kinetic, and orbital energy relationships. By considering this electron redistribution in the molecule comprising a $Si-O$ bond as well as the fact that the central field decreases by an integer for each successive electron of the shell, the radius $r_{Si-O3sp^3}$ of the $Si3sp^3$ shell may be calculated from the Coulombic energy using Eq. (15.18).

$$r_{Si-O3sp^3}=\left(\sum_{n=10}^{13}(Z-n)-0.5\right)\frac{e^2}{8\pi\varepsilon_0\left(e105.23554\ eV\right)}=\frac{9.5e^2}{8\pi\varepsilon_0\left(e105.23554\ eV\right)}=1.22825a_0 \tag{20.38}$$

Using Eqs. (15.19) and (20.38), the Coulombic energy $E_{Coulomb}\left(Si_{Si-O},3sp^3\right)$ of the outer electron of the $Si3sp^3$ shell is:

$$E_{Coulomb}\left(Si_{Si-O},3sp^3\right)=\frac{-e^2}{8\pi\varepsilon_0 r_{Si-O3sp^3}}=\frac{-e^2}{8\pi\varepsilon_0 1.22825a_0}=-11.07743\ eV \tag{20.39}$$

During hybridization, the spin-paired $3s$ electrons are promoted to the $Si3sp^3$ shell as unpaired electrons. The energy for the promotion is the magnetic energy given by Eq. (20.6). Using Eqs. (20.6) and (20.39), the energy $E\left(Si_{Si-O},3sp^3\right)$ of the outer electron of the $Si3sp^3$ shell is:

$$E\left(Si_{Si-O},3sp^3\right)=\frac{-e^2}{8\pi\varepsilon_0 r_{silane3sp^3}}+\frac{2\pi\mu_0 e^2\hbar^2}{m_e^2\left(r_{12}\right)^3}=-11.07743\ eV+0.05836\ eV=-11.01906\ eV \tag{20.40}$$

Thus, $E_T\left(Si-O,3sp^3\right)$, the energy change of each $Si3sp^3$ shell with the formation of the $Si-O$-bond MO is given by the difference between Eq. (20.40) and Eq. (20.7):

$$E_T\left(Si-O,3sp^3\right)=E\left(Si_{Si-O},3sp^3\right)-E\left(Si,3sp^3\right)=-11.01906\ eV-\left(-10.25487\ eV\right)=-0.76419\ eV \tag{20.41}$$

Using Eq. (15.28), to meet the energy matching condition in silanols and siloxanes for all σ MOs at the $Si3sp^3$ HO and $O2p$ AO of each $Si-O$-bond MO as well as with the $C2sp^3$ HOs of the molecule, the energy $E\left(Si_{RSi-OR'},3sp^3\right)$ (R,R' are alkyl or H) of the outer electron of the $Si3sp^3$ shell of the silicon atom must be the average of $E\left(Si_{silane},3sp^3\right)$ (Eq. (20.11)) and $E_T\left(Si-O,3sp^3\right)$ (Eq. (20.40)).

$$E\left(Si_{RSi-OR'},3sp^3\right)=\frac{E\left(Si_{silane},3sp^3\right)+E\left(Si_{Si-O},3sp^3\right)}{2}=\frac{\left(-10.73503\ eV\right)+\left(-11.01906\ eV\right)}{2}=-10.87705\ eV \tag{20.42}$$

Using Eq. (15.29), $E_{T_{silanol,siloxane}}\left(Si-O,3sp^3\right)$, the energy change of each $Si3sp^3$ shell with the formation of each $RSi-OR'$-bond MO, must be the average of $E_T\left(Si-Si,3sp^3\right)$ (Eq. (20.12)) and $E_T\left(Si-O,3sp^3\right)$ (Eq. (20.41)).

$$E_{T_{silanol,siloxane}}\left(Si-O,3sp^3\right)=\frac{E_T\left(Si-Si,3sp^3\right)+E_T\left(Si-O,3sp^3\right)}{2}=\frac{\left(-0.48015\ eV\right)+\left(-0.76419\ eV\right)}{2}=-0.62217\ eV \tag{20.43}$$

To meet the energy matching condition in silicic acids for all σ MOs at the $Si3sp^3$ HO and $O2p$ AO of each $Si-O$-bond MO as well as all H AOs, the energy $E\left(Si_{H_nSi-(OH)_{4-n}},3sp^3\right)$ of the outer electron of the $Si3sp^3$ shell of the silicon atom must be the average of $E\left(Si_{silane},3sp^3\right)$ (Eq. (20.15)) and $E_T\left(Si-O,3sp^3\right)$ (Eq. (20.40)).

$$E\left(Si_{H_nSi-(OH)_{4-n}},3sp^3\right)=\frac{E\left(Si_{silane},3sp^3\right)+E\left(Si_{Si-O},3sp^3\right)}{2}=\frac{\left(-11.37682\ eV\right)+\left(-11.01906\ eV\right)}{2}=-11.16876\ eV \tag{20.44}$$

Using Eq. (15.29), $E_{T_{silicic\ acid}}\left(Si-O,3sp^3\right)$, the energy change of each $Si3sp^3$ shell with the formation of each $RSi-OR'$-bond MO, must be the average of $E_T\left(Si-H,3sp^3\right)$ (Eq. (20.16)) and $E_T\left(Si-O,3sp^3\right)$ (Eq. (20.41)).

$$E_{T_{silicic\ acid}}\left(Si-O,3sp^3\right)=\frac{E_T\left(Si-H,3sp^3\right)+E_T\left(Si-O,3sp^3\right)}{2}=\frac{\left(-1.06358\ eV\right)+\left(-0.76419\ eV\right)}{2}=-0.91389\ eV \tag{20.45}$$

Using Eqs. (20.22-22.26), the general force balance equation for the σ-MO of the silicon to oxygen $Si-O$-bond MO in terms of n_e and $|L_i|$ corresponding to the angular momentum terms of the $3sp^3$ HO shell is:

$$\frac{\hbar^2}{m_e a^2 b^2}D=\frac{e^2}{8\pi\varepsilon_0 ab^2}D+\frac{\hbar^2}{2m_e a^2 b^2}D-\left(\frac{n_e}{2}+\sum_i\frac{|L_i|}{Z}\right)\frac{\hbar^2}{2m_e a^2 b^2}D \tag{20.46}$$

Having a solution for the semimajor axis a of:

$$a=\left(1+\frac{n_e}{2}+\sum_i\frac{|L_i|}{Z}\right)a_0 \tag{20.47}$$

In terms of the angular momentum L, the semimajor axis a is**:**

$$a=\left(1+\frac{n_e}{2}+\frac{L}{Z}\right)a_0 \tag{20.48}$$

Using the semimajor axis, the geometric and energy parameters of the MO are calculated using Eqs. (15.1-15.117) in the same manner as the organic functional groups given in the Organic Molecular Functional Groups and Molecules section. The semimajor axis a solutions given by Eq. (20.48) of the force balance equation, Eq. (20.46), for the σ-MO of the $Si-O$-bond MO of each functional group of silicon oxide, silicon dioxide, silicic acids, silanols, siloxanes, and disiloxanes are given in Table 20.15 with the force-equation parameters $Z=14$, n_e, and L corresponding to the angular momentum of the $Si3sp^3$ HO shell.

For the $Si-O$ functional groups, hybridization of the $3s$ and $3p$ AOs of Si to form a single $3sp^3$ shell forms an energy minimum, and the sharing of electrons between the $Si3sp^3$ HO and the O AO to form a MO permits each participating orbital to decrease in radius and energy. The O AO has an energy of $E(O)=-13.61805\ eV$, and the $Si3sp^3$ HO has an energy of $E\left(Si,3sp^3\right)=-10.25487\ eV$ (Eq. (20.7)). To meet the equipotential condition of the union of the $Si-O$ H_2-type-ellipsoidal-MO with these orbitals, the corresponding hybridization factors c_2 and C_2 of Eq. (15.61) for silicic acids, silanols, siloxanes, and disiloxanes and the hybridization factor C_2 of silicon oxide and silicon dioxide given by Eq. (15.77) are:

$$c_2\left(O\ to\ Si3sp^3HO\right)=C_2\left(O\ to\ Si3sp^3HO\right)=\frac{E\left(Si,3sp^3\right)}{E(O)}=\frac{-10.25487\ eV}{-13.61805\ eV}=0.75304 \tag{20.49}$$

Each bond of silicon oxide and silicon dioxide is a double bond such that $c_1=2$ and $C_1=0.75$ in the geometry relationships (Eqs. (15.2-15.5)) and the energy equation (Eq. (15.61)). Each $Si-O$ bond in silicic acids, silanols, siloxanes, and disiloxanes is a single bond corresponding to $c_1=1$ and $C_1=0.5$ as in the case of alkanes (Eq. (14.152)).

Since the energy of the MO is matched to that of the $Si3sp^3$ HO, $E\left(AO/HO\right)$ in Eq. (15.61) is $E\left(Si,3sp^3\right)$ given by Eq. (20.7) and twice this value for double bonds. $E_T\left(atom-atom,msp^3.AO\right)$ of the $Si-O$-bond MO of each functional group is determined by energy matching in the molecule while achieving an energy minimum. For silicon oxide and silicon dioxide, $E_T\left(atom-atom,msp^3.AO\right)$ is three and two times $-1.37960\ eV$ given by Eq. (20.20), respectively. $E_T\left(atom-atom,msp^3.AO\right)$ of silicic acids is two times $-0.91389\ eV$ given by Eq. (20.45). $E_T\left(atom-atom,msp^3.AO\right)$ of silanols, siloxanes, and disiloxanes is two times $-0.62217\ eV$ given by Eq. (20.43).

The symbols of the functional groups of silicon oxides, silicic acids, silanols, siloxanes, and disiloxanes are given in Table 20.14. The geometrical (Eqs. (15.1-15.5), (20.1-20.21), (20.29), (20.32-20.33), (20.37), and (20.46-20.49)) and intercept (Eqs. (15.80-15.87) and (20.21)) parameters are given in Tables 20.15 and 20.16, respectively. The energy (Eqs. (15.61), (20.1-20.20), (20.33-20.35), (20.37-45), and (20.49)) parameters are given in Table 20.17. The total energy of each silicon oxide, silicic acid, silanol, siloxane, or disiloxane given in Table 20.18 was calculated as the sum over the integer multiple of each $E_D(Group)$ of Table 20.17 corresponding to functional-group composition of the molecule. The bond angle parameters determined

using Eqs. (15.88-15.117) are given in Table 20.19. The charge-densities of exemplary siloxane, $\left(\left(CH_3\right)_2 SiO\right)_3$ and disiloxane, hexamethyldisiloxane comprising the concentric shells of atoms with the outer shell bridged by one or more H_2-type ellipsoidal MOs or joined with one or more hydrogen MOs are shown in Figures 20.4A and B, respectively.

Figure 20.4. (A) Color scale, translucent view of the charge-density of $\left(\left(CH_3\right)_2 SiO\right)_3$ showing the orbitals of the Si, O, and C atoms at their radii, the ellipsoidal surface of each H or H_2-type ellipsoidal MO that transitions to the corresponding outer shell of the atoms participating in each bond, and the nuclei (red, not to scale). (B) Color scale, translucent view of the charge-density of $\left(CH_3\right)_3 SiOSi\left(CH_3\right)_3$ showing the orbitals of the Si, O, and C atoms at their radii, the ellipsoidal surface of each H or H_2-type ellipsoidal MO that transitions to the corresponding outer shell of the atoms participating in each bond, and the nuclei (red, not to scale).

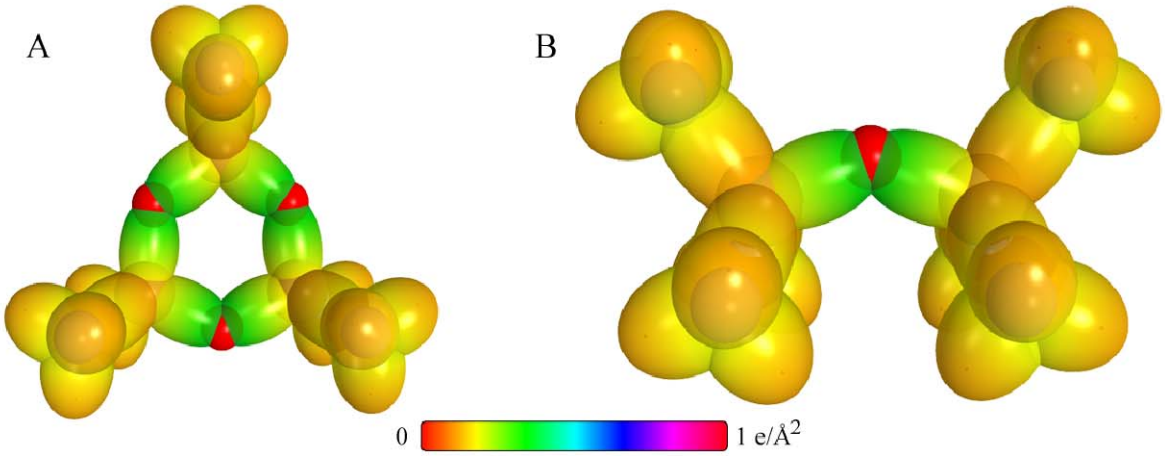

Table 20.14. The symbols of functional groups of silicon oxides, silicic acids, silanols, siloxanes and disiloxanes.

Functional Group	Group Symbol
SiO bond (silicon oxide)	$Si-O$ (i)
SiO bond (silicon dioxide)	$Si-O$ (ii)
SiO bond (silicic acid)	$Si-O$ (iii)
SiO bond (silanol and siloxane)	$Si-O$ (iv)
Si-OSi bond (disiloxane)	$Si-O$ (v)
SiH group of $SiH_{n=1,2,3}$	$Si-H$
CSi bond	$C-Si$ (i)
OH group	OH
CO (CH_3-O- and $\left(CH_3\right)_3 C-O-$)	$C-O$ (i)
CO (alkyl)	$C-O$ (ii)
CH_3 group	$C-H\ \left(CH_3\right)$
CH_2 group	$C-H\ \left(CH_2\right)$
CH	$C-H$
CC bond (n-C)	$C-C$ (a)
CC bond (iso-C)	$C-C$ (b)
CC bond (*tert-C*)	$C-C$ (c)
CC (*iso* to *iso-C*)	$C-C$ (d)
CC (*t* to *t-C*)	$C-C$ (e)
CC (*t* to *iso-C*)	$C-C$ (f)

Table 20.15. The geometrical bond parameters silicon oxides, silicic acids, silanols, siloxanes, disiloxanes and experimental values.

Parameter	$Si-O$ (i) Group	$Si-O$ (ii) Group	$Si-O$ (iii) Group	$Si-O$ (iv) Group	$Si-O$ (v) Group	$Si-H$ Group	$C-Si$ (i) Group	OH Group	$C-O$ (i) Group	$C-O$ (ii) Group	$C-H$ (CH_3) Group	$C-H$ (CH_2) Group	$C-H$ Group	$C-C$ (a) Group	$C=C$ Group
n_e	2	2	2	2	2										
L	$4\sqrt{\frac{3}{4}}$	$6\sqrt{\frac{3}{4}}$	0	0	0										
$a\ (a_0)$	2.24744	2.37115	2.00000	2.00000	2.00000	2.24744	2.20339	1.26430	1.80717	1.79473	1.64920	1.67122	1.67465	2.12499	1.47228
$c'\ (a_0)$	1.41056	1.44886	1.62970	1.62970	1.62970	1.40593	1.77327	0.91808	1.34431	1.33968	1.04856	1.05553	1.05661	1.45744	1.26661
Bond Length $2c'\ (\AA)$	1.49287	1.53341	1.72480	1.72480	1.72480	1.48797	1.87675	0.971651	1.42276	1.41785	1.10974	1.11713	1.11827	1.54280	1.34052
Exp. Bond Length $(\AA)$	1.509 (silicon oxide) [18]	1.55 (silicon dioxide) [19]	1.703 [20]	1.703 [20]	1.668 [20]	1.485 (methylsilane) [8] 1.492 (Si_2H_6) [8] 1.489 (trimethyl silane) [9]	1.867 (methylsilane) [8] 1.875 (tetramethyl silane) [8] 1.877 (methylsilane) [9] 1.871 (dimethylsilane) [9] 1.878 (trimethyl silane) [9]	0.971 (ethanol) 0.9451 (methanol) [8]	1.416 (dimethyl ether) [8]	1.418 (ethyl methyl ether (avg.)) [8]	1.093 (methylsilane) [8] 1.115 (tetramethyl silane) [8] 1.107 ($C-H$ propane) [8] 1.117 ($C-H$ butane) [8]	1.107 ($C-H$ propane) [8] 1.117 ($C-H$ butane) [8]	1.122 (isobutane) [8]	1.532 (propane) [8] 1.531 (butane) [8]	1.342 (2-methylpropene) [8] 1.346 (2-butene) [8] 1.349 (1,3-butadiene) [8]
$b,c\ (a_0)$	1.74966	1.87701	1.15935	1.15935	1.15935	1.75338	1.30783	0.86925	1.20776	1.19429	1.27295	1.29569	1.29924	1.54616	0.75055
e	0.62763	0.61104	0.81485	0.81485	0.81485	0.62557	0.80479	0.72615	0.74388	0.74645	0.63580	0.63159	0.63095	0.68600	0.86030

Table 20.16. The MO to HO intercept geometrical bond parameters of silicon oxides, silicic acids, silanols, siloxanes and disiloxanes. *R*, *R'*, *R''* are *H* or alkyl groups. E_T is E_T (*atom - atom msp*^{3}.*AO*).

Bond	Atom	E_T (eV) Bond 1	E_T (eV) Bond 2	E_T (eV) Bond 3	E_T (eV) Bond 4	Final Total Energy $Si3sp^3$ $C2sp^3$ (eV)	$r_{initial}$ (a_0)	r_{final} (a_0)	$E_{Coulomb}(C2sp^3)$ (eV) Final	$E(Si3sp^3)$ $E(C2sp^3)$ (eV) Final	θ' (°)	ϑ_1 (°)	θ_2 (°)	d_1 (a_0)	d_2 (a_0)
$Si=O(SiO)$ $(Si-O$ (i))	*Si*	-2.06940	0	0	0		1.31926	1.09878	-12.38264	-12.32428	67.55	112.45	35.48	1.83015	0.41959
$Si=O(SiO)$ $(Si-O$ (i))	*O*	-2.06940	0	0	0		1.00000	0.86730	-15.68745		24.63	155.37	11.92	2.19896	0.78840
$O=Si=O(SiO_2)$ $(Si-O$ (ii))	*Si*	-1.37960	-1.37960	0	0		1.31926	1.04080	-13.07244	-13.01408	45.59	134.41	23.33	2.17721	0.72835
$O=Si=O(SiO_2)$ $(Si-O$ (ii))	*O*	-1.37960	0	0	0		1.00000	0.90720	-14.99765						
$(HO)_3SiO-H$	*O*	-0.91389	0	0	0		1.00000	0.93627	-14.53194		119.87	60.13	69.07	0.45174	0.46634
R_3SiO-H	*O*	-0.62217	0	0	0		1.00000	0.95545	-14.24022		121.05	58.95	70.34	0.42532	0.49275
$(HO)_3Si-OH$ $(Si-O$ (iii))	*Si*	-0.91389	-0.91389	-0.91389	-0.91389		1.31926	0.97402	-13.96878	-13.91042	112.36	67.64	50.98	1.25911	0.37059
$(HO)_3Si-OH$ $(Si-O$ (iii))	*O*	-0.91389	0	0	0		1.00000	0.93627	-14.53194		110.26	69.74	49.25	1.30543	0.32427
$(CH_3)_3Si-OH$ $(Si-O$ (iv))	*Si*	-0.62217	-0.60236	-0.60236	-0.60236		1.31926	1.06775	-12.74250	-12.68414	117.05	62.95	55.11	1.14408	0.48562
$(CH_3)_3Si-OH$ $(Si-O$ (iv))	*O*	-0.62217	0	0	0		1.00000	0.95545	-14.24022		111.35	68.65	50.14	1.28189	0.34780
$C-H\ (OCH_3)$	*C*	-0.72457	0	0	0	-152.34026	0.91771	0.87495	-15.55033	-15.35946	78.85	101.15	42.40	1.21777	0.16921
$SiO-CH_3$ $SiO-C(CH_3)_3$ $(C-O$ (i))	*C*	-0.72457	0	0	0	-152.34026	0.91771	0.87495	-15.55033	-15.35946	95.98	84.02	46.10	1.25319	0.09112
$SiO-CH_3$ $SiO-C(CH_3)_3$ $(C-O$ (i)) $(Si-O$ (iv))	*O*	-0.72457	-0.62217	0	0		1.00000	0.84129	-16.17250		93.13	86.87	44.07	1.29844	0.04587
$-H_2C_a-OSi$ $(C-O$ (ii))	C_a	-0.82688	-0.92918	0	0	-153.37175	0.91771	0.82053	-16.58181	-16.39095	92.41	87.59	43.35	1.30512	0.03456
$-H_2C_a-OC_b(CH_3)_3$ $-H_2C_a-OC_bH_3$ $(C-O$ (ii)) $(Si-O$ (iv))	*O*	-0.82688	-0.62217	0	0		1.00000	0.83600	-16.27480		93.79	86.21	44.30	1.28438	0.05529
$(CH_3O)_3Si-OCH_3$ $(Si-O$ (iv))	*Si*	-0.62217	-0.62217	-0.62217	-0.62217		1.31926	1.06279	-12.80192	-12.74356	116.82	63.18	54.89	1.15016	0.47954
$(CH_3O)_3Si-OCH_3$ $(Si-O$ (iv))	*O*	-0.62217	-0.72457	0	0		1.00000	0.90919	-14.96480		108.67	71.33	47.98	1.33867	0.29103
$(CH_3)_3Si-OSi(CH_3)_3$ $(Si-O$ (v))	*Si*	-0.48015	-0.60236	-0.60236	-0.60236		1.31926	1.07978	-12.60048	-12.54212	117.61	62.39	55.62	1.12931	0.50039

Table 20.16 cont' d. The MO to HO intercept geometrical bond parameters of silicon oxides, silicic acids, silanols, siloxanes and disiloxanes. *R*, *R'*, *R''* are *H* or alkyl groups. E_T is E_T (*atom - atom msp*^{3}*.AO*).

Bond	Atom	E_T (eV) Bond 1	E_T (eV) Bond 2	E_T (eV) Bond 3	E_T (eV) Bond 4	Final Total Energy $Si3sp^3$ $C2sp^3$ (eV)	$r_{initial}$ (a_0)	r_{final} (a_0)	$E_{Coulomb}(C2sp^3)$ (eV) Final	$E(Si3sp^3)$ $E(C2sp^3)$ (eV) Final	θ' (°)	θ_1 (°)	θ_2 (°)	d_1 (a_0)	d_2 (a_0)
$(CH_3)_3Si-OSi(CH_3)_3$ $(Si-O$ (v))	O	-0.48015	-0.48015	0	0		1.00000	0.93329	-14.57836		110.09	69.91	49.11	1.30909	0.32061
$H_3Si_a-C_aH_2-$ $(C-Si$ (i))	Si_a	-0.60236	-1.06358	-1.06358	-1.06358		1.31926	0.73075	-18.61886	-18.56050	85.56	94.44	33.85	1.82982	0.05655
$H_2Si_a-(C_aH_2-)_2$ $(C-Si$ (i))	Si_a	-0.60236	-0.60236	-1.06358	-1.06358		1.31926	0.74932	-18.15764	-18.09928	87.44	92.56	34.92	1.80676	0.03349
$HSi_a-(C_aH_2-)_3$ $(C-Si$ (i))	Si_a	-0.60236	-0.60236	-0.60236	-1.06358		1.31926	0.76884	-17.69642	-17.63806	89.31	90.69	36.00	1.78249	0.00922
$Si_a-(C_aH_2-)_4$ $(C-Si$ (i))	Si_a	-0.60236	-0.60236	-0.60236	-0.60236		1.31926	0.78942	-17.23521	-17.17685	91.19	88.81	37.12	1.75693	0.01634
$-Si_aH_2-CH_3$ $(C-Si$ (i))	C	-0.60236	0	0	0	-152.21805	0.91771	0.88188	-15.42812	-15.23725	98.56	81.44	41.82	1.64204	0.13123
$-Si_aH_2-C_aH_2CH_2-$ $(C-Si$ (i))	C_a	-0.60236	-0.92918	0	0	-153.14724	0.91771	0.83179	-16.35730	-16.16643	94.76	85.24	39.33	1.70428	0.06899
$C-H$ (CH_3)	C	-0.92918	0	0	0	-152.54487	0.91771	0.86359	-15.75493	-15.56407	77.49	102.51	41.48	1.23564	0.18708
$C-H$ (CH_2)	C	-0.92918	-0.92918	0	0	-153.47406	0.91771	0.81549	-16.68412	-16.49325	68.47	111.53	35.84	1.35486	0.29933
$C-H$ (CH)	C	-0.92918	-0.92918	-0.92918	0	-154.40324	0.91771	0.77247	-17.61330	-17.42244	61.10	118.90	31.37	1.42988	0.37326
$H_3C_aC_bH_2CH_2-$ $(C-C$ (a))	C_a	-0.92918	0	0	0	-152.54487	0.91771	0.86359	-15.75493	-15.56407	63.82	116.18	30.08	1.83879	0.38106
$H_3C_aC_bH_2CH_2-$ $(C-C$ (a))	C_b	-0.92918	-0.92918	0	0	-153.47406	0.91771	0.81549	-16.68412	-16.49325	56.41	123.59	26.06	1.90890	0.45117
$R-H_2C_aC_b(H_2C_c-R')HCH_2-$ $(C-C$ (b))	C_b	-0.92918	-0.92918	-0.92918	0	-154.40324	0.91771	0.77247	-17.61330	-17.42244	48.30	131.70	21.90	1.97162	0.51388
$R-H_2C_a(R'-H_2C_d)C_b(R''-H_2C_c)CH_2-$ $(C-C$ (c))	C_b	-0.92918	-0.72457	-0.72457	-0.72457	-154.71860	0.91771	0.75889	-17.92866	-17.73779	48.21	131.79	21.74	1.95734	0.50570
$isoC_aC_b(H_2C_c-R')HCH_2-$ $(C-C$ (d))	C_b	-0.92918	-0.92918	-0.92918	0	-154.40324	0.91771	0.77247	-17.61330	-17.42244	48.30	131.70	21.90	1.97162	0.51388
$tertC_a(R'-H_2C_d)C_b(R''-H_2C_c)CH_2-$ $(C-C$ (e))	C_b	-0.72457	-0.72457	-0.72457	-0.72457	-154.51399	0.91771	0.76765	-17.92866	-17.73779	50.04	129.96	22.66	1.94462	0.49298
$tertC_aC_b(H_2C_c-R')HCH_2-$ $(C-C$ (f))	C_b	-0.72457	-0.92918	-0.92918	0-	-154.19863	0.91771	0.78155	-17.40869	-17.21783	52.78	127.22	24.04	1.92443	0.47279
$isoC_a(R'-H_2C_d)C_s(R''-H_2C_c)CH_2-$ $(C-C$ (f))	C_b	-0.72457	-0.72457	-0.72457	-0.72457	-154.51399	0.91771	0.76765	-17.92866	-17.73779	50.04	129.96	22.66	1.94462	0.49298

Table 20.17. The energy parameters (eV) of functional groups of silicon oxides, silicic acids, silanols, siloxanes and disiloxanes.

Parameters	$Si-O$ (i) Group	$Si-O$ (ii) Group	$Si-O$ (iii) Group	$Si-O$ (iv) Group	$Si-O$ (v) Group	$Si-H$ Group	$C-Si$ (i) Group	OH Group	$C-O$ (i) Group	$C-O$ (ii) Group	CH_3 Group	CH_2 Group	$C-H$ Group	$C-C$ (a) Group	$C=C$ Group
n_1	2	2	1	1	1	1	1	1	1	1	3	2	1	1	2
n_2	0	0	0	0	0	0	0	0	0	0	2	1	0	0	0
n_3	0	0	0	0	0	0	0	0	0	0	0	0	0	0	0
C_1	0.75	0.75	0.5	0.5	0.5	0.75	0.5	0.75	0.5	0.5	0.75	0.75	0.75	0.5	0.5
C_2	0.75304	0.75304	0.75304	0.75304	0.75304	0.75800	0.70071	1	1	1	1	1	1	1	0.91771
c_1	1	1	1	1	1	1	1	0.75	1	1	1	1	1	1	1
c_2	1	1	0.75304	0.75304	0.75304	1	1	1	0.85395	0.85395	0.91771	0.91771	0.91771	0.91771	0.91771
c_3	0	0	0	0	0	0	0	1	0	0	0	1	1	0	0
c_4	2	2	1	1	1	1	2	1	2	2	1	1	1	2	4
c_5	2	2	1	1	1	1	0	1	0	0	3	2	1	0	0
C_{1o}	0.75	0.75	0.5	0.5	0.5	0.75	0.5	0.75	0.5	0.5	0.75	0.75	0.75	0.5	0.5
C_{2o}	0.75304	0.75304	0.75304	0.75304	0.75304	0.75800	0.70071	1	1	1	1	1	1	1	0.91771
V_s (eV)	-56.90923	-53.38219	-28.70052	-28.70052	-28.70052	-28.41703	-34.13046	-40.92709	-33.15757	-33.47304	-107.32728	-70.41425	-35.12015	-28.79214	-102.08992
V_p (eV)	19.29141	18.78139	8.34866	8.34866	8.34866	9.67746	7.67272	14.81988	10.12103	10.15605	38.92728	25.78002	12.87680	9.33352	21.48386
T (eV)	12.66092	11.25659	7.17513	7.17513	7.17513	6.32210	7.74501	16.18567	9.17389	9.32537	32.53914	21.06675	10.48582	6.77464	34.67062
V_w (eV)	-6.33046	-5.62829	-3.58757	-3.58757	-3.58757	-3.16105	-3.87250	-8.09284	-4.58695	-4.66268	-16.26957	-10.53337	-5.24291	-3.38732	-17.33531
$E_{(AO/HO)}$ (eV)	-20.50975	-20.50975	-10.25487	-10.25487	-10.25487	-10.25487	-10.25487	-13.6181	-14.63489	-14.63489	-15.56407	-15.56407	-14.63489	-15.56407	0
$\Delta E_{H_2MO\,(AO/HO)}$ (eV)	0	0	0	0	0	0	-1.20473	0	-1.44915	-1.65376	0	0	0	0	0
E_T $_{(AO/HO)}$ (eV)	-20.50975	-20.50975	-10.25487	-10.25487	-10.25487	-10.25487	-9.05014	-13.6181	-13.18574	-12.98113	-15.56407	-15.56407	-14.63489	-15.56407	0
E_T $_{(H_2MO)}$ (eV)	-51.79710	-49.48226	-27.01917	-27.01917	-27.01917	-25.83339	-31.63538	-31.63247	-31.63533	-31.63544	-67.69451	-49.66493	-31.63533	-31.63537	-63.27075
$E_T\left(atom-atom, msp^3.AO\right)$ (eV)	-4.13881	-2.75921	-1.82777	-1.24434	-0.96031	-1.06358	-1.20473	0	-1.44915	-1.65376	0	0	0	-1.85836	-2.26759
E_T $_{(MO)}$ (eV)	-55.93591	-52.24146	-28.84694	-28.26351	-27.97947	-26.89697	-32.84010	-31.63537	-33.08452	-33.28912	-67.69450	-49.66493	-31.63537	-33.49373	-65.53833
$\omega\left(10^{15}\ rad/s\right)$	9.22130	12.0816	8.96876	8.96876	8.96876	13.4257	7.48178	44.1776	12.0329	12.1583	24.9286	24.2751	24.1759	9.43699	43.0680
E_K (eV)	6.06962	7.95229	5.90340	5.90340	5.90340	8.83703	4.92463	29.07844	7.92028	8.00277	16.40846	15.97831	15.91299	6.21159	28.34813
$\bar{E}_D$ (eV)	-0.13632	-0.14573	-0.13866	-0.13586	-0.13449	-0.15818	-0.14418	-0.33749	-0.18420	-0.18631	-0.25352	-0.25017	-0.24966	-0.16515	-0.34517
$\bar{E}_{Kvib}$ (eV)	0.15393 [3]	0.15393 [3]	0.15393 [3]	0.15393 [3]	0.15393 [3]	0.25315 [3]	0.10663 [10]	0.46311 [21-22]	0.13663 [23]	0.16118 [24]	0.35532 (Eq. (13.458))	0.35532 (Eq. (13.458))	0.35532 (Eq. (13.458))	0.12312 [25]	0.17897 [26]
$\bar{E}_{osc}$ (eV)	-0.05935	-0.06876	-0.06169	-0.05889	-0.05752	-0.03161	-0.09086	-0.10594	-0.11589	-0.10572	-0.22757	-0.14502	-0.07200	-0.10359	-0.25568
E_{mag} (eV)	0.04983	0.04983	0.04983	0.04983	0.04983	0.04983	0.04983	0.11441	0.14803	0.14803	0.14803	0.14803	0.14803	0.14803	0.14803
E_T $_{(Group)}$ (eV)	-56.05461	-52.37898	-28.90863	-28.32240	-28.03700	-26.92857	-32.93096	-31.74130	-33.20040	-33.39484	-67.92207	-49.80996	-31.70737	-33.59732	-66.04969
$E_{initial\,(s_A\,AO/HO)}$ (eV)	-10.25487	-10.25487	-10.25487	-10.25487	-10.25487	-10.25487	-14.63489	-13.6181	-14.63489	-14.63489	-14.63489	-14.63489	-14.63489	-14.63489	-14.63489
$E_{initial\,(s_A\,AO/HO)}$ (eV)	-13.61805	-13.61805	-13.61805	-13.61805	-13.61805	-13.59844	0	-13.59844	0	0	-13.59844	-13.59844	-13.59844	0	0
$E_{D\,(Group)}$ (eV)	8.30876	4.63313	5.03571	4.44948	4.16408	3.07526	3.66118	4.41035	3.93062	4.12506	12.49186	7.83016	3.32601	4.32754	7.51014

Table 20.18. The total bond energies of silicon oxides, silicic acids, silanols, siloxanes, and disiloxanes calculated using the functional group composition and the energies of Table 20.17 compared to the experimental values.

Formula	Name or Structure	*Si–O* (i) Group	*Si–O* (ii) Group	*Si–O* (iii) Group	*Si–O* (iv) Group	*Si–O* (v) Group	*Si–H* Group	*C–Si* (i) Group	*OH* Group	*C–O* (i) Group	*C–O* (ii) Group	CH_3	CH_2	*CH*	*C–C* (a)	*C=C*	Calculated Total Bond Energy (eV)	Experimental Total Bond Energy (eV)	Relative Error
SiO	Silicon oxide	1	0	0	0	0	0	0	0	0	0	0	0	0	0	0	8.30876	8.29905 [18]	-0.00117
SiO_2	Silicon dioxide	1	1	0	0	0	0	0	0	0	0	0	0	0	0	0	12.94190	12.98073 [19]	0.00299
SiH_4O	H_3SiOH	0	0	1	0	0	3	0	1	0	0	0	0	0	0	0	18.67184	19.00701[a] [27]	0.01763
SiH_4O_2	$H_2Si(OH)_2$	0	0	2	0	0	2	0	2	0	0	0	0	0	0	0	25.04264	25.04264[a] [27]	0.00563
SiH_4O_3	$HSi(OH)_3$	0	0	3	0	0	1	0	3	0	0	0	0	0	0	0	31.41344	31.47012[a] [27]	0.00180
SiH_4O_4	$Si(OH)_4$	0	0	4	0	0	0	0	4	0	0	0	0	0	0	0	37.78423	38.03638 [28]	0.00663
$C_3H_{10}SiO$	Trimethylsilanol	0	0	0	1	0	0	3	1	0	0	3	0	0	0	0	57.31895	57.30073 [29]	-0.00032
C_2H_6SiO	Vinylsilanol	0	0	0	1	0	2	1	1	0	0	0	1	1	0	1	37.33784		
CH_6SiO_4	$(HO)_3SiOCH_3$	0	0	0	4	0	0	0	3	1	0	1	0	0	0	0	47.45144	49.28171[a] [30]	0.03714
$C_4H_{12}SiO_4$	Tetramethoxysilioxane	0	0	0	4	0	0	0	0	4	0	4	0	0	0	0	83.48783	84.04681 [31]	0.00665
$C_6H_{16}SiO_3$	Triethoxysilioxane	0	0	0	3	0	1	0	0	0	3	3	3	0	3	0	102.74755	102.57961 [31]	-0.00164
$C_8H_{20}SiO_4$	Tetraethoxysilioxane	0	0	0	4	0	0	0	0	0	4	4	4	0	4	0	132.89639	133.23177 [31]	0.00252
$C_6H_{18}Si_3O_3$	$((CH_3)_2SiO)_3$	0	0	0	6	0	0	6	0	0	0	6	0	0	0	0	123.61510	123.22485 [31]	-0.00317
$C_8H_{24}Si_4O_4$	$((CH_3)_2SiO)_4$	0	0	0	8	0	0	8	0	0	0	8	0	0	0	0	164.82014	164.79037 [31]	-0.00018
$C_{10}H_{30}Si_5O_5$	$((CH_3)_2SiO)_5$	0	0	0	10	0	0	10	0	0	0	10	0	0	0	0	206.02517	206.35589 [31]	0.00160
$C_6H_{18}Si_2O$	Hexamethyldisiloxane	0	0	0	0	2	0	6	0	0	0	6	0	0	0	0	105.24639	105.20196 [31]	-0.00042

[a]theory

Table 20.19. The bond angle parameters of silicon oxides, silicic acids, silanols, siloxanes, disiloxanes and experimental values. In the calculation of θ_v, the parameters from the preceding angle were used. E_T is E_T (*atom - atom* msp^3*.AO*).

Atoms of Angle	2c' Bond 1 (a_0)	2c' Bond 2 (a_0)	2c' Terminal Atoms (a_0)	$E_{Coulombic}$ Atom 1	Atom 1 Hybridization Designation (Table)	$E_{Coulombic}$ Atom 2	Atom 2 Hybridization Designation (Table)	c_2 Atom 1	c_2 Atom 2	C_1	C_2	c_1	c_2'	E_v (eV)	θ_v (°)	θ_1 (°)	θ_2 (°)	Cal. θ (°)	Exp. θ (°)
$\angle SiOH$	3.25940	1.83616	4.3931	-10.25487 *Si*		H	H	0.75304 (Eq. (20.49))	1	0.75	0.75304	0.75	0.75304	-0.48015 (Eq. (20.12))				116.31	116.4 (H_3SiOH)[a] [32]
$\angle OSiO$	3.25940	3.25940	5.3292	14.96480		14.96480		0.90919	0.90919	1	1	1	0.90919	-1.65376				109.67	109 (polydimethyl siloxane) [33]
$\angle CSiO$	3.54654	3.25940	5.4955	-14.82575 *C*		-13.61805 *O*		0.91771	1	1	1	1	0.91771	-1.65376				107.62	
$\angle C_aSiC_b$	3.54654	3.54654	5.6921	-15.55033 C_a	5 (15.3.A)	-15.55033 C_b	5 (15.3.A)	0.87495	0.87495	1	1	1	0.87495	-1.85836				106.74	106 (polydimethyl siloxane) [33]
$\angle Si_aOSi_b$	3.25940	3.25940	6.0992	-10.25487 *Si*		-10.25487 *Si*		0.75304 (Eq. (20.49))	0.75304 (Eq. (20.49))	1	1	1	0.75304 (Eq. (20.49))					138.66	140 (hexamethyl disiloxane) [33]
$\angle C_aSiC_b$	3.54654	3.54654	5.8310	-15.55033 C_a	5 (15.3.A)	-15.55033 C_b	5 (15.3.A)	0.87495	0.87495	1	1	1	0.87495	-1.85836				110.58	111.0 (dimethylsilane) [9] 110.2 (trimethylsilane) [9]
$\angle C_aSiH$															71.67			108.33	108.8 (trimethylsilane) [9]
Methyl $\angle HC_cH$	2.09711	2.09711	3.4252	-15.75493	7 (15.3.A)	H	H	0.86359	1	1	1	0.75	1.15796	0				109.50	
$\angle HC_cSi$															70.56			109.44	
$\angle C_aC_bC_c$															70.56			109.44	
Methylene $\angle HC_cH$	2.11106	2.11106	3.4252	-15.75493	7 (15.3.A)	H	H	0.86359	1	1	1	0.75	1.15796	0				108.44	107 (propane) [8]
$\angle C_aC_bC_c$															69.51			110.49	112 (propane) [8] 113.8 (butane) [8] 110.8 (isobutane) [8]
$\angle C_aC_3H$															69.51			110.49	111.0 (butane) [8] 111.4 (isobutane) [8]
Methyl $\angle HC_cH$	2.09711	2.09711	3.4252	-15.75493	7 (15.3.A)	H	H	0.86359	1	1	1	0.75	1.15796	0				109.50	
$\angle C_aC_bC_c$															70.56			109.44	
$\angle C_aC_3H$															70.56			109.44	
$\angle C_bC_aC_c$ iso C_a	2.91547	2.91547	4.7958	-16.68412 C_b	26 (15.3.A)	-16.68412 C_c	26 (15.3.A)	0.81549	0.81549	1	1	1	0.81549	-1.85836				110.67	110.8 (isobutane) [8]
$\angle C_bC_aH$ iso C_a	2.91547	2.11323	4.1633	-15.55033 C_a	5 (15.3.A)	-14.82575 C_b	1 (15.3.A)	0.87495	0.91771	0.75	1	0.75	1.04887	0				110.76	
$\angle C_aC_3H$ iso C_a	2.91547	2.09711	4.1633	-15.55033 C_b	5 (15.3.A)	-14.82575 C_a	1 (15.3.A)	0.87495	0.91771	0.75	1	0.75	1.04887	0				111.27	111.4 (isobutane) [8]
$\angle C_bC_aC_b$ tert C_a	2.90327	2.90327	4.7958	-16.68412 C_b	26 (15.3.A)	-16.68412 C_b	26 (15.3.A)	0.81549	0.81549	1	1	1	0.81549	-1.85836				111.37	110.8 (isobutane) [8]
$\angle C_bC_aC_d$															72.50			107.50	

SUMMARY TABLES OF SILICON MOLECULES

The bond energies, calculated using closed-form equations having integers and fundamental constants only for classes of molecules whose designation is based on the main functional group, are given in the following tables with the experimental values.

Table 20.20.1. Summary results of silanes.

Formula	Name	Calculated Total Bond Energy (eV)	Experimental Total Bond Energy (eV)	Relative Error
SiH	silylidyne	3.07526	3.02008 [6]	-0.01827
SiH_2	silylene	6.15052	6.35523 [7]	0.03221
SiH_3	silyl	9.22578	9.36494 [7]	0.01486
SiH_4	silane	13.57257	13.34577 [6]	-0.01699
Si_2H_6	disilane	21.76713	22.05572 [7]	0.01308
Si_3H_8	trisilane	31.23322	30.81334 [7]	-0.01363

Table 20.20.2. Summary results of alkyl silanes and disilanes.

Formula	Name	Calculated Total Bond Energy (eV)	Experimental Total Bond Energy (eV)	Relative Error
CH_6Si	methylsilane	25.37882	25.99491 [9]	0.02370
C_2H_8Si	dimethylsilane	38.45660	38.64819 [9]	0.00496
$C_3H_{10}Si$	trimethylsilane	51.53438	51.33567 [9]	-0.00387
$C_4H_{12}Si$	tetramethylsilane	64.61216	64.22319 [14]	-0.00606
$C_4H_{12}Si$	diethylsilane	62.77200	63.37771 [15]	0.00956
$C_6H_{16}Si$	triethylsilane	88.00748	87.46141 [15]	-0.00624
$C_8H_{20}Si$	tetraethylsilane	113.24296	112.06547[15]	-0.01051
CH_8Si_2	methyldisilane	34.56739	34.73920 [16]	0.00495
$C_2H_{10}Si_2$	1,1-dimethyldisilane	47.36764	47.42283 [16]	0.00116
$C_2H_{10}Si_2$	1,2-dimethyldisilane	47.36764	47.42283 [16]	0.00116
$C_3H_{12}Si_2$	1,1,1-trimethyldisilane	60.16789	60.10646 [16]	-0.00102
$C_3H_{12}Si_2$	1,1,2-trimethyldisilane	60.16789	60.10646 [16]	-0.00102
$C_4H_{14}Si_2$	1,1,1,2-tetramethyldisilane	72.96815	72.79442 [16]	-0.00239
$C_4H_{14}Si_2$	1,1,2,2-tetramethyldisilane	72.96815	72.79442 [16]	-0.00239
$C_5H_{16}Si_2$	1,1,1,2,2-pentamethyldisilane	85.76840	85.47805 [16]	-0.00340
$C_6H_{18}Si_2$	hexamethyldisilane	98.56865	98.32646 [16]	-0.00246

Table 20.20.3. Summary results of silicon oxides, silicic acids, silanols, siloxanes, and disiloxanes.

Formula	Name	Calculated Total Bond Energy (eV)	Experimental Total Bond Energy (eV)	Relative Error
SiO	silicon oxide	8.30876	8.29905 [18]	-0.00117
SiO_2	silicon dioxide	12.94190	12.98073 [19]	0.00299
SiH_4O	H_3SiOH	18.67184	19.00701[a] [27]	0.01763
SiH_4O_2	$H_2Si(OH)_2$	25.04264	25.04264 [a] [27]	0.00563
SiH_4O_3	$HSi(OH)_3$	31.41344	31.47012[a] [27]	0.00180
SiH_4O_4	$Si(OH)_4$	37.78423	38.03638 [28]	0.00663
$C_3H_{10}SiO$	trimethylsilanol	57.31895	57.30073 [29]	-0.00032
C_2H_6SiO	vinylsilanol	37.33784		
CH_6SiO_4	$(HO)_3SiOCH_3$	47.45144	49.28171[a] [30]	0.03714
$C_4H_{12}SiO_4$	tetramethoxysilioxane	83.48783	84.04681 [31]	0.00665
$C_6H_{16}SiO_3$	triethoxysilioxane	102.74755	102.57961 [31]	-0.00164
$C_8H_{20}SiO_4$	tetraethoxysilioxane	132.89639	133.23177 [31]	0.00252
$C_6H_{18}Si_3O_3$	$((CH_3)_2SiO)_3$	123.61510	123.22485 [31]	-0.00317
$C_8H_{24}Si_4O_4$	$((CH_3)_2SiO)_4$	164.82014	164.79037 [31]	-0.00018
$C_{10}H_{30}Si_5O_5$	$((CH_3)_2SiO)_5$	206.02517	206.35589 [31]	0.00160
$C_6H_{18}Si_2O$	hexamethyldisiloxane	105.24639	105.20196 [31]	-0.00042

[a] theory

REFERENCES

1. D. R. Lide, *CRC Handbook of Chemistry and Physics*, 86th Edition, CRC Press, Taylor & Francis, Boca Raton, (2005-6), pp. 10-202 to 10-204.
2. D. R. Lide, *CRC Handbook of Chemistry and Physics*, 86th Edition, CRC Press, Taylor & Francis, Boca Raton, (2005-6), p. 9-26.
3. D. R. Lide, *CRC Handbook of Chemistry and Physics*, 86th Edition, CRC Press, Taylor & Francis, Boca Raton, (2005-6), p. 9-86.
4. D. R. Lide, *CRC Handbook of Chemistry and Physics*, 86th Edition, CRC Press, Taylor & Francis, Boca Raton, (2005-6), p. 9-57.
5. D. R. Lide, *CRC Handbook of Chemistry and Physics*, 86th Edition, CRC Press, Taylor & Francis, Boca Raton, (2005-6), p. 9-71.
6. B. H. Boo, P. B. Armentrout, "Reaction of silicon ion (^{2}P) with silane (SiH_4, SiD_4). Heats of formation of SiH_n, SiH_n^+ (n = 1, 2, 3), and $Si_2H_n^+$ (n = 0, 1, 2,3). Remarkable isotope exchange reaction involving four hydrogen shifts," J. Am. Chem. Soc., (1987), Vol. 109, pp. 3549–3559.
7. G. Katzer, M. C. Ernst, A. F. Sax, J. Kalcher, "Computational thermochemistry of medium-sized silicon hydrides," J. Phys. Chem. A, (1997), Vol. 101, pp. 3942–3958.
8. D. R. Lide, *CRC Handbook of Chemistry and Physics*, 86th Edition, CRC Press, Taylor & Francis, Boca Raton, (2005-6), pp. 9-19 to 9-45.
9. M. R. Frierson, M. R. Imam, V. B. Zalkow, N. L. Allinger, "The MM2 force field for silanes and polysilanes," J. Org. Chem., Vol. 53, (1988), pp. 5248–5258.
10. D. Lin-Vien. N. B. Colthup, W. G. Fateley, J. G. Grasselli, The *Handbook of Infrared and Raman Frequencies of Organic Molecules*, Academic Press, Inc., Harcourt Brace Jovanovich, Boston, (1991), p. 256.
11. G. Herzberg, *Molecular Spectra and Molecular Structure II. Infrared and Raman Spectra of Polyatomic Molecules*, Van Nostrand Reinhold Company, New York, New York, (1945), p. 344.
12. R. J. Fessenden, J. S. Fessenden, *Organic Chemistry*, Willard Grant Press. Boston, Massachusetts, (1979), p. 320.
13. "Cyclohexane," *NIST Chemistry Handbook.* http://webbook.nist.gov/.
14. D. R. Lide, *CRC Handbook of Chemistry and Physics*, 86th Ed., CRC Press, Taylor & Francis, Boca Raton, (2005-6), p. 5-28.
15. M. J. S. Dewar, C. Jie, "AM 1 calculations for compounds containing silicon," Organometallics, Vol. 6, (1987), pp. 1486-1490.
16. R. Walsh, "Certainties and uncertainties in the heats of formation of the methylsilylenes," Organometallics, Vol. 8, (1989), .pp. 1973-1978.
17. R. W. Kilb, L. Pierce, "Microwave spectrum, structure, and internal barrier of methyl silane," J. Chem. Phys., Vol. 27, No. 1, (1957), pp. 108–112.
18. M. W. Chase, Jr., C. A. Davies, J. R. Downey, Jr., D. J. Frurip, R. A. McDonald, A. N. Syverud, JANAF Thermochemical Tables, Third Edition, Part II, Cr-Zr, J. Phys. Chem. Ref. Data, Vol. 14, Suppl. 1, (1985), p. 1728.
19. M. W. Chase, Jr., C. A. Davies, J. R. Downey, Jr., D. J. Frurip, R. A. McDonald, A. N. Syverud, JANAF Thermochemical Tables, Third Edition, Part II, Cr-Zr, J. Phys. Chem. Ref. Data, Vol. 14, Suppl. 1, (1985), p. 1756.
20. D. Nyfeler, T. Armbruster, "Silanol groups in minerals and inorganic compounds," American Mineralogist, Vol. 83, (1998), pp. 119-125.
21. K. P. Huber, G. Herzberg, *Molecular Spectra and Molecular Structure, IV. Constants of Diatomic Molecules*, Van Nostrand Reinhold Company, New York, (1979).
22. J. Crovisier, Molecular Database—Constants for molecules of astrophysical interest in the gas phase: photodissociation, microwave and infrared spectra, Ver. 4.2, Observatoire de Paris, Section de Meudon, Meudon, France, May 2002, pp. 34–37, available at http://wwwusr.obspm.fr/~crovisie/.
23. "Dimethyl ether," *NIST Chemistry Handbook.* http://webbook.nist.gov/.
24. R. J. Fessenden, J. S. Fessenden, *Organic Chemistry*, Willard Grant Press. Boston, Massachusetts, (1979), p. 320.
25. "Fluoroethane," *NIST Chemistry Handbook.* http://webbook.nist.gov/.
26. G. Herzberg, *Molecular Spectra and Molecular Structure II. Infrared and Raman Spectra of Polyatomic Molecules*, Van Nostrand Reinhold Company, New York, New York, (1945), p. 326.
27. M. D. Allendorf, C. F. Melius, P. Ho, M. R. Zachariah, "Theoretical study of the thermochemistry of molecules in the Si–O–H system," J. Phys. Chem., Vol. 99, (1995), pp. 15285–15293.
28. N. S. Jacobson, E. J. Opila, D. L. Myers, E. H. Copeland, "Thermodynamics of gas phase species in the Si–O–H system," J. Chem. Thermodynamics, Vol. 37, (2005), pp. 1130–1137.
29. J. D. Cox, G. Pilcher, *Thermochemistry of Organometallic Compounds*, Academic Press, New York, (1970), pp. 468-469.
30. J. C. S. Chu, R. Soller, M. C. Lin, C. F. Melius, "Thermal decomposition of tetramethyl orthoscilicate in the gas phase: An experimental and theoretical study of the initiation process," J. Phys. Chem, Vol. 99, (1995), pp. 663–672.
31. R. Becerra, R. Walsh, In *The Chemistry of Organic Silicon Compounds*; Z. Rappaport, Y. Apeloig, Eds.; Thermochemistry, Vol. 2; Wiley, New York, (1998), Chp. 4.
32. C. L. Darling, H. B. Schlegel, "Heats of formation of SiH_nO and SiH_nO_2 calculated by ab initio molecular orbital methods at the G-2 level of theory," J. Phys. Chem. Vol. 97, (1993), 8207–8211.
33. A. C. M. Kuo, In *Polymer Data Handbook*; Poly(dimethylsiloxane); Oxford University Press, (1999), p 419.

Chapter 21

THE NATURE OF THE SEMICONDUCTOR BOND OF SILICON

GENERALIZATION OF THE NATURE OF THE SEMICONDUCTOR BOND

Semiconductors are solids that have properties intermediate between insulators and metals. For an insulator to conduct, high energy and power are required to excite electrons into a conducting state in sufficient numbers. Application of high energy to cause electron ionization to the continuum level or to cause electrons to transition to conducing molecular orbitals (MOs) will give rise to conduction when the power is adequate to maintain a high population density of such states. Only high temperatures or extremely high-strength electric fields will provide enough energy and power to achieve an excited state population permissive of conduction. In contrast, metals are highly conductive at essentially any field strength and power. Diamond and alkali metals given in the corresponding sections are representative of insulator and metal classes of solids at opposite extremes of conductivity. It is apparent from the bonding of diamond comprising a network of highly stable MOs that it is an insulator, and the planar free-electron membranes in metals give rise to their high conductivity.

Column IV elements silicon, germanium, and α-gray tin all have the diamond structure and are insulators under standard conditions. However, the electrons of these materials can be excited into a conducting excited state with modest amounts of energy compared to a pure insulator. As opposed to the $5.2\ eV$ excitation energy for carbon, silicon, germanium, and α-gray tin have excitation energies for conduction of only $1.1\ eV$, $0.61\ eV$, and $0.078\ eV$, respectively. Thus, a semiconductor can carry a current by providing the relatively small amount of energy required to excite electrons to conducting excited states. As in the case of insulators, excitation can occur thermally by a temperature increase. Since the number of excited electrons increases with temperature, a concomitant increase in conductance is observed. This behavior is the opposite of that of metals. Alternatively, the absorption of photons of light causes the electrons in the ground state to be excited to a conducting state that is the basis of conversion of solar power into electricity in solar cells and detection and reception in photodetectors and fiber optic communications, respectively. In certain semiconductors, rather than decay by internal conversion to phonons, the energy of excited-state electrons is emitted as light as the electrons transition from the excited conducting state to the ground state. This photon emission process is the basis of light emitting diodes (LEDs) and semiconductor lasers which have broad application in industry.

In addition to elemental materials such as silicon and germanium, semiconductors may be compound materials such as gallium arsenide and indium phosphide, or alloys such as silicon germanium or aluminum arsenide. Conduction in materials such as silicon and germanium crystals can be enhanced by adding small amounts (e.g. 1-10 parts per million) of dopants such as boron or phosphorus as the crystals are grown. Phosphorous with five valence electrons has a free electron even after contributing four electrons to four single bond-MOs of the diamond structure of silicon. Since this fifth electron can be ionized from a phosphorous atom with only $0.011\ eV$ provided by an applied electric field, phosphorous as an electron donor makes silicon a conductor.

In an opposite manner to that of the free electrons of the dopant carrying electricity, an electron acceptor may also transform silicon to a conductor. Atomic boron has only three valence electrons rather than the four needed to replace a silicon atom in the diamond structure of silicon. Consequently, a neighboring silicon atom has an unpaired electron per boron atom. These electrons can be ionized to carry electricity as well. Alternatively, a valence electron of a silicon atom neighboring a boron atom can be excited to ionize and bind to the boron. The resulting negative boron ion can remain stationary as the corresponding positive center on silicon migrates from atom to atom in response to an applied electric field. This occurs as an electron transfers from a silicon atom with four electrons to one with three to fill the vacant silicon orbital. Concomitantly, the positive center is transferred in the opposite direction. Thus, inter-atomic electron transfer can carry current in a cascade effect as the propagation of a “hole” in the opposite direction as the sequentially transferring electrons.

The ability of the conductivity of semiconductors to transition from that of insulators to that of metals with the application of sufficient excitation energy implies a transition of the excited electrons from covalent to metallic-bond electrons. The bonding in diamond shown in the Nature of the Molecular Bond of Diamond section is a network of covalent bonds.

Semiconductors comprise covalent bonds wherein the electrons are of sufficiently high energy that excitation creates an ion and a free electron. The free electron forms a membrane as in the case of metals given in the Nature of the Metallic Bond of Alkali Metals section. This membrane has the same planar structure throughout the crystal. This feature accounts for the high conductivity of semiconductors when the electrons are excited by the application of external fields or electromagnetic energy that causes ion-pair ($M^+ — e^-$) formation.

It was demonstrated in the Nature of the Metallic Bond of Alkali Metals section that the solutions of the external point charge at an infinite planar conductor are also those of the metal ions and free electrons of metals based on the uniqueness of solutions of Maxwell's equations and the constraint that the individual electrons in a metal conserve the classical physical laws of the macro-scale conductor. The nature of the metal bond is a lattice of metal ions with field lines that end on the corresponding lattice of electrons comprising two-dimensional charge density σ given by Eq. (19.6) where each is equivalent electrostatically to an image point charge at twice the distance from the point charge of $+e$ due to M^+. Thus, the metallic bond is equivalent to the ionic bond given in the Alkali-Hydride Crystal Structures section with a Madelung constant of one with each negative ion at a position of one half the distance between the corresponding positive ions, but electrostatically equivalent to being positioned at twice this distance, the M^+-M^+-separation distance. Then, the properties of semiconductors can be understood as due to the excitation of a bound electron from a covalent state such as that of the diamond structure to a metallic state such as that of an alkali metal. The equations are the same as those of the corresponding insulators and metals.

NATURE OF THE INSULATOR-TYPE SEMICONDUCTOR BOND

As given in the Nature of the Solid Molecular Bond of Diamond section, diamond *C* - *C* bonds are all equivalent, and each *C* - *C* bond can be considered bound to a t-butyl group at the corresponding vertex carbon. Thus, the parameters of the diamond *C* - *C* functional group are equivalent to those of the t-butyl *C* - *C* group of branched alkanes given in the Branched Alkanes section. Silicon also has the diamond structure. The diamond *Si* - *Si* bonds are all equivalent, and each *Si* - *Si* bond can be considered bound to three other *Si* - *Si* bonds at the corresponding vertex silicon. Thus, the parameters of the crystalline silicon *Si* - *Si* functional group are equivalent to those of the *Si* - *Si* group of silanes given in the Silanes (Si_nH_{2n+2}) section except for the $E_T\left(atom-atom,msp^3.AO\right)$ term of Eq. (15.61). Since bonds in pure crystalline silicon are only between $Si3sp^3$ HOs having energy less than the Coulombic energy between the electron and proton of H given by Eq. (1.264) $E_T\left(atom-atom,msp^3.AO\right)=0$. Also, as in the case of the *C* - *C* functional group of diamond, the $Si3sp^3$ HO magnetic energy E_{mag} is subtracted due to a set of unpaired electrons being created by bond breakage such that c_3 of Eq. (15.65) is one, and E_{mag} is given by Eqs. (15.15) and (20.3).

$$E_{mag}\left(Si3sp^3\right)=c_3\frac{8\pi\mu_0\mu_B^2}{r^3}=c_3\frac{8\pi\mu_0\mu_B^2}{\left(1.31926a_0\right)^3}=c_3\,0.04983\ eV \tag{21.1}$$

The symbols of the functional group of crystalline silicon is given in Table 21.1. The geometrical (Eqs. (15.1-15.5), (20.3-20.7), (20.29), and (20.33)) parameters of crystalline silicon are given in Table 21.2. Using the internuclear distance $2c'$, the lattice parameter a of crystalline silicon is given by Eq. (17.3). The intercept (Eqs. (15.80-15.87), (20.3), and (20.21)) and energy (Eqs. (15.61), (20.3-20.7), and (20.33)) parameters of crystalline silicon are given in Tables 21.2, 21.3, and 21.4, respectively. The total energy of crystalline silicon given in Table 21.5 was calculated as the sum over the integer multiple of each $E_D(Group)$ of Table 21.4 corresponding to functional-group composition of the solid. The bond angle parameters of crystalline silicon determined using Eqs. (15.88-15.117), (20.4), (20.33), and (21.1) are given in Table 21.6. The diamond structure of silicon in the insulator state is shown in Figure 21.1. The predicted structure matches the experimental images of silicon determined using STM [1] as shown in Figure 21.2.

Figure 21.1. The diamond structure of silicon in the insulator state. Axes indicate positions of additional bonds of the repeating structure. (A) Twenty six $C-C$-bond MOs. (B) Fifty one $C-C$-bond MOs.

(A)

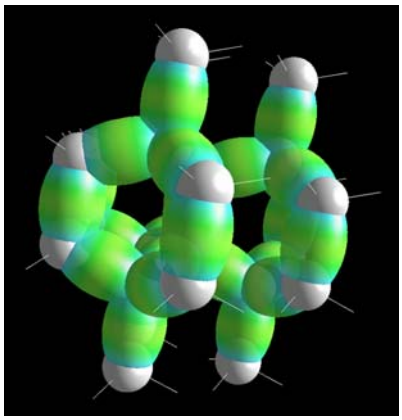

(B)

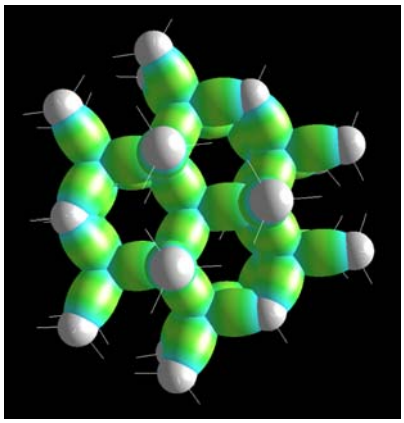

Figure 21.2. (A)-(B) STM topographs of the clean Si(111)-(7X7) surface. Reprinted with permission from Ref. [1]. Copyright 1995 American Chemical Society.

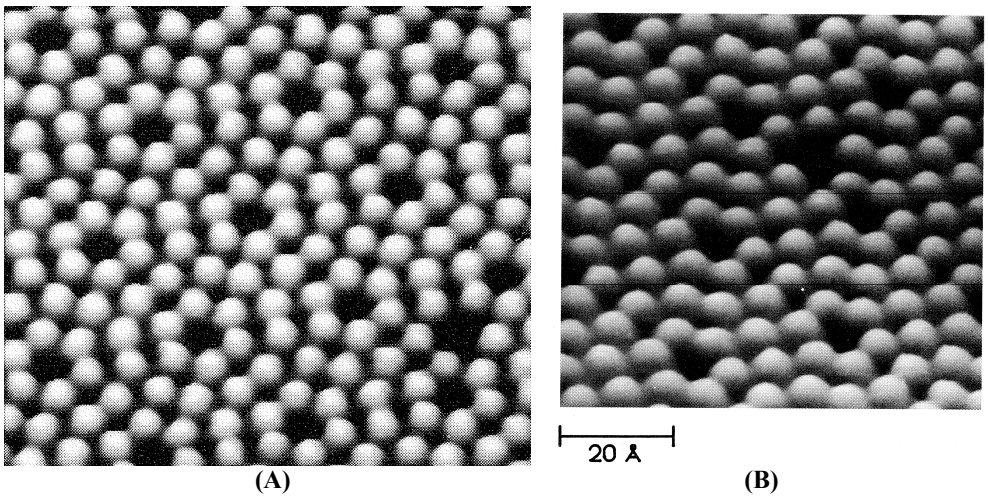

Table 21.1. The symbols of the functional group of crystalline silicon.

Functional Group	Group Symbol
SiSi bond (diamond-type-*Si*)	$Si-Si$

Table 21.2. The geometrical bond parameters of crystalline silicon and experimental values.

Parameter	$Si-Si$ Group
$a\ (a_0)$	2.74744
$c'\ (a_0)$	2.19835
Bond Length $2c'\ (\text{Å})$	2.32664
Exp. Bond Length (Å)	2.35 [2]
$b,c\ (a_0)$	1.64792
e	0.80015
Lattice Parameter $a_l\ (\text{Å})$	5.37409
Exp. Lattice Parameter $a_l\ (\text{Å})$	5.4306 [3]

Table 21.3. The MO to HO intercept geometrical bond parameters of crystalline silicon. E_T is E_T (*atom - atom* msp^3*.AO*).

Bond	Atom	E_T (eV) Bond 1	E_T (eV) Bond 2	E_T (eV) Bond 3	E_T (eV) Bond 4	Final Total Energy $Si3sp^3$ (eV)	$r_{initial}$ $\left(a_0\right)$	r_{final} $\left(a_0\right)$	$E_{Coulomb}\left(C2sp^3\right)$ (eV) Final	$E\left(C2sp^3\right)$ (eV) Final	θ' $\left(^\circ\right)$	θ_1 $\left(^\circ\right)$	θ_2 $\left(^\circ\right)$	d_1 $\left(a_0\right)$	d_2 $\left(a_0\right)$
$Si-Si$	Si	0	0	0	0	-105.23554	1.31926	1.31926	-10.31324	-10.25487	108.26	71.74	49.48	1.78489	0.41346

Table 21.4. The energy parameters (eV) of the functional group of crystalline silicon.

Parameters	$Si-Si$ Group
n_1	1
n_2	0
n_3	0
C_1	0.37500
C_2	0.75800
c_1	1
c_2	0.75800
c_3	0
c_4	2
c_5	0
C_{1o}	0.37500
C_{2o}	0.75800
$V_e\ (eV)$	-20.62357
$V_p\ (eV)$	6.18908
$T\ (eV)$	3.75324
$V_m\ (eV)$	-1.87662
$E_{(AO/HO)}\ (eV)$	-10.25487
$\Delta E_{H_2MO(AO/HO)}\ (eV)$	0
$E_{T(AO/HO)}\ (eV)$	-10.25487
$E_{T(H_2MO)}\ (eV)$	-22.81274
$E_T\left(atom-atom, msp^3.AO\right)\ (eV)$	0
$E_{T(MO)}\ (eV)$	-22.81274
$\omega\ \left(10^{15}\ rad/s\right)$	4.83999
$E_K\ (eV)$	3.18577
$\bar{E}_D\ (eV)$	-0.08055
$\bar{E}_{Kvib}\ (eV)$	0.06335 [4]
$\bar{E}_{osc}\ (eV)$	-0.04888
$E_{mag}\ (eV)$	0.04983
$F_{1(Group)}\ (eV)$	-22.86162
$E_{initial(c_4\ AO/HO)}\ (eV)$	-10.25487
$E_{initial(c_5\ AO/HO)}\ (eV)$	0
$E_{D(Group)}\ (eV)$	2.30204

Table 21.5. The total bond energy of crystalline silicon calculated using the functional group composition and the energy of Table 21.4 compared to the experimental value [5].

Formula	Name	$Si-Si$	Calculated Total Bond Energy (eV)	Experimental Total Bond Energy (eV)	Relative Error
Si_n	Crystalline silicon	1	2.30204	2.3095	0.003

Table 21.6. The bond angle parameters of crystalline silicon and experimental values [2]. In the calculation of $\theta_{v,}$ the parameters from the preceding angle were used. E_T is E_T (*atom - atom* msp^3*.AO*).

Atoms of Angle	2*c'* Bond 1 (a_0)	2*c'* Bond 2 (a_0)	2*c'* Terminal Atoms (a_0)	$E_{Coulombic}$ Atom 1	Atom 1 Hybridization Designation (Table 20.1)	$E_{Coulombic}$ Atom 2	Atom 2 Hybridization Designation (Table 20.1)	c_2 Atom 1	c_2 Atom 2	C_1	C_2	c_1	c_2'	E_T (eV)	θ_v (°)	θ_1 (°)	θ_2 (°)	Cal. θ (°)	Exp. θ (°)
$\angle Si_bSi_aSi_c$	4.39671	4.39671	7.1668	-10.31324 Si_b	1	-10.31324 Si_c	1	1	1	0.75	0.75800 Eq. (20.33)	1	1	-0.04983 (Eq. (21.1))				109.18	109.5
$\angle Si_bSi_aSi_d$															70.24			109.76	109.5

NATURE OF THE CONDUCTOR-TYPE SEMICONDUCTOR BOND

With the application of excitation energy equivalent to at least the *band gap* in the form of photons for example, electrons in silicon transition to conducting states. The nature of these states are equivalent to those of the electrons of metals with the appropriate lattice parameters and boundary conditions of silicon. Since the planar electron membranes are in contact throughout the crystalline matrix, the Maxwellian boundary condition that an equipotential must exist between contacted perfect conductors maintains that all of the planar electrons are at the energy of the highest energy state electron. This condition with the availability of a multitude of states with different ion separation distances and corresponding energies coupled with a near continuum of phonon states and corresponding energies gives rise to a continuum energy band or *conduction band* in the excitation spectrum. Thus, the conducting state of silicon comprises a background covalent diamond structure with free metal-type electrons and an equal number of silicon cations dispersed in the covalent lattice wherein excitation has occurred. The band gap can be calculated from the difference between the energy of the free electrons at the minimum electron-ion separation distance (the parameter d given in the Nature of the Metallic Bond of Alkali Metals section) and the energy of the covalent-type electrons of the diamond-type bonds given in the Nature of the Insulator-Type Semiconductor Bond section.

The band gap is the lowest energy possible to form free electrons and corresponding Si^+ ions. Since the gap is the energy difference between the total energy of the free electrons and the MO electrons, a minimum gap corresponds to the lowest energy state of the free electrons. With the ionization of silicon atoms, planar electron membranes form with the corresponding ions at initial positions of the corresponding bond in the silicon lattice. The potential energy between the electrons and ions is a maximum if the electron membrane comprises the superposition of the two electrons ionized from a corresponding $Si-Si$ bond, and the orientation of the membrane is the transverse bisector of the former bond axis such that the magnitude of the potential is four times that of a single $Si^+ \text{—} e^-$ pair. In this case, the potential is given by two times Eq. (19.21). Furthermore, all of the field lines of the silicon ions end on the intervening electrons. Thus, the repulsion energy between Si^+ ions is zero and the energy of the ionized state is a minimum. Using the parameters from Tables 21.1 and 21.6, the $Si^+ \text{—} e^-$ distance of $c' = 1.16332\ \text{Å}$, and the calculated Si^+ ionic radius of $r_{Si^+ 3sp^3} = 1.16360 a_0 = 0.61575\ \text{Å}$ (Eq. 20.17), the lattice structure of crystalline silicon in a conducting state is shown in Figure 21.3.

Figure 21.3. (A), (B), and (C) The conducting state of crystalline silicon showing the covalent diamond-structure network of the unit cell with two electrons ionized from a MO shown as a planar two-dimensional membrane of zero thickness that is the perpendicular bisector of the former $Si-Si$ bond axis. The corresponding two Si^+ ions (smaller radii) are centered at the positions of the atoms that contributed the ionized $Si3sp^3$-HO electrons. The electron equipotential energy surface may superimpose with multiple planar electron membranes. The surface charge density of each electron gives rise to an electric field equivalent to that of an image point charge for each corresponding positive ion of the lattice.

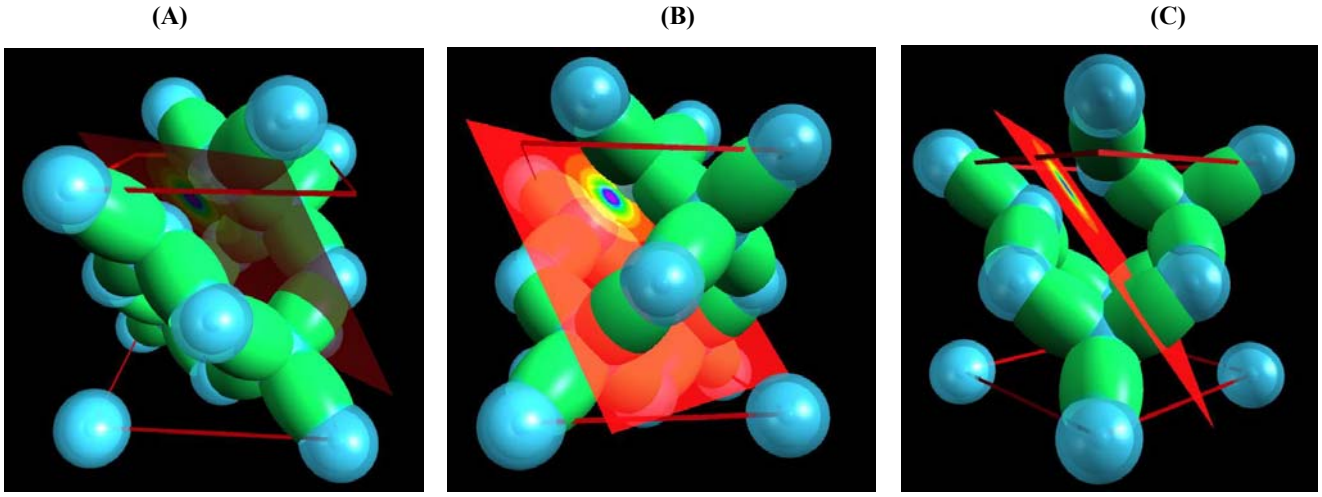

The optimal Si^+ ion-electron separation distance parameter d is given by:

$$d = c' = 2.19835 a_0 = 1.16332\ X\ 10^{-10}\ m \tag{21.2}$$

The band gap is given by the difference in the energy of the free electrons at the optimal Si^+-electron separation distance parameter d given by Eq. (21.2) and the energy of the electrons in the initial state of the $Si-Si$-bond MO. The total energy of electrons of a covalent $Si-Si$-bond MO $E_T\left(Si_{Si-SiMO}\right)$ given by Eq. (15.65) and Table 21.4 is:

$$E_T\left(Si_{Si-SiMO}\right) = E_T\left(MO\right) + \bar{E}_{osc} - E_{mag} = -22.81274\ eV + 0.04888 - 0.04983\ eV = -22.81369\ eV \tag{21.3}$$

The minimum energy of a free-conducting electron in silicon for the determination of the band gap $E_{T(band\ gap)}\left(\ free\ e^{-}\ in\ Si\right)$ is given by the sum of twice the potential energy and the kinetic energy given by Eqs. (19.21) and (19.24), respectively:

$$E_{T(band\ gap)}\left(\ free\ e^{-}\ in\ Si\right)=V+T=\frac{-2e^2}{4\pi\varepsilon_0 d}+\frac{4}{3}\left(\frac{1}{2}\frac{\hbar^2}{m_e d^2}\right) \tag{21.4}$$

In addition, the ionization of the MO electrons increases the charge on the two corresponding $Si3sp^3$ HO with a corresponding energy decrease, $E_T\left(atom-atom,msp^3.AO\right)$ given by one half that of Eq. (20.20). With d given by Eq. (21.2), $E_{T(band\ gap)}\left(\ free\ e^{-}\ in\ Si\right)$ is:

$$\begin{aligned}E_{T(band\ gap)}\left(\ free\ e^{-}\ in\ Si\right)&=\left(\begin{array}{l}\dfrac{-2e^2}{4\pi\varepsilon_0\left(1.16332\ X\ 10^{-10}\ m\right)}\\ +\dfrac{4}{3}\left(\dfrac{1}{2}\dfrac{\hbar^2}{m_e\left(1.16332\ X\ 10^{-10}\ m\right)^2}\right)\\ +E_T\left(atom-atom,msp^3.AO\right)\end{array}\right)\\ &=-24.75614\ eV+3.75374\ eV-\frac{1.37960}{2}\ eV\\ &=-21.69220\ eV\end{aligned} \tag{21.5}$$

The band gap in silicon E_g given by the difference between $E_{T(band\ gap)}\left(\ free\ e^{-}\ in\ Si\right)$ (Eq. (21.5)) and $E_T\left(Si_{Si-SiMO}\right)$ (Eq. (21.3)) is:

$$\begin{aligned}E_g&=E_{T(band\ gap)}\left(\ free\ e^{-}\ in\ Si\right)-E_T\left(Si_{Si-SiMO}\right)\\ &=-21.69220\ eV-\left(-22.81179\ eV\right)\\ &=1.120\ eV\end{aligned} \tag{21.6}$$

The experimental band gap for silicon [6] is:

$$E_g=1.12\ eV \tag{21.7}$$

The calculated band gap is in excellent agreement with the experimentally measured value. This result along with the prediction of the correct lattice parameters, cohesive energy, and bond angles given in Tables 21.2, 21.5, and 21.6, respectively, confirms that conductivity in silicon is due to the creation of discrete ions, Si^{+} and e^{-}, with the excitation of electrons from covalent bonds. The current carriers are free metal-type electrons that exist as planar membranes with current propagation along these structures shown in Figure 21.3. Since the conducting electrons are equivalent to those of metals, the resulting kinetic energy distribution over the population of electrons can be modeled using the statistics of electrons in metals, Fermi Dirac statistics given in the Fermi-Dirac section and the Physical Implications of Free Electrons in Metals section.

REFERENCES

1. H. N. Waltenburg, J. T. Yates, "Surface chemistry of silicon," Chem. Rev., Vol. 95, (1995), pp. 1589-1673.
2. D. W. Palmer, www.semiconductors.co.uk, (2006), September.
3. D. R. Lide, *CRC Handbook of Chemistry and Physics*, 86th Edition, CRC Press, Taylor & Francis, Boca Raton, (2005-6), p. 12-18.
4. D. R. Lide, *CRC Handbook of Chemistry and Physics*, 86th Edition, CRC Press, Taylor & Francis, Boca Raton, (2005-6), p. 9-86.
5. B. Farid, R. W. Godby, "Cohesive energies of crystals," Physical Review B, Vol. 43 (17), (1991), pp. 14248-14250.
6. D. R. Lide, *CRC Handbook of Chemistry and Physics*, 86th Edition, CRC Press, Taylor & Francis, Boca Raton, (2005-6), p. 12-82.

Chapter 22

BORON MOLECULAR FUNCTIONAL GROUPS AND MOLECULES

GENERAL CONSIDERATIONS OF THE BORON MOLECULAR BOND

Boron molecules comprising an arbitrary number of atoms can be solved using similar principles and procedures as those used to solve organic molecules of arbitrary length and complexity. Boron molecules can be considered to be comprised of functional groups such as $B-B$, $B-C$, $B-H$, $B-O$, $B-N$, $B-X$ (X is a halogen atom), and the alkyl functional groups of organic molecules. The solutions of these functional groups or any others corresponding to the particular boron molecule can be conveniently obtained by using generalized forms of the force balance equation given in the Force Balance of the σ MO of the Carbon Nitride Radical section for molecules comprised of boron and hydrogen only and the geometrical and energy equations given in the Derivation of the General Geometrical and Energy Equations of Organic Chemistry section for boron molecules further comprised of heteroatoms such as carbon. The appropriate functional groups with their geometrical parameters and energies can be added as a linear sum to give the solution of any molecule containing boron..

BORANES (B_xH_y)

As in the case of carbon, silicon, and aluminum, the bonding in the boron atom involves four sp^3 hybridized orbitals formed from the $2p$ and $2s$ electrons of the outer shells except that only three HOs are filled. Bonds form between the $B2sp^3$ HOs of two boron atoms and between a $B2sp^3$ HO and a $H1s$ AO to yield boranes. The geometrical parameters of each $B-H$ and $B-B$ functional group is solved from the force balance equation of the electrons of the corresponding σ-MO and the relationships between the prolate spheroidal axes. Then, the sum of the energies of the H_2-type ellipsoidal MOs is matched to that of the $B2sp^3$ shell as in the case of the corresponding carbon molecules. As in the case of ethane ($C-C$ functional group given in the Ethane Molecule section) and silane ($Si-Si$ functional group given in the Silanes section), the energy of the $B-B$ functional group is determined for the effect of the donation of 25% electron density from each participating $B2sp^3$ HO to the $B-B$-bond MO.

The energy of boron is less than the Coulombic energy between the electron and proton of *H* given by Eq. (1.264). A minimum energy is achieved while matching the potential, kinetic, and orbital energy relationships given in the Hydroxyl Radical (*OH*) section with the donation of 25% electron density from each participating $B2sp^3$ HO to each *B* - *H* and *B* - *B*-bond MO. As in the case of acetylene given in the Acetylene Molecule section, the energies of the *B* - *H* and *B* - *B* functional groups are determined for the effect of the charge donation.

The $2sp^3$ hybridized orbital arrangement is:

$2sp^3$ state

↑	↑	↑	
0,0	1,-1	1,0	1,1

(22.1)

where the quantum numbers (ℓ, m_ℓ) are below each electron. The total energy of the state is given by the sum over the four electrons. The sum $E_T\left(B,2sp^3\right)$ of experimental energies [1] of B, B^+, and B^{2+} is:

$$E_T\left(B,2sp^3\right)=37.93064\ eV+25.1548\ eV+8.29802\ eV=71.38346\ eV \tag{22.2}$$

By considering that the central field decreases by an integer for each successive electron of the shell, the radius r_{2sp^3} of the $B2sp^3$ shell may be calculated from the Coulombic energy using Eq. (15.13).

$$r_{2sp^3} = \sum_{n=2}^{4} \frac{(Z-n)e^2}{8\pi\varepsilon_0 \left(e71.38346\ eV\right)} = \frac{6e^2}{8\pi\varepsilon_0 \left(e71.38346\ eV\right)} = 1.14361a_0 \tag{22.3}$$

where $Z = 5$ for boron. Using Eq. (15.14), the Coulombic energy $E_{Coulomb}\left(B, 2sp^3\right)$ of the outer electron of the $B2sp^3$ shell is:

$$E_{Coulomb}\left(B, 2sp^3\right) = \frac{-e^2}{8\pi\varepsilon_0 r_{2sp^3}} = \frac{-e^2}{8\pi\varepsilon_0 1.14361a_0} = -11.89724\ eV \tag{22.4}$$

During hybridization, one of the spin-paired $2s$ electrons is promoted to the $B2sp^3$ shell as an unpaired electron. The energy for the promotion is the magnetic energy given by Eq. (15.15) at the initial radius of the $2s$ electrons. From Eq. (10.62) with $Z = 5$, the radius r_3 of $B2s$ shell is

$$r_3 = 1.07930a_0 \tag{22.5}$$

Using Eqs. (15.15) and (22.5), the unpairing energy is:

$$E(magnetic) = \frac{2\pi\mu_0 e^2\hbar^2}{m_e^2 \left(r_3\right)^3} = \frac{8\pi\mu_0\mu_B^2}{\left(1.07930a_0\right)^3} = 0.09100\ eV \tag{22.6}$$

Using Eqs. (24.4) and (22.6), the energy $E\left(B, 2sp^3\right)$ of the outer electron of the $B2sp^3$ shell is:

$$E\left(B, 2sp^3\right) = \frac{-e^2}{8\pi\varepsilon_0 r_{2sp^3}} + \frac{2\pi\mu_0 e^2\hbar^2}{m_e^2 \left(r_3\right)^3} = -11.89724\ eV + 0.09100\ eV = -11.80624\ eV \tag{22.7}$$

Next, consider the formation of the $B-H$ and $B-B$-bond MOs of boranes wherein each boron atom has a $B2sp^3$ electron with an energy given by Eq. (22.7). The total energy of the state of each boron atom is given by the sum over the three electrons. The sum $E_T\left(B_{borane}, 2sp^3\right)$ of energies of $B2sp^3$ (Eq. (22.7)), B^+, and B^{2+} is:

$$\begin{aligned} E_T\left(B_{borane}, 2sp^3\right) &= -\left(37.93064\ eV + 25.1548\ eV + E\left(B, 2sp^3\right)\right) \\ &= -\left(37.93064\ eV + 25.1548\ eV + 11.80624\ eV\right) = -74.89168\ eV \end{aligned} \tag{22.8}$$

where $E\left(B, 2sp^3\right)$ is the sum of the energy of B, $-8.29802\ eV$, and the hybridization energy.

Each *C* - *H*-bond MO forms with the sharing of electrons between each $B2sp^3$ HO and each $H1s$ AO. As in the case of *C* - *H*, the H_2-type ellipsoidal MO comprises 75% of the *B* - *H* -bond MO according to Eq. (13.429) and Eq. (13.59). Similarly to the case of *C* - *C*, the *B* - *B* H_2-type ellipsoidal MO comprises 50% contribution from the participating $B2sp^3$ HOs according to Eq. (14.152). The sharing of electrons between a $B2sp^3$ HO and one or more $H1s$ AOs to form *B* - *H* -bond MOs or between two $B2sp^3$ HOs to form a *B* - *B* -bond MO permits each participating orbital to decrease in size and energy. As shown below, the boron HOs have spin and orbital angular momentum terms in the force balance which determines the geometrical parameters of each σ MO. The angular momentum term requires that each σ MO be treated independently in terms of the charge donation. In order to further satisfy the potential, kinetic, and orbital energy relationships, each $B2sp^3$ HO donates an excess of 25% of its electron density to the *B* - *H* or *B* - *B* -bond MO to form an energy minimum. By considering this electron redistribution in the borane molecule as well as the fact that the central field decreases by an integer for each successive electron of the shell, the radius $r_{borane2sp^3}$ of the $B2sp^3$ shell may be calculated from the Coulombic energy using Eq. (15.18).

$$r_{borane2sp^3} = \left(\sum_{n=2}^{4}(Z-n) - 0.25\right)\frac{e^2}{8\pi\varepsilon_0 \left(e74.89168\ eV\right)} = \frac{5.75e^2}{8\pi\varepsilon_0 \left(e74.89168\ eV\right)} = 1.04462a_0 \tag{22.9}$$

Using Eqs. (15.19) and (22.9), the Coulombic energy $E_{Coulomb}\left(B_{borane}, 2sp^3\right)$ of the outer electron of the $B2sp^3$ shell is:

$$E_{Coulomb}\left(B_{borane}, 2sp^3\right) = \frac{-e^2}{8\pi\varepsilon_0 r_{borane2sp^3}} = \frac{-e^2}{8\pi\varepsilon_0 1.04462a_0} = -13.02464\ eV \tag{22.10}$$

During hybridization, one of the spin-paired $2s$ electrons are promoted to the $B2sp^3$ shell as an unpaired electron. The energy for the promotion is the magnetic energy given by Eq. (22.6). Using Eqs. (22.6) and (22.10), the energy $E\left(B_{borane}, 2sp^3\right)$ of the outer electron of the $B2sp^3$ shell is:

$$E\left(B_{borane}, 2sp^3\right) = \frac{-e^2}{8\pi\varepsilon_0 r_{borane2sp^3}} + \frac{2\pi\mu_0 e^2\hbar^2}{m_e^2 \left(r_3\right)^3} = -13.02464\ eV + 0.09100\ eV = -12.93364\ eV \tag{22.11}$$

Thus, $E_T\left(B-H, 2sp^3\right)$ and $E_T\left(B-B, 2sp^3\right)$, the energy change of each $B2sp^3$ shell with the formation of the $B-H$ and $B-B$-bond MO, respectively, is given by the difference between Eq. (22.11) and Eq. (22.7):

$$E_T\left(B-H,2sp^3\right)=E_T\left(B-B,2sp^3\right)=E\left(B_{borane},2sp^3\right)-E\left(B,2sp^3\right)$$
$$=-12.93364\ eV-\left(-11.80624\ eV\right)=-1.12740\ eV \tag{22.12}$$

Next, consider the case that each $B2sp^3$ HO donates an excess of 50% of its electron density to the σ MO to form an energy minimum. By considering this electron redistribution in the borane molecule as well as the fact that the central field decreases by an integer for each successive electron of the shell, the radius $r_{borane2sp^3}$ of the $B2sp^3$ shell may be calculated from the Coulombic energy using Eq. (15.18).

$$r_{borane2sp^3}=\left(\sum_{n=2}^{4}(Z-n)-0.5\right)\frac{e^2}{8\pi\varepsilon_0\left(e74.89168\ eV\right)}=\frac{5.5e^2}{8\pi\varepsilon_0\left(e74.89168\ eV\right)}=0.99920a_0 \tag{22.13}$$

Using Eqs. (15.19) and (22.13), the Coulombic energy $E_{Coulomb}\left(B_{borane},2sp^3\right)$ of the outer electron of the $B2sp^3$ shell is:

$$E_{Coulomb}\left(B_{borane},2sp^3\right)=\frac{-e^2}{8\pi\varepsilon_0 r_{borane2sp^3}}=\frac{-e^2}{8\pi\varepsilon_0 0.99920a_0}=-13.61667\ eV \tag{22.14}$$

During hybridization, one of the spin-paired $2s$ electrons is promoted to the $B2sp^3$ shell as an unpaired electron. The energy for the promotion is the magnetic energy given by Eq. (22.6). Using Eqs. (22.6) and (22.14), the energy $E\left(B_{borane},2sp^3\right)$ of the outer electron of the $B2sp^3$ shell is:

$$E\left(B_{borane},2sp^3\right)=\frac{-e^2}{8\pi\varepsilon_0 r_{borane2sp^3}}+\frac{2\pi\mu_0 e^2\hbar^2}{m_e^2\left(r_3\right)^3}=-13.61667\ eV+0.09100\ eV=-13.52567\ eV \tag{22.15}$$

Thus, $E_T\left(B-atom,2sp^3\right)$, the energy change of each $B2sp^3$ shell with the formation of the $B-atom$-bond MO is given by the difference between Eq. (22.15) and Eq. (22.7):

$$E_T\left(B-atom,2sp^3\right)=E\left(B_{borane},2sp^3\right)-E\left(B,2sp^3\right)=-13.52567\ eV-\left(-11.80624\ eV\right)=-1.71943\ eV \tag{22.16}$$

Consider next the radius of the HO due to the contribution of charge to more than one bond. The energy contribution due to the charge donation at each boron atom superimposes linearly. In general, the radius r_{mol2sp^3} of the $B2sp^3$ HO of a boron atom of a given borane molecule is calculated after Eq. (15.32) by considering $\sum E_{T_{mol}}\left(MO,2sp^3\right)$, the total energy donation to all bonds with which it participates in bonding. The general equation for the radius is given by:

$$r_{mol3sp^3}=\frac{-e^2}{8\pi\varepsilon_0\left(E_{Coulomb}\left(B,2sp^3\right)+\sum E_{T_{mol}}\left(MO,2sp^3\right)\right)}=\frac{e^2}{8\pi\varepsilon_0\left(e11.89724\ eV+\sum\left|E_{T_{mol}}\left(MO,2sp^3\right)\right|\right)} \tag{22.17}$$

where $E_{Coulomb}\left(B,2sp^3\right)$ is given by Eq. (22.4). The Coulombic energy $E_{Coulomb}\left(B,2sp^3\right)$ of the outer electron of the $B\,2sp^3$ shell considering the charge donation to all participating bonds is given by Eq. (15.14) with Eq. (22.4). The energy $E\left(B,2sp^3\right)$ of the outer electron of the $B\,2sp^3$ shell is given by the sum of $E_{Coulomb}\left(B,2sp^3\right)$ and $E(magnetic)$ (Eq. (22.6)). The final values of the radius of the $B2sp^3$ HO, r_{2sp^3}, $E_{Coulomb}\left(B,2sp^3\right)$, and $E\left(B_{borane}2sp^3\right)$ calculated using $\sum E_{T_{mol}}\left(MO,2sp^3\right)$, the total energy donation to each bond with which an atom participates in bonding are given in Table 22.1. These hybridization parameters are used in Eqs. (15.88-15.117) for the determination of bond angles given in Table 22.7.

Table 22.1. Atom hybridization designation (# first column) and hybridization parameters of atoms for determination of bond angles with final values of r_{2sp^3}, $E_{Coulomb}\left(B,2sp^3\right)$ (designated as $E_{Coulomb}$), and $E\left(B_{borane}2sp^3\right)$ (designated as E) calculated using the appropriate values of $\sum E_{T_{mol}}\left(MO,2sp^3\right)$ (designated as E_T) for each corresponding terminal bond spanning each angle.

#	E_T	E_T	E_T	E_T	E_T	r_{3sp^3} Final	$E_{Coulomb}$ (eV) Final	E (eV) Final
1	0	0	0	0	0	1.14361	11.89724	11.80624
2	-1.71943	0	0	0	0	0.99920	-13.61667	-13.52567
3	-1.18392	-1.18392	0	0	0	0.95378	-14.26508	-14.17408
4	-1.12740	-1.12740	-0.56370	0	0	0.92458	-14.71574	-14.62474

The MO semimajor axes of the $B-H$ and $B-B$ functional groups of boranes are determined from the force balance equation of the centrifugal, Coulombic, and magnetic forces as given in the Polyatomic Molecular Ions and Molecules section and the More Polyatomic Molecules and Hydrocarbons section. In each case, the distance from the origin of the H_2-type-ellipsoidal-MO to each focus c', the internuclear distance $2c'$, and the length of the semiminor axis of the prolate spheroidal

H_2-type MO $b=c$ are solved from the semimajor axis a. Then, the geometric and energy parameters of each MO are calculated using Eqs. (15.1-15.117).

The force balance of the centrifugal force equated to the Coulombic and magnetic forces is solved for the length of the semimajor axis. The Coulombic force on the pairing electron of the MO is**:**

$$\mathbf{F}_{Coulomb}=\frac{e^2}{8\pi\varepsilon_0 ab^2}D\mathbf{i}_\xi \tag{22.18}$$

The spin-pairing force is**:**

$$\mathbf{F}_{spin-pairing}=\frac{\hbar^2}{2m_e a^2b^2}D\mathbf{i}_\xi \tag{22.19}$$

The diamagnetic force is:

$$\mathbf{F}_{diamagneticMO1}=-\frac{n_e\hbar^2}{4m_e a^2b^2}D\mathbf{i}_\xi \tag{22.20}$$

where n_e is the total number of electrons that interact with the binding σ-MO electron. The diamagnetic force $\mathbf{F}_{diamagneticMO2}$ on the pairing electron of the σ MO is given by the sum of the contributions over the components of angular momentum:

$$\mathbf{F}_{diamagneticMO2}=-\sum_{i,j}\frac{|L_i|\hbar}{Z_j\,2m_e a^2b^2}D\mathbf{i}_\xi \tag{22.21}$$

where $|L|$ is the magnitude of the angular momentum of each atom at a focus that is the source of the diamagnetism at the σ-MO. The centrifugal force is:

$$\mathbf{F}_{centrifugalMO}=-\frac{\hbar^2}{m_e a^2b^2}D\mathbf{i}_\xi \tag{22.22}$$

The force balance equation for the σ-MO of the two-center $B-H$-bond MO is the given by centrifugal force given by Eq. (22.22) equated to the sum of the Coulombic (Eq. (22.18)), spin-pairing (Eq. (22.19)), and $\mathbf{F}_{diamagneticMO2}$ (Eq. (22.21)) with $|L|=4\sqrt{\frac{3}{4}}\hbar$ corresponding to the four $B2sp^3$ HOs:

$$\frac{\hbar^2}{m_e a^2b^2}D=\frac{e^2}{8\pi\varepsilon_0 ab^2}D+\frac{\hbar^2}{2m_e a^2b^2}D-\frac{4\sqrt{\frac{3}{4}}}{Z}\frac{\hbar^2}{2m_e a^2b^2}D \tag{22.23}$$

$$a=\left(1+\frac{4\sqrt{\frac{3}{4}}}{Z}\right)a_0 \tag{22.24}$$

With $Z=5$, the semimajor axis of the $B-H$-bond MO is:

$$a=1.69282a_0 \tag{22.25}$$

The force balance equation for each σ-MO of the $B-B$-bond MO with $n_e=2$ and $|L|=3\sqrt{\frac{3}{4}}\hbar$ corresponding to three electrons of the $B2sp^3$ shell is:

$$\frac{\hbar^2}{m_e a^2b^2}D=\frac{e^2}{8\pi\varepsilon_0 ab^2}D+\frac{\hbar^2}{2m_e a^2b^2}D-\left(1+\frac{3\sqrt{\frac{3}{4}}}{Z}\right)\frac{\hbar^2}{2m_e a^2b^2}D \tag{22.26}$$

$$a=\left(2+\frac{3\sqrt{\frac{3}{4}}}{Z}\right)a_0 \tag{22.27}$$

With $Z=5$, the semimajor axis of the $B-B$-bond MO is:

$$a=2.51962a_0 \tag{22.28}$$

Using the semimajor axis, the geometric and energy parameters of the MO are calculated using Eqs. (15.1-15.127) in the same manner as the organic functional groups given in the Organic Molecular Functional Groups and Molecules section. For the $B-H$ functional group, c_1 is one and $C_1=0.75$ based on the MO orbital composition as in the case of the $C-H$-bond MO. In boranes, the energy of boron is less than the Coulombic energy between the electron and proton of H given by Eq. (1.264). Thus, the energy matching condition is determined by the c_2 and C_2 parameters in Eqs. (15.51) and (15.61). Then, the hybridization factor for the $B-H$-bond MO given by the ratio of 11.89724 eV, the magnitude of $E_{Coulomb}\left(B_{borane},2sp^3\right)$ (Eq. (22.4)), and 13.605804 eV, the magnitude of the Coulombic energy between the electron and proton of H (Eq. (1.264)):

$$c_2 = C_2\left(borane2sp^3HO\right) = \frac{11.89724\ eV}{13.605804\ eV} = 0.87442 \tag{22.29}$$

Since the energy of the MO is matched to that of the $B2sp^3$ HO, $E\left(AO/HO\right)$ in Eqs. (15.51) and (15.61) is $E\left(B,2sp^3\right)$ given by Eq. (22.7), and $E_T\left(atom-atom,msp^3.AO\right)$ is one half of $-1.12740\ eV$ corresponding to the independent single-bond charge contribution (Eq. (22.12)) of one center.

For the $B-B$ functional group, c_1 is one and $C_1 = 0.5$ based on the MO orbital composition as in the case of the $C-C$-bond MO. The energy matching condition is determined by the c_2 and C_2 parameters in Eqs. (15.51) and (15.61), and the hybridization factor for the $B-B$-bond MO given is by Eq. (22.29). Since the energy of the MO is matched to that of the $B2sp^3$ HO, $E\left(AO/HO\right)$ in Eqs. (15.51) and (15.61) is $E\left(B,2sp^3\right)$ given by Eq. (22.7), and $E_T\left(atom-atom,msp^3.AO\right)$ is two times $-1.12740\ eV$ corresponding to the independent single-bond charge contributions (Eq. (22.12)) from each of the two $B2sp^3$ HOs.

BRIDGING BONDS OF BORANES ($B-H-B$ AND $B-B-B$)

As in the case of the $Al3sp^3$ HOs given in the Organoaluminum Hydrides ($Al-H-Al$ and $Al-C-Al$) section, the $B2sp^3$ HOs comprise four orbitals containing three electrons as given by Eq. (23.1) that can form three-center as well as two-center bonds. The designation for a three-center bond involving two $B2sp^3$ HOs and a $H1s$ AO is $B-H-B$, and the designation for a three-center bond involving three $B2sp^3$ HOs is $B-B-B$.

The parameters of the force balance equation for the σ-MO of the $B-H-B$-bond MO are $n_e = 2$ and $|L| = 0$ due to the cancellation of the angular momentum between borons:

$$\frac{\hbar^2}{m_e a^2 b^2} D = \frac{e^2}{8\pi\varepsilon_0 a b^2} D + \frac{\hbar^2}{2m_e a^2 b^2} D - \frac{\hbar^2}{2m_e a^2 b^2} D \tag{22.30}$$

From Eq. (22.30), the semimajor axis of the $B-H-B$-bond MO is

$$a = 2a_0 \tag{22.31}$$

The parameters in Eqs. (15.51) and (15.61) are the same as those of the $B-H-B$ functional group except that $E_T\left(atom-atom,msp^3.AO\right)$ is two times $-1.12740\ eV$ corresponding to the independent single-bond charge contributions (Eq. (22.12)) from each of the two $B2sp^3$ HOs.

The force balance equation and the semimajor axis for the σ-MO of the $B-B-B$-bond MO are the same as those of the $B-B$-bond MO given by Eqs. (22.30) and (22.31), respectively. The parameters in Eqs. (15.51) and (15.61) are the same as those of the $B-B$ functional group except that $E_T\left(atom-atom,msp^3.AO\right)$ is three times $-1.12740\ eV$ corresponding to the independent single-bond charge contributions (Eq. (22.12)) from each of the three $B2sp^3$ HOs.

The H_2-type ellipsoidal MOs of the $B-H-B$ three-center bond intersect and form a continuous single surface. However, in the case of the $B-B-B$-bond MO the current of each $B-B$ MO forms a bisector current described in the Methane Molecule (CH_4) section that is continuous with the center $B2sp^3$-HO shell (Eqs. (15.36-15.44)). Based on symmetry, the polar angle ϕ at which the $B-H-B$ H_2-type ellipsoidal MOs intersect is given by the bisector of the external angle between the $B-H$ bonds:

$$\phi = \frac{360° - \theta_{\angle BHB}}{2} = \frac{360° - 85.4°}{2} = 137.3° \tag{22.32}$$

where [2]

$$\theta_{\angle BHB} = 85.4° \tag{22.33}$$

The polar radius r_i at this angle is given by Eqs. (13.84-13.85).

$$r_i = \left(a - c'\right)\frac{1 + \frac{c'}{a}}{1 + \frac{c'}{a}\cos\phi'} \tag{22.34}$$

Substitution of the parameters of Table 22.2 into Eq. (22.34) gives:

$$r_i = 2.26561a_0 = 1.19891\ X\ 10^{-10}\ m \tag{22.35}$$

The polar angle ϕ at which the $B-B-B$ H_2-type ellipsoidal MOs intersect is given by the bisector of the external angle between the $B-B$ bonds:

$$\phi = \frac{360° - \theta_{\angle BBB}}{2} = \frac{360° - 58.9°}{2} = 150.6° \tag{22.36}$$

where [3]

$$\theta_{\angle BHB} = 58.9° \tag{22.37}$$

The polar radius r_i at this angle is given by Eqs. (13.84-13.85):

$$r_i = (a - c')\frac{1+\frac{c'}{a}}{1+\frac{c'}{a}\cos\phi'} \tag{22.38}$$

Substitution of the parameters of Table 22.2 into Eq. (22.38) gives:

$$r_i = 3.32895 a_0 = 1.76160\ X\ 10^{-10}\ m \tag{22.39}$$

The symbols of the functional groups of boranes are given in Table 22.2. The geometrical (Eqs. (15.1-15.5) and (22.23-22.39)), intercept (Eqs. (15.80-15.87) and (22.17)), and energy (Eq. (15.61), (22.4), (22.7), (22.12), and (22.29)) parameters of boranes are given in Tables 22.3, 22.4, and 22.5, respectively. In the case that the MO does not intercept the B HO due to the reduction of the radius from the donation of Bsp^3 HO charge to additional MOs, the energy of each MO is energy matched as a linear sum to the B HO by contacting it through the bisector current of the intersecting MOs as described in the Methane Molecule (CH_4) section. The total energy of each borane given in Table 22.6 was calculated as the sum over the integer multiple of each $E_{D\,(Group)}$ of Table 22.5 corresponding to functional-group composition of the molecule. E_{mag} of Table 22.5 is given by Eqs. (15.15) and (22.3). The bond angle parameters of boranes determined using Eqs. (15.88-15.117) and (20.36) with $B2sp^3$ replacing $Si3sp^3$ are given in Table 22.7. The charge-density in diborane is shown in Figure 22.1.

Figure 22.1. *Diborane.* Color scale, opaque view of the charge-density of B_2H_6 comprising the linear combination of two sets of two $B-H$-bond MOs and two $B-H-B$-bond MOs. For each $B-H$ and $B-H-B$ bond, the ellipsoidal surface of the H_2-type ellipsoidal MO transitions to the $B2sp^3$ HO shell with radius $0.89047a_0$ (Eq. (22.17)). The inner $B1s$ radius is $0.20670a_0$ (Eq. (10.51)).

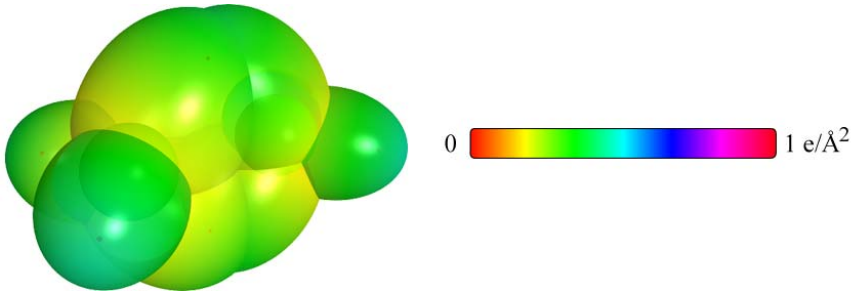

Table 22.2. The symbols of the functional groups of boranes.

Functional Group	Group Symbol
BH group	$B-H$
BHB (bridged *H*)	$B-H-B$
BB bond	$B-B$
BBB (bridged *B*)	$B-B-B$

Table 22.3. The geometrical bond parameters of boranes and experimental values.

Parameter	$B-H$ Group	$B-H-B$ Group	$B-B$ and $B-B-B$ Groups
$a\ (a_0)$	1.69282	2.00000	2.51962
$c'\ (a_0)$	1.13605	1.23483	1.69749
Bond Length $2c'\ (Å)$	1.20235	1.30689	1.79654
Exp. Bond Length $(Å)$	1.19 [4] (diborane)	1.32 [4] (diborane)	1.798 [3] ($B_{13}H_{19}$)
$b,c\ (a_0)$	1.25500	1.57327	1.86199
e	0.67110	0.61742	0.67371

Table 22.4. The MO to HO intercept geometrical bond parameters of boranes. H_t is a terminal or two-center H. H_b is a bridge or three-center H. B_b is a bridge or three-center B. E_T is E_T (*atom - atom msp³.AO*).

Bond	Atom	E_T (eV) Bond 1	E_T (eV) Bond 2	E_T (eV) Bond 3	E_T (eV) Bond 4	Final Total Energy $B2sp^3$ (eV)	$r_{initial}$ (a_0)	r_{final} (a_0)	$E_{Coulomb}(B2sp^3)$ (eV) Final	$E(B2sp^3)$ (eV) Final	θ' (°)	θ_1 (°)	θ_2 (°)	d_1 (a_0)	d_2 (a_0)
$B-H_t\ (H_{t2}BB-)$	B	-0.56370	-0.56370	-1.12740	0	-77.14647	1.14361	0.96140	-14.15203	-14.06103	92.75	87.25	49.92	1.08988	0.04618
$B-H_t\ (H_{t2}BH_{b2}-)$	B	-0.56370	-0.56370	-1.12740	-1.12740	-78.27387	1.14361	0.89047	-15.27943	-15.18843	86.17	93.83	45.07	1.19558	0.05953
$B-H_t\ (H_tH_{b2}BB_b-)$	B	-0.56370	-1.12740	-1.12740	-1.69110	-79.40127	1.14361	0.82928	-16.40683	-16.31583	79.53	100.47	40.52	1.28676	0.15070
$B-H_t\ (H_tH_bBBB_b-)$	B	-0.56370	-1.12740	-1.12740	-1.69110	-79.40127	1.14361	0.82928	-16.40683	-16.31583	79.53	100.47	40.52	1.28676	0.15070
$B-H_t\ (H_tH_bBB_{b2}-)$	B	-0.56370	-1.12740	-1.69110	-1.69110	-79.96497	1.14361	0.80173	-16.97053	-16.87953	76.16	103.84	38.34	1.32780	0.19175
$B-H_b\ (H_{t2}BH_{b2}-)$	B	-1.12740	-1.12740	-0.56370	-0.56370	-78.27387	1.14361	0.89047	-15.27943	-15.18843	50.85	129.15	26.03	1.79706	0.56223
$B-B\ (H_{t2}BB-)$	B	-1.12740	-0.56370	-0.56370	0	-77.14647	1.14361	0.96140	-14.15203	-14.06103	50.20	129.80	23.37	2.31289	0.61540
$B-B\ (H_{b2}H_tBB-)$	B	-1.12740	-1.12740	-1.12740	-0.56370	-78.83757	1.14361	0.85878	-15.84313	-15.75213	26.62	153.38	11.93	2.46521	0.76773
$B-B\ (H_{b2}H_tBB-)$	B	-1.12740	-0.56370	-1.69110	-1.12740	-79.40127	1.14361	0.82928	-16.40683	-16.31583	11.88	168.12	5.26	2.50901	0.81152
$B-B_b\ (H_{b2}H_tBB_b-)$	B	-1.69110	-0.56370	-1.12740	-1.12740	-79.40127	1.14361	0.82928	-16.40683	-16.31583	11.88	168.12	5.26	2.50901	0.81152
$B-B_b\ (H_bH_tBBB_b-)$	B	-1.69110	-0.56370	-1.12740	-1.12740	-79.40127	1.14361	0.82928	-16.40683	-16.31583	11.88	168.12	5.26	2.50901	0.81152
$B-B_b\ (H_bH_tB_bBB_b-)$	B	-1.69110	-1.69110	-0.56370	-1.12740	-79.96497	1.14361	0.80173	-16.97053	-16.87953					

Table 22.5. The energy parameters (eV) of functional groups of boranes.

Parameters	$B-H$ Group	$B-H-B$ Group	$B-B$ Group	$B-B-B$ Group
n_1	1	1	1	1
n_2	0	0	0	0
n_3	0	0	0	0
C_1	0.75	0.75	0.5	0.5
C_2	0.87442	0.87442	0.87442	0.87442
c_1	1	1	1	1
c_2	0.87442	0.87442	0.87442	0.87442
c_3	0	0	0	0
c_4	1	1	2	2
c_5	1	1	0	0
C_{1o}	0.75	0.75	0.5	0.5
C_{2o}	0.87442	0.87442	0.87442	0.87442
$V_e\ (eV)$	-34.04561	-27.77951	-22.91867	-22.91867
$V_p\ (eV)$	11.97638	11.01833	8.01527	8.01527
$T\ (eV)$	10.05589	6.94488	4.54805	4.54805
$V_m\ (eV)$	-5.02794	-3.47244	-2.27402	-2.27402
$E_{(AO/HO)}\ (eV)$	-11.80624	-11.80624	-11.80624	-11.80624
$\Delta E_{H_2MO(AO/HO)}\ (eV)$	0	0	0	0
$E_{T(AO/HO)}\ (eV)$	-11.80624	-11.80624	-11.80624	-11.80624
$E_{T(H_2MO)}\ (eV)$	-28.84754	-25.09498	-24.43561	-24.43561
$E_{I}\left(atom-atom, msp^3.AO\right)\ (eV)$	-0.56370	-2.25479	-2.25479	-3.38219
$E_{T(MO)}\ (eV)$	-29.41123	-29.60457	-26.69041	-27.81781
$\omega\ \left(10^{15}\ rad/s\right)$	15.2006	23.9931	6.83486	6.83486
$E_K\ (eV)$	10.00529	15.79265	4.49882	4.49882
$\overline{E}_D\ (eV)$	-0.18405	-0.23275	-0.11200	-0.11673
$\overline{E}_{Kvib}\ (eV)$	0.29346 [5]	0.09844 [6]	0.13035 [5]	0.13035 [5]
$\overline{E}_{osc}\ (eV)$	-0.03732	-0.18353	-0.04682	-0.05156
$E_{mag}\ (eV)$	0.07650	0.07650	0.07650	0.07650
$E_{T(Group)}\ (eV)$	-29.44855	-29.78809	-26.73723	-27.86936
$E_{initial(c_4\ AO/HO)}\ (eV)$	-11.80624	-11.80624	-11.80624	-11.80624
$E_{initial(c_5\ AO/HO)}\ (eV)$	-13.59844	-13.59844	0	0
$E_{D(Group)}\ (eV)$	4.04387	4.38341	3.12475	4.25687

Table 22.6. The total bond energies of boranes calculated using the functional group composition and the energies of Table 22.5 compared to the experimental values [7]. The structures are given in Refs. [8-9].

Formula	Name	$B-H$ Group	$B-H-B$ Group	$B-B$ Group	$B-B-B$ Group	Calculated Total Bond Energy (eV)	Experimental Total Bond Energy (eV)	Relative Error
BB	Diboron	0	0	1	0	3.12475	3.10405	-0.00667
B_2H_6	Diborane	4	2	0	0	24.94229	24.89030	-0.00209
B_4H_{10}	Tetraborane(10)	6	4	1	0	44.92160	45.33134	0.00904
B_5H_9	Pentaborane(9)	5	4	2	1	48.25462	48.85411	0.01227
B_5H_{11}	Pentaborane(11)	8	3	0	2	54.00546	53.06086	-0.01780
B_6H_{10}	Hexaborane(10)	6	4	2	2	56.55063	56.74739	0.00347
B_9H_{15}	Nonaborane(15)	10	5	2	4	85.61380	84.95008	-0.00781
$B_{10}H_{14}$	Decaborane(14)	10	4	2	6	89.73467	89.69790	-0.00041

Table 22.7. The bond angle parameters of boranes and experimental values. H_t is a terminal or two-center H. H_b is a bridge or three-center H. E_T is E_T (*atom - atom msp³.AO*).

Atoms of Angle	$2c'$ Bond 1 (a_0)	$2c'$ Bond 2 (a_0)	$2c'$ Terminal Atoms (a_0)	$E_{Coulombic}$ Atom 1	Atom 1 Hybridization Designation (Table)	$E_{Coulombic}$ Atom 2	Atom 2 Hybridization Designation (Table)	c_2 Atom 1	c_2 Atom 2	C_1	C_2	c_1	c_2'	E_T (eV)	θ_v (°)	θ_1 (°)	θ_2 (°)	Cal. θ (°)	Exp. θ (°)
$\angle H_tBH_t$	2.27211	2.27211	3.9623	-13.61667	2 (22.1)	H	H	0.99920	1	1	1	0.75	1.00080	-1.71943				121.37	122 [10] (diborane)
$\angle H_tBH_b$	2.27211	2.46967	3.8210	-14.71574	4 (22.1)	H	H	0.92458	1	1	1	0.75	1.08158	-1.12740				107.30	108.9 [2] (B_4H_{10})
$\angle H_bBH_b$	2.46967	2.46967	3.6606	-14.26508	3 (22.1)	H	H	0.95378	1	1	1	0.75	1.04846	-1.12740				95.65	95.0 [2] (B_4H_{10})
$\angle BH_bB$	2.46967	2.46967	3.4358	-11.89724 B_a	1 (22.1)	-11.89724 B_b	1 (22.1)	1	1	1	1.14361	1	1	0				88.15	87.7 [2] (B_4H_{10})

ALKYL BORANES ($R_xB_yH_z; R = alkyl$)

The alkyl boranes may comprise at least a terminal methyl group (CH_3) and at least one B bound by a carbon-boron single bond comprising a $C-B$ group, and may comprise methylene (CH_2), methylyne (CH), $C-C$, $B-H$, $B-B$, $B-H-B$, and $B-B-B$ functional groups. The methyl and methylene functional groups are equivalent to those of straight-chain alkanes. Six types of $C-C$ bonds can be identified. The n-alkane $C-C$ bond is the same as that of straight-chain alkanes. In addition, the $C-C$ bonds within isopropyl ($(CH_3)_2CH$) and t-butyl ($(CH_3)_3C$) groups and the isopropyl to isopropyl, isopropyl to t-butyl, and t-butyl to t-butyl $C-C$ bonds comprise functional groups. Additional groups include aromatics such as phenyl. These groups in alkyl boranes are equivalent to those in branched-chain alkanes and aromatics, and the $B-H$, $B-B$, $B-H-B$, and $B-B-B$ functional groups of alkyl boranes are equivalent to those in boranes.

For the $C-B$ functional group, hybridization of the $2s$ and $2p$ AOs of each C and B to form single $2sp^3$ shells forms an energy minimum, and the sharing of electrons between the $C2sp^3$ and $B2sp^3$ HOs to form a MO permits each participating orbital to decrease in radius and energy. In alkyl boranes, the energy of boron is less than the Coulombic energy between the electron and proton of H given by Eq. (1.264). Thus, c_1 in Eq. (15.61) is one, and the energy matching condition is determined by the c_2 and C_2 parameters. Then, the $C2sp^3$ HO has an energy of $E\left(C,2sp^3\right) = -14.63489\ eV$ (Eq. (15.25)), and the $B2sp^3$ HOs have an energy of $E\left(B,2sp^3\right) = -11.80624\ eV$ (Eq. (22.7)). To meet the equipotential condition of the union of the $C-B$ H_2-type-ellipsoidal-MO with these orbitals, the hybridization factors c_2 and C_2 of Eq. (15.61) for the $C-B$-bond MO given by Eq. (15.77) is:

$$c_2\left(C2sp^3HO\ to\ B2sp^3HO\right) = C_2\left(C2sp^3HO\ to\ B2sp^3HO\right) = \frac{E\left(B,2sp^3\right)}{E\left(C,2sp^3\right)} = \frac{-11.80624\ eV}{-14.63489\ eV} = 0.80672 \tag{22.40}$$

$E_T\left(atom-atom, msp^3.AO\right)$ of the $C-B$-bond MO is $-1.44915\ eV$ corresponding to the single-bond contributions of carbon and boron of $-0.72457\ eV$ given by Eq. (14.151). The energy of the $C-B$-bond MO is the sum of the component energies of the H_2-type ellipsoidal MO given in Eq. (15.51) with $E\left(AO/HO\right) = E\left(B,2sp^3\right)$ given by Eq. (22.7) and $\Delta E_{H_2MO}\left(AO/HO\right) = E_T\left(atom-atom, msp^3.AO\right)$ in order to match the energies of the carbon and boron HOs.

Consider next the radius of the HO due to the contribution of charge to more than one bond. The energy contribution due to the charge donation at each boron atom and carbon atom superimposes linearly. In general, since the energy of the $B2sp^3$ HO is matched to that of the $C2sp^3$ HO, the radius $r_{mol\,2sp^3}$ of the $B2sp^3$ HO of a boron atom and the $C2sp^3$ HO of a carbon atom of a given alkyl borane molecule is calculated after Eq. (15.32) by considering $\sum E_{T_{mol}}\left(MO,2sp^3\right)$, the total energy donation to all bonds with which it participates in bonding. The Coulombic energy $E_{Coulomb}\left(atom,2sp^3\right)$ of the outer electron of the $atom$ $2sp^3$ shell considering the charge donation to all participating bonds is given by Eq. (15.14). The hybridization parameters used in Eqs. (15.88-15.117) for the determination of bond angles of alkyl boranes are given in Table 22.8.

Table 22.8. Atom hybridization designation (# first column) and hybridization parameters of atoms for determination of bond angles with final values of r_{2sp^3}, $E_{Coulomb}(atom,2sp^3)$ (designated as $E_{Coulomb}$), and $E_{Coulomb}(atom_{alkylborane}2sp^3)$ (designated as E) calculated using the appropriate values of $\sum E_{T_{mol}}(MO,2sp^3)$ (designated as E_T) for each corresponding terminal bond spanning each angle.

#	E_T	E_T	E_T	E_T	E_T	r_{3sp^3} (a_0) Final	$E_{Coulomb}$ (eV) Final	E (eV) Final
1	-0.36229	-0.92918	0	0	0	0.84418	-16.11722	-15.92636

The symbols of the functional groups of alkyl boranes are given in Table 22.9. The geometrical (Eqs. (15.1-15.5) and (22.23-22.40)), intercept (Eqs. (15.32) and (15.80-15.87)), and energy (Eq. (15.61), (22.4), (22.7), (22.12), (22.29), and (22.40)) parameters of alkyl boranes are given in Tables 22.10, 22.11, and 22.12, respectively. In the case that the MO does not intercept the B HO due to the reduction of the radius from the donation of B $2sp^3$ HO charge to additional MOs, the energy of each MO is energy matched as a linear sum to the B HO by contacting it through the bisector current of the intersecting MOs as described in the Methane Molecule (CH_4) section. The total energy of each alkyl borane given in Table 22.13 was calculated as the sum over the integer multiple of each $E_D(Group)$ of Table 22.12 corresponding to functional-group composition of the molecule. E_{mag} of Table 22.13 is given by Eqs. (15.15) and (22.3) for $B-H$. The bond angle parameters of alkyl boranes determined using

Eqs. (15.88-15.117) are given in Table 22.14. The charge-densities of exemplary alkyl boranes, trimethylborane, tetramethyldiborane, and methyldecaborane comprising the concentric shells of atoms with the outer shell bridged by one or more H_2-type ellipsoidal MOs or joined with one or more hydrogen MOs are shown in Figures 22.2A-B and 22.3A-B, respectively.

Figure 22.2. A. *Trimethylborane.* Color scale, translucent views of the charge-density of $(H_3C)_3 B$ showing the orbitals of the B and C atoms at their radii, the ellipsoidal surface of each H or H_2-type ellipsoidal MO that transitions to the corresponding outer shell of the atoms participating in each bond, and the hydrogen nuclei (red, not to scale). B. *Tetramethyldiborane.* Color scale, opaque view of the charge-density of $(CH_3)_2 BH_2B(CH_3)_2$ showing the orbitals of the B and C atoms at their radii, the ellipsoidal surface of each H or H_2-type ellipsoidal MO that transitions to the corresponding outer shell of the atoms participating in each bond, and the hydrogen nuclei (red, not to scale).

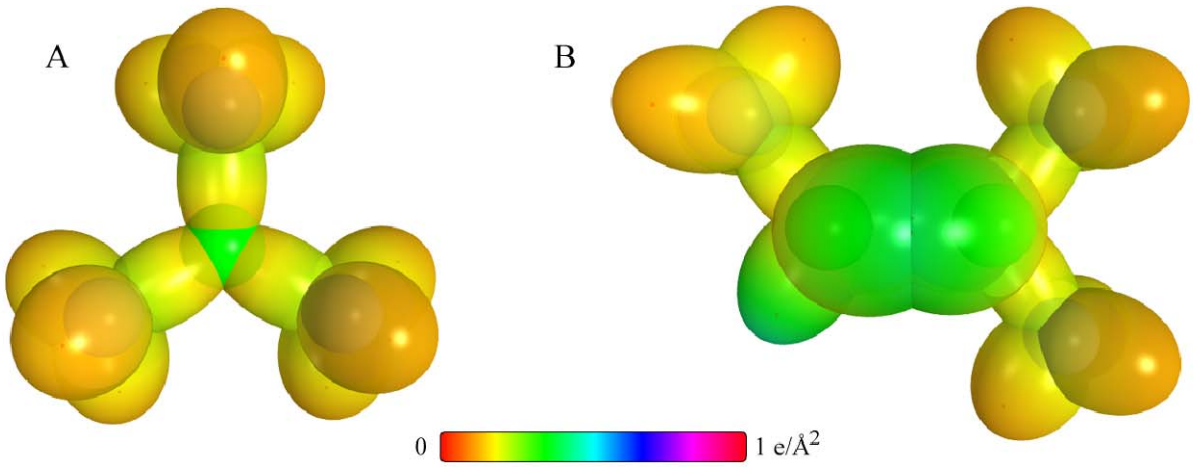

Figure 22.3. A-B. *Methyldecaborane*. Color scale, translucent view of the charge-density of methyldecaborane showing the orbitals of the *B* and *C* atoms at their radii, the ellipsoidal surface of each *H* or H_2-type ellipsoidal MO that transitions to the corresponding outer shell of the atoms participating in each bond, and the hydrogen nuclei (red, not to scale).

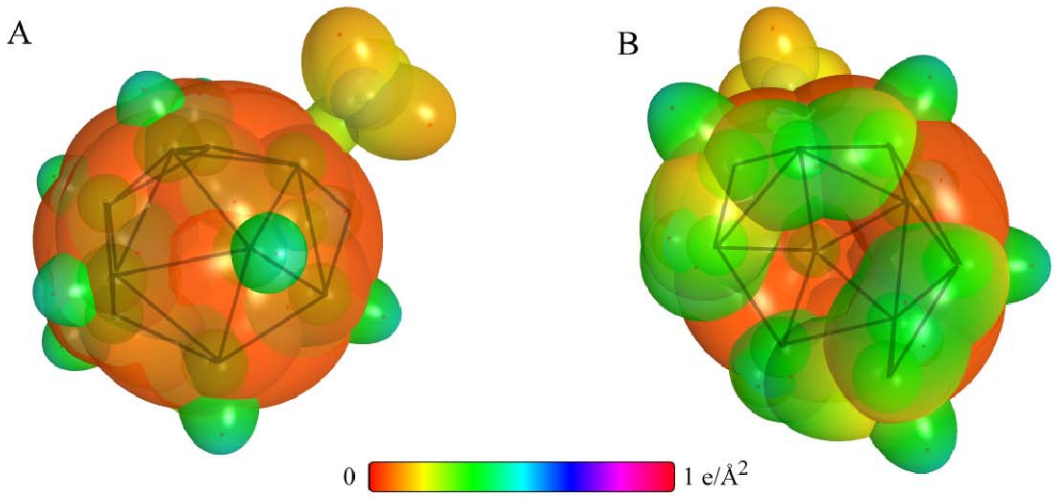

Table 22.9. The symbols of the functional groups of alkyl boranes.

Functional Group	Group Symbol
C-B bond	$C-B$
BH bond	$B-H$
BHB (bridged *H*)	$B-H-B$
BB bond	$B-B$
BBB (bridged *B*)	$B-B-B$
CC (aromatic bond)	$C\overset{3e}{=}C$
CH (aromatic)	CH (i)
CH_3 group	$C-H\ (CH_3)$
CH_2 group	$C-H\ (CH_2)$
CH	$C-H$ (ii)
CC bond (*n-C*)	$C-C$ (a)
CC bond (*iso-C*)	$C-C$ (b)
CC bond (*tert-C*)	$C-C$ (c)
CC (*iso* to *iso-C*)	$C-C$ (d)
CC (*t* to *t-C*)	$C-C$ (e)
CC (*t* to *iso-C*)	$C-C$ (f)

Table 22.10. The geometrical bond parameters of alkyl boranes and experimental values. The experimental alkyl distances from Ref. [10].

Parameter	$C-B$ Group	$B-H$ Group	$B-H-B$ Group	$B-B$ and $B-B-B$ Groups	$\overset{3v}{C=C}$ Group	CH (i) Group	$C-H\ (CH_3)$ Group	$C-H\ (CH_2)$ Group	$C-H$ (ii) Group	$C-C$ (a) Group	$C-C$ (b) Group	$C-C$ (c) Group	$C-C$ (d) Group	$C-C$ (e) Group	$C-C$ (f) Group
$a\ (a_0)$	1.78528	1.69282	2.00000	2.51962	1.47348	1.60061	1.64920	1.67122	1.67465	2.12499	2.12499	2.10725	2.12499	2.10725	2.10725
$c'\ (a_0)$	1.48762	1.13605	1.23483	1.69749	1.31468	1.03299	1.04856	1.05553	1.05661	1.45744	1.45744	1.45164	1.45744	1.45164	1.45164
Bond Length $2c'\ (\AA)$	1.57443	1.20235	1.30689	1.79654	1.39140	1.09327	1.10974	1.11713	1.11827	1.54280	1.54280	1.53635	1.54280	1.53635	1.53635
Exp. Bond Length $(\AA)$	1.578 [10] (trimethylborane) 1.580 [10] (1,2-dimethyldiborane)	1.19 [4] (diborane)	1.32 [4] (diborane)	1.798 [3] ($B_{15}H_{15}$)	1.399 (benzene)	1.101 (benzene)	1.114 ($C-H$ trimethylborane) 1.107 ($C-H$ propane) 1.117 ($C-H$ butane)	1.107 ($C-H$ propane) 1.117 ($C-H$ butane)	1.122 (isobutane)	1.532 (propane) 1.531 (butane)	1.532 (propane) 1.531 (butane)	1.532 (propane) 1.531 (butane)	1.532 (propane) 1.531 (butane)	1.532 (propane) 1.531 (butane)	1.532 (propane) 1.531 (butane)
$b,c\ (a_0)$	0.98702	1.25500	1.57327	1.86199	0.66540	1.22265	1.27295	1.29569	1.29924	1.54616	1.54616	1.52750	1.54616	1.52750	1.52750
e	0.83327	0.67110	0.61742	0.67371	0.89223	0.64537	0.63580	0.63159	0.63095	0.68600	0.68600	0.68888	0.68600	0.68888	0.68888

Table 22.11. The MO to HO intercept geometrical bond parameters of alkyl boranes. H_t is a terminal or two-center *H*. H_b is a bridge or three-center *H*. B_b is a bridge or three-center *B*. E_T is E_T (*atom - atom msp³.AO*).

Bond	Atom	E_1 (eV) Bond 1	E_2 (eV) Bond 2	E_3 (eV) Bond 3	E_4 (eV) Bond 4	Final Total Energy $B2sp^3$ (eV)	$r_{initial}$ (a_0)	r_{final} (a_0)	$E_{valence}(B2sp^3)$ (eV) Final	$E(B2sp^3)$ (eV) Final	θ' (°)	θ_1 (°)	θ_2 (°)	d_1 (a_0)	d_2 (a_0)
$B\ \ H_t\ (H_{t2}BB-)$	*B*	-0.56370	-0.56370	-1.12740	0	-77.14647	1.14361	0.96140	-14.15203	-14.06103	92.75	87.25	49.92	1.08988	0.01618
$B-H_t\ (H_{t2}BH_{b2}\ )$	*B*	-0.56370	-0.56370	-1.12740	-1.12740	-78.27387	1.14361	0.89047	-15.27943	-15.18843	86.17	93.83	45.07	1.19558	0.05953
$B-H_t\ (H_tH_{b2}BB_b-)$	*B*	-0.56370	-1.12740	-1.12740	-1.69110	-79.40127	1.14361	0.82928	-16.40683	-16.31583	79.53	100.47	40.52	1.28676	0.15070
$B\ H_t\ (H_tH_tBBB_b\ )$	*B*	-0.56370	-1.12740	-1.12740	-1.69110	-79.40127	1.14361	0.82928	-16.40683	-16.31583	79.53	100.47	40.52	1.28676	0.15070
$B\ H_t\ (H_tH_tBB_{b2}-)$	*B*	-0.56370	-1.12740	-1.69110	-1.69110	-79.96497	1.14361	0.80173	-16.97053	-16.87953	76.16	103.84	38.34	1.32780	0.19175
$B-H_b\ (H_{t2}BH_{b2}-)$	*B*	-1.12740	-1.12740	-0.56370	-0.56370	-78.27387	1.14361	0.89047	-15.27943	-15.18843	50.85	129.15	26.03	1.79706	0.56223
$B-B\ (H_{t2}BB-)$	*B*	-1.12740	-0.56370	-0.56370	0	-77.14647	1.14361	0.96140	-14.15203	-14.06103	50.20	129.80	23.37	2.31289	0.61540
$B\ B\ (H_{b2}H_tBB\ )$	*B*	-1.12740	-1.12740	-1.12740	-0.56370	-78.83757	1.14361	0.85878	-15.84313	-15.75213	26.62	153.38	11.93	2.46521	0.76773
$B-B\ (H_tH_tB_bBB-)$	*B*	-1.12740	-0.56370	-1.69110	-1.12740	-79.40127	1.14361	0.82928	-16.40683	-16.31583	11.88	168.12	5.26	2.50901	0.81152
$B-B_b\ (H_{t2}H_tBB_b-)$	*B*	-1.69110	-0.56370	-1.12740	-1.12740	-79.40127	1.14361	0.82928	-16.40683	-16.31583	11.88	168.12	5.26	2.50901	0.81152
$B-B_b\ (H_tH_tBBB_b-)$	*B*	-1.69110	-0.56370	-1.12740	-1.12740	-79.40127	1.14361	0.82928	-16.40683	-16.31583	11.88	168.12	5.26	2.50901	0.81152
$B-B_b\ (H_tH_tB_bBB_b-)$	*B*	-1.69110	-1.69110	-0.56370	-1.12740	-79.96497	1.14361	0.80173	-16.97053	-16.87953					
$B-H_t\ (H_{t2}BR)$	*B*	-0.56370	-0.56370	-0.72457	0		1.14361	0.81581	-16.67772	-16.58672	77.92	102.08	39.47	1.30683	0.17077
$B-H_t\ (H_tBR_t)$	*B*	-0.56370	-0.72457	-0.72457	0		1.14361	0.80801	-16.83860	-16.74760	76.95	103.05	38.85	1.31844	0.18239
$B\ \ H_t\ (H_tBBR)$	*B*	-0.56370	-1.12740	-0.72457	0		1.14361	0.78913	-17.24142	-17.15042	74.53	105.47	37.30	1.34657	0.21052
$B-H_b\ (H_tRBH_{b2}-)$	*B*	-1.12740	-1.12740	-0.56370	-0.72457	0	1.14361	0.74070	-18.36882	-18.27782					
$B-H_b\ (R_tBH_{b2}-)$	*B*	-1.12740	-1.12740	-0.72457	-0.72457	0	1.14361	0.73427	-18.52969	-18.43869					
$B\ B\ (H_tRBB\ )$	*B*	-1.12740	-0.56370	-0.72457	0	0	1.14361	0.78913	-17.24142	-17.15042					
$B-B\ (R_tBB-)$	*B*	-1.12740	-0.72457	-0.72457	0	0	1.14361	0.78184	-17.40230	-17.31130					
$B-B\ (H_{t2}RBB-)$	*B*	-1.12740	-1.12740	-1.12740	-0.72457		1.14361	0.71865	-18.93252	-18.84152					
$B-B\ (H_tRB_bBB-)$	*B*	-1.12740	-1.12740	-1.69110	-0.72457		1.14361	0.69787	-19.49622	-19.40522					
$B-B_b\ (H_{b2}RBB_b\ )$	*B*	-1.69110	-0.72457	-1.12740	-1.12740		1.14361	0.69787	-19.49622	-19.40522					
$B-B_b\ (H_tRBBB_b-)$	*B*	-1.69110	-0.72457	-1.12740	-1.12740		1.14361	0.69787	-19.49622	-19.40522					
$B-B_b\ (H_tRB_tBB_t-)$	*B*	-1.69110	-1.69110	-0.72457	-1.12740		1.14361	0.67826	-20.05991	-19.96891					
$C\ \ B\ (H_{t2}B-CH_3)$	*B*	-0.72457	-0.56370	-0.56370	0		1.14361	0.81581	-16.67772	-16.58672	113.41	66.59	49.33	1.16346	0.32416
$C-B\ (H_t(CH_3)B\ \ CH_3)$	*B*	-0.72457	-0.72457	-0.56370	0		1.14361	0.80801	-16.83860	-16.74760	112.93	67.07	48.93	1.17281	0.31481
$C-B\ ((CH_3)_2B-CH_3)$	*B*	-0.72457	-0.72457	-0.72457	0		1.14361	0.80037	-16.99947	-16.90847	112.45	67.55	48.54	1.18199	0.30563
$C-B\ (H_tRBB)$	*B*	-0.72457	-0.56370	-1.12740	0		1.14361	0.78913	-17.24142	-17.15042	111.73	68.27	47.96	1.19547	0.29215
$C-B\ (H_tRBH_{b2})$	*B*	-0.72457	-0.56370	-1.12740	-1.12740		1.14361	0.74070	-18.36882	-18.27782	108.42	71.58	45.40	1.25359	0.23403
$C-B\ (R_tBH_{b2})$	*B*	-0.72457	-0.72457	-1.12740	-1.12740		1.14361	0.73427	-18.52969	-18.43869	107.95	72.05	45.05	1.26131	0.22631

Table 22.11 cont'd. The MO to HO intercept geometrical bond parameters of alkyl boranes. H_t is a terminal or two-center *H*. H_b is a bridge or three-center *H*. B_b is a bridge or three-center *B*. E_T is E_T (*atom - atom msp³.AO*).

Bond	Atom	E_T (eV) Bond 1	E_T (eV) Bond 2	E_T (eV) Bond 3	E_T (eV) Bond 4	Final Total Energy $B2sp^3$ (eV)	$r_{initial}$ (a_0)	r_{final} (a_0)	$E_{Coulomb}(B2sp^3)$ (eV) Final	$E(B2sp^3)$ (eV) Final	θ' (°)	θ_1 (°)	θ_2 (°)	d_1 (a_0)	d_2 (a_0)
$C-B\ (R_2BB)$	*B*	-0.72457	-0.72457	-1.12740	0		1.14361	0.78184	-17.40230	-17.31130	111.25	68.75	47.58	1.20422	0.28340
$C-B\ (RBBH_{b2})$	*B*	-1.12740	-0.72457	-1.12740	-1.12740		1.14361	0.71865	-18.93252	-18.84152	106.79	73.21	44.19	1.28006	0.20756
$C-B\ (H_bB_bRBB)$	*B*	-0.72457	-1.12740	-1.12740	-1.69110		1.14361	0.69787	-19.49622	-19.40522	105.17	74.83	43.03	1.30499	0.18263
$C-B\ (H_bRBH_{b2})$	*B*	-0.72457	-1.69110	-1.12740	-1.12740		1.14361	0.69787	-19.49622	-19.40522	105.17	74.83	43.03	1.30499	0.18263
$C-B\ (H_bRBB_{b2})$	*B*	-0.72457	-1.12740	-1.69110	-1.69110		1.14361	0.67826	-20.05991	-19.96891	103.57	76.43	41.91	1.32853	0.15909
$C-H\ (BCH_3)$	*C*	-0.72457	0	0	0	-152.34026	0.91771	0.87495	-15.55033	-15.35946	78.85	101.15	42.40	1.21777	0.16921
$C-H\ (BCH_2-)$	*C*	-0.72457	-0.92918	0	0	-153.26945	0.91771	0.82562	-16.47951	-16.28865	69.93	110.07	36.76	1.33883	0.28330
$C-H\ (BCH-)$	*C*	-0.72457	-0.92918	-0.92918	0	-154.19863	0.91771	0.78155	-17.40869	-17.21783	62.67	117.33	32.30	1.41549	0.35888
$C-B\ (-B-CH_3)$	*C*	-0.72457	0	0	0	-152.34026	0.91771	0.87495	-15.55033	-15.35946	116.85	63.15	52.27	1.09248	0.39514
$C-B\ (-B-C_aH_2R)$	C_a	-0.72457	-0.92918	0	0	-153.26945	0.91771	0.82562	-16.47951	-16.28864	114.01	65.99	49.83	1.15168	0.33594
$C-H\ (CH_3)$	*C*	-0.92918	0	0	0	-152.54487	0.91771	0.86359	-15.75493	-15.56407	77.49	102.51	41.48	1.23564	0.18708
$C-H\ (CH_2)$	*C*	-0.92918	-0.92918	0	0	-153.47406	0.91771	0.81549	-16.68412	-16.49325	68.47	111.53	35.84	1.35486	0.29933
$C-H\ (CH)$	*C*	-0.92918	-0.92918	-0.92918	0	-154.40324	0.91771	0.77247	-17.61330	-17.42244	61.10	118.90	31.37	1.42988	0.37326
$H_3C_aC_bH_2CH_2-(C-C\ (a))$	C_a	-0.92918	0	0	0	-152.54487	0.91771	0.86359	-15.75493	-15.56407	63.82	116.18	30.08	1.83879	0.38106
$H_3C_aC_bH_2CH_2-(C-C\ (a))$	C_b	-0.92918	-0.92918	0	0	-153.47406	0.91771	0.81549	-16.68412	-16.49325	56.41	123.59	26.06	1.90890	0.45117
$R-H_2C_b(H_2C_c-R')HCH_2-$ $(C-C\ (b))$	C_b	-0.92918	-0.92918	-0.92918	0	-154.40324	0.91771	0.77247	-17.61330	-17.42244	48.30	131.70	21.90	1.97162	0.51388
$R-H_2C_a(R'-H_2C_d)C_b(R''-H_2C_c)CH_2-$ $(C-C\ (c))$	C_b	-0.92918	-0.72457	-0.72457	-0.72457	-154.71860	0.91771	0.75889	-17.92866	-17.73779	48.21	131.79	21.74	1.95734	0.50570
$isoC_aC_b(H_2C_c-R')HCH_2-$ $(C-C\ (d))$	C_b	-0.92918	-0.92918	-0.92918	0	-154.40324	0.91771	0.77247	-17.61330	-17.42244	48.30	131.70	21.90	1.97162	0.51388
$tertC_a(R'-H_2C_d)C_b(R''-H_2C_c)CH_2-$ $(C-C\ (e))$	C_b	-0.72457	-0.72457	-0.72457	-0.72457	-154.51399	0.91771	0.76765	-17.72417	-17.73779	50.04	129.96	22.66	1.94462	0.49298
$tertC_aC_b(H_2C_c-R')HCH_2-$ $(C-C\ (f))$	C_b	-0.72457	-0.92918	-0.92918	0-	-154.19863	0.91771	0.78155	-17.40869	-17.21783	52.78	127.22	24.04	1.92443	0.47279
$isoC_a(R'-H_2C_d)C_b(R''-H_2C_c)CH_2-$ $(C-C\ (f))$	C_b	-0.72457	-0.72457	-0.72457	-0.72457	-154.51399	0.91771	0.76765	-17.92866	-17.73779	50.04	129.96	22.66	1.94462	0.49298

Table 22.12. The energy parameters (*eV*) of functional groups of alkyl boranes.

Parameters	$C-B$ Group	$B-H$ Group	$B-H-B$ Group	$B-B$ Group	$B-B-B$ Group	$C\overset{3e}{=}C$ Group	CH (i) Group	CH_3 Group	CH_2 Group	$C-H$ (ii) Group	$C-C$ (a) Group	$C-C$ (b) Group	$C-C$ (c) Group	$C-C$ (d) Group	$C-C$ (e) Group	$C-C$ (f) Group
f_1	1	1	1	1	1	0.75	1	1	1	1	1	1	1	1	1	
n_1	1	1	1	1	1	2	1	3	2	1	1	1	1	1	1	1
n_2	0	0	0	0	0	0	0	2	1	0	0	0	0	0	0	0
n_3	0	0	0	0	0	0	0	0	0	0	0	0	0	0	0	0
C_1	0.5	0.75	0.75	0.5	0.5	0.5	0.75	0.75	0.75	0.75	0.5	0.5	0.5	0.5	0.5	0.5
C_2	0.80672	0.87442	0.87442	0.87442	0.87442	0.85252	1	1	1	1	1	1	1	1	1	1
c_1	1	1	1	1	1	1	1	1	1	1	1	1	1	1	1	1
c_2	0.80672	0.87442	0.87442	0.87442	0.87442	0.85252	0.91771	0.91771	0.91771	0.91771	0.91771	0.91771	0.91771	0.91771	0.91771	0.91771
c_3	0	0	0	0	0	0	1	0	1	1	0	0	0	1	1	0
c_4	2	1	1	2	2	3	1	1	1	1	2	2	2	2	2	2
c_5	0	1	1	0	0	0	1	3	2	1	0	0	0	0	0	0
C_{1o}	0.5	0.75	0.75	0.5	0.5	0.5	0.75	0.75	0.75	0.75	0.5	0.5	0.5	0.5	0.5	0.5
C_{2o}	0.80672	0.87442	0.87442	0.87442	0.87442	0.85252	1	1	1	1	1	1	1	1	1	1
V_e (eV)	-35.37850	-34.04561	-27.77951	-22.91867	-22.91867	-101.12679	-37.10024	-107.32728	-70.41425	-35.12015	-28.79214	-28.79214	-29.10112	-28.79214	-29.10112	-29.10112
V_p (eV)	9.14602	11.97638	11.01833	8.01527	8.01527	20.69825	13.17125	38.92728	25.78002	12.87680	9.33352	9.33352	9.37273	9.33352	9.37273	9.37273
T (eV)	9.90839	10.05589	6.94488	4.54805	4.54805	34.31559	11.58941	32.53914	21.06575	10.48582	6.77464	6.77464	6.90500	6.77464	6.90500	6.90500
V_m (eV)	-4.95420	-5.02794	-3.47244	-2.27402	-2.27402	-17.15779	-5.79470	-16.26957	-10.53337	-5.24291	-3.38732	-3.38732	-3.45250	-3.38732	-3.45250	-3.45250
$E(AO/HO)$ (eV)	-11.80624	-11.80624	-11.80624	-11.80624	-11.80624	0	-14.63489	-15.56407	-15.56407	-14.63489	-15.56407	-15.56407	-15.35946	-15.56407	-15.35946	-15.35946
$\Delta E_{H_2MO}(AO/HO)$ (eV)	-1.44915	0	0	0	0	0	-1.13379	0	0	0	0	0	0	0	0	0
$E_T(AO/HO)$ (eV)	-10.35710	-11.80624	-11.80624	-11.80624	-11.80624	0	-13.50110	-15.56407	-15.56407	-14.63489	-15.56407	-15.56407	-15.35946	-15.56407	-15.35946	-15.35946
$E_T(p_z MO)$ (eV)	-31.63538	-28.84754	-25.09498	-24.43561	-24.43561	-63.27075	-31.63539	-67.69451	-49.66493	-31.63533	-31.63537	-31.63537	-31.63535	-31.63537	-31.63535	-31.63535
$E_T\left(atom-atom, msp^3.AO\right)$ (eV)	-1.44915	-0.56370	-2.25479	-2.25479	-3.38219	-2.26759	-0.56690	0	0	0	-1.85836	-1.85836	-1.44915	-1.85836	-1.44915	-1.44915
$E_T(MO)$ (eV)	-33.08452	-29.41123	-29.60457	-26.69041	-27.81781	-65.53833	-32.20226	-67.69450	-49.66493	-31.63537	-33.49373	-33.49373	-33.08452	-33.49373	-33.08452	-33.08452
$\omega\ \left(10^{15}\ rad/s\right)$	26.7757	15.2006	23.9931	6.83486	6.83486	49.7272	26.4826	24.9286	24.2751	24.1759	9.43699	9.43699	15.4846	9.43699	9.55643	9.55643
E_K (eV)	17.62425	10.00529	15.79265	4.49882	4.49882	32.73133	17.43132	16.40846	15.97831	15.91299	6.21159	6.21159	10.19220	6.21159	6.29021	6.29021
$\overline{E}_D$ (eV)	-0.27478	-0.18405	-0.23275	-0.11200	-0.11673	-0.35806	-0.26130	-0.25352	-0.25017	-0.24966	-0.16515	-0.16515	-0.20896	-0.16515	-0.16416	-0.16416
$\overline{E}_{Kvib}$ (eV)	0.11841 [11]	0.29346 [5]	0.09844 [6]	0.13035 [5]	0.13035 [5]	0.19649 [12]	0.35532 Eq. (13.458)	0.35532 (Eq. (13.458))	0.35532 (Eq. (13.458))	0.35532 (Eq. (13.458))	0.12312 [13]	0.17978 [14]	0.09944 [15]	0.12312 [13]	0.12312 [13]	0.12312 [13]
$\overline{E}_{osc}$ (eV)	-0.21558	-0.03732	-0.18353	-0.04682	-0.05156	-0.25982	-0.08364	-0.22757	-0.14502	-0.07200	-0.10359	-0.07526	-0.15924	-0.10359	-0.10260	-0.10260
E_{mag} (eV)	0.14803	0.07650	0.07650	0.07650	0.07650	0.14803	0.14803	0.14803	0.14803	0.14803	0.14803	0.14803	0.14803	0.14803	0.14803	0.14803
$E_T(Group)$ (eV)	-33.30009	-29.44855	-29.78809	-26.73723	-27.86936	-49.54347	-32.28590	-67.92207	-49.80996	-31.70737	-33.59732	-33.49373	-33.24376	-33.59732	-33.18712	-33.18712
$E_{mitted}(c_1 AO/HO)$ (eV)	-14.63489	-11.80624	-11.80624	-11.80624	-11.80624	-14.63489	-14.63489	-14.63489	-14.63489	-14.63489	-14.63489	-14.63489	-14.63489	-14.63489	-14.63489	-14.63489
$E_{mitted}(c_5 AO/HO)$ (eV)	0	-13.59844	-13.59844	0	0	0	-13.59844	-13.59844	-13.59844	-13.59844	0	0	0	0	0	0
$E_D(Group)$ (eV)	4.03031	4.04387	4.38341	3.12475	4.25687	5.63881	3.90454	12.49186	7.83016	3.32601	4.32754	4.29921	3.97398	4.17951	3.62128	3.91734

Table 22.13. The total bond energies of alkyl boranes calculated using the functional group composition and the energies of Table 22.12 compared to the experimental values.

Formula	Name	C – B Group	B – H Group	B – H – B Group	B – B Group	B – B – B Group	^{1e} C=C Group	CH (i) Group	CH_3	CH_2	CH (ii)	C – C (a)	C – C (b)	C – C (c)	C – C (d)	C – C (e)	C – C (f)	Calculated Total Bond Energy (eV)	Experimental Total Bond Energy (eV)	Relative Error
CH_5B	methylborane	1	2	0	0	0	0	0	1	0	0	0	0	0	0	0	0	24.60991	24.49350 [16]	-0.00475
C_2H_7B	dimethylborane	2	1	0	0	0	0	0	2	0	0	0	0	0	0	0	0	37.08821	37.17713 [16]	0.00239
B_2CH_8	methyldiborane	1	3	2	0	0	0	0	1	0	0	0	0	0	0	0	0	37.42060	37.58259 [16]	0.00431
$B_2C_2H_{10}$	ethyldiborane	1	3	2	0	0	0	0	1	1	0	1	0	0	0	0	0	49.57830	49.50736 [16]	-0.00143
C_3H_9B	trimethylboron	3	0	0	0	0	0	0	3	0	0	0	0	0	0	0	0	49.56652	49.76102 [17]	0.00391
$B_2C_2H_{10}$	1,1-dimethyldiborane	2	2	2	0	0	0	0	2	0	0	0	0	0	0	0	0	49.89890	50.20118 [16]	0.00602
$B_2C_2H_{10}$	1,2-dimethyldiborane	2	2	2	0	0	0	0	2	0	0	0	0	0	0	0	0	49.89890	50.20118 [16]	0.00602
B_4CH_{12}	methyltetraborane	1	5	4	1	0	0	0	1	0	0	0	0	0	0	0	0	57.39990	57.74604 [16]	0.00599
B_5CH_{11}	methylpentaborane	1	4	4	2	1	0	0	1	0	0	0	0	0	0	0	0	60.73292	61.51585 [16]	0.01273
$B_2C_3H_{12}$	trimethyldiborane	3	1	2	0	0	0	0	3	0	0	0	0	0	0	0	0	62.37721	62.88481 [16]	0.00807
$B_4C_2H_{14}$	ethyltetraborane	1	5	4	1	0	0	0	1	1	0	1	0	0	0	0	0	69.55760	69.99603 [16]	0.00626
$B_5C_2H_{13}$	ethylpentaborane	1	4	4	2	1	0	0	1	1	0	1	0	0	0	0	0	72.89062	73.76585 [16]	0.01186
$B_2C_4H_{14}$	1,1-diethyldiborane	2	2	2	0	0	0	0	2	2	0	2	0	0	0	0	0	74.21430	74.34420 [16]	0.00175
$B_2C_4H_{14}$	tetramethyldiborane	4	0	2	0	0	0	0	4	0	0	0	0	0	0	0	0	74.85551	75.48171 [16]	0.00830
$B_5C_3H_{15}$	propylpentaborane	1	4	4	2	1	0	0	1	2	0	2	0	0	0	0	0	85.04832	85.84239 [16]	0.00925
$C_6H_{15}B$	triethylboron	3	0	0	0	0	0	0	3	3	0	3	0	0	0	0	0	86.03962	86.12941 [18]	0.00104
$B_2C_6H_{18}$	triethyldiborane	3	1	2	0	0	0	0	3	3	0	3	0	0	0	0	0	98.85031	98.59407 [16]	-0.00260
$B_{10}CH_{16}$	methyldecaborane	1	9	4	2	6	0	0	1	0	0	0	0	0	0	0	0	102.21298	101.91775 [16]	-0.00290
$C_8H_{17}B$	n-butylboracyclopentane	3	0	0	0	0	0	0	1	7	0	6	0	0	0	0	0	105.35916	105.69874[a] [18]	0.00321
$B_{10}C_2H_{18}$	ethyldecaborane	1	9	4	2	6	0	0	1	1	0	1	0	0	0	0	0	114.37068	113.56066 [16]	-0.00713
$C_9H_{21}B$	tripropylboron	3	0	0	0	0	0	0	3	6	0	6	0	0	0	0	0	122.51272	122.59753 [18]	0.00069
$C_9H_{21}B$	tri-isopropylboron	3	0	0	0	0	0	0	6	0	3	0	6	0	0	0	0	122.81539	122.75798 [18]	-0.00047
$B_2C_8H_{22}$	tetraethyldiborane	4	0	2	0	0	0	0	4	4	0	4	0	0	0	0	0	123.48631	123.74017 [16]	0.00205
$B_{10}C_3H_{20}$	propyldecaborane	1	9	4	2	6	0	0	1	2	0	2	0	0	0	0	0	126.52838	125.94075 [16]	-0.00467
$C_{12}H_{27}B$	tri-s-butylboron	3	0	0	0	0	0	0	6	3	3	3	6	0	0	0	0	159.28849	158.50627 [18]	-0.00493
$C_{12}H_{27}B$	tributylboron	3	0	0	0	0	0	0	3	9	0	9	0	0	0	0	0	158.98582	159.03530 [16]	0.00031
$C_{12}H_{27}B$	tri-isobutylboron	3	0	0	0	0	0	0	6	3	3	0	9	0	0	0	0	159.20350	159.34318 [16]	0.00088
$C_{18}H_{15}B$	triphenylboron	3	0	0	0	0	18	15	0	0	0	0	0	0	0	0	0	172.15755	172.09681 [18]	-0.00035
$C_{15}H_{33}B$	tri-3-methylbutylboron	3	0	0	0	0	0	0	6	6	3	3	9	0	0	0	0	195.67660	195.78095 [18]	0.00053
$C_{18}H_{33}B$	tricyclohexylboron	3	0	0	0	0	0	0	0	15	3	12	6	0	0	0	0	217.24711	218.23763 [18]	0.00454
$C_{18}H_{39}B$	tri-n-hexylboron	3	0	0	0	0	0	0	3	15	0	15	0	0	0	0	0	231.93202	231.76340 [18]	-0.00073
$C_{21}H_{45}B$	tri-n-heptylboron	3	0	0	0	0	0	0	3	18	0	18	0	0	0	0	0	268.40512	268.22285 [18]	-0.00068
$C_{24}H_{51}B$	tri-s-octylboron	3	0	0	0	0	0	0	6	15	3	15	6	0	0	0	0	305.18089	304.61292 [18]	-0.00186
$C_{24}H_{51}B$	tri-n-octylboron	3	0	0	0	0	0	0	3	21	0	21	0	0	0	0	0	304.87822	304.68230 [18]	-0.00064

[a] Crystal.

Table 22.14. The bond angle parameters of alkyl boranes and experimental values. H_t is a terminal or two-center *H*. H_b is a bridge or three-center *H*. In the calculation of θ_v, the parameters from the preceding angle were used. The experimental alkyl angle from Ref. [10]. E_T is E_T (*atom - atom msp³.AO*).

Atoms of Angle	2e' Bond 1 (a_1)	2e' Bond 2 (a_2)	2e' Terminal Atoms (a_3)	$E_{Coulombic}$ Atom 1	Atom 1 Hybridization Designation (Table)	$E_{Coulombic}$ Atom 2	Atom 2 Hybridization Designation (Table)	c_2 Atom 1	c_2 Atom 2	C_1	C_2	c_3	c_2'	E_T (eV)	θ_1 (°)	θ_2 (°)	θ_3 (°)	Cal. θ (°)	Exp. θ (°)
$\angle CBC$ $(CH_3)_3B$	2.97524	2.97524	5.1769	16.11722	1 (22.8)	16.11722	1 (22.8)	0.84418	0.84418	1	1	1	0.84418	-1.85836				120.92	120.0 [10] (trimethylborane)
Methyl $\angle HCH$	2.09711	2.09711	3.4252	-15.75493	7 (15.3A)	H	H	0.86359	1	1	1	0.75	1.15796	0				109.50	
$\angle BCH$															70.56			109.44	112.5 [10] (trimethylborane)
$\angle CBH_t$	2.97524	2.27211	4.5607	-15.55033	5 (15.3A)	H	H	0.87495	1	0.75	1	0.75	1.14292	0				120.12	
$\angle CBH_b$	2.97524	2.46967	4.6904	-15.55033	5 (15.3A)	H	H	0.87495	1	0.75	1	0.75	1.14292	0				118.66	
$\angle BBC$																120.12	118.66	121.22	122.6 [10] (1,2-dimethyldiborane)
$\angle H_tBH_t$	2.27211	2.27211	3.9623	-13.61667	2 (22.1)	H	H	0.99920	1	1	1	0.75	1.00080	-1.71543				121.37	122 [10] (diborane)
$\angle H_tBH_b$	2.27211	2.46967	3.8210	-14.71574	4 (22.1)	H	H	0.92458	1	1	1	0.75	1.08158	-1.12740				107.30	108.9 [2] (B_2H_6)
$\angle H_bBH_b$	2.46967	2.46967	3.6606	-14.26508	3 (22.1)	H	H	0.95378	1	1	1	0.75	1.04846	-1.12740				95.65	95.0 [2] (B_2H_6)
$\angle BH_bB$	2.46967	2.46967	3.4358	-11.89724 B_t	1 (22.1)	-11.89724 B_t	1 (22.1)	1	1	1	0.74361	1	1	0				88.15	87.7 [2] (B_2H_6)
$\angle CCC$ (aromatic)	2.62936	2.62936	4.5585	-17.17218	38 (15.3A)	-17.17218	38 (15.3A)	0.79232	0.79232	1	1	1	0.79232	-1.85836				120.19	120 [19-21] (benzene)
$\angle CCH$ (aromatic)																120.19		119.91	120 [19-21] (benzene)
Methylene $\angle HC_aH$	2.11106	2.11106	3.4252	-15.75493	7 (15.3A)	H	H	0.86359	1	1	1	0.75	1.15796	0				108.44	107 (dimethylamine) 107 (propane)
$\angle C_aC_bC_c$															69.51			110.49	112 (propane) 113.8 (butane) 110.8 (isobutane)
$\angle C_aC_aH$															69.51			110.49	111.0 (butane) 111.4 (isobutane)
Methyl $\angle HC_aH$	2.09711	2.09711	3.4252	-15.75493	7 (15.3A)	H	H	0.86359	1	1	1	0.75	1.15796	0				109.50	
$\angle C_bC_cC_c$															70.56			109.44	
$\angle C_aC_aH$															70.56			109.44	
$\angle C_bC_cC_c$ iso C_a	2.91547	2.91547	4.7958	-16.68412 C_c	26 (15.3A)	-16.68412 C_c	26 (15.3A)	0.81549	0.81549	1	1	1	0.81549	-1.85836				110.67	110.8 (isobutane)
$\angle C_bC_aH$ iso C_a	2.91547	2.11323	4.1633	-15.55033 C_a	5 (15.3A)	-14.82575 C_b	1 (15.3A)	0.87495	0.91771	0.75	1	0.75	1.04887	0				110.76	
$\angle C_aC_aH$ iso C_a	2.91547	2.09711	4.1633	-15.55033 C_a	5 (15.3A)	-14.82575 C_a	1 (15.3A)	0.87495	0.91771	0.75	1	0.75	1.04887	0				111.27	111.4 (isobutane)
$\angle C_aC_aC_b$ tert C_a	2.90327	2.90327	4.7958	-16.68412 C_b	26 (15.3A)	-16.68412 C_b	26 (15.3A)	0.81549	0.81549	1	1	1	0.81549	-1.85836				111.37	110.8 (isobutane)
$\angle C_bC_cC_a$															72.50			107.50	

ALKOXY BORANES ($(RO)_x B_y H_z; R = alkyl$) AND ALKYL BORINIC ACIDS ($(RO)_q B_r H_s (HO)_t$)

The alkoxy boranes and borinic acids each comprise a $B-O$ functional group, at least one boron-alkyl-ether moiety or one or more hydroxyl groups, respectively, and in some cases one or more alkyl groups and borane moieties. Each alkoxy moiety, $C_n H_{2n+1} O$, of alkoxy boranes comprises one of two types of $C-O$ functional groups that are equivalent to those given in the Ethers ($C_n H_{2n+2} O_m$, $n = 2,3,4,5...\infty$) section. One is for methyl or t-butyl groups, and the other is for general alkyl groups. Each hydroxyl functional group of borinic acids and alkyl borinic acids is equivalent to that given in the Alcohols ($C_n H_{2n+2} O_m$, $n = 1,2,3,4,5...\infty$) section. The alkyl portion may be part of the alkoxy moiety, or an alkyl group may be bound to the central boron atom by a carbon-boron single bond comprising the $C-B$ group of the Alkyl Boranes ($R_x B_y H_z; R = alkyl$) section. Each alkyl portion may comprise at least a terminal methyl group (CH_3) and methylene (CH_2), methylyne (CH), and $C-C$ functional groups. The methyl and methylene functional groups are equivalent to those of straight-chain alkanes. Six types of $C-C$ bonds can be identified. The n-alkane $C-C$ bond is the same as that of straight-chain alkanes. In addition, the $C-C$ bonds within isopropyl ($(CH_3)_2 CH$) and t-butyl ($(CH_3)_3 C$) groups and the isopropyl to isopropyl, isopropyl to t-butyl, and t-butyl to t-butyl $C-C$ bonds comprise functional groups. Additional R groups include aromatics such as phenyl. These groups in alkoxy boranes and alkyl borinic acids are equivalent to those in branched-chain alkanes and aromatics given in the corresponding sections. Furthermore, $B-H$, $B-B$, $B-H-B$, and $B-B-B$ groups may be present that are equivalent to those in boranes as given in the Boranes ($B_x H_y$) section.

The MO semimajor axes of the $B-O$ functional groups of alkoxy alkanes and borinic acids are determined from the force balance equation of the centrifugal, Coulombic, and magnetic forces as given in the Boranes ($B_x H_y$) section. In each case, the distance from the origin of the H_2-type-ellipsoidal-MO to each focus c', the internuclear distance $2c'$, and the length of the semiminor axis of the prolate spheroidal H_2-type MO $b = c$ are solved from the semimajor axis a. Then, the geometric and energy parameters of each MO are calculated using Eqs. (15.1-15.117).

The parameters of the force balance equation for the σ-MO of the $B-O$-bond MO in Eqs. (22.18-22.22) are $n_e = 2$ and $|L| = 0$:

$$\frac{\hbar^2}{m_e a^2 b^2} D = \frac{e^2}{8\pi\varepsilon_0 a b^2} D + \frac{\hbar^2}{2 m_e a^2 b^2} D - \frac{\hbar^2}{2 m_e a^2 b^2} D \tag{22.41}$$

From Eq. (22.41), the semimajor axis of the $B-O$-bond MO is:

$$a = 2a_0 \tag{22.42}$$

For the $B-O$ functional groups, hybridization of the $2s$ and $2p$ AOs of each C and B to form single $2sp^3$ shells forms an energy minimum, and the sharing of electrons between the $C2sp^3$ and $B2sp^3$ HOs to form a MO permits each participating orbital to decrease in radius and energy. The energy of boron is less than the Coulombic energy between the electron and proton of H given by Eq. (1.264). Thus, in c_1 and c_2 in Eq. (15.61) is one, and the energy matching condition is determined by the C_2 parameter. The approach to the hybridization factor of O to B in boric acids is similar to that of the O to S bonding in the SO group of sulfoxides. The O AO has an energy of $E(O) = -13.61805\ eV$, and the $B2sp^3$ HOs has an energy of $E(B, 2sp^3) = -11.80624\ eV$ (Eq. (22.7)). To meet the equipotential condition of the union of the $B-O$ H_2-type-ellipsoidal-MO with these orbitals in borinic acids and to energy match the OH group, the hybridization factor C_2 of Eq. (15.61) for the $B-O$-bond MO given by Eq. (15.77) is:

$$C_2(OAO\ to\ B2sp^3 HO) = \frac{E(OAO)}{E(B, 2sp^3)} = \frac{-13.61805\ eV}{-11.80624\ eV} = 1.15346 \tag{22.43}$$

Since the energy of the MO is matched to that of the $B2sp^3$ HO, $E(AO/HO)$ in Eqs. (15.51) and (15.61) is $E(B, 2sp^3)$ given by Eq. (22.7), and $E_T(atom-atom, msp^3.AO)$ is $-1.12740\ eV$ corresponding to the independent single-bond charge contribution (Eq. (22.12)) of one center.

The parameters of the $B-O$ functional group of alkoxy boranes are the same as those of borinic acids except for C_1 and C_2. Rather than being bound to an H, the oxygen is bound to a $C2sp^3$ HO, and consequently, the hybridization of the $C-O$ given by Eq. (15.133) includes the $C2sp^3$ HO hybridization factor of 0.91771 (Eq. (13.430)). To meet the equipotential condition of the union of the $B-O$ H_2-type-ellipsoidal-MO with the $B2sp^3$ HOs having an energy of $E(B, 2sp^3) = -11.80624\ eV$ (Eq. (22.7)) and the O AO having an energy of $E(O) = -13.61805\ eV$ such that the hybridization

matches that of the $C-O$-bond MO, the hybridization factor C_2 of Eq. (15.61) for the $B-O$-bond MO given by Eqs. (15.77) and (15.79) is:

$$C_2\left(B2sp^3HO\ to\ O\right)=\frac{E\left(B,2sp^3\right)}{E\left(O\right)}c_2\left(C2sp^3HO\right)=\frac{-11.80624\ eV}{-13.61805\ eV}\left(0.91771\right)=0.79562 \tag{22.44}$$

Furthermore, in order to form an energy minimum in the $B-O$-bond MO, oxygen acts as an H in bonding with B since the $2p$ shell of O is at the Coulomb energy between an electron and a proton (Eq. (10.163)). In this case, k' is 0.75 as given by Eq. (13.59) such that $C_1=0.75$ in Eq. (15.61).

Consider next the radius of the HO due to the contribution of charge to more than one bond. The energy contribution due to the charge donation at each boron atom and oxygen atom superimposes linearly. In general, since the energy of the $B2sp^3$ HO and O AO is matched to that of the $C2sp^3$ HO when the molecule contains a $C-B$-bond MO and a $C-O$-bond MO, respectively, the corresponding radius $r_{mol\,2sp^3}$ of the $B2sp^3$ HO of a boron atom, the $C2sp^3$ HO of a carbon atom, and the O AO of a given alkoxy borane or borinic acid molecule is calculated after Eq. (15.32) by considering $\sum E_{T_{mol}}\left(MO,2sp^3\right)$, the total energy donation to all bonds with which it participates in bonding. The Coulombic energy $E_{Coulomb}\left(atom,2sp^3\right)$ of the outer electron of the $atom$ $2sp^3$ shell considering the charge donation to all participating bonds is given by Eq. (15.14). In the case that the boron or oxygen atom is not bound to a $C2sp^3$ HO, $r_{mol\,2sp^3}$ is calculated using Eq. (15.31) where $E_{Coulomb}\left(atom,msp^3\right)$ is $E_{Coulomb}\left(B2sp^3\right)=-11.89724\ eV$ and $E\left(O\right)=-13.61805\ eV$, respectively.

The symbols of the functional groups of alkoxy boranes and borinic acids are given in Table 22.15. The geometrical (Eqs. (15.1-15.5) and (22.42-22.44)), intercept (Eqs. (15.31-15.32) and (15.80-15.87)), and energy (Eq. (15.61), (22.4), (22.7), (22.12), (22.29), and (22.43-22.44)) parameters of alkoxy boranes and borinic acids are given in Tables 22.16, 22.17, and 22.18, respectively. In the case that the MO does not intercept the B HO due to the reduction of the radius from the donation of B $2sp^3$ HO charge to additional MO's, the energy of each MO is energy matched as a linear sum to the B HO by contacting it through the bisector current of the intersecting MOs as described in the Methane Molecule (CH_4) section. The total energy of each alkyl borane given in Table 22.19 was calculated as the sum over the integer multiple of each $E_{D\,(Group)}$ of Table 22.18 corresponding to functional-group composition of the molecule. E_{mag} of Table 22.18 is given by Eqs. (15.15) and (22.3) for the $B-O$ groups and the $B-H$, $B-B$, $B-H-B$, and $B-B-B$ groups. E_{mag} of Table 22.18 is given by Eqs. (15.15) and (10.162) for the OH group. The bond angle parameters of alkoxy boranes and borinic acids determined using Eqs. (15.88-15.117) are given in Table 22.20. The charge-densities of exemplary alkoxy borane, trimethoxyborane, boric acid, and phenylborinic anhydride comprising the concentric shells of atoms with the outer shell bridged by one or more H_2-type ellipsoidal MOs or joined with one or more hydrogen MOs are shown in Figures 22.4, 22.5, and 22.6, respectively.

Figure 22.4. *Trimethoxyborane.* Color scale, translucent views of the charge-density of $\left(H_3CO\right)_3B$ showing the orbitals of the B, O, and C atoms at their radii, the ellipsoidal surface of each H or H_2-type ellipsoidal MO that transitions to the corresponding outer shell of the atoms participating in each bond, and the hydrogen nuclei (red, not to scale).

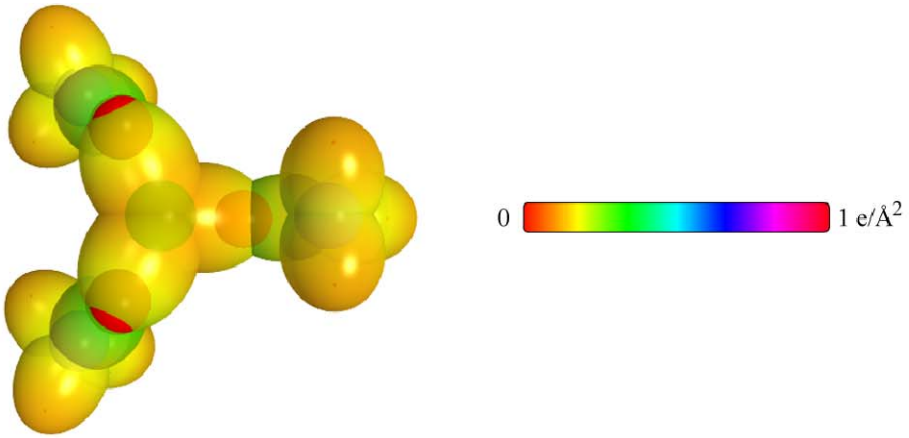

Figure 22.5. *Boric Acid.* Color scale, translucent view of the charge-density of $(HO)_3 B$ showing the orbitals of the B and O atoms at their radii, the ellipsoidal surface of each H or H_2-type ellipsoidal MO that transitions to the corresponding outer shell of the atoms participating in each bond, and the hydrogen nuclei (red, not to scale).

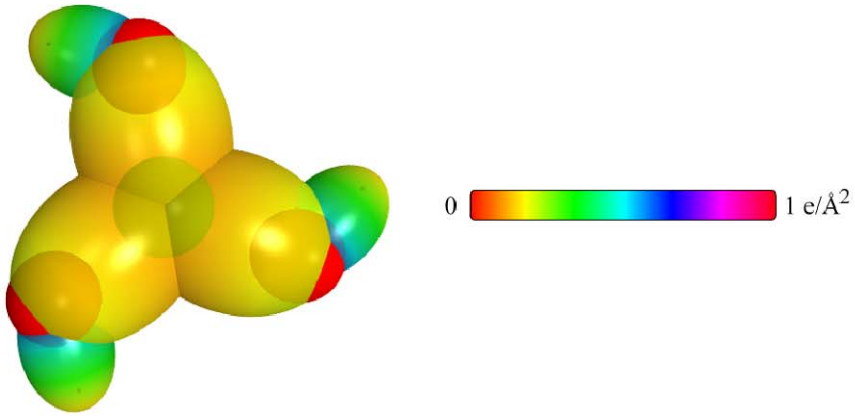

Figure 22.6. *Phenylborinic Anhydride.* Color scale, translucent view of the charge-density of phenylborinic anhydride showing the orbitals of the B and O atoms at their radii, the ellipsoidal surface of each H or H_2-type ellipsoidal MO that transitions to the corresponding outer shell of the atoms participating in each bond, and the hydrogen nuclei (red, not to scale).

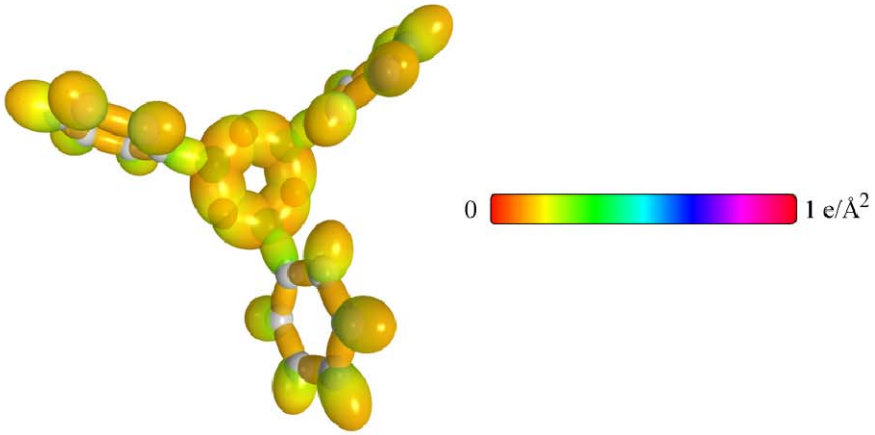

Table 22.15. The symbols of the functional groups of alkoxy boranes and borinic acids.

Functional Group	Group Symbol
B-O bond (borinic acid)	$B-O$ (i)
B-O bond (alkoxy borane)	$B-O$ (ii)
OH group	OH
C-O (CH_3-O- and $(CH_3)_3 C-O-$)	$C-O$ (i)
C-O (alkyl)	$C-O$ (ii)
C-B bond	$C-B$
BH bond	$B-H$
BHB (bridged *H*)	$B-H-B$
BB bond	$B-B$
BBB (bridged *B*)	$B-B-B$
CC (aromatic bond)	$C \overset{3e}{=} C$
CH (aromatic)	CH (i)
CH_3 group	$C-H\ (CH_3)$
CH_2 group	$C-H\ (CH_2)$
CH	$C-H$ (ii)
CC bond (*n-C*)	$C-C$ (a)
CC bond (*iso-C*)	$C-C$ (b)

Table 22.16. The geometrical bond parameters of alkoxy boranes and borinic acids and experimental values. The experimental alkyl distances from Ref. [10].

Parameter	$B-O$ (i) Group	$B-O$ (ii) Group	OH Group	$C-O$ (i) Group	$C-O$ (ii) Group	$C-B$ Group	$B-H$ Group	$B-H-B$ Group	$B-B$ and $B-B-B$ Groups	$C \overset{3e}{=} C$ Group	CH (i) Group	$C-H\ (CH_3)$ Group	$C-H\ (CH_2)$ Group	$C-H$ (ii) Group	$C-C$ (a) Group	$C-C$ (b) Group
$a\ (a_0)$	2.00000	2.00000	1.26430	1.80717	1.79473	1.78528	1.69282	2.00000	2.51962	1.47348	1.60061	1.64920	1.67122	1.67465	2.12499	2.12499
$c'\ (a_0)$	1.31678	1.29455	0.91808	1.34431	1.33968	1.48762	1.13605	1.23483	1.69749	1.31468	1.03299	1.04856	1.05553	1.05661	1.45744	1.45744
Bond Length $2c'\ (\AA)$	1.39362	1.37009	0.971651	1.42276	1.41785	1.57443	1.20235	1.30689	1.79654	1.39140	1.09327	1.10974	1.11713	1.11827	1.54280	1.54280
Exp. Bond Length $(\AA)$	1.376 [17] ($B(OH)_3$)	1.367 [17] ($B(OCH_3)_3$)	0.971 [10] (ethanol) 0.9451 [10] (methanol)	1.424 [17] ($B(OCH_3)_3$) 1.416 [10] (dimethyl ether)	1.418 [10] (ethyl methyl ether (avg.))	1.578 [10] (trimethylborane) 1.580 [10] (1,2-dimethyldiborane)	1.19 [4] (diborane)	1.32 [4] (diborane)	1.798 [3] ($B_{13}H_{19}$)	1.39 [10] (benzene)	1.101 [10] (benzene)	1.114 ($C-H$ trimethylborane) 1.107 ($C-H$ propane) 1.117 ($C-H$ butane)	1.107 ($C-H$ propane) 1.117 ($C-H$ butane)	1.122 (isobutane)	1.532 (propane) 1.531 (butane)	1.532 (propane) 1.531 (butane)
$b,c\ (a_0)$	1.50535	1.52452	0.86925	1.20776	1.19429	0.98702	1.25500	1.57327	1.86199	0.66540	1.22265	1.27295	1.29569	1.29924	1.54616	1.54616
e	0.65839	0.64727	0.72615	0.74388	0.74645	0.83327	0.67110	0.61742	0.67371	0.89223	0.64537	0.63580	0.63159	0.63095	0.68600	0.68600

Table 22.17. The MO to HO intercept geometrical bond parameters of alkoxy boranes and borinic acids. H_t is a terminal or two-center *H*. H_b is a bridge or three-center *H*. B_b is a bridge or three-center *B*. E_T is E_T (*atom - atom msp³.AO*).

Bond	Atom	E_1 (eV) Bond 1	E_2 (eV) Bond 2	E_3 (eV) Bond 3	E_4 (eV) Bond 4	Final Total Energy $B2sp^3$ (eV)	r_{Atom1} (a_0)	r_{Atom2} (a_0)	$E_{Conjugate}(B2sp^3)$ (eV) Final	$E(B2sp^3)$ (eV) Final	θ^1 (°)	θ_2 (°)	θ_3 (°)	d_1 (a_0)	d_2 (a_0)
$B-H_t$ $(H_{1/2}BOH)$ $(H_1B(OH)_2)$	*B*	-0.56370	-0.56370	-0.56370	0	-76.58278	1.14361	1.00129	-13.58834	-13.49734	96.05	83.95	52.50	1.03045	0.10561
$B-H_t$ $(H_{1/2}BOR)$ $(H_1B(OR)_2)$	*B*	-0.56370	-0.56370	-0.56370	0	-76.58278	1.14361	1.00129	-13.58834	-13.49734	96.05	83.95	52.50	1.03045	0.10561
$B-H_t$ (H_1CBOH) (H_1CBOR)	*B*	-0.56370	-0.72457	-0.56370	0		1.14361	0.81581	-16.67772	-16.58672	77.92	102.08	39.47	1.30683	0.17077
$C-B$ $(H_1(-O)B-C)$	*B*	-0.72457	-0.56370	-0.56370	0		1.14361	0.81581	-16.67772	-16.58672	113.41	66.59	49.33	1.16346	0.32416
$C-B$ $(C(-O)B-C)$	*B*	-0.72457	-0.72457	-0.56370	0		1.14361	0.80801	-16.83860	-16.74760	112.93	67.07	48.93	1.17281	0.31481
$C-B$ $((-O)_2B-C)$	*B*	-0.72457	-0.56370	-0.56370	0		1.14361	0.81581	-16.67772	-16.58672	113.41	66.59	49.33	1.16346	0.32416
$C-H$ (BCH_3)	*C*	-0.72457	0	0	0	-152.34026	0.91771	0.87495	-15.55033	-15.35946	78.85	101.15	42.40	1.21777	0.16921
$C-H$ (BCH_2-)	*C*	-0.72457	-0.92918	0	0	-153.26945	0.91771	0.82562	-16.47951	-16.28865	69.93	110.07	36.76	1.33883	0.28330
$C-H$ $(BCH-)$	*C*	-0.72457	-0.92918	-0.92918	0	-154.19863	0.91771	0.78155	-17.40869	-17.21783	62.67	117.33	32.30	1.41549	0.35888
$C-B$ $(-B-CH_3)$	*C*	-0.72457	0	0	0	-152.34026	0.91771	0.87495	-15.55033	-15.35946	116.85	63.15	52.27	1.09248	0.39514
$C-B$ $(B\ C_nH_2R)$	C_n	-0.72457	-0.92918	0	0	-153.26945	0.91771	0.82562	-16.47951	-16.28864	114.01	65.99	49.83	1.15168	0.33594
$BO-H$	*O*	-0.56370	0	0	0		1.00030	0.95939	-14.18175		121.28	58.72	70.60	0.41990	0.49818
$-BOH$ $(B-O\ (i))$	*O*	-0.56370	0	0	0		1.00030	0.95939	-14.18175		74.04	105.96	37.79	1.58054	0.26276
$H_{1/2}BOH$ $(B-O\ (i))$	*B*	-0.53670	-0.53670	-0.53670	0	-76.58278	1.14361	1.00129	-13.58834	-13.49734	78.47	101.53	40.67	1.51690	0.20012
$H_1B(OH)_2$ $(B-O\ (i))$	*B*	-0.53670	-0.53670	-0.53670	0	-76.58278	1.14361	1.00129	-13.58834	-13.49734	78.47	101.53	40.67	1.51690	0.20012
$B(OH)_3$ $(B-O\ (i))$	*B*	-0.53670	-0.53670	-0.53670	0	-76.58278	1.14361	1.00129	-13.58834	-13.49734	78.47	101.53	40.67	1.51690	0.20012
H_1RBOH $(B-O\ (i))$	*B*	-0.56370	-0.56370	-0.72457	0		1.14361	0.81581	-16.67772	-16.58672	53.80	126.20	25.93	1.79862	0.48184
R_2BOH $(B-O\ (i))$	*B*	-0.56370	-0.72457	-0.72457	0		1.14361	0.80801	-16.83860	-16.74760	52.34	127.66	25.15	1.81046	0.49368
$RB(OH)_2$ $(B-O\ (i))$	*B*	-0.56370	-0.56370	-0.72457	0		1.14361	0.81581	-16.67772	-16.58672	53.80	126.20	25.93	1.79862	0.48184

Table 22.17 cont' d. The MO to HO intercept geometrical bond parameters of alkoxy boranes and borinic acids. H_t is a terminal or two-center H. H_b is a bridge or three-center H. B_b is a bridge or three-center B. E_T is E_T (*atom - atom* msp^3*.AO*).

Bond	Atom	E_1 (eV) Bond 1	E_2 (eV) Bond 2	E_3 (eV) Bond 3	E_4 (eV) Bond 4	Final Total Energy $B2sp^3$ (eV)	r_{bond} (a_0)	r_{final} (a_0)	$E_{Coulomb}(B2sp^3)$ (eV) Final	$E(B2sp^3)$ (eV) Final	θ' (°)	θ (°)	θ_2 (°)	d_x (a_0)	d_z (a_0)
$H_{t2}BOR$ ($B-O$ (ii))	B	-0.56370	-0.56370	-0.56370	0	-76.58278	1.14361	1.00129	-13.58834	-13.49734	75.64	104.36	39.51	1.54296	0.24841
$H_tB(OR)_2$ ($B-O$ (ii))	B	-0.56370	-0.56370	-0.56370	0	-76.58278	1.14361	1.00129	-13.58834	-13.49734	75.64	104.36	39.51	1.54296	0.24841
$B(OR)_3$ ($B-O$ (ii))	B	-0.56370	-0.56370	-0.56370	0	-76.58278	1.14361	1.00129	-13.58834	-13.49734	75.64	104.36	39.51	1.54296	0.24841
H_tBBOR ($B-O$ (ii))	B	-0.56370	-0.56370	-0.72457	0		1.14361	0.81581	-16.67772	-16.58672	49.02	130.98	23.83	1.82951	0.53497
R_2BOR ($B-O$ (ii))	B	-0.56370	-0.72457	-0.72457	0		1.14361	0.80801	-16.83860	-16.74760	47.39	132.61	22.96	1.84155	0.54701
$RB(OR)_2$ ($B-O$ (ii))	B	-0.56370	-0.56370	-0.72457	0		1.14361	0.81581	-16.67772	-16.58672	49.02	130.98	23.83	1.82951	0.53497
$-B-OCH_3$ ($B-O$ (ii); $C-O$ (i))	O	-0.56370	-0.72457	0	0		1.00000	0.84435	-16.11402		54.45	125.55	26.78	1.78542	0.49088
$-B-OCH_2-$ ($B-O$ (ii); $C-O$ (ii))	O	-0.56370	-0.82688	0	0		1.00000	0.83902	-16.21633		53.50	126.50	26.26	1.79365	0.49911
$C-H$ (OC_eH_3)	C_e	-0.72457	0	0	0	-152.34026	0.91771	0.87495	-15.55033	-15.35946	78.85	101.15	42.40	1.21777	0.16921
$BO-C_eH_3$ $BO-C_e(CH_3)_2$ ($C-O$ (i))	C_e	-0.72457	0	0	0	-152.34026	0.91771	0.87495	-15.55033	-15.35946	95.98	84.02	46.10	1.25319	0.09112
$BO-C_eH_3$ $BO-C_e(CH_3)_2$ ($C-O$ (i))	O	-0.72457	-0.56370	0	0		1.00000	0.84435	-16.11402		93.39	86.61	44.26	1.29433	0.04998
$-H_2C_e-OB$ ($C-O$ (iii))	C_e	-0.82688	-0.92918	0	0	-153.37175	0.91771	0.82053	-16.58181	-16.39095	92.41	87.59	43.35	1.30512	0.03456
$-H_2C_e-OB$ ($C-O$ (iii))	O	-0.82688	-0.56370	0	0		1.00000	0.83902	-16.21633		94.06	85.94	44.49	1.28034	0.05933
$C-H$ (CH_3)	C	-0.92918	0	0	0	-152.54487	0.91771	0.86359	-15.75493	-15.56407	77.49	102.51	41.48	1.23564	0.18708
$C-H$ (CH_2)	C	-0.92918	-0.92918	0	0	-153.47406	0.91771	0.81549	-16.68412	-16.49325	68.47	111.53	35.84	1.35486	0.29953
$C-H$ (CH)	C	-0.92918	-0.92918	-0.92918	0	-154.40324	0.91771	0.77247	-17.61330	-17.42244	61.10	118.90	31.37	1.42988	0.37326
$H_3C_eC_3H_2CH_2$ ($C-C$ (a))	C_e	-0.92918	0	0	0	-152.54487	0.91771	0.86359	-15.75493	-15.56407	63.82	116.18	30.08	1.83879	0.38106
$H_3C_eC_3H_2CH_2$ ($C-C$ (a))	C_e	-0.92918	-0.92918	0	0	-153.47406	0.91771	0.81549	-16.68412	-16.49325	56.41	123.59	26.06	1.90890	0.45117
$R-H_2C_eC_2(H_2C_2-R')HCH_2-$ ($C-C$ (b))	C_e	-0.92918	-0.92918	-0.92918	0	-154.40324	0.91771	0.77247	-17.61330	-17.42244	48.30	131.70	21.90	1.97162	0.51388

Table 22.18. The energy parameters (eV) of functional groups of alkoxy boranes and borinic acids.

Parameters	$B-O$ (i) Group	$B-O$ (ii) Group	OH Group	$C-O$ (i) Group	$C-O$ (ii) Group	$C-B$ Group	$B-H$ Group	$B-H-B$ Group	$B-B$ Group	$B-B-B$ Group	$C\overset{3a}{=}C$ Group	CH (i) Group	CH_3 Group	CH_2 Group	$C-H$ (ii) Group	$C-C$ (a) Group	$C-C$ (b) Group
f_1	1	1	1	1	1	1	1	1	1	1	0.75	1	1	1	1	1	1
n_1	1	1	1	1	1	1	1	1	1	1	2	1	3	2	1	1	1
n_2	0	0	0	0	0	0	0	0	0	0	0	0	2	1	0	0	0
n_3	0	0	0	0	0	0	0	0	0	0	0	0	0	0	0	0	0
C_1	0.5	0.75	0.75	0.5	0.5	0.5	0.75	0.75	0.5	0.5	0.5	0.75	0.75	0.75	0.75	0.5	0.5
C_2	1.15346	0.79562	1	1	1	0.80672	0.87442	0.87442	0.87442	0.87442	0.85252	1	1	1	1	1	1
c_1	1	1	0.75	1	1	1	1	1	1	1	1	1	1	1	1	1	1
c_2	1	1	1	0.85395	0.85395	0.80672	0.87442	0.87442	0.87442	0.87442	0.85252	0.91771	0.91771	0.91771	0.91771	0.91771	0.91771
c_3	0	0	1	0	0	0	0	0	0	0	0	1	0	1	1	0	0
c_4	1	1	1	2	2	2	1	1	2	2	3	1	1	1	1	2	2
c_5	1	1	1	0	0	0	1	1	0	0	0	1	3	2	1	0	0
C_{1o}	0.5	0.75	0.75	0.5	0.5	0.5	0.75	0.75	0.5	0.5	0.5	0.75	0.75	0.75	0.75	0.5	0.5
C_{2o}	1.15346	0.79562	1	1	1	0.80672	0.87442	0.87442	0.87442	0.87442	0.85252	1	1	1	1	1	1
V_e (eV)	-32.64974	-32.39594	-40.92709	-33.15757	-33.47304	-35.37850	-34.04561	-27.77951	-22.91867	-22.91867	-101.12679	-37.10024	-107.32728	-70.41425	-35.12015	-28.79214	-28.79214
V_p (eV)	10.33263	10.51010	14.81988	10.12103	10.15605	9.14602	11.97638	11.01833	8.01527	8.01527	20.69825	13.17125	38.92728	25.78002	12.87680	9.33352	9.33352
T (eV)	8.16244	8.09899	16.18567	9.17389	9.32537	9.90839	10.05589	6.94488	4.54805	4.54805	34.31559	11.58941	32.53914	21.06675	10.48582	6.77464	6.77464
V_m (eV)	-4.08122	-4.04949	-8.09284	-4.58695	-4.66268	-4.95420	-5.02794	-3.47244	-2.27402	-2.27402	-17.15779	-5.79470	-16.26957	-10.53337	-5.24291	-3.38732	-3.38732
$E_{(AO/HO)}$ (eV)	-11.80624	-11.80624	-13.6181	-14.63489	-14.63489	-11.80624	-11.80624	-11.80624	-11.80624	-11.80624	0	-14.63489	-15.56407	-15.56407	-14.63489	-15.56407	-15.56407
$\Delta E_{H_2MO(AO/HO)}$ (eV)	0	0	0	-1.44915	-1.65376	-1.44915	0	0	0	0	0	-1.13379	0	0	0	0	0
E_T (AO/HO) (eV)	-11.80624	-11.80624	-13.6181	-13.18574	-12.98113	-10.35710	-11.80624	-11.80624	-11.80624	-11.80624	0	-13.50110	-15.56407	-15.56407	-14.63489	-15.56407	-15.56407
E_T (H_2MO) (eV)	-30.04213	-29.64258	-31.63247	-31.63533	-31.63544	-31.63538	-28.84754	-25.09498	-24.43561	-24.43561	-63.27075	-31.63539	-67.69451	-49.66493	-31.63533	-31.63537	-31.63537
$E_T\left(atom-atom, msp^3.AO\right)$ (eV)	-1.12740	-1.12740	0	-1.44915	-1.65376	-1.44915	-0.56370	-2.25479	-2.25479	-3.38219	-2.26759	-0.56690	0	0	0	-1.85836	-1.85836
E_T (MO) (eV)	-31.16953	-30.76998	-31.63537	-33.08452	-33.28912	-33.08452	-29.41123	-29.60457	-26.69041	-27.81781	-65.53833	-32.20226	-67.69450	-49.66493	-31.63537	-33.49373	-33.49373
$\omega\left(10^{15}\ rad/s\right)$	11.1001	16.9656	44.1776	12.0329	12.1583	26.7757	15.2006	23.9931	6.83486	6.83486	49.7272	26.4826	24.9286	24.2751	24.1759	9.43699	9.43699
E_K (eV)	7.30627	11.16705	29.07844	7.92028	8.00277	17.62425	10.00529	15.79265	4.49882	4.49882	32.73133	17.43132	16.40846	15.97831	15.91299	6.21159	6.21159
$\overline{E}_D$ (eV)	-0.16668	-0.20342	-0.33749	-0.18420	-0.18631	-0.27478	-0.18405	-0.23275	-0.11200	-0.11673	-0.35806	-0.26130	-0.25352	-0.25017	-0.24966	-0.16515	-0.16515
$\overline{E}_{Kvib}$ (eV)	0.23380 [5]	0.23380 [5]	0.46311 [22-23]	0.13663 [24]	0.16118 [14]	0.11841 [11]	0.29346 [5]	0.09844 [6]	0.13035 [5]	0.13035 [5]	0.19649 [12]	0.35532 Eq. (13.458)	0.35532 (Eq. (13.458))	0.35532 (Eq. (13.458))	0.35532 (Eq. (13.458))	0.12312 [13]	0.17978 [14]
$\overline{E}_{osc}$ (eV)	-0.04978	-0.08652	-0.10594	-0.11589	-0.10572	-0.21558	-0.03732	-0.18353	-0.04682	-0.05156	-0.25982	-0.08364	-0.22757	-0.14502	-0.07200	-0.10359	-0.07526
E_{mag} (eV)	0.07650	0.07650	0.11441	0.14803	0.14803	0.14803	0.07650	0.07650	0.07650	0.07650	0.14803	0.14803	0.14803	0.14803	0.14803	0.14803	0.14803
E_T $(Group)$ (eV)	-31.21931	-30.85651	-31.74130	-33.20040	-33.39484	-33.30009	-29.44855	-29.78809	-26.73723	-27.86936	-49.54347	-32.28590	-67.92207	-49.80996	-31.70737	-33.59732	-33.49373
$E_{initial}\left(c_4\ AO/HO\right)$ (eV)	-11.80624	-11.80624	-13.6181	-14.63489	-14.63489	-14.63489	-11.80624	-11.80624	-11.80624	-11.80624	-14.63489	-14.63489	-14.63489	-14.63489	-14.63489	-14.63489	-14.63489
$E_{initial}\left(c_5\ AO/HO\right)$ (eV)	-13.6181	-13.6181	-13.59844	0	0	0	-13.59844	-13.59844	0	0	0	-13.59844	-13.59844	-13.59844	-13.59844	0	0
E_D $(Group)$ (eV)	5.79502	5.43221	4.41035	3.93062	4.12506	4.03031	4.04387	4.38341	3.12475	4.25687	5.63881	3.90454	12.49186	7.83016	3.32601	4.32754	4.29921

Table 22.19. The total bond energies of alkoxy boranes and borinic acids calculated using the functional group composition and the energies of Table 22.18 compared to the experimental values.

Formula	Name	$B-O$ (i) Group	$B-O$ (ii) Group	OH Group	$C-O$ (i) Group	$C-O$ (ii) Group	$C-B$ Group	$B-H$ Group	$B-H-B$ Group	$B-B$ Group	$B-B-B$ Group	$^{3e}C=C$ Group	CH (i) Group	CH_3	CH_2	CH (ii)	$C-C$ (a)	$C-C$ (b)	Calculated Total Bond Energy (eV)	Experimental Total Bond Energy (eV)	Relative Error
BH_3O	hydroxyborane	1	0	1	0	0	0	2	0	0	0	0	0	0	0	0	0	0	18.29311	18.22572 [17]	-0.00370
BH_3O_2	dihydroxyborane	2	0	2	0	0	0	1	0	0	0	0	0	0	0	0	0	0	24.45460	24.43777 [17]	-0.00069
BH_3O_3	boric acid	3	0	3	0	0	0	0	0	0	0	0	0	0	0	0	0	0	30.61610	30.68431 [7]	0.00222
$BC_2H_7O_2$	dimethoxyborane	2	0	0	2	0	0	1	0	0	0	0	0	2	0	0	0	0	47.75325	47.72358 [16]	-0.00062
$BC_3H_9O_3$	trimethyl borate	0	3	0	3	0	0	0	0	0	0	0	0	3	0	0	0	0	65.56408	65.53950 [17]	-0.00037
$C_5H_{11}OB$	methoxyboracyclopentane	0	1	0	1	0	2	0	0	0	0	0	0	1	4	0	3	0	71.24858	74.47566[a] [18]	0.00345
$C_6H_7O_2B$	phenylborinic acid	2	0	2	0	0	1	0	0	0	0	6	0	0	0	5	0	0	77.79659	78.86121[a] [18]	0.01350
$C_6H_{15}O_2B$	di-isoproxyborane	0	2	0	0	2	0	1	0	0	0	0	0	4	0	2	0	4	96.97471	97.41737[a] [18]	0.00454
$BC_6H_{15}O_3$	triethyl borate	0	3	0	0	3	0	0	0	0	0	0	0	3	3	0	3	0	102.62050	102.50197 [16]	-0.00116
$C_8H_{19}OB$	di-n-butylborinic acid	1	0	1	0	0	2	0	0	0	0	0	0	2	6	0	6	0	116.19591	116.45117 [18]	0.00219
$BC_9H_{21}O_3$	tri-n-propyl borate	0	3	0	0	3	0	0	0	0	0	0	0	3	6	0	6	0	139.09360	139.11319 [16]	0.00014
$C_{12}H_{27}OB$	n-butyl di-n-butylborinate	0	1	0	0	1	2	0	0	0	0	0	0	3	9	0	9	0	164.51278	165.29504[a] [18]	0.00473
$C_{12}H_{27}O_2B$	di-n-butyl n-butylboronate	0	2	0	0	2	1	0	0	0	0	0	0	3	9	0	9	0	170.03974	170.86964[a] [18]	0.00486
$BC_{12}H_{27}O_3$	tri-n-butyl borate	0	3	0	0	3	0	0	0	0	0	0	0	3	9	0	9	0	175.56670	175.62901 [18]	0.00035
$C_{18}H_{15}O_3B_3$	phenylborinic anhydride	0	6	0	0	0	3	0	0	0	0	18	15	0	0	0	0	0	204.75082	205.96548[a] [18]	0.00590
$C_{16}H_{36}OB_2$	di-n-butylborinic anhydride	0	2	0	0	0	4	0	0	0	0	0	0	4	12	0	12	0	222.84551	223.70232[a] [18]	0.00383
$C_{24}H_{20}OB_2$	diphenylborinic anhydride	0	2	0	0	0	4	0	0	0	0	24	20	0	0	0	0	0	240.40782	241.38941[a] [18]	0.00407

[a] Crystal.

Table 22.20. The bond angle parameters of alkoxy boranes and borinic acids and experimental values. H_t is a terminal or two-center H. H_b is a bridge or three-center H. In the calculation of θ_v, the parameters from the preceding angle were used. The experimental alkyl angle from Ref. [10]. E_T is E_T (*atom - atom msp³.AO*).

Atoms of Angle	2c' Bond 1 (a_0)	2c' Bond 2 (a_0)	2c' Terminal Atoms (a_0)	$E_{Coulombic}$ Atom 1	Atom 1 Hybridization Designation (Table)	$E_{Coulombic}$ Atom 2	Atom 2 Hybridization Designation (Table)	c_2 Atom 1	c_2 Atom 2	C_1	C_2	c_1	c_2'	E_T (eV)	θ_v (°)	θ_1 (°)	θ_2 (°)	Cal. θ (°)	Exp. θ (°)
$\angle BOH$ ($B-O$ (i))	2.63356	1.83616	3.7771	-11.80624		-13.61805		1	0.87442 (Eq. (22.29))	0.75	1	0.75	0.87442	-0.56370 (Eq. (22.12))				114.17	114.1 [10] (F_2BOH)
$\angle O_aBO_b$ ($B-O$ (i))	2.63356	2.63356	4.5277	-15.75493 O_a	7 (15.3A)	-15.75493 O_b	7 (15.3A)	0.86359	0.86359	1	1	1	0.86359	-1.44915				118.55	120 [10] ($B_3H_3O_3$)
$\angle O_aBO_b$ ($B-O$ (ii))	2.58909	2.58909	4.4944	-15.75493 O_a	7 (15.3A)	-15.75493 O_b	7 (15.3A)	0.86359	0.86359	1	1	1	0.86359	-1.44915				120.44	120 [10] ($B_3H_3O_3$)
$\angle CBC$ $(CH_3)_3B$	2.97524	2.97524	5.1769	16.11722	1 (22.8)	16.11722	1 (22.8)	0.84418	0.84418	1	1	1	0.84418	-1.85836				120.92	120.0 [10] (trimethylborane)
Methyl $\angle HCH$	2.09711	2.09711	3.4252	-15.75493	7	H	H	0.86359	1	1	1	0.75	1.15796	0				109.50	
$\angle BCH$															70.56			109.44	112.5 [10] (trimethylborane)
$\angle CBH_t$	2.97524	2.27211	4.5607	-15.55033	5 (15.3A)	H	H	0.87495	1	0.75	1	0.75	1.14292	0				120.12	
$\angle CBH_b$	2.97524	2.46967	4.6904	-15.55033	5 (15.3A)	H	H	0.87495	1	0.75	1	0.75	1.14292	0				118.66	
$\angle BBC$																120.12	118.66	121.22	122.6 [10] (1,2-dimethyldiborane)
$\angle H_tBH_t$	2.27211	2.27211	3.9623	-13.61667	2 (22.1)	H	H	0.99920	1	1	1	0.75	1.00080	-1.71943				121.37	122 [10] (diborane)
$\angle H_tBH_b$	2.27211	2.46967	3.8210	-14.71574	4 (22.1)	H	H	0.92458	1	1	1	0.75	1.08158	-1.12740				107.30	108.9 [2] (B_4H_{10})
$\angle H_bBH_b$	2.46967	2.46967	3.6606	-14.26508	3 (22.1)	H	H	0.95378	1	1	1	0.75	1.04846	-1.12740				95.65	95.0 [2] (B_4H_{10})
$\angle BH_bB$	2.46967	2.46967	3.4358	-11.89724 B_a	1 (22.1)	-11.89724 B_b	1 (22.1)	1	1	1	1.14361	1	1	0				88.15	87.7 [2] (B_4H_{10})
$\angle CCC$ (aromatic)	2.62936	2.62936	4.5585	-17.17218	38 (15.3A)	-17.17218	38 (15.3A)	0.79232	0.79232	1	1	1	0.79232	-1.85836				120.19	120 [19-21] (benzene)
$\angle CCH$ (aromatic)																120.19		119.91	120 [19-21] (benzene)
Methylene $\angle HC_aH$	2.11106	2.11106	3.4252	-15.75493	7	H	H	0.86359	1	1	1	0.75	1.15796	0				108.44	107 (dimethylamine) (propane)
$\angle C_cC_bC_c$															69.51			110.49	112 (propane) 113.8 (butane) 110.8 (isobutane)
$\angle C_aC_bH$															69.51			110.49	111.0 (butane) 111.4 (isobutane)
Methyl $\angle HC_aH$	2.09711	2.09711	3.4252	-15.75493	7 (15.3A)	H	H	0.86359	1	1	1	0.75	1.15796	0				109.50	
$\angle C_cC_bC_c$															70.56			109.44	
$\angle C_aC_bH$															70.56			109.44	
$\angle C_cC_aC_c$ iso C_a	2.91547	2.91547	4.7958	-16.68412 C_b	26 (15.3A)	-16.68412 C_c	26 (15.3A)	0.81549	0.81549	1	1	1	0.81549	-1.85836				110.67	110.8 (isobutane)
$\angle C_bC_aH$ iso C_a	2.91547	2.11323	4.1633	-15.55033 C_a	5 (15.3A)	-14.82575 C_b	1 (15.3A)	0.87495	0.91771	0.75	1	0.75	1.04887	0				110.76	
$\angle C_aC_bH$ iso C_a	2.91547	2.09711	4.1633	-15.55033 C_b	5 (15.3A)	-14.82575 C_a	1 (15.3A)	0.87495	0.91771	0.75	1	0.75	1.04887	0				111.27	111.4 (isobutane)

TERTIARY AND QUATERNARY AMINOBORANES AND BORANE AMINES $(R_qB_rN_sR_t;R=H;alkyl)$

The tertiary and quaternary amino boranes and borane amines each comprise at least one B bound by a boron-nitrogen single bond comprising a $B-N$ group, and may comprise at least a terminal methyl group (CH_3), as well other alkyl and borane groups such as methylene (CH_2), methylyne (CH), $C-C$, $B-H$, $B-C$, $B-H$, $B-B$, $B-H-B$, and $B-B-B$ functional groups. The methyl and methylene functional groups are equivalent to those of straight-chain alkanes. Six types of $C-C$ bonds can be identified. The n-alkane $C-C$ bond is the same as that of straight-chain alkanes. In addition, the $C-C$ bonds within isopropyl ($(CH_3)_2CH$) and t-butyl ($(CH_3)_3C$) groups and the isopropyl to isopropyl, isopropyl to t-butyl, and t-butyl to t-butyl $C-C$ bonds comprise functional groups. These groups in tertiary and quaternary amino boranes and borane amines are equivalent to those in branched-chain alkanes, the $B-C$ group is equivalent to that of alkyl boranes, and the $B-H$, $B-B$, $B-H-B$, and $B-B-B$ functional groups are equivalent to those in boranes.

In tertiary amino boranes and borane amines, the nitrogen atom of each $B-N$ bond is bound to two other atoms such that there are a total of three bounds per atom. The amino or amine moiety may comprise NH_2, $N(H)R$, and NR_2. The corresponding functional group for the NH_2 moiety is the NH_2 functional group given in the Primary Amines $(C_nH_{2n+2+m}N_m,\ n=1,2,3,4,5...\infty)$ section. The $N(H)R$ moiety comprises the NH functional group of the Secondary Amines $(C_nH_{2n+2+m}N_m,\ n=2,3,4,5...\infty)$ section and the $C-N$ functional group of the Primary Amines $(C_nH_{2n+2+m}N_m,\ n=1,2,3,4,5...\infty)$ section. The NR_2 moiety comprises two types of $C-N$ functional groups, one for the methyl group corresponding to the C of $C-N$ and the other for general alkyl secondary amines given in the Secondary Amines $(C_nH_{2n+2+m}N_m,\ n=2,3,4,5...\infty)$ section.

In quaternary amino boranes and borane amines, the nitrogen atom of each $B-N$ bond is bound to three other atoms such that there are a total of four bonds per atom. The amino or amine moiety may comprise NH_3, $N(H_2)R$, $N(H)R_2$, and NR_3. The corresponding functional group for the NH_3 moiety is ammonia given in the Ammonia (NH_3) section. The $N(H_2)R$ moiety comprises the NH_2 and the $C-N$ functional groups given in the Primary Amines $(C_nH_{2n+2+m}N_m,\ n=1,2,3,4,5...\infty)$ section. The $N(H)R_2$ moiety comprises the NH functional group and two types of $C-N$ functional groups, one for the methyl group corresponding to the C of $C-N$ and the other for general alkyl secondary amines given in the Secondary Amines $(C_nH_{2n+2+m}N_m,\ n=2,3,4,5...\infty)$ section. The NR_3 moiety comprises the $C-N$ functional group of tertiary amines given in the Tertiary Amines $(C_nH_{2n+3}N,\ n=3,4,5...\infty)$ section.

The bonding in the $B-N$ functional groups of tertiary and quaternary amino boranes and borane amines is similar to that of the $B-O$ groups of alkoxy boranes and borinic acids given in the corresponding section. The MO semimajor axes of the $B-N$ functional groups are determined from the force balance equation of the centrifugal, Coulombic, and magnetic forces as given in the Boranes (B_xH_y) section. In each case, the distance from the origin of the H_2-type-ellipsoidal-MO to each focus c', the internuclear distance $2c'$, and the length of the semiminor axis of the prolate spheroidal H_2-type MO $b=c$ are solved from the semimajor axis a. Then, the geometric and energy parameters of each MO are calculated using Eqs. (15.1-15.117).

As in the case of the $B-O$-bond MOs, the σ-MOs of the tertiary and quaternary $B-N$-bond MOs is energy matched to the $B2sp^3$ HO which determines that the parameters of the force balance equation based on electron angular momentum are determined by those of the boron atom. Thus, the parameters of the force balance equation for the σ-MO of the $B-N$-bond MOs in Eqs. (22.18-22.22) are $n_e=1$ and $|L|=\frac{3\sqrt{\frac{3}{4}}}{Z}$ corresponding to the three electrons of the boron atom:

$$\frac{\hbar^2}{m_e a^2 b^2}D=\frac{e^2}{8\pi\varepsilon_0 ab^2}D+\frac{\hbar^2}{2m_e a^2 b^2}D-\left(\frac{1}{2}+\frac{3\sqrt{\frac{3}{4}}}{Z}\right)\frac{\hbar^2}{2m_e a^2 b^2}D \tag{22.45}$$

$$a=\left(\frac{3}{2}+\frac{3\sqrt{\frac{3}{4}}}{Z}\right)a_0 \tag{22.46}$$

With $Z=5$, the semimajor axis of the tertiary $B-N$-bond MO is:

$$a=2.01962a_0 \tag{22.47}$$

For the $B-N$ functional groups, hybridization of the $2s$ and $2p$ AOs of B to form single $2sp^3$ shells forms an energy minimum, and the sharing of electrons between the $B2sp^3$ HO and N AO to form a MO permits each participating orbital to decrease in radius and energy. The energy of boron is less than the Coulombic energy between the electron and proton of H given by Eq. (1.264). Thus, in c_1 and c_2 in Eq. (15.61) is one, and the energy matching condition is determined by the C_1 and

C_2 parameters. The N AO has an energy of $E(N) = -14.53414\ eV$, and the $B2sp^3$ HOs have an energy of $E(B, 2sp^3) = -11.80624\ eV$ (Eq. (22.7)). To meet the equipotential condition of the union of the $B-N$ H_2-type-ellipsoidal-MO with these orbitals, the hybridization factor C_2 of Eq. (15.61) for the $B-N$-bond MO given by Eq. (15.77) is:

$$C_2\left(NAO\ to\ B2sp^3HO\right) = \frac{E\left(B, 2sp^3\right)}{E\left(NAO\right)} = \frac{-11.80624\ eV}{-14.53414\ eV} = 0.81231 \tag{22.48}$$

Since the energy of the MO is matched to that of the $B2sp^3$ HO, $E(AO/HO)$ in Eqs. (15.51) and (15.61) is $E\left(B, 2sp^3\right)$ given by Eq. (22.7), and $E_T\left(atom-atom, msp^3.AO\right)$ for ternary $B-N$ is $-1.12740\ eV$ corresponding to the independent single-bond charge contribution (Eq. (22.12)) of one center as in the case of the alkoxy borane $B-O$ functional group. Furthermore, k' is 0.75 as given by Eq. (13.59) such that $C_1 = 0.75$ in Eq. (15.61) which is also equivalent to C_1 of the $B-O$ alkoxy borane group.

$E_T\left(atom-atom, msp^3.AO\right)$ of the quaternary $B-N$-bond MO is determined by considering that the bond involves an electron transfer from the nitrogen atom to the boron atom to form zwitterions such as $R_3N^+-B^-R'_3$. By considering the electron redistribution in the quaternary amino borane and borane amine molecule as well as the fact that the central field decreases by an integer for each successive electron of the shell, the radius $r_{B-Nborane2sp^3}$ of the $B2sp^3$ shell may be calculated from the Coulombic energy using Eq. (15.18) , except that the sign of the charge donation is positive:

$$r_{B-Nborane2sp^3} = \left(\sum_{n=2}^{4}(Z-n)+1\right)\frac{e^2}{8\pi\varepsilon_0\left(e74.89168\ eV\right)} = \frac{7e^2}{8\pi\varepsilon_0\left(e74.89168\ eV\right)} = 1.27171a_0 \tag{22.49}$$

Using Eqs. (15.19) and (22.49), the Coulombic energy $E_{Coulomb}\left(B_{B-Nborane}, 2sp^3\right)$ of the outer electron of the $B2sp^3$ shell is:

$$E_{Coulomb}\left(B_{B-Nborane}, 2sp^3\right) = \frac{-e^2}{8\pi\varepsilon_0 r_{B-Nborane2sp^3}} = \frac{-e^2}{8\pi\varepsilon_0 1.27171a_0} = -10.69881\ eV \tag{22.50}$$

During hybridization, one of the spin-paired $2s$ electrons is promoted to the $B2sp^3$ shell as an unpaired electron. The energy for the promotion is the magnetic energy given by Eq. (22.6). Using Eqs. (22.6) and (22.50), the energy $E\left(B_{B-Nborane}, 2sp^3\right)$ of the outer electron of the $B2sp^3$ shell is:

$$E\left(B_{B-Nborane}, 2sp^3\right) = \frac{-e^2}{8\pi\varepsilon_0 r_{B-Nborane2sp^3}} + \frac{2\pi\mu_0 e^2\hbar^2}{m_e^2\left(r_3\right)^3} = -10.69881\ eV + 0.09100\ eV = -10.60781\ eV \tag{22.51}$$

Thus, $E_T\left(B-N, 2sp^3\right)$, the energy change of each $B2sp^3$ shell with the formation of the $B-N$-bond MO is given by the difference between Eq. (22.51) and Eq. (22.7).

$$E_T\left(B-N, 2sp^3\right) = E\left(B_{B-Nborane}, 2sp^3\right) - E\left(B, 2sp^3\right) = -10.60781\ eV - \left(-11.80624\ eV\right) = 1.19843\ eV \tag{22.52}$$

Thus, $E_T\left(atom-atom, msp^3.AO\right)$ of the quaternary $B-N$-bond MO is $1.19843\ eV$.

Consider next the radius of the HO due to the contribution of charge to more than one bond. The energy contribution due to the charge donation at each boron atom and nitrogen atom superimposes linearly. In general, since the energy of the $B2sp^3$ HO and N AO is matched to that of the $C2sp^3$ HO when a molecule contains a $C-B$-bond MO and a $C-N$-bond MO, respectively, the corresponding radius r_{mol2sp^3} of the $B2sp^3$ HO of a boron atom, the $C2sp^3$ HO of a carbon atom, and the N AO of a given $B-N$-containing borane molecule is calculated after Eq. (15.32) by considering $\sum E_{T_{mol}}\left(MO, 2sp^3\right)$, the total energy donation to all bonds with which it participates in bonding. The Coulombic energy $E_{Coulomb}\left(atom, 2sp^3\right)$ of the outer electron of the $atom$ $2sp^3$ shell considering the charge donation to all participating bonds is given by Eq. (15.14). In the case that the boron or nitrogen atom is not bound to a $C2sp^3$ HO, r_{mol2sp^3} is calculated using Eq. (15.31) where $E_{Coulomb}\left(atom, msp^3\right)$ is $E_{Coulomb}\left(B2sp^3\right) = -11.89724\ eV$ and $E(N) = -14.53414\ eV$, respectively. The hybridization parameters used in Eqs. (15.88-15.117) for the determination of bond angles of tertiary and quaternary amino boranes and borane amines are given in Table 22.21.

Table 22.21. Atom hybridization designation (# first column) and hybridization parameters of atoms for determination of bond angles with final values of r_{2sp^3}, $E_{Coulomb}(atom,2sp^3)$ (designated as $E_{Coulomb}$), and $E(atom_{\ B\text{-}Nborane}\ 2sp^3)$ (designated as E) calculated using the appropriate values of $\sum E_{T_{mol}}(MO,2sp^3)$ (designated as E_T) for each corresponding terminal bond spanning each angle.

#	E_T	E_T	E_T	E_T	E_T	r_{3sp^3} Final	$E_{Coulomb}$ (eV) Final	E (eV) Final
1	-0.46459	0	0	0	0	0.88983 (Eq. (15.32))	-15.29034	-15.09948
2	-0.56370	-0.56370	-0.56370	0	0	0.82343 (Eq. (15.32))	-16.52324	

The symbols of the functional groups of tertiary and quaternary amino boranes and borane amines are given in Table 22.22. The geometrical (Eqs. (15.1-15.5) and (22.47)), intercept (Eqs. (15.31-15.32) and (15.80-15.87)), and energy (Eq. (15.61), (22.4), (22.7), (22.12), (22.48), and (22.52)) parameters of tertiary and quaternary amino boranes and borane amines are given in Tables 22.23, 22.24, and 22.25, respectively. In the case that the MO does not intercept the B HO due to the reduction of the radius from the donation of $B\ 2sp^3$ HO charge to additional MOs, the energy of each MO is energy matched as a linear sum to the B HO by contacting it through the bisector current of the intersecting MOs as described in the Methane Molecule (CH_4) section. The total energy of each tertiary and quaternary amino borane or borane amine given in Table 22.26 was calculated as the sum over the integer multiple of each $E_{D\,(Group)}$ of Table 22.25 corresponding to functional-group composition of the molecule. E_{mag} of Table 22.26 is given by Eqs. (15.15) and (22.3) for the $B-N$ groups and the $B-H$, $B-B$, $B-H-B$, and $B-B-B$ groups. E_{mag} of Table 22.26 is given by Eqs. (15.15) and (10.142) for NH_3. The bond angle parameters of tertiary and quaternary amino boranes and borane amines determined using Eqs. (15.88-15.117) are given in Table 22.27. The charge-densities of exemplary tertiary amino borane, tris(dimethylamino)borane and quaternary amino borane, trimethylaminotrimethylborane comprising the concentric shells of atoms with the outer shell bridged by one or more H_2-type ellipsoidal MOs or joined with one or more hydrogen MOs are shown in Figures 22.7 and 22.8, respectively.

Figure 22.7. *Trisdimethylaminoborane.* Color scale, opaque views of the charge-density of $\left(\left(H_3C\right)_2N\right)_3B$ showing the orbitals of the *B*, *N*, and *C* atoms at their radii, the ellipsoidal surface of each *H* or H_2-type ellipsoidal MO that transitions to the corresponding outer shell of the atoms participating in each bond, and the hydrogen nuclei (red, not to scale).

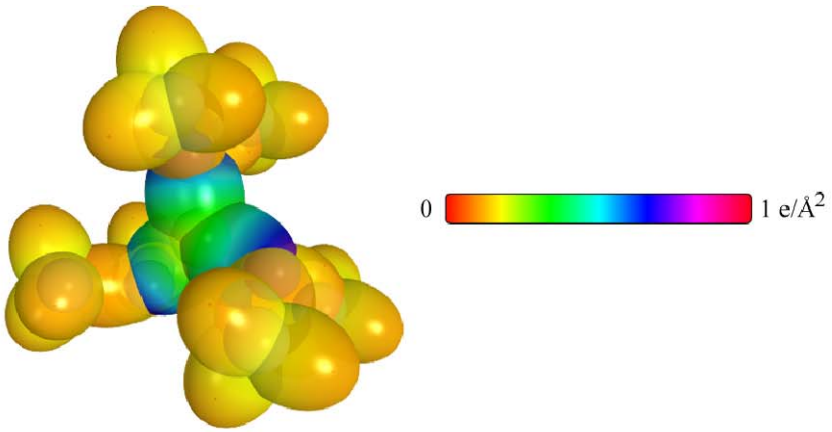

Figure 22.8. *Trimethylaminotrimethylborane.* Color scale, opaque view of the charge-density of $(CH_3)_3 BN(CH_3)_3$ showing the orbitals of the *B*, *N*, and *C* atoms at their radii, the ellipsoidal surface of each *H* or H_2-type ellipsoidal MO that transitions to the corresponding outer shell of the atoms participating in each bond, and the hydrogen nuclei (red, not to scale).

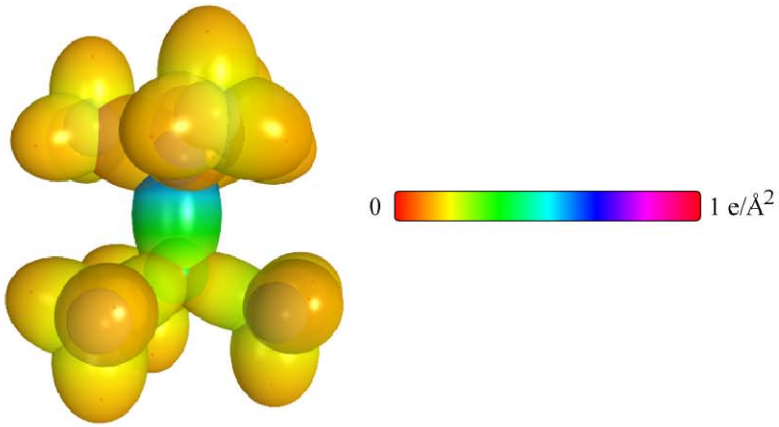

Table 22.22. The symbols of the functional groups of tertiary and quaternary amino boranes and borane amines.

Functional Group	Group Symbol
B-N bond 3°	$B-N$ (i)
B-N bond 4°	$B-N$ (ii)
C-N bond 1° amine	$C-N$ (i)
C-N bond 2° amine (methyl)	$C-N$ (ii)
C-N bond 2° amine (alkyl)	$C-N$ (iii)
C-N bond 3° amine	$C-N$ (iv)
NH_3 group	NH_3
NH_2 group	NH_2
NH group	*NH*
C-B bond	$C-B$
BH bond	$B-H$
BHB (bridged *H*)	$B-H-B$
BB bond	$B-B$
CH_3 group	$C-H\ (CH_3)$
CH_2 group	$C-H\ (CH_2)$
CH	$C-H$ (i)
CC bond (*n-C*)	$C-C$ (a)

Table 22.23. The geometrical bond parameters of tertiary and quaternary amino boranes and borane amines and experimental values.

Parameter	$B-N$ (i) Group	$B-N$ (ii) Group	$C-N$ (i) Group	$C-N$ (ii) Group	$C-N$ (iii) Group	$C-N$ (iv) Group	NH_3 Group	NH_2 Group	NH Group	$C-B$ Group	$B-H$ Group	$B-H-B$ Group	$B-B$ and $B-B-B$ Groups	$C-H\ (CH_3)$ Group	$C-H\ (CH_2)$ Group	$C-H$ (i) Group	$C-C$ (a) Group
$a\ (a_0)$	2.01962	2.01962	1.92682	1.94862	1.94862	1.96313	1.34750	1.28083	1.26224	1.78528	1.69282	2.00000	2.51962	1.64920	1.67122	1.67465	2.12499
$c'\ (a_0)$	1.28744	1.57679	1.38810	1.39593	1.39593	1.40112	0.97961	0.95506	0.94811	1.48762	1.13605	1.23483	1.69749	1.04856	1.05553	1.05661	1.45744
Bond Length $2c'\ (\AA)$	1.36257	1.66880	1.46910	1.47739	1.47739	1.48288	1.03677	1.0108	1.00343	1.57443	1.20235	1.30689	1.79654	1.10974	1.11713	1.11827	1.54280
Exp. Bond Length $(\AA)$	1.281 [5] (BN)	1.638 [17] ($(CH_3)_3NBH_3$)	1.471 [10] (methylamine)	1.455 [10] (dimethylamine)		1.458 [10] (trimethylamine)	1.0120 [10] (ammonia)	1.010 [10] (methylamine)	1.00 [10] (dimethylamine)	1.578 [10] (trimethylborane) 1.580 [10] (1,2-dimethyldiborane)	1.19 [4] (diborane)	1.32 [4] (diborane)	1.798 [3] ($B_{13}H_{19}$)	1.114 [10] ($C-H$ trimethylborane) 1.107 [10] ($C-H$ propane) 1.117 [10] ($C-H$ butane)	1.107 [10] ($C-H$ propane) 1.117 [10] ($C-H$ butane)	1.122 [10] (isobutane)	1.532 [10] (propane) 1.531 [10] (butane)
$b,c\ (a_0)$	1.55607	1.26198	1.33634	1.35960	1.35960	1.37505	0.92527	0.85345	0.83327	0.98702	1.25500	1.57327	1.86199	1.27295	1.29569	1.29924	1.54616
e	0.63747	0.78074	0.72041	0.71637	0.71637	0.71372	0.72698	0.74566	0.75113	0.83327	0.67110	0.61742	0.67371	0.63580	0.63159	0.63095	0.68600

Table 22.24. The MO to HO intercept geometrical bond parameters of tertiary and quaternary amino boranes and borane amines. H_t is a terminal or two-center H. H_b is a bridge or three-center H. B_b is a bridge or three-center B. E_T is E_T (*atom - atom msp³.AO*).

Bond	Atom	E_T (eV) Bond 1	E_T (eV) Bond 2	E_T (eV) Bond 3	E_T (eV) Bond 4	Final Total Energy (eV)	$r_{initial}$ (a_0)	r_{final} (a_0)	$E_{Coulomb}$ (eV) Final	E (eV) Final	θ' (°)	θ_1 (°)	θ_2 (°)	d_1 (a_0)	d_2 (a_0)
$N-H\ (-BNH_2)$ $(B-N$ (i))	N	-0.56370	0	0	0		0.93084	0.90118	-15.09784		119.66	60.34	66.58	0.50915	0.44591
$N-H\ (-BNHR)$ $(B-N$ (i); $C-N$ (i)); $R=CH_3$ *or alkyl*)	N	-0.56370	-0.72457	0	0		0.93084	0.84435	-16.11402		117.64	62.36	63.85	0.55635	0.39176
$C-N\ (H_3C_a-NHB-)$; $(-H_2C_a-NHB-)$ $(B-N$ (i); $C-N$ (i))	N	-0.72457	-0.56370	0	0		0.93084	0.84435	-16.11402		82.21	97.79	38.76	1.50258	0.11448
$C-N\ (H_3C_a-NHB-)$ $(B-N$ (i); $C-N$ (i))	C_a	-0.72457	0	0	0	-152.34026	0.91771	0.87495	-15.55033	-15.35946	85.28	94.72	40.73	1.46010	0.07200
$C-N\ (-H_2C_a-NHB-)$ $(B-N$ (i); $C-N$ (i))	C_a	-0.72457	-0.92918	0	0	-153.26945	0.91771	0.82562	-16.47951	-16.28864	80.20	99.80	37.50	1.52858	0.14048
$C-N\ (-BN-(C_aH_2)_2)$; $(-BN-(C_aH_2-)_2)$ $(B-N$ (i); $C-N$ (ii) or $C-N$ (iii))	N	-0.56690	-0.56690	-0.56370	0		0.93084	0.82343	-16.52324		77.75	102.25	36.29	1.57068	0.17475
$C-N\ (-BN-(C_aH_2)_2)$ $(B-N$ (i); $C-N$ (ii))	C_a	-0.56690	0	0	0	-152.18259	0.91771	0.88392	-15.39265	-15.20178	84.14	95.86	40.30	1.48625	0.09032
$C-N\ (-BN-(C_aH_2-)_2)$ $(B-N$ (i); $C-N$ (ii))	C_a	-0.56690	-0.92918	0	0	-153.11177	0.91771	0.83360	-16.32183	-16.13097	78.89	101.11	36.99	1.55650	0.16057
$B-N\ (B(N(CH_2)_2)_3)$ $(B-N$ (i); $C-N$ (ii))	B	-0.56370	-0.56370	-0.56370	0	-76.58278	1.14361	1.00129	-13.58834	-13.49734	71.96	108.04	37.72	1.59746	0.31002
$B-N\ (B(N(CH_2)_2)_3)$ $(B-N$ (i); $C-N$ (ii))	N	-0.56370	-0.56690	-0.56690	0		0.93084	0.82343	-16.52324		44.33	135.67	21.70	1.87645	0.58901
$B-N\ (R_2BNH_2)$ $(B-N$ (i))	B	-0.56370	-0.72457	-0.72457	0	-76.90453	1.14361	0.80801	-16.83860	-16.74760	40.63	139.37	19.76	1.90065	0.61320
$B-N\ (R_2BNH_2)$ $(B-N$ (i))	N	-0.56370	0	0	0		0.93084	0.90118	-15.09784		40.63	139.37	19.76	1.90065	0.61320
$B-N\ (R_2BNHR)$ $(B-N$ (i); $C-N$ (i); $R=CH_3$ *or alkyl*)	B	-0.56370	-0.72457	-0.72457	0	-76.90453	1.14361	0.80801	-16.83860	-16.74760	40.63	139.37	19.76	1.90065	0.61320
$B-N\ (R_2BNHR)$ $(B-N$ (i); $C-N$ (i); $R=CH_3$ *or alkyl*)	N	-0.56370	-0.72457	0	0		0.93084	0.84435	-16.11402		48.80	131.20	24.09	1.84365	0.55621
$B-N\ (B_2H_5NH_2)$ $(B-N$ (i))	B	-0.56370	-0.56370	-1.12740	-1.12740		1.14361	0.89047	-15.27943	-15.18843	57.09	122.91	28.71	1.77130	0.48386
$B-N\ (B_2H_5NH_2)$ $(B-N$ (i))	N	-0.56370	0	0	0		0.93084	0.90118	-15.09784		57.09	122.91	28.71	1.77130	0.48386
$B-N\ (B_2H_5NR_2)$ $(B-N$ (i); $C-N$ (ii) or (iii); $R=CH_3$ *or alkyl*)	B	-0.56370	-0.56370	-1.12740	-1.12740	-78.27387	1.14361	0.89047	-15.27943	-15.18843	57.09	122.91	28.71	1.77130	0.48386
$B-N\ (B_2H_5NR_2)$ $(B-N$ (i); $C-N$ (ii) or (iii); $R=CH_3$ *or alkyl*)	N	-0.56370	-0.56690	-0.56690	0		0.93084	0.82343	-16.52324		57.09	122.91	28.71	1.77130	0.48386
$C-B\ (R_2B-N-)$ $(B-N$ (i); $R=CH_3$ *or alkyl*))	B	-0.72457	-0.72457	-0.56370	0		1.14361	0.80801	-16.83860	-16.74760	112.93	67.07	48.93	1.17281	0.31481
$B-H_t\ (-N(H_t)BH_{b2}-)$ $(B-N$ (i))	B	-0.56370	-1.12740	-1.12740	-0.56370		1.14361	0.89047	-15.27943	-15.18843	86.17	93.83	45.07	1.19558	0.05983
$B-H_b\ (-N(H_t)BH_{b2}-)$ $(B-N$ (i))	B	-1.12740	-1.12740	-0.56370	-0.56370		1.14361	0.89047	-15.27943	-15.18843	50.85	129.15	26.03	1.79706	0.56223
$N-H\ (-BNH_3)$ $(B-N$ (ii))	N	0.59922	0	0	0		0.93084	0.97638	-13.93492		118.72	61.28	67.74	0.51049	0.46911
$N-H\ (-BNHR_2)$ $(B-N$ (ii); $C-N$ (ii) or $C-N$ (iii); $R=CH_3$ *or alkyl*)	N	0.59922	0.56690	0.56690	0		0.93084	0.88578	-15.36033		120.30	59.70	66.61	0.50119	0.44692
$C-N\ ((H_3C_a)_2-NHB-)$; $((-H_2C_a)_2-NHB-)$ $(B-N$ (ii); $C-N$ (ii) or $C-N$ (iii))	N	-0.56690	-0.56690	0.59922	0		0.93084	0.88578	-15.36033		84.32	95.68	40.41	1.48366	0.08773

Table 22.24 Cont' d. The MO to HO intercept geometrical bond parameters of tertiary and quaternary amino boranes and borane amines. H_t is a terminal or two-center *H*. H_b is a bridge or three-center *H*. B_b is a bridge or three-center *B*. E_T is E_T (*atom - atom msp*^{3}*.AO*).

Bond	Atom	E_T (eV) Bond 1	E_T (eV) Bond 2	E_T (eV) Bond 3	E_T (eV) Bond 4	Final Total Energy (eV)	$r_{initial}$ (a_0)	r_{final} (a_0)	$E_{Coulomb}$ (eV) Final	E (eV) Final	θ' (°)	θ_1 (°)	θ_2 (°)	d_1 (a_0)	d_2 (a_0)
$C-N\ \left(\left(H_3C_a\right)_2-NHB-\right)$ $(B-N$ (ii); $C-N$ (ii))	C_a	-0.56690	0	0	0	-152.18259	0.91771	0.88392	-15.39265	-15.20178	84.14	95.86	40.30	1.48625	0.09032
$C-N\ \left(\left(-H_2C_a\right)_2-NHB-\right)$ $(B-N$ (ii); $C-N$ (iii))	C_a	-0.56690	-0.92918	0	0	-153.11177	0.91771	0.83360	-16.32183	-16.13097	78.89	101.11	36.99	1.55650	0.16057
$C-N\ \left(-BN-\left(C_aH_3\right)_3\right)$; $\left(-BN-\left(C_aH_2-\right)_3\right)$ $(B-N$ (ii); $C-N$ (iv))	N	-0.46459	-0.46459	-0.46459	0.59922		0.93084	0.87103	-15.62031		81.48	98.52	38.79	1.53016	0.12904
$C-N\ \left(-BN-\left(C_aH_3\right)_3\right)$ $(B-N$ (ii); $C-N$ (iv))	C_a	-0.46459	0	0	0	-152.08028	0.91771	0.88983	-15.29034	-15.09948	83.37	96.63	40.00	1.50383	0.10271
$C-N\ \left(-BN-\left(C_aH_2-\right)_3\right)$ $(B-N$ (ii); $C-N$ (iv))	C_a	-0.46459	-0.92918	0	0	-153.00946	0.91771	0.83885	-16.21952	-16.02866	78.02	101.98	36.64	1.57525	0.17413
$B-N\ \left(R_3BNH_3\right)$ $(B-N$ (ii))	B	0.59922	-0.72457	-0.72457	-0.72457		1.14361	0.82961	-16.40026	-16.30926	93.63	86.37	41.00	1.52421	0.05258
$B-N\ \left(R_3BNH_3\right)$ $(B-N$ (ii))	N	0.59922	0	0	0		0.93084	0.95637	-14.22654		102.99	77.01	47.60	1.36185	0.21494
$B-N\ \left(H_3BNR_3\right)$ $(B-N$ (ii); $C-N$ (iv))	B	0.59922	-0.56370	-0.56370	-0.56370		1.14361	0.85476	-15.91763	-15.82663	95.69	84.31	42.37	1.49199	0.08480
$B-N\ \left(H_3BNR_3\right)$ $(B-N$ (ii); $C-N$ (iv))	N	0.59922	-0.46459	-0.46459	-0.46459		0.93084	0.87103	-15.62031		96.97	83.03	43.24	1.47115	0.10563
$B-N\ \left(H_3BNHR_2\right)$ $(B-N$ (ii); $C-N$ (ii) or $C-N$ (iii))	B	0.59922	-0.56370	-0.56370	-0.56370		1.14361	0.85476	-15.91763	-15.82663	95.69	84.31	42.37	1.49199	0.08480
$B-N\ \left(H_3BNHR_2\right)$ $(B-N$ (ii); $C-N$ (ii) or $C-N$ (iii))	N	0.59922	-0.56690	-0.56690	0		0.93084	0.88578	-15.36033		98.08	81.92	44.02	1.45227	0.12452
$B-N\ \left(R_3BNR_3\right)$ $(B-N$ (ii); $C-N$ (iv)))	B	0.59922	-0.72457	-0.72457	-0.72457		1.14361	0.82961	-16.40026	-16.30926	93.63	86.37	41.00	1.52421	0.05258
$B-N\ \left(R_3BNR_3\right)$ $(B-N$ (ii); $C-N$ (iv))	N	0.59922	-0.46459	-0.46459	-0.46459		0.93084	0.87103	-15.62031		96.97	83.03	43.24	1.47115	0.10563
$C-B\ \left(R_3B-N-\right)$ $(B-N$ (ii); $R=CH_3$ *or alkyl*))	B	-0.72457	-0.72457	-0.72457	0.59922		1.14361	0.82961	-16.40026	-16.30926	114.25	65.75	50.03	1.14689	0.34073
$B-H_t\ \left(H_{t3}BN-\right)$ $(B-N$ (ii))	B	-0.56370	-0.56370	-0.56370	0.59922		1.14361	1.04748	-12.98912	-12.89812	99.59	80.41	55.39	0.96162	0.17443
$B-H_b\ \left(R_2BH_{b2}-\right)$	B	-1.12740	-1.12740	-0.72457	-0.72457		1.14361	0.73427	-18.52969	-18.43869					
$B-B\ \left(H_tRBB-\right)$	B	-1.12740	-0.56370	-0.72457	0		1.14361	0.78913	-17.24142	-17.15042					
$B-B\ \left(R_2BB-\right)$	B	-1.12740	-0.72457	-0.72457	0		1.14361	0.78184	-17.40230	-17.31130					
$B-B\ \left(H_{b2}RBB-\right)$	B	-1.12740	-1.12740	-1.12740	-0.72457		1.14361	0.71865	-18.93252	-18.84152					
$B-B\ \left(H_bRB_bBB-\right)$	B	-1.12740	-1.12740	-1.69110	-0.72457		1.14361	0.69787	-19.49622	-19.40522					
$B-B_b\ \left(H_{b2}RBB_t-\right)$	B	-1.69110	-0.72457	-1.12740	-1.12740		1.14361	0.69787	-19.49622	-19.40522					
$B-B_b\ \left(H_tRBBB_b-\right)$	B	-1.69110	-0.72457	-1.12740	-1.12740		1.14361	0.69787	-19.49622	-19.40522					
$B-B_b\ \left(H_tRB_bBB_b-\right)$	B	-1.69110	-1.69110	-0.72457	-1.12740		1.14361	0.67826	-20.05991	-19.96891					
$C-H\ \left(BCH_3\right)$	C	-0.72457	0	0	0	-152.34026	0.91771	0.87495	-15.55033	-15.35946	78.85	101.15	42.40	1.21777	0.16921
$C-H\ \left(BCH_2-\right)$	C	-0.72457	-0.92918	0	0	-153.26945	0.91771	0.82562	-16.47951	-16.28865	69.93	110.07	36.76	1.33883	0.28330
$C-H\ \left(BCH-\right)$	C	-0.72457	-0.92918	-0.92918	0	-154.19863	0.91771	0.78155	-17.40869	-17.21783	62.67	117.33	32.30	1.41549	0.35888
$C-B\ \left(-B-CH_3\right)$	C	-0.72457	0	0	0	-152.34026	0.91771	0.87495	-15.55033	-15.35946	116.85	63.15	52.27	1.09248	0.39514
$C-B\ \left(-B-C_aH_2R\right)$	C_a	-0.72457	-0.92918	0	0	-153.26945	0.91771	0.82562	-16.47951	-16.28864	114.01	65.99	49.83	1.15168	0.33594
$C-H\ \left(RCH_3\right)$	C	-0.92918	0	0	0	-152.54487	0.91771	0.86359	-15.75493	-15.56407	77.49	102.51	41.48	1.23564	0.18708
$C-H\ \left(CH_2\right)$	C	-0.92918	-0.92918	0	0	-153.47406	0.91771	0.81549	-16.68412	-16.49325	68.47	111.53	35.84	1.35486	0.29933
$C-H\ \left(CH\right)$	C	-0.92918	-0.92918	-0.92918	0	-154.40324	0.91771	0.77247	-17.61330	-17.42244	61.10	118.90	31.37	1.42988	0.37326
$H_3C_aC_3H_2CH_2-$ $(C-C$ (a))	C_a	-0.92918	0	0	0	-152.54487	0.91771	0.86359	-15.75493	-15.56407	63.82	116.18	30.08	1.83879	0.38106
$H_3C_aC_3H_2CH_2-$ $(C-C$ (a))	C_b	-0.92918	-0.92918	0	0	-153.47406	0.91771	0.81549	-16.68412	-16.49325	56.41	123.59	26.06	1.90890	0.45117

Table 22.25. The energy parameters (eV) of functional groups of tertiary and quaternary amino boranes and borane amines.

Parameters	$B-N$ (i) Group	$B-N$ (ii) Group	$C-N$ (i) Group	$C-N$ (ii) Group	$C-N$ (iii) Group	$C-N$ (iv) Group	NH_3 Group	NH_2 Group	NH Group	$C-B$ Group	$B-H$ Group	$B-H-B$ Group	$B-B$ Group	$B-B-B$ Group	CH_3 Group	CH_2 Group	$C-H$ (i) Group	$C-C$ (a) Group
n_1	1	1	1	1	1	1	3	2	1	1	1	1	1	1	3	2	1	1
n_2	0	0	0	0	0	0	1	0	0	0	0	0	0	0	2	1	0	0
n_3	0	0	0	0	0	0	1	1	0	0	0	0	0	0	0	0	0	0
C_1	0.75	0.5	0.5	0.5	0.5	0.5	0.75	0.75	0.75	0.5	0.75	0.75	0.5	0.5	0.75	0.75	0.75	0.5
C_2	0.81231	0.81231	1	1	1	1	0.93613	0.93613	0.93613	0.80672	0.87442	0.87442	0.87442	0.87442	1	1	1	1
c_1	1	1	1	1	1	1	0.75	0.75	0.75	1	1	1	1	1	1	1	1	1
c_2	1	0.81231	0.91140	0.91140	0.91140	0.91140	1	0.94627	0.93383	0.80672	0.87442	0.87442	0.87442	0.87442	0.91771	0.91771	0.91771	0.91771
c_3	0	0	0	0	0	0	0	0	1	0	0	0	0	0	0	1	1	0
c_4	1	1	2	2	2	2	1	1	1	2	1	1	2	2	1	1	1	2
c_5	1	1	0	0	0	0	3	2	1	0	1	1	0	0	3	2	1	0
$C_{1\sigma}$	0.75	0.5	0.5	1	1	0.5	1	1.5	0.75	0.5	0.75	0.75	0.5	0.5	0.75	0.75	0.75	0.5
$C_{2\sigma}$	0.81231	0.81231	1	1	1	1	1.5	1	1	0.80672	0.87442	0.87442	0.87442	0.87442	1	1	1	1
V_e (eV)	-31.86906	-29.36199	-32.46339	-31.98456	-31.98456	-31.67393	-115.28799	-77.89897	-39.21967	-35.37850	-34.04561	-27.77951	-22.91867	-22.91867	-107.32728	-70.41425	-35.12015	-28.79214
V_p (eV)	10.56810	8.62881	9.80175	9.74677	9.74677	9.71067	41.66718	28.49191	14.35050	9.14602	11.97638	11.01833	8.01527	8.01527	38.92728	25.78002	12.87680	9.33352
T (eV)	7.88989	7.26921	8.42409	8.20698	8.20698	8.06719	42.77848	30.40957	15.53581	9.90839	10.05589	6.94488	4.54805	4.54805	32.53914	21.06675	10.48582	6.77464
V_m (eV)	-3.94494	-3.63460	-4.21204	-4.10349	-4.10349	-4.03359	-21.38924	-15.20478	-7.76790	-4.95420	-5.02794	-3.47244	-2.27402	-2.27402	-16.26957	-10.53337	-5.24291	-3.38732
$E_{(AO/HO)}$ (eV)	-11.80624	-11.80624	-14.63489	-14.63489	-14.63489	-14.63489	-14.53414	-14.53414	-14.53414	-11.80624	-11.80624	-11.80624	-11.80624	-11.80624	-15.56407	-15.56407	-14.63489	-15.56407
$\Delta E_{H_2MO(AO/HO)}$ (eV)	0	0	-1.44915	-1.13379	-1.13379	-0.92918	0	0	0	-1.44915	0	0	0	0	0	0	0	0
E_T $_{(AO/HO)}$ (eV)	-11.80624	-11.80624	-13.18574	-13.50110	-13.50110	-13.70571	-14.53414	-14.53414	-14.53414	-10.35710	-11.80624	-11.80624	-11.80624	-11.80624	-15.56407	-15.56407	-14.63489	-15.56407
$E_{(n_1AO/HO)}$ (eV)	0	0	0	0	0	0	-14.53414	-14.53414	0	0	0	0	0	0	0	0	0	0
E_T $_{(H_2MO)}$ (eV)	-29.16227	-28.90482	-31.63534	-31.63540	-31.63540	-31.63537	-66.76571	-48.73642	-31.63541	-31.63538	-28.84754	-25.09498	-24.43561	-24.43561	-67.69451	-49.66493	-31.63533	-31.63537
$E_T\left(atom-atom, nsp^3.AO\right)$ (eV)	-1.12740	1.19843	-1.44915	-1.13379	-1.13379	-0.92918	0	0	0	-1.44915	-0.56370	-2.25479	-2.25479	-3.38219	0	0	0	-1.85836
E_T $_{(MO)}$ (eV)	-30.28967	-27.70639	-33.08452	-32.76916	-32.76916	-32.56455	-66.76616	-48.73660	-31.63537	-33.08452	-29.41123	-29.60457	-26.69041	-27.81781	-67.69450	-49.66493	-31.63537	-33.49373
$\omega\left(10^{15}\ rad/s\right)$	16.6240	9.17969	18.9231	15.1983	26.0778	18.1298	56.8887	64.2189	47.0696	26.7757	15.2006	23.9931	6.83486	6.83486	24.9286	24.2751	24.1759	9.43699
E_K (eV)	10.94219	6.04223	12.45552	10.00377	17.16484	11.93333	37.44514	42.27003	30.98202	17.62425	10.00529	15.79265	4.49882	4.49882	16.40846	15.97831	15.91299	6.21159
$\bar{E}_D$ (eV)	-0.19822	-0.13474	-0.23100	-0.20505	-0.26859	-0.22255	-0.38298	-0.40690	-0.34836	-0.27478	-0.18405	-0.23275	-0.11200	-0.11673	-0.25352	-0.25017	-0.24966	-0.16515
$\bar{E}_{Kvib}$ (eV)	0.18779 [5]	0.18779 [5]	0.12944 [25]	0.12944 [25]	0.11159 [26]	0.12944 [25]	0.42695 [27]	0.40929 [28]	0.40696 [29]	0.11841 [11]	0.29346 [5]	0.09844 [6]	0.13035 [5]	0.13035 [5]	0.35532 (Eq. (13.458))	0.35532 (Eq. (13.458))	0.35532 (Eq. (13.458))	0.12312 [13]
$\bar{E}_{osc}$ (eV)	-0.10433	-0.04084	-0.16628	-0.14033	-0.21280	-0.15783	-0.16950	-0.20226	-0.14488	-0.21558	-0.03732	-0.18353	-0.04682	-0.05156	-0.22757	-0.14502	-0.07200	-0.10359
E_{mag} (eV)	0.07650	0.07650	0.14803	0.14803	0.14803	0.14803	0.14185	0.14803	0.14803	0.14803	0.07650	0.07650	0.07650	0.07650	0.14803	0.14803	0.14803	0.14803
E_T $_{(Group)}$ (eV)	-30.39399	-27.74723	-33.25079	-32.90949	-32.98196	-32.72238	-67.27466	-49.14112	-31.78025	-33.30009	-29.44855	-29.78809	-26.73723	-27.86936	-67.92207	-49.80996	-31.70737	-33.59732
$E_{initial(c_1AO/HO)}$ (eV)	-11.80624	-11.80624	-14.63489	-14.63489	-14.63489	-14.63489	-14.53414	-14.53414	-14.53414	-14.63489	-11.80624	-11.80624	-11.80624	-11.80624	-14.63489	-14.63489	-14.63489	-14.63489
$E_{initial(c_5AO/HO)}$ (eV)	-14.53414	-14.53414	0	0	0	0	-13.59844	-13.59844	-13.59844	0	-13.59844	-13.59844	0	0	-13.59844	-13.59844	-13.59844	0
$E_{D(Group)}$ (eV)	4.05361	1.40685	3.98101	3.63971	3.71218	3.45260	11.94520	7.41010	3.50582	4.03031	4.04387	4.38341	3.12475	4.25687	12.49186	7.83016	3.32601	4.32754
Exp. $E_{D(Group)}$ (eV)	4.03164 [9-55] (BN)																	

Table 22.26. The total bond energies of tertiary and quaternary amino boranes and borane amines calculated using the functional group composition and the energies of Table 22.25 compared to the experimental values.

Formula	Name	$B-N$ (i) Group	$B-N$ (ii) Group	$C-N$ (i) Group	$C-N$ (ii) Group	$C-N$ (iii) Group	$C-N$ (iv) Group	NH_2 Group	NH_2 Group	NH Group	$C-B$ Group	$B-H$ Group	$B-H-B$ Group	$B-B$ Group	CH_3	CH_2	CH (i)	$C-C$ (a)	Calculated Total Bond Energy (eV)	Experimental Total Bond Energy (eV)	Relative Error
B_2H_7N	aminodiborane	1	0	0	0	0	0	0	1	0	0	3	2	0	0	0	0	0	32.36213	31.99218 [16]	-0.01156
$B_2C_2H_{11}N$	n-dimethylaminodiborane	1	0	0	2	0	0	0	0	0	0	3	2	0	2	0	0	0	57.21517	57.52855 [17]	0.00545
$C_6H_{18}N_3B$	tris(dimethylamino)borane	3	0	0	6	0	0	0	0	0	0	0	0	0	6	0	0	0	108.95023	108.64490 [18]	-0.00281
$C_8H_{20}NB$	di-n-butylboronamine	1	0	0	0	0	0	0	1	0	2	0	0	0	2	6	0	6	117.45425	119.49184 [a] [18]	0.01705
$C_{12}H_{28}NB$	di-n-butylboron-n-butylamine	1	0	1	0	0	0	0	0	1	2	0	0	0	3	9	0	9	166.49595	167.83269 [a] [18]	0.00796
$C_2H_{10}NB$	dimethylaminoborane	0	1	0	2	0	0	0	0	1	0	3	0	0	2	0	0	0	49.30740	49.52189 [18]	0.00433
$BC_3H_{12}N$	trimethylaminoborane	0	1	0	0	0	3	0	0	0	0	3	0	0	3	0	0	0	61.37183	61.05205 [16]	-0.00524
$BC_3H_{12}N$	ammonia-trimethylborane	0	1	0	0	0	0	1	0	0	3	0	0	0	3	0	0	0	62.91857	62.52207 [16]	-0.00634
$C_6H_{18}NB$	triethylaminoborane	0	1	0	0	0	3	0	0	0	0	3	0	0	3	3	0	3	97.84493	97.42044 [18]	-0.00436
$BC_6H_{18}N$	trimethylaminotrimethylborane	0	1	0	0	0	3	0	0	0	3	0	0	0	6	0	0	0	98.80674	98.27036 [17]	-0.00546

[a] Crystal.

Table 22.27. The bond angle parameters of tertiary and quaternary amino boranes and borane amines and experimental values. H_t is a terminal or two-center H. H_b is a bridge or three-center H. In the calculation of θ_v, the parameters from the preceding angle were used. E_T is E_T (*atom - atom msp³.AO*).

Atoms of Angle	2c' Bond 1 (a_0)	2c' Bond 2 (a_0)	2c' Terminal Atoms (a_0)	$E_{Coulombic}$ Atom 1	Atom 1 Hybridization Designation (Table)	$E_{Coulombic}$ Atom 2	Atom 2 Hybridization Designation (Table)	c_2 Atom 1	c_2 Atom 2	C_1	C_2	c_1	c_2'	E_T (eV)	θ_v (°)	θ_1 (°)	θ_2 (°)	Cal. θ (°)	Exp. θ (°)
$\angle NBN$ ($B-N$ (i) & $C-N$ (ii))	2.57488	2.57488	4.4721	-16.52324	2 (22.21)	-16.52324	2 (22.21)	0.82343	0.82343	1	1	1	0.82343	-1.65376				120.55	
$\angle CNB$ ($B-N$ (ii) & $C-N$ (iv))	2.80224	3.15357	4.8531	-15.29034	1 (22.21)			0.88983	0.81231 (Eq. (22.48))	1	0.80672 (Eq. (22.40))	1	0.81508	-0.72457				109.00	109.9 [17] $((CH_3)_3NBH_3)$
$\angle HBN$ ($B-N$ (ii) & $C-N$ (iv))	2.27211	3.15357	4.2895	-11.89724	B	-14.53414	N	0.87442 (Eq. (22.29))	0.93613	0.75	1	0.75	1.07056	0				103.28	105.3 [17] $((CH_3)_3NBH_3)$
$\angle HNB$ ($B-N$ (ii)	1.95921	3.15357	4.2776	-14.53414	N	-11.89724	B	0.93613	0.87442 (Eq. (22.29))	0.75	0.87442 (Eq. (22.29))	0.75	0.93409	0				111.43	110.3 [17] (H_3NBH_3)
$\angle HNH$	1.91013	1.91013	3.0984	-14.53414	N	H	H	0.94627 Eq. (15.134))	1	1	1	0.75	1.05679	0				108.40	107.1 [10] (methylamine)
$\angle HNC_a$ ($C-N$ (i))	1.91013	2.77620	3.8816	-14.53414	N	-15.35946	5 (15.3A)	0.91140 (Eq. (15.135))	0.88583	0.75	1	0.75	0.97194	0				110.48	110.3 [10] (methylamine)
$\angle HCN$ ($C-N$ (i) & (ii))	2.09711	2.79186	4.0661	-14.82575	1 (15.3A)	-14.53414	N	0.91771	0.93383 (Eq. (15.136))	0.75	1	0.75	1.01756	0				111.76	112 [10] (dimethylamine)
$\angle HNC_a$ ($C-N$ (ii) & (iii))	1.89621	2.79186	3.8123	-14.53414	N	-15.56407 (Eq. (15.136))	7 (15.3A)	0.91140 (Eq. (15.135))	0.87418	0.75	1	0.75	0.95917	0				107.27	107 [10] (dimethylamine)
$\angle CNC$ ($C-N$ (ii) & (iii))	2.79186	2.79186	4.6260	-17.04640	33 (15.3A)	-17.04640	33 (15.3A)	0.79816	0.79816	1	1	1	0.79816	-1.85836				111.89	111.8 [10] (dimethylamine)
$\angle CNC$ ($C-N$ (iv))	2.80224	2.80224	4.6043	-17.14871	36 (15.3A)	-17.14871	36 (15.3A)	0.79340	0.79340	1	1	1	0.79340	-1.85836				110.48	110.9 [10] (trimethylamine)
$\angle H_tBH_t$	2.27211	2.27211	3.9623	-13.61667	2 (22.1)	H	H	0.99920	1	1	1	0.75	1.00080	-1.71943				121.37	122 [10] (diborane)
$\angle H_tBH_b$	2.27211	2.46967	3.8210	-14.71574	4 (22.1)	H	H	0.92458	1	1	1	0.75	1.08158	-1.12740				107.30	108.9 [2] (B_4H_{10})
$\angle H_bBH_b$	2.46967	2.46967	3.6606	-14.26508	3 (22.1)	H	H	0.95378	1	1	1	0.75	1.04846	-1.12740				95.65	95.0 [2] (B_4H_{10})
$\angle BH_bB$	2.46967	2.46967	3.4358	-11.89724 B_a	1 (22.1)	-11.89724 B_b	1 (22.1)	1	1	1	1.14361	1	1	0				88.15	87.7 [2] (B_4H_{10})
Methylene $\angle HC_aH$	2.11106	2.11106	3.4252	-15.75493	7 (15.3A)	H	H	0.86359	1	1	1	0.75	1.15796	0				108.44	107 [10] (dimethylamine) 107 [10] (propane)
$\angle C_aC_bC_c$															69.51			110.49	112 [10] (propane) 113.8 [10] (butane) 110.8 [10] (isobutane)
$\angle C_aC_bH$															69.51			110.49	111.0 [10] (butane) 111.4 [10] (isobutane)
Methyl $\angle HC_aH$	2.09711	2.09711	3.4252	-15.75493	7 (15.3A)	H	H	0.86359	1	1	1	0.75	1.15796	0				109.50	
$\angle C_aC_bC_c$															70.56			109.44	
$\angle C_aC_bH$															70.56			109.44	

HALIDOBORANES

The halidoboranes each comprise at least one B bound by a boron-halogen single bond comprising a $B-X$ group where $X=F,Cl,Br,I$, and may further comprise one or more alkyl groups and borane moieties. The latter comprise alkyl and aryl moieties and $B-C$, $B-H$, $B-B$, $B-H-B$, and $B-B-B$ functional groups wherein the $B-C$ group is equivalent to that of alkyl boranes, and the $B-H$, $B-B$, $B-H-B$, and $B-B-B$ functional groups are equivalent to those in boranes given in the corresponding sections. Alkoxy boranes and borinic acids moieties given in the Alkoxy Boranes and Alkyl Borinic Acids ($(RO)_q B_r H_s (HO)_t$) section may be bound to the $B-X$ group by a $B-O$ functional group. The former further comprise at least one boron-alkyl-ether moiety, and the latter comprise one or more hydroxyl groups, respectively. Each alkoxy moiety, $C_nH_{2n+1}O$, comprises one of two types of $C-O$ functional groups that are equivalent to those given in the Ethers ($C_nH_{2n+2}O_m,\ n=2,3,4,5...\infty$) section. One is for methyl or t-butyl groups, and the other is for general alkyl groups. Each borinic acid hydroxyl functional group is equivalent to that given in the Alcohols ($C_nH_{2n+2}O_m,\ n=1,2,3,4,5...\infty$) section.

Tertiary amino-borane and borane-amine moieties given in the Tertiary and Quaternary Aminoboranes and Borane Amines ($R_qB_rN_sR_t; R=H; alkyl$) section can be bound to the $B-X$ group by a $B-N$ functional group. The nitrogen atom of each $B-N$ functional group is bound to two other atoms such that there are a total of three bonds per atom. The amino or amine moiety may comprise NH_2, $N(H)R$, and NR_2. The corresponding functional group for the NH_2 moiety is the NH_2 functional group given in the Primary Amines **(**$C_nH_{2n+2+m}N_m,\ n=1,2,3,4,5...\infty$**)** section. The $N(H)R$ moiety comprises the NH functional group of the Secondary Amines ($C_nH_{2n+2+m}N_m,\ n=2,3,4,5...\infty$) section and the $C-N$ functional group of the Primary Amines **(**$C_nH_{2n+2+m}N_m,\ n=1,2,3,4,5...\infty$**)** section. The NR_2 moiety comprises two types of $C-N$ functional groups, one for the methyl group corresponding to the C of $C-N$ and the other for general alkyl secondary amines given in the Secondary Amines ($C_nH_{2n+2+m}N_m,\ n=2,3,4,5...\infty$) section.

Quaternary amino-borane and boraneamine moieties given in the Tertiary and Quaternary Aminoboranes and Borane Amines ($R_qB_rN_sR_t; R=H; alkyl$) section can be bound to the $B-X$ group by a $B-N$ functional group. The nitrogen atom of each $B-N$ bond is bound to three other atoms such that there are a total of four bonds per atom. The amino or amine moiety may comprise NH_3, $N(H_2)R$, $N(H)R_2$, and NR_3. The corresponding functional group for the NH_3 moiety is ammonia given in the Ammonia (NH_3) section. The $N(H_2)R$ moiety comprises the NH_2 and the $C-N$ functional groups given in the Primary Amines **(**$C_nH_{2n+2+m}N_m,\ n=1,2,3,4,5...\infty$**)** section. The $N(H)R_2$ moiety comprises the NH functional group and two types of $C-N$ functional groups, one for the methyl group corresponding to the C of $C-N$ and the other for general alkyl secondary amines given in the Secondary Amines ($C_nH_{2n+2+m}N_m,\ n=2,3,4,5...\infty$) section. The NR_3 moiety comprises the $C-N$ functional group of tertiary amines given in the Tertiary Amines ($C_nH_{2n+3}N,\ n=3,4,5...\infty$) section.

The alkyl portion may be part of the alkoxy moiety, amino or amine moiety, or an alkyl group, or it may be bound to the central boron atom by a carbon-boron single bond comprising the $C-B$ group of the Alkyl Boranes ($R_xB_yH_z; R=alkyl$) section. Each alkyl portion may comprise at least a terminal methyl group (CH_3) and methylene (CH_2), methylyne (CH), and $C-C$ functional groups. The methyl and methylene functional groups are equivalent to those of straight-chain alkanes. Six types of $C-C$ bonds can be identified. The n-alkane $C-C$ bond is the same as that of straight-chain alkanes. In addition, the $C-C$ bonds within isopropyl ($(CH_3)_2CH$) and t-butyl ($(CH_3)_3C$) groups and the isopropyl to isopropyl, isopropyl to t-butyl, and t-butyl to t-butyl $C-C$ bonds comprise functional groups. Additional R groups include aromatics such as phenyl and $-HC=CH_2$. These groups in halidobroanes are equivalent to those in branched-chain alkanes, aromatics, and alkenes given in the corresponding sections.

The bonding in the $B-X$ functional groups of halidoboranes is similar to that of the $B-O$ and $B-N$ groups of alkoxy boranes and borinic acids and tertiary and quaternary amino boranes and borane amines given in the corresponding sections. The MO semimajor axes of the $B-X$ functional groups are determined from the force balance equation of the centrifugal, Coulombic, and magnetic forces as given in the Boranes (B_xH_y) section. In each case, the distance from the origin of the H_2-type-ellipsoidal-MO to each focus c', the internuclear distance $2c'$, and the length of the semiminor axis of the prolate spheroidal H_2-type MO $b=c$ are solved from the semimajor axis a. Then, the geometric and energy parameters of each MO are calculated using Eqs. (15.1-15.117).

As in the case of the $B-O$- and $B-N$-bond MOs, the σ-MOs of the $B-X$-bond MOs are energy matched to the $B2sp^3$ HO which determines that the parameters of the force balance equation based on electron angular momentum are determined by those of the boron atom. The parameters of the force balance equation for the σ-MO of the $B-F$-bond MO in Eqs. (22.18-22.22) are $n_e=1$ and $|L|=0$:

$$\frac{\hbar^2}{m_e a^2 b^2}D=\frac{e^2}{8\pi\varepsilon_0 ab^2}D+\frac{\hbar^2}{2m_e a^2 b^2}D-\left(\frac{1}{2}\right)\frac{\hbar^2}{2m_e a^2 b^2}D \tag{22.53}$$

From Eq. (22.53), the semimajor axis of the tertiary *B* - *F* -bond MO is

$$a = 1.5a_0 \tag{22.54}$$

The force balance equation for each σ-MO of the $B-Cl$ is equivalent to that of the $B-B$-bond MO with $n_e = 2$ and $|L| = 3\sqrt{\frac{3}{4}}\hbar$ corresponding to three electrons of the $B2sp^3$ shell is**:**

$$\frac{\hbar^2}{m_e a^2 b^2} D = \frac{e^2}{8\pi\varepsilon_0 ab^2} D + \frac{\hbar^2}{2m_e a^2 b^2} D - \left(1 + \frac{3\sqrt{\frac{3}{4}}}{Z}\right) \frac{\hbar^2}{2m_e a^2 b^2} D \tag{22.55}$$

$$a = \left(2 + \frac{3\sqrt{\frac{3}{4}}}{Z}\right) a_0 \tag{22.56}$$

With $Z = 5$, the semimajor axis of the $B-Cl$ -bond MO is:

$$a = 2.51962a_0 \tag{22.57}$$

The hybridization of the bonding in the *B* - *X* functional groups of halidoboranes is similar to that of the *C* - *X* groups of alkyl halides given in the corresponding sections. For the *B* - *X* functional groups, hybridization of the 2*s* and 2*p* AOs of *B* to form single $2sp^3$ shells forms an energy minimum, and the sharing of electrons between the $B2sp^3$ HO and *X* AO to form a MO permits each participating orbital to decrease in radius and energy. The *F* AO has an energy of $E(F) = -17.42282\ eV$, and the $B2sp^3$ HOs have an energy of $E\left(B, 2sp^3\right) = -11.80624\ eV$ (Eq. (22.7)). To meet the equipotential condition of the union of the $B-F$ H_2-type-ellipsoidal-MO with these orbitals, the hybridization factor c_2 of Eq. (15.61) for the $B-F$ -bond MO given by Eq. (15.77) is:

$$c_2\left(FAO\ to\ B2sp^3 HO\right) = \frac{E\left(B, 2sp^3\right)}{E\left(FAO\right)} = \frac{-11.80624\ eV}{-17.42282\ eV} = 0.68285 \tag{22.58}$$

Since the energy of the MO is matched to that of the $B2sp^3$ HO, $E\left(AO/HO\right)$ in Eqs. (15.51) and (15.61) is $E\left(B, 2sp^3\right)$ given by Eq. (22.7).

$E_T\left(atom-atom, msp^3.AO\right)$ of the $B-F$ -bond MO is determined by considering that the bond involves an electron transfer from the boron atom to the fluorine atom to form zwitterions such as $H_2B^+ - F^-$. By considering the electron redistribution in the fluoroborane as well as the fact that the central field decreases by an integer for each successive electron of the shell, the radius $r_{B-Fborane2sp^3}$ of the $B2sp^3$ shell may be calculated from the Coulombic energy using Eq. (15.18).

$$r_{B-Fborane2sp^3} = \left(\sum_{n=2}^{4}(Z-n) - 1\right) \frac{e^2}{8\pi\varepsilon_0\left(e74.89168\ eV\right)} = \frac{5e^2}{8\pi\varepsilon_0\left(e74.89168\ eV\right)} = 0.90837a_0 \tag{22.59}$$

Using Eqs. (15.19) and (22.13), the Coulombic energy $E_{Coulomb}\left(B_{B-Fborane}, 2sp^3\right)$ of the outer electron of the $B2sp^3$ shell is:

$$E_{Coulomb}\left(B_{B-Fborane}, 2sp^3\right) = \frac{-e^2}{8\pi\varepsilon_0 r_{B-Fborane2sp^3}} = \frac{-e^2}{8\pi\varepsilon_0 0.90837a_0} = -14.97834\ eV \tag{22.60}$$

During hybridization, one of the spin-paired 2*s* electrons is promoted to the $B2sp^3$ shell as an unpaired electron. The energy for the promotion is the magnetic energy given by Eq. (22.6). Using Eqs. (22.6) and (22.60), the energy $E\left(B_{B-Xborane}, 2sp^3\right)$ of the outer electron of the $B2sp^3$ shell is:

$$E\left(B_{B-Fborane}, 2sp^3\right) = \frac{-e^2}{8\pi\varepsilon_0 r_{B-Fborane2sp^3}} + \frac{2\pi\mu_0 e^2\hbar^2}{m_e^2\left(r_3\right)^3} = -14.97834\ eV + 0.09100\ eV = -14.88734\ eV \tag{22.61}$$

Thus, $E_T\left(B-F, 2sp^3\right)$, the energy change of each $B2sp^3$ shell with the formation of the $B-F$ -bond MO is given by the difference between Eq. (22.15) and Eq. (22.7).

$$E_T\left(B-F, 2sp^3\right) = E\left(B_{B-Fborane}, 2sp^3\right) - E\left(B, 2sp^3\right) = -14.88734\ eV - \left(-11.80624\ eV\right) = -3.08109\ eV \tag{22.62}$$

Thus, $E_T\left(atom-atom, msp^3.AO\right)$ for ternary $B-F$ is $-6.16219\ eV$ corresponding to the maximum charge contribution of an electron given by two times Eq. (22.62).

In chloroboranes, the energies of chlorine and boron are less than the Coulombic energy between the electron and proton of *H* given by Eq. (1.264). Thus, c_1 and c_2 in Eq. (15.61) are one, and the energy matching condition is determined by the C_2 parameter. The *Cl* AO has an energy of $E(Cl) = -12.96764\ eV$, and the $B2sp^3$ HOs have an energy of $E(B,2sp^3) = -11.80624\ eV$ (Eq. (22.7)). To meet the equipotential condition of the union of the *B* - *Cl* H_2-type-ellipsoidal-MO with these orbitals, the hybridization factor c_2 of Eq. (15.61) for the *B* - *Cl* -bond MO given by Eq. (15.77) is:

$$C_2\left(ClAO\ to\ B2sp^3HO\right)=\frac{E\left(B,2sp^3\right)}{E\left(ClAO\right)}=\frac{-11.80624\ eV}{-12.96764\ eV}=0.91044 \tag{22.63}$$

Since the energy of the MO is matched to that of the $B2sp^3$ HO, $E\left(AO/HO\right)$ in Eqs. (15.51) and (15.61) is $E\left(B,2sp^3\right)$ given by Eq. (22.7), and $E_T\left(atom-atom,msp^3.AO\right)$ is given by two times Eq. (22.12) corresponding to the two centers.

Consider next the radius of the HO due to the contribution of charge to more than one bond. The energy contribution due to the charge donation at each boron atom and halogen atom superimposes linearly. In general, since the energy of the $B2sp^3$ HO and X AO is matched to that of the $C2sp^3$ HO when a molecule contains a $C-B$-bond MO and a $C-X$-bond MO, respectively, the corresponding radius $r_{mol\,2sp^3}$ of the $B2sp^3$ HO of a boron atom, the $C2sp^3$ HO of a carbon atom, and the X AO of a given halidoborane molecule is calculated after Eq. (15.32) by considering $\sum E_{T_{mol}}\left(MO,2sp^3\right)$, the total energy donation to all bonds with which it participates in bonding. The Coulombic energy $E_{Coulomb}\left(atom,2sp^3\right)$ of the outer electron of the $atom$ $2sp^3$ shell considering the charge donation to all participating bonds is given by Eq. (15.14). In the case that the boron or halogen atom is not bound to a $C2sp^3$ HO, $r_{mol\,2sp^3}$ is calculated using Eq. (15.31) where $E_{Coulomb}\left(atom,msp^3\right)$ is $E_{Coulomb}\left(B2sp^3\right)=-11.89724\ eV$, $E\left(F\right)=-17.42282\ eV$, or $E\left(Cl\right)=-12.96764\ eV$. The hybridization parameters used in Eqs. (15.88-15.117) for the determination of bond angles of halidoboranes are given in Table 22.28.

Table 22.28. Atom hybridization designation (# first column) and hybridization parameters of atoms for determination of bond angles with final values of r_{2sp^3}, $E_{Coulomb}\left(atom,2sp^3\right)$ (designated as $E_{Coulomb}$), and $E\left(atom_{B-Xborane}2sp^3\right)$ (designated as E) calculated using the appropriate values of $\sum E_{T_{mol}}\left(MO,2sp^3\right)$ (designated as E_T) for each corresponding terminal bond spanning each angle.

#	E_T	E_T	E_T	E_T	E_T	r_{3sp^3} Final	$E_{Coulomb}$ (eV) Final	E (eV) Final
1	-0.56370	0	0	0	0	0.95939 (Eq. (15.31))	-14.18175	
2	-3.08109	-3.08109	0	0	0	0.75339 (Eq. (15.31))	-18.05943	-17.96843
3	-3.08109	0	0		0	0.66357 (Eq. (15.31))	-20.50391	-20.26346

The symbols of the functional groups of halidoboranes are given in Table 22.29. The geometrical (Eqs. (15.1-15.5) and (22.47)), intercept (Eqs. (15.31-15.32) and (15.80-15.87)), and energy (Eq. (15.61), (22.4), (22.7), (22.12), (22.48), and (22.52)) parameters of halidoboranes are given in Tables 22.30, 22.31, and 22.32, respectively. In the case that the MO does not intercept the B HO due to the reduction of the radius from the donation of B $2sp^3$ HO charge to additional MOs, the energy of each MO is energy matched as a linear sum to the B HO by contacting it through the bisector current of the intersecting MOs as described in the Methane Molecule (CH_4) section. The total energy of each halidoborane given in Table 22.33 was calculated as the sum over the integer multiple of each $E_{D\,(Group)}$ of Table 22.32 corresponding to functional-group composition of the molecule. E_{mag} of Table 22.33 is given by Eqs. (15.15) and (22.3) for the $B-X$ groups and the $B-O$, $B-N$, $B-H$, $B-B$, $B-H-B$, and $B-B-B$ groups. E_{mag} of Table 22.33 is given by Eqs. (15.15) and (10.162) for the OH group. The bond angle parameters of halidoboranes determined using Eqs. (15.88-15.117) are given in Table 22.34. The charge-densities of exemplary fluoroborane, boron trifluoride and choloroborane, boron trichloride comprising the concentric shells of atoms with the outer shell bridged by one or more H_2-type ellipsoidal MOs or joined with one or more hydrogen MOs are shown in Figures 22.9 and 22.10, respectively.

Figure 22.10. (A) *Boron Trifluoride*. Color scale, translucent view of the charge-density of BF_3 showing the orbitals of the *B* and *F* atoms at their radii, and the ellipsoidal surface of each H_2-type ellipsoidal MO that transitions to the corresponding outer shell of the atoms participating in each bond. (B) *Boron Trichloride.* Color scale, translucent views of the charge-density of BCl_3 showing the orbitals of the *B* and *Cl* atoms at their radii, and the ellipsoidal surface of each H_2-type ellipsoidal MO that transitions to the corresponding outer shell of the atoms participating in each bond.

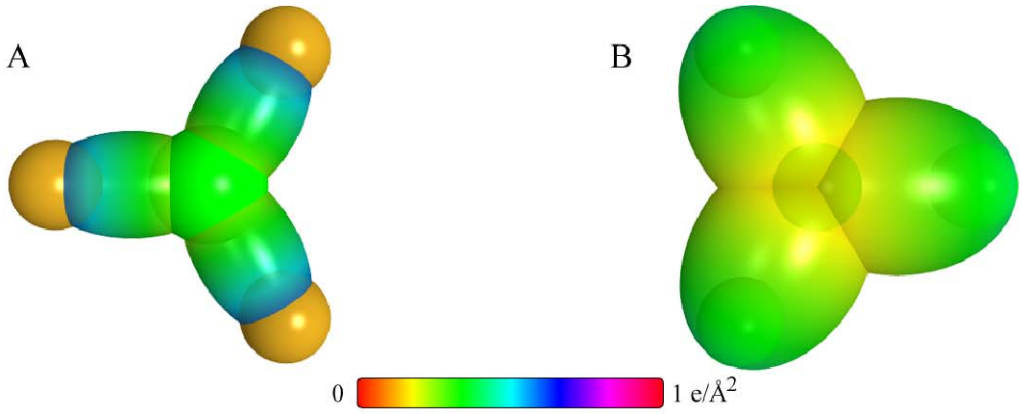

Table 22.29. The symbols of the functional groups of halidoboranes.

Functional Group	Group Symbol
B-F bond	$B-F$
B-Cl bond	$B-Cl$
B-N bond 3°	$B-N$ (i)
B-N bond 4°	$B-N$ (ii)
C-N bond 1° amine	$C-N$ (i)
C-N bond 2° amine (methyl)	$C-N$ (ii)
C-N bond 2° amine (alkyl)	$C-N$ (iii)
C-N bond 3° amine	$C-N$ (iv)
NH_3 group	NH_3
NH_2 group	NH_2
NH group	NH
B-O bond (borinic acid)	$B-O$ (i)
B-O bond (alkoxy borane)	$B-O$ (ii)
OH group	OH
C-O (CH_3-O- and $(CH_3)_3C-O-$)	$C-O$ (i)
C-O (alkyl)	$C-O$ (ii)
C-B bond	$C-B$
BH bond	$B-H$
BHB (bridged *H*)	$B-H-B$
BB bond	$B-B$
BBB (bridged *B*)	$B-B-B$
CC (aromatic bond)	$C\overset{3e}{=}C$
CH (aromatic)	CH (i)
CH_3 group	$C-H\ (CH_3)$
CH_2 alkyl group	$C-H\ (CH_2)$ (i)
CH	$C-H$ (ii)
CC bond (*n-C*)	$C-C$ (a)
CC bond (*iso-C*)	$C-C$ (b)
$HC = CH_2HC$ (ethylene bond)	$C=C$
CH_2 alkenyl group	CH_2 (ii)

Table 22.30A. The geometrical bond parameters of halidoboranes and experimental values.

Parameter	$B-F$ Group	$B-Cl$ Group	$B-N$ (i) Group	$B-N$ (ii) Group	$C-N$ (i) Group	$C-N$ (ii) Group	$C-N$ (iii) Group	$C-N$ (iv) Group	NH_3 Group	NH_2 Group	NH Group	$B-O$ (i) Group	$B-O$ (ii) Group	OH Group	$C-O$ (i) Group
$a\ (a_0)$	1.5	2.51962	2.01962	2.01962	1.92682	1.94862	1.94862	1.96313	1.34750	1.28083	1.26224	2.00000	2.00000	1.26430	1.80717
$c'\ (a_0)$	1.22474	1.66357	1.28744	1.57679	1.38810	1.39593	1.39593	1.40112	0.97961	0.95506	0.94811	1.31678	1.29455	0.91808	1.34431
Bond Length $2c'\ (\AA)$	1.29621	1.76065	1.36257	1.66880	1.46910	1.47739	1.47739	1.48288	1.03677	1.0108	1.00343	1.39362	1.37009	0.971651	1.42276
Exp. Bond Length $(\AA)$	1.313 [10] (BF_3)	1.761 [17] ($PhBCl_2$)	1.281 [5] (BN)	1.638 [17] ($(CH_3)_3NBH_3$)	1.471 [10] (methylamine)	1.455 [10] (dimethylamine)		1.458 [10] (trimethylamine)	1.0120 [10] (ammonia)	1.010 [10] (methylamine)	1.00 [10] (dimethylamine)	1.376 [17] ($B(OH)_3$)	1.367 [17] ($B(OCH_3)_3$)	0.971 [10] (ethanol) 0.9451 [10] (methanol)	1.424 [17] ($B(OCH_3)_3$) 1.416 [10] (dimethyl ether)
$b, c\ (a_0)$	0.86603	1.89235	1.55607	1.26198	1.33634	1.35960	1.35960	1.37505	0.92527	0.85345	0.83327	1.50535	1.52452	0.86925	1.20776
e	0.81650	0.66025	0.63747	0.78074	0.72041	0.71637	0.71637	0.71372	0.72698	0.74566	0.75113	0.65839	0.64727	0.72615	0.74388

Table 22.30B. The geometrical bond parameters of halidoboranes and experimental values.

Parameter	$C-O$ (ii) Group	$C-B$ Group	$B-H$ Group	$B-H-B$ Group	$B-B$ and $B-B-B$ Groups	$C^{3e}=C$ Group	CH (i) Group	$C-H\ (CH_3)$ Group	$C-H\ (CH_2)$ (i) Group	$C-H$ (ii) Group	$C-C$ (a) Group	$C-C$ (b) Group	$C=C$ Group	CH_2 (ii) Group
$a\ (a_0)$	1.79473	1.78528	1.69282	2.00000	2.51962	1.47348	1.60061	1.64920	1.67122	1.67465	2.12499	2.12499	1.47228	1.64010
$c'\ (a_0)$	1.33968	1.48762	1.13605	1.23483	1.69749	1.31468	1.03299	1.04856	1.05553	1.05661	1.45744	1.45744	1.26661	1.04566
Bond Length $2c'\ (\AA)$	1.41785	1.57443	1.20235	1.30689	1.79654	1.39140	1.09327	1.10974	1.11713	1.11827	1.54280	1.54280	1.34052	1.10668
Exp. Bond Length $(\AA)$	1.418 [10] (ethyl methyl ether (avg.))	1.578 [10] (trimethylborane) 1.580 [10] (1,2-dimethyldiborane)	1.19 [4] (diborane)	1.32 [4] (diborane)	1.798 [3] ($B_{13}H_{19}$)	1.39 [10] (benzene)	1.101 [10] (benzene)	1.114 [10] ($C-H$ trimethylborane) 1.107 [10] ($C-H$ propane) 1.117 [10] ($C-H$ butane)	1.107 [10] ($C-H$ propane) 1.117 [10] ($C-H$ butane)	1.122 [10] (isobutane)	1.532 [10] (propane) 1.531 [10] (butane)	1.532 [10] (propane) 1.531 [10] (butane)	1.342 [10] (2-methylpropene) 1.346 [10] (2-butene) 1.349 [10] (1,3-butadiene)	1.10 [10] (2-methylpropene) 1.108 (avg.) [10] (1,3-butadiene)
$b, c\ (a_0)$	1.19429	0.98702	1.25500	1.57327	1.86199	0.66540	1.22265	1.27295	1.29569	1.29924	1.54616	1.54616	0.75055	1.26354
e	0.74645	0.83327	0.67110	0.61742	0.67371	0.89223	0.64537	0.63580	0.63159	0.63095	0.68600	0.68600	0.86030	0.63756

Table 22.31. The MO to HO intercept geometrical bond parameters of exemplary halidoboranes F_2BOH, BF_3, F_2BCH_3, $(CH_3O)_2\,BCl$, and BCl. E_T is E_T (*atom - atom* msp^3.*AO*).

Bond	Atom	E_T (eV) Bond 1	E_T (eV) Bond 2	E_T (eV) Bond 3	E_T (eV) Bond 4	Final Tctal Energy $B2sp^3$ (eV)	$r_{initial}$ (a_0)	r_{final} (a_0)	$E_{Coulomb}\left(B2sp^3\right)$(eV) Final	$E\left(B2sp^3\right)$ (eV) Final	θ' (°)	θ_1 (°)	θ_2 (°)	d_1 (a_0)	d_2 (a_0)
$BO-H\ (F_2BOH)$	O	-0.56370	0	0	0		1.00000	0.95939	-14.18175		121.28	58.72	70.60	0.41990	0.49818
$-B-OH\ (F_2BOH)$ $(B-O$ (i))	O	-0.56370	0	0	0		1.00000	0.95939	-14.18175		74.04	105.96	37.79	1.58054	0.26376
$-B-OH\ (F_2BOH)$ $(B-O$ (i))	B	-0.56370	-3.08109	-3.08109	0	-81.61757	1.14361	0.73059	-18.62313	-18.53213	33.21	146.79	15.41	1.92806	0.61128
$B-F\ (F_2BOH)$	B	-3.08109	-3.08109	-0.56370	0		1.14361	0.73059	-18.62313	-18.53213	112.74	67.26	51.08	0.94234	0.28241
$B-F\ (F_2BOH)$	F	-3.08109	0	0	0		0.78069	0.66357	-20.50391	-20.26346	107.57	72.43	46.93	1.02441	0.20033
$B-F\ (BF_3)$	B	-3.08109	-3.08109	-3.08109	0		1.14361	0.64359	-21.14052	-21.04952	105.86	74.14	45.63	1.04889	0.17586
$B-F\ (BF_3)$	F	-3.08109	0	0	0		0.78069	0.66357	-20.50391	-20.26346	107.57	72.43	46.93	1.02441	0.20033
$C-H\ (BCH_3)$	C	-0.72457	0	0	0	-152.34026	0.91771	0.87495	-15.55033	-15.35946	78.85	101.15	42.40	1.21777	0.16921
$C-B\ (-B-CH_3)$	C	-0.72457	0	0	0	-152.34026	0.91771	0.87495	-15.55033	-15.35946	116.85	63.15	52.27	1.09248	0.39514
$C-B\ (-B-CH_3)$	B	-0.72457	-3.08109	-3.08109	0		1.14361	0.62663	-21.71251	-21.62151	98.92	81.08	38.84	1.39048	0.09714
$B-F\ (F_2BCH_3)$	B	-3.08109	-3.08109	-0.72457	0		1.14361	0.62663	-21.71251	-21.62151	104.33	75.67	44.51	1.06965	0.15509
$B-F\ (F_2BCH_3)$	F	-3.08109	0	0	0		0.78069	0.66357	-20.50391	-20.26346	107.52	72.43	46.93	1.02441	0.20033
$C-H\ (OC_aH_3)$	C_a	-0.72457	0	0	0	-152.34026	0.91771	0.87495	-15.55033	-15.35946	78.85	101.15	42.40	1.21777	0.16921
$BO-C_aH_3$ $BO-C_a(CH_3)_3$ $(C-O$ (i))	C_a	-0.72457	0	0	0	-152.34026	0.91771	0.87495	-15.55033	-15.35946	95.98	84.02	46.10	1.25319	0.09112
$BO-C_aH_3$ $BO-C_a(CH_3)_3$ $(C-O$ (i))	O	-0.72457	-0.56370	0	0		1.00000	0.84435	-16.11402		93.39	86.61	44.26	1.29433	0.04998
$ClB-(OCH_3)_2$ $(B-O$ (ii))	B	-0.56370	-0.56370	-1.12740	0	-77.14647	1.14361	0.96140	-14.15204	-14.06104	71.19	108.81	36.65	1.60458	0.31003
$ClB-(OCH_3)_2$ $(B-O$ (ii); $(C-O$ (i))	O	-0.56370	-0.72457	0	0		1.00000	0.84435	-16.11402		54.45	125.55	26.78	1.78542	0.49088
$B-Cl\ \left(ClB(OCH_3)_2\right)$	B	-1.12740	-0.56370	-0.56370	0		1.14361	0.96140	-14.15203	-14.06103	43.58	136.42	20.50	2.36004	0.69647
$B-Cl\ \left(ClB(OCH_3)_2\right)$	Cl	-1.12740	0	0	0		1.05158	0.96529	-14.09504	-13.99665	44.32	135.68	20.88	2.35415	0.69058
$B-Cl\ (BCl_3)$	B	-1.12740	-1.12740	-1.12740	0		1.14361	0.89047	-15.27943	-15.18843					
$B-Cl\ (BCl_3)$	Cl	-1.12740	0	0	0		1.05158	0.96529	-14.09504	-13.99665	44.32	135.68	20.88	2.35415	0.69058

Table 22.32A. The energy parameters (eV) of functional groups of halidoboranes.

Parameters	$B-F$ Group	$B-Cl$ Group	$B-N$ (i) Group	$B-N$ (ii) Group	$C-N$ (i) Group	$C-N$ (ii) Group	$C-N$ (iii) Group	$C-N$ (iv) Group	NH_3 Group	NH_2 Group	NH Group	$B-O$ (i) Group	$B-O$ (ii) Group	OH Group	$C-O$ (i) Group
n_1	1	1	1	1	1	1	1	1	3	2	1	1	1	1	1
n_2	0	0	0	0	0	0	0	0	1	0	0	0	0	0	0
n_3	0	0	0	0	0	0	0	0	1	1	0	0	0	0	0
C_1	0.5	0.5	0.75	0.5	0.5	0.5	0.5	0.5	0.75	0.75	0.75	0.5	0.75	0.75	0.5
C_2	1	0.91044	0.81231	0.81231	1	1	1	1	0.93613	0.93613	0.93613	1.15346	0.79562	1	1
c_1	1	1	1	1	1	1	1	1	0.75	0.75	0.75	1	1	0.75	1
c_2	0.68285	1	1	0.81231	0.91140	0.91140	0.91140	0.91140	1	0.94627	0.93383	1	1	1	0.85395
c_3	0	0	0	0	0	0	0	0	0	0	1	0	0	1	0
c_4	1	1	1	1	2	2	2	2	1	1	1	1	1	1	2
c_5	1	1	1	1	0	0	0	0	3	2	1	1	1	1	0
C_{1o}	0.5	0.5	0.75	0.5	0.5	1	1	0.5	1	1.5	0.75	0.5	0.75	0.75	0.5
C_{2o}	1	0.91044	0.81231	0.81231	1	1	1	1	1.5	1	1	1.15346	0.79562	1	1
V_e (eV)	-34.78026	-25.95105	-31.86906	-29.36199	-32.46339	-31.98456	-31.98456	-31.67393	-115.28799	-77.89897	-39.21967	-32.64974	-32.39594	-40.92709	-33.15757
V_p (eV)	11.10909	8.17867	10.56810	8.62881	9.80175	9.74677	9.74677	9.71067	41.66718	28.49191	14.35050	10.33263	10.51010	14.81988	10.12103
T (eV)	11.59342	5.14980	7.88989	7.26921	8.42409	8.20698	8.20698	8.06719	42.77848	30.40957	15.53581	8.16244	8.09899	16.18567	9.17389
V_m (eV)	-5.79671	-2.57490	-3.94494	-3.63460	-4.21204	-4.10349	-4.10349	-4.03359	-21.38924	-15.20478	-7.76790	-4.08122	-4.04949	-8.09284	-4.58695
$E_{(AO/HO)}$ (eV)	-11.80624	-11.80624	-11.80624	-11.80624	-14.63489	-14.63489	-14.63489	-14.63489	-14.53414	-14.53414	-14.53414	-11.80624	-11.80624	-13.6181	-14.63489
$\Delta E_{H_2MO\,(AO/HO)}$ (eV)	0	0	0	0	-1.44915	-1.13379	-1.13379	-0.92918	0	0	0	0	0	0	-1.44915
E_T $_{(AO/HO)}$ (eV)	-11.80624	-11.80624	-11.80624	-11.80624	-13.18574	-13.50110	-13.50110	-13.70571	-14.53414	-14.53414	-14.53414	-11.80624	-11.80624	-13.6181	-13.18574
$E_{[n_3\,AO/HO]}$ (eV)	0	0	0	0	0	0	0	0	-14.53414	-14.53414	0	0	0	0	0
E_T $_{(H_2MO)}$ (eV)	-29.68070	-27.00372	-29.16227	-28.90482	-31.63534	-31.63540	-31.63540	-31.63537	-66.76571	-48.73642	-31.63541	-30.04213	-29.64258	-31.63247	-31.63533
$E_T\left(atom-atom, msp^3.AO\right)$ (eV)	-6.16219	-2.25479	-1.12740	1.19843	-1.44915	-1.13379	-1.13379	-0.92918	0	0	0	-1.12740	-1.12740	0	-1.44915
E_T $_{(MO)}$ (eV)	-35.84289	-29.25852	-30.28967	-27.70639	-33.08452	-32.76916	-32.76916	-32.56455	-66.76616	-48.73660	-31.63537	-31.16953	-30.76998	-31.63537	-33.08452
$\omega\left(10^{15}\ rad/s\right)$	15.9123	10.7150	16.6240	9.17969	18.9231	15.1983	26.0778	18.1298	56.8887	64.2189	47.0696	11.1001	16.9656	44.1776	12.0329
E_K (eV)	10.47375	7.05282	10.94219	6.04223	12.45552	10.00377	17.16484	11.93333	37.44514	42.27003	30.98202	7.30627	11.16705	29.07844	7.92028
$\overline{E}_D$ (eV)	-0.22949	-0.15372	-0.19822	-0.13474	-0.23100	-0.20505	-0.26859	-0.22255	-0.38298	-0.40690	-0.34836	-0.16668	-0.20342	-0.33749	-0.18420
$\overline{E}_{Kvib}$ (eV)	0.17384 [5]	0.10418 [5]	0.18779 [5]	0.18779 [5]	0.12944 [25]	0.12944 [25]	0.11159 [26]	0.12944 [25]	0.42695 [26]	0.40929 [28]	0.40696 [29]	0.23380 [5]	0.23380 [5]	0.46311 [22-23]	0.13663 [24]
$\overline{E}_{osc}$ (eV)	-0.14257	-0.10163	-0.10433	-0.04084	-0.16628	-0.14033	-0.21280	-0.15783	-0.16950	-0.20226	-0.14488	-0.04978	-0.08652	-0.10594	-0.11589
E_{mag} (eV)	0.07650	0.07650	0.07650	0.07650	0.14803	0.14803	0.14803	0.14803	0.14185	0.14803	0.14803	0.07650	0.07650	0.11441	0.14803
E_T $_{(Group)}$ (eV)	-35.98546	-29.36015	-30.39399	-27.74723	-33.25079	-32.90949	-32.98196	-32.72238	-67.27466	-49.14112	-31.78025	-31.21931	-30.85651	-31.74130	-33.20040
$E_{initial\,(c_4\,AO/HO)}$ (eV)	-11.80624	-11.80624	-11.80624	-11.80624	-14.63489	-14.63489	-14.63489	-14.63489	-14.53414	-14.53414	-14.53414	-11.80624	-11.80624	-13.6181	-14.63489
$E_{initial\,(c_5\,AO/HO)}$ (eV)	-17.42282	-12.96764	-14.53414	-14.53414	0	0	0	0	-13.59844	-13.59844	-13.59844	-13.6181	-13.6181	-13.59844	0
E_D $_{(Group)}$ (eV)	6.75639	4.58626	4.05361	1.40685	3.98101	3.63971	3.71218	3.45260	11.94520	7.41010	3.50582	5.79502	5.43221	4.41035	3.93062

Table 22.32B. The energy parameters (eV) of functional groups of halidoboranes.

Parameters	$C-O$ (ii) Group	$C-B$ Group	$B-H$ Group	$B-H-B$ Group	$B-B$ Group	$B-B-B$ Group	$C\overset{2e}{=}C$ Group	CH (i) Group	CH_3 Group	CH_2 (i) Group	CH (ii) Group	$C-C$ (a) Group	$C-C$ (b) Group	$C=C$ Group	CH_2 (ii) Group
f_1	1	1	1	1	1	1	0.75	1	1	1	1	1	1	1	1
n_1	1	1	1	1	1	1	2	1	3	2	1	1	1	2	2
n_2	0	0	0	0	0	0	0	0	2	1	0	0	0	0	1
n_3	0	0	0	0	0	0	0	0	0	0	0	0	0	0	0
C_1	0.5	0.5	0.75	0.75	0.5	0.5	0.5	0.75	0.75	0.75	0.75	0.5	0.5	0.5	0.75
C_2	1	0.80672	0.87442	0.87442	0.87442	0.87442	0.85252	1	1	1	1	1	1	0.91771	1
c_1	1	1	1	1	1	1	1	1	1	1	1	1	1	1	1
c_2	0.85395	0.80672	0.87442	0.87442	0.87442	0.87442	0.85252	0.91771	0.91771	0.91771	0.91771	0.91771	0.91771	0.91771	0.91771
c_3	0	0	0	0	0	0	0	1	0	1	1	0	0	0	1
c_4	2	2	1	1	2	2	3	1	1	1	1	2	2	4	1
c_5	0	0	1	1	0	0	0	1	3	2	1	0	0	0	2
C_{1o}	0.5	0.5	0.75	0.75	0.5	0.5	0.5	0.75	0.75	0.75	0.75	0.5	0.5	0.5	0.75
C_{2o}	1	0.80672	0.87442	0.87442	0.87442	0.87442	0.85252	1	1	1	1	1	1	0.91771	1
$\bar{V}_e$ (eV)	-33.47304	-35.37850	-34.04561	-27.77951	-22.91867	-22.91867	-101.12679	-37.10024	-107.32728	-70.41425	-35.12015	-28.79214	-28.79214	-102.08992	-72.03287
$\bar{V}_p$ (eV)	10.15605	9.14602	11.97638	11.01833	8.01527	8.01527	20.69825	13.17125	38.92728	25.78002	12.87680	9.33352	9.33352	21.48386	26.02344
$\bar{T}$ (eV)	9.32537	9.90839	10.05589	6.94488	4.54805	4.54805	34.31559	11.58941	32.53914	21.06675	10.48582	6.77464	6.77464	34.67062	21.95990
$\bar{V}_m$ (eV)	-4.66268	-4.95420	-5.02794	-3.47244	-2.27402	-2.27402	-17.15779	-5.79470	-16.26957	-10.53337	-5.24291	-3.38732	-3.38732	-17.33531	-10.97995
$E_{(AO/HO)}$ (eV)	-14.63489	-11.80624	-11.80624	-11.80624	-11.80624	-11.80624	0	-14.63489	-15.56407	-15.56407	-14.63489	-15.56407	-15.56407	0	-14.63489
$\Delta E_{H_2MO\,(AO/HO)}$ (eV)	-1.65376	-1.44915	0	0	0	0	0	-1.13379	0	0	0	0	0	0	0
E_T $_{(AO/HO)}$ (eV)	-12.98113	-10.35710	-11.80624	-11.80624	-11.80624	-11.80624	0	-13.50110	-15.56407	-15.56407	-14.63489	-15.56407	-15.56407	0	-14.63489
E_T $_{(H_2MO)}$ (eV)	-31.63544	-31.63538	-28.84754	-25.09498	-24.43561	-24.43561	-63.27075	-31.63539	-67.69451	-49.66493	-31.63533	-31.63537	-31.63537	-63.27075	-49.66437
$E_T\left(atom-atom, msp^3.AO\right)$ (eV)	-1.65376	-1.44915	-0.56370	-2.25479	-2.25479	-3.38219	-2.26759	-0.56690	0	0	0	-1.85836	-1.85836	-2.26759	0
E_T $_{(MO)}$ (eV)	-33.28912	-33.08452	-29.41123	-29.60457	-26.69041	-27.81781	-65.53833	-32.20226	-67.69450	-49.66493	-31.63537	-33.49373	-33.49373	-65.53833	-49.66493
ω $\left(10^{15}\ rad/s\right)$	12.1583	26.7757	15.2006	23.9931	6.83486	6.83486	49.7272	26.4826	24.9286	24.2751	24.1759	9.43699	9.43699	43.0680	25.2077
E_K (eV)	8.00277	17.62425	10.00529	15.79265	4.49882	4.49882	32.73133	17.43132	16.40846	15.97831	15.91299	6.21159	6.21159	28.34813	16.59214
$\bar{E}_D$ (eV)	-0.18631	-0.27478	-0.18405	-0.23275	-0.11200	-0.11673	-0.35806	-0.26130	-0.25352	-0.25017	-0.24966	-0.16515	-0.16515	-0.34517	-0.25493
$\bar{E}_{Kvib}$ (eV)	0.16118 [14]	0.11841 [11]	0.29346 [5]	0.09844 [6]	0.13035 [5]	0.13035 [5]	0.19649 [12]	0.35532 Eq. (13.458)	0.35532 (Eq. (13.458))	0.35532 (Eq. (13.458))	0.35532 (Eq. (13.458))	0.12312 [13]	0.17978 [14]	0.17897 [31]	0.35532 Eq. (13.458)
$\bar{E}_{osc}$ (eV)	-0.10572	-0.21558	-0.03732	-0.18353	-0.04682	-0.05156	-0.25982	-0.08364	-0.22757	-0.14502	-0.07200	-0.10359	-0.07526	-0.25568	-0.07727
E_{mag} (eV)	0.14803	0.14803	0.07650	0.07650	0.07650	0.07650	0.14803	0.14803	0.14803	0.14803	0.14803	0.14803	0.14803	0.14803	0.14803
E_T $_{(Group)}$ (eV)	-33.39484	-33.30009	-29.44855	-29.78809	-26.73723	-27.86936	-49.54347	-32.28590	-67.92207	-49.80996	-31.70737	-33.59732	-33.49373	-66.04969	-49.81948
$E_{initial}$ $_{(c_4\ AO/HO)}$ (eV)	-14.63489	-14.63489	-11.80624	-11.80624	-11.80624	-11.80624	-14.63489	-14.63489	-14.63489	-14.63489	-14.63489	-14.63489	-14.63489	-14.63489	-14.63489
$E_{initial}$ $_{(c_5\ AO/HO)}$ (eV)	0	0	-13.59844	-13.59844	0	0	0	-13.59844	-13.59844	-13.59844	-13.59844	0	0	0	-13.59844
E_D $_{(Group)}$ (eV)	4.12506	4.03031	4.04387	4.38341	3.12475	4.25687	5.63881	3.90454	12.49186	7.83016	3.32601	4.32754	4.29921	7.51014	7.83968

Table 22.33. The total bond energies of halidoboranes calculated using the functional group composition and the energies of Tables 22.32 A and B compared to the experimental values.

Formula	Name	B – F Group	B – Cl Group	B – N (i) Group	B – N (ii) Group	C – N (ii) Group	C – N (iv) Group	B – O (i) Group	B – O (ii) Group	OH Group	C – O (i) Group	C – O (ii) Group	C – B Group	B – H Group	3e C=C Group	CH (i) Group	CH_3 Group	CH_2 (i) Group	CH (ii) Group	C – C (a) Group	C – C (b) Group	C=C Group	CH_2 (ii) Group	Calculated Total Bond Energy (eV)	Experimental Total Bond Energy (eV)	Relative Error
HBF_2	difluoroboron	2	0	0	0	0	0	0	0	0	0	0	0	1	0	0	0	0	0	0	0	0	0	17.55666	17.41845 [17]	-0.00793
BF_3	boron trifluoride	3	0	0	0	0	0	0	0	0	0	0	0	0	0	0	0	0	0	0	0	0	0	20.26918	20.09744 [7]	-0.00855
BF_2HO	difluoroborinic acid	2	0	0	0	0	0	1	0	1	0	0	0	0	0	0	0	0	0	0	0	0	0	23.71816	23.64784 [17]	-0.00297
BFH_2O_2	fluoroboronic acid	1	0	0	0	0	0	2	0	2	0	0	0	0	0	0	0	0	0	0	0	0	0	27.16713	27.18135 [17]	0.00052
BCH_3F_2	difluoro-methyl-borane	2	0	0	0	0	0	0	0	0	0	0	1	0	0	0	1	0	0	0	0	0	0	30.03496	30.33624 [17]	0.00993
$BC_2H_3F_2$	vinyldifluoroborane	2	0	0	0	0	0	0	0	0	0	0	1	0	0	0	0	0	1	0	0	1	1	36.21893	36.54981 [17]	0.00905
$BC_3H_9NF_3$	trimethylamine-trifluoroborane	3	0	0	1	0	3	0	0	0	0	0	0	0	0	0	3	0	0	0	0	0	0	69.50941	69.11368 [16]	-0.00573
$HBCl_2$	dichloroboron	0	2	0	0	0	0	0	0	0	0	0	0	1	0	0	0	0	0	0	0	0	0	13.21640	13.25291 [17]	0.00276
BCl_3	boron trichloride	0	3	0	0	0	0	0	0	0	0	0	0	0	0	0	0	0	0	0	0	0	0	13.75879	13.80748 [17]	0.00353
BCl_2F	dichlorofluoroborane	1	2	0	0	0	0	0	0	0	0	0	0	0	0	0	0	0	0	0	0	0	0	15.92892	15.87507 [17]	-0.00339
$BClF_2$	chlorodifluoroborane	2	1	0	0	0	0	0	0	0	0	0	0	0	0	0	0	0	0	0	0	0	0	18.09905	17.98169 [17]	-0.00653
$C_2H_5OCl_2B$	ethoxydichloroborane	0	2	0	0	0	0	0	1	0	0	1	0	0	0	0	1	1	0	0	1	0	0	43.37936	43.55732 [18]	0.00409
$C_2H_4O_2ClB$	2-chloro-1,3,2-dioxaborolan	0	1	0	0	0	0	0	2	0	0	2	0	0	0	0	0	2	0	1	0	0	0	43.68867	43.99361[a] [18]	0.00693
$C_2H_6NCl_2B$	dimethylaminodichloro borane	0	2	1	0	2	0	0	0	0	0	0	0	0	0	0	2	0	0	0	0	0	0	45.48927	45.73940 [16]	0.00547
$BC_2ClH_6O_2$	dimethoxychloroborane	0	1	0	0	0	0	0	2	0	2	0	0	0	0	0	2	0	0	0	0	0	0	48.29565	48.40390 [17]	0.00224
$C_3H_6O_2ClB$	4-methyl-2-chloro-1,3,2-dioxaborolan	0	1	0	0	0	0	0	2	0	0	2	0	0	0	0	1	1	1	0	2	0	0	55.94726	56.39537[a] [18]	0.00795
$BC_6H_5Cl_2$	phenylboron dichloride	0	2	0	0	0	0	0	0	0	0	0	1	0	6	5	0	0	0	0	0	0	0	66.55838	66.97820 [17]	0.00627
$C_4H_8O_2ClB$	4,5-dimethyl-2-chloro-1,3,2-dioxaborolan	0	1	0	0	0	0	0	2	0	0	2	0	0	0	0	2	0	2	0	3	0	0	68.23418	68.72342[a] [18]	0.00712
$C_4H_{10}O_2ClB$	diethoxychloroborane	0	1	0	0	0	0	0	2	0	0	2	0	0	0	0	2	2	0	2	0	0	0	72.99993	73.07735 [18]	0.00106
$C_4H_{12}N_2ClB$	bis(dimethlamino) chloroborane	0	1	2	0	4	0	0	0	0	0	0	0	0	0	0	4	0	0	0	0	0	0	77.21975	77.38078 [18]	0.00208
$C_8H_{18}ClB$	di-n-butylchloroborane	0	1	0	0	0	0	0	0	0	0	0	2	0	0	0	2	6	0	6	0	0	0	110.57681	110.99317 [18]	0.00375
$C_{12}H_{10}ClB$	diphenylchloroborane	0	1	0	0	0	0	0	0	0	0	0	2	0	12	10	0	0	0	0	0	0	0	119.35796	119.79335 [18]	0.00363

[a] Crystal.

Table 22.34. The bond angle parameters of halidoboranes and experimental values. H_t is a terminal or two-center *H*. H_b is a bridge or three-center *H*. In the calculation of θ_v, the parameters from the preceding angle were used. E_T is E_T (*atom - atom msp³.AO*).

Atoms of Angle	2c' Bond 1 (a_0)	2c' Bond 2 (a_0)	2c' Terminal Atoms (a_0)	$E_{Coulombic}$ Atom 1	Atom 1 Hybridization Designation (Table)	$E_{Coulombic}$ Atom 2	Atom 2 Hybridization Designation (Table)	c_2 Atom 1	c_2 Atom 2	C_1	C_2	c_1	c_2'	E_T (eV)	θ_v (°)	θ_1 (°)	θ_2 (°)	Cal. θ (°)	Exp. θ (°)
$\angle HBF$	2.27211	2.44949	4.0988	-18.05943 *B*	2 (22.28)	-17.42282 *F*	*F*	0.75339	0.78092 (Eq. 15.74)	0.75	1	1	1.03654	0				120.43	118.3 [17] (HBF_2)
$\angle FBF$	2.44949	2.44949	4.2426	-17.42282 *F*	*F*	-17.42282 *F*	*F*	0.78092 (Eq. 15.74)	0.78092 (Eq. 15.74)	1	1	1	0.78092 (Eq. 15.74)	-1.71943				120.00	118 [10] ($HOBF_2$) 118.3 [10] (HBF_2)
$\angle FBO$	2.44949	2.63356	4.4721	-20.50391	3 (22.28)	-14.18175	1 (22.28)	0.66357	0.95939	1	1	1	0.81148	-1.71943				123.20	123 [10] ($HOBF_2$)
$\angle CBCl$	2.97524	3.32714	5.4371	-14.82575	1 (15.3A)	-12.96764 *Cl*	*Cl*	0.91771	0.91044 (Eq. (22.63))	1	0.83552 (Eqs. (15.77), (22.63), (13.430))	1	0.81317 (Eq. (15.130))	-1.44915				119.14	
$\angle ClBCl$	3.32714	3.32714	5.7594	-12.96764 *Cl*	*Cl*	-12.96764 *Cl*	*Cl*	1	1	1	0.91044 (Eq. (22.63))	1	1	-1.12740				119.88	
$\angle NBN$ ($B-N$ (i) & $C-N$ (ii))	2.57488	2.57488	4.4721	-16.52324	2 (22.21)	-16.52324	2 (22.21)	0.82343	0.82343	1	1	1	0.82343	-1.65376				120.55	
$\angle CNB$ ($B-N$ (ii) & $C-N$ (iv))	2.80224	3.15357	4.8531	-15.29034	1 (22.21)			0.88983	0.81231 (Eq. (22.48))	1	0.80672 (Eq. (22.40))	1	0.81508	-0.72457				109.00	109.9 [17] ($(CH_3)_3NBH_3$)
$\angle HBN$ ($B-N$ (ii) & $C-N$ (iv))	2.27211	3.15357	4.2895	-11.89724	B	-14.53414	N	0.87442 (Eq. (22.29))	0.93613	0.75	1	0.75	1.07056	0				103.28	105.3 [17] ($(CH_3)_3NBH_3$)
$\angle HNB$ ($B-N$ (ii)	1.95921	3.15357	4.2776	-14.53414	N	-11.89724	B	0.93613	0.87442 (Eq. (22.29))	0.75	0.87442 (Eq. (22.29))	0.75	0.93409	0				111.43	110.3 [17] (H_3NBH_3)
$\angle HNH$	1.91013	1.91013	3.0984	-14.53414	N	H	H	0.94627 Eq. (15.134))	1	1	1	0.75	1.05679	0				108.40	107.1 [10] (methylamine)
$\angle HNC_\alpha$ ($C-N$ (i))	1.91013	2.77620	3.8816	-14.53414	N	-15.35946	5 (15.3A)	0.91140 (Eq. (15.135))	0.88583	0.75	1	0.75	0.97194	0				110.48	110.3 [10] (methylamine)
$\angle HCN$ ($C-N$ (i) & (ii))	2.09711	2.79186	4.0661	-14.82575	1 (15.3A)	-14.53414	N	0.91771	0.93383 (Eq. (15.136))	0.75	1	0.75	1.01756	0				111.76	112 [10] (dimethylamine)
$\angle HNC_\alpha$ ($C-N$ (ii) & (iii))	1.89621	2.79186	3.8123	-14.53414	N	-15.56407 (Eq. (15.136))	7 (15.3A)	0.91140 (Eq. (15.135))	0.87418	0.75	1	0.75	0.95917	0				107.27	107 [10] (dimethylamine)
$\angle CNC$ ($C-N$ (ii) & (iii))	2.79186	2.79186	4.6260	-17.04640	33 (15.3A)	-17.04640	331 (15.3A)	0.79816	0.79816	1	1	1	0.79816	-1.85836				111.89	111.8 [10] (dimethylamine)
$\angle BOH$ ($B-O$ (i))	2.63356	1.83616	3.7771	-11.80624		-13.61805		1	0.87442 (Eq. (22.29))	0.75	1	0.75	0.87442	-0.56370 (Eq. (22.12))				114.17	114.1 [10] (F_2BOH)
$\angle O_\alpha BO_b$ ($B-O$ (i))	2.63356	2.63356	4.5277	-15.75493 O_α	7 (15.3A)	-15.75493 O_b	7 (15.3A)	0.86359	0.86359	1	1	1	0.86359	-1.44915				118.55	120 [10] ($B_3H_3O_3$)
$\angle O_\alpha BO_b$ ($B-O$ (ii))	2.58909	2.58909	4.4944	-15.75493 O_α	7 (15.3A)	-15.75493 O_b	7 (15.3A)	0.86359	0.86359	1	1	1	0.86359	-1.44915				120.44	120 [10] ($B_3H_3O_3$)
$\angle CBC$ $(CH_3)_3B$	2.97524	2.97524	5.1769	16.11722	1 (22.8)	16.11722	1 (22.8)	0.84418	0.84418	1	1	1	0.84418	-1.85836				120.92	120.0 [10] (trimethylborane)
Methyl $\angle HCH$	2.09711	2.09711	3.4252	-15.75493	7 (15.3A)	H	H	0.86359	1	1	1	0.75	1.15796	0				109.50	
$\angle BCH$															70.56			109.44	112.5 [10] (trimethylborane)
$\angle CBH_t$	2.97524	2.27211	4.5607	-15.55033	5 (15.3A)	H	H	0.87495	1	0.75	1	0.75	1.14292	0				120.12	
$\angle CBH_b$	2.97524	2.46967	4.6904	-15.55033	5 (15.3A)	H	H	0.87495	1	0.75	1	0.75	1.14292	0				118.66	
$\angle BBC$																120.12	118.66	121.22	122.6 [10] (1,2-dimethyldiborane)
$\angle H_tBH_t$	2.27211	2.27211	3.9623	-13.61667	2 (22.1)	H	H	0.99920	1	1	1	0.75	1.00080	-1.71943				121.37	122 [10] (diborane)

Table 22.34 cont' d. The bond angle parameters of halidoboranes and experimental values. H_t is a terminal or two-center *H*. H_b is a bridge or three-center *H*. In the calculation of θ_v, the parameters from the preceding angle were used. E_T is E_T (*atom - atom msp³.AO*).

Atoms of Angle	2c' Bond 1 (a_0)	2c' Bond 2 (a_0)	2c' Terminal Atoms (a_0)	$E_{Coulombic}$ Atom 1	Atom 1 Hybridization Designation (Table)	$E_{Coulombic}$ Atom 2	Atom 2 Hybridization Designation (Table)	c_2 Atom 1	c_2 Atom 2	C_1	C_2	c_1	c_2'	E_T (eV)	θ_v (°)	θ_1 (°)	θ_2 (°)	Cal. θ (°)	Exp. θ (°)
$\angle H_t B H_b$	2.27211	2.46967	3.8210	-14.71574	4 (22.1)	H	H	0.92458	1	1	1	0.75	1.08158	-1.12740				107.30	108.9 [2] (B_4H_{10})
$\angle H_b B H_b$	2.46967	2.46967	3.6606	-14.26508	3 (22.1)	H	H	0.95378	1	1	1	0.75	1.04846	-1.12740				95.65	95.0 [2] (B_4H_{10})
$\angle B H_b B$	2.46967	2.46967	3.4358	-11.89724 B_a	1 (22.1)	-11.89724 B_b	1 (22.1)	1	1	1	1.14361	1	1	0				88.15	87.7 [2] (B_4H_{10})
Methylene $\angle HC_aH$	2.11106	2.11106	3.4252	-15.75493	7 (15.3A)	H	H	0.86359	1	1	1	0.75	1.15796	0				108.44	107 [10] (dimethylamine) 107 [10] (propane)
$\angle C_aC_bC_c$															69.51			110.49	112 [10] (propane) 113.8 [10] (butane) 110.8 [10] (isobutane)
$\angle C_aC_bH$															69.51			110.49	111.0 [10] (butane) 111.4 [10] (isobutane)
Methyl $\angle HC_aH$	2.09711	2.09711	3.4252	-15.75493	7 (15.3A)	H	H	0.86359	1	1	1	0.75	1.15796	0				109.50	
$\angle C_aC_bC_c$															70.56			109.44	
$\angle C_aC_bH$															70.56			109.44	

SUMMARY TABLES OF BORON MOLECULES

The bond energies, calculated using closed-form equations having integers and fundamental constants only for classes of molecules whose designation is based on the main functional group, are given in the following tables with the experimental values.

Table 22.35.1. Summary results of boranes.

Formula	Name	Calculated Total Bond Energy (eV)	Experimental Total Bond Energy (eV)	Relative Error
BB	diboron	3.12475	3.10405	-0.00667
B_2H_6	diborane	24.94229	24.89030	-0.00209
B_4H_{10}	tetraborane(10)	44.92160	45.33134	0.00904
B_5H_9	pentaborane(9)	48.25462	48.85411	0.01227
B_5H_{11}	pentaborane(11)	54.00546	53.06086	-0.01780
B_6H_{10}	hexaborane(10)	56.55063	56.74739	0.00347
B_9H_{15}	nonaborane(15)	85.61380	84.95008	-0.00781
$B_{10}H_{14}$	decaborane(14)	89.73467	89.69790	-0.00041

Table 22.35.2. Summary results of alkyl boranes.

Formula	Name	Calculated Total Bond Energy (eV)	Experimental Total Bond Energy (eV)	Relative Error
CH_5B	methylborane	24.60991	24.49350 [16]	-0.00475
C_2H_7B	dimethylborane	37.08821	37.17713 [16]	0.00239
B_2CH_8	methyldiborane	37.42060	37.58259 [16]	0.00431
$B_2C_2H_{10}$	ethyldiborane	49.57830	49.50736 [16]	-0.00143
C_3H_9B	trimethylboron	49.56652	49.76102 [17]	0.00391
$B_2C_2H_{10}$	1,1-dimethyldiborane	49.89890	50.20118 [16]	0.00602
$B_2C_2H_{10}$	1,2-dimethyldiborane	49.89890	50.20118 [16]	0.00602
B_4CH_{12}	methyltetraborane	57.39990	57.74604 [16]	0.00599
B_5CH_{11}	methylpentaborane	60.73292	61.51585 [16]	0.01273
$B_2C_3H_{12}$	trimethyldiborane	62.37721	62.88481 [16]	0.00807
$B_4C_2H_{14}$	ethyltetraborane	69.55760	69.99603 [16]	0.00626
$B_5C_2H_{13}$	ethylpentaborane	72.89062	73.76585 [16]	0.01186
$B_2C_4H_{14}$	1,1-diethyldiborane	74.21430	74.34420 [16]	0.00175
$B_2C_4H_{14}$	tetramethyldiborane	74.85551	75.48171 [16]	0.00830
$B_5C_3H_{15}$	propylpentaborane	85.04832	85.84239 [16]	0.00925
$C_6H_{15}B$	triethylboron	86.03962	86.12941 [18]	0.00104
$B_2C_6H_{18}$	triethyldiborane	98.85031	98.59407 [16]	-0.00260
$B_{10}CH_{16}$	methyldecaborane	102.21298	101.91775 [16]	-0.00290
$C_8H_{17}B$	n-butylboracyclopentane	105.35916	105.69874[a] [18]	0.00321
$B_{10}C_2H_{18}$	ethyldecaborane	114.37068	113.56066 [16]	-0.00713
$C_9H_{21}B$	tripropylboron	122.51272	122.59753 [18]	0.00069
$C_9H_{21}B$	tri-isopropylboron	122.81539	122.75798 [18]	-0.00047
$B_2C_8H_{22}$	tetraethyldiborane	123.48631	123.74017 [16]	0.00205
$B_{10}C_3H_{20}$	propyldecaborane	126.52838	125.94075 [16]	-0.00467
$C_{12}H_{27}B$	tri-s-butylboron	159.28849	158.50627 [18]	-0.00493
$C_{12}H_{27}B$	tributylboron	158.98582	159.03530 [16]	0.00031
$C_{12}H_{27}B$	tri-isobutylboron	159.20350	159.34318 [16]	0.00088
$C_{18}H_{15}B$	triphenylboron	172.15755	172.09681 [18]	-0.00035
$C_{15}H_{33}B$	tri-3-methylbutylboron	195.67660	195.78095 [18]	0.00053
$C_{18}H_{33}B$	tricyclohexylboron	217.24711	218.23763 [18]	0.00454
$C_{18}H_{39}B$	tri-n-hexylboron	231.93202	231.76340 [18]	-0.00073
$C_{21}H_{45}B$	tri-n-heptylboron	268.40512	268.22285 [18]	-0.00068
$C_{24}H_{51}B$	tri-s-octylboron	305.18089	304.61292 [18]	-0.00186
$C_{24}H_{51}B$	tri-n-octylboron	304.87822	304.68230 [18]	-0.00064

[a] Crystal.

Table 22.35.3. Summary results of alkoxy boranes and borinic acids.

Formula	Name	Calculated Total Bond Energy (eV)	Experimental Total Bond Energy (eV)	Relative Error
BH_3O	hydroxyborane	18.29311	18.22572 [17]	-0.00370
BH_3O_2	dihydroxyborane	24.45460	24.43777 [17]	-0.00069
BH_3O_3	boric acid	30.61610	30.68431 [7]	0.00222
$BC_2H_7O_2$	dimethoxyborane	47.75325	47.72358 [16]	-0.00062
$BC_3H_9O_3$	trimethyl borate	65.56408	65.53950 [17]	-0.00037
$C_5H_{11}OB$	methoxyboracyclopentane	74.21858	74.47566[a] [18]	0.00345
$C_6H_7O_2B$	phenylborinic acid	77.79659	78.86121[a] [18]	0.01350
$C_6H_{15}O_2B$	di-isoproxyborane	96.97471	97.41737[a] [18]	0.00454
$BC_6H_{15}O_3$	triethyl borate	102.62050	102.50197 [16]	-0.00116
$C_8H_{19}OB$	di-n-butylborinic acid	116.19591	116.45117 [18]	0.00219
$BC_9H_{21}O_3$	tri-n-propyl borate	139.09360	139.11319 [16]	0.00014
$C_{12}H_{27}OB$	n-butyl di-n-butylborinate	164.51278	165.29504[a] [18]	0.00473
$C_{12}H_{27}O_2B$	di-n-butyl n-butylboronate	170.03974	170.86964[a] [18]	0.00486
$BC_{12}H_{27}O_3$	tri-n-butyl borate	175.56670	175.62901 [18]	0.00035
$C_{18}H_{15}O_3B_3$	phenylborinic anhydride	204.75082	205.96548[a] [18]	0.00590
$C_{16}H_{36}OB_2$	di-n-butylborinic anhydride	222.84551	223.70232[a] [18]	0.00383
$C_{24}H_{20}OB_2$	diphenylborinic anhydride	240.40782	241.38941[a] [18]	0.00407

[a] Crystal.

Table 22.35.4. Summary results of tertiary and quaternary amino boranes and borane amines.

Formula	Name	Calculated Total Bond Energy (eV)	Experimental Total Bond Energy (eV)	Relative Error
B_2H_7N	aminodiborane	32.36213	31.99218 [16]	-0.01156
$B_2C_2H_{11}N$	n-dimethylaminodiborane	57.21517	57.52855 [17]	0.00545
$C_6H_{18}N_3B$	tris(dimethylamino)borane	108.95023	108.64490 [18]	-0.00281
$C_8H_{20}NB$	di-n-butylboronamine	117.45425	119.49184 [a] [18]	0.01705
$C_{12}H_{28}NB$	di-n-butylboron-n-butylamine	166.49595	167.83269 [a] [18]	0.00796
$C_2H_{10}NB$	dimethylaminoborane	49.30740	49.52189 [18]	0.00433
$BC_3H_{12}N$	trimethylaminoborane	61.37183	61.05205 [16]	-0.00524
$BC_3H_{12}N$	ammonia-trimethylborane	62.91857	62.52207 [16]	-0.00634
$C_6H_{18}NB$	triethylaminoborane	97.84493	97.42044 [18]	-0.00436
$BC_6H_{18}N$	trimethylaminotrimethylborane	98.80674	98.27036 [17]	-0.00546

[a] Crystal.

Table 22.35.5. Summary results of halidoboranes.

Formula	Name	Calculated Total Bond Energy (eV)	Experimental Total Bond Energy (eV)	Relative Error
HBF_2	difluoroboron	17.55666	17.41845 [17]	-0.00793
BF_3	boron trifluoride	20.26918	20.09744 [7]	-0.00855
BF_2HO	difluoroborinic acid	23.71816	23.64784 [17]	-0.00297
BFH_2O_2	fluoroboronic acid	27.16713	27.18135 [17]	0.00052
BCH_3F_2	difluoro-methyl-borane	30.03496	30.33624 [17]	0.00993
$BC_2H_3F_2$	vinyldifluoroborane	36.21893	36.54981 [17]	0.00905
$BC_3H_9NF_3$	trimethylamine-trifluoroborane	69.50941	69.11368 [16]	-0.00573
$HBCl_2$	dichloroboron	13.21640	13.25291 [17]	0.00276
BCl_3	boron trichloride	13.75879	13.80748 [17]	0.00353
BCl_2F	dichlorofluoroborane	15.92892	15.87507 [17]	-0.00339
$BClF_2$	chlorodifluoroborane	18.09905	17.98169 [17]	-0.00653
$C_2H_5OCl_2B$	ethoxydichloroborane	43.37936	43.55732 [18]	0.00409
$C_2H_4O_2ClB$	2-chloro-1,3,2-dioxaborolan	43.68867	43.99361[a] [18]	0.00693
$C_2H_6NCI_2B$	dimethylaminodichloroborane	45.48927	45.73940 [16]	0.00547
BC_2ClH_602	dimethoxychloroborane	48.29565	48.40390 [17]	0.00224
$C_3H_6O_2ClB$	4-methyl-2-chloro-1,3,2-dioxaborolan	55.94726	56.39537[a] [18]	0.00795
$BC_6H_5Cl_2$	phenylboron dichloride	66.55838	66.97820 [17]	0.00627
$C_4H_8O_2ClB$	4,5-dimethyl-2-chloro-1,3,2-dioxaborolan	68.23418	68.72342[a] [18]	0.00712
$C_4H_{10}O_2ClB$	diethoxychloroborane	72.99993	73.07735 [18]	0.00106
$C_4H_{12}N_2ClB$	bis(dimethlamino) chloroborane	77.21975	77.38078 [18]	0.00208

Formula	Name	Calculated Total Bond Energy (eV)	Experimental Total Bond Energy (eV)	Relative Error
$C_8H_{18}ClB$	di-n-butylchloroborane	110.57681	110.99317 [18]	0.00375
$C_{12}H_{10}ClB$	diphenylchloroborane	119.35796	119.79335 [18]	0.00363

[a] Crystal.

REFERENCES

1. D. R. Lide, *CRC Handbook of Chemistry and Physics*, 86th Edition, CRC Press, Taylor & Francis, Boca Raton, (2005-6), pp. 10-202 to 10-204.
2. V. Ramakrishna, B. J. Duke, "Can the bis(diboranyl) structure of $\left[B(4)H(10)\right]$ be observed? The story continues," Inorg. Chem., Vol. 43, No. 25, (2004), pp. 8176-8184.
3. J. C. Huffman, D. C. Moody, R. Schaeffer, "Studies of boranes. XLV. Crystal structure, improved synthesis, and reactions of tridecaborane(19)," Inorg. Chem., Vol. 15, No. 1. (1976), pp. 227-232.
4. K. Kuchitsu, "Comparison of molecular structures determined by electron diffraction and spectroscopy. Ethane and diborane," J. Chem. Phys., Vol. 49, No. 10, (1968), pp. 4456-4462.
5. D. R. Lide, *CRC Handbook of Chemistry and Physics*, 86th Ed., CRC Press, Taylor & Francis, Boca Raton, (2005-6), p. 9-82.
6. diborane ($^{11}B_2H_6$) at http://webbook.nist.gov/.
7. D. R. Lide, *CRC Handbook of Chemistry and Physics*, 86th Edition, CRC Press, Taylor & Francis, Boca Raton, (2005-6), pp. 9-63; 5-4 to 5-42.
8. W. N. Lipscomb, "The boranes and their relatives," Nobel Lecture, December 11, 1976.
9. A. B. Burg, R. Kratzer, "The synthesis of nonaborane, B_9H_{11}," Inorg. Chem., Vol. 1, No. 4, (1962), pp. 725-730.
10. D. R. Lide, *CRC Handbook of Chemistry and Physics*, 86th Edition, CRC Press, Taylor & Francis, Boca Raton, (2005-6), p. 9-19 to 9-45.
11. BCCB at http://webbook.nist.gov/.
12. G. Herzberg, *Molecular Spectra and Molecular Structure II. Infrared and Raman Spectra of Polyatomic Molecules*, Van Nostrand Reinhold Company, New York, New York, (1945), pp. 362-369.
13. G. Herzberg, *Molecular Spectra and Molecular Structure II. Infrared and Raman Spectra of Polyatomic Molecules*, Van Nostrand Reinhold Company, New York, New York, (1945), p. 344.
14. R. J. Fessenden, J. S. Fessenden, *Organic Chemistry*, Willard Grant Press. Boston, Massachusetts, (1979), p. 320.
15. cyclohexane at http://webbook.nist.gov/.
16. R. L. Hughes, I. C. Smith,, E. W. Lawless, *Production of the Boranes and Related Research*, Ed. R. T. Holzmann, Academic Press, New York, (1967), pp. 390-396.
17. M. J. S. Dewar, C. Jie, E. G. Zoebisch, "AM1 calculations for compounds containing boron," Organometallics, Vol. 7, (1988), pp. 513-521.
18. J. D. Cox, G. Pilcher, *Thermochemistry of Organometallic Compounds*, Academic Press, New York, (1970), pp. 454-465.
19. W. I. F. David, R. M. Ibberson, G. A. Jeffrey, J. R. Ruble, "The structure analysis of deuterated benzene and deuterated nitromethane by pulsed-neutron powder diffraction: a comparison with single crystal neutron analysis," Physica B (1992), 180 & 181, pp. 597-600.
20. G. A. Jeffrey, J. R. Ruble, R. K. McMullan, J. A. Pople, "The crystal structure of deuterated benzene," Proceedings of the Royal Society of London. Series A, Mathematical and Physical Sciences, Vol. 414, No. 1846, (Nov. 9, 1987), pp. 47-57.
21. H. B. Burgi, S. C. Capelli, "Getting more out of crystal-structure analyses," Helvet. Chim Acta, Vol. 86, (2003), pp. 1625-1640.
22. K. P. Huber, G. Herzberg, *Molecular Spectra and Molecular Structure, IV. Constants of Diatomic Molecules*, Van Nostrand Reinhold Company, New York, (1979).
23. J. Crovisier, Molecular Database—Constants for molecules of astrophysical interest in the gas phase: photodissociation, microwave and infrared spectra, Ver. 4.2, Observatoire de Paris, Section de Meudon, Meudon, France, May 2002, pp. 34–37, available at http://wwwusr.obspm.fr/~crovisie/.
24. dimethyl ether at http://webbook.nist.gov/.
25. methylamine at http://webbook.nist.gov/.
26. D. Lin-Vien. N. B. Colthup, W. G. Fateley, J. G. Grasselli, The *Handbook of Infrared and Raman Frequencies of Organic Molecules*, Academic Press, Inc., Harcourt Brace Jovanovich, Boston, (1991), p. 482.
27. W. S. Benedict, E. K. Plyler, "Vibration-rotation bands of ammonia," Can. J. Phys., Vol. 35, (1957), pp. 1235-1241.
28. T. Amano, P. F. Bernath, R. W. McKellar, "Direct observation of the ν_1 and ν_3 fundamental bands of NH_2 by difference frequency laser spectroscopy," J. Mol. Spectrosc., Vol. 94, (1982), pp. 100-113.
29. D. R. Lide, *CRC Handbook of Chemistry and Physics*, 79th Ed., CRC Press, Boca Raton, Florida, (1998-9), pp. 9-80 to 9-85.
30. D. R. Lide, *CRC Handbook of Chemistry and Physics*, 86th Ed., CRC Press, Taylor & Francis, Boca Raton, (2005-6), p. 9-55.
31. G. Herzberg, *Molecular Spectra and Molecular Structure II. Infrared and raman spectra of polyatomic molecules*, Van Nostrand Reinhold Company, New York, NY, (1945), p. 326.

Chapter 23

ORGANOMETALLIC AND COORDINATE FUNCTIONAL GROUPS AND MOLECULES

GENERAL CONSIDERATIONS OF THE ORGANOMETALLIC AND COORDINATE BOND

Organometallic and coordinate compounds comprising an arbitrary number of atoms can be solved using similar principles and procedures as those used to solve organic molecules of arbitrary length and complexity. Organometallic and coordinate compounds can be considered to be comprised of functional groups such as $M-C$, $M-H$, $M-X$ ($X=F,Cl,Br,I$), $M-OH$, $M-OR$, and the alkyl functional groups of organic molecules. The solutions of these functional groups or any others corresponding to the particular organometallic or coordinate compound can be conveniently obtained by using generalized forms of the force balance equation given in the Force Balance .of the σ MO of the Carbon Nitride Radical section for molecules comprised of metal and atoms other than carbon and the geometrical and energy equations given in the Derivation of the General Geometrical and Energy Equations of Organic Chemistry section for organometallic and coordinate compounds comprised of carbon. The appropriate functional groups with their geometrical parameters and energies can be added as a linear sum to give the solution of any organometallic or coordinate compound.

ALKYL ALUMINUM HYDRIDES (R_nAlH_{3-n})

Similar to the case of carbon and silicon, the bonding in the aluminum atom involves four sp^3 hybridized orbitals formed from the outer $3p$ and $3s$ shells except that only three HOs are filled. In organoaluminum compounds, bonds form between a $Al3sp^3$ HO and at least one $C2sp^3$ HO and one or more $H1s$ AOs. The geometrical parameters of each AlH functional group is solved from the force balance equation of the electrons of the corresponding σ-MO and the relationships between the prolate spheroidal axes. Then, the sum of the energies of the H_2-type ellipsoidal MOs is matched to that of the $Al3sp^3$ shell as in the case of the corresponding carbon and silicon molecules. As in the case of alkyl silanes given in the corresponding section, the sum of the energies of the H_2-type ellipsoidal MO of the $Al-C$ functional group is matched to that of the $Al3sp^3$ shell, and Eq. (15.51) is solved for the semimajor axis with $n_1=1$ in Eq. (15.50).

The energy of aluminum is less than the Coulombic energy between the electron and proton of H given by Eq. (1.264). A minimum energy is achieved while matching the potential, kinetic, and orbital energy relationships given in the Hydroxyl Radical (OH) section with the donation of 25% electron density from the participating $Al3sp^3$ HO to each $Al-H$-bond MO.

The $3sp^3$ hybridized orbital arrangement after Eq. (13.422) is

$$\begin{array}{cccc} & 3sp^3 \text{ state} & & \\ \underline{\uparrow} & \underline{\uparrow} & \underline{\uparrow} & \underline{\quad} \\ 0,0 & 1,-1 & 1,0 & 1,1 \end{array} \tag{23.1}$$

where the quantum numbers (ℓ,m_ℓ) are below each electron. The total energy of the state is given by the sum over the three electrons. The sum $E_T\left(Al,3sp^3\right)$ of experimental energies [1] of Al, Al^+, and Al^{2+} is

$$E_T\left(Al,3sp^3\right)=-\left(28.44765\ eV+18.82856\ eV+5.98577\ eV\right)=-53.26198\ eV \tag{23.2}$$

By considering that the central field decreases by an integer for each successive electron of the shell, the radius r_{3sp^3} of the

$Al3sp^3$ shell may be calculated from the Coulombic energy using Eq. (15.13):

$$r_{3sp^3} = \sum_{n=10}^{12} \frac{(Z-n)e^2}{8\pi\varepsilon_0 \left(e53.26198\ eV\right)} = \frac{6e^2}{8\pi\varepsilon_0 \left(e53.26198\ eV\right)} = 1.53270a_0 \tag{23.3}$$

where $Z = 13$ for aluminum. Using Eq. (15.14), the Coulombic energy $E_{Coulomb}\left(Al, 3sp^3\right)$ of the outer electron of the $Al3sp^3$ shell is:

$$E_{Coulomb}\left(Al, 3sp^3\right) = \frac{-e^2}{8\pi\varepsilon_0 r_{3sp^3}} = \frac{-e^2}{8\pi\varepsilon_0 1.53270a_0} = -8.87700\ eV \tag{23.4}$$

During hybridization, the spin-paired $3s$ electrons are promoted to the $Al3sp^3$ shell as unpaired electrons. The energy for the promotion is the magnetic energy given by Eq. (15.15) at the initial radius of the $3s$ electrons. From Eq. (10.255) with $Z = 13$, the radius r_{12} of the $Al3s$ shell is:

$$r_{12} = 1.41133a_0 \tag{23.5}$$

Using Eqs. (15.15) and (23.5), the unpairing energy is:

$$E(magnetic) = \frac{2\pi\mu_0 e^2\hbar^2}{m_e^2\left(r_{12}\right)^3} = \frac{8\pi\mu_o\mu_B^2}{\left(1.41133a_0\right)^3} = 0.04070\ eV \tag{23.6}$$

Using Eqs. (23.4) and (23.6), the energy $E\left(Al, 3sp^3\right)$ of the outer electron of the $Al3sp^3$ shell is:

$$E\left(Al, 3sp^3\right) = \frac{-e^2}{8\pi\varepsilon_0 r_{3sp^3}} + \frac{2\pi\mu_0 e^2\hbar^2}{m_e^2\left(r_{12}\right)^3} = -8.87700\ eV + 0.04070\ eV = -8.83630\ eV \tag{23.7}$$

Next, consider the formation of the $Al-H$ -bond MO of organoaluminum hydrides wherein each aluminum atom has an $Al3sp^3$ electron with an energy given by Eq. (23.7). The total energy of the state of each aluminum atom is given by the sum over the three electrons. The sum $E_T\left(Al_{organoAl}3sp^3\right)$ of energies of $Al3sp^3$ (Eq. (23.7)), Al^+, and Al^{2+} is:

$$\begin{aligned} E_T\left(Al_{organoAl}3sp^3\right) &= -\left(28.44765\ eV + 18.82856\ eV + E\left(Al, 3sp^3\right)\right) \\ &= -\left(28.44765\ eV + 18.82856\ eV + 8.83630\ eV\right) = -56.11251\ eV \end{aligned} \tag{23.8}$$

where $E\left(Al, 3sp^3\right)$ is the sum of the energy of Al, $-5.98577\ eV$, and the hybridization energy.

Each $Al-H$ -bond MO of each functional group $AlH_{n=1,2,3}$ forms with the sharing of electrons between each $Al3sp^3$ HO and each $H1s$ AO. As in the case of $C-H$, the H_2 -type ellipsoidal MO comprises 75% of the $Al-H$ -bond MO according to Eq. (13.429). Furthermore, the donation of electron density from each $Al3sp^3$ HO to each $Al-H$ -bond MO permits the participating orbital to decrease in size and energy. As shown below, the aluminum HOs have spin and orbital angular momentum terms in the force balance which determines the geometrical parameters of the σ MO. The angular momentum term requires that each $Al-H$ -bond MO be treated independently in terms of the charge donation. In order to further satisfy the potential, kinetic, and orbital energy relationships, each $Al3sp^3$ HO donates an excess of 25% of its electron density to each $Al-H$ -bond MO to form an energy minimum. By considering this electron redistribution in the organoaluminum hydride molecule as well as the fact that the central field decreases by an integer for each successive electron of the shell, the radius $r_{organoAlH3sp^3}$ of the $Al3sp^3$ shell may be calculated from the Coulombic energy using Eq. (15.18).

$$r_{organoAlH3sp^3} = \left(\sum_{n=10}^{12}(Z-n) - 0.25\right)\frac{e^2}{8\pi\varepsilon_0\left(e56.11251\ eV\right)} = \frac{5.75e^2}{8\pi\varepsilon_0\left(e56.11251\ eV\right)} = 1.39422a_0 \tag{23.9}$$

Using Eqs. (15.19) and (23.9), the Coulombic energy $E_{Coulomb}\left(Al_{organoAlH}, 3sp^3\right)$ of the outer electron of the $Al3sp^3$ shell is:

$$E_{Coulomb}\left(Al_{organoAlH}, 3sp^3\right) = \frac{-e^2}{8\pi\varepsilon_0 r_{organoAlH3sp^3}} = \frac{-e^2}{8\pi\varepsilon_0 1.39422a_0} = -9.75870\ eV \tag{23.10}$$

During hybridization, the spin-paired $3s$ electrons are promoted to the $Al3sp^3$ shell as unpaired electrons. The energy for the promotion is the magnetic energy given by Eq. (23.6). Using Eqs. (23.6) and (23.10), the energy $E\left(Al_{organoAlH}, 3sp^3\right)$ of the outer electron of the $Al3sp^3$ shell is:

$$E\left(Al_{organoAlH}, 3sp^3\right) = \frac{-e^2}{8\pi\varepsilon_0 r_{3sp^3}} + \frac{2\pi\mu_0 e^2\hbar^2}{m_e^2\left(r_{12}\right)^3} = -9.75870\ eV + 0.04070\ eV = -9.71800\ eV \tag{23.11}$$

Thus, $E_T\left(Al-H, 3sp^3\right)$, the energy change of each $Al3sp^3$ shell with the formation of the $Al-H$ -bond MO is given by the difference between Eq. (23.11) and Eq. (23.7):

$$E_T\left(Al-H,3sp^3\right)=E\left(Al_{organoAlH},3sp^3\right)-E\left(Al,3sp^3\right)=-9.71800\ eV-\left(-8.83630\ eV\right)=-0.88170\ eV \tag{23.12}$$

The MO semimajor axis of the $Al-H$ functional group of organoaluminum hydrides is determined from the force balance equation of the centrifugal, Coulombic, and magnetic forces as given in the Polyatomic Molecular Ions and Molecules section and the More Polyatomic Molecules and Hydrocarbons section. The distance from the origin of the H_2-type-ellipsoidal-MO to each focus c', the internuclear distance $2c'$, and the length of the semiminor axis of the prolate spheroidal H_2-type MO $b=c$ are solved from the semimajor axis a. Then, the geometric and energy parameters of the MO are calculated using Eqs. (15.1-15.117).

The force balance of the centrifugal force equated to the Coulombic and magnetic forces is solved for the length of the semimajor axis. The Coulombic force on the pairing electron of the MO is:

$$\mathbf{F}_{Coulomb}=\frac{e^2}{8\pi\varepsilon_0 ab^2}D\mathbf{i}_\xi \tag{23.13}$$

The spin pairing force is

$$\mathbf{F}_{spin-pairing}=\frac{\hbar^2}{2m_e a^2b^2}D\mathbf{i}_\xi \tag{23.14}$$

The diamagnetic force is:

$$\mathbf{F}_{diamagneticMO1}=-\frac{n_e\hbar^2}{4m_e a^2b^2}D\mathbf{i}_\xi \tag{23.15}$$

where n_e is the total number of electrons that interact with the binding σ-MO electron. The diamagnetic force $\mathbf{F}_{diamagneticMO2}$ on the pairing electron of the σ MO is given by the sum of the contributions over the components of angular momentum:

$$\mathbf{F}_{diamagneticMO2}=-\sum_{i,j}\frac{|L_i|\hbar}{Z_j 2m_e a^2b^2}D\mathbf{i}_\xi \tag{23.16}$$

where $|L|$ is the magnitude of the angular momentum of each atom at a focus that is the source of the diamagnetism at the σ-MO. The centrifugal force is:

$$\mathbf{F}_{centrifugalMO}=-\frac{\hbar^2}{m_e a^2b^2}D\mathbf{i}_\xi \tag{23.17}$$

The force balance equation for the σ-MO of the $Al-H$-bond MO is the same as that of the $Si-H$ except that $Z=13$ and there are three spin-unpaired electron in occupied orbitals rather than four, and the orbital with ℓ,m_ℓ angular momentum quantum numbers of (1,1) is unoccupied. With $n_e=2$ and $|L|=3\sqrt{\frac{3}{4}}\hbar$ and $|L|=3\sqrt{\frac{3}{4}}\hbar$ corresponding to the spin and orbital angular momentum of the three occupied HOs of the $Al3sp^3$ shell, the force balance equation is**:**

$$\frac{\hbar^2}{m_e a^2b^2}D=\frac{e^2}{8\pi\varepsilon_0 ab^2}D+\frac{\hbar^2}{2m_e a^2b^2}D-\left(1+\frac{6\sqrt{\frac{3}{4}}}{Z}\right)\frac{\hbar^2}{2m_e a^2b^2}D \tag{23.18}$$

$$a=\left(2+\frac{6\sqrt{\frac{3}{4}}}{Z}\right)a_0 \tag{23.19}$$

With $Z=13$, the semimajor axis of the $Al-H$-bond MO is:

$$a=2.39970a_0 \tag{23.20}$$

Using the semimajor axis, the geometric and energy parameters of the MO are calculated using Eqs. (15.1-15.127) in the same manner as the organic functional groups given in the Organic Molecular Functional Groups and Molecules section. For the $Al-H$ functional group, c_1 is one and $C_1=0.75$ based on the orbital composition as in the case of the $C-H$-bond MO. In organoaluminum hydrides, the energy of aluminum is less than the Coulombic energy between the electron and proton of H given by Eq. (1.264). Thus, c_2 in Eqs. (15.51) and (15.61) is also one, and the energy matching condition is determined by the C_2 parameter. Then, the hybridization factor for the $Al-H$-bond MO is given by the ratio of $8.87700\ eV$, the magnitude of $E_{Coulomb}\left(Al_{organoAlH},3sp^3\right)$ (Eq. (23.4)), and $13.605804\ eV$, the magnitude of the Coulombic energy between the electron and proton of H (Eq. (1.264)):

$$C_2\left(organoAlH3sp^3HO\right)=\frac{8.87700\ eV}{13.605804\ eV}=0.65244 \tag{23.21}$$

Since the energy of the MO is matched to that of the $Al3sp^3$ HO, $E\left(AO/HO\right)$ in Eqs. (15.51) and (15.61) is $E\left(Al,3sp^3\right)$ given by Eq. (23.7), and $E_T\left(atom-atom,msp^3.AO\right)$ is $-0.88170\ eV$ corresponding to the independent single-bond charge

contribution (Eq. (23.12)). The energies $E_D\left(AlH_{n=1,2}\right)$ of the functional groups $AlH_{n=1,2}$ of organoaluminum hydride molecules are each given by the corresponding integer n times that of $Al-H$:

$$E_D\left(AlH_{n=1,2}\right)=nE_D\left(AlH\right) \tag{23.22}$$

The branched-chain organoaluminum hydrides, R_nAlH_{3-n}, comprise at least a terminal methyl group (CH_3) and at least one Al bound by a carbon-aluminum single bond comprising a $C-Al$ group, and may comprise methylene (CH_2), methylyne (CH), $C-C$, and $AlH_{n=1,2}$ functional groups. The methyl and methylene functional groups are equivalent to those of straight-chain alkanes. Six types of $C-C$ bonds can be identified. The n-alkane $C-C$ bond is the same as that of straight-chain alkanes. In addition, the $C-C$ bonds within isopropyl ($\left(CH_3\right)_2CH$) and t-butyl ($\left(CH_3\right)_3C$) groups and the isopropyl to isopropyl, isopropyl to t-butyl, and t-butyl to t-butyl $C-C$ bonds comprise functional groups. These groups in branched-chain organoaluminum hydrides are equivalent to those in branched-chain alkanes.

For the $C-Al$ functional group, hybridization of the $2s$ and $2p$ AOs of each C and the $3s$ and $3p$ AOs of Al to form single $2sp^3$ and $3sp^3$ shells, respectively, forms an energy minimum, and the sharing of electrons between the $C2sp^3$ and $Al3sp^3$ HOs to form a MO permits each participating orbital to decrease in radius and energy. Furthermore, the energy of aluminum is less than the Coulombic energy between the electron and proton of H given by Eq. (1.264). Thus, in organoaluminum hydrides, the $C2sp^3$ HO has a hybridization factor of 0.91771 (Eq. (13.430)) with a corresponding energy of $E\left(C,2sp^3\right)=-14.63489\,eV$ (Eq. (15.25)), and the Al HO has an energy of $E\left(Al,3sp^3\right)=-8.83630\,eV$. To meet the equipotential, minimum-energy condition of the union of the $Al3sp^3$ and $C2sp^3$ HOs, c_2 and C_2 of Eqs. (15.2-15.5), (15.51), and (15.61) for the $Al-C$-bond MO given by Eqs. (15.77) and (15.79) is:

$$\begin{aligned}C_2\left(C2sp^3HO\ to\ Al3sp^3HO\right)&=c_2\left(C2sp^3HO\ to\ Al3sp^3HO\right)\\&=\frac{E\left(Al,3sp^3\right)}{E\left(C,2sp^3\right)}c_2\left(C2sp^3HO\right)=\frac{-8.83630\,eV}{-14.63489\,eV}\left(0.91771\right)=0.55410\end{aligned} \tag{23.23}$$

The energy of the $C-Al$-bond MO is the sum of the component energies of the H_2-type ellipsoidal MO given in Eq. (15.51). Since the energy of the MO is matched to that of the $Al3sp^3$ HO, $E\left(AO/HO\right)$ in Eqs. (15.51) and (15.61) is $E\left(Al,3sp^3\right)$ given by Eq. (23.7). Since the $C2sp^3$ HOs have four electrons with a corresponding total field of ten in Eq. (15.13); whereas, the $Al3sp^3$ HOs have three electrons with a corresponding total field of six, $E_T\left(atom-atom,msp^3.AO\right)$ is $-0.72457\,eV$ corresponding to the single-bond contributions of carbon (Eq. (14.151)). $\Delta E_{H_2MO}\left(AO/HO\right)=E_T\left(atom-atom,msp^3.AO\right)$ in order to match the energies of the carbon and aluminum HOs.

BRIDGING BONDS OF ORGANOALUMINUM HYDRIDES ($Al-H-Al$ AND $Al-C-Al$)

As given in the Nature of the Chemical Bond of Hydrogen-Type Molecules and Molecular Ions section, the Organic Molecular Functional Groups and Molecules section, and other sections on bonding in neutral molecules, the molecular chemical bond typically comprises an integer number of paired electrons. One exception given in the Benzene Molecule section and other sections on aromatic molecules such as naphthalene, toluene, chlorobenzene, phenol, aniline, nitrobenzene, benzoic acid, pyridine, pyrimidine, pyrazine, quinoline, isoquinoline, indole, adenine, fullerene, and graphite is that the paired electrons are distributed over a linear combination of bonds such that the bonding between two atoms involves less than an integer multiple of two electrons. In these aromatic cases, three electrons can be assigned to a given bond between two atoms wherein the electrons of the linear combination of bonded atoms are paired and comprise an integer multiple of two.

The $Al3sp^3$ HOs comprise four orbitals containing three electrons as given by Eq. (23.1). These three occupied orbitals can form three single bonds with other atoms wherein each $Al3sp^3$ HO and each orbital from the bonding atom contribute one electron each to the pair of the corresponding bond. However, an alternative bonding is possible that further lowers the energy of the resulting molecule wherein the remaining unoccupied orbital participates in bonding. (Actually an unoccupied orbital has no physical basis. It is only a convenient concept for the bonding electrons in this case additionally having the electron angular momentum state with ℓ,m_ℓ quantum numbers of (1,1)). In this case the set of two paired electrons are distributed over three atoms and belong to two bonds. Such an electron deficient bonding involving two paired electrons centered on three atoms is called a *three-center bond* as opposed to the typical single bond called a *two-center bond*. The designation for a three-center bond involving two $Al3sp^3$ HOs and a $H1s$ AO is $Al-H-Al$, and the designation for a three-center bond involving two $Al3sp^3$ HOs and a $C2sp^3$ HO is $Al-C-Al$.

Each $Al-H-Al$-bond MO and $Al-C-Al$-bond MO comprises the corresponding single bond and forms with further sharing of electrons between each $Al3sp^3$ HO and each $H1s$ AO and $C2sp^3$ HO, respectively. Thus, the geometrical and energy parameters of the three-center bond are equivalent to those of the corresponding two-center bonds except that the bond

energy is increased in the former case since the donation of electron density from the unoccupied $Al3sp^3$ HO to each $Al-H-Al$-bond MO and $Al-C-Al$-bond MO permits the participating orbital to decrease in size and energy. In order to further satisfy the potential, kinetic, and orbital energy relationships, the $Al3sp^3$ HO donates an additional excess of 25% of its electron density to form the bridge (three-center-bond MO) to decrease the energy in the multimer. By considering this electron redistribution in the organoaluminum hydride molecule as well as the fact that the central field decreases by an integer for each successive electron of the shell, the radius $r_{organoAlH3sp^3}$ of the $Al3sp^3$ shell calculated from the Coulombic energy, the Coulombic energy $E_{Coulomb}\left(Al_{organoAlH},3sp^3\right)$ of the outer electron of the $Al3sp^3$ shell, and the energy $E\left(Al_{organoAlH},3sp^3\right)$ of the outer electron of the $Al3sp^3$ shell are given by Eqs. (23.9), (23.10), and (23.11), respectively. Thus, $E_T\left(Al-H-Al,3sp^3\right)$ and $E_T\left(Al-C-Al,3sp^3\right)$, the energy change with the formation of the three-center-bond MO from the corresponding two-center-bond MO and the unoccupied $Al3sp^3$ HO is given by Eq. (23.12):

$$E_T\left(Al-H-Al,3sp^3\right)=E_T\left(Al-C-Al,3sp^3\right)=-0.88170\ eV \tag{23.24}$$

The upper range of the experimental association enthalpy per bridge for both of the reactions.

$$2AlH\left(CH_3\right)_2\rightarrow\left[AlH\left(CH_3\right)_2\right]_2 \tag{23.25}$$

and

$$2Al\left(CH_3\right)_3\rightarrow\left[Al\left(CH_3\right)_3\right]_2 \tag{23.26}$$

is [2]

$$E_T\left(Al-H-Al,3sp^3\right)=E_T\left(Al-C-Al,3sp^3\right)=-0.867\ eV \tag{23.27}$$

which agrees with Eq. (23.24) very well.

The symbols of the functional groups of alkyl organoaluminum hydrides are given in Table 23.1. The geometrical (Eqs. (15.1-15.5), (23.20), and (23.23)) and intercept (Eqs. (15.80-15.87)) parameters of alkyl organoaluminum hydrides are given in Tables 23.2 and 23.3, respectively. Since the energy of the $Al3sp^3$ HO is matched to that of the $C2sp^3$ HO, the radius r_{mol2sp^3} of the $Al3sp^3$ HO of the aluminum atom and the $C2sp^3$ HO of the carbon atom of a given $C-Al$-bond MO are calculated after Eq. (15.32) by considering $\sum E_{T_{mol}}\left(MO,2sp^3\right)$, the total energy donation to all bonds with which each atom participates in bonding. In the case that the MO does not intercept the Al HO due to the reduction of the radius from the donation of Al $3sp^3$ HO charge to additional MO's, the energy of each MO is energy matched as a linear sum to the Al HO by contacting it through the bisector current of the intersecting MOs as described in the Methane Molecule (CH_4) section. The energy (Eq. (15.61), (23.4), (23.7), and (23.21-23.23)) parameters of alkyl organoaluminum hydrides are given in Table 23.5. The total energy of each alkyl aluminum hydride given in Table 23.5 was calculated as the sum over the integer multiple of each $E_{D\,(Group)}$ of Table 23.4 corresponding to functional-group composition of the molecule. E_{mag} of Table 23.4 is given by Eqs. (15.15) and (23.3). The bond angle parameters of organoaluminum hydrides determined using Eqs. (15.88-15.117) are given in Table 23.6. The charge-density in trimethyl aluminum is shown in Figure 23.1.

Figure 23.1. *Trimethylaluminum*. Color scale, translucent view of the charge-density of $(H_3C)_3\,Al$ comprising the linear combination of three sets of three $C-H$ -bond MOs and three $C-Al$ -bond MOs with the $Al_{oganoAl}3sp^3$ HOs and $C2sp^3$ HOs shown transparently. Each $C-Al$ -bond MO comprises a H_2 -type ellipsoidal MO bridging $C2sp^3$ and $Al3sp^3$ HOs. For each $C-H$ and $C-Al$ bond, the ellipsoidal surface of the H_2 -type ellipsoidal MO that transitions to the $C2sp^3$ HO shell with radius $0.89582a_0$ (Eq. (15.32)) or $Al3sp^3$ HO, the $Al3sp^3$ HO shell with radius $0.85503a_0$ (Eq. (15.32)), inner $Al1s$, $Al2s$, and $Al2p$ shells with radii of $Al1s = 0.07778a_0$ (Eq. (10.51)), $Al2s = 0.33923a_0$ (Eq. (10.62)), and $Al2p = 0.45620a_0$ (Eq. (10.212)), respectively, and the nuclei (red, not to scale), are shown.

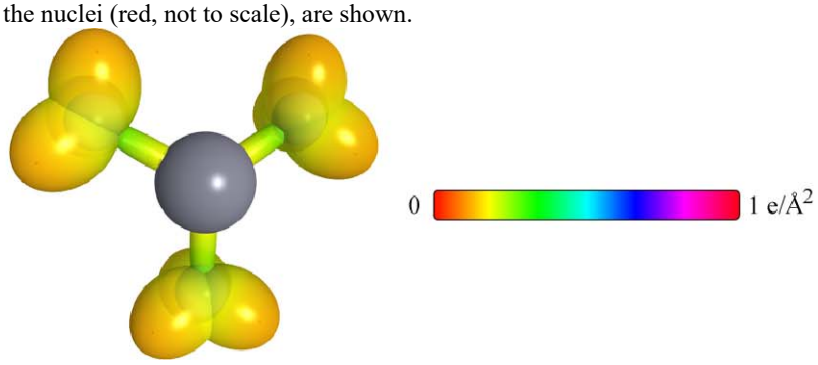

Table 23.1. The symbols of the functional groups of organoaluminum hydrides.

Functional Group	Group Symbol
AlH group of $AlH_{n=1,2}$	$Al-H$
AlHAl (bridged *H*)	$Al-H-Al$
CAl bond	$C-Al$
AlCAl (bridged *C*)	$Al-C-Al$
CH_3 group	$C-H\ (CH_3)$
CH_2 group	$C-H\ (CH_2)$
CH	$C-H$
CC bond (*n-C*)	$C-C$ (a)
CC bond (*iso-C*)	$C-C$ (b)
CC bond (*tert-C*)	$C-C$ (c)
CC (*iso* to *iso-C*)	$C-C$ (d)
CC (*t* to *t-C*)	$C-C$ (e)
CC (*t* to *iso-C*)	$C-C$ (f)

Table 23.2. The geometrical bond parameters of organoaluminum hydrides and experimental values [3].

Parameter	$C-Al$ and $Al-C-Al$ Groups	$Al-H$ and $Al-H-Al$ Groups	$C-H$ (CH_3) Group	$C-H$ (CH_2) Group	$C-H$ Group	$C-C$ (a) Group	$C-C$ (b) Group	$C-C$ (c) Group	$C-C$ (d) Group	$C-C$ (e) Group	$C-C$ (f) Group
a (a_0)	1.89887	2.39970	1.64920	1.67122	1.67465	2.12499	2.12499	2.10725	2.12499	2.10725	2.10725
c' (a_0)	1.85120	1.56589	1.04856	1.05553	1.05661	1.45744	1.45744	1.45164	1.45744	1.45164	1.45164
Bond Length $2c'$ (Å)	1.95923	1.65727	1.10974	1.11713	1.11827	1.54280	1.54280	1.53635	1.54280	1.53635	1.53635
Exp. Bond Length (Å)	1.957 (trimethylaluminum)	1.6482E-10 (AlH)	1.113 (trimethylaluminum) 1.107 ($C-H$ propane) 1.117 ($C-H$ butane)	1.107 ($C-H$ propane) 1.117 ($C-H$ butane)	1.122 (isobutane)	1.532 (propane) 1.531 (butane)	1.532 (propane) 1.531 (butane)	1.532 (propane) 1.531 (butane)	1.532 (propane) 1.531 (butane)	1.532 (propane) 1.531 (butane)	1.532 (propane) 1.531 (butane)
b, c (a_0)	0.42282	1.81839	1.27295	1.29569	1.29924	1.54616	1.54616	1.52750	1.54616	1.52750	1.52750
e	0.97489	0.65254	0.63580	0.63159	0.63095	0.68600	0.68600	0.68888	0.68600	0.68888	0.68888

Table 23.3. The MO to HO intercept geometrical bond parameters of organoaluminum hydrides. *R, R′, R″* are *H* or alkyl groups. E_T is E_T (*atom–atom,msp³.AO*).

Bond	Atom	E_T (eV) Bond 1	E_v (eV) Bond 2	E_T (eV) Bond 3	E_T (eV) Bond 4	Final Total Energy $Al3sp^3$ $C2sp^3$ (eV)	$r_{initial}$ (a_0)	r_{final} (a_0)	$E_{Coulomb}(Al3sp^3)$ $E_{Coulomb}(C2sp^3)$ (eV) Final	$E(Al3sp^3)$ $E(C2sp^3)$ (eV) Final	θ' (°)	θ_1 (°)	θ_2 (°)	d_1 (a_0)	d_2 (a_0)
$Al-H$ (AlH)	Al	-0.88170	0	0	0	-56.99421	1.53270	1.39422	-9.75870	-9.71800	91.03	88.97	50.05	1.54088	0.02501
$Al-H$ $(RAlH_2)$	Al	-0.88170	-0.88170	-0.36229	0		1.53270	0.80263	-16.95144	-16.91074					
$Al-H$ (R_2AlH)	Al	-0.88170	-0.36229	-0.36229	0		1.53270	0.82801	-16.43203	-16.39133					
$Al-H$ $(R_2Al(H_b)_2)$ (H_b =bridge H)	Al	-1.32255	-1.32255	-0.36229	-0.36229		1.53270	0.74776	-18.19543	-18.15473					
$H_2Al-C_aH_2-$	Al	-0.36229	-0.88170	-0.88170	0	-56.47480	1.53270	0.80263	-16.95144	-16.91074	154.88	25.12	53.69	1.12447	0.72673
$HAl-(C_aH_2-)_2$	Al	-0.36229	-0.36229	-0.88170	0	-55.95538	1.53270	0.82801	-16.43203	-16.39133	155.38	24.62	54.66	1.09845	0.75276
$Al-(C_aH_2-)_3$	Al	-0.36229	-0.36229	-0.36229	0	-56.47480	1.53270	0.85503	-15.91261	-15.87191	155.90	24.10	55.68	1.07072	0.78048
$(-C_aH_2)_2\,Al-(C_b)_2$ (C_b =bridge C)	Al	-0.36229	-0.36229	-0.36229	-0.80314	-57.27793	1.53270	0.81395	-16.71575	-16.67505	155.11	24.89	54.12	1.11286	0.73834
$Al-CH_3$	C	-0.36229	0	0	0	-151.97798	0.91771	0.89582	-15.18804	-14.99717	156.63	23.37	57.19	1.02888	0.82232
$Al-C_aH_2CH_2-$	C_a	-0.36229	-0.92918	0	0	-152.90716	0.91771	0.84418	-16.11722	-15.92636	155.69	24.31	55.27	1.08186	0.76935
$(-C_aH_2)_2(C_b)Al-C_b-Al$ (C_b =bridge C)	C_b	-0.80314	-0.80314	0	0	-153.22196	0.91771	0.82801	-16.43203	-16.24116	155.38	24.62	54.66	1.09845	0.75276
$C-H$ (CH_3)	C	-0.92918	0	0	0	-152.54487	0.91771	0.86359	-15.75493	-15.56407	77.49	102.51	41.48	1.23564	0.18708
$C-H$ (CH_2)	C	-0.92918	-0.92918	0	0	-153.47406	0.91771	0.81549	-16.68412	-16.49325	68.47	111.53	35.84	1.35486	0.29933
$C-H$ (CH)	C	-0.92918	-0.92918	-0.92918	0	-154.40324	0.91771	0.77247	-17.61330	-17.42244	61.10	118.90	31.37	1.42988	0.37326
$H_3C_aC_bH_2CH_2-$ ($C-C$ (a))	C_a	-0.92918	0	0	0	-152.54487	0.91771	0.86359	-15.75493	-15.56407	63.82	116.18	30.08	1.83879	0.38106
$H_3C_aC_bH_2CH_2-$ ($C-C$ (a))	C_b	-0.92918	-0.92918	0	0	-153.47406	0.91771	0.81549	-16.68412	-16.49325	56.41	123.59	26.06	1.90890	0.45117
$R-H_2C_aC_b(H_2C_c-R')HCH_2-$ ($C-C$ (b))	C_b	-0.92918	-0.92918	-0.92918	0	-154.40324	0.91771	0.77247	-17.61330	-17.42244	48.30	131.70	21.90	1.97162	0.51388
$R-H_2C_a(R'-H_2C_d)C_b(R''-H_2C_c)CH_2-$ ($C-C$ (c))	C_b	-0.92918	-0.72457	-0.72457	-0.72457	-154.71860	0.91771	0.75889	-17.92866	-17.73779	48.21	131.79	21.74	1.95734	0.50570
$isoC_aC_b(H_2C_c-R')HCH_2-$ ($C-C$ (d))	C_b	-0.92918	-0.92918	-0.92918	0	-154.40324	0.91771	0.77247	-17.61330	-17.42244	48.30	131.70	21.90	1.97162	0.51388
$tertC_a(R'-H_2C_d)C_b(R''-H_2C_c)CH_2-$ ($C-C$ (e))	C_b	-0.72457	-0.72457	-0.72457	-0.72457	-154.51399	0.91771	0.76765	-17.92866	-17.73779	50.04	129.96	22.66	1.94462	0.49298
$tertC_aC_b(H_2C_c-R')HCH_2-$ ($C-C$ (f))	C_b	-0.72457	-0.92918	-0.92918	0	-154.19863	0.91771	0.78155	-17.40869	-17.21783	52.78	127.22	24.04	1.92443	0.47279
$isoC_a(R'-H_2C_d)C_b(R''-H_2C_c)CH_2-$ ($C-C$ (f))	C_b	-0.72457	-0.72457	-0.72457	-0.72457	-154.51399	0.91771	0.76765	-17.92866	-17.73779	50.04	129.96	22.66	1.94462	0.49298

Table 23.4. The energy parameters (eV) of functional groups of organoaluminum hydrides.

Parameters	$C-Al$ and $Al-C-Al$ [a] Groups	$Al-H$ and $Al-H-Al$ [a] Groups	CH_3 Group	CH_2 Group	$C-H$ Group	$C-C$ (a) Group	$C-C$ (b) Group	$C-C$ (c) Group	$C-C$ (d) Group	$C-C$ (e) Group	$C-C$ (f) Group
n_1	1	1	3	2	1	1	1	1	1	1	1
n_2	0	0	2	1	0	0	0	0	0	0	0
n_3	0	0	0	0	0	0	0	0	0	0	0
C_1	0.5	0.75	0.75	0.75	0.75	0.5	0.5	0.5	0.5	0.5	0.5
C_2	0.55410	0.65244	1	1	1	1	1	1	1	1	1
c_1	1	1	1	1	1	1	1	1	1	1	1
c_2	0.55410	1	0.91771	0.91771	0.91771	0.91771	0.91771	0.91771	0.91771	0.91771	0.91771
c_3	0	0	0	1	1	0	0	0	1	1	0
c_4	2	1	1	1	1	2	2	2	2	2	2
c_5	0	1	3	2	1	0	0	0	0	0	0
C_{1o}	0.5	0.75	0.75	0.75	0.75	0.5	0.5	0.5	0.5	0.5	0.5
C_{2o}	0.55410	0.65244	1	1	1	1	1	1	1	1	1
V_e (eV)	-35.55430	-27.09887	-107.32728	-70.41425	-35.12015	-28.79214	-28.79214	-29.10112	-28.79214	-29.10112	-29.10112
V_p (eV)	7.34971	8.68884	38.92728	25.78002	12.87680	9.33352	9.33352	9.37273	9.33352	9.37273	9.37273
T (eV)	9.36194	5.64629	32.53914	21.06675	10.48582	6.77464	6.77464	6.90500	6.77464	6.90500	6.90500
V_m (eV)	-4.68097	-2.82315	-16.26957	-10.53337	-5.24291	-3.38732	-3.38732	-3.45250	-3.38732	-3.45250	-3.45250
$E_{(AO/HO)}$ (eV)	-8.83630	-8.83630	-15.56407	-15.56407	-14.63489	-15.56407	-15.56407	-15.35946	-15.56407	-15.35946	-15.35946
$\Delta E_{H_2MO\,(AO/HO)}$ (eV)	-0.72457	0	0	0	0	0	0	0	0	0	0
$E_{T\,(AO/HO)}$ (eV)	-8.11172	-8.83630	-15.56407	-15.56407	-14.63489	-15.56407	-15.56407	-15.35946	-15.56407	-15.35946	-15.35946
$E_{T\,(H_2MO)}$ (eV)	-31.63534	-24.42317	-67.69451	-49.66493	-31.63533	-31.63537	-31.63537	-31.63535	-31.63537	-31.63535	-31.63535
$E_T\left(atom-atom, msp^3, AO\right)$ (eV)	-0.72457	-0.88170	0	0	0	-1.85836	-1.85836	-1.44915	-1.85836	-1.44915	-1.44915
$E_{T\,(MO)}$ (eV)	-32.35994	-25.30487	-67.69450	-49.66493	-31.63537	-33.49373	-33.49373	-33.08452	-33.49373	-33.08452	-33.08452
$\omega\left(10^{15}\ rad/s\right)$	8.31610	11.7938	24.9286	24.2751	24.1759	9.43699	9.43699	15.4846	9.43699	9.55643	9.55643
E_K (eV)	5.47380	7.76290	16.40846	15.97831	15.91299	6.21159	6.21159	10.19220	6.21159	6.29021	6.29021
$\bar{E}_D$ (eV)	-0.14978	-0.13948	-0.25352	-0.25017	-0.24966	-0.16515	-0.16515	-0.20896	-0.16515	-0.16416	-0.16416
$\bar{E}_{Kvib}$ (eV)	0.05721 [4]	0.20861 [5]	0.35532 (Eq. (13.458))	0.35532 (Eq. (13.458))	0.35532 (Eq. (13.458))	0.12312 [6]	0.17978 [7]	0.09944 [8]	0.12312 [6]	0.12312 [6]	0.12312 [6]
$\bar{E}_{osc}$ (eV)	-0.12118	-0.03518	-0.22757	-0.14502	-0.07200	-0.10359	-0.07526	-0.15924	-0.10359	-0.10260	-0.10260
E_{mag} (eV)	0.14803	0.03178	0.14803	0.14803	0.14803	0.14803	0.14803	0.14803	0.14803	0.14803	0.14803
$E_{T\,(Group)}$ (eV)	-32.48112	-25.34005	-67.92207	-49.80996	-31.70737	-33.59732	-33.49373	-33.24376	-33.59732	-33.18712	-33.18712
$E_{initial\,(c_4\ AO/HO)}$ (eV)	-14.63489	-8.83630	-14.63489	-14.63489	-14.63489	-14.63489	-14.63489	-14.63489	-14.63489	-14.63489	-14.63489
$E_{initial\,(c_5\ AO/HO)}$ (eV)	0	-13.59844	-13.59844	-13.59844	-13.59844	0	0	0	0	0	0
$E_{D\,(Group)}$ (eV)	3.21134	2.90531	12.49186	7.83016	3.32601	4.32754	4.29921	3.97398	4.17951	3.62128	3.91734
Exp. $E_{D\,(Group)}$ (eV)		2.98 (AlH [9])									

[a] Additional association enthalpy given by Eq. (23.28).

Table 23.5. The total bond energies of gaseous-state organoaluminum hydrides calculated using the functional group composition and the energies of Table 23.4 compared to the gaseous-state experimental values [10] except where indicated.

Formula	Name	$Al-H$ Group	$C-Al$ Group	CH_3	CH_2	CH	$C-C$ (a)	$C-C$ (b)	$C-C$ (c)	$C-C$ (d)	$C-C$ (e)	$C-C$ (f)	Calculated Total Bond Energy (eV)	Experimental Total Bond Energy (eV)	Relative Error
C_2H_7Al	Dimethylaluminum hydride	1	2	2	0	0	0	0	0	0	0	0	34.31171	34.37797[a] [11]	0.00193
C_3H_9Al	Trimethyl aluminum	0	3	3	0	0	0	0	0	0	0	0	47.10960	46.95319	-0.00333
$C_4H_{11}Al$	Diethylaluminum hydride	1	2	2	2	0	2	0	0	0	0	0	58.62711	60.10948[b]	0.02466
$C_6H_{15}Al$	Triethylaluminum hydride	0	3	3	3	0	3	0	0	0	0	0	83.58270	83.58176	-0.00001
$C_6H_{15}Al$	Di-n-propylaluminum hydride	1	2	2	4	0	4	0	0	0	0	0	82.94251	84.40566[b]	0.01733
$C_9H_{21}Al$	Tri-n-propyl aluminum	0	3	3	6	0	6	0	0	0	0	0	120.05580	121.06458[b]	0.00833
$C_8H_{19}Al$	Di-n-butylaluminum hydride	1	2	2	6	0	6	0	0	0	0	0	107.25791	108.71051[b]	0.01336
$C_8H_{19}Al$	Di-isobutylaluminum hydride	1	2	4	2	2	0	6	0	0	0	0	107.40303	108.77556[b]	0.01262
$C_{12}H_{27}Al$	Tri-n-butyl aluminum	0	3	3	9	0	9	0	0	0	0	0	156.52890	157.42429[b]	0.00569
$C_{12}H_{27}Al$	Tri-isobutyl aluminum	0	3	6	3	3	0	9	0	0	0	0	156.74658	157.58908[b]	0.00535

[a] Estimated.
[b] Crystal.

Table 23.6. The bond angle parameters of organoaluminum hydrides and experimental values [3]. In the calculation of θ_v, the parameters from the preceding angle were used. E_T is E_T (*atom–atom,msp³.AO*).

Atoms of Angle	$2c'$ Bond 1 (a_0)	$2c'$ Bond 2 (a_0)	$2c'$ Terminal Atoms (a_0)	$E_{Coulombic}$ Atom 1	Atom 1 Hybridization Designation (Table 15.3A)	$E_{Coulombic}$ Atom 2	Atom 2 Hybridization Designation (Table 15.3A)	c_2 Atom 1	c_1 Atom 2	C_1	C_2	c_1	c_2'	E_T (eV)	θ_v (°)	θ_1 (°)	θ_2 (°)	Cal. θ (°)	Exp. θ (°)
$\angle C_aAlC_b$	3.70240	3.70240	6.4187	-14.82575 C_a	1	-15.18804 C_b	2	0.91771	0.89582	1	1	1	0.90677	-1.85836				120.19	120 (trimethylaluminum)
Methyl $\angle HC_aH$	2.09711	2.09711	3.4252	-15.75493	7	H	H	0.86359	1	1	1	0.75	1.15796	0				109.50	111.7 (trimethylaluminum)
$\angle HC_aAl$															70.56			109.44	
$\angle C_aC_bC_c$															70.56			109.44	
Methylene $\angle HC_aH$	2.11106	2.11106	3.4252	-15.75493	7	H	H	0.86359	1	1	1	0.75	1.15796	0				108.44	107 (propane)
$\angle C_aC_bC_c$															69.51			110.49	112 (propane) 113.8 (butane) 110.8 (isobutane)
$\angle C_aC_bH$															69.51			110.49	111.0 (butane) 111.4 (isobutane)
$\angle C_aC_bH$															70.56			109.44	
$\angle C_bC_aC_c$ iso C_a	2.91547	2.91547	4.7958	-16.68412 C_b	26	-16.68412 C_c	26	0.81549	0.81549	1	1	1	0.81549	-1.85836				110.67	110.8 (isobutane)
$\angle C_bC_aH$ iso C_a	2.91547	2.11323	4.1633	-15.55033 C_a	5	-14.82575 C_b	1	0.87495	0.91771	0.75	1	0.75	1.04887	0				110.76	
$\angle C_aC_bH$ iso C_a	2.91547	2.09711	4.1633	-15.55033 C_b	5	-14.82575 C_a	1	0.87495	0.91771	0.75	1	0.75	1.04887	0				111.27	111.4 (isobutane)
$\angle C_bC_aC_b$ tert C_a	2.90327	2.90327	4.7958	-16.68412 C_b	26	-16.68412 C_b	26	0.81549	0.81549	1	1	1	0.81549	-1.85836				111.37	110.8 (isobutane)
$\angle C_bC_aC_d$															72.50			107.50	

TRANSITION METAL ORGANOMETALLIC AND COORDINATE BOND

The transition-metal atoms fill the $3d$ orbitals in the series Sc to Zn. The $4s$ orbitals are filled except in the cases of Cr and Cu wherein one $4s$ electron occupies a $3d$ orbital to achieve a half-filled and filled $3d$ shell, respectively. Experimentally the transition-metal elements ionize successively from the $4s$ shell to the $3d$ shell [12]. Thus, bonding in the transition metals involves the hybridization of the $3d$ and $4s$ electrons to form the corresponding number of $3d4s$ HOs except for Cu and Zn which each have a filled inner $3d$ shell and one and two outer $4s$ electrons, respectively. Cu may form a single bond involving the $4s$ electron or the $3d$ and $4s$ shells may hybridize to form multiple bonds with one or more ligands. The $4s$ shell of Zn hybridizes to form two $4s$ HOs that provide for two possible bonds, typically two metal-alkyl bonds.

For organometallic and coordinate compounds comprised of carbon, the geometrical and energy equations are given in the Derivation of the General Geometrical and Energy Equations of Organic Chemistry section. For metal-ligand bonds other than to carbon, the force balance equation is that developed in the Force Balance of the σ MO of the Carbon Nitride Radical section wherein the diamagnetic force terms include orbital and spin angular momentum contributions. The electrons of the $3d4s$ HOs may pair such that the binding energy of the HO is increased. The hybridization factor accordingly changes which effects the bond distances and energies. The diamagnetic terms of the force balance equations of the electrons of the MOs formed between the $3d4s$ HOs and the AOs of the ligands also changes depending on whether the nonbonding HOs are occupied by paired or unpaired electrons. The orbital and spin angular momentum of the HOs and MOs is then determined by the state that achieves a minimum energy including that corresponding to the donation of electron charge from the HOs and AOs to the MOs. Historically, according to crystal field theory and molecular orbital theory [13] the possibility of a bonding metal atom achieving a so called "high-spin" or "low-spin" state having unpaired electrons occupying higher-energy orbitals versus paired electrons occupying lower-energy orbitals was due to the strength of the ligand crystal field or the interaction between metal orbitals and the ligands, respectively. Excited-state spectral data recorded on transition-metal organometallic and coordinate compounds has been misinterpreted. Excitation of an unpaired electron in a $3d4s$ HO to a $3d4s$ paired state is equivalent to an excitation of the molecule to a higher energy MO since the MOs change energy due to the corresponding change in the hybridization factor and diamagnetic force balance terms. But, levels misidentified as crystal field levels do not exist in the absence of excitation by a photon.

The parameters of the $3d4s$ HOs are determined using Eqs. (15.12-15.21). For transition metal atoms with electron configuration $3d^n4s^2$, the spin-paired $4s$ electrons are promoted to the $3d4s$ shell during hybridization as unpaired electrons. Also, for $n>5$ the electrons of the $3d$ shell are spin-paired and these electrons are promoted to the $3d4s$ shell during hybridization as unpaired electrons. The energy for each promotion is the magnetic energy given by Eq. (15.15) at the initial radius of the $4s$ electrons and the paired $3d$ electrons determined using Eq. (10.102) with the corresponding nuclear charge Z of the metal atom and the number of electrons, n, of the corresponding ion with the filled outer shell from which the pairing energy is determined. Typically, the electrons from the $4s$ and $3d$ shells successively fill unoccupied HOs until the HO shell is filled with unpaired electrons, then the electrons pair per HO. The magnetic energy of pairing given by Eqs. (15.13) and (15.15) is added to $E_{Coulomb}\left(atom,3d4s\right)$ the for each pair. Thus, after Eq. (15.16), the energy $E\left(atom,3d4s\right)$ of the outer electron of the $atom$ $3d4s$ shell is given by the sum of $E_{Coulomb}\left(atom,3d4s\right)$ and $E(magnetic)$:

$$E\left(atom,3d4s\right)=\frac{-e^2}{8\pi\varepsilon_0 r_{3d4s}}+\frac{2\pi\mu_0 e^2\hbar^2}{m_e^2 r_{4s}^3}+\sum_{3d\ pairs}\frac{2\pi\mu_0 e^2\hbar^2}{m_e^2 r_{3d}^3}-\sum_{HO\ pairs}\frac{2\pi\mu_0 e^2\hbar^2}{m_e^2 r_{3d4s}^3} \tag{23.28}$$

The sharing of electrons between the metal $3d4s$ HOs and the ligand AOs or HOs to form a $M-L$-bond MO (L not C) permits each participating hybridized or atomic orbital to decrease in radius and energy. Due to the low binding energy of the metal atom and the high electronegativity of the ligand, an energy minimum is achieved while further satisfying the potential, kinetic, and orbital energy relationships, each metal $3d4s$ HO donates an excess of an electron per bond of its electron density to the $M-L$-bond MO. In each case, the radius of the hybridized shell is calculated from the Coulombic energy equation by considering that the central field decreases by an integer for each successive electron of the shell and the total energy of the shell is equal to the total Coulombic energy of the initial AO electrons plus the hybridization energy. After Eq. (15.17), the total energy $E_T\left(mol.atom,3d4s\right)$ of the HO electrons is given by the sum of energies of successive ions of the atom over the n electrons comprising the total electrons of the initial AO shell and the hybridization energy:

$$E_T\left(mol.atom,3d4s\right)=E\left(atom,3d4s\right)-\sum_{m=2}^{n}IP_m \tag{23.29}$$

where IP_m is the mth ionization energy (positive) of the atom and the sum of $-IP_1$ plus the hybridization energy is $E\left(atom,3d4s\right)$. Thus, the radius r_{3d4s} of the hybridized shell due to its donation of a total charge $-Qe$ to the corresponding MO is given by:

$$r_{3d4s}=\left(\sum_{q=Z-n}^{Z-1}(Z-q)-Q\right)\frac{-e^2}{8\pi\varepsilon_0 E_T\left(mol.atom,3d4s\right)}=\left(\sum_{q=Z-n}^{Z-1}(Z-q)-s\left(0.25\right)\right)\frac{-e^2}{8\pi\varepsilon_0 E_T\left(mol.atom,3d4s\right)} \tag{23.30}$$

where $-e$ is the fundamental electron charge, $s=1,2,3$ for a single, double, and triple bond, respectively, and $s=4$ for typical coordinate and organometallic compounds wherein L is not carbon. The Coulombic energy $E_{Coulomb}\left(mol.atom,3d4s\right)$ of the outer electron of the $atom$ $3d4s$ shell is given by

$$E_{Coulomb}\left(mol.atom,3d4s\right)=\frac{-e^2}{8\pi\varepsilon_0 r_{3d4s}} \tag{23.31}$$

In the case that during hybridization the metal spin-paired $4s$ AO electrons are unpaired to contribute electrons to the $3d4s$ HO, the energy change for the promotion to the unpaired state is the magnetic energy $E(magnetic)$ at the initial radius r of the AO electron given by Eq. (15.15). In addition in the case that the $3d4s$ HO electrons are paired, the corresponding magnetic energy is added. Then, the energy $E\left(mol.atom,3d4s\right)$ of the outer electron of the $atom$ $3d4s$ shell is given by the sum of $E_{Coulomb}\left(mol.atom,3d4s\right)$ and $E(magnetic)$:

$$E\left(mol.atom,3d4s\right)=\frac{-e^2}{8\pi\varepsilon_0 r_{3d4s}}+\frac{2\pi\mu_0 e^2\hbar^2}{m_e^2 r_{4s}^3}-\sum_{HO\ pairs}\frac{2\pi\mu_0 e^2\hbar^2}{m_e^2 r_{3d4s}^3} \tag{23.32}$$

$E_T\left(atom-atom,3d4s\right)$, the energy change of each $atom$ msp^3 shell with the formation of the atom-atom-bond MO is given by the difference between $E\left(mol.atom,3d4s\right)$ and $E\left(atom,3d4s\right)$:

$$E_T\left(atom-atom,3d4s\right)=E\left(mol.atom,3d4s\right)-E\left(atom,3d4s\right) \tag{23.33}$$

Any unpaired electrons of ligands typically pair with unpaired HO electrons of the metal. In the case that no such electrons of the metal are available, the ligand electrons pair and form a bond with an unpaired metal HO when available. An unoccupied HO may form by the pairing of the corresponding HO electrons to form an energy minimum due to the effect on the bond parameters such as the diamagnetic force term, hybridization factor, and the $E_T\left(atom-atom,msp^3.AO\right)$ term. In the case of carbonyls, the two unpaired Csp^3 HO electrons on each carbonyl pair with any unpaired electrons of the metal HOs. Any excess carbonyl electrons pair in the formation of the corresponding MO and any remaining metal HO electrons pair where possible. In the latter case, the energy of the HO for the determination of the hybridization factor and other bonding parameters in Eqs. (15.51) and (15.65) is given by the Coulombic energy plus the pairing energy.

The force balance of the centrifugal force equated to the Coulombic and magnetic forces is solved for the length of the semimajor axis. The Coulombic force on the pairing electron of the MO is:

$$\mathbf{F}_{Coulomb}=\frac{e^2}{8\pi\varepsilon_0 ab^2}D\mathbf{i}_\xi \tag{23.34}$$

The spin pairing force is

$$\mathbf{F}_{spin-pairing}=\frac{\hbar^2}{2m_e a^2 b^2}D\mathbf{i}_\xi \tag{23.35}$$

The diamagnetic force is:

$$\mathbf{F}_{diamagneticMO1}=-\frac{n_e\hbar^2}{4m_e a^2 b^2}D\mathbf{i}_\xi \tag{23.36}$$

where n_e is the total number of electrons that interact with the binding σ-MO electron. The diamagnetic force $\mathbf{F}_{diamagneticMO2}$ on the pairing electron of the σ MO is given by the sum of the contributions over the components of angular momentum:

$$\mathbf{F}_{diamagneticMO2}=-\sum_i\frac{\left|L_i\right|\hbar^2}{Z2m_e a^2 b^2}D\mathbf{i}_\xi \tag{23.37}$$

where $\left|L_i\right|$ is the magnitude of the angular momentum component of the metal atom at a focus that is the source of the diamagnetism at the σ-MO. The centrifugal force is:

$$\mathbf{F}_{centrifugalMO}=-\frac{\hbar^2}{m_e a^2 b^2}D\mathbf{i}_\xi \tag{23.38}$$

The general force balance equation for the σ-MO of the metal (M) to ligand (L) $M-L$-bond MO in terms of n_e and $\left|L_i\right|$ corresponding to the orbital and spin angular momentum terms of the $3d4s$ HO shell is**:**

$$\frac{\hbar^2}{m_e a^2 b^2}D=\frac{e^2}{8\pi\varepsilon_0 ab^2}D+\frac{\hbar^2}{2m_e a^2 b^2}D-\left(\frac{n_e}{2}+\sum_i\frac{\left|L_i\right|}{Z}\right)\frac{\hbar^2}{2m_e a^2 b^2}D \tag{23.39}$$

Having a solution for the semimajor axis a of:

$$a=\left(1+\frac{n_e}{2}+\sum_i\frac{\left|L_i\right|}{Z}\right)a_0 \tag{23.40}$$

In term of the total angular momentum L, the semimajor axis a is**:**

$$a=\left(1+\frac{n_e}{2}+\frac{L}{Z}\right)a_0 \tag{23.41}$$

Using the semimajor axis, the geometric and energy parameters of the MO are calculated using Eqs. (15.1-15.117) in the same manner as the organic functional groups given in the Organic Molecular Functional Groups and Molecules section.

Bond angles in organometallic and coordinate compounds are determined using the standard Eqs. (15.70-15.79) and (15.88-15.117) with the appropriate $E_T\left(atom-atom, msp^3.AO\right)$ for energy matching with the $B-C$ terminal bond of the corresponding angle $\angle BAC$. For bond angles in general, if the groups can be maximally displaced in terms of steric interactions and magnitude of the residual E_T term is less that the steric energy, then the geometry that minimizes the steric interactions is the lowest energy. Steric-energy minimizing geometries include tetrahedral (T_d) and octahedral symmetry (O_h).

SCANDIUM FUNCTIONAL GROUPS AND MOLECULES

The electron configuration of scandium is $[Ar]4s^2 3d$ having the corresponding term $^2D_{3/2}$. The total energy of the state is given by the sum over the three electrons. The sum $E_T\left(Sc, 3d4s\right)$ of experimental energies [1] of Sc, Sc^+, and Sc^{2+} is:

$$E_T\left(Sc, 3d4s\right) = -\left(24.75666\ eV + 12.79977\ eV + 6.56149\ eV\right) = -44.11792\ eV \tag{23.42}$$

By considering that the central field decreases by an integer for each successive electron of the shell, the radius r_{3d4s} of the $Sc3d4s$ shell may be calculated from the Coulombic energy using Eq. (15.13).

$$r_{3d4s} = \sum_{n=18}^{20} \frac{(Z-n)e^2}{8\pi\varepsilon_0\left(e44.11792\ eV\right)} = \frac{6e^2}{8\pi\varepsilon_0\left(e44.11792\ eV\right)} = 1.85038a_0 \tag{23.43}$$

where $Z = 21$ for scandium. Using Eq. (15.14), the Coulombic energy $E_{Coulomb}\left(Sc, 3d4s\right)$ of the outer electron of the $Sc3d4s$ shell is:

$$E_{Coulomb}\left(Sc, 3d4s\right) = \frac{-e^2}{8\pi\varepsilon_0 r_{3d4s}} = \frac{-e^2}{8\pi\varepsilon_0 1.85038a_0} = -7.35299\ eV \tag{23.44}$$

During hybridization, the spin-paired $4s$ electrons are promoted to the $Sc3d4s$ shell as unpaired electrons. The energy for the promotion is the magnetic energy given by Eq. (15.15) at the initial radius of the $4s$ electrons. From Eq. (10.102) with $Z = 21$ and $n = 21$, the radius r_{21} of the $Sc4s$ shell is:

$$r_{21} = 2.07358a_0 \tag{23.45}$$

Using Eqs. (15.15) and (23.45), the unpairing energy is:

$$E(magnetic) = \frac{2\pi\mu_0 e^2\hbar^2}{m_e^2\left(r_{21}\right)^3} = \frac{8\pi\mu_0\mu_B^2}{\left(2.07358a_0\right)^3} = 0.01283\ eV \tag{23.46}$$

Using Eqs. (23.44) and (23.46), the energy $E\left(Sc, 3d4s\right)$ of the outer electron of the $Sc3d4s$ shell is:

$$E\left(Sc, 3d4s\right) = \frac{-e^2}{8\pi\varepsilon_0 r_{3d4s}} + \frac{2\pi\mu_0 e^2\hbar^2}{m_e^2\left(r_{21}\right)^3} = -7.352987\ eV + 0.01283\ eV = -7.34015\ eV \tag{23.47}$$

Next, consider the formation of the $Sc-L$-bond MO wherein each scandium atom has an $Sc3d4s$ electron with an energy given by Eq. (23.47). The total energy of the state of each scandium atom is given by the sum over the three electrons. The sum $E_T\left(Sc_{Sc-L}3d4s\right)$ of energies of $Sc3d4s$ (Eq. (23.47)), Sc^+, and Sc^{2+} is:

$$\begin{aligned} E_T\left(Sc_{Sc-L}3d4s\right) &= -\left(24.75666\ eV + 12.79977\ eV + E\left(Sc, 3d4s\right)\right) \\ &= -\left(24.75666\ eV + 12.79977\ eV + 7.34015\ eV\right) = -44.89658\ eV \end{aligned} \tag{23.48}$$

where $E\left(Sc, 3d4s\right)$ is the sum of the energy of Sc, $-6.56149\ eV$, and the hybridization energy.

The scandium HO donates an electron to each MO. Using Eq. (23.30), the radius r_{3d4s} of the $Sc3d4s$ shell calculated from the Coulombic energy is:

$$r_{Sc-L3d4s} = \left(\sum_{n=18}^{20}(Z-n) - 1\right)\frac{e^2}{8\pi\varepsilon_0\left(e44.89658\ eV\right)} = \frac{5e^2}{8\pi\varepsilon_0\left(e44.89658\ eV\right)} = 1.51524a_0 \tag{23.49}$$

Using Eqs. (15.19) and (23.49), the Coulombic energy $E_{Coulomb}\left(Sc_{Sc-L}, 3d4s\right)$ of the outer electron of the $Sc3d4s$ shell is:

$$E_{Coulomb}\left(Sc_{Sc-L}, 3d4s\right) = \frac{-e^2}{8\pi\varepsilon_0 r_{Sc-L3d4s}} = \frac{-e^2}{8\pi\varepsilon_0 1.51524a_0} = -8.97932\ eV \tag{23.50}$$

The only magnetic energy term is that for the unpairing of the $4s$ electrons given by Eq. (23.46). Using Eqs. (23.32), (23.46), and (23.50), the energy $E\left(Sc_{Sc-L}, 3d4s\right)$ of the outer electron of the $Sc3d4s$ shell is:

$$E\left(Sc_{Sc-L}, 3d4s\right) = \frac{-e^2}{8\pi\varepsilon_0 r_{Sc-L3d4s}} + \frac{2\pi\mu_0 e^2\hbar^2}{m_e^2\left(r_{21}\right)^3} = -8.97932\ eV + 0.01283\ eV = -8.96648\ eV \tag{23.51}$$

Thus, $E_T\left(Sc-L, 3d4s\right)$, the energy change of each $Sc3d4s$ shell with the formation of the $Sc-L$-bond MO is given by the difference between Eq. (23.51) and Eq. (23.47).

$$E_T\left(Sc-L, 3d4s\right) = E\left(Sc_{Sc-L}, 3d4s\right) - E\left(Sc, 3d4s\right) = -8.96648\ eV - \left(-7.34015\ eV\right) = -1.62633\ eV \tag{23.52}$$

The semimajor axis a solution given by Eq. (23.41) of the force balance equation, Eq. (23.39), for the σ-MO of the $Sc-L$-bond MO of ScL_n is given in Table 23.8 with the force-equation parameters $Z=21$, n_e, and L corresponding to the orbital and spin angular momentum terms of the $3d4s$ HO shell.

For the $Sc-L$ functional groups, hybridization of the $4s$ and $3d$ AOs of Sc to form a single $3d4s$ shell forms an energy minimum, and the sharing of electrons between the $Sc3d4s$ HO and L AO to form a MO permits each participating orbital to decrease in radius and energy. The F AO has an energy of $E(F)=-17.42282\ eV$, the Cl AO has an energy of $E(Cl)=-12.96764\ eV$, the O AO has an energy of $E(O)=-13.61805\ eV$, and the $Sc3d4s$ HOs have an energy of $E(Sc,3d4s)=-7.34015\ eV$ (Eq. (23.47)). To meet the equipotential condition of the union of the $Sc-L$ H_2-type-ellipsoidal-MO with these orbitals, the hybridization factor(s), at least one of c_2 and C_2 of Eq. (15.61) for the $Sc-L$-bond MO given by Eq. (15.77) is:

$$c_2(FAO\ to\ Sc3d4sHO)=C_2(FAO\ to\ Sc3d4sHO)=\frac{E(Sc,3d4s)}{E(FAO)}=\frac{-7.34015\ eV}{-17.42282\ eV}=0.42130 \tag{23.53}$$

$$c_2(ClAO\ to\ Sc3d4sHO)=C_2(ClAO\ to\ Sc3d4sHO)=\frac{E(Sc,3d4s)}{E(ClAO)}=\frac{-7.34015\ eV}{-12.96764\ eV}=0.56604 \tag{23.54}$$

$$c_2(O\ to\ Sc3d4sHO)=\frac{E(Sc,3d4s)}{E(O)}=\frac{-7.34015\ eV}{-13.61805\ eV}=0.53900 \tag{23.55}$$

Since the energy of the MO is matched to that of the $Sc3d4s$ HO, $E(AO/HO)$ in Eq. (15.61) is $E(Sc,3d4s)$ given by Eq. (23.47) and twice this value for double bonds. $E_T(atom-atom,msp^3.AO)$ of the $Sc-L$-bond MO is determined by considering that the bond involves an electron transfer from the scandium atom to the ligand atom to form partial ionic character in the bond as in the case of the zwitterions such as $H_2B^+-F^-$ given in the Halido Boranes section. $E_T(atom-atom,msp^3.AO)$ is $-3.25266\ eV$, two times the energy of Eq. (23.52) for single bonds, and $-6.50532\ eV$, four times the energy of Eq. (23.52) for double bonds.

The symbols of the functional groups of scandium coordinate compounds are given in Table 23.7. The geometrical (Eqs. (15.1-15.5) and (23.41)), intercept (Eqs. (15.31-15.32) and (15.80-15.87)), and energy (Eqs. (15.61) and (23.28-23.33)) parameters of scandium coordinate compounds are given in Tables 23.8, 23.9, and 23.10, respectively. The total energy of each scandium coordinate compound given in Table 23.11 was calculated as the sum over the integer multiple of each $E_{D(Group)}$ of Table 23.10 corresponding to functional-group composition of the compound. The charge-densities of exemplary scandium coordinate compound, scandium trifluoride comprising the concentric shells of atoms with the outer shell bridged by one or more H_2-type ellipsoidal MOs or joined with one or more hydrogen MOs is shown in Figure 23.2.

Figure 23.2. *Scandium Trifluoride.* Color scale, translucent view of the charge-density of ScF_3 showing the orbitals of the Sc and F atoms at their radii, the ellipsoidal surface of each H_2-type ellipsoidal MO that transitions to the corresponding outer shell of the atoms participating in each bond, and the nuclei (red, not to scale).

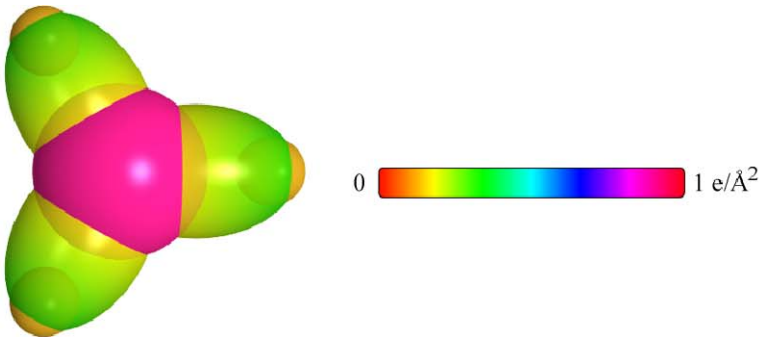

Table 23.7. The symbols of the functional groups of scandium coordinate compounds.

Functional Group	Group Symbol
ScF group of *ScF*	$Sc-F$ (a)
ScF group of ScF_2	$Sc-F$ (b)
ScF group of ScF_3	$Sc-F$ (c)
ScCl group of *ScCl*	$Sc-Cl$
ScO group of *ScO*	$Sc-O$

Table 23.8. The geometrical bond parameters of scandium coordinate compounds and experimental values.

Parameter	$Sc-F$ (a) Group	$Sc-F$ (b) Groups	$Sc-F$ (c) Group	$Sc-Cl$ Group	$Sc-O$ Group
n_e	1	2	2	2	1
L	$2+\sqrt{\frac{3}{4}}$	$4\sqrt{\frac{3}{4}}$	$2+\sqrt{\frac{3}{4}}$	$1+3\sqrt{\frac{3}{4}}$	$3+2\sqrt{\frac{3}{4}}$
$a\ (a_0)$	1.63648	2.16496	2.13648	2.17134	1.72534
$c'\ (a_0)$	1.60922	1.60294	1.59236	1.95858	1.51672
Bond Length $2c'\ (\text{Å})$	1.70313	1.69647	1.68528	2.07287	1.60523
Exp. Bond Length (Å)	1.788 [14] (scandium fluoride)	1.788 [14] (scandium fluoride)	1.788 [41] (scandium fluoride)	2.229 [15] (scandium chloride)	1.668 [15] (scandium oxide)
$b,c\ (a_0)$	0.29743	1.45521	1.45521	0.93737	0.82240
e	0.98335	0.74040	0.74040	0.90202	0.87909

Table 23.9. The MO to HO intercept geometrical bond parameters of scandium coordinate compounds. E_T is E_T (*atom–atom,msp³.AO*).

Bond	Atom	E_T (eV) Bond 1	E_T (eV) Bond 2	E_T (eV) Bond 3	E_T (eV) Bond 4	Final Total Energy $Sc3d4s$ (eV)	$r_{initial}$ (a_0)	r_{final} (a_0)	$E_{Coulomb}(Sc3d4s)$ (eV) Final	$E(Sc3d4s)$ (eV) Final	θ' (°)	θ_1 (°)	θ_2 (°)	d_1 (a_0)	d_2 (a_0)
$Sc-F$ (ScF)	Sc	-1.62633	0	0	0		1.85038	1.51524	-8.97932		168.71	11.29	85.68	0.12329	1.48593
$Sc-F$ (ScF)	F	-1.62633	0	0	0		0.78069	0.71425	-19.04915		160.05	19.95	55.03	0.93785	0.67137
$Sc-F$ (ScF_2)	Sc	-1.62633	-1.62633	0	0		1.85038	1.28288	-10.60565		108.71	71.29	56.61	1.19135	0.41159
$Sc-F$ (ScF_2)	F	-1.62633	0	0	0		0.78069	0.71425	-19.04915		60.07	119.93	25.17	1.95936	0.35642
$Sc-F$ (ScF_3)	Sc	-1.62633	-1.62633	-1.62633	0		1.85038	1.11231	-12.23198		101.31	78.69	49.97	1.37413	0.21823
$Sc-F$ (ScF_3)	F	-1.62633	0	0	0		0.78069	0.71425	-19.04915		63.75	116.25	26.73	1.90822	0.31586
$Sc-Cl$ $(ScCl)$	Sc	-1.62633	0	0	0		1.85038	1.51524	-8.97932		144.35	35.65	70.43	0.72737	1.23121
$Sc-Cl$ $(ScCl)$	Cl	-1.62633	0	0	0		1.05158	0.93229	-14.59397		128.86	51.14	50.76	1.37364	0.58494
$Sc-O$ (ScO)	Sc	-3.25266	0	0	0		1.85038	1.28288	-10.60565		142.18	37.82	73.04	0.50331	1.01341
$Sc-O$ (ScO)	O	-3.25266	0	0	0		1.00000	0.80647	-16.87072		125.78	54.22	52.71	1.04524	0.47148

Table 23.10. The energy parameters (eV) of functional groups of scandium coordinate compounds.

Parameters	$Sc-F$ (a) Groups	$Sc-F$ (b) Groups	$Sc-F$ (c) Group	$Sc-Cl$ Group	$Sc-O$ Group
n_1	1	1	1	1	2
n_2	0	0	0	0	0
n_3	0	0	0	0	0
C_1	0.75	1	1	0.5	0.375
C_2	0.42130	0.42130	0.42130	0.56604	1
c_1	1	1	1	1	1
c_2	0.42130	1	1	0.56604	0.53900
c_3	0	0	0	0	0
c_4	1	1	1	1	2
c_5	1	1	1	1	2
C_{1o}	0.75	1	1	0.5	0.375
C_{2o}	0.42130	0.42130	0.42130	0.56604	1
$V_e\ (eV)$	-34.05166	-32.30098	-32.89066	-23.32429	-53.06036
$V_p\ (eV)$	8.45489	8.48805	8.54444	6.94677	17.94106
$T\ (eV)$	10.40395	7.45996	7.69741	5.37095	15.37682
$V_m\ (eV)$	-5.20198	-3.72998	-3.84870	-2.68548	-7.68841
$E(AO/HO)\ (eV)$	-7.34015	-7.34015	-7.34015	-7.34015	-14.68031
$\Delta E_{H_2MO}(AO/HO)\ (eV)$	0	0	0	0	0
$E_T(AO/HO)\ (eV)$	-7.34015	-7.34015	-7.34015	-7.34015	-14.68031
$E_T(H_2MO)\ (eV)$	-27.73495	-27.42310	-27.83768	-21.03220	-42.11120
$E_T(atom-atom, msp^3.AO)\ (eV)$	-3.25266	-3.25266	-3.25266	-3.25266	-6.50532
$E_T(MO)\ (eV)$	-30.98761	-30.67576	-31.09034	-24.28486	-48.61652
$\omega\ (10^{15}\ rad/s)$	11.1005	15.2859	8.59272	6.87387	33.9452
$E_K\ (eV)$	7.30656	10.06142	5.65588	4.52450	22.34334
$\bar{E}_D\ (eV)$	-0.16571	-0.19250	-0.14628	-0.10219	-0.22732
$\bar{E}_{Kvib}\ (eV)$	0.09120 [14]	0.09120 [14]	0.09120 [14]	0.04823 [16]	0.12046 [17]
$\bar{E}_{osc}\ (eV)$	-0.12011	-0.14690	-0.10068	-0.07808	-0.16709
$E_T(Group)\ (eV)$	-31.10771	-30.82266	-31.19102	-24.36294	-48.95069
$E_{initial}(c_4\ AO/HO)\ (eV)$	-7.34015	-7.34015	-7.34015	-7.34015	-7.34015
$E_{initial}(c_5\ AO/HO)\ (eV)$	-17.42282	-17.42282	-17.42282	-12.96764	-13.61806
$E_D(Group)\ (eV)$	6.34474	6.05969	6.42804	4.05515	7.03426

Table 23.11. The total bond energies of gaseous-state scandium coordinate compounds calculated using the functional group composition and the energies of Table 23.10 compared to the gaseous-state experimental values [15].

Formula	Name	$Sc-F$ (a) Groups	$Sc-F$ (b) Groups	$Sc-F$ (c) Group	$Sc-Cl$ Group	$Sc-O$ Group	Calculated Total Bond Energy (eV)	Experimental Total Bond Energy (eV)	Relative Error
ScF	Scandium fluoride	1	0	0	0	0	6.34474	6.16925	-0.02845
ScF_2	Scandium difluoride	0	2	0	0	0	12.11937	12.19556	0.00625
ScF_3	Scandium trifluoride	0	0	3	0	0	19.28412	19.27994	-0.00022
ScCl	Scandium chloride	0	0	0	1	0	4.05515	4.00192	-0.01330
ScO	Scandium oxide	0	0	0	0	1	7.03426	7.08349	0.00695

TITANIUM FUNCTIONAL GROUPS AND MOLECULES

The electron configuration of titanium is $[Ar]4s^2 3d^2$ having the corresponding term ${}^3F_2$. The total energy of the state is given by the sum over the four electrons. The sum $E_T(Ti, 3d4s)$ of experimental energies [1] of Ti, Ti^+, Ti^{2+}, and Ti^{3+} is

$$E_T(Ti, 3d4s) = -(43.2672\ eV + 27.4917\ eV + 13.5755\ eV + 6.82812\ eV) = -91.16252\ eV \tag{23.56}$$

By considering that the central field decreases by an integer for each successive electron of the shell, the radius r_{3d4s} of the $Ti3d4s$ shell may be calculated from the Coulombic energy using Eq. (15.13):

$$r_{3d4s} = \sum_{n=18}^{21} \frac{(Z-n)e^2}{8\pi\varepsilon_0 (e91.16252\ eV)} = \frac{10e^2}{8\pi\varepsilon_0 (e91.16252\ eV)} = 1.49248a_0 \tag{23.57}$$

where $Z = 22$ for titanium. Using Eq. (15.14), the Coulombic energy $E_{Coulomb}(Ti, 3d4s)$ of the outer electron of the $Ti3d4s$ shell is:

$$E_{Coulomb}(Ti, 3d4s) = \frac{-e^2}{8\pi\varepsilon_0 r_{3d4s}} = \frac{-e^2}{8\pi\varepsilon_0 1.49248a_0} = -9.11625\ eV \tag{23.58}$$

During hybridization, the spin-paired $4s$ electrons are promoted to the $Ti3d4s$ shell as unpaired electrons. The energy for the promotion is the magnetic energy given by Eq. (15.15) at the initial radius of the $4s$ electrons. From Eq. (10.102) with $Z = 22$ and $n = 22$, the radius r_{22} of the $Ti4s$ shell is:

$$r_{22} = 1.99261a_0 \tag{23.59}$$

Using Eqs. (15.15) and (23.59), the unpairing energy is:

$$E(magnetic) = \frac{2\pi\mu_0 e^2\hbar^2}{m_e^2 (r_{22})^3} = \frac{8\pi\mu_0\mu_B^2}{(1.99261a_0)^3} = 0.01446\ eV \tag{23.60}$$

Using Eqs. (23.58) and (23.60), the energy $E(Ti, 3d4s)$ of the outer electron of the $Ti3d4s$ shell is:

$$E(Ti, 3d4s) = \frac{-e^2}{8\pi\varepsilon_0 r_{3d4s}} + \frac{2\pi\mu_0 e^2\hbar^2}{m_e^2 (r_{22})^3} = -9.11625\ eV + 0.01446\ eV = -9.10179\ eV \tag{23.61}$$

Next, consider the formation of the $Ti-L$-bond MO wherein each titanium atom has a $Ti3d4s$ electron with an energy given by Eq. (23.61). The total energy of the state of each titanium atom is given by the sum over the four electrons. The sum $E_T(Ti_{Ti-L}3d4s)$ of energies of $Ti3d4s$ (Eq. (23.61)), Ti^+, Ti^{2+}, and Ti^{3+} is:

$$\begin{aligned} E_T(Ti_{Ti-L}3d4s) &= -(43.2672\ eV + 27.4917\ eV + 13.5755\ eV + E(Ti, 3d4s)) \\ &= -(43.2672\ eV + 27.4917\ eV + 13.5755\ eV + 9.10179\ eV) \\ &= -93.43619\ eV \end{aligned} \tag{23.62}$$

where $E(Ti, 3d4s)$ is the sum of the energy of Ti, $-6.82812\ eV$, and the hybridization energy.

The titanium HO donates an electron to each MO. Using Eq. (23.30), the radius r_{3d4s} of the $Ti3d4s$ shell calculated from the Coulombic energy is:

$$r_{Ti-L3d4s} = \left(\sum_{n=18}^{21} (Z-n) - 1\right) \frac{e^2}{8\pi\varepsilon_0 (e93.43619\ eV)} = \frac{9e^2}{8\pi\varepsilon_0 (e93.43619\ eV)} = 1.31054a_0 \tag{23.63}$$

Using Eqs. (15.19) and (23.63), the Coulombic energy $E_{Coulomb}(Ti_{Ti-L}, 3d4s)$ of the outer electron of the $Ti3d4s$ shell is:

$$E_{Coulomb}(Ti_{Ti-L}, 3d4s) = \frac{-e^2}{8\pi\varepsilon_0 r_{Ti-L3d4s}} = \frac{-e^2}{8\pi\varepsilon_0 1.31054a_0} = -10.38180\ eV \tag{23.64}$$

The only magnetic energy term is that for the unpairing of the $4s$ electrons given by Eq. (23.60). Using Eqs. (23.32), (23.60), and (23.64), the energy $E(Ti_{Ti-L}, 3d4s)$ of the outer electron of the $Ti3d4s$ shell is:

$$E(Ti_{Ti-L}, 3d4s) = \frac{-e^2}{8\pi\varepsilon_0 r_{Ti-L3d4s}} + \frac{2\pi\mu_0 e^2\hbar^2}{m_e^2 (r_{22})^3} = -10.38180\ eV + 0.01446\ eV = -10.36734\ eV \tag{23.65}$$

Thus, $E_T(Ti-L, 3d4s)$, the energy change of each $Ti3d4s$ shell with the formation of the $Ti-L$-bond MO is given by the difference between Eq. (23.65) and Eq. (23.61).

$$E_T(Ti-L, 3d4s) = E(Ti_{Ti-L}, 3d4s) - E(Ti, 3d4s) = -10.36734\ eV - (-9.10179\ eV) = -1.26555\ eV \tag{23.66}$$

The semimajor axis a solution given by Eq. (23.41) of the force balance equation, Eq. (23.39), for the σ-MO of the $Ti-L$-bond MO of TiL_n is given in Table 23.13 with the force-equation parameters $Z = 22$, n_e, and L corresponding to the orbital and spin angular momentum terms of the $3d4s$ HO shell.

For the $Ti-L$ functional groups, hybridization of the $4s$ and $3d$ AOs of Ti to form a single $3d4s$ shell forms an energy minimum, and the sharing of electrons between the $Ti3d4s$ HO and L AO to form a MO permits each participating orbital to

decrease in radius and energy. The F AO has an energy of $E(F) = -17.42282\ eV$, the Cl AO has an energy of $E(Cl) = -12.96764\ eV$, the Br AO has an energy of $E(Br) = -11.8138\ eV$, the I AO has an energy of $E(I) = -10.45126\ eV$, the O AO has an energy of $E(O) = -13.61805\ eV$, and the $Ti3d4s$ HOs have an energy of $E(Ti,3d4s) = -9.10179\ eV$ (Eq. (23.61)). To meet the equipotential condition of the union of the $Ti-L$ H_2-type-ellipsoidal-MO with these orbitals, the hybridization factor(s), at least one of c_2 and C_2 of Eq. (15.61) for the $Ti-L$-bond MO given by Eq. (15.77) is:

$$C_2(FAO\ to\ Ti3d4sHO) = \frac{E(Ti,3d4s)}{E(FAO)} = \frac{-9.10179\ eV}{-17.42282\ eV} = 0.52241 \tag{23.67}$$

$$C_2(ClAO\ to\ Ti3d4sHO) = \frac{E(Ti,3d4s)}{E(ClAO)} = \frac{-9.10179\ eV}{-12.96764\ eV} = 0.70188 \tag{23.68}$$

$$c_2(BrAO\ to\ Ti3d4sHO) = C_2(BrAO\ to\ Ti3d4sHO) = \frac{E(Ti,3d4s)}{E(BrAO)} = \frac{-9.10179\ eV}{-11.8138\ eV} = 0.77044 \tag{23.69}$$

$$c_2(IAO\ to\ Ti3d4sHO) = C_2(IAO\ to\ Ti3d4sHO) = \frac{E(Ti,3d4s)}{E(IAO)} = \frac{-9.10179\ eV}{-10.45126\ eV} = 0.87088 \tag{23.70}$$

$$c_2(O\ to\ Ti3d4sHO) = \frac{E(Ti,3d4s)}{E(O)} = \frac{-9.10179\ eV}{-13.61805\ eV} = 0.66836 \tag{23.71}$$

Since the energy of the MO is matched to that of the $Ti3d4s$ HO, $E(AO/HO)$ in Eq. (15.61) is $E(Ti,3d4s)$ given by Eq. (23.61) and twice this value for double bonds. $E_T(atom-atom,msp^3.AO)$ of the $Ti-L$-bond MO is determined by considering that the bond involves an electron transfer from the titanium atom to the ligand atom to form partial ionic character in the bond as in the case of the zwitterions such as $H_2B^+-F^-$ given in the Halido Boranes section. $E_T(atom-atom,msp^3.AO)$ is $-2.53109\ eV$, two times the energy of Eq. (23.66).

The symbols of the functional groups of titanium coordinate compounds are given in Table 23.12. The geometrical (Eqs. (15.1-15.5) and (23.41)), intercept (Eqs. (15.31-15.32) and (15.80-15.87)), and energy (Eqs. (15.61) and (23.28-23.33)) parameters of titanium coordinate compound are given in Tables 23.13, 23.14, and 23.15, respectively. The total energy of each titanium coordinate compounds given in Table 23.16 was calculated as the sum over the integer multiple of each $E_{D(Group)}$ of Table 23.15 corresponding to functional-group composition of the compound. The bond angle parameters of titanium coordinate compounds determined using Eqs. (15.88-15.117) are given in Table 23.17. The $E_T(atom-atom,msp^3.AO)$ term for $TiOCl_2$ was calculated using Eqs. (23.30-23.33) as a linear combination of $s=1$ and $s=2$ for the energies of $E(Ti,3d4s)$ given by Eqs. (23.63-23.66) corresponding to a $Ti-Cl$ single bond and a $Ti=O$ double bond. The charge-densities of exemplary titanium coordinate compound, titanium tetrafluoride comprising the concentric shells of atoms with the outer shell bridged by one or more H_2-type ellipsoidal MOs or joined with one or more hydrogen MOs is shown in Figure 23.3.

Figure 23.3. *Titanium Tetrafluoride.* Color scale, translucent view of the charge-density of TiF_4 showing the orbitals of the Ti and F atoms at their radii, the ellipsoidal surface of each H_2-type ellipsoidal MO that transitions to the corresponding outer shell of the atoms participating in each bond, and the nuclei (red, not to scale).

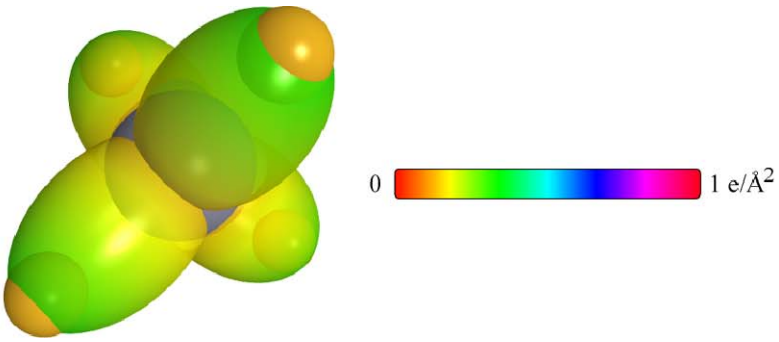

Table 23.12. The symbols of the functional groups of titanium coordinate compounds.

Functional Group	Group Symbol
TiF group of *TiF*	$Ti-F$ (a)
TiF group of TiF_2	$Ti-F$ (b)
TiF group of TiF_3	$Ti-F$ (c)
TiF group of TiF_4	$Ti-F$ (d)
TiCl group of *TiCl*	$Ti-Cl$ (a)
TiCl group of $TiCl_2$	$Ti-Cl$ (b)
TiCl group of $TiCl_3$	$Ti-Cl$ (c)
TiCl group of $TiCl_4$	$Ti-Cl$ (d)
TiBr group of *TiBr*	$Ti-Br$ (a)
TiBr group of $TiBr_2$	$Ti-Br$ (b)
TiBr group of $TiBr_3$	$Ti-Br$ (c)
TiBr group of $TiBr_4$	$Ti-Br$ (d)
TiI group of *TiI*	$Ti-I$ (a)
TiI group of TiI_2	$Ti-I$ (b)
TiI group of TiI_3	$Ti-I$ (c)
TiI group of TiI_4	$Ti-I$ (d)
TiO group of *TiO*	$Ti-O$ (a)
TiO group of TiO_2	$Ti-O$ (b)

Table 23.13. The geometrical bond parameters of titanium coordinate compounds and experimental values.

Parameter	$Ti-F$ (a) Group	$Ti-F$ (b) Group	$Ti-F$ (c) Group	$Ti-F$ (d) Group	$Ti-Cl$ (a) Group	$Ti-Cl$ (b) Group	$Ti-Cl$ (c) Group	$Ti-Cl$ (d) Group	$Ti-Br$ (a) Group	$Ti-Br$ (b) Group	$Ti-Br$ (c) Group	$Ti-Br$ (d) Group	$Ti-I$ (a) Groups	$Ti-I$ (b) Group	$Ti-I$ (c) Group	$Ti-I$ (d) Group	$Ti-O$ (a) Group	$Ti-O$ (b) Group
n_e	2	2	2	2	3	3	3	3	3	3	3	3	4	4	4	4	2	-2
L	$1+\sqrt{\frac{3}{4}}$	3	$4\sqrt{\frac{3}{4}}$	4	$9\sqrt{\frac{3}{4}}$	$4+3\sqrt{\frac{3}{4}}$	$3+5\sqrt{\frac{3}{4}}$	8	$2+3\sqrt{\frac{3}{4}}$	3	4	$3+2\sqrt{\frac{3}{4}}$	3	1	$3\sqrt{\frac{3}{4}}$	$4\sqrt{\frac{3}{4}}$	$9\sqrt{\frac{3}{4}}$	$3+6\sqrt{\frac{3}{4}}$
$a\ (a_0)$	2.16355	2.13636	2.15746	2.18182	2.85428	2.79991	2.83319	2.86364	2.70900	2.63636	2.68182	2.71509	3.13636	3.04545	3.11809	3.15746	2.35428	2.37255
$c'\ (a_0)$	1.66163	1.65115	1.65929	1.66863	2.01658	1.99728	2.00911	2.01988	2.16524	2.13601	2.15435	2.16767	2.19131	2.15932	2.18492	2.19867	1.53242	1.53835
Bond Length $2c'\ (A)$	1.75859	1.74751	1.75611	1.76600	2.13426	2.11383	2.12635	2.13775	2.29159	2.26066	2.28006	2.29416	2.31918	2.28532	2.31242	2.32697	1.62184	1.62812
Exp. Bond Length (A)	1.745 [15] (TiF_4)	1.745 [15] (TiF_4)	1.745 [15] (TiF_4)	1.745 [15] (TiF_4)	2.170 [18] ($TiCl_4$)	2.170 [18] ($TiCl_4$)	2.170 [81] ($TiCl_4$)	2.170 [18] ($TiCl_4$)	2.31 [19] ($TiBr_4$)	2.31 [19] ($TiBr_4$)	2.31 [19] ($TiBr_4$)	2.31 [19] ($TiBr_4$)	2.5 [20] (TiI_4)	2.5 [20] (TiI_4)	2.5 [20] (TiI_4)	2.5 [20] (TiI_4)	1.623 [15] (TiO)	1.62 [15] (TiO_2)
$b,c\ (a_0)$	1.38562	1.35563	1.37891	1.40571	2.01998	1.96224	1.99760	2.02990	1.62802	1.54527	1.59717	1.63491	2.24387	2.14759	2.22456	2.26615	1.78727	1.80623
e	0.76801	0.77288	0.76909	0.76479	0.70651	0.71334	0.70914	0.70536	0.79927	0.81021	0.80332	0.79838	0.69868	0.70903	0.70072	0.69634	0.65091	0.64840

Table 23.14. The MO to HO intercept geometrical bond parameters of titanium coordinate compounds. E_T is E_T (*atom–atom,HO.AO*).

Bond	Atom	E_T (eV) Bond 1	E_T (eV) Bond 2	E_T (eV) Bond 3	E_T (eV) Bond 4	Final Total Energy $Ti3d4s$ (eV)	$r_{initial}$ (a_0)	r_{final} (a_0)	$E_{Coulomb}(Ti3d4s)$ (eV) Final	$E(Ti3d4s)$ (eV) Final	θ' (°)	θ_1 (°)	θ_2 (°)	d_1 (a_0)	d_2 (a_0)
$Ti-F\ (TiF)$	Ti	-1.26555	0	0	0		1.49248	1.31054	-10.38180		114.86	65.14	59.11	1.11067	0.55096
$Ti-F\ (TiF)$	F	-1.26555	0	0	0		0.78069	0.72804	-18.68837		73.44	106.56	30.24	1.86913	0.20751
$Ti-F\ (TiF_2)$	Ti	-1.26555	-1.26555	0	0		1.49248	1.16815	-11.64735		109.94	70.06	54.10	1.25274	0.39842
$Ti-F\ (TiF_2)$	F	-1.26555	0	0	0		0.78069	0.72804	-18.68837		76.41	103.59	31.47	1.82218	0.17102
$Ti-F\ (TiF_3)$	Ti	-1.26555	-1.26555	-1.26555	0		1.49248	1.05366	-12.91289		102.28	77.72	48.30	1.43520	0.22409
$Ti-F\ (TiF_3)$	F	-1.26555	0	0	0		0.78069	0.72804	-18.68837		74.11	105.89	30.52	1.85858	0.19930
$Ti-F\ (TiF_4)$	Ti	-1.26555	-1.26555	-1.26555	-1.26555		1.49248	0.95961	-14.17844		94.21	85.79	42.91	1.59810	0.07053
$Ti-F\ (TiF_4)$	F	-1.26555	0	0	0		0.78069	0.72804	-18.68837		71.40	108.60	29.40	1.90090	0.23227
$Ti-Cl\ (TiCl)$	Ti	-1.26555	0	0	0		1.49248	1.31054	-10.38180		82.62	97.38	40.05	2.18502	0.16844
$Ti-Cl\ (TiCl)$	Cl	-1.26555	0	0	0		1.05158	0.95592	-14.23319		45.47	134.53	19.72	2.68696	0.67038
$Ti-Cl\ (TiCl_2)$	Ti	-1.26555	-1.26555	0	0		1.49248	1.16815	-11.64735		75.61	104.39	35.22	2.28751	0.29023
$Ti-Cl\ (TiCl_2)$	Cl	-1.26555	0	0	0		1.05158	0.95592	-14.23319		52.06	127.94	22.59	2.58502	0.58774
$Ti-Cl\ (TiCl_3)$	Ti	-1.26555	-1.26555	-1.26555	0		1.49248	1.05366	-12.91289		61.65	118.35	27.66	2.50943	0.50032
$Ti-Cl\ (TiCl_3)$	Cl	-1.26555	0	0	0		1.05158	0.95592	-14.23319		48.12	131.88	20.87	2.64726	0.63815
$Ti-Cl\ (TiCl_4)$	Ti	-1.26555	-1.26555	-1.26555	-1.26555		1.49248	0.95961	-14.17844		44.92	135.08	19.50	2.69938	0.67950
$Ti-Cl\ (TiCl_4)$	Cl	-1.26555	0	0	0		1.05158	0.95592	-14.23319		44.25	135.75	19.18	2.70461	0.68473
$Ti-Br\ (TiBr)$	Ti	-1.26555	0	0	0		1.49248	1.31054	-10.38180		108.49	71.51	49.77	1.74966	0.41558
$Ti-Br\ (TiBr)$	Br	-1.26555	0	0	0		1.15169	1.04025	-13.07935		94.27	85.73	39.58	2.08783	0.07740
$Ti-Br\ (TiBr_2)$	Ti	-1.26555	-1.26555	0	0		1.49248	1.16815	-11.64735		106.10	73.90	46.58	1.81214	0.32387
$Ti-Br\ (TiBr_2)$	Br	-1.26555	0	0	0		1.15169	1.04025	-13.07935		99.18	80.82	41.65	1.97000	0.16601
$Ti-Br\ (TiBr_3)$	Ti	-1.26555	-1.26555	-1.26555	0		1.49248	1.05366	-12.91289		96.95	83.05	40.91	2.02680	0.12755
$Ti-Br\ (TiBr_3)$	Br	-1.26555	0	0	0		1.15169	1.04025	-13.07935		96.12	83.88	40.36	2.04349	0.11086
$Ti-Br\ (TiBr_4)$	Ti	-1.26555	-1.26555	-1.26555	-1.26555		1.49248	0.95961	-14.17844		88.14	91.86	35.92	2.19881	0.03114
$Ti-Br\ (TiBr_4)$	Br	-1.26555	0	0	0		1.15169	1.04025	-13.07935		93.85	86.15	39.41	2.09781	0.06986
$Ti-I\ (TiI)$	Ti	-1.26555	0	0	0		1.49248	1.31054	-10.38180		71.22	108.78	33.57	2.61325	0.42194
$Ti-I\ (TiI)$	I	-1.26555	0	0	0		1.30183	1.16122	-11.71681		56.81	123.19	25.66	2.82697	0.63566
$Ti-I\ (TiI_2)$	Ti	-1.26555	-1.26555	0	0		1.49248	1.16815	-11.64735		65.29	114.71	29.61	2.64772	0.48840
$Ti-I\ (TiI_2)$	I	-1.26555	0	0	0		1.30183	1.16122	-11.71681		64.60	115.40	29.24	2.65748	0.49817
$Ti-I\ (TiI_3)$	Ti	-1.26555	-1.26555	-1.26555	0		1.49248	1.05366	-12.91289		43.74	136.26	19.12	2.94615	0.76124
$Ti-I\ (TiI_3)$	I	-1.26555	0	0	0		1.30183	1.16122	-11.71681		58.44	121.56	26.41	2.79265	0.60774
$Ti-I\ (TiI_4)$	Ti	-1.26555	-1.26555	-1.26555	-1.26555		1.49248	0.95961	-14.17844		3.69	176.31	1.56	3.15628	0.95762
$Ti-I\ (TiI_4)$	I	-1.26555	0	0	0		1.30183	1.16122	-11.71681		54.88	125.12	24.78	2.86676	0.66809
$Ti-O\ (TiO)$	Ti	-1.26555	0	0	0		1.49248	1.31054	-10.38180		86.89	93.11	47.07	1.60351	0.07109
$Ti-O\ (TiO)$	O	-1.26555	0	0	0		1.00000	0.91490	-14.87135		42.09	137.91	20.07	2.21135	0.67893
$Ti-O\ (TiO_2)$	Ti	-1.26555	0	0	0		1.49248	1.16815	-11.64734		74.14	105.86	38.47	1.85751	0.31916
$Ti-O\ (TiO_2)$	O	-1.26555	-1.26555	0	0		1.00000	0.91490	-14.87135		39.13	140.87	18.64	2.24809	0.70973

Table 23.15. The energy parameters (eV) of functional groups of titanium coordinate compounds.

Parameters	$Ti-F$ (a) Group	$Ti-F$ (b) Group	$Ti-F$ (c) Group	$Ti-F$ (d) Group	$Ti-Cl$ (a) Group	$Ti-Cl$ (b) Group	$Ti-Cl$ (c) Group	$Ti-Cl$ (d) Group	$Ti-Br$ (a) Group	$Ti-Br$ (b) Group	$Ti-Br$ (c) Group	$Ti-Br$ (d) Group	$Ti-I$ (a) Groups	$Ti-I$ (b) Group	$Ti-I$ (c) Group	$Ti-I$ (d) Group	$Ti-O$ (a) Group	$Ti-O$ (b) Group
n_1	1	1	1	1	1	1	1	1	1	1	1	1	1	1	1	1	2	2
n_2	0	0	0	0	0	0	0	0	0	0	0	0	0	0	0	0	0	0
n_3	0	0	0	0	0	0	0	0	0	0	0	0	0	0	0	0	0	0
C_1	0.75	0.75	0.75	0.75	0.5	0.5	0.5	0.5	0.375	0.375	0.375	0.375	0.375	0.375	0.375	0.375	0.75	0.75
C_2	0.52241	0.52241	0.52241	0.52241	0.70188	0.70188	0.70188	0.70188	0.77044	0.77044	0.77044	0.77044	0.87088	0.87088	0.87088	0.87088	0.66836	0.66836
c_1	1	1	1	1	1	1	1	1	1	1	1	1	1	1	1	1	1	1
c_2	1	1	1	1	1	1	1	1	0.77044	0.77044	0.77044	0.77044	0.87088	0.87088	0.87088	0.87088	1	1
c_3	0	0	0	0	0	0	0	0	0	0	0	0	0	0	0	0	0	0
c_4	1	1	1	1	1	1	1	1	1	1	1	1	1	1	1	1	2	2
c_5	1	1	1	1	1	1	1	1	1	1	1	1	1	1	1	1	2	2
C_{1o}	0.75	0.75	0.75	0.75	0.5	0.5	0.5	0.5	0.375	0.375	0.375	0.375	0.375	0.375	0.375	0.375	0.75	0.75
C_{2o}	0.52241	0.52241	0.52241	0.52241	0.70188	0.70188	0.70188	0.70188	0.77044	0.77044	0.77044	0.77044	0.87088	0.87088	0.87088	0.87088	0.66836	0.66836
V_e (eV)	-33.25925	-33.86525	-33.39295	-32.86502	-23.75423	-24.35881	-23.98503	-23.65338	-21.23559	-22.13551	-21.56268	-21.16382	-18.70299	-19.43040	-18.84456	-18.54225	-55.18049	-54.66023
V_p (eV)	8.18824	8.24018	8.19979	8.15389	6.74697	6.81216	6.77204	6.73594	6.28375	6.36973	6.31552	6.27670	6.20899	6.30098	6.22715	6.18821	17.75727	17.68877
T (eV)	7.68627	7.92591	7.73895	7.53157	4.16116	4.34992	4.23287	4.12996	3.91945	4.19811	4.02016	3.89744	2.98164	3.19007	3.02181	2.93626	11.71917	11.51929
V_m (eV)	-3.84314	-3.96296	-3.86948	-3.76578	-2.08058	-2.17496	-2.11643	-2.06498	-1.95972	-2.09906	-2.01008	-1.94872	-1.49082	-1.59503	-1.51090	-1.46813	-5.85959	-5.75964
$E_{(AO/HO)}$ (eV)	-9.10179	-9.10179	-9.10179	-9.10179	-9.10179	-9.10179	-9.10179	-9.10179	-9.10179	-9.10179	-9.10179	-9.10179	-9.10179	-9.10179	-9.10179	-9.10179	-18.20358	-18.20358
$\Delta E_{H_2MO_{(AO/HO)}}$ (eV)	0	0	0	0	0	0	0	0	0	0	0	0	0	0	0	0	0	0
$E_{T_{(AO/HO)}}$ (eV)	-9.10179	-9.10179	-9.10179	-9.10179	-9.10179	-9.10179	-9.10179	-9.10179	-9.10179	-9.10179	-9.10179	-9.10179	-9.10179	-9.10179	-9.10179	-9.10179	-18.20358	-18.20358
$E_{T_{(H_2MO)}}$ (eV)	-30.32966	-30.76391	-30.42547	-30.04713	-24.02848	-24.47348	-24.19834	-23.95426	-22.09391	-22.76852	-22.33888	-22.04019	-20.10497	-20.63618	-20.20830	-19.98770	-49.76721	-49.41539
$E_T\left(atom-atom, msp^3.AO\right)$ (eV)	-2.53109	-2.53109	-2.53109	-2.53109	-2.53109	-2.53109	-2.53109	-2.53109	-2.53109	-2.53109	-2.53109	-2.53109	-2.53109	-2.53109	-2.53109	-2.53109	-2.53109	-2.53109
$E_{T_{(MG)}}$ (eV)	-32.86076	-33.29501	-32.95657	-32.57823	-26.55957	-27.00457	-26.72944	-26.48535	-24.62500	-25.29961	-24.86997	-24.57129	-22.63607	-23.16728	-22.73939	-22.51880	-52.29830	-51.94648
$\omega\ \left(10^{15}\ rad/s\right)$	8.13148	8.28718	8.16593	8.02956	5.07876	5.22741	8.67440	5.05389	4.98373	5.19112	5.05970	4.96698	7.02884	4.44530	4.29087	4.21088	12.2500	8.00936
E_K (eV)	5.35228	5.45477	5.37496	5.28520	3.34292	3.44077	5.70964	3.32656	3.28038	3.41689	3.33039	3.26935	4.62650	2.92598	2.82433	2.77168	8.06316	5.27190
$\bar{E}_D$ (eV)	-0.15040	-0.15384	-0.15116	-0.14817	-0.09607	-0.09910	-0.12636	-0.09557	-0.08824	-0.09252	-0.08979	-0.08789	-0.09632	-0.07840	-0.07560	-0.07417	-0.14690	-0.11798
$\bar{E}_{Kvib}$ (eV)	0.07315 [21]	0.07315 [21]	0.07315 [21]	0.07315 [21]	0.04823 [16]	0.04823 [16]	0.04823 [16]	0.04823 [16]	0.03658 [19]	0.03658 [19]	0.03658 [19]	0.03658 [19]	0.02976 [20]	0.02976 [20]	0.02976 [20]	0.02976 [20]	0.12510 [14]	0.12510 [14]
$\bar{E}_{osc}$ (eV)	-0.11383	-0.11726	-0.11458	-0.11159	-0.07195	-0.07498	-0.10224	-0.07145	-0.06995	-0.07423	-0.07150	-0.06961	-0.08144	-0.06352	-0.06072	-0.05929	-0.08435	-0.05543
$E_{T_{(Group)}}$ (eV)	-32.97458	-33.41227	-33.07115	-32.68982	-26.63152	-27.07955	-26.83168	-26.55680	-24.69495	-25.37384	-24.94147	-24.64090	-22.71751	-23.23080	-22.80011	-22.57809	-52.46699	-52.05734
$E_{initial\ i_{c_4\ AO/HO)}}$ (eV)	-9.10179	-9.10179	-9.10179	-9.10179	-9.10179	-9.10179	-9.10179	-9.10179	-9.10179	-9.10179	-9.10179	-9.10179	-9.10179	-9.10179	-9.10179	-9.10179	-9.10179	-9.10179
$E_{initial\ i_{c_5\ AO/HO)}}$ (eV)	-17.42282	-17.42282	-17.42282	-17.42282	-12.96764	-12.96764	-12.96764	-12.96764	-11.8138	-11.8138	-11.8138	-11.8138	-10.45126	-10.45126	-10.45126	-10.45126	-13.61806	-13.61806
$E_{D_{(Group)}}$ (eV)	6.44997	6.88766	6.54654	6.16521	4.56209	5.01012	4.76225	4.48737	3.77936	4.45825	4.02588	3.72530	3.16446	3.67775	3.24706	3.02504	7.02729	6.61764

Table 23.16. The total bond energies of gaseous-state titanium coordinate compounds calculated using the functional group composition and the energies of Table 23.15 compared to the gaseous-state experimental values.

Formula	Name	$Ti-F$ (a) Group	$Ti-F$ (b) Group	$Ti-F$ (c) Group	$Ti-F$ (d) Group	$Ti-Cl$ (a) Group	$Ti-Cl$ (b) Group	$Ti-Cl$ (c) Group	$Ti-Cl$ (d) Group	$Ti-Br$ (a) Group	$Ti-Br$ (b) Group	$Ti-Br$ (c) Group	$Ti-Br$ (d) Group	$Ti-I$ (a) Groups	$Ti-I$ (b) Group	$Ti-I$ (c) Group	$Ti-I$ (d) Group	$Ti-O$ (a) Group	$Ti-O$ (b) Group	Calculated Total Bond Energy (eV)	Experimental Total Bond Energy (eV)	Relative Error
TiF	Titanium fluoride	1	0	0	0	0	0	0	0	0	0	0	0	0	0	0	0	0	0	6.44997	6.41871 [21]	-0.00487
TiF_2	Titanium difluoride	0	2	0	0	0	0	0	0	0	0	0	0	0	0	0	0	0	0	13.77532	13.66390 [21]	-0.00815
TiF_3	Titanium trifluoride	0	0	3	0	0	0	0	0	0	0	0	0	0	0	0	0	0	0	19.63961	19.64671 [21]	0.00036
TiF_4	Titanium tetrafluoride	0	0	0	4	0	0	0	0	0	0	0	0	0	0	0	0	0	0	24.66085	24.23470 [21]	-0.01758
TiCl	Titanium chloride	0	0	0	0	1	0	0	0	0	0	0	0	0	0	0	0	0	0	4.56209	4.56198 [22]	-0.00003
$TiCl_2$	Titanium dichoride	0	0	0	0	0	2	0	0	0	0	0	0	0	0	0	0	0	0	10.02025	9.87408 [22]	-0.01517
$TiCl_3$	Titanium trichloride	0	0	0	0	0	0	3	0	0	0	0	0	0	0	0	0	0	0	14.28674	14.22984 [22]	-0.00400
$TiCl_4$	Titanium tetrachloride	0	0	0	0	0	0	0	4	0	0	0	0	0	0	0	0	0	0	17.94949	17.82402 [22]	-0.00704
TiBr	Titanium bromide	0	0	0	0	0	0	0	0	1	0	0	0	0	0	0	0	0	0	3.77936	3.78466 [19]	0.00140
$TiBr_2$	Titanium dibromide	0	0	0	0	0	0	0	0	0	2	0	0	0	0	0	0	0	0	8.91650	8.93012 [19]	0.00153
$TiBr_3$	Titanium tribromide	0	0	0	0	0	0	0	0	0	0	3	0	0	0	0	0	0	0	12.07765	12.02246 [19]	-0.00459
$TiBr_4$	Titanium tetrabromide	0	0	0	0	0	0	0	0	0	0	0	4	0	0	0	0	0	0	14.90122	14.93239 [19]	0.00209
TiI	Titanium iodide	0	0	0	0	0	0	0	0	0	0	0	0	1	0	0	0	0	0	3.16446	3.15504 [20]	-0.00299
TiI_2	Titanium diiodide	0	0	0	0	0	0	0	0	0	0	0	0	0	2	0	0	0	0	7.35550	7.29291 [20]	-0.00858
TiI_3	Titanium triiodide	0	0	0	0	0	0	0	0	0	0	0	0	0	0	3	0	0	0	9.74119	9.71935 [20]	-0.00225
TiI_4	Titanium tetraiodide	0	0	0	0	0	0	0	0	0	0	0	0	0	0	0	4	0	0	12.10014	12.14569 [20]	0.00375
TiO	Titanium oxide	0	0	0	0	0	0	0	0	0	0	0	0	0	0	0	0	1	0	7.02729	7.00341 [23]	-0.00341
TiO_2	Titanium dioxide	0	0	0	0	0	0	0	0	0	0	0	0	0	0	0	0	0	2	13.23528	13.21050 [23]	-0.00188
TiOF	Titanium fluoride oxide	0	0	0	1	0	0	0	0	0	0	0	0	0	0	0	0	0	1	12.78285	12.77353 [23]	-0.00073
$TiOF_2$	Titanium difluoride oxide	0	0	0	2	0	0	0	0	0	0	0	0	0	0	0	0	0	1	18.94807	18.66983 [23]	-0.01490
TiOCl	Titanium chloride oxide	0	0	0	0	0	0	0	1	0	0	0	0	0	0	0	0	0	1	11.10501	11.25669 [23]	0.01347
$TiOCl_2$	Titanium dichloride oxide	0	0	0	0	0	0	0	2	0	0	0	0	0	0	0	0	0	1	15.59238	15.54295 [23]	-0.00318

Table 23.17. The bond angle parameters of titanium coordinate compounds and experimental values [15]. E_T is E_T (*atom–atom,HO.AO*).

Atoms of Angle	$2c'$ Bond 1 (a_0)	$2c'$ Bond 2 (a_0)	$2c'$ Terminal Atoms (a_0)	$E_{Coulombic}$ Atom 1	Atom 1 Hybridization Designation (Table 15.3A)	$E_{Coulombic}$ Atom 2	Atom 2 Hybridization Designation (Table 15.3A)	c_2 Atom 1	c_2 Atom 2	C_1	C_2	c_1	c_2'	E_T (eV)	θ_v (°)	θ_1 (°)	θ_2 (°)	Cal. θ (°)	Exp. θ (°)
$\angle OTiCl$	3.07671	4.03976	6.2075	-13.61806 *O*	O	-12.96764 *Cl*	Cl	0.66836 (Eq. (23.71))	0.70188 (Eq. (23.68))	0.75	0.68512	1	0.68512	-0.59304				120.85	120 ($TiOCl_2$)

VANADIUM FUNCTIONAL GROUPS AND MOLECULES

The electron configuration of vanadium is $[Ar]4s^2 3d^3$ having the corresponding term ${}^4F_{3/2}$. The total energy of the state is given by the sum over the five electrons. The sum $E_T(V,3d4s)$ of experimental energies [1] of V, V^+, V^{2+}, V^{3+}, and V^{4+} is

$$E_T(V,3d4s) = -(65.2817\ eV + 46.709\ eV + 29.311\ eV + 14.618\ eV + 6.74619\ eV) = -162.66589\ eV \tag{23.72}$$

By considering that the central field decreases by an integer for each successive electron of the shell, the radius r_{3d4s} of the $V3d4s$ shell may be calculated from the Coulombic energy using Eq. (15.13).

$$r_{3d4s} = \sum_{n=18}^{22} \frac{(Z-n)e^2}{8\pi\varepsilon_0 (e162.66589\ eV)} = \frac{15e^2}{8\pi\varepsilon_0 (e162.66589\ eV)} = 1.25464a_0 \tag{23.73}$$

where $Z = 23$ for vanadium. Using Eq. (15.14), the Coulombic energy $E_{Coulomb}(V,3d4s)$ of the outer electron of the $V3d4s$ shell is:

$$E_{Coulomb}(V,3d4s) = \frac{-e^2}{8\pi\varepsilon_0 r_{3d4s}} = \frac{-e^2}{8\pi\varepsilon_0 1.25464a_0} = -10.844393\ eV \tag{23.74}$$

During hybridization, the spin-paired $4s$ electrons are promoted to the $V3d4s$ shell as unpaired electrons. The energy for the promotion is the magnetic energy given by Eq. (15.15) at the initial radius of the $4s$ electrons. From Eq. (10.102) with $Z = 23$ and $n = 23$, the radius r_{23} of the $V4s$ shell is:

$$r_{23} = 2.01681a_0 \tag{23.75}$$

Using Eqs. (15.15) and (23.74), the unpairing energy is:

$$E(magnetic) = \frac{2\pi\mu_0 e^2\hbar^2}{m_e^2 (r_{23})^3} = \frac{8\pi\mu_0\mu_B^2}{(2.01681a_0)^3} = 0.01395\ eV \tag{23.76}$$

Using Eqs. (23.73) and (23.75), the energy $E(V,3d4s)$ of the outer electron of the $V3d4s$ shell is:

$$E(V,3d4s) = \frac{-e^2}{8\pi\varepsilon_0 r_{3d4s}} + \frac{2\pi\mu_0 e^2\hbar^2}{m_e^2 (r_{23})^3} = -10.844393\ eV + 0.01395\ eV = -10.83045\ eV \tag{23.77}$$

Next, consider the formation of the $V-L$-bond MO wherein each vanadium atom has a $V3d4s$ electron with an energy given by Eq. (23.76). The total energy of the state of each vanadium atom is given by the sum over the five electrons. The sum $E_T(V_{V-L}3d4s)$ of energies of $V3d4s$ (Eq. (23.76)), V^+, V^{2+}, V^{3+}, and V^{4+} is:

$$E_T(V_{V-L}3d4s) = -\begin{pmatrix} 65.2817\ eV + 46.709\ eV + 29.311\ eV \\ +14.618\ eV + E(V,3d4s) \end{pmatrix} = -\begin{pmatrix} 65.2817\ eV + 46.709\ eV + 29.311\ eV \\ +14.618\ eV + 10.83045 \end{pmatrix} \tag{23.78}$$
$$= -166.75015\ eV$$

where $E(V,3d4s)$ is the sum of the energy of V, $-6.74619\ eV$, and the hybridization energy.

The vanadium HO donates an electron to each MO. Using Eq. (23.30), the radius r_{3d4s} of the $V3d4s$ shell calculated from the Coulombic energy is:

$$r_{V-L3d4s} = \left(\sum_{n=18}^{22}(Z-n) - 1\right)\frac{e^2}{8\pi\varepsilon_0 (e166.75015\ eV)} = \frac{14e^2}{8\pi\varepsilon_0 (e166.75015\ eV)} = 1.14232a_0 \tag{23.79}$$

Using Eqs. (15.19) and (23.78), the Coulombic energy $E_{Coulomb}(V_{V-L},3d4s)$ of the outer electron of the $V3d4s$ shell is

$$E_{Coulomb}(V_{V-L},3d4s) = \frac{-e^2}{8\pi\varepsilon_0 r_{V-L3d4s}} = \frac{-e^2}{8\pi\varepsilon_0 1.14232a_0} = -11.91072\ eV \tag{23.80}$$

The only magnetic energy term is that for the unpairing of the $4s$ electrons given by Eq. (23.75). Using Eqs. (23.32), (23.73), and (23.79), the energy $E(V_{V-L},3d4s)$ of the outer electron of the $V3d4s$ shell is:

$$E(V_{V-L},3d4s) = \frac{-e^2}{8\pi\varepsilon_0 r_{V-L3d4s}} + \frac{2\pi\mu_0 e^2\hbar^2}{m_e^2 (r_{23})^3} = -11.91072\ eV + 0.01446\ eV = -11.89678\ eV \tag{23.81}$$

Thus, $E_T(V-L,3d4s)$, the energy change of each $V3d4s$ shell with the formation of the $V-L$-bond MO is given by the difference between Eq. (23.80) and Eq. (23.76):

$$E_T(V-L,3d4s) = E(V_{V-L},3d4s) - E(V,3d4s) = -11.89678\ eV - (-10.83045\ eV) = -1.06633\ eV \tag{23.82}$$

The semimajor axis a solution given by Eq. (23.41) of the force balance equation, Eq. (23.39), for the σ-MO of the $V-L$-bond MO of VL_n is given in Table 23.19 with the force-equation parameters $Z = 23$, n_e, and L corresponding to the orbital and spin angular momentum terms of the $3d4s$ HO shell. The semimajor axis a of carbonyl and organometallic compounds are solved using Eq. (15.51).

For the $V-L$ functional groups, hybridization of the $4s$ and $3d$ AOs of V to form a single $3d4s$ shell forms an energy

minimum, and the sharing of electrons between the $V3d4s$ HO and L AO to form a MO permits each participating orbital to decrease in radius and energy. The F AO has an energy of $E(F) = -17.42282\ eV$, the Cl AO has an energy of $E(Cl) = -12.96764\ eV$, the $C_{aryl}2sp^3$ HO has an energy of $E(C_{aryl}, 2sp^3) = -15.76868\ eV$ (Eq. (14.246)), the $C2sp^3$ HO has an energy of $E(C, 2sp^3) = -14.63489\ eV$ (Eq. (15.25)), the N AO has an energy of $E(N) = -14.53414\ eV$, the O AO has an energy of $E(O) = -13.61805\ eV$, and the $V3d4s$ HO has an energy of $E_{Coulomb}(V, 3d4s) = -10.84439\ eV$ (Eq. (23.75)) and $E(V, 3d4s) = -10.83045\ eV$ (Eq. (23.76)). To meet the equipotential condition of the union of the $V-L$ H_2-type-ellipsoidal-MO with these orbitals, the hybridization factor(s), at least one of c_2 and C_2 of Eq. (15.61) for the $V-L$-bond MO given by Eq. (15.77) is:

$$C_2(FAO\ to\ V3d4sHO) = \frac{E(V,3d4s)}{E(FAO)} = \frac{-10.83045\ eV}{-17.42282\ eV} = 0.62162 \tag{23.83}$$

$$C_2(ClAO\ to\ V3d4sHO) = \frac{E(V,3d4s)}{E(ClAO)} = \frac{-10.83045\ eV}{-12.96764\ eV} = 0.83519 \tag{23.84}$$

$$C_2(C2sp^3HO\ to\ V3d4sHO) = \frac{E_{Coulomb}(V,3d4s)}{E(C,2sp^3)} c_2(C2sp^3HO) = \frac{-10.84439\ eV}{-14.63489\ eV}(0.91771) = 0.68002 \tag{23.85}$$

$$c_2(C_{aryl}2sp^3HO\ to\ V3d4sHO) = C_2(C_{aryl}2sp^3HO\ to\ V3d4sHO) = \frac{E_{Coulomb}(V,3d4s)}{E(C_{aryl},2sp^3)} = \frac{-10.84439\ eV}{-15.76868\ eV} = 0.68772 \tag{23.86}$$

$$c_2(NAO\ to\ V3d4sHO) = C_2(NAO\ to\ V3d4sHO) = \frac{E(V,3d4s)}{E(NAO)} = \frac{-10.83045\ eV}{-14.53414\ eV} = 0.74517 \tag{23.87}$$

$$c_2(O\ to\ V3d4sHO) = \frac{E(V,3d4s)}{E(O)} = \frac{-10.83045\ eV}{-13.61805\ eV} = 0.79530 \tag{23.88}$$

where Eqs. (15.76), (15.79), and (13.430) were used in Eq. (23.84). Since the energy of the MO is matched to that of the $V3d4s$ HO of coordinate compounds, $E(AO/HO)$ in Eq. (15.61) is $E(V,3d4s)$ given by Eq. (23.76) and twice this value for double bonds. For carbonyls and organometallics, the energy of the MO is matched to that of the Coulomb energy of the $V3d4s$ HO such that $E(AO/HO)$ in Eq. (15.61) is $E_{Coulomb}(V,3d4s)$ given by Eq. (23.73). $E_T(atom-atom, msp^3.AO)$ of the $V-L$-bond MO is determined by considering that the bond involves an electron transfer from the vanadium atom to the ligand atom to form partial ionic character in the bond as in the case of the zwitterions such as $H_2B^+-F^-$ given in the Halido Boranes section. For coordinate compounds, $E_T(atom-atom, msp^3.AO)$ is $-2.53109\ eV$, two times the energy of Eq. (23.81). For carbonyl and organometallic compounds, $E_T(atom-atom, msp^3.AO)$ is $-1.65376\ eV$ and $-2.26759\ eV$, respectively. The former is based on the energy match between the $V3d4s$ HO and the $C2sp^3$ HO of a carbonyl group and is given by the linear combination of $-0.72457\ eV$ (Eq. (14.151)) and $-0.92918\ eV$ (Eq. (14.513)), respectively. The latter is equivalent to that of ethylene and the aryl group, $-2.26759\ eV$, given by Eq. (14.247). The $C=O$ functional group of carbonyls is equivalent to that of formic acid given in the Carboxylic Acids section except that $\bar{E}_{Kvib}$ corresponds to that of a metal carbonyl and $E_T(AO/HO)$ of Eq. (15.47) is:

$$E_T(AO/HO) = -\Delta E_{H_2MO}(AO/HO) = -(-14.63489\ eV - 3.58557\ eV) = 18.22046\ eV \tag{23.89}$$

wherein the additional $E(AO/HO) = -14.63489\ eV$ (Eq. (15.25)) component corresponds to the donation of both unpaired electrons of the $C2sp^3$ HO of the carbonyl group to the metal-carbonyl bond. The benzene groups of organometallic, $V(C_6H_6)_2$ are equivalent to those given in the Aromatic and Heterocyclic Compounds section.

The symbols of the functional groups of vanadium coordinate compounds are given in Table 23.18. The geometrical (Eqs. (15.1-15.5) and (23.41)), intercept (Eqs. (15.31-15.32) and (15.80-15.87)), and energy (Eqs. (15.61) and (23.28-23.33)) parameters of vanadium coordinate compounds are given in Tables 23.19, 23.20, and 23.21, respectively. The total energy of each vanadium coordinate compound given in Table 23.22 was calculated as the sum over the integer multiple of each $E_{D(Group)}$ of Table 23.21 corresponding to functional-group composition of the compound. The bond angle parameters of vanadium coordinate compounds determined using Eqs. (15.88-15.117) are given in Table 23.23. The $E_T(atom-atom, msp^3.AO)$ term for $VOCl_3$ was calculated using Eqs. (23.30-23.33) with $s=1$ for the energies of $E(V,3d4s)$ given by Eqs. (23.78-23.81). The charge-densities of exemplary vanadium carbonyl and organometallic compounds, vanadium hexacarbonyl ($V(CO)_6$) and dibenzene vanadium ($V(C_6H_6)_2$), respectively, comprising the concentric shells of atoms with the outer shell bridged by one or more H_2-type ellipsoidal MOs or joined with one or more hydrogen MOs are shown in Figures 23.4A and B.

Figure 23.4. (A) *Vanadium Hexacarbonyl*. Color scale, translucent view of the charge-density of $V(CO)_6$ showing the orbitals of the V, C, and O atoms at their radii, the ellipsoidal surface of each H_2-type ellipsoidal MO that transitions to the corresponding outer shell of the atoms participating in each bond, and the nuclei (red, not to scale). (B) *Dibenzene Vanadium*. Color scale, translucent view of the charge-density of $V(C_6H_6)_2$ showing the orbitals of the V and C atoms at their radii, the ellipsoidal surface of each H or H_2-type ellipsoidal MO that transitions to the corresponding outer shell of the atoms participating in each bond, and the hydrogen nuclei (red, not to scale).

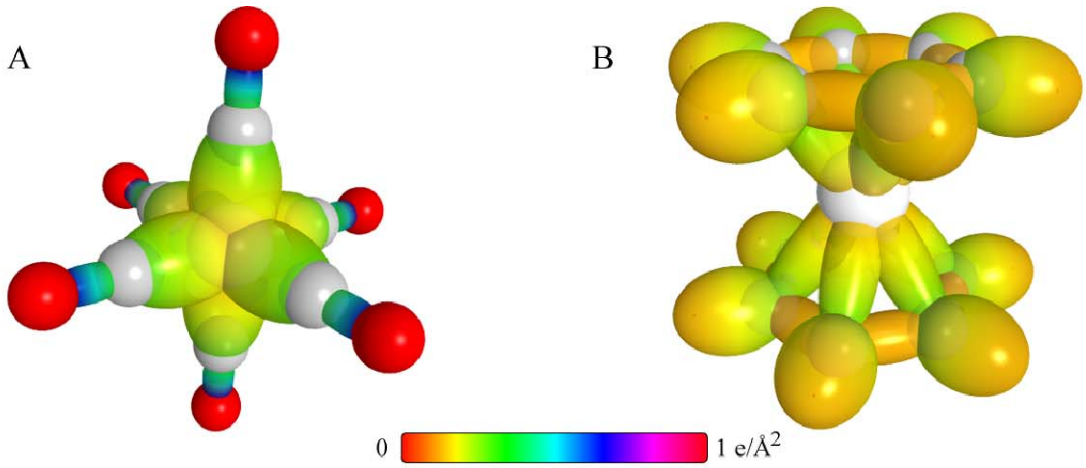

Table 23.18. The symbols of the functional groups of vanadium coordinate compounds.

Functional Group	Group Symbol
VF group of VF_5	$V-F$
VCl group of VCl_4	$V-Cl$
VN group of VN	$V-N$
VO group of VO and VO_2	$V-O$
VCO group of $V(CO)_6$	$V-CO$
C=O	$C=O$
VC_{aryl} group of $V(C_6H_6)_2$	$V-C_6H_6$
CC (aromatic bond)	$C\overset{3e}{=}C$
CH (aromatic)	CH

Table 23.19. The geometrical bond parameters of vanadium coordinate compounds and experimental values.

Parameter	$V-F$ Group	$V-Cl$ Group	$V-N$ Group	$V-O$ Group	$V-CO$ Group	$C=O$ Group	$V-C_6H_6$ Group	$C\overset{3e}{=}C$ Group	CH Group
n_e	2	3	1	2					
L	$2\sqrt{\frac{3}{4}}$	2	$4+8\sqrt{\frac{3}{4}}$	$3\sqrt{\frac{3}{4}}$					
$a\ (a_0)$	2.07531	2.58696	1.97514	2.11296	2.34957	1.184842	2.21181	1.47348	1.60061
$c'\ (a_0)$	1.49187	2.03222	1.62806	1.62997	1.85880	1.08850	2.07080	1.31468	1.03299
Bond Length $2c'\ (Å)$	1.57893	2.15081	1.72306	1.72509	1.96727	1.15202	2.19164	1.39140	1.09327
Exp. Bond Length $(Å)$	1.71 [18] (VF_5)	2.138 [18] (VCl_4)	1.612 [24] (VN)	1.890 [25] 1.5893 [18] (VO)	2.015 [18] $(V(CO)_6)$	1.138[18] $(V(CO)_6)$	2.17 [26] $(V(C_6H_6)_2)$	1.399 [3] (benzene)	1.101 [3] (benzene)
$b,c\ (a_0)$	1.44264	1.60075	1.11830	1.34454	1.43713	0.46798	0.77710	0.66540	1.22265
	0.71887	0.78556	0.82428	0.77142	0.79112	0.91869	0.93625	0.89223	0.64537

Table 23.20. The MO to HO intercept geometrical bond parameters of vanadium coordinate compounds. E_T is E_T (*atom–atom,HO.AO*).

Bond	Atom	E_T (eV) Bond 1	E_T (eV) Bond 2	E_T (eV) Bond 3	E_T (eV) Bond 4	E_T (eV) Bond 5	E_T (eV) Bond 6	Final Total Energy $V3d4s$ (eV)	$r_{initial}$ (a_0)	r_{final} (a_0)	$E_{Coulomb}(V3d4s)$ (eV) Final	$E(V3d4s)$ (eV) Final	θ' (°)	θ_1 (°)	θ_2 (°)	d_1 (a_0)	d_2 (a_0)
$V-F\ (VF_5)$	V	-1.06633	-1.06633	-1.06633	-1.06633	-1.06633	0		1.25464	0.84111	-16.17605		74.48	105.52	34.18	1.71686	0.22499
$V-F\ (VF_5)$	F	-1.06633	0	0	0	0	0		0.78069	0.73588	-18.48915		59.69	120.31	26.13	1.86324	0.37137
$V-Cl\ (VCl_4)$	V	-1.06633	-1.06633	-1.06633	-1.06633	0	0		1.25464	0.90047	-15.10972		82.69	97.31	33.91	2.14685	0.11463
$V-Cl\ (VCl_4)$	Cl	-1.06633	0	0	0	0	0		1.05158	0.96949	-14.03397		88.42	91.58	37.26	2.05898	0.02676
$V-N\ (VN)$	V	-1.26555	0	0	0	0	0		1.25464	1.14232	-11.91073		122.73	57.27	59.23	1.01037	0.61769
$V-N\ (VN)$	N	-1.26555	0	0	0	0	0		0.93084	0.87214	-15.60047		109.42	70.58	47.35	1.33814	0.28992
$V-O\ (VO)$	V	-1.26555	0	0	0	0	0		1.25464	1.14232	-11.91073		108.99	71.01	53.45	1.25826	0.37171
$V-O\ (VO)$	O	-1.26555	0	0	0	0	0		1.00000	0.92655	-14.68439		95.70	84.30	43.29	1.53796	0.09201
$V-O\ (VO_2)$	V	-1.26555	-1.26555	0	0	0	0		1.25464	1.14232	-11.91073		108.99	71.01	53.45	1.25826	0.37171
$V-O\ (VO_2)$	O	-1.26555	0	0	0	0	0		1.00000	0.92655	-14.68439		95.70	84.30	43.29	1.53796	0.09201
$VC=O$	O	-1.79278	0	0	0	0	0		1.00000	0.81871	-16.61853		147.43	32.57	70.34	0.39853	0.68997
$VC=O$	C	-1.79278	-0.82688	0	0	0	0	-154.23535	0.91771	0.77991	-17.44541	-17.25455	146.15	33.85	68.16	0.44077	0.64773
$V-CO\ (V(CO)_6)$	C	-0.82688	-1.79278	0	0	0	0		0.91771	0.77991	-17.44541	-17.25455	80.76	99.24	32.39	1.98409	1.85880
$V-CO\ (V(CO)_6)$	V	-0.82688	-0.82688	-0.82688	-0.82688	-0.82688	-0.82688		1.25464	0.686761	-19.78702		69.40	110.60	26.61	2.10076	0.24196
$C-H\ (CH)$	C	-0.85035	-0.85035	-0.56690	-0.18897	0	0	-154.07224	0.91771	0.78727	-17.28230	-17.09143	73.22	106.78	38.06	1.26026	0.22727
$C\overset{3e}{=}HC_a\overset{3e}{=}C$	C_a	-0.85035	-0.85035	-0.56690	-0.18897	0	0	-154.07225	0.91771	0.78727	-17.28231	-17.09144	133.87	46.13	58.54	0.76910	0.54558
$V-C_6H_6$	V	-1.13379	-1.13379	0	0	0	0		1.25464	0.79597	-17.09334		134.57	45.43	46.87	1.51225	0.55855
$V-C_6H_6$	C	-0.18897	-0.85035	-0.85035	-0.56690	0	0		0.91771	0.78727	-17.28231	-17.09144	134.24	45.76	46.53	1.52154	0.54926

Table 23.21. The energy parameters (eV) of functional groups of vanadium coordinate compounds.

Parameters	$V-F$ Group	$V-Cl$ Group	$V-N$ Group	$V-O$ Group	$V-CO$ Group	$C=O$ Group	$V-C_6H_6$ Group	$C\overset{3e}{=}C$ Group	CH Group
f_1	1	1	1	1	1	1	1	0.75	1
n_1	1	1	1	2	1	2	1	2	1
n_2	0	0	0	0	0	0	0	0	0
n_3	0	0	0	0	0	0	0	0	0
C_1	0.75	0.375	0.5	0.5	0.5	0.5	0.375	0.5	0.75
C_2	0.62162	0.83519	0.74517	0.79530	0.68002	1	0.68772	0.85252	1
c_1	1	1	1	1	1	1	1	1	1
c_2	1	0.83519	0.74517	0.79530	1	0.85395	0.68772	0.85252	0.91771
c_3	0	0	0	0	0	2	0	0	1
c_4	1	1	1	2	2	4	2	3	1
c_5	1	1	1	2	0	0	0	0	1
C_{1o}	0.75	0.375	0.5	0.5	0.5	0.5	0.375	0.5	0.75
C_{2o}	0.62162	0.83519	0.74517	0.79530	0.68002	1	0.68772	0.85252	1
$V_e\ (eV)$	-33.02514	-23.70273	-29.14480	-54.37349	-31.45782	-134.96850	-30.84785	-101.12679	-37.10024
$V_p\ (eV)$	9.11995	6.69504	8.35707	16.69453	7.31967	24.99908	6.57031	20.69825	13.17125
$T\ (eV)$	7.95669	4.58120	7.37791	12.86667	6.69438	56.95634	6.97344	34.31559	11.58941
$V_m\ (eV)$	-3.97835	-2.29060	-3.68896	-6.43333	-3.34719	-28.47817	-3.48672	-17.15779	-5.79470
$E_{(AO/HO)}\ (eV)$	-10.83045	-10.83045	-10.83045	-21.66089	-10.84439	0	-10.84439	0	-14.63489
$\Delta E_{H_2MO(AO/HO)}\ (eV)$	0	0	0	0	0	-18.22046	0	0	-1.13379
$E_{T(AO/HO)}\ (eV)$	-10.83045	-10.83045	-10.83045	-21.66089	-10.84439	18.22046	-10.84439	0	-13.50110
$E_{T(H_2MO)}\ (eV)$	-30.75729	-25.54754	-27.92923	-52.90652	-31.63535	-63.27080	-31.63521	-63.27075	-31.63539
$E_T\left(atom-atom, msp^3.AO\right)\ (eV)$	-2.13266	-2.13266	-2.13266	-2.13266	-1.65376	-3.58557	-2.26759	-2.26759	-0.56690
$E_{T(MO)}\ (eV)$	-32.88995	-27.68020	-30.06189	-55.03919	-33.28913	-66.85630	-33.90295	-65.53833	-32.20226
$\omega\ \left(10^{15}\ rad/s\right)$	16.2908	5.56044	21.3383	16.7215	13.9922	22.6662	30.6471	49.7272	26.4826
$E_K\ (eV)$	10.72287	3.65998	14.04526	11.00636	9.20994	14.91930	20.17243	32.73133	17.43132
$\bar{E}_D\ (eV)$	-0.21307	-0.10476	-0.22289	-0.18062	-0.19986	-0.25544	-0.30124	-0.35806	-0.26130
$\bar{E}_{Kvib}\ (eV)$	0.07538 [27]	0.05059 [28]	0.12708 [24]	0.12539 [14]	0.04749 [29]	0.24962 [29]	0.04749 [29]	0.19649 [30]	0.35532 Eq. (13.458)
$\bar{E}_{osc}\ (eV)$	-0.17538	-0.07947	-0.15934	-0.11793	-0.17612	-0.13063	-0.27750	-0.25982	-0.08364
$E_{mag}\ (eV)$	0.05793	0.05793	0.05793	0.05793	0.05793	0.11441	0.05793	0.14803	0.14803
$E_{T(Group)}\ (eV)$	-33.06533	-27.75967	-30.22123	-55.27504	-33.46525	-67.11757	-34.18046	-49.54347	-32.28590
$E_{initial(c_4\ AO/HO)}\ (eV)$	-10.83045	-10.83045	-10.83045	-10.83045	-14.63489	-14.63489	-15.76868	-14.63489	-14.63489
$E_{initial(c_5\ AO/HO)}\ (eV)$	-17.42282	-12.96764	-14.53414	-13.61806	0	0	0	0	-13.59844
$E_{D(Group)}\ (eV)$	4.81206	3.96159	4.85665	6.37803	4.19547	8.34918	2.64309	5.63881	3.90454
Exp. $E_{D(Group)}\ (eV)$				6.4 (VO [25])					

Table 23.22. The total bond energies of gaseous-state vanadium coordinate compounds calculated using the functional group composition and the energies of Table 23.21 compared to the gaseous-state experimental values except where indicated.

Formula	Name	$V-F$ Group	$V-Cl$ Group	$V-N$ Group	$V-O$ Group	$V-CO$ Group	$C=O$ Group	$V-C_6H_6$ Group	$^{3e}C=C$ Group	CH Group	Calculated Total Bond Energy (eV)	Experimental Total Bond Energy (eV)	Relative Error
VF_5	Vanadium pentafluoride	5	0	0	0	0	0	0	0	0	24.06031	24.24139 [15]	0.00747
VCl_4	Vanadium tetrachloride	0	4	0	0	0	0	0	0	0	15.84635	15.80570 [15]	-0.00257
VN	Vanadium nitride	0	0	1	0	0	0	0	0	0	4.85655	4.81931 [24]	-0.00775
VO	Vanadium oxide	0	0	0	1	0	0	0	0	0	6.37803	6.60264 [15]	0.03402
VO_2	Vanadium dioxide	0	0	0	2	0	0	0	0	0	12.75606	12.89729 [34]	0.01095
$VOCl_3$	Vanadium trichloride oxide	0	3	0	1	0	0	0	0	0	18.26279	18.87469 [15]	0.03242
$V(CO)_6$	Vanadium hexacarbonyl	0	0	0	0	6	6	0	0	0	75.26791	75.63369 [32]	0.00484
$V(C_6H_6))_2$	Dibenzene vanadium	0	0	0	0	0	0	2	12	12	119.80633	121.20193[a] [33]	0.01151

[a] Liquid.

Table 23.23. The bond angle parameters of vanadium coordinate compounds and experimental values. E_T is E_T (*atom–atom,HO.AO*).

Atoms of Angle	$2c'$ Bond 1 (a_0)	$2c'$ Bond 2 (a_0)	$2c'$ Terminal Atoms (a_0)	$E_{Coulombic}$ Atom 1	Atom 1 Hybridization Designation (Table 15.3A)	$E_{Coulombic}$ Atom 2	Atom 2 Hybridization Designation (Table 15.3A)	c_2 Atom 1	c_2 Atom 2	C_1	C_2	c_1	c_2'	E_T (eV)	θ_v (°)	θ_1 (°)	θ_2 (°)	Cal. θ (°)	Exp. θ (°)
$\angle OVCl$	2.88926	4.06444	5.9161	-13.61806 *O*	O	-12.96764 *Cl*	Cl	0.79530 (Eq. (23.87))	0.83519 (Eq. (23.83))	0.75	0.81525	1	0.81525	-0.46070				115.56	111.3 [15] ($VOCl_3$)
$\angle ClVCl$	4.06444	4.06444	6.7231	-12.96764 *Cl*	Cl	-12.96764 *Cl*	Cl	0.83519 (Eq. (23.83))	0.83519 (Eq. (23.83))	1	0.5	1	0.83519					111.60	111.3 [18] ($VOCl_3$)
$\angle CCC$ (aromatic)	2.62936	2.62936	4.5585	-17.17218	38	-17.17218	38	0.79232	0.79232	1	1	1	0.79232	-1.85836				120.19	120 [34-36] (benzene)
$\angle CCH$ (aromatic)																120.19		119.91	120 [34-36] (benzene)

CHROMIUM FUNCTIONAL GROUPS AND MOLECULES

The electron configuration of chromium is $[Ar]4s^1 3d^5$ having the corresponding term $^7S_3$. The total energy of the state is given by the sum over the six electrons. The sum $E_T(Cr,3d4s)$ of experimental energies [1] of Cr, Cr^+, Cr^{2+}, Cr^{3+}, Cr^{4+}, and Cr^{5+} is

$$E_T(Cr,3d4s) = -\begin{pmatrix} 90.6349\ eV + 69.46\ eV + 49.16\ eV \\ +30.96\ eV + 16.4857\ eV + 6.76651\ eV \end{pmatrix} = -263.46711\ eV \tag{23.90}$$

By considering that the central field decreases by an integer for each successive electron of the shell, the radius r_{3d4s} of the $Cr3d4s$ shell may be calculated from the Coulombic energy using Eq. (15.13).

$$r_{3d4s} = \sum_{n=18}^{23} \frac{(Z-n)e^2}{8\pi\varepsilon_0 (e263.46711\ eV)} = \frac{21e^2}{8\pi\varepsilon_0 (e263.46711\ eV)} = 1.08447a_0 \tag{23.91}$$

where $Z = 24$ for chromium. Using Eq. (15.14), the Coulombic energy $E_{Coulomb}(Cr,3d4s)$ of the outer electron of the $Cr3d4s$ shell is:

$$E_{Coulomb}(Cr,3d4s) = \frac{-e^2}{8\pi\varepsilon_0 r_{3d4s}} = \frac{-e^2}{8\pi\varepsilon_0 1.08447a_0} = -12.546053\ eV \tag{23.92}$$

Next, consider the formation of the $Cr-L$-bond MO wherein each chromium atom has a $Cr3d4s$ electron with an energy given by Eq. (23.91). The total energy of the state of each chromium atom is given by the sum over the six electrons. The sum $E_T(Cr_{Cr-L}3d4s)$ of energies of $Cr3d4s$ (Eq. (23.91)), Cr^+, Cr^{2+}, Cr^{3+}, Cr^{4+}, and Cr^{5+} is:

$$\begin{aligned} E_T(Cr_{Cr-L}3d4s) &= -\begin{pmatrix} 90.6349\ eV + 69.46\ eV + 49.16\ eV \\ +30.96\ eV + 16.4857\ eV + E_{Coulomb}(Cr,3d4s) \end{pmatrix} \\ &= -\begin{pmatrix} 90.6349\ eV + 69.46\ eV + 49.16\ eV \\ +30.96\ eV + 16.4857\ eV + 12.546053\ eV \end{pmatrix} = -269.24665\ eV \end{aligned} \tag{23.93}$$

where $E(Cr,3d4s)$ is the sum of the energy of Cr, $-6.76651\ eV$, and the hybridization energy.

The chromium HO donates an electron to each MO. Using Eq. (23.30), the radius r_{3d4s} of the $Cr3d4s$ shell calculated from the Coulombic energy is:

$$r_{Cr-L3d4s} = \left(\sum_{n=18}^{23}(Z-n)-1\right)\frac{e^2}{8\pi\varepsilon_0 (e269.24665\ eV)} = \frac{20e^2}{8\pi\varepsilon_0 (e269.24665\ eV)} = 1.01066a_0 \tag{23.94}$$

Using Eqs. (15.19) and (23.93), the Coulombic energy $E_{Coulomb}(Cr_{Cr-L},3d4s)$ of the outer electron of the $Cr3d4s$ shell is

$$E_{Coulomb}(Cr_{Cr-L},3d4s) = \frac{-e^2}{8\pi\varepsilon_0 r_{Cr-L3d4s}} = \frac{-e^2}{8\pi\varepsilon_0 1.01066a_0} = -13.46233\ eV \tag{23.95}$$

Thus, $E_T(Cr-L,3d4s)$, the energy change of each $Cr3d4s$ shell with the formation of the $Cr-L$-bond MO is given by the difference between Eq. (23.94) and Eq. (23.91):

$$E_T(Cr-L,3d4s) = E(Cr_{Cr-L},3d4s) - E(Cr,3d4s) = -13.46233\ eV - (-12.546053\ eV) = -0.91628\ eV \tag{23.96}$$

The semimajor axis a solution given by Eq. (23.41) of the force balance equation, Eq. (23.39), for the σ-MO of the $Cr-L$-bond MO of CrL_n is given in Table 23.25 with the force-equation parameters $Z = 24$, n_e, and L corresponding to the orbital and spin angular momentum terms of the $3d4s$ HO shell. The semimajor axis a of carbonyl and organometallic compounds are solved using Eq. (15.51).

For the $Cr-L$ functional groups, hybridization of the $4s$ and $3d$ AOs of Cr to form a single $3d4s$ shell forms an energy minimum, and the sharing of electrons between the $Cr3d4s$ HO and L AO to form a MO permits each participating orbital to decrease in radius and energy. The F AO has an energy of $E(F) = -17.42282\ eV$, the Cl AO has an energy of $E(Cl) = -12.96764\ eV$, the $C_{aryl}2sp^3$ HO has an energy of $E(C_{aryl},2sp^3) = -15.76868\ eV$ (Eq. (14.246)), the $C2sp^3$ HO has an energy of $E(C,2sp^3) = -14.63489\ eV$ (Eq. (15.25)), the O AO has an energy of $E(O) = -13.61805\ eV$, and the $Cr3d4s$ HO has an energy of $E_{Coulomb}(Cr,3d4s) = -12.54605\ eV$ (Eq. (23.91)). To meet the equipotential condition of the union of the $Cr-L$ H_2-type-ellipsoidal-MO with these orbitals, the hybridization factor(s), at least one of c_2 and C_2 of Eq. (15.61) for the $Cr-L$-bond MO given by Eq. (15.77) is:

$$c_2(FAO\ to\ Cr3d4sHO) = C_2(FAO\ to\ Cr3d4sHO) = \frac{E_{Coulomb}(Cr,3d4s)}{E(FAO)} = \frac{-12.54605\ eV}{-17.42282\ eV} = 0.72009 \tag{23.97}$$

$$c_2(ClAO\ to\ Cr3d4sHO) = C_2(ClAO\ to\ Cr3d4sHO) = \frac{E_{Coulomb}(Cr,3d4s)}{E(ClAO)} = \frac{-12.54605\ eV}{-12.96764\ eV} = 0.96749 \tag{23.98}$$

$$c_2\left(C2sp^3HO\ to\ Cr3d4sHO\right)=C_2\left(C2sp^3HO\ to\ Cr3d4sHO\right)=\frac{E_{Coulomb}\left(Cr,3d4s\right)}{E\left(C,2sp^3\right)}=\frac{-12.54605\ eV}{-14.63489\ eV}=0.85727 \quad (23.99)$$

$$C_2\left(C_{aryl}2sp^3HO\ to\ Cr3d4sHO\right)=\frac{E_{Coulomb}\left(Cr,3d4s\right)}{E\left(C_{aryl},2sp^3\right)}=\frac{-12.54605\ eV}{-15.76868\ eV}=0.79563 \quad (23.100)$$

$$c_2\left(O\ to\ Cr3d4sHO\right)=C_2\left(O\ to\ Cr3d4sHO\right)=\frac{E_{Coulomb}\left(Cr,3d4s\right)}{E\left(O\right)}=\frac{-12.54605\ eV}{-13.61805\ eV}=0.92128 \quad (23.101)$$

Since the energy of the MO is matched to that of the $Cr_{Coulomb}3d4s$ HO, $E\left(AO/HO\right)$ in Eq. (15.61) is $E_{Coulomb}\left(Cr,3d4s\right)$ given by Eq. (23.91) and twice this value for double bonds. $E_T\left(atom-atom,msp^3.AO\right)$ of the $Cr-L$-bond MO is determined by considering that the bond involves an electron transfer from the chromium atom to the ligand atom to form partial ionic character in the bond as in the case of the zwitterions such as $H_2B^+-F^-$ given in the Halido Boranes section. For coordinate compounds, $E_T\left(atom-atom,msp^3.AO\right)$ is $-1.83256\ eV$, two times the energy of Eq. (23.95). For carbonyl and organometallic compounds, $E_T\left(atom-atom,msp^3.AO\right)$ is $-1.44915\ eV$ (Eq. (14.151)), and the $C=O$ functional group of carbonyls is equivalent to that of vanadium carbonyls. The benzene and substituted benzene groups of organometallics are equivalent to those given in the Aromatic and Heterocyclic Compounds section.

The symbols of the functional groups of chromium coordinate compounds are given in Table 23.24. The corresponding designation of the structure of the $\left(CH_3\right)_3C_6H_3$ group of $Cr(\left(CH_3\right)_3C_6H_3)_2$ is equivalent to that of toluene shown in Figure 23.5B. The geometrical (Eqs. (15.1-15.5) and (23.41)), intercept (Eqs. (15.31-15.32) and (15.80-15.87)), and energy (Eqs. (15.61) and (23.28-23.33)) parameters of chromium coordinate compounds are given in Tables 23.25, 23.26, and 23.27, respectively. The total energy of each chromium coordinate compound given in Table 23.28 was calculated as the sum over the integer multiple of each $E_{D\,(Group)}$ of Table 23.27 corresponding to functional-group composition of the compound. The bond angle parameters of chromium coordinate compounds determined using Eqs. (15.88-15.117) are given in Table 23.29. The $E_T\left(atom-atom,msp^3.AO\right)$ term for $CrOCl_3$ was calculated using Eqs. (23.30-23.33) with $s=1$ for the energies of $E_{Coulomb}\left(Cr,3d4s\right)$ given by Eqs. (23.93-23.95). The charge-densities of exemplary chromium carbonyl and organometallic compounds, chromium hexacarbonyl ($Cr\left(CO\right)_6$) and di-(1,2,4-trimethylbenzene) chromium ($Cr(\left(CH_3\right)_3C_6H_3)_2$), respectively, comprising the concentric shells of atoms with the outer shell bridged by one or more H_2-type ellipsoidal MOs or joined with one or more hydrogen MOs are shown in Figures 23.5A and C.

Figure 23.5. (A) *Chromium Hexacarbonyl.* Color scale, translucent view of the charge-density of $Cr\left(CO\right)_6$ showing the orbitals of the Cr, C, and O atoms at their radii, the ellipsoidal surface of each H_2-type ellipsoidal MO that transitions to the corresponding outer shell of the atoms participating in each bond, and the nuclei (red, not to scale). (B) *Toluene.* (C) *Di-(1,2,4-trimethylbenzene) Chromium.* Color scale, opaque view of the charge-density of $Cr(\left(CH_3\right)_3C_6H_3)_2$ showing the orbitals of the Cr and C atoms at their radii and the ellipsoidal surface of each H or H_2-type ellipsoidal MO that transitions to the corresponding outer shell of the atoms participating in each bond.

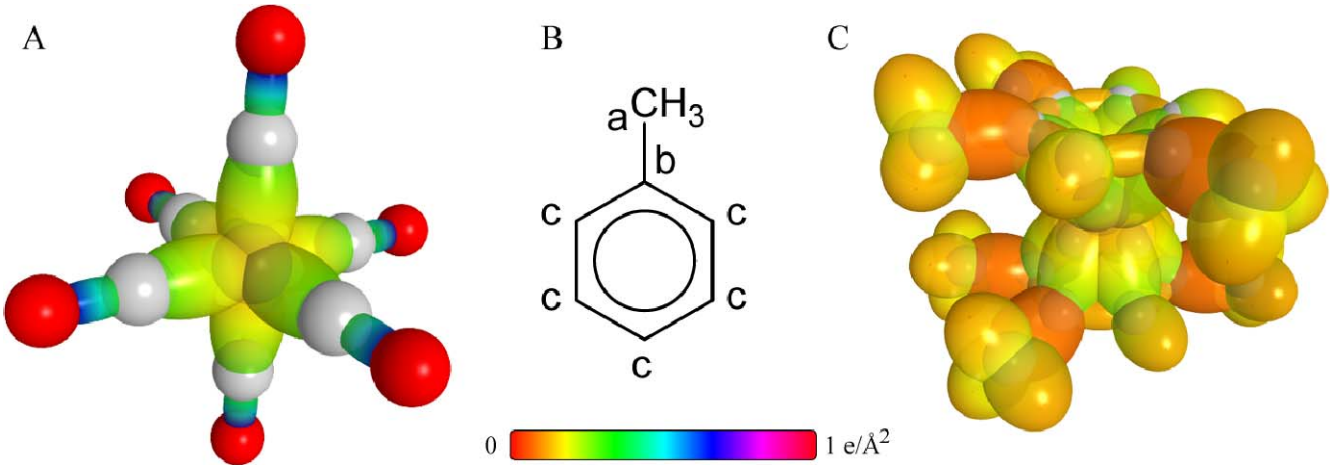

Table 23.24. The symbols of the functional groups of chromium coordinate compounds.

Functional Group	Group Symbol
CrF group of CrF_2	$Cr-F$
$CrCl$ group of $CrCl_2$	$Cr-Cl$
CrO group of CrO	$Cr-O$ (a)
CrO group of CrO_2	$Cr-O$ (b)
CrO group of CrO_3	$Cr-O$ (c)
$CrCO$ group of $Cr(CO)_6$	$Cr-CO$
C=O	$C=O$
CrC_{aryl} group of $Cr(C_6H_6)_2$ and $Cr((CH_3)_3C_6H_3)_2$	$Cr-C_6H_6$
CC (aromatic bond)	$C\overset{3e}{=}C$
CH (aromatic)	CH
C_a-C_b (CH_3 to aromatic bond)	$C-C$
CH_3 group	$C-H\ (CH_3)$

Table 23.25. The geometrical bond parameters of chromium coordinate compounds and experimental values.

Parameter	$Cr-F$ Group	$Cr-Cl$ Group	$Cr-O$ (a) Group	$Cr-O$ (b) Group	$Cr-O$ (c) Group	$Cr-CO$ Group	$C=O$ Group	$Cr-C_6H_6$ Group	$C\overset{3e}{=}C$ Group	CH Group	$C-C$ Group	$C-H\ (CH_3)$ Group
n_e	1	3	2	2	2							
L	$8\sqrt{\frac{3}{4}}$	$6\sqrt{\frac{3}{4}}$	$9\sqrt{\frac{3}{4}}$	$4+4\sqrt{\frac{3}{4}}$	$4+4\sqrt{\frac{3}{4}}$							
$a\ (a_0)$	1.78868	2.71651	2.32476	2.31100	2.31100	2.17050	1.184842	2.52782	1.47348	1.60061	2.06004	1.64920
$c'\ (a_0)$	1.57606	1.93487	1.58852	1.58381	1.58381	1.83734	1.08850	2.05820	1.31468	1.03299	1.43528	1.04856
Bond Length $2c'\ (\AA)$	1.66802	2.04778	1.68122	1.67624	1.67624	1.94456	1.15202	2.17830	1.39140	1.09327	1.51904	1.10974
Exp. Bond Length $(\AA)$	1.720 [15] (CrO_2F_2)	2.126 [15] (CrO_2Cl_2)	1.627 [37] (CrO_n n=1,2,3)	1.627 [37] (CrO_n n=1,2,3)	1.627 [37] (CrO_n n=1,2,3)	1.92 [3] ($Cr(CO)_6$)	1.16 [3] 1.141 [38] ($Cr(CO)_6$)	2.125 [39] ($Cr(C_6H_6)_2$)	1.399 [3] (benzene)	1.101 [3] (benzene)	1.524 [3] (toluene)	1.11 (avg.) [3] (toluene)
$b,c\ (a_0)$	0.84582	1.90675	1.69738	1.68294	1.68294	1.15552	0.46798	1.46755	0.66540	1.22265	1.47774	1.27295
e	0.88113	0.71226	0.68331	0.68534	0.68534	0.84651	0.91869	0.81422	0.89223	0.64537	0.69673	0.63580

Table 23.26. The MO to HO intercept geometrical bond parameters of chromium coordinate compounds. E_T is E_T (*atom–atom,HO.AO*).

Bond	Atom	E_T (eV) Bond 1	E_T (eV) Bond 2	E_T (eV) Bond 3	E_T (eV) Bond 4	E_T (eV) Bond 5	E_T (eV) Bond 6	Final Total Energy $Cr3d4s$ (eV)	$r_{initial}$ (a_0)	r_{final} (a_0)	$E_{Coulomb}(Cr3d4s)$ (eV) Final	$E(Cr3d4s)$ (eV) Final	θ' (°)	θ_1 (°)	θ_2 (°)	d_1 (a_0)	d_2 (a_0)
$Cr-F\ (CrF_1)$	Cr	-0.91628	-0.91628	0	0	0	0		1.08447	0.94625	-14.37861		130.93	49.07	57.69	0.95607	0.61998
$Cr-F\ (CrF_1)$	F	-0.91628	0	0	0	0	0		0.78069	0.74190	-18.33910		121.54	58.46	48.38	1.18799	0.38806
$Cr-Cl\ (CrCl_2)$	Cr	-0.91628	-0.91628	0	0	0	0		1.08447	0.94625	-14.37861		54.42	125.58	23.81	2.48539	0.55052
$Cr-Cl\ (CrCl_2)$	Cl	-0.91628	0	0	0	0	0		1.05158	0.97997	-13.88392		59.10	120.90	26.17	2.43805	0.50318
$Cr-O\ (CrO)$	Cr	-0.91628	0	0	0	0	0		1.08447	1.01066	-13.46233		70.66	109.34	34.18	1.92315	0.33463
$Cr-O\ (CrO)$	O	-0.91628	0	0	0	0	0		1.00000	0.93611	-14.53434		61.71	118.29	29.05	2.03225	0.44372
$Cr-O\ (CrO_2)$	Cr	-0.91628	-0.91628	0	0	0	0		1.08447	0.94625	-14.37861		64.49	115.51	30.49	1.99136	0.40754
$Cr-O\ (CrO_2)$	O	-0.91628	0	0	0	0	0		1.00000	0.93611	-14.53434		63.18	116.82	29.76	2.00615	0.42234
$Cr-O\ (CrO_3)$	Cr	-0.91628	-0.91628	-0.91628	0	0	0		1.08447	0.88957	-15.29489		56.56	123.44	26.17	2.07408	0.49026
$Cr-O\ (CrO_3)$	O	-0.91628	0	0	0	0	0		1.00000	0.93611	-14.53434		63.18	116.82	29.76	2.00615	0.42234
$CrC=O$	O	-1.79278	0	0	0	0	0		1.00000	0.81871	-16.61853		147.43	32.57	70.34	0.39853	0.68997
$CrC=O$	C	-1.79278	-0.72457	0	0	0	0	-154.13305	0.91771	0.78451	-17.34311	-17.15225	146.31	33.69	68.42	0.43577	0.65274
$Cr-CO\ (Cr(CO)_6)$	C	-0.72457	-1.79278	0	0	0	0		0.91771	0.78451	-17.34311	-17.15225	104.77	75.23	41.03	1.63731	0.20004
$Cr-CO\ (Cr(CO)_6)$	Cr	-0.72457	-0.72457	-0.72457	-0.72457	-0.72457	-0.72457		1.08447	0.70963	-19.17320		99.05	80.95	37.34	1.72577	0.11158
$C-H\ (CH)$ $(Cr(C_6H_6)_2)$	C	-0.85035	-0.85035	-0.56690	-0.12076	0	0		0.91771	0.79039	-17.21409	-17.02323	73.65	106.35	38.34	1.25543	0.22244
$\overset{3e}{C}=HC_a=\overset{3e}{C}$ $(Cr(C_6H_6)_2)$	C_a	-0.85035	-0.85035	-0.56690	-0.12076	0	0		0.91771	0.79039	-17.21410	-17.02324	134.00	46.00	58.70	0.76561	0.54908
$Cr-(C_6H_6)_2$	Cr	-0.72457	-0.72457	0	0	0	0		1.08447	0.83600	-16.27490		88.65	91.35	34.72	2.07785	0.01965
$Cr-(C_6H_6)_2$	C_a	-0.12076	-0.85035	-0.85035	-0.56690	0	0		0.91771	0.79039	-17.21410	-17.02324	84.51	95.49	32.42	2.13387	0.07567
$C-H\ (C_aH_3)$ $\left(Cr\left((CH_3)_3C_6H_3\right)_2\right)$	C_a	-0.56690	0	0	0	0	0	-152.18259	0.91771	0.88392	-15.39265	-15.20178	79.89	100.11	43.13	1.20367	0.15511
$C-H\ (C_cH)$ $\left(Cr\left((CH_3)_3C_6H_3\right)_2\right)$	C_c	-0.85035	-0.85035	-0.56690	-0.12076	0	0		0.91771	0.79039	-17.21409	-17.02323	73.65	106.35	38.34	1.25543	0.22244
$\overset{3e}{C}=HC_c=\overset{3e}{C}$ $\overset{3e}{C}=(H_3C_a)C_b=\overset{3e}{C}$ $\left(Cr\left((CH_3)_3C_6H_3\right)_2\right)$	C_c C_b	-0.85035	-0.85035	-0.56690	-0.12076	0	0		0.91771	0.79039	-17.21410	-17.02324	134.00	46.00	58.70	0.76561	0.54908
$\left(C=\right)_2C_b-C_aH_3$ $\left(Cr\left((CH_3)_3C_6H_3\right)_2\right)$	C_a	-0.56690	0	0	0	0	0	-152.18259	0.91771	0.88392	-15.39265	-15.20178	73.38	106.62	34.97	1.68807	0.25279
$\left(C=\right)_2C_b-C_aH_3$ $\left(Cr\left((CH_3)_3C_6H_3\right)_2\right)$	C_b	-0.56690	-0.85035	-0.85035	-0.12076	0	0	-154.00404	0.91771	0.79039	-17.21410	-17.02324	60.68	119.32	27.80	1.82231	0.38703
$Cr-\left((CH_3)_3C_6H_3\right)_2$	Cr	-0.72457	-0.72457	0	0	0	0		1.08447	0.83600	-16.27490		88.65	91.35	34.72	2.07785	0.01965
$Cr-C_b\ \ \overset{3e}{C}=(H_3C_a)C_b=\overset{3e}{C}$ $\left(Cr\left((CH_3)_3C_6H_3\right)_2\right)$	C_b	-0.12076	-0.85035	-0.85035	-0.56690	0	0		0.91771	0.79039	-17.21410	-17.02324	84.51	95.49	32.42	2.13387	0.07567
$Cr-C_c\ \ \overset{3e}{C}=HC_c=\overset{3e}{C}$ $\left(Cr\left((CH_3)_3C_6H_3\right)_2\right)$	C_c	-0.12076	-0.85035	-0.85035	-0.56690	0	0		0.91771	0.79039	-17.21410	-17.02324	84.51	95.49	32.42	2.13387	0.07567

Table 23.27. The energy parameters (eV) of functional groups of chromium coordinate compounds.

Parameters	$Cr-F$ Group	$Cr-Cl$ Group	$Cr-O$ (a) Group	$Cr-O$ (b) Group	$Cr-O$ (c) Group	$Cr-CO$ Group	$C=O$ Group	$Cr-C_6H_6$ Group	$C \overset{3e}{=} C$ Group	CH Group	$C-C$ Group	CH_3 Group
f_1	1	1	1	1	1	1	1	1	0.75	1		
n_1	1	1	2	2	2	1	2	1	2	1	1	3
n_2	0	0	0	0	0	0	0	0	0	0	0	2
n_3	0	0	0	0	0	0	0	0	0	0	0	0
C_1	0.5	0.375	0.5	0.5	0.5	0.375	0.5	0.375	0.5	0.75	0.5	0.75
C_2	0.72009	0.96749	0.92128	0.92128	0.92128	0.85727	1	0.79563	0.85252	1	1	1
c_1	1	1	1	1	1	1	1	1	1	1	1	1
c_2	0.72009	0.96749	0.92128	0.92128	0.92128	0.85727	0.85395	1	0.85252	0.91771	0.91771	0.91771
c_3	0	0	0	0	0	0	2	0	0	1	0	0
c_4	1	1	2	2	2	2	4	2	3	1	2	1
c_5	1	1	2	2	2	0	0	0	0	1	0	3
C_{1o}	0.5	0.375	0.5	0.5	0.5	0.375	0.5	0.375	0.5	0.75	0.5	0.75
C_{2o}	0.72009	0.96749	0.92128	0.92128	0.92128	0.85727	1	0.79563	0.85252	1	1	1
V_e (eV)	-34.33458	-24.26770	-52.72902	-53.12750	-53.12750	-31.58105	-134.96850	-30.12868	-101.12679	-37.10024	-29.95792	-107.32728
V_p (eV)	8.63282	7.03190	17.13015	17.18105	17.18105	7.40515	24.99908	6.61055	20.69825	13.17125	9.47952	38.92728
T (eV)	9.59777	4.46671	11.34075	11.49446	11.49446	7.27506	56.95634	5.95942	34.31559	11.58941	7.27120	32.53914
V_m (eV)	-4.79888	-2.23336	-5.67037	-5.74723	-5.74723	-3.63753	-28.47817	-2.97971	-17.15779	-5.79470	-3.63560	-16.26957
$E_{(AO/HO)}$ (eV)	-12.54605	-12.54605	-25.09211	-25.09211	-25.09211	-12.54605	0	-12.54605	0	-14.63489	-15.35946	-15.56407
$\Delta E_{H_2MO(AO/HO)}$ (eV)	0	0	0	0	0	-1.44915	-18.22046	-1.44915	0	-1.13379	-0.56690	0
$E_{T(AO/HO)}$ (eV)	-12.54605	-12.54605	-25.09211	-25.09211	-25.09211	-11.09690	18.22046	-11.09690	0	-13.50110	-14.79257	-15.56407
$E_{T(H_2MO)}$ (eV)	-33.44892	-27.54850	-55.02060	-55.29133	-55.29133	-31.63528	-63.27080	-31.63533	-63.27075	-31.63539	-31.63537	-67.69451
$E_T\left(atom-atom, msp^3.AO\right)$ (eV)	-1.83256	-1.83256	-1.83256	-1.83256	-1.83256	-1.44915	-3.58557	-1.44915	-2.26759	-0.56690	-1.13379	0
$E_{T(MO)}$ (eV)	-35.28148	-29.38106	-56.85316	-57.12389	-57.12389	-33.08452	-66.85630	-33.08452	-65.53833	-32.20226	-32.76916	-67.69450
$\omega\left(10^{15}\ rad/s\right)$	10.3697	9.45766	12.6881	12.8518	7.98665	18.8708	22.6662	12.7018	49.7272	26.4826	16.2731	24.9286
E_K (eV)	6.82553	6.22520	8.35152	8.45929	5.25695	12.42109	14.91930	8.36057	32.73133	17.43132	10.71127	16.40846
$\bar{E}_D$ (eV)	-0.18236	-0.14503	-0.16252	-0.16435	-0.12956	-0.23068	-0.25544	-0.18925	-0.35806	-0.26130	-0.21217	-0.25352
$\bar{E}_{Kvib}$ (eV)	0.07005 [40]	0.04030 [40]	0.11144 [37]	0.11144 [37]	0.11144 [37]	0.04724 [41]	0.24962 [29]	0.05951 [42]	0.19649 [30]	0.35532 Eq. (13.458)	0.14940 [43]	0.35532 (Eq. (13.458))
$\bar{E}_{osc}$ (eV)	-0.14733	-0.12488	-0.10680	-0.10863	-0.07384	-0.20706	-0.13063	-0.15950	-0.25982	-0.08364	-0.13747	-0.22757
E_{mag} (eV)	0.08971	0.08971	0.08971	0.08971	0.08971	0.14803	0.11441	0.14803	0.14803	0.14803	0.14803	0.14803
$E_{T(Group)}$ (eV)	-35.42881	-29.50594	-57.06677	-57.34114	-57.27156	-33.29158	-67.11757	-33.24401	-49.54347	-32.28590	-32.90663	-67.92207
$E_{initial(c_4\ AO/HO)}$ (eV)	-12.54605	-12.54605	-12.54605	-12.54605	-12.54605	-14.63489	-14.63489	-15.76868	-14.63489	-14.63489	-14.63489	-14.63489
$E_{initial(c_5\ AO/HO)}$ (eV)	-17.42282	-12.96764	-13.61806	-13.61806	-13.61806	0	0	0	0	-13.59844	0	-13.59844
$E_{D(Group)}$ (eV)	5.45994	3.99224	4.73854	5.01291	4.94333	4.02180	8.34918	1.70665	5.63881	3.90454	3.63685	12.49186

Table 23.28. The total bond energies of gaseous-state chromium coordinate compounds calculated using the functional group composition and the energies of Table 23.27 compared to the gaseous-state experimental values except where indicated.

Formula	Name	$Cr-F$ Group	$Cr-Cl$ Group	$Cr-O$ (a) Group	$Cr-O$ (b) Group	$Cr-O$ (c) Group	$Cr-CO$ Group	$C=O$ Group	$Cr-C_6H_6$ Group	$^{3c}C=C$ Group	CH Group	$C-C$ Group	CH_3 Group	Calculated Total Bond Energy (eV)	Experimental Total Bond Energy (eV)	Relative Error
CrF_2	Chromium difluoride	2	0	0	0	0	0	0	0	0	0	0	0	10.91988	10.92685 [15]	0.00064
$CrCl_2$	Chromium dichloride	0	2	0	0	0	0	0	0	0	0	0	0	7.98449	7.96513 [15]	-0.00243
CrO	Chromium oxide	0	0	1	2	0	0	0	0	0	0	0	0	4.73854	4.75515 [37]	0.00349
CrO_2	Chromium dioxide	0	0	0	0	3	0	0	0	0	0	0	0	10.02583	10.04924 [37]	0.00233
CrO_3	Chromium trioxide	0	0	0	0	0	0	0	0	0	0	0	0	14.83000	14.85404 [37]	0.00162
CrO_2Cl_2	Chromium dichloride dioxide	0	2	2	0	0	0	0	0	0	0	0	0	17.46158	17.30608 [15]	-0.00899
$Cr(CO)_6$	Chromium hexacarbonyl	0	0	0	0	0	6	6	0	0	0	0	0	74.22588	74.61872 [44]	0.00526
$Cr(C_6H_6)_2$	Dibenzene chromium	0	0	0	0	0	0	0	2	12	12	0	0	117.93345	117.97971 [44]	0.00039
$Cr((CH_3)_3C_6H_3)_2$	Di-(1,2,4-trimethylbenzene) chromium	0	0	0	0	0	0	0	2	12	6	6	6	191.27849	192.42933[a] [44]	0.00598

[a] Liquid.

Table 23.29. The bond angle parameters of chromium coordinate compounds and experimental values. E_T is E_T (*atom–atom,HO.AO*).

Atoms of Angle	$2c'$ Bond 1 (a_0)	$2c'$ Bond 2 (a_0)	$2c'$ Terminal Atoms (a_0)	$E_{Coulombic}$ Atom 1	Atom 1 Hybridization Designation (Table 15.3A)	$E_{Coulombic}$ Atom 2	Atom 2 Hybridization Designation (Table 15.3A)	c_2 Atom 1	c_2 Atom 2	C_1	C_2	c_1	c_2'	E_T (eV)	θ_v (°)	θ_1 (°)	θ_2 (°)	Cal. θ (°)	Exp. θ (°)
$\angle OCrO$	3.17704	3.17704	5.1463	-13.61806 *O*	O	-13.61806 *O*	O	1	1	1	0.92128 (Eq. (23.100))	1	1	-0.85938				108.18	108.7 [15] (CrO_2Cl_2)
$\angle ClCrCl$	3.86974	3.86974	6.4704	-12.96764 *Cl*	Cl	-12.96764 *Cl*	Cl	0.96749 (Eq. (23.97))	0.96749 (Eq. (23.97))	1	0.75	1	0.96749	-0.85938				113.45	113.0 [15] (CrO_2Cl_2)
$\angle CCC$ (aromatic)	2.62936	2.62936	4.5585	-17.17218	38	-17.17218	38	0.79232	0.79232	1	1	1	0.79232	-1.85836				120.19	120 [34-36] (benzene)
$\angle CCH$ (aromatic)																120.19		119.91	120 [34-36] (benzene)

MANGANESE FUNCTIONAL GROUPS AND MOLECULES

The electron configuration of manganese is $[Ar]4s^2 3d^5$ having the corresponding term ${}^6S_{5/2}$. The total energy of the state is given by the sum over the seven electrons. The sum $E_T(Mn, 3d4s)$ of experimental energies [1] of Mn, Mn^+, Mn^{2+}, Mn^{3+}, Mn^{4+}, Mn^{5+}, and Mn^{6+} is:

$$E_T(Mn, 3d4s) = -\begin{pmatrix} 119.203\ eV + 95.6\ eV + 72.4\ eV + 51.2\ eV \\ +33.668\ eV + 15.6400\ eV + 14.22133\ eV \end{pmatrix} = -401.93233\ eV \tag{23.102}$$

By considering that the central field decreases by an integer for each successive electron of the shell, the radius r_{3d4s} of the $Mn3d4s$ shell may be calculated from the Coulombic energy using Eq. (15.13).

$$r_{3d4s} = \sum_{n=18}^{24} \frac{(Z-n)e^2}{8\pi\varepsilon_0 (e395.14502\ eV)} = \frac{28e^2}{8\pi\varepsilon_0 (e395.14502\ eV)} = 0.96411a_0 \tag{23.103}$$

where $Z = 25$ for manganese. Using Eq. (15.14), the Coulombic energy $E_{Coulomb}(Mn, 3d4s)$ of the outer electron of the $Mn3d4s$ shell is:

$$E_{Coulomb}(Mn, 3d4s) = \frac{-e^2}{8\pi\varepsilon_0 r_{3d4s}} = \frac{-e^2}{8\pi\varepsilon_0 0.96411a_0} = -14.112322\ eV \tag{23.104}$$

During hybridization, the spin-paired $4s$ electrons are promoted to the $Mn3d4s$ shell as unpaired electrons. The energy for the promotion is the magnetic energy given by Eq. (15.15) at the initial radius of the $4s$ electrons. From Eq. (10.102) with $Z = 25$ and $n = 25$, the radius r_{25} of the $Mn4s$ shell is:

$$r_{25} = 1.83021a_0 \tag{23.105}$$

Using Eqs. (15.15) and (23.104), the unpairing energy is:

$$E_{4s}(magnetic) = \frac{2\pi\mu_0 e^2\hbar^2}{m_e^2 (r_{25})^3} = \frac{8\pi\mu_0\mu_B^2}{(1.83021a_0)^3} = 0.01866\ eV \tag{23.106}$$

The electrons from the $4s$ and $3d$ shells successively fill unoccupied HOs until the HO shell is filled with unpaired electrons, then the electrons pair per HO. In the case of the $Mn3d4s$ shell having seven electrons and six orbitals, one set of electrons is paired. Using Eqs. (15.15) and (23.102), the pairing energy is given by:

$$E_{3d4s}(magnetic) = -\frac{2\pi\mu_0 e^2\hbar^2}{m_e^2 (r_{3d4s})^3} = -\frac{8\pi\mu_0\mu_B^2}{(0.96411a_0)^3} = -0.12767\ eV \tag{23.107}$$

Thus, after Eq. (23.28), the energy $E(Mn, 3d4s)$ of the outer electron of the $Mn3d4s$ shell is given by adding the magnetic energy of unpairing the $4s$ electrons (Eq. (23.105)) and pairing of one set of $Mn3d4s$ electrons (Eq. (23.106)) to $E_{Coulomb}(Mn, 3d4s)$ (Eq. (23.103)).

$$\begin{aligned} E(Mn, 3d4s) &= \frac{-e^2}{8\pi\varepsilon_0 r_{3d4s}} + \frac{2\pi\mu_0 e^2\hbar^2}{m_e^2 r_{4s}^3} + \sum_{3d\ pairs} \frac{2\pi\mu_0 e^2\hbar^2}{m_e^2 r_{3d}^3} - \sum_{HO\ pairs} \frac{2\pi\mu_0 e^2\hbar^2}{m_e^2 r_{3d4s}^3} \\ &= -14.112322\ eV + 0.01866\ eV - 0.12767\ eV = -14.22133\ eV \end{aligned} \tag{23.108}$$

Next, consider the formation of the $Mn-L$-bond MO wherein each manganese atom has a $Mn3d4s$ electron with an energy given by Eq. (23.107). The total energy of the state of each manganese atom is given by the sum over the seven electrons. The sum $E_T(Mn_{Mn-L}3d4s)$ of energies of $Mn3d4s$ (Eq. (23.107)), Mn^+, Mn^{2+}, Mn^{3+}, Mn^{4+}, Mn^{5+}, and Mn^{6+} is:

$$\begin{aligned} E_T(Mn_{Mn-L}3d4s) &= -\begin{pmatrix} 119.203\ eV + 95.6\ eV + 72.4\ eV + 51.2\ eV \\ +33.668\ eV + 15.6400\ eV + E(Mn, 3d4s) \end{pmatrix} \\ &= -\begin{pmatrix} 119.203\ eV + 95.6\ eV + 72.4\ eV + 51.2\ eV \\ +33.668\ eV + 15.6400\ eV + 14.22133\ eV \end{pmatrix} \\ &= -401.93233\ eV \end{aligned} \tag{23.109}$$

where $E(Mn, 3d4s)$ is the sum of the energy of Mn, $-7.43402\ eV$, and the hybridization energy.

The manganese HO donates an electron to each MO. Using Eq. (23.30), the radius r_{3d4s} of the $Mn3d4s$ shell calculated from the Coulombic energy is:

$$r_{Mn-L3d4s} = \left(\sum_{n=18}^{24} (Z-n) - 1\right) \frac{e^2}{8\pi\varepsilon_0 (e401.93233\ eV)} = \frac{27e^2}{8\pi\varepsilon_0 (e401.93233\ eV)} = 0.91398a_0 \tag{23.110}$$

Using Eqs. (15.19) and (23.109), the Coulombic energy $E_{Coulomb}(Mn_{Mn-L}, 3d4s)$ of the outer electron of the $Mn3d4s$ shell is:

$$E_{Coulomb}(Mn_{Mn-L}, 3d4s) = \frac{-e^2}{8\pi\varepsilon_0 r_{Mn-L3d4s}} = \frac{-e^2}{8\pi\varepsilon_0 0.91398a_0} = -14.88638\ eV \tag{23.111}$$

The magnetic energy terms are those for the unpairing of the $4s$ electrons (Eq. (23.105)) and pairing one set of $Mn3d4s$ electrons (Eq. (23.106)). Using Eqs. (23.32), (23.105), (23.106), and (23.110), the energy $E\left(Mn_{Mn-L},3d4s\right)$ of the outer electron of the $Mn3d4s$ shell is:

$$\begin{aligned} E\left(Mn_{Mn-L},3d4s\right) &= \frac{-e^2}{8\pi\varepsilon_0 r_{Mn-L3d4s}} + \frac{2\pi\mu_0 e^2\hbar^2}{m_e^2\left(r_{25}\right)^3} - \frac{2\pi\mu_0 e^2\hbar^2}{m_e^2\left(r_{3d4s}\right)^3} \\ &= -14.88638\ eV + 0.01866\ eV - 0.12767\ eV = -14.99539\ eV \end{aligned} \tag{23.112}$$

Thus, $E_T\left(Mn-L,3d4s\right)$, the energy change of each $Mn3d4s$ shell with the formation of the $Mn-L$-bond MO is given by the difference between Eq. (23.111) and Eq. (23.107):

$$\begin{aligned} E_T\left(Mn-L,3d4s\right) &= E\left(Mn_{Mn-L},3d4s\right) - E\left(Mn,3d4s\right) \\ &= -14.99539\ eV - \left(-14.22133\ eV\right) = -0.77406\ eV \end{aligned} \tag{23.113}$$

The semimajor axis a solution given by Eq. (23.41) of the force balance equation, Eq. (23.39), for the σ-MO of the $Mn-L$-bond MO of MnL_n is given in Table 23.31 with the force-equation parameters $Z=25$, n_e, and L corresponding to the orbital and spin angular momentum terms of the $3d4s$ HO shell. The semimajor axis a of carbonyl and organometallic compounds are solved using Eq. (15.51).

For the $Mn-L$ functional groups, hybridization of the $4s$ and $3d$ AOs of Mn to form a single $3d4s$ shell forms an energy minimum, and the sharing of electrons between the $Mn3d4s$ HO and L AO to form a MO permits each participating orbital to decrease in radius and energy. The F AO has an energy of $E\left(F\right)=-17.42282\ eV$, the Cl AO has an energy of $E\left(Cl\right)=-12.96764\ eV$, the $C2sp^3$ HO has an energy of $E\left(C,2sp^3\right)=-14.63489\ eV$ (Eq. (15.25)), the Coulomb energy of $Mn3d4s$ HO is $E_{Coulomb}\left(Mn,3d4s\right)=-14.11232\ eV$ (Eq. (23.103)), the $Mn3d4s$ HO has an energy of $E\left(Mn,3d4s\right)=-14.22133\ eV$ (Eq. (23.107)), and $13.605804\ eV$ is the magnitude of the Coulombic energy between the electron and proton of H (Eq. (1.264)). To meet the equipotential condition of the union of the $Mn-L$ H_2-type-ellipsoidal-MO with these orbitals, the hybridization factor(s), at least one of c_2 and C_2 of Eq. (15.61) for the $Mn-L$-bond MO given by Eq. (15.77) is:

$$C_2\left(FAO\ to\ Mn3d4sHO\right)=\frac{E\left(Mn,3d4s\right)}{E\left(FAO\right)}=\frac{-14.22133\ eV}{-17.42282\ eV}=0.81625 \tag{23.114}$$

$$C_2\left(ClAO\ to\ Mn3d4sHO\right)=\frac{E\left(ClAO\right)}{E\left(Mn,3d4s\right)}=\frac{-12.96764\ eV}{-14.22133\ eV}=0.91184 \tag{23.115}$$

$$c_2\left(C2sp^3HO\ to\ Mn3d4sHO\right)=\frac{E_{Coulomb}\left(Mn,3d4s\right)}{E\left(C,2sp^3\right)}c_2\left(C2sp^3HO\right)=\frac{-14.11232\ eV}{-14.63489\ eV}\left(0.91771\right)=0.88495 \tag{23.116}$$

$$C_2\left(Mn3d4sHO\ to\ Mn3d4sHO\right)=\frac{E\left(H\right)}{E_{Coulomb}\left(Mn,3d4s\right)}=\frac{-13.605804\ eV}{-14.11232\ eV}=0.96411 \tag{23.117}$$

where Eqs. (15.76), (15.79), and (13.430) were used in Eq. (23.115) and Eq. (15.71) was used in Eq. (23.116). Since the energy of the MO is matched to that of the $Mn3d4s$ HO in coordinate compounds, $E\left(AO/HO\right)$ in Eq. (15.61) is $E\left(Mn,3d4s\right)$ given by Eq. (23.107) and $E\left(AO/HO\right)$ in Eq. (15.61) of carbonyl compounds is $E_{Coulomb}\left(Mn,3d4s\right)$ given by Eq. (23.103). $E_T\left(atom-atom,msp^3.AO\right)$ of the $Mn-L$-bond MO is determined by considering that the bond involves an electron transfer from the manganese atom to the ligand atom to form partial ionic character in the bond as in the case of the zwitterions such as $H_2B^+-F^-$ given in the Halido Boranes section. For the coordinate compounds, $E_T\left(atom-atom,msp^3.AO\right)$ is $-1.54812\ eV$, two times the energy of Eq. (23.112). For the $Mn-CO$ bonds of carbonyl compounds, $E_T\left(atom-atom,msp^3.AO\right)$ is $-1.44915\ eV$ (Eq. (14.151)), and the $C=O$ functional group of carbonyls is equivalent to that of vanadium carbonyls.

The symbols of the functional groups of manganese coordinate compounds are given in Table 23.30. The geometrical (Eqs. (15.1-15.5) and (23.41)), intercept (Eqs. (15.31-15.32) and (15.80-15.87)), and energy (Eqs. (15.61) and (23.28-23.33)) parameters of manganese coordinate compounds are given in Tables 23.31, 23.32, and 23.33, respectively. The total energy of each manganese coordinate compound given in Table 23.34 was calculated as the sum over the integer multiple of each $E_{D\,(Group)}$ of Table 23.33 corresponding to functional-group composition of the compound. The charge-densities of exemplary manganese carbonyl compound, dimanganese decacarbonyl ($Mn_2\left(CO\right)_{10}$) comprising the concentric shells of atoms with the outer shell bridged by one or more H_2-type ellipsoidal MOs or joined with one or more hydrogen MOs is shown in Figure 23.6.

Figure 23.6. *Diamanganese decacarbonyl*. Color scale, opaque view of the charge-density of $Mn_2(CO)_{10}$ showing the orbitals of the Mn, C, and O atoms at their radii and the ellipsoidal surface of each H_2-type ellipsoidal MO that transitions to the corresponding outer shell of the atoms participating in each bond.

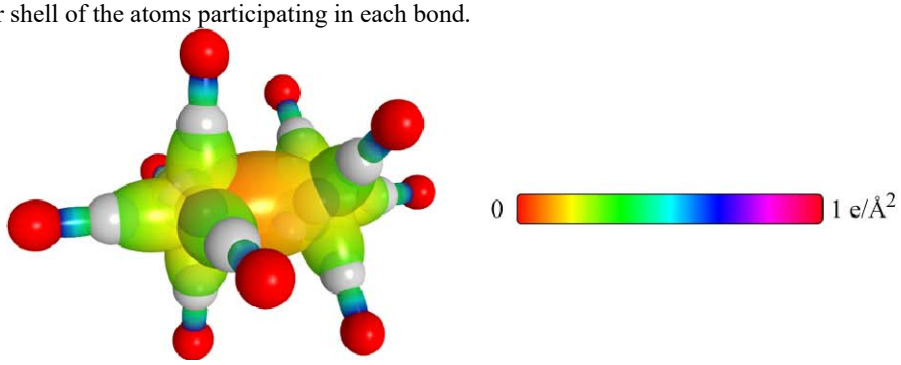

Table 23.30. The symbols of the functional groups of manganese coordinate compounds.

Functional Group	Group Symbol
MnF group of *MnF*	$Mn-F$
MnCl group of *MnCl*	$Mn-Cl$
MnCO group of $Mn_2(CO)_{10}$	$Mn-CO$
MnMn group of $Mn_2(CO)_{10}$	$Mn-Mn$
C=O	$C=O$

Table 23.31. The geometrical bond parameters of manganese coordinate compounds and experimental values.

Parameter	$Mn-F$ Group	$Mn-Cl$ Group	$Mn-CO$ Group	$Mn-Mn$ Group	$C=O$ Group
n_e	2	3		5	
L	$2+4\sqrt{\frac{3}{4}}$	$4+6\sqrt{\frac{3}{4}}$		$3\sqrt{\frac{3}{4}}$	
$a\ (a_0)$	2.21856	2.86785	2.23676	3.60392	1.184842
$c'\ (a_0)$	1.64864	2.04780	1.72695	2.73426	1.08850
Bond Length $2c'\ (\text{Å})$	1.74484	2.16729	1.82772	2.89382	1.15202
Exp. Bond Length (Å)	1.729 [45] (MnF_2)	2.202 [15] ($MnCl_2$)	1.830 [46] ($Mn_2(CO)_{10}$)	2.923 [46] ($Mn_2(CO)_{10}$)	1.151 [29, 46] ($Mn_2(CO)_{10}$)
$b,c\ (a_0)$	1.48459	2.00775	1.42153	2.34778	0.46798
e	0.74311	0.71405	0.77208	0.75869	0.91869

Table 23.32. The MO to HO intercept geometrical bond parameters of manganese coordinate compounds. E_T is E_T (*atom–atom,HO.AO*).

Bond	Atom	E_T (eV) Bond 1	E_T (eV) Bond 2	E_T (eV) Bond 3	E_T (eV) Bond 4	E_T (eV) Bond 5	E_T (eV) Bond 6	Final Total Energy *Mn3d4s* (eV)	$r_{initial}$ (a_0)	r_{final} (a_0)	$E_{Coulomb}(Mn3d4s)$ (eV) Final	$E(Mn3d4s)$ (eV) Final	θ' (°)	θ_1 (°)	θ_2 (°)	d_1 (a_0)	d_2 (a_0)
$Mn-F\ (MnF)$	*Mn*	-0.77406	0	0	0	0	0		0.96411	0.91398	-14.88638		83.28	96.72	37.69	1.75558	0.10694
$Mn-F\ (MnF)$	*F*	-0.77406	0	0	0	0	0		0.78069	0.74770	-18.19688		63.75	116.25	26.85	1.97934	0.33070
$Mn-Cl\ (MnCl)$	*Mn*	-0.77406	0	0	0	0	0		0.96411	0.91398	-14.88638		41.12	138.88	17.42	2.73630	0.68851
$Mn-Cl\ (MnCl)$	*Cl*	-0.77406	0	0	0	0	0		1.05158	0.99011	-13.74170		54.01	125.99	23.52	2.62968	0.58189
$MnC=O$	*O*	-1.79278	0	0	0	0	0		1.00000	0.81871	-16.61853		147.43	32.57	70.34	0.39853	0.68997
$MnC=O$	*C*	-1.79278	-0.72457	0	0	0	0	-154.13305	0.91771	0.78451	-17.34311	-17.15225	146.31	33.69	68.42	0.43577	0.65274
$Mn-CO\ \left((CO)_5\,MnMn(CO)_5\right)$	*C*	-0.72457	-1.79278	0	0	0	0		0.91771	0.78451	-17.34311	-17.15225	78.68	101.32	32.76	1.88097	0.15402
$Mn-CO\ \left((CO)_5\,MnMn(CO)_5\right)$	*Mn*	-0.72457	-0.72457	-0.72457	-0.72457	-0.72457	-0.77002		0.96411	0.70795	-19.21864		69.05	110.95	27.72	1.98013	0.25319
$Mn-Mn\ \left((CO)_5\,Mn-Mn(CO)_5\right)$	*Mn*	-0.72457	-0.72457	-0.72457	-0.72457	-0.72457	-0.77002		0.96411	0.73524	-18.50521						

Table 23.33. The energy parameters (eV) of functional groups of manganese coordinate compounds.

Parameters	$Mn-F$ Group	$Mn-Cl$ Group	$Mn-CO$ Group	$Mn-Mn$ Group	$C=O$ Group
f_1	1	1	1	1	1
n_1	1	1	1	1	2
n_2	0	0	0	0	0
n_3	0	0	0	0	0
C_1	0.5	0.375	0.375	0.25	0.5
C_2	0.81625	0.91184	1	0.96411	1
c_1	1	1	1	1	1
c_2	1	1	0.88495	1	0.85395
c_3	0	0	0	0	2
c_4	1	1	2	2	4
c_5	1	1	0	0	0
C_{1o}	0.5	0.375	0.375	0.25	0.5
C_{2o}	0.81625	0.91184	1	0.96411	1
$V_e\ (eV)$	-31.60440	-23.79675	-28.59791	-19.76726	-134.96850
$V_p\ (eV)$	8.25276	6.64412	7.87853	4.97605	24.99908
$T\ (eV)$	7.12272	4.14889	6.39271	2.74246	56.95634
$V_m\ (eV)$	-3.56136	-2.07445	-3.19636	-1.37123	-28.47817
$E_{(AO/HO)}\ (eV)$	-14.22133	-14.22133	-14.11232	-14.11232	0
$\Delta E_{H_2MO(AO/HO)}\ (eV)$	0	0	0	0	-18.22046
$E_{T(AO/HO)}\ (eV)$	-14.22133	-14.22133	-14.11232	-14.11232	18.22046
$E_{T(H_2MO)}\ (eV)$	-34.01162	-29.29952	-31.63535	-27.53231	-63.27080
$E_{T}\left(atom-atom, msp^3.AO\right)\ (eV)$	-1.54812	-1.54812	-1.44915	-1.54005	-3.58557
$E_{T(MO)}\ (eV)$	-35.55974	-30.84764	-33.08452	-29.07235	-66.85630
$\omega\ \left(10^{15}\ rad/s\right)$	7.99232	4.97768	7.56783	2.96657	22.6662
$E_K\ (eV)$	5.26068	3.27640	4.98128	1.95265	14.91930
$\bar{E}_D\ (eV)$	-0.16136	-0.11046	-0.14608	-0.08037	-0.25544
$\bar{E}_{Kvib}\ (eV)$	0.07672 [47]	0.04772 [47]	0.04749 [29]	0.01537 [48]	0.24962 [29]
$\bar{E}_{osc}\ (eV)$	-0.12299	-0.08660	-0.12234	-0.07268	-0.13063
$E_{mag}\ (eV)$	0.12767	0.12767	0.14803	0.12767	0.11441
$E_{T(Group)}\ (eV)$	-35.68273	-30.93425	-33.20686	-29.14504	-67.11757
$E_{initial(c_4\ AO/HO)}\ (eV)$	-14.22133	-14.22133	-14.63489	-14.11232	-14.63489
$E_{initial(c_5\ AO/HO)}\ (eV)$	-17.42282	-12.96764	0	0	0
$E_{D(Group)}\ (eV)$	4.03858	3.74528	3.93708	0.92039	8.34918

Table 23.34. The total bond energies of gaseous-state manganese coordinate compounds calculated using the functional group composition and the energies of Table 23.33 compared to the gaseous-state experimental values.

Formula	Name	$Mn-F$ Group	$Mn-Cl$ Group	$Mn-CO$ Group	$Mn-Mn$ Group	$C=O$ Group	Calculated Total Bond Energy (eV)	Experimental Total Bond Energy (eV)	Relative Error
MnF	Manganese fluoride	1	0	0	0	0	4.03858	3.97567 [15]	-0.01582
MnCl	Manganese chloride	0	1	0	0	0	3.74528	3.73801 [15]	-0.00194
$Mn_2(CO)_{10}$	Dimanganese decacarbonyl	0	0	10	1	0	123.78299	122.70895 [49]	-0.00875

IRON FUNCTIONAL GROUPS AND MOLECULES

The electron configuration of iron is $[Ar]4s^2 3d^6$ having the corresponding term ${}^5D_4$. The total energy of the state is given by the sum over the eight electrons. The sum $E_T(Fe,3d4s)$ of experimental energies [1] of Fe, Fe^+, Fe^{2+}, Fe^{3+}, Fe^{4+}, Fe^{5+}, Fe^{6+}, and Fe^{7+} is:

$$E_T(Fe,3d4s) = -\begin{pmatrix} 151.06\ eV + 124.98\ eV + 99.1\ eV + 75.0\ eV \\ +54.8\ eV + 30.652\ eV + 16.1877\ eV + 7.9024\ eV \end{pmatrix} = -559.68210\ eV \tag{23.118}$$

By considering that the central field decreases by an integer for each successive electron of the shell, the radius r_{3d4s} of the $Fe3d4s$ shell may be calculated from the Coulombic energy using Eq. (15.13).

$$r_{3d4s} = \sum_{n=18}^{25} \frac{(Z-n)e^2}{8\pi\varepsilon_0 (e559.68210\ eV)} = \frac{36e^2}{8\pi\varepsilon_0 (e559.68210\ eV)} = 0.87516a_0 \tag{23.119}$$

where $Z = 26$ for iron. Using Eq. (15.14), the Coulombic energy $E_{Coulomb}(Fe,3d4s)$ of the outer electron of the $Fe3d4s$ shell is

$$E_{Coulomb}(Fe,3d4s) = \frac{-e^2}{8\pi\varepsilon_0 r_{3d4s}} = \frac{-e^2}{8\pi\varepsilon_0 0.87516a_0} = -15.546725\ eV \tag{23.120}$$

During hybridization, the spin-paired $4s$ electrons and the one. set of paired $3d$ electrons are promoted to the $Fe3d4s$ shell as initially unpaired electrons. The energies for the promotions are given by Eq. (15.15) at the initial radii of the $4s$ and $3d$ electrons. From Eq. (10.102) with $Z = 26$ and $n = 26$, the radius r_{26} of the $Fe4s$ shell is

$$r_{26} = 1.72173a_0 \tag{23.121}$$

and with $Z = 26$ and $n = 24$, the radius r_{24} of the $Fe3d$ shell is:

$$r_{24} = 1.33164a_0 \tag{23.122}$$

Using Eqs. (15.15), (23.120), and (23.121), the unpairing energies are:

$$E_{4s}(magnetic) = \frac{2\pi\mu_0 e^2\hbar^2}{m_e^2 (r_{26})^3} = \frac{8\pi\mu_0\mu_B^2}{(1.72173a_0)^3} = 0.02242\ eV \tag{23.123}$$

$$E_{3d}(magnetic) = \frac{2\pi\mu_0 e^2\hbar^2}{m_e^2 (r_{24})^3} = \frac{8\pi\mu_0\mu_B^2}{(1.33164a_0)^3} = 0.04845\ eV \tag{23.124}$$

The electrons from the *4s* and 3*d* shells successively fill unoccupied HOs until the HO shell is filled with unpaired electrons, then the electrons pair per HO. In the case of the *Fe*3*d*4*s* shell having eight electrons and six orbitals, two sets of electrons are paired. Using Eqs. (15.15) and (23.118), the pairing energy is given by:

$$E_{3d4s}(magnetic) = -\frac{2\pi\mu_0 e^2\hbar^2}{m_e^2 (r_{3d4s})^3} = -\frac{8\pi\mu_0\mu_B^2}{(0.87516a_0)^3} = -0.17069\ eV \tag{23.125}$$

Thus, after Eq. (23.28), the energy $E(Fe,3d4s)$ of the outer electron of the $Fe3d4s$ shell is given by adding the magnetic energies of unpairing the $4s$ (Eq. (23.122)) and $3d$ electrons (Eq. (23.123)) and pairing of two sets of $Fe3d4s$ electrons (Eq. (23.124)) to $E_{Coulomb}(Fe,3d4s)$ (Eq. (23.119)).

$$\begin{aligned} E(Fe,3d4s) &= \frac{-e^2}{8\pi\varepsilon_0 r_{3d4s}} + \frac{2\pi\mu_0 e^2\hbar^2}{m_e^2 r_{4s}^3} + \sum_{3d\ pairs} \frac{2\pi\mu_0 e^2\hbar^2}{m_e^2 r_{3d}^3} - \sum_{HO\ pairs} \frac{2\pi\mu_0 e^2\hbar^2}{m_e^2 r_{3d4s}^3} \\ &= -15.546725\ eV + 0.02242\ eV + 0.04845\ eV - 2(0.17069\ eV) = -15.81724\ eV \end{aligned} \tag{23.126}$$

Next, consider the formation of the $Fe-L$-bond MO wherein each iron atom has an $Fe3d4s$ electron with an energy given by Eq. (23.125). The total energy of the state of each iron atom is given by the sum over the eight electrons. The sum $E_T(Fe_{Fe-L}3d4s)$ of energies of $Fe3d4s$ (Eq. (23.125)), Fe^+, Fe^{2+}, Fe^{3+}, Fe^{4+}, Fe^{5+}, Fe^{6+}, and Fe^{7+} is:

$$\begin{aligned} E_T(Fe_{Fe-L}3d4s) &= -\begin{pmatrix} 151.06\ eV + 124.98\ eV + 99.1\ eV + 75.0\ eV \\ +54.8\ eV + 30.652\ eV + 16.1877\ eV + E(Fe,3d4s) \end{pmatrix} \\ &= -\begin{pmatrix} 151.06\ eV + 124.98\ eV + 99.1\ eV + 75.0\ eV \\ +54.8\ eV + 30.652\ eV + 16.1877\ eV + 15.81724\ eV \end{pmatrix} = -567.59694\ eV \end{aligned} \tag{23.127}$$

where *E(Fe*, 3*d* 4*s)* is the sum of the energy of *Fe*, –7.9024 *eV,* and the hybridization energy.

The iron HO donates an electron to each MO. Using Eq. (23.30), the radius r_{3d4s} of the $Fe3d4s$ shell calculated from the Coulombic energy is:

$$r_{Fe-L3d4s} = \left(\sum_{n=18}^{25} (Z-n) - 1\right) \frac{e^2}{8\pi\varepsilon_0 (e567.59694\ eV)} = \frac{35e^2}{8\pi\varepsilon_0 (e567.59694\ eV)} = 0.83898a_0 \tag{23.128}$$

Using Eqs. (15.19) and (23.127), the Coulombic energy $E_{Coulomb}(Fe_{Fe-L},3d4s)$ of the outer electron of the $Fe3d4s$ shell is

$$E_{Coulomb}\left(Fe_{Fe-L},3d4s\right)=\frac{-e^2}{8\pi\varepsilon_0 r_{Fe-L3d4s}}=\frac{-e^2}{8\pi\varepsilon_0 0.83898a_0}=-16.21706\ eV \tag{23.129}$$

The magnetic energy terms are those for the unpairing of the $4s$ and $3d$ electrons (Eqs. (23.122) and (23.123), respectively) and paring two sets of $Fe3d4s$ electrons (Eq. (23.124)). Using Eqs. (23.32), (23.128) and (23.122-23.124), the energy $E\left(Fe_{Fe-L},3d4s\right)$ of the outer electron of the $Fe3d4s$ shell is:

$$\begin{aligned}E\left(Fe_{Fe-L},3d4s\right)&=\frac{-e^2}{8\pi\varepsilon_0 r_{Fe-L3d4s}}+\frac{2\pi\mu_0 e^2\hbar^2}{m_e^2\left(r_{26}\right)^3}+\frac{2\pi\mu_0 e^2\hbar^2}{m_e^2\left(r_{24}\right)^3}-2\frac{2\pi\mu_0 e^2\hbar^2}{m_e^2\left(r_{3d4s}\right)^3}\\&=-16.21706\ eV+0.02242\ eV+0.04845\ eV-2\left(0.17069\ eV\right)=-16.48757\ eV\end{aligned} \tag{23.130}$$

Thus, $E_T\left(Fe-L,3d4s\right)$, the energy change of each $Fe3d4s$ shell with the formation of the $Fe-L$-bond MO is given by the difference between Eq. (23.129) and Eq. (23.125):

$$E_T\left(Fe-L,3d4s\right)=E\left(Fe_{Fe-L},3d4s\right)-E\left(Fe,3d4s\right)=-16.48757\ eV-\left(-15.81724\ eV\right)=-0.67033\ eV \tag{23.131}$$

The semimajor axis a solution given by Eq. (23.41) of the force balance equation, Eq. (23.39), for the σ-MO of the $Fe-L$-bond MO of FeL_n is given in Table 23.36 with the force-equation parameters $Z=26$, n_e, and L corresponding to the orbital and spin angular momentum terms of the $3d4s$ HO shell. The semimajor axis a of carbonyl and organometallic compounds are solved using Eq. (15.51).

For the $Fe-L$ functional groups, hybridization of the $4s$ and $3d$ AOs of Fe to form a single $3d4s$ shell forms an energy minimum, and the sharing of electrons between the $Fe3d4s$ HO and L AO to form a MO permits each participating orbital to decrease in radius and energy. The F AO has an energy of $E\left(F\right)=-17.42282\ eV$, the Cl AO has an energy of $E\left(Cl\right)=-12.96764\ eV$, the $C_{aryl}2sp^3$ HO has an energy of $E\left(C_{aryl},2sp^3\right)=-15.76868\ eV$ (Eq. (14.246)), the $C2sp^3$ HO has an energy of $E\left(C,2sp^3\right)=-14.63489\ eV$ (Eq. (15.25)), the O AO has an energy of $E\left(O\right)=-13.61805\ eV$, the Coulomb energy of $Fe3d4s$ HO is $E_{Coulomb}\left(Fe,3d4s\right)=-15.546725\ eV$ (Eq. (23.119)), and the $Fe3d4s$ HO has an energy of $E\left(Fe,3d4s\right)=-15.81724\ eV$ (Eq. (23.125)). To meet the equipotential condition of the union of the $Fe-L$ H_2-type-ellipsoidal-MO with these orbitals, the hybridization factor(s), at least one of c_2 and C_2 of Eq. (15.61) for the $Fe-L$-bond MO given by Eq. (15.77) is:

$$c_2\left(FAO\ to\ Fe3d4sHO\right)=C_2\left(FAO\ to\ Fe3d4sHO\right)=\frac{E\left(Fe,3d4s\right)}{E\left(FAO\right)}=\frac{-15.81724\ eV}{-17.42282\ eV}=0.90785 \tag{23.132}$$

$$c_2\left(ClAO\ to\ Fe3d4sHO\right)=C_2\left(ClAO\ to\ Fe3d4sHO\right)=\frac{E\left(ClAO\right)}{E\left(Fe,3d4s\right)}=\frac{-12.96764\ eV}{-15.81724\ eV}=0.81984 \tag{23.133}$$

$$c_2\left(C2sp^3HO\ to\ Fe3d4sHO\right)=\frac{E\left(C,2sp^3\right)}{E_{Coulomb}\left(Fe,3d4s\right)}c_2\left(C2sp^3HO\right)=\frac{-14.63489\ eV}{-15.54673\ eV}\left(0.91771\right)=0.86389 \tag{23.134}$$

$$\begin{aligned}c_2\left(C_{aryl}2sp^3HO\ to\ Fe3d4sHO\right)&=C_2\left(C_{aryl}2sp^3HO\ to\ Fe3d4sHO\right)\\&=\frac{E\left(C,2sp^3\right)}{E_{Coulomb}\left(Fe,3d4s\right)}c_2\left(C_{aryl}2sp^3HO\right)=\frac{-14.63489\ eV}{-15.54673\ eV}\left(0.85252\right)=0.80252\end{aligned} \tag{23.135}$$

$$c_2\left(O\ to\ Fe3d4sHO\right)=C_2\left(O\ to\ Fe3d4sHO\right)=\frac{E\left(O\right)}{E\left(Fe,3d4s\right)}=\frac{-13.61805\ eV}{-15.81724\ eV}=0.86096 \tag{23.136}$$

where Eqs. (15.76), (15.79), and (13.430) were used in Eq. (23.133) and Eqs. (15.76), (15.79), and (14.417) were used in Eq. (23.134). Since the energy of the MO is matched to that of the $Fe3d4s$ HO in coordinate compounds, $E\left(AO/HO\right)$ in Eq. (15.61) is $E\left(Fe,3d4s\right)$ given by Eq. (23.125) and $E\left(AO/HO\right)$ in Eq. (15.61) of carbonyl and organometallic compounds is $E_{Coulomb}\left(Fe,3d4s\right)$ given by Eq. (23.119). $E_T\left(atom-atom,msp^3.AO\right)$ of the $Fe-L$-bond MO is determined by considering that the bond involves an electron transfer from the iron atom to the ligand atom to form partial ionic character in the bond as in the case of the zwitterions such as $H_2B^+-F^-$ given in the Halido Boranes section. For the coordinate compounds, $E_T\left(atom-atom,msp^3.AO\right)$ is $-1.34066\ eV$, two times the energy of Eq. (23.130). For the $Fe-C$ bonds of carbonyl and organometallic compounds, $E_T\left(atom-atom,msp^3.AO\right)$ is $-1.44915\ eV$ (Eq. (14.151)), and the $C=O$ functional group of carbonyls is equivalent to that of vanadium carbonyls. The aromatic cyclopentadienyl moieties of organometallic $Fe\left(C_5H_5\right)_2$ comprise $C\overset{3e}{=}C$ and CH functional groups that are equivalent to those given in the Aromatic and Heterocyclic Compounds section.

The symbols of the functional groups of iron coordinate compounds are given in Table 23.35. The geometrical (Eqs. (15.1-15.5) and (23.41)), intercept (Eqs. (15.31-15.32) and (15.80-15.87)), and energy (Eqs. (15.61) and (23.28-23.33)) parameters of iron coordinate compounds are given in Tables 23.36, 23.37, and 23.38, respectively. The total energy of each iron coordinate compound given in Table 23.39 was calculated as the sum over the integer multiple of each $E_D(Group)$ of Table 23.38 corresponding to functional-group composition of the compound. The charge-densities of exemplary iron carbonyl and organometallic compounds, iron pentacarbonyl ($Fe(CO)_5$) and bis-cylopentadienyl iron or ferrocene ($Fe(C_5H_5)_2$) comprising the concentric shells of atoms with the outer shell bridged by one or more H_2-type ellipsoidal MOs or joined with one or more hydrogen MOs are shown in Figures 23.7 and 23.8, respectively.

Figure 23.7. *Iron Pentacarbonyl.* Color scale, translucent view of the charge-density of $Fe(CO)_5$ showing the orbitals of the Fe, C, and O atoms at their radii, the ellipsoidal surface of each H_2-type ellipsoidal MO that transitions to the corresponding outer shell of the atoms participating in each bond, and the nuclei (red, not to scale).

Figure 23.8. *Bis-cylopentadienyl Iron.* Color scale, opaque view of the charge-density of $Fe(C_5H_5)_2$ showing the orbitals of the Fe and C atoms at their radii and the ellipsoidal surface of each H or H_2-type ellipsoidal MO that transitions to the corresponding outer shell of the atoms participating in each bond.

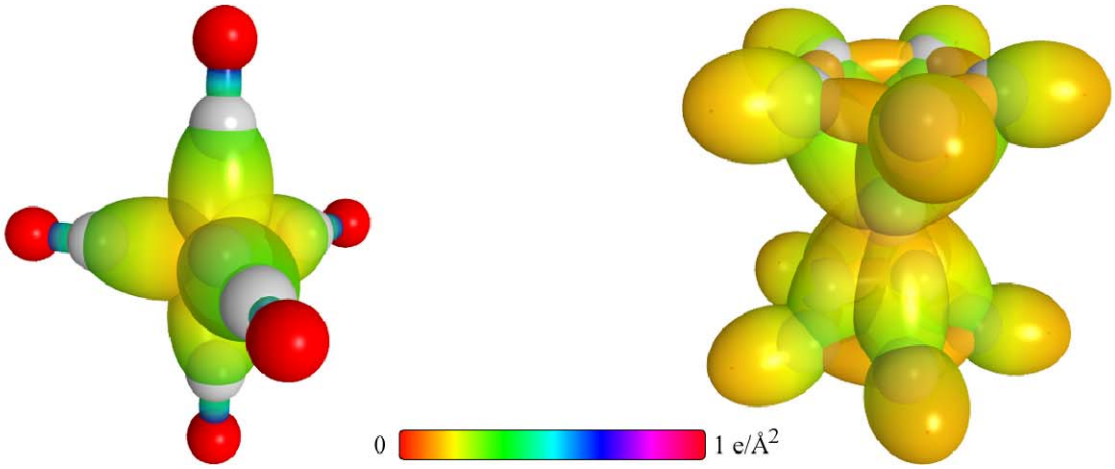

Table 23.35. The symbols of the functional groups of iron coordinate compounds.

Functional Group	Group Symbol
FeF group of FeF	$Fe-F$ (a)
FeF2 group of FeF_2	$Fe-F$ (b)
FeF3 group of FeF_3	$Fe-F$ (c)
FeCl group of $FeCl$	$Fe-Cl$ (a)
FeCl2 group of $FeCl_2$	$Fe-Cl$ (b)
FeCl3 group of $FeCl_3$	$Fe-Cl$ (c)
FeO group of FeO	$Fe-O$
FeCO group of $Fe(CO)_5$	$Fe-CO$
$C=O$	$C=O$
FeCaryl group of $Fe(C_5H_5)_2$	$Fe-C_5H_5$
CC (aromatic bond)	$C\overset{3e}{=}C$
CH (aromatic)	CH

Table 23.36. The geometrical bond parameters of iron coordinate compounds and experimental values.

Parameter	$Fe-F$ (a) Group	$Fe-F$ (b) Group	$Fe-F$ (c) Group	$Fe-Cl$ (a) Group	$Fe-Cl$ (b) Group	$Fe-Cl$ (c) Group	$Fe-O$ Group	$Fe-CO$ Group	$C=O$ Group	$Fe-C_5H_5$ Group	$C\overset{3e}{=}C$ Group	CH Group
n_e	2	2	2	3	3	3	2					
L	$4+\sqrt{\frac{3}{4}}$	$5\sqrt{\frac{3}{4}}$	$5\sqrt{\frac{3}{4}}$	$3\sqrt{\frac{3}{4}}$	0	$\sqrt{\frac{3}{4}}$	$4\sqrt{\frac{3}{4}}$					
$a\ (a_0)$	2.18715	2.16654	2.16654	2.59993	2.50000	2.53331	2.13323	2.18970	1.184842	2.33324	1.47348	1.60061
$c'\ (a_0)$	1.79227	1.78380	1.78380	2.05629	2.01639	2.02978	1.57408	1.70868	1.08850	1.96889	1.31468	1.03299
Bond Length $2c'\ (\AA)$	1.89685	1.88790	1.88790	2.17628	2.13405	2.14822	1.66594	1.80839	1.15202	2.08379	1.39140	1.09327
Exp. Bond Length $(\AA)$	1.80 [15] (FeF_n $n=1,2,3$)	1.80 [15] (FeF_n $n=1,2,3$)	1.80 [15] (FeF_n $n=1,2,3$)	2.09 [15] ($FeCl$)	2.09 [15] ($FeCl$) 2.17 [50] (FCl_n $n=2,3$)	2.09 [15] ($FeCl$) 2.17 [50] (FCl_n $n=2,3$)	1.619 [15] (FeO)	1.806 [29] ($Fe(CO)_5$ Fe-CO equatorial) 1.833 [29] ($Fe(CO)_5$ Fe-CO axial) 1.82 [9-22] ($Fe(CO)_5$ Fe-CO avg.) 0.020 [3] $Fe(CO)_5$ Fe-CO equatorial-Fe-CO axial	1.145 [29] ($Fe(CO)_5$)	2.064 [3] ($Fe(C_5H_5)_2$)	1.399 [3] (benzene)	1.101 [3] (benzene)
$b,c\ (a_0)$	1.25356	1.22962	1.22962	1.59100	1.47790	1.51580	1.43978	1.36937	0.46798	1.25199	0.66540	1.22265
e	0.81945	0.82334	0.82334	0.79090	0.80656	0.80124	0.73788	0.78033	0.91869	0.84384	0.89223	0.64537

Table 23.37. The MO to HO intercept geometrical bond parameters of iron coordinate compounds. E_T is E_T (*atom–atom,HO.AO*).

Bond	Atom	E_T (eV) Bond 1	E_T (eV) Bond 2	E_T (eV) Bond 3	E_T (eV) Bond 4	E_T (eV) Bond 5	Final Total Energy $Fe3d4s$ (eV)	$r_{initial}$ (a_0)	r_{final} (a_0)	$E_{Coulomb}(Fe3d4s)$ (eV) Final	$E(Fe3d4s)$ (eV) Final	θ' (°)	θ_1 (°)	θ_2 (°)	d_1 (a_0)	d_2 (a_0)
$Fe-F\ (FeF)$	Fe	-0.67033	0	0	0	0		0.87516	0.83898	-16.21706		100.09	79.91	41.22	1.64521	0.14705
$Fe-F\ (FeF)$	F	-0.67033	0	0	0	0		0.78069	0.75199	-18.09315		93.12	86.88	36.80	1.75138	0.04089
$Fe-F\ (FeF_2)$	Fe	-0.67033	-0.67033	0	0	0		0.87516	0.80568	-16.88739		99.35	80.65	40.28	1.65286	0.13095
$Fe-F\ (FeF_2)$	F	-0.67033	0	0	0	0		0.78069	0.75199	-18.09315		95.01	84.99	37.53	1.71807	0.06573
$Fe-F\ (FeF_3)$	Fe	-0.67033	-0.67033	-0.67033	0	0		0.87516	0.77492	-17.55772		96.94	83.06	38.73	1.69022	0.09359
$Fe-F\ (FeF_3)$	F	-0.67033	0	0	0	0		0.78069	0.75199	-18.09315		95.01	84.99	37.53	1.71807	0.06573
$Fe-Cl\ (FeCl)$	Fe	-0.67033	0	0	0	0		0.87516	0.83898	-16.21706		78.30	101.70	31.09	2.22650	0.17020
$Fe-Cl\ (FeCl)$	Cl	-0.67033	0	0	0	0		1.05158	0.99764	-13.63797		91.75	88.25	38.81	2.02589	0.03040
$Fe-Cl\ (FeCl_2)$	Fe	-0.67033	-0.67033	0	0	0		0.87516	0.80568	-16.88739		83.99	96.01	32.83	2.10069	0.08430
$Fe-Cl\ (FeCl_2)$	Cl	-0.67033	0	0	0	0		1.05158	0.99764	-13.63797		98.86	81.14	41.83	1.86268	0.15370
$Fe-Cl\ (FeCl_3)$	Fe	-0.67033	-0.67033	-0.67033	0	0		0.87516	0.77492	-17.55772		77.72	102.28	29.97	2.19460	0.16482
$Fe-Cl\ (FeCl_3)$	Cl	-0.67033	0	0	0	0		1.05158	0.99764	-13.63797		96.51	83.49	40.84	1.91662	0.11315
$Fe-O\ (FeO)$	Fe	-0.67033	0	0	0	0		0.87516	0.83898	-16.21706		77.62	102.38	34.69	1.75401	0.17992
$Fe-O\ (FeO)$	O	-0.67033	0	0	0	0		1.00000	0.95223	-14.28839		88.41	91.59	41.39	1.60053	0.02645
$FeC=O$	O	-1.79278	0	0	0	0		1.00000	0.81871	-16.61853		147.43	32.57	70.34	0.39853	0.68997
$FeC=O$	C	-1.79278	-0.72457	0	0	0	-154.13305	0.91771	0.78451	-17.34311	-17.15225	146.31	33.69	68.42	0.43577	0.65274
$Fe-CO\ (Fe(CO)_5)$	C	-0.72457	-1.79278	0	0	0		0.91771	0.78451	-17.34311	-17.15225	83.26	96.74	34.68	1.80077	0.09209
$Fe-CO\ (Fe(CO)_5)$	Fe	-0.72457	-0.72457	-0.72457	-0.72457	-0.72457		0.87516	0.73750	-18.44862		78.08	101.92	31.80	1.86102	0.15233
$C-H\ (CH)$	C	-0.85035	-0.85035	-0.56690	-0.14491	0		0.91771	0.78928	-17.23825	-17.04738	73.50	106.50	38.24	1.25715	0.22415
$C\overset{3e}{=}HC_a\overset{3e}{=}C$	C_a	-0.85035	-0.85035	-0.56690	-0.14491	0		0.91771	0.78928	-17.23826	-17.04739	133.96	46.04	58.64	0.76685	0.54783
$Fe-C_5H_5$	Fe	-0.72457	-0.72457	0	0	0		0.87516	0.83600	-16.27490		103.46	76.54	40.50	1.77431	0.19458
$Fe-C_5H_5$	C	-0.14491	-0.85035	-0.85035	-0.56690	0		0.91771	0.78928	-17.23826	-17.04739	100.16	79.84	38.36	1.82967	0.13922

Table 23.38. The energy parameters (eV) of functional groups of iron coordinate compounds.

Parameters	$Fe-F$ (a) Group	$Fe-F$ (b) Group	$Fe-F$ (c) Group	$Fe-Cl$ (a) Group	$Fe-Cl$ (b) Group	$Fe-Cl$ (c) Group	$Fe-O$ Group	$Fe-CO$ Group	$C=O$ Group	$Fe-C_5H_5$ Group	$C^{3e}=C$ Group	CH Group
f_1	1	1	1	1	1	1	1	1	1	1	0.75	1
n_1	1	1	1	1	1	1	1	1	2	1	2	1
n_2	0	0	0	0	0	0	0	0	0	0	0	0
n_3	0	0	0	0	0	0	0	0	0	0	0	0
C_1	0.375	0.375	0.375	0.375	0.375	0.375	0.5	0.375	0.5	0.375	0.5	0.75
C_2	0.90785	0.90785	0.90785	0.81984	0.81984	0.81984	0.86096	1	1	0.80252	0.85252	1
c_1	1	1	1	1	1	1	1	1	1	1	1	1
c_2	0.90785	0.90785	0.90785	0.81984	0.81984	0.81984	0.86096	0.86389	0.85395	0.80252	0.85252	0.91771
c_3	0	0	0	0	0	0	0	0	2	0	0	1
c_4	1	1	1	1	1	1	1	2	4	2	3	1
c_5	1	1	1	1	1	1	1	0	0	0	0	1
C_{1o}	0.375	0.375	0.375	0.375	0.375	0.375	0.5	0.375	0.5	0.375	0.5	0.75
C_{2o}	0.90785	0.90785	0.90785	0.81984	0.81984	0.81984	0.86096	1	1	0.80252	0.85252	1
$V_e\ (eV)$	-31.84422	-32.32645	-32.32645	-23.30074	-24.71893	-24.22529	-28.15464	-28.78715	-134.96850	-27.38198	-101.12679	-37.10024
$V_p\ (eV)$	7.59139	7.62741	7.62741	6.61667	6.74761	6.70310	8.64365	7.96274	24.99908	6.91038	20.69825	13.17125
$T\ (eV)$	7.27983	7.46038	7.46038	4.48104	4.94379	4.78135	6.59905	6.57331	56.95634	5.86780	34.31559	11.58941
$V_m\ (eV)$	-3.63991	-3.73019	-3.73019	-2.24052	-2.47189	-2.39068	-3.29952	-3.28665	-28.47817	-2.93390	-17.15779	-5.79470
$E_{(AO/HO)}\ (eV)$	-15.81724	-15.81724	-15.81724	-15.81724	-15.81724	-15.81724	-15.81724	-15.54673	0	-15.54673	0	-14.63489
$\Delta E_{H_2MO\,(AO/HO)}\ (eV)$	0	0	0	0	0	0	0	-1.44915	-18.22046	-1.44915	0	-1.13379
$E_{T\,(AO/HO)}\ (eV)$	-15.81724	-15.81724	-15.81724	-15.81724	-15.81724	-15.81724	-15.81724	-14.09758	-18.22046	-14.09758	0	-13.50110
$E_{T\,(H_2MO)}\ (eV)$	-36.43016	-36.78609	-36.78609	-30.26079	-31.31666	-30.94875	-32.02870	-31.63533	-63.27080	-31.63527	-63.27075	-31.63539
$E_T\left(atom-atom, msp^3.AO\right)\ (eV)$	-1.34066	-1.34066	-1.34066	-1.34066	-1.34066	-1.34066	-1.34066	-1.44915	-3.58557	-1.44915	-2.26759	-0.56690
$E_{T\,(MO)}\ (eV)$	-37.77082	-38.12675	-38.12675	-31.60145	-32.65732	-32.28941	-33.36936	-33.08452	-66.85630	-33.08452	-65.53833	-32.20226
$\omega\ \left(10^{15}\ rad/s\right)$	7.45740	7.56407	1.76910	1.14225	1.27585	5.68504	16.9210	15.7986	22.6662	16.1893	49.7272	26.4826
$E_K\ (eV)$	4.90859	4.97880	11.64452	7.51848	8.39787	3.74199	11.13772	10.39888	14.91930	10.65607	32.73133	17.43132
$\bar{E}_D\ (eV)$	-0.16555	-0.16830	-0.25739	-0.17143	-0.18723	-0.12357	-0.22032	-0.21107	-0.25544	-0.21366	-0.35805	-0.26130
$\bar{E}_{Kvib}\ (eV)$	0.07811 [51]	0.07811 [51]	0.07811 [51]	0.04054 [50]	0.04054 [50]	0.04054 [50]	0.10911 [52]	0.04749 [29]	0.24962 [29]	0.04749 [29]	0.19649 [30]	0.35532 Eq. (13.458)
$\bar{E}_{osc}\ (eV)$	-0.12650	-0.12925	-0.21834	-0.15115	-0.16696	-0.10330	-0.16576	-0.18732	-0.13063	-0.18992	-0.25982	-0.08364
$E_{mag}\ (eV)$	0.17069	0.17069	0.17069	0.17069	0.17069	0.17069	0.17069	0.14803	0.11441	0.14803	0.14803	0.14803
$E_{T\,(Group)}\ (eV)$	-37.89732	-38.25600	-38.34508	-31.75260	-32.82428	-32.39271	-33.53513	-33.27184	-67.11757	-33.27443	-49.54347	-32.28590
$E_{initial\,(c_4\ AO/HO)}\ (eV)$	-15.81724	-15.81724	-15.81724	-15.81724	-15.81724	-15.81724	-15.81724	-14.63489	-14.63489	-14.63489	-14.63489	-14.63489
$E_{initial\,(c_5\ AO/HO)}\ (eV)$	-17.42282	-17.42282	-17.42282	-12.96764	-12.96764	-12.96764	-13.61806	0	0	0	0	-13.59844
$E_{D\,(Group)}\ (eV)$	4.65726	5.01594	5.10503	2.96772	4.03940	3.60783	4.09983	4.00206	8.34918	1.73707	5.63881	3.90454

Table 23.39. The total bond energies of gaseous-state iron coordinate compounds calculated using the functional group composition and the energies of Table 23.38 compared to the gaseous-state experimental values.

Formula	Name	$Fe-F$ (a) Group	$Fe-F$ (b) Group	$Fe-F$ (c) Group	$Fe-Cl$ (a) Group	$Fe-Cl$ (b) Group	$Fe-Cl$ (c) Group	$Fe-O$ Group	$Fe-CO$ Group	$C=O$ Group	$Fe-C_5H_5$ Group	$C^{3e}=C$ Group	CH Group	Calculated Total Bond Energy (eV)	Experimental Total Bond Energy (eV)	Relative Error
FeF	Iron fluoride	1	0	0	0	0	0	0	0	0	0	0	0	4.65726	4.63464 [15]	-0.00488
FeF_2	Iron difluoride	0	2	0	0	0	0	0	0	0	0	0	0	10.03188	9.98015 [15]	-0.00518
FeF_3	Iron trifluoride	0	0	3	0	0	0	0	0	0	0	0	0	15.31508	15.25194 [15]	-0.00414
FeCl	Iron chloride	0	0	0	1	0	0	0	0	0	0	0	0	2.96772	2.97466 [15]	0.00233
$FeCl_2$	Iron dichoride	0	0	0	0	2	0	0	0	0	0	0	0	8.07880	8.28632 [15]	0.02504
$FeCl_3$	Iron trichloride	0	0	0	0	0	3	0	0	0	0	0	0	10.82348	10.70065 [50]	-0.01148
FeO	Iron oxide	0	0	0	0	0	0	1	0	0	0	0	0	4.09983	4.20895 [15]	0.02593
$Fe(CO)_5$	Iron pentacarbonyl	0	0	0	0	0	0	0	5	5	0	0	0	61.75623	61.91846 [29]	0.00262
$Fe(C_5H_5)_2$	Bis-cylopentadienyl iron (ferrocene)	0	0	0	0	0	0	0	0	0	2	10	10	98.90760	98.95272 [53]	0.00046

COBALT FUNCTIONAL GROUPS AND MOLECULES

The electron configuration of cobalt is $[Ar]4s^2 3d^7$ having the corresponding term ${}^4F_{9/2}$. The total energy of the state is given by the sum over the nine electrons. The sum $E_T(Co,3d4s)$ of experimental energies [1] of Co, Co^+, Co^{2+}, Co^{3+}, Co^{4+}, Co^{5+}, Co^{6+}, Co^{7+}, and Co^{8+} is:

$$E_T(Co,3d4s) = -\begin{pmatrix} 186.13\ eV + 157.8\ eV + 128.9\ eV + 102.0\ eV + 79.5\ eV \\ +51.3\ eV + 33.50\ eV + 17.084\ eV + 7.88101\ eV \end{pmatrix} = -764.09501\ eV \tag{23.137}$$

By considering that the central field decreases by an integer for each successive electron of the shell, the radius r_{3d4s} of the $Co3d4s$ shell may be calculated from the Coulombic energy using Eq. (15.13).

$$r_{3d4s} = \sum_{n=18}^{26} \frac{(Z-n)e^2}{8\pi\varepsilon_0 (e764.09501\ eV)} = \frac{45e^2}{8\pi\varepsilon_0 (e764.09501\ eV)} = 0.80129a_0 \tag{23.138}$$

where $Z = 27$ for cobalt. Using Eq. (15.14), the Coulombic energy $E_{Coulomb}(Co,3d4s)$ of the outer electron of the $Co3d4s$ shell is

$$E_{Coulomb}(Co,3d4s) = \frac{-e^2}{8\pi\varepsilon_0 r_{3d4s}} = \frac{-e^2}{8\pi\varepsilon_0 0.80129a_0} = -16.979889\ eV \tag{23.139}$$

During hybridization, the spin-paired $4s$ electrons and the two sets of paired $3d$ electrons are promoted to the $Co3d4s$ shell as initially unpaired electrons. The energies for the promotions are given by Eq. (15.15) at the initial radii of the $4s$ and $3d$ electrons. From Eq. (10.102) with $Z = 27$ and $n = 27$, the radius r_{27} of the $Co4s$ shell is:

$$r_{27} = 1.72640a_0 \tag{23.140}$$

and with $Z = 27$ and $n = 25$, the radius r_{25} of the $Co3d$ shell is:

$$r_{25} = 1.21843a_0 \tag{23.141}$$

Using Eqs. (15.15), (23.139), and (23.140), the unpairing energies are:

$$E_{4s}(magnetic) = \frac{2\pi\mu_0 e^2\hbar^2}{m_e^2 (r_{27})^3} = \frac{8\pi\mu_0\mu_B^2}{(1.72640a_0)^3} = 0.02224\ eV \tag{23.142}$$

$$E_{3d}(magnetic) = \frac{2\pi\mu_0 e^2\hbar^2}{m_e^2 (r_{25})^3} = \frac{8\pi\mu_0\mu_B^2}{(1.21843a_0)^3} = 0.06325\ eV \tag{23.143}$$

The electrons from the $4s$ and $3d$ shells successively fill unoccupied HOs until the HO shell is filled with unpaired electrons, then the electrons pair per HO. In the case of the $Co3d4s$ shell having nine electrons and six orbitals, three sets of electrons are paired. Using Eqs. (15.15) and (23.137), the pairing energy is given by:

$$E_{3d4s}(magnetic) = -\frac{2\pi\mu_0 e^2\hbar^2}{m_e^2 (r_{3d4s})^3} = -\frac{8\pi\mu_0\mu_B^2}{(0.80129a_0)^3} = -0.22238\ eV \tag{23.144}$$

Thus, after Eq. (23.28), the energy $E(Co,3d4s)$ of the outer electron of the $Co3d4s$ shell is given by adding the magnetic energies of unpairing the $4s$ (Eq. (23.141)) and $3d$ electrons (Eq. (23.142)) and pairing of three sets of $Co3d4s$ electrons (Eq. (23.143)) to $E_{Coulomb}(Co,3d4s)$ (Eq. (23.138)).

$$\begin{aligned} E(Co,3d4s) &= \frac{-e^2}{8\pi\varepsilon_0 r_{3d4s}} + \frac{2\pi\mu_0 e^2\hbar^2}{m_e^2 r_{4s}^3} + \sum_{3d\ pairs} \frac{2\pi\mu_0 e^2\hbar^2}{m_e^2 r_{3d}^3} - \sum_{HO\ pairs} \frac{2\pi\mu_0 e^2\hbar^2}{m_e^2 r_{3d4s}^3} \\ &= -16.979889\ eV + 0.02224\ eV + 2(0.06325\ eV) - 3(0.22238\ eV) = -17.49830\ eV \end{aligned} \tag{23.145}$$

Next, consider the formation of the $Co-L$-bond MO wherein each cobalt atom has an $Co3d4s$ electron with an energy given by Eq. (23.144). The total energy of the state of each cobalt atom is given by the sum over the nine electrons. The sum $E_T(Co_{Co-L}3d4s)$ of energies of $Co3d4s$ (Eq. (23.144)), Co^+, Co^{2+}, Co^{3+}, Co^{4+}, Co^{5+}, Co^{6+}, Co^{7+}, and Co^{8+} is:

$$\begin{aligned} E_T(Co_{Co-L}3d4s) &= -\begin{pmatrix} 186.13\ eV + 157.8\ eV + 128.9\ eV + 102.0\ eV + 79.5\ eV \\ +51.3\ eV + 33.50\ eV + 17.084\ eV + E(Co,3d4s) \end{pmatrix} \\ &= -\begin{pmatrix} 186.13\ eV + 157.8\ eV + 128.9\ eV + 102.0\ eV + 79.5\ eV \\ +51.3\ eV + 33.50\ eV + 17.084\ eV + 17.49830\ eV \end{pmatrix} = -773.71230\ eV \end{aligned} \tag{23.146}$$

where $E(Co,3d4s)$ is the sum of the energy of Co, $-7.88101\ eV$, and the hybridization energy.

The cobalt HO donates an electron to each MO. Using Eq. (23.30), the radius r_{3d4s} of the $Co3d4s$ shell calculated from the Coulombic energy is:

$$r_{Co-L3d4s} = \left(\sum_{n=18}^{26} (Z-n) - 1\right) \frac{e^2}{8\pi\varepsilon_0 (e773.71230\ eV)} = \frac{44e^2}{8\pi\varepsilon_0 (e773.71230\ eV)} = 0.77374a_0 \tag{23.147}$$

Using Eqs. (15.19) and (23.146), the Coulombic energy $E_{Coulomb}\left(Co_{Co-L},3d4s\right)$ of the outer electron of the $Co3d4s$ shell is:

$$E_{Coulomb}\left(Co_{Co-L},3d4s\right)=\frac{-e^2}{8\pi\varepsilon_0 r_{Co-L3d4s}}=\frac{-e^2}{8\pi\varepsilon_0 0.77374a_0}=-17.58437\ eV \tag{23.148}$$

The magnetic energy terms are those for the unpairing of the $4s$ and $3d$ electrons (Eqs. (23.141) and (23.142), respectively) and paring three sets of $Co3d4s$ electrons (Eq. (23.143)). Using Eqs. (23.32), (23.148) and (23.141-23.143), the energy $E\left(Co_{Co-L},3d4s\right)$ of the outer electron of the $Co3d4s$ shell is:

$$\begin{aligned}E\left(Co_{Co-L},3d4s\right)&=\frac{-e^2}{8\pi\varepsilon_0 r_{Fe-L3d4s}}+\frac{2\pi\mu_0 e^2\hbar^2}{m_e^2\left(r_{27}\right)^3}+\frac{2\pi\mu_0 e^2\hbar^2}{m_e^2\left(r_{25}\right)^3}-3\frac{2\pi\mu_0 e^2\hbar^2}{m_e^2\left(r_{3d4s}\right)^3}\\&=-17.58437\ eV+0.02224\ eV+2\left(0.06325\ eV\right)-3\left(0.22238\ eV\right)=-18.10278\ eV\end{aligned} \tag{23.149}$$

Thus, $E_T\left(Co-L,3d4s\right)$, the energy change of each $Co3d4s$ shell with the formation of the $Co-L$-bond MO is given by the difference between Eq. (23.148) and Eq. (23.144):

$$E_T\left(Co-L,3d4s\right)=E\left(Co_{Co-L},3d4s\right)-E\left(Co,3d4s\right)=-18.10278\ eV-\left(-17.49830\ eV\right)=-0.60448\ eV \tag{23.150}$$

The semimajor axis a solution given by Eq. (23.41) of the force balance equation, Eq. (23.39), for the σ-MO of the $Co-L$-bond MO of CoL_n is given in Table 23.41 with the force-equation parameters $Z=27$, n_e, and L corresponding to the orbital and spin angular momentum terms of the $3d4s$ HO shell. The semimajor axis a of carbonyl and organometallic compounds are solved using Eq. (15.51).

For the $Co-L$ functional groups, hybridization of the $4s$ and $3d$ AOs of Co to form a single $3d4s$ shell forms an energy minimum, and the sharing of electrons between the $Co3d4s$ HO and L AO to form a MO permits each participating orbital to decrease in radius and energy. The F AO has an energy of $E\left(F\right)=-17.42282\ eV$, the Cl AO has an energy of $E\left(Cl\right)=-12.96764\ eV$, the $C2sp^3$ HO has an energy of $E\left(C,2sp^3\right)=-14.63489\ eV$ (Eq. (15.25)), the Coulomb energy of $Co3d4s$ HO is $E_{Coulomb}\left(Co,3d4s\right)=-16.979889\ eV$ (Eq. (23.138)), $13.605804\ eV$ is the magnitude of the Coulombic energy between the electron and proton of H (Eq. (1.264)), and the $Co3d4s$ HO has an energy of $E\left(Co,3d4s\right)=-17.49830\ eV$ (Eq. (23.144)). To meet the equipotential condition of the union of the $Co-L$ H_2-type-ellipsoidal-MO with these orbitals, the hybridization factor(s), at least one of c_2 and C_2 of Eq. (15.61) for the $Co-L$-bond MO given by Eq. (15.77) is:

$$c_2\left(FAO\ to\ Co3d4sHO\right)=\frac{E\left(FAO\right)}{E\left(Co,3d4s\right)}=\frac{-17.42282\ eV}{-17.49830\ eV}=0.99569 \tag{23.151}$$

$$C_2\left(ClAO\ to\ Co3d4sHO\right)=\frac{E\left(ClAO\right)}{E\left(Co,3d4s\right)}=\frac{-12.96764\ eV}{-17.49830\ eV}=0.74108 \tag{23.152}$$

$$c_2\left(C2sp^3HO\ to\ Co3d4sHO\right)=\frac{E\left(C,2sp^3\right)}{E_{Coulomb}\left(Co,3d4s\right)}c_2\left(C2sp^3HO\right)=\frac{-14.63489\ eV}{-16.97989\ eV}\left(0.91771\right)=0.79097 \tag{23.153}$$

$$c_2\left(HAO\ to\ Co3d4sHO\right)=C_2\left(HAO\ to\ Co3d4sHO\right)=\frac{E\left(H\right)}{E_{Coulomb}\left(Co,3d4s\right)}=\frac{-13.605804\ eV}{-16.97989\ eV}=0.80129 \tag{23.154}$$

where Eqs. (15.76), (15.79), and (13.430) were used in Eq. (23.152) and Eq. (15.71) was used in Eq. (23.153). Since the energy of the MO is matched to that of the $Co3d4s$ HO in coordinate compounds, $E\left(AO/HO\right)$ in Eq. (15.61) is $E\left(Co,3d4s\right)$ given by Eq. (23.144) and $E\left(AO/HO\right)$ in Eq. (15.61) of carbonyl compounds is $E_{Coulomb}\left(Co,3d4s\right)$ given by Eq. (23.138). $E_T\left(atom-atom,msp^3.AO\right)$ of the $Co-L$-bond MO is determined by considering that the bond involves an electron transfer from the cobalt atom to the ligand atom to form partial ionic character in the bond as in the case of the zwitterions such as $H_2B^+-F^-$ given in the Halido Boranes section. For the coordinate compounds, $E_T\left(atom-atom,msp^3.AO\right)$ is $-1.20896\ eV$, two times the energy of Eq. (23.149). For the $Co-C$ bonds of carbonyl compounds, $E_T\left(atom-atom,msp^3.AO\right)$ is $-1.13379\ eV$ (Eq. (14.247)), and the $C=O$ functional group of carbonyls is equivalent to that of vanadium carbonyls.

The symbols of the functional groups of cobalt coordinate compounds are given in Table 23.40. The geometrical (Eqs. (15.1-15.5) and (23.41)), intercept (Eqs. (15.31-15.32) and (15.80-15.87)), and energy (Eqs. (15.61) and (23.28-23.33)) parameters of cobalt coordinate compounds are given in Tables 23.41, 23.42, and 23.43, respectively. The total energy of each cobalt coordinate compound given in Table 23.44 was calculated as the sum over the integer multiple of each $E_D\left(Group\right)$ of Table 23.43 corresponding to functional-group composition of the compound. The charge-densities of exemplary cobalt carbonyl compound, cobalt tetracarbonyl hydride ($CoH\left(CO\right)_4$) comprising the concentric shells of atoms with the outer shell bridged by one or more H_2-type ellipsoidal MOs or joined with one or more hydrogen MOs is shown in Figure 23.9.

Figure 23.9. *Cobalt Tetracarbonyl Hydride.* Color scale, translucent view of the charge-density of $CoH(CO)_4$ showing the orbitals of the Co, C, and O atoms at their radii, the ellipsoidal surface of each H or H_2-type ellipsoidal MO that transitions to the corresponding outer shell of the atoms participating in each bond, and the nuclei (red, not to scale).

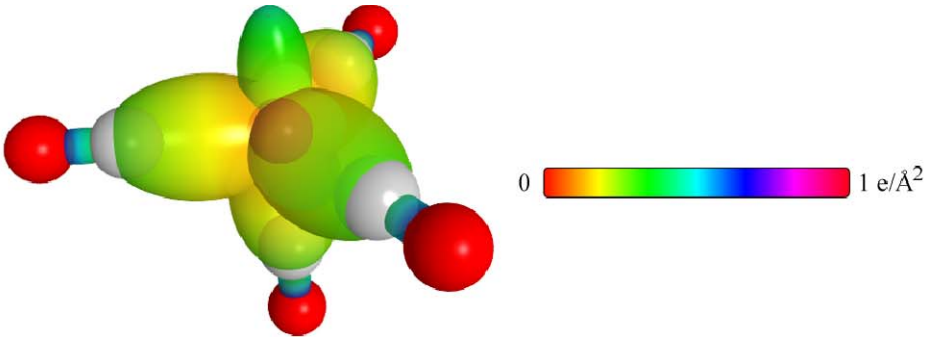

Table 23.40. The symbols of the functional groups of cobalt coordinate compounds.

Functional Group	Group Symbol
CoF_2 group of CoF_2	$Co-F$
$CoCl$ group of $CoCl$	$Co-Cl$ (a)
$CoCl_2$ group of $CoCl_2$	$Co-Cl$ (b)
$CoCl_3$ group of $CoCl_3$	$Co-Cl$ (c)
CoH group of $CoH(CO)_4$	$Co-H$
$CoCO$ group of $CoH(CO)_4$	$Co-CO$
$C=O$	$C=O$

Table 23.41. The geometrical bond parameters of cobalt coordinate compounds and experimental values.

Parameter	$Co-F$ Group	$Co-Cl$ (a) Group	$Co-Cl$ (b) Group	$Co-Cl$ (c) Group	$Co-H$ Group	$Co-CO$ Group	$C=O$ Group
n_e	2	3	3	3	1		
L	$7\sqrt{\frac{3}{4}}$	$4+3\sqrt{\frac{3}{4}}$	$2+4\sqrt{\frac{3}{4}}$	$6+2\sqrt{\frac{3}{4}}$	$5\sqrt{\frac{3}{4}}$		
$a\ (a_0)$	2.22453	2.74437	2.70237	2.78637	1.66038	2.25172	1.184842
$c'\ (a_0)$	1.72222	1.92437	1.90959	1.93904	1.43949	1.73271	1.08850
Bond Length $2c'\ (Å)$	1.82272	2.03667	2.02102	2.05219	1.52349	1.83382	1.15202
Exp. Bond Length $(Å)$	1.72 [54] (CoF_2)	2.09 [15] ($CoCl$)	2.09 [15] ($CoCl$)	2.09 [15] ($CoCl$)	1.542 [3] (CoH)	1.82 [55] ($Ni(CO)_4$)	1.145 [29] ($Fe(CO)_5$)
$b,c\ (a_0)$	1.40801	1.95662	1.91214	2.00100	0.82748	1.43804	0.46798
e	0.77420	0.70121	0.70663	0.69590	0.86697	0.76951	0.91869

Table 23.42. The MO to HO intercept geometrical bond parameters of cobalt coordinate compounds. E_T is E_T (*atom–atom,HO.AO*).

Bond	Atom	E_T (eV) Bond 1	E_T (eV) Bond 2	E_T (eV) Bond 3	E_T (eV) Bond 4	E_T (eV) Bond 5	Final Total Energy $Co3d4s$ (eV)	$r_{initial}$ (a_0)	r_{final} (a_0)	$E_{Coulomb}(Co3d4s)$ (eV) Final	$E(Co3d4s)$ (eV) Final	θ' (°)	θ_1 (°)	θ_2 (°)	d_1 (a_0)	d_2 (a_0)
$Co-F\ (CoF_2)$	Co	-0.60448	-0.60448	0	0	0		0.80129	0.74803	-18.18885		75.69	104.31	30.98	1.90713	0.18492
$Co-F\ (CoF_2)$	F	-0.60448	0	0	0	0		0.78069	0.75473	-18.02730		76.49	103.51	31.41	1.89848	0.17626
$Co-Cl\ (CoCl)$	Co	-0.60448	0	0	0	0		0.80129	0.77374	-17.58437						
$Co-Cl\ (CoCl)$	Cl	-0.60448	0	0	0	0		1.05158	1.00248	-13.57212		56.06	123.94	25.15	2.48414	0.55976
$Co-Cl\ (CoCl_2)$	Co	-0.60448	-0.60448	0	0	0		0.80129	0.74803	-18.18885						
$Co-Cl\ (CoCl_2)$	Cl	-0.60448	0	0	0	0		1.05158	1.00248	-13.57212		60.34	119.66	27.10	2.40562	0.49603
$Co-Cl\ (CoCl_3)$	Co	-0.60448	-0.60448	-0.60448	0	0		0.80129	0.72397	-18.79333						
$Co-Cl\ (CoCl_3)$	Cl	-0.60448	0	0	0	0		1.05158	1.00248	-13.57212		51.48	128.52	23.08	2.56342	0.62438
$CoC=O$	O	-1.79278	0	0	0	0		1.00000	0.81871	-16.61853		147.43	32.57	70.34	0.39853	0.68997
$CoC=O$	C	-1.79278	-0.56690	0	0	0	-153.97537	0.91771	0.79171	-17.18543	-16.99457	146.55	33.45	68.83	0.42793	0.66057
$Co-CO\ (CoH(CO)_4)$	C	-0.56690	-1.79278	0	0	0		0.91771	0.79171	-17.18543	-16.99457	78.00	102.00	32.58	1.89734	0.16463
$Co-CO\ (CoH(CO)_4)$	Co	-0.56690	-0.56690	-0.56690	-0.56690	0		0.80129	0.79597	-17.09334		78.47	101.53	32.84	1.89180	0.15908
$Co-H$	Co	0	-0.56690	-0.56690	-0.56690	-0.56690		0.80129	0.70689	-19.24748		118.72	61.28	48.52	1.09980	0.33969

Table 23.43. The energy parameters (eV) of functional groups of cobalt coordinate compounds.

Parameters	$Co-F$ Group	$Co-Cl$ (a) Group	$Co-Cl$ (b) Group	$Co-Cl$ (c) Group	$Co-H$ Group	$Co-CO$ Group	$C=O$ Group
f_1	1	1	1	1	1	1	1
n_1	1	1	1	1	1	1	2
n_2	0	0	0	0	0	0	0
n_3	0	0	0	0	0	0	0
C_1	0.375	0.5	0.5	0.5	0.5	0.375	0.5
C_2	1	0.74108	0.74108	0.74108	0.80129	1	1
c_1	1	1	1	1	0.75	1	1
c_2	0.99569	1	1	1	0.80129	0.79097	0.85395
c_3	0	0	0	0	0	0	2
c_4	1	1	1	1	1	2	4
c_5	1	1	1	1	1	0	0
C_{1o}	0.375	0.5	0.5	0.5	0.5	0.375	0.5
C_{2o}	1	0.74108	0.74108	0.74108	0.80129	1	1
$V_e\ (eV)$	-32.43083	-24.59516	-25.09218	-24.11830	-30.00832	-25.31882	-134.96850
$V_p\ (eV)$	7.90017	7.07026	7.12499	7.01677	9.45183	7.85231	24.99908
$T\ (eV)$	7.28938	4.48102	4.64262	4.32790	9.03661	5.62211	56.95634
$V_m\ (eV)$	-3.64469	-2.24051	-2.32131	-2.16395	-4.51831	-2.81105	-28.47817
$E_{(AO/HO)}\ (eV)$	-17.49830	-17.49830	-17.49830	-17.49830	-16.97989	-16.97989	0
$\Delta E_{H_2MO\,(AO/HO)}\ (eV)$	0	0	0	0	0	0	-18.22046
$E_{T\,(AO/HO)}\ (eV)$	-17.49830	-17.49830	-17.49830	-17.49830	-16.97989	-16.97989	18.22046
$E_{T\,(H_2MO)}\ (eV)$	-38.38427	-32.78269	-33.14419	-32.43588	-33.01808	-31.63534	-63.27080
$E_T\left(atom-atom, msp^3.AO\right)\ (eV)$	-1.20896	-1.20896	-1.20896	-1.20896	0	-1.13379	-3.58557
$E_{T\,(MO)}\ (eV)$	-39.59324	-33.99165	-34.35315	-33.64484	-33.01808	-32.76916	-66.85630
$\omega\ \left(10^{15}\ rad/s\right)$	15.1528	9.19478	5.66480	5.41058	12.2308	7.49254	22.6662
$E_K\ (eV)$	9.97387	6.05217	3.72867	3.56134	8.05053	4.93172	14.91930
$\bar{E}_D\ (eV)$	-0.24738	-0.16544	-0.13123	-0.12561	-0.18534	-0.14397	-0.25544
$\bar{E}_{Kvib}\ (eV)$	0.09448 [54]	0.05222 [56]	0.05222 [56]	0.05222 [56]	0.23887 [57]	0.07181 [58]	0.24962 [29]
$\bar{E}_{osc}\ (eV)$	-0.20014	-0.13933	-0.10512	-0.09950	-0.06590	-0.10806	-0.13063
$E_{mag}\ (eV)$	0.22238	0.22238	0.22238	0.22238	0.22238	0.14803	0.11441
$E_{T\,(Group)}\ (eV)$	-39.79337	-34.13098	-34.45827	-33.74434	-33.08398	-32.87722	-67.11757
$E_{initial\,(c_4\ AO/HO)}\ (eV)$	-17.49830	-17.49830	-17.49830	-17.49830	-16.97989	-14.63489	-14.63489
$E_{initial\,(c_5\ AO/HO)}\ (eV)$	-17.42282	-12.96764	-12.96764	-12.96764	-13.59844	0	0
$E_{D\,(Group)}\ (eV)$	4.87226	3.66504	3.99233	3.27840	2.50565	3.60744	8.34918

Table 23.44. The total bond energies of gaseous-state cobalt coordinate compounds calculated using the functional group composition and the energies of Table 23.43 compared to the gaseous-state experimental values.

Formula	Name	$Co-F$ Group	$Co-Cl$ (a) Group	$Co-Cl$ (b) Group	$Co-Cl$ (c) Group	$Co-H$ Group	$Co-CO$ Group	$C=O$ Group	Calculated Total Bond Energy (eV)	Experimental Total Bond Energy (eV)	Relative Error
CoF_2	Cobalt difluoride	1	0	0	0	0	0	0	9.45115	9.75552 [54]	0.03120
CoCl	Cobalt chloride	0	1	0	0	0	0	0	3.66504	3.68049 [15]	0.00420
CoI_2	Cobalt dichloride	0	0	2	0	0	0	0	7.98467	7.92106 [15]	-0.00803
$CoCl_3$	Cobalt trichloride	0	0	0	3	0	0	0	9.83521	9.87205 [15]	0.00373
$CoH(CO)_4$	Cobalt tetracarbonyl hydride	0	0	0	0	1	4	4	50.33217	50.36087 [53]	0.00057

NICKEL FUNCTIONAL GROUPS AND MOLECULES

The electron configuration of nickel is $[Ar]4s^2 3d^8$ having the corresponding term ${}^3F_4$. The total energy of the state is given by the sum over the ten electrons. The sum $E_T(Ni, 3d4s)$ of experimental energies [1] of Ni, Ni^+, Ni^{2+}, Ni^{3+}, Ni^{4+}, Ni^{5+}, Ni^{6+}, Ni^{7+}, Ni^{8+}, and Ni^{9+} is:

$$E_T(Ni, 3d4s) = -\begin{pmatrix} 224.6\ eV + 193\ eV + 162\ eV + 133\ eV + 108\ eV + 76.06\ eV \\ +54.9\ eV + 35.19\ eV + 18.16884\ eV + 7.6398\ eV \end{pmatrix} = -1012.55864\ eV \tag{23.155}$$

By considering that the central field decreases by an integer for each successive electron of the shell, the radius r_{3d4s} of the $Ni3d4s$ shell may be calculated from the Coulombic energy using Eq. (15.13).

$$r_{3d4s} = \sum_{n=18}^{27} \frac{(Z-n)e^2}{8\pi\varepsilon_0 (e1012.55864\ eV)} = \frac{55e^2}{8\pi\varepsilon_0 (e1012.55864\ eV)} = 0.73904a_0 \tag{23.156}$$

where $Z = 28$ for nickel. Using Eq. (15.14), the Coulombic energy $E_{Coulomb}(Ni, 3d4s)$ of the outer electron of the $Ni3d4s$ shell is:

$$E_{Coulomb}(Ni, 3d4s) = \frac{-e^2}{8\pi\varepsilon_0 r_{3d4s}} = \frac{-e^2}{8\pi\varepsilon_0 0.73904a_0} = -18.410157\ eV \tag{23.157}$$

During hybridization, the spin-paired $4s$ electrons and the three sets of paired $3d$ electrons are promoted to the $Ni3d4s$ shell as initially unpaired electrons. The energies for the promotions are given by Eq. (15.15) at the initial radii of the $4s$ and $3d$ electrons. From Eq. (10.102) with $Z = 28$ and $n = 28$, the radius r_{28} of the $Ni4s$ shell is

$$r_{28} = 1.78091a_0 \tag{23.158}$$

and with $Z = 28$ and $n = 26$, the radius r_{26} of the $Ni3d$ shell is:

$$r_{26} = 1.15992a_0 \tag{23.159}$$

Using Eqs. (15.15), (23.157), and (23.158), the unpairing energies are:

$$E_{4s}(magnetic) = \frac{2\pi\mu_0 e^2\hbar^2}{m_e^2 (r_{28})^3} = \frac{8\pi\mu_0\mu_B^2}{(1.78091a_0)^3} = 0.02026\ eV \tag{23.160}$$

$$E_{3d}(magnetic) = \frac{2\pi\mu_0 e^2\hbar^2}{m_e^2 (r_{26})^3} = \frac{8\pi\mu_0\mu_B^2}{(1.15992a_0)^3} = 0.07331\ eV \tag{23.161}$$

The electrons from the $4s$ and $3d$ shells successively fill unoccupied HOs until the HO shell is filled with unpaired electrons, then the electrons pair per HO. In the case of the $Ni3d4s$ shell having ten electrons and six orbitals, four sets of electrons are paired. Using Eqs. (15.15) and (23.155), the pairing energy is given by:

$$E_{3d4s}(magnetic) = -\frac{2\pi\mu_0 e^2\hbar^2}{m_e^2 (r_{3d4s})^3} = -\frac{8\pi\mu_0\mu_B^2}{(0.73904a_0)^3} = -0.28344\ eV \tag{23.162}$$

Thus, after Eq. (23.28), the energy $E(Ni, 3d4s)$ of the outer electron of the $Ni3d4s$ shell is given by adding the magnetic energies of unpairing the $4s$ (Eq. (23.159)) and $3d$ electrons (Eq. (23.160)) and pairing of four sets of $Ni3d4s$ electrons (Eq. (23.161)) to $E_{Coulomb}(Ni, 3d4s)$ (Eq. (23.156)).

$$\begin{aligned} E(Ni, 3d4s) &= \frac{-e^2}{8\pi\varepsilon_0 r_{3d4s}} + \frac{2\pi\mu_0 e^2\hbar^2}{m_e^2 r_{4s}^3} + \sum_{3d\ pairs} \frac{2\pi\mu_0 e^2\hbar^2}{m_e^2 r_{3d}^3} - \sum_{HO\ pairs} \frac{2\pi\mu_0 e^2\hbar^2}{m_e^2 r_{3d4s}^3} \\ &= -18.410157\ eV + 0.02026\ eV + 3(0.07331\ eV) - 4(0.28344\ eV) = -19.30374\ eV \end{aligned} \tag{23.163}$$

Next, consider the formation of the $Ni-L$-bond MO wherein each nickel atom has a $Ni3d4s$ electron with an energy given by Eq. (23.162). The total energy of the state of each nickel atom is given by the sum over the ten electrons. The sum $E_T(Ni_{Ni-L}3d4s)$ of energies of $Ni3d4s$ (Eq. (23.162)), Ni^+, Ni^{2+}, Ni^{3+}, Ni^{4+}, Ni^{5+}, Ni^{6+}, Ni^{7+}, Ni^{8+}, and Ni^{9+} is:

$$\begin{aligned} E_T(Ni_{Ni-L}3d4s) &= -\begin{pmatrix} 224.6\ eV + 193\ eV + 162\ eV + 133\ eV + 108\ eV + 76.06\ eV \\ +54.9\ eV + 35.19\ eV + 18.16884\ eV + E(Ni, 3d4s) \end{pmatrix} \\ &= -\begin{pmatrix} 224.6\ eV + 193\ eV + 162\ eV + 133\ eV + 108\ eV + 76.06\ eV \\ +54.9\ eV + 35.19\ eV + 18.16884\ eV + 19.30374\ eV \end{pmatrix} = -1024.22258\ eV \end{aligned} \tag{23.164}$$

where $E(Ni, 3d4s)$ is the sum of the energy of Ni, $-7.6398\ eV$, and the hybridization energy.

The nickel HO donates an electron to each MO. Using Eq. (23.30), the radius r_{3d4s} of the $Ni3d4s$ shell calculated from the Coulombic energy is:

$$r_{Ni-L3d4s}=\left(\sum_{n=18}^{27}(Z-n)-1\right)\frac{e^2}{8\pi\varepsilon_0\left(e1024.22258\ eV\right)}=\frac{54e^2}{8\pi\varepsilon_0\left(e1024.22258\ eV\right)}=0.71734a_0 \tag{23.165}$$

Using Eqs. (15.19) and (23.164), the Coulombic energy $E_{Coulomb}\left(Ni_{Ni-L},3d4s\right)$ of the outer electron of the $Ni3d4s$ shell is

$$E_{Coulomb}\left(Ni_{Ni-L},3d4s\right)=\frac{-e^2}{8\pi\varepsilon_0 r_{Ni-L3d4s}}=\frac{-e^2}{8\pi\varepsilon_0 0.71734a_0}=-18.96708\ eV \tag{23.166}$$

The magnetic energy terms are those for the unpairing of the $4s$ and $3d$ electrons (Eqs. (23.159) and (23.160), respectively) and paring four sets of $Ni3d4s$ electrons (Eq. (23.161)). Using Eqs. (23.32), (23.165) and (23.159-23.161), the energy $E\left(Ni_{Ni-L},3d4s\right)$ of the outer electron of the $Ni3d4s$ shell is:

$$\begin{aligned}E\left(Ni_{Ni-L},3d4s\right)&=\frac{-e^2}{8\pi\varepsilon_0 r_{Ni-L3d4s}}+\frac{2\pi\mu_0 e^2\hbar^2}{m_e^2\left(r_{28}\right)^3}+3\frac{2\pi\mu_0 e^2\hbar^2}{m_e^2\left(r_{26}\right)^3}-4\frac{2\pi\mu_0 e^2\hbar^2}{m_e^2\left(r_{3d4s}\right)^3}\\&=-18.96708\ eV+0.02026\ eV+3\left(0.07331\ eV\right)-4\left(0.28344\ eV\right)=-19.86066\ eV\end{aligned} \tag{23.167}$$

Thus, $E_T\left(Ni-L,3d4s\right)$, the energy change of each $Ni3d4s$ shell with the formation of the $Ni-L$-bond MO is given by the difference between Eq. (23.166) and Eq. (23.162):

$$E_T\left(Ni-L,3d4s\right)=E\left(Ni_{Ni-L},3d4s\right)-E\left(Ni,3d4s\right)=-19.86066\ eV-\left(-19.30374\ eV\right)=-0.55693\ eV \tag{23.168}$$

The semimajor axis a solution given by Eq. (23.41) of the force balance equation, Eq. (23.39), for the σ-MO of the $Ni-L$-bond MO of NiL_n is given in Table 23.46 with the force-equation parameters $Z=28$, n_e, and L corresponding to the orbital and spin angular momentum terms of the $3d4s$ HO shell. The semimajor axis a of carbonyl and organometallic compounds are solved using Eq. (15.51).

For the $Ni-L$ functional groups, hybridization of the $4s$ and $3d$ AOs of Ni to form a single $3d4s$ shell forms an energy minimum, and the sharing of electrons between the $Ni3d4s$ HO and L AO to form a MO permits each participating orbital to decrease in radius and energy. The Cl AO has an energy of $E\left(Cl\right)=-12.96764\ eV$, the $C_{aryl}2sp^3$ HO has an energy of $E\left(C_{aryl},2sp^3\right)=-15.76868\ eV$ (Eq. (14.246)), the $C2sp^3$ HO has an energy of $E\left(C,2sp^3\right)=-14.63489\ eV$ (Eq. (15.25)), the Coulomb energy of $Ni3d4s$ HO is $E_{Coulomb}\left(Ni,3d4s\right)=-18.41016\ eV$ (Eq. (23.156)), and the $Ni3d4s$ HO has an energy of $E\left(Ni,3d4s\right)=-19.30374\ eV$ (Eq. (23.162)). To meet the equipotential condition of the union of the $Ni-L$ H_2-type-ellipsoidal-MO with these orbitals, the hybridization factor(s), at least one of c_2 and C_2 of Eq. (15.61) for the $Ni-L$-bond MO given by Eq. (15.77) is:

$$C_2\left(ClAO\ to\ Ni3d4sHO\right)=\frac{E\left(ClAO\right)}{E\left(Ni,3d4s\right)}=\frac{-12.96764\ eV}{-19.30374\ eV}=0.67177 \tag{23.169}$$

$$c_2\left(C2sp^3HO\ to\ Ni3d4sHO\right)=\frac{E\left(C,2sp^3\right)}{E_{Coulomb}\left(Ni,3d4s\right)}c_2\left(C2sp^3HO\right)=\frac{-14.63489\ eV}{-18.41016\ eV}\left(0.91771\right)=0.72952 \tag{23.170}$$

$$C_2\left(C_{aryl}2sp^3HO\ to\ Ni3d4sHO\right)=\frac{E\left(C,2sp^3\right)}{E_{Coulomb}\left(Ni,3d4s\right)}c_2\left(C_{aryl}2sp^3HO\right)=\frac{-14.63489\ eV}{-18.41016\ eV}\left(0.85252\right)=0.67770 \tag{23.171}$$

where Eqs. (15.76), (15.79), and (13.430) were used in Eq. (23.169) and Eqs. (15.76), (15.79), and (14.417) were used in Eq. (23.170). Since the energy of the MO is matched to that of the $Ni3d4s$ HO in coordinate compounds, $E\left(AO/HO\right)$ in Eq. (15.61) is $E\left(Ni,3d4s\right)$ given by Eq. (23.162) and $E\left(AO/HO\right)$ in Eq. (15.61) of carbonyl compounds and organometallics is $E_{Coulomb}\left(Ni,3d4s\right)$ given by Eq. (23.156). $E_T\left(atom-atom,msp^3.AO\right)$ of the $Ni-L$-bond MO is determined by considering that the bond involves an electron transfer from the nickel atom to the ligand atom to form partial ionic character in the bond as in the case of the zwitterions such as $H_2B^+-F^-$ given in the Halido Boranes section. For the coordinate compounds, $E_T\left(atom-atom,msp^3.AO\right)$ is $-1.11386\ eV$, two times the energy of Eq. (23.167). For the $Ni-C$ bonds of carbonyl compound, $Ni\left(CO\right)_4$ and organometallic, nickelocene, $E_T\left(atom-atom,msp^3.AO\right)$ is $-1.85837\ eV$ (two times Eq. (14.513)) and $-0.92918\ eV$ (Eq. (14.513)), respectively. The $C=O$ functional group of $Ni\left(CO\right)_4$ is equivalent to that of vanadium carbonyls. The aromatic cyclopentadienyl moieties of organometallic $Ni\left(C_5H_5\right)_2$ comprise $C\overset{3e}{=}C$ and CH functional groups that are equivalent to those given in the Aromatic and Heterocyclic Compounds section.

The symbols of the functional groups of nickel coordinate compounds are given in Table 23.45. The geometrical (Eqs. (15.1-15.5) and (23.41)), intercept (Eqs. (15.31-15.32) and (15.80-15.87)), and energy (Eqs. (15.61) and (23.28-23.33)) parameters of nickel coordinate compounds are given in Tables 23.46, 23.47, and 23.48, respectively. The total energy of each nickel coordinate compound given in Table 23.49 was calculated as the sum over the integer multiple of each $E_D\left(Group\right)$ of Table

23.48 corresponding to functional-group composition of the compound. The charge-densities of exemplary nickel carbonyl and organometallic compounds, nickel tetracarbonyl ($Ni(CO)_4$) and bis-cylopentadienyl nickel or nickelocene ($Ni(C_5H_5)_2$) comprising the concentric shells of atoms with the outer shell bridged by one or more H_2-type ellipsoidal MOs or joined with one or more hydrogen MOs are shown in Figure 23.10A and B, respectively.

Figure 23.10. (A) *Nickel Tetracarbonyl.* Color scale, translucent view of the charge-density of $Ni(CO)_4$ showing the orbitals of the Ni, C, and O atoms at their radii, the ellipsoidal surface of each H_2-type ellipsoidal MO that transitions to the corresponding outer shell of the atoms participating in each bond, and the nuclei (red, not to scale). (B) *Nickelocene.* Color scale, opaque view of the charge-density of $Ni(C_5H_5)_2$ showing the orbitals of the Ni and C atoms at their radii and the ellipsoidal surface of each H or H_2-type ellipsoidal MO that transitions to the corresponding outer shell of the atoms participating in each bond.

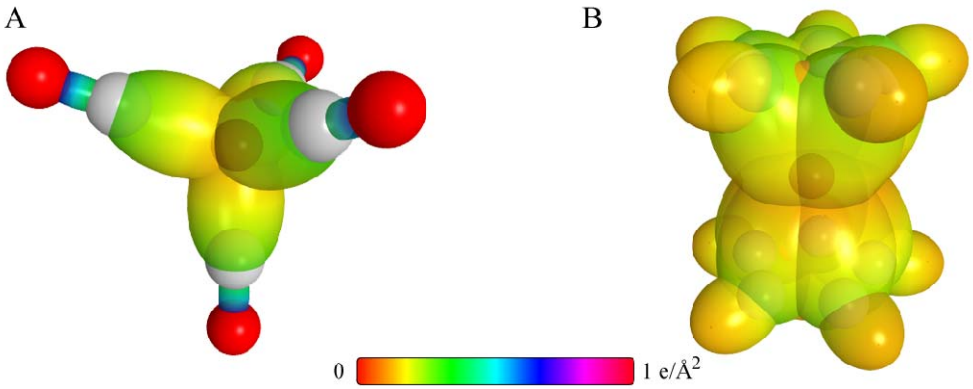

Table 23.45. The symbols of the functional groups of nickel coordinate compounds.

Functional Group	Group Symbol
$NiCl$ group of $NiCl$	$Ni-Cl$ (a)
$NiCl_2$ group of $NiCl_2$	$Ni-Cl$ (b)
$NiCO$ group of $Ni(CO)_4$	$Ni-CO$
$C=O$	$C=O$
NiC_{aryl} group of $Ni(C_5H_5)_2$	$Ni-C_5H_5$
CC (aromatic bond)	$C\overset{3e}{=}C$
CH (aromatic)	CH

Table 23.46. The geometrical bond parameters of nickel coordinate compounds and experimental values.

Parameter	$Ni-Cl$ (a) Group	$Ni-Cl$ (b) Group	$Ni-CO$ Group	$C=O$ Group	$Ni-C_5H_5$ Group	$C\overset{3e}{=}C$ Group	CH Group
n_e	3	3					
L	$5+5\sqrt{\frac{3}{4}}$	$4+6\sqrt{\frac{3}{4}}$					
$a\ (a_0)$	2.83322	2.82843	2.22132	1.184842	3.00077	1.47348	1.60061
$c'\ (a_0)$	2.05367	2.05193	1.72098	1.08850	2.10426	1.31468	1.03299
Bond Length $2c'\ (Å)$	2.17351	2.17167	1.82140	1.15202	2.22705	1.39140	1.09327
Exp. Bond Length $(Å)$	2.137 [15, 59] ($NiCl$) 2.09 [15, 59] ($NiCl_2$)	2.137 [15, 59] ($NiCl$) 2.09 [15, 59] ($NiCl_2$)	1.82 [55] ($Ni(CO)_4$)	1.15 [55] ($Ni(CO)_4$)	2.185 [60] ($Ni(C_5H_5)_2$)	1.399 [3] (benzene)	1.101 [3] (benzene)
$b,c\ (a_0)$	1.95181	1.94669	1.40446	0.46798	2.13933	0.66540	1.22265
e	0.72485	0.72547	0.77475	0.91869	0.70124	0.89223	0.64537

Table 23.47. The MO to HO intercept geometrical bond parameters of nickel coordinate compounds. E_T is E_T (*atom–atom,HO.AO*).

Bond	Atom	E_T (eV) Bond 1	E_T (eV) Bond 2	E_T (eV) Bond 3	E_T (eV) Bond 4	E_T (eV) Bond 5	Final Total Energy $Ni3d4s$ (eV)	$r_{initial}$ (a_0)	r_{final} (a_0)	$E_{Coulomb}(Ni3d4s)$ (eV) Final	$E(Ni3d4s)$ (eV) Final	θ' (°)	θ_1 (°)	θ_2 (°)	d_1 (a_0)	d_2 (a_0)
$Ni-Cl\ (NiCl)$	Ni	-0.55693	0	0	0	0		0.73904	0.71734	-18.96708						
$Ni-Cl\ (NiCl)$	Cl	-0.55693	0	0	0	0		1.05158	1.00601	-13.52457		62.33	117.67	27.16	2.52080	0.46713
$Ni-Cl\ (NiCl_2)$	Ni	-0.55693	-0.55693	0	0	0		0.73904	0.69688	-19.52401						
$Ni-Cl\ (NiCl_2)$	Cl	-0.55693	0	0	0	0		1.05158	1.00601	-13.52457		62.78	117.22	27.36	2.51208	0.46014
$NiC=O$	O	-1.79278	0	0	0	0		1.00000	0.81871	-16.61853		147.13	32.57	70.34	0.39853	0.68997
$NiC=O$	C	-1.79278	-0.92918	0	0	0	-154.33766	0.91771	0.77536	-17.54772	-17.35685	146.00	34.00	67.90	0.44572	0.64278
$Ni-CO\ (Ni(CO)_4)$	C	-0.92918	-1.79278	0	0	0		0.91771	0.77536	-17.54772	-17.35685	79.19	100.81	32.84	1.86635	0.14537
$Ni-CO\ (Ni(CO)_4)$	Ni	-0.92918	-0.92918	-0.92918	-0.92918	0		0.73904	0.73376	-18.54249		74.26	105.74	30.19	1.92004	0.19906
$C-H\ (CH)$	C	-0.85035	-0.85035	-0.56690	-0.09292	0	-153.97619	0.91771	0.79167	-17.18625	-16.99539	73.83	106.17	38.45	1.25345	0.22045
$C\overset{3e}{=}HC_a\overset{3e}{=}C$	C_a	-0.85035	-0.85035	-0.56690	-0.09292	0		0.91771	0.79167	-17.18625	-16.99539	134.06	45.94	58.76	0.76417	0.55051
$Ni-C_3H_5$	Ni	-0.46459	-0.46459	0	0	0		0.73904	0.86359	-15.75493						
$Ni-C_3H_5$	C	-0.09292	-0.85035	-0.85035	-0.56690	0		0.91771	0.79167	-17.18626	-16.99540					

Table 23.48. The energy parameters (eV) of functional groups of nickel coordinate compounds.

Parameters	$Ni-Cl$ (a) Group	$Ni-Cl$ (b) Group	$Ni-CO$ Group	$C=O$ Group	$Ni-C_5H_5$ Group	$^{3e}C=C$ Group	CH Group
f_1	1	1	1	1	1	0.75	1
n_1	1	1	1	2	1	2	1
n_2	0	0	0	0	0	0	0
n_3	0	0	0	0	0	0	0
C_1	0.5	0.5	0.375	0.5	0.5	0.5	0.75
C_2	0.67177	0.67177	1	1	0.67770	0.85252	1
c_1	1	1	1	1	1	1	1
c_2	1	1	0.72952	0.85395	1	0.85252	0.91771
c_3	0	0	0	2	0	0	1
c_4	1	1	2	4	2	3	1
c_5	1	1	0	0	0	0	1
C_{1o}	0.5	0.5	0.375	0.5	0.5	0.5	0.75
C_{2o}	0.67177	0.67177	1	1	0.67770	0.85252	1
$V_e\ (eV)$	-24.32206	-24.37691	-23.81088	-134.96850	-22.49426	-101.12679	-37.10024
$V_p\ (eV)$	6.62512	6.63072	7.90586	24.99908	6.46585	20.69825	13.17125
$T\ (eV)$	4.29230	4.30926	5.35963	56.95634	3.74808	34.31559	11.58941
$V_m\ (eV)$	-2.14615	-2.15463	-2.67981	-28.47817	-1.87404	-17.15779	-5.79470
$E_{(AO/HO)}\ (eV)$	-19.30374	-19.30374	-18.41016	0	-18.41016	0	-14.63489
$\Delta E_{H_2MO\,(AO/HO)}\ (eV)$	0	0	0	-18.22046	-0.92918	0	-1.13379
$E_{T\,(AO/HO)}\ (eV)$	-19.30374	-19.30374	-18.41016	18.22046	-17.48097	0	-13.50110
$E_{T\,(H_2MO)}\ (eV)$	-34.85452	-34.89529	-31.63537	-63.27080	-31.63535	-63.27075	-31.63539
$E_T\left(atom-atom, msp^3.AO\right)\ (eV)$	-1.11386	-1.11386	-1.85837	-3.58557	-0.92918	-2.26759	-0.56690
$E_{T\,(MO)}\ (eV)$	-35.96838	-36.00914	-33.49374	-66.85630	-32.56455	-65.53833	-32.20226
$\omega\ \left(10^{15}\ rad/s\right)$	8.78663	8.82133	7.64687	22.6662	7.69080	49.7272	26.4826
$E_K\ (eV)$	5.78351	5.80635	5.03330	14.91930	5.06222	32.73133	17.43132
$\bar{E}_D\ (eV)$	-0.17113	-0.17166	-0.14866	-0.25544	-0.14495	-0.35806	-0.26130
$\bar{E}_{Kvib}\ (eV)$	0.05257 [59]	0.05257 [59]	0.04711 [55]	0.24962 [29]	0.04711 [55]	0.19649 [30]	0.35532 Eq. (13.458)
$\bar{E}_{osc}\ (eV)$	-0.14484	-0.14537	-0.12510	-0.13063	-0.12139	-0.25982	-0.08364
$E_{mag}\ (eV)$	0.28344	0.28344	0.14803	0.11441	0.14803	0.14803	0.14803
$E_{T\,(Group)}\ (eV)$	-36.11322	-36.15452	-33.61884	-67.11757	-32.68594	-49.54347	-32.28590
$E_{initial\,(c_4\ AO/HO)}\ (eV)$	-19.30374	-19.30374	-14.63489	-14.63489	-14.63489	-14.63489	-14.63489
$E_{initial\,(c_5\ AO/HO)}\ (eV)$	-12.96764	-12.96764	0	0	0	0	-13.59844
$E_{D\,(Group)}\ (eV)$	3.84184	3.88314	4.34906	8.34918	1.14858	5.63881	3.90454

Table 23.49. The total bond energies of gaseous-state nickel coordinate compounds calculated using the functional group composition and the energies of Table 23.48 compared to the gaseous-state experimental values.

Formula	Name	$Ni-Cl$ (a) Group	$Ni-Cl$ (b) Group	$Ni-CO$ Group	$C=O$ Group	$Ni-C_5H_5$ Group	$C=C$ Group	CH Group	Calculated Total Bond Energy (eV)	Experimental Total Bond Energy (eV)	Relative Error
NiCl	Nickel chloride	1	0	0	0	0	0	0	3.84184	3.82934 [59]	-0.00327
$NiCl_2$	Nickel dichloride	0	2	0	0	0	0	0	7.76628	7.74066 [59]	-0.00331
$Ni(CO)_4$	Nickel tetracarbonyl	0	0	4	0	0	0	0	50.79297	50.77632 [55]	-0.00033
$Ni(C_5H_5)_2$	Bis-cylopentadienyl nickel (nickelocene)	0	0	0	0	2	10	10	97.73062	97.84649 [53]	0.00118

COPPER FUNCTIONAL GROUPS AND MOLECULES

The electron configuration of copper is $[Ar]4s^1 3d^{10}$ having the corresponding term ${}^2S_{1/2}$. The single outer $4s$ [61] electron having an energy of $-7.72638\ eV$ [1] forms a single bond to give an electron configuration with filled $3d$ and $4s$ shells. Additional bonding of copper is possible involving a double bond or two single bonds by the hybridization of the $3d$ and $4s$ shells to form a $Cu3d4s$ shell and the donation of an electron per bond. The total energy of the copper ${}^2S_{1/2}$ state is given by the sum over the eleven electrons. The sum $E_T(Cu,3d4s)$ of experimental energies [1] of Cu, Cu^+, Cu^{2+}, Cu^{3+}, Cu^{4+}, Cu^{5+}, Cu^{6+}, Cu^{7+}, Cu^{8+}, Cu^{9+}, and Cu^{10+} is

$$E_T(Cu,3d4s) = -\begin{pmatrix} 265.3\ eV + 232\ eV + 199\ eV + 166\ eV + 139\ eV + 103\ eV + 79.8\ eV \\ +57.38\ eV + 36.841\ eV + 20.2924\ eV + 7.72638\ eV \end{pmatrix} = -1306.33978\ eV \tag{23.172}$$

By considering that the central field decreases by an integer for each successive electron of the shell, the radius r_{3d4s} of the $Cu3d4s$ shell may be calculated from the Coulombic energy using Eq. (15.13).

$$r_{3d4s} = \sum_{n=18}^{28} \frac{(Z-n)e^2}{8\pi\varepsilon_0 (e1306.33978\ eV)} = \frac{66e^2}{8\pi\varepsilon_0 (e1306.33978\ eV)} = 0.68740a_0 \tag{23.173}$$

where $Z = 29$ for copper. Using Eq. (15.14), the Coulombic energy $E_{Coulomb}(Cu,3d4s)$ of the outer electron of the $Cu3d4s$ shell is:

$$E_{Coulomb}(Cu,3d4s) = \frac{-e^2}{8\pi\varepsilon_0 r_{3d4s}} = \frac{-e^2}{8\pi\varepsilon_0 0.68740a_0} = -19.793027\ eV \tag{23.174}$$

During hybridization, the unpaired $4s$ electron and five sets of spin-paired $3d$ electrons are promoted to the $Cu3d4s$ shell as initially unpaired electrons. The energies for the promotions of the initially paired electrons are given by Eq. (15.15) at the initial radius of the $3d$ electrons. From Eq. (10.102) with $Z = 29$ and $n = 28$, the radius r_{28} of the $Cu3d$ shell is:

$$r_{28} = 1.34098a_0 \tag{23.175}$$

Using Eqs. (15.15), and (23.174), the unpairing energy is:

$$E_{3d}(magnetic) = \frac{2\pi\mu_0 e^2\hbar^2}{m_e^2 (r_{28})^3} = \frac{8\pi\mu_0\mu_B^2}{(1.34098a_0)^3} = 0.04745\ eV \tag{23.176}$$

The electrons from the $4s$ and $3d$ shells successively fill unoccupied HOs until the HO shell is filled with unpaired electrons, then the electrons pair per HO. In the case of the $Cu3d4s$ shell having eleven electrons and six orbitals, five sets of electrons are paired. Using Eqs. (15.15) and (23.172), the pairing energy is given by:

$$E_{3d4s}(magnetic) = -\frac{2\pi\mu_0 e^2\hbar^2}{m_e^2 (r_{3d4s})^3} = -\frac{8\pi\mu_0\mu_B^2}{(0.68740a_0)^3} = -0.35223\ eV \tag{23.177}$$

Thus, after Eq. (23.28), the energy $E(Cu,3d4s)$ of the outer electron of the $Cu3d4s$ shell is given by adding the magnetic energies of unpairing five sets of $3d$ electrons (Eq. (23.175)) and pairing of five sets of $Cu3d4s$ electrons (Eq. (23.176)) to $E_{Coulomb}(Cu,3d4s)$ (Eq. (23.173)).

$$\begin{aligned} E(Cu,3d4s) &= \frac{-e^2}{8\pi\varepsilon_0 r_{3d4s}} + \frac{2\pi\mu_0 e^2\hbar^2}{m_e^2 r_{4s}^3} + \sum_{3d\ pairs} \frac{2\pi\mu_0 e^2\hbar^2}{m_e^2 r_{3d}^3} - \sum_{HO\ pairs} \frac{2\pi\mu_0 e^2\hbar^2}{m_e^2 r_{3d4s}^3} \\ &= -19.793027\ eV + 0\ eV + 5(0.04745\ eV) - 5(0.35223\ eV) = -21.31697\ eV \end{aligned} \tag{23.178}$$

Next, consider the formation of the $Cu-L$-bond MO wherein each copper atom has a $Cu3d4s$ electron with an energy given by Eq. (23.178). The total energy of the state of each copper atom is given by the sum over the eleven electrons. The sum $E_T(Cu_{Cu-L}3d4s)$ of energies of $Cu3d4s$ (Eq. (23.178)), Cu^+, Cu^{2+}, Cu^{3+}, Cu^{4+}, Cu^{5+}, Cu^{6+}, Cu^{7+}, Cu^{8+}, Cu^{9+}, and Cu^{10+} is:

$$\begin{aligned} E_T(Cu_{Cu-L}3d4s) &= -\begin{pmatrix} 265.3\ eV + 232\ eV + 199\ eV + 166\ eV \\ +139\ eV + 103\ eV + 79.8\ eV + 57.38\ eV \\ +36.841\ eV + 20.2924\ eV + E(Cu,3d4s) \end{pmatrix} \\ &= -\begin{pmatrix} 265.3\ eV + 232\ eV + 199\ eV + 166\ eV \\ +139\ eV + 103\ eV + 79.8\ eV + 57.38\ eV \\ +36.841\ eV + 20.2924\ eV + 21.31697\ eV \end{pmatrix} = -1319.93037\ eV \end{aligned} \tag{23.179}$$

where $E(Cu,3d4s)$ is the sum of the energy of Cu, $-7.72638\ eV$, and the hybridization energy.

The copper HO donates an electron to each MO. Using Eq. (23.30), the radius r_{3d4s} of the $Cu3d4s$ shell calculated from the Coulombic energy is:

$$r_{Cu-L3d4s}=\left(\sum_{n=18}^{28}(Z-n)-1\right)\frac{e^2}{8\pi\varepsilon_0\left(e1319.93037\ eV\right)}=\frac{65e^2}{8\pi\varepsilon_0\left(e1319.93037\ eV\right)}=0.67002a_0 \tag{23.180}$$

Using Eqs. (15.19) and (23.179), the Coulombic energy $E_{Coulomb}\left(Cu_{Cu-L},3d4s\right)$ of the outer electron of the $Cu3d4s$ shell is:

$$E_{Coulomb}\left(Cu_{Cu-L},3d4s\right)=\frac{-e^2}{8\pi\varepsilon_0 r_{Cu-L3d4s}}=\frac{-e^2}{8\pi\varepsilon_0 0.67002a_0}=-20.30662\ eV \tag{23.181}$$

The magnetic energy terms are those for the unpairing of the five sets of $3d$ electrons (Eq. (23.175)) and pairing of five sets of $Cu3d4s$ electrons (Eq. (23.176)). Using Eqs. (23.32), (23.180), and (23.175-23.176), the energy $E\left(Cu_{Cu-L},3d4s\right)$ of the outer electron of the $Cu3d4s$ shell is:

$$\begin{aligned}E\left(Cu_{Cu-L},3d4s\right)&=\frac{-e^2}{8\pi\varepsilon_0 r_{Cu-L3d4s}}+0\frac{2\pi\mu_0 e^2\hbar^2}{m_e^2\left(r_{29}\right)^3}+5\frac{2\pi\mu_0 e^2\hbar^2}{m_e^2\left(r_{28}\right)^3}-5\frac{2\pi\mu_0 e^2\hbar^2}{m_e^2\left(r_{3d4s}\right)^3}\\&=-20.30662\ eV+0\ eV+5\left(0.04745\ eV\right)-5\left(0.35223\ eV\right)=-21.83056\ eV\end{aligned} \tag{23.182}$$

Thus, $E_T\left(Cu-L,3d4s\right)$, the energy change of each $Cu3d4s$ shell with the formation of the $Cu-L$-bond MO is given by the difference between Eq. (23.181) and Eq. (23.177).

$$E_T\left(Cu-L,3d4s\right)=E\left(Cu_{Cu-L},3d4s\right)-E\left(Cu,3d4s\right)=-21.83056\ eV-\left(-21.31697\ eV\right)=-0.51359\ eV \tag{23.183}$$

The semimajor axis a solution given by Eq. (23.41) of the force balance equation, Eq. (23.39), for the σ-MO of the $Cu-L$-bond MO of CuL_n is given in Table 23.51 with the force-equation parameters $Z=29$, n_e, and L corresponding to the orbital and spin angular momentum terms of the $3d4s$ HO shell.

For the $Cu-L$ functional groups, hybridization of the $4s$ and $3d$ AOs of Cu to form a single $3d4s$ shell forms an energy minimum, and the sharing of electrons between the $Cu3d4s$ HO and L AO to form a MO permits each participating orbital to decrease in radius and energy. The F AO has an energy of $E\left(F\right)=-17.42282\ eV$, the Cl AO has an energy of $E\left(Cl\right)=-12.96764\ eV$, the O AO has an energy of $E\left(O\right)=-13.61805\ eV$, the Cu AO has an energy of $E\left(Cu\right)=-7.72638\ eV$, and the $Cu3d4s$ HO has an energy of $E\left(Cu,3d4s\right)=-21.31697\ eV$ (Eq. (23.177)). To meet the equipotential condition of the union of the $Cu-L$ H_2-type-ellipsoidal-MO with these orbitals, the hybridization factor(s), at least one of c_2 and C_2 of Eq. (15.61) for the $Cu-L$-bond MO given by Eq. (15.77) is:

$$C_2\left(FAO\ to\ CuAO\right)=\frac{E\left(CuAO\right)}{E\left(FAO\right)}=\frac{-7.72638\ eV}{-17.42282\ eV}=0.44346 \tag{23.184}$$

$$c_2\left(ClAO\ to\ CuAO\right)=C_2\left(ClAO\ to\ CuAO\right)=\frac{E\left(CuAO\right)}{E\left(ClAO\right)}=\frac{-7.72638\ eV}{-12.96764\ eV}=0.59582 \tag{23.185}$$

$$C_2\left(FAO\ to\ Cu3d4sHO\right)=\frac{E\left(FAO\right)}{E\left(Cu,3d4s\right)}=\frac{-17.42282\ eV}{-21.31697\ eV}=0.81732 \tag{23.186}$$

$$c_2\left(O\ to\ Cu3d4sHO\right)=\frac{E\left(O\right)}{E\left(Cu,3d4s\right)}=\frac{-13.61805\ eV}{-21.31697\ eV}=0.63884 \tag{23.187}$$

Since the energy of the MO is matched to that of the $Cu3d4s$ HO in coordinate compounds, $E\left(AO/HO\right)$ in Eq. (15.61) is $E\left(Cu,3d4s\right)$ given by Eq. (23.177) and twice this value for double bonds. $E_T\left(atom-atom,msp^3.AO\right)$ of the $Cu-L$-bond MO is determined by considering that the bond involves an electron transfer from the copper atom to the ligand atom to form partial ionic character in the bond as in the case of the zwitterions such as $H_2B^+-F^-$ given in the Halido Boranes section. For the two-bond coordinate compounds, $E_T\left(atom-atom,msp^3.AO\right)$ is $-1.02719\ eV$, two times the energy of Eq. (23.182).

The symbols of the functional groups of copper coordinate compounds are given in Table 23.50. The geometrical (Eqs. (15.1-15.5) and (23.41)), intercept (Eqs. (15.31-15.32) and (15.80-15.87)), and energy (Eqs. (15.61) and (23.28-23.33)) parameters of copper coordinate compounds are given in Tables 23.51, 23.52, and 23.53, respectively. The total energy of each copper coordinate compound given in Table 23.54 was calculated as the sum over the integer multiple of each $E_D\left(Group\right)$ of Table 23.53 corresponding to functional-group composition of the compound. The charge-densities of exemplary copper coordinate compounds, copper chloride ($CuCl$) and copper dichloride ($CuCl_2$) comprising the concentric shells of atoms with the outer shell bridged by one or more H_2-type ellipsoidal MOs or joined with one or more hydrogen MOs are shown in Figures 23.11A and B, respectively.

Figure 23.11. (A) *Copper Chloride.* Color scale, translucent view of the charge-density of $CuCl$ showing the orbitals of the Cu and Cl atoms at their radii, the ellipsoidal surface of each H_2-type ellipsoidal MO that transitions to the corresponding outer shell of the atoms participating in each bond, and the nuclei (red, not to scale). (B) *Copper Dichloride.* Color scale, translucent view of the charge-density of $CuCl_2$ showing the orbitals of the Cu and Cl atoms at their radii, the ellipsoidal surface of each H_2-type ellipsoidal MO that transitions to the corresponding outer shell of the atoms participating in each bond, and the nuclei (red, not to scale).

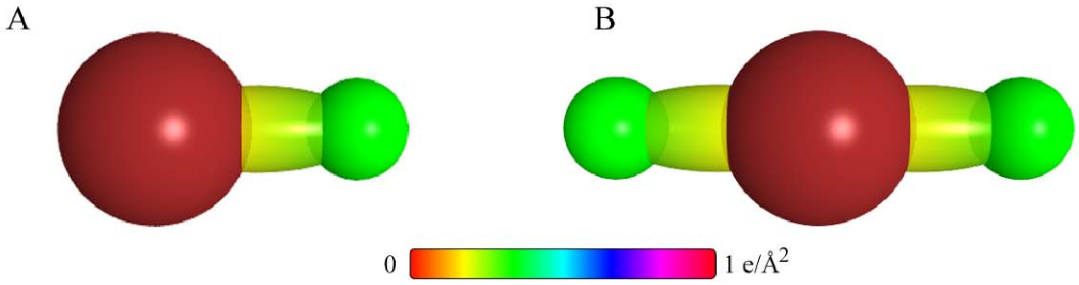

Table 23.50. The symbols of the functional groups of copper coordinate compounds.

Functional Group	Group Symbol
CuF group of *CuF*	$Cu-F$ (a)
CuF2 group of CuF_2	$Cu-F$ (b)
CuCl group of *CuCl*	$Cu-Cl$
CuO group of *CuO*	$Cu-O$

Table 23.51. The geometrical bond parameters of copper coordinate compounds and experimental values.

Parameter	$Cu-F$ (a) Group	$Cu-F$ (b) Group	$Cu-Cl$ Group	$Cu-O$ Group
n_e	1	2	2	1
L	$10+2\sqrt{\frac{3}{4}}$	$2+4\sqrt{\frac{3}{4}}$	0	$3+10\sqrt{\frac{3}{4}}$
$a\ (a_0)$	1.90455	2.18842	2.00000	1.90208
$c'\ (a_0)$	1.69208	1.63632	1.83213	1.59251
Bond Length $2c'\ (Å)$	1.79083	1.73181	1.93905	1.68544
Exp. Bond Length $(Å)$	1.7449 [3] (*CuF*)	1.7449 [3] (*CuF*)	2.051 [15] (*CuCl*)	1.724 [15] (*CuO*)
$b,c\ (a_0)$	0.87417	1.45314	0.80205	1.04009
e	0.88844	0.74772	0.91607	0.83725

Table 23.52. The MO to HO intercept geometrical bond parameters of copper coordinate compounds. E_T is E_T (*atom–atom,HO.AO*).

Bond	Atom	E_T (eV) Bond 1	E_T (eV) Bond 2	E_T (eV) Bond 3	E_T (eV) Bond 4	Final Total Energy *Cu3d4s* (eV)	$r_{initial}$ (a_0)	r_{final} (a_0)	$E_{Coulomb}(Cu3d4s)$ (eV) Final	$E(Cu3d4s)$ (eV) Final	θ' (°)	θ_1 (°)	θ_2 (°)	d_1 (a_0)	d_2 (a_0)
$Cu-F$ (CuF)	Cu	0	0	0	0		1.76095	1.76095	-7.72638		150.35	29.65	85.13	0.16163	1.53045
$Cu-F$ (CuF)	F	0	0	0	0		0.78069	0.78092	-17.42282		123.18	56.82	48.39	1.26473	0.42736
$Cu-F$ (CuF_2)	Cu	-0.51359	-0.51359	0	0		0.68740	0.65349	-20.82022		50.41	129.59	20.28	2.05281	0.41649
$Cu-F$ (CuF_2)	F	-0.51359	0	0	0		0.78069	0.75856	-17.93641		68.67	111.33	29.09	1.91230	0.27597
$Cu-Cl$ $(CuCl)$	Cu	0	0	0	0		1.76095	1.76095	-7.72638		153.16	26.84	82.50	0.26095	1.57119
$Cu-Cl$ $(CuCl)$	Cl	0	0	0	0		1.05158	1.05158	-12.96764		139.26	40.74	58.82	1.03532	0.79682
$Cu-O$ (CuO)	Cu	-0.51359	0	0	0		0.68740	0.67002	-20.30662		100.40	79.60	39.32	1.47156	0.12096
$Cu-O$ (CuO)	O	-0.51359	0	0	0		1.00000	0.96279	-14.13165		119.26	60.74	53.86	1.12187	0.47064

Table 23.53. The energy parameters (eV) of functional groups of copper coordinate compounds.

Parameters	$Cu-F$ (a) Group	$Cu-F$ (b) Group	$Cu-Cl$ Group	$Cu-O$ Group
n_1	1	1	1	2
n_2	0	0	0	0
n_3	0	0	0	0
C_1	0.75	0.5	0.5	0.375
C_2	0.44346	0.81732	0.59582	1
c_1	0.75	1	1	1
c_2	1	1	0.59582	0.63884
c_3	0	0	0	0
c_4	1	1	1	2
c_5	1	1	1	2
C_{1o}	0.75	0.5	0.5	0.375
C_{2o}	0.44346	0.81732	0.59582	1
$V_e\ (eV)$	-34.12088	-32.18726	-27.68094	-52.91628
$V_p\ (eV)$	8.04085	8.31487	7.42620	17.08719
$T\ (eV)$	8.95771	7.35401	6.92024	13.91013
$V_m\ (eV)$	-4.47886	-3.67700	-3.46012	-6.95506
$E_{(AO/HO)}\ (eV)$	-7.72638	-21.31697	-7.72638	-42.633933
$\Delta E_{H_2MO\,(AO/HO)}\ (eV)$	0	0	0	0
$E_{T\,(AO/HO)}\ (eV)$	-7.72638	-21.31697	-7.72638	-42.633933
$E_{T\,(H_2MO)}\ (eV)$	-29.32755	-41.51235	-24.52100	-68.46008
$E_T\left(atom-atom, msp^3.AO\right)\ (eV)$	0	-1.02719	0	-1.02719
$E_{T\,(MO)}\ (eV)$	-29.32755	-42.53954	-24.52100	-69.48726
$\omega\ \left(10^{15}\ rad/s\right)$	29.1710	8.16340	7.97779	9.65069
$E_K\ (eV)$	19.20083	5.37329	5.25112	6.35225
$\bar{E}_D\ (eV)$	-0.25424	-0.19508	-0.11116	-0.17324
$\bar{E}_{Kvib}\ (eV)$	0.07721 [62]	0.07721 [62]	0.05149 [62]	0.07937 [62]
$\bar{E}_{osc}\ (eV)$	-0.21563	-0.15648	-0.08542	-0.13355
$E_{mag}\ (eV)$	0	0.35223	0	0.35223
$E_{T\,(Group)}\ (eV)$	-29.54319	-42.69602	-24.60642	-69.75437
$E_{initial\,(c_4\ AO/HO)}\ (eV)$	-7.72638	-21.31697	-7.72638	-21.31697
$E_{initial\,(c_5\ AO/HO)}\ (eV)$	-17.42282	-17.42282	-12.96764	-13.61806
$E_{D\,(Group)}\ (eV)$	4.39399	3.95623	3.91240	2.93219

Table 23.54. The total bond energies of gaseous-state copper coordinate compounds calculated using the functional group composition and the energies of Table 23.53 compared to the gaseous-state experimental values.

Formula	Name	$Cu-F$ (a) Group	$Cu-F$ (b) Group	$Cu-Cl$ Group	$Cu-O$ Group	Calculated Total Bond Energy (eV)	Experimental Total Bond Energy (eV)	Relative Error
CuF	Copper fluoride	1	0	0	0	4.39399	4.44620 [63]	0.01174
CuF_2	Copper difluoride	0	2	0	0	7.91246	7.89040 [63]	-0.00280
CuCl	Copper chloride	0	0	1	0	3.91240	3.80870 [15]	-0.02723
CuO	Copper oxide	0	0	0	1	2.93219	2.90931 [63]	-0.00787

ZINC FUNCTIONAL GROUPS AND MOLECULES

The electron configuration of zinc is $[Ar]4s^2 3d^{10}$ having the corresponding term $^1S_0$. The two outer $4s$ [61] electrons having energies of $-9.394199\ eV$ and $-17.96439\ eV$ [1] hybridize to form a single shell comprising two HOs. Each HO donates an electron to any single bond that participates in bonding with the HO such that two single bonds with ligands are possible to achieve a filled, spin-paired outer electron shell. Then, the total energy of the $^1S_0$ state of the bonding zinc atom is given by the sum over the two electrons. The sum $E_T(Zn, 4sHO)$ of experimental energies [1] of Zn, and Zn^+, is:

$$E_T(Zn, 4sHO) = -(17.96439\ eV + 9.394199\ eV) = -27.35859\ eV \tag{23.188}$$

By considering that the central field decreases by an integer for each successive electron of the shell, the radius r_{4sHO} of the $Zn4s$ HO shell may be calculated from the Coulombic energy using Eq. (15.13).

$$r_{4sHO} = \sum_{n=28}^{29} \frac{(Z-n)e^2}{8\pi\varepsilon_0 (e27.35859\ eV)} = \frac{3e^2}{8\pi\varepsilon_0 (e27.35859\ eV)} = 1.49194a_0 \tag{23.189}$$

where $Z = 30$ for zinc. Using Eq. (15.14), the Coulombic energy $E_{Coulomb}(Zn, 4sHO)$ of the outer electron of the $Zn4s$ shell is

$$E_{Coulomb}(Zn, 4sHO) = \frac{-e^2}{8\pi\varepsilon_0 r_{4sHO}} = \frac{-e^2}{8\pi\varepsilon_0 1.49194a_0} = -9.119530\ eV \tag{23.190}$$

During hybridization, the spin-paired $4s$ AO electrons are promoted to the $Zn4s$ HO shell as unpaired electrons. The energy for the promotion is given by Eq. (15.15) at the initial radius of the $4s$ electrons. From Eq. (10.102) with $Z = 30$ and $n = 30$, the radius r_{30} of the $Zn4s$ AO shell is:

$$r_{30} = 1.44832a_0 \tag{23.191}$$

Using Eqs. (15.15) and (23.190), the unpairing energy is:

$$E_{4s}(magnetic) = \frac{2\pi\mu_0 e^2\hbar^2}{m_e^2 (r_{30})^3} = \frac{8\pi\mu_o\mu_B^2}{(1.44832a_0)^3} = 0.03766\ eV \tag{23.192}$$

Using Eqs. (23.189) and (23.191), the energy $E(Zn, 4sHO)$ of the outer electron of the $Zn4s$ HO shell is:

$$E(Zn, 4sHO) = \frac{-e^2}{8\pi\varepsilon_0 r_{4sHO}} + \frac{2\pi\mu_0 e^2\hbar^2}{m_e^2 (r_{30})^3} = -9.119530\ eV + 0.03766\ eV = -9.08187\ eV \tag{23.193}$$

Next, consider the formation of the $Zn-L$-bond MO wherein each zinc atom has a $Zn4sHO$ electron with an energy given by Eq. (23.192). The total energy of the state of each zinc atom is given by the sum over the two electrons. The sum $E_T(Zn_{Zn-L}4sHO)$ of energies of $Zn4sHO$ (Eq. (23.192)) and Zn^+ is:

$$E_T(Zn_{Zn-L}4sHO) = -(17.96439\ eV + E(Zn, 4sHO)) = -(17.96439\ eV + 9.08187\ eV) = -27.04626\ eV \tag{23.194}$$

where $E(Zn, 4sHO)$ is the sum of the energy of Zn, $-9.394199\ eV\ eV$, and the hybridization energy.

The zinc HO donates an electron to each MO. Using Eq. (23.30), the radius r_{4sHO} of the $Zn4sHO$ shell calculated from the Coulombic energy is:

$$r_{Zn-L4sHO} = \left(\sum_{n=28}^{29} (Z-n) - 1\right) \frac{e^2}{8\pi\varepsilon_0 (e27.04626\ eV)} = \frac{2e^2}{8\pi\varepsilon_0 (e27.04626\ eV)} = 1.00611a_0 \tag{23.195}$$

Using Eqs. (15.19) and (23.194), the Coulombic energy $E_{Coulomb}(Zn_{Zn-L}, 4sHO)$ of the outer electron of the $Zn4sHO$ shell is:

$$E_{Coulomb}(Zn_{Zn-L}, 4sHO) = \frac{-e^2}{8\pi\varepsilon_0 r_{Zn-L4sHO}} = \frac{-e^2}{8\pi\varepsilon_0 1.00611a_0} = -13.52313\ eV \tag{23.196}$$

During hybridization, the spin-paired $2s$ electrons are promoted to the $Zn4sHO$ shell as unpaired electrons. The energy for the promotion is the magnetic energy given by Eq. (23.191). Using Eqs. (23.195) and (23.191), the energy $E(Zn_{Zn-L}, 4sHO)$ of the outer electron of the $Zn4s$ HO shell is:

$$E(Zn_{Zn-L}, 4sHO) = \frac{-e^2}{8\pi\varepsilon_0 r_{Zn-L4sHO}} + \frac{2\pi\mu_0 e^2\hbar^2}{m_e^2 (r_{30})^3} = -13.52313\ eV + 0.03766\ eV = -13.48547\ eV \tag{23.197}$$

Thus, $E_T(Zn-L, 4sHO)$, the energy change of each $Zn4sHO$ shell with the formation of the $Zn-L$-bond MO is given by the difference between Eq. (23.196) and Eq. (23.192):

$$E_T(Zn-L, 4sHO) = E(Zn_{Zn-L}, 4sHO) - E(Zn, 4sHO) = -13.48547\ eV - (-9.08187\ eV) = -4.40360\ eV \tag{23.198}$$

The semimajor axis a solution given by Eq. (23.41) of the force balance equation, Eq. (23.39), for the σ-MO of the $Zn-L$-bond MO of ZnL_n is given in Table 23.56 with the force-equation parameters $Z = 30$, n_e, and L corresponding to the orbital and spin angular momentum terms of the $4s$ HO shell. The semimajor axis a of organometallic compounds are solved using Eq. (15.51).

For the $Zn-L$ functional groups, hybridization of the $4s$ AOs of Zn to form a single $4s$ HO shell forms an energy minimum, and the sharing of electrons between the $Zn4s$ HO and L AO to form a MO permits each participating orbital to decrease in radius and energy. The Cl AO has an energy of $E(Cl) = -12.96764\ eV$, the $C2sp^3$ HO has an energy of $E(C,2sp^3) = -14.63489\ eV$ (Eq. (15.25)), the Coulomb energy of the $Zn4s$ HO is $E_{Coulomb}(Zn,4sHO) = -9.119530\ eV$ (Eq. (23.189)), and the $Zn4s$ HO has an energy of $E(Zn,4sHO) = -9.08187\ eV$ (Eq. (23.192)). To meet the equipotential condition of the union of the $Zn-L$ H_2-type-ellipsoidal-MO with these orbitals, the hybridization factor(s), at least one of c_2 and C_2 of Eq. (15.61) for the $Zn-L$-bond MO given by Eq. (15.77) is:

$$C_2(ClAO\ to\ Zn4sHO) = \frac{E(Zn,34sHO)}{E(ClAO)} = \frac{-9.08187\ eV}{-12.96764\ eV} = 0.70035 \tag{23.199}$$

$$\begin{aligned} c_2(C2sp^3HO\ to\ Zn4sHO) &= C_2(C2sp^3HO\ to\ Zn4sHO) \\ &= \frac{E_{Coulomb}(Zn,4sHO)}{E(C,2sp^3)} c_2(C2sp^3HO) = \frac{-9.11953\ eV}{-14.63489\ eV}(0.91771) = 0.57186 \end{aligned} \tag{23.200}$$

where Eqs. (15.76), (15.79), and (13.430) were used in Eq. (23.199). Since the energy of the MO is matched to that of the $Zn4sHO$ in coordinate compounds, $E(AO/HO)$ in Eq. (15.61) is $E(Zn,4sHO)$ given by Eq. (23.192) and $E(Zn,4sHO)$ for organometallics is $E_{Coulomb}(Zn,4sHO)$ given by Eq. (23.189). $E_T(atom-atom,msp^3.AO)$ of the $Zn-L$-bond MO is determined by considering that the bond involves an electron transfer from the zinc atom to the ligand atom to form partial ionic character in the bond as in the case of the zwitterions such as $H_2B^+-F^-$ given in the Halido Boranes section. For the coordinate compounds, $E_T(atom-atom,msp^3.AO)$ is $-8.80720\ eV$, two times the energy of Eq. (23.197).

The symbols of the functional groups of zinc coordinate compounds are given in Table 23.55. The geometrical (Eqs. (15.1-15.5) and (23.41)), intercept (Eqs. (15.31-15.32) and (15.80-15.87)), and energy (Eqs. (15.61) and (23.28-23.33)) parameters of zinc coordinate compounds are given in Tables 23.56, 23.57, and 23.58, respectively. The total energy of each zinc coordinate compound given in Table 22.59 was calculated as the sum over the integer multiple of each $E_{D\,(Group)}$ of Table 23.58 corresponding to functional-group composition of the compound. The charge-densities of exemplary zinc coordinate and organometallic compounds, zinc chloride ($ZnCl$) and di-n-butylzinc ($Zn(C_4H_9)_2$) comprising the concentric shells of atoms with the outer shell bridged by one or more H_2-type ellipsoidal MOs or joined with one or more hydrogen MOs are shown in Figures 23.12A and B, respectively.

Figure 23.12. (A) *Zinc Chloride.* Color scale, translucent view of the charge-density of $ZnCl$ showing the orbitals of the Zn and Cl atoms at their radii, the ellipsoidal surface of each H_2-type ellipsoidal MO that transitions to the corresponding outer shell of the atoms participating in each bond, and the nuclei (red, not to scale). (B) *Di-n-butylzinc.* Color scale, translucent view of the charge-density of $Zn(C_4H_9)_2$ showing the orbitals of the Zn and C atoms at their radii, the ellipsoidal surface of each H or H_2-type ellipsoidal MO that transitions to the corresponding outer shell of the atoms participating in each bond, and the nuclei (red, not to scale).

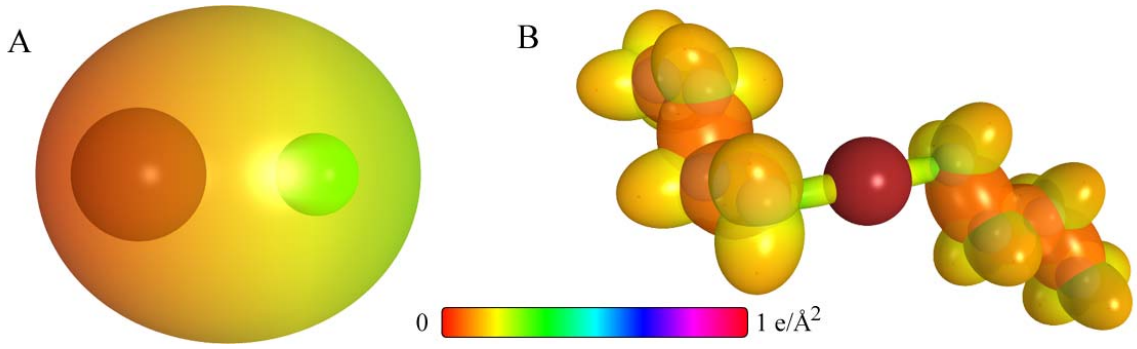

Table 23.55. The symbols of the functional groups of zinc coordinate compounds.

Functional Group	Group Symbol
ZnCl group of *ZnCl*	$Zn-Cl$ (a)
$ZnCl_2$ group of $ZnCl_2$	$Zn-Cl$ (b)
ZnC_{alkyl} group of $RZnR'$	$Zn-C$
CH_3 group	$C-H\ (CH_3)$
CH_2 group	$C-H\ (CH_2)$
CC bond (*n*-*C*)	$C-C$

Table 23.56. The geometrical bond parameters of zinc coordinate compounds and experimental values.

Parameter	$Zn-Cl$ (a) Group	$Zn-Cl$ (b) Group	$Zn-C$ Group	$C-H\ (CH_3)$ Group	$C-H\ (CH_2)$ Group	$C-C$ Group
n_e	6	5				
L	$4\sqrt{\frac{3}{4}}$	10				
$a\ (a_0)$	4.11547	3.83333	1.87715	1.64920	1.67122	2.12499
$c'\ (a_0)$	1.97928	1.91023	1.81177	1.04856	1.05553	1.45744
Bond Length $2c'\ (\text{Å})$	2.09478	2.02170	1.91750	1.10974	1.11713	1.54280
Exp. Bond Length (Å)	2.05 [15] ($ZnCl_2$)	2.05 [15] ($ZnCl_2$)	1.930 [15] (CH_3ZnCH_3)	1.113 [3] (trimethylaluminum) 1.107 [3] ($C-H$ propane) 1.117 [3] ($C-H$ butane)	1.107 [3] ($C-H$ propane) 1.117 [3] ($C-H$ butane)	1.532 [3] (propane) 1.531 [3] (butane)
$b,c\ (a_0)$	3.60826	3.32347	0.49108	1.27295	1.29569	1.54616
e	0.48094	0.49832	0.96517	0.63580	0.63159	0.68600

Table 23. 57. The MO to HO intercept geometrical bond parameters of zinc coordinate compounds. E_T is E_T $(atom\text{–}atom, HO.AO)$.

Bond	Atom	E_T (eV) Bond 1	E_T (eV) Bond 2	E_T (eV) Bond 3	E_T (eV) Bond 4	Final Total Energy $Zn4sHO$ (eV)	$r_{initial}$ (a_0)	r_{final} (a_0)	$E_{Coulomb}(Zn4sHO)$ (eV) Final	$E(Zn4sHO)$ (eV) Final	θ' (°)	θ_1 (°)	θ_2 (°)	d_1 (a_0)	d_2 (a_0)
$Zn-Cl\ (ZnCl)$	Zn	-4.40360	0	0	0		1.49194	1.00611	-13.52313						
$Zn-Cl\ (ZnCl)$	Cl	-4.40360	0	0	0		1.05158	0.78324	-17.37124						
$Zn-Cl\ (ZnCl_2)$	Zn	-4.40360	-4.40360	0	0		1.49194	0.75897	-17.92673						
$Zn-Cl\ (ZnCl_2)$	Cl	-4.40360	0	0	0		1.05158	0.78324	-17.37124						
$Zn-(CH_3)_2$	Zn	0	0	0	0		1.49194	1.49194	-14.82575		153.00	27.00	58.02	0.99406	0.81772
$Zn-(CH_3)_2$	C	0	0	0	0		0.91771	0.91771	-14.82575	-14.63489	153.00	27.00	58.02	0.99406	0.81772
$Zn-(C_aH_2CH_2-)_2$	Zn	0	0	0	0		1.49194	1.49194	-14.82575		153.00	27.00	58.02	0.99406	0.81772
$Zn-(C_aH_2CH_2-)_2$	C	0	0	0	0		0.91771	0.91771	-14.82575	-14.63489	153.00	27.00	58.02	0.99406	0.81772
$C-H\ (CH_3)$	C	-0.92918	0	0	0	-152.54487	0.91771	0.86359	-15.75493	-15.56407	77.49	102.51	41.48	1.23564	0.18708
$C-H\ (CH_2)$	C	-0.92918	-0.92918	0	0	-153.47406	0.91771	0.81549	-16.68412	-16.49325	68.47	111.53	35.84	1.35486	0.29933
$H_3C_aC_bH_2CH_2-$	C_a	-0.92918	0	0	0	-152.54487	0.91771	0.86359	-15.75493	-15.56407	63.82	116.18	30.08	1.83879	0.38106
$H_3C_aC_bH_2CH_2-$	C_b	-0.92918	-0.92918	0	0	-153.47406	0.91771	0.81549	-16.68412	-16.49325	56.41	123.59	26.06	1.90890	0.45117

Table 23.58. The energy parameters (eV) of functional groups of zinc coordinate compounds.

Parameters	$Zn-Cl$ (a) Group	$Zn-Cl$ (b) Group	$Zn-C$ Group	CH_3 Group	CH_2 Group	$C-C$ Group
n_1	1	1	1	3	2	1
n_2	0	0	0	2	1	0
n_3	0	0	0	0	0	0
C_1	0.75	0.75	0.5	0.75	0.75	0.5
C_2	0.70035	0.70035	0.57186	1	1	1
c_1	1	1	1	1	1	1
c_2	1	1	0.57186	0.91771	0.91771	0.91771
c_3	0	0	2	0	1	0
c_4	1	1	2	1	1	2
c_5	1	1	0	3	2	0
C_{1o}	0.75	0.75	0.5	0.75	0.75	0.5
C_{2o}	0.70035	0.70035	0.57186	1	1	1
$V_e\ (eV)$	-14.41370	-15.58624	-34.63883	-107.32728	-70.41425	-28.79214
$V_p\ (eV)$	6.87412	7.12260	7.50965	38.92728	25.78002	9.33352
$T\ (eV)$	1.75116	2.03299	9.22644	32.53914	21.06675	6.77464
$V_m\ (eV)$	-0.87558	-1.01649	-4.61322	-16.26957	-10.53337	-3.38732
$E_{(AO/HO)}\ (eV)$	-9.08187	-9.08187	-9.11953	-15.56407	-15.56407	-15.56407
$\Delta E_{H_2MO\,(AO/HO)}\ (eV)$	0	0	0	0	0	0
$E_{T\,(AO/HO)}\ (eV)$	-9.08187	-9.08187	-9.11953	-15.56407	-15.56407	-15.56407
$E_{T\,(H_2MO)}\ (eV)$	-15.74587	-16.52901	-31.63548	-67.69451	-49.66493	-31.63537
$E_T\left(atom-atom, msp^3.AO\right)\ (eV)$	-8.80720	-8.80720	0	0	0	-1.85836
$E_{T\,(MO)}\ (eV)$	-24.55307	-25.33621	-31.63537	-67.69450	-49.66493	-33.49373
$\omega\ \left(10^{15}\ rad/s\right)$	4.37145	3.99216	8.59541	24.9286	24.2751	9.43699
$E_K\ (eV)$	2.87737	2.62771	5.65765	16.40846	15.97831	6.21159
$\bar{E}_D\ (eV)$	-0.08240	-0.08125	-0.14887	-0.25352	-0.25017	-0.16515
$\bar{E}_{Kvib}\ (eV)$	0.04842 [14]	0.04842 [14]	0.06236 [64]	0.35532 (Eq. (13.458))	0.35532 (Eq. (13.458))	0.12312 [6]
$\bar{E}_{osc}\ (eV)$	-0.05819	-0.05704	-0.11768	-0.22757	-0.14502	-0.10359
$E_{mag}\ (eV)$	0.03445	0.03445	0.14803	0.14803	0.14803	0.14803
$E_{T\,(Group)}\ (eV)$	-24.61126	-25.39325	-31.75305	-67.92207	-49.80996	-33.59732
$E_{initial\,(c_4\ AO/HO)}\ (eV)$	-9.08187	-9.08187	-14.63489	-14.63489	-14.63489	-14.63489
$E_{initial\,(c_5\ AO/HO)}\ (eV)$	-12.96764	-12.96764	0	-13.59844	-13.59844	0
$E_{D\,(Group)}\ (eV)$	2.56175	3.34374	2.18721	12.49186	7.83016	4.32754

Table 23.59. The total bond energies of gaseous-state zinc coordinate compounds calculated using the functional group composition and the energies of Table 23.58 compared to the gaseous-state experimental values.

Formula	Name	*Zn–Cl* (a) Group	*Zn–Cl* (b) Group	*Zn–C* Group	CH_3 Group	CH_2 Group	*C–C* Group	Calculated Total Bond Energy (eV)	Experimental Total Bond Energy (eV)	Relative Error
ZnCl	Zinc chloride	1	0	0	0	0	0	2.56175	2.56529 [15]	0.00138
$ZnCl_2$	Zinc dichloride	0	2	0	0	0	0	6.68749	6.63675 [15]	-0.00764
$Zn(CH_3)_2$	Dimethylzinc	0	0	2	2	0	0	29.35815	29.21367 [15]	-0.00495
$(CH_3CH_2)_2Zn$	Diethylzinc	0	0	2	2	2	2	53.67355	53.00987 [65]	-0.01252
$(CH_3CH_2CH_2)_2Zn$	Di-n-propylzinc			2	2	4	4	77.98895	77.67464 [65]	-0.00405
$(CH_3CH_2CH_2CH_2)_2Zn$	Di-n-butylzinc			2	2	6	6	102.30435	101.95782 [65]	-0.00340

GERMANIUM ORGANOMETALLIC FUNCTIONAL GROUPS AND MOLECULES

The branched-chain alkyl germanium molecules, GeC_nH_{2n-2}, comprise at least one Ge bound by a carbon-germanium single bond comprising a $C-Ge$ group, and the digermanium molecules further comprise a $Ge-Ge$ functional group. Both comprise at least a terminal methyl group (CH_3) and may comprise methylene (CH_2), methylyne (CH), and $C-C$ functional groups. The methyl and methylene functional groups are equivalent to those of straight-chain alkanes. Six types of $C-C$ bonds can be identified. The n-alkane $C-C$ bond is the same as that of straight-chain alkanes. In addition, the $C-C$ bonds within isopropyl ($(CH_3)_2 CH$) and t-butyl ($(CH_3)_3 C$) groups and the isopropyl to isopropyl, isopropyl to t-butyl, and t-butyl to t-butyl $C-C$ bonds comprise functional groups.

As in the cases of carbon, silicon, and tin, the bonding in the germanium atom involves four sp^3 hybridized orbitals. For germanium, they are formed from the $4p$ and $4s$ electrons of the outer shells. $Ge-C$ bonds form between a $Ge4sp^3$ HO and a $C3sp^3$ HO, and $Ge-Ge$ bonds form between between $Ge4sp^3$ HOs to yield germanes and digermanes, respectively. The geometrical parameters of each $Ge-C$ and $Ge-Ge$ functional group is solved using Eq. (15.51) and the relationships between the prolate spheroidal axes. Then, the sum of the energies of the H_2-type ellipsoidal MOs is matched to that of the $Ge4sp^3$ shell as in the case of the corresponding carbon, silicon, and tin molecules. As in the case of the transition metals, the energy of each functional group is determined for the effect of the electron density donation from each participating $C3sp^3$ HO and $Ge4sp^3$ HO to the corresponding MO that maximizes the bond energy.

The Ge electron configuration is $[Ar]4s^2 3d^{10} 4p^2$, and the orbital arrangement is:

4p state

$$\begin{array}{ccc} \uparrow & \uparrow & \\ \hline 1 & 0 & -1 \end{array} \qquad (23.201)$$

corresponding to the ground state ${}^3P_0$. The energy of the germanium $4p$ shell is the negative of the ionization energy of the germanium atom [1] given by

$$E(Ge, 4p\ shell) = -E(ionization;\ Ge) = -7.89943\ eV \qquad (23.202)$$

The energy of germanium is less than the Coulombic energy between the electron and proton of H given by Eq. (1.264), but the atomic orbital may hybridize in order to achieve a bond at an energy minimum. After Eq. (13.422), the $Ge4s$ atomic orbital (AO) combines with the $Ge4p$ AOs to form a single $Ge4sp^3$ hybridized orbital (HO) with the orbital arrangement:

$4sp^3$ state

$$\begin{array}{cccc} \uparrow & \uparrow & \uparrow & \uparrow \\ \hline 0,0 & 1,-1 & 1,0 & 1,1 \end{array} \qquad (23.203)$$

where the quantum numbers (ℓ, m_ℓ) are below each electron. The total energy of the state is given by the sum over the four electrons. The sum $E_T(Ge, 4sp^3)$ of experimental energies [1] of Ge, Ge^+, Ge^{2+}, and Ge^{3+} is:

$$E_T(Ge, 4sp^3) = 45.7131\ eV + 34.2241\ eV + 15.93461\ eV + 7.89943\ eV = 103.77124\ eV \qquad (23.204)$$

By considering that the central field decreases by an integer for each successive electron of the shell, the radius r_{4sp^3} of the $Ge4sp^3$ shell may be calculated from the Coulombic energy using Eq. (15.13).

$$r_{4sp^3} = \sum_{n=28}^{31} \frac{(Z-n)e^2}{8\pi\varepsilon_0 (e103.77124\ eV)} = \frac{10e^2}{8\pi\varepsilon_0 (e103.77124\ eV)} = 1.31113 a_0 \qquad (23.205)$$

where $Z = 32$ for germanium. Using Eq. (15.14), the Coulombic energy $E_{Coulomb}(Ge, 4sp^3)$ of the outer electron of the $Ge4sp^3$ shell is:

$$E_{Coulomb}(Ge, 4sp^3) = \frac{-e^2}{8\pi\varepsilon_0 r_{4sp^3}} = \frac{-e^2}{8\pi\varepsilon_0 1.31113 a_0} = -10.37712\ eV \qquad (23.206)$$

During hybridization, the spin-paired $4s$ electrons are promoted to the $Ge4sp^3$ shell as unpaired electrons. The energy for the promotion is the magnetic energy given by Eq. (15.15) at the initial radius of the $4s$ electrons. From Eq. (10.102) with $Z = 32$ and $n = 30$, the radius r_{30} of the $Ge4s$ shell is:

$$r_{30} = 1.19265 a_0 \qquad (23.207)$$

Using Eqs. (15.15) and (23.207), the unpairing energy is:

$$E(magnetic)=\frac{2\pi\mu_0 e^2\hbar^2}{m_e^2\left(r_{30}\right)^3}=\frac{8\pi\mu_o\mu_B^2}{\left(1.19265a_0\right)^3}=0.06744\ eV \tag{23.208}$$

Using Eqs. (23.206) and (23.208), the energy $E\left(Ge,4sp^3\right)$ of the outer electron of the $Ge4sp^3$ shell is:

$$E\left(Ge,4sp^3\right)=\frac{-e^2}{8\pi\varepsilon_0 r_{4sp^3}}+\frac{2\pi\mu_0 e^2\hbar^2}{m_e^2\left(r_{30}\right)^3}=-10.37712\ eV+0.06744\ eV=-10.30968\ eV \tag{23.209}$$

Next, consider the formation of the $Ge-L$-bond MO of gernmanium compounds wherein L is a ligand including germanium and carbon and each gemanium atom has a $Ge4sp^3$ electron with an energy given by Eq. (23.209). The total energy of the state of each germanium atom is given by the sum over the four electrons. The sum $E_T\left(Ge_{Ge-L},4sp^3\right)$ of energies of $Ge4sp^3$ (Eq. (23.209)), Ge^+, Ge^{2+}, and Ge^{3+} is:

$$\begin{aligned}E_T\left(Ge_{Ge-L},4sp^3\right)&=-\left(45.7131\ eV+34.2241\ eV+15.93461\ eV+E\left(Ge,4sp^3\right)\right)\\&=-\left(45.7131\ eV+34.2241\ eV+15.93461\ eV+10.30968\ eV\right)\\&=-106.18149\ eV\end{aligned} \tag{23.210}$$

where $E\left(Ge,4sp^3\right)$ is the sum of the energy of Ge, $-7.89943\ eV$, and the hybridization energy.

A minimum energy is achieved while matching the potential, kinetic, and orbital energy relationships given in the Hydroxyl Radical (OH) section with the donation of electron density from the participating $Ge4sp^3$ HO to each $Ge-L$-bond MO. Consider the case wherein each $Ge4sp^3$ HO donates an excess of 25% of its electron density to the $Ge-L$-bond MO to form an energy minimum. By considering this electron redistribution in the germanium molecule as well as the fact that the central field decreases by an integer for each successive electron of the shell, in general terms, the radius $r_{Ge-L4sp^3}$ of the $Ge4sp^3$ shell may be calculated from the Coulombic energy using Eq. (15.18).

$$r_{Ge-L4sp^3}=\left(\sum_{n=28}^{31}(Z-n)-0.25\right)\frac{e^2}{8\pi\varepsilon_0\left(e106.18149\ eV\right)}=\frac{9.75e^2}{8\pi\varepsilon_0\left(e106.18149\ eV\right)}=1.24934a_0 \tag{23.211}$$

Using Eqs. (15.19) and (23.211), the Coulombic energy $E_{Coulomb}\left(Ge_{Ge-L},4sp^3\right)$ of the outer electron of the $Ge4sp^3$ shell is:

$$E_{Coulomb}\left(Ge_{Ge-L},4sp^3\right)=\frac{-e^2}{8\pi\varepsilon_0 r_{Ge-L4sp^3}}=\frac{-e^2}{8\pi\varepsilon_0 1.24934a_0}=-10.89041\ eV \tag{23.212}$$

During hybridization, the spin-paired $4s$ electrons are promoted to the $Ge4sp^3$ shell as unpaired electrons. The energy for the promotion is the magnetic energy given by Eq. (23.208). Using Eqs. (23.208) and (23.212), the energy $E\left(Ge_{Ge-L},4sp^3\right)$ of the outer electron of the $Ge4sp^3$ shell is:

$$E\left(Ge_{Ge-L},4sp^3\right)=\frac{-e^2}{8\pi\varepsilon_0 r_{Ge-L4sp^3}}+\frac{2\pi\mu_0 e^2\hbar^2}{m_e^2\left(r_{30}\right)^3}=-10.89041\ eV+0.06744\ eV=-10.82297\ eV \tag{23.213}$$

Thus, $E_T\left(Ge-L,4sp^3\right)$, the energy change of each $Ge4sp^3$ shell with the formation of the $Ge-L$-bond MO is given by the difference between Eq. (23.213) and Eq. (23.209):

$$E_T\left(Ge-L,4sp^3\right)=E\left(Ge_{Ge-L},4sp^3\right)-E\left(Ge,4sp^3\right)=-10.82297\ eV-\left(-10.30968\ eV\right)=-0.51329\ eV \tag{23.214}$$

Now, consider the formation of the $Ge-L$-bond MO of gernmanium compounds wherein L is a ligand including germanium and carbon. For the $Ge-L$ functional groups, hybridization of the $4p$ and $4s$ AOs of Ge to form a single $Ge4sp^3$ HO shell forms an energy minimum, and the sharing of electrons between the $Ge4sp^3$ HO and L HO to form a MO permits each participating orbital to decrease in radius and energy. The $C2sp^3$ HO has an energy of $E\left(C,2sp^3\right)=-14.63489\ eV$ (Eq. (15.25)) and the $Ge4sp^3$ HO has an energy of $E\left(Ge,4sp^3\right)=-10.30968\ eV$ (Eq. (23.209)). To meet the equipotential condition of the union of the $Ge-L$ H_2-type-ellipsoidal-MO with these orbitals, the hybridization factor C_2 of Eq. (15.61) for the $Ge-L$-bond MO given by Eq. (15.77) is:

$$C_2\left(Ge4sp^3HO\ to\ Ge4sp^3HO\right)=C_2\left(C2sp^3HO\ to\ Ge4sp^3HO\right)=\frac{E\left(Ge,4sp^3HO\right)}{E\left(C,2sp^3\right)}=\frac{-10.30968\ eV}{-14.63489\ eV}=0.70446 \tag{23.215}$$

Since the energy of the MO is matched to that of the $Ge4sp^3$ HO, $E\left(AO/HO\right)$ in Eq. (15.61) is $E\left(Ge,4sp^3HO\right)$ given by Eq. (23.209). In order to match the energies of the HOs within the molecule, $E_T\left(atom-atom,msp^3.AO\right)$ of the $Ge-L$-bond MO for the ligands carbon or germanium is $\frac{-0.72457}{2}$ (Eq. (14.151)).

The symbols of the functional groups of germanium compounds are given in Table 23.60. The geometrical (Eqs. (15.1-15.5)), intercept (Eqs. (15.31-15.32) and (15.80-15.87)), and energy (Eqs. (15.61) and (23.28-23.33)) parameters of germanium compounds are given in Tables 23.61, 23.62, and 23.63, respectively. The total energy of each germanium compounds given in Table 22.64 was calculated as the sum over the integer multiple of each $E_{D\,(Group)}$ of Table 23.63 corresponding to functional-group composition of the compound. The bond angle parameters of germanium compounds determined using Eqs. (15.88-15.117) are given in Table 23.65. The charge-densities of exemplary germanium and digermanium compounds, tetraethylgermanium ($Ge\left(CH_2CH_3\right)_4$) and hexaethyldigermanium ($\left(C_2H_5\right)_3GeGe\left(C_2H_5\right)_3$) comprising atoms with the outer shell bridged by one or more H_2-type ellipsoidal MOs or joined with one or more hydrogen MOs are shown in Figures 23.13A and B, respectively.

Figure 23.13. (A) Color scale, charge-density of $Ge\left(CH_2CH_3\right)_4$ showing the orbitals of the Ge and C atoms at their radii, the ellipsoidal surface of each H or H_2-type ellipsoidal MO that transitions to the corresponding outer shell of the atoms participating in each bond, and the hydrogen nuclei. (B) Color scale, charge-density of $\left(C_2H_5\right)_3GeGe\left(C_2H_5\right)_3$ showing the orbitals of the Ge and C atoms at their radii, the ellipsoidal surface of each H or H_2-type ellipsoidal MO that transitions to the corresponding outer shell of the atoms participating in each bond, and the hydrogen nuclei.

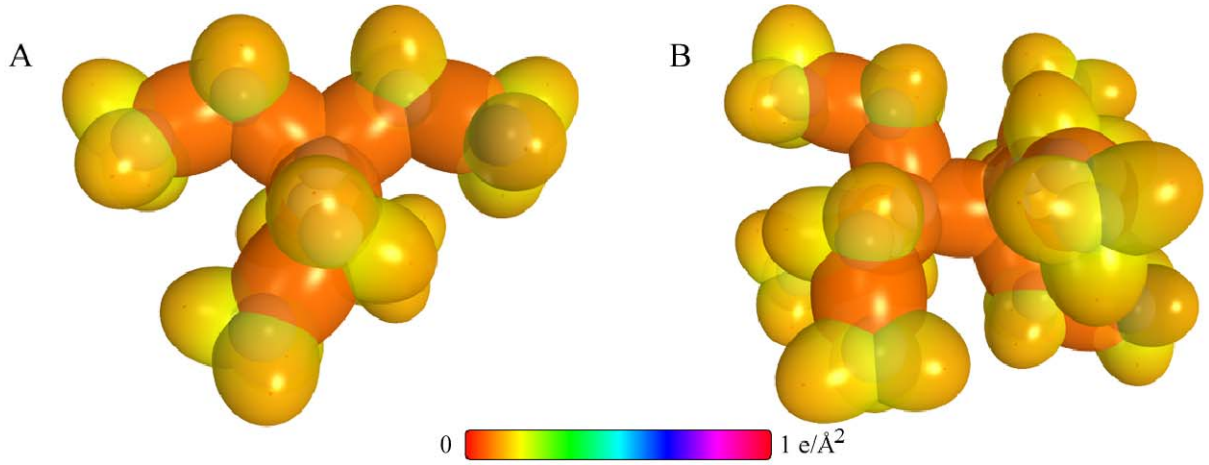

Table 23.60. The symbols of functional groups of germanium compounds.

Functional Group	Group Symbol
GeC group	$Ge-C$
GeGe group	$Ge-Ge$
CH_3 group	$C-H\ \left(CH_3\right)$
CH_2 alkyl group	$C-H\ \left(CH_2\right)$
CH alkyl	$C-H$
CC bond (*n-C*)	$C-C$ (a)
CC bond (*iso-C*)	$C-C$ (b)
CC bond (*tert-C*)	$C-C$ (c)
CC (*iso* to *iso-C*)	$C-C$ (d)
CC (*t* to *t-C*)	$C-C$ (e)
CC (*t* to *iso-C*)	$C-C$ (f)

Table 23.61. The geometrical bond parameters of germanium compounds and experimental values [3].

Parameter	$Ge-C$ Group	$Ge-Ge$ Group	$C-H\ (CH_3)$ Group	$C-H\ (CH_2)$ Group	$C-H$ Group	$C-C$ (a) Group	$C-C$ (b) Group	$C-C$ (c) Group	$C-C$ (d) Group	$C-C$ (e) Group	$C-C$ (f) Group
$a\ (a_0)$	2.27367	2.27367	1.64920	1.67122	1.67465	2.12499	2.12499	2.10725	2.12499	2.10725	2.10725
$c'\ (a_0)$	1.79654	1.79654	1.04856	1.05553	1.05661	1.45744	1.45744	1.45164	1.45744	1.45164	1.45164
Bond Length $2c'\ (\AA)$	1.90137	1.90137	1.10974	1.11713	1.11827	1.54280	1.54280	1.53635	1.54280	1.53635	1.53635
Exp. Bond Length $(\AA)$	1.945 $((CH_3)_4Ge)$ 1.945 (CH_3GeH_3) 1.89 (CH_3GeCl_3)		1.107 ($C-H$ propane) 1.117 ($C-H$ butane)	1.107 ($C-H$ propane) 1.117 ($C-H$ butane)	1.122 (isobutane)	1.532 (propane) 1.531 (butane)	1.532 (propane) 1.531 (butane)	1.532 (propane) 1.531 (butane)	1.532 (propane) 1.531 (butane)	1.532 (propane) 1.531 (butane)	1.532 (propane) 1.531 (butane)
$b,c\ (a_0)$	1.39357	1.39357	1.27295	1.29569	1.29924	1.54616	1.54616	1.52750	1.54616	1.52750	1.52750
e	0.79015	0.79015	0.63580	0.63159	0.63095	0.68600	0.68600	0.68888	0.68600	0.68888	0.68888

Table 23.62. The MO to HO intercept geometrical bond parameters of germanium compounds. *R, R′, R″* are *H* or alkyl groups. E_T is E_T (*atom–atom,msp³.AO*).

Bond	Atom	E_T (eV) Bond 1	E_T (eV) Bond 2	E_T (eV) Bond 3	E_T (eV) Bond 4	Final Total Energy $Ge4sp^3$ $C2sp^3$ (eV)	$r_{initial}$ (a_0)	r_{final} (a_0)	$E_{Coulomb}(C2sp^3)$ (eV) Final	$E(Ge4sp^3)$ $E(C2sp^3)$ (eV) Final	θ' (°)	θ_1 (°)	θ_2 (°)	d_1 (a_0)	d_2 (a_0)
$C-H\ (CH_3)$	C	-0.18114	0	0	0	-151.79683	0.91771	0.90664	-15.00689	-14.81603	82.43	97.57	44.91	1.16793	0.11938
$(CH_3)_3Ge-CH_3$	Ge	-0.18114	-0.18114	-0.18114	-0.18114		1.31113	0.87495	-15.55033		91.73	88.27	38.87	1.77020	0.02634
$(CH_3)_3Ge-CH_3$	C	-0.18114	0	0	0		0.91771	0.90664	-15.00689	-14.81603	94.20	85.80	40.45	1.73010	0.06644
$(CH_3)_3Ge-Ge(CH_3)_3$	Ge	-0.18114	-0.18114	-0.18114	-0.18114		1.31113	0.87495	-15.55033		91.73	88.27	38.87	1.77020	0.02634
$C-H\ (CH_3)$	C	-0.92918	0	0	0	-152.54487	0.91771	0.86359	-15.75493	-15.56407	77.49	102.51	41.48	1.23564	0.18708
$C-H\ (CH_2)$ (i)	C	-0.92918	-0.92918	0	0	-153.47406	0.91771	0.81549	-16.68412	-16.49325	68.47	111.53	35.84	1.35486	0.29933
$C-H\ (CH)$ (i)	C	-0.92918	-0.92918	-0.92918	0	-154.40324	0.91771	0.77247	-17.61330	-17.42244	61.10	118.90	31.37	1.42988	0.37326
$H_3C_aC_bH_2CH_2-$ $(C-C$ (a))	C_a	-0.92918	0	0	0	-152.54487	0.91771	0.86359	-15.75493	-15.56407	63.82	116.18	30.08	1.83879	0.38106
$H_3C_aC_bH_2CH_2-$ $(C-C$ (a))	C_b	-0.92918	-0.92918	0	0	-153.47406	0.91771	0.81549	-16.68412	-16.49325	56.41	123.59	26.06	1.90890	0.45117
$R-H_2C_aC_b(H_2C_c-R')HCH_2-$ $(C-C$ (b))	C_b	-0.92918	-0.92918	-0.92918	0	-154.40324	0.91771	0.77247	-17.61330	-17.42244	48.30	131.70	21.90	1.97162	0.51388
$R-H_2C_a(R'-H_2C_d)C_b(R''-H_2C_c)CH_2-$ $(C-C$ (e))	C_b	-0.92918	-0.72457	-0.72457	-0.72457	-154.71860	0.91771	0.75889	-17.92866	-17.73779	48.21	131.79	21.74	1.95734	0.50570
$isoC_aC_b(H_2C_c-R')HCH_2-$ $(C-C$ (d))	C_b	-0.92918	-0.92918	-0.92918	0	-154.40324	0.91771	0.77247	-17.61330	-17.42244	48.30	131.70	21.90	1.97162	0.51388
$tertC_a(R'-H_2C_d)C_b(R''-H_2C_c)CH_2-$ $(C-C$ (e))	C_b	-0.72457	-0.72457	-0.72457	-0.72457	-154.51399	0.91771	0.76765	-17.92866	-17.73779	50.04	129.96	22.66	1.94462	0.49298
$tertC_aC_b(H_2C_c-R')HCH_2-$ $(C-C$ (f))	C_b	-0.72457	-0.92918	-0.92918	0	-154.19863	0.91771	0.78155	-17.40869	-17.21783	52.78	127.22	24.04	1.92443	0.47279
$isoC_a(R'-H_2C_d)C_b(R''-H_2C_c)CH_2-$ $(C-C$ (f))	C_b	-0.72457	-0.72457	-0.72457	-0.72457	-154.51399	0.91771	0.76765	-17.92866	-17.73779	50.04	129.96	22.66	1.94462	0.49298

Table 23.63. The energy parameters (eV) of functional groups of germanium compounds.

Parameters	$Ge-C$ Group	$Ge-Ge$ Group	CH_3 Group	CH_2 Group	CH Group	$C-C$ (a) Group	$C-C$ (b) Group	$C-C$ (c) Group	$C-C$ (d) Group	$C-C$ (e) Group	$C-C$ (f) Group
n_1	1	1	3	2	1	1	1	1	1	1	1
n_2	0	0	2	1	0	0	0	0	0	0	0
n_3	0	0	0	0	0	0	0	0	0	0	0
C_1	0.5	0.5	0.75	0.75	0.75	0.5	0.5	0.5	0.5	0.5	0.5
C_2	0.70446	0.70446	1	1	1	1	1	1	1	1	1
c_1	1	1	1	1	1	1	1	1	1	1	1
c_2	1	1	0.91771	0.91771	0.91771	0.91771	0.91771	0.91771	0.91771	0.91771	0.91771
c_3	0	0	0	1	1	0	0	0	1	1	0
c_4	2	2	1	1	1	2	2	2	2	2	2
c_5	0	0	3	2	1	0	0	0	0	0	0
C_{1o}	0.5	0.5	0.75	0.75	0.75	0.5	0.5	0.5	0.5	0.5	0.5
C_{2o}	0.70446	0.70446	1	1	1	1	1	1	1	1	1
V_e (eV)	-32.46926	-32.46926	-107.32728	-70.41425	-35.12015	-28.79214	-28.79214	-29.10112	-28.79214	-29.10112	-29.10112
V_p (eV)	7.57336	7.57336	38.92728	25.78002	12.87680	9.33352	9.33352	9.37273	9.33352	9.37273	9.37273
T (eV)	7.14028	7.14028	32.53914	21.06675	10.48582	6.77464	6.77464	6.90500	6.77464	6.90500	6.90500
V_m (eV)	-3.57014	-3.57014	-16.26957	-10.53337	-5.24291	-3.38732	-3.38732	-3.45250	-3.38732	-3.45250	-3.45250
$E_{(AO/HO)}$ (eV)	-10.30968	-10.30968	-15.56407	-15.56407	-14.63489	-15.56407	-15.56407	-15.35946	-15.56407	-15.35946	-15.35946
$\Delta E_{H_2MO\,(AO/HO)}$ (eV)	0	0	0	0	0	0	0	0	0	0	0
E_T $_{(AO/HO)}$ (eV)	-10.30968	-10.30968	-15.56407	-15.56407	-14.63489	-15.56407	-15.56407	-15.35946	-15.56407	-15.35946	-15.35946
E_T $_{(H_2MO)}$ (eV)	-31.63544	-31.63544	-67.69451	-49.66493	-31.63533	-31.63537	-31.63537	-31.63535	-31.63537	-31.63535	-31.63535
$E_I\left(atom-atom, msp^3.AO\right)$ (eV)	-0.36229	-0.36229	0	0	0	-1.85836	-1.85836	-1.44915	-1.85836	-1.44915	-1.44915
E_T $_{(MO)}$ (eV)	-31.99766	-31.99766	-67.69450	-49.66493	-31.63537	-33.49373	-33.49373	-33.08452	-33.49373	-33.08452	-33.08452
$\omega\ \left(10^{15}\ rad/s\right)$	14.9144	14.9144	24.9286	24.2751	24.1759	9.43699	9.43699	15.4846	9.43699	9.55643	9.55643
E_K (eV)	9.81690	9.81690	16.40846	15.97831	15.91299	6.21159	6.21159	10.19220	6.21159	6.29021	6.29021
$\bar{E}_D$ (eV)	-0.19834	-0.19834	-0.25352	-0.25017	-0.24966	-0.16515	-0.16515	-0.20896	-0.16515	-0.16416	-0.16416
$\bar{E}_{Kvit}$ (eV)	0.15312 [66]	0.06335 [14]	0.35532 Eq. (13.458)	0.35532 Eq. (13.458)	0.35532 Eq. (13.458)	0.12312 [6]	0.17978 [7]	0.09944 [8]	0.12312 [6]	0.12312 [6]	0.12312 [6]
$\bar{E}_{osc}$ (eV)	-0.12178	-0.16666	-0.22757	-0.14502	-0.07200	-0.10359	-0.07526	-0.15924	-0.10359	-0.10260	-0.10260
E_{mag} (eV)	0.14803	0.14803	0.14803	0.14803	0.14803	0.14803	0.14803	0.14803	0.14803	0.14803	0.14803
E_T $_{(Group)}$ (eV)	-32.11943	-32.16432	-67.92207	-49.80996	-31.70737	-33.59732	-33.49373	-33.24376	-33.59732	-33.18712	-33.18712
$E_{initial\,(c_4\ AO/HO)}$ (eV)	-14.63489	-14.63489	-14.63489	-14.63489	-14.63489	-14.63489	-14.63489	-14.63489	-14.63489	-14.63489	-14.63489
$E_{initial\,(c_5\ AO/HO)}$ (eV)	0	0	-13.59844	-13.59844	-13.59844	0	0	0	0	0	0
$E_{D\,(Group)}$ (eV)	2.84965	2.89454	12.49186	7.83016	3.32601	4.32754	4.29921	3.97398	4.17951	3.62128	3.91734

Table 23.64. The total bond energies of gaseous-state germanium compounds calculated using the functional group composition (separate functional groups designated in the first row) and the energies of Table 23.63 compared to the gaseous-state experimental values [67].

Formula	Name	$Ge-C$	$Ge-Ge$	CH_3	CH_2	CH	$C-C$ (a)	Calculated Total Bond Energy (eV)	Experimental Total Bond Energy (eV)	Relative Error
$C_8H_{20}Ge$	Tetraethylgermanium	4	0	4	4	0	4	109.99686	110.18166	0.00168
$C_{12}H_{28}Ge$	Tetra-n-propylgermanium	4	0	4	8	0	8	158.62766	158.63092	0.00002
$C_{12}H_{30}Ge_2$	Hexaethyldigermanium	6	1	6	6	0	6	167.88982	167.89836	0.00005

Table 23.65. The bond angle parameters of germanium compounds and experimental values [3]. In the calculation of θ_v, the parameters from the preceding angle were used. E_T is E_T (*atom–atom,msp³.AO*).

Atoms of Angle	2c' Bond 1 (a_0)	2c' Bond 2 (a_0)	2c' Terminal Atoms (a_0)	$E_{Coulombic}$ Atom 1	Atom 1 Hybridization Designation (Table 15.3.A)	$E_{Coulombic}$ Atom 2	Atom 2 Hybridization Designation (Table 15.3.A)	c_2 Atom 1	c_2 Atom 2	C_1	C_2	c_1	c_2'	E_T (eV)	θ_v (°)	θ_1 (°)	θ_2 (°)	Cal. θ (°)	Exp. θ (°)
Methyl $\angle HC_aH$	2.09711	2.09711	3.4252	-15.75493	7	H	H	0.86359	1	1	1	0.75	1.15796	0				109.50	
$\angle H_aC_aGe$															70.56			109.44	108 (tetramethyl germanium)
$\angle C_aGeC_b$	3.59307	3.59307	5.7446	-15.55033	5	-15.55033	5	0.87495	0.87495	1	1	1	0.87495	-1.85836				106.14	109.5 (tetramethyl germanium)
Methylene $\angle HC_aH$	2.11106	2.11106	3.4252	-15.75493	7	H	H	0.86359	1	1	1	0.75	1.15796	0				108.44	107 (propane)
$\angle C_aC_bC_c$															69.51			110.49	112 (propane) 113.8 (butane) 110.8 (isobutane)
$\angle C_aC_bH$															69.51			110.49	111.0 (butane) 111.4 (isobutane)
Methyl $\angle HC_aH$	2.09711	2.09711	3.4252	-15.75493	7	H	H	0.86359	1	1	1	0.75	1.15796	0				109.50	
$\angle C_aC_bC_c$															70.56			109.44	
$\angle C_aC_bH$															70.56			109.44	
$\angle C_bC_aC_c$ iso C_a	2.91547	2.91547	4.7958	-16.68412 C_b	26	-16.68412 C_c	26	0.81549	0.81549	1	1	1	0.81549	-1.85836				110.67	110.8 (isobutane)
$\angle C_bC_aH$ iso C_a	2.91547	2.11323	4.1633	-15.55033 C_a	5	-14.82575 C_b	1	0.87495	0.91771	0.75	1	0.75	1.04887	0				110.76	
$\angle C_aC_bH$ iso C_a	2.91547	2.09711	4.1633	-15.55033 C_b	5	-14.82575 C_a	1	0.87495	0.91771	0.75	1	0.75	1.04887	0				111.27	111.4 (isobutane)
$\angle C_bC_aC_b$ tert C_a	2.90327	2.90327	4.7958	-16.68412 C_b	26	-16.68412 C_b	26	0.81549	0.81549	1	1	1	0.81549	-1.85836				111.37	110.8 (isobutane)
$\angle C_bC_aC_d$															72.50			107.50	

TIN FUNCTIONAL GROUPS AND MOLECULES

As in the cases of carbon, silicon and germanium, the bonding in the tin atom involves four sp^3 hybridized orbitals formed from the $5p$ and $5s$ electrons of the outer shells. $Sn-X$ $X=halide,oxide$, $Sn-H$, and $Sn-Sn$ bonds form between $Sn5sp^3$ HOs and between a halide or oxide AO, a $H1s$ AO, and a $Sn5sp^3$ HO, respectively to yield tin halides and oxides, stannanes, and distannanes, respectively. The geometrical parameters of each $Sn-X$ $X=halide,oxide$, $Sn-H$, and $Sn-Sn$ functional group is solved from the force balance equation of the electrons of the corresponding σ-MO and the relationships between the prolate spheroidal axes. Then, the sum of the energies of the H_2-type ellipsoidal MOs is matched to that of the $Sn5sp^3$ shell as in the case of the corresponding carbon and tin molecules. As in the case of the transition metals, the energy of each functional group is determined for the effect of the electron density donation from each participating $Sn5sp^3$ HO and AO to the corresponding MO that maximizes the bond energy.

The branched-chain alkyl stannanes and distannanes, $Sn_mC_nH_{2(m+n)+2}$, comprise at least a terminal methyl group (CH_3) and at least one Sn bound by a carbon-tin single bond comprising a $C-Sn$ group, and may comprise methylene (CH_2), methylyne (CH), $C-C$, $SnH_{n=1,2,3}$, and $Sn-Sn$ functional groups. The methyl and methylene functional groups are equivalent to those of straight-chain alkanes. Six types of $C-C$ bonds can be identified. The n-alkane $C-C$ bond is the same as that of straight-chain alkanes. In addition, the $C-C$ bonds within isopropyl ($(CH_3)_2CH$) and t-butyl ($(CH_3)_3C$) groups and the isopropyl to isopropyl, isopropyl to t-butyl, and t-butyl to t-butyl $C-C$ bonds comprise functional groups.

The Sn electron configuration is $[Kr]5s^24d^{10}5p^2$, and the orbital arrangement is:

$$\begin{array}{c} \text{5p state} \\ \underline{\uparrow} \quad \underline{\uparrow} \quad \underline{} \\ 1 \quad 0 \quad -1 \end{array} \tag{23.216}$$

corresponding to the ground state ${}^3P_0$. The energy of the carbon $5p$ shell is the negative of the ionization energy of the tin atom [1] given by:

$$E(Sn,5p\ shell)=-E(ionization;\ Sn)=-7.34392\ eV \tag{23.217}$$

The energy of tin is less than the Coulombic energy between the electron and proton of H given by Eq. (1.264), but the atomic orbital may hybridize in order to achieve a bond at an energy minimum. After Eq. (13.422), the $Sn5s$ atomic orbital (AO) combines with the $Sn5p$ AOs to form a single $Sn5sp^3$ hybridized orbital (HO) with the orbital arrangement is:

$$\begin{array}{c} \text{5sp}^3\text{ state} \\ \underline{\uparrow} \quad \underline{\uparrow} \quad \underline{\uparrow} \quad \underline{\uparrow} \\ 0,0 \quad 1,-1 \quad 1,0 \quad 1,1 \end{array} \tag{23.218}$$

where the quantum numbers (ℓ,m_ℓ) are below each electron. The total energy of the state is given by the sum over the four electrons. The sum $E_T(Sn,4sp^3)$ of experimental energies [1] of Sn, Sn^+, Sn^{2+}, and Sn^{3+} is:

$$E_T(Sn,5sp^3)=40.73502\ eV+30.50260\ eV+14.6322\ eV+7.34392\ eV=93.21374\ eV \tag{23.219}$$

By considering that the central field decreases by an integer for each successive electron of the shell, the radius r_{5sp^3} of the $Sn5sp^3$ shell may be calculated from the Coulombic energy using Eq. (15.13).

$$r_{5sp^3}=\sum_{n=46}^{49}\frac{(Z-n)e^2}{8\pi\varepsilon_0(e93.21374\ eV)}=\frac{10e^2}{8\pi\varepsilon_0(e93.21374\ eV)}=1.45964a_0 \tag{23.220}$$

where $Z=50$ for tin. Using Eq. (15.14), the Coulombic energy $E_{Coulomb}(Sn,5sp^3)$ of the outer electron of the $Sn5sp^3$ shell is:

$$E_{Coulomb}(Sn,5sp^3)=\frac{-e^2}{8\pi\varepsilon_0 r_{5sp^3}}=\frac{-e^2}{8\pi\varepsilon_0 1.45964a_0}=-9.321374\ eV \tag{23.221}$$

During hybridization, the spin-paired $5s$ electrons are promoted to the $Sn5sp^3$ shell as unpaired electrons. The energy for the promotion is the magnetic energy given by Eq. (15.15) at the initial radius of the $5s$ electrons. From Eq. (10.255) with $Z=50$, the radius r_{48} of the $Sn5s$ shell is:

$$r_{48}=1.33816a_0 \tag{23.222}$$

Using Eqs. (15.15) and (23.206), the unpairing energy is:

$$E(magnetic)=\frac{2\pi\mu_0 e^2\hbar^2}{m_e^2(r_{48})^3}=\frac{8\pi\mu_o\mu_B^2}{(1.33816a_0)^3}=0.04775\ eV \tag{23.223}$$

Using Eqs. (23.203) and (23.207), the energy $E\left(Sn,5sp^3\right)$ of the outer electron of the $Sn5sp^3$ shell is:

$$E\left(Sn,5sp^3\right)=\frac{-e^2}{8\pi\varepsilon_0 r_{5sp^3}}+\frac{2\pi\mu_0 e^2\hbar^2}{m_e^2\left(r_{48}\right)^3}=-9.321374\ eV+0.04775\ eV=-9.27363\ eV \tag{23.224}$$

Next, consider the formation of the $Sn-L$-bond MO of tin compounds wherein L is a ligand including tin and each tin atom has a $Sn5sp^3$ electron with an energy given by Eq. (23.224). The total energy of the state of each tin atom is given by the sum over the four electrons. The sum $E_T\left(Sn_{Sn-L},5sp^3\right)$ of energies of $Sn5sp^3$ (Eq. (23.224)), Sn^+, Sn^{2+}, and Sn^{3+} is:

$$\begin{aligned}E_T\left(Sn_{Sn-L},5sp^3\right)&=-\left(40.73502\ eV+30.50260\ eV+14.6322\ eV+E\left(Sn,5sp^3\right)\right)\\&=-\left(40.73502\ eV+30.50260\ eV+14.6322\ eV+9.27363\ eV\right)=-95.14345\ eV\end{aligned} \tag{23.225}$$

where $E\left(Sn,5sp^3\right)$ is the sum of the energy of Sn, $-7.34392\ eV$, and the hybridization energy.

A minimum energy is achieved while matching the potential, kinetic, and orbital energy relationships given in the Hydroxyl Radical (OH) section with the donation of electron density from the participating $Sn5sp^3$ HO to each $Sn-L$-bond MO. As in the case of acetylene given in the Acetylene Molecule section, the energy of each $Sn-L$ functional group is determined for the effect of the charge donation. For example, as in the case of the $Si-Si$-bond MO given in the Alkyl Silanes and Disilanes section, the sharing of electrons between two $Sn5sp^3$ HOs to form a $Sn-Sn$-bond MO permits each participating orbital to decrease in size and energy. In order to further satisfy the potential, kinetic, and orbital energy relationships, each $Sn5sp^3$ HO donates an excess of 25% of its electron density to the $Sn-Sn$-bond MO to form an energy minimum. By considering this electron redistribution in the distannane molecule as well as the fact that the central field decreases by an integer for each successive electron of the shell, in general terms, the radius $r_{Sn-L5sp^3}$ of the $Sn5sp^3$ shell may be calculated from the Coulombic energy using Eq. (15.18).

$$r_{Sn-L5sp^3}=\left(\sum_{n=46}^{49}(Z-n)-0.25\right)\frac{e^2}{8\pi\varepsilon_0\left(e95.14345\ eV\right)}=\frac{9.75e^2}{8\pi\varepsilon_0\left(e95.14345\ eV\right)}=1.39428a_0 \tag{23.226}$$

Using Eqs. (15.19) and (23.210), the Coulombic energy $E_{Coulomb}\left(Sn_{Sn-L},5sp^3\right)$ of the outer electron of the $Sn5sp^3$ shell is:

$$E_{Coulomb}\left(Sn_{Sn-L},5sp^3\right)=\frac{-e^2}{8\pi\varepsilon_0 r_{Sn-L5sp^3}}=\frac{-e^2}{8\pi\varepsilon_0 1.39428a_0}=-9.75830\ eV \tag{23.227}$$

During hybridization, the spin-paired $5s$ electrons are promoted to the $Sn5sp^3$ shell as unpaired electrons. The energy for the promotion is the magnetic energy given by Eq. (23.223). Using Eqs. (23.223) and (23.227), the energy $E\left(Sn_{Sn-L},5sp^3\right)$ of the outer electron of the $Sn5sp^3$ shell is:

$$E\left(Sn_{Sn-L},5sp^3\right)=\frac{-e^2}{8\pi\varepsilon_0 r_{Sn-L5sp^3}}+\frac{2\pi\mu_0 e^2\hbar^2}{m_e^2\left(r_{48}\right)^3}=-9.75830\ eV+0.04775\ eV=-9.71056eV \tag{23.228}$$

Thus, $E_T\left(Sn-L,5sp^3\right)$, the energy change of each $Sn5sp^3$ shell with the formation of the $Sn-L$-bond MO is given by the difference between Eq. (23.228) and Eq. (23.224).

$$E_T\left(Sn-L,5sp^3\right)=E\left(Sn_{Sn-L},5sp^3\right)-E\left(Sn,5sp^3\right)=-0.43693\ eV \tag{23.229}$$

Next, consider the formation of the $Sn-L$-bond MO of additional functional groups wherein each tin atom contributes a $Sn5sp^3$ electron having the sum $E_T\left(Sn_{Sn-L},5sp^3\right)$ of energies of $Sn5sp^3$ (Eq. (23.224)), Sn^+, Sn^{2+}, and Sn^{3+} given by Eq. (23.209). Each $Sn-L$-bond MO of each functional group $Sn-L$ forms with the sharing of electrons between a $Sn5sp^3$ HO and a AO or HO of L, and the donation of electron density from the $Sn5sp^3$ HO to the $Sn-L$-bond MO permits the participating orbitals to decrease in size and energy. In order to further satisfy the potential, kinetic, and orbital energy relationships while forming an energy minimum, the permitted values of the excess fractional charge of its electron density that the $Sn5sp^3$ HO donates to the $Sn-L$-bond MO given by Eq. (15.18) is $s\left(0.25\right);\quad s=1,2,3,4$ and linear combinations thereof. By considering this electron redistribution in the tin molecule as well as the fact that the central field decreases by an integer for each successive electron of the shell, the radius $r_{Sn-L5sp^3}$ of the $Sn5sp^3$ shell may be calculated from the Coulombic energy using Eq. (15.18).

$$r_{Sn-L5sp^3}=\left(\sum_{n=46}^{49}(Z-n)-s\left(0.25\right)\right)\frac{e^2}{8\pi\varepsilon_0\left(e95.14345\ eV\right)}=\frac{\left(10-s\left(0.25\right)\right)e^2}{8\pi\varepsilon_0\left(e95.14345\ eV\right)} \tag{23.230}$$

Using Eqs. (15.19) and (23.230), the Coulombic energy $E_{Coulomb}\left(Sn_{Sn-L},5sp^3\right)$ of the outer electron of the $Sn5sp^3$ shell is

$$E_{Coulomb}\left(Sn_{Sn-L},5sp^3\right)=\frac{-e^2}{8\pi\varepsilon_0 r_{Sn-L5sp^3}}=\frac{-e^2}{8\pi\varepsilon_0\dfrac{\left(10-s\left(0.25\right)\right)e^2}{8\pi\varepsilon_0\left(e95.14345\ eV\right)}}=\frac{95.14345\ eV}{\left(10-s\left(0.25\right)\right)} \tag{23.231}$$

During hybridization, the spin-paired $5s$ electrons are promoted to the $Sn5sp^3$ shell as unpaired electrons. The energy for the promotion is the magnetic energy given by Eq. (23.223). Using Eqs. (23.223) and (23.231), the energy $E\left(Sn_{Sn-L},5sp^3\right)$ of the outer electron of the $Sn5sp^3$ shell is:

$$E\left(Sn_{Sn-L},5sp^3\right)=\frac{-e^2}{8\pi\varepsilon_0 r_{Sn-L5sp^3}}+\frac{2\pi\mu_0 e^2\hbar^2}{m_e^2\left(r_{48}\right)^3}=\frac{95.14345\ eV}{\left(10-s\left(0.25\right)\right)}+0.04775\ eV \tag{23.232}$$

Thus, $E_T\left(Sn-L,5sp^3\right)$, the energy change of each $Sn5sp^3$ shell with the formation of the $Sn-L$-bond MO is given by the difference between Eq. (23.232) and Eq. (23.224).

$$E_T\left(Sn-L,5sp^3\right)=E\left(Sn_{Sn-L},5sp^3\right)-E\left(Sn,5sp^3\right)=-\frac{95.14345}{\left(10-s\left(0.25\right)\right)}\ eV+0.04775\ eV\ -\left(-9.27363\ eV\right) \tag{23.233}$$

Using Eq. (15.28) for the case that the energy matching and energy minimum conditions of the MOs in the tin molecule are met by a linear combination of values of s (s_1 and s_2) in Eqs. (23.230-23.233), the energy $E\left(Sn_{Sn-L},5sp^3\right)$ of the outer electron of the $Sn5sp^3$ shell is:

$$E\left(Sn_{Sn-L},5sp^3\right)=\frac{\dfrac{95.14345\ eV}{\left(10-s_1\left(0.25\right)\right)}+\dfrac{95.14345\ eV}{\left(10-s_2\left(0.25\right)\right)}+2\left(0.04775\ eV\right)}{2} \tag{23.234}$$

Using Eqs. (15.13) and (23.234), the radius corresponding to Eq. (23.234) is:

$$r_{5sp^3}=\frac{e^2}{8\pi\varepsilon_0 E\left(Sn_{Sn-L},5sp^3\right)}=\frac{e^2}{8\pi\varepsilon_0\left(e\left(\dfrac{\dfrac{95.14345\ eV}{\left(10-s_1\left(0.25\right)\right)}+\dfrac{95.14345\ eV}{\left(10-s_2\left(0.25\right)\right)}+2\left(0.04775\ eV\right)}{2}\right)\right)} \tag{23.235}$$

$E_T\left(Sn-L,5sp^3\right)$, the energy change of each $Sn5sp^3$ shell with the formation of the $Sn-L$-bond MO is given by the difference between Eq. (23.235) and Eq. (23.224).

$$\begin{aligned}E_T\left(Sn-L,5sp^3\right)&=E\left(Sn_{Sn-L},5sp^3\right)-E\left(Sn,5sp^3\right)\\&=\frac{\dfrac{95.14345\ eV}{\left(10-s_1\left(0.25\right)\right)}+\dfrac{95.14345\ eV}{\left(10-s_2\left(0.25\right)\right)}+2\left(0.04775\ eV\right)}{2}\ -\left(-9.27363\ eV\right)\end{aligned} \tag{23.236}$$

$E_T\left(Sn-L,5sp^3\right)$ is also given by Eq. (15.29). Bonding parameters for the $Sn-L$-bond MO of tin functional groups due to charge donation from the HO to the MO are given in Table 23.66.

Table 23.66. The values of r_{Sn5sp^3}, $E_{Coulomb}\left(Sn_{Sn-L},5sp^3\right)$, and $E\left(Sn_{Sn-L},5sp^3\right)$ and the resulting $E_T\left(Sn-L,5sp^3\right)$ of the MO due to charge donation from the HO to the MO.

MO Bond Type	s 1	s 2	$r_{Sn5sp^3}\left(a_0\right)$ Final	$E_{Coulomb}\left(Sn_{Sn-L},5sp^3\right)$ (eV) Final	$E\left(Sn_{Sn-L},5sp^3\right)$ (eV) Final	$E_T\left(Sn-L,5sp^3\right)$ (eV)
0	0	0	1.45964	-9.321374	-9.27363	0
I	1	0	1.39428	-9.75830	-9.71056	-0.43693
II	2	0	1.35853	-10.01510	-9.96735	-0.69373
III	3	0	1.32278	-10.28578	-10.23803	-0.96440
IV	4	0	1.28703	-10.57149	-10.52375	-1.25012
I+II	1	2	1.37617	-9.88670	-9.83895	-0.56533
II+III	2	3	1.34042	-10.15044	-10.10269	-0.82906

The semimajor axis a solution given by Eq. (23.41) of the force balance equation, Eq. (23.39), for the σ-MO of the $Sn-L$-bond MO of SnL_n is given in Table 23.68 with the force-equation parameters $Z=50$, n_e, and L corresponding to the orbital and spin angular momentum terms of the $4s$ HO shell. The semimajor axis a of organometallic compounds, stannanes and distannanes, are solved using Eq. (15.51).

For the $Sn-L$ functional groups, hybridization of the $5p$ and $5s$ AOs of Sn to form a single $Sn5sp^3$ HO shell forms an energy minimum, and the sharing of electrons between the $Sn5sp^3$ HO and L AO to form a MO permits each participating orbital to decrease in radius and energy. The Cl AO has an energy of $E(Cl)=-12.96764\ eV$, the Br AO has an energy of $E(Br)=-11.8138\ eV$, the I AO has an energy of $E(I)=-10.45126\ eV$, the O AO has an energy of $E(O)=-13.61805\ eV$, the $C2sp^3$ HO has an energy of $E(C,2sp^3)=-14.63489\ eV$ (Eq. (15.25)), $13.605804\ eV$ is the magnitude of the Coulombic energy between the electron and proton of H (Eq. (1.264)), the Coulomb energy of the $Sn5sp^3$ HO is $E_{Coulomb}(Sn,5sp^3HO)=-9.32137\ eV$ (Eq. (23.205)), and the $Sn5sp^3$ HO has an energy of $E(Sn,5sp^3HO)=-9.27363\ eV$ (Eq. (23.208)). To meet the equipotential condition of the union of the $Sn-L$ H_2-type-ellipsoidal-MO with these orbitals, the hybridization factor(s), at least one of c_2 and C_2 of Eq. (15.61) for the $Sn-L$-bond MO given by Eq. (15.77) is:

$$c_2(ClAO\ to\ Sn5sp^3HO)=C_2(ClAO\ to\ Sn5sp^3HO)=\frac{E(Sn,5sp^3)}{E(ClAO)}=\frac{-9.27363\ eV}{-12.96764\ eV}=0.71514 \tag{23.237}$$

$$C_2(BrAO\ to\ Sn5sp^3HO)=\frac{E(Sn,5sp^3)}{E(BrAO)}=\frac{-9.27363\ eV}{-11.8138\ eV}=0.78498 \tag{23.238}$$

$$c_2(IAO\ to\ Sn5sp^3HO)=\frac{E(Sn,Sn5sp^3)}{E(IAO)}=\frac{-9.27363\ eV}{-10.45126\ eV}=0.88732 \tag{23.239}$$

$$c_2(O\ to\ Sn5sp^3HO)=C_2(O\ to\ Sn5sp^3HO)=\frac{E(Sn,5sp^3)}{E(O)}=\frac{-9.27363\ eV}{-13.61805\ eV}=0.68098 \tag{23.240}$$

$$c_2(HAO\ to\ Sn5sp^3HO)=\frac{E_{Coulomb}(Sn,5sp^3)}{E(H)}=\frac{-9.32137\ eV}{-13.605804\ eV}=0.68510 \tag{23.241}$$

$$C_2(C2sp^3HO\ to\ \mathrm{S}n5sp^3HO)=\frac{E(Sn,5sp^3HO)}{E(C,2sp^3)}c_2(C2sp^3HO)=\frac{-9.27363\ eV}{-14.63489\ eV}(0.91771)=0.58152 \tag{23.242}$$

$$c_2(Sn5sp^3HO\ to\ Sn5sp^3HO)=\frac{E_{Coulomb}(Sn,5sp^3)}{E(H)}=\frac{-9.32137\ eV}{-13.605804\ eV}=0.68510 \tag{23.243}$$

where Eq. (15.71) was used in Eqs. (23.241) and (23.243) and Eqs. (15.76), (15.79), and (13.430) were used in Eq. (23.242). Since the energy of the MO is matched to that of the $Sn5sp^3$ HO, $E(AO/HO)$ in Eq. (15.61) is $E(Sn,5sp^3HO)$ given by Eq. (23.224) for single bonds and twice this value for double bonds. $E_T(atom-atom,msp^3.AO)$ of the $Sn-L$-bond MO is determined by considering that the bond involves up to an electron transfer from the tin atom to the ligand atom to form partial ionic character in the bond as in the case of the zwitterions such as $H_2B^+-F^-$ given in the Halido Boranes section. For the tin compounds, $E_T(atom-atom,msp^3.AO)$ is that which forms an energy minimum for the hybridization and other bond parameter. The general values of Table 23.66 are given by Eqs. (23.233) and (23.226), and the specific values for the tin functional groups are given in Table 23. 70.

The symbols of the functional groups of tin compounds are given in Table 23.67. The geometrical (Eqs. (15.1-15.5) and (23.41)), intercept (Eqs. (15.31-15.32) and (15.80-15.87)), and energy (Eqs. (15.61) and (23.28-23.33)) parameters of tin compounds are given in Tables 23.68, 23.69, and 23.70, respectively. The total energy of each tin compound given in Table 22.71 was calculated as the sum over the integer multiple of each $E_{D(Group)}$ of Table 23.70 corresponding to functional-group composition of the compound. The bond angle parameters of tin compounds determined using Eqs. (15.88-15.117) are given in Table 23.72. The $E_T(atom-atom,msp^3.AO)$ term for $SnCl_4$ was calculated using Eqs. (23.230-23.277) with $s=1$ for the energies of $E(Sn,5sp^3)$. The charge-densities of exemplary tin coordinate and organometallic compounds, tin tetrachloride ($SnCl_4$) and hexaphenyldistannane ($(C_6H_5)_3SnSn(C_6H_5)_3$) comprising the concentric shells of atoms with the outer shell bridged by one or more H_2-type ellipsoidal MOs or joined with one or more hydrogen MOs are shown in Figures 23.14 and 23.15, respectively.

Figure 23.14. *Tin Tetrachloride.* Color scale, translucent view of the charge-density of $SnCl_4$ showing the orbitals of the *Sn* and *Cl* atoms at their radii, the ellipsoidal surface of each H_2-type ellipsoidal MO that transitions to the corresponding outer shell of the atoms participating in each bond, and the nuclei (red, not to scale).

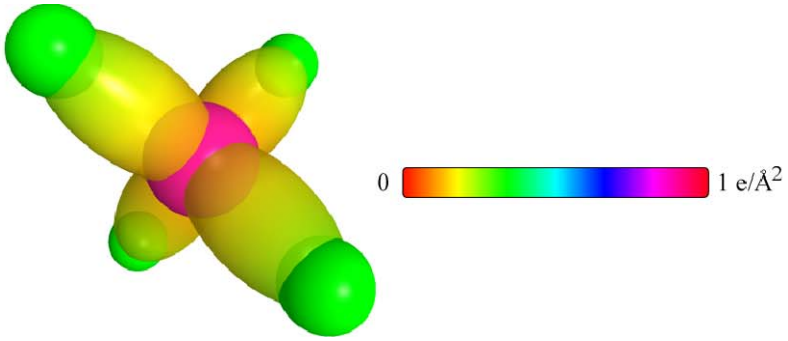

Figure 23.15. (A) and (B) *Hexaphenyldistannane.* Color scale, opaque view of the charge-density of $(C_6H_5)_3SnSn(C_6H_5)_3$ showing the orbitals of the *Sn* and *C* atoms at their radii and the ellipsoidal surface of each *H* or H_2-type ellipsoidal MO that transitions to the corresponding outer shell of the atoms participating in each bond.

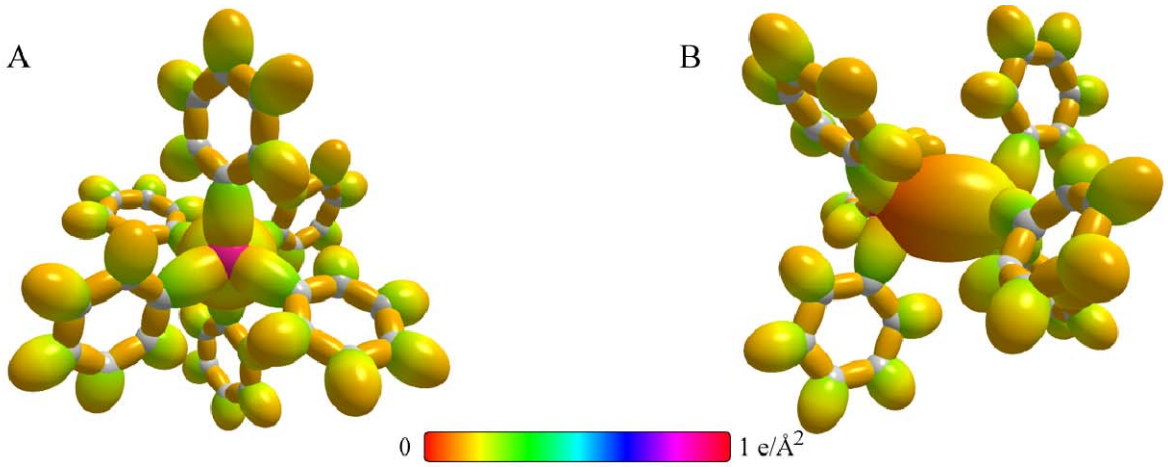

Table 23.67. The symbols of functional groups of tin compounds.

Functional Group	Group Symbol
SnCl group	$Sn-Cl$
SnBr group	$Sn-Br$
SnI group	$Sn-I$
SnO group	$Sn-O$
SnH group	$Sn-H$
SnC group	$Sn-C$
SnSn group	$Sn-Sn$
CH_3 group	$C-H\ (CH_3)$
CH_2 alkyl group	$C-H\ (CH_2)$ (i)
CH alkyl	$C-H$ (i)
CC bond (*n*-*C*)	$C-C$ (a)
CC bond (*iso*-*C*)	$C-C$ (b)
CC bond (*tert*-*C*)	$C-C$ (c)
CC (*iso* to *iso*-*C*)	$C-C$ (d)
CC (*t* to *t*-*C*)	$C-C$ (e)
CC (*t* to *iso*-*C*)	$C-C$ (f)
CC double bond	$C=C$
C vinyl single bond to -*C(C)=C*	$C-C$ (i)
C vinyl single bond to -*C(H)=C*	$C-C$ (ii)
C vinyl single bond to -*C(C)=CH*$_2$	$C-C$ (iii)
CH_2 alkenyl group	$C-H\ (CH_2)$ (ii)
CC (aromatic bond)	$C\overset{3e}{=}C$
CH (aromatic)	CH (ii)
C_a-C_b (CH_3 to aromatic bond)	$C-C$ (iv)
C-*C*(*O*)	$C-C(O)$
C=*O* (aryl carboxylic acid)	$C=O$
(*O*)*C*-*O*	$C-O$
OH group	OH

Table 23.68A. The geometrical bond parameters of tin compounds and experimental values [3].

Parameter	$Sn-Cl$ Group	$Sn-Br$ Group	$Sn-I$ Group	$Sn-O$ Group	$Sn-H$ Group	$Sn-C$ Group	$Sn-Sn$ Group	$C-H$ (CH_3) Group	$C-H$ (CH_3) (i) Group	$C-H$ (i) Group	$C-C$ (a) Group	$C-C$ (b) Group	$C-C$ (c) Group	$C-C$ (d) Group
n_c	3	5	5	2	2		6							
L	$\sqrt[3]{\frac{3}{2}}$	$3\sqrt[3]{\frac{3}{4}}$	0	$2\sqrt[3]{\frac{3}{4}}$	0		0							
a (a_0)	2.51732	3.55196	3.50000	2.03464	2.00000	2.44449	4.00000	1.64920	1.57122	1.67465	2.12499	2.12499	2.10725	2.12499
c' (a_0)	2.16643	2.45926	2.64575	1.72853	1.63299	2.35027	2.79011	1.04856	1.05553	1.05661	1.45744	1.45744	1.45164	1.45744
Bond Length $2c'$ (Å)	2.2928	2.59959	2.80014	1.82940	1.72829	2.16991	2.95293	1.10974	1.11713	1.11827	1.54280	1.54280	1.53635	1.54280
Exp. Bond Length (Å)	2.280 ($SnCl_4$)	2.495 [68] ($(C_6H_5)_3SnBr$)	2.708 [69] ($(C_6H_5)_3SnI$)	1.8325 (SnO)	1.711 (SnH_4)	2.144 ($Sn(CH_3)_4$)	2.79–2.70] ($(CH_3)_3SnSn(CH_3)_3$)	1.107 ($C-H$ propane) 1.117 ($C-H$ butane)	1.107 ($C-H$ propene) 1.117 ($C-H$ butane)	1.122 (isobutane)	1.532 (propane) 1.531 (butane)	1.532 (propane) 1.531 (butane)	1.532 (propene) 1.531 (butane)	1.532 (propene) 1.531 (butane)
$b.e$ (a_0)	1.28199	2.56578	2.29129	1.07326	1.15470	1.33114	2.80623	1.27295	1.29569	1.29924	1.54616	1.54616	1.52750	1.54616
e	0.86051	0.69152	0.75593	0.84955	0.81650	0.83873	0.69753	0.63580	0.63159	0.63095	0.68600	0.68600	0.68888	0.68600

Table 23.68B. The geometrical bond parameters of tin compounds and experimental values [3].

Parameter	$C-C$ (e) Group	$C-C$ (f) Group	$C=C$ Group	$C-C$ (i) Group	$C-C$ (ii) Group	$C-C$ (iii) Group	$C-H$ (CH_2) (ii) Group	$C=C$ Group	CH (ii) Group	$C-C$ (iv) Group	$C-C(O)$ Group	$C=O$ Group	$C-O$ Group	OH Group
a (a_0)	2.10725	2.10725	2.47228	2.04740	2.04740	2.04740	1.66010	1.47348	1.60061	2.06004	1.95111	1.29907	2.73490	1.26430
c' (a_0)	1.45164	1.45164	1.26661	1.43087	1.43087	1.43087	1.04566	1.31468	1.03299	1.45528	1.39682	1.13977	2.31716	2.91808
Bond Length $2c'$ (Å)	1.53635	1.53535	1.34052	1.51437	1.51437	1.51437	1.10668	1.39140	1.09227	1.51907	1.47833	1.20628	2.36402	0.971651
Exp. Bond Length (Å)	1.532 (propane) 1.531 (butane)	1.532 (propene) 1.531 (butane)	1.342 (2-methylpropene) 1.346 (2-butene) 1.349 (1,3-butadiene)		1.508 (2-butene)	1.508 (2-methylpropene)	1.10 (2-methylpropane) 1.108 (avg.) (1,3-butadiene)	1.399 (benzene)	1.101 (benzene)	1.524 (toluene)	1.48 [71] (benzoic acid)	1.214 (acetic acid)	1.393 (methyl formate)	0.972 (formic acid)
$b.e$ (a_0)	1.52750	1.52750	0.75055	1.46439	1.46439	1.46439	1.26354	0.66540	1.22265	1.47774	1.36225	0.62331	2.12915	0.86925
e	0.68888	0.68888	0.86030	0.69887	0.69887	0.69887	0.63756	0.89223	0.64537	0.69673	0.71591	0.87737	0.75921	0.72615

Table 23.69. The MO to HO intercept geometrical bond parameters of tin compounds. *R, R′, R″* are *H* or alkyl groups. E_T is E_T (*atom–atom,msp*^{3}*.AO*).

Bond	Atom	E_T (eV) Bond 1	E_T (eV) Bond 2	E_T (eV) Bond 3	E_T (eV) Bond 4	Final Total Energy $Sn5sp^3$ $C2sp^3$ (eV)	$r_{initial}$ (a_0)	r_{final} (a_0)	$E_{Coulomb}(C2sp^3)$ (eV) Final	$E(Sn5sp^3)$ $E(C2sp^3)$ (eV) Final	θ' (°)	θ_1 (°)	θ_2 (°)	d_1 (a_0)	d_2 (a_0)
$Sn-Cl\ (SnCl_4)$	Sn	-0.69373	-0.69373	-0.69373	-0.69373		1.45964	1.12479	-12.09627		119.18	60.82	50.00	1.61807	0.54836
$Sn-Cl\ (SnCl_4)$	Cl	-0.69373	0	0	0		1.05158	0.99593	-13.66137		113.59	66.41	45.39	1.76780	0.39862
$Sn-Br\ (SnBr_4)$	Sn	-1.25012	-1.25012	-1.25012	-1.25012		1.45964	0.95000	-14.32185						
$Sn-Br\ (SnBr_4)$	Br	-1.25012	0	0	0		1.15169	1.04148	-13.06392						
$Sn-I\ (SnI_4)$	Sn	-0.62506	-0.62506	-0.62506	-0.62506		1.45964	1.15093	-11.82161		66.35	113.65	27.39	3.10753	0.46178
$Sn-I\ (SnI_4)$	I	-0.62506	0	0	0		1.30183	1.22837	-11.07632		72.99	107.01	30.84	3.00509	0.35933
$Sn-O\ (SnO)$	Sn	-0.56533	0	0	0		1.45964	1.37617	-9.88670		133.85	46.15	67.61	0.77508	0.41569
$Sn-O\ (SnO)$	O	-0.56533	0	0	0		1.00000	0.95928	-14.18339		118.84	61.16	51.53	1.26580	0.46831
$Sn-H\ (SnH_4)$	Sn	-0.82906	-0.82906	-0.82906	-0.82906		1.45964	1.07661	-12.63763		117.80	62.20	55.57	1.13092	0.50208
$Sn-(CH_3)_4$	Sn	0	0	0	0		1.45964	0.91771	-14.82575		104.51	75.49	41.87	1.82034	0.22992
$Sn-(CH_3)_4$	C	0	0	0	0		0.91771	0.91771	-14.82575	-14.63489	104.51	75.49	41.87	1.82034	0.22992
$(CH_3)_3Sn-Sn(CH_3)_3$	Sn	-0.21846	0	0	0		1.45964	1.42621	-9.53983		50.89	129.11	22.71	3.68987	0.89976
$C-H\ (CH_3)$	C	-0.92918	0	0	0	-152.54487	0.91771	0.86359	-15.75493	-15.56407	77.49	102.51	41.48	1.23564	0.18708
$C-H\ (CH_2)$ (i)	C	-0.92918	-0.92918	0	0	-153.47406	0.91771	0.81549	-16.68412	-16.49325	68.47	111.53	35.84	1.35486	0.29933
$C-H\ (CH)$ (i)	C	-0.92918	-0.92918	-0.92918	0	-154.40324	0.91771	0.77247	-17.61330	-17.42244	61.10	118.90	31.37	1.42988	0.37326
$H_3C_aC_bH_2CH_2-$ $(C-C$ (a))	C_a	-0.92918	0	0	0	-152.54487	0.91771	0.86359	-15.75493	-15.56407	63.82	116.18	30.08	1.83879	0.38106
$H_3C_aC_bH_2CH_2-$ $(C-C$ (a))	C_b	-0.92918	-0.92918	0	0	-153.47406	0.91771	0.81549	-16.68412	-16.49325	56.41	123.59	26.06	1.90890	0.45117
$R-H_2C_aC_b(H_2C_c-R')HCH_2-$ $(C-C$ (b))	C_b	-0.92918	-0.92918	-0.92918	0	-154.40324	0.91771	0.77247	-17.61330	-17.42244	48.30	131.70	21.90	1.97162	0.51388
$R-H_2C_a(R'-H_2C_d)C_b(R''-H_2C_c)CH_2-$ $(C-C$ (c))	C_b	-0.92918	-0.72457	-0.72457	-0.72457	-154.71860	0.91771	0.75889	-17.92866	-17.73779	48.21	131.79	21.74	1.95734	0.50570
$isoC_aC_b(H_2C_c-R')HCH_2-$ $(C-C$ (d))	C_b	-0.92918	-0.92918	-0.92918	0	-154.40324	0.91771	0.77247	-17.61330	-17.42244	48.30	131.70	21.90	1.97162	0.51388
$teriC_a(R'-H_2C_d)C_b(R''-H_2C_c)CH_2-$ $(C-C$ (e))	C_b	-0.72457	-0.72457	-0.72457	-0.72457	-154.51399	0.91771	0.76765	-17.92866	-17.73779	50.04	129.96	22.66	1.94462	0.49298
$teriC_aC_b(H_2C_c-R')HCH_2-$ $(C-C$ (f))	C_b	-0.72457	-0.92918	-0.92918	0	-154.19863	0.91771	0.78155	-17.40869	-17.21783	52.78	127.22	24.04	1.92443	0.47279
$isoC_a(R'-H_2C_d)C_b(R''-H_2C_c)CH_2-$ $(C-C$ (f))	C_b	-0.72457	-0.72457	-0.72457	-0.72457	-154.51399	0.91771	0.76765	-17.92866	-17.73779	50.04	129.96	22.66	1.94462	0.49298
$C_c(H)C_a=C_a(H)C_d$	C_a	-1.13380	-0.92918	0	0	-153.67867	0.91771	0.80561	-16.88873	-16.69786	127.61	52.39	58.24	0.77492	0.49168
$C_c(H)C_a=C_bH_2$	C_b	-1.13380	0	0	0	-152.74949	0.91771	0.85252	-15.95955	-15.76868	129.84	50.16	60.70	0.72040	0.54620
$C_c(C_d)C_a=C_bH,C_e$	C_a	-1.13380	-0.72457	-0.72457	0	-154.19863	0.91771	0.78155	-17.40869	-17.21783	126.39	53.61	56.95	0.80289	0.46371
$R_1C_bH_2-C_a(C)=C$ $(C-C$ (i))	C_a	-1.13380	-0.72457	-0.72457	0	-154.19863	0.91771	0.78155	-17.40869	-17.21783	60.88	119.12	27.79	1.81127	0.38039

Table 23.69 cont' d. The MO to HO intercept geometrical bond parameters of tin compounds. *R, R′, R″* are *H* or alkyl groups. E_T is E_T (*atom–atom,msp*^{3}*.AO*).

Bond	Atom	E_T (eV) Bond 1	E_T (eV) Bond 2	E_T (eV) Bond 3	E_T (eV) Bond 4	Final Total Energy $Sn5sp^3$ $C2sp^3$ (eV)	$r_{initial}$ (a_0)	r_{final} (a_0)	$E_{Coulomb}\left(C2sp^3\right)$ (eV) Final	$E\left(Sn5sp^3\right)$ $E\left(C2sp^3\right)$ (eV) Final	θ' (°)	θ_1 (°)	θ_2 (°)	d_1 (a_0)	d_2 (a_0)
$R_1C_bH_2-C_a(C)=C$ $(C-C$ (i)) $R_1C_bH_2-C_a(C)=CH_2$ $(C-C$ (iii))	C_b	-0.72457	-0.92918	0	0	-153.26945	0.91771	0.82562	-16.47951	-16.28864	67.40	112.60	31.36	1.74821	0.31734
$R_1C_bH_2-C_a(H)=C$ $(C-C$ (ii))	C_a	-1.13380	-0.92918	0	0	-153.67866	0.91771	0.80561	-16.88873	-16.69786	64.57	115.43	29.79	1.77684	0.34596
$R_1C_bH_2-C_a(H)=C$ $(C-C$ (i))	C_b	-0.92918	-0.92918	0	0	-153.47405	0.91771	0.81549	-16.68411	-16.49325	65.99	114.01	30.58	1.76270	0.33183
$C-H$ (CH_2) (ii)	C	-1.13380	0	0	0	-152.74949	0.91771	0.85252	-15.95955	-15.76868	77.15	102.85	41.13	1.23531	0.18965
$C^{3e}=(Sn)C_a^{3e}=C$	C_a	-0.85035	-0.85035	0	0	-153.31638	0.91771	0.82327	-16.52644	-16.33558	135.37	44.63	60.36	0.72875	0.58594
$C-H$ (CH) (ii)	C	-0.85035	-0.85035	-0.56690	0	-153.88327	0.91771	0.79597	-17.09334	-16.90248	74.42	105.58	38.84	1.24678	0.21379
$C^{3e}=HC_b^{3e}=C$	C_b	-0.85035	-0.85035	-0.56690	0	-153.88327	0.91771	0.79597	-17.09334	-16.90248	134.24	45.76	58.98	0.75935	0.55533
$C-H$ (C_aH_3)	C_a	-0.56690	0	0	0	-152.18259	0.91771	0.88392	-15.39265	-15.20178	79.89	101.11	43.13	1.20367	0.15511
$C-H$ (C_cH)	C_c	-0.85035	-0.85035	-0.56690	0	-153.88327	0.91771	0.79597	-17.09334	-16.90248	74.42	105.58	38.84	1.24678	0.21379
$C^{3e}=HC_c^{3e}=C$ $C^{3e}=(H_3C_a)C_b^{3e}=C$	C_c C_b	-0.85035	-0.85035	-0.56690	0	-153.88327	0.91771	0.79597	-17.09334	-16.90248	134.24	45.76	58.98	0.75935	0.55533
$\left(C^{3e}=\right)_2 C_b-C_aH_3$	C_a	-0.56690	0	0	0	-152.18259	0.91771	0.88392	-15.39265	-15.20178	73.38	106.62	34.97	1.68807	0.25279
$\left(C^{3e}=\right)_2 C_b-C_aH_3$	C_b	-0.56690	-0.85035	-0.85035	0	-153.88328	0.91771	0.79597	-17.09334	-16.90247	61.56	118.44	28.27	1.81430	0.37901
$C^{3e}=HC_b^{3e}=C$ $C^{3e}=(HOOC_a)C_b^{3e}=C_c(H)$ $C^{3e}=(Cl)C_a^{3e}=C_b(H)$ $C^{3e}=(H_2N)C_a^{3e}=C_b(H)$	C_b C_c C_b C_b	-0.85035	-0.85035	-0.56690	0	-153.88327	0.91771	0.79597	-17.09334	-16.90248	134.24	45.76	58.98	0.75935	0.55533
$C_bC_a(O)O-H$	O	-0.92918	0	0	0		1.00000	0.86359	-15.75493		115.09	64.91	64.12	0.55182	0.36625
$C_bC_a(O)-OH$	O	-0.92918	0	0	0		1.00000	0.86359	-15.75493		101.32	78.68	48.58	1.14765	0.16950
$C_bC_a(O)-OH$	C_a	-0.92918	-1.34946	-0.64574	0	-154.54007	0.91771	0.76652	-17.75013	-17.55927	93.11	86.89	42.68	1.27551	0.04165
$C_bC_a(OH)=O$	O	-1.34946	0	0	0		1.00000	0.84115	-16.17521		137.27	42.73	66.31	0.52193	0.61784
$C_bC_a(OH)=O$	C_a	-1.34946	-0.64574	-0.92918	0	-154.54007	0.91771	0.76652	-17.75013	-17.55927	134.03	45.97	62.14	0.60699	0.53278
$C_b-C_a(O)OH$	C_a	-0.64574	-1.34946	-0.92918	0	-154.54007	0.91771	0.76652	-17.75013	-17.55927	70.34	109.66	32.00	1.65466	0.25784
$C_b-C_a(O)OH$	C_b	-0.64574	-0.85035	-0.85035	0	-153.96212	0.91771	0.79232	-17.17218	-16.98131	73.74	106.26	33.94	1.61863	0.22181

Table 23.70A. The energy parameters (eV) of functional groups of tin compounds.

Parameters	$Sn-Cl$ Group	$Sn-Br$ Group	$Sn-I$ Group	$Sn-O$ Group	$Sn-H$ Group	$Sn-C$ Group	$Sn-Sn$ Group	CH_3 Group	CH_2 (i) Group	CH (i) Group	$C-C$ (a) Group	$C-C$ (b) Group	$C-C$ (c) Group	$C-C$ (d) Group
n_1	1	1	1	2	1	1	1	3	2	1	1	1	1	1
n_2	0	0	0	0	0	0	0	2	1	0	0	0	0	0
n_3	0	0	0	0	0	0	0	0	0	0	0	0	0	0
C_1	0.375	0.375	0.25	0.5	0.375	0.5	0.375	0.75	0.75	0.75	0.5	0.5	0.5	0.5
C_2	0.71514	0.78498	1	0.68098	1	0.58152	0.68510	1	1	1	1	1	1	1
c_1	1	1	1	1	1	1	1	1	1	1	1	1	1	1
c_2	0.71514	1	0.88732	0.68098	0.68510	1	1	0.91771	0.91771	0.91771	0.91771	0.91771	0.91771	0.91771
c_3	0	0	0	0	0	0	0	0	1	1	0	0	0	1
c_4	1	1	1	2	1	2	2	1	1	1	2	2	2	2
c_5	1	1	1	2	1	0	0	3	2	1	0	0	0	0
C_{1b}	0.375	0.375	0.25	0.5	0.375	0.5	0.375	0.75	0.75	0.75	0.5	0.5	0.5	0.5
C_{2b}	0.71514	0.78498	1	0.68098	1	0.58152	0.68510	1	1	1	1	1	1	1
V_σ (eV)	-23.27710	-18.85259	-18.00852	-53.79650	-26.17110	-32.30127	-16.82311	-107.32728	-70.41425	-35.12015	-28.79214	-28.79214	-29.10112	-28.79214
V_π (eV)	6.28029	5.53925	5.14251	15.74264	8.33182	6.63612	4.87644	38.92728	25.78002	12.87680	9.33352	9.33352	9.37273	9.33352
T (eV)	4.62339	2.65383	2.57265	13.22015	6.54278	6.60696	2.10289	32.53914	21.06675	10.48582	6.77464	6.77464	6.90500	6.77464
V_m (eV)	-2.31169	-1.32691	-1.28632	-6.61007	-3.27139	-3.30348	-1.05144	-16.26957	-10.53337	-5.24291	-3.38732	-3.38732	-3.45250	-3.38732
$E_{(AO:BO)}$ (eV)	-9.27363	-9.27363	-9.27363	-18.54725	-9.27363	-9.27363	-9.27363	-15.56407	-15.56407	-14.63489	-15.56407	-15.56407	-15.35946	-15.56407
$\Delta E_{(AO:BO)}$ (eV)	0	0	0	0	0	0	0	0	0	0	0	0	0	0
E_2 (eV)	-9.27363	-9.27363	-9.27363	-18.54725	-9.27363	-9.27363	-9.27363	-15.56407	-15.56407	-14.63489	-15.56407	-15.56407	-15.35946	-15.56407
E_1 (eV)	-23.95874	-21.26006	-20.85531	-49.99104	-23.84152	-31.63530	-20.16886	-67.69451	-49.66493	-31.63533	-31.63537	-31.63537	-31.63535	-31.63537
$E_T\left(atom\ \ atom, nsp^3, AO\right)$ (eV)	-1.38745	-2.50024	-1.25012	-1.13065	-1.65813	0	-0.43693	0	0	0	-1.85836	-1.85836	-1.44915	-1.85836
E_2 (sol) (eV)	-25.34619	-23.76030	-22.10343	-51.12170	-25.49965	-31.63537	-20.60579	-67.59450	-49.66493	-31.63537	-33.49373	-33.49373	-33.08452	-33.49373
$\omega\left(10^5\ rad/s\right)$	14.7492	5.45759	3.15684	21.6951	8.95067	14.5150	2.61932	24.9286	24.2751	24.1759	9.43699	9.43699	15.4846	9.43699
F_N (eV)	9.70820	3.59228	2.07789	14.28009	5.89149	9.55403	1.72408	16.40846	15.97831	15.91299	6.21159	6.21159	10.19220	6.21159
$\bar{E}_D$ (eV)	-0.15624	-0.08909	-0.06303	-0.19109	-0.12245	-0.19345	-0.05353	-0.25352	-0.25017	-0.24966	-0.16515	-0.16515	-0.20896	-0.16515
$\bar{E}_{Nuc}$ (eV)	0.04353 [14]	0.03065 [14]	0.02467 [14]	0.10193 [14]	0.22937 [72]	0.14754 [72]	0.02343 [73]	0.35532 Eq. (13.458)	0.35532 Eq. (13.458)	0.35532 Eq. (13.458)	0.12312 [6]	0.17978 [7]	0.09944 [8]	0.12312 [6]
$\bar{E}_{ee}$ (eV)	-0.13447	-0.07377	-0.05070	-0.14013	-0.00776	-0.11968	-0.04181	-0.22757	-0.14502	-0.07200	-0.10359	-0.07526	-0.15924	-0.10359
E_{mag} (eV)	0.03679	0.03679	0.03679	0.03679	0.03679	0.14803	0.03679	0.14803	0.14803	0.14803	0.14803	0.14803	0.14803	0.14803
E_2 (corr) (eV)	-25.48066	-23.83407	-22.15413	-51.40195	-25.50741	-31.75505	-20.64760	-67.92207	-49.80996	-31.70737	-33.59732	-33.49373	-33.24376	-33.59732
E_{proton} (sol AO:BO) (eV)	-9.27363	-9.27363	-9.27363	-9.27363	-9.27363	-14.63489	-9.27362	-14.63489	-14.63489	-14.63489	-14.63489	-14.63489	-14.63489	-14.63489
E_{proton} (sol AO:BO) (eV)	-12.96764	-11.8138	-10.45126	-13.61806	-13.59844	0	0	-13.59844	-13.59844	-13.59844	0	0	0	0
E_D (corr) (eV)	3.23939	2.74664	2.42924	5.61858	2.63534	2.48527	2.10034	12.49186	7.83016	3.32601	4.32754	4.29921	3.97398	4.17951

Table 23.70B. The energy parameters (eV) of functional groups of tin compounds.

Parameters	$C-C$ (e) Group	$C-C$ (f) Group	$C=C$ Group	$C-C$ (i) Group	$C-C$ (ii) Group	$C-C$ (iii) Group	CH_2 (ii) Group	$^{3e}C=C$ Group	CH (ii) Group	$C-C$ (iv) Group	$C-C(O)$ Group	$C=O$ Group	$C-O$ Group	OH Group
f_1	1	1	1	1	1	1	1	0.75	1	1	1	1	1	1
n_1	1	1	2	1	1	1	2	2	1	1	1	2	1	1
n_2	0	0	0	0	0	0	1	0	0	0	0	0	0	0
n_3	0	0	0	0	0	0	0	0	0	0	0	0	0	0
C_1	0.5	0.5	0.5	0.5	0.5	0.5	0.75	0.5	0.75	0.5	0.5	0.5	0.5	0.75
C_2	1	1	0.91771	1	1	1	1	0.85252	1	1	1	1	1	1
c_1	1	1	1	1	1	1	1	1	1	1	1	1	1	0.75
c_2	0.91771	0.91771	0.91771	0.91771	0.91771	0.91771	0.91771	0.85252	0.91771	0.91771	0.91771	0.85395	0.85395	1
c_3	1	0	0	1	0	1	1	0	1	0	0	2	0	1
c_4	2	2	4	2	2	2	1	3	1	2	2	4	2	1
c_5	0	0	0	0	0	0	2	0	1	0	0	0	0	1
C_{1o}	0.5	0.5	0.5	0.5	0.5	0.5	0.75	0.5	0.75	0.5	0.5	0.5	0.5	0.75
C_{2o}	1	1	0.91771	1	1	1	1	0.85252	1	1	1	1	1	1
V_e (eV)	-29.10112	-29.10112	-102.08992	-30.19634	-30.19634	-30.19634	-72.03287	-101.12679	-37.10024	-29.95792	-32.15216	-111.25473	-35.08488	-40.92709
V_p (eV)	9.37273	9.37273	21.48386	9.50874	9.50874	9.50874	26.02344	20.69825	13.17125	9.47952	9.74055	23.87467	10.32968	14.81988
T (eV)	6.90500	6.90500	34.67062	7.37432	7.37432	7.37432	21.95990	34.31559	11.58941	7.27120	8.23945	42.82081	10.11150	16.18567
V_m (eV)	-3.45250	-3.45250	-17.33531	-3.68716	-3.68716	-3.68716	-10.97995	-17.15779	-5.79470	-3.63560	-4.11973	-21.41040	-5.05575	-8.09284
$E_{(AO/HO)}$ (eV)	-15.35946	-15.35946	0	-14.63489	-14.63489	-14.63489	-14.63489	0	-14.63489	-15.35946	-14.63489	0	-14.63489	-13.6181
$\Delta E_{H_2MO(AO/HO)}$ (eV)	0	0	0	0	0	0	0	0	-1.13379	-0.56690	-1.29147	-2.69893	-2.69893	0
$E_{T(AO/HO)}$ (eV)	-15.35946	-15.35946	0	-14.63489	-14.63489	-14.63489	-14.63489	0	-13.50110	-14.79257	-13.34342	2.69893	-11.93596	-13.6181
$E_{T(H_2MO)}$ (eV)	-31.63535	-31.63535	-63.27075	-31.63534	-31.63534	-31.63534	-49.66437	-63.27075	-31.63539	-31.63537	-31.63530	-63.27074	-31.63541	-31.63247
$E_T\left(atom-atom, msp^3.AO\right)$ (eV)	-1.44915	-1.44915	-2.26759	-1.44915	-1.85836	-1.44915	0	-2.26759	-0.56690	-1.13379	-1.29147	-2.69893	-1.85836	0
$E_{T(MO)}$ (eV)	-33.08452	-33.08452	-65.53833	-33.08452	-33.49373	-33.08452	-49.66493	-65.53833	-32.20226	-32.76916	-32.92684	-65.96966	-33.49373	-31.63537
$\omega\left(10^{15}\ rad/s\right)$	9.55643	9.55643	43.0680	9.97851	16.4962	9.97851	25.2077	49.7272	26.4826	16.2731	10.7262	59.4034	24.3637	44.1776
E_K (eV)	6.29021	6.29021	28.34813	6.56803	10.85807	6.56803	16.59214	32.73133	17.43132	10.71127	7.06019	39.10034	16.03660	29.07844
$\bar{E}_D$ (eV)	-0.16416	-0.16416	-0.34517	-0.16774	-0.21834	-0.16774	-0.25493	-0.35806	-0.26130	-0.21217	-0.17309	-0.40804	-0.26535	-0.33749
$\bar{E}_{Kvib}$ (eV)	0.12312 [6]	0.12312 [6]	0.17897 [72]	0.15895 [73]	0.09931 [74]	0.09931 [74]	0.35532 Eq. (13.458)	0.19649 [30]	0.35532 Eq. (13.458)	0.14940 [43]	0.10502 [75]	0.21077 [76]	0.14010 [77]	0.46311 [78-79]
$\bar{E}_{osc}$ (eV)	-0.10260	-0.10260	-0.25568	-0.08827	-0.16869	-0.11809	-0.07727	-0.25982	-0.08364	-0.13747	-0.12058	-0.30266	-0.19530	-0.10594
E_{mag} (eV)	0.14803	0.14803	0.14803	0.14803	0.14803	0.14803	0.14803	0.14803	0.14803	0.14803	0.14803	0.11441	0.14803	0.11441
$E_{T(Group)}$ (eV)	-33.18712	-33.18712	-66.04969	-33.17279	-33.66242	-33.20260	-49.81948	-49.54347	-32.28590	-32.90663	-33.04742	-66.57498	-33.68903	-31.74130
$E_{initial\ (c_4\ AO/HO)}$ (eV)	-14.63489	-14.63489	-14.63489	-14.63489	-14.63489	-14.63489	-14.63489	-14.63489	-14.63489	-14.63489	-14.63489	-14.63489	-14.63489	-13.6181
$E_{initial\ (c_5\ AO/HO)}$ (eV)	0	0	0	0	0	0	-13.59844	0	-13.59844	0	0	0	0	-13.59844
$E_{D(Group)}$ (eV)	3.62128	3.91734	7.51014	3.75498	4.39264	3.78480	7.83968	5.63881	3.90454	3.63685	3.77764	7.80660	4.41925	4.41035

Table 23.71. The total bond energies of gaseous-state tin compounds calculated using the functional group composition (separate functional groups designated in the first row) and the energies of Tables 23.70 A and B compared to the gaseous-state experimental values except where indicated.

Formula	Name	*SnCl*	*SnBr*	*SnI*	*SnO*	*SnH*	*SnC*	*SnSn*	CH_3	CH_2 (i)	*CH* (i)	*C–C* (a)	*C–C* (b)	*C–C* (c)	*C=C*	*C–C* (ii)	CH_2 (ii)	$^{3c}C{=}C$	*CH* (ii)	*C–C* (iv)	*C–C(O)*	*C=O*	*C–O*	*OH*	Calculated Total Bond Energy (eV)	Experimental Total Bond Energy (eV)	Relative Error
$SnCl_4$	Tin tetrachloride	4	0	0	0	0	0	0	0	0	0	0	0	0	0	0	0	0	0	0	0	0	0	0	12.95756	13.03704 [82]	0.00610
CH_3Cl_3Sn	Methyltin trichloride	3	0	0	0	0	1	0	1	0	0	0	0	0	0	0	0	0	0	0	0	0	0	0	24.69530	25.69118[a] [83]	0.03876
$C_2H_6Cl_2Sn$	Dimethyltin dichloride	2	0	0	0	0	2	0	2	0	0	0	0	0	0	0	0	0	0	0	0	0	0	0	36.43304	37.12369 [84]	0.01860
C_3H_9ClSn	Trimethylin Chloride	1	0	0	0	0	3	0	3	0	0	0	0	0	0	0	0	0	0	0	0	0	0	0	48.17077	49.00689 [84]	0.01706
$SnBr_4$	Tin tetrabromide	0	4	0	0	0	0	0	0	0	0	0	0	0	0	0	0	0	0	0	0	0	0	0	10.98655	11.01994 [82]	0.00303
C_3H_9BrSn	Trimethyltin bromide	0	1	0	0	0	3	0	3	0	0	0	0	0	0	0	0	0	0	0	0	0	0	0	47.67802	48.35363 [84]	0.01397
$C_{12}H_{10}Br_2Sn$	Diphenyltin dibromide	0	2	0	0	0	2	0	0	0	0	0	0	0	0	0	0	12	10	0	0	0	0	0	117.17489	117.36647[a] [83]	0.00163
$C_{12}H_{27}BrSn$	Tri-n-butyltin bromide	0	1	0	0	0	3	0	3	9	0	9	0	0	0	0	0	0	0	0	0	0	0	0	157.09732	157.26555[a] [83]	0.00107
$C_{18}H_{15}BrSn$	Triphenyltin bromide	0	1	0	0	0	3	0	0	0	0	0	0	0	0	0	0	18	15	0	0	0	0	0	170.26905	169.91511[a] [83]	-0.00208
SnI_4	Tin tetraiodide	0	0	4	0	0	0	0	0	0	0	0	0	0	0	0	0	0	0	0	0	0	0	0	9.71697	9.73305 [85]	0.00165
C_3H_9ISn	Trimethyltin iodide	0	0	1	0	0	3	0	3	0	0	0	0	0	0	0	0	0	0	0	0	0	0	0	47.36062	47.69852 [84]	0.00708
$C_{18}H_{15}SnI$	Triphenyltin iodide	0	0	1	0	0	3	0	0	0	0	0	0	0	0	0	0	18	15	0	0	0	0	0	169.95165	167.87948[a] [84]	-0.01234
SnO	Tin oxide	0	0	0	1	0	0	0	0	0	0	0	0	0	0	0	0	0	0	0	0	0	0	0	5.61858	5.54770 [82]	-0.01278
SnH_4	Stannane	0	0	0	0	4	0	0	0	0	0	0	0	0	0	0	0	0	0	0	0	0	0	0	10.54137	10.47181 [82]	-0.00664
C_2H_8Sn	Dimethylstannane	0	0	0	0	2	2	0	2	0	0	0	0	0	0	0	0	0	0	0	0	0	0	0	35.22494	35.14201 [84]	-0.00236
$C_3H_{10}Sn$	Trimethylstannane	0	0	0	0	1	3	0	3	0	0	0	0	0	0	0	0	0	0	0	0	0	0	0	47.56673	47.77353 [84]	0.00433
$C_4H_{12}Sn$	Diethylstannane	0	0	0	0	2	2	0	2	2	0	2	0	0	0	0	0	0	0	0	0	0	0	0	59.54034	59.50337 [84]	-0.00062
$C_4H_{12}Sn$	Tetramethyltin	0	0	0	0	0	4	0	4	0	0	0	0	0	0	0	0	0	0	0	0	0	0	0	59.90851	60.13973 [82]	0.00384
$C_5H_{12}Sn$	Trimethylvinyltin	0	0	0	0	0	4	0	3	0	1	0	0	0	1	0	1	0	0	0	0	0	0	0	66.09248	66.43260 [84]	0.00526
$C_5H_{14}Sn$	Trimethylethyltin	0	0	0	0	0	4	0	4	1	0	1	0	0	0	0	0	0	0	0	0	0	0	0	72.06621	72.19922 [83]	0.00184
$C_6H_{16}Sn$	Trimethylisopropyltin	0	0	0	0	0	4	0	5	0	1	0	2	0	0	0	0	0	0	0	0	0	0	0	84.32480	84.32346 [83]	-0.00002
$C_8H_{12}Sn$	Tetravinyltin	0	0	0	0	0	4	0	0	0	4	0	0	0	4	0	4	0	0	0	0	0	0	0	84.64438	86.53803[a] [83]	0.02188
$C_6H_{18}Sn_2$	Hexamethyldistannane	0	0	0	0	0	6	1	6	0	0	0	0	0	0	0	0	0	0	0	0	0	0	0	91.96311	91.75569 [83]	-0.00226
$C_7H_{18}Sn$	Trimethyl-t-butyltin	0	0	0	0	0	4	0	6	0	0	0	0	3	0	0	0	0	0	0	0	0	0	0	96.81417	96.47805 [82]	-0.00348
$C_9H_{14}Sn$	Trimethylphenyltin	0	0	0	0	0	4	0	3	0	0	0	0	0	0	0	0	6	5	0	0	0	0	0	100.77219	100.42716 [83]	-0.00344
$C_8H_{18}Sn$	Triethylvinyltin	0	0	0	0	0	4	0	3	3	1	3	0	0	1	0	1	0	0	0	0	0	0	0	102.56558	102.83906[a] [83]	-0.00266
$C_8H_{20}Sn$	Tetraethyltin	0	0	0	0	0	4	0	4	4	0	4	0	0	0	0	0	0	0	0	0	0	0	0	108.53931	108.43751 [83]	-0.00094
$C_{10}H_{16}Sn$	Trimethylbenzyltin	0	0	0	0	0	4	0	3	1	0	0	0	0	0	0	0	6	5	1	0	0	0	0	112.23920	112.61211 [83]	0.00331
$C_{10}H_{14}O_2Sn$	Trimethyltin benzoate	0	0	0	0	0	4	0	3	0	0	0	0	0	0	0	0	6	4	0	1	1	1	1	117.28149	119.31199[a] [83]	0.01702
$C_{10}H_{20}Sn$	Tetra-allyltin	0	0	0	0	0	4	0	0	4	4	0	0	0	4	0	4	0	0	4	0	0	0	0	133.53558	139.20655[a] [83]	0.04074
$C_{12}H_{28}Sn$	Tetra-n-propyltin	0	0	0	0	0	4	0	4	8	0	8	0	0	0	0	0	0	0	0	0	0	0	0	157.17011	157.01253 [83]	-0.00100
$C_{12}H_{28}Sn$	Tetraisopropyltin	0	0	0	0	0	4	0	8	0	4	0	4	0	0	0	0	0	0	0	0	0	0	0	157.57367	156.9952 [83]	-0.00366
$C_{12}H_{30}Sn_2$	Hexaethyldistannane	0	0	0	0	0	6	1	6	6	0	6	0	0	0	0	0	0	0	0	0	0	0	0	164.90931	164.76131[a] [83]	-0.00090
$C_{19}H_{18}Sn$	Triphenylmethyltin	0	0	0	0	0	4	0	1	0	0	0	0	0	0	0	0	18	15	0	0	0	0	0	182.49954	180.97881[a] [84]	-0.00840
$C_{20}H_{20}Sn$	Triphenylethyltin	0	0	0	0	0	4	0	1	1	0	1	0	0	0	0	0	18	15	0	0	0	0	0	194.65724	192.92526[a] [84]	-0.00898
$C_{16}H_{36}Sn$	Tetra-n-butyltin	0	0	0	0	0	4	0	4	12	0	12	0	0	0	0	0	0	0	0	0	0	0	0	205.80091	205.60055 [83]	-0.00097
$C_{16}H_{36}Sn$	Tetraisobutyltin	0	0	0	0	0	4	0	8	4	4	0	12	0	0	0	0	0	0	0	0	0	0	0	206.09115	206.73234 [83]	0.00310
$C_{21}H_{24}Sn_2$	Triphenyl-trimethyldistannane	0	0	0	0	0	6	1	3	0	0	0	0	0	0	0	0	18	15	0	0	0	0	0	214.55414	212.72973[a] [84]	-0.00858
$C_{24}H_{20}Sn$	Tetraphenyltin	0	0	0	0	0	4	0	0	0	0	0	0	0	0	0	0	24	20	0	0	0	0	0	223.36322	221.61425 [83]	-0.00789
$C_{24}H_{44}Sn$	Tetracyclohexyltin	0	0	0	0	0	4	0	0	20	4	24	0	0	0	0	0	0	0	0	0	0	0	0	283.70927	284.57603 [83]	0.00305
$C_{36}H_{30}Sn_2$	Hexaphenyldistannane	0	0	0	0	0	6	1	0	0	0	0	0	0	0	0	0	36	30	0	0	0	0	0	337.14517	333.27041 [83]	-0.01163

[a] Crystal.

Table 23.72. The bond angle parameters of tin compounds and experimental values [3]. In the calculation of θ_v, the parameters from the preceding angle were used. E_T is E_T (*atom–atom,msp*^{3}*.AO*).

Atoms of Angle	2c' Bond 1 (a_0)	2c' Bond 2 (a_0)	2c' Terminal Atoms (a_0)	$E_{Coulombic}$ Atom 1	Atom 1 Hybridization Designation (Table 15.3A)	$E_{Coulombic}$ Atom 2	Atom 2 Hybridization Designation (Table 15.3A)	c_2 Atom 1	c_2 Atom 2	C_1	C_2	c_1	c_2'	E_T (eV)	θ_v (°)	θ_1 (°)	θ_2 (°)	Cal. θ (°)	Exp. θ (°)
$\angle ClSnCl$	4.33286	4.33286	6.9892	-12.96764 *Cl*	Cl	-12.96764 *Cl*	Cl	0.71514	0.71514	0.75	0.71514	1	0.71514	-0.87386				107.52	109.5 (tin tetrachloride)
$\angle HSnH$	3.26599	3.26599	5.3417	-9.32137 *Sn*	(Eq. 23.221)	H	H	0.68510	1	0.75	1	1	0.68510	-1.65813 (Eq. 23.236)				109.72	109.5 (stannane)
$\angle CSnC$	4.10053	4.10053	6.7082	-14.82575	1	-14.82575	1	0.91771	0.91771	1	1	1	0.91771	0				109.76	109.5 (tetramethyltin)
Methyl $\angle HC_aH$	2.09711	2.09711	3.4252	-15.75493	7	H	H	0.86359	1	1	1	0.75	1.15796	0				109.50	
$\angle HC_aSn$															70.56			109.44	
$\angle C_aC_bC_c$															70.56			109.44	
Methylene $\angle HC_aH$	2.11106	2.11106	3.4252	-15.75493	7	H	H	0.86359	1	1	1	0.75	1.15796	0				108.44	107 (propane)
$\angle C_aC_bC_c$															69.51			110.49	112 (propane) 113.8 (butane) 110.8 (isobutane)
$\angle C_aC_bH$															69.51			110.49	111.0 (butane) 111.4 (isobutane)
Methyl $\angle HC_aH$	2.09711	2.09711	3.4252	-15.75493	7	H	H	0.86359	1	1	1	0.75	1.15796	0				109.50	
$\angle C_aC_bC_c$															70.56			109.44	
$\angle C_aC_bH$															70.56			109.44	
$\angle C_bC_aC_c$ iso C_a	2.91547	2.91547	4.7958	-16.68412 C_b	26	-16.68412 C_c	26	0.81549	0.81549	1	1	1	0.81549	-1.85836				110.67	110.8 (isobutane)
$\angle C_bC_aH$ iso C_a	2.91547	2.11323	4.1633	-15.55033 C_a	5	-14.82575 C_b	1	0.87495	0.91771	0.75	1	0.75	1.04887	0				110.76	
$\angle C_aC_bH$ iso C_a	2.91547	2.09711	4.1633	-15.55033 C_b	5	-14.82575 C_a	1	0.87495	0.91771	0.75	1	0.75	1.04887	0				111.27	111.4 (isobutane)
$\angle C_bC_aC_b$ tert C_a	2.90327	2.90327	4.7958	-16.68412 C_b	26	-16.68412 C_b	26	0.81549	0.81549	1	1	1	0.81549	-1.85836				111.37	110.8 (isobutane)
$\angle C_bC_aC_d$															72.50			107.50	
$\angle HC_aC_c$ $(C_c(H)C_a = C_b)$	2.11323	2.86175	4.2895	-15.95954 C_a	10	-14.82575 C_c	1	0.85252	0.91771	0.75	1	0.75	1.07647	0				118.36	
$\angle C_cC_aC_c$ $(C_c(C_c)C_a = C_b)$	2.86175	2.86175	4.7958	-16.68411 C_c	25	-16.68411 C_c	25	0.81549	0.81549	1	1	1	0.81549	-1.85836				113.84	
$\angle C_bC_aC_c$ $(C_b = C_aC_c)$	2.53321	2.86175	4.7539	-16.88873 C_b	30	-16.68411 C_c	25	0.80561	0.81549	1	1	1	0.81055	-1.85836				123.46	124.4 (1,3,5-hexatriene CbCcCc) 121.7 (1,3,5-hexatriene CaCbCc) 124.4 (1,3-butadiene CCC) 125.3 (2-butene CbCaCc)

Table 23.72 cont' d. The bond angle parameters of tin compounds and experimental values [3]. In the calculation of θ_v, the parameters from the preceding angle were used. E_T is E_T (*atom–atom,msp*^{3}*.AO*).

Atoms of Angle	2c' Bond 1 (a_0)	2c' Bond 2 (a_0)	2c' Terminal Atoms (a_0)	$E_{Coulombic}$ Atom 1	Atom 1 Hybridization Designation (Table 15.3A)	$E_{Coulombic}$ Atom 2	Atom 2 Hybridization Designation (Table 15.3A)	c_2 Atom 1	c_2 Atom 2	C_1	C_2	c_1	c_2'	E_T (eV)	θ_v (°)	θ_1 (°)	θ_2 (°)	Cal. θ (°)	Exp. θ (°)
$\angle HC_aC_b$																118.36	123.46	118.19	
$\angle HC_aH$ $(H_2C_a=C_bC_c)$	2.04578	2.04578	3.4756	-15.95955	10	H	H	0.85252	1	1	1	0.75	1.17300	0				116.31	118.5 (2-methylpropene)
$\angle C_bC_aH$ $(H_2C_a=C_bC_c)$																116.31		121.85	121 (2-methylpropene)
$\angle CCC$ (aromatic)	2.62936	2.62936	4.5585	-17.17218	38	-17.17218	38	0.79232	0.79232	1	1	1	0.79232	-1.85836				120.19	120 [34-36] (benzene)
$\angle CCH$ (aromatic)																120.19		119.91	120 [34-36] (benzene)
$\angle C_aO_bH$	2.63431	1.83616	3.6405	-14.82575	1	-14.82575	1	1	0.91771	0.75	1	0.75	0.91771	0				107.71	
$\angle C_bC_aO_a$	2.82796	2.27954	4.4721	-17.17218	38	-13.61806	O	0.79232	0.85395 (Eq. (15.133))	1	1	1	0.82313	-1.65376				121.86	122 [55] (benzoic acid)
$\angle C_bC_aO_b$	2.82796	2.63431	4.6690	-16.40067	20	-13.61806	O	0.82959	0.85395 (Eq. (15.133))	1	1	1	0.84177	-1.65376				117.43	118 [55] (benzoic acid)
$\angle O_aC_aO_b$	2.27954	2.63431	4.3818	-16.17521 O_a	13	-15.75493 O_b	7	0.84115	0.86359	1	1	1	0.85237	-1.44915				126.03	122 [55] (benzoic acid)

LEAD ORGANOMETALLIC FUNCTIONAL GROUPS AND MOLECULES

The branched-chain alkyl lead molecules, PbC_nH_{2n-2}, comprise at least one Pb bound by a carbon-lead single bond comprising a $C-Pb$ group, at least a terminal methyl group (CH_3), and may comprise methylene (CH_2), methylyne (CH), and $C-C$ functional groups. The methyl and methylene functional groups are equivalent to those of straight-chain alkanes. Six types of $C-C$ bonds can be identified. The n-alkane $C-C$ bond is the same as that of straight-chain alkanes. In addition, the $C-C$ bonds within isopropyl ($(CH_3)_2CH$) and t-butyl ($(CH_3)_3C$) groups and the isopropyl to isopropyl, isopropyl to t-butyl, and t-butyl to t-butyl $C-C$ bonds comprise functional groups.

As in the cases of carbon, silicon, tin, and germanium, the bonding in the lead atom involves four sp^3 hybridized orbitals. For lead, they are formed from the $6p$ and $6s$ electrons of the outer shells. $Pb-C$ bonds form between a $Pb6sp^3$ HO and a $C3sp^3$ HO to yield alkyl leads. The geometrical parameters of the $Pb-C$ functional group are solved using Eq. (15.51) and the relationships between the prolate spheroidal axes. Then, the sum of the energies of the H_2-type ellipsoidal MOs is matched to that of the $Pb6sp^3$ shell as in the case of the corresponding carbon, silicon, tin, germanium molecules. As in the case of the transition metals, the energy of each functional group is determined for the effect of the electron density donation from each participating $C3sp^3$ HO and $Pb6sp^3$ HO to the corresponding MO that maximizes the bond energy.

The Pb electron configuration is $[Xe]6s^24f^{14}5d^{10}6p^2$, and the orbital arrangement is:

$$\begin{array}{ccc} & \text{6p state} & \\ \underline{\uparrow} & \underline{\uparrow} & \underline{\quad} \\ 1 & 0 & -1 \end{array} \tag{23.244}$$

corresponding to the ground state $^3P_0$. The energy of the lead $6p$ shell is the negative of the ionization energy of the lead atom [1] given by:

$$E\left(Pb,6p\ shell\right) = -E(ionization;\ Pb) = -7.41663\ eV \tag{23.245}$$

The energy of lead is less than the Coulombic energy between the electron and proton of H given by Eq. (1.264), but the atomic orbital may hybridize in order to achieve a bond at an energy minimum. After Eq. (13.422), the $Pb6s$ atomic orbital (AO) combines with the $Pb6p$ AOs to form a single $Pb6sp^3$ hybridized orbital (HO) with the orbital arrangement

$$\begin{array}{cccc} & & \text{6sp}^3\text{ state} & \\ \underline{\uparrow} & \underline{\uparrow} & \underline{\uparrow} & \underline{\uparrow} \\ 0,0 & 1,-1 & 1,0 & 1,1 \end{array} \tag{23.246}$$

where the quantum numbers (ℓ, m_ℓ) are below each electron. The total energy of the state is given by the sum over the four electrons. The sum $E_T\left(Pb,6sp^3\right)$ of experimental energies [1] of Pb, Pb^+, Pb^{2+}, and Pb^{3+} is:

$$E_T\left(Pb,6sp^3\right) = 42.32\ eV + 31.9373\ eV + 15.03248\ eV + 7.41663\ eV = 96.70641\ eV \tag{23.247}$$

By considering that the central field decreases by an integer for each successive electron of the shell, the radius r_{6sp^3} of the $Pb6sp^3$ shell may be calculated from the Coulombic energy using Eq. (15.13).

$$r_{6sp^3} = \sum_{n=78}^{81} \frac{(Z-n)e^2}{8\pi\varepsilon_0\left(e96.70641\ eV\right)} = \frac{10e^2}{8\pi\varepsilon_0\left(e96.70641\ eV\right)} = 1.40692a_0 \tag{23.248}$$

where $Z = 82$ for lead. Using Eq. (15.14), the Coulombic energy $E_{Coulomb}\left(Pb,6sp^3\right)$ of the outer electron of the $Pb6sp^3$ shell is

$$E_{Coulomb}\left(Pb,6sp^3\right) = \frac{-e^2}{8\pi\varepsilon_0 r_{6sp^3}} = \frac{-e^2}{8\pi\varepsilon_0 1.40692a_0} = -9.67064\ eV \tag{23.249}$$

During hybridization, the spin-paired $6s$ electrons are promoted to the $Pb6sp^3$ shell as unpaired electrons. The energy for the promotion is the magnetic energy given by Eq. (15.15) at the initial radius of the $6s$ electrons. From Eq. (10.102) with $Z = 82$ and $n = 80$, the radius r_{80} of the $Pb6s$ shell is:

$$r_{80} = 1.27805a_0 \tag{23.250}$$

Using Eqs. (15.15) and (23.250), the unpairing energy is:

$$E(magnetic) = \frac{2\pi\mu_0 e^2\hbar^2}{m_e^2\left(r_{80}\right)^3} = \frac{8\pi\mu_o\mu_B^2}{\left(1.27805a_0\right)^3} = 0.05481\ eV \tag{23.251}$$

Using Eqs. (23.249) and (23.251), the energy $E\left(Pb,6sp^3\right)$ of the outer electron of the $Pb6sp^3$ shell is:

$$E\left(Pb,6sp^3\right)=\frac{-e^2}{8\pi\varepsilon_0 r_{6sp^3}}+\frac{2\pi\mu_0 e^2\hbar^2}{m_e^2\left(r_{80}\right)^3}=-9.67064\ eV+0.05481\ eV=-9.61584\ eV \tag{23.252}$$

Next, consider the formation of the $Pb-L$-bond MO of lead compounds wherein L is a ligand including carbon and each lead atom has a $Pb6sp^3$ electron with an energy given by Eq. (23.252). The total energy of the state of each lead atom is given by the sum over the four electrons. The sum $E_T\left(Pb_{Pb-L},6sp^3\right)$ of energies of $Pb6sp^3$ (Eq. (23.252)), Pb^+, Pb^{2+}, and Pb^{3+} is:

$$\begin{aligned}E_T\left(Pb_{Pb-L},6sp^3\right)&=-\left(42.32\ eV+31.9373\ eV+15.03248\ eV+E\left(Pb,6sp^3\right)\right)\\&=-\left(42.32\ eV+31.9373\ eV+15.03248\ eV+9.61584\ eV\right)=-98.90562\ eV\end{aligned} \tag{23.253}$$

where $E\left(Pb,6sp^3\right)$ is the sum of the energy of Pb, $-7.41663\ eV$, and the hybridization energy.

A minimum energy is achieved while matching the potential, kinetic, and orbital energy relationships given in the Hydroxyl Radical (OH) section with the donation of electron density from the participating $Pb6sp^3$ HO to each $Pb-L$-bond MO. Consider the case wherein each $Pb6sp^3$ HO donates an excess of 25% of its electron density to the $Pb-L$-bond MO to form an energy minimum. By considering this electron redistribution in the lead molecule as well as the fact that the central field decreases by an integer for each successive electron of the shell, in general terms, the radius $r_{Pb-L6sp^3}$ of the $Pb6sp^3$ shell may be calculated from the Coulombic energy using Eq. (15.18).

$$r_{Pb-L6sp^3}=\left(\sum_{n=78}^{81}(Z-n)-0.25\right)\frac{e^2}{8\pi\varepsilon_0\left(e98.90562\ eV\right)}=\frac{9.75e^2}{8\pi\varepsilon_0\left(e98.90562\ eV\right)}=1.34124a_0 \tag{23.254}$$

Using Eqs. (15.19) and (23.254), the Coulombic energy $E_{Coulomb}\left(Pb_{Pb-L},6sp^3\right)$ of the outer electron of the $Pb6sp^3$ shell is:

$$E_{Coulomb}\left(Pb_{Pb-L},6sp^3\right)=\frac{-e^2}{8\pi\varepsilon_0 r_{Pb-L6sp^3}}=\frac{-e^2}{8\pi\varepsilon_0 1.34124a_0}=-10.14417\ eV \tag{23.255}$$

During hybridization, the spin-paired $6s$ electrons are promoted to the $Pb6sp^3$ shell as unpaired electrons. The energy for the promotion is the magnetic energy given by Eq. (23.251). Using Eqs. (23.251) and (23.255), the energy $E\left(Pb_{Pb-L},6sp^3\right)$ of the outer electron of the $Pb6sp^3$ shell is:

$$E\left(Pb_{Pb-L},6sp^3\right)=\frac{-e^2}{8\pi\varepsilon_0 r_{Pb-L6sp^3}}+\frac{2\pi\mu_0 e^2\hbar^2}{m_e^2\left(r_{80}\right)^3}=-10.14417\ eV+0.05481\ eV=-10.08936\ eV \tag{23.256}$$

Thus, $E_T\left(Pb-L,6sp^3\right)$, the energy change of each $Pb6sp^3$ shell with the formation of the $Pb-L$-bond MO is given by the difference between Eq. (23.256) and Eq. (23.252).

$$E_T\left(Pb-L,6sp^3\right)=E\left(Pb_{Pb-L},6sp^3\right)-E\left(Pb,6sp^3\right)=-10.08936\ eV-\left(-9.61584\ eV\right)=-0.47352\ eV \tag{23.257}$$

Next, consider the formation of the $Pb-C$-bond MO by bonding with a carbon having a $C2sp^3$ electron with an energy given by Eq. (14.146). The total energy of the state is given by the sum over the four electrons. The sum $E_T\left(C_{ethane},2sp^3\right)$ of calculated energies of $C2sp^3$, C^+, C^{2+}, and C^{3+} from Eqs. (10.123), (10.113-10.114), (10.68), and (10.48), respectively, is:

$$\begin{aligned}E_T\left(C_{ethane},2sp^3\right)&=-\left(64.3921\ eV+48.3125\ eV+24.2762\ eV+E\left(C,2sp^3\right)\right)\\&=-\left(64.3921\ eV+48.3125\ eV+24.2762\ eV+14.63489\ eV\right)=-151.61569\ eV\end{aligned} \tag{23.258}$$

where $E\left(C,2sp^3\right)$ is the sum of the energy of C, $-11.27671\ eV$, and the hybridization energy.

The sharing of electrons between the $Pb6sp^3$ HO and $C2sp^3$ HOs to form a $Pb-C$-bond MO permits each participating hybridized orbital to decrease in radius and energy. A minimum energy is achieved while satisfying the potential, kinetic, and orbital energy relationships, when the $Pb6sp^3$ HO donates, and the $C2sp^3$ HO receives, excess electron density equivalent to an electron within the $Pb-C$-bond MO. By considering this electron redistribution in the alkyl lead molecule as well as the fact that the central field decreases by an integer for each successive electron of the shell, the radius $r_{Pb-C2sp^3}$ of the $C2sp^3$ shell of the $Pb-C$-bond MO may be calculated from the Coulombic energy using Eqs. (15.18) and (23.258).

$$r_{Pb-C2sp^3}=\left(\sum_{n=2}^{5}(Z-n)+1\right)\frac{e^2}{8\pi\varepsilon_0\left(e151.61569\ eV\right)}=\frac{11e^2}{8\pi\varepsilon_0\left(e151.61569\ eV\right)}=0.98713a_0 \tag{23.259}$$

Using Eqs. (15.19) and (23.259), the Coulombic energy $E_{Coulomb}\left(C_{Pb-C},2sp^3\right)$ of the outer electron of the $C2sp^3$ shell is

$$E_{Coulomb}\left(C_{Pb-C},2sp^3\right)=\frac{-e^2}{8\pi\varepsilon_0 r_{Pb-C2sp^3}}=\frac{-e^2}{8\pi\varepsilon_0 0.98713a_0}=-13.78324\ eV \tag{23.260}$$

During hybridization, the spin-paired $2s$ electrons are promoted to the $C2sp^3$ shell as unpaired electrons. The energy for the promotion is the magnetic energy given by Eq. (14.145). Using Eqs. (14.145) and (23.260), the energy $E\left(C_{Pb-C},2sp^3\right)$ of the outer electron of the $C2sp^3$ shell is:

$$E\left(C_{Pb-C},2sp^3\right)=\frac{-e^2}{8\pi\varepsilon_0 r_{Pb-C2sp^3}}+\frac{2\pi\mu_0 e^2\hbar^2}{m_e^2\left(r_3\right)^3}=-13.78324\ eV+0.19086\ eV=-13.59238\ eV \tag{23.261}$$

Thus, $E_T\left(Pb-C,2sp^3\right)$, the energy change of each $C2sp^3$ shell with the formation of the $Pb-C$-bond MO is given by the difference between Eq. (23.261) and Eq. (14.146).

$$E_T\left(Pb-C,2sp^3\right)=E\left(C_{Pb-C},2sp^3\right)-E\left(C,2sp^3\right)=-13.59238\ eV-\left(-14.63489\ eV\right)=1.04251\ eV \tag{23.262}$$

Now, consider the formation of the $Pb-L$-bond MO of lead compounds wherein L is a ligand including carbon. For the $Pb-L$ functional groups, hybridization of the $6p$ and $6s$ AOs of Pb to form a single $Pb6sp^3$ HO shell forms an energy minimum, and the sharing of electrons between the $Pb6sp^3$ HO and L HO to form a MO permits each participating orbital to decrease in radius and energy. The $C2sp^3$ HO has an energy of $E\left(C,2sp^3\right)=-14.63489\ eV$ (Eq. (15.25)) and the $Pb6sp^3$ HO has an energy of $E\left(Pb,6sp^3\right)=-9.61584\ eV$ (Eq. (23.252)). To meet the equipotential condition of the union of the $Pb-L$ H_2-type-ellipsoidal-MO with these orbitals, the hybridization factors c_2 and C_2 of Eq. (15.61) for the $Pb-L$-bond MO given by Eq. (15.77) are:

$$c_2\left(C2sp^3HO\ to\ Pb6sp^3HO\right)=C_2\left(C2sp^3HO\ to\ Pb6sp^3HO\right)=\frac{E\left(Pb,6sp^3HO\right)}{E\left(C,2sp^3\right)}=\frac{-9.61584\ eV}{-14.63489\ eV}=0.65705 \tag{23.263}$$

Since the energy of the MO is matched to that of the $Pb6sp^3$ HO, $E\left(AO/HO\right)$ in Eq. (15.61) is $E\left(Pb,6sp^3HO\right)$ given by Eq. (23.252). In order to match the energies of the carbon and lead HOs within the molecule, $E_T\left(atom-atom,msp^3.AO\right)$ of the $Pb-L$-bond MO for the ligand carbon is one half $E_T\left(Pb-C,2sp^3\right)$ (Eq. (23.262)).

The symbols of the functional groups of lead compounds are given in Table 23.73. The geometrical (Eqs. (15.1-15.5)), intercept (Eqs. (15.31-15.32) and (15.80-15.87)), and energy (Eqs. (15.61) and (23.28-23.33)) parameters of lead compounds are given in Tables 23.74, 23.75, and 23.76, respectively. The total energy of each lead compound given in Table 22.77 was calculated as the sum over the integer multiple of each $E_D(Group)$ of Table 23.76 corresponding to functional-group composition of the compound. The bond angle parameters of lead compounds determined using Eqs. (15.88-15.117) are given in Table 23.78. The charge-densities of exemplary lead compound, tetraethyl lead ($Pb\left(CH_2CH_3\right)_4$) comprising atoms with the outer shell bridged by one or more H_2-type ellipsoidal MOs or joined with one or more hydrogen MOs are shown in Figure 23.16.

Figure 23.16. Color scale, charge-density of $Pb(CH_2CH_3)_4$ showing the orbitals of the Pb and C atoms at their radii, the ellipsoidal surface of each H or H_2-type ellipsoidal MO that transitions to the corresponding outer shell of the atoms participating in each bond, and the hydrogen nuclei.

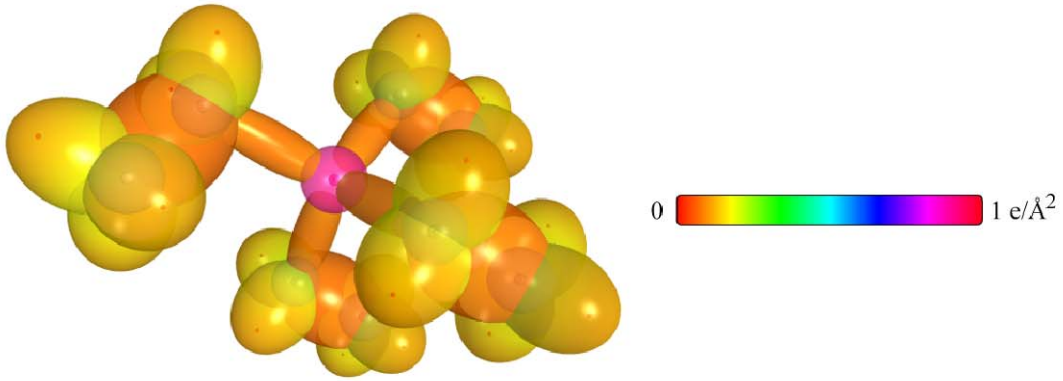

Table 23.73. The symbols of functional groups of lead compounds.

Functional Group	Group Symbol
PbC group	$Pb-C$
CH_3 group	$C-H\ (CH_3)$
CH_2 alkyl group	$C-H\ (CH_2)$
CH alkyl	$C-H$
CC bond (*n-C*)	$C-C$ (a)
CC bond (*iso-C*)	$C-C$ (b)
CC bond (*tert-C*)	$C-C$ (c)
CC (*iso* to *iso-C*)	$C-C$ (d)
CC (*t* to *t-C*)	$C-C$ (e)
CC (*t* to *iso-C*)	$C-C$ (f)

Table 23.74. The geometrical bond parameters of lead compounds and experimental values [3].

Parameter	$Pb-C$ Group	$C-H\ (CH_3)$ Group	$C-H\ (CH_2)$ Group	$C-H$ Group	$C-C$ (a) Group	$C-C$ (b) Group	$C-C$ (c) Group	$C-C$ (d) Group	$C-C$ (e) Group	$C-C$ (f) Group
$a\ (a_0)$	2.21873	1.64920	1.67122	1.67465	2.12499	2.12499	2.10725	2.12499	2.10725	2.10725
$c'\ (a_0)$	2.12189	1.04856	1.05553	1.05661	1.45744	1.45744	1.45164	1.45744	1.45164	1.45164
Bond Length $2c'\ (Å)$	2.24571	1.10974	1.11713	1.11827	1.54280	1.54280	1.53635	1.54280	1.53635	1.53635
Exp. Bond Length $(Å)$	2.238 $((CH_3)_4 Pb)$	1.107 ($C-H$ propane) 1.117 ($C-H$ butane)	1.107 ($C-H$ propane) 1.117 ($C-H$ butane)	1.122 (isobutane)	1.532 (propane) 1.531 (butane)	1.532 (propane) 1.531 (butane)	1.532 (propane) 1.531 (butane)	1.532 (propane) 1.531 (butane)	1.532 (propane) 1.531 (butane)	1.532 (propane) 1.531 (butane)
$b,c\ (a_0)$	0.64834	1.27295	1.29569	1.29924	1.54616	1.54616	1.52750	1.54616	1.52750	1.52750
e	0.95635	0.63580	0.63159	0.63095	0.68600	0.68600	0.68888	0.68600	0.68888	0.68888

Table 23.75. The MO to HO intercept geometrical bond parameters of lead compounds. *R, R′, R″* are *H* or alkyl groups. E_T is E_T (*atom–atom,msp*^{3}*.AO*).

Bond	Atom	E_T (eV) Bond 1	E_T (eV) Bond 2	E_T (eV) Bond 3	E_T (eV) Bond 4	Final Total Energy $Pb6sp^3$ $C2sp^3$ (eV)	$r_{initial}$ (a_0)	r_{final} (a_0)	$E_{Coulomb}(C2sp^3)$ (eV) Final	$E(Pb6sp^3)$ $E(C2sp^3)$ (eV) Final	θ' (°)	θ_1 (°)	θ_2 (°)	d_1 (a_0)	d_2 (a_0)
$C-H\ (CH_3)$	C	0.26063	0	0	0	-151.35506	0.91771	0.93414	-14.56512	-14.37426	85.33	94.67	47.00	1.12468	0.07613
$(CH_3)_3\,Pb-CH_3$	Pb	0.26063	0.26063	0.26063	0.26063		1.40692	0.98713	-13.78324		147.67	32.33	54.52	1.28781	0.83408
$(CH_3)_3\,Pb-CH_3$	C	0.26063	0	0	0		0.91771	0.93414	-14.56512	-14.37426	146.47	33.53	52.74	1.34322	0.77867
$C-H\ (CH_3)$	C	-0.92918	0	0	0	-152.54487	0.91771	0.86359	-15.75493	-15.56407	77.49	102.51	41.48	1.23564	0.18708
$C-H\ (CH_2)$ (i)	C	-0.92918	-0.92918	0	0	-153.47406	0.91771	0.81549	-16.68412	-16.49325	68.47	111.53	35.84	1.35486	0.29933
$C-H\ (CH)$ (i)	C	-0.92918	-0.92918	-0.92918	0	-154.40324	0.91771	0.77247	-17.61330	-17.42244	61.10	118.90	31.37	1.42988	0.37326
$H_3C_aC_bH_2CH_2-$ $(C-C$ (a))	C_a	-0.92918	0	0	0	-152.54487	0.91771	0.86359	-15.75493	-15.56407	63.82	116.18	30.08	1.83879	0.38106
$H_3C_aC_bH_2CH_2-$ $(C-C$ (a))	C_b	-0.92918	-0.92918	0	0	-153.47406	0.91771	0.81549	-16.68412	-16.49325	56.41	123.59	26.06	1.90890	0.45117
$R-H_2C_aC_b(H_2C_c-R')HCH_2-$ $(C-C$ (b))	C_b	-0.92918	-0.92918	-0.92918	0	-154.40324	0.91771	0.77247	-17.61330	-17.42244	48.30	131.70	21.90	1.97162	0.51388
$R-H_2C_a(R'-H_2C_d)C_b(R'-H_2C_c)CH_2-$ $(C-C$ (c))	C_b	-0.92918	-0.72457	-0.72457	-0.72457	-154.71860	0.91771	0.75889	-17.92866	-17.73779	48.21	131.79	21.74	1.95734	0.50570
$isoC_aC_b(H_2C_c-R')HCH_2-$ $(C-C$ (d))	C_b	-0.92918	-0.92918	-0.92918	0	-154.40324	0.91771	0.77247	-17.61330	-17.42244	48.30	131.70	21.90	1.97162	0.51388
$tertC_a(R'-H_2C_d)C_b(R''-H_2C_c)CH_2-$ $(C-C$ (e))	C_b	-0.72457	-0.72457	-0.72457	-0.72457	-154.51399	0.91771	0.76765	-17.92866	-17.73779	50.04	129.96	22.66	1.94462	0.49298
$tertC_aC_b(H_2C_c-R')HCH_2-$ $(C-C$ (f))	C_b	-0.72457	-0.92918	-0.92918	0	-154.19863	0.91771	0.78155	-17.40869	-17.21783	52.78	127.22	24.04	1.92443	0.47279
$isoC_a(R'-H_2C_d)C_b(R''-H_2C_c)CH_2-$ $(C-C$ (f))	C_b	-0.72457	-0.72457	-0.72457	-0.72457	-154.51399	0.91771	0.76765	-17.92866	-17.73779	50.04	129.96	22.66	1.94462	0.49298

Table 23.76. The energy parameters (eV) of functional groups of lead compounds.

Parameters	$Pb-C$ Group	CH_3 Group	CH_2 Group	CH Group	$C-C$ (a) Group	$C-C$ (b) Group	$C-C$ (c) Group	$C-C$ (d) Group	$C-C$ (e) Group	$C-C$ (f) Group
n_1	1	3	2	1	1	1	1	1	1	1
n_2	0	2	1	0	0	0	0	0	0	0
n_3	0	0	0	0	0	0	0	0	0	0
C_1	0.375	0.75	0.75	0.75	0.5	0.5	0.5	0.5	0.5	0.5
C_2	0.65705	1	1	1	1	1	1	1	1	1
c_1	1	1	1	1	1	1	1	1	1	1
c_2	0.65705	0.91771	0.91771	0.91771	0.91771	0.91771	0.91771	0.91771	0.91771	0.91771
c_3	0	0	1	1	0	0	0	1	1	0
c_4	2	1	1	1	2	2	2	2	2	2
c_5	0	3	2	1	0	0	0	0	0	0
C_{1o}	0.375	0.75	0.75	0.75	0.5	0.5	0.5	0.5	0.5	0.5
C_{2o}	0.65705	1	1	1	1	1	1	1	1	1
V_e (eV)	-32.04219	-107.32728	-70.41425	-35.12015	-28.79214	-28.79214	-29.10112	-28.79214	-29.10112	-29.10112
V_p (eV)	6.41212	38.92728	25.78002	12.87680	9.33352	9.33352	9.37273	9.33352	9.37273	9.37273
T (eV)	7.22084	32.53914	21.06675	10.48582	6.77464	6.77464	6.90500	6.77464	6.90500	6.90500
V_m (eV)	-3.61042	-16.26957	-10.53337	-5.24291	-3.38732	-3.38732	-3.45250	-3.38732	-3.45250	-3.45250
$E_{(AO/HO)}$ (eV)	-9.61584	-15.56407	-15.56407	-14.63489	-15.56407	-15.56407	-15.35946	-15.56407	-15.35946	-15.35946
$\Delta E_{H_2MO\,(AO/HO)}$ (eV)	0	0	0	0	0	0	0	0	0	0
$E_{T\,(AO/HO)}$ (eV)	-9.61584	-15.56407	-15.56407	-14.63489	-15.56407	-15.56407	-15.35946	-15.56407	-15.35946	-15.35946
$E_{T\,(H_2MO)}$ (eV)	-31.63548	-67.69451	-49.66493	-31.63533	-31.63537	-31.63537	-31.63535	-31.63537	-31.63535	-31.63535
$E_T\left(atom-atom, msp^3.AO\right)$ (eV)	0.52125	0	0	0	-1.85836	-1.85836	-1.44915	-1.85836	-1.44915	-1.44915
$E_{T\,(MO)}$ (eV)	-31.11411	-67.69450	-49.66493	-31.63537	-33.49373	-33.49373	-33.08452	-33.49373	-33.08452	-33.08452
$\omega\ \left(10^{15}\ rad/s\right)$	6.20930	24.9286	24.2751	24.1759	9.43699	9.43699	15.4846	9.43699	9.55643	9.55643
E_K (eV)	4.08707	16.40846	15.97831	15.91299	6.21159	6.21159	10.19220	6.21159	6.29021	6.29021
$\overline{E}_D$ (eV)	-0.12444	-0.25352	-0.25017	-0.24966	-0.16515	-0.16515	-0.20896	-0.16515	-0.16416	-0.16416
$\overline{E}_{Kvib}$ (eV)	0.14444 [66]	0.35532 Eq. (13.458)	0.35532 Eq. (13.458)	0.35532 Eq. (13.458)	0.12312 [6]	0.17978 [7]	0.09944 [8]	0.12312 [6]	0.12312 [6]	0.12312 [6]
$\overline{E}_{osc}$ (eV)	-0.05222	-0.22757	-0.14502	-0.07200	-0.10359	-0.07526	-0.15924	-0.10359	-0.10260	-0.10260
E_{mag} (eV)	0.14803	0.14803	0.14803	0.14803	0.14803	0.14803	0.14803	0.14803	0.14803	0.14803
$E_{T\,(Group)}$ (eV)	-31.16633	-67.92207	-49.80996	-31.70737	-33.59732	-33.49373	-33.24376	-33.59732	-33.18712	-33.18712
$E_{initial\,(c_4\ AO/HO)}$ (eV)	-14.63489	-14.63489	-14.63489	-14.63489	-14.63489	-14.63489	-14.63489	-14.63489	-14.63489	-14.63489
$E_{initial\,(c_5\ AO/HO)}$ (eV)	0	-13.59844	-13.59844	-13.59844	0	0	0	0	0	0
$E_{D\,(Group)}$ (eV)	1.89655	12.49186	7.83016	3.32601	4.32754	4.29921	3.97398	4.17951	3.62128	3.91734

Table 23.77. The total bond energies of gaseous-state lead compounds calculated using the functional group composition (separate functional groups designated in the first row) and the energies of Table 23.76 compared to the gaseous-state experimental values [86].

Formula	Name	$Pb-C$	CH_3	CH_2	CH	$C-C$ (a)	Calculated Total Bond Energy (eV)	Experimental Total Bond Energy (eV)	Relative Error
$C_4H_{12}Pb$	Tetramethyl-lead	4	4	0	0	0	57.55366	57.43264	-0.00211
$C_8H_{20}Pb$	Tetraethyl-lead	4	4	4	0	4	106.18446	105.49164	-0.00657

Table 23.78. The bond angle parameters of lead compounds and experimental values [3]. In the calculation of θ_v, the parameters from the preceding angle were used. E_T is E_T ($atom$–$atom$,msp^3.AO).

Atoms of Angle	2c' Bond 1 (a_0)	2c' Bond 2 (a_0)	2c' Terminal Atoms (a_0)	$E_{Coulombic}$ Atom 1	Atom 1 Hybridization Designation (Table 15.3.A)	$E_{Coulombic}$ Atom 2	Atom 2 Hybridization Designation (Table 15.3.A)	c_2 Atom 1	c_2 Atom 2	C_1	C_2	c_1	c_2'	E_T (eV)	θ_v (°)	θ_1 (°)	θ_2 (°)	Cal. θ (°)	Exp. θ (°)
Methyl $\angle HC_aH$	2.09711	2.09711	3.4252	-15.75493	7	H	H	0.86359	1	1	1	0.75	1.15796	0				109.50	
$\angle H_aC_aPb$															70.56			109.44	
$\angle C_aPbC_b$	4.24378	4.24378	6.9282	-14.82575	1	-14.82575	1	0.91771	0.91771	1	1	1	0.91771	-1.85836				109.43	109.5 (tetramethyllead)
Methylene $\angle HC_aH$	2.11106	2.11106	3.4252	-15.75493	7	H	H	0.86359	1	1	1	0.75	1.15796	0				108.44	107 (propane)
$\angle C_aC_bC_c$															69.51			110.49	112 (propane) 113.8 (butane) 110.8 (isobutane)
$\angle C_aC_bH$															69.51			110.49	111.0 (butane) 111.4 (isobutane)
Methyl $\angle HC_aH$	2.09711	2.09711	3.4252	-15.75493	7	H	H	0.86359	1	1	1	0.75	1.15796	0				109.50	
$\angle C_aC_bC_c$															70.56			109.44	
$\angle C_aC_bH$															70.56			109.44	
$\angle C_bC_aC_c$ iso C_a	2.91547	2.91547	4.7958	-16.68412 C_b	26	-16.68412 C_c	26	0.81549	0.81549	1	1	1	0.81549	-1.85836				110.67	110.8 (isobutane)
$\angle C_bC_aH$ iso C_a	2.91547	2.11323	4.1633	-15.55033 C_a	5	-14.82575 C_b	1	0.87495	0.91771	0.75	1	0.75	1.04887	0				110.76	
$\angle C_aC_bH$ iso C_a	2.91547	2.09711	4.1633	-15.55033 C_b	5	-14.82575 C_a	1	0.87495	0.91771	0.75	1	0.75	1.04887	0				111.27	111.4 (isobutane)
$\angle C_bC_aC_b$ tert C_a	2.90327	2.90327	4.7958	-16.68412 C_b	26	-16.68412 C_b	26	0.81549	0.81549	1	1	1	0.81549	-1.85836				111.37	110.8 (isobutane)
$\angle C_bC_aC_d$															72.50			107.50	

ALKYL ARSINES ($\left(C_nH_{2n+1}\right)_3 As,\ \ n=1,2,3,4,5...\infty$)

The alkyl arsines, $\left(C_nH_{2n+1}\right)_3 As$, comprise a $As-C$ functional group. The alkyl portion of the alkyl arsine may comprise at least two terminal methyl groups (CH_3) at each end of each chain, and may comprise methylene (CH_2), and methylyne (CH) functional groups as well as C bound by carbon-carbon single bonds. The methyl and methylene functional groups are equivalent to those of straight-chain alkanes. Six types of $C-C$ bonds can be identified. The n-alkane $C-C$ bond is the same as that of straight-chain alkanes. In addition, the $C-C$ bonds within isopropyl ($\left(CH_3\right)_2 CH$) and t-butyl ($\left(CH_3\right)_3 C$) groups and the isopropyl to isopropyl, isopropyl to t-butyl, and t-butyl to t-butyl $C-C$ bonds comprise functional groups. The branched-chain-alkane groups in alkyl arsines are equivalent to those in branched-chain alkanes. The $As-C$ group may further join the $As4sp^3$ HO to an aryl HO.

As in the case of phosphorous, the bonding in the arsenic atom involves sp^3 hybridized orbitals formed, in this case, from the $4p$ and $4s$ electrons of the outer shells. The $As-C$ bond forms between $As4sp^3$ and $C2sp^3$ HOs to yield arsines. The semimajor axis a of the $As-C$ functional group is solved using Eq. (15.51). Using the semimajor axis and the relationships between the prolate spheroidal axes, the geometric and energy parameters of the MO are calculated using Eqs. (15.1-15.117) in the same manner as the organic functional groups given in the Organic Molecular Functional Groups and Molecules section.

The energy of arsenic is less than the Coulombic energy between the electron and proton of H given by Eq. (1.264). A minimum energy is achieved while matching the potential, kinetic, and orbital energy relationships given in the Hydroxyl Radical (OH) section with hybridization of the arsenic atom such that in Eqs. (15.51) and (15.61), the sum of the energies of the H_2-type ellipsoidal MOs is matched to that of the $As4sp^3$ shell as in the case of the corresponding phosphine molecules.

The As electron configuration is $[Ar]4s^2 3d^{10} 4p^3$ corresponding to the ground state ${}^4S_{3/2}$, and the $4sp^3$ hybridized orbital arrangement after Eq. (13.422) is:

$$\begin{array}{cccc} & 4\text{sp}^3 \text{ state} & & \\ \underline{\uparrow\downarrow} & \underline{\uparrow} & \underline{\uparrow} & \underline{\uparrow} \\ 0,0 & 1,-1 & 1,0 & 1,1 \end{array} \tag{23.264}$$

where the quantum numbers (ℓ, m_ℓ) are below each electron. The total energy of the state is given by the sum over the five electrons. The sum $E_T\left(As,4sp^3\right)$ of experimental energies [1] of As, As^+, As^{2+}, As^{3+}, and As^{4+} is:

$$E_T\left(As,4sp^3\right)=62.63\ eV+50.13\ eV+28.351\ eV+18.5892\ eV+9.7886\ eV=169.48880\ eV \tag{23.265}$$

By considering that the central field decreases by an integer for each successive electron of the shell, the radius r_{4sp^3} of the $As4sp^3$ shell may be calculated from the Coulombic energy using Eq. (15.13).

$$r_{4sp^3}=\sum_{n=28}^{32}\frac{(Z-n)e^2}{8\pi\varepsilon_0\left(e169.48880\ eV\right)}=\frac{15e^2}{8\pi\varepsilon_0\left(e169.48880\ eV\right)}=1.20413a_0 \tag{23.266}$$

where $Z=33$ for arsenic. Using Eq. (15.14), the Coulombic energy $E_{Coulomb}\left(As,4sp^3\right)$ of the outer electron of the $As4sp^3$ shell is:

$$E_{Coulomb}\left(As,4sp^3\right)=\frac{-e^2}{8\pi\varepsilon_0 r_{4sp^3}}=\frac{-e^2}{8\pi\varepsilon_0 1.20413a_0}=-11.29925\ eV \tag{23.267}$$

During hybridization, the spin-paired $4s$ electrons are promoted to the $As4sp^3$ shell as paired electrons at the radius r_{4sp^3} of the $As4sp^3$ shell. The energy for the promotion is the difference in the magnetic energy given by Eq. (15.15) at the initial radius of the $4s$ electrons and the final radius of the $As4sp^3$ electrons. From Eq. (10.102) with $Z=33$ and $n=30$, the radius r_{30} of the $As4s$ shell is:

$$r_{30}=1.08564a_0 \tag{23.268}$$

Using Eqs. (15.15) and (23.268), the unpairing energy is:

$$E(magnetic)=\frac{2\pi\mu_0 e^2\hbar^2}{m_e^2}\left(\frac{1}{\left(r_{30}\right)^3}-\frac{1}{\left(r_{4sp^3}\right)^3}\right)=8\pi\mu_o\mu_B^2\left(\frac{1}{\left(1.08564a_0\right)^3}-\frac{1}{\left(1.20413a_0\right)^3}\right)=0.02388\ eV \tag{23.269}$$

Using Eqs. (23.267) and (23.269), the energy $E\left(As,4sp^3\right)$ of the outer electron of the $As4sp^3$ shell is:

$$E\left(As,4sp^3\right)=\frac{-e^2}{8\pi\varepsilon_0 r_{4sp^3}}+\frac{2\pi\mu_0 e^2\hbar^2}{m_e^2}\left(\frac{1}{\left(r_{30}\right)^3}-\frac{1}{\left(r_{4sp^3}\right)^3}\right)=-11.29925\ eV+0.02388\ eV=-11.27537\ eV \tag{23.270}$$

For the $As-C$ functional group, hybridization of the $2s$ and $2p$ AOs of each C and the $4s$ and $4p$ AOs of each As to form single $2sp^3$ and $4sp^3$ shells, respectively, forms an energy minimum, and the sharing of electrons between the $C2sp^3$ and $As4sp^3$ HOs to form a MO permits each participating orbital to decrease in radius and energy. In branched-chain alkyl arsines, the energy of arsenic is less than the Coulombic energy between the electron and proton of H given by Eq. (1.264). Thus, c_2 in Eq. (15.61) is one, and the energy matching condition is determined by the C_2 parameter. Then, the $C2sp^3$ HO has an energy of $E\left(C,2sp^3\right)=-14.63489\ eV$ (Eq. (15.25)), and the $As4sp^3$ HO has an energy of $E\left(As,4sp^3\right)=-11.27537\ eV$ (Eq. (23.270)). To meet the equipotential condition of the union of the $As-C$ H_2-type-ellipsoidal-MO with these orbitals, the hybridization factor C_2 of Eq. (15.61) for the $As-C$-bond MO given by Eqs. (15.77), (15.79), and (13.430) is:

$$C_2\left(C2sp^3HO\ to\ As4sp^3HO\right)=\frac{E\left(As,4sp^3\right)}{E\left(C,2sp^3\right)}c_2\left(C2sp^3HO\right)=\frac{-11.27537\ eV}{-14.63489\ eV}\left(0.91771\right)=0.70705 \tag{23.271}$$

The energy of the $As-C$-bond MO is the sum of the component energies of the H_2-type ellipsoidal MO given in Eq. (15.51) with $E\left(AO/HO\right)=E\left(As,4sp^3\right)$ given by Eq. (23.270), and $E_T\left(atom-atom,msp^3.AO\right)$ is zero in order to match the energies of the carbon and arsenic HOs.

The symbols of the functional groups of branched-chain alkyl arsines are given in Table 23.79. The geometrical (Eqs. (15.1-15.5) and (15.51)), intercept (Eqs. (15.80-15.87)), and energy (Eqs. (15.6-15.11) and (15.17-15.65)) parameters of alkyl arsines are given in Tables 23.80, 23.81, and 23.82, respectively. The total energy of each alkyl arsine given in Table 23.83 was calculated as the sum over the integer multiple of each $E_{D\,(Group)}$ of Table 23.82 corresponding to functional-group composition of the molecule. The bond angle parameters of alkyl arsines determined using Eqs. (15.88-15.117) are given in Table 23.84. The color scale, charge-density of exemplary alkyl arsine, triphenylarsine, comprising atoms with the outer shell bridged by one or more H_2-type ellipsoidal MOs or joined with one or more hydrogen MOs is shown in Figure 23.17.

Figure 23.17. Color scale, charge-density of triphenylarsine showing the orbitals of the atoms at their radii, the ellipsoidal surface of each H or H_2-type ellipsoidal MO that transitions to the corresponding outer shell of the atom(s) participating in each bond, and the hydrogen nuclei.

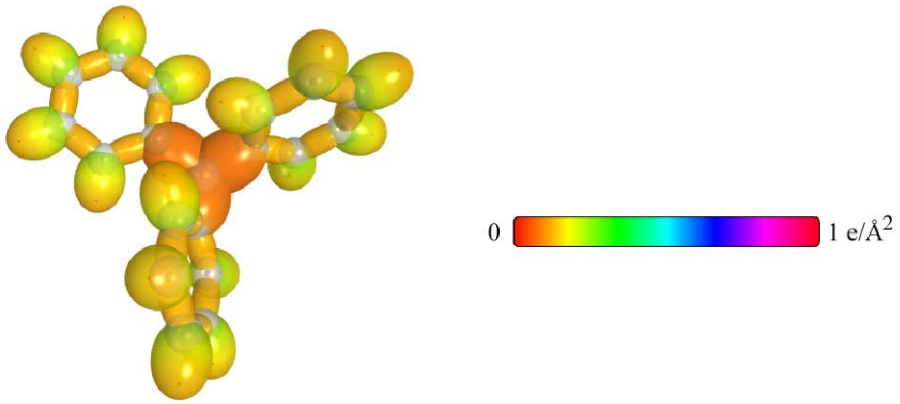

Table 23.79. The symbols of functional groups of alkyl arsines.

Functional Group	Group Symbol
As-C	$As-C$
CH_3 group	$C-H\ (CH_3)$
CH_2 group	$C-H\ (CH_2)$
CH	$C-H$ (i)
CC bond (*n-C*)	$C-C$ (a)
CC bond (*iso-C*)	$C-C$ (b)
CC bond (*tert-C*)	$C-C$ (c)
CC (*iso* to *iso-C*)	$C-C$ (d)
CC (*t* to *t-C*)	$C-C$ (e)
CC (*t* to *iso-C*)	$C-C$ (f)
CC (aromatic bond)	$C\overset{3e}{=}C$
CH (aromatic)	CH (ii)

Table 23.80. The geometrical bond parameters of alkyl arsines and experimental values [3].

Parameter	$As-C$ Group	$C-H\ (CH_3)$ Group	$C-H\ (CH_2)$ Group	$C-H$ (i) Group	$C-C$ (a) Group	$C-C$ (b) Group	$C-C$ (c) Group	$C-C$ (d) Group	$C-C$ (e) Group	$C-C$ (f) Group	$^{3e}C=C$ Group	CH (ii) Group
$a\ (a_0)$	2.33431	1.64920	1.67122	1.67465	2.12499	2.12499	2.10725	2.12499	2.10725	2.10725	1.47348	1.60061
$c'\ (a_0)$	1.81700	1.04856	1.05553	1.05661	1.45744	1.45744	1.45164	1.45744	1.45164	1.45164	1.31468	1.03299
Bond Length $2c'\ (A)$	1.92303	1.10974	1.11713	1.11827	1.54280	1.54280	1.53635	1.54280	1.53635	1.53635	1.39140	1.09327
Exp. Bond Length (A)	1.979 $((CH_3)_2AsCH_3)$	1.107 ($C-H$ propane) 1.117 ($C-H$ butane)	1.107 ($C-H$ propane) 1.117 ($C-H$ butane)	1.122 (isobutane)	1.532 (propane) 1.531 (butane)	1.532 (propane) 1.531 (butane)	1.532 (propane) 1.531 (butane)	1.532 (propane) 1.531 (butane)	1.532 (propane) 1.531 (butane)	1.532 (propane) 1.531 (butane)	1.399 (benzene)	1.101 (benzene)
$b,c\ (a_0)$	1.46544	1.27295	1.29569	1.29924	1.54616	1.54616	1.52750	1.54616	1.52750	1.52750	0.66540	1.22265
e	0.77839	0.63580	0.63159	0.63095	0.68600	0.68600	0.68888	0.68600	0.68888	0.68888	0.89223	0.64537

Table 23.81. The MO to HO intercept geometrical bond parameters of alkyl arsines. *R, R′, R″* are *H* or alkyl groups. E_T is E_T (*atom–atom,msp*^{3}*.AO*.

Bond	Atom	E_T (eV) Bond 1	E_T (eV) Bond 2	E_T (eV) Bond 3	E_T (eV) Bond 4	Final Total Energy $C2sp^3$ (eV)	$r_{initial}\ (a_0)$	$r_{final}\ (a_0)$	$E_{Coulomb}$ (eV) Final	$E(C2sp^3)$ (eV) Final	θ' (°)	θ_1 (°)	θ_2 (°)	$d_1\ (a_0)$	$d_2\ (a_0)$
$C-H\ (CH_3)$	C	0	0	0	0	-151.61569	0.91771	0.91771	-14.82575	-14.63489	83.62	96.38	45.76	1.15051	0.10195
$(CH_3)_2\ As-CH_3$	C	0	0	0	0		0.91771	0.91771	-14.82575	-14.63489	89.82	90.18	38.77	1.81991	0.00291
$(CH_3)_2\ As-CH_3$	As	0	0	0	0		0.91771	0.91771	-14.82575		89.82	90.18	38.77	1.81991	0.00291
$C-H\ (CH_3)$	C	-0.92918	0	0	0	-152.54487	0.91771	0.86359	-15.75493	-15.56407	77.49	102.51	41.48	1.23564	0.18708
$C-H\ (CH_2)$	C	-0.92918	-0.92918	0	0	-153.47406	0.91771	0.81549	-16.68412	-16.49325	68.47	111.53	35.84	1.35486	0.29933
$C-H\ (CH)$	C	-0.92918	-0.92918	-0.92918	0	-154.40324	0.91771	0.77247	-17.61330	-17.42244	61.10	118.90	31.37	1.42988	0.37326
$H_3C_aC_bH_2CH_2-$ ($C-C$ (a))	C_a	-0.92918	0	0	0	-152.54487	0.91771	0.86359	-15.75493	-15.56407	63.82	116.18	30.08	1.83879	0.38106
$H_3C_aC_bH_2CH_2-$ ($C-C$ (a))	C_b	-0.92918	-0.92918	0	0	-153.47406	0.91771	0.81549	-16.68412	-16.49325	56.41	123.59	26.06	1.90890	0.45117
$R-H_2C_aC_b(H_2C_c-R')HCH_2-$ ($C-C$ (b))	C_b	-0.92918	-0.92918	-0.92918	0	-154.40324	0.91771	0.77247	-17.61330	-17.42244	48.30	131.70	21.90	1.97162	0.51388
$R-H_2C_a(R'-H_2C_d)C_b(R''-H_2C_c)CH_2-$ ($C-C$ (c))	C_b	-0.92918	-0.72457	-0.72457	-0.72457	-154.71860	0.91771	0.75889	-17.92866	-17.73779	48.21	131.79	21.74	1.95734	0.50570
$isoC_aC_b(H_2C_c-R')HCH_2-$ ($C-C$ (d))	C_b	-0.92918	-0.92918	-0.92918	0	-154.40324	0.91771	0.77247	-17.61330	-17.42244	48.30	131.70	21.90	1.97162	0.51388
$tertC_a(R'-H_2C_d)C_b(R''-H_2C_c)CH_2-$ ($C-C$ (e))	C_b	-0.72457	-0.72457	-0.72457	-0.72457	-154.51399	0.91771	0.76765	-17.92866	-17.73779	50.04	129.96	22.66	1.94462	0.49298
$tertC_aC_b(H_2C_c-R')HCH_2-$ ($C-C$ (f))	C_b	-0.72457	-0.92918	-0.92918	0	-154.19863	0.91771	0.78155	-17.40869	-17.21783	52.78	127.22	24.04	1.92443	0.47279
$isoC_a(R'-H_2C_d)C_b(R''-H_2C_c)CH_2-$ ($C-C$ (f))	C_b	-0.72457	-0.72457	-0.72457	-0.72457	-154.51399	0.91771	0.76765	-17.92866	-17.73779	50.04	129.96	22.66	1.94462	0.49298

Table 23.82. The energy parameters (eV) of functional groups of alkyl arsines.

Parameters	$As-C$ Group	CH_3 Group	CH_2 Group	CH (i) Group	$C-C$ (a) Group	$C-C$ (b) Group	$C-C$ (c) Group	$C-C$ (d) Group	$C-C$ (e) Group	$C-C$ (f) Group	$C=C$ Group	CH (ii) Group
f_1	1	1	1	1	1	1	1	1	1	1	0.75	1
n_1	1	3	2	1	1	1	1	1	1	1	2	1
n_2	0	2	1	0	0	0	0	0	0	0	0	0
n_3	0	0	0	0	0	0	0	0	0	0	0	0
C_1	0.5	0.75	0.75	0.75	0.5	0.5	0.5	0.5	0.5	0.5	0.5	0.75
C_2	0.70705	1	1	1	1	1	1	1	1	1	0.85252	1
c_1	1	1	1	1	1	1	1	1	1	1	1	1
c_2	1	0.91771	0.91771	0.91771	0.91771	0.91771	0.91771	0.91771	0.91771	0.91771	0.85252	0.91771
c_3	0	0	1	1	0	0	0	1	1	0	0	1
c_4	2	1	1	1	2	2	2	2	2	2	3	1
c_5	0	3	2	1	0	0	0	0	0	0	0	1
C_{1o}	0.5	0.75	0.75	0.75	0.5	0.5	0.5	0.5	0.5	0.5	0.5	0.75
C_{2o}	0.70705	1	1	1	1	1	1	1	1	1	0.85252	1
$V_s\ (eV)$	-31.18832	-107.32728	-70.41425	-35.12015	-28.79214	-28.79214	-29.10112	-28.79214	-29.10112	-29.10112	-101.12679	-37.10024
$V_p\ (eV)$	7.48806	38.92728	25.78002	12.87680	9.33352	9.33352	9.37273	9.33352	9.37273	9.37273	20.69825	13.17125
$T\ (eV)$	6.68041	32.53914	21.06675	10.48582	6.77464	6.77464	6.90500	6.77464	6.90500	6.90500	34.31559	11.58941
$V_m\ (eV)$	-3.34021	-16.26957	-10.53337	-5.24291	-3.38732	-3.38732	-3.45250	-3.38732	-3.45250	-3.45250	-17.15779	-5.79470
$E_{(AO/HO)}\ (eV)$	-11.27537	-15.56407	-15.56407	-14.63489	-15.56407	-15.56407	-15.35946	-15.56407	-15.35946	-15.35946	0	-14.63489
$\Delta E_{H_2MO(AO/HO)}\ (eV)$	0	0	0	0	0	0	0	0	0	0	0	-1.13379
$E_{T(AO/HO)}\ (eV)$	-11.27537	-15.56407	-15.56407	-14.63489	-15.56407	-15.56407	-15.35946	-15.56407	-15.35946	-15.35946	0	-13.50110
$E_{T(H_2MO)}\ (eV)$	-31.63542	-67.69451	-49.66493	-31.63533	-31.63537	-31.63537	-31.63535	-31.63537	-31.63535	-31.63535	-63.27075	-31.63539
$E_T\left(atom-atom, msp^3.AO\right)\ (eV)$	0	0	0	0	-1.85836	-1.85836	-1.44915	-1.85836	-1.44915	-1.44915	-2.26759	-0.56690
$E_{T(MO)}\ (eV)$	-31.63537	-67.69450	-49.66493	-31.63537	-33.49373	-33.49373	-33.08452	-33.49373	-33.08452	-33.08452	-65.53833	-32.20226
$\omega\ \left(10^{15}\ rad/s\right)$	6.89218	24.9286	24.2751	24.1759	9.43699	9.43699	15.4846	9.43699	9.55643	9.55643	49.7272	26.4826
$E_K\ (eV)$	4.53655	16.40846	15.97831	15.91299	6.21159	6.21159	10.19220	6.21159	6.29021	6.29021	32.73133	17.43132
$\bar{E}_D\ (eV)$	-0.13330	-0.25352	-0.25017	-0.24966	-0.16515	-0.16515	-0.20896	-0.16515	-0.16416	-0.16416	-0.35806	-0.26130
$\bar{E}_{Kvib}\ (eV)$	0.15498 [66]	0.35532 (Eq. (13.458))	0.35532 (Eq. (13.458))	0.35532 (Eq. (13.458))	0.12312 [6]	0.17978 [7]	0.09944 [8]	0.12312 [6]	0.12312 [6]	0.12312 [6]	0.19649 [30]	0.35532 Eq. (13.458)
$\bar{E}_{osc}\ (eV)$	-0.05581	-0.22757	-0.14502	-0.07200	-0.10359	-0.07526	-0.15924	-0.10359	-0.10260	-0.10260	-0.25982	-0.08364
$E_{mag}\ (eV)$	0.14803	0.14803	0.14803	0.14803	0.14803	0.14803	0.14803	0.14803	0.14803	0.14803	0.14803	0.14803
$E_{T(Group)}\ (eV)$	-31.69118	-67.92207	-49.80996	-31.70737	-33.59732	-33.49373	-33.24376	-33.59732	-33.18712	-33.18712	-49.54347	-32.28590
$E_{initial\ (c_1\ AO/HO)}\ (eV)$	-14.63489	-14.63489	-14.63489	-14.63489	-14.63489	-14.63489	-14.63489	-14.63489	-14.63489	-14.63489	-14.63489	-14.63489
$E_{initial\ (c_5\ AO/HO)}\ (eV)$	0	-13.59844	-13.59844	-13.59844	0	0	0	0	0	0	0	-13.59844
$E_{D(Group)}\ (eV)$	2.42140	12.49186	7.83016	3.32601	4.32754	4.29921	3.97398	4.17951	3.62128	3.91734	5.63881	3.90454

Table 23.83. The total bond energies of alkyl arsines calculated using the functional group composition and the energies of Table 23.82 compared to the experimental values [87].

Formula	Name	$As-C$	CH_3	CH_2	CH (i)	$C-C$ (a)	$C-C$ (b)	$C-C$ (c)	$C-C$ (d)	$C-C$ (e)	$C-C$ (f)	$C=C$	CH (ii)	Calculated Total Bond Energy (eV)	Experimental Total Bond Energy (eV)	Relative Error
C_3H_9As	Trimethylarsine	3	3	0	0	0	0	0	0	0	0	0	0	44.73978	45.63114	0.01953
$C_6H_{15}As$	Triethylarsine	3	3	3	0	3	0	0	0	0	0	0	0	81.21288	81.01084	-0.00249
$C_{18}H_{15}As$	Triphenylarsine	3	0	0	0	0	0	0	0	0	0	18	15	167.33081	166.49257	-0.00503

Table 23.84. The bond angle parameters of alkyl arsines and experimental values [3]. In the calculation of θ_v, the parameters from the preceding angle were used. E_T is E_T (*atom–atom,msp*^{3}*.AO*).

Atoms of Angle	2*c'* Bond 1 (a_0)	2*c'* Bond 2 (a_0)	2*c'* Terminal Atoms (a_0)	$E_{Coulombic}$ or *E* Atom 1	Atom 1 Hybridization Designation (Table 15.3.A)	$E_{Coulombic}$ Atom 2	Atom 2 Hybridization Designation (Table 15.3.A)	c_2 Atom 1	c_2 Atom 2	C_1	C_2	c_1	c_2'	E_T (eV)	θ_v (°)	θ_1 (°)	θ_2 (°)	Cal. θ (°)	Exp. θ (°)
Methyl $\angle HC_aH$	2.09711	2.09711	3.4252	-15.75493	7	H	H	0.86359	1	1	1	0.75	1.15796	0				109.50	
$\angle H_aC_aAs$															70.56			109.44	111.4 (trimethylarsine)
$\angle C_aAsC_b$	3.63400	3.63400	5.5136	-15.75493	7	-15.75493	7	0.86359	0.86359	1	1	1	0.86359	-1.85836				98.68	98.8 (trimethylarsine)
Methylene $\angle HC_aH$	2.11106	2.11106	3.4252	-15.75493	7	H	H	0.86359	1	1	1	0.75	1.15796	0				108.44	107 (propane)
$\angle C_aC_bC_c$															69.51			110.49	112 (propane) 113.8 (butane) 110.8 (isobutane)
$\angle C_aC_bH$															69.51			110.49	111.0 (butane) 111.4 (isobutane)
Methyl $\angle HC_aH$	2.09711	2.09711	3.4252	-15.75493	7	H	H	0.86359	1	1	1	0.75	1.15796	0				109.50	
$\angle C_aC_bC_c$															70.56			109.44	
$\angle C_aC_bH$															70.56			109.44	
$\angle C_bC_aC_c$ iso C_a	2.91547	2.91547	4.7958	-16.68412 C_b	26	-16.68412 C_c	26	0.81549	0.81549	1	1	1	0.81549	-1.85836				110.67	110.8 (isobutane)
$\angle C_bC_aH$ iso C_a	2.91547	2.11323	4.1633	-15.55033 C_a	5	-14.82575 C_b	1	0.87495	0.91771	0.75	1	0.75	1.04887	0				110.76	
$\angle C_aC_bH$ iso C_a	2.91547	2.09711	4.1633	-15.55033 C_b	5	-14.82575 C_a	1	0.87495	0.91771	0.75	1	0.75	1.04887	0				111.27	111.4 (isobutane)
$\angle C_bC_aC_b$ tert C_a	2.90327	2.90327	4.7958	-16.68412 C_b	26	-16.68412 C_b	26	0.81549	0.81549	1	1	1	0.81549	-1.85836				111.37	110.8 (isobutane)
$\angle C_bC_aC_d$															72.50			107.50	

ALKYL STIBINES ($\left(C_nH_{2n+1}\right)_3 Sb,\ \ n=1,2,3,4,5...\infty$)

The alkyl stibines, $\left(C_nH_{2n+1}\right)_3 Sb$, comprise a $Sb-C$ functional group. The alkyl portion of the alkyl stibine may comprise at least two terminal methyl groups (CH_3) at each end of each chain, and may comprise methylene (CH_2), and methylyne (CH) functional groups as well as C bound by carbon-carbon single bonds. The methyl and methylene functional groups are equivalent to those of straight-chain alkanes. Six types of $C-C$ bonds can be identified. The n-alkane $C-C$ bond is the same as that of straight-chain alkanes. In addition, the $C-C$ bonds within isopropyl ($\left(CH_3\right)_2 CH$) and t-butyl ($\left(CH_3\right)_3 C$) groups and the isopropyl to isopropyl, isopropyl to t-butyl, and t-butyl to t-butyl $C-C$ bonds comprise functional groups. The branched-chain-alkane groups in alkyl stibines are equivalent to those in branched-chain alkanes. The $Sb-C$ group may further join the $Sb5sp^3$ HO to an aryl HO.

As in the case of phosphorous, the bonding in the antimony atom involves sp^3 hybridized orbitals formed, in this case, from the $5p$ and $5s$ electrons of the outer shells. The $Sb-C$ bond forms between $Sb5sp^3$ and $C2sp^3$ HOs to yield stibines. The semimajor axis a of the $Sb-C$ functional group is solved using Eq. (15.51). Using the semimajor axis and the relationships between the prolate spheroidal axes, the geometric and energy parameters of the MO are calculated using Eqs. (15.1-15.117) in the same manner as the organic functional groups given in the Organic Molecular Functional Groups and Molecules section.

The energy of antimony is less than the Coulombic energy between the electron and proton of H given by Eq. (1.264). A minimum energy is achieved while matching the potential, kinetic, and orbital energy relationships given in the Hydroxyl Radical (OH) section with hybridization of the antimony atom such that in Eqs. (15.51) and (15.61), the sum of the energies of the H_2-type ellipsoidal MOs is matched to that of the $Sb5sp^3$ shell as in the case of the corresponding phosphine and arsine molecules.

The Sb electron configuration is $[Kr]5s^2 4d^{10} 5p^3$ corresponding to the ground state ${}^4S_{3/2}$, and the $5sp^3$ hybridized orbital arrangement after Eq. (13.422) is:

$$\begin{array}{cccc} & 5\mathrm{sp}^3 \text{ state} & & \\ \underline{\uparrow\downarrow} & \underline{\uparrow} & \underline{\uparrow} & \underline{\uparrow} \\ 0,0 & 1,-1 & 1,0 & 1,1 \end{array} \tag{23.272}$$

where the quantum numbers (ℓ, m_ℓ) are below each electron. The total energy of the state is given by the sum over the five electrons. The sum $E_T\left(Sb,5sp^3\right)$ of experimental energies [1] of Sb, Sb^+, Sb^{2+}, Sb^{3+}, and Sb^{4+} is:

$$E_T\left(Sb,5sp^3\right)=56.0\ eV+44.2\ eV+25.3\ eV+16.63\ eV+8.60839\ eV=150.73839\ eV \tag{23.273}$$

By considering that the central field decreases by an integer for each successive electron of the shell, the radius r_{5sp^3} of the $Sb5sp^3$ shell may be calculated from the Coulombic energy using Eq. (15.13).

$$r_{5sp^3}=\sum_{n=46}^{50}\frac{(Z-n)e^2}{8\pi\varepsilon_0\left(e150.73839\ eV\right)}=\frac{15e^2}{8\pi\varepsilon_0\left(e150.73839\ eV\right)}=1.35392a_0 \tag{23.274}$$

where $Z=51$ for antimony. Using Eq. (15.14), the Coulombic energy $E_{Coulomb}\left(Sb,5sp^3\right)$ of the outer electron of the $Sb5sp^3$ shell is:

$$E_{Coulomb}\left(Sb,5sp^3\right)=\frac{-e^2}{8\pi\varepsilon_0 r_{5sp^3}}=\frac{-e^2}{8\pi\varepsilon_0 1.35392a_0}=-10.04923\ eV \tag{23.275}$$

During hybridization, the spin-paired $5s$ electrons are promoted to the $Sb5sp^3$ shell as paired electrons at the radius r_{5sp^3} of the $Sb5sp^3$ shell. The energy for the promotion is the difference in the magnetic energy given by Eq. (15.15) at the initial radius of the $5s$ electrons and the final radius of the $Sb5sp^3$ electrons. From Eq. (10.102) with $Z=51$ and $n=48$, the radius r_{48} of the $Sb5s$ shell is:

$$r_{48}=1.23129a_0 \tag{23.276}$$

Using Eqs. (15.15) and (23.276), the unpairing energy is:

$$E(magnetic)=\frac{2\pi\mu_0 e^2\hbar^2}{m_e^2}\left(\frac{1}{\left(r_{48}\right)^3}-\frac{1}{\left(r_{5sp^3}\right)^3}\right)=8\pi\mu_0\mu_B^2\left(\frac{1}{\left(1.23129a_0\right)^3}-\frac{1}{\left(1.35392a_0\right)^3}\right)=0.01519\ eV \tag{23.277}$$

Using Eqs. (23.275) and (23.277), the energy $E\left(Sb,5sp^3\right)$ of the outer electron of the $Sb5sp^3$ shell is:

$$E\left(Sb,5sp^3\right)=\frac{-e^2}{8\pi\varepsilon_0 r_{5sp^3}}+\frac{2\pi\mu_0 e^2\hbar^2}{m_e^2}=-10.04923\ eV+0.01519\ eV=-10.03404\ eV \tag{23.278}$$

For the $Sb-C$ functional group, hybridization of the $2s$ and $2p$ AOs of each C and the $5s$ and $5p$ AOs of each Sb to form single $2sp^3$ and $5sp^3$ shells, respectively, forms an energy minimum, and the sharing of electrons between the $C2sp^3$ and $Sb5sp^3$ HOs to form a MO permits each participating orbital to decrease in radius and energy. In branched-chain alkyl stibines, the energy of antimony is less than the Coulombic energy between the electron and proton of H given by Eq. (1.264). Thus, c_2 in Eq. (15.61) is one, and the energy matching condition is determined by the C_2 parameter. Then, the $C2sp^3$ HO has an energy of $E\left(C,2sp^3\right)=-14.63489\ eV$ (Eq. (15.25)), and the $Sb5sp^3$ HO has an energy of $E\left(Sb,5sp^3\right)=-10.03404\ eV$ (Eq. (23.278)). To meet the equipotential condition of the union of the $Sb-C$ H_2-type-ellipsoidal-MO with these orbitals, the hybridization factor C_2 of Eq. (15.61) for the $Sb-C$-bond MO given by Eqs. (15.77), (15.79), and (13.430) is:

$$C_2\left(C2sp^3HO\ to\ Sb5sp^3HO\right)=\frac{E\left(Sb,5sp^3\right)}{E\left(C,2sp^3\right)}c_2\left(C2sp^3HO\right)=\frac{-10.03404\ eV}{-14.63489\ eV}\left(0.91771\right)=0.62921 \tag{23.279}$$

The energy of the $Sb-C$-bond MO is the sum of the component energies of the H_2-type ellipsoidal MO given in Eq. (15.51) with $E\left(AO/HO\right)=E\left(Sb,5sp^3\right)$ given by Eq. (23.278), and $E_T\left(atom-atom,msp^3.AO\right)$ is zero in order to match the energies of the carbon and antimony HOs.

The symbols of the functional groups of branched-chain alkyl stibines are given in Table 123.85. The geometrical (Eqs. (15.1-15.5) and (15.51)), intercept (Eqs. (15.80-15.87)), and energy (Eqs. (15.6-15.11) and (15.17-15.65)) parameters of alkyl stibines are given in Tables 23.86, 23.87, and 23.88, respectively. The total energy of each alkyl stibine given in Table 23.89 was calculated as the sum over the integer multiple of each $E_D\left(Group\right)$ of Table 23.88 corresponding to functional-group composition of the molecule. The bond angle parameters of alkyl stibines determined using Eqs. (15.88-15.117) are given in Table 23.90. The color scale, charge-density of exemplary alkyl stibine, triphenylstibine, comprising atoms with the outer shell bridged by one or more H_2-type ellipsoidal MOs or joined with one or more hydrogen MOs is shown in Figure 23.18.

Figure 23.18. Color scale, charge-density of triphenylstibine showing the orbitals of the atoms at their radii, the ellipsoidal surface of each H or H_2-type ellipsoidal MO that transitions to the corresponding outer shell of the atom(s) participating in each bond, and the hydrogen nuclei.

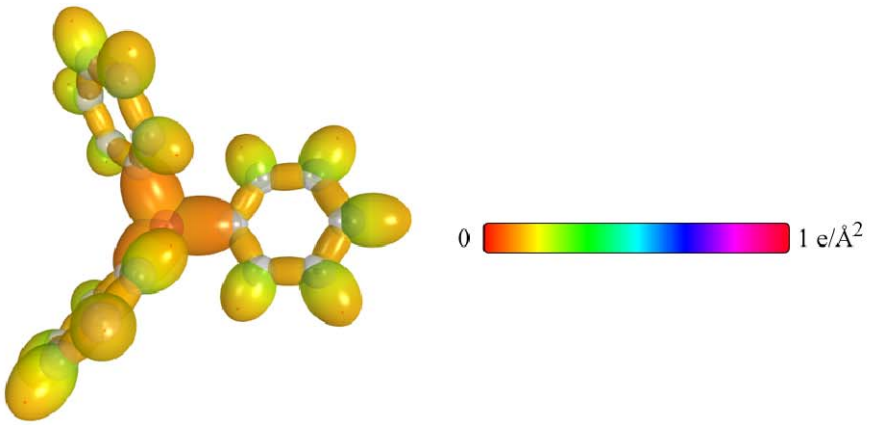

Table 23.85. The symbols of functional groups of alkyl stibines.

Functional Group	Group Symbol
Sb-C	$Sb-C$
CH_3 group	$C-H\ (CH_3)$
CH_2 group	$C-H\ (CH_2)$
CH	$C-H$ (i)
CC bond (*n-C*)	$C-C$ (a)
CC bond (*iso-C*)	$C-C$ (b)
CC bond (*tert-C*)	$C-C$ (c)
CC (*iso* to *iso-C*)	$C-C$ (d)
CC (*t* to *t-C*)	$C-C$ (e)
CC (*t* to *iso-C*)	$C-C$ (f)
CC (aromatic bond)	$C\overset{3e}{=}C$
CH (aromatic)	CH (ii)

Table 23.86. The geometrical bond parameters of alkyl stibines and experimental values [3].

Parameter	$Sb-C$ Group	$C-H\ (CH_3)$ Group	$C-H\ (CH_2)$ Group	$C-H$ (i) Group	$C-C$ (a) Group	$C-C$ (b) Group	$C-C$ (c) Group	$C-C$ (d) Group	$C-C$ (e) Group	$C-C$ (f) Group	$C^{3e}=C$ Group	CH (ii) Group
$a\ (a_0)$	2.38997	1.64920	1.67122	1.67465	2.12499	2.12499	2.10725	2.12499	2.10725	2.10725	1.47348	1.60061
$c'\ (a_0)$	1.94894	1.04856	1.05553	1.05661	1.45744	1.45744	1.45164	1.45744	1.45164	1.45164	1.31468	1.03299
Bond Length $2c'\ (\AA)$	2.06267	1.10974	1.11713	1.11827	1.54280	1.54280	1.53635	1.54280	1.53635	1.53635	1.39140	1.09327
Exp. Bond Length $(\AA)$		1.107 ($C-H$ propane) 1.117 ($C-H$ butane)	1.107 ($C-H$ propane) 1.117 ($C-H$ butane)	1.122 (isobutane)	1.532 (propane) 1.531 (butane)	1.532 (propane) 1.531 (butane)	1.532 (propane) 1.531 (butane)	1.532 (propane) 1.531 (butane)	1.532 (propane) 1.531 (butane)	1.532 (propane) 1.531 (butane)	1.399 (benzene)	1.101 (benzene)
$b,c\ (a_0)$	1.38332	1.27295	1.29569	1.29924	1.54616	1.54616	1.52750	1.54616	1.52750	1.52750	0.66540	1.22265
e	0.81547	0.63580	0.63159	0.63095	0.68600	0.68600	0.68888	0.68600	0.68888	0.68888	0.89223	0.64537

Table 23.87. The MO to HO intercept geometrical bond parameters of alkyl stibines. *R, R', R"* are *H* or alkyl groups. E_T is E_T (*atom–atom,*msp^3*.AO)*.

Bond	Atom	E_T (eV) Bond 1	E_T (eV) Bond 2	E_T (eV) Bond 3	E_T (eV) Bond 4	Final Total Energy $C2sp^3$ (eV)	$r_{initial}$ (a_0)	r_{final} (a_0)	$E_{Coulomb}$ (eV) Final	$E(C2sp^3)$ (eV) Final	θ' (°)	θ_1 (°)	θ_2 (°)	d_1 (a_0)	d_2 (a_0)
$C-H\ (CH_3)$	C	0	0	0	0	-151.61569	0.91771	0.91771	-14.82575	-14.63489	83.62	96.38	45.76	1.15051	0.10195
$(CH_3)_2\,Sb-CH_3$	C	0	0	0	0		0.91771	0.91771	-14.82575	-14.63489	99.00	81.00	40.94	1.80541	0.14353
$(CH_3)_2\,Sb-CH_3$	Sb	0	0	0	0		1.35392	0.91771	-14.82575		99.00	81.00	40.94	1.80541	0.14353
$C-H\ (CH_3)$	C	-0.92918	0	0	0	-152.54487	0.91771	0.86359	-15.75493	-15.56407	77.49	102.51	41.48	1.23564	0.18708
$C-H\ (CH_2)$	C	-0.92918	-0.92918	0	0	-153.47406	0.91771	0.81549	-16.68412	-16.49325	68.47	111.53	35.84	1.35486	0.29933
$C-H\ (CH)$	C	-0.92918	-0.92918	-0.92918	0	-154.40324	0.91771	0.77247	-17.61330	-17.42244	61.10	118.90	31.37	1.42988	0.37326
$H_3C_aC_bH_2CH_2-$ ($C-C$ (a))	C_a	-0.92918	0	0	0	-152.54487	0.91771	0.86359	-15.75493	-15.56407	63.82	116.18	30.08	1.83879	0.38106
$H_3C_aC_bH_2CH_2-$ ($C-C$ (a))	C_b	-0.92918	-0.92918	0	0	-153.47406	0.91771	0.81549	-16.68412	-16.49325	56.41	123.59	26.06	1.90890	0.45117
$R-H_2C_aC_b(H_2C_c-R')HCH_2-$ ($C-C$ (b))	C_b	-0.92918	-0.92918	-0.92918	0	-154.40324	0.91771	0.77247	-17.61330	-17.42244	48.30	131.70	21.90	1.97162	0.51388
$R-H_2C_a(R'-H_2C_d)C_b(R"-H_2C_c)CH_2-$ ($C-C$ (c))	C_b	-0.92918	-0.72457	-0.72457	-0.72457	-154.71860	0.91771	0.75889	-17.92865	-17.73779	48.21	131.79	21.74	1.95734	0.50570
$isoC_aC_b(H_2C_c-R')HCH_2-$ ($C-C$ (d))	C_b	-0.92918	-0.92918	-0.92918	0	-154.40324	0.91771	0.77247	-17.61330	-17.42244	48.30	131.70	21.90	1.97162	0.51388
$teriC_a(R'-H_2C_d)C_b(R"-H_2C_c)CH_2-$ ($C-C$ (e))	C_b	-0.72457	-0.72457	-0.72457	-0.72457	-154.51399	0.91771	0.76765	-17.92865	-17.73779	50.04	129.96	22.66	1.94462	0.49298
$teriC_aC_b(H_2C_c-R')HCH_2-$ ($C-C$ (f))	C_b	-0.72457	-0.92918	-0.92918	0	-154.19863	0.91771	0.78155	-17.40869	-17.21783	52.78	127.22	24.04	1.92443	0.47279
$isoC_a(R'-H_2C_d)C_b(R"-H_2C_c)CH_2-$ ($C-C$ (f))	C_b	-0.72457	-0.72457	-0.72457	-0.72457	-154.51399	0.91771	0.76765	-17.92865	-17.73779	50.04	129.96	22.66	1.94462	0.49298

Table 23.88. The energy parameters (eV) of functional groups of alkyl stibines.

Parameters	$Sb-C$ Group	CH_3 Group	CH_2 Group	CH (i) Group	$C-C$ (a) Group	$C-C$ (b) Group	$C-C$ (c) Group	$C-C$ (d) Group	$C-C$ (e) Group	$C-C$ (f) Group	$C^{3e}=C$ Group	CH (ii) Group
f_1	1	1	1	1	1	1	1	1	1	1	0.75	1
n_1	1	3	2	1	1	1	1	1	1	1	2	1
n_2	0	2	1	0	0	0	0	0	0	0	0	0
n_3	0	0	0	0	0	0	0	0	0	0	0	0
C_1	0.5	0.75	0.75	0.75	0.5	0.5	0.5	0.5	0.5	0.5	0.5	0.75
C_2	0.62921	1	1	1	1	1	1	1	1	1	0.85252	1
c_1	1	1	1	1	1	1	1	1	1	1	1	1
c_2	1	0.91771	0.91771	0.91771	0.91771	0.91771	0.91771	0.91771	0.91771	0.91771	0.85252	0.91771
c_3	0	0	1	1	0	0	0	1	1	0	0	1
c_4	2	1	1	1	2	2	2	2	2	2	3	1
c_5	0	3	2	1	0	0	0	0	0	0	0	1
C_{1o}	0.5	0.75	0.75	0.75	0.5	0.5	0.5	0.5	0.5	0.5	0.5	0.75
C_{2o}	0.62921	1	1	1	1	1	1	1	1	1	0.85252	1
V_e (eV)	-31.92151	-107.32728	-70.41425	-35.12015	-28.79214	-28.79214	-29.10112	-28.79214	-29.10112	-29.10112	-101.12679	-37.10024
V_p (eV)	6.98112	38.92728	25.78002	12.87680	9.33352	9.33352	9.37273	9.33352	9.37273	9.37273	20.69825	13.17125
T (eV)	6.67822	32.53914	21.06675	10.48582	6.77464	6.77464	6.90500	6.77464	6.90500	6.90500	34.31559	11.58941
V_m (eV)	-3.33911	-16.26957	-10.53337	-5.24291	-3.38732	-3.38732	-3.45250	-3.38732	-3.45250	-3.45250	-17.15779	-5.79470
$E_{(AO/HO)}$ (eV)	-10.03404	-15.56407	-15.56407	-14.63489	-15.56407	-15.56407	-15.35946	-15.56407	-15.35946	-15.35946	0	-14.63489
$\Delta E_{H_2MO\,(AO/HO)}$ (eV)	0	0	0	0	0	0	0	0	0	0	0	-1.13379
$E_T{}_{(AO/HO)}$ (eV)	-10.03404	-15.56407	-15.56407	-14.63489	-15.56407	-15.56407	-15.35946	-15.56407	-15.35946	-15.35946	0	-13.50110
$E_T{}_{(H_2MO)}$ (eV)	-31.63532	-67.69451	-49.66493	-31.63533	-31.63537	-31.63537	-31.63535	-31.63537	-31.63535	-31.63535	-63.27075	-31.63539
$E_T\left(atom-atom, msp^3.AO\right)$ (eV)	0	0	0	0	-1.85836	-1.85836	-1.44915	-1.85836	-1.44915	-1.44915	-2.26759	-0.56690
$E_T{}_{(MO)}$ (eV)	-31.63537	-67.69450	-49.66493	-31.63537	-33.49373	-33.49373	-33.08452	-33.49373	-33.08452	-33.08452	-65.53833	-32.20226
$\omega\left(10^{15}\ rad/s\right)$	6.27593	24.9286	24.2751	24.1759	9.43699	9.43699	15.4846	9.43699	9.55643	9.55643	49.7272	26.4826
E_K (eV)	4.13093	16.40846	15.97831	15.91299	6.21159	6.21159	10.19220	6.21159	6.29021	6.29021	32.73133	17.43132
$\overline{E}_D$ (eV)	-0.12720	-0.25352	-0.25017	-0.24966	-0.16515	-0.16515	-0.20896	-0.16515	-0.16416	-0.16416	-0.35806	-0.26130
$\overline{E}_{Kvib}$ (eV)	0.14878 [66]	0.35532 (Eq. (13.458))	0.35532 (Eq. (13.458))	0.35532 (Eq. (13.458))	0.12312 [6]	0.17978 [7]	0.09944 [8]	0.12312 [6]	0.12312 [6]	0.12312 [6]	0.19649 [30]	0.35532 Eq. (13.458)
$\overline{E}_{osc}$ (eV)	-0.05281	-0.22757	-0.14502	-0.07200	-0.10359	-0.07526	-0.15924	-0.10359	-0.10260	-0.10260	-0.25982	-0.08364
E_{mag} (eV)	0.14803	0.14803	0.14803	0.14803	0.14803	0.14803	0.14803	0.14803	0.14803	0.14803	0.14803	0.14803
$E_T{}_{(Group)}$ (eV)	-31.68818	-67.92207	-49.80996	-31.70737	-33.59732	-33.49373	-33.24376	-33.59732	-33.18712	-33.18712	-49.54347	-32.28590
$E_{initial\ (c_4\ AO/HO)}$ (eV)	-14.63489	-14.63489	-14.63489	-14.63489	-14.63489	-14.63489	-14.63489	-14.63489	-14.63489	-14.63489	-14.63489	-14.63489
$E_{initial\ (c_5\ AO/HO)}$ (eV)	0	-13.59844	-13.59844	-13.59844	0	0	0	0	0	0	0	-13.59844
$E_D{}_{(Group)}$ (eV)	2.41840	12.49186	7.83016	3.32601	4.32754	4.29921	3.97398	4.17951	3.62128	3.91734	5.63881	3.90454

Table 23.89. The total bond energies of alkyl stibines calculated using the functional group composition and the energies of Table 23.88 compared to the experimental values [88].

Formula	Name	$Sb-C$	CH_3	CH_2	CH (i)	$C-C$ (a)	$C-C$ (b)	$C-C$ (c)	$C-C$ (d)	$C-C$ (e)	$C-C$ (f)	$C^{3e}=C$	CH (ii)	Calculated Total Bond Energy (eV)	Experimental Total Bond Energy (eV)	Relative Error
C_3H_9Sb	Trimethylstibine	3	3	0	0	0	0	0	0	0	0	0	0	44.73078	45.02378	0.00651
$C_6H_{15}Sb$	Triethylstibine	3	3	3	0	3	0	0	0	0	0	0	0	81.20388	80.69402	-0.00632
$C_{18}H_{15}Sb$	Triphenylstibine	3	0	0	0	0	0	0	0	0	0	18	15	167.32181	165.81583	-0.00908

Table 23.90. The bond angle parameters of alkyl stibines and experimental values [3]. In the calculation of θ_v, the parameters from the preceding angle were used. E_T is E_T (*atom–atom,msp*^{3}*.AO*).

Atoms of Angle	2c' Bond 1 (a_0)	2c' Bond 2 (a_0)	2c' Terminal Atoms (a_0)	$E_{Coulombic}$ or E Atom 1	Atom 1 Hybridization Designation (Table 15.3.A)	$E_{Coulombic}$ Atom 2	Atom 2 Hybridization Designation (Table 15.3.A)	c_2 Atom 1	c_2 Atom 2	C_1	C_2	c_1	c_2'	E_T (eV)	θ_v (°)	θ (°)	θ_2 (°)	Cal. θ (°)	Exp. θ (°)
Methyl $\angle HC_aH$	2.09711	2.09711	3.4252	-15.75493	7	H	H	0.86359	1	1	1	0.75	1.15796	0				109.50	
$\angle H_aC_aSb$															70.56			109.44	
$\angle C_aSbC_b$	3.89789	3.89789	5.7446	-15.55033	5	-15.55033	5	0.87495	0.87495	1	1	1	0.87495	-1.85836				94.93	94.2 (trimethylstibine)
Methylene $\angle HC_aH$	2.11106	2.11106	3.4252	-15.75493	7	H	H	0.86359	1	1	1	0.75	1.15796	0				108.44	107 (propane)
$\angle C_aC_bC_c$															69.51			110.49	112 (propane) 113.8 (butane) 110.8 (isobutane)
$\angle C_aC_bH$															69.51			110.49	111.0 (butane) 111.4 (isobutane)
Methyl $\angle HC_aH$	2.09711	2.09711	3.4252	-15.75493	7	H	H	0.86359	1	1	1	0.75	1.15796	0				109.50	
$\angle C_aC_bC_c$															70.56			109.44	
$\angle C_aC_bH$															70.56			109.44	
$\angle C_bC_aC_c$ iso C_a	2.91547	2.91547	4.7958	-16.68412 C_b	26	-16.68412 C_c	26	0.81549	0.81549	1	1	1	0.81549	-1.85836				110.67	110.8 (isobutane)
$\angle C_bC_aH$ iso C_a	2.91547	2.11323	4.1633	-15.55033 C_a	5	-14.82575 C_b	1	0.87495	0.91771	0.75	1	0.75	1.04887	0				110.76	
$\angle C_aC_bH$ iso C_a	2.91547	2.09711	4.1633	-15.55033 C_b	5	-14.82575 C_a	1	0.87495	0.91771	0.75	1	0.75	1.04887	0				111.27	111.4 (isobutane)
$\angle C_bC_aC_b$ tert C_a	2.90327	2.90327	4.7958	-16.68412 C_b	26	-16.68412 C_b	26	0.81549	0.81549	1	1	1	0.81549	-1.85836				111.37	110.8 (isobutane)
$\angle C_bC_aC_d$															72.50			107.50	

ALKYL BISMUTHS ($\left(C_nH_{2n+1}\right)_3 Bi,\ \ n=1,2,3,4,5...\infty$)

The alkyl bismuths, $\left(C_nH_{2n+1}\right)_3 Bi$, comprise a $Bi-C$ functional group. The alkyl portion of the alkyl bismuth may comprise at least two terminal methyl groups (CH_3) at each end of each chain, and may comprise methylene (CH_2), and methylyne (CH) functional groups as well as C bound by carbon-carbon single bonds. The methyl and methylene functional groups are equivalent to those of straight-chain alkanes. Six types of $C-C$ bonds can be identified. The n-alkane $C-C$ bond is the same as that of straight-chain alkanes. In addition, the $C-C$ bonds within isopropyl ($\left(CH_3\right)_2 CH$) and t-butyl ($\left(CH_3\right)_3 C$) groups and the isopropyl to isopropyl, isopropyl to t-butyl, and t-butyl to t-butyl $C-C$ bonds comprise functional groups. The branched-chain-alkane groups in alkyl bismuths are equivalent to those in branched-chain alkanes. The $Bi-C$ group may further join the $Bi6sp^3$ HO to an aryl HO.

As in the case of phosphorous, arsenic, and antimony, the bonding in the bismuth atom involves sp^3 hybridized orbitals formed, in this case, from the $6p$ and $6s$ electrons of the outer shells. The $Bi-C$ bond forms between $Bi6sp^3$ and $C2sp^3$ HOs to yield bismuths. The semimajor axis a of the $Bi-C$ functional group is solved using Eq. (15.51). Using the semimajor axis and the relationships between the prolate spheroidal axes, the geometric and energy parameters of the MO are calculated using Eqs. (15.1-15.117) in the same manner as the organic functional groups given in the Organic Molecular Functional Groups and Molecules section.

The energy of bismuth is less than the Coulombic energy between the electron and proton of H given by Eq. (1.264). A minimum energy is achieved while matching the potential, kinetic, and orbital energy relationships given in the Hydroxyl Radical (OH) section with hybridization of the bismuth atom such that in Eqs. (15.51) and (15.61), the sum of the energies of the H_2-type ellipsoidal MOs is matched to that of the $Bi6sp^3$ shell as in the case of the corresponding phosphines, arsines, and stibines.

The Bi electron configuration is $[Xe]6s^2 4f^{14} 5d^{10} 6p^3$ corresponding to the ground state ${}^4S_{3/2}$, and the $6sp^3$ hybridized orbital arrangement after Eq. (13.422) is:

$$\begin{array}{cccc} & 6sp^3 \text{ state} & & \\ \underline{\uparrow\downarrow} & \underline{\uparrow} & \underline{\uparrow} & \underline{\uparrow} \\ 0,0 & 1,-1 & 1,0 & 1,1 \end{array} \tag{23.280}$$

where the quantum numbers (ℓ, m_ℓ) are below each electron. The total energy of the state is given by the sum over the five electrons. The sum $E_T\left(Bi,6sp^3\right)$ of experimental energies [1] of Bi, Bi^+, Bi^{2+}, Bi^{3+}, and Bi^{4+} is:

$$E_T\left(Bi,6sp^3\right)=56.0\ eV+45.3\ eV+25.56\ eV+16.703\ eV+7.2855\ eV=150.84850\ eV \tag{23.281}$$

By considering that the central field decreases by an integer for each successive electron of the shell, the radius r_{6sp^3} of the $Bi6sp^3$ shell may be calculated from the Coulombic energy using Eq. (15.13).

$$r_{6sp^3}=\sum_{n=78}^{82}\frac{(Z-n)e^2}{8\pi\varepsilon_0\left(e150.84850\ eV\right)}=\frac{15e^2}{8\pi\varepsilon_0\left(e150.84850\ eV\right)}=1.35293a_0 \tag{23.282}$$

where $Z=83$ for bismuth. Using Eq. (15.14), the Coulombic energy $E_{Coulomb}\left(Bi,6sp^3\right)$ of the outer electron of the $Bi6sp^3$ shell is:

$$E_{Coulomb}\left(Bi,6sp^3\right)=\frac{-e^2}{8\pi\varepsilon_0 r_{6sp^3}}=\frac{-e^2}{8\pi\varepsilon_0 1.35293a_0}=-10.05657\ eV \tag{23.283}$$

During hybridization, the spin-paired $6s$ electrons are promoted to the $Bi6sp^3$ shell as paired electrons at the radius r_{6sp^3} of the $Bi6sp^3$ shell. The energy for the promotion is the difference in the magnetic energy given by Eq. (15.15) at the initial radius of the $6s$ electrons and the final radius of the $Bi6sp^3$ electrons. From Eq. (10.102) with $Z=83$ and $n=80$, the radius r_{80} of the $Bi6s$ shell is:

$$r_{80}=1.20140a_0 \tag{23.284}$$

Using Eqs. (15.15) and (23.284), the unpairing energy is:

$$E(magnetic)=\frac{2\pi\mu_0 e^2\hbar^2}{m_e^2}\left(\frac{1}{\left(r_{80}\right)^3}-\frac{1}{\left(r_{6sp^3}\right)^3}\right)=8\pi\mu_o\mu_B^2\left(\frac{1}{\left(1.20140a_0\right)^3}-\frac{1}{\left(1.35293a_0\right)^3}\right)=0.01978\ eV \tag{23.285}$$

Using Eqs. (23.283) and (23.285), the energy $E\left(Bi,6sp^3\right)$ of the outer electron of the $Bi6sp^3$ shell is:

$$E\left(Bi,6sp^3\right)=\frac{-e^2}{8\pi\varepsilon_0 r_{6sp^3}}+\frac{2\pi\mu_0 e^2\hbar^2}{m_e^2}\left(\frac{1}{\left(r_{80}\right)^3}-\frac{1}{\left(r_{6sp^3}\right)^3}\right)=-10.05657\ eV+0.01978\ eV=-10.03679\ eV \tag{23.286}$$

Next, consider the formation of the $Bi-L$-bond MO of bismuth compounds wherein L is a very stable ligand and each bismuth atom has a $Bi6sp^3$ electron with an energy given by Eq. (23.286). The total energy of the state of each bismuth atom is given by the sum over the five electrons. The sum $E_T\left(Bi_{Bi-L},6sp^3\right)$ of energies of $Bi6sp^3$ (Eq. (23.286)), Bi^+, Bi^{2+}, Bi^{3+}, and Bi^{4+} is:

$$\begin{aligned}E_T\left(Bi_{Bi-L},6sp^3\right)&=-\left(56.0\ eV+45.3\ eV+25.56\ eV+16.703\ eV+E\left(Bi,6sp^3\right)\right)\\&=-\left(56.0\ eV+45.3\ eV+25.56\ eV+16.703\ eV+10.03679\ eV\right)=-153.59979\ eV\end{aligned} \tag{23.287}$$

where $E\left(Bi,6sp^3\right)$ is the sum of the energy of Bi, $-7.2855\ eV$, and the hybridization energy.

A minimum energy is achieved while matching the potential, kinetic, and orbital energy relationships given in the Hydroxyl Radical (OH) section with the donation of electron density from the participating $Bi6sp^3$ HO to each $Bi-L$-bond MO. Consider the case wherein each $Bi6sp^3$ HO donates an excess of 25% of its electron density to the $Bi-L$-bond MO to form an energy minimum. By considering this electron redistribution in the bismuth molecule as well as the fact that the central field decreases by an integer for each successive electron of the shell, in general terms, the radius $r_{Bi-L6sp^3}$ of the $Bi6sp^3$ shell may be calculated from the Coulombic energy using Eq. (15.18).

$$r_{Bi-L6sp^3}=\left(\sum_{n=78}^{82}(Z-n)-0.25\right)\frac{e^2}{8\pi\varepsilon_0\left(e153.59979\ eV\right)}=\frac{14.75e^2}{8\pi\varepsilon_0\left(e153.59979\ eV\right)}=1.30655a_0 \tag{23.288}$$

Using Eqs. (15.19) and (23.288), the Coulombic energy $E_{Coulomb}\left(Bi_{Bi-L},6sp^3\right)$ of the outer electron of the $Bi6sp^3$ shell is:

$$\begin{aligned}E_{Coulomb}\left(Bi_{Bi-L},6sp^3\right)&=\frac{-e^2}{8\pi\varepsilon_0 r_{Bi-L6sp^3}}\\&=\frac{-e^2}{8\pi\varepsilon_0 1.30655a_0}\\&=-10.41354\ eV\end{aligned} \tag{23.289}$$

During hybridization, the spin-paired $6s$ electrons are promoted to the $Bi6sp^3$ shell as paired electrons at the radius r_{6sp^3} of the $Bi6sp^3$ shell. The energy for the promotion is the difference in the magnetic energy given by Eq. (15.15) at the initial radius of the $6s$ electrons and the final radius of the $Bi6sp^3$ electrons. Using Eqs. (23.285) and (23.289), the energy $E\left(Bi_{Bi-L},6sp^3\right)$ of the outer electron of the $Bi6sp^3$ shell is:

$$E\left(Bi_{Bi-L},6sp^3\right)=\frac{-e^2}{8\pi\varepsilon_0 r_{Bi-L6sp^3}}+\frac{2\pi\mu_0 e^2\hbar^2}{m_e^2\left(r_{80}\right)^3}=-10.41354\ eV+0.01978\ eV=-10.39377\ eV \tag{23.290}$$

Thus, $E_T\left(Bi-L,6sp^3\right)$, the energy change of each $Bi6sp^3$ shell with the formation of the $Bi-L$-bond MO is given by the difference between Eq. (23.290) and Eq. (23.286).

$$E_T\left(Bi-L,6sp^3\right)=E\left(Bi_{Bi-L},6sp^3\right)-E\left(Bi,6sp^3\right)=-10.39377\ eV-\left(-10.03679\ eV\right)=-0.35698\ eV \tag{23.291}$$

Next, consider the formation of the $Bi-C$-bond MO by bonding with a carbon having a $C2sp^3$ electron with an energy given by Eq. (14.146). The total energy of the state is given by the sum over the five electrons. The sum $E_T\left(C_{ethane},2sp^3\right)$ of calculated energies of $C2sp^3$, C^+, C^{2+}, and C^{3+} from Eqs. (10.123), (10.113-10.114), (10.68), and (10.48), respectively, is:

$$\begin{aligned}E_T\left(C_{ethane},2sp^3\right)&=-\left(64.3921\ eV+48.3125\ eV+24.2762\ eV+E\left(C,2sp^3\right)\right)\\&=-\left(64.3921\ eV+48.3125\ eV+24.2762\ eV+14.63489\ eV\right)=-151.61569\ eV\end{aligned} \tag{23.292}$$

where $E\left(C,2sp^3\right)$ is the sum of the energy of C, $-11.27671\ eV$, and the hybridization energy.

The sharing of electrons between the $Bi6sp^3$ HO and $C2sp^3$ HOs to form a $Bi-C$-bond MO permits each participating hybridized orbital to decrease in radius and energy. A minimum energy is achieved while satisfying the potential, kinetic, and orbital energy relationships, when the $Bi6sp^3$ HO donates, and the $C2sp^3$ HO receives, excess electron density equivalent to an electron within the $Bi-C$-bond MO. By considering this electron redistribution in the alkyl bismuth molecule as well as the fact that the central field decreases by an integer for each successive electron of the shell, the radius $r_{Bi-C2sp^3}$ of the $C2sp^3$ shell of the $Bi-C$-bond MO may be calculated from the Coulombic energy using Eqs. (15.18) and (23.292):

$$r_{Bi-C2sp^3}=\left(\sum_{n=2}^{5}(Z-n)+1\right)\frac{e^2}{8\pi\varepsilon_0\left(e151.61569\ eV\right)}=\frac{11e^2}{8\pi\varepsilon_0\left(e151.61569\ eV\right)}=0.98713a_0 \tag{23.293}$$

Using Eqs. (15.19) and (23.293), the Coulombic energy $E_{Coulomb}\left(C_{Bi-C},2sp^3\right)$ of the outer electron of the $C2sp^3$ shell is:

$$E_{Coulomb}\left(C_{Bi-C},2sp^3\right)=\frac{-e^2}{8\pi\varepsilon_0 r_{Bi-C2sp^3}}=\frac{-e^2}{8\pi\varepsilon_0 0.98713a_0}=-13.78324\ eV \tag{23.294}$$

During hybridization, the spin-paired $2s$ electrons are promoted to the $C2sp^3$ shell as unpaired electrons. The energy for the promotion is the magnetic energy given by Eq. (14.145). Using Eqs. (14.145) and (23.294), the energy $E\left(C_{Bi-C},2sp^3\right)$ of the outer electron of the $C2sp^3$ shell is:

$$E\left(C_{Bi-C},2sp^3\right)=\frac{-e^2}{8\pi\varepsilon_0 r_{Bi-C2sp^3}}+\frac{2\pi\mu_0 e^2\hbar^2}{m_e^2\left(r_3\right)^3}=-13.78324\ eV+0.19086\ eV=-13.59238\ eV \tag{23.295}$$

Thus, $E_T\left(Bi-C,2sp^3\right)$, the energy change of each $C2sp^3$ shell with the formation of the $Bi-C$-bond MO is given by the difference between Eq. (23.295) and Eq. (14.146).

$$E_T\left(Bi-C,2sp^3\right)=E\left(C_{Bi-C},2sp^3\right)-E\left(C,2sp^3\right)=-13.59238\ eV-\left(-14.63489\ eV\right)=1.04251\ eV \tag{23.296}$$

Now, consider the formation of the $Bi-L$-bond MO of bismuth compounds wherein L is a ligand including carbon. For the $Bi-C$ functional group, hybridization of the $2s$ and $2p$ AOs of each C and the $6s$ and $6p$ AOs of each Bi to form single $2sp^3$ and $6sp^3$ shells, respectively, forms an energy minimum, and the sharing of electrons between the $C2sp^3$ and $Bi6sp^3$ HOs to form a MO permits each participating orbital to decrease in radius and energy. In branched-chain alkyl bismuths, the energy of bismuth is less than the Coulombic energy between the electron and proton of H given by Eq. (1.264). Thus, the energy matching condition is determined by the c_2 and C_2 parameters in Eq. (15.61). Then, the $C2sp^3$ HO has an energy of $E\left(C,2sp^3\right)=-14.63489\ eV$ (Eq. (15.25)), and the $Bi6sp^3$ HO has an energy of $E\left(Bi,6sp^3\right)=-10.03679\ eV$ (Eq. (23.286)). To meet the equipotential condition of the union of the $Bi-C$ H_2-type-ellipsoidal-MO with these orbitals, the hybridization factors c_2 and C_2 of Eq. (15.61) for the $Bi-C$-bond MO given by Eqs. (15.77) are:

$$c_2\left(C2sp^3HO\ to\ Bi6sp^3HO\right)=C_2\left(C2sp^3HO\ to\ Bi6sp^3HO\right)=\frac{E\left(Bi,6sp^3\right)}{E\left(C,2sp^3\right)}=\frac{-10.03679\ eV}{-14.63489\ eV}=0.68581 \tag{23.297}$$

The energy of the $Bi-C$-bond MO is the sum of the component energies of the H_2-type ellipsoidal MO given in Eq. (15.51) with $E\left(AO/HO\right)=E\left(Bi,6sp^3\right)$ given by Eq. (23.286), and $E_T\left(atom-atom,msp^3.AO\right)$ is $E_T\left(Bi-C,2sp^3\right)$ (Eq. (23.296)) in order to match the energies of the carbon and bismuth HOs.

The symbols of the functional groups of branched-chain alkyl bismuths are given in Table 23.91. The geometrical (Eqs. (15.1-15.5) and (15.51)), intercept (Eqs. (15.80-15.87)), and energy (Eqs. (15.6-15.11) and (15.17-15.65)) parameters of alkyl bismuths are given in Tables 23.92, 23.93, and 23.94, respectively. The total energy of each alkyl bismuth given in Table 23.95 was calculated as the sum over the integer multiple of each $E_{D\,(Group)}$ of Table 23.94 corresponding to functional-group composition of the molecule. The bond angle parameters of alkyl bismuths determined using Eqs. (15.88-15.117) are given in Table 23.96. The color scale, charge-density of exemplary alkyl bismuth, triphenylbismuth, comprising atoms with the outer shell bridged by one or more H_2-type ellipsoidal MOs or joined with one or more hydrogen MOs is shown in Figure 23.19.

Figure 23.19. Color scale, charge-density of triphenylbismuth showing the orbitals of the atoms at their radii, the ellipsoidal surface of each H or H_2-type ellipsoidal MO that transitions to the corresponding outer shell of the atom(s) participating in each bond, and the hydrogen nuclei.

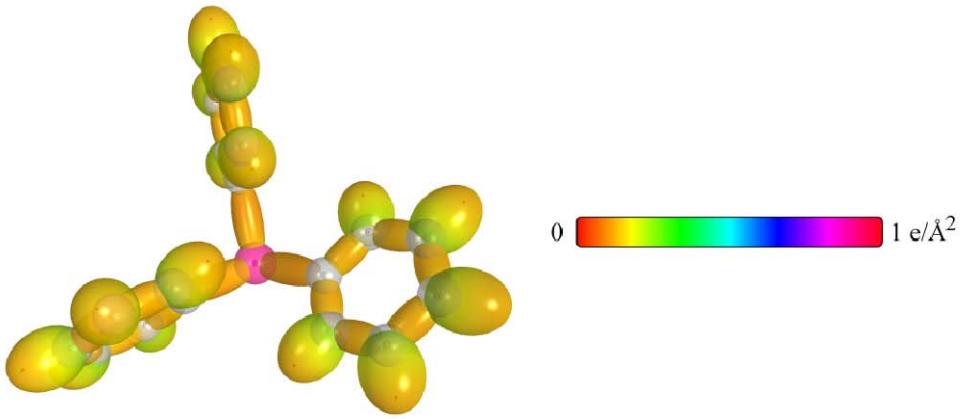

Table 23.91. The symbols of functional groups of alkyl bismuths.

Functional Group	Group Symbol
Bi-C	$Bi-C$
CH_3 group	$C-H\ (CH_3)$
CH_2 group	$C-H\ (CH_2)$
CH	$C-H$ (i)
CC bond (*n-C*)	$C-C$ (a)
CC bond (*iso-C*)	$C-C$ (b)
CC bond (*tert-C*)	$C-C$ (c)
CC (*iso* to *iso-C*)	$C-C$ (d)
CC (*t* to *t-C*)	$C-C$ (e)
CC (*t* to *iso-C*)	$C-C$ (f)
CC (aromatic bond)	$C\overset{3e}{=}C$
CH (aromatic)	*CH* (ii)

Table 23.92. The geometrical bond parameters of alkyl bismuths and experimental values [3].

Parameter	$Bi-C$ Group	$C-H\ (CH_3)$ Group	$C-H\ (CH_2)$ Group	$C-H$ (i) Group	$C-C$ (a) Group	$C-C$ (b) Group	$C-C$ (c) Group	$C-C$ (d) Group	$C-C$ (e) Group	$C-C$ (f) Group	$C^{3e}=C$ Group	CH (ii) Group
$a\ (a_0)$	2.18901	1.64920	1.67122	1.67465	2.12499	2.12499	2.10725	2.12499	2.10725	2.10725	1.47348	1.60061
$c'\ (a_0)$	2.06296	1.04856	1.05553	1.05661	1.45744	1.45744	1.45164	1.45744	1.45164	1.45164	1.31468	1.03299
Bond Length $2c'\ (\AA)$	2.18334	1.10974	1.11713	1.11827	1.54280	1.54280	1.53635	1.54280	1.53635	1.53635	1.39140	1.09327
Exp. Bond Length $(\AA)$	2.263 $(Bi(CH_3)_3)$	1.107 ($C-H$ propane) 1.117 ($C-H$ butane)	1.107 ($C-H$ propane) 1.117 ($C-H$ butane)	1.122 (isobutane)	1.532 (propane) 1.531 (butane)	1.532 (propane) 1.531 (butane)	1.532 (propane) 1.531 (butane)	1.532 (propane) 1.531 (butane)	1.532 (propane) 1.531 (butane)	1.532 (propane) 1.531 (butane)	1.399 (benzene)	1.101 (benzene)
$b,c\ (a_0)$	0.73210	1.27295	1.29569	1.29924	1.54616	1.54616	1.52750	1.54616	1.52750	1.52750	0.66540	1.22265
e	0.94242	0.63580	0.63159	0.63095	0.68600	0.68600	0.68888	0.68600	0.68888	0.68888	0.89223	0.64537

Table 23.93. The MO to HO intercept geometrical bond parameters of alkyl bismuths. *R, R′, R″* are *H* or alkyl groups. E_T is $E_T\,(atom–atom,msp^3.AO)$.

Bond	Atom	E_T (eV) Bond 1	E_T (eV) Bond 2	E_T (eV) Bond 3	E_T (eV) Bond 4	Final Total Energy $C2sp^3$ (eV)	$r_{initial}$ (a_0)	r_{final} (a_0)	$E_{Coulomb}$ (eV) Final	$E(C2sp^3)$ (eV) Final	θ' (°)	θ_1 (°)	θ_2 (°)	d_1 (a_0)	d_2 (a_0)
$C-H\ (CH_3)$	C	0.52125	0	0	0	-151.09444	0.91771	0.95116	-14.30450	-14.11363	87.03	92.97	48.26	1.09791	0.04936
$(CH_3)_2\,Bi-CH_3$	C	0.52125	0	0	0		0.91771	0.95116	-14.30450	-14.11363	141.99	38.01	53.13	1.31349	0.74947
$(CH_3)_2\,Bi-CH_3$	Bi	0.52125	0.52125	0.52125	0		1.35293	1.02592	-13.26199		143.89	36.11	55.68	1.23415	0.82881
$C-H\ (CH_3)$	C	-0.92918	0	0	0	-152.54487	0.91771	0.86359	-15.75493	-15.56407	77.49	102.51	41.48	1.23564	0.18708
$C-H\ (CH_2)$	C	-0.92918	-0.92918	0	0	-153.47406	0.91771	0.81549	-16.68412	-16.49325	68.47	111.53	35.84	1.35486	0.29933
$C-H\ (CH)$	C	-0.92918	-0.92918	-0.92918	0	-154.40324	0.91771	0.77247	-17.61330	-17.42244	61.10	118.90	31.37	1.42988	0.37326
$iH_3C_aC_bH_2CH_2-$ $(C-C$ (a))	C_a	-0.92918	0	0	0	-152.54487	0.91771	0.86359	-15.75493	-15.56407	63.82	116.18	30.08	1.83879	0.38106
$iH_3C_aC_bH_2CH_2-$ $(C-C$ (a))	C_b	-0.92918	-0.92918	0	0	-153.47406	0.91771	0.81549	-16.68412	-16.49325	56.41	123.59	26.06	1.90890	0.45117
$R-H_2C_aC_b(H_2C_c-R')HCH_2-$ $(C-C$ (b))	C_b	-0.92918	-0.92918	-0.92918	0	-154.40324	0.91771	0.77247	-17.61330	-17.42244	48.30	131.70	21.90	1.97162	0.51388
$R-H_2C_a(R'-H_2C_d)C_b(R''-H_2C_c)CH_2-$ $(C-C$ (c))	C_b	-0.92918	-0.72457	-0.72457	-0.72457	-154.71860	0.91771	0.75889	-17.92866	-17.73779	48.21	131.79	21.74	1.95734	0.50570
$isoC_aC_b(H_2C_c-R')HCH_2-$ $(C-C$ (d))	C_b	-0.92918	-0.92918	-0.92918	0	-154.40324	0.91771	0.77247	-17.61330	-17.42244	48.30	131.70	21.90	1.97162	0.51388
$tertC_a(R'-H_2C_d)C_b(R''-H_2C_c)CH_2-$ $(C-C$ (e))	C_b	-0.72457	-0.72457	-0.72457	-0.72457	-154.51399	0.91771	0.76765	-17.92866	-17.73779	50.04	129.96	22.66	1.94462	0.49298
$tertC_aC_b(H_2C_c-R')HCH_2-$ $(C-C$ (f))	C_b	-0.72457	-0.92918	-0.92918	0	-154.19863	0.91771	0.78155	-17.40869	-17.21783	52.78	127.22	24.04	1.92443	0.47279
$isoC_a(R'-H_2C_d)C_b(R''-H_2C_c)CH_2-$ $(C-C$ (f))	C_b	-0.72457	-0.72457	-0.72457	-0.72457	-154.51399	0.91771	0.76765	-17.92866	-17.73779	50.04	129.96	22.66	1.94462	0.49298

Table 23.94. The energy parameters (eV) of functional groups of alkyl bismuths.

Parameters	$Bi-C$ Group	CH_3 Group	CH_2 Group	CH (i) Group	$C-C$ (a) Group	$C-C$ (b) Group	$C-C$ (c) Group	$C-C$ (d) Group	$C-C$ (e) Group	$C-C$ (f) Group	$C^{3e}=C$ Group	CH (ii) Group
f_1	1	1	1	1	1	1	1	1	1	1	0.75	1
n_1	1	3	2	1	1	1	1	1	1	1	2	1
n_2	0	2	1	0	0	0	0	0	0	0	0	0
n_3	0	0	0	0	0	0	0	0	0	0	0	0
C_1	0.375	0.75	0.75	0.75	0.5	0.5	0.5	0.5	0.5	0.5	0.5	0.75
C_2	0.68581	1	1	1	1	1	1	1	1	1	0.85252	1
c_1	1	1	1	1	1	1	1	1	1	1	1	1
c_2	0.68581	0.91771	0.91771	0.91771	0.91771	0.91771	0.91771	0.91771	0.91771	0.91771	0.85252	0.91771
c_3	0	0	1	1	0	0	0	1	1	0	0	1
c_4	2	1	1	1	2	2	2	2	2	2	3	1
c_5	0	3	2	1	0	0	0	0	0	0	0	1
C_{1o}	0.375	0.75	0.75	0.75	0.5	0.5	0.5	0.5	0.5	0.5	0.5	0.75
C_{2o}	0.68581	1	1	1	1	1	1	1	1	1	0.85252	1
V_e (eV)	-31.82881	-107.32728	-70.41425	-35.12015	-28.79214	-28.79214	-29.10112	-28.79214	-29.10112	-29.10112	-101.12679	-37.10024
V_p (eV)	6.59529	38.92728	25.78002	12.87680	9.33352	9.33352	9.37273	9.33352	9.37273	9.37273	20.69825	13.17125
T (eV)	7.27014	32.53914	21.06675	10.48582	6.77464	6.77464	6.90500	6.77464	6.90500	6.90500	34.31559	11.58941
V_m (eV)	-3.63507	-16.26957	-10.53337	-5.24291	-3.38732	-3.38732	-3.45250	-3.38732	-3.45250	-3.45250	-17.15779	-5.79470
$E_{(AO/HO)}$ (eV)	-10.03679	-15.56407	-15.56407	-14.63489	-15.56407	-15.56407	-15.35946	-15.56407	-15.35946	-15.35946	0	-14.63489
$\Delta E_{H_2MO\,(AO/HO)}$ (eV)	0	0	0	0	0	0	0	0	0	0	0	-1.13379
$E_{T\,(AO/HO)}$ (eV)	-10.03679	-15.56407	-15.56407	-14.63489	-15.56407	-15.56407	-15.35946	-15.56407	-15.35946	-15.35946	0	-13.50110
$E_{T\,(H_2MO)}$ (eV)	-31.63524	-67.69451	-49.66493	-31.63533	-31.63537	-31.63537	-31.63535	-31.63537	-31.63535	-31.63535	-63.27075	-31.63539
$E_T\left(atom-atom,msp^3.AO\right)$ (eV)	1.04251	0	0	0	-1.85836	-1.85836	-1.44915	-1.85836	-1.44915	-1.44915	-2.26759	-0.56690
$E_{T\,(MO)}$ (eV)	-30.59286	-67.69450	-49.66493	-31.63537	-33.49373	-33.49373	-33.08452	-33.49373	-33.08452	-33.08452	-65.53833	-32.20226
$\omega\left(10^{15}\ rad/s\right)$	33.4696	24.9286	24.2751	24.1759	9.43699	9.43699	15.4846	9.43699	9.55643	9.55643	49.7272	26.4826
E_K (eV)	22.03030	16.40846	15.97831	15.91299	6.21159	6.21159	10.19220	6.21159	6.29021	6.29021	32.73133	17.43132
$\bar{E}_D$ (eV)	-0.28408	-0.25352	-0.25017	-0.24966	-0.16515	-0.16515	-0.20896	-0.16515	-0.16416	-0.16416	-0.35806	-0.26130
$\bar{E}_{Kvib}$ (eV)	0.14878 [66]	0.35532 (Eq. (13.458))	0.35532 (Eq. (13.458))	0.35532 (Eq. (13.458))	0.12312 [6]	0.17978 [7]	0.09944 [8]	0.12312 [6]	0.12312 [6]	0.12312 [6]	0.19649 [30]	0.35532 Eq. (13.458)
$\bar{E}_{osc}$ (eV)	-0.20968	-0.22757	-0.14502	-0.07200	-0.10359	-0.07526	-0.15924	-0.10359	-0.10260	-0.10260	-0.25982	-0.08364
E_{mag} (eV)	0.14803	0.14803	0.14803	0.14803	0.14803	0.14803	0.14803	0.14803	0.14803	0.14803	0.14803	0.14803
$E_{T\,(Group)}$ (eV)	-30.80254	-67.92207	-49.80996	-31.70737	-33.59732	-33.49373	-33.24376	-33.59732	-33.18712	-33.18712	-49.54347	-32.28590
$E_{initial\,(c_4\ AO/HO)}$ (eV)	-14.63489	-14.63489	-14.63489	-14.63489	-14.63489	-14.63489	-14.63489	-14.63489	-14.63489	-14.63489	-14.63489	-14.63489
$E_{initial\,(c_5\ AO/HO)}$ (eV)	0	-13.59844	-13.59844	-13.59844	0	0	0	0	0	0	0	-13.59844
$E_{D\,(Group)}$ (eV)	1.53276	12.49186	7.83016	3.32601	4.32754	4.29921	3.97398	4.17951	3.62128	3.91734	5.63881	3.90454

Table 23.95. The total bond energies of alkyl bismuths calculated using the functional group composition and the energies of Table 23.94 compared to the experimental values [88].

Formula	Name	$Bi-C$	CH_3	CH_2	CH (i)	$C-C$ (a)	$C-C$ (b)	$C-C$ (c)	$C-C$ (d)	$C-C$ (e)	$C-C$ (f)	$C^{3e}=C$	CH (ii)	Calculated Total Bond Energy (eV)	Experimental Total Bond Energy (eV)	Relative Error
C_3H_9Bi	Trimethylbismuth	3	3	0	0	0	0	0	0	0	0	0	0	42.07387	42.79068	0.01675
$C_6H_{15}Bi$	Triethylbismuth	3	3	3	0	3	0	0	0	0	0	0	0	78.54697	78.39153	-0.00198
$C_{18}H_{15}Bi$	Triphenylbismuth	3	0	0	0	0	0	0	0	0	0	18	15	164.66490	163.75184	-0.00558

Table 23.96. The bond angle parameters of alkyl bismuths and experimental values [3]. In the calculation of θ_v, the parameters from the preceding angle were used. E_T is E_T (*atom–atom,msp*^{3}*.AO*).

Atoms of Angle	2*c'* Bond 1 (a_0)	2*c'* Bond 2 (a_0)	2*c'* Terminal Atoms (a_0)	$E_{Coulombic}$ or *E* Atom 1	Atom 1 Hybridization Designation (Table 15.3.A)	$E_{Coulombic}$ Atom 2	Atom 2 Hybridization Designation (Table 15.3.A)	c_2 Atom 1	c_2 Atom 2	C_1	C_2	c_1	c'_2	E_T (eV)	θ_v (°)	θ (°)	θ_2 (°)	Cal. θ (°)	Exp. θ (°)
Methyl $\angle HC_aH$	2.09711	2.09711	3.4252	-15.75493	7	H	H	0.86359	1	1	1	0.75	1.15796	0				109.50	
$\angle H_aC_aBi$															70.56			109.44	
$\angle C_aBiC_b$	4.12592	4.12592	6.1806	-15.18804	2	-15.18804	2	0.89582	0.89582	1	1	1	0.89582	-1.85836				97.01	97.1 (trimethylbismuth)
Methylene $\angle HC_aH$	2.11106	2.11106	3.4252	-15.75493	7	H	H	0.86359	1	1	1	0.75	1.15796	0				108.44	107 (propane)
$\angle C_aC_bC_c$															69.51			110.49	112 (propane) 113.8 (butane) 110.8 (isobutane)
$\angle C_aC_bH$															69.51			110.49	111.0 (butane) 111.4 (isobutane)
Methyl $\angle HC_aH$	2.09711	2.09711	3.4252	-15.75493	7	H	H	0.86359	1	1	1	0.75	1.15796	0				109.50	
$\angle C_aC_bC_c$															70.56			109.44	
$\angle C_aC_bH$															70.56			109.44	
$\angle C_bC_aC_c$ iso C_a	2.91547	2.91547	4.7958	-16.68412 C_b	26	-16.68412 C_c	26	0.81549	0.81549	1	1	1	0.81549	-1.85836				110.67	110.8 (isobutane)
$\angle C_bC_aH$ iso C_a	2.91547	2.11323	4.1633	-15.55033 C_a	5	-14.82575 C_b	1	0.87495	0.91771	0.75	1	0.75	1.04887	0				110.76	
$\angle C_aC_bH$ iso C_a	2.91547	2.09711	4.1633	-15.55033 C_b	5	-14.82575 C_a	1	0.87495	0.91771	0.75	1	0.75	1.04887	0				111.27	111.4 (isobutane)
$\angle C_bC_aC_b$ tert C_a	2.90327	2.90327	4.7958	-16.68412 C_b	26	-16.68412 C_b	26	0.81549	0.81549	1	1	1	0.81549	-1.85836				111.37	110.8 (isobutane)
$\angle C_bC_aC_d$															72.50			107.50	

SUMMARY TABLES OF ORGANOMETALLIC AND COORDINATE MOLECULES

The bond energies, calculated using closed-form equations having integers and fundamental constants only for classes of molecules whose designation is based on the main functional group, are given in the following tables with the experimental values.

Table 23.97.1. Summary results of organoaluminum compounds.

Formula	Name	Calculated Total Bond Energy (eV)	Experimental Total Bond Energy (eV)	Relative Error
C_2H_7Al	dimethylaluminum hydride	34.31171	34.37797[a] [11]	0.00193
C_3H_9Al	trimethyl aluminum	47.10960	46.95319 [10]	-0.00333
$C_4H_{11}Al$	diethylaluminum hydride	58.62711	60.10948[b] [10]	0.02466
$C_6H_{15}Al$	triethylaluminum hydride	83.58270	83.58176 [10]	-0.00001
$C_6H_{15}Al$	di-n-propylaluminum hydride	82.94251	84.40566[b] [10]	0.01733
$C_9H_{21}Al$	tri-n-propyl aluminum	120.05580	121.06458[b] [10]	0.00833
$C_8H_{19}Al$	di-n-butylaluminum hydride	107.25791	108.71051[b] [10]	0.01336
$C_8H_{19}Al$	di-isobutylaluminum hydride	107.40303	108.77556[b] [10]	0.01262
$C_{12}H_{27}Al$	tri-n-butyl aluminum	156.52890	157.42429[b] [10]	0.00569
$C_{12}H_{27}Al$	tri-isobutyl aluminum	156.74658	157.58908[b] [10]	0.00535

[a] Estimated.
[b] Crystal

Table 23.97.2. Summary results of scandium coordinate compounds.

Formula	Name	Calculated Total Bond Energy (eV)	Experimental Total Bond Energy (eV)	Relative Error
ScF	scandium fluoride	6.34474	6.16925 [15]	-0.02845
ScF_2	scandium difluoride	12.11937	12.19556 [15]	0.00625
ScF_3	scandium trifluoride	19.28412	19.27994 [15]	-0.00022
ScCl	scandium chloride	4.05515	4.00192 [15]	-0.01330
ScO	scandium oxide	7.03426	7.08349 [15]	0.00695

Table 23.97.3. Summary results of titanium coordinate compounds.

Formula	Name	Calculated Total Bond Energy (eV)	Experimental Total Bond Energy (eV)	Relative Error
TiF	titanium fluoride	6.44997	6.41871 [21]	-0.00487
TiF_2	titanium difluoride	13.77532	13.66390 [21]	-0.00815
TiF_3	titanium trifluoride	19.63961	19.64671 [21]	0.00036
TiF_4	titanium tetrafluoride	24.66085	24.23470 [21]	-0.01758
TiCl	titanium chloride	4.56209	4.56198 [22]	-0.00003
$TiCl_2$	titanium dichloride	10.02025	9.87408 [22]	-0.01517
$TiCl_3$	titanium trichloride	14.28674	14.22984 [22]	-0.00400
$TiCl_4$	titanium tetrachloride	17.94949	17.82402 [22]	-0.00704
TiBr	titanium bromide	3.77936	3.78466 [19]	0.00140
$TiBr_2$	titanium dibromide	8.91650	8.93012 [19]	0.00153
$TiBr_3$	titanium tribromide	12.07765	12.02246 [19]	-0.00459
$TiBr_4$	titanium tetrabromide	14.90122	14.93239 [19]	0.00209
TiI	titanium iodide	3.16446	3.15504 [20]	-0.00299
TiI_2	titanium diiodide	7.35550	7.29291 [20]	-0.00858
TiI_3	titanium triiodide	9.74119	9.71935 [20]	-0.00225
TiI_4	titanium tetraiodide	12.10014	12.14569 [20]	0.00375
TiO	titanium oxide	7.02729	7.00341 [23]	-0.00341
TiO_2	titanium dioxide	13.23528	13.21050 [23]	-0.00188
TiOF	titanium fluoride oxide	12.78285	12.77353 [23]	-0.00073
$TiOF_2$	titanium difluoride oxide	18.94807	18.66983 [23]	-0.01490
TiOCl	titanium chloride oxide	11.10501	11.25669 [23]	0.01347
$TiOCl_2$	titanium dichloride oxide	15.59238	15.54295 [23]	-0.00318

Table 23.97.4. Summary results of vanadium coordinate compounds.

Formula	Name	Calculated Total Bond Energy (eV)	Experimental Total Bond Energy (eV)	Relative Error
VF_5	vanadium pentafluoride	24.06031	24.24139 [15]	0.00747
VCl_4	vanadium tetrachloride	15.84635	15.80570 [15]	-0.00257
VN	vanadium nitride	4.85655	4.81931 [24]	-0.00775
VO	vanadium oxide	6.37803	6.60264 [15]	0.03402
VO_2	vanadium dioxide	12.75606	12.89729 [34]	0.01095
$VOCl_3$	vanadium trichloride oxide	18.26279	18.87469 [15]	0.03242
$V(CO)_6$	vanadium hexacarbonyl	75.26791	75.63369 [32]	0.00484
$V(C_6H_6))_2$	dibenzene vanadium	119.80633	121.20193[a] [33]	0.01151

[a] Liquid.

Table 23.97.5. Summary results of chromium coordinate compounds.

Formula	Name	Calculated Total Bond Energy (eV)	Experimental Total Bond Energy (eV)	Relative Error
CrF_2	chromium difluoride	10.91988	10.92685 [15]	0.00064
$CrCl_2$	chromium dichloride	7.98449	7.96513 [15]	-0.00243
CrO	chromium oxide	4.73854	4.75515 [37]	0.00349
CrO_2	chromium dioxide	10.02583	10.04924 [37]	0.00233
CrO_3	chromium trioxide	14.83000	14.85404 [37]	0.00162
CrO_2Cl_2	chromium dichloride dioxide	17.46158	17.30608 [15]	-0.00899
$Cr(CO)_6$	chromium hexacarbonyl	74.22588	74.61872 [44]	0.00526
$Cr(C_6H_6)_2$	dibenzene chromium	117.93345	117.97971 [44]	0.00039
$Cr((CH_3)_3C_6H_3)_2$	di-(1,2,4-trimethylbenzene) chromium	191.27849	192.42933[a] [44]	0.00598

[a] Liquid.

Table 23.97.6. Summary results of manganese coordinate compounds.

Formula	Name	Calculated Total Bond Energy (eV)	Experimental Total Bond Energy (eV)	Relative Error
MnF	manganese fluoride	4.03858	3.97567 [15]	-0.01582
MnCl	manganese chloride	3.74528	3.73801 [15]	-0.00194
$Mn_2(CO)_{10}$	dimanganese decacarbonyl	123.78299	122.70895 [49]	-0.00875

Table 23.97.7. Summary results of iron coordinate compounds.

Formula	Name	Calculated Total Bond Energy (eV)	Experimental Total Bond Energy (eV)	Relative Error
FeF	iron fluoride	4.65726	4.63464 [15]	-0.00488
FeF_2	iron difluoride	10.03188	9.98015 [15]	-0.00518
FeF_3	iron trifluoride	15.31508	15.25194 [15]	-0.00414
FeCl	iron chloride	2.96772	2.97466 [15]	0.00233
$FeCl_2$	iron dichloride	8.07880	8.28632 [15]	0.02504
$FeCl_3$	iron trichloride	10.82348	10.70065 [50]	-0.01148
FeO	iron oxide	4.09983	4.20895 [15]	0.02593
$Fe(CO)_5$	iron pentacarbonyl	61.75623	61.91846 [29]	0.00262
$Fe(C_5H_5)_2$	bis-cyclopentadienyl iron (ferrocene)	98.90760	98.95272 [53]	0.00046

Table 23.97.8. Summary results of cobalt coordinate compounds.

Formula	Name	Calculated Total Bond Energy (eV)	Experimental Total Bond Energy (eV)	Relative Error
CoF_2	cobalt difluoride	9.45115	9.75552 [54]	0.03120
CoCl	cobalt chloride	3.66504	3.68049 [15]	0.00420
CoI_2	cobalt dichloride	7.98467	7.92106 [15]	-0.00803
$CoCl_3$	cobalt trichloride	9.83521	9.87205 [15]	0.00373
$CoH(CO)_4$	cobalt tetracarbonyl hydride	50.33217	50.36087 [53]	0.00057

Table 23.97.9. Summary results of nickel coordinate compounds.

Formula	Name	Calculated Total Bond Energy (eV)	Experimental Total Bond Energy (eV)	Relative Error
NiCl	nickel chloride	3.84184	3.82934 [59]	-0.00327
$NiCl_2$	nickel dichloride	7.76628	7.74066 [59]	-0.00331
$Ni(CO)_4$	nickel tetracarbonyl	50.79297	50.77632 [55]	-0.00033
$Ni(C_5H_5)_2$	bis-cyclopentadienyl nickel (nickelocene)	97.73062	97.84649 [53]	0.00118

Table 23.97.10. Summary results of copper coordinate compounds.

Formula	Name	Calculated Total Bond Energy (eV)	Experimental Total Bond Energy (eV)	Relative Error
CuF	copper fluoride	4.39399	4.44620 [63]	0.01174
CuF_2	copper difluoride	7.91246	7.89040 [63]	-0.00280
CuCl	copper chloride	3.91240	3.80870 [15]	-0.02723
CuO	copper oxide	2.93219	2.90931 [63]	-0.00787

Table 23.97.11. Summary results of zinc coordinate compounds.

Formula	Name	Calculated Total Bond Energy (eV)	Experimental Total Bond Energy (eV)	Relative Error
ZnCl	zinc chloride	2.56175	2.56529 [15]	0.00138
$ZnCl_2$	zinc dichloride	6.68749	6.63675 [15]	-0.00764
$Zn(CH_3)_2$	dimethylzinc	29.35815	29.21367 [15]	-0.00495
$(CH_3CH_2)_2Zn$	diethylzinc	53.67355	53.00987 [65]	-0.01252
$(CH_3CH_2CH_2)_2Zn$	di-n-propylzinc	77.98895	77.67464 [65]	-0.00405
$(CH_3CH_2CH_2CH_2)_2Zn$	di-n-butylzinc	102.30435	101.95782 [65]	-0.00340

Table 23.97.12. Summary results of germanium compounds.

Formula	Name	Calculated Total Bond Energy (eV)	Experimental Total Bond Energy (eV)	Relative Error
$C_8H_{20}Ge$	tetraethylgermanium	109.99686	110.18166 [67]	0.00168
$C_{12}H_{28}Ge$	tetra-n-propylgermanium	158.62766	158.63092 [67]	0.00002
$C_{12}H_{30}Ge_2$	hexaethyldigermanium	167.88982	167.89836 [67]	0.00005

Table 23.97.13. Summary results of tin compounds.

Formula	Name	Calculated Total Bond Energy (eV)	Experimental Total Bond Energy (eV)	Relative Error
$SnCl_4$	tin tetrachloride	12.95756	13.03704 [82]	0.00610
CH_3Cl_3Sn	methyltin trichloride	24.69530	25.69118[a] [83]	0.03876
$C_2H_6Cl_2Sn$	dimethyltin dichloride	36.43304	37.12369 [84]	0.01860
C_3H_9ClSn	trimethyltin chloride	48.17077	49.00689 [84]	0.01706
$SnBr_4$	tin tetrabromide	10.98655	11.01994 [82]	0.00303
C_3H_9BrSn	trimethyltin bromide	47.67802	48.35363 [84]	0.01397
$C_{12}H_{10}Br_2Sn$	diphenyltin dibromide	117.17489	117.36647[a] [83]	0.00163
$C_{12}H_{27}BrSn$	tri-n-butyltin bromide	157.09732	157.26555[a] [83]	0.00107
$C_{18}H_{15}BrSn$	triphenyltin bromide	170.26905	169.91511[a] [83]	-0.00208
SnI_4	tin tetraiodide	9.71697	9.73306 [85]	0.00165
C_3H_9ISn	trimethyltin iodide	47.36062	47.69852 [84]	0.00708
$C_{18}H_{15}SnI$	triphenyltin iodide	169.95165	167.87948[a] [84]	-0.01234
SnO	tin oxide	5.61858	5.54770 [82]	-0.01278
SnH_4	stannane	10.54137	10.47181 [82]	-0.00664
C_2H_8Sn	dimethylstannane	35.22494	35.14201 [84]	-0.00236
$C_3H_{10}Sn$	trimethylstannane	47.56673	47.77353 [84]	0.00433
$C_4H_{12}Sn$	diethylstannane	59.54034	59.50337 [84]	-0.00062
$C_4H_{12}Sn$	tetramethyltin	59.90851	60.13973 [82]	0.00384
$C_5H_{12}Sn$	trimethylvinyltin	66.08296	66.43260 [84]	0.00526
$C_5H_{14}Sn$	trimethylethyltin	72.06621	72.19922 [83]	0.00184
$C_6H_{16}Sn$	trimethylisopropyltin	84.32480	84.32346 [83]	-0.00002
$C_8H_{12}Sn$	tetravinyltin	84.64438	86.53803[a] [83]	0.02188
$C_6H_{18}Sn_2$	hexamethyldistannane	91.96311	91.75569 [83]	-0.00226
$C_7H_{18}Sn$	trimethyl-t-butyltin	96.81417	96.47805 [82]	-0.00348
$C_9H_{14}Sn$	trimethylphenyltin	100.77219	100.42716 [83]	-0.00344
$C_8H_{18}Sn$	triethylvinyltin	102.56558	102.83906[a] [83]	0.00266
$C_8H_{20}Sn$	tetraethyltin	108.53931	108.43751 [83]	-0.00094
$C_{10}H_{16}Sn$	trimethylbenzyltin	112.23920	112.61211 [83]	0.00331
$C_{10}H_{14}O_2Sn$	trimethyltin benzoate	117.28149	119.31199[a] [83]	0.01702
$C_{10}H_{20}Sn$	tetra-allyltin	133.53558	139.20655[a] [83]	0.04074
$C_{12}H_{28}Sn$	tetra-n-propyltin	157.17011	157.01253 [83]	-0.00100
$C_{12}H_{28}Sn$	tetraisopropyltin	157.57367	156.9952 [83]	-0.00366
$C_{12}H_{30}Sn_2$	hexaethyldistannane	164.90931	164.76131[a] [83]	-0.00090
$C_{19}H_{18}Sn$	triphenylmethyltin	182.49954	180.97881[a] [84]	-0.00840
$C_{20}H_{20}Sn$	triphenylethyltin	194.65724	192.92526[a] [84]	-0.00898
$C_{16}H_{36}Sn$	tetra-n-butyltin	205.80091	205.60055 [83]	-0.00097
$C_{16}H_{36}Sn$	tetraisobutyltin	206.09115	206.73234 [83]	0.00310
$C_{21}H_{24}Sn_2$	triphenyl-trimethyldistannane	214.55414	212.72973[a] [84]	-0.00858
$C_{24}H_{20}Sn$	tetraphenyltin	223.36322	221.61425 [83]	-0.00789
$C_{24}H_{44}Sn$	tetracyclohexyltin	283.70927	284.57603 [83]	0.00305
$C_{36}H_{30}Sn_2$	hexaphenyldistannane	337.14517	333.27041 [83]	-0.01163

[a] Crystal.

Table 23.97.14. Summary results of lead compounds.

Formula	Name	Calculated Total Bond Energy (eV)	Experimental Total Bond Energy (eV)	Relative Error
$C_4H_{12}Pb$	tetramethyl-lead	57.55366	57.43264 [86]	-0.00211
$C_8H_{20}Pb$	tetraethyl-lead	106.18446	105.49164 [86]	-0.00657

Table 23.97.15. Summary results of alkyl arsines.

Formula	Name	Calculated Total Bond Energy (eV)	Experimental Total Bond Energy (eV)	Relative Error
C_3H_9As	trimethylarsine	44.73978	45.63114 [87]	0.01953
$C_6H_{15}As$	triethylarsine	81.21288	81.01084 [87]	-0.00249
$C_{18}H_{15}As$	triphenylarsine	167.33081	166.49257 [87]	-0.00503

Table 23.97.16. Summary results of alkyl stibines.

Formula	Name	Calculated Total Bond Energy (eV)	Experimental Total Bond Energy (eV)	Relative Error
C_3H_9Sb	trimethylstibine	44.73078	45.02378 [88]	0.00651
$C_6H_{15}Sb$	triethylstibine	81.20388	80.69402 [88]	-0.00632
$C_{18}H_{15}Sb$	triphenylstibine	167.32181	165.81583 [88]	-0.00908

Table 23.97.17. Summary results of alkyl bismuths.

Formula	Name	Calculated Total Bond Energy (eV)	Experimental Total Bond Energy (eV)	Relative Error
C_3H_9Bi	trimethylbismuth	42.07387	42.79068 [88]	0.01675
$C_6H_{15}Bi$	triethylbismuth	78.54697	78.39153 [88]	-0.00198
$C_{18}H_{15}Bi$	triphenylbismuth	164.66490	163.75184 [88]	-0.00558

REFERENCES

1. D. R. Lide, *CRC Handbook of Chemistry and Physics*, 86th Edition, CRC Press, Taylor & Francis, Boca Raton, (2005-6), pp. 10-202 to 10-204.
2. B. G. Willis, K. F. Jensen, "An evaluation of density functional theory and ab initio predictions for bridge-bonded aluminum compounds," J. Phys. Chem. A, Vol. 102, (1998), pp. 2613-2623.
3. D. R. Lide, *CRC Handbook of Chemistry and Physics*, 86th Edition, CRC Press, Taylor & Francis, Boca Raton, (2005-6), pp. 9-19 to 9-45.
4. T. Shinzawa, F. Uesugi, I. Nishiyama, K. Sugai, S. Kishida, H. Okabayashi, "New molecular compound precursor for aluminum chemical vapor deposition," Applied Organometallic Chem., Vol. 14, (2000), pp. 14-24.
5. D. R. Lide, *CRC Handbook of Chemistry and Physics*, 86th Edition, CRC Press, Taylor & Francis, Boca Raton, (2005-6), p. 9-82.
6. G. Herzberg, *Molecular Spectra and Molecular Structure II. Infrared and Raman Spectra of Polyatomic Molecules*, Van Nostrand Reinhold Company, New York, New York, (1945), p. 344.
7. R. J. Fessenden, J. S. Fessenden, *Organic Chemistry*, Willard Grant Press. Boston, Massachusetts, (1979), p. 320.
8. cyclohexane at http://webbook.nist.gov/.
9. D. R. Lide, *CRC Handbook of Chemistry and Physics*, 86th Ed., CRC Press, Taylor & Francis, Boca Raton, (2005-6), p. 9-54.
10. J. D. Cox, G. Pilcher, *Thermochemistry of Organic and Organometallic Compounds*, Academic Press, New York, (1970).
11. M. B. J. Smith, J. Organometal. Chem., Vol. 76, (1974), pp. 171-201.
12. NIST Atomic Spectra Database, www.physics.nist.gov/cgi-bin/AtData/display.ksh.
13. J. E. Huheey, *Inorganic Chemistry Principles of Structure and Reactivity*, 2nd Ed., Harper & Row, New York, (1978), Chp. 9.
14. D. R. Lide, *CRC Handbook of Chemistry and Physics*, 86th Edition, CRC Press, Taylor & Francis, Boca Raton, (2005-6), p. 9-86.
15. J. Li, P. C. de Mello, K. Jug, "Extension of SINDO1 to transition metal compounds," J. Comput. Chem., Vol. 13(1), (1992), pp. 85-92.
16. D. R. Lide, *CRC Handbook of Chemistry and Physics*, 86th Edition, CRC Press, Taylor & Francis, Boca Raton, (2005-6), p. 9-81.
17. G. Herzberg, *Molecular Spectra and Molecular Structure II. Infrared and Raman Spectra of Polyatomic Molecules*, Van Nostrand Reinhold Company, New York, New York, (1945), p. 567.
18. D. R. Lide, *CRC Handbook of Chemistry and Physics*, 86th Edition, CRC Press, Taylor & Francis, Boca Raton, (2005-6), p. 9-27.
19. M. W. Chase, Jr., C. A. Davies, J. R. Downey, Jr., D. J. Frurip, R. A. McDonald, A. N. Syverud, JANAF Thermochemical Tables, Third Edition, Part I, Al-Co, J. Phys. Chem. Ref. Data, Vol. 14, Suppl. 1, (1985), pp. 467, 509, 522, 535.
20. M. W. Chase, Jr., C. A. Davies, J. R. Downey, Jr., D. J. Frurip, R. A. McDonald, A. N. Syverud, JANAF Thermochemical Tables, Third Edition, Part II, Cr-Zr, J. Phys. Chem. Ref. Data, Vol. 14, Suppl. 1, (1985), pp. 1411, 1438, 1447, 1460.
21. M. W. Chase, Jr., C. A. Davies, J. R. Downey, Jr., D. J. Frurip, R. A. McDonald, A. N. Syverud, JANAF Thermochemical Tables, Third Edition, Part II, Cr-Zr, J. Phys. Chem. Ref. Data, Vol. 14, Suppl. 1, (1985), pp. 1096, 1153, 1174, 1192.

22. M. W. Chase, Jr., C. A. Davies, J. R. Downey, Jr., D. J. Frurip, R. A. McDonald, A. N. Syverud, JANAF Thermochemical Tables, Third Edition, Part I, Al-Co, J. Phys. Chem. Ref. Data, Vol. 14, Suppl. 1, (1985), pp. 808, 866, 887, 906.
23. M. W. Chase, Jr., C. A. Davies, J. R. Downey, Jr., D. J. Frurip, R. A. McDonald, A. N. Syverud, JANAF Thermochemical Tables, 3rd Edition, Part I, Al-Co & Part II, Cr-Zr, J. Phys. Chem. Ref. Data, Vol. 14, Suppl. 1, (1985), pp. 796, 843, 1082, 1132, 1738, 1762.
24. M. W. Chase, Jr., C. A. Davies, J. R. Downey, Jr., D. J. Frurip, R. A. McDonald, A. N. Syverud, JANAF Thermochemical Tables, Third Edition, Part II, Cr-Zr, J. Phys. Chem. Ref. Data, Vol. 14, Suppl. 1, (1985), p. 1616.
25. G. Herzberg, Molecular Spectra and Molecular Structure. I. Spectra of Diatomic Molecules, Krieger Publishing Company, Malabar, FL, (1950), p. 578.
26. E. L. Muetterties, J. R. Bleeke, E. J. Wucherer, "Structural, stereochemical, and electronic features of arene-metal complexes," Chem. Rev., Vol. 82, No. 5, (1982), pp. 499-525.
27. vanadium pentafluoride at http://webbook.nist.gov/.
28. vanadium oxytrichloride at http://webbook.nist.gov/.
29. M. W. Chase, Jr., C. A. Davies, J. R. Downey, Jr., D. J. Frurip, R. A. McDonald, A. N. Syverud, JANAF Thermochemical Tables, Third Edition, Part I, Al-Co & Part II, Cr-Zr, J. Phys. Chem. Ref. Data, Vol. 14, Suppl. 1, (1985), p. 698.
30. G. Herzberg, *Molecular Spectra and Molecular Structure II. Infrared and Raman Spectra of Polyatomic Molecules*, Van Nostrand Reinhold Company, New York, New York, (1945), pp. 362-369.
31. M. W. Chase, Jr., C. A. Davies, J. R. Downey, Jr., D. J. Frurip, R. A. McDonald, A. N. Syverud, JANAF Thermochemical Tables, Third Edition, Part II, Cr-Zr, J. Phys. Chem. Ref. Data, Vol. 14, Suppl. 1, (1985), p. 1763.
32. Wagman, D. D.; Evans, W. H.; Parker, V. B.; Halow, I.; Bailey, .S. .M.; Schumm, R. L.; Nuttall, R. H. The NBS Tables of Chemical. Thermodynamic Properties, J. Phys. Chem. Ref. Data, Vol. 11, Suppl. 2 (1982)Wagman, D. D.; Evans, W. H.; Parker, V. B.; Halow, I.; Bailey, .S. .M.; Schumm, R. L.; Nuttall, R. H. The NBS Tables of Chemical. Thermodynamic Properties, J. Phys. Chem. Ref. Data, Vol. 11, Suppl. 2 (1982)Wagman, D. D.; Evans, W. H.; Parker, V. B.; Halow, I.; Bailey, .S. .M.; Schumm, R. L.; Nuttall, R. H. The NBS Tables of Chemical. Thermodynamic Properties, J. Phys. Chem. Ref. Data, Vol. 11, Suppl. 2 (1982)Wagman, D. D.; Evans, W. H.; Parker, V. B.; Halow, I.; Bailey, .S. .M.; Schumm, R. L.; Nuttall, R. H. The NBS Tables of Chemical. Thermodynamic Properties, J. Phys. Chem. Ref. Data, Vol. 11, Suppl. 2 (1982).
33. J. D. Cox, G. Pilcher, *Thermochemistry of Organometallic Compounds*, Academic Press, New York, (1970), p. 478.
34. W. I. F. David, R. M. Ibberson, G. A. Jeffrey, J. R. Ruble, "The structure analysis of deuterated benzene and deuterated nitromethane by pulsed-neutron powder diffraction: a comparison with single crystal neutron analysis," Physica B (1992), 180 & 181, pp. 597-600.
35. G. A. Jeffrey, J. R. Ruble, R. K. McMullan, J. A. Pople, "The crystal structure of deuterated benzene," Proceedings of the Royal Society of London. Series A, Mathematical and Physical Sciences, Vol. 414, No. 1846, (Nov. 9, 1987), pp. 47-57.
36. H. B. Burgi, S. C. Capelli, "Getting more out of crystal-structure analyses," Helv. Chim. Acta, Vol. 86, (2003), pp. 1625-1640.
37. M. W. Chase, Jr., C. A. Davies, J. R. Downey, Jr., D. J. Frurip, R. A. McDonald, A. N. Syverud, JANAF Thermochemical Tables, Third Edition, Part II, Cr-Zr, J. Phys. Chem. Ref. Data, Vol. 14, Suppl. 1, (1985), pp. 968, 969, 970.
38. A. Jost, B. Rees, "Electronic structure of chromium hexacarbonyl at 78K. I. Neutron diffraction study, Acta. Cryst. Vol. B31 (1975), pp. 2649-2658.
39. J. A. Ibers, "The structure of dibenzene chromium," J. Phys. Chem., Vol. 40, (1964), pp.3129-3130.
40. B.B. Ebbinghaus, "Thermodynamics of gas phase chromium species: The chromium chlorides, oxychlorides, fluorides, oxyfluorides, hydroxides, oxyhydroxides, mixed oxyfluorochlorohydroxides, and volatility calculations in waste incineration processes," Combustion and Flame, Vol. 101, (1995), pp. 311-338.
41. "Hexacarbonylnickel," *NIST Chemistry Handbook.* http://webbook.nist.gov/.
42. "CrCC," *NIST Chemistry Handbook.* http://webbook.nist.gov/.
43. D. Lin-Vien. N. B. Colthup, W. G. Fateley, J. G. Grasselli, The *Handbook of Infrared and Raman Frequencies of Organic Molecules*, Academic Press, Inc., Harcourt Brace Jovanovich, Boston, (1991), p. 481.
44. J. D. Cox, G. Pilcher, *Thermochemistry of Organometallic Compounds*, Academic Press, New York, (1970), p. 489.
45. N. Vogt, "Equilibrium bond lengths, force constants and vibrational frequencies of MnF_2, FeF_2, CoF_2, NiF_2, and ZnF_2 from least-squares analysis of gas-phase electron diffraction data," J. Molecular Structure, Vol. 570, (2001), pp. 189-195.
46. L. F. Dahl, "The structure of dimanganese decacarbonyl, $Mn_2(CO)_{10}$," Acta. Cryst., Vol. 16, (1963), pp. 419-426.
47. G. Herzberg, Molecular Spectra and Molecular Structure. I. Spectra of Diatomic Molecules, Krieger Publishing Company, Malabar, FL, (1950), p. 550.
48. "Mn_3," *NIST Chemistry Handbook.* http://webbook.nist.gov/.
49. J. D. Cox, G. Pilcher, *Thermochemistry of Organometallic Compounds*, Academic Press, New York, (1970), p. 491.
50. M. W. Chase, Jr., C. A. Davies, J. R. Downey, Jr., D. J. Frurip, R. A. McDonald, A. N. Syverud, JANAF Thermochemical Tables, Third Edition, Part I, Al-Co, J. Phys. Chem. Ref. Data, Vol. 14, Suppl. 1, (1985), pp. 822, 879.
51. M. W. Chase, Jr., C. A. Davies, J. R. Downey, Jr., D. J. Frurip, R. A. McDonald, A. N. Syverud, JANAF Thermochemical Tables, Third Edition, Part II, Cr-Zr, J. Phys. Chem. Ref. Data, Vol. 14, Suppl. 1, (1985), p. 1054.
52. M. W. Chase, Jr., C. A. Davies, J. R. Downey, Jr., D. J. Frurip, R. A. McDonald, A. N. Syverud, JANAF Thermochemical Tables, Third Edition, Part II, Cr-Zr, J. Phys. Chem. Ref. Data, Vol. 14, Suppl. 1, (1985), p. 1239.
53. J. D. Cox, G. Pilcher, *Thermochemistry of Organometallic Compounds*, Academic Press, New York, (1970), p. 493.

54. M. W. Chase, Jr., C. A. Davies, J. R. Downey, Jr., D. J. Frurip, R. A. McDonald, A. N. Syverud, JANAF Thermochemical Tables, Third Edition, Part II, Cr-Zr, J. Phys. Chem. Ref. Data, Vol. 14, Suppl. 1, (1985), p. 953.
55. M. W. Chase, Jr., C. A. Davies, J. R. Downey, Jr., D. J. Frurip, R. A. McDonald, A. N. Syverud, JANAF Thermochemical Tables, Third Edition, Part II, Cr-Zr, J. Phys. Chem. Ref. Data, Vol. 14, Suppl. 1, (1985), p. 695.
56. G. Herzberg, Molecular Spectra and Molecular Structure. I. Spectra of Diatomic Molecules, Krieger Publishing Company, Malabar, FL, (1950), p. 522.
57. D. R. Lide, *CRC Handbook of Chemistry and Physics*, 86th Ed., CRC Press, Taylor & Francis, Boca Raton, (2005-6), p. 9-85.
58. "Co(CO)," *NIST Chemistry Handbook.* http://webbook.nist.gov/.
59. M. W. Chase, Jr., C. A. Davies, J. R. Downey, Jr., D. J. Frurip, R. A. McDonald, A. N. Syverud, JANAF Thermochemical Tables, Third Edition, Part II, Cr-Zr, J. Phys. Chem. Ref. Data, Vol. 14, Suppl. 1, (1985), pp. 794, 840.
60. P. Seiler, J. D. Dunitz, "The structure of nickelocene at room temperature and at 101 K," Acta. Cryst., Vol. B36, (1980), pp. 2255-2260.
61. NIST Atomic Spectra Database, www.physics.nist.gov/cgi-bin/AtData/display.ksh.
62. D. R. Lide, *CRC Handbook of Chemistry and Physics*, 86th Edition, CRC Press, Taylor & Francis, Boca Raton, (2005-6), pp. 9-83 to 9-84.
63. M. W. Chase, Jr., C. A. Davies, J. R. Downey, Jr., D. J. Frurip, R. A. McDonald, A. N. Syverud, JANAF Thermochemical Tables, Third Edition, Part II, Cr-Zr, J. Phys. Chem. Ref. Data, Vol. 14, Suppl. 1, (1985), pp. 1013, 1017, 1020.
64. "Dimethylzinc," *NIST Chemistry Handbook.* http://webbook.nist.gov/.
65. J. D. Cox, G. Pilcher, *Thermochemistry of Organometallic Compounds*, Academic Press, New York, (1970), pp. 446-447.
66. D. Lin-Vien. N. B. Colthup, W. G. Fateley, J. G. Grasselli, The *Handbook of Infrared and Raman Frequencies of Organic Molecules*, Academic Press, Inc., Harcourt Brace Jovanovich, Boston, (1991), p. 13.
67. J. D. Cox, G. Pilcher, *Thermochemistry of Organic and Organometallic Compounds*, Academic Press, New York, (1970), pp. 470-471.
68. H. Preut, "Structure of triphenyltin bromide," Acta. Cryst., Vol. B35, (1979), pp. 744-746.
69. S. W. Ng, "Triphenyltin iodide," Acta. Cryst., Vol. C51, (1995), pp. 629-631.
70. Von H. Preut, H.-J. Haupt, F. Huber, "Die Kristall-und molekularstruktur des hexaphenyl-distannans," Zeitschrift für anorganische und allgemeine Chemie, Vol. 396, Issue 1, January, (1973), pp. 81-89.
71. G. A. Sim, J. M. Robertson, T. H. Goodwin, "The crystal and molecular structure of benzoic acid," Acta Cryst., Vol. 8, (1955), pp.157-164.
72. D. Lin-Vien. N. B. Colthup, W. G. Fateley, J. G. Grasselli, The *Handbook of Infrared and Raman Frequencies of Organic Molecules*, Academic Press, Inc., Harcourt Brace Jovanovich, Boston, (1991), pp 5,14.
73. J. F. Sanz, A. Marquez, "Molecular structure and vibrational analysis of distannane from ab initio second-order perturbation calculations. A theoretical approach to the tin-X bond (X=Cl, Si, Ge, Sn)," J. Phys. Chem., Vol. 93, (1989), pp. 7328-7333.
74. G. Herzberg, *Molecular Spectra and Molecular Structure II. Infrared and Raman Spectra of Polyatomic Molecules*, Van Nostrand Reinhold Company, New York, New York, (1945), p. 326.
75. "b1 2-methyl-1-propene," *NIST Chemistry Handbook.* http://webbook.nist.gov/.
76. "a1 2-methyl-1-propene," *NIST Chemistry Handbook.* http://webbook.nist.gov/.
77. "Acetic acid," *NIST Chemistry Handbook.* http://webbook.nist.gov/.
78. G. Herzberg, *Molecular Spectra and Molecular Structure II. Infrared and Raman Spectra of Polyatomic Molecules*, Krieger Publishing Company, Malabar, FL, (1991), p. 195.
79. D. Lin-Vien. N. B. Colthup, W. G. Fateley, J. G. Grasselli, The *Handbook of Infrared and Raman Frequencies of Organic Molecules*, Academic Press, Inc., Harcourt Brace Jovanovich, Boston, (1991), p. 138.
80. K. P. Huber, G. Herzberg, *Molecular Spectra and Molecular Structure, IV. Constants of Diatomic Molecules*, Van Nostrand Reinhold Company, New York, (1979).
81. J. Crovisier, Molecular Database—Constants for molecules of astrophysical interest in the gas phase: photodissociation, microwave and infrared spectra, Ver. 4.2, Observatoire de Paris, Section de Meudon, Meudon, France, May 2002, pp. 34–37, available at http://wwwusr.obspm.fr/~crovisie/.
82. D. R. Lide, *CRC Handbook of Chemistry and Physics*, 86th Edition, CRC Press, Taylor & Francis, Boca Raton, (2005-6), pp. 5-8, 5-10, 5-14, 5-16, 5-28.
83. J. D. Cox, G. Pilcher, *Thermochemistry of Organometallic Compounds*, Academic Press, New York, (1970), pp. 472-477.
84. P. G. Harrison, *Chemistry of Tin*, Blackie, Glasgow, (1989), pp. 10-12.
85. O. Knacke, O. Kubaschewski, K. Hesselmann, *Thermochemical Properties of Inorganic Substances*, 2nd Edition, Vol. II, Springer, New York (1991), pp. 1888-1889.
86. J. D. Cox, G. Pilcher, *Thermochemistry of Organometallic Compounds*, Academic Press, New York, (1970), pp. 476-477.
87. J. D. Cox, G. Pilcher, *Thermochemistry of Organometallic Compounds*, Academic Press, New York, (1970), pp. 484-485.
88. J. D. Cox, G. Pilcher, *Thermochemistry of Organometallic Compounds*, Academic Press, New York, (1970), pp. 486-487.

The Grand Unified Theory of Classical Physics

Dr. Randell L. Mills

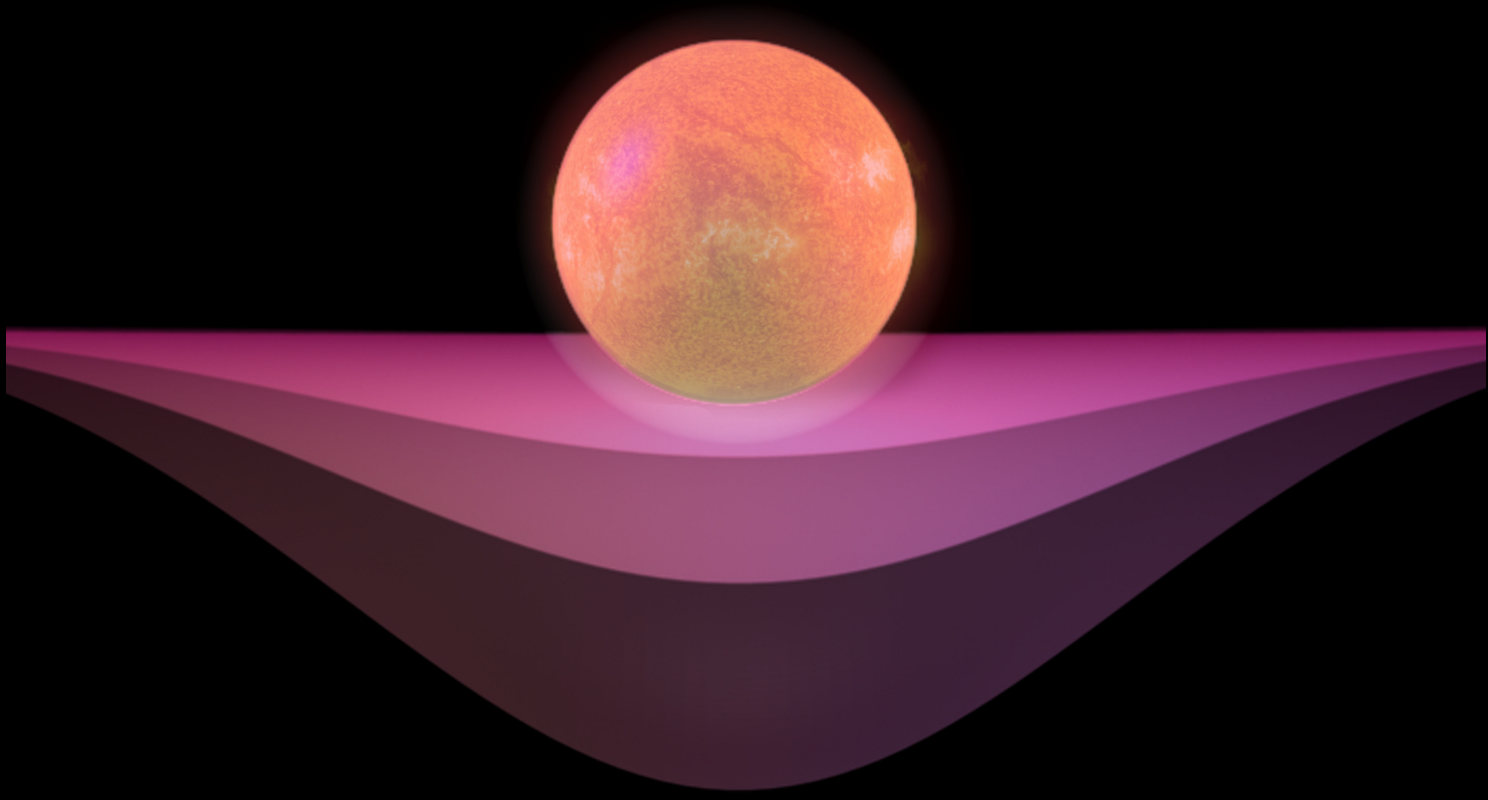

Volume III:

Collective Phenomena, High-Energy Physics, & Cosmology

THE GRAND UNIFIED THEORY OF CLASSICAL PHYSICS

Volume 3 of 3

THE GRAND UNIFIED THEORY OF CLASSICAL PHYSICS

BY

Dr. Randell L. Mills

April 2023 Edition
Volume 3 of 3

ISBN 979-8-218-17988-5
Library of Congress Control Number 2023905641

TABLE OF CONTENTS

VOLUME 3 COLLECTIVE PHENOMENA, HIGH-ENERGY PHYSICS, & COSMOLOGY

APPENDICES

Chapter 24

STATISTICAL MECHANICS

Large systems of particles are ubiquitous in nature. The physics of each particle of a large system is determined by physical laws considering its initial conditions and history. However, the amount of information to follow even 2 grams of hydrogen gas having Avogadro's number of molecules ($N_A = 6.022045\ X\ 10^{23}\ mol^{-1}$) is overwhelming. Statistical models typically deal with insufficient information for an underlying deterministic macrosystem such as the determination of an average property of a population with the accuracy only limited by the number of independent samples[1]. Fortunately for the cases of atomic systems, it is also possible to determine the bulk properties of many systems using statistical models. The modeling of aggregate behavior of a large ensemble of atoms, electrons, or photons obeying classical physics such as molecules in a gas, photons in a cavity, and free electrons in a metal is the branch of physics called statistical mechanics. Statistical mechanics gives state properties of a system of many particles that are a manifestation of the properties of the particles themselves. The necessity to be concerned with the actual motions and interactions of individual particles is avoided. Instead, such models give predictions for the probability that the particle has a certain amount of energy at a certain moment. It gives statistical distributions for all of the particles rather than the exact value for a specific particle.

THREE DIFFERENT KINDS OF ATOMIC-SCALE STATISTICAL DISTRIBUTIONS [5]

It was shown in the State Lifetimes and Line Intensities section, that a mean lifetime arises due to the superposition of transitions over an ensemble of individual atoms. Each atom has an exact lifetime due to an exact transition involving specific initial, final, and any intermediate ℓ, m states and the corresponding exact photon in space relative to the states. The mean lifetime arises from the mean current given by Eq. (2.87) and the spherical radiation field due to the superposition of emitted photons. Similarly, Maxwell's equations apply to macroscopic electromagnetic fields that are in actuality the superposition of quantized photons traveling at the speed of light. Furthermore, using Maxwell's equations, the reduced speed of light in a transparent medium can be shown to be due to the radiation from many induced dipoles that produce a single wave propagating at the reduced speed [6]. Thus, deterministic physics arises as the aggregate behavior of entities that also in turn obey deterministic physics. The same principle applies in the case of statistical mechanical models.

In previous sections, the exact nature of individual particles (e.g. atoms, electrons, and photons) were solved. The interactions of two separate individual particles demonstrated three types of behavior that are correctly modeled by three types of corresponding statistical models. Each statistical model with a corresponding probability distribution function is based on the properties of the particle and their corresponding interactions.

According to statistical thermodynamics [7], a macroscopic thermodynamic system is viewed as an assembly of myriad submicroscopic entities in ever changing quantum states. Consider the number of distinct ways that a set number of energy

[1] Quantum theory is incompatible with probability theory since the latter is based on underlying unknown, but determined outcomes, and the former is not [1]. Wavefunction solutions of the Schrödinger equation are interpreted as probability-density functions. Quantum theory confuses the concepts of a wave and a probability-density function that are based on totally different mathematical and physical principles. The use of "probability" in this instance does not conform to the mathematical rules and principles of probability theory. Statistical theory is based on an existing deterministic reality with incomplete information; whereas, quantum measurement acts on a "probability-density function" to determine a reality that did not exist before the measurement. Additionally, it is nonsensical to treat a single particle such as an electron as if it was a population of electrons and to assign the single electron to a statistical distribution over many states. The electron has conjugate degrees of freedom such as position, momentum, and energy that obey conservation laws in an inverse-r Coulomb field. A single electron cannot have multiple positions and momenta or energies simultaneously. The decision to treat the electron as a point-particle-probability wave, a point with no volume with a vague probability wave requiring that the electron have an infinite number of positions and energies including negative and infinite energies simultaneously was a turning point in physics. The adoption of the probabilistic versus deterministic nature of atomic particles violates all physical laws including special relativity with violation of causality as pointed out by Einstein [2] and de Broglie [3]. Consequently, it was rejected even by Schrödinger [4]. Pure mathematics took the place of physics, but even so, the mathematics is not even consistent with probability theory.

quanta can be distributed between a set number of energy levels each called a microstate. The total number of microstates W associated with any configuration involving N distinguishable units is

$$W = \frac{N!}{(\eta_a!)(\eta_b!)\cdots} \tag{24.1}$$

where η_a represents the number of units assigned the same number of energy quanta (and, hence, occupying the same quantum number), and η_b represents the number of units occupying some other quantum level. As the number of units increases, the total number of microstates skyrockets to unimaginable magnitudes. Thus, one can calculate that an assembly of 1000 localized harmonic oscillators sharing 1000 energy quanta possesses more than 10^{600} different microstates. This explosive expansion of the total number of microstates with increasing N is a direct consequence of the mathematics of permutations, from which arises also a second consequence of no less importance. Statistical analysis shows that the emergence of a *predominant configuration* is characteristic of any assembly with a large number (N) of units. Of the immense total number of microstates that can be assumed by a large assembly, an overwhelming proportion arises from one comparatively, small set of configurations centered on, and only minutely different from, the predominant configuration—with which they share an empirically identical set of macroscopic properties.

The first step in the program of statistical mechanics is to find a general expression for W for the kind of particles being considered. Then W is maximized subject to the conditions that the system consists of a fixed number of N particles (except when they are photons or their acoustic equivalents called *phonons* where the total energy is conserved, but the number can change since the individual energies are given by Planck's equation, $E = h\nu$) and that the system contains a fixed amount of energy E *that is conserved in populating the conserved number of states where applicable*. The result in each case is an expression for $n(\varepsilon)$, the number of particles with the energy ε, that has the form:

$$n(\varepsilon) = g(\varepsilon)\, f(\varepsilon) \tag{24.2}$$

where $g(\varepsilon)$ = number of states of energy ε
= statistical weight corresponding to energy ε
$f(\varepsilon)$ = distribution function
= average number of particles in each state of energy ε
= probability of occupancy of each state of energy ε

When a continuous rather than a discrete distribution of energies is involved, $g(\varepsilon)$ is replaced by $g(\varepsilon)d\varepsilon$, the number of states with energies between ε and $\varepsilon + d\varepsilon$.

Each of the three models is based upon the determination of the most probable way in which a certain total amount of energy E is distributed among the N members of a system of particles in thermal equilibrium at the absolute temperature T. Then, it is possible to statistically predict aggregate properties such as the number of particles having an energy ε_1, ε_2, and so on, based on the model. The particle interactions are assumed to be at thermal equilibrium between themselves and the walls of their container in the absence of strongly correlated motion. More than one particle state may have a certain energy ε. In the case of Maxwell-Boltzmann and Bose-Einstein statistics more than one particle may be in a certain state. In the case of Fermi-Dirac statistics each particle must be in different state since Fermi-Dirac statistics treats particles such as electrons that spin pair. A fundamental assumption of all statistical mechanical models that is supported by experimentation and consistent with physical laws, is that the greater the number W of different ways in which the particles can be arranged among the available states to yield a particular distribution of energies, the more probable the distribution. It is assumed that each state of a certain energy is equally likely to be occupied. The atomic scale distributions derived from deterministic, conditional probability theory [8] are:

MAXWELL-BOLTZMANN—identical, discrete particles such as molecules are separated and act independently such that they possess a continuum of momenta with exchange by the predominant interaction of collisional scattering. Atoms and molecules have exact dimensions as shown in the and One-Electron Atom section, Two-Electron Atoms section, Three- Through Twenty-Electron Atoms section, Nature of the Chemical Bond of Hydrogen-Type Molecules and Molecular Ions section, Polyatomic Molecular Ions and Molecules section, and More Polyatomic Molecules and Hydrocarbons section. Neutral particles such as atoms and molecules undergo one-on-one collisional interactions, which are conservative; otherwise, there is no correlation between the separated particles. Maxwell-Boltzmann statistics is used to model the aggregate properties of a gas at a given temperature. The corresponding Maxwell-Boltzmann distribution function states that the average number of particles $f_{MB}(\varepsilon)$ in a state of energy ε in a system of particles at the absolute temperature T is:

$$f_{MB}(\varepsilon) = Ae^{-\varepsilon/kT} \tag{24.3}$$

where the value of A depends of the number of particles in the system and serves to scale the distribution to the number of particles and, $k = 1.381\times10^{-23}\ J/K = 8.617\times10^{-5}\ eV/K$ is Boltzmann's constant.

BOSE-EINSTEIN—indistinguishable photons called bosons having $\hbar$ of angular momentum excite quantized energy levels of electron resonator cavities where superposition and conservation of angular momentum are obeyed. As shown in the Excited States of the One-Electron Atom (Quantization) and the Excited States of Helium sections, each bound electron is a resonator cavity, which traps single photons of discrete frequencies. Thus, photon absorption occurs as an excitation of a resonator mode. The angular momentum of the free space photon given by $\mathbf{m} = \int \frac{1}{8\pi c} \mathrm{Re}\left[\mathbf{r} \times (\mathbf{E} \times \mathbf{B}^*)\right] dx^4 = \hbar$ in the Photon section is conserved [9] for the solutions for the resonant photons and excited-state electron functions. The change in angular frequency of the electron is equal to the angular frequency of the resonant photon that excites the resonator cavity mode corresponding to the transition, and the energy is given by Planck's equation. An ensemble of a large number of photons in equilibrium with a material comprised of many electron states having resonant transitions excited by the photons may be correlated in order to conserve angular momentum. Certain solid materials have essentially a continuum of discrete excited states wherein excitation of any state increases the cross section for the absorption of additional photons of the same energy by changing the angular momentum of the electron during excitation to permit further excitation. In each case, the excited-state electron can undergo further transitions by resonant excitation with photons of the same energy, but different polarizations having the required angular momentum. An ensemble of a large number of photons in equilibrium, with such a solid material comprised of many electron states having correlated resonant transitions excited by the photons, gives rise to blackbody radiation. The statistics of this model is based on the physics that the presence of a particle in a certain quantum state *increases* the probability that other particles are to be found in the same state. Bose-Einstein statistics is used to model photons in equilibrium with a cavity to account for the spectrum of radiation from a blackbody. It is also used to model phonons in a solid. The corresponding Bose-Einstein distribution function states that the probability $f(\varepsilon)$ that a boson occupies a state of energy ε in a system of particles at the absolute temperature T is:

$$f_{BE}(\varepsilon) = \frac{1}{e^{\alpha} e^{\varepsilon/kT} - 1} \tag{24.4}$$

FERMI-DIRAC—identical, indistinguishable electrons called fermions occupy the lowest energy configuration as given in the Two Electron Atom section. The Pauli Exclusion Principle arises as a minimum of energy for interacting electrons each having a Bohr magneton of magnetic moment. Electrons pair as opposite mirror-image currents such that the occupation of one spin state by a first electron (e.g. $s = 1/2$) causes a second to occupy the opposite spin state ($s = -1/2$). Thus, the statistics of this model is based on physics that the presence of a particle in a certain state *prevents* any other particles from being in that state. Fermi-Dirac statistics is used to model the behavior of electrons in a metal to explain the ability of metals to conduct electricity. The corresponding Fermi-Dirac distribution function states that the probability $f(\varepsilon)$ that a fermion occupies a state of energy ε in a system of particles at the absolute temperature T is:

$$f_{FD}(\varepsilon) = \frac{1}{e^{\alpha} e^{\varepsilon/kT} + 1} \tag{24.5}$$

The quantity α depends on the properties of the particular system and may be a function of T.

The Maxwell-Boltzmann distribution function holds for systems of identical particles that can be distinguished one from another and there is no conditional-probability factor corresponding to the physics of the occupation of a given quantum state influencing the probability that other particles are found in the same state. In contrast, the –1 term in the denominator of Eq. (24.4) expresses the increased likelihood of multiple occupancy of an energy state by bosons compared with the likelihood for distinguishable particles such as molecules. The +1 term in the denominator in Eq. (24.5) is a consequence of the minimization of energy corresponding to spin pairing: no matter what the values of α, ε, and T, $f(\varepsilon)$ can never exceed one. In both cases, when $\varepsilon \gg kT$, the functions $f(\varepsilon)$ approach that of the Maxwell-Boltzmann statistics, Eq. (24.3). Figure 24.1 is a comparison of the three distribution functions for $\alpha = -1$. For a given value of $\frac{\varepsilon}{kT}$, $f_{BE}(\varepsilon)$, which models bosons (photons and phonons), is always greater than $f_{MB}(\varepsilon)$, and $f_{FD}(\varepsilon)$, which models fermions (electrons), is always smaller.

From Eq. (24.5), $f_{FD}(\varepsilon) = \frac{1}{2}$ when the energy is:

$$\varepsilon_F = -\alpha kT \tag{24.6}$$

This energy defined as the *Fermi energy*, has significance in analyzing the behavior of a system of fermions, such as the conduction electrons in a metal. The Fermi-Dirac distribution function, expressed in terms of ε_F is:

$$f_{FD}(\varepsilon) = \frac{1}{e^{(\varepsilon - \varepsilon_F)/kT} + 1} \tag{24.7}$$

Figure 24.1. A comparison of the three statistical functions that give the probability of occupancy of a state of energy ε at the absolute temperature T for $\alpha = -1$. The Maxwell-Boltzmann is pure exponential. The Bose-Einstein function is always higher and the Fermi-Dirac function is always lower.

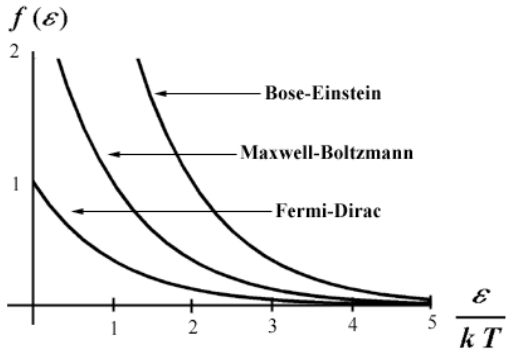

The significance of the Fermi energy can be appreciated by comparing the occupancy of the states a system of fermions at $T = 0$ whose energies are less than ε_F with those that are greater than ε_F:

$$T = 0,\ \varepsilon < \varepsilon_F:\ f_{FD}(\varepsilon) = \frac{1}{e^{(\varepsilon-\varepsilon_F)/kT}+1} = \frac{1}{e^{-\infty}+1} = \frac{1}{0+1} = 1$$
$$T = 0,\ \varepsilon > \varepsilon_F:\ f_{FD}(\varepsilon) = \frac{1}{e^{(\varepsilon-\varepsilon_F)/kT}+1} = \frac{1}{e^{\infty}+1} = 0 \tag{24.8}$$

At absolute zero, all energy states up to ε_F are occupied, but none above ε_F as shown in Figure 24.2 for $T = 0$. As given in the Free Electrons in a Metal Section (Eq. (24.60)), the Fermi energy ε_F of a system containing N fermions can be calculated by filling up its energy states with the N particles in order of increasing energy starting from $\varepsilon = 0$. The highest state to be occupied will then have the energy $\varepsilon = \varepsilon_F$.

The distribution functions for fermions at $T = 0$, $T = 0.1\frac{\varepsilon_F}{k}$, and $T = 1.0\frac{\varepsilon_F}{k}$ are shown in Figure 24.2. As the temperature is increased above $T = 0$ with $0 < kT < \varepsilon_F$, fermions shift their population of states from those just below ε_F to states just above it as shown in Figure 24.2 for $T = 0.1\frac{\varepsilon_F}{k}$. At higher temperatures, even fermions in the lowest states will begin to be excited to higher ones, so $f_{FD}(0)$ will drop below 1. In these circumstances $f_{FD}(\varepsilon)$ will assume a shape like that in the lowest curve in Figure 24.2 corresponding to $T = 1.0\frac{\varepsilon_F}{k}$. The properties of the three distribution functions are summarized in Table 24.1 wherein to obtain the *actual number* $n(\varepsilon)$ of particles with an energy ε, the functions $f(\varepsilon)$ are multiplied by $g(\varepsilon)$, the number of states of energy (ε):

$$n(\varepsilon) = g(\varepsilon)\, f(\varepsilon) \tag{24.9}$$

Figure 24.2. Distribution function for fermions at three different temperatures. At $T = 0$, all the energy states up to the Fermi energy ε_F are occupied. At low temperature ($T = 0.1\frac{\varepsilon_F}{k}$), some fermions will leave states just below ε_F and move into states just above ε_F. At a higher temperature ($T = 1.0\frac{\varepsilon_F}{k}$), fermions from any state below ε_F may move into states above ε_F.

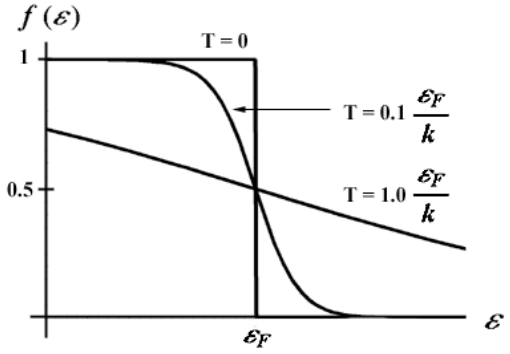

Table 24.1. The Three Statistical Distribution Functions

	Maxwell-Boltzmann	Bose-Einstein	Fermi-Dirac
Applies to systems of	Identical, distinguishable particles	Identical, indistinguishable particles that do not spin pair	Identical, indistinguishable particles that spin pair
Categories of particles	Collisional	Bosons	Fermions
Properties of particles	Any spin	Spin 0, 1, 2,	Spin $\frac{1}{2}, \frac{3}{2}, \frac{5}{2}$
Examples	Molecules of gas	Photons in a cavity; phonons in a solid; liquid helium at low temperatures	Free electrons in a metal
Distribution function (number of particles in each state of energy ε at the temperature T)	$f_{MB}(\varepsilon) = Ae^{-\varepsilon/kT}$	$f_{BE}(\varepsilon) = \frac{1}{e^{\alpha}e^{\varepsilon/kT} - 1}$	$f_{FD}(\varepsilon) = \frac{1}{e^{(\varepsilon-\varepsilon_F)/kT} + 1}$
Properties of distribution	No limit to number of particles per state	No limit to number of particles per state; more particles per state than f_{MB} at low energies; approaches f_{MB} at high energies	Never more than 1 particle per state; fewer particles per state than f_{MB} at low energies; approaches f_{MB} at high energies

APPLICATION OF MAXWELL-BOLTZMANN STATISTICS TO MODEL MOLECULAR ENERGIES IN AN IDEAL GAS

Combining Eqs. (24.2) and (24.3) gives us the number $n(\varepsilon)$ of identical, distinguishable particles in an assembly at the temperature T that have the energy ε:

$$n(\varepsilon) = Ag(\varepsilon)e^{-\varepsilon/kT} \tag{24.10}$$

Eq. (24.3) predicts that $f_{MB}(\varepsilon)$ decreases with ε and increases with increasing T consistent with observations. A more definite test of the validity of Eq. (24.3) including the $1/kT$ factor in the exponent is to use it to calculate the total internal energy E of a system of particles for which E is known. An appropriate test system is a sample of an ideal gas that contains N molecules. The elementary kinetic theory of gases shows that the ideal-gas law will have the correct form $PV = NkT$ only if the average molecular kinetic energy is $\frac{3}{2}kT$, so that the total molecular energy must be $E = \frac{3}{2}NkT$. As shown by Eq. (24.24), Eq. (24.3) does give this result validating the model, which is developed next.

The translational motion of gas molecules is continuous, and the total number of molecules N in a sample is usually very large. Therefore, a continuous distribution of molecular energies is used instead of the discrete set $\varepsilon_1, \varepsilon_2, \varepsilon_3, \ldots$. If $n(\varepsilon)d\varepsilon$ is the number of molecules whose energies lie between ε and $\varepsilon + d\varepsilon$, Eq. (24.3) can be written:

$$n(\varepsilon)d\varepsilon = \left[g(\varepsilon)d\varepsilon\right]\left[f(\varepsilon)\right] = Ag(\varepsilon)e^{-\varepsilon/kT}d\varepsilon \tag{24.11}$$

To find $g(\varepsilon)d\varepsilon$, the number of states that have energies between ε and $\varepsilon + d\varepsilon$, first consider that a molecule of energy ε has a momentum **p** whose magnitude p is specified by:

$$p = \sqrt{2m\varepsilon} = \sqrt{p_x^2 + p_y^2 + p_z^2} \tag{24.12}$$

Each set of momentum components p_x, p_y, p_z specifies a different state of motion. Further consider a *momentum space* whose coordinate axes are p_x, p_y, p_z, as in Figure 24.3. The number of states $g(p)dp$ with momenta whose magnitudes are between p and $p + dp$ are proportional to the volume of a spherical shell in momentum space p in radius and dp thick, which is $4\pi p^2 dp$. Hence

$$g(p)dp = Bp^2 dp \tag{24.13}$$

where B is some constant. Since each momentum magnitude p corresponds to a single energy ε, the number of energy states $g(\varepsilon)d\varepsilon$ between ε and $\varepsilon + d\varepsilon$ is the same as the number of momentum states $g(p)dp$ between p and $p + dp$. Thus, Eq. (24.13) becomes:

$$g(\varepsilon)d\varepsilon = Bp^2 dp \tag{24.14}$$

Figure 24.3. The coordinates in momentum space are p_x, p_y, p_z. The number of momentum states available to a particle with a momentum whose magnitude is between p and $p + dp$ is proportional to the volume of a spherical shell in momentum space of radius p and thickness dp.

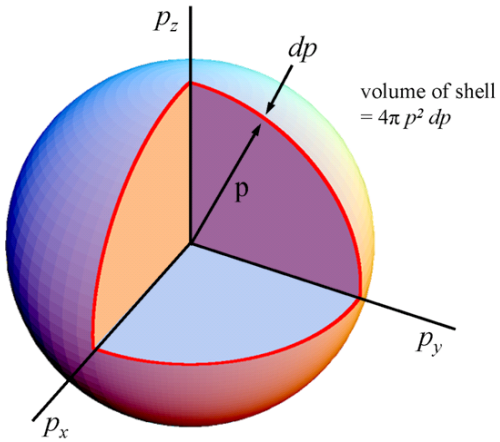

Since

$$p^2 = 2m\varepsilon \text{ and } dp = \frac{m\, d\varepsilon}{\sqrt{2m\varepsilon}} \tag{24.15}$$

Eq. (24.14) becomes

$$g(\varepsilon)\, d\varepsilon = \sqrt{2}m^{3/2} B\sqrt{\varepsilon}\, d\varepsilon \tag{24.16}$$

The number of molecules with energies between ε and $d\varepsilon$ is therefore,

$$n(\varepsilon)\, d\varepsilon = C\sqrt{\varepsilon} e^{-\varepsilon/kT} d\varepsilon \tag{24.17}$$

where $C\left(=\sqrt{2}m^{3/2}AB\right)$ is a constant to be evaluated. To find C we make use of the normalization condition that the total number of molecules is N, so that

$$N = \int_0^\infty n(\varepsilon) d\varepsilon = C\int_0^\infty \sqrt{\varepsilon} e^{-\varepsilon/kT} d\varepsilon \tag{24.18}$$

From integral # 670 of Lide [10] we find that

$$\int_0^\infty \sqrt{x} e^{-ax} dx = \frac{1}{2a}\sqrt{\frac{\pi}{a}} \tag{24.19}$$

where $a = 1/kT$, such that

$$N = \frac{C}{2}\sqrt{\pi}\,(kT)^{3/2}$$
$$C = \frac{2\pi N}{(\pi kT)^{3/2}} \tag{24.20}$$

Substitution of Eq. (24.20) into Eq. (24.17) gives:

$$n(\varepsilon)\, d\varepsilon = \frac{2\pi N}{(\pi kT)^{3/2}}\sqrt{\varepsilon} e^{-\varepsilon/kT} d\varepsilon \tag{24.21}$$

Eq. (24.21) gives the number of molecules with energies between ε and $\varepsilon + d\varepsilon$ in a sample of an ideal gas that contains N molecules at absolute temperature T.

Figure 24.4. Maxwell-Boltzmann energy distribution for the molecules of an ideal gas.

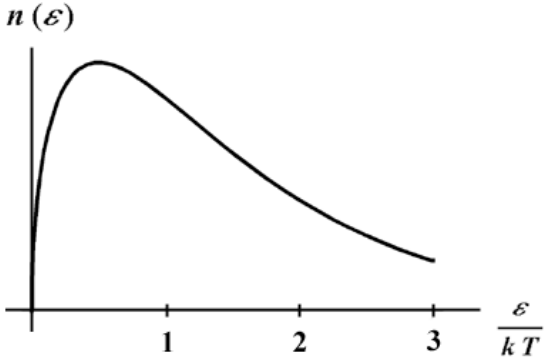

The curve of Equation (24.21) plotted in terms of kT (Figure 24.4) is not symmetrical about the most probable energy. This is because $\varepsilon = 0$ is the lower limit to ε while the upper limit is $\varepsilon \to \infty$; although, the probability of particles with energies many times greater than kT is small.

The total internal energy of the system is calculated by integrating the product of $n(\varepsilon)d\varepsilon$ and the energy ε over all energies from 0 to ∞:

$$E = \int_0^\infty \varepsilon n(\varepsilon) d\varepsilon = \frac{2\pi N}{(\pi kT)^{3/2}}\int_0^\infty \varepsilon^{3/2} e^{-\varepsilon/kT} d\varepsilon \tag{24.22}$$

Using integral #521 and #670 of Lide [11]:

$$\int_0^\infty x^{3/2} e^{-ax} dx = \frac{3}{4a^2}\sqrt{\frac{\pi}{a}} \tag{24.23}$$

gives

$$E = \frac{2\pi N}{(\pi kT)^{3/2}}\left(\frac{3}{4}\right)(kT)^2\sqrt{\pi kT} = \frac{3}{2}NkT \tag{24.24}$$

This is the correct result based on the ideal-gas law's dependence on the average molecular kinetic energy being $\frac{3}{2}kT$. Eq. (24.24) confirms that the $1/kT$ factor in the exponent of the Maxwell-Boltzmann distribution function of Eq. (24.3) properly describes the dependence of $n(\varepsilon)d\varepsilon$ on T. Also, from Eq. (24.24), the average energy of an ideal-gas molecule is $\frac{E}{N}$, or

$$\bar{\varepsilon} = \frac{3}{2}kT \tag{24.25}$$

which is independent of the molecule's mass; however, a light molecule has a greater average speed at a given temperature than a heavy one. The value of $\bar{\varepsilon}$ at room temperature is about 0.04eV.

A gas molecule can be excited to translate in three directions such that it possesses energy in three translational modes or *degrees of freedom* corresponding to motions in the x, y, and z directions. $\frac{1}{2}kT$ of energy can be associated with each degree of freedom. This association turns out to be a quite general one; the average energy per degree of freedom of any Newtonian entity modeled by Maxwell-Boltzmann statistics that is part of a system of such entities in thermal equilibrium at the temperature T is $\frac{1}{2}kT$.

For example, a harmonic oscillator has two degrees of freedom, one corresponding to its kinetic energy and the other to its potential energy. Each oscillator of a system of harmonic oscillators thus has an average energy of $(2)\left(\frac{1}{2}\right)kT = kT$. To a first approximation, the atoms of a solid behave like a system of Newtonian harmonic oscillators, as shown in the Application of Bose-Einstein Statistics to Model Specific Heats of Solids section.

The distribution of molecular speeds can be found from Eq. (24.21) by making the substitution

$$\varepsilon = \frac{1}{2}mv^2$$
$$d\varepsilon = mv\,dv \tag{24.26}$$

First obtained by Maxwell in 1859, the result for the number of molecules with speeds between v and $v + dv$ is:

$$n(v)\,dv = \frac{\sqrt{2}\pi N m^{3/2}}{(\pi kT)^{3/2}} v^2 e^{-mv^2/2kT}\,dv \tag{24.27}$$

Eq. (24.27) is plotted in Figure 24.5.

Figure 24.5. Maxwell-Boltzmann speed distribution.

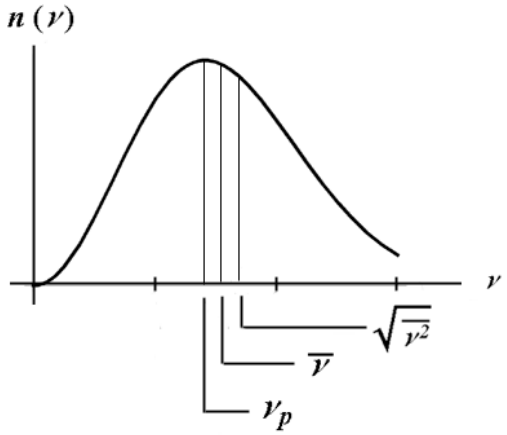

v_{rms}, the square root of the average of the squared molecular speed of a molecule with an average energy of $\frac{3}{2}kT$ is

$$v_{rms} = \sqrt{\overline{v^2}} = \sqrt{\frac{3kT}{m}} \tag{24.28}$$

since $\overline{\frac{1}{2}mv^2} = \frac{3}{2}kT$. This speed is denoted as the root-mean-square speed which is not the same as the simple arithmetic average speed $\bar{v}$. The relationship between $\bar{v}$ and v_{rms} depends on the distribution law that governs the molecular speeds in a particular system. For a Maxwell-Boltzmann distribution,

$$v_{rms} = \sqrt{\frac{3\pi}{8}}\bar{v} \approx 1.09\bar{v} \tag{24.29}$$

so that the rms speed is about 9 percent greater than the arithmetical average speed. Due to the asymmetry of the speed distribution given by Eq. (24.27), the most probable speed v_p is smaller than either $\bar{v}$ or v_{rms}. To find v_p, the derivative of $n(v)$ with respect to v is set equal to zero and the resulting equation is solved for v:

$$v_p = \sqrt{\frac{2kT}{m}} \tag{24.30}$$

Molecular speeds in a gas may vary considerably about v_p as shown (Figure 24.6) by the distributions of speeds in oxygen at 73 K (–200°C), in oxygen at 273 K (0°C), and in hydrogen at 273 K. The most probable speed increases with temperature and decreases with molecular mass such that molecular speeds in oxygen at 73 K are in totality less than at 273 K. Furthermore, the average molecular energy is the same in both oxygen and hydrogen at 273 K, but the molecular speeds in hydrogen at 273 K are in totality greater than those in oxygen at the same temperature.

Figure 24.6. The distributions of molecular speeds in oxygen at 73 K, in oxygen at 273 K, and in hydrogen at 273 K.

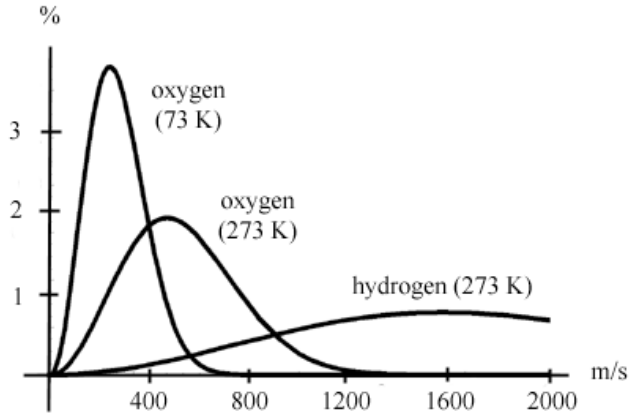

APPLICATION OF BOSE-EINSTEIN STATISTICS TO MODEL BLACKBODY RADIATION

Every substance emits electromagnetic radiation with a spectrum that depends on the nature and temperature of the substance. The discrete electronic-excited-state spectra of isolated atoms of gases such as hydrogen and helium are given in the Excited States of the One-Electron Atom (Quantization) and the Excited States of Helium sections. At the other extreme, continuum spectra are observed from dense bodies such as solids. As expected, the ability of a body to radiate is closely related to its ability to absorb radiation, since a body at a constant temperature is in thermal equilibrium with its surroundings and must absorb energy from them at the same rate as it emits energy. It is convenient to consider a *blackbody* as an ideal body that absorbs *all* radiation incident upon it, independent of frequency.

Figure 24.7. Two pairs of Identical Surfaces in Thermal Equilibrium. Surfaces I and I' are identical to each other and are different from the identical pair of surfaces II and II'.

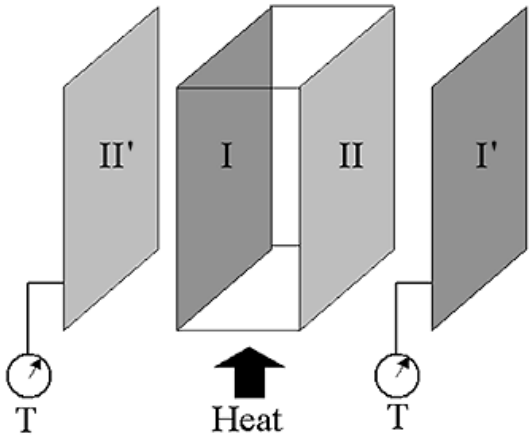

An experiment, illustrated in Figure 24.7, to demonstrate that a blackbody is the best emitter of radiation involves two identical pairs (I, I' and II, II') of dissimilar surfaces with no temperature difference observed between two of the surfaces I' and II'. At a given temperature, the surfaces I and I' radiate at the rate of e_1 while the dissimilar surfaces II and II' radiate at the different rate e_2. The surfaces I and I' absorb some fraction a_1 of the incident radiation, while the dissimilar surfaces II and II' absorb some other fraction a_2. Hence I' absorbs energy from II at a rate proportional to $a_1 e_2$, and II' absorbs energy from I at a rate proportional to $a_2 e_1$. For I' and II' to remain at the same temperature,

$$a_1 e_2 = a_2 e_1 \text{ and } \frac{e_1}{a_1} = \frac{e_2}{a_2} \tag{24.31}$$

Eq. (24.31) shows that the ability of a body to emit radiation is proportional to its ability to absorb radiation.

Next, consider that I and I' are blackbodies such that $a_1 = 1$, and II and II' are not with $a_2 < 1$. Eq. (24.31) becomes:

$$e_1 = \frac{e_2}{a_2} \tag{24.32}$$

Since $a_2 < 1$, Eq. (24.32) gives:

$$e_1 > e_2 \tag{24.33}$$

A blackbody at a given temperature is the most effective radiator of energy.

In the analysis of thermal radiation, the concept of an idealized blackbody permits the precise nature of whatever is radiating to be disregarded, since all blackbodies behave identically. A laboratory blackbody can be approximated by a hollow object with a very small hole leading to its interior as shown in Figure 24.8. Any radiation striking the hole enters the cavity, where it is trapped by reflecting from the walls until it is absorbed. The cavity walls are constantly emitting and absorbing radiation, and the properties of this radiation (*blackbody radiation*) can be modeled using Bose-Einstein statistics.

Figure 24.8. A hole in the wall of a hollow object is an excellent approximation of a blackbody.

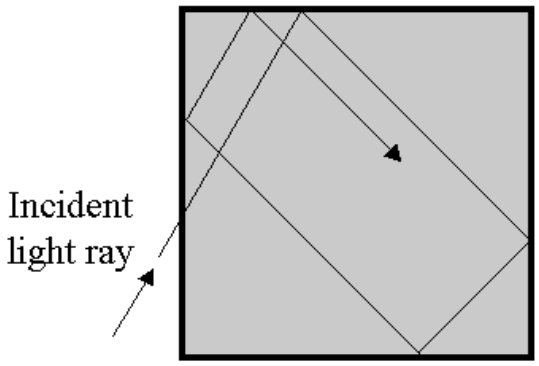

Blackbody radiation can be experimentally sampled by recording the spectrum of the light emitted from the hole in the cavity, and the results agree with our everyday experience. Blackbody radiation increases with temperature, and the spectrum of a hot blackbody has its peak at a higher frequency than the peak of the spectrum of a cooler one. For example, as an iron bar is heated to progressively higher temperature, it first glows dull red, then bright orange-red, and eventually becomes "white hot." The spectrum of blackbody radiation for two temperatures is shown in Figure 24.9.

PLANCK RADIATION LAW

As shown in the Excited States of the One-Electron Atom (Quantization) and the Excited States of Helium sections, each bound electron is a resonator cavity, which traps single photons of discrete frequencies. Thus, photon absorption occurs as an excitation of a resonator mode. The angular momentum of the free space photon given by $\mathbf{m} = \int \frac{1}{8\pi c} \mathrm{Re}\left[\mathbf{r} \times (\mathbf{E} \times \mathbf{B}^*)\right] dx^4 = \hbar$ in the Photon section is conserved [9] for the solutions for the resonant photons and excited state electron functions. The change in angular frequency of the electron is equal to the angular frequency of the resonant photon that excites the resonator cavity mode corresponding to the transition, and the energy is given by Planck's equation. The equation of the blackbody spectrum shown in Figure 24.9 is derived using the quantization of electromagnetic radiation.

Figure 24.9. Blackbody spectra. The spectral distribution of energy in the radiation depends only on the temperature of the body.

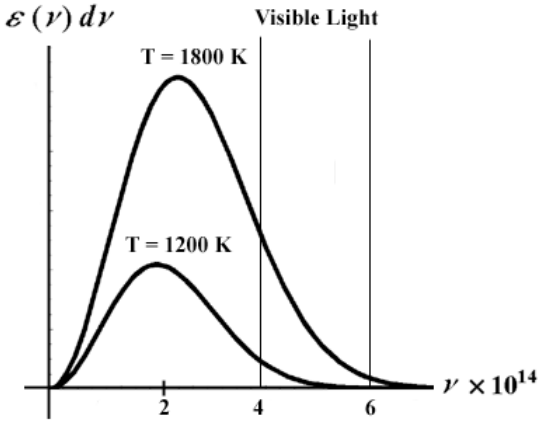

The superposition of photons gives rise to electromagnetic waves that obey the macro Maxwell's equations. The radiation inside a cavity of temperature T whose walls are perfect reflectors exists as a series of three-dimensional standing electromagnetic waves.

The condition for standing waves in such a cavity is that the path length from wall to wall in any x, y, or z direction must be an integral number j of half-wavelengths such that a node occurs at each reflecting surface.

$$\begin{aligned} j_x &= \frac{2L}{\lambda} = 1,2,3\ldots = \text{ number of half-wavelengths in } x \text{ direction} \\ j_y &= \frac{2L}{\lambda} = 1,2,3\ldots = \text{ number of half-wavelengths in } y \text{ direction} \\ j_z &= \frac{2L}{\lambda} = 1,2,3\ldots = \text{ number of half-wavelengths in } z \text{ direction} \end{aligned} \tag{24.34}$$

Combining the components for a standing wave in any arbitrary direction gives:

$$j_x^2 + j_y^2 + j_z^2 = \left(\frac{2L^2}{\lambda}\right) \qquad \begin{aligned} j_x &= 0,1,2,\ldots \\ j_y &= 0,1,2,\ldots \\ j_z &= 0,1,2,\ldots \end{aligned} \tag{24.35}$$

in order that the wave terminate in a node at its ends.

The number of standing waves $g(\lambda)d\lambda$ within the cavity whose wavelengths lie between λ and $\lambda + d\lambda$ can be counted as the number of permissible sets of j_x, j_y, j_z values that yield wavelengths in this interval. Consider a three-dimensional *j*-space whose coordinate axes are j_x, j_y, and j_z where Figure 24.10 shows part of the j_x - j_y plane of such a space. Each point in the *j*-space corresponds to a standing wave having a permissible set of j_x, j_y, j_z values. The magnitude of each vector j defined from the origin to a particular point j_x, j_y, j_z is:

$$j = \sqrt{j_x^2 + j_y^2 + j_z^2} \tag{24.36}$$

The total number of wavelengths between λ and $\lambda + d\lambda$ is equivalent to the number of points in j space whose distances from the origin lie between j and $j + dj$, the volume of a spherical shell of radius j and thickness dj is $4\pi j^2 dj$. Taking the octant of this shell having positive values of j_x, j_y, and j_z as physical and considering the two perpendicular directions of polarization of each standing electromagnetic wave, the number of independent standing waves in the cavity is:

$$g(j)dj = (2)\left(\frac{1}{8}\right)\left(4\pi j^2 dj\right) = \pi j^2 dj \tag{24.37}$$

Figure 24.10. Each point in *j* space corresponds to a possible standing electromagnetic wave.

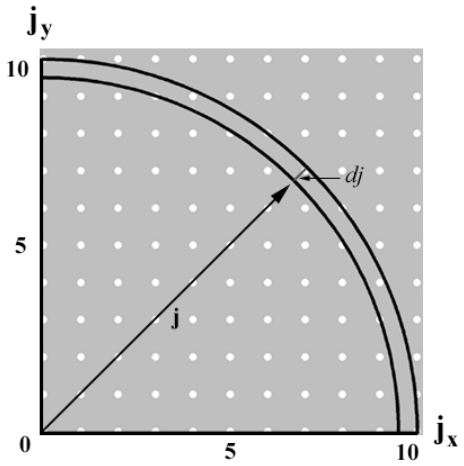

The number of standing waves in the cavity as a function of j is converted into their frequency (ν) dependence. From Eqs. (24.35) and (24.36):

$$j = \frac{2L}{\lambda} = \frac{2L\nu}{c} \tag{24.38}$$

$$dj = \frac{2L}{c} d\nu \tag{24.39}$$

Substitution of Eqs. (24.38) and (24.39) into Eq. (24.37) gives:

$$g(\nu)\, d\nu = \pi \left(\frac{2L\nu}{c} \right)^2 \frac{2L}{c}\, d\nu = \frac{8\pi L^3}{c^3} \nu^2\, d\nu \tag{24.40}$$

The cavity volume is L^3; thus, from Eq. (24.40), the number of independent standing waves per unit volume is:

$$G(\nu)\, d\nu = \frac{1}{L^3} g(\nu)\, d\nu = \frac{8\pi\nu^2\, d\nu}{c^3} \tag{24.41}$$

To determine the average energy per standing wave, Bose-Einstein statistics are used. The energy of each photon of frequency ν is quantized in units of $h\nu$. The average number of photons $f(\nu)$ in each state of energy $\varepsilon = h\nu$ is given by the Bose-Einstein distribution function of Eq. (24.4). The value of α in Eq. (24.4) depends on the number of particles in the system being considered, but unlike gas molecules or electrons, photons of different frequencies (energies) are continuously emitted and absorbed. Although the total radiant energy in the cavity must remain constant, the number of free photons having this total energy can change. Because of the way in which α is defined in the derivation of Eq. (24.4) as given by Beiser [8], the nonconservation of the total number of photons means that $\alpha = 0$ such that the Bose-Einstein distribution function for photons is

$$f(\nu) = \frac{1}{e^{h\nu/kT} - 1} \tag{24.42}$$

Equation (24.41) for the number of standing waves of frequency ν per unit volume in a cavity is valid for the number of quantum states of frequency ν since photons each have two possible directions of polarization, right-hand and left-hand circular polarization. Thus, the energy density of photons in a cavity is:

$$u(\nu)\, d\nu = h\nu G(\nu) f(\nu)\, d\nu \tag{24.43}$$

$$= \frac{8\pi h}{c^3} \frac{\nu^3\, d\nu}{e^{h\nu/kT} - 1} \tag{24.44}$$

Equation (24.44) is the *Planck radiation formula* for the spectral energy density of blackbody radiation, which agrees with experimental spectra such as those of Figure 24.9.

An object need not be so hot that it glows conspicuously in the visible region in order to be radiating. Every body of condensed matter radiates according to Eq. (24.44), regardless of its temperature. For example, an object at room temperature radiates predominantly in the infrared part of the spectrum, which are nonvisible frequencies.

Wien's displacement law and the *Stefan-Boltzmann law* can be obtained from the Planck radiation formula. The wavelength whose energy density is the greatest is obtained by expressing Eq. (24.44) in terms of wavelength and solving $du(\lambda)/d\lambda = 0$ for $\lambda = \lambda_{\max}$:

$$\frac{hc}{kT\lambda_{\max}} = 4.965 \tag{24.45}$$

Eq. (24.45) can be more conveniently expressed as:

$$\lambda_{\max} T = \frac{hc}{4.965k} = 2.898\times10^{-3}\,\mathrm{m\cdot K} \tag{24.46}$$

Equation (24.46) known as *Wien's displacement law* quantitatively expresses the observation that the peak in the blackbody spectrum shifts to progressively shorter wavelengths (higher frequencies) as the temperature is increased as shown in Figure 24.9.

The total energy density u within the cavity we can also be obtained from Eq. (24.44) by integrating the energy density over all frequencies:

$$u = \int_0^\infty u(\nu)\, d\nu = \frac{8\pi^5 k^4}{15c^3h^3} T^4 = aT^4 \tag{24.47}$$

where a is a universal constant. The total energy density is proportional to the fourth power of the absolute temperature of the cavity walls. Similarly, the energy R radiated by an object per second per unit area is also proportional to T^4. This result is shown by the *Stefan-Boltzmann law*:

$$R = e\sigma T^4 \tag{24.48}$$

where Stefan's constant σ is given by $\sigma = \frac{ac}{4} = 5.670\times10^{-8}\ \mathrm{W/m^2\cdot K^4}$.

The emissivity e depends on the nature of the radiating surface and ranges from 0, for a perfect reflector with zero radiation, to 1, for a blackbody. Some exemplary values of e are 0.07 for polished steel, 0.06 for oxidized copper and brass, and 0.97 for matte black paint.

APPLICATION OF BOSE-EINSTEIN STATISTICS TO MODEL SPECIFIC HEATS OF SOLIDS

Consider, C_V, the molar specific heat of a solid at constant volume which is the energy that must be added to 1 kmole of the substance at fixed volume to raise its temperature by 1 K. C_P, the specific heat at constant pressure, is 3 to 5 percent higher than C_V in solids because it includes the work associated with a volume change as well as the change in internal energy. The internal energy of a solid resides in the vibrations of its constituent particles, which may be atoms, ions, or molecules. These vibrations may be resolved into components along three perpendicular axes, such that each particle (designated as an atom for convenience) can be represented by three harmonic oscillators. Using Bose-Einstein statistics, the probability $f(\nu)$ that an oscillator has the frequency ν is given by Eq. (24.42), $f(\nu) = 1\Big/\left(e^{h\nu/kT} - 1\right)$. Hence, the average energy for an oscillator whose frequency of vibration is ν is:

$$\bar{\varepsilon} = h\nu f(\nu) = \frac{h\nu}{e^{h\nu/kT} - 1} \tag{24.49}$$

Therefore, the total internal energy of a kilomole of a solid is given by:

$$E = 3N_0\bar{\varepsilon} = \frac{3N_0 h\nu}{e^{h\nu/kT} - 1} \tag{24.50}$$

and its molar specific heat is:

$$C_V = \left(\frac{\partial E}{\partial T}\right)_V = 3R\left(\frac{h\nu}{kT}\right)^2 \frac{e^{h\nu/kT}}{\left(e^{h\nu/kT} - 1\right)^2} \tag{24.51}$$

Thus, at high temperatures $h\nu \ll kT$, and

$$e^{h\nu/kT} \approx 1 + \frac{h\nu}{kT} \tag{24.52}$$

since

$$e^x = 1 + x + \frac{x^2}{2!} + \frac{x^3}{3!} + \ldots \tag{24.53}$$

Hence Eq. (24.49) becomes:

$$\bar{\varepsilon} \approx h\nu\big/(h\nu/kT) = kT \tag{24.54}$$

which leads to $C_V \approx 3R$. At high temperatures the spacing $h\nu$ between possible energies is small relative to kT, so ε is effectively continuous and Maxwell-Boltzmann statistics applies.

As the temperature decreases, the value of C_V given by Eq. (24.51) decreases. The deviation from Maxwell Boltzmann behavior arises as the spacing between possible energies becomes large relative to kT. The natural frequency ν for a particular solid can be determined by comparing Eq. (24.51) with an empirical curve of C_V versus T. The result in the case of aluminum is $\nu = 6.4\times10^{12}$ Hz, which agrees with estimates made in other ways, for instance on the basis of elastic moduli [5].

Eq. (24.51) predicts that $C_V \to 0$ as $T \to 0$ in agreement with observations. However, better models to the actual behavior of C_V as $T \to 0$ such as Debye's [5] take into account that a solid is a continuous elastic body wherein the internal energy of a solid resides in elastic standing waves, rather than vibrations of individual atoms. The elastic waves in a solid are of two kinds, longitudinal and transverse, and range in frequency from 0 to a maximum ν_m. (The interatomic spacing in a solid sets a lower limit to the possible wavelengths and hence an upper limit to the frequencies.) Typically, the total number of different standing waves in a mole of a solid is equal to its $3N_A$ degrees of freedom. These waves, like electromagnetic waves, have energies quantized in units of $h\nu$. A quantum of acoustic energy in a solid is called a *phonon*, and it travels with the speed of sound since sound waves are elastic in nature. The concept of phonons is quite general and has applications other than in connection with specific heats. A phonon gas has the same statistical behavior as a photon gas or a system of harmonic oscillators in thermal equilibrium, so that the average energy $\bar{\varepsilon}$ per standing wave is the same as in Eq. (24.49). The resulting formula for C_V, which is fairly complicated, reproduces the curves of C_V versus T quite well at all temperatures.

APPLICATION OF FERMI-DIRAC STATISTICS TO MODEL FREE ELECTRONS IN A METAL

Fermi-Dirac statistics corresponds to the physics of electrons wherein no more than one electron can occupy each quantum state. Although systems of bosons and fermions both approach Maxwell-Boltzmann statistics with average energies $\bar{\varepsilon} = \frac{1}{2}kT$ per degree of freedom at "high" temperatures, in a metal, the transition temperature range for Maxwell-Boltzmann behavior is not necessarily the same for the two kinds of systems. According to Eq. (24.7), the distribution function that gives the average occupancy of a quantum state of energy ε in a system of fermions is

$$f_{FD}(\varepsilon) = \frac{1}{e^{(\varepsilon - \varepsilon_F)/kT} + 1} \tag{24.55}$$

An expression for $g(\varepsilon)\, d\varepsilon$, the number of quantum states available to electrons with energies between ε and $\varepsilon + d\varepsilon$, is obtained using the same approach as that used to determine the number of standing waves in a cavity with the wavelength λ in the Planck Radiation Law section. The correspondence is exact because there are two possible spin states, $m_s = +\frac{1}{2}$ and $m_s = -\frac{1}{2}$ ("up" and "down"), for electrons, just as there are two independent directions of polarization for otherwise identical standing waves.

Using Eq. (24.37), the number of standing waves in a cubical cavity L on a side is:

$$g(j)\, dj = \pi j^2\, dj \tag{24.56}$$

where $j = 2L/\lambda$. In the case of an electron, λ is its de Broglie wavelength of $\lambda = \frac{h}{p}$. Electrons in a metal have nonrelativistic velocities, so $p = \sqrt{2m_e\varepsilon}$ and

$$\begin{aligned} j &= \frac{2L}{\lambda} = \frac{2Lp}{h} = \frac{2L\sqrt{2m_e\varepsilon}}{h} \\ dj &= \frac{L}{h}\sqrt{\frac{2m_e}{\varepsilon}}\, d\varepsilon \end{aligned} \tag{24.57}$$

Using these expressions for j and dj in Eq. (24.37) gives:

$$g(\varepsilon)\, d\varepsilon = \frac{8\sqrt{2}\pi L^3 m_e^{3/2}}{h^3}\sqrt{\varepsilon}\, d\varepsilon \tag{24.58}$$

As in the case of standing waves in a cavity the exact shape of the metal sample does not matter; so, its volume V can substituted for L^3 to give:

$$g(\varepsilon)\, d\varepsilon = \frac{8\sqrt{2}\pi V m_e^{3/2}}{h^3}\sqrt{\varepsilon}\, d\varepsilon \tag{24.59}$$

Using Eq. (24.59), the Fermi energy ε_F can be calculated by filling up the energy states in the metal sample with the N free electrons it contains in order of increasing energy starting from $\varepsilon = 0$ such that the highest state to be filled has the energy $\varepsilon = \varepsilon_F$. This is the definition of ε_F as given in the Three Different Kinds of Atomic-Scale Statistical Distributions section. The number of electrons that can have the same energy ε is equal to the number of states that have this energy, since each state is limited to one electron.

$$N = \int_0^{\varepsilon_F} g(\varepsilon)\, d\varepsilon = \frac{8\sqrt{2}\pi V m_e^{3/2}}{h^3}\int_0^{\varepsilon_F}\sqrt{\varepsilon}\, d\varepsilon = \frac{16\sqrt{2}\pi V m_e^{3/2}}{3h^3}\varepsilon_F^{3/2} \tag{24.60}$$

and

$$\varepsilon_F = \frac{h^2}{2m_e}\left(\frac{3N}{8\pi V}\right)^{2/3} = \frac{h^2}{2m_e}\left(\frac{3}{8\pi}\right)^{2/3} n^{2/3} \tag{24.61}$$

The quantity $\frac{N}{V}$ is the density of free electrons.

ELECTRON-ENERGY DISTRIBUTION

Using Eqs. (24.7) and (24.59), the number of electrons in an electron gas that have energies between ε and $\varepsilon + d\varepsilon$ is

$$n(\varepsilon)\, d\varepsilon = g(\varepsilon)\, f(\varepsilon)\, d\varepsilon = \frac{\left(\frac{8\sqrt{2}\pi V m_e^{3/2}}{h^3}\right)\sqrt{\varepsilon}\, d\varepsilon}{e^{(\varepsilon-\varepsilon_F)/kT}+1} \tag{24.62}$$

Expressing the numerator of Eq. (24.62) in terms of the Fermi energy ε_F (Eq. (24.61)) gives :

$$n(\varepsilon)\, d\varepsilon = \frac{\left(\frac{3N}{2}\right)\varepsilon_F^{-3/2}\sqrt{\varepsilon}\, d\varepsilon}{e^{(\varepsilon-\varepsilon_F)/kT}+1} \tag{24.63}$$

Eq. (24.63) is plotted in Figure 24.11 for $T = 0,\ 300$, and 1200 K .

Figure 24.11. Distribution of electron energies in a metal at various temperatures.

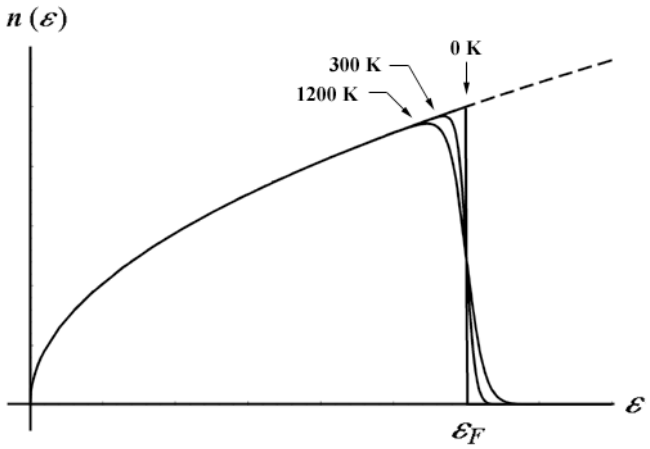

To determine the average electron energy at 0 K, the total energy E_0 at 0 K is first obtained by the following integral:

$$E_0 = \int_0^{\varepsilon_F} \varepsilon n(\varepsilon)\, d\varepsilon \tag{24.64}$$

Since at $T = 0$ K, all of the electrons have energies less than or equal to the Fermi energy ε_F, the temperature-dependent term becomes:

$$e^{(\varepsilon-\varepsilon_F)/kT} = e^{-\infty} = 0 \tag{24.65}$$

and Eqs. (24.63) and (24.64) gives:

$$E_0 = \frac{3N}{2}\varepsilon_F^{-3/2}\int_0^{\varepsilon_F} \varepsilon^{3/2}\, d\varepsilon = \frac{3}{5}N\varepsilon_F \tag{24.66}$$

The average electron energy $\bar{\varepsilon}_0$ is this total energy divided by the number of electrons present N, which gives:

$$\bar{\varepsilon}_0 = \frac{3}{5}\varepsilon_F \tag{24.67}$$

Since Fermi energies for metals are usually several eVs (Table 24.2), the average electron energy in them at 0 K will also be of this order of magnitude. In contrast, the temperature of an ideal gas whose molecules have an average kinetic energy of 1 eV is 11,600 K.

Table 24.2. Some Fermi energies.

Metal		Fermi energy, *eV*
Lithium	Li	4.72
Sodium	Na	3.12
Aluminum	Al	11.8
Potassium	K	2.14
Cesium	Cs	1.53
Copper	Cu	7.04
Zinc	Zn	11.0
Silver	Ag	5.51
Gold	Au	5.54

The failure of the free electrons in a metal to contribute appreciably to its specific heat is due to the behavior of the electron energy distribution. When a metal is heated, only those electrons with thermal energy near the very top of the energy distribution—those within about kT of the Fermi energy—are excited to the higher energy states while the less energetic electrons cannot absorb more energy because the states above them are already filled. An electron with a low energy ε in the range of 0.5 eV below ε_F is unlikely to undergo a transition to the nearest vacant state above the intervening states that are already filled since *kT* at room temperature is 0.025 eV and even at 500 K it is only 0.043 eV.

A detailed calculation shows that the specific heat of the electron gas in a metal is given by [5] :

$$C_{Ve} = \frac{\pi^2}{2}\left(\frac{kT}{\varepsilon_F}\right)R \tag{24.68}$$

For the metals listed in Table 24.2, $\frac{kT}{\varepsilon_F}$ at room temperature ranges from 0.016 for cesium to 0.0021 for aluminum; so, the coefficient of *R* is very much smaller than the Maxwell Boltzmann figure of $\frac{3}{2}$. The atomic specific heat C_V in a metal is much greater than the electronic specific heat over a wide temperature range. However, at very low temperatures C_{Ve} becomes significant because C_V is then approximately proportional to T^3 whereas C_{Ve} is proportional to T. At very high temperatures, C_V approaches the value of about $3R$ while C_{Ve} continues to increase such that the contribution of C_{Ve} to the total specific heat is detectable.

REFERENCES

1. R. L. Mills, "The Nature of Free Electrons in Superfluid Helium--a Test of Quantum Mechanics and a Basis to Review its Foundations and Make a Comparison to Classical Theory," Int. J. Hydrogen Energy, Vol. 26, No. 10, (2001), pp. 1059-1096.
2. A. Einstein, B. Podolsky, N. Rosen, Phys. Rev., Vol. 47, (1935), p. 777.
3. L. de Broglie, "On the true ideas underlying wave mechanics," *Old and New Questions in Physics, Cosmology, Philosophy, and Theoretical Biology*, A. van der Merwe, Editor, Plenum Press, New York, (1983), pp. 83-86.
4. D. C. Cassidy, *Uncertainty: the Life and Science of Werner Heisenberg*, W. H. Freeman and Company, New York, (1992), pp. 224-225.
5. A. Beiser, *Concepts of Modern Physics*, Fourth Edition, McGraw-Hill Book Company, New York, (1978), pp. 312-354.
6. M. B. James, D. J. Griffiths, "Why the speed of light is reduced in a transparent medium," Am. J. Phys., Vol. 60, No. 4, (1992), pp. 309-313.
7. L. K. Nash, Chemthermo: *A Statistical approach to Classical Chemical Thermodynamics*, Addison-Wesley Publishing Company, Reading Massachusetts, (1976), pp. 1-44.
8. A. Beiser, *Concepts of Modern Physics*, Fourth Edition, McGraw-Hill Book Company, New York, (1978), Appendix IV.
9. J. D. Jackson, *Classical Electrodynamics*, Second Edition, John Wiley & Sons, New York, (1975), pp. 739-779.
10. D. R. Lide, *CRC Handbook of Chemistry and Physics*, 79th Edition, CRC Press, Boca Raton, Florida, (1998-9), p. A-62.
11. D. R. Lide, *CRC Handbook of Chemistry and Physics*, 79th Edition, CRC Press, Boca Raton, Florida, (1998-9), pp. A52 and A-62.

Chapter 25

SUPERCONDUCTIVITY

In the case of a superconductor, an applied voltage gives rise to a transient constant electric field in the z direction

$$\mathbf{E}_z = E_0 \cos\theta \mathbf{i}_z \tag{25.1}$$

$$\mathbf{E}_z = E_0 \mathbf{i}_z \tag{25.2}$$

where $\mathbf{i}_z$ is the unit vector along the z-axis.

The applied field polarizes the material into a superconducting current comprised of current dipoles, i.e. magnetic dipoles. In Cartesian coordinates, the magnetic field, $\mathbf{H}$, at the point (x, y, z) due to a magnetic dipole having a magnetic dipole moment of a Bohr magneton, μ_B, at the position (x_0, y_0, z_0) is:

$$\mathbf{H} = \frac{\mu_B\left(2(z-z_0)^2 - (x-x_0)^2 - (y-y_0)^2\right)}{[(x-x_0)^2 + (y-y_0)^2 + (z-z_0)^2]^{5/2}}\mathbf{i}_z \tag{25.3}$$

$$\mathbf{H} = \frac{\left(2z^2 - x^2 - y^2\right)}{[x^2 + y^2 + z^2]^{5/2}} \otimes \mu_B \delta(x - x_0, y - y_0, z - z_0)\mathbf{i}_z \tag{25.4}$$

The field is the convolution of the system function, $h(x, y, z)$ *or* $h(\rho, \phi, z)$, (the left-handed part of Eq. (25.4)) with the delta function (the right-hand part of Eq. (25.4)) at the position (x_0, y_0, z_0). A very important theorem of Fourier analysis states that the Fourier transform of a convolution is the product of the individual Fourier transforms [1]. The Fourier transform of the system function, $h(x, y, z)$ or $h(\rho, \phi, z)$, is given in Box 25.1.

BOX 25.1 FOURIER TRANSFORM OF THE SYSTEM FUNCTION

The system function, $h(\rho, \phi, z)$, in cylindrical coordinates is

$$h(\rho, \phi, z) = \frac{2z^2 - x^2 - y^2}{[x^2 + y^2 + z^2]^{5/2}} = \frac{2z^2 - \rho^2}{[\rho^2 + z^2]^{5/2}} \tag{1}$$

The spacetime Fourier transform in three dimensions in cylindrical coordinates, $H(k_\rho, \Phi, k_z)$, is given [1] as follows:

$$H(k_\rho, \Phi, k_z) = \int_{-\infty}^{\infty}\int_{0}^{2\pi}\int_{0}^{\infty} h(\rho, \phi, z)\exp\left(-i2\pi\left[k_\rho \rho\cos(\Phi - \phi) + k_z z\right]\right)\rho d\rho d\phi dz \tag{2}$$

With circular symmetry [1] :

$$H(k_\rho, k_z) = 2\pi\int_{0}^{\infty}\int_{-\infty}^{\infty} h(\rho, z) J_0(k_\rho \rho) e^{-iwz}\rho d\rho dz \tag{3}$$

The Fourier transform of the system function is given by the substitution of Eq. (1) into Eq. (3).

$$H = \int_{-\infty}^{\infty} 2\pi \int_{0}^{\infty} \frac{2z^2 - \rho^2}{[\rho^2 + z^2]^{5/2}} J_0[k_\rho \rho]\rho d\rho e^{-jk_z z} dz \tag{4}$$

Consider the integral of Eq. (4) with respect to $d\rho$ only. Factorization of $h(\rho,\phi,z)$ gives:

$$2\pi\int_0^\infty\left[\frac{2z^2\rho}{[\rho^2+z^2]^{5/2}}-\frac{\rho^3}{[\rho^2+z^2]^{5/2}}\right]J_0[k_\rho\rho]d\rho \tag{5}$$

Consider the definite integral

$$\int_0^\infty\frac{t^{v+1}J_v[at]dt}{[t^2+z^2]^{u+1}}=\frac{a^u z^{v-u}K_{v-u}[az]}{2^u\Gamma[u+1]} \tag{6}$$

and the relationship between modified Bessel functions of the third kind where:

$$K_{-\upsilon}[x]=K_\upsilon[x] \tag{7}$$

The first factor of Eq. (5) is the same form as Eq. (6) with $\nu=0;\ u=\frac{3}{2}$, thus,

$$2z^2(2\pi)\int_0^\infty\frac{\rho}{[\rho^2+z^2]^{5/2}}J_0[k_\rho\rho]d\rho=\frac{2z^2(2\pi)k_\rho^{3/2}z^{-3/2}}{2^{3/2}\Gamma[5/2]}K_{-3/2}[k_\rho z]=\frac{[2^{1/2}]\pi z^{1/2}k_\rho^{3/2}}{\Gamma[5/2]}K_{3/2}[k_\rho z] \tag{8}$$

where $K_{-3/2}[k_\rho z]=K_{3/2}[k_\rho z]$ (Eq. (7)). The second factor of Eq. (5) can be made into the same form as Eq. (6) using the recurrence relationship of Bessel functions of the first kind:

$$J_{v-1}[x]+J_{v+1}[x]=\frac{2v}{x}J_v[x] \tag{9}$$

Consider the second factor of the integral of Eq. (5) thus,

$$-2\pi\int_0^\infty\frac{\rho^3}{[\rho^2+z^2]^{5/2}}J_0[k_p\rho]d\rho \tag{10}$$

Eq. (9) with $\upsilon=1$ is:

$$J_0[x]+J_2[x]=\frac{2}{x}J_1[x] \tag{11}$$

$$J_0[x]=\frac{2}{x}J_1[x]-J_2[x] \tag{12}$$

Let

$$x=k_\rho\rho \tag{13}$$

Substitution of Eq. (13) into Eq. (12) is:

$$J_0[k_\rho\rho]=\frac{2}{k_\rho\rho}J_1[k_\rho\rho]-J_2[k_\rho\rho] \tag{14}$$

Substitution of Eq. (10) into Eq. (14) is:

$$\begin{aligned}-2\pi\int_0^\infty\frac{\rho^3}{[\rho^2+z^2]}J_0[k_\rho\rho]d\rho&=-2\pi\int_0^\infty\frac{\rho^3}{[\rho^2+z^2]^{5/2}}\left[\frac{2}{k_\rho\rho}J_1[k_\rho\rho]-J_2[k_\rho\rho]\right]d\rho\\&=-2\pi\int_0^\infty\frac{2\rho^2}{k_\rho[\rho^2+z^2]^{5/2}}J_1[k_\rho\rho]d\rho+2\pi\int_0^\infty\frac{\rho^3}{[\rho^2+z^2]^{5/2}}J_2[k_\rho\rho]d\rho\end{aligned} \tag{15}$$

The first factor of the right-hand side of Eq. (15) is the same form as Eq. (6) with $\nu=1;\ u=\frac{3}{2}$, thus,

$$-2\pi\int_0^\infty\frac{2\rho^2}{k_\rho[\rho^2+z^2]^{5/2}}J_1[k_\rho\rho]d\rho=\frac{-(4\pi)k_\rho^{3/2}z^{-1/2}}{k_\rho 2^{3/2}\Gamma[5/2]}K_{-1/2}[k_\rho z]=-\frac{[2^{1/2}]\pi z^{-1/2}k_\rho^{1/2}}{\Gamma[5/2]}K_{1/2}[k_\rho z] \tag{16}$$

where $K_{-1/2}[k_\rho z]=K_{1/2}[k_\rho z]$ (Eq. (7)). The second factor of the right-hand side of Eq. (15) is the same form as Eq. (6) with $\nu=2;\ u=\frac{3}{2}$, thus,

$$2\pi\int_0^\infty\frac{\rho^3}{[\rho^2+z^2]^{5/2}}J_2[k_\rho\rho]d\rho=\frac{(2\pi)k_\rho^{3/2}z^{1/2}}{2^{3/2}\Gamma[5/2]}K_{1/2}[k_\rho z]=\frac{\pi z^{1/2}k_\rho^{3/2}}{[2^{1/2}]\Gamma[5/2]}K_{1/2}[k_\rho z] \tag{17}$$

Combining the parts of the integration with respect to $d\rho$ of Eq. (4) by adding Eq. (8), Eq. (16), and Eq. (17) gives:

$$\int_{-\infty}^\infty\left[\frac{[2^{1/2}]\pi z^{1/2}k_\rho^{3/2}}{\Gamma[5/2]}K_{3/2}[k_\rho z]-\frac{[2^{1/2}]\pi z^{-1/2}k_\rho^{1/2}}{\Gamma[5/2]}K_{1/2}[k_\rho z]+\frac{\pi z^{1/2}k_\rho^{3/2}}{[2^{1/2}]\Gamma[5/2]}K_{1/2}[k_\rho z]\right]e^{-jk_z z}dz \tag{18}$$

The modified Bessel functions of the third kind may be expressed as:

$$K_{n+1/2}[x]=\left[\frac{\pi}{2x}\right]^{1/2}e^{-x}\sum_{m=0}^{n}[2x]^{-m}\frac{\Gamma[n+m+1]}{m!\Gamma[n+1-m]} \tag{19}$$

Substitution of Eq. (13) into Eq. (19) with $\upsilon = 1$ is:

$$K_{3/2}[k_\rho z] = \left[\frac{\pi}{2k_\rho z}\right]^{1/2} e^{-k_\rho z}\left[1+\frac{1}{2k_\rho z}\Gamma[3]\right] \tag{20}$$

Substitution of Eq. (13) into Eq. (19) with $\upsilon = 0$ is:

$$K_{1/2}[k_\rho z] = \left[\frac{\pi}{2k_\rho z}\right]^{1/2} e^{-k_\rho z} \tag{21}$$

Substitution of Eq. (20) and Eq. (21) into Eq. (18) is:

$$\int_{-\infty}^{\infty}\left\{\left[\frac{(2^{1/2})\pi z^{1/2}k_\rho^{3/2}}{\Gamma[5/2]}\left[1+\frac{1}{2k_\rho z}\Gamma[3]\right]-\frac{(2^{1/2})\pi z^{1/2}k_\rho^{1/2}}{\Gamma[5/2]}+\frac{\pi z^{-1/2}k_\rho^{3/2}}{(2^{1/2})\Gamma[5/2]}\right]\left[\frac{\pi}{2k_\rho z}\right]^{1/2} e^{-k_\rho z}\right\}e^{-jk_z z}dz \tag{22}$$

$$\int_{-\infty}^{\infty}\left\{\frac{\pi^{3/2}}{\Gamma[5/2]}k_\rho e^{-[jk_z+k_\rho]z}+\frac{z^{-1}\pi^{3/2}\Gamma[3]}{\Gamma[5/2]2}e^{-[jk_z+k_\rho]z}-\frac{z^{-1}\pi^{3/2}}{\Gamma[5/2]}e^{-[jk_z+k_\rho]z}+\frac{\pi^{3/2}}{\Gamma[5/2]2}k_\rho e^{-[jk_z+k_\rho]z}\right\}dz \tag{23}$$

Collecting terms gives:

$$\int_{-\infty}^{\infty}\frac{\pi^{3/2}}{\Gamma[5/2]}\left\{k_\rho[1+1/2]+\left[\frac{\Gamma[3]}{2}-1\right]z^{-1}\right\}e^{-[jk_z+k_\rho]z}dz \tag{24}$$

With $\Gamma[3]=2$ and $\Gamma\left[5/2\right]=3/4\pi^{1/2}$, Eq. (24) is:

$$\int_{-\infty}^{\infty}\frac{\pi^{3/2}}{\Gamma[5/2]}\left\{k_\rho[3/2]+[1-1]z^{-1}\right\}e^{-k_\rho z}e^{-jk_z z}dz \tag{25}$$

$$\int_{-\infty}^{\infty}\frac{\pi^{3/2}}{3/4\pi^{1/2}}3/2k_\rho e^{-k_\rho z}e^{-jk_z z}dz \tag{26}$$

$$2\pi k_\rho\int_{-\infty}^{\infty}e^{-k_\rho z}e^{-jk_z z}dz \tag{27}$$

$$4\pi k_\rho\int_{0}^{\infty}e^{-k_\rho z}e^{-jk_z z}dz \tag{28}$$

$$4\pi k_\rho\int_{0}^{\infty}e^{-[jk_z+k_\rho]z}dz \tag{29}$$

Integration of Eq. (29) with respect to dz gives:

$$4\pi k_\rho\left\{\frac{-1}{jk_z+k_\rho}e^{-[jk_z+k_\rho]z}\Big|_0^\infty\right\} \tag{30}$$

$$4\pi k_\rho\left[\frac{1}{jk_z+k_\rho}\right] \tag{31}$$

Multiplication of Eq. (31) by:

$$1=\left[\frac{-jk_z+k_\rho}{-jk_z+k_\rho}\right] \tag{32}$$

gives:

$$4\pi k_\rho\left[\frac{-jk_z+k_\rho}{{k_z}^2+{k_\rho}^2}\right] \tag{33}$$

The system function (Eq. (1)) is an even function; thus, the spacetime Fourier transform in three dimensions in cylindrical coordinates, $H(k_\rho,k_z)$, is given by taking the real part of Eq. (33) [2]:

$$H[k_\rho,k_z]=\frac{4\pi{k_\rho}^2}{{k_z}^2+{k_\rho}^2} \tag{34}$$

The spacetime Fourier transform in three dimensions in Cartesian coordinates, $H(k_\rho,k_z)$, is:

$$H[k_x,k_y,k_z]=\frac{4\pi[{k_x}^2+{k_y}^2]}{[{k_x}^2+{k_y}^2+{k_z}^2]} \tag{35}$$

where the relationship between the wave numbers and the spatial Cartesian coordinates is as follows:

$$k_x=\frac{2\pi}{\lambda_x}=\frac{1}{x} \tag{36}$$

$$k_y=\frac{2\pi}{\lambda_y}=\frac{1}{y} \tag{37}$$

$$k_z = \frac{2\pi}{\lambda_z} = \frac{1}{z} \tag{38}$$

REFERENCES

1. R. N. Bracewell, *The Fourier Transform and Its Applications*, McGraw-Hill Book Company, New York, (1978), pp. 252-253.
2. W. McC. Siebert, *Circuits, Signals, and Systems*, The MIT Press, Cambridge, Massachusetts, (1986), p. 399.

BAND-PASS FILTER

The z component of a magnetic dipole oriented in the z direction has the system function, $h(x,y,z)$, which has the Fourier transform, $H[k_x,k_y,k_z]$, which is shown in Figure 25.1.

$$H[k_x,k_y,k_z] = \frac{4\pi[k_x{}^2 + k_y{}^2]}{[k_x{}^2 + k_y{}^2 + k_z{}^2]} \tag{25.5}$$

$$= H[k_\rho,k_z] = \frac{4\pi k_\rho{}^2}{k_z{}^2 + k_\rho{}^2} = \frac{4\pi}{1 + \frac{k_z{}^2}{k_\rho{}^2}} \tag{25.6}$$

Figure 25.1. The Fourier transform $H[k_x,k_y,k_z]$ of the system function $h(x,y,z)$ corresponding to the z component of a magnetic dipole oriented in the z direction.

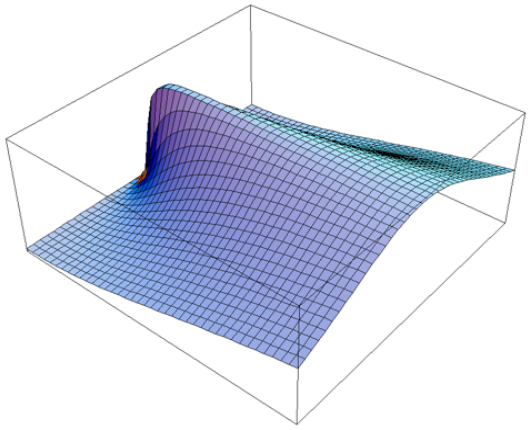

As shown in the Electron Scattering by Helium section, in the far field, the amplitude of the scattered electromagnetic radiation or scattered electron flux density is the Fourier transform of the aperture function. In the case of a superconductor, the electric field is zero—no voltage drop occurs; however, a magnetic field is present. The relationship between the amplitude of the scattered energy and the Fourier transform of the aperture function can be applied to the present case of the scattering of magnetic energy by the lattice of the potential superconductor. The spatial aperture function is the convolution of the array pattern with the elemental pattern. The elemental pattern is the system function, $h(x,y,z)$, which is the geometric transfer function for the z component of a z oriented magnetic dipole. And, the array pattern is a periodic array of delta functions each at the position of a magnetic dipole corresponding to a current carrying electron.

$$\frac{\left(2z^2 - x^2 - y^2\right)}{\left[x^2 + y^2 + z^2\right]^{5/2}} \otimes \sum_{n=-\infty}^{\infty} \mu_B \delta\left(x - nx_0, y - ny_0, z - nz_0\right) \tag{25.7}$$

The Fourier transform of a periodic array of delta functions (the right-hand side of Eq. (25.7)) is also a periodic array of delta functions in k-space:

$$\frac{1}{x_0 y_0 z_0} \sum_{n=-\infty}^{\infty} \mu_B \delta\left(k_x - \frac{n}{x_0}, k_y - \frac{n}{y_0}, k_z - \frac{n}{z_0}\right) \tag{25.8}$$

By the Fourier Theorem, the Fourier transform of the spatial aperture function, Eq. (25.7), is the product of the Fourier transform of the elemental function, system function given by Eq. (25.6), and the Fourier transform of the array function given by Eq. (25.8):

$$\frac{4\pi}{1+\frac{k_z^2}{k_\rho^2}}\frac{1}{x_0 y_0 z_0}\sum_{n=-\infty}^{\infty}\mu_B\delta\left(k_x-\frac{n}{x_0},k_y-\frac{n}{y_0},k_z-\frac{n}{z_0}\right) \tag{25.9}$$

The spacetime aperture function corresponding to the current-density function is given by multiplying the spatial aperture function (Eq. (25.7)) by a time harmonic function

$$\exp\left(-i\omega t\right) \tag{25.10}$$

Thus, the spacetime aperture function is:

$$\frac{\left(2z^2-x^2-y^2\right)}{\left[x^2+y^2+z^2\right]^{5/2}}\otimes\sum_{n=-\infty}^{\infty}\mu_B\delta\left(x-nx_0,y-ny_0,z-nz_0\right)\exp\left(-i\omega t\right) \tag{25.11}$$

The Fourier transform of the time harmonic function (Eq. (25.10)) is:

$$\frac{\left[\delta\left(\omega-\omega_z\right)+\delta\left(\omega-\omega_z\right)\right]}{2} \tag{25.12}$$

A very important theorem of Fourier analysis states that the Fourier transform of a product is the convolution of the individual Fourier transforms. Thus, the Fourier transform of Eq. (25.11) is the convolution of Eqs. (25.9) and (25.12) :

$$\frac{4\pi}{1+\frac{k_z^2}{k_\rho^2}}\frac{1}{x_0 y_0 z_0}\sum_{n=-\infty}^{\infty}\mu_B\delta\left(k_x-\frac{n}{x_0},k_y-\frac{n}{y_0},k_z-\frac{n}{z_0}\right)\otimes\frac{\left[\delta\left(\omega-\omega_z\right)+\delta\left(\omega-\omega_z\right)\right]}{2} \tag{25.13}$$

In the special case that:

$$k_\rho = k_z \tag{25.14}$$

the Fourier transform of the system function (the left-hand side of Eq. (25.13)) is given by:

$$H = 4\pi \tag{25.15}$$

Thus, the Fourier transform of the system function band-passes the Fourier transform of the time dependent array function. Both the spacetime aperture function, Eq. (25.11) and its Fourier transform, Eq. (25.13), are a periodic array of delta functions. No frequencies of the Fourier transform of the spacetime aperture function are attenuated; thus, no energy is lost in this special case where Eq. (25.14) holds. (This result is also central to a powerful new medical imaging technology—4 Dimensional Magnetic Resonance Imaging (4D-MRI [2]). No energy loss corresponds to a superconducting state. And the relationship between k-space and real space is:

$$k_x = \frac{2\pi}{\lambda_x} = \frac{1}{x}$$

$$k_y = \frac{2\pi}{\lambda_y} = \frac{1}{y} \tag{25.16}$$

$$k_z = \frac{2\pi}{\lambda_z} = \frac{1}{z}$$

From Eqs. (25.14) and (25.16), it follows that a cubic array ($x_0 = y_0 = z_0$) of magnetic dipoles centered on the nuclei of the lattice is a superconductor when the temperature is less than the critical temperature such that the superconducting electrons can propagate. Propagating electrons that carry the superconducting current and comprise magnetic dipoles form standing waves centered on the nuclear centers of the cubic lattice. Fermi-Dirac statistics apply to electrons as given in the Statistical Mechanics section. It follows from Eqs. (25.14) and (25.16) that the Fermi energy is calculated for a *cubical* cavity L on a side. The number of standing waves in a cubical cavity L on a side is given by Eq. (9.33) of Beiser [3] :

$$g\left(j\right)dj = \pi j^2 dj \tag{25.17}$$

where

$$j = \frac{2L}{\lambda} \tag{25.18}$$

The de Broglie wavelength of an electron is:

$$\lambda = \frac{h}{p} \tag{25.19}$$

Electrons in superconductors have non-relativistic velocities; so,

$$p = \sqrt{2m_e\varepsilon} \tag{25.20}$$

where ε is the kinetic energy and

$$j = \frac{2L}{\lambda} = \frac{2Lp}{h} = \frac{2L\sqrt{2m_e\varepsilon}}{h} \tag{25.21}$$

$$dj = \frac{L}{h}\sqrt{\frac{2m_e}{\varepsilon}}d\varepsilon \tag{25.22}$$

Using these expressions for j and dj in Eq. (25.17) gives:

$$g(\varepsilon)d\varepsilon = \frac{8\sqrt{2}\pi L^3 m_e^{3/2}}{h^3}\sqrt{\varepsilon}d\varepsilon \tag{25.23}$$

Substitution of V for L^3 gives the number of electron states, $g(\varepsilon)$

$$g(\varepsilon)d\varepsilon = \frac{8\sqrt{2}\pi V m_e^{3/2}}{h^3}\sqrt{\varepsilon}d\varepsilon \tag{25.24}$$

The Fermi energy, E_F, is calculated by equating the number of free electrons, N, to the integral over the electron states of energy ε from zero to the highest energy, the Fermi energy, $E = E_F$.

$$N = \int_0^{E_F} g(\varepsilon)d\varepsilon = \frac{8\sqrt{2}\pi V m_e^{3/2}}{h^3}\int_0^{E_F}\sqrt{\varepsilon}d\varepsilon \tag{25.25}$$

$$= \frac{16\sqrt{2}\pi V m_e^{3/2}}{3h^3}E_F^{3/2} \tag{25.26}$$

and the Fermi energy is:

$$E_F = \frac{h^2}{2m_e}\left(\frac{3N}{8\pi V}\right)^{2/3} = \frac{h^2}{2m_e}\left(\frac{3}{8\pi}\right)^{2/3} n^{2/3} \tag{25.27}$$

The quantity $N/V = n$ is the density of free electrons.

In the case of superconducting electrons, comprising an array of magnetic dipoles (each dipole in the xy-plane and oriented along the z-axis), the dimensions of Eq. (9.33) of Beiser [3] is reduced to 2 from 3.

$$2\frac{1}{4}2\pi j = g(j) \tag{25.28}$$

For $g(j) = 1$ with the substitution of Eq. (25.18),

$$2\pi L = \lambda \tag{25.29}$$

As the temperature of a superconducting material rises from a temperature below the critical temperature, T_c, the number density, n_s, of superconducting electrons decreases. At the transition temperature, the superconducting electrons condense into a nondissipative electron current ensemble, which obeys the statistics of a Bose gas (each electron is identical and indistinguishable as indicated in Eq. (25.8) with the constraint of Eq. (25.14)), and Eqs. (25.28) and (25.29) apply:

$$\left(\frac{2\pi}{\lambda}\right)^3 = \left(\frac{1}{L}\right)^3 = n_s \tag{25.30}$$

where

$$n_s E_F = nk_B T_c \tag{25.31}$$

n_s is the number density of superconducting electrons within $k_B T_c$ of the Fermi energy and n is the number density of free electrons. The current carried by each superconducting electron corresponds to a translational or kinetic energy. The relationship between the electron de Broglie wavelength (Eqs. (25.19) and (25.20)) and the average electron energy, $\bar{\varepsilon}$, per degree of freedom, f, given by Beiser [4]:

$$\bar{\varepsilon} = \frac{f}{2}k_B T_c = \Delta \qquad f = 3,\ 2,\ or\ 1 \tag{25.32}$$

is

$$\lambda = \frac{h}{\left(2m_e\left(\frac{1}{2}fk_B T_c\right)\right)^{1/2}} = \frac{h}{\left(m_e f k_B T_c\right)^{1/2}} \tag{25.33}$$

where in the present case of an inverse squared central field, the binding energy or energy gap of the superconducting state, Δ, is one half the negative of the potential energy and equal to the kinetic energy [5]. Consider the case wherein the Fermi energy is that of a three dimensional system, but the motion of superconducting electrons is restricted to 3, 2, *or* 1 directions corresponding to $f = 3,\ 2,\ or\ 1$, respectively. Combining Eqs. (25.30-25.33) gives the transition temperature,

$$T_c = \frac{8}{(2\pi)^6}\left(\frac{8\pi}{3}\right)^2 \frac{E_F}{k_B f^3} \tag{25.34}$$

where the Fermi energy, E_F, is given by Eq. (25.27). An isotope effect can be manifested indirectly by changing the rms. position of atoms which effects the condition of Eq. (25.14) or the Fermi energy by changing the bond and vibrational energies. The superconducting electrons are equivalent to those of metals and semiconductors in the conduction state given in the Nature

of the Metallic Bond of Alkali Metals section and the Nature of the Semiconductor Bond of Silicon section, respectively. The electron supercurrents confined to two-dimensions corresponding to $f = 2$ in Eq. (25.32) are shown pictorially in Figures 25.2A-25.2F. Except for their distribution in the lattice, the individual electron planes of superconductors are the same as those of metals. This aspect has been experimentally confirmed by using high-intensity pulsed magnetic fields that cause the superconducting electrons to behave the same as those in metals [6].

Figure 25.2A-F. A superconductor comprising covalent bonds and metallic (free) electrons showing the superconducting current as two-dimensional membranes of zero thickness that are each an equipotential energy surface comprised of the superposition of multiple electrons. The membranes called bands carry the current along two axes in the plane. Such a band is shown separately in (B).

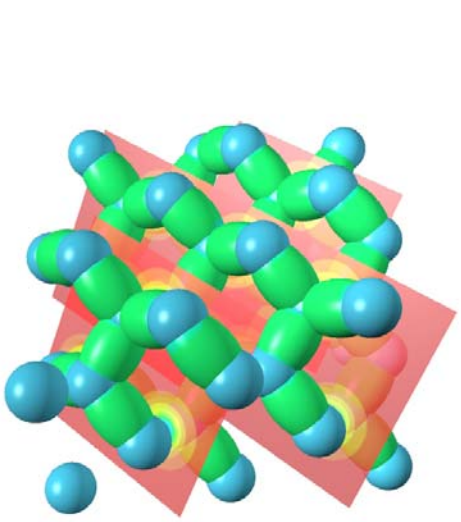

A

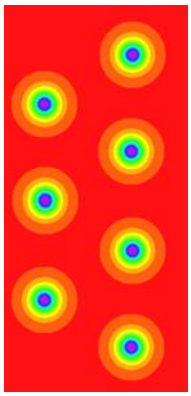

B

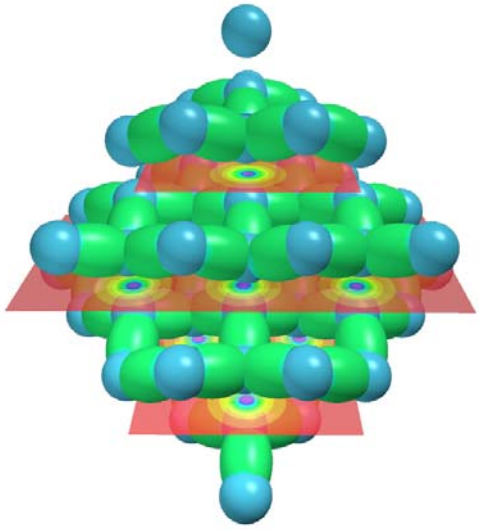

C

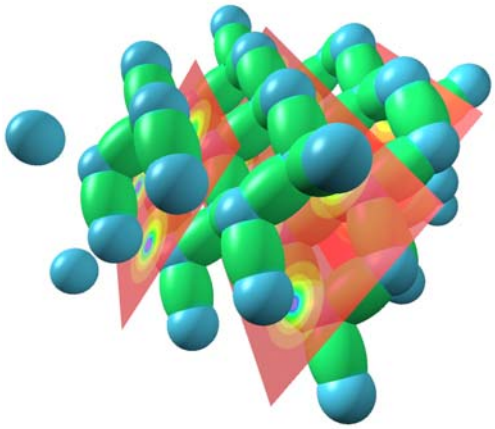

D

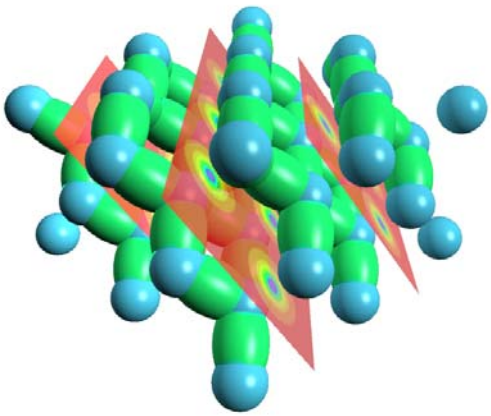

E

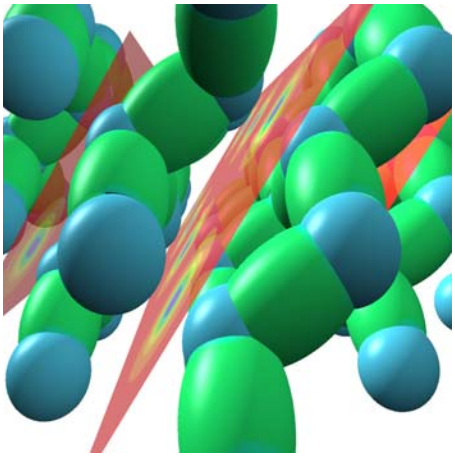

F

CRITICAL TEMPERATURE, T_C

T_C FOR CONVENTIONAL THREE DIMENSIONAL METALLIC SUPERCONDUCTORS

In the case of conventional three dimensional metallic superconductors, the number density of conduction electrons is comparable to the number density of atoms—approximately $10^{29} / m^3$.

Thus, the calculated transition temperature (Eq. (25.34)) is

$T_c = 30.8\ K$

As a comparison, the material of this class with the highest known transition of $23.2\ K$ is Nb_3Ge [7].

T_C FOR ONE, TWO, OR THREE DIMENSIONAL CERAMIC OXIDE SUPERCONDUCTORS

In the case of ceramic oxide superconductors, one, two, and three-dimensional conduction mechanisms are possible. The number density of conduction electrons is less than that of metallic superconductors—approximately $10^{28} / m^3$. For the three-dimensional case, the calculated transition temperature (Eq. (25.34)) is:

$T_c = 7\ K$

As a comparison, a possible material of this class, Li_2TiO_3 has a transition temperature of 13.7 K [8].

For the two-dimensional case,

$T_c = 22\ K$

As a comparison, a possible material of this class, the original Bednorz and Muller $Ba - La - Cu - O$ material has a transition temperature of 35 K [7].

For the one-dimensional case,

$T_c = 180\ K$

As a comparison, a possible material of this class, $Tl - Ca - Ba - Cu - O$ has a transition temperature of $120 - 125\ K$ [9]. The existence of superconductivity confined to stripes has been observed experimentally by neutron scattering [10].

Transition temperatures which are intermediate of each of these limiting cases are possible where combinations of conduction mechanisms are present.

JOSEPHSON JUNCTION, WEAK LINK

As shown in the Electron g Factor section, the electron links flux in units of the magnetic flux quantum. Thus, the magnetic flux that links a superconducting loop with a weak link is the magnetic flux quantum, Φ_0.

$$\Phi_0 = \frac{h}{2e} \tag{25.35}$$

The factor of $2e$ in the denominator has been erroneously interpreted [11] as evidence that Cooper pairs are the superconducting current carriers, which is central to the BCS theory of superconductors. This theory fails to explain so called High Temperature Superconductors. These materials have a transition temperature, which corresponds to an internal electron energy that is well above the energy limits at which the BCS theory permits conduction electron pairing. According to CP, Cooper pairs do not exist, and CP is consistent with the existence of High Temperature Superconductors as well as the experimental result that the magnetic flux that links a superconducting loop with a weak link is the magnetic flux quantum, Φ_0. Cooper pairs are also disproved by the existence of a spin triplet supercurrent [12].

REFERENCES

1. G. O. Reynolds, J. B. DeVelis, G. B. Parrent, B. J. Thompson, *The New Physical Optics Notebook*, SPIE Optical Engineering Press, (1990).
2. R. Mills, Magnetic Susceptibility Imaging (MSI), U.S. Patent No. 5,073,858 (1991); Mills, R., Resonant Magnetic Susceptibility Imaging (ReMSI), US Patent Application No. 60/065,318, filed November 12, 1998; Mills, R., 4 Dimensional Magnetic Resonance Imaging, PCT/US01/25954, August 21, 2001.
3. A. Beiser, *Concepts of Modern Physics*, Fourth Edition, McGraw-Hill, New York, (1987), p. 333.
4. A. Beiser, *Concepts of Modern Physics*, Fourth Edition, McGraw-Hill, New York, (1987), p. 344.
5. G. R. Fowles, *Analytical Mechanics*, Third Edition, Holt, Rinehart, and Winston, New York, (1977), pp. 154-156.
6. N. Doiron-Leyraud, C. Proust, D. LeBoeuf, J. Levallois, Jean-Baptiste Bonnemaison, R. Liang, D. A. Bonn, W. N. Hardy, L. Taillefer, "Quantum oscillations and the Fermi surface in an underdoped high-Tc superconductor," Nature, Vol. 447, (2007), pp. 565-568.
7. J. G. Bednorz, K. A. Muller, Science, Vol. 237, (1987), pp. 1133-1139.
8. D. C. Johnston, H. Prakash, W. H. Zachariasen, and V. Viswanathan, Materials Research Bulletin, Vol. 8, (1973), pp. 777.
9. Z. Z. Sheng, A. M. Hermann, Nature, Vol. 322, (1988), pp. 55.
10. R. F. Service, Science, Vol. 283, (1999), pp. 1106-1108.
11. C. E. Gough, M. S. Colclough, E. M. Forgan, R. G. Jordan, M. Keene, C. M. Muirhead, A. I. M. Rae, N. Thomas, J. S. Abell, S. Sutton, Nature, Vol. 326, (1987), p. 855.
12. R. S. Keizer, S. T. B. Goennenwein, T. M. Klapwijk, G. Miao, G. Xiao, A. Gupta, "A spin triplet supercurrent through the half-metallic ferromagnet CrO_2," Nature, Vol. 439, No. 16, (2006), pp. 825-827.

Chapter 26

QUANTUM HALL EFFECT

GENERAL CONSIDERATIONS

When confined to two dimensions and subjected to a magnetic field, electrons exhibit a range of extraordinary behavior, most notably the Quantum Hall Effect (QHE). Two distinct versions of this phenomenon are observed, the Integral Quantum Hall Effect (IQHE) and the Fractional Quantum Hall Effect (FQHE). The former involves the condition for re-establishment of a superconducting state of one well in the presence of a magnetic field; whereas, the latter involves the condition for re-establishment of a superconducting state of two magnetically linked wells in the presence of a magnetic field.

Consider a conductor in a uniform magnetic field and assume that it carries a current driven by an electric field perpendicular to the magnetic field. The current in this case is not parallel to the electric field, but is deflected at an angle to it by the magnetic field. This is the Hall Effect, and it occurs in most conductors.

In the Quantum Hall Effect, the applied magnetic field quantizes the Hall conductance. The current is then precisely perpendicular to the magnetic field, so that no dissipation (that is no ohmic loss) occurs. This is seen in two-dimensional systems, at cryogenic temperatures, in quite high magnetic fields. Furthermore, the ratio of the total electric potential drop to the total current, the Hall resistance, R_H, is precisely equal to:

$$R_H = \frac{h}{ne^2} = \frac{25812.807\Omega}{n} \tag{26.1}$$

The factor n is an integer in the case of the Integral Quantum Hall Effect, and n is a small rational fraction in the case of the Fractional Quantum Hall Effect. In an experimental plot [1] as the function of the magnetic field, the Hall resistance exhibits flat steps precisely at these quantized resistance values; whereas, the regular resistance vanishes (or is very small) at these Hall steps. Thus, the quantized Hall resistance steps occur for a transverse superconducting state.

As shown in the Superconductivity section, superconductivity arises for an array of current carrying magnetic dipoles when:

$$k_p = k_z \tag{26.2}$$

Thus, the Fourier transform of the system function band-passes the Fourier transform of the time dependent array function. Both the spacetime aperture function and its Fourier transform are a periodic array of delta functions. No frequencies of the Fourier transform of the spacetime aperture function are attenuated; thus, no energy is lost in this special case where Eq. (26.2) holds. Consider the case that an external magnetic field is applied along the x-axis to a two-dimensional superconductor in the yz-plane, which exhibits the Integral Quantum Hall Effect. (See Figure 26.1.) The magnetic field is expelled from the bulk of the superconductor by the supercurrent (Meissner Effect). The supercurrent-density function is a minimum energy surface; thus, the magnetic flux decays exponentially at the surface as given by the London Equation [2]. The Meissner current increases as a function of the applied flux. The energy of the superconducting electrons increases with flux. This energy increase is equivalent to lowering the critical temperature in Eq. (25.31) of the Superconductivity section which is given by:

$$n_s E_F = nkT_c \tag{26.3}$$

where n_s is the number density of superconducting electrons within kT_c of the Fermi energy and n is the number density of free electrons. At the critical current, the material loses superconductivity and becomes normal at a temperature below that of the critical temperature in the absence of an applied field. Conduction electrons align with the applied field in the x direction as the field permeates the material. The normal current carrying electrons experience a Lorentz force, $\mathbf{F}_L$, due to the magnetic flux. The y directed Lorentz force on an electron having a velocity **v** in the z direction by an x directed applied flux, **B**, is

$$\mathbf{F}_L = e\mathbf{v}\times\mathbf{B} \tag{26.4}$$

The electron motion is a cycloid where the center of mass experiences an $\mathbf{E}\times\mathbf{B}$ drift [3]. Consequently, the normal Hall Effect occurs. Conduction electron energy states are altered by the applied field and by the electric field corresponding to the Hall Effect. The electric force, $\mathbf{F}_H$, due to the Hall electric field, $\mathbf{E}_y$, is:

$$\mathbf{F}_L = e\mathbf{E}_y \tag{26.5}$$

When these two forces are equal and opposite, conduction electrons propagate in the z direction alone. For this special case, it is demonstrated in Jackson [3] that the ratio of the corresponding Hall electric field and the applied magnetic flux is:

$$E/B = v \tag{26.6}$$

where $\mathbf{v}$ is the electron velocity. At a temperature below T_c, given by Eq. (26.3) where E_F is the Fermi energy, Eq. (26.6) is satisfied. The further conditions for superconductivity are:

$$n\omega_\rho = \omega_z \tag{26.7}$$

$$nk_\rho = k_z \tag{26.8}$$

And, it is demonstrated in the Integral Quantum Hall Effect section that the Hall resistance, R_H, in the superconducting state is given by:

$$R_H = \frac{h}{ne^2} \tag{26.9}$$

where n of Eqs. (26.7), (26.8), and (26.9) is the same integer for the case of a single superconducting well. It is demonstrated in the Fractional Quantum Hall Effect section that electrons in different superconducting wells can interact when the two wells are separated by a distance comparable to the magnetic length, ℓ_0:

$$\ell_0 = \left(\frac{\hbar c}{eB}\right)^{1/2} \tag{26.10}$$

In this case, it is further demonstrated that the Hall resistance, R_H, in the superconductivity state is given by Eq. (26.9) where n is a fraction.

INTEGRAL QUANTUM HALL EFFECT

A superconducting current-density function is nonradiative and does not dissipate energy as was the case for single electron current-density functions described previously in the One-Electron Atom section, the Two Electron Atom section, the Three Electron Atom section, the Electron in Free Space section, and the Nature of the Chemical Bond section. Furthermore, a superconducting current-density function is the superposition of single electron current-density functions which are spatially two dimensional in nature. Thus, a superconducting current-density function is an electric and magnetic equipotential energy surface. The nature of electrons in materials as such extended surfaces is observed by scanning tunneling electron microscopy (STM) [4].

From Eq. (1.36), the angular frequency in spherical coordinates which satisfies the boundary condition for nonradiation is:

$$\omega = \frac{\hbar}{m_e r^2} = \frac{(2\pi)^2\hbar}{m_e(2\pi r)^2} \tag{26.11}$$

The relationship between the electron wavelength and the radius, which satisfies the nonradiative boundary condition in spherical coordinates is given by Eq. (1.15):

$$2\pi r = \lambda \tag{26.12}$$

Substitution of Eq. (26.12) into Eq. (26.11) gives:

$$\omega = \frac{\hbar}{m_e}k^2 \tag{26.13}$$

where

$$k = \frac{2\pi}{\lambda} \tag{26.14}$$

It follows from Eq. (1.35) where:

$$v = \frac{\hbar}{m_e r} = \frac{\hbar}{m_e}k \tag{26.15}$$

In a solid lattice, the coordinates are Cartesian rather than spherical. The relationship between the wavelength of a standing wave of a superconducting electron and the length, x, of a cubical unit cell follows from Eqs. (25.28) and (25.29) of the

Superconductivity section

$$\lambda = 2\pi r \tag{26.16}$$

The de Broglie wavelength, λ is given by:

$$\lambda = \frac{h}{m_e v} \tag{26.17}$$

It follows from Eqs. (26.14), (26.16), and (26.17) that the angular velocity, ω, and linear velocity, v, for an electron held in force balance by a periodic array of nuclei comprising a cubical unit cell with internuclear spacing x are given by Eqs. (26.13) and (26.15) where:

$$k = \frac{2\pi}{\lambda} = \frac{1}{x} \tag{26.18}$$

In general, the Cartesian coordinate wavenumber, *k*, given by Eq. (26.18) replaces $\frac{1}{r}$ of spherical coordinates.

In the case of an exact balance between the Lorentz force (Eq. (26.4)) and the electric force corresponding to the Hall voltage (Eq. (26.5)), each superconducting electron propagates along the z-axis where:

$$E/B = v \tag{26.19}$$

where v is given by Eq. (26.15). Substitution of Eqs. (26.15) and (26.18) into Eq. (26.19) gives:

$$E/B = \frac{\hbar}{m_e} k = \frac{\hbar}{m_e x} \tag{26.20}$$

Eq. (26.20) is the condition for superconductivity in the presence of crossed electric and magnetic fields. The Hall resistance for this superconducting state is derived as follows using the coordinate system shown in Figure 26.1.

Figure 26.1. Coordinate system of crossed electric field, $\mathbf{E}_y$, corresponding to the Hall voltage, magnetic flux, $\mathbf{B}_x$, due to applied field, and superconducting current, $\mathbf{i}_z$.

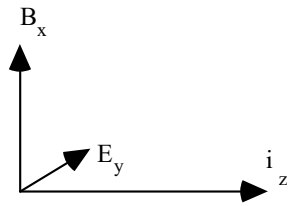

The current is perpendicular to $\mathbf{E}_y$, thus there is no dissipation. This occurs when,

$$e\mathbf{E} = e\mathbf{v} \times \mathbf{B} \tag{26.21}$$

or

$$E/B = v \tag{26.22}$$

The magnetic flux, **B**, is quantized in terms of the Bohr magneton because an electron, and therefore a superconductor, links flux in units of the magnetic flux quantum,

$$\Phi_0 = \frac{h}{2e} \tag{26.23}$$

The electric field, $\mathbf{E}_y$, corresponding to the Hall voltage, V_H, is quantized in units of e because this electric field arises from conduction electrons-each of charge *e*. The energy, E_H, corresponding to the Hall voltage is calculated using the Poynting Power Theorem. The Hall energy of an integer number of electrons, *Z*, each in the presence of a magnetic dipole and an electric field of magnitude *Ze* due to the *Z* electrons follows for Eqs. (7.46) and (7.63) of the Two Electron Atom section where

$$E_H = ZE_{mag} = \frac{Z\pi\mu_0 e^2 \hbar^2 k^3}{Z m_e^{\,2}} \tag{26.24}$$

where k is given by Eq. (26.13) and where the electric energy of Eq. (7.63) is zero because each electron is a conduction electron. In the limit to a superconducting state, the trajectory of each electron is a cycloid where ω_p is the angular frequency in the xy-plane and ω_z is angular the frequency along the z-axis. In this case, the dipole array function given in the Superconductivity section is multiplied by a time harmonic function with argument ω_p

$$\frac{\left(2z^2-x^2-y^2\right)}{\left[x^2+y^2+z^2\right]^{5/2}} \otimes \sum_{n=-\infty}^{\infty} \mu_B \delta\left(x-nx_0, y-ny_0, z-nz_0\right) \exp\left(-i\omega t\right) \tag{26.25}$$

where

$$\omega = \omega_\rho + \omega_z \tag{26.26}$$

The Fourier transform of the convolved functions of Eq. (26.25) is given in the Superconductivity section as:

$$\frac{4\pi}{1+\frac{k_z^2}{k_\rho^2}} \frac{1}{x_0 y_0 z_0} \sum_{n=-\infty}^{\infty} \mu_B \delta\left(k_x - \frac{n}{x_0}, k_y - \frac{n}{y_0}, k_z - \frac{n}{z_0}\right) \tag{26.27}$$

The Fourier transform of the time harmonic function is:

$$\frac{\left[\delta\left(\omega-\left(\omega_p-\omega_z\right)\right)+\delta\left(\omega+\left(\omega_p-\omega_z\right)\right)\right]}{2} \tag{26.28}$$

A very important theorem of Fourier analysis states that the Fourier transform of a product is the convolution of the individual Fourier transforms. Thus, the Fourier transform of Eq. (26.25) is the convolution of Eqs. (26.27) and (26.28) where

$$\frac{4\pi}{1+\frac{k_z^2}{k_\rho^2}} \frac{1}{x_0 y_0 z_0} \sum_{n=-\infty}^{\infty} \mu_B \delta\left(k_x - \frac{n}{x_0}, k_y - \frac{n}{y_0}, k_z - \frac{n}{z_0}\right) \otimes \frac{\left[\delta\left(\omega-\left(\omega_p-\omega_z\right)\right)+\delta\left(\omega+\left(\omega_p-\omega_z\right)\right)\right]}{2} \tag{26.29}$$

Eq. (26.29) is a band-pass when

$$nk_p = k_z \tag{26.30}$$

and when

$$\frac{\omega_z}{\omega_\rho} = n \tag{26.31}$$

where n is an integer. The cyclotron angular frequency, ω_p, is derived as follows:

The force balance between the Lorentz force and the centrifugal force is:

$$\frac{m_e \mathbf{v}^2}{r} = e\mathbf{v} \times \mathbf{B} \tag{26.32}$$

The magnetic flux, **B**, from a magnetic moment of a Bohr magneton is:

$$B = \frac{\mu_0 e\hbar}{2m_e} k^3 \tag{26.33}$$

Cancellation of $\mathbf{v}$ on both sides of Eq. (26.32) gives:

$$m_e \omega = e \times \mathbf{B} \tag{26.34}$$

$$\omega_\rho = \frac{eB}{m_e} \tag{26.35}$$

Substitution of Eq. (26.33) into Eq. (26.35) gives:

$$\omega_\rho = \frac{\mu_0 e^2 \hbar}{2m_e^2} k^3 \tag{26.36}$$

Substitution of Eq. (26.31) into Eq. (26.36) gives:

$$\omega_z = \frac{n\mu_0 e^2 \hbar}{2m_e^2} k^3 \tag{26.37}$$

The current, $\mathbf{i}_z$, along the z-axis is given as the product of the charge, e, and ω_z, the angular frequency along the z-axis where:

$$\mathbf{i}_z = e\omega_z = \frac{n\mu_0 e^3 \hbar}{2m_e^2} k^3 \tag{26.38}$$

The Hall voltage is given as the energy per coulomb:

$$V_H = \frac{E_{mag}}{e} = \frac{\pi \mu_0 e \hbar^2 k^3}{m_e^2} \tag{26.39}$$

Thus, the Hall resistance, R_H, is given as the ratio of the Hall voltage (Eq. (26.39)) and the current, $\mathbf{i}_z$, (Eq. (26.38))

$$R_H = \frac{V_H}{i_z} = \frac{\frac{\pi\mu_0 e\hbar^2 k^3}{m_e^{\,2}}}{\frac{n\mu_0 e^3\hbar k^3}{2m_e^{\,2}}} = \frac{h}{ne^2} \tag{26.40}$$

The velocity of each superconducting electron according to Eq. (26.22) is:

$$E/B = v \tag{26.41}$$

which is derived as follows:

The Hall electric field, $\mathbf{E}_y$, is given by the ratio of the Hall voltage and the distance of the cyclotron orbit, $2\pi x$, where the unit cell distance, x, and the wavenumber, k, are related by Eq. (26.18) where:

$$\mathbf{E}_y = V_H \frac{k}{2\pi} \tag{26.42}$$

where V_H is given by Eq. (26.39):

$$\mathbf{E}_y = \frac{\pi\mu_0 e\hbar^2 k^4}{2\pi m_e^{\,2}} \tag{26.43}$$

The magnetic field, **B**, is given by Eq. (26.33); thus the velocity $\mathbf{v}$ is given as:

$$\mathbf{v} = \frac{\frac{\pi\mu_0 e\hbar^2 k^4}{2\pi m_e^{\,2}}}{\frac{\mu_0 e\hbar k^3}{2m_e}} = \frac{\hbar}{m_e} k \tag{26.44}$$

Eq. (26.44) is equivalent to the velocity for nonradiation given by Eq. (1.35), where:

$$\frac{2\pi}{2\pi r} = \frac{2\pi}{\lambda} = k \tag{26.45}$$

This superconducting phenomenon whereby the Hall resistance occurs as inverse integer multiples of:

$$\frac{h}{e^2} \tag{26.46}$$

is the Integral Quantum Hall Effect (IQHE).

FRACTIONAL QUANTUM HALL EFFECT

For two superconducting wells separated by the magnetic length, ℓ_0,

$$\ell_0 = \left(\frac{\hbar c}{eB}\right)^{1/2} = \left(\frac{c}{\pi}\frac{\Phi_0}{B}\right)^{1/2} \tag{26.47}$$

where Φ_0 given by Eq. (26.23) is the magnetic flux quantum, the wells are linked. Electrons can propagate from one well to the other with activation energy where:

$$\left|\frac{\Delta E_{mag}}{E_{mag}}\right| \propto \frac{e^2}{\ell_0} \tag{26.48}$$

In the case that a magnetic field is applied to both well one and well two, and that an exact balance between the Lorentz force (Eq. (26.4)) and the electric force corresponding to the Hall voltage (Eq. (26.5)) exists, each superconducting electron propagates along the z-axis where

$$\frac{E_1}{B_1} = v_1 \tag{26.49}$$

$$\frac{E_2}{B_2} = v_2 \tag{26.50}$$

Because the two wells are linked,

$$v_1 = jv_2 \tag{26.51}$$

where j is an integer. Eq. (26.51) provides that the electrons are in phase with:

$$\frac{2\pi}{\lambda_1} = k_1 = j \cdot k_2 = j\frac{2\pi}{\lambda_2} \tag{26.52}$$

where the de Broglie wavelength is given by Eq. (26.17). Otherwise, $E_z \neq 0$, and the state is not superconducting. It follows from the derivation of Eq. (26.41) of the Integral Quantum Hall Effect section that:

$$\frac{E_1}{n_1 B_{01}} = v_1 \tag{26.53}$$

and,

$$\frac{E_2}{n_2 B_{01}} = v_2 \tag{26.54}$$

where n_1 and n_2 are integers. From Eqs. (26.52), (26.53), and (26.54) where:

$$E_1 = j\frac{n_1}{n_2}\frac{E_2}{B_{01}}B_{01} \tag{26.55}$$

The resistance of each well is proportional to the transverse velocity as shown previously, and the resistance across both linked wells which are in series is the sum of the individual resistances. Thus, the total resistance is proportional to the sum of the individual velocities.

$$R \propto \left(\frac{E_1}{n_1 B_{01}} + \frac{E_2}{n_2 B_{01}}\right) \tag{26.56}$$

Substitution of Eq. (26.55) into Eq. (26.56) gives:

$$R \propto \frac{E_2}{B_{01}}\frac{1}{n_2}\left(j+1\right) \tag{26.57}$$

It follows from the derivation of Eq. (26.40) of the Integral Quantum Hall Effect section that Hall resistance, R_H, is:

$$R_H = \frac{V_H}{i_z} = \frac{\left(j+1\right)\dfrac{\pi\mu_0 e\hbar^2 k^3}{m_e^{\,2}}}{\dfrac{n_2\mu_0 e^3\hbar k^3}{2m_e^{\,2}}} = \frac{h}{ne^2} \tag{26.58}$$

where n is a fraction. This superconducting phenomenon whereby the Hall resistance occurs as inverse fractional multiples of

$$\frac{h}{e^2} \tag{26.59}$$

is the Fractional Quantum Hall Effect (FQHE).

REFERENCES

1. S. Das Sarma, R. E. Prange, Science, Vol. 256, (1992), pp. 1284-1285.
2. F. A. Matsen, Journal of Chemical Education, Vol. 64, No. 10, (1987), pp. 842-845.
3. J. D. Jackson, *Classical Electrodynamics*, Second Edition, John Wiley & Sons, New York, (1975), pp. 582-584.
4. W. A. Hofer, "Unraveling electron mysteries," Materials Today, October, (2002), pp. 24-31.

Chapter 27

AHARONOV-BOHM EFFECT

The resistance of a circuit corresponds to the decrease in the energy of the current carrying electrons as they propagate through the circuit. Scattering of the electrons is a principal mechanism. In the case where a magnetic field is applied such that the field lines are perpendicular to the plane of a current carrying ring, the current carrying electrons lose energy through the effect of the field on the current.

The application of the magnetic field to the current carrying ring initially gives rise to a changing flux through the ring. The changing flux gives rise to an electric field that reduces the current in the ring; thus, the magnetic field contributes a term called magnetoresistance to the resistance of the ring. This term can be derived from the change in velocity (assuming no scattering) of a current carrying electron of charge, e, and mass, m_e, by the application of a magnetic field of strength, **B**, which is given as Eq. (29) of Purcell [1] :

$$\frac{\Delta \mathbf{v}}{r} = \frac{e\mathbf{B}}{2m_e} \tag{27.1}$$

where r is the radius of the ring. The changes in the force on the electron due to the electric field is:

$$\Delta \mathbf{F} = e\Delta \mathbf{E} \tag{27.2}$$

The change in kinetic energy of the electron over length, s, is:

$$\frac{1}{2} m_e \Delta \mathbf{v}^2 = \Delta \mathbf{F} s = e\Delta \mathbf{E} s = e\Delta V \tag{27.3}$$

where ΔV is the change in voltage over the distance, s. From Eq. (27.3), the voltage change is:

$$\Delta V = \frac{m_e \Delta v^2}{2e} \tag{27.4}$$

The change in current, $\Delta \mathbf{i}$, per electron due to the change in velocity, $\Delta \mathbf{v}$, is given by Eq. (20) of Purcell [1].

$$\Delta \mathbf{i} = \frac{e\Delta \mathbf{v}}{2\pi r} \tag{27.5}$$

And, the total change in current, $\Delta \mathbf{i}$, is:

$$\Delta \mathbf{i} = NWt\frac{e\Delta \mathbf{v}}{2\pi r} \tag{27.6}$$

where N is the density of current carrying electrons in the current ring cross section, W is the width of the current ring, and t is the thickness of the ring.

The resistance change, ΔR, follows from Eqs. (27.4) and (27.6) where

$$\Delta R = \frac{\Delta V}{\Delta i} = \frac{2\pi r m_e \Delta v^2}{NWt2ee\Delta v} = \frac{\pi r m_e \Delta v}{NWte^2} \tag{27.7}$$

Substitution of Δv given by Eq. (27.1) into Eq. (27.7) gives the change in resistance corresponding to the magnetoresistance:

$$\Delta R = \frac{\pi r^2 B}{NWt2e} \tag{27.8}$$

An additional critically damped, overdamped, or underdamped oscillatory resistive term may arise due to both the magnetoresistance and the vector potential of the electron. The electron possesses an angular momentum of $\hbar$. As shown in the Electron g Factor section, the electron angular momentum comprises kinetic and vector potential components. Angular momentum is conserved in the presence of an applied magnetic field when the electron links flux in units of the magnetic flux quantum, Φ_0.

$$\Phi_0 = \frac{h}{2e} \tag{27.9}$$

This occurs when the electron rotates by $\frac{\pi}{2}$ radians about an axis perpendicular to the axis parallel to the magnetic flux lines. This electron rotation corresponds to an $\frac{\hbar}{2}$ magnitude, 180° , rotation of the electron's angular momentum vector. In the case that the electrons carry current, this change in momentum of a given current carrying electron increases or decreases the current depending on the vector projection of the momentum change onto the direction of the current. Recently, it has been demonstrated that 50-nm-diameter rings of *InAs* on a *GaAs* surface can host a single circulating electron in a pure quantum state, that is easily controlled by magnetic fields and voltages on nearby plates. The electrons were observed to link flux in the unit of the magnetic flux quantum with a gain in a unit of angular momentum in a specific direction with the linkage [2].

At low temperature, the de Broglie wavelength of an electron,

$$\lambda = \frac{h}{m_e v} \tag{27.10}$$

has macroscopic dimensions, and the electron scattering length for a given electron in a current carrying ring may be comparable to the dimensions of the ring. A current carrying ring having a magnetic field applied perpendicularly to the plane of the ring may be constructed and operated at a temperature, current, and applied magnetic field strength such that resonance occurs between the vector potential of a current carrying electron and the flux of the applied magnetic field. This coupling can give rise to a contribution to the resistance, which behaves as an underdamped harmonic oscillator in response to the applied magnetic flux. The general form of the equation for this component of the resistance is the product of an exponential dampening function and a harmonic function as given by Fowles [3]. Each electron links flux only in units of the magnetic flux quantum, Φ_0, given by Eq. (27.9). Thus, the natural frequency in terms of the applied flux, Φ, is the magnetic flux quantum, Φ_0. According to Eq. (27.8), the magnetoresistance is proportional to the applied flux Φ where:

$$\Phi = \pi r^2 B \tag{27.11}$$

Thus, the argument of the dampening function is proportional to $\frac{\Phi}{\Phi_0}$. Furthermore, the magnetoresistance gives rise to a distribution of electron velocity changes centered about the average velocity change given by Eq. (27.1) where each electron's current contributing drift velocity along the ring contributes a component to the kinetic term of the electron's angular momentum. The distribution of velocity changes, dampens the coupling between each electron vector potential and the applied magnetic flux at the natural frequency corresponding to the average electron velocity. And, each electron de Broglie wavelength change corresponding to its velocity change alters the electron-lattice scattering cross section, which also contributes to the dampening of the oscillatory resistance behavior. The argument of the dampening function is the product of $\frac{\Phi}{\Phi_0}$ and the corresponding dimensionless damping factor, α_D, which incorporates both dampening effects. The underdamped oscillatory resistance change due to the applied magnetic field is:

$$\Delta R = \frac{\pi r^2 B}{NWt2e} e^{-\alpha_D\left[\frac{\Phi}{\Phi_0}\right]} \cos 2\pi \frac{\Phi}{\Phi_0} \tag{27.12}$$

The total resistance change due to the applied field is the sum of the magnetoresistance and the underdamped oscillatory resistance where:

$$\Delta R = \frac{\pi r^2 B}{NWt2e}\left[1 + e^{-\alpha_D\left[\frac{\Phi}{\Phi_0}\right]} \cos 2\pi \frac{\Phi}{\Phi_0}\right] \tag{27.13}$$

This type of contribution to the resistance that is an oscillatory function of the applied flux with a period of $\Phi_0 = \frac{h}{2e}$ is known as the Aharonov-Bohm Effect. The resistance contribution given by Eq. (27.13) is consistent with the observed behavior [4] as shown in Figure 27.1.

Figure 27.1. The change in the resistance divided by the resistance as a function of the applied flux that demonstrates the Aharonov-Bohm effect.

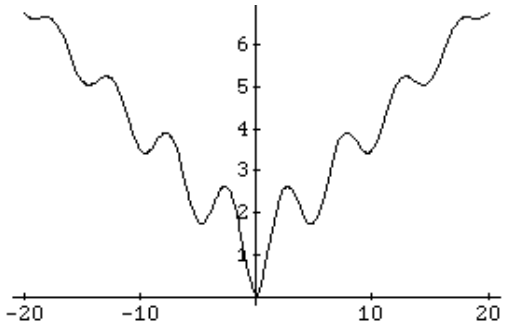

REFERENCES

1. E. Purcell, *Electricity and Magnetism*, McGraw-Hill, New York, (1965), pp. 373.
2. A. Lorke, R. J. Luyken, A. O. Govorov, J. P. Kotthaus, J. M. Garcia, and P. M. Petroff, Phys. Rev. Lett., Vol. 84, March 6, (2000), p. 2223.
3. G. R. Fowles, *Analytical Mechanics*, Third Edition, Holt, Rinehart, and Winston, New York, (1977), pp. 62-66.
4. V. Chandrasekhar, M. J. Rooks, S. Wind, D. E. Prober, Physical Review Letters, Vol. 55, No. 15, (1985), pp. 1610-161.

Chapter 28

CREATION OF MATTER FROM ENERGY

[The general result of particle production equations and relationships derived in the Pair Production and Gravity sections are given herein.]

Matter and energy are interconvertible and are in essence different *states* of the same entity. The state, matter or energy, is determined by the laws of nature and the properties of spacetime. A photon propagates according to Maxwell's Equations at the speed of light in spacetime having intrinsic impedance η. Matter, as a fundamental particle, is created in spacetime from a photon. Matter obeys the laws of Special Relativity, the relationship of motion to spacetime, and spacetime is curved by matter according to the laws of General Relativity. Relationships must exist between these laws and the implicit fundamental constants. The fundamental elements which determine the evolution of the Universe are the fundamental constants of spacetime, ε_o and μ_o with the property of charge; the capacity of spacetime to be curved by mass-energy; and the photon's angular momentum of $\hbar$. The conversion of energy into matter requires a transition state for which the identification of the entity as matter or energy is impossible. From the properties of the entity, as matter or energy, and from the physical laws and the properties of spacetime, the transition state hereafter called a transition state atomic orbital are derived. Concomitantly, the equations for the interconversion of matter and energy are determined, and the fundamental constant relationships are determined exactly. The results are: matter and energy possess mass; matter possesses charge, and energy is stored in the electric and magnetic fields of matter as a consequence of its charge and the motion of its charge. Matter can trap photons as an absorption event. The mass of the matter possessing a "trapped photon" increases by the mass-energy of the photon, and the photon acts as if it possesses charge. (The electric field of "trapped photons" is given in the Excited States of the One-Electron Atom (Quantization) section). Photons obey Maxwell's Equations. At the two-dimensional surface of the atomic orbital containing a "trapped photon," the relationship between the photon's electric field and its charge at the atomic orbital (See Eq. 2.10) is:

$$\mathbf{n} \bullet \left(\mathbf{E}_1 - \mathbf{E}_2 \right) = \frac{\sigma}{\varepsilon_0} \tag{28.1}$$

Thus, the photon's electric field acts as surface charge. This property of a photon is essential because *charge arises from electromagnetic radiation in the creation of matter*. Furthermore, energy is proportional to the mass of matter as given by:

$$E = mc^2 \tag{28.2}$$

And, energy is proportional to angular frequency as given by Planck's equation,

$$E = \hbar\omega \tag{28.3}$$

It is shown in the Gravity section (Eq. (32.29)) that the de Broglie relationship can be derived from Planck's equation,

$$\lambda = \frac{h}{mv} \tag{28.4}$$

Matter and light obey the wave equation relationship,

$$v = \lambda \frac{\omega}{2\pi} \tag{28.5}$$

and Eqs. (28.2) through (28.4). Light and matter exist as atomic orbitals, as given in the Photon Equation section and the One-Electron Atom section, respectively.

The boundary condition for nonradiation by *a transition state atomic orbital* is:

$$2\pi(r_n^*) = 2\pi(nr_1^*) = n\lambda_1^* = \lambda_n^* \tag{28.6}$$

where r^* and λ^* are allowed radii and allowed wavelengths for the transition state matter in question, and n is a positive real number. A general relationship derived for the electron in the Pair Production section is that when $r = \alpha a_o$, v of Eq. (28.5) of a transition state atomic orbital equals the velocity of light in the inertial reference frame of the photon of angular frequency ω^* and energy $\hbar\omega^* = m_e c^2$ which forms the transition state atomic orbital of rest mass m_e. Substitution of Eq. (28.4) into Eq. (28.6) with $v = c$ and $r^* = \alpha a_0$ (See Spacetime Fourier Transform of the Electron Function and the Determination of Atomic Orbital Radii sections) gives the result that the radius of the transition state atomic orbital is the Compton wavelength bar, $\lambda\!\!\!^{-}_c$, which gives the general condition for particle production where:

$$r^*_{\alpha} = \alpha a_0 = \lambda\!\!\!^{-}_c = \frac{\hbar}{m_0 c} \tag{28.7}$$

With the substitution of Eq. (28.7) and the appropriate special relativistic corrections into the atomic orbital energy equations, the following energies, written in general form, are equal to:

$$E = \hbar\omega^* = m_0 c^2 = V \tag{28.8}$$

where V is the potential energy. In the case of an electron atomic orbital, the rest mass $m_0 = m_e$, the radius $r^*_{\alpha} = \alpha a_o$, and the electron and positron each experience an effective charge of:
$\alpha^{-1} e$.

$$V = \frac{\alpha^{-1} e^2}{4\pi\varepsilon_0 \alpha a_0} \tag{28.9}$$

This energy and mass are that of the transition state atomic orbital which can be considered to be created from the photon of angular frequency ω^*. Furthermore, the relativistic factor, γ,

$$\gamma = \frac{1}{\sqrt{1 - \left(\frac{v}{c}\right)^2}} \tag{28.10}$$

for the lab frame relative to the photon frame of the transition state atomic orbital of radius αa_0 is 2π where Eq. (28.10) is transformed from Cartesian coordinates to spherical coordinates[1]. (For example, the relativistic mass of the electron transition state atomic orbital of radius αa_0 is $2\pi m_e$. See the Special Relativistic Correction to the Ionization Energies section.) Using the relativistic mass, the Lorentz invariance of charge, and the radius of the transition state atomic orbital as αa_0, it is demonstrated in the Pair Production section that the electrical potential energy is equal to the energy stored in the magnetic field which gives the following equalities of energies written in general form where:

$$E = V = E_{mag} = \hbar\omega^* = m_0 c^2 \tag{28.11}$$

The energy stored in the electric and magnetic fields of any photon are equal, and equivalence of these energies occurs for an LC circuit excited at its resonance angular frequency,

$$\omega^* = \frac{1}{\sqrt{LC}} \tag{28.12}$$

where L is the inductance and C is the capacitance of the circuit. Spacetime is an LC circuit with resonance angular frequency

---

[1] For time harmonic motion, with angular velocity, ω, the relationship between the radius and the wavelength given Eq. (1.15) by is

$$2\pi r_n = \lambda_n$$

The de Broglie wave length is given by Eq. (1.38)

$$\lambda_n = \frac{h}{p_n} = \frac{h}{m_e v_n}$$

In the relativistically corrected case given by Eq. (1.16),

$$r_n = \lambda_n$$

Then from Eq. (1.38),

$$r_n = \lambda_n = \frac{h}{p_n} = \frac{h}{(2\pi m_e) v_n}$$

Thus, the relativistically corrected electron mass in the mass density is $2\pi m_e$. Alternatively, with the wavelength in the speed of light frame given by Eq. (1.16), the relativistic invariance of the angular momentum of the electron of $\hbar$ (Eq. (1.37)) gives the corresponding electron mass as $2\pi m_e$.

$$\omega^* = \frac{1}{\sqrt{LC}} = \frac{1}{\sqrt{\varepsilon_0 \mu_0 d^2}} = \frac{1}{\sqrt{\varepsilon_0 \mu_0 \lambda\!\!\!^{-2}_C}} \tag{28.13}$$

where d is the circuit dimensions. (This equation is derived in the Pair Production section.) For $d = \alpha a_o$, this frequency is equivalent to that of a photon of energy $m_e c^2$. When the resonance frequency of an LC circuit is excited, the impedance becomes infinite. Thus, spacetime is excited at its resonance frequency when a photon of angular frequency ω^* forms a transition state atomic orbital of mass-energy $m_e c^2$. At this event, the equivalence of all energies given previously provides that matter and energy are indistinguishable. (For the transition state atomic orbital, the potential energy corresponds to the stored electrical energy of an LC circuit, which in turn corresponds to the energy stored in the electric field of a photon.) The impedance for the propagation of electromagnetic radiation becomes infinite and a photon of energy $m_e c^2$ becomes a fundamental particle as the transition state atomic orbital becomes real. The energy of the photon is equal to the rest mass of the particle at zero potential energy. Therefore, in the case of charged particle production, a particle and an antiparticle each of mass $\frac{\hbar\omega^*}{c^2}$ are produced at infinity relative to the mutual central field of:

$$\mathbf{E} = \frac{+e}{4\pi\varepsilon_0 r^2} \tag{28.14}$$

And momentum is conserved by a third body, such as an atomic nucleus.

The boundary condition, Eq. (1.15) and Eq. (28.6), precludes the existence of the Fourier components of the current-density function of the atomic orbital that are synchronous with waves traveling at the speed of light. The nonradiative condition is Lorentz invariant because the velocity is perpendicular to the radius. However, the constancy of the speed of light must also hold which requires relativistic corrections to spacetime. The Schwarzschild metric gives the relationship whereby matter causes relativistic corrections to spacetime that determines the curvature of spacetime and is the origin of gravity. Thus, the creation of matter causes local spacetime to become curved. The geometry of spacetime is transformed from flat (Euclidean) to curved (Riemannian). Time and distances are distorted. At particle production, the proper time of the particle must equal the coordinate time given by Special Relativity for Riemannian geometry affected by the creation of matter of mass m_0 where the metric of spacetime is given by the Schwarzschild metric. This boundary condition determines the masses of the fundamental particles.

The gravitational radius, α_G or r_G, which arises from the solution of the Schwarzschild metric is defined as

$$\alpha_G = \frac{G m_0}{c^2} = r_G \tag{28.15}$$

where G is the gravitational constant. The radius of the transition state atomic orbital is:

$$r_\alpha^* = \lambda\!\!\!^{-}_c = \frac{\hbar}{m_0 c} \tag{28.16}$$

These radii are equal when the gravitational potential, E_{grav}, is:

$$E_{grav} = \frac{G m_0^2}{r_\alpha^*} = \frac{G m_0^2}{\lambda\!\!\!^{-}_c} = \hbar\omega^* = V = E_{mag} \tag{28.17}$$

These relationships represent the unification of the fundamental laws of the Universe, Maxwell's Equations, Newtonian Mechanics, Special and General Relativity, and the Planck equation and the de Broglie relationship where the latter two can be derived from Maxwell's Equations as demonstrated in the Gravity section.

Chapter 29

PAIR PRODUCTION

The conversion of energy into matter requires a transition state for which the identification of the entity as matter or energy is impossible. From the properties of the entity, as matter or energy, and from the physical laws and the properties of spacetime, the transition state hereafter called a transition state atomic orbital is derived. For example, a photon of energy 1.02 *MeV* in the presence of a third particle becomes a positron and an electron. This phenomenon, called pair production, involves the conservation of mass-energy, charge, and angular and linear momentum. Pair production occurs as an event in spacetime where all boundary conditions are met according to the physical laws: Maxwell's Equations, Newton's Laws, and Special and General Relativity, where matter and energy are indistinguishable by any physical property. Matter and photons exist as atomic orbitals; thus, the conversion of energy to matter must involve the atomic orbital equations derived in the previous sections. It must also depend on the equations of electromagnetic radiation and the properties of spacetime because matter is created from electromagnetic radiation as an event in spacetime.

Matter and light obey the wave equation relationship,

$$v = \lambda \frac{\omega}{2\pi} \tag{29.1}$$

The boundary condition for nonradiation by a transition state atomic orbital is:

$$2\pi(r_n^*) = 2\pi(nr_1^*) = n\lambda_1^* = \lambda_n^* \tag{29.2}$$

where r^* and λ^* are allowed radii and allowed wavelengths for the transition state matter in question, and n is a positive real number.

Consider the production of an electron and a positron providing a mutual central field. The relationship between the potential energy of an electron atomic orbital and the angular velocity of the atomic orbital is:

$$V = \hbar\omega* = \frac{1}{n}\frac{e^2}{4\pi\varepsilon_0 n a_0} \tag{29.3}$$

It can be demonstrated that the velocity of the electron atomic orbital satisfies the relationship for the velocity of a wave by substitution of Eqs. (1.15) and (1.36) into Eq. (29.1), which gives Eq. (1.35). Similarly, the relationship between c, the velocity of light in free space, and angular frequency, ω, and wavelength, λ, is:

$$c = \lambda \frac{\omega}{2\pi} \tag{29.4}$$

And, the energy of a photon of angular frequency, ω, is:

$$E = \hbar\omega \tag{29.5}$$

Recall from the Excited States of the One Electron (Quantization) section that a photon of discrete angular frequency, ω, can be trapped in the atomic orbital of an electron which serves as a resonator cavity of radius r_n where the resonance excitation energy of the cavity is given by Eq. (29.3).

As demonstrated in the Excited States of the One-Electron Atom (Quantization) section, with the inclusion of the contribution of the electron kinetic energy change, the change in the atomic orbital angular velocity is equal to the angular velocity of the resonant photon of the corresponding electron transition. For the initial conditions of an unbound electron at rest, the ratio of the linear velocity of the subsequently bound electron to the emitted free-space photon is given by Eq. (29.4).

$$\frac{v_n}{c_{photon}} = \frac{\lambda_n \frac{\omega_n}{2\pi}}{\lambda_{photon}\frac{\omega_{photon}}{2\pi}} = \frac{\lambda_n}{\lambda_{photon}} = \frac{\pi r_n}{r_{photon}} \tag{29.6}$$

where the n subscripts refer to atomic orbital quantities and the far-right-hand-side relationship follows from Eq. (2.2) and Eq. (4.12).

Consider a transition state electron atomic orbital, which is defined as the transition state between light and matter where light and matter are indistinguishable and the linearly propagating photon becomes a stationary spherical standing wave that only possesses light speed of rotation along field lines[1]. For this case, the velocity of the electron transition state atomic orbital is the speed of light in the inertial reference frame of the photon, which formed the transition state atomic orbital. The result of the substitution into Eq. (29.1) of c for v, of λ_n given by Eq. (2.2) where r_1 is given by Eq. (1.257) for λ, and of ω_n given by Eq. (1.36) for ω is:

$$c = 2\pi n a_0 \frac{\hbar}{m_e (n a_0)^2 2\pi} \tag{29.7}$$

Maxwell's Equations provide that

$$c = \sqrt{\frac{1}{\varepsilon_0 \mu_0}} \tag{29.8}$$

The result of substitution of Eqs. (1.256) and (29.8) into Eq. (29.7) is:

$$n^{-1} = \frac{m_e c a_0}{\hbar} = \frac{m_e}{\hbar\sqrt{\varepsilon_0 \mu_0}} \frac{4\pi\varepsilon_0 \hbar^2}{e^2 m_e} = 4\pi \sqrt{\frac{\varepsilon_0}{\mu_0}} \frac{\hbar}{e^2} = \alpha^{-1} \tag{29.9}$$

In fact, α is the fine structure constant (a dimensionless constant for pair production) [1]. The experimental value is 0.0072973506. Recently, alterations to the most up-to-date, self consistent set of the recommended values of the MKS basic constants and conversion factors of physics and chemistry resulting from the 1986 least-squares adjustment have been proposed [2]. Eq. (29.9), the equations of pair production given below, and the equations in the Unification of Spacetime, the Forces, Matter, and Energy section and Gravity section permit the derivation of a more accurate self-consistent set.

Continuing with the present MKS units, the radius of the transition state electron atomic orbital is αa_0, and the potential energy, V, is given by Eq. (29.3) where $n = \alpha$ where α arises from Gauss' law surface integral and the relativistic invariance of charge where:

$$V = \frac{-\alpha^{-2} e^2}{4\pi\varepsilon_0 a_0} \tag{29.10}$$

$$V = m_e c^2 \tag{29.11}$$

Furthermore, the result of the multiplication of both sides of Eq. (1.36) by $\hbar$, $r_n = n a_0$, and the substitution of $n = \alpha$ yields

$$\hbar\omega_\alpha^* = m_e c^2 \tag{29.12}$$

The relativistic factor,

$$\gamma = \frac{1}{\sqrt{1 - \left(\frac{v}{c}\right)^2}} \tag{29.13}$$

for an atomic orbital at radius r_α^* (αa_0 in the case of the electron) is 2π where Eq. (29.13) is transformed from Cartesian coordinates to spherical coordinates. (See the Special Relativistic Correction to the Ionization Energies section.) The energy stored in the magnetic field of the electron atomic orbital is:

$$E_{mag} = \frac{\pi\mu_0 e^2 \hbar^2}{(m_e)^2 r_n^3} \tag{29.14}$$

Eq. (29.15) is the result of the substitution of αa_0 for r_n, the relativistic mass, $2\pi m_e$, for m_e, and multiplication by the relativistic correction, α^{-1}, which arises from Gauss' law surface integral and the relativistic invariance of charge.

---

[1] The relationship between the angular frequency ω, radius r_{photon}, and speed c is

$$\omega r_{photon} = c \tag{1}$$

It follows from Eq. (1) that

$$\frac{2\pi}{T} r_{photon} = c \tag{2}$$

where T is the period of motion such that

$$2\pi r_{photon} = cT = \lambda \tag{3}$$

corresponding to a match with the particle radius and wavelength in the transition state.

$$E_{mag} = m_e c^2 \tag{29.15}$$

Thus, the energy stored in the magnetic field of the transition state electron atomic orbital equals the electrical potential energy of the transition state atomic orbital. The magnetic field is a relativistic effect of the electrical field; thus, equivalence of the potential and magnetic energies when $v = c$ is given by Special Relativity where these energies are calculated using Maxwell's Equations. The energy stored in the electric and magnetic fields of a photon are equivalent. The corresponding equivalent energies of the transition state atomic orbital are the electrical potential energy and the energy stored in the magnetic field of the atomic orbital.

Spacetime is an electrical LC circuit with an intrinsic impedance of exactly,

$$\eta = \sqrt{\frac{\mu_0}{\varepsilon_0}} = 376.730\ 519\ \Omega \tag{29.16}$$

The lab frame circumference of the transition state electron atomic orbital is $2\pi\alpha a_0$; whereas, the circumference for the $v = c$ inertial frame is αa_0. The relativistic factor for the radius of αa_0 is 2π as shown in the Spacetime Fourier Transform of the Electron Function section, the Relativistic Correction to the Ionization Energies section, and the Spin-Orbit Coupling section; thus, due to relativistic length contraction, the total capacitance of free space of the transition state atomic orbital of radius αa_0 is:

$$C = \frac{2\pi\alpha a_0 \varepsilon_0}{2\pi} = \varepsilon_0 \alpha a_0 \tag{29.17}$$

where ε_0 is the capacitance of spacetime per unit length (F / m). Similarly, the inductance is:

$$L = \frac{2\pi\alpha a_0 \mu_0}{2\pi} = \mu_0 \alpha a_0 \tag{29.18}$$

where μ_0 is the inductance per unit length (H / m).

Thus, the resonance angular frequency of a transition state electron atomic orbital is:

$$\omega^* = \frac{1}{\sqrt{LC}} = \frac{1}{\sqrt{\varepsilon_0 \alpha a_0 \mu_0 \alpha a_0}} \tag{29.19}$$

Thus,

$$\omega^* = \frac{m_e c^2}{\hbar} \tag{29.20}$$

Thus, the LC resonance frequency of free space for a transition state electron atomic orbital equals the frequency of the photon, which forms the transition state atomic orbital.

The impedance of any LC circuit goes to infinity when it is excited at the resonance frequency. Thus, the electron transition state atomic orbital is an LC circuit excited at the corresponding resonance frequency of free space. The impedance of free space becomes infinite, and electromagnetic radiation cannot propagate. At this event, the frequency, wavelength, velocity, and energy of the transition state atomic orbital equal that of the photon. The energy of the photon is equal to the rest mass-energy of the particle at zero potential energy, and charge is conserved. Therefore, a free electron and a free positron each of mass $\frac{\hbar\omega^*}{c^2}$ are produced at infinity relative to the mutual central field of:

$$\mathbf{E} = \frac{+e}{4\pi\varepsilon_0 r^2} \tag{29.21}$$

where all of the electron transition state atomic orbital equations developed herein apply to this central field. The equation of the free electron is given in the Electron in Free Space section. The transition state is equivalent to the equation of the photon given in the Photon Equation section. Photons superimpose; thus, pair production occurs with a single photon of energy equal to twice the rest mass of an electron. Linear momentum is conserved by a third body such as a nucleus which recoils in the opposite direction as the particle pair; thus, permitting pair production to occur.

For pair production, angular momentum is conserved. All photons carry $\pm\hbar$ of angular momentum, and the angular momentum of all matter as atomic orbitals is $\pm\hbar$; see Eq. (1.37). The radius of particle creation is αr_1^*. This radius is equal to $\lambda\!\!\!^{-}_c$, the Compton wavelength bar, where $\lambda\!\!\!^{-}_c = \frac{\hbar}{m_e c}$. It arises naturally from the boundary condition of no radiation, Eq. (1.15) and Eq. (29.2) where $n = \alpha$, the de Broglie relationship, Eq. (1.38), and that the velocity of the transition state atomic orbital equals c.

$$r_\alpha^* = \frac{\hbar}{m_e c} = \lambda\!\!\!^{-}_c \tag{29.22}$$

A schematic of the pair-production process of photon to transition state to free electron-positron pair is shown in Figure 29.1A-E. In addition, a free positron and electron may form a bound state with a radius of $2a_0$ called positronium that exists for a fraction of a second before decaying into two 510 keV photons in opposite directions. Positronium is discussed in the corresponding section.

Figure 29.1. Pair Production. (A) A linearly polarized photon of energy 1.02 MeV comprising the superposition of two oppositely circularly-polarized photons collides with a third body such as a proton. (B) The photon transforms into a transition state intermediate between matter and energy. (C) The photon forms a two-dimensional spherical shell of mass $2m_e$ with the same radius as the photon, the electron Compton-wavelength bar ($\lambda\!\!\!^{-}_c$). The shell comprises the superposition of the positron and the electron of opposite charges and each having $\hbar$ of total angular momentum. (D) The transition state ionizes. (E) Free particles propagate in different directions with linear momentum conserved.

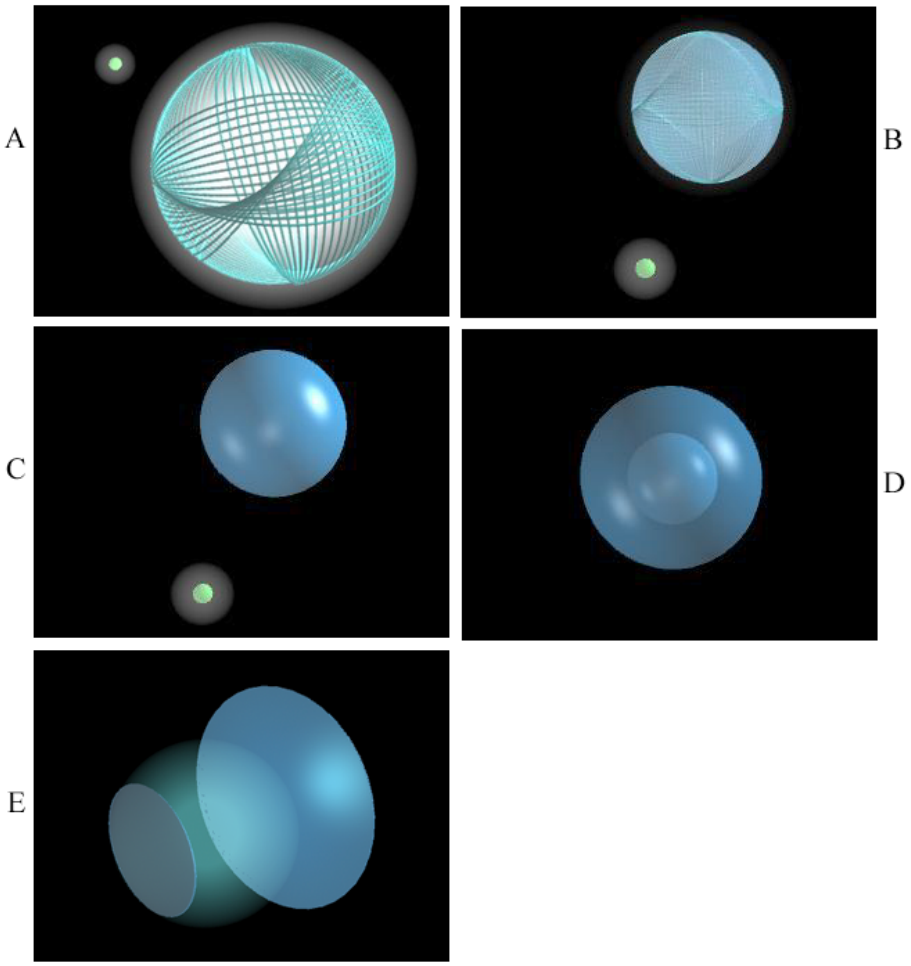

The equations derived for the electron in the present section are generally applicable to all fundamental particles, and it is shown in the Gravity section that the masses of the fundamental particles are determined by these equations and the curvature of spacetime by matter. During the creation of matter, the constancy of the speed of light must hold which requires relativistic corrections to spacetime. The Schwarzschild metric gives the relationship whereby matter causes relativistic corrections to spacetime that determines the curvature of spacetime and is the origin of gravity. Thus, the creation of matter causes local spacetime to become curved. The geometry of spacetime is transformed from flat (Euclidean) to curved (Riemannian). Time and distances are distorted. At particle production, the proper time of the particle must equal the coordinate time given by Special Relativity for Riemannian geometry affected by the creation of matter of mass m_0 (in the case of pair production, $m_0 = m_e$) where the metric of spacetime is given by the Schwarzschild metric. This boundary condition determines the masses of the fundamental particles.

REFERENCES

1. I. S. Hughes, *Elementary Particles*, Cambridge University Press, (1972), pp. 100-102.
2. B. Cohen, B. Taylor, “The fundamental physical constants”, Physics Today, August, (1991), BG 9-BG13.

Chapter 30

POSITRONIUM

Pair production, the creation of a positron/electron pair, occurs such that the radius of one atomic orbital has a radius infinitesimally greater than the radius of the antiparticle atomic orbital as discussed in the Pair Production section and the Leptons section. In addition, a free positron and electron may form a bound state with a radius of $2a_0$ called positronium that exists for a fraction of a second before decaying into two 510 keV photons in opposite directions. The sequence of events is shown in Figures 30.1 A-F.

As shown in Figures 30.1A-B, a minimum energy is obtained by the binding of a positron and an electron as concentric atomic orbitals at the same radius form a short-lived hydrogen-like atom wherein the electric fields mutually cancel and the $\hbar$ of angular momentum of each lepton is conserved. Before annihilation, positronium can exist with the electron and positron spins parallel or antiparallel called orthopositronium ($^3S_1$) and parapositronium ($^1S_0$), respectively. Due to the opposite charge of the positron, the magnetic moments are opposed to the spin orientations. The respective decay times are 1 ns and 1 μs. The splitting of the spectral lines due to spin orientations is called the hyperfine structure of positronium.

The forces of positronium are central, and the radius of the outer atomic orbital (electron or positron) is calculated as follows. The centrifugal force is given by Eq. (1.241). The centripetal electric force of the inner atomic orbital on the outer atomic orbital is given by Eq. (1.242). A second centripetal force is the relativistic corrected magnetic force, $\mathbf{F}_{mag}$, between each point of the particle and the antiparticle given by Eq. (1.252) with m_e substituted for m. The force balance equation is given by Eq. (1.253) with m_e substituted for m. The balance between the centrifugal and electric and magnetic forces is given in the Excited States of the One-Electron Atom (Quantization) section and the Excited States of Helium section:

$$\frac{m_e v^2}{r_1} = \frac{\hbar^2}{m_e r_1^3} = \frac{e^2}{4\pi\varepsilon_0 r_1^2} - \frac{\hbar^2}{m_e r_1^3} \tag{30.1}$$

$$r_1 = \frac{4\pi\varepsilon_0 \hbar^2}{e^2 \mu} \tag{30.2}$$

where $r_1 = r_2$ is the radius of the positron and the electron and where the reduced mass , μ, is:

$$\mu = \frac{m_e}{2} \tag{30.3}$$

The Bohr radius given by:

$$a_0 = \frac{4\pi\varepsilon_0 \hbar^2}{e^2 m_e} \tag{30.4}$$

and Eq. (30.3) is substituted into Eq. (30.2) to give the ground-state radius of positronium:

$$r_1 = 2a_0 \tag{30.5}$$

Figure 30.1. Formation and Annihilation of Positronium. (A) A free positron and electron are mutually attracted by the Coulombic force. (B) A positron and an electron form a bound state called positronium that exists as a two-dimensional spherical shell of mass $2m_e$ with a radius of $2a_0$. The particle provides the central force for the antiparticle. The shell comprises the superposition of the positron and the electron of opposite charges and each having $\hbar$ of total angular momentum. Transitions between ortho and para magnetic states may occur. (C) The pair transforms into a transition state intermediate between matter and energy. (D-F) The annihilation is complete as two oppositely circularly-polarized photons each of 510 keV and having a radius of twice the electron Compton-wavelength bar ($\lambda\!\!\!^{-}_C$) (not to scale) propagate in opposite directions.

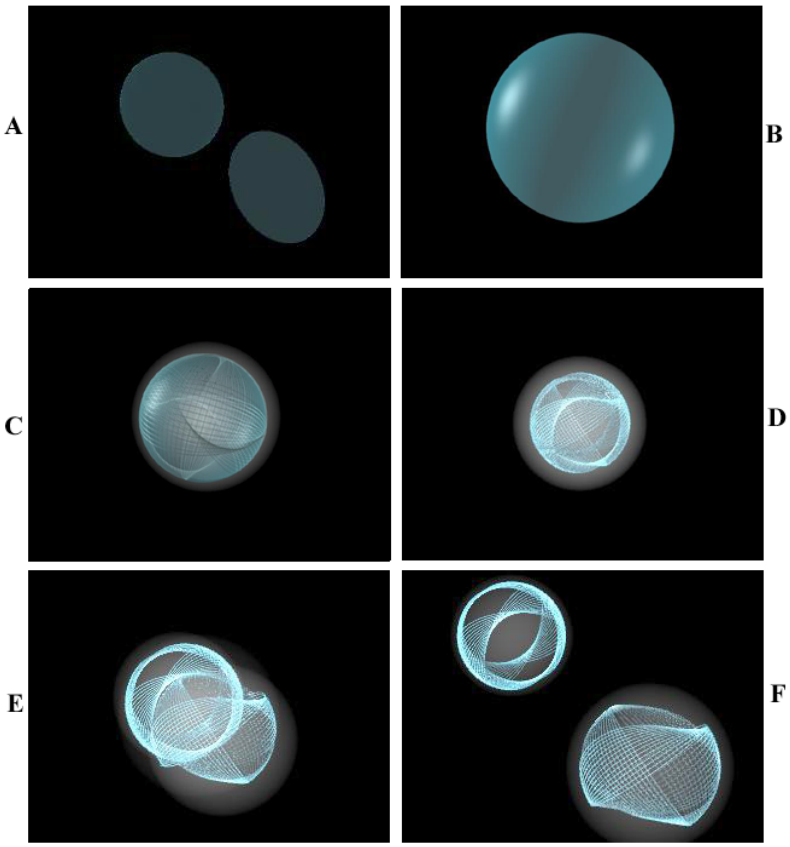

EXCITED STATE ENERGIES

The potential energy V between the particle and the antiparticle having the radius r_1 given by Eq. (1.261) is:

$$V = \frac{-e^2}{4\pi\varepsilon_0 r_1} = \frac{-Z^2e^2}{8\pi\varepsilon_0 a_0} = -2.18375\ X\ 10^{-18}\ J = -13.59\ eV \tag{30.6}$$

The calculated ionization energy is $\frac{1}{2}V$ (Eqs. (1.262-1.264)) which is:

$$E_{ele} = 6.795\ eV \tag{30.7}$$

The experimental ionization energy is $6.795\ eV$.

Parapositronium, a singlet state hydrogen-like atom comprising an electron and a positron, can absorb a photon which excites the atom to the first triplet state, orthopositronium. In parapositronium, the electron and positron angular momentum vectors are antiparallel; whereas, the magnetic moment vectors are parallel. The opposite relationships exist for orthopositronium. The balance between the centrifugal and electric and magnetic forces is:

$$\frac{m_e v^2}{r_n} = \frac{\hbar^2}{m_e r_n^3} = \frac{1}{n}\frac{e^2}{4\pi\varepsilon_0 r_n^2} - \frac{\hbar^2}{m_e r_n^3} \tag{30.8}$$

$$r_n = n2a_0 \tag{30.9}$$

where n is an integer and both electrons are at the same excited state radius of $r_n = n2a_0$. The principal energy levels for the singlet excited states are given by Eq. (2.22) and Eq. (9.12) with the electron reduced mass (Eq. (30.3)) substituted for the mass of the electron where

$$E_n = \frac{1}{n}\frac{e^2\mu}{8\pi\varepsilon_0 r_n} = \frac{1}{n}\frac{e^2\mu}{8\pi\varepsilon_0 n a_0} = \frac{6.795}{n^2}\ eV \tag{30.10}$$

The levels given by Eq. (30.10) match the experimental energy levels.

HYPERFINE STRUCTURE

As shown in the Atomic Orbital Equation of Motion For $\ell = 0$ Based on the Current Vector Field (CVF) section, the angular momentum of the electron or positron atomic orbital in a magnetic field comprises the initial $\frac{\hbar}{2}$ projection on the z-axis and the initial $\frac{\hbar}{4}$ vector component in the xy-plane that precesses about the z-axis. As further shown in the Magnetic Parameters of the Electron (Bohr Magneton) section, a resonant excitation of the Larmor precession frequency gives rise to an additional component of angular momentum which is consistent with Maxwell's equations. As shown in the Excited States of the One-Electron Atom (Quantization) section, conservation of the $\hbar$ of angular momentum of a trapped photon can give rise to $\hbar$ of electron angular momentum along the $\mathbf{S}$-axis. The photon standing waves of excited states are spherical harmonic functions which satisfy Laplace's equation in spherical coordinates and provide the force balance for the corresponding charge (mass)-density waves. Consider the photon in the case of the precessing electron with a Bohr magneton of magnetic moment along the $\mathbf{S}$-axis. The radius of the atomic orbital is unchanged, and the photon gives rise to current on the surface that satisfies the condition:

$$\nabla \cdot J = 0 \tag{30.11}$$

corresponding to a rotating spherical harmonic dipole [1] that phase-matches the current (mass) density of Eq. (1.144). Thus, the electrostatic energy is constant, and only the magnetic energy need be considered as given by Eqs. (30.14-30.15). The corresponding central field at the atomic orbital surface given by the superposition of the central field of the lepton and that of the photon follows from Eqs. (2.10-2.17) and Eq. (17) of Box 1.1:

$$\mathbf{E} = \frac{e}{4\pi\varepsilon_0 r^2}\left[Y_0^0(\theta,\phi)\mathbf{i}_\mathbf{r} + \mathrm{Re}\left\{Y_\ell^m(\theta,\phi)e^{i\omega_n t}\right\}\mathbf{i}_\mathbf{y}\delta(r-r_1)\right] \tag{30.12}$$

where the spherical harmonic dipole $Y_\ell^m(\theta,\phi) = \sin\theta$ is with respect to the $\mathbf{S}$-axis. The dipole spins about the $\mathbf{S}$-axis at the angular velocity given by Eq. (1.36). The resulting current is nonradiative as shown in Appendix I: Nonradiation Condition. Thus, the field in the RF rotating frame is magnetostatic, as shown in Figures 1.28 and 1.29, but directed along the $\mathbf{S}$-axis.

The application of a magnetic field with a resonant Larmor excitation gives rise to a precessing angular momentum vector $\mathbf{S}$ of magnitude $\hbar$ directed from the origin of the atomic orbital at an angle of $\theta = \frac{\pi}{3}$ relative to the applied magnetic field. $\mathbf{S}$ rotates about the axis of the applied field at the Larmor frequency. The magnitude of the components of $\mathbf{S}$ that are parallel and orthogonal to the applied field (Eqs (1.129-1.130)) are $\frac{\hbar}{2}$ and $\sqrt{\frac{3}{4}}\hbar$, respectively. Since both the RF field and the orthogonal components shown in Figure 1.25 rotate at the Larmor frequency, the RF field that causes a Stern Gerlach transition produces a stationary magnetic field with respect to these components as described by Patz [2].

The component of Eq. (1.130) adds to the initial $\frac{\hbar}{2}$ parallel component to give a total of $\hbar$ in the stationary frame corresponding to a Bohr magneton, μ_B, of magnetic moment. The potential energy of a magnetic moment $\mathbf{m}$ in the presence of flux $\mathbf{B}$ [3] is:

$$E = \mathbf{m} \cdot \mathbf{B} \tag{30.13}$$

The angular momentum of the electron gives rise to a magnetic moment of μ_B. Thus, the energy ΔE_{mag}^{spin} to switch from parallel to antiparallel to the field is given by Eq. (1.168) :

$$\Delta E_{mag}^{spin} = 2\mu_\mathbf{B}\,\mathbf{i}_\mathbf{z} \cdot \mathbf{B} = 2\mu_B B\cos\theta = 2\mu_B B \tag{30.14}$$

ΔE_{mag}^{spin} is also given by Planck's equation. It can be shown from conservation of angular momentum considerations (Eqs. (26-32) of Box 1.1) that the Zeeman splitting is given by Planck's equation and the Larmor frequency based on the gyromagnetic ratio (Eq. (2) of Box 1.1). The electron's magnetic moment may only be parallel or antiparallel to the magnetic field rather than at a continuum of angles including perpendicular according to Eq. (30.13). No continuum of energies predicted by Eq. (30.13) for a pure magnetic dipole is possible. The energy difference for the magnetic moment to flip from parallel to antiparallel to the applied field is:

$$\Delta E_{mag}^{spin} = 2\hbar\omega_L \tag{30.15}$$

corresponding to magnetic dipole radiation wherein ω_L is the Larmor angular frequency.

Eq. (30.13) implies a continuum of energies; whereas, Eq. (29) of Box 1.1 shows that the static-kinetic and dynamic vector potential components of the angular momentum are quantized at $\frac{\hbar}{2}$. Consequently, as shown in the Electron g Factor section, the flux linked during a spin transition is quantized as the magnetic flux quantum:

$$\Phi_0 = \frac{h}{2e} \tag{30.16}$$

Only the states corresponding to:

$$m_s = \pm\frac{1}{2} \tag{30.17}$$

are possible due to conservation of angular momentum. It is further shown using the Poynting power vector with the requirement that flux is linked in units of the magnetic flux quantum, that the factor 2 of Eqs. (30.14) and (30.15) is replaced by the electron g factor. From Eqs. (1.226-1.227), the energy ΔE_{mag}^{spin} to flip the electron's magnetic moment from parallel to antiparallel to the applied field is:

$$\Delta E_{mag}^{spin} = 2\left(1+\frac{\alpha}{2\pi}+\frac{2}{3}\alpha^2\left(\frac{\alpha}{2\pi}\right)-\frac{4}{3}\left(\frac{\alpha}{2\pi}\right)^2\right)\mu_B B \tag{30.18}$$

$$\Delta E_{mag}^{spin} = g\,\mu_B B \tag{30.19}$$

The spin-flip transition can be considered as involving a magnetic moment of g times that of a Bohr magneton. The calculated value of $\frac{g}{2}$ is $1.001\ 159\ 652\ 137$. The experimental value [4] of $\frac{g}{2}$ is $1.001\ 159\ 652\ 188(4)$.

Positronium undergoes a Stern-Gerlach transition. The energy of the transition from orthopositronium ($^3S_1$) to parapositronium ($^1S_0$) is the hyperfine structure interval. The angular momentum of the photon given by $\mathbf{m} = \int \frac{1}{8\pi c}\mathrm{Re}\left[\mathbf{r}\times(\mathbf{E}\times\mathbf{B}^*)\right]dx^4 = \hbar$ in the Photon section is conserved [5] for the solutions for the resonant photons and hyperfine-state lepton functions as shown for the cases of one-electron atoms and helium in the Excited States of the One-Electron Atom (Quantization) section and the Excited States of Helium section, respectively. To conserve the $\hbar$ of angular momentum of each lepton and the photon, orthopositronium possesses orbital angular momentum states corresponding to $m_\ell = 0, \pm 1$; whereas, parapositronium possesses orbital angular momentum states corresponding to the quantum number $m_\ell = 0$. The orbital angular momentum states of orthopositronium are degenerate in the absence of an applied magnetic field. As in the case of the electron Stern-Gerlach transition, the radius of both leptons remains at the same radius of $r = 2a_0$ given by Eq. (30.5).

The hyperfine structure interval of positronium can be calculated from the spin-spin and spin-orbit coupling energies of the $^3S_1 \rightarrow {}^1S_0$ transition using the procedure given in the Two-Electron Atoms section and Appendix VI. The vector projection of the atomic orbital angular momentum on the z-axis is $\mathbf{L}_z = \frac{\hbar}{2}$ (Eq. (1.128)) with an orthogonal component of $\mathbf{L}_{xy} = \frac{\hbar}{4}$ (Eq. (1.127)). The magnetic flux, $\mathbf{B}$, of the electron (positron) at the positron (electron) due to $\mathbf{L}_z$ after McQuarrie [3] (Eqs. (2.183) and (7.6)) is:

$$\mathbf{B} = \frac{\mu_0 e\hbar}{2m_e r^3} \tag{30.20}$$

where μ_0 is the permeability of free-space ($4\pi\ X\ 10^{-7}\ N/A^2$). The spin-spin coupling energy $\Delta E_{\text{spin-spin}}$ between the inner atomic orbital and the outer atomic orbital is given by Eq. (1.227) where μ_B, the magnetic moment of the outer atomic orbital is given by Eq. (1.169). Substitution of Eqs. (1.169) and (30.20) into Eq. (30.19) gives:

$$\Delta E_{\text{spin-spin}} = \frac{1}{2}\frac{g\mu_0 e^2\hbar^2}{4m_e^2 r_1^3} = \frac{g\mu_0 e^2\hbar^2}{8m_e^2\left(2a_0\right)^3} = \frac{1}{8\pi\alpha}\frac{g\alpha^5\left(2\pi\right)^2}{8}m_e c^2 \tag{30.21}$$

where the factor of $1/2$ arises from Eq. (30.13) with the presence of the magnetic flux only for the $^1S_0$ state, the radius is given by Eq. (30.5), and Eqs. (2.183-2.194) were used to convert Eq. (30.21) to the electron mass-energy form of Eq. (30.22).

In the case of atomic hydrogen with $n = 2$, the radius given by Eq. (2.2) is $r = 2a_0$, and the predicted energy difference

between the $^2P_{3/2}$ and $^2P_{1/2}$ levels of the hydrogen atom, $E_{s/o}$, is:

$$E_{s/o} = \frac{\alpha^5 (2\pi)^2}{8} m_e c^2 \sqrt{\frac{3}{4}} \tag{30.22}$$

In the case of the hyperfine transition of positronium, the spin-orbit coupling energy $\Delta E_{s/o}(^3S_1 \rightarrow {}^1S_0)$ having $r = 2a_0$ is given by Eq. (2.194) with the requirement that the flux from the partner lepton is linked in units of the magnetic flux quantum corresponding to the anomalous g factor (Eqs. (30.18-30.19)), the source current given by Eq. (30.12) gives rise to a factor of $3/2$, and each lepton contributes to the energy:

$$\Delta E_{s/o}(^3S_1 \rightarrow {}^1S_0) = 2\frac{3}{2}\frac{g\alpha^5 (2\pi)^2}{8} m_e c^2 \sqrt{\frac{3}{4}} \tag{30.23}$$

The hyperfine structure interval of positronium ($^3S_1 \rightarrow {}^1S_0$) is given by the sum of Eqs. (30.21) and (30.23).

$$\begin{aligned}
\Delta E_{\text{Ps hyperfine}} &= \Delta E_{\text{spin-spin}} + \Delta E_{s/o}(^3S_1 \rightarrow {}^1S_0) \\
&= \frac{g\mu_0 e^2 \hbar^2}{8m_e^2 (2a_0)^3} + \frac{3g\alpha^5 (2\pi)^2}{8} m_e c^2 \sqrt{\frac{3}{4}} \\
&= \frac{g\alpha^5 (2\pi)^2}{8} m_e c^2 \left(\frac{1}{8\pi\alpha} + \frac{3\sqrt{3}}{2} \right) \\
&= 8.41155110\ X\ 10^{-4}\ eV
\end{aligned} \tag{30.24}$$

Using Planck's equation (Eq. (2.148)), the interval in frequency, $\Delta\upsilon$, is:

$$\Delta\upsilon = 203.39041\ GHz \tag{30.25}$$

The experimental ground-state hyperfine structure interval [6] is:

$$\begin{aligned}
&\Delta E_{\text{Ps hyperfine}}(\text{experimental}) = 8.41143\ X\ 10^{-4}\ eV \\
&\Delta\upsilon(\text{experimental}) = 203.38910(74)\ GHz\ \ (3.6\,ppm)
\end{aligned} \tag{30.26}$$

There is remarkable (six significant figure) agreement between the calculated and experimental values of $\Delta\upsilon$ that is only limited by the accuracy of the fundamental constants [7].

REFERENCES

1. J. D. Jackson, *Classical Electrodynamics*, Second Edition, John Wiley & Sons, New York, (1975), pp. 84-102; 752-763.
2. S. Patz, Cardiovasc Interven Radiol, (1986), 8:25, pp. 225-237.
3. D. A. McQuarrie, *Quantum Chemistry*, University Science Books, Mill Valley, CA, (1983), pp. 238-241.
4. R. S. Van Dyck, Jr., P. Schwinberg, H. Dehmelt, "New high precision comparison of electron and positron g factors," Phys. Rev. Lett., Vol. 59, (1987), p. 26-29.
5. J. D. Jackson, *Classical Electrodynamics*, Second Edition, John Wiley & Sons, New York, (1975), pp. 739-779.
6. M. W. Ritter, P. O. Egan, V. W. Hughes, K. A. Woodle, "Precision determination of the hyperfine structure interval in the ground state of positronium. V," Phys. Rev. A, Vol. 30, No. 3, (1984), pp. 1331-1338.
7. P. J. Mohr, B. N. Taylor, "CODATA recommended values of the fundamental physical constants: 2002," Reviews of Modern Physics, Vol. 77, No. 1, (2005), pp. 1-107.

Chapter 31

RELATIVITY

BASIS OF A THEORY OF RELATIVITY[1]

To describe any phenomenon such as the motion of a body or the propagation of light, a definite frame of reference is required. A frame is a certain base consisting of a defined origin and three axes equipped with graduated rulers and clocks. Bodies in motion then have definite positions and definite motions with respect to the base. The motion of planets is commonly described in the heliocentric system. The origin is defined as the mass center, and the three axes are chosen to point to three fixed stars to establish the fixed orientation of the axes. In general, the mathematical form of the laws of nature will be different in different frames. For example, the motion of bodies relative to the Earth may be described either in a frame with axes pointing to three fixed stars or in one rigidly fixed to the Earth. In the latter case, Coriolis forces arise in the equations of motion. There exist frames of reference in which the equations of motion have a particular simple form; in a certain sense these are the most "natural" frames of reference. They are the *inertial* frames in which the motion of a body is uniform and rectilinear, provided no forces act on it[2]. In pre-relativistic physics the notion of an inertial system was related only to the laws of mechanics. Newton's first law of motion is, in fact, nothing but a definition of an inertial frame. Similarly, Newton's second law gives the relationship of a force acting on a mass and its acceleration relative to a certain frame of reference. Newton introduced the concept of absolute space to provide an absolute frame for acceleration and rotation as well as uniform motion. According to Newton, acceleration and rotation relative to absolute space are detected by simple experiments. But, it was believed that there is no such means to identify an absolute frame for uniform motion[3].

The relativity principle is postulated on the basis of the impossibility of measuring absolute velocity. This assumption is incorrect. Absolute space can be defined based on the solution of the exact conserved relationships between matter, energy, and spacetime given in the Equivalence of Inertial and Gravitational Masses Due to Absolute Space and Absolute Light Velocity section. Specifically, the production of an isolated particle from a photon of identically the production energy defines the absolute inertial frame at rest for the particle and could, in principle, define absolute space that conserves the energy inventory of the Universe and resolves paradoxes such as the twin paradox [1-2]. But, even though any motion, or parameter of inertia or electromagnetism can ultimately be measured in principle (but perhaps not always in practice) relative to absolute space, a principle of relativity based on physical laws can be derived that has great utility. The principle of relativity given next treats relative motion, and the transforms of relativity are Lorentzian.

Since the constant speed of light is the absolute limiting conversion factor from time to length, it is reasonable to expect that the laws of light propagation play a fundamental part in the definition of the basic concepts relating to space and time in terms of inertial frames defined according to uniform relative motion. Therefore it proves more correct to relate the notion of an inertial frame not only to the laws of mechanics but also to those of light propagation.

The usual form of Maxwell's equations refers to some inertial frame. It is obvious and has always been assumed, even before relativity, that at least one reference frame exists that is inertial with respect to mechanics and in which at the same time Maxwell's equations are true. The law of propagation of an electromagnetic wave front in the form:

---

[1] A good reference for the historical concepts of the theory of special relativity, which are partially included herein, is Fock [3].

[2] Regarding the consequences of the motion such as time dilation, mass increase, and length contraction while maintaining energy conservation, the constitution of an inertial frame as a frame of reference possessing constant relative rectilinear velocity and absence of forces is generalized to one possessing constant relative speed and force balance as discussed in the Equivalence of Inertial and Gravitational Masses Due to Absolute Space and Absolute Light Velocity section. This generalization, supported by experimental data [4-5], is applied in the Special Relativistic Effect on the Electron Radius and the Relativistic Ionization Energies section.

[3] Even relative uniform motion is an approximation since it is impossible for any two objects to maintain an exact (infinite precision) relative velocity even for a brief time. Inherently, there are always deviations, and acceleration or deceleration is always present even at very short time scales of measurement.

$$\frac{1}{c^2}\left(\frac{\partial^2\omega}{\partial t^2}\right)-\left[\left(\frac{\partial^2\omega}{\partial x^2}\right)+\left(\frac{\partial^2\omega}{\partial y^2}\right)+\left(\frac{\partial^2\omega}{\partial z^2}\right)\right]=0 \tag{31.1}$$

also refers to this inertial frame. A frame for which Eq. (31.1) is valid may be called inertial in the electromagnetic sense. A frame that is inertial both in the mechanical and in the electromagnetic senses will be simply called inertial.

Thus, by the definition we have adopted, an inertial frame is characterized by the following two properties:

1. In an inertial frame, a body moves uniformly and in a straight line, provided no forces act on it. (The usual mechanical inertial property.)

2. In an inertial frame, the equation of propagation of an electromagnetic wave front has the form Eq. (31.1). (The inertial property for the field.)

Eq. (31.1) applies not only to the propagation of an electromagnetic wave. The electromagnetic field has no preference over other fields. The maximum speed of propagation of all fields must be the same such that Eq. (31.1) is of universal validity.

The fundamental postulate of the theory of relativity, also called the principle of relativity, asserts that phenomena occurring in a closed system are independent of any non-accelerated motion of the system as a whole. The principle of relativity asserts that the two sequences of events will be exactly the same (at least insofar as they are determined at all). If a process in the original systems can be described in terms of certain functions of the space and time coordinates of the first frame, the same functions of the space and time coordinates of the second frame will describe a process occurring in the copy. *The uniform rectilinear motion of a material system as a whole has no influence on the course of any process occurring within it*.

The theory of relativity is based on two postulates, namely, the principle of relativity and another principle that states that the velocity of light is independent of the velocity of its source. The latter principle is a consequence of the first. The latter principle is implicit in the law of the propagation of an electromagnetic wave front given by Eq. (31.1). The basis for defining inertial reference frames is Eq. (31.1) together with the fact of the uniform rectilinear motion of a body not subject to forces. The principle of relativity holds in the case that the reference frames are inertial.

It is appropriate to give a generalized interpretation of the law of wave front propagation and to formulate the following general postulate:

There exists a maximum speed for the propagation of any kind of action—the speed of light in free space.

This principle is very significant because the transmission of signals with greatest possible speed plays a fundamental part in the definition of concepts concerning space and time. The very notion of a definite frame of reference for describing events in space and time depends on the existence of such signals. The principle formulated above, by asserting the existence of a general upper limit for all kinds of action and signal, endows the speed of light with a universal significance, independent of the particular properties of the agency of transmission and reflecting a certain objective property of spacetime. This principle has a logical connection with the principle of relativity. For if there was no single limiting velocity but instead different agents, e.g. light and gravitation, propagated in vacuum with different speeds, then the principle of relativity would necessarily be violated as regards at least one of the agents. The principle of the universal limiting velocity can be made mathematically precise as follows:

For any kind of wave advancing with limiting velocity and capable of transmitting signals, the equation of front propagation is the same as the equation for the front of a light wave.

Thus, the equation:

$$\frac{1}{c^2}\left(\frac{\partial^2\omega}{\partial t^2}\right)-\left(grad^2\omega\right)=0 \tag{31.2}$$

acquires a general character; it is more general than Maxwell's equations from which Maxwell originally derived it. As a consequence of the principle of the existence of a universal limiting velocity one can assert the following: the differential equations describing any field that is capable of transmitting signals must be of such a kind that the equation of their characteristics is the same as the equation for the characteristics of light waves. In addition to governing the propagation of any form of energy, the wave equation governs fundamental particles created from energy and vice versa, the associated effects of mass on spacetime, and the evolution of the Universe itself. The equation that describes the electron rotational energy and angular momentum given by Eqs. (1.56-1.65) is the wave equation, the relativistic correction of spacetime due to particle production travels according to the wave equation as given in the Gravity section, and the evolution of the Universe is according to the wave equation as given in the Gravity section and the Unification of Spacetime, the Forces, Matter, and Energy section (Eqs. (33.45-33.36)).

The presence of a gravitational field somewhat alters the appearance of the equation of the characteristics from the form of Eq. (31.2), but in this case one and the same equation still governs the propagation of all kinds of wave fronts traveling with limiting velocity, including electromagnetic and gravitational ones. The basis for defining inertial reference frames is Eq. (31.2) asserting the universality of the equation together with the fact of the uniform rectilinear motion of a body not subject to forces.

Let one and the same phenomenon be described in two inertial frames of reference. The question arises of relating measurements in one frame to those in another. For example, consider transforming radar data obtained by a satellite circling the Earth to that recorded on the ground. For such a transformation, the relationship between the space and time coordinates x, y, z and t in the first frame and the corresponding x', y', z' and t' in the second. Before relativity one accepted as self-evident the existence of a universal time t that was the same for all frames. In this case $t' = t$ or $t' = t - t_0$, if a change of time origin was used. Considering two events occurring at t' and τ, the old point of view required the time elapsed between them to be the same in all reference frames so that:

$$t - \tau = t' - \tau' \tag{31.3}$$

Furthermore, it was considered to be evident that the length of a rigid rod, measured in the two frames, would have the same value. (This applies equally to the distance between the "simultaneous" positions of two points that need not necessarily be rigidly connected.) Denoting the spatial coordinates of the two ends of the rod (or the two points) by (x, y, z) and (ξ, η, ζ) in the one frame and by (x', y', z') and (ξ', η', ζ') in the other, the old theory required:

$$(x-\xi)^2 + (y-\eta)^2 + (z-\zeta)^2 = (x'-\xi')^2 + (y'-\eta')^2 + (z'-\zeta')^2 \tag{31.4}$$

Eqs. (31.3) and (31.4) determine uniquely the general form of the transformation connecting x, y, z and t with x', y', z' and t'. It consists of a change in origin of spatial coordinates and of time, of a rotation of the spherical axes, and of a transformation such as:

$$\begin{aligned} x' &= x - V_x t \\ y' &= y - V_y t \\ z' &= z - V_z t \\ t' &= t \end{aligned} \tag{31.5}$$

where V_x, V_x, and V_x are the constants of velocity with which the primed frame moves relative to the unprimed one; more exactly they are the components of this velocity in the unprimed frame. The transformation (Eq. (31.5)) is known as a Galileo transformation. Thus, pre-relativistic physics asserted that, given an inertial frame (x, y, z), space and time coordinates in any other frame moving uniformly and rectilinearly relative to the former are connected by a Galileo transformation, apart from a displacement of the origin.

Galileo transformations satisfy the principle of relativity as far as the laws of (Newtonian) mechanics are concerned, but not in relation to the propagation of light. Indeed the wave front equation changes its appearance when subjected to a Galileo transformation. If Galileo transformations were valid and the Principle of Relativity in its generalized form was not, then there would exist only one inertial system as defined above. The changed form of the wave front equation in any other frame would allow one to detect even uniform rectilinear motion relative to the single inertial system—the "immobile ether"—and to determine the velocity of this motion. Experiments devised to discover such motion relative to the "ether" have unquestionably eliminated the "ether" as a possibility and confirm that the form of the law of wave front propagation is the same in all non-accelerated frames[4]. Therefore the principle of relativity is certainly also applicable to electromagnetic phenomena. It also follows that the Galileo transformation is in general wrong and should be replaced by another. The problem can be stated as follows. Let a reference frame be given which is inertial according to the definition given above (i.e. both mechanically and electromagnetically). The space time coordinates in this frame are given by x, y, z and t. Let the space time coordinates in another inertial frame be given by (x', y', z', t'). The connection between (x, y, z, t) and (x', y', z', t') is to be found. The problem of finding a transformation between two inertial frames is purely mathematical; it can be solved without any further physical assumptions other than the definition of an inertial frame given above. The transformations are given by Lorentz.

[4] The most famous of such experiments is the Michelson-Morley experiment. In 1887 in collaboration with Edward Morley, Albert Michelson performed an experiment to measure the motion of the Earth through the "ether," a hypothetical medium pervading the Universe in which light waves propagated. The notion of the ether was carried over from the days before light waves were recognized as electromagnetic. At that time, the physics community was unwilling to discard the idea that light propagates relative to some universal frame of reference. The extremely sensitive Michelson-Morley experiment could find no motion through an ether, which meant that there could be no ether and no principle of "absolute motion" relative to it. All motion is relative to a specific frame of reference, not a universal one. The experiment which in essence compared the speeds of light parallel to and perpendicular to the Earth's motion around the Sun, also showed that the speed of light is the same for all observers. This is not true in the case of waves that need a material medium in which to occur such as sound and water waves. The experimental results of the Michelson-Morley experiment as well as those of Fizeau comprised the basis of a theory proposed in 1904 by Poincaré [6-8] that stated the impossibility of an absolute reference frame and that the speed of light is a constant maximum for all observers. Thus, the Michelson-Morley experiment set the stage for the special theory of relativity as Michelson was reluctant to accept this result.

LORENTZ TRANSFORMATIONS

A Lorentz transformation is a set of equations for transforming the space and time coordinates in one inertial frame into those of another that moves uniformly and in a straight line relative to the first. The transformation can be characterized by the fact that the quantity,

$$ds^2 = dx_0^2 - \left(dx_1^2 + dx_2^2 + dx_3^2\right) \tag{31.6}$$

or

$$ds^2 = c^2dt^2 - \left(dx^2 + dy^2 + dz^2\right) \tag{31.7}$$

remains invariant in the strict sense (not only the numerical value, but also the mathematical form of the expression remain unchanged). Newtonian mechanics is corrected by Lorentz transformations of the time, length, mass, momentum, and energy of an object. Newtonian mechanics with Galileo transforms give mechanical forces for $v << c$:

$$\mathbf{F} = \frac{d\mathbf{p}}{dt} = \frac{d(m\mathbf{v})}{dt} = m\frac{d\mathbf{v}}{dt} = m\mathbf{a} \tag{31.8}$$

$$T = \frac{1}{2}mv^2 \tag{31.9}$$

In the case that v approaches c, Lorentz transforms apply.

TIME DILATION

THE RELATIVITY OF TIME

The postulates of relativity may be used to derive the Lorentz transformation that described how relative motion affects measurements of time intervals.

A clock that moves with respect to an observer appears to tick less rapidly than it does when at rest with respect to him. That is, if someone in a spacecraft finds that the time interval between two events in the spacecraft is t_0, we on the ground would find that the same interval has the longer duration t. The quantity t_0, which is determined by events that occur *at the same place* in a observer's frame of reference, is called the *proper time* of the interval between the events. When witnessed from the ground, the events that mark the beginning and end of the time interval occur at different places, and as a consequence the duration of the interval appears longer than the proper time. This effect is called time dilation (to dilate is to become larger).

To see how time dilation comes about, let us consider two clocks of the particularly simple kind shown in Figure 31.1.

Figure 31.1. A simple clock. Each "tick" corresponds to a round trip of the light pulse from the lower mirror to the upper one and back.

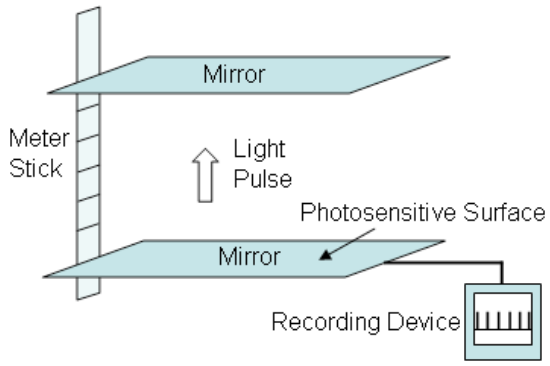

Such a clock consists of a stick L_0 long with a mirror at each end. A pulse of light is reflected up and down between the mirrors, and a device attached to one of them produces a "tick" of some kind each time the light pulse strikes it. Such a device might be a photosensitive coating on the mirror that gives an electric signal when the pulse arrives.

One clock is at rest in a laboratory on the ground and the other is in a spacecraft that moves at the velocity v relative to the ground. An observer in the laboratory watches both clocks and finds that they tick at different rates.

Figure 31.2 shows the laboratory clock in operation. The time interval between ticks is the proper time t_0. The time needed for the light pulse to travel between the mirrors at the speed of light, c, is $\frac{t_0}{2}$; hence $\frac{t_0}{2} = \frac{L_0}{c}$ and

$$t_0 = \frac{2L_0}{c} \tag{31.10}$$

Figure 31.3 shows the moving clock with its mirrors perpendicular to the direction of motion relative to the ground.

Figure 31.2. A light-pulse clock at rest on the ground as seen by an observer on the ground. The dial represents a conventional clock on the ground.

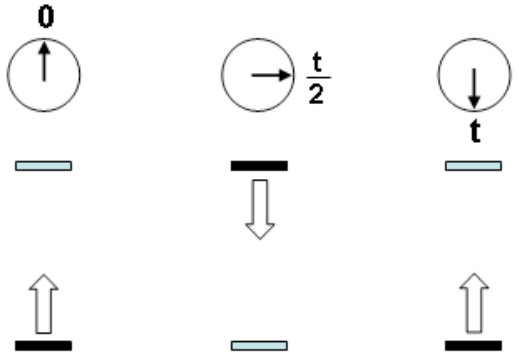

Figure 31.3. A light-pulse clock in a spacecraft as seen by an observer on the ground. The mirrors are parallel to the direction of motion of the spacecraft. The dial represents a conventional clock on the ground.

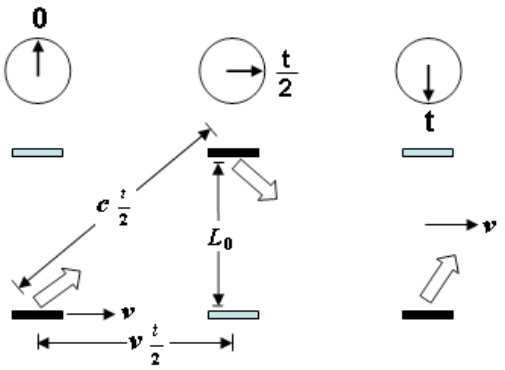

The time interval between ticks is *t*. Because the clock is moving, the light pulse, as seen from the ground, follows a zigzag path. On its way from the lower mirror to the upper one in the time $\frac{t}{2}$, the pulse travels a horizontal distance of $v\frac{t}{2}$ and a total distance of $c\frac{t}{2}$. Since L_0 is the vertical distance between the mirrors,

$$\left(c\frac{t}{2}\right)^2 = L_0^2 + \left(v\frac{t}{2}\right)^2 \tag{31.11}$$

$$\frac{t^2}{4}\left(c^2 - v^2\right) = L_0^2 \tag{31.12}$$

$$t^2 = \frac{4L_0^2}{c^2 - v^2} = \frac{\left(2L_0\right)^2}{c^2\left(1 - \frac{v^2}{c^2}\right)} \tag{31.13}$$

$$t = \frac{\frac{2L_0}{c}}{\sqrt{1 - \frac{v^2}{c^2}}} \tag{31.14}$$

But $\frac{2L_0}{c}$ is the time interval t_0 between ticks on the clock on the ground, as in Eq. (31.10), and so the **time dilation relationship** is:

$$t = \frac{t_0}{\sqrt{1 - \frac{v^2}{c^2}}} \tag{31.15}$$

wherein the parameters are:

t_0 = time interval on clock at rest relative to an observer
t = time interval on clock in motion relative to an observer
v = speed of relative motion
c = speed of light

Because the quantity $\sqrt{1 - \frac{v^2}{c^2}}$ is always smaller than 1 for a moving object, *t* is always greater than t_0. The moving clock in the spacecraft appears to tick at a slower rate than the stationary one on the ground, as seen by an observer on the ground.

Exactly the same analysis holds for measurements of the clock on the ground by the pilot of the spacecraft. To him, the light pulse of the ground clock follows a zigzag path that requires a total time *t* per round trip. His own clock, at rest in the spacecraft, ticks at intervals of t_0. He too finds that

$$t = \frac{t_0}{\sqrt{1-\frac{v^2}{c^2}}} \tag{31.16}$$

so the effect is reciprocal: Every observer finds that clocks in motion relative to him tick more slowly than clocks at rest relative to him.

The Lorentz transformation of time, length, mass, momentum, and energy which are significant when v approaches c can be derived by a similar procedure [2]. The Lorentz transformations are:

$$t = \frac{t_0}{\sqrt{1-\frac{v^2}{c^2}}} \tag{31.17}$$

$$l = l_o\sqrt{1-\frac{v^2}{c^2}} \tag{31.18}$$

$$m = \frac{m_0}{\sqrt{1-\frac{v^2}{c^2}}} \tag{31.19}$$

$$p = \frac{m_0 v}{\sqrt{1-\frac{v^2}{c^2}}} \tag{31.20}$$

$$E = mc^2 = \frac{m_0 c^2}{\sqrt{1-\frac{v^2}{c^2}}} \tag{31.21}$$

$$E^2 = m_0^2 c^4 + p^2 c^2 \tag{31.22}$$

When speaking of the relativity of a frame of reference or simply of relativity, one usually means that there exist identical physical processes in different frames of reference. According to the generalized Galilean principle of relativity identical processes are possible in all inertial frames of reference related by Lorentz transformations. On the other hand, Lorentz transformations characterize the uniformity of Galilean spacetime.

THE RELATIVITY PRINCIPLE AND THE COVARIANCE OF EQUATIONS IN GALILEAN OR EUCLIDEAN SPACETIME AND RIEMANN SPACETIME

From the geometrical point of view the theory of space and time naturally divides into the theory of uniform, Galilean, space and the theory of non-uniform, Riemannian, space.

Galilean space is of maximal uniformity. This means that in it:

(a) All points in space and instants in time are equivalent

(b) All directions are equivalent, and

(c) All inertial systems, moving uniformly and in a straight line relative to one another, are equivalent (Galilean principle of relativity).

The uniformity of space and time manifests itself in the existence of a group of transformations which leave the four-dimensional interval between two points (distance) invariant. The expression for this interval plays an important part in the theory of space and time because its form is directly related to the form taken by the basic laws of physics, viz. the law of motion of a free mass-point and the law of propagation in free space of the front of a light wave.

The indications (a), (b) and (c) of the uniformity of Galilean space are related to the following transformations:

(a) To the equivalence of all points and instants corresponds to the transformation of displacing the origins of the spatial coordinates and of time; the transformation involves four parameters, namely, the three space coordinates and the time coordinate of the origin.

(b) To the equivalence of all directions corresponds to the transformation of rotating the spatial coordinate axes; this involves three parameters, the three angles of rotation.

(c) To the equivalence of inertial frames corresponds to a change from one frame of reference to another moving uniformly in a straight line with respect to the first; this transformation involves three parameters, the three components of relative velocity.

The most general transformation involves ten parameters. This is the Lorentz transformation. It is well known that in a space of n dimensions the group of transformations which leave invariant the expression for the squared distance between infinitely near points, can contain at most $\frac{1}{2}n(n+1)$ parameters. If there is a group involving all $\frac{1}{2}n(n+1)$ parameters then the

space is of maximal uniformity; it may be a space of constant curvature, or, if the curvature vanishes, a Euclidean or pseudo-Euclidean space.

In the case of spacetime, the number of dimensions is four and therefore the greatest possible number of parameters is ten. This is also the number of parameters in the Lorentz transformation, so that Galilean space, to which the transformation relates, is indeed of maximal uniformity. It is customary to call the theory based on the Lorentz transformations the special theory of relativity. More precisely, the subject of that theory is the formulation of physical laws in accordance with the properties of Galilean space.

A formulation of the principle of relativity given *supra,* which together with the postulate that the velocity of light has a limiting character, may be made the basis of relativity theory. We shall now investigate in more detail the question of the connection of the physical principle of relativity with the requirement that the equations be covariant.

In the first place, we shall attempt to give a generally covariant formulation of the principle of relativity, without as yet making this concept more precise. In its most general form, the principle of relativity states the equivalence of the coordinate systems (or frames of reference) that belong to a certain class and are related by transformations of the form:

$$x'_\alpha = f_\alpha(x_0, x_1, x_2, x_3) \tag{31.23}$$

which may be stated more briefly as:

$$x' = f(x) \tag{31.24}$$

It is essential to remember that, in addition to the group of permissible transformations, the class of coordinate systems must be characterized by certain supplementary conditions. Thus, for instance, if we consider Lorentz transformations, it is self-evident that these linear transformations must connect not any arbitrary coordinates, but only the Galilean coordinates in two inertial reference frames. To consider linear transformations between any other (non-Galilean) coordinates has no sense, because the Galilean principle of relativity has no validity in relation to such artificial linear transformations. On the other hand, if one introduces any other variables in place of the Galilean coordinates, a Lorentz transformation can evidently be expressed in terms of these variables, but then the transformation formulae will have a more complicated form.

The formulation of the principle of relativity based on the equivalence of reference frames depends on the ability to call two reference frames (x) and (x') physically equivalent if phenomena proceed in the same way in them. Specifically, if a possible process is described in the coordinates (x) by the functions:

$$\phi_1(x),\ \phi_2(x),\ ...,\ \phi_n(x) \tag{31.25}$$

then there is another possible process which is describable by the same functions

$$\phi_1(x'),\ \phi_2(x'),\ ...,\ \phi_n(x') \tag{31.26}$$

in the coordinates (x'). Conversely any process of the form Eq. (31.26) in the second system corresponds to a possible process of the form Eq. (31.25) in the first system. Thus, a relativity principle is a statement concerning the existence of corresponding processes in a set of reference frames of a certain class wherein the corresponding systems are accepted as equivalent. It is clear from this definition that both the principle of relativity itself and the equivalence of two reference frames are physical concepts, and validity of either involves a definite physical hypothesis rather than convention. In addition, it follows that the very notion of a "principle of relativity" becomes well defined only when a definite class of frames of reference has been singled out. In the usual theory of relativity, this class is that of inertial systems.

The functions Eq. (31.25) or Eq. (31.26) describing a physical process will be called field functions or functions of state. In a generally covariant formulation of the equations describing physical processes the components $g_{\mu\nu}$ of the metric tensor must be included among the functions of state such as the collection of field functions:

$$F_{\mu\nu}(x), \qquad j_\nu(x), \qquad g_{\mu\nu}(x) \tag{31.27}$$

i.e. the electromagnetic field, the current vector, and the metric tensor, respectively. The requirement for the formulation of a principle of relativity that in two equivalent reference frames corresponding phenomena should proceed in the same way applies equally to the metric tensor. Thus, if we compare two corresponding phenomena in two physically equivalent reference frames, then for the first phenomenon, described in the old coordinates, not only the components of electromagnetic field and of current density, but also the components of the metric tensor must have the same mathematical form as for the second phenomenon described in the new coordinates.

Further conclusions depend on whether the metric is assumed to be fixed or whether phenomena that influence the metric are considered. In the usual theory of relativity, it is assumed that the metric is given, and it does not depend on any physical processes. This is also the case for the generally covariant formulation of the theory of relativity. As long as the assumption remains in force that the character of spacetime is Galilean and the $g_{\mu\nu}$ are introduced only to achieve general covariance, these quantities will depend only on the choice of coordinate system, not on the nature of the physical process discussed. They are functions of state only in a formula sense. In the theory of gravitation on the other hand, a different assumption is made concerning the nature of spacetime. There the $g_{\mu\nu}$ are functions of state, not only in a formal sense, but in fact: they describe a certain physical field, namely the field of gravitation.

To give a definite meaning to the principle of relativity in such circumstances, it is essential to specify more closely not only the class of coordinate systems, but also the nature of the physical processes for which the principle is being formulated. Starting from the assumption that the metric is fixed ("rigid"), or that it may be considered as fixed for a certain class of physical processes, consider the above definition of corresponding phenomena in two physically equivalent coordinate systems, wherein all field functions, including the components of the metric tensor, must have the same mathematical form for the first process described in the old coordinates as for the second process described in the new coordinates. If the $g_{\mu\nu}$ are independent of the nature of the physical phenomenon, then a distinction must be made between the first and second process relative to those quantities, and only transformations of the coordinates need to be considered. Thus, the quantities

$$g_{\mu\nu}(x) \quad \text{and} \quad g'_{\mu\nu}(x') \tag{31.28}$$

will be connected by the tensor transformation rule, and the requirement of the relativity principle that they should have one and the same mathematical form reduces (for infinitesimal coordinate transformations) to the equations $\delta g_{\mu\nu} = 0$.

The most general class of transformations that satisfies these equations contains 10 parameters and is possible only in uniform spacetime, where the relation,

$$R_{\mu\nu,\alpha\beta} = K \cdot (g_{\nu\alpha} g_{\mu\beta} - g_{\mu\alpha} g_{\nu\beta}) \tag{31.29}$$

is valid. (A space in which the curvature tensor $R_{\mu\nu,\alpha\beta}$ has the form of Eq. (31.29) is called a space of constant curvature; it is a four-dimensional generalization of Friedmann-Lobachevsky space. The constant *K* is called the constant of curvature.) If in these relations, *K* is zero, the spacetime is Galilean and the transformations in question are Lorentz transformations, except when other (non-Galilean) coordinates are used.

Thus, with the rigidity assumption for the metric, the principle of relativity implies the uniformity of spacetime. And, if the additional condition $K = 0$ holds, we obtain a Galilean metric in appropriate coordinates. The relativity principle in general form then reduces to the Galilean relativity principle. As for the condition $K = 0$, it results in an additional uniformity of spacetime. If the scale of the Galilean coordinates is changed, then the scale of the elementary interval changes in the same proportion. This property implies in turn that there is no absolute scale for spacetime, unlike the absolute scale that exists for velocities in terms of the velocity of light. The absence of an absolute scale for spacetime leads conversely to the equation $K = 0$.

Furthermore, taking into account phenomena that may influence the metric gives rise to the possibility that under certain conditions the principle of relativity will be valid in non-uniform space also. In this case, it is necessary that the motion of the masses producing the non-uniformity be included in the description of the phenomena.

It can be shown that under the assumption that spacetime is uniform at infinity (where it must be Galilean), a class of coordinate systems exist that are analogous to inertial systems and defined up to a Lorentz transformation. A principle of relativity will hold with respect to this class of coordinate systems in the same form as in the usual theory of relativity, despite the fact that at a finite distance from the masses the space is non-uniform. However, ultimately, this relativity principle is also a result of uniformity forced by the boundary conditions that require uniformity at infinity.

Since the greatest possible uniformity is expressed by Lorentz transformations, there is no more general principle of relativity than that discussed in ordinary relativity theory. Moreover, there cannot be a general principle of relativity, as a physical principle, which would hold with respect to arbitrary frames of reference. In order to make this fact clear, it is essential to distinguish sharply between a physical principle that postulates the existence of corresponding phenomena in different frames of reference and the simple requirement that equations should be covariant transforming from one frame of reference to another. It is clear that a principle of relativity implies a covariance of equations, but the converse is not true: covariance of differential equations is also possible when no principle of relativity is satisfied.

Covariance of equations in itself is in no way the expression of any kind of physical law. For instance, consider the mechanics of systems of mass-points. Lagrange's equations of the second kind are covariant with respect to arbitrary transformations of the coordinates. However, they do not express any new physical law compared to, for example, Lagrange's equations of the first kind, which are stated in Cartesian coordinates and are not covariant. In the case of Lagrange's equations, covariance is achieved by introducing the coefficients of the Lagrangian as new auxiliary functions considered as a quadratic expression, but not necessarily homogeneous in the velocities.

Independently considering that not all laws of nature reduce to differential equations, even fields described by differential equations not only require these equations for their definitions, but also all kinds of initial, boundary, and other conditions. These conditions are not covariant. Therefore, the preservation of their physical content requires a change in their mathematical form and, conversely, preservation of their mathematical form implies a change of their physical content. But, the realization of a process with a new physical content is an independent question that cannot be solved *a priori*. If "corresponding" physical processes within a given class of reference systems are possible, then a principle of relativity holds. In the opposite case, it does not. It is clear, however, that such a model representative of physical processes, and in particular such a model representative of the metric, is possible at most for a narrow class of reference systems of limited number. This argument shows once again (without invoking the concept of uniformity) that a general principle of relativity, as a physical principle, holding in relation to arbitrary frames of reference, is impossible.

A desire to find a general principle of relativity is unnecessary as a basis of the requirement of the covariance of the equations. The covariance requirement can be justified independently. It is a self-evident, purely logical requirement that in all cases in which the coordinate system is not fixed in advance, equations written down in different coordinate systems should be mathematically equivalent. The class of transformations with respect to which the equations must be covariant must correspond to the class of coordinate systems considered. Thus, if one deals with inertial systems related by Lorentz transformations and if Galilean coordinates are used, it is sufficient to require covariance with respect to Lorentz transformations. If, however, arbitrary coordinates are employed, it is necessary to demand general covariance.

It should be noted that covariance of coordinate systems acquires definite physical meaning if, and only if, a principle of relativity exists for the class of reference frames used. Such is the covariance with respect to Lorentz transformations. This concept was so useful in the formulation of physical laws because it contains concrete temporal and geometric elements (rectilinearity and uniformity of motion) and also dynamic elements (the concept of inertia in the mechanical and the electromagnetic sense). Because of this, it is related to the physical principle of relativity and itself becomes concrete and physical.

However, if arbitrary transformations are considered rather than the Lorentz transformations, one ceases to single out that class of coordinate systems relative to which the principle of relativity exists, and by doing this one destroys the connection between physics and the concept of covariance. There remains a purely logical side to the concept of covariance as a consistency requirement on equations written in different coordinate systems. Naturally this requirement is necessary, and it can always be satisfied.

In dealing with classes of reference frames that are more general than that relative to which a principle of relativity holds, the necessity arises of replacing the explicit formulation of the principle by some other statement. The explicit formulation consists of indicating a class of physically equivalent frames of reference. The new formulation must express those properties of space and time by which the principle of relativity is possible. With the assumption of a rigid metric this is achieved by introducing an additional Eq. (31.29). With the additional assumption of the absence of a universal scale ($K = 0$) these equations lead to a generally covariant formulation of the theory of relativity, without any alteration of its physical content. The Galileo-Lorentz principle of relativity is then maintained to its full extent.

The very possibility of formulating the ordinary theory of relativity in a general covariant form clearly demonstrates the difference between the principle of relativity as a physical principle and the covariance of the equations as a logical requirement. In addition, such a formulation opens the way to generalizations based on a relaxation of the assumption of a rigid metric. This relaxation provides the possibility of replacing the supplementary conditions Eq. (31.29) by others that reflect better the properties of space and time corresponding to the theory of gravitation.

Universal gravitation does not fit into the framework of uniform Galilean space because the gravitational mass of a body as well as the inertial mass depends on its energy. In the latter case, Einstein felt that it was possible to eliminate the effects of gravity by transforming to an accelerating frame of reference that defined his "Equivalence Principle." A theory of universal gravitation is derived in the Gravity section wherein Euclidean, or rather pseudo-Euclidean, geometry is abandoned in favor of the geometry of Riemann. But the derivation does not involve the traditional approach based on the Equivalence Principle; rather it is based on Eq. (31.2).

In Riemannian geometry, the coefficients $g_{\mu\nu}$ of the quadratic form for the squared infinitesimal distance are mechanics functions. These functions establish a law regarding their transformation from one coordinate frame to another based on their definition as coefficients of a quadratic form, together with the condition that this form is an invariant. Thus, a transformation of the coordinates is accompanied by a transformation of the metric $g_{\mu\nu}$ according to this law. The set of quantities $g_{\mu\nu}$ is called the metric tensor.

With the introduction of a metric tensor, expressions can be formed that are covariant with respect to any coordinate transformation. Nothing other than the covariance of equations is implicit in the metric tensors that may be obtainable from a particular one (e.g. from the Galilean tensor) by coordinate transformation. But, metric tensors of a more general form that cannot be transformed into one another by coordinate transformations are fundamentally different. In each case, the metric tensor will express not only properties of the coordinate system but also properties of space, and the latter can be related to the phenomenon of gravitation. It is shown below that the origin of gravity is the relativistic correction of spacetime itself as opposed to the relativistic correction of mass, length, and time of objects of inertial frames in constant relative motion. The production of a particle having an inertial and gravitational mass from a photon traveling at the speed of light requires time dilation and length contraction of spacetime. The present theory of gravity also maintains the constant maximum speed of light for the propagation of any form of energy including the gravitational field.

Having clarified the concept of covariance as applied to Riemannian geometry, consider it together with the previously discussed concept of the uniformity of space. As was shown above, the property of uniformity in Galilean space manifests itself in the existence of transformations that leave unchanged the expression for the four-dimensional distance between two points. More precisely, these transformations leave unchanged the coefficients of this expression, i.e. the quantities $g_{\mu\nu}$. $g_{\mu\nu}$ are functions of the coordinates which means that the mathematical form of these functions is unchanged: The dependence of the new $g_{\mu\nu}$ on the new coordinates has the same mathematical form as that of the old $g_{\mu\nu}$ on the old coordinates. In the general case of Riemannian geometry, there are no transformations that leave the $g_{\mu\nu}$ unchanged because Riemannian space is not uniform. One deals with transformations of coordinates accompanied by transformations of the $g_{\mu\nu}$, and neither such a combined transformation nor covariance with respect to it has any relation to the uniformity or non-uniformity of space.

The geometrical properties of real physical space and time correspond not to Euclidean but to Riemannian geometry. Any deviation of geometrical properties from their Euclidean, or to be precise, pseudo-Euclidean form appears in Nature as a gravitational field. The geometrical properties are inseparably linked with the distribution and motion of ponderable matter. This relationship is mutual. On the one hand the deviations of geometrical properties from the Euclidean are determined by the presence of gravitating masses, on the other, the motion of masses in the gravitational field is determined by these deviations. In short, masses determine the geometrical properties of space and time, and these properties determine the movement of the masses. The description of the gravitational field demands the introduction of no functions other than the metric tensor itself which is uniquely determined by the presence and motion of matter. Differing from other kinds of forces, gravity which influences the motion of the matter by determining the properties of spacetime, is itself described by the metric of spacetime. For this principle of relativity, the class of coordinate systems relative to which the principle of relativity exists is the spherical coordinate systems. Spherical harmonic coordinates arise naturally due to the spherical symmetry of the particle production (energy/matter conversion) event and its effect on spacetime and provide the connection between physics and the concept of covariance as shown in the Gravity section. The corresponding metric is the Schwarzschild metric derived in the Gravity section.

The Schwarzschild metric gives the relationship whereby matter causes relativistic corrections to spacetime that determines the curvature of spacetime and is the origin of gravity. The correction is based on the boundary conditions that no signal can travel faster that the speed of light including the gravitational field that propagates following particle production from a photon wherein the particle has a finite gravitational velocity given by Newton's Law of Gravitation. The spacetime contraction during particle production is analogous to Lorentz length contraction and time dilation of an object in one inertial frame relative to another moving at constant relative velocity. In the former case, the corresponding correction is a function of the square of the ratio of the gravitational velocity to the speed of light. In the latter case, the corresponding correction is a function of the square of the ratio of the relative velocity of two inertial frames to the speed of light. Thus, the relativity principle for both Euclidean and Riemannian geometries is based on the light wave front propagation equation, specifically Eq. (31.2).

REFERENCES

1. S. Kak, "Moving observers in an isotropic universe," International Journal of Theoretical Physics, Vol. 46, (2007).
2. A. Beiser, *Concepts of Modern Physics*, Fourth Edition, McGraw-Hill Book Company, New York, (1978), pp. 2-40.
3. V. Fock, *The Theory of Space, Time, and Gravitation*, The MacMillan Company, (1964).
4. J. Bailey et al., "Final report on the CERN muon storage ring including the anomalous magnetic moment and the electric dipole moment of the muon, and a direct test of relativistic time dilation, Nuclear Physics B150, (1979), pp. 1-75.
5. P. Sprangle, A. T. Drobot, "The linear and self-consistent nonlinear theory of the electron cyclotron maser instability," IEEE Transactions on Microwave Theory and Techniques, Vol. MTT-25, No. 6, June, (1977), pp. 528-544.
6. E. Giannetto, The rise of special relativity: Henri Poincaré's works before Einstein. Atti del 18 Congresso di Storia della Fisica e dell'Astronomia, (1998).
7. H. Poincaré, "L'etat actuel et l'avenir de la physique mathematique," *Bulletin des sciences mathematiques*, Vol. 28, (1904), pp. 302-324; quoted in Whittaker (1987), p. 30.
8. E. Whittaker, *A History of the Theories of Aether and Electricity*, Vol. 2, Modern Theories, Chapter 2, "The Relativity Theories of Poincaré and Lorentz," Nelson, London, (1987), Reprinted, American Institute of Physics, pp. 30–31.

Chapter 32

GRAVITY

QUANTUM GRAVITY OF FUNDAMENTAL PARTICLES

The attractive gravitational force has been the subject of investigation for centuries. Traditionally, gravitational attraction has been investigated in the field of astrophysics applying a large-scale perspective of cosmological spacetime, as distinguished from currently held theories of atomic and subatomic structure. However, gravity originates on the atomic scale. In Newtonian gravitation, the mutual attraction between two particles of masses m_1 and m_2 separated by a distance r is:

$$\mathbf{F} = G\frac{m_1 m_2}{r^2} \tag{32.1}$$

where G is the gravitational constant, its value being $6.67\ X\ 10^{-11}\ Nm^2kg^{-2}$. Although Newton's theory gives a correct quantitative description of the gravitational force, the most elementary feature of gravitation is still not well defined. What is the most important feature of gravitation in terms of fundamental principles? By comparing Newton's second law,

$$\mathbf{F} = m\mathbf{a} \tag{32.2}$$

with his law of gravitation, we can describe the motion of a freely falling object by using the following equation:

$$m_i\mathbf{a} = m_g\frac{GM_\oplus}{r^3}\mathbf{r} \tag{32.3}$$

where m_i and m_g represent respectively the object's inertial mass (inversely proportional to acceleration) and the gravitational mass (directly proportional to gravitational force), $M_\oplus$ is the gravitational mass of the Earth, and **r** is the position vector of the object taken from the center of the Earth. The above equation can be rewritten as:

$$\mathrm{a} = \frac{m_g}{m_i}\left(\frac{GM_\oplus}{r^2}\right) \tag{32.4}$$

Extensive experimentation dating from Galileo Galilei's Pisa experiment to the present has shown that irrespective of the object chosen, the acceleration of an object produced by the gravitational force is the same, which from Eq. (32.4) implies that the value of m_g / m_i should be the same for all objects. In other words, we have

$$\frac{m_g}{m_i} = \text{universal constant} \tag{32.5}$$

the equivalence of the gravitational mass and the inertial mass. The fractional deviation of Eq. (32.5) from a constant is experimentally confirmed to less $1\ X\ 10^{-11}$ [1]. In physics, the discovery of a universal constant often leads to the development of an entirely new theory. From the universal constancy of the velocity of light, *c*, the special theory of relativity was derived; and from Planck's constant, *h*, the quantum theory was deduced. Therefore, the universal constant m_g / m_i should be the key to the gravitational problem. The theoretical difficulty with Newtonian gravitation is to explain just why relation, Eq. (32.5), exists implicitly in Newton's theory as a separate law of nature besides Eqs. (32.1) and (32.2). Furthermore, discrepancies between certain astronomical observations and predictions based on Newtonian celestial mechanics exist, and they apparently could not be reconciled until the development of Einstein's theory of general relativity which can be transformed to Newtonian gravitation on the scale in which Newton's theory holds.

General relativity is the geometric theory of gravitation developed by Albert Einstein, whereby he intended to incorporate and extend the special theory of relativity to accelerated frames of reference. Einstein's theory of general relativity is based on a flawed dynamic formulation of Galileo Galilei's law. Einstein took as the basis to postulate his gravitational field equations a certain kinematical consequence of a law, which he called the "Principle of Equivalence," which states that it is impossible to

distinguish a uniform gravitational field from an accelerated frame. However, the two are not equivalent since they obviously depend on the direction of acceleration relative to the gravitating body and the distance from the gravitating body since the gravitational force is a central force. (In the latter case, only a line of a massive body may be exactly radial, not the entire mass.) And, this assumption leads to conflicts with special relativity. The success of Einstein's gravity equation can be traced to a successful solution which arises from assumptions and approximations whereby the form of the solution ultimately conflicts with the properties of the original equation; no solution is consistent with the experimental data in the case of the possible cosmological solutions of Einstein's general relativity. Furthermore, Einstein's general relativity is a partial theory in that it deals with matter on the scale of celestial objects, but not on an atomic scale. And, it fails on the cosmological scale. All gravitating bodies are composed of matter and are collections of atoms that are composed of fundamental particles such as electrons, which are leptons, and quarks, which make up protons and neutrons. Gravity originates from the fundamental particles.

Einstein's theory has as its foundation that gravity is a force unique from electromagnetism. The magnetic force was unified with the Coulomb force by Maxwell. Lorentz derived the transformations named after him which formalize the origin of the magnetic force as a relativistic correction of the Coulomb force. The unification of electricity and magnetism by Maxwell permitted him to derive a wave equation that predicted the propagation of electromagnetic waves at the speed of light. Maxwell's wave equation defines a four-dimensional spacetime and the speed of light as a maximum permitted according to the permeability and permittivity of spacetime. Minkowski originated the concept of a four-dimensional spacetime formally expressed as the Minkowski tensor [2]. The Minkowski tensor corresponds to the electromagnetic wave equation derived by Maxwell and can be derived from it [3]. Special relativity is implicit in the wave equation of electromagnetic waves that travel at the speed of light. As given in the Relativity section and the Equivalence of Inertial and Gravitational Masses Due to Absolute Space and Absolute Light Velocity section, the generalization of this metric to mass as well as charge requiring application of Lorentz transformations comprises the theory of special relativity invented by Poincaré in 1904 [4-6][1]. The Lorentz transformations quantify the measurement of the increase in mass, length contraction, and time dilation in the direction of constant relative motion of separate inertial frames due to the finite maximum speed of light. The goal of Einstein, who worked on special relativity, was to generalize it to accelerated frames of reference as well as inertial frames moving at constant relative velocity. But, gravity is not a force separable from electromagnetism. The true origin of gravity is the relativistic correction of spacetime itself as opposed to the relativistic correction of mass, length, and time of objects of inertial frames in constant relative motion. The production of a massive particle from a photon with zero rest mass traveling at the speed of light requires time dilation and length contraction of spacetime. The present theory of gravity also maintains the constant maximum speed of light for the propagation of any form of energy. (Recently the speed of gravity has been measured to be the speed of light [7].) And, the origin of the gravitational force is also a relativistic correction. In the metric which arises due to the presence of mass, spacetime itself must be relativistically corrected as a consequence of the presence of mass in order that (i) the speed of light is constant and a maximum, (ii) the angular momentum of a photon, $\hbar$, is conserved, and (iii) the energy of the photon is conserved as mass. Spacetime must undergo time dilation and length contraction due to the production event. The event must be spacelike even though the photon of the particle production event travels at the speed of light and the particle must travel at a velocity less than the speed of light. The relativistically altered spacetime gives rise to a gravitational force between separated masses. Thus, the production of matter and its motion alters spacetime and the altered spacetime affects the motion of matter, which must follow geodesics.

When speaking of the relativity of a frame of reference or simply of relativity, one usually means that there exist identical physical processes in different frames of reference. According to the generalized Galilean principle of relativity identical processes are possible in all inertial frames of reference related by Lorentz transformations. On the other hand, Lorentz transformations characterize the uniformity of Galilean spacetime. Using the four-dimensional coordinates x^μ for describing the events and the world-line in spacetime the separation of proper time between two events x^μ and $x^\mu + dx^\mu$ is:

$$d\tau^2 = -g_{\mu\nu} dx^\mu dx^\nu \tag{32.6}$$

where $g_{\mu\nu}$ is the metric tensor which determines the geometric character of spacetime. For different coordinate systems, the dx^μ may not be the same, but the separation $d\tau^2$ remains unchanged. The metric $g_{\mu\nu}$ for Euclidean space called the Minkowski tensor $\eta_{\mu\nu}$ is:

[1] In 1900, Lorentz conjectured that gravitation could be attributed to actions that propagate with the velocity of light. Poincaré, in a paper in July 1905 (submitted days before Einstein's special relativity paper), suggested that all forces should transform according to Lorentz transformations. In this case, he notes that Newton's Law of Gravitation is not valid and proposed gravitational waves that propagated with the velocity of light. Specifically, Poincaré pointed out that all forces must propagate with the finite light velocity, that interaction implies a time delay, and it is mediated by field waves. Thus, Poincaré made for the first time the hypothesis of the existence of gravitational waves [4].

$$\eta_{\mu\nu} = \begin{pmatrix} -1 & 0 & 0 & 0 \\ 0 & \frac{1}{c^2} & 0 & 0 \\ 0 & 0 & \frac{1}{c^2} & 0 \\ 0 & 0 & 0 & \frac{1}{c^2} \end{pmatrix} \tag{32.7}$$

In this case, the separation of proper time between two events x^μ and $x^\mu + dx^\mu$ is:

$$d\tau^2 = -\eta_{\mu\nu} dx^\mu dx^\nu \tag{32.8}$$

A spherically symmetrical system of mass m_0 applies to the production of a particle which implies spherical coordinates with the origin at 0. Thus, a family of curved surfaces, each with constant *r*, is a series of concentric spheres on which it is natural to adopt the coordinate *r* so that a sphere with constant *r* has area $4\pi r^2$, and the metric on the surface of the sphere would then be:

$$ds^2 = r^2 d\theta^2 + r^2 \sin^2\theta d\phi^2 \tag{32.9}$$

Such a definition of *r* is no longer the distance from the origin to the surface, because of the spacetime contraction caused by the mass m_0. The form of the outgoing gravitational field front traveling at the speed of light is:

$$f\left(t - \frac{r}{c}\right) \tag{32.10}$$

Therefore the spatial metric should be expressed as

$$ds^2 = f(r)^{-1} dr^2 + r^2 d\theta^2 + r^2 \sin^2\theta d\phi^2 \tag{32.11}$$

In addition, **the existence of mass m_0 also causes time dilation of spacetime** such that the clock on each r-sphere is no longer observed from each r-sphere to run at the same rate. That is, clocks slow down in a gravitational field [8]. Therefore, the general form of the metric due to the relativistic effect on spacetime due to mass m_0 is:

$$d\tau^2 = f(r) dt^2 - \frac{1}{c^2}\left[f(r)^{-1} dr^2 + r^2 d\theta^2 + r^2 \sin^2\theta d\phi^2 \right] \tag{32.12}$$

In the case where $m_0 = 0$, space would be flat which corresponds to:

$$f(r) = f(r)^{-1} = 1 \tag{32.13}$$

Then the spacetime metric is the Minkowski tensor. In the case that the mass m_0 is finite, the Minkowski tensor is corrected by the time dilation and length contraction of spacetime.

The creation of a particle from light requires the event to be spacelike; yet, particle production arises from a photon traveling at the speed of light. At production, the particle must have a finite velocity called the Newtonian gravitational velocity (according to Newton's Law of Gravitation) that may not exceed the speed of light. The Newtonian gravitational velocity must have an associated gravitational energy. The photon initially traveling at the speed of light undergoes particle production and must produce a gravitational field that travels at the speed of light. The gravitational energy associated with the field must have an inverse radius dependence according to the spreading wave. Since the gradient of the gravitational energy gives rise to the gravitational field, the gravitational field must have an inverse radius squared dependence. In order that the velocity of light does not exceed *c* in any frame including that of the particle having a finite Newtonian gravitational velocity, v_g, the laboratory frame of an incident photon, and that of a gravitational field propagating outward at the speed of light, spacetime must undergo time dilation and length contraction due to the production event. During particle production the speed of light as a constant maximum as well as phase matching and continuity conditions require the following form of the squared displacements due to constant motion along two orthogonal axes in polar coordinates:

$$(c\tau)^2 + (v_g t)^2 = (ct)^2 \tag{32.14}$$

$$(c\tau)^2 = (ct)^2 - (v_g t)^2 \tag{32.15}$$

$$\tau^2 = t^2\left(1 - \left(\frac{v_g}{c}\right)^2\right) \tag{32.16}$$

Thus,

$$f(r) = \left(1 - \left(\frac{v_g}{c}\right)^2\right) \tag{32.17}$$

(The derivation and result of spacetime time dilation is analogous to the derivation and result of special relativistic time dilation given by Eqs. (30.11-30.15).) Therefore, the general form of the metric due to the relativistic effect on spacetime due to mass $\frac{\text{proper time}}{\text{coordinate time}} = \frac{m_0}{m_u} = \alpha^{-1}\frac{\mu_0 e^2 c}{2h}\frac{\sqrt{\frac{Gm_0}{\lambda\!\!\!^{-}_C}}}{c} = \alpha^{-1}\frac{\mu_0 e^2 c}{2h}\sqrt{\frac{Gm_0}{c^2\lambda\!\!\!^{-}_C}} = \alpha^{-1}\frac{\mu_0 e^2 c}{2h}\frac{v_G}{c} = \frac{v_G}{c}$ is:

$$d\tau^2 = \left(1-\left(\frac{v_g}{c}\right)^2\right)dt^2 - \frac{1}{c^2}\left[\left(1-\left(\frac{v_g}{c}\right)^2\right)^{-1} dr^2 + r^2 d\theta^2 + r^2\sin^2\theta d\phi^2\right] \tag{32.18}$$

The gravitational energy of a particle during production given by Newton's Law of Gravitation may be unified with the inertial and electromagnetic energies given by Planck's equation and Maxwell's equations, respectively. The physical basis is the law of Galileo that in the absence of a resistive medium all bodies fall equally fast, or, more accurately, with equal acceleration. The law of Galileo can be stated in generalized form as the law of the equality of inertial and gravitational mass. The equivalence of the Planck equation, electric potential, and the stored magnetic energies occurs for a transition state atomic orbital during pair production as shown in the Pair Production section. During particle production the transition state atomic orbital has a charge-density function σ given by

$$\sigma = \frac{e}{4\pi r^2}\delta(r - r_n) \tag{32.19}$$

where e is the fundamental charge. The corresponding mass-density function is:

$$\mu = \frac{m_0}{4\pi r^2}\delta(r - r_n) \tag{32.20}$$

where mass, m_0, is the rest mass of the particle produced. In both cases, the radius, r_n, is the Compton wavelength bar, $\lambda\!\!\!^{-}_C$, given by

$$\lambda\!\!\!^{-}_C = \frac{\hbar}{m_0 c} = r_\alpha^* \tag{32.21}$$

Consider the gravitational radius, α_G or r_G, of an atomic orbital of mass, m_0, defined as:

$$\alpha_G = r_G = \frac{Gm_0}{c^2} \tag{32.22}$$

where G is the Newtonian gravitational constant. Notice that as m_0 increases the gravitational radius, r_G, increases (i.e. the curvature of spacetime increases), and the radius of the transition state atomic orbital, r_α^*, decreases. Remarkably, when $r_G = r_\alpha^* = \lambda\!\!\!^{-}_C$, the gravitational potential energy equals $m_0 c^2$ where m_0 is the rest mass of the fundamental particle created as the transition state atomic orbital becomes real. This is shown by equating the gravitational radius, r_G, to the Compton wavelength bar, $\lambda\!\!\!^{-}_C$, given by Eq. (29.22):

$$\frac{Gm_0}{c^2} = \lambda\!\!\!^{-}_c = \frac{\hbar}{m_0 c} \tag{32.23}$$

Multiplication of both sides of Eq. (32.23) by $m_0 c^2$ and division of both sides by λ^* gives:

$$\frac{Gm_0^2}{\lambda^*} = \frac{\hbar c}{\lambda^*} \tag{32.24}$$

Since $\hbar = h/2\pi$:

$$\frac{Gm_0^2}{\frac{\lambda^*}{2\pi}} = \frac{hc}{\lambda^*} \tag{32.25}$$

Since $\lambda\!\!\!^{-}_C = \lambda_C / 2\pi$ and from Eqs. (27.3) and (27.5), $\frac{hc}{\lambda^*} = \hbar\omega$:

$$\frac{Gm_0^2}{\lambda\!\!\!^{-}_C} = \frac{Gm_0^2}{r_\alpha^*} = \hbar\omega^* \tag{32.26}$$

The left-hand side of Eq. (32.26) is the gravitational potential energy and the right-hand side is the energy of the particle-production photon. Thus, from Eq. (28.11) and Eq. (32.26), the following energies are equivalent

$$E = m_0 c^2 = V = \hbar\omega^* = E_{mag} = \frac{Gm_0^2}{\lambda\!\!\!^{-}_C^*} \tag{32.27}$$

where $\omega*$ is the angular frequency of the photon which forms the transition state atomic orbital, and $\omega*$ is also the spacetime resonance angular frequency for this particle. Furthermore, given

$$E = m_0 c^2 = \hbar \omega^* = \frac{hc}{\lambda^*} \tag{32.28}$$

It follows that

$$\lambda^* = \frac{h}{m_0 c} = \frac{h}{m_0 v} = \frac{h}{p} \tag{32.29a}$$

and in general,

$$\lambda = \frac{h}{mv} = \frac{h}{p} \tag{32.29b}$$

This equation is the de Broglie relationship; it must hold for matter and energy. In fact, this was de Broglie's original insight [9] which led him to postulate the relationship named after him. The mass-energy which causes the gravitational radius, r_G, to equal $\lambda\!\!\!^{-}_C$ is hereafter called the Grand Unification Mass-Energy which is equal to $\hbar$ times the angular frequency of the photon which becomes the transition state atomic orbital. This angular frequency is also the spacetime resonance angular frequency of the Grand Unification Mass-Energy as given by Eq. (28.13). The Grand Unification Mass-Energy is further equal to the corresponding electric potential, stored magnetic, and gravitational potential energy. The equality of radii unifies de Broglie's equation, Planck's equation, Maxwell's equations, Newton's equations, and Special and General Relativity, which comprise the fundamental laws of the Universe.

The Grand Unification Mass-Energy, m_u, can be expressed in terms of Planck's constant.

$$m_u c^2 = \frac{G m_u^2}{\lambda\!\!\!^{-*}_C} = G m_u^2 \cdot \frac{m_u c}{\hbar} \tag{32.30}$$

$$m_u = \sqrt{\frac{\hbar c}{G}} \tag{32.31}$$

The Grand Unification Mass-Energy, m_u, given by Eq. (32.31) is the ***Planck mass***. From Eq. (28.11), the relationship of the equivalent particle production energies (mass energy = Planck equation energy = electric potential energy = magnetic energy = gravitational potential energy) is

$$m_0 c^2 = \hbar \omega^* = V = E_{mag} = E_{grav} \tag{32.32a}$$

where m_0 is the rest mass of a fundamental particle of the Planck mass m_u when the gravitational energy is the gravitational potential energy given by Eq. (32.30). A corresponding general relationship of the equivalent particle production energies (mass energy = Planck equation energy = electric potential energy = magnetic energy = gravitational energy) is:

$$m_0 c^2 = \left(\hbar \omega^* = \frac{\hbar^2}{m_0 \lambda\!\!\!^{-2}_C} \right) = \alpha^{-1} \frac{e^2}{4\pi \varepsilon_0 \lambda\!\!\!^{-}_C} = \alpha^{-1} \frac{\pi \mu_0 e^2 \hbar^2}{\left(2\pi m_0\right)^2 \lambda\!\!\!^{-3}_C} = \alpha^{-1} \frac{\mu_0 e^2 c^2}{2h} \sqrt{\frac{G m_0}{\lambda\!\!\!^{-}_C}} \sqrt{\frac{\hbar c}{G}} \tag{32.32b}$$

where m_0 is the rest mass of a fundamental particle. For particle production, the gravitational velocity, v_G, is defined as

$$v_G = \sqrt{\frac{G m_0}{r}} = \sqrt{\frac{G m_0}{\lambda\!\!\!^{-}_C}} \tag{32.33}$$

Substitution of the gravitational velocity, v_G, given by Eq. (32.33) and the Planck mass, m_u, given by Eq. (32.31) into Eq. (32.32) followed by division by the speed of light squared gives the mass of a fundamental particle in terms of the Planck mass where:

$$m_0 = \alpha^{-1} \frac{\mu_0 e^2 c}{2h} \frac{\sqrt{\frac{G m_0}{\lambda\!\!\!^{-}_C}}}{c} m_u = \alpha^{-1} \frac{\mu_0 e^2 c}{2h} \sqrt{\frac{G m_0}{c^2 \lambda\!\!\!^{-}_C}} m_u = \alpha^{-1} \frac{\mu_0 e^2 c}{2h} \frac{v_G}{c} m_u = \frac{v_G}{c} m_u \tag{32.34}$$

The equivalence of the gravitational and inertial masses according to experiments and Eq. (32.32) prove that Newton's Gravitational Law is exact on a local scale. The production of a particle requires that the velocity of each of the point masses of the particle is equivalent to the Newtonian gravitational escape velocity v_g of the superposition of the point masses of the antiparticle. According to Newton's Law of Gravitation the eccentricity is one (Eqs. (35.17-35.22)) and the particle production trajectory is a parabola relative to the center of mass of the antiparticle. The correction to Newton's Gravitational Law due to the relativistic effect of the presence of mass on spacetime may be determined by substitution of the gravitational escape velocity, v_g, given by [10]:

$$v_g = \sqrt{\frac{2 G m_0}{r}} = \sqrt{\frac{2 G m_0}{\lambda\!\!\!^{-}_C}} \tag{32.35}$$

into Eq. (32.18) for v_g. The corresponding Newtonian gravitational radius is given by:

$$r_g = \frac{2 G m_0}{c^2} \tag{32.36}$$

In the case of the boundary conditions of Eq. (32.32), Eq. (32.35) and Eq (32.36), three families of leptons and quarks are predicted wherein each particle corresponds to a unique atomic orbital radius equal to its Compton wavelength bar. At particle production, a photon having a radius and a wavelength equal to the Compton wavelength bar of the particle forms a transition state atomic orbital of the particle of the same wavelength.

A fourth family is not observed. A pair of particles each of the Planck mass corresponding to the conditions of Eq. (32.22), Eq. (32.32), and Eq. (32.33), is not observed since the velocity of each of the point masses of the transition state atomic orbital is the gravitational velocity v_G that in this case is the speed of light; whereas, the Newtonian gravitational escape velocity v_g of the superposition of the point masses of the antiparticle would be $\sqrt{2}$ the speed of light (Eq. (32.35)). In this case, an electromagnetic wave of mass energy equivalent to the Planck mass travels in a circular orbit around the center of mass of another electromagnetic wave of mass energy equivalent to the Planck mass wherein the eccentricity is equal to zero (Eq. (35.21)), and the escape velocity can never be reached. The Planck mass is a "measuring stick." The extraordinarily high Planck mass ($\sqrt{\frac{\hbar c}{G}} = 2.18\ X\ 10^{-8}\ kg$) is the unobtainable mass bound imposed by the angular momentum and speed of the photon relative to the gravitational constant. It is analogous to the unattainable bound of the speed of light for a particle possessing finite rest mass imposed by the Minkowski tensor. It has a physical significance for the fate of blackholes as given in the Composition of the Universe section.

Eq. (32.34) gives the relationship between the mass of each fundamental particle and the ratio of the gravitational velocity v_G to the speed of light times the Planck mass, the mass at which the gravitational radius r_G is the Compton wavelength bar and the production energy is equal to the gravitational potential energy given by Eq. (32.30). The square of the ratio of the gravitational escape velocity v_g of each particle relative to the speed of light gives the corresponding spacetime contraction according to Eqs. (32.17-32.18). During particle production, a particle having the gravitational escape velocity v_g is formed from a photon traveling at the speed of light. The spacetime contraction during particle production is analogous to Lorentz length contraction and time dilation of an object in one inertial frame relative to another moving at constant relative velocity. In the latter case, the correction is the square of the ratio of the relative velocity of two inertial frames to the speed of light according to Eqs. (31.17-31.18). The theory of the masses of fundamental particles is given in the Particle Production section, the Leptons section, and The Quarks section.

The resulting metric is valid for the external region of particles and spherically symmetric bodies comprised of fundamental particles such as the celestial bodies. The metric $g_{\mu\nu}$ for non-Euclidean space due to the relativistic effect on spacetime due to mass m_0 is:

$$g_{\mu\nu} = \begin{pmatrix} -\left(1-\frac{2Gm_0}{c^2 r}\right) & 0 & 0 & 0 \\ 0 & \frac{1}{c^2}\left(1-\frac{2Gm_0}{c^2 r}\right)^{-1} & 0 & 0 \\ 0 & 0 & \frac{1}{c^2}r^2 & 0 \\ 0 & 0 & 0 & \frac{1}{c^2}r^2\sin^2\theta \end{pmatrix} \tag{32.37}$$

In this case, the separation of proper time between two events x^μ and $x^\mu + dx^\mu$ is:

$$d\tau^2 = \left(1-\frac{2Gm_0}{c^2 r}\right)dt^2 - \frac{1}{c^2}\left[\left(1-\frac{2Gm_0}{c^2 r}\right)^{-1} dr^2 + r^2 d\theta^2 + r^2\sin^2\theta d\phi^2\right] \tag{32.38}$$

The origin of gravity is fundamental particles, and the masses and fields from particles superimpose. So, m_0, the mass of a fundamental particle, may be replaced by *M*, the sum of the masses of the particles which make up a massive body. In this case, Eq. (32.38) is equivalent to a modified version of the Schwarzschild metric [8 and footnote 7].

One interpretation of the relativistic correction of spacetime due to conversion of energy into matter and matter into energy is that spacetime contracts and expands, respectively, in the radial and time dimensions. Thus, matter-energy conversion can be considered to conserve spacetime. Also, since matter causes spacetime to deviate from flat or Euclidean, matter-energy conversion can be considered to curve spacetime. The result is that spacetime is positively curved to match the boundary condition of the positive curvature of particles during production. The two-dimensional nature of fundamental particles requires that the radial and time dimensions are distinct from the angular dimensions. The curvature of spacetime results from a discontinuity of matter having curvature confined to two spatial dimensions. This is the property of all matter as an atomic orbital. A space in which the curvature tensor has the following form:

$$R_{\mu\nu,\alpha\beta} = K\cdot(g_{\nu\alpha}g_{\mu\beta} - g_{\mu\alpha}g_{\nu\beta}) \tag{32.39}$$

is called a space of constant curvature; it is a four-dimensional generalization of Friedmann-Lobachevsky space. The constant *K* is called the constant of curvature. Consider an isolated atomic orbital and radial distances, *r*, from its center. For *r* less than r_n there is no mass; thus, spacetime is flat or Euclidean. The curvature tensor applies to all space of the inertial frame considered; thus, for *r* less than r_n, $K = 0$. At $r = r_n$ there exists a discontinuity of mass of the atomic orbital. This results in a discontinuity of the metric tensor for radial distances greater than or equal to r_n which defines the curvature tensor given by Eq. (32.39).

Gauss and Riemann [8, 11] developed the theory of curved spacetime and proposed that our Universe may be curved rather than flat. A generation later, Einstein formalized the ideas of Gauss, Riemann, and Clifford [8, 11, 12] that matter curved spacetime to give rise to a gravitational field[2]. Einstein proposed the principle of equivalence as the basis that gravity could be explained in terms of a spacetime metric that is different from Euclidean [8, 11]. According to Einstein's theory of general relativity, his field equations give the relationship whereby matter determines the curvature of spacetime[3], which is the origin of gravity. The definitive form of the equations are as follows[4]:

$$R_{\mu\nu} - \frac{1}{2} g_{\mu\nu} R = \frac{-8\pi G}{c^4} T_{\mu\nu} \tag{32.40}$$

where $R_{\mu\nu} = g^{\alpha\beta} R_{\mu\alpha\nu\beta}$, $R = g^{\mu\nu} R_{\mu\nu}$, the left-half of Eq. (32.40) is Einstein's Tensor $G_{\mu\nu}$, and $T_{\mu\nu}$ is the stress-energy-momentum tensor. Einstein proposed Eq. (32.40) starting with the assumption of the local equivalence of accelerated and gravitational inertial reference frames called the Principle of Equivalence. Einstein's equation postulates that a conservative Riemannian tensor is proportional to a conservative stress energy momentum tensor wherein the proportionality constant contains Newton's gravitational constant. The uniqueness of the radial and time dimensions for particle production (Eq. (32.32) and Eqs. (32.37-32.38)) and the corresponding effect on spacetime reveals a fatal flaw in Einstein's gravity equations. The tensors cannot be conservative. All cosmological solutions of general relativity predict a decelerating Universe from a postulated initial condition of a "Big Bang" expansion [13]. The astrophysical data reveals an accelerating cosmos [14] that invalidates Einstein's equation, as discussed in the Cosmology section. *Recently Lieu and Hillman [15] and Ragazzoni et al. [16] have shown using the Hubble space telescope that the infinities in the quantum singularity, which became the Universe with the big bang, cannot be reconciled by invoking uncertainty on the Planck-time scale. Time is continuous rather than quantized, the concept of the big bang is experimentally fatally flawed.*

It has been shown that the correct basis of gravitation is not according to Einstein's equation (Eq. (32.40)); instead the origin of gravity is the relativistic correction of spacetime itself which is analogous to the special relativistic corrections of inertial parameters—increase in mass, dilation in time, and contraction in length in the direction of constant relative motion of separate inertial frames. On this basis, the observed acceleration of the cosmos is predicted as given in the Cosmology section.

The popular terms for these effects, general relativity and special relativity, respectively, are confusing at best. The special relativistic corrections of an object corresponding to Newton's law of mechanics applied to inertial frames with constant relative motion are more appropriately named Newtonian Inertial Corrections or Newtonian Corrections of the First Kind. The gravitational relativistic corrections of spacetime, which correspond to Newton's Laws of Gravitation applied to massive bodies are more appropriately named Newtonian Gravitational Corrections or Newtonian Corrections of the Second Kind. The nomenclature used herein will adhere to tradition, but it is implicit that Special Relativity refers to spacetime defined by the Minkowski tensor, and General Relativity refers not to Einstein's equations but to the spacetime defined by the Schwarzschild metric wherein the physical basis for the latter is the time dilation and length contraction of spacetime due to particle production[5]. Furthermore, in the use of traditional nomenclature of the magnetic force as a relativistic correction of the Coulomb

---

[2] It is easy to discuss two-dimensional surfaces since we live in a three-dimensional space. Gauss considered the problem of whether a being that lives in and measures only in a two dimensional surface and can not travel in a three dimensional space can determine whether the surface in which it exists is curved or flat. The solution is not obvious. "One cannot be sure of the true sights of Lu mountain, since one is on it." Gauss found the solution that the two dimensional being could determine whether the surface on which it exists is curved by measuring the angle sum of a "geodesic triangle" on the surface. Euclidean plane geometry asserts that in a plane, the sum of the angles of a triangle add up to 180°. On the surface of a sphere, however, the sum of the angles of a "geodesic triangle" exceeds 180°. Gauss reasoned that the question of whether the three dimensional space in which we live is curved or flat could be resolved analogously. Gauss himself measured the angle sum of a triangle formed by three mountains as vertices, but failed to detect any departure from 180° within the limits of accuracy of his experiments. A generation later Einstein paraphrased this concept, "When a blind beetle crawls over the surface of the globe, he doesn't realize that the track he has covered is curved. I was lucky enough to have spotted it."

[3] It is important to realize the distinction between the rationalization that the origin of gravity is by virtue of matter causing spacetime to be curved, and a physical basis consistent with Maxwell's equations and special relativity that the origin of gravity is time dilation and length contraction of spacetime based on the speed of light which is a constant maximum for the propagation of any form of energy at particle production. The relativistic correction of spacetime may be viewed as matter causing spacetime to be curved, but this is a consequence rather than the cause of the origin of gravity.

[4] Although historically Einstein is credited with Eq. (32.40), David Hilbert discovered the same form of the field equations days before Einstein. Einstein had reached his final version of general relativity after a slow road with progress but many errors along the way. In December 1915, he said of himself, "That fellow Einstein suits his convenience. Each year he retracts what he wrote the year before." A reference describing the tremendous broad-based effort to develop the theory of general relativity in the early 20th century is the web site: http://www-history.mcs.st-andrews.ac.uk/HistTopics/General_relativity.html. Also see D. Overbye, "Einstein, Confused in Love, and Sometimes, Physics," New York Times, August 31, 1999, F4.

[5] The Schwarzschild metric was originally derived from Einstein's field equations and is widely used in astrophysical calculations. This metric is widely regarded as a triumph of Einstein's theory of gravitation. Implicit in the Schwarzschild solution is a privileged system of coordinates. Yet, Einstein denied the existence of a privileged system of coordinates in all cases based on his view of the local method of discussing properties of space. The equivalence principle used by Einstein as the basis for Riemannian geometry of space is only valid locally. Einstein underestimated the importance of considering

space as a whole. Having obtained his equation based on the Principle of Equivalence, Einstein realized that the mass of the Universe would cause it to collapse. He would accept only a static Universe. Thus, he added a cosmological constant to his equation. This type of antigravity of spacetime was intended to exactly balance the tendency of matter to cause spacetime to collapse. But, according to his basic postulates, the absence of a gravitational field signifies the absence of deviations of the geometry of spacetime from Euclidean, and therefore, also vanishing of the curvature tensor $R^{\mu\nu}$ and of its invariant *R*. Also, the gravitational field will be absent if the mass tensor $T^{\mu\nu}$ is zero everywhere. Therefore, the equations $T^{\mu\nu}=0$ and $R^{\mu\nu}=0$ must certainly be compatible, and this is only possible if the equations relating $G^{\mu\nu}=R^{\mu\nu}-\frac{1}{2}g^{\mu\nu}R$ to $T^{\mu\nu}$ do not contain the term $\lambda g^{\mu\nu}$. The cosmological constant must be zero. This is also the case in order to obtain consistency with Newton's Law of Gravitation in the same limit. After Hubble's redshift observations in 1929 demonstrated the expansion of the Universe, the original motivation for the introduction of Λ was lost. Nevertheless, Λ has been reintroduced on numerous occasions when discrepancies have arisen between theory and observations, only to be abandoned again when these discrepancies have been resolved. Einstein abandoned the constant calling it the greatest mistake of his life. Einstein failed to notice two other tremendously important features of the Universe, which further undermines his view of a static Universe. A positively curved spacetime has a finite radius based on the mass and energy. And, the Universe is converting about 10^{33} kilograms of matter into energy per second. He also failed to develop an atomic theory of gravity, which is the means to determine the impact of matter to energy conversion on the expansion of the Universe.

In Einstein's equation in its original form, a conservative tensor (the divergence of the tensor is zero) which expresses the curvature of spacetime is equated with a conservative stress-energy-momentum tensor of matter. This approach conserves momentum, matter, and energy. The Schwarzschild metric given as Eq. (57.54) of Fock [17]:

$$ds^2=c^2\left(\frac{r-\frac{GM}{c^2}}{r+\frac{GM}{c^2}}\right)dt^2-\left(\frac{r-\frac{GM}{c^2}}{r+\frac{GM}{c^2}}\right)^{-1}dr^2-\left(r+\frac{GM}{c^2}\right)^2\left(d\theta^2+\sin^2\theta d\phi^2\right) \tag{32.41}$$

is an exact solution of the Einstein's equation based on a preferred system of coordinates. According to a theorem by Birkoff [18] the Schwarzschild metric is the only solution of Einstein's gravity equations for the corresponding boundary conditions of a spherically symmetric time-independent or dynamic solution with zero cosmological constant for the metric of a space which is empty apart from a central spherical body.

The Schwarzschild metric is consistent with observations wherein the radius applies to distances between gravitating bodies. For example, it solves the precession of the perihelion of Mercury and the deflection of light in a gravitational field. However, Einstein's equation with general coordinates has an infinite number of solutions, and none of the possible solutions are consistent with cosmological observations as shown in the Cosmology Section. These solutions are all conservative (the divergence of each metric tensor is zero). The Schwarzschild metric given by Eq. (32.41) is also conservative; whereas, the Schwarzschild metric in the form given by Eq. (32.38) is not conservative.

The Schwarzschild metric (Eq. (32.38)) gives the relationship whereby matter (energy) causes relativistic corrections to spacetime that determines the curvature of spacetime and is the origin of gravity. The Minkowski space is obtained in the limit of no mass at infinity. Eq. (32.41) may be transformed into Eq. (32.38) by the substitution of the radial coordinate *r* with the reduced radial coordinate, $r-\frac{GM}{c^2}$.

The origin of gravity is fundamental particles, and the masses and fields from particles superimpose. The derivation of the correct form of the Schwarzschild metric (Eq. (32.38)) is based on contraction of spacetime during particle production that requires a privileged system of coordinates. Einstein's approach to his equation conserves momentum, matter, and energy. Derivation of the Schwarzschild metric is based on the wave equation that conserves momentum, matter, and energy and additionally requires a maximum constant velocity for the propagation of any signal including a gravitational field at particle production. As a consequence of particle production the radius of the Universe contracts by 2π times the gravitational radius of each particle with the gravitational radius given by Eq. (32.36) which applies to the observed leptons and quarks formed at the gravitational velocity v_g which is the escape velocity given by Eq. (32.35). Thus, *Q*, the mass-energy-to-expansion-contraction quotient of spacetime (Eq. (32.140)), is given by the ratio of the mass of a particle at production divided by *T* the period of the gravitational radius as given by Eq. (32.149) wherein the gravitational radius is the Newtonian gravitational radius given by Eq. (32.36). Thus, *T* is the period of the orbit of the particle relative to the antiparticle during production. By superposition, obtaining the correct solution of the Schwarzschild metric (Eq. (32.38)) requires that the radius of the metric (Eq. (32.41)) be replaced by the radius decreased by the gravitational radius of the central mass (Eq. (32.22) which applies to a particle of the Planck mass). The gravitational radius which gives the spacetime dilation at particle production may be considered the "effective thickness" of fundamental particles which are two dimensional.

It is shown in the Cosmology Based on the Relativistic Effects of Matter/Energy Conversion on Spacetime Section that a 3-sphere spatial geometry describes the Universe which is finite but has no boundary. The radius of the Universe oscillates harmonically between two finite radii. It expands as matter is transformed into energy, and it contracts as the radiation filled Universe reverts back to a matter filled Universe. Matter causes spacetime to become curved like a dimple on a ball, but in three spatial dimensions plus time. Consider such a dimple as shown in Figure 32.3 caused by the Sun which is converting 5 *billion kg* of matter into energy per second. If the conversion persisted indefinitely, the Sun would vanish. The local spacetime dimple would vanish also. Thus, spacetime must expand as matter is converted into energy. The same applies to the Universe as a whole. Due to matter converting to energy the radius of the Universe expands by 2π times the gravitational radius of the converted matter (Eq. (32.140)) with the gravitational radius given by Eq. (32.36) wherein m_0, the mass of a fundamental particle, is replaced by *M*, the sum of the masses of the particles which make up the massive body). The Hubble constant is consistent with the experimental mass to energy conversion rate of the Universe calculated from the number of galaxies (400 *billion*) times the number of stars per galaxy (400 *billion*) times the average mass to energy conversion rate per star (5 *billion kg / sec star*). The Schwarzschild metric (Eq. (32.38)) is shown to explain all current cosmological observations as well as permit the derivation of an equation which correctly predicts the masses of fundamental particles. It is proposed that the Schwarzschild metric (Eq. (32.38)) is an exact description of reality which has as its basis the gravitational velocity v_g of a massive object according to Newton's Law of Gravitation and the constant maximum speed of light. It provides that any discontinuities in the gravitational field caused by matter to energy conversion or vice versa must propagate as a front like a light wave in empty space. This equation does not conserve matter, energy, and momentum separately from spacetime. In this case, matter, energy, momentum, and spacetime are conserved as a totality. The wave equation conserves matter, energy, and momentum. It further provides for the conservation of these physical entities with spacetime and provides a unifying physical principle that gives an oscillating Universe as given in the Wave Equation Section.

force and now the origin of gravity as the relativistic correction of spacetime, magnetism and gravity should be considered more than *corrections*, rather they are *fundamental relativistic effects*.

PARTICLE PRODUCTION

The equations which *unify de Broglie's Equation, Planck's Equation, Maxwell's Equations, Newton's Equations, and Special and General Relativity define the mass of fundamental particles in terms of the spacetime metric*. Eq. (32.32) (Eq. (32.48) *infra.*) gives the equivalence of particle production energies corresponding to mass, charge, current, and gravity according to the proportionality constants which are given in terms of a self-consistent set of units. This equivalence is a consequence of equivalence of the gravitational mass and the inertial mass together with special relativity. Charge is relativistically invariant; whereas, mass and spacetime are not. The fine structure constant is dimensionless and is the proportionality constant corresponding to the relativistic invariance of charge. Thus, it is absolute. All the other constants are not, and any property of mass-energy or spacetime is measurable only in terms of the remaining properties where the metrics and definitions of the properties are in terms of experiments which define a self-consistent circular system of units. In addition to the equivalence of particle production energies corresponding to mass, charge, current, and gravity according to the proportionality constants which are given in terms of a self-consistent set of units, general relativity further provides for the further proportional equivalence with the metric of spacetime of the same self-consistent system of units. The metric of spacetime is used to calculate the mass of the fundamental particles in terms of the same consistent system of units.

Satisfaction of the nonradiative boundary condition precludes emission of electromagnetic radiation. Continuity of boundary conditions requires that particle production gives rise to a gravitational field front which satisfies the same wave equation as electromagnetic radiation and travels at the speed of light. The charge and mass-density functions of an atomic orbital are interchangeable by interchanging the fundamental charge and the particle mass; thus, satisfaction of the boundary condition of no Fourier components of the current-density function which are synchronous with waves traveling at the speed of light also holds for the mass-density function. The transverse electric field of the photon of zero rest mass is replaced by a central electric and gravitational field and a particle and antiparticle. For Euclidean spacetime, the radius of the boundary condition is invariant because the velocity is perpendicular to the radius of the atomic orbital. (The radius of the boundary condition is not length-contracted by special relativistic effects.) However, the nonradiative boundary condition and the constancy of the speed of light must hold which requires relativistic corrections to spacetime.

Mass and charge are concomitantly created with the transition of a photon to a particle and antiparticle. Thus, the energies, which are equal to the mass energies apply for the proper time of the particle (antiparticle) given by general relativity, Eq. (32.38). The transition state from a photon to a particle and antiparticle pair comprises two concentric atomic orbitals called transition state atomic orbitals. The gravitational effect of a spherical shell on an object outside of the radius of the shell is equivalent to that of a point of equal mass at the origin. Thus, the proper time of the concentric transition state atomic orbital with radius ${}^{+}r^{*}$ (the radius is infinitesimally greater than that of the inner transition state atomic orbital with radius r^{*}) is given by the Schwarzschild metric, Eq. (32.38). The proper time applies to each point on the atomic orbital. Therefore, consider a general point in the xy-plane having $r = \lambda\!\!\!^{-}_{C}$; $dr = 0$; $d\theta = 0$; $\sin^2\theta = 1$. Substitution of these parameters into Eq. (32.38) gives:

$$d\tau = dt\left(1 - \frac{2Gm_0}{c^2 r_\alpha^*} - \frac{v^2}{c^2}\right)^{\frac{1}{2}} \tag{32.42}$$

With $v^2 = c^2$, Eq. (32.42) becomes:

$$\tau = ti\sqrt{\frac{2GM}{c^2 r_\alpha^*}} = ti\sqrt{\frac{2GM}{c^2 \lambda\!\!\!^{-}_{c}}} = ti\sqrt{\frac{r_g}{\lambda\!\!\!^{-}_{c}}} = ti\frac{v_g}{c} \tag{32.43}$$

where the gravitational radius, r_g, and the gravitational velocity, v_g, are given by Eqs. (32.35) and (32.36), respectively. The production of a real particle from a transition state atomic orbital is a spacelike event in terms of special relativity wherein spacetime is contracted by the gravitational radius of the particle during its production. Thus, the coordinate time is imaginary as given by Eq. (32.43). On a cosmological scale, imaginary time corresponds to spacetime expansion and contraction as a consequence of the harmonic interconversion of matter and energy as given by Eq. (32.140). The left-hand side of Eq. (32.43) represents the proper time of the particle/antiparticle as the photon atomic orbital becomes matter. The right-hand side of Eq. (32.43) represents the correction to the laboratory coordinate metric for time corresponding to the relativistic correction of spacetime by the particle production event. Riemannian space is conservative, and only changes in the metric of spacetime during particle production must be considered. The changes must be conservative. For example, pair production occurs in the presence of a heavy body. A nucleus which existed before the production event only serves to conserve momentum but is not a factor in determining the change in the properties of spacetime as a consequence of the pair production event. The effect of this and other external gravitating bodies are equal on the photon and resulting particle and antiparticle and do not affect the boundary conditions for particle production. For particle production to occur, the particle must possess the escape velocity relative to the antiparticle where Eqs. (32.34), (32.48), and (32.140) apply.

Eq. (32.43) is valid in the case that $v_g < c$ [6]. The velocity of each mass-density element of the extended particle is equivalent to the gravitational escape velocity v_g of the mass of the antiparticle (Eq. (32.43)). According to Newton's Law of Gravitation the eccentricity is one and the particle production trajectory is a parabola relative to the center of mass of the antiparticle. The mass of each member of a lepton pair corresponds to an energy of Eq. (32.32). The electron and antielectron correspond to the Planck equation energy. The muon and antimuon correspond to the electric energy. And, the tau and antitau correspond to the magnetic energy. However, a pair of particles each of the Planck mass corresponding to the conditions of Eq. (32.22), Eq. (32.32), and Eq. (32.33), is not observed since the velocity of each of the point masses of the transition state atomic orbital is the gravitational velocity v_G that in this case is the speed of light; whereas, the Newtonian gravitational escape velocity v_g of the superposition of the point masses of the antiparticle would be $\sqrt{2}$ the speed of light (Eq. (32.35)). In this case, an electromagnetic wave of mass energy equivalent to the Planck mass travels in a circular orbit around the center of mass of another electromagnetic wave of mass energy equivalent to the Planck mass wherein the eccentricity is equal to zero (Eq. (26.20)), and the escape velocity can never be reached. The relative velocity of Eq. (32.18) given by the velocity addition formula of special relativity for two photons corresponding to a particle and an antiparticle each of the Planck mass is c. In this case, the Compton wavelength bar is the gravitational radius given by Eq. (32.22) where the mass m is the Planck mass, and no matter can escape. Thus, for example, only three pairs of leptons are observed. And, a lepton having the Planck mass is not observed. From Eq. (32.43), the masses of fundamental particles are calculated in the Leptons and Quarks sections.

As stated in the Relativity section, to describe any phenomenon such as the motion of a body or the propagation of light, a definite frame of reference is required. A frame of reference is a certain base consisting of a defined origin and three axes equipped with graduated rulers and clocks. Given the unified relationships between the mass energy, the Planck equation energy, electric potential, magnetic energy, the gravitational potential energy, and the mass/spacetime metric energy given by Eqs. (32.32-32.34) and Eq. (32.48) *infra*., it is possible to reduce the graduated rulers and clocks to a clock alone. The units of measure are interdependent. Eqs. (32.32-32.34) and Eq. (32.48) *infra* which unify the energies also unify the relationships of the units of measurement. *A measure of spacetime does not exist a priori. Thus, one must be defined.* Based on the unification, only the metric of time need be set in the equations such that the other calculable parameters of matter and energy may be expressed relative to the time metric in terms of an internally consistent system of units such as the MKS units. The permeability of free space, μ_0, is defined in terms of the MKS unit NA^{-2} as

$$\mu_0 = 4\pi \ X \ 10^{-7} \ NA^{-2} \tag{32.44}$$

The permeability of free space, μ_0, and the permittivity of free space, ε_0, are derived by converting the Coulombic force law and the magnetic force law from CGS units to MKS units. In CGS units, the unit of charge is defined such that the Coulomb force equation is:

$$F\left(dynes\right) = k\frac{e^2\left(esu^2\right)}{r^2\left(cm^2\right)} \text{ where } k = 1 \tag{32.45}$$

From the magnetic force per unit length law, μ_0 is given by the conversion of:

$$F\left(dynes/cm\right) = k\frac{2I^2\left(esu/\sec\right)^2}{rc^2\left(cm^3/\sec^2\right)} \text{ where } k = 1 \tag{32.46}$$

to

$$F\left(dynes/cm\right) = \frac{\mu_0}{4\pi}\frac{2I^2}{r}\left(\frac{A^2}{m}\right) \tag{32.47}$$

and defined exactly as $\mu_0 = 4\pi \ X \ 10^{-7} \ NA^{-2}$. The experimental definition of charge in MKS units is based on the speed of light. The Coulomb force law gives ε_0 in terms of the MKS charge; thus, ε_0 in terms of MKS units is based on the experimentally measured speed of light. The speed of light is the conversion factor from time to length. Time can also be converted to inertial and gravitational mass and charge according to Eqs. (32.32-32.34) and Eq. (32.48) *infra.* MKS units are selected. In the case of MKS units, the time metric is the second which is substituted for the variable *t* of Eq. (32.43). (See Box 32.1.) Eq. (32.43) which gives the equivalence of time in the proper and coordinate frames according to a dimensionless correction factor provides a definition of the unit of time in terms of fundamental constants. And, the unification equation provides a superior means to define a self-consistent set of units based only on time where

$$m_0c^2 = \hbar\omega^* = V = E_{mag} = E_{grav} = E_{spacetime} \tag{32.48a}$$

---

[6] Eq. (32.42) becomes the special case where $\frac{v_0}{c} = \sqrt{1 - \frac{2Gm_0}{c^2 r_\alpha^*}} = \sqrt{1 - \left(\frac{v_{g0}}{c}\right)^2}$ when $v_0 = v_{g0} = c$ and $\tau_0 = 0$. No particle can form when the proper time, τ_0, is not finite.

$$m_0c^2 = \hbar\omega^* = \frac{\hbar^2}{m_0\lambda\!\!\!^{-2}_C} = \alpha^{-1}\frac{e^2}{4\pi\varepsilon_0\lambda\!\!\!^{-}_C} = \alpha^{-1}\frac{\pi\mu_0 e^2\hbar^2}{(2\pi m_0)^2\lambda\!\!\!^{-3}_C} = \alpha^{-1}\frac{\mu_0 e^2c^2}{2h}\sqrt{\frac{Gm_0}{\lambda\!\!\!^{-}_C}}\sqrt{\frac{\hbar c}{G}} = \frac{\alpha h}{1\text{ sec}}\sqrt{\frac{\lambda\!\!\!^{-}_C c^2}{2Gm_0}} \tag{32.48b}$$

where the mass, m_0, of the relationship containing the time ruler sec must be corrected for the energy of the particle fields corresponding to neutrinos as given in the Leptons section. A superior measure of time is an atomic standard. Using Eq. (32.48b) all other standards are determined according to the metric of time defined by Eq. (32.43).

BOX 32.1 DEFINITION OF TIME UNIT SEC, AND CALCULATION AND MEASUREMENT OF OBSERVABLES OVER ALL SCALES THEREUPON

A unit of time may be defined arbitrarily in terms of how it is measured (such as the time for a defined number of "clicks" of a Cs 133 atom), but mass, charge, energy, spacetime, and other observables are not generalities. The result of unification is that each arises from and is dependent on the other and may be measured on this basis only. The relationships between observables depend on fundamental constants. So, generalities are lost after a clock is defined in terms of the constants. The relationships are circular since no phenomenon is independent of another.

The metric of time, sec, is defined by Eq. (36.2) in terms of fundamental constants and the electron mass with the implicit contraction of spacetime due to the formation of the electron from energy. Eq. (32.29) is equivalent to Eq. (36.2) which is the definition of the sec. However, the form given by Eq. (32.29) gives a method of experimentally determining the metric of time (sec) which does not require the measurement of the electron mass. The electron Compton wavelength, $\lambda\!\!\!^{-}_C$, is equal to the wavelength of the photon which gives rise to the electron, and the velocity of each mass-density element of the extended particle is equivalent to the gravitational escape velocity, v_g, of the mass of the antiparticle (Eq. (32.43)). According to Newton's Law of Gravitation the eccentricity is one and the particle production trajectory is a parabola relative to the center of mass of the antiparticle. Both parameters, $\lambda\!\!\!^{-}_C$ and v_g, may be measured independently of the electron mass. The resulting determination of the unit of the metric of spacetime, sec, may be used to calculate the electron mass (Eq. (36.3)).

Another example that follows from Eq. (32.48) with Eq. (28.15) is:

$$\alpha^{-1}\frac{e^2}{4\pi\varepsilon_0\lambda\!\!\!^{-}_C} = \frac{\alpha h}{1\text{ sec}}\sqrt{\frac{\lambda\!\!\!^{-}_C c^2}{2Gm}}\left(1+\frac{2\pi\alpha^2}{2}\right)^{-2} \tag{32.1.1}$$

$$1\text{ sec} = \frac{4\pi\varepsilon_0\lambda\!\!\!^{-2}_C\alpha^2 2\pi c}{e^2}\sqrt{\frac{\hbar c}{2G}}\left(1+\frac{2\pi\alpha^2}{2}\right)^{-2} = 0.9975\text{ second} \tag{32.1.2}$$

which is based on the time definition of Eq. (36.2), but does not require knowledge of the electron mass for the determination of the unit sec.

The electron mass is not a fundamental constant since it can be derived in terms of the actual fundamental constants given in the Relationship of Spacetime, Matter, and Charge section. The electron mass is given by Eq. (36.3) wherein the time unit sec may be determined independently of any parameter measured directly on the electron. The production (annihilation) of a particle requires that spacetime contract (expand). *The relationship of matter to energy conversion and space time expansion given by Eq. (32.140) is*:

$$Q = \frac{m_0}{\tau} = \frac{m_0}{\frac{2\pi r_g}{c}} = \frac{m_0}{2\pi\frac{2Gm_0}{c^2}} = \frac{c^3}{4\pi G} = 3.22\ X\ 10^{34}\ \frac{kg}{\text{sec}} \tag{32.1.3}$$

That is the conversion of $3.22\ X\ 10^{34}$ kg of matter into energy results in the expansion of the 3-sphere Universe-(Riemannian three-dimensional hyperspace plus time of constant positive curvature at each r-sphere) by one sec. Based on this result with the inherent time unit sec, the Universe is time harmonically oscillatory in matter energy and spacetime expansion and contraction with a minimum radius that is the gravitational radius. With the origin of gravity being the contraction of spacetime during particle production, the masses of particles and the cosmological parameters such as the Hubble constant, the age of the Universe, the observed acceleration of the expansion, the power of the Universe, the mass-density, the power spectrum of the Universe, the microwave background temperature, the uniformity of the microwave background radiation, the microkelvin spatial variation of the microwave background radiation, and the large scale structure of the Universe are given in terms of sec as the definition of the spacetime metric. The harmonic oscillation period, T, of the Universe given by Eq. (32.149) is:

$$T = \frac{2\pi r_G}{c} = \frac{2\pi Gm_U}{c^3} = \frac{2\pi G\left(2\ X\ 10^{54}\ kg\right)}{c^3} = 3.10\ X\ 10^{19}\ \text{sec} \tag{32.1.4}$$

where the mass of the Universe, m_U, is approximately $2\ X\ 10^{54}\ kg$. The mass of the Universe is a fundamental constant which may be measured by internal consistency of the cosmological parameters. From Eq. (32.1.4), the time unit sec is given by the time required for the Universe to complete $\left|\frac{1}{T}\right|$ of a cycle. Thus, the converse of the definition given by Eq. (36.2) holds—cosmological observables each serve as a clock to give a measurement of and circularly define the time unit sec.

The laws of nature are self contained and self consistent such that any phenomena can be described only in terms of all the others, but cannot be described in isolation. A force is simply the change in energy with distance. When matter decays to energy, the energy content of spacetime increases and it expands. This can be thought of in terms of a corresponding force called the "Q force" after Eq. (32.140). The process can only be described in terms of its relationship to Maxwell's equations and other first principles. The interdependencies are summarized in Eq. (32.48).

Eq. (32.48b) gives the circular relationships between matter, energy, and spacetime based on the definition of time given by Eq. (36.2). A unified theory can only provide the relationships between all measurable observables in terms of a clock defined according to those observables and used to measure them. The so ***defined "clock" measures "clicks" on an observable in one aspect, and in another, it is the ruler of spacetime of the Universe with the implicit dependence of spacetime on matter-energy conversion***. In this case, fundamental physical constants and observables calculated in terms of the fundamental constants have no meaning except with regard to the definition of time in terms of the constants. Then all observables such as the excited states of atoms, ionization energies of atoms, chemical bond energies, scattering of electrons from atoms, nuclear parameters, cosmological parameters, etc. are given in terms of the definition of the sec (Eq. (36.2)) which is extremely close to the MKS second. Internal consistency is given with a high degree of precision over the scalar range of 85 orders of magnitude (mass of the electron to mass of the Universe). To achieve exact predictions of particle masses and cosmological parameters which requires the introduction of the spacetime metric as a fundamental constant, a slight modification of the experimental definition of the second may be required. Presently, all fundamental constants including masses are determined in a self-consistent manner involving definitions and measurements. With time defined by Eq. (36.2) and the Compton wavelength bar given by Eq. (32.21), the unit system will ultimately have to be revised according to Eq. (32.48b) which gives the exact relationships between the measurable constants. Then from the definition of the metric of time, sec, in terms of fundamental constants given by Eq. (36.2) and the relationships between the fundamental constants given by Eq. (32.48b), the periods of spacetime expansion (contraction) and particle decay (production) for the Universe are equal as shown in the Period Equivalence section, and the atomic, thermodynamic, and cosmological arrows of time discussed in the Arrow of Time and Entropy section are based on the same time unit**.**

For convenience, the masses of particles derived from Eq. (32.43) and given in the Leptons and Quarks sections as well as the cosmological parameters given in The Expanding Universe and the Microwave Background, The Period of Oscillation Based on Closed Propagation of Light, Equations of the Evolution of the Universe, Power Spectrum of the Cosmos, The Differential Equation of the Radius of the Universe, and Power Spectrum of the Cosmic Microwave Background sections are calculated based on the approximation of the sec to the MKS second wherein MKS units are used. However, the sec may be converted to MKS second based on the deviation of Eq. (36.2) from one second (also Eq. (32.1.2)). The accuracy of the conversion factor of 0.9975 second/sec is limited by the error in the value of the gravitational constant (See Box 32.2). A new system of units would eliminate the need for conversion and permit a more accurate determination of the constants including the definition of time based on internal consistency.

BOX 32.2 RELATIONSHIPS BETWEEN THE EARTH MEAN SOLAR DAY DEFINITION OF THE SECOND, THE DEFINITION OF SEC BASED ON PAIR PRODUCTION AND ITS EFFECT ON SPACETIME, AND THE DEFINITION OF SEC AND THE FUNDAMENTAL CONSTANTS

The definition of the time unit sec is given in terms of the mass of the electron and fundamental constants in Eq. (36.2).

$$2\pi\frac{\hbar}{mc^2}=\sec\sqrt{\frac{2Gm^2}{c\alpha^2\hbar}} \tag{32.2.1}$$

Substitution of the MKS values for the fundamental constants and the electron mass for m including the correction due to the particle fields given by Eq. (36.15) into Eq. (32.2.1) gives $\sec = 0.9975$ MKS seconds. One scenario of how the MKS second (presently defined as the time required for 9,192,631,770 vibrations within the cesium-133 atom) evolved such that it matches the sec to within a ppt follows from Eq. (32.39).

$$\frac{2\pi\lambda\!\!\!^{-}_C}{\sqrt{\frac{2Gm_e}{\lambda\!\!\!^{-}_C}}}=\frac{2\pi\lambda\!\!\!^{-}_C}{v_g}=i\alpha^{-1}\sec \tag{32.2.2}$$

The electron Compton wavelength, $\lambda\!\!\!^{-}_C$, is equal to the wavelength of the photon which gives rise to the electron, and the velocity of each mass-density element of the extended particle is equivalent to the gravitational escape velocity, v_g, of the mass of the antiparticle (Eq. (32.43)). According to Newton's Law of Gravitation, the eccentricity is one and the particle production trajectory is a parabola relative to the center of mass of the antiparticle. In the case of particle production, Eq. (1.16) gives

$$r_n=\lambda_n \tag{32.2.3}$$

Substitution of Eq. (32.2.3) into Eq. (32.2.2) gives:

$$\frac{2\pi r}{\sqrt{\frac{2Gm_e}{r}}} = \frac{2\pi r}{v_g} = i\alpha^{-1} \text{ sec} \tag{32.2.4}$$

which gives the definition of sec in terms of traveling the distance corresponding to one particle orbit at the gravitational velocity.

The Mean Solar Day (1956) definition of the time unit second was based on the day-night cycle of the Earth defined as the time for 1/86,400 th of a rotation of the Earth. This definition was the predecessor to the MKS definition of time which is also based on the second. The exact number, 86,400, permits the day-night cycle to be expressed in terms of 24 hours per day, 60 minutes per hour, and 60 second per minute. One method of advancing the definition of second is to develop a relationship between the fundamental constants and Newton's Law of Gravitation regarding the Earth. The gravitational velocity of the Earth, v_{g_E}, is:

$$v_{g_E} = \sqrt{\frac{2GM}{R}} = 1.1\ X\ 10^4\ m/s \tag{32.2.5}$$

where $R = 6\ X\ 10^6\ m$ is the radius of the Earth, and $M = 6\ X\ 10^{24}\ kg$ is the mass of the Earth. Eq. (32.2.5) is also the gravitational escape velocity. A Mean Solar Day definition of the second based on constants and gravity is:

$$\frac{L}{2K_{g_E}} = \frac{L}{m\left(v_{g_E}\right)^2} = \frac{L/m}{\left(v_{g_E}\right)^2} = \alpha^{-1}\ s \tag{32.2.6}$$

where the fine structure constant, α, is dimensionless, L/m is the angular momentum per unit mass over 2π radians, K_{g_E} is the kinetic energy corresponding to the gravitational escape velocity, and the escape velocity, v_{g_E}, is given by Eq. (32.2.5). L/m is given by

$$\mathbf{L}/m = 2\pi\mathbf{R}\times\mathbf{v} \tag{32.2.7}$$

Substitution of Eq. (32.2.7) into Eq. (32.2.6) gives:

$$\frac{L/m}{\left(v_{g_E}\right)^2} = \frac{2\pi R}{v_{g_E}}\frac{v}{v_{g_E}} = \alpha^{-1}\ s \tag{32.2.8}$$

where the linear velocity of the Earth at the equator due to rotation is given by:

$$v = \frac{2\pi R}{T} \tag{32.2.9}$$

where T is the period of rotation. From the Mean Solar Day (1956) definition

$$T = 86,400\ s \tag{32.2.10}$$

Substitution of Eqs. (32.2.9) and (32.2.10) into Eq. (32.2.8) gives:

$$\frac{L/m}{\left(v_{g_E}\right)^2} = \frac{2\pi R}{v_{g_E}}\frac{\frac{2\pi R}{86,400\ s}}{v_{g_E}} = \alpha^{-1}\ s \tag{32.2.11}$$

Substitution of Eq. (32.2.5) into Eq. (32.2.11) gives:

$$\frac{\frac{\left(2\pi R\right)^2}{86,400\ s}}{\left(1.1\ X\ 10^4\ m/s\right)^2} = \frac{\frac{\left(2\pi\left(6\ X\ 10^6\ m\right)\right)^2}{86,400\ s}}{\left(1.1\ X\ 10^4\ m/s\right)^2} = 136\ s \approx \alpha^{-1}\ s \tag{32.2.12}$$

This close identity may have played a role in choosing the number 86,400 in the definition of the second.

Now consider the relationship between Eq. (32.2.8) and Eq. (32.2.2). In the case of pair production, the electron linear velocity is the gravitational escape velocity, and the radius is the Compton wavelength bar, $\lambda\!\!\!^{-}_C$, as given by Eqs. (32.2.2-32.2.4). Thus, Eq. (32.2.8) may be written as

$$\frac{L/m}{\left(v_{g_E}\right)^2} = \frac{2\pi R}{v_g}\frac{v}{v_g} = \frac{2\pi R}{v_g}\frac{v_g}{v_g} = \frac{2\pi\lambda\!\!\!^{-}_C}{v_g} = \frac{2\pi\lambda\!\!\!^{-}_C}{\sqrt{\frac{2Gm_e}{\lambda\!\!\!^{-}_C}}} = i\alpha^{-1}\ s \tag{32.2.13}$$

where the imaginary number indicates that pair production is spacelike. Eq. (32.2.13) is identical to Eq. (32.2.2). Thus, the Mean Solar Day definition of the second and the definition of sec given by Eq. (32.2.2) are identical to the extent that Eq. (32.2.12) is identically the reciprocal of the fine structure constant. And, other equivalent parallels between Eq. (32.2.2) and (32.2.8) are given in terms of other fundamental constants using Eq. (32.48b) and (Eq. (33.21)) which give the relationships between the constants and the time unit sec.

ORBITAL MECHANICS

Newton's differential equations of motion in the case of the central field are:

$$m(\ddot{r} - r\dot{\theta}^2) = f(r) \tag{32.49}$$

$$m(2\dot{r}\dot{\theta} + r\ddot{\theta}) = 0 \tag{32.50}$$

where $f(r)$ is the central force. The second or transverse equation, Eq. (32.50), gives the result that the angular momentum is constant,

$$r^2\dot{\theta} = \text{constant} = L/m \tag{32.51}$$

where L is the angular momentum. The central force equations can be transformed into an orbital equation by the substitution, $u = \frac{1}{r}$. The differential equation of the orbit of a particle moving under a central force is:

$$\frac{\partial^2 u}{\partial\theta^2} + u = \frac{-1}{\frac{mL^2u^2}{m^2}} f(u^{-1}) \tag{32.52}$$

Because the angular momentum is constant, motion in only one plane need be considered; thus, the orbital equation is given in polar coordinates. The solution of Eq. (32.52) for an inverse square force,

$$f(r) = -\frac{k}{r^2} \tag{32.53}$$

is

$$r = r_0 \frac{1+e}{1+e\cos\theta} \tag{32.54}$$

$$e = A\frac{m\frac{L^2}{m^2}}{k} \tag{32.55}$$

$$r_0 = \frac{m\frac{L^2}{m^2}}{k(1+e)} \tag{32.56}$$

where e is the eccentricity and A is a constant. The equation of motion due to a central force can also be expressed in terms of the energies of the orbit. The square of the speed in polar coordinates is

$$v^2 = (\dot{r}^2 + r^2\dot{\theta}^2) \tag{32.57}$$

Since a central force is conservative, the total energy, E, is equal to the sum of the kinetic, T, and the potential, V, and is constant. The total energy is

$$\frac{1}{2}m(\dot{r}^2 + r^2\dot{\theta}^2) + V(r) = E = \text{ constant} \tag{32.58}$$

Substitution of the variable $u = \frac{1}{r}$ and Eq. (32.51) into Eq. (32.58) gives the orbital energy equation.

$$\frac{1}{2}m\frac{L^2}{m^2}[(\frac{\partial^2 u}{\partial\theta^2}) + u^2] + V(u^{-1}) = E \tag{32.59}$$

Because the potential energy function $V(r)$ for an inverse square force field is:

$$V(r) = -\frac{k}{r} = -ku \tag{32.60}$$

the energy equation of the orbit, Eq. (32.59),

$$\frac{1}{2}m\frac{L^2}{m^2}[(\frac{\partial^2 u}{\partial\theta^2}) + u^2] - ku = E \tag{32.61}$$

which has the solution

$$r = \frac{m\frac{L^2}{m^2}k^{-1}}{1 + [1 + 2Em\frac{L^2}{m^2}k^{-2}]^{1/2}\ \cos\theta} \tag{32.62}$$

where the eccentricity, *e*, is:

$$e = [1 + 2Em\frac{L^2}{m^2}k^{-2}]^{1/2} \tag{32.63}$$

Eq. (32.63) permits the classification of the orbits according to the total energy, *E*, as follows:

$$\begin{array}{lll} E<0, & e<1 & \text{ellipse} \\ E<0, & e=0 & \text{circle (special case of ellipse)} \\ E=0, & e=1 & \text{parabolic orbit} \\ E>0, & e>1 & \text{hyperbolic orbit} \end{array} \tag{32.64}$$

Since $E = T + V$ and is constant, the closed orbits are those for which $T < |V|$, and the open orbits are those for which $T \geq |V|$. It can be shown that the time average of the kinetic energy, $< T >$, for elliptic motion in an inverse square field is $1/2$ that of the time average of the potential energy, $< V >$: $< T >= 1/2 < V >$.

In Newtonian gravitation, the central force between two particles of masses m_1 and m_2 separated by a distance r is:

$$F = G\frac{m_1 m_2}{r^2} \tag{32.65}$$

where G is the gravitational constant, its value being $6.67\ X\ 10^{-11}\ Nm^2kg^{-2}$. The theoretical difficulty with Newtonian gravitation is to explain just why Eq. (32.5) exists implicitly in Newton's theory as a separate law of nature besides Eq. (32.1) and Eq. (32.2). Even so, Newtonian gravitation and mechanics was the first truly successful dynamics, and its most well-known application was in celestial mechanics. The verification of the prediction of the existence of Neptune marked the peak of the success of celestial mechanics, but the first real difficulty was also met here. It was first pointed out in 1850, based on astronomical observations, that there was a discrepancy between certain observations of the orbit of Mercury and the predictions made by Newtonian mechanics. According to Newton's theory of gravitation, the Sun's gravitational force acting on Mercury causes its orbit to be a closed ellipse. In fact it is not a precise ellipse: with every revolution, its major axis rotates slightly. The observed rate of Mercury's precession (rotation) of the perihelion (major axis) is 1° 33'20" per century. This value ought to be due to the gravitational perturbations of all other planets and the effect of rotation of our Earth-based coordinate system. However, the value calculated from Newtonian mechanics is 1° 32'37" per century. The discrepancy between them of

$$1°\ 33'20" - 1°\ 32'37 = 43" \tag{32.66}$$

is extremely small, but it has been observed with a negligible amount of observational error, and it represents a tremendous outstanding problem for Newtonian mechanics.

RELATIVISTIC CORRECTIONS OF NEWTONIAN MECHANICS AND NEWTONIAN GRAVITY

Newtonian mechanics (Eqs. (32.2)) is corrected by Lorentz transformations of the time, length, mass, momentum, and energy of an object (Eqs. (30.17-30.22)). Similarly Newtonian gravitation is corrected by relativistic corrections of the metric. The Schwarzschild metric is relativistically correct and may be solved to provide the orbital equation. The force is central; therefore, the angular momentum per unit mass is constant. The transverse differential equation of motion in the case of the central field,

$$m(2\dot{r}\dot{\phi} + r\ddot{\phi}) = 0 \tag{32.67}$$

gives the result that the angular momentum is constant

$$r^2\dot{\phi} = \text{constant} = L_\phi / m \tag{32.68}$$

where L_ϕ is the ϕ component of the angular momentum of an orbiting body of mass m. Eq. (32.38) may be expressed as:

$$1 = \left(1 - \frac{2Gm_0}{c^2 r}\right)\left(\frac{dt}{d\tau}\right)^2 - \frac{1}{c^2}\left[\left(1 - \frac{2Gm_0}{c^2 r}\right)^{-1}\left(\frac{dr}{d\tau}\right)^2 + r^2\left(\frac{d\phi}{d\tau}\right)^2\right] \tag{32.69}$$

The relativistic correction for time is:

$$\tau^2 = t^2\left(1 - \left(\frac{v_g}{c}\right)^2\right) \tag{32.70}$$

It has the same form as the special relativistic correction for time with v_g in place of v. This correction may be determined by considering an object of mass m orbiting an object of mass M. The gravitational force is central; thus the angular momentum is constant. Consider that a radial force is applied to increase the radius r of the object's orbit with a change of its energy E. The angular momentum is conserved; thus,

$$mr_i^2\left(\frac{d\phi}{dt}\right)_i = mr_f^2\left(\frac{d\phi}{dt}\right)_f \tag{32.71}$$

where $\left(\frac{d\phi}{dt}\right)_i$ is the initial angular velocity, $\left(\frac{d\phi}{dt}\right)_f$ is the final angular velocity, r_i is the initial radius and r_f is the final radius. At fixed radius, dr^2 is zero, but dt^2 is finite. Applying the time relativistic correction given by Eq. (32.38) and Eqs. (32.14-32.17) gives the mass m_f at r_f with respect to the mass m_i of the inertial frame of r_i as:

$$m_i\sqrt{\left(1-\frac{2GM}{rc^2}\right)}=m_f \tag{32.72}$$

where r is the increase in the radius. The proper energy E_p of the object is given by:

$$m_ic^2\sqrt{\left(1-\frac{2GM}{rc^2}\right)}=E_p \tag{32.73}$$

The relativistic correction for energy is of the same form as the special relativistic correction for mass (Eq. (31.21)) with v_g in place of v.

$$\frac{E}{\sqrt{1-\left(\frac{v_g}{c}\right)^2}}=mc^2 \tag{32.74}$$

where m is the coordinate mass of the orbiting body and E is the energy of the orbiting object. In the case that the gravitational velocity is much less than the speed of light ($v_g << c$), the gravitational energy E_g converges to that given by Newton.

$$E\approx mc^2\left(1-\frac{1}{2}\left(\frac{2GM}{rc^2}\right)\right) \tag{32.75}$$

$$E\approx mc^2-\frac{GMm}{r} \tag{32.76}$$

$$E_g=-\frac{GMm}{r} \tag{32.77}$$

PRECESSION OF THE PERIHELION

Combining Eq. (32.73) and Eq. (32.38) in terms of the time differentials gives:

$$\left(1-\frac{2GM}{rc^2}\right)\frac{dt}{d\tau}=\frac{E}{mc^2} \tag{32.78}$$

Eq. (32.78) is herein derived from first principles. It is ***postulated*** in previous solutions [8, 11]. Having arrived at the basis for the orbital equation using the correct physics, the derivation follows from Fang and Ruffini [8]. Eqs. (32.69), (32.78) and (32.68) are the equations of motion of the geodesic, which give

$$\left(\frac{dr}{d\phi}\right)^2=\frac{r^4}{L_\phi^2}\left[\left(\frac{E}{c}\right)^2-\left(1-\frac{2GM}{c^2r}\right)\left(\frac{L_\phi^2}{r^2}+m^2c^2\right)\right] \tag{32.79}$$

The central force equations can be transformed into an orbital equation by the substitution, $u=\frac{1}{r}$. The relativistically corrected differential equation of the orbit of a particle moving under a central force is:

$$\left(\frac{du}{d\phi}\right)^2+u^2=\frac{\left(\frac{E}{c}\right)^2-m^2c^2}{L_\phi^2}+\frac{m^2c^2}{L_\phi^2}\left(\frac{2GM}{c^2}\right)u+\left(\frac{2GM}{c^2}\right)u^3 \tag{32.80}$$

By differentiating with respect to ϕ, noting that $u=u(\phi)$ gives

$$\frac{d^2u}{d\phi^2}+u=\frac{GM}{a^2}+\frac{3}{2}\left(\frac{2GM}{c^2}\right)u^2 \tag{32.81}$$

where

$$a=\frac{L_\phi}{m} \tag{32.82}$$

In the case of a weak field,

$$\left(\frac{2GM}{c^2}\right)u<<1 \tag{32.83}$$

and the second term on the right-hand of Eq. (32.81) can then be neglected in the zero-order. In such a case the solution is

$$u_0 - \frac{GM}{a^2} = A\cos\left(\phi + \phi_0\right) \tag{32.84}$$

where A and ϕ_0 denote the constants of integration. The orbits of Eq. (32.84) are conic sections and are specified in terms of eccentricity

$$e = \frac{Aa^2}{GM} \tag{32.85}$$

and perihelion distance

$$r_{\min} = \frac{a^2}{GM\left(1+e\right)} \tag{32.86}$$

If $e<1$, the orbits are bound and elliptical in shape. In the case for which the minor axis is parallel to $\phi = 0$ (i.e. $\phi_0 = 0$), the ellipse can be written as:

$$u_0 = \frac{1}{r} = \frac{GM}{a^2}\left(1 + e\cos\phi\right) \tag{32.87}$$

The correction to the elliptical orbits caused by the relativistic term $\frac{3}{2}\left(\frac{2GM}{c^2}\right)u^2$ in Eq. (32.81) is calculated. The value of this term is only about 10^{-7} for Mercury and far less for other planets, so that it is only necessary to calculate the lowest order corrections, called the ***post-Newtonian corrections***. Substituting Eq. (32.87) into the second term on the right-hand side of Eq. (32.81), gives:

$$\frac{d^2u}{d\phi^2} + u = \frac{GM}{a^2} + \varepsilon\frac{3GM}{a^2}\left[2e\cos\phi + \left(1 + e^2\cos^2\phi\right)\right] \tag{32.88}$$

where $\varepsilon = \left(\frac{GM}{ca}\right)^2 << 1$. Let $u = u_0 + u_1$. Then the equation for the first-order correction function u_1 is:

$$\frac{d^2u_1}{d\phi^2} + u_1 = \varepsilon\frac{3GM}{a^2}\left[2e\cos\phi + \left(1 + e^2\cos^2\phi\right)\right] \tag{32.89}$$

This is an equation for forced oscillations. In Eq. (32.89), the only important term on the right-hand side is the first one, which is resonant, while the second non-resonant term will only cause a slight periodic variation in the position of the perihelion. Thus, after neglecting the non-resonant term, Eq. (32.87) becomes:

$$\frac{d^2u_1}{d\phi^2} + u_1 = \varepsilon\frac{6GM}{a^2}e\cos\phi \tag{32.90}$$

A solution can be obtained as:

$$u_1 = \varepsilon\frac{3GMe}{a^2}\phi\sin\phi \tag{32.91}$$

The presence of a multiplicative factor ϕ in the solution causes a cumulative effect which can be observed clearly after a sufficiently large number of revolutions.

Using the above solution, by considering the relativistic correction up to the first order, the orbit is:

$$u = u_0 + u_1 = \frac{GM}{a^2}\left[1 + e\left(\cos\phi + 3\varepsilon\phi\sin\phi\right)\right] \tag{32.92}$$

or

$$r \approx \frac{\frac{a^2}{GM}}{\left\{1 + e\cos\left[\phi\left(1-3\varepsilon\right)\right]\right\}} \tag{32.93}$$

as ε is small.

Perihelia occur when the cosine is unity; thus, they are given by the following condition:

$$\phi\left(1-3\varepsilon\right) = 2\pi n \tag{32.94}$$

where n is any integer. This can be approximated as:

$$\phi = 2\pi n + 6\pi n\varepsilon \tag{32.95}$$

Therefore, the azimuth angle ϕ increases with increasing n, corresponding to a precession of the major axis of the ellipse. The angular precession $\Delta\phi_1$ per revolution is:

$$\Delta\phi_1 = \frac{6\pi GM}{c^2 r_{\min}\left(1+e\right)} \tag{32.96}$$

and the centennial precession $\Delta\phi$ is:

$$\Delta\phi = \frac{6\pi GMN}{c^2 r_{\min}(1+e)} \tag{32.97}$$

where N is the number of revolutions per century.

Only for the planets Mercury, Venus, and the Earth, and the asteroid Icarus, is $r_{\min}$ small enough and M large enough for $\Delta\phi$ to be measured. The results are as shown in Table 32.1. The large uncertainty in the measured precession of Venus arises from the near-circularity of the orbit (e is only 0.0068), which makes it difficult to locate the precession. These results support that the Schwarzschild metric derived from Maxwell's equations is the correct theory of gravitation.

Table 32.1. Observed and theoretical angle of precession of the perihelion of Mercury, Venus, Earth, and Icarus.

Planet	Observed $\Delta\phi^{100}$ (seconds of arc)	Theoretical $\Delta\phi^{100}$ (seconds of arc)
Mercury	43.11 ± 0.45	43.03
Venus	8.4 ± 4.8	8.6
Earth	5.0 ± 1.2	3.8
Icarus	9.8 ± 0.8	10.3

Other sources of precession must be ruled out in order to definitely assign the remaining precession to a Newtonian correction based on the Schwarzschild metric. The most important source of some precession is the non-spherical symmetry of the Sun. If the Sun is slightly oblate, its gravitational potential would be:

$$V = \frac{GM}{r}\left[1 - J_2 \frac{R_{Sun}^2}{r^2}\left(\frac{3\cos^2\theta - 1}{2}\right)\right] \tag{32.98}$$

where J_2 is the oblateness of the Sun. The corresponding rotation of the perihelion per revolution of the Sun is:

$$\Delta\phi = \frac{6\pi GM}{r_{\min}(1+e)} J_2 \frac{\frac{R_{Sun}^2}{MG}}{2r_{\min}(1+e)} \tag{32.99}$$

The lack of data of J_2 is the major limitation in determining the Sun's contribution if any. Measurement of J_2 from the visual oblateness of the Sun is difficult, and the results are in dispute. Dicke and Goldenberg have claimed that this oblateness is as large as $J_2 = 5\ X\ 10^{-5}$ [8], corresponding to about 20% of the remaining precession. However, recent observations indicate that the oblateness of the Sun is far less corresponding to $J_2 = (1.84 \pm 1.25)\ X\ 10^{-6}$. Inference of J_2 by comparing results for Mercury and Mars is also difficult. The effect for Mars is very small, and the influences of the asteroid belt on the orbit of Mars make the interpretation of a measured precession difficult. J_2 should be directly measured by tracking a spacecraft that passes close to the Sun. In one scenario, the spacecraft would be sent from the Earth to pass by Jupiter to obtain a "gravity assist." Due to the Jupiter encounter, the spacecraft would be made to travel perpendicular to the ecliptic. After several years of flight, the spacecraft would pass by the Sun in less than a day and J_2 would be estimated from that brief encounter.

DEFLECTION OF LIGHT

The photon has $\hbar$ of angular momentum, which must be conserved while light passes a gravitating body. In addition, particle production causes contraction of spacetime. According to the Schwarzschild metric matter causes relativistic corrections to the spacetime metric that determines the curvature of spacetime and is the origin of gravity. Due to conservation of angular momentum, *Newtonian mechanics predicts the bending of the trajectory of light in a gravitational field.* The deflection predicted by Newtonian gravitation is less than the experimental value, but closely matches the experimental value when relativistically corrected. As early as 1801, Soldner calculated the deflection of light in gravitational fields using Newtonian mechanics. Eq. (32.87) corresponds to unbound hyperbolic orbits if the eccentricity e exceeds unity. The asymptotes, where $r \to \infty$, correspond to the angles shown in Figure 32.1 having the following relationship

$$\phi_{\pm} = \pm\left(\frac{\pi}{2} + \frac{1}{2}\delta\right) \tag{32.100}$$

where δ is the total Newtonian deflection of the ray, given by:

$$\cos\phi_{\pm} = -\frac{1}{e} \tag{32.101}$$

which is equivalent to:

$$\sin\frac{1}{2}\delta=\frac{1}{e} \tag{32.102}$$

Figure 32.1. The coordinate parameters of the deflection of light in the gravitational field of the Sun.

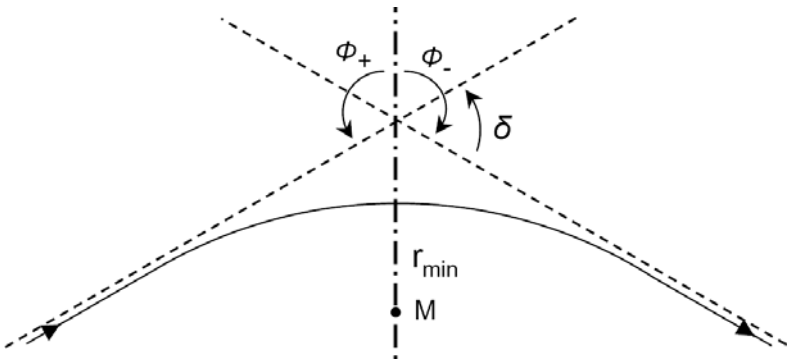

Using the speed of light c, Eq. (32.51) and $a=\frac{L_\phi}{m}$, the angular momentum per unit mass of the photon, a, is approximately

$$a\approx r_{\min}c \tag{32.103}$$

The eccentricity follows from Eq. (32.85) and Eq. (32.86).

$$e=\frac{a^2}{GMr_{\min}}-1\approx\frac{c^2r_{\min}}{GM}-1\approx\frac{c^2r_{\min}}{GM} \tag{32.104}$$

Since $\frac{c^2r_{\min}}{GM}>>1$, e is very large and δ is very small, so that we have approximately,

$$\sin\left(\frac{1}{2}\delta\right)\approx\frac{1}{2}\delta=\frac{1}{e} \tag{32.105}$$

that is

$$\delta=\frac{2GM}{c^2r_{\min}} \tag{32.106}$$

For light grazing the surface of the Sun, $r_{\min}=R_{Sun}$ and $M=M_{Sun}$, giving:

$$\delta=0".875 \tag{32.107}$$

The Newtonian deflection must be corrected relativistically to calculate the true deflection δ. The results obtained in the Precession of the Perihelion section can be applied to light propagation in gravitational fields wherein the *gravitational mass of light is zero* (rather than the rest mass of light is zero as typically given [8])[7]. Substitution of $m=0$ in Eq. (32.81) gives

$$\frac{d^2u}{d\phi^2}+u=\frac{3GM}{c^2}u^2 \tag{32.108}$$

If $M=0$, the path of the light would be a straight line with the orbit equation,

$$u_0=\frac{1}{r_{\min}}\cos\left(\phi+\phi_0\right) \tag{32.109}$$

where $r_{\min}$ and ϕ_0 are constants of integration. By making $\phi_0=0$, up to the first order correction, Eq. (32.108) gives:

$$\frac{d^2u}{d\phi^2}+u=\frac{3GM}{c^2r_{\min}^2}\cos^2\phi \tag{32.110}$$

which has the solution:

$$u=\frac{1}{r_{\min}}\cos\phi+\frac{GM}{c^2r_{\min}^2}\left(1+\sin^2\phi\right) \tag{32.111}$$

[7] According to standard general relativity, the solution of the deflection of light in a gravitational field requires that the gravitational mass of the photon be zero. To avoid an inconsistency with the equivalence principle, a hand-waving argument is offered wherein the parameter *m* in Eq. (32.81) which is unequivocally the gravitational mass somehow becomes the photon rest mass. As shown in the Cosmology section, since the gravitational field and the photon both travel at the speed of light, the photon cannot give rise to a gravitational field without violating causality. The zero rest mass argument is made further internally inconsistent by invoking special relativity to magically make the rest mass of the photon be zero, but special relativity absolutely requires that the speed of the photon be c for all inertial frames with the absence of a special frame. Specifically, the frame in terms of the historical data is that of an Earth observer, not a photon rest frame.

The asymptote is determined by taking $r \to \infty$, namely,

$$0 = -\frac{1}{r_{\min}} \sin\frac{\delta}{2} + \frac{GM}{c^2 r_{\min}^2}\left(1 + \cos^2\frac{\delta}{2}\right) \tag{32.112}$$

Since $\delta \approx 0$ and $\frac{GM}{c^2 r_{\min}} << 1$, the deflection δ is:

$$\delta \approx \frac{4GM}{c^2 r_{\min}} \tag{32.113}$$

This is twice the unrelativistically corrected Newtonian value. For light grazing the Sun,

$$\delta = 1".75 \tag{32.114}$$

It is only possible to measure the deflection of light from a star during a total eclipse of the Sun. A comparison between the measured relative positions of the stars around the Sun during an eclipse and six months later (i.e. in the absence of the Sun's gravitational field in the region), gives $\Delta\phi$, the Sun's deflection of light from these stars. $\Delta\phi$ has been measured for about 400 stars since 1919. The experimental results all lie within the limits 1".57-2".37 with a mean value of 1".89. These results disagree with the prediction of unrelativistically corrected Newtonian theory. But, ***the predicted and experimentally observed values agree quite well after general relativistic correction of Newton's Law of Gravitation.***

Observation of deflections is experimentally difficult. For example, the effect of the solar corona limits measurements of the star with $r_{\min} > 2R_{Sun}$. Total eclipses of the Sun are not usually observable at locations where large telescopes are available. The accuracy of the measurement is restricted by the size of the diffraction disc of the telescope (e.g. a 10 cm diameter telescope has a diffraction disc of about $5\ X\ 10^{-6}$ arc). Moreover, exposures and developing made at different times give rise to systematic errors.

Recently, radiosources have been used for detecting the deflection of light. Since the precision of the direction measurements made by very long baseline interferometry can be very high compared to telescopes, the corresponding data is superior. For example, QSO 3C279 is occulted annually by the Sun. The deflection results are obtained by measuring the angle between 3C279 and 3C273 before and after an occultation. Some of these results are listed in Table 32.2.

Table 32.2. The angle of deflection of the propagation of a light ray $\Delta\phi$ by a gravitating body.

Name of Observatory	Frequency (MHz)	Length of Baseline (km)	$\Delta\phi$
OWENSVALLEY	9602	1	1".7 ± 0".20
GOLDSTONE	2388	21.566	1".82 ± 0".24 0".17
GOLDSTONE HAYSTACK	7840	3899.22	1".80 ± 0".2
NRAO	2695		
	8085	2.7	1".57 ± 0".08
NRAO	2697		
	4993.8	1.41	1".87 ± 0".3

In addition, radiosources 0119+11, 0116+08, and 0111+02 are collinear such that when the ecliptic of the Sun crosses 0116+08, 0119+11 and 0111+02 are each on one side of the ecliptic, making angles of 4° and 6° with the ecliptic, respectively. The Sun passes through the celestial region near 0116+08 in the first ten days of April. The effects of the corona are eliminated using two frequencies, 2695 and 8085 MHz. Fomaleont and Sramek have obtained the result $\Delta\phi = 1".761 \pm 0".010$ by measuring the change in the relative positions of the three radiosources using the 35 km baseline interferometry at NRAO when the Sun passed 0116+08.

COSMOLOGY

The development of the cosmological solutions of Einstein's general relativity with big bang theory are from Wald [13]. The failings of this theory and a discussion of solutions by the author of this book are given in this section in italicized text to distinguish the author's work from that of Wald.

A space in which the curvature tensor $R_{\mu\nu,\alpha\beta}$ having the form:

$$R_{\mu\nu,\alpha\beta} = K \cdot (g_{\nu\alpha} g_{\mu\beta} - g_{\mu\alpha} g_{\nu\beta}) \tag{32.115}$$

is satisfied (with $K = \text{constant}$) is called a space of constant curvature; it is a four-dimensional generalization of Friedmann-Lobachevsky space. The constant *K* is called the constant of curvature. If in these relations *K* is zero, the spacetime is Galilean and the transformations in questions are Lorentz transformations, except when other (non-Galilean) coordinates are used. It can be shown [19] that any two spaces of constant curvature of the same dimension and metric signature which have equal values of

K must be (locally) isometric. Thus, our task of determining the possible spatial geometries of a hypersurface Σ_t will be completed if we enumerate spaces of constant curvature encompassing all values of K. This is easily done. All positive values of K are attained by the 3-spheres, defined as the surfaces in four-dimensional flat Euclidean space R^4 whose Cartesian coordinates satisfy

$$x^2 + y^2 + z^2 + w^2 = R^2 \tag{32.116}$$

In spherical coordinates, the metric of the unit 3-sphere is:

$$ds^2 = d\psi^2 + \sin^2\psi\left(d\theta^2 + \sin^2\theta d\phi^2\right) \tag{32.117}$$

The value $K = 0$ is attained by ordinary three-dimensional flat space. In Cartesian coordinates, this metric is

$$ds^2 = dx^2 + dy^2 + dz^2 \tag{32.118}$$

Finally, all negative values of K are attained by the three-dimensional hyperboloids, defined as the surfaces in a four-dimensional flat Lorentz signature spaces (i.e., Minkowski spacetime) whose global inertial coordinates satisfy

$$t^2 - x^2 - y^2 - z^2 = R^2 \tag{32.119}$$

In hyperbolic coordinates, the metric of the unit hyperboloid is:

$$ds^2 = d\psi^2 + \sinh^2\psi\left(d\theta^2 + \sin^2\theta d\phi^2\right) \tag{32.120}$$

The new possibilities for the global spatial structure of our Universe should be stressed. In prerelativity physics, as well as in special relativity, it was assumed that space had the flat structure given by the possibility $K = 0$ above. But even under the very restrictive assumptions of homogeneity and isotropy, the framework of general relativity admits two other distinct possibilities. The possibility of a 3-sphere spatial geometry is particularly interesting, as it is a compact manifold and thus describes a Universe which is finite but has no boundary. Such a Universe is called "closed," while the Universes with noncompact spatial sections such as those given by flat and hyperboloid geometries are called "open." (One could construct closed Universes with flat or hyperboloid geometries by making topological identifications, but it does not appear to be natural to do so.) Thus, an intriguing question raised by general relativity is whether our Universe is closed or open.

Consider isotropic observers orthogonal to the homogeneous hypersurfaces Σ_t. In this case, we may express the four-dimensional spacetime metric g_{ab} as:

$$g_{ab} = -u_a u_b + h_{ab}(t) \tag{32.121}$$

where for each t, $h_{ab}(t)$ is the metric of either (a) a sphere, (b) flat Euclidean space, or (c) a hyperboloid, on Σ_t. We can choose, respectively, either (a) spherical coordinates, (b) Cartesian coordinates, or (c) hyperbolic coordinates on one of the homogeneous hypersurfaces. We then "carry" these coordinates to each of the other homogeneous hypersurfaces by means of our isotropic observers; i.e., we assign a fixed spatial coordinate label to each observer. Finally, we label each hypersurface by the proper time, τ, of a clock carried by any of the isotropic observers. (By homogeneity, all the isotropic observes must agree on the time difference between any two hypersurfaces.) Thus, τ and our spatial coordinates label each event in the Universe.

Expressed in these coordinates, the spacetime metric takes the form:

$$ds^2 = -d\tau^2 + a^2(\tau)\begin{cases} d\psi^2 + \sin^2\psi\left(d\theta^2 + \sin^2\theta d\phi^2\right) \\ dx^2 + dy^2 + dz^2 \\ d\psi^2 + \sinh^2\psi\left(d\theta^2 + \sin^2\theta d\phi^2\right) \end{cases} \tag{32.122}$$

where the three possibilities in the bracket correspond to the three possible spatial geometries. The metric for the spatially flat case could be made to look more similar to the other cases by writing it in spherical coordinates as:

$$d\psi^2 + \psi^2\left(d\theta^2 + \sin^2\theta d\phi^2\right) \tag{32.123}$$

The general form of the metric, Eq. (32.122) is called a Robertson-Walker cosmological model. The assumptions of homogeneity and isotropy alone determine the spacetime metric up to three discrete possibilities of spatial geometry and arbitrary positive function $a(\tau)$. Einstein's equation can be solved for the spatial geometry and $a(\tau)$. As shown *infra* the result is that all possible solutions of Einstein's equation are inconsistent with the observation that the expansion of the cosmos accelerates.

FAILED COSMOLOGICAL PREDICTIONS REVEAL EINSTEIN'S INCORRECT PHYSICAL BASIS OF GENERAL RELATIVITY

Dynamical predictions for the evolution of the Universe according to Einstein's equation based on the Equivalence Principle may be found by substituting the metric into Eq. (32.40). In the cases of spherical, flat, and hyperbolic geometries, the general evolution equations for homogeneous, isotropic cosmology are:

$$3\frac{\dot{a}^2}{a^2} = 8\pi\rho - 3\frac{k}{a^2} \tag{32.124}$$

$$3\frac{\ddot{a}}{a} = -4\pi(\rho + 3P) \tag{32.125}$$

where $k = +1$ for the 3-sphere, $k = 0$ for flat space, and $k = -1$ for the hyperboloid and ρ is the (average) mass-density of matter, $\dot{a} = \frac{da}{d\tau}$, and P is the pressure. The exact solutions of these equations for the cases of dust ($P = 0$) and radiation ($P = \frac{\rho}{3}$) are given below in Table 32.3.

Table 32.3. Dust and Radiation Filled Robertson-Walker Cosmologies.

	TYPE OF MATTER	
	"Dust"	Radiation
SPATIAL GEOMETRY	$P = 0$	$P = \frac{\rho}{3}$
3-sphere, $k = +1$	$a = \frac{1}{2}C(1-\cos\eta)$ $\tau = \frac{1}{2}C(\eta - \sin\eta)$	$a = \sqrt{C'}\left[1-\left(1-\frac{\tau}{\sqrt{C'}}\right)^2\right]^{\frac{1}{2}}$
Flat, $k = 0$	$a = \left(\frac{9C}{4}\right)^{\frac{1}{3}}\tau^{\frac{2}{3}}$	$a = (4C')^{\frac{1}{4}}\tau^{\frac{1}{2}}$
Hyperboloid, $k = -1$	$a = \frac{1}{2}C(\cosh\eta - 1)$ $\tau = \frac{1}{2}C(\sinh\eta - \eta)$	$a = \sqrt{C'}\left[\left(1+\frac{\tau}{\sqrt{C'}}\right)^2 - 1\right]^{\frac{1}{2}}$

Consider some of the important qualitative properties of the solutions. The first striking result is that the Universe cannot be static, provided only that $\rho > 0$ and $P \geq 0$. This conclusion follows immediately from ***Eq. (32.125) which tells us that*** $\ddot{a} < 0$**.** Thus, the Universe must always either be expanding ($\dot{a} > 0$) or contracting ($\dot{a} < 0$) (with the possible exception of an instant of time when expansion changes over to contraction). Note the nature of this expansion or contraction: The distance scale between all isotropic observers (in particular, between galaxies) changes with time, but there is no preferred center of expansion or contraction. Indeed, if the distance (measured on the homogeneous surface) between two isotropic observers at time τ is R, the rate of change of R is:

$$v \equiv \frac{dR}{d\tau} = \frac{R}{a}\frac{da}{d\tau} = HR \tag{32.126}$$

where $H(\tau) = \frac{\dot{a}}{a}$ is called Hubble's constant. (Note, however, that the value of H changes with time.) Eq. (32.126) is known as Hubble's law.

Note that v can be much greater than the speed of light if $H(\tau) = \frac{\dot{a}}{a}$ is large enough. This represents a contradiction of special relativity that no signal may travel faster than c, the speed of light, for any observer. The maximum expansion rate for a 3-sphere is $4\pi c$ which is given in Eq. (32.186). In this case a photon traveling at the speed of light may complete identically one revolution of the Universe per cycle as shown infra.

The expansion of the Universe in accordance with Eq. (32.126) has been confirmed by the observation of the redshifts of distant galaxies. The confirmation of this striking prediction of Einstein's general relativity is regarded as a dramatic success of the theory. Unfortunately, the historical development of events clouded this success and recent data reveals a fatal flaw in the nature of the expansion. Einstein was sufficiently unhappy with the prediction of a dynamic Universe that he proposed a modification of his equation, the addition of a new term, as follows:

$$G_{ab} + \Lambda g_{ab} = 8\pi T_{ab} \tag{32.127}$$

where Λ is a new fundamental constant of nature, called the cosmological constant. (It can be shown [20] that a linear combination of G_{ab} and g_{ab} is the most general two-index symmetric tensor which is divergence-free and can be constructed locally from the metric and its derivatives up to second order; so, Eq. (32.127) gives the most general modification which does not grossly alter the basic properties of Einstein's equation. If $\Lambda \neq 0$, *one does* ***not*** *obtain Newtonian theory* in the slow motion, weak field limit; but if Λ is small enough, the deviations from Newtonian theory would not be noticed.) With this additional one-parameter degree of freedom, static solutions exist, though they require exact adjustment of the parameters and are unstable, much like a pencil standing on its point. Thus, Einstein was able to modify the theory to yield static solutions. After Hubble's redshift observations in 1929 demonstrated the expansion of the Universe, the original motivation for the introduction of Λ was lost. Nevertheless, Λ has been reintroduced on numerous occasions when discrepancies have arisen between theory and observations, only to be abandoned again when these discrepancies have been resolved. In the following, we shall assume that $\Lambda = 0$.

Given that the Universe is expanding, $\dot{a} > 0$, we know from Eq. (32.125) that $\ddot{a} < 0$, so the Universe must have been expanding at a faster and faster rate as one goes backward in time. Einstein's equation predicts that the Universe must be decelerating for all time.

In fact, the opposite is observed experimentally [14].

If the Universe had always expanded at its present rate, then at the time $T = \frac{a}{\dot{a}} = H^{-1}$ ago, we would have had $a = 0$. Since its expansion actually was faster, the time at which a was zero was even closer to the present. Thus, under the assumption of homogeneity and isotropy, Einstein's general relativity makes the prediction that at a time less than H^{-1} ago, the Universe was in a singular state: The distance between all "points of space" was zero; the density of matter and the curvature of spacetime was infinite. This singular state of the Universe is referred to as the *big bang*.

Such a spacetime structure makes no physical sense. Furthermore, big bang theory requires the existence of a center of the Universe from which the Universe originated. No such point of origin is observed. Recently Lieu and Hillman [15] and Ragazzoni [16] have shown, using the Hubble space telescope, that the infinities in the quantum singularity that became the Universe with the big bang can not be reconciled by invoking uncertainty on the Planck-time scale. Time is continuous rather than quantized, the concepts of the graviton and the big bang are experimentally fatally flawed.

For many years it was generally believed that the prediction of a singular origin of the Universe was due merely to the assumptions of exact homogeneity and isotropy, that if these assumptions were relaxed one would get a non-singular "bounce" at small a rather than a singularity. However, the singularity theorems of general relativity [21] show that singularities are generic features of cosmological solutions; they have ruled out the possibility of "bounce" models close to the homogeneous, isotropic modes.

In order to determine the qualitative predictions of Einstein's general relativity for the future evolution of the Universe, it is useful to first obtain an equation for the evolution of the mass-density. Multiplying Eq. (32.124) by a^2, differentiating it with respect to τ, and then eliminating $\ddot{a}$ via Eq. (32.125) gives an equation for the evolution of the mass-density.

$$\dot{\rho} + 3(\rho + P)\frac{\dot{a}}{a} = 0 \tag{32.128}$$

In the case of a dust filled Universe ($P = 0$), the equation for the predicted evolution of the mass-density of the Universe is:

$$\rho a^3 = \text{constant} \tag{32.129}$$

which expresses conservation of rest mass, while in the case of a radiation filled Universe ($P = \frac{\rho}{3}$)

$$\rho a^4 = \text{constant} \tag{32.130}$$

In this case, the explanation is that the energy density decreases more rapidly as a increases than by the volume factor a^3, since the radiation in each volume element does work on its surroundings as the Universe expands. (Alternatively, in terms of photons, the photon number density decreases as a^{-3}, but each photon loses energy as a^{-1} because of redshift.) Comparison of Eq. (32.129) and Eq. (32.130) shows that although the radiation content of the present Universe may be negligible, its contribution to the total mass-density far enough into the past ($a \to 0$) should dominate over that of ordinary matter.

In Einstein's gravity equation, the Einstein tensor and the stress-energy-momentum tensor are each conservative. This forces conservation of curvature and conservation of mass-energy and momentum. Consequentially, a photon and a gravitational field with corresponding energies must each produce a gravitational field corresponding to the equivalent mass. However, for any kind of wave advancing with limiting velocity and capable of transmitting signals, the equation of front propagation is the same as the equation for the front of a light wave. If gravity propagates at the speed of light, light travels at c in all inertial frames, and light gives rise to a gravitation field, then an internal inconsistency arises regarding causality.

Conservation of mass-energy and momentum under the law of the limiting propagation velocity based on Maxwell's equations requires conservation of spacetime with matter-energy and momentum but ***nonconservation of curvature****. Thus, the wave equation conserves matter, energy, and momentum. It further provides for the conservation of these physical entities with spacetime and provides a unifying physical principle that gives an oscillating Universe with predictions that are consistent with observation.*

Furthermore, in the calculation of the deflection of light by a gravitational field, the mass of the photon was set equal to zero in the Deflection of Light section at Eq. (32.108). The agreement of the observed deflection with that predicted with $m = 0$ confirms that the photon has zero gravitational mass.

The qualitative features of the future evolution of the Universe predicted by Einstein's general relativity may now be determined. If $k = 0$ or -1, Eq. (32.124) shows that $\dot{a}$ never can become zero. Thus, if the Universe is presently expanding, it must continue to expand forever. Indeed, for any matter with $P \geq 0$, ρ must decrease as a increases at least as rapidly as a^{-3}, the value for dust. Thus, $\rho a^2 \to 0$ as $a \to \infty$. Hence, if $k = 0$, the "expansion velocity" $\dot{a}$ asymptotically approaches zero as $\tau \to \infty$, while if $k = -1$ we have $\dot{a} \to 1$ as $\tau \to \infty$.

However, if $k = +1$, the Universe cannot expand forever. The first term on the right hand of Eq. (32.124) decreases with a more rapidly than the second term, and thus, since the left-hand side must be positive, there is a critical value, a_c such that $a \leq a_c$. Furthermore, a cannot asymptotically approach a_c as $\tau \to \infty$ because the magnitude of $\ddot{a}$ is bounded from below on account of Eq. (32.125). Thus, if $k = +1$, then at a finite time after the big bang origin of the Universe, the Universe will achieve a maximum size a_c and then will begin to recontract. The same argument as given above for the occurrence of a big bang of the Universe now shows that a finite time after recontraction begins, a "big crunch" end of the Universe will occur. Thus, the dynamical equations of Einstein's general relativity show that the spatially closed 3-sphere Universe will exist for only a finite span of time.

Let us now turn our attention to solving Eq. (32.124) and Eq. (32.125) exactly for the cases of dust and radiation. The most efficient procedure for doing this is to eliminate ρ using Eq. (32.129) or, respectively, Eq. (32.130), and substitute into Eq. (32.124). The result for dust is:

$$\dot{a}^2 - \frac{C}{a} + k = 0 \tag{32.131}$$

where $C = \dfrac{8\pi\rho a^3}{3}$ is constant; and for radiation,

$$\dot{a}^2 - \frac{C'}{a^2} + k = 0 \tag{32.132}$$

where $C' = \dfrac{8\pi\rho a^4}{3}$. Given Eq. (32.129) (or Eq. (32.130)), Eq. (32.125) is redundant; so, the only first order ordinary differential Eq. (32.131) (or, respectively, Eq. (32.132)) need be solved. The solutions for $a(\tau)$ are readily obtained by elementary methods. These solutions for the six cases of interest are given in Table 32.3. Graphs of $a(\tau)$ versus τ for dust-filled Robertson-Walker Universes are shown in Figure 32.2. Similar graphs are obtained for radiation-filled Robertson-Walker Universes. The solution for the dust-filled Universe with 3-sphere geometry was first given by Friedmann (1922) and is called the Friedmann cosmology, although in some references all the solutions in Table 32.3 are referred to as Friedmann solutions.

Figure 32.2. The dynamics of dust-filled Robertson-Walker Universes.

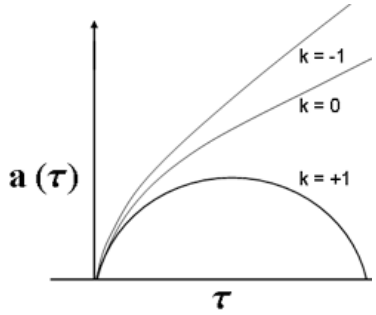

Solutions to Einstein's general relativity yield multiple possible outcomes of $a(\tau)$ with regard to future evolution such as whether our Universe is "open" or "closed," i.e., whether it corresponds to the cases $k=0$, $k=-1$, or the case $k=+1$. If the Universe is open, it will expand forever, while if it is closed it will eventually recontract. The basic equations (Eq. (32.124) and Eq. (32.125)) governing the dynamics of the Universe may be expressed in terms of Hubble's constant, $H=\frac{\dot{a}}{a}$, and the deceleration parameter, q, defined by:

$$q=-\ddot{a}\frac{a}{(\dot{a})^2} \tag{32.133}$$

Assuming $P\approx 0$ in the present Universe, gives:

$$H^2=\frac{8\pi G\rho}{3}-\frac{kc^2}{a^2} \tag{32.134}$$

$$q=\frac{4\pi G\rho}{3H^2} \tag{32.135}$$

Defining Ω as:

$$\Omega=\frac{8\pi G\rho}{3H^2} \tag{32.136}$$

gives the result:

$$q=\frac{\Omega}{2} \tag{32.137}$$

and the Universe is closed ($k=+1$) if and only if $\Omega>1$, i.e., $\rho>\rho_c\equiv\frac{3H^2}{8\pi G}$.

Dynamical predictions for the evolution of the Universe according to Einstein's equation are consistent with the expansion of the cosmos; but are fatally flawed since they predict the possibility of an expansion velocity that greatly exceeds the speed of light such that a cosmology inconsistent with special relativity is possible, and all cosmological solutions of Einstein's general relativity predict a decelerating Universe from a postulated initial condition of a "big bang" expansion [13][8]*. The astrophysical data reveal an accelerating cosmos [14], which invalidates Einstein's equation. Furthermore, multiple solutions with dramatically different consequences are equally valid. The solutions to Einstein's equation cannot account for the power spectrum of the cosmos or the nature or uniformity of the cosmic microwave background radiation. Einstein's Universe is static with expanding dust, expanding radiation, or a static expanding mixture. In actuality, the Universe comprises predominantly matter which is undergoing conversion into radiation with a concomitant expansion of spacetime. The Einstein solutions predict the opposite of the actual evolution of the cosmos wherein radiation dominates in the early Universe with matter dominant later. The equations are derived infra. They reconcile the shortcomings of Einstein's general relativity. The correct basis of gravitation is not according to Einstein's equation (Eq. (32.40)); instead the origin of gravity is the relativistic correction of spacetime itself which is analogous to the special relativistic corrections of inertial parameters—increase in mass, dilation in time, and contraction in length in the direction of constant relative motion of separate inertial frames. As matter converts into energy spacetime undergoes expansion. On this basis, the observed acceleration of the expansion of the cosmos is predicted.*

[8] Some of the failings of the "Big Bang" model as well as an even more far-fetched model are given by Linde [22].

COSMOLOGY BASED ON THE RELATIVISTIC EFFECTS OF MATTER/ENERGY CONVERSION ON SPACETIME

THE ARROW OF TIME AND ENTROPY

The first principle laws are time symmetrical. They are equally valid for reverse time as they are for forward time. The principle of entropy was invented to provide an explanation for the direction of time as it pertains to macroscopic processes. And, it is not based on first principles. It does not provide an atomic arrow of time or provide insight into its existence. It is not clear whether entropy applies to the entire Universe, and the relationship of entropy to the observed large-scale expansion of the Universe is not obvious.

The following retrospect of entropy is adapted from Levine [23]. Consider the spontaneous mixing of two different gases. In the mixing process, the molecules move according to Newton's second law, Eq. (32.2). This law is symmetric with respect to time, meaning that if t is replaced by $-t$ and $\mathbf{v}$ by $-\mathbf{v}$, the law is unchanged. Thus, a reversal of all particle motions gives a set of motions that is also a valid solution of Newton's equation. Hence it is possible for the molecules to become spontaneously unmixed, and this unmixing does not violate the laws of motion. However, motions that correspond to a detectable degree of unmixing are extremely improbable (even though not absolutely impossible). Although Newton's laws of motion (which govern the motion of individual molecules) do not single out a direction of time, when the behavior of a very large number of molecules is considered, the second law of thermodynamics (which is a statistical law) tells us that states of an isolated system with lower entropy must precede in time states with higher entropy. The second law is not time-symmetric but singles out the direction of increasing time; we have $\frac{dS}{dt} > 0$ for an isolated system, so that the signs of dS and dt are the same. If someone showed us a film of two gases mixing spontaneously and then ran the film backward, we would not see any violation of $\mathbf{F} = m\mathbf{a}$ in the unmixing process, but the second law would tell us which showing of the film corresponded to how things actually happened. Likewise, if we saw a film of someone being spontaneously propelled out of a swimming pool of water, with the concurrent subsidence of waves in the pool, we would know that we were watching a film run backward; although tiny pressure fluctuations in a fluid can propel colloidal particles about, the Brownian motion of an object the size of a person is too improbable to occur.

The second law of thermodynamics singles out the direction of increasing time. The astrophysicist Eddington puts things nicely with his statement that "entropy is time's arrow." The fact that $\frac{dS}{dt} > 0$ for an isolated system gives us the *thermodynamic arrow of time*. Besides the thermodynamic arrow, there is a *cosmological arrow of time*. Spectral lines in light reaching us from other galaxies show wavelengths that are longer than the corresponding wavelengths of light from objects at rest (the famous redshift). This redshift indicates that all galaxies are moving away from us. Thus, the Universe is expanding with increasing time, and this expansion gives the cosmological arrow. Many physicists believe that the thermodynamic and the cosmological arrows are directly related, but this question is still undecided [24].

Particle physicists feel that there is strong (but not conclusive) evidence that the decay of one of the elementary particles (the neutral K meson) follows a law that is not symmetric with respect to time reversal. Thus, they speculate that there may also be a *microscopic arrow of time*, in addition to the thermodynamic and cosmological arrows [25-27].

The second law of thermodynamics shows that S increases with time for an isolated system. Can this statement be applied to the entire physical Universe? Scientists use Universe to mean the system plus those parts of the world which interact with the system. In the present contexts, Universe shall mean everything that exists—the entire cosmos of galaxies, intergalactic matter, electromagnetic radiation, etc. Physicists in the late nineteenth century generally believed that the second law is valid for the entire Universe, but presently they are not so sure. Scientists make the point that experimental thermodynamic observations are on systems that are not of astronomic size, and hence they are cautious about extrapolating thermodynamic results to encompass the entire Universe. They feel that there is no guarantee that laws that hold on a terrestrial scale must also hold on a cosmic scale. Although there is no evidence for a cosmic violation of the second law, their experience is insufficient to rule out such a violation.

THE ARROW OF TIME

The present theory provides an alternative explanation for the expanding Universe which unifies the ***microscopic, thermodynamic, and cosmological arrows of time***.

Physical phenomena involve exchange of energy between matter and spacetime. The relationship between mass-energy and spacetime provides the arrow of time. The particle production equations which unify de Broglie's Equation, Planck's Equation, Maxwell's Equations, Newton's Equations, and Special and General Relativity, Eq. (32.48a) and Eq. (32.48b), give the equivalence of particle production energies corresponding to mass, charge, current, gravity, and spacetime according to the proportionality constants which are given in terms of a self-consistent set of units. As shown by Eq. (32.38), particle production requires radial length contraction and time dilation that results in the curvature of spacetime. Thus, the creation of mass from energy causes an infinitesimal contraction or collapse of spacetime much like a dimple in a plastic ball but in three dimensions plus time; whereas, the release of energy causes an expansion of spacetime. Time goes forward in the direction of lower energy states and greater entropy because these states correspond to an expansion of spacetime relative to the higher energy states of

matter. Expanded space corresponds to a smaller cross section for reverse time as opposed to forward time. Thus, the arrow of time arising on the subatomic and atomic level gives rise to the Second Law of thermodynamics;

In an isolated system, spontaneous processes occur in the direction of increasing entropy.

Stated mathematically:

The entropy change, dS, which is equal to the change in heat, dq, divided by the temperature, T, is greater than zero.

$$dS = \frac{dq}{T} > 0 \tag{32.138}$$

THE EXPANDING UNIVERSE AND THE MICROWAVE BACKGROUND

The atomic arrow of time also applies to cosmology and provides for the expansion of spacetime on a cosmological scale. As fundamental particles, atoms, molecules, and macroscopic configurations of fundamental particles, atoms, and molecules release energy, spacetime increases. The superposition of expanding spacetime arising at the atomic level over all scales of dimensions from the atomic to the cosmological gives rise to the observed expanding Universe which continues to increase in entropy. However, due to conservation of mass-energy and spacetime as given by Eqs. (32.43), (32.48a), and (32.48b), the change in entropy of the Universe over all spacetime is zero.

$$\langle dS \rangle_{spacetime} = 0 \tag{32.139}$$

Thus, regions of the world line of the Universe exist wherein entropy decreases. The implications that are developed *supra.* are that:

- ***The Universe is closed*** **(**it is ***finite but with no boundary*****)**
- The total matter in the Universe is sufficient to eventually stop the expansion and is less than that which would result in permanent collapse (a 3-sphere Universe-Riemannian three-dimensional hyperspace plus time of constant positive curvature at each r-sphere), and
- ***The Universe is oscillatory in matter/energy and spacetime.***

As shown in the Particle Production section, the gravitational equations with the equivalence of the particle production energies require the ***conservation relationship of mass-energy,*** $E = mc^2$***, and spacetime,*** $\frac{c^3}{4\pi G} = 3.22\ X\ 10^{34}\ \frac{kg}{\sec}$. Spacetime expands as mass is released as energy which provides the basis of the atomic, thermodynamic, and cosmological arrows of time. Entropy and the expansion of the Universe are large scale consequences. It is further shown *infra.* that the Universe is closed independently of the total mass of the Universe, and different regions of space are isothermal even though they are separated by greater distances than that over which light could travel during the time of the expansion of the Universe. The Universe is oscillatory in matter/energy and spacetime with a finite minimum radius, the gravitational radius; thus, the gravitational force causes celestial structures to evolve on a time scale corresponding to the period of oscillation. The equation of the radius of the Universe, $\aleph$, is $\aleph = \left(\frac{2Gm_U}{c^2} + \frac{cm_U}{\frac{c^3}{4\pi G}} \right) - \frac{cm_U}{\frac{c^3}{4\pi G}} \cos\left(\frac{2\pi t}{\frac{2\pi G m_U}{c^3}} \right)$ which predicts the observed acceleration of the expansion. The calculated Hubble constant is $H_0 = 78.5\ \frac{km}{\sec \cdot Mpc}$. Presently, stars and large-scale structures exist that are older than the elapsed time of the present expansion as stellar and celestial evolution occurred during the contraction phase. The maximum energy release of the Universe which occurs at the beginning of the expansion phase is $P_U = \frac{c^5}{4\pi G} = 2.88\ X\ 10^{51}\ W$.

Figure 32.3. Shown below are three increasing times in the evolution of an illustrative "star." As the star converts matter into energy spacetime expands.

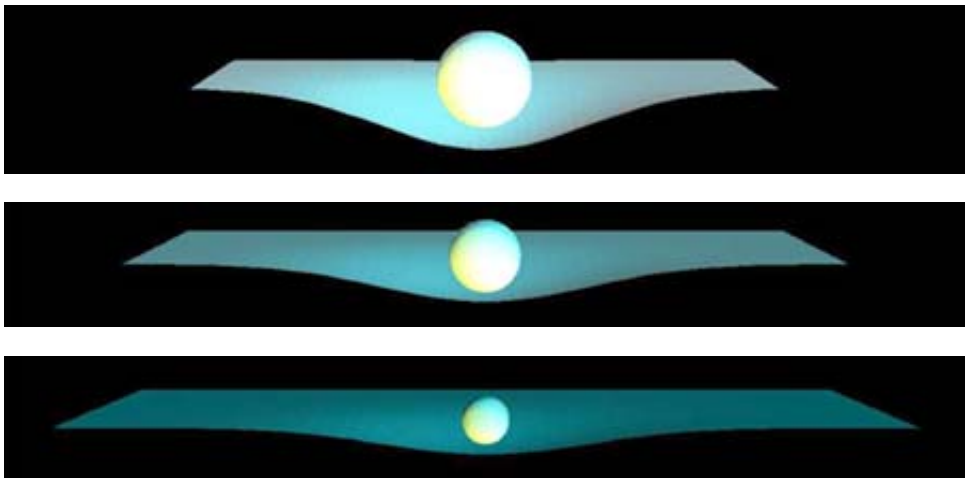

The amount of mass which is released as energy to cause spacetime to expand by one second can be calculated in the following way: Consider the conversion of an electron of mass m_e into energy $E = m_e c^2$. Eq. (32.43) represents the relationship between ***the equivalence of mass-energy conversion and the contraction/expansion of spacetime*** and gives the relativistic factor $\beta_g = \frac{v_g}{c}$, which divides the electron mass m_e and multiplies the electron proper time τ to give the corresponding spacetime expansion. Thus, Q, the mass-energy-to-expansion-contraction quotient of spacetime is given by:

$$Q = \frac{\beta_g^{-1} m_e}{\tau \cdot \beta_g} = \frac{\frac{m_e}{\frac{v_g}{c}}}{\tau \cdot \frac{v_g}{c}} = \frac{\frac{m_e}{\sqrt{\frac{2Gm_e}{c^2 \lambda\!\!\!^{-}_c}}}}{\tau \cdot \sqrt{\frac{2Gm_e}{c^2 \lambda\!\!\!^{-}_c}}} = \frac{m_e}{\tau} \cdot \frac{c^2 \lambda\!\!\!^{-}_c}{2Gm_e} = \frac{m_e}{2\pi \frac{\hbar}{m_e c^2}} \cdot \frac{c^2 \frac{\hbar}{m_e c}}{2Gm_e} = \frac{c^3}{4\pi G} = 3.22\ X\ 10^{34}\ \frac{kg}{\text{sec}} \tag{32.140a}$$

where τ and $\lambda\!\!\!^{-}_c$ are given by Eq. (36.1) of the Lepton section and Eq. (28.7), respectively.

Alternatively, Q may be calculated as follows: As a consequence of particle production the radius of the Universe contracts by 2π times the gravitational radius of each particle with the gravitational radius as given by Eq. (32.36) which applies to the observed leptons and quarks formed at the gravitational velocity v_g which is the escape velocity given by Eq. (32.35). Thus, Q the mass-energy-to-expansion-contraction quotient of spacetime is also given by the ratio of the mass of a particle at production divided by τ the period of the gravitational radius as given by Eq. (32.149) wherein the gravitational radius is the Newtonian gravitational radius is given by Eq. (32.36). Thus, τ is the period of the orbit of the particle relative to: the antiparticle during production. Then Q is given by:

$$Q = \frac{m_0}{\tau} = \frac{m_0}{\frac{2\pi r_g}{c}} = \frac{m_0}{2\pi \frac{\frac{2Gm_0}{c^2}}{c}} = \frac{c^3}{4\pi G} = 3.22\ X\ 10^{34}\ \frac{kg}{\text{sec}} \tag{32.140b}$$

As shown infra. the minimum radius of the universe is the gravitational radius of 3.12 X 10^{11} light years given by Eq. (32.147), and the maximum radius given by Eq. (32.150) is 1.97 X 10^{12} light years. The Universe oscillates between the extremes of matter filled and light filled as it correspondingly oscillates between expansion and contraction between these extrema. Throughout its oscillatory cycle the universe always contains both matter and light or energy wherein the exact spacetime points of the matter filled condition and the light filled condition only regard one r-sphere at each of the extrema. In the derivations given infra., a matter filled universe regards the maximum matter content, and light filled universe regards the maximum light content. At the beginning of its expansion from its gravitational radius, the Universe is matter filled, and at the middle of the cycle, the universe is light filled. For an observer in an expanding (contracting) universe, observations looking backward on evolution of the cosmos can be achieved using light signals with redshift (blueshift) time stamps corresponding to the extent of spacetime expansion between the observer and observed. Consider that the Earth is in an expanding universe at about 10 billion years from the cycle clock beginning at zero as contraction transitioned to expansion. ***The Universe is not observable by using increasing redshift measurements for earlier times***. An Earth observer's window on the universe is also

limited by the dimness of distant spacetime objects so only a small portion of the evolution of the cosmos is accessible to direct observation. Fortunately, the entire cycle of the evolution of the universe can be derived from physical laws as shown infra.

Regarding the phenomenon involved with the state parameters of a matter filled and light filled universe and the corresponding transition, consider a radioactive isotope. At the instance of ½ life, ½ of the atoms will have decayed. What happens to the decayed atoms is another issue. Similarly with the universe, after 500B years all the matter of the cycle will have decayed to light corresponding to the light filled state. At this instance, the universe stops expanding and begins contracting. After another 500B years, all the light of the cycle will have converted to matter corresponding to the matter filled state. At this instance, the universe stops contracting and begins expanding. The state of the entire observable universe at any time in the oscillatory cycle is given in the radius, velocity, acceleration, Hubble constant, power, mass density, and temperature equations and plots derived infra. Looking to the earliest times possible by increasing redshift, the matter filled state, the size of the universe is a minimum and the power is a maximum corresponding to a maximum temperature (a measure of the photon density and inventory). The matter inventory of the universe is a maximum with huge structures and old stars formed during the contraction phase to the limit of the observable horizon, the radius since the beginning of the expansion. The matter and light filled extrema only occur for an instant at one r-sphere in the history of the oscillation. Neither are exactly observable for humans, only a record of the evolutionary history with a timeline from the current into the past wherein all natural processes including the conversion of matter to energy and corresponding spacetime expansion proceed continuously and universally corresponding to a phase factor between observers based on spacetime separation.

Considering Earth as the frame of reference, the observable mass to energy conversion rate of the Universe calculated from the number of galaxies (400 *billion*) times the number of stars per galaxy (400 *billion*) times the average mass to energy conversion rate per star (5 *billion kg / sec star*) is $8\ X\ 10^{32}\ \frac{kg}{\text{sec}}$ which is 2.5% of Q given by Eq. (32.140). The time of the present expansion calculated from the observed Hubble constant and the maximum redshift is approximately 10 billion years [28]. Assuming the presently observed mass to energy conversion rate was approximately constant over this time, the amount of mass to energy released during this time is:

$$3.2\ X\ 10^{34}\ \frac{kg}{\text{sec}}\ X\ 3.2\ X\ 10^{17}\ \text{sec}\ =\ 1\ X\ 10^{52}\ kg \tag{32.141}$$

The mass of the Universe is approximately $2\ X\ 10^{54}\ kg$ [Eq. (32.147) with ref. 30-32]; thus, 0.5% of the maximum mass of the Universe has been converted to energy within the Earth's redshift and intensity window. The present Universe is predominantly comprised of matter, and according to Eq. (32.158) the mass of the matter of the Universe is close to its maximum. Given time harmonic behavior, the observable Universe is approximately at its minimum size. The wavefront of energy and spacetime from matter to energy conversion travel at the speed of light. Consider Eq. (32.43). At the present time in the cycle of the Universe, the world line of the expanding spacetime and the released energy are approximately coincident. In terms of Eq. (32.38), the proper time and the coordinate time are approximately equal. The ratio of the gravitational radius, r_g given by Eq. (32.36), and the radius of the Universe equal to one and the gravitational escape velocity given by Eq. (32.35) is the speed of light. And, Q, (Eq. (32.140)) is equal to the matter to energy conversion rate of the time harmonic expansion-contraction cycle of the entire Universe (versus the observable Universe) which permits light energy (photons) to propagate (escape the gravitational hole of the Universe).

When the gravitational radius r_g is the radius of the Universe, the proper time is equal to the coordinate time (Eq. (32.43)), and the gravitational escape velocity v_g of the Universe is the speed of light.

The cosmic microwave background radiation dominates the total radiation density of the Universe. The microwave background spectrum obtained by COBE is well fitted by a blackbody with a temperature of $2.735 \pm 0.06\ K$, and the deviation from a blackbody is less than 1% of the peak intensity over the range $1 - 20\ cm^{-1}$ [33]. From the isothermal temperature of the ubiquitous microwave background radiation and the Stefan-Boltzmann law, the minimum size of the Universe is calculated. Presently, the mass to energy conversion rate of the Universe is approximately equal to Q, the mass-energy-to-expansion-contraction quotient of spacetime given by Eq. (32.140). At the beginning of the cycle of the Universe, the world line of the expanding spacetime and the released energy are coincident. In terms of Eq. (32.38), the proper time and the coordinate time are equal. Therefore, the mass to energy conversion rate of the entire Universe is equated with Q. Thus, P_U, ***the maximum power radiated by the Universe*** is given by Eqs. (32.27) and (32.140).

$$P_U = \frac{\frac{m_e c^2}{\sqrt{\frac{2GM}{c^2 \lambda\!\!\!^{-}_c}}}}{\tau\sqrt{\frac{2GM}{c^2 \lambda\!\!\!^{-}_c}}} = \frac{c^5}{4\pi G} = 2.89\ X\ 10^{51}\ W \tag{32.142}$$

The observable mass to energy conversion rate of the Universe calculated from the number of galaxies (400 *billion*) times the number of stars per galaxy (400 *billion*) times the average mass to energy conversion rate per star (5 *billion kg / sec star*) is $7.2\ X\ 10^{49}\ W$ which is 2.5% of P_U given by Eq. (32.142).

The Stefan-Boltzmann law [34] equates the power radiated by an object per unit area, *R*, to the emissivity, *e*, times the Stefan-Boltzmann constant, σ, times the fourth power of the temperature, T^4.

$$R = e\sigma T^4 \tag{32.143}$$

The area, A_U, of the Universe of radius $\aleph$ is:

$$A_U = 4\pi\aleph^2 \tag{32.144}$$

The power radiated by the Universe per unit area, R_U, is given by the ratio of Eq. (32.142) and Eq. (32.144:

$$R_U = \frac{\frac{c^5}{4\pi G}}{4\pi\aleph^2} = \frac{2.89\ X\ 10^{51}\ W}{4\pi\aleph^2} \tag{32.145}$$

The minimum radius of the Universe, $\aleph_{\min}$, is calculated in terms of the temperature of the cosmic microwave background radiation by the substitution of Eq. (32.145) into Eq. (32.143):

$$\aleph_{\min} = \sqrt{\frac{c^5}{(4\pi)^2 Ge\sigma T^4}} = 8.52\ X\ 10^{27}\ m \tag{32.146}$$

$$\aleph_{\min} = \frac{8.52\ X\ 10^{27}\ m}{c} = 9.01\ X\ 10^{11}\ light\ years$$

where $T = 2.735\ ^\circ K$, $e = 1$ for a blackbody, and $\sigma = 5.67\ X\ 10^{-8}\ Wm^{-2}K^{-4}$. Given that the present expansion age is 10 billion years [28] and that the power used to calculate Eq. (32.146) is an upper bound, the ***minimum radius of the Universe***, $\aleph_{\min}$, given by Eq. (32.146) ***is equal to the gravitational radius of the Universe***, r_g, given by Eq. (32.36) and Eq. (32.38) where the experimental mass of the Universe is $2\ X\ 10^{54}\ kg$ [Eq. (32.147) with ref. 30-32].

$$r_g = \frac{2Gm_U}{c^2} = 2.96\ X\ 10^{27}\ m = 3.12\ X\ 10^{11}\ light\ years \tag{32.147}$$

Eq. (32.147) is consistent with the mass of the Universe being that which gives the ratio of the gravitational radius, r_g, and the radius of the Universe equal to one and the gravitational escape velocity given by Eq. (32.35) equal to the speed of light.

The gravitational equation (Eq. (32.38)) with the equivalence of the particle production energies (Eqs. (32.48a) and (32.48b)) permit the equivalence of mass-energy ($E = mc^2$) and spacetime ($\frac{c^3}{4\pi G} = 3.22\ X\ 10^{34}\ \frac{kg}{\sec}$). Spacetime expands as mass is released as energy which provides the basis of the atomic, thermodynamic, and cosmological arrows of time. Entropy and the expansion of the Universe are large scale consequences. ***The Universe is closed independently of the total mass of the Universe***. Because Eq. (32.140) gives a constant as the ratio of energy to spacetime expansion, the energy density is constant throughout the inhomogeneous Universe for a given r-sphere; thus, ***different regions of space are isothermal even though they are separated by greater distances than that over which light could travel during the time of the expansion of the Universe***. The spacetime expansion and the energy released travel spherically outward at the speed of light. The sum of the spacetime expansion over all points in the Universe and the sum of the energy release over all points in the Universe are each equivalent to that of a point source at the observer's position of magnitude equal to the corresponding sum. The cosmic microwave background radiation is an average temperature of 2.7°K, with deviations of 30 or so μK in different parts of the sky representing slight variations in the density of matter. Peaks in the power spectrum from the temperature fluctuations of the cosmic microwave background radiation appear at certain values of ℓ of spherical harmonics [35] as shown in the Power Spectrum of the Cosmic Microwave Background section. The origin of the microwave background radiation (CMBR) as the power from the Universe rather than from a Big Bang creation event is demonstrated by the absence of the shadows in the CMBR required for the Big Bang model [36].

THE PERIOD OF OSCILLATION BASED ON CLOSED PROPAGATION OF LIGHT

Mass-energy must be conserved during the harmonic cycle of expansion and contraction. The gravitational potential energy E_{grav} of the Universe follows that given by Eq. (32.26)

$$E_{grav} = \frac{Gm_U^2}{\aleph} \tag{32.148}$$

In the case that the radius of the Universe $\aleph$ is the gravitational radius r_G given by Eq. (32.22), the gravitational potential energy is equal to $m_U c^2$ which follows that given by Eq. (32.27)[9]. The gravitational velocity v_G is given by Eq. (32.33) wherein an electromagnetic wave of mass-energy equivalent to the mass of the Universe travels in a circular orbit wherein the eccentricity is equal to zero (Eq. (35.21)), and the escape velocity from the Universe can never be reached. The wavelength of the oscillation of the Universe and the wavelength corresponding to the gravitational radius r_G must be equal. Both spacetime expansion and contraction travel at the speed of light and obey the wave relationship given by Eq. (29.4). The wavelength is given in terms of the radius by Eq. (2.2). Thus, ***the harmonic oscillation period***, T_U, is:

$$T_U = \frac{2\pi r_G}{c} = \frac{2\pi G m_U}{c^3} = \frac{2\pi G\left(2\ X\ 10^{54}\ kg\right)}{c^3} = 3.10\ X\ 10^{19}\ \text{sec} = 9.83\ X\ 10^{11}\ years \tag{32.149}$$

where the mass of the Universe, m_U, is approximately $2\ X\ 10^{54}\ kg$ [Eq. (32.147) with ref. 30-32]. Thus, the observed Universe will expand as mass is released as photons for $4.92\ X\ 10^{11}\ years$. At this point in its world line, the Universe will obtain its maximum size and begin to contract.

EQUATIONS OF THE EVOLUTION OF THE UNIVERSE

The Universe is oscillatory in matter/energy and spacetime with a finite minimum radius, the gravitational radius r_g. The minimum radius of the Universe, 300 billion light years [32], is larger than that provided by the current expansion, approximately 10 billion light years [28]; even though, presently the spacetime expansion and the released energy world lines are coincident as a consequence of the equality of Eq. (32.140) and the rate of matter to energy conversion. In terms of Eq. (32.38), the proper time and the coordinate time are approximately equal. Consequently, the radius of the Universe does not go negative during the contraction phase of the oscillatory cycle.

The ***maximum excursion of the radius of the Universe***, the amplitude, $\aleph_o$, of the time harmonic variation in the radius of the Universe, is given by the quotient of the total mass of the Universe and Q, the mass-energy-to-expansion-contraction, given by Eq. (32.140):

$$\aleph_0 = \frac{m_U}{Q} = \frac{m_U}{\frac{c^3}{4\pi G}} = \frac{2\ X\ 10^{54}\ kg}{3.22\ X\ 10^{34}\ \frac{kg}{\text{sec}}} = 6.20\ X\ 10^{19}\ \text{sec} = 1.97\ X\ 10^{12}\ light\ years = 1.86\ X\ 10^{28}\ m \tag{32.150}$$

where the conversion factor of space to time is the speed of light according to Minkowski's tensor [8]. The equation for $\aleph$, the radius of the Universe is:

$$\aleph = \left(r_U - \aleph_0 \cos\left(\frac{2\pi t}{T_U}\right)\right) = \left(r_U - \frac{c m_U}{\frac{c^3}{4\pi G}} \cos\left(\frac{2\pi t}{T_U}\right)\right)$$

$$\aleph = \left(r_U - 1.97\ X\ 10^{12} \cos\left(\frac{2\pi t}{3.10\ X\ 10^{19}\ \text{sec}}\right)\right) light\ years = \left(r_U - 1.86\ X\ 10^{28} \cos\left(\frac{2\pi t}{3.10\ X\ 10^{19}\ \text{sec}}\right)\right) m \tag{32.151}$$

where r_U is the average size of the Universe and T_U is given by Eq. (32.149).

The Universe has a finite minimum radius equal to its gravitational radius r_g according to Eq. (32.147) and a maximum excursion of the radius given by Eq. (32.150). Therefore, the Universe has an average size which represents an offset of an oscillatory cycle of expansion and contraction. The average size of the Universe, r_U, is determined by substitution of Eq. (32.147) into Eq. (32.151) with $t = 0$.

$$r_U = \aleph_0 + r_g = \left(1.97\ X\ 10^{12} + 3.12\ X\ 10^{11}\right) light\ years = 2.28\ X\ 10^{12}\ light\ years = 2.16\ X\ 10^{28}\ m \tag{32.152}$$

---

[9] The ratio of v_g to v_G is $\sqrt{2}$. The total angle which is traversed twice in the generation of the atomic orbital of the electron as shown in the Atomic Orbital Equation of Motion for $\ell = 0$ Based on the Current Vector Field (CVF) section is $\sqrt{2}\pi$. Thus, $\sqrt{2}$ is also the ratio of the angular sum of the rotations to generate the atomic orbital to the angle spanned by a great circle of the atomic orbital. $\sqrt{2}\pi$ is the hypotenuse of the triangle having the sides of π radians corresponding to x-axis rotations and π radians corresponding to y-axis rotations. Similarly, the result that $\frac{v_g}{v_G} = \sqrt{2}$ can be considered as the projection of two degrees of freedom of a spherical wave to one at the speed of light.

Substitution of Eq. (32.152) into Eq. (32.151) gives ***the radius of the Universe as a function of time***.

$$\aleph = r_U - \frac{cm_U}{\frac{c^3}{4\pi G}}\cos\left(\frac{2\pi t}{T_U}\right) = \left(\aleph_0 + r_g\right) - \frac{cm_U}{\frac{c^3}{4\pi G}}\cos\left(\frac{2\pi t}{T_U}\right) = \left(\frac{2Gm_U}{c^2} + \frac{cm_U}{\frac{c^3}{4\pi G}}\right) - \frac{cm_U}{\frac{c^3}{4\pi G}}\cos\left(\frac{2\pi t}{\frac{2\pi G m_U}{c^3}}\right)$$

$$\aleph = \left(2.16\ X\ 10^{28} - 1.86\ X\ 10^{28}\ \cos\left(\frac{2\pi t}{9.83\ X\ 10^{11}\ yrs}\right)\right) m \tag{32.153}$$

$$\aleph = \left(2.28\ X\ 10^{12} - 1.97\ X\ 10^{12}\ \cos\left(\frac{2\pi t}{9.83\ X\ 10^{11}\ \text{yrs}}\right)\right)\ light\ years$$

The expansion/contraction rate, $\dot{\aleph}$, is given by taking the derivative with respect to time of Eq. (32.153).

$$\dot{\aleph} = 4\pi c \cdot \sin\left(\frac{2\pi t}{\frac{2\pi G m_U}{c^3}}\right) \tag{32.154}$$

$$\dot{\aleph} = 3.77\ X\ 10^{6}\ \sin\left(\frac{2\pi t}{9.83\ X\ 10^{11}\ yrs}\right)\ \frac{km}{\text{sec}}$$

The expansion/contraction acceleration, $\ddot{\aleph}$, is given by taking the derivative with respect to time of Eq. (32.154).

$$\ddot{\aleph} = 4\pi \frac{c^4}{Gm_U} \cdot \cos\left(\frac{2\pi t}{\frac{2\pi G m_U}{c^3}}\right) \tag{32.155}$$

$$\ddot{\aleph} = 7.64\ X\ 10^{-13}\ \cos\left(\frac{2\pi t}{9.83\ X\ 10^{11}\ yrs}\right)\ \frac{km}{\text{sec}^2} = 78.6\ \cos\left(\frac{2\pi t}{9.83\ X\ 10^{11}\ yrs}\right)\ \frac{km}{\text{sec} \cdot Mpc}$$

where 1 Megaparsec (Mpc) is $3.258\ X\ 10^6$ light years. ***Eq. (32.155) and Figure 32.5 are consistent with the experimental observation that the rate of the expansion of the Universe is increasing [37-39].***

The ***time harmonic radius of the Universe*** is shown graphically in Figure 32.4. The ***time harmonic expansion/contraction rate of the radius of the Universe*** is shown graphically in Figure 32.5.

Figure 32.4. The radius of the Universe as a function of time.

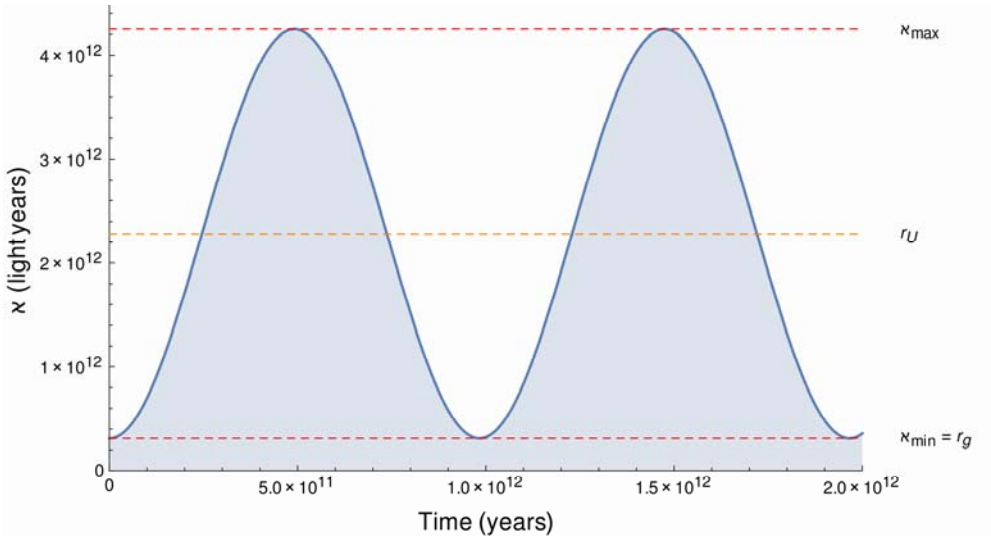

Figure 32.5. The expansion/contraction rate of the Universe as a function of time.

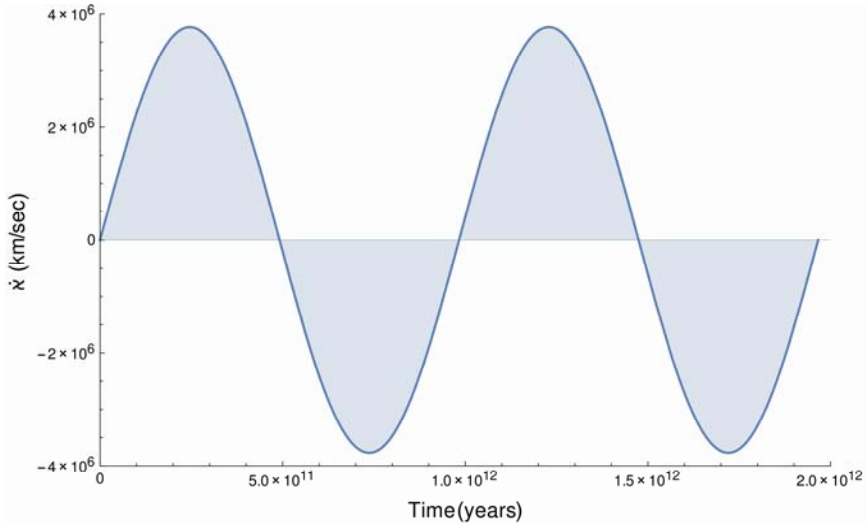

The ***Hubble constant*** defined by Eq. (32.126) is given by the ratio of the expansion rate given in units of $\frac{km}{\sec}$ divided by the radius of the expansion in units of Mpc (1 Megaparsec (Mpc) is $3.258\ X\ 10^6$ light years). The radius of expansion is equivalent to the radius of the light sphere with an origin at the time point when the Universe stopped contracting and started to expand. Thus, the radius of Eq. (32.126) is given by the time of expansion times the speed of light, c. From Eq. (32.154), the ***Hubble constant*** is:

$$H = \frac{\dot{\aleph}}{ct} = \frac{4\pi c \cdot \sin\left(\frac{2\pi t}{\frac{2\pi G m_U}{c^3}}\right)}{ct} = \frac{3.77\ X\ 10^6\ \sin\left(\frac{2\pi t}{9.83\ X\ 10^{11}\ yrs}\right)\ \frac{km}{\sec}}{ct} \tag{32.156}$$

For small t, the Hubble constant is also equivalent to the acceleration as given by Eq. (32.155). For $t = 10^{10}\ light\ years;\quad ct = 3.069\ X\ 10^3 Mpc$,

$$H = \frac{3.77\ X\ 10^6\ \sin\left(\frac{2\pi\left(10^{10}\ yrs\right)}{9.83\ X\ 10^{11}\ yrs}\right)\ \frac{km}{\sec}}{3.069\ X\ 10^3\ M\text{pc}} = 78.5\frac{km}{\sec \cdot M\text{pc}} \tag{32.157}$$

Thus, from Eqs. (32.156-32.157), the Hubble, H_0, constant is $H_0 = 78.5\ \frac{km}{\sec \cdot Mpc}$. The experimental value is $H_0 = 80 \pm 17\ \frac{km}{\sec \cdot Mpc}$ [28], or more recently $H_0 = 72 \pm 8\ \frac{km}{\sec \cdot Mpc}$ [29]. The ***Hubble constant as a function of time*** is shown graphically in Figure 32.6. Due to the possibility of observing galaxies at greater distances than the time at which the universe stopped contacting and started expanding, the measurement of the Hubble constant based on redshifts is prone to error due the ancient light undergoing partial blue-shifting as well as red-shifting during the corresponding phases.

Figure 32.6. The Hubble constant of the Universe as a function of time.

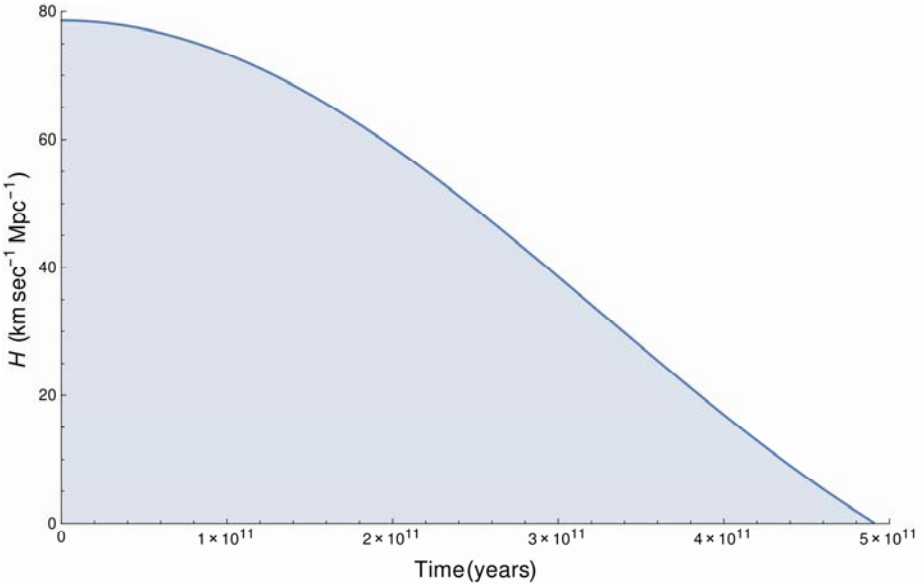

The mass of the Universe as a function of time, $m_U(t)$, follows from the initial mass of $2\ X\ 10^{54}\ kg$ (based on internal consistency with the size, age, Hubble constant, temperature, density of matter, and power spectrum of the Universe given herein) and Eq. (32.153). The positive definite harmonic function that matches the boundary conditions at the extrema is given by:

$$m_U(t) = \frac{m_U}{2}\left(1+\cos\left(\frac{2\pi t}{\frac{2\pi G m_U}{c^3}}\right)\right) = 1\ X\ 10^{57}\left(1+\cos\left(\frac{2\pi t}{9.83\ X\ 10^{11}\ yrs}\right)\right) g \tag{32.158}$$

The volume of the Universe as a function of time $V(t)$ follows from Eq. (32.153).

$$V(t) = \frac{4}{3}\pi \aleph(t)^3 = \frac{4}{3}\pi\left[\left(\frac{2Gm_U}{c^2}+\frac{cm_U}{\frac{c^3}{4\pi G}}\right)-\frac{cm_U}{\frac{c^3}{4\pi G}}\cos\left(\frac{2\pi t}{\frac{2\pi G m_U}{c^3}}\right)\right]^3$$

$$V(t) = \frac{4}{3}\pi\left(2.16\ X\ 10^{30} cm - 1.86\ X\ 10^{30}\cos\left(\frac{2\pi t}{9.83\ X\ 10^{11}\ yrs}\right) cm\right)^3 \tag{32.159}$$

The mass density of the Universe as a function of time $\rho_U(t)$ is given by the ratio of the mass as a function of time given by Eq. (32.158) and the volume as a function of time given by Eq. (32.159):

$$\rho_U(t)=\frac{m_U(t)}{V(t)}=\frac{m_U(t)}{\frac{4}{3}\pi\aleph(t)^3}=\frac{\frac{m_U}{2}\left(1+\cos\left(\frac{2\pi t}{\frac{2\pi G m_U}{c^3}}\right)\right)}{\frac{4}{3}\pi\left[\left(\frac{2Gm_U}{c^2}+\frac{cm_U}{\frac{c^3}{4\pi G}}\right)-\frac{cm_U}{\frac{c^3}{4\pi G}}\cos\left(\frac{2\pi t}{\frac{2\pi G m_U}{c^3}}\right)\right]^3} \tag{32.160}$$

$$\rho_U(t)=\frac{1\ X\ 10^{57}\left(1+\cos\left(\frac{2\pi t}{9.83\ X\ 10^{11}\ yrs}\right)\right)g}{\frac{4}{3}\pi\left(2.16\ X\ 10^{30}cm-1.86\ X\ 10^{30}\cos\left(\frac{2\pi t}{9.83\ X\ 10^{11}\ yrs}\right)cm\right)^3}$$

For $t=10^{10}\ light\ years=3.069\ X\ 10^3 Mpc$, $\rho_U=1.7\ X\ 10^{-32}\ g/cm^3$. The density of luminous matter of stars and gas of galaxies is about $\rho_U=2\ X\ 10^{-31}\ g/cm^3$ [40, 41]. The ***time harmonic density of the Universe***, $\rho_U(t)$, is shown graphically in Figure 32.7.

Figure 32.7. The mass density of the Universe as a function of time.

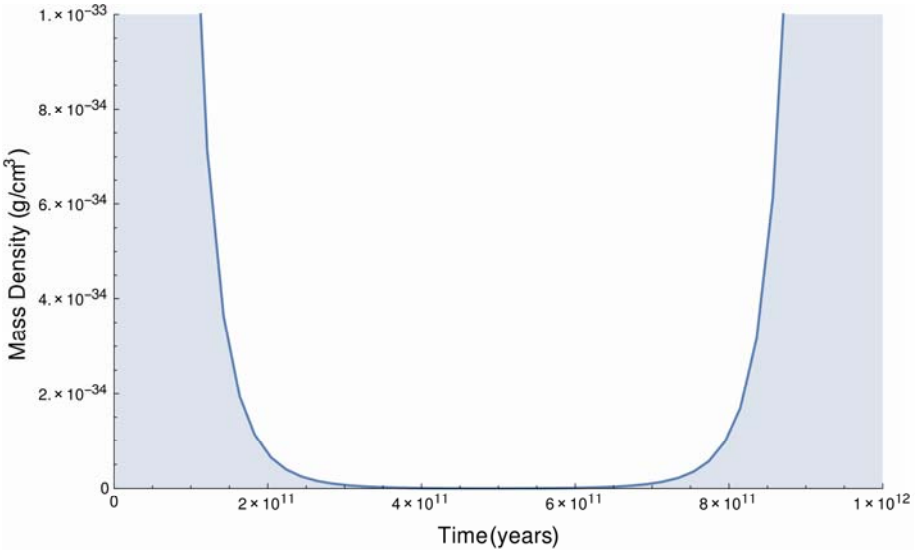

The power of the Universe as a function of time, $P_U(t)$, follows from Eq. (32.142) and Eq. (32.151) with matching the boundary conditions at the extrema.

$$P_U(t)=\frac{c^5}{8\pi G}\left(1+\cos\left(\frac{2\pi t}{\frac{2\pi G m_U}{c^3}}\right)\right) \tag{32.161}$$

$$P_U(t)=1.45\ X\ 10^{51}\left(1+\cos\left(\frac{2\pi t}{9.83\ X\ 10^{11}\ yrs}\right)\right)W$$

The ***time harmonic power of the Universe***, $P_U(t)$, is shown graphically in Figure 32.8.

Figure 32.8. The power of the Universe as a function of time.

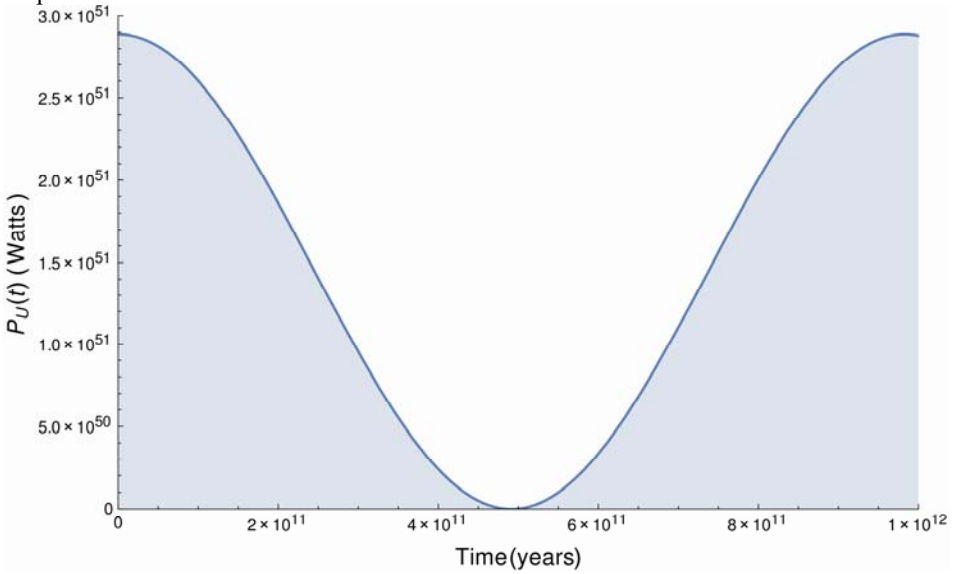

The temperature of the Universe as a function of time can be derived from the Stefan-Boltzmann law. The Stefan-Boltzmann law (Eq. (32.143)) equates the power radiated by an object per unit area, *R*, to the emissivity, *e*, times the Stefan-Boltzmann constant, σ, times the fourth power of the temperature, T^4. The area of the Universe as a function of time, $A_U(t)$, is approximately given by substitution of Eq. (32.153) into Eq. (32.144). (The Universe is a four-dimensional hyperspace of constant positive curvature at each r-sphere. In the case that the radius of the Universe is equal to the gravitational radius r_g, the area is given by Eq. (32.144); otherwise, the area of the sphere corresponding to the radius of the Universe is less than that given by Eq. (32.144). The proper area is given by solving Eq. (32.38) for the coordinate radius as a function of the proper radius followed by the substitution of the coordinate radius into Eq. (32.144)).

$$A_U(t) = 4\pi\aleph^2 = 4\pi\left[\left(\frac{2Gm_U}{c^2}+\frac{cm_U}{\frac{c^3}{4\pi G}}\right)-\frac{cm_U}{\frac{c^3}{4\pi G}}\cos\left(\frac{2\pi t}{\frac{2\pi Gm_U}{c^3}}\right)\right]^2 \tag{32.162}$$

$$A_U(t) = 4\pi\left[2.16\ X\ 10^{28}-1.86\ X\ 10^{28}\cos\left(\frac{2\pi t}{3.10\ X\ 10^{19}\ \text{sec}}\right)\right]^2 m^2$$

The power radiated by the Universe per unit area as a function of time, $R_U(t)$, is given by the ratio of Eq. (32.161) and Eq. (32.162):

$$R_U(t) = \frac{P_U(t)}{A_U(t)} = \frac{\frac{c^5}{8\pi G}\left(1+\cos\left(\frac{2\pi t}{\frac{2\pi Gm_U}{c^3}}\right)\right)}{4\pi\left[\left(\frac{2Gm_U}{c^2}+\frac{cm_U}{\frac{c^3}{4\pi G}}\right)-\frac{cm_U}{\frac{c^3}{4\pi G}}\cos\left(\frac{2\pi t}{\frac{2\pi Gm_U}{c^3}}\right)\right]^2} \tag{32.163}$$

$$R_U(t) = \frac{1.45\ X\ 10^{51}\left(1+\cos\left(\frac{2\pi t}{3.10\ X\ 10^{19}\ \text{sec}}\right)\right) W}{4\pi\left[2.16\ X\ 10^{28}-1.86\ X\ 10^{28}\cos\left(\frac{2\pi t}{3.10\ X\ 10^{19}\ \text{sec}}\right)\right]^2 m^2}$$

The ***temperature of the Universe as a function of time***, $T_U(t)$, follows from the Stefan-Boltzmann law (Eq. (32.143)) and Eq. (32.163).

$$T_U(t) = \left[\frac{R_U(t)}{e\sigma}\right]^{\frac{1}{4}} = \left[\frac{\dfrac{\dfrac{c^5}{8\pi G}\left(1+\cos\left(\dfrac{2\pi t}{\dfrac{2\pi G m_U}{c^3}}\right)\right)}{4\pi\left[\left(\dfrac{2Gm_U}{c^2}+\dfrac{cm_U}{\dfrac{c^3}{4\pi G}}\right)-\dfrac{cm_U}{\dfrac{c^3}{4\pi G}}\cos\left(\dfrac{2\pi t}{\dfrac{2\pi G m_U}{c^3}}\right)\right]^2}}{e\sigma}\right]^{\frac{1}{4}} \tag{32.164}$$

$$T_U(t) = \left[\frac{\dfrac{1.45\ X\ 10^{51}\left(1+\cos\left(\dfrac{2\pi t}{3.10\ X\ 10^{19}\ \text{sec}}\right)\right)\ W}{4\pi\left[2.16\ X\ 10^{28}-1.86\ X\ 10^{28}\cos\left(\dfrac{2\pi t}{3.10\ X\ 10^{19}\ \text{sec}}\right)\right]^2\ m^2}}{5.67 X 10^{-8}\ Wm^{-2}K^{-4}}\right]^{\frac{1}{4}}$$

where the emissivity, e, for a blackbody is one, and $\sigma = 5.67\ X\ 10^{-8}\ Wm^{-2}K^{-4}$.

The Universe is a four-dimensional hyperspace of constant positive curvature at each r-sphere. The coordinates are spherical, and the space can be described as a series of spheres each of constant radius r whose centers coincide at the origin. The existence of the mass m_U causes the area of the spheres to be less than $4\pi r^2$ and causes the clock of each r-sphere to run so that it is no longer observed from other r-spheres to be at the same rate. The Schwarzschild metric given by Eq. (32.38) is the general form of the metric which allows for these effects. Fang and Ruffini [8] show that the time effect is equivalent to a gravitational redshift of a photon. The shifted wavelength due to the gravitational field of a mass m_U is:

$$\lambda(\infty) = \lambda(r)\left(1+\frac{Gm_U}{c^2 r}\right) \tag{32.165}$$

Wien's displacement law gives the relationship between temperature and wavelength [34].

$$\lambda_{\max} T = 2.898\ X\ 10^{-3}\ m \cdot K \tag{32.166}$$

Thus, the temperature of the Universe as a function of time, $T_U(t)$, is:

$$T_U(t)=\left(\frac{1}{1+\frac{Gm_U(t)}{c^2\aleph(t)}}\right)\left[\frac{R_U(t)}{e\sigma}\right]^{\frac{1}{4}}=\left(\frac{1}{1+\frac{Gm_U(t)}{c^2\aleph(t)}}\right)\left[\frac{\frac{P_U(t)}{4\pi\aleph(t)^2}}{e\sigma}\right]^{\frac{1}{4}}$$

$$T_U(t)=\left(1+\frac{\frac{Gm_U}{2}\left(1+\cos\left(\frac{2\pi t}{\frac{2\pi Gm_U}{c^3}}\right)\right)}{c^2\left[\left(\frac{2Gm_U}{c^2}+\frac{cm_U}{\frac{c^3}{4\pi G}}\right)-\frac{cm_U}{\frac{c^3}{4\pi G}}\cos\left(\frac{2\pi t}{\frac{2\pi Gm_U}{c^3}}\right)\right]}\right)^{-1}X$$

$$\left[\frac{\frac{\frac{c^5}{8\pi G}\left(1+\cos\left(\frac{2\pi t}{\frac{2\pi Gm_U}{c^3}}\right)\right)}{4\pi\left(\left(\frac{2Gm_U}{c^2}+\frac{cm_U}{\frac{c^3}{4\pi G}}\right)-\frac{cm_U}{\frac{c^3}{4\pi G}}\cos\left(\frac{2\pi t}{\frac{2\pi Gm_U}{c^3}}\right)\right)^2}}{e\sigma}\right]^{\frac{1}{4}} \tag{32.167}$$

$$T_U(t)=\left(1+\frac{0.74\ X\ 10^{27}\left(1+\cos\left(\frac{2\pi t}{9.83\ X\ 10^{11}\ yrs}\right)\right)m}{\left[2.16\ X\ 10^{28}-1.86\ X\ 10^{28}\cos\left(\frac{2\pi t}{9.83\ X\ 10^{11}\ yrs}\right)m\right]}\right)^{-1}X$$

$$\left[\frac{\frac{1.45\ X\ 10^{51}\left(1+\cos\left(\frac{2\pi t}{9.83\ X\ 10^{11}\ yrs}\right)\right)W}{4\pi\left[2.16\ X\ 10^{28}-1.86\ X\ 10^{28}\cos\left(\frac{2\pi t}{9.83\ X\ 10^{11}\ yrs}\right)m\right]^2}}{5.67X10^{-8}\ Wm^{-2}K^{-4}}\right]^{\frac{1}{4}} \tag{32.168}$$

The temperature of the Universe as a function of time, $T_U(t)$, during the expansion phase is shown graphically in Figure 32.9.

Figure 32.9. The temperature of the Universe as a function of time during the expansion phase.

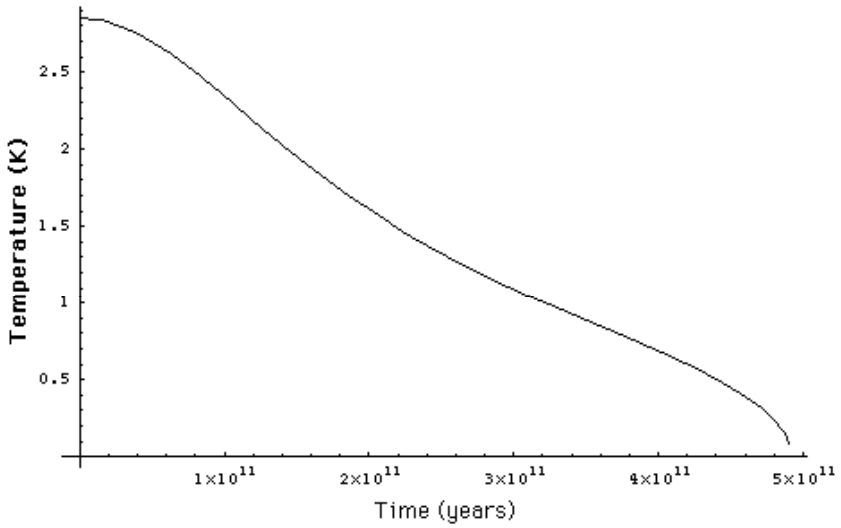

BOX 32.3 SIMPLIFIED SET OF COSMOLOGICAL EQUATIONS [42]

$$Q = \frac{c^3}{4\pi G} = \frac{m_U}{2T}$$

$$r_G = \frac{Gm_U}{c^2} = \frac{m_U c}{4\pi Q} = \frac{cT}{2\pi} = \frac{c}{\omega_U}$$

where $\omega_U = 2\pi / T$ is the angular frequency of the Universe:

$$r_g = \frac{2Gm_U}{c^2} = \frac{m_U c}{2\pi Q} = \frac{cT}{\pi}$$

Period of the Universe:

$$T = 2\pi \frac{r_G}{c} = \frac{2\pi G m_U}{c^3} = \frac{m_U}{2Q}$$

$$\aleph_0 = \frac{m_U c}{Q} = 2cT$$

$$r_U = r_g + \aleph_0 = \frac{m_U c}{2\pi Q}(1+2\pi) = \frac{cT}{\pi}(1+2\pi) = 2cT(1+2\pi)$$

$$\frac{\aleph_0}{r_U} = \frac{2\pi}{1+2\pi} \approx 0.8627$$

$$\aleph = r_g\left[(1+2\pi) - 2\pi\cos\left(2\pi\frac{t}{T}\right)\right] = \frac{cT}{\pi}\left[(1+2\pi) - 2\pi\cos\left(2\pi\frac{t}{T}\right)\right] \quad = \frac{m_U c}{2\pi Q}\cdot\left[(1+2\pi) - 2\pi\cos\left(\frac{4\pi Q}{m_U}t\right)\right]$$

$$\dot{\aleph} = \frac{d\aleph}{dt} = \frac{cT}{\pi}\cdot 2\pi\cdot\frac{2\pi}{T}\cdot\sin\left(\frac{4\pi Q}{m_U}t\right) = 4\pi c\cdot\sin\left(2\pi\frac{t}{T}\right) = 4\pi c\sin\left(\frac{4\pi Q}{m_U}t\right)$$

$$\rho_U(t)=\frac{m_U(t)}{\frac{4}{3}\pi\aleph^3}=\frac{\frac{1}{2}m_U\left[1+\cos\left(2\pi\frac{t}{T}\right)\right]}{\frac{4}{3}\pi\left(\frac{m_Uc}{2\pi Q}\right)^3\cdot\left[(1+2\pi)-2\pi\cos\left(2\pi\frac{t}{T}\right)\right]^3}$$

$$=\frac{3\pi^2Q^3}{m_U^2c_3}\cdot\frac{1+\cos\left(\frac{4\pi Q}{m_U}t\right)}{\left[(1+2\pi)-2\pi\cos\left(\frac{4\pi Q}{m_U}t\right)\right]^3}$$

$$\rho_{U\max}=\rho_U(t)\big|_{t=0}=\frac{6\pi^2Q^3}{m_U^2c^3}=6\pi^2\frac{m_U}{r_0^3}=\frac{3}{4\pi}\frac{m_U}{r_g^3}=\frac{3\pi^2m_U}{4(cT)^3}$$

$$\rho_U(t)=\frac{c^5}{8\pi G}\left[1+\cos\left(\frac{4\pi Q}{m_U}t\right)\right]=\frac{1}{2}Qc^2\left[1+\cos\left(\frac{4\pi Q}{m_U}t\right)\right]=\frac{m_Uc^2}{4T}\left[1+\cos\left(2\pi\frac{t}{T}\right)\right]$$

$$T_U(t)=\frac{1}{1+\frac{G}{c^2}\cdot\frac{m_U(t)}{\aleph(t)}}\cdot\sqrt[4]{\frac{R_U(t)}{e\sigma}};\quad e=1;\quad \sigma=\frac{\pi^2k^4}{60\hbar^3c^2}=5.6704\cdot10^{-8}Wm^{-2}K^{-4}$$

$$\frac{G}{c^2}\cdot\frac{m_U(t)}{\aleph(t)}=\frac{G}{c^2}\cdot\frac{\frac{1}{2}m_U\left[1+\cos\left(\frac{4\pi Q}{m_U}t\right)\right]}{\frac{2Gm_U}{c^2}\cdot\left[(1+2\pi)-2\pi\cos\left(\frac{4\pi Q}{m_U}t\right)\right]}=\frac{1}{4}\cdot\frac{1+\cos\left(\frac{4\pi Q}{m_U}t\right)}{(1+2\pi)-2\pi\cos\left(\frac{4\pi Q}{m_U}t\right)}$$

$$R_U(t)=\frac{P_U(t)}{4\pi\aleph(t)^2}=\frac{\frac{1}{2}Qc^2}{4\pi\left(\frac{m_Uc}{2\pi Q}\right)^2}\cdot\frac{1+\cos\left(\frac{4\pi Q}{m_U}t\right)}{\left[(1+2\pi)-2\pi\cos\left(\frac{4\pi Q}{m_U}t\right)\right]^2}$$

$$=\frac{\pi Q^3}{2m_U^2}\cdot\frac{1+\cos\left(\frac{4\pi Q}{m_U}t\right)}{\left[(1+2\pi)-2\pi\cos\left(\frac{4\pi Q}{m_U}t\right)\right]^2}$$

$$T_U(t)=\frac{\sqrt[4]{\frac{30\hbar^3c^2Q^3}{\pi k^4m_U^2}}}{1+\frac{1}{4}\cdot\frac{1+\cos\left(\frac{4\pi Q}{m_U}t\right)}{(1+2\pi)-2\pi\cos\left(\frac{4\pi Q}{m_U}t\right)}}\cdot\frac{\sqrt[4]{1+\cos\left(\frac{4\pi Q}{m_U}t\right)}}{\sqrt{(1+2\pi)-2\pi\cos\left(\frac{4\pi Q}{m_U}t\right)}}$$

$$\frac{30\hbar^3c^2Q^3}{\pi k^4m_U^2}=\frac{30\hbar^3m_Uc^2}{8\pi T^3k^4}$$

$$m_U(t) = 1 \cdot 10^{54} \left[1 + \cos\left(2\pi \frac{t}{T} \right) \right] kg$$

$$V_U(t) = \frac{4}{3} \pi \aleph(t)^3 = 4.22 \cdot 10^{85} \cdot \left[1 - 0.863 \cdot \cos\left(2\pi \frac{t}{T_U} \right) \right]^3 mm^3$$

$$\rho_U(t) = \frac{m_U(t)}{V_U(t)} = 2.37 \cdot 10^{-35} \cdot \frac{1 + \cos\left(2\pi \frac{t}{T_U} \right)}{\left[1 - 0.863 \cdot \cos\left(2\pi \frac{t}{T_U} \right) \right]^3} \frac{g}{m^3}$$

$$\rho_U(t) = \frac{c^5}{8\pi G} = \left[1 + \cos\left(2\pi \frac{t}{T_U} \right) \right] = 1.444 \cdot 10^{51} \left[1 + \cos\left(2\pi \frac{t}{T_U} \right) \right] W$$

$$A_U = 4\pi \aleph^2$$

$$A_U(t) = 4\pi \aleph^2 = 5.86 \cdot 10^{57} \cdot \left[1 - 0.863 \cdot \cos\left(2\pi \frac{t}{T_U} \right) \right]^2 m^2$$

$$R_U(t) = \frac{P_U(t)}{A_U(t)} = 2.46 \cdot 10^{-7} \cdot \frac{1 + \cos\left(2\pi \frac{t}{T_U} \right)}{\left[1 - 0.863 \cdot \cos\left(2\pi \frac{t}{T_U} \right) \right]^2} \frac{W}{m^2}$$

$$T_U(t) = \left[\frac{R_U(t)}{e\sigma} \right]^{\frac{1}{4}} = 1.444 \cdot \frac{\left[1 + \cos\left(2\pi \frac{t}{T_U} \right) \right]^{\frac{1}{4}}}{\left[1 - 0.863 \cdot \cos\left(2\pi \frac{t}{T_U} \right) \right]^{\frac{1}{2}}} K$$

$$T_U(t) = \frac{1}{1 + \frac{G}{c^2} \cdot \frac{m_U(t)}{\aleph(t)}} \cdot \left[\frac{R_U(t)}{e\sigma} \right]^{\frac{1}{4}}$$

$$= \frac{1}{1 + 3.44 \cdot 10^{-2} \cdot \frac{1 + \cos\left(2\pi \frac{t}{T_U} \right)}{1 - 0.863 \cdot \cos\left(2\pi \frac{t}{T_U} \right)}} \cdot \frac{1.444 \cdot \left[1 + \cos\left(2\pi \frac{t}{T_U} \right) \right]^{\frac{1}{4}}}{\left[1 - 0.863 \cdot \cos\left(2\pi \frac{t}{T_U} \right) \right]^{\frac{1}{2}}} K$$

$$T_U(t)\big|_{t=0} = T_{U\max} = \frac{1}{1 + 0.502} \cdot 1.444 \cdot \frac{1.1892}{0.3701} K = \frac{4.639}{1.502} K = 3.089 K$$

COMPOSITION OF THE UNIVERSE

In the case that ***lower-energy hydrogen, hydrinos, comprises the dark matter***, all matter is ordinary (baryonic) matter, and the mass of the Universe is sufficient for it to be closed [30, 31]. Whereas, the standard theory of big bang nucleosynthesis explains the observed abundance of light elements (H, He, and Li) only if the present density of ordinary (baryonic) matter is less than 10 % of the critical value [43, 44]. Recently, the missing mass has been showed to be baryonic rather than strange matter [45]. According to classical physics (CP), ***the abundance of the lighter elements, H, He, and Li can be explained by neutron, proton, and electron production during the contraction phase and stellar nucleosynthesis during the contraction as well as the expansion phase of the expansion-contraction cycle***. In the latter case, stellar and galaxy evolution occurred during the contraction phase as revealed by high-redshift radio galaxies and galaxies associated with extremely distant, luminous quasars that date back to the beginning of the expansion [46, 47]. The presence of metal lines in quasars demand a previous generation of stars (two generations for nitrogen) that is consistent with the stellar nucleosynthesis origin of the light elements [46].

The abundance of light elements for any r-sphere may be calculated using the power of the Universe as a function of time (Eq. (32.161)) and the stellar nucleosynthesis rates. During the contraction phase of the oscillatory cycle, the electron neutrino causes neutron production from a photon. Planck's equation and special and general relativity define the mass of the neutron in terms of the spacetime metric as given in the Quarks section. The Planck equation energy, which is equal to the mass energy, applies for the proper time of the neutron given by general relativity (Eq. (32.38)) that is created with the transition of a photon to a neutron.

As discussed previously in the Quantum Gravity of Fundamental Particles section, ordinarily, a photon gives rise to a particle and an antiparticle. The event must be spacelike or annihilation would occur. The event must also conserve energy, momentum, charge, and satisfy the condition that the speed of light is a constant maximum. Eqs. (32.14-32.17) give the relationship whereby matter causes relativistic corrections to spacetime that determines the curvature of spacetime and is the origin of gravity. To satisfy the boundary conditions, particle production from a single photon requires the production of an antimatter particle as well as a particle. The transition state from a photon to a particle and antiparticle comprises two concentric atomic orbitals called transition state atomic orbitals. The gravitational effect of a spherical shell on an object outside of the radius of the shell is equivalent to that of a point of equal mass at the origin. Thus, the proper time of the concentric atomic orbital with radius ${}^{+}r^{*}$ (the radius is infinitesimally greater than that of the inner transition state atomic orbital with radius r^{*}) is given by the Schwarzschild metric, Eq. (32.38). The proper time applies to each point on the atomic orbital. Therefore, consider a general point in the xy-plane having $r = \lambda\!\!\!^{-}_{C}$; $dr = 0$; $d\theta = 0$; $\sin^2\theta = 1$. Substitution of these parameters into Eq. (32.38) gives:

$$d\tau = dt\left(1 - \frac{2Gm_0}{c^2 r_\alpha^*} - \frac{v^2}{c^2}\right)^{\frac{1}{2}} \tag{32.169}$$

with $v^2 = c^2$, Eq. (32.169) becomes

$$\tau = ti\sqrt{\frac{2GM}{c^2 r_\alpha^*}} = ti\sqrt{\frac{2GM}{c^2 \lambda\!\!\!^{-}_{c}}} \tag{32.170}$$

The coordinate time is imaginary because particle/antiparticle production is spacelike. The left-hand side of Eq. (32.170) represents the proper time of the particle/antiparticle as the photon atomic orbital becomes matter. The right-hand side of Eq. (32.170) represents the correction to the laboratory coordinate metric for time corresponding to the curvature of spacetime by the particle production event.

In contrast to the familiar particle production event involving production of particles in matter-antimatter pairs, it is possible to form a particle without production of the corresponding antimatter partner. During the contraction phase, electron neutrinos cause neutron production from photons. In this case, the event must also be spacelike or annihilation would occur. Similarly, the event must also conserve energy, momentum, charge, and satisfy the condition that the speed of light is a constant maximum. Eqs. (32.14-32.17) also apply. They give the relationship whereby matter causes relativistic corrections to spacetime that determines the curvature of spacetime and is the origin of gravity.

Astrophysical observations discussed *infra* confirm that Hydrino is the dark matter of the universe which comprises the total mass of the universe except for a few percent non-hydrino hydrogen and traces of other elements. Hydrino states, atomic dominance during expansion and molecular dominance during contraction, are central to the matter decay to energy and energy to matter production reactions which drive the corresponding expansion and contraction phases of the universe. The nuclear reaction for the beta decay of the neutron is given by Eqs. (39.1-39.11) and Eq. (32.173). From Eq. (32.173), it can be appreciated by time reversal symmetry that the product of the reaction of an electron antineutrino with atomic hydrino comprising a proton and a beta particle (electron) is a neutron except for the energy deficit of hydrino. In the absence MeV scale hydrino collisional or antineutrino energy, the corresponding reverse beta decay transition state to a neutron is unstable and decays ultimately to gamma rays. To conserve spin (angular momentum), the reaction is:

$$\bar{\nu}_e + {}^1H\left[\frac{a_H}{p}\right] \rightarrow \gamma + \nu_e \tag{32.171}$$

where ν_e is the electron neutrino and $\bar{\nu}_e$ is the electron antineutrino. A branch of the decay path may be similar to that of the

π^0 meson. Gamma and pair-production decay result in characteristic 511 keV annihilation energy emission. This emission has been recently been identified with dark matter [48,49]. Disproportionation reactions to the lowest-energy states of hydrogen followed by reverse beta decay with gamma ray emission may be *a source of nonthermal γ-ray bursts from interstellar regions* [50]. The energy peak of the gamma ray spectrum of the universe is about 1 GeV, the mass/energy of a hydrino atom consistent with Eq. (32.171) [51]. An extreme excess of gamma rays of non-cosmic ray origin is emitted by the Sun. The energy cutoff is at the atomic hydrino annihilation energy consistent with Eq. (32.171) [52] and consistent with the independent hypothesis that the source of the Sun's gamma rays is decaying dark matter [53].

Consider the impact of the hydrino electron-proton annihilation reaction on spacetime mechanics. Hydrinos which comprises the dark matter, essentially all of the mass of the universe, annihilate to photons and electron neutrinos as given by Eq. (32,173) and in the New "Ground" State section. The annihilation reaction dominates over matter production reactions during the expansion phase due to the relative competing kinetics. Specifically, during the expansion phase the power and temperature of the universe start at a maximum with a consequence that the dominant inventory of hydrino is in atomic form rather than the molecular hydrino form. Moreover, the population and density of electron antineutrinos formed during the contraction phase also start at a maximum during spacetime expansion, and the corresponding atomic hydrino nuclear reactions dominate those involving molecular hydrino discussed *infra*.

In addition to those corresponding to Eq. (32.171), another source of nonthermal γ-ray bursts from interstellar regions [50] is the conversion of matter to photons of the Planck mass-energy, which may also give rise to cosmic rays. When the gravitational potential energy density of a massive body such as a blackhole equals that of a particle having the Planck mass as given by Eqs. (32.22-32.32), the matter may transition to photons of the Planck mass given by Eq. (32.31). In the case of the Planck mass, the gravitational potential energy (Eq, (32.30)) is equal to the Planck, electric, and magnetic energies which equal mc^2 (Eq. (32.32)), and the coordinate time is equal to the proper time (Eqs. (32.33-32.34) and Eq. (32.43)). However, the particle corresponding to the Planck mass may not form since its gravitational velocity (Eq. (32.33)) is the speed of light.

> *The limiting speed of light eliminates the singularity problem of Einstein's equation that arises as the radius of a blackhole equals the Schwarzschild radius. General relativity with the singularity eliminated resolves the paradox of the infinite propagation velocity required for the gravitational force in order to explain why the angular momentum of objects orbiting a gravitating body does not increase due to the finite propagation delay of the gravitational force according to special relativity [54].*

Thus, it remains a photon. Even light from a blackhole will escape when the decay rate of the trapped matter with the concomitant spacetime expansion is greater than the effects of gravity that oppose this expansion. The annihilation of a blackhole may be the source of *γ-ray bursts*. Gamma-ray bursts are the most energetic phenomenon known that can release an explosion of gamma rays packing 100 times more energy than a supernova explosion [55]. Cosmic rays are the most energetic particles known, and their origin is also a mystery [56]. In 1966, Cornell University's Kenneth Greisen predicted that interaction with the ubiquitous photons of the cosmic microwave background would result in a smooth power-law cosmic-ray energy spectrum being sharply cutoff close to $5\ X\ 10^{19}\ eV$. However, in 1998, Schwarzschild reported [57] that the *Akeno Giant Air Shower Array (AGASA) in Japan has collected data that show the cosmic-ray energy spectrum is extending beyond the Greisen-Zatsepin-Kuzmin (GZK) cutoff.* According to the GZK cutoff, the cosmic spectrum cannot extend beyond $5\ X\ 10^{19}\ eV$, but AGASA, the world's largest air shower array, has shown that the spectrum is extending beyond without any clear sign of cutoff. Similarly, the Utah Fly's Eye had detected cosmic rays with energy up to $3\ X\ 10^{20}\ eV$ [58,59]. *Photons, each of the Planck mass, may be the source of these inexplicably energetic cosmic rays* corresponding to tremendous power and concomitant spacetime expansion. The Planck mass conversion of matter into energy may also be the unprecedented X-ray power of the ultraluminous pulsar: NuSTAR [60]. The gamma ray burst energy may undergo energy down conversion by interaction with matter due to higher energy absorption and re-emission of lower energy gamma rays. The gamma rays from each of the sources may convert back into matter during the contraction phase due to a unique molecular hydrino-catalyzed reaction of an electron neutrino and a gamma photon.

Rather than being particles with non-zero rest mass, neutrinos such as the electron neutrino and the electron antineutrino are special types of photons as given in the Neutrino section. Massless neutrinos travel at light speed for all observers. In addition, neutrinos have spin which must be conserved. To satisfy the boundary conditions, particle production from an electron neutrino and a photon requires the production of a single neutral particle, a neutron. In this case, the transition state only comprises a single particle transition state atomic orbital with the antiparticle partner one absent. The left-hand side of Eq. (32.170) represents the proper time of the neutron as the photon atomic orbital becomes matter. The right-hand side of Eq. (32.170) represents the correction to the laboratory coordinate metric for time corresponding to the relativistic correction of spacetime by the particle production. Thus, ***during the contraction phase of the oscillatory cycle, the electron neutrino causes neutron production from a gamma photon, and the production of protons and electrons occurs by neutron beta decay. From Eq. (32.173), the number of electrons exactly balances the number of protons. Thus, the Universe is electrically neutral.***

Typically, antimatter and matter are created in the laboratory in equal amounts; yet ***celestial antimatter is not observed***. The reason is that electron neutrinos of only one type (electron neutrinos versus electron antineutrinos) dominate the kinetics of matter production over antimatter production. Specially, spin conservation requires that antineutron production does not occur

as a separate symmetrical reaction, and particle production from an electron neutrino and a photon prohibits production of the antimatter twin. From Eq. (38.6), the neutron mass is

$$m_{ddu\ \ calculated} = (3)(2\pi)\left(\frac{1}{1-\alpha}\right)\left(\frac{2\pi h}{\sec\ c^2}\right)^{\frac{1}{2}}\left(\frac{2\pi(3)ch}{2G}\right)^{\frac{1}{4}} = 1.674\ X\ 10^{-27}\ kg \tag{32.172}$$

The neutron production reaction and the nuclear reaction for the beta decay of a neutron are:

$$\gamma + \nu_e \rightarrow {}^1n$$

$$^1n \rightarrow {}^1H + \beta + \overline{\nu}_e + 0.7835\ MeV \tag{32.173}$$

where ν_e is the electron neutrino and $\overline{\nu}_e$ is the electron antineutrino. The molecular orbital of molecular hydrino comprises a paired and an unpaired electron whereby ro-vibrational states may undergo transitions involving absorption and emission via one-photon, two-photon, and electron neutrino absorption and emission [61]. Thus, molecular hydrino may catalyze neutron production by the reaction of Eq. (32.173) when a gamma ray strikes a molecular hydrino in an excited ro-vibrational state such that it undergoes de-excitation by emitting an electron neutrino during the gamma-ray collisional event. During the cold contraction phase the molecular hydrino population and its corresponding nuclear reactions dominate over those of atomic hydrino. Moreover, the energy of cosmic gammas rays may be blue shifted during spacetime contraction to further enable the production of neutrons by Eq. (32.173). Consistent with Eq. (32.173), characteristic neutral pion decay gamma rays were detected in 2013 originating in two supernova remnants confirm that pions are produced copiously after supernovas, most probably in conjunction with production of high-energy protons that are detected on Earth as cosmic rays [62]. In fact, essentially all cosmic rays comprise protons followed in abundance by electrons [63,64].

Since the atomic radius and the semi-major and semi-minor axes of atomic hydrino and molecular hydrino, respectively, are inversely related to the p quantum number, the p quantum state inventory of the atomic hydrino and molecular hydrino as well as the relative ratio of the atomic to molecular hydrino in the universe affects the rates that atomic hydrino causes proton-electron decay to create an inventory of gamma ray photons and molecular hydrino catalyzes proton-electron production from cosmic gamma-rays. As time increases in the expansion phase, the atomic hydrino states comprise high p quantum numbers such the reverse beta decay reaction becomes more probable with an antineutrino collision. In addition, the rovibrational levels of the corresponding molecular hydrino may contribute to any mismatch between the gamma ray energy and the resonant neutron production energy wherein molecular hydrino further serves as the required third body to conserve momentum during the particle production event. The decay rate is dominant during the expansion phase when the hydrino atomic population of high p quantum number overwhelms molecular hydrino population of high p quantum number, whereas the opposite is the case during the contraction phase. A third factor affecting the dominance of the rate of proton-electron decay versus proton-electron production is the range of the p quantum number of hydrinos that also varies during the expansion-contraction cycle.

In addition to these novel mechanisms for the conversion of matter into energy, a light filled from a matter filled universe may be the result from a subtle change in the fundamental constants due to spacetime expansion to the maximum radius. There is evidence that with time evolution (spacetime expansion and contraction) the fine structure constant changes as an inherent property [65-68]. This would have a profound effect on stability and the inter-conversion rates of matter and energy.

Thus, the Universe is oscillatory in matter, energy, and spacetime without the existence of antimatter due to conservation of spin of the electron neutrino and the relationship of particle production to spacetime contraction. During the expansion phase, ***the arrow of time runs forward*** to lower mass and higher entropy states; whereas, during collapse, ***the arrow of time runs backwards*** relative to the case of the Universe in a state of expansion. Recent particle physics experiments demonstrate that the decay of kaons and antikaons follows a law that is not symmetric with respect to time reversal [39]. The data reveals that there is a microscopic arrow of time, in addition to the thermodynamic and cosmological arrows.

The Universe evolves to higher mass and lower entropy states. Thus, biological organisms such as humans, which rely on the spontaneity of chemical reactions with respect to the forward arrow of time cannot exist in the contracting phase of the Universe. And, compared to the period of the Universe, the ***origins of life*** occurred at a time very close to the beginning of the expansion of the Universe when the direction of the spontaneity of reactions changed to the direction of increasing entropy and the rate of the increase in entropy of the Universe was a maximum.

The origin of the microwave background radiation (CMBR) as the power from the Universe rather than from a Big Bang creation event is demonstrated by the absence of the shadows in the CMBR required for the Big Bang model [36]. As shown in the Power Spectrum of the Cosmic Microwave Background section, when the Universe reaches the maximum radius of the time harmonic variation in the radius of the Universe, (Eq. (32.150)), it is radiation filled. Since the photon has no gravitational mass, the radiation is uniform. As energy converts into matter the power of the Universe may be considered negative for the first quarter cycle starting from the point of maximum expansion as given by Eq. (32.195), and spacetime contracts according to Eq. (32.140). The gravitational field from particle production travels as a light wave front. As the Universe contracts to a minimum radius, the gravitational radius given by Eq. (32.147), constructive interference of the gravitational fields occurs. The resulting slight variations in the density of matter are observed from our present r-sphere. As shown in the Power Spectrum of the Cosmic Microwave Background section, the cosmic microwave background radiation is an average temperature of 2.725 K, with deviations of 30 or so μK in different parts of the sky representing these slight variations in the density of matter. By this

mechanism, the production of particles over time from a photon-filled Universe gave rise to centers that eventually aggregated by gravitational attraction into a hierarchy of more massive structures to eventually form the large-scale structure of the cosmos.

Galaxies formed during the collapsing stage of the evolution of the Universe wherein the mass perturbations occurred due to gravity wave interference as demonstrated by the DASI and WMAP data as shown in the Power Spectrum of the Cosmic Microwave Background section. These perturbations resulted in collapsing gas clouds that formed quasars. Then each of these quasars erupted into a supernova and formed a blackhole. The expelled gas eventually formed galaxies. The observation of a blackhole in the center of each galaxy is consistent with the origin of galaxies from a quasar supernova [69, 70]. Furthermore, since angular momentum must be conserved in the rotation of the founding quasar and the resulting blackhole and galactic rotating stars, a linear relationship of the plot of the velocity of the outer stars of a given galaxy to the blackhole mass is expected. This ratio called sigma is indeed observed to be linear [69,70].

The Universe is oscillatory with a finite minimum radius, the gravitational radius. Thus, stellar and celestial structures evolve on a time scale that is greater than the observed time of expansion. ***Stars exist which are older than the elapsed time of the present expansion*** as stellar evolution occurred during the contraction phase [71,72]. Galaxy evolution also occurred during the contraction phase as revealed by high-redshift radio galaxies and galaxies associated with extremely distant, luminous quasars that date back to the beginning of the expansion [46, 47]. The Gemini Deep Deep Survey confirmed the predicted existence of old galaxies at the beginning of the expansion at 10 billion light years and further directly disprove the Big Bang theory of cosmology [73-75]. These results were confirmed by a spectroscopic redshift survey that probed the most massive and quiescent galaxies back at 10 billion light years [76,77]. It was found that a significant fraction of the massive old galaxies observed over all of time since the expansion were in place in the early Universe. This is also shown by the Hubble Ultra Deep Field (HUDF) given in Figure 32.10. A definitive validation of the classical predictions is provided by the Keck survey for gravitationally lensed Lyα emitters that found galaxies back at over 13 billion light years [78]. The absence of red dwarf stars that contain no metals is another indication of the ancient nature of the universe that is much older than the 10 billion years of expansion. Further confirmation of the older age of the universe is the existence of the brightest quasar in the early universe powered by the most massive black hole yet known [79] and that dust, a signature of an old galaxy, has been observed in a young universe [80]. Furthermore, the recent unanticipated Webb telescope images confirm additional GUTCP predictions of fully formed galaxies and old galaxies at the beginning of the expansion of the universe that disprove the long held metaphysical Big Bang and related theories of cosmology [81-84]. In fact, even massive old blackholes [85, 86] and carbon molecules [87] are observed to the beginning of expansion, 13.7 B light years from present-day Earth.

Figure 32.10. The Hubble Ultra Deep Field (HUDF) shows mature galaxies at the time of the beginning of the expansion of the Universe. The "Big Bang" is NOT observed. This image is a composite of two separate images taken by the Hubble's Advanced Camera for Surveys (ACS) and the Near Infrared Camera and Multiobject Spectrometer (NICMOS), the result of over eleven and a half days of exposure. It contains an estimated ten thousand galaxies. Released on 9 March 2004. Courtesy of NASA, ESA, S. Beck with STScI and the HUDF Team.

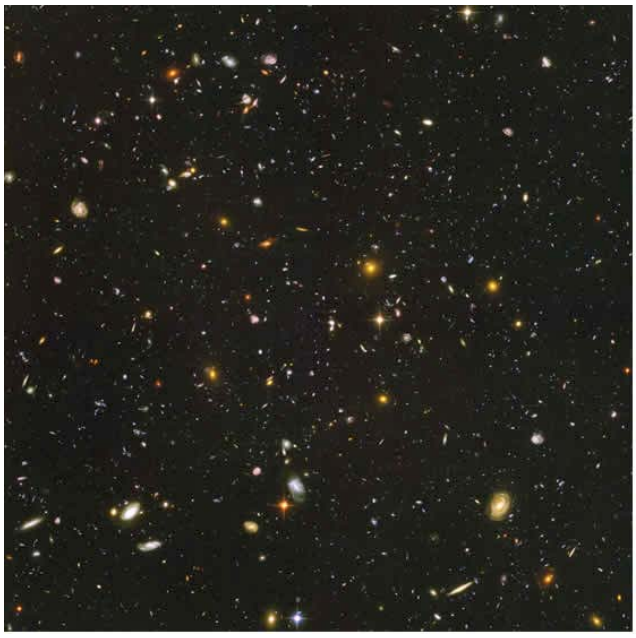

In addition to fusion reactions in stars, hydrino transitions to lower energy hydrino states is a source of power contribution to the CMBR as well as a source of spacetime expansion as matter is converted into energy. As given in the Disproportionation of Energy States section, classical physical laws predict that atomic hydrogen may undergo a catalytic

reaction with certain species, including itself, that can accept energy in integer multiples of the potential energy of atomic hydrogen, $m \cdot 27.2$ eV, wherein m is an integer. The predicted reaction involves a resonant, nonradiative energy transfer from otherwise stable atomic hydrogen to the catalyst capable of accepting the energy. The product is H(1/p), fractional Rydberg states of atomic hydrogen called "hydrino atoms," wherein n = 1/2, 1/3, 1/4,…, 1/p (p≤137 is an integer) replaces the well-known parameter n = integer in the Rydberg equation for hydrogen excited states. Each hydrino state also comprises an electron, a proton, and a photon, but the field contribution from the photon increases the binding energy rather than decreasing it corresponding to energy desorption rather than absorption. Since the potential energy of atomic hydrogen is 27.2 eV, $m\ H$ atoms serve as a catalyst of $m \cdot 27.2\ eV$ for another $(m+1)$th H atom (See BlackLight Process section). For example, a H atom can act as a catalyst for another H by accepting 27.2 eV from it via through-space energy transfer such as by magnetic or induced electric dipole-dipole coupling to form an intermediate that decays with the emission of continuum bands with short wavelength cutoffs and energies of $m^2 \cdot 13.6\ eV\ \left(\frac{91.2}{m^2}\ nm\right)$. The continuum radiation band at 10.1 nm and going to longer wavelengths for theoretically predicted transitions of H to lower-energy, so called "hydrino" state H(1/4), was observed only arising from pulsed pinch gas discharges comprising some hydrogen and oxygen as an oxide, first at Brilliant Light Power, Inc. (BLP) and reproduced at the Harvard Center for Astrophysics (CfA) [88-94]. HOH was shown to be the catalyst in these pinch plasma continua as well as in the 10-30 nm EUV continuum observed from plasma having essentially no field. The latter plasma was formed by igniting a solid fuel source of H and HOH catalyst by passing an ultra-low voltage, high current through the fuel to produce an explosive plasma [88]. Moreover, $m\ H$ catalyst (Eqs. (5.48-5.61)) was identified to be active in astronomical sources such as the Sun, stars, and interstellar medium wherein the characteristics of hydrino product match those of the dark matter of the Universe [88]. Hydrogen continua from transitions to form hydrinos matches the emission from white dwarfs, provides a possible mechanism of linking the temperature and density conditions of the different discrete layers of the coronal/chromospheric sources, and provides a source of the diffuse ubiquitous EUV cosmic background with the 10.1 nm continuum matching the observed intense 11.0-16.0 nm band in addition to resolving other cosmological mysteries [88,92,95,96]. Given the seeding by the anisotropic gravitational forces in a contracting Universe, expansion of the Universe depends on the rate of energy release, which varies throughout the Universe; thus, clusters of galaxies, huge voids, and other ***large features which are observed*** [97-101] are caused by the interaction between the rate of energy release with concomitant spacetime expansion and gravitational attraction. Hydrogen-type atoms and molecules comprise most of the matter of the Universe. The distinction between hydrogen and hydrinos with respect to the interaction with electromagnetic radiation and release of energy by transitioning to lower energy states (See Disproportionation of Energy States section) also has an influence on the formation of large voids and walls of matter. Lower-energy atomic hydrogen atoms, hydrinos, each have the same mass and a similar interaction as the neutron. According to Steinhardt and Spergel of Princeton University [101], these are the properties of dark matter that are necessary in order for the theory of the structure of galaxies to work out on all scales. The observation that galaxy clusters arrange themselves as predicted for cold dark matter except that the cores are less dense than expected is explained. Hydrinos further account for the observation that small halos of dark matter are evaporated when they approach larger ones and that dark matter is easily influenced by black holes, explaining how they grew so large.

Laboratory EUV continuum results [88] offer resolution to many otherwise inexplicable celestial observations with (a) the energy and radiation from the hydrino transitions being the source of extraordinary temperatures and power regarding the solar corona problem, the cause of sunspots and other solar activity, and why the Sun emits X-rays [92], (b) the hydrino-transition radiation being the radiation source heating the WHIM and behind the observation that diffuse Hα emission is ubiquitous throughout the Galaxy requiring widespread sources of flux shortward of 912 $\AA$, and (c) the identity of dark matter being hydrinos.

Stars also comprise plasmas of hydrogen with surfaces comprised of essentially dense atomic hydrogen permissive of multi-body H interactions to propagate transition of H to H(1/(m +1)) wherein $m\ H$ serves as the catalyst. Such transitions are predicted to emit EUV continuum radiation according to Eqs. (5.48-5.61). The emission from white dwarfs arising from an extremely high concentration of hydrogen is modeled as an optically thick blackbody of ~ 50,000 K gas comprising predominantly hydrogen and helium. A modeled composite spectrum of the full spectral range from 10 nm to >91.2 nm with an abundance He/H=10^{-5} from Barstow and Holberg [95] is shown in Figure 10 of Ref. [88]. Albeit, while white dwarf spectra can be curve fitted using stratification and adjustable He and H column densities and ionization fractions to remove some inconsistencies between optical and EUV spectra [103] and independent measurements of the latter, matching the spectrum at the short-wavelengths is problematic. Alternatively, combining the laboratory-observed emission continuum bands gives a spectrum with continua having edges at 10.1 nm, 22.8, nm, and 91.2 nm, a match to the white dwarf spectrum [88]. However, the proposed nature of the plasmas and the mechanisms are very different. The emission in our studies is assigned to hydrino transitions in cold-gas, optically-thin plasmas absent any helium. White-dwarf and celestial models may need revision and benefit from our discovery of high-energy H continua emission.

For example, there is no existing physical model that can couple the temperature and density conditions in different discrete regions of the outer atmosphere (chromosphere, transition region, and corona) of coronal/chromospheric sources [103]. Typically, the corona is modeled to be three orders of magnitude hotter than the surface that is the source of coronal heating seemingly in defiance of the second law of thermodynamics. Reconciliation is offered by the mechanism of line absorption and re-emission of the $m^2 \cdot 13.6\ eV$ (Eq. (5.57)) continuum radiation. The 91.2 nm continuum to longer wavelengths is expected to be prominent (less attenuated than the 10.1 nm and 22.8 nm bands) and is observed in the solar extreme ultraviolet spectrum as

shown in Figure 11 of Ref. [88] and Ref. [104] despite attenuation by the coronal gas. High-energy-photon excitation is more plausible than a thermal mechanism with T~10^6 given the 4000 K surface temperature and the observation of the CO absorption band at 4.7 μm in the solar atmosphere wherein CO cannot exist above 4000 K [105]. Considering the 10.1 nm band as a source, the upper limit of coronal temperature based on excitation of about 10^6 K is an energy match. In addition to the temperature, another extraordinary observation is that although the total average energy output of the outer layers of the Sun is $\cong 0.01\ \%$ of the photospheric radiation, local transient events can produce an energy flux that exceeds the photospheric flux [106]. The energy source of the latter may be magnetic in nature, but identity of the highly ionizing coronal source is not established. Nor, has the total energy balance of the Sun been reconciled. The possibility of a revolutionary discovery of a new source of energy in the Sun based on a prior undiscovered process is an open question [107]. That $m\ H$ catalyzed hydrino transitions occur in stars and the Sun [108] as evident by corresponding continua in its spectrum resolves the solar corona problem, the cause of sunspots and other solar activity, and why the Sun emits X-rays [92].

The laboratory EUV continuum results [88] have further implications for the resolution of the identity of dark matter and the identity of the radiation source behind the observation that diffuse Hα emission is ubiquitous throughout the Galaxy and widespread sources of flux shortward of 912 $\AA$ are required [109]. The identity of dark matter has been a cosmological mystery. It is anticipated that the emission spectrum of the extreme ultraviolet background of interstellar matter possesses the spectral signature of dark matter. Labov and Bowyer designed a grazing incidence spectrometer to measure and record the diffuse extreme ultraviolet background [109]. The instrument was carried aboard a sounding rocket, and data were obtained between 80 $\AA$ and 650 $\AA$ (data points approximately every 1.5 $\AA$). Several lines including an intense 635 $\AA$ emission associated with dark matter were observed [109] which has considerable astrophysical importance as indicated by the authors:

> "Regardless of the origin, the 635 $\AA$ emission observed could be a major source of ionization. Reynolds (1983, 1984, 1985) has shown that diffuse Hα emission is ubiquitous throughout the Galaxy, and widespread sources of flux shortward of 912 $\AA$ are required. Pulsar dispersion measures (Reynolds 1989) indicate a high scale height for the associated ionized material. Since the path length for radiation shortward of 912 $\AA$ is low, this implies that the ionizing source must also have a large scale height and be widespread. Transient heating appears unlikely, and the steady state ionization rate is more than can be provided by cosmic rays, the soft X-ray background, B stars, or hot white dwarfs (Reynolds 1986; Brushweiler & Cheng 1988). Sciama (1990) and Salucci & Sciama (1990) have argued that a variety of observations can be explained by the presence of dark matter in the galaxy which decays with the emission of radiation below 912 $\AA$.
>
> The flux of 635 $\AA$ radiation required to produce hydrogen ionization is given by $F = \zeta_H / \sigma_\lambda = 4.3\ X\ 10^4 \zeta_{-13}\ photons\ cm^{-2} s^{-1}$, where ζ_{-13} is the ionizing rate in units of $10^{-13} s^{-1}$ per H atom. Reynolds (1986) estimates that in the immediate vicinity of the Sun, a steady state ionizing rate of ζ_{-13} between 0.4 and 3.0 is required. To produce this range of ionization, the 635 $\AA$ intensity we observe would have to be distributed over 7% - 54% of the sky."

The 63.5 ± 0.47 nm line [109] matches a hydrino transition predicted for H undergoing catalysis with H (m=1) as the catalyst giving rise to a concerted energy exchange of the total energy of 40.8 eV with the excitation of the He $1s^2$ to $1s^1 2p^1$ transition. The predicted 63.3 nm emission associated with dark matter was observed with the addition of hydrogen to helium microwave plasma as shown previously [92,110]. An alternative assignment suggested by Labov and Bowyer [109] is the 63.0 nm line of O V requiring a large-scale non-thermal source of ionization. Continuum radiation from transitions to low-level hydrino states can provide this radiation. Indeed, the observation of the 63.3 nm line is also associated with the presence of an interstellar X-ray background.

The first soft X-ray background was detected and reported [111] about 25 years ago. Quite naturally, it was assumed that these soft X-ray emissions were from ionized atoms within hot gases. Labov and Bowyer also interpreted the data as emissions from hot gases. However, the authors left the door open for some other interpretation with the following statement from their introduction:

> *"It is now generally believed that this diffuse soft X-ray background is produced by a high-temperature component of the interstellar medium. However, evidence of the thermal nature of this emission is indirect in that it is based not on observations of line emission, but on indirect evidence that no plausible non-thermal mechanism has been suggested which does not conflict with some component of the observational evidence."*

The authors also state "if this interpretation is correct, gas at several temperatures is present." Specifically, emissions were attributed to gases in three ranges: $5.5 < \log T < 5.7$; $\log T = 6$; $6.6 < \log T < 6.8$. Observations in the ultraviolet with HST and FUSE [112] and also XMM-Newton [113] confirm these extraordinary temperatures of diffuse intergalactic medium (IGM) and reveal that a large component of the baryonic matter of the Universe is in the form of WHIM (warm-hot ionized media) [112,113]. The mysteries of the identity of dark matter, the observed dark interstellar medium spectrum, the source of the diffuse X-ray background, and the source of ionization of the IGM [112,113] are resolved by the formation of hydrinos that emit EUV and X-ray continua depending on the state transition and conditions; the continua create highly ionized ions that emit ion

radiation of non-thermal origin; the hydrino transition H to H(1/2) results in a 63.3 nm line [92,110], and He^+ acting as a catalyst of 54.4 eV ($2 \cdot 27.2\ eV$) pumps the intensity of helium ion lines such as the 30.4 nm line [90, 92].

As shown in the Disproportionation of Energy States section, the products of the catalysis reactions (e.g. Eqs. (5.48-5.51)) have binding energies of $m \cdot 27.2\ eV$, such that they may further serve as catalysts. Thus, further catalytic transitions may occur: $n = \frac{1}{3} \rightarrow \frac{1}{4}$, $\frac{1}{4} \rightarrow \frac{1}{5}$, and so on. Thus, lower-energy hydrogen atoms, *hydrinos*, can act as catalysts by resonantly and nonradiatively accepting energy of $m \cdot 27.2\ eV$ from another H or hydrino atom (Eq. (5.24)). Such disproportionation reactions of hydrinos are predicted to give rise to features in the X-ray region. As shown by Eqs. (5.40-5.43) the reaction product of HOH catalyst is $H\left[\frac{a_H}{4}\right]$. A likely transition reaction in hydrogen clouds containing H_2O gas is the transition of a H atom to $H\left[\frac{a_H}{17}\right]$ wherein $H\left[\frac{a_H}{4}\right]$ serves as a catalyst to give a broad peak having a short wavelength cutoff at $E = 3481.6\ eV;\ 0.35625\ nm$. A broad X-ray peak with a 3.48 keV cutoff was recently observed in the Perseus Cluster by NASA's Chandra X-ray Observatory and by the XMM-Newton [114,115] that has no match to any known atomic transition. The 3.48 keV feature assigned to dark matter of unknown identity by BulBul et al. [114] matches the $H\left[\frac{a_H}{4}\right] + H\left[\frac{a_H}{1}\right] \rightarrow H\left[\frac{a_H}{17}\right]$ transition and further confirms hydrinos as the identity of dark matter.

Evidence for EUV emission from hydrino transitions also comes from the interstellar medium (ISM) since it provides a source of the diffuse ubiquitous EUV cosmic background. Specifically, the 10.1 nm continuum matches the observed intense 11.0-16.0 nm band [95,96]. Furthermore, it provides a mechanism for the high ionization of helium of the ISM and the excess EUV radiation from galaxy clusters that cannot be explained thermally [114]. Moreover, recent data reveals that X-rays from distant active galactic nuclei sources are absorbed selectively by oxygen ions in the vicinity of the galaxy [115]. The temperature of the absorbing halo is between 1 million and 2.5 million Kelvin, or a few hundred times hotter than the surface of the Sun. The corresponding energy range is 86 eV to 215 eV which is in the realm of the energy released for the transition of H to H(1/4). Additional astrophysical evidence such as the observation that a large component of the baryonic matter of the Universe is in the form of WHIM (warm-hot ionized media) in the absence of a conventional source and the match of hydrinos to the identity of dark matter was presented previously [116,117]. The latter case is further supported by observations of signature electron-positron annihilation energy.

Dark matter comprises a majority of the mass of the Universe as well as intra-galactic mass [118,119]. It would be anticipated to concentrate at the center of the Milky Way galaxy due to the high gravity from the presence of a super massive blackhole at the center that emits gamma rays as matter falls into it. Since hydrinos are each a state of hydrogen having a proton nucleus, high-energy gamma rays impinging on dark matter will result in pair production. The corresponding observed characteristic signature being the emission of the 511 keV annihilation energy of pair production identifies dark matter as hydrino [120-122]. Another hydrino decay pathway for this radiation is given by Eq. (32.171). The interstellar medium [122-125], gamma-ray bursts [125,126], and solar flares [105, 125,127] also emit 511 keV line radiation. The dominant source of positrons in gamma-ray bursts is likely pair production by photon on photons or on strong magnetic fields [125]. The solar-flare emission is likely due to production of radioactive positron emitters in accelerated charge interactions [125],whereas the diffuse 511 keV radiation by interstellar medium is consistent with the role of hydrino as dark matter in pair production from incident cosmic radiation [123-125].

The characteristic spectral signatures and properties of hydrino match those attributed to the dark matter of the Universe. The Universe is predominantly comprised of hydrogen and a small amount of helium. These elements exist in interstellar regions of space, and they are expected to comprise the majority of interstellar matter. However, the observed constant angular velocity of many galaxies as the distance from the luminous galactic center increases can only be accounted for by the existence of nonluminous weakly interacting matter, dark matter. It was previously accepted that dark matter exists at the cold fringes of galaxies and in cold interstellar space. This has since been disproved by the observation of Bournaud et al. [118,119] that demonstrated that galaxies are mostly comprised of dark matter, and the data persistently supports that dark matter probably accounts for the majority of the universal mass.

The best evidence yet for the existence of dark matter is its direct observation as a source of massive gravitational mass evidenced by gravitational lensing of background galaxies that does not emit or absorb light as shown in Figure 32.11 [128]. There has been the announcement of some unexpected astrophysical results that support the existence of hydrinos. In 1995, Mills published the GUTCP prediction [129] that the expansion of the Universe was accelerating from the same equations that correctly predicted the mass of the top quark before it was measured. To the astonishment of cosmologists, this was confirmed by 2000. Mills made another prediction about the nature of dark matter based on GUTCP that may be close to being confirmed. Bournaud et al. [118,119] suggest that dark matter is hydrogen in dense molecular form that somehow behaves differently in terms of being unobservable except by its gravitational effects. Theoretical models predict that dwarfs formed from collisional debris of massive galaxies should be free of nonbaryonic dark matter. So, their gravity should tally with the stars and gas within them. By analyzing the observed gas kinematics of such recycled galaxies, Bournaud et al. [118,119] have measured the gravitational masses of a series of dwarf galaxies lying in a ring around a massive galaxy that has recently experienced a collision. Contrary to the predictions of Cold-Dark-Matter (CDM) theories, their results demonstrate that they contain a massive

dark component amounting to about twice the visible matter. This baryonic dark matter is argued to be cold molecular hydrogen, but it is distinguished from ordinary molecular hydrogen in that it is not traced at all by traditional methods, such as emission of CO lines. These results match the predictions of the dark matter being molecular hydrino.

Figure 32.11. Dark matter ring in galaxy cluster. This Hubble Space Telescope composite image shows a ghostly "ring" of dark matter in the galaxy cluster Cl 0024+17. The ring is one of the strongest pieces of evidence to date for the existence of dark matter, a prior unknown substance that pervades the Universe. Courtesy of NASA, M.J. Jee and H. Ford (Johns Hopkins University).

Additionally, astronomers Jee at al. [130] using data from NASA's Hubble Telescope have mapped the distribution of dark matter, galaxies, and hot gas in the core of the merging galaxy cluster Abell 520 formed from a violent collision of massive galaxy clusters and have determined that the dark matter had collected in a dark core containing far fewer galaxies than would be expected if dark matter was collsionless with dark matter and galaxies anchored together. The collisional debris left behind by the galaxies departing the impact zone behaved as hydrogen did, another indication that the identity of dark matter is molecular hydrino. Moreover, detection of alternative hypothesized identities for dark matter such as super-symmetry particles such as neutalinos has failed at the Large Hadron Collider; nor, has a single event been observed for weakly interacting massive particles or wimps at the Large Underground Xenon (LUX) experiment [131]. The HADES search for dark matter eliminated the leading candidate, "Dark Photon" or U Boson, as a possibility. This failure also undermines the Standard Model of particle physics [126].

POWER SPECTRUM OF THE COSMOS

The maximum energy release of the Universe given by Eq. (32.142) occurred at the beginning of the expansion phase, and the power spectrum is a function of the r-sphere of the observer. The power spectrum of the cosmos, as measured by the Las Campanas survey, generally follows the prediction of cold dark matter on the scales of 200 million to 600 million light-years. However, the power increases dramatically on scales of 600 million to 900 million light-years [70]. This discrepancy means that the Universe is much more structured on those scales than current theories can explain. The Universe is oscillatory in matter/energy and spacetime with a finite minimum radius. The minimum radius of the Universe, 300 billion light years [32], is larger than that provided by the current expansion, approximately 10 billion light years [28]. The Universe is a four-dimensional hyperspace of constant positive curvature at each r-sphere. The coordinates are spherical, and the space can be described as a series of spheres each of constant radius r whose centers coincide at the origin. The existence of the mass m_U causes the area of the spheres to be less than $4\pi r^2$ and causes the clock of each r-sphere to run so that it is no longer observed from other r-spheres to be at the same rate. The Schwarzschild metric given by Eq. (32.38) is the general form of the metric that allows for these effects. Consider the present observable Universe that has undergone expansion for 10 billion years. The radius of the Universe as a function of time from the coordinate r-sphere is of the same form as Eq. (32.153). The average size of the Universe, r_U, is given as the sum of the gravitational radius, r_g, and the observed radius, 10 billion light years.

$$r_U = r_g + 10^{10}\ light\ years$$

$$r_U = 3.12\ X\ 10^{11}\ light\ years + 10^{10}\ light\ years \tag{32.174}$$

$$r_U = 3.22\ X\ 10^{11}\ light\ years$$

The frequency of Eq. (32.153) is one half the amplitude of spacetime expansion from the conversion of the mass of Universe into energy according to Eq. (32.140). Thus, keeping the same relationships, the frequency of the current expansion function is the reciprocal of one half the current age. Substitution of the average size of the Universe, the frequency of expansion, and the amplitude of expansion, 10 billion light years, into Eq. (32.153) gives ***the radius of the Universe as a function of time for the coordinate r-sphere***.

$$\aleph = \left(3.22\ X\ 10^{11}\ light\ years - 1\ X\ 10^{10}\ \cos\left(\frac{2\pi t}{5\ X\ 10^{9}\ light\ years} \right) \right) light\ years \tag{32.175}$$

The Schwarzschild metric gives the relationship between the proper time and the coordinate time (Eq. (32.38)). The infinitesimal temporal displacement, $d\tau^2$, is:

$$d\tau^2 = \left(1 - \frac{2Gm_U}{c^2 r} \right) dt^2 - \frac{1}{c^2} \left[\left(\frac{dr^2}{1 - \frac{2Gm_U}{c^2 r}} \right) + r^2 d\theta^2 + r^2 \sin^2\theta d\phi^2 \right] \tag{32.176}$$

In the case that $dr^2 = d\theta^2 = d\phi^2 = 0$, the relationship between the proper time and the coordinate time is:

$$d\tau^2 = \left(1 - \frac{2Gm_U}{c^2 r} \right) dt^2 \tag{32.177}$$

$$\tau = t \sqrt{1 - \frac{2Gm_U}{c^2 r}} \tag{32.178}$$

$$\tau = t \sqrt{1 - \frac{r_g}{r}} \tag{32.179}$$

The maximum power radiated by the Universe is given by Eq. (32.142) and occurs when the proper radius, the coordinate radius, and the gravitational radius r_g are equal. For the present Universe, the coordinate radius is given by Eq. (32.174). The gravitational radius is given by Eq. (32.147). The maximum of the power spectrum of a trigonometric function occurs at its frequency [133]. Thus, the coordinate maximum power according to Eq. (32.175) occurs at $5\ X\ 10^9\ light\ years$. The maximum power corresponding to the proper time is given by the substitution of the coordinate radius, the gravitational radius r_g, and the coordinate power maximum into Eq. (32.179). The power maximum in the proper frame occurs at:

$$\tau = 5\ X\ 10^9\ light\ years \sqrt{1 - \frac{3.12\ X\ 10^{11}\ light\ years}{3.22\ X\ 10^{11}\ light\ years}} \tag{32.180}$$

$$\tau = 880\ X\ 10^6\ light\ years$$

The power maximum of the current observable Universe is predicted to occur on the scale of $880\ X\ 10^6\ light\ years$. There is excellent agreement between the predicted value and the experimental value of between 600 million to 900 million light years [134].

THE DIFFERENTIAL EQUATION OF THE RADIUS OF THE UNIVERSE

The differential equation of the radius of the Universe, $\aleph$, can be derived as a conservative simple harmonic oscillator having a restoring force, $\mathbf{F}$, which is proportional to the radius. The proportionality constant, k, is given in terms of the potential energy, E, gained as the radius decreases from the maximum expansion to the minimum contraction.

$$\frac{E}{\aleph^2} = k \tag{32.181}$$

The Universe oscillates between a minimum and maximum radius as matter is created into energy and then energy is converted to matter. At the minimum radius, the gravitational velocity, v_G, is given by Eq. (32.33) and the gravitational radius r_G, is given by Eq. (32.22) wherein an electromagnetic wave of mass energy equivalent to the mass of the Universe travels in a circular orbit wherein the eccentricity is equal to zero (Eq. (35.21)), and the escape velocity from the Universe can never be reached. At this point in time, all of the energy of the Universe is in the form of matter, and the gravitational energy (Eq. (32.148)) is equal to $m_U c^2$. Thus, the proportionality constant of the restoring force with respect to the radius is:

$$F = -k\aleph = -\frac{m_U c^2}{r_G^2}\aleph = -\frac{m_U c^2}{\left(\frac{Gm_U}{c^2}\right)^2}\aleph \tag{32.182}$$

Considering the oscillation, the differential equation of the radius of the Universe, $\aleph$, follows from Eq. (32.182) as given by Fowles [135]:

$$\begin{aligned} m_U \ddot{\aleph} + \frac{m_U c^2}{r_G^2}\aleph = 0 \\ m_U \ddot{\aleph} + \frac{m_U c^2}{\left(\frac{Gm_U}{c^2}\right)^2}\aleph = 0 \end{aligned} \tag{32.183}$$

The solution of Eq. (32.183) which gives the radius of the Universe as a function of time follows from Fowles [135]:

$$\begin{aligned} \aleph &= \left(r_g + \frac{cm_U}{Q}\right) - \frac{cm_U}{Q}\cos\left(\frac{2\pi t}{\frac{2\pi r_G}{c}}\right) \\ \aleph &= \left(\frac{2Gm_U}{c^2} + \frac{cm_U}{\frac{c^3}{4\pi G}}\right) - \frac{cm_U}{\frac{c^3}{4\pi G}}\cos\left(\frac{2\pi t}{\frac{2\pi Gm_U}{c^3}}\right) \end{aligned} \tag{32.184}$$

The gravitation force causes the radius of Eq. (32.184) to be offset [135]. After Eq. (32.38), the force equations of general relativity give the offset radius, r_U. The minimum radius corresponds to the gravitational radius r_g whereby the proper time is equal to the coordinate time. The offset radius, r_U, is:

$$r_U = r_g + \frac{cm_U}{\frac{c^3}{4\pi G}} \tag{32.185}$$

The expansion/contraction rate, $\dot{\aleph}$, is given by taking the derivative with respect to time of Eq. (32.184):

$$\dot{\aleph} = 4\pi c \cdot \sin\left(\frac{2\pi t}{\frac{2\pi Gm_U}{c^3}}\right) \tag{32.186}$$

According to special relativity no signal may travel faster than c, the speed of light for any observer. The maximum expansion rate for a 3-sphere is $4\pi c$ which is given in Eq. (32.186). The expansion/contraction acceleration, $\ddot{\aleph}$, is given by taking the derivative with respect to time of Eq. (32.186).:

$$\ddot{\aleph} = 4\pi \frac{c^4}{Gm_U} \cdot \cos\left(\frac{2\pi t}{\frac{2\pi Gm_U}{c^3}}\right) \tag{32.187}$$

Consistent with the vast time difference in spacetime scale between an Earth observer's view of the universe through a redshifted window and the period of oscillation between the matter filled and the light or energy filled universe, ancient stars and the large-scale structure of the cosmos comprising galactic superclusters and voids are visible that could not have formed within the elapsed time of expansion [70-77,97-101,136,137]. Recently, a uniform cosmic infrared background has been discovered which is consistent with the heating of dust with reradiation over a much longer period than the elapsed time of expansion [138]. The size of the Universe may be detected by observing the early curvature, the power spectrum, and the microwave background temperature. In the latter case, the power released as a function of time over the entire Universe is given by Eq. (32.161). The size of the Universe as a function of time is given by Eq. (32.153). The microwave background temperature corresponds to the power density over the entire Universe that is to within a few parts per million uniform on the scale of the entire Universe. Thus, the microwave background temperature as a function of time for each observer within his light sphere is given by Eq. (32.168).

The Hubble constant is given by the ratio of the expansion rate (Eq. (32.186)) given in units of $\frac{km}{\text{sec}}$ and the radius of the expansion (Eq. (32.126)) in units of Mpc (1 Megaparsec (Mpc) is $3.258\ X\ 10^6$ light years).

$$H = \frac{\dot{\aleph}}{ct} = \frac{4\pi \sin\left(\frac{2\pi t}{\frac{2\pi Gm_U}{c^3}}\right)}{t} \tag{32.188a}$$

Using

$$1\ Gyr = 3.1358\ X\ 10^{16} s \rightarrow \frac{3.1358\ X\ 10^{16} s}{1\ Gyr} = 1$$
$$1\ Mpc = 3.0857\ X\ 10^{19} km \rightarrow \frac{3.0857\ X\ 10^{19} km}{1\ Mpc} = 1 \quad (32.188b)$$

and $t = 10\ Gyr$, Eq. (32.188a) is given by:

$$H = \frac{4\pi \sin\left(2\pi \frac{t}{983\ Gyr}\right) \cdot \frac{3.0857\ X\ 10^{19} km}{1\ Mpc}}{t \cdot \frac{3.1358\ X\ 10^{16} s}{1\ Gyr}}$$

$$= 1229 \frac{km}{s \cdot Mpc} \cdot \frac{\sin\left(2\pi \frac{t}{983\ Gyr}\right)}{\frac{t}{1\ Gyr}} \quad (32.188c)$$

$$H\Big|_{t=10\ Gyr} = 1229 \frac{km}{s \cdot Mpc} \cdot \frac{\sin\left(2\pi \frac{10\ Gyr}{983\ Gyr}\right)}{\frac{10\ Gyr}{1\ Gyr}} \approx 78.5 \frac{km}{s \cdot Mpc}$$

The differential in the radius of the Universe $\Delta\aleph$ due to its acceleration is given by:

$$\Delta\aleph = 1/2 \ddot{\aleph} t^2 \quad (32.189)$$

The ***expansion of the light sphere due to the acceleration of the expansion of the cosmos*** given by Eq. (32.155) and Eq. (32.187) is shown graphically in Figure 32.12. The observed brightness of supernovae as standard candles is inversely proportional to their distance squared. As shown in Figure 32.12, $\Delta\aleph$ increases by a factor of about three as the time of expansion increases from the midpoint to a time comparable to the elapsed time of expansion, $t = 10^{10}\ light\ years = 3.069\ X\ 10^3 Mpc$. As an approximation, this differential in expanded radius corresponds to a decease in brightness of a supernovae standard candle of about an order of magnitude of that expected where the distance is taken as $\Delta\aleph$. This result is consistent with the experimental observation [37-39]. Recently, the BOOMERANG telescope [139] imaged the microwave background radiation covering about 2.5% of the sky with an angular resolution of 35 times that of COBE [33]. The image revealed hundreds of complex structures that were visible as tiny fluctuations—typically only 100 millionths of a degree (0.0001 °C)—in temperature of the Cosmic Microwave Background. Structures of about 1° in size were observed that are consistent with a Universe of nearly flat geometry since the commencement of its expansion. The data is consistent with a large offset radius of the Universe as given by Eq. (32.147) with a fractional increase in size (Eq. (32.153)) since the commencement of expansion about 10 billion years ago.

Figure 32.12. The differential expansion of the light sphere due to the acceleration of the expansion of the cosmos as a function of time.

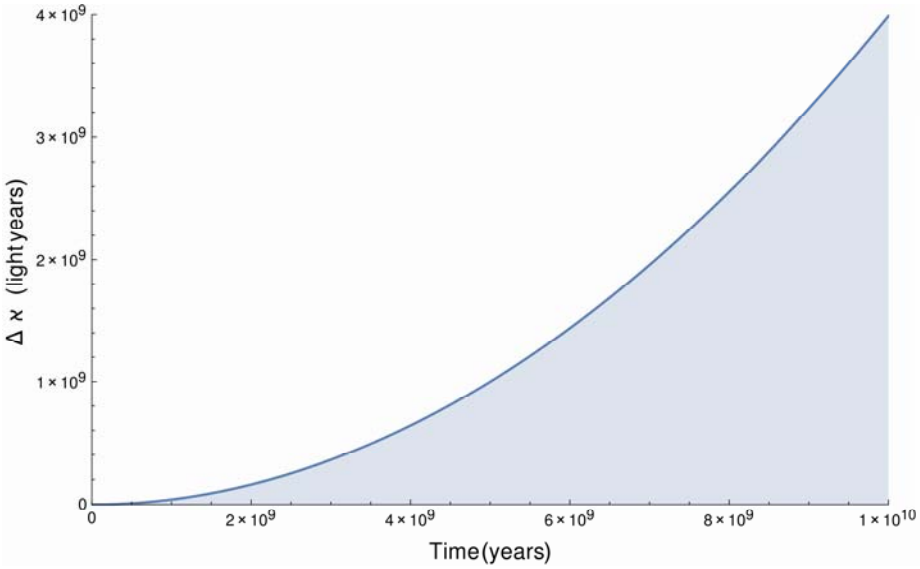

Recently NASA announced Hubble Space telescope results taken on the most distant supernova ever at a distance of 10 billion light years [140,141]. The extraordinary brightness of this standard candle compared to other such closer supernovas indicates that the Universe accelerated from a stationary state 10 billion years ago. This result is in agreement with the predictions of Eqs. (32.15-32.154) and Figure 32.5 presented before 1995 which predated the startling discovery that the Universe is accelerating.

POWER SPECTRUM OF THE COSMIC MICROWAVE BACKGROUND

The cosmic microwave background radiation (CMBR) corresponds to an average temperature of 2.725 K, with deviations of 30 μK or so in different parts of the sky representing slight variations in the density of matter. Early detailed measurements of the anisotropy as well as the discovery of polarization of the CMBR were achieved by the Degree Angular Scale Interferometer (DASI) [35]. The angular power spectrum was measured in the range $100 < \ell < 900$, and peaks in the power spectrum from the temperature fluctuations of the cosmic microwave background radiation appear at certain values of ℓ of spherical harmonics [35]. Peaks were observed at $\ell \approx 200$, $\ell \approx 550$, and $\ell \approx 800$ with relative intensities of 1, 0.5, and 0.3, respectively. Many subsequent missions have confirmed these peaks and mapped other higher multipoles of the temperature and polarization fluctuations of the CMBR. These measurements are considered essential to cosmological models. The standard model is a piecemeal set of inferences about the evolution of the cosmos. First, there is an inflation piece wherein a random infinitesimally small region of an infinitesimally small Universe of essentially infinite energy density that for an unknown reason ballooned to relative gargantuan size instantaneously by an unknown mechanism and stopped for some unknown reason. It remains inexplicable why inflation doesn't happen again at any point in the Universe. Gravity waves existed in whatever underwent inflation, but it is inexplicable whether matter, energy, gravity, known forces, or the current properties of spacetime held in the inflation state to manifest the gravity waves. After inflation stopped, for an unknown reason, there was a Big Bang with gravity-driven acoustic standing wave oscillations of the fireball plasma. Everything was created in the Big Bang as whatever it was expanded. But, rather than slow down, the Universe was observed to be accelerating in its expansion. So, at some point, dark energy took over; even though, there is no evidence of the identity of dark energy, and its mechanism of causing the accelerated expansion is unknown. The rate of the acceleration caused by dark energy cannot be predicted by the model. Another challenge is that the amount of mass of the Universe that is observable is only a small percentage based on gravity effects of the predominantly unseen mass of the Universe. Thus, nonbaryonic dark matter—exotic unidentified matter that exerts a gravitational attraction but has essentially no other interaction observed for normal matter such as absorption of light, is added as another parameter in the models. Many adjustable parameters were invented to try to meld the inhomogeneous pieces into continuity of the creation, appearance, behavior, and fate of the Universe.

The fluctuations in the CMBR are believed to be key since they are attributed to signatures from the early pieces, inflation and Big Bang. Specifically, the CMBR peaks are incorporated into adiabatic inflationary cosmology models wherein the at least 10 parameters are fully adjustable to fit the data supposedly corresponding to gravity waves during inflation, gravity-driven acoustic oscillations in the primordial plasma, and nonbaryonic dark matter. Yet, there is no guarantee that these occurred or that the CMBR is such a signature. There are many variants of the four-piece standard theory that are no more than models comprising conjectures about the state and occurrences of the early Universe. The four principle conjectures are not based on physical laws or mechanisms. Inflation occurred at infinitely faster than light speed that defies the laws of wave propagation of any kind. But, consider the gravity waves of inflation with the conjecture that the laws of gravity existed under the conditions of infinite energy density of unknown composition expanding at an near infinite rate as proposed. As given in the

Absolute Space Confirmed Experimentally section, there is no physical basis for a transverse light-speed propagating gravity field to comprise a gravity wave consistent with the absence of the direct experimental observation of gravity waves [142,143]. Next, consider the gravity-driven acoustic oscillations in the primordial Big Bang plasma. Acoustic waves are not observed in plasmas, and if the Sun were analogous to the primordial plasma, helioseismology data shows no resemblance to orderly spherical harmonic waves [144]. Such acoustic waves in plasma, if they could exist, could not seed the structure of the Universe since acoustic waves would have a propagation velocity far less than the speed of light. Acoustic waves would be perturbed by plasma instabilities due to electromagnetic forces that dominate plasma physics. Furthermore, standing waves are precluded in rapidly expanding plasma. Consider that these inflationary models require the assignment of dark matter, which is essentially all of the matter in the Universe, as exotic nonbaryonic matter. The identity of dark matter has been a cosmological mystery. Postulated assignments include τ neutrinos, but a detailed search for signature emissions has yielded nil [145]. The search for signatures by the Cryogenic Dark Matter Search (CDMS) developed to detect theorized Weakly Interacting Massive Particles (WIMPs) has similarly yielded nil [146,147]. Moreover, detection of alternative hypothesized identities for dark matter such as super-symmetry particles such as neutalinos has failed at the Large Hadron Collider; nor, has a single event been observed for weakly interacting massive particles or WIMPs at the Large Underground Xenon (LUX) experiment [131] or the upgrade Gran Sasso's XENON1T [148]. China's PandaX experiment and IceCube sterile neutrino detector recorded nil as well [148-150]. WIMP theory's main competitor known as MACHO theory assigns the Dark Matter to Massive Compact Halo Objects (MACHOs) which rather than elusive subatomic particles comprises ordinary baryonic matter in the form of burned-out dark stars, stray planets, and other large, heavy, but dark objects that must be ubiquitous throughout the Universe. However, MACHO theory has also recently been ruled out based on lack of evidence of these dark objects observable by the brief ellipses caused by them moving in front of distant stars. Only a few such objects have been observed after exhaustively searching for over five years [146,147].

As given in the Disproportionation of Energy States section, since the potential energy of atomic hydrogen is 27.2 eV, $m\ H$ atoms serve as a catalyst of $m \cdot 27.2\ eV$ for another $(m+1)$th H atom to form hydrino to H(1/(m +1)). For example, a H atom can act as a catalyst for another H by accepting 27.2 eV from it via through-space energy transfer such as by magnetic or induced electric dipole-dipole coupling to form an intermediate that decays with the emission of continuum bands with short wavelength cutoffs and energies of $m^2 \cdot 13.6\ eV \left(\frac{91.2}{m^2}\ nm \right)$. The recording of high-energy continuum radiation from hydrogen as it forms hydrinos in the laboratory [88-94] has astrophysical implications such as hydrino being a candidate for the identity of dark matter and the corresponding emission being the source of high-energy celestial and stellar continuum radiation [88-94,95,96]. $m\ H$ catalyst (Eqs. (5.48-5.61)) was shown to be active in astronomical sources [88]. Hydrogen continua from transitions to form hydrinos provides a possible mechanism of linking the temperature and density conditions of the different discrete layers of the coronal/chromospheric sources. EUV spectra of white dwarfs matches the continua for H(1/2), H(1/3), and H(1/4), and the 10.1 nm continuum is observed from interstellar medium. The hydrino continuum radiation matches the diffuse ubiquitous EUV and soft X-ray cosmic background [109,111] with the 10.1 nm continuum matching the observed intense 11.0-16.0 nm band, the radiation source behind the observation that diffuse Hα emission is ubiquitous throughout the Galaxy and widespread sources of flux shortward of 912 $\AA$ are required [109], and the source of ionization of the interstellar medium (ISM) wherein a large component of the baryonic matter of the Universe is in the form of WHIM (warm-hot ionized media) in the absence of a conventional source [112,113,115]. Moreover, recent X-ray absorption data reveals that the temperature of galactic halo gas is in the range of 86 eV to 215 eV which is in the realm of the energy released for the transition of H to H(1/4) [115]. Indirect emission from ions of nonthermal origin is a feature of the continuum radiation emitted from hydrino transitions in celestial sources as well as hydrogen pinch plasmas at oxidized electrodes and solid fuel plasmas in the laboratory [88].

Hydrogen is known to comprise about 95% of the visible matter of the Universe. Recently, the missing mass has been showed to be baryonic rather than strange matter [45] (See Composition of the Universe section). Astrophysical [118,119,128,130] and direct laboratory spectroscopic data [61, 88-94] indicate that the dark matter is also hydrogen, but in a lower-energy state. Thus, it comprises ordinary baryonic matter. Hydrogen atoms in these states exert a gravitational force, but do not resonantly absorb photons. Lower-energy atomic hydrogen atoms, hydrinos, each have the same mass and a similar interaction as the neutron. According to Steinhardt and Spergel of Princeton University [102], these are the properties of dark matter that are necessary in order for the theory of the structure of galaxies to work out on all scales. Rather than curve fitting the peaks corresponding to the anisotropy in the CMBR, the data is predicted due to the time harmonic oscillation of the Universe due to the relationship between energy-matter (matter-energy) conversion and spacetime contraction (expansion) without requiring that the Universe is almost entirely comprised of exotic unidentified matter. A classical, closed-form solution of the CMBR using physical laws provides a rational alternative explanation to inflation-Big Bang-dark energy-exotic nonbaryonic dark matter cosmology.

Molecular hydrino possesses a magnetic moment and is EPR active [61,151]. Dispersion of molecular hydrino in vacuum, gases, or liquids results in self-assembly of web structures (Figure 32.13A). Assembly mechanisms and natural phenomena that demonstrate fractal behavior such as crystal growth, fluid turbulence, and galaxy formation are ubiquitous in nature. The ability of molecular hydrino to self-assemble into webs provides an organizing mechanism to seed first gas clouds, galaxies, and then clusters of galaxies into a cosmic web wherein ordinary hydrogen and initially gravitational interactions are too weak to provide an organizing mechanism for celestial objects and the cosmic web structure (Figure 32.13B). In this process, the catalysis of H by at least another H to from hydrino with further reaction to molecular hydrino initiates the mass

aggregation towards large scale cosmic structure.

Figures 32.13A-B. A. Molecular hydrino uniquely possesses an unpaired electron resulting in the ability to self-assemble into webs due to the corresponding magnetic attractive force. B. Fractal growth provides an organizing mechanism to seed first gas clouds, galaxies, and then clusters of galaxies into a cosmic web. (Courtesy of ESA.)

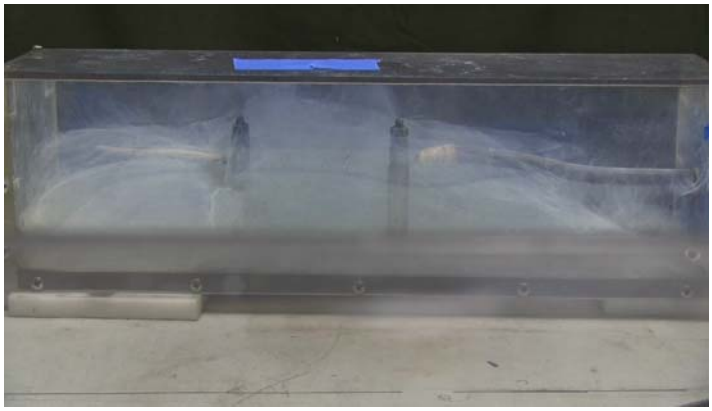

(A)

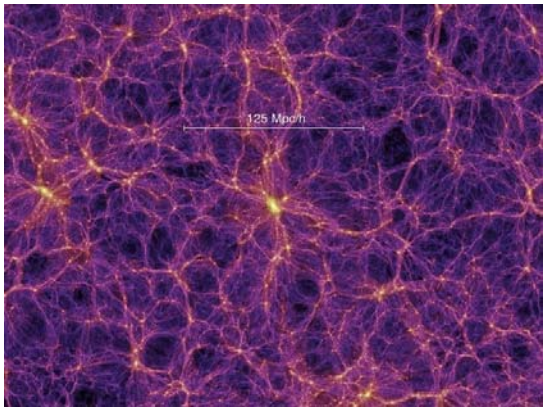

(B)

When the Universe reaches the maximum radius corresponding to the maximum contribution of the amplitude, $\aleph_o$, of the time harmonic variation in the radius of the Universe, (Eq. (32.150)), it is radiation-filled. Since the photon has no gravitational mass, the radiation is uniform. As energy converts into matter the power of the Universe may be considered negative for the first quarter cycle starting from the point of maximum expansion as given by Eq. (32.161), and spacetime contracts according to Eq. (32.140). The gravitational field from particle production travels as a light wave front. As the Universe contracts to a minimum radius, the gravitational radius given by Eq. (32.147), constructive interference of the gravitational fields occurs. The resulting slight variations in the density of matter are observed from our present r-sphere. The observed radius of expansion is equivalent to the radius of the light sphere with an origin at the time point when the Universe stopped contracting and started to expand.

Consider the effect of the expansion and contraction of the Universe on the unperturbed condition of uniform energy-matter density and a static Universe. The radius of the Universe time and spatially oscillates wherein the radius as a function of time is given by Eqs. (32.153) and (32.184). The Universe is a 3-sphere hyperspace of constant positive curvature that expands and contracts cyclically in all directions relative to an embedded space-time observer at his r-sphere. The harmonic oscillation of the radius of the Universe and thus its volume gives rise to delays and advances to light spheres of the continuum of r-spheres of the Universe that would otherwise propagate at relative velocity c. The gravitational field from particle production travels as a light wave front. As the radius of the Universe changes constructive interference of the gravitational fields occurs as the distance between r-spheres changes such that the fronts are advanced or delayed to interfere with each other. The resulting slight variations in the density of matter are observed from our present r-sphere. These variations would be observed as spherical harmonics corresponding to the spherical contraction and expansion in all directions. For each r-sphere, the angular variation in density corresponds to an angular distribution of the power of the Universe (Eq. (32.161)) and thus the temperature of the Universe according to the Stefan-Boltzmann law (Eq. (32.168)). These angular harmonic temperature variations are predominantly unpolarized, but posses a slight E-mode polarization and a lesser and B-mode polarization (Figure 32.14).

Figure 32.14. Color scale temperature variations and temperature variations of the E-mode and B-mode polarization of the CMBR of the Universe in degrees μK. Courtesy of NASA, G. Hinshaw, *et al*.

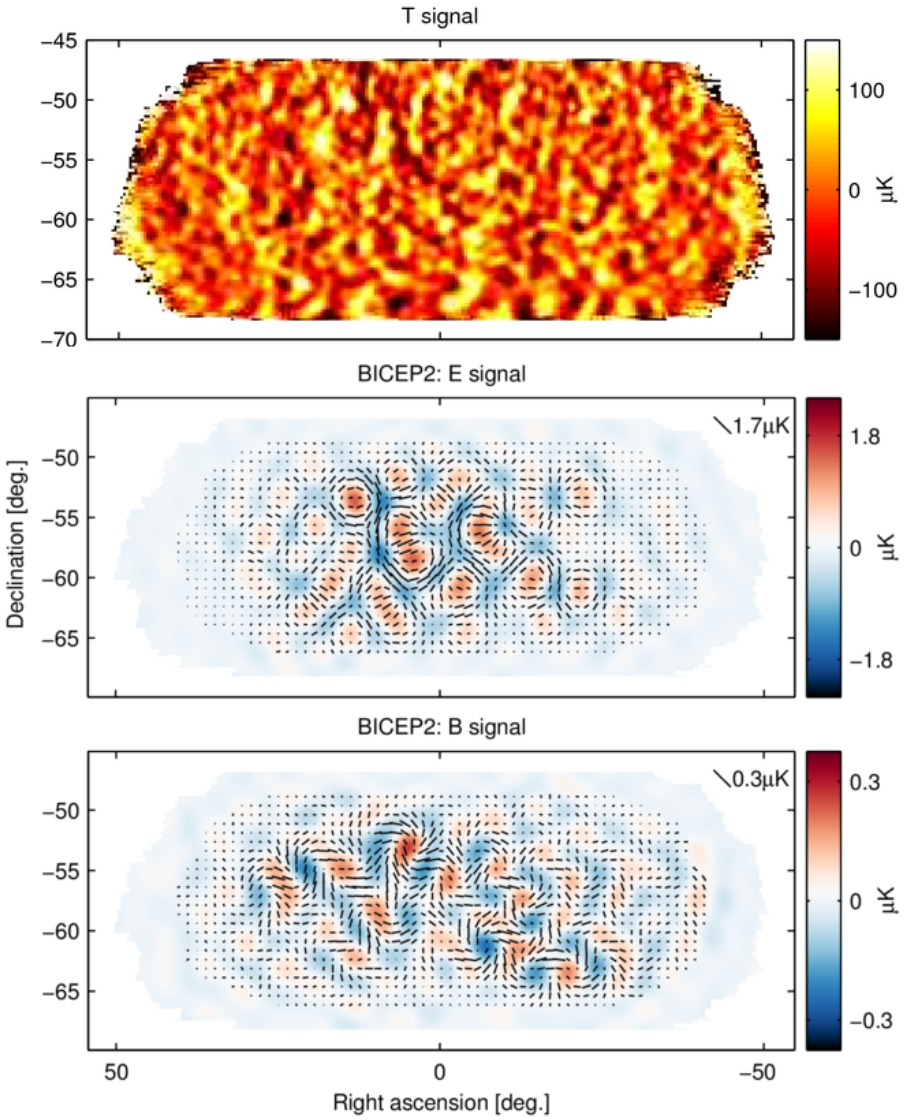

The angular variation in temperature is given by the Fourier transform of the observer's r-sphere temperature over the oscillatory period starting at matter formation at the initial time of contraction through the initiation of expansion to the present time in the expansion cycle. The temperature of the Universe at each r-sphere $T_U(t)$ as a function of time is given by Eq. (32.168). The present r-sphere corresponds to a radial delta function ($f(r)=\frac{1}{r_{sphere}^2}\delta(r-r_{sphere})$) having the radius r_{sphere}. The temperature variation ΔT given by the spacetime Fourier transform of $T_U(t)$ in three dimensions in spherical coordinates plus time is given [152,153] as follows:

$$\Delta T(s,\Theta,\Phi,\omega)=$$

$$\int_0^{\infty}\int_0^{2\pi}\int_0^{\pi}\int_0^{\infty}\left[\begin{array}{l} T_U(t)\frac{1}{r_{sphere}^2}\delta(r-r_{sphere}) \\ \exp\left(-i2\pi sr[\cos\Theta\cos\theta+\sin\Theta\sin\theta\cos(\phi-\Phi)]\right)\exp(-i\omega t)\end{array}\right] r^2\sin\theta\,dr\,d\theta\,d\phi\,dt \tag{32.190}$$

With spherical symmetry [152],

$$\Delta T(s,\omega) = 4\pi \int_0^\infty \int_0^\infty T_U(t) \frac{1}{r_{sphere}^2} \delta(r - r_{sphere}) \text{sinc}(sr) r^2 \exp(-i\omega t) dr dt \tag{32.191}$$

$$\begin{aligned} \Delta T(s,\omega) &= 4\pi \int_0^\infty T_U(t) \text{sinc}(s r_{sphere}) \exp(-i\omega t) dt \\ \Delta T(\ell,\omega) &= 4\pi \int_0^\infty T_U(t) \text{sinc}\left(\frac{\pi}{140}\ell\right) \exp(-i\omega t) dt \end{aligned} \tag{32.192}$$

where the Fourier wavenumber s is the multipole moment $\ell = \frac{2\pi}{\theta}$ due to the observable angular variations at the observer's (present) r-sphere due to radius, power, area, and temperature oscillations is all directions of the four-dimensional hyperspace of constant positive curvature. The corresponding angular multipole of the radius of the present expansion r-sphere after the half-period of contraction $\frac{\pi}{\ell_{sphere}}$ is substituted for r_{sphere}. The spherical harmonic parameter ℓ_{sphere} of the interference is given by the ratio of the amplitude, $\aleph_o$, of the time harmonic variation in the radius of the Universe, (Eq. (32.150)) divided by the observer's present r-sphere radius. The latter is given by the sum of ct (the light sphere due to light speed for $t = 10^{10}\ light\ years = 3.069\ X\ 10^3 Mpc$) and the differential in the radius of the Universe $\Delta\aleph$ due to its acceleration is given by Eq. (32.189) wherein $\ddot{\aleph}$ is given by Eq. (32.155). As shown in Figure 32.11 the differential in the radius of the Universe $\Delta\aleph$ due to its acceleration is:

$$\begin{aligned} \Delta\aleph &= 1/2 \ddot{\aleph} t^2 \\ &= \frac{1}{2}\left(8.04\ X\ 10^{-11}\right) \cos\left(\frac{2\pi\left(1\ X\ 10^{10}\ yrs\right)}{9.83\ X\ 10^{11}\ yrs}\right) \frac{light\ years}{yrs^2}\left(1\ X\ 10^{10}\ yrs\right)^2 \\ &= 4.02\ X\ 10^9\ light\ years \end{aligned} \tag{32.193}$$

The radius r_{sphere} of the currently observed Universe is, thus

$$\begin{aligned} r_{sphere} &= ct + \Delta\aleph \\ &= 10^{10}\ light\ years + 4.02\ X\ 10^9\ light\ years \\ &= 14.02\ X\ 10^9\ light\ years \end{aligned} \tag{32.194}$$

The angular scale or spherical harmonic parameter ℓ_{sphere} is:

$$\ell_{sphere} = \frac{\aleph_0}{r_{sphere}} = \frac{\aleph_0}{ct + \Delta\aleph} = \frac{1.97\ X\ 10^{12}\ light\ years}{10^{10}\ light\ years + 4.02\ X\ 10^9\ light\ years} = 140 \tag{32.195}$$

$T_U(t)$ given by Eq. (32.168) is a complicated function of ratios of sums of constants and trigonometric equations to different exponents. However, from Figure 32.9, it can be appreciated that $T_U(t)$ during the contraction phase is represented to good approximation by the equation:

$$T_U(t) = \left(0.01 + 5.98\ X\ 10^{-12}\ yrs^{-1} t\right) K \tag{32.196}$$

Substitution of Eqs. (32.195) and (32.196) into Eq. (32.192) with the proper limits on the contraction time and considering the incremental solid angle gives:

$$\Delta T(\ell,\omega) = \omega \int_{T/2}^{T} \left(0.01 + 5.98\ X\ 10^{-12}\ yrs^{-1} t\right) \text{sinc}\left(\frac{\pi}{140}\ell\right) \exp(-i\omega t) dt\ K \tag{32.197}$$

$$\begin{aligned} \Delta T(\ell) &= \left(0.01 + \left(5.9\ X\ 10^{-12}\ yrs^{-1}\right)\left(\left(\frac{9.83\ X\ 10^{11}\ yrs}{2}\right)\right)\right) \text{sinc}\left(\frac{\pi}{140}\ell\right) K \\ \Delta T(\ell) &= 3\,\text{sinc}\left(\frac{\pi}{140}\ell\right) K \end{aligned} \tag{32.198}$$

The amplitude of the temperature fluctuations are dependent on the relative areas of the current r-sphere to that of the radius of the initiation of contraction. The scaling factor $C_{Tsphere}$ is given by:

$$C_{Tsphere}=\left(\frac{ct}{\aleph_0}\right)^{-2}=\left(\frac{ct}{\frac{m_U c}{Q}}\right)^{-2}=\left(\frac{t}{2T}\right)^{-2}$$
$$=\left(\frac{ct}{\frac{2\ X\ 10^{54}\ kg}{\frac{c^3}{4\pi G}}}\right)^{-2}=\left(\frac{10^{10}\ light\ years}{1.97\ X\ 10^{12}\ light\ years}\right)^{-2}=(197)^{-2} \quad (32.199)$$

Using Eq. (32.199), the correction of the temperature for the current r-sphere area relative to the maximum area gives:

$$\Delta T(\ell)=C_{Tsphere}\,3\mathrm{sinc}\left(\frac{\pi}{140}\ell\right)\ K=77\mathrm{sinc}\left(\frac{\pi}{140}\ell\right)\ \mu K \quad (32.200)$$

The temperature variation is shifted by the relative position of the current light sphere with the limiting one. Specifically, the ℓ_0 shift is given by the ratio of the amplitude, $\aleph_o$, of the time harmonic variation in the radius of the Universe (Eq. (32.150)), divided by the present radius of the light sphere, $ct=10^{10}\ light\ years=3.069\ X\ 10^3 Mpc$. Using Eq. (32.199), the shift is given by

$$\ell_0=\frac{\aleph_0}{ct}=\frac{\frac{m_U c}{Q}}{ct}=\frac{2T}{t}=\frac{\frac{2\ X\ 10^{54}\ kg}{\frac{c^3}{4\pi G}}}{ct}=\frac{1.97\ X\ 10^{12}\ light\ years}{10^{10}\ light\ years}=197 \quad (32.201)$$

Substitution of the shift given by Eq. (32.201) into Eq. (32.200) gives the temperature variations in degrees μK as a function of multipole moment ℓ:

$$\Delta T(\ell)=77\mathrm{sinc}\left(\frac{\pi}{140}(\ell-197)\right)\ \mu K \quad (32.202)$$

for $\ell>0$. A plot of Eq. (32.202) is given in Figure 32.15. The predictions match the DASI observed amplitude of $77\mu K$ and the peaks at $\ell\approx 200$, $\ell\approx 550$, and $\ell\approx 800$ with relative intensities of 1, 0.5, and 0.3, respectively [35,154-157]. The plot of the corresponding power spectrum comprising spherical harmonic coefficient $\frac{\ell(\ell+1)C_\ell}{2\pi}\left[\mu K^2\right]$ amplitudes as a function of multipole ℓ is shown in Figure 32.16. The power spectrum plot is the square of Eq. (32.202) made positive-definite by first adding the corresponding constant to it before squaring. The amplitude was normalized to 77 μK squared. The experimental power spectrum of WMAP with the data of SPT and ACT [158], and best curve fit comprising spherical harmonic coefficient $\frac{\ell(\ell+1)C_\ell}{2\pi}\left[\mu K^2\right]$ amplitudes as a function of multipole ℓ for the temperature variations of the CMBR of the Universe is shown in Figure 32.16. There is excellent agreement between the predicted and experimental multipole temperature fluctuation curves.

Figure 32.15. The temperature variations and temperature variations of the E-mode and B-mode polarization of the CMBR of the Universe in degrees μK as a function of multipole moment ℓ.

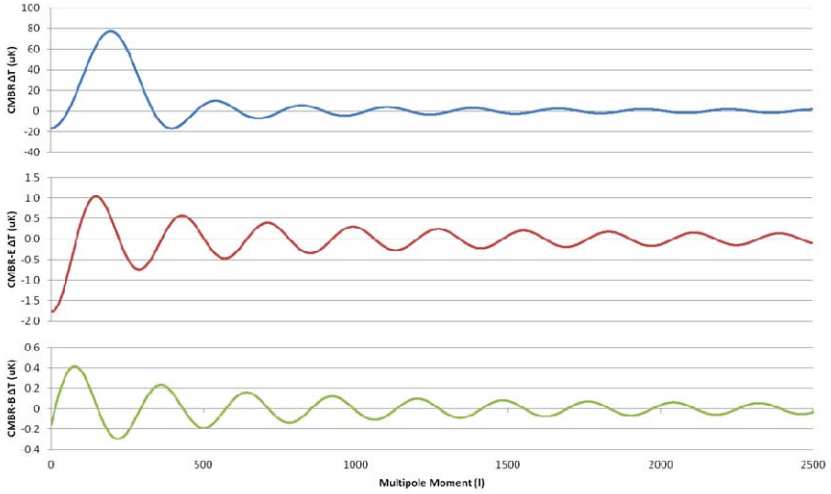

Figures 32.16A-B. The power spectrum comprising spherical harmonic coefficient $\frac{\ell(\ell+1)C_\ell}{2\pi}\left[\mu K^2\right]$ amplitudes as a function of multipole ℓ for the temperature variations and temperature variations of the E-mode and B-mode polarization of the CMBR of the Universe. The experimental data points of BICEP2 [159,160] for the E-mode peak at $\ell = 140$ and the B-mode peak at $\ell = 70$, $r = 0.20^{+0.07}_{-0.05}$ are superimposed. A. Plot over the range $0 \le \ell \le 2500$. B. Plot over the range $0 \le \ell \le 200$.

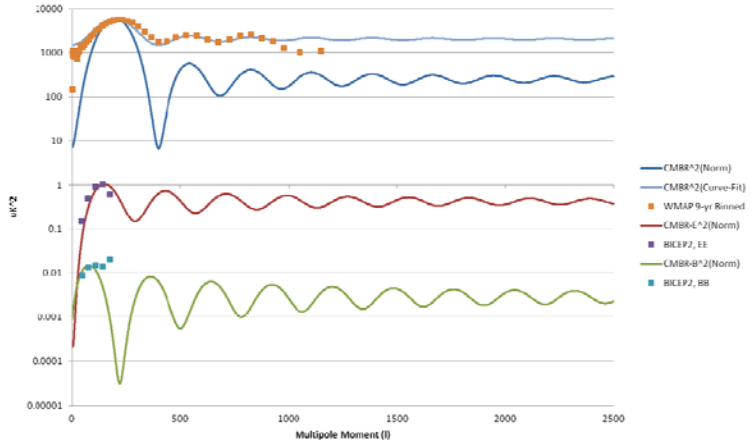

(A)

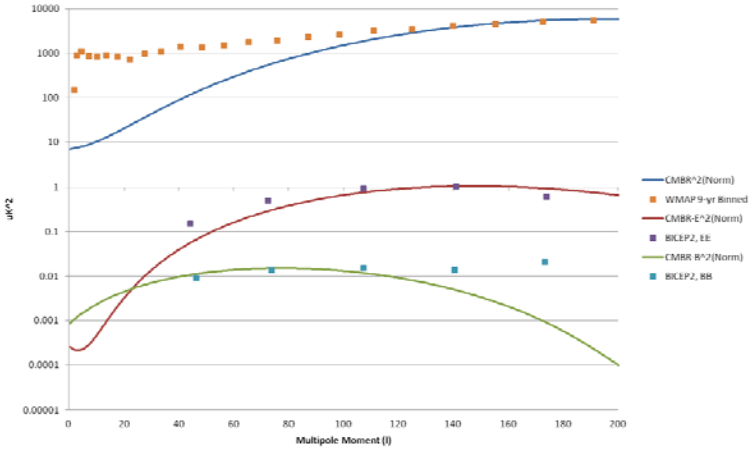

(B)

Figure 32.17. The experimental power spectrum of WMAP with the data of SPT and ACT [158] and best curve fit comprising spherical harmonic coefficient $\frac{\ell(\ell+1)C_\ell}{2\pi}\left[\mu K^2\right]$ amplitudes as a function of multipole ℓ for the temperature variations of the CMBR of the Universe. Courtesy of NASA, G. Hinshaw, *et al*.

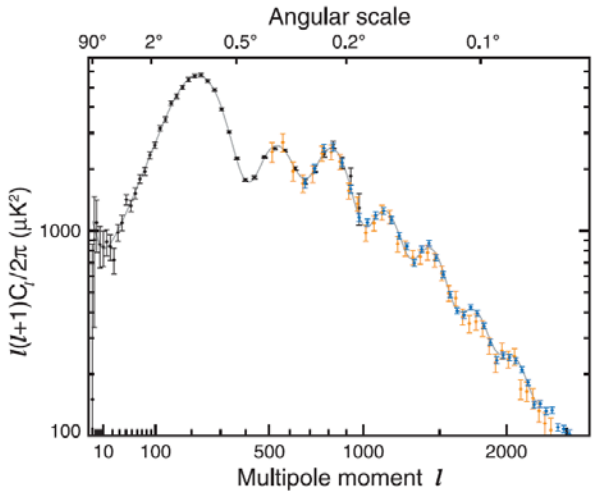

Polarized light is produced as correlation multipoles of the CMBR temperature fluctuations by Thompson scattering of the CMBR by stellar and interstellar medium plasma electrons (essentially ionized hydrogen) over the half period of contraction $T_U/2 = 4.92\ X\ 10^{11}\ years$ plus the time of expansion $t = 10^{10}\ years$. The phase shift corresponds to an opposite sign of the shift of Eq. (32.202), an advance in the cosmic microwave background radiation temperature modulation rather than a delay:

$$\Delta T_{\text{E-mode}}(\ell) = C_{\text{effThompson}}\, 77\text{sinc}\left(\frac{\pi}{140}(\ell+197)\right)\ \mu K \tag{32.203}$$

wherein $\ell > 0$ and C_{eff} is the Thompson polarization constant that is a small fraction corresponding to the weakness of Thompson scattering. The constant may be calculated from the temperature fluctuations, the blackbody electromagnetic radiation spectrum, and the plasma density of the Universe over the cycle from the commencement of contraction to the present r-sphere. The first peak is predicted at $\ell = 140$ which matches that observed by BICEP2 [159,160].

The polarization pattern of the Thompson scattered CMBR comprises a curl free component call E-mode since it is electric-field-like or gradient-mode with no handedness. Gravitational lensing causes E-mode polarization to convert to a gradient free component call B-mode since it is magnetic-field-like or curl-mode with handedness. Another mechanism to achieve polarized B-mode angular variations in the CMBR is based on the acceleration of the expansion of spacetime. The Universe is matter-filled at the transition time point from contraction to expansion. Thus, the light sphere propagates into a Universe that is much older and larger according to Eq. (32.153) with time equal to the elapsed time from the commencement of expansion. The light sphere expands at light speed, but into spacetime that is accelerating in its expansion. Due to the acceleration of the light-speed propagating light sphere, E-mode light experiences the same spacetime gradients as in the case of gravitational lensing; consequently, E-mode is converted to B-mode polarization. The B-mode radiation is shifted by $\frac{\pi}{2}$ relative to the E-mode radiation. Thus, Eq. (32.203) gives the B-mode radiation pattern as:

$$\Delta T_{\text{B-mode}}(\ell) = r^{1/2} C_{\text{effThompson}}\, 77\text{sinc}\left(\frac{\pi}{140}(\ell+197+70)\right)\ \mu K \tag{32.204}$$

for $\ell > 0$. The first peak is predicted at $\ell = 70$. The E-mode polarized radiation should be substantially less intense than fluctuations in the CMBR since it is Thompson scattered radiation. Furthermore, the B-mode radiation should been a fraction of the E-mode since the latter is converted from the former. Consider that the mode conversion by accelerating spacetime is limited by the relative extent of the acceleration. The ratio $r^{1/2}$ of the amplitude ΔT of the B-mode to E-mode components is given by the ratio of the differential radius due to acceleration $\Delta\aleph$ and the radius due to light sphere expansion ct. Thus, using Eq. (32.193), the ratio $r^{1/2} = \frac{\Delta T(\text{B-mode})}{\Delta T(E\text{-mode})}$ is:

$$r^{1/2} = \frac{\Delta T(B\text{-mode})}{\Delta T(E\text{-mode})} = \frac{\Delta\aleph}{(ct)} = \left(\frac{4.02\ X\ 10^9\ light\ years}{10^{10}\ light\ years}\right) = 0.40 \tag{32.205}$$

The ratio r of the amplitude ΔT^2 of the B-mode to E-mode power spectral components is:

$$r = \left[\frac{\Delta T\left(B\text{-mode}\right)}{\Delta T\left(E\text{-mode}\right)}\right]^2 = 0.16 \tag{32.206}$$

Substitution of Eq. (32.206) into Eq. (32.204) gives:

$$\Delta T_{\text{B-mode}}(\ell) = C_{\text{effThompson}}\, 31 \text{sinc}\left(\frac{\pi}{140}\left(\ell + 197 + 70\right)\right)\ \mu K \tag{32.207}$$

BICEP2 [160] reports a value of $r = 0.20^{+0.07}_{-0.05}$ $\ell = 70$ that is in good agreement with predictions. The plots of the corresponding E-mode and B-mode power spectra comprising spherical harmonic coefficient $\frac{\ell(\ell+1)C_\ell}{2\pi}\left[\mu K^2\right]$ amplitudes as a function of multipole ℓ are shown in Figure 32.16. The E-mode and B-mode power spectral plots are the square of Eqs. (32.203) and (32.207), respectively, each made positive-definite by first adding the corresponding constant to it before squaring. Each plot was normalized by the corresponding squared amplitude of the ΔT plot. $C_{\text{effThompson}}$ can be calculated, but for convenience it was taken as the experimental ratio of $\Delta T_{\text{E-mode}}(\ell)$ to $\Delta T(\ell)$. The BICEP2 [160] experimental data points for the E-mode peak at $\ell = 140$ and the B-mode peak at $\ell = 70$ are shown. There is excellent agreement between the predicted and experimental multipole polarization temperature fluctuation curves.

The definitive form of the field equations of general relativity follow from the Schwarzschild metric (Eq. (32.38)) and can be expressed in terms of ***the contraction of spacetime by the special relativistic mass of a fundamental particle*** (Eq. (32.140)). The masses and charges of the fundamental particles are determined by the equations of the transition state atomic orbital herein derived where the nonradiative boundary condition and the constancy of the speed of light must hold which requires relativistic corrections to spacetime. Fundamental particles can decay or interact to form an energy minimum. Thus, each stable particle arises from a photon directly or from a decaying particle, which arose from a photon. The photon, and the corresponding fundamental particle, possess $\hbar$ of angular momentum. Nuclei form as binding energy is released as the atomic orbitals of participating nucleons overlap. Atoms form as the potential energy of the fields of electrons and nuclei is released as the fields are partially annihilated. Molecules form as the energy stored in the fields of atoms is minimized. Planets and celestial bodies form as the gravitational potential energy is minimized. All of these energies correspond to forces, and the equations of the forces are given in the Unification of Spacetime, the Forces, Matter, and Energy section.

REFERENCES

1. E. G. Adelberger, C. W. Stubbs, B. R. Heckel, Y. Su, H. E. Swanson, G. Smith, J. H. Gundlach, Phys. Rev. D, Vol. 42, No. 10, (1990), pp. 3267-3292.
2. H. Minkowski's interpretation of special relativity in terms of a four dimensional space time was presented in the form of a lecture in Cologne, Germany in September 1908. An English translation, entitled "Space and Time," can be found in the collection *The Principle of Relativity*, Dover, New York, 1952.
3. V. Fock, *The Theory of Space, Time, and Gravitation*, The MacMillan Company, (1964), pp. 14-15.
4. E. Giannetto, The rise of special relativity: Henri Poincaré's works before Einstein. Atti del 18 Congresso di Storia della Fisica e dell'Astronomia, (1998), pp. 171-207, [http://www.brera.unimi.it/old/Atti-Como-98/Giannetto.pdf].
5. H. Poincaré, "L'etat actuel et l'avenir de la physique mathematique," *Bulletin des sciences mathematiques*, Vol. 28, (1904), pp.302-324; quoted in Whittaker (1987), p. 30.
6. E. Whittaker, *A History of the Theories of Aether and Electricity*, Vol. 2, Modern Theories, Chapter 2, "The Relativity Theories of Poincaré and Lorentz," Nelson, London, (1987), Reprinted, American Institute of Physics, pp. 30–31.
7. E. Fomalont, S. Kopeikin, "How fast is gravity," New Scientist, Vol. 177, Issue 2377, Jan. 11, (2003), pp. 32.
8. L. Z. Fang, and R. *Ruffini, Basic Concepts in Relativistic Astrophysics*, World Scientific, (1983).
9. A. Beiser, *Concepts of Modern Physics*, Fourth Edition, McGraw-Hill Book Company, New York, (1978), pp. 88-89.
10. G. R. Fowles, *Analytical Mechanics*, Third Edition, Holt, Rinehart, and Winston, New York, (1977), pp. 154-155.
11. V. Fock, *The Theory of Space, Time, and Gravitation*, The MacMillan Company, (1964).
12. W. K. Clifford, *The Common Sense of the Exact Sciences*, Mathematical Papers, p. 21, presented to the Cambridge Philosophical Society in 1870.
13. R. M. Wald, *General Relativity*, University of Chicago Press, Chicago, (1984), pp. 91-101.
14. N. A. Bahcall, J. P. Ostriker, S. Perlmutter, P. J. Steinhardt, Science, May 28, 1999, Vol. 284, pp. 1481-1488.
15. R. Lieu, L. W. Hillman, "The phase coherence of light from extragalactic sources—direct evidence against first order Planck scale fluctuations in time and space," Astrophysical Journal Letters, March 10, (2003).
16. R. Ragazzoni, M. Turatto, W. Gaessler, "The lack of evidence for quantum structure of spacetime at Planck scales," Astrophysical Journal, April 10, (2003), Vol. 587, L1-L4.
17. V. Fock, *The Theory of Space, Time, and Gravitation*, The MacMillan Company, (1964), pp. 209-215.
18. S. Weinberg, *Gravitation and Cosmology: Principles and Applications of the General Theory of Relativity*, John Wiley & Sons, New York, (1972), Sect. 11/7, pp. 335 ff.
19. L. P. Eisenhart, *Riemannian Geometry*, Princeton: Princeton University Press, (1949).
20. D. Lovelock, "The Four Dimensionality of Space and the Einstein Tensor," J. Math. Phys., Vol. 13, (1972), pp. 874-876.
21. R. M. Wald, *General Relativity*, University of Chicago Press, Chicago, (1984), Chp. 9 and Chp. 14.
22. A. Linde, "The Self Reproducing Inflationary Universe," Scientific American Presents, Spring (1998), Vol. 9 pp. 98-104.
23. I. Levine, *Physical Chemistry*, McGraw-Hill Book Company, (1978).
24. T. Gold, Am. J. Phys., 30, 403 (1962).
25. R. S. Casella, Phys. Rev. Lett., 21, 1128 (1968).
26. R. S. Casella, Phys. Rev. Lett., 22, 554 (1969).
27. Y. Ne'eman, Int. J. Theoret. Phys., 3, 1 (1970).
28. W. L. Freeman, et. al., Nature, 371, pp. 757-762, (1994).
29. W. L. Freeman et. al., "Final Results from the Hubble Space Telescope Key Project to measure the Hubble constant," Astrophysical Journal, Vol. 553, May 20, (2001), pp. 47-72.
30. R. F. Mushotzky, Meeting of the American Astronomical Society, Phoenix, AZ, (January 4, 1994).
31. D. N. Schramm, Physics Today, April, (1983), pp. 27-33.
32. S. W. Hawking, *A Brief History of Time*, Bantam Books, Toronto, (1988), p. 11.
33. J. C. Mather, et. al., The Astrophysical Journal, 354, L37-L40, (1990).
34. A. Beiser, *Concepts of Modern Physics*, Fourth Edition, McGraw-Hill Book Company, New York, (1978), pp. 329-339.
35. N. W. Halverson, E. M. Leitch, C. Pryke, J. Kovac, J. E. Carlstrom, W. L. Holzapfel, M. Dragovan, J. K. Cartwright, B. S. Mason, S. Padin, T. J. Pearson, M. C. Shepard, and A. C. S. Readhead, "DASI first results: a measurement of the cosmic microwave background angular power spectrum," arXiv:astro-ph/0104489, 30 April, (2001).
36. R. Lieu, J. P. D. Mittaz, S-N Zhang, "The Sunyaev-zel'dovich effect in a sample of 31 clusters: a comparison between the X-ray predicted and WMAP observed cosmic microwave background temperature decrement," The Astrophysical Journal, Vol. 648, (2006), pp. 176-199.
37. Science, Vol. 279, Feb., (1998), pp. 1298-1299.
38. Science News, Vol. 153, May, (1998), p. 344.
39. Science News, Vol. 154, October 31, (1998), p. 277.
40. R. M. Wald, *General Relativity*, University of Chicago Press, Chicago, (1984), pp. 114-116.
41. P. J. E. Peebles, J. Silk, Nature, Vol. 346, July, 19, (1990), p. 233-239.
42. Personal communication, Dr.-Ing. Günther Landvogt, Hamburg, Germany, January, (2003).
43. M. Davis, et. al., Nature, 356, (1992), pp. 489-493.
44. K. A. Olive, D. N. Schramm, G. Steigman, and T. P. Walker, Phys. Lett., B236, (1990), pp. 454-460.

45. F. Nicastro, A. Zezas, M. Elvis, S. Mathur, F. Fiore, C. Cecchi-Pestellini, D. Burke, J. Drake, P. Casella, "The far-ultraviolet signature of the 'missing' baryons in the local group of galaxies," Nature, Vol. 421, No. 13, pp. 719-721.
46. D. Stern, H. Spinrad, P. Eisenhardt, A. J. Bunker, S. Dawson, S. A. Stanford, R. Elston, "Discovery of a color-selected quasar at $z = 5.5$," Astrophysical Journal, Vol. 533, April 20, (2000), pp. L75-L78.
47. X. Fan, et al., "A survey of $z > 5.8$ quasars in the Sloan Digital Sky Survey I: discovery of three new quasars and the spatial density of luminous quasars at $z \approx 6$," Astrophysical Journal, December, (2001).
48. M. Chown, "Astronomers claim dark matter breakthrough," NewScientist.com, Oct. 3, (2003), http://www.newscientist.com/article/dn4214-astronomers-claim-dark-matter-breakthrough.html.
49. C. Boehm, D. Hooper, J. Silk, M. Casse, J. Paul, "MeV dark matter: Has it been detected," Phys. Rev. Lett., Vol. 92, (2004), p. 101301.
50. Hurley, K., et. al., Nature, 372, (1994), pp. 652-654.
51. National Aeronautics and Space Administration, Goddard Space Flight Center, Fermi Gamma-ray Space Telescope, "Overview of GRB spectral analysis", https://fermi.gsfc.nasa.gov/ssc/data/analysis/documentation/Cicerone/Cicerone_GRBs/Overview_GRB_Spec_Anal.html.
52. G. Share, R. Murphy, "Solar Gamma-Ray Line Spectroscopy - Physics of a Flaring Star", Part 4: High Energy Phenomena in Sun and Stars, Symposium - International Astronomical Union, Vol. 219: Stars as Suns : Activity, Evolution and Planets, (2004), pp. 133 – 144; DOI: https://doi.org/10.1017/S0074180900182051.
53. N. Wolchover, "The Sun Is Stranger Than Astrophysicists Imagined", Quanta Magazine, May 1, 2019, https://www.quantamagazine.org/gamma-ray-data-reveal-surprises-about-the-sun-20190501/.
54. T. Van Flandern, "The Speed of Gravity—What the Experiments Say," Physics Letters A, 250 (1998), pp. 1-11.
55. R. Cowen, Science News, May 9, (1998), p. 292.
56. M. Chown, New Scientist, May 10, (1997), p. 21.
57. B. Schwarzschild, Physics Today, Vol. 51, No. 10, October, (1998), pp. 19-21.
58. G. Taubes, "Pattern emerges in cosmic ray mystery," Science, News Series, Vol. 262, No. 5140, (Dec. 10, 1993), p. 1649.
59. D. J. Bird, et al., "Evidence for correlated changes in the spectrum and composition of cosmic rays at extremely high energies," Physical Review Letters, Vol. 71, No. 21, (1993), pp. 3401-3404.
60. F. Harrison, "An ultraluminous X-ray source powered by an accrediting neutron star", Nature, (2014), dx.doi.org/10.1038/nature13791189.
61. R. Mills, Hydrino States of Hydrogen, (2023), https://brilliantlightpower.com/pdf/Hydrino_States_of_Hydrogen.pdf.
62. Ackermann, M.; et al. (2013). "Detection of the characteristic pion-decay signature in supernova remnants". Science. 339 (6424): 807–811. arXiv:1302.3307. Bibcode:2013Sci…339..807A. doi:10.1126/science.1231160. PMID 23413352. S2CID 29815601.
63. CERN, "Cosmic rays from outer space", https://home.cern/science/physics/cosmic-rays-particles-outer-space#:~:text=He%20had%20discovered%20cosmic%20rays,the%20way%20up%20to%20uranium.
64. IceCube MasterClass, "Cosmic-ray energy spectrum", https://masterclass.icecube.wisc.edu/en/analyses/cosmic-ray-energy-spectrum#:~:text=The%20energy%20spectrum%20of%20cosmic,very%20high%20energy%20cosmic%20rays.
65. J.K. Webb et al. (1999). "Search for Time Variation of the Fine Structure Constant". Physical Review Letters82 (5): 884–887. arXiv:astro-ph/9803165. Bibcode:1999PhRvL..82..884W. doi:10.1103/PhysRevLett.82.884.
66. M.T. Murphy et al. (2001). "Possible evidence for a variable fine-structure constant from QSO absorption lines: motivations, analysis and results". Monthly Notices of the Royal Astronomical Society327 (4): 1208. arXiv:astro-ph/0012419. Bibcode:2001MNRAS.327.1208M. doi:10.1046/j.1365-8711.2001.04840.x.
67. J.K. Webb et al. (2001). "Further Evidence for Cosmological Evolution of the Fine Structure Constant".Physical Review Letters87 (9): 091301. arXiv:astro-ph/0012539. Bibcode:2001PhRvL..87i1301W. doi:10.1103/PhysRevLett.87.091301. PMID 11531558.
68. M.T. Murphy, J.K. Webb, V.V. Flambaum (2003). "Further Evidence for a Variable Fine-Structure Constant from Keck/HIRES QSO Absorption Spectra". Monthly Notices of the Royal Astronomical Society345 (2): 609. arXiv:astro-ph/0306483.Bibcode:2003MNRAS.345..609M. doi:10.1046/j.1365-8711.2003.06970.x.
69. L. Farrarese, D. Merritt, Astrophysical Journal, Vol. 539, (2000) p. L9.
70. K. Gebhardt, et al., Astrophysical Journal, Vol. 539, (2000) p. L13.
71. S. Flamsteed, Discover, Vol. 16, Number 3, March, (1995), pp. 66-77.
72. J. Glanz, Science, Vol. 273, (1996), p. 581.
73. http://www.eurekalert.org/pub_releases/2004-01/ci-ogi010504.php.
74. http://www.eurekalert.org/pub_releases/2004-01/nsf-ase010804.php.
75. http://www.gemini.edu/gdds/.
76. K. Glazebrook, R. G. Abraham, P. J. McCarthy, S. Savaglio, H-W Chen , D. Crampton, R. Murowinski, I. Jorgensen, K. Roth, I. Hook, R. O. Marzke, R. G. Carlberg, "A high abundance of massive galaxies 3-6 billion years after the Big Bang," Nature, Vol. 430, (2004) pp. 181-184.
77. A. Cimatti, E. Daddi, A. Renzini, P. Cassata, E. Vanzella, L. Pozzetti, S. Cristiani, A. Fontana, G. Rodighiero, M. Mignoli, G. Zamorani, "Old galaxies in the young Universe," Nature, Vol. 430, (2004), pp. 184-187.

78. D. Stark, R. S. Ellis, J. Richard, J-P. Kneib, G. P. Smith, M. R. Santos, "A Keck survey for gravitationally lensed Lyα emitters in the redshift range 8.5 < z < 10.4: New constraints on the contribution of low-luminosity sources to cosmic reionization," The Astrophysical Journal, Vol. 663, No. 10, (2007), pp. 10-28.
79. X. Wu, F. Wang, X. Fan, W. Yi, W. Zuo, F. Bian, L. Jiang, I. D. McGreer, R. Wang, J. Yang, Q. Yang, D. Thompson, Y. Beletsky, "An ultraluminous quasar with a twelve-billion-solar-mass black hole at redshift 6.30", Nature, Vol. 518, (2015), (7540): 512 DOI: 10.1038/nature14241.
80. D. Watson, L. Christensen, K .K. Knudsen, J. Richard, A. Gallazzi, M. J. Michalowski, "A dusty, normal galaxy in the epoch of reionization", Nature, March 2,(2015); http://dx.doi.org/10.1038/nature14164.
81. B. Lewis, "James Webb telescope discovers the 4 oldest galaxies in the universe, born just 300 million years after the Big Bang", LiveScience, April 2, 2023, https://www.livescience.com/james-webb-telescope-discovers-the-4-oldest-galaxies-in-the-universe-born-just-300-million-years-after-the-big-bang.
82. H. Devlin, "James Webb telescope detects evidence of ancient 'universe breaker' galaxies", Guardian, February 22, 2023, https://www.theguardian.com/science/2023/feb/22/universe-breakers-james-webb-telescope-detects-six-ancient-galaxies.
83. B. Specktor, "James Webb telescope discovers 2 of the oldest galaxies in the universe", LiveScience, November 22, 2023, https://www.livescience.com/space/astronomy/james-webb-telescope-discovers-2-of-the-oldest-galaxies-in-the-universe.
84. B. Wang, et al, "UNCOVER: Illuminating the Early Universe—JWST/NIRSpec Confirmation of z > 12 Galaxies", The Astrophysical Journal Letters, Vol. 957, (2023), p. L34, DOI 10.3847/2041-8213/acfe07, https://iopscience.iop.org/article/10.3847/2041-8213/acfe07.
85. R. Lea, "Universe's oldest X-ray-spitting quasar could reveal how the biggest black holes were born", LiveScience, November 8, 2023, https://www.livescience.com/space/black-holes/universes-oldest-x-ray-spitting-quasar-could-reveal-how-the-biggest-black-holes-were-born.
86. B. Turner, "James Webb Space Telescope discovers oldest black hole in the universe — a cosmic monster 10 million times heavier than the sun", LiveScience, April 5, 2023, /www.livescience.com/james-webb-space-telescope-discovers-oldest-black-hole-in-the-universe-a-cosmic-monster-ten-million-times-heavier-than-the-sun.
87. J. Thompson, "James Webb Space Telescope discovers oldest organic molecules in the known universe, 12 billion light-years from Earth", LiveScience, June 7, 2023, https://www.livescience.com/space/cosmology/james-webb-space-telescope-discovers-oldest-organic-molecules-in-the-known-universe-12-billion-light-years-from-earth.
88. R. Mills, Y. Lu, R. Frazer, "Power Determination and Hydrino Product Characterization of Ultra-low Field Ignition of Hydrated Silver Shots", Chinese Journal of Physics, Vol. 56, (2018), pp. 1667-1717.
89. R. L. Mills, Y. Lu, "Hydrino continuum transitions with cutoffs at 22.8 nm and 10.1 nm," Int. J. Hydrogen Energy, 35 (2010), pp. 8446-8456, doi: 10.1016/j.ijhydene.2010.05.098.
90. R. L. Mills, Y. Lu, K. Akhtar, "Spectroscopic observation of helium-ion- and hydrogen-catalyzed hydrino transitions," Cent. Eur. J. Phys., 8 (2010), pp. 318-339, doi: 10.2478/s11534-009-0106-9.
91. R. L. Mills, Y. Lu, "Time-resolved hydrino continuum transitions with cutoffs at 22.8 nm and 10.1 nm," Eur. Phys. J. D, Vol. 64, (2011), pp. 65, DOI: 10.1140/epjd/e2011-20246-5.
92. R. L. Mills, R. Booker, Y. Lu, "Soft X-ray Continuum Radiation from Low-Energy Pinch Discharges of Hydrogen," J. Plasma Physics, Vol. 79, (2013), pp 489-507; doi: 10.1017/S0022377812001109.
93. A. Bykanov, "Validation of the observation of soft X-ray continuum radiation from low energy pinch discharges in the presence of molecular hydrogen," http://www.blacklightpower.com/wp-content/uploads/pdf/GEN3_Harvard.pdf.
94. R. Mills, J. Lotoski, Y. Lu, "Mechanism of soft X-ray continuum radiation from low-energy pinch discharges of hydrogen and ultra-low field ignition of solid fuels", Plasma Science and Technology, Vol. 19, (2017), pp. 1-28.
95. M. A. Barstow and J. B. Holberg, *Extreme Ultraviolet Astronomy*, Cambridge Astrophysics Series 37, Cambridge University Press, Cambridge, (2003).
96. R. Stern, S. Bowyer, "Apollo-Soyuz survey of the extreme-ultraviolet/soft X-ray background", Astrophys. J., Vol. 230, (1979), pp. 755-767.
97. W. Sanders, et. al. Nature, 349, (1991), pp. 32-38.
98. R. P. Kirshner, A. J. Oemler, P. L. Schecter, and A. S. Schectman, AJ, (1983), 88,1285.
99. V. de Lapparent, V., M. J. Geller, and J. P. Huchra, ApJ, (1988), 332, 44.
100. A. Dressler, et. al., (1987), Ap. J., 313, L37.
101. S. A. Thomas, F. B. Abdalla, O. Lahav, "Excess clustering on large scales in the MegaZ DR7 Photometric Redshift Survey", Physical Review Letters, Vol. 106, (2011), pp. 241301-1-24310-4.
102. G. Musser, Scientific American, May, (2000), p. 24.
103. M. A. Barstow and J. B. Holberg, *Extreme Ultraviolet Astronomy*, Cambridge Astrophysics Series 37, Cambridge University Press, Cambridge, (2003), Chp 8.
104. M. Stix, *The Sun*, Springer-Verlag, Berlin, (1991), Figure 9.5, p. 321.
105. Phillips, J. H., *Guide to the Sun*, Cambridge University Press, Cambridge, Great Britain, (1992), pp. 126-127.
106. M. Stix, *The Sun*, Springer-Verlag, Berlin, (1991), pp. 351-356.
107. http://nobelprize.org/nobel_prizes/physics/articles/bahcall/.
108. N. Craig, M. Abbott, D. Finley, H. Jessop, S. B. Howell, M. Mathioudakis, J. Sommers, J. V. Vallerga, R. F. Malina, "The Extreme Ultraviolet Explorer stellar spectral atlas", The Astrophysical Journal Supplement Series, Vol. 113, (1997), pp. 131-193.

109. S. Labov, S. Bowyer, "Spectral observations of the extreme ultraviolet background", The Astrophysical Journal, 371, (1991), pp. 810-819.
110. A. F. H. van Gessel, Masters Thesis: *EUV spectroscopy of hydrogen plasmas*, April (2009), Eindhoven University of Technology, Department of Applied Physics, Group of Elementary Processes in Gas Discharges, EPG 09-02, pp. 61-70.
111. S. Bower, G. Field, and J. Mack, "Detection of an anisotrophic soft X-ray background flux," Nature, Vol. 217, (1968), p. 32.
112. C. W. Danforth, J. M. Shull, "The low-z intergalactic medium. III. H I and metal absorbers at z<0.4", The Astrophysical Journal, Vol. 679, (2008), pp. 194-219.
113. N. Werner, A. Finoguenov, J. S. Kaastra, A. Simionescu, J. P. Dietrich, J Vink, H. Böhringer, "Detection of hot gas in the filament connecting the clusters of galaxies Abell 222 and Abell 223", Astronomy & Astrophysics Letters, Vol. 482, (2008), pp. L29-L33.
114. E. Bulbul, M. Markevitch, A. Foster, R. K. Smith, M. Loewenstein, S. W. Randall, "Detection of an unidentified emission line in the stacked X-Ray spectrum of galaxy clusters," The Astrophysical Journal,Volume 789, Number 1, (2014).
115. A. Boyarsky, O. Ruchayskiy, D. Iakubovskyi, J. Franse, "An unidentified line in X-ray spectra of the Andromeda galaxy and Perseus galaxy cluster," (2014), arXiv:1402.4119 [astro-ph.CO].
116. S. Bowyer, J. J. Drake, S. Vennes, "Extreme ultraviolet spectroscopy", Ann. Rev. Astron. Astrophys., Vol. 38, (2000), pp. 231-288.
117. A. Gupta, S. Mathur, Y. Krongold, F. Nicastro, M. Galeazzi, "A huge reservoir of ionized gas around the Milky Way: Accounting for the missing mass?" The Astrophysical Journal Letters, Volume 756, Number 1, (2012), P. L8, doi:10.1088/2041-8205/756/1/L8.
118. F. Bournaud, P. A. Duc, E. Brinks, M. Boquien, P. Amram, U. Lisenfeld, B. Koribalski, F. Walter, V. Charmandaris, "Missing mass in collisional debris from galaxies", Science, Vol. 316, (2007), pp. 1166–1169.
119. B. G. Elmegreen, "Dark matter in galactic collisional debris", Science, Vol. 316, (2007), pp. 32-33.
120. P. Jean, et al., "Early SPI/INTEGRAL measurements of 511 keV line emission from the 4th quadrant of the Galaxy", Astron, Astrophys., Vol. 407, (2003), pp. L55-L58.
121. M. Chown, "Astronomers claim dark matter breakthrough," NewScientist.com, Oct. 3, (2003), http://www.newscientist.com/ article/dn4214-astronomers-claim-dark-matter-breakthrough.html.
122. C. Boehm, D. Hooper, J. Silk, M. Casse, J. Paul, "MeV dark matter: Has it been detected," Phys. Rev. Lett., Vol. 92, (2004), p. 101301.
123. G. H. Share, "Recent results on celestial gamma radiation from SMM", Advances in Space Research, Vol.11, Issue 8, (1991), pp. 85-94.
124. G. H. Share, R. L. Kinzer, D. C. Messina, W. R. Purcell, E. L. Chupp, D. J. Forrest, E. Rieger, "Observations of galactic gamma-radiation with the SMM spectrometer", Advances in Space Research, Vol. 6, Issue 4, (1986), pp. 145-148.
125. B. Kozlovsky, R. E. Lingenfelter, R. Ramaty, "Positrons from accelerated particle interactions," The Astrophysical Journal, Vol. 316, (1987), pp. 801-818.
126. E. P. Mazets, S. V. Golenetskii, V. N. Il'inskii, R. L. Aptekar', Y. A. Guryan, "Observations of a flaring X-ray pulsar in Dorado," Nature, Vol. 282, No. 5739, (1979), pp. 587-589.
127. G. H. Share, E. L. Chupp, D. J. Forrest, E. Rieger in Positron and Electron Pairs in Astrophysics, ed. M. L. Burns, A. K. Harding, R. Ramaty, "Positron annihilation radiation from Solar flares", (1983), New York: AIP, pp. 15-20.
128. M. J. Jee, et al., "Discovery of a ringlike dark matter structure in the core of the galaxy cluster C1 0024+17," Astrophysical Journal, Vol. 661, (2007), pp. 728-749.
129. R. L. Mills, *The Grand Unified Theory of Classical Quantum Mechanics*, November 1995 Edition, HydroCatalysis Power Corp., Malvern, PA, Library of Congress Catalog Number 94-077780, ISBN number ISBN 0-9635171-1-2, Chp. 22.
130. M. J. Jee, A. Mahdavi, H. Hoekstra, A. Babul, J. J. Dalcanton, P. Carroll, P. Capak, "A study of the dark core in A520 with the Hubble Space Telescope: The mystery deepens," Astrophys. J., Vol. 747, No.96, (2012), pp. 96-103.
131. D. S. Akerib, et al., "First results from the LUX dark matter experiment at the Stanford Underground Research Facility", (2014), http://arxiv.org/abs/1310.8214.
132. G. Agakishiev, A. Balanda, D. Belver, A. Belyaev, J.C. Berger-Chen, A. Blanco, M. Böhmer, J.L. Boyard, P. Cabanelas, S. Chernenko, A. Dybczak, E. Epple, L. Fabbietti, O. Fateev, P. Finocchiaro, P. Fonte, J. Friese, I. Fröhlich, T. Galatyuk, J.A. Garzón, R. Gernhäuser, K. Göbel, M. Golubeva, D. González-Díaz, F. Guber, M. Gumberidze, T. Heinz, T. Hennino, R. Holzmann, A. Ierusalimov, I. Iori, A. Ivashkin, M. Jurkovic, B. Kämpfer, T. Karavicheva, I. Koenig, W. Koenig, B.W. Kolb, G. Kornakov, R. Kotte, A. Krása, F. Krizek, R. Krücken, H. Kuc, W. Kühn, A. Kugler, A. Kurepin, V. Ladygin, R. Lalik, S. Lang, K. Lapidus, A. Lebedev, T. Liu, L. Lopes, M. Lorenz, L. Maier, A. Mangiarotti, J. Markert, V. Metag, B. Michalska, J. Michel, C. Müntz, L. Naumann, Y.C. Pachmayer, M. Palka, Y. Parpottas, V. Pechenov, O. Pechenova, V. Petousis, J. Pietraszko, W. Przygoda, B. Ramstein, A. Reshetin, A. Rustamov, A. Sadovsky, P. Salabura, T. Scheib, H. Schuldes, A. Schmah, E. Schwab, J. Siebenson, Yu.G. Sobolev, S. Spataro, B. Spruck, H. Ströbele, J. Stroth, C. Sturm, A. Tarantola, K. Teilab, P. Tlusty, M. Traxler, R. Trebacz, H. Tsertos, T. Vasiliev, V. Wagner, M. Weber, C. Wendisch, J. Wüstenfeld, S. Yurevich, Y. Zanevsky, "Searching a dark photon with HADES", Physics Letters B, Vol. 731, (2014), p. 265 DOI: 10.1016/j.physletb.2014.02.035.
133. W. McC. Siebert, *Circuits, Signals, and Systems*, The MIT Press, Cambridge, Massachusetts, (1986), pp. 597-603.
134. S. D. Landy, Scientific American, June, (1999), pp. 38-45.

135. G. R. Fowles, *Analytical Mechanics*, Third Edition, Holt, Rinehart, and Winston, New York, (1977), pp. 57-60.
136. C. Willott, "A monster in the early Universe," Nature, Vol. 474, (2011), pp.583-584.
137. D.J. Mortlock,et al., "A luminous quasar at a redshift of z=7.085," Nature, Vol. 474, (2011), pp. 616-619.
138. G. Musser, Scientific American, Vol. 278, No. 3, March, (1998), p. 18.
139. P. de Bernardis, et al., A flat universe from high-resolution maps of the cosmic microwave background radiation, Nature,Vol. 404, (2000), p. 955; http://cmb.phys.cwru.edu/boomerang.
140. K. Sawyer, "Supernova observations bolster dark energy theory," April 3, (2001), washingtonpost.com.
141. A. G. Riess, et. al. "The farthest known supernova: support for an accelerating universe and a glimpse of the epoch of deceleration," Astrophysical Journal, Vol. 560, (2001), pp. 49-71.
142. B. P. Abbott, R Abbott, R. Adhikari, P. Ajith, B. Allen, G. Allen, R. S. Amin, S. B. Anderson, W. G. Anderson, M. A. Arain; et al., "LIGO: the Laser Interferometer Gravitational-Wave Observatory," Rep. Prog. Phys. 72 (2009) 076901 (25pp).
143. P. Shawhan, "Gravitational-wave astronomy: observational results and their impact," Class. Quantum Grav., Vol. 27 (2010) 084017 (14 pp).
144. J. H. Phillips, *Guide to the Sun*, Cambridge University Press, Cambridge, Great Britain, (1992), pp. 58-67.
145. A. Davidsen, et al., "Test of the decaying dark matter hypothesis using the Hopkins ultraviolet telescope," Nature, 351, (1991), pp. 128-130.
146. W. Milan, "Shall the WIMPs Inherit the Universe," SPACE.com, 28, February, 2000, http://space.com/scienceastronomy/ generalscience/dark_matter_000228.html.
147. R. Abusaidi, et al., "Exclusion limits on the WIMP-nucleon cross section from the cryogenic dark matter search," Physical Review Letters, Vol. 84, No. 25, 19, June, (2000), pp. 5699-5703.
148. E. Gibney, "Dark-matter hunt fails to find the elusive particles, "Nature, Vol. 551, (2017), pp. 153–154, doi:10.1038/551153a.
149. E. Aprile et al., "First Dark Matter Search Results from the XENON1T Experiment," Phys. Rev. Lett., Vol. 119, (2017), pp. 181301-1-181301-6.
150. M. G. Aartsen et al. (IceCube Collaboration), "Searches for Sterile Neutrinos with the IceCube Detector," Phys. Rev. Lett., Vol. 117, (2016), pp. 071801-1-071801-9.
151. Wilfred R. Hagen, Randell L. Mills, "Electron Paramagnetic Resonance Proof for the Existence of Molecular Hydrino", Vol. 47, No. 56, (2022), pp. 23751-23761; https://www.sciencedirect.com/science/article/pii/S0360319922022406.
152. R. N. Bracewell, *The Fourier Transform and Its Applications*, McGraw-Hill Book Company, New York, (1978), pp. 252-253.
153. W. McC. *Siebert, Circuits, Signals, and Systems*, The MIT Press, Cambridge, Massachusetts, (1986), p. 415.
154. B. R. Oppenheimer, N. C. Hambly, A. P. Digby, S. T. Hodgkin, and D. Saumon, "Direct detection of galactic halo dark matter," Science, Vol. 292, 27, April, (2000), pp. 698-702.
155. M. Zaldarriaga, "Background comes to the fore," Nature, Vol. 420, No. 6917, (2002), pp. 747-748.
156. E. M. Leitch, J. M. Kovac, C. Pryke, J. E. Carlstrom, N. W. Halverson, W. L. Holzapfel, M. Dragovan, B. Reddall, E. S. Sandberg, "Measurement of the polarization with the Degree Angular Scale Interferometer," Nature, Vol. 420, No. 6917, (2002), pp. 763-771.
157. J. M. Kovac, E. M. Leitch, C. Pryke, J. E. Carlstrom, N. W. Halverson, W. L. Holzapfel, "Detection of polarization in the cosmic microwave background using DASI," Nature, Vol. 420, No. 6917, (2002), pp. 772-787.
158. G. Hinshaw, et al., "Nine-year Wilkinson Microwave Anisotropy Probe (WMAP) observations: Cosmological parameters results", The Astrophysical Journal Supplement Series, Vol. 208. No.19, (2013), pp. 1-25.
159. H. C. Chiang, P. A. R. Ade, D. Barkats, J. O. Battle, E. M. Bierman, J. J. Bock, C. D. Dowell, L. Duband, E. F. Hivon, W. L. Holzapfel, V. V. Hristov, W. C. Jones, B. G. Keating, J. M. Kovac, C. L. Kuo, A. E. Lange, E. M. Leitch, P. V. Mason, T. Matsumura, H. T. Nguyen, N. Ponthieu, C. Pryke, S. Richter, G. Rocha, C. Sheehy, Y. D. Takahashi, J. E. Tolan, K. W. Yoon, "Measurement of cosmic microwave background polarization power spectra from two years of BICEP data", The Astrophysical Journal, Vol. 711, pp. 1123-1140.
160. Bicep2 Collaboration – P. A. R. Ade, R. W. Aikin, D. Barkats, S. J. Benton, C. A. Bischoff, J. J. Bock, J. A. Brevik, I. Buder, E. Bullock, C. D. Dowell, L. Duband, J. P. Filippini, S. Fliescher, S. R. Golwala, M. Halpern, M. Hasselfield, S. R. Hildebrandt, G. C. Hilton, V. V. Hristov, K. D. Irwin, K. S. Karkare, J. P. Kaufman, B. G. Keating, S. A. Kernasovskiy, J. M. Kovac, C. L. Kuo, E. M. Leitch, M. Lueker, P. Mason, C. B. Netterfield, H. T. Nguyen, R. O'Brient, R. W. Ogburn IV, A. Orlando, C. Pryke, C. D. Reintsema, S. Richter, R. Schwarz, C. D. Sheehy, Z. K. Staniszewski, R. V. Sudiwala, G. P. Teply, J. E. Tolan, A. D. Turner, A. G. Vieregg, C. L. Wong, K. W. Yoon, "Bicep2 I: Detection of B-mode polarization at degree angular scales, http://arxiv.org/pdf/1403.3985.pdf.

Chapter 33

UNIFICATION OF SPACETIME, THE FORCES, MATTER, AND ENERGY

RELATIONSHIP OF SPACETIME AND THE FORCES

Spacetime has an intrinsic impedance of η. It provides a limiting speed of c for the propagation of any wave, including gravitational and electromagnetic waves. It further provides fields that match boundary conditions. Matter/energy acts on spacetime and spacetime acts on matter/energy. Thus, a spatial two-dimensional manifold of matter results in a gravitational field in spacetime; a three-dimensional spacetime manifold of current gives rise to a magnetic field in spacetime; a spatial two-dimensional manifold of charge gives rise to an electric field in spacetime. Thus, General Relativity and Maxwell's Equations are valid on any scale. Furthermore, the existence of matter with a determined mass as a three-dimensional spacetime manifold that is charged maximizes the volume of spacetime to the surface area of matter. This gives an energy minimum of the resulting gravitational, electric, and magnetic fields.

Matter/energy are interchangeable and are, in essence, the same entity with different boundary values imposed by spacetime where the matter/energy has a reaction effect on spacetime. The intricacy of the action/reaction is evident in that all matter/energy obeys the four-dimensional wave equation, and the magnetic, electric, photonic, and gravitational fields can be derived as boundary value problems of the wave equation of spacetime where space provides the respective force fields for the matter/energy. That spacetime is four-dimensional is evident because the fundamental forces of gravity and electric attraction which are time dependent have a one-over-distance-squared relationship. This relationship is equivalent to the distance dependence of the area of a spherically symmetric wavefront which carries the forces. The force at the wavefront is nonradial and has an inverse r-dependence, traveling at the limiting speed of light provided by spacetime in accordance with Special Relativity.

The action/reaction relationships of the third fundamental force, the mechanical force, are given by Newton's Laws. They provide the motion of matter including charged matter, which can give rise to gravitational, magnetic, and photonic fields. The action/reaction provided by forces in one inertial frame is given in a different inertial frame by the Lorentz transformations of Special Relativity, which are valid for Euclidean spacetime and are a consequence of the limiting speed of light. For example, the magnetic field in one inertial frame is given as electric field in another inertial frame as a consequence of their relative motion. The presence of matter causes the geometry of spacetime to deviate from Euclidean, which is manifest as a gravitational field. The gravitational equation is derived for all scales from the present atomic orbital model where spacetime is Riemannian.

The provision of the equivalence of inertial and gravitational mass by the CP theory of fundamental particles permits the correct derivation of the General Theory. And, the former provision of the two-dimensional nature of matter permits the unification of atomic, subatomic, and cosmological gravitation. The unified theory of gravitation is derived by first establishing a metric.

A space in which the curvature tensor has the following form:

$$R_{\mu\nu,\alpha\beta} = K \cdot (g_{\nu\alpha} g_{\mu\beta} - g_{\mu\alpha} g_{\nu\beta}) \tag{33.1}$$

is called a space of constant curvature; it is a four-dimensional generalization of Friedmann-Lobachevsky space. The constant K is called the constant of curvature. *The curvature of spacetime will be shown to result from a discontinuity of matter having curvature confined to two spatial dimensions. This is the property of all matter as an atomic orbital.* Consider an isolated atomic orbital and radial distances, r, from its center. *For r less than r_n there is no mass; thus, spacetime is flat or Euclidean.* The curvature tensor applies to all space of the inertial frame considered; thus, for r less than r_n, $K = 0$. At $r = r_n$ there exists a discontinuity of mass of the atomic orbital. This results in a discontinuity of the curvature tensor for radial distances greater than or equal to r_n. The discontinuity requires relativistic corrections to spacetime itself. It requires radial length contraction and

time dilation that results in the curvature of spacetime. The gravitational radius r_g of the atomic orbital and infinitesimal temporal displacement in spacetime, which is curved by the presence of the atomic orbital, are derived in the Gravity section.

The Schwarzschild metric gives the relationship whereby matter causes relativistic corrections to spacetime that determines the curvature of spacetime and is the origin of gravity. The separation of proper time between two events x^μ and $x^\mu + dx^\mu$ given by the Schwarzschild metric is:

$$d\tau^2 = \left(1 - \frac{2Gm_0}{c^2 r}\right) dt^2 - \frac{1}{c^2}\left[\left(1 - \frac{2Gm_0}{c^2 r}\right)^{-1} dr^2 + r^2 d\theta^2 + r^2 \sin^2\theta d\phi^2\right] \tag{33.2}$$

Eq. (33.2) can be reduced to Newton's Law of Gravitation for $\frac{r_g}{r_\alpha^*} << 1$, where $r_\alpha^* = \lambda\!\!\!^{-}_c$

$$\mathbf{F} = \frac{Gm_1 m_2}{r^2} \tag{33.3}$$

where G is the Newtonian gravitational constant. Eq. (33.2) relativistically corrects Newton's gravitational theory. In an analogous manner, Lorentz transformations correct Newton's Laws of Mechanics.

Maxwell's Equations give the electromagnetic forces:

$$\nabla \times \mathbf{E} = -\frac{\partial \mu_0 \mathbf{H}}{\partial t} \tag{33.4}$$

$$\nabla \times \mathbf{H} = \mathbf{J} + \frac{\partial \varepsilon_0 \mathbf{E}}{\partial t} \tag{33.5}$$

$$\nabla \bullet \varepsilon_0 \mathbf{E} = \rho \tag{33.6}$$

$$\nabla \bullet \mu_0 \mathbf{H} = 0 \tag{33.7}$$

Maxwell's Integral Laws in Free Space are:

Ampere's Law

$$\oint_C \mathbf{H} \bullet d\mathbf{s} = \int_S \mathbf{J} \bullet d\mathbf{a} + \frac{d}{dt}\int_S \varepsilon_0 \mathbf{E} \bullet d\mathbf{a} \tag{33.8}$$

Faraday's Law

$$\oint_C \mathbf{E} \bullet d\mathbf{s} = -\frac{d}{dt}\int_S \mu_0 \mathbf{H} \bullet d\mathbf{a} \tag{33.9}$$

Power flow is governed by the Poynting power theorem:

$$\nabla \bullet (\mathbf{E} \times \mathbf{H}) = -\frac{\partial}{\partial t}\left[\frac{1}{2}\mu_0 \mathbf{H} \bullet \mathbf{H}\right] - \frac{\partial}{\partial t}\left[\frac{1}{2}\varepsilon_0 \mathbf{E} \bullet \mathbf{E}\right] - \mathbf{J} \bullet \mathbf{E} \tag{33.10}$$

Newtonian mechanics gives mechanical forces for $v << c$:

$$\mathbf{F} = \frac{d\mathbf{p}}{dt} = \frac{d(m\mathbf{v})}{dt} = m\frac{d\mathbf{v}}{dt} = m\mathbf{a} \tag{33.11}$$

$$T = \frac{1}{2}mv^2 \tag{33.12}$$

Special Relativity applies when v approaches c:

$$E = mc^2 \tag{33.13}$$

$$m = \frac{m_0}{\sqrt{1 - \frac{v^2}{c^2}}} \tag{33.14}$$

$$l = l_0\sqrt{1 - \frac{v^2}{c^2}} \tag{33.15}$$

$$t = \frac{t_0}{\sqrt{1-\frac{v^2}{c^2}}} \tag{33.16}$$

where the subscript denotes the value in the rest frame.

The following equations are boundary conditions:

$$2\pi(nr_1) = 2\pi r_n = n\lambda_1 = \lambda_n \tag{33.17}$$

where

λ_1 is the allowed wavelength for $n = 1$

r_1 is the allowed radius for $n = 1$

For pair production:

$n = \alpha$

For hydrogen:

$n = 1, 2, 3, 4, ...$

$n = \frac{1}{2}, \frac{1}{3}, \frac{1}{4}, ...$

$$v_n = \frac{\hbar}{m_e r_n} \tag{33.18}$$

The weak and strong nuclear forces are discussed in the Weak Nuclear Force: Beta Decay of the Neutron section and the Strong Nuclear Force section. These forces are electromagnetic in nature. They arise as a minimization of the stored field energies. This also applies for the case of the force of the chemical bond as described in the Nature of the Chemical Bond section.

RELATIONSHIP OF SPACETIME, MATTER, AND CHARGE

In addition to the force laws, the nature of the Universe is determined by the following experimentally observed parameters:

- Four dimensional spacetime (the only dimensionality consistent with observations [1]);
- The fundamental constants which comprise the fine structure constant;
- Fundamental particles including photons have $\hbar$ of angular momentum;
- The Newtonian gravitational constant, G;
- The mass of the Universe, and
- The spin of the electron neutrino.

General Relativity gives the relationship between the proper time and the coordinate time of particle production.

$$\tau = ti\sqrt{\frac{2GM}{c^2 r_\alpha^*}} = ti\sqrt{\frac{2GM}{c^2 \lambda\!\!\!^{-}_c}} \tag{33.19}$$

The following boundary condition applies at the creation of matter from energy:

$$2\pi r_n = \lambda_n \qquad n = \alpha \tag{33.20}$$

The particle production energies given in the Gravity section are the mass energy, the Planck equation energy, the electric potential energy, the magnetic energy, the gravitational potential energy, and the mass/spacetime metric energy[1].

$$m_0 c^2 = \hbar\omega^* = V = E_{mag} = E_{grav} = E_{spacetime}$$

$$m_0 c^2 = \hbar\omega^* = \frac{\hbar^2}{m_0 \lambda\!\!\!^{-2}_C} = \alpha^{-1}\frac{e^2}{4\pi\varepsilon_0 \lambda\!\!\!^{-}_C} = \alpha^{-1}\frac{\pi\mu_0 e^2\hbar^2}{\left(2\pi m_0\right)^2 \lambda\!\!\!^{-3}_C} = \alpha^{-1}\frac{\mu_0 e^2 c^2}{2h}\sqrt{\frac{Gm_0}{\lambda\!\!\!^{-}_C}}\sqrt{\frac{\hbar c}{G}} = \frac{\alpha h}{1\ \text{sec}}\sqrt{\frac{\lambda\!\!\!^{-}_C c^2}{2Gm_0}} \tag{33.21}$$

When m_o is the Grand Unification Mass or Planck mass, m_u,

[1] Eq. (33.21) is the relationship between matter and energy with an implicit physical basis for particle production. The current understanding of the matter-energy relationship $E = m_0 c^2$ first recognized by Poincaré [2-4] is based on the derivation of the kinetic energy from Newton's force equation [5] or by applying special relativistic principles to conservation of energy and momentum during particle scattering [6]. These approaches have nothing to do with particle production. Eq. (33.21) is the mass-energy for particle production and is the correct physics for the popular equation $E = m_0 c^2$ and the version including relative motion given by Eq. (34.17).

$$m_u c^2 = \hbar\omega^* = V = E_{mag} = \frac{Gm_u^2}{\lambda\!\!\!^{-}_C^*}$$
$$m_u = m_0 = \sqrt{\frac{\hbar c}{G}} \tag{33.22}$$

The gravitational velocity, v_G, is defined as:

$$v_G = \sqrt{\frac{Gm_0}{\lambda\!\!\!^{-}_C}} \tag{33.23}$$

Substitution of the gravitational velocity, v_G, given by Eq. (33.23) and the Planck mass, m_u, given by Eq. (33.22) into Eq. (33.21) followed by division by the speed of light squared gives the particle mass in terms of the Planck mass.

$$m_0 = \alpha^{-1}\frac{\mu_0 e^2 c}{2h}\frac{\sqrt{\frac{Gm_0}{\lambda\!\!\!^{-}_C}}}{c}m_u = \alpha^{-1}\frac{\mu_0 e^2 c}{2h}\sqrt{\frac{Gm_0}{c^2\lambda\!\!\!^{-}_C}}m_u = \alpha^{-1}\frac{\mu_0 e^2 c}{2h}\frac{v_G}{c}m_u = \frac{v_G}{c}m_u \tag{33.24}$$

The relationships between the fundamental constants are given by the equivalence of the particle production energies. The magnitude of the quantized angular momentum of the photon and fundamental particles is Planck's constant bar, $\hbar$. The wave equation gives the relationship between the velocity, wavelength, and frequency of the wave.

$$v = \lambda\frac{\omega}{2\pi} \tag{33.25}$$

When $v = c$ the radius at particle production is given by Eq. (29.22).

$$r_\alpha = \frac{\hbar}{m_o c} = \lambda\!\!\!^{-}_C \tag{33.26}$$

Substitution of Eq. (33.25) and (33.26) into Eq. (33.21) with $v = c$ gives the relationship between $\hbar$ and the fundamental charge squared.

$$\hbar\omega^* = h\frac{c}{\lambda} = \alpha^{-1}\frac{e^2}{4\pi\varepsilon_0\lambda\!\!\!^{-}_C}$$
$$\hbar\frac{c}{\lambda\!\!\!^{-}_C} = \alpha^{-1}\frac{e^2}{4\pi\varepsilon_0\lambda\!\!\!^{-}_C} \tag{33.27}$$
$$\hbar c = \alpha^{-1}\frac{e^2}{4\pi\varepsilon_0}$$

Thus, charge is quantized as a consequence of the quantization of the angular momentum of the photon. The relationship between the speed of light, c, and the permittivity of free space, ε_0, and the permeability of free space, μ_0, is:

$$c = \frac{1}{\sqrt{\mu_0\varepsilon_0}} \tag{33.28}$$

The fine structure constant, given by Eqs. (1.179) and (29.9), is the dimensionless factor that corresponds to the relativistic invariance of charge.

$$\alpha = \frac{1}{4\pi}\sqrt{\frac{\mu_0}{\varepsilon_0}}\frac{e^2}{\hbar} = \frac{1}{2}\frac{\sqrt{\frac{\mu_0}{\varepsilon_0}}}{\frac{h}{e^2}} = \frac{\mu_0 e^2 c}{2h} \tag{33.29}$$

It is equivalent to one half the ratio of the radiation resistance of free space, $\sqrt{\frac{\mu_0}{\varepsilon_0}}$, and the hall resistance, $\frac{h}{e^2}$. The radiation resistance of free space is equal to the ratio of the electric field and the magnetic field of the photon (Eq. (4.10)). The Hall resistance is given by Eq. (26.46). Substitution of Eq. (33.28) into Eq. (33.27) gives the relationship for the radiation resistance of free space, η.

$$\eta = \sqrt{\frac{\mu_0}{\varepsilon_0}} = 4\pi\alpha\frac{\hbar}{e^2} \tag{33.30}$$

It provides a limiting speed of c for the propagation of any wave, including gravitational and electromagnetic waves and expanding spacetime.

PERIOD EQUIVALENCE

The Universe undergoes time harmonic expansion and contraction corresponding to matter/energy conversion. The equation of the radius of the Universe, $\aleph$, which is derived in the Gravity section is

$$\aleph = \left(\frac{2Gm_U}{c^2} + \frac{cm_U}{\frac{c^3}{4\pi G}} \right) - \frac{cm_U}{\frac{c^3}{4\pi G}} \cos\left(\frac{2\pi t}{\frac{2\pi G m_U}{c^3}} \right) \tag{33.31}$$

The gravitational equation (Eq. (31.38)) with the equivalence of the particle production energies (Eqs. (31.48a-31.48b)) permit the equivalence of mass-energy ($E = mc^2$) and spacetime ($\frac{c^3}{4\pi G} = 3.22\ X\ 10^{34}\ \frac{kg}{\sec}$). Spacetime expands as mass is released as energy according to Eq. (32.140) which provides the basis of the atomic, thermodynamic, and cosmological arrows of time. Q, the mass-energy-to-expansion-contraction quotient of spacetime is given by the ratio of the electron mass m_e and the electron proper time τ wherein Eq. (32.43) gives the relativistic correction $\beta_g = \frac{v_g}{c}$ to give the corresponding spacetime expansion for the conversion of matter into energy.

$$Q = \frac{\beta_g^{-1} m_e}{\tau \cdot \beta_g} = \frac{\frac{m_e}{\frac{v_g}{c}}}{\tau \cdot \frac{v_g}{c}} = \frac{\frac{m_e}{\sqrt{\frac{2Gm_e}{c^2 \lambda\!\!\!^{-}_c}}}}{\tau \cdot \sqrt{\frac{2Gm_e}{c^2 \lambda\!\!\!^{-}_c}}} = \frac{m_e}{\tau} \cdot \frac{c^2 \lambda\!\!\!^{-}_c}{2Gm_e} = \frac{m_e}{2\pi \frac{\hbar}{m_e c^2}} \cdot \frac{c^2 \frac{\hbar}{m_e c}}{2Gm_e} = \frac{c^3}{4\pi G} = 3.22\ X\ 10^{34}\ \frac{kg}{\sec} \tag{33.32}$$

From Eq. (33.31), the period of the expansion-contraction cycle of the radius of the Universe, T, is:

$$T = \frac{2\pi G m_U}{c^3} \tag{33.33}$$

It is herein derived that ***the periods of spacetime expansion/contraction and particle decay/production for the Universe are equal***. It follows from the Poynting Power Theorem (Eq. (7.43)) with spherical radiation that the transition lifetimes are given by the ratio of energy and the power of the transition [7]. Magnetic energy is a Special Relativistic consequence of electric energy and kinetic energy. Thus, only transitions involving electric energy need be considered. The transition lifetime, τ, in the case of the electric multipole moment given by Jackson [7] as:

$$Q_{lm} = \frac{3}{\ell + 3} e \left(r_n \right)^{\ell} \tag{33.34}$$

is [7]

$$\tau = \frac{energy}{power}$$

$$\tau = \frac{\left[\hbar \omega \right]}{\left[\frac{2\pi c}{\left[(2l+1)!! \right]^2} \left(\frac{l+1}{l} \right) k^{2(l+1)} \left| Q_{lm} + Q'_{lm} \right|^2 \right]} = \frac{1}{2\pi} \left(\frac{h}{e^2} \right) \sqrt{\frac{\varepsilon_0}{\mu_0}} \frac{\left[(2l+1)!! \right]^2}{2\pi} \left(\frac{l}{l+1} \right) \left(\frac{l+3}{3} \right)^2 \frac{1}{\left(k r_n \right)^{2l} \omega} \tag{33.35}$$

where in the exemplary case of an excited state of atomic hydrogen r_n is the radius of the electron atomic orbital which is na_0 (Eq. (33.17)). From Eq. (33.35), the transition lifetime is proportional to the ratio of $\frac{h}{e^2}$, the Quantum Hall resistance, and η, the radiation resistance of free space where:

$$\eta = \sqrt{\frac{\mu_0}{\varepsilon_0}} \tag{33.36}$$

The Quantum Hall resistance given in the Quantum Hall Effect section was derived using the Poynting Power Theorem. Also, from Eq. (33.35), the transition lifetime is proportional to the fine structure constant, α,

$$\alpha = \frac{1}{4\pi} \sqrt{\frac{\mu_0}{\varepsilon_0}} \frac{e^2}{\hbar} \tag{33.37}$$

From Eq. (33.35), the lifetime of an excited state of a hydrogen atom is inversely proportional to the frequency of the transition. This is also the case for the Universe that is a 3-sphere Universe. (More explicitly, the Universe is a Riemannian three-

dimensional hyperspace plus time with a constant positive curvature at each r-sphere). During an electromagnetic transition, the total energy of the system decays exponentially. Applying Eqs. (2.119) and (2.120) to the case of exponential decay,

$$h(t) = e^{-\alpha t}u(t) = e^{-\frac{2\pi}{T}t}u(t) \tag{33.38}$$

However, Eq. (33.19) determines that ***the coordinate time is imaginary*** because energy transitions are spacelike due to General Relativistic effects. For example, Eq. (36.2) gives the mass of the electron (a fundamental particle) in accordance with Eq. (33.19) :

$$\frac{2\pi \lambda\!\!\!^{-}_C}{\sqrt{\frac{2Gm_e}{\lambda\!\!\!^{-}_C}}} = \frac{2\pi \lambda\!\!\!^{-}_C}{v_g} = i\alpha^{-1}\sec \tag{33.39}$$

where Newtonian gravitational velocity v_g is given by Eq. (32.35). Replacement of the coordinate time, t, of Eq. (33.38) by the spacelike time, it, gives:

$$h(t) = \mathrm{Re}\left\{e^{-i\frac{2\pi}{T}t}\right\} = \cos\frac{2\pi}{T}t \tag{33.40}$$

where the period is *T*. The periods of spacetime expansion/contraction and particle decay/production for the Universe are equal due to Eq. (33.19) which determines the masses of fundamental particles, the equivalence of inertial and gravitational mass, the phase matching condition of mass to the speed of light and charge to the speed of light, and that the coordinate time is imaginary because energy transitions are spacelike due to general relativistic effects. From Eq. (33.19),

$$\frac{\text{proper time}}{\text{coordinate time}} = \frac{\text{gravitational wave condition}}{\text{electromagnetic wave condition}} = \frac{\text{gravitational mass phase matching}}{\text{charge/inertial mass phase matching}}$$

$$\frac{\text{proper time}}{\text{coordinate time}} = i\frac{\sqrt{\frac{2Gm}{c^2 \lambda\!\!\!^{-}_C}}}{\alpha} = i\frac{v_g}{\alpha c} \tag{33.41}$$

where Newtonian gravitational velocity, v_g, is given by Eq. (32.35). Eq. (33.24) gives the ratio of Eq. (33.41) in terms of the coordinate particle mass, m_0, and the Planck mass, m_u:

$$\frac{\text{proper time}}{\text{coordinate time}} = \frac{m_0}{m_u} = \alpha^{-1}\frac{\mu_0 e^2 c}{2h}\frac{\sqrt{\frac{Gm_0}{\lambda\!\!\!^{-}_C}}}{c} = \alpha^{-1}\frac{\mu_0 e^2 c}{2h}\sqrt{\frac{Gm_0}{c^2 \lambda\!\!\!^{-}_C}} = \alpha^{-1}\frac{\mu_0 e^2 c}{2h}\frac{v_G}{c} = \frac{v_G}{c} \tag{33.42}$$

As fundamental particles, atoms, molecules, and macroscopic configurations of fundamental particles, atoms, and molecules release energy, spacetime increases. The superposition of expanding spacetime arising at the atomic level over all scales of dimensions from the atomic to the cosmological gives rise to the observed expanding Universe. The wavefront of energy and spacetime from matter to energy conversion travel at the speed of light. Consider Eq. (32.43). As given in the Gravity section, at the present time in the cycle of the Universe, the world line of the expanding spacetime and the released energy are approximately coincident. In terms of Eq. (32.38), the proper time and the coordinate time are approximately equal. The ratio of the gravitational radius, r_g, given by Eq. (32.36), and the radius of the Universe are about equal to one and the gravitational escape velocity given by Eq. (32.35) is the speed of light. And, Q, (Eq. (32.140)) is equal to the matter to energy conversion rate of the time harmonic expansion-contraction cycle of the Universe which permits light energy (photons) to propagate (escape the gravitational hole of the Universe).

When the gravitational radius r_g is the radius of the Universe, the proper time is equal to the coordinate time (Eq. (31.43)), and the gravitational escape velocity v_g of the Universe is the speed of light.

Mass-energy must be conserved during the harmonic cycle of expansion and contraction. The gravitational potential energy E_{grav} of the Universe follows that given by Eq. (32.26).

$$E_{grav} = \frac{Gm_U^2}{r} \tag{33.43}$$

In the case that the radius of the Universe *r* is the gravitational radius r_G given by Eq. (32.22), the gravitational potential energy is equal to $m_U c^2$ which follows that given by Eq. (32.27). The gravitational velocity v_G is given by Eq. (32.33) wherein an electromagnetic wave of mass-energy equivalent to the mass of the Universe travels in a circular orbit wherein the eccentricity is equal to zero (Eq. (35.21)), and the escape velocity from the Universe can never be reached. The wavelength of the oscillation of the Universe and the wavelength corresponding to the gravitational radius r_G must be equal. Electromagnetic energy and gravitational mass obey superposition, and both spacetime expansion/contraction and electromagnetic energy corresponding to particle decay/production travel at the speed of light and obey the wave relationship given by Eq. (29.4). The wavelength is given in terms of the radius by Eq. (2.2). Thus, ***the harmonic oscillation period***, *T*, is:

$$T = \frac{2\pi r_G}{c} = \frac{2\pi G m_U}{c^3} = \frac{2\pi G\left(2\ X\ 10^{54}\ kg\right)}{c^3} = \ 3.10\ X\ 10^{19}\ \text{sec}\ = 9.83\ X\ 10^{11}\ \text{years} \tag{33.44}$$

where the mass of the Universe, m_U .

WAVE EQUATION

The equation

$$\frac{1}{c^2}\frac{\partial^2 \omega}{\partial t^2} - grad^2 \omega = 0 \tag{33.45}$$

acquires a general character; it is more general than Maxwell's equations from which Maxwell originally derived it. As a consequence of the principle of the existence of a universal limiting velocity one can assert the following: the differential equations describing any field that is capable of transmitting signals must be of such a kind that the equation of their characteristics is the same as the equation for the characteristics of light waves. In addition to governing the propagation of any form of energy, the wave equation governs fundamental particles created from energy and vice versa, the associated effects of mass on spacetime, and the evolution the Universe itself. The equation that describes the rotational motion of the charge-density wave of the electron given by Eqs. (1.56-1.65) is the wave equation, the relativistic correction of spacetime due to particle production travels according to the wave equation as given in the Gravity section, and the evolution of the Universe is according to the wave equation. The speed of light is the conversion factor from time to distance. Thus, the equation of the radius of the Universe, $\aleph$, (Eq. (33.31)) may be written as:

$$\aleph = \left(\frac{2Gm_U}{c^2} + \frac{cm_U}{\frac{c^3}{4\pi G}}\right) - \frac{cm_U}{\frac{c^3}{4\pi G}}\ \cos\left(\frac{2\pi}{\frac{2\pi G m_U}{c^3}\ \text{sec}}\left(t - \frac{\aleph}{c}\right)\right) \tag{33.46}$$

which is a solution to the wave equation.

REFERENCES

1. M. Tegmark, "On the dimensionality of spacetime," Class. Quantum Grav., Vol. 14, (1997), pp. L69-L75.
2. E. Giannetto, The rise of special relativity: Henri Poincaré's works before Einstein. Atti del 18 Congresso di Storia della Fisica e dell'Astronomia, (1998), pp. 171-207, [http://www.brera.unimi.it/old/Atti-Como-98/Giannetto.pdf].
3. H. Poincaré, "L'etat actuel et l'avenir de la physique mathematique," *Bulletin des sciences mathematiques*, Vol. 28, (1904), pp.302-324; quoted in Whittaker (1987), p. 30.
4. E. Whittaker, *A History of the Theories of Aether and Electricity*, Vol. 2, Modern Theories, Chapter 2, "The Relativity Theories of Poincaré and Lorentz," Nelson, London, (1987), Reprinted, American Institute of Physics, pp. 30–31.
5. A. Beiser, *Concepts of Modern Physics*, Fourth Edition, McGraw-Hill Book Company, New York, (1978), pp. 27-30.
6. J. D. Jackson, *Classical Electrodynamics*, Second Edition, John Wiley & Sons, New York, (1975), pp. 525-532.
7. J. D. Jackson, *Classical Electrodynamics*, Second Edition, John Wiley & Sons, New York, (1975), pp. 758-763.

Chapter 34

EQUIVALENCE OF INERTIAL AND GRAVITATIONAL MASSES DUE TO ABSOLUTE SPACE AND ABSOLUTE LIGHT VELOCITY

NEWTON'S ABSOLUTE SPACE WAS ABANDONED BY SPECIAL RELATIVITY BECAUSE ITS NATURE WAS UNKNOWN

Maxwell's electrodynamic equations predict electromagnetic waves and their propagation velocity of the speed of light c that is determined by the permittivity ε_0 and permeability μ_0 of free space such that

$$c = 1/\sqrt{\varepsilon_0 \mu_0} \tag{34.1}$$

Thus, if these spacetime properties were independent of the motion of emitters and observers, then, the speed of light is a constant. This result was proven by the Michelson-Morley experiment in 1887. The covariance or invariance of form of Maxwell's electrodynamic equations under Lorentz transformations was shown by Lorentz and Poincaré before the formulation of special relativity. The various parameters ρ, $\mathbf{J}$, $\mathbf{E}$, and $\mathbf{B}$ that are operated on in these equations transform in well-defined ways under Lorentz transformations such that the laws of electricity, magnetism, and electrodynamics have the same form independent of relative constant motion of observers. In 1904 [1-4], Poincaré achieved the similar covariance of the equations of Newton's laws of mechanics under Lorentz transformation of the corresponding spatial-temporal and mechanical parameters with the invention of special relativity based on his two postulates [1]:

> The principle of relativity, according to which the laws of physical phenomena should be the same, whether for an observer fixed, or for an observer carried along in a uniform movement of translation; so that we have not and could not have any means of discerning whether or not we are carried along in such a motion.
>
> From all these results, if they are confirmed, would arise an entirely new mechanics, which would be, above all, characterized by this fact, that no velocity could surpass that of light. Poincaré added that consistency of the descriptions of different inertial reference frames implies that the limiting light velocity is invariant for inertial reference frames.

Poincaré recognized that the inertia of material bodies would become infinite when one approached the velocity of light and predicted the relationship of matter to energy: $E = mc^2$ [2]. He further pointed out that all forces must propagate with the finite light velocity, that interaction implies a time delay, and it is mediated by field waves. Thus, Poincaré made for the first time the hypothesis of the existence of gravitational waves [1]. He and others who worked on special relativity developed the principles and mathematics to make the laws of nature covariant, correctly modeled the propagation of light, particles, and forces including the gravitational force, and recognized the relationship between matter and energy. But, they did not realize or even consider the nature of the gravitational force or the relationship between matter-energy and spacetime. Nor, did they consider the implications of relativity as a description of the physical nature of spacetime. Relativity was developed for a Universe that was empty (devoid of matter and light) and infinite in extent. Yet, the Universe is not only filled with matter and light, it is also dynamic in the conversion of matter to light. Furthermore, it is finite rather than infinite, and its size is also dynamic and determined by the inter-conversion of matter to energy as shown in the Gravity section.

Shortcomings, problems, and paradoxes arise with special relativity. Since relativity is simply a set of postulates and mathematical rules for transformation of coordinates and mechanical parameters, it provides no physical basis for the conversion of matter into energy, the absolute loss of time in experiments such as those regarding the twin paradox, the equivalence of the inertial and gravitational masses, the masses of fundamental particles, and the limiting velocity c for the propagation of matter in the same sense that Maxwell's equations do for electromagnetic-waves in terms like Eq. (34.1). Furthermore, the basis of

defining an inertial frame of reference based on relative motion ignores the kinetic energy of the objects in motion. Indeed, the potential for an infinite number of Universes with total kinetic energies from zero to infinities of infinite energy are all equally permissible. For example, a single celestial object could be translating at say $0.99999c$ relative to the balance of the objects of the Universe, or all of the celestial objects of the Universe could be translating at $0.99999c$ relative to the single object. In terms of special relativity, both situations are equivalent, simultaneously. But the *kinetic energy inventory and mass-energy inventory is not conserved* between the two cases. By selecting different inertial frames that are all equivalent under special relativity, the energy in the former case with 10^{23} objects weighing a total of $2\ X\ 10^{54}\ kg$ is:

$$E = \sum_{i=2}^{10^{23}} m_i c^2 + m_1 c^2 = \sum_{i=2}^{10^{23}} m_{0i} c^2 + \frac{m_{01} c^2}{\sqrt{1 - \left(\frac{0.99999c}{c}\right)^2}} \tag{34.2}$$

And, in the latter case the energy is:

$$E = \sum_{i=2}^{10^{23}} m_i c^2 + m_1 c^2 = \sum_{i=2}^{10^{23}} \frac{m_{0i} c^2}{\sqrt{1 - \left(\frac{0.99999c}{c}\right)^2}} + m_{01} c^2 \tag{34.3}$$

corresponding to essentially zero kinetic energy in the first case compared to the equivalent of over two hundred times the rest mass of the Universe mass or $(223.6)\left(2\ X\ 10^{54}\ kg\right)c^2 = 4.02\ X\ 10^{73}\ J$ in the latter case!

The obvious question is how can the mass-energy of the Universe be increased up to arbitrary orders of magnitude by simply selecting an inertial frame? The set of equivalent inertial frames extends over an infinite range of kinetic energies relative to even one body for example. Since the Universe is finite and closed, and matter, energy, and spacetime are conserved these infinite possibilities for equivalent inertial frames for the Universe with its unique inventories is untenable[1]. The frames of reference regarding relative uniform motion are only convenient means to compare measurements in those frames when absolute values are not important in the determination, and it is not necessary to determine the relative rank of the frames (e.g. the stationary versus the moving one). These conditions may break down, and paradoxes arise that can only be resolved by abandoning the simplified frames of special relativity and invoking an absolute frame of reference.

Specifically, in addition to the lack of energy conservation and physical mechanism for many of its consequences, another problem that arises is the inability to determine which body is in motion when comparing relative motion in order to arrive at consistent predictions. The limitation in uniquely and unequivocally identifying inertial frames centrally impacts the ability to interpret and apply special relativity. This is particularly acute when objects initially in the same inertial frame separate and rejoin. A famous example is the case of the twin paradox. Here two twins separate and are rejoined with intervening periods of acceleration and reversal of physical displacement. A failure of special relativity is that upon rejoining the traveling twin is younger relative to the stationary twin in contradiction to his expectations since to him, it is the stationary twin who had been in motion. Although strained "resolutions" to the asymmetrical time dilation of the traveling twin have been put forward including a far-fetched one by Einstein regarding gravitational time dilation of the general relativity theory, none are tenable [5]. The fundamental impasse is inherent in the consideration that motion is arbitrarily relative. There must be an absolute frame for each object in order to conserve the mass/energy inventory of the Universe as well as resolve paradoxes such as the twin paradox.

To develop an understanding of spacetime that is described by relativity and to correct its deficiencies, it is insightful to consider the history of the laws of mechanics starting with Newton. The second law is represented by:

$$\mathbf{F} = \frac{d\mathbf{p}}{dt} = \frac{d(m\mathbf{v})}{dt} = m\frac{d\mathbf{v}}{dt} = m\mathbf{a} \tag{34.4}$$

where m is the mass of the body, $\mathbf{a}$ is its acceleration relative to a certain frame of reference, and $\mathbf{F}$ is the resultant force acting on the body due to all other bodies that apply the force. Newton's laws are valid in frames of reference called inertial frames, moving relative to each other with uniform velocities. Experimentally, the laws of physics are the same in all such inertial frames which provides a means to identify a frame as inertial. By this criterion, inertial frames are unaccelerating and nonrotating. Otherwise, all objects would be accelerating or rotating relative to some other frame. Such a reference frame must exist for all cases. Newton introduced the concept of absolute space to provide such an absolute frame for acceleration and rotation as well as uniform motion. According to Newton, acceleration and rotation relative to absolute space are detected by simple experiments. For example, an observer accelerated relative to the Earth sees the Earth accelerate in the opposite direction. Since there is no force acting on the Earth, the apparent acceleration is not a consequence of the Newton's second law, rather it is due to the acceleration of the observer relative to absolute space. Another example is rotation wherein the object rotating relative to absolute space can be identified by the measurement of centrifugal forces. Thus, it can be appreciated that observations consistent with physical laws permit identifying acceleration and rotation relative to absolute space, but consequences of the forces of acceleration or rotation cannot be used to determine an absolute frame for two bodies in uniform

[1] Einstein's interpretation of relativity predicts the existence of "parallel universes" each with a different energy inventory based on measurement as basis of reality and eliminates inertial mass and Newton's Second Law. This consequence may be considered the origin of the misguided interpretation of reality in terms of an observer's measurement. This philosophy originally from Mach evolved into quantum mechanics theory with its inherent uncertainty principle involving simultaneity of infinite states for a single particle with a "collapse" into a single state with measurement. Thus, single-valued exact properties were deemed impossibilities due to perturbations with measurement, and the development of the theory became a discourse regarding measurement.

motion. Although Newton could give the criterion for absolute acceleration and absolute rotation, he could not do so for absolute velocity. Locally, motion can only be defined as relative. So, it seems impossible to define an absolute frame, and in particular, the absolute frame at rest could not be identified. Newton's absolute space was abandoned by special relativity due to this limitation of being unable to reference an inertial frame in an absolute sense. However, this inability to identify or understand the nature of absolute space and an absolute frame at rest should not be confused with the lack of their existence and the consequences for the nature of spacetime, matter, and energy.

The relativity principle is postulated on the basis of the impossibility of measuring absolute velocity. This assumption is incorrect. Absolute space can be defined based on the solution of the exact conserved relationships between matter, energy, and spacetime given in the Gravity section. Specifically, the production of an isolated particle from a photon of identically the production energy defines the absolute inertial frame at rest for the particle and could, in principle, define absolute space that conserves the energy inventory of the Universe and resolves paradoxes such as the twin paradox. The rate at which ones clock is ticking can be determined in terms of the absolute time unit defined in the Gravity section as the "sec" of each particle. It is possible as discussed *infra.* to slow the clock of an object by expending energy to increase its velocity with a consequent and concomitant acceleration of the clocks of parts of the object's surroundings such that the absolute time of the Universe is conserved overall.

A relativity principle based only on frames in uniform motion excludes all of the dynamic properties of the Universe. And, no two independent objects can maintain infinitely exact constant relative motion. Furthermore, matter is dynamic, either gaining or losing energy with changing velocities and directions, and, all of the matter in the Universe is accelerating as spacetime expands. The physics of essentially all forms of motion of matter including acceleration, rotation, and motion of any type in a gravitational field[2] cannot be dealt with within the context of relative space. However, even though any motion, or parameter of inertia or electromagnetism can ultimately be measured in principle (but perhaps not always in practice) relative to absolute space as discussed *infra*., a principle of relativity based on physical laws can be derived that has great utility. The principle of relativity given next treats relative uniform rectilinear motion, and the transforms of relativity are Lorentzian[3].

Since the constant speed of light is the absolute limiting conversion factor from time to length, it is reasonable to expect that the laws of light propagation play a fundamental part in the definition of the basic concepts relating to space and time in terms of inertial frames defined according to uniform relative motion. Therefore it proves more correct to relate the notion of an inertial frame not only to the laws of mechanics but also to those of light propagation as given in the Relativity section.

The usual form of Maxwell's equations refers to some inertial frame. It is obvious and has always been assumed, even before relativity, that at least one reference frame exists that is inertial with respect to mechanics and in which at the same time Maxwell's equations are true. The law of propagation of an electromagnetic wave front in the form of:

$$\frac{1}{c^2}\left(\frac{\partial^2\omega}{\partial t^2}\right)-\left[\left(\frac{\partial^2\omega}{\partial x^2}\right)+\left(\frac{\partial^2\omega}{\partial y^2}\right)+\left(\frac{\partial^2\omega}{\partial z^2}\right)\right]=0 \tag{34.5}$$

also refers to this inertial frame. A frame for which Eq. (34.5) is valid may be called inertial in the electromagnetic sense. A frame that is inertial both in the mechanical and in the electromagnetic senses will be simply called inertial. Thus, by the definition we have adopted, an inertial frame is characterized by the following two properties:

1. In an inertial frame, a body moves uniformly and in a straight line, provided no forces act on it. (The usual mechanical inertial property.)

2. In an inertial frame, the equation of propagation of an electromagnetic wave front has the form Eq. (34.5). (The inertial property for the field.)

Eq. (34.5) applies not only to the propagation of an electromagnetic wave. The electromagnetic field has no preference over other fields. The maximum speed of propagation of all fields must be the same such that Eq. (34.5) is of universal validity.

The fundamental postulate of the theory of relativity, also called the principle of relativity, asserts that phenomena occurring in a closed system are independent of any non-accelerated motion of the system as a whole. The principle of relativity asserts that the two sequences of events will be exactly the same (at least insofar as they are determined at all). If a process in the original systems can be described in terms of certain functions of the space and time coordinates of the first frame, the same functions of the space and time coordinates of the second frame will describe a process occurring in the copy. *The uniform rectilinear motion of a material system as a whole has no influence on the course of any process occurring within it.*

The theory of relativity is based on two postulates, namely, the principle of relativity and another principle that states that the velocity of light is independent of the velocity of its source. The latter principle is a consequence of the first. The latter principle is implicit in the law of the propagation of an electromagnetic wave front given by Eq. (34.5). The basis for defining inertial reference frames is Eq. (34.5) together with the fact of the uniform rectilinear motion of a body not subject to forces. The principle of relativity holds in the case that the reference frames are inertial.

---

[2] Another mistake regarding relativity was made by Einstein in the consideration of the extension of relativity to accelerating frames with the postulate of the equivalence of a uniform gravitational field and an accelerating frame. As shown in the Gravity section, in addition to being physically flawed, Einstein's version of general relativity is disproved experimentally with the observation that the expansion of the cosmos is accelerating in contradiction with the predictions of decelerating cosmologies by all solutions of Einstein's equations.

[3] Ironically, some of the most cited experimental validations of special relativity such as the dilation of the half-life of particles such as muons moving at near light speed in cyclotrons involve constant acceleration in the storage ring rather than constant uniform rectilinear motion.

It is appropriate to give a generalized interpretation of the law of wave front propagation and to formulate the following general postulate:

There exists a maximum speed for the propagation of any kind of action—the speed of light in free space.

This principle is very significant because the transmission of signals with greatest possible speed plays a fundamental part in the definition of concepts concerning space and time. The very notion of a definite frame of reference for describing events in space and time depends on the existence of such signals. The principle formulated above, by asserting the existence of a general upper limit for all kinds of action and signal, endows the speed of light with a universal significance, independent of the particular properties of the agency of transmission and reflecting a certain objective property of spacetime. This principle has a logical connection with the principle of relativity. For if there was no single limiting velocity, but instead different agents, e.g. light and gravitation, propagated in vacuum with different speeds, then the principle of relativity would necessarily be violated as regards at least one of the agents. The principle of the universal limiting velocity can be made mathematically precise as follows:

For any kind of wave advancing with limiting velocity and capable of transmitting signals, the equation of front propagation is the same as the equation for the front of a light wave.

Thus, the equation:

$$\frac{1}{c^2}\left(\frac{\partial^2\omega}{\partial t^2}\right)-\left(grad^2\omega\right)=0 \tag{34.6}$$

acquires a general character; it is more general than Maxwell's equations from which Maxwell originally derived it. As a consequence of the principle of the existence of a universal limiting velocity one can assert the following: the differential equations describing any field that is capable of transmitting signals must be of such a kind that the equation of their characteristics is the same as the equation for the characteristics of light waves. In addition to governing the propagation of any form of energy, the wave equation governs fundamental particles created from energy and vice versa, the associated effects of mass on spacetime, and the evolution of the Universe itself. Specially, the equation that describes the electron dynamics of the rotational energy and angular momentum with $\ell \neq 0$ given by Eqs. (1.56-1.65) is the wave equation, the relativistic correction of spacetime due to particle production travels according to the wave equation as given in the Gravity section, and the evolution of the Universe is according to the wave equation as given in the Gravity section and the Unification of Spacetime, the Forces, Matter, and Energy section (Eqs. (33.45-33.46)).

RELATIONSHIP OF THE PROPERTIES OF SPACETIME AND THE PHOTON TO THE INERTIAL AND GRAVITATIONAL MASSES

LORENTZ TRANSFORMS BASED ON CONSTANT RELATIVE VELOCITY

The magnetic force was unified with the Coulombic force by Maxwell. Lorentz derived the transformations named after him which formalize the origin of the magnetic force as a relativistic correction of the Coulomb force. The unification of electricity and magnetism by Maxwell permitted him to derive a wave equation, which predicted the propagation of electromagnetic waves at the speed of light (Eq. (34.1)). Maxwell's wave equation defines a four-dimensional spacetime with the speed of light as a maximum permitted according to the permeability and permittivity of spacetime. Minkowski originated the concept of a four-dimensional spacetime formally expressed as the Minkowski tensor [6]. The Minkowski tensor corresponds to the electromagnetic wave equation derived by Maxwell and can be derived from it [7]. Special relativity is implicit in the wave equation of electromagnetic waves that travel at the speed of light. The generalization of this metric to mass as well as charge requiring application of Lorentz transformations to relative parameters comprises the theory of special relativity. The Lorentz transformations quantify the measurement of the increase in mass, length contraction, and time dilation in the direction of constant relative motion of separate inertial frames due to the finite maximum speed of light.

Using the principle that light velocity is the constant maximum c in all inertial frames, the relationships between distances in two frames with one moving a constant velocity relative to the other are shown in the Relativity section to be [8] :

$$\left(c\frac{t}{2}\right)^2=L_0^2+\left(v\frac{t}{2}\right)^2 \tag{34.7}$$

$$t=\frac{\frac{2L_0}{c}}{\sqrt{1-\frac{v^2}{c^2}}} \tag{34.8}$$

$$t=\frac{t_0}{\sqrt{1-\frac{v^2}{c^2}}} \tag{34.9}$$

The Lorentz transformation of the other spatial-temporal and mechanical parameters that maintain the covariance of mechanical laws gives the following relationships between the parameters of inertial frames [8]:

$$l = l_0\sqrt{1-\frac{v^2}{c^2}} \tag{34.10}$$

$$m = \frac{m_0}{\sqrt{1-\frac{v^2}{c^2}}} \tag{34.11}$$

$$p = \frac{m_0 v}{\sqrt{1-\frac{v^2}{c^2}}} \tag{34.12}$$

Using the Lorentz transformation of the energy of particle production given by Eq. (34.49) gives:

$$E = mc^2 = \frac{m_0 c^2}{\sqrt{1-\frac{v^2}{c^2}}} \tag{34.13}$$

Squaring the energy given in Eq. (34.13) gives:

$$E^2 = \frac{m_0^2 c^4}{1-\frac{v^2}{c^2}} \tag{34.14}$$

The square of the Lorentz momentum given by Eq. (34.12) multiplied by c^2 is:

$$p^2c^2 = \frac{m_0^2 v^2 c^2}{1-\frac{v^2}{c^2}} \tag{34.15}$$

Subtracting p^2c^2 from E^2 gives:

$$E^2 - p^2c^2 = \frac{m_0^2c^4 - m_0^2v^2c^2}{1-\frac{v^2}{c^2}} = \frac{m_0^2c^4\left(1-\frac{v^2}{c^2}\right)}{1-\frac{v^2}{c^2}} = m_0^2c^4 \tag{34.16}$$

Thus,

$$E^2 = m_0^2c^4 + p^2c^2 \tag{34.17}$$

MINKOWSKI SPACE

When speaking of the relativity of a frame of reference or simply of relativity, one usually means that there exist identical physical processes in different frames of reference. According to the generalized Galilean principle of relativity, identical processes are possible in all inertial frames of reference related by Lorentz transformations. On the other hand, Lorentz transformations characterize the uniformity of Galilean spacetime. Using the four-dimensional coordinates x^μ for describing the events and the world-line in spacetime the separation of proper time between two events x^μ and $x^\mu + dx^\mu$ is:

$$d\tau^2 = -g_{\mu\nu}dx^\mu dx^\nu \tag{34.18}$$

where $g_{\mu\nu}$ is the metric tensor which determines the geometric character of spacetime. For different coordinate systems, the dx^μ may not be the same, but the separation $d\tau^2$ remains unchanged. The metric $g_{\mu\nu}$ for Euclidean space called the Minkowski tensor $\eta_{\mu\nu}$ is:

$$\eta_{\mu\nu} = \begin{pmatrix} -1 & 0 & 0 & 0 \\ 0 & \frac{1}{c^2} & 0 & 0 \\ 0 & 0 & \frac{1}{c^2} & 0 \\ 0 & 0 & 0 & \frac{1}{c^2} \end{pmatrix} \tag{34.19}$$

In this case, the separation of proper time between two events x^μ and $x^\mu + dx^\mu$ is:

$$d\tau^2 = -\eta_{\mu\nu}dx^\mu dx^\nu \tag{34.20}$$

Relativity deals with definitions and tensor mathematics in space devoid of matter. To cast relative measurements for

bodies in relative motion in physical terms, the relationships of matter to spacetime and spacetime to matter must be included.

ORIGIN OF GRAVITY WITH PARTICLE PRODUCTION

Gravity is not a force separable from electromagnetism. The production of a particle having an inertial mass and a gravitational mass from a photon initially traveling at the speed of light requires time dilation and length contraction of spacetime itself as opposed to the relativistic correction of mass, length, and time of objects of inertial frames in constant relative motion. The derivation of the gravity equations and the inherent masses of particles maintains the relativity principle of Eq. (34.6): the constant maximum speed of light for the propagation of light and gravity wave fronts. The gravity metric corresponding to spacetime time dilation and length contraction due to the production event is derived with the boundary conditions: (i) the speed of light is constant and a maximum, (ii) the angular momentum of a photon, $\hbar$, is conserved, and (iii) the energy of the photon is conserved as mass. The event must be spacelike even though the photon of the particle production event travels at the speed of light and the particle must travel at a velocity less than the speed of light. The relativistically altered spacetime gives rise to a gravitational force between separated masses. Thus, the production of matter and its motion alters spacetime, and the altered spacetime affects the motion of matter, which must follow geodesics. The spacetime contraction and time dilation derivation based on the same principle as special relativity has a similar form as that of its Lorentz transformations relating observations from different inertial frames of reference.

SCHWARZSCHILD SPACE AND LORENTZ-TYPE TRANSFORMS BASED ON THE GRAVITATIONAL VELOCITY AT PARTICLE PRODUCTION

A spherically symmetrical system of mass m_0 applies to the production of a particle which implies spherical coordinates with the origin at 0. Thus, a family of curved surfaces, each with constant r, is a series of concentric spheres on which it is natural to adopt the coordinate r so that a sphere with constant r has area $4\pi r^2$, and the metric on the surface of the sphere would then be

$$ds^2 = r^2 d\theta^2 + r^2 \sin^2\theta d\phi^2 \tag{34.21}$$

Such a definition of r is no longer the distance from the origin to the surface, because of the spacetime contraction caused by the mass m_0. The form of the outgoing gravitational field front traveling at the speed of light is:

$$f\left(t - \frac{r}{c}\right) \tag{34.22}$$

Therefore the spatial metric should be expressed as:

$$ds^2 = f(r)^{-1} dr^2 + r^2 d\theta^2 + r^2 \sin^2\theta d\phi^2 \tag{34.23}$$

In addition, **the existence of mass m_0 also causes time dilation and length contraction of spacetime** such that the clock on each r-sphere is no longer observed from each r-sphere to run at the same rate. That is, clocks slow down in a gravitational field [9]. Therefore, the general form of the metric due to the relativistic effect on spacetime due to mass m_0 is

$$d\tau^2 = f(r)dt^2 - \frac{1}{c^2}\left[f(r)^{-1} dr^2 + r^2 d\theta^2 + r^2 \sin^2\theta d\phi^2 \right] \tag{34.24}$$

In the case where $m_0 = 0$, space would be flat which corresponds to:

$$f(r) = f(r)^{-1} = 1 \tag{34.25}$$

Then the spacetime metric is the Minkowski tensor. In the case that the mass m_0 is finite, the Minkowski tensor is corrected by the time dilation and length contraction of spacetime.

The photon initially traveling at the speed of light undergoes particle production and must produce a gravitational field that travels at the speed of light. According to Newton's Law of Gravitation, the particle must have a finite velocity relative to the antiparticle called the Newtonian gravitational velocity, v_g, (Eq. (32.35)) that may not exceed the speed of light and has an associated gravitational energy given in the Gravity section. The eccentricity is one (Eqs. (35.17-35.22)), the total energy is zero, and the particle production trajectory is a parabola relative to the center of mass of the antiparticle. In order that the velocity of light does not exceed c in any frame including that of the particle having a finite Newtonian gravitational velocity, v_g, the laboratory frame of an incident photon, and that of a gravitational field propagating outward at the speed of light, spacetime must undergo time dilation and length contraction due to the production event. During particle production the speed of light as a constant maximum as well as phase matching and continuity conditions require the following form of the squared displacements due to constant motion along two orthogonal axes in polar coordinates:

$$(c\tau)^2 + (v_g t)^2 = (ct)^2 \tag{34.26}$$

$$\tau^2 = t^2\left(1-\left(\frac{v_g}{c}\right)^2\right) \tag{34.27}$$

Thus,

$$f(r) = \left(1-\left(\frac{v_g}{c}\right)^2\right) \tag{34.28}$$

The derivation and result of spacetime time dilation is analogous to the derivation and result of special relativistic time dilation given by Eqs. (31.11-31.15) wherein the gravitational velocity replaces the relative velocity of two inertial frames in the Lorentz factor. The general form of the metric due to the relativistic effect on spacetime due to mass m_0 is:

$$d\tau^2 = \left(1-\left(\frac{v_g}{c}\right)^2\right)dt^2 - \frac{1}{c^2}\left[\left(1-\left(\frac{v_g}{c}\right)^2\right)^{-1} dr^2 + r^2 d\theta^2 + r^2\sin^2\theta d\phi^2\right] \tag{34.29}$$

The equivalence of the gravitational and inertial masses, according to experiments and Eqs. (34.49) and (34.67-34.68), prove that Newton's Gravitational Law is exact on a local scale. The correction to Newton's Gravitational Law due to the relativistic effect of the presence of mass on spacetime may be determined by substitution of the gravitational escape velocity, v_g, given by:

$$v_g = \sqrt{\frac{2Gm_0}{r}} = \sqrt{\frac{2Gm_0}{\lambda\!\!\!^{-}_C}} \tag{34.30}$$

into Eq. (34.29) for v_g. The corresponding Newtonian gravitational radius is given by [10]:

$$r_g = \frac{2Gm_0}{c^2} \tag{34.31}$$

Thus, Eq. (34.29) can also be expressed as:

$$d\tau^2 = \left(1-\frac{r_g}{r}\right)dt^2 - \frac{1}{c^2}\left[\left(1-\frac{r_g}{r}\right)^{-1} dr^2 + r^2 d\theta^2 + r^2\sin^2\theta d\phi^2\right] \tag{34.32}$$

In the case of the boundary conditions of Eqs. (34.48-34.49), Eq. (34.30) and Eq. (34.31), three families of leptons and quarks are predicted in the corresponding sections wherein each particle corresponds to a unique atomic orbital radius equal to its Compton wavelength bar. At particle production, a photon having a radius and a wavelength equal to the Compton wavelength bar of the particle forms a transition state atomic orbital of the particle of the same wavelength.

$$r = \lambda\!\!\!^{-}_C = \frac{\hbar}{mc} = r_\alpha^* \tag{34.33}$$

The resulting metric $g_{\mu\nu}$ for non-Euclidean space due to the relativistic effect on spacetime due to mass m_0 with v_g given by Eq. (34.30) is

$$g_{\mu\nu} = \begin{pmatrix} -\left(1-\frac{2Gm_0}{c^2 r}\right) & 0 & 0 & 0 \\ 0 & \frac{1}{c^2}\left(1-\frac{2Gm_0}{c^2 r}\right)^{-1} & 0 & 0 \\ 0 & 0 & \frac{1}{c^2}r^2 & 0 \\ 0 & 0 & 0 & \frac{1}{c^2}r^2\sin^2\theta \end{pmatrix} \tag{34.34}$$

In this case, the separation of proper time between two events x^μ and $x^\mu + dx^\mu$ is:

$$d\tau^2 = \left(1-\frac{2Gm_0}{c^2 r}\right)dt^2 - \frac{1}{c^2}\left[\left(1-\frac{2Gm_0}{c^2 r}\right)^{-1} dr^2 + r^2 d\theta^2 + r^2\sin^2\theta d\phi^2\right] \tag{34.35}$$

The *Schwarzschild-type metric (Eq. (34.35)) gives the relationship whereby matter causes relativistic corrections to spacetime that determines the curvature of spacetime and is the origin of gravity.*

The origin of gravity is fundamental particles, and the masses and fields from particles superimpose. So, m_0, the mass of a

fundamental particle, may be replaced by M, the sum of the masses of the particles which make up a massive body. In this case, Eq. (34.35) is equivalent to a modified version of the Schwarzschild metric that is conservative of matter, energy, and spacetime and lacking the reduced radial coordinate, $r - \frac{GM}{c^2}$, and singularity issues of general relativity.

The Schwarzschild metric provides transforms of the spacetime and mass-energy parameters based on the effect of gravity in an analogous manner as the Minkowski tensor provides the Lorentz transforms for the corresponding inertial parameters. As shown in Eq. (32.70), the relativistic correction for time is:

$$t = \frac{\tau}{\sqrt{1 - \frac{v_g^2}{c^2}}} \tag{34.36}$$

Then,

$$l = l_o \sqrt{1 - \frac{v_g^2}{c^2}} \tag{34.37}$$

The spacetime corrections have the same form as the special relativistic corrections for time and length with v_g in place of v. Consider the relationship between proper and coordinate mass derived in the Gravity section by considering an object of mass m orbiting an object of mass M. The gravitational force is central; thus the angular momentum is constant. Consider that a radial force is applied to increase the radius r of the object's orbit with a change of its energy E. The angular momentum is conserved; thus,

$$m r_i^2 \left(\frac{d\phi}{dt} \right)_i = m r_f^2 \left(\frac{d\phi}{dt} \right)_f \tag{34.38}$$

where $\left(\frac{d\phi}{dt} \right)_i$ is the initial angular velocity, $\left(\frac{d\phi}{dt} \right)_f$ is the final angular velocity, r_i is the initial radius and r_f is the final radius. At fixed radius, dr^2 is zero, but dt^2 is finite. Applying the time relativistic correction given by Eq. (34.35) and Eqs. (34.26-34.28) gives the mass m_f at r_f with respect to the mass m_i of the inertial frame of r_i as:

$$m_i \sqrt{\left(1 - \frac{2GM}{rc^2} \right)} = m_f \tag{34.39}$$

where r is the increase in the radius. The proper energy E_p of the object is given by:

$$m_i c^2 \sqrt{\left(1 - \frac{2GM}{rc^2} \right)} = E_p \tag{34.40}$$

The relativistic correction for energy is of the same form as the special relativistic correction for mass (Eq. (31.21)) with v_g in place of v.

$$\frac{E_p}{\sqrt{1 - \left(\frac{v_g}{c} \right)^2}} = mc^2 \tag{34.41}$$

where m is the coordinate mass of the orbiting body and E is the energy of the orbiting object. In the case that the gravitational velocity is much less than the speed of light ($v_g << c$), the gravitational energy E_g converges to that given by Newton's law of Gravitation.

$$E_p \approx mc^2 \left(1 - \frac{1}{2} \left(\frac{2GM}{rc^2} \right) \right) \tag{34.42}$$

$$E_p \approx mc^2 - \frac{GMm}{r} \tag{34.43}$$

$$E_g = -\frac{GMm}{r} \tag{34.44}$$

PARTICLE PRODUCTION CONTINUITY CONDITIONS FROM MAXWELL'S EQUATIONS, AND THE SCHWARZSCHILD METRIC GIVE RISE TO CHARGE, MOMENTUM AND MASS

The photon possesses electric and magnetic fields and the corresponding energies and momentum. The angular momentum of the photon given by:

$$\mathbf{m} = \int \frac{1}{8\pi c} \mathrm{Re}\left[\mathbf{r} \times (\mathbf{E} \times \mathbf{B}^*)\right] dx^4 = \hbar \tag{34.45}$$

in the Photon section is conserved [11] during particle production. The energy due to the angular frequency of the photon according to Planck's equation and those of its electric and magnetic fields match those of the particle to which it gives rise. The transition state has dimensions of the particle's Compton wavelength bar such that the speed matches light speed at the photon's frequency as a further constraint of Maxwell's equations and the inherent special relativity. This limiting speed is set by the permittivity and permeability of spacetime. Spacetime undergoes time dilation and length contraction at the particle production event as a gravitation-field front propagates out as a light-wave front at light speed. The photon's effect on spacetime and spacetime's effect on the corresponding production particle then determine its inertial and gravitational mass m_0 and the fundamental charge e where the momentum and energies of the photon are continuous with those of the particle during the production event.

The photon to particle event requires a transition state that is continuous wherein the velocity of a transition state atomic orbital is the speed of light. The radius, r, is the Compton wavelength bar, $\lambda\!\!\!^{-}_C$, given by Eq. (34.33). At production, the Planck equation energy, the electric potential energy, and the magnetic energy are equal to $m_0 c^2$.

The Schwarzschild metric gives the relationship whereby matter causes relativistic corrections to spacetime that determines the masses of fundamental particles. Substitution of $r = \lambda\!\!\!^{-}_C$; $dr = 0$; $d\theta = 0$; $\sin^2\theta = 1$ into the Schwarzschild metric gives:

$$d\tau = dt\left(1 - \frac{2Gm_0}{c^2 r_\alpha^*} - \frac{v^2}{c^2}\right)^{\frac{1}{2}} \tag{34.46}$$

with $v^2 = c^2$, the relationship between the proper time and the coordinate time is:

$$\tau = ti\sqrt{\frac{2GM}{c^2 r_\alpha^*}} = ti\sqrt{\frac{2GM}{c^2 \lambda\!\!\!^{-}_c}} = ti\frac{v_g}{c} \tag{34.47}$$

When the atomic orbital velocity is the speed of light, continuity conditions based on the constant maximum speed of light given by Maxwell's equations are mass energy = Planck equation energy = electric potential energy = magnetic energy = mass/spacetime metric energy. Therefore,

$$m_o c^2 = \hbar\omega^* = V = E_{mag} = E_{spacetime} \tag{34.48}$$

$$m_0 c^2 = \hbar\omega^* = \frac{\hbar^2}{m_0 \lambda\!\!\!^{-2}_C} = \alpha^{-1}\frac{e^2}{4\pi\varepsilon_0 \lambda\!\!\!^{-}_C} = \alpha^{-1}\frac{\pi\mu_0 e^2\hbar^2}{\left(2\pi m_0\right)^2 \lambda\!\!\!^{-3}_C} = \frac{\alpha h}{1\ \mathrm{sec}}\sqrt{\frac{\lambda\!\!\!^{-}_C c^2}{2Gm}} \tag{34.49}$$

The continuity conditions based on the constant maximum speed of light given by the Schwarzschild metric are:

$$\frac{\text{proper time}}{\text{coordinate time}} = \frac{\text{gravitational wave condition}}{\text{electromagnetic wave condition}} = \frac{\text{gravitational mass phase matching}}{\text{charge/inertial mass phase matching}} \tag{34.50}$$

$$\frac{\text{proper time}}{\text{coordinate time}} = i\frac{\sqrt{\frac{2Gm}{c^2 \lambda\!\!\!^{-}_C}}}{\alpha} = i\frac{v_g}{\alpha c}$$

Each of the Planck equation energy, electric energy, and magnetic energy corresponds to a particle given by the relationship between the proper time and the coordinate time. The electron and down-down-up neutron correspond to the Planck equation energy. The muon and strange-strange-charmed neutron correspond to the electric energy. The tau and bottom-bottom-top neutron correspond to the magnetic energy. The particle must possess the escape velocity v_g relative to the antiparticle where $v_g < c$. According to Newton's law of gravitation, the eccentricity is one and the particle production trajectory is a parabola relative to the center of mass of the antiparticle. The masses of the three families of leptons and quarks are given in the corresponding sections. Exemplary relations between fundamental particles are shown in Table 34.1.

Table 34.1. The calculated relations between the lepton masses and neutron to electron mass ratio are given in terms of the dimensionless fine structure constant α only and compared to experimental values from the 1998 CODATA and the Particle Data Group given in parentheses [12-13].

$\frac{m_\mu}{m_e}=\left(\frac{\alpha^{-2}}{2\pi}\right)^{\frac{2}{3}}\frac{\left(1+2\pi\frac{\alpha^2}{2}\right)}{\left(1+\frac{\alpha}{2}\right)}=206.76828$	(206.76827)
$\frac{m_\tau}{m_\mu}=\left(\frac{\alpha^{-1}}{2}\right)^{\frac{2}{3}}\frac{\left(1+\frac{\alpha}{2}\right)}{\left(1-4\pi\alpha^2\right)}=16.817$	(16.817)
$\frac{m_\tau}{m_e}=\left(\frac{\alpha^{-3}}{4\pi}\right)^{\frac{2}{3}}\frac{\left(1+2\pi\frac{\alpha^2}{2}\right)}{\left(1-4\pi\alpha^2\right)}=3477.2$	(3477.3)
$\frac{m_N}{m_e}=\frac{12\pi^2}{1-\alpha}\sqrt{\frac{\sqrt{3}}{\alpha}}\frac{\left(1+2\pi\frac{\alpha^2}{2}\right)}{\left(1-2\pi\frac{\alpha^2}{2}\right)}=1838.67$	(1838.68)

Consider pair production. The proper time of the particle is equated with the coordinate time according to the Schwarzschild metric corresponding to light speed. The special relativistic condition corresponding to the Planck energy (Eq. (34.49)) gives the mass of the electron [12-13]:

$$2\pi\frac{\hbar}{mc^2}=\sec\sqrt{\frac{2Gm^2}{c\alpha^2\hbar}} \tag{34.51}$$

$$m_e=\left(\frac{h\alpha}{\sec c^2}\right)^{\frac{1}{2}}\left(\frac{c\hbar}{2G}\right)^{\frac{1}{4}}=9.0998\ X\ 10^{-31}\ kg \tag{34.52}$$

where $m_{e\ \text{experimental}}=9.10945455\ X\ 10^{-31}\ kg$. A clock is defined in terms of a self-consistent system of units used to measure the particle mass. Presently the second is defined as the time required for 9,192,631,770 vibrations within the cesium-133 atom. The "sec" as defined in Eqs. (34.49) and (34.51) is a fundamental constant, namely, the metric of spacetime (it is almost identically equal to the present value of the MKS second for reasons explained in the Gravity section). A unified theory can only provide the relationships between all measurable observables in terms of a clock defined in terms of fundamental constants according to those observables and used to measure them. The so *defined "clock" measures "clicks" on an observable in one aspect, and in another, it is the ruler of spacetime of the Universe with the implicit dependence of spacetime on matter-energy conversion* as shown in the Gravity and Relationship of Matter to Energy and Spacetime Expansion sections.

RELATIONSHIP OF MATTER TO ENERGY AND SPACETIME EXPANSION

The Schwarzschild metric gives the relationship whereby matter causes relativistic corrections to spacetime. The limiting velocity c results in the contraction of spacetime due to particle production, which is given by $2\pi r_g$ where r_g is the gravitational radius of the particle. This has implications for the expansion of spacetime when matter converts to energy. Q the mass/energy to expansion/contraction quotient of spacetime is given by the ratio of the mass of a particle at production divided by T, the period of production where:

$$Q = \frac{m_0}{T} = \frac{m_0}{\frac{2\pi r_g}{c}} = \frac{m_0}{\frac{2\pi \frac{2Gm_0}{c^2}}{c}} = \frac{c^3}{4\pi G} = 3.22\ X\ 10^{34}\ \frac{kg}{\sec} \tag{34.53}$$

The gravitational equations with the equivalence of the particle production energies (Eq. (34.49)) permit the conservation of mass/energy ($E = mc^2$) and spacetime ($\frac{c^3}{4\pi G} = 3.22\ X\ 10^{34}\ \frac{kg}{\sec}$). With the conversion of $3.22\ X\ 10^{34}$ *kg* of matter to energy, spacetime expands by 1 *sec*. The photon has inertial mass and angular momentum, but due to Maxwell's equations and the implicit special relativity it does not have a gravitational mass. The observed gravitational deflection of light is predicted as given in the Gravity section.

COSMOLOGICAL CONSEQUENCES

The Universe is closed (it is *finite but with no boundary*). It is a 3-sphere Universe-Riemannian three-dimensional hyperspace plus time of constant positive curvature at each r-sphere. The *Universe is oscillatory in matter/energy and spacetime* with a finite minimum radius, the gravitational radius. Spacetime expands as mass is released as energy which provides the basis of the *atomic, thermodynamic, and cosmological arrows of time*. Different regions of space are isothermal even though they are separated by greater distances than that over which light could travel during the time of the expansion of the Universe [14]. Presently, stars and large scale structures exist which are older than the elapsed time of the present expansion as stellar, galaxy, and supercluster evolution occurred during the contraction phase [15–21]. The maximum power radiated by the Universe, which occurs at the beginning of the expansion phase, is $P_U = \frac{c^5}{4\pi G} = 2.89\ X\ 10^{51}\ W$.

THE PERIOD OF OSCILLATION OF THE UNIVERSE BASED ON CLOSED PROPAGATION OF LIGHT

Mass/energy is conserved during harmonic expansion and contraction. The gravitational potential energy E_{grav} given by Eq. (32.148) with $m_0 = m_U$ is equal to $m_U c^2$ when the radius of the Universe r is the gravitational radius r_G (Eq. (32.22)). The gravitational velocity v_G (Eq. (32.33) with $r = r_G$ and $m_0 = m_U$) is the speed of light in a circular orbit wherein the eccentricity is equal to zero and the escape velocity from the Universe can never be reached. The period of the oscillation of the Universe and the period for light to transverse the Universe corresponding to the gravitational radius r_G must be equal. The harmonic oscillation period, T, is:

$$\begin{aligned} T &= \frac{2\pi r_G}{c} = \frac{2\pi G m_U}{c^3} = \frac{2\pi G\left(2\ X\ 10^{54}\ kg\right)}{c^3} \\ &= 3.10\ X\ 10^{19}\ \sec\ = 9.83\ X\ 10^{11}\ years \end{aligned} \tag{34.54}$$

where the mass of the Universe, m_U, is approximately $2\ X\ 10^{54}\ kg$. (The initial mass of the Universe of $2\ X\ 10^{54}\ kg$ is based on internal consistency with the size, age, Hubble constant, temperature, density of matter, and power spectrum.) Thus, the observed Universe will expand as mass is released as photons for $4.92\ X\ 10^{11}\ years$. At this point in its world line, the Universe will obtain its maximum size and begin to contract.

THE DIFFERENTIAL EQUATION OF THE RADIUS OF THE UNIVERSE

Based on conservation of mass/energy ($E = mc^2$) and spacetime ($\frac{c^3}{4\pi G} = 3.22\ X\ 10^{34}\ \frac{kg}{\sec}$), the Universe behaves as a simple harmonic oscillator having a restoring force, $\mathbf{F}$, which is proportional to the radius. The proportionality constant, k, is given in terms of the potential energy, E, gained as the radius decreases from the maximum expansion to the minimum contraction.

$$\frac{E}{\aleph^2} = k \tag{34.55}$$

Since the gravitational potential energy E_{grav} is equal to $m_U c^2$ when the radius of the Universe r is the gravitational radius r_G

$$F = -k\aleph = -\frac{m_U c^2}{r_G^2}\aleph = -\frac{m_U c^2}{\left(\frac{Gm_U}{c^2}\right)^2}\aleph \tag{34.56}$$

and, considering the oscillation, the differential equation of the radius of the Universe, $\aleph$ is:

$$m_U \ddot{\aleph} + \frac{m_U c^2}{r_G^2}\aleph = m_U \ddot{\aleph} + \frac{m_U c^2}{\left(\frac{Gm_U}{c^2}\right)^2}\aleph = 0 \tag{34.57}$$

The *maximum radius of the Universe*, the amplitude, r_o, of the time harmonic variation in the radius of the Universe, is given by the quotient of the total mass of the Universe and Q (Eq. (34.53)), the mass/energy to expansion/contraction quotient.

$$r_0 = \frac{m_U}{Q} = \frac{m_U}{\frac{c^3}{4\pi G}} = \frac{2\ X\ 10^{54}\ kg}{\frac{c^3}{4\pi G}} = 1.97\ X\ 10^{12}\ \textit{light years} \tag{34.58}$$

The *minimum radius* which corresponds to the gravitational radius, r_g, given by Eq. (32.36) with $m_0 = m_U$ is

$$r_g = \frac{2Gm_U}{c^2} = 2.96\ X\ 10^{27}\ m = 3.12\ X\ 10^{11}\ \textit{light years} \tag{34.59}$$

When the radius of the Universe is the gravitational radius, r_g, the proper time is equal to the coordinate time by Eq. (34.47), and the gravitational escape velocity v_g of the Universe is the speed of light. The radius of the Universe as a function of time is

$$\aleph = \left(r_g + \frac{cm_U}{Q}\right) - \frac{cm_U}{Q}\cos\left(\frac{2\pi t}{\frac{2\pi r_G}{c}}\right) = \left(\frac{2Gm_U}{c^2} + \frac{cm_U}{\frac{c^3}{4\pi G}}\right) - \frac{cm_U}{\frac{c^3}{4\pi G}}\cos\left(\frac{2\pi t}{\frac{2\pi G m_U}{c^3}}\right) \tag{34.60}$$

As shown in the Gravity section, Eq. (34.60) correctly predicts the observed size, age, Hubble constant, temperature, density of matter, power spectrum, large-scale structure, and *acceleration rate of the expansion of the Universe*. The latter astonishing observation was predicted years before it was observed [22].

THE PERIODS OF SPACETIME EXPANSION/CONTRACTION AND PARTICLE DECAY/PRODUCTION FOR THE UNIVERSE ARE EQUAL

The period of the expansion/contraction cycle of the radius of the Universe, T, is given by Eq. (34.54). It follows from the Poynting power theorem with spherical radiation that the transition lifetimes are given by the ratio of energy and the power of the transition (Eq. (33.35)). Exponential decay applies to electromagnetic energy decay,

$$h(t) = e^{-\alpha t}u(t) = e^{-\frac{2\pi}{T}t}u(t) \tag{34.61}$$

The coordinate time is imaginary because energy transitions are spacelike due to spacetime expansion from matter to energy conversion. For example, the mass of the electron (a fundamental particle) is given by:

$$\frac{2\pi \lambda\!\!\!^{-}_C}{\sqrt{\frac{2Gm_e}{\lambda\!\!\!^{-}_C}}} = \frac{2\pi \lambda\!\!\!^{-}_C}{v_g} = i\alpha^{-1}\sec \tag{34.62}$$

where v_g is the Newtonian gravitational velocity (Eq. (34.30)). When the gravitational radius r_g is the radius of the Universe, the proper time is equal to the coordinate time by Eq. (34.47), and the gravitational escape velocity v_g of the Universe is the speed of light. Replacement of the coordinate time, t, by the spacelike time, it, gives:

$$h(t) = \mathrm{Re}\left[e^{-i\frac{2\pi}{T}t}\right] = \cos\frac{2\pi}{T}t \tag{34.63}$$

where the period is T (Eq. (34.54)). The continuity conditions based on the constant maximum speed of light (Maxwell's equations) are given by Eqs. (34.48-34.49). The continuity conditions based on the constant maximum speed of light (Schwarzschild metric) are given by Eq. (34.50). The periods of spacetime expansion/contraction and particle decay/production for the Universe are equal because only the particles which satisfy Maxwell's equations and the relationship between proper time and coordinate time imposed by the Schwarzschild metric may exist.

The general form of the light front wave equation is given by Eq. (34.5). The equation of the radius of the Universe, $\aleph$, may be written as:

$$\aleph = \left(\frac{2Gm_U}{c^2} + \frac{cm_U}{\frac{c^3}{4\pi G}} \right) - \frac{cm_U}{\frac{c^3}{4\pi G}} \cos\left(\frac{2\pi}{\frac{2\pi G m_U}{c^3}} \left(t - \frac{\aleph}{c} \right) \right) \tag{34.64}$$

which is a solution of the wave equation for a light wave front. Maxwell's equations, Planck's equation, the de Broglie equation, Newton's laws, and special relativity, and gravity are unified. Classical physical laws apply on all scales wherein space is finite-absolute rather than infinite-relative[4].

EQUIVALENCE OF THE GRAVITATIONAL AND INERTIAL MASSES

The relationships of relativity and gravity have the same form with the interchange of the inertial and gravitational velocities (Compare Eqs. (34.7-34.17) with Eqs. (34.26), and (34.36-34.41)). The relationships are reciprocal due to the nature of absolute space that is produced or annihilated with particle annihilation or production, respectively. Due to the finite propagation time for signals set by the speed of light which is in turn set by the finite permeability and permittivity of free space the mechanics parameters are corrected by Lorentz transformations or their equivalent with the gravitational velocity replacing the constant kinetic velocity in the case of gravitating bodies.

Extensive experimentation dating from Galileo Galilei's Pisa experiment to the present has shown that irrespective of the object chosen, the acceleration of an object produced by the gravitational force is the same, which from Eq. (32.4) implies that the value of m_g / m_i should be the same for all objects. In other words, we have:

$$\frac{m_g}{m_i} = \text{universal constant} \tag{34.65}$$

the equivalence of the gravitational mass and the inertial mass. The fractional deviation of Eq. (34.65) from a constant is experimentally confirmed to less $1\,X\,10^{-11}$ [23]. The equivalence of the gravitational mass and the inertial mass is a conservation statement of the mass, energy, and spacetime of the Universe. The overall inventory is a constant with the inter-conversion related by the ratios of fundamental constants of spacetime.

At particle production, the outgoing gravitational field, traveling as a wave front, carries the change in the curvature of spacetime. The front must travel at light speed since the permittivity ε_0 and permeability μ_0 of free spacetime are and must remain independent of curvature in order for the laws of physics to be covariant and the physics of the Universe to be conservative. Thus, any perturbation must travel at the speed of light c given by Eq. (34.1). The justification for Eq. (34.26) is the relativity principle based on Eq. (34.6) and the invariance of the light speed due to the invariance of the permittivity ε_0 and permeability μ_0 of free spacetime.

From Eqs. (34.35) and (34.47-34.53), each r-sphere of the Universe comprising a finite, closed 3-sphere Universe-(Riemannian three-dimensional hyperspace plus time of constant positive curvature at each r-sphere) is determined by a clock set by the conservation relationship of mass-energy, $E = mc^2$, and spacetime, $\frac{c^3}{4\pi G} = 3.22\,X\,10^{34}\,\frac{kg}{\sec}$. Spacetime expands at light speed as mass is released as energy which provides the basis of the atomic, thermodynamic, and cosmological arrows of time.

Consider the relationship (Eq. (34.41)) between gravitational mass m_g and proper energy E_p of a gravitating object based on the absolute light speed and absolute space:

$$\frac{E_p}{\sqrt{1 - \left(\frac{v_g}{c} \right)^2}} = m_g c^2 \tag{34.66}$$

Similarly, based on the absolute light speed and absolute space, the relationship (Eq. (34.13)) between inertial mass m_i and energy is:

---

[4] The views that all phenomena in the universe are purely relative, the basis of gravity is the equivalence principle, and light has a wave-particle duality nature determined by the act of measurement were the seeds for the abandonment of the testable physical laws of Newton and Maxwell. Subsequent missteps of the interpretation of the electron as a nonphysical point-particle probability wave with intrinsic spin, the use of mathematics for circumventing intrinsic infinites while engendering the vacuum with infinities of virtual particles, and the pursuit of compactified extra dimensions, nonbaryonic dark matter and dark energy gave rise to the pure mathematics and the metaphysics of current quantum mechanics and string theory. This path has been a complete failure at achieving the goal of unification of the forces and laws of nature.

$$E_p = m_i c^2 = \frac{m_0 c^2}{\sqrt{1-\frac{v^2}{c^2}}} \tag{34.67}$$

At particle production $v = v_g$ and Eqs. (34.47-34.49) are continuously satisfied with a final free state at rest, such that:

$$E_p = m_g c^2 \sqrt{1-\left(\frac{v_g}{c}\right)^2} = m_i c^2 \sqrt{1-\frac{v^2}{c^2}} = m_0 c^2 \tag{34.68}$$

thus,

$$m_g = m_i = m_0 \tag{34.69}$$

wherein a particle's absolute frame of reference is determined by the production event having production mass m_0 (e.g. Eq. (34.52)), energy $m_0 c^2$ (Eq. (34.49)), velocity v_g (Eq. (34.30)) in the photon-particle transition state and zero as a free particle, and the proper time defined in terms of the unit *sec* of its proper clock which depends on its gravitational and inertial masses (Eqs. (34.47), (34.49), (34.51)) which are equivalent. Following production, conservation of mass-energy relative to absolute space and consequently relative space in Eqs. (34.13) and (34.41) requires that:

$$m_g = m_i \tag{34.70}$$

where the energy is a Lorentz scalar and the contributions due to kinetic energy and gravitational energy corresponding to v and v_g, respectively, superimpose. The validity of the gravity metric under interchange of the masses of gravitating bodies requires that Eqs. (34.69-34.70) apply in general.

The absolute gravitational and inertial masses are equivalent since they both obey the relativity principle and conservation of mass-energy-spacetime. With regard to gravitational effects, clocks and rulers are affected by the acquisition of translational velocity. The gravitational mass increases by the kinetic energy increase. This causes a gravitating particle's internal clock to undergo gravitational dilation such that its proper time with respect to the absolute time unit *sec* is synchronized with the mass-energy expansion-contraction cycle of the Universe. Since the same physical relationships hold for all frames of reference (Relativity Principle), the relative inertial and gravitational masses are equivalent in their effects from the perspective of the corresponding frames. This result also provides a gravitational causality constraint regarding the maximum particle speed that matches that imposed by the particle's equivalent gravitational and inertial masses. In addition to the impossible result that the inertia of the particle would become infinite when it approached the velocity of light as first recognized by Poincaré [1], the principle that the particle velocity cannot exceed c also arises from the existence of absolute space. A particle's gravitational mass cannot become infinite, and the particle's position cannot outdistance the spacetime perturbation created by its production or any mass increase from the acquisition of kinetic energy.

Regarding the inertial implications, based on the absolute speed of light, measurements by clocks in different inertial frames deviate in a manner independent of that due to spacetime curvature caused by gravitating bodies. These effects are also due to an absolute change in the particle's mass-energy-spacetime parameters. They are not due to different relative perceptions of time measurement as inherent in the current interpretations of special relativity. For example, the appearance that a stick immersed in water appears to bend can be understood in terms of the difference in the speed of light propagation in air and water. The molecules are not really forming new bonds. But, clocks that were initially synchronized and at relative rest, have undergone relative translation, and were rejoined, measure different times in an absolute sense, not just a relative one. And, thereafter the relative velocity is zero, the increase in kinetic energy has gone to zero, and any contraction of physical dimensions due to relativity is not observed. Time has been absolutely lost due to motion. This conclusion is in agreement with the results of the twin paradox and differences in the observation of the simultaneity of events due to motion. It is possible to slow the clock of an object by expending energy to increase its velocity with a consequent and concomitant acceleration of the clocks of parts of the object's surroundings such that the absolute time of the Universe is conserved overall. As shown *supra.*, spacetime expands as mass is released as energy which provides the basis of the *atomic, thermodynamic, and cosmological arrows of time*. The resulting object's kinetic energy is also an absolute as opposed to a relative parameter. It represents a conservative physical change in the mass-energy-spacetime inventory of the Universe. It can be quantified in terms of absolutes with the inertial and gravitational masses being equivalent as a requirement of the conservation of mass, energy, and spacetime.

The equivalence of the inertial and gravitational masses is due to mass-energy conservation relative to absolute space whose permittivity and permeability and gravitational constant determine the conversion factor between mass and energy and the mass and curvature, respectively. Since the gravitational and inertial mass are equivalent, the same mass value for a gravitating body with inertia is used in both the gravitational and inertial equations of motion. Given that a particle's mass is absolute relative to absolute space according to Eq. (34.11) wherein v is the absolute velocity, the factor of resistance to any change in velocity due to an applied force corresponding to a change in kinetic energy and therefore mass-energy inventory over space and time is the inertial mass. Thus, conservation of mass-energy when there is any change is the basis of an absolute law, namely Newton's second law.

NEWTON'S SECOND LAW

All matter is comprised of charged fundamental particles such as quarks and leptons. Charge is relativistically invariant. Consider a particle that acquires a finite constant velocity. In the case of the electron atomic orbital, the radius undergoes relativistic contraction in the direction of constant velocity relative to a stationary observer according to Eq. (34.10). Thus, as v approaches c, the radius goes to zero, and the Coulomb potential density along the axis of propagation goes to infinity (Eq. (1.261)). However, as the velocity increases, the electric field lines of the particle increase in density relative to the stationary observer in a direction perpendicular to the direction of motion of the particle. The field lines of a stationary proton, electron, and hydrogen atom are shown in Figure 1.32. The field lines in the lab frame follow from the relativistic invariance of charge as given by Purcell [24]. The relationship between the relativistic velocity and the electric field of a moving point charge at two velocities is shown schematically in Figures 34.1A and 34.1B.

Figure 34.1A. The electric field lines of a moving point charge ($v = \frac{1}{3}c$).

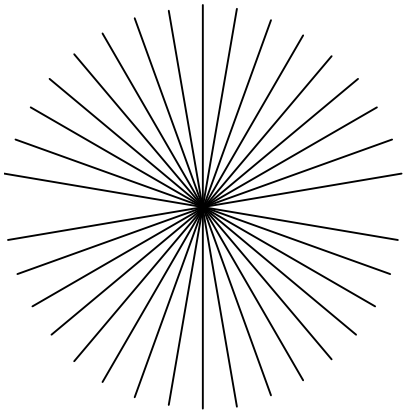

Figure 34.1B. The electric field lines of a moving point charge ($v = \frac{4}{5}c$).

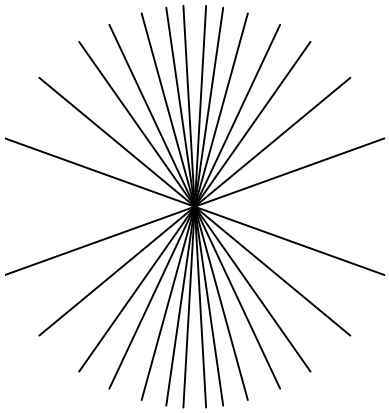

The Lorentz correction to maintain the invariance of the field lines identically cancels the Lorentz contraction of the atomic orbital such that the Coulomb potential is unchanged. Thus, inertial mass is purely kinematics, except for *radiation from moving charges* and *radiation reaction effects of charged particles* given by Jackson [25] where these later effects also arise from Maxwell's equations and special relativity. The inertial mass is related to the gravitational mass and the momentum of the photon corresponding to its electric and magnetic fields as well as the corresponding energies as given by Eq. (34.49) for the particle production event. Thereafter, the constant maximum velocity of the speed of light maintains that the relationships between parameters of observers moving at constant relative velocity are given by the Minkowski tensor. The *inertial mass* arises from the impedance of spacetime of $\eta = \sqrt{\frac{\mu_0}{\varepsilon_0}} = 4\pi\alpha\frac{\hbar}{e^2} = 377\Omega$ for the motion of light or matter at production according to Eq. (34.49) wherein matter can be considered a special case of light from which it is formed. The resistance of mass to motion is thereafter based on absolute energy conservation. Thus, from Eq. (34.49), Newton's force law can be derived.

$$F = \frac{dE}{ds} = \frac{d\left(mc^2\right)}{ds} = \frac{d\left(\frac{m_0c^2}{\sqrt{1-\frac{v^2}{c^2}}}\right)}{ds} = \frac{1}{2}\frac{m_0c^2}{\left(1-\frac{v^2}{c^2}\right)^{3/2}}\frac{2v}{c^2}\frac{dv}{ds} = \frac{1}{2}\frac{m_0c^2}{\left(1-\frac{v^2}{c^2}\right)^{3/2}}\frac{2}{c^2}\frac{ds}{dt}\frac{dv}{ds} = \frac{m_0}{\left(1-\frac{v^2}{c^2}\right)^{3/2}}\frac{dv}{dt} \tag{34.71}$$

Consider the invariant momentum given by Eq. (34.12). The time derivative is given by:

$$\frac{dp}{dt} = \frac{d}{dt}\left(\frac{m_0v}{\sqrt{1-\frac{v^2}{c^2}}}\right) = \frac{m_0}{\left(1-\frac{v^2}{c^2}\right)^{3/2}}\frac{dv}{dt} \tag{34.72}$$

Comparison of Eq. (34.71) with Eq. (34.72) gives Newton's force law (Eq. (34.4)).

$$F = \frac{d}{dt}\left(\frac{m_0v}{\sqrt{1-\frac{v^2}{c^2}}}\right) = \frac{d\mathbf{p}}{dt} \tag{34.73}$$

Thus, the application of a force causes acceleration to a new final absolute velocity corresponding to the final absolute mass where the mass difference is the increased kinetic energy. Since the absolute-mass-energy of the source of force identically decreases by that of the increase of the accelerated body, the mass-energy inventory of the Universe is conserved. This result is contrasted to the case in special relativity wherein there are infinites of inertial frames corresponding to infinities of different energy inventories. It is no more tenable that mass-energy can be created by simply selecting an alternative inertial frame, than matter can be created from the vacuum as predicted by the Heisenberg Uncertainty principle of quantum mechanics. Both have no basis in physical reality. In addition to restoring conservation to the Universe, the determination of absolute space resolves inconsistencies of special relativity such as the twin paradox as well as other confusing issues in the interpretation of special relativity.

RETURN TO THE TWIN PARADOX

It was discussed *supra*. that the framers of special relativity were incorrect in their conclusion of the absence of an absolute frame based on their limited understanding of the nature of spacetime and their inability to identify such a frame. In fact, an absolute frame at rest exists for each particle at the moment of its creation from a photon wherein its absolute proper time is based on the time unit *sec*. Newton's second law and Newton's Law of Gravitation may be understood in terms of the nature of spacetime in the relationship of the photon and the corresponding particle. Spacetime has a limiting speed of light for the propagation of fields including the electromagnetic and gravitational fields with the requirement that the production of matter having inertial mass gives rise to the corresponding equivalent gravitational mass. Mass energy and spacetime are conserved, and the clocks for the transition of matter to energy and the expansion of the cosmos are absolute overall and are synchronized.

The production of a particle from a photon of identically the production energy defines the absolute inertial frame at rest for the particle. Since a typical laboratory object is comprised of trillions of trillions of particles, it is impossible to determine the kinetic energy inventory exactly. However, since the electromagnetic forces dominate the gravitational force by about forty orders of magnitude, and accelerated and hot particles typically thermalize by radiation and collisional exchange, the temperature of space at each r-sphere is a reasonable measure of the average kinetic energy inventory with space modeled as a blackbody as given in the Statistical Mechanics section. The current absolute temperature is about 4 K; thus, on average, the kinetic energy of the mass of the Universe can be assumed near rest relative to an absolute frame. Thus, the twin paradox is easily resolved in that the Earth is identifiable as a good approximation to an absolute frame at rest for near-light-speed space travel by the traveling twin[5]. For relative motion, the inertial frames are easily ranked based on relative expenditure of energy to increase the corresponding spaceship's absolute energy. The kinetic energy imparted to the spaceship of the traveling twin causes its clock to slow down relative to the Earth-bound one's to maintain the conservation of matter, energy, and spacetime of the Universe. Recall that the *defined "clock" measures "clicks" in units of sec on an observable in one aspect, and in another, it is the ruler of spacetime of the Universe with the implicit dependence of spacetime on matter-energy conversion* as shown in the Gravity and Relationship of Matter to Energy and Spacetime Expansion sections. Even though the twins are rejoined and their clocks read identically thereafter, the returning twin is younger since his proper absolute clock underwent dilation. His retarded clock was at the expense of advancing the clocks of parts of his surroundings in the expenditure of the energy required for the acceleration and deceleration of his spaceship. Overall, the absolute periods of particle decay/production (Maxwell's equations) and spacetime expansion/contraction (Schwarzschild metric) for the Universe are equal and conserved. The synchronized periods are based on the corresponding continuity conditions given by Eq. (34.49) and Eq. (34.50), respectively, that arise from the relativity principle (Eq. (34.6)).

In summary, the relationship between inertial and gravitational mass is based on the result that only fundamental particles having an equivalence of the inertial and gravitational masses at particle production are permitted to exist since only in these cases are Maxwell's equations and the conditions inherent in the Schwarzschild metric of spacetime satisfied simultaneously wherein space must be absolute. The equivalence is maintained for any velocity thereafter due to the absolute nature of space and the absolute speed of light. The invariant speed c is set by the permittivity and permeability of absolute space which determines the relativity principle based on propagation of fields and signals as light-wave fronts. The predicted twin-paradox result based on Poincaré's postulates, Lorentz transforms, and absolute space has been verified by experiments in which extremely precise and accurate clocks are synchronized, divided into identical Earth-bound and traveling clocks, and the times of stationary members are compared with ones flown around the world on airplanes [8].

[5] Other celestial objects will also suffice. A suitable practical object as a reference of absolute space at rest for relativistic astrophysical measurements is a bright celestial body that has a zero translational velocity within its r-sphere, or this component is corrected for. A point at rest on the surface of a given r-sphere including the expansion horizon corresponding to absolute space can be observed in approximation by identifying a Cepheid of the corresponding calculated age (distance) relative to the current r-sphere. Measurement of the change in angular diameter over its pulsation cycle when combined with spectroscopic radial velocity measurements, permits the distance to be determined very accurately in a quasi-geometrical way, and permits the zero-point of the Cepheid Period-Luminosity empirical law to be calibrated.

ABSOLUTE SPACE CONFIRMED EXPERIMENTALLY

The absolute nature of spacetime is confirmed by the observation that the power spectra of quasars do not exhibit time dilation [26-29]. The power spectra of quasars are identical at high and low redshift. Clocks at earlier r-spheres run slower than those at later r-spheres due to spacetime dilation/expansion. But internal processes being time independent of redshift due to the expansion of spacetime is expected since time dilation arises from motion relative to an object's absolute space and not relative to an arbitrary observer such as an Earth observer whose position has relatively receded at a corresponding velocity due to spacetime expansion. The independence of time dilation for internal processes due to spacetime expansion is also supported by the spacetime-expansion independence of the fundamental constants which determine the clocks of internal processes. Furthermore, time dilation is not predicted due to an apparent relativistic motion due to expansion. Given that a quasar's velocity relative to its absolute space is not expected to be substantial even though its velocity relative to an Earth observer corresponding to its redshift may be relativistic, the power spectrum that arises from internal emission processes is predicted not to show time dilation. This consequence of absolute space is unequivocally experimentally confirmed for quasars that are each essentially stationary relative to their absolute space [26-29][6].

In contrast, the ejected matter of a supernova is accelerated to close to light speed relative to its absolute space and is predicted to exhibit time dilation observable by the dilation of its spectral evolution. Indeed, observational results are inconsistent with the null, no time dilation, hypothesis at a confidence level of 99.0% [30].

In addition to providing for (i) the uniqueness of the energy inventory of the universe, (ii) the basis of inertial and gravitational masses and their equivalence, (iii) the restoration of Newton's laws as well as their relationship to Maxwell's equations, pillars of modern technological society, (iv) the resolution of the twin paradox, and (v) the predictions of the acceleration of the cosmic expansion and the mass of the top quark as well providing the means for calculating the masses of the other fundamental particles, the nature of absolute space and absolute light velocity resolves the observation of the absence of time dilation in quasars and its presence in supernovas. These results demonstrate that a hypothetical particle dubbed the Higgs boson whose properties are coupled to the 19 semiempirical parameters of the Standard Model requiring 32 significant figure precision to prevent nonsensical outcomes in the corresponding computer algorithms is not the basis of inertial mass. Such a mass conveying particle will not be observed in experiments performed at Fermi National Accelerator Laboratory (Fermilab), the Large Hadron Collider (LHC), or any future collider [31]. Recent Higgs hunt results from CERN of a 126 GeV boson match predictions for a high-energy neutron resonance predicted in the Intermediate Vector and Higgs Bosons section.

The nature of spacetime also has implications regarding the possibility of gravity waves analogous to electromagnetic waves. As shown in the Period Equivalence section, the only particles that can exist are those that obey the condition of period equivalence of spacetime expansion and contraction and electromagnetic decay such that matter-energy and spacetime are conserved. However, the natures of the electromagnetic and gravitational fields are distinct. Only matter-energy conversion is capable of causing a change to the curvature of spacetime and the corresponding gravitational field. Charges can emit photons that superpose to form an electromagnetic wave; whereas, gravitating bodies cannot emit a particle that similarly forms a transverse light-speed wave. Any oscillation or change in motion of a gravitating body must conserve the relationship between matter-energy and spacetime with a change in time dependent curvature propagating inwards and outwards during the corresponding phase of the period of periodic motion to maintain the conservation. The time dependent gravitational field fluctuations would only be experienced radially in the near field with no transverse time-dependent gravity wave effect in the far field consistent with the absence of the observation of gravity waves [32-33].

REFERENCES

1. E. Giannetto, The rise of special relativity: Henri Poincaré's works before Einstein. Atti del 18 Congresso di Storia della Fisica e Dell'Astronomia, (1998), pp. 171-207.
2. E. Giannetto, The rise of special relativity: Henri Poincaré's works before Einstein. Atti del 18 Congresso di Storia della Fisica e Dell'Astronomia, (1998), p. 179.
3. H. Poincaré, "L'etat actuel et l'avenir de la physique mathematique," *Bulletin des sciences mathematiques*, Vol. 28, (1904), pp. 302-324; quoted in Whittaker (1987), p. 30.
4. E. Whittaker, *A History of the Theories of Aether and Electricity*, Vol. 2, Modern Theories, Chapter 2, "The Relativity Theories of Poincaré and Lorentz," Nelson, London, (1987), Reprinted, American Institute of Physics, pp. 30–31.
5. S. Kak, "Moving observers in an isotropic universe," International Journal of Theoretical Physics, Vol. 46, No. 5, (2007), pp. 1424-1430.
6. H. Minkowski's interpretation of special relativity in terms of a four dimensional space time was presented in the form of a lecture in Cologne, Germany in September 1908. An English translation, entitled "Space and Time," can be found in the collection *The Principle of Relativity*, Dover, New York, 1952.
7. V. Fock, *The Theory of Space, Time, and Gravitation*, The MacMillan Company, (1964), pp. 14-15.
8. A. Beiser, *Concepts of Modern Physics*, Fourth Edition, McGraw-Hill Book Company, New York, (1978), pp. 2-40.
9. L. Z. Fang, and R. Ruffini, *Basic Concepts in Relativistic Astrophysics*, World Scientific, (1983).
10. G. R. Fowles, *Analytical Mechanics*, Third Edition, Holt, Rinehart, and Winston, New York, (1977), pp. 154-155.
11. J. D. Jackson, *Classical Electrodynamics*, Second Edition, John Wiley & Sons, New York, (1975), pp. 739-779.
12. K. Hagiwara et al., Phys. Rev. D 66, 010001 (2002); http://pdg.lbl.gov/2002/s035.pdf.

[6] There is no time dilation corresponding to any potential blue-shift in contraction either. The oscillation of the universe is evidenced by the parts-per-million angular-harmonic anisotropy in the microwave background radiation given in the Power Spectrum of the Cosmic Microwave Background section.

13. P. J. Mohr and B. N. Taylor, "CODATA recommended values of the fundamental physical constants: 1998," Reviews of Modern Physics, Vol. 72, No. 2, April, (2000), pp. 351-495.
14. J. C. Mather, E. S. Cheng, A preliminary measurement of the cosmic microwave background spectrum by the Cosmic Background Explorer (COBE) satellite, *Astrophysical Journal Letters*, 354, L37–L40 (May 10, 1990).
15. W. Saunders, C. Frenk, The density field of the local universe; *Nature*, 349(6304), 32–38 (1991).
16. R. P. Kirshner, A. Oemler, Jr., P. L. Schechter, S. A. Shectman, A deep survey of galaxies, *Astronomical Journal*, 88, 1285–1300 (September 1983).
17. V. de Lapparent, M. J. Geller, J. P. Huchra, The mean density and two-point correlation function for the CfA redshift survey slices, *Astrophysical Journal*, 332(9) 44–56 (1988).
18. A. Dressler, S. M. Faber, D. Burstein, R. L. Davies, D. Lynden-Bell, R. J. Terlevich, G. Wegner, "Spectroscopy and photometry of elliptical galaxies—A large-scale streaming motion in the local universe," *Astrophysical Journal*, 313, L37-L42, (1987).
19. S. Flamsteed, Crisis in the Cosmos, *Discover*, 16(3), 66(1995).
20. J. Glanz, CO in the early universe clouds cosmologists' views, *Science*, 273(5275), 581 (1996)
21. S. D. Landy, Mapping the Universe, *Scientific American*, 280(6), 38–45 (1999).
22. R. L. Mills, *The Grand Unified Theory of Classical Quantum Mechanics*, November 1995 Edition, HydroCatalysis Power Corp., Malvern, PA, Library of Congress Catalog Number 94-077780, ISBN number ISBN 0-9635171-1-2, Chp. 22.
23. E. G. Adelberger, C. W. Stubbs, B. R. Heckel, Y. Su, H. E. Swanson, G. Smith, J. H. Gundlach, Phys. Rev. D, Vol. 42, No. 10, (1990), pp. 3267-3292.
24. E. Purcell, *Electricity and Magnetism*, McGraw-Hill, New York, (1965), pp. 156-167.
25. J. D. Jackson, *Classical Electrodynamics*, Second Edition, John Wiley & Sons, New York, (1975), Chps. 14 and 17.
26. M. R. S. Hawkins, "On time dilation in quasar light curves," Monthly Notices of the Royal Astronomical Society, Vol. 405, 2010, 1940–1946, July 2010 doi: 10.1111/j.1365-2966.2010.16581.x.
27. http://www.physorg.com/news190027752.html.
28. M. R. S. Hawkins, "Time dilation and quasar variability," The Astrophysical Journal, 553, (2001), L97-L100.
29. M. R. S. Hawkins, "Gravitational microlensing, quasar variability and missing matter," Nature, 366, (1993), 242-245.
30. R. J. Foley, A. V. Filippenko, D. C. Leonard, A. G. Riess, P. Nugent, and S. Perlmutter, "A definitive measurement of time dilation in the spectral evolution of the moderate-redshift type Ia Supernova 1997ex," The Astrophysical Journal, 626(1), (2005), pp. L11–L14.
31. A. Cho, "Fermilab physicists don't see Higgs, argue they should keep looking", Science, Vol. 329, (2010), pp. 498-499.
32. B. P. Abbott, R Abbott, R. Adhikari, P. Ajith, B. Allen, G. Allen, R. S. Amin, S. B. Anderson, W. G. Anderson, M. A. Arain; et al., "LIGO: the Laser Interferometer Gravitational-Wave Observatory," Rep. Prog. Phys. 72 (2009) 076901 (25pp).
33. P. Shawhan, "Gravitational-wave astronomy: observational results and their impact," Class. Quantum Grav., Vol. 27 (2010) 084017 (14 pp).

Chapter 35

THE FIFTH FORCE

GENERAL CONSIDERATIONS

The physical basis of the equivalence of inertial and gravitational mass of fundamental particles is given in the Equivalence of Inertial and Gravitational Masses Due to Absolute Space and Absolute Light Velocity section wherein spacetime is Riemannian due to a relativistic correction to spacetime with particle production. The Schwarzschild metric gives the relationship whereby matter causes relativistic corrections to spacetime that determines the curvature of spacetime and is the origin of gravity. Matter arises during particle production from a photon and comprises mass and charge confined to a two dimensional surface. Matter of fundamental particles such as an electron has zero thickness. But, in order that the speed of light is a constant maximum in any frame including that of the gravitational field that propagates out as a light-wave front at particle production, the production event gives rise to a spacetime dilation equal to 2π times the Newtonian gravitational or Schwarzschild radius $r_g = \frac{2Gm_e}{c^2} = 1.3525\ X\ 10^{-57}\ m$ of the particle according to Eqs. (32.36) and (32.140b) and the discussion at the footnote after Eq. (32.40). For the electron, this corresponds to a spacetime dilation of $8.4980\ X\ 10^{-57}\ m$ or $2.8346\ X\ 10^{-65}\ s$. Although the electron does not occupy space in the third spatial dimension, its mass discontinuity effectively "displaces" spacetime wherein the spacetime dilation can be considered a "thickness" associated with its gravitational field. Matter and the motion of matter effects the curvature of spacetime which in turn influences the motion of matter. Consider the angular motion of matter of a fundamental particle. The angular momentum of the photon is $\hbar$. An electron is formed from a photon, and it can only change its bound states in discrete quantized steps caused by a photon at each step. Thus, the electron angular momentum is always quantized in terms of $\hbar$. But this intrinsic motion comprises a two-dimensional current surface of the motion of the matter through space that may be positively curved, flat, or negatively curved. The first and second cases correspond to the bound and free electron, respectively. The third case corresponds to an extraordinary state of matter called a ***pseudoelectron*** given *infra*. Due to interplay between the motion of matter and spacetime in terms of their respective geometries, only in the first case are the inertial and gravitational masses of the electron equivalent. In the second case, the gravitational mass is zero. ***The experimental mass of the free electron measured by Witteborn [1] using a free fall technique is less than*** $0.09\ m_e$***, where*** m_e ***is the inertial mass of the free electron*** $\left(9.109534\ X\ 10^{-31}\ kg\right)$ ***consistent with the Classical Physics theoretical prediction.*** In the third case, the gravitational mass is negative in the equations of extrinsic or translational motion. The negative gravitational mass of a fundamental particle is the basis of and is manifested as a ***fifth force*** that acts on the fundamental particle in the presence of a gravitating body in a direction opposite to that of the gravitational force with far greater magnitude[1].

The two-dimensional nature of matter permits the unification of subatomic, atomic, and cosmological gravitation. The theory of gravitation that applies on all scales from quarks to cosmos as shown in the Gravity section is derived by first establishing a metric. A space in which the curvature tensor has the following form:

$$R_{\mu\nu,\alpha\beta} = K \cdot (g_{\nu\alpha} g_{\mu\beta} - g_{\mu\alpha} g_{\nu\beta}) \tag{35.1}$$

is called a space of constant curvature; it is a four-dimensional generalization of Friedmann-Lobachevsky space. The constant

[1] In the case of Einstein's gravity equation (Eq. (32.40)), the Einstein Tensor $G_{\mu\nu}$, is equal to the stress-energy-momentum tensor $T_{\mu\nu}$. The only possibility is for the gravitational mass to be equivalent to the inertial mass. A particle of zero or negative gravitational mass is not possible. However, it is shown in the Gravity section that the correct basis of gravitation is not according to Einstein's equation Eq. (32.40); instead, the origin of gravity is the relativistic correction of spacetime itself which is analogous to the special relativistic corrections of inertial parameters—increase in mass, dilation in time, and contraction in length in the direction of constant relative motion of separate inertial frames. On this basis, the observed acceleration of the cosmos is predicted as given in the Cosmology section.

K is called the constant of curvature. *The curvature of spacetime results from a discontinuity of matter having curvature confined to two spatial dimensions. This is the property of all matter at the fundamental-particle scale.* Consider an isolated bound electron comprising an atomic orbital with a radius r_n as given in the One-Electron Atom section. For radial distances, r, from its center with $r < r_n$, there *is no mass; thus, spacetime is flat or Euclidean.* The curvature tensor applies to all space of the inertial frame considered; thus, for $r < r_n$, $K = 0$. At $r = r_n$ there exists a discontinuity of mass in constant motion within the atomic orbital as a positively curved surface. This results in a discontinuity in the curvature tensor for radial distances $\geq r_n$. The discontinuity requires relativistic corrections to spacetime itself. It requires radial length contraction and time dilation corresponding to the curvature of spacetime. The gravitational radius of the atomic orbital and infinitesimal temporal displacement corresponding to the contribution to the curvature in spacetime caused by the presence of the atomic orbital are derived in the Gravity section.

The Schwarzschild metric gives the relationship whereby matter causes relativistic corrections to spacetime that determines the curvature of spacetime and is the origin of gravity. The correction is based on the boundary conditions that no signal can travel faster than the speed of light including the gravitational field that propagates following particle production from a photon wherein the particle has a finite gravitational velocity given by Newton's Law of Gravitation. The separation of proper time between two events x^μ and $x^\mu + dx^\mu$ given by Eq. (32.38), the Schwarzschild metric [2-3], is:

$$d\tau^2 = \left(1 - \frac{2Gm_0}{c^2 r}\right) dt^2 - \frac{1}{c^2}\left[\left(1 - \frac{2Gm_0}{c^2 r}\right)^{-1} dr^2 + r^2 d\theta^2 + r^2 \sin^2\theta d\phi^2\right] \tag{35.2}$$

Eq. (35.2) can be reduced to Newton's Law of Gravitation for r_g, the gravitational radius of the particle, much less than r_α^*, the radius of the particle at production ($\frac{r_g}{r_\alpha^*} << 1$), where the radius of the particle is its Compton wavelength bar ($r_\alpha^* = \lambda\!\!\!^{-}_c$):

$$F = \frac{Gm_1 m_2}{r^2} \tag{35.3}$$

where G is the Newtonian gravitational constant. Eq. (35.2) relativistically corrects Newton's gravitational theory. In an analogous manner, Lorentz transformations correct Newton's laws of mechanics.

The effects of gravity preclude the existence of inertial frames in a large region, and only local inertial frames, between which relationships are determined by gravity are possible. In short, the effects of gravity are only in the determination of the local inertial frames. The frames depend on gravity, and the frames describe the spacetime background of the motion of matter. Therefore, differing from other kinds of forces, gravity which influences the motion of matter by determining the properties of spacetime is itself described by the metric of spacetime. It was demonstrated in the Gravity section that gravity arises from the two spatial dimensional mass-density functions of the fundamental particles.

It is demonstrated in the One-Electron Atom section that a bound electron is a two-dimensional spherical shell—an atomic orbital. On the atomic scale, the curvature, *K*, is given by $\frac{1}{r_n^2}$, where r_n is the radius of the radial delta function of the atomic orbital. The velocity of the electron is a constant on this two-dimensional sphere. It is this local, positive curvature of the electron that causes gravity due to the corresponding physical contraction of spacetime due to its presence as shown in the Gravity section. It is worth noting that all ordinary matter, comprised of leptons and quarks, has positive curvature. Euclidean plane geometry asserts that (in a plane) the sum of the angles of a triangle equals 180°. In fact, this is the definition of a flat surface. For a triangle on an atomic orbital the sum of the angles is greater than 180°, and the atomic orbital has *positive curvature*. For some surfaces the sum of the angles of a triangle is less than 180°; these are said to have *negative curvature*.

sum of angles of triangles	type of surface
> 180°	positive curvature
= 180°	flat
< 180°	negative curvature

The measure of Gaussian curvature, *K*, at a point on a two-dimensional surface is:

$$K = \frac{1}{r_1 r_2} \tag{35.4}$$

the inverse product of the radius of the maximum and minimum circles, r_1 and r_2, which fit the surface at the point, and the radii are normal to the surface at the point. By a theorem of Euler, these two circles lie in orthogonal planes. For a sphere, the radii of the two circles of curvature are the same at every point and are equivalent to the radius of a great circle of the sphere. Thus, the sphere is a surface of constant curvature;

$$K = \frac{1}{r^2} \tag{35.5}$$

at every point. In the case of positive curvature of which the sphere is an example, the circles fall on the same side of the surface, but when the circles are on opposite sides, the curve has negative curvature. A saddle, a cantenoid, a hyperboloid, and a

pseudosphere are negatively curved. The general equation of a saddle is:

$$z = \frac{x^2}{a^2} - \frac{y^2}{b^2} \tag{35.6}$$

where a and b are constants. The curvature of the surface of Eq. (35.6) is:

$$K = \frac{-1}{4a^2b^2}\left[\frac{x^2}{a^4} + \frac{y^2}{b^4} + \frac{1}{4}\right]^{-2} \tag{35.7}$$

A saddle is shown schematically in Figure 35.1, a hyperboloid is shown in Figure 35.2, and a conic is shown in Figure 35.3.

Figure 35.1. A saddle.

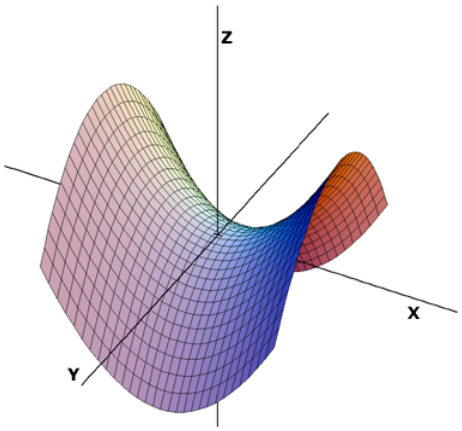

Figure 35.2. A hyperboloid.

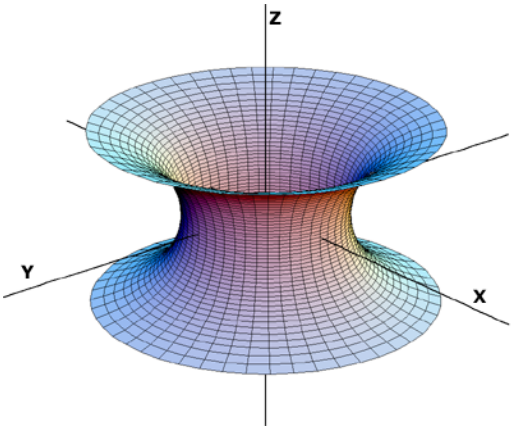

Figure 35.3. A conic.

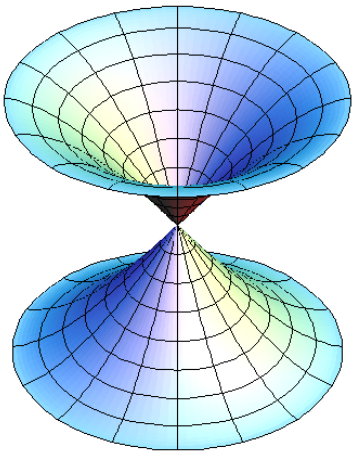

Figure 35.4. A pseudosphere.

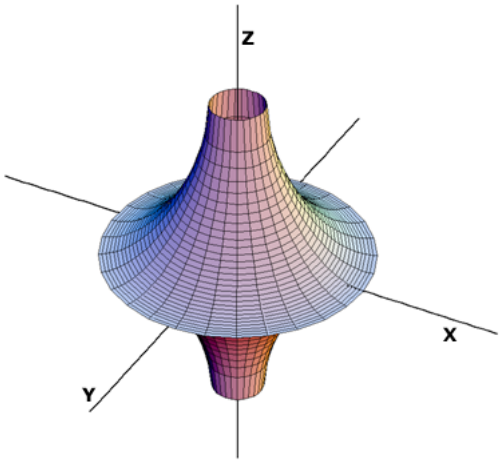

A pseudosphere is constructed by revolving the tractrix about its asymptote. For the tractrix, the length of any tangent measured from the point of tangency to the x-axis is equal to the height R of the curve from its asymptote—in this case the x-axis. The pseudosphere is a surface of constant negative curvature. The curvature, K

$$K = \frac{-1}{r_1 r_2} = \frac{-1}{R^2} \tag{35.8}$$

given by the product of the two principal curvatures on opposite sides of the surface is equal to the inverse of R squared at every point where R is the equitangent. R is also known as the radius of the pseudosphere. A pseudosphere is shown schematically in Figure 35.4.

In the case of a sphere, surfaces of constant potential are concentric spherical shells. The general law of potential for

surfaces of constant curvature is:

$$V = \frac{1}{4\pi\varepsilon_0}\sqrt{\frac{1}{r_1 r_2}} = \frac{1}{4\pi\varepsilon_0 R} \tag{35.9}$$

In the case of a pseudosphere the radii r_1 and r_2, the two principal curvatures, represent the distances measured along the normal from the negative potential surface to the two sheets of its evolute, envelop of normals (cantenoid and x-axis). The force is given as the gradient of the potential that is proportional to $\frac{1}{r^2}$ in the case of a sphere.

All matter is comprised of fundamental particles, and all fundamental particles exist as mass confined to two spatial dimensions. The particle's current surface is positively curved in the case of an atomic orbital, flat in the case of a free electron, and negatively curved in the case of an electron as a pseudosphere hereafter called a pseudoelectron. The effect of this "local" curvature on the non-local spacetime is to cause it to be Riemannian in the case of an atomic orbital, or hyperbolic, in the case of a pseudoelectron, as opposed to Euclidean in the case of the free electron. Each curvature is manifest as a gravitational field, a repulsive gravitational field, or the absence of a gravitational field, respectively. Thus, the spacetime is curved with constant spherical curvature in the case of an atomic orbital, or spacetime is curved with negative curvature in the case of a pseudoelectron.

Matter arises during particle production from a photon. The limiting velocity c results in the contraction of spacetime due to particle production. The contraction is given by $2\pi r_g$ where r_g is the gravitational radius of the particle. This has implications for the physics of gravitation. By applying the condition to electromagnetic and gravitational fields at particle production, the Schwarzschild metric (SM) is derived from the classical wave equation, which modifies general relativity to include conservation of spacetime in addition to momentum and matter/energy. The result gives a natural relationship between Maxwell's equations, special relativity, and general relativity. It gives gravitation from the atom to the cosmos. The Schwarzschild metric gives the relationship whereby matter causes relativistic corrections to spacetime that determines the curvature of spacetime and is the origin of gravity. The gravitational equations with the equivalence of the particle production energies permit the equivalence of mass-energy and the spacetime wherein a *"clock" is defined which measures "clicks" on an observable in one aspect, and in another, it is the ruler of spacetime of the Universe with the implicit dependence of spacetime on matter-energy conversion*. The masses of the leptons, the quarks, and nucleons are derived from this metric of spacetime.

The relativistic correction for spacetime dilation and contraction due to the production of a particle with positive curvature is given by Eq. (32.17):

$$f(r) = \left(1 - \left(\frac{v_g}{c}\right)^2\right) \tag{35.10}$$

As shown in the Gravity section (Eq. (32.35)), the derivation of the relativistic correction factor of spacetime was based on the constant maximum velocity of light and a finite positive Newtonian gravitational velocity v_g of the particle. The production of a particle requires that the velocity of the particle is equivalent to the Newtonian gravitational escape velocity, v_g, of the antiparticle:

$$v_g = \sqrt{\frac{2Gm_0}{r}} = \sqrt{\frac{2Gm_0}{\lambda\!\!\!^{-}_C}} \tag{35.11}$$

From Eq. (35.22) and Eqs. (35.18-35.19), the eccentricity is one and the particle production trajectory is a parabola relative to the center of mass of the antiparticle. The right-hand side of Eq. (32.43) represents the correction to the laboratory coordinate metric for time corresponding to the relativistic correction of spacetime by the particle production event. Consider a Newtonian gravitational radius, r_g, of each atomic orbital of the particle production event, each of mass m_0

$$r_g = \frac{2Gm_0}{c^2} \tag{35.12}$$

where G is the Newtonian gravitational constant. The substitution of each of Eq. (35.11) and Eq. (35.12) into the Schwarzschild metric Eq. (35.2) gives:

$$d\tau^2 = \left(1 - \left(\frac{v_g}{c}\right)^2\right)dt^2 - \frac{1}{c^2}\left[\left(1 - \left(\frac{v_g}{c}\right)^2\right)^{-1} dr^2 + r^2 d\theta^2 + r^2 \sin^2\theta d\phi^2\right] \tag{35.13}$$

and

$$d\tau^2 = \left(1 - \frac{r_g}{r}\right)dt^2 - \frac{1}{c^2}\left[\left(1 - \frac{r_g}{r}\right)^{-1} dr^2 + r^2 d\theta^2 + r^2 \sin^2\theta d\phi^2\right] \tag{35.14}$$

respectively. The solutions for the Schwarzschild metric exist wherein the relativistic correction to the gravitational velocity v_g and the gravitational radius r_g are of the opposite sign (i.e. negative). In these cases, the Schwarzschild metric (Eq. (35.2)) is:

$$d\tau^2 = \left(1 + \left(\frac{v_g}{c}\right)^2\right)dt^2 - \frac{1}{c^2}\left[\left(1 + \left(\frac{v_g}{c}\right)^2\right)^{-1} dr^2 + r^2 d\theta^2 + r^2 \sin^2\theta d\phi^2\right] \tag{35.15}$$

and

$$d\tau^2 = \left(1 + \frac{r_g}{r}\right)dt^2 - \frac{1}{c^2}\left[\left(1 + \frac{r_g}{r}\right)^{-1} dr^2 + r^2 d\theta^2 + r^2 \sin^2\theta d\phi^2\right] \tag{35.16}$$

The metric given by Eqs. (35.13-35.14) corresponds to positive curvature. The metric given by Eqs. (35.15-35.16) corresponds to negative curvature. The positive curvature of spacetime arises from the conversion of a photon traveling at light speed and having no gravitational mass into a bound particle-antiparticle pair such as an electron-positron pair each having its inertial rest mass relative to the corresponding particle's absolute space (Equivalence of Inertial and Gravitational Masses Due to Absolute Space and Absolute Light Velocity section). The escape velocity is the gravitational velocity v_g following a parabolic orbit with both particles traveling to an unbound state with relative velocity with respect to the absolute space corresponding to the excess energy over the mass energy of the particles (Gravity section). Both free particles such as leptons and antileptons exist with zero curvature. Each zero-curvature particle is predicted to have a zero gravitational mass and a zero gravitational radius based on continuity of the spacetime metric relationships given by Eqs. (35.13-35.14).

The equations that govern the production and trajectories of fundamental particles (Quantum Gravity of Fundamental Particles section and Particle Production section) also apply to the mechanical equations of existing particles. Bound and free electrons are natural states for inverse-r potentials. Yet, a third extraordinary state is possible for the correspondence between the geometrical form of the mass and the intrinsic motion of particles and their effect on spacetime which in turn affects the extrinsic motion of the particles. Specifically, the particle may possess a negative gravitation radius and a corresponding imaginary velocity. The metric given by Eqs. (35.13-35.14) corresponds to positive curvature; whereas, the metric given by Eqs. (35.15-35.16) corresponds to the extraordinary case of negative curvature. Spacetime having positive curvature in turn affects the extrinsic motion of the negatively curved particle such as one having mass and intrinsic motion confined to a negatively curved two-dimensional membrane in the form of a pseudosphere, pseudoelectron, to give rise to an imaginary translational velocity corresponding to a hyperbolic orbit along the gradient of the positive curvature. Thus, negative gravity (***fifth force***) can be created by forcing matter into negative curvature. A fundamental particle such as an electron with negative curvature, a pseudoelectron, would experience a central but repulsive force with a gravitating body comprised of matter of positive curvature. In this case, the fifth force deflects the pseudoelectron upward such that the negatively curved electron has the translational kinetic energy that causes the coordinate and proper times to be equivalent according to the Schwarzschild metric. Masses and their effects on spacetime superimpose; thus, the metric corresponding to the Earth is given by substitution of the mass of the Earth, M, for m_0 in Eqs. (35.11-35.16). The corresponding Schwarzschild metric Eq. (35.2) is:

$$d\tau^2 = \left(1 \pm \frac{2GM}{c^2 r}\right)dt^2 - \frac{1}{c^2}\left[\left(1 \pm \frac{2GM}{c^2 r}\right)^{-1} dr^2 + r^2 d\theta^2 + r^2 \sin^2\theta d\phi^2\right] \tag{35.17}$$

which is the gravitational mechanics equation that can be expressed in terms of the gravitational velocity v_g and the gravitational radius r_g as given by Eqs. (35.13-35.16) with the mass being that of the Earth $M = 5.98\ X\ 10^{24}\ kg$.

POSITIVE, ZERO, AND NEGATIVE GRAVITATIONAL MASS

The geometry of an electron's 2-dimensional mass surface determines that the electron may have a gravitational mass different from its inertial mass. A bound electron comprising a positively curved mass with its intrinsic surface velocity corresponds to a positive gravitational mass equal to the inertial mass (e.g. particle production or a bound electron). An absolutely free electron comprising a flat surface corresponds to zero gravitational mass with inertial mass m_e. A pseudoelectron comprising negatively curved mass with its intrinsic surface velocity corresponds to a negative gravitational mass with inertial mass m_e. Each case is considered in turn *infra*.

According to Newton's Law of Gravitation, the production of a particle of finite mass gives rise to a gravitational velocity of the particle that is essential in the determination of the particle masses as given in the Quantum Gravity of Fundamental Particles section and Particle Production section. The gravitational velocity of a gravitating body such as the Earth, the velocity of an existing particle, and the nature of its gravitational mass determines the energy, eccentricity, and trajectory of

the gravitational orbit of the particle. Consider the case of the equivalence of inertial and gravitational masses. The eccentricity, *e*, given by Newton's differential equations of motion in the case of the central field (Eq. (32.49-32.50)) permits the classification of the orbits according to the total energy, *E*, and according to the orbital velocity, v_0, relative to the Newtonian gravitational escape velocity, v_g, as follows [4]. The same relationships hold for trajectories during particle production and motion of existing particles:

$$\begin{array}{lll} E<0 & e<1 & \text{ellipse} \\ E<0 & e=0 & \text{circle (special case of ellipse)} \\ E=0 & e=1 & \text{parabolic orbit} \\ E>0 & e>1 & \text{hyperbolic orbit} \end{array} \tag{35.18}$$

$$\begin{array}{lll} v_0^2 < v_g^2 = \dfrac{2GM}{r_0} & e<1 & \text{ellipse} \\ v_0^2 < v_g^2 = \dfrac{2GM}{r_0} & e=0 & \text{circle (special case of ellipse)} \\ v_0^2 = v_g^2 = \dfrac{2GM}{r_0} & e=1 & \text{parabolic orbit} \\ v_0^2 > v_g^2 = \dfrac{2GM}{r_0} & e>1 & \text{hyperbolic orbit} \end{array} \tag{35.19}$$

Since $E = T + V$ and is constant, the closed orbits are those for which $T < |V|$, and the open orbits are those for which $T \geq |V|$. It can be shown that the time average of the kinetic energy, $< T >$, for elliptic motion in an inverse square field is $1/2$ that of the time average of the potential energy, $< V >$: $< T >= 1/2 < V >$.

In the case that a particle of inertial mass, m, is observed to have a speed, v_0, a distance from a massive object, r_0, and a direction of motion that makes an angle, ϕ, with the radius vector from the object (including a particle) of mass, *M*, the total energy is given by:

$$E = \frac{1}{2}mv^2 - \frac{GMm}{r} = \frac{1}{2}mv_0^2 - \frac{GMm}{r_0} = \text{constant} \tag{35.20}$$

The orbit will be elliptic, parabolic, or hyperbolic, according to whether E is negative, zero, or positive. Accordingly, if v_0^2 is less than, equal to, or greater than $\dfrac{2GM}{r_0}$, the orbit will be an ellipse, a parabola, or a hyperbola, respectively. Since h, the angular momentum per unit mass, is:

$$h = L/m = |\mathbf{r} \times \mathbf{v}| = r_0 v_0 \sin\phi \tag{35.21}$$

the eccentricity, *e*, from Eq. (32.63) may be written as:

$$e = [1 + \left(v_0^2 - \frac{2GM}{r_0} \right) \frac{r_0^2 v_0^2 \sin^2\phi}{G^2 M^2}]^{1/2} \tag{35.22}$$

The nature of the sign of the parameters v_g^2 and r_g (Eqs. (35.13-35.16)) with the corresponding mechanics equations determine the behavior of the electron of a given curvature in terms of the classification of the gravitational mass being positive, zero, or negative in the historical Newtonian or general relativistic view. In the last two cases, the inertial and gravitational masses are not equivalent. Consider the first case. The particle production equation (Eq. (32.43)) is for isolated particles at infinity wherein the gravitational and inertial masses are equal. A discontinuity in mass in positive curvature gives rise to a discontinuity in the positive curvature of spacetime that is the origin of gravity. Even at infinity relative to each other, each member of a production pair of particles is still in positive curvature due to the charge neutrality condition that requires that the field lines of one particle terminate on the other. The central field exists and maintains a positive curvature that maintains the equivalence of inertial and gravitational masses. The electric and magnetic fields of a particle are considered part of its inertial mass. This inertial mass is released as photons corresponding to the binding energy E_B of the oppositely charged particle. So, the sum of the masses of bound particles is less by $\dfrac{E_B}{c^2}$. The gravitational mass also decreases by this amount since the released photons have no gravitational mass as given in the Deflection of Light section. In a special case, a free electron can be maintained in the essential

absence of fields and without spin angular momentum by cancellation with orbital angular momentum such that the curvature is no longer positive, and the inertial and gravitational masses are no longer equivalent.

Minkowski space applies to the free electron. In the Electron in Free Space section, a free electron is shown to be a two-dimensional plane wave—a flat surface. Because the gravitational mass depends on the positive curvature of a particle, a free electron has inertial mass but not gravitational mass. If the electric and magnetic fields are essentially eliminated from a region of vacuum space containing an electron such that the electron is completely free and unbound and the spin angular momentum is cancelled, it may be possible to measure an electron gravitational mass that is less than the inertial mass m_e. The gravitational mass is zero in the limit of the electron being absolutely free. With the exclusion of electromagnetic fields and the cancelation of the spin angular momentum, Witteborn [1] experimentally measured the gravitational mass of the free electron using a free fall technique. The reported result was less than $0.09\ m_e$, where m_e is the inertial mass of the free electron $\left(9.109534\ X\ 10^{-31}\ kg\right)$. Thus, ***a free electron is not gravitationally attracted to ordinary matter, and the gravitational and inertial masses are not equivalent.*** Witteborn [1] explains the observation that free electrons floated in the drift tube by a postulated Schiff—Barnhill effect wherein the electrons in the metal of the drift tube fall in the Earth's gravitational field to produce an electric field which identically balances the force of gravity on the free electrons in the drift tube. This explanation is untenable. The binding energy of electrons in metals is typically 5 eV; whereas, the gravitational potential energy over atomic dimensions is over 20 orders of magnitude less and is given by $E = m_e gh$ where m_e is the mass of the electron, g is the acceleration of gravity, and h is the metal internuclear spacing, about $10^{-10}\ m$. The positive nuclei weigh 4,000 times the mass of the electrons. And, this zero mass equivalent electrical force requires the achievement of a perfect Penning trap having 11 orders of magnitude strength match at six-figure accuracy using gravity as the source of the trapping field by pure chance!

The reluctance to accept the experimental results of the free electron gravitational mass is that it would violate the Equivalence Principle and disprove general relativity[2]. This bias is evident in the presentation of the findings of the 2nd International Workshop on Antimatter and Gravity that took place on November 13–15, 2013 at the Albert Einstein Center for Fundamental Physics of the University of Bern. One of the main topics was on the results of the measurement of the gravitational mass of the free electron. The CERN Courier [5] reports:

"Free-fall experiments with charged particles are notoriously difficult because they must be carefully shielded from electromagnetic fields. For example, the sagging of the gas of free electrons in metallic shielding induces an electric field that can counterbalance the effect of gravity. Indeed, measurements based on dropping electrons led to a value of the acceleration of gravity, g, consistent with zero (instead of $g = 9.8$ m/s^2)."

Indeed the predicted gravitational mass of the free electron is zero.

Another reservation against the acceptance of the measurement of the zero gravitational mass of the free electron is that under the equivalence principle a perpetual motion scheme could be devised: (1) the free electron is formed with the application of a 13.6 eV photon to a hydrogen atom, (2) the proton and free electron are transported to infinity relative to the Earth, (3) the free electron binds with the proton to return the 13.6 eV photon, (4) the atom comprising a bound electron having a gravitational mass equivalent to the inertial mass falls to the Earth to net produce "free energy" from the added gravitational energy with the free electron now bound becoming gravitationally massive on the return trip. This scenario is an infinitely repeatable cycle; thus, it comprises perpetual motion. The reason why this is not the case is that it requires exactly the gravitation potential energy of the electron's inertial mass to exclude all fields, cancel spin, and form an absolutely free electron. The gravitational energy to completely eliminate any electric field termination on its surface and cancel the spin angular momentum such that it is absolutely free is given by:

$$V_G = -\frac{GMm}{r} = -\frac{6.67\ X\ 10^{-11}\ N\cdot m^2/kg^2\left(9.11\ X\ 10^{-31}\ kg\right)\left(5.98\ X\ 10^{24}\ kg\right)}{\left(6.37\ X\ 10^{6}\ m\right)} \tag{35.23}$$

$$= -5.70\ X\ 10^{-23}\ J = -3.56\ X\ 10^{-4}\ eV$$

wherein $r = 6.37\ X\ 10^{6}\ m$ is the radius of the Earth.

Furthermore, it is possible to give the electron negative curvature to cause a fifth force with negative gravitational mass behavior. Hereto, energy must be applied to form this state so no perpetual motion scheme is possible. The negative mass behavior can be modeled as a hyperbolic trajectory of a pseudoelectron. A particle comprising a gravitating body is the source of local spacetime curvature that is negative in the case of a pseudoelectron. In the presence of the large positive curvature of the Earth, the corresponding gravitational velocity is imaginary, the energy of the orbit of the pseudoelectron must always be greater than zero, the eccentricity is always greater than one, and the trajectory is a hyperbola (Eqs. (35.18-35.19) and (35.22)). The gravitational mass of the pseudoelectron behaves as negative and the inertial mass m_e is constant (e.g. equivalent to its mass energy given by Eq. (33.13)). The trajectory of pseudoelectrons can be found by solving the Newtonian inverse-square gravitational force equations for the case of a repulsive force caused by pseudoelectron production. The trajectory follows from the Newtonian gravitational force and the solution of motion in an inverse-square repulsive field is given by Fowles [6]. The

[2] The original Equivalence Principle put forth by Einstein was the equivalence of an accelerating inertial frame and a gravitational field that was shown to be incorrect and modified by others.

trajectory can be calculated rigorously by solving the orbital equation from the Schwarzschild metric (Eqs. (35.15-35.16)) for a two-dimensional spatial mass-density function of negative curvature which is repelled by the Earth. The rigorous solution is equivalent to that given for the case of a positive gravitational velocity given in the Orbital Mechanics section except that the gravitational velocity is imaginary and the magnitude is determined by the negative curvature.

In the case of a mass of negative curvature, Eq. (32.77) becomes

$$E_g = +\frac{GMm}{r} \tag{35.24}$$

where M is the mass of the Earth and m ***is the gravitational mass of the pseudoelectron that is negative, different from its inertial mass, and depends on the negative curvature***. The negative curvature is determined by the Gaussian curvature, *K*, at a point on a two-dimensional surface given by Eqs. (35.4-35.5) and (35.8). According to Eqs. (32.48), (32.140) and (32.43), matter, energy, and spacetime are conserved with respect to creation of the pseudoelectron which is repelled from a gravitating body (e.g. the Earth). The ejection of a pseudoelectron having a negatively curved mass surface from the Earth must result in an infinitesimal decrease in the radius of the Earth (e.g. r of the Schwarzschild metric given by Eq. (35.2) where $m_0 = M$ is the mass of the Earth, $5.98\ X\ 10^{24}\ kg$). The amount that the gravitational potential energy of the Earth is lowered is equivalent to the total energy gained by the repelled pseudoelectron. As an offsetting contribution to the curvature inventory, the conversion of matter to energy to produce the photon that excites the pseudoelectron state causes spacetime expansion according to Eq. (32.140). Upon decay, the energy is available to be absorbed to increase the equivalent inertial and gravitational masses of matter in positive curvature. Momentum is also conserved for the pseudoelectron and Earth, wherein the latter gravitating body that repels the pseudoelectron, receives an equal and opposite change of momentum with respect to that of the electron. As a familiar example, causing a satellite to follow a hyperbolic trajectory about a gravitating body is a common technique to achieve a gravity assist to further propel the satellite. In this case, the energy and momentum gained by the satellite are also equal and opposite those lost by the gravitating body. Next, the mathematical structure, nature, and energies of the pseudoelectron will be elucidated.

DETERMINATION OF THE PROPERTIES OF ELECTRONS, THOSE OF CONSTANT NEGATIVE CURVATURE, AND THOSE OF PSEUDOELECTRONS

The candidates for a negatively curved electron state are shown in Figures 35.1-35.4. By rotating a curve in the xz-plane about the z-axis, an exemplary surface of revolution with constant Gaussian curvature having $K = -1$ is generated. Consider that the Cartesian coordinate curve profile is given by:

$$c(t) = \left(x(t), 0, z(t)\right) \tag{35.25}$$

parameterized by arc length

$$x'(t)^2 + z'(t)^2 = 1 \tag{35.26}$$

The Gaussian curvature of the corresponding surface of revolution

$$f(u,v) = \left(x(u)\cos v, x(u)\sin v, z(u)\right) \tag{35.27}$$

is then given by

$$K(u,v) = \frac{x''(u)}{x(u)} = -1 \tag{35.28}$$

Since $K = -1$ is a constant, Eq. (35.28) gives rise to the second-order differential equation:

$$x''(t) + x(t) = 0 \tag{35.29}$$

that is solved analytically to give:

$$x(t) = ae^{t} + be^{-t} \tag{35.30}$$

where a and b are constants to match boundary conditions. The corresponding function z is then calculated from Eq. (35.26) by numerical integration to give the surface shown in Figure 35.5 [7]. Alternatively, the analytical expressions are given by M. Spivak [8] for the case of $a = -b$:

$$x(t) = a\left(e^{t} - e^{-t}\right) = 2a\sinh t \tag{35.31}$$

$$z(t) = \pm\int_0^t \sqrt{1 - 4a^2\cosh^2 t}\,dt \tag{35.32}$$

wherein $0 < 2a < 1$ and $1 \le \cosh t \le 1/2a$, so that $0 \le \cosh^{-1} 1/2a$ and $0 \le g(t) \le \sqrt{1-4a^2}$. These are functions that can be expressed in terms of elliptic integrals with results shown in Figure 35.5.

A free electron avoids a singularity by having the current density approach zero at the extrema. A nonphysical aspect of the candidate shown in Figure 35.5 having a negatively curved surface are the singularities at the extrema. In contrast, the pseudosphere (Figure 35.6) generated by rotating the tractrix about the asymptote avoids such a singularity and maintains current continuity at infinity. The mass goes to zero at the extrema at infinity since the corresponding area goes to zero, the current has an increasing azimuthal component at the extrema at infinity to maintain continuity, and relativistic effects cause the asymptotic span to be finite. Moreover, the constant radius R of the pseudosphere is permissive of a central force balance that is stable to radiation and conserves the electron angular momentum of $\hbar$ as shown in the Fourier Transform of the Pseudoelectron Current Density section and the Force Balance and Electrical Energies of Pseudoelectron States section. The nature of a pseudoelectron comprising an autonomous electron with a bound photon to maintain its surface of constant negative curvature can be appreciated by comparing it to other photon-electron states and the nature of the unnormalized atomic orbital current density distribution shown in Figure 1.20 and the normalized one shown in Figure 1.21.

Figure 35.5. The half-space surface rendering of a constant Gaussian curvature $K = -1$. The complete surface comprises additionally the mirror image.

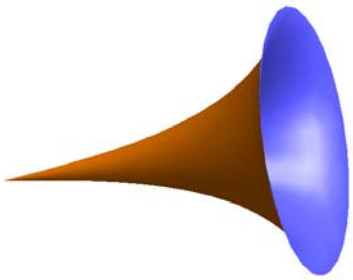

Figure 35.6. A pseudosphere showing rulings of the tractrix along the asymptote axis.

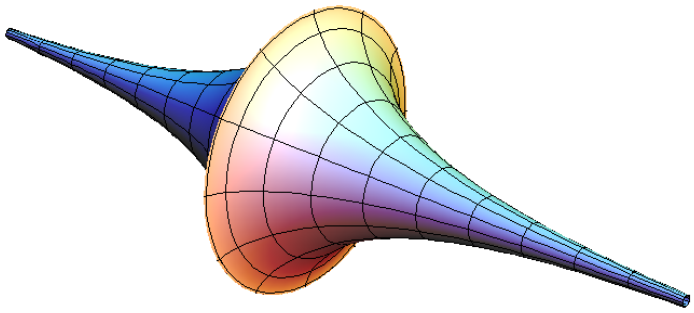

NATURE OF PHOTONIC SUPER BOUND HYDROGEN STATES AND THE CORRESPONDING CONTINUUM EXTREME ULTRAVIOLET (EUV) TRANSITION EMISSION AND SUPER FAST ATOMIC HYDROGEN

J. R. Rydberg showed that all of the spectral lines of atomic hydrogen were given by a completely empirical relationship:

$$\bar{\nu} = R\left(\frac{1}{n_f^2} - \frac{1}{n_i^2}\right) \tag{35.33}$$

where $R = 109,677\ cm^{-1}$, $n_f = 1,2,3,...$, $n_i = 2,3,4,...$ and $n_i > n_f$. Bohr, Schrödinger, and Heisenberg, each developed a theory for atomic hydrogen that gave the energy levels in agreement with Rydberg's equation:

$$E_n = -\frac{e^2}{n^2 8\pi\varepsilon_o a_H} = -\frac{13.598\ eV}{n^2} \tag{35.34}$$

$$n = 1,2,3,... \tag{35.35}$$

where e is the elementary charge, ε_o is the permittivity of vacuum, and a_H is the radius of the hydrogen atom. The Rydberg equation is a simple integer formula that empirically represents the Rydberg series of spectral lines, the entire hydrogen spectrum given in terms of the differences between all of the principal energy levels of the hydrogen atom.

The excited energy states of atomic hydrogen are given by Eq. (35.35) for $n > 1$ in Eq. (35.34). The $n = 1$ state is the "ground" state for "pure" photon transitions (i.e. the $n = 1$ state can absorb a photon and go to an excited electronic state, but it cannot release a photon and go to a lower-energy electronic state). However, an electron transition from the ground state to a lower-energy state may be possible by a resonant nonradiative energy transfer such as multipole coupling or a resonant collision mechanism. Processes such as hydrogen molecular bond formation that occur without photons and that require collisions are common [9]. Also, some commercial phosphors are based on resonant nonradiative energy transfer involving multipole coupling [10]. Specifically, atomic hydrogen may undergo a catalytic reaction with certain atomized elements and ions which

singly or multiply ionize at integer multiples of the potential energy of atomic hydrogen, $m \cdot 27.2\ eV$ wherein m is an integer. The predicted reaction involves a resonant, nonradiative energy transfer from otherwise stable atomic hydrogen to the catalyst capable of accepting the energy. The product is $H\left(1/p\right)$, fractional Rydberg states of atomic hydrogen called "hydrino atoms" wherein $n = \frac{1}{2}, \frac{1}{3}, \frac{1}{4}, ..., \frac{1}{p}$ ($p \le 137$ is an integer) replaces the well-known parameter $n = \text{integer}$ in the Rydberg equation for hydrogen excited states.

The $n = 1$ state of hydrogen and the $n = \frac{1}{\text{integer}}$ states of hydrogen are nonradiative, but a transition between two nonradiative states, say $n = 1$ to $n = 1/2$, is possible via a nonradiative energy transfer. Hydrogen is a special case of the stable states given by Eqs. (35.34) wherein the corresponding radius of the hydrogen or hydrino atom is given by:

$$r = \frac{a_H}{p}, \tag{35.36}$$

where $p = 1, 2, 3, ...$. In order to conserve energy, energy must be transferred from the hydrogen atom to the catalyst in units of

$$m \cdot 27.2\ eV,\ m = 1, 2, 3, 4, ... \tag{35.37}$$

and the radius transitions to $\frac{a_H}{m+p}$. The catalyst reactions involve two steps of energy release: a nonradiative energy transfer to the catalyst followed by additional energy release as the radius decreases to the corresponding stable final state. Thus, the general reaction is given by:

$$m \cdot 27.2\ eV + Cat^{q+} + H\left[\frac{a_H}{p}\right] \rightarrow Cat_{fast}^{(q+r)+} + re^- + H*\left[\frac{a_H}{(m+p)}\right] + m \cdot 27.2\ eV \tag{35.38}$$

$$H*\left[\frac{a_H}{(m+p)}\right] \rightarrow H\left[\frac{a_H}{(m+p)}\right] + [(p+m)^2 - p^2] \cdot 13.6\ eV - m \cdot 27.2\ eV \tag{35.39}$$

$$Cat_{fast}^{(q+r)+} + re^- \rightarrow Cat^{q+} + m \cdot 27.2\ eV \tag{35.40}$$

And, the overall reaction is:

$$H\left[\frac{a_H}{p}\right] \rightarrow H\left[\frac{a_H}{(m+p)}\right] + [(p+m)^2 - p^2] \cdot 13.6\ eV \tag{35.41}$$

q, r, m, and p are integers. $H*\left[\frac{a_H}{(m+p)}\right]$ has the radius of the hydrogen atom (corresponding to 1 in the denominator) and a central field equivalent to $(m+p)$ times that of a proton, and $H\left[\frac{a_H}{(m+p)}\right]$ is the corresponding stable state with the radius of $\frac{1}{(m+p)}$ that of H. As the electron undergoes radial acceleration from the radius of the hydrogen atom to a radius of $\frac{1}{(m+p)}$ this distance, energy is released as characteristic light emission or as third-body kinetic energy. The emission may be in the form of an extreme-ultraviolet continuum radiation having an edge at $[(p+m)^2 - p^2 - 2m] \cdot 13.6\ eV$ or $\frac{91.2}{[(p+m)^2 - p^2 - 2m]}\ nm$ and extending to longer wavelengths [11-17]. In addition to radiation, a resonant kinetic energy transfer from $H*\left[\frac{a_H}{(m+p)}\right]$ to form fast H may occur by an inverse Franck-Hertz mechanism [18] involving H atoms rather than electrons that are selective for H based on resonant dipole induction and H being the most efficient momentum acceptor having the least mass of any atom (See the Dipole-Dipole Coupling section). Subsequent excitation of these fast $H\left(n=1\right)$ atoms by collisions with the background gases followed by emission of the corresponding $H\left(n=3\right)$ atoms gives rise to broadened Balmer α emission. Fast H may also arise from the production of fast protons that conserve the potential energy of the catalyst that is ionized during the energy transfer wherein the catalyst comprises a source of H such as HOH or nH (n is an integer) catalyst. The fast protons recombine with electrons to give the characteristic Doppler broadened atomic H lines such as broadened Balmer alpha emission observed experimentally [19-25].

Visible photons and extremely high-energy photons, respectively, may excite the formation of photon bound, autonomous electron states such as spherical states in liquid media and inverse spherical states in vacuum or gas. The former case regards the formation of photon bonding of an atomic orbital current density function as given in the One Electron Atom section. In the latter case, a free electron is in a nonradiative bound state comprising geometry that is the inverse of a bound excited state. Specifically, a free electron may form an inverse spherical bound state of pseudospherical mass, charge, and surface current density bound by a trapped photon that travels along the two-dimensional electron surface as in the case of the

excited states, but the photon field is repulsive rather than attractive, such that the direction of the centrifugal forces is also opposite the spherical case. Here, the energy to form the stable bound state is not due to a negative electrostatic potential. Rather, the binding energy is due to the negative gravitational potential energy that arises from the mass, charge, and current density surface in negative curvature. The pseudospherical electron state is referred to as a ***pseudoelectron***. The formation of a pseudoelectron requires the presence of a gravitating body wherein the gravitational energy is conserved between the gravitating body and the pseudoelectron. Specifically, the positive curvature of spacetime due to the gravitating body is increased causing a more negative gravitational energy in response to the negative curvature contribution of the pseudoelectron that consequently experiences a force to eject it from the spacetime in proximity to the gravitating body. The change in positive curvature and corresponding gravitational field propagate as a light-like wave as in the case with particle production given in the Quantum Gravity of Fundamental Particles section.

NATURE OF PHOTON-BOUND AUTONOMOUS ELECTRON STATES

As shown in the Free Electrons in Superfluid Helium are Real in the Absence of Measurement Requiring a Connection of Ψ(x) to Physical Reality section, free electrons are trapped in superfluid helium as autonomous electron bubbles interloped between helium atoms that have been excluded from the space occupied by the bubble [26-29]. The surrounding helium atoms maintain the spherical bubble through van der Waals forces. Each spherical electron cavity comprises an atomic orbital that can act as a resonator cavity. The excitation of the Maxwellian resonator cavity modes by resonant photons forms bubbles with radii of reciprocal integer multiples of that of the unexcited $n = 1$ state. The central force that results in a fractional electron radius compared to the unexcited electron is provided by the absorbed photon. Each stable excited state electron bubble that has a radius of $\frac{r_1}{\text{integer}}$ may migrate in an applied electric field. The photo-conductivity absorption spectrum of free electrons in superfluid helium and their mobilities predicted from the corresponding size and multipolarity of these long-lived bubble-like states with quantum numbers n, ℓ, and m_ℓ matched the experimental results of the 15 identified ions [26].

In addition to superfluid helium, free electrons also form bubbles devoid of any atoms in other fluids such as oils and liquid ammonia. In the operation of an electrostatic atomizing device, Kelly [30] observed that with plasma light irradiation the mobility of free electrons in oil increased by an integer factor rather than continuously. Certain metals such as alkali metals that have low ionization energy dissolve as ions and free electrons in liquid ammonia and certain other solvents. As in the case of free electrons in superfluid helium, ammoniated free electrons form cavities devoid of ammonia molecules having a typical diameter of 3-3.4 Å. The cavities are evidenced by the observation that the solutions are of much lower density than the pure solvent. From another perspective, they occupy far too great a volume than that predicted from the sum of the volumes of the metal and solvent. The electrolytically conductive solutions have free electrons of extraordinary mobility as their main charge carriers [31]. In very pure liquid ammonia the lifetime of free electrons can be significant with less than 1% decomposition per day. The confirmation of their existence as free entities is given by their broad absorption around 15,000 Å that can only be assigned to free electrons in the solution that is blue due to the absorption. In addition, magnetic and electron spin resonance studies show the presence of free electrons, and a decrease in paramagnetism with increasing concentration is consistent with spin pairing of electrons to form diamagnetic pairs.

In the case of vacuum, there is no solvent sphere; consequently, new physics may be observed with high energy irradiation of electrons, namely the formation of pseudoelectrons each comprising a pseudospherical charge and current density membrane held in force balance by a trapped photon. In the case of free electrons in a liquid medium such as superfluid helium, ammonia, or oil, the geometry is driven by minimization of the surface to volume ratio similar to the case with surface tension of bubble films. In contrast, the formation of a pseudoelectron depends on maximizing the negative gravitational potential energy that also results in the further minor energy contribution to stability of the minimization of the electric self-field energy. This occurs by maximizing the surface to volume ratio to diffuse the electric field. By both mechanisms, the energy stability is achieved by minimizing the pseudosphere volume (Eq. (35.100)) that also maximizes the curvature K of pseudoelectron having a R^{-2} dependency where R is the pseudoelectron radius (Eq. (35.8)). In addition, the nature of the absorbed photon of the particular electronic state determines its stability or instability wherein the nature of the absorbed photon is dependent on the geometry or curvature of the electron comprising a 2-D current membrane, any nuclear field, and the energy of the state.

As shown by Eqs. (35.38-35.41), the photonic contribution to the central field of a hydrino is positive. Specifically, at the position of the electron, the photon field provides the equivalent of a positive integer increase to the central field of the proton (Eq. (5.27)) that gives rise to a radial monopole (Eq. (6.9)). Conversely, at the position of the electron, the excited state photon field comprises the superposition of two components, the negative equivalent of the central field of the proton and a positive reciprocal integer times the equivalent of the central field of the proton (Eqs. (2.12-2.17)). The opposing components give rise to the sum of a radial dipole (Eq. (2.25))) and a positive spherical and time harmonic monopole having the field equivalents of the fundamental charge and a fraction of the fundamental charge, respectively. The photonic central field of the pseudoelectron is purely negative; thus, the photon field gives rise to a corresponding pure radial monopole at the position of the electron. The stability of the pseudoelectron (Eqs. (35.72)) versus the instability of an electronic excited state (Eqs. (2.29-2.35)) arises from the different states having negative curvature versus positive curvature, respectively. The different geometries cause the corresponding current densities to be absent and possess Fourier components synchronous with waves traveling at the speed

of light, respectively, that determine stability to radiation as given in the Fourier Transform of the Pseudosphere Current Density section.

The radiative states comprise the hydrino intermediate (atomic hydrogen following energy transfer to a catalyst), excited states, and free electron states undergoing acceleration wherein the mechanism of charge acceleration may be generalized to all three cases. The nonradiative cases are hydrogen ($n=1$ state), hydrino states, spherical states in a liquid medium, these states with an absorbed photon, and free electrons at rest or constant velocity. The lifetime of the pseudoelectron state may be long as it is in the case of the continuum excited states of free electrons comprising a bound photon and negative gravitational potential energy to maintain the state with kinetic energy equal to ½ the excitation energy as shown in the Classical Physics of the de Broglie Relation section.

PSEUDOELECTRONS

Surfaces shown in Figures 35.1-35.4 are candidates for a negatively curved electron state to produce the sought negative gravitational force according to Eqs. (35.15-35.16). The boundary constraints are a surface of constant negative Gaussian curvature and capable of binding a photon and maintaining mechanical and electrical force balance with the relativistic photon field normal to the electron surface as given in the Equation of the Electric Field inside the Atomic Orbital section, relativistic invariance and total energy conservation of the equation of motion on the surface, and stability of the current to radiation. Let's first solve the equivalent of the great circle current loop of the Atomic Orbital Equation of Motion for $\ell=0$ Based on the Current Vector Field (CVF) section in hyperbolic coordinates. By rotating a curve in the xz-plane about the z-axis, an exemplary surface of revolution with constant Gaussian curvature having $K=-1$ is generated. Consider that the alternative Cartesian coordinate curve profile given by Eqs. (35.25-35.30) for the case of $a=1$ and $b=0$. Eq. (35.30) becomes:

$$x(t)=ae^{t} \tag{35.42}$$

Using Eq. (35.26), Eq. (35.32) becomes:

$$z(t)=\pm\int_0^t\sqrt{1-e^{2t}}\,dt=\sqrt{1-e^{2t}}-\cosh^{-1}\left(e^{-t}\right) \tag{35.43}$$

replacing some variables gives the xz-cross section of a pseudosphere shown in Figure 35.6 having the equation:

$$z=\sqrt{1-x^2}-\cosh^{-1}\frac{1}{x} \tag{35.44}$$

A pseudosphere, also called a tractroid, tractricoid, antisphere, or tractrisoid, comprises a negative-Gaussian curvature surface $K=-1$ of revolution generated by a tractrix in the xy-plane about its asymptote, the z-axis. The pseudosphere of radius $r>0$ is the image $R(\mathrm{R}\times[0,2\pi[)$ having Cartesian parametric equations of:

$$\mathbf{r}(u,v)=\underline{\mathbf{e}}\begin{pmatrix} r\,\mathrm{sech}(u)\cos(v)\\ r\,\mathrm{sech}(u)\sin(v)\\ ru-r\tanh^2(u)\end{pmatrix} \tag{35.45}$$

for $u\in(-\infty,\infty)$ and $v\in[0,2\pi)$. Alternatively, the pseudosphere can be expressed in Cartesian form as:

$$z^2=\left[R\,\mathrm{sech}^{-1}\left(\frac{\sqrt{x^2+y^2}}{R}\right)-\sqrt{R^2-x^2-y^2}\right]^2 \tag{35.46}$$

A pseudoelectron shown in Figures 35.6 and 35.7 comprises a pseudospherical plane lamina of charge and current density comprising a minimum total energy surface having constant negative curvature of $K=-1$. The pseudospherical membrane is bound by a photon. The absorbed photon of the pseudoelectron provides a repulsive central electric field that maintains the pseudoelectron in force balance between the centrifugal and corresponding electrostatic force wherein the directions of the centrifugal and electrostatic forces relative to the direction along the central radius are opposite those of hydrino and excited states, and negative binding energy is from the negative gravitational potential energy of the state of constant negative curvature.

Figure 35.7. A representation of a pseudoelectron.

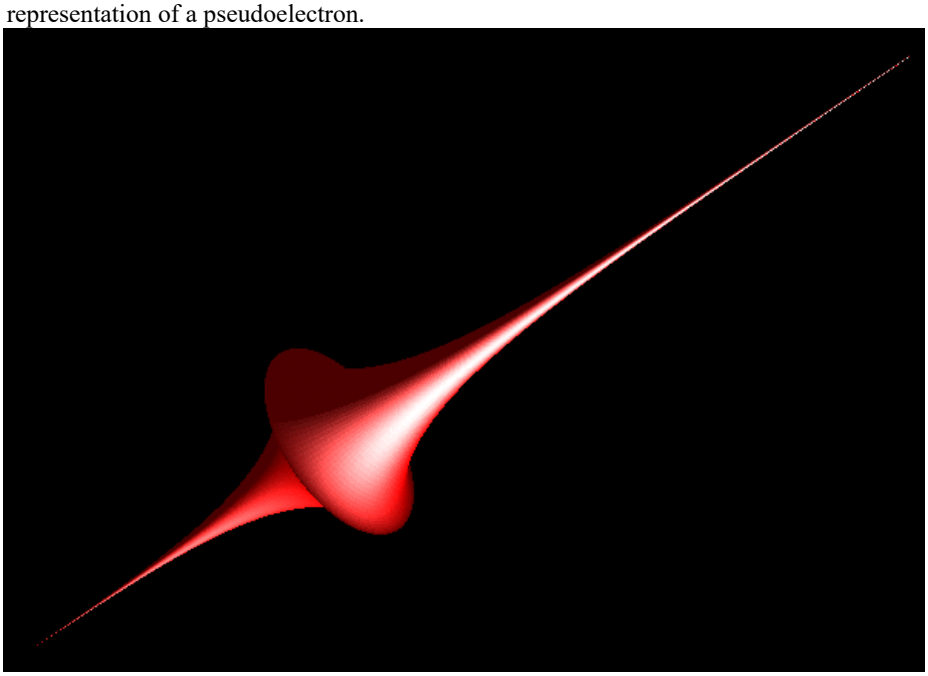

The pseudosphere is a solution of the sine-Gordon equation. Consider that the pseudosphere may be described as a map $\vec{x}(u,v)$ from a patch to the surface. If the map is parametrized by arclength along asymptotic lines, then the first fundamental form for the pseudosphere is:

$$\mathbf{I} = d\vec{x} \cdot d\vec{x} = du^2 + 2\cos\phi dudv + dv^2 \tag{35.47}$$

Similarly, the second fundamental form is:

$$\mathbf{II} = d\vec{x} \cdot d\vec{N} = \frac{2}{\rho}\sin\phi dudv \tag{35.48}$$

Application of the Codazzi-Mainardi equations then yields [32]

$$\phi_{uv} = \frac{1}{\rho^2}\sin\phi \tag{35.49}$$

which is the sine-Gordon equation that can be written as:

$$\frac{\delta^2}{\delta t^2}\phi - \frac{\delta^2}{\delta x^2}\phi + \sin\phi = 0 \tag{35.50}$$

The sine-Gordon equation also meets the prerequisite of being invariant under Lorentz transforms. The relevant Lorentz transforms are:

$$t' = \gamma\left(t - \frac{vx}{c^2}\right) \tag{35.51}$$

$$x' = \gamma\left(x - vt\right) \tag{35.52}$$

$$y' = y \tag{35.53}$$

$$z' = z \tag{35.54}$$

wherein the inverse Lorentz transformations are given by interchanging the primed and unprimed variables and changing the sign of the velocity. The spacetime sine-Gordon equation (Eq. (35.50)) can be expressed in spacetime coordinates as:

$$\varphi_{tt} - \varphi_{xx} + \sin\phi = 0 \tag{35.55}$$

Using the consideration that γ is a constant, Eq. (35.55) can be expressed in the primed coordinates using the following relationships of the time-coordinate:

$$\varphi_{t'} = \varphi_t \frac{dt}{dt'} = \gamma\varphi_t \tag{35.56}$$

$$\varphi_{t't'} = \frac{\delta\gamma}{\delta t'}\phi_t + \gamma\varphi_{tt}\frac{\delta\gamma}{\delta t'} = \gamma^2\varphi_{tt} \tag{35.57}$$

The corresponding space-coordinate relationship is:

$$\varphi_{x'x'} = \gamma^2\varphi_{xx} \tag{35.58}$$

Using Eqs. (35.55-35.58), the transformed sine-Gordon equation is:

$$\varphi_{t't'} - \varphi_{x'x'} + \frac{1}{\gamma^2}\sin\phi = 0 \tag{35.59}$$

The equations of motion of matter and energy that are a solution of the sine-Gordon equation obey the laws of the universe wherein higher velocity gives rise to relativistic length contraction and mass increase of the electron mass density function as given in the Special Relativistic Effect on the Electron Radius and the Relativistic Ionization Energies section.

The sine-Gordon equation can be derived from the Lagrangian with the proper setting of the potential energy function. The general physical energy equations of the current and mass density of the electron are given by the classical Lagrangian that obeys the principle of least action corresponding to conservation of the total energy:

$$L = \delta_u\delta^u\phi - U(\phi) \tag{35.60}$$

The corresponding general physical equations of motion are:

$$\delta_u\delta^u\phi + \left(\frac{\delta U}{\delta\phi}\right) = 0 \tag{35.61}$$

The function ϕ is the spacetime mass and current density function of the negatively curved electron. It is also the spacetime function of the photon field that is in phase with the electron density functions and maintains the force balance. The surface is equal energy, but not equipotential. The potential is given by:

$$U = \cos\phi \tag{35.62}$$

Considering one spatial and time dimension corresponding to one current loop the equation of motion becomes the sine-Gordon equation given by Eq. (35.50).

The sine-Gordon equation meets the prerequisite of being of the proper form for governing motion of mass and electromagnetic fields comprising a surface of negative curvature. The sine-Gordon equation is a hyperbolic, nonlinear wave equation in 1 + 1 dimensions having solutions of surfaces with constant negative Gaussian curvature K = −1, also called pseudospherical surfaces. The solutions $\varphi(x,t)$ of Eq. (35.50) determine the internal Riemannian geometry of surfaces of constant negative scalar curvature R = −2, given by the line-element:

$$ds^2 = \sin^2\left(\frac{\phi}{2}\right)dt^2 + \cos^2\left(\frac{\phi}{2}\right)dx^2 \tag{35.63}$$

where the angle ϕ describes the embedding of the surface into Euclidean space R^3 [33]. Another common terminology regarding the pseudosphere is the hyperboloid model of the hyperbolic plane wherein the hyperboloid is referred to as a pseudosphere since the hyperboloid can be thought of as a sphere of imaginary radius, embedded in a Minkowski space. Like the atomic orbital of centrally bound states, the pseudoelectron is stable to radiation; thus, it satisfies all of the boundary conditions.

FOURIER TRANSFORM OF THE PSEUDOELECTRON CURRENT DENSITY

Both the atomic excited state photon and the pseudoelectron photon have at least a component of negative radially directed central field that gives rise to a radiative electric dipole in the case of an excited state as shown by Fourier transform analysis in the Instability of Excited States section. However, in contrast to the atomic excited state electron, the radial field corresponds to a monopole, and the radiative stability of the pseudoelectron can be shown by the absence of Fourier components $k = \omega/c$ of the spacetime Fourier transform of the pseudoelectron current density function given by Eq. (35.72) with the constant current having angular frequency given by Eq. (35.85) integrated over the parameter u. Due to the constancy of the current that is required to maintain a constant total energy, the time dependent local current fluctuations are zero such that the corresponding Fourier transform is zero. Thus, radiative components $k = \omega/c$ do not exist.

Consider the alternative pseudospherical Cartesian parametric equations of:

$$x = R\cos(u)\sin(v) \tag{35.64}$$

$$y = R\sin(u)\sin(v) \tag{35.65}$$

$$z = R\left(\cos(v) + \ln\left[\tan\left(\frac{1}{2}v\right)\right]\right) \tag{35.66}$$

for $u \in (0, 2\pi)$ and $v \in (0, \pi)$. The Fourier transform of the pseudosphere $K(s)$ may be obtained by expressing the Fourier transform in pseudospherical coordinates using (Eqs. (35.64-35.66)) and the Jacobian:

$$J(v) = -R^2 \cos(v) \ln\left[\tan\left(\frac{v}{2}\right)\right] \sin(v) \tag{35.67}$$

The integrals over the parametric variables u and v are:

$$K(s) = -R^2 \int_0^{\pi} \int_0^{2\pi} \cos(v) \ln\left[\tan\left(\frac{v}{2}\right)\right] \sin(v) \exp\left[-2\pi i s R \cos(u) \sin(v)\right] du dv \tag{35.68}$$

The integration over u given by Mathematica is:

$$K(s) = -2\pi R^2 \int_0^{\pi} J_0\left(2\pi s R \sin(v)\right) \cos(v) \ln\left[\tan\left(\frac{v}{2}\right)\right] \sin(v)\, dv \tag{35.69}$$

The integration over v is not analytically computable by Mathematica. However, Eq. (35.69) may be integrated as a power series expansion about $v = 0$:

$$K(s) = -2\pi R^2 \left(\begin{array}{l} \frac{1}{4}\left(-1 - 2\ln 2 + 2\ln \pi\right)\pi^2 \\ +\frac{1}{192}\left(\begin{array}{l} 12 + 3\left(2\pi s R\right)^2 + 4\left(2\pi s R\right)^2 \ln 8 \\ +4\ln 256 - 32\ln \pi - 12\left(2\pi s R\right)^2 \ln \pi \end{array} \right)\pi^4 \\ +O\left[\pi\right]^5 \end{array} \right) \tag{35.70}$$

Next, the constant time function must be considered. The constant current is given by the charge density multiplied by the constant angular frequency and a constant time function. The Fourier transform of a constant time function [34] is:

$$\begin{array}{ccc} x(t) = \int_{-\infty}^{\infty} X(f)\, e^{j2\pi ft} df & & X(t) = \int_{-\infty}^{\infty} x(t)\, e^{-j2\pi ft} dt \\ \hline 1 & \Leftrightarrow & \delta(f) \end{array} \tag{35.71}$$

A very important theorem of Fourier analysis states that the Fourier transform of a product is the convolution of the individual Fourier transforms [35]. Treating the radial monopole due to the pseudoelectron photon-electron interface, the spacetime Fourier transform of the pseudoelectron current density function $P(s)$ is given by the convolution of the Fourier transforms of the current density alone (Eq. (35.70)) and the time function alone (Eq. (35.71)). The convolution of the frequency delta function of Eq. (35.71) with $P(s)$ (Eq. (35.72)) replaces the frequency variable with zero and produces zero resultant:

$$P(s) = \omega K(s) \otimes \delta(\omega) = 0 K(s) = 0 \tag{35.72}$$

Thus, when the light-like condition of Eq. (Ap.I.43) is applied, the spacetime Fourier transform of the pseudoelectron current density function (Eq. (35.72)) is absent Fourier components $k = \omega / c$ due to the absence of the equivalent of time and spherically harmonic current components of atomic electronic excited states. There are no time fluctuations of the current. Rather, it is constant in spacetime having zero as the corresponding Fourier transform.

FORCE BALANCE AND ELECTRICAL ENERGIES OF PSEUDOELECTRONS STATES

Unlike the case wherein photons are released spontaneously by minimization of the energy in a positive R^{-2} field such as during emission of an excited state or during a hydrino transition corresponding to the inverse of an excited state, the potential energy and kinetic energy of the pseudoelectron are both positive. The total energy must be negative in order for the pseudoelectron to be stable, and the negative energy requirement for stability is satisfied when the negative gravitational energy exceeds the total energy according to Eq. (35.97).

The force balance of the pseudoelectron is provided by a trapped photon having an electric field at the inner pseudospherical surface corresponding to the electric potential given by Eqs. (35.74) and (35.77). The far-field of the free electron and the far-field of a pseudoelectron are each that of a point charge at the origin along the z-axis, the axis perpendicular to the plane of the free electron and the axis in the plane perpendicular to the asymptote of the pseudoelectron, respectively. The pseudoelectron (PE) transition is excited by a linearly polarized photon corresponding to zero angular momentum. The transition is similar to the spherical transition with $\Delta m_\ell = 0$ (Eq. (2.71)). Based on the symmetry of the pseudoelectron across the plane perpendicular to the asymptote (yz-plane), the cross section is highest for the photon propagating along the z-axis. The angular dependence of the pseudoelectron excitation can be calculated by substituting the photon-e&mvf for the helium atom in

the elastic scattering of a free electron from helium as given in the Electron Scattering for Helium Based on the Atomic Orbital Model section. The photon electric field is predominantly forward scattered as shown by Eq. (8.57) and Figure 8.8.

The photon that maintains the force balance of the pseudoelectron exists only at the inner surface of the pseudoelectron described by a Dirac delta function such as given by Eq. (2.15) with the spherical radius replaced by the pseudospherical radius $\mathbf{r}(u,v)$ (Eq. (35.45)). The charge, current, and angular momentum are finite integratable without incurring infinites at the extrema of the asymptote such that the average electric field density due to the trapped photon is the same as that of a spherical excited electronic state. Specifically, the area A of the electron atomic orbital and the pseudoelectron are equivalent:

$$A = 4\pi R^2 \tag{35.73}$$

wherein R is the radius of the electron atomic orbital and also the pseudoelectron. A Gauss's-law approach gives an average wherein the average electric field density due to the trapped photon matches that of a spherical excited electronic state.

$$\mathbf{E}_{photon} = \frac{-Ze}{4\pi\varepsilon_0 R^2}\delta\left(r-\mathbf{r}(u,v)\right)\hat{\mathrm{N}} \tag{35.74}$$

However, unlike the case of a sphere, the surface area of the pseudosphere is not independent of the position on the surface. The area element dA is

$$dA = R^2 \operatorname{sech} u\left|\tanh u\right| du dv = 2\pi R^2 \operatorname{sech} u\left|\tanh u\right| du \tag{35.75}$$

The normalized area element variation along the pseudosphere current loop is:

$$dA = \frac{R^2 \operatorname{sech} u\left|\tanh u\right| du}{2} \tag{35.76}$$

Thus, the normal electric field as a function of area position on the current loop of the pseudosphere is:

$$\mathbf{E}_{photon}(u) = \frac{-Ze}{4\pi\varepsilon_0 R^2}\frac{2}{\operatorname{sech} u\left|\tanh u\right| du}\delta\left(r-\mathbf{r}(u,v)\right)\hat{\mathrm{N}} \tag{35.77}$$

wherein $\hat{\mathbf{N}}$ is the pseudosphere surface normal vector and $\mathbf{r}(u,v)$ is given by Eq. (35.45). The photon travels on the inner surface of the pseudoelectron at light speed such that the relativistic electric field at each point of contact with the pseudoelectron is perpendicular to the tangent at that point and the radius R is tangential. The parameter-curve tangent vectors are:

$$r_u(u,v) = \underline{\mathbf{e}}\begin{pmatrix} -r\,tanh(u)\operatorname{sech}(u)\cos(v) \\ -r\,tanh(u)\operatorname{sech}(u)\sin(v) \\ r - r\operatorname{sech}^2(u) \end{pmatrix}, \qquad r_v(u,v) = \underline{\mathbf{e}}\begin{pmatrix} -r\operatorname{sech}(u)\cos(v) \\ r\operatorname{sech}(u)\sin(v) \\ 0 \end{pmatrix} \tag{35.78}$$

Such a field is a solution to the sine-Gordon equation and is relativistically invariant. The set of perpendicular field lines extended to infinity form a catenoid that is a minimum surface, one having no mean curvature. The electric fields of the pseudosphere or anti-sphere are in the opposite direction than in the case of a bound electron having spherical geometry. The relativistic electric field is negative in sign and perpendicular to the pseudosphere radius $\mathbf{r}(u,v)$ rather than being positive in sign and directed along the spherical central radius. The standard unit normal vector field of the electric field shown in Figure 35.8 is:

$$\hat{\mathbf{N}}(u,v) = \left|\coth u\right|\underline{\mathbf{e}}\begin{pmatrix} \left(\operatorname{sech}^2(u)-1\right)\cos(v) \\ \left(\operatorname{sech}^2(u)-1\right)\sin(v) \\ -\operatorname{sech}(u)\tanh u \end{pmatrix} \tag{35.79}$$

Figure 35.8. A representation of the standard unit normal vector field of the electric field of a pseudoelectron.

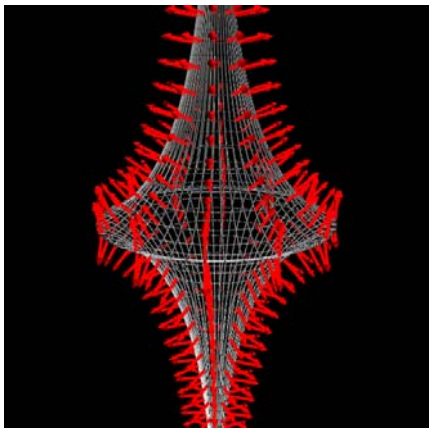

The hyperbolic function of the photon electric field (Eq. (35.77)) that gives the outward directed force integrates or averages to 2 over one cycle. Thus, for the pseudosphere as a whole the electric force $\mathbf{F}_{ele}$ is equivalent to that of a point charge of $-e$ at the origin of a sphere having the pseudosphere radius. The photon is phase locked with the current, and the force due to the mass motion corresponding to the current balances the electric force due to the photon. The centrifugal force that is normal to the surface of the pseudosphere is given by the general equation of force of an object in rotation. The general force in a rotating system is [36]:

$$\mathbf{F}_{centrifugal} = m_e \frac{d^2 R}{dt^2} + m_e \frac{d\omega}{dt} \times R - 2m_e \omega \times \frac{dR}{dt} + m_e \omega \times (\omega \times R) \tag{35.80}$$

In force balance between the electric and centrifugal forces, the overall frequency ω and radius R are constants such that Eq. (35.80) becomes:

$$\mathbf{F}_{centrifugal} = m_e \omega \times (\omega \times R) \tag{35.81}$$

The gravitational mass is zero for a free electron having zero net angular momentum such that it is completely unbounded. Otherwise, it is equivalent to an infinite excited state electron. The scalar angular momentum of a pseudoelectron due to the current is $\hbar$, and it is constant in force balance. Consider the generator functions of the pseudospherical surface that comprises the pseudoelectron current density function. A tractrix is a curve with the property that the radius hyperbolic R being the segment of the tangent line between the point of tangency and a fixed line called the asymptote is constant, and the revolution of the tractrix about the asymptote by 2π forms a pseudosphere. Both of the electric and centrifugal forces are only normal to the surface of the pseudosphere surface, also corresponding to being only normal to the tangent line. Consider the constancy of the integrated, time averaged angular momentum of $\hbar$ along all current loops that possess hyperbolic geometry, the constancy of the angular momentum per unit mass of the pseudoelectron, and the effect of the variation of the cylindrical coordinate radii ρ and the corresponding cross sectional area elements along the current path. The areal velocity as a function of the variable u is equal to one half the angular momentum per unit mass [37]:

$$\frac{dA(u)}{dt} = \frac{L}{m} = \frac{\hbar}{2m_e} \tag{35.82}$$

The areal velocity as a function of the parameter u is given by the product of the frequency and π times the differential cylindrical coordinate radius squared, the area element of Eq. (35.76):

$$\frac{dA(u)}{dt} = \frac{\omega_u}{2\pi} \pi R^2 \frac{\operatorname{sech} u \left|\tanh u\right| du}{2} \tag{35.83}$$

Using Eqs. (35.82) and (35.83), the position dependent angular velocity ω_u is given by [38]:

$$\frac{\omega_u}{2\pi} \pi R^2 \frac{\operatorname{sech} u \left|\tanh u\right| du}{2} = \frac{\hbar}{2m_e} \tag{35.84}$$

$$\omega_u = \frac{\hbar}{m_e R^2} \frac{2}{\operatorname{sech} u \left|\tanh u\right| du} \tag{35.85}$$

Using Eq. (35.81) and (35.85), the centrifugal force $\mathbf{F}_{centrifugal}(u)$ becomes:

$$\begin{aligned}\mathbf{F}_{centrifugal}(u) &= m_e\left(\frac{\hbar}{m_e R^2}\frac{2}{\operatorname{sech} u\left|\tanh u\right| du}\right)^2 R\frac{2}{\operatorname{sech} u\left|\tanh u\right| du}\hat{\mathbf{N}} \\ &= \frac{\hbar^2}{m_e R^3}\left(\frac{2}{\operatorname{sech} u\left|\tanh u\right| du}\right)\hat{\mathbf{N}}\end{aligned} \tag{35.86}$$

wherein the radius is corrected for position as a function of the parameter u (Eq. (35.76)). The opposing electric force $\mathbf{F}_{ele}(u)$ follows from Eq. (35.77):

$$\mathbf{F}_{ele}(u) = \frac{Ze^2}{4\pi\varepsilon_0 R^2}\frac{2}{\operatorname{sech} u\left|\tanh u\right| du}\hat{\mathrm{N}} \tag{35.87}$$

Equating the outward electric force (Eq. (35.87)) to the inward centrifugal force (Eq. (35.86)) gives the pseudoelectron force balance equation:

$$\frac{\hbar^2}{m_e R^3}\left(\frac{2}{\operatorname{sech} u\left|\tanh u\right| du}\right) = \frac{Ze^2}{4\pi\varepsilon_0 R^2}\left(\frac{2}{\operatorname{sech} u\left|\tanh u\right| du}\right) \tag{35.88}$$

From the force balance equation:

$$R = \frac{4\pi\varepsilon_o\hbar^2}{Ze^2 m_e} = \frac{a_0}{Z} \tag{35.89}$$

where the Bohr radius a_0 is given by Eq. (1.256) and Z is the effective charge that may be a rational positive number and corresponds to the energy of the photon that determines the electric field strength of the trapped photon such as that given by Eqs. (5.26-5.28). The electric potential energy given by Eqs. (1.261) and (1.293) is:

$$V = \frac{Ze^2}{4\pi\varepsilon_0 R} = m_{e0}c^2\frac{(\alpha Z)^2}{\sqrt{1-(\alpha Z)^2}} \tag{35.90}$$

The relativistic kinetic energy is (Eq. (1.291)):

$$T = m_{e0}c^2\left(\frac{1}{\sqrt{1-\left(\frac{v}{c}\right)^2}}-1\right) = m_{e0}c^2\left(\frac{1}{\sqrt{1-(\alpha Z)^2}}-1\right) \tag{35.91}$$

The binding energy E_B is given by the sum of the potential V energy and kinetic energy T, Eq. (1.293) with both contributions positive:

$$E_B = V + T = m_{e0}c^2\frac{(\alpha Z)^2}{\sqrt{1-(\alpha Z)^2}} + m_{e0}c^2\left(\frac{1}{\sqrt{1-(\alpha Z)^2}}-1\right) = m_{e0}c^2\left(\frac{(\alpha Z)^2+1}{\sqrt{1-(\alpha Z)^2}}-1\right) \tag{35.92}$$

Consider equipotential, minimum energy surfaces with constant positive curvature such as those of spherical H ($n=1$), excited, and hydrino states. The self-field energy E_{self} is the energy in the electric fields $\mathbf{E}$ of the electron alone, E_{ele}, given by (Eqs. (1.263) and (AII.55)):

$$E_{self} = E_{ele} = \frac{1}{2}\varepsilon_0\int_0^\infty \mathbf{E}^2 dv = \frac{1}{2}m_{e0}c^2\frac{(\alpha Z)^2}{\sqrt{1-(\alpha Z)^2}} \tag{35.93}$$

The same self-energy considerations apply to spherical autonomous photon-bound electron states in liquid media. In contrast, the pseudoelectron exists in vacuum. Rather than the physical principles of spherical electron bubbles surrounded by species of a liquid, the opposite ones apply in vacuum. Here, each electron does not exist as an interloper in a cage of atoms or molecules wherein their interaction energy is disrupted. The binding energy of the pseudoelectron arises from the negative gravitational potential energy overcoming the positive potential, the kinetic, and the self-energy. The photon fields acting at the electron surface provide the negative central electrostatic force to balance the inward centrifugal force (Eq. (35.88)). The corresponding potential and kinetic energies are given by Eqs. (35.90) and (35.91), respectively. Next consider the self-energy in the pseudoelectron electric fields. The pseudospherical surface area to volume is twice that of the spherical case (Eqs. (35.73) and (35.103)). For a central field photon of a given energy and corresponding field strength (Eqs. (35.77) and (35.87)), the charge density is reduced by a factor of two by Gauss' law. In this case the self-field energy E_{self} comprising the energy in the electric fields $\mathbf{E}$ of the electron alone E_{ele} is ¼ that given by Eq. (35.93):

$$E_{self}\left(\,pseudoelectron\right)=\frac{1}{8}m_{e0}c^2\frac{\left(\alpha Z\right)^2}{\sqrt{1-\left(\alpha Z\right)^2}} \tag{35.94}$$

The total energy E_T to form the pseudoelectron is the sum of the binding energy E_B and self energy E_{self} given by Eqs. (35.92) and (35.94), respectively:

$$E_T=E_B+E_{self}=m_{e0}c^2\left(\frac{(\alpha Z)^2+1}{\sqrt{1-(\alpha Z)^2}}-1\right)+\frac{1}{8}m_{e0}c^2\frac{(\alpha Z)^2}{\sqrt{1-(\alpha Z)^2}}=m_{e0}c^2\left(\frac{\frac{9}{8}(\alpha Z)^2+1}{\sqrt{1-(\alpha Z)^2}}-1\right) \tag{35.95}$$

Using Planck's equation for the relationship of the photon's energy to frequency, the photon energy of state Z given by Eq. (35.95) is:

$$E_{photon}=\hbar\omega_{photon}=E_T=m_{e0}c^2\left(\frac{\frac{9}{8}\left(\alpha Z\right)^2+1}{\sqrt{1-\left(\alpha Z\right)^2}}-1\right) \tag{35.96}$$

wherein ω_{photon} is the frequency of the photon that is trapped by the free electron to form the pseudoelectron state.

Since the electric potential, kinetic, and self-energies are positive, the total energy is positive with the negative binding energy provided by the negative gravitational energy provided by the state of negative curvature. In order for the total energy of the pseudoelectron to be negative and consequently energetically stable, the negative gravitational energy must be at least greater in magnitude than the total energy E_T (Eqs. (35.95) and (35.96)). The minimum value of the mass M to radius R ratio of a massive gravitating body for a photon central field equivalent of Z, for which the negative gravitational potential energy exceeds the positive total energy of the pseudoelectron photon, follows from Eqs. (35.95), (35.96), (32.1), (1.285), and (1.286):

$$\left|V_G\right|\geq E_T$$

$$\frac{GM}{R}\frac{m_{e0}}{\sqrt{1-\left(\alpha Z\right)^2}}\geq m_{e0}c^2\left(\frac{\frac{9}{8}\left(\alpha Z\right)^2+1}{\sqrt{1-\left(\alpha Z\right)^2}}-1\right) \tag{35.97}$$

$$\frac{GM}{Rc^2}\geq\left(\frac{9}{8}\left(\alpha Z\right)^2+1-\sqrt{1-\left(\alpha Z\right)^2}\right)$$

Eq. (35.97) can be solved reiteratively. There is no solution using the Newtonian gravitational constant $G=6.67\ X\ 10^{-11}\ N\cdot m^2/kg^2$, Earth mass $M=5.98\ X\ 10^{24}\ kg$, Earth radius $R=6.37\ X\ 10^6\ m$, and the limiting value of $Z=1$. The ratio of the mass to the radius of the Earth is $\frac{M}{R}=9.39\ X\ 10^{17}\ kg/m$. Consider the lowest energy case with $Z=1$, then the reiterative solution for the mass to radius ratio of the massive object to support the formation of pseudoelectrons is $\frac{M}{R}=9.39\ X\ 10^{17}\ kg/m$. Black holes are celestial objects that have such mass density and corresponding extreme gravitational fields. Thus, the minimum energy photon to excite a stable pseudoelectron state is given Eqs. (35.96) and (35.97) is:

$$E_{photon}=E_T=m_{e0}c^2\left(\frac{\frac{9}{8}\left(\alpha Z\right)^2+1}{\sqrt{1-\left(\alpha Z\right)^2}}-1\right)=m_{e0}c^2\left(\frac{\frac{9}{8}\left(\alpha\right)^2+1}{\sqrt{1-\left(\alpha\right)^2}}-1\right) \tag{35.98}$$

$$=7.08\ X\ 10^{-18}\ J=44.2\ eV$$

The electric potential energy given by Eqs. (35.90) and (35.97) is:

$$V=m_{e0}c^2\frac{\left(\alpha Z\right)^2}{\sqrt{1-\left(\alpha Z\right)^2}}=m_{e0}c^2\frac{\left(\alpha\right)^2}{\sqrt{1-\left(\alpha\right)^2}}=4.36\ X\ 10^{-18}\ J=27.2\ eV \tag{35.99}$$

The kinetic energy T given by Eqs. (35.91) and (35.97) is:

$$T=m_{e0}c^2\left(\frac{1}{\sqrt{1-\left(\alpha Z\right)^2}}-1\right)=m_{e0}c^2\left(\frac{1}{\sqrt{1-\left(\alpha\right)^2}}-1\right)=2.18\ X\ 10^{-18}\ J=13.6\ eV \tag{35.100}$$

The binding energy E_B given by Eqs. (35.92) and (35.97) is:

$$E_B = m_{e0}c^2\left(\frac{(\alpha Z)^2+1}{\sqrt{1-(\alpha Z)^2}}-1\right) = m_{e0}c^2\left(\frac{(\alpha)^2+1}{\sqrt{1-(\alpha)^2}}-1\right) = 6.54\ X\ 10^{-18}\ J = 40.8\ eV \tag{35.101}$$

The self-field energy E_{self} comprising given by Eqs. (35.94) and Eq. (35.97) is:

$$E_{self} = \frac{1}{8}m_{e0}c^2\frac{(\alpha Z)^2}{\sqrt{1-(\alpha Z)^2}} = \frac{1}{8}m_{e0}c^2\frac{(\alpha)^2}{\sqrt{1-(\alpha)^2}} = 5.45\ X\ 10^{-19}\ J = 3.4\ eV \tag{35.102}$$

Pseudoelectron production may be achieved by irradiating electrons having zero gravitational mass m_g with photons of energy of at least $44.2\ eV$ in the presence of a black hole wherein the incident photons excite the electrons to pseudoelectrons.

Tri-Hydrogen Cation Electron Collision Pseudoelectron Mechanism

In an alternative mechanism, pseudoelectrons may be formed by collision of free electrons with a partner that conserves the total angular momentum of the partners as the pseudoelectron production energy is derived from electron kinetic energy as the electron kinetic energy converts to comprise the pseudoelectron excitation photon. The angular momentum conservation must occur between the incident free electron, the collision partner, and the leaving pseudoelectron. One mechanism for angular momentum conservation regards an incident free electron having zero net angular momentum due to cancelation of the intrinsic spin angular momentum by interaction of the electron spin and orbital angular momentum. The cancellation may be achieved in a high magnetic field and by a source of microwaves that causes the free electrons of a beam to undergo a transition to the ground spin state wherein the spin and orbital magnetic moments essentially cancel.

Alternatively, the tri-hydrogen cation (H_3^+) may serve as a means to convert incident electrons into pseudoelectrons due to spin and orbital angular momentum exchange between the incident electron and the H_3^+ ion and the product pseudoelectron, H_2, and a proton. As shown in Figures 35.9 and 35.10, the free electron has the geometry of a two-dimensional planar disc and H_3^+ has the geometry of an equilateral triangle inside of a circle.

Figure 35.9. The angular-momentum-axis view of the magnitude of the continuous mass(charge)-density function in the xy-plane of a polarized free electron propagating along the z-axis and the side view of this electron. For the polarized electron, the angular momentum axis is aligned along the direction of propagation, the z-axis.

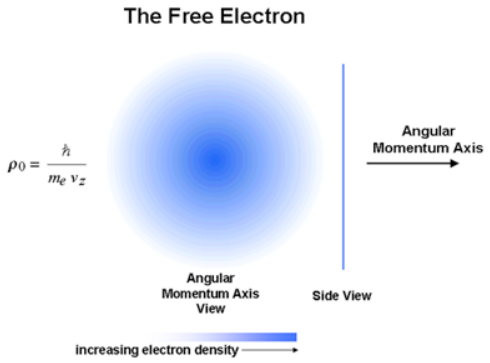

Figure 35.10. The equilateral triangular $H_3^+(1/p)$ MO formed by the superposition of three $H_2(1/p)$-type ellipsoidal MOs with the protons at the foci. (A)-(C) Oblique, top, and side views of the circular and equilateral triangular geometry. (D)-(E) Oblique and top views of the charge-density shown in color scale showing the ellipsoid surfaces and the nuclei (red, not to scale). (F) Cross sectional view with one proton cut away.

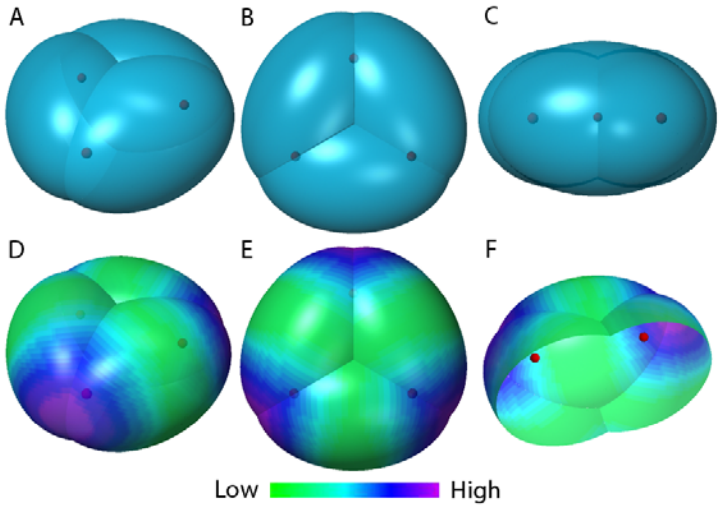

Two different nuclear spin configurations for H_3^+ are possible, called ortho and para. Ortho-H_3^+ has all three proton spins parallel, yielding a total nuclear spin of $3/2$. Para-H_3^+ has two proton spins parallel while the other is anti-parallel, yielding a total nuclear spin of $1/2$. Similarly, H_2 also has ortho and para states, with ortho-H_2 having a total nuclear spin 1 and para-H_2 having a total nuclear spin of 0. When an ortho-H_3^+ and a para-H_2 collide, the transferred proton changes the total spins of the molecules, yielding instead a para-H_3^+ and an ortho-H_2. Nuclear spin transfer and conservation may occur more readily between a spin polarized electron and a nucleus.

Electron-nuclear and nuclear-nuclear spin exchanges are exploited in creating spin-polarized nuclei for proton nuclear magnetic resonance studies. In an exemplary method to form electron spin polarized rubidium atoms and transfer the spin to form nuclear spin polarized ^{129}Xe [39], the polarizer may comprise a rubidium spin exchange optical pumping system such as one based on a fiber coupled laser diode array the produces circularly polarized light at the pumping cell [40,41]. The spin-polarized xenon-129 may undergo nuclear spin exchange to form hyperpolarization in proton spins. Paramagnetic spin catalysts, each comprising a species comprising a paramagnetic ion may spin polarize species comprising protons [42,43]. The nuclear spin polarization may be controlled by controlling the electron spin polarization by means such as laser or electron spin excitation with a specific energy and polarization to excite the spin polarized state that may transfer the electron spin polarization to a nucleus such as a proton to spin polarize a species comprising protons. A method called dynamic nuclear polarization (DNP) comprises electron spin resonance (ESR) excitation of an ESR active species in a magnetic field at its ESR resonance frequency wherein the spin polarized electron transfers the spin polarization to a nucleus to form a nuclear magnetic resonance polarization [44]. Conversely, due to time reversal symmetry of the spin exchange, such an exchange during a collision between an electron and H_3^+ with spin conservation in the colliding species and the resulting products supports collisional pseudoelectron production.

Consider the event of an electron colliding with H_3^+ to form a pseudoelectron where the initial incident electron possesses kinetic energy greater than that required for forming a pseudoelectron in the massive body's gravitational field wherein the threshold energy for pseudoelectron production is given by Eqs. (35.97) and (35.98). The large mass difference between the electron and H_3^+, and the large interaction cross section between the collisional partners may effectively stop the electron during a collision wherein the ground spin state of a magnetically polarized electron may be formed from an interaction with irradiating microwaves. Then, the kinetic energy of the incident electron provides the photon to excite the pseudoelectron state.

The photon absorption mechanism of the transition of a free electron to a pseudoelectron states obeys selection rules based on conservation of the photon and electron angular momentum. Based on the vector multipolarity of the corresponding source currents and the quantization of the angular momentum of photons in terms of $\hbar$, the selection rules for the electric dipole transition after Jackson((Eq. (2.71)) are:

$$\Delta\ell = \pm 1$$
$$\Delta m_\ell = 0, \pm 1 \tag{35.103}$$
$$\Delta m_s = 0$$

The transition is allowed by a collision that obeys the selection rules wherein the total angular momentum before and after the collision to form a pseudoelectron may be conserved between the colliding partners with electron-nuclear angular momentum exchange. A collisional partner for incident electrons having a total angular momentum of zero to form a pseudoelectron having an angular momentum of ± 1 according to the selection rules (Eq. (35.103)) is H_3^+.

Pseudoelectrons may be formed from inelastic scattering of energetic electrons in an H_3^+ medium or from a H_3^+ molecular ion beam wherein the electrons possess kinetic energy over the threshold of the pseudoelectron production energy. H_3^+ generation may be achieved in hydrogen plasma. The H_3^+ reactions are

$$H_2 + e^- \rightarrow H_2^+ + 2e^- \tag{35.104}$$
$$H_2^+ + H_2 \rightarrow H_3^+ + H \tag{35.105}$$

The pseudoelectron reaction is

$$H_3^+ + e^-\left(E > E_T\right) \rightarrow H^+ + H_2 + e^-\left(pe\right) \tag{35.106}$$

wherein E_T is the threshold pseudoelectron production energy and pe designates pseudoelectron. The hydrogen plasma to maintain an inventory of H_3^+ may be found in celestial objects such as black hole jets. At elevated H_2 pressure such as above 0.01 mbar, H_3^+ dominates the ion inventory [45]. H_3^+ may collide with electrons having zero total angular momentum. The collision may occur in a region having a magnetic field to align the angular momentum vectors of the colliding partners that may also be polaized by microwaves. Black holes produce both high magnetic fields and microwaves.

Consider that incident electron e^- possesses a total angular momentum of 0 and that the incident magnetic-field aligned electron may collide with ortho-H_3^+ having a total nuclear spin of $\pm 3/2$ to form para-H_2 having a total nuclear spin of 0 and a free proton that may have a nuclear spin of $\pm 1/2$ (Eq. (35.106)). The electron may transition to a pseudoelectron state having an angular momentum state comprising spin and orbital components such that the total angular momentum is ± 1 (Eq. (35.103)). The pseudoelectron transition may achieve conservation of angular momentum of the species before and after the collision by momentum exchange between the incident e^- and H_3^+ and the resulting $e^-\left(pe\right)$, H_2, and H^+. In this exemplary case, the magnitude of the total angular momentum sum of the species before and after the collision to form a pseudoelectron is $3/2$. Due to the equilateral symmetry (point group D_{3h}) there is no electronic polarization in H_3^+, and there are no unpaired electrons in the product H_2.

Alternatively, the incident electron e^- possesses a total angular momentum of 0, and the incident magnetic-field aligned electron may collide with ortho-H_2 having a total nuclear spin of ± 1 to form para-H_2 having a total nuclear spin of 0. The electron may transition to a pseudoelectron state having an angular momentum state comprising spin and orbital components such that the total angular momentum is ± 1 (Eq. (35.103)). The pseudoelectron transition may achieve conservation of angular momentum of the species before and after the collision by momentum exchange between the incident e^- and ortho-H_2 and the resulting $e^-\left(pe\right)$ and para-H_2. In this exemplary case, the magnitude of the total angular momentum sum of the species before and after the collision to form a pseudoelectron is 1. However, the reaction with the larger cross section involving energetic free electrons is given by Eq. (35.106)) [46].

There are natural phenomena that defy conventional explanation that comprise observable manifestations of fifth force effects. Relativistic electrons are ejected from the center of black holes that produce jets along the poles wherein the accretion disc has the strongest gravitational field (Figure 35.11). These ejected electrons are extraordinary since the gravitation field is so strong that even light can't escape. Gamma ray light has been observed at the poles where these jets originate. Pseudoelectrons may form in black holes by free electron absorption of high intensity gamma rays present therein. The strong magnetic field present may facilitate the transition of the abundant free electrons to their ground spin state to allow the transition to the gravitationally repulsive pseudoelectrons state. Alternatively, pseudoelectrons may form by the collision of high-energy electrons with H_3^+, both present in abundances in black holes. The observed electron plasma jets emitted from black holes comprising electrons moving at close to the speed of light are assigned to pseudoelectrons since no other physical mechanism is known to permit mass to escape from a black hole.

Figure 35.11. Jet of electrons accelerated to near light speed from the center of black hole.

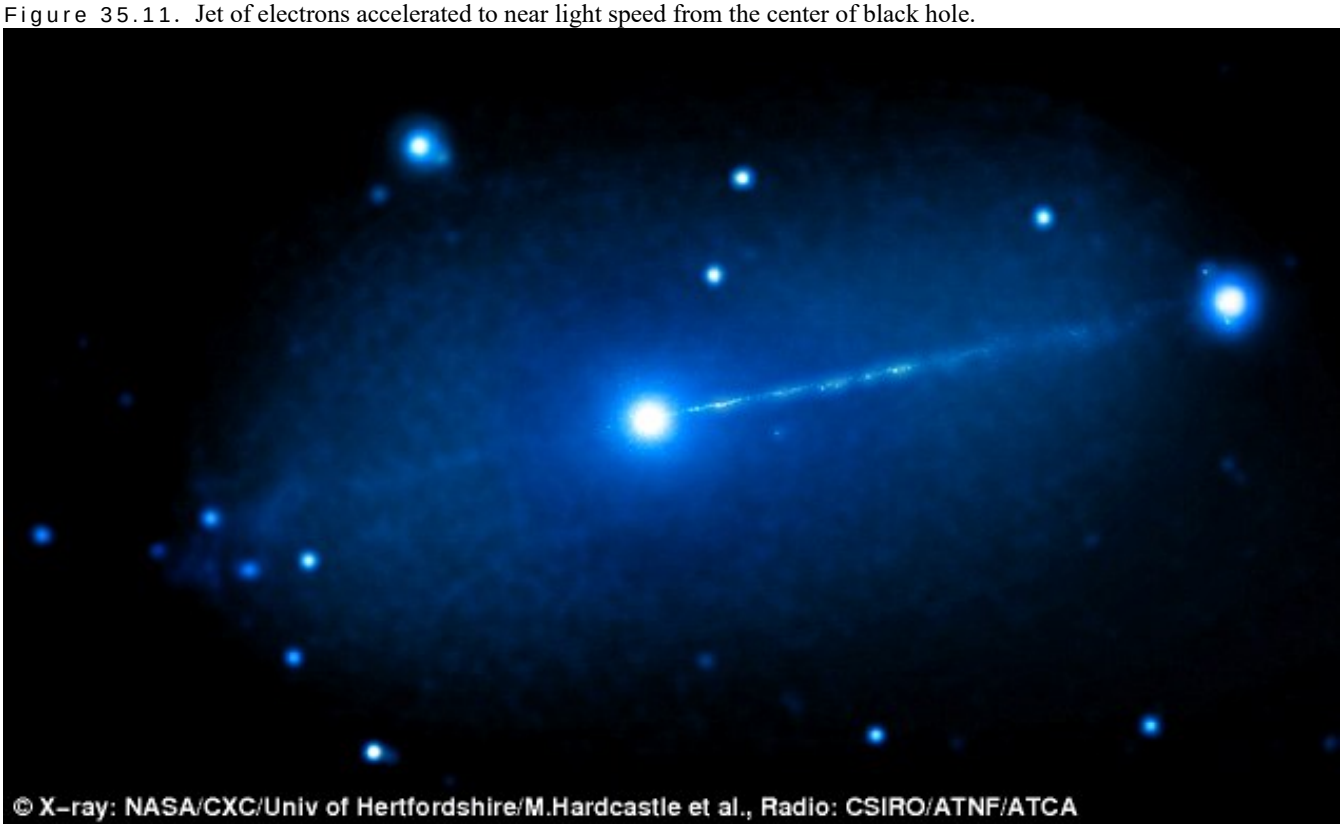

The black hole plasma jets have been implicated as the source of molecular hydrogen gas moving at extraordinary speeds of 1 million kilometers per hour observed at the locations in the galaxy where its jets are impacting regions of dense gas [47]. However, H_2 is fragile in the sense that it is destroyed at relatively low energies. It is extraordinary that the molecular gas can survive being accelerated by jets of electrons moving at close to the speed of light. The paradox may be resolved by three aspects of pseudoelectrons: fast H_2 may be formed by the reaction of H_3^+ to H_2 and H^+ by high energy electron collision wherein the colliding electron forms a pseudoelectron with momentum conservation in the collisional products, pseudoelectrons may have a low cross section for ionization and bond breakage of H_2 during collisional momentum transfer, and a relativistic pseudoelectron may collide with H_3^+ to produce H^+ and fast H_2 (Eq. (35.106)).

REFERENCES

1. F. C. Witteborn, W. M. Fairbank, Physical Review Letters, Vol. 19, No. 18, (1967), pp. 1049-1052.
2. V. Fock, The Theory of Space, Time, and Gravitation, The MacMillan Company, (1964).
3. L. Z. Fang, and R. Ruffini, Basic Concepts in Relativistic Astrophysics, World Scientific, (1983).
4. G. R. Fowles, Analytical Mechanics, Third Edition, Holt, Rinehart, and Winston, New York, (1977), pp. 154-155.
5. C. Amsler, CERN Courier, "Antigravity matters at WAG 2013", March 2014.
6. G. R. Fowles, Analytical Mechanics, Third Edition, Holt, Rinehart, and Winston, New York, (1977), pp. 140-164.
7. http://demonstrations.wolfram.com/SurfacesOfRevolutionWithConstantGaussianCurvature/.
8. M. Spivak, A Comprehensive Introduction to Differential Geometry, Vol. 3, 3rd ed., Houston: Publish or Perish, 1999, Chp 3.
9. N. V. Sidgwick, The Chemical Elements and Their Compounds, Volume I, Oxford, Clarendon Press, (1950), p.1
10. M. D. Lamb, Luminescence Spectroscopy, Academic Press, London, (1978), p. 68.
11. R. Mills, J. Lotoski, Y. Lu. "Mechanism of Soft X-ray Continuum Radiation from Low-Energy Pinch Discharges of Hydrogen and Ultra-low Field Ignition of Solid Fuels", (2015), submitted.
12. R. L. Mills, Y. Lu, "Hydrino continuum transitions with cutoffs at 22.8 nm and 10.1 nm," Int. J. Hydrogen Energy, 35 (2010), pp. 8446-8456, doi: 10.1016/j.ijhydene.2010.05.098.
13. R. L. Mills, Y. Lu, K. Akhtar, "Spectroscopic observation of helium-ion- and hydrogen-catalyzed hydrino transitions," Cent. Eur. J. Phys., 8 (2010), pp. 318-339, doi: 10.2478/s11534-009-0106-9.
14. R. L. Mills, Y. Lu, "Time-resolved hydrino continuum transitions with cutoffs at 22.8 nm and 10.1 nm," Eur. Phys. J. D, Vol. 64, (2011), pp. 65, DOI: 10.1140/epjd/e2011-20246-5.

15. R. L. Mills, R. Booker, Y. Lu, "Soft X-ray Continuum Radiation from Low-Energy Pinch Discharges of Hydrogen," J. Plasma Physics, Vol. 79, (2013), pp 489-507; doi:10.1017/S0022377812001109.
16. A. Bykanov, "Validation of the observation of soft X-ray continuum radiation from low energy pinch discharges in the presence of molecular hydrogen," http://www.blacklightpower.com/wp-content/uploads/pdf/GEN3_Harvard.pdf.
17. R. Mills J. Lotoski, "H_2O-based solid fuel power source based on the catalysis of H by HOH catalyst", Int'l J. Hydrogen Energy, Vol. 40, (2015), pp. 25-37.
18. A. Beiser, Concepts of Modern Physics, Fourth Edition, McGraw-Hill Book Company, New York, (1978), pp. 153-155.
19. K. Akhtar, J. Scharer, R. L. Mills, "Substantial Doppler broadening of atomic-hydrogen lines in DC and capacitively coupled RF plasmas**,"** J. Phys. D, Applied Physics, Vol. 42, (2009), 42 135207 (2009) doi:10.1088/0022-3727/42/13/135207.
20. R. Mills, K. Akhtar, "Tests of features of field-acceleration models for the extraordinary selective H Balmer α broadening in certain hydrogen mixed plasmas," Int. J. Hydrogen Energy, Vol. 34, (2009), pp. 6465-6477.
21. R. L. Mills, B. Dhandapani, K. Akhtar, "Excessive Balmer α line broadening of water-vapor capacitively-coupled RF discharge plasmas," Int. J. Hydrogen Energy, Vol. 33, (2008), pp. 802-815.
22. R. Mills, P. Ray, B. Dhandapani, "Evidence of an energy transfer reaction between atomic hydrogen and argon II or helium II as the source of excessively hot H atoms in RF plasmas," Journal of Plasma Physics, (2006), Vol. 72, Issue 4, pp. 469-484.
23. J. Phillips, C-K Chen, K. Akhtar, B. Dhandapani, R. Mills, "Evidence of catalytic production of hot hydrogen in RF generated hydrogen/argon plasmas," International Journal of Hydrogen Energy, Vol. 32(14), (2007), 3010-3025.
24. R. L. Mills, P. C. Ray, R. M. Mayo, M. Nansteel, B. Dhandapani, J. Phillips, "Spectroscopic study of unique line broadening and inversion in low pressure microwave generated water plasmas," J. Plasma Physics, Vol. 71, Part 6, (2005), pp. 877-888.
25. R. L. Mills, K. Akhtar, "Fast H in hydrogen mixed gas microwave plasmas when an atomic hydrogen supporting surface was present," Int. J. Hydrogen Energy, 35 (2010), pp. 2546-2555, doi:10.1016/j.ijhydene.2009.12.148.
26. P. Weiss, Science News, Vol. 158, No. 14, September 30, (2000), p. 216.
27. P. Ball, Nature, http://helix.nature.com/nsu/000921/000921-1.html.
28. M. Chown, New Scientist, October 14, (2000), Vol. 168, Issue 2260, pp. 24, 33.
29. H. J. Maris, Journal of Low Temperature Physics, Vol. 120, (2000), p. 173.
30. Arnold J. Kelly, "Electrostatic Atomizing Device," United States Patent No. 4,581,675, April 8, 1986.
31. F. A. Cotton, G. Wilkinson, Advanced Inorganic Chemistry A Comprehensive Text, Interscience Publishers, New York, NY, (1962), pp. 193-194.
32. J. Lyons, H. Kippenhan, E. Wildforster, "Modeling soliton solutions to the sine-Gordon equation," Dynamics at the Horsetooth, Volume 2, (2010), pp. 1-5.
33. R. K. Bullough, P. J. Caudrey (Eds.), Solitons, Springer-Verlag, Berlin, (1980).
34. W. McC. Siebert, Circuits, Signals, and Systems, The MIT Press, Cambridge, Massachusetts, (1986), pp. 415-416.
35. G. O. Reynolds, J. B. DeVelis, G. B. Parrent, B. J. Thompson, The New Physical Optics Notebook, SPIE Optical Engineering Press, (1990).
36. G. R. Fowles, *Analytical Mechanics*, Third Edition, Holt, Rinehart, and Winston, New York, (1977), pp. 117-135.
37. G. R. Fowles, *Analytical Mechanics*, Third Edition, Holt, Rinehart, and Winston, New York, (1977), pp. 146-147.
38. D.P. Hardin, E.B. Saff, "Discretizing manifolds via minimum energy points," Notices of the AMS, Vol. 51, No. 10, pp. 1186-1194.
39. "Hyperpolarized Xe", Optical Spin-Polarization & Magnetic Resonance, Department of Physics and Astronomy, University of Utah, http://www.physics.utah.edu/~hpgas/production.html.
40. A. Zook, B. B. Adhyaru, C. R. Bowers, "High capacity production of >65% spin polarized xenon-129 for NMR spectroscopy and imaging", J Magn Reson, 2002 December, Vol. 159(2), pp. 175-182, https://www.ncbi.nlm.nih.gov/pubmed/12482697.
41. G. Navon, Y. Q. Song, T. Room, S. Appelt, R. E. Taylor, A. Pines, "Enhancement of Solution NMR and MRI with Laser-Polarized Xenon", Science, Vol. 27, 29 March, 1996, pp. 1848-1851.
42. C. Terenz, S. Bouguet-Bonnet, D. Canet, "Electron spin polarization transfer to ortho-H_2 by interaction of para-H_2 with paramagnetic species: A key to a novel para → ortho conversion mechanism", J. Phys. Chem. Lett., (2015), Vol. 6 (9), pp. 1611–1615, DOI: 10.1021/acs.jpclett.5b00518.
43. M. Matsumoto, J. H. Espenson, "Kinetics of the interconversion of parahydrogen and orthohydrogen catalyzed by paramagnetic complex ions", J. Am. Chem. Soc., (2005), Vol. 127 (32), pp. 11447–11453, DOI: 10.1021/ja0524292.
44. A. J. Rossini, A. Zagdoun, M. Lelli, A. Lesage, C. Coperet, L. Emsley, "Dynamic Nuclear Polarization Surface Enhanced NMR Spectroscopy, Accounts of Chemical Research, Vol. 46, No. 9, (2013), pp. 1942–1951.
45. I. Mendez, F. J. Gordillo-Vazquez, V. J. Herrero, I. Tanarro, "Atom and ion chemistry in low pressure hydrogen DC plasmas", J. Phys. Chem. A, (2006), Vol. 110, pp. 6060-6066.
46. H. Tawara, Y. Itikawa, H. Nishimura, M. Yoshino, "Cross sections and related data for electron collisions with hydrogen molecules and molecular ions, J. Phys. Chem. Ref. Data, Vol. 19, No. 3, (1990), pp. 617-636.
47. C. Tadhunter, R. Morganti, M. Rose, J. B. R. Oonk, T. Oosterloo, "Jet acceleration of the fast molecular outflows in the Seyfert galaxy", IC 5063. Nature, 2014; DOI: 10.1038/nature 13520.

Chapter 36

LEPTONS

Only three lepton particles can be formed from photons corresponding to the Planck equation energy, the potential energy, and the magnetic energy, where each is equal to the mass energy (Eq. (32.27)). As opposed to a continuum of energies, leptons arise from photons of only three energies. Each "resonant" photon can be considered to be the superposition of two photons—each possessing the energy given by Planck's equation, Eq. (32.28), which is equal to the mass energy of the lepton or antilepton, each possessing $\hbar$ of angular momentum, and each traveling at the speed of light in the lab inertial frame.

At particle production, a photon having a radius and a wavelength equal to the Compton wavelength bar of the particle forms a transition state atomic orbital of the particle of the same wavelength. Eq. (32.43) equates the proper and coordinate times at particle production wherein the velocity of the transition state atomic orbital in the coordinate frame is the speed of light and the relationships between the mass energies given by Eq. (32.32) hold. To describe any phenomenon such as the motion of a body or the propagation of light, a definite frame of reference is required. A frame of reference is a certain base consisting of a defined origin and three axes equipped with graduated rules and clocks as described in the Relativity section. In the case of particle production wherein the velocity is the speed of light, only the time ruler need be defined. By defining a standard ruler for time in the coordinate frame, the mass of the particle is then given in terms of the self-consistent system of units based on the definition of the time ruler. The mass of the particle must be experimentally measured with the same time ruler as part of a consistent system of units. In the case that MKS units are used, the permeability of free space is a fundamental constant defined as exactly $\mu_0 = 4\pi\ X\ 10^{-7}\ Hm^{-1}$. Similarly, the coordinate time (Eq. (36.2)) is defined as the "second[1]," and the mass of the particle is given in kilograms based on this definition of the "second" (See Particle Production section). The production of a real particle from a transition state atomic orbital is a spacelike event in terms of special relativity wherein spacetime is contracted by the gravitational radius of the particle during its production as given in the Gravity section. Thus, the coordinate time is imaginary as given by Eq. (32.43). On a cosmological scale, imaginary time corresponds to spacetime expansion and contraction as a consequence of the harmonic interconversion of matter and energy as given by Eq. (33.40).

The mass of each member of a lepton pair corresponds to an energy of Eq. (32.32). The electron and antielectron

[1] Using an atom to define the unit of time is a means to set a more universal standard. Presently the second is defined as the time required for 9,192,631,770 vibrations within the cesium-133 atom. The "second" as defined in Eq. (36.2) is a fundamental constant, namely, the metric of spacetime. This definition gives the relationship of energy to matter conversion to spacetime contraction, and it sets the clock (ruler of time) to the conversion rate of matter into energy and the corresponding rate of spacetime expansion of the Universe. A theory that unifies all physics must ultimately be able to describe all observations in terms of the definition of time only. All other measurable parameters of matter, energy, charge, spacetime, etc. are ultimately expressed in terms of the unit of time. If coordinate time is defined by Eq. (36.2), then Eq. (32.43) gives the masses of "allowed particles" in terms of that definition. Eq. (32.39) gives another method of experimentally determining the metric of time (sec) which does not require the measurement of the electron mass. The electron Compton wavelength $\lambda\!\!\!^{-}_C$ is equal to the wavelength of the photon which gives rise to the electron, and the velocity of each mass-density element of the extended particle is equivalent to the gravitational escape velocity, v_g, of the mass of the antiparticle (Eq. (32.43)). Eq. (33.21) gives the circular relationships between matter, energy, and spacetime based on this definition of time. A unified theory can only provide the relationships between all measurable observables in terms of a clock defined according to those observables and used to measure them.

In this case, fundamental physical constants and observables calculated in terms of the fundamental constants have no meaning except with regard to the definition of time in terms of the constants. Then all observables such as the excited states of atoms, ionization energies of atoms, chemical bond energies, scattering of electrons from atoms, nuclear parameters, cosmological parameters, etc. are given in terms of the definition of the "second" (Eq. (36.2) which is extremely close to the MKS second (**See Box 32.1.**). Internal consistency is given with a high degree of accuracy over the scalar range of 85 orders of magnitude (mass of the electron to mass of the Universe). To achieve exact predictions of particle masses and cosmological parameters that require the introduction of the spacetime metric as a fundamental constant, a slight modification of the experimental definition of the second may be required. Presently, all fundamental constants including masses are determined in a self-consistent manner involving definitions and measurements. Ultimately the unit system will have to be revised according to Eq. (33.21), which gives the exact relationships between the measurable constants.

correspond to the Planck equation energy. The muon and antimuon correspond to the electric energy. And, the tau and antitau correspond to the magnetic energy. It is shown that the masses are given by Eq. (32.43) and the relative masses differ in their specific function of the fine structure constant α only. These functions are determined by relativistic coefficients given by Eq. (32.32) according to the kind of energy that is responsible for the respective level (e, μ, τ) of the particular particle within its family.

A neutrino/antineutrino pair is formed in each of three cases of lepton/anti-lepton production to conserve linear and angular momentum during the separation of the world lines of each particle and its antiparticle. The neutrino and antineutrino are photons that travel at velocity c and have energy, but are mass-less. Equations of such photons are given in the Neutrinos section.

THE ELECTRON-ANTIELECTRON LEPTON PAIR

From Eq. (32.43), when the gravitational radius r_g (Eq. (32.36)) is equal to the radius of the transition state atomic orbital, the corresponding gravitational velocity v_g (Eq. (32.35)) is the speed of light c, and the proper time is equal to the coordinate time. Thus, the special relativistic corrections to r_g are the same as those of the transition state radius which gives the energy of the particle equal to its mass times the speed of light squared as given by Eqs. (32.32a-32.32b).

Consider the Planck energy equation, Eq. (32.28). The proper time τ is given by:

$$\tau = \frac{2\pi}{\omega} = 2\pi\frac{\hbar}{mc^2} \tag{36.1}$$

In the lab frame, the relativistic correction of the radius in the derivation of the Planck's equation for the transition state atomic orbital (Eq. (29.12)) is α^{-2}. Substitution of (i) $\alpha^{-2}r_g$, the relativistically corrected gravitational radius (Eq. (32.36)) for r_g, (ii) the sec which is essentially the second—the definition for the coordinate time in MKS units, for *ti*, and (iii) the Compton wavelength bar for the radius r of the transition state atomic orbital, (Eq. (32.21)), into Eq. (32.43) gives:

$$2\pi\frac{\hbar}{m_e c^2} = \sec\sqrt{\frac{2Gm_e^2}{c\alpha^2\hbar}} \tag{36.2}$$

The left-hand side of Eq. (36.2) is the general relativistic correction of the coordinate time. The special relativistic factor, α^{-1} (factored out of the square root), also follows from Eq. (32.34), from Eqs. (2.118) and (2.123), and from Eq. (5.45) of Fowles [1]. The mass of the electron/antielectron in MKS units based on the definition of the coordinate time in terms of the sec is:

$$m_e = \left(\frac{h\alpha}{\sec c^2}\right)^{\frac{1}{2}}\left(\frac{c\hbar}{2G}\right)^{\frac{1}{4}} = \left(\frac{h\alpha}{\sqrt{2}\sec c^2}\right)^{\frac{1}{2}} m_u^{\frac{1}{2}} = 9.0998\ X\ 10^{-31}\ kg \tag{36.3}$$

where m_u is the Planck mass given by Eq. (32.31) and $m_{e\ \text{experimental}} = 9.10945455\ X\ 10^{-31}\ kg$ [3-4].

With lepton production a particle of electrostatic charge $-e$ and an antiparticle of electrostatic charge $+e$ are produced. The corresponding fields travel at the speed of light and interact with each other. In order to conserve mass-energy, the electromagnetic fields of the particles must be included in the mass determination. The correction to the electron mass is given by Eq. (36.15). The corresponding lepton neutrinos carry any energy not accounted for as binding energy, kinetic energy, or carried by photons, and they further conserve linear and angular momentum including the angular momentum of the electromagnetic field fronts (Eq. (4.1)) which propagate at the speed of light to give the electrostatic fields of the particles as discussed in the Neutrinos section.

The difference between the calculated and experimental values of the electron mass is due to the very slight difference between the present MKS second and the definition of the corresponding time unit defined by Eq. (36.2). Eq. (33.21) gives the circular relationships between matter, energy, and spacetime based on the definition of time given by Eq. (36.2). Any fundamental constant is exactly given in terms of the other members of these relationships and may be determined to the experimental accuracy that they are known. An exact value for the imaginary time ruler *ti* given by Eq. (32.43) can be obtained by using Eq. (36.2) with the results of Eqs. (36.9-36.22).

$$1\ \sec = m_e^{-2}\left(\frac{h\alpha}{c^2}\right)\left(\frac{c\hbar}{2G}\right)^{\frac{1}{2}}\left(1+\frac{2\pi\alpha^2}{2}\right)^{-2} = 0.9975(46714)\ \text{MKS second} \tag{36.4}$$

The accuracy of the conversion factor of 0.9975 second/sec is limited by the error in the value of the gravitational constant (See Boxes 32.1 and 32.2). A new system of units would eliminate the need for conversion and permit a more accurate determination of the constants including the definition of time based on internal consistency.

THE MUON-ANTIMUON LEPTON PAIR

The muon (antimuon) decays to the electron (antielectron) and may be considered a transient resonance which decays to the stable lepton, the electron (antielectron). Given that the electron is "allowed" by the Planck energy equation (Eq. (32.28)) and that the proper time is given by general relativity (Eq. (32.38)), the muon (antimuon) mass can be calculated from the potential energy, *V*, (Eq. (32.27)) and the proper time relative to the electron inertial frame. In this case, the special relativistic corrections to r_g are the inverse of those of the radius of the transition state atomic orbital, which gives the energy of the particle equal to its mass times the speed of light squared as given by Eqs. (32.32a-32.32b). For the lab inertial frame, the relativistic correction of the radius of the transition state atomic orbital given by the potential energy equations (Eq. (29.10) and (29.11)) is α^{-2}. For the electron inertial frame, the relativistic correction of the gravitational radius relative to the proper frame is the inverse, α^2. Furthermore, the potential energy equation gives an electrostatic energy; thus, the electron inertial time must be corrected by the relativistic factor of 2π relative to the proper time. (See the Special Relativistic Correction to the Ionization Energies section.) Multiplication of the right side of Eq. (32.43) by 2π and substitution of (i) m_e, the mass of the electron, for *M*, (ii) the sec which is essentially the second—the definition for the coordinate time in MKS units, for *ti*, (iii) $\alpha^2 r_g$, the relativistically corrected gravitational radius, for r_g (Eq. (32.36)), and the Compton wavelength bar for the transition state atomic orbital radius *r*, (Eq. (32.21)), into Eq. (32.43) gives the relationship between the proper time and the electron coordinate time:

$$2\pi \frac{\hbar}{m_\mu c^2} = 2\pi \sec \sqrt{\frac{2Gm_e \alpha^2 m_\mu}{c\hbar}} \tag{36.5}$$

The mass of the muon/antimuon using the MKS second is:

$$m_\mu = \frac{\hbar}{c}\left(\frac{1}{2Gm_e(\alpha \sec)^2}\right)^{\frac{1}{3}} = 1.8874\ X\ 10^{-28}\ kg \tag{36.6}$$

where $m_{\mu \text{experimental}} = 1.88355\ X\ 10^{-28}\ kg$ [3].

THE TAU-ANTITAU LEPTON PAIR

Given that the electron is "allowed" by the Planck energy equation (Eq. (32.28)) and that the proper time is given by general relativity (Eq. (32.38)), the tau (antitau) mass can be calculated from the magnetic energy (Eq. (32.27)) and the proper time relative to the electron inertial frame. For the lab inertial frame, the relativistic correction of the radius of the transition state atomic orbital given by the magnetic energy equations (Eq. (29.14) and (29.15)) is $\frac{1}{(2\pi)^2\alpha^4}$[2]. For the electron inertial frame, the relativistic correction of the gravitational radius relative to the proper frame is the inverse, $(2\pi)^2\alpha^4$. Furthermore, the transition state comprises two magnetic moments. For $v = c$, the magnetic energy equals, the potential energy, equals the Planck equation energy, equals mc^2. The magnetic energy is given by the square of the magnetic field as given by Eqs. (1.154-1.162). The magnetic energy corresponding to particle production is given by Eq. (32.32). Because two magnetic moments are produced the magnetic energy (and corresponding photon frequency) in the proper frame is two times that of the electron frame. Thus, the electron time is corrected by a factor of two relative to the proper time. Multiplication of the right side of Eq. (32.43) by 2 and substitution of (i) m_e, the mass of the electron, for M, (ii) the sec which is essentially the second—the definition for the coordinate time in MKS units, for ti, (iii) $(2\pi)^2\alpha^4 r_g$, the relativistically corrected gravitational radius, for r_g (Eq. (32.36)), and the Compton wavelength bar for the transition state atomic orbital radius r, (Eq. (32.21)), into Eq. (32.43) gives the relationship between the proper time and the electron coordinate time:

$$2\pi \frac{\hbar}{m_\tau c^2} = 2 \sec \sqrt{\frac{2Gm_e(2\pi)^2\alpha^4 m_\tau}{c\hbar}} \tag{36.7}$$

The mass of the tau/antitau is:

$$m_\tau = \frac{\hbar}{c}\left(\frac{1}{2Gm_e}\right)^{\frac{1}{3}}\left(\frac{1}{2\sec\alpha^2}\right)^{\frac{2}{3}} = 3.1604\ X\ 10^{-27}\ kg \tag{36.8}$$

where $m_{\tau\ \text{experimental}} = 3.1676\ X\ 10^{-27}\ kg\ \left(1776.9\ MeV/c^2\right)$ [3].

In the case of the production of each lepton a nucleus is present during particle/antiparticle production to conserve momentum. A fourth particle/antiparticle pair can arise by the gravitational potential energy of Eq. (32.27). However, a pair of particles each of the Planck mass corresponding to the conditions of Eq. (32.22), Eq. (32.32), and Eq. (32.33) is not observed since the velocity of each of the point masses of the transition state atomic orbital is the gravitational velocity v_G that in this case

[2] The special relativistic correction of the particle masses in the transition state given by Eq. (1.273) avoids the situation of encountering an infinite mass at light speed as given by Eq. (33.14).

is the speed of light; whereas, the Newtonian gravitational escape velocity v_g of the superposition of the point masses of the antiparticle would be $\sqrt{2}$ times the speed of light (Eq. (32.35)). In this case, an electromagnetic wave of mass energy equivalent to the Planck mass travels in a circular orbit around the center of mass of another electromagnetic wave of mass energy equivalent to the Planck mass wherein the eccentricity is equal to zero (Eq. (35.21)), and the escape velocity can never be reached. The Planck mass is a "measuring stick." The extraordinarily high Planck mass ($\sqrt{\frac{\hbar c}{G}} = 2.18\ X\ 10^{-8}\ kg$) is the unobtainable mass bound imposed by the angular momentum and speed of the photon relative to the gravitational constant. It is analogous to the unattainable bound of the speed of light for a particle possessing finite rest mass imposed by the Minkowski tensor. It has a physical significance for the fate of blackholes as given in the Composition of the Universe section.

RELATIONS BETWEEN THE LEPTONS

Based on Eqs. (36.3), (36.6), and (36.8), the relations between the lepton masses which are independent of the definition of the imaginary time ruler ti given by Eq. (32.43) are [2] :

$$\frac{m_\mu}{m_e} = \left(\frac{\alpha^{-2}}{2\pi}\right)^{\frac{2}{3}} = 207.48800 \qquad (206.76827) \tag{36.9}$$

$$\frac{m_\tau}{m_\mu} = \left(\frac{\alpha^{-1}}{2}\right)^{\frac{2}{3}} = 16.744 \qquad (16.817) \tag{36.10}$$

$$\frac{m_\tau}{m_e} = \left(\frac{\alpha^{-3}}{4\pi}\right)^{\frac{2}{3}} = 3474.3 \qquad (3477.3) \tag{36.11}$$

The respective experimental lepton mass ratios according to the 1998 CODATA and the Particle Data Group are given in parentheses [3-4]. Eqs. (36.9-36.11) do not include the neutrino energies and the coulomb and magnetic field energies.

With lepton production a particle of electrostatic charge $-e$ and an antiparticle of electrostatic charge $+e$ are produced. The corresponding fields travel at the speed of light and interact with each other. In order to conserve mass-energy, the electromagnetic fields of the particles must be included in the mass determination. Consider the electron given by Eq. (36.3). The coulomb field of the electron and positron correspond to a potential energy. As given in the Positronium section (Eq. (30.5)), the potential energy V between the particle and the antiparticle having the radius r_1 is,

$$V = \frac{-e^2}{4\pi\varepsilon_0 r_1} = \frac{-Z^2e^2}{8\pi\varepsilon_0 a_0} = -2.18375\ X\ 10^{-18}\ J = -13.59\ eV \tag{36.12}$$

The calculated ionization energy is $\frac{1}{2}V$ which is:

$$E_{ele} = 6.795\ eV\ . \tag{36.13}$$

The experimental ionization energy is $6.795\ eV$.

Eq. (36.12) may be written in terms of the mass-energy of the electron:

$$V = \frac{-e^2}{4\pi\varepsilon_0 r_1} = \frac{-Z^2e^2}{8\pi\varepsilon_0 a_0} = -\frac{\alpha^2}{2} m_e c^2 = -2.18375\ X\ 10^{-18}\ J = -13.59\ eV \tag{36.14}$$

Since the electron mass-energy is given by the Planck energy equation given by Eqs. (29.12) and (32.32), the special relativistic factor for the bound particle-antiparticle state relative to the particle-production transition state given in Eq. (36.14) is α^2. In addition, due to time dilation at $v = c$ relative to the velocity of the bound state, the frequency and thus the energy increases by 2π as given by Eq. (1.281). From Eqs. (1.281) and (36.14) the electron mass is corrected by a factor γ^* of:

$$\gamma^* = \left(1 + 2\pi\frac{\alpha^2}{2}\right)^{-1} \tag{36.15}$$

Similarly to the positron and following Eq. (36.12), the muon mass must be corrected due to the particle fields. Since the muon is given by the electrostatic coulomb energy equation given by Eqs. (28.9) and (32.32), the special relativistic factor for the bound particle-antiparticle state relative to the transition state frame given in Eqs. (28.9), (32.32), and (36.5) is α corresponding to the relative radii where the corresponding potential energy is given by:

$$V = -\frac{\alpha}{2} m_\mu c^2 = -6.17671\ X\ 10^{-14}\ J = -3.85517\ X\ 10^5\ eV \tag{36.16}$$

From Eq. (36.16) the muon mass is corrected by a factor γ^* of:

$$\gamma^* = \left(1 + \frac{\alpha}{2}\right)^{-1} \tag{36.17}$$

From Eqs. (36.15) and (36.17), the ratio of the differential relativistic correction of the electron mass to that of the muon mass due to charge interactions is given by Eq. (1.281).

Similarly to the positron and following Eq. (36.12), the tau mass must be corrected due to the particle fields where the tau is given by the magnetic energy equation given by Eqs. (29.14) and (32.32). In this case, two magnetic dipoles are formed that are spin paired in order to conserve angular momentum. Since the particle and antiparticle are oppositely charged and the magnetic dipoles are antiparallel, the force is repulsive rather than attractive. In this case, the corresponding energy increases the mass of the tau and antitau since the corresponding special relativistic factor for the bound particle-antiparticle state relative to the transition state frame is negative. The magnitude is four times that of the electron correction corresponding to replacing the reduced mass in Eq. (36.12) by the mass (Eqs. (30.1-30.4) where the force is purely magnetic) and a factor of two corresponding to the interaction of two magnetic dipoles rather than electric monopoles as given by Eqs. (1.154-1.162). The corresponding potential energy is given by:

$$V = 4\pi\alpha^2 m_\tau c^2 = 1.905\ X\ 10^{-13}\ J = 1.189\ X\ 10^6\ eV \tag{36.18}$$

From Eq. (36.16) the tau mass is corrected by a factor γ^* of:

$$\gamma^* = \left(1 - 4\pi\alpha^2\right)^{-1} \tag{36.19}$$

Based on Eqs. (36.3), (36.6), (36.15), and (36.17), the relation between the muon and electron masses (Eq. (36.9)) which is independent of the definition of the imaginary time ruler ti given by Eq. (32.43) including the contribution of the fields due to charge production of magnitude e is:

$$\frac{m_\mu}{m_e} = \left(\frac{\alpha^{-2}}{2\pi}\right)^{\frac{2}{3}} \frac{\left(1 + 2\pi\frac{\alpha^2}{2}\right)}{\left(1 + \frac{\alpha}{2}\right)} = 206.76828 \qquad (206.76827) \tag{36.20}$$

Based on Eqs. (36.6), (36.8), (36.17), and (36.19), the relation between the tau and muon masses (Eq. (36.10)) which is independent of the definition of the imaginary time ruler ti given by Eq. (32.43) including the contribution of the fields due to charge production of magnitude e is:

$$\frac{m_\tau}{m_\mu} = \left(\frac{\alpha^{-1}}{2}\right)^{\frac{2}{3}} \frac{\left(1 + \frac{\alpha}{2}\right)}{\left(1 - 4\pi\alpha^2\right)} = 16.817 \qquad (16.817) \tag{36.21}$$

Based on Eqs. (36.3), (36.8), (36.15), and (36.19), the relation between the tau and electron masses (Eq. (36.11)) which is independent of the definition of the imaginary time ruler *ti* given by Eq. (32.43) including the contribution of the fields due to charge production of magnitude *e* is:

$$\frac{m_\tau}{m_e} = \left(\frac{\alpha^{-3}}{4\pi}\right)^{\frac{2}{3}} \frac{\left(1 + 2\pi\frac{\alpha^2}{2}\right)}{\left(1 - 4\pi\alpha^2\right)} = 3477.2 \qquad (3477.3) \tag{36.22}$$

For Eqs. (36.20-36.22), the respective experimental lepton mass ratios according to the 1998 CODATA and Particle Data Group tables are given in parentheses [3-4]. There is remarkable agreement. The corresponding lepton neutrinos carry any energy not accounted for as binding energy, kinetic energy, or carried by photons, and they further conserve linear and angular momentum including the angular momentum of the electromagnetic field fronts (Eq. (4.1)) which propagate at the speed of light to give the electrostatic fields of the particles as discussed in the Neutrinos section.

X17 PARTICLE

As shown in this section, the electron, muon, and tau masses are based on the relativistic corrections of the Planck, electric, and magnetic energies, respectively, as given in Eq. (32.48) wherein, the masses of the heavier leptons, the muon and tau are dependent on the first lepton's mass, the electron mass, and each can be considered a relativistic effect of the electron mass. As shown in the Muonic Hydrogen Lamb shift section, the radiation reaction force F_{RR} of muonic hydrogen comprises three terms that follow from Eq. (2.135) and arise from lepton-photon-momentum transfer during the ${}^2P_{1/2} \rightarrow {}^2S_{1/2}$ transition wherein the photon couples with the three possible states of the electron mass corresponding to the three possible leptons. The radiation reaction force of relativistic origin is determined by the action on the electron mass with each mass hierarchy having a corresponding force component. Similarly, neutral mass-energy resonances arising from simultaneous satisfaction of Maxwell's equations and the spacetime particle-production condition (Eq. 32.43)) involve the higher mass-energy muon and tau leptons states and give rise to particles that may decay to an electron-positron pair e^+e^-. A resonance exists for the tau relativistic correction of the muon resonance of the electron mass given by the ratio of the muon to tau masses (Eq. (36.10)) times the mass

of the electron. The neutral electromagnetic production of the tau-to-muon resonance predicts a neutral particle of 16.744 times the mass of the electron-positron pair e^+e^-. Since the electron mass is 511 keV, the predicted mass is 17.11 MeV.

$$m_{X17} = 2\left(\frac{\alpha^{-1}}{2}\right)^{\frac{2}{3}} m_e = 17.11 MeV \tag{36.23}$$

Krasznahorkay et al. have reported a particle of 17 MeV that decays to e^+e^- [5]. Specifically, when protons were fired at thin targets of lithium-7 to create unstable beryllium-8 nuclei that then decayed to pairs of electrons and positrons excess decays were observed at an opening angle of 140° between the e^+ and e^- having a combined energy of approximately 17 MeV, which indicated that a small fraction of beryllium-8 nuclei each lost excess energy in the form of a new particle. Recently, a 17 MeV particle also was evident by the discovery of a e^+e^- angular correlation of 115 ° and a combined energy of approximately 17 MeV from the decay of the 21 MeV excited nuclear state of helium-4 formed by the firing of 900 keV protons at helium-3 [6]. The authors speculate that the existence of a 17 MeV particle missed by the Standard Model regards a new so-called fifth force with further speculation that it has relevance to dark matter. But particles do not mediate forces according to classical laws; rather all forces are either electromagnetic in nature or arise from the curvature of spacetime. Furthermore, the 17 MeV particle is not dark matter; rather dark matter is hydrogen in lower chemical energy states as shown in the Composition of the Universe section [7].

REFERENCES

1. G. R. Fowles, *Analytical Mechanics*, Third Edition, Holt, Rinehart, and Winston, New York, (1977), p. 157.
2. Personal communication, Dr.-Ing. Günther Landvogt, Hamburg, Germany, February, (2003).
3. K. Hagiwara et al., Phys. Rev. D 66, 010001 (2002); http://pdg.lbl.gov/2002/s035.pdf.
4. P. J. Mohr and B. N. Taylor, "CODATA recommended values of the fundamental physical constants: 1998," Reviews of Modern Physics, Vol. 72, No. 2, April, (2000), pp. 351-495.
5. A. J. Krasznahorkay, M. Csatlós, L. Csige, Z. Gácsi, J. Gulyás, M. Hunyadi, I. Kuti, B. M. Nyakó, L. Stuhl, J. Timár, T. G. Tornyi, Zs. Vajta, T. J. Ketel, A. Krasznahorkay, "Observation of anomalous internal pair creation in 8Be: A possible indication of a light, neutral boson", Physical Review Letters, Vol. 116, (2016), p. 42501.
6. A.J. Krasznahorkay, M. Csatlos, L. Csige, J. Gulyas, M. Koszta, B. Szihalmi, J. Timar, D.S. Firak, A. Nagy, N.J. Sas, A. Krasznahorkay, "New evidence supporting the existence of the hypothetic X17 particle", (2019), arXiv:1910.10459 [nucl-ex].
7. R. Mills, J. Lotoski, Y. Lu, "Mechanism of soft X-ray continuum radiation from low-energy pinch discharges of hydrogen and ultra-low field ignition of solid fuels", Plasma Science and Technology, Vol. 19, (2017), pp. 1-28.

Chapter 37

PROTON AND NEUTRON

Experimental evidence [1] indicates that the proton and neutron each comprise three charged fundamental particles called quarks and three massive photons called gluons. Each quark is found in combination with a gluon. It is demonstrated in the Excited States of the One-Electron Atom (Quantization) section and by Eq. (2.11) that photons trapped inside of an atomic orbital resonator cavity provide an effective charge at the two-dimensional atomic orbital. A model of the nucleons which is consistent with experimentation and the present theory is a transition state atomic orbital of mass and charge comprised of three superimposed quasiparticles (quarks) held in force balance on a spherical two-dimensional shell by the corresponding matched photons (gluons) trapped inside of the atomic orbital. This model explains the experimental result that 1/3 of the total proton spin [2] is due to the spin angular momentum of the quarks and the remaining 2/3 is predicted to be due to quark orbital angular momentum. The neutron angular momentum is based on that of the proton. The magnetic moments calculated from the model as well as the masses of the quarks, gluons, and nucleons in simple closed-form equations containing fundamental constants only match the experimental values extraordinarily well. QCD depends on virtual particles and renormalization of intractable infinities and is incapable of such calculations.

The experimental radius of the proton is $1.3\ X\ 10^{-15}\ m$ [3]:

$$r_p = 1.3\ X\ 10^{-15}\ m \tag{37.1}$$

The Compton wavelength of the proton, $\lambda_{C,p}$, is:

$$\lambda_{C,p} = \frac{h}{m_p c} = 1.3214\ X\ 10^{-15}\ m \tag{37.2}$$

Substitution of Eq. (1.249) and using Eq. (1.256) yields:

$$\lambda_{C,p} = \frac{2\pi a_o m_e}{\alpha^{-1} m_p} = 1.3214\ X\ 10^{-15}\ m \tag{37.3}$$

It appears that $\lambda_{C,p} = r_p$. To test this assumption we proceed as follows. We know that a proton is comprised of three quarks and three gluons ("trapped photons"). The quarks superimpose to form an atomic orbital of radius r_q such that:

$$r_p = r_q, \text{ and that} \tag{37.4}$$

$$m_p = m_q + m_g'' = m_q'', \tag{37.5}$$

where r_q is the radius of the quarks, m_q is the rest mass of the quarks, m_g'' is the relativistic mass of the gluons, and m_q'' is the relativistic mass of the quarks. The proton is in the ground state and,

$$2\pi r_{1,p} = \lambda_{1,p} = 2\pi\lambda_{C,p} \tag{37.6}$$

The boundary condition for the quarks is:

$$2\pi r_{n,q} = \lambda_{n,q} = \frac{h}{m_q v_{nq}} = 2\pi r_{1,p} = 2\pi \frac{h}{m_p c} = 2\pi\lambda_{C,p} \tag{37.7}$$

A solution to Eq. (37.7) is $v_{nq} = c$ and $m_q = \frac{m_p}{2\pi}$. When the quark velocity is the speed of light in the photon frame (gluon frame in this case), the relativistic factor, γ, for the lab frame is 2π. (See the Special Relativistic Correction to the Ionization Energies section and the Spin Orbit Coupling section.) Thus, the mass of the quarks in the lab frame (the relativistic mass) is:

$$2\pi m_q = 2\pi\ X\ \frac{m_p}{2\pi} = m_p = m_q^{"} \tag{37.8}$$

Furthermore, the (relativistic) mass of the gluons can be determined when:

$$m_g^{"} = m_p - m_q = m_p\left[1-\frac{1}{2\pi}\right] \tag{37.9}$$

The radius of the atomic orbital for $v_{nq} = c$ is then:

$$r_{n,q} = r_{1,p} = \lambda_{C,p} = \frac{h}{m_p c} = \frac{\hbar}{m_q c} = 2\pi\ \text{x}\ \frac{a_o m_e}{\alpha^{-1} m_p} = \lambda\!\!\!^{-}_{C,q} \tag{37.10}$$

where $\lambda\!\!\!^{-}_{c,q}$ is the Compton wavelength bar for the quarks. This result is internally consistent and represents the solution of the boundary value problem of the rest mass of the proton.

The quark mass/charge functions and the gluon mass/charge functions must have the same angular dependence. Thus, the force balance equation is:

$$\frac{m_q v_n^2}{r_n} = \frac{Z_{eff} e^2}{4\pi\varepsilon_0 r_n^2} = \frac{m_q v_n^2}{r_{1p}} = \frac{Z_{eff} e^2}{4\pi\varepsilon_0 r_{1p}^2}, \text{ where} \tag{37.11}$$

$$v_n = \frac{\hbar}{m_q r_{1p}} \tag{37.12}$$

The result of the substitution of Eq. (37.12) in Eq. (37.11), $r_{1,p} = \lambda_{C,p}$, and $m_q = \frac{m_p}{2\pi}$ is that $Z_{eff} = \alpha^{-1}$, and $n = \alpha$. Thus, Z_{eff}, the magnitude of the gluon field is α^{-1}. The potential energy of the quarks is then:

$$V_q = \frac{\alpha^{-1} e^2}{4\pi\varepsilon_0 r_{1p}} = \frac{m_p}{2\pi} c^2 \tag{37.13}$$

Thus, the total energy of the proton is:

$$E = m_q c^2 + m_g c^2 = \frac{m_p}{2\pi} c^2 + m_p\left[1-\frac{1}{2\pi}\right] c^2 = m_p c^2 \tag{37.14}$$

The neutron rest mass, m_n, the rest mass for the neutron quarks, the Compton wavelength of the neutron, and the Compton wavelength bar of the neutron quarks are obtained in a similar fashion,

$$\lambda_{C,n} = \lambda\!\!\!^{-}_{c,q} = \frac{2\pi a_0 m_e}{\alpha^{-1} m_n} = 1.3196\ X\ 10^{-15}\ m = r_{1,n} \tag{37.15}$$

$$m_q = \frac{m_n}{2\pi} \tag{37.16}$$

$$m_g^{"} = m_n - m_q = m_n\left[1-\frac{1}{2\pi}\right] \tag{37.17}$$

QUARK AND GLUON FUNCTIONS

Spherical harmonics are solutions to Laplace's Equations in spherical coordinates, and the constant atomic orbital is also a solution. All matter and energy is a linear combination of these functions. Thus, matter is created as an atomic orbital with mass/charge being linear combinations of spherical harmonics and constant functions. And, photons whose electric fields are linear combinations of solutions to Laplace's Equation, spherical harmonics and constant angular functions, can be trapped in the atomic orbital at the creation of matter from energy. (See the Excited States of the One-Electron Atom (Quantization) section and Hydrino Theory—BlackLight Process section for the equations of these photons.) The proton and the neutron are such hybrids of matter and energy. The proton and neutron can each be viewed as being comprised of a linear combination of three quarks possessing mass and charge and three gluons (photons) which hold the atomic orbital comprised of three quarks per nucleon in force balance on a spherical two-dimensional shell. The proton atomic orbital is comprised of two up quarks and a down quark, and the neutron is comprised of two down quarks and an up quark where the charge of an up quark is $+\frac{2}{3}e$ and the charge of a down quark is $-\frac{1}{3}e$. Each quark is associated with its gluon where the quark mass/charge function has the same angular dependence as the gluon mass/charge function.

To be consistent with experimentation, we choose a solution that is a linear combination of the three spherical harmonic functions, corresponding to $\ell = 1$, and three constant atomic orbitals. This resultant function can be viewed as being comprised of three separate particles. The three functions are orthogonal, and the corresponding gluon potentials have the same angular dependence as each other and each quark where there exists a one-to-one correspondence between each quark and each gluon.

THE PROTON

The proton functions can be viewed as a linear combination of three fundamental particles, three quarks, of $+\frac{2}{3}e$, $+\frac{2}{3}e$, $-\frac{1}{3}e$.

The magnitude of Z_{eff} of the radial gluon electric field for a proton is given by the solution of Eq. (37.11) as α^{-1}, and $r_1 = \frac{2\pi a_0 m_e}{\alpha^{-1} m_p}$. The normalized quark mass-density function of a proton is:

$$\frac{m_p}{2\pi}\left[\frac{1}{3}(1+\sin\theta\sin\phi)+\frac{1}{3}(1+\sin\theta\cos\phi)+\frac{1}{3}(1+\cos\theta)\right]\frac{\delta\left(r-\lambda_{C,p}\right)}{4\pi\left(\lambda_{C,p}\right)^2} \tag{37.18}$$

The normalized charge-density function of the quarks of a proton is:

$$e\left[\frac{2}{3}(1+\sin\theta\sin\phi)+\frac{2}{3}(1+\sin\theta\cos\phi)-\frac{1}{3}(1+\cos\theta)\right]\frac{\delta\left(r-\lambda_{C,p}\right)}{4\pi\left(\lambda_{C,p}\right)^2} \tag{37.19}$$

The gluons comprise three trapped orthogonal elliptical polarized photon atomic orbitals as given in the Equation of the Photon section and the Excited States of the One-Electron Atom (Quantization) section. Each gluon travels with the corresponding quark at $v = c$ (Eq. (37.7)) as a uniform component with a superimposed light speed spherical harmonic dependent component. The quark temporal mass/charge modulation is the same as that of an elliptically polarized photon with $v = c$ at any position on the nucleon surface according to the relativistic velocity addition formula. The gluons are inseparable from the corresponding quarks wherein the gluons provide the central field that maintains force balance. The potential function of the gluons of a proton is:

$$\Phi(r,\theta,\phi) = \frac{\alpha^{-1}e}{8\pi\varepsilon_0 r^2}\left[\frac{3}{2}(1+\sin\theta\sin\phi)+\frac{3}{2}(1+\sin\theta\cos\phi)-3(1+\cos\theta)\right]\delta\left(r-\lambda_{C,p}\right) \tag{37.20}$$

The radial electric field of the gluons of a proton is

$$E_r = \frac{-\alpha^{-1}e}{4\pi\varepsilon_0 r^3}\frac{2\pi a_0}{\frac{m_p}{m_e}\alpha^{-1}}\left[\frac{3}{2}(1+\sin\theta\sin\phi)+\frac{3}{2}(1+\sin\theta\cos\phi)-3(1+\cos\theta)\right]\delta\left(r-\lambda_{C,p}\right) \tag{37.21}$$

Recent experiments at the Thomas Jefferson National Accelerator Facility, using polarized electrons have shown that the proton charge may actually increase with distance from the center at certain radii [4-5] consistent with Eq. (37.19). The proton is shown in Figures 37.1 and 37.2.

Figure 37.1. The proton mass-density function in its inertial frame shown with the low and high mass-density proportional to red intensity and blue intensity, respectively. The proton is comprised of a linear combination of three orthogonal quarks, up, up, and down, of equal mass, $\frac{1}{3}\frac{m_p}{2\pi}$, that form a two-dimensional spherical shell of mass having a radius of the Compton wavelength of the proton. Each quark, in turn, comprises a constant function modulated by a spherically harmonic function. The quarks which have the properties of an energy-to-matter transition state spin about the z-axis at the speed of light. The centrifugal force of each quark is balanced by the electric field of its gluon, a heavy photon, each of mass $m_p\left[1-\frac{1}{2\pi}\right]$, that is phase-locked to the spinning quark and inseparable from it and exists at the radius of the quarks. The brightness corresponds to the intensity of the two-dimensional radial gluon field.

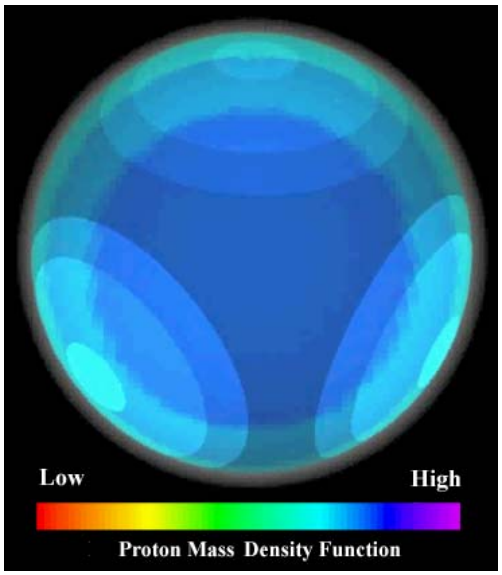

Figure 37.2. The proton charge-density function in its inertial frame shown with positive and negative charge-density proportional to red intensity and blue intensity, respectively. The proton is comprised of a linear combination of three orthogonal quarks, up, up, and down, of charge +2/3, +2/3, and -1/3, respectively, that form a two-dimensional spherical shell of charge having a radius of the Compton wavelength of the proton. Each quark, in turn, comprises a constant function modulated by a spherically harmonic function. The quarks, which have the properties of an energy-to-matter transition state, spin about the z-axis at the speed of light. The centrifugal force of each quark is balanced by the electric field of its gluon, a heavy photon, that is phase-locked to the spinning quark, is inseparable from it, and exists at the radius of the quarks.

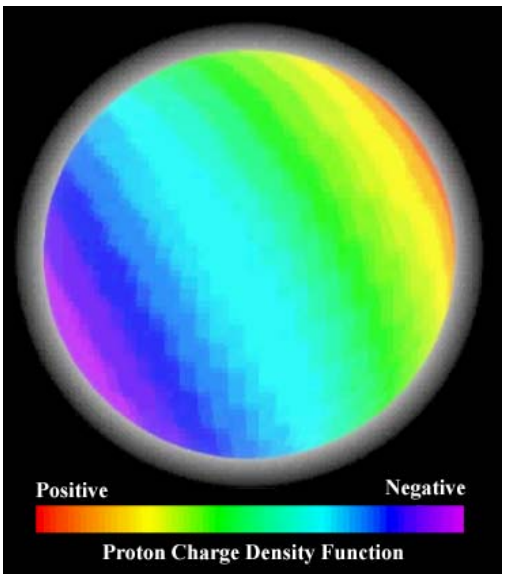

THE NEUTRON

The neutron functions can be viewed as a linear combination of three fundamental particles, three quarks, of charge $+\frac{2}{3}e$, $-\frac{1}{3}e$, and $-\frac{1}{3}e$. The magnitude of Z_{eff} of the radial gluon electric field for a neutron is given by the solution of Eq. (37.11) as α^{-1}, and $r_1 = \frac{2\pi a_0 m_e}{\alpha^{-1} m_n}$ where m_n is the rest mass of the neutron. The normalized quark mass-density function of a neutron is:

$$\frac{m_n}{2\pi}\left[\frac{1}{3}(1+\sin\theta\sin\phi)+\frac{1}{3}(1+\sin\theta\cos\phi)+\frac{1}{3}(1+\cos\theta)\right]\frac{\delta\left(r-\lambda_{C,n}\right)}{4\pi\left(\lambda_{C,n}\right)^2} \tag{37.22}$$

The normalized charge-density function of the quarks of a neutron is:

$$e\left[\frac{2}{3}(1+\sin\theta\sin\phi)-\frac{1}{3}(1+\sin\theta\cos\phi)-\frac{1}{3}(1+\cos\theta)\right]\frac{\delta\left(r-\lambda_{C,n}\right)}{4\pi\left(\lambda_{C,n}\right)^2} \tag{37.23}$$

The gluons comprise three trapped orthogonal elliptical polarized photon atomic orbitals as given in the Equation of the Photon section and the Excited States of the One-Electron Atom (Quantization) section. The gluons travel with the quarks at $v = c$ (Eq. (37.15)); thus, the gluons provide the central field that maintains force balance. The potential function of the gluons of a neutron is:

$$\Phi(r,\theta,\phi) = \frac{\alpha^{-1}e}{8\pi\varepsilon_0 r^2}\left[\frac{3}{2}(1+\sin\theta\sin\phi)-3(1+\sin\theta\cos\phi)-3(1+\cos\theta)\right]\delta\left(r-\lambda_{C,n}\right) \tag{37.24}$$

The radial electric field of the gluons of a neutron is:

$$E_r = \frac{-\alpha^{-1}e}{4\pi\varepsilon_0 r^3}\frac{2\pi a_0}{\frac{m_n}{m_e}\alpha^{-1}}\left[\frac{3}{2}(1+\sin\theta\sin\phi)-3(1+\sin\theta\cos\phi)-3(1+\cos\theta)\right]\delta\left(r-\lambda_{C,n}\right) \tag{37.25}$$

The neutron is shown in Figures 37.3 and 37.4.

Figure 37.3. The neutron mass-density function in its inertial frame shown with the low and high mass-density proportional to red intensity and blue intensity, respectively. The neutron is comprised of a linear combination of three orthogonal quarks, up, down, and down, of equal mass, $\frac{1}{3}\frac{m_n}{2\pi}$, that form a two-dimensional spherical shell of mass having a radius of the Compton wavelength of the neutron. Each quark, in turn, comprises a constant function modulated by a spherically harmonic function. The quarks which have the properties of an energy-to-matter transition state spin about the z-axis at the speed of light. The centrifugal force of each quark is balanced by the electric field of its gluon, a heavy photon, each of mass $m_n\left[1-\frac{1}{2\pi}\right]$, that is phase-locked to the spinning quark and inseparable from it and exists at the radius of the quarks. The brightness corresponds to the intensity of the two-dimensional radial gluon field.

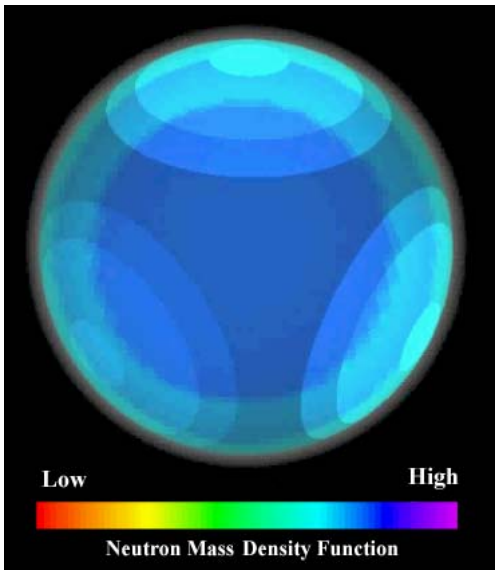

Figure 37.4. The neutron charge-density function in its inertial frame shown with positive and negative charge-density proportional to red intensity and blue intensity, respectively. The neutron is comprised of a linear combination of three orthogonal quarks, up, down, and down, of charge +2/3, -1/3, and -1/3, respectively, that form a two-dimensional spherical shell of charge having a radius of the Compton wavelength of the neutron. Each quark, in turn, comprises a constant function modulated by a spherically harmonic function. The quarks that have the properties of an energy-to-matter transition state spin about the z-axis at the speed of light. The centrifugal force of each quark is balanced by the electric field of its gluon, a heavy photon, that is phase-locked to the spinning quark, is inseparable from it, and exists at the radius of the quarks.

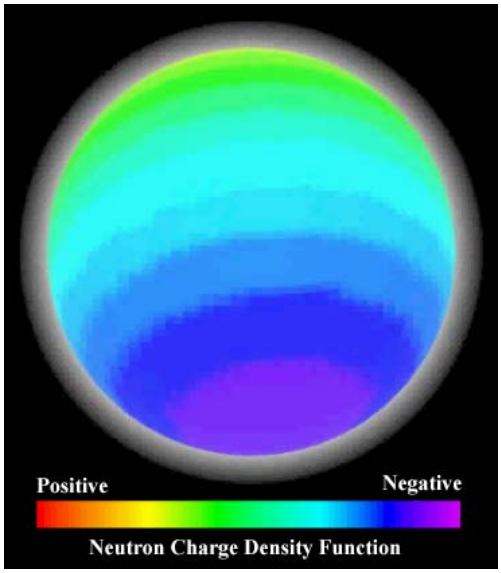

MAGNETIC MOMENTS

The spatial-temporal current and corresponding angular momentum distributions of the proton and the neutron give rise to magnetic dipole and quadrupole moments. It is demonstrated in the derivations of the magnetic moments that follow that 1/3 of the total angular momentum of the proton is due to the spin angular momentum of the quarks and the remaining 2/3 is due to the quark orbital angular momentum. The spin contribution has been confirmed experimentally [2]. Then, the neutron angular momentum follows from that of the proton and the angular momentum change due to conversion of an up quark/gluon to a down quark/gluon.

PROTON MAGNETIC MOMENT

The proton is comprised of three orthogonal mass functions—spherical harmonics with $\ell = 1$; these are the quarks. In addition, the proton is comprised of three "trapped orthogonal photons" called gluons of the same angular dependence as the quarks. Each gluon is in phase with a quark. The combination of a quark and its associated gluon is hereafter referred to as a quark/gluon. The projection of the quark/gluon angular momentum onto the z-axis is given by the sum of the independent projections. The angular momentum of the photon is $\hbar$, and the proton is generated from a photon as demonstrated in the Neutron and Proton Production section. Thus, the $\hbar$ of angular momentum of the production photon is conserved in the sum of the magnitude of the angular momentum of the three quarks, and the magnitude of the angular momentum of each quark held in force balance by the corresponding gluon is $\frac{\hbar}{3}$. As demonstrated in the Orbital and Spin Splitting section, the z component of

the angular momentum of an excited state electron atomic orbital corresponding to a multipole of order (ℓ , m) is:

$$L_z = m\hbar \tag{37.26}$$

Thus, the z projection of the angular momentum of a quark/gluon corresponding to $m_\ell = \pm 1$ is $\pm\frac{\hbar}{3}$. In the case that the two orthogonal up quark/gluons each of charge $+\frac{2}{3}$ are in the xy-plane with $m_\ell = 1$ and the down quark/gluon of charge $-\frac{1}{3}$ is along the z-axis, the magnetic moment is aligned along the z-axis. The former is time independent and the latter corresponds to a time-harmonic current-density wave. Thus, 1/3 and 2/3 of the total proton angular momentum is associated with quark spin and quark orbital angular momentum, respectively.

The magnetic moment is defined [6] as:

$$\mu = \frac{\text{charge X angular momentum}}{\text{2 X mass}} \tag{37.27}$$

The down quark corresponding to quantum number $m_\ell = 0$ has no magnetic projection on the z-axis that couple to an electromagnetic field. From Eq. (37.7), the mass of the quark function comprising the superposition of the three quarks is $\frac{m_p}{2\pi}$ and the charge of each up quark is $+\frac{2}{3}e$. The angular momentum of Eq. (37.27) for the proton is the sum of the z projections of the two up quarks[1] thus,

$$L_z = \frac{1}{3}\hbar + \frac{1}{3}\hbar = \frac{2}{3}\hbar \tag{37.28}$$

Therefore, the magnetic moment of the proton μ_p given by the sum of the contributions due to each quark of angular momentum $\frac{\hbar}{3}$ is:

$$\mu_p = \frac{\frac{2}{3}e\frac{1}{3}\hbar}{2\frac{m_p}{2\pi}} + \frac{\frac{2}{3}e\frac{1}{3}\hbar}{2\frac{m_p}{2\pi}} = \frac{\frac{2}{3}e\frac{2}{3}\hbar}{2\frac{m_p}{2\pi}} = \frac{4}{9}2\pi\frac{e\hbar}{2m_p} = 2.79253\mu_N \tag{37.29}$$

where μ_N is the nuclear magneton $\frac{e\hbar}{2m_p}$. The experimental magnetic moment of the proton is $\mu_p = 2.79268\mu_N$.

NEUTRON MAGNETIC MOMENT

The neutron is unstable and undergoes beta decay with a half-life of 10.2 minutes. Thus, the neutron can be viewed as the sum of an electron, a proton, and the beta decay energy. (The calculation of the energy of beta decay of a neutron is given below.) The magnetic moment of a neutron can be calculated as the sum of the following: $-\mu_N$, the magnetic moment of a constant atomic orbital of charge $-e$ corresponding to the beta particle at the initial radius of the neutron, $\frac{4}{9}2\pi\mu_N$, the magnetic moment of a proton, and the magnetic moment associated with changing an up quark/gluon to a down quark/gluon [See Quark and Gluon Functions of the Proton and Neutron section]. The contribution due to the transformation of an up quark/gluon to a down quark/gluon is determined as follows:

The fractional change in the quark functions equals the fractional change in the gluon function where:

$$\frac{3/2}{3+3+3/2} = \frac{1}{5} \tag{37.30}$$

Substitution of the equation for the time-averaged angular-momentum density, **m**, of a photon (Eq. (4.1)).

$$\mathbf{m} = \frac{1}{8\pi c}\text{Re}\left[\mathbf{r}\times(\mathbf{E}\times\mathbf{B}^*)\right] \tag{37.31}$$

into the vector identity:

---

[1] The projection of the angular momentum is analogous to that of a globe, where $I = \frac{2}{3}mr^2$, spinning about some axis [7].

$$\mathbf{A}\times\left(\mathbf{B}\times\mathbf{C}\right)=\mathbf{B}\left(\mathbf{A}\cdot\mathbf{C}\right)-\mathbf{C}\left(\mathbf{A}\cdot\mathbf{B}\right) \tag{37.32}$$

gives

$$\mathbf{m}=\frac{1}{8\pi c}\mathrm{Re}\left[\mathbf{E}\left(\mathbf{r}\cdot\mathbf{B}^{*}\right)-\mathbf{B}^{*}\left(\mathbf{r}\cdot\mathbf{E}\right)\right] \tag{37.33}$$

The first term of Eq. (37.33) is zero wherein the electric field is radial and the magnetic field is transverse. Using the relationship between the photon electric and magnetic fields from Appendix V ($|\mathbf{B}^{*}|=|\mathbf{B}|=|\mathbf{E}|$ in cgs units):

$$\mathbf{m}=\frac{1}{8\pi c}\mathrm{Re}\left[-\mathbf{E}\left(\mathbf{r}\cdot\mathbf{E}\right)\right]=-\frac{1}{8\pi c}\mathrm{Re}\left[-\mathbf{r}\left(\mathbf{E}\cdot\mathbf{E}\right)\right] \tag{37.34}$$

The gluon is a photon that is phase-matched to a quark. The quark/gluon is analogous to the case of an absorbed photon and the corresponding electron in an excited state as described in the Excited States of the One-Electron Atom (Quantization) section. From Eq. (37.27), Eq. (37.30), and Eq. (37.34), the contribution to the change in the magnetic moment of the nucleon from the quark/gluon function is proportional to the dot product of the change in the electric field of the quark/gluon,

$$\frac{1}{5}\cdot\frac{1}{5}=\frac{1}{25} \tag{37.35}$$

The contribution to the change in the nucleon magnetic moment from a quark/gluon with $\ell = 1$ is a factor of three times greater than that of a constant angular distribution of mass ($\ell = 0$). The integral of the dot product of the modulation functions (spherical harmonic functions) of each quark/gluon function with itself over all space for all three orthogonal quark/gluons is one, and the integral of the modulation function of the mass of each quark/gluon over the nucleon is zero. The change of an up quark/gluon to a down quark/gluon involves one of the three where $\ell = 1$. With the mass of parameter of Eq. (37.27) equal to one third the mass of the nucleon, the contribution to the change in the magnetic moment due to the transformation of an up quark/gluon to a down quark/gluon is:

$$3\ X\ \frac{1}{25}\ X\ \mu_N \tag{37.36}$$

The sum of the three components, the magnetic moment of the neutron, μ_n, is:

$$\mu_n=\left[1-\frac{4}{9}2\pi-\frac{3}{25}\right]\mu_N=-1.91253\mu_N \tag{37.37}$$

The direction of the positive z-axis is taken as the spin part of the magnetic moment. The experimental magnetic moment of the neutron is $\mu_n=-1.913043\mu_N$.

NEUTRON AND PROTON PRODUCTION

Eq. (32.43) equates the proper and coordinate times in the special case that the velocity of the transition state atomic orbital in the coordinate frame is the speed of light. In this case, the mass of the particle is given by defining a standard ruler for time in the coordinate frame whereby the mass of the particle must be experimentally measured with the same time ruler as part of a consistent system of units. In the case that MKS units are used, the coordinate time is defined as the sec which is essentially the MKS second (See Leptons section.), the permeability of free space is defined as $\mu_0=4\pi\ X\ 10^{-7}\ Hm^{-1}$, and the mass of the particle is given in kilograms. The production of a real particle from a transition state atomic orbital is a space-like event in terms of special relativity wherein spacetime is contracted by the gravitational radius of the particle during its production as given in the Gravity section. Thus, the coordinate time is imaginary as given by Eq. (32.43).

The considerations for the production of leptons and baryons are the same as those for leptons as described in the Leptons section. Consider the relativistic corrections of the variables of the relationship between the proper and coordinate times, Eq. (32.43), for the production of a neutral particle/antiparticle pair, each comprised of three quarks and three gluons of equivalent mass. The charges of each set of three quarks must sum to zero and the lowest energy nonuniform spherical harmonics are those corresponding to $\ell = 1$; thus, the charges are $-\frac{1}{3}$, $-\frac{1}{3}$, and $+\frac{2}{3}$ for the neutron quarks and $+\frac{1}{3}$, $+\frac{1}{3}$, $-\frac{2}{3}$ for the antineutron quarks. The neutron possesses three quarks of total mass $\frac{m_n}{2\pi}$ (Eq. (37.16)); thus, the mass of each quark is:

$$m_{1q}=\frac{m_n}{(3)2\pi} \tag{37.38}$$

The quarks/gluons possess magnetic stored energy. Concomitant with the "capture" of the gluons by the quark resonator cavity, the magnetic flux of the gluons is "captured." To conserve the total quark angular momentum, $\hbar$, the flux is trapped in quanta of the magnetic quantum of flux (See Electron g factor section.). The quark/gluon velocity is $v=c$; thus, the stored magnetic energy is m_nc^2 (Eqs. (29.14) and (29.15) with m_e replaced by m_n). The mass (energy) released due to magnetic flux "capture"

(gluon "capture") follows from Eq. (1.181) :

$$mass\ deficit = m_n \frac{\alpha}{2\pi} \tag{37.39}$$

The force corresponding to this mass deficit is the strong nuclear force (which is calculated for the deuterium nucleus in the Strong Nuclear Force section). Combining Eqs. (37.38) and (37.39) gives the bound individual quark mass where:

$$m_{1q} = \frac{m_n}{3}\left[\frac{1}{2\pi} - \frac{\alpha}{2\pi}\right] \tag{37.40}$$

The radius of the quark atomic orbital at neutron production thereafter is given by Eq. (37.15). No particles or fields propagate out from the event radius at the speed of light; thus, the lab frame transition state radius being the Compton wavelength of the neutron and the Compton wavelength bar of the neutron quarks is relativistically corrected relative to the $v = c$ inertial frame by the factor 2π (Eq. (1.281) with interchange of frames of reference). Moreover, the mass in the Compton wavelength bar is reduced by the factor 2π (Eq. (1.281) or (1.273) with interchange of frames of reference) such that the relativistic radius can be identified as $(2\pi)^2 r$. The radius r is the Compton wavelength bar of the neutron quarks given by Eq. (32.21) wherein three fundamental composite particles each comprising a quark-gluon pair of angular momentum $\hbar$ superimpose to form the baryon of resultant total angular momentum $\hbar$. Additionally, since the velocity of the quarks in the proper frame is $v = c$ (Proton and Neutron section), the proper time is relativistically dilated by a factor of 2π (Eq. (1.273)). Multiplication of the left side of Eq. (32.43) by 2π, and making the following substitutions: (i) Eq. (36.1) for τ, (ii) the sec which is essentially the second—the definition for the coordinate time in MKS units, for ti, (iii) $(2\pi)^2 r$ for the transition state radius r which is also the final particle radius, (iv) the Compton wavelength bar for the transition state radius r (Eq. (32.21)) times three due to the superposition of the three fundamental particles each of angular momentum $\hbar$, and (v) the mass of Eq. (37.40) for M as well as this mass in the Compton wavelength bar formula, gives the relationship between the neutron proper time and the coordinate time:

$$2\pi \frac{2\pi\hbar}{\frac{m_n}{3}\left[\frac{1}{2\pi} - \frac{\alpha}{2\pi}\right]c^2} = \sec\sqrt{\frac{2G\left[\frac{m_n}{3}\left[\frac{1}{2\pi} - \frac{\alpha}{2\pi}\right]\right]^2}{3c(2\pi)^2\hbar}} \tag{37.41}$$

The neutron mass in MKS units based on the definition of the coordinate time in terms of the sec is:

$$m_{\text{n } calculated} = (3)(2\pi)\left(\frac{1}{1-\alpha}\right)\left(\frac{2\pi h}{\sec c^2}\right)^{\frac{1}{2}}\left(\frac{2\pi(3)ch}{2G}\right)^{\frac{1}{4}} = 1.6726X10^{-27}\ kg \tag{37.42}$$

where $m_{\text{n experimental}} = 1.6749X10^{-27}\ kg$. The difference between the calculated and experimental values of the neutron mass is due to the very slight difference between the MKS second and the definition of the corresponding time unit defined by Eq. (36.2). The relationship between the neutron and electron masses which is independent of the definition of the imaginary time ruler ti given by Eqs. (32.43) and (36.2) including the contribution of the fields due to charge production is given by Eq. (38.31). Three families of quarks arise from Eq. (32.27) as given in the case of the leptons in the Leptons section.

Proton production is given in the Weak Nuclear Force: Beta Decay of the Neutron section via beta decay of the neutron. The energy of the neutron can be lowered by neutron decay to a proton and a beta. The proton mass calculated from the neutron decay reaction given in the Weak Nuclear Force: Beta Decay of the Neutron section is $1.672648\ X\ 10^{-27}\ kg$. The experimental proton mass is $1.672648\ X\ 10^{-27}\ kg$.

INTERMEDIATE VECTOR AND HIGGS BOSONS

The only fundamental matter particles that can exist are the three leptons, three sets of quarks, and their antiparticles. However, linear combinations of these fundamental particles may comprise more complicated species beyond neutrons and protons. Particle energies in collisions may exceed the particle production energies and consequently exceed the corresponding spacetime resonance frequencies during particle production and decay reactions. The relationship between proper and coordinate time has higher order or over-energy resonances due to the same principles regarding the relationship between proper and coordinate time that is the basis of production of the fundamental particles. Then, an increase in the intensity of particle reactions events is predicted at the over-energy resonance frequencies. However, the associated peak at the resonance energy does not represent a new fundamental particle. Nor, does this phenomenon have any association with mediating forces such as the weak nuclear force or the conveyance of inertial mass. The former is due to the electromagnetic force and the latter is due to the absolute nature of spacetime and the conservation of matter, energy, and spacetime with satisfaction of Maxwell's equations and the conditions inherent in the Schwarzschild metric of spacetime required for particle production.

The additional resonances can be predicted by applying these principles to energy exceeding the production energy of a given particle. Specifically, using the spatial dimensions and the velocity at the electron production event, the scaling factor between the proper and coordinate time is given by Eq. (34.62) wherein the latter is imaginary because energy transitions are spacelike due to spacetime expansion from matter to energy conversion:

$$\frac{2\pi\lambda\!\!\!^{-}_{C}}{\sqrt{\frac{2Gm_e}{\lambda\!\!\!^{-}_{C}}}} = \frac{2\pi\lambda\!\!\!^{-}_{C}}{v_g} = i\alpha^{-1}\sec \tag{37.43}$$

where v_g is Newtonian gravitational velocity (Eq. (34.30)). Consider the muon that is a lepton arising from a resonance involving the electron wherein in addition to pair production, the latter is a product of beta decay. The correction between proper and coordinate time based on the Coulombic potential as the basis of the muonic production energy is 2π (Eqs. (36.5) and (1.281)), and further applying Eq. (34.62) , the resonance coupling factor g_C is:

$$g_C = 2\pi\alpha^{-1} \tag{37.44}$$

Using the relationship between the proper time and the electron coordinate time for the Coulomb potential energy as the production energy, the mass of the muon/antimuon using the MKS second is (Eqs. (36.5-36.6)):

$$m_\mu = \frac{\hbar}{c}\left(\frac{1}{2Gm_e(\alpha\sec)^2}\right)^{\frac{1}{3}} = 1.8874\ X\ 10^{-28}\ kg\ \left(0.10587\ GeV\right) \tag{37.45}$$

Applying resonance coupling factor g_C (Eq. (37.44)) to the muon production mass (Eq. (37.45)) having its inherent lepton member, the electron, gives an over-energy resonance E_{Z^0} at:

$$E_{Z^0} = g_C m_\mu = 2\pi\alpha^{-1}\frac{\hbar}{c}\left(\frac{1}{2Gm_e(\alpha\sec)^2}\right)^{\frac{1}{3}} = 2\pi\alpha^{-1}\left(0.10587\ GeV\right) = 91.16\ GeV \tag{37.46}$$

Experimentally, the event excess called the intermediate vector boson Z^0 occurs at 91.1876 GeV [8]. This signature is deemed a manifestation of the weak force regarding an ad hoc postulated Standard Model treatment of beta decay.

In contrast, based on Maxwell's equations and the conditions inherent in the Schwarzschild metric of spacetime required for particle production, the neutron mass is given by Eq. (37.42) in terms of fundamental constants and MKS units based on the definition of the coordinate time in terms of the sec. An over-energy absolute spacetime resonance of the electrically neutral neutron E_{H^0} due to the relationship between proper and coordinate time given by Eq. (37.43) is predicted at:

$$E_{H^0} = \alpha^{-1}m_n = \alpha^{-1}(3)(2\pi)\left(\frac{1}{1-\alpha}\right)\left(\frac{2\pi h}{\sec c^2}\right)^{\frac{1}{2}}\left(\frac{2\pi(3)ch}{2G}\right)^{\frac{1}{4}} = \alpha^{-1}\left(0.93956536\ GeV\right) = 128.75\ GeV \tag{37.47}$$

High-energy proton-proton collisions that produce neutron-antineutron pairs decay to two gamma ray photons or correspondingly two pairs of electron-positron or muon-antimuon pairs. Such an excess of events at 126 GeV has recently been announced by CERN [9]. Specifically, the corresponding excess of events at the neutron over-energy spacetime resonance energy has been announced as the discovery the Higgs boson H^0 that conveys mass to particles according to an ad hoc postulate of the Standard Model. However, there is no physical evidence that this slight excess of events at 126 GeV conveys mass to particles, and the energy of the excess events deemed the Higgs boson cannot and was not directly observed as a real particle due to the extraordinarily small mean lifetime of the resonance.

As given in the Weak Nuclear Force: Beta Decay of the Neutron section, a proton is formed via beta decay of the neutron. This requires the initial step of the conversion of a down quark to an up quark having charges -1/3 and +2/3, respectively, with the concomitant formation of an electron of the lepton family having a charge of -1. Considering that the

transition occurs on a time scale of $10^{-25} s$, the radius of the baryon is unchanged, and the energy change is that of the electric energy decrease given by Eq. (1.170). Using 1/3, the magnitude of the change in charge normalized to that of the proton, and $(2\pi)^{-2}$, the relativistic correction term of the neutron production condition of Eq. (37.41) with the equivalence of the correction for charge and mass density since they are interchangeable by the ratio e/m, an over-energy resonance E_{W^-} corresponding to E_{Z^0} of Eq. (37.46) is predicted at:

$$\begin{aligned} E_{W^-} &= g_C m_\mu \left\{1-\left[\frac{1}{3}\left(1+(2\pi)^{-2}\right)\right]^2\right\} = 2\pi\alpha^{-1}\frac{\hbar}{c}\left(\frac{1}{2Gm_e(\alpha \sec)^2}\right)^{\frac{1}{3}}\left\{1-\left[\frac{1}{3}\left(1+(2\pi)^{-2}\right)\right]^2\right\} \\ &= 2\pi\alpha^{-1}(0.10587\ GeV)\left\{1-\left[\frac{1}{3}\left(1+(2\pi)^{-2}\right)\right]^2\right\} = 80.51\ GeV \end{aligned} \tag{37.48}$$

Then, by the symmetry of antiparticles, the positron decay of the antineutron corresponds to W^+. Experimentally, the event excess called the intermediate vector bosons $W^\pm$ occurs at $80.423\ GeV$ [8]. These particles convey the weak nuclear force according to an ad hoc postulate of the Standard Model that seems nonsensical since each weighs 80 times the mass of the neutron. There is no physical evidence that these particles produce a nuclear force. Moreover, the intermediate vector bosons $W^\pm$ are not real particles in that they cannot and were not directly observed since the experimental mean lifetime of the resonance is $3.076\ X\ 10^{-25}\ s$ [10]. Similarly, the experimental mean lifetime of the Z^0 spacetime resonance is $2.6379\ X\ 10^{-25}\ s$ [11].

REFERENCES

1. R. Hasty et al., "Strange magnetism and the anapole structure of the proton," Science, Vol. 290, (2000), pp. 2117-2119.
2. E. S. Ageev et al., "Measurement of the spin structure of the deuteron in the DIS region," Phys. Lett. B, Vol. 612, (2005), pp. 154-164.
3. K. K. Seth, D. J. Hughes, R. L. Zimmerman, R. C. Grant, "Nuclear radii by scattering of low-energy neutrons," Phys. Rev., Vol. 110, No. 3, (1958), pp. 692-700.
4. P. Weiss, "New probe reveals unfamiliar inner proton," Science News, Vol. 159, May, 5, (2001), p. 277.
5. M. K. Jones, et al., "G_{E_p} / G_{M_p} ratio by polarization transfer in $\vec{e}p \to e\vec{p}$," Physical Review Letters, Vol. 84, No. 7, February, 14, (2000), pp. 1398-1402.
6. D. A. McQuarrie, *Quantum Chemistry*, University Science Books, Mill Valley, CA, (1983), pp. 238-241.
7. G. R. Fowles, *Analytical Mechanics*, Third Edition, Holt, Rinehart, and Winston, New York, (1977), pp. 195-196.
8. K. Hagiwara, et al., (Particle Data Group), Phys Rev. D, Vol. 66, 010001, (2002) (URL:http://pdg.lbl.gov).
9. "CERN experiments observe particle consistent with long-sought Higgs boson," CERN press release, 4 July 2012, http://press.web.cern.ch/press/PressReleases/Releases2012/PR17.12E.html.
10. http://www.wolframalpha.com/input/?i=W+boson.
11. http://www.wolframalpha.com/input/?i=Z+boson.

Chapter 38

QUARKS

Only three quark families can be formed from photons corresponding to the Planck equation energy, the potential energy, and the magnetic energy, where each is equal to the mass energy (Eq. (32.27)). As opposed to a continuum of energies, fundamental quark families arise from photons of only three energies. The considerations for the production of baryons are described in the Neutron and Proton Production section. Consider the relativistic corrections of the variables of the relationship between the proper and coordinate times, Eq. (32.43), for the production of three types of neutral baryon/antibaryon pairs, each comprised of three quarks and three gluons. The charges of each set of three quarks must sum to zero and the lowest energy nonuniform spherical harmonics are those corresponding to $\ell = 1$; thus, the charges are $-\frac{1}{3}$, $-\frac{1}{3}$, and $+\frac{2}{3}$ for the baryon quarks and $+\frac{1}{3}$, $+\frac{1}{3}$, $-\frac{2}{3}$ for the antibaryon quarks. The radius of the quark atomic orbital at baryon production and thereafter follows from by Eq. (37.15). The baryon possesses three quarks of total mass $\frac{m_B}{2\pi}$ (Eq. (37.16)); thus, the mass of each quark is:

$$m_{1q} = \frac{m_B}{(3)2\pi} \tag{38.1}$$

The quarks/gluons possess magnetic stored energy. Concomitant with the "capture" of the gluons by the quark resonator cavity, the magnetic flux of the gluons is "captured." To conserve the total quark angular momentum, $\hbar$, the flux is trapped in quanta of the magnetic quantum of flux (See Electron g Factor section.). The quark/gluon velocity is $v = c$; thus, the magnetic stored energy is $m_B c^2$ (Eq. (29.14) and (29.15) with m_e replaced by m_B). The mass (energy) released due to magnetic flux "capture" (gluon "capture") follows from Eq. (1.181).

$$mass\ deficit = m_B \frac{\alpha}{2\pi} \tag{38.2}$$

The force corresponding to this mass deficit is the strong nuclear force (which is calculated for the deuterium nucleus in the Strong Nuclear Force section). Combining Eqs. (38.1) and (38.2) gives the bound individual quark mass:

$$m_{1q} = \frac{m_B}{3}\left[\frac{1}{2\pi} - \frac{\alpha}{2\pi}\right] \tag{38.3}$$

No particles or fields propagate out from the event radius at the speed of light; thus, the lab frame transition state radius being the Compton wavelength of the neutron and the Compton wavelength bar of the neutron quarks is relativistically corrected relative to the $v = c$ inertial frame by the factor 2π (Eq. (1.281) with interchange of frames of reference). Moreover, the mass in the Compton wavelength bar is reduced by the factor 2π (Eq. (1.281) or (1.273) with interchange of frames of reference) such that the relativistic radius can be identified as $(2\pi)^2 r$. The radius r is the Compton wavelength bar of the neutron quarks given by Eq. (32.21) wherein three fundamental composite particles each comprising a quark-gluon pair of angular momentum $\hbar$ superimpose to form the baryon of resultant total angular momentum $\hbar$. Additionally, since the velocity of the quarks in the proper frame is $v = c$ (Proton and Neutron section), the proper time is relativistically dilated by a factor of 2π (Eq. (1.273)). Multiplication of the left side of Eq. (32.43) by 2π, and making the following substitutions: (i) Eq. (36.1) for τ, (ii) the sec which is essentially the second—the definition for the coordinate time in MKS units, for ti, (iii) $(2\pi)^2 r$ for the transition state radius r which is also the final particle radius, (iv) the Compton wavelength bar for the transition state radius r (Eq. (32.21))

times three due to the superposition of the three fundamental particles each of angular momentum $\hbar$, gives the relationship between the neutron proper time and the coordinate time:

$$2\pi\frac{2\pi\hbar}{\frac{m_B}{3}\left[\frac{1}{2\pi}-\frac{\alpha}{2\pi}\right]c^2}=\sec\sqrt{\frac{2GM\left[\frac{m_B}{3}\left[\frac{1}{2\pi}-\frac{\alpha}{2\pi}\right]\right]}{3c(2\pi)^2\hbar}} \tag{38.4}$$

The mass of each member of a quark pair corresponds to an energy of Eq. (32.32) where the production state goes through the corresponding neutron comprising quarks and gluons. The down-down-up neutron (ddu) and anti-ddu correspond to the Planck equation energy. The strange-strange-charm neutron (ssc) and anti-ssc correspond to the electric energy. And, the bottom-bottom-top neutron (bbt) and anti-bbt correspond to the magnetic energy. It is shown that the masses are given by Eq. (32.43) and the relative masses differ in their specific function of the fine structure constant α only. These functions are determined by relativistic coefficients in Eq. (38.4) given by Eq. (32.32) according to the kind of energy that is responsible for the respective level (*ddu* , *ssc* , *bbt*) of the particular particle within its family.

DOWN-DOWN-UP NEUTRON (DDU)

The down-down-up neutron is comprised of a down, down, and an up quark where the charge of a down quark is $-\frac{1}{3}e$, and the charge of an up quark is $+\frac{2}{3}e$. The mass of the down-down-up neutron corresponds to the Planck equation energy given by Eq. (32.28). Substitution of the mass of Eq. (38.3) for M as well as this mass in the Compton wavelength bar formula, gives the relationship between the down-down-up neutron proper time and the coordinate time:

$$2\pi\frac{2\pi\hbar}{\frac{m_{ddu}}{3}\left[\frac{1}{2\pi}-\frac{\alpha}{2\pi}\right]c^2}=\sec\sqrt{\frac{2G\left[\frac{m_{ddu}}{3}\left[\frac{1}{2\pi}-\frac{\alpha}{2\pi}\right]\right]^2}{3c(2\pi)^2\hbar}} \tag{38.5}$$

The neutron mass in MKS units based on the definition of the coordinate time in terms of the sec is:

$$m_{ddu\ \ calculated}=(3)(2\pi)\left(\frac{1}{1-\alpha}\right)\left(\frac{2\pi h}{\sec c^2}\right)^{\frac{1}{2}}\left(\frac{2\pi(3)ch}{2G}\right)^{\frac{1}{4}} \tag{38.6}$$

$$m_{ddu\ \ calculated}=1.6726\ X\ 10^{-27}\ kg \tag{38.7}$$

$$m_{ddu\ \ experimental}=1.6749\ X\ 10^{-27}\ kg \tag{38.8}$$

The difference between the calculated and experimental values of the neutron mass is due to the very slight difference between the MKS second and the definition of the corresponding time unit defined by Eq. (36.2) and the slight contribution due to the field energies of the quarks' charges. The relation between the ddu neutron and electron masses which is independent of the definition of the imaginary time ruler *ti* given by Eqs. (32.43) and (36.2) including the contribution of the fields due to charge production is given by Eq. (38.31).

STRANGE-STRANGE-CHARM NEUTRON (SSC)

The strange-strange-charm neutron is comprised of a strange, strange, and a charm quark where the charge of a strange quark is $-\frac{1}{3}e$, and the charge of a charm quark is $+\frac{2}{3}e$. Given that the down-down-up neutron is a solution to Eq. (38.4), other solutions follow from this solution and the other energy solutions.

Consider the case of the potential energy. Given that the down-down-up neutron is "allowed" by the Planck energy equation (Eq. (32.28)) and that the proper time is given by general relativity (Eq. (32.38)), the strange-strange-charm neutron mass can be calculated from the potential energy, V, (Eq. (32.27)) and the proper time relative to the down-down-up neutron inertial frame.

Baryons comprised of charm and strange quarks (antiquarks) decay to baryons of up and down quarks (antiquarks) and may be considered a transient resonance which decays to the stable baryons, the neutron or proton (antineutron or antiproton). For the lab inertial frame, the relativistic correction of the radius of the transition state atomic orbital given by the potential energy equations (Eq. (29.10) and (29.11)) is α^{-2}. As shown in the Muon-Antimuon Lepton Pair section, for the down-down-up neutron inertial frame, the relativistic correction of the gravitational radius r_g (Eq. (32.36)) relative to the proper frame is the inverse, α^2. Furthermore, the potential energy equation gives an electrostatic energy; thus, the down-down-up neutron inertial time must be corrected by the relativistic factor of 2π relative to the proper time. (See the Special Relativistic Correction to the Ionization Energies section.) Multiplication of the right side of Eq. (38.4) by 2π and substitution of (i) $\alpha^2 r_g$, the relativistically

corrected gravitational radius for r_g (Eq. (32.36)), and (ii) m_{ddu}, the mass of the down-down-up neutron, for M into Eq. (38.4) gives the relationship between the proper time and the down-down-up neutron coordinate time:

$$2\pi \frac{2\pi\hbar}{\frac{m_{ssc}}{3}\left[\frac{1}{2\pi}-\frac{\alpha}{2\pi}\right]c^2} = 2\pi \sec\sqrt{\frac{2G\alpha^2 m_{ddu}\left[\frac{m_{ssc}}{3}\left[\frac{1}{2\pi}-\frac{\alpha}{2\pi}\right]\right]}{3c(2\pi)^2\hbar}} \tag{38.9}$$

The strange-strange-charm neutron mass in MKS units based on the definition of the coordinate time in terms of the sec is:

$$m_{ssc\ calculated} = (3)(2\pi)\left(\frac{1}{1-\alpha}\right)\left(\frac{h}{\sec c^2}\right)^{\frac{2}{3}}\left(\frac{2\pi(3)ch}{2m_{ddu}G\alpha^2}\right)^{\frac{1}{3}} \tag{38.10}$$

$$m_{ssc\ calculated} = 4.89X10^{-27}\ kg = 2.74\ GeV/c^2 \tag{38.11}$$

The observed mass of the Ω^- hyperon that contains three strange quarks (sss) is [1]:

$$m_{\Omega^-} = 1673\ MeV/c^2 \tag{38.12}$$

Thus, an estimate for the dynamical mass of the strange quark, m_s, is:

$$m_s = \frac{m_{\Omega^-}}{3} = \frac{1673\ MeV/c^2}{3} = 558\ MeV/c^2 \tag{38.13}$$

The dynamical mass of the charm quark, m_c, has been determined by fitting quarkonia spectra, and from the observed masses of the charm pseudoscalar mesons $D^0(1865)$ and $D^+(1869)$ [2]:

$$m_c = 1.580\ GeV/c^2 \tag{38.14}$$

Thus,

$$m_{ssc\,experimental} = 2m_s + m_c = 2(558\ MeV/c^2) + 1580\ MeV/c^2 \tag{38.15}$$

$$m_{ssc\,experimental} = 2.70\ GeV/c^2 \tag{38.16}$$

Eqs. (38.11) and (38.16) are in agreement.

BOTTOM-BOTTOM-TOP NEUTRON (BBT)

The bottom-bottom-top neutron is comprised of a bottom, bottom, and a top quark where the charge of a bottom quark is $-\frac{1}{3}e$, and the charge of a top quark is $+\frac{2}{3}e$. Given that the down-down-up neutron is a solution to Eq. (38.4), other solutions follow from this solution and the other energy solutions.

Consider the case of the magnetic energy. Given that the down-down-up neutron is "allowed" by the Planck energy equation (Eq. (32.28)) and that the proper time is given by general relativity (Eq. (32.38)), the bottom-bottom-top neutron mass can be calculated from the magnetic energy (Eq. (32.27)) and the proper time relative to the down-down-up neutron inertial frame. As given in the Proton and Neutron section for the neutron and proton, the bottom-bottom-top neutron and the antibottom-bottom-top neutron radius, r, is given by the Compton wavelength:

$$r = \lambda_{C,bbt} = \frac{h}{m_{bbt}\,c} \tag{38.17}$$

Furthermore, the transition state comprises two magnetic moments. For $v = c$, the magnetic energy equals the potential energy, equals the Planck equation energy, equals mc^2. The magnetic energy is given by the square of the magnetic field as given by Eqs. (1.154-1.162). As in the case of the tau-mass calculation given in the Leptons sections, the magnetic energy corresponding to particle production is given by Eq. (32.32). Because two magnetic moments are produced, the magnetic energy (and corresponding photon frequency) in the proper frame is two times that of the down-down-up neutron frame. Thus, the down-down-up neutron time is corrected by a factor of two relative to the proper time. Both the bottom-bottom-top neutron and the antibottom-bottom-top neutron undergo and exit the production event with a radius given by Eq. (38.17). Whereas, in the case of tau-antitau production given in the Leptons section, the radius of the lepton and antilepton increased symmetrically to produce lepton plane waves at infinity relative to each other. Thus, in the lab frame, the gravitational radius r_g (Eq. (32.36)) is not corrected by $(2\pi)^2$. Furthermore, a mutual central magnetic field exists for the particles of fixed radius. The corresponding electrodynamic special relativistic correction is given by Eqs. (1.241-1.260) where the mass of each particle in Eq. (1.255) is m_{bbt}. Thus, as a consequence of the mutual magnetic dipole interaction, the mass m_{bbt} is replaced by the corresponding reduced mass μ_{bbt} of the two baryonic magnetic dipoles:

$$\mu_{bbt} = \frac{m_{bbt}}{2} \tag{38.18}$$

Furthermore, for the lab inertial frame, the relativistic correction of the radius of the transition state atomic orbital given by the

magnetic energy equations (Eq. (29.14) and (29.15)) is $\frac{1}{\alpha^4}$. As shown in the Tau-Antitau Lepton Pair section, for the down-down-up neutron inertial frame, the relativistic correction of the gravitational radius r_g relative to the proper frame is the inverse, α^4. Multiplication of the right side of Eq. (38.4) by 2 and substitution of (i) m_{ddu}, the mass of the down-down-up neutron, for M, (ii) $\alpha^4 r_g$, the relativistically corrected gravitational radius for r_g (Eq. (32.36)), and (iii) the reduced mass μ_{bbt} (Eq. (38.18)) for m_{bbt} into Eq. (38.4) gives the relationship between the proper time and the down-down-up neutron coordinate time:

$$2\pi \frac{2\pi\hbar}{\frac{m_{bbt}}{3}\left[\frac{1}{2\pi}-\frac{\alpha}{2\pi}\right]c^2} = 2\sec\sqrt{\frac{2G\alpha^4 m_{ddu}\left[\frac{m_{bbt}}{3}\left[\frac{1}{2\pi}-\frac{\alpha}{2\pi}\right]\right]}{3c2(2\pi)^2\hbar}} \tag{38.19}$$

The bottom-bottom-top neutron mass in MKS units based on the definition of the coordinate time in terms of the sec is:

$$m_{bbt\ \ calculated} = (3)(2\pi)\left(\frac{1}{1-\alpha}\right)\left(\frac{2\pi h}{2\sec c^2}\right)^{\frac{2}{3}}\left(\frac{2\pi(3)ch}{m_{ddu}G\alpha^4}\right)^{\frac{1}{3}} \tag{38.20}$$

$$m_{bbt\ \ calculated} = 3.50\ X\ 10^{-25}\ kg = 196\ GeV/c^2$$

The dynamical mass of the bottom quark, m_b, has been determined by fitting quarkonia spectra; and from the observed masses of the bottom pseudoscalar mesons $B^0(5275)$ and $B^+(5271)$ [2]:

$$m_b = 4.580\ GeV/c^2 \tag{38.21}$$

Thus, the predicted dynamical mass of the top quark based on the dynamical mass of the bottom quark is:

$$m_{t\ calculated} = m_{bbt\ \ calculated} - 2m_b = 196\ GeV/c^2 - 2(4.580\ GeV/c^2) \tag{38.22}$$

$$m_{t\ calculated} = 187\ GeV/c^2$$

Considering all jets, the CDF collaboration determined the mass of the top quark to be $186 \pm 10\ GeV/c^2$ [3].

All other hadrons comprise linear combinations of the fundamental quarks.

RELATIONS BETWEEN MEMBERS OF THE NEUTRON FAMILY AND THE LEPTONS

As shown in the Leptons section (Eqs. (36.9-36.11)), the mass ratios of the members of the lepton family are based solely on the fine structure constant α. Based on Eqs. (36.3), (38.6), (38.10), and (38.20), the relations between the electron and neutron masses which are independent of the definition of the imaginary time ruler ti given by Eq. (32.43) are [4]:

$$\frac{m_N}{m_e} = \frac{12\pi^2}{1-\alpha}\sqrt{\frac{\sqrt{3}}{\alpha}} = 1838.06 \qquad (1838.68) \tag{38.23}$$

$$\frac{m_{ssc}}{m_{ddu}} = \frac{m_{ssc}}{m_N} = \frac{1}{2\pi}\left(\frac{1-\alpha}{3\alpha^2}\right)^{\frac{1}{3}} = 2.926 \tag{38.24}$$

$$\frac{m_{bbt}}{m_{ssc}} = \left(\frac{2\pi^2}{\alpha^2}\right)^{\frac{1}{3}} = 71.8 \tag{38.25}$$

$$\frac{m_{bbt}}{m_{ddu}} = \frac{m_{bbt}}{m_N} = \left(\frac{1-\alpha}{12\pi\alpha^4}\right)^{\frac{1}{3}} = 210 \tag{38.26}$$

The respective experimental neutron/electron mass ratio according to the 1998 CODATA is given in parentheses [5]. Remarkably, all of the quarks as well as leptons are related by the fine structure constant α only which demonstrates that the masses arise as a consequence of special relativity. This result is analogous to the magnetic field that is a special relativistic consequence of the electric field.

Eq. (38.23) does not include the electron neutrino energy or the coulomb and magnetic field energies. As shown in the Relations Between the Leptons section, in order to conserve mass-energy, the electromagnetic fields of the particles must be included in the mass determination. The correction γ^* to the electron mass given by Eq. (36.15) is:

$$\gamma^* = \left(1 + 2\pi\frac{\alpha^2}{2}\right)^{-1} \tag{38.27}$$

Similar to the electron-positron pair, the ddu-neutron-anti-ddu-neutron pair depends on the Planck energy equation. The latter is exceptional in that the radius of the charged quarks does not change following particle production. Since the energy in the electrostatic fields of the electron-positron pair are released as photons during binding and photons have no gravitational mass as

shown in the Gravity section, the relativistic correction decreases each lepton mass as shown in Eq. (36.15). However, in the case of the neutron, the electrostatic field, for radial distance greater than the radius of the quarks, is zero, and the gluons result in a relativistically corrected quark mass as given in the Proton and Neutron section. In this case, the corresponding correction γ^* has the opposite sign as that of Eq. (38.27) and is given by:

$$\gamma^* = \left(1 - 2\pi\frac{\alpha^2}{2}\right)^{-1} \tag{38.28}$$

Substitution of the relationship between the definition of the imaginary time ruler ti given by Eq. (36.4) and the correction due to the contribution of the fields due to charged quark production given by Eq. (38.28) into Eq. (38.6) gives the ddu neutron mass as:

$$m_{ddu\ \ calculated} = (3)(2\pi)\left(\frac{1}{1-\alpha}\right)\left(\frac{2\pi h}{0.9975(46714)\ \text{MKS second}c^2}\right)^{\frac{1}{2}}\left(\frac{2\pi(3)ch}{2G}\right)^{\frac{1}{4}}\left(1 - 2\pi\frac{\alpha^2}{2}\right)^{-1} \tag{38.29}$$

$$m_{ddu\ \ calculated} = 1.6749\ X\ 10^{-27}\ kg \tag{38.30}$$

To the appropriate number of significant figures, there is good agreement with the experimental value of $m_{ddu\ \text{experimental}} = 1.6749\ X\ 10^{-27}\ kg$.

Based on Eqs. (36.3), (38.6), (38.27), and (38.28), the relation between the ddu neutron and electron masses (Eq. ((38.23)) which is independent of the definition of the imaginary time ruler ti given by Eq. (36.43) including the contribution of the fields due to charge production is:

$$\frac{m_N}{m_e} = \frac{12\pi^2}{1-\alpha}\sqrt{\frac{\sqrt{3}}{\alpha}}\frac{\left(1 + 2\pi\frac{\alpha^2}{2}\right)}{\left(1 - 2\pi\frac{\alpha^2}{2}\right)} = 1838.67 \qquad (1838.68) \tag{38.31}$$

The experimental ddu neutron-electron mass ratio according to the 1998 CODATA given in parentheses matches the predicted value very well.

REFERENCES

1. I. S. Hughes, *Elementary Particles*, Cambridge University Press, (1972), pp. 124-125.
2. I. R. Kenyon, *Elementary Particle Physics*, Routledge & Kegan Paul, London, (1987), p.196.
3. K. Hagiwara et al., Phys. Rev. D66, 010001 (2002); http://pdg.lbl.gov; http://pdg.lbl.gov/2002/topquark_q007.pdf.
4. Personal communication, Dr.-Ing. Günther Landvogt, Hamburg, Germany, February, (2003).
5. P. J. Mohr and B. N. Taylor, "CODATA recommended values of the fundamental physical constants: 1998," Reviews of Modern Physics, Vol. 72, No. 2, April, (2000), pp. 351-495.

Chapter 39

NUCLEAR FORCES AND RADIOACTIVITY

THE WEAK NUCLEAR FORCE: BETA DECAY OF THE NEUTRON

BETA DECAY ENERGY

The nuclear reaction for the beta decay of a neutron is:

$$^1n \rightarrow {}^1H + \beta + \bar{\nu}_e + \gamma \tag{39.1}$$

where $\bar{\nu}_e$ is the electron antineutrino. The beta decay energy, E_β, can be calculated from conservation of mass-energy

$$E_\beta = E_n - E_p - E_e \tag{39.2}$$

where E_n, E_p, and E_e are the mass-energy of the neutron, proton, and electron. Thus,

$$E_{beta\ decay} = (m_n - m_P - m_e)c^2 = 0.7824 MeV \tag{39.3}$$

The experimental value is $0.782\ MeV$ [1].

Neutron decay results in the change of the nuclear moment from that of a neutron $\left(\left[1-\frac{4}{9}2\pi-\frac{3}{25}\right]\mu_N\right)$ to that of a proton $(\frac{4}{9}2\pi\ \mu_N)$ where these terms were determined in the Magnetic Moment section. The radii of the proton and the neutron are the corresponding Compton wavelengths given by Eqs. (37.3) and (37.15), respectively:

$$\lambda_{C,p} = \frac{2\pi a_0 m_e}{\alpha^{-1} m_P} = 1.32141\ X\ 10^{-15}\ m = r_p \tag{39.4}$$

$$\lambda_{C,n} = \frac{2\pi a_0 m_e}{\alpha^{-1} m_N} = 1.31959\ X\ 10^{-15}\ m = r_n \tag{39.5}$$

The beta decay energy can be calculated from the magnetic, electric, and kinetic energy transformations which occur during the decay. The energy components are the sum of the following:

- the release of E_{mag}, the magnetic energy stored in one μ_N, since the corresponding beta particle no longer contains the magnetic fields of the gluons at a radius of $\lambda_{C,p}$, the radius of the proton, following beta decay;
- minus E_{mag} (gluon), the energy to change the gluon field corresponding to a down quark to that corresponding to an up quark;
- minus E_{ele}, the electric energy stored in the electric field of the proton;
- minus $E_v\left(\lambda_{C,n},\lambda_{C,p}\right)$, the electric potential energy change in going from the radius of the neutron to that of the proton;
- plus T, the initial kinetic energy of the electron in its frame at production with $v = c$ at a radius of the electron Compton wavelength bar.

The magnitude of the beta decay energy contributions are given as follows:

From the Strong Nuclear Force section, and using Eq. (37.39) with Eqs. (33.13) and (39.40), E_{mag} is given by:

$$E_{mag} = m_p c^2 \frac{\alpha}{2\pi} = 1.089727\ X\ 10^6\ eV \tag{39.6}$$

Since the change in the magnetic moment contribution of quark/gluon function is $\frac{3}{25}$ (Eq. (37.36)) and the change in the energy stored in the magnetic field is proportional to the change in magnetic moment squared (Eq. (1.154)), $E_{mag}(gluon)$ is given by:

$$E_{mag}(gluon) = \left[\frac{3}{25}\right]^2 E_{mag} = 1.569207\ X\ 10^4\ eV \tag{39.7}$$

where E_{mag} is given by Eq. (39.6). From Eqs. (1.264) and (39.5), E_{ele} is given by:

$$E_{ele} = \frac{e^2}{8\pi\varepsilon_0 \lambda_{C,n}} = 5.456145\ X\ 10^5\ eV \tag{39.8}$$

From Eqs. (1.261), (39.4), and (39.5), $E_v\left(\lambda_{C,n},\lambda_{C,p}\right)$ is given by:

$$E_v\left(\lambda_{C,n},\lambda_{C,p}\right) = \frac{e^2}{4\pi\varepsilon_0}\left(\frac{1}{\lambda_{C,n}} - \frac{1}{\lambda_{C,p}}\right) = 1502.2\ eV \tag{39.9}$$

From the Creation of Matter from Energy and Pair Production sections, and using Eq. (1.35), T is given by:

$$T = \frac{1}{2}mv^2 = \frac{1}{2}\frac{m_e\hbar^2}{\left[\frac{m_N}{2\pi}\right]^2\left(\frac{2\pi a_0 m_e}{\alpha^{-1}m_N}\right)^2} = \frac{1}{2}m_e\left(\frac{\hbar}{m_e \lambda\!\!\!^{-}_C}\right)^2 = \frac{1}{2}m_e c^2 = 2.555017\ X\ 10^5\ eV \tag{39.10}$$

wherein the electron Compton wavelength bar is given by Eq. (28.7). The beta decay energy, E_β, given by the sum of the energies of Eqs. (39.6-39.10) is:

$$\begin{aligned} E_\beta &= E_{mag} - E_{mag}(gluon) - E_{ele} - E_v\left(\lambda_{C,n},\lambda_{C,p}\right) + T \\ E_\beta &= 0.7824\ MeV \end{aligned} \tag{39.11}$$

The calculated result is in good agreement with Eq. (39.3). Then the weak force is the negative gradient of the weak energy given by Eq. (39.11).

NEUTRINOS

Photons carry $\hbar$ of angular momentum in their electric and magnetic fields as shown in the Photon section. All electronic transitions require $\hbar$ of angular momentum photons. Nuclear reactions such as beta decay require emission of neutrinos with $\frac{\hbar}{2}$ of angular momentum. Thus, they may be photons with different electric and magnetic fields that give $\frac{\hbar}{2}$ of angular momentum. Then different trigonometric functions of the electric and magnetic fields would correspond to the different flavor neutrinos, the energy of each would depend on its frequency since the speed is light speed, and the cross sections would depend on the particular fields and energy.

To conserve energy and linear and angular momentum an electron antineutrino, $\bar{\nu}_e$, is emitted with the beta particle. The antineutrino is a ***unique elliptically polarized photon*** that has handedness (the neutrino and antineutrino have opposite handedness), is massless, and travels at the speed c. Consider the photon atomic orbital given in the Equation of the Photon section. It may comprise magnetic and electric field lines basis elements that are constant in magnitude as a function of angle over the surface. Or, the magnitude may vary as a function of angular position (ϕ,θ) on the atomic orbital which corresponds to an elliptically polarized photon. The general photon equation for the electric field is

$$\mathbf{E}_{\phi,\theta} = \frac{e}{4\pi\varepsilon_0 r_{photon}^2}\left(-1 + \frac{1}{n}\left[Y_0^0(\theta,\phi) + \mathrm{Re}\left\{Y_\ell^m(\theta,\phi)e^{im\omega_n t}\right\}\right]\right)\delta\left(r - \frac{\lambda}{2\pi}\right) \tag{39.12}$$

For the particle-production or emission event, r_{photon} is the radius of the photon atomic orbital which is equal to $\pi\Delta n a_H$, the change in electron atomic orbital radius given by Eq. (2.21), λ is the photon wavelength which is equal to $\Delta\lambda$, the change in the de Broglie wavelength of the atomic orbital given by Eqs. (2.21), (1.34), and (1.38), and $\omega_n = \frac{2\pi c}{\lambda}$ is the photon angular velocity which is equal to $\Delta\omega$, the change in atomic orbital angular velocity given by Eqs. (2.21). The magnetic field photon

atomic orbital is given by Eqs. (4.14) and (4.2). The nature of the unique elliptically polarized photon atomic orbital which is the antineutrino (neutrino) is determined by the nature of quark/gluon functions and the change in the quark/gluon angular harmonic functions during the transition from a neutron to a proton (proton to a neutron) with the emission of a beta particle (positron). A free quark or a free gluon is not a stable state of matter, and both are precluded from existence in isolation. Quarks and gluons can only exist in pairs, each comprising a quark and a gluon. In the case of beta decay, a down quark/gluon is converted to an up quark/gluon. Energy and linear momentum are conserved by the emission of an electron antineutrino, $\overline{\nu}_e$, with the beta particle where the maximum energy of the antineutrino is that of the mass deficit. To conserve angular momentum, the electric field, $\mathbf{E}_\theta$, of the electron antineutrino has an angular dependence given by a harmonic function squared corresponding to the change between the initial and final quark/gluon functions where the electric field of each gluon and its corresponding quark are radial and Eq. (37.34) applies.

$$\begin{aligned}\mathbf{E}_\theta &\propto \mathrm{Re}\left\{\left(Y_\ell^m(\theta,\phi)\right)^2\left(1+e^{i\omega_n t}\right)\right\}\delta\left(r-\frac{\lambda}{2\pi}\right)\\ &\propto \cos^2\theta\,\mathrm{Re}\left(1+e^{i\omega_n t}\right)\delta\left(r-\frac{\lambda}{2\pi}\right)=\left(\frac{1}{2}+\frac{\cos 2\theta}{2}\right)\mathrm{Re}\left(1+e^{i\omega_n t}\right)\delta\left(r-\frac{\lambda}{2\pi}\right)\end{aligned} \tag{39.13}$$

where $\ell=1$ and the power is given by Eq. (4.16). In contrast, the electric field of a photon corresponding to electronic transitions (Eq. (39.12)) is given by the sum of a constant function plus a spherical harmonic modulation function which averages to zero over a period. The angular momentum of an antineutrino (neutrino) is $-\frac{\hbar}{2}$ ($\frac{\hbar}{2}$)

$$|\mathbf{m}| = \int \frac{1}{8\pi c}\mathrm{Re}\left[\mathbf{r}\times(\mathbf{E}\times\mathbf{B}^*)\right]dx^4 = \frac{\hbar}{2} \tag{39.14}$$

compared to that of a photon corresponding to an electronic transition of $\pm\hbar$ (Eq. (4.1)).

The matrices to generate the electric and magnetic vector fields (e&mvf) of neutrinos are the same as those of the right- and left-circularly-polarized and linearly-polarized photons with the exception that the magnitude of the basis element field is not constant over the spherical surface, but is modulated by a trigonometric function squared. The right- and left-$\cos^2\theta$ or $\sin^2\theta$-polarized neutrinos are mirror images of opposite spin corresponding to a neutrino-antineutrino pair. The right-hand-$\cos^2\theta$-polarized neutrino (RHC^2P) is given by:

$$\begin{bmatrix}x'\\y'\\z'\end{bmatrix} = \cos^2\theta\,\delta\left(r-r_{photon}\right)\begin{bmatrix}\frac{1}{2}+\frac{\cos\theta}{2} & \frac{1}{2}-\frac{\cos\theta}{2} & -\frac{\sin\theta}{\sqrt{2}}\\ \frac{1}{2}-\frac{\cos\theta}{2} & \frac{1}{2}+\frac{\cos\theta}{2} & \frac{\sin\theta}{\sqrt{2}}\\ \frac{\sin\theta}{\sqrt{2}} & -\frac{\sin\theta}{\sqrt{2}} & \cos\theta\end{bmatrix}\bullet\left(E_0\begin{bmatrix}0\\ r_n\cos\phi\\ r_n\sin\phi\end{bmatrix}_{\mathrm{Red}}+B_0\begin{bmatrix}r_n\cos\phi\\ 0\\ r_n\sin\phi\end{bmatrix}_{\mathrm{Blue}}\right) \tag{39.15}$$

The RHC^2P neutrino-e&mvf that is generated by the rotation of the great-circle basis elements in the xz- and yz-planes about the $\left(\mathbf{i}_x,\mathbf{i}_y,0\mathbf{i}_z\right)$-axis by $\frac{\pi}{2}$ corresponding to the output of the matrix given by Eq. (39.15) is shown in Figure 39.1 wherein the magnitude of each field line is according to $\cos^2\theta$.

Figure 39.1. The field-line pattern given by Eq. (39.15) from three orthogonal perspectives of a RHC^2P neutrino-e&mvf corresponding to the first great circle magnetic field line and the second great circle electric field line shown with 6 degree increments of the angle θ. (Electric field lines red; Magnetic field lines blue).

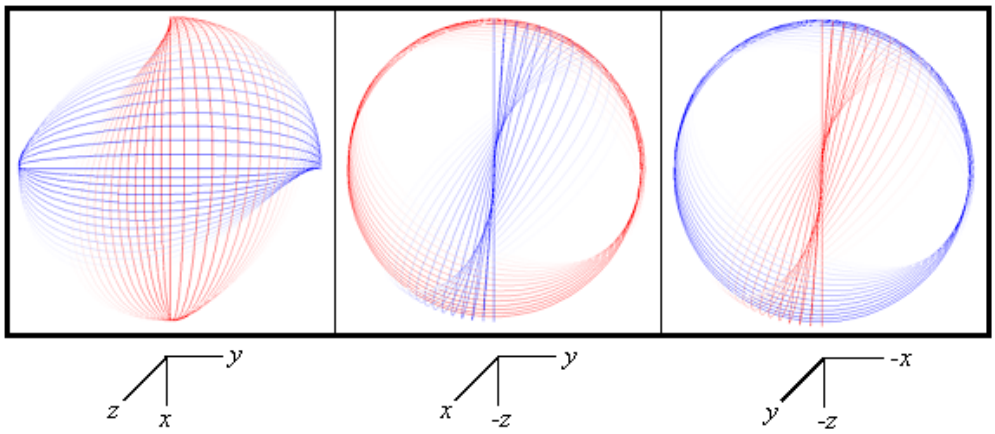

The corresponding antineutrino, the left-hand-$\cos^2\theta$-polarized neutrino (LHC^2P), is given by is given by:

$$\begin{bmatrix} x' \\ y' \\ z' \end{bmatrix} = \cos^2\theta\,\delta\left(r - r_{photon}\right) \begin{bmatrix} \frac{1}{2}+\frac{\cos\theta}{2} & -\frac{1}{2}+\frac{\cos\theta}{2} & \frac{\sin\theta}{\sqrt{2}} \\ -\frac{1}{2}+\frac{\cos\theta}{2} & \frac{1}{2}+\frac{\cos\theta}{2} & \frac{\sin\theta}{\sqrt{2}} \\ -\frac{\sin\theta}{\sqrt{2}} & -\frac{\sin\theta}{\sqrt{2}} & \cos\theta \end{bmatrix} \bullet \left(E_0 \begin{bmatrix} 0 \\ r_n\cos\phi \\ r_n\sin\phi \end{bmatrix}_{\text{Red}} + B_0 \begin{bmatrix} r_n\cos\phi \\ 0 \\ r_n\sin\phi \end{bmatrix}_{\text{Blue}} \right) \tag{39.16}$$

The LHC^2P neutrino-e&mvf that is generated by the rotation of the great-circle basis elements in the xz- and yz-planes about the $\left(\mathbf{i}_x, -\mathbf{i}_y, 0\mathbf{i}_z\right)$-axis by $\frac{\pi}{2}$ corresponding to the output of the matrix given by Eq. (39.16) is shown in Figure 39.2.

Figure 39.2. The field-line pattern given by Eq. (39.16) from three orthogonal perspectives of a LHC^2P neutrino-e&mvf corresponding to the first great circle magnetic field line and the second great circle electric field line shown with 6 degree increments of the angle θ. (Electric field lines red; Magnetic field lines blue).

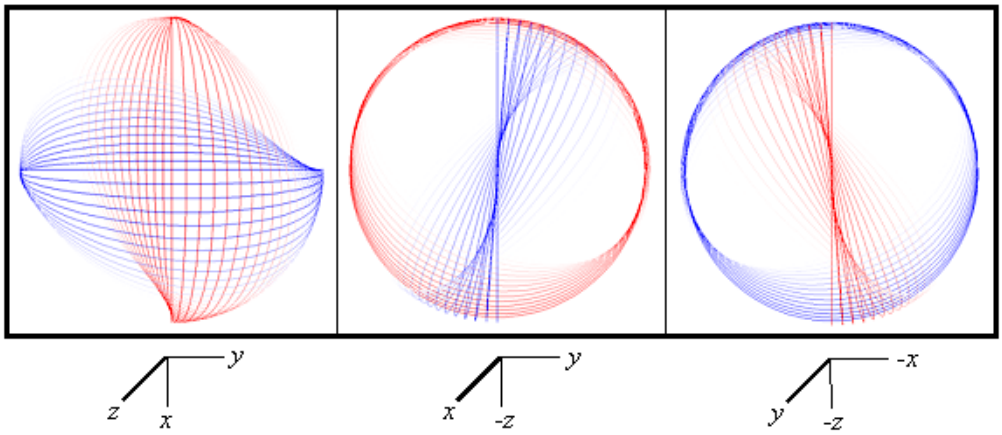

Based on the invariance of the field lines under Gauss' Integral Law as given in the Photon section, the spatial distribution of the field lines of a cosine-squared neutrino (Eq. (39.13)) in the inertial frame for the stationary observer or laboratory frame is shown in Figure 39.3.

Figure 39.3. The electric (red) and magnetic (blue) field lines of a cosine-squared neutrino given by Eq. (39.13) as seen along the axis of propagation in the lab inertial reference frame at a fixed time. A and B. Views transverse to the axis of propagation, the z-axis, wherein $2r_{neutrino} = \lambda$. C and D. Off z-axis views showing field aspects both along and transverse to the axis of propagation.

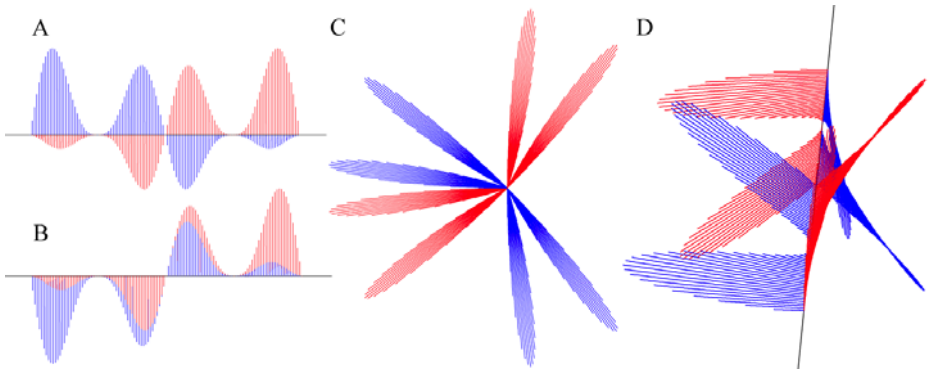

Eq. (39.13) is the equation of the neutrino's electric field in its frame. The neutrino's field called the neutrino electric and magnetic vector field (neutrino-e&mvf) follows from that of the photon. Eq. (25) of Appendix V: Analytical-Equation Derivation of the Photon Electric and Magnetic Fields which gives the laboratory-frame relationship of the fields and the angular momentum then becomes:

$$\frac{1}{8\pi c}\sqrt{\frac{\varepsilon_0}{\mu_0}}\frac{E_0^2}{4}\frac{2\pi}{2\omega}2\pi r_{photon}^3\int_0^\pi \sin^2 2\theta\cos^2\theta\sin^4\theta d\theta = \frac{\hbar}{2} \tag{39.17}$$

$$\sqrt{\frac{\varepsilon_0}{\mu_0}}\frac{E_0^2}{32c}\frac{2\pi}{\omega}r_{photon}^3\int_0^\pi \sin^2 2\theta\left(\frac{1+\cos 2\theta}{2}\right)\left(\frac{1-\cos 2\theta}{2}\right)^2 d\theta = \frac{\hbar}{2} \tag{39.18}$$

$$\sqrt{\frac{\varepsilon_0}{\mu_0}}\frac{E_0^2}{256c}\frac{2\pi}{\omega}r_{photon}^3\int_0^\pi \sin^2 2\theta\left(1-\cos 2\theta-\cos^2 2\theta+\cos^3 2\theta\right)d\theta = \frac{\hbar}{2} \tag{39.19}$$

Using the wave equation relationship and the relationship between the wavelength and the radius of the photon-e&mvf given by Eq. (21) and Eq. (22) of Appendix V, respectively, gives

$$\sqrt{\frac{\varepsilon_0}{\mu_0}}\frac{E_0^2}{128}\frac{\pi^4}{\omega^4}c^2\left(\begin{array}{l}\int_0^\pi \sin^2 2\theta d\theta-\int_0^\pi \sin^2 2\theta\cos 2\theta d\theta\\ -\int_0^\pi \sin^2 2\theta\cos^2 2\theta d\theta+\int_0^\pi \sin^2 2\theta\cos^3 2\theta d\theta\end{array}\right) = \frac{\hbar}{2} \tag{39.20}$$

The integrals by Lide [2] give

$$\sqrt{\frac{\varepsilon_0}{\mu_0}}\frac{E_0^2}{128}\frac{\pi^4}{\omega^4}c^2\left(\begin{array}{l}\left(\frac{\theta}{2}-\frac{1}{8}\sin 4\theta\right)_0^\pi-\left(\frac{\sin^3 2\theta}{6}\right)_0^\pi\\ -\left(-64\sin 8\theta+\frac{\theta}{8}\right)_0^\pi+\left(-\frac{\sin 2\theta\cos^4 2\theta}{10}\right)_0^\pi\\ +\frac{1}{5}\int_0^\pi \cos^3 2\theta d\theta\end{array}\right) = \frac{\hbar}{2} \tag{39.21}$$

$$\sqrt{\frac{\varepsilon_0}{\mu_0}}\frac{E_0^2}{128}\frac{\pi^4}{\omega^4\sqrt{\varepsilon_0\mu_0}}c\left(\frac{\pi}{2}-\frac{\pi}{8}+\frac{1}{30}\left(\sin 2\theta\left(\cos^2 2\theta+2\right)\right)_0^\pi\right) = \frac{\hbar}{2} \tag{39.22}$$

$$\sqrt{\frac{\varepsilon_0}{\mu_0}}\frac{E_0^2}{128}\frac{\pi^4}{\omega^4\sqrt{\varepsilon_0\mu_0}}c\left(\frac{\pi}{2}-\frac{\pi}{8}\right)=\frac{\hbar}{2} \tag{39.23}$$

$$\frac{3E_0^2}{1024}\frac{\pi^5}{\omega^4\mu_0}c=\frac{\hbar}{2} \tag{39.24}$$

Thus,

$$E_0=\sqrt{\frac{512\omega^4\mu_0\hbar}{3c\pi^5}}=\omega^2\sqrt{\frac{512\mu_0\hbar}{3c\pi^5}} \tag{39.25}$$

which has the required MKS units of Vm^{-1}. From Planck's law, the energy is given by:

$$E=L\omega=\frac{\hbar}{2}\omega=\frac{3E_0^2}{1024}\frac{\pi^5}{\omega^4\mu_0}c\omega \tag{39.26}$$

In the case of Eq. (39.13), a neutrino of a different flavor can also have an electric field in its frame of:

$$\begin{aligned}\mathbf{E}_\theta &\propto \mathrm{Re}\left\{\left(Y_\ell^m(\theta,\phi)\right)^2\left(1+e^{i\omega_n t}\right)\right\}\delta\left(r-\frac{\lambda}{2\pi}\right)\\ &\propto \sin^2\theta\,\mathrm{Re}\left(1+e^{i\omega_n t}\right)\delta\left(r-\frac{\lambda}{2\pi}\right)=\left(\frac{1}{2}-\frac{\cos 2\theta}{2}\right)\mathrm{Re}\left(1+e^{i\omega_n t}\right)\delta\left(r-\frac{\lambda}{2\pi}\right)\end{aligned} \tag{39.27}$$

The right-hand-$\sin^2\theta$-polarized neutrino (RHS^2P) is given by:

$$\begin{bmatrix}x'\\y'\\z'\end{bmatrix}=\sin^2\theta\,\delta\left(r-r_{photon}\right)\begin{bmatrix}\frac{1}{2}+\frac{\cos\theta}{2} & \frac{1}{2}-\frac{\cos\theta}{2} & -\frac{\sin\theta}{\sqrt{2}}\\ \frac{1}{2}-\frac{\cos\theta}{2} & \frac{1}{2}+\frac{\cos\theta}{2} & \frac{\sin\theta}{\sqrt{2}}\\ \frac{\sin\theta}{\sqrt{2}} & -\frac{\sin\theta}{\sqrt{2}} & \cos\theta\end{bmatrix}\bullet\left(E_0\begin{bmatrix}0\\r_n\cos\phi\\r_n\sin\phi\end{bmatrix}_{\mathrm{Red}}+B_0\begin{bmatrix}r_n\cos\phi\\0\\r_n\sin\phi\end{bmatrix}_{\mathrm{Blue}}\right) \tag{39.28}$$

The RHS^2P neutrino-e&mvf that is generated by the rotation of the great-circle basis elements in the xz- and yz-planes about the $\left(\mathbf{i}_x,\mathbf{i}_y,0\mathbf{i}_z\right)$-axis by $\frac{\pi}{2}$ corresponding to the output of the matrix given by Eq. (39.28) is shown in Figure 39.4.

Figure 39.4. The field-line pattern given by Eq. (39.28) from three orthogonal perspectives of a RHS^2P neutrino-e&mvf corresponding to the first great circle magnetic field line and the second great circle electric field line shown with 6 degree increments of the angle θ. (Electric field lines red; Magnetic field lines blue).

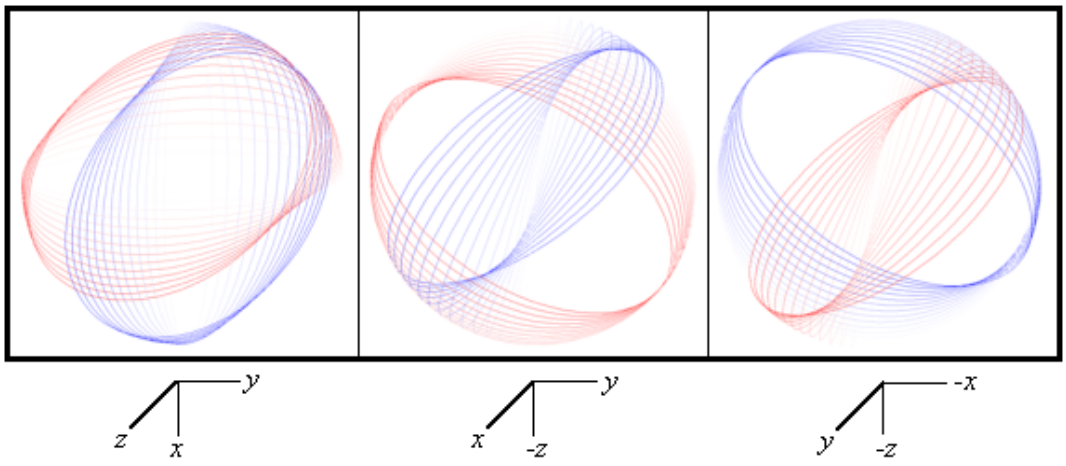

The corresponding antineutrino, the left-hand-$\sin^2\theta$-polarized neutrino (LHS^2P), is given by is given by:

$$\begin{bmatrix} x' \\ y' \\ z' \end{bmatrix} = \sin^2\theta\delta\left(r - r_{photon}\right) \begin{bmatrix} \frac{1}{2}+\frac{\cos\theta}{2} & -\frac{1}{2}+\frac{\cos\theta}{2} & \frac{\sin\theta}{\sqrt{2}} \\ -\frac{1}{2}+\frac{\cos\theta}{2} & \frac{1}{2}+\frac{\cos\theta}{2} & \frac{\sin\theta}{\sqrt{2}} \\ -\frac{\sin\theta}{\sqrt{2}} & -\frac{\sin\theta}{\sqrt{2}} & \cos\theta \end{bmatrix} \bullet \left(E_0 \begin{bmatrix} 0 \\ r_n\cos\phi \\ r_n\sin\phi \end{bmatrix}_{\text{Red}} + B_0 \begin{bmatrix} r_n\cos\phi \\ 0 \\ r_n\sin\phi \end{bmatrix}_{\text{Blue}} \right) \tag{39.29}$$

The LHS^2P neutrino-e&mvf that is generated by the rotation of the great-circle basis elements in the xz- and yz-planes about the $\left(\mathbf{i}_x, -\mathbf{i}_y, 0\mathbf{i}_z\right)$-axis by $\frac{\pi}{2}$ corresponding to the output of the matrix given by Eq. (39.29) is shown in Figure 39.5.

Figure 39.5. The field-line pattern given by Eq. (39.29) from three orthogonal perspectives of a LHS^2P neutrino-e&mvf corresponding to the first great circle magnetic field line and the second great circle electric field line shown with 6 degree increments of the angle θ. (Electric field lines red; Magnetic field lines blue).

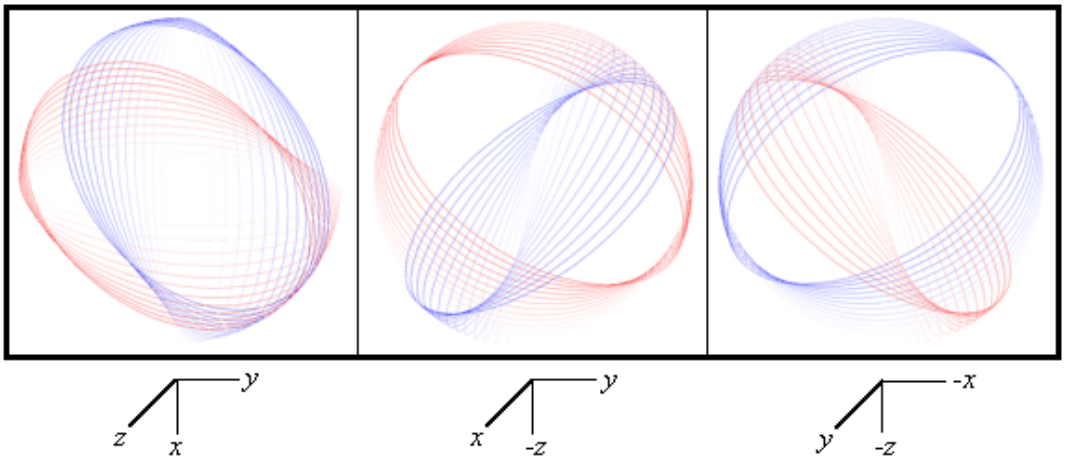

The spatial distribution of the field lines of a sine-squared neutrino (Eq. (39.27)) in the inertial frame for the stationary observer or laboratory frame is shown in Figure 39.6.

Figure 39.6. The electric (red) and magnetic (blue) field lines of a sine-squared neutrino given by Eq. (39.27) as seen along the axis of propagation in the lab inertial reference frame at a fixed time. A and B. Views transverse to the axis of propagation, the z-axis, wherein $2r_{neutrino} = \lambda$. C and D. Off z-axis views showing field aspects both along and transverse to the axis of propagation.

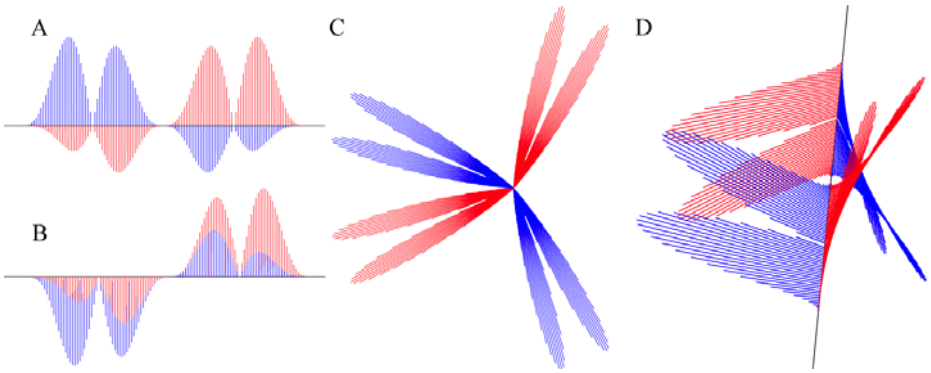

In this case, Eq. (25) of Appendix V: Analytical-Equation Derivation of the Photon Electric and Magnetic Fields then becomes:

$$\frac{1}{8\pi c}\sqrt{\frac{\varepsilon_0}{\mu_0}}\frac{E_0^2}{4}\frac{2\pi}{2\omega}2\pi r_{photon}^3\int_0^{\pi}\sin^2 2\theta\sin^6\theta d\theta=\frac{\hbar}{2} \tag{39.30}$$

$$\sqrt{\frac{\varepsilon_0}{\mu_0}}\frac{E_0^2}{32c}\frac{2\pi}{\omega}r_{photon}^3\int_0^{\pi}\sin^2 2\theta\left(\frac{1-\cos 2\theta}{2}\right)^3 d\theta=\frac{\hbar}{2} \tag{39.31}$$

$$\sqrt{\frac{\varepsilon_0}{\mu_0}}\frac{E_0^2}{256c}\frac{2\pi}{\omega}r_{photon}^3\int_0^{\pi}\sin^2 2\theta\left(1-3\cos 2\theta+3\cos^2 2\theta-\cos^3 2\theta\right)d\theta=\frac{\hbar}{2} \tag{39.32}$$

Using the wave equation relationship and the relationship between the wavelength and the radius of the photon-e&mvf given by Eq. (21) and Eq. (22) of Appendix V, respectively, with the integral by Lide [2] gives

$$\sqrt{\frac{\varepsilon_0}{\mu_0}}\frac{E_0^2}{128}\frac{\pi^4}{\omega^4}c^2\left(\begin{array}{l}\int_0^{\pi}\sin^2 2\theta d\theta-3\int_0^{\pi}\sin^2 2\theta\cos 2\theta d\theta\\ +3\int_0^{\pi}\sin^2 2\theta\cos^2 2\theta d\theta-\int_0^{\pi}\sin^2 2\theta\cos^3 2\theta d\theta\end{array}\right)=\frac{\hbar}{2} \tag{39.33}$$

Using the integral #322 and #320 of Lide [2] gives

$$\sqrt{\frac{\varepsilon_0}{\mu_0}}\frac{E_0^2}{128}\frac{\pi^4}{\omega^4}c^2\left(\begin{array}{l}\left(\frac{\theta}{2}-\frac{1}{8}\sin 4\theta\right)_0^{\pi}-3\left(\frac{\sin^3 2\theta}{6}\right)_0^{\pi}\\ +3\left(-64\sin 8\theta+\frac{\theta}{8}\right)_0^{\pi}-\left(-\frac{\sin 2\theta\cos^4 2\theta}{10}\right)_0^{\pi}\\ -\frac{1}{5}\int_0^{\pi}\cos^3 2\theta d\theta\end{array}\right)=\frac{\hbar}{2} \tag{39.34}$$

$$\sqrt{\frac{\varepsilon_0}{\mu_0}}\frac{E_0^2}{128}\frac{\pi^4}{\omega^4\sqrt{\varepsilon_0\mu_0}}c\left(\frac{\pi}{2}+\frac{3\pi}{8}-\frac{1}{30}\left(\sin 2\theta\left(\cos^2 2\theta+2\right)\right)_0^{\pi}\right)=\frac{\hbar}{2} \tag{39.35}$$

$$\sqrt{\frac{\varepsilon_0}{\mu_0}}\frac{E_0^2}{128}\frac{\pi^4}{\omega^4\sqrt{\varepsilon_0\mu_0}}c\left(\frac{\pi}{2}+\frac{3\pi}{8}\right)=\frac{\hbar}{2} \tag{39.36}$$

$$\frac{7E_0^2}{1024}\frac{\pi^5}{\omega^4\mu_0}c=\frac{\hbar}{2} \tag{39.37}$$

Thus,

$$E_0 = \sqrt{\frac{512\omega^4\mu_0\hbar}{7c\pi^5}} = \omega^2\sqrt{\frac{512\mu_0\hbar}{7c\pi^5}} \tag{39.38}$$

Due to its unusual angular momentum, the antineutrino and neutrino interact extremely weakly with matter. Essentially, it only has a finite cross-section for processes which involve transitions of two fundamental particles simultaneously. Such cases include beta decay, inverse beta decay, and the hydrino decay reaction (Eq. (32.171)).

$$\overline{\nu}_e + {}^1H\left[\frac{a_H}{p}\right] \rightarrow \gamma + \nu_e \tag{39.39}$$

where ν_e is the electron neutrino and $\overline{\nu}_e$ is the electron antineutrino. There are three classes of neutrinos (antineutrinos) corresponding to the electron (antielectron), muon (antimuon), and tau (antitau) as described in the Leptons section. Each flavor corresponds to its multipolarity and polarization, $\cos^2\theta$, $\sin^2\theta$, and the superposition of $\cos^2\theta$ and $\sin^2\theta$. Its particle versus antiparticle type corresponds to its handedness. The determination of the flavor and type assignment can be determined by the multipolarity and polarization and handedness of the particle reaction that gives rise to the neutrino that conserves these aspects as well as energy and linear momentum. The energy of the electric and magnetic fields given by Eq. (1.154) and Eq. (1.263), respectively, equals the energy given by the Planck equation (Eq. (4.8)). The multipolarities and polarizations of photons of visible light change upon interacting with a dichroic material through which they propagate. Similar to dichroism, interconversion of neutrinos may be possible via interaction with matter that causes corresponding changes in multipolarities and polarizations.

Thus, neutrinos are each a photon that has an exceptional $\frac{\hbar}{2}$ angular momentum in its electric and magnetic fields giving rise to an intrinsic weak interaction limited to nuclei, travels at the speed of light, and can change polarization in condensed matter in a manner that may appear as "oscillation between flavors". Light speed is characteristic of and identifies photons. Neutrinos have been confirmed to be photons by the measurement of the neutrino velocity with the OPERA detector to be the speed of light to within a relative difference of $\left(2.48 \pm 0.28(sat) \pm 0.30(sys)\right) X10^{-5}$ [3]. Moreover, the speeds of photons and neutrinos are identical within a part per billion from the coincidence of optical and neutrino detection of supernova 1987A [4].

THE STRONG NUCLEAR FORCE

THE DEUTERIUM NUCLEUS

The bonding in multi-nucleon nuclei involves the superposition of the quark and gluon functions of the constituent nucleons to form the nuclear version of atomic orbitals wherein the gluons provide the central force and the quarks comprise the two-dimensional current-density surfaces. The nuclear bonding gives rise to spherical shells comprising equipotential minimum-energy surfaces as a linear combination of the nucleons. For example, the deuterium nucleus is a minimum energy superposition of a neutron and a proton. Thus, the deuterium quark/gluon function is a spherical coordinate atomic orbital solution of Laplace's equation (Eq. (I.44)). The neutron is electrically neutral; thus, no electric term arises in the energy calculation. The neutron and proton quarks of the same kind or flavor are indistinguishable and superimpose to form the deuterium atomic orbital. The gluon electric and magnetic fields of each nucleon superimpose with conservation of stored electric energy density (Eq. (1.263)) and stored magnetic energy density (Eq. (1.154)); however, gluon mass-energy is released as the proton and neutron gluon fields superimpose to provide the central field of the deuterium atomic orbital comprising the linear combination of quarks from both nucleons. The quark/gluons possess magnetic stored energy. Concomitant with the superposition of the neutron with the proton, the quark resonator cavity of the proton traps the magnetic flux of the neutron gluons, and the neutron quark resonator cavity captures the flux of the proton gluons. To conserve the total quark angular momentum of each nucleon, $\hbar$, the flux is trapped in quanta of the quantum of magnetic flux. As shown in the Quark and Gluon Functions of the Proton and Neutron section, the quark/gluon proper velocity is c. Therefore, the quark/gluon stored magnetic energy is $m_P c^2$ and $m_N c^2$ for the proton and the neutron, respectively (Eqs. (29.14) and (29.15) with m_e replaced by the nucleon mass). The energy released due to the magnetic flux capture, the deuterium binding energy ($E_{Binding}$), follows from Eq. (1.181) :

$$E_{Binding} = \left(\frac{\alpha}{2\pi}m_P + \frac{\alpha}{2\pi}m_N\right)c^2 \tag{39.40}$$

$$E_{Binding} = \left(m_P + m_N\right)\frac{\alpha}{2\pi}c^2 \tag{39.41}$$

The calculated mass of deuterium is

$$Mass = m_e + \left(m_P + m_N\right)\left(1 - \frac{\alpha}{2\pi}\right) = 2.014149\ AMU \tag{39.42}$$

The NIST experimental mass of deuterium is $2.0141017778\ AMU$ [5].

NUCLEAR AND X-RAY MULTIPOLE RADIATION

Using Maxwell's equations, the essential features of multipole radiation in nuclei can be presented with simple arguments developed by Jackson [6]. By using Jackson's Eq. (16.97) and the multipole coefficients (Jackson's Eqs. (16.92) and (16.93)), the total power radiated by a multipole of order (ℓ , m) is:

$$\left.\begin{aligned} P_E(\ell,m) &= \frac{2\pi c}{[(2\ell+1)!!]^2}\left(\frac{\ell+1}{\ell}\right)k^{2\ell+2}\left|Q_{\ell m}+Q'_{\ell m}\right|^2 \\ P_M(\ell,m) &= \frac{2\pi c}{[(2\ell+1)!!]^2}\left(\frac{\ell+1}{\ell}\right)k^{2\ell+2}\left|M_{\ell m}+M'_{\ell m}\right|^2 \end{aligned}\right\} \tag{39.43}$$

The transition probability (reciprocal mean life) is defined as the power divided by the energy of a photon:

$$\frac{1}{\tau}=\frac{P}{\hbar\omega} \tag{39.44}$$

Using the source structure given in the Proton and Neutron sections, the oscillating nuclear charge density of a nucleus comprised of many nucleons may be modeled as being of the form

$$\rho(\mathrm{x})=\begin{cases}\dfrac{3e}{a^3}Y_{\ell m}(\theta,\phi), & r<a\\ 0, & r>a\end{cases} \tag{39.45}$$

The corresponding electric multipole moment Q_{lm} is:

$$Q_{\ell m}=\frac{3}{\ell+3}ea^{\ell} \tag{39.46}$$

independent of m. Based on the spherical-shell structure of the nucleons, the divergences of the magnetizations are:

$$\nabla\cdot\mathbf{M}+\frac{1}{\ell+1}\nabla\bullet\left(\frac{\mathrm{r}\times\mathrm{J}}{c}\right)=\begin{cases}\dfrac{2g}{a^3}Y_{\ell m}(\theta,\phi)\left(\dfrac{e\hbar}{mcr}\right), & r<a\\ 0, & r>a\end{cases} \tag{39.47}$$

where g is the effective g factor for the magnetic moments of the particles in the nuclear system, and $e\hbar/mc$ is twice the Bohr magneton for those particles. The sum of magnetic multipole moments is:

$$M_{\ell m}+M'_{\ell m}\simeq-\frac{2}{\ell+2}ea^{\ell}\left(\frac{g\hbar}{mca}\right) \tag{39.48}$$

The definitions of the multipole moments $Q_{\ell m}$ and $Q'_{\ell m}$ given by Jackson's Eq. (16.94) are:

$$Q_{\ell m}=\int r^{\ell}Y^*_{\ell m}\rho d^3x \tag{39.49}$$

$$Q'_{\ell m}=\frac{-ik}{\ell+1}\int r^{\ell}Y^*_{\ell m}\nabla\bullet\left(\mathbf{r}\times\mathbf{M}\right)d^3x \tag{39.50}$$

Using Eqs. (39.48) and (39.50) gives:

$$Q'_{lm}\simeq g\left(\frac{\hbar\omega}{mc^2}\right)Q_{lm} \tag{39.51}$$

Since the energies of radiative transitions in nuclei are always very small compared to the rest energies of the particles involved (i.e. $\hbar\omega<<mc^2$), $Q'_{\ell m}$ is always completely negligible compared to $Q_{\ell m}$. However, using Eqs. (39.43), (39.44), and (39.46), the transition probability for electrical multipole transitions of order ℓ are:

$$\frac{1}{\tau_E(\ell)}\simeq\left(\frac{e^2}{\hbar c}\right)\frac{2\pi}{[(2\ell+1)!!]^2}\left(\frac{\ell+1}{\ell}\right)\left(\frac{3}{\ell+3}\right)^2(ka)^{2\ell}\omega \tag{39.52}$$

Using Eqs. (39.43), (39.44), (39.48), and (39.50–39.52), the transition probability for magnetic multipoles is:

$$\frac{1}{\tau_{\mathrm{M}}(\ell)}=\left(\frac{\dfrac{2}{\ell+2}}{\dfrac{3}{\ell+3}}\right)^2\left(\frac{g\hbar}{mca}\right)^2\frac{1}{\tau_{\mathrm{E}}(\ell)} \tag{39.53}$$

In the long-wavelength limit $(ka\ll1)$, the transition rate predicted by Eq. (39.52) falls off rapidly with increasing multipole order, for a fixed frequency due to the $(ka)^{2l}$ factor in the transition probability. Consequently, the lowest nonvanishing

multipole will generally be the only one having a significant rate in the radioactive decay. Omitting numerical factors of relative order $(1/\ell)$, the ratio of transition probabilities for successive orders of either electric or magnetic multipoles of the same frequency is:

$$\frac{\left[\tau(\ell+1)\right]^{-1}}{\left[\tau(\ell)\right]^{-1}} \sim \frac{(ka)^2}{4\ell^2} \tag{39.54}$$

The transition rates of electric dipole transitions of single-electron-excited-state atoms were given in the State Lifetimes and Line Intensities section. Consider an Auger transition due to a multipole central field created by an inner shell vacancy. The dimensions of the source due to the initial to final state current may be taken as having the same multipolarity as the central field and can be approximated as $a \simeq (a_0/\mathrm{Z})$, where a_0 is the Bohr radius and Z is the nuclear charge. The energy of any atomic transition obeys the relationship:

$$\hbar\omega \lesssim \mathrm{Z}^2 \frac{e^2}{a_0} \tag{39.55}$$

where the right-hand side of Eq. (39.55) only holds for one electron atoms as shown in the One-Electron Atom section, Two-Electron Atoms section, and Three- Through Twenty-Electron Atoms section. Thus, an estimate of ka is given by:

$$ka \lesssim \alpha\mathrm{Z} \tag{39.56}$$

where α is the fine structure constant. According to Eq. (39.54) the transition rates of successive multipoles have the ratio $(\alpha\mathrm{Z})^2$. Using $a \simeq a_0/\mathrm{Z} = \alpha^{-1}(\hbar/mc\mathrm{Z})$ in Eq. (39.53), the magnetic ℓ^{th} multipole transition rate is about a factor of $(\alpha\mathrm{Z})^2$ smaller than the corresponding electric multipole rate. The electric dipole transitions are predicted to be the most intense, with electric quadrupole and magnetic dipole transitions a factor $(\alpha\mathrm{Z})^2$ weaker. Competition from transitions other than that of the lowest-order electric multipole is only possible with X-ray transitions in heavy elements.

Eq. (39.52) can be used to characterize radiative transitions in atomic nuclei as well, but the values of ka cover a wide range because nuclear radiative transition energies vary greatly (from ~10 keV to several MeV). Consequently, for a given multipole order, the transition probabilities (or mean lifetimes) will range over many orders of magnitude depending on the energy release, overlapping the multipoles on either side. However, because of the strong dependency on ℓ, rate behavior at a fixed energy release can be obtained from Eqs. (39.52) and (39.53) that is useful in cataloging nuclear multipole transitions. Using Eq. (39.52) with the proton charge e and $a \simeq 5.6\,\mathrm{x}\,10^{-13}$ cm (nuclear radius appropriate to mass number $\mathrm{A} \simeq 100$), a log-log plot of lifetimes of electric multipole transitions versus energy is shown in Figure 39.7. Although the curves tend to converge at high energies, the predicted lifetimes for different multipoles at the same energy differ by factors typically of order 10^5 that is permissive of assigning multipole orders. The experimentally observed lifetime-energy diagram [7] shows broad, but well-defined, bands lying in the vicinity of the straight lines shown in Figure 39.7. With Eq. (39.46) being an upper bound on the multipole moment, there is a general tendency for the corresponding estimate given by Eq. (39.52) to serve as a lower bound on the lifetime. But, for certain so-called "enhanced" electric quadrupole transitions the lifetimes can be as much as 100 times shorter than those shown in Figure 39.7.

Figure 39.7. Log-log plot of lifetimes of electric multipole transitions versus energy from Eq. (39.52).

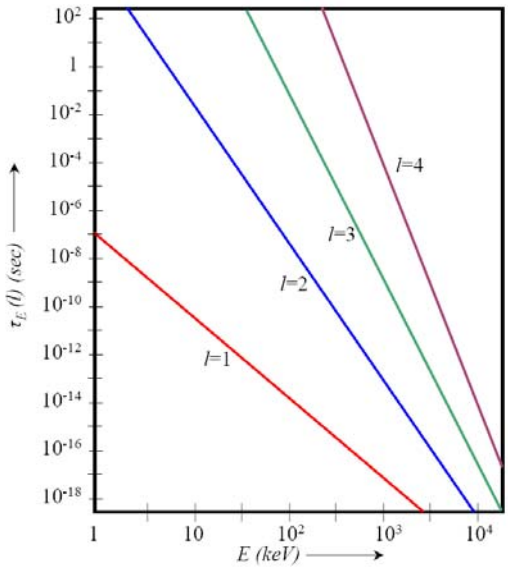

Using a typical nucleon g factor of g~3 and source size of $a \simeq R = 1.2A^{1/3} X\ 10^{-13}\ cm$ in Eq. (39.53), the relationship between magnetic and electric multipoles of the same order is:

$$\frac{1}{\tau_M(\ell)} \simeq \frac{0.3}{\mathrm{A}^{2/3}} \frac{1}{\tau_E(\ell)} \tag{39.57}$$

Since the numerical factor $\frac{0.3}{\mathrm{A}^{2/3}}$ ranges from $4X10^{-2}$ *to* $0.8\ X\ 10^{-2}$ *for* $20 < A < 250$, given multipole order electric transitions are predicted to be 25-120 times more intense than the magnetic transitions. For most multipoles, this relationship is experimentally confirmed. But, for $\ell = 1$, there are special circumstances in nuclei at least at low energies whereby strongly attractive, charge-independent forces inhibit electric dipole transitions. In these cases, Eq. (39.57) does not hold, and magnetic dipole transitions are far commoner and equally intense as electric dipole transitions. The weak and strong nuclear forces given in the Beta Decay section and the Strong Nuclear Force section, respectively, are examples of where the magnetic energy is dominant and Eq. (39.57) with Eq. (39.46) does not apply.

Based on selection rules corresponding to conservation of angular momentum in the initial and final states and the radiation of multipolarity ℓ as shown in the Selection Rules section, a transition between two quantum states involving a mixture of multipoles, such as magnetic $\ell, (\ell+2), ...$pole and electric $(\ell+1), (\ell+3), ...$pole, can occur. In the long-wavelength limit, only the lowest multipole of each type is significant. Combining the ratios (39.105) and (39.106) gives the relative transition rates of electric $(\ell+1)$ pole to magnetic ℓ pole (most commonly used for $\ell = 1$):

$$\frac{\left[\tau E(\ell+1)\right]^{-1}}{\left[\tau_M(\ell)\right]^{-1}} \simeq \left(\frac{\mathrm{A}^{1/3}E}{200\ell}\right)^2 \tag{39.58}$$

where E is the photon energy in MeV. For energetic transitions in heavy elements, the electric quadrupole *amplitude* is ~5 per cent of the magnetic dipole amplitude. If there is an enhancement of the effective quadrupole moment by a factor of 10 as observed in the rare earth and transuranic nuclei, the electric quadrupole transition competes favorably with the magnetic dipole transition. Even for energetic transitions, a magnetic $(\ell+1)$ pole never comes close to competing with an electric ℓ pole because for a mixture, the ratio of transition rates is:

$$\frac{\left[\tau_M(\ell+1)\right]^{-1}}{\left[\tau_E(\ell)\right]^{-1}} \simeq \left(\frac{E}{600\ell}\right)^2 \tag{39.59}$$

In addition to emission, resonant absorption of nuclear radiation is possible. The gluon fields of a nucleon such as a proton or a neutron are given in the Proton and Neutron section. A resonant photon having gamma-ray energy and $\hbar$ of angular momentum in its electric and magnetic fields (Eq. (4.1)) can cause an excited nuclear state with a corresponding source-current component induced in the quarks of the same multipolarity as that of the gamma ray. The process is akin to that of the formation of an excited atomic state as given in the Excited States of the One-Electron Atom (Quantization) section. The absorption of a gamma ray gives rise to a trapped-photon standing wave inside the resonator cavity provided by the quarks of the nucleon. Both the photon standing wave and the source current to which it is phase-matched are spherical and time harmonics. The resonant absorption of gamma rays is the *Mössbauer Effect*. The nuclear size may increase or decrease depending on the effect of the excitation on the strong nuclear force via the absorbed photon field superposing with the gluon field. Similarly to the case of excited atomic states given in the Excited States of the One-Electron Atom (Quantization) section, the change in the total nucleon binding energy corresponding to the strong nuclear force is equal to the energy of the gamma ray, and the angular frequency change of the quark source current matches that of the gamma ray.

K-CAPTURE

The nuclear charge produces a high electric field at the radius of the inner shell electrons of heavy atoms. In addition, the nuclear magnetic moment of a nucleus produces a magnetic field at these positions that is substantial. The electron can also produce a magnetic field at the nucleus due to its spin and orbital angular momentum as shown in the Atomic Orbital Equation of Motion For ℓ = 0 Based on the Current Vector Field (CVF) and Orbital and Spin Splitting sections. Thus, in addition to nuclear radiation from the nuclear source current directly, Eq. (39.52) also can be applied to the case of K capture. Here, $|Q_{lm} + Q'_{lm}|^2$ and $|M_{lm} + M'_{lm}|^2$ are, respectively, the magnitudes of the electric and magnetic multipole moments between the electron and the nucleus, which correspond to equivalent multipole components of the two dimensional current-density functions of the electron and the nucleus.

ALPHA DECAY

ELECTRON TRANSMISSION AND REFLECTION AT A POTENTIAL ENERGY STEP [8]

The electron in free space has its charge-density in a two-dimensional plane as given in the Electron in Free Space section. Electron transition and reflection can be modeled as a plane wave at a potential energy barrier. An electron of total energy E is incident at an angle θ_i upon a potential energy barrier of height V_B as shown in Figure 39.8. The incident and transmitted electron wave vectors are shown in Figure 39.9a.

Figure 39.8. An electron plane wave of wave vector k_i incident at an angle θ_i upon a potential barrier of height V_B.

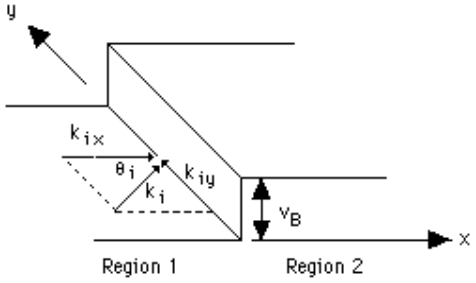

Figure 39.9. Electron wave-vector components in the parallel (y) and perpendicular (x) directions to the potential barrier for (a) incident and transmitted electron plane waves and (b) incident and reflected electron plane waves.

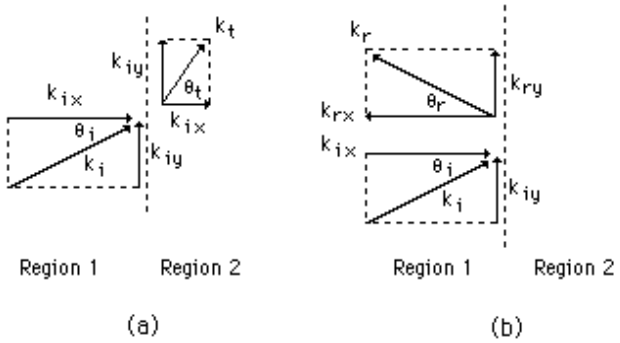

The kinetic energy of an incident electron (region 1) is:

$$E = \left(\hbar^2 / 2m_1^*\right)\left(k_{ix}^2 + k_{iy}^2\right) = \left(\hbar^2 / 2m_1^*\right)k_i^2, \tag{39.60}$$

where, m^* is the electron effective mass, k_{ix} and k_{iy} are the components of the incident electron wave vector normal and parallel to the boundary, respectively, and k_i, is the magnitude of the incident electron wave vector which is given by

$$k_i = \left(2m_1^* E\right)^{1/2} / \hbar \tag{39.61}$$

The incident and reflected electron wave vectors are shown in Figure 39.9b. The kinetic energy of a transmitted electron (region 2) is:

$$E - V_B = \left(\hbar^2 / 2m_2^*\right)\left(k_{tx}^2 + k_{ty}^2\right) = \left(\hbar^2 / 2m_2^*\right)k_t^2, \tag{39.62}$$

where k_{tx} and k_{ty} are the components of the transmitted electron wave vector normal and parallel to the boundary, respectively, and k_t is the magnitude of the transmitted wave vector which is given by:

$$k_t = \left[2m_2^*\left(E - V_B\right)\right]^{1/2} / \hbar \tag{39.63}$$

The phase of the transmitted electron along the boundary must be identical to that of the incident electron wave. This requirement of the continuity of the instantaneous phase at a boundary is commonly referred to as "phase matching." For the transmitted electron wave, the component of the wave parallel to the boundary is

$$k_{ty} = k_{iy} \tag{39.64}$$

The transmitted wave vector normal to the boundary can be obtained by combining Eqs. (39.61), (39.63), and (39.64). The result is:

$$k_{tx} = \left[\left(m_2^* / m_1^*\right)\left(k_{ix}^2 + k_{iy}^2\right) - k_{iv}^2 - \left(2m_2^* / \hbar^2\right)V_B\right]^{1/2} \tag{39.65}$$

The kinetic energy of the reflected electron wave (region 1) is:

$$E = \left(\hbar^2 / 2m_1^*\right)\left(k_{rx}^2 + k_{ry}^2\right) = \left(\hbar^2 / 2m_1^*\right)k_r^2 \tag{39.66}$$

where k_{rx} and k_{ry} are the components of the reflected electron wave vector normal and parallel to the boundary, respectively, and k_r, is the magnitude of the reflected wave vector which is given by:

$$k_r = \left(2m_1^* E\right)^{1/2} / \hbar \tag{39.67}$$

The requirement that the reflected wave also be phase-matched to the incident wave means that

$$k_{ry} = k_{iy} \tag{39.68}$$

Since the kinetic energy of a reflected electron is the same as that of an incident electron, then

$$k_{rx} = -k_{ix} \tag{39.69}$$

and thus implies the angle of reflection, θ_r, is equal to the angle of incidence, θ_i. That is:

$$\theta_r = \theta_i \tag{39.70}$$

Equation (39.64) represents the equivalent of Snell's law for electrons. It can be rewritten as:

$$k_t \sin\theta_t = k_i \sin\theta_i \tag{39.71}$$

In terms of the electron energies, Eq. (39.64) becomes:

$$\frac{\sin\theta_t}{\sin\theta_i} = \frac{k_i}{k_t} = \left(\frac{m_1^* E}{m_2^*\left(E - V_B\right)}\right)^{1/2} \tag{39.72}$$

For isotropic materials, the electron-allowed wave-vector surfaces are spheres. For an electron wave obliquely incident upon an infinitely thick potential barrier as shown in Figure 39.8, the allowed wave-vector surfaces may be depicted as shown in Figure 39.10.

Figure 39.10. Allowed wave-vector surfaces for the incident and reflected electron plane wave vectors and for the transmitted plane wave vector.

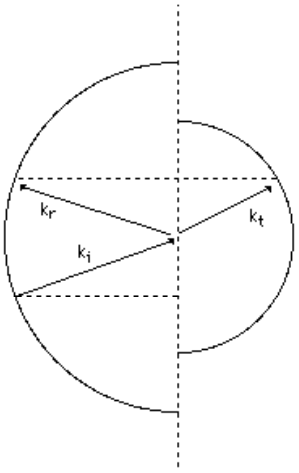

In general the radius of the allowed wave vector surface is:

$$k = \left[2m^*\left(E - V\right)\right]^{1/2} / \hbar, \tag{39.73}$$

where $E - V$ is the kinetic energy of the electron. The onset of total internal reflection occurs when $\theta_t = 90°$. This happens when the angle of incidence is equal to the critical angle, θ_{ic}. Thus from Eq. (39.72), the critical angle is:

$$\theta_{ic} = \begin{cases} \sin^{-1}\left[m_2^*\left[E - V_B\right] / m_1^* E\right]^{1/2} & \text{for } E - V_B > 0 \\ 0 & \text{for } E - V_B \le 0 \end{cases} \tag{39.74}$$

For an electron wave incident at an angle greater than θ_{ic}, the wave is totally internally reflected for an infinitely thick barrier. At steady state, all of the electron current is reflected back into region 1. The electron wave function decays exponentially into region 2. If the kinetic energy $E - V_B \le 0$, then total internal reflection occurs for any angle of incidence including normal incidence. This is in contrast to the electromagnetic case where total internal reflection can never occur at normal incidence due to the non-zero value of the minimum (free-space) wave-vector magnitude.

TRANSMISSION (TUNNELING) OUT OF A NUCLEUS—ALPHA DECAY [9]

Fundamental particles can demonstrate a phenomenon known as *tunneling*—they can overcome a potential energy barrier greater than that of their total energy. This is possible because the fundamental particles are extended such that a part of the particle that extends to a region of opposite potential energy as the rest can contribute sufficiently to the total energy of the particle to exceed that required for the particle to transverse the barrier. An example is the transmission of alpha particles from a nucleus.

Consider the equation for the propagation of the electron in free space, a two-dimensional plane, given by the plane wave equation Eq. (3.1):

$$E = E_0 e^{-ik_z z} \tag{39.75}$$

In the case where electrons of kinetic energy K are incident on a rectangular potential barrier whose height V_B is greater than K. V is substituted for V_B and K is substituted for E and the wave vector given by Eq. (39.63) becomes imaginary. An approximate value of T, the transmission probability—the ratio between the number of electrons that pass through the barrier and the number that arrive is given by

$$T = \left[\frac{E}{E_0}\right]^2 \tag{39.76}$$

From Eqs. (39.63), (39.75), and (39.76) the transmission probability is:

$$T = e^{-2k_2 L} \tag{39.77}$$

where

$$k_2 = \frac{\sqrt{2m(V-K)}}{\hbar} \tag{39.78}$$

and L is the width of the barrier. Eqs. (39.77) and (39.78) were derived for electrons. However, protons and neutrons are also two-dimensional in nature, and alpha particles are comprised of protons and neutrons. Thus, the model applies to alpha particles. Furthermore, Eqs. (39.77) and (39.78) were derived for electrons incident on a rectangular potential barrier; whereas, an alpha particle inside a nucleus is faced with a barrier of varying height, as shown in Figure 39.11.

Figure 39.11. The potential energy of an alpha particle as a function of its distance from the center of the nucleus.

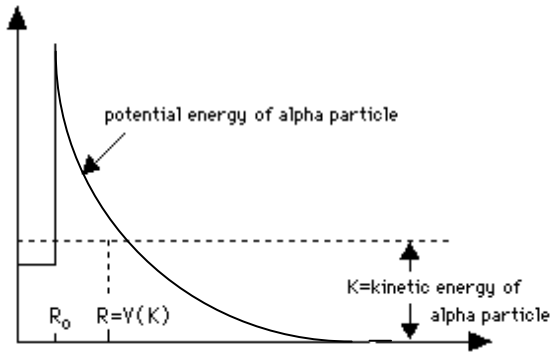

Eqs. (39.77) and (39.78) can be adapted to the case of a nuclear alpha particle. The first step is to rewrite Eqs. (39.77) and (39.78) in the form:

$$\ln T = -2k_2 L \tag{39.79}$$

and then express them as the integral:

$$\ln T = -2\int_0^L k_2(x)\,dx = -2\int_{R_0}^R k_2(x)\,dx \tag{39.80}$$

where R_0 is the radius of the nucleus and R is the distance from its center at which $V = K$. The kinetic energy K is greater than the potential energy V for $x > R$; so, if it can get past R, the alpha particle will have permanently escaped from the nucleus.

The electrical potential energy of an alpha particle at the distance x from the center of a nucleus of charge Ze is given by:

$$V(x) = \frac{2Ze^2}{4\pi\varepsilon_0 x} \tag{39.81}$$

Here Ze is the nuclear charge minus the alpha-particle charge of $2e$; thus, Z is the atomic number of the daughter nucleus.

We therefore have

$$k_2 = \frac{\sqrt{2m(V-K)}}{\hbar} = \left(\frac{2m}{\hbar^2}\right)^{1/2}\left(\frac{2Ze^2}{4\pi\varepsilon_0 x} - K\right)^{1/2} \tag{39.82}$$

Since $V = K$ when $x = R$,

$$K = \frac{2Ze^2}{4\pi\varepsilon_0 x} \tag{39.83}$$

and we can express k_2 in the form:

$$k_2 = \left(\frac{2mK}{\hbar^2}\right)^{1/2}\left(\frac{R}{x} - 1\right)^{1/2} \tag{39.84}$$

Hence

$$\ln T = -2\int_{R_0}^{R} k_2(x)\,dx \tag{39.85}$$

$$= -2\left(\frac{2mK}{\hbar^2}\right)^{1/2}\int_{R_0}^{R}\left(\frac{R}{x} - 1\right)^{1/2} dx$$

$$= -2\left(\frac{2mK}{\hbar^2}\right)^{1/2} R\left[\cos^{-1}\left(\frac{R_0}{R}\right)^{1/2} - \left(\frac{R_0}{R}\right)^{1/2}\left(1 - \frac{R_0}{R}\right)^{1/2}\right] \tag{39.86}$$

Because the potential barrier is relatively wide, $R >> R_o$, and

$$\cos^{-1}\left(\frac{R_0}{R}\right)^{1/2} \approx \frac{\pi}{2} - \left(\frac{R_0}{R}\right)^{1/2}$$

$$\left(1 - \frac{R_0}{R}\right)^{1/2} \approx 1 \tag{39.87}$$

with the result that

$$\ln T = -2\left(\frac{2mK}{\hbar^2}\right)^{1/2} R\left[\frac{\pi}{2} - 2\left(\frac{R_0}{R}\right)^{1/2}\right] \tag{39.88}$$

From the Eq. (39.83)

$$R = \frac{2Ze^2}{4\pi\varepsilon_0 K} \tag{39.89}$$

and so

$$\ln T = \frac{4e}{\hbar}\left(\frac{m}{\pi\varepsilon_0}\right)^{1/2} Z^{1/2} R_0^{1/2} - \frac{e^2}{\hbar\varepsilon_0}\left(\frac{m}{2}\right)^{1/2} ZK^{-1/2} \tag{39.90}$$

The result of evaluating the various constants in Eq. (39.90) is

$$\ln T = 2.97 Z^{1/2} R_0^{1/2} - 3.95 ZK^{-1/2} \tag{39.91}$$

where K (alpha-particle kinetic energy) is expressed in MeV, R_o (the nuclear radius) is expressed in fermis ($1\,fm = 10^{-15}\,m$), and Z is the atomic number of the nucleus minus the alpha particle. The decay probability per unit time, λ, can be expressed as the product of the number of times per second, υ, that an alpha particle within the nucleus strikes the potential barrier and the probability, T, that a particle will be transmitted through the barrier. And, υ can be expressed as the alpha particle velocity divided by the nuclear distance. Thus, the decay constant, λ, is given by

$$\lambda = \upsilon T = \frac{v}{2R_0} T \tag{39.92}$$

Taking the natural logarithm of both sides and substituting for the transmission probability T, gives:

$$\ln\lambda = \ln\left(\frac{v}{2R_0}\right) + 2.97 Z^{1/2} R_0^{1/2} - 3.95 ZK^{-1/2} \tag{39.93}$$

To express Eq. (39.93) in terms of common logarithms, we note that:

$$\ln A = \frac{\log_{10} A}{\log_{10} e} = \frac{\log_{10} A}{0.4343} \tag{39.94}$$

and so

$$\log_{10} \lambda = \log_{10}\left(\frac{v}{2R_0}\right) + 0.4343\left(2.97Z^{1/2}R_0^{1/2} - 3.95ZK^{-1/2}\right) \tag{39.95}$$

$$\text{Alpha Decay Constant} = \log_{10}\left(\frac{v}{2R_0}\right) + 1.29Z^{1/2}R_0^{1/2} - 1.72ZK^{-1/2} \tag{39.96}$$

Figure 39.12 Plot of $\log_{10}\lambda$ *versus* $ZK^{-1/2}$ for a number of alpha-radioactive nuclides.

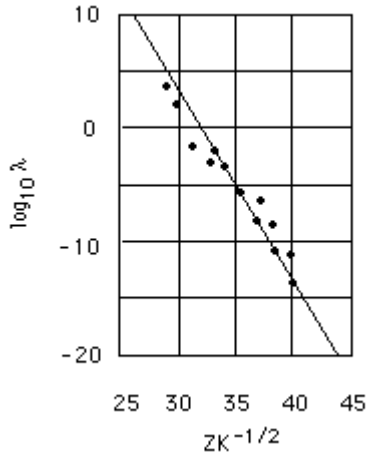

The straight line fitted to the experimental data has the -1.72 slope predicted throughout the entire range of decay constants that is in excellent agreement with the experimental data. We can use the position of the line to determine R_o, the nuclear radius. The result agrees with the results obtained from nuclear scattering experiments [9]. This approach thus constitutes an independent means of determining nuclear sizes.

REFERENCES

1. D. R. Lide, *CRC Handbook of Chemistry and Physics*, 79th Edition, CRC Press, Boca Raton, Florida, (1998-9), pp. 11-42.
2. D. R. Lide, *CRC Handbook of Chemistry and Physics*, 79th Edition, CRC Press, Boca Raton, Florida, (1998-9), pp. A-38 to A-40.
3. T. Adam, et. al., "Measurement of the neutrino velocity with the OPERA detector in the CNGS beam", Sept., (2011), http://arxiv.org/abs/1109.4897.
4. L. M. Krauss, S. Tremaine, "Test of the weak equivalence principle for neutrinos and photons", Phys. Rev. Lett., Vol. 60, (1988), pp. 176-177.
5. http://physics.nist.gov/cgi-bin/Compositions/stand_alone.pl?ele=H&ascii=html&isotype=some.
6. J. D. Jackson, *Classical Electrodynamics*, Second Edition, John Wiley & Sons, New York, (1975), pp. 758-763.
7. M. Goldhaber, J. Weneser, *Annual Review of Nuclear Science*, Vol. 5, ed., J. G. Beckerley, Annual Reviews, Stanford (1955), pp. 1-24.
8. T. K. Gaylord, K. F. Brennan, J. Appl. Phys., Vol. 65 (2), (1989), pp. 814-820.
9. A. Beiser, *Concepts of Modern Physics*, Fourth Edition, McGraw-Hill, New York, (1987), pp. 462-467.

Chapter 40

RETROSPECT: THE SCHRÖDINGER WAVE FUNCTION IN VIOLATION OF MAXWELL'S EQUATIONS

The Schrödinger equation implicitly postulates time harmonic motion of the spatial charge function of the electron. A wave equation was assumed, and time-harmonic motion was eliminated by Schrödinger [1], by substituting de Broglie waves, kinetic and potential energy relationships, and the equation,

$$v = \lambda f \tag{40.1}$$

The solution to the Schrödinger equation is a wave function $\psi(x)$. An interpretation of $\psi(x)$ is required. Schrödinger postulated that $\psi(x)$ represents the amplitude of the particle in some sense, and because the intensity of a wave is the square of the amplitude the "intensity of the particle" is proportional to $\psi^*(x)\psi(x)$ [$\psi^*(x)$ is the complex conjugate of $\psi(x)$]. A controversy arose over the meaning of intensity. Schrödinger considered $e\psi^*(x)\psi(x)$ to be the charge-density or $e\psi^*(x)\psi(x)$ to be the amount of charge between x and $x+dx$. Thus, he presumed the electron to be spread all over the region. The electron has kinetic energy and angular momentum and energy must be conserved; thus, the motion of an electron must be time harmonic. It is demonstrated in the One-Electron Atom section that emission of electromagnetic radiation occurs if the spacetime Fourier transform possesses waves that are synchronous with waves traveling at the speed of light. It is demonstrated below that the Schrödinger wave equations have such components; thus, they must radiate. That no radiation is observed demonstrates the invalidity of these equations as an accurate description of an electron.

The angular functions of Schrödinger wave equations are spherical harmonics and their spacetime Fourier transform is given in the One-Electron Atom section (Spacetime Fourier Transform of the Electron Function) as the transforms of $g(\theta)$, $h(\phi)$, and $k(t)$. The radial solutions (solutions which are a function of the radial variable *r*) are of the form of *r* raised to a power times a negative exponential of *r*. Thus, it is appropriate to take the spacetime Fourier transform of the general solution for psi squared times a time harmonic function (which is proportional to qdr/dt) and apply Haus' nonradiative condition [2]. The most fundamental solution is chosen for analysis. Additional powers of the radial functions would give rise to convolution integrals in Fourier space and additional terms that do not go to zero. The same applies to additional linear terms. It is only necessary to demonstrate that one component does not vanish for $k = \frac{\omega}{c}$.

The spacetime Fourier transform of the radial function $f(r) = re^{-r/a_0}$ follows:

With spherical symmetry [3]:

$$G(s) = 4\pi \int_0^\infty g(r)\mathrm{sinc}(2sr)r^2 dr \tag{40.2}$$

$$G(s) = 4\pi \int_0^\infty re^{-r/a_0}\mathrm{sinc}(2sr)r^2 dr \tag{40.3}$$

Using the definition of the function:

$$Sinc\ x = \frac{\sin \pi x}{\pi x} \tag{40.4}$$

Eq. (40.3) becomes:

$$= 4\pi \int_0^\infty r^3 e^{-r/a_0} \frac{\sin 2\pi sr dr}{\pi sr} \tag{40.5}$$

$$= \frac{4}{s} \int_0^\infty r^2 e^{-r/a_0} \sin 2\pi sr dr \tag{40.6}$$

Let

$$r = \frac{r'}{2\pi} \quad and \quad dr = \frac{dr'}{2\pi} \tag{40.7}$$

$$G(s) = \frac{1}{2s\pi^3} \int_0^\infty r'^2 \exp(\frac{-r'}{2\pi a_0}) \sin sr' dr' \tag{40.8}$$

From Bateman [4]:

$$\int_0^\infty x^n e^{-\alpha x} \sin(xy) dx = n! \left(\frac{\alpha}{\alpha^2 + y^2} \right)^{n+1} \sum_{m=0}^{\frac{n}{2}} (-1)^m \left(\binom{n+1}{2m+1} \left(\frac{y}{\alpha} \right)^{2m+1} \right) \tag{40.9}$$

Let

$$x = r,\ s = y,\ \alpha = \frac{1}{2\pi a_0},\ n = 2 \tag{40.10}$$

and apply Eq. (40.9) to Eq. (40.8).

$$G(s) = \frac{1}{2s\pi^3} \int_0^\infty r'^2 \exp\left(\frac{-r'}{2\pi a_0} \right) \sin sr' dr' = \frac{1}{2s\pi^3} 2! \left(\frac{\frac{1}{2\pi a_0}}{\left(\frac{1}{2\pi a_0} \right)^2 + s^2} \right)^3 \sum_{m=0}^{1} (-1)^m \left(\binom{3}{2m+1} \left(\frac{s}{\frac{1}{2\pi a_0}} \right)^{2m+1} \right) \tag{40.11}$$

In Appendix I, the Fourier transforms of the angular functions are given by Eqs. (26) and (27), and the Fourier transform of the time harmonic function is given by Eq. (34). By Eq. (35), the complete spacetime Fourier transform of a Schrödinger wave equation, $W(s, \Theta, \Phi, \omega)$, is the convolution of Eqs. (40.11), (26), (27), and (34) where:

$$\begin{aligned} W(s,\Theta,\Phi,\omega) = {} & \frac{1}{2s\pi^3} 2! \left(\frac{\frac{1}{2\pi a_0}}{\left(\frac{1}{2\pi a_0} \right)^2 + s^2} \right)^3 \sum_{m=0}^{1} (-1)^m \left(\binom{3}{2m+1} \left(\frac{s}{\frac{1}{2\pi a_0}} \right)^{2m+1} \right) \\ & \otimes 2\pi \sum_{\upsilon=1}^{\infty} \frac{(-1)^{\upsilon-1} (\pi \sin\Theta)^{2(\upsilon-1)}}{\upsilon(\upsilon-1)!} \frac{\Gamma\left(\frac{1}{2}\right)\Gamma\left(\upsilon+\frac{1}{2}\right)}{(\pi\cos\Theta)^{2\upsilon+1} 2^{\upsilon+1}} \frac{2\upsilon!}{\upsilon!} s^{-2\upsilon} \\ & \otimes 2\pi \sum_{\upsilon=1}^{\infty} \frac{(-1)^{\upsilon-1} (\pi \sin\Phi)^{2(\upsilon-1)}}{\upsilon(\upsilon-1)!} \frac{\Gamma\left(\frac{1}{2}\right)\Gamma\left(\upsilon+\frac{1}{2}\right)}{(\pi\cos\Phi)^{2\upsilon+1} 2^{\upsilon+1}} \frac{2\upsilon!}{\upsilon!} s^{-2\upsilon} \\ & \frac{1}{4\pi} \left[\delta(\omega - \omega_n) + \delta(\omega + \omega_n) \right] \end{aligned} \tag{40.12}$$

This transform has components $\frac{\omega_n}{c} = k$ that are not zero and are synchronous with waves traveling at the speed of light. Thus, a charge-density function given by the Schrödinger wave equation must radiate in accordance with Maxwell's Equations.

REFERENCES

1. D. A. McQuarrie, *Quantum Chemistry*, University Science Books, Mill Valley, CA, (1983), pp. 78-79.
2. H. A. Haus, "On the radiation from point charges," American Journal of Physics, 54, (1986), pp. 1126-1129.
3. R. N. Bracewell, *The Fourier Transform and Its Applications*, McGraw-Hill Book Company, New York, (1978), pp. 252-253.
4. H. Bateman, *Tables of Integral Transforms*, Vol. III, McGraw-Hill, New York, (1954), p. 72.

Chapter 41

RETROSPECT: CLASSICAL ELECTRON RADIUS

Electron scattering from neutral atoms and the classical electron radius are tests of the nature of bound electrons as atomic orbitals of the classical model as opposed to point particles of the Schrödinger-Born model.

Electron scattering experiments support the nature of bound electrons as atomic orbitals of the classical model, and the data is inconsistent with the probability point particle model of Schrödinger and Born. Consider the case given in the Classical Photon and Electron Scattering section wherein experimental results by Bromberg [1] were presented. Quoting from Bromberg [1], "At smaller angles; however, the Born approximation calculation fails utterly, the experimental curve rising much more steeply than the theoretical." This point is explicitly demonstrated in Figure 8.6. In contrast, the closed form function (Eqs. (8.57) and (8.58)) for the elastic differential cross section for the elastic scattering of electrons by helium atoms is in agreement with the data of Bromberg as demonstrated in Figure 8.7. In principle, Quantum mechanics cannot adequately describe the results of electron scattering from neutral atoms or the results of the Davidson-Germer experiment. An assembly of point particles cannot give rise to neutral scattering in the absence of the violation of Special Relativity. Otherwise, an internal inconsistency arises—namely violation of the Uncertainty Principle. Rutherford scattering would be predicted from a point particle model.

Furthermore, the radius of the electron according to quantum mechanics is zero; whereas, the minimum classical electron radius is the Compton wavelength bar as required by conservation of mass-energy and relativity as shown in the Gravity section. The electron must spin in one dimension and give rise to a Bohr magneton, μ_B,

$$\mu_B = \frac{e\hbar}{2m_e} = 9.274\ X\ 10^{-24}\ JT^{-1}, \tag{41.1}$$

The magnetic energy corresponding to the magnetic moment of Eq. (41.1) is:

$$E_{mag} = \frac{1}{2}\mu_0 \int_0^{2\pi}\int_0^{\pi}\int_0^{\infty} H^2 r^2 \sin\theta dr d\theta d\Phi \tag{41.2}$$

$$\mathbf{H} = \frac{e\hbar}{2m_e r^3}(\mathbf{i}_r 2\cos\theta - \mathbf{i}_\theta \sin\theta) \quad for \quad r > r_n \tag{41.3}$$

which in the present case is infinity (by substitution of $r = 0$ for the model that the electron is a point particle) not the required mc^2. This interpretation is in violation of Special Relativity [2].

Eq. (29.14) of the Pair Production section gives the magnetic energy correctly as mc^2. The "effective" atomic orbital radius to be used to calculate the cross section for pair production using the electric energy of Eq. (29.10) and Eq. (29.11) is the classical electron radius,

$$\alpha^2 a_o = \alpha \lambda\!\!\!^{-}_c = 2.82X10^{-13}\ cm\ (CGS\ units) \tag{41.4}$$
$$= 2.82X10^{-15}\ m\ (MKS\ units)$$

$$V = -\frac{\alpha^{-2}e^2}{4\pi\varepsilon_0 a_0} \tag{41.5}$$

$$V = m_e c^2 \tag{41.6}$$

Based on Eqs. (41.5) and (41.6), σ, the geometric cross section of the electron can be derived using the classical electron radius.

$$\sigma = \pi\left[\frac{e^2}{m_e c^2}\right]^2 \tag{41.7}$$

$$\sigma = \pi\left[\alpha \lambda\!\!\!^{-}_{C}\right]^2 \tag{41.8}$$

From the geometric cross section of the electron, the equation for radiation scattering follows from the equation for radiation by a Hertzian dipole where:

$$I = I_o \frac{8\pi}{3}\frac{\sigma}{\pi} = I_o \frac{8\pi}{3}\left[\frac{e^2}{m_e c^2}\right]^2 \ (CGS\ units) \tag{41.9}$$

Electron-proton force balance exists and the atomic orbital is nonradiative. Mechanics and electrodynamics can both be satisfied simultaneously to achieve these conditions of force balance with cancellation of all radiation fields. Directional antennae arrays are designed using identical principles of achieving cancellation of desired radiation fields. For the electron atomic orbital,

$$\left[\nabla^2 - \frac{1}{v^2}\frac{\partial^2}{\partial t^2}\right]\rho(r,\theta,\phi,t) = 0 \tag{41.10}$$

And, the Fourier transform of the atomic orbital is zero when:

$$\left[k^2 - \left[\frac{\omega^2}{c}\right]^2\right] = 0 \tag{41.11}$$

In contrast, the electron described by a Schrödinger one-electron wave function would radiate. (See The Schrödinger Wavefunction in Violation of Maxwell's Equation section).

Furthermore, the correct prediction of the elastic scattering of electrons by helium atoms wherein the electron radius is a crucial parameter (Eq. (8.57)), the results of the Stern-Gerlach experiment, the results of the Davisson-Germer experiment, as well as the correct derivation of the electron (fluxon) g factor, the resonant line shape, the Lamb Shift, spin-orbit coupling energies, and the excited state spectrum of hydrogen wherein ***the correspondence principle holds*** are direct verifications that the electron is an atomic orbital with the calculated radius. Quantum mechanics has failings in each of these cases.

Two-dimensional distributions are common in classical physics. A two-dimensional discontinuity in surface current gives rise to a magnetic field; a discontinuity in surface charge gives rise to an electric field. Ampere's and Gauss' Laws also apply in the present theory with respect to the electron. Furthermore, a two-dimensional discontinuity in mass according to the classical model gives rise to a gravitational field which is consistent with General Relativity which leads to the correct prediction of the masses of leptons (Leptons section), the quarks (Quarks section), and the classical electron radius as given in Eq. (29.14) of the Pair Production section wherein the magnetic energy is correctly given as $m_e c^2$ as shown previously.

Furthermore, Born postulated that the electron is a one dimensional delta function—zero volume and infinite mass-density. The Schrödinger solutions for the hydrogen atom exclude the existence of energy levels below the "ground" state corresponding to $n = \frac{1}{\text{integer}}$ in the Rydberg formula [3]:

$$\bar{\nu} = R\left(\frac{1}{n_f^2} - \frac{1}{n_i^2}\right) \tag{41.12}$$

where $R = 10,967,758\ m^{-1}$, $n = \frac{1}{2}, \frac{1}{3}, \frac{1}{4}, ...$, and $n_i > n_f$. The data given in the Foreword section and the Astrophysics section proves that the Schrödinger-Born model is incorrect because it is clearly inconsistent with the experimental findings. The two-dimensional function given for a bound electron in the One-Electron Atom section and for a free electron in the Electron in Free Space section is the correct description of the electron. Also, the two-dimensional function given in the Photon Equation section is the correct description for electromagnetic radiation that can give rise to the electron. The models of classical physics are supported by the close agreement between experimental observation and theoretical predictions.

REFERENCES

1. P. J. Bromberg, "Absolute differential cross sections of elastically scattered electrons. I. He, N_2, and CO at 500 eV," The Journal of Chemical Physics, Vol. 50, No. 9, (1969), pp. 3906-3921.
2. A. Pais, "George Uhlenbeck and the discovery of electron spin," Physics Today, 40, (1989), pp. 34-40
3. J. A. Maly, J. Vavra, Fusion Tech., Vol. 24, Nov. (1993), pp. 307-318.

Chapter 42

RETROSPECT: WAVE-PARTICLE DUALITY

> [My father] said, "I understand that they say that light is emitted from an atom when it goes from one state to another, from an excited state to a state of lower energy."
> I said, "That's right."
> "And light is kind of a particle, a photon, I think they call it."
> "Yes."
> "So if the photon comes out of the atom when it goes from the excited to the lower state, the photon must have been in the atom in the excited state."
> I said, "Well no."
> He said, "Well, how do you look at it so you can think of a particle photon coming out without it having been there in the excited state?"
> I thought a few minutes, and I said, "I'm sorry; I don't know. I can't explain it to you."
> -Richard P. Feynman, *The Physics Teacher* (September 1969).

Many great physicists rejected Quantum Mechanics. Feynman also attempted to use first principles including Maxwell's Equations to discover new physics to replace quantum mechanics [1]. Other great physicists of the 20th century searched. "Einstein [...] insisted [...] that a more detailed, wholly deterministic theory must underlie the vagaries of quantum mechanics [2]." He felt that scientists were misinterpreting the data. In fact, this is the case. Experiments by the early part of the 20th century had revealed that both light and electrons behave as waves in certain instances and as particles in others. This was unanticipated from preconceptions held regarding the nature of light and the electron. Early 20th century theoreticians proclaimed that light and atomic particles have a wave-particle duality that was unlike anything in our common everyday experience. The wave-particle duality is the central mystery of quantum mechanics–the one to which all others could ultimately be reduced. Consider the two-slit experiment. A gun (obeying classical physics) sprays bullets towards a target. Before they reach the target, they must pass through a screen with two slits. The pattern they make shows how their probability of arrival varies from place to place. They are more likely to strike directly behind the one slit that they went through as shown in Figure 42.1. The pattern happens to be simply the sum of the patterns for each slit considered separately: if half the bullets were fired with only the left slit open and then half were fired with just the right slit open, the result would be the same.

Figure 42.1. Two-slit experiment with macroscopic particles gives an image of each slit.

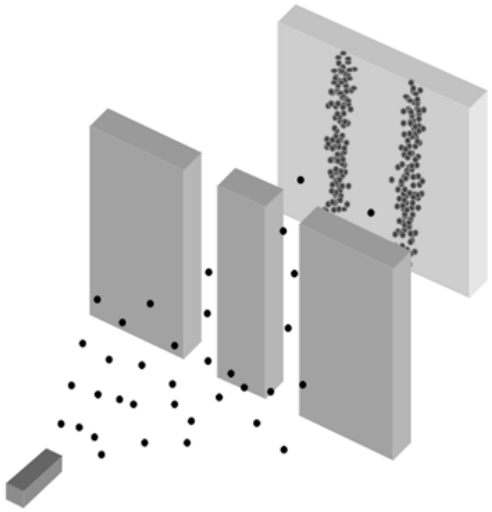

Figure 42.2. Two-slit experiment with waves gives an interference pattern.

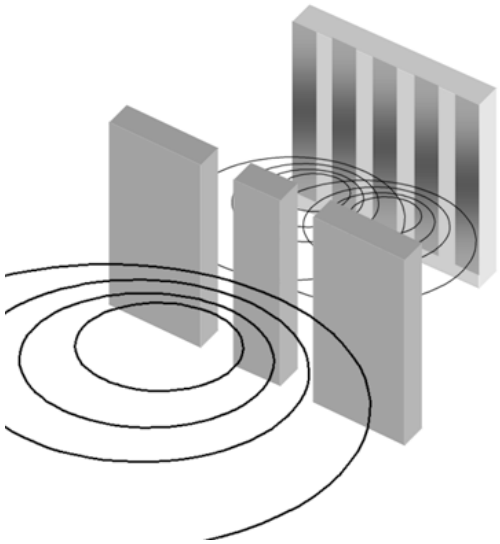

With waves, however, the result is very different, because of interference. If the slits were opened one at a time, the pattern would resemble the pattern for bullets: two distinct peaks. But, when the slits are open at the same time, the waves pass through both slits at once and interfere with each other: where they are in phase they reinforce each other; where they are out of phase they cancel each other out as shown in Figure 42.2.

Now the quantum paradox: Electrons, like bullets, strike the target one at a time. Yet, like waves, they create an interference pattern as shown in Figure 42.3.

If each electron passes individually through one slit, with what does it "interfere"? Although each electron arrives at the target at a single place and a single time, it seems that each has passed through–or somehow felt the presence of both slits at once. Thus, the electron is understood in terms of a wave-particle duality as represented in Figure 42.4.

Figure 42.3. Two-slit experiment with electrons also gives an interference pattern.

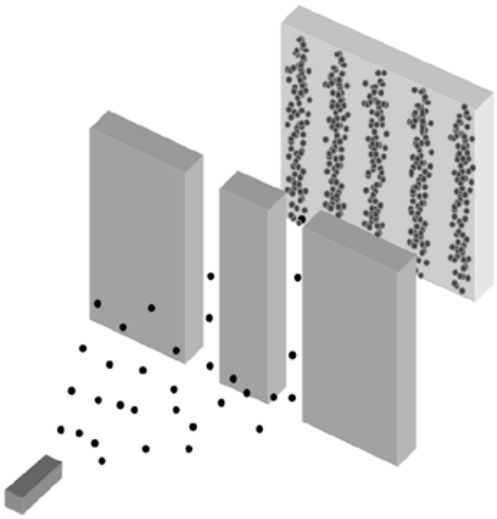

Figure 42.4. The interpretation of the observed wave interference pattern of the two-slit experiment with electrons was in terms of a wave-particle duality to the nature of the electron.

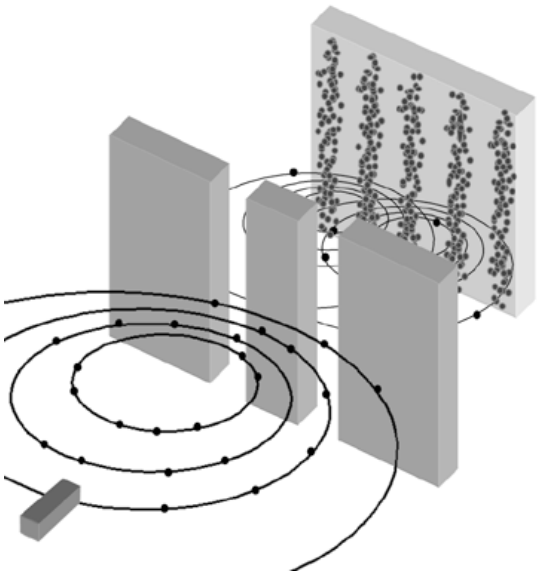

The mistake in the direction of the development of the theory of light and the atom occurred when theoreticians

concluded: The laws of physics that are valid in the macroworld do not hold true in the microworld of the atom. In contrast, as shown in previous chapters **classical physics** was applied correctly to solve the structures of the electron and photon demonstrating that the laws of physics that are valid in the macroworld *do hold true* in the microworld of the atom. The predictions, which arise from the equations of light and atomic particles, are completely consistent with observation, including the wave-particle duality of light and atomic particles as shown explicitly in the Classical Photon and Electron Scattering section. Furthermore, the quantization of atomic energy levels arises classically without invoking new physics. Continuous motion such as electronic transitions between quantized states and translational motion restores continuity and causality with the continuous nature of spacetime itself restored consistent with first principles and observation. The postulates and mathematical constructs of quantum mechanics are erroneous. Physical laws apply to the atomic scale in refutation to quantum mechanics.

Maxwell unified electricity and magnetism by proposing the existence of electromagnetic waves that travel at the velocity c. In 1888, Hertz showed that electromagnetic waves exist and behave exactly as Maxwell had predicted—they had electric and magnetic components, and they could be reflected, refracted, and diffracted. Toward the end of the 19th century, many physicists believed that all of the principles of physics had been discovered. The accepted principles, now called ***classical physics***, included laws relating to Newton's mechanics, Gibbs' thermodynamics, LaGrange's and Hamilton's elasticity and hydrodynamics, Maxwell-Boltzmann molecular statistics, and Maxwell's Equations. However, the discovery that the intensity of blackbody radiation goes to zero, rather than infinity as predicted by the prevailing laws of electromagnetism, led theoreticians to question the validity of Maxwell's Equations on the atomic scale. In 1900, Planck made the revolutionary assumption that energy levels were quantized, and that atoms of the blackbody could emit light energy only in amounts given by $h\nu$, where ν is the radiation's frequency and h is a proportionality constant (now called Planck's constant). This assumption does not conflict with the notion that light is a wave. However, Hertz's experiments with light further revealed that photoelectrons were emitted from illuminated metals, and the photoelectron energy increases with the frequency of incident light and not its intensity. Einstein explained this photoelectron effect by proposing that light of a given frequency is composed of individual photons whose energy is proportional to that frequency according to Planck's relationship[1]. Einstein's proposal that light has a particle nature in that it travels through space as distinct photons[2] is opposed to the wave view whereby light waves spread out from a source, and the energy is spread continuously throughout the wave pattern. Thus, light has since been regarded as both a wave and a particle which exhibits one feature or the other during observation but never both simultaneously. Early 20th century theoreticians proclaimed that light has a wave-particle duality that was unlike anything in our common everyday experience [3].

A similar course arose in the development of the model of the atom. J. J. Balmer showed, in 1885, that the frequencies for some of the lines observed in the emission spectrum of atomic hydrogen could be expressed with a completely empirical relationship. This approach was later extended by J. R. Rydberg, who showed that all of the spectral lines of atomic hydrogen were given by the equation:

$$\bar{\nu} = R\left(\frac{1}{n_f^2} - \frac{1}{n_i^2}\right) \tag{42.1}$$

where $R = 10,967,758\ m^{-1}$, $n_f = 1,2,3,\ldots$, $n_i = 2,3,4,\ldots$, and $n_i > n_f$. Niels Bohr, in 1913, developed a theory for atomic hydrogen based on an unprecedented postulate of stable circular orbits that do not radiate. Although no explanation was offered for the existence of stability for these orbits, the results gave energy levels in agreement with Rydberg's equation. Bohr's theory was a straightforward application of Newton's laws of motion and Coulomb's law of electric force—both pillars of classical physics and is in accord with the experimental observation that atoms are stable. However, it is not in accord with electromagnetic theory—another pillar of classical physics, which predicts that accelerated charges radiate energy in the form of electromagnetic waves. An electron pursuing a curved path is accelerated and therefore should continuously lose energy, spiraling into the nucleus in a fraction of a second. The predictions of electromagnetic theory have always agreed with experiment, yet atoms do not collapse. To the early 20th century theoreticians, this contradiction could mean only one thing: The laws of physics that are valid in the macroworld do not hold true in the microworld of the atom. In 1923, de Broglie suggested that the motion of an electron has a wave aspect—$\lambda = \frac{h}{p}$. This concept seemed unlikely according to the familiar properties of electrons such as charge, mass and adherence to the laws of particle mechanics. But, the wave nature of the electron was confirmed by Davisson and Germer in 1927 by observing diffraction effects when electrons were reflected from metals. Schrödinger reasoned that if electrons have wave properties, there must be a wave equation that governs their motion. And in 1926, he proposed the Schrödinger equation, $H\Psi = E\Psi$, where Ψ is the wave function, H is the wave operator, and E is the energy of the wave. This equation, and its associated postulates, is now the basis of ***quantum mechanics***, and it is the basis for the worldview that the atomic realm including the electron and photon cannot be described in terms of "pure" wave and "pure" particle but in terms of a wave-particle duality. The wave-particle duality based on the fundamental principle that physics on an atomic scale is very different from physics on a macroscopic scale is central to present day atomic theory [4].

The hydrogen atom is the only real problem for which the Schrödinger equation can be solved without approximations; however, it only provides three quantum numbers–not four. Nevertheless, the application of the Schrödinger equation to real

[1] In 1900, Planck made the revolutionary assumption that energy levels were quantized, and that atoms of the blackbody could emit light energy only in amounts given by $h\nu$, where ν is the radiation's frequency and h is a proportionality constant (now called Planck's constant). This assumption also led to our understanding of the photoelectric effect and ultimately to the concept of light as a particle called a photon.

[2] This view was first proposed by Newton. Einstein was the founder of the erroneous wave-particle duality concept that's the source of "weirdness" in quantum mechanics.

problems has provided useful approximations for physicists and chemists. Schrödinger interpreted $e\Psi^*(x)\Psi(x)$ as the charge-density or the amount of charge between x and $x+dx$ (Ψ^* is the complex conjugate of Ψ) wherein he pictured the electron to be spread over large regions of space. Three years after Schrödinger's interpretation, Max Born, who was working with scattering theory, found that this interpretation led to inconsistencies and he replaced the Schrödinger interpretation with the probability of finding the electron between x and $x+dx$ as:

$$\int \Psi(x)\Psi^*(x)dx \tag{42.2}$$

Born's interpretation is generally accepted. Nonetheless, interpretation of the wave function is a never-ending source of confusion and conflict. Many scientists have solved this problem by conveniently adopting the Schrödinger interpretation for some problems and the Born interpretation for others. This duality allows the electron to be everywhere at one time—yet have no volume. Alternatively, the electron can be viewed as a discrete particle that moves here and there (from $r=0$ to $r=\infty$), and $\Psi\Psi^*$ gives the time average of this motion.

According to the quantum mechanical view, a moving particle is regarded as a wave group. To regard a moving particle as a wave group implies that there are fundamental limits to the accuracy with which such "particle" properties as position and momentum can be measured. Quantum mechanics predicts that the particle may be located anywhere within its wave group with a probability $|\Psi|^2$. An isolated wave group is the result of superposing an infinite number of waves with different wavelengths. The narrower the wave group is, the greater range of wavelengths involved. A narrow de Broglie wave group thus means a well-defined position (Δx smaller) but a poorly defined wavelength and a large uncertainty $\Delta\mathbf{p}$ in the momentum of the particle the group represents. A wide wave group means a more precise momentum but a less precise position. The infamous Heisenberg Uncertainty Principle is a formal statement of the standard deviations of properties implicit in the probability model of fundamental particles.

$$\Delta x \Delta \mathbf{p} \geq \frac{\hbar}{2} \tag{42.3}$$

According to the standard interpretation of quantum mechanics, the act of measuring the position or momentum of a quantum mechanical entity collapses the wave-particle duality because the principle forbids both quantities to be simultaneously known with precision. (The Resonant Line Shape and Lamb Shift section discusses the erroneous nature of the Uncertainty Principle.)

THE WAVE-PARTICLE DUALITY IS NOT DUE TO THE UNCERTAINTY PRINCIPLE

Quantum entities can behave like particles or waves, depending on how they are observed. They can be diffracted and produce interference patterns (wave behavior) when they are allowed to take different paths from some source to a detector—in the usual example, electrons or photons go through two slits and form an interference pattern on the screen behind. On the other hand, with an appropriate detector put along one of the paths (at a slit, say), the quantum entities can be detected at a particular place and time, as if they are point-like particles. But any attempt to determine which path a quantum object takes destroys the interference pattern. Richard Feynman described this as the central mystery of quantum physics.

Bohr called this vague principle "complementarity," and explained it in terms of the uncertainty principle, put forward by Werner Heisenberg, his postdoc at the time. In an attempt to persuade Einstein that wave-particle duality is an essential part of quantum mechanics, Bohr constructed models of quantum measurements that showed the futility of trying to determine which path was taken by a quantum object in an interference experiment. As soon as enough information is acquired for this determination, the quantum interferences must vanish, said Bohr, because any act of observing will impart uncontrollable momentum kicks to the quantum object. This is quantified by Heisenberg's uncertainty principle, which relates uncertainty in positional information to uncertainty in momentum—when the position of an entity is constrained, the momentum must be randomized to a certain degree.

More than 60 years after the famous debate between Niels Bohr and Albert Einstein on the nature of quantum reality, a question central to their debate—the nature of quantum interference—has resurfaced. The usual textbook explanation of wave-particle duality in terms of unavoidable "measurement disturbances" is experimentally proven incorrect by an experiment reported in the September 3, 1998 issue of *Nature* [5] by Durr, Nonn, and Rempe. Durr, Nonn, and Rempe report on the interference fringes produced when a beam of cold atoms is diffracted by standing waves of light. Their interferometer displayed fringes of high contrast—but when they manipulated the electronic state within the atoms with a microwave field according to which path was taken, the fringes disappeared entirely. The interferometer produced a spatial distribution of electronic populations that were observed via fluorescence. The microwave field canceled the spatial distribution of electronic populations. The key to this new experiment was that although the interferences are destroyed, the initially imposed atomic momentum distribution left an envelope pattern (in which the fringes used to reside) at the detector. A careful analysis of the pattern demonstrated that it had not been measurably distorted by a momentum kick of the type invoked by Bohr, and therefore that any locally realistic momentum kicks imparted by the manipulation of the internal atomic state according to the particular path of the atom are too small to be responsible for destroying interference.

Durr et al. conclude that the "Heisenberg Uncertainty relationship has nothing to do with wave-particle duality" and further conclude that the phenomenon is based on entanglement and correlation. Their interpretation of the principles of the experiment is that directional information is encoded by manipulating the internal state of an atom with a microwave field, which entangles the atom's momentum with its internal electronic state. Like all such entangled states, the constituent parts lose

their separate identity. But the attachment of a distinguishable electronic label to each path means that the total electronic-plus-path wavefunction along one path becomes orthogonal to that along the other, and so the paths can't interfere. By encoding information as to which path is taken within the atoms, the fringes disappear entirely. The internal labeling of paths does not even need to be read out to destroy the interferences: all you need is the option of being able to read it out.

According to Durr et al., the mere existence of information about an entity's path causes its wave nature to disappear. But, correlations are observations about relationships between quantities and do not cause physical processes to occur. **The existence of information about an entity's path is a consequence of the manipulation of the momentum states of the atoms which resulted in cancellation of the interference pattern. It was not the cause of the cancellation. The cancellation is predicted by classical atomic theory.**

The explanation for the loss of interference in which-way experiments that endured and is present in essentially all quantum physics textbooks is that based on Heisenberg's position-momentum uncertainty relation. This has been illustrated in famous gedanken experiments like Einstein's recoiling slit [6] or Feynman's light microscope [7]. In the light microscope, electrons are illuminated with light immediately after they have passed through a double slit with slit separation d. A scattered photon localizes the electron with a position uncertainty of the order of the light wavelength, $\Delta z = \lambda_{light}$. Owing to Heisenberg's position-momentum uncertainty relation, this localization must produce a momentum uncertainty of the order of $\Delta p_z \approx h/\lambda_{light}$. This momentum uncertainty arises from the momentum kick transferred by the scattered photon. For $\lambda_{light} < d$, which-way information is obtained, but the momentum kick is so large that it completely washes out the spatial interference pattern.

The issue of whether momentum kicks are necessary to explain the two-slit experiment is revisited. Obviously, momentum is involved, because a diffraction pattern is a map of the momentum distribution in the experiment. But how is it involved? Is it everything, as Bohr would have claimed?

This is the question addressed by Durr et al. [5] who report on a which-way experiment with an atom interferometer wherein an incoming beam of atoms passes through two separated standing wave light beams. The detuning of the light frequency from the atomic resonance, $\Delta = \omega_{light} - \omega_{atom}$, is large so that spontaneous emission can be neglected. The light fields each create a conservative potential U for the atoms, the so-called light shift, with $U \propto I/\Delta$, where I is the light intensity. In a standing wave, the light intensity is a function of position where,

$$I(z) = I_0 \cos^2\left(k_{light} z\right) \tag{42.4}$$

where k_{light} is the wavevector of the light. Hence the light shift potential takes the form of:

$$U(z) = U_0 \cos^2\left(k_{light} z\right) \tag{42.5}$$

with $U_0 \propto I_0/\Delta$.

The atoms are Bragg-reflected from this periodic potential, if they enter the standing light wave at a Bragg angle. This process is similar to Bragg reflection of X-rays from the periodic structure of a solid-state crystal, but with the role of matter and light exchanged. The light creates the periodic structure, from which the matter wave is reflected.

The scheme of the interferometer is shown in Figure 42.5. The standing light wave splits the incoming atomic beam A into two beams, a transmitted beam C and a first-order Bragg-reflected beam B. The angle between the beams B and C corresponds to a momentum transfer of exactly $2\hbar k_{light}$ as determined by the spatial period of $U(z)$. By varying the light intensity, the fraction of reflected atoms can be adjusted to any arbitrary value. Durr et al. tune the reflectivity of the beam splitter to about 50%.

Figure 42.5. Scheme of the atom interferometer. The incoming atomic beam A is split into two beams: beam C is transmitted and beam B is Bragg-reflected from a standing light wave. The beams are not exactly vertical because a Bragg condition must be fulfilled. After free propagation for a time t_{sep}, the beams are displaced by a distance d. Then the beams are split again with a second standing light wave. In the far field, a spatial interference pattern is observed.

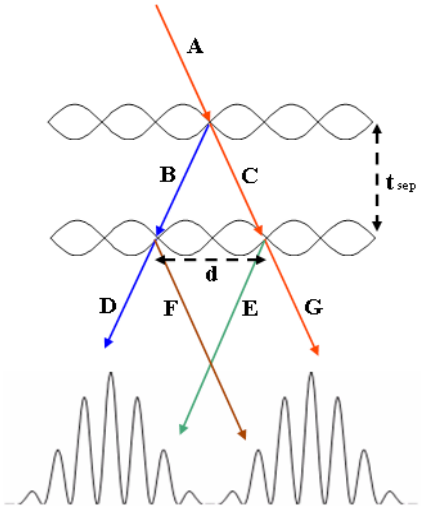

After switching off the first standing light wave, the two beams are allowed to propagate freely for a time interval t_{sep}. During this time, beam B moves a horizontal distance $d/2$ to the left, and beam C moves $d/2$ to the right. The longitudinal velocities (direction normal to the standing light wave of Figure 42.5) of the two beams are not affected by the light field. Then a second standing light wave is switched on, which also serves as a 50% beam splitter. Now two atomic beams D and E are traveling to the left, while beams F and G are traveling to the right. In the far field, each pair of overlapping beams produces a spatial interference pattern. The fringe period is the same as in a double-slit experiment with slit separation d as given in the Two-Beam Interference section. The intensity is given by Eq. (8.23) :

$$I(\mathrm{x}) = 16a^2C^2\mathrm{sinc}^2\left(\frac{2\pi a\mathrm{x}}{\lambda f}\right)\cos^2\left(\frac{2\pi d\mathrm{x}}{\lambda f}\right) \tag{42.6}$$

From Eq. (42.6), it is clear that the resulting pattern has the appearance of cosine^2 fringes of period $\lambda f/d$ with an envelope $\mathrm{sinc}^2(2\pi a\mathrm{x}/\lambda f)$ where f is the focal length and a is the slit width. In the present case, the envelope of the fringe pattern is given by the collimation properties of the initial atomic beam A. Note that Eq. (42.6) corresponds to an amplitude transmission of a plane wave. The bound unpaired electron of each ^{85}Rb atom behaves as a plane wave of wavelength $\lambda = h/p$ as shown in the Free Electron section. The relevant wavelength λ of Eq. (42.6) is the de Broglie wavelength associated with the momentum of the atoms (Eq. (1.38)) which is transferred to the electrons through atomic interactions.

The atomic position distribution is observed by exciting atoms with a resonant laser and detecting the fluorescence photons. The observed far-field position distribution is a picture of the atomic transverse momentum distribution after the interaction. The pattern is given by Eq. (42.6). The pattern may be altered by application of microwave pulses which transfer momentum to the electrons of the ^{85}Rb atoms which add vectorially to that transferred from the interactions with the standing light field and atomic interactions.

Microwave pulses are now added to manipulate the two internal electronic states of the atom according to whether it moved along pathway B or C. A simplified level scheme of ^{85}Rb is shown in Figure 42.6. The manipulation of internal states by two microwave fields which each apply a $\pi/2$ pulse is shown in Figure 42.7. Rabi oscillations between states $|2\rangle$ and $|3\rangle$ can be induced by applying a microwave field of about 3 GHz. To describe the manipulation of the two internal electronic states of the atom, we first investigate the properties of a single Bragg beam splitter.

Figure 42.6. Simplified level scheme of ^{85}Rb. The excited state $\left(5^2P_{3/2}\right)$ is labeled $|e\rangle$. The ground state $\left(5^2P_{1/2}\right)$ is split into two hyperfine states with total angular momentum $F=2$ and $F=3$, which are labeled $|2\rangle$ and $|3\rangle$, respectively. The standing light wave has angular frequency ω_{light}.

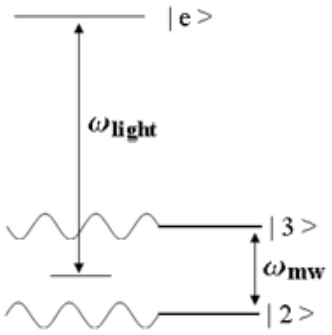

Figure 42.7. Scheme of the manipulation of internal states of ^{85}Rb by two microwave fields which each apply a $\pi/2$ pulse. The standing light wave with angular frequency ω_{light} induces a light shift for both ground states, which is given as a function of position. The beam splitter produces a phase shift that depends on the internal and external degree of freedom. A Ramsey scheme, consisting of two microwave $\pi/2$ pulses, converts this phase shift into a population difference.

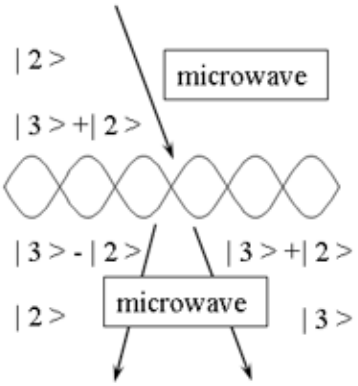

The frequency of the standing light wave, ω_{light} is tuned halfway between the $|2\rangle \rightarrow |e\rangle$ and $|3\rangle \rightarrow |e\rangle$ transitions. Hence the detunings from these transitions, Δ_{2e}, and Δ_{3e}, have the same absolute value but opposite sign. The reflectivity of the beam splitter, that is, the probability of reflecting an atom, depends on $t_{Bragg} X |U_0|$, and it is independent of the internal state.

However, the amplitude of the wavefunction experiences a phase shift which depends on the internal atomic state. A simple analogy for this phase shift can be found in light optics: a light wave reflected from an optically thicker medium experiences a phase shift of π, while reflection from an optical thinner medium or transmission into an arbitrary medium does not cause any phase shift. This argument also applies in atomic optics: in the present experiment, an atom in $|2\rangle$ sees a negative light shift potential (because $\Delta_{2e} < 0$), corresponding to an optically thicker medium, while an atom in $|3\rangle$ sees a positive potential (because $\Delta_{3e} > 0$), corresponding to an optically thinner medium. Hence an atom will experience a π phase shift only if it is reflected in $|2\rangle$.

This phase shift can be converted into a population difference between the hyperfine levels. For that purpose, two microwave $\pi/2$ pulses resonant with the hyperfine transition are applied. They form a Ramsey scheme as shown in Figure 42.7. The atom is initially prepared in state $|2\rangle$. Then a $\pi/2$ microwave pulse is applied, converting the beam into an equal mixture of internal states of $|2\rangle + |3\rangle$. After this, each atom interacts with the standing light wave. As explained above, each atom will experience a π phase shift only if it is reflected and in state $|2\rangle$. Thus the internal state of the reflected beam is changed to an equal mixture of internal states of $|3\rangle - |2\rangle$, while the internal state of the transmitted beam is not affected. As a result, the momentum of each atom is a superposition of the internal and external degree of freedom of the atom which is specific to the path. The state vector of the system becomes:

$$|\psi\rangle \propto |\psi_B\rangle \otimes \left(|3\rangle - |2\rangle\right) + |\psi_C\rangle \otimes \left(|3\rangle + |2\rangle\right) \tag{42.7}$$

where $|\psi_B\rangle$ and $|\psi_C\rangle$ describe the center-of-mass motion for the reflected and transmitted beams (see Figure 42.5), respectively. The second microwave pulse action on both beams (the transmitted and the reflected), converts the internal state of the transmitted beam to state $|3\rangle$, while the reflected beam is converted to state $-|2\rangle$. Thus, the state vector after the pulse sequence shown in Figure 42.7 becomes:

$$|\psi\rangle \propto -|\psi_B\rangle \otimes |2\rangle + |\psi_C\rangle \otimes |3\rangle \tag{42.8}$$

Eq. (42.8) shows that the internal state is correlated with the way taken by the atom. The which-way information can be read out later by performing a measurement of the internal atomic state. The result of this measurement reveals which way the atom took: if the internal state is found to be $|2\rangle$, the atom moved along beam B, otherwise it moved along beam C.

After considering a single beam splitter, now consider the complete interferometer. Sandwiching the first Bragg beam splitter between two $\pi/2$ microwave pulses produces a reflected and transmitted beam each of a single internal atomic state, as described above. We note that the second Bragg beam splitter does not change the internal state. **No fringes are**

experimentally observed in this case. The data is recorded with the same parameters with the only difference being that two microwave pulses are added to produce a single internal atomic state according to the particular path of the atom. Atoms in both hyperfine states are detected. The interference pattern is also not observed when only atoms in state $|2\rangle$ or only atoms in state $|3\rangle$ are detected. Of course, the absolute size of the signal is reduced by a factor of two in these cases. The key to this new experiment is that although the interferences are destroyed, the initially imposed atomic momentum distribution leaves an envelope pattern (in which the fringes used to reside) at the detector. **A careful analysis of the pattern finds that it has not been measurably distorted by a momentum kick of the type invoked by Bohr, and therefore that any locally realistic momentum kicks imparted by the manipulation of the internal atomic state according to the particular path of the atom are too small to be responsible for destroying interference.**

In order to investigate why the interference is lost, we consider the state vector for the interaction sequence used which causes the disappearance of the fringes. The state vector after the interaction with the first beam splitter sandwiched between the two microwave pulses is given by Eq. (42.8). The second beam splitter transforms this state vector into a left peak and a right peak given by:

$$|\psi_{left}\rangle \propto -|\psi_D\rangle \otimes |2\rangle + |\psi_E\rangle \otimes |3\rangle \tag{42.9}$$

and

$$|\psi_{right}\rangle \propto |\psi_F\rangle \otimes |2\rangle + |\psi_G\rangle \otimes |3\rangle \tag{42.10}$$

where the sign of $|\psi_F\rangle$ is positive due to the π phase shift during the reflection from the second beam splitter. Each peak is a superposition of atoms which follow separate paths and comprise atoms of a single internal state. In each case atoms which interfere have internal states which are orthogonal; thus, in the far field, the atomic position distribution under each peak of the envelope is given by the superposition of two single slit patterns rather than the double slit pattern in the absence of the application of the $\pi/2$ microwave pulses. In the far field, the amplitude of the atomic position distribution under each peak of the envelope $\tilde{\Psi}(\mathrm{x})$ is the sum of the independent Fraunhofer planes and the intensity of the atomic position distribution under each peak of the envelope $\tilde{\Psi}^2(\mathrm{x})$ is given by:

$$\tilde{\Psi}^2(\mathrm{x}) = (2aC)^2 \ \mathrm{sinc}^2\left(\frac{ka\mathrm{x}}{\mathrm{f}}\right) \tag{42.11}$$

where f is the focal length and a is the slit width. In the present case, the envelope of the fringe pattern is given by the collimation properties of the initial atomic beam A.

A dramatic change in the spatial momentum distribution occurs when adding the microwave fields to the interferometer that manifests itself as loss of interference; even though, the microwave itself does not transfer enough momentum to the atom to wash out the fringes according to the Heisenberg Uncertainty Principle. The addition of the microwave fields modifies the probability for momentum transfer by the light fields. This modification of the momentum transfer probability is due to the manipulation of the internal atomic state according to the particular path of the atom. The disappearance of interference is explained by classical physics. In addition to the invalidation of the HUP as the basis of the wave particle duality, the other aspect of the HUP, the measurement-disturbance relationship of the HUP, has been tested for the first time and experimentally disproved [L. A. Rozema, A. Darabi, D. H. Mahler, A. Hayat, Y. Soudagar, A. M. Steinberg, "Violation of Heisenberg's Measurement-Disturbance Relationship by Weak Measurements," Phys. Rev. Lett., 109 (2012), 100404.].

INCONSISTENCIES OF QUANTUM MECHANICS

Quantum mechanics failed to predict the results of the Stern-Gerlach experiment which indicated the need for an additional quantum number. Quantum electrodynamics was proposed by Dirac in 1926 to provide a generalization of quantum mechanics for high energies in conformity with the theory of Special Relativity and to provide a consistent treatment of the interaction of matter with radiation. From Weisskopf [8], "Dirac's quantum electrodynamics gave a more consistent derivation of the results of the correspondence principle, but it also brought about a number of new and serious difficulties." Quantum electrodynamics: (1) does not explain nonradiation of bound electrons; (2) contains an internal inconsistency with Special Relativity regarding the classical electron radius–the electron mass corresponding to its electric energy is infinite; (3) it admits solutions of negative rest mass and negative kinetic energy; (4) the interaction of the electron with the predicted zero-point field fluctuations leads to infinite kinetic energy and infinite electron mass; (5) Dirac used the unacceptable states of negative mass for the description of the vacuum; yet, infinities still arise. In 1947, Lamb discovered a 1000 *MHz* shift between the $^2S_{1/2}$ state and the $^2P_{1/2}$ state of the hydrogen atom. This so called Lamb Shift marked the beginning of modern quantum electrodynamics. In the words of Dirac [9], "No progress was made for 20 years. Then a development came initiated by Lamb's discovery and explanation of the Lamb Shift, which fundamentally changed the character of theoretical physics. It involved setting up rules for discarding ...infinities..." Renormalization is presently believed to be required of any fundamental theory of physics [10]. However, dissatisfaction with renormalization has been expressed at various times by many physicists including Dirac [11]. who felt that, "This is just not sensible mathematics. Sensible mathematics involves neglecting a quantity when it turns out to be small—not neglecting it just because it is infinitely great and you do not want it!"

Modern quantum mechanics has encountered several obstacles that have proved insurmountable as pointed out previously in the General Considerations section and the Classical Electron Radius section. It is not based on physical laws, and is not predictive as discussed previously [8, 12–24]. SQM has never dealt with the nature or structure of fundamental particles.

They are treated as zero-dimensional points that occupy no volume and are everywhere at once. This view is impossible since occupying no volume would preclude their existence; the inherent infinities are not observed nor are they possible, and the possibility of a particle being everywhere at once violates all physical laws including conservation of energy and causality. Furthermore, it leads to certain philosophical interpretations [25] which are not sensible. Some conjure up multitudes of Universes including "mind" Universes; others require belief in a logic that allows two contradictory statements to be true. The question addressed is whether the Universe is determined or influenced by the possibility of our being conscious of it. The meaning of quantum mechanics is debated, but the Copenhagen interpretation is predominant. Its asserts that "what we observe is all we can know; any speculation about what a photon, an atom or even a SQUID (Superconducting Quantum Interference Device) really is or what it is doing when we are not looking is just that speculation [26]." According to this interpretation every observable exists in a state of superposition of possible states, and observation or the potential for knowledge causes the wavefunction corresponding to the possibilities to collapse into a definite one. As shown by Platt [27] in the case of the Stern-Gerlach experiment, "the postulate of quantum measurement [which] asserts that the process of measuring an observable forces the state vector of the system into an eigenvector of that observable, and the value measured will be the eigenvalue of that eigenvector."

According to the Zeno no-go theorem which is a consequence of the postulate of quantum measurement, observation of an atom collapses its state into a definite; thus, transitions cannot occur under continuous observation. Recently, it has become possible to test this postulate via an experiment involving transitions of a single atom, and the results are inconsistent with the predictions. Quoting from the caption of Figure 10 of the article, by Dehmelt [28],

> *"Shelving" the Ba^+ optical electron in the metastable D level. Illuminating the ion with a laser tuned close to its resonance line produces strong resonance fluorescence and an easily detectable photon count of 1600 photons/sec. When later an auxiliary, weak Ba^+ spectral lamp is turned on, the ion is randomly transported into the metastable $D_{5/2}$ level for 30-s lifetime and becomes invisible. After dwelling in this shelving level for 30 s on average, it drops down to the S ground state spontaneously and becomes visible again. This cycle repeats randomly. According to the Zeno no-go theorem, no quantum jumps should occur under continuous observation.*

The Copenhagen interpretation equally applies to witnessing the presence of the moon. According to quantum mechanics the moon is not there until it is observed. Since the act of measuring is relative to each individual observer and it is "entangled" with each observer, the "collapse" must result in different realities for different observers of presumably the same object. Thus, Man's consciousness has a special position in the most popular interpretation of quantum mechanics as the engine of reality and individualism results in the conjuring up of multitudes of Universes including parallel "mind" Universes [25].

Of course this is nonsense and is a consequence of the mistake of originally postulating that fundamental particles are probability waves rather than real. Furthermore, the brain obeys the same physical laws as the rest of the matter of the Universe. Sodium, potassium, and chloride ions in the brain are obtained from the ambient environment and are constantly being interchanged with that environment. The same rules apply irrespective of where that matter is found. In fact, the phenomena of the ability of the brain to reason and to produce a state called consciousness has nothing to do with god-like properties unique to humans that are deeply seated in quantum folklore. Rather, it can be traced to simple properties of excitable neurons, their organization, and simple thermodynamic principles exploited by biological systems to more or lesser extents over millions of years of evolution.

At the most fundamental level, a conscious being is made of energy, quarks, gluons, electrons, atoms, molecules, etc. that originate from and are part of the Universe. For example, the elements of humans other than hydrogen originate in stars. Therefore, in broader terms, the physics of the Universe dynamically gives rise to a conscious being, and it is implicit that the Universe is aware of itself. Then, distinctions exist between animate beings and inanimate objects that must follow first principles. Consciousness, the ability of a chemical reaction to be aware of itself arises from the relationship of energy changes to entropy. If the brain chemistry of conscious beings behaved as typical chemical reactions following an arrow of time according to typical enthalpy and concomitant entropy changes, then any information stored and processed by the brain would decrease over time, and consciousness would not be possible. The brain chemistry comprising ion channel conductance changes, ion flows, ion pump activity, metabolic reactions, etc., comprise an energy state in opposition to the thermodynamic arrow of time. Living beings produce negative entropy at the expense of their surroundings. In other words, consciousness is achieved against the arrow of time discussed in the Arrow of Time and Entropy section by increasing the entropy of the surroundings to offset its relatively low entropic state. Consciousness is shaped by and requires the environment with which the brain interacts and depends for a source of energy and materials to maintain the local-temporal high entropic state relative to its surroundings.

A previous publication [29-30] showed that the brain is governed by the entropy principle of thermodynamics whereby the wet-chemistry-based system comprising excitable neurons arranged in a spatial-temporal hierarchy of ensembles in a dynamical state of activation and connectivity dependent on present and past activation rates, influenced by past and present input from the environment, achieves a state representative of a predominant configuration, the most probable state in time. ***The brain must be active continuously as a predominant configuration. This time-dependent state based on the second law of thermodynamics and comprising representations of aspects of the physical Universe is the basis of consciousness.***

In addition to exploiting the second law of thermodynamics with the formation of a predominant configuration, the brain has evolved to exploit several fundamental signal processing principles to achieve consciousness. For example, the brain functions as an analog Fourier processor which transduces and processes information representative of physical characteristics or

representations of physical characteristics as Fourier series in Fourier space. The brain also exploits time using spatial segregation of stored information as a means to encode context of the physical characteristics of the information. Specific time delays arising from the spatial separation of propagating signals correspond to modulation of the Fourier series at corresponding frequencies to encode the context. The brain associates information by exploiting the principle that cascaded stages such as association neurons give rise to delayed Gaussian filters. And, filtered signals may be associated based on the physics of energy exchange between two or more harmonic states. Given the evolutionary ascension of multicellular organisms each producing negative entropic states and having specialized cells with excitable membranes, the progress to consciousness and intelligence was inevitable. The first-principles-based theory of the signal processing mechanism of the brain and the origin of consciousness was published previously with a means to computer-simulate these phenomena [29-30].

Specifically, a method and system for pattern recognition and processing involving processing information in Fourier space was reported [29-30]. The theoretical results given previously are that (1) action potentials carry information with digital and analog aspects that allows the brain to operate as a Fourier processor in Fourier space with encoding of context in the structure of transducers mapping one-to-one with corresponding structural elements of the memory, (2) an ensemble of interlinked neurons can filter information as delayed Gaussian filters, (3) the neuronal ensembles propagating cascaded action potentials may couple with Poisson probability to form associations of information encoded in the action potentials, (4) ensembles of neurons as delayed Gaussian filters may order format information by forming associations of the corresponding filtered action potentials with memory elements, and (5) a predominant configuration of activation may arise that is analogous to that of interacting quantum levels with partition of energy as given by statistical thermodynamics. These aspects are modeled such that a simulation may be programmable on digital processing systems.

This novel approach anticipates the signal processing action of an ensemble of neurons as a unit and intends to simulate aspects of the brain that give rise to capabilities such as intelligence, pattern recognition, reasoning, and ultimately consciousness that have not been reproduced with past approaches such as neural networks that are based on individual simulated "neuronal units." Information representative of physical characteristics or representations of physical characteristics is transformed into a Fourier series in Fourier space within an input context of the physical characteristics that is encoded in time as delays corresponding to modulation of the Fourier series at corresponding frequencies. Associations are formed between Fourier series by filtering the Fourier series and by using a spectral similarity between the filtered Fourier series to determine the association based on Poissonian probability. The associated Fourier series are added to form strings of Fourier series. Each string is ordered by filtering it with multiple selected filters to form multiple time order formatted subset Fourier series, and by establishing the order through associations with one or more initially ordered strings to form an ordered string. Associations are formed between the ordered strings to form complex ordered strings that relate similar items of interest. The components of the system based on the algorithm are active based on probability using weighting factors based on activation rates. The probabilistic activation, based on past activation rates, gives rise to a system state akin to a time-dependent predominate configuration of statistical thermodynamics that can be associated with consciousness.

THE ASPECT EXPERIMENT—NO SPOOKY ACTIONS AT A DISTANCE

In addition to the interpretation that photons, electrons, neutrons, and even human beings [25] have no definite form until they are measured, a more disturbing interpretation of quantum mechanics is that a measurement of a quantum entity can instantaneously influence another light years away. Einstein argued that a probabilistic versus deterministic nature of atomic particles leads to disagreement with Special Relativity. In fact, the nonlocality result of the Copenhagen interpretation violates causality. As a consequence of the indefinite nature of the Universe according to quantum mechanics and the implied Uncertainty Principle, Einstein, Podolsky, and Rosen (EPR) in a classic paper [31] presented a paradox which led them to infer that quantum mechanics is not a complete theory. They concluded that the quantum-mechanical description of a physical system should be supplemented by postulating the existence of "hidden variables," the specification of which would predetermine the result of measuring any observable of the system. They believed the predictions of quantum mechanics to be correct, but only as consequences of statistical distribution of the hidden variables. But, Bell [32] showed that in a Gedanken experiment of Bohm [34] (a variant of that of EPR) no local hidden-variable theory can reproduce all of the statistical predictions of quantum mechanics. Thus, a paradox arises from Einstein's conviction that quantum-mechanical predictions concerning spatially separated systems are incompatible with his condition for locality unless hidden variables exist. Bell's theorem provides a decisive test of the family of local hidden-variable theories (LHVT). In a classic experiment involving measurement of coincident photons at spatially separated detectors, Aspect [34] showed that local hidden-variable theories are inconsistent with the experimental results. Although Aspect's results are touted as a triumph of the predictions of quantum mechanics, the correct coincidence rate of detection of photons emitted from a doubly excited state of calcium requires that the z component of the angular momentum is conserved on a photon pair basis. As a consequence, a paradox arises between the deterministic conservation of angular momentum and the Uncertainty Principle. The prediction derived from the quantum nature of the electromagnetic fields for a single photon is inconsistent with Aspect's results, and Bell's theorem also disproves quantum mechanics. However, the results of Aspect's experiment are predicted by classical physics wherein locality and causality hold.

The Aspect experiment is often invoked as the proof of the quantum-mechanical nature of reality [34-42]. According to the quantum explanation of the Aspect experiment [34], the polarization of each photon of a pair is not determined until a measurement is made, and the act of measuring the polarization of one photon causes an action at a distance with regard to the measurement of the polarization of the other member of a given pair. These results are interpreted as proof of a spooky action at a distance. Thus, information travels faster than the speed of light in violation of Special Relativity, or nonlocality and noncausality are implicit.

Bell's theorem is a simple proof of statistical inequalities of expectation values of observables given that quantum

statistics are correct and that the physical system possesses "hidden variables." Classical physics does not possess hidden-variables. It is deterministic, and Bell's theorem does not apply to it. The correct interpretation of the results of the Aspect experiment follows from a classical derivation from the physical nature of excited-state atoms and the corresponding emitted photons. The expectation value of the coincidence rate at separated randomly oriented polarization analyzers for pairs of photons emitted from a doubly excited state atom is derived from the equation of the photon which appears in the Equation of the Photon section.

Aspect [34] reports the measurement of polarization correlation (coincidence count rate) of visible photons ($\nu_1 = 551.3\ nm$; $\nu_2 = 422.7\ nm$) emitted in a $(J=0)\rightarrow(J=1)\rightarrow(J=0)$ calcium atomic cascade $\left(4p^2\ {}^1S_0 - 4s4p\ {}^1P_1 - 4s^2\ {}^1S_0\right)$. The calcium atoms were selectively pumped to the upper level of the cascade from the ground state by the two photon absorption via two lasers, a single-mode krypton ion laser and a cw single-mode Rhodamine 6G dye laser tuned to the resonance for the two photon process. The fluorescent light was collected by lenses and made incident on two detectors–one at position -z and the other at position +z relative to the emitting calcium atoms. The polarizers were independently rotated in the xy-plane, and the coincidence count rate was measured.

The equation for the transmission of an electromagnetic wave through a barrier as given in any text of classical electrodynamics such as that of Kong [43] is:

$$\mathbf{E}_T = TE_i e^{i\mathbf{k}_z z} \tag{42.12}$$

where $\mathbf{E}_T$ is the transmitted wave, E_i is the incident wave, and T is the transmission coefficient. For a wave that propagates at an angle with respect to the z-axis, the transmitted photon is given by a sum of equations of the form of Eq. (42.12) for each vector component. Using the convention of Horne [39], the vector transmission efficiencies (coefficients) can be written in matrix form with a matrix corresponding to each linear polarizer. In a basis of linear polarizations along x_1 and y_1 in the coordinates of photon 1, the most general linear polarizer with axis along x_1 is described by an efficiency matrix

$$\varepsilon(1) = \begin{pmatrix} \varepsilon_M^1 & 0 \\ 0 & \varepsilon_m^1 \end{pmatrix} \tag{42.13}$$

where ε_M^1 is the probability of transmitting an x_1 linearly polarized photon and ε_m^1 is the probability of transmitting a y_1 linearly polarized photon (leakage). In the ideal case $\varepsilon_M^1 = 1$ and $\varepsilon_m^1 = 0$. If the polarizer is not parallel to the x_1-axis but rotated in the plane perpendicular to the interdetector axis by an angle ϕ_1 from x_1, and $\varepsilon(1)$ is expressed in the basis of right hand circular (RHC) and left hand circular (LHC) photon states formed from x_1 and y_1, then the elementary transformations give the elements of $\varepsilon(1)$ as a function of ϕ_1 in matrix form:

$$\varepsilon^1\left(\sigma_1^{'},\sigma_1\right) \equiv \left\langle \sigma_1^{'} \middle| \varepsilon(1) \middle| \sigma_1 \right\rangle = \frac{1}{2}\begin{pmatrix} \varepsilon_M^1 + \varepsilon_m^1 & -\left(\varepsilon_M^1 - \varepsilon_m^1\right)e^{-2i\phi_1} \\ -\left(\varepsilon_M^1 - \varepsilon_m^1\right)e^{2i\phi_1} & \varepsilon_M^1 - \varepsilon_m^1 \end{pmatrix} \tag{42.14}$$

where $\left\langle \sigma_1^{'} \middle| \varepsilon(1) \middle| \sigma_1 \right\rangle$ is defined as the expectation value of the transmission of the photon 1 with polarization σ_1, $\sigma_1 = \pm 1$ are RHC and LHC, respectively, and the angle between polarizer 1 (P_1) and x_1 is:

$$\Delta\phi_1 = \phi_1 \tag{42.15}$$

Similarly, $\varepsilon(2)$, the efficiency matrix as a function of $\phi - \phi_2$ of the second polarizer (P_2) in the circular polarization basis of photon 2, is

$$\varepsilon^2\left(\sigma_2^{'},\sigma_2\right) \equiv \left\langle \sigma_2^{'} \middle| \varepsilon(1) \middle| \sigma_2 \right\rangle = \frac{1}{2}\begin{pmatrix} \varepsilon_M^2 + \varepsilon_m^2 & -\left(\varepsilon_M^2 - \varepsilon_m^2\right)e^{-2i(\phi-\phi_2)} \\ -\left(\varepsilon_M^2 - \varepsilon_m^2\right)e^{2i(\phi-\phi_2)} & \varepsilon_M^2 - \varepsilon_m^2 \end{pmatrix} \tag{42.16}$$

where the angle between polarizer 2 and the x-polarization of photon 2 (i.e. the angle between P_2 and x_2) is:

$$\Delta\phi_2 = \phi - \phi_2 \tag{42.17}$$

The efficiency matrix for coincidence transmission of photon 1 and photon 2 is given by the product of their independent probabilities, $\varepsilon(1)\varepsilon(2)$. The normalized coincidence counting rate is

$$\frac{R(\phi)}{R_0} = \frac{Tr\left[\varepsilon(1)\varepsilon(2)\,p_f\right]}{Tr\left(Ip_f\right)} \tag{42.18}$$

The normalized coincidence counting rate with polarizer 2 removed, $\frac{R_1}{R_0}$, is

$$\frac{R_1}{R_0}=\frac{Tr\left[\varepsilon(1)\,p_f\right]}{Tr\left(Ip_f\right)} \tag{42.19}$$

The normalized coincidence counting rate with polarizer 1 removed, $\frac{R_2}{R_0}$, is:

$$\frac{R_2}{R_0}=\frac{Tr\left[\varepsilon(2)\,p_f\right]}{Tr\left(Ip_f\right)} \tag{42.20}$$

where I is the identity matrix and p_f is the probability that photon 1 and photon 2 have the same polarization and is a function of solid angle of the projection of the propagation vector of each photon onto the z-axis. In terms of Eq. (42.12), p_f corresponds to the vector correlated electric field incident on the opposed detectors. It is given by the normalized electric field of photons of matched momentum projected onto the z-axis over the solid angle of the detectors.

The Excited States of the One-Electron Atom (Quantization) section gives the method to calculate the Einstein A coefficient in terms of the electric field based on classical electrodynamics that is applicable to each photon of the two photon $\left(J=0\right)\rightarrow\left(J=1\right)\rightarrow\left(J=0\right)$ cascade of calcium. The Excited States of Helium section further applies the dependence of the transition energy, and Jackson [44] applies the transition probability, on the integral of the product of the multipole of the photon, ${}^{p}X_{l,m}\left(\theta,\phi\right)$, and the initial, ${}^{i}X_{l,m}\left(\theta,\phi\right)$, and final, ${}^{f}X_{l,m}\left(\theta,\phi\right)$, states as is the case with classical electrodynamics calculations involving antennas. The transition probability $\frac{1}{\tau}$ is given by the power of the transition divided by the energy:

$$\frac{1}{\tau}=\frac{power}{energy}=\frac{\int\langle\mathbf{S}\rangle\,d\Omega}{\hbar\omega}=\frac{\int\frac{1}{2}\mathrm{Re}\left[\mathbf{E}\times\mathbf{H}^{*}\right]d\Omega}{\hbar\omega} \tag{42.21}$$

The distribution of multipole radiation and the multipole moments of the electron for absorption and emission are given in the Excited States of the One-Electron Atom (Quantization) section and in Jackson [44]. The electric-field amplitude of the emitted photon follows from that given in the Equation of the Photon section.

Horne postulates the emission as a plane wave which is replaced by a spherical multipole expansion. The spherical multipole expansion of a plane wave such as given in Jackson [45] is consistent with the Green Function as the function which corresponds to the superposition of an ensemble of photons given classically by Eqs. (4.18-4.23). Using classical Eqs. (2.64-2.65), the projection of the photon pair propagation vector onto the axis perpendicular to the plane of each detector gives a factor of one corresponding to the conservation of angular momentum for each photon pair times a solid angle correction. The result for the numerator of Eq. (42.18) is:

$$Tr\left[\varepsilon(1)\varepsilon(2)\,p_f\right]=\sum_{\sigma_1\sigma_1'\sigma_2\sigma_2'}\sigma_1\sigma_1'\sigma_2\sigma_2'\varepsilon^{1}\left(\sigma_1',\sigma_1\right)\varepsilon^{2}\left(\sigma_2',\sigma_2\right)g\left(\sigma_1,\sigma_2\right)g^{*}\left(\sigma_1',\sigma_2'\right) \tag{42.22}$$

where $g\left(\sigma_1,\sigma_2\right)g^{*}\left(\sigma_1',\sigma_2'\right)$ is a factor corresponding to the solid angle.

Eq. (42.22) is equivalent to Eq. (5.17) of Horne. To obtain this result, Horne suppressed the integration over $d\Omega_1$ and $d\Omega_2$ as well as the explicit dependence on the photon propagation vectors, $\mathbf{k}_1$ and $\mathbf{k}_2$, respectively. (The integration was also suppressed over frequency space as well as the explicit dependence on the photon propagation vectors, $\mathbf{k}_1$ and $\mathbf{k}_2$ in the case that QED holds.) This is only valid if the z component of angular momentum is conserved on a photon by photon basis such that the polarization correlation distribution function is independent of angle. Otherwise, it **cannot** be removed from the integral. HORNE'S CALCULATION IS NOT CONSISTENT WITH THE QUANTUM-MECHANICAL NATURE OF THE ELECTROMAGNETIC FIELDS FOR A SINGLE PHOTON as described below.

Substitution of Eq. (42.14) and (42.15) and the results of the solid angle term of Eq. (42.22) into Eq. (42.18) gives the normalized coincidence count rate.

$$\frac{R(\phi)}{R_0}=\frac{1}{4}\left(\varepsilon_M^{1}+\varepsilon_m^{1}\right)\left(\varepsilon_M^{2}+\varepsilon_m^{2}\right)+\frac{1}{4}\left(\varepsilon_M^{1}-\varepsilon_m^{1}\right)\left(\varepsilon_M^{2}-\varepsilon_m^{2}\right)F_1(\theta)\cos 2\phi \tag{42.23}$$

where the solid angle factor, $F_1(\theta)$, for the $0-1-0$ electric dipole cascade is:

$$F_1(\theta)=2G_1^{2}(\theta)\left[G_2^{2}(\theta)+\frac{1}{2}G_3^{2}(\theta)\right]^{-1} \tag{42.24}$$

The normalized coincidence count rate with polarizer 2 removed, $\frac{R_1}{R_0}$, is:

$$\frac{R_1}{R_0}=\frac{1}{2}\left(\varepsilon_M^{1}+\varepsilon_m^{1}\right) \tag{42.25}$$

The normalized coincidence count rate with polarizer 1 removed, $\frac{R_2}{R_0}$, is:

$$\frac{R_2}{R_0} = \frac{1}{2}\left(\varepsilon_M^2 + \varepsilon_m^2\right) \tag{42.26}$$

The transmittances ε_M^i and ε_m^i of the polarizers (i=1 or 2) for light polarized parallel or perpendicular to the polarization axis were measured by Aspect [34]:

$$\varepsilon_M^1 = 0.971 \pm 0.005,\ \varepsilon_m^1 = 0.029 \pm 0.005,$$
$$\varepsilon_M^2 = 0.968 \pm 0.005,\ \varepsilon_m^2 = 0.028 \pm 0.005 \tag{42.27}$$

And, the solid angle factor, $F_1(\theta)$, for the $0-1-0$ electric dipole cascade which accounts for the solid angles subtended by the collecting lenses of the Aspect experiment is:

$$F_1(\theta) = F_2(\theta) = 0.984 \tag{42.28}$$

Substitution of Eqs. (42.27) and (42.28) into Eq. (42.23) gives the normalized coincidence count rate as a function of the relative angle between the polarizers.

$$\frac{R(\phi)}{R_0} = 0.2490 + 0.2178\cos 2\phi \tag{42.29}$$

ASPECT EXPERIMENTAL RESULTS ARE PREDICTED CLASSICALLY

The sequence of events based on physical laws for Aspect's measurement of the polarization correlation (coincidence count rate) of visible photons ($\nu_1 = 551.3\ nm;\ \ \nu_2 = 422.7\ nm$) emitted in a $(J=0)\rightarrow(J=1)\rightarrow(J=0)$ calcium atomic cascade $\left(4p^2\ {}^1S_0 - 4s4p\ {}^1P_1 - 4s^2\ {}^1S_0\right)$ is shown in Figures 42.8A-E.

The expectation value of the coincidence rate at separated randomly oriented polarization analyzers for pairs of photons emitted from a doubly-excited state atom was derived from the equation of the photon in Eqs. (42.12-42.29). Rather than a point that obeys a probability-density wave, the photon is an extended particle with a radius given by $r = \frac{\lambda}{2\pi}$ wherein λ is the wavelength of the photon. Consequently, the photon's electric field vector has a projection onto the axis of each rotated polarizer's axis. Angular momentum of the doubly excited-state atom is conserved by emitting photons of the same linear polarization in opposite directions. Thus, the photon polarization is exactly correlated based on physics. Based on these physical attributes of the emitted photons, the normalized coincidence count rate, $\frac{R(\phi)}{R_0}$, as a function of the relative polarizer orientation, ϕ, given by Eq. (42.29) matches with the results of Aspect [34] as shown in Figure 42.9. A computer simulation is given in Ref. [46].

Figure 42.8. (A) Calcium atoms were selectively pumped to the upper level of the cascade from the ground state by a two photon absorption via two lasers (blue beam). The fluorescent light was collected by lenses and made incident on two detectors (smooth plates)—one at position -z and the other at position +z relative to the emitting calcium atoms (blue sphere). The polarizers (plates with lines along each optical axis) were independently rotated in the xy-plane, and the coincidence count rate was measured (box connected to both detectors). (B) The source current of the doubly-excited state atom gives rise to electromagnetic fields that become emitted photons in opposite directions wherein the radius of each photon is given by the ratio of the speed of light to the velocity change of the excited state electron upon de-excitation. (C) The plane (green) of polarization of each photon pair is exactly correlated to conserve the angular momentum of the excited state. (D) The transmittance of each photon at each detector depends on the alignment or angle of the plane of polarization of the photons (random but matched) and the axis of each polarizer (rotated relative to each other by the experimenter). When the polarizers are parallel, the photons are both transmitted if each is sufficiently aligned with the polarizer. (E) Or, both are blocked if the transmittance is low due to a condition of crossed polarization of each photon and polarizer. Intermediate cases depend on the relative angle of each photon and its polarizer as shown in (C).

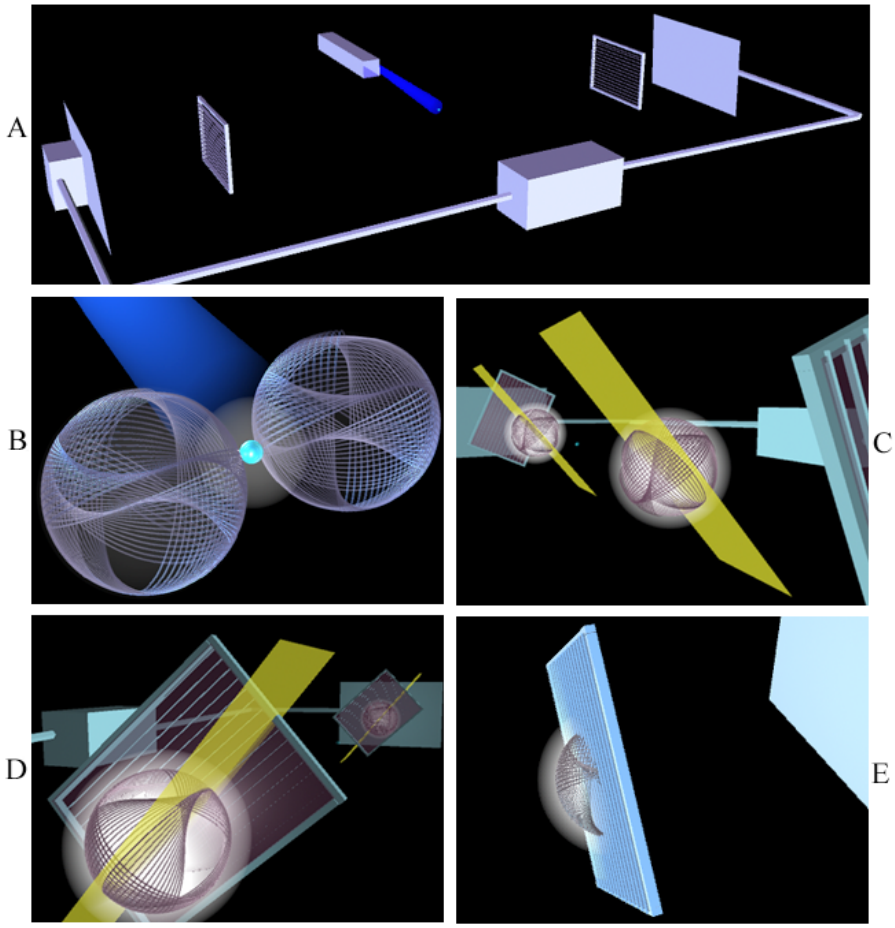

Figure 42.9. The normalized coincidence count rate as a function of the relative polarizer orientation as given by Eqs. (42.23), (42.24), and Eq. (42.29) (solid curve) with the results of Aspect [34] (•) match. This result is based on the physical treatment of the photon as an extended particle that obeys Maxwell's equations with conservation of angular momentum of the doubly-excited state calcium atom and the corresponding emission of two photons of the same linear polarization in opposite directions.

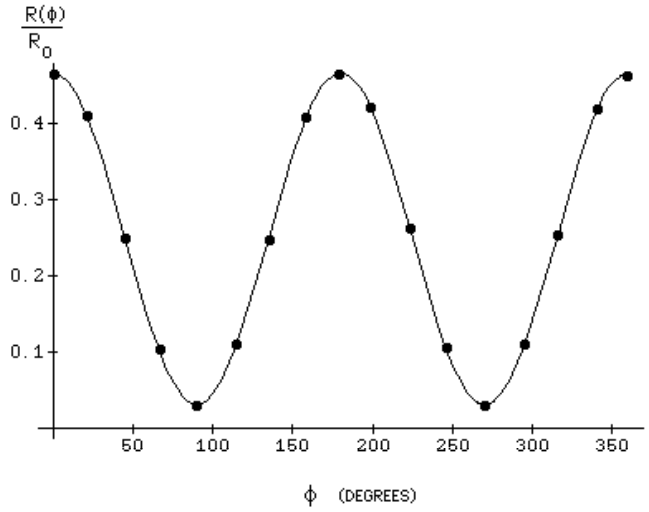

ASPECT EXPERIMENTAL RESULTS ARE NOT PREDICTED BY QUANTUM MECHANICS

Eq. (5.17) of Horne (same as Eq. (42.22)) is the sum over the product of the transmission efficiencies of photon pairs of identical polarization at two independent detectors and a correction for the solid angle of the detectors for the photon pairs emitted from a remote isotropic source. The probability integral over momentum space was "suppressed" and set equal to one. Thus, the calculation is a deterministic equation. It does ***not correspond*** to the equation for coincident detection predicted ***by quantum mechanics***. According to Jackson [47]:

> For a multipole with a single m value, M_x and M_y vanish, while a comparison of (17.67) and (17.60) shows that:
>
> $$\frac{dM_z}{dr} = \frac{m}{\omega}\frac{dU}{dr} \tag{17.68}$$
>
> independent of r. This has the obvious quantum interpretation that the radiation from a multipole of order (l,m) carries off $m\hbar$ units of z component of angular momentum per photon of energy $\hbar\omega$. Even with a superposition of different m values, the same interpretation of (17.67) holds, with each multipole of definite m contributing incoherently its share of the z component of angular momentum. Now, however the x and y components are in general nonvanishing, with multipoles of adjacent m values contributing in a weighed coherent sum. The behavior continued in (17.64) and exhibited explicitly in (17.65)-(17.67) is familiar in the quantum mechanics of a vector operator and its representation with respect to basis states of J^2 and J_z*. The angular momentum of multipole fields affords a classical example of this behavior, with the z component being diagonal in the (l,m) multipole basis and the x and y components not.
>
> The characteristics of the angular momentum just presented hold true generally, even though our example (17.57) was somewhat specialized. For a superposition of both electric and magnetic multipoles of various (l,m) values, the angular momentum expression (16.63) is generalized to:
>
> $$\begin{aligned}\frac{d\mathbf{M}}{dr} = \frac{1}{8\pi\omega k^2}\mathrm{Re}\sum_{\substack{l,m\\ l',m'}}\Big\{&\Big[a_E^*(l',m')a_E(l,m)+a_M^*(l',m')a_M(l,m)\Big]\int(\mathbf{L}\cdot\mathbf{X}_{l'm'})^*\mathbf{X}_{l,m}d\Omega\\ &+i^{l'-l}\Big[a_E^*(l',m')a_M(l,m)-a_M^*(l',m')a_E(l,m)\Big]\int(\mathbf{L}\cdot\mathbf{X}_{l'm'})^*\mathbf{n}\times\mathbf{X}_{l,m}d\Omega\Big\}\end{aligned} \tag{17.69}$$
>
> The first term in (17.69) is of the same form as (17.63) and represents the sum of the electric and magnetic multipoles separately. The second term is an interference between electric and magnetic multipoles. Examination of the structure of its angular integral shows that the interference is between electric and magnetic multipoles whose l values differ by unity. This is a necessary consequence of the parity properties of the multipole fields (see below). Apart from this complication of interference, the properties of $\frac{d\mathbf{M}}{dr}$ are as before.
>
> The quantum-mechanical interpretation of (17.68) concerned the z component of angular momentum carried off by each

photon. In further analogy with quantum mechanics, we would expect the ratio of the square of the angular momentum to the square of the energy to have the value,

$$\frac{M^{(q)^2}}{U^2}=\frac{\left(M_x^2+M_y^2+M_z^2\right)_q}{U^2}=\frac{l(l+1)}{\omega^2} \tag{17.70}$$

But from (17.60) and (17.65)-(17.67), the classical result for a pure (l,m) multipole is:

$$\frac{M^{(c)^2}}{U^2}=\frac{|M_z|^2}{U^2}=\frac{m^2}{\omega^2} \tag{17.71}$$

The reason for this difference lies in the quantum nature of the electromagnetic fields for a single photon. If the z component of angular momentum of a single photon is known precisely, the uncertainty principle requires that the other components be uncertain, with mean square values such that (17.70) holds. On the other hand, for a state of the radiation field containing many photons (the classical limit) the mean square values of the transverse components of angular momentum can be made negligible compared to the square of the z component. Then the classical limit (17.71) applies. For a (l,m) multipole field containing N photons it can be shown* that:

$$\frac{\left[M^{(q)}(N)\right]^2}{\left[U(N)\right]^2}=\frac{N^2m^2+Nl(l+1)-m^2}{N^2\omega^2} \tag{17.72}$$

This contains (17.70) and (17.71) as limiting cases.

Consider the quantum nature of the electromagnetic fields for a single photon. According to Eqs. (17.70-17.72) of Jackson, photon pairs cannot have identical z components of angular momentum; therefore, each pair cannot have identical polarization. Each quantum-mechanical photon is a superposition of RHC, LHC, linear, and elliptic polarization. And, in the case of Quantum Electrodynamics (QED), each photon is also a superposition over frequency space. In the quantum-mechanical case Eq. (17.71) of Jackson applies–the z component of angular momentum is conserved on the average of many photons. Probability applies to the emission of a pair of photons of identical polarizations (the correlation of polarizations cannot be one ($P(A,B)\neq 1$)) as well as to the detection of the photons of equal polarizations. Furthermore, QED requires that the probability associated with emission as well as detection applies to a distribution of photon wavelengths with expectation values of $\nu_1=551.3\ nm$ and $\nu_2=422.7\ nm$. The coincidence count rate is a function of the dot product of the electric field vector of each photon pair having correlated polarization onto the z-axis, and the probability of detection of the separate members of each pair at the separate detectors where the associated probabilities are independent. Thus, the probability of detecting a coincident event is given by the product of their independent probabilities. The quantum nature of the electromagnetic fields for a single photon requires a p_f of Eq. (42.18) that includes all distributions. Thus, the coincident rate predicted by quantum mechanics is less than the experimental rate. The extent of the error, which is a function of the relative angle of the polarizers, is given by Bell's theorem.

BELL'S THEOREM TEST OF LOCAL HIDDEN VARIABLE THEORIES (LHVT) AND QUANTUM MECHANICS

Using the convention of Clauser and Horne [37, 39], consider an ensemble of correlated pairs of photons emitted from the $0-1-0$ cascade of excited state calcium atoms each moving so that one enters polarizer 1 (P_1) and the other polarizer 2 (P_2), where ϕ_1 and ϕ_2 are adjustable angles of polarizer 1 and 2. In each polarizer a photon is recorded as ± 1 corresponding to RHC and LHC polarized, respectively. Let the results of these selections be represented by $A(a)$ and $B(b)$, each of which equals ± 1 according as the RHC or LHC is recorded.

Suppose now that a statistical correlation of $A(a)$ and $B(b)$ is due to information carried by and localized within each photon, and that at some time in the past the photons constituting one pair were in contact and in communication regarding this information. The information is quantum mechanical or is part of the content of a set of hidden variables, denoted collectively by λ. The results of the two polarization outcomes are then to be functions $A(a,\lambda)$ and $B(b,\lambda)$. Locality reasonably requires $A(a,\lambda)$ to be independent of the parameter b and $B(b,\lambda)$ to be likewise independent of a, since the two outcomes may occur at an arbitrarily great distance from each other. Finally, since the pair of photons is generally emitted by a source in a manner physically independent of the adjustable parameters a and b, we assume that the normalized probability distribution $\rho(\lambda)$ characterizing the ensemble is independent of a and b. The requirement that the expectation value of a and b is equal to one ($E(a,b)=1$) (on the average, the polarization of photons incident on each polarizer are equal) implies $B(a,\lambda)=A(a,\lambda)$. Defining the correlation function $P(a,b)\equiv\int_\Gamma A(a,\lambda)B(b,\lambda)\rho(\lambda)d\lambda$ where Γ is the total λ space, generalization of Bell's theorem gives

$$\begin{aligned}\left|P(a,b)-P(a,c)\right| &\le \int_\Gamma \left|A(a,\lambda)B(b,\lambda)-A(a,\lambda)B(c,\lambda)\right|\rho(\lambda)d\lambda \\ &= \int_\Gamma \left|A(a,\lambda)B(b,\lambda)\right|\ \left[1-B(b,\lambda)B(c,\lambda)\right]\rho(\lambda)d\lambda \\ &= \int_\Gamma \left[1-B(b,\lambda)B(c,\lambda)\right]\rho(\lambda)d\lambda \\ &= 1-\int_\Gamma B(b,\lambda)B(c,\lambda)\rho(\lambda)d\lambda\end{aligned} \tag{42.30}$$

In the case of the $0-1-0$ cascade, the coincidence count rate, $R(\mathbf{a},\mathbf{b})$, replaces the correlation function, $P(a,b)$, of the generalization of Bell's theorem which then yields the following inequalities [34]:

$$-1 \le S = \frac{\left[R(\mathbf{a},\mathbf{b})-R(\mathbf{a},\mathbf{b}')+R(\mathbf{a}',\mathbf{b})+R(\mathbf{a}',\mathbf{b}')-R_1(\mathbf{a}')-R_2(\mathbf{b}')\right]}{R_0} \le 0 \tag{42.31}$$

where $R(\mathbf{a},\mathbf{b})$ is the rate of coincidences with polarizer 1 in orientation $\mathbf{a}$ and polarizer 2 in orientation $\mathbf{b}$, $R_1(\mathbf{a}')$ is the coincidence rate with polarizer 2 removed and polarizer 1 in orientation $\mathbf{a}'$, $R_2(\mathbf{b}')$ is the coincidence rate with polarizer 1 removed and polarizer 2 in orientation $\mathbf{b}'$, and R_0 is the coincidence rate with the two polarizers removed. The maximum violation of Bell's inequalities (Eq. (42.31)) is predicted by substituting Eqs. (42.23-42.26) into Eq. (42.31) and by taking derivatives with respect to the orientation angles and setting them equal to zero [39]. Assuming the rotational invariance of $R(\mathbf{a},\mathbf{b})$, the inequalities (Eq. (42.31)) contract to [34] :

$$\delta = \frac{\left|R(22.5°)-R(67.5°)\right|}{R_0}-\frac{1}{4} \le 0 \tag{42.32}$$

The calculated value, δ_{cal}, from Eqs. (42.23) and Eq. (42.32) is:

$$\delta_{cal} = 5.8\ X\ 10^{-2} \pm 0.2\ X\ 10^{-2} \tag{42.33}$$

The experimental value, $\delta_{\exp}$, is [34]:

$$\delta_{\exp} = 5.72 X 10^{-2} \pm 0.43 X 10^{-2} \tag{42.34}$$

The experimental value is in agreement with the calculated value and violates the inequality of Eq. (42.32) by 13 standard deviations. From Eq. (42.23) and Eq. (42.31), the inequality parameter, S_{cal}, corresponding to orientations:

$$-1 \le S = \frac{\left[R(22.5°)-R(67.5°)+R(22.5°)+R(22.5°)-R_1(44.8°)-R_2(67.5°)\right]}{R_0} \le 0 \tag{42.35}$$

is

$$S_{cal} = 0.118 \pm 0.005 \tag{42.36}$$

The experimental value, $S_{\exp}$, is [34]:

$$S_{\exp} = 0.126 \pm 0.014 \tag{42.37}$$

The experimental value is in agreement with the calculated value and violates the inequality of Eq. (42.31) by 9 standard deviations. These results refute LHVT and quantum mechanics because both theories require a distribution function of correlated angular momentum. Only classical physics correctly predicts the coincidence count rate as a function of the relative orientation of the polarizers.

A fundamental difference exists between classical physics versus quantum mechanics and quantum electrodynamics (QED). In the case of classical physics, Eq. (17.70) of Jackson applies–the z component of angular momentum is conserved on a photon by photon basis. Whereas, in the quantum mechanical case, Eq. (17.71) of Jackson–the z component of angular momentum is conserved on the average of many photons. The photon is the cause of quantization in the deterministic classical physics; whereas, quantization arises from the expectation values of probability distribution functions in quantum mechanics and QED. Bell's theorem accepts quantum-mechanical statistics and hidden variables as correct simultaneously. The resulting inequalities predicted for the measurement of two spatially separated observables that were historically in communication with the condition that local hidden variables theories (LHVT) are correct is inconsistent with experimental results. Thus, the data refute LHVT. Furthermore, the calculation of Horne is ***not quantum mechanical***, the implicit physics is deterministic with the statistics of the measurement associated with two independent, inefficient detectors. For a true quantum-mechanical and QED calculation, the z component of angular momentum is only conserved on average over momentum space, and in the case of QED, the z component of angular momentum is only conserved on average over momentum space as well as over a continuum of frequencies centered about the expectation values of ν_1 and ν_2. (The expectation value of the z component of angular momentum must include an integral over all momentum space and over all frequency space.) Bell's inequalities apply not only

to LHVT, but also to quantum mechanics and QED. Consider the consequences of the postulate of quantum mechanics that photon momentum has a distribution function, and the change in the z component of angular momentum is zero on the average of many emission events. The associated average momentum distribution function is equivalent to a hidden variable distribution function in Eqs. (42.18) and (42.30). The observed coincidence count rate of Aspect [34] is equal to that predicted classically from the statistics of measurement at an inefficient detector only. The additional finite distribution function required in the case of quantum mechanics and QED results in incorrect predictions as demonstrated in the Bell's Theorem Test of Local Hidden Variable Theories (LHVT) and Quantum Mechanics section. The observed results disprove LHVT, quantum mechanics, and QED and support classical physics that is deterministic, not statistical.

As a further consideration discussed by Mills [12], Bell's theorem is just an inequality relationship between ARBITRARY probability-density functions with certain assumptions about independence, expectation value equal to one, etc. wherein an additional probability distribution function is introduced which may represent local hidden variables or something else for that matter. And, the initial functions may correspond to quantum mechanical statistics or something else for that matter. Standard probability rules are accepted such as the probability of two independent events occurring simultaneously is the product of their independent probabilities. What is calculated and plugged into the formula for the functions and whether the substitutions are valid are the issues that determine what Bell's inequality tests when compared with data. Historically, Bell's inequality is a simple proof of statistical inequalities of expectation values of observables given that quantum statistics is correct and that the physical system possesses "hidden variables." However, if deterministic statistics are actually calculated and quantum statistics is equivalent to deterministic statistics (e.g. detection of a wave at an inefficient detector) but possesses further statistics based on the probability nature of the theory (statistical conservation of photon angular momentum), then Bell's inequality actually tested and confirmed determinism versus quantum theory when compared to the data.

The arbitrary nature of Bell's probability inequality equation has fundamental ramifications regarding its validity in the first place as pointed out by Mills [12]. Hess and Phillips [48] have recently published on the results of considering the arbitrary assumptions Bell proposed in his probability inequality equation. In addition to the assumption that hidden variables exist, Bell tacitly made a variety of other assumptions such as the assumption that the proposed hidden variables are governed by a single probability measure independent of the analyzer settings. Hess and Phillips show that the mathematical model of Bell excludes a large set of local hidden variables and a large variety of probability densities such as time correlated parameters and generalized probability density. Their extended space of local hidden variables does permit deviation of the quantum result and is consistent with all known experiments. The results of Hess and Phillips further eliminates the need to default to spooky actions at a distance to explain the results of EPR experiments.

WHEELER: BACK TO REALITY NOT BACK TO THE FUTURE

Another version of the Aspect experiment called Wheeler's delayed-choice gedanken experiment has been realized according to a group comprising Aspect and others [49, 50]. It involves the single-photon detection of the random input of orthogonally polarized photons at two independent output detectors. When an electro-optical modulator (EOM) is not active each photon can be assigned to a specific path of an interferometer at the corresponding detector that is determined by the input polarization. But, the path is presumed unknown when the EOM is activated after a given photon has entered the interferometer. In the EOM-not-active case, the output at each detector is random and equal over many photons, but in the EOM-active case, output is observed at only one detector. Furthermore, when the relative path length of the two paths of the interferometer is varied to cause a correspondingly proportional phase angle, photon detection is then observed to occur at both detectors wherein the output demonstrates a modulation having a trigonometric dependence on the phase angle with a relative phase angle of π between the output of the two orthogonal detectors. The EOM-not-active output is recognized as the expected classical result with adherence to causality with each photon propagating along a single path and detected by the corresponding detector wherein the path and detector are determined by the input polarization state of the single photon. The phase independence is interpreted as due to the possession of knowledge of each single-photon propagation path based on the measurement of the corresponding detector output. The knowledge, in turn, determines the photon path, and with single-path propagation, interference associated with phase dependency is not deemed possible. Conversely, in the EOM-active case, the absence of knowledge determines that each photon must travel along two paths simultaneously, even when the device is activated when the photon is traveling at light speed along a path in route to the corresponding detector. Thus, the EOM-active results are interpreted as being due to each single photon traveling at light speed through the two possible paths simultaneously requiring that it had to first go back in time after the EOM was turned on and change history from one path to two-path propagation. The subsequent inference from the dual-flight path of the single photon explains the inference. This metaphysical interpretation is despite the authors' contradictory view on "the intuitive image that a single particle cannot be detected simultaneously in the two paths of the interferometer [49]."

In reality, these results can be explained in terms of classical physical laws based on the nature of the photon and the hardware of the experiment. The experimental device is shown in Figure 42.10. Linearly polarized single photons emitted by a single N-V color center are transmitted by a polarization beamsplitter (BS_{input}) to an interferometer having two spatially separated paths 1 and 2 associated with orthogonal S and P polarizations, respectively, wherein the propagation path is determined by the initial state of the two permitted orthogonal polarization states of each single photon. The tiltable output beamsplitter BS_{output} comprises the combination of (i.) a half-wave plate that interchanges the S or P polarization state, (ii.) a second polarization beamsplitter BS' that merges the propagation paths, (iii.) an EOM that is randomly in an open or half-wave-plate state for each photon according to the output voltage of a quantum random number generator (QRNG) ($V_{EOM} = 0$ or $V_{EOM} = V_{\pi}$, respectively) wherein the input polarizations are rotated by 45° when the EOM is in the active state ($V_{EOM} = V_{\pi}$)

since the EOM optical axis is at 22.5° from the input polarizations, and (iv.) a Wollaston prism (WP) aligned such that the initial S or P polarization state associated with each separate path 1 or 2 is selectively transmitted to detector D_1 or D_2, respectively.

Figure 42.10. A schematic of the single-photon, two-path interferometer that operates in EOM-not-active and EOM-active modes to give different detection statistics at two independent output detectors that are selective for a given path of propagation determined by the initial linear polarization state of the single photon.

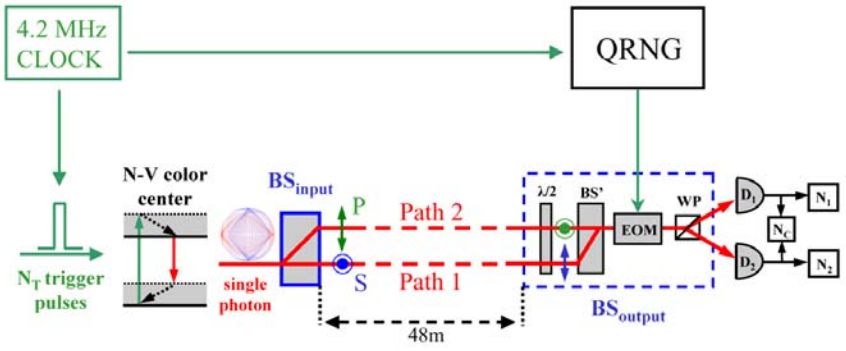

Now, the results of the Aspect group can be predicted based on the physics of the optical components and the nature of linearly polarized single photons wherein each is comprised of inseparable right hand circular polarized (RHCP) and left hand circular polarized (LHCP) components that must conserve the $\hbar$ of angular momentum associated with its electric and magnetic fields as given by Eq. (4.1). The EOM rotates the RHCP and LHCP components to tilt the angle of linear polarization by $\frac{\pi}{4}$ with a relative phase angle of π between the components. As the beam splitter BS' is tilted the orientation and path length changes by Δz which corresponds to the tilt-phase angle ϕ:

$$\phi = k\Delta z \tag{42.38}$$

Then, the WP adds the two components to give an output having the appearance of interference between separate linearly polarized photons or a linear combination of circular polarized photons when there is a relative tilt-phase angle ϕ between the original RHCP and LHCP components. As shown *infra*. the predicted modulated output at the polarization-selective detectors matches the observed modulated output shown in Figure of the Aspect group [49].

Consider the components of the input photon linearly polarized along the y-axis as given in the Equation of the Photon section. Since the photon is an extended particle comprised of spatially varying fields, the action of the EOM and WP for the transmission of the oppositely rotating RHCP or LHCP components for the determination of the detection statistics depends on the orientation and the corresponding tilt-phase of the beam splitter BS'. The components having a dependency on the relative tilt-phase angle ϕ are:

RHCP component

$$E_x = a\sin(\omega t - kz + \phi) \tag{42.39}$$

$$E_y = a\cos(\omega t - kz + \phi) \tag{42.40}$$

LHCP component

$$E_x = -a\sin(\omega t - kz) \tag{42.41}$$

$$E_y = a\cos(\omega t - kz) \tag{42.42}$$

To conserve angular momentum during the response to the EOM, the vectors of the oppositely polarized photon components rotate in the opposite directions corresponding to a relative phase angle of π corresponding to $\frac{\pi}{2}$ per component:

RHCP component

$$E_x = a\sin(\omega t - kz + \phi) \tag{42.43}$$

$$E_y = a\cos(\omega t - kz + \phi) \tag{42.44}$$

LHCP component

$$E_x = -a\sin(\omega t - kz + \pi) \tag{42.45}$$

$$E_y = a\cos(\omega t - kz + \pi) \tag{42.46}$$

At the WP, the superposition is

$$E_x = a\sin(\omega t - kz + \phi) + a\sin(\omega t - kz) \tag{42.47}$$

$$E_y = a\cos(\omega t - kz + \phi) - a\cos(\omega t - kz) \tag{42.48}$$

Next, consider the components of the input photon linearly polarized along the x-axis:

RHCP component

$$E_x = a\cos(\omega t - kz + \phi) \tag{42.49}$$

$$E_y = a\sin(\omega t - kz + \phi) \tag{42.50}$$

LHCP component

$$E_x = a\cos(\omega t - kz) \tag{42.51}$$

$$E_y = -a\sin(\omega t - kz) \tag{42.52}$$

The action of the EOM on the opposite circular polarized component vectors is antisymmetrical about the axes with the interchange of initial direction of the linear polarization from E_y to E_x. Again, to conserve angular momentum during the response to the EOM, the vectors of the oppositely polarized photon components rotate in the opposite directions corresponding to a relative phase angle of π corresponding to $\frac{\pi}{2}$ per component. In addition, for the initially x-polarized case, there is a change to the opposite parity for the E_x (RHCP) and E_y (LHCP) components corresponding to the electric-dipole selection rules with the rotated photon field vector having a projection in the opposite direction as that of the initially y-axis-polarized case [51]:

RHCP component

$$E_x = -a\cos(\omega t - kz + \phi) \tag{42.53}$$

$$E_y = a\sin(\omega t - kz + \phi) \tag{42.54}$$

LHCP component

$$E_x = a\cos(\omega t - kz + \pi) \tag{42.55}$$

$$E_y = a\sin(\omega t - kz + \pi) \tag{42.56}$$

At the WP, the superposition is

$$E_x = -a\cos(\omega t - kz + \phi) - a\cos(\omega t - kz) \tag{42.57}$$

$$E_y = a\sin(\omega t - kz + \phi) - a\sin(\omega t - kz) \tag{42.58}$$

With a tilt-phase angle $\phi = 0, n2\pi$ where n is an integer, the WP output is totally E_x giving rise to the maximum output at D_2 only, and with a phase angle $\phi = n\pi$ where n is an integer, the WP output is totally E_y giving rise to the maximum output at D_1 only. Thus, the detection rate corresponding to the detection probabilities at the outputs 1 and 2 are given by an equation of the same form as that of the Aspect experiment give by Eq. (42.29). The normalized EOM-active D_2 and D_1 count rates, $R_2(\phi)$ and $R_1(\phi)$, as a function of the tilt-phase angle ϕ are:

$$\frac{R_2(\phi)}{R_0} = (0.5 + 0.5\cos 2\phi_{1/2}) \tag{42.59}$$

$$\frac{R_1(\phi)}{R_0} = (0.5 - 0.5\cos 2\phi_{1/2}) \tag{42.60}$$

where the angular variable of $\phi_{1/2} = 0.5\phi$ corresponds to the effect of the rotation of the EOM and R_0 is the total EOM-not-active count rate (sum of D_2 and D_1 count rates). Without the antisymmetrical rotational effect of the EOM, the detection rates at the orthogonal detectors for random E_x and E_y polarized input are constant as a function of ϕ. This is because the output at each detector over time is due to the superposition of two sets of RHCP and LHCP components, each comprised of E_x and E_y components wherein only one term of each of the latter is phase dependent. The phase independent term of each E_x and E_y component gives an equal detection contribution at both detectors corresponding to the detection of circularly polarized light at the detectors, and the phase-dependent terms statistically balance since the sum of the phase dependency at each detector is unity ($\cos^2\phi + \sin^2\phi$). That is, the crossover between E_x input to E_y output with D_2 detection is statistically balanced by E_y input to E_x output with D_1 detection such that the detection rate at both detectors is constant, independent of phase angle. Thus, the normalized EOM-not-active D_2 and D_1 count rates, $R_2(\phi)$ and $R_1(\phi)$, as a function of the tilt-phase angle ϕ are:

$$\frac{R_2(\phi)}{0.5R_0} = 0.25 + (0.25 + 0.25\cos 2\phi) + 0.25 + (0.25 - 0.25\cos 2\phi) = 1 \tag{42.61}$$

$$\frac{R_1(\phi)}{0.5R_0} = 0.25 + (0.25 - 0.25\cos 2\phi) + 0.25 + (0.25 + 0.25\cos 2\phi) = 1 \tag{42.62}$$

The predicted results are shown in Figure 42.11.

Figure 42.11. The normalized D_2 (red curve) and D_1 (blue curve) count rates, $R_2(\phi)$ and $R_1(\phi)$, as a function of the tilt-phase angle ϕ. (A) EOM-active count rates as given by Eqs. (42.59) and (42.60), respectively. (B) EOM-not-active count rates as given by Eqs. (42.61) and (42.62), respectively. These results are based on the physical treatment of the linearly polarized single photon comprised of RHCP and LHCP components that obey conservation of angular momentum at the EOM.

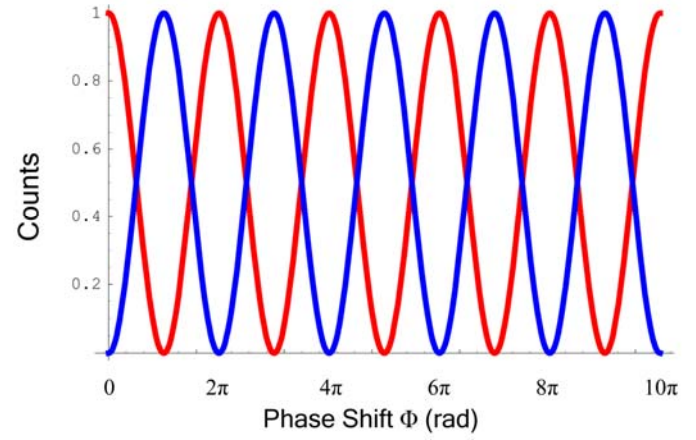

(**A**)

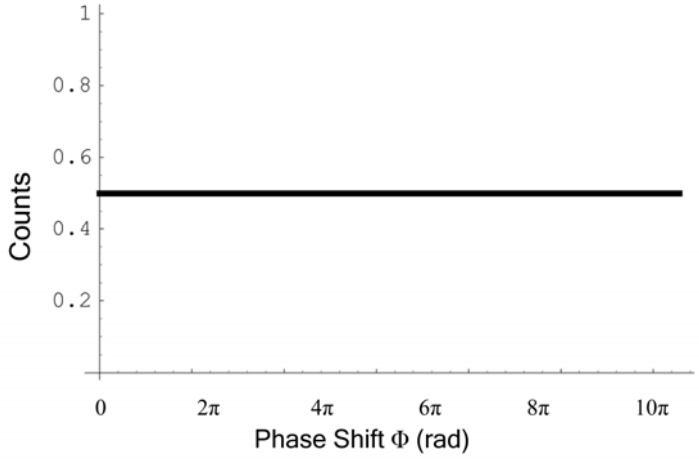

(**B**)

These physical results match the experimental observations of the Aspect group [49] without requiring the photon traveling back in time, changing history, and being in two places at the same time. Physics is restored, and an EOM is not a time machine.

SCHRÖDINGER "BLACK" CATS

A recent report in New York Times [52] entitled "Physicists Put Atom in 2 Places at Once" states, "a team of physicists has proved that an entire atom can simultaneously exist in two widely separated places." The article further states, "In the quantum 'microscale' world, objects can tunnel magically through impenetrable barriers. A single object can exist in a multiplicity of forms and places. In principle, two quantum-mechanically 'entangled' objects can respond instantly to each other's experiences, even when the two objects are at the opposite ends of the Universe." (This quantum mechanical prediction of the Spooky Actions at a Distance was disproved in the previous sections—Aspect Experiment-No Spooky Action at a Distance and Bell's Theorem Test of Local Hidden Variable Theories (LHVT) and Quantum Mechanics). Experimentally, interference patterns were observed by Monroe et al. [53] for a single $^9Be^+$ ion in a trap in a continuous Stern-Gerlach experiment. The phenomenon is similar to that of the Aharonov-Bohm Effect which was erroneously interpreted as interference of electron wave-functions as given in the Aharonov-Bohm Effect section. In this case, the erroneous interpretation of the experimental observation was that the ion wave-function interfered with itself wherein the ion was at two separate places at the same time corresponding to a wave function state called a "Schrödinger cat" state [52-54]. According to Monroe et al. [53],

> "A 'Schrödinger cat'-like state of matter was generated at the single atom level. A trapped $^9Be^+$ ion was laser-cooled to the zero-point energy and then prepared in a superposition of spatially separated coherent oscillator states. This state was created by application of a sequence of laser pulses, which entangles internal (electronic) and external (motional) states of the ion. The 'Schrödinger cat' superposition was verified by detection of the quantum mechanical interference between the localized wave packets. This mesoscopic system may provide insight into the fuzzy boundary between the classical and quantum worlds by allowing controlled studies of quantum measurement and quantum decoherence."

The "Schrödinger cat" state analysis relies on the postulate that the Pauli Exclusion Principle applies to Rabi states

wherein a rotation of the magnetic moment of the unpaired electron of an RF-trapped $^9Be^+$ ion is represented by a linear combination of spin 1/2 ($\left|\uparrow\right\rangle_i$) and spin -1/2 ($\left|\downarrow\right\rangle_i$) states. Three steps of rotation of the spin magnetic moment by a time harmonic field provided by pairs of copropagating off-resonant laser beams which drove two-photon-stimulated Raman magnetic resonance transitions were each separated by displacement laser pulses which excited a resonant translational harmonic oscillator level of the trapped ion by coupling only with the $\left|\uparrow\right\rangle_i$ state. According to Monroe, "this selectivity of the displacement force provides quantum entanglement of the internal state with the external motional state. Although the motional state can be thought of as nearly classical, its entanglement with the internal atomic quantum levels precludes any type of semiclassical analysis." The interference was detected by exciting a fluorescent transition, which only appreciatively coupled to the $\left|\downarrow\right\rangle_i$ state. Thus, the fluorescence reading was proportional to the probability $P_\downarrow$ the ion was in state $\left|\downarrow\right\rangle_i$. The "Schrödinger cat" superposition was supposedly verified by detection of the quantum mechanical interference between the localized wave packets.

However, the interference arises not from the existence of the ion at two places at once. The positively charged ion was excited to a time harmonic translational energy state, and the spin quantization axis was defined by an applied $0.20\ mT$ magnetostatic field at an angle of $\frac{\pi}{4}$ with respect to the x-axis of the RF-trap. **The frequency of the energy to "flip" the spin state was equivalent to the projection of that of the translational harmonic oscillator onto the spin axis**

$$\frac{\omega_x}{2\pi}\cos^2\frac{\pi}{4} = (11.2\ MHz)(0.5) = 5.605\ MHz = \frac{\Delta E_{mag}^{spin}}{h} \tag{42.63}$$

given by Eqs. (42.70-42.73), *infra*. Thus, interference occurred between the Stern-Gerlach transition and the synchrotron radiation corresponding to the charged harmonic oscillator. Since the displacement beams affected only motion correlated with the $\left|\uparrow\right\rangle_i$ state, a rotation of the magnetic moment such that $\delta \neq 0$ with application of the displacement beams gives rise to a phase shift of the interference pattern.

EXPERIMENTAL APPROACH

A classical approach to the description of the experiment and the results of Monroe [53] are given herein. The corresponding description according to a "Schrödinger cat" state is given by Monroe [53].

A single $^9Be^+$ ion was confined in a coaxial-resonator radio frequency (RF)-ion trap [55] that provided harmonic oscillation frequencies of $(\omega_x, \omega_y, \omega_z)/2\pi \approx (11.2,\ 18.2,\ 29.8)\ MHz$ along the principal axes of the trap. The ion was laser-cooled to the quantum ground state of motion [56], and then the electronic and motional states were coherently manipulated by applying pairs of off-resonant laser beams, which drove two-photon stimulated Raman transitions. The two internal states of interest were the stable $^2S_{1/2}(F=2, m_F=-2)$ and $^2S_{1/2}(F=1, m_F=-1)$ hyperfine ground states (denoted by $\left|\downarrow\right\rangle_i$ and $\left|\uparrow\right\rangle_i$, respectively), separated in frequency by $\omega_{HF}/2\pi \approx 1.250\ GHz$. Here, F and m_F are quantum numbers representing the total internal angular momentum of the atom and its projection along a quantization axis. The Raman beams were detuned by $\Delta \approx -12\ GHz$ from the $^2P_{1/2}(F=2, m_F=-2)$ excited state, which acted as the virtual level, providing the Raman coupling. The external motional states were characterized by the quantized vibrational harmonic oscillator states $\left|n\right\rangle_e$ in the x dimension, separated in frequency by $\omega_x/2\pi \approx 11.2\ MHz$.

When the Raman beam difference frequency was tuned near ω_{HF} and the "carrier beams" a and b were applied, the magnetic moment of the ion was rotated away from the spin axis as described by Slichter [57]. By adjusting the exposure time of the carrier beams, for example, the electronic state was "flipped"—a $\left|\downarrow\right\rangle_i$ to $\left|\uparrow\right\rangle_i$ transition by a π-pulse or rotated into the x'y'-plane (the plane perpendicular to the spin axis) of the rotating coordinate system by a $\frac{\pi}{2}$-pulse. Transitions on the carrier did not significantly affect the state of motion, because beams a and b were copropagating. When the Raman beam difference frequency was tuned near ω_x, and the "displacement" beams b and c were applied, the displacement beams produced a "walking wave" pattern whose time-dependent dipole force resonantly excited the harmonic motion. According to Monroe [53], this force promoted an initial zero-point state of motion $\left|0\right\rangle_e$ to a coherent state expressed as:

$$\left|\beta\right\rangle_e = \exp\left(\frac{-\left|\beta\right|^2}{2}\right)\sum_n \frac{\beta^n}{(n!)^{1/2}}\left|n\right\rangle_e \tag{42.64}$$

where $\beta = \alpha e^{i\theta}$ is a dimensionless complex number that represents the amplitude and phase of the motion in the harmonic potential. The probability distribution of vibrational levels in a coherent state is Poissonian with mean number of vibrational quanta

$$\left\langle n\right\rangle = \alpha^2 \tag{42.65}$$

The coherent state of motion is much like classical motion in a harmonic potential with amplitude

$$2\alpha x_0 \tag{42.66}$$

where

$$x_0 = \left(\frac{\hbar}{2M\omega_x} \right)^{1/2} = 7.1\ nm \tag{42.67}$$

was the root mean square Gaussian amplitude of the oscillating ion and M was the mass of the ion.

The polarizations of the three Raman beams, a, b, and c produced π, σ^+ / σ^-, and σ^- couplings, respectively, with respect to a quantization axis defined by an applied $0.20\ mT$ magnetic field which was at an angle of $\frac{\pi}{4}$ with respect to the x-axis of the RF-trap. As a result, the displacement beams (b and c) affected only the motional state correlated with the $\left|\uparrow\right\rangle_i$ state, because the σ^- polarized beam c could not couple the $\left|\downarrow\right\rangle_i$ state to any virtual ${}^2P_{1/2}$ states.

The energy to flip the orientation of the atomic orbital due to its magnetic moment of a Bohr magneton, μ_B, given by Eq. (1.227) is:

$$\Delta E_{mag}^{spin} = 2\frac{g}{2}\mu_B \mathbf{B} \tag{42.68}$$

where

$$\mu_B = \frac{e\hbar}{2m_e} \tag{42.69}$$

In the case that the magnetic flux density was $0.2\ mT$, the energy was:

$$\Delta E_{mag}^{spin} = 2g\mu_B \mathbf{B} = 2(1.00116)\left(9.2741\times10^{-24}\ \frac{J}{T} \right)\left(0.2\times10^{-3}\ T \right) = 3.714\times10^{-27}\ J \tag{42.70}$$

The resonance frequency is given by Planck's equation

$$\omega = \frac{\Delta E_{mag}^{spin}}{\hbar} = \frac{3.714\times10^{-27}\ J}{\hbar} = 3.522\times10^{7}\ \frac{rads}{s} = 5.605\ MHz \tag{42.71}$$

As demonstrated by Eq. (42.97) and Eq. (42.98), *infra.*, energy is exchanged between the harmonic oscillator state and the spin state according to the dot product of the wavenumber vector of the spin transition and the harmonic displacement vector

$$\left[\mathbf{k}\cdot\mathbf{u}(l,\phi) \right]^2 \propto \cos^2\frac{\pi}{4} = 0.5 \tag{42.72}$$

Because the positively charged ion was excited to a time harmonic translational energy state along the x-axis, and the spin quantization axis was defined by an applied $0.20\ mT$ magnetostatic field at an angle of $\frac{\pi}{4}$ with respect to the x-axis of the RF-trap the frequency of the energy to "flip" the spin state was equivalent to the projection of that of the translational harmonic oscillator onto the spin axis

$$\frac{\omega_x}{2\pi}\cos^2\frac{\pi}{4} = (11.2\ MHz)(0.5) = 5.605\ MHz = \frac{\Delta E_{mag}^{spin}}{h} \tag{42.73}$$

Each Raman beam contained $\approx 1\ mW$ of power at $\approx 313\ nm$. This resulted in a two-photon Rabi frequency of $\frac{\Omega}{2\pi} = 250\ kHz$ for the copropagating Raman carrier beams a and b, or a π-pulse exposure time of about $1\ \mu s$. The displacement Raman beams (b and c) were applied to the ion in directions such that their wave vector difference **dk** pointed nearly along the x-axis of the trap. Motion in the y or z dimensions was therefore highly insensitive to the displacement beams. When the displacement beams were applied to a zero-point translational state (correlated with the $\left|\uparrow\right\rangle_i$ state) for time τ on average a harmonic oscillator state of amplitude,

$$\alpha = \eta\Omega_d\tau \tag{42.74}$$

was created. Here, $\eta = 0.205$ is the Lamb-Dicke parameter and $\frac{\Omega_d}{2\pi} \approx 300\ kHz$ is the coupling strength of the displacement beams. After each preparation cycle (described below), which spin state ($\left|\downarrow\right\rangle_i$ or $\left|\uparrow\right\rangle_i$) the ion occupied was detected independent of its state of motion. This was accomplished by applying a few microwatts of σ^--polarized light ("detection" beam d) resonant with the cycling $\left|\downarrow\right\rangle_i \rightarrow {}^2P_{3/2}(F=3,\ m_F=-3)$ transition [radiative linewidth $\frac{\gamma}{2\pi} \approx 19.4\ MHz$ at wavelength $(\lambda) \approx 313\ nm$] and observing the resulting ion fluorescence. Because this radiation does not appreciably couple to the $\left|\uparrow\right\rangle_i$ state, the fluorescence reading was proportional to the probability $P_\downarrow$ the ion was in state $\left|\downarrow\right\rangle_i$. The experiment was

continuously repeated—cooling, state preparation, detection—while slowly sweeping the harmonic oscillator phase ϕ.

STATE PREPARATION AND DETECTION

The ion was first laser-cooled so that the $\left|\downarrow\right\rangle_i \left|n_x = 0\right\rangle_e$ state was occupied about 95% of the time. Then, five sequential pulses of Raman beams were applied. In step 1, a $\frac{\pi}{2}$-pulse on the carrier rotated the magnetic moment into the plane perpendicular to the spin axis (z'-axis) in a coordinate system which rotates around the z'-axis. The moment precessed about the x'-axis of the rotating coordinate frame described by Slichter [57]. The precessing moment had a time averaged projection onto the z'-axis equivalent to an equal superposition of states $\left|\downarrow\right\rangle_i \left|0\right\rangle_e$ and $\left|\uparrow\right\rangle_i \left|0\right\rangle_e$. In step 2, the displacement beams excited the motion correlated with the $\left|\uparrow\right\rangle_i$ component to a harmonic oscillator state $\left|\alpha e^{-i\phi/2}\right\rangle_e$. In step 3, a π-pulse rotated the magnetic moment in the plane perpendicular to the spin axis such that the moment precessed about the negative x'-axis of the rotating coordinate frame described by Slichter [57]. The precessing moment was equivalent to the swap of the superposition of states $\left|\downarrow\right\rangle_i \left|0\right\rangle_e$ and $\left|\uparrow\right\rangle_i \left|n\right\rangle_e$ produced in step 1 to give component states $\left|\downarrow\right\rangle_i \left|n\right\rangle_e$ and $\left|\uparrow\right\rangle_i \left|0\right\rangle_e$. In step 4, the displacement beams excited the motion correlated with the $\left|\uparrow\right\rangle_i$ component to a second harmonic oscillator state $\left|\alpha e^{i\phi/2}\right\rangle_e$. In step 5, a final $\frac{\pi}{2}$-pulse on the carrier rotated the magnetic moment to the spin axis to give $\left|\downarrow\right\rangle_i \left|n\right\rangle_e$, the initial spin state excited to an oscillator state of quantum number n, or $\left|\uparrow\right\rangle_i \left|n\right\rangle_e$, the flipped spin state excited to an oscillator state of quantum number n. In the absence of interference between the oscillatory state and the spin state, $\left|\downarrow\right\rangle_i \left|n\right\rangle_e$ and $\left|\uparrow\right\rangle_i \left|n\right\rangle_e$ occur with equal probability. The relative phases of the above steps were determined by the phases of the RF difference frequencies of the Raman beams which were easily controlled by phase-locking RF sources. The experiment was continuously repeated—cooling, state preparation, detection—while slowly sweeping the harmonic oscillator phase ϕ. The relative populations of $\left|\downarrow\right\rangle_i$ and $\left|\uparrow\right\rangle_i$ depended on the phase difference ϕ between the two oscillator states because of the interference of these states, and each coupled (interfered) with the Stern-Gerlach transition. The state $\left|\downarrow\right\rangle_i \left|n\right\rangle_e$ underwent a transition to the higher energy spin state $\left|\uparrow\right\rangle_i$ by coupling to the energy of the oscillator state. The amplitude of the oscillation, α, given by Eq. (42.74) is modulated by the interference between the displacement beam of step 2 having a phase $\frac{\phi}{2}$ and step 4 having a phase $\frac{\phi}{2}$. The resultant amplitude, $\left\langle \alpha(\phi) \right\rangle$, of the oscillation as a function of harmonic oscillator phase $\frac{\phi}{2}$ was given by:

$$\left\langle \alpha(\phi) \right\rangle = \sqrt{\left(\alpha e^{i\frac{\phi}{2}}\right)^2} = \sqrt{\left(\alpha e^{-i\frac{\phi}{2}}\right)^2} = \alpha \sin\frac{\phi}{2} \tag{42.75}$$

where the probability (Eq. (42.106), *infra.*) of detecting the $\left|\downarrow\right\rangle_i$ was $\phi = \frac{\pi}{2}$ out of phase with the probability of the ion oscillatory state $\left|n\right\rangle_e$ because the spin flip to the higher energy state occurred—$\left|\downarrow\right\rangle_i \rightarrow \left|\uparrow\right\rangle_i$. The interference of the oscillator states with the Stern-Gerlach transition was measured by detecting the probability $P_\downarrow(\phi)$ that the ion was in the $\left|\downarrow\right\rangle_i$ state for a given value of ϕ. The magnitude of the harmonic oscillator state was controlled by the duration of the applied displacement beams (Eq. (42.74)) in steps 2 and 4. The phase of the harmonic oscillator state was controlled by the phase of the applied displacement beams in steps 2 and 4. Monroe et al. report [53] on average the detection of one photon per measurement cycle when the ion was in the $\left|\downarrow\right\rangle_i$ state. The data represented an average of about 4000 measurements, or 1 second of integration.

The physical behavior of a large number of continuous Stern-Gerlach experiments (an ensemble) each detecting the spin state of a harmonic oscillating RF-trapped ion is equivalent to that of the interaction of ultrasound with Mössbauer gamma rays (interference of an electronic transition and an oscillator transition). Consider the Lamb-Mössbauer formula for the absorption of a γ ray of energy E by a nucleus in a crystal given by Maradudin [58] where,

$$\sigma_a(E) = \frac{1}{4}\sigma_0 \Gamma^2 \sum_{mn} \frac{e^{-\beta E_m}}{Z} \times \frac{\left\langle m \left| e^{i\left(\frac{\mathbf{p}}{\hbar}\right)\cdot\mathbf{R}(l)} \right| n \right\rangle \left\langle n \left| e^{-i\left(\frac{\mathbf{p}}{\hbar}\right)\cdot\mathbf{R}(l)} \right| m \right\rangle}{\left(E_0 - E + E_n - E_m\right)^2 + \frac{1}{4}\Gamma^2} \tag{42.76}$$

In this equation, E_0 is the energy difference between the final and initial nuclear states of the absorbing nucleus, E_m and E_n are the energies of the eigenstates $\left|m\right\rangle$ and $\left|n\right\rangle$ of the crystal, respectively, Γ is the natural width of the excited state of the nucleus,

p is the momentum of the γ ray, $\mathbf{R}(l)$ is the instantaneous position vector of the absorbing nucleus, Z is the crystal's partition function, $T=(k\beta)^{-1}$, and σ_0 is the resonance absorption cross section for the absorbing nucleus. By expressing the denominator of Eq. (42.76) as an integral, Eq. (42.76) is equivalent to:

$$\sigma_a(E)=\frac{1}{2}\sigma_0\gamma\int_{-\infty}^{\infty}dte^{i\omega t-\gamma|t|}\times\left\langle\exp\left[-i\mathbf{k}\cdot\mathbf{u}(l;t)\right]\exp\left[i\mathbf{k}\cdot\mathbf{u}(l;0)\right]\right\rangle \tag{42.77}$$

wherein the position vector $\mathbf{R}(l)$ is

$$\mathbf{R}(l)=\mathbf{x}(l)+\mathbf{u}(l) \tag{42.78}$$

For, Eq. (42.78), $\mathbf{x}(l)$ is the position vector of the mean position of the absorbing nucleus, and $\mathbf{u}(l)$ is its displacement from the mean position. Eq. (42.77) follows from Eq. (42.76) with the following substitutions:

$$\left(\frac{1}{\hbar}\right)\mathbf{p}=\mathbf{k} \tag{42.79}$$

$$\hbar\omega=E-E_0 \tag{42.80}$$

$$\gamma=\frac{\Gamma}{2\hbar} \tag{42.81}$$

and $\mathbf{u}(l;t)$ denotes the Heisenberg operator,

$$\mathbf{u}(l;t)=e^{i\left(\frac{t}{\hbar}\right)H}\mathbf{u}(l;0)e^{-i\left(\frac{t}{\hbar}\right)H} \tag{42.82}$$

where H is the Hamiltonian. The angular brackets in Eq. (42.77) denote an average over the canonical ensemble of the crystal.

The probability $P_{\downarrow}(\phi)$ that the ion of the experiments of Monroe et al. [53] was in the $\left|\downarrow\right\rangle_i$ state for a given value of ϕ is herein derived from the correlation function for the statistical average of large number of continuous Stern-Gerlach experiments (an ensemble) each detecting the spin state of a harmonic oscillating RF-trapped ion which is equivalent to that of the interaction of ultrasound with Mössbauer gamma rays. From Eq. (42.77), the correlation function $Q(t)$ of acoustically modulated gamma ray absorption by Mössbauer nuclei is

$$Q(t)=\left\langle\exp\left[-i\mathbf{k}\cdot\mathbf{u}(l;t)\right]\exp\left[i\mathbf{k}\cdot\mathbf{u}(l;0)\right]\right\rangle \tag{42.83}$$

In the present case, the position vector is given by Eq. (42.78) where $\mathbf{x}(l)$ is the position vector of the mean position of the trapped ion, and $\mathbf{u}(l)$ is its displacement from the mean position. In this case, **p** and **k** of Eq. (42.79) are the momentum and the wavenumber, respectively, of the ion corresponding to the spin flip, E of Eq. (42.80) is the energy of the harmonic oscillator, E_0 is the difference in energy between the $\left|\uparrow\right\rangle_i$ and $\left|\downarrow\right\rangle_i$ states, and $\mathbf{u}(l;t)$ of Eq. (42.82) is:

$$\mathbf{u}(l;t)=e^{i\left(\frac{t}{\hbar}\right)E}\mathbf{u}(l;0)e^{-i\left(\frac{t}{\hbar}\right)E} \tag{42.84}$$

The matrix elements of Eq. (42.83) are calculated by using the theorem [59]:

$$e^Ae^B=e^{A+B}e^{\frac{1}{2}[A,B]}\qquad\text{if }\left[[A,B],A\right]=\left[[A,B],B\right]=0 \tag{42.85}$$

For a harmonic oscillator, the commutator of $\mathbf{k}\cdot\mathbf{u}(l;t)$ and $\mathbf{k}\cdot\mathbf{u}(l;0)$ is a c number; thus,

$$\begin{aligned}Q(t)&=\left\langle\exp\left[-i\mathbf{k}\cdot\mathbf{u}(l;t)\right]\exp\left[i\mathbf{k}\cdot\mathbf{u}(l;0)\right]\right\rangle\\&=\left\langle\exp\left[-i\mathbf{k}\cdot\left[\mathbf{u}(l;t)-\mathbf{u}(l;0)\right]\right]\right\rangle\times\exp\left[\frac{1}{2}\left\langle\left[\mathbf{k}\cdot\mathbf{u}(l;t),\ \mathbf{k}\cdot\mathbf{u}(l;0)\right]\right\rangle\right]\end{aligned} \tag{42.86}$$

Since the correlation function applies to an ensemble of harmonic oscillator states, the first thermodynamic average can be simplified as follows:

$$\left\langle\exp\left[-i\mathbf{k}\cdot\left[\mathbf{u}(l;t)-\mathbf{u}(l;0)\right]\right]\right\rangle=\exp\left[-\frac{1}{2}\left\langle\left\{\mathbf{k}\cdot\left[\mathbf{u}(l;t)-\mathbf{u}(l;0)\right]\right\}^2\right\rangle\right] \tag{42.87}$$

This theorem is known in lattice dynamics as Ott's theorem [60] or sometimes as Bloch's theorem [61]. Using the time independence of the harmonic potential, Eq. (42.87) is:

$$\exp\left[-\frac{1}{2}\left\langle\left\{\mathbf{k}\cdot\left[\mathbf{u}(l;t)-\mathbf{u}(l;0)\right]\right\}^2\right\rangle\right]=\exp-\left[\frac{1}{2}\left\langle\left[\mathbf{k}\cdot\mathbf{u}(l;t)\right]^2\right\rangle+\frac{1}{2}\left\langle\left[\mathbf{k}\cdot\mathbf{u}(l;0)\right]^2\right\rangle\right] \tag{42.88}$$

$$=\exp-\left\langle\left[\mathbf{k}\cdot\mathbf{u}(l)\right]^2\right\rangle \tag{42.89}$$

Substitution of Eqs. (42.87-42.89) into Eq. (42.86) gives

$$Q(t)=\exp\left\langle -\left[\mathbf{k}\cdot\mathbf{u}(l;t)\right]^2\right\rangle\times\exp\left[\frac{1}{2}\left\langle\left[\mathbf{k}\cdot\mathbf{u}(l;t),\ \ \mathbf{k}\cdot\mathbf{u}(l;0)\right]\right\rangle\right] \tag{42.90}$$

Expanding $\mathbf{u}_\alpha(l;t)$ in terms of the normal coordinates of the harmonic potential and the phonon operators of that harmonic potential gives:

$$u_\alpha(l;t)=\left(\frac{\hbar}{2M_l}\right)^{\frac{1}{2}}\sum_s\frac{B_\alpha^{(s)}(l)}{(\omega_s)^{\frac{1}{2}}}\left(b_s e^{-i\omega_s t}+b_s^\dagger e^{i\omega_s t}\right) \tag{42.91}$$

where α labels the Cartesian components, M_l is the mass of the ion in the lth experiment, ω_s is the frequency of the sth normal mode, $B^{(s)}(l)$ is the associated unit eigenvector, and $b_s^\dagger$ and b_s are the phonon creation and destruction operators for the sth normal mode. By use of the coordinate expansion, the exponential of the correlation function appearing in Eq. (42.90) can be written as

$$\begin{aligned}e^{\langle\mathbf{k}\cdot\mathbf{u}(l;t)\mathbf{k}\cdot\mathbf{u}(l;0)\rangle}&=e^{\sum_s -c_s^2\left(\frac{e^{i\omega_s t}}{(\gamma_s)^{\frac{1}{2}}}+(\gamma_s)^{\frac{1}{2}}e^{-i\omega_s t}\right)}\\&=\prod_s e^{-c_s^2\left(\frac{e^{i\omega_s t}}{(\gamma_s)^{\frac{1}{2}}}+(\gamma_s)^{\frac{1}{2}}e^{-i\omega_s t}\right)}\\&=\prod_s\left[J_0\left(2c_s^2\right)+\sum_{n=1}^{\infty}J_n\left(2c_s^2\right)\left(\frac{e^{i\omega_s t}}{(\gamma_s)^{\frac{1}{2}}}+(\gamma_s)^{\frac{1}{2}}e^{-i\omega_s t}\right)\right]\end{aligned} \tag{42.92}$$

where the following substitutions were made:

$$\gamma_s=\frac{n_s+1}{n_s}=e^{\frac{\hbar\omega_s}{kT}} \tag{42.93}$$

$$n_s=\frac{1}{e^{\frac{\hbar\omega_s}{kT}}-1} \tag{42.94}$$

$$c_s^2=\frac{\hbar}{2M_l}\frac{\left[k\cdot B^{(s)}(l)\right]^2}{\omega_s}\frac{e^{\frac{\hbar\omega_s}{2kT}}}{e^{\frac{\hbar\omega_s}{kT}}-1} \tag{42.95}$$

and where the Bessel function relationship [62]:

$$e^{\frac{1}{2}x\left(y+y^{-1}\right)}=\sum_{n=-\infty}^{\infty}J_n(x)\,y^n \tag{42.96}$$

was used. n_s is the mean number of phonons in the sth mode at temperature T. In the case of Monroe's experiments [53], the correlation function for the exchange of energy between a harmonic oscillator state and a spin state was independent of time—not a function of $e^{i\omega_s t}$ and $e^{-i\omega_s t}$. Thus, the time dependent factors are dropped in Eq. (42.92), and combining Eqs. (42.90-42.92) and Eq. (42.92) gives the correlation function as

$$Q\left(c_s^2\right)=\exp-\left[c_s^2\right]\prod_s J_0\left(2c_s^2\right) \tag{42.97}$$

For the experiment of Monroe et al. [53], the ion was laser-cooled so that the $\left|\downarrow\right\rangle_i\left|n_x=0\right\rangle_e$ state was occupied about 95% of the time; thus, the partition function of Eq. (42.76) is equal to one. Eq. (42.95) is

$$c_s^2=\frac{\hbar}{2M}\frac{\left[k\cdot B^{(s)}(l)\right]^2}{\omega_s} \tag{42.98}$$

The harmonic frequency was $\omega_s=\omega_x$ with $s=1$ in Eq. (42.92) where the sum is over the ensemble of translational harmonic oscillator modes for a series of "Schrödinger cat" state experiments—each a specific Raman beam pulse sequence with measurement; therefore, the correlation function is

$$Q\left(c_s^2\right)=\exp-\left[c_s^2\right]J_0\left(2c_s^2\right) \tag{42.99}$$

Monroe et al. [53] measured the probability of spin state $\left|\downarrow\right\rangle_i$ as a function of the phase angle of the displacement lasers of steps 2 and 4. The probability $P_\downarrow(\phi)$ of detecting the $\left|\downarrow\right\rangle_i$ state as a function of phase angle, ϕ, can be derived from the correlation

function, Eq. (42.99). The expansion of the Bessel function is:

$$J_\nu(x) = \left(\frac{x}{2}\right)^\nu \sum_{m=0}^{\infty} \frac{\left(\frac{-x^2}{4}\right)^m}{\left[m!\Gamma(m+\nu+1)\right]}$$
$$J_0(x) = \sum_{m=0}^{\infty} \frac{\left(\frac{-x^2}{4}\right)^m}{\left[m!\Gamma(m+1)\right]} = \sum_{m=0}^{\infty} \frac{\left(\frac{-x^2}{4}\right)^m}{\left[m!m!\right]} \tag{42.100}$$

where $\Gamma(m+1) = m!$ was used. The probability distribution function of vibrational levels in a coherent state is Poissonian. The probability [63] of a spin flip with the emission of m phonons is:

$$P_m = \frac{\langle n\rangle^m e^{-\langle n\rangle}}{m!} = \frac{\left(\alpha^2\right)^m e^{-\alpha^2}}{m!} = \frac{\alpha^{2m} e^{-\alpha^2}}{m!} \tag{42.101}$$

with mean number of vibrational quanta $\langle n\rangle = \alpha^2$ (Eq. (42.65)). The probability $P_\downarrow(\phi)$ can be derived by factoring Eq. (42.101) from the Bessel function of the correlation function (Eq. (42.99)) and its expansion which follows from Eq. (42.100).

$$J_0(x) = \sum_{m=0}^{\infty} \frac{\left(\frac{-x^2}{4}\right)^m}{\left[m!m!\right]};$$
$$J_0(\alpha x) = \sum_{m=0}^{\infty} \frac{\left(\frac{-(\alpha x)^2}{4}\right)^m}{m!m!} = \frac{1}{e^{-\alpha^2}} \sum_{m=0}^{\infty} \frac{\left(\frac{-x^2}{4}\right)^m}{m!} \frac{\alpha^{2m} e^{-\alpha^2}}{m!} \tag{42.102}$$

Combining Eq. (42.101) and Eq. (42.102) demonstrates that the probability $P_\downarrow(\phi)$ is proportional to:

$$P_\downarrow(\alpha x) \propto \sum_{m=0}^{\infty} \frac{\left(\frac{-x^2}{4}\right)^m}{m!} \tag{42.103}$$

Let $x = y^2$, then the change of variable in Eq. (42.103) is:

$$P_\downarrow(\alpha y) \propto \sum_{m=0}^{\infty} \frac{\left(\frac{-x}{4}\right)^m}{m!} = \sum_{m=0}^{\infty} \frac{\left(\frac{-x^2}{4}\right)^{m/2}}{m!} \tag{42.104}$$

Let $m' = m/2$, then the change of variable in Eq. (42.104) is:

$$P_\downarrow(\alpha y) \propto \sum_{m=0}^{\infty} \frac{\left(\frac{-x^2}{4}\right)^{m/2}}{m!} \propto \sum_{m=0}^{\infty} \frac{\left(\frac{-x^2}{4}\right)^{m'}}{(2m')!} \tag{42.105}$$

The series expansion of $\cos(x)$ is:

$$\cos(x) = \sum_{m=0}^{\infty} \frac{\left(-x^2\right)^m}{(2m)!} \tag{42.106}$$

Combining Eq. (42.99) and Eqs. (42.103-42.106) gives the probability $P_\downarrow(\phi)$ proportional to:

$$P_\downarrow(\phi) \propto \cos\left(2\alpha\sqrt{c_s^2}\right) \tag{42.107}$$

where $y = \sqrt{x} = \sqrt{c_s^2}$. The quantization axis was at an angle of $\frac{\pi}{4}$ with respect to the x-axis. From Eqs. (42.65-42.67), Eq. (42.75), and Eq. (42.98),

$$c_s^2 = \alpha^2 \sin^2\frac{\phi}{2} \tag{42.108}$$

Combining Eq. (42.107) and Eq. (42.108) gives the probability $P_\downarrow(\phi)$ proportional to:

$$P_{\downarrow}(\phi) \propto \cos\left(2\alpha^2 \sin\frac{\phi}{2}\right) \tag{42.109}$$

Combining Eq. (42.99), Eq. (42.108), and Eq. (42.109) gives the probability $P_{\downarrow}(\phi)$ proportional to:

$$P_{\downarrow}(\phi) \propto \exp\left[-\alpha^2 \sin^2\phi\right]\cos\left(2\alpha^2 \sin\frac{\phi}{2}\right) = \exp\left[-\alpha^2\left(\frac{1-\cos\phi}{2}\right)\right]\cos\left(2\alpha^2 \sin\frac{\phi}{2}\right) \tag{42.110}$$

The rotation of the magnetic moment with RF fields such that $\delta \neq 0$ with application of the displacement beams is equivalent to a phase shift of the correlation function given by Eq. (42.83).

$$Q(t) = \left\langle \exp i\delta \exp\left[-i\mathbf{k}\cdot\mathbf{u}(l;t)\right]\exp\left[i\mathbf{k}\cdot\mathbf{u}(l;0)\right]\right\rangle \tag{42.111}$$

Thus, Eq. (42.110) is phase shifted.

$$P_{\downarrow}(\phi,\delta) \propto \exp\left[-\alpha^2\left(\frac{1-\cos\phi}{2}\right)\right]\cos\left(\delta + 2\alpha^2 \sin\frac{\phi}{2}\right) \tag{42.112}$$

The probability of detecting either $\left|\downarrow\right\rangle_i$ or $\left|\uparrow\right\rangle_i$ is one. The initial state of the ion for each cycle is $\left|\downarrow\right\rangle_i$. Consider the $\frac{\pi}{2}$-pulses (steps 2 and 5). In the absence of interference between the oscillator states and the Stern-Gerlach transition with $\alpha \neq 0$, the probability of detecting $\left|\downarrow\right\rangle_i$ or $\left|\uparrow\right\rangle_i$ is the same—1/2. However, with interference, the spin flip to the higher energy state occurs, $\left|\downarrow\right\rangle_i \rightarrow \left|\uparrow\right\rangle_i$. The probability of detecting $\left|\downarrow\right\rangle_i$ with interference is given by 1/2 minus the probability function, Eq. (42.112), normalized to 1/2. The probability function for the detection of $\left|\downarrow\right\rangle_i$ with interference as a function of phase angle, ϕ, harmonic oscillator amplitude, α, and phase shift, δ, is:

$$P_{\downarrow}(\phi,\delta) = \frac{1-\exp\left[-\alpha^2\left(\frac{1-\cos\phi}{2}\right)\right]\cos\left(\delta + 2\alpha^2 \sin\frac{\phi}{2}\right)}{2} \tag{42.113}$$

The plot of the probability $P_{\downarrow}(\phi)$ of detecting the $\left|\downarrow\right\rangle_i$ state as a function of phase angle, ϕ, harmonic oscillator amplitude, α, and phase shift, δ, using the values of the curve fit parameters of Monroe et al. [53] are given in Figures 42.12 and 42.13. Monroe et al. report [53] on average the detection of one photon per measurement cycle when the ion is in the $\left|\downarrow\right\rangle_i$ state. The data represented an average of about 4000 measurements, or 1 second of integration.

Figure 42.12. The plot of the probability $P_{\downarrow}(\phi)$ (Eq. (42.113)) of detecting the $\left|\downarrow\right\rangle_i$ state as a function of phase angle, ϕ, for the harmonic oscillator amplitude, α, and phase shift, $\delta = 0$. Curves in (**A**) to (**D**) represent experiments with various values of τ (2, 3, 5, and 15 μs, respectively). The curves are fits of the measurements to the values of Monroe et al. [53] for the parameter α of α=0.84, 1.20, 1.92, and 2.97, respectively.

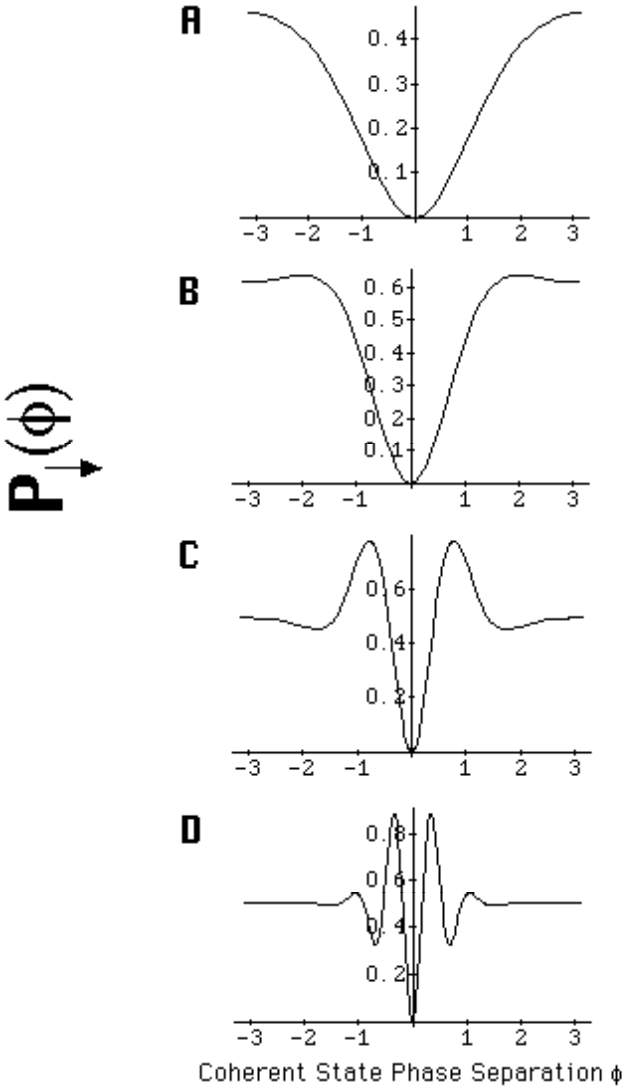

Figure 42.13. The plot of the probability $P_{\downarrow}(\phi)$ (Eq. (42.113)) of detecting the $|\downarrow\rangle_i$ state as a function of phase angle, ϕ, for the harmonic oscillator amplitude, $\alpha = 1.5$, and phase shift, δ. Curves in (**A**) to (**C**) are fits of the measurements to the values of Monroe et al. [53] for the parameter δ of $\delta = 1.03\pi$, 0.48π, and 0.06π, respectively.

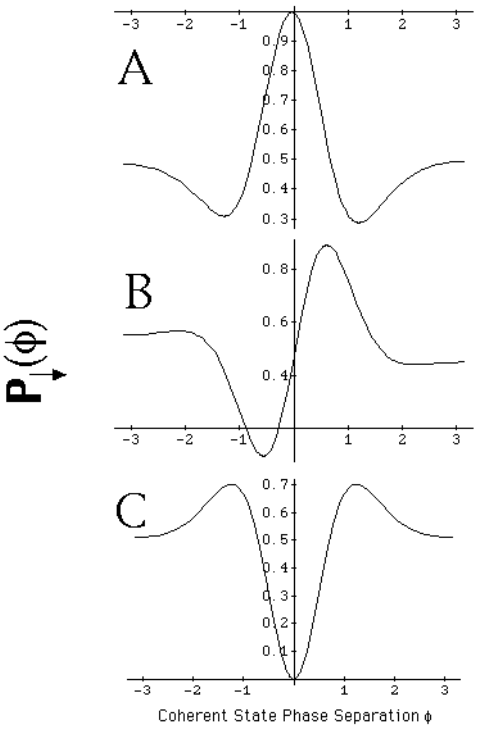

These results confirm that classical physics predicts the interference patterns observed by Monroe et al. [53] for a single $^9Be^+$ ion in a trap in a continuous Stern-Gerlach experiment without the requirement of Monroe [53] or Browne [52], "that an entire atom can simultaneously exist in two widely separated places."

SCHRÖDINGER FAT CATS—ANOTHER FLAWED INTERPRETATION

In 1935, Schrödinger [65] proposed a famous thought experiment in an attempt to demonstrate the limitations of quantum mechanics. He proposed a preposterous situation predicted by quantum mechanics in which a cat is put in a quantum superposition of alive and dead states. Believing in the validity of quantum mechanics has repetitively caused theoreticians to misinterpret and misrepresent physical observations as supporting such notions that lie outside the bounds of common sense or physical reality. For example, a recent report in The New York Times [64] entitled "Here, There and Everywhere: A Quantum State of Mind" states, "Physicists at Delft University of Technology have put a 5-micrometer-wide loop of superconducting wire into a 'quantum superposition' of two contradictory possibilities: in one, the current flows clockwise; in the other, current flows counterclockwise." The article further states, "In the realm of atoms and smaller particles, objects exist not so much as objects as mists of possibilities being here there and everywhere at the same time–and then someone looks and the possibilities suddenly collapse into definite locations." The experiment was a simplified version of the concept of Schrödinger's cat.

Instead of a cat, Friedman et al. [66], a Stony-Brook group working separately from the researchers at Delft, used a small square loop of superconducting wire linked to a SQUID (Superconducting Quantum Interference Device). A SQUID comprises a superconducting loop with a Josephson junction, a weak link that causes magnetic flux to be linked in integer units of the magnetic flux quantum. When the loop is placed in an external magnetic field, the loop spontaneously sets up an electrical current to cancel the field or generate an additional magnetic field, adjusting the magnetic field to a unit of the magnetic flux quantum, one of the allowed values. In the experiment of Friedman et al. [66], the loop was placed in a magnetic field equal to one half of the first allowed value, a magnetic flux quantum. Thus, the loop could set up either a current to raise the field strength to the first allowed value, or with equal probability, a current of equal magnitude flowing in the opposite direction to cancel out the external field. A pulse of microwaves was applied at the frequency to cause a transition of the magnetic moment of the current loop as an entirety. The absorption of microwaves caused the magnetic state of the SQUID to change and the current to reverse its direction.

Experimentally, a measurement always gave one of the two possible answers, clockwise or counterclockwise, never a zero cancellation. A difference in energy at which the flip transition occurred between the two possibilities was detected by a group led by J. Lukens and J. Friedman at the State University of New York (SUNY) [66]. A simple explanation was that the microwaves simply flipped the current direction which had an energy bias in one direction versus the opposite based on the corresponding presence or absence of a magnetic flux quantum within the SQUID. Rather, they interpreted the results as

experimental evidence that a SQUID can be put into a superposition of two magnetic flux states: one corresponding to a few microamperes of current flowing clockwise and the other corresponding to the same amount of current flowing anticlockwise. "Just as the cat is neither alive nor dead but a ghostly mix of the two possibilities, the current flows neither clockwise or counterclockwise, but is a mix of the two possibilities [64]." According to Friedman, "we can have two of these macroscopically well-defined states at the same time. Which is something of an affront to our classical intuitions about the world [64]."

Current running in both directions simultaneously is nonsensical. Current is a vector and must have only one direction. ***The energy difference observed by Friedman et al. can be explained CLASSICALLY.*** The experimental apparatus comprised a small SQUID coupled to a large current loop. A second SQUID magnetometer read the flux state of the first sample SQUID. The energy difference was not due to superposition of flux states. Rather, it was due to the nature of the electron which carries the superconducting current and links flux in units of the magnetic flux quantum. Consequently, the sample SQUID linked zero or one magnetic flux quantum. When excited by electromagnetic radiation of a resonant frequency, individual electrons undergo a spin-flip or Stern-Gerlach transition corresponding to a reversal of the electron magnetic moment, angular moment, and current. The Stern-Gerlach transition energies of electrons superimpose. ***The energy difference observed by Friedman et al. matches the energy corresponding to the flux linkage of the magnetic flux quantum by the ensemble of superconducting electrons in their entirety with a reversal of the corresponding macroscopic current.*** The linkage was caused by high power microwave excitation of a Stern-Gerlach transition of the magnetically biased loop which caused a concomitant change in the flux state of the separately magnetically biased sample SQUID. In this case, the microwave frequency was kept constant, and the bias flux of the loop was scanned at a fixed magnetic bias of the sample SQUID until the resonance with the superposition of the Stern-Gerlach transitions of the superconducting electrons in their entirety was achieved.

SUPERCONDUCTING QUANTUM INTERFERENCE DEVICE (SQUID)

The electron possesses an angular momentum of $\hbar$. As shown in the Electron g Factor section, the electron angular momentum comprises kinetic and vector potential components. Angular momentum is conserved in the presence of an applied magnetic field when the electron links flux in units of the magnetic flux quantum, Φ_0.

$$\Phi_0 = \frac{h}{2e} \tag{42.114}$$

This occurs when the electron rotates by $\frac{\pi}{2}$ radians about an axis perpendicular to the axis parallel to the magnetic flux lines. This electron rotation corresponds to an $\frac{\hbar}{2}$ magnitude, 180° rotation of the electron's angular momentum vector. In the case that the electrons carry current, this change in momentum of a given current-carrying electron increases or decreases the current depending on the vector projection of the momentum change onto the direction of the current. Recently, it has been demonstrated that 50-nm-diameter rings of *InAs* on a *GaAs* surface can host a single circulating electron in a pure quantum state, that is easily controlled by magnetic fields and voltages on nearby plates. The electrons were observed to link flux in the unit of the magnetic flux quantum with a gain in a unit of angular momentum in a specific direction with the linkage [67] as given in the Aharonov-Bohm Effect section. Since the electron links flux in units of the magnetic flux quantum, the magnetic flux that links a superconducting loop with a weak link called a Josephson junction is the magnetic flux quantum. The factor of $2e$ in the denominator of the magnetic flux quantum (Eq. (42.114)) has been erroneously interpreted [68] as evidence that Cooper pairs are the superconducting current carriers which is central to the BCS theory of superconductors. However, single electrons, not electron pairs, are the carriers of the superconducting current.

The supercurrent and the linkage of flux is dissipationless; thus, the general form of the equation for the energy of a Josephson junction is a harmonic function as given by Fowles [69]. Each electron links flux only in units of the magnetic flux quantum, Φ_0, given by Eq. (42.114). Thus, the parameter in terms of the applied flux, Φ, that corresponds to the natural frequency of a harmonic oscillator is the magnetic flux quantum, Φ_0. From Friedman et al. [66]:

> The simplest SQUID (the radio frequency (r.f.) SQUID) is a superconducting loop of inductance L broken by a Josephson junction with capacitance C and critical current I_c. In equilibrium, a dissipationless supercurrent can flow around this loop, driven by the difference between the flux Φ that threads the loops and the external flux Φ_x applied to the loop. The dynamics of the SQUID can be described in terms of the variable Φ and are analogous to those of a particle of "mass" C (and kinetic energy $\frac{1}{2}C\dot{\Phi}^2$) moving in a one-dimensional potential given by the sum of the magnetic energy of the loop and the Josephson coupling energy of the junction.
>
> $$U = U_0\left[\frac{1}{2}\left(\frac{2\pi(\Phi-\Phi_x)}{\Phi_0}\right)^2 - \beta_L\cos\left(2\pi\frac{\Phi}{\Phi_0}\right)\right] \tag{42.115}$$
>
> where Φ_0 is the flux quantum,
>
> $$U_0 \equiv \frac{\Phi_0^2}{4\pi^2 L} \tag{42.116}$$

and

$$\beta_L \equiv \frac{2\pi L I_C}{\Phi_0} \tag{42.117}$$

For the parameters of our experiment, this is a double-well potential separated by a barrier with a height depending on I_c. When $\Phi_x = \frac{\Phi_0}{2}$ the potential is symmetric. Any change in Φ_x then tilts the potential [...].

In the experiment of Friedman et al. [66], the flux state of the sample SQUID was zero or one fluxon. A static current flowed either clockwise or counterclockwise around the loop to cancel or augment Φ_x such that an allowed fluxon state was maintained.

EXPERIMENTAL APPROACH

The SUNY experiment was a macroscopic Stern-Gerlach experiment on a macroscopic current loop coupled to a small d.c. SQUID (sample SQUID). The SQUID and the current loop were independently biased with externally applied flux. From Friedman et al. [66]:

> The SQUID used in these experiments was made up of two $Nb/AlO_x/Nb$ tunnel junctions in parallel as shown in Figure 42.14. This essentially acts as a tunable junction in which I_c can be adjusted with a flux $\Phi_{xd.c.}$ applied to the small loop of the d.c. SQUID. Another flux Φ_x applied to the loop tuned the tilt ε of the potential wherein $\Phi_{xd.c.}$ tuned the barrier height ΔU_0 at $\varepsilon = 0$. The SQUID was biased such that it was in a zero or one fluxon state. A separate d.c. SQUID inductively coupled to the sample acted as a magnetometer, measuring the flux state of the sample SQUID: zero or one fluxon.
>
> The sample SQUID used in the experiments was characterized by the following three energies:

the charging energy

$$E_c \equiv \frac{e^2}{2C} = 9.0\ mK \tag{42.118}$$

the inductive energy

$$E_L \equiv \frac{\Phi_0^2}{2L} = 645\ K \tag{42.119}$$

and a tunable Josephson coupling energy

$$E_J \equiv \left(I_c \frac{\Phi_0}{2\pi}\right)\cos\left(\frac{\pi\Phi_{xd.c.}}{\Phi_0}\right) = 76\ K\cos\left(\frac{\pi\Phi_{xd.c.}}{\Phi_0}\right) \tag{42.120}$$

The angular frequency of the plasma, ω_J, associated with these parameters was $1.5-1.8\ X\ 10^{11}\ rad\ s^{-1}(24-29\ GHz)$ depending on the value of $\Phi_{xd.c.}$. The fact that $E_c << E_L,\ E_J$ confirms that flux was the proper basis to describe the SQUID's dynamics.

The sample was encased in a PdAu radiation shield with a coaxial cable entering the shield to provide for the controlled application of external microwaves. The apparatus was carefully filtered and cooled to about 40 mK in a dilution refrigerator.

The flux Φ_x tilted the potential from being symmetric at $\Phi_x = \frac{\Phi_0}{2}$ according to Eq. (42.115). It was varied over the range $\frac{\Phi_0}{2} + 11.5\ m\Phi_0 < \Phi_0 < \frac{\Phi_0}{2} + 15.5\ m\Phi_0$. The barrier height ΔU_0 was varied over the range $8.559\ K \le \Delta U_0 \le 9.117\ K$. The SQUID was established in one state and excited with a pulse of high power 96.0 *GHz* (4.61 *K*) microwaves as Φ_x was scanned. The values of Φ_x at which photon absorption occurred with a change of flux state of the SQUID was recorded at a fixed barrier height ΔU_0. The experiment was repeated with ΔU_0 changed.

The system was initially prepared in a zero or one fluxon state with an energy barrier ΔU_0 and a tilt energy ε. Millisecond pulses of 96 GHz microwave radiation at a fixed power were then applied. When the energy difference between the initial and final states matched the resonance frequency as ε was varied for a given ΔU_0, the system had an appreciable probability of changing flux state which was detected by the magnetometer. The experiment was repeated for different values of ΔU_0.

Figure 42.14. The experimental set-up.

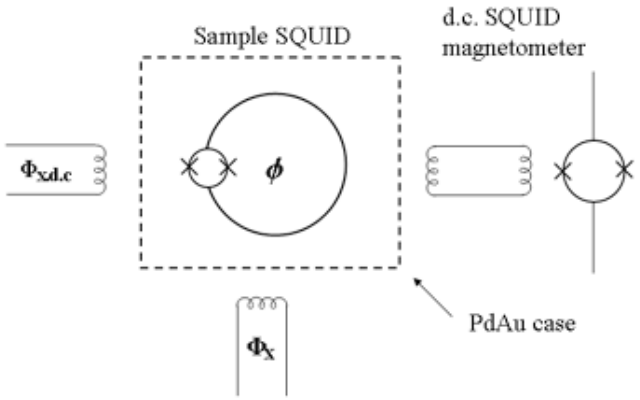

DATA

The probability of the sample SQUID making a flux state transition when a millisecond pulse of $96.0\,GHz$ $(4.61\,K)$ microwaves was applied was recorded as shown in Figure 42.15. For each ΔU_0, two peaks were observed as Φ_x was varied. As the energy barrier ΔU_0 was reduced, the observed peaks moved closer together and then separated without crossing. For $\Delta U_0 = 9.117\,K$ (thick solid curve), the right peak corresponds to level $|0\rangle$ which has a greater relative amplitude than the left peak which corresponds to level $|1\rangle$. When ΔU_0 was decreased to $8.956\,K$ (dotted curve), the peaks moved closer, and the asymmetry disappeared. As the barrier was decreased further ($8.797\,K$ is the dashed curve), the peaks moved apart again, and the asymmetry reappeared. But, in this case, the left larger peak corresponded to level $|0\rangle$. Thus, with a barrier change of about $2\,X\ 0.14\,K$, the two levels passed through the point at which the levels were symmetrical according to Eq. (42.115) at about $\Delta U_0 = 8.956\,K$ and changed roles without actually intersecting. The insert shows the position of the peaks in the main figure (as well as other peaks) in the $\Delta U_0 - \Phi_x$ plane. Two examples of the convergence and divergence of the peaks in the $\Delta U_0 - \Phi_x$ plane at point where the levels were symmetrical according to Eq. (42.115) were observed. The dashed line in the insert represents the locus of points where the calculated top of the energy barrier was 96 GHz above state $|i\rangle$. All of the data lies to the left of the dashed line and therefore, corresponds to levels that are below the top of the barrier according to Eq. (42.115).

Figure 42.15. The probability P_{switch} of making a flux state transition when a millisecond pulse of 96-GHz microwave radiation is applied. For clarity, each curve is shifted vertically by 0.3 relative to the previous one. The insert shows the position of the observed peaks in the $\Delta U_0 - \Phi_x$ plane. This image reproduced with permission from Nature.

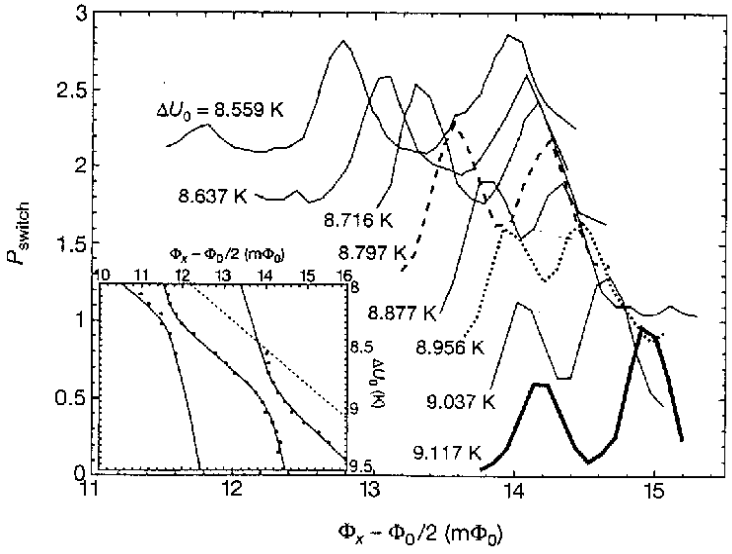

The inductance L and the impedance $Z \equiv \sqrt{L/C}$ of the loop, and the Josephson coupling parameter β_L of the sample SQUID were measured independently. The values were $L = 240 \pm 15\,pH$, $Z = 48.0 \pm 0.1\,\Omega$, and $\beta_L = 2.33 \pm 0.01$. The energy

levels of the flux states $|0\rangle$ and $|1\rangle$ E_{level} as a function of ε relative to their mean energy $E_{mean}(\Delta U_0, \Phi_x)$ using the experimentally measured *L*, *Z*, and β_L are shown in Figure 42.16. At the middle at which point the levels were symmetrical according to Eq. (42.115), the two levels have a splitting of about $\Delta = 0.14\ K$ in energy and the upper level is about $\Delta = 0.14\ K$ below the top of the energy barrier as calculated from Eq. (42.115).

Figure 42.16. Energy of the measured peaks relative to the calculated mean of the two levels as a function of ε. This image reproduced with permission from Nature.

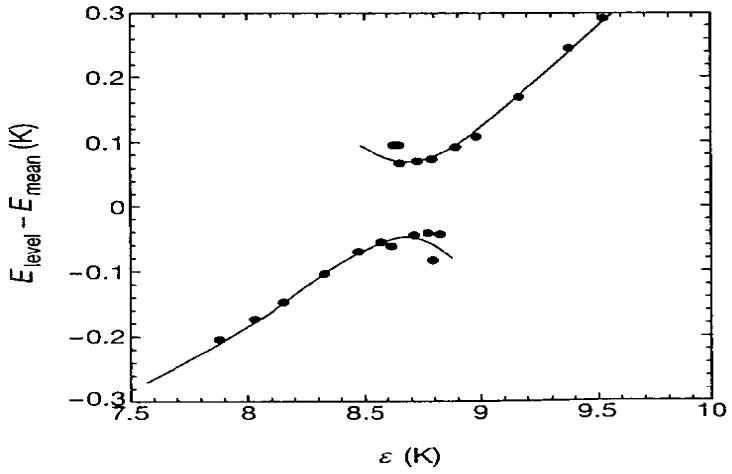

The quantum dynamics of the SQUID was determined by the flux through the loop, a collective phenomenon representing the superposition of about 10^{10} electrons acting in tandem. Since the experimental temperature was about 500 times smaller than the superconducting gap, almost all of the microscopic degrees of freedom were frozen out, and only the collective flux transition retained any dynamic relevance. The flux states $|0\rangle$ and $|1\rangle$ differed in flux by Φ_0 and differed in current by $2-3\ \mu A$. Given the geometry of the SQUID this corresponded to a local magnetic moment of $10^{10}\ \mu_B$.

QUANTUM INTERPRETATION

According to quantum theory, a superposition of fluxoid states $|0\rangle$ and $|1\rangle$ would manifest itself in an anticrossing defined as the lifting of the degeneracy of the energy levels of the two states at the point at which the states would be degenerate in the absence of coherence. Coherent tunneling lifts the degeneracy so that at the degeneracy point, the energy eigenstates are the symmetric and antisymmetric superposition of flux-basis states: $\frac{1}{\sqrt{2}}(|0\rangle + |1\rangle)$ and $\frac{1}{\sqrt{2}}(|0\rangle - |1\rangle)$. The energy difference ΔE between the two states is given approximately by

$$\Delta E = \sqrt{\varepsilon^2 + \Delta^2} \tag{42.121}$$

where Δ is known as the tunnel spitting. For a given ΔU_0, Eq. (42.115) predicts that two peaks would be observed as ε is varied by varying Φ_x. It further predicts that the peak separation should decrease and cross as the experiment is repeated for different values of ΔU_0. The lifting of degeneracy or splitting was anticipated to be observed as a decrease in peak separation and a reversal of the flux states in the $\Delta U_0 - \Phi_x$ plane without crossing. Friedman et al. sought to demonstrate the existence of such a splitting to support the notion of superposition of flux states corresponding to clockwise and counterclockwise currents simultaneously.

CLASSICAL INTERPRETATION

Two sets of peaks are given by Eq. (42.115) which is derived from CLASSICAL PHYSICS. The nondegeneracy of the energy levels and the absence of crossing of the peaks was due to the linkage of flux by the electrons of the supercurrent.

As given in the Electron g Factor section (Eq. (1.164)), the angular momentum of the electron in the presence of an applied magnetic field is

$$\mathbf{L} = \mathbf{r} \times (m_e \mathbf{v} + e\mathbf{A}) \tag{42.122}$$

where $\mathbf{A}$ is the vector potential of the external field evaluated at the location of the electron. Conservation of angular momentum of the electron permits a discrete change of its "kinetic angular momentum" $(\mathbf{r} \times m\mathbf{v})$ by the field of $\frac{\hbar}{2}$, and

concomitantly the "potential angular momentum" ($\mathbf{r}\times e\mathbf{A}$) must change by $-\frac{\hbar}{2}$. To conserve angular momentum in the presence of an applied magnetic field, the electron magnetic moment can be parallel or antiparallel to an applied field as observed with the Stern-Gerlach experiment, and the flip between orientations (a rotation of $\frac{\pi}{2}$) is accompanied by the "capture" of the magnetic flux quantum by the electron.

According to Eq. (1.168), the energy to flip the orientation of the atomic orbital due to its magnetic moment of a Bohr magneton, μ_B, is

$$\Delta E_{mag}^{spin\ moment} = 2\mu_B B \tag{42.123}$$

where

$$\mu_B = \frac{e\hbar}{2m_e} \tag{42.124}$$

The energy change corresponding to the "capture" of the magnetic flux quantum is derived below. From Eq. (1.171), the energy stored in the magnetic field of the electron is:

$$E_{mag} = \frac{\pi\mu_0 e^2\hbar^2}{(m_e)^2 r_n^3} \tag{42.125}$$

The atomic orbital is equivalent to a Josephson junction which can trap integer numbers of fluxons where the quantum of magnetic flux is $\Phi_0 = \frac{h}{2e}$. Thus, Eq. (1.181) gives:

$$\Delta E_{mag}^{fluxon} = 2\frac{\alpha}{2\pi}\mu_B B \tag{42.126}$$

The principal energy of the transition of reorientation of the atomic orbital is given by Eq. (1.168). And, the total energy of the flip transition is the sum of Eq. (1.181), the energy of a fluxon treading the atomic orbital and Eq. (1.168), the energy of reorientation of the magnetic moment (Eqs. (1.226-1.227)). Considering only the magnetic energy term,

$$\Delta E_{mag}^{spin} = 2\left(\mu_B B + \frac{\alpha}{2\pi}\mu_B B\right) \tag{42.127}$$

$$\Delta E_{mag}^{spin} = 2(1+\frac{\alpha}{2\pi})\mu_B B \tag{42.128}$$

$$\Delta E_{mag}^{spin} = g\mu_B B \tag{42.129}$$

The spin-flip transition can be considered as involving a magnetic moment of g times that of a Bohr magneton. The g factor is redesignated the fluxon g factor as opposed to the anomalous g factor. The value of $\frac{g}{2}$ considering only the first term is 1.00116. The experimental value is 1.00116. (See Eqs. (1.236-1.237)).

The energy difference Δ of the flux states $|0\rangle$ and $|1\rangle$ was not the tunnel spitting energy sought by Friedman et al. to support the notion of superposition of flux states corresponding to clockwise and counterclockwise currents simultaneously. The microwaves simply flipped the current direction which had an energy bias in one direction versus the opposite based on the corresponding presence or absence of a magnetic flux quantum within the SQUID. The energy difference was due to the linkage of flux by the current carrying superconducting electrons with a reversal of the current direction and a corresponding change in the flux state of the sample SQUID. The loop and SQUID transition resulted from a Stern-Gerlach transition of a magnetic moment of 10^{10} μ_B that was equivalent to the superposition of 10^{10} electrons. The macroscopic spin-flip occurred by the absorption of high power microwave energy at the 96 GHz resonance frequency of the equivalent macroscopic magnetic moment. The energy of the 10^{10} electrons linking flux of $\frac{1}{2}\Phi_0$ is calculated from Eq. (42.126) by determining the magnetic flux due to 10^{10} electrons.

The magnetic moment of 10^{10} electrons, μ, is given by the number of electrons times a Bohr magneton μ_B of magnetic moment per electron.

$$\mu = 10^{10}\mu_B \tag{42.130}$$

The magnetic moment is equal to the current of the loop I times the area of the loop A.

$$\mu = 10^{10}\mu_B = IA \tag{42.131}$$

The magnetic flux B is given by one half the magnetic flux quantum Φ_0 divided by the area of the loop which is given by Eq. (42.131).

$$B = \frac{\frac{1}{2}\Phi_0}{A} = \frac{\frac{1}{2}\Phi_0}{\frac{\mu}{I}} = \frac{\frac{1}{2}\Phi_0}{\frac{10^{10}\mu_B}{I}} \tag{42.132}$$

The energy of the 10^{10} electrons linking flux of $\frac{1}{2}\Phi_0$ by reversing the direction of supercurrent is calculated from Eq. (42.126) and Eq. (42.132) wherein the energy is one half that given by Eq. (42.126) because the flux state of the loop is initially biased at about the symmetrical point.

$$\Delta E_{mag}^{fluxon} = 10^{10}\frac{\alpha}{2\pi}\mu_B B = 10^{10}\frac{\alpha}{2\pi}\mu_B\frac{\frac{1}{2}\Phi_0}{\frac{\mu}{I}} = 10^{10}\frac{\alpha}{2\pi}\mu_B\frac{\frac{1}{2}\Phi_0}{\frac{10^{10}\mu_B}{I}} = \frac{\alpha}{4\pi}I\Phi_0 \tag{42.133}$$

The linkage of $\frac{1}{2}\Phi_0$ occurs when the electron rotates by $\frac{\pi}{2}$ radians about an axis perpendicular to the axis parallel to the magnetic flux lines. This electron rotation corresponds to an $\frac{\hbar}{2}$ magnitude, 180° rotation of the electron's angular momentum vector. Since the electrons carry current, this reversal in momentum reverses the current according to the vector projection of the momentum change onto the direction of the current. Since the current reverses direction when a magnetic fluxon treads the loop of the SQUID, the current I is given by one half of the critical current I_c. The critical current I_c may be calculated from the Josephson coupling parameter β_L of the sample SQUID given by Eq. (42.117) using the independently measured value of $\beta_L = 2.33 \pm 0.01$ and the inductance $L = 240 \pm 15\ pH$.

$$I_C \equiv \frac{\beta_L\Phi_0}{2\pi L} = \frac{(2.33)\Phi_0}{2\pi\left(240\times10^{-12}\ H\right)} = 3.2\ \mu A \tag{42.134}$$

Substitution of one half I_c given by Eq. (42.134) into Eq. (42.133) gives the energy difference between the flux states.

$$\Delta E_{mag}^{fluxon} = \frac{1}{2}\left(\frac{\alpha}{2\pi}\right)\left(\frac{1}{2}I_c\right)\Phi_0 = \frac{1}{4}\left(\frac{\alpha}{2\pi}\right)I_c\Phi_0 = \frac{1}{4}\alpha\frac{I_c\Phi_0}{2\pi}$$

$$\Delta E_{mag}^{fluxon} = \frac{\alpha}{4\pi}\frac{\beta_L\Phi_0}{4\pi L}\Phi_0 = \frac{\alpha(2.33)(\Phi_0)^2}{(4\pi)^2\left(240\times10^{-12}\ H\right)} = 0.012\ meV = 0.139\ K \tag{42.135}$$

Using Eqs. (42.115-42.117), the Josephson coupling energy of the junction U_J can be written in a form that is similar to that given by Eq. (42.135). From Eq. (42.115),

$$U_J = U_0\beta_L\cos\left(2\pi\frac{\Phi}{\Phi_0}\right) \tag{42.136}$$

Substitution of Eq. (42.116) for U_0 and Eq. (42.117) for β_L gives

$$U_J = U_0\beta_L\cos\left(2\pi\frac{\Phi}{\Phi_0}\right) = \frac{\Phi_0^2}{4\pi^2 L}\beta_L\cos\left(2\pi\frac{\Phi}{\Phi_0}\right) = \frac{\Phi_0^2}{4\pi^2 L}\frac{2\pi L I_C}{\Phi_0}\cos\left(2\pi\frac{\Phi}{\Phi_0}\right) = \frac{I_C\Phi_0}{2\pi}\cos\left(2\pi\frac{\Phi}{\Phi_0}\right) \tag{42.137}$$

The SQUID links flux in integer units of the magnetic flux quantum; thus, the Josephson coupling energy of the junction U_J is

$$U_J = \frac{I_C\Phi_0}{2\pi} \tag{42.138}$$

The switch between Stern-Gerlach states is predicted to be Lorentz with a maximum transition intensity or probability at the energy level of 96 GHz difference between the states. The energy of the magnetic level $|0\rangle$ or $|1\rangle$ was tuned by the flux $\Phi_{xd.c.}$ which was tilted by flux Φ_x applied to the large current loop. In the case that the flux $\Phi_{xd.c.}$ corresponded to an energy level above the symmetrical case according to Eq. (42.115), the initial flux state $|0\rangle$ underwent a transition to the state $|1\rangle$ at a higher flux Φ_x than in the case that $|1\rangle$ under went a transition to the state $|0\rangle$. In the case that the flux $\Phi_{xd.c.}$ corresponded to an energy level above the symmetrical case according to Eq. (42.115), the situation was reversed. The states were nondegenerate at the symmetrical point according to Eq. (42.115) because an energy bias existed based on the presence or

absence of a magnetic flux quantum within the SQUID. Consequently, the energy difference of the peaks decreased to a minimum as the symmetrical point was approached, reversed assignments without crossing, and separated again. The data demonstrate a difference in the energies of the flux states even at the point at which they were symmetrical according to Eq. (42.115). The difference was due to linking of flux by the superconducting electrons. The transition probability of state $|0\rangle$ to the state $|1\rangle$ occurred with slightly greater probability than the later since the potential energy of the state $|0\rangle$ was greater than of the state $|1\rangle$. Thus, the intensity ratios of the peaks reversed also with the interchange of the assignments of the peaks as shown in Figure 42.15.

The energy of the 10^{10} electrons linking flux of $\frac{1}{2}\Phi_0$ is equivalent to the energy difference Δ of the flux states $|0\rangle$ and $|1\rangle$ of about $\Delta = 0.14\ K$ measured by Friedman et al as shown in Figure 42.16. The energy of the highest energy level is predicted to be about $\Delta = 0.14\ K$ below that given by Eq. (42.115) since the SQUID is biased by about $\frac{1}{2}\Phi_0$ with flux $\Phi_{xd.c.}$ which is perturbed by flux Φ_x. The measured value of about $\Delta = 0.14\ K$ is in good agreement with the predicted value.

The phenomenon observed by Friedman et al. [66] is similar to that of the Aharonov-Bohm Effect and the results of Monroe et al. [53] given in the Aharonov-Bohm Effect section and the Schrödinger "Black" Cats section, respectively. In the first case, the results of a damped harmonic oscillatory behavior of the ratio of the change in resistance and the resistance as a function of the flux applied to a current loop was erroneously interpreted as interference of electron wave-functions. The results were due to the linkage of flux by electrons in units of the magnetic flux quantum. In the latter case, the results were erroneously interpreted as demonstrating that an entire atom can simultaneously exist in two widely separated places and interfere with itself. The results were due to an interference between an oscillatory translational mode and a Stern-Gerlach transition of the electron of a trapped charged ion. Similarly, the SUNY results confirm that classical physics predicts the splitting or difference in energy between flux states observed by Friedman et al. The behavior of a biased SQUID coupled to a biased macroscopic loop having the possibility of either clockwise or counterclockwise current that is interchanged by a Stern-Gerlach experiment is predicted quantitatively. The prediction is without the requirement of Friedman et al. [66] or Chang [64], that "Physicists have put a loop of superconducting wire into a 'quantum superposition' of two contradictory possibilities: in one, the current flows clockwise; in the other, current flows counterclockwise."

CLASSICAL ALL THE WAY UP

Since a SQUID is quantized in its excited-energy states according to the magnetic flux quantum imposed by the intrinsic z-component of angular momentum of each electron of $\frac{\hbar}{2}$, it can be integrated into instrumentation that has unique capabilities such as extreme measurement sensitivity or control via exploiting this quantization. For example, SQUID magnetometers employ a resonant RF tank circuit that is inductively coupled to the SQUID as the primary flux-sensing component that has extreme sensitivity due to the flux quantization of the measured field at the fine level of the magnetic flux quantum Φ_0. The characteristic frequency of a SQUID based on the Josephson effect called the Josephson constant is precisely reproducible independent of device design, material, measurement setup, etc. The recommended value is [70]:

$$K_J = \frac{2e}{h} = 0.483597879\ GHz / \mu V \tag{42.139}$$

No correction terms are required in a practical implementation of using the Josephson effect and constant as a standard for calibrating or defining the volt by an exact voltage-to-frequency conversion, combined with the cesium-133 time reference, as decided by the 18th General Conference on Weights and Measures. Typically an array of several thousand or tens of thousands of junctions are used, excited by microwave signals between 10 and 80 GHz depending on the array design [71]. A Josephson junction qbit is another device comprising a SQUID. The qbit, in principle, can accept energy in quantized units from an excited resonator. Conversely, by exploiting the SQUID quantization of energy levels, the qbit is also permissive of driving systems, even macroscopic systems, with quantized excitation when such as system is capable of quantized resonances. The resonance energy exchanges between the energy levels of the two systems, qbit and macroresonator, may occur when the pair are tuned to be coupled. Familiar quantized macrodevice candidates are lasers, masers, resonators, and waveguides. The list of candidate quantization-capable devices may even be extended to those that employ mechanical with optoelectronic elements that are inherently quantized. Both of the resonantly coupled systems must obey the same physical laws in order to exchange energy. Such a classical-physics based tunable resonance energy coupling between qbit and an optoelectronics-mechanical macrodevice has been achieved experimentally [72] again demonstrating that classical physics applies to all levels, atomic to macroscale. Lacking the knowledge of the classical solutions and behavior of electrons, the device has been mischaracterized in terms of quantum mechanics.

Recently O'Connell et al. [72] claimed to have achieved a quantum state of motion for a mechanical object by causing a Josephson junction qbit to be entangled with a macroscopic mechanical resonator and thereby extending, in their opinion, the weird rules of quantum mechanics such as zero-order vibration and entanglement to the macroworld. In reality, O'Connell's team has only shown that classical physics applies to the macroworld by a mechanism that also proves that it applies to the atomic scale; moreover, zero-order vibration is experimentally shown to be nonexistent. Based on the experimental data

provided [72], it is easy to confirm that the device that they fabricated and tested is no more than a variant of a SQUID, a known macrodevice. However, it uniquely exploits piezoelectricity to form the weak link of a superconducting loop to enable the device. Specifically, the device comprised a superconducting microwave circuit having a circuit element of a capacitor with aluminum electrodes filled with an AlN piezoelectric dielectric wherein the assembly was attached only by aluminum leads such that it was mechanically free to vibrate by contraction and expansion of the piezoelectric layer. The mechanical resonator produced and responded to an electric field due to the correspondence between the mechanical distortion manifested as vibration and the piezoelectric field. The constraint of quantized flux linkage in units of the magnetic flux quantum, $\Phi_0 = h/2e$, correspondingly quantized the mechanical vibrational frequency. The circuit dimensions and resonant circuit including excitation electronics were typically of those of prior SQUIDs.

As shown in the exemplary corresponding sections regarding macrocurrent loops that comprise SQUIDs and demonstrate the Aharonov-Bohm Effect, the physics of single electrons can be manifest on the macroscale when the metal becomes a superconductor. The operating temperature of 25 mK of O'Connell et al. [72] was well below critical temperature T_c of Al (1.175 K) [73]. The piezoelectric vibration of their mechanical resonator gives rise to an oscillatory electric field that carries an electric displacement current in the dielectric and acts as a weak link of a superconducting current loop. Thus, the piezoelectric device comprises a SQUID with a characteristic resonance frequency for linkage of flux in quantized units of the magnetic flux quantum. The resonance frequency may be determined from the magnetic flux quantum, $\Phi_0 = h/2e$, the corresponding fundamental charge that carries the linkage current, $2e$, and the measured inductance of the circuit element, $L_m = 1.043\ \mu H$:

$$f = \frac{\Phi_0}{L2e} = \frac{2.0678506\ X\ 10^{-15}\ Wb}{\left(1.043X\ 10^{-6}\ H\right)(2)\left(1.6021892X\ 10^{-19}\ C\right)} = 6.187\ GHz \tag{42.140}$$

This frequency is shifted slightly due to the other RLC components of the circuit. The mechanical frequency of vibration is given by

$$f = \frac{v}{2t} = \frac{9100\ m/s}{2((150+130+330+130)\ X\ 10^{-9}\ m)} = 6\ GHz \tag{42.141}$$

where v is the average sound speed and t is the resonator thickness that is also the length of the displacement current and weak link portion of the superconducting loop. The existence of a mechanical frequency that can support the quantized SQUID resonance frequency is a necessary condition for the operation of the circuit element as a quantized macrodevice.

O'Connell et al. [72] experimentally measured the reactive and resistive microwave circuit elements according to their inductance, capacitance, and resistance, and performed classical circuit analysis. An open circuit condition between the two SQUIDS was achieved via detuning the qbit to cause an impendence mismatch between them. Then, O'Connell et al. [72] applied microwaves to the first mechanical SQUID independently of the second (qbit) and demonstrated that the first was excited in a quantized manner. This independent quantized excitability feature of the resonator shown experimentally with classical direct microwave excitation of the mechanical resonator disproved entanglement. Furthermore, no RF reactive signal was detectable in the qbit when it was set to interact with the mechanical SQUID in its "ground" vibrational state. This confirmed that the mechanical vibrator was at rest; otherwise, an electric field must be generated based on the correspondence of the mechanical vibration and the piezoelectric oscillatory electric field. That is, a reactive electric field must be present for a vibrating oscillator, and it was absent. Moreover, no motion is possible in the "ground" state of vibration. The mechanical resonator element comprises a SQUID that links flux only with the corresponding required vibrational excitation. Conversely, since the flux of the SQUID ground state is known to be zero, the corresponding state of the mechanical resonator must be in the rest state. Thus, zero order vibration was proved to be nonexistent.

Conversely to uncoupled measurements, the qbit SQUID tank circuit microwave excitation and flux bias were tuned to impedance match the mechanical SQUID resonance to cause exchange of quanta of energy determined by the quantized flux linkage of each SQUID. The excitations, exchange behavior with tuning, transition times, cross-sections, and dynamic coupling involving linear combinations of the SQUID energy states matched those predicted by classical circuit modeling. Thus, classical laws were shown to apply on the macroscale based on their validity on the atomic scale. In future experiments, the classical behavior of the mechanical resonator circuit comprising a SQUID can be further confirmed by the testing of the predicted effect of flux bias on the resonance behavior uncoupled and coupled to the qbit. This will provide more insight into the linkage of classical physics between different orders of magnitude of scale.

FREE ELECTRONS IN SUPERFLUID HELIUM ARE REAL IN THE ABSENCE OF MEASUREMENT REQUIRING A CONNECTION OF $\Psi(x)$ TO PHYSICAL REALITY

A challenge to the fundamental foundations of quantum mechanics has arisen based on experiments of free electrons injected into superfluid helium [12]. From the time of its inception, the quantum mechanical meaning of the electron wave function has been enigmatic, debated, and fluid. A now popular interpretation is a zero or one-dimensional point in an all-space probability-wave function $\Psi(x)$ that only becomes "real" by act of measurement. However, the behavior of free electrons in superfluid helium has again forced the issue of the meaning of the wavefunction and its connection with reality. Electrons form bubbles in superfluid helium, which reveal that the electron is real and that a physical interpretation of the wavefunction is necessary. Furthermore, when irradiated with low energy light, the electrons carry increased current at different rates as if they exist with at least 15 different sizes.

Interpretations of quantum mechanics such as hidden variables, multiple worlds, consistency rules, and spontaneous collapse have been put forward in an attempt to base the theory in reality. The Copenhagen interpretation asserts that what we observe is all we can know; any speculation about what an electron, photon, atom, or other atomic-sized entity really is or what it is doing when we are not looking is just that—speculation. The postulate of quantum measurement asserts that the process of measuring an observable forces it into a state of reality. In other words, reality is irrelevant until a measurement is made. In the case of electrons in helium, the fallacy with this position is that the "ticks" (migration times of electron bubbles) reveal that the electron is real before a measurement is made. Maris and other experimental physicists believe that the data on electrons in liquid helium reveals that the electron is real and physical and exposes a fundamental flaw in quantum theory [74–76]. Physicists have always been content to think of the wave function, the immeasurable entity which describes quantum systems, as a mathematical device with observable consequences. The time has come for the idea to be grounded in reality. For the electron bubbles in helium, Maris' position is that the size of the bubble is determined by how much of the wave function is trapped inside the bubble. "If there is no part of the wave function inside the bubble, the bubble will collapse. This makes the wave function seem to be a tangible object. Theoreticians are going to have to address the question: what is a wave function? Is it a real thing, or just a mathematical convenience? [74]"

In the 111 years since its discovery, there has been no evidence whatsoever that the electron is divisible. But, in order to explain the increase in conductivity of free electrons in superfluid helium when irradiated with low energy light and the observation of an unexpected plethora of exotic negative charge carriers in superfluid helium with mobilities greater than that of the normal electron Maris has proposed [77] that the electron breaks into equal-sized fragments which he calls "electrinos." According to Maris, this process of division of the electron may continue to such that the electron breaks into two and then the 1/2 electrons may divide into two forming 1/4 electrons, and the process may repeat indefinitely. Maris argues that the Schrödinger equation solution of the wavefunction of the $1p$ state, an excited state, will break into two following the $1s$ to $1p$ transition of an electron in superfluid helium. This result is a consequence of the localization of the maximum electron probability density, $\Psi(x)$, in the extremes of the dumb-bell shaped $1p$ orbital with the existence of a node at the center of the orbital. Maris likens $\Psi(x)$ to a physical electron density bubble. The large differences in time scales of the motion of the electron and the motion of the bubble wall means that the Franck-Condon principle should apply and that the wave function of the electron will deform adiabatically (Born-Oppenheimer principle) at this node to result in electron fission. Following the break, one half of the electron's wave function is trapped in each of the two daughter bubbles. As the wave function is the essence of an electron, the electron splits into two. One piece acquires all of the charge and the other is neutral.

Of course the electron cannot break into two or more pieces, and $\Psi(x)$ can not be an electron density function based on scattering experiments as pointed out by Max Born who formulated the currently accepted probability wave interpretation of $\Psi(x)$. The physical explanation for the free-electron photoconductivity and mobility observations is provided by the nature of the free electron as an atomic orbital in liquid helium and by the nature of its excited states. The nature of these states follows from the solution of the bound electron and its excited states given in One-Electron Atom and the Excited States of the One-Electron Atom (Quantization) sections, respectively. Free electrons in liquid helium form physical hollow bubbles that serve as resonator cavities that transition to long-lived metastable states of fractional (1/integer) sizes that migrate at different rates when an electric field is applied as shown in Figure 42.17. The predicted behavior for allowed fractional-principal-quantum-energy states of the electron in liquid helium matches the formerly inexplicable photoconductivity and mobility observations.

Figure 42.17. Free electrons in liquid helium form physical hollow bubbles that serve as resonator cavities that transition to fractional (1/integer) sizes and migrate at different rates when an electric field is applied. (A) Free electrons are trapped in superfluid helium as autonomous hollow electron bubbles. (B) Photons are absorbed by the *bubble-like* atomic orbital that serve as resonator cavities. (C) The excitation of the Maxwellian resonator cavity modes by resonant photons form long-lived states having quantum numbers n, ℓ, and m_ℓ with radii of reciprocal integer multiples that of the unexcited $n=1$ state. (D-F) The normal bubble (F) with the radius, r_1, and each stable excited state electron bubble with radius $\frac{r_1}{\text{integer}}$ (D-E) may migrate in an applied electric field, and the time of flight to a detector decreases with the size of the bubble. The absorption spectrum of free electrons in superfluid helium and their mobilities predicted from the corresponding size and multipolarity of these bubble-like states with quantum numbers n, ℓ, and m_ℓ matched the experimental results of 15 identified ions.

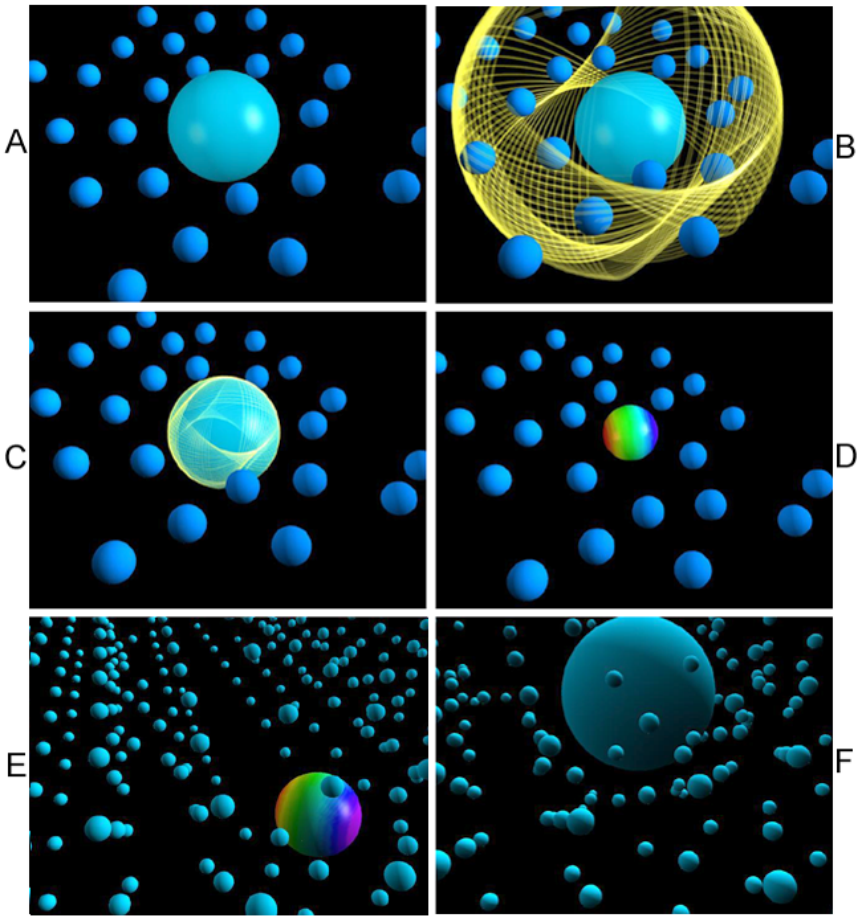

Specifically, free electrons are trapped in superfluid helium as autonomous electron bubbles interloped between helium atoms that have been excluded from the space occupied by the bubble. The surrounding helium atoms maintain the spherical bubble through van der Waals forces. The *bubble-like* "*wavefunction*" called an atomic orbital can act as a resonator cavity. The excitation of the Maxwellian resonator cavity modes by resonant photons form bubbles with radii of reciprocal integer multiples of that of the unexcited $n=1$ state. The central force that results in a fractional electron radius compared to the unexcited electron is provided by the absorbed photon. Each stable excited state electron bubble which has a radius of $\frac{r_1}{\text{integer}}$ may migrate in an applied electric field. Superfluid helium is an ideal medium to study individual trapped electrons in much the same way that individual ions may be studied in Penning traps. An equation for the electron bubble mobility is based on a well known roton-bubble momentum transfer cross section using the geometrical cross section and the multipolarity of the different electron states. Experiments to study the effect of light on ion mobility have been conducted [12, 74]. The photo-conductivity absorption spectrum of free electrons in superfluid helium and their mobilities predicted from the corresponding size and multipolarity of these long-lived bubble-like states with quantum numbers n, ℓ, and m_ℓ matched the experimental results of the 15 identified ions. Electrons bubbles in superfluid helium reveal that the electron is real and that a physical interpretation of the wavefunction is necessary. The concept of probability waves of quantum mechanics must be abandoned and atomic theory must be based in reality.

STABILITY OF FRACTIONAL-PRINCIPAL-QUANTUM STATES OF FREE ELECTRONS IN LIQUID HELIUM

Photon absorption occurs as an excitation of a resonator mode; consequently, the hydrogen atomic energy states are quantized as a function of the parameter n as shown in the Excited States (Quantization) section. Each value of n corresponds to an allowed transition caused by a resonant photon that excites the transition of the atomic orbital resonator cavity. In the case of free electrons in superfluid helium, the central field of the proton is absent; however, the electron is maintained as an atomic orbital by the pressure of the surrounding helium atoms. In this case, rather than the traditional integer values (1, 2, 3,...,) of n, values of reciprocal integers are allowed according to Eq. (2.2) where both the radii and wavelengths of the states are reciprocal integer multiples of that of the $n=1$ state and correspond to transitions with an increase in the effective central field that decreases the radius of the atomic orbital. In these cases, the electron undergoes a transition to a nonradiative higher-energy state. The trapped photon electric field which provides force balance for the atomic orbital is a solution of Laplace's equation in spherical coordinates and is given by Eq. (42.144).

In each case, the "trapped photon" is a "standing electromagnetic wave" which actually is a circulating wave that propagates around the z-axis, and its source current superimposes with each great circle current loop of the atomic orbital. The time-function factor, $k(t)$, for the "standing wave" is identical to the time-function factor of the atomic orbital in order to satisfy the boundary (phase) condition at the atomic orbital surface. Thus, the angular frequency of the "trapped photon" has to be identical to the angular frequency of the electron atomic orbital, ω_n, given by Eq. (1.36). Furthermore, the phase condition requires that the angular functions of the "trapped photon" have to be identical to the spherical harmonic angular functions of the electron atomic orbital. Combining $k(t)$ with the ϕ-function factor of the spherical harmonic gives $e^{i(m\phi-\omega_n t)}$ for both the electron and the "trapped photon" function. The angular functions in phase with the corresponding photon functions are the spherical harmonics. The charge-density functions including the time-function factor (Eq. (1.27-1.29)) are:

$\ell = 0$

$$\rho(r,\theta,\phi,t) = \frac{e}{8\pi r^2}[\delta(r-r_n)]\left[Y_0^0(\theta,\phi)+Y_\ell^m(\theta,\phi)\right] \tag{42.142}$$

$\ell \neq 0$

$$\rho(r,\theta,\phi,t) = \frac{e}{4\pi r^2}[\delta(r-r_n)]\left[Y_0^0(\theta,\phi)+\mathrm{Re}\left\{Y_\ell^m(\theta,\phi)e^{im\omega_n t}\right\}\right] \tag{42.143}$$

where $Y_\ell^m(\theta,\phi)$ are the spherical harmonic functions that spin about the z-axis with angular frequency ω_n with $Y_0^0(\theta,\phi)$ the constant function and $\mathrm{Re}\left\{Y_\ell^m(\theta,\phi)e^{im\omega_n t}\right\} = P_\ell^m(\cos\theta)\cos(m\phi+m\omega_n t)$. The solution of the "trapped photon" field of electrons in helium that is analogous to those of hydrogen excited states given by Eq. (2.15) is

$$\mathbf{E}_{r\ photon\ n,\ell,m} = C\frac{e(na)^\ell}{4\pi\varepsilon_o}\frac{1}{r^{(\ell+2)}}\left[\frac{1}{n}\left[Y_0^0(\theta,\phi)+\mathrm{Re}\left\{Y_\ell^m(\theta,\phi)e^{im\omega_n t}\right\}\right]\right]\delta(r-r_n)\mathbf{i}_r \tag{42.144}$$

$$n = 1,\frac{1}{2},\frac{1}{3},\frac{1}{4},...,\frac{1}{p}$$
$$\ell = 0,1,2,...,n-1$$
$$m = -\ell,-\ell+1,...,0,...,+\ell$$

In Eq. (42.144), a is the radius of the electron in helium without an absorbed photon. C is a constant expressed in terms of an equivalent central charge. It is determined by the force balance between the centrifugal force of the electron atomic orbital and the radial force provided by the pressure from the van der Waals force of attraction between helium atoms given *infra*.

For fractional quantum energy states of the electron, σ_{photon}, the two-dimensional surface charge density due to the "trapped photon" at the electron atomic orbital, follows from Eqs. (5.27) and (2.11).

$$\sigma_{photon} = \frac{e}{4\pi(r_n)^2}\left[-\frac{1}{n}\left[Y_0^0(\theta,\phi)+\mathrm{Re}\left\{Y_\ell^m(\theta,\phi)e^{im\omega_n t}\right\}\right]\right]\delta(r-r_n) \quad n=1,\frac{1}{2},\frac{1}{3},\frac{1}{4},..., \tag{42.145}$$

And, $\sigma_{electron}$, the two-dimensional surface charge density of the electron atomic orbital is

$$\sigma_{electron} = \frac{-e}{4\pi(r_n)^2}\left[Y_0^0(\theta,\phi)+\mathrm{Re}\left\{Y_\ell^m(\theta,\phi)e^{im\omega_n t}\right\}\right]\delta(r-r_n) \tag{42.146}$$

The superposition of σ_{photon} (Eq. (42.145)) and $\sigma_{electron}$, (Eq. (42.146)) where the spherical harmonic functions satisfy the conditions given in the Bound Electron "Atomic Orbital" section gives a radial electric monopole represented by a delta function.

$$\sigma_{photon}+\sigma_{electron} = \frac{-e}{4\pi(r_n)^2}\frac{1}{n}\left[Y_0^0(\theta,\phi)+\mathrm{Re}\left\{Y_\ell^m(\theta,\phi)e^{im\omega_n t}\right\}\right]\delta(r-r_n) \quad n=1,\frac{1}{2},\frac{1}{3},\frac{1}{4},..., \tag{42.147}$$

The radial delta function does not possess spacetime Fourier components synchronous with waves traveling at the speed of light [78–80]. Thus, the fractional quantum energy states are stable as given in the Boundary Condition of Nonradiation and the Radial Function—the Concept of the "Atomic Orbital" section.

The speed of light in vacuum c is given by

$$c = \frac{1}{\sqrt{\mu_0 \varepsilon_0}} \tag{42.148}$$

where μ_o is the permeability of free-space and ε_0 is the permittivity of free-space. The wavenumber is given by:

$$k_{vacuum} = \frac{2\pi}{\lambda} = \omega\sqrt{\mu_0 \varepsilon_0} \tag{42.149}$$

The speed of light in a medium such as superfluid helium v is given by:

$$v = \frac{1}{\sqrt{\mu_0 \varepsilon}} \tag{42.150}$$

where μ_o is the permeability of free-space and ε is the permittivity of the medium. The wavenumber is given by:

$$k_{medium} = \frac{2\pi}{\lambda} = \omega\sqrt{\mu_0 \varepsilon} \tag{42.151}$$

The ratio of the wavenumber in vacuum and the wavenumber in superfluid helium is given by:

$$\frac{k_{helium}}{k_{vacuum}} = \frac{\frac{2\pi}{\lambda_{helium}}}{\frac{2\pi}{\lambda_{vacuum}}} = \frac{\omega\sqrt{\mu_0 \varepsilon}}{\omega\sqrt{\mu_0 \varepsilon_0}} \tag{42.152}$$

The frequency of the photon in free space and in helium at the electron must be the same. Thus,

$$k_{helium} = k_{vacuum}\frac{\varepsilon}{\varepsilon_0} \tag{42.153}$$

Since $\varepsilon > \varepsilon_0$, the wavenumber in helium is greater than the wavenumber in vacuum. Thus, a photon traveling in liquid helium may excite a mode in an electron bubble which is nonradiative. In this case, spacetime harmonics of $\frac{\omega_n}{c} = k$ or $\frac{\omega_n}{c}\sqrt{\frac{\varepsilon}{\varepsilon_o}} = k$ for which the Fourier transform of the current-density function is nonzero do not exist. Radiation due to charge motion does not occur in any medium when this boundary condition is met.

As discussed *infra.*, the phenomenon of photon absorption by electrons in superfluid helium to give rise to an increase in conductivity is temperature dependent. This temperature dependence may be explained on the basis of the loss of viscosity of superfluid helium that is permissive of an electron supercurrent. That is, at 1.7 K, the viscosity is sufficiently close to zero such that the angular current of the electron may propagate without energy loss. Roton scattering dominates over phonon scattering at this temperature and below [81]. Then, the two dimensional surface charge due to a "trapped photon" at the electron atomic orbital of a free electron in helium is given by Eq. (42.147) such that the corresponding state is stable. Resonant photon absorption may occur between these stable states. The central force which results in a fractional electron radius compared to the unexcited electron is provided by the absorbed photon as discussed in the Ion Mobility Results in Superfluid Helium Match Predictions section.

ION MOBILITY RESULTS IN SUPERFLUID HELIUM MATCH PREDICTIONS

Experiments to study the effect of light on ion mobility have been conducted by Northby and Sanders [82, 83], Zipfel and Sanders [84, 85], and Grimes and Adams [86, 87]. For example, in the Northby and Sanders experiments [82, 83], ions were introduced into the liquid from a radioactive source, and had to pass through two grids in order to reach the detector. The voltages on the grids were varied in time in a way such that normal negative ions could not reach the detector. It was found that when the liquid was illuminated, a small ion current reached the detector. Thus, they observed an increase in ion mobility under illumination, but recognized that the origin of the effect was unclear. It appears that the absorption of a photon by an electron bubble or atomic orbital in superfluid helium provides a natural explanation for the majority of the photo-conductivity results.

The photon absorption is determined by the correspondence principle—the conservation of the $\hbar$ of angular momentum of the free space photon and the equivalent change in the angular momentum of the electron upon excitation. Thus, the radius of the electron following the absorption of a resonant photon is given by $n = \frac{1}{\text{integer}}$ times that of the original radius.

$$r = nr_1 \tag{42.154}$$

where $n = \frac{1}{\text{integer}}$ and r_1 is the radius of the electron in superfluid helium which has not absorbed a photon. This radius is determined by a force balance between the van der Waals pressure (force per unit area) of superfluid helium and the centrifugal force of the electron. The latter is given by

$$\mathbf{F}_{centrifugal} = \frac{m_e}{4\pi r_1^2}\frac{\mathbf{v}_1^{\,2}}{r_1} \tag{42.155}$$

where $\frac{m_e}{4\pi r_1^2}$ is the mass density of the atomic orbital and $\mathbf{v}_1$ is given by Eq. (1.35). The radius r_1 can be determined from the photo-conductivity experiments of Zipfel and Sanders [85]. At zero pressure a photo-conductivity peak was observed at approximately $0.5\ eV$. From Eqs. (2.18-2.22), the change in the frequency of the electron which matches the frequency of the exciting photon is given by:

$$\omega_{photon} = \frac{\hbar}{m_e r_1^2}\left[\frac{1}{n^2} - 1\right] \tag{42.156}$$

where $n = \frac{1}{\text{integer}}$. The radius r_1 is given by

$$r_1 = \sqrt{\frac{\hbar}{m_e \omega_{photon}}\left(\frac{1}{n^2} - 1\right)} \tag{42.157}$$

The relationship between energy and angular frequency of a photon is given by Planck's equation.

$$E = \hbar\omega_{photon} \tag{42.158}$$

The angular frequency corresponding to a photon of $0.5\ eV$ is:

$$\omega_{photon} = \frac{8.0\times10^{-20}\ J}{\hbar} = 7.6\times10^{14}\ rad/\sec \tag{42.159}$$

In the case that $0.5\ eV$ is the lowest energy transition for an electron in superfluid helium, the $n = 1 \to n = \frac{1}{2}$ transition corresponds to $n = \frac{1}{2}$ in Eq. (42.156). From Eq. (42.156) and Eq. (42.159), the radius r_1 is:

$$r_1 = \sqrt{\frac{\hbar}{m_e\left(7.6\times10^{14}\ rad/\sec\right)}\left(\frac{1}{\left(\frac{1}{2}\right)^2} - 1\right)} = 6.7\times10^{-10}\ m = 6.7\ \text{Å} \tag{42.160}$$

where $n = \frac{1}{2}$. Comparing the case of the electron of a hydrogen atom to the case of an electron in helium, no initial central Coulomb field due to a proton is present, and the electron increases in kinetic energy upon photon absorption. Thus, the energy required to cause a transition in the latter case is twice that of the former. The photon stores energy in the electric field of the resonator mode and increases the potential energy of the electron. The potential is the sum of the binding energy and the kinetic energy. The corresponding photon wavelength that will be absorbed by the electron is $2.5\ \mu m$.

The radius calculated in Eq. (42.160), is an approximation since the energy due to the pressure volume work and the surface energy change of the bubble were neglected. The former is given by:

$$P\int dV = \frac{4}{3}\pi\left(r_1^3 - r_n^3\right)P \tag{42.161}$$

where P is the applied pressure, the integral is over the volume of the bubble, and r_1 and r_n are the initial and final radii of the electron bubble. The latter is given by

$$\alpha\int dA = 4\pi\left(r_1^2 - r_n^2\right)\alpha \tag{42.162}$$

where α is the surface energy of helium per unit area, the integral is over the surface of the bubble, and r_1 and r_n are the initial and final radii of the electron bubble.

The contribution of these terms can be estimated by comparing the next experimental photo-conductivity peak at higher energy compared to the prediction given by Eqs. (42.156) and (42.158). Northby and Sanders [82, 83] found that in the range of $0.7\ eV$ to $3\ eV$ the photo-induced current had a peak when the photon energy was $1.21\ eV$ at zero pressure. Zipfel and Sanders [84, 85] confirmed the peak at $1.21\ eV$. In experiments similar to those of Northby and Sanders [82, 83], Zipfel and Sanders [84, 85] made measurements of the photo-conductivity as a function of pressure up to 16 bars. The photo-conductivity peak detected by Northby and Sanders [82, 83] was found to shift to higher photon energies as the pressure increased. This is expected since the radius of the normal electron decreases and the corresponding initial angular frequency increases with increasing pressure. Thus, the transition angular frequencies and energies increase (Eq. (42.156)).

The next higher energy transition for an electron in superfluid helium is $n = 1 \to n = \frac{1}{3}$. The transition energy corresponds to $n = \frac{1}{3}$ in Eqs. (42.156) and (42.158). The calculated energy neglecting the energy due to the pressure volume work and the surface energy change of the bubble is:

$$E = \hbar\omega_{photon} = \frac{\hbar^2}{m_e r_1^2}\left[\frac{1}{\left(\frac{1}{3}\right)^2} - 1\right] = \frac{\hbar^2}{m_e\left(6.7\times10^{-10}\ m\right)^2}\left[\frac{1}{\left(\frac{1}{3}\right)^2} - 1\right] = 1.3\ eV \tag{42.163}$$

where r_1 is given by Eq. (42.160). Given the experimental uncertainty of the energy of the lowest energy transition, 1.21 eV, this result confirms that the contributions due to pressure volume work and the surface energy change of the bubble may be neglected.

In the experiments of Northby and Sanders [82, 83], Zipfel and Sanders [84, 85], and Grimes and Adams [86, 87], it was noted that the photo-conductivity effect was absent above a critical temperature. This temperature was approximately 1.7 K at zero pressure, and decreased to 1.2 K at 20 bars. Roton scattering dominates over phonon scattering at 1.7 K and below [81]. The photo-conductivity signal disappears because of phonon excitation of the bubble motion which causes the excited electron state to decay. As the pressure is increased, the roton energy gap goes down, and so the phonon scattering increases. Thus, it is to be expected that the critical temperature decreases with increasing pressure.

Each stable excited state electron bubble, which has a radius of $\frac{r_1}{\text{integer}}$ may migrate in an applied electric field. The bubble may be scattered by rotons, phonons, and He^3 impurities. At temperatures less than 1.7 K, roton scattering dominates [81]. An equation for the electron bubble mobility is derived by Baym, Barrera, and Pethick [88] in terms of the roton-bubble momentum transfer cross section by calculating the rate of roton-bubble momentum transfer using a statistical mechanical approach. In the case of an elementary excitation $\vec{k}$ scattered by the bubble with a differential cross section $\sigma(k,\theta)$ and obeying $|\vec{k}'| \cong |\vec{k}|$, their result may be written,

$$\frac{e}{\mu} = -\frac{\hbar^2}{6\pi^2}\int_0^\infty k^4 \frac{\partial n}{\partial \varepsilon} v_g(k)\sigma_T(k)\,dk \tag{42.164}$$

where μ is the bubble mobility, n is the distribution function of the excitation, $v_g(k)$ is the group velocity of the excitation, and $\sigma_T(k)$ is the momentum-transfer cross section defined by:

$$\sigma_T(k) = \int (1-\cos\theta)\sigma(k,\theta)\,d\Omega \tag{42.165}$$

Schwarz and Stark [81] made the reasonable assumption that $\sigma_T(k)$ is a weak function of $k - k_0$. Because of the strong minimum at $k_0 = 1.91$ Å^{-1} in the roton energy spectrum, Eq. (42.164) then gives to a good approximation:

$$\mu = \frac{3\pi^2 e}{\hbar k_0^4 \sigma_T(k_0)} \exp(\Delta / k_B T) = \frac{3.38\times10^{-25}\ m^4 V^{-1}\sec^{-1}}{\sigma_T(k_0)} \exp(8.65\ K/T) \tag{42.166}$$

where $\Delta / k_B = 8.65 \pm 0.04\ K$ is the roton energy gap derived from neutron scattering [89]. Schwarz and Stark [81] propose that the roton de Broglie wavelength corresponding to $k_0 = 1.91$ Å^{-1} is $\lambda_0 = 3.3$ Å, which is small compared with $\sqrt{\frac{\sigma_T(k_0)}{\pi}}$; thus, the collision cross section may be nearly geometrical. Although the roton carries a great deal of energy and momentum, its effective mass is much less than that of the ion. Assume that the scattering is elastic, then $|\vec{k}'| \cong |\vec{k}|$ is satisfied. They conclude a hard-sphere cross section given by:

$$\sigma_T(k_0) \cong \pi(a_+ + a_r)^2 \tag{42.167}$$

where a_+ is the radius of the ion and a_r is the effective collision radius of the roton. Using experimental values for a_+ and $\sigma_T(k)$, they find that

$$a_r = 3.7 \pm 0.2\ \text{Å} \tag{42.168}$$

They surmise from this that the roton is localized within a region of radius $\approx 3.7 - 4.0$ Å, and that it interacts strongly with any disturbance, which penetrates this region. They point out that $\approx 3.7 - 4.0$ Å is only slightly larger than the nearest neighbor distance in liquid helium [90] and that a roton may thus be pictured as a highly correlated motion of an energetic He^4 atom and its nearest neighbors only.

The geometric cross-section of the normal electron bubble σ_e is given as:

$$\sigma_e = \pi r_1^2 \tag{42.169}$$

where r_1 is the radius of the unexcited electron bubble given by Eq. (42.160). From Eq. (42.160) and Eqs. (42.166-42.169), the mobility of the normal electron bubble is given by

$$\mu = \frac{3\pi^2 e}{\hbar k_0^4 \pi (a_r + r_1)^2} \exp(\Delta / k_B T) = \frac{3.38\times10^{-25}\ m^4 V^{-1}\sec^{-1}}{\pi\left(3.7\times10^{-10}\ m + 6.7\times10^{-10}\ m\right)^2} \exp(8.65\ K/T) \tag{42.170}$$

At 1 K, Eq. (42.170) gives $\mu = 5.7\ cm^2 V^{-1}\sec^{-1}$ for the mobility of the normal electron bubble ($n = 1$), which is in reasonable agreement with the experimental value of 5 $cm^2 V^{-1}\sec^{-1}$ [77, 91].

The normal electron bubble has a uniform constant spherical charge density. This charge density may be modulated by a time and spherically harmonic function as given by Eq. (42.143). In the case of excited state electron bubbles, the contribution to the roton scattering cross section given by Eq. (42.165) is larger than the geometric cross section given in Eq. (42.169) where

the radius is given by Eq. (42.154). In this case, $\sigma_T(k)$ given by Eq. (42.165) follows the derivation of Baym, Barrera, and Pethick [88] where the spherical harmonic angular function causes a gain in the scattering cross section that may be modeled after that of a Hertzian dipole antenna. The radiation power pattern of a Hertzian dipole is given by Shen and Kong [92]. The radiation power pattern is

$$\langle \mathbf{S} \rangle = \frac{1}{2}\mathrm{Re}\left[\mathbf{E}\times\mathbf{H}\right] = \hat{\mathbf{r}}\frac{\eta}{2}\left(\frac{k|I|\Delta z}{4\pi r}\right)\sin^2\theta \tag{42.171}$$

where I is the current, Δz is the length of the dipole, and η is the impedance of free space. The antenna directive gain $D(\theta,\varphi)$ is defined as the radiation of the Poynting power density $\langle S_r \rangle$ over the power P, divided by the area of the sphere:

$$D(\theta,\phi) = \frac{\langle S_r \rangle}{P/4\pi r^2} = \frac{3}{2}\sin^2\theta \tag{42.172}$$

The plot of $D(\theta,\varphi)$ given by Eq. (42.172) is known as the gain pattern. The directivity of an antenna is defined as the value of the gain in the direction of its maximum value. For the Hertzian dipole the maximum of 1.5 occurs at $\theta = \frac{\pi}{2}$. Thus, the directivity of a Hertzian dipole is 1.5.

The spherical harmonic angular functions are

$$Y_{\ell m}(\theta,\phi) = \sqrt{\frac{(2\ell+1)(\ell-m)!}{4\pi(\ell+m)!}}P_\ell^m(\cos\theta)e^{im\phi} = N_{\ell,m_\ell}P_\ell^m(\cos\theta)e^{im\phi} \tag{42.173}$$

where is the normalization constant given by

$$N_{\ell,m_\ell} = \sqrt{\frac{(2\ell+1)(\ell-m)!}{4\pi(\ell+m)!}} \tag{42.174}$$

In the case of excited states, $\sigma(k,\theta)$ of Eq. (42.165) is

$$\sigma(k,\theta) = k^{-2}\left|\frac{\int P_0^0(\cos\theta)e^{i0\phi}d\Omega}{\int P_\ell^m(\cos\theta)e^{im\phi}d\Omega}\right|^2 = k^{-2}\left(\frac{N_{\ell.m_\ell}}{N_{0,0}}\right)^2 \tag{42.175}$$

For excited states, the geometric cross-section of the electron bubble σ_e is then given as

$$\sigma_e = \pi n r_{n,\ell,m_\ell}^2 \tag{42.176}$$

where

$$r_{n,\ell,m_\ell} = \frac{N_{\ell,m_\ell}}{N_{0,0}}nr_1 \tag{42.177}$$

r_1 is the radius of the unexcited electron bubble given by Eq. (42.132) and $n = \frac{1}{\text{integer}}$. The angular parameters $\frac{N_{\ell,m_\ell}}{N_{0,0}}$ are given with the first few spherical harmonics in Table 42.1. In this case, $\sigma_T(k)$ is given by Eq. (42.165) where r_1 is replaced by r_{n,ℓ,m_ℓ} (Eq. (42.177)). The roton scattering cross section given by the hard-sphere cross section is then:

$$\sigma_T(k_0) \cong \pi\left(r_{n,\ell,m_\ell} + a_r\right)^2 \tag{42.178}$$

where a_r is the effective collision radius of the roton given by Eq. (42.168). From Eq. (42.170) and Eqs. (42.173-42.178), the mobilities of electron bubbles are given by:

$$\begin{aligned}\mu &= \frac{3\pi^2 e}{\hbar k_0^4 \pi\left(a_r + r_{n,\ell,m_\ell}\right)^2}\exp\left(\Delta/k_BT\right) \\ &= \frac{3.38\times10^{-25}\ m^4V^{-1}\sec^{-1}}{\pi\left(3.7\times10^{-10}\ m + n\frac{N_{\ell,m_\ell}}{N_{0,0}}6.7\times10^{-10}\ m\right)^2}\exp\left(8.65\ K/T\right)\end{aligned} \tag{42.179}$$

where $n = \frac{1}{\text{integer}}$. The mobility of an excited state electron bubble having a fractional principal quantum number ($n = \frac{1}{\text{integer}}$) relative to the normal electron bubble as a function of quantum numbers n, ℓ, and m_ℓ is given in Table 42.2. The temperature dependence of the mobility predicted by Eq. (42.179) is in good agreement with the data of Ihas [91] and the plots of Maris [77].

Table 42.1. The first few spherical harmonics and $\frac{N_{\ell,m_\ell}}{N_{0,0}}$ of Eq. (42.174) as a function of ℓ, and m_ℓ.

Spherical Harmonics

$Y_{m_\ell}^{\ell}$	ℓ	m_ℓ	$\frac{N_{\ell,m_\ell}}{N_{0,0}}$
$Y_0^0 = \frac{1}{(4\pi)^{1/2}}$	0	0	1
$Y_1^0 = \left(\frac{3}{4\pi}\right)^{1/2} \cos\theta$	1	0	$\sqrt{3}$
$Y_1^1 = \left(\frac{3}{8\pi}\right)^{1/2} \sin\theta e^{i\phi}$	1	1	$\sqrt{\frac{3}{2}}$
$Y_1^{-1} = \left(\frac{3}{8\pi}\right)^{1/2} \sin\theta e^{-i\phi}$	1	-1	$\sqrt{\frac{3}{2}}$
$Y_2^0 = \left(\frac{5}{16\pi}\right)^{1/2} \left(3\cos^2\theta - 1\right)$	2	0	$\sqrt{\frac{5}{4}}$
$Y_2^1 = \left(\frac{15}{8\pi}\right)^{1/2} \left(\sin\theta\cos\theta e^{i\phi}\right)$	2	1	$\sqrt{\frac{15}{2}}$
$Y_2^{-1} = \left(\frac{15}{8\pi}\right)^{1/2} \left(\sin\theta\cos\theta e^{-i\phi}\right)$	2	-1	$\sqrt{\frac{15}{2}}$
$Y_2^2 = \left(\frac{15}{32\pi}\right)^{1/2} \sin^2\theta e^{2i\phi}$	2	2	$\sqrt{\frac{15}{8}}$
$Y_2^{-2} = \left(\frac{15}{32\pi}\right)^{1/2} \sin^2\theta e^{-2i\phi}$	2	-2	$\sqrt{\frac{15}{8}}$

Table 42.2. The mobility of an excited state electron bubble having a fraction principal quantum number ($n = \frac{1}{\text{integer}}$) relative to the normal electron bubble as a function of quantum numbers n, ℓ, and m_ℓ given by Eq. (42.179). The peaks that appear in Figure 42.18 and Table 42.3 are indicated.

n	$\ell = 0$	$\ell = 1$ $m_\ell = 0$	$\ell = 1$ $m_\ell = \pm 1$	$\ell = 2$ $m_\ell = 0$	$\ell = 2$ $m_\ell = \pm 1$	$\ell = 2$ $m_\ell = \pm 2$
$\frac{1}{2}$	2.21 peak # 8	1.22 peak # 3	1.81 peak # 5			
$\frac{1}{3}$	3.12 peak # 10	1.92 peak # 6	2.66	2.86	1.14 peak # 2	2.41
$\frac{1}{4}$	3.81 peak # 11	2.52 peak # 9	3.33	3.54	1.60 peak # 4	3.06
$\frac{1}{5}$	4.33 peak # 12	3.03	3.86	4.07	2.03 peak # 7	3.59
$\frac{1}{6}$	4.74 peak # 13	3.47	4.28	4.49	2.41	4.02
$\frac{1}{7}$	5.07 peak # 14	3.83	4.63	4.83	2.75	4.38
$\frac{1}{8}$	5.34 peak # 15	4.15	4.93	5.12	3.06	4.68
$\frac{1}{9}$	5.57 peak # 15	4.42	5.17	5.35	3.34	4.94
$\frac{1}{10}$	5.76 peak # 15	4.66	5.38	5.56	3.59	5.16
$\frac{1}{11}$	5.92 peak # 15	4.87	5.56	5.73	3.82	5.35
$\frac{1}{12}$	6.07 peak # 15	5.05	5.72	5.88	4.02	5.52
$\frac{1}{100}$	7.75 peak # 15	7.55	7.69	7.72	7.29	7.65

Using time-of-flight, Doake and Gribbon [93] detected negatively-charged ions that had a mobility substantially higher than the normal electron bubble negative ion. This ion, which has become known as the "fast ion," was next seen in another time-of-flight experiment by Ihas and Sanders in 1971 [94]. They showed that the fast ion could be produced by an α or β source, or by an electrical discharge in the helium vapor above the liquid. In addition, they reported the existence of two additional negative carriers, referred to as "exotic ions," that had mobilities larger than the mobility of the normal negative ion, but less than the mobility of the fast ion. These exotic ions were detected only when there was an electrical discharge above the liquid surface. In a paper the following year [95], Ihas and Sanders reported on further experiments in which at least 13 carriers with different mobilities were detected. The experimental details are described in the thesis of Ihas [91]. Eden and McClintock [96, 97] also detected as many as 13 ions with different mobilities. Both Ihas and Sanders and Eden and McClintock put forward a number of proposals to explain the exotic ions, but all of these proposals were shown to be unsatisfactory by Maris [77]. It is significant that the exotic ions appear only when an electrical discharge takes place close to the free surface of the liquid. Under these conditions, the electrons that enter the liquid and form bubbles may absorb light emitted from the discharge. Thus, it is natural to consider the possibility that the exotic ions are electron bubbles in fractional energy states.

Following a pulse discharge with an electric field applied to superfluid helium, Ihas [91] recorded ion peaks using time of flight. Fifteen ion peaks recorded by Ihas and Sanders are identified in Figure 42.18. The mobilities relative to the normal electron bubble ($n = 1$) are given in Table 42.3. The assignments of the mobilities of excited state electron bubbles having fractional principal quantum number ($n = \frac{1}{\text{integer}}$) relative to the normal electron bubble as a function of quantum numbers n, ℓ, and m_ℓ are also given in Table 42.3 based on the theoretical values given in Table 42.2. The agreement between theory and experiment is excellent.

Figure 42.18. Data trace from Ihas [91] showing the detected ion signal as a function of time. N and F denote the normal and fast ion peaks. The peaks labeled 1 to 15 are assigned in Table 42.3. For a description of experimental condition see Ihas [91].

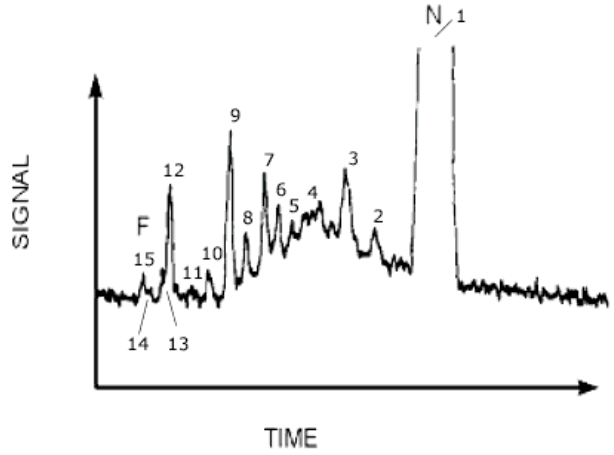

Table 42.3. The migration times and experimental mobilities of the 15 ion peaks shown in Figure 42.18 relative to the normal ion with their assignments to excited state electron bubbles with quantum numbers n, ℓ, and m_ℓ and theoretical mobilities given in Table 42.2.

Peak #	Migration Time (Arbitrary Units)	Mobility Relative to Peak #1	Theoretical Mobility Relative to Peak #1	Assignment n, ℓ, and m_ℓ.
1	9.8	1.00	1	$n=1\ \ell=0\ \ m_\ell=0$
2	8.2	1.20	1.14	$n=\frac{1}{3}\ \ell=2\ \ m_\ell=\pm1$
3	7.6	1.29	1.22	$n=\frac{1}{2}\ \ell=1\ \ m_\ell=0$
4	6.2	1.58	1.6	$n=\frac{1}{4}\ \ell=2\ \ m_\ell=\pm1$
5	5.4	1.81	1.81	$n=\frac{1}{2}\ \ell=1\ \ m_\ell=\pm1$
6	5	1.96	1.92	$n=\frac{1}{3}\ \ell=1\ \ m_\ell=0$
7	4.85	2.02	2.03	$n=\frac{1}{5}\ \ell=2\ \ m_\ell=\pm1$
8	4.35	2.25	2.21	$n=\frac{1}{2}\ \ell=0\ \ m_\ell=0$
9	3.9	2.51	2.52	$n=\frac{1}{4}\ \ell=1\ \ m_\ell=0$
10	3.3	2.97	3.12	$n=\frac{1}{3}\ \ell=0\ \ m_\ell=0$
11	2.8	3.50	3.81	$n=\frac{1}{4}\ \ell=0\ \ m_\ell=0$
12	2.1	4.67	4.33	$n=\frac{1}{5}\ \ell=0\ \ m_\ell=0$
13	2	4.90	4.74	$n=\frac{1}{6}\ \ell=0\ \ m_\ell=0$
14	1.8	5.44	5.07	$n=\frac{1}{7}\ \ell=0\ \ m_\ell=0$
15	1.3	7.54	7.75	$n=\frac{1}{100}\ \ell=0\ \ m_\ell=0$

Peaks 14-15 of Figure 42.18 and Table 42.3 represent a band with a cutoff at a migration velocity of about 7.5 times the velocity of the normal ion as $n = \frac{1}{\text{integer}}$ approaches zero ($n = \frac{1}{100}$ was used to calculate this limiting case). The electron radius is predicted to decrease such that the effective collision radius of the roton determines the maximum mobility as given by Eq. (42.179). The theoretically predicted maximum of electron bubble mobility of about seven times that of the normal ion is confirmed by the Ihas data [91] where the band comprising peaks 14-15 correspond to $n \le \frac{1}{7}$. Furthermore, Eden and McClintock [96] and Doake and Gribbon [93] measured the drift velocity as a function of applied electric field. The fast ion showed a slope of the drift velocity versus applied electric field of about seven times that of the normal ion. Thus, these results agree with the data of Ihas and with theoretical predictions.

The agreement between the experimental data and theoretical mobilities is excellent. The existence of multiple peaks under the fast peak such as peak #14 and #15 of Figure 42.18 is also supported by the data of Eden and McClintock [96] because the peak of highest mobility split into the two peaks at higher fields.

In summary, the photo-conductivity absorption spectrum of free electrons in superfluid helium and their mobilities predicted from the corresponding bubble-like wavefunctions matched the experimental results of the 15 identified ions. The data support the existence of fractional-principal-quantum-energy states of free electrons in superfluid helium. The implications to atomic hydrogen states were discussed previously [98]. These results also have implications that the concept of probability waves of quantum mechanics must be abandoned and atomic theory must be based in reality.

In addition to superfluid helium, free electrons also form bubbles devoid of any atoms in other fluids such as oils and liquid ammonia. In the operation of an electrostatic atomizing device Kelly [99] observed that the mobility of free electrons in oil increased by an integer factor rather that continuously. Above the breakdown of the discharge device, the slope of the current versus electric field was discontinuous. It shifted to one half that before breakdown. This corresponds to a higher mobility of electrons to the grounded electrode of a triode of the atomizer, with a concomitant reduction in charging of the moving oil and the corresponding charged fluid current at the outlet of the dispersion device. As in the case of the discharge effect on the mobility of free electrons in superfluid helium, the breakdown current is a light source which excites the electron to transition from the $n = 1$ to the $n = \frac{1}{2}$ state given by Eq. (42.154). Excitation of electrons to fractional states is a method to increase their mobility to more effectively charge a fluid in order to form a dispersed fluid. The apparatus patented by Kelly [99] may be improved by a modification to include a source of light to cause the electron transitions to fractional states.

Alkali metals, and to a lesser extent other metals such as Ca, Sr, Ba, Eu, and Yb are soluble in liquid ammonia and certain other solvents. The electrolytically conductive solutions have free electrons of extraordinary mobility as their main charge carriers [100]. In very pure liquid ammonia the lifetime of free electrons can be significant with less than 1% decomposition per day. The confirmation of their existence as free entities is given by their broad absorption around 15,000 Å that can only be assigned to free electrons in the solution that is blue due to the absorption. In addition, magnetic and electron spin resonance studies show the presence of free electrons, and a decrease in paramagnetism with increasing concentration is consistent with spin pairing of electrons to form diamagnetic pairs. As in the case of free electrons in superfluid helium, ammoniated free electrons form cavities devoid of ammonia molecules having a typical diameter of 3-3.4 Å. The cavities are evidenced by the observation that the solutions are of much lower density than the pure solvent. From another perspective, they occupy far too great a volume than that predicted from the sum of the volumes of the metal and solvent. An understanding of the structure of free electrons in other fluids such as liquid ammonia may further lead to means to control the electron mobility and reactivity by controlling the fractional state using light.

ONE DIMENSION GRAVITY WELL—ANOTHER FLAWED INTERPRETATION

Nesvizhevsky et al. [101] claim that they created a potential well for falling neutrons formed by the Earth's gravitational field and a horizontal mirror. According to Nesvizhevsky et al., "we now consider how to demonstrate that bound states exist for neutrons trapped in the Earth's gravitational field. The gravitational field alone does not create a potential well, it can only confine particles by forcing them to fall along field lines. We need a second 'wall' to create the well." Supposedly, a neutron falling in the Earth's gravitational field hits the bottom mirror, is reflected, and the neutron wavefunction interferes with itself. The self-interference creates a standing wave in the neutron density: the probability of finding a neutron at a given height exhibits maxima and minima along the vertical direction which is a function of the quantum number of the bound states. The quantum mechanical probability wave problem is solved as a particle on a box or one-dimensional well problem [102].

Nesvizhevsky et al. [101] give the standing waves as asymmetric sinusoidal waves—the claimed distortion due to the argument that "the gravitational field is much softer than an infinite sharp wall; as a result, the gravitational well extends in the opposite direction to the gravity with increasing quantum number."[3] Consequently, the neutron wavefunctions are deformed upwards, and the energy differences between states become very slightly smaller as the quantum numbers increase. For example, the energy of the n=1 state is 1.4 peV, and that of the n=4 state is 4.1 peV, rather than 5.6 peV for a linear relationship.

[3] How the particle "knows" that "the field extends beyond the reflecting barrier" is not addressed. Nor is the internal inconsistency that the Standard Model attributes the force of gravity to exchange of gravitons and not to a classical field. Ironically, even though gravity is a ubiquitous force, gravitons have never been observed after 70 years of searching. In addition, quantum electrodynamics requires that the vacuum be filled with an infinite number of virtual particles that occupy quantum states. The consequences such as the prediction of an infinite cosmological constant and the failure of quantum mechanics to provide a successful quantum gravitational theory are also not addressed. See Mills article [12].

For comparison, the classical potential energy V of a neutron lifted a height of $z = 15\ \mu\ m$ against the Earth's gravitational field is given by:

$$V = m_n gz = \left(1.67\times10^{-27}\ kg\right)\left(9.8\ m/s^2\right)\left(15\times10^{-6}\ m\right) = 1.5\ \times10^{-12}\ eV = 1.5\ peV \tag{42.180}$$

where m_n is the mass of the neutron and g is the acceleration due to gravity.

Nesvizhevsky et al. [101] directed ultracold neutrons with a horizontal velocity of $\approx 10\ m/s$ through a parallel plate channel wherein the top plate was a neutron absorber and the bottom plate was a neutron mirror. The neutrons were selected by a collimator that projected the neutrons at a slightly upward angle such that they followed a parabolic trajectory in the Earth's gravitational field. The neutron's vertical velocity at the peak height of the parabola corresponded to classical result of zero, and increased as the neutron fell to the bottom mirror. The vertical velocity component was limited by the variable height of the vertical neutron absorber. For example, a vertical velocity of $\approx 1.7\ \text{X}10^{-2}\ m/s$ corresponded to a parabolic height of $z = 15\ \mu m$ wherein the kinetic energy K given by:

$$K = 1/2 m_n v^2 = \left(1.67\times10^{-27}\ kg\right)\left(1.7\times10^{-2}\ m/s\right)^2 = 1.5\ peV \tag{42.181}$$

was converted to gravitational potential energy given by Eq. (42.180).

The neutron as well as the proton and electron are fundamental particles with a de Broglie wavelength. They demonstrate interference patterns during diffraction as given in the Electron Scattering by Helium section. The observed far-field position distribution is a picture of the particle's transverse momentum distribution after the interaction. The momentum transfer is given by $\hbar k$ where k is the wavenumber ($\frac{2\pi}{\lambda}$). The relevant wavelength lambda is the de Broglie wavelength associated with the momenta of the particles which is transferred through interactions. An example is the interference pattern for rubidium atoms given in the Wave-Particle Duality is Not Due to the Uncertainty Principle section. Also see the Electron in Free Space section.

The de Broglie wavelength λ is given by:

$$\lambda = \frac{h}{p} = \frac{h}{m_n v} \tag{42.182}$$

where h is Planck's constant, m_n is the mass of the neutron, and v is the neutron velocity in the direction of the wavelength. In the Nesvizhevsky experiment, a neutron with an initial vertical velocity of $\approx 1.7\ \text{X}10^{-2}\ m/s$ has zero velocity at the top of the parabolic trajectory. The corresponding velocity of the falling neutron at the mirror before reflection is negative $\approx 1.7\ \text{X}10^{-2}\ m/s$, and after reflection, it is positive $\approx 1.7\ \text{X}10^{-2}\ m/s$. The de Broglie wavelength of the neutron in the vertical direction corresponding to the momentum acquired by falling from the top of the trajectory and undergoing momentum reversal at the mirror is given by

$$\lambda = \frac{h}{\Delta p} = \frac{h}{2m_n v} = \frac{6.63\times10^{-34} J\cdot s}{(2)\left(1.67\times10^{-27} kg\right)\left(1.7\times10^{-2}\ m/s\right)} = 11.7\times10^{-6}\ m = 12\ \mu m \tag{42.183}$$

which is less than $z = 15\ \mu m$ corresponding to the initial vertical velocity of $\approx 1.7\ \text{X}10^{-2}\ m/s$.

The time scale for the collision of a neutron with the bottom mirror was much less than the transit time t_t of the neutron through the slits which is given by the ratio of the channel length ($0.1\ m$) and the horizontal speed ($\approx 10\ m/s$).

$$t_t = \frac{0.1\ m}{10\ m/s} = 0.01\ s \tag{42.184}$$

The time scale t_d for the fall of a neutron with a parabolic height of $z = 15\ \mu m$ was also much less than the transit time of a neutron through the slits.

$$t_d = \sqrt{\frac{2z}{g}} = \sqrt{\frac{(2)\left(15\times10^{-6}\ m\right)}{9.8\ m/s^2}} = 1.7\times10^{-3}\ s \tag{42.185}$$

The interaction scale in the vertical direction is the de Broglie wavelength for the neutron-mirror collision; thus, neutron transmission through the slits is limited by the height of the absorber relative to the de Broglie wavelength. The de Broglie wavelength is inversely proportional to the initial velocity (Eq. (42.183)). And, from Eqs. (42.180) and (42.181) the parabolic height increases as v^2. Then, the slit-width for transmission threshold z_1 is the de Broglie wavelength that equals the parabolic height corresponding to the initial kinetic energy. The de Broglie wavelength is larger than the slit width for widths less than z_1, and the opposite relationship occurs for slits wider than z_1. The velocity given by equating the initial kinetic energy (Eq. (42.181)) and the corresponding gravitational potential energy (Eq. (42.180)) is:

$$v = \sqrt{2gz_1} \tag{42.186}$$

The corresponding de Broglie wavelength given by Eqs. (42.183) and (42.186) is:

$$\lambda = z_1 = \frac{1}{2}\left(\frac{h}{m_n}\right)^{2/3}\left(g\right)^{-1/3} = 12.6\ \mu m \tag{42.187}$$

Nesvizhevsky et al. [101] flowed neutrons between the mirror below and the absorber above and recorded the

transmission N (counts/s) as a function of the width Δz of the slit formed by the mirror and the absorber. Thus, the width Δz acted as a vertical velocity selector. The expected classical prediction is that there is some transmission at a slit width greater that of the neutron cross section for neutrons propagating with no vertical velocity component. This was in fact observed. For neutrons with a vertical velocity component, no transmission of neutrons is expected until the slit width is greater than the vertical de Broglie wavelength corresponding to momentum reversal at the mirror. This is due to the interaction of the reflected neutrons with the absorber with a separation less than this length. From Eq. (42.187), the slit height at which neutrons are predicted to be transmitted is about $13\ \mu m$. This was exactly what was observed. At this point, the detection rate N should increase as a linear function of the slit width corrected for any changes in the vertical component of the neutron velocity due to changes in the acceptance angle for neutrons. Nesvizhevsky et al. [101] give a correction factor of $z^{0.5}$ to N due to the increase in the accepted spread of velocities. Thus, the classically predicted transmission as a function of slit width Δz is:

$$N = c\left(z - z_1\right)^{1.5} \tag{42.188}$$

where c is a constant dependent on the neutron flux and z_1 is the vertical de Broglie wavelength given by Eq. (42.187). There was remarkable agreement between the experimental data of Nesvizhevsky et al. and the classical prediction given by Eq. (42.188).

In contrast, the experimental data did not match critical predictions of quantum mechanics. According to Nesvizhevsky et al. [101], "we expect a stepwise dependence of N as a function of Δz. If Δz is smaller than the spatial width of the lowest quantum state, then N should be zero. When Δz is equal to the spatial width of the lowest quantum state, then N should increase sharply. Further increase in Δz s*hould not increase* N as long as Δz is smaller than the spatial width of the second quantum state. Then N should again increase stepwise." In contrast to these predictions, some transmission was observed at a slit width of an order of magnitude less than that of the predicted transmission threshold. Also, *no stepwise transmission between quantum states was observed*. Nesvizhevsky et al. [101] erred by not considering the vertical de Broglie wavelength in the cutoff for transmission.

Moreover, at sufficiently large slit width Δz, Nesvizhevsky et al. [101] predict that the classical dependence $N \approx \Delta z$ should be approached. Their data shows that their erred classical prediction actually coincides with the data at the n=3 state—a far cry from the point at which the quantum and classical results are expected to coincide based on the one-dimensional-well problem of quantum mechanics. (The two are not to converge until the quantum number n becomes very large and approaches infinity [103].) Their results further point to the tendency to misinterpret data in order to support quantum theory when in fact the data disproves it.

PHYSICS IS NOT DIFFERENT ON THE ATOMIC SCALE

The central feature of nature is that all particles (atomic-size particles and macroscopic particles) obey the same physical laws. Whereas Schrödinger postulated the boundary condition: "$\Psi \to 0$ as $r \to \infty$," which leads to a purely mathematical model of the electron, the boundary condition in classical physics was derived from Maxwell's equations by Haus [78]:

> *For non-radiative states, the current-density function must not possess spacetime Fourier components that are synchronous with waves traveling at the speed of light.*

Application of the latter boundary condition leads to an entirely different model of particles, atoms, molecules, and to a very different concept of the nature of the physical Universe. ***The classical physical laws are unified and are shown to apply on all scales.***

The seemingly esoteric wave-particle duality of light and particles including the experimentally observed de Broglie relationship can be simply understood in terms of first principles. The independent variables of four-dimensional spacetime, the fundamental constants comprising the fine structure constant, α,

$$\alpha = \frac{1}{4\pi}\sqrt{\frac{\mu_o}{\varepsilon_0}}\frac{e^2}{\hbar} \tag{42.189}$$

the gravitational constant, *G*, the mass of the Universe, and the spin of the electron neutrino determine the nature of the Universe as shown in particular in the Gravity section and the Unification of Spacetime, the Forces, Matter, and Energy section. Photons and fundamental particles which arise from photons possess $\hbar$ of angular momentum and are two-dimensional. As a consequence of this nature with first principle laws, absorption and emission of photons occurs in units or quanta of energy according to the Planck equation as described in particular in the One-Electron Atom section. Photons and electromagnetic fields arise from fundamental particles as given in the Photon Equation section and superimpose due to the linearity of Maxwell's Equations and spacetime. Interference patterns, surface waves, diffraction, reflection, standing waves, and/or corpuscular behavior can be observed depending on the means of observation. These phenomena are explained according to first principles [104].

The wave-particle duality of the photon can be understood in terms of classical physics from the equation of the photon (Eq. (4.14)), a two-dimensional atomic orbital, given in the Photon Equation section. This function provides a photon angular momentum of $\hbar$, an energy given by the Planck relationship, a solution to the wave equation and Maxwell's Equations, a velocity of c, a zero rest mass, and linearly, circularly, or elliptically polarized light. Furthermore, photons superimpose in space and time to give a spherical wave described by the Green Function (Eq. (4.23)) which is consistent with the Airy pattern (Eq. (8.23)) in double slit diffraction experiments.

The wave-particle duality of the electron can be understood in terms of classical physics from the equation of the bound electron, a two-dimensional atomic orbital, given in the One-Electron Atom section and from the equation of the free electron given in the Electron in Free Space section. In both cases, the electron has an electric field equivalent to a point charge, e, has mass, m_e, the electron wavelength is given by the de Broglie relationship, the angular momentum of the electron is $\hbar$ (Two possible orientations are possible in a magnetic field as observed in the Stern-Gerlach experiment, and the energy of the flip transition is proportional to the electron (fluxon) g factor (Eq. (1.227)). The ionized electron has its electron density in a plane (Eq. (3.7)), and the superposition of electrons provides a plane wave having the de Broglie wavelength which is consistent with the Davisson-Germer experiment given in the Electron Scattering by Helium section. Furthermore, the correct prediction of the elastic scattering of electrons by helium atoms given in the Electron Scattering by Helium section wherein the electron radius is a crucial parameter (Eq. (8.57)), and the excited state spectrum of hydrogen given in the Excited States of the One-Electron atom (Quantization) section (wherein ***the correspondence principle holds***) are direct verifications that the electron is an atomic orbital with the calculated radius.

Atoms are stable according to classical principles as shown in the Spacetime Fourier Transform of the Electron Function section, Appendix I, and the Stability of Atoms and Hydrinos section. The infinities of quantum electrodynamics are removed at once by having a finite electron radius as given in the One-Electron Atom section and the Electron in Free Space section. In addition, the Lamb Shift is due to conservation of energy and linear momentum and arises from the radiation reaction force between the electron and the photon as given in the Resonant Line Shape and Lamb Shift section. The negative result of the Michelson-Morley experiment rendered untenable the hypothesis of the ether by demonstrating that the ether had no measurable properties. And, the more recent related concepts of vacuum fluctuations, vacuum polarization, and virtual particles which are a source of infinities have no basis in physical reality; so, they are discarded.

REFERENCES

1. F. Dyson, "Feynman's proof of Maxwell equations," Am. J. Phys., Vol. 58, (1990), pp. 209-211.
2. J. Horgan, "Quantum Philosophy," Scientific American, July, (1992), p. 96.
3. A. Beiser, *Concepts of Modern Physics*, Fourth Edition, McGraw-Hill, New York, (1987), pp. 44-86.
4. A. Beiser, *Concepts of Modern Physics*, Fourth Edition, McGraw-Hill, New York, (1987), pp. 87-117.
5. S. Durr, T. Nonn, G. Rempe, Nature, September 3, (1998), Vol. 395, pp. 33-37.
6. N. Bohr, in *Albert Einstein: Philosopher-Scientist* (ed. Schilpp, P.A.) 200-241 (Library of Living Philosophers, Evanston, 1949); reprinted in *Quantum Theory and Measurement* (eds. J. A. Wheeler, and W. H. & Zurek) 9-49 (Princeton University Press 1983).
7. R. Feynman, R. Leighton, M. Sands, in *Feynman Lectures on Physics*, Vol. III, Ch. I (Addison Wesley, Reading, 1965).
8. V. F. Weisskopf, Reviews of Modern Physics, Vol. 21, No. 2, (1949), pp. 305-315.
9. P. A. M. Dirac, *From a Life of Physics*, ed. A. Salam, et al., World Scientific, Singapore, (1989).
10. P. W. Milonni, *The Quantum Vacuum*, Academic Press, Inc., Boston, p. 90.
11. P. A. M. Dirac, *Directions in Physics*, ed. H. Hora and J. R. Shepanski, Wiley, New York, (1978), p. 36.
12. R. Mills, The Nature of Free Electrons in Superfluid Helium—a Test of Quantum Mechanics and a Basis to Review its Foundations and Make a Comparison to Classical Theory, Int. J. Hydrogen Energy, Vol. 26, No. 10, (2001), pp. 1059-1096.
13. R. L. Mills, "Classical Quantum Mechanics," Physics Essays, Vol. 16, No. 4, (2003), pp. 433-498; posted with spreadsheets at http://www.blacklightpower.com/techpapers.shtml.
14. R. L. Mills, "Physical Solutions of the Nature of the Atom, Photon, and Their Interactions to Form Excited and Predicted Hydrino States," Phys. Essays, Vol. 20, No. 3, (2007), pp.403-460.
15. R. L. Mills, "Exact Classical Quantum Mechanical Solutions for One- Through Twenty-Electron Atoms," Phys. Essays, Vol. 18, No. 3 (2005), 321-361.
16. R. L. Mills, "The Nature of the Chemical Bond Revisited and an Alternative Maxwellian Approach," Physics Essays, Vol. 17, (2004), pp. 342-389, posted with spreadsheets at http://www.blacklightpower.com/techpapers.shtml.
17. R. L. Mills, "Maxwell's Equations and QED: Which is Fact and Which is Fiction," Physics Essays, Vol. 19, (2006), pp. 225-262.
18. R. L. Mills, "Exact Classical Quantum Mechanical Solution for Atomic Helium Which Predicts Conjugate Parameters from a Unique Solution for the First Time," Phys. Essays, Vol. 21, No. 2, (2008), pp.103-141.
19. R. L. Mills, "The Fallacy of Feynman's Argument on the Stability of the Hydrogen Atom According to Quantum Mechanics," Annales de la Fondation Louis de Broglie, Vol. 30, No. 2, (2005), pp. 129-151; posted at http://www.blacklightpower.com/theory/theory.shtml.
20. R. Mills, "The Grand Unified Theory of Classical Quantum Mechanics," Int. J. Hydrogen Energy, Vol. 27, No. 5, (2002), pp. 565-590.
21. R. Mills, "The Hydrogen Atom Revisited," Int. J. of Hydrogen Energy, Vol. 25, Issue 12, (2000), pp. 1171-1183.
22. P. Pearle, Foundations of Physics, "Absence of radiationless motions of relativistically rigid classical electron," Vol. 7, Nos. 11/12, (1977), pp. 931-945.
23. H. Wergeland, "The Klein Paradox Revisited," *Old and New Questions in Physics, Cosmology, Philosophy, and Theoretical Biology*, A. van der Merwe, Editor, Plenum Press, New York, (1983), pp. 503-515.
24. F. Laloë, "Do we really understand quantum mechanics? Strange correlations, paradoxes, and theorems," Am. J. Phys. 69 (6), June 2001, 655-701.
25. J. Horgan, "Quantum Philosophy," Scientific American, Vol. 276, July, (1992), pp. 94-104.

26. J. Horgan, "Quantum Philosophy," Scientific American, Vol. 267, July, (1992), p. 101.
27. D. E. Platt, Am. J. Phys., 60 (4), April, 1992, pp. 306-308.
28. H. J. Dehmelt, American Journal of Physics, Vol. 58, No. 1, January, (1990). pp. 17-27.
29. R. L. Mills, US Patent Application No. 09/220,970, "A Method and System for Pattern Recognition and Processing" filed December 23, 1998; R. L. Mills, International Patent Application No. PCT/US98/27624, "A Method and System for Pattern Recognition and Processing," filed December 23, 1998.
30. R. L. Mills, "Novel Method and System for Pattern Recognition and Processing Using Data Encoded as Fourier Series in Fourier Space," International Scientific Journal Engineering Applications of Artificial Intelligence, Vol. 19, (2006), pp. 219-234.
31. A. Einstein, B. Podolsky, N. Rosen, Phys. Rev., Vol. 47, (1935), p. 777.
32. J. S. Bell, Physics, Vol. 1, (1965), p. 195.
33. D. Bohm, *Quantum Theory*, Prentice-Hall, Inc., Englewood Cliffs, NJ, (1951), p. 614.
34. A. Aspect, P. Grangier, R. Gerard, Phys. Rev. Lett., Vol. 47, No. 7, (1981), pp. 460-463.
35. A. Aspect, P. Grangier, R. Gerard, Phys. Rev. Lett., Vol. 49, No. 2, (1982), pp. 91-94.
36. A. Aspect, J. Dalibard, R. Gerard, Phys. Rev. Lett., Vol. 49, No. 25, (1982), pp. 1804-1807.
37. J. F. Clauser, et al., Phys. Rev. Lett., Vol. 23, No. 15, (1969), pp. 880-884.
38. J. F. Clauser, M. Horne, Physical Review D, Vol. 10, No. 2, (1974), pp. 526-535.
39. M. A. Horne, "Experimental Consequences of Local Hidden Variable Theories," thesis, Boston University, (1969).
40. N. D. Mermin, Physics Today, April , (1995), pp. 38-47.
41. N. D. Mermin, Physics Today, June, (1994), pp. 9-11.
42. N. D. Mermin, Physics Today, June, (1990), pp. 9-11.
43. J. A. Kong, *Electromagnetic Wave Theory*, Second Edition, John Wiley & Sons, Inc., New York, (1990).
44. J. D. Jackson, *Classical Electrodynamics*, Second Edition, John Wiley & Sons, New York, (1975), pp. 752-763.
45. J. D. Jackson, *Classical Electrodynamics*, Second Edition, John Wiley & Sons, New York, (1975), pp. 739-779.
46. Maya modeling of R. Mills' theory by B. Holverstott in "Computer Simulation of The Aspect Experiment—No Spooky Actions at a Distance," posted at www.blacklightpower.com.
47. J. D. Jackson, *Classical Electrodynamics*, Second Edition, John Wiley & Sons, New York, (1975), pp. 750-751.
48. K. Hess, W. Phillips, "Bell's theorem and the problem of decidability between the views of Einstein and Bohr," PNAS, Vol. 98, No. 25, December, (2000), pp. 14228-14233.
49. V. Jacques, E. Wu, F. Grosshans, F. Treussart, P. Grangier, A. Aspect, J-F. Roch, "Experimental realization of Wheeler's delayed-choice gedanken experiment," Science, Vol. 315, (2007), pp. 966-968.
50. A. Miller is acknowledged for bringing to my attention Wheeler's delayed-choice gedanken experiment and its significance to the quantum mechanical theory community, March, 2008.
51. J. D. Jackson, *Classical Electrodynamics*, Second Edition, John Wiley & Sons, New York, (1975), pp. 751-752.
52. M. W. Browne, "Physicist Put Atom in Two Places at Once," New York Times, Tuesday, May 28,1996, pp. B5-B6.
53. C. Monroe, D. M. Meekhof, B. E. King, D. J. Wineland, Science, Vol. 272, (1996), pp. 1131-1135.
54. G. Taubes, Science, Vol. 272, (1996), p. 1134.
55. S. R. Jefferts, C. Monroe, E. W. Bell, D. J. Wineland, Physical Review A, Vol. 51, No. 4, (1995), pp. 3112-3116.
56. C. Monroe, D. M. Meekhof, B. E. King, S. R. Jefferts, W. M. Itano, D. J. Wineland, Physical Review Letters, Vol. 75, No. 22, (1995), pp. 4011-4014.
57. C. P. Slichter, *Principles of Magnetic Resonance*, Harper & Row, New York, (1963), pp. 1-44.
58. A. A. Maradudin, Rev. Mod. Phys., Vol. 36, (1964), pp. 417-432.2.
59. A. Messiah, Quantum Mechanics, Vol. I, North-Holland Publishing Company, Amsterdam, (1961), p. 442.
60. H. Ott, Ann. Physik, Vol. 23, (1935), p. 169.
61. F. Bloch, Z. Physik, Vol. 74, (1932), p. 295.
62. G. N. Watson, *Bessel Functions*, Cambridge University Press, Cambridge, (1944), p. 14.
63. R. V. Hogg, E. A. Tanis, *Probability and Statistical Inference*, MacMillan Publishing Co., Inc., New York, (1977), pp. 78-82.
64. K. Chang, The New York Times, Tuesday, July 11, 2000, p. F3.
65. E. Schrödinger, "Die gegenwärtige situation in der quantenmechanik," Naturwissenschaften, Vol. 23, (1935), pp. 807-812, 823-828, 844-849.
66. J. R. Friedman, V. Patella, W. Hen, S. K. Tolpygo, J. E. Lukens, "Quantum superposition of distinct macroscopic states," Nature, Vol. 406, July, 6, (2000), pp. 43-45.
67. A. Lorke, R. J. Luyken, A. O. Govorov, J. P. Kotthaus, J. M. Garcia, P. M. Petroff, Phys. Rev. Lett., Vol. 84, March 6, (2000), p. 2223.
68. C. E. Gough, M. S. Colclough, E. M. Forgan, R. G. Jordan, M. Keene, C. M. Muirhead, A. I. M. Rae, N. Thomas, J. S. Abell, S. Sutton, Nature, Vol. 326, (1987), P. 855.
69. G. R. Fowles, *Analytical Mechanics*, Third Edition, Holt, Rinehart, and Winston, New York, (1977), pp. 62-66.
70. D. R. Lide, CRC Handbook of Chemistry and Physics, 86th Edition, CRC Press, Taylor & Francis, Boca Raton, (2005-6), pp. 1-1 to 1-6.
71. Burroughs, Charles J.; Benz, Samuel P. (1999-06-01), "1 volt DC programmable Josephson voltage standard", IEEE Transactions on Applied Superconductivity, Vol. 9 (3), pp. 4145–4149, ISSN 1051-8223.

72. A. D. O'Connell, M. Hofheinz, M. Ansmann, R. C. Bialczak, M. Lenander, E. Lucero, M. Neeley, D. Sank, H. Wang, M. Weides, J. Wenner, J. M. Martinis, A. N. Cleland, "Quantum ground state and single-phonon control of a mechanical resonator", Nature, Vol. 464, (2010), pp. 697-703.
73. D. R. Lide, CRC Handbook of Chemistry and Physics, 86th Edition, CRC Press, Taylor & Francis, Boca Raton, (2005-6), p. 12-57.
74. P. Weiss, Science News, Vol. 158, No. 14, September 30, (2000), p. 216.
75. P. Ball, Nature, http://helix.nature.com/nsu/000921/000921-1.html.
76. M. Chown, New Scientist, October 14, (2000), Vol. 168, Issue 2260, pp. 24, 33.
77. H. J. Maris, Journal of Low Temperature Physics, Vol. 120, (2000), p. 173.
78. H. A. Haus, "On the radiation from point charges," Am. J. Phys., 54, (1986), pp. 1126-1129.
79. T. A. Abbott, D. J. Griffiths, , Am. J. Phys., Vol. 153, No. 12, (1985), pp. 1203-1211.
80. G. Goedecke, Phys. Rev., 135B, (1964), p. 281.
81. K. W. Schwarz, R. W. Stark, Phys. Rev. Lett., Vol. 22, No. 24, (1969), pp. 1278-1280.
82. J. A. Northby, Ph.D. thesis, University of Minnesota, 1966, (unpublished).
83. J. A. Northby, T. M. Sanders, Phys. Rev. Lett., Vol. 18, (1967), p. 1184.
84. C. L. Zipfel, Ph.D. thesis, University of Michigan, 1969, unpublished.
85. C. L. Zipfel, T. M. Sanders, in Proceedings of the 11th International Conference on Low Temperature Physics, edited by J. F. Allen, D. M. Finlayson, and D. M. McCall (St. Andrews University, St. Andrews, Scotland, (1969), p. 296.
86. C. C. Grimes, G. Adams, Phys. Rev., Vol. B41, (1990), p. 6366.
87. C. C. Grimes, G. Adams, Phys. Rev., Vol. B45, (1992), p. 2305.
88. G. Baym, R. G. Barrera, C. J. Pethick, Phys. Rev. Letters, Vol. 22, No. 1, (1969), pp. 20-23.
89. D. G. Henshaw, A. D. B. Woods, Phys. Rev. Lett., Vol. 121, (1961), p. 1266.
90. F. London, *Superfluids* (Dover Publications, New York, 1964), Vol. III.
91. G. G. Ihas, Ph.D. thesis, University of Michigan, 1971.
92. L. C. Shen, J. A. Kong, *Applied Electromagnetism*, Brooks/Cole Engineering Division, Monterey, CA, (1983), pp. 210-215.
93. C. S. M. Doake, P. W. F. Gribbon, Phys. Lett., Vol. 30A, No. 4, (1969), pp. 251-253.
94. G. G. Ihas, T. M. Sanders, Phys. Rev. Lett., Vol. 27, (1971), p. 383.
95. G. G. Ihas, T. M. Sanders, in Proceedings of the 13 th International Conference on Low Temperature Physics, editors K. D. Timmerhaus, W. J. O'Sullivan and E. F. Hammel, Plenum, New York, (1972), Vol. 1, p. 477.
96. V. L. Eden, P. V. E. McClintock, Phys. Lett., Vol. 102A, No. 4, (1984), pp. 197-200.
97. V. L. Eden, M. Phil. thesis, University of Lancaster, 1986.
98. R. Mills, P. Ray, B. Dhandapani, W. Good, P. Jansson, M. Nansteel, J. He, A. Voigt, "Spectroscopic and NMR Identification of Novel Hydride Ions in Fractional Quantum Energy States Formed by an Exothermic Reaction of Atomic Hydrogen with Certain Catalysts," European Physical Journal-Applied Physics, Vol. 28, (2004), pp. 83-104.
99. Arnold J. Kelly, "Electrostatic Atomizing Device," United States Patent No. 4,581,675, April 8, 1986.
100. F. A. Cotton, G. Wilkinson, *Advanced Inorganic Chemistry A Comprehensive Text*, Interscience Publishers, New York, NY, (1962), pp. 193-194.
101. V. V. Nesvizhevsky, H. G. Borner, A. K. Petukhov, H. Abele, S. Baebler, F. J. Rueb, T. Stoferele, A. Westphal, A. M. Gagarski, G. A. Petrov, A. V. Strelkov, "Quantum states of neutron's in the Earth's gravitational field," Nature, Vol. 415, (2002), pp. 297-299.
102. D. A. McQuarrie, *Quantum Chemistry*, University Science Books, Mill Valley, CA, (1983), pp 77-101.
103. A. Beiser, *Concepts of Modern Physics*, Fourth Edition, McGraw-Hill, New York, (1987), pp. 147-149.
104. M. B. James, D. J. Griffiths, Am. J. Phys., 60 (4), April, (1992), pp. 309-313.

Appendix I

NONRADIATION CONDITION

DERIVATION OF THE CONDITION FOR NONRADIATION

The condition for radiation by a moving point charge given by Haus [1] is that its spacetime Fourier transform does possess components that are synchronous with waves traveling at the speed of light. Conversely, it is proposed that the condition for nonradiation by an ensemble of moving charge that comprises a charge-density function is that its spacetime Fourier transform does NOT possess components that are synchronous with waves traveling at the speed of light. The Haus derivation applies to a moving charge-density function as well because charge obeys superposition. The Haus derivation is summarized below.

The Fourier components of the current produced by the moving charge are derived. The electric field is found from the vector equation in Fourier space ($\mathbf{k}$, ω-space). The inverse Fourier transform is carried over the magnitude of $\mathbf{k}$. The resulting expression demonstrates that the radiation field is proportional to $\mathbf{J}_\perp(\frac{\omega}{c}\mathbf{n},\omega)$ where $\mathbf{J}_\perp(\mathbf{k},\omega)$ is the spacetime Fourier transform of the current perpendicular to $\mathbf{k}$ and $\mathbf{n}\equiv\frac{\mathbf{k}}{|k|}$. Specifically,

$$\mathbf{E}_\perp(\mathbf{r},\omega)\frac{d\omega}{2\pi}=\frac{c}{2\pi}\int\rho(\omega,\Omega)d\omega d\Omega\sqrt{\frac{\mu_0}{\varepsilon_0}}\mathbf{n}\ X\ \left(\mathbf{n}\ X\ \mathbf{J}_\perp\left(\frac{\omega}{c}\mathbf{n},\omega\right)e^{i\left(\frac{\omega}{c}\right)\mathbf{n}\bullet\mathbf{r}}\right) \tag{1}$$

The field $\mathbf{E}_\perp(\mathbf{r},\omega)\frac{d\omega}{2\pi}$ is proportional to $\mathbf{J}_\perp\left(\frac{\omega}{c}\mathbf{n},\omega\right)$, namely, the Fourier component for which $\mathbf{k}=\frac{\omega}{c}$. Factors of ω that multiply the Fourier component of the current are due to the density of modes per unit volume and unit solid angle. An unaccelerated charge does not radiate in free space, not because it experiences no acceleration, but because it has no Fourier component $\mathbf{J}_\perp\left(\frac{\omega}{c}\mathbf{n},\omega\right)$.

SPACETIME FOURIER TRANSFORM OF THE ELECTRON FUNCTION

The electron charge-density (mass-density) function is the product of a radial delta function $(f(r)=\frac{1}{r^2}\delta(r-r_n))$, two angular functions (spherical harmonic functions), and a time-harmonic function. The spacetime Fourier transform of the spherical current membrane in three dimensions in spherical coordinates plus time is given [2, 3] as follows:

$$M(s,\Theta,\Phi,\omega)=\int_0^\infty\int_0^\infty\int_0^\pi\int_0^{2\pi}\rho(r,\theta,\phi,t)\exp(-i2\pi sr[\cos\Theta\cos\theta+\sin\Theta\sin\theta\cos(\phi-\Phi)])\exp(-i\omega t)r^2\sin\theta d\phi d\theta drdt \tag{2}$$

With circular symmetry [2]

$$M(s,\Theta,\omega)=2\pi\int_0^\infty\int_0^\infty\int_0^\pi\rho(r,\theta,t)J_0\left(2\pi sr\sin\Theta\sin\theta\right)\exp\left(-i2\pi sr\cos\Theta\cos\theta\right)r^2\sin\theta\exp\left(-i\omega t\right)d\theta drdt \tag{3}$$

With spherical symmetry [2],

$$M(s,\omega)=4\pi\int_0^\infty\int_0^\infty\rho(r,t)\mathrm{sinc}(2sr)r^2\exp(-i\omega t)drdt \tag{4}$$

The functions that model the electron charge density are separable.

$$\rho(r,\theta,\phi,t) = f(r)g(\theta)h(\phi)k(t) \tag{5}$$

The atomic orbital function is separable into a product of functions of independent variables, $r, \theta, \phi,$ and t. The radial function, that satisfies the boundary condition is a delta function. The time functions are of the form $e^{i\omega t}$, the angular functions are spherical harmonics, sine or cosine trigonometric functions or sums of these functions, each raised to various powers. The spacetime Fourier transform is derived of the separable variables for the angular space function of $\sin\phi$ and $\sin\theta$. It follows from the spacetime Fourier transform given below that other possible spherical harmonic angular functions give the same form of result as the transform of $\sin\theta$ and $\sin\phi$. Using Eq. (4), $F(s)$, the space Fourier transform of $f(r) = \frac{1}{r^2}\delta(r - r_n)$ is given as follows:

$$F(s) = 4\pi\int_0^\infty \frac{1}{r^2}\delta(r - r_n)\text{sinc}(2sr)r^2 dr \tag{6}$$

$$F(s) = 4\pi\text{sinc}(2sr_n) \tag{7}$$

The subscript n is used hereafter; however, the quantization condition appears in the Excited States of the One-Electron Atom (Quantization) section. Quantization arises as "allowed" Maxwellian solutions corresponding to a resonance between the electron and a photon.

Using Eq. (3), $G_1^1(s,\Theta)$, the space Fourier transform of $g(\theta) = \sin\theta$ is given as follows where there is no dependence on ϕ:

$$G_1^1(s,\Theta) = 2\pi\int_0^\infty\int_0^\pi \sin\theta J_0\left(2\pi sr\sin\Theta\sin\theta\right)\exp\left(-i2\pi sr\cos\Theta\cos\theta\right)\sin\theta r^2 d\theta dr \tag{8}$$

$$G_1^1(s,\Theta) = 2\pi\int_0^\infty\int_0^\pi r^2\sin^2\theta J_0\left(2\pi sr\sin\Theta\sin\theta\right)\cos\left(2\pi sr\cos\Theta\cos\theta\right)d\theta dr \tag{9}$$

From Luke [4] and Abramowitz and Stegun [5]:

$$J_\upsilon(z) = \left(\frac{1}{2}z\right)^\nu\sum_{n=0}^\infty\frac{(-1)^n\left(\frac{z}{2}\right)^{2n}}{n!\Gamma(\nu+n+1)} = \left(\frac{1}{2}z\right)^\nu\sum_{n=0}^\infty\frac{(-1)^n\left(\frac{z}{2}\right)^{2n}}{n!(\nu+n)!} \tag{10}$$

Let

$$z = 2\pi sr\sin\Theta\sin\theta \tag{11}$$

With the substitution of Eqs. (11) and (10) into Eq. (9),

$$G_1^1(s,\Theta) = 2\pi\int_0^\infty\int_0^\pi r^2\sin^2\theta\left[\sum_{n=0}^\infty\frac{(-1)^n\left(\pi sr\sin\Theta\sin\theta\right)^{2n}}{n!n!}\right]\cos(2\pi sr\cos\Theta\cos\theta)d\theta dr \tag{12}$$

$$G_1^1(s,\Theta) = 2\pi\int_0^\infty r^2\int_0^\pi\sum_{n=0}^\infty\frac{(-1)^n\left(\pi sr\sin\Theta\right)^{2n}}{n!n!}\sin^{2(n+1)}\theta\cos\left(2\pi sr\cos\Theta\cos\theta\right)d\theta dr \tag{13}$$

$$G_1^1(s,\Theta) = 2\pi\int_0^\infty r^2\int_0^\pi\sum_{n=1}^\infty\frac{(-1)^{n-1}\left(\pi sr\sin\Theta\right)^{2(n-1)}}{(n-1)!(n-1)!}\sin^{2n}\theta\cos(2\pi sr\cos\Theta\cos\theta)d\theta dr \tag{14}$$

From Luke [6], with $\text{Re}(\upsilon) > -\frac{1}{2}$:

$$J_\upsilon(z) = \frac{\left(\frac{1}{2}z\right)^\upsilon}{\Gamma\left(\frac{1}{2}\right)\Gamma\left(\upsilon+\frac{1}{2}\right)}\int_0^\pi\cos\left(z\cos\theta\right)\sin^{2\upsilon}\theta d\theta \tag{15}$$

Let

$$z = 2\pi sr\cos\theta \text{ and } n = \upsilon \tag{16}$$

Applying the relationship, the integral of a sum is equal to the sum of the integrals to Eq. (14), and transforming Eq. (14) into the form of Eq. (15) by multiplication by:

$$1 = \frac{\Gamma\left(\frac{1}{2}\right)\Gamma\left(\upsilon+\frac{1}{2}\right)\left(\pi sr\cos\Theta\right)^\upsilon}{\left(\pi sr\cos\Theta\right)^\upsilon\Gamma\left(\frac{1}{2}\right)\Gamma\left(\upsilon+\frac{1}{2}\right)} \tag{17}$$

and by moving the constant outside of the integral gives:

$$G_1^1(s,\Theta)=2\pi\int_0^\infty r^2\sum_{\upsilon=1}^\infty\int_0^\pi\frac{(-1)^{\upsilon-1}\left(\pi sr\sin\Theta\right)^{2(\upsilon-1)}}{(\upsilon-1)!(\upsilon-1)!}\,\frac{\Gamma\left(\frac{1}{2}\right)\Gamma\left(\upsilon+\frac{1}{2}\right)\left(\pi sr\cos\Theta\right)^{\upsilon}}{\left(\pi sr\cos\Theta\right)^{\upsilon}\Gamma\left(\frac{1}{2}\right)\Gamma\left(\upsilon+\frac{1}{2}\right)}\sin^{2\upsilon}\theta\cos(2\pi sr\cos\Theta\cos\theta)d\theta dr \tag{18}$$

$$G_1^1\left(s,\Theta\right)=2\pi\int_0^\infty r^2\sum_{\upsilon=1}^\infty\frac{(-1)^{\upsilon-1}\left(\pi sr\sin\Theta\right)^{2(\upsilon-1)}}{(\upsilon-1)!(\upsilon-1)!}\,\frac{\Gamma\left(\frac{1}{2}\right)\Gamma\left(\upsilon+\frac{1}{2}\right)\left(\pi sr\cos\Theta\right)^{\upsilon}}{\left(\pi sr\cos\Theta\right)^{\upsilon}\Gamma\left(\frac{1}{2}\right)\Gamma\left(\upsilon+\frac{1}{2}\right)}\int_0^\pi\sin^{2\upsilon}\theta\cos(2\pi sr\cos\Theta\cos\theta)d\theta dr \tag{19}$$

Applying Eq. (15),

$$G_1^1\left(s,\Theta\right)=2\pi\int_0^\infty r^2\sum_{\upsilon=1}^\infty\frac{(-1)^{\upsilon-1}\left(\pi sr\sin\Theta\right)^{2(\upsilon-1)}}{(\upsilon-1)!(\upsilon-1)!}\,\frac{\Gamma\left(\frac{1}{2}\right)\Gamma\left(\upsilon+\frac{1}{2}\right)}{\left(\pi sr\cos\Theta\right)^{\upsilon}}J_\upsilon\left(2\pi sr\cos\Theta\right)dr \tag{20}$$

Collecting the r raised to a power terms, Eq. (20) becomes,

$$G_1^1(s,\Theta)=2\pi\sum_{\upsilon=1}^\infty\int_0^\infty\frac{(-1)^{\upsilon-1}\left(\pi s\sin\Theta\right)^{2(\upsilon-1)}}{(\upsilon-1)!(\upsilon-1)!}\,\frac{\Gamma\left(\frac{1}{2}\right)\Gamma\left(\upsilon+\frac{1}{2}\right)}{\left(\pi s\cos\Theta\right)^{\upsilon}}r^\upsilon J_\upsilon(2\pi sr\cos\Theta)dr \tag{21}$$

Let $r=\dfrac{r'}{2\pi\cos\Theta}$; $dr=\dfrac{dr'}{2\pi\cos\Theta}$,

$$G_1^1(s,\Theta)=2\pi\sum_{\upsilon=1}^\infty\int_0^\infty\frac{(-1)^{\upsilon-1}\left(\pi s\sin\Theta\right)^{2(\upsilon-1)}}{(\upsilon-1)!(\upsilon-1)!}\,\frac{\Gamma\left(\frac{1}{2}\right)\Gamma\left(\upsilon+\frac{1}{2}\right)}{\left(\pi s\cos\Theta\right)^{\upsilon}\left(2\pi\cos\Theta\right)^{\upsilon+1}}r'^{\upsilon}J_\upsilon(sr')dr' \tag{22}$$

Consider the Hankel transform formula from Bateman [7]:

$$\begin{aligned}&\int_0^\infty r^\upsilon J_\upsilon(rs)dr\\&=s^{-\left(\frac{1}{2}\right)}\int_0^\infty r^{\upsilon-\frac{1}{2}}\left(rs\right)^{\left(\frac{1}{2}\right)}J_\upsilon(rs)dr\\&=2^{\upsilon-1}\pi^{\left(\frac{1}{2}\right)}\Gamma\left(\frac{1}{2}+\upsilon\right)s^{-\upsilon}\left[J_\upsilon\left(s\right)\mathbf{H}_{\upsilon-1}\left(s\right)-\mathbf{H}_\upsilon\left(s\right)J_{\upsilon-1}\left(s\right)\right]\end{aligned} \tag{23}$$

where the radius is normalized to the dimensionless parameter r that satisfies the conditions,

$$\begin{aligned}&r^{\upsilon-\frac{1}{2}},\ 0<r<1\\&0,\ r>1\\&\mathrm{Re}\,\upsilon>-\frac{1}{2}\end{aligned} \tag{24}$$

By applying Eq. (23), Eq. (22) becomes,

$$G_1^1(s,\Theta)=2\pi\sum_{\upsilon=1}^\infty\frac{(-1)^{\upsilon-1}\left(\pi s\sin\Theta\right)^{2(\upsilon-1)}}{(\upsilon-1)!(\upsilon-1)!}\,\frac{\Gamma\left(\frac{1}{2}\right)\Gamma\left(\upsilon+\frac{1}{2}\right)}{\left(\pi s\cos\Theta\right)^{\upsilon}\left(2\pi\cos\Theta\right)^{\upsilon+1}}2^{\upsilon-1}\pi^{\left(\frac{1}{2}\right)}\Gamma\left(\frac{1}{2}+\upsilon\right)s^{-\upsilon}\begin{bmatrix}J_\upsilon\left(s\right)\mathbf{H}_{\upsilon-1}\left(s\right)\\-\mathbf{H}_\upsilon\left(s\right)J_{\upsilon-1}\left(s\right)\end{bmatrix} \tag{25}$$

By collecting power terms of s gives

$$G_1^1(s,\Theta)=2\pi\sum_{\upsilon=1}^\infty\frac{(-1)^{\upsilon-1}\left(\pi\sin\Theta\right)^{2(\upsilon-1)}}{(\upsilon-1)!(\upsilon-1)!}\,\frac{\Gamma\left(\frac{1}{2}\right)\Gamma\left(\upsilon+\frac{1}{2}\right)}{\left(\pi\cos\Theta\right)^{2\upsilon+1}2^{\upsilon+1}}2^{\upsilon-1}\pi^{\left(\frac{1}{2}\right)}\Gamma\left(\frac{1}{2}+\upsilon\right)s^{-2}\left[J_\upsilon\left(s\right)\mathbf{H}_{\upsilon-1}\left(s\right)-\mathbf{H}_\upsilon\left(s\right)J_{\upsilon-1}\left(s\right)\right] \tag{26}$$

Next, $H_1^1(s,\Theta,\Phi)$, the space Fourier transform of $h(\phi)=\sin\phi$, is considered wherein the radius is normalized to the dimensionless parameter r as given in Eq. (24). Using Eq. (2) $H_1^1(s,\Theta,\Phi)$ is

$$H_1^1(s,\Theta,\Phi)=\int_0^\pi\int_0^{2\pi}\int_0^1\sin\phi\exp(-i2\pi sr[\cos\Theta\cos\theta+\sin\Theta\sin\theta\cos(\phi-\Phi)])r^2\sin\theta dr d\phi d\theta \tag{27}$$

By setting

$$\alpha = \alpha(s,\theta,\phi,\Theta,\Phi) = 2\pi s[\cos\Theta\cos\theta + \sin\Theta\sin\theta\cos(\phi - \Phi)] \tag{28}$$

Eq. (28) simplifies to:

$$H_1^1(s,\Theta,\Phi) = \int_0^{\pi}\int_0^{2\pi}\int_0^1 \sin\phi\sin\theta e^{-i\alpha r} r^2 dr d\phi d\theta \tag{29}$$

Following the radial integration [8], $H_1^1(s,\Theta,\Phi)$ is:

$$H_1^1(s,\Theta,\Phi) = \int_0^{\pi}\int_0^{2\pi} \sin\phi\sin\theta\left[\frac{2\cos\alpha}{\alpha^2} + \frac{\sin\alpha}{\alpha} - \frac{2\sin\alpha}{\alpha^3} + i\left(\frac{\cos\alpha}{\alpha} - \frac{2\cos\alpha}{\alpha^3} - \frac{2\sin\alpha}{\alpha^2} + \frac{2}{\alpha^3}\right)\right] d\phi d\theta \tag{30}$$

Based on the spatial similarity of $h(\phi) = \sin\phi$ and $g(\theta) = \sin\theta$, the respective Fourier transforms are similar and considered nonzero since the inverse Fourier transforms are the original trigonometric functions.

The time Fourier transform of $q(t) = \mathrm{Re}\{\exp(i\omega_n t)\}$ is given as follows [3]:

$$Q(\omega) = \int_0^{\infty} \cos\omega_n t \exp(-i\omega t) dt = \frac{1}{2\pi}\frac{1}{2}[\delta(\omega - \omega_n) + \delta(\omega + \omega_n)] \tag{31}$$

where ω_n is the angular frequency given by Eq. (1.36) corresponding to the frequency of a potentially emitted photon as given in Chp. 2.

A very important theorem of Fourier analysis states that the Fourier transform of a product is the convolution of the individual Fourier transforms [9]. By applying this theorem, the spacetime Fourier transform of an atomic orbital, $M_\ell^{m_\ell}(s,\Theta,\Phi,\omega)$ is of the following form:

$$M_\ell^{m_\ell}(s,\Theta,\Phi,\omega) = F(s) \otimes G_\ell^{m_\ell}(s,\Theta) \otimes H_\ell^{m_\ell}(s,\Theta,\Phi) \otimes Q(\omega) \tag{32}$$

Therefore, the spacetime Fourier transform, $M_1^1(s,\Theta,\Phi,\omega)$, is the convolution of Eqs. (7), (26), and (30-31).

$$M_1^1(s,\Theta,\Phi,\omega) = 4\pi\,\mathrm{sinc}(2sr_n) \otimes H_1^1(s,\Theta,\Phi)$$
$$\otimes 2\pi\sum_{\upsilon=1}^{\infty}\left\{2\pi\sum_{\upsilon=1}^{\infty}\frac{(-1)^{\upsilon-1}\left(\pi\sin\Theta\right)^{2(\upsilon-1)}}{(\upsilon-1)!(\upsilon-1)!}\frac{\Gamma\left(\frac{1}{2}\right)\Gamma\left(\upsilon+\frac{1}{2}\right)}{\left(\pi\cos\Theta\right)^{2\upsilon+1}2^{\upsilon+1}}\right.$$
$$\left.\cdot 2^{\upsilon-1}\pi^{\left(\frac{1}{2}\right)}\Gamma\left(\frac{1}{2}+\upsilon\right)s^{-2}\left[J_\upsilon(s)\mathbf{H}_{\upsilon-1}(s) - \mathbf{H}_\upsilon(s)J_{\upsilon-1}(s)\right]\right\} \tag{33}$$
$$\otimes\frac{1}{4\pi}[\delta(\omega-\omega_n) + \delta(\omega+\omega_n)]$$

The spherical harmonics functions are:

$$Y_\ell^m(\theta,\phi) = N_{\ell,m}P_\ell^m(\cos\theta)e^{im\phi} \tag{34}$$

Generalizing the exemplary functions $\sin\theta$ and $\sin\phi$, the Fourier transforms of the spherical harmonics expressed in terms of the respective integrals are given by:

$$G_\ell^{m_\ell}(s,\Theta) = 2\pi N_{\ell,m}\int_0^{\infty}\int_0^{\pi} P_\ell^m(\cos\theta)J_0(2\pi sr\sin\Theta\sin\theta)\exp(-i2\pi sr\cos\Theta\cos\theta)\sin\theta r^2 d\theta dr \tag{35}$$

and

$$H_\ell^{m_\ell}(s,\Theta,\Phi) = \int_0^{\infty}\int_0^{\pi}\int_0^{2\pi} e^{im\phi}\exp(-i2\pi sr[\cos\Theta\cos\theta + \sin\Theta\sin\theta\cos(\phi-\Phi)])r^2\sin\theta d\phi d\theta dr \tag{36}$$

In the general case, the spacetime Fourier transform, $M_\ell^{m_\ell}(s,\Theta,\Phi,\omega)$, is the convolution of Eqs. (7), (31), and (35-36).

$$M_\ell^{m_\ell}(s,\Theta,\Phi,\omega) = 4\pi\,\mathrm{sinc}(2sr_n) \otimes G_\ell^{m_\ell}(s,\Theta) \otimes H_\ell^{m_\ell}(s,\Theta,\Phi) \otimes \frac{1}{4\pi}[\delta(\omega-\omega_n) + \delta(\omega+\omega_n)] \tag{37}$$

wherein $G_\ell^{m_\ell}(s,\Theta)$ and $H_\ell^{m_\ell}(s,\Theta,\Phi)$ are the spherical-coordinate Fourier transforms of $N_{\ell,m}P_\ell^m(\cos\theta)$ and $e^{im\phi}$, respectively. The condition for nonradiation of a moving charge-density function is that the spacetime Fourier transform of the current-density function must not have waves synchronous with waves traveling at the speed of light, that is synchronous with $\frac{\omega_n}{c}$ or synchronous with $\frac{\omega_n}{c}\sqrt{\frac{\varepsilon}{\varepsilon_0}}$ where ε is the dielectric constant of the medium. The Fourier transform of the charge-density function of the atomic orbital (membrane bubble of radius r) is given by Eq. (37). In the case of time-harmonic motion, the current-density function is given by the time derivative of the charge-density function. Thus, the current-density function is given by the product of the constant angular velocity and the charge-density function. The Fourier transform of the current-density function of the atomic orbital is given by the product of the constant angular velocity and Eq. (37). Consider the radial

and time parts of $K_\ell^{m_\ell}(s,\Theta,\Phi,\omega)$, the Fourier transform of the current-density function, where the angular transforms $G_\ell^{m_\ell}(s,\Theta)\otimes H_\ell^{m_\ell}(s,\Theta,\Phi)$ are taken as not zero:

$$K_\ell^{m_\ell}(s,\Theta,\Phi,\omega)=4\pi\omega_n\frac{\sin(2sr_n)}{2sr_n}\otimes G_\ell^{m_\ell}(s,\Theta)\otimes H_\ell^{m_\ell}(s,\Theta,\Phi)\otimes\frac{1}{4\pi}[\delta(\omega-\omega_n)+\delta(\omega+\omega_n)] \tag{38}$$

For the case that the current-density function is constant corresponding to $Y_0^0(\theta,\phi)$, the proceeding factor ω_n of the RHS of Eq. (38) is zero. For time harmonic motion, with angular velocity, ω, Eq. (38) is nonzero only for $\omega=\omega_n$; thus, $-\infty<s<\infty$ becomes finite only for the corresponding wavenumber, s_n. The relationship between the radius and the wavelength is:

$$v_n=\lambda_n f_n \tag{39}$$

$$v_n=2\pi r_n f_n=\lambda_n f_n \tag{40}$$

$$2\pi r_n=\lambda_n \tag{41}$$

Radiation of the bound electron requires an excited state wherein a potentially emitted photon circulates along the atomic orbital at light speed. The nature of an excited state as shown in the Excited States of the One-Electron Atom (Quantization) section is a superposition of an electron and a photon comprising two-dimensional shells of current and field lines, respectively, at the same radius as defined by $\delta(r-r_n)$[1]. Due to the further nature of the photon possessing light-speed angular motion, the electron motion and corresponding spatial and temporal parameters may be considered relative to light-speed for the laboratory frame of the electron's constant angular velocity. A radial correction exists due to Special Relativistic effects. Consider the wave vector of the sinc function. When the velocity is c corresponding to a potentially emitted photon,

$$\mathbf{s}_n\bullet\mathbf{v}_n=\mathbf{s}_n\bullet\mathbf{c}=\omega_n \tag{42}$$

the relativistically corrected wavelength given by Eq. (1.279) is[2]:

$$\lambda_n=r_n \tag{43}$$

The charge-density functions in spherical coordinates plus time are given by Eqs. (1.27-1.29). In the case of Eq. (1.27), the wavelength of Eq. (42) is independent of θ; whereas, in the case of Eqs. (1.28-1.29), the wavelength in Eq. (42) is a function of $\sin\theta$. Thus, in the latter case, Eq. (43) holds wherein the relationship of wavelength and the radius as a function of θ are given by $r_n\sin\theta=\lambda_n\sin\theta$.

Substitution of Eq. (43) into the sinc function (Eq. (38)) results in the vanishing of the entire Fourier transform of the current-density function. Thus, spacetime harmonics of $\frac{\omega_n}{c}=k$ or $\frac{\omega_n}{c}\sqrt{\frac{\varepsilon}{\varepsilon_0}}=k$ do not exist for which the Fourier transform of the current-density function is nonzero. Radiation due to charge motion does not occur in any medium when this boundary condition is met. Note that the boundary condition for the solution of the radial function of the hydrogen atom with the Schrödinger equation is $\Psi\to 0$ as $r\to\infty$. Here, however, the boundary condition is derived from Maxwell's equations: For non-radiative states, the current-density function must not possess spacetime Fourier components that are synchronous with waves traveling at the speed of light. An alternative derivation to that of Haus [1] considering the macro-Maxwellian case and boundary conditions that provides acceleration without radiation is given by Abbott [10].

NONRADIATION BASED ON THE ELECTROMAGNETIC FIELDS AND THE POYNTING POWER VECTOR

A point charge undergoing periodic motion accelerates and as a consequence radiates power P according to the Larmor formula:

$$P=\frac{1}{4\pi\varepsilon_0}\frac{2e^2}{3c^3}a^2 \tag{44}$$

where e is the charge, a is its acceleration, ε_0 is the permittivity of free space, and c is the speed of light. Although an accelerated *point* particle radiates, an *extended distribution* modeled as a superposition of accelerating charges does not have to radiate [1, 10-13]. An ensemble of charges, all oscillating at the same frequency, create a radiation pattern with a number of

[1] Note that the equations of exited state photons given by Eq. (2.15) are not the macro-Maxwellian spherical resonator cavity solutions. The latter is the superposition of many photons comprising a three-dimensional electromagnetic wave in the cavity with the associated macro-boundary conditions. Haus [1] does not address the quantization of single-photon radiation of a bound state that conserves the angular momentum of the photon and single bound electron based on their respective natures. However, the superposition of many photons obeying the quantization condition on a single electron converges to the macro-Maxwellian result. Haus considers an example of rectilinear oscillation of a free point charge that would radiate many photons of many frequencies. It is the macro-Maxwellian case and boundary conditions that Haus addresses in his paper [1] on radiation from point charges. Since Maxwell's equations are obeyed on all scales, the converse of the condition for radiation gives rise to the condition of nonradiation of the bound electron.

[2] In the frame synchronous with waves traveling at the speed of light, the lab-frame electron motion is on a sphere with a radius contracted by the factor 2π. The derivation is given in the Special Relativistic Effect on the Electron Radius and the Relativistic Ionization Energies section. With the wavelength in the speed of light frame given by Eq. (43), the relativistic invariance of the angular momentum of the electron of $\hbar$ (Eq. (1.37)) provides that the corresponding relativistic electron mass (integral of the mass density over the surface) is $2\pi m_e$.

nodes. The same applies to current patterns in phased array antenna design [14]. It is possible to have an infinite number of charges oscillating in such as way as to cause destructive interference or nodes in all directions. The electromagnetic far field is determined from the current distribution in order to obtain the condition, if it exists, that the electron current distribution given by Eq. (49) must satisfy such that the electron does not radiate.

The charge-density functions of the electron atomic orbital in spherical coordinates plus time are given by Eqs. (1.27-1.29). For $\ell = 0,\ N = \frac{-e}{8\pi r_n^2}$, and the charge-density function is:

$\ell = \mathbf{0}$

$$\rho(r,\theta,\phi,t) = \frac{e}{8\pi r_n^2}[\delta(r-r_n)]\left[Y_0^0(\theta,\phi) + Y_\ell^m(\theta,\phi)\right] \tag{45}$$

The equipotential, uniform or constant charge-density function (Eq. (1.27) and Eq. (49)) further comprises a current pattern given in the Atomic Orbital Equation of Motion for $\ell = 0$ Based on the Current Vector Field (CVF) section. It also corresponds to the nonradiative $n = 1$, $\ell = 0$ state of atomic hydrogen and to the spin function of the electron. The current-density function is given by multiplying Eq. (47) by the modulation frequency corresponding to the constant angular velocity ω_n. There is acceleration without radiation, in this case, centripetal acceleration. A static charge distribution exists even though each point on the surface is accelerating along a great circle. Haus' condition predicts no radiation for the entire ensemble. The same result is trivially predicted from consideration of the fields and the radiated power. Since the current is not time dependent, the fields are given by:

$$\nabla \times \mathbf{H} = \mathbf{J} \tag{46}$$

and

$$\nabla \times \mathbf{E} = 0 \tag{47}$$

which are the electrostatic and magnetostatic cases, respectively, with no radiation.

In cases of orbitals of heavier elements and excited states of one electron-atoms and atoms or ions of heavier elements that are not constant as given by Eqs. (1.28-1.29), the constant spin function is modulated by a time and spherical harmonic function. The modulation or traveling charge-density wave corresponds to an orbital angular momentum in addition to a spin angular momentum. These states are typically referred to as p, d, f, etc. orbitals and correspond to an ℓ quantum number not equal to zero. Haus' condition also predicts nonradiation for a constant spin function modulated by a time and spherically harmonic orbital function. However, in the case that such a state arises as an excited state by photon absorption, it is radiative due to a radial dipole term in its current-density function since it possesses spacetime Fourier transform components synchronous with waves traveling at the speed of light as given in the Instability of Excited States section.

The nonradiation condition given by Eqs. (38) and (42-43) may be confirmed by determining the fields and the current distribution condition that is nonradiative based on Maxwell's equations.

For $\ell \neq 0,\ N = \frac{-e}{4\pi r_n^2}$. The charge-density functions including the time-function factor are:

$\ell \neq \mathbf{0}$

$$\rho(r,\theta,\phi,t) = \frac{e}{4\pi r^2}[\delta(r-r_n)]\left[Y_0^0(\theta,\phi) + \mathrm{Re}\left\{Y_\ell^m(\theta,\phi)e^{im\omega_n t}\right\}\right] \tag{48}$$

where $\mathrm{Re}\left\{Y_\ell^m(\theta,\phi)e^{im\omega_n t}\right\} = P_\ell^m(\cos\theta)\cos(m\phi + m\omega_n t)$. In the cases that $m \neq 0$, Eqs. (1.28-1.29) and Eq. (48) is a spherical harmonic traveling charge-density wave of quantum number m that moves on the surface of the atomic orbital about the z-axis at angular frequency ω_n and modulates the atomic orbital corresponding to $\ell = 0$ at $m\omega_n$. Since the charge is modulated time harmonically about the z-axis with the frequency $m\omega_n$ and the current-density function is given by the time derivative of the charge-density function, the current-density function is given by the normalized product of the constant modulation angular velocity and the charge-density function. The first current term of Eq. (48) is static. Thus, it is trivially nonradiative. The current due to the time dependent term is

$$\mathbf{J} = \frac{m\omega_n}{2\pi}\frac{e}{4\pi r_n^2} N[\delta(r-r_n)]\,\mathrm{Re}\left\{Y_\ell^m(\theta,\phi)\right\}\left[\mathbf{u}(t)\times\mathbf{r}\right]$$

$$= \frac{m\omega_n}{2\pi}\frac{e}{4\pi r_n^2} N[\delta(r-r_n)]\,\mathrm{Re}\left\{Y_\ell^m(\theta,\phi)e^{im\omega_n t}\right\}\left[\mathbf{u}\times\mathbf{r}\right]$$

$$= \frac{m\omega_n}{2\pi}\frac{e}{4\pi r_n^2} N'[\delta(r-r_n)]\,\mathrm{Re}\left(P_\ell^m(\cos\theta)e^{im\phi}e^{im\omega_n t}\right)\left[\mathbf{u}\times\mathbf{r}\right] \tag{49}$$

$$= \frac{m\omega_n}{2\pi}\frac{e}{4\pi r_n^2} N'[\delta(r-r_n)]\left(P_\ell^m(\cos\theta)\cos\left(m\phi+m\omega_n t\right)\right)\left[\mathbf{u}\times\mathbf{r}\right]$$

$$= \frac{m\omega_n}{2\pi}\frac{e}{4\pi r_n^2} N'[\delta(r-r_n)]\left(P_\ell^m(\cos\theta)\cos\left(m\phi+m\omega_n t\right)\right)\sin\theta\hat{\phi}$$

where N and N' are normalization constants. The vectors are defined as:

$$\hat{\phi} = \frac{\hat{u}\times\hat{r}}{\left|\hat{u}\times\hat{r}\right|} = \frac{\hat{u}\times\hat{r}}{\sin\theta}; \qquad \hat{u} = \hat{z} = orbital\ axis \tag{50}$$

$$\hat{\theta} = \hat{\phi}\times\hat{r} \tag{51}$$

"^" denotes the unit vectors $\hat{u} \equiv \dfrac{\mathbf{u}}{|\mathbf{u}|}$, non-unit vectors are designed in bold, and the current function is normalized. For time-varying electromagnetic fields, Jackson [15] gives a generalized expansion in vector spherical waves that are convenient for electromagnetic boundary-value problems possessing spherical symmetry properties and for analyzing multipole radiation from a localized source distribution. The Green function $G(\mathbf{x}',\mathbf{x})$ which is appropriate to the equation:

$$\left(\nabla^2 + k^2\right)G(\mathbf{x}',\mathbf{x}) = -\delta(\mathbf{x}'-\mathbf{x}) \tag{52}$$

in the infinite domain with the spherical wave expansion for the outgoing wave Green function is:

$$G(\mathbf{x}',\mathbf{x}) = \frac{e^{-ik|\mathbf{x}-\mathbf{x}'|}}{4\pi|\mathbf{x}-\mathbf{x}'|} = ik\sum_{\ell=0}^{\infty} j_\ell(kr_<)h_\ell^{(1)}(kr_>)\sum_{m=-\ell}^{\ell} Y_{\ell,m}^*(\theta',\phi')Y_{\ell,m}(\theta,\phi) \tag{53}$$

General spherical coordinates are shown in Figure AI.1.

Figure AI.1. Far field approximation.

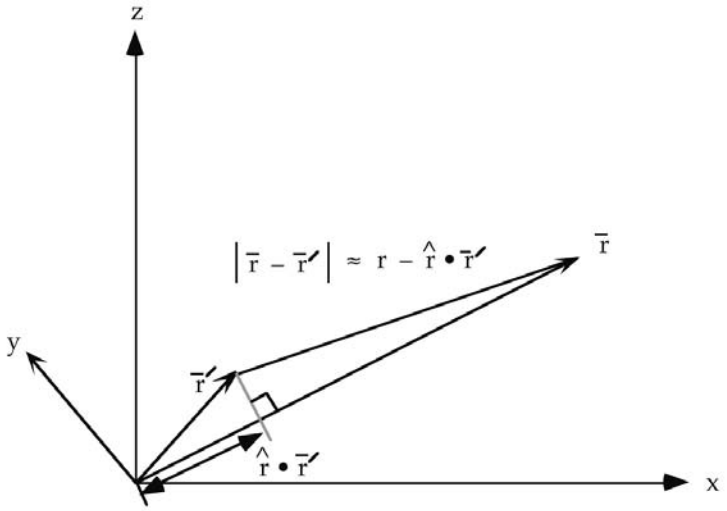

Jackson [15] further gives the general multipole field solution to Maxwell's equations in a source-free region of empty space with the assumption of a time dependence $e^{i\omega t}$.

$$\begin{aligned}\mathbf{B} &= \sum_{\ell,m}\left[a_E(\ell,m) f_\ell(kr)\mathbf{X}_{\ell,m} - \frac{i}{k}a_M(\ell,m)\nabla\times g_\ell(kr)\mathbf{X}_{\ell,m}\right]\\ \mathbf{E} &= \sum_{\ell,m}\left[\frac{i}{k}a_E(\ell,m)\nabla\times f_\ell(kr)\mathbf{X}_{\ell,m} + a_M(\ell,m) g_\ell(kr)\mathbf{X}_{\ell,m}\right]\end{aligned} \tag{54}$$

where the cgs units used by Jackson are retained in this section. The radial functions $f_\ell(kr)$ and $g_\ell(kr)$ are of the form:

$$g_\ell(kr) = A_\ell^{(1)} h_\ell^{(1)} + A_\ell^{(2)} h_\ell^{(2)} \tag{55}$$

$\mathbf{X}_{\ell,m}$ is the vector spherical harmonic defined by:

$$\mathbf{X}_{\ell,m}(\theta,\phi) = \frac{1}{\sqrt{\ell(\ell+1)}}\mathbf{L}Y_{\ell,m}(\theta,\phi) \tag{56}$$

where

$$\mathbf{L} = \frac{1}{i}(\mathbf{r}\times\nabla) \tag{57}$$

The coefficients $a_E(\ell,m)$ and $a_M(\ell,m)$ of Eq. (54) specify the amounts of electric (ℓ,m) multipole and magnetic (ℓ,m) multipole fields, and are determined by sources and boundary conditions as are the relative proportions in Eq. (55). Jackson gives the result of the electric and magnetic coefficients from the sources as:

$$a_E(\ell,m) = \frac{4\pi k^2}{i\sqrt{\ell(\ell+1)}}\int Y_\ell^{m*}(\theta,\phi)\left\{\rho\frac{\partial}{\partial r}\left[rj_\ell(kr)\right] + \frac{ik}{c}(\mathbf{r}\cdot\mathbf{J})j_\ell(kr) - ik\nabla\cdot(r\times\boldsymbol{M})j_\ell(kr)\right\}d^3x \tag{58}$$

and

$$a_M(\ell,m) = \frac{-4\pi k^2}{\sqrt{\ell(\ell+1)}}\int j_\ell(kr)Y_\ell^{m*}(\theta,\phi)\mathbf{L}\cdot\left(\frac{\mathbf{J}}{c} + \nabla\times\boldsymbol{M}\right)d^3x \tag{59}$$

respectively, where the distribution of charge $\rho(\mathbf{x},t)$, current $\mathbf{J}(\mathbf{x},t)$, and intrinsic magnetization $\boldsymbol{M}(\mathbf{x},t)$ are harmonically varying sources: $\rho(\mathbf{x})e^{-\omega t}$, $\mathbf{J}(\mathbf{x})e^{-\omega t}$, and $\boldsymbol{M}(\mathbf{x})e^{-\omega t}$. From Eq. (49), the charge and intrinsic magnetization terms are zero. Also, the current $\mathbf{J}(\mathbf{x},t)$ is in the $\hat{\phi}$ direction; thus, the $a_E(\ell,m)$ coefficient given by Eq. (58) is zero since $\mathbf{r}\cdot\mathbf{J} = 0$. Substitution of Eq. (49) into Eq. (59) gives the magnetic multipole coefficient $a_M(\ell,m)$:

$$a_M(\ell,m) = \frac{-4\pi k^2}{\sqrt{\ell(\ell+1)}}\int j_\ell(kr)Y_\ell^{m*}(\theta,\phi)\mathbf{L}\cdot\left(\frac{\frac{m\omega_n}{2\pi}\frac{e}{4\pi r_n^2}N\delta(r-r_n)Y_\ell^m(\theta,\phi)\sin\theta\hat{\phi}}{c}\right)d^3x \tag{60}$$

wherein the separable time harmonic function of the current is considered separately in Eq. (81). Each mass-density element of the electron moves about the z-axis along a circular orbit of radius $r_n\sin\theta$ in such a way that ϕ changes at a constant rate. That is $\phi = \omega t$ at time t where $m\omega_n$ is the constant angular modulation frequency given in Eq. (49), and

$$r(t) = \mathbf{i}r_n\sin\theta\cos\omega t + \mathbf{j}r_n\sin\theta\sin\omega t \tag{61}$$

is the parametric equation of the circular orbit. The relationships between the Cartesian ($\mathbf{ijk}$) and spherical ($\mathbf{e}_r\mathbf{e}_\theta\mathbf{e}_\phi$) coordinates are [16]:

$$\begin{aligned}\mathbf{e}_r &= \mathbf{i}\sin\theta\cos\phi + \mathbf{j}\sin\theta\sin\phi + \mathbf{k}\cos\theta\\ \mathbf{e}_\theta &= \mathbf{i}\cos\theta\cos\phi + \mathbf{j}\cos\theta\sin\phi - \mathbf{k}\sin\theta\\ \mathbf{e}_\phi &= -\mathbf{i}\sin\phi + \mathbf{j}\cos\phi\end{aligned} \tag{62}$$

The selection rules (Eq. (2.86)) for the conservation of angular momentum must be satisfied during the emission of a single photon of angular momentum $\hbar$:

$$\Delta\ell = \pm 1 \tag{63}$$

The photon's angular momentum given by Eq. (4.1) is:

$$\mathbf{m} = \int\frac{1}{8\pi c}\mathrm{Re}\left[\mathbf{r}\times(\mathbf{E}\times\mathbf{B}^*)\right]dx^4 = \hbar \tag{64}$$

requiring a matching change in the electron's angular momentum. With emission, the radius must decrease in order to conserve

the photon's energy

$$E = \hbar\omega \tag{65}$$

and the electron's energy in the inverse-radius Coulomb potential:

$$V = \frac{-Ze^2}{4\pi\varepsilon_0 r} \tag{66}$$

The radial electric dipole current for a potentially emitted photon for the selection-rule condition of Eq. (2.86) given by Eq. (2.90) is

$$\frac{\mathbf{r}}{|\mathbf{r}|}\cdot\mathbf{J} = J\mathbf{k} = J\left(\cos\theta\mathbf{e}_r - \sin\theta\mathbf{e}_\theta\right) \tag{67}$$

Then, for radiation to occur from the rotating spherical harmonic current (Eq. (49)) while obeying the selection rules and the requirement of an allowed azimuthal-only $\mathbf{B}$ (Eq. (2.102)) pertaining to the emission of a single photon, the radiated magnetic field must have $\mathbf{e}_\phi$ only dependence. Further given Jackson's Eq. (16.84-16.89) [15] for the relationship of $a_M(\ell,m)$ to $\mathbf{B}$, the components of L in Eq. (60) are restricted to those in the xy-plane, the L_x and L_y components. It can easily be appreciated that this result also arises from application of $\mathbf{L}\cdot\mathbf{J}$ to Eq. (67) with the use of the vector identity given by Eq. (16.90) of Jackson [15]:

$$\mathbf{L}\cdot\mathbf{J} = i\nabla\cdot(\mathbf{r}\times\mathbf{J}) \tag{68}$$

Then, the nonradiation condition tests whether the components of the rotating spherical harmonic current that are parallel to those of Eq. (67) give rise to radiation.

Jackson gives the operator in the xy-plane corresponding to the current motion in this plane and the relations for $Y_\ell^m(\theta,\phi)$ [15]:

$$L_+ = L_x + iL_y = e^{i\phi}\left(\frac{\partial}{\partial\theta} + i\cot\theta\frac{\partial}{\partial\phi}\right) \tag{69}$$

$$L_+ Y_\ell^m(\theta,\phi) = \sqrt{(\ell-m)(\ell+m+1)}\,Y_\ell^{m+1}(\theta,\phi) \tag{70}$$

Using Eq. (69), $\mathbf{L}\cdot\mathbf{J}$ of Eq. (59) is

$$\begin{aligned} L_+\left(Y_\ell^m(\theta,\phi)\sin\theta\right) &= e^{i\phi}\left(\frac{\partial}{\partial\theta} + i\cot\theta\frac{\partial}{\partial\phi}\right)Y_\ell^m(\theta,\phi)\sin\theta \\ &= e^{i\phi}Y_\ell^m(\theta,\phi)\left(\frac{\partial}{\partial\theta} + i\cot\theta\frac{\partial}{\partial\phi}\right)\sin\theta + e^{i\phi}\sin\theta\left(\frac{\partial}{\partial\theta} + i\cot\theta\frac{\partial}{\partial\phi}\right)Y_\ell^m(\theta,\phi) \end{aligned} \tag{71}$$

Using Eq. (70) in Eq. (71) gives:

$$L_+\left(Y_\ell^m(\theta,\phi)\sin\theta\right) = e^{i\phi}Y_\ell^m(\theta,\phi)\cos\theta + \sin\theta\sqrt{(\ell-m)(\ell+m+1)}\,Y_\ell^{m+1}(\theta,\phi) \tag{72}$$

The spherical harmonic is given as

$$Y_\ell^m(\theta,\phi) = \sqrt{\frac{2\ell+1}{4\pi}\frac{(\ell-m)!}{(\ell+m)!}}P_\ell^m(\cos\theta)e^{im\phi} = N_{\ell,m}P_\ell^m(\cos\theta)e^{im\phi} \tag{73}$$

Thus, Eq. (72) is given as:

$$L_+\left(Y_\ell^m(\theta,\phi)\sin\theta\right) = e^{i\phi}N_{\ell,m}P_\ell^m(\cos\theta)e^{im\phi}\cos\theta + \sin\theta\sqrt{(\ell-m)(\ell+m+1)}N_{\ell,m+1}P_\ell^{m+1}(\cos\theta)e^{i(m+1)\phi} \tag{74}$$

Substitution of Eq. (74) into Eq. (60) gives:

$$\begin{aligned} a_M(\ell,m) = {} & \frac{-k^2}{c\sqrt{\ell(\ell+1)}}\frac{\omega_n}{2\pi}\frac{e}{r_n^2}N \\ & \int j_\ell(kr)Y_\ell^{m*}(\theta,\phi)\delta(r-r_n)\left\{\begin{array}{l} e^{i\phi}N_{\ell,m}P_\ell^m(\cos\theta)e^{im\phi}\cos\theta \\ \\ +\sin\theta\sqrt{(\ell-m)(\ell+m+1)}N_{\ell,m+1}P_\ell^{m+1}(\cos\theta)e^{i(m+1)\phi} \end{array}\right\}d^3x \end{aligned} \tag{75}$$

Substitution of $Y_\ell^{-m}(\theta,\phi) = (-1)^m Y_\ell^{m*}(\theta,\phi)$ and Eq. (73) into Eq. (75) and integration with respect to dr gives:

$$a_M(\ell,m)=\frac{-ek^2}{c\sqrt{\ell(\ell+1)}}\frac{\omega_n}{2\pi}Nj_\ell(kr_n)$$
$$\int_0^{2\pi}\int_0^{\pi}(-1)^m N_{\ell,-m}P_\ell^{-m}(\cos\theta)e^{-im\phi}\begin{Bmatrix}e^{i\phi}N_{\ell,m}P_\ell^m(\cos\theta)e^{im\phi}\cos\theta\\ +\sin\theta\sqrt{(\ell-m)(\ell+m+1)}N_{\ell,m+1}P_\ell^{m+1}(\cos\theta)e^{i(m+1)\phi}\end{Bmatrix}\sin\theta d\theta d\phi \tag{76}$$

The integral in Eq. (76) separated in terms of $d\theta$ and $d\phi$ is:

$$a_M(\ell,m)=\frac{-ek^2}{c\sqrt{\ell(\ell+1)}}\frac{\omega_n}{2\pi}Nj_\ell(kr_n)$$
$$\int_0^{\pi}(-1)^m N_{\ell,-m}P_\ell^{-m}(\cos\theta)\begin{Bmatrix}N_{\ell,m}P_\ell^m(\cos\theta)\cos\theta\\ +\sin\theta\sqrt{(\ell-m)(\ell+m+1)}N_{\ell,m+1}P_\ell^{m+1}(\cos\theta)\end{Bmatrix}\sin\theta d\theta\int_0^{2\pi}e^{i\phi}d\phi \tag{77}$$

Consider that the $d\theta$ integral is finite and designated by Θ, then Eq. (77) is given as:

$$a_M(\ell,m)=\frac{-ek^2}{c\sqrt{\ell(\ell+1)}}\frac{\omega_n}{2\pi}Nj_\ell(kr_n)\Theta\int_0^{2\pi}e^{i\phi}d\phi \tag{78}$$

From Eq. (54), the far fields are given by:

$$\begin{aligned}\mathbf{B}&=-\frac{i}{k}a_M(\ell,m)\nabla\times g_\ell(kr)\mathbf{X}_{\ell,m}\\ \mathbf{E}&=a_M(\ell,m)g_\ell(kr)\mathbf{X}_{\ell,m}\end{aligned} \tag{79}$$

where $a_M(\ell,m)$ is given by Eq. (78).

The power density $P(t)$ given by the Poynting power vector is:

$$P(t)=\mathbf{E}\times\mathbf{H} \tag{80}$$

For a pure multipole of order (ℓ,m), the time-averaged power radiated per solid angle $\frac{dP(\ell,m)}{d\Omega}$ given by Eqs. (16.74) and (16.75) of Jackson [15] is:

$$\frac{dP(\ell,m)}{d\Omega}=\frac{c}{8\pi k^2}\left|a_M(\ell,m)\right|^2\left|\mathbf{X}_{\ell,m}\right|^2 \tag{81}$$

where $a_M(\ell,m)$ is given by Eq. (78).

The modulation function $Y_{\ell,m}(\theta,\phi)$ is a traveling charge-density wave that moves time harmonically on the surface of the atomic orbital, spins about the z-axis with frequency ω_n, and modulates at $m\omega_n$ corresponding to the term $m\omega_n t$ in Eq. (49). The independent variable ϕ is also a term of the argument of the spherical harmonic function as shown in Eq. (49). Consider the entire potentially radiating surface and the single quantized potentially emitted photon that carries all of the conserved angular momentum of $\hbar$ and energy given by Planck's equation. The time dependence of the power is eliminated in Eq. (81), but the boundary condition of the azimuthal spatial integral for $a_M(\ell,m)$ over its ϕ dependence can also be evaluated in Eqs. (78) and (81) according to the source current's space and time dependence using a substitution of variable for ϕ. From the azimuthal dependency of the source current corresponding to one period, Eq. (78) that can be written as:

$$a_M(\ell,m)=\frac{-ek^2}{c\sqrt{\ell(\ell+1)}}\frac{\omega_n}{2\pi}Nj_\ell(kr_n)\Theta\int_0^{vT_n}\cos(ks)ds \tag{82}$$

where s is the distance along a current path with the corresponding limit of integration being the angular displacement of the rotating modulation function during one period T_n at the linear velocity in the $\hat{\phi}$ direction of v, and k is the wavenumber corresponding to the angular frequency. Thus,

$$a_M(\ell,m)=\frac{-ek^2}{c\sqrt{\ell(\ell+1)}}\frac{\omega_n}{2\pi}Nj_\ell(kr_n)\Theta\sin(kvT_n) \tag{83}$$

$$a_M(\ell,m)=\frac{-ek^2}{c\sqrt{\ell(\ell+1)}}\frac{\omega_n}{2\pi}Nj_\ell(kr_n)\Theta\sin(ks) \tag{84}$$

In the case that k is the light-like k^0, then $k=\omega_n/c$, and the $\sin(ks)$ term in Eq. (84) vanishes for,

$$R=cT_n \tag{85}$$

$$RT_n^{-1}=c \tag{86}$$

$$Rf=c \tag{87}$$

Here ω_n refers to Eq. (48) regarding the angular frequency given by Eq. (1.36) corresponding to the frequency of a potentially emitted photon as given in Chp. 2. Thus,

$$s=vT_n=R=r_n=\lambda_n \tag{88}$$

as given by Eq. (1.279) which is identical to the Haus condition for nonradiation given by Eq. (43), and the photon emission condition given by Eq. (88) is equivalent to that of Eq. (67). Then, the multipole coefficient $a_M(\ell,m)$ is zero as it also has to be according to Eq. (78). For the condition given by Eq. (88), the time-averaged power radiated per solid angle $\frac{dP(\ell,m)}{d\Omega}$ given by Eqs (81) and (84) is zero. *There is no radiation*.

REFERENCES

1. H. A. Haus, "On the radiation from point charges," American Journal of Physics, 54, (1986), pp. 1126-1129.
2. R. N. Bracewell, *The Fourier Transform and Its Applications*, McGraw-Hill Book Company, New York, (1978), pp. 252-253.
3. W. McC. Siebert, *Circuits, Signals, and Systems*, The MIT Press, Cambridge, Massachusetts, (1986), p. 415.
4. Y. L. Luke, *Integrals of Bessel Functions*, McGraw-Hill, New York, (1962), p.22.
5. M. Abramowitz, I. Stegun (3rd Printing 1965), p. 366, Eq. 9.1.10, and p. 255, Eq. 6.1.6.
6. Y. L. Luke, *Integrals of Bessel Functions*, McGraw-Hill, New York, (1962), p.30.
7. H. Bateman, *Tables of Integral Transforms*, Vol. III, McGraw-Hill, New York, (1954), p. 33.
8. Personal communication from M. Nansteel February 2011, confirmed by Mathematica™ by J. Lotoski.
9. G. O. Reynolds, J. B. DeVelis, G. B. Parrent, B. J. Thompson, *The New Physical Optics Notebook,* SPIE Optical Engineering Press, (1990).
10. T. A. Abbott, D. J. Griffiths, Am. J. Phys., Vol. 53, No. 12, (1985), pp. 1203-1211.
11. P. Pearle, Foundations of Physics, "Absence of radiationless motions of relativistically rigid classical electron," Vol. 7, Nos. 11/12, (1977), pp. 931-945.
12. G. Goedecke, Phys. Rev 135B, (1964), p. 281.
13. J. Daboul and J. H. D. Jensen, Z. Physik, Vol. 265, (1973), pp. 455-478.
14. L. C. Shi, J. A. Kong, *Applied Electromagnetism*, Brooks/Cole Engineering Division, Monterey, CA, (1983), pp. 170-209.
15. J. D. Jackson, *Classical Electrodynamics*, Second Edition, John Wiley & Sons, New York, (1975), pp. 739-779.
16. G. R. Fowles, *Analytical Mechanics*, Third Edition, Holt, Rinehart, and Winston, New York, (1977), p. 35.

Appendix II

STABILITY AND ABSENCE OF SELF INTERACTION AND SELF ENERGY

STABILITY

Quantum mechanics does not provide for the stability of matter. The Schrödinger and Dirac solutions violate Maxwell's equations [1-3] and the textbook argument for stability based on the Heisenberg Uncertainty Principle is false [4-5]. Dirac originally attempted to solve the bound electron physically with stability with respect to radiation according to Maxwell's equations with the further constraints that it was relativistically invariant and gave rise to electron spin [74]. He and many founders of QM such as Sommerfeld, Bohm, and Weinstein wrongly pursued a planetary model, were unsuccessful, and resorted to the current mathematical-probability-wave model that has many problems [2, 5-18] such as violation of causality and locality, negative kinetic energy states, violation of conservation of energy as shown by the Klein Paradox with an infinite self energy in the electric and magnetic fields as well as instability to radiation.

In contrast, the atomic orbital is stable to radiation as given in Appendix I, and the current pattern is a uniform, minimum-energy equipotential surface, $Y_0^0(\theta,\phi)$, that gives rise to electron spin. The uniformity proof of the current density and the corresponding angular momentum that gives rise to electron spin is derived in the Atomic Orbital Equation of Motion For $\ell = 0$ Based on the Current Vector Field (CVF) section. The atomic orbital geometry and its intrinsic angular momentum of $\hbar$ are relativistically invariant as given in the Classical Physics of the de Broglie Relation section and Special Relativistic Correction to the Ionization Energies section, respectively. Furthermore, the centrifugal and Coulombic force-densities that are in balance according to Eq. (1.253) are enormous. From Eqs. (1.35), (1.253), and (1.259), the equivalent pressure P_H is:

$$P_H = \frac{1}{4\pi r_1^2}\frac{\hbar^2}{m_e r_1^3} = \frac{\hbar^2}{4\pi m_e a_H^5} = 2.33\ X\ 10^{12}\ N\cdot m^{-2} \tag{1}$$

This is equivalent to twenty million atmospheres. But, even given the incredible forces of the bound atomic orbital, the energy state can be altered by atomic events such as a resonant collision or the absorption of a resonant photon to form an excited state; whereas, non-resonant collisions and photons cannot change the energy state. Only resonant photons are emitted or absorbed according to the Maxwellian-based conservation rules given in the Excited States section and the Equation of the Photon section to result in an energy state change. No states exist between the resonant states. Moreover, state stability to minor perturbations is an inherent electron property.

Specifically, the electron can only exist as a particle that has mass m_e with a total magnitude of intrinsic angular momentum of $\hbar$ based on the physical laws and constants of the universe (Eqs. (36.1-36.4)). Only specific masses that obey the physical laws of Maxwell's equations and those of spacetime while satisfying the conservation conditions can exist. The possible particles can be inter-converted, but not broken into smaller particles that do not satisfy these conditions. (See Introduction, Table I.1, and Chapters 32-38.) Chapter 36 (Leptons) provides the conditions for the creation of an electron from a photon that alters spacetime corresponding to a gravitational field contribution. *Leptons such as the electron are indivisible, perfectly conducting, and possess an inalienable $\hbar$ of intrinsic angular momentum such that any inelastic perturbation involves the entire particle wherein the intrinsic angular momentum remains unchanged. Bound state transitions are allowed involving the exchange of photons between states, each having $\hbar$ of angular momentum in their fields.* Thus, changes in electron state involve photons that carry the quantized conserved energy and $\hbar$ of angular momentum in their fields. A physical approach to solving the structure of the bound electron was followed in Chapter 1 and Appendix I based on the principles of radiation and the corresponding electron state change. These properties maintain the stability of a bound electron to perturbations that do not cause a transition between states and provide that the integral of the physical properties such as the angular momentum of $\hbar$ and

energies in the inverse r-squared electric field originating at the nucleus over the entire electron match the boundary conditions. Consequently, the electron atomic orbital behaves as if it has rigidity based on the integrated conserved angular momentum of $\hbar$ as well as kinetic energy T wherein T is one-half the magnitude of the potential V_e as required for an inverse-squared force wherein V_e is the source of T. Based on the same physical principles, molecular orbitals are stable to non-state-changing perturbations as given in Chapter 11.

It was shown in the Electron g Factor section that as a requirement of the conservation of the electron's intrinsic angular momentum corresponding to spin, the magnetic momentum of the electron can only be parallel or antiparallel to an applied magnetic field, and it must link flux in units of the magnetic flux quantum that is the origin of the electron g factor. Similarly, in order to maintain the electron's intrinsic angular momentum with photon induced states that conserve the photon's orbital angular momentum by inducing a time harmonic orbital distribution in the electron current, the electron orbital angular momentum integrates to zero over each cycle (Eqs. (1.72) and (1.76)). Moreover, the electron's velocity changes in at least one of magnitude and direction during a transition. Then, further considering photons that change the electron's orbital angular momentum and those that don't, all excited state photons carry angular momentum in their electric and magnetic fields only in quantized units of $\hbar$ (Equation of the Photon section) with a corresponding energy of $\hbar\omega$ due to the inalienable electron intrinsic angular momentum of $\hbar$. The electron atomic orbital cannot change its state in a continuous manner. Rather any change is quantized (Excited States of the One-Electron Atom (Quantization) section). This condition also applies to any state change mediated by a collision as well as those mediated by photons wherein the collision creates the resonant photon of the excited state with angular momentum and energy conserved. Thus, any potential self interaction of the elements of the current density distribution of the bound electron associated with its intrinsic angular momentum (Atomic Orbital Equation of Motion For $\ell = 0$ Based on the Current Vector Field (CVF) section) requires the emission of a photon having an angular momentum that is a fraction of $\hbar$ and a commensurate fractional change in the electron's intrinsic angular momentum. This possibility is not allowed as a condition for the existence of the electron.

Furthermore, any allowed self interaction is a radiation-reaction type wherein k is also the lightlike k^0 such that $k = \omega_n / c$. Any such light-like interaction can only be central. Since the velocity of each point of the electron is the same, the current of the atomic orbital is confined to a two-dimensional shell in the $v = c$ frame as well as the lab frame as given by Eq. (1.280). Since the current is orthogonal to the radial vector at the same radius for each great circle current density element, there is no self interaction. However, as shown in the Electron in Free Space section a radiation-reaction force results when the current is confined to a plane lamina. This force and the conservation of the angular momentum of the free electron and the photon in quantized units of $\hbar$ gives rise to the de Broglie relationship as shown in the Classical Physics of the de Broglie Relationship section.

There is *no electrostatic self-energy* as shown *infra*, and there is also *no magnetic self-energy* for the bound electron according to Maxwell's equations. The magnetic moment is invariant for all states as given in the Special Relativistic Correction to the Ionization Energies section, and the surface current is the source of the discontinuous field that does not exist inside of the electron as given by Eq. (1.136).

$$\mathbf{n}\ X\ (\mathbf{H}_a - \mathbf{H}_b) = \mathbf{K} \tag{2}$$

No energy term is associated with the magnetic field unless another source of magnetic field is present.

SELF INTERACTION

In addition to the electrodynamic interaction between the electron and the nucleus, the self interaction of the electron must be considered in the derivation of Eq. (1.253). The bubble-like geometry of the atomic orbital requires the presence of the proton; otherwise, the electron would exist in the free-electron geometry. As given in the Free Electron section, a free electron comprises a two-dimensional planar lamina with field lines that are discontinuous and orthogonal from opposite surfaces of the lamina such that the Maxwellian condition

$$\mathbf{n} \bullet \left(\mathbf{E}_1 - \mathbf{E}_2\right) = \frac{\sigma}{\varepsilon_0} \tag{3}$$

is satisfied where $\mathbf{n}$ is the radial normal unit vector, $\mathbf{E}_1$ and $\mathbf{E}_2$ are the electric field vectors that are discontinuous at the opposite surfaces, and σ is the charge density of the electron corresponding to a total charge of e. There is no self interaction for the free electron that behaves as a two-dimensional perfect conductor. Consider the transformation of the electron's field lines during binding due to the central field of the proton. The spherical symmetry requires that the field lines of the proton and the bound electron are radial. In order to minimize the energy, the continuous charge density function is a two-dimensional equipotential energy surface with an electric field that is strictly normal-radial (Eq. (2.11)) for $r > r_1$ according to Gauss' law and Faraday's law given in the Gauss' Law in Two Dimensions Equates a Discontinuous Field Due to a Discontinuous Charge Layer Source section. The relationship between the electric field equation and the electron source charge-density function is also given by Eq. (3), Maxwell's equation in two dimensions [19-21]. As shown in Figure 1.32, $\mathbf{E}_1$, the electric field inside of the atomic orbital, is zero, $\mathbf{E}_2$, the electric field outside of the atomic orbital, is equivalent to that of a point charge at the origin, and σ is the surface charge density corresponding to a total charge of e.

Eq. (3) applies to a perfect conductor. *The electron is a perfect conductor, and zero field inside of a perfect conductor is confirmed experimentally.* This relation shows that only a 2-D geometry meets the criterion for a fundamental particle and is required for particle production in order to satisfy Maxwell's equations, special and general relativity, and other first principles such as conservation of energy and momentum as shown in the Gravity, Leptons, and Quarks sections. 2-D is the non-singularity geometry, which is no longer divisible. It is the dimension from which it is not possible to lower the dimensionality without encountering intrinsic field infinities. In this case, there is no electrostatic self interaction since the corresponding potential is discontinuous radially across the surface according to Faraday's law in the electrostatic limit, and the field is discontinuous, normal, and radial to the charge according to Gauss' law [19-21]. Thus, only the continuous current density function need be considered.

GAUSS' LAW IN TWO DIMENSIONS EQUATES A DISCONTINUOUS FIELD DUE TO A DISCONTINUOUS CHARGE LAYER SOURCE

Haus [19], Jackson [20], and Stratton [21], give the derivation for Gauss' law in two dimensions. In the electrostatic limit, the pertinent laws are Faraday's law without magnetic induction and Gauss' law. The corresponding continuity conditions are:

$$\mathbf{n}\times\left[\mathbf{E}^{\mathbf{a}}-\mathbf{E}^{\mathbf{b}}\right]=0 \tag{4}$$

$$\mathbf{n}\bullet\left(\varepsilon_0\mathbf{E}^{a}-\varepsilon_0\mathbf{E}^{b}\right)=\sigma_s \tag{5}$$

where $\mathbf{n}$ is the normal unit vector, $\mathbf{E}^a$ and $\mathbf{E}^b$ are the electric field vectors that are discontinuous at the opposite surfaces, and σ_s is the discontinuous two-dimensional surface charge density. The contour enclosing the integration surface over which Faraday's law is integrated to obtain Eq. (4) and the integration volume used to obtain Eq. (5) from Gauss' law are shown in Figures AII.1 and 2, respectively.

Figure AII.1. The differential contour intersecting the surface charge density σ enclosing the integration surface over which Faraday's law is integrated to obtain Eq. (4) (positive charge is shown by convention).

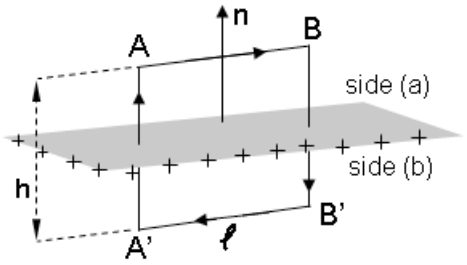

Figure AII.2. The differential integration volume enclosing the surface charge density σ having normal $\mathbf{n}$ used to obtain Eq. (5) from Gauss' law.

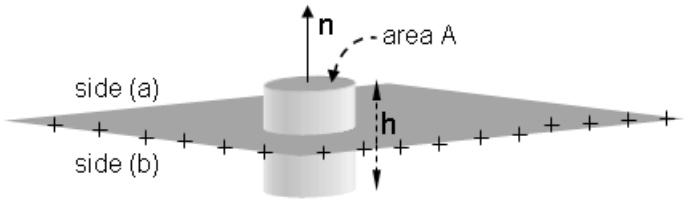

The conditions that the tangential components of the electric field on either side of the interface are the same according to Eq. (4) requires that the potential is continuous over a surface of discontinuity even if that surface carries a surface charge density. Specifically, as shown for the integration of $\mathbf{E}$ around the contour in Figure AII.1, the contributions from $A\to B$ cancel those from $B'\to A'$. Thus, the line integral of $\mathbf{E}$ from $A'\to A$ must be the same as that from $B'\to B$.

$$\int_{A'}^{A}\mathbf{E}\cdot d\mathbf{s}=\int_{B'}^{B}\mathbf{E}\cdot d\mathbf{s}=\Phi_{A'}-\Phi_A=\text{constant} \tag{6}$$

If the potential difference across the surface of discontinuity is constant, then the tangential component of $\mathbf{E}$ is continuous. Furthermore, since the thickness of the layer $h\to 0$, any finite constant potential requires that $\mathbf{E}$ is infinite. To avoid this infinity, the continuity condition on Φ is required to be

$$\Phi^a-\Phi^b=0 \tag{7}$$

From Haus [19]:

"*Continuity of tangential* ***E*** *is equivalent to continuity of* Φ."

To determine the Gauss' law jump condition through the surface of discontinuity, Gauss' law is integrated over the

volume shown intersecting the surface in Figure AII.2. The resulting continuity condition (Eq. (5)) is given in terms of the potential using the electrostatic limit where:

$$\mathbf{E} = -\nabla\Phi \tag{8}$$

Eqs. (3) and (5) become

$$\mathbf{n}\cdot\left[\left(\nabla\Phi\right)^{a} - \left(\nabla\Phi\right)^{b}\right] = -\frac{\sigma_s}{\varepsilon_0} \tag{9}$$

From Haus [91]:

"At a surface of discontinuity that carries a surface charge density, the normal derivative of the potential is discontinuous."

SELF FORCE DUE TO A LAYER OF CHARGE WITH NONZERO THICKNESS

It is shown by Purcell [22] that a self force does arise in the case of a charge layer that has thickness which is an inescapable problem for the quantum mechanical electron; whereas, the two-dimensional electron atomic orbital has no self interaction. Following the example given by Purcell, consider a spherical surface such as that of a balloon of radius 10 cm charged with about $4\ X\ 10^{10}$ additional electrons. Each additional electron is stuck to a rubber molecule that fixes it to the balloon surface where the separation between electrons is about $10^{-4}\ cm$. The electric field inside of the sphere is zero according to Gauss' law since there is no charge here. Outside of the sphere, the electric field given by Gauss' law is:

$$\mathbf{E} = \frac{Q}{4\pi\varepsilon_0 r^2} = \frac{4\pi R^2\sigma}{4\pi\varepsilon_0 r^2}\mathbf{i}_{\mathbf{r}} = \frac{57.6\ V\cdot m}{r^2}\mathbf{i}_{\mathbf{r}} \tag{10}$$

where the total charge on the sphere of radius $R = 0.01\ m$ and the charge density $\sigma = 5.10\ X\ 10^{-6}\ C/m^2$ gives~~is~~ $Q = 6.41\ X\ 10^{-9}\ C$. In the case of a two dimensional layer of charge, there is no self force since there is no self charge for this field to act on. But, in the case that the charges of the layer are distributed such that there is a radial distribution, there exists a corresponding radial self force. A fundamental particle is two dimensional, but the layer of the charged balloon and other such charged surfaces cannot be two dimensional and must have finite thickness.

Regarding aggregates of charges on macroscopic objects Purcell [22] states that "real charge layers do not have zero thickness." He obviously missed the implications for electrons as fundamental particles, even though the absence of self interaction at each radial position was involved in his derivation. And, he states that the self energy corresponding to self force is eliminated "when we replace the actual distribution of discrete elementary charges (the electrons on the rubber balloon) by a perfectly continuous charge distribution [23]."

Purcell uses Gauss' law in two dimensions as well as Newton's third law to conclude that there cannot be any charge-charge interaction for charges at the same radial position. According to Purcell, the force within ~~of~~ any two-dimensional spherical shell must be zero. "Coulomb repulsion between charges in the patch is just another example of Newton's law; the patch as a whole cannot push on itself." Purcell gives the force on each n^{th} shell as

$$d\mathbf{F} = \mathbf{E}dq = \mathbf{E}\sigma_n dA_n \tag{11}$$

where the electric field **E** is external to the shell—not from the shell itself. Purcell affirms that the correct form of Gauss' law for the two-dimensional spherical shell is:

$$\mathbf{n}\bullet\left(\mathbf{E}_1 - \mathbf{E}_2\right) = \frac{\sigma}{\varepsilon_0} \tag{12}$$

and that the proper form in the case of the charge layer of finite thickness is:

$$\nabla\cdot E = \frac{\rho}{\varepsilon_0} \tag{13}$$

The radial distribution of charge is the source of an external field to act on each shell of increasing radius wherein the original charge layer given in Eq. (3) is now considered to have thickness and is modeled as a series of radial subshells corresponding to a radial charge density distribution shown in Figure AII.3.

Figure AII.3. Charge pushes against charge in the radial direction such that within the charge layer of density $\rho(x)$, $E(x+dx)-E(x)=\rho dx$.

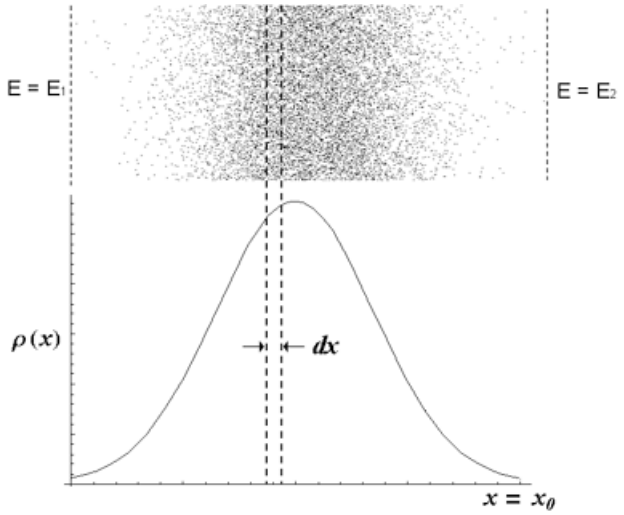

Consider that the field is continuously increasing from $\mathbf{E}_1 = 0\mathbf{i}_\mathbf{r}$ to that at the radius of the largest shell now redefined as *R*:

$$\mathbf{E}_2 = \frac{Q}{4\pi\varepsilon_0 R^2} = \frac{4\pi R^2\sigma}{4\pi\varepsilon_0 R^2}\mathbf{i}_\mathbf{r} = \frac{\sigma}{\varepsilon_0}\mathbf{i}_\mathbf{r} \tag{14}$$

The total force per unit area $\mathbf{F}'$ on the three-dimensional layer of radial thickness x_0 is:

$$\mathbf{F}' = \int_0^{x_0} \mathbf{E}\rho dx \tag{15}$$

Using Eq. (13) gives *dE*, the change in *E* through each increment in the radial direction, *dx*, as ρdx. Thus, ρdx in Eq. (15) may be replaced with *dE* to give:

$$\mathbf{F} = \int_0^{E_2} \mathbf{E}dE = \frac{1}{2}E_2^2 = \frac{1}{2}\left(\frac{\sigma}{\varepsilon_0}+0\right)\frac{\sigma}{\varepsilon_0} = \frac{1}{2}\left(\frac{Q}{4\pi\varepsilon_0 R^2}+0\right)\frac{Q}{4\pi\varepsilon_0 R^2} \tag{16}$$

where Eq. (10) was used. The self force per unit area of a three-dimensional layer of charge is then proportional to the average of the field inside and outside of the layer of charge which is zero and given by Eq. (10), respectively. Here, the charge density given by Purcell is:

$$\sigma = \int_0^{x_0} \rho dx \tag{17}$$

This usage is misleading and should not be confused with a two-dimensional charge density according to Eq. (3). In the case of the charged balloon, the force per unit area is:

$$\mathbf{F}' = \frac{1}{2}\frac{\sigma^2}{\varepsilon_0} = 1.47\ N/m^2 \tag{18}$$

An expression similar to that given Eq. (16) arises when using Coulomb's law to calculate the field of a spherical layer of charge at the radius of the shell. The calculation of the field inside of the shell alone implies that the layer must have thickness so that the field of $\frac{1}{2}Q$ and self interaction applies. This situation does not arise if Coulomb's law is applied correctly for regions outside of a two-dimensional charge discontinuity as given in the Conditions for the Absence or Presence of a Self Force Using Coulomb's Law section.

Quantum mechanics is internally inconsistent. Electron shielding or self interaction of the electron cloud is ignored in cases involving one electron such as *H* and H_2^+, but electron-electron repulsion terms as well as shielding are considered in multielectron problems such as *He* and H_2; even though, the charge densities occupy the same space whether there is one or more electrons—the only difference being the magnitude. The electron cloud model is also mandatory to achieve neutral scattering despite the internal inconsistency with scattering experiments that the momentum transfer is with the entire mass of the electron as pointed out by Max Born. The subsequent probability-wave model violates special relativity and causality by requiring a point electron to be over all space at once, weighted according to a "guiding" probability density function.

The electron spread over all space must interact with itself since Gauss' law applied to the volumetric charge density

gives rise to a radial electric field from zero to infinity. Consequently, there is the inescapable problem that the electron cloud is unstable, not to mention the nonphysical nature of the infinities in the electric and magnetic fields of the point electron manifested as a probability cloud distribution.

CONDITIONS FOR THE ABSENCE OR PRESENCE OF A SELF FORCE USING COULOMB'S LAW

Following the derivation by Fowles [24] for the inverse r-squared gravitational force on a point test mass due to a shell of mass, the electric force of a spherical shell of charge on a test charge q is derived using Coulomb's law, which is also an inverse r-squared force. The charge-density is integrated over the spherical surface rather than the mass, but the results are of the same form. The Coulomb derivation is also given by Nansteel [25].

Figure AII.4. Coordinates for calculating the field of a spherical shell of charge e of zero thickness.

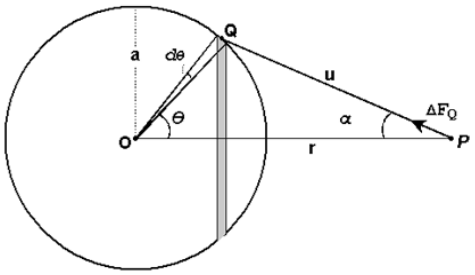

The shell of zero thickness, total charge $-e$, and radius a shown in Figure AII.4 has a uniform, two-dimensional charge density of:

$$\sigma = -\frac{e}{4\pi a^2} \tag{19}$$

centered on the origin *O*. Based on symmetry, the r-axis is defined as the z-axis, and the azimuthal directions are defined as the xy-plane.

The incremental force $d\mathbf{F}$ on the test charge at point P on the z-axis at a distance *r* from the center *O* of the spherical shell due to the incremental charge σdA at a point Q of the shell is given by:

$$d\mathbf{F} = \frac{1}{4\pi\varepsilon_0}\frac{q(\sigma dA)}{u^3}\mathbf{u} \tag{20}$$

where the test charge may lie inside ($r < a$) or outside ($r > a$) of the 2-D sphere and the force at $r = a$ is given by $r_> \to a$ since Coulomb's and Gauss' laws are only defined outside of the charge that is the source of the field, the angle $\angle POQ$ between the z-axis and point Q is defined as θ, $\mathbf{u}$ is the vector $\vec{PQ}$, $u = |\mathbf{u}|$, and the area increment *dA* on the surface at Q is given by:

$$dA = a^2 \sin\theta d\phi d\theta \tag{21}$$

where ϕ is the azimuthal angle about the z-axis. The vector projections of $\mathbf{u}$ from the triangle POQ are:

$$\mathbf{u} = (r - a\cos\theta)\mathbf{i}_\mathbf{z} + a\sin\theta\mathbf{i}_\mathbf{xy} \tag{22}$$

where $\mathbf{i}_\mathbf{z}$ is the unit vector along the z-axis and $\mathbf{i}_\mathbf{xy}$ is the unit vector lying in the plane of POQ and perpendicular to the z-axis. With the substitution of Eq. (22) into Eq. (20) the incremental force on the test charge is:

$$d\mathbf{F} = \frac{q\sigma a^2}{4\pi\varepsilon_0}\frac{\sin\theta}{u^3}\left[(r - a\cos\theta)\mathbf{i}_\mathbf{z} + a\sin\theta\mathbf{i}_\mathbf{xy}\right]d\phi d\theta \tag{23}$$

and the total force is

$$\mathbf{F} = \int_{Spherical\ Shell} d\mathbf{F} = \frac{q\sigma a^2}{4\pi\varepsilon_0}\int_{\theta=0}^{\pi}\left(\frac{\sin\theta}{u^3}\int_{\phi=0}^{2\pi}\left[(r - a\cos\theta)\mathbf{i}_\mathbf{z} + a\sin\theta\mathbf{i}_\mathbf{xy}\right]d\phi\right)d\theta \tag{24}$$

Due to symmetry the azimuthal forces cancel out over each circular integral:

$$\int_{\phi=0}^{2\pi}\mathbf{i}_\mathbf{xy}d\phi = 0 \tag{25}$$

Thus, the force is only a function of θ:

$$\mathbf{F} = \frac{q\sigma a^2}{2\varepsilon_0}\mathbf{i}_z \int_{\theta=0}^{\pi} \frac{\sin\theta(r - a\cos\theta)}{u^3} d\theta \tag{26}$$

The integration variable may be changed to u by obtaining the scalar by squaring Eq. (22):

$$u^2 = (r - a\cos\theta)^2 + (a\sin\theta)^2 \tag{27}$$

and then differentiating with respect to θ:

$$2udu = 2(r - a\cos\theta)(a\sin\theta)d\theta + 2(a\sin\theta)a\cos\theta d\theta \tag{28}$$

Then,

$$udu = (ra\sin\theta - a^2\cos\theta\sin\theta)d\theta + a^2\cos\theta\sin\theta d\theta = ra\sin\theta d\theta \tag{29}$$

From triangle POQ, the law of cosines gives:

$$u^2 + r^2 - 2ur\cos\alpha = a^2 \tag{30}$$

where

$$r - a\cos\theta = u\cos\alpha \tag{31}$$

Substitution of Eq. (31) into Eq. (30) gives:

$$u^2 + r^2 - 2r(r - a\cos\theta) = a^2 \tag{32}$$

$$r - a\cos\theta = \frac{u^2 + r^2 - a^2}{2r} \tag{33}$$

Multiplication of the right-hand side of Eq. (33) by $1 = \frac{u}{u}$ gives:

$$r - a\cos\theta = u\left(\frac{r^2 + u^2 - a^2}{2ru}\right) \tag{34}$$

Substitution of Eqs. (29) and (34) into Eq. (26) gives

$$\mathbf{F} = \frac{q\sigma a^2}{\varepsilon_0 r^2}\mathbf{i}_z I(r) \tag{35}$$

where

$$I(r) = \frac{1}{4a}\int_{u=|r-a|}^{r+a} \frac{(r-a)(r+a)}{u^2} + 1 \; du \tag{36}$$

Evaluation of Eq. (36) for $I(r)$ gives

$$I(r) = \frac{1}{4a}\left(-\frac{(r-a)(r+a)}{u} + u\right)_{u=|r-a|}^{u=r+a} = \frac{1}{4a}\left(-\frac{(r-a)(r+a)}{r+a} + \frac{(r-a)(r+a)}{r-a} + (r+a) - (r-a)\right)$$

$$= \frac{1}{4a}\left(-(r-a) + (r+a) + 2a\right) = \frac{1}{4a}(2a + 2a) = 1 \tag{37}$$

Thus, the force on the test charge given by Coulomb's law is:

$$\mathbf{F} = \frac{qe}{4\pi\varepsilon_0}\mathbf{i}_z \begin{cases} \frac{1}{r^2}, & r > a \\ 0, & r < a \end{cases} \tag{38}$$

which is the field of a point charge at the origin for radial distances greater than or equal to the radius. This result is consistent with Gauss' and Faraday's laws at a two-dimensional layer of charge given by Eq. (3). Then, $I(r)$ increases by unity as the test charge is moved from the inside of the sphere ($r < a$) to outside ($r > a$).

But, the behavior of $I(r)$:

$$I(r) = \begin{cases} 1, & r > a \\ 0, & r < a \end{cases} \tag{39}$$

suggests the definition

$$I(a)=\frac{1}{2}\left\{\lim_{r\to a+0} I(r)+\lim_{r\to a-0} I(r)\right\}=\frac{1}{2} \tag{40}$$

for the case that the test charge lies at the spherical shell. The corresponding force is:

$$\mathbf{F}=\frac{qe}{4\pi\varepsilon_0}\mathbf{i}_z\begin{cases}\dfrac{1}{r^2},\ r>a\\ \dfrac{1}{2a^2},\ r=a\\ 0,\ r<a\end{cases} \tag{41}$$

in conflict with the result of Eq. (3). Although, mathematically Eq. (24) leads to the result of Eq. (41), it is nonphysical, applicable to a charged insulator. To achieve a minimum energy for the bound electron, a perfect conductor, the electric field lines are radial from the surface. The Eq. (38) result is obtained trivially by application of Gauss' law. A perfectly conducting cavity acts as a Faraday cage wherein experimentally the field inside is zero since the interior contains no charge. The following Gauss-law result holds,

$$\int_S \mathbf{E}\cdot dA=\int_V \frac{\rho}{\varepsilon_0}dV \tag{42}$$

$$\mathbf{E}=\frac{0}{4\pi\varepsilon_0 r_n^2}\mathbf{i}_r=0 \tag{43}$$

For a two-dimensional spherical shell that is a perfect conductor the field inside of the spherical cavity, or any hollow conductor for that matter, is zero as shown by Bueche [26]. Thus, the integral given by Eq. (24) is trivially zero since there is no remote action[1] of any surface point on another[2]. Using Eq. (3), the field is given by Eq. (38).

In contrast to the bound-electron case, an ensemble of point charges that are on the surface of a spherical shell insulator gives rise to the result of Eq. (41) with an inherent self interaction due to the remote action of each other surface point charge on any given point charge. An additional self interaction arises when the spherical layer of point charges possesses thickness. A charge density of nonzero thickness is of the form considered by Purcell with:

$$\sigma=\int_{a-\frac{x_0}{2}}^{a+\frac{x_0}{2}}\rho dx \tag{44}$$

Specifically, for a linear radial distribution, Gauss' law gives the force as:

$$\int_{Spherical\ Shell,\ r=a} E\cdot dA=\int_{a-\frac{x_0}{2}}^{a}\frac{\frac{e}{x_0}}{\varepsilon_0}dx \tag{45}$$

$$E4\pi a^2=\frac{\frac{e}{2}}{\varepsilon_0} \tag{46}$$

Thus,

$$E=\frac{1}{2}\frac{e}{4\pi a^2\varepsilon_0} \tag{47}$$

And, the corresponding force on the test charge q at $r=a$ is:

$$F=qE=\frac{1}{2}\frac{qe}{4\pi a^2\varepsilon_0} \tag{48}$$

This result is also equivalent to the self force given by Purcell in Eq. (16). It is also important to notice that the electric field in both cases is a continuous function of the radial displacement dx such that the final force with the test charge outside of the charge layer is equivalent to that given by Eq. (38) with the exception that the radius includes the thickness of the layer. The *caution of confusing the use of σ as defined in Eqs. (12) and (19) with that given in Eqs. (17) and (44) was also discussed in the Self Force Due to a Layer of Charge with Nonzero Thickness section*.

---

[1] Remote action refers to that of a point with a different (θ,ϕ) from a selected point.

[2] The same result arises with the consideration of the cancellation of the bound electron's field by that of the proton.

In the case that the test charge is a proton at the origin and the charge layer is the electron cloud of the hydrogen atom according to quantum mechanics, the factor of 1/2 must also be considered with the requirement that field lines of the proton end on the electron charge. The proton's field is continuous and must end in a continuous manner throughout the electron cloud, which results in an infinite-body problem to solve for the form of the cloud and the corresponding energy. Another fatal flaw in quantum mechanics is the corresponding self energy. This problem does not arise in the case of the electron atomic orbital as shown in the Self Energy section.

SELF ENERGY

The force balance equation can also be arrived at by the familiar minimization of the energy, which demonstrates the absence of a self-energy term for the atomic orbital and the presence of an infinite term for the quantum mechanical solutions. The atomic orbital electron kinetic energy T_1 obtained by integration over the mass density at spherical position $r = r'$ (Eq. (1.27)) is:

$$T_1 = \frac{1}{2}v^2 \int_0^{2\pi}\int_0^{\pi}\int_0^{\infty} \frac{m_e}{4\pi r'^2}\delta(r-r')r^2 \sin\theta dr d\theta d\phi = \frac{1}{2}m_e v^2 = \frac{1}{2}\frac{\hbar^2}{m_e r^2} \tag{49}$$

where the velocity is given by Eq. (1.35). The electron atomic orbital is a two-dimensional equipotential energy surface at spherical position $r = r'$. The potential energy is given by integrating Poisson's equation over the continuous two-dimensional surface charge density given by Eq. (1.27) at the equipotential due to the proton at spherical position $r = r'$ where the electric field of the electron is strictly normal-radial (Eq. (2.11)) for $r > r_1$ according to Gauss' law, and the potential is continuous across the surface according to Faraday's law in the electrostatic limit.

$$V = -\frac{Ze}{4\pi\varepsilon_0 r}\int_0^{2\pi}\int_0^{\pi}\int_0^{\infty} \frac{e}{4\pi r'^2}\delta(r-r')r^2 \sin\theta dr d\theta d\phi = -\frac{Ze^2}{4\pi\varepsilon_0 r} \tag{50}$$

And, the energy due to the electrodynamic interaction of the electron and the proton T_2 due to their relative motion given by Eq. (1.35) is

$$T_2 = \frac{1}{2}mv^2 = \frac{1}{2}\frac{\hbar^2}{mr^2} \tag{51}$$

The total energy E is the sum of Eqs. (49-51).

$$E = T_1 + V + T_2 = \frac{1}{2}\frac{\hbar^2}{m_e r^2} - \frac{Ze^2}{4\pi\varepsilon_0 r} + \frac{1}{2}\frac{\hbar^2}{mr^2} \tag{52}$$

Then, the minimum energy is obtained by taking the derivative of Eq. (52) and setting it to zero, which is

$$\frac{\hbar^2}{m_e r^3} = \frac{Ze^2}{4\pi\varepsilon_0 r^2} - \frac{\hbar^2}{mr^3} \tag{53}$$

Eq. (53) can be written in terms of the densities:

$$\frac{m_e}{4\pi r_1^2}\frac{v_1^2}{r_1} = \frac{e}{4\pi r_1^2}\frac{Ze}{4\pi\varepsilon_0 r_1^2} - \frac{1}{4\pi r_1^2}\frac{\hbar^2}{mr_1^3} \tag{54}$$

where $Z = 1$ and $m = m_p$ for the hydrogen atom. Then, Eq. (54) is the same as Eq. (1.253).

As shown in Figure 1.32, the electric field of the proton alone is over all space, and the electric field of the bound electron alone is finite only for $r > r_1$. The radius goes to infinity in the case of the ionized or free electron, and the corresponding charge and current density functions are given in the Free Electron Section. During binding of the free electron which is a two-dimensional disc lamina, the electron charge distribution becomes that of a 2-D uniform spherical shell of charge, and the electric field of the electron superimposes and cancels part of that of the proton for $r > r_1$ as shown in Figure 1.32. The energy in the electric fields of each of the proton and the electron alone is given as

$$E_{ele} = \frac{1}{2}\varepsilon_0 \int_0^{\infty} \mathbf{E}^2 dv \tag{55}$$

where $\mathbf{E}$ is the electric field of each independently. The binding energy of the hydrogen atom, which is released as photons is given as the change in the electric field energy due to the change in the electric field due to the superposition of the fields of the electron and proton.

$$T = \Delta E_{ele} = \frac{1}{2}\varepsilon_0 \int_0^\infty (\Delta \mathbf{E})^2 dv = -\frac{1}{2}\varepsilon_0 \int_\infty^{r_1} \left(\frac{e}{4\pi\varepsilon_0 r^2}\right)^2 dv \quad = -\frac{1}{2}\varepsilon_0 \int_0^{2\pi}\int_0^{\pi}\int_\infty^{r_1} \left(\frac{e}{4\pi\varepsilon_0 r^2}\right)^2 r^2 \sin\theta dr d\theta d\Phi$$
$$= -\int_\infty^{r_1} \frac{e^2}{8\pi\varepsilon_0 r^2} dr \quad = \frac{e^2}{8\pi\varepsilon_0 r_1} \tag{56}$$

For $r_1 = a_H$ as given by Eq. (1.260),

$$T = \Delta E_{ele} = \frac{e^2}{8\pi\varepsilon_0 a_H} = 13.5984\ eV \tag{57}$$

In the case of nuclear charge Z, ΔE_{ele} increases by a factor of Z, and the radius given by Eq. (1.260) is $r_1 = \frac{a_H}{Z}$. These substitutions in Eq. (57) give Eq. (1.264).

Eq. (57), matches the experimental binding energy. In contrast, the corresponding energy does not match in the case of the solutions of the Schrödinger equation. Even if it is assumed that the electron is everywhere at once in order to achieve electroneutrality, which is impossible, the energy stored in the electric field of the electron does not match the binding energy since the average radius of the hydrogen atom in this case is 3/2 the Bohr radius. Even more problematic is that the self-energy in the quantum mechanical electron is infinite wherein the radius in Eq. (56) goes to zero as given by Purcell [27].

REFERENCES

1. V. F. Weisskopf, Reviews of Modern Physics, Vol. 21, No. 2, (1949), pp. 305-315.
2. P. Pearle, Foundations of Physics, "Absence of radiationless motions of relativistically rigid classical electron," Vol. 7, Nos. 11/12, (1977), pp. 931-945.
3. R. L. Mills, "The fallacy of Feynman's argument on the stability of the hydrogen atom according to quantum mechanics," Annales de la Fondation Louis de Broglie, Vol. 30, No. 2, (2005), pp.129-151; posted at http://www.blacklightpower.com/techpapers.shtml.
4. E. H. Lieb, "The stability of matter," Reviews of Modern Physics, Vol. 48, No. 4, (1976), pp, 553-569.
5. R. L. Mills, "The fallacy of Feynman's argument on the stability of the hydrogen atom according to quantum mechanics," Annales de la Fondation Louis de Broglie, Vol. 30, No. 2, (2005), pp. 129-151; posted at http://www.blacklightpower.com/techpapers.shtml.
6. F. Laloë, "Do we really understand quantum mechanics? Strange correlations, paradoxes, and theorems," Am. J. Phys. 69 (6), June 2001, 655-701.
7. R. L. Mills, "Classical quantum mechanics," Physics Essays, Vol. 16, No. 4, December, (2003), pp. 433-498; posted at http://www.blacklightpower.com/techpapers.shtml.
8. R. L. Mills, "Exact classical quantum mechanical solutions for one- through twenty-electron atoms," Phys. Essays, Vol. 18, No.3 (2005), 321-361.
9. R. L. Mills, "The Nature of the chemical bond revisited and an alternative Maxwellian approach," Physics Essays, Vol. 17, (2004), pp. 342-389; posted at http://www.blacklightpower.com/techpapers.shtml.
10. R. L. Mills, "Exact classical quantum mechanical solution for atomic helium which predicts conjugate parameters from a unique solution for the first time," Phys. Essays, Vol. 21, No. 2, (2008), pp. 103-141.
11. R. L. Mills, *The Grand Unified Theory of Classical Quantum Mechanics*, May 2005 Edition posted at http://www.blacklightpower.com/theory/bookdownload.shtml.
12. R. L. Mills, "The Grand Unified Theory of Classical Quantum Mechanics," Int. J. Hydrogen Energy, Vol. 27, No. 5, (2002), pp. 565-590.
13. R. L. Mills, "The nature of free electrons in superfluid helium--a test of quantum mechanics and a basis to review its foundations and make a comparison to classical theory," Int. J. Hydrogen Energy, Vol. 26, No. 10, (2001), pp. 1059-1096.
14. R. L. Mills, "The hydrogen atom revisited," Int. J. of Hydrogen Energy, Vol. 25, Issue 12, December, (2000), pp. 1171-1183.
15. R. L. Mills, "Maxwell's equations and QED: Which is fact and which is fiction," Physics Essays, Vol. 19, No. 2, (2006), 225-262S.
16. V. F. Weisskopf, Reviews of Modern Physics, Vol. 21, No. 2, (1949), pp. 305-315.
17. A. Einstein, B. Podolsky, N. Rosen, Phys. Rev., Vol. 47, (1935), p. 777.
18. H. Wergeland, "The Klein Paradox Revisited," *Old and New Questions in Physics, Cosmology, Philosophy, and Theoretical Biology*, A. van der Merwe, Editor, Plenum Press, New York, (1983), pp. 503-515.
19. H. A. Haus, J. R. Melcher, "Electromagnetic Fields and Energy," Department of Electrical Engineering and Computer Science, Massachusetts Institute of Technology, (1985), Sec. 5.3.
20. J. D. Jackson, Classical Electrodynamics, Second Edition, John Wiley & Sons, New York, (1975), pp. 17-22.
21. J. A. Stratton, *Electromagnetic Theory,* McGraw-Hill Book Company, (1941), p. 195.
22. E. Purcell, *Electricity and Magnetism,* McGraw-Hill, New York, (1985), pp. 29-31.
23. E. Purcell, *Electricity and Magnetism,* McGraw-Hill, New York, (1985), p. 33.
24. G. R. Fowles, *Analytical Mechanics,* Third Edition, Holt, Rinehart, and Winston, New York, (1977), pp. 138-140.

25. M. Nansteel, available at http://www.blacklightpower.com/pdf/Electrical_Field_Due_to_Spherical_Surface_Charge.pdf.
26. F. J. Bueche, *Introduction to Physics for Scientists and Engineers,* McGraw-Hill, New York, (1975), pp. 351-356.
27. E. Purcell, *Electricity and Magnetism,* McGraw-Hill, New York, (1985), pp. 31-33.

Appendix III

MUON g FACTOR

The muon, like the electron, is a lepton with $\hbar$ of angular momentum. The magnetic moment of the muon is given by Eq. (1.169) with the electron mass replaced by the muon mass. It is twice that predicted using the gyromagnetic ratio (given in Eq. (2) of Box 1.2) in Eq. (2.65) of the Orbital and Spin Splitting section wherein the intrinsic angular momentum for the spin 1/2 fermion is $\frac{\hbar}{2}$. As is the case with the electron, the magnetic moment of the muon is the sum of the component corresponding to the kinetic angular momentum, $\frac{\hbar}{2}$, and the component corresponding to the vector potential angular momentum, $\frac{\hbar}{2}$, (Eq. (1.164)). The spin-flip transition can be considered as involving a magnetic moment of g times that of a Bohr magneton of the muon. The g factor (Eq. (1.261)) is:

$$\frac{g}{2} = 1 + \frac{\alpha}{2\pi} + \frac{2}{3}\alpha^2\left(\frac{\alpha}{2\pi}\right) - \frac{4}{3}\left(\frac{\alpha}{2\pi}\right)^2 \tag{1}$$

For $\alpha^{-1} = 137.03603(82)$ (Eq. (1.235)),

$$\frac{g}{2} = 1.001\ 159\ 652\ 137 \tag{2}$$

The muon anomalous magnetic moment has been measured in a new experiment at Brookhaven National Laboratory (BNL) [1]. Polarized muons were stored in a superferric ring, and the angular frequency difference ω_a between the spin precession and orbital frequencies was determined by measuring the time distribution of high-energy decay positrons. The ratio R of ω_a to the Larmor precession frequency of free protons ω_p in the storage-ring magnetic field was measured. R is given by

$$R = \frac{\omega_a}{\omega_p} \tag{3}$$

The anomalous g value a_μ of the μ^+ was determined where the anomalous g value is related to the gyromagnetic ratio by

$$a_\mu = \frac{(g-2)}{2} \tag{4}$$

and

$$a_\mu = \frac{R}{\lambda - R} \tag{5}$$

where λ is the ratio of the muon and proton magnetic moments:

$$\lambda = \frac{\mu_\mu}{\mu_p} \tag{6}$$

According to Carey et al. [1], "For polarized muons moving in a uniform magnetic field $\vec{B}$, which is perpendicular to the muon spin direction and to the plane of the orbit, and with an electric quadrupole field $\vec{E}$ for vertical focusing, the angular frequency difference, ω_a, between the spin precession frequency ω_s and the cyclotron frequency ω_c is given by:

$$\vec{\omega}_a = -\frac{e}{mc}\left[a_\mu \vec{\mathbf{B}} - \left(a_\mu - \frac{1}{\gamma^2 - 1}\right)\hat{\beta} \times \vec{\mathbf{E}}\right] \tag{7}$$

The dependence of ω_a on the electric field is eliminated by storing muons with the 'magic' $\gamma = 29.3$, which corresponds to a muon momentum $p = 3.09\ GeV/c$. Hence measurement of ω_a and of B determines a_μ."

Based on Lorentz covariance Jackson [2] gives the BMT equation which is the relativistic equation of motion for spin in uniform or slowly varying external fields. The rate of change of the component of spin **s** parallel to the velocity may be determined from the BMT equation. This is the longitudinal polarization or net helicity of the particle. If $\hat{\beta}$ is a unit vector in the direction of $\beta = \frac{\mathbf{v}}{\mathbf{c}}$, the longitudinal polarization is $\hat{\beta} \cdot \mathbf{s}$. It changes in time because **s** changes and also β changes. The BMT equation in cgs units gives:

$$\frac{d}{dt}\left(\hat{\beta} \cdot \mathbf{s}\right) = -\frac{e}{mc}\mathbf{s}_\perp \cdot \left[\left(\frac{g}{2} - 1\right)\hat{\beta} \times \mathbf{B} + \left(\frac{g\beta}{2} - \frac{1}{\beta}\right)\mathbf{E}\right] \tag{8}$$

where $\mathbf{s}_\perp$ is the component of **s** perpendicular to the velocity. Eq. (8) demonstrates a remarkable property of a particle with $g = 2$. In a purely magnetic field, the spin precesses in such a manner that the longitudinal polarization remains constant, whatever the motion of the particle. If the particle is relativistic ($\beta \to 1$), even the presence of an electric field causes the longitudinal polarization to change only very slowly, at a rate proportional to γ^{-2} times the electric field component perpendicular to **v**.

The "magic" γ given by Eq. (8) wherein the contribution to the change of the longitudinal polarization by the electric quadrupole focusing fields are eliminated occurs when:

$$\frac{g_\mu \beta}{2} - \frac{1}{\beta} = 0 \tag{9}$$

where g_μ is the muon g factor which is required to be different from the electron g factor in the standard model due to the dependence of the mass dependent interaction of each lepton with vacuum polarizations due to virtual particles. For example, the muon is much heavier than the electron, and so high energy (short distance) effects due to strong and weak interactions are more important here [3]. Also, according to the BNL collaboration [1]:

> "The hadronic contribution and uncertainty are dominated by the single vacuum polarization loop with hadrons present, which is determined from a dispersion relationship using data from annihilation to hadrons and from hadronic decay. A contribution from higher order hadronic vacuum polarization and light-by-light scattering must be included"

The BNL Muon (g-2) Collaboration [1] used a "magic" $\gamma = 29.3$ which satisfied Eq. (9) identically for $\frac{g_\mu}{2}$; however, their assumption that this condition eliminated the affect of the electrostatic field on ω_a is flawed as shown below. The relativistic factor γ is given by:

$$\gamma = \frac{1}{\sqrt{1 - \beta^2}} \tag{10}$$

where

$$\beta = \frac{v}{c} \tag{11}$$

Substitution of Eq. (9) into Eq. (10) gives:

$$\gamma = \frac{1}{\sqrt{1 - \frac{2}{g_\mu}}} \tag{12}$$

and

$$\beta_\mu = \sqrt{\frac{2}{g_\mu}} = \sqrt{1 - \frac{1}{\gamma^2}} \tag{13}$$

From the BNL99 results and the average of the CERN and BNL97 results [1] an estimated value of $\frac{g_\mu}{2}$ is:

$$\frac{g_\mu}{2} = 1.00116593 \tag{14}$$

Substitution of Eq. (14) into Eq. (12) gives the "magic" γ as:

$$\gamma = 29.3033176 \tag{15}$$

and from Eq. (13),

$$\beta_\mu = 0.999417544 \tag{16}$$

As shown in the Electron g Factor section, in the case of an exact balance between the Lorentz force (Eq. (1.183)) and the electric force corresponding to the Hall voltage (Eq. (1.184)), the superconducting condition is met when:

$$\frac{E}{B} = v \tag{17}$$

which in cgs units is:

$$E = \frac{Bv}{c} = B\beta_\mu \tag{18}$$

Consider the case that the g factor for the muon and the electron are the same and the "magic" $\gamma = 29.3$ selected by the BNL Muon (g-2) Collaboration which satisfied Eq. (9) identically for $\frac{g_\mu}{2}$ (Eq. (1.229)) does not satisfy Eq. (9) for $\frac{g_e}{2}$ given by the experimental value (Eq. (27)). In this case, the second term of Eq. (8) contributes to ω_a. With $g = g_e$ and $\beta = \beta_\mu$, the BMT equation is:

$$\frac{d}{dt}\left(\hat{\beta}\cdot\mathbf{s}\right) = -\frac{e}{mc}\mathbf{s}_\perp \cdot \left[\left(\frac{g_e}{2}-1\right)\hat{\beta}\times\mathbf{B} + \left(\frac{g_e\beta_\mu}{2} - \frac{1}{\beta_\mu}\right)\mathbf{E}\right] \tag{19}$$

Since **B** is parallel to $\mathbf{s}_\perp \times \hat{\beta}$ and since **E** and $\mathbf{s}_\perp$ are anti-parallel, the electric field from Eq. (18) is:

$$\mathbf{E} = -\beta_\mu \hat{\beta}\times\mathbf{B} \tag{20}$$

Figure AIII.1. Coordinate system of crossed electric field, $\mathbf{E}_x$, corresponding to the Hall voltage, magnetic flux, $\mathbf{B}_z$, due to the applied field, the velocity, $\mathbf{v}_y$, in the $\hat{\beta}$ direction, and $\mathbf{s}_\perp$ where $|\mathbf{E}| = \beta B$.

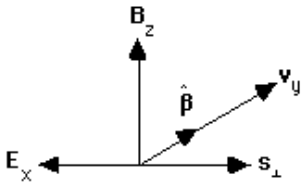

Then

$$\frac{d}{dt}\left(\hat{\beta}\cdot\mathbf{s}\right) = -\frac{e}{mc}\mathbf{s}_\perp \cdot \left[\left(\frac{g_e}{2}-1\right) - \left(\frac{g_e\beta_\mu^2}{2}-1\right)\right]\hat{\beta}\times\mathbf{B} \tag{21}$$

$$= -\frac{e}{mc}\left[\frac{g_e}{2} - \frac{g_e\beta_\mu^2}{2}\right]\mathbf{s}_\perp \cdot \left(\hat{\beta}\times\mathbf{B}\right) \tag{22}$$

$$= -\frac{e}{mc}\left[\frac{g_e}{2}\left(1-\beta_\mu^2\right)\right]\mathbf{s}_\perp \cdot \left(\hat{\beta}\times\mathbf{B}\right) \tag{23}$$

In the case that $g = g_\mu \neq g_e$, the term in **E** of Eq. (8)

$$\frac{d}{dt}\left(\hat{\beta}\cdot\mathbf{s}\right)=-\frac{e}{mc}\left[\frac{g_\mu}{2}-1\right]\mathbf{s}_\perp\cdot\left(\hat{\beta}\times\mathbf{B}\right) \tag{24}$$

vanishes and a change in longitudinal polarization due to the finite electric term can be considered as an additional term to the electron g factor which gives rise to an effective g factor corresponding to $\frac{g_\mu}{2}$. Comparison of Eq. (23) and Eq. (24) gives the effective value of $\frac{g_\mu}{2}$ which is the predicted experimental value for $\frac{g_\mu}{2}$:

$$\frac{g_\mu}{2}-1=\frac{g_e}{2}\left(1-\beta_\mu^2\right) \tag{25}$$

$$\frac{g_\mu}{2}=1+\frac{g_e}{2}\left(1-\beta_\mu^2\right) \tag{26}$$

Eq. (19), which gives the predicted experimental value for $\frac{g_\mu}{2}$ (Eq. (26)), corresponds to the experimental situation of the BNL measurement of $\frac{g_\mu}{2}$. The experimental value of $\frac{g_e}{2}$ [4] is:

$$\frac{g_e}{2}=1.001\ \ 159\ \ 652\ \ 188(4) \tag{27}$$

Substitution of $\frac{g_e}{2}$ and β_μ given by Eq. (27) and Eq. (16), respectively, into Eq. (26) gives the calculated effective muon g factor which is:

$$\frac{g_\mu}{2}=1.001\ 165\ 923 \tag{28}$$

The calculated result based on the equivalence of the muon and electron g factors is in agreement with the result of Carey et al. [1]:

$$\frac{g_\mu}{2}=1.001\ 165\ 925\ (15) \tag{29}$$

Rather than indicating an expanded plethora of postulated super-symmetry virtual particles which make contributions such as smuon-neutralino and sneutrino-chargino loops as suggested by Brown et al. [5], the deviation of the experimental value of $\frac{g_\mu}{2}$ from that of the standard model prediction simply indicates that the muon g factor is identical to the electron g factor. This could have been spotted immediately had the objectivity of the experimental design been given precedence over the assumption of the validity of the standard model. Given the ad hoc nonphysical nature of QED (See Refs. [6-7]) and the internal inconsistency of the theoretical basis of this experiment regarding using the classical BMT equation in a test of nonclassical QED, more scrutiny was especially warranted.

From Eqs. (26), (27), and (16), the difference between $\frac{g_\mu}{2}$ and $\frac{g_e}{2}$ due to the finite electric term of Eqs. (8) and (19) with $g=g_e$ is:

$$\frac{g_\mu}{2}-\frac{g_e}{2}=1-\frac{g_e}{2}\beta_\mu^2=0.0000062705 \tag{30}$$

With the equivalence of the muon g factor and the electron g factor, the possibilities are limited for the occurrence of internal consistency during the determination of $\frac{g_\mu}{2}$ using the BMT equation with the flawed assumption that $\frac{g_\mu}{2}\neq\frac{g_e}{2}$. Consider the case of Eq. (9) with $g=g_e=g_\mu$ and $\beta=\beta_u$ with the corresponding "magic" γ given by Eqs. (10-13). An equation equivalent to Eq. (30) that gives rise to an internally consistent experimental observation of an effective muon g factor corresponding to $\beta=\beta_u$ is:

$$\left[\frac{1}{\sqrt{\frac{2}{g_{\mu\gamma}}}}-\frac{g_e\sqrt{\frac{2}{g_{\mu\gamma}}}}{2}\right]\sqrt{\frac{2}{g_{\mu\gamma}}}=0.0000062705 \tag{31}$$

$$1-\frac{\frac{g_e}{2}}{\frac{g_{\mu\gamma}}{2}}=0.0000062705 \tag{32}$$

where $g_{\mu\gamma}$ is the muon anomalous g factor selected before the experiment to fix the "magic" γ, 0.0000062705 given by Eq. (32) (also see Eq. (30)) is the difference between the projected experimental value of $\frac{g_\mu}{2}$ and the experimentally measured value of $\frac{g_e}{2}$. The experimental value of $\frac{g_e}{2}$ from Eq. (27) and the selected value of $\frac{g_{\mu\gamma}}{2}$ from Eq. (14) satisfy Eqs. (31-32) and are in close agreement with the experimental value of $\frac{g_\mu}{2}$ determined by Carey et al. [1] (Eqs. (28-29)). The "magic" γ of BNL which gave an internally consistent but misinterpreted result was most likely arrived at by trial and error. Consider the following relationship between δ and $\frac{\left(g_{\mu y}-2\right)}{2}$ of the "magic" γ that follows from Eq. (32):

$$1-\frac{\frac{g_e}{2}}{\frac{g_{\mu y}}{2}}=\delta \tag{33}$$

where

$$\frac{\left(g_e-2\right)}{2}+\delta=\frac{\left(g_\mu-2\right)}{2} \tag{34}$$

and g_e is the experimentally measured electron anomalous g factor and g_μ is the projected experimental value of the muon anomalous g factor based on $g_{\mu\gamma}$, the selected value of the muon anomalous g factor to fix the "magic" γ. A plot of δ versus $\frac{\left(g_{\mu y}-2\right)}{2}$ from Eq. (33) is shown in Figure AIII.2.

Figure AIII.2. Plot of δ versus $\frac{\left(g_{\mu\gamma}-2\right)}{2}$ of the "magic" γ from Eq. (33).

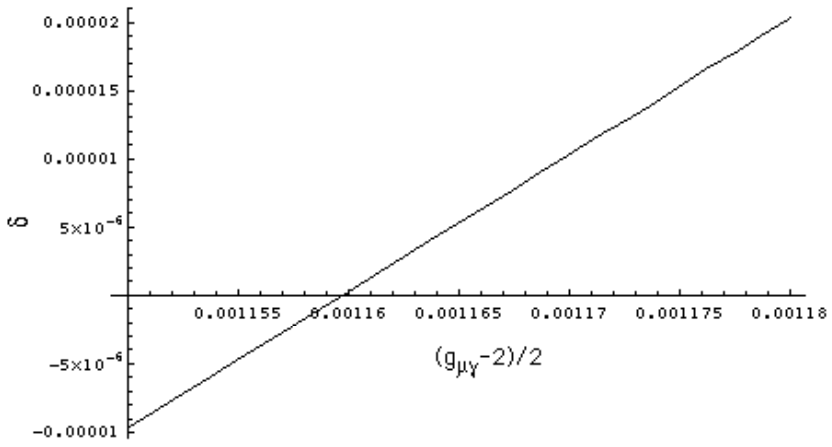

Only a narrow range of values of $\frac{\left(g_{\mu\gamma}-2\right)}{2}$ about the value of $\frac{\left(g_\mu-2\right)}{2}$ measured by Carey et al. [1] are internally consistent.

Similar misinterpretations of data based on a bias towards quantum theory are described in the Schrödinger "Black" Cats section. For example, NIST claimed to have placed a $^9Be^+$ ion in two places at once when in reality an applied magnetic field and a potential well were found which forced a resonance between an oscillatory and a Stern-Gerlach transition. And, the resulting interference pattern in the fluorescence emission was misinterpreted as indicating that the ion was in two widely separated positions simultaneously [8]. The BNL experiment should be repeated to determine the dependence of ω_a on the "magic" γ. The current BNL results and classical theory support the equivalence of the electron and muon g factors.

EXPERIMENTAL DETERMINATION OF THE PROPER β [9]

The angular frequency difference between the spin procession frequency and the cyclotron frequency, [4], is:

$$\vec{\omega}_a = -\frac{e}{mc}\left[a_\mu \vec{\mathbf{B}} - \left(a_\mu - \frac{1}{\gamma^2 - 1}\right)\hat{\beta} \times \vec{\mathbf{E}}\right] \tag{35}$$

Introducing the velocity ratio, β, and g,

$$\gamma^2 - 1 = \frac{\beta^2}{1-\beta^2}, \qquad a_\mu = \frac{g}{2} - 1 \tag{36}$$

yields

$$\vec{\omega}_a = -\frac{e}{mc}\left[\left(\frac{g}{2} - 1\right)\vec{\mathbf{B}} - \left(\frac{g}{2} - \frac{1}{\beta^2}\right)\hat{\beta} \times \vec{\mathbf{E}}\right] \tag{37}$$

The unique value of β for which the term in **E** vanishes is β^*:

$$\frac{g}{2} = \frac{1}{\beta^{*2}} \tag{38}$$

For $\beta = \beta^*$

$$\vec{\omega}_a\left(\beta^*\right) = -\frac{e}{mc}\left(\frac{1}{\beta^{*2}} - 1\right)\vec{\mathbf{B}} \tag{39}$$

Taking the magnitude results in

$$\omega_a\left(\beta^*\right) = \frac{e}{mc}\left(\frac{1}{\beta^{*2}} - 1\right)B \tag{40}$$

The experimental measurement of the frequency difference for various β allows the graphical determination of β^*, (See Figure AIII.3), with no assumption regarding g.

Figure AIII.3. Plot of the experimental measurement of the frequency difference for various β which allows the graphical determination of β^*.

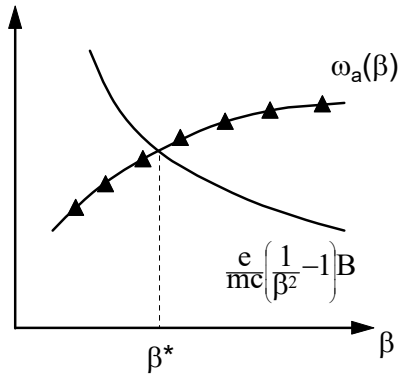

REFERENCES

1. R. M. Carey et al., Muon (g-2) Collaboration, "New measurement of the anomalous magnetic moment of the positive muon," Phys. Rev. Lett., Vol. 82, (1999), pp. 1632-1635.
2. J. D. Jackson, *Classical Electrodynamics*, Second Edition, John Wiley & Sons, New York, (1975), pp. 556-560.
3. G. P. Lepage, Theoretical advances in quantum electrodynamics, International Conference on Atomic Physics, Atomic Physics Proceedings, Singapore, World Scientific, Vol. 7, (1981), pp. 297-311.
4. R. S. Van Dyck, Jr., P. Schwinberg, H. Dehmelt, "New high precision comparison of electron and positron g factors," Phys. Rev. Lett., Vol. 59, (1987), p. 26-29.
5. H. N. Brown et al., Muon (g-2) Collaboration, "Precise measurement of the positive muon anomalous magnetic moment," Phys. Rev. D62, 091101, (2000).
6. R. L. Mills, "Maxwell's Equations and QED: Which is Fact and Which is Fiction," Physics Essays, Vol. 19, (2006), pp. 225-262.
7. R. L. Mills, "The Fallacy of Feynman's Argument on the Stability of the Hydrogen Atom According to Quantum Mechanics," Annales de la Fondation Louis de Broglie, Vol. 30, No. 2, (2005), pp. 129-151.
8. C. Monroe, D. M. Meekhof, B. E. King, D. J. Wineland, Science, Vol. 272, (1996), pp. 1131-1135.
9. M. Nansteel, BlackLight Power, Inc., Cranbury, NJ, Personal Communication, May, (2001).

Appendix IV

ANALYTICAL EQUATIONS TO GENERATE THE FREE ELECTRON CURRENT-VECTOR FIELD AND THE ANGULAR-MOMENTUM-DENSITY FUNCTION $Y_0^0(\theta,\phi)$

ROTATION OF A GREAT CIRCLE IN THE XY-PLANE ABOUT THE $(\mathbf{i}_x,0\mathbf{i}_y,\mathbf{i}_z)$-AXIS BY 2π

With the electron current in the counter clockwise direction, the Larmor precession of the angular momentum vector of the free electron is about two axes simultaneously, the $(\mathbf{i}_x,0\mathbf{i}_y,\mathbf{i}_z)$-axis and the laboratory-frame z-axis defined by the direction of the applied magnetic field. The precessions are about the opposite axes with the current in the opposite direction. The motion generates CVFs equivalent to those of the bound electron given in the Atomic Orbital Equation of Motion for $\ell = 0$ Based on the Current Vector Field (CVF) section. Over one time period, the first motion sweeps out the equivalent of a BECVF, and the rotation about the z-axis sweeps out the equivalent of an OCVF. The combined motions sweep out the equivalent of the convolution of the BECVF with the OCVF, a distribution having the angular momentum equivalent of $Y_0^0(\theta,\phi)$ of the bound electron. The electron may flip between the two states wherein the BECVF, OCVF, and $Y_0^0(\theta,\phi)$ precession distributions developed *infra* apply to both states, but the currents are opposite.

Specifically, the Larmor precession of the free electron with the current in the counter clockwise direction corresponds to the two superimposed independent time-harmonic rotations of the plane-lamina disc initially in the xy-plane. One is about the $(\mathbf{i}_x,0\mathbf{i}_y,\mathbf{i}_z)$-axis by 2π wherein the angular momentum vector of the free electron that is perpendicular to the plane-lamina of its current sweeps out a cone about the $(\mathbf{i}_x,0\mathbf{i}_y,\mathbf{i}_z)$-axis. The plane-lamina is comprised of concentric great circle current loops each of a radius given by the continuous variable ρ for $0 \le \rho \le \rho_0$. For each great circle, the first Larmor precession generates the equivalent vector-field pattern as that of a BECVF. Simultaneously, the distribution corresponding to the first rotation precesses or rotates about the laboratory z-axis defined by the applied magnetic field direction wherein the $(\mathbf{i}_x,0\mathbf{i}_y,\mathbf{i}_z)$-axis sweeps out a cone about the z-axis. Over one time period, the rotational motion about the z-axis generates the equivalent vector-field pattern as that of an OCVF of the bound electron. The combined motions over time generate the equivalent distribution and angular momentum as those of $Y_0^0(\theta,\phi)$ of the bound electron given by the convolution of the OCVF with the BECVF.

The rotation of a great circle in the xy-plane about the $(\mathbf{i}_x,0_y,\mathbf{i}_z)$-axis by 2π generates a free electron BECVF corresponding to the precession motion with its resultant angular momentum of $\sqrt{2}\hbar$ along the $(\mathbf{i}_x,0\mathbf{i}_y,\mathbf{i}_z)$-axis having components of $\mathbf{L}_{xy} = \hbar$ and $\mathbf{L}_z = \hbar$. Equally valid is the substitution of the $(-\mathbf{i}_x,0\mathbf{i}_y,\mathbf{i}_z)$-axis for the $(\mathbf{i}_x,0_y,\mathbf{i}_z)$-axis since the corresponding orthogonal BECVFs have the same distribution and are simply related by a half cycle of precession motion about the z-axis. Both will be considered.

The BECVF corresponding to the $\left(\mathbf{i}_x, 0\mathbf{i}_y, \mathbf{i}_z\right)$-axis over 2π will be generated first following the procedure given in Fowles [1] and using the matrices given by Eqs. (1.80-1.82). The rotational matrix about the $\left(\mathbf{i}_x, 0\mathbf{i}_y, \mathbf{i}_z\right)$-axis by θ, $R_{(\mathbf{i}_x, 0\mathbf{i}_y, \mathbf{i}_z)}(\theta)$, is given by:

$$R_{(\mathbf{i}_x, 0\mathbf{i}_y, \mathbf{i}_z)}(\theta) = R_y\left(-\frac{\pi}{4}\right) R_z(\theta) R_y\left(\frac{\pi}{4}\right) \tag{1}$$

Then, using Eqs. (1) and Eqs. (1.81-1.82), the great circle basis elements and rotational matrix are given by:

BECVF MATRICES ($R_{(\mathbf{i}_x, 0\mathbf{i}_y, \mathbf{i}_z)}(\theta)$)

$$\begin{bmatrix} x' \\ y' \\ z' \end{bmatrix} = \begin{bmatrix} \frac{1}{2}+\frac{\cos\theta}{2} & \frac{\sin\theta}{\sqrt{2}} & \frac{1}{2}-\frac{\cos\theta}{2} \\ -\frac{\sin\theta}{\sqrt{2}} & \cos\theta & \frac{\sin\theta}{\sqrt{2}} \\ \frac{1}{2}-\frac{\cos\theta}{2} & -\frac{\sin\theta}{\sqrt{2}} & \frac{1}{2}+\frac{\cos\theta}{2} \end{bmatrix} \begin{bmatrix} \rho\cos\phi \\ \rho\sin\phi \\ 0 \end{bmatrix} \tag{2}$$

Using Eq. (2), the BECVF matrix representation of the convolution is given by:

$$BECVF = \lim_{\Delta\theta\to 0} \sum_{m=1}^{m=\frac{2\pi}{|\Delta\theta|}} \left[\left(R_{(\mathbf{i}_x, 0\mathbf{i}_y, \mathbf{i}_z)}(\theta) \bullet GC^{basis}_{(\mathbf{i}_x, \mathbf{i}_y, 0\mathbf{i}_z)} \right) \otimes \delta\left(\theta - m\Delta\theta_M\right) \right] \tag{3}$$

wherein $R_{(\mathbf{i}_x, 0\mathbf{i}_y, \mathbf{i}_z)}(\theta)$ is the rotational matrix about the $R_{(\mathbf{i}_x, 0\mathbf{i}_y, \mathbf{i}_z)}(\theta)$-axis, $GC^{basis}_{(\mathbf{i}_x, \mathbf{i}_y, 0\mathbf{i}_z)}$ is the great circle basis element initially in the xy-plane, and $\otimes$ designates the convolution with the delta function of the infinitesimal incremental angle $m\Delta\theta_M$. The integral form of the convolution is

$$BECVF = \int_0^{2\pi} \left(R_{(\mathbf{i}_x, 0\mathbf{i}_y, \mathbf{i}_z)}(\theta) \bullet GC^{basis}_{(\mathbf{i}_x, \mathbf{i}_y, 0\mathbf{i}_z)} \right) \lim_{\Delta\theta\to 0} \sum_{m=1}^{m=\frac{2\pi}{|\Delta\theta|}} \delta\left(\theta - m\Delta\theta_M\right) d\theta \tag{4}$$

The integration gives the infinite sum of great circles that constitute the BECVF:

$$BECVF = \lim_{\Delta\theta\to 0} \sum_{m=1}^{m=\frac{2\pi}{|\Delta\theta|}} \left[\left(R_{(\mathbf{i}_x, 0\mathbf{i}_y, \mathbf{i}_z)}(m\Delta\theta_M) \bullet GC^{basis}_{(\mathbf{i}_x, \mathbf{i}_y, 0\mathbf{i}_z)} \right) \right] \tag{5}$$

The current pattern for the rotation of the xy-plane great circle about the $\left(\mathbf{i}_x, 0\mathbf{i}_y, \mathbf{i}_z\right)$-axis is shown in Figure IV.1 wherein θ is varied from 0 to 2π.

Figure IV.1. The current pattern for the rotation of the xy-plane great circle about the $\left(\mathbf{i}_x, 0\mathbf{i}_y, \mathbf{i}_z\right)$-axis (Eqs. (2) and (5)) shown with 6 degree increments of θ from the perspective of looking along the z-axis. The great circle current loop that served as a basis element that was initially in the xy-plane is shown as red.

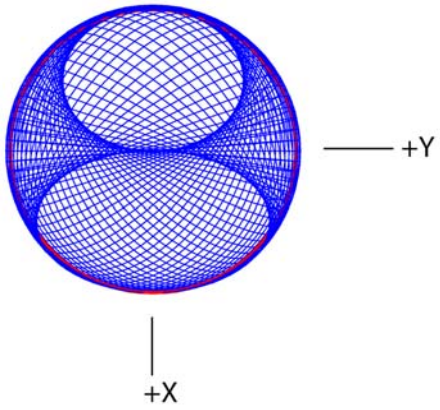

CONICAL SURFACES FORMED BY VARIATION OF ρ

The rotation of the free-electron disc having a continuous progression of larger current loops along ρ forms two conical surfaces over a period that join at the origin and face in the opposite directions along the $\left(\mathbf{i}_x, 0\mathbf{i}_y, \mathbf{i}_z\right)$-axis, the axis of rotation, as shown in Figure IV.2. At each position of $0 < \rho$, there exists a BECVF of that radius that is concentric to the one of infinitesimally larger radius to the limit at $\rho = \rho_0$. The BECVF at each position ρ generated over a period by the Larmor precession about the $\left(\mathbf{i}_x, 0\mathbf{i}_y, \mathbf{i}_z\right)$- axis by 2π is given by Eqs. (2) and (5). The conical surfaces were generated by varying ρ in Eqs. (2) and (5).

Figure IV.2. The two conical surfaces formed by rotation of the plane-lamina disc comprised of concentric great circles about the $\left(\mathbf{i}_x, 0\mathbf{i}_y, \mathbf{i}_z\right)$-axis that join at the origin and face in the opposite directions along the axis of rotation, the $\left(\mathbf{i}_x, 0\mathbf{i}_y, \mathbf{i}_z\right)$-axis.

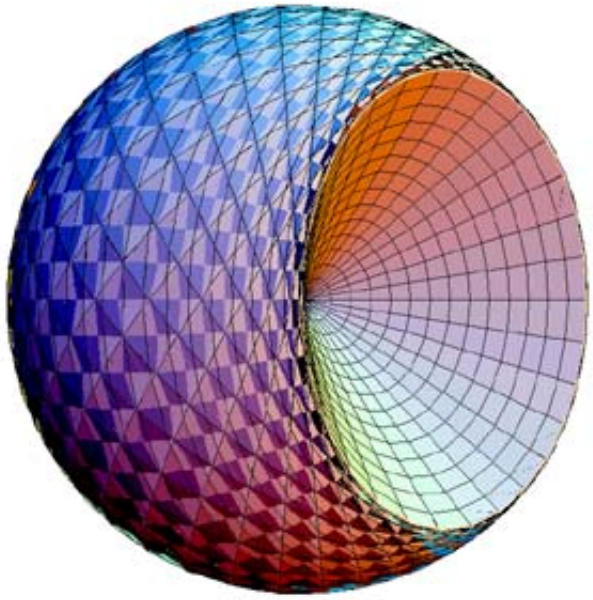

ROTATION OF A GREAT CIRCLE IN THE XY-PLANE ABOUT THE $\left(-\mathbf{i}_x, 0\mathbf{i}_y, \mathbf{i}_z\right)$-AXIS BY 2π

Similarly, the Larmor precession of the free electron about the z-axis also corresponds to the time-harmonic rotation of the plane-lamina disc about the $\left(-\mathbf{i}_x, 0\mathbf{i}_y, \mathbf{i}_z\right)$-axis by 2π. The Larmor precession of the plane-lamina comprised of concentric great-circle current loops each of a radius given by the continuous variable ρ for $0 \le \rho \le \rho_0$ generates the equivalent BECVF. The rotational matrix about the $\left(-\mathbf{i}_x, 0\mathbf{i}_y, \mathbf{i}_z\right)$-axis by θ, $R_{\left(-\mathbf{i}_x, 0\mathbf{i}_y, \mathbf{i}_z\right)}(\theta)$, is given by

$$R_{\left(-\mathbf{i}_x, 0\mathbf{i}_y, \mathbf{i}_z\right)}(\theta) = R_y\left(\frac{\pi}{4}\right) R_z(\theta) R_y\left(\frac{-\pi}{4}\right) \tag{6}$$

Then, using Eqs. (6) and Eqs. (1.81-1.82), the great circle basis elements and rotational matrix are given by

BECVF MATRICES ($R_{(-\mathbf{i}_x,0\mathbf{i}_y,\mathbf{i}_z)}(\theta)$)

$$\begin{bmatrix} x' \\ y' \\ z' \end{bmatrix} = \begin{bmatrix} \frac{1}{2}+\frac{\cos\theta}{2} & \frac{\sin\theta}{\sqrt{2}} & -\frac{1}{2}+\frac{\cos\theta}{2} \\ -\frac{\sin\theta}{\sqrt{2}} & \cos\theta & -\frac{\sin\theta}{\sqrt{2}} \\ -\frac{1}{2}+\frac{\cos\theta}{2} & \frac{\sin\theta}{\sqrt{2}} & \frac{1}{2}+\frac{\cos\theta}{2} \end{bmatrix} \begin{bmatrix} \rho\cos\phi \\ \rho\sin\phi \\ 0 \end{bmatrix} \tag{7}$$

Using Eq. (7), the BECVF matrix representation of the convolution is given by:

$$BECVF = \lim_{\Delta\theta\to 0} \sum_{m=1}^{m=\frac{2\pi}{|\Delta\theta|}} \left[\left(R_{(-\mathbf{i}_x,0\mathbf{i}_y,\mathbf{i}_z)}(\theta) \bullet GC^{basis}_{(\mathbf{i}_x,\mathbf{i}_y,0\mathbf{i}_z)} \right) \otimes \delta(\theta - m\Delta\theta_M) \right] \tag{8}$$

wherein $R_{(-\mathbf{i}_x,0\mathbf{i}_y,\mathbf{i}_z)}(\theta)$ is the rotational matrix about the $R_{(-\mathbf{i}_x,0\mathbf{i}_y,\mathbf{i}_z)}(\theta)$-axis, $GC^{basis}_{(\mathbf{i}_x,\mathbf{i}_y,0\mathbf{i}_z)}$ is the great circle basis element initially in the xy-plane, and $\otimes$ designates the convolution with the delta function of the infinitesimal incremental angle $m\Delta\theta_M$. The integral form of the convolution is

$$BECVF = \int_0^{2\pi} \left(R_{(-\mathbf{i}_x,0\mathbf{i}_y,\mathbf{i}_z)}(\theta) \bullet GC^{basis}_{(\mathbf{i}_x,\mathbf{i}_y,0\mathbf{i}_z)} \right) \lim_{\Delta\theta\to 0} \sum_{m=1}^{m=\frac{2\pi}{|\Delta\theta|}} \delta(\theta - m\Delta\theta_M) d\theta \tag{9}$$

The integration gives the infinite sum of great circles that constitute the BECVF:

$$BECVF = \lim_{\Delta\theta\to 0} \sum_{m=1}^{m=\frac{2\pi}{|\Delta\theta|}} \left[\left(R_{(-\mathbf{i}_x,0\mathbf{i}_y,\mathbf{i}_z)}(m\Delta\theta_M) \bullet GC^{basis}_{(\mathbf{i}_x,\mathbf{i}_y,0\mathbf{i}_z)} \right) \right] \tag{10}$$

The current pattern for the rotation of the xy-plane great circle about the $(-\mathbf{i}_x,0\mathbf{i}_y,\mathbf{i}_z)$-axis is shown in Figure IV.3 wherein θ is varied from 0 to 2π.

Figure IV.3. The current pattern for the rotation of the xy-plane great circle about the $(-\mathbf{i}_x,0\mathbf{i}_y,\mathbf{i}_z)$-axis (Eqs. (7) and (10)) shown with 6 degree increments of θ from the perspective of looking along the z-axis. The great circle current loop that served as a basis element that was initially in the xy-plane is shown as red.

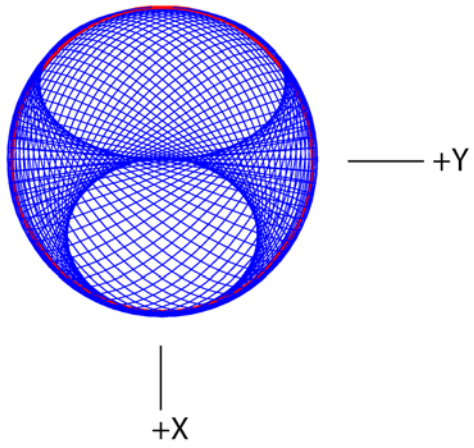

CONICAL SURFACES FORMED BY VARIATION OF ρ

The rotation of the free-electron disc having a continuous progression of larger current loops along ρ forms two conical surfaces over a period that join at the origin and face in the opposite directions along the $\left(-\mathbf{i}_x, 0\mathbf{i}_y, \mathbf{i}_z\right)$-axis, the axis of rotation, as shown in Figure IV.4. At each position of $0 < \rho$, there exists a BECVF of that radius that is concentric to the one of infinitesimally larger radius to the limit at $\rho = \rho_0$. The BECVF at each position ρ generated over a period by the Larmor precession about the $\left(-\mathbf{i}_x, 0\mathbf{i}_y, \mathbf{i}_z\right)$- axis by 2π is given by Eqs. (7) and (10). The conical surfaces were generated by varying ρ in Eqs. (7) and (10).

Figure IV.4. The two conical surfaces formed by rotation of the plane-lamina disc comprised of concentric great circles about the $\left(-\mathbf{i}_x, 0\mathbf{i}_y, \mathbf{i}_z\right)$-axis that join at the origin and face in the opposite directions along the axis of rotation, the $\left(-\mathbf{i}_x, 0\mathbf{i}_y, \mathbf{i}_z\right)$-axis.

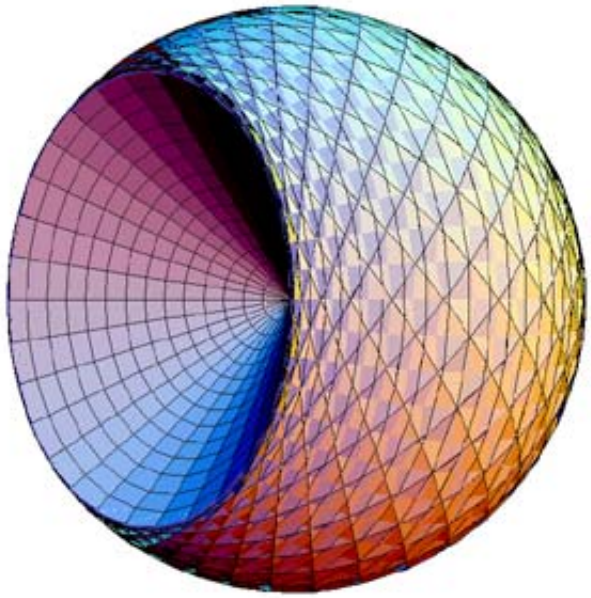

THE MOMENTUM-DENSITY FUNCTION $Y_0{}^0(\theta,\phi)$

Each basis-element great circle of the plane lamina current-density function of the free electron at a position ρ generates the BECVF that is perpendicular to the rotation axis used for the generation of the distribution of great circles. The rotation of a great circle in the xy-plane about the $\left(\mathbf{i}_x, 0_y, \mathbf{i}_z\right)$-axis by 2π generates a precessing free electron BECVF corresponding to a Bohr magneton of magnetic moment about the z-axis as given in the Rotation of a Great Circle in the xy-Plane about the $\left(\mathbf{i}_x, 0\mathbf{i}_y, \mathbf{i}_z\right)$-Axis by 2π section. An OCVF is formed by the 2π rotation of a great circle perpendicular to the $\left(\mathbf{i}_x, 0_y, \mathbf{i}_z\right)$-axis about the z-axis. Using the same type of convolution of CVFs as in the Atomic Orbital Equation of Motion for ℓ = 0 Based on the Current Vector Field (CVF) section, the function $Y_0^0\left(\theta,\phi\right)$ corresponding to the motion of a free electron is obtained by convolving the BECVF given by Eqs. (2) and (5) as the basis element with the OCVF. This operation is equivalent to incrementally rotating the BECVF about the z-axis by 2π.

Similarly, the rotation of a great circle in the xy-plane about the $\left(-\mathbf{i}_x, 0_y, \mathbf{i}_z\right)$-axis by 2π generates the orthogonal BECVF given in the Rotation of a Great Circle in the xy-Plane about the $\left(-\mathbf{i}_x, 0_y, \mathbf{i}_z\right)$-Axis by 2π section. An OCVF is also formed by the 2π rotation of a great circle perpendicular to the $\left(-\mathbf{i}_x, 0_y, \mathbf{i}_z\right)$-axis about the z-axis. The function $Y_0^0\left(\theta,\phi\right)$ corresponding to the motion of a free electron is obtained by convolving the BECVF given by Eqs. (7) and (10) as the basis element with the OCVF. This operation is equivalent to incrementally rotating the BECVF about the z-axis by 2π.

MATRICES TO VISUALIZE THE MOMENTUM-DENSITY OF $Y_0^0(\theta,\phi)$ FOR THE COMBINED PRECESSION MOTION OF THE FREE ELECTRON ABOUT THE $(\mathbf{i}_x,0\mathbf{i}_y,\mathbf{i}_z)$-AXIS AND Z-AXIS

The free BECVFs are given by Eqs. (2) and (5) and Eqs. (7) and (10). Consider the case of the $Y_0^0(\theta,\phi)$ momentum-density pattern for the combined precessional motion of the free electron about the $(\mathbf{i}_x,0\mathbf{i}_y,\mathbf{i}_z)$-axis and z-axis having the magnetic moment of μ_B on the z-axis. The free electron OCVF is given by rotating a basis-element great circle that is perpendicular to the $(\mathbf{i}_x,0\mathbf{i}_y,\mathbf{i}_z)$-axis about the z-axis by 2π. The transformation matrix to give the OCVF is generated by the combined rotation of a great circle in the xy-plane about the y-axis by $-\frac{\pi}{4}$ then about the z-axis by θ. The coordinates of the great circle basis element to generate the OCVF are given by the matrix that rotates a great circle in the xy-plane about the y-axis by $-\frac{\pi}{4}$:

$$[x',y',z']^{\mathrm{T}}=\left[\frac{\rho\cos\phi}{\sqrt{2}},\rho\sin\phi,-\frac{\rho\cos\phi}{\sqrt{2}}\right]^{\mathrm{T}}=R_y\left(\frac{-\pi}{4}\right)\bullet[\rho\cos\phi,\rho\sin\phi,0]^{\mathrm{T}} \tag{11}$$

The OCVF is generated by rotating the basis element great circle given by Eq. (11) about the z-axis using $R_z(\theta)$ over the span of 2π. Using Eqs. (11) and Eq. (1.82), the great circle basis elements and rotational matrix are given by:

OCVF MATRICES ($R_z(\theta)$)

$$\begin{bmatrix}x'\\y'\\z'\end{bmatrix}=\begin{bmatrix}\cos(\theta) & \sin(\theta) & 0\\ -\sin(\theta) & \cos(\theta) & 0\\ 0 & 0 & 1\end{bmatrix}\begin{bmatrix}\frac{\rho\cos\phi}{\sqrt{2}}\\ \rho\sin\phi\\ -\frac{\rho\cos\phi}{\sqrt{2}}\end{bmatrix} \tag{12}$$

Using Eq. (12), the infinite sum of great circles representation of the OCVF is given by:

$$OCVF=\lim_{\Delta\theta\to 0}\sum_{m=1}^{m=\frac{2\pi}{|\Delta\theta|}}\left[\left(R_z(m\Delta\theta_M)\bullet GC^{basis}_{\left(\frac{1}{\sqrt{2}}\mathbf{i}_x,\mathbf{i}_y,-\frac{1}{\sqrt{2}}\mathbf{i}_z\right)}\right)\right] \tag{13}$$

The current pattern for the 2π rotation of the great circle perpendicular to the $(\mathbf{i}_x,0\mathbf{i}_y,\mathbf{i}_z)$-axis about the z-axis is shown in Figure IV.5 wherein θ is varied from 0 to 2π.

Figure IV.5. The current pattern given by Eqs. (12) and (13) shown with 6 degree increments of θ from the perspective of looking along the z-axis. The great circle current loop that served as a basis element that was initially in the xy-plane before applying Eq. (11) and then Eq. (12) is shown as red.

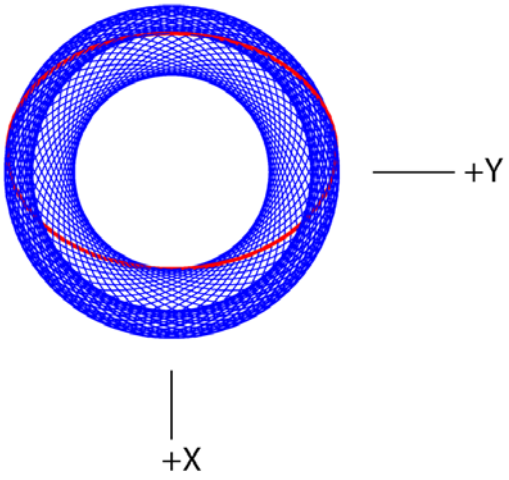

CONVOLUTION GENERATION OF $Y_0^0(\theta,\phi)$

The great-circle distribution $Y_0^0(\theta,\phi)$ is generated by the convolution of either BECVF with the corresponding OCVF over a 2π span. The convolution operator treats each CVF independently and results in the placement of a BECVF at each great circle of the OCVF such that momentum density pattern over time matches the bound-electron current pattern $Y_0^0(\theta,\phi)$, the initial angular momentum matches that of the great circle basis element of the OCVF, and the angular momentum rotates about the z-axis along the initial resultant angular momentum axis. This is achieved by rotating the orientation, phase, and vector-matched basis-element, the BECVF, about the same axis as that which generated the OCVF from the corresponding basis element great circle. Thus, the corresponding BECVF replaces the great circle basis element initially perpendicular to one of the orthogonal axes such as the $\left(\mathbf{i}_x, 0\mathbf{i}_y, \mathbf{i}_z\right)$-axis and matches its resultant angular momentum of $\sqrt{2}\hbar$ along the $\left(\mathbf{i}_x, 0\mathbf{i}_y, \mathbf{i}_z\right)$-axis having components of $\mathbf{L}_{xy} = \hbar$ and $\mathbf{L}_z = \hbar$. Then, $Y_0^0(\theta,\phi)$ is generated by rotation of the BECVF about the z-axis by an infinite set of infinitesimal increments of the rotational angle over the 2π span such that coverage of the spherical surface is complete. The corresponding convolution operator comprises an autocorrelation-type function that demonstrates the resulting azimuthal uniformity of the distribution when the orthonormality of the operator matrices is utilized as shown in the Azimuthal Uniformity Proof of $Y_0^0(\theta,\phi)$ section.

The operator to form $Y_0^0(\theta,\phi)$ comprises the BECVF convolution [2] of the rotational matrix of the great circles basis element about the $\left(\mathbf{i}_x, 0\mathbf{i}_y, \mathbf{i}_z\right)$-axis with an infinite series of delta functions of argument of the infinitesimal angular increment that is further convolved with the OCVF convolution of the rotational matrix of the great circles basis element about the z-axis with an infinite series of delta functions of argument of the infinitesimal angular increment. Using the BECVF matrix representation of its convolution operation (Eqs. (2) and (5)) and the OCVF matrix representation of its convolution operation (Eqs. (12) and (13)), the $Y_0^0(\theta,\phi)$ matrix representation of the convolution is given by:

$$Y_0^0(\theta,\phi) = OCVF \otimes BECVF = \left\{ \begin{array}{l} \left(\lim\limits_{\Delta\theta\to 0} \sum\limits_{m=1}^{m=\frac{2\pi}{|\Delta\theta|}} \left[\left(R_z(\theta) \bullet GC^{basis}_{\left(\frac{1}{\sqrt{2}}\mathbf{i}_x, \mathbf{i}_y, -\frac{1}{\sqrt{2}}\mathbf{i}_z\right)} \right) \otimes \delta\left(\theta - m\Delta\theta_M\right) \right] \right) \\ \otimes \left(\lim\limits_{\Delta\theta\to 0} \sum\limits_{n=1}^{n=\frac{2\pi}{|\Delta\theta|}} \left[\left(R_{\left(\mathbf{i}_x, 0\mathbf{i}_y, \mathbf{i}_z\right)}(\theta) \bullet GC^{basis}_{\left(\mathbf{i}_x, \mathbf{i}_y, 0\mathbf{i}_z\right)} \right) \otimes \delta\left(\theta - n\Delta\theta_N\right) \right] \right) \end{array} \right\} \tag{14}$$

where the commutative property of convolutions [2] allows for the interchange of the order of CVFs, but the rotational matrices are noncommutative [1]. The integral form of the convolution is:

$$Y_0^0(\theta,\phi) = \left\{ \begin{array}{l} \left[\int_0^{2\pi} \left(R_z(\theta) \bullet GC^{basis}_{\left(\frac{1}{\sqrt{2}}\mathbf{i}_x, \mathbf{i}_y, -\frac{1}{\sqrt{2}}\mathbf{i}_z\right)} \right) \lim\limits_{\Delta\theta\to 0} \sum\limits_{m=1}^{m=\frac{2\pi}{|\Delta\theta|}} \delta\left(\theta - m\Delta\theta_M^{OCVF}\right) d\theta \right] \\ \otimes \left[\int_0^{2\pi} \left(R_{\left(\mathbf{i}_x, 0\mathbf{i}_y, \mathbf{i}_z\right)}(\theta) \bullet GC^{basis}_{\left(\mathbf{i}_x, \mathbf{i}_y, 0\mathbf{i}_z\right)} \right) \left(\lim\limits_{\Delta\theta\to 0} \sum\limits_{n=1}^{n=\frac{2\pi}{|\Delta\theta|}} \delta\left(\theta - n\Delta\theta_N^{BECVF}\right) \right) d\theta \right] \end{array} \right\} \tag{15}$$

$$Y_0^0(\theta,\phi) = \lim_{\Delta\theta\to 0} \sum_{m=1}^{m=\frac{2\pi}{|\Delta\theta|}} \lim_{\Delta\theta\to 0} \sum_{n=1}^{n=\frac{2\pi}{|\Delta\theta|}} \int_0^{2\pi} d\theta_1 \int_0^{2\pi} d\theta_2 R_z(\theta_1) \bullet R_{\left(\mathbf{i}_x, 0\mathbf{i}_y, \mathbf{i}_z\right)}(\theta_2) \bullet GC^{basis}_{\left(\mathbf{i}_x, \mathbf{i}_y, 0\mathbf{i}_z\right)} \delta\left(\theta_1 - m\Delta\theta_M^{OCVF}\right) \delta\left(\theta_2 - n\Delta\theta_N^{BECVF}\right) \tag{16}$$

The integration gives the infinite double sum of great circles that constitute $Y_0^0(\theta,\phi)$:

$$Y_0^0(\theta,\phi) = \lim_{\Delta\theta\to 0} \sum_{m=1}^{m=\frac{2\pi}{|\Delta\theta|}} \left[R_z\left(m\Delta\theta_M^{OCVF}\right) \bullet \lim_{\Delta\theta\to 0} \sum_{n=1}^{n=\frac{2\pi}{|\Delta\theta|}} \left[R_{\left(\mathbf{i}_x, 0\mathbf{i}_y, \mathbf{i}_z\right)}\left(n\Delta\theta_N^{BECVF}\right) \bullet GC^{basis}_{\left(\mathbf{i}_x, \mathbf{i}_y, 0\mathbf{i}_z\right)} \right] \right] \tag{17}$$

The positions of the basis-element great circle over time comprises a continuous distribution. However, using Eq. (17), a discrete representation of the current distribution $Y_0^0(\theta,\phi)$ that shows a finite number of current elements over time can be generated by showing the BECVF as a finite sum of the convolved great circle elements using Eqs. (2) and (5) and by showing the continuous convolution of the BECVF with the OCVF as a superposition of discrete incremental rotations of the position of the BECVF rotated according to Eqs. (12) and (13) corresponding to the matrix which generated the OCVF. In the case that the discrete representation of the BECVF comprises N great circles and the number of convolved BECVF elements is M, the representation of the azimuthally uniform current density function showing current loops is given by Eq. (18) and shown in Figures IV.6 and IV.7. The corresponding mass(momentum) density is also represented by Figures IV.6 and IV.7 wherein the

charge and mass are interchangeable by the conversion factor m_e / e. Computer modeling of the analytical equations to generate the free electron current vector fields and the azimuthally uniform momentum-density function $Y_0^0(\theta,\phi)$ is available on the web [3]:

$$\begin{bmatrix} x' \\ y' \\ z' \end{bmatrix} = \sum_{m=1}^{m=M} \begin{bmatrix} \cos\left(\frac{m2\pi}{M}\right) & \sin\left(\frac{m2\pi}{M}\right) & 0 \\ -\sin\left(\frac{m2\pi}{M}\right) & \cos\left(\frac{m2\pi}{M}\right) & 0 \\ 0 & 0 & 1 \end{bmatrix}$$

$$\bullet \sum_{n=1}^{n=N} \begin{bmatrix} \frac{1}{2}+\frac{\cos\left(\frac{n2\pi}{N}\right)}{2} & \frac{\sin\left(\frac{n2\pi}{N}\right)}{\sqrt{2}} & \frac{1}{2}-\frac{\cos\left(\frac{n2\pi}{N}\right)}{2} \\ -\frac{\sin\left(\frac{n2\pi}{N}\right)}{\sqrt{2}} & \cos\left(\frac{n2\pi}{N}\right) & \frac{\sin\left(\frac{n2\pi}{N}\right)}{\sqrt{2}} \\ \frac{1}{2}-\frac{\cos\left(\frac{n2\pi}{N}\right)}{2} & -\frac{\sin\left(\frac{n2\pi}{N}\right)}{\sqrt{2}} & \frac{1}{2}+\frac{\cos\left(\frac{n2\pi}{N}\right)}{2} \end{bmatrix} \begin{bmatrix} \rho\cos\phi \\ \rho\sin\phi \\ 0 \end{bmatrix} \tag{18}$$

Figures IV.6 and IV.7. Representations of the current pattern of the $Y_0^0(\theta,\phi)$ free electron motion over a period of both precessional motions shown with 30 degree increments ($N = M = 12$ in Eq. (18)) of the angle to generate the free electron BECVF corresponding to Eqs. (2) and (5) and 30 degree increments of the rotation of this basis element about the z-axis corresponding to Eqs. (12) and (13). The great circle current loop that served as a basis element that was initially in the xy-plane of each free electron BECVF is shown as red

Figure IV.6 The perspective is along the z-axis.

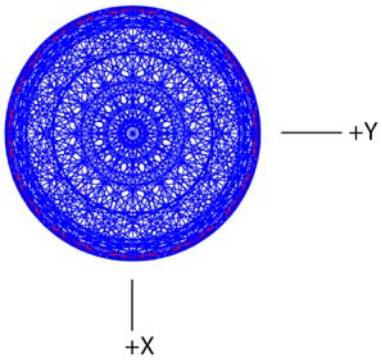

Figure IV.7 The perspective is along the x-axis.

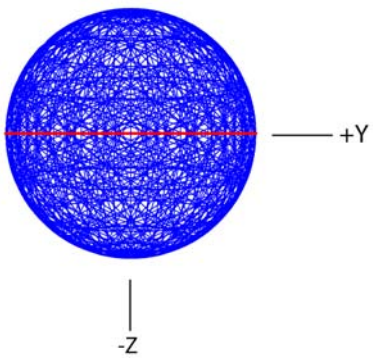

MATRICES TO VISUALIZE THE MOMENTUM-DENSITY OF $Y_0^0(\theta,\phi)$ FOR THE COMBINED PRECESSION MOTION OF THE FREE ELECTRON ABOUT THE $(-\mathbf{i}_x, 0\mathbf{i}_y, \mathbf{i}_z)$-AXIS AND Z-AXIS

Consider the case of the $Y_0^0(\theta,\phi)$ momentum-density pattern for the combined precessional motion of the free electron about the $(-\mathbf{i}_x, 0\mathbf{i}_y, \mathbf{i}_z)$-axis and z-axis having the magnetic moment of μ_B on the z-axis. The corresponding free BECVF is given by Eqs. (7) and (10). The free electron OCVF is given by rotating a basis-element great circle that is perpendicular to the $(-\mathbf{i}_x, 0\mathbf{i}_y, \mathbf{i}_z)$-axis about the z-axis by 2π. The transformation matrix to give the OCVF is generated by the combined rotation of a great circle in the xy-plane about the y-axis by $\frac{\pi}{4}$ then about the z-axis by θ. The coordinates of the great circle basis element to generate the OCVF are given by the matrix that rotates a great circle in the xy-plane about the y-axis by $\frac{\pi}{4}$:

$$[x', y', z']^{\mathrm{T}} = \left[\frac{\rho\cos\phi}{\sqrt{2}}, \rho\sin\phi, \frac{\rho\cos\phi}{\sqrt{2}}\right]^{\mathrm{T}} = R_y\left(\frac{\pi}{4}\right)\bullet[\rho\cos\phi, \rho\sin\phi, 0]^{\mathrm{T}} \tag{19}$$

The OCVF is generated by rotating the basis element great circle given by Eq. (19) about the z-axis using $R_z(\theta)$ over the span of 2π. Using Eqs. (19) and Eq. (1.82), the great circle basis elements and rotational matrix are given by:

OCVF MATRICES ($R_z(\theta)$)

$$\begin{bmatrix} x' \\ y' \\ z' \end{bmatrix} = \begin{bmatrix} \cos(\theta) & \sin(\theta) & 0 \\ -\sin(\theta) & \cos(\theta) & 0 \\ 0 & 0 & 1 \end{bmatrix} \begin{bmatrix} \frac{\rho\cos\phi}{\sqrt{2}} \\ \rho\sin\phi \\ \frac{\rho\cos\phi}{\sqrt{2}} \end{bmatrix} \tag{20}$$

Using Eq. (20) and the procedure of Eqs, (3-5), the infinite sum of great circles that constitute the OCVF is given by:

$$OCVF = \lim_{\Delta\theta\to 0}\sum_{m=1}^{m=\frac{2\pi}{|\Delta\theta|}}\left[\left(R_z(m\Delta\theta_M)\bullet GC^{basis}_{\left(\frac{1}{\sqrt{2}}\mathbf{i}_x, \mathbf{i}_y, \frac{1}{\sqrt{2}}\mathbf{i}_z\right)}\right)\right] \tag{21}$$

The current pattern for the 2π rotation of the great circle perpendicular to the $(-\mathbf{i}_x, 0\mathbf{i}_y, \mathbf{i}_z)$-axis about the z-axis is shown in Figure IV.8 wherein θ is varied from 0 to 2π.

Figure IV.8. The current pattern given by Eqs. (20) and (21) shown with 6 degree increments of θ from the perspective of looking along the z-axis. The great circle current loop that served as a basis element that was initially in the xy-plane before applying Eq. (19) and then Eq. (20) is shown as red.

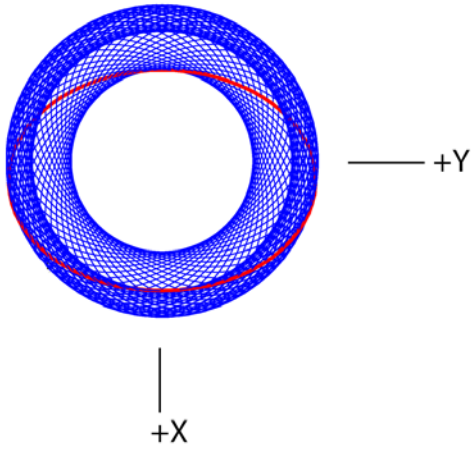

The great-circle distribution $Y_0^{\,0}(\theta,\phi)$ is generated by the convolution of the BECVF with the OCVF over a 2π span. The corresponding BECVF replaces the great circle basis element initially perpendicular to the $\left(-\mathbf{i}_x, 0\mathbf{i}_y, \mathbf{i}_z\right)$-axis and matches its resultant angular momentum of $\sqrt{2}\hbar$ along the $\left(-\mathbf{i}_x, 0\mathbf{i}_y, \mathbf{i}_z\right)$-axis having components of $\mathbf{L}_{xy} = \hbar$ and $\mathbf{L}_z = \hbar$. Then, $Y_0^{\,0}(\theta,\phi)$ is generated by rotation of the BECVF, about the z-axis by an infinite set of infinitesimal increments of the rotational angle over the 2π span such that coverage of the spherical surface is complete and azimuthally uniform. Using the BECVF given by Eqs. (7) and (10), the OCVF given by Eqs. (20) and (21), and the procedure given by Eqs. (14-17), the infinite double sum of great circles that constitute $Y_0^{\,0}(\theta,\phi)$ is given by:

$$Y_0^{\,0}(\theta,\phi) = \lim_{\Delta\theta\to 0}\sum_{m=1}^{m=\frac{2\pi}{|\Delta\theta|}}\left[R_z\left(m\Delta\theta_M^{OCVF}\right) \bullet \lim_{\Delta\theta\to 0}\sum_{n=1}^{n=\frac{2\pi}{|\Delta\theta|}}\left[R_{\left(-\mathbf{i}_x,0\mathbf{i}_y,\mathbf{i}_z\right)}\left(n\Delta\theta_N^{BECVF}\right) \bullet GC^{basis}_{\left(\mathbf{i}_x,\mathbf{i}_y,0\mathbf{i}_z\right)}\right]\right] \tag{22}$$

The positions of the basis-element great circle over time comprises a continuous distribution. However, using Eq. (22), a discrete representation of the current distribution $Y_0^{\,0}(\theta,\phi)$ that shows a finite number of current elements over time can be generated by showing the BECVF as a finite sum of the convolved great circle elements using Eqs. (7) and (10) and by showing the continuous convolution of the BECVF with the OCVF as a superposition of discrete incremental rotations of the position of the BECVF rotated according to Eqs. (20) and (21) corresponding to the matrix which generated the OCVF. In the case that the discrete representation of the BECVF comprises N great circles and the number of convolved BECVF elements is M, the representation of the azimuthally uniform current density function showing current loops is given by Eq. (23). The corresponding mass(momentum) density is given by Eq. (23) wherein the charge and mass are interchangeable by the conversion factor m_e / e.

$$\begin{bmatrix} x' \\ y' \\ z' \end{bmatrix} = \sum_{m=1}^{m=M}\begin{bmatrix} \cos\left(\frac{m2\pi}{M}\right) & \sin\left(\frac{m2\pi}{M}\right) & 0 \\ -\sin\left(\frac{m2\pi}{M}\right) & \cos\left(\frac{m2\pi}{M}\right) & 0 \\ 0 & 0 & 1 \end{bmatrix}$$

$$\bullet\sum_{n=1}^{n=N}\begin{bmatrix} \frac{1}{2}+\frac{\cos\left(\frac{n2\pi}{N}\right)}{2} & \frac{\sin\left(\frac{n2\pi}{N}\right)}{\sqrt{2}} & -\frac{1}{2}+\frac{\cos\left(\frac{n2\pi}{N}\right)}{2} \\ -\frac{\sin\left(\frac{n2\pi}{N}\right)}{\sqrt{2}} & \cos\left(\frac{n2\pi}{N}\right) & -\frac{\sin\left(\frac{n2\pi}{N}\right)}{\sqrt{2}} \\ -\frac{1}{2}+\frac{\cos\left(\frac{n2\pi}{N}\right)}{2} & \frac{\sin\left(\frac{n2\pi}{N}\right)}{\sqrt{2}} & \frac{1}{2}+\frac{\cos\left(\frac{n2\pi}{N}\right)}{2} \end{bmatrix}\begin{bmatrix} \rho\cos\phi \\ \rho\sin\phi \\ 0 \end{bmatrix} \tag{23}$$

Representations of the $Y_0^{\,0}(\theta,\phi)$ current pattern of the free electron motion over a period of both precessions shown with 30 degree increments ($N = M = 12$ in Eq. (23)) of the angle to generate the free electron BECVF corresponding to Eqs. (7) and (10) and 30 degree increments of the rotation of this basis element about the z-axis corresponding to Eqs. (20) and (21) are equivalent to those shown in Figures IV.6 and IV.7. As shown in these figures, the distribution generated by the precessional motion of the free electron over time in the presence of an applied magnetic field matches that of $Y_0^{\,0}(\theta,\phi)$ of the bound electron given in the Atomic Orbital Equation of Motion for $\ell = 0$ Based on the Current Vector Field (CVF) section.

AZIMUTHAL UNIFORMITY PROOF OF $Y_0^0(\theta,\phi)$

By using the matrices to generate $Y_0^0(\theta,\phi)$, it is shown to be azimuthally uniform about the z-axis. Consider the $Y_0^0(\theta,\phi)$ convolution in summation form given by Eqs. (14) and (17):

$$\begin{bmatrix} x' \\ y' \\ z' \end{bmatrix} = \left(\lim_{\Delta\theta\to 0} \sum_{m=1}^{m=\frac{2\pi}{|\Delta\theta|}} \left[\left(R_z\left(m\Delta\theta_M^{OCVF}\right) \bullet BECVF^{basis}_{\left(\frac{1}{\sqrt{2}}\mathbf{i}_x,\mathbf{i}_y,-\frac{1}{\sqrt{2}}\mathbf{i}_z\right)} \right) \right] \right) \tag{24}$$

wherein $BECVF^{basis}_{\left(\frac{1}{\sqrt{2}}\mathbf{i}_x,\mathbf{i}_y,-\frac{1}{\sqrt{2}}\mathbf{i}_z\right)}$ is the distribution that replaced the great circle basis element of the OCVF distribution in the convolution given by Eqs. (5), (11), (13), and (14), respectively. Consider the rotation of both sides of Eq. (24) about the y-axis (Eq. (1.81)), the orthogonal axis to that which generated the OCVF, by $-\frac{\pi}{4}$.

$$R_y\left(-\frac{\pi}{4}\right)\begin{bmatrix} x' \\ y' \\ z' \end{bmatrix} = \left(R_y\left(-\frac{\pi}{4}\right) \lim_{\Delta\theta\to 0} \sum_{m=1}^{m=\frac{2\pi}{|\Delta\theta|}} \left[\left(R_z\left(m\Delta\theta_M^{OCVF}\right) \bullet BECVF^{basis}_{\left(\frac{1}{\sqrt{2}}\mathbf{i}_x,\mathbf{i}_y,-\frac{1}{\sqrt{2}}\mathbf{i}_z\right)} \right) \right] \right) \tag{25}$$

The rotation of a sum is the same as the sum of the rotations

$$R_y\left(-\frac{\pi}{4}\right)\begin{bmatrix} x' \\ y' \\ z' \end{bmatrix} = \left(\lim_{\Delta\theta\to 0} \sum_{m=1}^{m=\frac{2\pi}{|\Delta\theta|}} \left[\left(R_y\left(-\frac{\pi}{4}\right) \bullet R_z\left(m\Delta\theta_M^{OCVF}\right) \bullet BECVF^{basis}_{\left(\frac{1}{\sqrt{2}}\mathbf{i}_x,\mathbf{i}_y,-\frac{1}{\sqrt{2}}\mathbf{i}_z\right)} \right) \right] \right) \tag{26}$$

When the distribution given by Eq. (21) having its C_∞-axis along the z-axis is rotated about the y-axis by $-\frac{\pi}{4}$, the resulting distribution having the C_∞-axis along the $\left(\mathbf{i}_x, 0\mathbf{i}_y, \mathbf{i}_z\right)$-axis is equivalent to the distribution given by Eq. (5) of matching C_∞-axis. Substitution of Eq. (5) into Eq. (26) gives:

$$R_y\left(-\frac{\pi}{4}\right)\begin{bmatrix} x' \\ y' \\ z' \end{bmatrix} = \left(\lim_{\Delta\theta\to 0} \sum_{m=1}^{m=\frac{2\pi}{|\Delta\theta|}} \left[\left(R_{(\mathbf{i}_x,0\mathbf{i}_y,\mathbf{i}_z)}\left(m\Delta\theta_M^{OCVF}\right) \bullet BECVF^{basis}_{\left(\frac{1}{\sqrt{2}}\mathbf{i}_x,\mathbf{i}_y,-\frac{1}{\sqrt{2}}\mathbf{i}_z\right)} \right) \right] \right) \tag{27}$$

Substitution of Eq. (5) for BECVF gives:

$$R_y\left(-\frac{\pi}{4}\right)\begin{bmatrix} x' \\ y' \\ z' \end{bmatrix} = \left(\lim_{\Delta\theta\to 0} \sum_{m=1}^{m=\frac{2\pi}{|\Delta\theta|}} \left[\left(R_{(\mathbf{i}_x,0\mathbf{i}_y,\mathbf{i}_z)}\left(m\Delta\theta_M\right) \bullet \lim_{\Delta\theta\to 0} \sum_{n=1}^{n=\frac{2\pi}{|\Delta\theta|}} \left[\left(R_{(\mathbf{i}_x,0\mathbf{i}_y,\mathbf{i}_z)}\left(n\Delta\theta_N\right) \bullet GC^{basis}_{(\mathbf{i}_x,\mathbf{i}_y,0\mathbf{i}_z)} \right) \right] \right) \right] \right) \tag{28}$$

Using the distributive property of the double sum gives:

$$R_y\left(-\frac{\pi}{4}\right)\begin{bmatrix} x' \\ y' \\ z' \end{bmatrix} = \lim_{\Delta\theta\to 0}\sum_{m=1}^{m=\frac{2\pi}{|\Delta\theta|}} \lim_{\Delta\theta\to 0}\sum_{n=1}^{n=\frac{2\pi}{|\Delta\theta|}} R_{(\mathbf{i}_x,0\mathbf{i}_y,\mathbf{i}_z)}\left(m\Delta\theta_M\right)\bullet R_{(\mathbf{i}_x,0\mathbf{i}_y,\mathbf{i}_z)}\left(n\Delta\theta_N\right)\bullet GC^{basis}_{(\mathbf{i}_x,\mathbf{i}_y,0\mathbf{i}_z)} \tag{29}$$

Rotation of the BECVF about its C_∞-axis, the $\left(\mathbf{i}_x,0\mathbf{i}_y,\mathbf{i}_z\right)$-axis, leaves the BECVF distribution unchanged.

$$R_y\left(-\frac{\pi}{4}\right)\begin{bmatrix} x' \\ y' \\ z' \end{bmatrix} = BECVF^{basis}_{\left(\frac{1}{\sqrt{2}}\mathbf{i}_x,\mathbf{i}_y,-\frac{1}{\sqrt{2}}\mathbf{i}_z\right)} \tag{30}$$

Eq. (30) represents the properties of the distribution perpendicular to the z-axis since the distribution was rotated about the y-axis to align the z-axis with the $\left(\mathbf{i}_x,0\mathbf{i}_y,\mathbf{i}_z\right)$-axis. This result confirms that the distribution is uniform about the z-axis since the $BECVF^{basis}_{\left(\frac{1}{\sqrt{2}}\mathbf{i}_x,\mathbf{i}_y,-\frac{1}{\sqrt{2}}\mathbf{i}_z\right)}$ that served to generate the distribution of $Y_0^{\,0}(\theta,\phi)$ is azimuthally uniform. Furthermore, as shown in the Electron in Free Space section the angular momentum distribution swept out during a period of both precessional motions for each position ρ of the free electron is equivalent that of the bound electron.

SPIN-FLIP TRANSITIONS

Consider the momentum-density pattern for the combined precessional motion of the free electron about either the $\left(\mathbf{i}_x,0\mathbf{i}_y,\mathbf{i}_z\right)$-axis or the $\left(-\mathbf{i}_x,0\mathbf{i}_y,\mathbf{i}_z\right)$-axis and z-axis. The corresponding free BECVFs are given by Eqs. (2) and (5) and Eqs. (7) and (10). As shown in Figures IV.1 and IV.3, respectively, the great circle basis element is in the xy-plane and the counterclockwise current together with the counter clockwise precession of the $\left(\mathbf{i}_x,0\mathbf{i}_y,\mathbf{i}_z\right)$-axis or the $\left(-\mathbf{i}_x,0\mathbf{i}_y,\mathbf{i}_z\right)$-axis about the z-axis gives rise to a resultant angular momentum of $\sqrt{2}\hbar$ along the $\left(\mathbf{i}_x,0\mathbf{i}_y,\mathbf{i}_z\right)$ or $\left(-\mathbf{i}_x,0\mathbf{i}_y,\mathbf{i}_z\right)$-axis having components of $\mathbf{L}_{xy}=\hbar$ and $\mathbf{L}_z=\hbar$ and a corresponding magnetic moment of μ_B on the z-axis. As shown in Figures IV.6 and IV.7, the corresponding distribution over time due to both components of motion is equivalent to the current pattern and angular momentum of $Y_0^{\,0}(\theta,\phi)$ of the bound electron. The electron may flip between the two spin states having the magnetic moment parallel to the z-axis or antiparallel to the z-axis. This spin flip transition corresponds to a reversal of the orientation of the electron magnetic moment with the applied magnetic field. The BECVFs, OCVF, and $Y_0^{\,0}(\theta,\phi)$ precession distributions developed *supra* apply to both states, but the currents are opposite. Based on symmetry, the transition corresponds to a $\pm\pi$ rotation of the distribution $Y_0^{\,0}(\theta,\phi)$ (designated $Y_0^{\,0}(\theta,\phi)_z$) given by Eqs. (17) and (22) about the x-axis using $R_x\left(\theta\right)$ given by Eq. (1.80).

Using Eqs. (17) and (1.80) for the z to –z-axis spin transition, the infinite double sum of great circles that constitute the corresponding $Y_0^{\,0}(\theta,\phi)_{-z}$ from flipping $Y_0^{\,0}(\theta,\phi)_z$ is given by:

$$\begin{aligned} Y_0^{\,0}(\theta,\phi)_{-z} &= R_x\left(\pi\right)Y_0^{\,0}(\theta,\phi)_z \\ &= R_x\left(\pi\right)\lim_{\Delta\theta\to 0}\sum_{m=1}^{m=\frac{2\pi}{|\Delta\theta|}}\left[R_z\left(m\Delta\theta_M^{OCVF}\right)\bullet\lim_{\Delta\theta\to 0}\sum_{n=1}^{n=\frac{2\pi}{|\Delta\theta|}}\left[R_{(\mathbf{i}_x,0\mathbf{i}_y,\mathbf{i}_z)}\left(n\Delta\theta_N^{BECVF}\right)\bullet GC^{basis}_{(\mathbf{i}_x,\mathbf{i}_y,0\mathbf{i}_z)}\right]\right] \\ &= \lim_{\Delta\theta\to 0}\sum_{m=1}^{m=\frac{2\pi}{|\Delta\theta|}}\left[R_z\left(-m\Delta\theta_M^{OCVF}\right)\bullet\lim_{\Delta\theta\to 0}\sum_{n=1}^{n=\frac{2\pi}{|\Delta\theta|}}\left[R_{(\mathbf{i}_x,0\mathbf{i}_y,\mathbf{i}_z)}\left(n\Delta\theta_N^{BECVF}\right)\bullet GC^{basis}_{(\mathbf{i}_x,\mathbf{i}_y,0\mathbf{i}_z)}\right]\right] \end{aligned} \tag{31}$$

The positions of the basis-element great circle over time comprises a continuous distribution. However, using Eq. (31), a discrete representation of the current distribution $Y_0^{\,0}(\theta,\phi)_{-z}$ that shows a finite number of current elements over time can be generated by showing the BECVF as a finite sum of the convolved great circle elements using Eqs. (2) and (5) and by showing the continuous convolution of the BECVF with the OCVF as a superposition of discrete incremental rotations of the position of the BECVF rotated according to Eqs. (12) and (13) corresponding to the matrix which generated the OCVF. In the case that the

discrete representation of the BECVF comprises N great circles and the number of convolved BECVF elements is M, the representation of the flipped azimuthally uniform current density function showing current loops given by Eq. (32) is equivalent to that shown in Figures IV.6 and IV.7 but the current direction is reversed.

$$\begin{bmatrix} x' \\ y' \\ z' \end{bmatrix} = \sum_{m=1}^{m=M} \begin{bmatrix} \cos\left(\frac{m2\pi}{M}\right) & -\sin\left(\frac{m2\pi}{M}\right) & 0 \\ \sin\left(\frac{m2\pi}{M}\right) & \cos\left(\frac{m2\pi}{M}\right) & 0 \\ 0 & 0 & 1 \end{bmatrix}$$

$$\bullet \sum_{n=1}^{n=N} \begin{bmatrix} \frac{1}{2}+\frac{\cos\left(\frac{n2\pi}{N}\right)}{2} & \frac{\sin\left(\frac{n2\pi}{N}\right)}{\sqrt{2}} & \frac{1}{2}-\frac{\cos\left(\frac{n2\pi}{N}\right)}{2} \\ -\frac{\sin\left(\frac{n2\pi}{N}\right)}{\sqrt{2}} & \cos\left(\frac{n2\pi}{N}\right) & \frac{\sin\left(\frac{n2\pi}{N}\right)}{\sqrt{2}} \\ \frac{1}{2}-\frac{\cos\left(\frac{n2\pi}{N}\right)}{2} & -\frac{\sin\left(\frac{n2\pi}{N}\right)}{\sqrt{2}} & \frac{1}{2}+\frac{\cos\left(\frac{n2\pi}{N}\right)}{2} \end{bmatrix} \begin{bmatrix} \rho\cos\phi \\ \rho\sin\phi \\ 0 \end{bmatrix} \tag{32}$$

REFERENCES

1. G. R. Fowles, *Analytical Mechanics*, Third Edition, Holt, Rinehart, and Winston, New York, (1977), pp. 17-20.
2. W. McC. Siebert, *Circuits, Signals, and Systems*, The MIT Press, Cambridge, Massachusetts, (1986), pp. 261, 272, 286, 287, 290, 410, 569, 599.
3. Mathematica modeling of R. Mills' theory by B. Holverstott in "Modeling the Analytical Equations to Generate the Free Electron Current-Vector Field and the Uniform Angular-Momentum-Density Function $Y_0^0(\theta,\phi)$," posted at www.brilliantlightpower.com.

Appendix V

ANALYTICAL-EQUATION DERIVATION OF THE PHOTON ELECTRIC AND MAGNETIC FIELDS

ANALYTICAL EQUATIONS TO GENERATE THE RIGHT-HANDED CIRCULARLY POLARIZED PHOTON ELECTRIC AND MAGNETIC VECTOR FIELD BY ROTATION OF THE GREAT-CIRCLE BASIS ELEMENTS ABOUT THE $\left(\mathbf{i}_x,\mathbf{i}_y,0\mathbf{i}_z\right)$ -AXIS BY $\frac{\pi}{2}$

The right-handed circularly polarized (RHCP) photon electric and magnetic vector field (photon-e&mvf) is also generated following a similar procedure as that used to generate the atomic orbital in the Atomic Orbital Equation of Motion for $\ell = 0$ Based on the Current Vector Field (CVF) section using the rotational matrices given therein. The RHCP photon-e&mvf is generated by the rotation of the basis elements comprising the great circle magnetic field line in the xz-plane and the great circle electric field line in the yz-plane about the $\left(\mathbf{i}_x,\mathbf{i}_y,0\mathbf{i}_z\right)$-axis by $\frac{\pi}{2}$. A first transformation matrix is generated by the combined rotation of the great circles about the z-axis by $\frac{\pi}{4}$ then about the x-axis by θ where positive rotations about an axis are defined as clockwise:

$$\begin{bmatrix} x' \\ y' \\ z' \end{bmatrix} = \begin{bmatrix} \cos\left(\frac{\pi}{4}\right) & \sin\left(\frac{\pi}{4}\right) & 0 \\ -\sin\left(\frac{\pi}{4}\right)\cos\theta & \cos\left(\frac{\pi}{4}\right)\cos\theta & \sin\theta \\ \sin\left(\frac{\pi}{4}\right)\sin\theta & -\cos\left(\frac{\pi}{4}\right)\sin\theta & \cos\theta \end{bmatrix} \bullet \left(\begin{bmatrix} 0 \\ r_n\cos\phi \\ r_n\sin\phi \end{bmatrix}_{\text{Red}} + \begin{bmatrix} r_n\cos\phi \\ 0 \\ r_n\sin\phi \end{bmatrix}_{\text{Blue}} \right) \tag{1}$$

The transformation matrix about $\left(\mathbf{i}_x,\mathbf{i}_y,0\mathbf{i}_z\right)$ is given by multiplication of the output of the matrix given by Eq. (1) by the matrix corresponding to a rotation about the z-axis of $-\frac{\pi}{4}$. The output of the matrix given by Eq. (1) is shown in Figure AV.1 wherein θ is varied from 0 to $\frac{\pi}{2}$.

Figure AV.1. The electric, magnetic, and combined field-line pattern given by Eq. (1) from the perspective of looking along the z-axis corresponding to the first great circle magnetic field line and the second great circle electric field line shown with 6 degree increments of the angle θ. (Electric field lines red; Magnetic field lines blue).

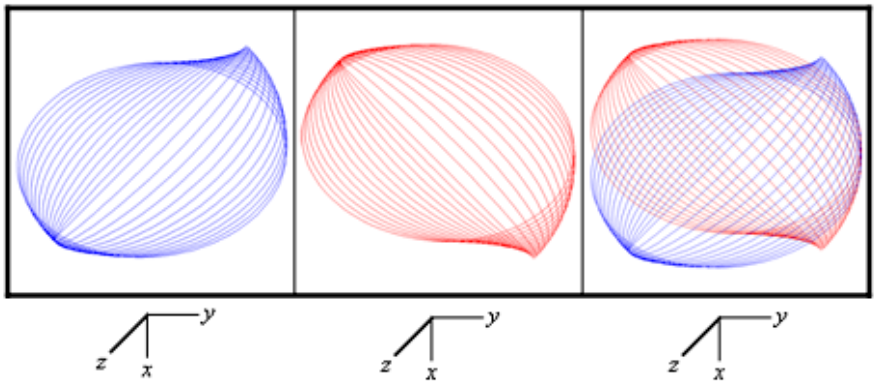

The rotation matrix about the z-axis by $-\frac{\pi}{4}$, $R_z\left(-\frac{\pi}{4}\right)$, is given by:

$$R_z\left(-\frac{\pi}{4}\right)=\begin{bmatrix}\cos\left(\frac{\pi}{4}\right) & -\sin\left(\frac{\pi}{4}\right) & 0\\ \sin\left(\frac{\pi}{4}\right) & \cos\left(\frac{\pi}{4}\right) & 0\\ 0 & 0 & 1\end{bmatrix} \tag{2}$$

Thus,

$$\begin{bmatrix}x'\\ y'\\ z'\end{bmatrix}=R_z\left(-\frac{\pi}{4}\right)\bullet\begin{bmatrix}\cos\left(\frac{\pi}{4}\right) & \sin\left(\frac{\pi}{4}\right) & 0\\ -\sin\left(\frac{\pi}{4}\right)\cos\theta & \cos\left(\frac{\pi}{4}\right)\cos\theta & \sin\theta\\ \sin\left(\frac{\pi}{4}\right)\sin\theta & -\cos\left(\frac{\pi}{4}\right)\sin\theta & \cos\theta\end{bmatrix}\bullet\left(\begin{bmatrix}0\\ r_n\cos\phi\\ r_n\sin\phi\end{bmatrix}_{\text{Red}}+\begin{bmatrix}r_n\cos\phi\\ 0\\ r_n\sin\phi\end{bmatrix}_{\text{Blue}}\right) \tag{3}$$

Substitution of the matrix given by Eq. (2) into Eq. (3) gives:

$$\begin{bmatrix}x'\\ y'\\ z'\end{bmatrix}=\begin{bmatrix}\frac{1}{2}+\frac{\cos\theta}{2} & \frac{1}{2}-\frac{\cos\theta}{2} & -\frac{\sin\theta}{\sqrt{2}}\\ \frac{1}{2}-\frac{\cos\theta}{2} & \frac{1}{2}+\frac{\cos\theta}{2} & \frac{\sin\theta}{\sqrt{2}}\\ \frac{\sin\theta}{\sqrt{2}} & -\frac{\sin\theta}{\sqrt{2}} & \cos\theta\end{bmatrix}\bullet\left(\begin{bmatrix}0\\ r_n\cos\phi\\ r_n\sin\phi\end{bmatrix}_{\text{Red}}+\begin{bmatrix}r_n\cos\phi\\ 0\\ r_n\sin\phi\end{bmatrix}_{\text{Blue}}\right) \tag{4}$$

$$\begin{bmatrix} x' \\ y' \\ z' \end{bmatrix} = \begin{bmatrix} \left(\left(\frac{1}{2}-\frac{\cos\theta}{2}\right)r_n\cos\phi-\frac{\sin\theta}{\sqrt{2}}r_n\sin\phi\right)_{\text{Red}}+\left(\left(\frac{1}{2}+\frac{\cos\theta}{2}\right)r_n\cos\phi-\frac{\sin\theta}{\sqrt{2}}r_n\sin\phi\right)_{\text{Blue}} \\ \left(\left(\frac{1}{2}+\frac{\cos\theta}{2}\right)r_n\cos\phi+\frac{\sin\theta}{\sqrt{2}}r_n\sin\phi\right)_{\text{Red}}+\left(\left(\frac{1}{2}-\frac{\cos\theta}{2}\right)r_n\cos\phi+\frac{\sin\theta}{\sqrt{2}}r_n\sin\phi\right)_{\text{Blue}} \\ \left(-\frac{\sin\theta}{\sqrt{2}}r_n\cos\phi+\cos\theta r_n\sin\phi\right)_{\text{Red}}+\left(\frac{\sin\theta}{\sqrt{2}}r_n\cos\phi+\cos\theta r_n\sin\phi\right)_{\text{Blue}} \end{bmatrix} \tag{5}$$

The RHCP photon-e&mvf that is generated by the rotation of the great-circle basis elements in the xz- and yz-planes about the $(\mathbf{i}_x,\mathbf{i}_y,0\mathbf{i}_z)$-axis by $\frac{\pi}{2}$ corresponding to the output of the matrix given by Eq. (5) is shown in Figure AV.2.

Figure AV.2. The field-line pattern given by Eq. (5) from three orthogonal perspectives of a RHCP photon-e&mvf corresponding to the first great circle magnetic field line and the second great circle electric field line shown with 6 degree increments of the angle θ. (Electric field lines red; Magnetic field lines blue).

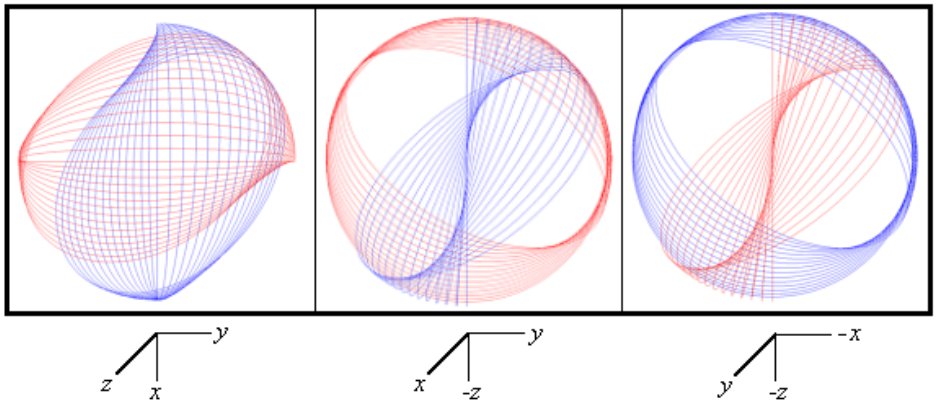

ANALYTICAL EQUATIONS TO GENERATE THE LEFT-HANDED CIRCULARLY POLARIZED PHOTON ELECTRIC AND MAGNETIC VECTOR FIELD BY ROTATION OF THE GREAT-CIRCLE BASIS ELEMENTS ABOUT THE $(\mathbf{i}_x,-\mathbf{i}_y,0\mathbf{i}_z)$-AXIS BY $\frac{\pi}{2}$

The left-handed circularly polarized (LHCP) photon electric and magnetic vector field (photon-e&mvf) is also generated following a similar procedure as that used to generate the atomic orbital in the Atomic Orbital Equation of Motion for $\ell=0$ Based on the Current Vector Field (CVF) section using the rotational matrices given therein. The LHCP photon-e&mvf is generated by the rotation of the basis elements comprising the great circle magnetic field line in the xz-plane and the great circle electric field line in the yz-plane about the $(\mathbf{i}_x,-\mathbf{i}_y,0\mathbf{i}_z)$-axis by $\frac{\pi}{2}$. A first transformation matrix is generated by the combined rotation of the great circles about the z-axis by $\frac{\pi}{4}$ then about the x-axis by θ where positive rotations about an axis are defined as clockwise:

$$\begin{bmatrix} x' \\ y' \\ z' \end{bmatrix} = \begin{bmatrix} \cos\left(\frac{\pi}{4}\right) & -\sin\left(\frac{\pi}{4}\right) & 0 \\ \sin\left(\frac{\pi}{4}\right)\cos\theta & \cos\left(\frac{\pi}{4}\right)\cos\theta & \sin\theta \\ -\sin\left(\frac{\pi}{4}\right)\sin\theta & -\cos\left(\frac{\pi}{4}\right)\sin\theta & \cos\theta \end{bmatrix} \bullet \left(\begin{bmatrix} 0 \\ r_n\cos\phi \\ r_n\sin\phi \end{bmatrix}_{\text{Red}} + \begin{bmatrix} r_n\cos\phi \\ 0 \\ r_n\sin\phi \end{bmatrix}_{\text{Blue}} \right) \tag{6}$$

The transformation matrix about $\left(\mathbf{i}_x, -\mathbf{i}_y, 0\mathbf{i}_z\right)$ is given by multiplication of the output of the matrix given by Eq. (6) by the matrix corresponding to a rotation about the z-axis of $\frac{\pi}{4}$. The output of the matrix given by Eq. (6) is shown in Figure AV.3 wherein θ is varied from 0 to $\frac{\pi}{2}$.

Figure AV.3. The electric, magnetic, and combined field-line pattern given by Eq. (6) from the perspective of looking along the z-axis corresponding to the first great circle magnetic field line and the second great circle electric field line shown with 6 degree increments of the angle θ. (Electric field lines red; Magnetic field lines blue).

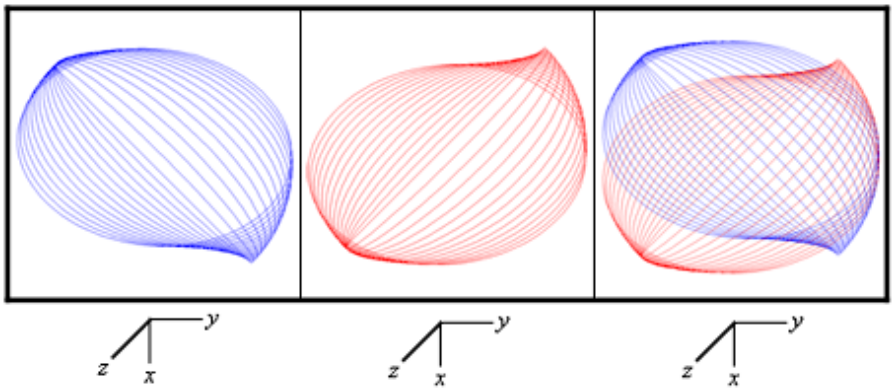

The rotation matrix about the z-axis by $\frac{\pi}{4}$, $R_z\left(\frac{\pi}{4}\right)$, is given by:

$$R_z\left(\frac{\pi}{4}\right) = \begin{bmatrix} \cos\left(\frac{\pi}{4}\right) & \sin\left(\frac{\pi}{4}\right) & 0 \\ -\sin\left(\frac{\pi}{4}\right) & \cos\left(\frac{\pi}{4}\right) & 0 \\ 0 & 0 & 1 \end{bmatrix} \tag{7}$$

Thus,

$$\begin{bmatrix} x' \\ y' \\ z' \end{bmatrix} = R_z\left(\frac{\pi}{4}\right) \bullet \begin{bmatrix} \cos\left(\frac{\pi}{4}\right) & -\sin\left(\frac{\pi}{4}\right) & 0 \\ \sin\left(\frac{\pi}{4}\right)\cos\theta & \cos\left(\frac{\pi}{4}\right)\cos\theta & \sin\theta \\ -\sin\left(\frac{\pi}{4}\right)\sin\theta & -\cos\left(\frac{\pi}{4}\right)\sin\theta & \cos\theta \end{bmatrix} \bullet \left(\begin{bmatrix} 0 \\ r_n\cos\phi \\ r_n\sin\phi \end{bmatrix}_{\text{Red}} + \begin{bmatrix} r_n\cos\phi \\ 0 \\ r_n\sin\phi \end{bmatrix}_{\text{Blue}} \right) \tag{8}$$

Substitution of the matrix given by Eq. (7) into Eq. (8) gives:

$$\begin{bmatrix} x' \\ y' \\ z' \end{bmatrix} = \begin{bmatrix} \frac{1}{2}+\frac{\cos\theta}{2} & -\frac{1}{2}+\frac{\cos\theta}{2} & \frac{\sin\theta}{\sqrt{2}} \\ -\frac{1}{2}+\frac{\cos\theta}{2} & \frac{1}{2}+\frac{\cos\theta}{2} & \frac{\sin\theta}{\sqrt{2}} \\ -\frac{\sin\theta}{\sqrt{2}} & -\frac{\sin\theta}{\sqrt{2}} & \cos\theta \end{bmatrix} \cdot \left(\begin{bmatrix} 0 \\ r_n\cos\phi \\ r_n\sin\phi \end{bmatrix}_{\text{Red}} + \begin{bmatrix} r_n\cos\phi \\ 0 \\ r_n\sin\phi \end{bmatrix}_{\text{Blue}} \right) \tag{9}$$

$$\begin{bmatrix} x' \\ y' \\ z' \end{bmatrix} = \begin{bmatrix} \left(\left(-\frac{1}{2}+\frac{\cos\theta}{2}\right)r_n\cos\phi+\frac{\sin\theta}{\sqrt{2}}r_n\sin\phi\right)_{\text{Red}} + \left(\left(\frac{1}{2}+\frac{\cos\theta}{2}\right)r_n\cos\phi+\frac{\sin\theta}{\sqrt{2}}r_n\sin\phi\right)_{\text{Blue}} \\ \left(\left(\frac{1}{2}+\frac{\cos\theta}{2}\right)r_n\cos\phi+\frac{\sin\theta}{\sqrt{2}}r_n\sin\phi\right)_{\text{Red}} + \left(\left(-\frac{1}{2}+\frac{\cos\theta}{2}\right)r_n\cos\phi+\frac{\sin\theta}{\sqrt{2}}r_n\sin\phi\right)_{\text{Blue}} \\ \left(-\frac{\sin\theta}{\sqrt{2}}r_n\cos\phi+\cos\theta r_n\sin\phi\right)_{\text{Red}} + \left(-\frac{\sin\theta}{\sqrt{2}}r_n\cos\phi+\cos\theta r_n\sin\phi\right)_{\text{Blue}} \end{bmatrix} \tag{10}$$

The LHCP photon-e&mvf that is generated by the rotation of the great-circle basis elements in the xz- and yz-planes about the $(\mathbf{i}_x, -\mathbf{i}_y, 0\mathbf{i}_z)$-axis by $\frac{\pi}{2}$ corresponding to the output of the matrix given by Eq. (10) is shown in Figure AV.4.

Figure AV.4. The field-line pattern given by Eq. (10) from three orthogonal perspectives of a LHCP photon-e&mvf corresponding to the first great circle magnetic field line and the second great circle electric field line shown with 6 degree increments of the angle θ. (Electric field lines red; Magnetic field lines blue).

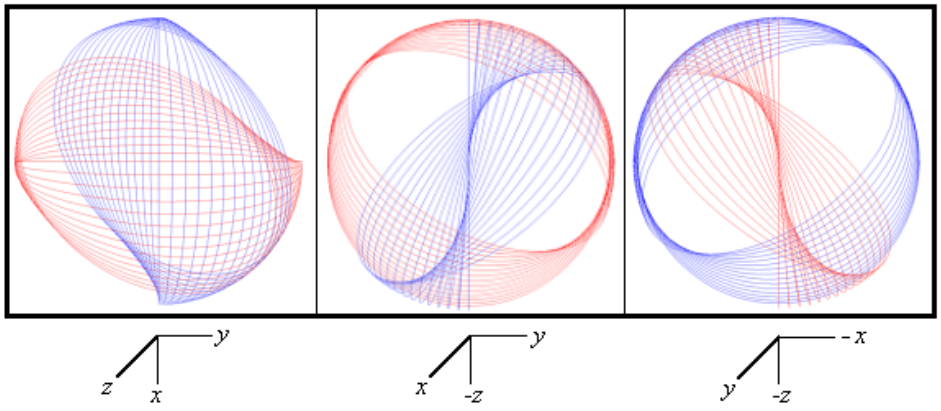

GENERATION OF THE LINEARLY-POLARIZED PHOTON ELECTRIC AND MAGNETIC VECTOR FIELD

The linearly polarized (LP) photon-e&mvf is generated by the superposition of the RHCP photon-e&mvf and the LHCP photon-e&mvf as shown in Figure AV.5.

Figure AV.5. The field-line pattern given by Eqs. (5) and (10) from three orthogonal perspectives of a LP photon-e&mvf corresponding to the first great circle magnetic field line and the second great circle electric field line shown with 6 degree increments of the angle θ about each of the $(\mathbf{i}_x, \mathbf{i}_y, 0\mathbf{i}_z)$- and $(\mathbf{i}_x, -\mathbf{i}_y, 0\mathbf{i}_z)$-axes. (Electric field lines red; Magnetic field lines blue).

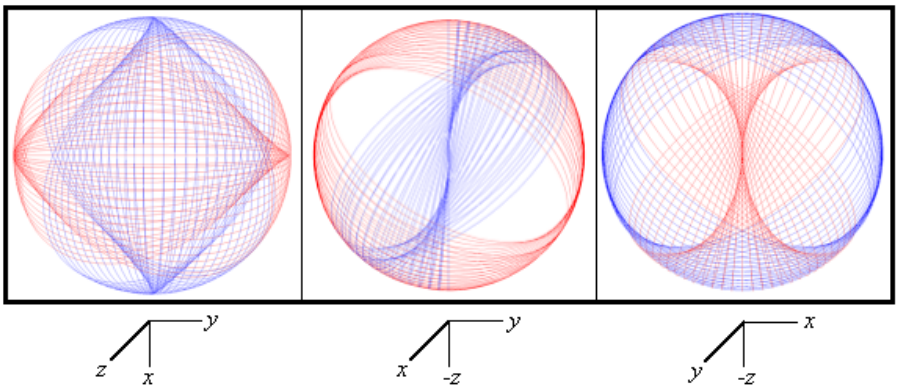

PHOTON FIELDS IN THE LABORATORY FRAME

Since the power flow, **P**, is governed by the Poynting power theorem given by:

$$\mathbf{P} = \nabla \bullet (\mathbf{E} \times \mathbf{H}) \tag{11}$$

and the time-averaged angular momentum density is given by Eq. (4.1), $\mathbf{m} = \int \frac{1}{8\pi c} \mathrm{Re}\left[\mathbf{r} \times (\mathbf{E} \times \mathbf{B}^*)\right] dx^4 = \hbar$, it is apparent that the photon propagation axis is along the $\mathbf{E} \times \mathbf{H}$-vector at the intersection point of the basis elements, the orthogonal great-circle electric and magnetic field lines. Consider the RHCP photon-e&mvf. The primary intersection occurs at the z-axis of the stationary xyz-coordinate system as shown in Figure 4.1. This point is also the initial position of the z'-axis of the x'y'z'-coordinate system that is rotated about the $(\mathbf{i}_x, \mathbf{i}_y, 0\mathbf{i}_z)$-axis by $\frac{\pi}{2}$ wherein the great-circle field lines are stationary with respect to this system. Then, as the photon-e&mvf is generated by rotation of the basis elements about the $(\mathbf{i}_x, \mathbf{i}_y, 0\mathbf{i}_z)$-axis, the z' and -z'-intersection of the two orthogonal great-circle field lines move along great quarter circles in the (-x+y+z)-octant and (+x-y-z)-octant, respectively, each in a plane that is parallel with the z-and $(-\mathbf{i}_x, \mathbf{i}_y, 0\mathbf{i}_z)$-axes. Alternatively, the intersection point that gives rise to the $\mathbf{E} \times \mathbf{H}$-vector of the RHCP photon-e&mvf is always on a quarter circle in a plane orthogonal to the $\frac{\pi}{2}$-rotational axis, the $(\mathbf{i}_x, \mathbf{i}_y, 0\mathbf{i}_z)$-axis.

Consider the resulting curve formed by the intersection point of the basis elements, the orthogonal great-circle electric and magnetic field lines, when considering that the RHCP photon-e&mvf propagates through a plane perpendicular to the z-axis as shown in Figure 4.1. From this perspective using the coordinates shown in Figure 4.1, the two quarter circles add in time to give a trajectory that always follows a circle that initiates at (0,0,1) and ends at (0,0,-1). Additionally, since the density of the intersection points over the spherical surface in the (-x+y+z)-octant and (+x-y-z)-octant is constant, the pitch of the intersection point viewed along the z-axis is constant. It is shown *infra*, that the magnitude of the transverse electric and magnetic fields vary at twice the frequency along the z-axis as the circular rotation of the intersection point. When the vector projection on the transverse fields is superimposed on the manifold of circular rotation at constant pitch, the form is a right handed-helix. Thus, geometrically the set of all such intersection points over the spherical surface of the RHCP photon-e&mvf defines a parametric helical curve relative to the z-axis for the field lines when their projections in times are considered. The orthogonally-related electric and magnetic fields observed in the laboratory frame are transverse to the z-axis along this right-handed helical curve as shown *infra*, and the LHCP photon-e&mvf has the opposite handedness.

Consider the Fields Based on Invariance Under Gauss' Integral Law section [1]. As shown in the Excited States of the One-Electron Atom (Quantization) section, since the linear velocity at each point along a great circle of the photon-e&mvf is c, the field on the spherical surface of the photon-e&mvf at each point is radially inward in its frame. In addition, this law requires that the electric and magnetic field lines are perpendicular to the direction of power flow, the direction of photon propagation,

being the z-axis. The electric and magnetic field basis elements that transfer power according to $\mathbf{E}\times\mathbf{H}$ are $\frac{\pi}{2}$ out of phase in the photon frame as shown in Figure 4.1 and must also be perpendicular in all frames that transfer power in order to conserve power transfer. The field vectors in a stationary laboratory frame are determined by the projection onto the two orthogonal axes in the transverse directions and one in the parallel direction relative to the propagation axis, the z-axis. Thus, the natural coordinates are Cartesian used *infra* wherein the transform is given by considering total field invariance under Gauss' integral law.

Consider an observer at the origin of his frame with the photon propagating by at light-speed c along the z-axis relative to him as shown in Figure AV.6. Since the photon field is purely radial in its frame, and the observer sees the transverse component of this radial field with respect to the z-axis, the observer sees a field with a $\sin\theta$ dependence over time along the z-axis wherein θ is the spherical coordinate with respect to the z-axis. This corresponds to the transverse projection of the radial photon field along the z-axis. In addition, the distribution of E and B fields on the spherical surface has a vector $\cos\theta$ dependence corresponding to an inversion center in the distribution formed by the $\left(\mathbf{i}_x,\mathbf{i}_y,0\mathbf{i}_z\right)$-axis rotation by $\frac{\pi}{2}$ and matching the continuity condition of the transverse field. Thus the transverse electric field has the following trigonometric dependence:

$$\mathbf{E} = E_0 \cos\theta \sin\theta \, \mathbf{i}_{xy} \tag{12}$$

Using a trigonometric identity

$$\cos\theta \sin\theta = \frac{1}{2}\sin 2\theta \tag{13}$$

gives

$$\mathbf{E} = \frac{E_0}{2}\sin 2\theta \mathbf{i}_{xy} \tag{14}$$

Since the magnetic field is perpendicular to the electric field according to Maxwell's equations (Eqs. (4.2-4.3)), Eq. (4.10) follows from Eq. (14), and the magnetic field $\mathbf{H}$ is given by:

$$\mathbf{H} = \sqrt{\frac{\varepsilon_0}{\mu_0}}\frac{E_0}{2}\sin 2\theta \mathbf{i}_z \times \mathbf{i}_{xy} \tag{15}$$

Figure AV.6. An observer at the origin of his frame with the photon-e&mvf stationary in its own frame propagating at light-speed c relative to the observer along its z-axis ($z_{photon-e\&mvf}$) that is collinear to the z-axis of the observer, $z_{laboratory}$.

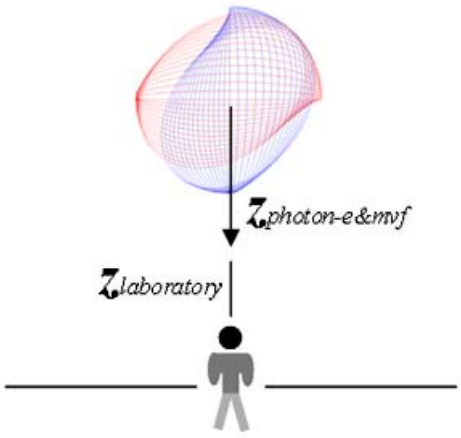

The photon-e&mvf, the electric and magnetic field lines make a helical trajectory relative to an observer who is passed at the light speed (Eqs. (4.10) and (4.11)). The transverse-plane-projected electric and magnetic fields rotate about the z-axis over a 2π angular span of the arguments of Eqs. (14) and (15) corresponding to the $\Delta z = 2r_{photon}$ span along the z-axis. The electric and magnetic fields also rotate time harmonically transverse to and about the z-axis according to the time function $k(t)$ given by

$$k(t) = e^{-j\omega t} \tag{16}$$

over the time span of one period, $\frac{\lambda}{c}$. For example, the spatial distribution of the fields of a right-handed circularly polarized photon-e&mvf in the laboratory frame is shown in Figures 4.5 and 4.6. More specifically, Figure AV.7 shows the visualization of the fields in the laboratory frame for the observer shown in Figure AV.6. The rotation about the z-axis requires that the photon angular momentum is along the z-axis. Using the time-averaged angular momentum density give by Eq. (4.1), the direction of $\mathbf{E}\times\mathbf{B}^*$ is the z-axis, and the vector rotates at angular frequency ω about the z-axis in the direction of $\mathbf{i}_\phi$ (cylindrical coordinates). Thus, the corresponding time-averaged integral of the unit-vector cross products of Eq. (4.1) is given by:

$$\mathbf{i}_\rho \times \mathbf{i}_\phi = \mathbf{i}_z \tag{17}$$

Figure AV.7. The electric (red) and magnetic (blue) field lines of a right-handed circularly polarized photon-e&mvf as seen in the lab inertial reference frame at a fixed time. A and B. Views transverse to the axis of propagation, the z-axis, wherein $2r_{photon} = \lambda$. C and D. Off z-axis views showing field aspects both along and transverse to the axis of propagation.

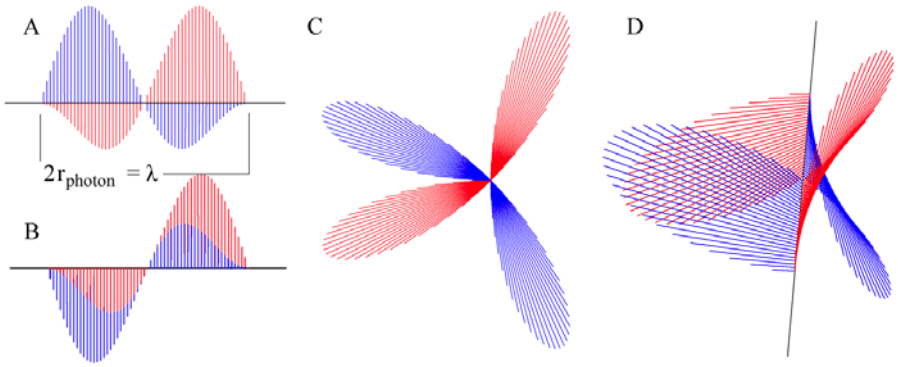

The corresponding photon-e&mvf equation in the lab frame is:

$$\mathbf{E} = E_0\left[\mathbf{x} - i\mathbf{y}\right]e^{-jk_z z}e^{-j\omega t} \tag{18}$$

$$\mathbf{H} = \left(\frac{E_0}{\eta}\right)\left[\mathbf{y} - i\mathbf{x}\right]e^{-jk_z z}e^{-j\omega t} = E_0\sqrt{\frac{\varepsilon}{\mu}}\left[\mathbf{y} - i\mathbf{x}\right]e^{-jk_z z}e^{-j\omega t} \tag{19}$$

with a wavelength of

$$\lambda = 2\pi\frac{c}{\omega} \tag{20}$$

The relationship between the photon atomic orbital radius and wavelength is:

$$2r_{photon} = \lambda \tag{21}$$

Using Eqs. (4.1), and (14-17) with

$$\rho = r_{photon}\sin\theta \tag{22}$$

the electric and magnetic-field parameter E_0 can be solved:

$$\frac{1}{8\pi c}\int_0^{\frac{2\pi}{\omega}}\int_0^{2\pi}\int_0^{\pi}\int_0^{\infty} r\sin\theta\sqrt{\frac{\varepsilon_0}{\mu_0}}\frac{E_0^2}{4}\sin^2 2\theta\sin^2\omega t r^2\delta\left(r - r_{photon}\right)\sin\theta\, dr\, d\theta\, d\phi\, dt = \hbar \tag{23}$$

where Eq. (4.1) was converted to MKS units. The integration over the period and the surface gives:

$$\frac{1}{8\pi c}\sqrt{\frac{\varepsilon_0}{\mu_0}}\frac{E_0^2}{4}\frac{2\pi}{2\omega}2\pi r_{photon}^3\int_0^{\pi}\sin^2 2\theta\sin^2\theta\, d\theta = \hbar \tag{24}$$

$$\sqrt{\frac{\varepsilon_0}{\mu_0}}\frac{E_0^2}{32c}\frac{2\pi}{\omega}r_{photon}^3\int_0^{\pi}\sin^2 2\theta\left(\frac{1-\cos 2\theta}{2}\right)d\theta = \hbar \tag{25}$$

Using the wave equation relationship and the relationship between the wavelength and the radius of the photon-e&mvf given by:

Eq. (20) and Eq. (21), respectively, with the integral by Lide [2] gives:

$$\sqrt{\frac{\varepsilon_0}{\mu_0}}\frac{E_0^2}{32}\frac{\pi^4}{\omega^4}c^2\left(\left(\frac{\theta}{2}-\frac{1}{8}\sin 4\theta\right)_0^{\pi}-\int_0^{\pi}\sin^2 2\theta\cos 2\theta d\theta\right)=\hbar \tag{26}$$

The second integral by Lide [1] gives:

$$\sqrt{\frac{\varepsilon_0}{\mu_0}}\frac{E_0^2}{32}\frac{\pi^4}{\omega^4\sqrt{\varepsilon_0\mu_0}}c\left(\frac{\pi}{2}-\left(\frac{\sin^3 2\theta}{6}\right)_0^{\pi}\right)=\hbar \tag{27}$$

$$\frac{E_0^2}{64}\frac{\pi^5}{\omega^4\mu_0}c=\hbar \tag{28}$$

Thus,

$$E_0=\sqrt{\frac{64\omega^4\mu_0\hbar}{c\pi^5}}=8\omega^2\sqrt{\frac{\mu_0\hbar}{c\pi^5}} \tag{29}$$

which has the required MKS units of Vm^{-1}. From Planck's law, the energy is given by:

$$E=L\omega=\hbar\omega=\frac{E_0^2}{64}\frac{\pi^5}{\omega^4\mu_0}c\omega \tag{30}$$

The z-axial electric and magnetic fields cancel over time in agreement with relativistic effects of no field in the direction of propagation at light speed further satisfying required equivalence of the electric and magnetic stored energy given by Eqs. (1.263) and (1.154), respectively, and the energy given by Eq. (30) corresponding to the transverse field.

REFERENCES

1. E. Purcell, *Electricity and Magnetism*, McGraw-Hill, New York, (1965), pp. 156-167.
2. D. R. Lide, *CRC Handbook of Chemistry and Physics*, 79th Edition, CRC Press, Boca Raton, Florida, (1998-9), pp. A-38; A-40.

Appendix VI

THE RELATIVE ANGULAR MOMENTUM COMPONENTS OF ELECTRON 1 AND ELECTRON 2 OF HELIUM TO DETERMINE THE MAGNETIC INTERACTIONS AND THE CENTRAL MAGNETIC FORCE

The vector orientations and the corresponding magnetic moments of two-electron atoms to determine the radius of the two bound electrons are given in the Two-Electron Atoms section. From the corresponding ground state, the momentum-vector orientations for the two possible types of excited spin states, singlet and triplet, as well as each of these states with and without orbital angular momentum in addition to spin angular momentum is determined from conservation of angular momentum and torque balance. The central magnetic force is derived and is used in the Excited States of Helium section to calculate all of the excited states of the helium atom. Similar forces arise in the interaction of multi-electron atoms as shown in the Three- Through Twenty-Electron Atoms section.

SINGLET EXCITED STATES WITH ℓ = 0 ($1s^2 \rightarrow 1s^1(ns)^1$)

Due to the relative motion of the charge-density elements of each electron of the helium atom, a radiation reaction force arises between the two electrons. This force given in Sections 6.6, 12.10, and 17.3 of Jackson [1] achieves the condition that the sum of the mechanical momentum and electromagnetic momentum is conserved. The magnetic central force $\mathbf{F}_{\text{mag}}$ is derived from the Lorentz force which is relativistically corrected following the same procedure as given in the Two-Electron Atoms section. The magnetic force is derived by first determining the interaction of the two electrons due to the field of the outer electron 2 acting on the magnetic moments of electron 1 and vice versa. Insight to the behavior is given by considering the physics of a single bound electron in an externally applied uniform magnetic field as shown in the Resonant Precession of the Spin-1/2-Current-Density Function Gives Rise to the Bohr Magneton section and the physics of the binding of the two electrons of two-electron atoms given in the Two-Electron Atoms section. As discussed in the latter section, each of the two interacting electrons have two orthogonal components of angular momentum which give rise to a purely radial net magnetic force.

With $\ell = 0$ of the helium atom, the excited-state photon carries $\hbar$ of angular momentum that gives rise to a spin state in electron 1 to balance the dipole current about the $\mathbf{S}_2$-axis in electron 2 to achieve torque balance. Then, the electron source current of electron 2 in the excited state is a constant function given by Eq. (1.27) that spins as a globe about an axis. The angular momentum, $\mathbf{L}_{S_2}$, of the atomic orbital due to rotation about an axis defined as the $\mathbf{S}_2$-axis at angular velocity ω_2 is given by:

$$\mathbf{L}\mathbf{i}_{z_{S_2}} = I\omega\mathbf{i}_{z_{S_2}} = \int m_e\rho^2\omega_2 d\Omega = m_e\omega_2 \frac{\int_{-r_1}^{r_1}\left(r_2^2 - z_{S_2}^2\right)dz_{S_2}}{2r_2} = \frac{2}{3}m_e r_2^2\omega_2 \tag{1}$$

where the $\mathbf{i}_{z_{S_2}}$ is the unit vector along the $\mathbf{S}_2$-axis.

In the ground state, the magnetic moments of electrons 1 and 2 cancel as they are spin paired to form an energy minimum at the radius (i.e. $r_1 = r_2$). As shown in the Exact Generation of $Y_0^0(\theta,\phi)$ from the Atomic Orbital-cvf section, the atomic orbital uniform current density function $Y_0^0(\theta,\phi)$ comprises $\frac{\hbar}{4}$ (Eq. (1.127)) and $\frac{\hbar}{2}$ (Eq. (1.128)) components of angular momentum. In the excited singlet state, these components of electron 2 spin in the plane perpendicular to the $\mathbf{S}_2$-axis and time-average to zero. The spin state of electron 1 comprises a photon standing wave that is phase-matched to a spherical harmonic source current, a spherical harmonic dipole $Y_\ell^m(\theta,\phi) = \sin\theta$ with respect to the **S**-axis. The dipole spins about the **S**-axis at the angular velocity given by Eq. (1.36) with $\hbar$ of angular momentum. The intrinsic spin and photon angular momentum vectors are shown in Figure AVI.1.

In the stationary coordinate system of electron 2 (denoted by the axes labeled *X*, *Y*, and *Z* in Figure AVI.1A), the angular momentum vector $\mathbf{S}_2$ of magnitude $\frac{2}{3}\hbar$ is in the *YZ*-plane at an angle of $\theta = \frac{\pi}{6}$ relative to the *Z*-axis. The *Z*-axis projection of: $\mathbf{S}_2$ is $\frac{2}{3}\sqrt{\frac{3}{4}}\hbar$, and the *Y*-axis projection of $\mathbf{S}_2$ is $\frac{2}{3}\frac{\hbar}{2}$.

In the stationary coordinate system of electron 1 (denoted by the axes labeled X', Y', and Z' in Figure AVI.1B), the $\frac{\hbar}{4}$ of intrinsic angular momentum is along X', the $\frac{\hbar}{2}$ of intrinsic angular momentum is along Y', and the photon angular momentum vector $\mathbf{S}_1$ of magnitude $\hbar$ is in the $Y'Z'$-plane at an angle of $\theta = \frac{\pi}{3}$ relative to the Y'-axis. The Z'-axis projection of $\mathbf{S}_1$ is $\sqrt{\frac{3}{4}}\hbar$, and the Y'-axis projection of $\mathbf{S}_1$ is $\frac{\hbar}{2}$.

The torque from the corresponding magnetic moments given by Eq. (2.65) is balanced in the absence of Larmor precession for the angular momentum projections of electron 2 shown in Figure AVI.1A relative to those of electron 1 shown in Figure AVI.1B. The $\frac{\hbar}{4}$ of intrinsic angular momentum of electron 1 X' is orthogonal to the other components such that there is no net central force contribution. The $\frac{2}{3}\frac{\hbar}{2}$ Y-axis projection of $\mathbf{S}_2$ of electron 2 gives rise to a magnetic field corresponding to $\frac{2}{3}\frac{\mu_B}{2}$ in the direction of the $\sqrt{\frac{3}{4}}\hbar$ Z'-axis projection of $\mathbf{S}_1$ of electron 1. The $\frac{\hbar}{2}$ of intrinsic angular momentum of electron 1 along Y' and the Y'-axis projection of $\mathbf{S}_1$ of $\frac{\hbar}{2}$ gives rise to a magnetic field corresponding to μ_B in the direction of the $\frac{2}{3}\sqrt{\frac{3}{4}}\hbar$ Z-axis projection of $\mathbf{S}_2$ of electron 2.

Figure AVI.1. The relative angular momentum components of electron 1 and electron 2 to determine the magnetic interactions and the central magnetic force. (A) The atomic orbital and $\mathbf{S}_2$ of electron 2 in the stationary coordinate system X,Y,Z that is designated the unprimed spherical coordinate system relative to the Z-axis as shown. The rotational angular momentum vector $\mathbf{S}_2$ of magnitude $\frac{2}{3}\hbar$ is in the YZ-plane at an angle of $\theta = \frac{\pi}{6}$ relative to the Z-axis. (B) The angular momentum components of the atomic orbital and $\mathbf{S}_1$ of electron 1 in the stationary coordinate system X',Y',Z' that is designated the primed spherical coordinate system relative to the Z'-axis as shown. The photon angular momentum vector $\mathbf{S}_1$ of magnitude $\hbar$ is in the $Y'Z'$-plane at an angle of $\theta = \frac{\pi}{3}$ relative to the Y'-axis.

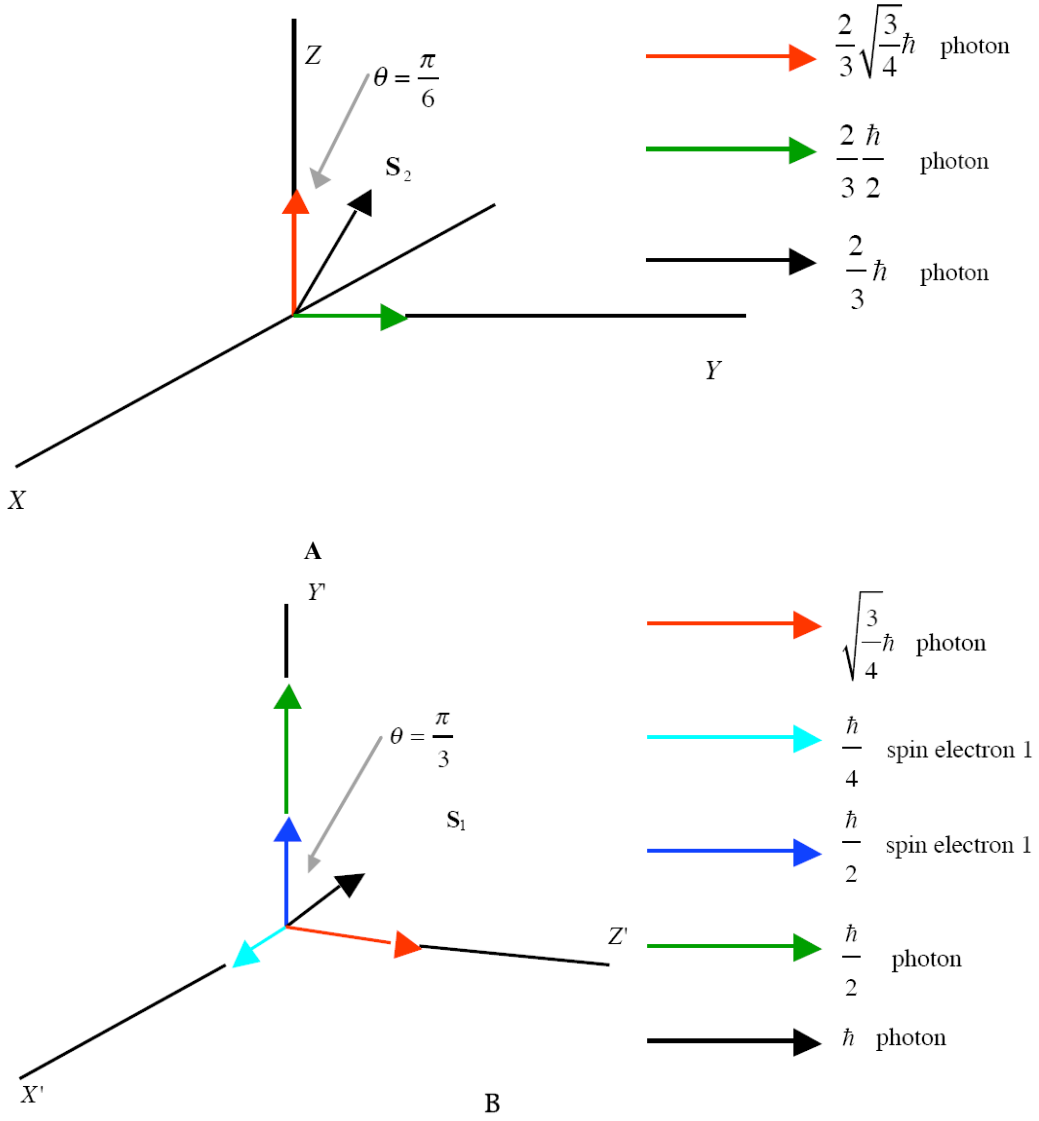

The magnetic central force is due to the interaction of the magnetic field of the electron 2 and the current dipole of the photon at the radius of electron 1 and vice versa. Considering the angular momentum vectors given in Figures AVI.1A and AVI.1B, the magnetostatic magnetic flux of electron 2 and electron 1 corresponding to $\frac{2}{3}\frac{\mu_B}{2}$ and μ_B, respectively, follow from Eqs. (1.132) and (1.133) and after McQuarrie [2]:

$$\mathbf{B} = \frac{2}{3}\frac{\mu_0 e\hbar}{2m_e r_2^3}(\mathbf{i}_{r'}\cos\theta - \mathbf{i}_{\theta'}\sin\theta) \tag{2}$$

$$\mathbf{B} = \frac{e\hbar}{2m_e r^3}(\mathbf{i}_r 2\cos\theta + \mathbf{i}_\theta \sin\theta) \tag{3}$$

where μ_0 is the permeability of free space ($4\pi\ X\ 10^{-7}\ N/A^2$) and the coordinates of the magnetic field due to electron 2 acting on the magnetic moments of electron 1 is designated as the primed system and the magnetic field of electron 1 acting on the magnetic moments of electron 2 is designated as the unprimed system. It follows from Eq. (1.131), the relationship for the Bohr magneton, and relationship between the magnetic dipole field and the magnetic moment **m** [3] that Eqs. (1.132) and (1.133) are the equations for the magnetic field due to a magnetic moment of one third of a Bohr magneton, $\mathbf{m} = \frac{2}{3}\frac{\mu_B}{2}\mathbf{i}_\mathbf{z}$ and one Bohr magneton, $\mathbf{m} = \mu_B \mathbf{i}_\mathbf{z}$, respectively, where $\mathbf{i}_\mathbf{z} = \mathbf{i}_\mathbf{r}\cos\theta - \mathbf{i}_\theta \sin\theta$. The spherical harmonic dipole $Y_\ell^m(\theta,\phi) = \sin\theta$ spins about the **S**-axis at the angular velocity given by Eq. (1.36). Thus, angular velocity $\hat{\omega}$ and linear velocity **v** projections onto each *Z*(*Z*′)-axis are:

$$\hat{\omega} = \frac{\hbar}{m_e r_2^2}\frac{2}{3}\sqrt{\frac{3}{4}}\mathbf{i}_Z \tag{4}$$

$$\mathbf{v} = \frac{\hbar}{m_e r_2}\frac{2}{3}\sqrt{\frac{3}{4}}\sin\theta\mathbf{i}_\phi \tag{5}$$

$$\hat{\omega} = \frac{\hbar}{m_e r_1^2}\sqrt{\frac{3}{4}}\mathbf{i}_{Z'} \tag{6}$$

$$\mathbf{v} = \frac{\hbar}{m_e r_1}\sqrt{\frac{3}{4}}\sin\theta\mathbf{i}_{\phi'} \tag{7}$$

The Lorentz force density at each point moving at velocity **v** given by Eq. (7.10) is

$$\mathbf{F}_{mag} = \frac{e}{4\pi r_2^2}\mathbf{v}\times\mathbf{B} \tag{8}$$

Substitution of Eqs. (2-3), (5), and (7) into Eq. (8) while maintaining the designation of the coordinates of the magnetic field of electron 2 acting on the magnetic moments of electron 1 as the primed system and the coordinates of the magnetic field of electron 1 acting on the magnetic moments of electron 2 as the unprimed system gives:

$$\mathbf{F}_{mag} = -\frac{e}{4\pi r_2^2}\begin{pmatrix}\frac{\hbar}{m_e r_1}\sqrt{\frac{3}{4}}\sin\theta\mathbf{i}_{\phi'}\times\frac{2}{3}\frac{\mu_0 e\hbar}{2m_e r_2^3}(\mathbf{i}_{r'}\cos\theta - \mathbf{i}_{\theta'}\sin\theta)\\ +\frac{\hbar}{m_e r_2}\frac{2}{3}\sqrt{\frac{3}{4}}\sin\theta\mathbf{i}_\phi\times\frac{\mu_0 e\hbar}{2m_e r_2^3}(\mathbf{i}_r 2\cos\theta + \mathbf{i}_\theta\sin\theta)\end{pmatrix} \tag{9}$$

As shown in Eqs. (7.16-7.24), the relativistic form of Eq. (9) results in the equivalence of the velocity at the two radii; thus, r_1 may be substituted for r_2 in the velocity factor of the second term to give:

$$\begin{aligned}\mathbf{F}_{mag} &= -\frac{1}{4\pi r_2^2}\frac{\mu_0 e^2\hbar^2}{2r_1 m_e^2 r_2^3}\frac{2}{3}\sqrt{\frac{3}{4}}\begin{pmatrix}\sin\theta\mathbf{i}_{\phi'}\times(\mathbf{i}_{r'}\cos\theta - \mathbf{i}_{\theta'}\sin\theta)\\ +\sin\theta\mathbf{i}_\phi\times(\mathbf{i}_r 2\cos\theta + \mathbf{i}_\theta\sin\theta)\end{pmatrix}\\ &= -\frac{1}{4\pi r_2^2}\frac{\mu_0 e^2\hbar^2}{2r_1 m_e^2 r_2^3}\frac{2}{3}\sqrt{\frac{3}{4}}\begin{pmatrix}-\sin\theta\cos\theta\mathbf{i}_{\theta'} + \sin^2\theta\mathbf{i}_{r'}\\ +2\sin\theta\cos\theta\mathbf{i}_\theta + \sin^2\theta\mathbf{i}_r\end{pmatrix}\end{aligned} \tag{10}$$

The $\mathbf{i}_{r'}$ unit vector is transformed to $\mathbf{i}_r$ by substituting θ with $\theta + \frac{\pi}{2}$ in the second term of Eq. (10):

$$\begin{aligned}\mathbf{F}_{mag} &= -\frac{1}{4\pi r_2^2}\frac{\mu_0 e^2\hbar^2}{2r_1 m_e^2 r_2^3}\frac{2}{3}\sqrt{\frac{3}{4}}\begin{pmatrix}-\sin\theta\cos\theta\mathbf{i}_{\theta'} + \sin^2\left(\theta+\frac{\pi}{2}\right)\mathbf{i}_{r'}\\ +2\sin\theta\cos\theta\mathbf{i}_\theta + \sin^2\theta\mathbf{i}_r\end{pmatrix}\\ &= -\frac{1}{4\pi r_2^2}\frac{\mu_0 e^2\hbar^2}{2r_1 m_e^2 r_2^3}\frac{2}{3}\sqrt{\frac{3}{4}}\begin{pmatrix}-\sin\theta\cos\theta\mathbf{i}_{\theta'} + (\sin^2\theta + \cos^2\theta)\mathbf{i}_r\\ +2\sin\theta\cos\theta\mathbf{i}_\theta\end{pmatrix}\\ &= -\frac{1}{4\pi r_2^2}\frac{\mu_0 e^2\hbar^2}{2r_1 m_e^2 r_2^3}\frac{2}{3}\sqrt{\frac{3}{4}}(-\sin\theta\cos\theta\mathbf{i}_{\theta'} + 2\sin\theta\cos\theta\mathbf{i}_\theta + \mathbf{i}_r)\\ &= -\frac{1}{4\pi r_2^2}\frac{\mu_0 e^2\hbar^2}{2r_1 m_e^2 r_2^3}\frac{2}{3}\sqrt{\frac{3}{4}}\left(-\frac{1}{2}\sin 2\theta\mathbf{i}_{\theta'} + \sin 2\theta\mathbf{i}_\theta + \mathbf{i}_r\right)\end{aligned} \tag{11}$$

The $F_{mag}\mathbf{i}_\theta$ and $F_{mag}\mathbf{i}_{\theta'}$ average to zero over the surface for $0 \le \theta \le \pi$. The relativistic correction given by Eq. (7.23) is based on quantized-angular-momentum conservation with the emission of a photon. The relativistic correction for the lightlike frame causes the circumferential distances on the surface to dilate to the radial dimension alone as given in the Two-Electron Atoms section. This causes the angular force to vanish since it averages to zero such that only the radial force remains. Since there is no net angular force on the electron, only the resultant radial force need be considered:

$$\mathbf{F}_{mag} = -\frac{1}{4\pi r_2^{\,2}}\frac{\mu_0 e^2\hbar^2}{2r_1 m_e^2 r_2^3}\frac{2}{3}\sqrt{\frac{3}{4}}\mathbf{i}_r \tag{12}$$

Eq. (12) may be written in the form

$$\mathbf{F}_{mag} = -\frac{1}{4\pi r_2^{\,2}}\frac{\mu_0 e^2\hbar^2}{2r_1 m_e^2 r_2^3}\frac{2}{3}\sqrt{s(s+1)}\mathbf{i}_r \tag{13}$$

where $s = 1/2$ and $\sqrt{s(s+1)} = \sqrt{\frac{3}{4}}$ is the historical designation of the spin-angular momentum magnitude. Then, the balance between the centrifugal and electric and magnetic forces is given by the Eq. (9.10):

$$\frac{m_e v^2}{r_2} = \frac{\hbar^2}{m_e r_2^3} = \frac{1}{n}\frac{e^2}{4\pi\varepsilon_0 r_2^2} + \frac{2}{3}\frac{1}{n}\frac{\hbar^2}{2m_e r_2^3}\sqrt{s(s+1)} \tag{14}$$

TRIPLET EXCITED STATES WITH $\ell = 0$ ($1s^2 \rightarrow 1s^1(ns)^1$)

For the $\ell = 0$ singlet state, the time-averaged spin angular momentum of electron 2 is zero. The $\ell = 0$ triplet state requires a further excitation to unpair the spin states of the two electrons. The angular momentum corresponding to the excited state is $\hbar$, and the angular momentum change corresponding to the spin-flip is also $\hbar$ as given in the Magnetic Parameters of the Electron (Bohr Magneton) section. Then, the triplet state comprises spin interaction terms between the two electrons plus a contribution from the unpairing photon. As shown in the Resonant Precession of the Spin-1/2-Current-Density Function Gives Rise to the Bohr Magneton section, the electron spin angular momentum gives rise to a trapped photon with $\hbar$ of angular momentum along an **S**-axis. Then, the spin state of each of electron 1 and 2 comprises a photon standing wave that is phase-matched to a spherical harmonic source current, a spherical harmonic dipole $Y_\ell^m(\theta,\phi) = \sin\theta$ with respect to the **S**-axis. The dipole spins about the **S**-axis at the angular velocity given by Eq. (1.55) with $\hbar$ of angular momentum. To conserve angular momentum, electron 2 rotates in the opposite direction about **S**, the axis of the photon angular momentum due to the spin, and this rotation corresponds to $-\frac{2}{3}\hbar$ of angular momentum relative to **S**. The intrinsic spin and photon angular momentum vectors are shown in Figure AVI.2.

In the stationary coordinate system of electron 2 (denoted by the axes labeled *X*, *Y*, and *Z* in Figure AVI.2A), the $\frac{\hbar}{4}$ of intrinsic angular momentum is along *X*, the $\frac{\hbar}{2}$ of intrinsic angular momentum is along *Y*, and $\mathbf{S}_3$, the $\hbar$ photon angular momentum vector due to spin interaction, is in the *YZ*-plane at an angle of $\theta = \frac{\pi}{3}$ relative to the *Y*-axis. The *Z*-axis projection of $\mathbf{S}_3$ is $\sqrt{\frac{3}{4}}\hbar$, and the *Y*-axis projection of $\mathbf{S}_3$ is $\frac{\hbar}{2}$.

Electron 2 is excited by the additional spin-unpairing photon. The angular momentum vector $\mathbf{S}_4$ of magnitude $\hbar$ in the *XZ*-plane is aligned in the plane perpendicular to $\mathbf{S}_3$ at an angle of $\theta = \frac{\pi}{6}$ relative to the *Z*-axis. The *Z*-axis projection of $\mathbf{S}_4$ is $\sqrt{\frac{3}{4}}\hbar$, and the *X*-axis projection of $\mathbf{S}_4$ is $-\frac{\hbar}{2}$.

In order to conserve angular momentum, the rotational angular momentum vector of the singlet state $\mathbf{S}_2$ is now aligned in the opposite direction to that of the photonic spin vector $\mathbf{S}_3$. The angular momentum vector $\mathbf{S}_2$ of magnitude $\frac{2}{3}\hbar$ is in the *YZ*-plane at an angle of $\theta = \frac{\pi}{6}$ relative to the $-Z$-axis. The *Z*-axis projection of $\mathbf{S}_2$ is $-\frac{2}{3}\sqrt{\frac{3}{4}}\hbar$, and the *Y*-axis projection of $\mathbf{S}_2$ is $-\frac{2}{3}\frac{\hbar}{2}$. Then, the total angular momentum along the *Z*-axis due to spin, unpairing, and rotation is:

$$\mathbf{S} = \left(\sqrt{\frac{3}{4}}\hbar + \sqrt{\frac{3}{4}}\hbar - \frac{2}{3}\sqrt{\frac{3}{4}}\hbar \right)\mathbf{i}_Z = \frac{4}{3}\sqrt{\frac{3}{4}}\hbar\mathbf{i}_Z \tag{15}$$

and the total angular momentum along the *Y*-axis comprising the sum of the initial $\frac{\hbar}{2}$ intrinsic angular momentum, the *Y*-axis projection of $\mathbf{S}_3$ of $\frac{\hbar}{2}$, and the *Y*-axis projection of $\mathbf{S}_2$ of $-\frac{2}{3}\frac{\hbar}{2}$ is:

$$\mathbf{S} = \left(\frac{\hbar}{2} + \frac{\hbar}{2} - \frac{2}{3}\frac{\hbar}{2} \right)\mathbf{i}_Y = \frac{4}{3}\frac{\hbar}{2}\mathbf{i}_Y \tag{16}$$

In the stationary coordinate system of electron 1 (denoted by the axes labeled *X'*, *Y'*, and *Z'* in Figure AVI.2B), the $\frac{\hbar}{4}$ of intrinsic angular momentum is along *X'*, the $\frac{\hbar}{2}$ of intrinsic angular momentum is along Y', and the photon angular momentum vector $\mathbf{S}_1$ of magnitude $\hbar$ is in the *Y'Z'*-plane at an angle of $\theta = \frac{\pi}{3}$ relative to the *Y'*-axis. The *Z'*-axis projection of $\mathbf{S}_1$ is $\sqrt{\frac{3}{4}}\hbar$, and the *Y'*-axis projection of $\mathbf{S}_1$ is $\frac{\hbar}{2}$.

The torque from the corresponding magnetic moments is given by Eq. (2.65) are balanced in the absence of Larmor precession for the angular momentum projections of electron 2 shown in Figure AVI.2A relative to those of electron 1 shown in Figure AVI.2B. The superposition of the $\frac{\hbar}{4}$ of intrinsic angular momentum of electrons 1 and 2 along *X'* and *X*, respectively, each with a corresponding magnetic moment of $\frac{\mu_B}{4}$ (Eq. (2.65)) cancel the *X*-axis projection of $\mathbf{S}_4$ of $-\frac{\hbar}{2}$ with a corresponding magnetic moment of $-\frac{\mu_B}{2}$. The $\frac{4}{3}\frac{\hbar}{2}$ of total angular momentum of electron 2 along *Y* gives rise to magnetic field corresponding to $\frac{4}{3}\frac{\mu_B}{2}$ in the direction of the $\sqrt{\frac{3}{4}}\hbar$ Z'-axis projection of $\mathbf{S}_1$ of electron 1. The $\frac{\hbar}{2}$ of intrinsic angular momentum of electron 1 along *Y'* and the *Y'*-axis projection of $\mathbf{S}_1$ of $\frac{\hbar}{2}$ gives rise to a total of $\hbar$ with a magnetic field corresponding to μ_B in the direction of the $\frac{4}{3}\sqrt{\frac{3}{4}}\hbar$ total *Z*-axis projection of electron 2.

Figure AVI.2. The relative angular momentum components of electron 1 and electron 2 to determine the magnetic interactions and the central magnetic force. (A) The atomic orbital and $\mathbf{S}_2$, $\mathbf{S}_3$, and $\mathbf{S}_4$ of electron 2 in the stationary coordinate system X,Y,Z that is designated the unprimed spherical coordinate system relative to the Z-axis as shown. The rotational angular momentum vector $\mathbf{S}_2$ of magnitude $\frac{2}{3}\hbar$ is in the YZ-plane at an angle of $\theta = \frac{\pi}{6}$ relative to the –Z-axis. $\mathbf{S}_3$, the $\hbar$ photon angular momentum vector due to spin interaction, is in the YZ-plane at an angle of $\theta = \frac{\pi}{6}$ relative to the Z-axis. $\mathbf{S}_4$, the $\hbar$ photon angular momentum vector due to spin unpairing, is in the XZ-plane at an angle of $\theta = \frac{\pi}{6}$ relative to the Z-axis. (B) The angular momentum components of the atomic orbital and $\mathbf{S}_1$ of electron 1 in the stationary coordinate system X',Y',Z' that is designated the primed spherical coordinate system relative to the Z'-axis as shown. The photon angular momentum vector $\mathbf{S}_1$ of magnitude $\hbar$ is in the $Y'Z'$-plane at an angle of $\theta = \frac{\pi}{3}$ relative to the Y'-axis.

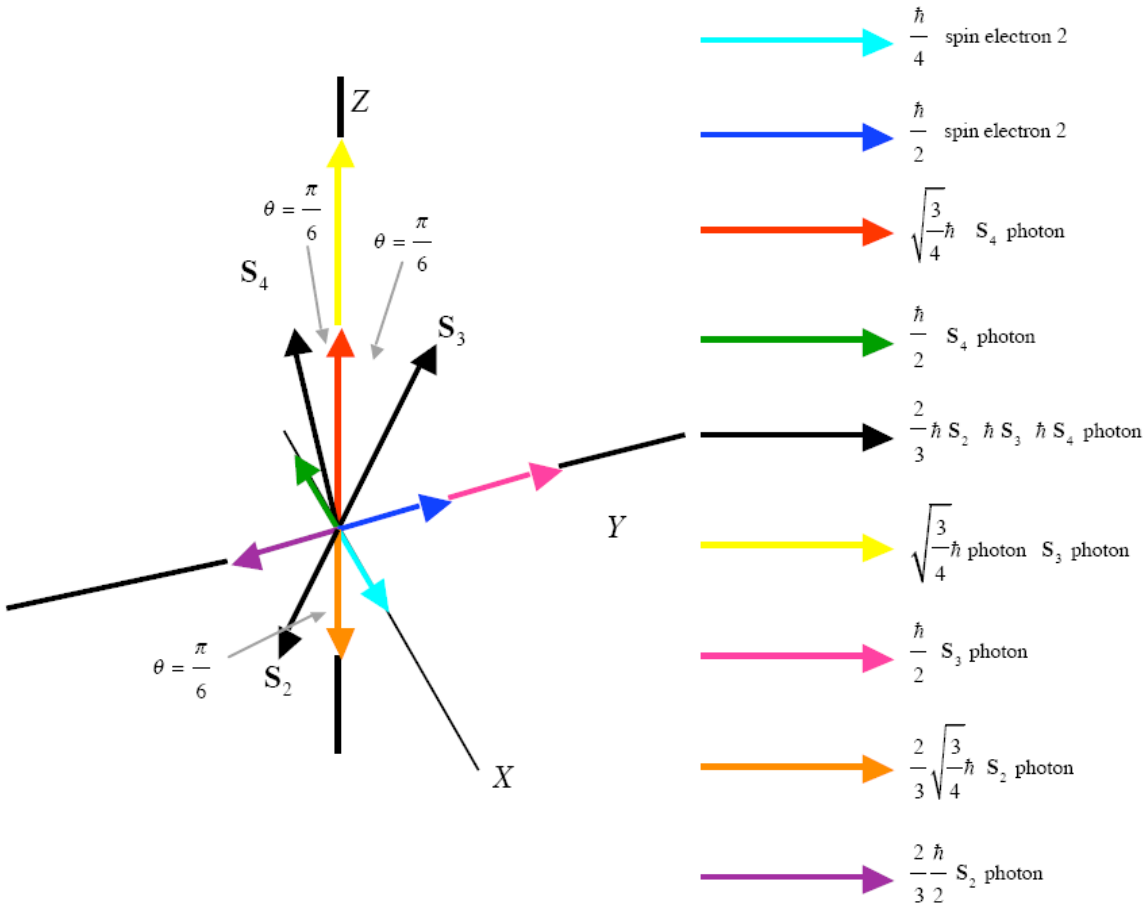

A

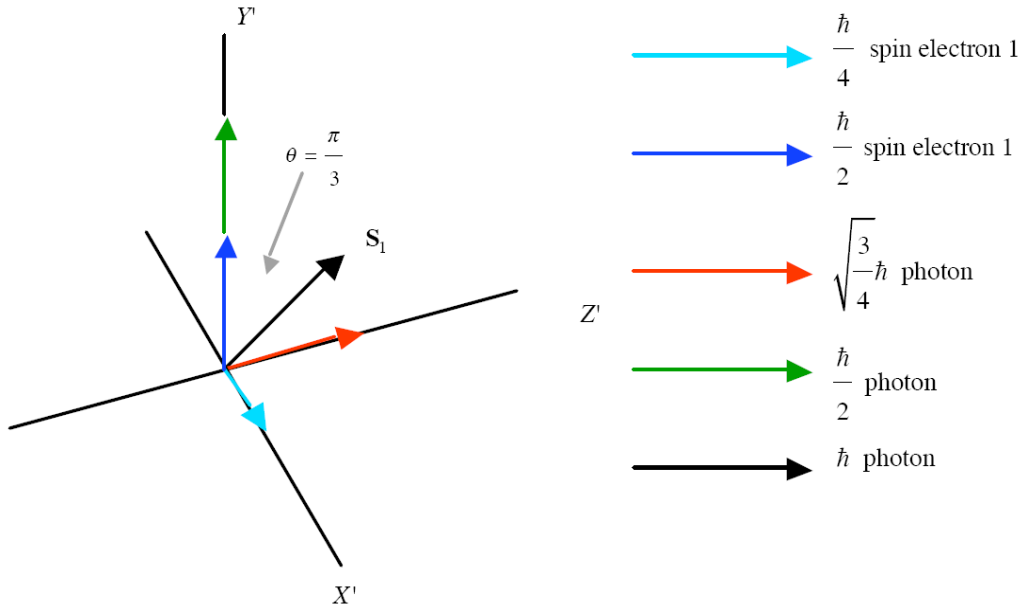

B

For each electron, the magnetic field corresponding to a magnetic moment of μ_B interacting with an aligned magnetic momentum of $\frac{4}{3}\sqrt{\frac{3}{4}}\mu_B$ gives the magnetic force for electron 2 that is twice that of the singlet states. The magnetic central force is due to the interaction of the magnetic field of electron 2 and the current dipole of the photon at the radius of electron 1 and vice versa. Considering the angular momentum vectors given in Figures AVI.2A and AVI.2B, the magnetostatic magnetic flux of electron 2 and electron 1 corresponding to $\frac{4}{3}\frac{\mu_B}{2}$ and μ_B, respectively, follow from Eqs. (1.132) and (1.133) and after McQuarrie [2]:

$$\mathbf{B} = \frac{4}{3}\frac{\mu_0 e\hbar}{2m_e r_2^3}(\mathbf{i}_{r'}\cos\theta - \mathbf{i}_{\theta'}\sin\theta) \tag{17}$$

$$\mathbf{B} = \frac{e\hbar}{m_e r^3}(\mathbf{i}_r 2\cos\theta + \mathbf{i}_\theta \sin\theta) \tag{18}$$

where μ_0 is the permeability of free space ($4\pi\ X\ 10^{-7}\ N/A^2$) and the coordinates of the magnetic field due to electron 2 acting on the magnetic moments of electron 1 is designated as the primed system and the magnetic field of electron 1 acting on the magnetic moments of electron 2 is designated as the unprimed system. The angular velocity $\hat{\omega}$ and linear velocity $\mathbf{v}$ projections onto each $Z(Z')$-axis are:

$$\hat{\omega} = \frac{\hbar}{m_e r_2^2}\frac{4}{3}\sqrt{\frac{3}{4}}\mathbf{i}_Z \tag{19}$$

$$\mathbf{v} = \frac{\hbar}{m_e r_2}\frac{4}{3}\sqrt{\frac{3}{4}}\sin\theta\mathbf{i}_\phi \tag{20}$$

$$\hat{\omega} = \frac{\hbar}{m_e r_1^2}\sqrt{\frac{3}{4}}\mathbf{i}_{Z'} \tag{21}$$

$$\mathbf{v} = \frac{\hbar}{m_e r_1}\sqrt{\frac{3}{4}}\sin\theta\mathbf{i}_{\phi'} \tag{22}$$

The Lorentz force density at each point moving at velocity $\mathbf{v}$ is given by Eq. (8). Substitution of Eqs. (17-18), (20), and (22) into Eq. (8) while maintaining the designation of the coordinates of the magnetic field of electron 2 acting on the magnetic moments of electron 1 as the primed system and the coordinates of the magnetic field of electron 1 acting on the magnetic moments of electron 2 as the unprimed system gives

$$\mathbf{F}_{mag} = -\frac{e}{4\pi r_2^2}\left(\begin{array}{l}\frac{\hbar}{m_e r_1}\sqrt{\frac{3}{4}}\sin\theta\mathbf{i}_{\phi'}\times\frac{4}{3}\frac{\mu_0 e\hbar}{2m_e r_2^3}\left(\mathbf{i}_{r'}\cos\theta-\mathbf{i}_{\theta'}\sin\theta\right)\\ +\frac{\hbar}{m_e r_2}\frac{4}{3}\sqrt{\frac{3}{4}}\sin\theta\mathbf{i}_{\phi}\times\frac{\mu_0 e\hbar}{2m_e r_2^3}\left(\mathbf{i}_{r}2\cos\theta+\mathbf{i}_{\theta}\sin\theta\right)\end{array}\right) \tag{23}$$

From Eqs. (10-13), the magnetic force is:

$$\mathbf{F}_{mag} = -\frac{e}{4\pi r_2^2}\frac{4}{3}\frac{1}{n}\frac{\hbar^2}{2m_e r_2^3}\sqrt{s(s+1)}\mathbf{i}_r \tag{24}$$

The force balance between the centrifugal and electric and magnetic forces given by Eq. (9.31) is:

$$\frac{m_e v^2}{r_2} = \frac{\hbar^2}{m_e r_2^3} = \frac{1}{n}\frac{e^2}{4\pi\varepsilon_0 r_2^2} + \frac{4}{3}\frac{1}{n}\frac{\hbar^2}{2m_e r_2^3}\sqrt{s(s+1)} \tag{25}$$

SINGLET EXCITED STATES WITH $\ell \neq 0$

With $\ell \neq 0$, the electron source current in the singlet excited state is the sum of constant and time-dependent functions where the latter, given by Eqs. (1.28-1.29), travels about the *Z*-axis in the case of electron 2. The corresponding angular momentum along the rotational axis of $\sqrt{\frac{\ell}{\ell+1}}\hbar$ superimposes with the projection of the spin angular momentum of $\sqrt{\frac{3}{4}}\hbar$. The vectors are in opposite directions in order to conserve angular momentum during excitation. The intrinsic spin and photon angular momentum vectors are shown in Figure AVI.3.

In the stationary coordinate system of electron 2 (denoted by the axes labeled *X*, *Y*, and *Z* in Figure AVI.3A), the $\frac{\hbar}{4}$ of intrinsic angular momentum is along X, the $\frac{\hbar}{2}$ of intrinsic angular momentum is along –*Y*, and $\mathbf{S}_3$, the $\hbar$ photon angular momentum vector due to spin interaction, is in the *XZ*-plane at an angle of $\theta = \frac{\pi}{6}$ relative to the –*Z*-axis. The *Z*-axis projection of $\mathbf{S}_3$ is $-\sqrt{\frac{3}{4}}\hbar$, and the *X*-axis projection of $\mathbf{S}_3$ is $-\frac{\hbar}{2}$. $\mathbf{S}_4$, the orbital angular momentum of $\sqrt{\frac{\ell}{\ell+1}}\hbar$, is directed along the *Z*-axis in the opposite direction of the *Z*-axis component of $\mathbf{S}_3$. Thus, in order to conserve angular momentum, the orbital angular momentum vector $\mathbf{S}_4$ corresponding to the rotational angular momentum vector of the $\ell = 0$ singlet and triplet states is now aligned in the opposite direction to that of the *Z*-axis component of the photonic spin vector $\mathbf{S}_3$, and the total angular momentum along the *Z*-axis due to spin and orbital contributions is:

$$\mathbf{S} = \left(\sqrt{\frac{\ell}{\ell+1}}\hbar - \sqrt{\frac{3}{4}}\hbar\right)\mathbf{i}_Z \tag{26}$$

In the stationary coordinate system of electron 1 (denoted by the axes labeled *X*′, *Y*′, and *Z*′ in Figure AVI.3B), the $\frac{\hbar}{4}$ of intrinsic angular momentum is along *X*′, the $\frac{\hbar}{2}$ of intrinsic angular momentum is along *Y*′, and the photon angular momentum vector $\mathbf{S}_1$ of magnitude $\hbar$ is in the *Y*′*Z*′-plane at an angle of $\theta = \frac{\pi}{3}$ relative to the *Y*′-axis. The *Z*′-axis projection of $\mathbf{S}_1$ is $\sqrt{\frac{3}{4}}\hbar$, and the Y'-axis projection of $\mathbf{S}_1$ is $\frac{\hbar}{2}$. $\mathbf{S}_2$, the orbital angular momentum of $\sqrt{\frac{\ell}{\ell+1}}\hbar$, is directed along the –*Z*′-axis in the opposite direction of the *Z*-axis component of $\mathbf{S}_1$. Thus, in order to conserve angular momentum, the orbital angular momentum vector $\mathbf{S}_2$ is aligned in the opposite direction to that of the *Z*′-axis component of the photonic spin vector $\mathbf{S}_1$, and the total angular momentum along the *Z*′-axis due to spin and orbital contributions is:

$$\mathbf{S} = \left(\sqrt{\frac{3}{4}}\hbar - \sqrt{\frac{\ell}{\ell+1}}\hbar\right)\mathbf{i}_{Z'} \tag{27}$$

The torque from the corresponding magnetic moments given by Eq. (2.65) are balanced in the absence of Larmor precession for the angular momentum projections of electron 2 shown in Figure AVI.3A relative to those of electron 1 shown in Figure AVI.3B. The superposition of the $\frac{\hbar}{4}$ of intrinsic angular momentum of electrons 1 and 2 along X' and X, respectively, each with a corresponding magnetic moment of $\frac{\mu_B}{4}$ (Eq. (2.65)) cancel the X -axis projection of $\mathbf{S}_3$ of $-\frac{\hbar}{2}$ with a corresponding magnetic moment of $-\frac{\mu_B}{2}$. The $-\frac{\hbar}{2}$ of total angular momentum of electron 2 along Y gives rise to magnetic field corresponding to $-\frac{\mu_B}{2}$ in the direction of the $\left(\sqrt{\frac{3}{4}}\hbar - \sqrt{\frac{\ell}{\ell+1}}\hbar\right)$ total Z-axis projection of electron 1. The $\frac{\hbar}{2}$ of intrinsic angular momentum of electron 1 along Y' and the Y'-axis projection of $\mathbf{S}_1$ of $\frac{\hbar}{2}$ gives rise to a total of $\hbar$ with a magnetic field corresponding to μ_B in the direction of the $\left(\sqrt{\frac{\ell}{\ell+1}}\hbar - \sqrt{\frac{3}{4}}\hbar\right)$ total Z-axis projection of electron 2.

Figure AVI.3. The relative angular momentum components of electron 1 and electron 2 to determine the magnetic interactions and the central magnetic force. (A) The atomic orbital and $\mathbf{S}_3$ and $\mathbf{S}_4$ of electron 2 in the stationary coordinate system X,Y,Z that is designated the unprimed spherical coordinate system relative to the Z-axis as shown. $\mathbf{S}_3$, the $\hbar$ photon angular momentum vector due to spin interaction, is in the XZ-plane at an angle of $\theta = \frac{\pi}{6}$ relative to the $-Z$-axis. $\mathbf{S}_4$, the orbital angular momentum of $\sqrt{\frac{\ell}{\ell+1}}\hbar$, is directed along the Z-axis in the opposite direction of the Z-axis component of $\mathbf{S}_3$. (B) The angular momentum components of the atomic orbital and $\mathbf{S}_1$ of electron 1 in the stationary coordinate system X',Y',Z' that is designated the primed spherical coordinate system relative to the Z'-axis as shown. The photon angular momentum vector $\mathbf{S}_1$ of magnitude $\hbar$ is in the $Y'Z'$-plane at an angle of $\theta = \frac{\pi}{3}$ relative to the Y'-axis. $\mathbf{S}_2$, the orbital angular momentum of $\sqrt{\frac{\ell}{\ell+1}}\hbar$, is directed along the $-Z'$-axis in the opposite direction of the Z-axis component of $\mathbf{S}_1$.

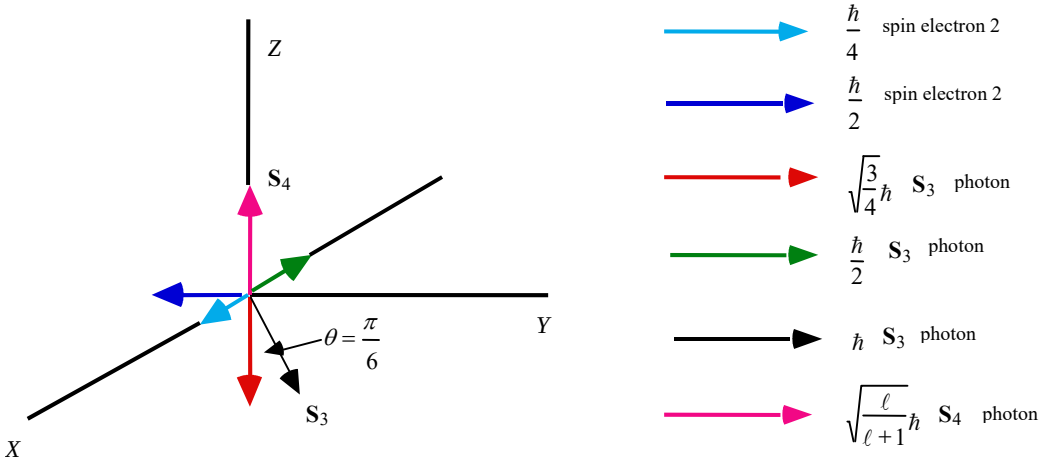

A

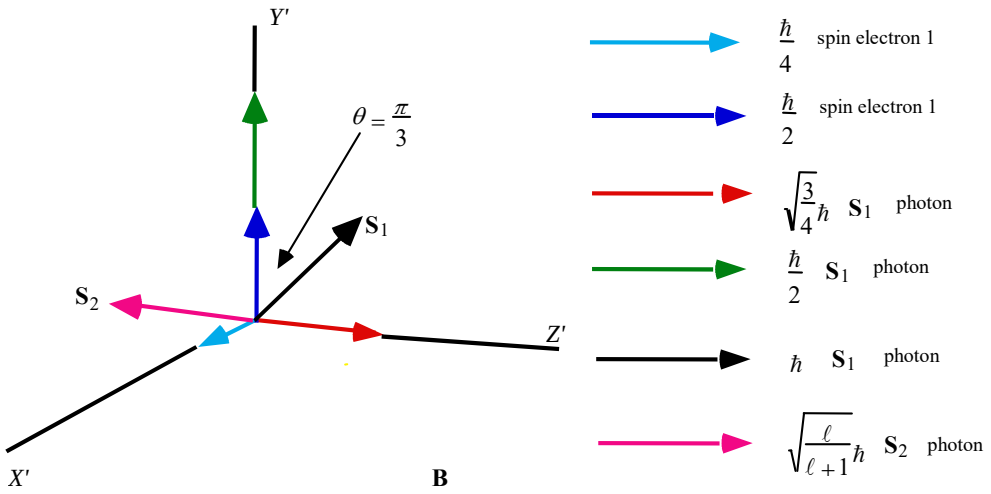

The magnetic central force is due to the interaction of the magnetic field of the electron 2 and the current dipole of the photon at the radius of electron 1 and vice versa. Considering the angular momentum vectors given in Figures AVI.3A and AVI.3B, the magnetostatic magnetic flux of electron 2 and electron 1 corresponding to $-\frac{\mu_B}{2}$ and μ_B, respectively, follow from Eqs. (1.132) and (1.133) and after McQuarrie [2]:

$$\mathbf{B} = -\frac{\mu_0 e\hbar}{2m_e r_2^3}(\mathbf{i}_{r'}\cos\theta - \mathbf{i}_{\theta'}\sin\theta) \tag{28}$$

$$\mathbf{B} = \frac{e\hbar}{2m_e r^3}(\mathbf{i}_r 2\cos\theta + \mathbf{i}_\theta \sin\theta) \tag{29}$$

where μ_0 is the permeability of free space ($4\pi\ X\ 10^{-7}\ N/A^2$) and the coordinates of the magnetic field due to electron 2 acting on the magnetic moments of electron 1 is designated as the primed system and the magnetic field of electron 1 acting on the magnetic moments of electron 2 is designated as the unprimed system. The angular velocity $\hat{\omega}$ and linear velocity $\mathbf{v}$ projections onto each $Z(Z')$-axis are:

$$\hat{\omega} = \frac{\hbar}{m_e r_2^2}\left(\sqrt{\frac{\ell}{\ell+1}} - \sqrt{\frac{3}{4}}\right)\mathbf{i}_Z \tag{30}$$

$$\mathbf{v} = \frac{\hbar}{m_e r_2}\left(\sqrt{\frac{\ell}{\ell+1}} - \sqrt{\frac{3}{4}}\right)\sin\theta\mathbf{i}_\phi \tag{31}$$

$$\hat{\omega} = \frac{\hbar}{m_e r_1^2}\left(\sqrt{\frac{3}{4}}\hbar - \sqrt{\frac{\ell}{\ell+1}}\hbar\right)\mathbf{i}_{Z'} \tag{32}$$

$$\mathbf{v} = \frac{\hbar}{m_e r_1}\left(\sqrt{\frac{3}{4}}\hbar - \sqrt{\frac{\ell}{\ell+1}}\hbar\right)\sin\theta\mathbf{i}_{\phi'} \tag{33}$$

The Lorentz force density at each point moving at velocity $\mathbf{v}$ is given by Eq. (8). Substitution of Eqs. (28-29), (31), and (33) into Eq. (8) while maintaining the designation of the coordinates of the magnetic field of electron 2 acting on the magnetic moments of electron 1 as the primed system and the coordinates of the magnetic field of electron 1 acting on the magnetic moments of electron 2 as the unprimed system gives

$$\mathbf{F}_{mag} = -\frac{e}{4\pi r_2^2}\left(\begin{array}{l}\frac{\hbar}{m_e r_1}\left(\sqrt{\frac{3}{4}} - \sqrt{\frac{\ell}{\ell+1}}\right)\sin\theta\mathbf{i}_{\phi'} \times \left(-\frac{\mu_0 e\hbar}{2m_e r_2^3}\right)(\mathbf{i}_{r'}\cos\theta - \mathbf{i}_{\theta'}\sin\theta) \\ + \frac{\hbar}{m_e r_2}\left(\sqrt{\frac{\ell}{\ell+1}} - \sqrt{\frac{3}{4}}\right)\sin\theta\mathbf{i}_\phi \times \frac{\mu_0 e\hbar}{2m_e r_2^3}(\mathbf{i}_r 2\cos\theta + \mathbf{i}_\theta \sin\theta)\end{array}\right) \tag{34}$$

From Eqs. (10-13), the magnetic force is

$$\mathbf{F}_{mag} = \frac{e}{4\pi r_2^2}\frac{1}{n}\frac{\hbar^2}{2m_e r_2^3}\left(\sqrt{s(s+1)} - \sqrt{\frac{\ell}{\ell+1}}\right)\mathbf{i}_r \tag{35}$$

The magnetic force between the two electrons is given by the product of magnetic multipole coefficient $a_M(\ell, m)$ given by Eq. (9.49) and the sum of the relativistically corrected Lorentz force terms due to the spin angular and orbital angular momenta of $\sqrt{s(s+1)}\hbar$ and $\sqrt{\frac{\ell}{\ell+1}}\hbar$, respectively:

$$\mathbf{F}_{mag} = \frac{1}{n}\frac{\frac{3}{2}}{(2\ell+1)!!}\frac{1}{\ell+2}\left(\frac{\ell+1}{\ell}\right)^{1/2}\frac{1}{2}\frac{\hbar^2}{m_e r^3}\left(\sqrt{s(s+1)} - \sqrt{\frac{\ell}{\ell+1}}\right)\mathbf{i}_r \tag{36}$$

The force balance between the centrifugal and electric and magnetic forces given by Eq. (9.52) is:

$$\frac{m_e v^2}{r_2} = \frac{\hbar^2}{m_e r_2^3} = \frac{1}{n}\frac{e^2}{4\pi\varepsilon_0 r_2^2} - \frac{1}{n}\frac{\frac{3}{2}}{(2\ell+1)!!}\left(\frac{\ell+1}{\ell}\right)^{1/2}\frac{1}{\ell+2}\frac{1}{2}\frac{\hbar^2}{m_e r^3}\left(\sqrt{s(s+1)} - \sqrt{\frac{\ell}{\ell+1}}\right) \tag{37}$$

TRIPLET EXCITED STATES WITH $\ell \neq 0$

With $\ell \neq 0$, the electron source current in the singlet excited state is the sum of orbital and spin components. The $\sqrt{\frac{\ell}{\ell+1}}\hbar$ of orbital angular momentum of electron 2 superimposes with the projection of the spin angular momentum that is twice that of the $\ell \neq 0$ singlet state. The vectors are in opposite directions in order to conserve angular momentum during excitation.

The $\ell \neq 0$ triplet state requires a further excitation to unpair the spin states of the two electrons. The angular momentum corresponding to the excited state is $\hbar$ and the angular momentum change corresponding to the spin-flip is also $\hbar$ as given in the Magnetic Parameters of the Electron (Bohr Magneton) section. Then, the triplet state comprises spin interaction terms between the two electrons plus a contribution from the unpairing photon. As shown in the Resonant Precession of the Spin-1/2-Current-Density Function Gives Rise to the Bohr Magneton section, the electron spin angular momentum gives rise to a trapped photon with $\hbar$ of angular momentum along an **S**-axis. Then, the spin state of each of electron 1 and 2 comprises a photon standing wave that is phase-matched to a spherical harmonic source current, a spherical harmonic dipole $Y_\ell^m(\theta,\phi) = \sin\theta$ with respect to the **S**-axis. The dipole spins about the **S**-axis at the angular velocity given by Eq. (1.36) with $\hbar$ of angular momentum. To conserve angular momentum, the orbital angular momentum is in the opposite direction of each *Z*-axis component of **S**, the axis of the photon angular momentum due to spin and the axis of the photon angular momentum due to unpairing, and the corresponding opposite current rotation corresponds to $-\frac{1}{2}\sqrt{\frac{\ell}{\ell+1}}\hbar$ of angular momentum relative to each photon vector **S**. The intrinsic spin and photon angular momentum vectors are shown in Figure AVI.4.

In the stationary coordinate system of electron 2 (denoted by the axes labeled *X*, *Y*, and *Z* in Figure AVI.4A), the $\frac{\hbar}{4}$ of intrinsic angular momentum is along *X*, the $\frac{\hbar}{2}$ of intrinsic angular momentum is along *Y*, and $\mathbf{S}_3$, the $\hbar$ photon angular momentum vector due to spin interaction, is in the *YZ*-plane at an angle of $\theta = \frac{\pi}{6}$ relative to the *Z*-axis. The *Z*-axis projection of $\mathbf{S}_3$ is $\sqrt{\frac{3}{4}}\hbar$, and the *Y*-axis projection of $\mathbf{S}_3$ is $\frac{\hbar}{2}$.

Electron 2 is excited by the additional spin-unpairing photon. The angular momentum vector $\mathbf{S}_4$ of magnitude $\hbar$ in the *XZ*-plane is aligned in the plane perpendicular to $\mathbf{S}_3$ at an angle of $\theta = \frac{\pi}{6}$ relative to the *Z*-axis. The *Z*-axis projection of $\mathbf{S}_4$ is $\sqrt{\frac{3}{4}}\hbar$, and the *X*-axis projection of $\mathbf{S}_4$ is $-\frac{\hbar}{2}$.

In order to conserve angular momentum, the orbital angular momentum vector $\mathbf{S}_2$ corresponding to the rotational angular momentum vector of the $\ell = 0$ singlet and triplet states state is now aligned in the opposite direction to that of the photonic spin

vectors $\mathbf{S}_3$ and $\mathbf{S}_4$. $\mathbf{S}_2$, the orbital angular momentum of $\sqrt{\frac{\ell}{\ell+1}}\hbar$, is directed along the –*Z*-axis in the opposite direction of the *Z*-axis component of $\mathbf{S}_3$ and $\mathbf{S}_4$. The total angular momentum along the *Z*-axis due to spin, unpairing, and orbital components is

$$\mathbf{S}=\left(\sqrt{\frac{3}{4}}\hbar+\sqrt{\frac{3}{4}}\hbar-\sqrt{\frac{\ell}{\ell+1}}\hbar\right)\mathbf{i}_Z=\left(2\sqrt{\frac{3}{4}}\hbar-\sqrt{\frac{\ell}{\ell+1}}\hbar\right)\mathbf{i}_Z \tag{38}$$

and the total angular momentum along the *Y*-axis comprising the sum of the initial $\frac{\hbar}{2}$ intrinsic angular momentum and the *Y*-axis projection of $\mathbf{S}_3$ of $\frac{\hbar}{2}$ is:

$$\mathbf{S}=\left(\frac{\hbar}{2}+\frac{\hbar}{2}\right)\mathbf{i}_Y=\hbar\mathbf{i}_Y \tag{39}$$

In the stationary coordinate system of electron 1 (denoted by the axes labeled *X*′, *Y*′, and *Z*′ in Figure AVI.4B), the $\frac{\hbar}{4}$ of intrinsic angular momentum is along *X*', the $\frac{\hbar}{2}$ of intrinsic angular momentum is along *Y*', and the photon angular momentum vector $\mathbf{S}_1$ of magnitude $\hbar$ is in the *Y*′*Z*′-plane at an angle of $\theta=\frac{\pi}{3}$ relative to the *Y*′-axis. The *Z*′-axis projection of $\mathbf{S}_1$ is $\sqrt{\frac{3}{4}}\hbar$, and the *Y*′-axis projection of $\mathbf{S}_1$ is $\frac{\hbar}{2}$. Since the $\sqrt{\frac{3}{4}}\hbar$ Z'-axis projection of $\mathbf{S}_1$ is one half that of the *Z*-axis component of $\mathbf{S}_3$ and $\mathbf{S}_4$, the orbital angular momentum $\mathbf{S}_2$ is $\frac{1}{2}\sqrt{\frac{\ell}{\ell+1}}\hbar$ and is directed along the –*Z*′-axis in the opposite direction of the *Z*-axis component of $\mathbf{S}_1$. Thus, in order to conserve angular momentum, the orbital angular momentum vector of the triplet state $\mathbf{S}_2$ is aligned in the opposite direction to that of the *Z*′-axis component of the photonic spin vector $\mathbf{S}_1$, and the total angular momentum along the *Z*′-axis due to spin and orbital contributions is

$$\mathbf{S}=\left(\sqrt{\frac{3}{4}}\hbar-\frac{1}{2}\sqrt{\frac{\ell}{\ell+1}}\hbar\right)\mathbf{i}_{Z'} \tag{40}$$

The torque from the corresponding magnetic moments given by Eq. (2.65) is balanced in the absence of Larmor precession for the angular momentum projections of electron 2 shown in Figure AVI.4A relative to those of electron 1 shown in Figure AVI.4B. The superposition of the $\frac{\hbar}{4}$ of intrinsic angular momentum of electrons 1 and 2 along *X*′ and *X*, respectively, each with a corresponding magnetic moment of $\frac{\mu_B}{4}$ (Eq. (2.65)) cancel the *X*-axis projection of $\mathbf{S}_4$ of $-\frac{\hbar}{2}$ with a corresponding magnetic moment of $-\frac{\mu_B}{2}$. The $\hbar$ of total angular momentum of electron 2 along *Y* gives rise to magnetic field corresponding to μ_B in the direction of the $\left(\sqrt{\frac{3}{4}}\hbar-\frac{1}{2}\sqrt{\frac{\ell}{\ell+1}}\hbar\right)$ total *Z*-axis projection of electron 1. The $\frac{\hbar}{2}$ of intrinsic angular momentum of electron 1 along *Y*′ and the *Y*′-axis projection of $\mathbf{S}_1$ of $\frac{\hbar}{2}$ gives rise to a total of $\hbar$ with a magnetic field corresponding to μ_B in the direction of the $\left(2\sqrt{\frac{3}{4}}\hbar-\sqrt{\frac{\ell}{\ell+1}}\hbar\right)$ total *Z*-axis projection of electron 2.

Figure AVI.4. The relative angular momentum components of electron 1 and electron 2 to determine the magnetic interactions and the central magnetic force. (A) The atomic orbital and $\mathbf{S}_2$, $\mathbf{S}_3$, and $\mathbf{S}_4$ of electron 2 in the stationary coordinate system *X*,*Y*,*Z* that is designated the unprimed spherical coordinate system relative to the *Z*-axis as shown. The orbital angular momentum vector $\mathbf{S}_2$ of magnitude $\sqrt{\frac{\ell}{\ell+1}}\hbar$ is along the –*Z*-axis. $\mathbf{S}_3$, the $\hbar$ photon angular momentum vector due to spin interaction, is in the *YZ*-plane at an angle of $\theta = \frac{\pi}{6}$ relative to the *Z*-axis. $\mathbf{S}_4$, the $\hbar$ photon angular momentum vector due to spin unpairing, is in the *XZ*-plane at an angle of $\theta = \frac{\pi}{6}$ relative to the *Z*-axis. (B) The angular momentum components of the atomic orbital and $\mathbf{S}_1$ of electron 1 in the stationary coordinate system *X*′,*Y*′,*Z*′ that is designated the primed spherical coordinate system relative to the *Z*′-axis as shown. The photon angular momentum vector $\mathbf{S}_1$ of magnitude $\hbar$ is in the *Y*′*Z*′-plane at an angle of $\theta = \frac{\pi}{3}$ relative to the *Y*′-axis. $\mathbf{S}_2$, the orbital angular momentum of $\frac{1}{2}\sqrt{\frac{\ell}{\ell+1}}\hbar$, is directed along the –*Z*′-axis in the opposite direction of the *Z*-axis component of $\mathbf{S}_1$.

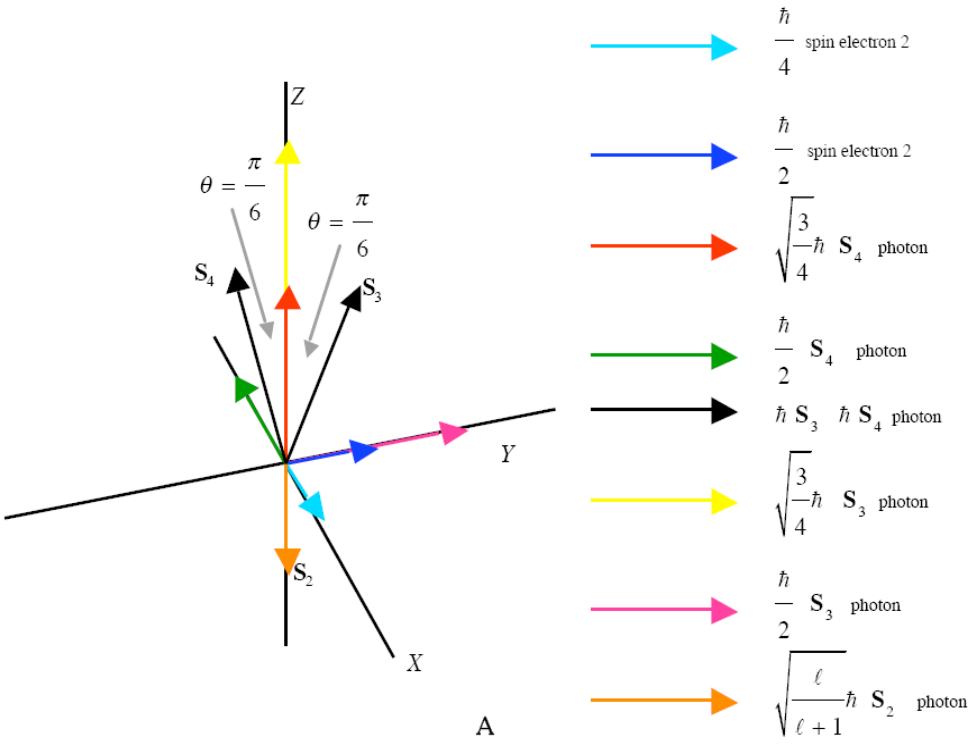

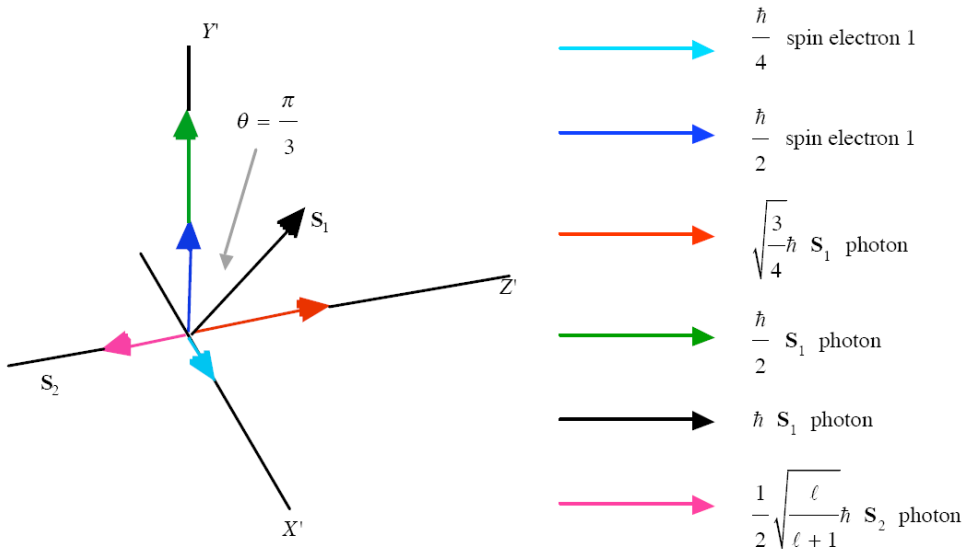

B

The magnetic central force is due to the interaction of the magnetic field of electron 2 and the current dipole of the photon at the radius of electron 1 and vice versa. Considering the angular momentum vectors given in Figures AVI.4A and AVI.4B, the magnetostatic magnetic flux of electron 2 and electron 1 corresponding to μ_B and μ_B, respectively, follow from Eqs. (1.132) and (1.133) and after McQuarrie [2]:

$$\mathbf{B} = \frac{\mu_0 e\hbar}{m_e r_2^3}(\mathbf{i}_{r'}\cos\theta - \mathbf{i}_{\theta'}\sin\theta) \tag{41}$$

$$\mathbf{B} = \frac{e\hbar}{2m_e r^3}(\mathbf{i}_r 2\cos\theta + \mathbf{i}_\theta \sin\theta) \tag{42}$$

where μ_0 is the permeability of free space ($4\pi\ X\ 10^{-7}\ N/A^2$) and the coordinates of the magnetic field due to electron 2 acting on the magnetic moments of electron 1 is designated as the primed system and the magnetic field of electron 1 acting on the magnetic moments of electron 2 is designated as the unprimed system. The angular velocity $\hat{\omega}$ and linear velocity **v** projections onto each $Z(Z')$ -axis are:

$$\hat{\omega} = \frac{\hbar}{m_e r_2^2}\left(2\sqrt{\frac{3}{4}} - \sqrt{\frac{\ell}{\ell+1}}\right)\mathbf{i}_Z \tag{43}$$

$$\mathbf{v} = \frac{\hbar}{m_e r_2}\left(2\sqrt{\frac{3}{4}} - \sqrt{\frac{\ell}{\ell+1}}\right)\sin\theta\mathbf{i}_\phi \tag{44}$$

$$\hat{\omega} = \frac{\hbar}{m_e r_1^2}\left(\sqrt{\frac{3}{4}}\hbar - \frac{1}{2}\sqrt{\frac{\ell}{\ell+1}}\hbar\right)\mathbf{i}_{Z'} \tag{45}$$

$$\mathbf{v} = \frac{\hbar}{m_e r_1}\left(\sqrt{\frac{3}{4}}\hbar - \frac{1}{2}\sqrt{\frac{\ell}{\ell+1}}\hbar\right)\sin\theta\mathbf{i}_{\phi'} \tag{46}$$

The Lorentz force density at each point moving at velocity **v** is given by Eq. (8). Substitution of Eqs. (41-42), (44), and (46) into Eq. (8) while maintaining the designation of the coordinates of the magnetic field of electron 2 acting on the magnetic moments of electron 1 as the primed system and the coordinates of the magnetic field of electron 1 acting on the magnetic moments of electron 2 as the unprimed system gives

$$\mathbf{F}_{mag} = -\frac{e}{4\pi r_2^{\,2}}\left(\begin{array}{l}\dfrac{\hbar}{m_e r_1}\left(\sqrt{\dfrac{3}{4}}-\dfrac{1}{2}\sqrt{\dfrac{\ell}{\ell+1}}\right)\sin\theta\mathbf{i}_{\phi'}\times\dfrac{\mu_0 e\hbar}{m_e r_2^3}\left(\mathbf{i}_{r'}\cos\theta-\mathbf{i}_{\theta'}\sin\theta\right)\\ +\dfrac{\hbar}{m_e r_2}\left(2\sqrt{\dfrac{3}{4}}-\sqrt{\dfrac{\ell}{\ell+1}}\right)\sin\theta\mathbf{i}_{\phi}\times\dfrac{\mu_0 e\hbar}{2m_e r_2^3}\left(\mathbf{i}_{r}2\cos\theta+\mathbf{i}_{\theta}\sin\theta\right)\end{array}\right) \tag{47}$$

From Eqs. (10-13), the magnetic force is

$$\mathbf{F}_{mag} = -\frac{e}{4\pi r_2^{\,2}}\frac{1}{n}\frac{\hbar^2}{2m_e r_2^3}\left(2\sqrt{s(s+1)}-\sqrt{\frac{\ell}{\ell+1}}\right)\mathbf{i}_r \tag{48}$$

The magnetic force between the two electrons is given by the product of magnetic multipole coefficient $a_M\left(\ell,m\right)$ given by Eq. (9.49) and the sum of the relativistically corrected Lorentz force terms due to the spin angular and orbital angular momenta of $\sqrt{s\left(s+1\right)}\hbar$ and $\sqrt{\dfrac{\ell}{\ell+1}}\hbar$, respectively:

$$\mathbf{F}_{mag} = -\frac{1}{n}\frac{\frac{3}{2}}{\left(2\ell+1\right)!!}\left(\frac{\ell+1}{\ell}\right)^{1/2}\frac{1}{\ell+2}\frac{1}{2}\frac{\hbar^2}{m_e r^3}\left(2\sqrt{s(s+1)}-\sqrt{\frac{\ell}{\ell+1}}\right)\mathbf{i}_r \tag{49}$$

The force balance between the centrifugal and electric and magnetic forces given by Eq. (9.63) is

$$\frac{m_e v^2}{r_2} = \frac{\hbar^2}{m_e r_2^3} = \frac{1}{n}\frac{e^2}{4\pi\varepsilon_0 r_2^2} + \frac{1}{n}\frac{\frac{3}{2}}{\left(2\ell+1\right)!!}\left(\frac{\ell+1}{\ell}\right)^{1/2}\frac{1}{\ell+2}\frac{1}{2}\frac{\hbar^2}{m_e r^3}\left(2\sqrt{s(s+1)}-\sqrt{\frac{\ell}{\ell+1}}\right) \tag{50}$$

REFERENCES

1. J. D. Jackson, *Classical Electrodynamics*, Second Edition, John Wiley & Sons, New York, (1975), pp. 236-240, 601-608, 786-790.
2. D. A. McQuarrie, *Quantum Chemistry*, University Science Books, Mill Valley, CA, (1983), pp. 238-241.
3. J. D. Jackson, *Classical Electrodynamics*, Second Edition, John Wiley & Sons, New York, (1975), p. 178.

POSTFACE

GUTCP REVIEW COMPLETED, WEBB SHOWS PREDICTED BIG BANG BUST

Dr. Randy Booker, Professor of Physics, University of North Carolina, Asheville recently completed the peer review [1] of the entire Grand Unified Theory of Classical Physics (GUTCP), involving a five-year effort. All the final derivations, computations, and comparisons with experimental observations were confirmed correct. Rather than assuming that the electron was a singularity, yet exists over all space simultaneously, the origins of Mills GUTCP was based on first seeking a physical solution of the electron by treating it as a source current for the absorption and emission of discrete electromagnetic waves, photons. This starting point revisits the stability of the atom to radiation.

In the atom such as the simplest one, hydrogen, the electron is constantly accelerating around the proton in an atomic orbit. Yet, classical physics requires that accelerating charges radiate energy, which would cause the electron to spiral into the nucleus in a fraction of a second. This seminal problem of the stability of the atom was one of the key obstacles that physicists faced early in the 20th century, and their inability to solve it led to the construction of quantum theory. Mills solved the structure of the electron using classical physical laws, such that electron orbits were stable to radiation. This allowed Mills to construct a new theory of atoms and molecules that was based entirely on classical physics that provides exact solutions for core phenomena and observables of chemistry and physics over the scale of quarks to cosmos, 85 orders of magnitude. These results confirm that it was a colossal mistake to assume that physical laws do not apply to the atomic scale, the founding postulate of quantum theory. The same is true on the cosmological scale regarding the quantum-fluctuation-singularity to Big Bang to inflation to dark-energy origin and evolution theories of the universe recently observationally disproved.

Physical laws such as those of mechanics (Newton-Lorentz) and those of electrodynamics (Maxwell) require that as matter converts into energy according to $E = mc^2$, spacetime expands according to $\frac{c^3}{4\pi G}$ wherein G is the Newtonian gravitational constant. The resulting dynamic behavior is a universe that oscillates between matter-filled and energy-filled with a period of one trillion years. In 1995, Mills published an earlier GUTCP prediction [2] that the expansion of the universe was accelerating from the same equations that correctly predicted the present Hubble constant and the mass of the top quark before they were measured as well as those of the other fundamental particles and cosmological parameters. To the astonishment of cosmologists, Mills acceleration prediction was confirmed by 2000. Moreover, Mills GUTCP value for the Hubble constant matches the present observed value which has created another crisis in astrophysics regarding cosmological models that inescapably predict an unacceptable fitted value of Hubble constant from other fitted terms. Mills made another prediction based on GUTCP that the identity of dark matter is Hydrino, a more stable allotrope of molecular hydrogen, now isolated and confirmed by 23 spectroscopic methods [3-5]. Furthermore, the recent unanticipated Webb telescope images confirm additional GUTCP predictions of fully formed galaxies and old galaxies at the beginning of the expansion of the universe that disprove the long held metaphysical Big Bang and related theories of cosmology.

REFERENCES

1. https://brilliantlightpower.com/theory/.
2. R. L. Mills *The Grand Unified Theory of Classical Quantum Mechanics*, November 1995 Edition, Library of Congress Catalog Number 94-077780 Chp.22 ISBN number ISBN 0-9635171-1-2.
3. https://www.sciencedirect.com/science/article/pii/S0360319922022406.
4. https://brilliantlightpower.com/pdf/Hydrino_States_of_Hydrogen.pdf.
5. https://brilliantlightpower.com/pdf/Analytical_Presentation.pdf.

ABOUT THE AUTHOR

Randell L. Mills received a Bachelor of Arts Degree in chemistry, summa cum laude and Phi Beta Kappa from Franklin & Marshall College and a Doctor of Medicine Degree from Harvard Medical School with a concentration on technology while also studying electrical engineering at the Massachusetts Institute of Technology. He is the Founder and President of Brilliant Light Power, Inc., based in the Princeton, New Jersey area that is developing technologies based on novel hydrogen chemistry. He has authored or co-authored over a hundred (100) articles and a book in this field. He is also active in a number of other areas of technology. He has received or filed patent applications in the following areas: (1) hydrino/SunCell power source; (2) computational chemical design technology; (3) magnetic resonance imaging; (4) Mossbauer cancer therapy; (5) Luminide class of drug delivery molecules; (6) genomic sequencing method, (7) artificial intelligence, and (8) fifth force technology. He is a member of the American Chemical Society.

Dr. Mills has replaced the field generally known as Quantum Mechanics which postulates that classical physical laws do not apply at the atomic scale by deriving a new atomic theory of from those first principles, which unifies Maxwell's Equations, Newton's Laws, and General and Special Relativity. The central feature is that physical laws hold over all scales, from the scale of subatomic particles to that of the cosmos.

Quantum Mechanics has remained mysterious to all who have encountered it. Schrödinger postulated a boundary condition $\Psi \rightarrow 0$ as $r \rightarrow \infty$ of a wavelike positional probability for a singularity that is everywhere at once until measurement. The result was a purely algorithmic mathematical model of the hydrogen atom. In contrast, Mills solved the exact structure of matter and energy and related phenomena from known classical physics, (e.g. Maxwell's Equations wherein under special conditions, an extended distribution of charge may accelerate without radiating energy). This leads to a physical model of subatomic particles, atoms, and molecules. The closed-form solutions containing fundamental constants only agree with experimental observations demonstrating that the fundamental quantum mechanical postulate, "classical physical laws do not apply to the atomic scale", was erroneous.

From two basic equations, the key building blocks of organic chemistry have been solved, allowing the true physical structure and parameters of an infinite number of organic molecules up to infinite length and complexity to be obtained. These equations were also applied to bulk forms of matter, such as the allotropes of carbon, the solid bond of silicon and the semiconductor bond; as well as fundamental forms of matter such as the ionic bond and the metallic bond; and major fields of chemistry such as that of silicon, tin, aluminum, boron, and coordinate compounds.

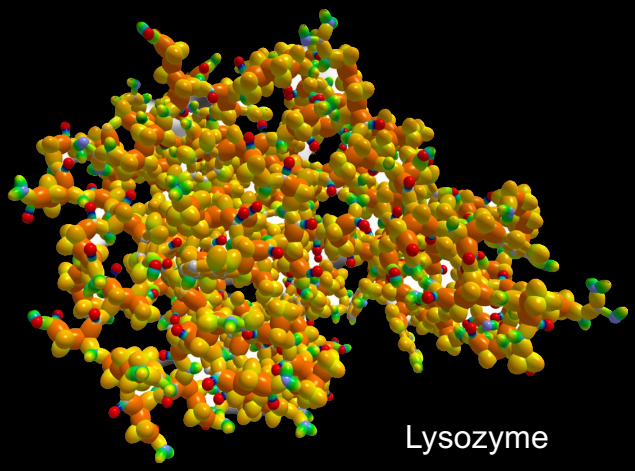

Lysozyme

Further, the Schwarzschild Metric is derived by applying Maxwell's Equations to electromagnetic and gravitational fields at particle production. This modifies General Relativity to include the conservation of spacetime and gives the origin of gravity, the families and masses of fundamental particles, the acceleration of the expansion of the universe (predicted by Dr. Mills in 1995 and since confirmed experimentally), and overturns the Big Bang model of the origin of the universe.

"Mills' theory explains the answers to some very old scientific questions, such as 'what happens to a photon upon absorption' and some very modern ones, such as 'what is dark matter.' ...Lastly, Mills has made an extremely important contribution to the philosophy of science. He has reestablished cause and effect as the basic principle of science." - **Dr. John J. Farrell**, former Chair of the Dept. of Chemistry, Franklin & Marshall College

"Mills' ingenious way of thinking creates in different physical areas astonishing results with fascinating mathematical simplicity and harmony. And his theory is strongly supported by the fact that nearly all these results are in comfortable accordance with experimental findings, sometimes with breathtaking accuracy." - **Dr Günther Landvogt,** Retired Scientist, Philips Research Lab

"Dr. Mills has apparently completed Einstein's quest for a unified field theory… without largesse from the US Government, and without the benediction of the US scientific priesthood." - **Shelby T. Brewer**, former Assistant Secretary of Energy, former CEO of ABB Combustion Engineering, MS/Ph.D. MIT - Nuclear Engineering.

"Mills proposes such a basic approach to quantum theory that it deserves considerably more attention from the general scientific community than it has received so far. The new theory appears to be a realization of Einstein's vision and a fitting closure of the "Quantum Century" that started in 1900..." - **Dr. Reinhart Engelmann**, Professor of Electrical Engineering, Oregon Graduate Institute of Science and Technology

Dr. Randell Mills holds a Doctor of Medicine degree from Harvard, a BA degree in Chemistry from Franklin and Marshall College, and studied Electrical Engineering at MIT. He is President, Chairman and CEO of Brilliant Light Power, Inc.